Aluminium Atoms at High Connectivity Sites in Polyhedral Polyborane Analogous Clusters: From Aluminaboranes to Carbaalanes

Werner Uhl*[a] and Frank Breher[a]

Keywords: Carbaalanes / Cluster compounds / Electron deficiency / Aluminium / Boron

Cluster chemistry in the third main group has long been restricted to compounds of the lightest element boron. However, about 30 years ago the first compounds were synthesized and characterized in which single aluminium atoms adopted positions of high connectivity in polyhedral borane or carbaborane clusters. The next successful step in these efforts to establish a chemistry analogous to that of the polyboranes with the heavier elements of the third main-group was the synthesis of *closo*-dodecaaluminate $[Al_{12}iBu_{12}]^{2-}$ at the beginning of the nineties, which was the first homonuclear aluminium analogue of a polyborate anion and had a core exclusively formed by aluminium atoms. Another class of interesting new aluminium compounds was formed by the carbaalanes, which were synthesized and characterized for the first time only recently. They have clusters of aluminium and carbon atoms, and are similar to the carbaborane analogues in that their structures seem to be determined by the number of electron pairs in their molecular centers in accordance with the Wade rules.

Introduction

Polyhedral compounds containing clusters of boron atoms have been well-known since the pioneering work of Alfred Stock at the beginning of this century.[1] Usually, the boron atoms in these clusters have a high connectivity[2] and are attached to up to six other boron atoms, as observed for a boron atom located above a boat-shaped six-membered ring in $[B_{11}H_{11}]^{2-}$.[3] Essentially, the configuration of these clusters is determined by the number of electron pairs delocalized in their molecular cores;[2][4] the addition of more electrons gives more open clusters. They can all be derived from the corresponding *closo* polyborate anions, in which the number of electron pairs exceeds the number of vertices by one. Two and three extra electron pairs are required for the electron count in *nido* or *arachno* compounds, respectively. The syntheses[5] of those polyborate anions or polyborane molecules often starts with diborane(6) (B_2H_6) or the borate anion $[BH_4]^-$, but in many cases the very sophisticated procedures yield the products in only poor yields. Nevertheless, these polyboron compounds form a class of well-characterized and highly interesting species with fascinating structures and bonding situations

[a] Fachbereich Chemie der Universität,
Postfach 2503, D-26111 Oldenburg, Germany
Fax: (internat.) +49-441/798-3352



Werner Uhl studied chemistry at the Technical University, Karlsruhe (Germany) where he obtained his PhD, after two years at the University of Marburg (Germany) under the supervision of Professor Gerd Becker, in 1980. Thereafter he undertook two years of industrial experience in the research and development department at the NUKEM company in Hanau (Germany), before he followed G. Becker to the University of Stuttgart (Germany) in 1983. He completed his "habilitation" in inorganic chemistry in 1989 and became a Professor of Inorganic Chemistry at the University of Oldenburg in 1992. In October 1999, he moved to the Philipps University of Marburg.



Frank Breher studied chemistry at the University of Oldenburg (Germany) where he graduated in 1998. After one year in the research group of Professor Uhl he moved with his group to the Philipps University of Marburg in September 1999. His research activities are focused on the synthesis of carbaalane cluster compounds.

MICROREVIEWS: This feature introduces the readers to the authors' research through a concise overview of the selected topic. Reference to important work from others in the field is included.

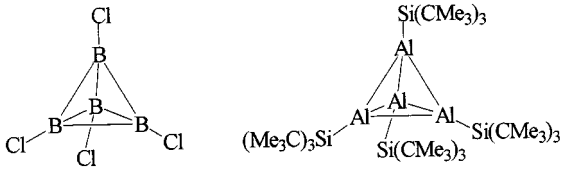
 © WILEY-VCH Verlag GmbH, D-69451 Weinheim, 2000 1434–1948/00/0101–0001 $ 17.50+.50/0

in their clusters, and were thoroughly investigated by conventional physical methods of structure determinations and quantum chemical calculations.[2]

Many years after the first synthesis of polyhedral polyboranes the carbaboranes were obtained as a new class of compounds; they have one or more boron atoms of the clusters replaced by carbon atoms. Often, they were synthesized by the reaction of polyboranes or some activated derivatives with alkynes,[2,5,6] but once again the yields are very low in most cases. The hydroboration of borylalkynes as a facile method for the synthesis of carbaboranes will be discussed in more detail later on. The structures and the bonding situation of these carbaboranes are quite similar to those of the pure boranes and this became clearer after the isolobality between the fragments BH^- and CH was recognized in the Sixties.[2] Carbaboranes are now known in huge numbers with a large variety of different structures and of carbon to boron ratios. They have been used to synthesize many fascinating derivatives with elements of the main group or transition metals enclosed in their clusters,[5] of which, as an example, only the dicarbollide ligand[7] will be mentioned, which gives coordination compounds similar to cyclopentadienyl complexes.

In contrast to these well-established classes of polyhedral cluster compounds, no comparable chemistry has been developed with aluminium which is the next heavier homologue of boron in the third main group. Only a few compounds have been described in the literature, in which one aluminium atom occupies a vertex in a borane or carbaborane cluster or which has a skeleton of aluminium atoms similar to the *closo* borate anions. Both these classes of compounds will be described in the next sections in more detail. Carbaalanes, which have clusters exclusively formed by aluminium and carbon atoms, analogous to the carbaboranes, have been obtained and completely characterized for the first time only recently by our group, they will be discussed in the last section of this Microreview.

Tetrahedral and neutral cluster compounds such as the rare examples containing boron, B_4Cl_4[8] (Scheme 1) or $B_4(CMe_3)_4$,[9] will not be considered here as they do not fit in the classic scheme of ordering in borane or carbaborane chemistry. This type of clusters has found considerable interest in current organoaluminium chemistry and several remarkable compounds with tetrahedra of aluminium atoms such as $Al_4Cp^*_4$[10] (Cp^* = pentamethylcyclopentadienyl), $Al_4[Si(CMe_3)_3]_4$[11] (Scheme 1), $Al_4[C(SiMe_3)_3]_4$,[12] or $Al_4[Si(SiMe_3)_3]_4$[13] have been reported in the literature. The cluster compound $[Al_{77}\{N(SiMe_3)_2\}_{20}]^{2-}$ was synthesized starting with aluminium(I) chloride and has three polyhedral shells of Al atoms and will also not be considered here.[14] The rapidly growing and fascinating chemistry of monovalent aluminium as well as the similar chemistry of the heavier homologues gallium, indium and thallium has been reviewed several times before.[15–17] Furthermore, we will not discuss compounds derived from these Al^I derivatives, which formally obey the Wade rules[4] for *closo* clusters like $Al_3Cp^*_3As_2$ with a trigonal bipyramidal Al_3As_2 cluster[18] and which, from quantum chemical calculations, have a delocalized electronic system in their molecular cores.

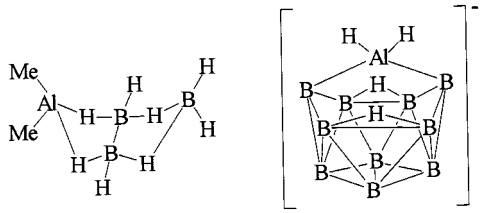


Scheme 1

Aluminaboranes and Aluminacarbaboranes

Few compounds are known in which single aluminium atoms occupy the positions of boron atoms in polyboranes. The simplest one (**1**) is derived from tetraborane(10), in which one bridging BH_2 group is replaced by an $AlMe_2$ group (Scheme 2). This compound was synthesized in high yield by the reaction of $[B_3H_8]^-$ with dimethylaluminium chloride,[19][20] and its structure was confirmed by an electron diffraction experiment in the gas phase.[20][21] Its conformation is quite similar to that of tetraborane(10),[22] although the inner B–B bond is lengthened. The Al–B distance of the Al–H–B three center bonds was found to be 231.6 pm which, as expected, is much longer than the Al–B distances observed in the other cage compounds discussed here. Decaborane(14) gave the aluminapolyborate anion $[AlH_2B_{10}H_{12}]^-$ (**2**) upon treatment with trimethylamine alane or monochloroalane adducts $AlXH_2{\cdot}NMe_3$ (X = H, Cl).[23][24] The structure is derived from that of $B_{10}H_{14}$ with the aluminium atom bridging the boron atoms in the 2,6 position of the boron polyhedron (Scheme 2). Compound **2** was claimed in 1965 to be the first compound containing a direct Al–B bond. Aluminium boranate $Al(BH_4)_3$ was reported to react with diborane(6), pentaborane(9) or tetraborane(10) with the formation of three different polyhedral aluminaboranes, for which the compositions AlB_4H_{11}, AlB_5H_{12}, and, after a decomposition reaction, AlB_6H_{13} were given.[25] The structures of these compounds are uncertain, although a polymeric structure with Al–H bridges was suggested from some physical and chemical properties. A *closo* aluminaboranate anion (**3**) analogous to $[B_{12}H_{12}]^{2-}$ was obtained according to Equation 1.[26] It possesses an icosahedron of eleven boron atoms and one aluminium atom (Figure 1). The B–B distances (176.0 to 185.6 pm) are within the normal range reported for polyboranes, the longer ones were observed for the pentagon bridged by the Al atom. As expected, the five B–Al distances are almost equidistant (213.1 to 214.0 pm) and the Al–C vector is only slightly tilted (by 2°) from the normal of that plane, which is formed by the five nearest boron atoms.

Much more information is available concerning carbaborane derivatives containing one aluminium atom, and much of the work has been done by the group of Hawthorne. A 3-alumina-1,2-dicarba-*closo*-dodecaborane **(4)**, obtained by the treatment of 1,2-dicarbaundecaborane with triethylaluminium (Equation 2),[27] has an icosahedral



1 **2**

Scheme 2

$$Na_2[B_{11}H_{13}] + Al(CH_3)_3 \xrightarrow[4\ days]{110°C} Na_2[B_{11}H_{11}AlCH_3] + 2\ CH_4 \quad (1)$$

3

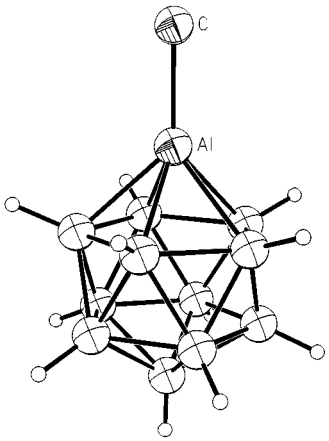


Figure 1. Molecular structure of $[MeAlB_{11}H_{11}]^{2-}$ **3**;[26] hydrogen atoms of the methyl group are omitted; boron atoms (not shaded) are not labelled

structure with the Al atom coordinated to both carbon atoms and three boron atoms as well as the terminal ethyl group (Figure 2). The Al−B and Al−C bond lengths in the cluster are 217.3 and 213.7 pm, respectively. As expected, the terminal Al−C bond is much shorter and has a length of 193.0 pm. The terminal Al−C bond is tilted from the normal of the B_3C_2 plane by 19.5°, so that the methylene group of the disordered ethyl substituent approaches both carbon atoms of the cluster. Compound **4** may be described as a dicarbollyl complex with a carbaboranate ligand coordinated to an Al atom; indeed, such compounds were later used as dicarbollyl transfer reagents.[28] The Al atom of **4** is electrophilic and, upon treatment with THF[29] or phosphanes,[30] adducts are formed in which the connectivity of the Al atoms is reduced to a normal value of four as shown by a crystal structure determination of a phosphane derivative (Figure 3). The cluster is attached to the Al atom by only one boron atom, and the Al−B distance is 212.8 pm, which is shorter than the three Al−B separations observed in the *closo* cluster **4**. The contacts of the Al atom to both remaining boron atoms are much longer (248.0 pm on average) and indicate no further significant bonding interaction. A similar reduction of the connectivity of the Al atoms was observed in some other cluster compounds, which had AlR_2 or AlRL (L = Et_2O) groups in bridging positions[29,30−33] and which are not discussed here in detail.

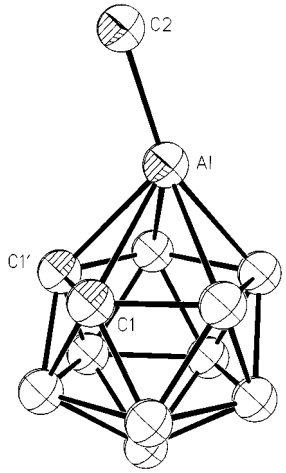


Figure 2. Molecular structure of $[EtAlB_9C_2H_{11}]$ **4**;[27] hydrogen atoms and the methyl group of the ethyl substituent are omitted; boron atoms (not shaded) are not labelled

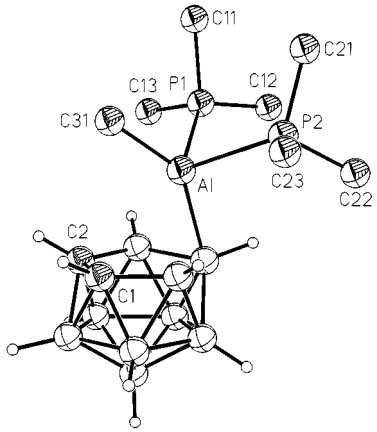


Figure 3. Molecular structure of $[EtAl(PEt_3)_2B_9C_2H_{11}]$;[30] hydrogen atoms of the alkyl groups are omitted; only the α carbon atoms of the ethyl groups are drawn; boron atoms (not shaded) are not labelled

$$(3)\text{-}1,2\text{-}B_9C_2H_{13} + Et_3Al \xrightarrow{50°C\ /\ 1\ h} 1,2\text{-}B_9C_2H_{12}AlEt_2 + C_2H_6 \quad (2)$$

$$1,2\text{-}B_9C_2H_{12}AlEt_2 \xrightarrow{77°C\ /\ 25\ h} 1,2\text{-}B_9C_2H_{11}AlEt + C_2H_6$$

4

Two remarkable bis(dicarbollide)aluminium sandwich compounds were described by the group of Hawthorne,[30,34–36] and may be named as *commo*-3,3′-bis(3-alumina-1,2-dicarba-*closo*-dodecaboranate) (Figure 4). One compound was obtained by the treatment of the aluminacarbaborane **4** with carbon monoxide.[30][34] It has an *exo* diethylaluminium group coordinated by two hydrogen atoms to one of the carbaborane clusters. The second compound (**5**) was synthesized by the reaction of diethylaluminium chloride with a thallium salt of the corresponding carbaborane (Equation 3).[30][35] An anionic symmetric sandwich compound (**5**, Figure 4) was isolated, in which

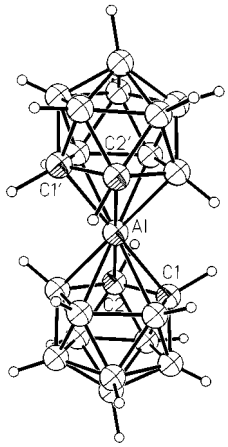


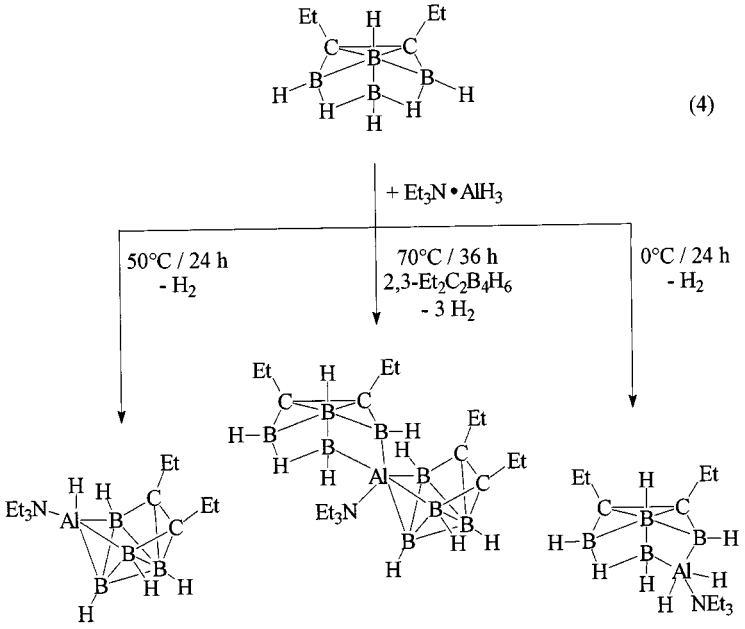
Figure 4. Molecular structure of $[Al(B_9C_2H_{11})_2]^-$ **5**;[34] boron atoms (not shaded) are not labelled

$$2\ Tl_2[7,8\text{-}C_2B_9H_{11}] + 4\ Et_2AlCl \longrightarrow Tl[Al(C_2B_9H_{11})_2] + 2\ Tl[AlEt_3Cl] + Tl[AlEt_2Cl_2] \quad (3)$$

5

two *closo* aluminacarbaboranes have a common Al atom. As expected, the Al–C and Al–B distances (224 to 230 pm and 214 to 229 pm, respectively) are longer than the distances observed in the monodicarbollyl compound **4**, which is probably caused by the greater connectivity of the Al atom (ten in **5**, six in **4**). Further *commo* derivatives with smaller carbaborane moieties are also known from the literature.[30,37,38] The aluminium atoms in these compounds have, however, normal coordination numbers of four. In one compound, the Al atom bridges two *nido*-6,9-dicarbadecaboranate ligands via their carbon atoms.[37] The metal atom resides above the six-membered B_4C_2 heterocycles with a boat conformation and is tetrahedrally coordinated by all four carbon atoms. The Al–C distances are 206 pm, which is longer than expected for tetracoordinated Al atoms. The Al–B distances are much longer (253 pm) indicating a very weak bonding interaction. In the second compound two *nido*-2,7-dicarba-octaboranate units are bridged by a common Al atom.[38] Once again the metal atom is tetrahedrally coordinated by the four carbon atoms of the ligands. The distance between both carbon atoms of one ligand is smaller than that in the carbaborate cage discussed before and, probably due to the lower steric strain, the Al–C distances are shorter (201.8 pm). Two of the Al–B distances are quite short (228 pm on average) and may indicate a further bonding interaction.

Small aluminacarbaborane clusters not stabilized by donor atoms, beside the *commo* compounds just cited, are rare. One article reported the reaction of the anionic cababorane $[2,3\text{-}C_2B_4H_7]^-$ with dimethylaluminium chloride,[39] which should yield μ-dimethylaluminium-2,3-*nido*-dicarbahexaborane(8). It was described as a very unstable compound in the liquid form or in solution and was thermolyzed in the gas phase to yield the unstable *closo* compound $MeAlC_2B_4H_6$. Remarkably, the gallium analogues of both compounds are much more stable and were isolated and



(4)

characterized.[39][40] Another reaction has been published, in which *nido*-$Et_2C_2B_4H_6$ was treated with the triethylamine alane adduct and from which, depending on the reaction conditions, three different products were obtained (Equation 4).[41] In accordance with the NMR and IR spectroscopic data, as well as elemental analyses, the authors suggested the structures given in Equation 4, which all have Al atoms with a higher connectivity than four.

The Icosahedral Compound $[Al_{12}iBu_{12}]^{2-}$ (6)

Compound **6** is the only known polyhedral organoelement compound containing only aluminium atoms which obeys the Wade rules for a *closo* cluster. It was obtained and characterized by a crystal structure determination in our group in 1991.[42] In 1976 the reduction of di(isobutyl)-aluminium chloride with elemental potassium was reported to yield tetra(isobutyl)dialane(4) with an Al−Al bond.[43] The compound was isolated as a brown oil and characterized by a hydrolysis experiment. However, in our experience, very large substituents are required to stabilize such dialuminium compounds, which contain bivalent aluminium atoms, against disproportionation reactions; we succeeded in isolating the first stable and completely characterized dialane(4), when we employed bulky bis(trimethylsilyl)methyl groups.[44] Therefore, we reinvestigated the synthesis of the isobutyl derivative and found a completely different result (Equation 5).[15] The main product is not the dialumium derivative originally proposed, but a potassium chloride adduct of tri(isobutyl)aluminium, which may be formed by a disproportionation reaction. A solid precipitated out of the reaction mixture, from which two products were extracted by treatment with toluene. One of these was identified as $K[Cl_2AliBu_2]$. The other one (**6**) was isolated as dark red crystals in a very low, but reproducible, yield of about 2%, and was identified as $K_2[Al_{12}iBu_{12}]$ by a crystal structure determination (Figure 5).[42] Compound **6** possesses an almost undistorted icosahedron of twelve aluminium atoms and is isoelectronic with the *closo*-borate anion $[B_{12}H_{12}]^{2-}$. The Al−Al distances are in a narrow range of 267.9 to 269.6 pm and are only slightly lengthened relative to the Al−Al single bonds in tetraalkyldialane(4) compounds (264 to 266 pm).[44][45] As shown in Figure 5, four triangles of each Al_{12} cluster are bridged by potassium ions to give a three-dimensional network in the solid state with tetrahedrally coordinated cluster anions and linearly coordinated potassium cations. Thus, the arrangement of anions and cations is quite different to that in solid $K_2[B_{12}H_{12}]$.[46]

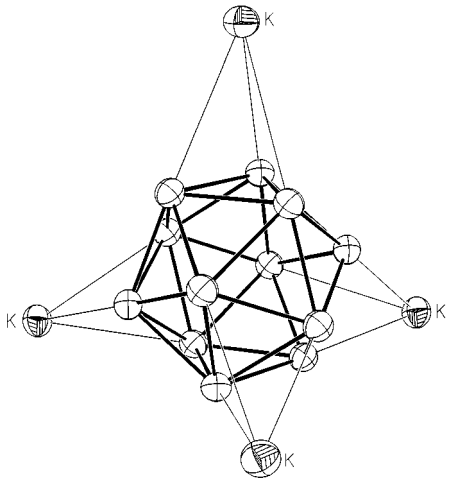
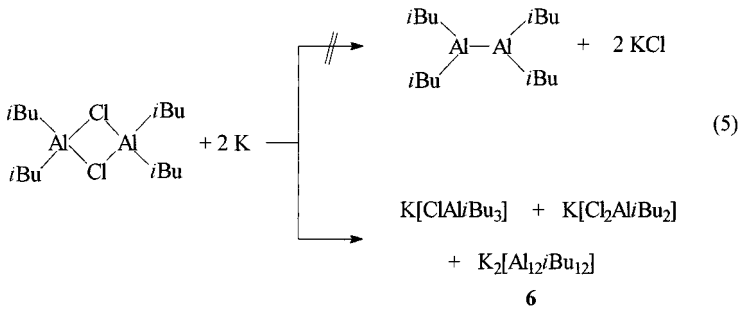


Figure 5. Crystal structure of $K_2[Al_{12}iBu_{12}]$ **6**;[42] isobutyl groups are omitted; each icosahedron is surrounded by four potassium ions to give a three-dimensional network

Compound **6** is only moderately stable in solution and decomposes slowly with the precipitation of elemental aluminium. In the crystalline form, it is much more stable with a decomposition point of 150 °C. The crystals can be stored in air for about two hours with no obvious signs of decomposition, but then slowly a colorless substance, probably aluminium hydroxide, is formed on their surfaces. Cyclovoltammetry revealed a reversible one-electron oxidation process, followed by a second irreversible oxidation.[47] In this respect the dodecaaluminate is similar to the corresponding boron compounds.[48]

A further anionic polyhedral cluster compound formed exclusively from aluminium atoms has been postulated by the group of Schnöckel, but until now it has not been isolated in a pure form or structurally characterized.[49] The reaction of aluminium(I) chloride with *tert*-butyllithium yielded a dark red, quite stable product of, presumably, a neutral oligomeric *tert*-butylaluminium(I) compound. Treatment of this intermediate with sodium/potassium alloy gave a radical anion (Equation 6) which, from an ESR spectroscopic characterization and quantum chemical calculations, was identified as the octahedral hexaaluminium compound $[Al_6(CMe_3)_6]^-$.[49] Furthermore, theory showed that the hypothetical neutral hexamer is much more stable



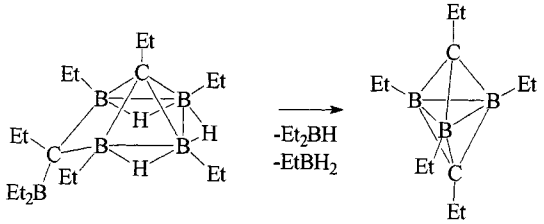
than the monomeric fragments (540 kJ/mol), and that the molecule is further stabilized by the addition of an electron and the formation of the radical anion by 140 kJ/mol.[16][49]

$$n\,AlCl + n\,LiCMe_3 \longrightarrow Al_n(CMe_3)_n \xrightarrow{Na/K} [Al_6(CMe_3)_6]^{\bullet -} \quad (6)$$

Hydroboration for the Synthesis of Carbaboranes; Some Remarks on Hydroalumination

The reaction of polyboranes with alkynes is the standard method for the synthesis of polyhedral carbaboranes.[5] However, mixtures are often formed and the isolation of pure products, even in a poor yield, is extremely difficult. The hydroboration of dialkylborylalkynes or bis(dialkylboryl)ethynes, followed by condensation reactions, offers an alternative route for the synthesis of carbaboranes, and several recent reports described such reactions, which yielded the products in some cases in a moderate to high yield.[50–57] For instance, treatment of diethylborylethyne with a large excess of diethylboron hydride afforded 1-carba-*arachno*-pentaborane(10) **(7)** (Equation 7), which by loss of diethylboron hydride and ethylboron dihydride gave *closo* dicarba-pentaborane(5) **(8)**.[51] Other products were identified, when the selectivity of the reaction was reduced.[55]

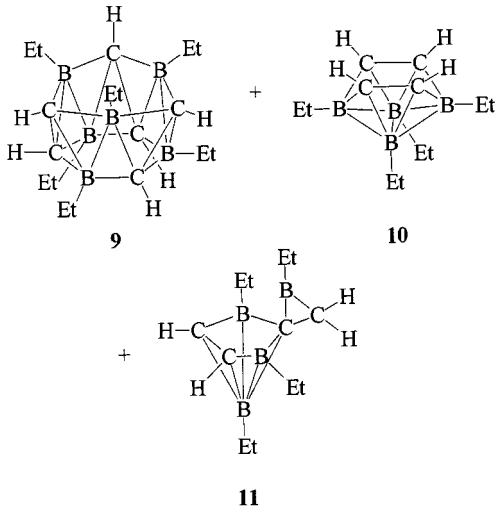
$$Et_2B{-}C{\equiv}C{-}Me + Et_2BH\ (excess) \xrightarrow[-Et_3B]{} \quad (7)$$



7 **8**

A mixture of carbaboranes was formed by the reaction of a diborylethyne with an excess of dialkylboron hydride (Equation 8), from which three products were isolated and characterized by NMR spectroscopy, one crystal structure determination and comparison of the observed data with those obtained by quantum chemical calculations.[54,56,57] Compound **9** was identified as a hexacarba-*arachno*-dodecaborane(12), which has a hexagonal antiprism of carbon and boron atoms.[56] The tetracarba-*nido*-octaborane(8) derivative **(10)** was isolated in a yield of 9% and contains a hexagonal face in a boat form, which has two pairs of carbon atoms bridged by two boron atoms.[54] The third compound **11** was isolated and characterized as a mixture with **10**. It was identified as a spiro compound, in which a 2,3,5-tricarba-*nido*-hexaborane cluster was connected to a three-membered C_2B heterocycle by a common carbon atom.[57] Some further examples, which are not discussed here in detail, show that the hydroboration reaction is a powerful method for the synthesis of such carbaborane clusters.

$$Et_2B{-}C{\equiv}C{-}BEt_2 + Et_2BH\ (excess) \xrightarrow[-Et_3B]{} \quad (8)$$



9 **10**

11

Similar to hydroboration is hydroalumination, which has been used in the synthesis of alkylaluminium derivatives and in preparative organic chemistry.[58][59] In many cases, the products obtained by the addition of Al–H bonds to alkynes were, however, not isolated and characterized, but hydrolyzed to liberate the corresponding hydrocarbons.[59] Thus, only poor information concerning the structure of most of the organoaluminium intermediates is available in the literature. To the best of our knowledge, the hydroalumination of aluminium alkynides, which is similar to the reactions of the boron compounds cited above, and may open the route to the formation of cluster compounds, has been described in only two papers. In a conference report, Wilke and Schneider described the reaction of diethylaluminium hydride with diethylaluminium butynide,[60] which in a first step yielded the product of a twofold hydroalumination $(Et_2Al)_3C{-}CH_2{-}C_2H_5$. This compound was characterized by deuterolysis and oxidation and decomposes upon heating to 50 or 60 °C with the formation of triethylalane and an unknown residue. A similar reaction with dimethylaluminium hydride and dimethylaluminium propynide afforded a solid which, in addition to hydrolysis, was characterized by elemental analysis and molar mass determination. These results were interpreted in terms of the formation of an adamantane-like cage compound ("pseudo-aluminoadamantane"), which has seven Al atoms and four C atoms. Two of the Al atoms should be bridged by hydride ions. Remarkably, this compound showed no tendency to form adducts with diethyl ether.[60] The hydroalumination of dimethylaluminium ethynide, generated in situ, with dimethylaluminium hydride was reported to afford $(AlMe)_6(CCH_3)_4$ with a true adamantane structure in which the tricoordinated Al atoms occupy the bridging po-

sitions.[60] In view of the results discussed below, it seems probable that the Wilke group had synthesized the first carbaalanes in 1963 without recognizing, however, their true structure and the importance of their particular and fascinating bonding situation.

Similar reactions were carried out by a Russian group in 1988.[61] They treated some diethylaluminium alkynides with isobutylaluminium hydride and obtained oily residues, which by hydrolysis experiments were identified as the products of the twofold hydroalumination, similar to the intermediate discussed in the preceding paragraph. In our opinion, however, it is not clear from these experiments whether they indeed had these trialuminium compounds or whether their reactions already gave cluster derivatives. In our experience, the reactions of differently substituted aluminium starting compounds, as described in ref.,[61] afford complicated mixtures of products by dismutation reactions. Thus, we suppose that they never had a pure component in their oily residues.

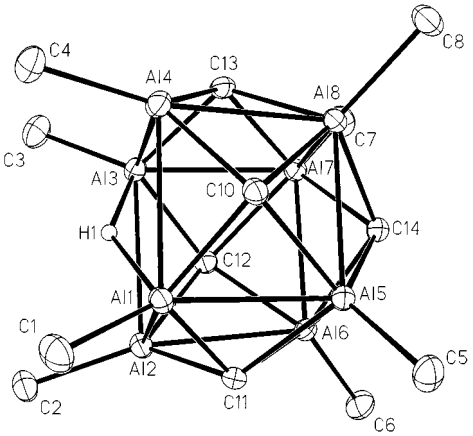
Carbaalanes

We began to investigate hydroalumination reactions because we were interested in an effective method for the synthesis of polyaluminium compounds, which are useful as chelating Lewis-acids in phase transfer processes or in anion recognition.[62] We succeeded in synthesizing these compounds by the reaction of polyalkynes with dialkylaluminium hydrides. The trialuminium derivatives, which were obtained by a twofold hydroalumination of aluminium alkynides as cited above, are of particular interest for such investigations, although we never observed a reaction at room temperature or in solution when we employed aluminium phenylethynides as starting compounds.

A hydroalumination reaction was observed when we dissolved dimethylaluminium phenylethynide in a slight excess of dimethylaluminium hydride (Equation 9) and heated the mixture to 80 °C for two days.[63] As shown by NMR spectroscopy, a large quantity of trimethylaluminium was formed, which was distilled off at room temperature in vacuo. Recrystallization of the residue afforded the colorless product $(AlMe)_8(CCH_2Ph)_5H$ (**12**). Compound **12** possesses a unique molecular structure (Figure 6), which comprises a cluster of eight aluminium and five carbon atoms. The aluminium atoms occupy the vertices of a slightly distorted cube, of which five faces are bridged by carbon atoms. The sixth face is bridged by a hydrogen atom. Each aluminium atom is further coordinated to one methyl group, and each carbon atom of the cluster is further attached to a benzyl group. Long Al−Al distances are observed for the hydrogen bonded face (279.7 pm), while the remaining eight edges of the cube are shorter (260.5 pm). The short distances are similar to those found in dimeric trimethylaluminium $(AlMe_3)_2$ (261 pm)[64] containing a 3c-2e Al−C−Al bond, and they are shorter than the Al−Al single bond in tetraalkyl compounds $R_2Al-AlR_2$.[44][45] Thus, they are consistent with a multicenter bonding interaction in the cluster. The Al−C separations within the cluster range between 201.8 pm and 214.1 pm and depend on the coordination sphere of the aluminium atoms. The shortest ones are observed to the Al atoms of the hydrogen bonded face and the longest to the carbon atom C14 at the opposite site of the cube. All are longer than the terminal Al−Me distances (195.0 pm). The formation of **12** may be described by the repeated hydroalumination of the starting aluminium ethynide and by condensation reactions with the release of trimethylalane. Furthermore, methylaluminium dihydride may be formed by the dismutation equilibrium of dimethylaluminium hydride and may be important at least for the introduction of the bridging hydride ion.

$$11\ Me_2AlH + 5\ Me_2Al{-}C{\equiv}C{-}Ph \longrightarrow (AlMe)_8(CCH_2Ph)_5H + 8\ AlMe_3 \quad (9)$$

12



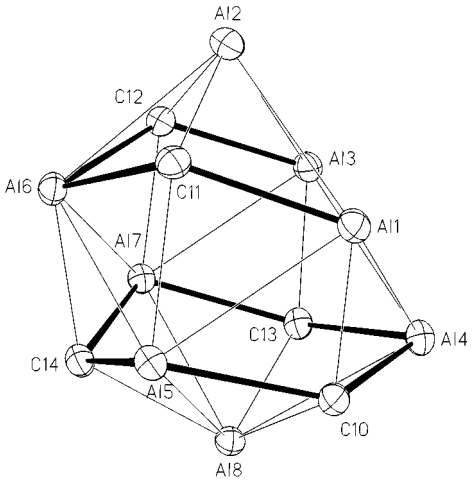


Figure 6. (a) Molecular structure of $(AlMe)_8(CCH_2C_6H_5)_5H$ **12**;[63] hydrogen atoms with the exception of H1 and benzyl groups are omitted. (b) The carbon and aluminium atoms of the rotated cluster with Al8 at the bottom, the bold lines characterize the planes discussed in the text

Each aluminium atom contributes two electrons and each carbon atom three electrons to the bonding in the cluster. Including the electron of the bridging hydrogen atom, a to-

tal electron count of 16 electron pairs results, which, in accordance with Wade's rules, gives an *arachno* configuration for the 13 vertex cluster of **12**. The corresponding *closo* polyborate $[B_{15}H_{15}]^{2-}$ is known only from quantum chemical calculations.[65] It has a hexagonal antiprism in its molecular center, of which the hexagonal faces are bridged by one and two boron atoms, respectively. The cluster of **12** can be derived from this structure, which is best recognized when it is placed on the aluminium atom Al8 (Figure 6). This atom bridges a six-membered heterocycle (Al4, Al5, Al7, C10, C13 and C14) in a chair form. The next plane comprises only five atoms (Al1, Al3, Al6, C11 and C12), and one vertex remains unoccupied, which is the approximate position of the bridging hydrogen atom H1. The atom Al2 resides above this plane. Thus, two vertices are unoccupied in comparison with *closo* $[B_{15}H_{15}]^{2-}$, which is in accordance with an *arachno* structure. However, **12** does not adopt an antiprismatic molecular center − owing to the large differences between the Al−Al and Al−C distances the planes are in an almost eclipsed conformation. Compound **12** was the first well-characterized cluster compound containing exclusively aluminium and carbon atoms to be reported in the literature. Owing to the obvious similarity between this compound and polyboranes or carbaboranes with respect to its structure and electronic configuration, we suggested the name carbaalanes[66] for this new class of organoaluminium derivatives.

When we reduced the excess of dimethylaluminium hydride, **12** was formed only as a minor by-product,[67] and a dark red compound $(AlMe)_8(CCH_2Ph)_5(C{\equiv}CPh)$ **(13)** was isolated in a yield of 40%; this compound has no hydrogen atoms attached to aluminium (Equation 10). The molecular structure of **13** (Figure 7) is quite similar to that of the colorless hydrido-bridged cluster **12**, except that the sixth face of the Al_8 cube is bridged by a phenylethynido ligand. Despite the different bridging atoms, the bond lengths in the cluster are almost indistinguishable from those of **12**, and the Al−Al separations of the ethynido-bridged face are longer (282.9 pm) than the remaining Al−Al distances (258.2 to 262.2 pm). The hydrido- or ethynido-bridged face of each cube is distorted to a rhombus with different distances between aluminium and the bridging atoms (Al−H: 191 and 221 pm in **12**; Al−C: 217.4 and 241.1 pm in **13**). Thus, these bridges may be interpreted as 3c-2e bonds with weak secondary interactions. The C−C bond length of the ethynide group (124.1 pm) is slightly longer than the standard bond length of a C≡C triple bond (120 pm[68]), and accordingly the absorption of the C≡C triple bond in the IR spectrum is shifted to 1956 cm^{-1}, which is more than 100 cm^{-1} lower than usually observed (e.g. in compound **15** discussed below with an exo ethynide group). These observations verify a particular bonding and electronic situation at the open face of the cluster, which may be compared with that of carbaboranes. Thus, we expect that, similar to the carbaboranes, the carbaalanes may show an interesting and unprecedented chemical reactivity.

Other products were formed when diethylaluminium derivatives were employed for the hydroalumination reaction.

$$10\ Me_2AlH + 6\ Me_2Al{-}C{\equiv}C{-}Ph \longrightarrow (AlMe)_8(CCH_2Ph)_5(C{\equiv}CPh) + 8\ AlMe_3 \quad (10)$$

13

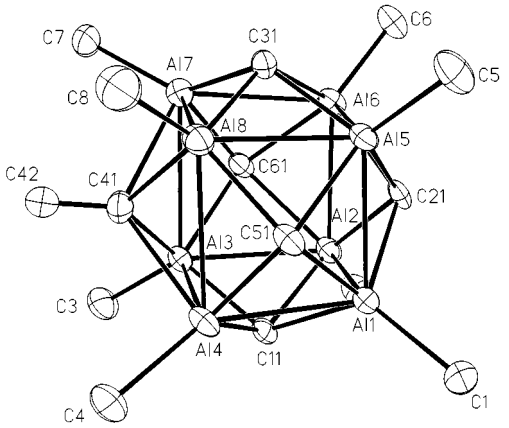


Figure 7. Molecular structure of $(AlMe)_8(CCH_2C_6H_5)_5(C{\equiv}C{-}C_6H_5)$ **13**;[67] hydrogen atoms, the phenyl group attached to C42 and benzyl groups are omitted

An orange-red product (**14**) was isolated after heating a mixture of the corresponding ethynide and hydride to 50°C for 18 hours (Equation 11).[69] Once again, trialkylaluminium ($AlEt_3$) was detected as a main product, which was distilled off in vacuo. Although the crude product contained **14** in a high concentration, the crystalline compound was obtained in only a 36% yield. A crystal structure determination confirmed the compound to be $(AlEt)_7(C{=}CHPh)_2(CCH_2Ph)_3H$ (Figure 8), which has seven Al and five carbon atoms in its cluster and may be derived from compound **12** with one vertex of the Al_8 cube unoccupied. The five carbon atoms are in two different positions: three of them bridge four Al atoms, while two reside above a triangle of Al atoms. The first ones belong to $C{-}CH_2{-}C_6H_5$ groups, similar to the bridging groups in compound **12**, while the second ones (C3,C3′) are alkenylidene carbon atoms of C=C double bonds. One further Al_3 triangle is bridged by a hydrogen atom. Thus, only one hydroalumination step with $EtAlH_2$ is missing to obtain a compound analogous to **12**. The Al−Al distances of the carbon- or hydrogen-bonded faces (268.2 and 270.7 pm, respectively) are shorter than those observed for the hydrogen-bonded face in **12**, while the remaining Al−Al separations are quite similar (256.9 and 260.0 pm). The C=C double bonds (136.0 pm on average) are only slightly lengthened relative to the standard bond length.[68] The alkenylidene groups adopt an orientation, in which a part of the π-orbitals overlaps the open face of the cluster. If the π-electrons are added to the number of cluster electrons, 16 electron pairs are obtained, which are in accordance with a *hypho* structure. Indeed, the cluster of **14** can be derived from that of the *closo*-borate $[B_{15}H_{15}]^{2-}$[65] with three vertices unoccupied. The molecular structure has five different ethyl groups, two different benzyl groups and the ethenylidene groups, and some

of the CH_2 groups are diastereotopic. Thus, very complicated NMR spectra resulted, some of their more important aspects are discussed later on.

$$9\ Et_2AlH + 5\ Et_2Al{-}C{\equiv}C{-}Ph \longrightarrow (AlEt)_7(C{=}CHPh)_2(CCH_2Ph)_3H + 7\ AlEt_3 + \mathbf{(15)} \quad (11)$$

14

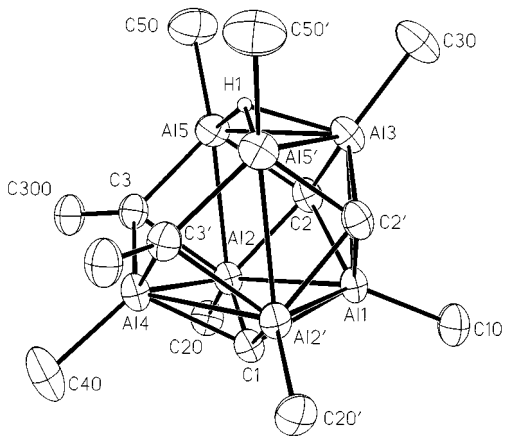


Figure 8. Molecular structure of $(AlEt)_7(CCH_2C_6H_5)_3(C{=}CHC_6H_5)_2H$ **14**;[69] hydrogen atoms with the exception of H1, phenyl and benzyl groups and the methyl groups of the ethyl substituents are omitted; the molecule is located on a crystallographic mirror plane

A second product (**15**) was isolated from the mother liquor after the separation of **14**.[69] Compound **14** was completely converted into **15** by heating a benzene solution to 60°C for several days. Monitoring of the rearrangement by NMR spectroscopy gave a first order reaction, which has an estimated rate constant of $k \approx 4 \times 10^{-5}$ sec^{-1} and a free enthalpy of activation of $\Delta G^{\neq} \approx 110$ kJ/mol. A much faster reaction was observed when the crude product from the reaction was heated to 110°C for one hour (Equation 12). Compound **15** is isomeric with **14**, but has a different structure with a cluster of seven Al and four C atoms [$(AlEt)_7(CCH_2Ph)_4(C{\equiv}CPh)H$, Figure 9]. One edge of the cluster (Al3−Al6) is bridged by a hydrogen atom and a second one (Al2−Al5) by an ethynide group. The Al_7C_4 molecular core has twelve electron pairs, which is in accordance with a *closo* configuration. Indeed, the structure of the cluster is analogous to that of *closo*-$[B_{11}H_{11}]^{2-}$[3] and has a six-membered heterocycle in a boat conformation bridged by an Al atom as a very characteristic structural motif. With the exception of the distances to the unique Al atom Al7, short Al−Al separations were observed, which are between 258.1 and 259.4 pm for the unsupported Al−Al edges, while they are little lengthened for the bridged ones (261.2 and 267.5 pm). Much longer distances of 281.8 to 292.1 pm were observed to the atom Al7 above the boat shaped Al_4C_2 heterocycle. A similar lengthening of the B−B distances to that unique position was observed in the undecaborate dianion (B−B = 200.9 pm).

$$(AlEt)_7(C{=}CHPh)_2(CCH_2Ph)_3H \xrightarrow{\Delta} (AlEt)_7(CCH_2Ph)_4(C{\equiv}CPh)H \quad (12)$$

14 **15**

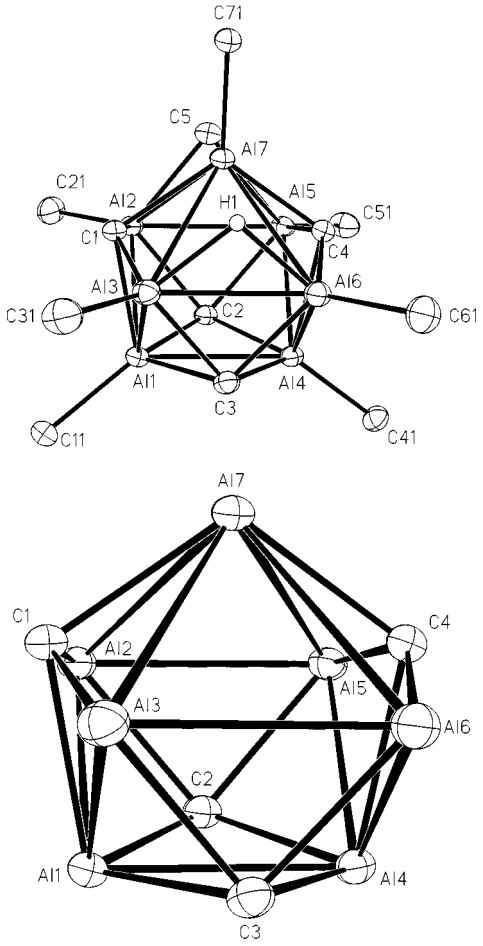


Figure 9. Molecular structure of $(AlEt)_7(CCH_2C_6H_5)_4(C{\equiv}C{-}C_6H_5)H$ **15**;[69] (a) shows the cluster with the exo hydrogen and ethyne (C5) ligands and the α carbon atoms of the ethyl substituents; (b) gives the naked cluster and shows the remarkable analogy to $[B_{11}H_{11}]^{2-}$

As described above, compound **14** containing seven Al atoms and two C=C double bonds may be converted into an *arachno* derivative analogous to **12** by a single hydroalumination step with $EtAlH_2$. However, only alkyl or aryl aluminium dihydrides with very bulky substituents are available.[70] Dihydrides bearing smaller substituents may be formed in trace amounts by the dismutation equilibrium of dialkylaluminium hydrides, and we suppose that they are intermediates in the hydroalumination reactions described here. Therefore, we treated compound **14** with an excess of diethylaluminium hydride in order to hydroaluminate **14** and to synthesize the corresponding *arachno* compound. The mixture of the starting materials was heated to 60°C

for 18 hours without additional solvent, and triethylaluminium was formed as detected by NMR spectroscopy. All volatile components were removed in vacuo, and recrystallization of the residue from *n*-pentane afforded colorless crystals of product **16** in a yield of 69% (Equation 13). The molecular structure is analogous to that of **12** containing a cube of eight Al atoms, of which five faces are bridged by carbon atoms and one face is occupied by a hydrogen atom. The reaction according to Equation (13) gives an important insight into the mechanism of the formation of these carbaalane clusters.

$$\underset{\mathbf{14}}{(AlEt)_7(C{=}CHPh)_2(CCH_2Ph)_3H} + Et_2AlH \text{ (excess)} \xrightarrow[-\ Et_3Al]{} \underset{\mathbf{16}}{(AlEt)_8(CCH_2Ph)_5H} \quad (13)$$

The complete characterization by NMR spectroscopy and assignment of resonances to all atoms of these compounds was extremely difficult, and despite the application of advanced NMR spectroscopic techniques (H,H COSY, HMQC and HMBC NMR spectra) not all resonances could clearly be assigned to particular atoms. However, those resonances which are important for the discussion of these clusters, were clearly resolved and assigned. ^{27}Al NMR spectroscopic data have not yet been recorded. The ^{13}C NMR resonances of the cluster carbon atoms show a strong shift to low field (δ = 21 to 35). Similar shifts were calculated for a carbaborane cluster which has an alternating arrangement of boron and carbon atoms (see above).[56] A chemical shift of 0 ppm is usually observed for compounds which have carbon atoms attached to aluminium with a higher coordination number than three. Those shifts were detected here for the α-carbon atoms of the terminally coordinated methyl or ethyl substituents. Similarly, the bridging hydrogen atoms show a low-field shift in the ^1H NMR spectra and resonate at about 4.7 to 5.3 ppm, while in the starting dimethyl or diethyl aluminium hydrides the hydrido bridges have resonances of δ = 2.92 and 2.79, respectively. The resonances of the CH_2 protons of the benzyl groups are also shifted to a lower field (δ = 3.0 to 3.7). We have not yet succeeded in the unambiguous assignment of absorptions in the IR spectra to cluster vibrations. All IR spectra show some weak absorptions in the typical range for Al−C bonds (≈ 450 to 550 cm^{-1}) and intense, broad absorptions at 660 to 710 cm^{-1}, which, however, is the range of deformation vibrations of the phenyl groups. Thus, their more intuitive assignment to cluster vibrations can only be discussed with reservation. Polyhedral carbaalanes without phenyl groups may help to clarify this point.

Concluding Remarks

A deficiency of electrons causes the singular property of boron to form clusters which require a delocalized bonding description. As described here, similar compounds are now available with its heavier homologue aluminium, in which Al atoms occupy positions of high connectivity in delocalized electronic systems; these compounds obey the same rules concerning structure and electron count. Nevertheless differences between both kinds of compounds should not be ignored. The aluminium derivatives are often more reactive and less stable than the boron clusters. This may be due to the low electronegativity of aluminium, which leads to a significant charge separation in all heteronuclear bonds. Steric shielding, which has been used for the preparation of so many compounds with unusual structures in main group chemistry, seems to have only a minor influence here, instead the stabilization of these clusters may be caused mainly by the delocalization of electron density. The investigation of the chemical reactivity of the carbaalanes as a new class of compounds is just beginning, but a broad application in research such as in catalytic processes seems to be possible, in particular due to their facile synthesis. Future work will show whether this type of aluminium chemistry will reach a similar importance and diversity as that of boron

Acknowledgments

We are grateful to the Deutsche Forschungsgemeinschaft and the Fonds der Chemischen Industrie for generous financial support.

[1] A. Stock, *Hydrides of Boron and Silicon*, Cornell University Press, Ithaca, NY, **1933**; A. Stock, C. Massenez, *Ber. Dtsch. Chem. Ges.* **1912**, *45*, 3539−3568.
[2] *The Borane, Carborane, Carbocation Continuum* (Ed.: J. Casanova), Wiley, New York, **1998**.
[3] O. Volkov, W. Dirk, U. Englert, P. Paetzold, *Z. Anorg. Allg. Chem.*, **1999**, *625*, 1193−1201; E. H. Wong, L. Prasad, E. J. Gabe, M. G. Gatter, *Inorg. Chem.* **1983**, *22*, 1143−1146.
[4] K. Wade, *Adv. Inorg. Chem. Radiochem*. **1976**, 18, 1−66.
[5] N. N. Greenwood, A. Earnshaw, *Chemie der Elemente*, VCH, Weinheim, **1990**.
[6] R. Köster, M. A. Grassberger, *Angew. Chem.* **1967**, *79*, 197−219; *Angew. Chem. Int. Ed. Engl.* **1967**, *6*, 218; T. Onak, *Comprehensive Organometallic Chemistry* (Ed. G. Wilkinson, F. G. A. Stone, E. W. Abel), Vol. 1, Pergamon, Oxford, **1982**, p. 411−457.
[7] K. P. Callahan, M. F. Hawthorne, *Adv. Organomet. Chem.* **1976**, *14*, 145−186.
[8] G. Urry, T. Wartik, H. I. Schlesinger, *J. Am. Chem. Soc.* **1952**, *74*, 5809. A. G. Massey, *Adv. Inorg. Chem. Radiochem.* **1983**, *26*, 1−54; J. A. Morrison, *Chem. Rev.* **1991**, *91*, 35−48.
[9] T. Mennekes, P. Paetzold, R. Boese, D. Bläser, *Angew. Chem.* **1991**, *103*, 199−200; *Angew. Chem. Int. Ed. Engl.* **1991**, *30*, 173−175; D. Hnyk, *Polyhedron* **1997**, *16*, 603−606.
[10] C. Dohmeier, C. Robl, M. Tacke, H. Schnöckel, *Angew. Chem.* **1991**, *103*, 594−595; *Angew. Chem. Int. Ed. Engl.* **1991**, *30*, 564−565; S. Schulz, H. W. Roesky, H. J. Koch, G. M. Sheldrick, D. Stalke, A. Kuhn, *Angew. Chem.* **1993**, *105*, 1828−1830; *Angew. Chem. Int. Ed. Engl.* **1993**, *32*, 1729−1731.
[11] N. Wiberg, K. Amelunxen, H. Nöth, M. Schmidt, H. Schwenk, *Angew. Chem.* **1996**, *108*, 110−112; *Angew. Chem. Int. Ed. Engl.* **1996**, *35*, 65−67; A. Purath, C. Dohmeier, A. Ecker, H. Schnöckel, K. Amelunxen, T. Passler, N. Wiberg, *Organometallics* **1998**, *17*, 1894−1896.
[12] C. Schnitter, H. W. Roesky, C. Röpken, R. Herbst-Irmer, H.-G. Schmidt, M. Noltemeyer, *Angew. Chem.* **1998**, *110*, 2059−2062; *Angew. Chem. Int. Ed.* **1998**, *37*, 1952−1955.
[13] A. Purath, H. Schnöckel, *J. Organomet. Chem.* **1999**, *579*, 373−375.

[14] A. Ecker, E. Weckert, H. Schnöckel, *Nature* **1997**, *387*, 379−381.
[15] W. Uhl, *Angew. Chem.* **1993**, *105*, 1449−1461; *Angew. Chem. Int. Ed. Engl.* **1993**, *32*, 1386−1397.
[16] C. Dohmeier, D. Loos, H. Schnöckel, *Angew. Chem.* **1996**, *108*, 141−161; *Angew. Chem. Int. Ed. Engl.* **1996**, *35*, 129−149.
[17] W. Uhl, *Rev. Inorg. Chem.* **1998**, *18*, 240−282.
[18] C. K. F. von Hänisch, C. Üffing, M. A. Junker, A. Ecker, B. O. Kneisel, H. Schnöckel, *Angew. Chem.* **1996**, *108*, 3003−3005; *Angew. Chem. Int. Ed. Engl.* **1996**, *35*, 2875−2877; the corresponding Sb derivative: S. Schulz, T. Schoop, H. W. Roesky, L. Häming, A. Steiner, R. Herbst-Irmer, *Angew. Chem.* **1995**, *107*, 1015−1016; *Angew. Chem. Int. Ed. Engl.* **1995**, *34*, 919−920.
[19] J. J. Borlin, D. F. Gaines, *J. Am. Chem. Soc.* **1972**, *94*, 1367−1369.
[20] C. J. Dain, A. J. Downs, D. W. H. Rankin, *J. Chem. Soc., Dalton Trans.* **1981**, 2465−2470.
[21] C. A. Morrison, B. A. Smart, P. T. Brain, D. W. H. Rankin, A. J. Downs, *J. Chem. Soc., Dalton Trans.* **1998**, 2155−2162.
[22] P. T. Brain, C. A. Morrison, S. Parsons, D. W. H. Rankin. *J. Chem. Soc., Dalton Trans.* **1996**, 4589−4596. C. J. Dain, A. J. Downs, G. S. Laurenson, D. W. H. Rankin, *J. Chem. Soc., Dalton Trans.* **1981**, 472−477.
[23] N. N. Greenwood, J. A. McGinnety, *J. Chem. Soc., Chem. Commun.* **1965**, 331−332.
[24] N. N. Greenwood, J. A. McGinnety, *J. Chem. Soc., A* **1966**, 1090−1095.
[25] F. L. Himpsl, Jr., A. C. Bond, *J. Am. Chem. Soc.* **1981**, *103*, 1098−1102.
[26] T. D. Getman, S. G. Shore, *Inorg. Chem.* **1988**, *27*, 3440−3442.
[27] D. A. T. Young, G. R. Willey, M. F. Hawthorne, M. R. Churchill, A. H. Reis, Jr., *J. Am. Chem. Soc.* **1970**, *92*, 6663−6664. M. R. Churchill, A. H. Reis, Jr., *J. Chem. Soc., Dalton Trans.* **1972**, 1317−1320.
[28] P. Jutzi, P. Galow, *J. Organomet. Chem.* **1987**, *319*, 139−147.
[29] D. A. T. Young, R. J. Wiersema, M. F. Hawthorne, *J. Am. Chem. Soc.* **1971**, *93*, 5687−5694. B. M. Mikhailov, T. V. Potapova, *Izv. Akad. Nauk. SSSR, Ser. Khim.* **1968**, *5*, 1153.
[30] D. M. Schubert, M. A. Bandman, W. S. Rees, Jr., C. B. Knobler, P. Lu, W. Nam, M. F. Hawthorne, *Organometallics* **1990**, *9*, 2046−2061.
[31] M. R. Churchill, A. H. Reis, Jr., D. A. T. Young, G. R. Willey, M. F. Hawthorne, *J. Chem. Soc., Chem. Commun.* **1971**, 298−299.
[32] M. R. Churchill, A. H. Reis, Jr., *J. Chem. Soc., Dalton Trans.* **1972**, 1314−1317.
[33] D. M. Schubert, C. B. Knobler, W. S. Rees, Jr., M. F. Hawthorne, *Organometallics* **1987**, *6*, 201−202.
[34] W. S. Rees, Jr., D. M. Schubert, C. B. Knobler, M. F. Hawthorne, *J. Am. Chem. Soc.* **1986**, *108*, 5367−5368.
[35] M. A. Bandman, C. B. Knobler, M. F. Hawthorne, *Inorg. Chem.* **1988**, *27*, 2399−2400.
[36] Gallium carbaborane sandwich: M. A. Bandman, C. B. Knobler, M. F. Hawthorne, *Inorg. Chem.* **1989**, *28*, 1204−1206.
[37] D. M. Schubert, C. B. Knobler, W. S. Rees, Jr., M. F. Hawthorne, *Organometallics* **1987**, *6*, 203- 204.
[38] D. M. Schubert, C. B. Knobler, M. F. Hawthorne, *Organometallics* **1987**, *6*, 1353−1356.
[39] C. P. Magee, L. G. Sneddon, D. C. Beer, R. N. Grimes, *J. Organomet. Chem.* **1975**, *86*, 159−167.
[40] R. N. Grimes, W. J. Rademaker, *J. Am. Chem. Soc.* **1969**, *91*, 6498−6499; R. N. Grimes, W. J. Rademaker, M. L. Denniston, R. F. Bryan, P. T. Greene, *J. Am. Chem. Soc.* **1972**, *94*, 1865−1869.
[41] J. S. Beck, L. G. Sneddon, *J. Am. Chem. Soc.* **1988**, *110*, 3467−3472.
[42] W. Hiller, K.-W. Klinkhammer, W. Uhl, J. Wagner, *Angew. Chem.* **1991**, *103*, 182−183; *Angew. Chem. Int. Ed. Engl.* **1991**, *30*, 179 −180.
[43] H. Hoberg, S. Krause, *Angew. Chem.* **1976**, *88*, 760−761; *Angew. Chem. Int. Ed. Engl.* **1976**, *15*, 694−695.
[44] W. Uhl, *Z. Naturforsch., B. Chem. Sci.* **1988**, *43*, 1113−1118.
[45] R. J. Wehmschulte, K. Ruhlandt-Senge, M. M. Olmstead, H. Hope, B. E. Sturgeon, P. P. Power, *Inorg. Chem.* **1993**, *32*, 2983−2984; a long Al−Al bond (275.1 pm) was observed in the silyl derivative tetrakis[tri(*tert*-butyl)silyl]dialane(4): N. Wiberg, K. Amelunxen, T. Blank, H. Nöth, J. Knizek, *Organometallics* **1998**, *17*, 5431−5433.
[46] J. A. Wunderlich, W. N. Lipscomb, *J. Am. Chem. Soc.* **1960**, *82*, 4427−4428.
[47] W. Uhl, J. Wagner, unpublished results.
[48] J. H. Morris, H. J. Gysling, D. Reed, *Chem. Rev.* **1985**, *85*, 51−76; R. L. Middaugh, F. Farha, Jr., *J. Am. Chem. Soc.* **1966**, *88*, 4147−4149; R. J. Wiersema, R. L. Middaugh, *J. Am. Chem. Soc.* **1967**, *89*, 5078−5079; A. P. Schmitt, R. L. Middaugh, *Inorg. Chem.* **1974**, *13*, 163−169; R. J. Wiersema, R. L. Middaugh, *Inorg. Chem.* **1969**, *8*, 2074−2079.
[49] C. Dohmeier, M. Mocker, H. Schnöckel, A. Lötz, U. Schneider, R. Ahlrichs, *Angew. Chem.* **1993**, *105*, 1491−1493; *Angew. Chem. Int. Ed. Engl.* **1993**, *32*, 1428−1430.
[50] R. Köster, G. Seidel, B. Wrackmeyer, *Angew. Chem.* **1994**, *106*, 2380−2382; *Angew. Chem. Int. Ed. Engl.* **1994**, *33*, 2294−2296.
[51] R. Köster, R. Boese, B. Wrackmeyer, H.-J. Schanz, *J. Chem. Soc., Chem. Commun.* **1995**, 1691−1692.
[52] B. Wrackmeyer, H.-J. Schanz, *Collect. Czech. Chem. Commun.* **1997**, *62*, 1254−1262.
[53] B. Wrackmeyer, H.-J. Schanz, W. Milius, *Angew. Chem.* **1997**, *109*, 98−99; *Angew. Chem. Int. Ed. Engl.* **1997**, *36*, 75−77.
[54] B. Wrackmeyer, H.-J. Schanz, W. Milius, *Angew. Chem.* **1997**, *109*, 1145−1147; *Angew. Chem. Int. Ed. Engl.* **1997**, *36*, 1117−1119.
[55] B. Wrackmeyer, H.-J. Schanz, M. Hofmann, P. von Ragué Schleyer, *Eur. J. Inorg. Chem.* **1998**, 633−637.
[56] B. Wrackmeyer, H.-J. Schanz, M. Hofmann, P. von Ragué Schleyer, *Angew. Chem.* **1998**, *110*, 1329−1331; *Angew. Chem. Int. Ed.* **1998**, *37*, 1245−1247.
[57] B. Wrackmeyer, H.-J. Schanz, M. Hofmann, P. von Ragué Schleyer, R. Boese, *Eur. J. Inorg. Chem.* **1999**, 533−537.
[58] J. J. Eisch, *Comprehensive Organometallic Chemistry* (Ed. G. Wilkinson, F. G. A. Stone, E. W. Abel), Vol. 1, Pergamon, Oxford, **1982**, p. 555−682.
[59] E. Winterfeldt, *Synthesis* **1975**, 617−630. I. Marek, J.-F. Normant, *Chem. Rev.* **1996**, *96*, 3241−3267.
[60] G. Wilke, W. Schneider, *Bull. Soc. Chim. Fr.* **1963**, 1462−1467.
[61] A. V. Kuchin, S. A. Markova, S. I. Lomakina, G. A. Tolstikov, *J. Gen. Chem. USSR*, **1988**, *58*, 1395−1397; *Zh. Obshch. Khim.* **1988**, *58*, 1567−1571.
[62] J. M. Lehn, *Supramolecular Chemistry*, VCH, Weinheim, **1995**. W. Uhl, F. Hannemann, W. Saak, R. Wartchow, *Eur. J. Inorg. Chem.* **1998**, 921−926.
[63] W. Uhl, F. Breher, *Angew. Chem.* **1999**, *111*, 1578−1580; *Angew. Chem. Int. Ed.* **1999**, *38*, 1477−1479.
[64] R. G. Vranka, E. L. Amma, *J. Am. Chem. Soc.* **1967**, *89*, 3121−3126; J. C. Huffman, W. E. Streib, *J. Chem. Soc., Chem. Commun.* **1971**, 911−912.
[65] J. Bicerano, D. S. Marynick, W. N. Lipscomb, *Inorg. Chem.* **1978**, *17*, 3443−3453; M. Gielen, *Polyhedron*, **1988**, *7*, 363−368; P. von Ragué Schleyer, K. Najafian, A. M. Mebel, *Inorg. Chem.* **1998**, *37*, 6765−6772.
[66] The term carbalane has been used before for Al−C compounds, which were, however, not analogues of carbaboranes: C. Üffing, A. Ecker, R. Köppe, K. Merzweiler, H. Schnöckel, *Chem. Eur. J.* **1998**, 2142−2147.
[67] W. Uhl, F. Breher, unpublished results.
[68] J. March, *Advanced Organic Chemistry*, third edition, Wiley, New York, **1985**.
[69] W. Uhl, F. Breher, A. Lützen, W. Saak, *Angew. Chem.*, in press.
[70] R. J. Wehmschulte, W. J. Grigsby, B. Schiemenz, R. A. Bartlett, P. P. Power, *Inorg. Chem.* **1996**, *35*, 6694−6702. R. J. Wehmschulte, P. P. Power, *Inorg. Chem.* **1994**, *33*, 5611−5612. R. J. Wehmschulte, J. F. Ellison, K. Ruhlandt-Senge, P. P. Power, *Inorg. Chem.* **1994**, *33*, 6300−6306.

Received August 3, 1999
[I99285]

Electrophilic Attack of $[I(py)_2]^+(NO_3^-)$ on Three-Coordinate Pt^0 Precursors: Synthesis and In Vitro Antitumor Activity of Water-Soluble, Five-Coordinate Pt^{II} Complexes

Mario Bigioni,*[a] Paolo Ganis,[b] Achille Panunzi,*[c] Francesco Ruffo,[b] Carmela Salvatore,[a] and Antonio Vito[d]

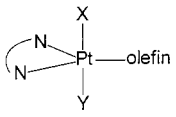
Keywords: Platinum / N ligands / Water soluble complexes / Antitumor agents / Electrophilic additions

$[I(py)_2]^+(NO_3^-)$ oxidatively adds to the three-coordinate platinum(0) precursors [Pt(*N*,*N*-chelate)(olefin)] affording the cationic five-coordinate products [Pt(*N*,*N*-chelate)I(py)(olefin)]$^+(NO_3^-)$ (**1**) {*N*,*N*-chelate = 2,9-Me_2-1,10-phenanthroline (dmphen), 2-methyl-6-[(phenylimino)methyl]pyridine (pimpy) and 2-methyl-6-[(4-methoxyphenylimino)methyl]pyridine (mpimpy)}. The crystal structure of [Pt(pimpy)I(py)(dimethyl fumarate)]$^+(NO_3^-)$ is reported. The crystals are triclinic, space group *P*1(bar), with *a* = 13.511(2), *b* = 13.754(2), *c* = 8.678(1) Å, α = 95.2(1)°, β = 92.5(2)°, γ = 64.7(1)°, *Z* = 2. Type **I** complexes, which are soluble both in chlorinated solvents and in water, were tested for cytotoxicity against a panel of tumour cell lines of various histotypes including NSCLC H460, leukaemic HL-60, ovarian A 2780, IGROV-1, SKOV-3, and an ovarian carcinoma A 2780/CP selected for resistance to *cis*-platin [DDP = *cis*-diamminedichloroplatinum(II)]. [Pt(dmphen)I(py)(methyl acrylate)]$^+(NO_3^-)$ was the most active in all cell lines tested, its antitumoural activity in vitro being comparable to that of DDP.

Introduction

Cisplatin [DDP = *cis*-diamminedichloroplatinum(II)] is an extensively investigated anticancer drug used in the treatment of some solid tumours such as ovarian, testicular and bladder cancers.[1] Its therapeutic efficacy is often limited by its dose-related nephrotoxicity and by the development of drug resistance, depending on the increase of intracellular glutathione,[2] increased tolerance to DNA damage or increased DNA repair.

Many analogues have been synthesised in an attempt to either decrease the toxic side effects of the parent drug or to overcome the intrinsic and induced resistant phenotype and so broaden the clinical spectrum of antitumour activity.



I

Figure 1. General formula for type **I** complexes

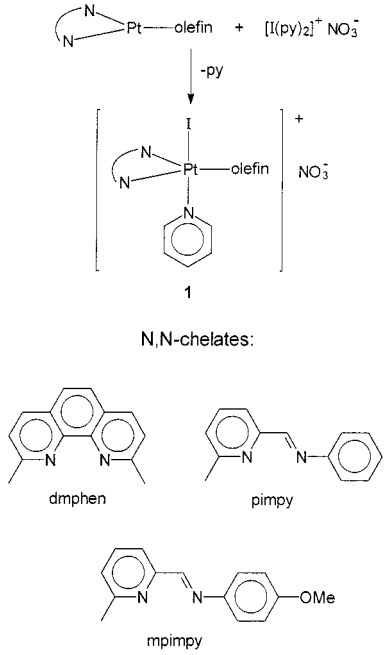
In the last few decades interest in five-coordinate platinum(II) complexes (**I**) (Figure 1) has increased.[3]

The stability of these species is prompted by the presence of sterically hindered nitrogen chelates, e.g. 2,9-Me_2-1,10-phenanthroline (dmphen). Such ligands inhibit olefin loss because the resulting square-planar product would suffer severe constraints in the coordination plane.[3] Some type **I** complexes of formula [PtCl(Me)(dmphen)(olefin)]BF_4[4] and [PtCl($SnMe_nCl_{4-n}$)(dmphen)(dimethyl fumarate)][5] have been tested in vitro against some tumour cell lines with promising results. As far as we know, this was the first investigation on coordinatively saturated platinum(II) derivatives, since a literature search shows that other studies have been concerned with square-planar platinum(II)[6] or octahedral platinum(IV) species.[7] The insolubility in water of the above-mentioned species of type **I** limits a further development of these studies. Thus, we were prompted to investigate the feasibility of related compounds with properties more suitable to pharmacological uses. Keeping in mind that a charged complex may display a good solubility in water without loss of pharmacological activity,[8] we aimed to prepare cationic water-soluble complexes of type **I**. A straightforward procedure was found to be the oxidative addition of the readily available iodonium salt $[I(py)_2]^+(NO_3^-)$[9] to three-coordinate platinum(0) precursors[10] (Scheme 1).

Herein we describe the synthesis of novel type **I** species, their NMR characterisation and the crystal structure of a

[a] Pharmacology Department, Menarini Ricerche S.p.A., via Tito Speri 10, I-00040 Pomezia, Italy
[b] Dipartimento di Chimica, Università di Napoli "Federico II", via Mezzocannone 4, I-80134 Napoli, Italy
[c] Facoltà di Agraria and Dipartimento di Chimica, Università di Napoli "Federico II", via Mezzocannone 4, I-80134 Napoli, Italy
Fax: (internat.) + 39-081/552-7771
E-mail: panunzi@chemna.dichi.unina.it
[d] Algalite, via Leonardo da Vinci 277, I-20090 Trezzano sul Naviglio, Italy

 © WILEY-VCH Verlag GmbH, D-69451 Weinheim, 2000 1434−1948/00/0808−1717 $ 17.50+.50/0



Scheme 1. Synthesis of type-**1** complexes and used *N,N* ligands

representative complex. This paper reports the pharmacological advantages of new modifications introduced in the type **I** species on the inhibitory effect of the growth of selected tumoural DDP resistant and sensitive cell lines.

Results and Discussion

Synthesis, NMR Characterisation and Reactivity of Type I Complexes

Cationic five-coordinate Pt^{II} complexes are known.[11,12] They were obtained by chloride abstraction starting from a suitable precursor in the presence of a silver salt [Equation (1) and Equation (2)]:

$$[PtCl(R)(N,N\text{-chelate})(olefin)] + AgBF_4 + MeCN \rightarrow [Pt(R)(MeCN)(N,N\text{-chelate})(olefin)](BF_4) + AgCl \quad (1)$$

$$cis\text{-}[PtCl_2(MeCN)(olefin)] + AgBF_4 + N,N\text{-chelate} \rightarrow [PtCl(MeCN)(N,N\text{-chelate})(olefin)](BF_4) + AgCl \quad (2)$$

Route 1 allowed the synthesis of type **I** derivatives containing a hydrocarbyl group R and a neutral ligand (e.g. MeCN) in the axial positions. The second procedure afforded the related chloro derivatives. In the latter case, only products with electron-rich olefins could be obtained, since the required precursors *cis*-$[PtCl_2(L)(olefin)]$ are not available when the olefin bears electron-withdrawing substituents. The synthetic procedure herein described bypasses this obstacle and allows the attainment of several cationic halo complexes containing electron-acceptor olefins.

The method is based on the well-known ability of three-coordinate platinum(0) complexes of general formula [Pt(*N,N*-chelate)(olefin)] to undergo electrophilic attack.[10] Thus, the iodonium(I) salt $[I(py)_2]^+(NO_3^-)$[9] oxidatively adds to the suitable Pt^0 complexes with formation of pyridine and of the corresponding five-coordinate complexes, which contain a pyridine and an iodide in the axial positions (Scheme 1).

The N,N ligands used in this work are shown in Scheme 1. The products **1** are listed in Table 1 with their labels. The reactions were performed in chloroform, which is a good solvent for both reagents and products. The only exception was the addition to [Pt(dmphen)(maleic anhydride)], which required the use of tetrachloroethane due to the poor solubility of the Pt^0 precursor.

Type **I** complexes could be crystallised by slow addition of diethyl ether to the reaction mixture. They are soluble both in water and chlorinated solvents, except for the dibenzoylethylene derivative, which is only soluble in chlorinated solvents. The products are fairly stable in solution, and no appreciable decomposition could be seen even after several hours.

The possibility that water may substitute iodide in one of the apical positions has been ruled out by conductivity measurements. Actually, if hydrolysis occurred, the dipositive cation $[Pt(N,N\text{-chelate})(H_2O)(py)(olefin)]^{2+}(I^-)(NO_3^-)$ should form. However, the molar conductivities of type **I** complexes in water are in the range $1.0-1.3 \times 10^2$ $ohm^{-1}\cdot cm^2\cdot mol^{-1}$. These values are close to that measured (1.4×10^2 $ohm^{-1}\cdot cm^2\cdot mol^{-1}$) for an authentic 1:1 salt, i.e. $K[PtCl_3(C_2H_4)]$. On the other hand, the conductivity of a 2:1 salt such as K_2PtCl_4 in water is significantly higher (2.3×10^2 $ohm^{-1}\cdot cm^2\cdot mol^{-1}$).

The NMR spectra were recorded in D_2O in most cases (Table 1). It is possible to assign unequivocally a trigonal bipyramidal geometry to the products on the basis of arguments already thoroughly discussed for related species.[3] As for the dmphen derivatives **1a-e**, the number of isomers theoretically predicted depends on the symmetry of the alkene. Dimethyl maleate and maleic anhydride can afford two rotamers, while methyl acrylate could afford two enantiomeric pairs. In all cases, only one spectral pattern was observed, indicating that the olefins coordinate with a high degree of stereoselectivity. Dimethyl fumarate gives rise to a pair of enantiomers, obviously not distinguishable by NMR spectroscopy in the absence of chiral interference.

In the case of pimpy (**1h**), we observed the expected two diastereomers (each one a pair of enantiomers) for the complex with dimethyl fumarate. Slow recrystallization of the complex affords only one pair whose X-ray crystal structure is described below. Finally, complex **1i** with mpimpy and dimethyl maleate should also exist as two diastereomers (pairs of enantiomers). The high degree of stereoselectivity in olefin coordination allows us to detect only one pair in solution.

Description of the Molecular Structure of 1h

A view of the structure of the cation giving the atom numbering scheme is shown in Figure 2. Selected bond lengths and angles and torsion angles are listed in Table 2.

The bipyramidal trigonal coordination about the metal is as expected and does not differ substantially from that found for similar five-coordinate Pt^{II} complexes.[3] The li-

Table 1. Selected spectroscopic and analytical data for type **I** complexes

Compound	^{1}H NMR[a]			Analysis (%) found (calcd)		
	H-olefin[b]	Me-chelate	Other selected signals	C	H	N
1a [PtI(py)(dmphen) (dimethyl maleate)](NO_3)	5.19 (s, 2 H, 80)	3.53 (6 H)	7.92 (d, 2 H, 2,6-H-py) 3.64 (s, 6 H, OMe)	36.61 (36.82)	3.15 (3.09)	6.69 (6.87)
1b[PtI(py)(dmphen) (dimethyl fumarate)](NO_3)	5.52 (d, 1 H) 4.95 (d, 1 H)	3.55 (3 H) 3.38 (3 H)	7.90 (d, 2 H, 2,6-H-py) 3.86 (s, 3 H, OMe) 3.55 (s, 3 H, OMe)	36.88 (36.82)	3.18 (3.09)	7.02 (6.87)
1c [PtI(py)(dmphen) (maleic anhydride)](NO_3)	5.16 (s, 2 H, 76)	3.56 (6 H)		35.75 (35.90)	2.60 (2.49)	7.41 (7.28)
1d [PtI(py)(dmphen) (methyl acrylate)](NO_3)	5.12 (dd, 1 H, 65) 4.17 (d, 1 H, 59) 3.82 (d, 1 H, 55)	3.51(3 H) 3.36 (3 H)	7.98 (d, 2 H, 2,6-H-py) 3.54 (s, 3 H, OMe)	36.28 (36.47)	2.98 (3.06)	7.24 (7.40)
1e[c] [PtI(py)(dmphen) (dibenzoylethylene)](NO_3)	5.15 (s, 2 H, 78)	2.71 (6 H)	8.20 (d, 2 H, 2,6-H-py)	46.36 (46.32)	3.27 (3.22)	6.29 (6.17)
1f [PtI(py)(dmphen) (diethylmaleate)](NO_3)	5.06 (s, 2 H, 76)	3.48 (6 H)	7.92 (d, 2 H, 2,6-H-py) 4.05 (m, 4 H, OCH_2) 1.14 (t, 6 H, CH_2*Me*)	38.57 (38.44)	3.38 (3.47)	6.78 (6.64)
1g [PtI(py)(dmphen) (diethyl fumarate)](NO_3)	5.51 (d, 1 H, 70) 4.95 (d, 1 H, 68)	3.56 (6 H)	8.03 (d, 2 H, 2,6-H-py) 4.30 (q, 2 H,OCH_2) 3.91 (m, 1 H, OCH_2) 3.65 (m, 1 H,OCH_2) 1.38 (t, 3 H, CH_2*Me*) 1.14 (t, 3 H, CH_2*Me*)	38.22 (38.44)	3.33 (3.47)	6.50 (6.64)
1h [PtI(py)(pimpy) (dimethyl fumarate)](NO_3) (more abundant isomer)	5.50 (d, 1 H) 4.48 (d, 1 H)	3.41 (3 H)	9.31 (s, 1 H, CH=N) 3.87 (s, 3 H, OMe) 3.39 (s, 3 H, OMe)	36.04 (35.88)	3.11 (3.14)	7.12 (6.97)
1i [PtI(py)(mpimpy) (dimethylmaleate)](NO_3)	5.25 (ABq, 2 H)	3.37 (3 H)	9.19 (s, 1 H, CH=N) 3.94 (s, 3 H, OMe) 3.55 (s, 3 H, OMe) 3.46 (s, 3 H, OMe)	36.28 (36.03)	3.19 (3.26)	6.57 (6.72)

[a] At 250 or 200 MHz and 298 K; in D_2O, HDO (δ = 4.8) as internal standard; abbreviations: ABq: AB quadruplet; d: doublet; dd: doublet of doublets; m: multiplet; s: singlet; q: quadruplet; t: triplet. – [b] $^2J_{Pt-H}$ (Hz) in parentheses (when measurable). – [c] In $CDCl_3$, $CHCl_3$ (δ = 7.26) as internal standard.

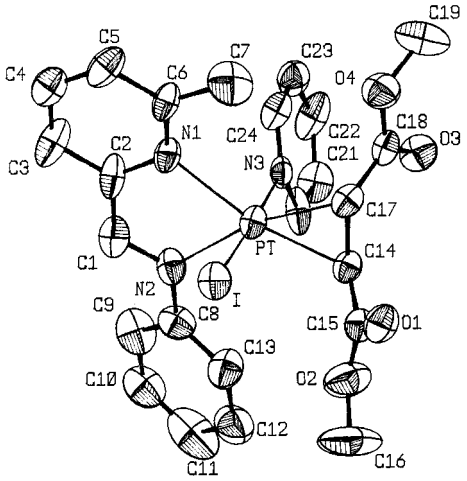


Figure 2. The molecular structure of the cation [PtI(py)(pimpy)(dimethyl fumarate)]$^+$ with the atom numbering scheme; the trigonal bipyramidal coordination sphere is clearly shown

gands iodide and pyridine occupy the axial positions, the pimpy ligand and the fumarate double bond are in the equatorial coordination sites. All the atoms of pimpy, except those of the phenyl group bonded to N2, lie in a plane almost coincidental with the equatorial coordination plane of Pt (the corresponding dihedral angle is ca. 3°). Also C14 and C17 of the olefin bond of dimethyl fumarate are contained in this plane with deviations of less than 0.01–0.02 Å. The phenyl group bonded to N2 is rotated about the

Table 2. Selected geometrical parameters for **1h**

Bond lengths (Å)	
Pt–I	2.616(2)
Pt–N(1)	2.209(8)
Pt–N(2)	2.21(1)
Pt–N(3)	2.08(1)
Pt–C(17)	2.10(1)
Pt–C(14)	2.116(9)
C(14)–C(17)	1.44(1)
Bond angles (°)	
C(14)–Pt–I	92.1(3)
N(1)–Pt–N(3)	91.9(4)
C(17)–Pt–I	93.2(3)
N(2)–Pt–N(3)	88.4(4)
N(1)–Pt–I	85.5(3)
C(17)–Pt–N(1)	122.2(4)
N(2)–Pt–I	90.5(3)
C(14)–Pt–N(2)	123.1(4)
C(14)–Pt–N(3)	90.5(4)
N(1)–Pt–N(2)	75.1(4)
C(17)–Pt–N(3)	88.5(5)
I–Pt–N(3)	177.4(4)
Torsion angles(°)	
C(18)–C(17)–C(14)–C(15)	133.6
C(1)–N(2)–C(8)–C(9)	26.9
C(14)–C(15)–O(2)–C(16)	–175.1
C(17)–C(18)–O(4)–C(19)	177.8

bond C8−N2 in order to relieve short contact interactions between HC9 and HC1 (here at 2.1 Å). The rotation is imposed by the pyridine group in the apical position on Pt such as to produce the most favourable contact distances between these two groups. The atoms C17 and C14, at distances of 1.44 Å, reveal, as found in several similar complexes,[13,14] a sharp dehybridization $sp^2 \rightarrow sp^3$ due to a consistent platinum-to-olefin back-donation. As a consequence, a rotation about the bond C14−C17 is allowed (here it is ca. 132°, i.e. 48° from a *trans* conformation). This rotation is imposed by stereochemical requirements in order to relieve intramolecular interactions, with I on one side (I···O1 = 3.4 Å; I···C15 = 3.3 Å) and the pyridine group on the other side (N3···C18 = 2.88 Å; N3···O3 = 2.95 Å). Repulsions between pimpy and dimethyl fumarate also cooperate to this effect, in particular C7 with O4, and C18 and C13 with O2. These interactions cannot be avoided through a rotation about the coordination axis of the olefin owing to demands imposed by the coordination geometry about the metal.[14] Dimethyl fumarate in its observed configuration seems to have no influence on the conformation or on the choice of coordination isomerism by the Schiff base at Pt (or vice versa, the Schiff base does not appear to induce any preference for the coordination of dimethyl fumarate in either of its prochiral configurations). Thus, we believe that the diastereoisomer examined here is the one favoured in the crystal only because of crystal field forces. All the other geometrical parameters are normal and have been exhaustively discussed in our previous structural reports.[12−14]

Cytotoxic Activity

The cytotoxic activity of six cisplatin (DDP) analogues were studied on a panel of three human carcinoma cell lines in comparison with the parent compound. The drugs were dissolved in DMSO and diluted with 0.9% NaCl solution. After further dilution in culture, DMSO is present at a concentration ranging from 0.01 to 1%. The pattern of cellular response is shown in Table 3.

Table 3. Cytotoxicity (IC_{50} μM) of type **I** compounds in comparison to DDP

Compound	A-2780	GLC-4	H-460
DDP	0.33 ± 0.06	0.53 ± 0.10	0.67 ± 0.10
1a	0.49 ± 0.18	1.59 ± 0.12	1.28 ± 0.49
1b	4.41 ± 0.02	1.96 ± 0.25	2.69 ± 0.60
1d	0.40 ± 0.07	0.40 ± 0.13	0.092 ± 0.003
1f	0.25 ± 0.16	0.58 ± 0.21	3.08 ± 0.95
1g	1.30 ± 0.12	1.85 ± 0.27	2.96 ± 0.59
1i	4.2 ± 0.6	2.39 ± 0.48	4.43 ± 1.44

Compound **1d** showed an activity similar to DDP on A2780 and GLC-4 cell lines, while on the H460 cell line the IC_{50} value was at least three orders of magnitude greater than that of the parent compound. The other analogues exhibited a cytotoxic potency lower or, at best, similar to that of DDP. The cytotoxic activity of **1d** was further evaluated on two additional ovarian cell lines (IGROV and SKOV-3) and on two leukaemia cell lines (human HL-60 and murine L1210). It exhibited a cytotoxic activity similar to (SKOV-3 cells) or three times higher (IGROV cells) than DDP, whereas on HL-60 and L1210 leukaemia its potency was lower (Table 4).

Table 4. Cytotoxicity (IC_{50} μM) of **1d** in comparison to DDP

Cell lines	DDP	**1d**
A 2780	0.33 ± 0.07	0.40 ± 0.07
A 2780/CP	3.3 ± 0.1	1.32 ± 0.03
H460	0.67 ± 0.10	0.09 ± 0.003
SKOV-3	4.2 ± 2.5	1.45 ± 0.33
IGROV	1.0 ± 0.7	0.13 ± 0.03
HL-60	0.40 ± 0.10	1.08 ± 0.35
L1210	1.0 ± 0.13	1.65 ± 0.07
GLC-4	0.53 ± 0.10	0.40 ± 0.13

In the A2780 sub-line selected for resistance to DDP (A2780/CP), characterised by an increased ability to repair drug-induced DNA damage, compound **1d** was cross-resistant to DDP with a Resistance Index (RI) value of 3 (vs. 10).

Conclusion

New cationic, water-soluble, trigonal bipyramidal complexes of platinum(II) were prepared by oxidative addition of $[I(py)_2]^+(NO_3^-)$ to suitable platinum(0) precursors. The products were tested for cytotoxicity against a panel of tumour cell lines of various histotypes. The data show that the new class of Pt^{II} five-coordinate complexes is endowed with promising antitumor properties. The next step will therefore be the characterisation of the antitumour efficacy of the compounds in vivo. In the meantime, studies evaluating the potential nephrotoxic effects of the molecule will be performed.

Experimental Section

General: NMR spectra were recorded at 250 or 200 MHz on a Bruker AC-250 or a Varian XL-200 spectrometer. The three-coordinate precursors [Pt(*N*,*N*-chelate)(olefin)][10] and $[I(py)_2]^+(NO_3^-)$[9] were prepared according to literature procedures. Solvents and reagents were of analytical grade and were used without further purification.

Type-1 Complexes: To a solution of the appropriate [Pt(*N*,*N*-chelate)(olefin)] precursor (0.20 mmol) in chloroform (1 mL) was added $[I(py)_2]^+(NO_3^-)$ (0.20 mmol) previously dissolved in the minimum amount of chloroform. Careful addition of diethyl ether prompted the crystallisation of the product, which was washed with diethyl ether and dried under vacuum (yield: 80−90%). In the case of the precursor [Pt(dmphen)(maleic anhydride)] the reaction was performed in tetrachloroethane.

X-ray Data Collection and Refinement of the Structure of 1h: A crystal of **1h** suitable for X-ray analysis was obtained from dichloro-

Table 5. Crystal data and experimental details for **1h**

Formula	$C_{24}H_{25}IN_4O_7Pt$[a]
M (g/mol)	803.5
Cryst. Syst.	Triclinic
Space group	*P*1(bar)
a, Å	13.511(2)
b, Å	13.754(2)
c, Å	8.678(1)
α (°)	95.2(1)
β (°)	92.5(1)
γ (°)	64.7(1)
Z	2
D (g/cm^3)	1.84
μ (Mo-*K*α) (cm^{-1})	56.67
F(000)	768
Cryst. Size (mm)	0.2×0.2×0.3
Scan speed (°/min)	2.0 in 2θ scan mode
2θ range (°)	3.0 ≤ 2θ ≤ 45
Measd. reflns.	6927
Scan width (°)	1.2
No. of data used [$I > 2\sigma(I)$]	5721
No. of params. refined	383
R[b], R_w[c]	0.060, 0.064
GOF[d]	1.11
Highest map residues (e/Å^3)	1.2[e]

[a] The probable presence of water of crystallization has not been considered. See text. – [b] $R = \Sigma||F_o| - |F_c||/\Sigma|F_o|$. – [c] $R_w = [\Sigma w(|F_o| - |F_c|)^2/\Sigma w|F_o|^2]^{1/2}$. – [d] GOF = $[\Sigma w(|F_o| - |F_c|)^2/(ND - NU)^2]^{1/2}$. – [e] This value is explained in the Experimental Section.

methane/diethyl ether. Crystal data, intensity data and processing details for **1h** are shown in Table 5.

The data were obtained with a Philips PW-100 four-circle automated diffractometer with graphite monochromator. Intensity data were collected at 25 °C using the θ−2θ scan method. Two reference reflections, monitored periodically, showed no significant variations in intensity. Data were corrected for Lorentz and polarization effects and an empirical absorption correction was applied (Ψ scan). The position of Pt was determined from a three-dimensional Patterson function. All the remaining atoms, except for the hydrogens, were located from successive Fourier maps using SHELX-76. The hydrogen atoms were located at calculated positions and refined with a fixed geometry with respect to their carrier atoms (C−H = 1.08 Å). Anisotropic thermal parameters were used for all the atoms except for the anion NO_3^- and the hydrogens. Blocked-cascade least-square refinements converged to $R = 0.060$.

Actually, the structure shows an appreciable degree of disorder due to the high libration of the anionic NO_3^- group which seems also to be solvated with one (or more likely less) water molecule through hydrogen bonds. This question could not be resolved through density measurements. The corresponding disorder could not be established with certainty from structure refinements and difference Fourier syntheses. These facts explain the relatively high value of the *R* index and the highest map residuals (see Table 5). Nonetheless, they do not invalidate the most relevant structural features here described.

Crystallographic data (excluding structure factors) for the structure reported in this paper have been deposited with the Cambridge Crystallographic Data Centre as supplementary publication no CCDC-143825. Copies of the data can be obtained free of charge on application to CCDC, 12 Union Road, Cambridge CB2 1EZ, UK [Fax: (internat.) + 44-1223/336-003; E-mail: deposit@ccdc.cam.ac.uk].

Evaluation of Cytotoxic Activity: The cytotoxicity of all compounds was studied on a variety of human tumour cell lines of different types, using the SRB assay.[15] Briefly, the A 2780 (1.0×10^4 cells/mL), A 2780/CP (7.0×10^3 cells/mL), SKOV-3 (4.0×10^4 cells/mL), IGROV-1 (2.5×10^4 cells/mL), L1210 (5.0×10^3 cells/mL), HL-60 (5×10^3 cells/mL), H460 (7×10^3 cells/mL) or GLC-4 (7×10^3 cells/mL) cell line was seeded in 96-well microtiter plates and incubated for 24 h at 37 °C in a 5% CO_2 incubator. Drugs were then added to the wells to achieve final drug concentrations ranging from 0.1 to 100 μM. After 24 h of drug exposure, the cells were washed twice with PBS and incubated in a drug-free medium for about three doubling times (72 h). The cells were then fixed with 16% TCA, incubated at 4 °C for 1 h and finally rinsed five times with tap water and dried thoroughly. The cells were stained with 100μL/well of SRB (0.4% in 1% acetic acid) for 15 min, rinsed five times in 1% glacial acetic acid and suspended in 10 mM TRIS-HCl (pH = 10.5) buffer solution. The absorbance was measured with Microplate Reader (BioRad MR 3550) at 570 nm. The results were expressed as IC_{50}, calculated from dose-response curves, and defined as the drug concentration required for a 50% reduction of absorbance compared to control cells. Each experiment was repeated at least three times.

Acknowledgments

We thank the Consiglio Nazionale delle Ricerche and the Ministero dell'Università e della Ricerca Scientifica (Programmi di Ricerca Scientifica di Rilevante Interesse Nazionale, Cofinanziamento 1998−1999) for financial support and the Centro Interdipartimentale di Metodologie Chimico-Fisiche, Università di Napoli "Federico II", for NMR facilities. A. P. and F. R. thank the Menarini for financial support. We thank also Prof. G. Valle for helpful assistance.

[1] C. Bonadonna, G. Robustelli Della Cuna, *Manuale di Oncologia Medica*, Masson Milan, **1992**.
[2] C. Meijer, N. H. Mulder, J. A. P. Hospers, D. R. A. Uges, E. G. E. De Vries, *British J. Cancer* **1990**, *62*, 72−77.
[3] V. G. Albano, G. Natile, A. Panunzi, *Coord. Chem. Rev.* **1994**, *133*, 67−114.
[4] S. Bartolucci, P. Carpinelli, V. De Felice, B. Giovannitti, A. De Renzi, *Inorg. Chim. Acta* **1992**, *197*, 51−57.
[5] S. Bartolucci, P. Carpinelli, F. Ruffo, *Anti Cancer Drug Design* **1995**, *10*, 43−49.
[6] E. Wong, C. M. Giandomenico, *Chem. Rev.* **1999**, *99*, 2451−2466.
[7] L. R. Kelland, C. F. J. Barnard, I. G. Evans, B. A. Murrer, B. C. Theobald, S. B. Wyer, P. M. Goddard, M. Jones, M. Valenti, A. Bryant, P. M. Rogers, K. R. Harrap, *J. Med. Chem.* **1995**, *38*, 3016−3024.
[8] J. Matsumani, H. Urata, K. Matsumoto, *Inorg. Chem.* **1995**, *34*, 202−208.
[9] R. A. Garrett, R. J. Gillespie, J. B. Senior, *Inorg. Chem.* **1965**, 563−566.
[10] A. De Renzi, V. De Felice, F. Ruffo, D. Tesauro, *Inorg. Chim. Acta* **1994**, *219*, 169−178.
[11] C. Castellari, V. De Felice, A. Panunzi, A. Vitagliano, A. Sanchez, *J. Organomet. Chem.* **1990**, *388*, 243−252.
[12] V. G. Albano, C. Castellari, V. De Felice, M. Monari, A. Panunzi, F. Ruffo, *Organometallics* **1992**, *11*, 3665−3669.
[13] L. Mantovani, A. Ceccon, A. Gambaro, S. Santi, P. Ganis, A. Venzo, *Organometallics* **1997**, *16*, 2682−2690.
[14] M. F. C. Guedes da Silva, J. J. R. Fraùsto da Silva, A. J. L. Pombeiro, R. Bertani, R. A. Michelin, M. Mozzon, F. Benetollo, G. Bombieri, *Inorg. Chim. Acta* **1993**, *214*, 85−95.
[15] P. Skehan, R. Storeng, D. A. Scudiero, A. Monks, J. McMahon, D. Vistica, J. T. Warren, H. Bokesh, S. Kenney, M. R. Boyd, *J. Nat. Cancer Institute* **1990**, *82*, 1107−1112.

Received January 25, 2000
[I00025]

Simple Preparations of the Anhydrous and Solvent-Free Uranyl and Cerium(IV) Triflates $UO_2(OTf)_2$ and $Ce(OTf)_4$ − Crystal Structures of $UO_2(OTf)_2(py)_3$ and $[\{UO_2(py)_4\}_2(\mu\text{-}O)][OTf]_2$

Jean Claude Berthet,*[a] Monique Lance,[b] Martine Nierlich,[b] and Michel Ephritikhine[a]

Keywords: Uranium / Cerium / Triflate complexes / Oxo complexes / Structure elucidation

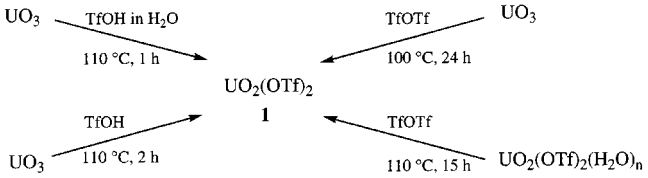
Treatment of UO_3 with pure triflic acid TfOH at 110 °C or with boiling triflic anhydride TfOTf afforded $[UO_2(OTf)_2]$ (**1**) in high yields. The latter was also prepared by the reaction of UO_3 with TfOH in water, or by dehydration of $[UO_2(OTf)_2(H_2O)_n]$ in boiling TfOTf. Anhydrous $[Ce(OTf)_4]$ (**2**) was similarly obtained from the commercially hydrated compound. X-ray analysis revealed that in $[UO_2(OTf)_2(py)_3]$ (**3**), the triflate ligands are monodentate whereas they are dissociated in $[\{UO_2(py)_4\}_2(\mu\text{-}O)][OTf]_2$ (**4**).

Introduction

Complexes of the uranyl moiety UO_2^{2+} are very familiar in actinide chemistry since considerable attention has been paid to their structure, physico-chemical properties and catalytic behaviour in a number of organic transformations.[1] It is interesting to note that most of these studies have been performed on compounds which were isolated from aqueous media. The development of anhydrous uranyl chemistry has long been impeded by the lack of easily available starting materials[2] and hence it is only very recently that a convenient preparation of $[UO_2Cl_2(THF)_3]$ has been reported.[3] In view of the major interest of metallic triflates in both organic[4] and inorganic syntheses,[5] and following our recent work on uranium triflates,[6] we decided to prepare the anhydrous and solvent-free uranyl and cerium (IV) triflates $[UO_2(OTf)_2]$ (**1**) and $[Ce(OTf)_4]$ (**2**). This will also be useful for further studies on the high oxidation-state chemistry of the f-block elements. Here we present convenient and large scale preparations of **1** and **2**; we also describe the X-ray crystal structures of the pyridine adduct $[UO_2(OTf)_2(py)_3]$ (**3**) (py = pyridine) and the μ-oxo derivative $[\{UO_2(py)_4\}_2(\mu\text{-}O)][OTf]_2$ (**4**).

Results and Discussion

Synthesis of the hydrated uranyl triflate $[UO_2(OTf)_2(H_2O)_n]$ was first performed by treating UO_3 with two equivalents of triflic acid in water.[7] Difficulties were encountered in the dehydration of this complex by the Kumagawa method, forming the acetonitrile adduct $[UO_2(OTf)_2(NCMe)_n]$ which was then used for the synthesis of inclusion compounds with crown-ethers. The anhydrous and solvent-free uranyl triflate **1** can be prepared by a number of different routes, as described in Scheme 1.



Scheme 1. Syntheses of the uranyl triflate **1**

A pale yellow solution was rapidly obtained by treating a suspension of uranium trioxide in water with a 10-fold excess of freshly distilled triflic acid. After evaporation and drying under vacuum at 200 °C, compound **1** was isolated as a pale yellow powder; the yields varied from 65 to 90%. This synthesis of **1** is analogous to that of UO_2Cl_2 by reaction of UO_3 with HCl.[8] However, thermal dehydration of uranyl triflate is straightforward whereas that of $[UO_2Cl_2(H_2O)_n]$ requires further treatment with dry HCl at 300 °C.[8] This was previously exploited in the preparation of anhydrous lanthanide(III) triflates,[9] and is related to the final sublimation of the triflic acid monohydrate [TfO][H_3O]. The synthesis of **1** can be described by Equation (1) and (2).

$$UO_3 + (2+x)\,TfOH \xrightarrow{H_2O} UO_2(OTf)_2.xL \quad (1)$$

$$UO_2(OTf)_2.xL \xrightarrow[\text{vacuum}]{200\ ^\circ C} UO_2(OTf)_2 + xL \quad (2)$$

1 L = [TfO][H_3O]

While UO_3 was found to react with HCl only in the presence of moisture,[8] it also reacted in suspension in pure TfOH to give **1,** which was recovered in almost quantitative yield after evaporation and prolonged heating at 200 °C under vacuum. However, direct reaction of metal oxides with anhydrous triflic acid may sometimes lead to the

[a] Laboratoire de Chimie de l'Uranium, Service de Chimie Moléculaire, DSM, DRECAM, CNRS URA 331,
CEA Saclay, Bat. 125, F-91191 Gif sur Yvette, France
Fax: (internat.) +33-1/6908-6640
E-mail: berthet@drecam.cea.fr
[b] Laboratoire de Cristallochimie, Service de Chimie Moléculaire, DSM, DRECAM, CNRS URA 331, CEA Saclay,
F-91191 Gif sur Yvette, France

 © WILEY-VCH Verlag GmbH, D-69451 Weinheim, 2000 1434−1948/00/0909−1969 $ 17.50+.50/0

formation of complexes solvated with the excess acid,[9] which can easily induce polymerization of THF,[10] a common solvent in uranium chemistry. Thus, the reaction of UO_3 with TfOH in aqueous solution should be preferred for the synthesis of **1**.

Nevertheless, the most convenient and efficient synthesis to **1** proved to be the reaction of uranium trioxide with triflic anhydride. A suspension of UO_3 in pure TfOTf was quantitatively transformed, after 24 h at 100 °C, into **1** which was easily recovered after evaporation of excess anhydride. The superiority of this synthetic route, shown in Equation (3), is related to the facile elimination of excess TfOTf, which is a poor coordinating reagent and has a lower boiling point (81−83 °C, 745 Torr) than triflic acid (162 °C, 760 Torr). In addition, reaction (3) does not generate side products, whereas sublimation of triflic acid hydrate, formed from reaction (2), requires a higher temperature (200 °C) and is time consuming.

$$UO_3 + TfOTf \xrightarrow{100\ ^\circ C} \underset{\mathbf{1}}{UO_2(OTf)_2} \quad (3)$$

Uranyl triflate **1**, like the other uranyl salts, is very hygroscopic and a practical dehydration method would be highly desirable. Triflic anhydride can also be used as a dehydrating agent and **1** was conveniently obtained by heating a suspension of $[UO_2(OTf)_2(H_2O)_n]$ in pure TfOTf at 110 °C for 15 h, according to Equation (4). Triflic acid is the only side product released during the process and was evaporated off with the excess anhydride.

$$UO_2(OTf)_2(H_2O)_n + n\ TfOTf \xrightarrow{110\ ^\circ C} \underset{\mathbf{1}}{UO_2(OTf)_2} + 2n\ TfOH \quad (4)$$

Irrespective of its mode of preparation, compound **1** was obtained in a pure state, as shown by the elemental analyses and the IR spectra, which confirm the absence of hydrated species.

In a similar way, with TfOTf as a dehydrating agent, the anhydrous cerium(IV) triflate $Ce(OTf)_4$ (**2**) was isolated as a pale yellow powder from the commercially available bright yellow compound $[Ce(OTf)_4(H_2O)_n]$ (n = 2−5) [Equation (5)]. After drying for 15 h at 100 °C, no reduction to Ce^{III} species was observed; the purity of **2** was established by elemental analyses as well as from IR and NMR spectra. $[Ce(OTf)_4(H_2O)_{1.5}]$ was previously prepared by successive treatment of cerium(IV) ammonium nitrate with potassium carbonate and triflic acid in water but could not be further dehydrated because of its decomposition above 120 °C into a trivalent cerium(III) species.[11] In addition to its applications in organic synthesis as a strong Lewis acid and oxidizing agent, compound **2** would be considered as a valuable precursor for the preparation of new cerium(IV) derivatives, while $CeCl_4$ is not stable, and its chemistry could be compared to that of its 5f analogue $U(OTf)_4$.[6b]

$$Ce(OTf)_4(H_2O)_n + n\ TfOTf \xrightarrow{20\ ^\circ C} \underset{\mathbf{2}}{Ce(OTf)_4} + 2n\ TfOH \quad (5)$$

In the solid state, compounds **1** and **2** are likely to adopt a polymeric structure with OTf bridges; such a structure has previously been found in some uranyl alkylsulfonate compounds which form infinite chains with bidentate bridging RSO_3 groups.[12,13] Compounds **1** and **2** are soluble in coordinating solvents like pyridine, THF and diethyl ether, giving stable Lewis base adducts.

The X-ray crystal structure of the mononuclear complex $[UO_2(OTf)_2(py)_3]$ (**3**) is shown in Figure 1 together with selected bond lengths and angles. The uranium atom is found in the most common pentagonal bipyramidal configuration of uranyl complexes with the equatorial plane defined by three nitrogen atoms of the pyridine ligands and two oxygen atoms of the triflate groups that are monodentate and non-adjacent. The U−O(triflate) bond lengths of 2.370(2) and 2.394(2) Å are identical to those found in $[UO_2(OTf)_2(H_2O)_3{\cdot}2benzo\text{-}15\text{-}crown\text{-}5]$ [2.38(1) and 2.392(9) Å][14] and in the monomeric sulfonato complexes $[UO_2(O_3SR)_2(H_2O)_3]$ (R = *p*-tolyl or mesityl) which vary from 2.355(6) to 2.406(7) Å.[13] The structural parameters of the OTf ligand are unexceptional. The structure of $[UO_2(OTf)_2(THF)_3]$, which could not be solved with good accuracy because of the poor quality of the crystals, shows the same arrangement of the equatorial ligands as in the above pyridine adduct **3** or the bromide analogue $[UO_2Br_2(THF)_3]$.[15]

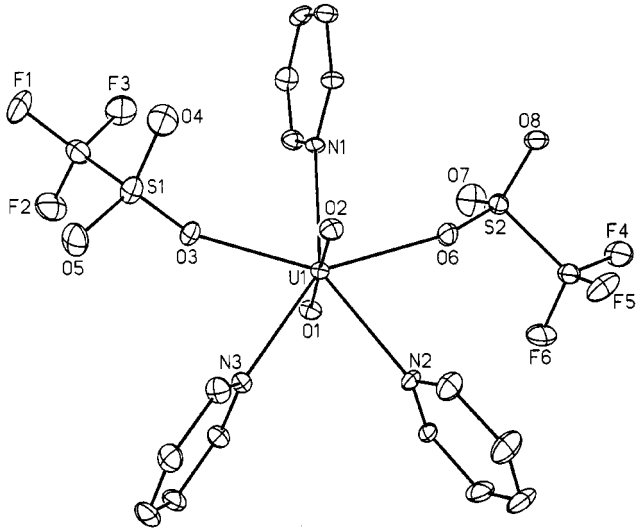


Figure 1. X-ray crystal structure of $UO_2(OTf)_2(py)_3$ (**3**) with thermal ellipsoids at the 40% probability level; selected bond lengths (Å) and angles (°): U−O(1) 1.744(2), U−O(2) 1.747(2), U−O(3) 2.370(2), U−O(6) 2.394(2), U−N(1) 2.529(2), U−N(2) 2.541(2), U−N(3) 2.518(2); O(1)−U−O(2) 178.49(9), N(1)−U−O(3) 72.82(7), N(1)−U−O(6) 73.00(8), N(3)−U−O(3) 73.47(7), N(2)−U−O(6) 71.06(8), N(2)−U−N(3) 69.71(8)

During one of the crystallizations of the bright yellow needles of **3**, a few round, yellow-green crystals were also deposited. X-ray analysis revealed that the μ-oxo complex $[\{UO_2(py)_4\}_2(\mu\text{-}O)][OTf]_2$ (**4**) had been formed, almost certainly after partial hydrolysis of **3** with adventitious traces

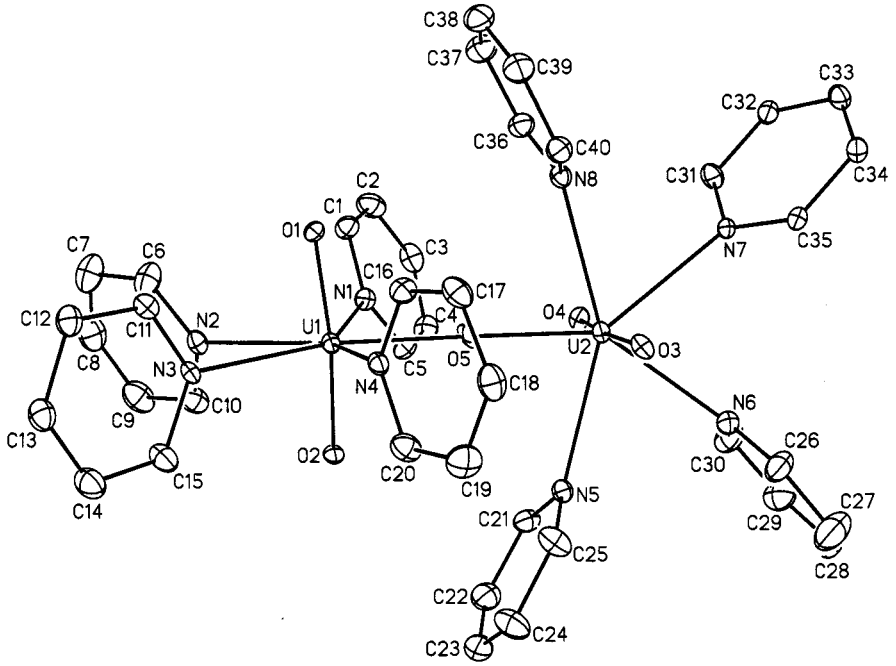


Figure 2. X-ray crystal structure of $[\{UO_2(py)_4\}_2(\mu\text{-}O)][OTf]_2$ (**4**) with thermal ellipsoids at the 15% probability level; selected bond lengths (Å) and angles (°): U(1)−O(1) 1.765(5), U(1)−O(2) 1.778(4), U(1)−N(1) 2.615(5), U(1)−N(2) 2.609(6), U(1)−N(3) 2.589(5), U(1)−N(4) 2.579(5), U(1)−O(5) 2.105(5), U(2)−O(3) 1.779(4), U(2)−O(4) 1.777(4), U(2)−N(5) 2.572(6), U(2)−N(6) 2.610(6), U(2)−N(7) 2.601(6), U(2)−N(8) 2.582(6), U(2)−O(5) 2.085(5); O(1)−U(1)−O(2) 173.1(2), N(1)−U(1)−N(2) 68.33(18), N(2)−U(1)−N(3) 71.88(17), N(3)−U(1)−N(4) 68.33(17), N(4)−U(1)−O(5) 74.81(17), N(1)−U(1)−O(5) 77.27(18), O(3)−U(2)−O(4) 171.5(2), N(5)−U(2)−N(6) 68.1(2), N(6)−U(2)−N(7) 73.35(19), N(7)−U(2)−N(8) 69.73(18), N(8)−U(2)−O(5) 74.3(2), N(5)−U(2)−O(5) 75.7(2), U(1)−O(5)−U(2) 173.7(2)

of water in the solvent. Compound **4** was obtained in larger quantities by crystallization of $[UO_2(OTf)_2(H_2O)_n]$ from pyridine/diethyl ether. The crystals of **4** are composed of discrete OTf anions, which display the expected geometry, and of $[\{UO_2(py)_4\}_2(\mu\text{-}O)]$ dications, the structure of which is shown in Figure 2 with selected bond lengths and angles. The pentagonal bases of each uranyl moiety, composed of the four nitrogen atoms of the pyridine ligands and the common oxygen atom of the μ-oxo group, are nearly orthogonal, intersecting at an angle of 88.3(1)°. The U(1)−O(5)−U(2) bridge is almost linear [173.7(2)°] with short metal−oxygen bond lengths which average 2.09(1) Å, reflecting a π interaction between the bridging oxygen and the metal.[16] This geometry of pseudo-D_{2d} symmetry is the best for the minimization of steric interactions between the two metallic fragments. It is interesting to note that, while linearly oxo-bridged binuclear compounds of early transition metals, lanthanides(III) and actinides(IV) are well documented,[17] compound **4** represents, to the best of our knowledge and from a search of the data of the Cambridge Crystallography Centre, the first example of such a uranyl complex. The other oxo bridged derivatives of uranyl exhibit a higher nuclearity ensured by μ_3-O bridges.[18]

In both **3** and **4**, the U−O bond lengths of the UO_2 moieties are unexceptional, ranging from 1.744(2) Å to 1.780(3) Å, as are the U−N(py) bond lengths which vary from 2.518(2) to 2.614(3) Å. These values compare well with those found in $[UO_2(NO_3)_2(py)_2]$ [<U−O> = 1.751(15) Å, U−N = 2.543(15) Å],[19a] $[UO_2(C_{15}H_{11}O_2)_2(py)]$ [<U−O> = 1.75(1) Å, U−N = 2.569(6) Å][19b] and $[UO_2(C_8H_{13}O_3)_2(py)]$ [<U−O> = 1.76(2) Å, U−N = 2.595(24) Å].[19b] It is noteworthy that, in contrast to **3**, the OTf groups of **4** are totally dissociated, having been replaced with pyridine ligands. This distinct behaviour is difficult to explain. More generally, the triflate ligands in $[UO_2(OTf)_2(H_2O)_3\cdot 2benzo\text{-}15\text{-}crown\text{-}5]$[14] and all the crystallographically characterized triflates of U^{III} and U^{IV} − $[U(OTf)_2(OPPh_3)_4][OTf]$,[6b] $[U(OTf)_4(OPPh_3)_3]$,[6c] $[U(C_5H_5)_3(OTf)(CNtBu)]$,[6a] $[U(C_5Me_5)_2(OTf)_2(H_2O)]$,[6a] and $[U(C_8H_8)(OTf)_2(OPPh_3)_2]$[6c] − were found not to have been displaced by strong oxygen and nitrogen Lewis bases. This clearly indicates that the uranium−triflate bond, whatever the metal oxidation state, is not as weak as could be expected.

Experimental Section

All preparations were carried out under argon (less than 2 ppm oxygen and water) using standard Schlenk- and vacuum-line techniques, or in a glove box. Solvents were thoroughly dried and deoxygenated by standard methods and distilled immediately before use. $[D_8]$THF was dried over Na-K alloy. IR spectra were obtained on a Perkin−Elmer 1725X spectrometer. Elemental analyses were performed by Analytische Laboratorien at Lindlar (Germany). The yellow powder of UO_3 was supplied by the Commissariat à l'Energie Atomique. $[Ce(OTf)_4(H_2O)_n]$ was supplied by Aldrich. Triflic acid (98 or 99%, Aldrich) and triflic anhydride (99%, Aldrich) were

distilled before use. $[UO_2(OTf)_2(H_2O)_n]$ was synthesized as previously reported.[7]

Uranyl Triflate $UO_2(OTf)_2$ (1). − From UO_3 and TfOH in Water: In the glove box, freshly distilled triflic acid (620 mL, 7 mmol) was added with a microsyringe into a 100 mL round-bottomed flask containing a suspension of UO_3 (210 mg, 0.7 mmol) in deoxygenated and demineralized water (15 mL). The trioxide was dissolved in a few minutes and the pale yellow solution was then refluxed for one hour to ensure complete reaction. Water was then evaporated off under vacuum and collected in a trap connected between the flask and the vacuum line and cooled in liquid nitrogen. The pale yellow residue was further heated at ca 200 °C under vacuum for 24 h and the white solid of $[TfO][H_3O]$ was eliminated by sublimation. During this step, the viscous drops that appeared on the upper walls of the flask were heated with a hot air stripper. Compound **1** was isolated as a pale yellow powder with yields varying from 65 to 90%; it turned bright yellow in air because of rapid hydration. − $C_2F_6O_8S_2U$ (568): calcd. C 4.22, F 20.06, S 11.28; found C 4.40, F 19.85, S 11.43. − IR (KBr in air): $\tilde{\nu}$ = 3593 (m), 3509 (m), 3217 (s) 1598 (s), 1262 (s), 1179 (s), 1034 (s), 950 (w), 905 (U=O, s), 769 (s), 643 (s), 581 (w), 519 (w), 478 (m); the IR spectrum of **1** in nujol between KBr plates shows no bands for water in the region 3600−3000 cm^{-1}.

From UO_3 and Pure TfOH: Triflic acid (ca 3 mL) was distilled into a 100 mL round-bottomed flask containing UO_3 (320 mg, 1.1 mmol) and the mixture was magnetically stirred for 2 h at 110 °C. The excess TfOH was distilled under vacuum into a trap cooled in liquid nitrogen and connected between the flask and the vacuum line. Compound **1** was obtained in 87% yield (550 mg) after drying for 24 h at 200 °C under vacuum. The IR spectra were identical to those described above.

From UO_3 and TfOTf: Freshly distilled triflic anhydride (ca 3 mL) was added in the glove box into a 100 mL round-bottomed flask containing UO_3 (205 mg, 0.7 mmol). The suspension was refluxed for 24 h whilst magnetically stirring. The excess TfOTf was distilled under vacuum into a trap connected between the flask and the vacuum line and cooled in liquid nitrogen. Further drying of the residue for 1 h at 100 °C under vacuum afforded **1** in 96% yield (340 mg). − $C_2F_6O_8S_2U$ (568): calcd. C 4.22, F 20.06, S 11.28; found C 4.37, F 19.81, S 11.37. The IR spectra were identical to those described above.

By Dehydration of $UO_2(OTf)_2(H_2O)_n$ with TfOTf: Triflic anhydride (ca 3 mL) was distilled under vacuum into a 100 mL round-bottomed flask containing the hydrated uranyl triflate $[UO_2(OTf)_2(H_2O)_n]$ (352 mg) and the bright yellow suspension was magnetically stirred at 110 °C for 15 h; the initial colour of the solid turned pale yellow. After cooling to room temperature, excess TfOTf was distilled off and **1** was obtained in almost quantitative yield (330 mg) after drying at 200 °C for 20 h under vacuum. − $C_2F_6O_8S_2U$ (568): calcd. C 4.22, F 20.06, S 11.28; found C 4.29, F 19.94, S 11.32. The IR spectra were identical to those described above.

Cerium(IV) Triflate $Ce(OTf)_4$ (2): Triflic anhydride (ca 3 mL) was distilled under vacuum into a 50 mL round-bottomed flask containing the hydrated cerium(IV) triflate $[Ce(OTf)_4(H_2O)_n]$ (500 mg). The yellow suspension was magnetically stirred for 1 h at 50 °C and then for 15 h at room temperature. The excess TfOTf was evaporated off and the pale yellow residue was dried under vacuum, first at room temperature for 10 h and then at 100 °C for 15 h. Compound **2** was obtained in almost quantitative yield (450 mg); its colour turned bright yellow upon exposure to air. − $C_4CeF_{12}O_{12}S_4$ (736): calcd. C 6.52, S 17.42; found C 6.39, S 17.25. Whereas the ^1H NMR spectrum of the commercially available $[Ce(OTf)_4(H_2O)_n]$ shows a broad signal at δ = 13.6 corresponding to H_2O, the spectrum of **2** in $[D_8]$THF confirms the absence of water and traces of triflic acid; polymerization of the solvent was not observed after 10 days. IR of $Ce(OTf)_4(H_2O)_n$ (KBr): $\tilde{\nu}$ = 3443 (s), 1660 (m), 1636 (m), 1244 (s), 1187 (m), 1031 (s), 771 (w), 640 (s), 582 (m), 524 (s). The IR spectrum of **2** in nujol between KBr plates shows no bands for H_2O; the IR spectrum of **2** in KBr pellet carried out in air is identical to that of $[Ce(OTf)_4(H_2O)_n]$.

X-ray Crystallography of 3: Single crystals were obtained by slow diffusion of diethyl ether into a solution of **3** in pyridine. A yellow crystal of approximate dimensions 0.30 × 0.20 × 0.15 mm was selected. Diffraction collection was carried out on a Nonius diffractometer equipped with a CCD detector. The lattice parameters were determined from ten images recorded with 1° Φ-scans and later refined on all data. The data were recorded at 173 K. A 180° Φ-range was scanned with 2° steps with a crystal-to-detector distance fixed at 35 mm. Data were corrected for Lorentz-polarization and absorption[20] effects. The structure was solved by the heavy-atom method and refined by full-matrix least-squares on F^2 with anisotropic thermal parameters for all non-H atoms. H atoms were introduced at calculated positions and constrained to ride on their parent C atom. $C_{17}H_{15}F_6N_3O_8S_2U$ (805.47), monoclinic, space group $P2_1/n$, a = 8.5920(17), b = 15.733(3), c = 18.687(4) Å, β = 94.73(3)°, V = 2517.5(9) $Å^3$, Z = 4, D_c = 2.125 g cm^{-1}, Mo-$K\alpha$ (λ = 0.71073 Å), μ_{Mo} = 6.705 mm^{-1}, $F(000)$ = 1520, total reflections = 12022, independent reflections = 3361 (R_{int} = 0.077), observed reflections [$I > 2\sigma(I)$] = 2864, R_1 = 0.0334, wR_2 = 0.0890. All calculations were performed on an O2 Silicon Graphics Station with the SHELXTL package.[21]

X-ray Crystallography of 4: During one of the crystallizations of **3**, a few single crystals of **4** were deposited. A yellow crystal of approximate dimensions 0.35 × 0.25 × 0.20 mm was selected. Diffraction collection was carried out on a Nonius diffractometer equipped with a CCD detector. The lattice parameters were determined from ten images recorded with 1° Φ-scans and later refined on all data. The data were recorded at 173 K. A 180° Φ-range was scanned with 2° steps with a crystal to detector distance fixed at 35 mm. Data were corrected for Lorentz-polarization and absorption [20] effects. The structure was solved by the heavy-atom method and refined by full-matrix least-squares on F^2 with anisotropic thermal parameters for all non-H atoms. H atoms were introduced at calculated positions and constrained to ride on their parent C atom. Due to imperfect absorption corrections and rather poor quality of data, the U−O−U angles of the uranyl fragments deviate from linearity. $C_{42}H_{40}F_6N_8O_{11}S_2U_2$ (1487.0), monoclinic, space group $P2_1/c$, a = 19.352(4), b = 13.248(3), c = 19.631(4) Å, β = 91.12(3)°, V = 5031.9(17) $Å^3$, Z = 4, D_c = 1.963 g cm^{-1}, Mo-K_α (λ = 0.71073 Å), μ_{Mo} = 6.597 mm^{-1}, $F(000)$ = 2824, total reflections = 12163, independent reflections = 6686 (R_{int} = 0.073), observed reflections [$I > 2\sigma(I)$] = 4744, R_1 = 0.047, wR_2 = 0.102. All calculations were performed on an O2 Silicon Graphics Station with the SHELXTL package.[21]

Crystallographic data (excluding structure factors) for the structures reported in this paper have been deposited with the Cambridge Crystallographic Data Centre as supplementary publication nos. CCDC-138645 **(3)** and -138646 **(4)**. Copies of the data can be obtained free of charge on application to CCDC, 12 Union Road, Cambridge CB2 1EZ, UK [Fax: (internat.) +44-1223/336-033; E-mail: deposit@ccdc.cam.ac.uk].

[1] [1a] A. F. Wells, in *Structural Inorganic Chemistry*, chapter 28, Clarendon Press, Oxford, **1995**. – [1b] J. H. Burns, in *The Chemistry of the Actinide Elements* (Eds.: J. J. Katz, G. T. Seaborg and L. R. Morss) vol. 2, Chapman and Hall, New York, **1986**. – [1c] V. van Axel Castelli, R. Cacciapaglia, G. Chiosis, F. C. J. M. van Veggel, L. Mandolini, D. N. Reinhoudt, *Inorg. Chim. Acta* **1996**, *246*, 181. – [1d] W. D. Wang, A. Bakac, J. H. Espenson, *Inorg. Chem*. **1995**, *34*, 6034. – [1e] M. Shimazu, K. Shinozuka, *Angew. Chem. Int. Ed. Engl*. **1993**, *32*, 870.

[2] [2a] J. A. Leary, J. F. Suttle, *Inorg. Synth*. **1957**, *5*, 148. – [2b] C. J. Burns, D. C. Smith, A. P. Sattelberger, H. B. Gray, *Inorg. Chem*. **1992**, *31*, 3724.

[3] M. P. Wilkerson, C. J. Burns, R. T. Paine, B. L. Scott, *Inorg. Chem.* **1999**, *38*, 4156.

[4] [4a] S. Kobayashi, M. Moriwaki, I. Hachiya, *Bull. Chem. Soc. Jap.* **1997**, *70*, 267. – [4b] S. Kobayashi, *Synlett.* **1994**, 689.

[5] [5a] G. A. Lawrance, *Chem. Rev.* **1986**, *86*, 17. – [5b] U. Kilimann, M. Schäfer, R. Herbst-Irmer, F. T. Edelman, *J. Organomet. Chem*. **1994**, *469*, C5, C10. – [5c] S. Y. Liu, G. H. Maunder, A. Sella, M. Stevenson, D. A. Tocher, *Inorg. Chem*. **1996**, *35*, 76.

[6] [6a]J. C. Berthet, M. Lance, M. Nierlich, M. Ephritikhine, *Chem. Commun*. **1998**, 1373. – [6b] J. C. Berthet, M. Lance, M. Nierlich, M. Ephritikhine, *Eur. J. Inorg. Chem*. **1999**, 2005. – [6c] J. C. Berthet, M. Lance, M. Nierlich, M. Ephritikhine, unpublished results.

[7] [7a] J. M. Sabattié, Internal Report, CEA Saclay, **1992**. – [7b] L. Deshayes, N. Keller, M. Lance, A. Navaza, M. Nierlich, J. Vigner, *Polyhedron* **1994**, *13*, 1725.

[8] [8a] J. J. Katz and E. Rabinowitch, in *The Chemistry of Uranium: the Element, its Binary and Related Compounds*, chapter 16, Dover Publications, New York, **1961**. – [8b] G. Prins, in *Uranyl Chloride, its Hydrates and Basic Salts*, RCN-186, Reactor Centrum Nederlands, **1973**.

[9] M. El M. Hamidi, J. L. Pascal, *Polyhedron* **1994**, *13*, 1787.

[10] F. Calderazzo, G. E. De Benedetto, S. Detti, G. Pampaloni, *J. Chem. Soc., Dalton Trans.* **1997**, 3319 and references herein.

[11] T. Imamoto, Y. Koide, S. Hiyama, *Chem. Lett.* **1990**, 1445.

[12] A. S. Wilson, *Acta Crystallogr., Sect. B* **1978**, *34*, 2302.

[13] N. W. Alcock, T. J. Kemp, J. Leciejewicz, *Inorg. Chim. Acta* **1993**, *203*, 81.

[14] P. Thuéry, M. Nierlich, N. Keller, M. Lance, J. D. Vigner, *Acta Crystallogr., Sect. C* **1995**, *51*, 1300.

[15] J. Rebizant, G. Van den Bossche, M. R. Spirlet, J. Goffart, *Acta Crystallogr., Sect. C* **1987**, *43*, 1298.

[16] F. A. Cotton, D. O. Marler, W. Schwotzer, *Inorg. Chem*. **1984**, *23*, 4211.

[17] J. C. Berthet, J. F. Le Maréchal, M. Nierlich, M. Lance, J. Vigner, M. Ephritikhine, *J. Organomet. Chem.* **1991**, *408*, 335 and references herein.

[18] [18a] R. L. Lintvedt, M. J. Heeg, N. Ahmad, M. D. Glick, *Inorg. Chem*. **1982**, *21*, 2350. – [18b] P. Charpin, M. Lance, M. Nierlich, J. D. Vigner, J. Livet, C. Musikas, *Acta Crystallogr., Sect. C* **1986**, *42*, 1691. – [18c] G. Van den Bossche, M. R. Spirlet, J. Rebizant, J. Goffart, *Acta Crystallogr., Sect. C* **1987**, *43*, 837. – [18d] U. Turpeinien, R. Hamalainen, I. Mutikainen, O. Orama, *Acta Crystallogr., Sect. C* **1996**, *52*, 1169. – [18e] P. Thuéry, M. Nierlich, B. Souley, Z. Asfari, J. Vicens, *J. Chem. Soc., Dalton Trans.* **1999**, 2589.

[19] [19a] M. Pennington, N. W. Alcock, D. J. Flanders, *Acta Crystallogr., Sect. C* **1988**, *44*, 1664. – [19b] N. W. Alcock, D. J. Flanders, M. Pennington, D. Brown, *Acta Crystallogr., Sect. C* **1987**, *43*, 1476.

[20] A. L. Spek, MULABS. *PLATON*, University of Utrecht, The Netherlands, **1997**.

[21] *SHELXTL*: Sheldrick **1999**, Bruker-AXS, Madison, WI, USA.

Received January 17, 2000
[I00008]

Transition Metal Complexes with Sulfur Ligands, 142[‡]

Inert and Labile [Ru(L)('pyS_4')] Complexes with Rigid [$RuNS_4$] Cores and *trans*-Thiolate Donors [L = PPh_3, PEt_3, DMSO, CO, NO^+, N_2H_4; 'pyS_4'$^{2-}$ = 2,6-Bis(2-mercaptophenylthio)dimethylpyridine(2–)]

Dieter Sellmann,*[a] Klaus Engl,[a] and Frank W. Heinemann[a]

Dedicated to Professor Wilhelm Preetz on the occasion of his 65th birthday

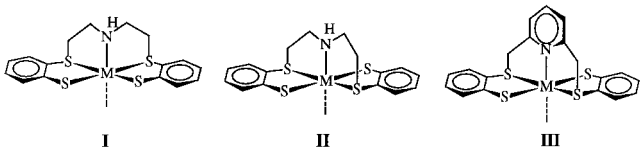
Keywords: Ruthenium / Sulfur ligands / Exchange reactions

In a quest for ruthenium complexes having [$RuNS_4$] cores, a non-fluxional configuration, *trans*-thiolate donors, and exchangeable coligands L, [Ru(L)('pyS_4')] complexes have been synthesized ['pyS_4'$^{2-}$ = 2,6-bis(2-mercaptophenylthio)dimethylpyridine(2–)]. Treatment of [$RuCl_2(PPh_3)_3$] with 'pyS_4'$^{2-}$ gave [Ru(PPh_3)('pyS_4')] (**1**). Alkylation of **1** with excess MeI yielded [Ru(PPh_3)('pyS_4'–Me_2)]I_2 (**2**). [Ru(DMSO)('pyS_4')] (**3**) was obtained from [$RuCl_2(DMSO)_4$] and 'pyS_4'$^{2-}$. The PPh_3 or DMSO coligands in **1**, **2**, and **3** proved to be very inert to substitution. Only the DMSO could be displaced by CO under drastic conditions yielding [Ru(CO)('pyS_4')] (**4**). Treatment of [$RuCl_2(CH_3CN)_4$] with 'pyS_4'$^{2-}$ yielded [Ru('pyS_4')]$_2$ (**5**); in the presence of PEt_3 or N_2H_4 mononuclear [Ru(PEt_3)('pyS_4')] (**6**) and [Ru(N_2H_4)('pyS_4')] (**7**) were formed. Template alkylation of NBu_4[Ru(NO)($S_2C_6H_4$)$_2$] with 2,6-bis(tosyloxymethyl)pyridine gave [Ru(NO)('pyS_4')]Tos (**8**). Complex **8** proved to be the best suited precursor for L exchange reactions. Under reducing conditions, **8** releases its NO ligand and the resulting [Ru('pyS_4')] fragments can combine either with each other to give **5**, or with PEt_3 and N_2H_4 to yield **6** and **7**, respectively. All complexes have been characterized by spectroscopic methods and elemental analysis; **1**, **2**, **3**, and **4** have also been submitted to X-ray structure analysis.

Introduction

Transition metals in sulfur-dominated coordination spheres form the active centers of numerous oxidoreductases, e.g. of nitrogenases, hydrogenases, and CO dehydrogenases.[1] Efforts to elucidate the molecular mechanisms of the enzyme reactions and to find competitive catalysts with enzyme-like activity are a major impetus in the search for low molecular weight complexes that combine structure and reactivity features of the enzyme metal–sulfur [MS] centers.[2] An important aspect of this search is the design of new ligands that meet specific requirements with regard to donor atom sets, configurations, stability, and reactivity of the resulting complexes.[3]

In this respect, the 'N_HS_4'$^{2-}$ [= 2,2'-bis(2-mercaptophenylthio)diethylamine(2–)] ligand has proved particularly versatile.[4] It has yielded a large number of [Fe(L)('N_HS_4')] complexes with L comprising the nitrogenase-relevant molecules CO, NO, N_2H_2, N_2H_4, and NH_3, although not N_2. This prompted us to investigate the coordination behaviour of 'N_HS_4'$^{2-}$ towards ruthenium as well; it was anticipated that with the kinetically more inert ruthenium, species that are labile with iron would become isolable. However, practically all our experiments in this area proved unsuccessful. Besides the problem of finding [Ru(L)('N_HS_4')] complexes with exchangeable coligands L, the diastereoisomerism of the [M('N_HS_4')] fragments led to the formation of inseparable mixtures of diastereomeric [Ru(L)('N_HS_4')] species. In [M(L)('N_HS_4')] complexes, the [M('N_HS_4')] fragments can exist in two diastereomeric forms, indicated by formulae I and II (Scheme 1).



Scheme 1. Configurations of [MNS_4] complexes

While in the case of iron these diastereomers isomerize via five-coordinate intermediates to yield, depending on the coligand L, either I or II,[4,5] the ruthenium analogues do not isomerize, due to the inert nature of the ruthenium donor bonds. In order to eliminate this problem, we replaced the flexible $N(C_2H_4)_2$ bridge of the 'N_HS_4'$^{2-}$ ligand by the rigid 2,6-bis(methylene)pyridine bridge and synthesized the ligand 'pyS_4'$^{2-}$ [= 2,6-bis(2-mercaptophenylthio)-dimethylpyridine(2–)].[6] This 'pyS_4'$^{2-}$ ligand indeed yielded iron complexes consistently containing the fragment III.[6,7] It is also noteworthy that the hydrazine complex [Fe(N_2H_4)('pyS_4')] contains a low-spin Fe^{II} center,[7] in con-

[‡] Part 141: D. Sellmann, F. Geipel, M. Moll, *Angew. Chem.*, in press.

[a] Institut für Anorganische Chemie der Universität Erlangen-Nürnberg,
Egerlandstrasse 1, D-91058 Erlangen, Germany
Fax: (internat.) +49(0)9131/852 7367
E-mail: sellmann@anorganik.chemie.uni-erlangen.de

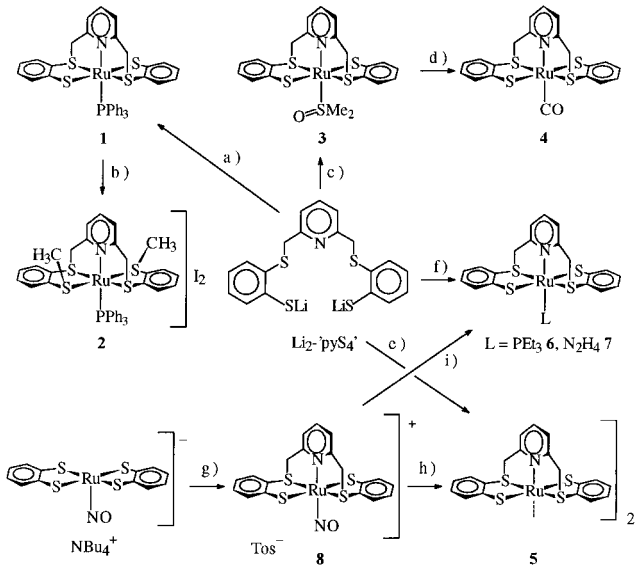
 © WILEY-VCH Verlag GmbH, D-69451 Weinheim, 2000 1434–1948/00/0303–423 $ 17.50+.50/0

trast to the [Fe(N_2H_4)('N_HS_4')] complex, which has the core structure I and a high-spin Fe^{II} center.

In this paper we report our efforts to synthesize [Ru(L)('pyS_4')] complexes and to find species in which the L coligands may be displaced by nitrogenase-relevant small molecules. The exchange of L proved to be the major problem.

Results

The HCl adduct ('pyS_4'–H_2) · HCl served as the starting material for preparing the ligand. It was routinely deprotonated with three equivalents of LiOMe to give Li_2'pyS_4'. The subsequent reactions of Li_2'pyS_4' with suitable Ru precursor complexes are summarized in Scheme 2.



Scheme 2. Syntheses and reactions of [Ru('pyS_4')] complexes; (a) + [$RuCl_2(PPh_3)_3$]/MeOH/15 h/room temp.; (b) + exc. CH_3I/THF/2 d/room temp.; (c) + [$RuCl_2(DMSO)_4$]/MeOH/15 h/room temp.; (d) + CO, 120 bar/THF/110 °C/3 d; (e) + [$RuCl_2(CH_3CN)_4$]/MeOH/4 h reflux; (f) + [$RuCl_2(CH_3CN)_4$]/exc. L (L = PEt_3, N_2H_4)/MeOH/4 h reflux; (g) + 'pyTos'/THF/4 h reflux; (h) + 2.5 $LiBEt_3H$/THF/2.5 d room temp.; (i) + exc. L (L = PEt_3, N_2H_4)/THF/room temp.

The PPh_3 complex [Ru(PPh_3)('pyS_4')] (**1**) was found to be readily soluble in CH_2Cl_2 or THF. Although PPh_3 is a relatively bulky ligand, it proved practically inert to substitution. As yet, we have not been able to exchange it by N_2H_4 or even CO, neither under standard conditions nor at elevated temperatures. Attempts to labilize the Ru–PPh_3 bond of **1** by alkylation of the thiolate donors using excess CH_3I gave [Ru(PPh_3)('pyS_4'–Me_2)]I_2 (**2**), which contains the 'pyS_4'–Me_2 ligand. Complex **2** was formed in diastereomerically pure form. The PPh_3 ligand in **2** has proved to be as substitution inert as that in **1**. Our next target complex was [Ru(DMSO)('pyS_4')] (**3**) as we anticipated that the DMSO ligand would be as labile as that in the related [Ru(DMSO)(PR_3)('S_4')] complexes with R = Cy, *i*Pr; 'S_4'$^{2-}$ = 1,2-bis(2-mercaptophenylthio)ethane(2–).[8a] However, the DMSO ligand in **3** also proved very inert and could not be exchanged for CO at room temperature at pressures ranging from 1–100 bar. Only under very drastic conditions in an autoclave (120 bar CO, 110 °C, THF) did a slow reaction (3 d) take place to give [Ru(CO)('pyS_4')] (**4**). Another potentially labile target complex was [Ru(CH_3CN)('pyS_4')]. Its synthesis was attempted starting from [$RuCl_2(CH_3CN)_4$] and Li_2'pyS_4'. However, heating in MeOH proved necessary in order to observe a reaction, and the resulting product was found not to contain CH_3CN. A red-brown solid precipitated, which was found to be practically insoluble in all common solvents. Its IR spectrum, elemental analysis, and mass spectrum, which featured an ion peak at *m/z* = 973, were compatible with the dinuclear [Ru('pyS_4')]$_2$ (**5**). Complex **5** was found not to react with boiling DMSO, pyridine, or with CO in these solvents. The reaction of [$RuCl_2(CH_3CN)_4$] with Li_2'pyS_4' took a different course when potential ligands such as PEt_3 or N_2H_4 were present. In these cases, the mononuclear complexes [Ru(PEt_3)('pyS_4')] (**6**) and [Ru(N_2H_4)('pyS_4')] (**7**) were formed. This might be indicative of the formation of a labile [Ru(CH_3CN)('pyS_4')] intermediate, which loses CH_3CN in boiling MeOH and either dimerizes to give **5** or adds PEt_3 and N_2H_4 to yield **6** and **7**, respectively. Complex **6** proved as inert to substitution as the PPh_3 complex **1**. Complex **7** demonstrates that the [Ru('pyS_4')] fragment can bind "hard" σ coligands. The purification of complexes **6** and **7** synthesized by this method proved troublesome. They were more easily obtained from reactions of the nitrosyl complex [Ru(NO)('pyS_4')]Tos (**8**). Complex **8** was obtained by template alkylation of NBu_4[Ru(NO)($S_2C_6H_4$)$_2$] with 2,6-bis(tosyloxymethyl)pyridine ('pyTos') in boiling THF. Pure **8** was precipitated from the reaction solution in good yield. It was found to be soluble in MeOH, DMF, and DMSO, but insoluble in THF, CH_2Cl_2, Et_2O, and *n*-hexane. The relatively high frequency of the ν(NO) absorption of **8** (1892 cm^{-1}) suggested that nucleophiles could be added to the NO ligand.[9] Indeed, rapid reactions occurred upon treatment of **8** with equimolar amounts of NH_3 or LiOMe in MeOH. Green-brown solids were immediately precipitated, which exhibited strong bands in their IR spectra at around 1800 cm^{-1}, consistent with the formation of ligands derived from NO. However, these products were so insoluble in all common solvents that they could not be adequately characterized.

In order to probe the reducibility of **8**, a cyclic voltammogram was recorded (Figure 1). The quasi-reversible (–275 mV) and irreversible (–1200 mV) redox waves in the cathodic region could tentatively be assigned to the formation of neutral [Ru(NO)('pyS_4')]^0 and anionic [Ru(NO)('pyS_4')]$^-$ complexes, which formally represent 19 and 20 valence electron [VE] species.

In order to achieve chemical reductions, **8** was treated with $LiBEt_3H$ and N_2H_4. On addition of $LiBEt_3H$ to a red-brown suspension of **8** in THF, gas was evolved and a deep-red solution was produced, from which red [Ru('pyS_4')]$_2$ (**5**) precipitated. The IR spectrum of the deep-red solution did not feature any bands attributable to an NO ligand. When a red-brown THF suspension of **8** was treated with an excess of N_2H_4, gas was again evolved and a deep-red solu-

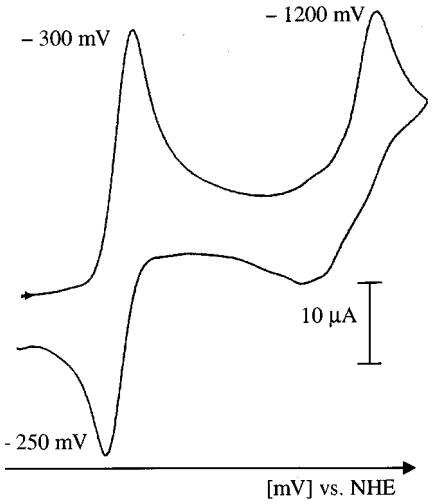


Figure 1. Cyclic voltammogram of [Ru(NO)('pyS$_4$')]Tos (**8**) in DMF (10^{-3} M **8**, 10^{-1} M NBu_4PF_6, $v = 0.02$ Vs^{-1})

tion was produced. Red microcrystals of the hydrazine complex **7** were precipitated upon addition of MeOH and Et_2O. In another experiment, a THF suspension of **8** was treated with excess PEt_3. A red-orange solid formed, which was characterized as the pure PEt_3 complex **6**. Phosphanes frequently act as reductants[10] and hence these results suggest that reduction of **8** gives a substitution labile species that releases NO to yield [Ru('pyS$_4$')] fragments. In the absence of suitable ligands, these fragments dimerize to give [Ru('pyS$_4$')]$_2$ (**5**), while in the presence of such ligands the corresponding [Ru(L)('pyS$_4$')] derivatives are formed.

Characterization and General Properties of the Complexes

As far as possible, all the complexes have been characterized by standard spectroscopic methods and by elemental analysis. The molecular structures of **1**, **2**, **3**, and **4** have been determined by X-ray diffraction analysis. All complexes are colored yellow-red to deep-red. The neutral complexes **1**, **3**, **4**, **6**, and **7** show moderate to good solubility in CH_2Cl_2 and THF, while the ionic complexes **2** and **8** are soluble in DMSO and DMF. The dinuclear species [Ru('pyS$_4$')]$_2$ (**5**) was found to be insoluble in all common solvents. Consequently, no NMR spectra of **5** could be recorded, and this complex could only be characterized by its IR and mass spectra and elemental analysis.

In the FD mass spectra, either the respective molecular ions or the [Ru('pyS$_4$')]$_2^+$ ion arising from dissociation of the coligand L and dimerization of the resulting [Ru('pyS$_4$')] fragments could be observed. The FD mass spectrum of [Ru(PPh$_3$)('pyS$_4$'–Me$_2$)]I$_2$ (**2**) exhibited only fragment ions resulting from demethylation, e.g. [Ru(PPh$_3$)('pyS$_4$'–Me)]$^+$ and [Ru(PPh$_3$)('pyS$_4$')]$^+$. The IR spectra in KBr featured the typical bands attributable to the [Ru('pyS$_4$')] fragment besides the characteristic bands of the coligands. For example, the ν(SO) band at 1015 cm^{-1} indicates *S*-coordination of the DMSO ligand in [Ru(DMSO)('pyS$_4$')] (**3**). Characteristic strong ν(CO) and ν(NO) bands are seen for **4** (1954 cm^{-1}) and **8** (1892 cm^{-1}), respectively, while ν(NH) bands at 3335, 3207, and 3042 cm^{-1} give evidence of the coordination of N_2H_4 in [Ru(N_2H_4)('pyS$_4$')] (**7**).

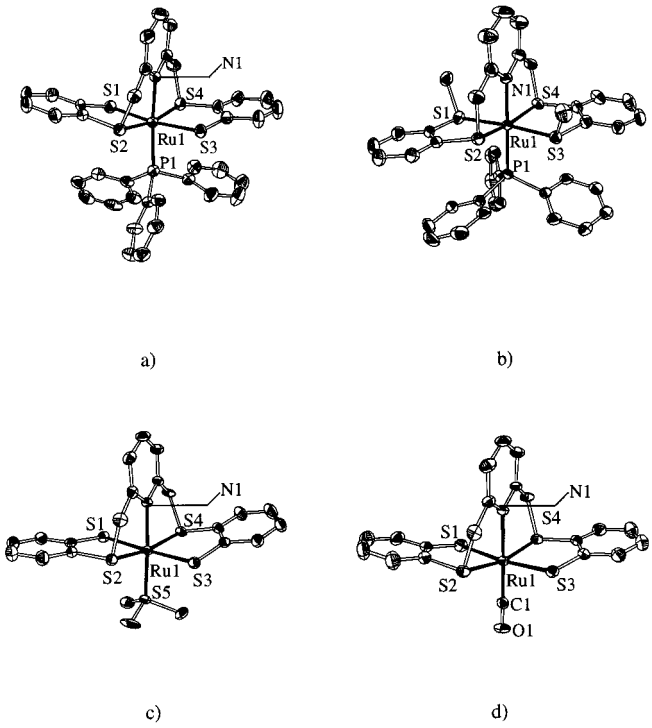


Figure 2. Molecular structures of [Ru(PPh$_3$)('pyS$_4$')] (**1**), [Ru(PPh$_3$)('pyS$_4$'-Me$_2$)]I$_2$ · 2 CH_2Cl_2 (**2** · 2 CH_2Cl_2), [Ru(DMSO)-('pyS$_4$')] · MeOH (**3** · MeOH), and [Ru(CO)('pyS$_4$')] · MeOH (**4** · MeOH) (50% probability ellipsoids; H atoms and solvent molecules omitted for clarity)

The $^{13}C\{^1H\}$-NMR spectra proved particularly helpful in establishing the diastereomeric purity of the complexes and the twofold symmetry of the [Ru('pyS$_4$')] fragments. The seventeen aromatic and two aliphatic C atoms of the [Ru('pyS$_4$')] fragments give rise to only ten ^{13}C signals. This is compatible with C_2 or C_S symmetry of the fragments. Steric considerations and the X-ray structure analyses show that in all cases the C_2-symmetric [Ru('pyS$_4$')] configuration with *trans*-thiolate donors is adopted. The singlet ^{13}C-NMR signal due to the two SCH_3 groups in [Ru(PPh$_3$)('pyS$_4$'–Me$_2$)]I$_2$ (**2**) proves that the thiolate alkylation of **1** yields only one diastereomer of **2**.

The AB splitting of the diastereotopic CH_2 protons, giving rise to two pseudo doublets is a characteristic feature of the [Ru('pyS$_4$')] pattern in the ^1H-NMR spectra. In some cases, a triplet due to the pyridine H_γ proton can also be observed. Usually, this triplet is superimposed by the signals of either the pyridine H_β, benzenedithiolate, or PPh_3 protons. Two DMSO methyl group singlets are seen for the DMSO complex **3**, while two N_2H_4 singlets are seen in the spectrum of the hydrazine complex **7**.

Table 1. Selected distances (pm) and angles (°) in [Ru(PPh_3)('pyS_4')] (**1**), [Ru(PPh_3)('pyS_4'–Me_2)]$I_2 \cdot 2\ CH_2Cl_2$ (**2** · 2 CH_2Cl_2), [Ru(DMSO)('pyS_4')] · MeOH (**3** · MeOH), and [Ru(CO)('pyS_4')] · MeOH (**4** · MeOH)

Complex (L)	**1** (PPh_3)	**2** · 2 CH_2Cl_2 (PPh_3)	**3** · MeOH (DMSO)	**4** · MeOH (CO)
Ru1–N1	211.1(4)	211.8(4)	208.8(3)	212.0(4)
Ru1–S1	238.8(1)	238.5(1)	239.1(1)	240.1(1)
Ru1–S2	231.0(1)	232.4(1)	230.3(1)	231.7(1)
Ru1–S3	239.8(1)	234.7(1)	239.3(1)	237.5(1)
Ru1–S4	231.4(1)	234.1(1)	231.7(1)	232.0(1)
Ru1–L	231.0(1)	234.9(1)	225.6(1)	185.3(5)
S1–Ru1–S2	87.46(4)	86.08(5)	87.18(4)	87.58(5)
S1–Ru1–S4	88.33(4)	99.43(5)	94.77(4)	94.10(5)
S3–Ru1–S4	86.85(4)	86.72(5)	87.08(4)	87.94(5)
S2–Ru1–S3	95.69(4)	88.37(5)	90.25(4)	89.06(5)
N1–Ru1–S1	86.57(10)	90.31(12)	85.62(9)	87.08(11)
N1–Ru1–S2	83.41(10)	84.19(12)	84.17(9)	83.43(12)
N1–Ru1–L	174.37(10)	178.18(11)	177.05(9)	178.6(2)

X-ray Structure Analysis

X-ray structure analyses of **1**, **2**, **3**, and **4** corroborated the spectroscopic conclusions with regard to the structures. Figure 2 depicts the molecular structures of [Ru(PPh_3)('pyS_4')] (**1**), [Ru(PPh_3)('pyS_4'–Me_2)]$I_2 \cdot 2\ CH_2Cl_2$ (**2** · 2 CH_2Cl_2), [Ru(DMSO)('pyS_4')] · MeOH (**3** · MeOH), and [Ru(CO)('pyS_4')] · MeOH (**4** · MeOH). Table 1 lists selected distances and angles.

In all the complexes, the ruthenium centers exhibit pseudo-octahedral coordination. The [Ru('pyS_4')] fragments are pseudo-C_2 symmetrical. The thiolate donors occupy positions *trans* to one another, and the coligands L occupy the positions *trans* to the pyridine N donor. Distances and angles show no anomalies.[8] The Ru–S(thiolate) distances are usually slightly longer than the Ru–S(thioether) distances. The Ru–N(pyridine) distances in all four complexes are almost identical. The molecular structure of **3** proves the *S*-coordination of the DMSO ligand, as had been concluded from the IR spectrum.

The results further indicate that the [Ru('pyS_4')] core is structurally very robust. This is also evidenced by a direct comparison of **1** and **2**. The Ru–N distances and the average Ru–S distances in **1** (235.3 pm) and the twofold methylated derivative **2** (234.9 pm) are practically identical. This demonstrates that the [$RuNS_4$] cores remain unaffected even when the electronic situation changes, as must occur upon alkylation of the thiolate donors. These results support the structure–function relationship of metal–sulfur complexes described in several previous papers.[2,11]

Discussion and Conclusion

The results reported herein demonstrate that the 'pyS_4'$^{2-}$ ligand forms ruthenium complexes possessing [Ru('pyS_4')] cores that (i) exhibit the desired configuration, having *trans*-thiolate donors, and (ii) are structurally robust. The new complexes were obtained either by direct reaction of 'pyS_4'$^{2-}$ with suitable Ru precursor complexes or by template alkylation of [Ru(NO)($S_2C_6H_4$)$_2$]$^-$ yielding [Ru(NO)('pyS_4')]Tos (**8**). In comparison with analogous [Fe(L)('pyS_4')] complexes, which are usually synthesized at room temperature, the synthesis of the corresponding [Ru(L)('pyS_4')] complexes has in many cases been found to require heating or very drastic conditions as, for example, in the case of the CO complex **4**. This reflects the more inert nature of Ru complexes as compared to their Fe counterparts. It also accounts for the fact that it is difficult to find complexes with labile L ligands that can serve as precursors for other [Ru(L)('pyS_4')] complexes. For example, the PPh_3 ligand in **1** is inert and could not be labilized by thiolate methylation, which can be expected to withdraw electron density from the Ru center and to weaken the Ru–PPh_3 bond.[11] Even the DMSO complex **3** proved virtually inert; only under very drastic conditions could a DMSO/CO exchange be achieved. Attempts to obtain labile [Ru(CH_3CN)('pyS_4')] complexes were unsuccessful, yielding only insoluble [Ru('pyS_4')]$_2$ (**5**) or, in the presence of PEt_3 or N_2H_4, the corresponding [Ru(L)('pyS_4')] complexes with L = PEt_3 (**6**) and N_2H_4 (**7**). Complexes **6** and **7** obtained by this method proved difficult to purify, probably due to the formation of side-products as a result of the drastic reaction conditions.

The best suited precursor complex for exchange reactions was ultimately found to be [Ru(NO)('pyS_4')]Tos (**8**). Cyclic voltammetry demonstrated the reducibility of **8**. The resulting 19 or even 20 valence electron species can be expected to be labile as antibonding orbitals must be populated.[4] Indeed, reduction of **8** with $LiBEt_3H$ leads to loss of the NO ligand with the formation of [Ru('pyS_4')]$_2$ (**5**). Reduction of **8** with excess N_2H_4 likewise releases NO, but the excess N_2H_4 adds as a ligand and the hydrazine complex **7** can be isolated in high yield in analytically pure form.

The potential of this method for the synthesis of [Ru(L)('pyS_4')] complexes with nitrogenase-relevant L ligands is currently being investigated.

Experimental Section

General Methods: Unless noted otherwise, all reactions and operations were carried out at room temperature under nitrogen using standard Schlenk techniques. Solvents were dried and distilled

prior to use. As far as possible, reactions were monitored by IR or NMR spectroscopy. Spectra were recorded with the following instruments: IR (KBr discs or CaF_2 cuvettes; solvent bands were compensated): Perkin–Elmer 983, 1620 FT-IR, and 16PC FT-IR. – NMR: Jeol FT-JNM-GX 270, EX 270, and Lambda LA 400; spectra were referenced to residual protio-solvent signals; chemical shifts are quoted on the δ scale (downfield shifts are positive) with respect to tetramethylsilane (^1H, $^{13}C\{^1H\}$ NMR) or 85% H_3PO_4 ($^{31}P\{^1H\}$ NMR); spectra were recorded at 25 °C. – Mass spectra: Jeol MSTATION 700 spectrometer. – Elemental analysis: Carlo Erba EA 1106 or 1108 analyzer. – Cyclic voltammetry was performed with a PAR 264A potentiostat using a three-electrode cell with a glassy carbon ROTEL A working electrode and Pt reference and counterelectrodes. Solutions were 10^{-3} M in the substance under investigation; TBA[PF_6] (10^{-1} M) was used as the supporting electrolyte. Potentials were referenced to the normal hydrogen electrode (NHE) using Fc/Fc^+ as an internal standard ($E_{Fc/Fc+} = +0.4$ V vs. NHE).[12]

$[RuCl_2(PPh_3)_3]$,[13] $[RuCl_2(DMSO)_4]$,[14] $[RuCl_2(CH_3CN)_4]$,[15] $NBu_4[Ru(NO)(S_2C_6H_4)_2]$,[16] 'pyTos' = 2,6-bis(tosyloxymethyl)pyridine),[17] and 'pyS_4'-H_2HCl[6] were prepared as described in the literature; LiOMe was purchased from Aldrich.

[Ru(PPh_3)('pyS_4')] (1): Solid $[RuCl_2(PPh_3)_3]$ (959 mg, 1.0 mmol) was added to a stirred MeOH solution (20 mL) of 'pyS_4'–$H_2 \cdot HCl$ (424 mg, 1.0 mmol) and LiOMe (3.0 mL of a 1 M solution in MeOH, 3.0 mmol). In the course of 15 h, a red-brown suspension was produced. The red-brown solid was separated, washed with MeOH (20 mL) and Et_2O (40 mL), dried, and dissolved in hot pyridine (40 mL). The resulting solution was cooled to room temperature and layered with MeOH (100 mL). Orange crystals precipitated, which were separated after 1 d, washed with MeOH (20 mL) and Et_2O (30 mL), and dried in vacuo. Yield: 615 mg of **1** (82%). – $C_{37}H_{30}NPRuS_4$ (748.94): calcd. C 59.34, H 4.04, N 1.87, S 17.12; found C 59.25, H 4.08, N 1.94, S 17.16. – MS (FD, CH_2Cl_2, ^{102}Ru); *m/z* = 749 [Ru(PPh_3)('pyS_4')]$^+$. – ^1H NMR (269.6 MHz, CD_2Cl_2): δ = 7.46–7.01 [m, 22 H, C_6H_4, P(C_6H_5) and pyridine], 6.87–6.76 (m, 4 H, C_6H_4), 4.94 (d, 2 H, CH_2), 4.46 (d, 2 H, CH_2). – $^{13}C\{^1H\}$ NMR (67.8 MHz, CD_2Cl_2): δ = 157.69, 157.45, 137.42, 136.81, 134.59 (arom. C), 133.85 [d, P(C_6H_5)], 132.40, 131.60, 130.87 (arom. C), 129.10 [d, P(C_6H_5)], 128.06 (arom. C), 127.71 [d, P(C_6H_5)], 121.31 [d, P(C_6H_5)], 58.68 (d, CH_2). – $^{31}P\{^1H\}$ NMR (109.38 MHz, CD_2Cl_2): δ = 49.0 (s).

[Ru(PPh_3)('pyS_4'–Me_2)]I_2 (2): 2 mL (32.13 mmol) of CH_3I was added to a stirred orange THF suspension (30 mL) of [Ru(PPh_3)('pyS_4')] (**1**) (350 mg, 0.47 mmol). A beige solid formed, which was separated after 2 d, washed with THF (80 mL) and Et_2O (40 mL), and dried in vacuo. Recrystallization from CH_2Cl_2/Et_2O yielded yellow crystals, which were separated, washed with Et_2O (20 mL), and dried in vacuo. Yield: 395 mg of **2** · 2 CH_2Cl_2 (70%). – $C_{41}H_{40}Cl_4I_2NPRuS_4$ (1202.68): calcd. C 40.95, H 3.35, N 1.16, S 10.66; found C 41.07, H 3.17, N 1.20, S 10.78. – MS (FD, CH_2Cl_2, ^{102}Ru); *m/z* = 749 [Ru(PPh_3)('pyS_4')]$^+$. – ^1H NMR (269.6 MHz, [D_6]DMSO): δ = 8.00 (d, 2 H, C_6H_4), 7.92 (t, 1 H, H_γ, pyridine), 7.83 (d, 2 H, C_6H_4), 7.64–7.52 [m, 6 H, C_6H_4, P(C_6H_5)], 7.30–7.17 [m, 15 H, C_6H_4, P(C_6H_5), H_β, pyridine], 5.80 (d, 2 H, CH_2), 5.23 (d, 2 H, CH_2), 2.12 (s, 6 H, CH_3). – $^{13}C\{^1H\}$ NMR (67.8 MHz, [D_6]DMSO): δ = 158.67, 138.06, 135.78, 133.78, 133.12 (arom. C), 132.76 [d, P(C_6H_5)], 131.99 [t, P(C_6H_5)], 130.96, 130.57, 130.27 (arom. C), 128.37 [d, P(C_6H_5)], 123.23, (arom. C), 55.54 (CH_2), 24.36 (CH_3). – $^{31}P\{^1H\}$ NMR (109.38 MHz, [D_6]DMSO): δ = 36.0 (s).

[Ru(DMSO)('pyS_4')] (3): Solid $[RuCl_2(DMSO)_4]$ (485 mg, 1.0 mmol) was added to a stirred MeOH solution (20 mL) of 'pyS_4'–$H_2 \cdot HCl$ (424 mg, 1.0 mmol) and LiOMe (3.0 mL of a 1 M solution in MeOH, 3.0 mmol). In the course of 15 h, a yellow suspension resulted. The yellow solid was separated, washed with MeOH (20 mL), dried, and dissolved in hot DMSO (20 mL). The resulting solution was cooled to room temperature and layered with MeOH (60 mL). Yellow crystals precipitated, which were separated after 2 d, washed with MeOH (20 mL) and Et_2O (30 mL), and dried in vacuo. Yield: 325 mg of **3** · MeOH (54%). – $C_{22}H_{25}NO_2RuS_5$ (596.82): calcd. C 44.28, H 4.22, N 2.35, S 26.86; found C 44.16, H 4.40, N 2.37, S 26.86. – IR (KBr): $\tilde{\nu}$ = 1015 cm^{-1} ν(SO). – MS (FD, CH_2Cl_2, ^{102}Ru); *m/z* = 565 [Ru(DMSO)('pyS_4')]$^+$. – ^1H NMR (269.6 MHz, [D_6]DMSO): δ = 7.70 (d, 2 H, C_6H_4), 7.45 (t, 1 H, H_γ, pyridine), 7.35 (d, 2 H, C_6H_4), 7.25 (d, 2 H, H_β, pyridine), 6.95–6.85 (m, 4 H, C_6H_4), 4.7 (s, 4 H, CH_2), 3.05 [s, 3 H, $CH_3S(O)CH_3$], 2.8 [s, 3 H, $CH_3S(O)CH_3$]. – $^{13}C\{^1H\}$ NMR (67.8 MHz, [D_6]DMSO): δ = 157.40, 155.60, 135.30, 132.60, 130.60, 130.10, 128.00, 121.50, 121.30, (arom. C), 55.70 (CH_2), 46.80, 46.30 (CH_3).

[Ru(CO)('pyS_4')] (4): In an autoclave, a yellow suspension of [Ru(DMSO)('pyS_4')] · MeOH (**3**) (330 mg, 0.55 mmol) in 30 mL of THF was exposed to CO gas (120 bar) for 3 d at 110 °C. The resulting yellow solution was then concentrated to dryness, the yellow residue was digested with MeOH (60 mL) and Et_2O (20 mL), and the product was dried in vacuo. Yield: 170 mg of **4** · MeOH (57%). – $C_{21}H_{19}NO_2RuS_4$ (546.70): calcd. C 46.14, H 3.50, N 2.56, S 23.46; found C 45.92, H 3.72, N 2.59, S 23.60. – IR (KBr): $\tilde{\nu}$ = 1954 cm^{-1} ν(CO). – MS (FD, CH_2Cl_2, ^{102}Ru); *m/z* = 515 [Ru(CO)('pyS_4')]$^+$. – ^1H NMR (269.6 MHz, CD_2Cl_2): δ = 7.63–7.60 (m, 2 H, C_6H_4), 7.46–7.43 (m, 3 H, C_6H_4, H_γ, pyridine), 7.19 (d, 2 H, H_β, pyridine), 7.02–6.91 (m, 4 H, C_6H_4), 5.07 (d, 2 H, CH_2), 4.59 (d, 2 H, CH_2). – $^{13}C\{^1H\}$ NMR (100.40 MHz, CD_2Cl_2): δ = 201.62 (CO), 156.23, 155.91, 136.76, 132.48, 131.02, 129.12, 122.60, 121.99 (arom. C), 58.11 (CH_2).

[Ru('pyS_4')]$_2$ (5): $LiBEt_3H$ (1.375 mL of a 1 M solution in THF, 1.375 mmol) was added to a red-brown suspension of [Ru(NO)('pyS_4')]Tos (**8**) (380 mg, 0.55 mmol) in 15 mL of THF. Gas was evolved and a deep-red solution was produced, from which a red-brown solid precipitated in the course of 2.5 d. This solid was separated, washed with MeOH (10 mL), THF (10 mL), and Et_2O (10 mL), and dried in vacuo. Yield: 120 mg of **5** · MeOH (43%). – $C_{39}H_{34}N_2ORu_2S_8$ (1005.33): calcd. C 46.59, H 3.41, N 2.79, S 25.51; found C 46.20, H 3.20, N 2.89, S 25.42. – MS (FD, DMSO, ^{102}Ru); *m/z* = 973 [Ru('pyS_4')]$_2^+$.

[Ru(PEt_3)('pyS_4')] (6): PEt_3 (0.5 mL, 3.40 mmol) was added to a red-brown suspension of [Ru(NO)('pyS_4')]Tos (**8**) (300 mg, 0.44 mmol) in 12 mL of THF. In the course of 20 h, an orange solid precipitated, which was separated, washed with MeOH (20 mL) and *n*-hexane (25 mL), and dried in vacuo. Yield: 100 mg of **6** (38%). – $C_{25}H_{30}NPRuS_4$ (604.80): calcd. C 49.65, H 5.00, N 2.32, S 21.20; found C 49.89, H 5.03, N 2.42, S 21.20. – MS (FD, CH_2Cl_2, ^{102}Ru); *m/z* = 605 [Ru(PEt_3)('pyS_4')]$^+$. – ^1H NMR (399.65 MHz, CD_2Cl_2): δ = 7.63–7.61 (m, 2 H, C_6H_4), 7.42–7.40 (m, 2 H, C_6H_4), 7.27 (t, 1 H, H_γ, pyridine), 7.10 (d, 2 H, H_β, pyridine), 6.90–6.82 (m, 4 H, C_6H_4), 4.78 (d, 2 H, CH_2), 4.42 (d, 2 H, CH_2), 1.90–1.79 (m, 3 H, P-CH_2CH_3), 1.57–1.46 (m, 3 H, P-CH_2CH_3), 0.97–0.89 (m, 9 H, P-CH_2CH_3). – $^{13}C\{^1H\}$ NMR (67.8 MHz, CD_2Cl_2): δ = 157.87, 156.39, 133.85, 132.34, 131.98, 130.69, 127.81, 120.90, 120.85 (arom. C), 59.26 (d, CH_2), 18.34 (d, P-CH_2CH_3), 7.70 (d, P-CH_2CH_3). – $^{31}P\{^1H\}$ NMR (161.70 MHz, CD_2Cl_2): δ = 34.7 (s).

Table 2. Selected crystallographic data for [Ru(PPh_3)('pyS_4')] (**1**), [Ru(PPh_3)('pyS_4'–Me_2)]$I_2 \cdot 2\,CH_2Cl_2$ (**2** · 2 CH_2Cl_2), [Ru(DMSO)('pyS_4')] · MeOH (**3** · MeOH), and [Ru(CO)('pyS_4')] · MeOH (**4** · MeOH)

Compound	**1**	**2** · 2 CH_2Cl_2	**3** · MeOH	**4** · MeOH
Formula	$C_{37}H_{30}NPRuS_4$	$C_{41}H_{40}Cl_4I_2NPRuS_4$	$C_{22}H_{24}NO_2RuS_5$	$C_{21}H_{19}NO_2RuS_4$
M_r [g/mol]	748.90	1202.62	595.79	546.68
Crystal size [mm]	0.50 × 0.30 × 0.12	0.60 × 0.54 × 0.38	0.35 × 0.20 × 0.10	0.50 × 0.20 × 0.10
F(000)	1528	1180	606	552
Crystal system	triclinic	triclinic	triclinic	triclinic
Space group	$P\bar{1}$	$P\bar{1}$	$P\bar{1}$	$P\bar{1}$
a [pm]	1315.8(3)	1136.9(1)	921.3(2)	837.7(2)
b [pm]	1381.2(3)	1143.2(2)	1113.5(1)	1132.3(2)
c [pm]	1868.3(4)	1783.2(2)	1247.9(2)	1220.3(2)
α [°]	83.98(2)	94.13(1)	90.35(1)	68.05(1)
β [°]	81.80(2)	96.38(1)	102.92(1)	84.18(2)
γ [°]	78.42(2)	94.83(1)	106.64(1)	87.79(2)
V [nm^3]	3.2821(12)	2.2873(5)	1.1921(3)	1.0680(4)
Z	4	2	2	2
$d_{calcd.}$ [g/cm^3]	1.516	1.746	1.660	1.700
μ [mm^{-1}]	0.809	2.174	1.116	1.143
Diffractometer	Nicolet R3m/V	Siemens P4	Siemens P4	Siemens P4
Radiation [pm]		Mo-K_α (λ = 71.073)		
Temperature [K]	293(2)	200(2)	200(2)	200(2)
Scan technique	ω scan	ω scan	ω scan	ω scan
2Θ range [°]	3.6–54.0	3.6–54.0	3.8–54.0	3.6–56.0
Scan speed [°/min]	10	8.0	4.0–40.0	5.0
Meas. reflections	15392	11544	6196	5949
Indep. reflections	14316	10003	5207	4958
R_{int} [%]	9.46	19.24	3.70	5.69
Obsd. reflections	8063	7518	3925	3602
σ criterion	$F_o \geq 4\sigma(F)$	$F_o \geq 4\sigma(F)$	$F_o \geq 4\sigma(F)$	$F_o \geq 4\sigma(F)$
$R1$; $wR2$ [%]	4.24, 9.06	4.86, 13.82	4.22, 11.15	4.92, 12.20
ref. parameters	973	607	352	319

[Ru(N_2H_4)('pyS_4')] (7): N_2H_4 (1.0 mL, 31.86 mmol) was added to a red-brown suspension of [Ru(NO)('pyS_4')]Tos (**8**) (200 mg, 0.29 mmol) in 20 mL of THF. Gas was evolved and a red solution was produced, from which a red oil separated. It was redissolved by the addition of MeOH (20 mL). Subsequent addition of Et_2O (40 mL) led to the precipitation of a microcrystalline red solid, which was separated, washed with MeOH (20 mL), THF (15 mL), and Et_2O (20 mL), and dried in vacuo. Yield: 50 mg of **7** (33%). – $C_{19}H_{19}N_3RuS_4$ (518.69): calcd. C 44.00, H 3.69, N 8.10, S 24.72; found C 43.97, H 3.70, N 7.56, S 24.53. – IR (KBr): $\tilde{\nu}$ = 3335, 3208, 3105 cm^{-1} ν(NH). – MS (FD, DMF, ^{102}Ru); *m/z* = 973 [Ru('pyS_4')]$_2^+$. – ^{1}H NMR (269.6 MHz, [D_7]DMF): δ = 7.75–7.72 (m, 2 H, C_6H_4), 7.46–7.42 (m, 2 H, C_6H_4), 7.12–7.07 (m, 3 H, pyridine), 6.92–6.81 (m, 4 H, C_6H_4), 4.86 (s, 2 H, –NH_2NH$_2$), 4.73 (d, 2 H, CH_2), 4.52 (d, 2 H, CH_2), 3.62 (s, 2 H, –NH$_2$NH_2). – ^{13}C{^{1}H} NMR (67.8 MHz, [D_7]DMF): δ = 159.60, 158.03, 133.09, 132.90, 131.85, 131.23, 127.86, 121.19, 120.77 (arom. C), 56.32 (CH_2).

[Ru(NO)('pyS_4')]Tos (8): A solution of 'pyTos' (2.27 g, 5.07 mmol) in 60 mL of THF was added dropwise to a stirred green solution of NBu_4[Ru(NO)($S_2C_6H_4)_2$] (3.32 g, 5.08 mmol) in 30 mL of THF and the resulting mixture was heated under reflux for 4 h. After cooling to room temperature, the precipitated red-brown solid was separated, washed with THF (60 mL) and Et_2O (30 mL), and dried in vacuo. Yield 1.96 g of **8** (56%). – $C_{26}H_{22}N_2O_4RuS_5$ (687.87): calcd. C 45.40, H 3.22, N 4.07, S 23.31; found C 45.45, H 3.38, N 4.04, S 22.98. – IR (KBr): $\tilde{\nu}$ = 1892 cm^{-1} ν(NO). – MS (FD, DMSO, ^{102}Ru); *m/z* = 517 [Ru(NO)('pyS_4')]$^+$. – ^{1}H NMR (269.6 MHz, [D_6]DMSO): δ = 8.01 (d, 2 H, C_6H_4), 7.79 (t, 1 H, H_γ, pyridine), 7.55 (d, 2 H, H_β, pyridine), 7.50–7.45 (m, 4 H, C_6H_4), 7.31–7.21 (m, 4 H, C_6H_4), 7.08 (d, 2 H, C_6H_4), 5.50 (d, 2 H CH_2), 5.29 (d, 2 H, CH_2), 2.25 (s, 3 H, CH_3). – ^{13}C{^{1}H} NMR (67.8 MHz, [D_6]DMSO): δ = 157.90, 149.12, 145.67, 140.22, 137.64, 132.95, 130.81, 129.58, 128.68, 128.07, 125.49, 125.24, 124.29 (arom. C), 55.22 (CH_2), 20.80 (CH_3).

X-ray Structure Analyses of [Ru(PPh_3)('pyS_4')] (1), [Ru(PPh_3)('pyS_4'-Me_2)]$I_2 \cdot 2\,CH_2Cl_2$ (2 · 2 CH_2Cl_2), [Ru(DMSO)('pyS_4')] · MeOH (3 · MeOH), and [Ru(CO)('pyS_4')] · MeOH (4 · MeOH): Orange platelets of [Ru(PPh_3)('pyS_4')] (**1**) were grown by layering a hot pyridine solution (8 mL) of **1** (110 mg, 0.15 mmol) with MeOH. Yellow rhombs of **2** · 2 CH_2Cl_2 formed upon layering a saturated CH_2Cl_2 solution of **2** with Et_2O. Yellow block-shaped crystals of **3** · MeOH were deposited from a saturated DMSO/MeOH solution at –30 °C. Yellow-orange needles of **4** · MeOH crystallized from a saturated CH_2Cl_2 solution of **4** upon layering with MeOH. Suitable single crystals were either sealed under N_2 in glass capillaries (**1**) or coated with inert perfluoropolyalkyl ether (**2** · CH_2Cl_2, **3** · MeOH, and **4** · MeOH). Data were corrected for Lorentz and polarization effects. An absorption correction was applied for **2** · CH_2Cl_2 using ΔF^2 methods (XABS2, T_{min} = 0.0644, T_{max} = 0.1740),[18] as well as for **3** · MeOH (T_{min} = 0.5690, T_{max} = 0.6561), and **4** · MeOH (T_{min} = 0.5707, T_{max} = 0.7288) on the basis of psi-scans.[19] The structures were solved by direct methods and refined using full-matrix least-squares procedures on F^2 (SHELXTL 5.03).[20] All non-hydrogen atoms were refined anisotropically. The positions of the hydrogen atoms were taken from difference Fourier maps and their positional parameters were refined. Complex **1** was found to contain two crystallographically independent molecules in the asymmetric unit. Selected crystallographic data are summarized in Table .[21]

Acknowledgments

Financial support of this work by the Deutsche Forschungsgemeinschaft and the Fonds der Chemischen Industrie is gratefully acknowledged.

[1] [1a] J. Reedijk (Ed.), *Bioinorganic Chemistry*, 2nd edition, M. Dekker, New York, **1999**. – [1b] J. B. Howard, D. C. Rees, *Chem. Rev.* **1996**, *96*, 2965–2982. – [1c] R. K. Thauer, A. R. Klein, G. C. Hartmann, *Chem. Rev.* **1996**, *96*, 3031–3042. – [1d] S. W. Ragsdale, M. Kumar, *Chem. Rev.* **1996**, *96*, 2515–2539.
[2] D. Sellmann, J. Sutter, *Acc. Chem. Res.* **1997**, *30*, 460–469.
[3] D. Sellmann, J. Sutter, in: *Molybdenum Enzymes, Cofactors and Model Systems* (Eds.: E. I. Stiefel, D. Coucouvanis, W. E. Newton), A.C.S. Symp. Ser. **1993**, *535*, 332–345.
[4] D. Sellmann, W. Soglowek, F. Knoch, G. Ritter, J. Dengler, *Inorg. Chem.* **1992**, *31*, 3711–3717.
[5] D. Sellmann, Th. Hofmann, F. Knoch, *Inorg. Chim. Acta* **1994**, *224*, 61–71.
[6] D. Sellmann, J. Utz, F. W. Heinemann, *Inorg. Chem.*, **1999**, *38*, 5314–5322.
[7] N. Blum, Diploma Thesis, University of Erlangen-Nürnberg, **1997**.
[8] [8a] D. Sellmann, T. Gottschalk-Gaudig, F. W. Heinemann, F. Knoch, *Chem. Ber.* **1997**, *130*, 571–579. – [8b] D. Sellmann, T. Gottschalk-Gaudig, F. W. Heinemann, *Inorg. Chem.* **1998**, *37*, 3982–3988.
[9] F. Bottomley, *Acc. Chem. Res.* **1978**, *11*, 158–163.
[10] [10a] J. Chatt, in: *Homogeneous Catalysis with Metal Phosphine Complexes* (Ed.: L. H. Pignolet), Plenum Press, New York, **1983**, 1–11. – [10b] A. Cahours, H. Gal, *Compt. Rend.* **1870**, *70*, 897–903. – [10c] A. Cahours, H. Gal, *Jahresber.* **1870**, 808–814.
[11] D. Sellmann, Th. Becker, F. Knoch, *Chem. Eur. J.* **1996**, *2*, 1092–1098.
[12] H. M. Koepp, H. Wendt, H. Strehlow, *Z. Elektrochem.* **1960**, *64*, 483–491.
[13] T. A. Stephenson, G. Wilkinson, *J. Inorg. Nucl. Chem.* **1966**, *28*, 945–956.
[14] I. P. Evans, A. Spencer, G. Wilkinson, *J. Chem. Soc., Dalton Trans.* **1973**, 204–209.
[15] J. D. Gilbert, D. Rose, G. Wilkinson, *J. Chem. Soc. (A)* **1970**, 2765–2769.
[16] D. Sellmann, G. Binker, *Z. Naturforsch.* **1987**, *42b*, 341–347.
[17] J. S. Bradshaw, P. Huszthy, C. W. McDaniel, J. Y. Zhu, N. K. Dalley, R. M. Izatt, *J. Org. Chem.* **1990**, *55*, 3129–3137.
[18] S. Parkin, B. Moezzi, H. Hope, *J. Appl. Cryst.* **1995**, *28*, 53–56.
[19] A. C. T. North, D. C. Phillips, F. S. Mathews, *Acta Cryst.* **1968**, *A24*, 351–359.
[20] SHELXTL 5.03 *for Siemens Crystallographic Research Systems*, Copyright **1995** by Siemens Analytical X-ray Instruments Inc., Madison WI.
[21] Crystallographic data (excluding structure factors) for the structures reported in this paper have been deposited with the Cambridge Crystallographic Data Centre as CCDC-119398 (**1**), 119399 (**2** · 2 CH_2Cl_2), 119400 (**3** · MeOH), and 119401 (**4** · MeOH). Copies of the data can be obtained free of charge on application to The Director, CCDC, 12 Union Road, Cambridge CB2 1EZ, U.K. [Fax: (internat.) +44 (0)1223 336033; E-mail: deposit@chemcrys.cam.ac.uk].

Received August 12, 1999
[I99299]

Titanium(III) Compounds with η^2-Pyrazolato Ligands

Nadia C. Mösch-Zanetti,*[a] Ralph Krätzner,[a] Christopher Lehmann,[a] Thomas R. Schneider,[a] and Isabel Usón[a]

Keywords: Pyrazole / Titanium / Redox reaction / Mercury / Amalgams

The reduction of $[L_2TiCl_2]$ (**1**) (L = 3,5-*tert*-butylpyrazolate) with 1% Na/Hg in tetrahydrofuran (THF) affords the complex $[L_2TiCl(THF)_2]$ (**2**), which crystallizes from hexane in moderate yield. The analogous reduction carried out in toluene gives dimeric $[(L_2TiCl)_2]$ (**3**) in high yield. If the reduction time is extended to 3 days, the complex $[L_3Ti]$ (**4**) is isolated as light blue crystals in low yield. An alternative procedure for preparing compound **4** requires mixing $[TiCl_3(THF)_3]$ with 3 equivalents of potassium 3,5-*tert*-butylpyrazolate in toluene. Crystallization from hexane affords **4** in high yield. Crystallographic data for **2**, **3** and **4** are presented.

Introduction

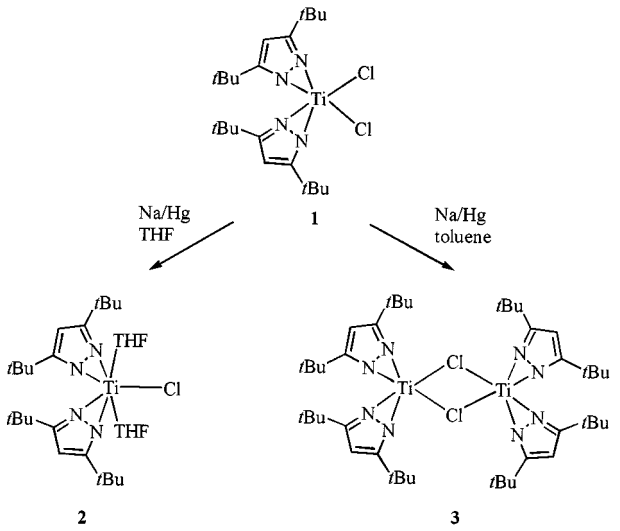
In the search for alternatives to the ubiquitous cyclopentadienyl ligand there has been considerable interest in other monoanionic species that may serve as ancillary ligands for early transition metals and that allow a better control of the electronic and steric properties. In particular, nitrogen-based systems have received considerable attention such as trispyrazolylborates,[1] amides,[2][3] amidinates,[4] aminoiminophosphoranates[5] and others.[6–8] A recent example that has caught our attention is the use of 3,5-disubstituted pyrazoles as ancillary ligands in early transition metal chemistry.[9–11] The coordination of pyrazole derivatives to mid- and late transition metals has been thoroughly investigated over many years. Of the four possible modes (bridging, η^1, η^2 and η^5), mainly bridging and η^1 have been observed.[12] The work of two research groups indicates that η^2-coordination towards early transition metals is favorable as they were able to isolate and structurally characterize several Ti^{IV}, Zr^{IV} and Ta^{V} complexes containing η^2-pyrazolato ligands.[10,13–15] According to a theoretical study[10] the presence of empty d-orbitals seems to be an important feature for η^2-coordination and, so far, all of the reported systems are d^0 metal complexes. Very recently, η^5-coordination has been reported for a late transition metal.[16] For a better understanding of the electronic features of these interesting systems we started to investigate the reduction chemistry of $[L_2TiCl_2]$. Our results can be compared to related Ti^{III} systems that contain other N-donor ligands such as amides,[3][17] N_4-macrocycles[18][19] or amidinates.[20][21]

Herein we report the synthesis and the molecular structure of three titanium(III) complexes that contain pyrazolato ligands. In all of these compounds the coordination mode of the pyrazolato ligand is exclusively η^2 and, to our knowledge, these represent the first d^1 metal complexes that contain η^2-pyrazolato ligands.

[a] Institut für Anorganische Chemie der Georg-August-Universität Göttingen,
Tammannstrasse 4, D-37077 Göttingen, Germany
E-mail: nmoesch@gwdg.de

Results and Discussion

The starting material for our reduction chemistry is $[L_2TiCl_2]$ (L = 3,5-*tert*-butylpyrazolato = 3,5-tBu$_2$pz) **(1)**, first reported by Guzei and Winter.[22] We found that this compound can be conveniently synthesized by the addition of two equivalents of 3,5-tBu$_2$pzH to $TiCl_4(THF)_2$ in the presence of triethylamine in dichloromethane. Removal of the solvent, extraction and crystallization from hexane gave the product as yellow crystals in high yield. This synthetic route represents a slight modification to an improved procedure recently described.[13]



Scheme 1. Reduction of $[L_2TiCl_2]$

A 1% Na/Hg amalgam reduction of compound **1** at 0°C in THF gave paramagnetic $[L_2TiCl(THF)_2]$ **(2)** after 2 h, in moderate yield, which was isolated as blue crystals from hexane as shown in Scheme 1. The ^{1}H NMR spectrum shows broad signals in the range 1.55–2.16 ppm for $(CCH_3)_3$ and the β-protons of the coordinated THF molecules, and at 4.8 ppm for the α-protons of THF. Infrared spectroscopy also indicates the presence of THF, since in comparison to $[(L_2TiCl)_2]$ (vide infra) the IR spectrum

 © WILEY-VCH Verlag GmbH, D-69451 Weinheim, 2000 1434–1948/00/0101–0013 $ 17.50+.50/0

shows two additional absorptions (1029 and 872 cm^{-1}). X-ray crystallography reveals a monomeric species with a pentacoordinated titanium atom in a trigonal bipyramidal environment, considering the pyrazolato ligands as occupying one coordination site each. The metal is further coordinated to two THF molecules and a Cl atom. Figure 1 shows an ORTEP view of the molecule, along with selected bond lengths and angles. The two THF molecules occupy the apical positions with an O1−Ti1−O2 angle of 176.2°. The four nitrogen atoms, the chloride and the titanium atom are in the equatorial plane to within a few degrees. The angles between each of these atoms and O1 or O2 vary within the range 86−93°. As expected, the length of the titanium chloride bond [2.4143(8) Å] is slightly longer than that in the titanium(IV) compound [L_2TiCl_2] [2.247(4) and 2.251(3) Å][22] due both to the larger covalent radius of Ti^{III} vs. Ti^{IV} and the higher coordination number. The structure is similar to the related compound [$(BTBA)_2TiCl(THF)$][20] [BTBA = *N*,*N*′-bis(trimethylsilyl)benzamidinate], where only one THF molecule is coordinated to Ti. In addition, it is noteworthy that the reduction of [Cp_2TiCl_2] in THF yields the base-free [$(Cp_2TiCl)_2$][23] suggesting that not only steric factors are responsible for the structure of compound **2**. The more electrophilic nature of the pyrazolato ligand relative to the cyclopentadienyl ligand leads to a rather electrophilic metal center which is stabilized by the coordination of additional base (two THF molecules).

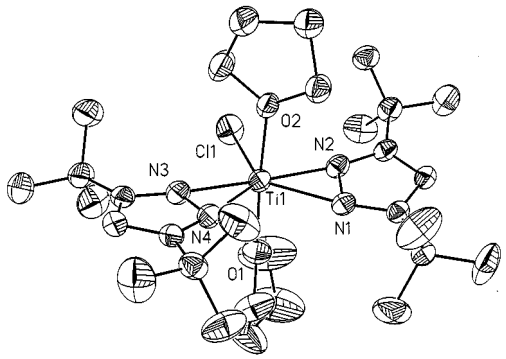


Figure 1. ORTEP view of [$L_2TiCl(THF)_2$] **(2)** drawn with 50% thermal ellipsoids; selected bond lengths (Å) and angles (°): Ti1−Cl1 2.4143(8); N1−Ti1−O1 86.67(8), N2−Ti1−O1 91.91(8), N3−Ti1−O1 89.91(8), N4−Ti1−O1 93.36(8), Cl1−Ti1−O1 91.26(6), N1−Ti1−O2 89.54(7), N2−Ti1−O2 85.50(7), N3−Ti1−O2 92.71(8), N4−Ti1−O2 86.96(8), Cl1−Ti1−O2 91.60(5).

In an analogous reaction, 1% Na/Hg amalgam reduction of compound **1** at 0°C in toluene followed by workup in hexane gave blue-green crystals in high yield. X-ray crystallography reveals the species to be the base-free dimer [$(L_2TiCl)_2$] **(3)**. Figure 2 shows an ORTEP view of the molecule, along with selected bond lengths and angles. The structure is similar to the related titanocene derivative [$(Cp_2TiCl)_2$], which is also dimeric.[24] The Ti−Cl bonds [2.4265(8) Å and 2.4299(8) Å] are slightly shorter than in [$(Cp_2TiCl)_2$] (average 2.543 Å). However, the bond angles in the Ti_2Cl_2 core [Cl−Ti−Cl 89.59(2)° and Ti−Cl−Ti 90.41(2)°] contrast sharply with those in [$(Cp_2TiCl)_2$] (average Cl−Ti−Cl 77.98°, average Ti−Cl−Ti 101.96°). These trends (the shorter M−Cl bond length and the different angles in the Ti_2Cl_2 core) can be attributed to the smaller steric constraint in the molecule. The bite angle between the two ligands (considering the center of the N−N bond as the coordination site) is in the same range for compound **3** (116.6°) and [L_2TiCl_2] (113°).[22]

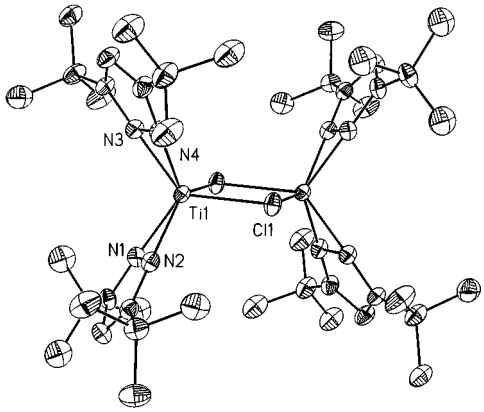
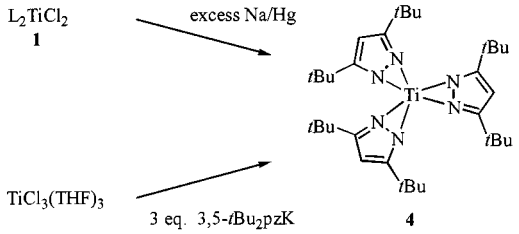


Figure 2. ORTEP view of [$(L_2TiCl)_2$] **(3)** drawn with 50% thermal ellipsoids; selected bond lengths (Å) and angles (°): Ti1−N1 2.027(2), Ti−N2 2.043(2), Ti−N3 2.040(2), Ti−N4 2.029(2), Ti1−Cl1 2.4265(8), Ti1−Cl1a 2.4299(8); Cl1−Ti−Cl1a 89.59(2), Ti1−Cl1−Ti1a 90.41(2); equivalent atoms "a" generated with: $-x + 1, -y, -z - 1$.

Reduction with an excess of Na/Hg over 3 days gave a black reaction mixture, from which, after extraction with hexane, light blue crystals could be isolated in low yield. X-ray crystallography revealed a titanium(III) species [L_3Ti] **(4)** containing three η^2-pyrazolato ligands. Alternatively, complex **4** has been synthesized conveniently and in high yield directly from $TiCl_3(THF)_3$ by the addition of 3 equivalents of *t*Bu_2PzK in toluene. Figure 3 shows an ORTEP view of the molecule, along with selected bond lengths and angles. The molecule has a crystallographic threefold axis running through Ti^{III}. The TiN_6 core is almost perfectly trigonal prismatic with a small deviation of 6° (angle between the projection of N1 and N2 onto a plane perpendicular to the C_3 axis). This is in contrast to the structure of [$(PhNC(H)NPh)_3Ti$], a related Ti^{III} compound with a TiN_6 core.[21] Its structure is best described as distorted trigonal antiprismatic. Due to the constraint imposed by the pyrazolato ring on the 1,2-*N*,*N*-bond length, a further tilting of the ligand cannot achieve an antiprismatic environment of the metal and leads to a higher steric repulsion between neighboring ligands.



Scheme 2. Formation of [L_3Ti]

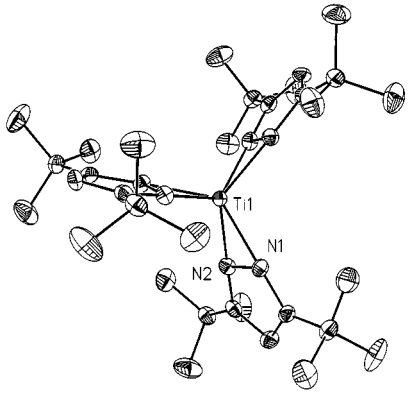


Figure 3. ORTEP view of [L_3Ti] **4** drawn with 50% thermal ellipsoids. Selected bond lengths (Å) and angles (°): Ti1−N1 2.034(3), Ti1−N2 2.038(3), N1−Ti1−N1b 109.37(1), N1−Ti−N1c 109.37(1), N1b−Ti−N1c 109.37(1); equivalent atoms "b" and "c" generated with: b = $-x + 1, -x + y, z$; c = $x - y + 1, -y + 1, z$).

In reactions with other reducing agents such as Mg, Zn or KC_8 the only isolable product was the homoleptic [L_3Ti] (**4**). The mechanism of formation of compound **4** in the reduction reaction is unclear. We assume that, initially, the system is reduced to Ti^{II}, but that bridging η^1-coordination then starts to compete with η^2-coordination at the large and electron-rich metal center. In addition, for steric reasons η^1-coordination is less favorable, although one example of a late transition metal has been reported.[25] Therefore such a bridging η^1 titanium(II) species is presumably not stable and disproportionates to [L_3Ti] and insoluble elemental titanium indicated by the black reaction mixtures. On these grounds it is less surprising that in several reduction reactions of [L_2TiCl_2] under 1 bar of N_2, C_2H_4 or CO the homoleptic titanium(III) species **4** has been isolated exclusively.

We have shown that η^2-coordination of pyrazolato ligands is favored for titanium centers with partially filled d-orbitals. However, very low oxidation states are not favored because, presumably, η^1-coordination starts to compete. So far, no reactivity at the ligands itself (such as C−H bond activation) has been observed. Therefore, as long as oxidation states are high to medium, η^2-pyrazolates may prove to serve as innocent ancillary ligands for a variety of metal centers.

Experimental Section

All reactions were carried out under dry nitrogen using standard Schlenk techniques. Solvents were dried by distillation from sodium/benzophenone or sodium/potassium alloy. [L_2TiCl_2] was prepared according to a literature procedure.[13] NMR spectra were recorded with a Bruker AC 250 spectrometer. IR samples were prepared as mineral oil mull, taken between KBr plates and obtained with a Bio-Rad FTS7 spectrometer. Mass spectra were obtained with a Finnigan MAT 8200 or MAT 95 spectrometer. Elemental analyses were performed in our institute.

[$L_2TiCl(THF)_2$] (2): A solution of **1** (0.71 g, 1.45 mmol) in THF (30 mL) was treated with one equivalent of 1% Na/Hg (0.037 g Na) at 0 °C for 2 h. The solvent was removed under reduced pressure, the resulting blue-green mixture extracted with hexane (30 mL) and filtered through Celite. Complex **2** was isolated at −25 °C as blue crystals (0.45 g, 53%). − ^{1}H NMR (C_6D_6): δ = 4.8 (br s, 8 H, α-H of THF), 2.16 (br s, 8 H, THF), 1.55 [br s, 36 H, C(CH_3)$_3$]. − IR (CsI): $\tilde{\nu}$ = 1508, 1361, 1252, 1233, 1029, 1020, 993, 872, 802, 720, 500, 478, 395, 322, 282 cm^{-1}. − MS: *m*/*z* = 441 [M^+ − 2THF]. − $C_{30}H_{54}ClN_4O_2Ti$ (586.10): calcd. C 61.48, H 9.29, N 9.56; found C 60.06, H 9.13, N 9.41.

[$L_2TiCl]_2$ (3): A solution of **1** (0.37 g, 0.78 mmol) in toluene (30 mL) was treated with 1% Na/Hg (0.023 g Na) at 0 °C for 2 h. The solvent was removed under reduced pressure, the resulting blue-green mixture extracted with hexane (30 mL) and filtered through Celite. Complex **3** was isolated at −25 °C as green crystals (0.29 g, 83%). − ^{1}H NMR (250 MHz, C_6D_6): δ = 6.04 (s, 2 H, C*H*), 1.30 [s, 36 H, C(CH_3)$_3$]. − IR (CsI): $\tilde{\nu}$ = 1506, 1364, 1253, 1233, 1018, 982, 820, 806, 719, 492, 399, 387, 323 cm^{-1}. − MS: *m*/*z* = 441 [M^+/2]. − $C_{44}H_{76}N_8Cl_2Ti_2$ (883.77): calcd. C 59.80, H 8.67, N 12.68; found C 59.40, H 8.85, N 12.59.

[L_3Ti] (4). Method 1: A solution of **1** (0.47 g, 0.98 mmol) in toluene (30 mL) was treated with an excess of 1% Na/Hg (0.113 g Na) for 3 days. The solvent was removed under reduced pressure, the resulting dark brown mixture extracted with hexane (30 mL) and filtered through Celite. Complex **4** was isolated at −25 °C as light blue crystals (0.15 g, 26%).

Method 2: $TiCl_3(THF)_3$ (0.62 g, 1.7 mmol) and *t*Bu$_2$pzK[26] (1.15 g, 5.3 mmol) were placed in a Schlenk flask and toluene was added. The mixture was stirred at room temperature for 5 h. The volatiles were removed under reduced pressure and the residue was extracted with 30 mL of hexane. Complex **4** was isolated at −25 °C as light blue crystals (0.80 g, 82%). − ^{1}H NMR (250 MHz, C_6D_6): δ = 2.05 [br s, C(CH_3)$_3$]. − IR (CsI): $\tilde{\nu}$ = 1529, 1364, 1252, 1232, 1020, 991, 808, 721, 501, 408 cm^{-1}. − MS: *m*/*z* = 585 [M^+]. − $C_{33}H_{57}N_6Ti$ (585.71): calcd. C 67.67, H 9.81, N 14.35; found C 67.53 H 10.39 N 14.29.

X-ray Crystal Structure Analysis

The crystals were mounted on a glass fiber in a rapidly cooled perfluoropolyether.[27] Diffraction data were collected on a Stoe-Siemens-Huber four-circle diffractometer coupled to a Siemens CCD area-detector at 153(2) K for **2** and 133(2) K for **3** and **4**, with graphite-monochromated Mo-K_α radiation (λ = 0.71073 Å), performing φ- and ω scans. The structures were solved by direct methods using SHELXS-97[28] and refined against F^2 on all data by full-matrix least-squares with SHELXL-97.[29] All non-hydrogen atoms were refined anisotropically. All hydrogen atoms were included in the model at geometrically calculated positions and refined using a riding model.

Compound 2: The single-crystal X-ray structure shows **2** to crystallize in the tetragonal space group $P4_2/n$ with one molecule in the asymmetric unit. One of the coordinated THF molecules is heavily disordered and was refined on two positions. Three difference electron density peaks near the inversion center at 0.25, 0.25, 0.25 were refined as a THF molecule with an occupancy of 0.25, using similarity restraints for 1−2 and 1−3 interatomic distances (bond lengths and angles) and displacement parameters.

Compound 3: The asymmetric unit contains half a molecule of compound **3** and a partially occupied molecule of toluene, which is disordered over the inversion center. Two of the four *t*Bu groups are heavily disordered and were refined on three positions.

Compound 4: The data for compound **4** were modeled as merohedrally twinned using the twin matrix (-1,0,0; 0,-1,0; 0,0,1). The twinning parameter refined to a value of 0.457(3). The three highest

Table 1. Crystal data and data collection parameters

Compound	**2**	**3**	**4**
Empirical formula	$C_{30}H_{54}ClN_4O_2Ti$·0.25THF	$C_{22}H_{38}ClN_4Ti$·0.5toluene	$C_{33}H_{57}N_6Ti$
Formula weight [g/mol]	602.13	487.98	474.78
Crystal size [mm]	0.3 × 0.3 × 0.2	0.4 × 0.4 × 0.3	0.4 × 0.3 × 0.3
Crystal system	tetragonal	triclinic	trigonal
Space group	$P4_2/n$	$P\bar{1}$	$P\bar{3}$
Unit cell	a = 25.577(4) Å	a = 10.202(2) Å	a = 14.582(3) Å
	b = 25.577(4) Å	b = 10.338(2) Å	b = 14.582(3) Å
	c = 10.652(2) Å	c = 14.686(3) Å	c = 10.453(5) Å
	α = 90°	α = 70.945(3)°	α = 90°
	β = 90°	β = 70.738(3)°	β = 90°
	γ = 90°	γ = 84.110(3)°	γ = 120°
Volume [Å^3]	V = 6968(2)	V = 1382.1(5)	V = 1924.8(11)
Z	8	2	2
Density [Mg/m^3]	1.148	1.173	1.011
Absorption coefficient	0.354 mm^{-1}	0.425 mm^{-1}	0.249 mm^{-1}
F(000)	2600	524	638
Reflections collected	108057	9473	28131
Reflections unique	6139 (R_{int} = 0.0941)	4847 (R_{int} = 0.0289)	2278 (R_{int} = 0.0710)
Data/Restr./Param.	6139 /210/437	4847/176/354	2278/0/122
Data collection range	2.07 ≤ 2&*Theta;* ≤ 25.00°	2.17 ≤ 2&*Theta;* ≤ 25.18°	2.53 ≤ 2&*Theta;* ≤ 25.00°
Final R indices [$I>2\sigma(I)$][a]	$R1$ = 0.0431	$R1$ = 0.0405	$R1$ = 0.0566
	$wR2$ = 0.1071	$wR2$ = 0.0981	$wR2$ = 0.1908
Final R indices (all data)	$R1$ = 0.0747	$R1$ = 0.0644	$R1$ = 0.0637
	$wR2$ = 0.1219	$wR2$ = 0.1046	$wR2$ = 0.1846
Goodness-of-fit on F^2 [b]	1.008	1.010	1.336
Largest diff. peak and hole	0.390 and −0.242 eÅ^{-3}	0.462 and −0.366 eÅ^{-3}	1.905 and −0.338 eÅ^{-3}

[a] $R1 = \Sigma|F_o - F_c|/\Sigma|F_o|$; $wR2 = [\Sigma w(F_o^2 - F_c^2)^2/\Sigma wF_o^4]^{1/2}$. − [b] Goodness of fit $S = [\Sigma w(F_o^2 - F_c^2)^2/\Sigma (n\text{-}p)]^{1/2}$).

difference density peaks are located on the threefold axis and result from a disordered hexane molecule.

Crystallographic data (excluding structure factors) for the structures reported in this paper have been deposited with the Cambridge Crystallographic Data Centre as supplementary publication nos. CCDC-129633 (**2**), -129627 (**3**) and -129636 (**4**). Copies of the data can be obtained free of charge on application to CCDC, 12 Union Road, Cambridge CB2 1EZ, UK [Fax: (internat.) + 44−1223/336−033; E-mail: deposit@ccdc.cam.ac.uk].

Acknowledgments

We are grateful to the Swiss National Foundation for support of this work and we thank Professor H. W. Roesky for many helpful discussions.

[1] S. Trofimenko, *Chem. Rev.* **1993**, *93*, 943.
[2] P. P. Power, *Comments Inorg. Chem.* **1989**, *8*, 177.
[3] C. C. Cummins, *Prog. Inorg. Chem.* **1998**, *47*, 685.
[4] F. T. Edelmann, *Coord. Chem. Rev.* **1994**, *137*, 403.
[5] J. Richter, F. T. Edelmann, M. Noltemeyer, H.-G. Schmidt, M. Shmulinson, M. S. Eisen, *J. Mol. Catal. A: Chem.* **1998**, *130*, 149.
[6] M. R. Bürgstein, H. Berberich, P. W. Roesky, *Organometallics* **1998**, *17*, 1452.
[7] H. V. R. Dias, W. Jin, Z. Wang, *Inorg. Chem.* **1996**, *35*, 6074.
[8] R. Kempe, P. Arndt, *Inorg. Chem.* **1996**, *35*, 2644.
[9] C. Yélamos, M. J. Heeg, C. H. Winter, *Organometallics* **1999**, *18*, 1168.
[10] I. A. Guzei, A. G. Baboul, G. P. A. Yap, A. L. Rheingold, H. B. Schlegel, C. H. Winter, *J. Am. Chem. Soc.* **1997**, *119*, 3387.
[11] J. E. Cosgriff, G. B. Deacon, *Angew. Chem.* **1998**, *110*, 298; *Angew. Chem. Int. Ed.* **1998**, *37*, 286.
[12] S. Trofimenko, *Chem. Rev.* **1972**, *72*, 497.
[13] C. Yélamos, M. J. Heeg, C. H. Winter, *Inorg. Chem.* **1999**, *38*, 1871.
[14] D. Röttger, G. Erker, M. Grehl, R. Fröhlich, *Organometallics* **1994**, *13*, 3897.
[15] I. A. Guzei, G. P. A. Yap, C. H. Winter, *Inorg. Chem.* **1997**, *36*, 1738.
[16] J. R. Perera, M. J. Heeg, H. B. Schlegel, C. H. Winter, *J. Am. Chem. Soc.* **1999**, *121*, 4536.
[17] P. W. Wanandi, W. M. Davis, C. C. Cummins, *J. Am. Chem. Soc.* **1995**, *117*, 2110.
[18] S. Ciurli, C. Floriani, A. Chiesi-Villa, C. Guastini, *J. Chem. Soc., Chem. Commun.* **1986**, 1401.
[19] C.-H. Yang, V. L. Goedken, *J. Chem. Soc., Chem. Commun.* **1986**, 1101.
[20] J. R. Hagadorn, J. Arnold, *Organometallics* **1998**, *17*, 1355.
[21] F. A. Cotton, W. A. Wojtczak, *Polyhedron* **1994**, *13*, 1337.
[22] I. A. Guzei, C. H. Winter, *Inorg. Chem.* **1997**, *36*, 4415.
[23] R. S. P. Coutts, P. C. Wailes, R. L. Martin, *J. Organomet. Chem.* **1973**, *47*, 375.
[24] R. Jungst, D. Sekutowski, J. Davis, M. Luly, G. Stucky, *Inorg. Chem.* **1977**, *16*, 1645.
[25] K. S. Chong, S. J. Rettig, A. Storr, J. Trotter, *Can. J. Chem.* **1979**, *57*, 3090.
[26] C. Yélamos, M. J. Heeg, C. H. Winter, *Inorg. Chem.* **1998**, *37*, 3892.
[27] T. Kottke, D. Stalke, *J. Appl. Crystallogr.* **1993**, *26*, 615.
[28] G. M. Sheldrick, *Acta Crystallogr., Sect. A* **1990**, *46*, 467.
[29] G. M. Sheldrick, Universität Göttingen, **1997**.

Received July 19, 1999
[I99263]

Microwave-Assisted Rapid Incorporation of Ruthenium into Lacunary Keggin-Type Polyoxotungstates: One-Step Synthesis, ^{99}Ru, ^{183}W NMR Characterization and Catalytic Activity of $[PW_{11}O_{39}Ru^{II}(DMSO)]^{5-}$

Alessandro Bagno,[a] Marcella Bonchio,*[a] Andrea Sartorel,[a] and Gianfranco Scorrano[a]

Keywords: Polyoxometalates / Ruthenium / Homogeneous catalysis / Oxidations / Microwaves

Microwave irradiation for 15 minutes allowed the highly selective hydrothermal synthesis of the diamagnetic, air-stable oxidation catalyst $[PW_{11}O_{39}Ru^{II}(DMSO)]^{5-}$, as confirmed by ^{1}H, ^{31}P, ^{99}Ru and ^{183}W NMR techniques.

Introduction

The design of transition metal based catalysts is finding new resources within the field of polyoxometalate chemistry.[1] In this respect, Keggin-type polyoxotungstates with mono-lacunary structures of formula $[XW_{11}O_{39}]^{n-}$ (X = B, Si, Ge, P, As), represent a unique class of ligands.[1][2] Properly referred to as inorganic porphyrin analogs,[2] they provide a rigid, hydrolytically stable, thermally robust, nonoxidizable framework that behaves as a pentadentate environment to include a catalytically active transition metal center.[1][2] Derivatization of such species with ruthenium retains a major interest in the field of homogeneous catalysis, especially within the domain of metal-mediated oxidations.[3−7] In fact, ruthenium porphyrin-based systems have been proved to carry out dioxygen activation,[8] to react with N_2O[9] and, in general, to promote highly chemo- and stereoselective oxidative transformations in the presence of various oxygen donors.[3][10] Despite their appealing potential, the synthesis of ruthenium-substituted polyoxotungstates is not straightforward and presents a series of problems, as indicated by the few literature reports published to date.[4−7] In particular: (i) use of the commercially available ruthenium source "$RuCl_3{\cdot}nH_2O$" produces either a mixture of undefined species or a low yield of the target compound; (ii) high temperatures and prolonged reaction times are generally needed; (iii) the formation of paramagnetic Ru^{III} complexes hampers both the NMR monitoring of the reaction and the structural elucidation of the final product.

Herein we report that $[RuCl_2(DMSO)_4]$ (**1**)[11] reacts with the lacunary tungstate ligand $[PW_{11}O_{39}]^{7-}$ (**2**)[12] in water at 200°C under microwave irradiation,[13] leading, after 15 minutes, to the complete incorporation of a ruthenium atom into the polyoxometalate framework, and to the selective production of the diamagnetic, air-stable, complex $[PW_{11}O_{39}Ru^{II}(DMSO)]^{5-}$ (**3**). Scheme 1 illustrates the synthetic approach described above and presents the optimized geometries of both **2** and **3** obtained with PM3(tm) semiempirical calculations.

^{183}W NMR spectroscopy provides an elegant tool to monitor the progress of the reaction. In Figure 1, spectra (a) and (b) allow us to examine the outcome of the metalation performed in water under conventional heating (100°C, 1 atm, 48 hours), or under microwave irradiation (200°C, 15 atm, 15 min), respectively.

As expected,[5] the formation of a Ru^{II} complex leads to a marked deshielding of the signals relative to the two W atoms adjacent to the substituted center (W_1 and W_4 in Scheme 1). The new set of six resonances is consistent with the formation of a unique species **3**.[5] This can be easily seen in Figure 1a, where the resonances of both **3** and of the unreacted **2** are present in a ca. 50:50 ratio. Therefore, the spectroscopic analysis of both reaction mixtures highlights the remarkable acceleration of the process achieved by the microwave irradiation, as it results in the complete disappearance of the ligand signals after only 15 minutes (Figure 1b).

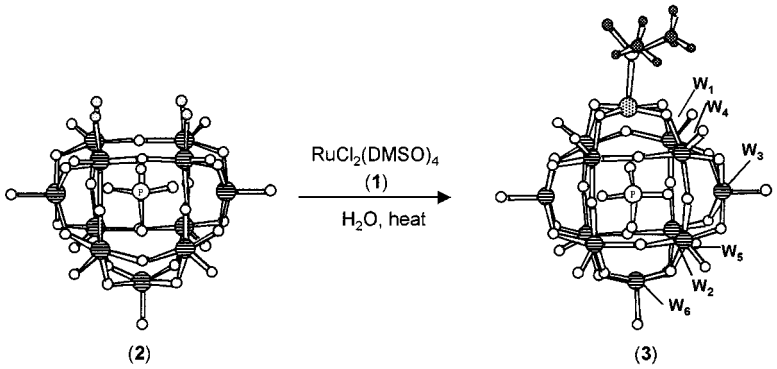
The assignment of the six resonances pertaining to the ruthenium complex **3** (W atom labels are shown in Scheme 1) is based on the analysis of W−W connectivities and $^{2}J_{WOW}$ scalar couplings determined from ^{183}W NMR COSY experiments with selective excitation (see Experimental Section). A sample spectrum is shown in Figure 2, while the complete set of results is collected in Table 1.

Homonuclear ^{183}W 2D COSY or INADEQUATE techniques have been employed for the structural elucidation of polyoxotungstates.[12] However, since the number of scalar couplings present in such systems is relatively small, the 1D COSY technique with selective excitation[14] provides an attractive alternative, since it allows for the collection of all connectivity information in separate experiments (whose number will not exceed the number of tungsten resonances) retaining the high resolution typical of 1D spectra.

As further evidence confirming the complete substitution and the selectivity of the process, analysis of the reaction mixture by ^{99}Ru NMR spectroscopy revealed a single signal, relative to **3**, at $\delta = 7737$ (Figure 3), whereas the signal for the precursor **1** is found at $\delta = 3976$. To the best of our

[a] Centro CNR Meccanismi Reazioni Organiche, Dipartimento di Chimica Organica, Università di Padova,
via Marzolo 1, I-35131 Padova, Italy
Fax: (internat.) + 39-049/827-5239
E-mail: marcella@chor.unipd.it

 © WILEY-VCH Verlag GmbH, D-69451 Weinheim, 2000 1434−1948/00/0101−0017 $ 17.50+.50/0



Scheme 1. W hatched, O white, Ru dotted; dark pattern spheres represent the atoms of the DMSO residue; W atoms are labelled according to the ^{183}W NMR assignments (see text)

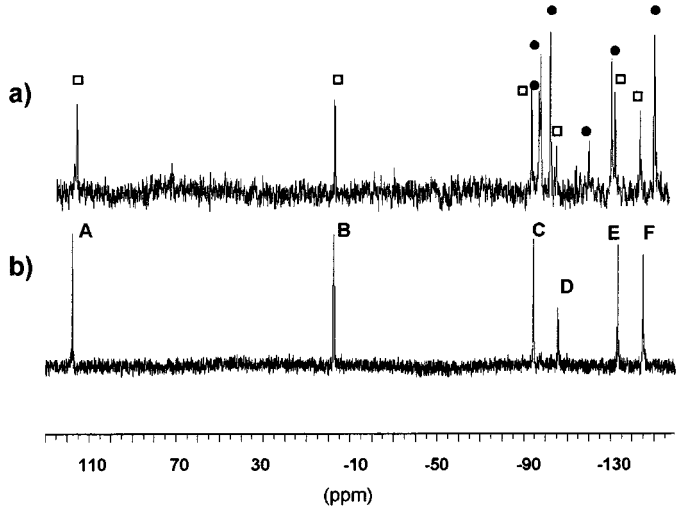


Figure 1. ^{183}W NMR spectra of the reaction mixtures (a) conventional heating, filled circles: signals of the unchanged **2**; open squares: signals of (**3**); (b) MW irradiation; letters indicate the resonances of **3** as reported in Table 1

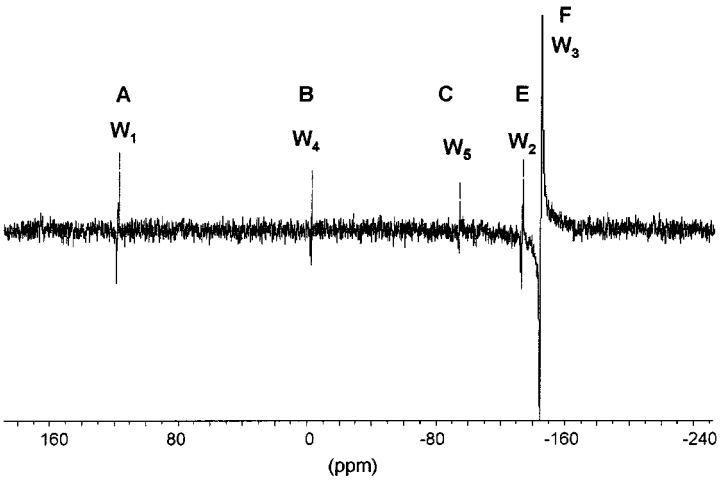


Figure 2. ^{183}W selective COSY spectrum carried out upon excitation of the resonance at $\delta = -145$

knowledge this is the first observation of a ^{99}Ru signal in a polyoxometalate inorganic matrix.

Complex **3** displays a remarkable catalytic activity in the presence of sodium periodate ($NaIO_4$) or potassium monopersulfate ($KHSO_5$) which were used as primary oxidants in the oxidation of cyclooctene and adamantane, respectively.[15] Particularly interesting is the ruthenium-promoted cleavage of the olefinic double bond which proceeds in water, with no need of organic solvent or phase transfer agent, leading to 90% conversion of the substrate in 4 hours

Table 1. ^{183}W NMR data for (**3**) as lithium salt in D_2O

W[a]	δ[b]	assign.	$^2J_{WOW}$ (Hz)[c] A	B	C	D	E	F	$^2J_{WOP}$[d]
A(2)	117.39	W1	–	–	–	–	16.1	26.2	1.23
B(2)	−2.66	W4	–	–	10.0	–	–	10.4	1.46
C(2)	−94.43	W5	–	–	–	18.5	–	10.0	1.01
D(1)	−105.76	W6	–	–	–	–	8.7	–	1.35
E(2)	−133.30	W2	–	–	–	–	–	20.3	1.23
F(2)	−145.14	W3	–	–	–	–	–	–	1.12

[a] Letters indicate resonances as shown in Figure 1b (integration ratio). – [b] ± 0.02 ppm. – [c] ± 0.2 Hz. – [d] ± 0.3 Hz. δ(^{31}P) = −10.8 (D_2O), δ(^1H) = 3.40 (D_2O) (s).

and ^{99}Ru NMR spectroscopic analysis, the reaction mixture was passed through a Li^+-form resin (Amberlite IR 120). Further purification of **3** can be achieved by chromatography on a Sephadex G-15 column with water as eluent. – IR (KBr): $\tilde{\nu}$ = 1067, 1049, 1018, 964, 885, 793, 691, 589, 513 cm^{-1}. – MS (FAB); *m/z*: 2893−2891 [$(M + H)^+$, $HLi_5PW_{11}O_{39}Ru(DMSO)^+$], calcd. 2893.

The reported procedure for the synthesis of **3** involves a two-step reaction requiring the reduction of $[PW_{11}O_{39}Ru^{III}(H_2O)]^{4-}$ by electrolysis or prolonged heating in DMSO.[5]

NMR Characterization: ^{183}W and ^{99}Ru spectra were obtained at 9.4 T (16.67 and 18.43 MHz, respectively) on a Bruker Avance DRX 400 instrument, equipped with a standard (^{31}P-^{109}Ag) 10-mm broadband probe which could be tuned below its specifications. The π/2 pulse duration was ca. 50 μs for both nuclei. ^{183}W and ^{99}Ru chemical shifts are externally referenced to 2 M aq. Na_2WO_4 or 0.3 M aq. $K_4Ru(CN)_6$, respectively. Typically, ca. 10^3 transients were collected in 32K or 1K data points, respectively. Selective COSY spectra were carried out with the standard sequence,[14] employing a 20-ms Gaussian-shaped selective pulse (π/2) at the desired offset and a 10-ms delay (the total evolution delay being ca. 20 ms). This value was found to be the optimum compromise between the need to emphasize the smallest couplings (4−5 Hz) and the relatively fast longitudinal relaxation (T_1 values being between 0.7−1.1 s). In order to gain insight into the molecular structure and the magnetic properties of the catalytically active ruthenium nucleus, ab initio calculations of the NMR properties of **3** are being performed.

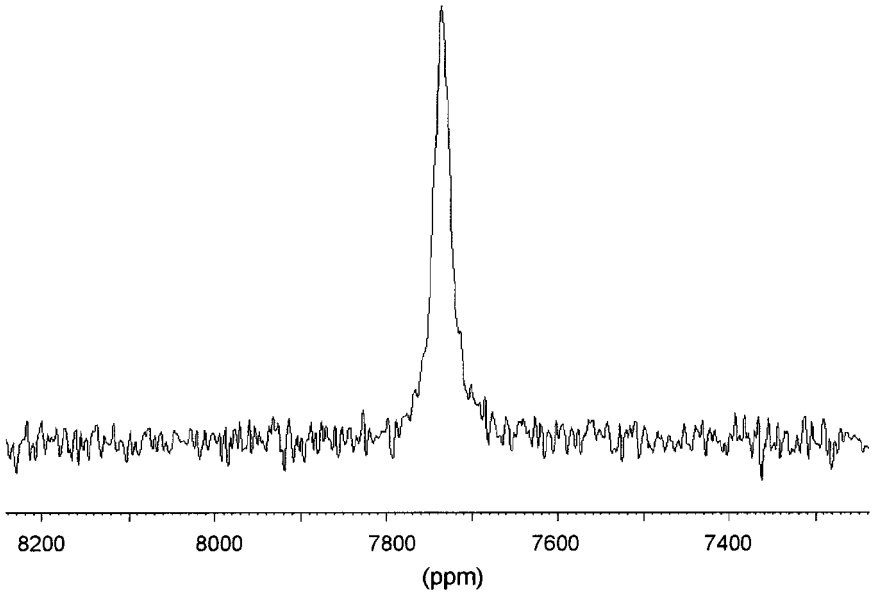


Figure 3. ^{99}Ru NMR spectrum of (**3**)

at 50 °C, 1,8-octanedioic acid (suberic acid) being formed in 83% yield. In the hydroxylation of adamantane, complex **3** exhibits the high selectivity typical of ruthenium-based catalysts.[3][10] The reaction occurs smoothly at 50 °C in a two-phase medium (1,2-dichloroethane/H_2O) and performs the preferential attack at the tertiary C−H site of the substrate (54% conversion after 20 hours) affording 1-adamantanol and 1-chloroadamantane as major products.[16] Further studies concerning the synthesis of tungstoruthenate catalysts together with the scope and mechanism of their promoted oxidations are currently in progress, especially with the aim to devise environmentally sustainable oxidation processes.[17]

Experimental Section

Preparation of $[PW_{11}O_{39}Ru^{II}(DMSO)]^{5-}$ (3): $K_7PW_{11}O_{39}$ (2.0 g) and $RuCl_2(DMSO)_4$ (0.3 g) in 50 mL of water were placed in a closed reactor (HPR-1000/10S, Milestone) equipped with temperature and pressure control units and irradiated inside the cavity of the MW Ethos-1600 labstation (Milestone) according to the following parameters: initial power, 350 W; initial time, 2 min; final power, 300 W; T_{max} = 200 °C; reaction time, 15 min. Before ^{183}W

Catalytic Oxidations: Cyclooctene (0.51 mmol) was suspended in 5 mL deionized water containing $NaIO_4$ (1.95 mmol) and **3** (5 μmol). After 4 hours, the unreacted olefin and the products were extracted with Et_2O (5 × 5 mL) from the acidified reaction mixture and analyzed by GC and ^1H and ^{13}C NMR spectroscopy.

Adamantane (0.195 mmol) and Bu_4NHSO_4 (0.096 mmol) were dissolved in 1,2-dichloroethane (2 mL) and reacted at 50 °C with an aqueous solution (2 mL) containing **3** (0.01 mol) and Oxone (0.4 mmol, added in 3 portions over 3 hours). The reaction was monitored by GC and products were identified by GC-MS analysis and by comparison with authentic samples. The observed product

distribution was as follows: 1-adamantanol (53%), 1-chloroadamantane (32%), adamantanone (10%), 2-chloroadamantane (5%); 2-adamantanol was detected only in traces.

Acknowledgments

We thank A. Agazzi and F. De Luca (F.K.V. Bergamo, Italy) for the technical assistance with the Ethos 1600 MW labstation, and the Centro NMR Università di Firenze (Italy) for running tests with a low frequency 600 MHz NMR probe. Mass spectrometry was provided by the Washington University Mass Spectrometry Resource, an NIH Research Resource (Grant no. P41RR0954).

[1] Recent reviews on polyoxometalates: [1a] M. T. Pope, A. Muller, *Angew. Chem. Int. Ed. Engl.* **1991**, *30*, 34−48. − [1b] C. L. Hill, C. M. Prosser-McCharta, *Coord. Chem. Rev.* **1995**, *143*, 407−455. − [1c] Polyoxometalates (Ed.: C. L. Hill), Chem. Rev. (Special Issue) **1998**, 98, 1−390.

[2] [2a] L. C. W. Baker, J. S. Figgis, *J. Am. Chem. Soc.* **1970**, *92*, 3794−3797. − [2b] C. L. Hill, R. B. Brown, *J. Am. Chem. Soc.* **1986**, *108*, 536−538.

[3] [3a] W. P. Griffith, *Chem. Soc. Rev.* **1992**, *21*, 179−185. − [3b] T. Naota, H. Takaya, S.-I. Murahashi, *Chem. Rev.* **1998**, *98*, 2599−2660.

[4] [4a] R. Neumann, C. J. Abu-Gnim, *J. Chem. Soc., Chem. Commun.* **1989**, 1324−1325. − [4b] R. Neumann, C. J. Abu-Gnim, *J. Am. Chem. Soc.* **1990**, *112*, 6025−6031.

[5] [5a] C. Rong, M. T. Pope, *J. Am. Chem. Soc.* **1992**, *114*, 2932−2938. − [5b] M. Bressan, A. Morvillo, G. Romanello, *J. Mol. Catal.* **1992**, *77*, 283−288.

[6] W. J. Randall, T. J. R. Weakley, R. G. Finke, *Inorg. Chem.* **1993**, *32*, 1068−1071.

[7] [7a] R. Neumann, A. M. Khenkin, *Inorg. Chem.* **1995**, *34*, 5753−5760. − [7b] R. Neumann, M. Dahan, *J. Am. Chem. Soc.* **1998**, *120*, 11969−11976 and references therein.

[8] J. T. Groves, R. Quinn, *J. Am. Chem. Soc.* **1985**, *107*, 5790.

[9] J. T. Groves, J. S. Roman, *J. Am. Chem. Soc.* **1995**, *117*, 5594−5595.

[10] [10a] J. T. Groves, M. Bonchio, T. Carofiglio, K. Shalyaev, *J. Am. Chem. Soc.* **1996**, *118*, 8961−8962. − [10b] J. T. Groves, M. Bonchio, T. Carofiglio, K. Shalyaev, in *Studies in Surface Science and Catalysis* vol. 110 (Eds.: R. K. Grasselli, S. T. Oyama, A. M. Gaffney, J. E. Lions), Elsevier, Amsterdam, **1997**, 865−872. − [10c] J. T. Groves, T. Carofiglio, M. Bonchio, A. Sauve, *PCT Int. Appl.*, WO 9804538 A1 19980205, patent 48 pp.

[11] E. Alessio, G. Mestroni, G. Nardin, W. M. Attia, M. Calligaris, G. Sava, S. Zorzet, *Inorg. Chem.* **1988**, *27*, 4099−4106 and references therein.

[12] C. Brevard, R. Schimpf, G. Tourné, C. M. Tourné, *J. Am. Chem. Soc.* **1983**, *105*, 7059−7063.

[13] [13a] D. M. P. Mingos, D. R. Baghurst, *Chem. Soc. Rev.* **1991**, *20*, 1−47. − [13b] S. Caddick, *Tetrahedron* **1995**, *51*, 10403−10432. − [13c] R. S. Varma, *Green Chemistry* **1999**, *1*, 43−55.

[14] H. Kessler, H. Oschkinat, C. Griesinger, W. Bermel, *J. Magn. Reson.* **1986**, *70*, 106−133.

[15] Related ruthenium catalysts have previously been employed in oxidation reactions.[4][5] However, because of the different experimental conditions (catalyst, oxygen donor and substrate) such results are not directly comparable to our own.

[16] During catalytic oxidation the DMSO ligand is oxidized to dimethyl sulfone, as shown by the ^{1}H NMR spectrum (singlet at $\delta = 3.17$) of the reaction mixtures.

[17] J. H. Clark, *Green Chemistry* **1999**, *1*, 1−8.

Received June 17, 1999
[I99221]

Tripodal Oxygen Ligand Supported Palladium(II) Complexes: Alkylation, Carboxymethylation, and CO Insertion Reactions – X-ray Crystal Structure Determination of $[PdL_2]$, $L^- = [(C_5H_5)Co\{P(O)(OMe)_2\}_3]^-$, a Novel Homoleptic Oxygen Ligand Palladium Complex

Wolfgang Kläui,*[a] Marcus Glaum,[a] Ekkehardt Hahn,[b] and Thomas Lügger[b]

Dedicated to Prof. Dr. H. Werner on the occasion of his 65th birthday

Keywords: Palladium / Tripodal ligands / O ligands / Fluxionality

The reaction of $[PdCl_2(CH_3CN)_2]$ with the silver salt of the tripodal oxygen ligand $L^- = [(C_5H_5)Co\{P(O)(OMe)_2\}_3]^-$ yields the homoleptic oxygen ligand complex $[PdL_2]$ (**1**). The molecular structure of **1** was determined by single-crystal X-ray diffraction: monoclinic space group $P2_1/n$; a = 8.515(1), b = 13.627(2), c = 15.828(2) Å; β = 92.44(1)°; V = 1834.9(7) Å^3; Z = 2. The complexes $[Pd(PPh_3)XL]$ [X = Cl (**2a**), Br (**2b**), I (**2c**)] have been prepared starting from **1**. Complex **2a** reacts with PPh_3 to form $[Pd(PPh_3)_2L]Cl$ (**3a**) and $[Pd(PPh_3)_2L]L$ (**3b**). Treatment of **2a** with CO in MeOH yields the carboxymethyl complex $[\{(PPh_3)(COOMe)Pd(\mu\text{-}Cl)\}_2]$ (**4**) and the protonated ligand HL. The carboxymethyl complex **4** shows some catalytic activity for the copolymerization of CO and ethene. Complex **4** reacts with AgL to yield $[Pd(PPh_3)(COOMe)L]$ (**6**). Alkylation of **2a** with Me_4Sn leads to the methyl complexes $[Pd(PPh_3)MeL]$ (**7**) and $[Me_2ClSnL]$ (**8**). CO insertion in the palladium–carbon bond of **7** gives the stable acetyl complex $[Pd(PPh_3)\{C(O)Me\}L]$ (**10**). The palladium(II) complexes **1**, **2**, **3**, **6**, **7**, and **10** of the tripodal oxygen ligand L are all fluxional molecules that have been studied by temperature-dependent ^{1}H- and ^{31}P-NMR spectroscopy.

Introduction

Palladium coordination chemistry is dominated by phosphorus and nitrogen donor ligands. Due to their backbonding ability, phosphorus donor ligands stabilize not only palladium in the oxidation state II but also zero-valent palladium.[1] Stable palladium(IV) complexes of phosphorus donor ligands are rarely described in the literature.[2][3] Nitrogen donor ligands usually stabilize palladium in the oxidation state II. Organometallic palladium(IV) complexes with nitrogen ligands were reported by Byers et al. in 1986.[4] Until recently, the organometallic chemistry of palladium with oxygen donor ligands was limited to palladium(II). In 1993 we reported the first organopalladium(IV) complex with oxygen donor ligands.[5] The oxygen ligands used are the mono-anionic half-sandwich complexes $[(C_5H_5)Co\{P(O)R_2\}_3]^-$ (short: L_R^-),[6] which can coordinate by means of three P=O units (Figure 1). The steric and electronic properties of L_R^- are adjustable through different substituents R (R = −alkyl, −O−alkyl, −O−phenyl). The electronic properties of this class of ligands are similar to those of fluoride and oxide ions, which makes them a useful model for metal oxide surfaces.

We became interested in the question whether palladium complexes of L_R^- are catalytically active. Reactions which involve a change of the palladium oxidation state from II to IV have been discussed recently.[7,8,9] The previously-described palladium(II) chemistry of L_R^- is limited to a few allyl−[10][11] and aryl−palladium complexes that are catalytically inactive.[12] We now report the preparation of new organopalladium(II) complexes of the tripodal oxygen ligand L_{OMe}^-, stereochemically nonrigid, methyl, acetyl, and carboxymethyl complexes and their possible role in catalytic reactions.

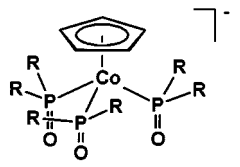


Figure 1. Schematic representation of the tripodal oxygen ligand L^-

Results and Discussion

$[PdL_2]$ (1), a Novel Homoleptic Palladium Complex

According to the HSAB concept, the palladium(II) ion is a soft metal ion.[13] Consequently, it prefers softer ligands to harder ones on complex formation. From this point of view, it makes sense that homoleptic palladium(II) complexes with hard oxygen donors are rarely observed. Known examples for homoleptic oxygen donor ligand Pd complexes are the palladium tetraaqua ion,[14] palladium carboxylate,[15] and palladium acetylacetonate.[16] All of these

[a] Institut für Anorganische Chemie und Strukturchemie der Universität Düsseldorf,
Universitätsstraße 1, D-40225 Düsseldorf, Germany
E-mail: klaeui@uni-duesseldorf.de
[b] Anorganisch-Chemisches Institut der Universität Münster,
Wilhelm-Klemm-Str. 8, D-48149 Münster, Germany

 © WILEY-VCH Verlag GmbH, D-69451 Weinheim, 2000 1434−1948/00/0101−0021 $ 17.50+.50/0

complexes feature labile oxygen palladium bonds and this explains the popularity of such complexes as starting material for new palladium complexes, as catalysts or catalyst precursors.

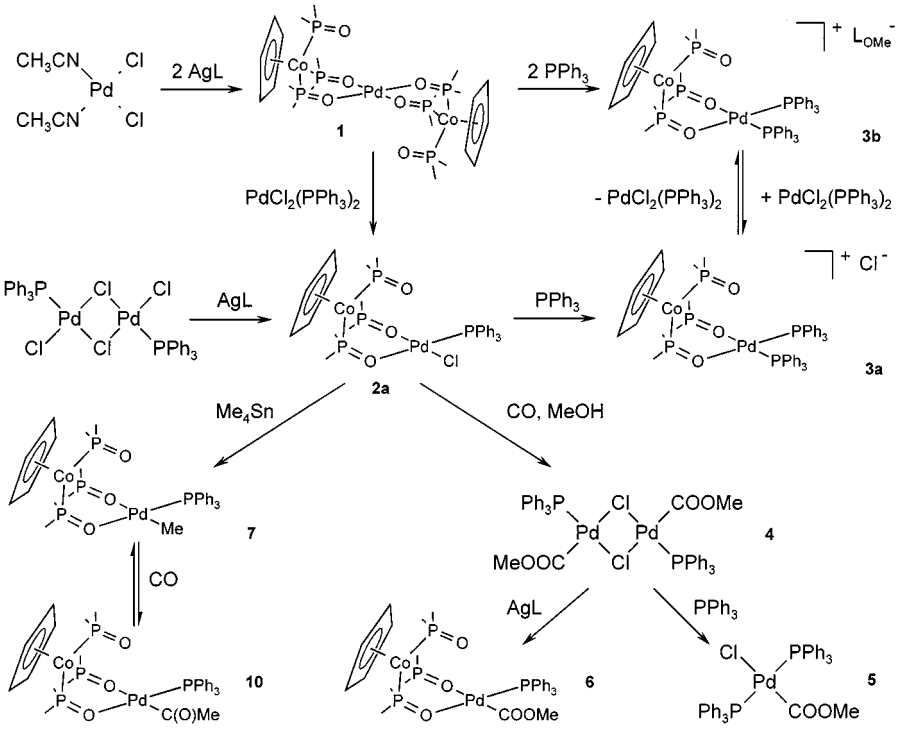
We have synthesized the new homoleptic Pd complex $[PdL_2]$ (**1**) (L = $[(C_5H_5)Co\{P(O)(OMe)_2\}_3]$) from $[PdCl_2(CH_3CN)_2]$ and AgL in dichloromethane (Scheme 1). Recrystallization from acetonitrile yielded dark red crystals of **1**. ^1H- and $^{31}P\{^1H\}$-NMR spectra of **1** in solution indicated that it was a fluxional molecule on the NMR time scale. The $^{31}P\{^1H\}$-NMR spectrum at room temperature (Figure 2) revealed a broad singlet for the three phosphorus atoms of each of the two ligands. Due to rapid site exchange reactions, all six phosphorus atoms appear equivalent. Upon cooling of the sample to 193 K a splitting of the signal into two AM_2 systems was observed, which gave evidence for the presence of two isomers. The observed spin system revealed that the tridentate ligands coordinate in these isomers only with two of the three donor groups. Based on the NMR data only, it is not possible to determine the exact underlying configuration. One can think of a "*cis*" and "*trans*" isomer in which the non-coordinating P=O units are positioned on either the same or on opposite sides of the palladium coordination plane (Figure 3).

Due to the rapid rearrangement process and hence equivalence of all methyl groups, the room-temperature ^1H-NMR spectrum (Figure 4) showed a poorly-resolved "virtual quadruplet" at δ = 3.8. On cooling to 193 K, the molecular symmetry changed from C_{3V} to C_S. The resulting $A[MX_3(Y_3)_2]_2$ spin system (A, M = ^{31}P; X, Y = ^1H) gave rise to one doublet and two "virtual triplets". The presence of two isomers that did not interconvert at low temperature was again shown by the doubling of signals. In the ^1H-NMR spectrum, two doublets ($^3J_{HP}$ = 11 Hz) could be clearly distinguished while the expected four "virtual triplets" superimposed in a way that left only two distinguishable multiplets. The two cyclopentadienyl signals at around δ = 5.1 indicated that the two isomers were formed in nearly equal amounts.

The stereochemical non-rigidity can be regarded as a fast nucleophilic substitution of a non-coordinating P=O unit for a coordinating one. Numerous investigations showed that the nucleophilic substitution at palladium(II) complexes[17] and other square planar d^8-complexes[18] follows an associative mechanism through a five coordinate transition state. It has been shown that this associative mechanism is also operative in the water exchange reaction at the palladium tetraaqua ion.[19][20] The rearrangement process of the ligands in **1** probably occurs via a five-coordinate transition state too. The alternative dissociative mechanism would feature a three-coordinated transition state with one mono-coordinated ligand. A coordination number of three is highly unlikely for a palladium(II) centre with hard ligands.

X-ray Crystal Structure of $[PdL_2]$ (1)

Complex $[PdL_2]$ (**1**) crystallized in the monoclinic space group $P2_1/n$ with a = 851.5(1), b = 1362.7(2), c = 1582.8(2) pm, β = 92.44(1)°. Data collection parameters, selected bond lengths and angles are listed in Tables 1−3. The palladium atom in **1** is coordinated by four oxygen atoms in a square planar fashion. The two tripodal ligands each use



Scheme 1. Synthesis and reactions of tripodal oxygen ligand supported palladium(II) complexes

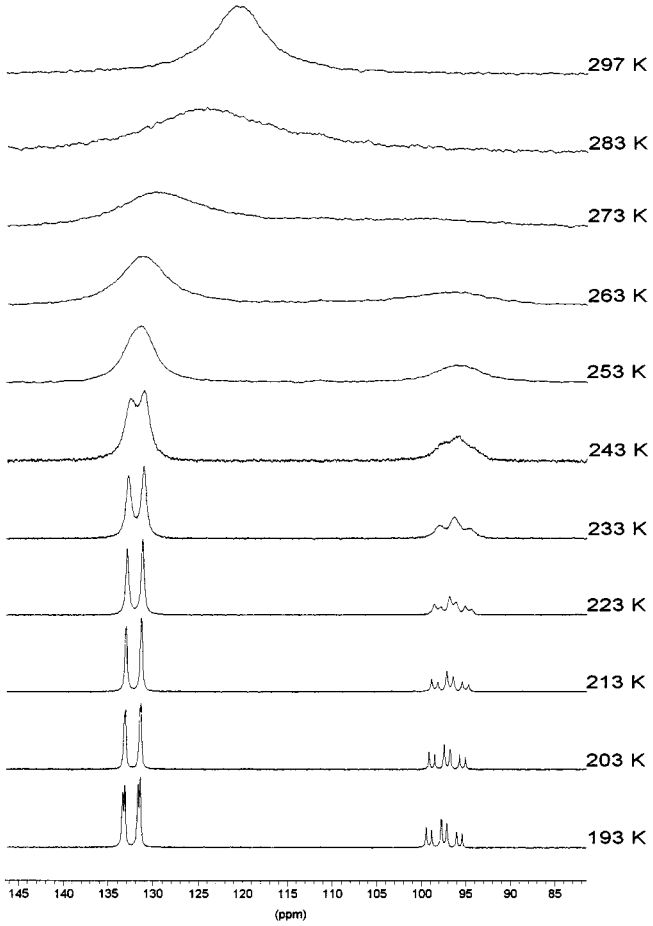


Figure 2. $^{31}P\{^{1}H\}$-NMR spectrum of **1** in CD_2Cl_2 at various temperatures

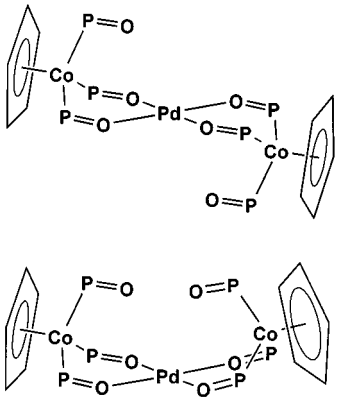


Figure 3. Possible configurations of **1** in solution at low temperature

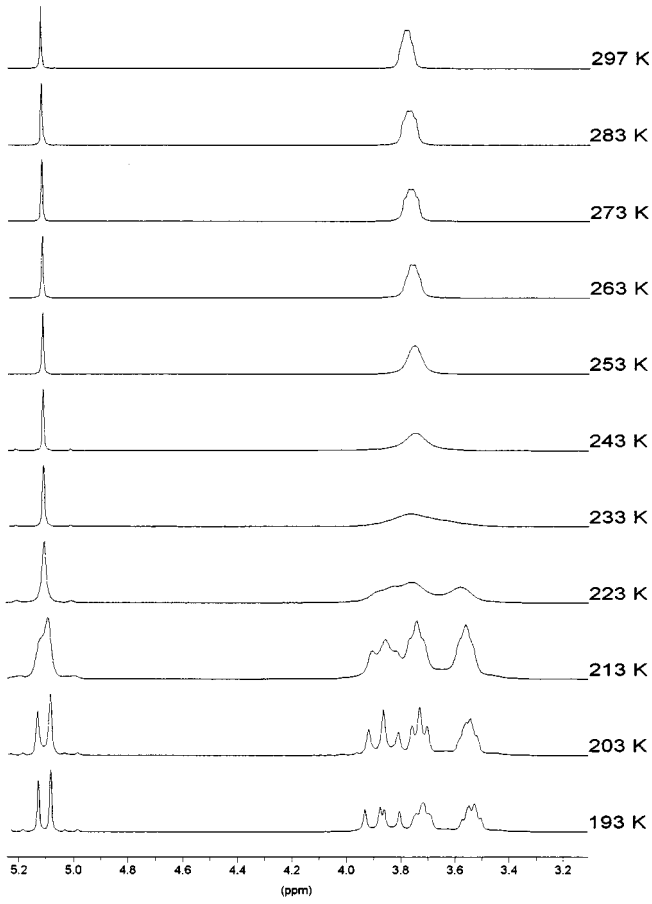


Figure 4. ^{1}H-NMR spectrum of **1** in CD_2Cl_2 at various temperatures

only two donor groups to coordinate the Pd^{II} ion (Figure 5). The measured O1−Pd−O4 chelate angle of 92.6(1)° deviates only slightly from the ideal value (90°) for a square planar geometry. The observed palladium−oxygen bond lengths are equal within experimental error [Pd−O 199.6(3), 199.4(3) pm] and fall in the expected range.[22] The distances are similar to the reported Pd−O contacts in palladium acetate (197.3−201.4 pm)[15] and are slightly longer than the corresponding bonds in $[Pd(acac)_2]$ (196(1) pm).[16]

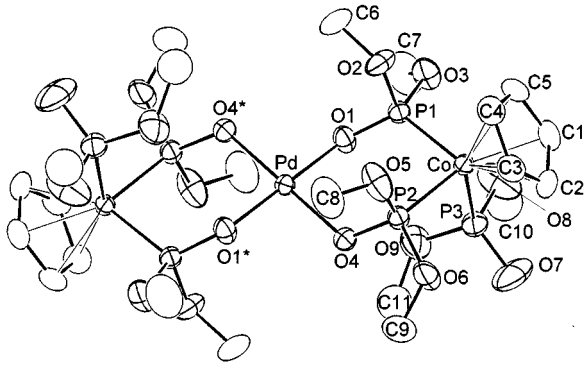


Figure 5. ORTEP plot of **1** showing 50% probability ellipsoids and the atomic numbering scheme; starred atoms represent transformed coordinates of the type $1 - x$, $1 - y$, $1 - z$

Due to the bidentate coordination mode of the tripodal ligand L^- the bond lengths and angles differ slightly in each of the $P(O)(OMe)_2$ groups. The coordinating P=O units show longer phosphorus−oxygen bond lengths [P−O 151.5(3), 151.7(3) pm] than the non-coordinating one [P=O 145.9(4) pm], which corresponds to a partial loss of double bond character of the phosphoryl units. In the solid state, the non-coordinating P=O units are twisted away

Table 1. Selected bond lengths for **1**

atom 1	atom 2	distance [pm]	atom 1	atom 2	distance [pm]
Pd	O1	199.6(3)	Co	C4	209.1(4)
Pd	O4	199.4(3)	Co	C5	209.1(4)
Co	P1	215.2(1)	P1	O1	151.5(3)
Co	P2	214.4(1)	P1	O2	159.7(3)
Co	P3	220.4(1)	P1	O3	159.4(3)
Co	C1	207.8(4)	P2	O4	151.7(3)
Co	C2	207.4(4)	P2	O5	158.8(3)
Co	C3	207.6(4)	P2	O6	158.3(3)
			P3	O7	145.9(4)
			P3	O8	160.6(4)
			P3	O9	158.7(3)

Table 2. Selected bond angles for **1**

			angle [°]				angle [°]
O1	Pd	O1*	180.(0)	O4	P2	O5	108.4(2)
O1	Pd	O4	92.6(1)	O4	P2	O6	104.5(2)
O1	Pd	O4*	87.4(1)	O5	P2	O6	104.8(2)
P1	Co	P2	91.75(4)	Co	P3	O7	116.4(2)
P1	Co	P3	93.62(5)	Co	P3	O8	103.0(1)
P2	Co	P3	94.20(5)	Co	P3	O9	114.8(1)
Co	P1	O1	121.5(1)	O7	P3	O8	111.6(3)
Co	P1	O2	106.2(1)	O7	P3	O9	111.1(2)
Co	P1	O3	111.7(1)	O8	P3	O9	97.9(2)
O1	P1	O2	108.7(2)	Pd	O1	P1	124.9(2)
O1	P1	O3	104.9(2)	P1	O2	C6	118.2(3)
O2	P1	O3	102.1(2)	P1	O3	C7	123.9(3)
Co	P2	O4	122.0(1)	Pd	O4	P2	122.6(2)
Co	P2	O5	106.0(1)	P2	O5	C8	122.8(3)
Co	P2	O6	110.1(1)	P2	O6	C9	126.4(3)
				P3	O8	C10	120.7(4)
				P3	O9	C11	120.8(4)

from the palladium centre. A similar orientation was observed in the analogous trispyrazolylborate complex $[Pd\{HB(pz)_3\}_2]$,[21] where the two tripodal ligands also bind with two donor groups only.

Reaction of PdL_2 with $[PdCl_2(PPh_3)_2]$

Complex **1** undergoes a metathesis reaction with $[PdCl_2(PPh_3)_2]$ to form the new chloro complex $[Pd(PPh_3)ClL]$ (**2a**) that was isolated as air-stable red crystals (Scheme 1). Reaction of $[\{(PPh_3)ClPd(\mu\text{-}Cl)\}_2]$ with the silver salt AgL (Scheme 1) was an alternative route to **2a**. The homologous, dark brown iodo complex $[Pd(PPh_3)IL]$ (**2c**) is similarly available from PdI_2 in acetonitrile with PPh_3 and subsequent addition of AgL. The deep red bromo complex $[Pd(PPh_3)BrL]$ (**2b**) was prepared by halide exchange from **2a** with silver triflate and $[NBu_4]Br$.

Room-temperature 500 MHz $^{31}P\{^1H\}$-NMR spectra of **2a**−**c** showed local C_{3v} symmetry for the tripodal oxygen ligands L which corroborated the fluxionality of these molecules. Below 223 K the singlet was split into a triplet and a singlet, a fact that can be explained by two different exchange rates of the two coordinated $P(O)(OMe)_2$ groups with the non-coordinated $P(O)(OMe)_2$ group. The triplet is assigned to the $P(O)(OMe)_2$ group in a *trans* position to the chloride ligand that exerts a much weaker *trans* effect than triphenylphosphane. At 173 K, the rearrangement process of **2a** became so slow on the NMR time scale that the $^{31}P\{^1H\}$-NMR spectrum revealed one broad signal for each of the three phosphorus atoms which was consistent with the expected C_1 symmetry.

Again we have no direct evidence for the mechanism of the ligand rearrangement process. We can exclude dissociation of the triphenylphosphane ligand since the triphenylphosphane phosphorus nucleus in **2a**−**c** showed coupling to the phosphorus nuclei of the ligand L. We assumed a transition state with coordination number five at the palladium centre to explain the dynamic NMR behaviour of complex **1.** The coalescence temperature for **2a** was significantly lower than for **1**. A possible explanation for this observation is the presence of a triphenylphosphane ligand in **2a**. Square planar d^8-metal complexes with soft ligands are more likely to form five-coordinate species than compounds with hard donors.[23] Consequently it would be easier for the palladium centre in **2a** to form a five-coordinate complex which in turn would decrease the energy barrier for the observed interconversion.

Reaction of $[Pd(PPh_3)ClL]$ (2a) with Triphenylphosphane

The reaction of **2a** with one equivalent of PPh_3 was complex. The first step was chloride ligand displacement and formation of the complex $[Pd(PPh_3)_2L]Cl$ (**3a**). Complex **3a** dismutated partly to form $[Pd(PPh_3)_2L]L$ (**3b**) and $[PdCl_2(PPh_3)_2]$ (Scheme 1). The same equilibrium mixture was obtained when we treat **3b** with one equivalent $[PdCl_2(PPh_3)_2]$. Compounds **3a**, **b** were identified by their ^{31}P-NMR spectrum. The formation of an ionic compound were followed by conductivity measurements during the reaction of **2a** with PPh_3. The molar conductivity of a dichloromethane solution of **2a** (c = 0.001 mol·l^{-1}) increased upon the addition of one equivalent PPh_3 from 0.2 to 49 $\mu\Omega^{-1}\cdot cm^{-2}\cdot mol^{-1}$.

The analogous reaction of the cyclopentadienyl complex $[Pd(PEt_3)BrCp]$ with triphenylphosphane has been reported to yield the ionic complex $[Pd(PEt_3)(PPh_3)Cp]Br$.[24] According to this observation, only the formation of **3a** would have been expected. The fact that we observed the formation of **3a** and **3b** demonstrates the much lower affinity of palladium(II) towards the oxygen ligand L than towards the carbon ligand Cp.

Reactivity of $[Pd(PPh_3)ClL]$ (2a) towards Carbon Monoxide and Ethene in Methanol

Alkoxycarbonyl palladium complexes are an interesting class of compounds. They are discussed as important intermediates during the synthesis of oxalic acid esters from carbon monoxide and alcohols.[25] Furthermore they are assumed to form as intermediates during the ester forming

hydrocarboxylation of olefins and the copolymerization of olefins with carbon monoxide to yield polyketones.[26–28]

We have therefore looked at the reactivity of the tripodal oxygen ligand palladium complex **2a** toward carbon monoxide, ethene, and methanol. Compound **2a** is stable in methanol. However, under carbon monoxide at 40 bar, the methoxycarbonyl complex $[\{(PPh_3)(COOMe)Pd(\mu\text{-}Cl)\}_2]$ (**4**) (Equation 1) was formed. The oxygen ligand took up the proton and was displaced as HL. According to our knowledge, **4** is the first halide-bridged methoxycarbonyl palladium complex. Its IR spectrum showed strong C=O and C–O–C valence vibrations that are characteristic of methoxycarbonyl complexes.[25] From the $^{31}P\{^1H\}$-NMR spectrum one must conclude that the dinuclear complex **4** exists as a *cis*/*trans* isomer mixture in solution.[29] The analogous reaction of $[Pd(PPh_3)Cl(acac)]$ with CO in methanol also led to the methoxycarbonyl palladium complex **4** (Equation 2). PPh_3 cleaved the chloride bridge in **4** and yielded the mononuclear complex $[PdCl(COOMe)(PPh_3)_2]$ (**5**), which was identified by comparison of its IR- and NMR data with the values reported in the literature.[25]

$$[Pd(PPh_3)ClL]\ (\mathbf{2a}) + CO + MeOH \rightarrow [\{(PPh_3)(COOMe)Pd(\mu\text{-}Cl)\}_2]\ (\mathbf{4}) + 2\ HL \quad (1)$$

$$[Pd(PPh_3)Cl(acac)] + CO + MeOH \rightarrow [\{(PPh_3)(COOMe)Pd(\mu\text{-}Cl)\}_2]\ (\mathbf{4}) + 2\ Hacac \quad (2)$$

Synthesis of $[Pd(PPh_3)(COOMe)L]$ (6)

We wondered whether the loss of the oxygen ligand–palladium bond during the formation of the methoxycarbonyl group meant that a complex with both the ligand L and a methoxycarbonyl group coordinated to palladium was unstable. We found that this type of compound was perfectly stable. It could be obtained in a clean reaction starting from the chloride bridged methoxycarbonyl complex **4** and AgL (Scheme 1). The product $[Pd(PPh_3)(COOMe)L]$ (**6**) is a yellow crystalline material, stable in moist air and soluble in polar solvents. It showed the same non-rigidity as the chloride complex **2a**, i.e. it exhibited the same type of dynamic NMR behaviour. Apart from the signal of the methoxycarbonyl group, the NMR spectra of the complexes **6** and **2** are identical. However, down to 203 K it was not possible to reach the slow exchange limit. Absorption bands at 1672 cm^{-1} [ν(C=O)] and 1078 cm^{-1} [ν(O–C–O)], characteristic of methoxycarbonyl complexes, were visible in the IR spectrum of **6**.[25]

The palladium complex **2a** is a catalyst precursor for the copolymerization of carbon monoxide with ethene. The reaction in methanol at 80°C under 25 bar each of ethene and CO produced a perfectly alternating polyketone. Under these reaction conditions, complex **2a** was transformed into the methoxycarbonyl complex **4**. We do not know whether **4** was the catalytically active compound or just another catalyst precursor. The system was not stable towards formation of metallic palladium and the polyketone yields were low.

Alkylation Reaction of 2a with Me_4Sn

The treatment of palladium halide complexes with organotin reagents is a standard procedure to form palladium–carbon bonds.[31] The attempted alkylation of the palladium chloride compound **2a** with Me_4Sn turned out to be a complex reaction. The reaction yielded the expected methyl palladium compound $[Pd(PPh_3)MeL]$ (**7**) together with the oxygen ligand tin complex $[Me_2ClSnL]$ (**8**) and the dinuclear palladium complex $[\{(PPh_3)MePd(\mu\text{-}Cl)\}_2]$ (**9**). Complex **9** is a known compound. It has been prepared form [PdMeCl(cod)] with one equivalent of PPh_3[30] and by alkylation of $[\{(PPh_3)ClPd(\mu\text{-}Cl)\}_2]$ with tetramethyltin.[32] The oxygen ligand tin complex **8** can be synthesized from Me_2SnCl_2 and the sodium salt of the ligand NaL (Equation 3).

$$Me_2SnCl_2 + NaL \rightarrow [Me_2ClSnL]\ (\mathbf{8}) \quad (3)$$

At room temperature, compound **8** exhibited fluxional behaviour in the ^1H-NMR spectrum: The tripodal ligand shows local C_{3v} symmetry. The tin methyl groups appeared as expected as a singlet with the typical $^2J_{HSn}$ satellites due to their coupling with the tin isotopes ^{117}Sn (72 Hz) and ^{119}Sn (75 Hz). These coupling constants were similar to reported values for analogous trispyrazolylborate complexes like $[SnMe_2ClTp]$ ($^2J_{119Sn\text{-}H}$ = 66 Hz)[33] and $[SnMe_2ClTp^{Me,Me}]$ ($^2J_{117Sn\text{-}H}$ = 67 Hz, $^2J_{119Sn\text{-}H}$ = 72 Hz).[34] It is possible to slow down the exchange process on cooling the sample to 203 K. The proton NMR signals of L revealed the expected lowering of symmetry from C_{3v} to C_s and the $^{31}P\{^1H\}$-NMR spectrum accordingly displayed an AM_2-spin system at the slow exchange limit. In the $^{119}Sn\{^1H\}$-NMR spectrum of **8** the slow exchange limit was already reached at 253 K. The quadruplet signal observed at room temperature ($^2J_{Sn\text{-}P}$ = 88±1 Hz) was split into a multiplet that could be interpreted as the A-part of an AXY_2-spin system.

Insertion of Carbon Monoxide in $[Pd(PPh_3)MeL]$ (7)

We were interested to see whether the methylpalladium complex **7** catalyzed the formation of polyketones. Our experiments show that **7** was able to reversibly insert carbon monoxide to yield the acetyl palladium complex $[Pd(PPh_3)\{C(O)Me\}L]$ (**10**). However, the acetyl palladium complex did not react further under an ethene atmosphere. The acetyl complex **10** possessed remarkable stability. Heating in high boiling solvents under vacuum led to deinsertion of carbon monoxide and to the formation of the methyl complex **7** in a clean reaction. A dichloromethane or acetonitrile solution of **10** could be stored for several weeks without decomposition. Analogous acetyl complexes of palladium with acetylacetonate as oxygen ligand decomposed easily in solution with the formation of metallic palladium. The ^1H-, ^{13}C-, and ^{31}P-NMR data of the $[Pd(PPh_3)L]$ part of **10** were similar to the ones of the complexes discussed above. The proton NMR signal of the acetyl group was

observed at δ = 2.18. A characteristic ^{13}C-signature was given by the carbonyl carbon atom, which appeared as a doublet at δ = 226 ($^2J_{C\text{-}P}$ = 2 Hz). The ν(C=O) IR-absorption occurred at 1703 cm^{-1}.

Concluding Remarks

The tripodal oxygen ligand L seemed to be more efficient than most other oxygen ligands in stabilizing organopalladium fragments. The reactions of the complexes that we have observed are probably reasonable models of reactions that occur or have been postulated to occur at palladium−metal oxide surface species. The pronounced non-rigid behaviour of the palladium complexes described here has its equivalent in the high mobility of Pd on silica and alumina surfaces.

Experimental Section

General: All reactions were carried out under nitrogen using standard Schlenk techniques. Filtration was done with 1-μm membrane filters (regenerated cellulose, Schleicher & Schuell). Acetonitrile was used as purchased (p.a. quality); all other solvents were dried by standard methods and distilled prior to use. − NMR spectra were recorded with a Bruker DRX 200 spectrometer, chemical shifts are given in ppm using the solvent signal as reference. Signal multiplicity is indicated by the following abbreviations: s = singlet, d = doublet, t = triplet, q = quadruplet, vq = "virtual quadruplet". − IR spectra were taken with a Bruker IFS 66 FT spectrometer. − Elemental analyses were performed in the Institut für Pharmazeutische Chemie, Universität Düsseldorf, using a Perkin−Elmer CHN-2400/II elemental analyzer.

[PdL$_2$] (1): To a suspension of [$PdCl_2(CH_3CN)_2$] (0.43 g, 1.7 mmol) in dichloromethane (30 mL) was added slowly at −30°C a solution of AgL[35] (2.2 g, 3.9 mmol) in CH_2Cl_2 (20 mL). The reaction mixture was warmed slowly to room temperature and heated at reflux for 1 h. Filtration of the black suspension through a membrane yielded a clear yellow solution. Removal of the solvent and recrystallization from a small amount of acetonitrile gave 1.20 g of yellow crystals (69%). − ^1H NMR ($CDCl_3$): δ = 3.80 (vq, $^3J_{HP}$ = 10 Hz, 18 H, OCH_3), 5.12 (s, 5 H, C_5H_5). − $^{31}P\{^1H\}$ NMR ($CDCl_3$): δ = 126 (br. s, P_{ligand}). − $^{13}C\{^1H\}$ NMR ($CDCl_3$): δ = 52.6 (s, OCH_3), 90.6 (s, C_5H_5). − IR (KBr): $\tilde{\nu}$ = 2992 cm^{-1} (w), 2944 (m), 2839 (w), 1423 (m), 1165 (s, P=O), 1117 (vs), 1067 (vs), 1007 (vs), 828 (m), 777 (s), 750 (s), 724 (s), 563 (m, P=O). − $C_{22}H_{46}Co_2O_{18}P_6Pd$ (1008.7): found C 26.42, H 4.42, Pd 10.73; calcd. C 26.20 H 4.60 Pd 10.52. − FAB-MS: positive ions: *m/z* (%) = 1031.7 (15) [M + Na]$^+$, 1009.7 (88) [M + 2]$^+$, 510.2 (100) [CoL$^+$]; negative ions: *m/z* = 1008.3 (11) [M$^-$], 451.1 (100) [L$^-$].

[Pd(PPh$_3$)ClL] (2a): $PdCl_2$ (1.41 g, 7.95 mmol) and PPh_3 (2.09 g, 7.95 mmol) were suspended in acetonitrile (100 mL) and heated at reflux for 2 h. The solvent was removed in vacuo and the orange precipitate of [$PdCl_2(PPh_3)]_2$ was dissolved in of dichloromethane (80 mL). A solution of AgL (4.45 g, 7.95 mmol) in dichloromethane (40 mL) was added slowly at −50°C. The reaction mixture was allowed to warm to −30°C when the mixture turned black. The suspension was stirred for an additional 2 h at room temperature and filtered through a membrane to give a red solution. The solvent was removed in vacuo and the residue was recrystallized from acetonitrile (ca. 200 mL) to yield 4.85 g of red crystals (72%). − ^1H NMR ($CDCl_3$): δ = 3.59 (vq, $^3J_{HP}$ = 11 Hz, 18 H, OCH_3), 5.09 (s, 5 H, C_5H_5), 7.3−7.7 [m, 15 H, P(C_6H_5)$_3$]. − $^{31}P\{^1H\}$ NMR ($CDCl_3$): δ = 115 (s, P_{ligand}), 26.7 [q, $^3J_{PP}$ = 5 Hz, $P(C_6H_5)_3$]. − $^{13}C\{^1H\}$ NMR ($CDCl_3$): δ = 52.4 (s, OCH_3), 90.3 (s, C_5H_5), 128.7 [d, J_{CP} = 12 Hz, P(C_6H_5)$_3$], 128.9 [d, J_{CP} = 58 Hz, P(C_6H_5)$_3$], 131.5 [s, P(C_6H_5)$_3$], 135.2 [d, J_{CP} = 11 Hz, P(C_6H_5)$_3$]. − IR (nujol): $\tilde{\nu}$ = 1462 cm^{-1} (vs), 1436 (m), 1175 (sh), 1154 (s, P=O), 1089 (s), 1041 (vs), 1008 (vs), 771 (m), 712 (s), 562 (m, P=O). − $C_{29}H_{38}ClCoO_9P_4Pd$ (855.3): found C 40.55, H 4.69; calcd. C 40.72, H 4.48. − MS (EI); *m/z* (%): 961 (10.8) [Co(L)$_2$]$^+$, 856 (3.7) [M$^+$ + 2], 262 (100) [PPh_3^+], 183 (60.3) [PPh_2^+ − 2], 108 (26.5) [PPh^+].

[Pd(PPh$_3$)BrL] (2b): Compound **2a** (0.31 g, 0.37 mmol) and AgOTf (0.11 g, 0.43 mmol) were dissolved in acetonitrile (10 mL) and stirred for 15 min. The AgCl precipitate was separated by membrane filtration and the clear solution was treated with [NBu_4]Br (0.12 g, 0.37 mmol). After about 60 minutes the red−brown precipitate was separated by filtration, dried, and recrystallized from a small amount of acetonitrile. Yield 0.10 g (30%). − ^1H NMR ($CDCl_3$): δ = 3.59 (vq, $^3J_{HP}$ = 11 Hz, 18 H, OCH_3), 5.10 (s, 5 H, C_5H_5), 7.3−7.9 [m, 15 H, P(C_6H_5)$_3$]. − $^{31}P\{^1H\}$ NMR ($CDCl_3$): δ = 114.4 (s, P_{ligand}), 28.5 [q, $^3J_{PP}$ = 5 Hz, $P(C_6H_5)_3$]. − IR (nujol): $\tilde{\nu}$ = 1463 cm^{-1} (s), 1377 (m), 1161 (s, P=O), 1089 (vs), 1043 (vs), 1006 (vs), 770 (s), 560 (m, P=O). − $C_{29}H_{38}BrCoO_9P_4Pd$ (899.8): found C 38.39, H 4.23; calcd. C 38.71, H 4.26.

[Pd(PPh$_3$)IL] (2c): Prepared analogously to **2a** using PdI_2 (0.52 g, 1.4 mmol), PPh_3 (0.38 g, 1.4 mmol) and AgL (0.80 g, 1.4 mmol). Yield 1.10 g (80%). − ^1H NMR ($CDCl_3$): δ = 3.59 (vq, $^3J_{HP}$ = 11 Hz, 18 H, OCH_3), 5.10 (s, 5 H, C_5H_5), 7.4−7.9 (m, 15 H, P(C_6H_5)$_3$). − $^{31}P\{^1H\}$ NMR ($CDCl_3$): δ = 112.6 (s, P_{ligand}), 28.9 [q, $^3J_{PP}$ = 5 Hz, $P(C_6H_5)_3$]. − IR (nujol): $\tilde{\nu}$ = 1463 (s), 1377 (m), 1160 (s, P=O), 1089 (vs), 1043 (vs), 1005 (vs), 768 (s), 706 (s), 538 (s). − $C_{29}H_{38}CoIO_9P_4Pd$ (946.8): found C 36.68, H 3.74; calcd. C 36.79, H 4.05.

[Pd(PPh$_3$)$_2$L]L (3b): Compound **1** (0.10 g, 0.10 mmol) and PPh_3 (53 mg, 0.20 mmol) were dissolved in dichloromethane (10 mL). After 30 min, the solvent was removed in vacuo leaving a brown−red wax that could not be crystallized. − ^1H NMR ($CDCl_3$): δ = 3.27 (vq, $^3J_{HP}$ = 11 Hz, 18 H, OCH_3 of L$^-$), 3.67 {vq, $^3J_{HP}$ = 11 Hz, 18 H, OCH_3 of [Pd(PPh_3)$_2$L]$^+$}, 4.95 (s, 5 H, C_5H_5 of L$^-$), 5.14 {s, 5 H, C_5H_5 of [Pd(PPh_3)$_2$L]$^+$}, 7.1−7.6 [m, 30 H, P(C_6H_5)$_3$], $^{31}P\{^1H\}$ NMR ($CDCl_3$): δ = 117 {s, P_{ligand} of [Pd(PPh_3)$_2$L]$^+$}, 105 (s, P_{ligand} of L$^-$), 34.5 {q, $^3J_{PP}$ = 4 Hz, [Pd(*P*Ph_3)$_2$L]$^+$}. − IR (KBr): $\tilde{\nu}$ = 3052 cm^{-1} (w), 2939 (w), 1436 (m), 1147 (s, P=O), 1076 (s), 1040 (vs), 1007 (vs), 834 (w), 748 (m), 706 (m), 562 (m, P=O).

[{(PPh$_3$)(COOMe)Pd(μ-Cl)}$_2$] (4): A solution of **2a** (0.35 g, 0.41 mmol) in methanol (5 mL) was placed in an autoclave and kept for 1 h under a CO pressure of 40 bar. The formation of a yellow solution and a white precipitate was observed. The white solid was separated by membrane filtration, washed with a small amount of methanol and dried in vacuo. Yield 0.11 g (58%). − ^1H NMR (CD_2Cl_2): δ = 3.14 (s, 3 H, COOCH_3), 7.5−7.8 [m, 15 H, P(C_6H_5)$_3$]. − $^{31}P\{^1H\}$ NMR (CD_2Cl_2): δ = 27.6 [s, $P(C_6H_5)_3$], 26.8 [s, $P(C_6H_5)_3$]. − IR (KBr): $\tilde{\nu}$ = 2943 cm^{-1} (w), 1672 (vs, C=O), 1479 (m), 1433 (s), 1417 (m), 1083 (vs, C−O−C), 750 (s), 697 (s), 533 (s).

[PdCl(COOMe)(PPh$_3$)$_2$] (5): Compound **4** (70 mg, 0.075 mmol) and PPh_3 (40 mg, 0.15 mmol) were dissolved in dichloromethane (10 mL). The mixture was stirred for 30 min and the solvent was removed in vacuo. The residue was treated with a little acetonitrile to give a white solid, which was filtered off and dried under vacuum. Yield 68 mg (60%). − ^1H NMR (CD_2Cl_2): δ = 2.50 (s, 3 H,

COOCH_3), 7.3−7.9 [m, 30 H, P(C_6H_5)$_3$]. − ^{31}P{^{1}H} NMR (CD_2Cl_2): δ = 20.4 [s, P(C_6H_5)$_3$]. − IR (KBr): ṽ = 3051 cm^{-1} (w), 1672 (vs, C=O), 1656 (s, C=O), 1433 (s), 1095 (m, C−O−C), 1064 (s), 693 (s), 519 (s). $C_{38}H_{33}ClO_2P_2Pd$ (725.5): found C 61.11, H 6.50; calcd. C 62.91, H 4.58.

[Pd(PPh$_3$)Cl(acac)]: [{(PPh$_3$)ClPd(μ-Cl)}$_2$] (1.0 g, 1.1 mmol) and [Ag(acac)] (0.47 g, 2.3 mmol) were stirred in acetonitrile (20 mL) for 1.5 h at room temperature. The reaction mixture was filtered through a membrane. The residue was extracted with dichloromethane. Both solutions were combined and the solvent was removed in vacuo. The yellow residue was recrystallized from acetone. Yield 0.72 g (63%). − ^{1}H NMR ($CDCl_3$): δ = 1.60 (s, 3 H, CH_3), 2.14 (s, 3 H, CH_3), 5.35 (s, 1 H, CH), 7.4−7.9 [m, 15 H, P(C_6H_5)$_3$]. − ^{31}P{^{1}H} NMR ($CDCl_3$): δ = 30.2 [s, P(C_6H_5)$_3$]. − IR (KBr): ṽ = 1575 cm^{-1} (s, C=O), 1565 (s, C=O), 1513 (s), 1434 (m), 1378 (m), 1097 (m), 691 (m), 536 (m), 515 (m), 497 (m). − $C_{23}H_{22}ClO_2PPd$ (503.7): found C 54.93, H 4.46; calcd. C 54.89, H 4.41.

[{(PPh$_3$)(COOMe)Pd(μ-Cl)}$_2$] (4) from [Pd(PPh$_3$)Cl(acac)]: [Pd(PPh$_3$)Cl(acac)] (0.30 g, 0.60 mmol) in methanol (5 mL) were treated for 60 min at room temperature with a CO pressure of 10 bar. Yield: 0.23 g (84%) grey-white precipitate, spectroscopic data as reported above.

Copolymerization of CO/Ethene with [Pd(PPh$_3$)ClL$_{OMe}$] (2a) and [{(PPh$_3$)(COOMe)PdCl}$_2$] (4): Compound **2a** (50 mg, 0.06 mmol) in methanol (20 mL) was pressurized in a 50-mL autoclave with 25 bar of CO and 25 bar of ethene at 80°C. Yield: 90 mg of polyketone as a grey precipitate. − TON = 16 g polyketone·(g Pd·h)$^{-1}$; IR (KBr): ṽ = 1692 cm^{-1} [ṽ(C=O)]. An analogous experiment with **4** (27 mg, 0.03 mmol) yielded polyketone (0.11 g). − TON = 18 g polyketone·(g Pd·h)$^{-1}$.

[Pd(PPh$_3$)(COOMe)L] (6): Compound **4** (0.10 g, 0.11 mmol) and AgL (0.12 g, 0.22 mmol) were dissolved in dichloromethane (10 mL) and stirred for 2 h. The precipitated AgCl was filtered off and the solvent was removed in vacuo. The yellow residue was recrystallized with a little acetonitrile. Yield 0.13 g (66%). − ^{1}H NMR ($CDCl_3$): δ = 3.15 (s, 3 H, COOCH_3), 3.59 (vq, 18 H, $^3J_{PH}$ = 11 Hz, OCH_3), 5.10 (s, 5 H, C_5H_5), 7.3−7.8 [m, 15 H, P(C_6H_5)$_3$]. − ^{31}P{^{1}H} NMR ($CDCl_3$): δ = 112.7 (s, P_{ligand}), 27.3 [q, $^3J_{PP}$ = 4 Hz, P(C_6H_5)$_3$]. − ^{13}C{^{1}H} NMR (CD_2Cl_2): δ = 51.9 (vq, OCH$_3$), 53.2 (s, COOCH$_3$), 90.1 (s, C_5H_5), 128.8 [d, J_{CP} = 11 Hz, P(C_6H_5)$_3$, 131.1 [d, J_{CP} = 3 Hz, P(C_6H_5)$_3$], 132.2 [d, J_{CP} = 52 Hz, P(C_6H_5)$_3$], 134.9 [d, J_{CP} = 12 Hz, P(C_6H_5)$_3$]. − IR (KBr): ṽ = 2935 cm^{-1} (m), 2827 (w), 1672 (vs, C=O), 1437 (s), 1175 (vs, P=O), 1078 (vs, C−O−C), 1047 (vs), 1002 (vs), 833 (m), 695 (s), 575 (s, P=O). $C_{31}H_{41}CoO_{11}P_4Pd$ (878.9): found C 42.65, H 4.63; calcd. C 42.36, H 4.70.

[Pd(PPh$_3$)MeL] (7): Compound **2a** (1.0 g, 1.2 mmol) and Me_4Sn (0.23 g, 1.3 mmol) were dissolved in dichloromethane (10 mL) and stirred for 4 h at room temperature. The reaction mixture became opaque and turned yellow almost instantly. The white precipitate formed [{(PPh$_3$)MePd(μ-Cl)}$_2$] (**9**) was isolated by centrifugation, washed with dichloromethane and dried. The yellow supernatant was reduced in volume and the residue was recrystallized twice from a small amount of acetonitrile. Yellow crystals of **7** were isolated and dried. The mother liquor was reduced in volume and stored at −20°C, which resulted in the formation of yellow crystals of [Me_2ClSnL] (**8**). Yields: 0.24 g of **9** (49%), 0.32 g of **7** (33%), and 0.14 g of **8** (22%). − Selected spectroscopic data for **7**: ^{1}H NMR ($CDCl_3$): δ = 0.48 (d, $^3J_{HP}$ = 2 Hz, 3 H, PdCH_3), 3.61 (vq, $^3J_{HP}$ = 11 Hz, 18 H, OCH_3), 5.12 (s, 5 H, C_5H_5), 7.3−7.7 [m, 15 H, P(C_6H_5)$_3$]. − ^{31}P{^{1}H} NMR ($CDCl_3$): δ = 112.2 (s, P_{Ligand}), 39.6 [q, $^3J_{PP}$ = 4 Hz, P(C_6H_5)$_3$]. − For **8**: ^{1}H NMR ($CDCl_3$): δ = 0.54 [s, $^2J_{HSn}$ = 74 Hz, 6 H, Sn(CH_3)$_2$], 3.72 (vq, $^3J_{HP}$ = 11 Hz, 18 H, OCH_3), 5.14 (s, 5 H, C_5H_5). − ^{31}P{^{1}H} NMR ($CDCl_3$): δ = 115.3 (s, P_{ligand}). − For **9**: ^{1}H NMR ($CDCl_3$): δ = 0.67 (broad s, 3H, PdCH_3), 7.2−7.8 [m, 15H, P(C_6H_5)$_3$]. − $C_{38}H_{36}Cl_2P_2Pd_2$ (838.4): found C 54.47, H 4.41; calcd. C 54.44, H 4.33. − IR (KBr): ṽ = 3072 cm^{-1} (w, C−H), 3049 (w, C−H), 2977 (w, C−H), 2893 (w, C−H), 1479 (m, C−C), 1435 (s, C−C), 1097 (s), 743 (m, C−H), 705 (s, C−H), 538 (s), 525 (m), 511 (s), 493 (m).

[Me_2ClSnL] (8): Me_2SnCl_2 (0.31 g, 1.4 mmol) and NaL (0.67 g, 1.4 mmol) were stirred in dichloromethane (10 mL). The yellow crystals of NaL dissolved slowly and a white precipitate was formed (NaCl). After 16 h, the mixture was filtered and the yellow filtrate was concentrated in vacuo to give a yellow powder (0.72 g, 81%) which was recrystallized from acetonitrile. Yield 0.49 g of yellow crystals (54%). − ^{1}H NMR ($CDCl_3$): δ = 0.55 [s, $^2J_{H\text{-}119Sn}$ = 75 Hz, $^2J_{H117Sn}$ = 72 Hz, 6 H, Sn(CH_3)$_2$], 3.73 (vq, $^3J_{HP}$ = 11 Hz, 18 H, OCH_3), 5.14 (s, 5 H, C_5H_5). − ^{1}H NMR (CD_2Cl_2, 203 K): δ = 0.38 [s, $^2J_{H\text{-}119Sn}$ = 74 Hz, $^2J_{H\text{-}117Sn}$ = 72 Hz, 6 H, Sn(CH_3)$_2$], 3.63 (d and vt superimposed, OCH_3), 3.70 (vt, $^3J_{HP}$ = 11 Hz, 18 H, OCH_3), 5.15 (s, 5 H, C_5H_5). − ^{31}P{^{1}H} NMR ($CDCl_3$): δ = 115.3 (s, P_{ligand}). − ^{31}P{^{1}H} NMR (CD_2Cl_2, 203 K): AB_2-spin system, ν_A = 119.5, ν_B = 116.5, J_{AB} = 146 Hz. − ^{119}Sn{^{1}H} NMR (CD_2Cl_2): δ = −344.3 (q, $^2J_{P\text{-}119Sn}$ = 86±1 Hz). − ^{119}Sn{^{1}H} NMR (CD_2Cl_2, 253 K): δ = −346.7 [dt (AXY_2-spin system), $^2J_{119SnP}$ (J_{AX}) = 107±1 Hz, $^2J_{119SnP}$ (J_{AY}) = 73±1 Hz]. − $C_{13}H_{29}ClCoO_9P_3Sn$ (635.4): found C 24.69, H 4.64; calcd. C 24.57, H 4.60. − IR (KBr): ṽ = 2988 cm^{-1} (w), 2948 (m), 2912 (w), 2841 (w), 1459 (m), 1424 (m), 1175 (s), 1120 (vs) (P=O), 1029 (vs), 833 (m), 785 (s), 735 (m), 591 (vs, P=O). − MS (EI); *m/z* (%): 621 (100) [SnMeClL]$^+$, 601 (28) [SnMe$_2$L]$^+$, 571 (8) [SnL]$^+$, 497 (7), 480 (13), 418 (12).

[Pd(PPh$_3$){C(O)Me}L] (10): Carbon monoxide was bubbled for 30 min through a solution of **7** (0.19 g, 0.23 mmol) in dichloromethane (10 mL). The solvent was removed at room temperature in vacuo and the residue was recrystallized from acetonitrile. Yield: 0.12 g (61%). − ^{1}H NMR ($CDCl_3$): δ = 2.18 [d, $^4J_{HP}$ = 1 Hz, 3 H, C(O)CH_3], 3.61 (vq, $^3J_{HP}$ = 11 Hz, 18 H, OCH_3), 5.10 (s, 5 H, C_5H_5). − ^{31}P{^{1}H} NMR ($CDCl_3$): δ = 111.5 (s, P_{ligand}), 27.4 [q, $^3J_{PP}$ = 3 Hz, P(C_6H_5)$_3$]. − ^{13}C{^{1}H} NMR ($CDCl_3$): δ = 34.9 [s, C(O)CH$_3$], 51.9 (vq, $^2J_{CP}$ = 9 Hz, OCH$_3$), 90.2 (s, C_5H_5), 128.8 [d, J_{CP} = 11 Hz, P(C_6H_5)$_3$], 130.9 [d, J_{CP} not resolved, P(C_6H_5)$_3$], 132.4 [d, J_{CP} = 47 Hz, P(C_6H_5)$_3$], 135.0 [d, J_{CP} = 13 Hz, P(C_6H_5)$_3$], 225.9 [d, $^2J_{CP}$ = 2 Hz, C(O)CH$_3$]. − IR (KBr): ṽ = 3048 cm^{-1} (w), 2974 (w), 2936 (m), 2829 (w), 1703 (vs, C=O), 1439 (m), 1162 (vs, P=O), 1115 (s), 1034 (vs), 1006 (vs), 833 (w), 706 (s), 582 (m, P=O). − $C_{31}H_{41}CoO_{10}P_4Pd$ (862.9): found C 43.42, H 4.89; calcd. C 43.15, H 4.79.

X-ray Crystal Structure Determination of [PdL$_2$] (1): A suitable crystal of **1** was selected and mounted on an Enraf−Nonius CAD-4 diffractometer. Important crystal and data collection details are listed in Table 3. Data for **1** were collected at room temperature using ω-2Θ scans. Raw data were reduced to structure factors[36] (and their esd′s) by correcting for scan speed, Lorentz and polarization effects. No crystal decay was detected and no absorption corrections were applied at this stage. The systematically absent reflections showed the space group to be $P2_1/n$. The positional parameters for Pd and Co were obtained from a three-dimensional Patterson map. Positional parameters for all other non-hydrogen atoms were found in subsequent difference Fourier maps. The positional parameters for all non-hydrogen atoms were refined by using first isotropic, and later anisotropic thermal parameters. An em-

pirical absorption correction (DIFABS[37]) was applied after refinement of the positional parameters of all non-hydrogen atoms with isotropic thermal parameters. A difference Fourier map calculated after refinement of the positional parameters with anisotropic thermal parameters showed the positional parameters of almost all hydrogen atoms. However, hydrogen atoms were added to the structure model at calculated positions [d(C−H) = 95 pm][38] and are unrefined. The isotropic temperature factors for hydrogen atoms were fixed to be 1.3 times the B_{eq} of the parent atom. All calculations were carried out with the MolEN[39] package. ORTEP[40] was used for molecular drawings. The Pd atoms reside on a crystallographic inversion centre. The asymmetric unit contains 1/2 molecule of **1**. Crystallographic data for the structure of **1** have been deposited with the Cambridge Crystallographic Data Centre as supplementary publication no. CCDC-118725. Copies of the data can be obtained free of charge on application to CCDC, 12 Union Road, Cambridge CB2 1EZ, UK [Fax: (internat.) + 44-1223/336-033; E-mail: deposit@ccdc.cam.ac.uk]. Figure 5 shows one molecule of **1** (the contents of two asymmetric units) with the employed crystallographic numbering scheme.

Table 3. Crystal and data collection details for **1**

Crystal size	0.50 × 0.41 × 0.32 mm
Empirical formula	$C_{22}H_{46}Co_2O_{18}P_6Pd$
Molecular mass	1008.71 amu
a	8.515(1) Å
b	13.627(2) Å
c	15.828(2) Å
β	92.44(1)°
V	1834.9(7) Å^3
Space group	$P2_1/n$
Z	2
$d_{calcd.}$	1.826 g/cm^3
$d_{obsd.}$	1.83 g/cm^3
μ	1.70 mm^{-1}
Data-coll. temp.	298(2) K
2Θ range	2° to 45°
Measured intensities	2694
Unique data	2386
Observed data	2188
Observation criterion	$Fo^2 \geq 3\sigma(F_o^2)$
Absorption correction	DIFABS
R	4.32%
R_w	6.00%
GOF	1.431
No. of variables	224
Resid. electr. dens.	0.79/−0.97 e/Å^3 (near Pd)

Acknowledgments

We thank Dr. W. Peters for his help with the dynamic NMR spectra, Prof. Dr. K. Jurkschat for measuring Sn-NMR spectra, the Fonds der Chemischen Industrie for financial support, and Degussa AG, Hanau, for a loan of palladium chloride.

[1] P. M. Maitlis, *The Organic Chemistry of Palladium*, vol. 1, Academic Press, New York, London, **1971**.
[2] D. Milstein, J. K. Stille, *J. Am. Chem. Soc.* **1979**, *101*, 4981−4991.
[3] A. Gillie, J. K. Stille, *J. Am. Chem. Soc.* **1980**, *102*, 4933−4941.
[4] P. K. Byers, A. J. Canty, B. W. Skelton, A. H. White, *J. Chem. Soc., Chem. Commun.* **1986**, 1722−1724.
[5] W. Kläui, M. Glaum, T. Wagner, M. A. Bennett, *J. Organomet. Chem.* **1994**, *472*, 355−358.
[6] W. Kläui, *Angew. Chem.* **1990**, *102*, 661−670; *Angew. Chem. Int. Ed. Engl.* **1990**, *29*, 627−637.
[7] A. J. Canty, *Platinum Met. Rev.* **1993**, *37*, 2−7.
[8] M. Catellani, G. P. Chiusoli, *J. Organomet. Chem.* **1988**, *346*, C27−C30.
[9] P. Brechot, Y. Chauvin, D. Commereuc, L. Saussine, *Organometallics* **1990**, *9*, 26−30.
[10] B. Domhöver, H. Hamers, W. Kläui, M. Pfeffer, *J. Organomet. Chem.* **1996**, *522*, 197−206.
[11] B. Domhöver, W. Kläui, *J. Organomet. Chem.* **1996**, *522*, 207−212.
[12] M. Glaum, W. Kläui, B. W. Skelton, A. H. White, *Aust. J. Chem.* **1997**, *50*, 1047−1052.
[13] J. A. Davies, F. R. Hartley, *Chem. Rev.* **1981**, *81*, 79−90.
[14] W. P. Griffith, K. Swars (Eds.), *Gmelin Handbook of Inorganic Chemistry*, Gmelin Handbook Pd Main, **1989**, vol. B 2, p. 218.
[15] A. C. Skapski, M. L. Smart, *Chem. Commun.* **1970**, 658−659.
[16] A. N. Knyazeva, E. A. Shugam, L. M. Shkol′nikova, *J. Struct. Chem.* **1970**, *11*, 875−876.
[17] P. M. Maitlis, P. Espinet, M. J. H. Russell, *Comprehensive Organometallic Chemistry* (Eds.: G. Wilkinson, F. G. A. Stone, E. W. Abel), Pergamon Press Oxford, England, **1982**, vol. 6, p. 233.
[18] J. E. Huheey, E. A. Keiter, R. L. Keiter, *Anorganische Chemie*, 2nd ed., Walter de Gruyter, Berlin, **1995**.
[19] L. Helm, L. I. Elding, A. E. Merbach, *Helv. Chim. Acta* **1984**, *67*, 1453−1460.
[20] R. J. Deeth, L. I. Elding, *Inorg. Chem.* **1996**, *35*, 5019−5026.
[21] A. J. Canty, N. J. Minchin, L. M. Engelhardt, B. W. Skelton, A. H. White, *J. Chem. Soc., Dalton Trans.* **1986**, 645−650.
[22] P. M. Maitlis, *The organic chemistry of palladium*, vol. 1, Academic Press, New York, **1971**.
[23] J. P. Collman, F. D. Vastine, W. R. Koper, *J. Am. Chem. Soc.* **1968**, *90*, 2282−2287.
[24] R. J. Cross, R. Wardle, *J. Chem. Soc. A* **1971**, 2000−2007.
[25] R. Bertani, G. Cavinato, L. Toniolo, G. Vasapollo, *Journal of Molecular Catalysis* **1993**, *84*, 165−176.
[26] K. Bittler, N. v. Kutepow, D. Neubauer, H. Reis, *Angew. Chem.*, **1968**, *80*, 352−359; *Angew. Chem. Int. Ed. Engl.* **1968**, *7*, 329−335.
[27] E. Drent, J. A. M. van Broekhoven, M. J. Doyle, *J. Organomet. Chem.* **1991**, *417*, 235−251.
[28] Z. Jiang, G. M. Dahlen, K. Housknecht, S. Sen, *Macromolecules* **1992**, *25*, 2999−3001.
[29] This is not unusual. The $^{31}P\{^1H\}$-NMR spectrum of the analogous complex $[\{(PEt_3)MePd(\mu\text{-}Cl)\}_2]$ reveals also the presence of a *cis*/*trans* isomer mixture.[30]
[30] F. T. Ladipo, G. K. Anderson, *Organometallics* **1994**, *13*, 303−306.
[31] J. K. Stille, *Angew. Chem.* **1986**, *98*, 504−519; *Angew. Chem. Int. Ed. Engl.* **1986**, *25*, 508−524.
[32] A. Singhal, V. K. Jain, *J. Chem. Soc., Dalton Trans.* **1993**, 1515−1517.
[33] G. G. Lobbia, F. Bonati, P. Cecchi, A. Cingolani, A. Lorenzotti, *J. Organomet. Chem.* **1989**, *378*, 139−146.
[34] G. G. Lobbia, F. Bonati, P. Cecchi, A. Lorenzotti, C. Pettinari, *J. Organomet. Chem.* **1991**, *403*, 317−323.
[35] B. Domhöver, Dissertation, Düsseldorf, **1996**.
[36] Neutral scattering factors were used: *International Tables for X-Ray Crystallography*, Kynoch Press: Birmingham, England, **1974**, vol. IV, Table 2.2B. Terms of anomalous dispersion from *International Tables for X-Ray Crystallography*, Kynoch Press, Birmingham, England, **1974**, vol. IV, Table 2.3.1.
[37] DIFABS: N. Walker, D. Stuart, *Acta Crystallogr., Sect A* **1983**, *39*, 158−166.
[38] M. R. Churchill, *Inorg. Chem.* **1973**, *12*, 1213−1214.
[39] MolEN: Molecular Structure Solution Procedures. Program Descriptions, Enraf−Nonius, Delft, **1990**. Definition of residuals: $R = \Sigma||F_o| - |F_c||/\Sigma|F_o|$, $R_w = [\Sigma w||F_o| - |F_c||^2/\Sigma w|F_o|^2]^{1/2}$, GOF = $[\Sigma w||F_o| - |F_c||^2/(n_o - n_p)]^{1/2}$ with n_o = number of structure factors and n_p = number of parameters, $w = 1/[\sigma_{(F)}]^2$.
[40] C. K. Johnson, *ORTEP II. Report ORNL-5138*, Oak Ridge National Laboratory, Oak Ridge, TN, **1971**.

Received April 22, 1999
[I99142]

Benzimidazole, Benzothiazole and Benzoxazole Ruthenium(II) Complexes; Catalytic Synthesis of 2,3-Dimethylfuran

Bekir Çetinkaya,[a] Ismail Özdemir,*[a] Christian Bruneau,[b] and Pierre H. Dixneuf*[b]

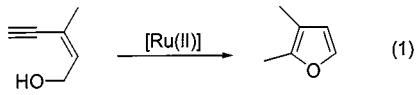
Dedicated to Professor W. P. Fehlhammer for his scientific contribution and on the occasion of his 60th birthday

Keywords: Arene complexes / Ruthenium / Benzimidazole / Benzothiazole / Benzoxazole / Cycloisomerisation

Fourteen ruthenium(II) complexes of the type $[RuCl_2(\eta^6\text{-arene})L]$, (arene = 1,4-$MeC_6H_4Pr^i$ or C_6Me_6; L = benzimidazole derivative in which the NH group is substituted by *N*-alkyl or isoelectronic O or S atoms) have been prepared by cleavage of $[RuCl_2(\eta^6\text{-arene})]_2$ with the *N*-heterocycle L. Their spectroscopic and electrochemical properties are described. The effect of the nature of the benzazole (L) on the catalytic activity of these complexes for the intramolecular cyclization of (Z)-3-methylpent-2-en-4-yn-1-ol into 2,3-dimethylfuran has also been studied; the benzimidazole complexes were found to be the most active.

Introduction

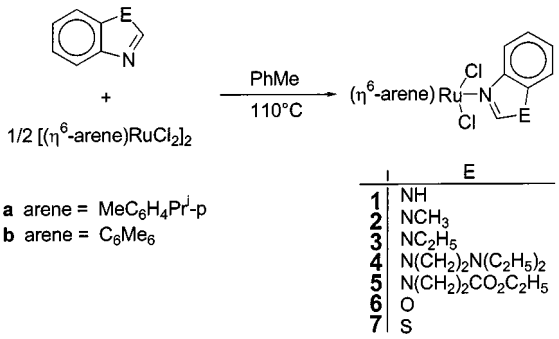
Transition metal complexes with ligands containing nitrogen-donor atoms have recently shown their potential to successfully promote the catalytic transformation of organic compounds.[1] These discoveries motivate the search for new metal complexes with *N*-coordinated ligands and the evaluation of their catalytic properties. In this context, Rh^I complexes of 1-alkyl-2-imidazoline in which the imidazoline coordinates through the N(3) atom of the ring have already been shown to catalyse the cyclopropanation of styrene with ethyl diazoacetate in good yield.[2] Our contribution to this field has recently started with the syntheses of the 2-imidazoline and 1,4,5,6-tetrahydropyrimidine complexes of Ru^{II} which are capable of catalyzing the intramolecular cyclization of (*Z*)-3-methylpent-2-en-4-yn-1-ol into 2,3-dimethylfuran (Equation 1) and the observation of the higher efficiency of the tetrahydropyrimidine complexes.[3]



(1)

In this paper we report the straightforward preparation of a series of (η^6-arene)ruthenium complexes of *N*-coordinated benzimidazole derivatives in which the NH group is substituted by *N*-alkyl or isoelectronic O or S atoms (Scheme 1). Their spectroscopic and electrochemical properties are described and the influence of the nature of the benzazole ligand L on the catalytic activity of these complexes in the formation of 2,3-dimethylfuran has also been studied.

[a] Inönü Üniversitesi Fen-Edebiyat Fakültesi, 44280 Malatya, Turkey
[b] UMR 6509 CNRS-Université de Rennes, Laboratoire de Chimie de Coordination et Catalyse, Campus de Beaulieu, F-35042 Rennes, France



Scheme 1. Synthetic route to benzazole complexes of Ru^{II}

Results and Discussion

The complexes **1**−**7** were prepared in 74−89% yield by simply heating the appropriate benzazole (L) with $[RuCl_2(\eta^6\text{-arene})]_2$ in toluene (Scheme 1). The compounds **1**−**7** were precipitated as red-brown crystalline solids upon cooling the reaction mixture, isolated by filtration and washed with *n*-hexane (see Table 1). The complexes **1**−**7** are perfectly stable in the solid state and show spectroscopic properties indicating that they all are N(3)-bonded. However, the reaction of benzimidazole with $[Ru(H_2O)(NH_3)_5)]^{2+}$, followed by HCl-catalyzed hydrolysis, has been reported to form C(2)-bonded benzimidazole ligand.[4] On the other hand, X-ray crystallographic studies revealed that 2,5-dimethylbenzoxazole, potentially an ambidentate ligand, coordinates to the Pt^{II} centre through the *N*-donor atom.[5] An X-ray structure of cyclopalladated complexes of *N*-acetyl-2-phenyl-benzimidazole has also been described.[6]

The nature of the bonding in the benzazole complexes **1**−**7** was readily shown by NMR spectroscopy (Tables 2 and 3). ^{13}C NMR spectroscopy was the most useful tool for structure elucidation. Thus, from our previous experience,[6][7] we expected that *C*-coordination would result in a shift of the carbene carbon nucleus to high frequency i.e. 190−210 ppm, while *N*-coordination would result in a low

 © WILEY-VCH Verlag GmbH, D-69451 Weinheim, 2000 1434−1948/00/0101−0029 $ 17.50+.50/0

Table 1. Physical measurement of new benzimidazole, benzothiazole and benzoxazole ruthenium complexes **(1−7)**

Compound	M.p. (°C)	Yield (%)	Micro Analysis Found (Calculated) (%)		
			C	H	N
1a	249−250	87	48.02 (48.11)	4.73 (4.75)	6.29 (6.61)
1b	373−374	89	50.71 (50.45)	5.41 (5.35)	6.33 (6.19)
2a	248−249	89	48.98 (49.31)	5.05 (5.06)	6.47 (6.39)
2b	345−346	83	51.41 (51.50)	5.76 (5.62)	5.98 (6.01)
3a	228−229	79	50.12 (50.44)	5.27 (5.35)	6.28 (6.20)
3b	317−318	85	52.25 (52.49)	5.87 (5.88)	6.03 (5.83)
4a	253−254	75	52.38 (52.76)	6.26 (6.36)	7.84 (8.03)
4b	359−361	80	53.99 (54.43)	6.35 (6.77)	7.24 (7.62)
5a	172−173	87	50.08 (50.38)	5.22 (5.38)	5.21 (5.34)
5b	240−241	89	52.34 (52.17)	5.41 (5.84)	4.89 (5.07)
6a	194−195	74	47.69 (48.00)	4.54 (4.51)	3.23 (3.76)
6b	378−378	78	49.92 (50.33)	5.39 (5.12)	3.03 (3.53)
7a	219−220	83	46.21 (46.26)	4.34 (4.34)	3.11 (3.18)
7b	369−370	77	48.15 (48.61)	4.96 (4.94)	2.54 (2.99)

frequency shift towards 160 ppm. The signal pattern for the nitrogen donor ligands and ^{13}C NMR chemical shifts were consistent with the proposed structure; the imino carbon appeared as a typical singlet in the ^{1}H-decoupled mode in the 142.6−160.6 ppm range. The ^{1}H NMR spectra of the complexes further supported the assigned structures; the resonances for C(2)−H were observed as sharp singlets in the 7.3−9.7 ppm range. An electrochemical study by cyclic voltammetry showed that these new complexes present one reversible redox wave for the system Ru^{II}/Ru^{III} located in the range 1−1.3V/ECS (Table 4). For the electron releasing C_6Me_6 ligand the redox process takes place at lower potential.

Catalytic Studies

Although various ruthenium catalysts have been reported[3,8,9] for the intramolecular cyclization of (*Z*)-enynols (Equation 1), the search for more efficient catalysts is necessary. Therefore, we evaluated the new ruthenium complexes **1−7** for this reaction. With 1 mol-% of Ru catalyst at 80°C (*Z*)-3-methylpent-2-en-4-yn-1-ol gave moderate to good yields of the cyclization product. These results are summarized in Table 5. They show that the most efficient complexes are **3a** and **5a** (Table 5, entries 7, 12, 13). The best yields were obtained at 80°C for 2−4 h. Comparison of the catalysts containing *p*-cymene (**a** type) and hexa-

Table 2. IR and ^{1}H NMR spectroscopic data for compounds **1−7**[a]

Compound	ν (CN) cm^{-1}	C(2)−*H*	Others
1a	1489	8.0 (s)	2.0 N*H*; 6.61−6.99 (m) C_6H_4; 5.3 and 5.5 (d, *J* 6 Hz)) [$(CH_3)_2CHC_6H_4$ (CH_3)-*p*]; 1.2 (d, *J* 7 Hz) [$(CH_3)_2CHC_6H_4$ (CH_3)-*p*]; 2.0 (s) [$(CH_3)_2CHC_6H_4$ (CH_3)-*p*]; 2.8 (sept. *J* 7) [$(CH_3)_2CHC_6H_4$ (CH_3)-*p*]
1b	1484	7.8 (s)	2.0 N*H*; 5.5−5.8 C_6H_4; 1.5 (s) $C_6(CH_3)_6$
2a	1610	8.4 (s)	3.7 (s) CH_3; 7.3−7.9 C_6H_4; 5.3 and 5.5 (d, *J* 6 Hz)) [$(CH_3)_2CHC_6H_4$ (CH_3)-*p*]; 1.2 (d, *J* 7 Hz) [$(CH_3)_2CHC_6H_4$ (CH_3)-*p*]; 2.1 (s) [$(CH_3)_2CHC_6H_4$ (CH_3)-*p*]; 2.8 (sept. *J* 7) [$(CH_3)_2CHC_6H_4$ (CH_3)-*p*]
2b	1608	8.2 (s)	3.8 (s) CH_3; 7.3−8.0 (m) C_6H_4; 2.0 (s) $C_6(CH_3)_6$
3a	1610	8.4 (s)	4.1 (q, *J* 7 Hz) CH_2CH_3; 1.4 (t, *J* 7 Hz) CH_2CH_3; 7.2−8.0 (m) C_6H_4; 5.3 and 5.5 (d, *J* 6 Hz)) [$(CH_3)_2CHC_6H_4$ (CH_3)-*p*]; 1.2 (d, *J* 7 Hz) [$(CH_3)_2CHC_6H_4$ (CH_3)-*p*]; 2.1 (s) [$(CH_3)_2CHC_6H_4$ (CH_3)-*p*]; 2.8 (sept. *J* 7) [$(CH_3)_2CHC_6H_4$ (CH_3)-*p*]
3b	1611	8.1 (s)	4.1 (q, *J* 7 Hz) CH_2CH_3; 1.4 (t, *J* 7 Hz) CH_2CH_3; 7.2−7.4 (m) C_6H_4; 1.9 (s) $C_6(CH_3)_6$
4a	1513	8.5 (s)	4.1 (t, *J* 6 Hz) $CH_2CH_2N(CH_2CH_3)_2$; 2.8 (t, *J* 6 Hz) $CH_2CH_2N(CH_2CH_3)_2$; 2.7 (q, *J* 6 Hz) $CH_2CH_2N(CH_2CH_3)_2$; 1.0 (t, *J* 7 Hz) $CH_2CH_2N(CH_2CH_3)_2$; 7.3−8.1 (m) C_6H_4; 5.4 and 5.6 (d, *J* 6 Hz) [$(CH_3)_2CHC_6H_4$ (CH_3)-*p*]; 1.3 (d, *J* 7 Hz) [$(CH_3)_2CHC_6H_4$ (CH_3)-*p*]; 2.1 (s) [$(CH_3)_2CHC_6H_4$ (CH_3)-*p*]; 3.0 (sept. *J* 7) [$(CH_3)_2CHC_6H_4$ (CH_3)-*p*]
4b	1490	7.3 (s)	1.8 (qu *J* 6 Hz) $NCH_2CH_2CH_2N$; 4.2 (s) $CH_2C_6H_5$; 7.1−7.3 (m) $CH_2C_6H_5$; 2.0 (s) $C_6(CH_3)_6$
5a	1508	8.3 (s)	2.7 and 4.2 (t, *J* 7 Hz) $CH_2CH_2COOCH_2CH_3$; 4.0 (q, *J* 6 Hz) $CH_2CH_2COOCH_2CH_3$; 1.2 (q, *J* 6 Hz) $CH_2CH_2COOCH_2CH_3$; 6.7−8.1 (m) C_6H_4; 5.3 and 5.5 (d, *J* 6 Hz) [$(CH_3)_2CHC_6H_4$ (CH_3)-*p*]; 1.2 (d, *J* 7 Hz) [$(CH_3)_2CHC_6H_4$ (CH_3)-*p*]; 2.1 (s) [$(CH_3)_2CHC_6H_4$ (CH_3)-*p*]; 2.0 (sept. *J* 7) [$(CH_3)_2CHC_6H_4$ (CH_3)-*p*]
5b	1506	8.0 (s)	2.6 and 4.0 (t, *J* 7 Hz) $CH_2CH_2COOCH_2CH_3$; 3.9 (q, *J* 6 Hz) $CH_2CH_2COOCH_2CH_3$; 1.1 (q, *J* 6 Hz) $CH_2CH_2COOCH_2CH_3$; 7.1−7.9 (m) C_6H_4; 1.9 (s) $C_6(CH_3)_6$
6a	1471	8.7(s)	7.4−8.0 (m) C_6H_4; 5.4 and 5.5 (d, *J* 6 Hz) [$(CH_3)_2CHC_6H_4$ (CH_3)-*p*]; 1.2 (d, *J* 7 Hz) [$(CH_3)_2CHC_6H_4$ (CH_3)-*p*]; 2.1 (s) [$(CH_3)_2CHC_6H_4$ (CH_3)-*p*]; 2.9 (sept. *J* 7) [$(CH_3)_2CHC_6H_4$ (CH_3)-*p*]
6b	1502	8.9 (s)	7.2−7.9 (m) C_6H_4; 2.0 (s) $C_6(CH_3)_6$
7a	1413	9.7 (s)	7.5−8.7 (m) C_6H_4; 5.4 and 5.6 (d, *J* 6 Hz) [$(CH_3)_2CHC_6H_4$ (CH_3)-*p*]; 1.2 (d, *J* 7 Hz) [$(CH_3)_2CHC_6H_4$ (CH_3)-*p*]; 2.0 (s) [$(CH_3)_2CHC_6H_4$ (CH_3)-*p*]; 2.8 (sept. *J* 7) [$(CH_3)_2CHC_6H_4$ (CH_3)-*p*]
7b	1413	9.2 (s)	7.4 and 8.4 (m) C_6H_4; 1.9 (s) $C_6(CH_3)_6$

s: singlet, d: doublet, t: triplet, q: quadruplet, qu: quintet, sept: septet, chemical shifts referenced to residual solvent $CDCl_3$.

Table 3. ^{1}C NMR spectroscopic data for compounds **1**−**7**[a]

Compound	*C*2	Others
1a	142.6	109.6, 113.4, 115.4, 122.9, 132.3, 138.8 C_6H_4; 81.1 81.7, 97.6, 102.3 [$(CH_3)_2CHC_6H_4(CH_3)$-*p*]; 22.1 [($CH_3)_2CHC_6H_4$ (CH_3)-*p*]; 19.1 [$(CH_3)_2CHC_6H_4$ (CH_3)-*p*]; 30.3 [$(CH_3)_2C$ HC_6H_4 (CH_3)-*p*]
1b	142.7	110.1, 112.9, 117.4, 122.9, 133.1, 137.4 C_6H_4; 90.7 $C_6(CH_3)_6$; 17.6 $C_6(CH_3)_6$
2a	145.7	32.3 CH_3; 110.9, 120.9, 123.9 124.5 134.8 142.7 C_6H_4; 81.5, 83.3, 98.1, 103.1 [$(CH_3)_2CHC_6H_4(CH_3)$-*p*]; 22.7 [($CH_3)_2CHC_6H_4$ (CH_3)-*p*]; 18.9 [$(CH_3)_2CHC_6H_4$ (CH_3)-*p*]; 31.1 [$(CH_3)_2C$ HC_6H_4 (CH_3)-*p*]
2b	145.6	31.8 CH_3; 110.2, 121.3, 122.9, 123.9, 134.5 C_6H_4; 16.3 $C_6(CH_3)_6$; 90.9 $C_6(CH_3)_6$
3a	144.1	15.2, 41.1 CH_2CH_3; 111.0, 120.5, 123.4, 124.0, 133.5, 142.6 C_6H_4; 81.2, 82.9, 97.7, 102.5 [$(CH_3)_2CHC_6H_4(CH_3)$-*p*]; 22.4 [($CH_3)_2CHC_6H_4$ (CH_3)-*p*]; 18.6 [$(CH_3)_2CHC_6H_4$ (CH_3)-*p*]; 30.7 [$(CH_3)_2C$ $HC_6H_4(CH_3)$-*p*]
3b	144.5	15.3, 40.1 CH_2CH_3; 110.6, 121.2, 122.7, 123.8, 133.5, 141.0 C_6H_4; 15.3 $C_6(CH_3)_6$; 90.8 $C_6(CH_3)_6$,
4a	145.6	47.1 $CH_2CH_2NCH_2CH_3$; 10.9, 51.3 $CH_2CH_2N(CH_2CH_3)_2$; 111.0, 120.5, 123.4, 124.2, 133.4, 142.2 C_6H_4; 81.1, 82.9, 97.6, 102.7 [$(CH_3)_2CHC_6H_4(CH_3)$-*p*]; 22.4 [($CH_3)_2CHC_6H_4$ (CH_3)-*p*]; 18.5 [$(CH_3)_2CHC_6H_4$ (CH_3)-*p*]; 30.7 [$(CH_3)_2C$ $HC_6H_4(CH_3)$-*p*]
4b	145.4	46.9 $CH_2CH_2NCH_2CH_3$; 11.0, 51.1 $CH_2CH_2N(CH_2CH_3)_2$; 109.1, 120.2, 122.9, 124.2, 133.6, 142.6 C_6H_4; 15.6 $C_6(CH_3)_6$; 90.5 $C_6(CH_3)_6$,
5a	145.5	41.1, 60.9 $CH_2CH_2CO_2CH_2CH_3$; 14.1, 33.5 $CH_2CH_2CO_2CH_2CH_3$; 170.6 $CH_2CH_2CO_2CH_2CH_3$; 111.1, 120.4, 123.3, 132.9, 142.1, C_6H_4, 81.1, 82.9, 97.5, 102.5 [$(CH_3)_2CHC_6H_4(CH_3)$-*p*]; 22.3 [($CH_3)_2CHC_6H_4$ (CH_3)-*p*]; 18.4 [$(CH_3)_2CHC_6H_4$ (CH_3)-*p*]; 30.4 [$(CH_3)_2C$ $HC_6H_4(CH_3)$-*p*]
5b	146.1	40.8, 60.9 $CH_2CH_2CO_2CH_2CH_3$; 14.1, 33.5 $CH_2CH_2CO_2CH_2CH_3$; 170.7 $CH_2CH_2CO_2CH_2CH_3$; 111.0, 120.9, 122.6, 124.1, 140.5, C_6H_4; 15.8 $C_6(CH_3)_6$; 90.8 $C_6(CH_3)_6$
6a	156.0	111.9, 121.0, 125.9, 126.9, 150.0 C_6H_4; 81.1, 82.9, 97.9, 103.1 [$(CH_3)_2CHC_6H_4(CH_3)$-*p*]; 22.3 [($CH_3)_2CHC_6H_4$ (CH_3)-*p*]; 18.6 [$(CH_3)_2CHC_6H_4$ (CH_3)-*p*]; 30.8 [$(CH_3)_2C$ $HC_6H_4(CH_3)$-*p*]
6b	156.1	112.0, 121.1, 125.3, 127.2, 149.8 C_6H_4; 15.6 $C_6(CH_3)_6$; 90.5 $C_6(CH_3)_6$
7a	160.4	97.6, 122.9, 125.6, 126.9, 127.5 C_6H_4; 81.9, 83.6, 98.4, 103.3 [$(CH_3)_2CHC_6H_4(CH_3)$-*p*]; 22.7 [($CH_3)_2CHC_6H_4$ (CH_3)-*p*]; 18.8 [$(CH_3)_2CHC_6H_4$ (CH_3)-*p*]; 31.1 [$(CH_3)_2C$ $HC_6H_4(CH_3)$-*p*]
7b	160.6	97.8, 123.0, 125.5, 126.8, 128.1 C_6H_4; 15.6 $C_6(CH_3)_6$; 90.6 $C_6(CH_3)_6$

[a] Chemical shifts referenced to residual solvent $CDCl_3$.

Table 4. Cyclic voltammetric data of ruthenium(II) complexes[a]

Compound	$E_{1/2}$ vs. SCE	E_p, mV
1a	1.29	87
3a	1.29	195
3b	1.03	104
4a	1.38	90
4b	1.05	100
5a	1.28	109
5b	1.04	114
6a	1.42	110
6b	1.17	100
7a	1.18	90

[a] *E* versus SCE, Pt working electrode, 100 mV/s. Recorded in CH_2Cl_2 solution 0.05M *n*-Bu_4NPF_6 as supporting electrolyte.

methylbenzene (**b** type) indicates that the presence of the *p*-cymene ligand gives a much better catalyst precursor. This may be due to the higher lability of the *p*-cymene ligand. The nature of the nitrogen ligand also has a strong influence on the catalytic activity as the ruthenium benzimidazole complexes **3** and **5** are the best catalysts and are much more efficient than the benzoxazole or benzothiazole complexes.

In conclusion, the preparation of ruthenium(II)-benzazole (L) complexes (**1**−**7**) is straightforward from the benzazole ligand and commercially available $[RuCl_2(arene)]_2$. The benzazoles behave as *N*-centered nucleophiles and all the complexes showed moderate to good catalytic activity for the cyclization of (*Z*)-3-methylpent-2-en-4-yn-1-ol into 2,3-dimethyfuran at 80°C, but (*p*-cymene)$RuCl_2$(benzimidole) appeared to give the best catalyst precursors.

Table 5. Catalytic synthesis of 2,3-dimethylfuran at 80°C

Entry	Catalyst	Time (h)	Yield (%)[a,b]
1	**1a**	2	75
2	**1a**	12	96 (82)[b]
3	**1b**	32	65
4	**1b**	40	79 (69)[b]
5	**2a**	8	83 (75)[b]
6	**2b**	40	84 (73)[b]
7	**3a**	1	90
8	**3a**	4	97 (89)[b]
9	**3b**	24	90 (78)[b]
10	**4a**	14	83 (75)[b]
11	**4b**	25	81 (69)[b]
12	**5a**	2.5	93
13	**5a**	12	98 (87)[b]
14	**5b**	30	90 (78)[b]
15	**6a**	32	83 (73)[b]
16	**6b**	20	81 (69)[b]
17	**7a**	36	76 (65)[b]
18	**7b**	13	81 (70)[b]

[a] Determined by gas chromatography. − [b] Isolated yield after distillation.

Experimental Section

General: Unless otherwise stated, manipulations were performed under an oxygen-free nitrogen atmosphere with previously dried solvents and standard Schlenk techniques. The complexes $[RuCl_2(p-MeC_6H_4CHMe_2)]_2$ and $[RuCl_2(C_6Me_6)]_2$ were prepared according to literature methods.[10] 1-Substituted benzimidazoles, used for the synthesis of **2**−**5**, were prepared from the potassium salt of benzimidazole by following the literature procedure.[11] Infrared spectra were recorded as KBr pellets in the range 4000−400 cm^{-1} on a ATI UNICAM systems 2000 Fourier Transform spectrometer. ^{1}H NMR spectra (300.131 MHz) and ^{13}C NMR spectra (75.5 MHz) were recorded on a Bruker AM 300

WB FT spectrometer with δ referenced to residual solvent $CDCl_3$. Microanalyses were performed by the TÜBITAK (Ankara−Turkey) or Service Central D′analyses du Centre National de la Recherche Scientifique (Vernaison-France).

General Procedure for the Preparation of Ruthenium(II) Benzazole Complexes 1−7: A solution of the azole (2.1 mmol) in toluene (20 mL) and $[RuCl_2(p-MeC_6H_4CHMe_2)]_2$ or $[RuCl_2(C_6Me_6)]_2$ (1.0 mmol) were heated for 2 h under reflux. Upon cooling to room temperature, orange crystals of **1−7** were obtained. The crystals were filtered, washed with *n*-hexane (2 × 15 mL) and dried under vacuum. The reported yields are based on $[RuCl_2(\eta^6\text{-arene})]_2$ and relevant physical data are compiled in Tables 1−4.

Catalytic Reaction Conditions: Ruthenium catalyst (0.1 mmol) was added to 10 mmol of neat (*Z*)-3-methylpent-2-en-4-yn-1-ol without a solvent. The mixture was stirred in an oil bath at 80°C for 1−32 hours. The conversion of the starting enynol was determined by gas chromatography and the pure furan was isolated by distillation under reduced pressure.

Acknowledgments

The authors are grateful to TÜBITAK and CNRS for financial support (cooperative program 2504).

[1] A. Togni and C. M. Venanzi, *Angew. Chem.* **1994**, *106*, 517; *Angew. Chem. Int. Ed. Eng.* **1994**, *33*, 497; C. Gemel, G. Trimmel, C. Slugovc, S. Kremel, K. Mereiter, R. Schmid, K. Kirchner, *Organometallics* **1996**, **15**, 3998; C.-P. Lan, L. Cheng, *J. Mol. Catal.* **1993**, *84*, 39; F. Simal, A. Demonceau, A. F. Noels, *Tetrahedron Lett*. **1998**, *39*, 3493; E. Galardon, P. Le Maux, L. Toupet, G. Simonneaux, *Organometallics* **1998**, *17*, 565; S.-B. Park, N. Sakata, H. Nishiyama, *Chem. Eur. J.* **1996**, *2*, 303.
[2] B. Çetinkaya, E. Çetinkaya, P. B. Hitchcock, M. F. Lappert, I. Özdemir, *J. Chem. Soc., Dalton Trans.* **1997**, 1359.
[3] B. Çetinkaya, B. Alici, I. Özdemir, C Bruneau, P. H. Dixneuf, *J. Organomet. Chem.* **1999**, *575*, 187.
[4] R. J. Sundberg, R. F. Bryan, I. F. Taylor, H. Taube, *J. Am. Chem. Soc.* **1974**, *96*, 381.
[5] G. F. Restrepo, C. L. Barnes, M. E. Cadz, E. Olivero, S. D. Huang, *Acta Cryst. C* **1998**, 15.
[6] F. Zamora, S. Luna, P. A. Ochoa, L. A. M.-Cruz, A. Vegas, *J. Organomet. Chem.* **1996**, *522*, 97.
[7] B. Çetinkaya, I. Özdemir, P. H. Dixneuf, *J. Organomet. Chem.* **1997**, *534*, 153.
[8] B. Çetinkaya, I. Özdemir, C. Bruneau, P. H. Dixneuf, *J. Mol. Catal. A* **1997**, *118*, L1; H. Küçükbay, B. Çetinkaya, S. Guesmi, P. H. Dixneuf, *Organometallic,* **1996**, *15*, 2334.
[9] B. Seiller, C. Bruneau, P. H. Dixneuf, *J. Chem. Soc., Chem. Commun.* **1994**, 493; B. Seiller, C. Bruneau, P. H. Dixneuf, *Tetrahedron* **1995**, *51*, 13089.
[10] M. A. Bennett, T. N. Huang, T. W. Matheson, A. K. Smith, *Inorg. Synth.* **1982**, *21*, 74.
[11] A. F. Pozharskii, A. M. Simanov, *Zh. Obsch. Khim.* **1963**, *33*, 179.

Received June 7, 1999
[I99204]

Neopentane-Based Tripodal CpL_2 Ligands: Synthesis and Reactions of $CH_3C(CH_2\text{-}\eta^5\text{-}C_5H_4)(CH_2\text{-}\eta^1\text{-}PPh_2)_2RuCl$; Hindered Rotation of Vinylidene Ligands

Katrin Urtel,[a] Axel Frick,[a] Gottfried Huttner,*[a] Laszlo Zsolnai,[a] Peter Kircher,[a] Peter Rutsch,[a] Elisabeth Kaifer,[a] and Albrecht Jacobi[a]

Dedicated to Prof. Helmut Werner on the occasion of his 65th birthday

Keywords: Tripod ligands / Hindered rotation of vinylidene ligands / $CpML_2$ chelate ligands / Ruthenium / Carbenes / Carbene-type ligands / Cyclic voltammetry

The tripodal ligand $[CH_3C(CH_2C_5H_4)(CH_2PPh_2)_2]^-$ reacts with $RuCl_2(PPh_3)_3$ to produce $CH_3C(CH_2\text{-}\eta^5\text{-}C_5H_4)(CH_2\text{-}\eta^1\text{-}PPh_2)_2RuCl$, [*tripod*$CpL_2RuCl$], **1**. Complex **1** undergoes substitution of the chlorine function with various nucleophiles L′ to produce [*tripod*CpL_2RuL']$^+$. The carbonyl derivative (L′ = CO) **2**, isonitrile (L′ = RNC) **3**, nitrile compounds (L′ = RCN) **4**, and a tolane adduct (L′ = η^2-PhC≡CPh) **5** are obtained when **1** is treated with the appropriate ligands in polar solvents. Halide acceptors (e.g. $TlPF_6$) are generally needed to promote these reactions. The cyanide derivative *tripod*CpL_2RuCN (**3a**) is alkylated by $F_3CSO_3CH_3$ to give the isonitrile derivative [*tripod*$CpL_2RuCNMe$]$^+$ **3b**. Terminal alkynes HC≡CR produce vinylidene compounds [*tripod*CpL_2RuL']$^+$, where L′ = C=CHR (R = *t*Bu, **7b**; R = Ph, **7c**), or allenylidene derivatives, L′ = C=C=CPh_2 (**6**), depending on the nature of R (R = CPh_2OH for synthesis of **6**). Trimethylsilylacetylene gives the parent vinylidene species, L′ = C=CH_2 (**7a**), which is transformed to the Fischer-type carbene compound, L′ = C(OMe)Me (**8**), upon treatment with methanol. The vinylidene species **7** are deprotonated by NaOMe to produce the alkynyl compounds *tripod*$CpL_2RuC{\equiv}CR$ (**9**). Methylation of **9** with $F_3CSO_3CH_3$ results in the vinylidene derivatives L′ = C=C(Me)R (R = *t*Bu, **7d**; R = Ph, **7e**), having two organic substituents at the terminal carbon centre. For all vinylidene compounds with two different substituents at their terminal carbon atom, hindered rotation of the single-faced vinylidene π-ligand about its Ru–C bond is observed. Analysis by ^{31}P-NMR spectroscopic coalescence measurements as well as line-shape analyses reveals activation enthalpies of around 40 kJmol^{-1} for this rotation, with small activation entropies of around ±10 Jmol^{-1}K^{-1}. Solid-state structures of nine compounds of the type [*tripod*CpL_2RuL']$^{+n}$ (n = 0, 1) demonstrate the remarkable conformational rigidity of the *tripod*CpL_2Ru template. They also show that the possible strain imposed by linking the Cp ligand and the two donor groups L in one and the same chelate scaffolding does not appear to impose a serious steric strain on these templates.

Introduction

$CpML_2$ compounds have played an important role in the development of organometallic chemistry as a tool for organic synthesis.[1] The $CpFe(CO)_2$ template and the $CpFeL_2$ species have been extensively studied[2] with regard to their interactions with organic substrates and many organic transformations mediated by this type of template have been reported.[2][3] Many of the organometallic derivatives that are rather unstable with $CpFeL_2$ as the organometallic group, making them non-isolable, are comparatively stable with the $CpRuL_2$ fragment as the organometallic moiety. Accordingly, there is a considerable volume of literature concerning the structure and properties of organic derivatives of the $CpRuL_2$ template.[3][4]

An inherent problem in the stereochemical interpretation of the reactions of such templates is the potential non-rigidity of $CpML_2$ fragments.[3−6] Quite early on in their seminal contributions, Brunner et al.[3][6] demonstrated that in the course of a reaction, CpMLL′ templates (M = Mn, Fe) may undergo inversion of configuration in a process geometrically similar to the inversion of ammonia. This type of behaviour tends to reduce the applicability of such CpMLL′ templates in diastereoselective organic transformations.

It thus appears that $CpML_2$ templates in which this type of configurational instability is prevented through appropriate design of the ligands might be of some use for the further development of this branch of chemistry. An appropriate design would impose a geometrical constraint upon the mutual positions of the Cp and L donors. Such a constraint is inherent in tripodal ligands, where the three donor groups, the Cp residue, and the L donors are bridged by a covalent framework. If the covalent linkers are sufficiently short, inversion of such a $CpML_2$ entity, once formed, becomes geometrically impossible.

As part of a strategy centred on the synthesis of a wide variety of neopentane-based tripod ligands $CH_3C(CH_2X)(CH_2Y)(CH_2Z)$ (X, Y, Z = donor groups), ligands of the

[a] Anorganisch Chemisches Institut der Universität Heidelberg, Im Neuenheimer Feld 270, D-69120 Heidelberg, Germany
Fax: (internat.) +49 (0)6221/545707

 © WILEY-VCH Verlag GmbH, D-69451 Weinheim, 2000 1434−1948/00/0101−0033 $ 17.50+.50/0

type $[CH_3C(CH_2C_5H_4)(CH_2PR_2)(CH_2PR'_2)]^-$ have been prepared.[7] It was shown that this type of ligand is capable of producing $CpML_2$ entities (M = Mn, Mo, Fe, Co) with the Cp residue and the phosphorus donor entities linked via the neopentane framework.[7][8]

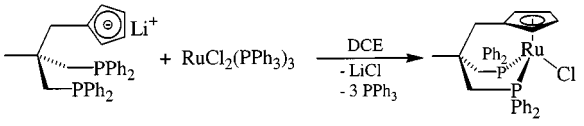
In this paper, we report on the synthesis of a variety of compounds containing the $CH_3C(CH_2C_5H_4)$-$(CH_2PPh_2)_2Ru$ template. Derivatives of this template incorporating nitrile, isonitrile, carbene, vinylidene, and allenylidene moieties, amongst others, are described. Their mutual transformations as well as their structures and redox properties are discussed. The dynamic behaviour of the corresponding vinylidene species is analysed.

Results and Discussion

1. Synthesis of $CH_3C(CH_2$-η^5-$C_5H_4)$-$(CH_2$-η^1-$PPh_2)_2RuCl$ (1)

The ligand $CH_3C(CH_2C_5H_4)(CH_2PPh_2)_2Li$ is accessible from $CH_3C(CH_2OH)_3$ in a few steps.[7] It had previously been observed that its tripodal coordination to metals may necessitate some specialized reaction procedures in order to avoid the formation of coordination polymers as well as of Cp_2M compounds.[7][8] Thus, it was not surprising that reaction of $RuCl_3 \cdot n\,H_2O$ with the ligand in ethanol, which represents a standard protocol for the preparation of $Cp(PPh_3)_2RuCl$,[9] did not work with the tripodal ligand. Either no reaction or decomposition of the ligand was observed under these conditions.

Using $RuCl_2(dmso)_4$ as the starting material[10] was found to lead to the desired *tripod*CpL_2RuCl compound **1**, albeit only in small yields [$CH_3C(CH_2C_5H_4)(CH_2PPh_2)_2Ru$ will henceforth be abbreviated as *tripod*CpL_2Ru]. It was eventually found that $RuCl_2(PPh_3)_3$, prepared from $RuCl_3 \cdot n\,H_2O$ and PPh_3 in methanol,[11] reacts with [*tripod*$CpL_2]^-$ in 1,2-dichloroethane (DCE) at 90°C to produce a fair yield of **1**.



1

Chromatographic separation of **1** from PPh_3 on Al_2O_3, using diethyl ether/CH_2Cl_2 as the mobile phase, gives the desired product in yields of up to 60%. The identity of **1**, already apparent from its analytical and spectroscopic data (Table 8), was further corroborated by its X-ray analysis (Figure 1; Tables 4, 5, and 7).

The primary reason for analyzing the structure of **1** was, however, to gain insight into the steric encumbrance imposed on the $CpML_2$ entity by the fixed tripodal arrangement of its ligand constituents.

Figure 2b shows a spacefilling model of **1**, which indicates that the chlorine function is well protected by the constituents of the ligand. For comparison, the spacefilling model of $Cp[PPh_2CH(CH_3)CH_2PPh_2]RuCl$[12] is shown in Figure 2a. It is evident that in this compound, where there is no covalent link between the Cp group and the diphosphane ligand, the PPh_2 groups adopt a different orientation that makes the chlorine function more accessible. It therefore seems likely that associatively initiated reactions should be problematic with **1**, while dissociative initiation, i.e. removal of the chlorine in a first step, might well be favorable. In this respect, it is interesting to compare **1** with $Cp(PPh_3)_2RuCl$[13] (Figure 2c). The potentially reactive chlorine position appears to be even less accessible in the latter PPh_3 derivative as compared to **1** (Figure 2b). Nevertheless, $Cp(PPh_3)_2RuCl$ has in fact been found to be quite reactive with respect to chlorine substitution. A reaction of $Cp(PPh_3)_2RuCl$ initiated by an associative process is difficult to imagine (Figure 2c). Dissociative activation of this compound might, however, follow from PPh_3 as well as from Cl^- dissociation, which may account for its reactivity.[13] Dissociative activation of **1** by cleavage of one of the M−P bonds should be largely disfavoured by the chelate nature of the ligand. It thus appears that the only low energy pathway leading to chlorine substitution in **1** should

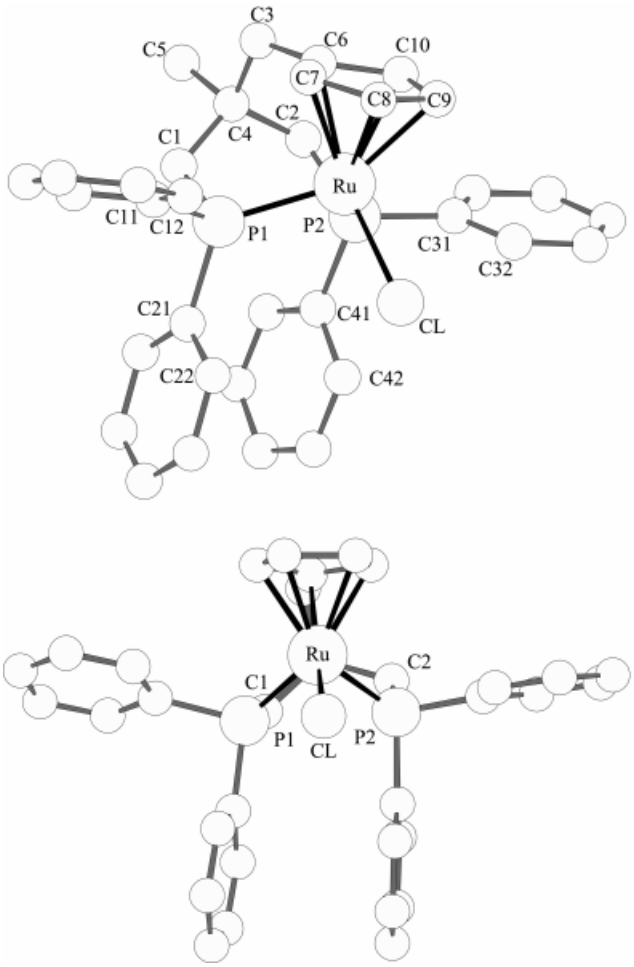


Figure 1. The structure of **1** in two different projections: top − general view; bottom − view along the Ru−C4 axis (the labelling scheme adopted for atoms of the tripodal ligand, as shown here for **1**, is consistently used for all structures reported in this paper)

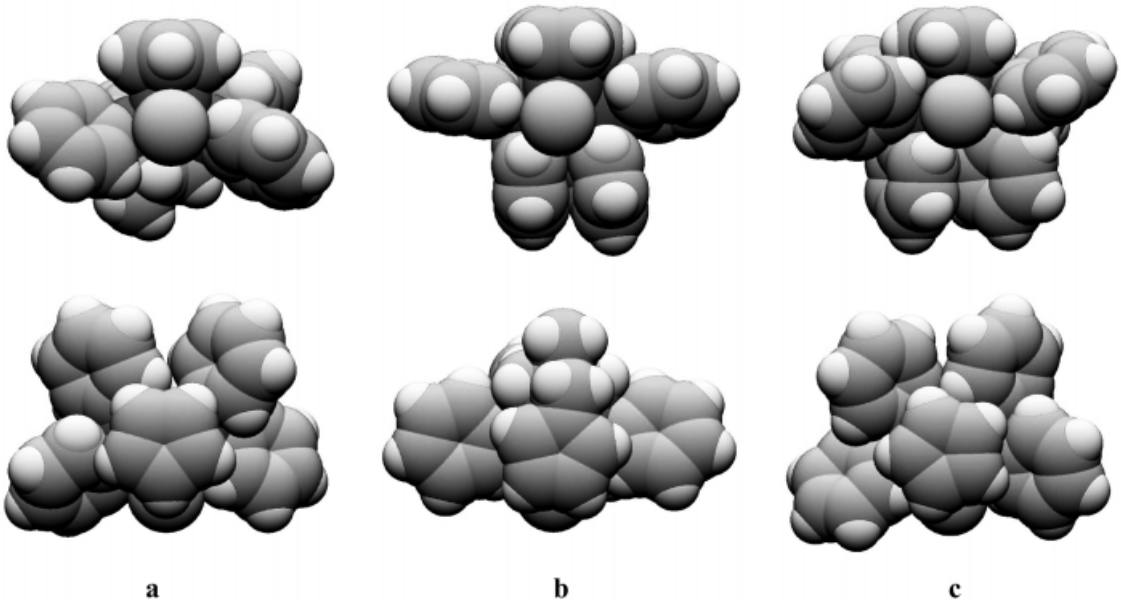
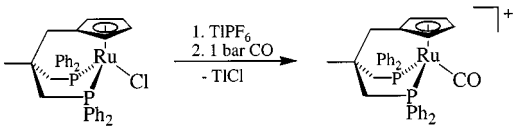


Figure 2. Spacefilling models of CpL_2Ru compounds as seen along the Cl−Ru axis (top) and in a projection onto the Cp planes (bottom); a: $Cp[PPh_2CH(CH_3)CH_2PPh_2]RuCl$; b: **1**; c: $Cp(PPh_3)_2RuCl$

be that involving heterolytic cleavage of the Ru−Cl bond. Bearing this in mind, the optimum conditions for substituting the chlorine function in **1** should be realized by using polar solvents and by carrying out the reactions in the presence of halide acceptors. In this way, a series of transformations of **1** has been achieved.

2. Substitution Reactions of 1

The cationic carbon monoxide derivative **2** is obtained when a solution of **1** in CH_2Cl_2 is treated with $TlPF_6$ under CO at 1 bar.



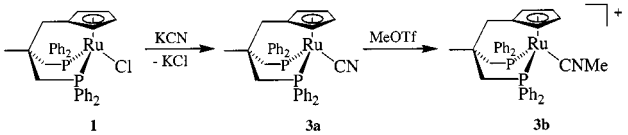
1 **2**

Analytically pure $\mathbf{2} \cdot PF_6$ can subsequently be isolated as a yellow microcrystalline powder (Table 8). Its $\tilde{\nu}_{CO}$ absorption is observed at 1966 cm^{-1}, in the region characteristic for $[CpL_2RuCO]^+$ compounds.[14] The pattern of NMR signals observed for the coordinated *tripod*CpL_2 ligand (Table 8) unequivocally proves its identity. The ^{31}P-NMR resonance is observed at $\delta = 45.3$. ^{13}C-NMR resonances are observed for all the individual carbon atoms of the ligand as well as for the coordinated CO group (Table 8).

Due to the rigid chelate framework, there are two distinct types of phenyl groups. Figure 2b (top) clearly shows these two classes: with respect to an idealized C_s symmetry (vertical mirror plane in Figure 2b), two phenyl groups, one at each of the two phosphorus nuclei, lie closely parallel to this plane. The remaining two phenyl groups are closely parallel to one another and lie in a "horizontal" plane at right angles to the idealized mirror plane. The *ipso* carbons of these two classes of phenyl residues give rise to two distinct NMR signals, which appear as pseudo triplets due to ^{31}P coupling. The carbon atoms in the *para* position show no apparent ^{31}P coupling. The pattern due to the carbon atoms of the coordinated cyclopentadienyl system is clearly resolved (Table 8).

In the ^1H-NMR spectrum, the Cp protons show the expected AA′XX′ pattern. The methylene protons of the CH_2 groups bonded to phosphorus give rise to two distinct doublets in the $^1H\{^{31}P\}$-NMR spectrum, while the CH_2 group linked to the Cp entity is seen as a broad singlet (Table 8). These NMR spectroscopic observations are in agreement with analogous findings reported for other compounds containing the same type of *tripod*CpL_2 ligand.[7][8] The same general features of the NMR spectra of **2**, as discussed above, also hold true for the other ruthenium derivatives of the same ligand described in this paper. The relevant data are collected in Tables 8−13 (Experimental Section); in the following paragraphs the discussion will be limited to references to these tables, except for compounds **7a−e**, where dynamic processes are observed.

1 reacts with KCN in methanol to produce **3a**, which is obtained as a yellow microcrystalline powder in analytically pure form after chromatographic workup.



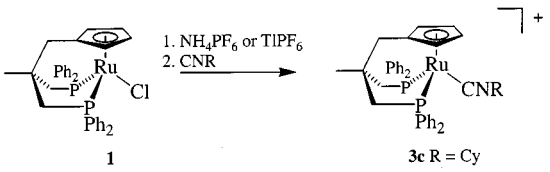
1 **3a** **3b**

The identity of **3a** was confirmed by its spectroscopic data (Table 8) as well as by an X-ray analysis (Figure 3; there are two crystallographically independent species **3a** in

the crystal, only one of which is depicted in Figure 3; Tables 4, 5, and 7).

As a derivative of **3a**, the isonitrile compound **3b** was obtained by treating **3a** in CH_2Cl_2 with $F_3CSO_3CH_3$. The triflate salt of **3b**, obtained as a pale-yellow powder, has been fully characterized (Table 9) by its spectroscopic and analytical data.

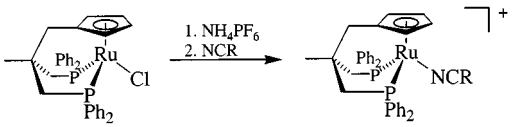
When methanolic solutions of **1** are treated with isonitriles, substitution does not take place spontaneously. Only when $TlPF_6$ is added to these solutions is complete substitution observed.



1 **3c** R = Cy

Instead of $TlPF_6$, NH_4PF_6 may also be used as an activator. The PF_6 salt of **3c** is obtained as a pale-yellow powder in analytically pure form, with all the spectroscopic data being consistent with the given constitution (Table 9). As is often found for isonitrile derivatives, the ^{13}C-NMR signal of the isonitrile carbon cannot be detected[15] while the signals of all the other carbon atoms are clearly evident (Table 9).

The chlorine function in **1** may also be replaced by nitriles.



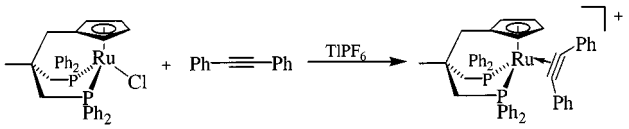
1 **4a** R = Me **4b** R = Ph

A methanolic solution of **1** reacts smoothly with acetonitrile in the presence of NH_4PF_6 to produce the PF_6 salt of **4a**. The benzonitrile derivative **4b** is accessible by the same type of procedure. Compounds **4** are obtained as yellow microcrystalline salts and have been fully characterized by their spectroscopic and analytical data (Tables 9 and 10). X-ray analysis of **4b** · PF_6 leaves no doubt as to its constitution (Figure 3; Tables 4, 5, and 7).

The substitution reactions of **1** leading to **2**–**4** are analogous to corresponding reactions in the chemistry of conventional CpL_2Ru compounds, i.e. compounds where the Cp ligand is not covalently linked to the donor groups L.[14–16] It appears that chlorine substitution in **1** is not drastically impeded by the reduced flexibility of the cage-type *tripod*CpL_2Ru template. This is an important observation with regard to the analysis of the reactivity of **1** towards alkynes, since all of the many transformations known for the system CpL_2Ru/alkyne necessarily start with a substitution reaction.

3. Transformation of Alkynes by the *tripod*CpL_2Ru Template

Solutions of **1** in CH_2Cl_2 react with 1,2-diphenylacetylene when the reaction mixture is activated with $TlPF_6$. Substitution of the chlorine function of **1** by the alkyne function is a slow process requiring many hours at 25°C to reach completion.



1 **5**

The PF_6 salt of **5** is obtained as an orange-yellow powder. Crystals may be obtained by slow diffusion of diethyl ether into DCE solutions of **5** · PF_6. The constitution of the compound has been verified by HR-FAB analysis (see Experimental Section, Table 14) and NMR spectroscopy (Table 10), and furthermore by an X-ray structure determination (Figure 3, Tables 4, 5, and 7). Despite the fact that the determined structure is not very accurate, due to the rather poor quality of the crystals obtained, the constitution of **5**·PF_6 is clear beyond doubt (Figure 3). The rotational orientation of the alkyne entity relative to the *tripod*CpL_2Ru template is close to orthogonal to the idealized mirror plane (Figure 3) and thus corresponds to the geometry anticipated by MO reasoning.[17] The length of the coordinated C–C triple bond (127.2 pm) as well as the bond angles C(alkyne)–C(alkyne)–C_i(phenyl) (148.1°, 147.8°) fall within the ranges normally observed for η^2-bonded alkynes.[18] It appears that the phenyl substituents at the alkyne ligand and the horizontal pair of phenyl substituents at the phosphorus centres are subject to some interference, which is manifested in a torsional position of the latter phenyl groups significantly different from the average (Figure 3; Tables 4 and 5).

Whenever terminal alkynes are reacted with a CpL_2Ru precursor, rearrangements tend to occur.[19] Although it has always been thought highly probable that the first step in such reactions is again η^2-coordination of the alkyne,[20] this has only recently been proved to be the case.[19–21] Mechanistic alternatives based on oxidative addition with C–H bond cleavage as the first step have also been proposed[20,22,23] and have in fact been verified with templates other than $CpRuL_2$.[23][24] For $CpRuL_2$, theoretical reasoning[20] tends to disfavour this latter hypothesis[20–24] and the observation that η^2-coordination does in fact occur gives additional credit to the suggestion that the transformation undergone by alkynes HC≡CR at $CpRuL_2$ templates involves η^2-coordination of the alkyne as the first step.

Since the characterization of **5** shows that the *tripod*CpL_2Ru template is capable of η^2-bonding of alkynes, alkynes HC≡CR can be expected to undergo transformations similar to those that have been observed with traditional $CpRuL_2$ entities.[19]

One of the standard transformations mediated by $CpRuL_2$ templates is the generation of allenylidene ligands

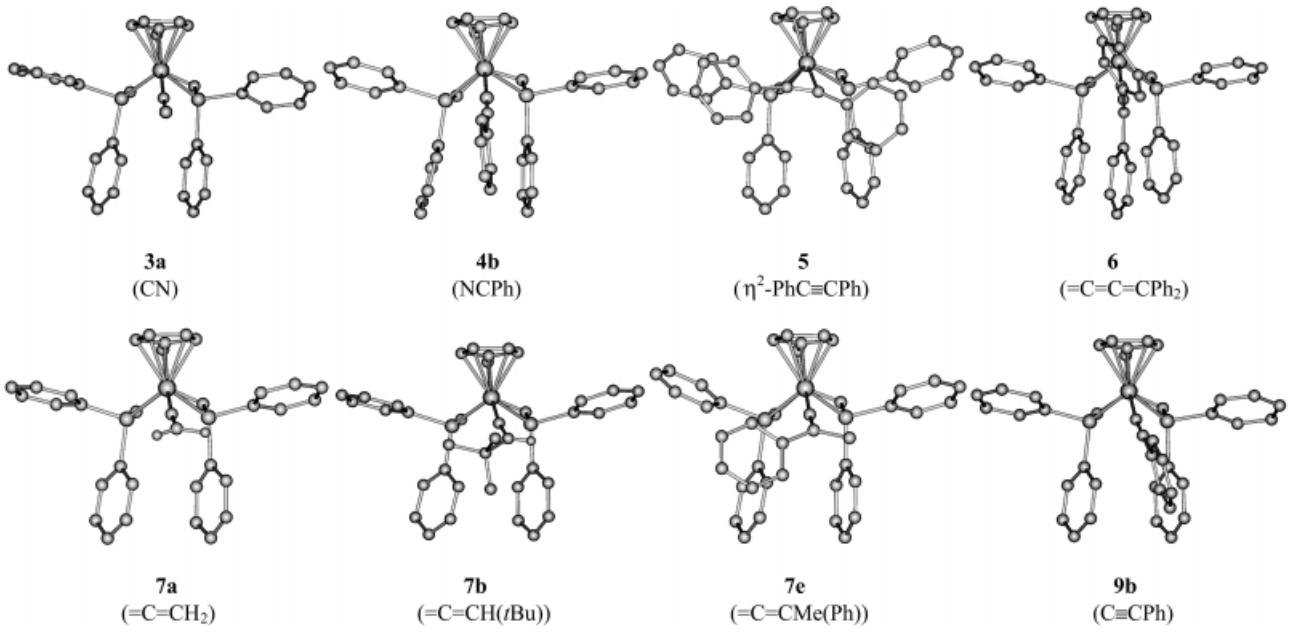
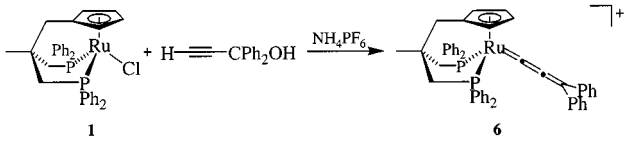


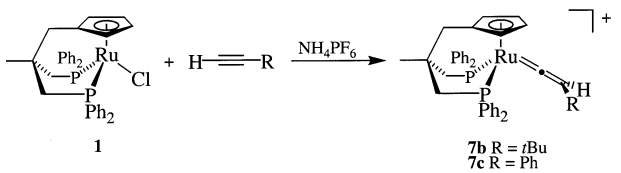
Figure 3. X-ray structures of compounds **3−9**; view along the Ru−C4 axis; coligands are shown in brackets

from $HC{\equiv}C{-}CR_2OH$.[25] This type of transformation is found to proceed equally well with *tripod*CpL_2Ru as the template. An orange suspension of **1** in methanol containing NH_4PF_6 reacts with $HC{\equiv}C{-}CPh_2OH$ to produce a purple solution of **6**, the PF_6 salt of which can be isolated as a microcrystalline purple solid.



A correct elemental analysis and the spectroscopic signature of **6** (Table 10) leave no doubt as to its identity. An X-ray analysis of the PF_6 salt of **6** (Figure 3, Tables 4, 5, and 7) reveals an almost linear arrangement of the $Ru{-}C_3$ chain of the allenylidene fragment (Table 5). The coordination plane of the terminal sp^2 carbons of the ligand is almost coincident with the idealized mirror plane of the coordination polyhedron (Figure 3). The rotational position of the phenyl groups at the terminal carbon of the allenylidene ligand also tends to be close to this orientation (Figure 3).

Terminal alkynes lacking the reactive group at the γ-carbon that leads to the allenylidene ligand in **6**, produce vinylidene species **7b/c** when reacted with **1** under appropriate activation.



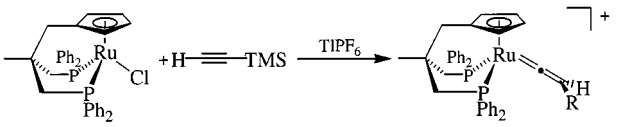
Products **7b/c** can be isolated as their PF_6 salts. Orange-brown **7b** · PF_6 and red-brown **7c** · PF_6 have been fully characterized by their analytical and spectroscopic data (Table 11). X-ray analysis of **7b**·PF_6 [Tables 4, 6, and 7; Figure 3 (there are two crystallographically independent species **7b** in the crystal, only one of which is shown in Figure 3)] shows that the orientation of the vinylidene ligand with respect to the $CpML_2$ template is such that the coordination plane about the β-carbon of the vinylidene group is "horizontal". This type of orientation is in line with expectation, considering the different π-bonding capabilities of the d-type orbitals of the $CpML_2$ unit.[17][26] The differentiation between these two π-bonding metal orbitals − that in the idealized mirror plane leading to a weaker π-interaction and the other, vertical to it, having better π-bonding capabilities − is generally not sufficient to lead to just one rigid conformation. Nevertheless, the preferred orientation, as predicted by theory,[17,19,26] is generally found to be adopted in solid-state structures. This also holds true for all the structurally characterized vinylidene compounds described in this paper. It is also the case for the allenylidene species **6** where, due to one additional carbon atom in the unsaturated chain, the sp^2 plane of the terminal carbon atom should lie within the idealized mirror plane of the template, as is indeed found (Figure 3, **6**).[17][26]

The barrier to ligand rotation imposed by this type of π-bonding has been estimated to be around 10−20 $kJmol^{-1}$ by theory,[17][26] while experimentally determined values have amounted to 29−42 $kJmol^{-1}$ for CpL_2Fe compounds[27] and to around 40 $kJmol^{-1}$ for $CpRuL_2$ compounds.[19][28] It would appear that the conformational rigidity of the *tripod*CpL_2Ru framework and the use of ^{31}P-NMR spectroscopy as the means of monitoring may allow

experimental estimation of this barrier for compounds **7**. On cooling, CD_2Cl_2 solutions of **7c** are found to show a broadening of the ^{31}P-NMR signal at $\delta = 51.4$ (178 K), such that at 170 K a splitting of this single resonance into two components ($\delta = 51.5, 51.6$) is observed (Table 1). Solubility problems prohibit analysis at lower temperatures in this case.

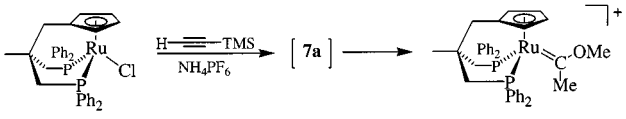
One sharp ^{31}P-NMR signal ($\delta \approx 51.5$) is observed for **7b** at temperatures above 178 K. Some broadening of the signal is apparent around 178 K ($\delta = 51.5$). At 159 K, two doublets are observed ($\delta = 51.4$ and 52.3; $^2J_{AB} = 45$ Hz). Coalescence occurs at 170 K ($\delta = 51.8$).

The above observations indicate that a dynamic process is operative, rendering the two phosphorus nuclei non-equivalent at low temperature while, in a dynamic sense, they are equivalent at higher temperatures. In order to further elucidate the nature of this dynamic process, the parent vinylidene compound **7a** was synthesized by reacting a suspension of **1** in CH_2Cl_2 containing $TlPF_6$ with $HC{\equiv}CSiMe_3$ to give **7a** · PF_6.



1 **7a** R = H

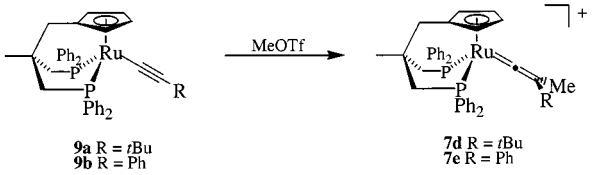
7a · PF_6 was isolated as a yellow microcrystalline solid and has been characterized by all the standard analytical tools (Table 11), including by an X-ray structural analysis (Figure 3; Tables 4, 6, and 7). An analogous reaction of **1** in methanol in the presence of NH_4PF_6, although initially producing **7a** (NMR control), ultimately led to the formation of the carbene compound **8**.



1 **8**

The transformation of vinylidene ligands into carbene ligands is not without precedence,[29] although it has been reported that in some cases the transformation is sufficiently slow to allow the isolation of the intermediate vinylidene species, even in the presence of methanol.[29b] The yellow-brown salt **8** · PF_6 has been fully characterized by a complete set of standard analytical data (Table 12).

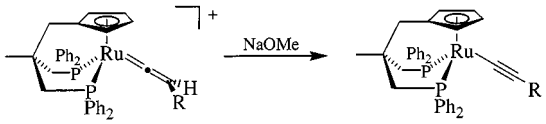
In relation to the dynamic behaviour observed for **7b/c**, the ^{31}P-NMR spectroscopic behaviour of **7a** is of interest. If the appearance of two ^{31}P-NMR signals for **7b/c** at low temperatures were to stem from a differentiation of the surroundings of the two phosphorus nuclei by a helical twist of the chelate scaffolding − which would be dynamic at high temperatures and frozen out at low temperatures − this splitting should also be observed for **7a** (assuming that the activation barrier for the twist of the cage is largely independent of the nature of the substituents at the terminal carbon of the vinylidene ligand). It is found, however, that down to 170 K, which represents the lowest accessible temperature, the ^{31}P-NMR resonance of **7a** remains as a sharp singlet. Freezing out of the twist of the cage can therefore be ruled out as the basis of the dynamic phenomena observed for **7b/c**. Due to the symmetry of the ligand, analysis of **7a** cannot of course provide data that might allow to answer the question as to whether it is the rotation of the vinylidene ligand about its ligand−metal bond that forms the basis of the phenomena observed for **7b/c**. This question might be addressed if it were possible to slow down this rotation to such an extent that the phenomena might be observed at higher temperatures, thereby circumventing the aforementioned solubility problems. Substitution of the terminal carbon of the vinylidene unit by two different organic groups can be expected to effectively serve this purpose. With this in mind, procedures allowing the synthesis of **7d/e** were developed, which were ultimately obtained from the alkynyl species as shown.



9a R = *t*Bu
9b R = Ph

7d R = *t*Bu
7e R = Ph

The alkynyl species **9a/b** are themselves available by deprotonation of the corresponding vinylidene compounds **7b/c**.



7b R = *t*Bu
7c R = Ph

9a R = *t*Bu
9b R = Ph

Compounds **9** are obtained as lemon-yellow materials of a somewhat waxy consistency. Their analytical data correspond to the depicted formulae and their spectroscopic data are in full agreement with the assigned constitutions (Table 13). X-ray analysis of **9b** gave independent confirmation of its identity (Figure 3; Tables 4, 6, and 7).

4. Model Compounds for the Analysis of Vinylidene Rotation

The alkynyl derivatives **9** are found to react smoothly with $F_3CSO_3CH_3$ as an alkylating agent in a type of reaction well-established in CpL_2Ru chemistry.[30] The triflate salts of **7d/e** are obtained as microcrystalline solids (**7d** orange-red, **7e** brick-red). Their analytical and spectroscopic data (Table 12), as well as an X-ray analysis of **7e** (Figure 3; Tables 4, 6, and 7) leave no doubt as to their constitutions. The orientation of the coordination plane of the terminal carbon of the vinylidene group is again as in **7b** (and **7a**, see above), such that this plane is vertical to the idealized mirror plane of the *tripod*CpL_2Ru template (Figure 3).

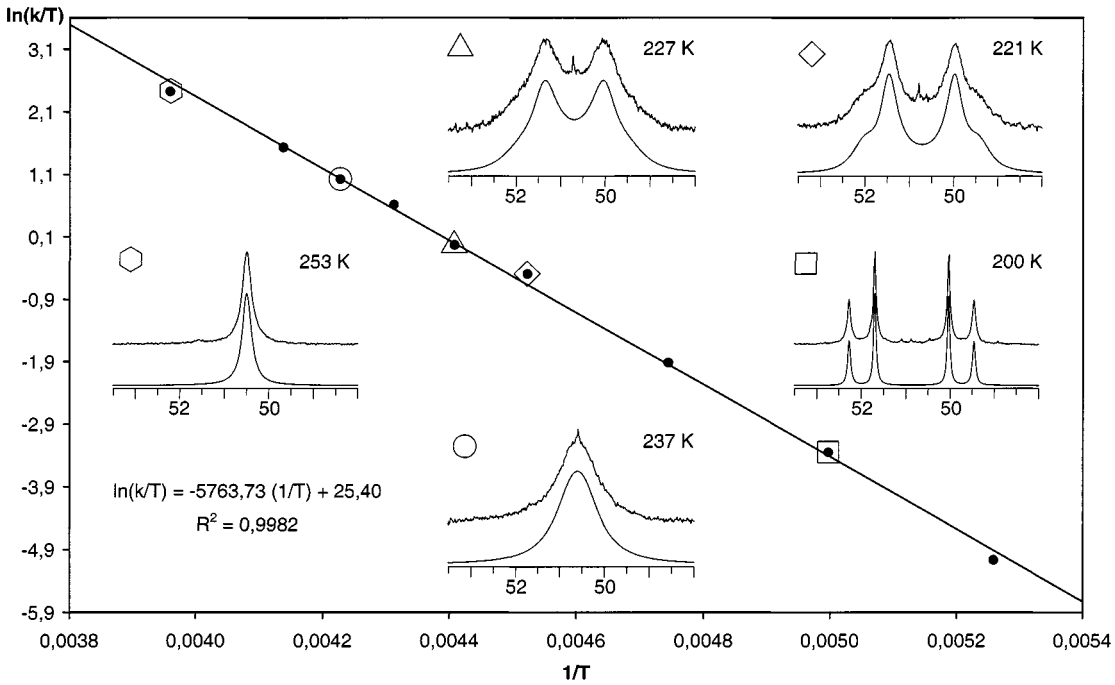


Figure 4. Eyring plot and examples of experimental (top) and simulated spectra (bottom) for compound **7e**

The ^{31}P-NMR spectrum of the triflate salt of **7e** shows one sharp signal at $\delta = 50.5$ at temperatures down to 253 K. At 242 K, significant broadening is observed, with two individual signals evolving at 227 K and a sharp pair of doublets being evident at 211 K. From the coalescence temperature of 232 K, $\Delta G^{\ddagger}_{232}$ may be estimated to be 44.5 kJmol^{-1}, corresponding to a rate constant of $k_{232} = 452$ s^{-1} (Table 1). Line shape analysis[31] of the complete set of spectra obtained at the specific temperatures given in Table 2 neatly reproduces the observed patterns (Figure 4).

The corresponding Eyring plot shows no significant deviation from linearity over the whole range of temperatures from 253 K to 190 K (Table 2; Figure 4). From this, the activation enthalpy $\Delta H^{\ddagger}$ can be estimated to be 47.9 kJmol^{-1}; $\Delta S^{\ddagger}$ is found to be 13.6 Jmol^{-1}K^{-1} (Table 2; Figure 4).

Table 1. Rotational barriers estimated from coalescence temperatures

	T [K]	P_A [ppm]	P_B [ppm]	J_{AB}[Hz]	Tc [K][a]	ΔG_{Tc} [kJ mol^{-1}]
7b	178	51.5			170	32.7[b]
	159	51.4	52.3	45		
7c	178	51.4			175	34.0[b]
	170	51.5	51.6	n.d.		
7d	253	50.3			227	43.1[b]
	200	49.8	52.0	48.6		
7e	253	50.5			232	44.5[b]
	211	49.8	52.0	48.6		

[a] Tc = coalescence temperature. – [b] $k_{Tc} = 303$ s^{-1} for **7b**; 254 s^{-1} for **7c**; 566 s^{-1} for **7d**; 452 s^{-1} for **7e**.

The same type of experiments were performed with **7d** (see data in Table 2). The fit obtained by line shape analysis[31] was equally good and the corresponding Eyring plot was again linear over the whole temperature range [$\ln(k/T) = -4849.09(1/T) + 22.3$; $R^2 = 0.9935$]. The thermodynamic data estimated from line shape analysis are given in Table 2, along with the estimates from the coalescence temperature (227 K) of k_{227} (566 s^{-1}) and $\Delta G^{\ddagger}_{227}$ (43.1 kJmol^{-1}) (see Table 1). For **7d** and **7e**, the respective $\Delta H^{\ddagger}$ values are found to be 40.3 kJmol^{-1} and 47.9 kJmol^{-1} (Table 2).

Table 2. Calculated rotational barriers and thermodynamic parameters from line shape analyses

T [K]	**7d** k [s^{-1}]	**7e** K [s^{-1}]
253	5300	2850
242	2650	1120
237	–	660
232	1025	430
227	–	220
221	340	135
211	95	31
200	24	7
190	5.5	1.2
178	2	–
Thermodynamic data	$\Delta H^{\ddagger} = 40.3$ kJ mol^{-1}	$\Delta H^{\ddagger} = 47.9$ kJ mol^{-1}
	$\Delta S^{\ddagger} = -12.12$ J mol^{-1}K^{-1}	$\Delta S^{\ddagger} = 13.60$ J mol^{-1}K^{-1}
	$\Delta G_{298}{}^{\ddagger} = 43.9$ kJ mol^{-1}	$\Delta G_{298}{}^{\ddagger} = 43.9$ kJ mol^{-1}

The activation entropies are small for both compounds (Table 2). Since a conservative estimate of the standard deviation of $\Delta S^{\ddagger}$ is around 7 Jmol^{-1}K^{-1}, the $\Delta S^{\ddagger}$ values (**7d**: $\Delta S^{\ddagger} = -12$ Jmol^{-1}K^{-1}; **7e**; $\Delta S^{\ddagger} = +14$ Jmol^{-1}K^{-1}) do not warrant a detailed discussion. However, the small magnitude of these values indicates that the steric crowding and

strain within the molecule are not subject to any great changes along the reaction coordinate.

7b/c can be thought of as analogues of **7d/e** having a hydrogen substituent at the terminal position where **7d/e** bear a methyl group. As mentioned above, the low temperature limit of the rotational exchange process cannot be reached experimentally with **7b/c**. Line shape analysis is therefore not possible for these compounds due to the fact that the shifts and coupling constants of the $P_{A/B}$ system are not experimentally accessible. From the coalescence temperatures, the parameters given in Table 1 can be deduced; the $\Delta G^{\neq}$ values at these temperatures are about 10 kJmol^{-1} smaller than the values estimated for **7d/e** at their coalescence temperatures (Table 1). Of course, this cannot be solely attributed to the steric relief caused by substituting a methyl group for a hydrogen since electronic factors are also likely to come into play.

Barriers to rotation of around 10−20 kJmol^{-1} for processes of the type analysed have been predicted by theoretical methods.[17][26] The experimental data for $CpL_2Fe{=}C{=}CRR'$ indicate barriers of 29−42 kJmol^{-1} and corresponding experiments on $CpL_2Ru{=}C{=}CRR'$ lead to activation barriers of around 40 kJmol^{-1}.[27][28] The activation barriers for the *tripod*CpL_2Ru−vinylidene compounds **7** (Tables 1 and 2) are thus in favorable agreement with the theoretical predictions as well as with data obtained for similar compounds.

5. Cyclic Voltammetry

The broad variation of the coligands in compounds **1**−**9** allows for some kind of systematic comparison of their electrochemical behaviour (Table 3).

The first four entries in Table 3 correspond to neutral species. Oxidation is reversible for the first three compounds (**1**, **9a**, **9b**) and occurs in the range 20−200 mV (SCE). The oxidation process can be attributed to the Ru^{II}/Ru^{III} redox couple, since, at least for **1** with the simple chlorine ligand, there is no other plausible explanation. Since the reversible oxidation of the two alkynyl compounds (**9a/b**) occurs in the same range as found for the chloro derivative **1**, the electrochemical process responsible for this oxidation wave should still be the reversible Ru^{II}/Ru^{III} oxidation. The organic substituents are only of secondary influence and are clearly not oxidized themselves in the potential range below 200 mV. At higher potentials, around 1100 mV, a second irreversible oxidation of compounds **9** is observed (Table 3), the probable nature of which will be discussed alongside the discussion of the redox behaviour of compounds **7** and **8** (see below).

With CN as the ligand, as in **3a**, the first oxidation is irreversible. Although comparison of this irreversible process at $E_P^A = 660$ mV with the reversible processes at $E_{1/2} \leq 220$ mV observed for **1**, **9a/b** is not strictly valid in a thermodynamic sense, the CN group would be expected to shift the oxidation potential to higher values, as is observed. The first irreversible oxidation of **3a** leads to a product that is − again irreversibly − reduced at $E_P^C = -190$ mV. The nature of this product is not known. At $E_{1/2} = 1164$ mV, a second oxidation of **3a** is observed, which is reversible. The nature of the product responsible for this signal is again unknown. It is highly improbable that this feature corresponds to the formal +IV oxidation state of ruthenium. On the other hand, the observed $E_{1/2}$ is close to that observed for the oxidation of the cationic isonitrile species **3b/c**, and hence some similar structure − possibly a coordinated CNH ligand − cannot be ruled out.

The next group of compounds comprises the cationic species **2**, **3b/c**, **4**, **5**, which, in contrast to the members of the final group, do not have carbene, vinylidene, or allenylidene ligands. The carbon monoxide derivative **2** is difficult

Table 3. Electrochemical data for compounds **1** to **9**[a]

compound	ligand	potential	$E_{1/2\ (Fc)}$	ΔE_{Fc}
1	Cl	$E_{1/2} = 220$; $\Delta E = 100$	434	132
9a	C≡C*t*Bu	$E_{1/2} = 20$; $\Delta E = 100$ $E_P^A = 1100$	436	139
9b	C≡CPh	$E_{1/2} = 132$; $\Delta E = 105$ $E_P^A = 1070$	433	143
3a	CN	$E_P^A = 660$; $E_P^C = -190$ $E_{1/2} = 1164$, $\Delta E = 97$	456	126
2	CO	$E_P^A = 1700$ $E_P^C = -2000$	393	75
3b [b]	CNMe	$E_{1/2} = 1240$; $\Delta E = 150$	438	135
3c	CNCy	$E_{1/2} = 1264$; $\Delta E = 172$	435	120
4a	NCMe	$E_{1/2} = 922$; $\Delta E = 114$ $E_P^A = 1600$	414	133
4b	NCPh	$E_{1/2} = 967$; $\Delta E = 105$	431	129
5	η^2-PhC≡CPh	$E_{1/2} = 986$; $\Delta E = 105$	413	135
6	C=C=CPh$_2$	$E_{1/2} = 1203$; $\Delta E = 119$ $E_{1/2} = -730$; $\Delta E = 106$	434	108
7a	C=CH$_2$	$E_P^A = 1410$ $E_P^C = -1765$	421	138
7b	C=CH(*t*Bu)	$E_P^A = 1330$ $E_P^C = -1920$	403	125
7c	C=CH(Ph)	$E_P^A = 1215$ $E_P^C = -1690$	418	119
7d	C=CMe(*t*Bu)	$E_{1/2} = 1187$; $\Delta E = 123$ $E_P^A = 1740$	416	142
7e	C=CMe(Ph)	$E_{1/2} = 1133$; $\Delta E = 116$ $E_P^C = -1880$	412	128
8	COMe(Me)	$E_{1/2} = 1066$; $\Delta E = 103$	442	127

[a] All potentials are given in mV vs. SCE. The data refer to a scan rate of 200 mV/s. To check the reversibility, scan rates of 50, 100, 200, 400, 600, and 800 mV/s were also applied. The square-root relationship between peak height and scan rate expected for reversible processes was observed in each case. For ease of comparison, the compounds are sorted into blocks, the order of which does not necessarily correspond to the sequence of numbers used for designating the compounds. With the exception of compound **2**, which was analyzed in CH_3CN solution, all measurements were performed in CH_2Cl_2 solution. In each case, the first line of data refers to an oxidative process. The second line, where relating to irreversible processes, refers to the anodic potential of a second oxidation wave at higher potentials. If the potential is less positive (**3a**, **2**, **7a**−**7c**) than that required for the oxidation (first line), the second line refers to the cathodic potentials of the reduction waves corresponding to the products generated by the oxidation (ECE). Only for compound **6** are both oxidation and reduction found to be reversible. For reversible processes, the separation $\Delta E = E_P^A - E_P^C$ is given, together with the ΔE_{Fc} observed in the same experiment for the electrochemically reversible ferrocene redox couple at around 430 mV. − [b] Quasi-reversible oxidation.

to oxidize and reduce. Both processes are irreversible. The isonitrile analogues **3b/c** are reversibly or quasi-reversibly oxidized at around 1250 mV. With nitriles as coligands, as in **4a/b**, reversible oxidation at somewhat lower potentials is observed.

The 1,2-diphenylacetylene derivative **5** shows a reversible oxidation at 986 mV, in the same region as observed for the oxidation of the nitrile derivatives (**4a/b**). It can be seen that oxidation of these cationic compounds occurs at markedly higher potentials than found for the neutral species of the first group. This is well in accord with expectation, since abstracting an electron from a cation clearly requires more energy than ionizing a neutral species. The relatively narrow range of oxidation potentials observed for the compounds of this group (Table 3) again points to an Ru^{II}/Ru^{III} redox process similar in nature to that inferred for compounds of the first group.

The cationic compounds **6**–**8**, containing carbene ligands, form a class of their own. Of the vinylidene species **7**, compounds **7a**–**c** show irreversible oxidations around 1200–1400 mV, while the oxidations of **7d/e** are reversible and occur at $E_{1/2}$ = 1187 mV and $E_{1/2}$ = 1133 mV, respectively. Since **7a**–**c** have at least one hydrogen atom bonded to the terminal sp^2 carbon, while in **7d/e** these positions are both blocked by organic groups, it is reasonable to assume that the presence of a hydrogen in the β-position of the coligands is responsible for the irreversibility of the oxidation process observed for **7a**–**c**. In other words, deprotonation of the oxidized species may be at the basis of the observation that first oxidations of **7d/e** are reversible while those of **7a**–**c** are not. As an indication of the plausibility of this argument, the narrow range of potentials over which the oxidations of **7a**–**e** are observed (ca. 1100 to 1400 mV) may be invoked. If the primary oxidation products of the compounds **7b/c**, $[tripodCpL_2RuC{\equiv}C(H)tBu]^{2+}$ ($\mathbf{7b}^+$) and $[tripodCpL_2RuC{\equiv}C(H)Ph]^{2+}$ ($\mathbf{7c}^+$), were to undergo deprotonation, they would be transformed into $\mathbf{9a}^+$ and $\mathbf{9b}^+$, respectively. However, these compounds are known to be irreversibly oxidized at potentials around 1100 mV (Table 3), which are lower than those needed for the oxidation of **7b** and **7c**. If a process as described for **7b/c** occurs, the signals of the redox process **9a**/$\mathbf{9a}^+$ would not be expected to be observed in the voltammogram of **7b**/$\mathbf{7b}^+$ (nor analogously signals due to **9b**/$\mathbf{9b}^+$ in the voltammogram **7c**/$\mathbf{7c}^+$) and indeed no such signals are found.

Irreversible reduction at rather negative potentials is observed for **7a/b/c/e** (−1900 to −1700 mV, Table 3) and a second irreversible oxidation is seen for **7d**. The potentials at which compounds **7d/e** are reversibly oxidized are in approximately the same region as those at which reversible or quasi-reversible oxidation of compounds **3**, **4**, **5** takes place. They are also close to the potential measured for the reversible oxidation of the carbene compound **8** (1066 mV). Thus, it is obvious that the first oxidation potentials of cationic compounds in the second group (**3**–**5**) and the third group (**7**–**8**) fall in a rather narrow range, irrespective of the broad variation in the nature of the coligands. This implies that for all these cationic species the oxidation process is adequately described by the Ru^{II}/Ru^{III} redox couple. The allenylidene compound **6** also fits into this scheme, since it shows a reversible oxidation at $E_{1/2}$ = 1203 mV (Table 3). As expected for an allenylidene species, it may also be reversibly reduced (Table 3), with the extra electron being delocalized over the cumulenic system.

Table 4. Bond lengths in compounds **1**–**9** [pm][a]

	1	**3a** [b]	**4b** · PF_6[c]	**5** · PF_6[c]	**6** · PF_6	**7a** · PF_6	**7b** · PF_6[b]	**7e** · PF_6[c]	**9b**
Ru–P1	226.47(10)	227.0(3)/227.3(3)	228.1(2)	229.9(3)	229.3(2)	229.80(12)	229.71(18)/229.44(19)	231.01(13)	225.1(1)
Ru–P2	225.65(10)	224.3(3)/225.0(3)	227.5(2)	232.3(3)	228.1(2)	228.52(13)	227.55(17)/226.54(18)	227.55(13)	224.1(1)
Ru–C6	215.4(3)	219.6(10)/219.8(9)	215.9(6)	217.8(9)	222.5(5)	222.2(4)	223.3(7)/223.2(7)	223.0(4)	220.4(4)
Ru–C7	221.1(3)	222.6(10)/221.4(9)	222.5(5)	222.0(9)	223.1(6)	223.8(4)	223.7(8)/225.1(6)	225.8(4)	222.9(4)
Ru–C8	225.6(3)	227.5(9)/225.8(9)	226.9(6)	228.5(9)	226.5(6)	227.3(4)	229.1(6)/229.3(6)	228.2(4)	226.2(4)
Ru–C9	224.3(3)	225.1(10)/224.9(9)	223.9(5)	229.6(9)	226.3(6)	226.7(4)	225.8(6)/226.5(7)	225.0(4)	224.9(4)
Ru–C10	219.4(3)	220.5(9)/223.6(9)	218.9(5)	221.4(9)	223.0(5)	224.1(4)	223.1(6)/223.5(7)	221.1(4)	223.3(4)
Ru–Z	185.0	187.8/187.1	185.8	188.4	189.2	189.2	190.1/190.3	189.3	188.0
Ru–X	245.53(10)	201.2(11)/199.3(11)	205.2(5)	[d]	190.7(6)	186.7(5)	189.4(8)/188.3(8)	186.1(5)	202.2(4)
C3–C6	149.0(4)	147.9(14)/151.2(14)	151.6(8)	150.4(13)	149.9(8)	150.4(6)	151.0(9)/150.1(9)	150.5(6)	151.2(6)
C6–C7	144.8(5)	143.4(14)/143.2(13)	143.8(8)	145.0(13)	143.4(8)	143.4(6)	142.7(9)/143.8(9)	142.6(6)	141.1(6)
C7–C8	139.1(5)	139.1(14)/139.2(14)	139.9(8)	141.5(13)	140.9(8)	142.7(6)	138.9(9)/140.9(9)	140.9(6)	142.7(6)
C8–C9	143.3(5)	143.9(14)/143.2(13)	143.2(8)	141.8(13)	141.8(8)	141.5(6)	142.3(9)/142.5(9)	142.7(6)	143.0(6)
C9–C10	141.9(5)	139.1(14)/141.4(14)	141.5(8)	140.4(13)	140.1(8)	142.4(6)	141.4(9)/141.5(10)	141.1(6)	139.6(6)
C10–C6	144.1(5)	141.9(14)/147.4(13)	142.4(8)	142.8(12)	142.0(8)	143.5(6)	142.3(9)/142.8(9)	143.7(6)	144.2(6)
X–Y	–	116.8(12)/117.4(12)	114.2(7)	[d]	127.0(8)	128.1(7)	130.1(9)/128.4(9)	132.3(6)	121.0(6)
Y–W	–	–	142.7(8)	[d]	135.8(8)	–	[d]	[d]	144.1(6)
d	10.0	7.5/6.4	9.8	12.2	5.0	5.4	6.0/5.6	4.6	5.1

[a] All hydrogen atoms were identified by X-ray methods (including those at C52 in **7**). Standard deviations in units of the least significant digit given in each case. Z represents the centre of the Cp ring; X, Y, W refer to the organic residues at Ru in the sequence Ru-X-Y-W. The numbering scheme corresponds to that used in Figure 1 throughout; *d* denotes the in-plane component of the shift of the Ru atom in the direction of the carbon atom C6 with respect to the geometric centre of the 5-membered ring; C6 is the carbon atom linking the Cp residue to the ligand scaffolding. – [b] As footnote [c] with respect to the second independent molecule. – [c] For the sake of comparison, the configuration has been inverted with respect to the deposited data. – [d] Some additional distances: **5**: Ru–C(sp) 218.4(9), 221.1(9); C(sp)–C(sp) 127.2(13); C(sp)–C(*i*-Ph) 146.1(10), 146.4(11). **6**: C(γ)–C(*i*-Ph) 149.7(6), 150.0(6). **7b**: C(β)–C(*t*Bu) 152.0(9)/152.7(9); **7e**: C(β)–C(Me) 152.4(9); C(β)–C(Ph) 148.7 (6).

Table 5. Bond angles and torsion angles in **1**–**6** [°][a]

	1	**3a** [b]	**4b** · PF_6[c]	**5** · PF_6	**6** · PF_6
P1–Ru–P2	84.40(3)	86.61(10)/86.44(10)	85.81(5)	85.56(9)	85.6(6)
P1–Ru–Z	120.4	117.3/118.5	119.3	112.9	117.1
P2–Ru–Z	117.6	119.6/118.1	116.0	118.6	116.0
P1–Ru–X	100.32(3)	99.1(3)/101.0(3)	97.8(1)	120.9(3)/94.2(3)	101.4(2)
P2–Ru–X	98.82(3)	94.7(3)/95.8(3)	98.3(1)	88.2(3)/107.1(3)	98.3(2)
Z–Ru–X	126.1	129.6/127.7	129.6	121.4/127.5	128.9
Ru–X–Y	–	175.0(9)/172.9(8)	177.8(5)	[d]	173.4(5)
X–Y–W	–	–	177.0(6)	[d]	175.9(6)[d]
C4–C1–P1–Ru	−4.3	1.1/0.3	−8.6	−4.2	3.7
C4–C2–P2–Ru	−33.8	−23.9/−23.6	−29.2	−23.7	−18.0
C4–C3–C6–Ru	−16.1	−7.1/−7.4	−15.6	−14.6	−5.4
C3–C6–C7–C8	177.7	177.3/176.3	178.2	−177.9	177.6
C3–C6–C10–C9	−177.5	−176.8/−175.9	−177.8	177.8	−177.3
C12–C11–P1–Hc1	18.78	−3.98/−1.3	16.46	45.0	17.03
C22–C21–P1–Hc1	10.82	−23.50/−21.32	0.03	37.98	−16.19
C32–C31–P2–Hc2	−0.28	−25.60/−16.21	−9.68	37.88	−13.07
C42–C41–P2–Hc2	2.19	−18.17/−16.89	−6.33	25.19	−28.12

[a] Standard deviations in units of the least significant digit given in each case. Z represents the centre of the Cp ring; X, Y, W refer to the organic residues at Ru in the sequence Ru-X-Y-W; Hc represents an auxiliary point, fixed at the phosphorus atoms such that it points towards the observer (Figure 1, bottom) and is parallel to the C4–Ru axis (Figure 1). – [b] As footnote [c] with respect to the second independent molecule. – [c] For the sake of comparison, the configuration has been inverted with respect to the deposited data. – [d] Some additional angles: **5**: C(sp)–C(sp)–C(*i*-Ph) 148.1(9), 147.8(9). **6**: C(β)–C(γ)–C(*i*-Ph) 117.1(5), 121.1(5).

6. Structural Characteristics of the *tripod*CpL_2Ru Template

The structures of nine compounds derived from the *tripod*CpL_2Ru template are shown in Figures 1 and 3, with the geometrical data being collected in Tables 4–6. The data in Table 4 shows that the distances within the *tripod*CpL_2Ru template are not significantly influenced by the coligands bound to this template. The Ru–P distances are found to range only from 224 to 232 pm (Table 4). The Ru–C_{Cp} distances fall within a range from 215 to 230 pm, while the C–C distances within the Cp residue lie between 139 and 145 pm.

The P–Ru–P angles (Tables 5 and 6) are found in the narrow range from 84° to 88°. The angles subtended at the ruthenium centre by the centre of the Cp residue and the phosphorus atoms show a similarly small degree of scatter (112 to 120°, Tables 5 and 6). The position at which the coligand is bound to the template is likewise defined by a narrow range of P–Ru–X (X = coligand; 87 to 104°) and Z–Ru–X angles (Z = centre of the Cp molecule; 126 to 132°).

The coordination polyhedron around the ruthenium centre is thus fairly constant in shape (Figure 3) and is not significantly influenced by the various types of coligands

Table 6. Bond angles and torsion angles in **7**–**9** [°][a]

	7a·PF_6	**7b** · PF_6 [b]	**7e** · PF_6 [c]	**9b**
P1–Ru–P2	86.22(5)	87.03(6)/87.71(6)	85.47(5)	86.05(4)
P1–Ru–Z	116.5	115.7/114.9	116.4	118.8
P2–Ru–Z	116.2	116.1/115.7	116.8	118.7
P1–Ru–X	103.23(15)	103.98(18)/103.86(19)	102.5(13)	101.2(1)
P2–Ru–X	96.68(15)	92.87(19)/91.9(2)	96.88(12)	91.7(1)
Z–Ru–X	128.7	130.8/132.1	129.1	129.6
Ru–X–Y	172.5(4)	172.1(5)/170.6(5)	174.4(4)	174.7(4)
X–Y–W	–	[d]	[d]	178.2(4)
C4–C1–P1–Ru	0.4	0.5/−4.6	−5.8	5.7
C4–C2–P2–Ru	−20.3	−20.6/−22.3	−25.7	−22.6
C4–C3–C6–Ru	−7.5	−4.5/−6.7	−11.4	−4.5
C3–C6–C7–C8	178.2	178.9/176.9	176.3	176.0
C3–C6–C10–C9	−178.0	−177.7/−176.8	−176.3	−175.9
C12–C11–P1–Hc1	5.31	1.16/−8.37	−18.81	13.37
C22–C21–P1–Hc1	−28.10	−32.60/−38.95	−23.79	−25.02
C32–C31–P2–Hc2	−14.61	−13.52/−14.18	−20.47	17.85
C42–C41–P2–Hc2	−26.69	−28.09/−29.55	−16.55	−25.07

[a] Standard deviations in units of the least significant digit given in each case. Z represents the centre of the Cp ring; X, Y, W refer to the organic residues at Ru in the sequence Ru-X-Y-W; Hc represents an auxiliary point, fixed at the phosphorus atoms such that it points towards the observer (Figure 1, bottom) and is parallel to the C4–Ru axis (Figure 1). – [b] As footnote [c] with respect to the second independent molecule. – [c] For the sake of comparison, the configuration has been inverted with respect to the deposited data. – [d] Some additional angles: **7b**: C(α)–C(β)–C(*i*-*t*Bu) 127.2(6)/129.1(6). **7e**: C(α)–C(β)–C(*i*-Ph) 118.9(4); C(α)–C(β)–C(Me) 121.8(4).

Table 7. Crystal data for compounds **1**−**9**[a]

Compound	**1**	**3a** · 6 $CDCl_3$	**4b** · PF_6 · 0.5 CH_2Cl_2	**5** · PF_6	**6** · PF_6 · 3 CD_2Cl_2
Formula	$C_{34}H_{33}ClP_2Ru$	$C_{35}H_{33}P_2NRu$	$C_{42}H_{38}Cl_{1.5}F_6P_3NO_{0.5}$ Ru	$C_{48}H_{43}F_6P_3Ru$	$C_{49}H_{43}F_6P_3Ru$
Molecular mass	640.060	329.580	925.89	1855.610	2357.100
Crystal system	orthorhombic	triclinic	monoclinic	monoclinic	orthorhombic
Space group	$P2_12_12_1$	$P\bar{1}$	$C2/c$	$P2_1/n$	$Pbca$
Lattice constants	a = 1063.1 (2) pm	a = 1232.2 (2) pm	a = 2616.8 (5) pm	a = 934.4 (2) pm	a = 1521.3 (3) pm
	b = 1498.2 (5) pm	b = 1816.0 (4) pm	b = 2148.1 (4) pm	b = 2441.3 (5) pm	b = 2536.4 (5) pm
	c = 1748.4 (4) pm	c = 1991.4 (4) pm	c = 1904.7 (4) pm	c = 2101.6 (4) pm	c = 2637.3 (5) pm
	α = 90.00°	α = 86.71(2)°	α = 90.00(0)°	α = 90.00(0)°	α = 90.00(0)°
	β = 90.00°	β = 78.90(1)°	β = 132.02(3)°	β = 100.38(3)°	β = 90.00(0)°
	γ = 90.00°	γ = 78.30(1)°	γ = 90.00(0)°	γ = 90.00(0)°	γ = 90.00(0)°
Cell volume	2785·10^6 pm^3	4282·10^6 pm^3	7954·10^6 pm^3	4716 × 10^6 pm^3	10176 × 10^6 pm^3
Molecular units per cell	Z = 4	Z = 4	Z = 8	Z = 4	Z = 8
Density (calculated)	1.527 g/cm^3	1.534 g/cm^3	1.546 g/cm^3	1.307 g/cm^3	1.538 g/cm^3
Measuring device	Nonius Kappa CCD	Siemens Nicolet-Syntex	Nonius Kappa CCD	Nonius Kappa CCD	Nonius Kappa CCD
Temperature	200 K	200 K	200 K	200 K	200 K
Number of reflections for cell refinement		36			
Scan range	3.6° < 2θ < 52.0°	3.1° < 2θ < 47.0°	3.8° < 2θ < 51.9°	3.9° < 2θ < 48.0°	3.1° < 2θ < 52.1°
Method	ω-scan, Δω = 1.0°	ω-scan, Δω = 0.60°	ω-scan, Δω = 1.0°	ω-scan, Δω = 1.0°	ω-scan, Δω = 2.0°
Scan speed	15 sec/frame	12° min^{-1}	20 sec/frame	18 sec/frame	10 sec/frame
Measured reflections	58132	13349	40070	73701	142716
Unique reflections	5440	12672	7630	7396	10001
Observed reflections [$I \geq 2\sigma(I)$]	4642	6929	5202	5033	5301
Number of parameters refined	297	926	504	455	543
Maximum of residual electron density	0.76 × 10^{-6} e/pm^3	1.29 × 10^{-6} e/pm^3	1.19 × 10^{-6} e/pm^3	2.54 × 10^{-6} e/pm^3	0.98 × 10^{-6} e/pm^3
Agreement factors	R_1 = 0.032	R_1 = 0.072	R_1 = 0.060	R_1 = 0.085	R_1 = 0.068
(F^2 refinement)	R_w = 0.072	R_w = 0.172	R_w = 0.177	R_w = 0.275	R_w = 0.137

Compound	**7a** · PF_6 · 1.75 CH_2Cl_2	**7b** · PF_6 · CH_2Cl_2	**7e** · OTf · CH_2Cl_2	**9b**
Formula	$C_{36}H_{35}F_6P_3Ru$	$C_{40}H_{43}P_3F_6Ru$	$C_{44}H_{41}P_2F_3O_3S$ Ru	$C_{42}H_{38}P_2Ru$
Molecular mass	1845.460	458.325	954.760	795.160
Crystal system	triclinic	monoclinic	triclinic	monoclinic
Space group	$P\bar{1}$	Pn	$P\bar{1}$	$P2_1/n$
Lattice constants	a = 1283.9 (3) pm	a = 1004.7 (2) pm	a = 1006.0 (2) pm	a = 1088.3 (2) pm
	b = 1316.1 (3) pm	b = 1935.2 (4) pm	b = 1162.2 (2) pm	b = 1890.2 (4) pm
	c = 1398.8 (3) pm	c = 2056.3 (4) pm	c = 1847.1 (4) pm	c = 1795.5 (4) pm
	α = 82.55(3)°	α = 90.00(0)°	α = 75.13(3)°	α = 90.00(0)°
	β = 63.39(3)°	β = 90.66(3)°	β = 83.98(3)°	β = 95.55(3)°
	γ = 67.95(3)°	γ = 90.00(0)°	γ = 81.70(3)°	γ = 90.00(0)°
Cell volume	1957·10^6 pm^3	3998·10^6 pm^3	2060·10^6 pm^3	3676·10^6 pm^3
Molecular units per cell	Z = 2	Z = 4	Z = 2	Z = 4
Density (calculated)	1.566 g/cm^3	1.523 g/cm^3	1.539 g/cm^3	1.437 g/cm^3
Measuring device	Nonius Kappa CCD	Nonius Kappa CCD	Nonius Kappa CCD	Nonius Kappa CCD
Temperature	200 K	200 K	200 K	200 K
Number of reflections for cell refinement				
Scan range	3.8° < 2θ < 52.0°	4.5° < 2θ < 52.1°	3.7° < 2θ < 49.0°	3.1° < 2θ < 52.1°
Method	ω-scan, Δω = 1.0°	ω-scan, Δω = 1.0°	ω-scan, Δω = 1.0°	ω-scan, Δω = 1.0°
Scan speed	5 sec/frame	10 sec/frame	6 sec/frame	30 sec/frame
Measured reflections	31037	17579	32432	127717
Unique reflections	7645	11424	6865	7242
Observed reflections [$I \geq 2\sigma(I)$]	5789	8873	5503	5117
Number of parameters refined	484	872	519	446
Maximum of residual electron density	1.75 × 10^{-6} e/pm^3	0.88 × 10^{-6} e/pm^3	2.06 × 10^{-6} e/pm^3	0.97 × 10^{-6} e/pm^3
Agreement factors	R_1 = 0.049	R_1 = 0.044	R_1 = 0.044	R_1 = 0.047
(F^2 refinement)	R_w = 0.137	R_w = 0.102	R_w = 0.114	R_w = 0.126

[a] The crystals tend to contain solvate molecules. The number and type of solvate molecules found per formula unit is given in the column header.

(Figure 3). The secondary interaction within the *tripod*CpL_2Ru templates, which governs their conformation, will be closely similar in all of its *tripod*CpL_2RuL' compounds (L′ = coligand) due to the fact that the distances and valence angles within the templates are also closely similar. It can be seen from Figures 1 and 3 that the conformations adopted by the *tripod*CpL_2Ru templates are in fact rather similar for the whole group of compounds. This is shown in a quantitative way by the torsion angles C_o−C_i−P−Hc (where Hc denotes an auxiliary point fixed to

Table 8. Analytical data for compounds **1**−**3a**

	1	**2**	**3a**
IR: $\tilde{\nu}$ [$^{-1}$]	−	CO: 1966 vs; PF: 839 vs	CN: 2070 m
$^1H\{^{31}P\}$ NMR	CD_2Cl_2	CD_2Cl_2	$CDCl_3$
CH$_3$	1.53 s, 3 H	1.83 s, 3 H	1.58 s, 3 H
CH$_2$Cp	1.67 s, 2 H	2.22 s, 2 H	1.91 s, 2 H
CH$_2$P(H$_a$) [a]	2.15 d ($^2J_{HH}$ = 15 Hz), 2 H	2.39 d ($^2J_{HH}$ = 15.8 Hz), 2 H	2.07 d ($^2J_{HH}$ = 15.4 Hz), 2 H
CH$_2$P(H$_b$) [a]	2.47 d ($^2J_{HH}$ = 15 Hz), 2 H	2.78 d ($^2J_{HH}$ = 15.8 Hz), 2 H	2.44 d ($^2J_{HH}$ = 15.4 Hz), 2 H
Cp**H**$_\alpha$; Cp**H**$_\beta$	4.19 s, 2 H; 5.09 s, 2 H	4.75 s, 2 H; 5.70 s, 2 H	4.19 s, 2 H; 5.19 s, 2 H
arom. H	6.85−8.01 m, 20 H	7.07−7.58 m, 20 H	6.84−8.0 m, 20 H
R *isonitrile*	−	−	−
^{31}P NMR (PPh_2; PF_6)	34.98 s	45.3 s; −144.1, $^1J_{PF}$ = 713 Hz	44.61 s
$^{13}C\{^1H\}$ NMR [b]	CD_2Cl_2	CD_2Cl_2	$CDCl_3$
CH$_3$	34.1 t ($^3J_{CP}$ = 13 Hz)	33.9 m	34.6 t ($^3J_{CP}$ = 10 Hz)
CH$_3$**C**	49.3 m	51.1 br. s	50.6 m
CH$_2$Cp	37.3 s	36.7 s	38.5 s
CH$_2$P	35.1 ps. t ($^1J_{CP}$ = $^3J_{CP}$ = 20 Hz)	33.2 ps. t ($^1J_{CP}$ = $^3J_{CP}$ = 18 Hz)	35.0 ps. t ($^1J_{CP}$ = $^3J_{CP}$ = 18 Hz)
C$_i$*Cp*	68.7 s	88.7 s	81.1 s
C$_\beta$*Cp*; **C**$_\alpha$*Cp*	83.3 s; 94.1 s	84.9 s; 101.2 s	80.6 s; 96.3 s
C$^{m1/2}$H*arom.* [c]	127.8; 128.5 ps. t ($^3J_{CP}$ = $^5J_{CP}$ = 5 Hz)	129.4; 129.7, ps. t ($^3J_{CP}$ = $^5J_{CP}$ = 5 Hz)	128.1; 128.8 ps. t ($^3J_{CP}$ = $^5J_{CP}$ = 5 Hz)
C$^{o1/2}$H*arom.* [c]	131.6−132.0 m	130.5; 131.3 m	131.3−131.9 m
C$^{p1/2}$H*arom.* [c]	129.3 s	130.8 s	128.8 s; 129.5 s
C^{i1}*arom.*	138.8 ps. t ($^1J_{CP}$ = $^3J_{CP}$ = 15 Hz)	132.7 ps. t ($^1J_{CP}$ = $^3J_{CP}$ = 27 Hz)	136.9 ps. t ($^1J_{CP}$ = $^3J_{CP}$ = 19.5 Hz)
C^{i2}*arom.*	144.4 ps. t ($^1J_{CP}$ = $^3J_{CP}$ = 15 Hz)	139.3 t ($^1J_{CP}$ = $^3J_{CP}$ = 27.5 Hz)	143.4 ps. t ($^1J_{CP}$ = $^3J_{CP}$ = 23 Hz)
CN /**C**O	−	203.2 m	146.4
elemental analysis	C 63.80 *64.09*, H 5.20 *5.62*, P 9.67	C 54.06 *54.50*, H 4.28 *4.86*, P 11.95	C 66.66 *65.37*, H 5.27 *5.58*, N 2.22
calculated/*found*	*9.34*	*11.83*	*2.01*, P 9.82 *9.30*
mass spectrometry	EI: 640 [M$^+$]; 605 [M$^+$ − Cl]	FAB: 633 [M$^+$]; 605 [M$^+$ − CO]	EI: 631 [M$^+$]; 605 [M$^+$ − CN]

[a] Diastereotopic hydrogen atoms at CH_2P groups. − [b] CH_3, CH_2, CH, and C carbons were assigned by means of a 135° DEPT experiment. − [c] Individual assignment of the resonances to the different classes of phenyl rings was not possible.

the phosphorus atom with the resulting vector pointing in the direction C4−Ru towards the observer), which indicate that − with the exception of **5** − the phenyl rings tend to be aligned parallel to this auxiliary vector within a maximum deviation of 39° and with an average deviation of only 18° (Tables 5 and 6).

It is apparent from Figure 3 (**5**) that the η^2-coordinated 1,2-diphenylacetylene coligand interferes with the orientation of the phenyl groups of the template. The data in Table 5 reveals correspondingly large torsion angles up to a maximum value of 45°. Whereas constitutionally the templates *tripod*CpL_2Ru have mirror symmetry, conformationally this cannot be so due to the skew within the chelate scaffolding. The entries in Figures 1 and 3 and Tables 4−6 have been arranged such that the torsion of the scaffolding has the same sense in all the structures. It can be seen from Figure 3 as well as from Tables 5 and 6 that the most prominent torsion occurs with respect to the C4−C2−P2−Ru part of the scaffolding (−18 to −34°). The least prominent skew is consistently observed for the C4−C1−P1−Ru part (+1 to −9°), with the skew of the part bearing the cyclopentadienyl molecule, C4−C3−C6−Ru, being intermediate −5 to −16° (Figures 1 and 3; Tables 5 and 6). It appears that the difference in the torsion angles C4−C1−P1−Ru (small) and C4−C2−P2−Ru (large) is mirrored in the Ru−P distances, which, although similar, are systematically larger for Ru−P1 (mean 228.5 pm) than for Ru−P2 (mean 227.0 pm) in all the compounds studied (Table 4). This may be taken as an indication of some strain within the chelate cage, which is also evident from the $Ru-C_{Cp}$ distances. The sequence of these distances is such that the bond to the carbon atom C6 (mean 220.3 pm), which is linked to the chelate cage, tends to be the shortest, while the bonds to C8/C9 are systematically longer (mean values 227.4 and 225.7 pm, respectively); the Ru−C7/C10 bonds have intermediate lengths (mean values 223.1 and 222 pm). This pattern of bond distances corresponds to a shift of the ruthenium atom parallel to the plane of the Cp ligand in the direction of C6, away from its ideal position below the centre of this ring (*d* in Table 4). The distances within the Cp ligand respond to this asymmetry in a systematic way. The C6−C7/C6−C10 bonds are longer (mean 143.3 pm) than the C7−C8/C9−C10 bonds (mean 140.7 pm), with the remaining C8−C9 bond also being rather long (mean 142.7 pm). This pattern is seen in all the individual compounds investigated and thus represents a general trend. In a few cases where at first glance this pattern appears to be contradicted by the numerical values, the standard deviations of these values make the apparent contradiction insignificant.

Taken together, the indications of strain within the chelate scaffolding are only minor since the variance in the geometrical parameters, which would be expected to have equal values in an unstrained system, is not significantly larger than that observed in compounds where there is no steric strain imposed by a chelate cage.[4,12,19] The chemical behaviour of the *tripod*CpL_2Ru template can thus be expected to be similar to that exhibited by the non-chelate templates of the type CpL_2Ru, as has indeed been observed.

Table 9. Analytical data for compounds **3b**−**4a**

	3b·OTf	**3c**·PF_6	**4a**·PF_6
IR: $\tilde{\nu}$ [$^{-1}$]	CN: 2127 s; OTf: 1265 s, 1152 m, 1030 m	CN: 2143 br, 836 vs	CN: 2266 vw; PF: 839 vs
$^1H\{^{31}P\}$ NMR	CD_2Cl_2	CD_2Cl_2	CD_2Cl_2
C**H**$_3$	1.73 s, 3 H	1.71 s, 3 H	1.62 s, 3 H
C**H**$_2$Cp	2.07 s, 2 H	2.08 s, 2 H	1.80 s, 2 H
C**H**$_2$P(H$_a$) [a]	2.25 d ($^2J_{HH}$ = 15.8 Hz), 2 H	2.26 d ($^2J_{HH}$ = 15.6 Hz), 2 H	2.20 d (J_{HH} = 15.6 Hz), 2 H
C**H**$_2$P(H$_b$) [a]	2.65 d ($^2J_{HH}$ = 15.8 Hz), 2 H	2.61 d ($^2J_{HH}$ = 15.6 Hz), 2 H	2.57 d (J_{HH} = 15.6 Hz), 2 H
Cp**H**$_\alpha$; Cp**H**$_\beta$	4.52 s, 2 H; 5.45 s, 2 H	4.52 s, 2 H; 5.39 s, 2 H	4.40 s, 2 H; 5.38 (+ solv.) s
arom. H	6.93−7.80 m, 20 H	6.86−7.62 m, 20 H	6.83−7.77 m, 20 H
R *isonitrile*	3.70 s, 3 H, CN*Me*	1.53, 1.88, 2.17, 4.15, 11H	2.56 s, 3 H, NC*Me*
^{31}P NMR (PPh_2; PF_6)	47.03 s	46.7 s; −144.2 $^1J_{PF}$ = 713 Hz	39.3 s; −144.1 $^1J_{PF}$ = 713 Hz
$^{13}C\{^1H\}$ NMR [b]	CD_2Cl_2	CD_2Cl_2	CD_2Cl_2
CH$_3$	34.0 m	34.2 m	33.9 t ($^3J_{CP}$ = 13 Hz)
CH$_3$**C**	50.9 t ($^2J_{CP}$ = 5 Hz)	51.0 m	49.8 t ($^2J_{CP}$ = 5 Hz)
CH$_2$Cp	37.3 s	37.6 s	36.5 s
CH$_2$P	34.1 ps. t ($^1J_{CP}$ = $^3J_{CP}$ = 20 Hz)	34.4 ps. t ($^1J_{CP}$ = $^3J_{CP}$ = 20 Hz)	34.4 ps. t ($^1J_{CP}$ = $^3J_{CP}$ = 19 Hz)
C$_i$*Cp*; **C**$_\alpha$*Cp*	84.2 s	84.4 s	72.5 s
C$_\beta$*Cp*; **C**$_\alpha$*Cp*	82.2 s; 98.5 s	82.4 s; 98.6 s	82.4 s; 95.9 s
C$^{m1/2}$H*arom.* [c]	128.7; 129.2 ps. t ($^3J_{CP}$ = $^5J_{CP}$ = 5 Hz)	128.6; 129.3 ps. t ($^3J_{CP}$ = $^5J_{CP}$ = 5 Hz)	128.6; 129.2 ps. t ($^3J_{CP}$ = $^5J_{CP}$ = 5 Hz)
C$^{o1/2}$H*arom.* [c]	130.5; 131.6 ps. t ($^2J_{CP}$ = $^4J_{CP}$ = 5 Hz)	130.9; 131.5 ps. t ($^2J_{CP}$ = $^4J_{CP}$ = 5 Hz)	130.6; 131.6 ps. t ($^2J_{CP}$ = $^4J_{CP}$ = 5 Hz)
C$^{p1/2}$H*arom.* [c]	129.9 s, 130.6 s	129.8; 130.6 s	129.6; 130.3 s
C^{i1}*arom.*	135.0 ps. t ($^1J_{CP}$ = $^3J_{CP}$ = 23 Hz)	135.3 ps. t ($^1J_{CP}$ = $^3J_{CP}$ = 23 Hz)	136.3 ps. t ($^1J_{CP}$ = $^3J_{CP}$ = 19 Hz)
C^{i2}*arom.*	141.1 ps. t ($^1J_{CP}$ = $^3J_{CP}$ = 25 Hz)	141.3 ps. t ($^1J_{CP}$ = $^3J_{CP}$ = 25 Hz)	141.8 ps. t ($^1J_{CP}$ = $^3J_{CP}$ = 19 Hz)
CN or N**C**	**C**F_3: 118.3 s; **C**N: 124.7	n. f.	127.7 s
CN**R** or NC**R**	31.0, CN***Me***	24.0, 25.5, 33.9 **C**H_2; 55.9 **C**H	4.8 NC**Me**
elemental analysis	C 55.92 *56.22*, H 4.57 *5.14*, N 1.76 *1.79*, P	C 57.34 *57.57*, H 5.16 *5.56*, N 1.63 *1.87*, P	C 54.69 *55.61*, H 4.59 *5.28*, N 1.77 *1.73*, P
calculated/*found*	7.79 *7.49*	10.82 *10.72*	11.75 *11.20*
mass spectrometry	FAB: 646 [M^+]; 605 [M^+ − CNMe]	FAB: 714 [M^+]; 605 [M^+ − CNCy]	FAB: 646 [M^+]; 604 [M^+ − NCMe]

[a] Diastereotopic hydrogen atoms at CH_2P groups. − [b] CH_3, CH_2, CH, and C carbons were assigned by means of a 135° DEPT experiment. − [c] Individual assignment of the resonances to the different classes of phenyl rings was not possible.

Conclusion

The chelate ligand $CH_3C(CH_2C_5H_4)(CH_2PPh_2)_2Li$ forms templates $CH_3C(CH_2\text{-}\eta^5\text{-}C_5H_4)(CH_2\text{-}\eta^1\text{-}PPh_2)_2Ru$, *tripod*$CpL_2Ru$, which bind to coligands L′ in a similar manner as known for the non-chelate analogues $CpRuL_2$. With anionic ligands (L′ = Cl^-, CN^-, acetylides), neutral compounds *tripod*CpL_2RuL' are obtained. With neutral ligands (L′ = nitriles, isonitriles, vinylidenes, allenylidenes) cationic species [*tripod*$CpL_2RuL']^+$ are formed. The reactivity of the template and its coordination compounds is similar to that reported for the non-chelate analogues $CpRuL_2$.[4][19]

Structural analyses of nine coordination compounds containing the *tripod*CpL_2Ru entity show that the conformation of the template is little affected by the nature of coligand bonded to it. The results also demonstrate that there is no great strain within the chelate cage. Nevertheless, the cage is rather rigid, such that inversion − which may be a problem in the reaction of non-chelate compounds of this type − cannot occur. Reactions of chiral versions of this template can thus be expected to allow for undisturbed diastereochemical control.

The barriers to rotation of the vinylidene fragments about their bonds to the *tripod*CpL_2Ru template amount to $\Delta H^{\neq}$ = 40.3 kJmol^{-1} in C=CMe(*t*Bu) and $\Delta H^{\neq}$ = 47.9 kJmol^{-1} in C=CMe(Ph), as estimated by means of ^{31}P-NMR spectroscopy. These values lie in a range typical for the rotation of such single-faced π-acceptors about their Ru−C bond in unstrained CpL_2Ru vinylidene compounds.

Experimental Section

General Remarks: Unless noted otherwise, all manipulations were carried out under argon by means of standard Schlenk techniques. All solvents were dried by standard methods[32] and distilled under argon. The solvents $CDCl_3$ and CD_2Cl_2 used for NMR spectroscopic measurements were degassed by three successive "freeze-pump-thaw" cycles and dried over 4 Å molecular sieves. − NMR: Bruker Avance DPX 200 at 200.12 MHz (^1H), 50.323 MHz ($^{13}C\{^1H\}$), 81.015 MHz ($^{31}P\{^1H\}$) or Bruker Avance DRX 500 at 500.13 MHz (^1H), 125.76 MHz ($^{13}C\{^1H\}$), 202.46 MHz ($^{31}P\{^1H\}$); at 303 K unless stated otherwise; chemical shifts (δ) in ppm with respect to residual solvent peaks as internal standards: $CDCl_3$ (^1H: δ = 7.27; ^{13}C: δ = 77.0); CD_2Cl_2 (^1H: δ = 5.32; ^{13}C: δ = 53.8). ^{31}P chemical shifts (δ) in ppm with respect to 85% H_3PO_4 (^{31}P: δ = 0) as external standard. − IR: Bruker IFS-66 spectrophotometer; KBr discs. − MS (EI): Finnigan MAT 8230: Fast-atom bombardment (FAB) with xenon; matrix: 4-nitrobenzyl alcohol. − HR-MS (EI): VG ZAB 2F and HR-MS (FAB) JEOL JMS 700; matrix: 4-nitrobenzyl alcohol. − Elemental analyses: Microanalytical Laboratory of the Organisch-Chemisches Institut, Universität Heidelberg. − Melting points: Gallenkamp MFB-595 010; values are not corrected. − Cyclic voltammetry: Metrohm "Universal Meß- und Titriergefäß", Metrohm GC electrode RDE 628, platinum electrode, SCE electrode, Princeton Applied Research potentiostat Model 273; substrate concentration 10^{-3} M in 0.1 M nBu$_4$NPF_6/CH_2Cl_2.

Crystallographic Structure Determinations: The measurements were carried out on a Siemens P4 four-circle diffractometer (for **3a**) or on an Enraf−Nonius Kappa CCD diffractometer, using graphite-monochromated Mo-K_α radiation throughout. In the case of the Siemens P4 four-circle diffractometer measurements, the intensities

Table 10. Analytical data for compounds **4b**−**6**

	4b·PF_6	**5**·PF_6	**6**·PF_6
IR: $\tilde{\nu}$ [$^{-1}$]	CN: 2218 s; PF: 843 vs	PF: 1905 vw; 838 vs	CC: 1919 br; PF: 838 vs
$^1H\{^{31}P\}$ NMR	CD_2Cl_2	CD_2Cl_2	CD_2Cl_2
C**H**$_3$	1.61 s, 3 H	1.17 s, 3 H	1.86 s, 3 H
C**H**$_2$Cp	1.81 s, 2 H	2.55 s, 2 H	2.39 s, 2 H
C**H**$_2$P(H_a) [a]	2.21 d (J_{HH} = 15.6 Hz), 2 H	2.34 d ($^2J_{HH}$ = 16 Hz), 2 H	2.40 d ($^2J_{HH}$ = 16 Hz), 2 H
C**H**$_2$P(H_b) [a]	2.63 d (J_{HH} = 15.6 Hz), 2 H	2.55 d ($^2J_{HH}$ = 16 Hz), 2 H	2.83 d ($^2J_{HH}$ = 16 Hz), 2 H
Cp**H**$_\alpha$; Cp**H**$_\beta$	4.45 s, 2 H; 5.47 s, 2 H	5.51 s, 2 H; 5.68 s, 2 H	4.79 s, 2 H; 5.86 s, 2 H
arom. H	6.85−7.78 m, 25 H	6.61−7.44 m, 30 H	7.79−8.00 m, 30 H
coligand	[d]	[d]	[d]
^{31}P NMR (PPh_2; PF_6)	39.5 s; −144.1 $^1J_{PF}$ = 713 Hz	38.80 s; −144.1 $^1J_{PF}$ = 713 Hz	50.4 s; −144.1 $^1J_{PF}$ = 713 Hz
$^{13}C\{^1H\}$ NMR [b]	CD_2Cl_2	CD_2Cl_2	CD_2Cl_2
CH$_3$	33.9 m	33.9 t ($^3J_{CP}$ = 13 Hz)	34.1 m
CH$_3$**C**	49.9 m	47.9 m	50.9 t ($^2J_{CP}$ = 3.7 Hz)
CH$_2$Cp	36.5 s	35.9 s	37.9 s
CH$_2$P	34.3 ps. t ($^1J_{CP}$ = $^3J_{CP}$ = 18.5 Hz)	39.0 ps. t ($^1J_{CP}$ = $^3J_{CP}$ = 17 Hz)	33.4 pt ($^1J_{CP}$ = $^3J_{CP}$ = 17 Hz)
C$_i$*Cp*	73.8 s	86.1 s	93.5 s
C$_\beta$*Cp*; **C**$_\alpha$*Cp*	82.9 s; 96.4 s	89.2 s; 95.3 s	91.3 s; 100.1 s
C$^{m1/2}$H*arom.* [c]	128.7; 129.2 ps. t ($^3J_{CP}$ = $^5J_{CP}$ = 5 Hz)	128.2; 128.8 ps. t ($^3J_{CP}$ = $^5J_{CP}$ = 5 Hz)	128.8; 129.4 ps. t ($^3J_{CP}$ = $^5J_{CP}$ = 5 Hz)
C$^{o1/2}$H*arom.* [c]	130.7; 131.6 ps. t ($^1J_{CP}$ = $^3J_{CP}$ = 5 Hz)	132.9; 133.4 ps. t ($^2J_{CP}$ = $^4J_{CP}$ = 5 Hz)	131.3 ps. t ($^2J_{CP}$ = $^4J_{CP}$ = 5 Hz)
C$^{p1/2}$H*arom.* [c]	129.8; 130.6 s	128.5, 129.1, 131.1, 130.7[d]	129.6, 130.4, 130.7, 130.9[d]
C^{i1}*arom.*	136.2 ps. t ($^1J_{CP}$ = $^3J_{CP}$ = 20 Hz)	134.4 ps. t ($^1J_{CP}$ = $^3J_{CP}$ = 25 Hz)	133.6 ps. t ($^1J_{CP}$ = $^3J_{CP}$ = 26 Hz)
C^{i2}*arom.*	141.5 ps. t ($^1J_{CP}$ = $^3J_{CP}$ = 25.5 Hz)	139.6 ps. t ($^1J_{CP}$ = $^3J_{CP}$ = 27 Hz)	140.1 ps. t ($^1J_{CP}$ = $^3J_{CP}$ = 27 Hz)
C$_\alpha$, **C**$_\beta$, **C**$_\gamma$	112.3 s, N**C**Ph	80.5 s, η^2-**CC**	291.9 m; 211.1, 152.0
coligand arom. **C**H	128.1 **C**^{i}; 130.2, 132.5, 134.1	132.0, **C**^{i}(**Ph**CC**Ph**)[d]	144.0, **C**^{i}Ph[d]
elemental analysis	C 57.75 *58.94*, H 4.49 *4.94*, N 1.64 *1.68*,	C 62.14 *60.82*, H 4.67 *4.98*, P 10.01 *n.b.*	C 62.92 *62.42*, H 4.61 *4.85*, P 9.89 *9.95*
calculated/*found*	P 10.90 *10.97*		
mass spectrometry	FAB: 708 [M$^+$]; 605 [M$^+$ − NCPh]	FAB: 783 [M$^+$]; 605 [M$^+$ − C_2Ph_2]	FAB: 796 [M$^+$]; 605 [M$^+$ − R]

[a] Diastereotopic hydrogen atoms at CH_2P groups. − [b] CH_3, CH_2, CH, and C carbons were assigned by means of a 135° DEPT experiment. − [c] Individual assignment of the resonances to the different classes of phenyl rings was not possible. − [d] Differentiation between the phenyl resonances of the coligand and the phenyl resonances of the tripodal ligand was not possible.

Table 11. Analytical data for compounds **7a**−**7c**

	7a·PF_6	**7b**·PF_6	**7c**·PF_6
IR: $\tilde{\nu}$ [$^{-1}$]	CC: 1624 m; PF: 840 vs	CC: 1638 m; PF: 840 vs	CC: 1641 m; PF: 840 vs
$^1H\{^{31}P\}$ NMR	CD_2Cl_2	CD_2Cl_2	CD_2Cl_2
C**H**$_3$	1.81 s, 3 H	1.73 s, 3 H	1.84 s, 3 H
C**H**$_2$Cp	2.22 s, 2 H	2.17 s, 2 H	2.31 s, 2 H
C**H**$_2$P(H_a) [a]	2.37 d ($^2J_{HH}$ = 16 Hz), 2 H	2.36 d ($^2J_{HH}$ = 15.8 Hz), 2 H	2.40 d ($^2J_{HH}$ = 16 Hz), 2 H
C**H**$_2$P(H_b) [a]	2.82 d ($^2J_{HH}$ = 16 Hz), 2 H	2.75 d ($^2J_{HH}$ = 15.8 Hz), 2 H	2.83, d ($^2J_{HH}$ = 16 Hz), 2 H
Cp**H**$_\alpha$; Cp**H**$_\beta$	4.75 s, 2 H; 5.88 s, 2 H	4.72 s, 2 H; 5.72 s, 2 H	4.89 s 2 H; 5.99 s, 2 H
arom. H	6.93−7.47 m, 20 H	6.81−7.65 m, 20 H	6.51−7.51 m, 25 H
=C**H**(R)	4.65 t ($^4J_{HP}$ = 4 Hz), 2 H	4.91 t ($^4J_{HP}$ = 4 Hz), 1 H	6.2 t ($^4J_{HP}$ = 3.4 Hz), 1 H
=C**R**(H)	−	1.31 s, 9 H	[d]
^{31}P NMR (PPh_2; PF_6)	48.8 s; −144.1 $^1J_{PF}$ = 713 Hz	48.9 s; −144.1 $^1J_{PF}$ = 713 Hz	48.8 s; −144.1 $^1J_{PF}$ = 713 Hz
$^{13}C\{^1H\}$ NMR [b]	CD_2Cl_2	CD_2Cl_2 (500 MHz)	CD_2Cl_2
CH$_3$	33.9 m	33.9 t ($^3J_{CP}$ = 13 Hz)	33.6 m
CH$_3$**C**	50.8 m	50.5 br. s	50. 6 t ($^2J_{CP}$ = 3.6 Hz)
CH$_2$Cp	37.5 s	37.4	37.3
CH$_2$P	33.4 ps. t ($^1J_{CP}$ = $^3J_{CP}$ = 15 Hz)	34.5 ps. t ($^1J_{CP}$ = $^3J_{CP}$ = 20 Hz)	33.8 ps. t ($^1J_{CP}$ = $^3J_{CP}$ = 17 Hz)
C$_i$*Cp*	92.8 s	92.2	93.1
C$_\beta$*Cp*; **C**$_\alpha$*Cp*	90.8 s; 101.3 s	90.7 s; 100.9 s	91.3 s; 101.5 s
C$^{m1/2}$H*arom.*[c]	128.8; 129.5 ps. t ($^3J_{CP}$ = $^5J_{CP}$ = 5 Hz)	128.6; 129.4 ps. t ($^3J_{CP}$ = $^5J_{CP}$ = 5 Hz)	128.8; 129.5 ps. t ($^3J_{CP}$ = $^5J_{CP}$ = 5 Hz)
C$^{o1/2}$H*arom.* [c]	131.3 m	131.6 m	131.5 m
C$^{p1/2}$H*arom.* [c]	130.6 s	130.6; 131.1 s	130.7; 131.3 s
C^{i1}*arom.*	132.2 ps. t ($^1J_{CP}$ = $^3J_{CP}$ = 27.5 Hz)	133.0 ps. t ($^1J_{CP}$ = $^3J_{CP}$ = 25 Hz)	134.2 ps. t ($^1J_{CP}$ = $^3J_{CP}$ = 20 Hz)
C^{i2}*arom.*	139.4 ps. t ($^1J_{CP}$ = $^3J_{CP}$ = 27.5 Hz)	139.6 ps. t ($^1J_{CP}$ = $^3J_{CP}$ = 25 Hz)	139.7 ps. t ($^1J_{CP}$ = $^3J_{CP}$ = 25 Hz)
C$_\alpha$; **C**$_\beta$	346.5 m; 98.7 s	348.8 m; 126.7 s	353.8 m; 119.3 s
=C**R**(H)	−	32.4 *t*Bu; 32.3 C_q*t*Bu	126.8, 127.0 s, 129.4 **C**H*Ph*
elemental analysis	C 55.75 *55.75*, H 4.55 *4.83*, P 11.98 *11.96*	C 57.76 *58.38*, H 5.21 *5.24*, P 11.17 *10.68*	C 59.23 *59.99*, H 4.26 *4.82*, P 10.91 *10.92*
calculated/*found*			
mass spectrometry	FAB: 631 [M$^+$]; 605 [M$^+$ − R]	FAB: 687 [M$^+$]; 605 [M$^+$ − R]	FAB: 707 [M$^+$]; 605 [M$^+$ − R]

[a] Diastereotopic hydrogen atoms at CH_2P groups. − [b] CH_3, CH_2, CH, and C carbons were assigned by means of a 135° DEPT experiment. − [c] Individual assignment of the resonances to the different classes of phenyl rings was not possible.

Table 12. Analytical data for compounds **7d**−**8**

	7d·OTf	**7e**·OTf	**8**·PF_6
IR: $\tilde{\nu}$ [$^{-1}$]	CC: 1649 br; OTf: 1264 s, 1147, 1030	CC: 1647 br; OTf: 1265 s, 1147, 1030	CO: 1246 m; PF: 840 vs
$^1H\{^{31}P\}$ NMR	CD_2Cl_2	CD_2Cl_2	CD_2Cl_2
C**H**$_3$	1.75 s, 3 H	1.84 s, 3 H	1.67 s, 3 H
C**H**$_2$Cp	2.24 s, 2 H	2.32 s, 2 H	2.06 s, 2 H
C**H**$_2$P(H$_a$) [a]	2.28 d ($^2J_{HH}$ = 16 Hz), 2 H	2.37 d ($^2J_{HH}$ = 16 Hz), 2 H	2.22 d ($^2J_{HH}$ = 16 Hz), 2 H
C**H**$_2$P(H$_b$) [a]	2.74 d ($^2J_{HH}$ = 16 Hz), 2 H	2.81 d ($^2J_{HH}$ = 16 Hz), 2 H	2.71 d ($^2J_{HH}$ = 16 Hz), 2 H
Cp**H**$_\alpha$; Cp**H**$_\beta$	4.93 s, 2 H; 5.84 s, 2 H	4.92 s, 2 H; 6.03 s, 2 H	4.74 s; 5.56 s
arom. H	6.95−7.45 m; 20 H	6.83−7.45 m, 25 H	6.7−7.9 m, 20 H
=CC**H**$_3$(R)	2.09 s, 3 H	2.52 s, 3 H	3.31 s *Me*, 3 H; 3.95 s *OMe*, 3 H
=C(Me)**R**	1.32 s, 9 H, *t*Bu	[d]	
^{31}P NMR (PPh$_2$; PF_6)	48.7 s	49.3 s	47.8 s; −144.1 $^1J_{PF}$ = 713 Hz
$^{13}C\{^1H\}$ NMR [b]	CD_2Cl_2	CD_2Cl_2	CD_2Cl_2
CH$_3$	33.9 t ($^3J_{CP}$ = 13 Hz)	33.8 m	34.2 t ($^3J_{CP}$ = 13 Hz)
CH$_3$**C**	50.0 br. s	50.4 m	50.1 br. s
CH$_2$Cp	37.3 s	37.2 s	38.6 s
CH$_2$P	35.9 ps. t ($^1J_{CP}$ = $^3J_{CP}$ = 17 Hz)	34.2 ps. t ($^1J_{CP}$ = $^3J_{CP}$ = 17 Hz)	35.8 ps. t ($^1J_{CP}$ = $^3J_{CP}$ = 17 Hz)
C$_i$*Cp*	91.6	92.9	87.4 s
C$_\beta$*Cp*; **C**$_\alpha$*Cp*	90.3 s; 100.5 s	90.8 s; 101.2 s	88.2 s; 100.8 s
C$^{m1/2}$H*arom.* [c]	128.7; 129.2 ps. t ($^3J_{CP}$ = $^5J_{CP}$ = 5 Hz)	128.8; 129.3 ps. t ($^3J_{CP}$ = $^5J_{CP}$ = 5 Hz)	127.9; 129.0 ps. t ($^3J_{CP}$ = $^5J_{CP}$ = 5 Hz)
C$^{o1/2}$H*arom.* [c]	131.9; 132.2 ps. t ($^2J_{CP}$ = $^4J_{CP}$ = 5 Hz)	131.5; 131.8 ps. t ($^2J_{CP}$ = $^4J_{CP}$ = 5 Hz)	131.8; 132.1 ps. t ($^1J_{CP}$ = $^3J_{CP}$ = 5 Hz)
C$^{p1/2}$H*arom.* [c]	130.7; 131.2 s	130.6; 131.2 s	129.6; 130.6 s
C^{i1}*arom.*	133.8 ps. t ($^1J_{CP}$ = $^3J_{CP}$ = 27 Hz)	133.1 ps. t ($^1J_{CP}$ = $^3J_{CP}$ = 30 Hz)	134.5 ps. t ($^1J_{CP}$ = $^3J_{CP}$ = 23 Hz)
C^{i2}*arom.*	139.8 ps. t ($^1J_{CP}$ = $^3J_{CP}$ = 27.5 Hz)	139.5 ps. t ($^1J_{CP}$ = $^3J_{CP}$ = 27.5 Hz)	141.5 ps. t ($^1J_{CP}$ = $^3J_{CP}$ = 25.5 Hz)
=**C**$_\alpha$; =**C**$_\beta$	352.1 m; n.f.	353.8 m; n.f.	308.2 m
=C**C**H$_3$(R); =C**R**(Me)	9.5 Me; 30.5 *t*Bu; 32.7 C^q	12.3 *Me*; 125.0 C^i*Ph*; 127.2, 127.5 **C**H	59.8 *O***C**H$_3$; 47.6 **C**H$_3$
elemental analysis calculated/*found*	C 59.36 *59.16*, H 5.34 *5.44*, P 7.29 *7.82*	C 60.75 *61.21*, H 4.75 *5.32*, P 7.12 *7.85*	C 55.02 *56.16*, H 4.87 *5.21*, P 11.50 *11.10*
mass spectrometry	FAB: 701 [M$^+$]; 605 [M$^+$ − R]	FAB: 721 [M$^+$]; 605 [M$^+$ − R]	FAB: 664 [M$^+$]; 605 [M$^+$ − R]

[a] Diastereotopic hydrogen atoms at CH_2P groups. − [b] CH_3, CH_2, CH, and C carbons were assigned by means of a 135° DEPT experiment. − [c] Individual assignment of the resonances to the different classes of phenyl rings was not possible.

Table 13. Analytical data for compound **9**

	9a	**9b**
IR: $\tilde{\nu}$ [$^{-1}$]	CC: 2071 m	CC: 2056 m
$^1H\{^{31}P\}$ NMR	CD_2Cl_2	CD_2Cl_2
C**H**$_3$	1.57 s, 3 H	1.54 t ($^4J_{HP}$ = 3 Hz), 3 H
C**H**$_2$Cp	1.94 s, 2 H	1.91 s, 2 H
C**H**$_2$P(H$_a$) [a]	2.08 d ($^2J_{HH}$ = 15.4 Hz), 2 H	2.11 d ($^2J_{HH}$ = 15.4 Hz), 2 H
C**H**$_2$P(H$_b$) [a]	2.37 d ($^2J_{HH}$ = 15.4 Hz), 2 H	2.46 d ($^2J_{HH}$ = 15.4 Hz), 2 H
Cp**H**$_\alpha$; Cp**H**$_\beta$	4.15 s, 2 H; 4.95 s, 2 H	4.20 s, 2 H; 5.10 s, 2 H
arom. H	6.84−7.88 m, 20 H	6.8−7.88 m, 25 H
C≡C**R**	1.38 s, 9 H	*cf.* arom. H
^{31}P NMR (PPh$_2$)	45.1 s	45.6 s
$^{13}C\{^1H\}$ NMR [b]	CD_2Cl_2	CD_2Cl_2
CH$_3$	34.2 m	34.2 t ($^3J_{CP}$ = 12.4 Hz)
CH$_3$**C**	50.3 m	50.5 t ($^2J_{CP}$ = 5.5 Hz)
CH$_2$Cp	38.8 s	38.8 s
CH$_2$P	35.3 ps. t ($^1J_{CP}$ = $^3J_{CP}$ = 20 Hz)	35.1 ps. t ($^1J_{CP}$ = $^3J_{CP}$ = 18 Hz)
C$_i$*Cp*	80.8 s	81.7 s
C$_\beta$*Cp*; **C**$_\alpha$*Cp*	80.2 s; 95.7 s	80.5 s; 96.0 s
C$^{m1/2}$H*arom.* [c]	127.3; 128.2 ps. t ($^3J_{CP}$ = $^5J_{CP}$ = 5 Hz)	127.7; 128.4 ps. t ($^3J_{CP}$ = $^5J_{CP}$ = 5 Hz)
C$^{o1/2}$H*arom.* [c]	131.7; 132.2 ps. t ($^2J_{CP}$ = $^4J_{CP}$ = 5 Hz)	131.7; 131.8 ps. t ($^2J_{CP}$ = $^4J_{CP}$ = 5 Hz)
C$^{p1/2}$H*arom.* [c]	128.3; 128.9 s	122.8, 129.1, 130.7[d]
C^{i1}*arom.*	138.9 ps. t ($^1J_{CP}$ = $^3J_{CP}$ = 17 Hz)	138.3 ps. t ($^1J_{CP}$ = $^3J_{CP}$ = 18 Hz)
C^{i2}*arom.*	145.3 ps. t ($^1J_{CP}$ = $^3J_{CP}$ = 21 Hz)	144.6 ps. t ($^1J_{CP}$ = $^3J_{CP}$ = 22 Hz)
C$_\alpha$≡; ≡**C**$_\beta$	92.2 m; 117.4 s	134.2 m; 112.2 s
C≡C**R**	33.8 *t*Bu; 32.4 **C**$_q$*t*Bu	[d]
elemental analysis calculated/*found*	C 70.06 *68.60*, H 6.17 *6.63*, P 9.03 *9.02*	C 71.48 *70.05*, H 5.43 *5.99*, P 8.78 *8.11*
mass spectrometry	EI: 687 [M$^+$]; 672 [M$^+$ − Me]	EI: 706 [M$^+$]; 604 [M$^+$ − C_2Ph]

[a] Diastereotopic hydrogen atoms at CH_2P groups. − [b] CH_3, CH_2, CH, and C carbons were assigned by means of a 135° DEPT experiment. − [c] Individual assignment of the resonances to the different classes of phenyl rings was not possible. − [d] Differentiation between the phenyl resonances of the coligand and the phenyl resonances of the tripodal ligand was not possible.

Table 14. Synthesis of complexes **3**−**9**

compound	coligand/procedure	reaction time/temp.	colour	yield [%]	m.p. [°C][a]	HR-MS (*m/z*) calcd.; *found*	crystallization method[d]
3b	MeO_3SCF_3 (0.07 mL, 0.7 mmol)/D	15 min/25°C	pale yellow	80	213 (dec.)	646.1366; *646.1407*[b]	–
3c	cyclohexyl isocyanide (0.08 mL, 0.8 mmol)/A	1 h/25°C	light yellow	95	230 (dec.)	–	–
4a	acetonitrile (7 mL)/A	6 h/25°C	yellow	88	188 (dec.)	646.1366; *646.1353*[b] 605.1101; *605.1149*	–
4b	benzonitrile (0.2 mL)/A	4 h/25°C	yellow	90	193 (dec.)	708.1523; *708.1624*[b] 707.1626; *707.1635*	I
5	1,2-diphenylacetylene (270 mg, 1.5 mmol)/B	18 h/25°C	yellow	92	180 (dec.)	783.1884; *783.1827*[b]	Ia
6	1,1-diphenyl-2-propynol (350 mg, 1.7 mmol)/A	18 h /25°C	purple	70−80[e]	187 (dec.)	–	II
7a	trimethylsilylacetylene (0.36 mL, 2.4 mmol)/B	18 h/25°C	yellow	90	210 (dec.)	–	III
7b	3,3-dimethyl-1-butyne/A (0.19 mL, 1.5 mmol)/A	15 min/reflux	yellow-brown	72	213 (dec.)	687.1884; *687.1899*[b] 605.1101; *605.1187*	III
7c	phenylacetylene (0.1 mL, 0.9 mmol)/A	15 min/reflux	red-brown	86	209 (dec.)	707.1571; *707.1579* [b] 605.1101; *605.1137*	–
7d	MeO_3SCF_3 (0.05 mL, 0.5 mmol)/D	20 min/25°C	orange-red	70	232	–	–
7e	MeO_3SCF_3 (0.05 mL, 0.5 mmol)/D	20 min /25°C	brick red	86	155	721.1727; *721.1722*[b] 605.1101; *605.1115*	I
8	trimethylsilylacetylene (0.23 mL, 1.5 mmol)/A	18 h /25°C	yellow-brown	95	198 (dec.)	663.1520; *663.1584*[b] 605.1101; *605.1178*	–
9a	NaOMe (10 mL)/C	1 h/25°C	yellow	75	190	686.1805; *686.1779*[c] 671.1571; *671.1577*	–
9b	NaOMe (10 mL)/C	1 h/25°C	yellow	71	155	706.1492; *706.1531*[c]	III

[a] dec. = decomposition. – [b] HR-FAB. – [c] HR-EI. – [d] I: vapour diffusion of diethyl ether into a CH_2Cl_2 solution of the complex, 25°C. Ia: slow diffusion of diethyl ether into a DCE solution of the complex, 25°C. II: slow evaporation of the solvent from a $CDCl_3$ solution of the complex. III: a saturated CH_2Cl_2 solution of the complex (at 25°C) was crystallized at −20°C. – [e] As found in 4 different experiments.

of three check reflections (measured every 100 reflections) remained constant throughout the data collection, thus indicating crystal and electronic stability. The data collected on the Siemens P4 diffractometer were corrected as usual, including an experimental absorption correction. The data from the Enraf−Nonius Kappa CCD device were processed using the standard Nonius software.[33] All calculations were performed using the SHELXT PLUS software package. Structures were solved by direct methods with the SHELXS-97 program and refined with the SHELXL-97 program.[34] Graphical handling of the structural data during solution and refinement was performed with XPMA.[35] Atomic coordinates and anisotropic thermal parameters of the non-hydrogen atoms were refined by full-matrix least-squares calculations. Data relating to the structure determinations are collected in Table 7. Crystallographic data (excluding structure factors) for the structures reported in this paper have been deposited with the Cambridge Crystallographic Data Centre as supplementary publication nos. CCDC-127499 to CCDC-127507. Copies of the data can be obtained free of charge on application to the CCDC, 12 Union Road, Cambridge CB2 1EZ, U.K. [Fax: (internat.) +44 (0)1223/336033; E-mail: deposit@ccdc.cam.ac.uk].

Preparation of *tripod*CpL_2RuCl (1): $CH_3C(CH_2C_5H_4)(CH_2PPh_2)_2Li$ (613 mg, 1.2 mmol) was added to a solution of $RuCl_2(PPh_3)_3$[11] (959 mg, 1.0 mmol) in 1,2-dichloroethane[36] (20 mL). After heating for 3 h at 90°C, the solvent was evaporated in vacuo and the orange-brown residue was purified by chromatography on Al_2O_3 (Brockmann activity grade III). Elution with 500 mL of diethyl ether removed the PPh_3. Using a 1:1 mixture of CH_2Cl_2/diethyl ether, the product was then eluted in an orange fraction. Chromatography on SiO_2 using diethyl ether/CH_2Cl_2, 10:1, as eluent also afforded **1**, but it was not possible to remove traces of non-reacted $RuCl_2(PPh_3)_3$ and PPh_3 (produced during the reaction) by this method. The purity of the $RuCl_2(PPh_3)_3$ was seen to play an important role in determining the yields; 40−60% of **1** could be obtained as an orange powder, which was found to decompose at 228°C. For all other analytical data, see Table 8. From a CH_2Cl_2 solution of **1** saturated at 30°C, orange crystals could be collected after 8 weeks at 25°C.

Preparation of *tripod*CpL_2RuCO^+ (2): $TlPF_6$ (89 mg, 0.26 mmol) was added to a solution of **1** (144 mg, 0.23 mmol) in 10 mL of CH_2Cl_2. The solution was completely degassed by performing several freeze-pump-thaw cycles and was then saturated with CO. After 18 h, the mixture had become yellow, TlCl was filtered off, and the solvent was removed in vacuo. The residual yellow solid was washed with diethyl ether (3 × 20 mL) and dried in vacuo to give **2** (96%) as a yellow powder (decomposing at 248°C). For analytical data, see Table 8. – HR-FAB: calcd. 633.1050; found 633.1072.

Preparation of *tripod*CpL_2RuCN (3a): KCN (20 mg, 0.31 mmol) was added to a solution of **1** (150 mg, 0.23 mmol) in 10 mL of CH_3OH. After refluxing for 15 min, the solution became lemon-yellow. The solvent was then removed and the residue was filtered through a plug of SiO_2 (∅: 2 cm, *l*: 5 cm) using < 300 mL of ethanol. Removal of the solvent from the filtrate afforded **3a** (81%) as a lemon-yellow powder, which was found to decompose above 242°C. Crystals suitable for X-ray analysis were obtained by solvent diffusion from a saturated $CDCl_3$ solution of **3a** at 25°C. For analytical data, see Table 8. – HR-EI: calcd. 631.1132; found 631.1170.

A: General Procedure for the Synthesis of [*tripod*$CpL_2RuL']^+$ Complexes (L′ = nitrile, isonitrile, allenylidene, vinylidene, and carbene;

3c, 4a, 4b, 6, 7b, 7c, and 8): To methanol (20 mL) were added *tripod*CpL_2RuCl **1** (190 mg, 0.3 mmol) and NH_4PF_6 (100 mg, 0.61 mmol) to give an orange suspension. An excess of the appropriate nitrile, isonitrile, or alkyne (Table 14) was then added to the solution, which was subsequently stirred for up to 18 h at 25°C or for up to 1 h under reflux. When the reaction was complete, the reaction mixture had changed colour − yellow in the case of nitriles and isonitriles, red-brown or purple with alkynes. The solvent was then evaporated in vacuo and the residue was redissolved in CH_2Cl_2. The resulting solution was filtered to remove NH_4Cl and the excess NH_4PF_6. The solvent was then evaporated once more and the residual solid was washed with diethyl ether (3 × 10 mL) to give the PF_6 salt of [*tripod*CpL_2RuL']$^+$ in analytically pure form. For analytical data, see Tables 9 to 12.

B: General Procedure for the Synthesis of [*tripod*CpL_2RuL']$^+$ Complexes (L′ = vinylidene, η²-alkynyl; 7a, 5): To a suspension of *tripod*CpL_2RuCl **1** (190 mg, 0.3 mmol) and $TlPF_6$ (115 mg, 0.31 mmol) in CH_2Cl_2 (15 mL) was added a fivefold excess of the appropriate alkyne (Table 14). Upon stirring at 25 °C for 18 h, the initially orange solution became yellow. The reaction mixture was then filtered, the filtrate was concentrated in vacuo, and the residue was washed with diethyl ether (3 × 10 mL) to give the PF_6 salts of the corresponding [*tripod*CpL_2RuL']$^+$ complexes in analytically pure form. For analytical data, see Tables 10, 11, and 14.

C: General Procedure for Transformation of Vinylidene Compounds (7) into Alkynyl Compounds (9): To a solution of 0.25 mmol of the appropriate vinylidene compound in 10 mL of methanol, sodium methoxide solution (prepared by treating 5 mg of Na with 10 mL of methanol) was added dropwise over a period of 1 min. The solution immediately turned yellow. After stirring for 1 h at 25°C, the solvent was removed in vacuo. The residue was redissolved in CH_2Cl_2, the resulting solution was filtered, and the solvent was removed once more. The product was extracted with diethyl ether (3 × 10 mL) and was in each case obtained as a lemon-yellow waxy powder (Table 14). For analytical data, see Tables 13 and 14.

D: General Procedure for Alkylations: To a solution of 0.3 mmol of **3a** or **9** in 10 mL of CH_2Cl_2 was added 0.05 mL of $F_3CSO_3CH_3$. After stirring for 15−30 min at 25 °C, the resulting mixture became almost colourless in the case of **3a** and red in the case of **9**. After filtration, the filtrate was concentrated in vacuo and the residue was washed with diethyl ether (3 × 10 mL). For analytical data, see Tables 9, 12, and 14.

Acknowledgments

This work was supported by the German Science Foundation (SFB 247) and the Fonds der Chemischen Industrie. A generous loan of ruthenium(III) chloride from Degussa AG, Frankfurt, is gratefully acknowledged. We are indebted to Dr. J. Groß and Mr. T. Jannack for performing mass spectrometric measurements, to Mr. D. Günauer for carrying out cyclovoltammetric experiments, and to the staff of the microanalytical laboratory of the Organisch-Chemisches Institut der Universität Heidelberg for providing elemental analyses.

[1] [1a] See for example: H. Brunner, *Top. Curr. Chem.* **1975**, *56*, 67−90. − [1b] H. Brunner, *Acc. Chem. Res.* **1979**, *12*, 250−257. − [1c] W. E. Watts, in: *Comprehensive Organomet. Chem.* **1982**, *Vol. 8*, 1013−1071 and references therein. − [1d] J. M. O′Connor, C. P. Casey, *Chem. Rev.* **1987**, *87*, 307−318.

[2] [2a] A. R. Cutler, K. Hanna, J. C. Vites, *Chem. Rev.* **1988**, *88*, 1363−1403. − [2b] M. Brookhart, W. B. Studabaker, *Chem. Rev.* **1987**, *87*, 411−432. − [2c] S. G. Davies, I. M. Dordor-Hedgecock, P. J. C. Easton, S. C. Preston, K. H. Sutton, J. C. Walker, *Bull. Soc. Chim. Fr.* **1987**, *124*, 608−630.

[3] H. Brunner, *Adv. Organomet. Chem.* **1980**, *18*, 151−206.

[4] S. G. Davies, J. P. McNally, A. J. Smallridge, *Adv. Organomet. Chem.* **1990**, *30*, 1−76.

[5] This problem has been analysed by quantum chemical modelling: T. Ward, O. Schafer, C. Daul, P. Hofmann, *Organometallics* **1997**, *16*, 3207−3215. It is found experimentally that compounds with 3d metals are less rigid than those containing 4d metals; cf. ref.[28a]

[6] [6a] H. Brunner, *Angew. Chem.* **1969**, *81*, 395; *Angew. Chem. Int. Ed. Engl.* **1969**, *8*, 382. − [6b] H. Brunner, *Angew. Chem.* **1971**, *83*, 274−285; *Angew. Chem. Int. Ed. Engl.* **1971**, *10*, 249. − [6c] H. Brunner, J. Aclasis, M. Langer, W. Steger, *Angew. Chem.* **1974**, *86*, 864−865; *Angew. Chem. Int. Ed. Engl.* **1974**, *13*, 810. − [6d] H. Brunner, K. Fisch, P. G. Jones, J. Salbeck, *Angew. Chem.* **1989**, *101*, 1558−1559; *Angew. Chem. Int. Ed. Engl.* **1989**, *28*, 1521.

[7] [7a] B. Antelmann, U. Winterhalter, G. Huttner, B. C. Janssen, J. Vogelgesang, *J. Organomet. Chem.* **1997**, *545−546*, 407−420. − [7b] B. Antelmann, G. Huttner U. Winterhalter, *J. Organomet. Chem.* **1998**, *553*, 433−441.

[8] [8a] B. Antelmann, G. Huttner, J. Vogelgesang, O. Walter, U. Winterhalter, *J. Organomet. Chem.* **1997**, *549*, 139−148. − [8b] B. Antelmann, G. Huttner U. Winterhalter, *J. Organomet. Chem.* **1998**, *555*, 119−125. − [8c] J. Vogelgesang, Diplomarbeit, **1996**, Heidelberg.

[9] M. I. Bruce, C. Hameister, A. G. Swincer, R. C. Wallis, *Inorg. Synth.* **1982**, *21*, 78−80.

[10] I. P. Evans, A. Spencer, G. Wilkinson, *J. Chem. Soc., Dalton Trans.* **1973**, 204−209.

[11] P. S. Hallmann, T. A. Stephenson, G. Wilkinson, *Inorg. Synth.* **1970**, *12*, 238−240.

[12] F. Morandini, G. Consiglio, B. Straub, G. Ciani, A. Sironi, *J. Chem. Soc., Dalton Trans.* **1983**, 2293−2298.

[13] Structure: [13a] M. I. Bruce, F. S. Wong, B. W. Skelton, A. H. White, *J. Chem. Soc., Dalton Trans.* **1981**, 1398−1405. − Reactivity: [13b] P. M. Treichel, D. A. Komar, P. J. Vincenti, *Inorg. Chim. Acta* **1984**, *88*, 151−152. − [13c] P. M. Treichel, P. J. Vincenti, *Inorg. Chem.* **1985**, *24*, 228−230. − [13d] H. E. Bryndza, P. J. Domaille, R. A. Paciello, J. E. Bercaw, *Organometallics* **1989**, *8*, 379−385.

[14] T. Blackmore, M. I. Bruce, F. G. A. Stone, *J. Chem. Soc., A* **1971**, 2376−2382.

[15] M. I. Bruce, R. C. Wallis, *Aust. J. Chem.* **1981**, *34*, 209−213.

[16] G. S. Ashby, M. I. Bruce, I. B. Tomkins, R. C. Wallis, *Aust. J. Chem.* **1979**, *32*, 1003−1016.

[17] B. E. R. Schilling, R. Hoffmann, D. L. Lichtenberger, *J. Am. Chem. Soc.* **1979**, *101*, 585−591.

[18] [18a] N. G. Bokiy, Yu. V. Gatilov, Yu. T. Struchkov, N. A. Ustynyuk, *J. Organomet. Chem.* **1973**, *54*, 213−219. − [18b] R. G. Ball, M. R. Burke, J. Takats, *Organometallics* **1987**, *6*, 1918−1924. − [18c] J. R. Lomprey, J. P. Selegue, *J. Am. Chem. Soc.* **1992**, *114*, 5518−5523.

[19] [19a] M. I. Bruce, A. G. Swincer, *Adv. Organomet. Chem.* **1983**, *22*, 59−127. − [19b] M. I. Bruce, *Chem. Rev.* **1991**, *91*, 197−257.

[20] J. Silvestre, R. Hoffmann, *Helv. Chim. Acta* **1985**, *68*, 1461−1506.

[21] Y. Wakatsuki, N. Koga, H. Yamazaki, K. Morokuma, *J. Am. Chem. Soc.* **1994**, *116*, 8105−8111.

[22] I. de los Ríos, M. J. Tenorio, M. C. Puerta, P. Valerga, *J. Am. Chem. Soc.* **1997**, *119*, 6529−6538.

[23] Y. Wakatsuki, N. Koga, H. Werner, K. Morokuma, *J. Am. Chem. Soc.* **1997**, *119*, 360−366.

[24] [24a] H. Werner, *Angew. Chem.* **1990**, *102*, 1109−1212, *Angew. Chem. Int. Ed. Engl.* **1990**, *29*, 1077. − [24b] H. Werner, *Nachr. Chem. Tech. Lab.* **1992**, *40*, 435−444. H. Werner, *J. Organomet. Chem.* **1994**, *475*, 45−55. − [24c] A. Höhn, H. Otto, M. Dziallas, H. Werner *J. Chem. Soc., Chem. Commun.* **1987**, 852−854. − [24d] A. Höhn, H. Werner, *J. Organomet. Chem.* **1990**, *382*, 255. − [24e] F. J. Garcia Alonso, A. Höhn, J. Wolf, H. Otto, H. Werner, *Angew. Chem.* **1985**, *97*, 401−402, *Angew. Chem. Int. Ed. Engl.* **1985**, *24*, 406.

[25] [25a] J. P. Selegue, *Organometallics* **1982**, *1*, 217−218. − [25b] H. Le Bozec, K. Ouzzine, P. H. Dixneuf, *J. Chem. Soc., Chem. Commun.* **1989**, 219−221.

[26] N. M. Kostic, R. F. Fenske, *Organometallics* **1982**, *1*, 974−982.

[27] [27a] G. Consiglio, F. Bangeter, C. Darpin, *Organometallics* **1984**,

3, 1446−1448. − [27b] M. P. Gamasa, J. Gimeno, E. Lastra, B. M. Martin, *Organometallics* **1992**, *11*, 1373−1381.
[28] [28a] G. Consiglio, F. Morandini, *Chem Rev.* **1987**, *87*, 761−778. − [28b] G. Consiglio, F. Morandini, *Inorg. Chim. Acta* **1987**, *127*, 79−85.
[29] [29a] S. Abott, S. G. Davies, P. Warner, *J. Organomet. Chem.* **1983**, *246*, C65−C68. − [29b] R. M. Bullock, *J. Chem. Soc., Chem. Commun.* **1989**, 165−167. − [29c] M. I. Bruce, G. A. Koutsantonis, *Aust. J. Chem.* **1991**, *44*, 207−217.
[30] M. I. Bruce, R. C. Wallis, *Aust. J. Chem.* **1979**, *32*, 1471−1485.
[31] WIN-DYNAMICS 1.0 Release 951220, *NMR Dynamic Spectra Simulation and Iteration*, Bruker-Fanzen Analytik GmbH and K. Ill′yasow, O. Nedopekin, Bremen, Germany.
[32] *Organikum*, Deutscher Verlag der Wissenschaften, Berlin, **1990**.
[33] "Collect" data collection software, Nonius, **1998**.
[34] [34a] G. M. Sheldrick, *SHELXS-97, Program for Crystal Structure Solution*, University of Göttingen, **1997**. − [34b] G. M. Sheldrick, *SHELXL-97, Program for Crystal Structure Refinement,* University of Göttingen, **1997**. − [34c] *International Tables for X-ray Crystallography*, vol. 4, Kynoch Press, Birmingham, U.K., **1974**.
[35] L. Zsolnai, G. Huttner, *XPMA, http://www.rzuser.uni-heidelberg.de/v54/xpm.html,* Universität Heidelberg, **1994**.
[36] A. M. Z. Slawin, D. J. Williams, J. Crosby, J. A. Ramsden, C. White, *J. Chem. Soc., Dalton Trans.* **1988**, 2491−2494.

Received June 23, 1999
[I99229]

Synthesis, Crystal Structures and Lithium Encapsulation by Some Phenolic Aza Cages

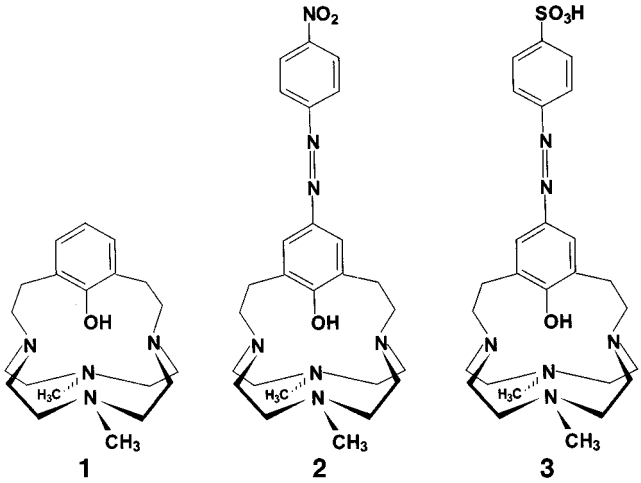
Mauro Micheloni,*[a] Mauro Formica,[a] Vieri Fusi,*[a] Paolo Romani,[a] Roberto Pontellini,[a] Paolo Dapporto,[b] Paola Paoli,[b] Patrizia Rossi,[b] and Barbara Valtancoli[c]

Keywords: Cages / Synthesis / Lithium / Crystal structures / Chromophores

Three new macrocyclic cages **1**, **2** and **3**, able to selectively encapsulate the lithium ion, were studied. The synthesis and characterization of **2** and **3** are reported. The basicity behaviour of the three cages was investigated by spectrophotometry and by ^{1}H and ^{13}C NMR spectroscopy. The protonation constants were determined by potentiometric methods in aqueous solution (I = 0.15 mol dm^{-3} NMe_4Cl, T = 298 ± 0.1 K) and were found to be logK_1 = 11.67(5), 10.77(7), 11.17(7); logK_2 = 7.76(5), 5.7(1), 5.6(1); logK_3 = 1.3(1), 2.4(1), 1.9(1) for **1**, **2**, and **3**, respectively. The lithium equilibrium complex formation $Li^+ + L = LiL_{H-1} + H^+$ was monitored by ^{13}C and ^{7}Li NMR spectroscopy, as well as by spectrophotometric and potentiometric techniques; log values of –9.1(1) and –8.0(1) were found for **1** and **3**, respectively. For **2**, precipitation of the lithium complex occurs. UV/Vis studies in aqueous solution show a significant shift towards high energy of the λ_{max} in the lithium complex, indicating the potential for application of these ligands in colourimetric analysis. The crystal structure of **1** was examined by single crystal X-ray diffraction. Data collection was performed on two samples, namely **1a** and **1b**, obtained from two different crystallization procedures. Crystals of **1a** are monoclinic, space group $P2_1/n$, while **1b** crystallized in an orthorhombic space group $Pc2_1b$. The cell parameters are a = 12.423(3), b = 14.378(9), c = 28.436(7) Å, β = 93.74(2)° for **1a**, and a = 10.674(4), b = 14.408(2), c = 17.034(2) Å for **1b**. Molecular simulations were carried out on both conformational isomers **1a** and **1b**, with results indicating that the two isomers have essentially the same flexibility.

Introduction

Lithium is a very important element and is certainly one of the most studied alkaline earth metals.[1] Lithium derivatives are important in many fields, ranging from high-performance batteries to the treatment of patients affected by manic depression.[2–5] Lithium ions have also been shown to exert antiviral activity against DNA-type viruses,[6] although the mechanisms by which Li^+ is involved in biological systems are unknown. Neither the natural nor the synthetic molecules available to date are selective enough to preferentially bind lithium ions under physiological conditions. Furthermore, the similarity of their chemical behaviour to that of other alkaline metal ions[7] makes the design of ligands able to selectively bind the lithium ion in the presence of sodium in aqueous solution very challenging. In this paper, we report a study of three new compounds **1**, **2** and **3** (see Scheme 1) able to encapsulate the lithium ion in aqueous solution. These novel chromoionophores exhibit high selectivity for Li^+ over the other alkaline ions in water and in alcohol solutions, leading to changes in the optical properties of the chromophore. Compound **1** can be considered as the precursor of compounds **2** and **3** in which azo chromophores external to the molecular cavity have been added. The aim of this work was to investigate whether or not the chromophores were sensitive to the Li^+ binding.



Scheme 1. Ligand drawing

Results and Discussion

Equilibrium Studies

All macrocycles behave as triprotic bases (see Table 1), although they possess five protonation sites. One proton cannot be removed even at very high pH values. The ^{1}H NMR spectra of the neutral species carried out in $CDCl_3$

[a] Institute of Chemical Sciences, University of Urbino, Piazza Rinascimento No. 6, I-61029 Urbino, Italy, Fax: (internat.) + 39-0722/350032
E-mail: mauro@chim.uniurb.it
[b] Department of Energetics "Sergio Stecco", University of Florence, Italy
[c] Chemistry Department, University of Florence, Italy

 © WILEY-VCH Verlag GmbH, D-69451 Weinheim, 2000 1434–1948/00/0101–0051 $ 17.50+.50/0

show a peak at δ = 10.1, 9.8 and 9.6 for the species **1**, **2**, and **3**, respectively, each integrating for one proton. These resonances were assigned to the deshielded acidic proton.[8−10] Upon addition of H_2O or CH_3OH to the chloroform solution, the signals did not disappear, indicating a slow exchange on the NMR time scale with the mobile protons of the solvent. Instead, the resonance disappeared when D_2O or CD_3OD was added. The value of the resonances, together with the experimental evidence, suggest that the proton is stabilized inside the macrocyclic cavity by a network of hydrogen bonds involving the phenolic and amine functional groups. The values of the stepwise basicity constants (see Table 1) indicate that all compounds are rather strong bases in the first, measurable step of protonation. Cage **1** is only slightly more basic than **2** and **3**; this is also true in the second basicity step: $\log K_2 = 7.76$ for **1** (see Table 1) versus $\log K_2 = 5.7$ and $\log K_2 = 5.6$ for **2** and **3**, respectively. The presence of bulky electron-withdrawing substituents on the aromatic ring in **2** and **3** but not in **1** may explain this moderate difference in basicity. In all three compounds, there is a marked decrease in the basic strength as the degree of protonation increases. This behaviour is expected for all aza cages,[11] in which positive charges are forced close to each other as a result of the molecular topology, thus making further addition of protons less energetically favoured.

The ^{13}C NMR spectrum recorded in D_2O at pH = 4, where the $[H_2\mathbf{1}]^{2+}$ species is prevalent in solution, showed twelve peaks, due to a reduced C_s symmetry in solution on the NMR time scale, instead of the expected C_{2v}.[12] Analysis of the spectrum revealed that the symmetry element lost is the plane passing through the bridgehead nitrogen atoms, while the other plane containing the nitrogen atoms, the methyl group and the phenolic oxygen atom is preserved. The ^{13}C NMR spectra of the triprotonated species of the other two ligands showed a similar pattern. This feature was attributed to the stiffened conformation of the protonated ligand that hinders the free interconversion of the phenolic fragment inside the macrocyclic cavity.

The involvement of the phenolic group in the protonation steps is well demonstrated by the UV/Vis absorption spectra of the ligands recorded at different pH values in water, as shown in Table 2. This spectral feature suggests that in the neutral species (L), the acidic proton is located on the tetraaza base, while the chromophore is in its anionic form. In fact, for all the ligands it was possible to observe a bathochromatic shift of the main wavelength from the acidic to the basic field. This different behaviour of the chromophore in the opposite pH fields for all the ligands can be attributed to the deprotonation of the phenolic group. The change in λ_{max} is due to the presence of the phenol hydroxy form at low pH values and to the phenolate form for **1**, or to the tautomeric hydrazone form for **2** and **3**.

Cage **1** shows a different behaviour in methanolic solution: The absorption spectra for the phenolic group do not change when the pH is varied from acidic to alkaline values, and the same wavelength and molar absorptivity (λ = 272 nm, ε = 1400 M^{-1} cm^{-1}) are conserved. In other words, the phenolic group always appears in its hydroxy form. This behaviour could be explained by the different solvation power of the two media, allowing the charge separation in water that is less favourable in methanol.

Table 1. Protonation and lithium equilibrium constants of **1**, **2** and **3** ($\log K$) in aqueous solution (298 ± 0.1 K, I = 0.15 mol dm^{-3} NMe_4Cl)

Reaction	**1**	**2**	**3**
$L + H^+ = HL^+$	11.67(5)[a]	10.77(7)	11.17(7)
$HL^+ + H^+ = H_2L^{2+}$	7.76(5)	5.7(1)	5.6(1)
$H_2L^{2+} + H^+ = H_3L^{3+}$	1.3(1)	2.4(1)	1.9(1)
$Li^+ + L = LiL_{H-1} + H^+$	−9.1(1)		−8.0(1)

[a] Values in parentheses are the standard deviation in the last significant figure.

Lithium Complexation

Direct potentiometric measurements indicate that compounds **1** and **3** bind lithium selectively (see Table 1). In the case of **2**, precipitation of the lithium complex prevents any equilibrium constant determination. The equilibrium constants reported in Table 1 for **1** and **3** refer to an overall process in which the Li^+ is bound and, at the same time, the last proton present in the cage is removed, yielding a neutral LiL_{H-1} species ($Li^+ + L = LiL_{H-1} + H^+$). Because the protonation constant involved is too high to be measurable in the absence of Li^+, as stated in the previous section, the stability constants relative to the neat complexation process $Li^+ + L_{H-1}{}^- = LiL_{H-1}$ can only be estimated. The $\log K$ for the process $H^+ + L_{H-1}{}^- = L$ should be significantly greater than 11.67 and 11.17 for **1** and **3**, respectively, and, because values of 9.1 and 8.1 (see Table 1) should be subtracted, a $\log K > 3$ is expected for the neat complexation process ($Li^+ + L_{H-1}{}^- = LiL$) for both cages.

The coordination of the alkaline metal ions by ligands **1**, **2** and **3** was also investigated by ^1H, ^{13}C and ^7Li NMR techniques. Using ^1H and ^{13}C NMR spectroscopy as a diagnostic technique, no evidence was found for complex formation with sodium and potassium ions in both aqueous and alcoholic solution. Instead, all the ligands readily bind the smallest Li^+ and the solid complexes were isolated as reported in the Experimental Section.

These solid compounds are soluble in organic solvents such as $CDCl_3$ and their ^7Li NMR spectra present a sharp peak, shifted by 1.0, 0.9, and 0.9 ppm downfield for **1**, **2**, and **3**, respectively, relative to that of the free ion. The ^7Li NMR spectrum of the $Li[Li\mathbf{3}_{H-2}]$ species in $CDCl_3$ presents another resonance at δ = 0, attributed to the lithium ion, which is not complexed due to the stoichiometry of the species; these chemical shift values were preserved in other solvents such as CD_3OD or CD_3CN. When an excess of Li^+ was added to an alkaline alcohol solution of **1** or **2**, the ^7Li NMR spectra also contained two peaks, one for the complexed and one for the free solvated ion. The presence of two types of lithium ion resonances indicates that the

ions do not exchange their positions on the NMR time scale.

The UV/Vis electronic experiments in aqueous solution revealed a shift toward higher energy of the maximum wavelength (λ_{max}) in the lithium complexes relative to those of the free amine (Table 2). The difference between the λ_{max} of the two spectra is 25 nm (see Table 2) for **2**, allowing a visible colour change. For **3**, the difference is smaller (18 nm), but still significant.

The UV/Vis absorption spectra demonstrated that for **1**, the last acidic proton is not removed even in strongly alkaline media. If we compare the ^{13}C NMR spectrum of the [Li**1**$_{H-1}$] species with that recorded in alkaline alcoholic solution for ligand **1** (see Figure 1), it is possible to observe the large downfield shift of a signal that can be assigned to the carbon atoms C-9 in the α position to the phenolic oxygen atom. An upfield shift of the aromatic signals of C-6 and C-8, β and γ, respectively, to the phenolic function in the complex was also evident. This behaviour confirms that in order to interact with the lithium ion, the macrocycles must lose the last acidic proton that in other conditions remains on the cage. This is also shown by the UV/Vis spectrum of the [Li**1**$_{H-1}$] compared with that of the free amine recorded in methanol solution. In fact, the free amine shows a λ_{max} at 272 nm while the [Li**1**$_{H-1}$] complex exhibits its λ_{max} at 302 nm. These data can be explained again by the deprotonation of the hydroxy group. It should be stressed once again that when other alkali metal ions were added to an alkaline alcoholic solution no changes in the spectral feature of the ligands were detected. In other words, the complexation does not occur in the presence of alkali ions different from Li^+, even at high concentrations, indicating that ligands **1**−**3** are able to completely discriminate Li^+ from the other alkali ions. This selectivity could be related to the small dimensions of the macrobicyclic cavity, in which larger ions cannot be encapsulated.

Table 2. UV/Vis spectra characteristics (λ_{max} and $\varepsilon[\lambda_{max}]$) of compounds **1**, **2** and **3** in aqueous solution at pH = 2, 12, > 12 and their lithium complexes

Compound	λ_{max} [nm] pH = 2	pH = 12	pH > 12	$\varepsilon[\lambda_{max}]$ M^{-1} cm^{-1} pH = 2	pH = 12	pH > 12
1	278	294	294	760	1540	1540
[Li**1**$_{H-1}$]			292			2000
2	486	512	550	9400	20900	21100
[Li**2**$_{H-1}$]			525			18800
3	347	464	490	16700	13600	13700
[Li**3**$_{H-2}$]			472			11000

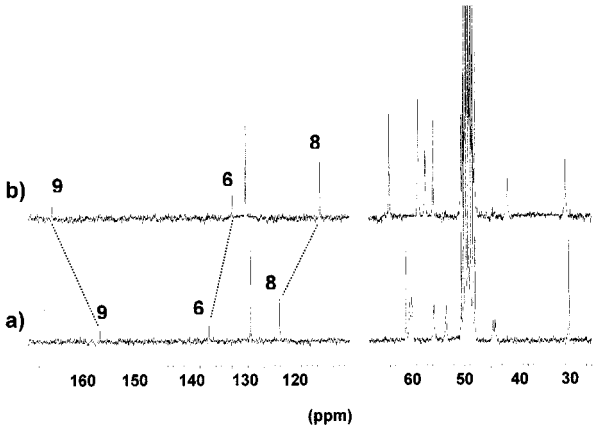


Figure 1. ^{13}C NMR spectra in methanol solution of the free ligand **1** (a) and of the [Li**1**$_{H-1}$] complex (b)

X-ray Structures

$C_{20}H_{38}N_4O{\cdot}2HClO_4$ (1a)

The crystal lattice is made up of $C_{20}H_{34}N_4O^{2+}$ cations $[H_2\mathbf{1}]^{2+}$ and perchlorate counterions; two independent $[H_2\mathbf{1}]^{2+}$ protonated ligands are present in the asymmetric unit. Several geometrical parameters characterising the 3D-arrangement of the two macrobicycles are reported in Table 3. The overall shapes of the two independent cations appear to be identical. As a consequence Figure 2 shows only one independent $[H_2\mathbf{1}]^{2+}$ cation. Interestingly, both cations show the same unusual sequence of torsion angles defining the conformation of the [12]aneN_4 ring, which was found to be of the [2334] type.[13] Analysis of the solid-state structures[14] collected in the Cambridge Structural Database[15] revealed that the [12]aneN_4 diprotonated ring always adopts a square C-corner[3333] conformation with only one exception ([2424] type[14b]), and as expected all the retrieved species are *trans*-diprotonated. In our case, the acidic hydrogen atoms were not localized; however, considering a *trans* disposition, the methylated nitrogen atoms appear to be the sites most likely to undergo protonation. In fact, taking into account the geometry of the fourth position at the nitrogen atoms, i.e. the distance between the two protons, this is the arrangement that best minimizes the electrostatic repulsion of the two positive charges. Given this disposition of the two protons, there would be, besides two pairs of N−H···N hydrogen bonds, an N4···O1 (N6···O2) hydrogen bond and a favourable interaction between the hydrogen atom on N2 (N8) and the aromatic ring. The line connecting the N2 (N8) with the C_6 centre of mass is almost perpendicular to the phenyl ring [80.2(5)°, 81.6(4)°] for the two independent cations.

Each oxygen atom of both the phenol moieties interacts with two oxygen atoms provided by two perchlorate counterions (O1···O16 3.23(2), O1···O18 2.87(2), O2···O12 3.11(2), O2···O11 2.93(2) Å).

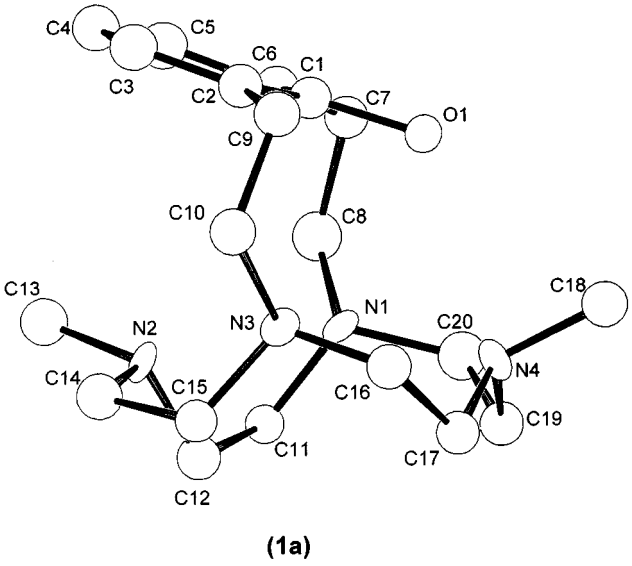
$C_{20}H_{34}N_4O{\cdot}2HClO_4{\cdot}H_2O$ (1b)

The asymmetric unit is composed of one $C_{20}H_{34}N_4O^{2+}$ cation ($H_2\mathbf{1}^{2+}$), two ClO_4^- counterions and one water molecule. Figure 2 shows the structure of **1b** as determined by X-ray diffraction. The four nitrogen atoms N1, N2, N3 and

Table 3. Geometrical parameters characterizing compounds **1a** and **1b**[a]

Selected distances [Å]	**1a**	**1a′**	**1b**
N2−phenyl plane	3.55(1)	3.58(1)	3.359(5)
H2N−phenyl plane	−	−	2.3(1)
H4N−O1	−	−	1.92(7)
N4−O1	2.79(2)	2.77(2)	2.756(7)
N4−N1	3.05(2)	3.01(2)	2.899(7)
N4−N3	3.02(2)	3.03(2)	3.070(7)
N2−N1	2.85(2)	2.86(2	3.116(6)
N2−N3	2.91(2)	2.87(2)	2.992(7)
H2N−N3	−	−	2.8(1)
H2N−N1	−	−	2.8(1)
H4N−N1	−	−	2.41(5)
H4N−N3	−	−	2.59(5)
N1−N3	4.10(2)	4.08(2)	3.848(6)
Angles [°]			
phenyl plane−$N_1N_2N_3N_4$ plane	17.7(1)	19.4(4)	15.1(1)
N2−phenyl[b]	80.2(5)	81.6(4)	87.96(2)

[a] For the **1a′** cation we have: N5, N8, N7 and N6 instead of N1, N2, N3 and N4, respectively. − [b] Angle between the vector N2−centre of the phenol ring and the C_6H_5 plane.



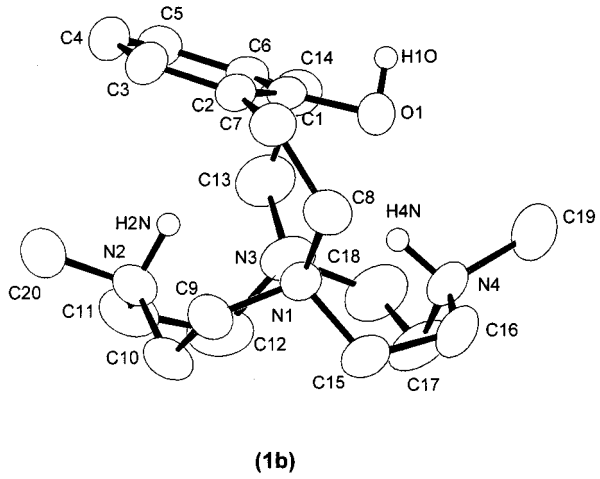


Figure 2. ORTEP view of the cations **1a** and **1b**; for sake of clarity, only one independent cation of the **1a** species is reported

N4 lie in a plane, with a maximum deviation of 0.121(6) Å (for N4) from the mean plane. The angle between the N_4 mean plane and that described by the phenyl ring is 15.5(1), with the hydrogen atom H1O directed out of the macrocyclic cavity.

Some short hydrogen bonds, involving the hydrogen atoms bonded to the N2 and N4 atoms, ranging from 1.92(7) to 2.8(1) Å (see Table 3) are present. In particular, the distance between the hydrogen atom H2N and the phenyl plane is rather short [2.3(1) Å] and the N2−H2N bond direction is almost perpendicular to the phenyl ring [87.96(2)°].[16] These interactions could confer a certain rigidity to the cation (see Figure 2). The macrocycle assumes a [3333] conformation, the most common for this type of ligand. The hydrogen atom H1O is outside the cavity and interacts with the oxygen atom of a water molecule [H1O···O10 2.46(8) Å] and with an oxygen atom of a perchlorate ion [H1O···O4 2.79(8) Å].

The shapes of the two conformational isomers (**1a** and **1b**) are similar, despite the different conformation of the [12]aneN_4 ring, as proved by the very similar values for the angles between the phenyl plane and the N_4 mean plane (see Table 3). The distance from N2 (N8 in **1a′**) to the phenyl plane is almost similar in all the structures, and the vector (N2−centre of the ring) is quite perpendicular to this plane for every isomer. Given this 3D similarity between **1a** and **1b**, the hypothesis about the localization of the protons in isomer **1a** appears to be likely.

Molecular Modelling Results

The first goal of the molecular modeling study was to gain some idea of the relative stability of the two conformational isomers of $[H_2\mathbf{1}]^{2+}$ found from the X-ray analyses. Geometric optimizations of **1a** and **1b**, starting from their solid-state structures and performed with both the force fields (CVFF and CFF91), maintained the original arrangement for the tetraaza ring as well as the orientation of the phenol arm. The two isomers were found to be almost isoenergetic once optimized by using CVFF, while the CFF91 potential shows a slight preference for the [3333] sequences of dihedrals which appears to be more stable by ca. 3 kcal.

Concerning the dynamics study, Table 4 reports the temperature of several MD runs performed on **1a** and **1b** using both the above-mentioned potential types. The aim was to test the conformational freedom of this cage, which could appear rather rigid, both due to the steric hindrance of the

phenol group and the network of hydrogen bonds. The analysis of the trajectories extracted during the MD runs underlined the fact that, in both the conformers, the phenol moiety can oscillate above the tetraaza ring, thus taking the hydroxy group into the other part of the cage in an equivalent position. It is worth noting that these results are in agreement with that found in the NMR solution experiments: the neutral species is more flexible than the triprotonated species.

Vacuum results show that using the CVFF force field, both **1a** and **1b** interconvert at 800 K. With the CFF91 force field, on the other hand, we noted that while **1a** already interconverts at 1300 K, 1400 K is needed to rearrange **1b**. Interestingly, the transition state reached during the rearranging of the [3333] cage (**1b**) was detected (T = 900 K, force field CVFF) (Figure 3). It is characterized by a [2334] sequence of torsions in the N_4-cyclododecane moiety, the phenol moiety being almost perpendicular to the N_4 mean plane (89°), with the hydrogen atom of the hydroxy group lying 0.3 Å out of the plane described by the bonded oxygen atom and the two bridgehead nitrogen atoms. Finally, the hydrogen atom of the hydroxy group is involved in a hydrogen bond interaction with one of the bridgehead nitrogen atoms (1.73 Å), while the oxygen atom comes into close contact with both the hydrogen atoms of the *N*-methylated groups (1.73 and 1.86 Å).

MD calculations performed in water show that both the conformational isomers interconvert at 1100 K with the CVFF force field and at 1300 K with the CFF91 one. It is noteworthy that the "umbrella" inversion affects a methylated nitrogen atom of both cations already at 800 K with the force field CVFF, 900 K with CFF91. To obtain some information about the relative flexibility of the two isomers, the mean square displacement (MSD) of two pseudoatoms defined as the geometric centre of the $N_4(CH_3)_2$ moiety and of the C_6H_5O group was monitored during each MD run: No significant trend was detected either in vacuo or in solvent, i.e., the flexibility of the two conformational isomers is nearly identical.

Table 4. Temperatures of the MD simulations performed with the CVFF and CFF91 force fields; the temperature at which the "interconversion" of the phenol group (see text) takes place is reported in bold

Compound	CVFF		CFF91	
	Vacuum	Water	Vacuum	Water
1a	300	300	300	900
	600	600	900	1100
	750	700	1200	**1300**
	770	800	**1300**	1500
	800	900	1500	
	900	**1100**	1800	
1b	300	300	300	900
	600	600	900	1100
	750	700	1200	**1300**
	770	800	1300	1500
	800	900	1350	
	900	**1100**	**1400**	
			1500	
			1800	

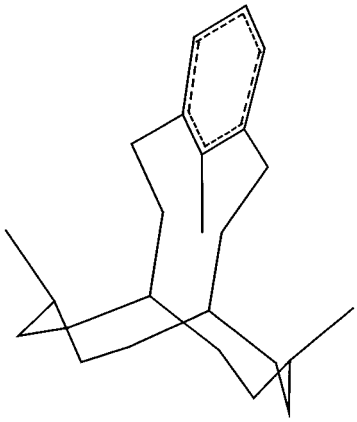


Figure 3. View of the transition state of cation **1b** (MD at 900 K, force field: CVFF) obtained by using the InsightII (MSI) graphics program

Conclusions

The molecular topology of compounds **1**−**3** is characterized by the presence of a three-dimensional macrocyclic cavity and of a chromophoric group sensitive to the lithium complexation and to the protonation step. It was possible to show that **1**−**3** do not lose the last acidic proton in aqueous solution under the experimental conditions used. Compound **1** shows different proton location in the neutral species in water or in alcoholic solution. All three ligands are able to selectively bind the lithium ion in either aqueous or alcoholic solution, exhibiting selectivity over the other alkaline metal ions. This remarkable selectivity is attributed to the small dimensions of the macrocyclic cavity, in which alkali metals larger than lithium cannot be encapsulated. The coordination of Li^+ perturbs the optical properties of the chromophore in solution, leading to a modification in the electronic absorption spectra. The colour change in aqueous solution for compounds **2** and **3** is in the range of the visible frequencies, while **1** undergoes a better variation in methanol solution. This behaviour provides an opportunity to use compounds **1**−**3** in reagents for colourimetric analysis. In instances where the extraction mode is applicable, all the chromoionophores can be used. In fact, all the solid lithium complexes isolated and characterized show high solubility in organic solvents such as $CHCl_3$.

Experimental Section

General Remarks: ^1H, ^{13}C and ^7Li NMR spectra were recorded with a Bruker AC-200 instrument, operating at 200.13, 50.33 and 77.78 MHz, respectively. In ^1H NMR experiments peak positions are reported relative to HOD (δ = 4.75) and dioxane was used as reference in ^{13}C NMR spectra (δ = 67.4). ^7Li peaks are reported relative to free $LiClO_4$. ^1H-^1H and ^1H-^{13}C correlation experiments were performed to assign the signals. Solvents and starting products were used as purchased. − Spectrophotometric measurements: Absorption spectra were recorded at 298 K with a Varian Cary-100 equipped with a temperature control unit. − Potentiometric measurements: All potentiometric measurements were carried out in 0.15 mol dm^{-3} Me_4NCl at 298.0 ± 0.1 K, in the pH range 2−11,

using the fully automatic equipment that has been already described.[17] The emf data were acquired with the PASAT computer program.[17] The electrode was calibrated as a hydrogen concentration probe by titrating known amounts of HCl with CO_2-free Me_4NOH solutions and determining the equivalence point by Gran's method,[18] which gives the standard potential $E°$ and the ionic product of water K_w. At least two or three measurements were performed. The HYPERQUAD[19] computer program was used to process the potentiometric data and to calculate the protonation constants. − Ligand synthesis: The synthesis of **1** has been already reported in ref.[12] For compounds **2** and **3**, the diazonium salts for the coupling reactions were freshly prepared and utilized following standard methods, starting from 4-nitroaniline or sulfanilic acid.

Synthesis of 2: A solution of **1** (346 mg, 1 mmol) in HCl (5 M, 20 mL) was cooled to 0° C and slowly added to a suspension at 0° C of diazonitrobenzene salt, freshly prepared from *p*-nitroaniline (138 mg, 1 mmol) in 30 mL of acidic water. The reaction was kept at room temperature and stirred for 2 h. The solution was made alkaline with an NaOH solution, and extracted with $CHCl_3$ (6 × 50 mL). The organic layers were collected, dried with anhydrous Na_2SO_4 and vacuum-concentrated to give an orange solid which was dissolved in ethanol and treated with 65% perchloric acid to give the diperchlorate salt of **2** as an orange solid. It was recrystallized from hot ethanol. Yield: 543 mg (78%). − ^{1}H NMR (D_2O, pH = 3): δ = 2.23 (s, 3 H), 2.71 (s, 3 H), 2.90 (m, 4 H), 3.25 (br., 8 H), 3.36 (br., 8 H), 3.45 (m, 4 H), 7.92 (s, 2 H), 7.93 (d, 2 H), 7.40 (d, 2 H). − ^{13}C NMR (D_2O, pH = 3): δ = 28.4, 43.8, 44.2, 49.4, 51.0, 55.0, 56.8, 58.0, 122.6, 126.5, 127.1, 135.3, 146.7, 148.4, 154.7, 157.4. − $C_{26}H_{39}Cl_2N_7O_{11}$ (695.21): calcd. C 44.83, H 5.64, N 14.08; found C 44.7, H 5.7, N 14.0.

Synthesis of 3: A solution of **1** (346 mg, 1 mmol) in HCl (5 M, 20 mL) was cooled to 0° C and slowly added to a suspension at 0° C of diazobenzensulfonate, freshly prepared from sulfanilic acid (173 mg, 1 mmol) in 30 mL of acidic water. The reaction was kept at room temperature for 2 h under constant stirring. The pH was adjusted to 9 and an orange solid was separated from the solution. The solid was dissolved in the minimum amount of ethanol and the solution treated with 65% perchloric acid to give the diperchlorate salt of **3** as an orange solid. It was recrystallized from hot ethanol. Yield: 534 mg (73%). − ^{1}H NMR (D_2O, pH = 3): δ = 2.04 (s, 3 H), 2.49 (br., 4 H), 2.79 (br., 8 H), 3.08 (br., 11 H), 3.38 (br., 4 H), 7.59 (s, 2 H), 7.69 (d, 2 H), 7.81 (d, 2 H). − ^{13}C NMR (D_2O, pH = 3): δ = 28.3, 42.3, 42.9, 49.6, 51.2, 55.4, 57.1, 58.8, 123.8, 125.2, 128.1, 134.5, 145.6, 148.7, 154.2, 159.1. − $C_{26}H_{40}Cl_2N_6O_{12}S$ (730.18): calcd. C 42.69, H 5.51, N 11.49; found C 42.6, H 5.6, N 11.3.

Preparation of the Complexes

[Li1] (4): A solution of LiOH (10 mg, 0.44 mmol) in methanol (15 mL) was added to a solution of **1**·2$HClO_4$ (55 mg, 0.1 mmol) in methanol (15 mL). The reaction mixture was stirred for 15 min and then concentrated to dryness. The yellow solid was suspended in $CHCl_3$ (20 mL) and the mixture was filtered to separate the inorganic excess. The organic solution was dried with Na_2SO_4. On addition of cyclohexane (25 mL), a white precipitate formed, yield 28 mg (79%). − ^{13}C NMR ($CDCl_3$): δ = 28.3, 42.7, 51.6, 56.3, 60.3, 122.7, 128.0, 134.2, 159.9. − $C_{20}H_{33}LiN_4O$ (352.28): calcd. C 68.16, H 9.44, N 15.90; found C 68.0, H 9.5, N 15.7.

[Li2] (5): This compound was synthesized from **2**·2$HClO_4$ (35 mg, 0.05 mmol) following the same procedure reported for **4** giving **5** as an orange solid, yield 21 mg (83%). − ^{13}C NMR ($CDCl_3$): δ = 28.5, 42.3, 43.4, 52.2, 55.7, 59.3, 61.4, 61.7, 123.5, 127.1, 127.6, 135.1, 145.3, 150.5 155.0, 161.2. − $C_{26}H_{36}LiN_7O_3$ (501.30): calcd. C 62.26, H 7.23, N 19.55; found C 62.1, H 7.1, N 19.3.

[$Li_2$3] (6): This compound was synthesized from **3**·2$HClO_4$ (37 mg, 0.05 mmol) following the same procedure reported for **4**, giving **6** as a violet solid, yield 19 mg (70%). − ^{13}C NMR ($CDCl_3$): δ = 30.8, 45.1, 52.0, 56.6, 59.3, 124.0, 126.9, 129.2, 134.2, 146.6, 148.2, 156.5, 160.4. − $C_{26}H_{36}Li_2N_6O_4S$ (542.28): calcd. C 57.56, H 6.69, N 15.49; found C 57.4, H 6.5, N 15.3.

Caution! Perchlorate salts of organic compounds are potentially explosive; these compounds must be handled with great care.

X-ray Crystallographic Studies: Crystallization procedure: Several attempts to obtain single crystals of $[H_2\mathbf{1}]^{2+}$ suitable for X-ray diffraction analysis were made. Finally, by slow concentration of an acidic H_2O/CH_3OH solution of $C_{20}H_{34}N_4O$(**1**)/$NaClO_4$, $[H_2\mathbf{1}]^{2+}$ single crystals were obtained. Unfortunately, the quality of the data was rather poor and a second crystallization attempt was needed. $C_{20}H_{34}N_4O$(**1**)/$NaClO_4$ was dissolved in an acidic water solution ($HClO_4$) and the solution was concentrated, affording single crystals suitable for X-ray analysis. − Crystal data and refinement details of structures **1a** and **1b** are reported in Table 5. Unit cell parameters and intensity data for compound **1a** were obtained with a Nonius CAD4 diffractometer, while for the second compound a Siemens P4 was used. Cell parameters were determined by least-squares fitting of 25 centered reflections for both structures. Intensity data were corrected for Lorentz and polarization effects. The structures were solved using the SIR-97 program[20] and subsequently refined by the full-matrix least-squares program SHELXL-93.[21] After this, absorption corrections were made using the Walker and Stuart's method.[22] The hydrogen atoms bonded to the carbon atoms were introduced in calculated positions in both cases, and their coordinates were refined in agreement with those of the linked atoms. For both structures, these hydrogen atoms were refined with an overall isotropic temperature factor [U = 0.089(7) Å^2 for **1a** and 0.074(4) Å^2 for **1b**]; the hydrogen atoms bonded to the oxygen atom and the two hydrogen atoms of the cation were not determined in structure **1a**, while in compound **1b** they were detected in difference syntheses and their positions were refined, as was the isotropic displacement parameter which converged to 0.09(3), 0.03(1) and 0.07(2) Å^2, for H2N, H4N and H1O, respectively. The hydrogen atoms of the water molecule in compound **1b** were not introduced. Atomic scattering factors and anomalous dispersion corrections for all the atoms were taken from ref.[23] Geometrical calculations were performed by PARST93.[24] The molecular plots were produced by the ORTEP program.[25] Crystallographic data (excluding structural factors) for the structures reported in this paper have been deposited with the Cambridge Crystallographic Data Centre as supplementary publication no. CCDC-128541, -128542 for **1a** and **1b**. Copies may be obtained without charge from CCDC, Union Road, Cambridge CB2 1EZ, UK [Fax: (internat.) + 44-1223/336-033; E-mail: deposit@ccdc.cam.ac.uk].

Molecular Simulations: Geometric optimizations (MM) and molecular dynamics (MD) simulations were performed on both the conformational isomers **1a** and **1b** found in the two X-ray diffraction measurements. In all cases, calculations were made by using two different force fields, CVFF and CFF91, both provided by Discover®,[26] with the aim of verifying that the behaviour of **1a** and **1b** does not depend on the force field used. Before starting the MD simulation, the geometry of each compound was optimized using the following routines: steepest descent, conjugate gradient and fi-

Table 5. Crystal data and structure refinement for **1a** and **1b**

	1a	**1b**
Empirical formula	$C_{40}H_{72}Cl_4N_8O_{18}$	$C_{20}H_{38}Cl_2N_4O_{10}$
Molecular mass	1094.86	565.44
Dimensions [mm]	0.2 × 0.4 × 0.5	0.4 × 0.5 × 0.7
Space group	$P2_1/n$	$Pc2_1b$
a [Å]	12.423(3)	10.647(4)
b [Å]	14.378(9)	14.408(2)
c [Å]	28.436(7)	17.034(2)
β [°]	93.74(2)	
V [Å^3]	5068(4)	2613(1)
Z	4	4
$\rho_{calcd.}$ [g cm^{-3}]	1.435	1.437
Radiation	0.71069	1.54180
F (000)	2320	1200
μ [mm^{-1}]	0.312	2.761
T [K]	293	293
2θ range [°]	5−36	8−130
Scan mode	θ-2θ	θ-2θ
Total reflections measured	3547	2829
Unique observed reflections	3446	2380
Reflections used	3433 [$I \geq 2\sigma(I)$]	2379 [$I \geq 2\sigma(I)$]
Refined parameters	436	341
$R(F)$,[a] for $I \geq 2\sigma(I)$	0.0852	0.0616
wR_2,[b] for $I \geq 2\sigma(I)$	0.2128	0.1669
S	0.925	0.998
a, b (weighting scheme)	0.1349, 46.65.	0.1553, 0.26
Δρ(max,min) [eÅ^{-3}]	0.343, −0.312	0.750, −0.398
Max shift/e.s.d.	0.039	0.133

[a] $R(F) = \Sigma||F_o| - |F_c||/\Sigma|F_o|$. − [b] $wR_2 = \{\Sigma[w(F_o^2-F_c^2)^2]/\Sigma[w(F_o^2)^2]\}^{0.5}$.

nally Newton-Raphson. The same sequence of algorithms was used for the molecular mechanics calculations. In the molecular dynamics, the equilibration procedure lasted 15 ps in all runs, after which the trajectories were monitored for 1500 ps, and snapshot conformations were saved every ps. MD simulations were carried out, under vacuum and in water, at different temperatures to gain some insight into the conformational freedom, i.e. the flexibility, of the two isomers (see Table 4); water calculations were performed mimicking the solvent by using a distance-dependent dielectric constant of 80.0. − Calculations were performed using the InsightII-Discover package supplied by MSI.[26] Molecular dynamics trajectories were analyzed and visualized by means of the Analysis module also provided by MSI. The computer program was implemented on a 3AT IBM computer.

Acknowledgments

Support for this research by MURST (Ministero per l'Università e la Ricerca Scientifica e Tecnologica, COFIN98) and CNR (Consiglio Nazionale delle Ricerche) is gratefully acknowledged.

[1] M. Formica, V. Fusi, M. Micheloni, R. Pontellini, P. Romani, *Coord. Chem. Rev.* **1999**, *184*, 347.
[2] R.O. Bach, *Lithium-Current Applications in Science, Medicine and Technology*, Wiley-Intercience, New York, **1985**.
[3] D. Tosteson, *Sci. Am.* **1981,** *244*, 164.
[4] J. H. Lazarus, K.J. Collard, *Endocrine and Metabolic Effects of Lithium*, Plenum, New York, **1986**.
[5] R. O. Bach, *Med. Hypotheses* **1987**, *23*, 157.
[6] R. P. Hanzlik, *Inorganic Aspects of Biological and Organic Chemistry,* Academic Press, New York, **1976.**
[7] F. A. Cotton, G. Wilkinson, *Advanced Inorganic Chemistry*, Wiley-Interscience, New York, **1988**.
[8] A. Bencini, A. Bianchi, M. Ciampolini, P. Dapporto, E. Garcia-España, M. Micheloni, P. Paoli, J. A. Ramirez, B. Valtancoli, *J. Chem. Soc., Chem. Commun.* **1989,** 701.
[9] A. Bencini, A. Bianchi, A. Borselli, M. Ciampolini, P. Dapporto, E. Garcia-España, M. Micheloni, P. Paoli, J. A. Ramirez, B. Valtancoli, *Inorg. Chem*. **1989**, *28*, 4279.
[10] A. Bencini, V. Fusi, C. Giorgi, M. Micheloni, N. Nardi, B. Valtancoli, *J. Chem. Soc., Perkin Trans. 2* **1996**, 2297.
[11] A. Bianchi, M. Micheloni, P. Paoletti, *Coord. Chem. Rev.* **1991**, *110*, 17.
[12] E. Bardazzi, M. Ciampolini, V. Fusi, M. Micheloni, N. Nardi, R. Pontellini, P. Romani, *J. Org. Chem.* **1999**, 64, 1335.
[13] I. Bernal (Ed.), *Stereochemical and Stereophysical Behaviour of Macrocycles*, Elsevier, Amsterdam, **1987**, p. 34.
[14] [14a] K. Kobayashi, S. Tsuboyama, K. Tsuboyama, T. Sakurai, T., *Acta Crystallogr., Sect. C: Cryst. Struct. Commun.* **1994**, *50*, 306. − [14b] A. Bencini, A. Bianchi, C. Bazzicalupi, M. Ciampolini, P. Dapporto, V. Fusi, M. Micheloni, N. Nardi, P. Paoli, B. Valtancoli, *J. Chem. Soc., Perkin Trans. 2* **1993**, 115. − [14c] S. Aime, A. S. Batsanov, M. Botta, J. A. K Howard, D. Parker, K. Senanayake, G. Williams, *Inorg. Chem*. **1994**, *33*, 4696. − [14d] A. Bencini, A. Bianchi, C. Bazzicalupi, M. Ciampolini, P. Dapporto, V. Fusi, M. Micheloni, N. Nardi, P. Paoli, B. Valtancoli, *J. Chem. Soc., Perkin Trans. 2* **1993**, 715. − [14e] C. Bazzicalupi, A. Bencini, A. Bianchi, V. Fusi, P. Paoletti, B. Valtancoli, *J. Chem. Soc., Perkin Trans. 2* **1994**, 815. − [14f] K. Kumar, C. A. Chang, L. C. Francesconi, D. D. Dischino, M. F. Malley, J. Z. Gougoutas, M. F. Tweedle, *Inorg. Chem*. **1994**, *33*, 3567. − [14g] A. Bianchi, M. Ciampolini, M. Micheloni, N. Nardi, B. Valtancoli, S. Mangani, J. A. Garcia-Espana, E. Ramirez, *J. Chem. Soc., Perkin Trans. 2* **1989**, 1131.
[15] F. H. Allen, O. Kennard, Cambridge Structural Database, *Chem. Des. Autom. News* **1993**, *8*, 31.
[16] J. F. Malone, C. M. Murray, M. H. Chalton, R. Docherty, A. J. Lavery, *J. Chem. Soc., Faraday Trans.* **1997**, 3429.
[17] M. Fontanelli, M. Micheloni, *1st Spanish−Italian Congr. Thermodynamics of Metal Complexes*, Peñiscola, June 3−6, **1990**, Univ. of Valencia, Spain, p. 4.
[18] [18a] G.Gran, *Analyst* **1952**, *77*, 661. − [18b] F.J. Rossetti, H. Rossotti, *J. Chem. Educ.* **1965**, *42*, 375.
[19] P. Gans, A. Sabatini, A. Vacca, *Talanta* **1996**, *43*, 1739.
[20] A. Altomare, G. Cascarano, C. Giacovazzo, A. Guagliardi, M. C. Burla, M. C. G. Polidori, M. Camalli, *J. Appl. Crystallogr.* **1994**, *27*, 435.
[21] G. M. Sheldrick, *SHELX 93, Program for crystal structure determination*, Univ. of Göttingen, Germany, **1994**.
[22] N. Walker, D. D. Stuart, *Acta Crystallogr., Sect. A* **1983**, *39*, 158.
[23] *International Tables for X-ray Crystallography*, vol.4, Kynoch Press, Birmingham, UK, **1974**.
[24] M. Nardelli, *Comput. Chem*. **1983**, *7*, 95.
[25] C. K. Johnson, ORTEP, Rep. ORNL 3794, Oak Ridge National Laboratory, TN, USA, **1971**.
[26] MSI 9685 Scranton Road, San Diego, CA 92121-3752, USA.

Received July 9, 1999
[I99252]

Transition Metal Complexes with Sulfur Ligands, 140[+]

Mononuclear Ni, Pd and Pt Complexes with $'S_3'^{2-}$ Thioether Thiolate and $HNPnPr_3$ Phosphorane Imine Ligands [$'S_3'^{2-}$ = Bis(2-mercaptophenyl)sulfide (2–)]

Dieter Sellmann,*[a] Franz Geipel,[a] and Frank W. Heinemann[a]

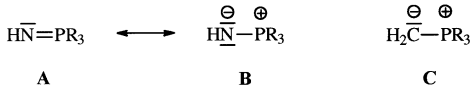
Dedicated to Professor Dirk Walther on the occasion of his 60th birthday

Keywords: Phosphorane imine / Sulfur ligands / Nickel / Palladium / Platinum

Reaction of the trinuclear $[M('S_3')]_3$ complexes {M = Ni (**4**), Pd (**5**), Pt (**6**); $'S_3'^{2-}$ = bis(2-mercaptophenyl)sulfide (2–)} with $HNPnPr_3$ yielded the new phosphorane imine complexes $[M(NHPnPr_3)('S_3')]$ {M = Ni (**1**), Pd (**2**), Pt (**3**)}. The complexes **1**–**3** have been completely characterized and are rare examples of mononuclear phosphorane imine complexes with late transition metals. Spectroscopic and structural results indicate that the $HNPnPr_3$ ligands favor the ylidic structure when binding to $[M('S_3')]$ fragments. X-ray structure determinations showed that $[M(NHPnPr_3)('S_3')]$ complexes associate through N–H···S(thiolate) bridges to give centrosymmetric dimers.

Introduction

Phosphorane imines $HNPR_3$ (R = alkyl, aryl), their *N*-organosubstituted $RNPR_3$ analogues and deprotonated phosphorane imide derivatives $[NPR_3]^-$ have proved to be versatile ligands. For example, $HNPR_3$ ligands can bind to metal centers in high, medium or low oxidation states, e.g. $[TiF_3(NPPh_3)(NHPPh_3)]_2$,[1] $[Zr_2Cl_4(NPMe_3)_4(NHPMe_3)]$,[2] $[Cp^*TaF_4(NHPPh_3)]$,[3] $[CoCl_2(NHPMe_3)_2]$,[4] $[PdCl(\eta^3\text{-}C_3H_5)(NHPPh_3)]$, $[Rh(CO)_2Cl(NHPPh_3)]$[5] and $[Mo_2(CO)_6(\mu\text{-}NHPPh_3)_3]$.[6] Phosphorane imides $[NPR_3]^-$, which are unstable in the free state and which can act as building blocks in numerous metal clusters, form as PR_3 adducts of nitrido or intermediary nitrene ligands, or can result from deoxygenation of nitrosylligands by phosphanes as demonstrated by complexes of the type $[MX(NPR_3)]_4$ (M = Mn, Co, Ni, Zn; X = Cl, Br, I),[7] $[NiCl(\mu^3\text{-}NH)(\mu^3\text{-}NPMe_3)(PMe_3)]$[8] and $[Mo(NPR_3)(NO)('S_4')]$[9] {R = alkyl, aryl, $'S_4'^{2-}$ = 1,2-bis(2-mercaptophenylthio)ethane (2−)}. The coordination chemistry of phosphorane imides has recently been reviewed.[10] Phosphorane imido metal complexes with terminal $[M-NPR_3]$ groups exhibit an interesting peculiarity which is still poorly understood. The M−N−P angle of such complexes can vary over a wide range from nearly 180° to almost 120°[10] as demonstrated by $[MoCl_4(NPPh_3)(pyridine)]$ {176.6(6)°}[11] and $[Mo(NPMePh_2)(NO)('S_4')]$ {129.7(4)°}.[12] As yet, it has not been possible to correlate unambiguously these angles with properties such as coordination number or oxidation state of the metal centers. Nevertheless, the structural variability of M−N−PR_3 groups suggests that NPR_3^- ligands are electronically flexible in the sense that they can act as two- or four-electron donors.[10] Electronic flexibility or ambiguity is also suggested for free $HNPR_3$ compounds by the valence bond formulae **A** and **B**.



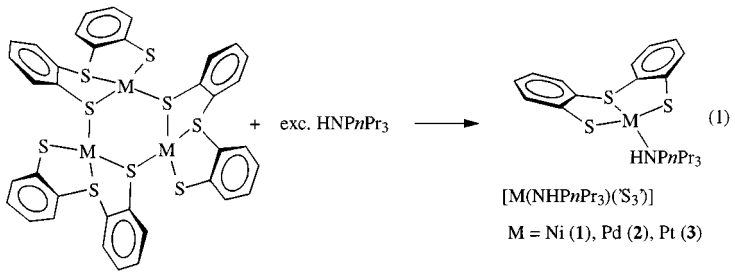
A **B** **C**

While formula **A** indicates a double bond character for the PN bond, the dipolar formula **B** exhibits a PN single bond and emphasizes the isoelectronic nature of phosphorane imines and the phosphorane ylides **C**. A high-precision low-temperature neutron and X-ray diffraction study of $HNPPh_3$[13] did not yield structural evidence for the preference of either formula **A** or formula **B**. Our interest in phosphorane imine or imido complexes originates from reactions that transform small nitrogen-containing molecules into other compounds in the coordination sphere of sulfur rich molecules.[14] In this context, we noted that phosphorane imine complexes of the late transition metals are rare. The few examples known usually contain *N*-substituted $RNPR_3$ ligands such as in $[CuCl_2(Me_3SiNPMe_3)]_2$,[15] where removal of the nitrogen substituent leads to phosphorane imido clusters, for example, $[Cu_6Cl_6(NPMe_3)_4]^+$.[16] $[NiCl(PMe_3)(Ph_2P(o\text{-}C_6H_4)-N=PMe_3)]^+$ appears to be the first mononuclear nickel phosphorane imine complex described in the literature.[17] It was obtained only recently and contains an $N=PMe_3$ entity as part of a chelate ligand. $[NiBr_2\{HNP(NMe_2)_3\}_2]$ is the second example of mononuclear nickel phosphorane imine complexes

[+] Part 39: Ref.[18b]

[a] Institut für Anorganische Chemie der Universität Erlangen-Nürnberg,
Egerlandstraße 1, D-91058 Erlangen, Germany
Fax: (internat.) + 49-9131/852-7367
E-mail: sellmann@anorganik.chemie.uni-erlangen.de

 © WILEY-VCH Verlag GmbH, D-69451 Weinheim, 2000 1434−1948/00/0101−0059 $ 17.50+.50/0



and was mentioned in the review article cited above.[10] Other mononuclear complexes of nickel, palladium and platinum with parent $HNPR_3$ imine ligands are unknown. We have now obtained such complexes from reactions of the trinuclear $[M('S_3')]_3$ complexes[18] {M = Ni, Pd, Pt, $'S_3'^{2-}$ = bis(2-mercaptophenyl)sulfide(2−)} with $HNPnPr_3$. The resulting $[M(NHPnPr_3)('S_3')]$ complexes were fully characterized and are described here.

Results and Discussion

Treatment of the trinuclear $[M('S_3')]_3$ (M = Ni, Pd, Pt) complexes with a slight excess of $HNPnPr_3$ yielded the mononuclear $[M(NHPnPr_3)('S_3')]$ complexes {M = Ni (**1**), Pd (**2**), Pt (**3**)} according to Equation 1.

In the course of the reactions, the black $[Ni('S_3')]_3$ or dark-red $[Pt('S_3')]_3$ complexes slowly dissolved and red-purple (Ni) or yellow (Pt) solutions formed, from which the corresponding $[M(NHPnPr_3)('S_3')]$ complexes were isolated in an analytically pure form. The complexes **1**−**3** readily dissolve in THF, acetone or CH_2Cl_2, but are only sparingly soluble in Et_2O, *n*-hexane, or CH_3CN. The IR spectra of **1**−**3** (KBr discs) exhibit the typical absorption patterns for the $[M('S_3')]$ fragments and, in addition, sharp ν(NH) bands of the $HNPnPr_3$ ligands in the region of 3273−3292 cm^{-1}. In comparison to the ν(NH) of free $HNPnPr_3$ (3367 cm^{-1}), the ν(NH) bands are slightly red-shifted. The complexes **1**−**3** are diamagnetic and yielded high-resolution NMR spectra. Figure 1 shows the ^1H NMR spectrum of **1**. The splitting pattern in the aromatic region is characteristic for $[M('S_3')]$ fragments and can be used as a diagnostic probe for monitoring these reactions.

The chemical shifts of the NH protons depend on the metal center binding the $HNPnPr_3$ ligand. In comparison to uncoordinated $HNPnPr_3$ with an NH signal at δ = −0.59 (CD_2Cl_2), the NH signals of the complexes (CD_2Cl_2) are either high-field shifted (**1**: δ = −1.85) or low-field shifted (**2**: δ = −0.03; **3**: δ = +0.54). Thus, within the series of complexes **1**−**3**, the NH protons are increasingly deshielded, possibly indicating an increasing NH acidity of the $HNPnPr_3$ ligands. The NH signals are slightly broadened and not split by $^2J_{H-P}$ coupling (down to temperatures of −60°C), although the NH signal of complex **3** exhibits a $^2J_{H-Pt}$ coupling constant of 41.5 Hz. The $^{13}C\{^1H\}$ NMR spectra exhibit only six signals for the twelve aromatic C atoms of the $'S_3'$ ligand, indicating a twofold symmetry of the $[M('S_3')]$ fragments. The NH chemical shifts are of interest with regard to the ylene structure **A** or ylide structure **B**. Protons at sp^2 hybridized N atoms in HN=X compounds (X = NH, CH_2, CR_2) such as diazenes, methylene imines or ketimines, are usually strongly low-field shifted (δ = 10−15), regardless of whether the HN=X species are in the free state or are coordinated to metal centers.[19] The NH signals of **1**−**3**, and of other diamagnetic $HNPR_3$ com-

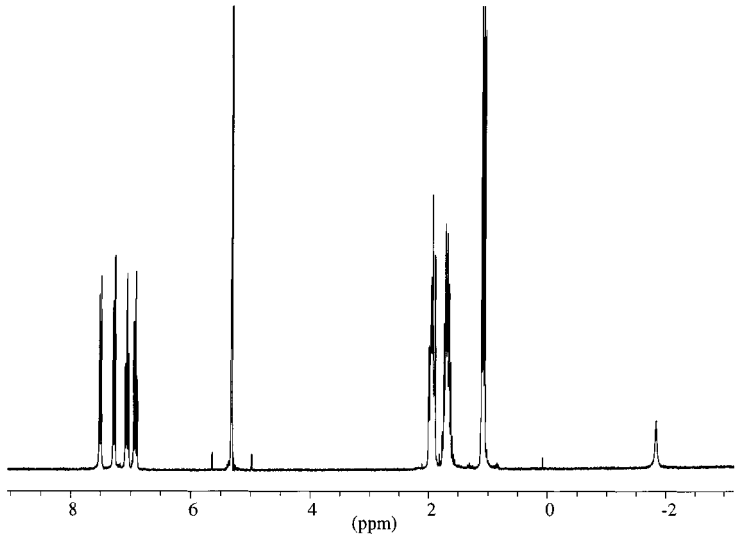


Figure 1. ^1H NMR spectrum of $[Ni(NHPnPr_3)('S_3')]$ (**1**) in CD_2Cl_2

plexes,[3,5,6] however, appear in the shift range typical of ammonia, amines, hydrazines etc. Thus the NH shifts of **1**−**3** seem to suggest the single bond formula **B** rather than the double bond structure **A** for complexed HNP*n*Pr$_3$.

X-ray Structure Determinations of 1−3

The molecular structures of all three complexes were determined by X-ray structure analyses. The crystals contain discrete molecules which, however, form dimers through N−H···S(thiolate) contacts. Figure 2 depicts their molecular structures and Table 1 lists selected distances and angles.

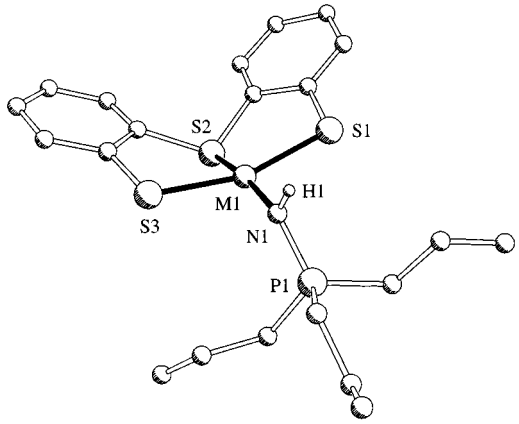


Figure 2. Molecular structure of [M(NHP*n*Pr$_3$)('S$_3$')] {M = Ni (**1**), Pd (**2**), Pt (**3**)}, (C bonded H atoms omitted)

Table 1. Selected distances (pm) and angles (°) of [Ni(NHP*n*Pr$_3$)('S$_3$')] (**1**), [Pd(NHP*n*Pr$_3$)('S$_3$')] (**2**) and [Pt(NHP*n*Pr$_3$)('S$_3$')] (**3**)

Complex (M)	**1** (Ni)	**2** (Pd)	**3** (Pt)
M1−N1	191.7(5)	206.3(3)	205.0(1)
M1−S1	217.4(2)	229.47(10)	229.5(5)
M1−S2	211.6(2)	221.75(9)	220.8(4)
M1−S3	218.4(2)	230.52(10)	230.2(5)
N1−P1	159.5(5)	159.6(3)	163(2)
N1−H1	78(5)	79(5)	86
N1−M1−S2	170.9(2)	175.26(9)	176.2(5)
S1−M1−S3	161.77(6)	163.46(4)	164.4(2)
M1−N1−P1	127.1(3)	123.5(2)	122.0(9)
M1−N1−H1	118(5)	116(4)	119
P1−N1−H1	110(4)	115(4)	119
N1···S3a[a]	366.0(5)	368.7(3)	367(2)
H1···S3a[a]	289(6)	296(5)	296
N1−H1···S3a[a]	169(5)	165(5)	141

[a] Symmetry code: −x + 1, −y + 2, −z + 1

Complexes **1**−**3** are isostructural. The HNP*n*Pr$_3$ ligands coordinate through their N donors to the [M('S$_3$')] fragments. The resulting [MNS$_3$] core geometries are considerably tetrahedrally distorted and not strictly planar as would be expected for four-coordinate low-spin d^8 M^{II} centers. A comparison of the [N1−M1−S2] and [S1−M1−S3] angles in complexes **1**−**3** demonstrates that this distortion is most pronounced in the nickel complex **1**, which exhibits angles of 170.9(2)° and 161.77(6)°, respectively. This distortion is to a major extent caused by the topology of the 'S$_3$' ligand. The sp^3 hybridization of the central thioether S donor (S2) forces the [M('S$_3$')] fragments to adopt a butterfly-like conformation, in which the two 'S$_3$' benzene ring planes exhibit an average dihedral angle of 109°.

The M−S distances in the [M('S$_3$')] fragments lie in the ranges observed also for other Ni^{II}, Pd^{II} and Pt^{II} thioether thiolate complexes.[20] However, it should be noted that the M−S2(thioether) distances of **1** {211.6(2) pm}, **2** {221.75(9) pm} and **3** {220.8(4) pm} are relatively short and are smaller than the corresponding M−S(thiolate) distances. This is a significant feature of [M('S$_3$')] fragments and is probably caused by the steric constraints of the 'S$_3$' ligand.[18] The M−N distances of **1** {191.7(5) pm}, **2** {206.3(3) pm} and **3** {205.0(14) pm} indicate M−N single bonds, but are also relatively short. This is shown by comparing, for example, the Ni−N distances in **1** {191.7(5) pm}, the phosphorane imine complex [NiCl(PMe$_3$)(Ph$_2$P(*o*-C$_6$H$_4$)−N=PMe$_3$)]$^+$ {201.1(7) pm}[17] and the oligonuclear phosphorane imido complex [NiBr(NPMe$_3$)]$_4$ (av. 202.1 pm).[7c] The P−N distances of **1** {159.5(5) pm}, **2** {159.6(3) pm} and **3** {163(2) pm} are identical within the 3 σ criterion. Calculations on HNPMe$_3$[21] and the above mentioned diffraction study of HNPPh$_3$[13] indicate that such distances are compatible with formulae **A** and **B**. The M−N−P and the (less accurate) M−N−H angles of **1** {127.1(3)°, 118(5)°}, **2** {123.5(2)°, 116(4)°} and **3** {122.0(9)°} suggest, at first glance, sp^2 hybridization of the N donors. However, the angle sums around the N atoms of **1** (355.1°) and **2** (354.5°) show that the coordination geometry of the three-coordinate N donors is not strictly planar but slightly distorted to trigonal pyramidal.

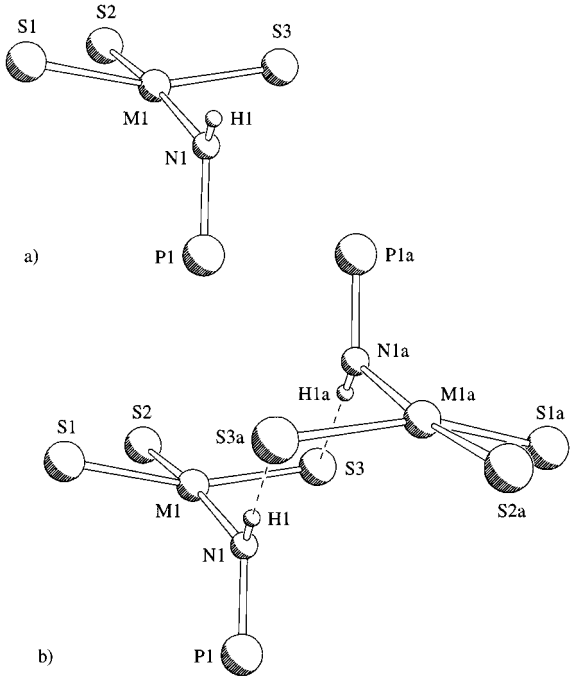


Figure 3. Views of (a) the core atoms of [M(NHP*n*Pr$_3$)('S$_3$')] (**1**−**3**), and (b) their dimerization through N−H···S(thiolate) bridges

Figure 3 illustrates the dimerization of [M(NHP*n*Pr$_3$)-($'S_3'$)] complexes through N−H···S(thiolate) bridges. The resulting dimers possess crystallographically imposed centers of inversion. The HNP*n*Pr$_3$ ligands coordinate to the [M($'S_3'$)] fragments in such a way that the NH bonds are approximately orthogonal to the [MNS$_3$] cores giving rise to N···S(thiolate) distances between two adjacent molecules of 366.0(5) pm in **1**, 368.7(3) pm in **2** and 367(2) pm in **3**. The corresponding H···S(thiolate) distances, which are shorter than the sum of the van der Waals radii (N = 155 pm, H = 120 pm, S = 180 pm),[22] and the N−H···S directionality (see Table 1), indicate hydrogen bonding. Inter- and intramolecular hydrogen bonds between HNPR$_3$ and chloride or iodide co-ligands have previously been suggested in [CdI$_2$(NHPPh$_3$)$_2$]$_2$[23] and [Cp*$_2$UCl$_2$-(NHPPh$_3$)].[24]

Conclusions

Three new phosphorane imine complexes have been synthesized and characterized. The complexes **1**−**3** are rare examples of mononuclear phosphorane imine complexes containing late transition metals. In addition, **1**−**3** contrast with previously reported complexes as their metal coordination spheres contain only sulfur donors, apart from the HNPR$_3$ ligand. Coordination of HNP*n*Pr$_3$ to the [M($'S_3'$)] fragments causes a considerable stabilization of HNP*n*Pr$_3$ towards hydrolysis. ^{1}H NMR spectroscopic data and the X-ray crystal structures indicate that HNP*n*Pr$_3$ favors the ylidic structure **B** when binding to [M($'S_3'$)] fragments. Studies are underway to evaluate the synthetic potential of the NH group and the influence of the electron-rich sulfur donors upon the reactivity of the HNP*n*Pr$_3$ ligands

Experimental Section

General: Unless stated otherwise, all reactions and manipulations were carried out under nitrogen using standard Schlenk techniques. Solvents were dried and distilled before use. As far as possible, reactions were monitored by IR or NMR spectroscopy. Spectra were recorded on the following instruments: IR (KBr discs or CaF_2 cuvettes, solvent bands were compensated) Perkin−Elmer 983, 1620 FT IR or 16PC FT-IR. NMR: Jeol-JNM-GX 270, EX 270 or Lambda LA 400 with the protio-solvent signal used as an internal reference. Chemical shifts are quoted on the δ scale (downfield shifts are positive) relative to tetramethylsilane (^{1}H, ^{13}C{^{1}H} NMR) or 85% H_3PO_4 (^{31}P{^{1}H} NMR). Spectra were recorded at 25°C. Mass spectra: Jeol MSTATION 700 spectrometer. Elemental analyses: Carlo Erba EA 1106 or 1108 analyzer. The starting [M($'S_3'$)]$_3$ complexes {M = Ni (**4**), Pd (**5**), Pt (**6**)}[18] and HNP*n*Pr$_3$ (**7**)[25] were prepared by literature methods.

[M(NHP*n*Pr$_3$)($'S_3'$)] (M = Ni, Pd, Pt). − General Procedure: HNP*n*Pr$_3$ (**7**) was added to suspensions of **4**−**6** in 10 mL of THF. The reaction mixtures were stirred for 12 h at room temperature yielding red-purple, red-brown, or yellow solutions. Undissolved traces of white material were removed by centrifugation. The solutions were reduced in volume to about 2 mL, layered with 10 mL of acetonitrile and cooled to −30°C. Precipitated microcrystals were separated after one week, washed with 10 mL of acetonitrile and dried in vacuo.

[Ni(NHP*n*Pr$_3$)($'S_3'$)] (1): Synthesised from **4** (510 mg, 0.55 mmol) and **7** (0.48 mL, 2.20 mmol) to give **1** as red-purple microcrystals. Yield: 424 mg (53%). − $C_{21}H_{30}NNiPS_3$ (482.32): calcd. C 52.30, H 6.27, N 2.90, S 19.94; found C 52.69, H 6.36, N 3.08, S 18.34. −

Table 2. Selected crystallographic data of [Ni(NHP*n*Pr$_3$)($'S_3'$)] (**1**), [Pd(NHP*n*Pr$_3$)($'S_3'$)] (**2**) and [Pt(NHP*n*Pr$_3$)($'S_3'$)] (**3**)

Compound	**1**	**2**	**3**
Formula	$C_{21}H_{30}NNiPS_3$	$C_{21}H_{30}NPPdS_3$	$C_{21}H_{30}NPPtS_3$
M_r [g/mol]	482.32	530.01	618.70
Crystal size [mm]	0.50 × 0.50 × 0.30	0.42 × 0.35 × 0.25	0.40 × 0.30 × 0.14
F(000)	2032	2176	2432
Crystal system	orthorhombic	orthorhombic	orthorhombic
Space group	*Pbca*	*Pbca*	*Pbca*
a [pm]	1290.3(2)	1311.4(1)	1310.1(4)
b [pm]	1824.1(2)	1813.5(1)	1819.3(6)
c [pm]	1959.8(3)	1965.0(2)	1960.7(5)
V [nm^3]	4.6127(11)	4.6732(6)	4.673(2)
Z	8	8	8
$D_{calcd.}$ [g/cm^3]	1.389	1.507	1.759
μ [mm^{-1}]	1.189	1.138	6.349
Diffractometer	Siemens P4	Siemens P4	Siemens P4
Radiation [pm]	Mo-*Kα* (λ = 71.073)	Mo-*Kα* (λ = 71.073)	Mo-*Kα* (λ = 71.073)
Temperature [K]	200	200	200
Scan technique	ωscan	ωscan	ωscan
2Θ range [°]	4.1−54.0	4.1−54.0	4.1−52.1
Scan speed [°/min]	6.0−60.0	5.0−50.0	4.0−40.0
Meas. reflections	4260	6224	4689
Indep. reflections	3374	5103	3750
R_{int} [%]	4.93	2.73	10.55
Obs. reflections	2330	3653	2177
σ criterion	$F_0 > 4\sigma$ (F_0)	$F_0 > 4\sigma$ (F_0)	$F_0 > 4\sigma$ (F_0)
R1; wR2 [%]	4.92; 11.83	3.64; 9.39	7.31; 20.85
Ref. parameters	364	334	247
Abs. correct. T_{min}/T_{max}	−	0.3611, 0.4017	0.0045, 0.0210

IR (KBr): $\tilde{\nu}$ = 3273 cm^{-1} (NH). – ^1H NMR (269.6 MHz, CD_2Cl_2): δ = 7.50 (d, 2 H, C_6H_4), 7.28 (d, 2 H, C_6H_4), 7.06 (m, 2 H, C_6H_4), 6.92 (m, 2 H, C_6H_4), 1.94 (m, 6 H, PCH_2), 1.69 (m, 6 H, PCH_2CH_2), 1.05 (t, 9 H, $P(CH_2)_2CH_3$), −1.85 (s, br, 1 H, N*H*). – $^{13}C\{^1H\}$ NMR (100.4 MHz, CD_2Cl_2): δ = 152.2, 133.5, 129.4, 128.7, 127.5, 122.2 [C(aryl)], 29.5 (d, $^1J_{P-C}$ = 60.3 Hz), 16.0 (d, J_{P-C} = 3.3 Hz), 15.8 (d, J_{P-C} = 16.6 Hz) [$P(C_3H_7)_3$]. – $^{31}P\{^1H\}$ NMR (161.7 MHz, CD_2Cl_2): δ = 51.38 [s, $P(C_3H_7)_3$]. – MS (FD, THF); *m*/*z*: 482 $[Ni(NHPnPr_3)(′S_3′)]^+$.

[Pd(NHP*n*Pr$_3$)(′S$_3$′)] (2): Synthesised from **5** (355 mg, 0.33 mmol) and **7** (0.33 mL, 1.50 mmol) to give **2** as red-brown microcrystals. Yield: 216 mg (41%). – $C_{21}H_{30}NPPdS_3$ (530.01): calcd. C 47.59, H 5.70, N 2.64, S 18.15; found C 47.90, H 5.95, N 2.73, S 17.08 – IR (KBr): $\tilde{\nu}$ = 3292 cm^{-1} (NH). – ^1H NMR (399.7 MHz, CD_2Cl_2): δ = 7.52 (d, 2 H, C_6H_4), 7.29 (d, 2 H, C_6H_4), 7.11 (m, 2 H, C_6H_4), 6.98 (m, 2 H, C_6H_4), 1.93 (m, 6 H, PCH_2), 1.66 (m, 6 H, PCH_2CH_2), 1.10 (t, 9 H, $P(CH_2)_2CH_3$), −0.03 (s, br, 1 H, N*H*). – $^{13}C\{^1H\}$ NMR (100.4 MHz, CD_2Cl_2): δ = 152.6, 133.4, 130.6, 129.2, 128.6, 122.5 [C(aryl)], 29.4 (d, $^1J_{P-C}$ = 60.3 Hz), 16.0 (d, J_{P-C} = 4.2 Hz), 15.8 (d, J_{P-C} = 15.7 Hz) [$P(C_3H_7)_3$]. – $^{31}P\{^1H\}$ NMR (161.7 MHz, CD_2Cl_2): δ = 51.27 [s, $P(C_3H_7)_3$]. – MS (FD, THF); *m*/*z*: 530 $[Pd(NHPnPr_3)(′S_3′)]^+$.

[Pt(NHP*n*Pr$_3$)(′S$_3$′)] (3): Synthesised from **6** (1.01 g, 0.77 mmol) and **7** (0.76 mL, 3.47 mmol) to give **3** as yellow microcrystals. Yield: 590 mg (41%). – $C_{21}H_{30}NPPtS_3$ (618.70): calcd. C 40.77, H 4.89, N 2.26, S 15.55; found C 40.91, H 5.04, N 2.46, S 15.42 – IR (KBr): $\tilde{\nu}$ = 3287 cm^{-1} (NH). – ^1H NMR (269.6 MHz, CD_2Cl_2): δ = 7.64 (d, 2 H, C_6H_4), 7.41 (d, 2 H, C_6H_4), 7.05 (m, 2 H, C_6H_4), 6.91 (m, 2 H, C_6H_4), 1.94 (m, 6 H, PCH_2), 1.64 (m, 6 H, PCH_2CH_2), 1.07 (t, 9 H, $P(CH_2)_2CH_3$), 0.54 (s + d, $^2J_{H-Pt}$ = 41.5 Hz, br, 1 H, N*H*). – $^{13}C\{^1H\}$ NMR (100.4 MHz, CD_2Cl_2): δ = 152.2, 133.9, 130.8 (s + d, $^3J_{C-Pt}$ = 63.2 Hz), 128.8, 128.4 (s + d, $^3J_{C-Pt}$ = 57.4 Hz), 122.2 [C(aryl)], 28.4 (d, $^1J_{P-C}$ = 59.8 Hz), 15.6 (d, J_{P-C} = 4.1 Hz), 15.4 (d, J_{P-C} = 16.2 Hz) [$P(C_3H_7)_3$]. – $^{31}P\{^1H\}$ NMR (161.7 MHz, CD_2Cl_2): δ = 51.27 (s + d, $^2J_{Pt-P}$ = 36.7 Hz, $P(C_3H_7)_3$). – MS (FD, THF); *m*/*z*: 619 $[Pt(NHPnPr_3)(′S_3′)]^+$.

X-ray Structure Analyses of [Ni(NHP*n*Pr$_3$)(′S$_3$′)] (1), [Pd(NHP*n*Pr$_3$)(′S$_3$′)] (2) and [Pt(NHP*n*Pr$_3$)(′S$_3$′)] (3): Dark red rhombohedra were obtained by slowly evaporating a concentrated acetone solution of **1**. Red single crystals were formed by layering a CD_2Cl_2 solution of **2** with *n*-hexane. Yellow single crystals were grown by slowly evaporating a concentrated THF solution of **3**. Suitable single crystals were sealed under N_2 in glass capillaries. Data were corrected for Lorentz and polarization effects. For **2** and **3** absorption effects have been corrected using Psi-scans (see Table 2), while for **1** absorption effects have been neglected. The structures were solved by direct methods (SHELXTL 5.03[26]). Full-matrix least-squares refinement was carried out on F^2 (SHELXTL 5.03). All non-hydrogen atoms were refined anisotropically. The positions of the hydrogen atoms of **1** and **2** were taken from the difference Fourier map and were either refined isotropically **1** or kept fixed with a common isotropic displacement parameter **2**. In the case of **3** the hydrogen atoms were geometrically positioned with isotropic displacement parameters fixed at 1.5 times *U*(eq) of the preceding carbon atom. Selected crystallographic data are summarized in Table 2.[27]

Acknowledgments

Support of these investigations by the Deutsche Forschungsgemeinschaft and Fonds der Chemischen Industrie is gratefully acknowledged.

[1] M. Grün, K. Harms, R. Meyer zu Köcker, K. Dehnicke, H. Goesmann, *Z. Anorg. Allg. Chem.* **1996**, *622*, 1091–1096.
[2] M. M. Stahl, N. Faza, W. Massa, K. Dehnicke, *Z. Anorg. Allg. Chem.* **1997**, *623*, 1855–1856.
[3] F. Schrumpf, H. W. Roesky, M. Noltemeyer, *Z. Naturforsch.* **1990**, *45b*, 1600–1602.
[4] R. Meyer zu Köcker, G. Frenzen, B. Neumüller, K. Dehnicke, J. Magull, *Z. Anorg. Allg. Chem.* **1994**, *620*, 431–437.
[5] E. W. Abel, S. A. Mucklejohn, *Inorg. Chim. Acta.* **1979**, *37*, 107–111.
[6] J. S. Miller, M. O. Visscher, K. G. Caulton, *Inorg. Chem.* **1974**, *13*, 1632–1639.
[7] [7a] H.-J. Mai, H.-C. Kang, S. Wocadlo, W. Massa, K. Dehnicke, *Z. Anorg. Allg. Chem.* **1995**, *621*, 1963–1968. – [7b] S. Abram, U. Abram, R. Meyer zu Köcker, K. Dehnicke, *Z. Anorg. Allg. Chem.* **1996**, *622*, 867–872. – [7c] M. Krieger, R. O. Gould, J. Pebler, K. Dehnicke, *Z. Anorg. Allg. Chem.* **1998**, *624*, 781–786.
[8] H.-F. Klein, S. Haller, H. König, M. Dartiguenave, Y. Dartiguenave, M.-J. Menu, *J. Am. Chem. Soc.* **1991**, *113*, 4673–4675.
[9] D. Sellmann, J. Keller, M. Moll, H. P. Beck, W. Milius, *Z. Naturforsch.* **1986**, *41b*, 1551–1560.
[10] K. Dehnicke, M. Krieger, W. Massa, *Coord. Chem. Rev.* **1999**, *182*, 19–65.
[11] K. Völp, F. Weller, K. Dehnicke, *Z. Naturforsch.* **1987**, *42b*, 947–950.
[12] D. Sellmann, J. Keller, M. Moll, C. F. Campana, M. Haase, *Inorg. Chim. Acta* **1988**, *141*, 243–252.
[13] M. G. Davidson, A. E. Goeta, J. A. K. Howard, C. W. Lehmann, G. M. McIntyre, R. D. Price, *J. Organomet. Chem.* **1998**, *550*, 449–452.
[14] D. Sellmann, M. W. Wemple, W. Donaubauer, F. W. Heinemann, *Inorg. Chem.* **1997**, *36*, 1397–1402.
[15] T. Miekisch, H. J. Mai, R. Meyer zu Köcker, K. Dehnicke, *Z. Anorg. Allg. Chem.* **1996**, *622*, 583–588.
[16] R. Meyer zu Köcker, A. Behrendt, K. Dehnicke, D. Fenske, *Z. Naturforsch.* **1994**, *49b*, 301–308.
[17] L. Crociani, F. Tisato, F. Refosco, G. Bandoli, B. Corain, L. M. Venanzi, *J. Am. Chem. Soc.* **1998**, *120*, 2973–2974.
[18] [18a] D. Sellmann, D. Häußinger, F. W. Heinemann, *Eur. J. Inorg. Chem.* in press. – [18b] D. Sellmann, F. Geipel, F. W. Heinemann, *Eur. J. Inorg. Chem.* submitted.
[19] [19a] D. Sellmann, E. Thallmair, *J. Organomet. Chem.* **1979**, *164*, 337–352. – [19b] B. Kersting, P. Suter, H. Vahrenkamp, *Z. Anorg. Allg. Chem.* **1998**, *624*, 787–791.
[20] [20a] D. Sellmann, W. Prechtel, F. Knoch, M. Moll, *Inorg. Chem.* **1993**, *32*, 538–546. – [20b] D. Sellmann, S. Fünfgelder, G. Pöhlmann, F. Knoch, M. Moll, *Inorg. Chem.* **1990**, *29*, 4772–4778. – [20c] D. Sellmann, S. Fünfgelder, F. Knoch, M. Moll, *Z. Naturforsch.* **1991**, *46b*, 1601–1608. – [20d] D. Sellmann, H. Schillinger, F. Knoch, M. Moll, *Z. Naturforsch.* **1992**, *47b*, 748–753. – [20e] D. Sellmann, D. Häußinger, F. Knoch, M. Moll, *J. Am. Chem. Soc.* **1996**, *118*, 5368–5374. – [20f] D. Sellmann, C. Allmann, F. W. Heinemann, F. Knoch, J. Sutter, *J. Organomet. Chem.* **1997**, *541*, 291–305.
[21] K. A. O. Starzewski, H. tom Dieck, *Inorg. Chem.* **1979**, *18*, 3307–3316.
[22] A. Bondi, *J. Phys. Chem.* **1964**, *68*, 441–451.
[23] E. W. Abel, S. A. Mucklejohn, *Z. Naturforsch.* **1978**, *33b*, 339–340.
[24] R. E. Cramer, S. Roth, J. W. Gilje, *Organometallics* **1989**, *8*, 2327–2330.
[25] [25a] W. Buchner, W. Wolfsberger, *Z. Naturforsch.* **1974**, *29b*, 328–334. – [25b] L. Birkofer, S. M. Kim, *Chem. Ber.* **1964**, *97*, 2100–2101.
[26] SHELXTL 5.03 for Siemens Crystallographic Research Systems, Copyright **1995** by Siemens Analytical X-Ray Instruments Inc., Madison, WI, U.S.A.
[27] Crystallographic data (excluding structure factors) for the structures reported in this paper have been deposited with the Cambridge Crystallographic Data Centre as supplementary publication no. CCDC-130662 (**1**), -130663 (**2**), -130664 (**3**). Copies of the data can be obtained free of charge on application to The Director, CCDC, 12 Union Road, Cambridge CB2 1EZ, UK [Fax: (internat.) + 44-1223/336-033, E-mail: deposit@ccdc.cam.ac.uk].

Received July 15, 1999
[I99260]

Water-Soluble Phosphanes, 11[+]

Syntheses and Coordination Chemistry of Chiral Phosphanyl Glycerols and Their Derivatives – X-ray Structure of (*R*)-$Ph_2P–CH_2–C^aH–O–B(Ph)–O–C^bH_2$($C^a$–$C^b$)

David J. Brauer,[a] Peter Machnitzki,[a] Thomas Nickel,[a] and Othmar Stelzer*[a]

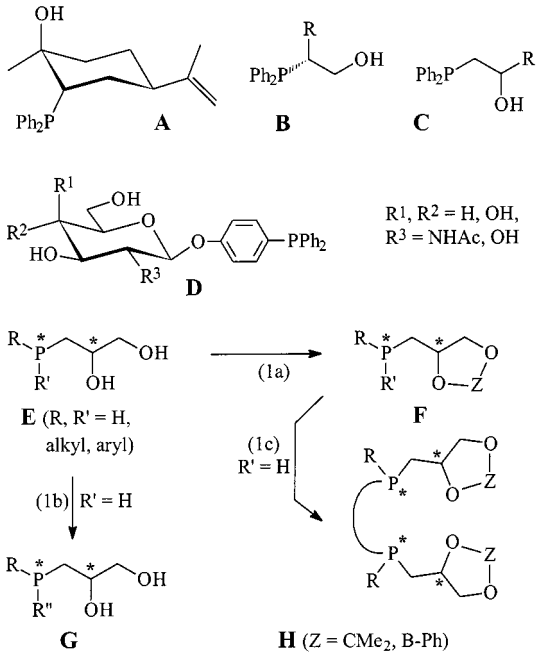
Dedicated to Professor Dr. R. Schmutzler on the occasion of his 65th birthday

Keywords: (*R*)-(+)-2,3-Epoxy-1-propanol / 2,3-Dihydroxyalkyl phosphanes / 1,3,2-Dioxaborolane / 1,3-Dioxolane ring / Enantiopure phosphanes / Complexes

Reaction of (*R*)-(+)-2,3-epoxy-1-propanol with Ph_2PH, Ph(Me)PH, or $PhPH_2$ in the superbasic medium KOH/DMSO affords the novel chiral phosphanes **1a**–**1c**. While **1a** is obtained enantiomerically pure, **1b** and the secondary phosphane **1c** are formed as mixtures of diastereoisomers (R_PR_C, S_PR_C) with homochiral β carbon atoms. Derivatization of **1a** with phenylboronic acid or 2,2-dimethoxypropane yields **2a** and **3a** with 1,3,2-dioxaborolane and 1,3-dioxolane ring systems, respectively. The X-ray structure of **2a** (space group $P2_1$) reveals the presence of four molecules of *R* configuration in the unit cell. Nucleophilic phosphanylation of (*R*)-(–)-2,3-*O*-isopropylideneglycerol tosylate with Ph_2PH, Ph(Me)PH, or $PhPH_2$ yields chiral **3a**–**3d**. Compound **3b** was obtained enantiomerically pure. The secondary phosphane **3c** has been employed in syntheses of the hydrophilic tertiary phosphanes **3e**, **3f** and of the novel bidentate phosphane ligands **3g**, **3h**, all of which have homochiral β carbon atoms. Pd^{II} complexes PdL_2Cl_2 of **1a**, **2a**, **3a** (L) are formed as mixtures of *cis*/*trans* isomers. Rh^I complexes of **1a**, **3a**, and bidentate **3h** have also been synthesized.

Functionalized hydrophilic phosphanes have attracted considerable interest in recent years, mainly because of their application as ligands in catalytically active coordination compounds and organometallic complexes.[2] The hydrophilic character was introduced by modification of the neutral phosphane ligands with polar groups.[3–5] The concept of attaining hydrophilicity by incorporation of hydroxyl groups at the periphery of the ligands has attracted much less attention.[6a] Chiral and achiral ligands containing monohydroxylated alkyl groups, e.g. **A**, have been obtained by addition of phosphides to oxiranes.[6b,6c] These reactions proceed with high regioselectivity,[7a,7b] i.e. the phosphorus nucleophile attacks preferentially at the least substituted carbon atom of the epoxide ring system. Using enantiopure epoxides obtained by Sharpless epoxidation[6d] of allyl alcohols, optically active hydroxylated phosphanes have been obtained by this method.[6e] The experimentally observed preference for inversion of configuration at the carbon atom attacked in the nucleophilic ring-opening of epoxides has been supported by theoretical studies.[7b]

Enders and Berg[8] developed a multi-step synthesis of optically active 2-hydroxyalkyl diphenylphosphanes (*R*)-$Ph_2P–CH(R)–CH_2–OH$ (**B**) starting from simple aldehydes. Kinetic resolution of the racemate of $Ph_2P–CH_2–CH(OH)R$ (**C**) (R = Me, Et, *n*Pr) through acylation with isopropenyl acetate under rabbit gastric lipase catalysis yielded the corresponding ligands in enantiomerically enriched form. Hydrophilic hydroxyalkylphosphanes containing carbohydrate moieties (**D**) have also been reported.[10]



[+] Part 10: Ref.[1]

[a] Fachbereich 9, Anorganische Chemie, Bergische Universität-GH Wuppertal,
Gaußstraße 20, D-42097 Wuppertal, Germany

 © WILEY-VCH Verlag GmbH, D-69451 Weinheim, 2000 1434–1948/00/0101–0065 $ 17.50+.50/0

Their dual functionality renders hydroxyalkylphosphanes hemilabile (P,O) ligands,[11] which are of great potential in homogeneous catalysis. Their physical properties may be tuned by derivatization of the OH groups.[12] The introduction of additional OH groups in vicinal positions and functionalization of the phosphorus atoms (**E**, R′ = H) add further interesting possibilities in the context of a systematic ligand tailoring, allowing the formation of 1,3-dioxolane and 1,3-dioxaborolane ring systems at the 1,2-diol moieties (**F**) (Equation 1a) and P−C coupling reactions to yield chiral mono- or bidentate tertiary phosphane ligands (**G**, **H**) (Equations 1b, 1c).

We report herein on the synthesis of ligands of type **E** and their derivatives **F**−**H**, which may formally be derived from glycerol by replacement of a terminal OH group by a phosphanyl substituent ("phosphanyl glycerols").

Results

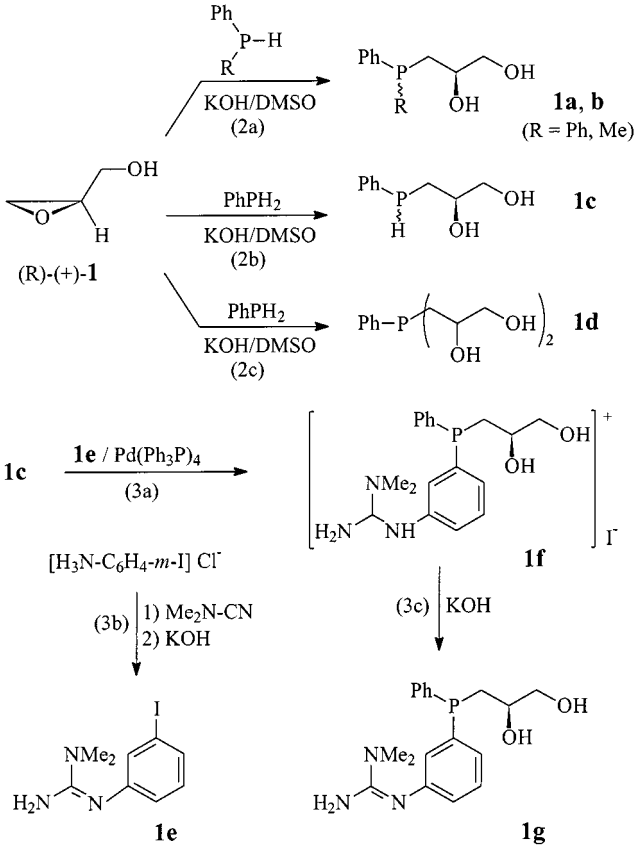
Chiral Phosphane Ligands with 2,3-Dihydroxypropyl Substituents

The synthesis of type **E** ligands containing 2,3-dihydroxypropyl substituents was achieved by nucleophilic opening of the epoxide ring system in glycidol (2,3-epoxy-1-propanol, **1**) using primary or secondary phosphanes in the superbasic medium DMSO/KOH.[13] Thus, **1a** and **1b** were formed in high yields by reaction of Ph_2PH[14a] or Ph(Me)PH[14b] with racemic **1** under these conditions (Equation 2a).

While **1a** shows only one signal at δP = −21.2 in its $^{31}P\{^1H\}$-NMR spectrum, **1b** with two centers of chirality (P, β-C) exhibits two resonances (δP = −39.1, −41.0, intensity ratio 1:1), which may be assigned to the *erythro* and *threo* isomers (R_PR_C/S_PS_C and R_PS_C/S_PR_C). Optically active **1a** {$[\alpha]_D^{20}$ = −19.4° (*c* = 1.3, CH_2Cl_2), δP = −21.2} is formed if commercially available (*R*)-(+)-**1** ($[\alpha]_D^{23}$ = +12°, neat, enantiomeric purity ≈98% *ee*) is employed in this reaction. This has been established from analysis of the $^{31}P\{^1H\}$-NMR spectrum of the disubstituted Pd complex **4** of **1a** (see below). Due to the chiral carbon atom in the β-position, the phenyl groups of the Ph_2P substituent in **1a** are non-equivalent, as indicated by the observation of two sets of resonances for the *ipso*, *ortho*, and *meta* carbon atoms in the $^{13}C\{^1H\}$-NMR spectrum.

The technique developed for the syntheses of **1a** and **1b** can also be used to prepare secondary phosphanes containing 2,3-dihydroxypropyl substituents with chiral β carbon atoms. Thus, reaction of $PhPH_2$[14c] with one equivalent (*R*)-(+)-glycidol gave **1c** in high yields (Equation 2b). The $^{31}P\{^1H\}$-NMR spectrum of **1c** features two resonances of about equal intensity at δP = −63.05 and −63.39, which may be assigned to the *erythro* and *threo* isomers. Under proton coupling, these signals are split into doublets [$^1J(^{31}P\text{-}^1H)$ = 212 Hz] showing additional fine structure [^nJ(PH), *n* = 2, 3].

Treatment of $PhPH_2$ with two equivalents of racemic **1** gave the tertiary phosphane **1d** as a mixture of three diastereoisomers (two *meso* forms and an enantiomeric pair; $^{31}P\{^1H\}$-NMR spectrum: δP = −32.8, −33.8, −34.4, intensity ratio 1:2:1) (Equation 2c). An analogous effect of two asymmetric carbon centers in the α- or β-positions on the $^{31}P\{^1H\}$-NMR spectra of chiral secondary phosphanes with $H-P(-C^*-C-)_2$ or $H-P(-C-C^*-)_2$ skeletons has been reported.[15] If (*R*)-(+)-**1** is employed instead of racemic **1**, one diastereoisomer of **1d** with homochiral β carbon atoms is formed {$[\alpha]_D^{20}$ = −25.7° (neat); −11.0° (*c* = 10, MeOH)}, which shows a single resonance at δP = −33.8 in its $^{31}P\{^1H\}$-NMR spectrum. Signals of low intensity (ca. 3% of the main signal) at δ = −32.8 and −34.4 may be assigned to the *meso* forms obtained, since the enantiomeric purity of (*R*)-(+)-**1** was only 97% *ee*. The formation of **1d** evidently proceeds with high stereoselectivity. However, in order to achieve a complete transformation of $PhPH_2$ and the intermediate secondary phosphane **1c** to **1d**, an excess of **1** or (*R*)-(+)-**1** (ca. 10−15%) had to be applied. The excess **1** and side-products formed during the reaction could not be completely separated by distillation due to the thermal instability of **1d**.



Scheme 1

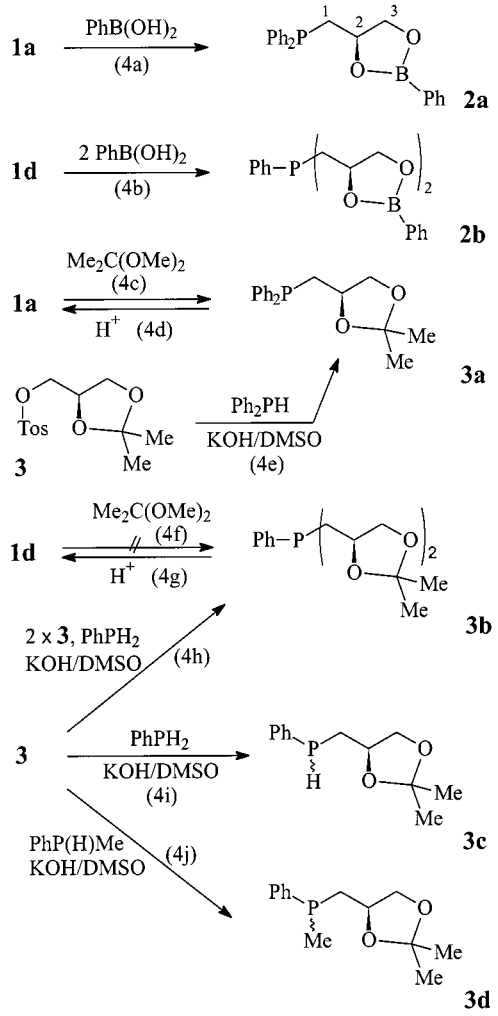
The secondary phosphane **1c** can be used as a building block for the synthesis of tertiary phosphanes containing dihydroxylated propyl substituents with chiral carbon and phosphorus atoms. In the context of a research program aimed at the development of chiral, water-soluble phosphanes for two-phase catalysis, the introduction of substituents bearing polar cationic or anionic groups was of pri-

mary interest.[5b] Nucleophilic phosphanylation[16a] or Pd-catalyzed P−C coupling,[16b,17] as developed earlier by us, could be used as the fundamental synthetic principles. Thus, reaction of **1c** with the iodophenyl guanidine **1e**[18] in the presence of a catalytic amount of $Pd(Ph_3P)_4$[19] gave the guanidinium phosphane **1f** (Equation 3a). In order to isolate it from the reaction mixture and to allow its further purification, **1f** was deprotonated with KOH to give the neutral guanidinophosphane ligand **1g** (Equation 3c). **1e** was obtained from 3-iodoanilinium chloride by reaction with Me_2NCN and subsequent deprotonation of the intermediate guanidinium salt with KOH.[18]

Direct and Indirect Derivatization of 1a, 1c, and 1d

The 2,3-dihydroxypropyl substituents and the PH functionality in **1a**−**1d** offer numerous possibilities for fine tuning of their ligand properties.

Chiral ligands **2a**, **2b** bearing Lewis acidic sites are accessible by reaction of enantiomerically pure **1a** or **1d**, respectively, with phenylboronic acid (Equation 4a, 4b). This access to aromatic boronate esters has been exploited in the synthesis of boron analogues of DIOP by Fields and Jacobsen.[20]



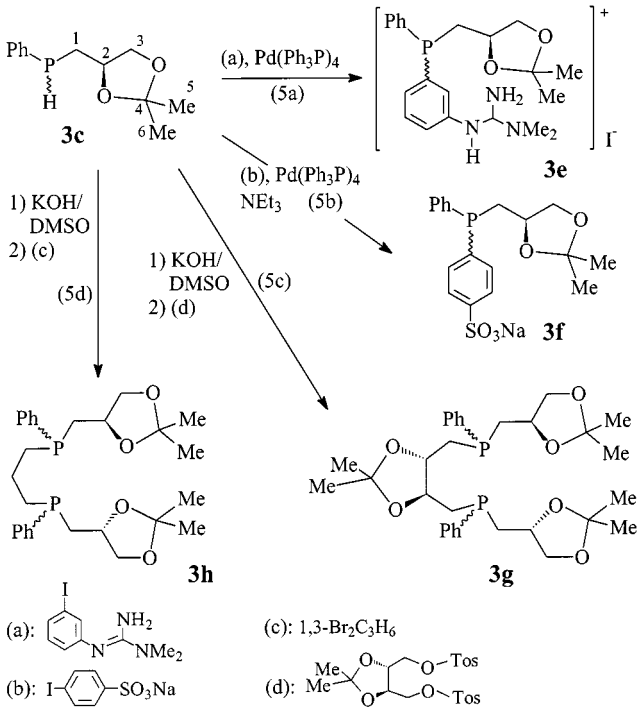
Scheme 2

The formation of **2a** from enantiopure (*R*)-(−)-**1a** proceeds with retention of configuration at the β carbon atom (see X-ray structural analysis of **2a**). The $^{31}P\{^1H\}$-NMR spectrum of **2b** features an intense signal at δP = −37.39 corresponding to the main (*RR*)-isomer. Additional resonances of low intensity at δP = −36.41 and −39.57 may be assigned to the two *meso* forms of **2b**, derived from the *meso* isomers present in the starting material **1d** (see above). If racemic **1d** is employed in this reaction (Equation 4b), a 1:2:1 mixture of three diastereoisomers of **2b** is obtained, which gives rise to resonances at δP = −36.46, −37.42, and −39.60 in the $^{31}P\{^1H\}$-NMR spectrum.

Ketalization of optically active **1a** with 2,2-dimethoxypropane using *p*-toluenesulfonic acid as catalyst yields (*R*)-(+)-2,3-*O*-isopropylideneglycerol-1-diphenylphosphane **3a** (Equation 4c). However, attempts to synthesize oligofunctional **3b** by ketalization of **1d** were not successful, a multi-component mixture being formed (Equation 4f). The phosphane ligand (*R*)-(+)-Glyphos (**3a**) was first prepared by Brunner and Leyerer[21a] in moderate yield by reaction of Ph_2PK in dioxane with (*R*)-(−)-2,3-*O*-isopropylidene-1-glycerol tosylate **3**. Very recently, Kerr et al.[21b] published an analogous synthetic procedure for (*R*)-(+)-Glyphos starting from D-mannitol. We have now found that this ligand may be obtained much more easily and in substantially higher yields by nucleophilic phosphanylation of enantiomerically pure (*R*)-(−)-**3** with Ph_2PH in the superbasic medium DMSO/KOH (Equation 4e). Using this methodology, the tertiary and secondary phosphanes **3b**−**3d** have also been prepared by employing $PhPH_2$ or Ph(Me)PH and (*R*)-(−)-**3** as the starting materials (Equations 4h−4j). **3b** shows only one signal (δP = −35.57) in its $^{31}P\{^1H\}$-NMR spectrum, indicating that it is formed stereoselectively [(*R,R*)-isomer] according to Equation 4h. In **3b**, with homochiral β carbon atoms, the two CH_2−P, CH−O, and CH_2O groups are non-equivalent. Compared with the spectra of **3a**, a doubling of the line patterns in the ^1H- and $^{13}C\{^1H\}$-NMR spectra is therefore observed.

The phosphanes **3c** and **3d** with two centers of chirality give rise to two $^{31}P\{^1H\}$-NMR signals [δP = −62.94, −63.44 (**3c**): δP = −38.96, −41.22 (**3d**)], which, in the case of **3c**, are split into doublets under proton coupling [^1J(PH) = 211.1 or 208.6 Hz]. The isopropylidene protecting group in **3a** may be cleaved by reaction with small amounts of *p*-toluenesulfonic acid, leading to the formation of **1a** without loss of optical activity (Equation 4d). Very recently, this method has been used by Brunner and Rückert[22] for the synthesis of **1a** using **3a** as starting material.

The PH functionality renders **3c** a valuable synthon for the preparation of further functionalized mono- or bidentate phosphanes. The bidentate ligand **3h** was thus obtained by alkylation of **3c** using 1,3-dibromopropane in the superbasic medium DMSO/KOH (Equation 5d). As evidenced by the $^{31}P\{^1H\}$-NMR spectrum, **3h**, with homochiral β carbon atoms, is formed as a mixture of three diastereoisomers ($R_CR_PR_PR_C$, $R_CS_PS_PR_C$, and $R_CR_PS_PR_C$), two of them ($R_CR_PR_PR_C$, $R_CS_PS_PR_C$) with equivalent (δP =



Scheme 3

−29.81, −31.46, respectively) and one ($R_CR_PS_PR_C$) with chemically non-equivalent phosphorus atoms [δP = −29.68, −31.32, ^4J(PP) = 1.0 Hz]. The value observed for ^4J(PP) is typical for long-range coupling constants (0−5 Hz) in trimethylene-bridged diphosphorus compounds.[23] If (*R,R*)-(+)-1,4-di-*O*-*p*-toluenesulfonyl-2,3-*O*-isopropylidene-D-threitol is used instead of 1,3-dibromopropane for coupling to **3c**, the bidentate ligand **3g** is obtained as a mixture of three diastereoisomers [$R_CR_P(S_C)_2R_PR_C$, $R_CS_P(S_C)_2S_PR_C$, $R_CR_P(S_C)_2S_PR_C$], in one of which [$R_CR_P(S_C)_2S_PR_C$] the P atoms are non-equivalent, as reflected in the $^{31}P\{^1H\}$-NMR spectrum (Equation 5c).

Derivatization of **3c** is also possible by means of Pd-catalyzed P−C coupling reactions with iodoaromatic compounds.[16b,17] Thus, on reaction of **3c** with iodophenyl guanidine **1e**, the cationic phosphane ligand **3e** is obtained in high yield (Equation 5a). Using sodium *p*-iodobenzenesulfonate[24] in the presence of NEt_3, the anionic phosphane **3f** is formed (Equation 5b). **3e** and **3f** are obtained as mixtures of diastereoisomers.

X-ray Structure of (*R*)-$Ph_2P-CH_2-C^aH-O-B(Ph)-O-C^bH_2$ [*C*^{a}−*C*^{b}]

Crystals suitable for X-ray structural analysis were obtained by recrystallization of (*R*)-(+)-**2a** from ethanol. The unit cell of the crystal of **2a** (space group $P2_1$) used for the X-ray analysis contains two crystallographically independent molecules forming pairs of antiparallel oriented molecules A and B both showing (*R*) configuration at the β carbon atom. The numbering scheme for **2a** and selected bond lengths and angles are collected in Figure 1.

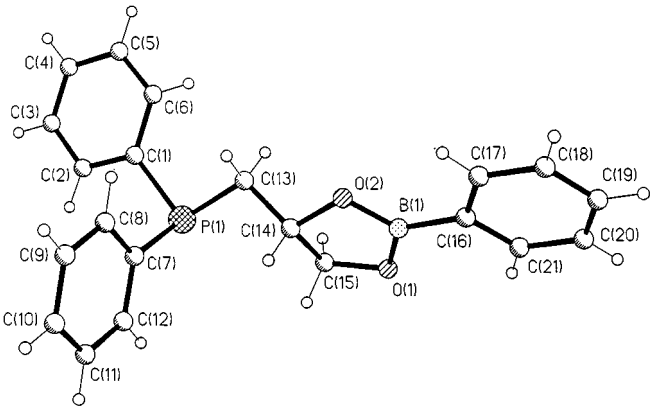


Figure 1. Molecular structure of **2a**; selected interatomic distances [Å] and angles [°]: P(1)−C(1) 1.836(6), P(1)−C(7) 1.822 (7), P(1)−C(13) 1.851(6), C(14)−O(2) 1.463(7), C(15)−O(1) 1.443(7), C(14)−C(15) 1.525, B(1)−O(1) 1.384(8), B(1)−O(2) 1.369(8), B(1)−C(16) 1.509(9); C(1)−P(1)−C(7) 101.76(29), C(1)−P(1)−C(13) 101.83(30), C(7)−P(1)−C(13) 101.46(28), O(1)−B(1)−O(2) 111.9(5)

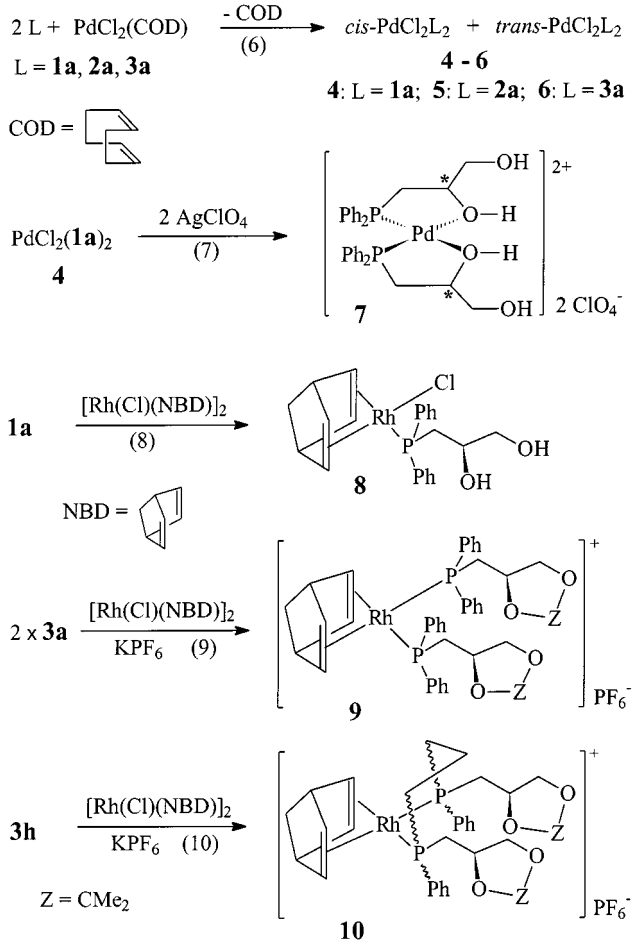
In the two independent molecules (A, B), the geometrical parameters of the PC_3 skeleton are slightly different, the P−C distances [P(1)−C(1) 1.836(6), P(1)−C(7) 1.822(7), P(1a)−C(1a) 1.805(7), P(1a)−C(7a) 1.836(6) Å] and C−P−C bond angles [C(1)−P(1)−C(7) 101.8(3), C(1a)−P(1a)−C(7a) 101.2(3)°] within the Ph_2P groups being comparable to those in Ph_3P.[25,26] The torsional arrangements of the aromatic ring planes within the Ph_2P units of the two independent molecules A and B are also different.

The atoms within the cyclic boronic diester moieties O(1)−C(14)−C(15)−O(2)−B(1)[*O(1)−B(1)*] are coplanar to within 0.084 Å, the coordination at B(1) or B(1a) being distorted trigonal planar [O(1)−B(1)−O(2) 111.9(5), O(2)−B(1)−C(16) 123.0(6), O(1)−B(1)−C(16) 125.1(6)°]. The aromatic substituent at B(1) or B(1a) and the BO_2C_2 cyclic boronic diester unit are arranged in an almost coplanar fashion, the interplanar angle between the plane of the aromatic ring system and the plane defined by B(1), O(1), O(2), and C(16) being just 4.42°. Similar coplanarity of the BO_2 group with the aromatic ring has been found in other aromatic boronic acids and their esters.[27]

Palladium(II) and Rhodium(I) Complexes of 1a, 2a, 3a, 3h

On reaction of enantiomerically pure **1a**, **2a**, or **3a** with $PdCl_2$(COD) in a 2:1 molar ratio, complexes of the composition $PdCl_2L_2$ are formed (Equation 6), which show two signals in their $^{31}P\{^1H\}$-NMR spectra in the ranges δ = 40−28 and δ = 15−13. By analogy with literature data for *cis*- and *trans*-Cl_2PdL_2 complexes,[28,29] the low field signals are assigned to the *cis* isomers and the high field resonances to the *trans* isomers of **4**−**6**. The relative intensities of the $^{31}P\{^1H\}$-NMR signals of both isomers (*cis*/*trans*) vary from 10:1 (**4**), through 1:1 (**6**), to 1:7 (**5**). The assignment of the $^{31}P\{^1H\}$-NMR resonances to *cis*/*trans* isomers is corroborated by analysis of the $^{13}C\{^1H\}$-NMR spectra, which fea-

ture signals (e.g. for C1, C3, C_{ipso}, C_{ortho}, C_{meta}) of corresponding intensity with doublet or triplet fine structures (for the numbering of the aliphatic C atoms, see Scheme 3). Thus, **4**, which exists predominantly as the *cis* isomer, shows signals with doublet fine structure for C1 and C3, while a singlet is observed for C2. In the case of **6**, two $^{13}C\{^1H\}$-NMR resonances are observed for the carbon atoms C1 and C_o, C_m of the phenyl substituents with doublet or triplet fine structures (X parts of ABX spin systems,[30] A, B = ^{31}P, X = ^{13}C) for the *cis* and *trans* isomers, respectively. Each of the two isomers show singlets for C2, C3, and C4. The Me groups of the CMe_2 units (C5, C6) in the two isomers of **6** (*cis*, *trans*) are diastereotopic due to the center of asymmetry at the β carbon. The same applies to the two Ph substituents of the Ph_2P groups in **5** (existing mainly as the *trans* isomer) and **6**; two sets of $^{13}C\{^1H\}$-NMR resonances with triplet fine structure are observed for the aromatic carbon atoms C_{ipso}, C_{ortho}, and C_{meta} of the *trans* isomer.



Scheme 4

Treatment of a toluene solution of **4** with $AgClO_4$ gave the dicationic complex **7** (Equation 7). Similar types of reactions have been reported by Pringle et al.[31–33] for palladium(II) and platinum(II) complexes of phosphanyl alcohols $Ph_2P-CH_2-CRR'-OH$ (R, R′ = H, Me). Complex **7** shows one signal at δP = 52.46 in its $^{31}P\{^1H\}$-NMR spectrum, in a range consistent with a *cis* geometry. A resonance of low intensity at δP = 47.63 may possibly be due to the *trans* isomer of **7**. The assignment of the main signal to the *cis* isomer is in accord with the filled-in doublet appearance of the $^{13}C\{^1H\}$-NMR resonances of the aromatic carbon atoms (C_o, C_m) at δC = 136.48, 134.59, 131.28, 130.83 (X parts of ABX-type spin systems,[30] A, B = ^{31}P, X = ^{13}C) in the $^{13}C\{^1H\}$-NMR spectrum.

On reaction of $[RhCl(NBD)Cl]_2$ with **1a**, complex **8** is formed (Equation 8). A signal at δP = 23.54 observed in the $^{31}P\{^1H\}$-NMR spectrum of **8** is split into a doublet by ^{103}Rh-^{31}P coupling [$J(^{103}Rh$-$^{31}P)$ = 168.7 Hz]. If **3a** is treated with $[RhCl(NBD)Cl]_2$ in a 2:1 molar ratio in the presence of KPF_6 using acetone as solvent, the cationic complex **9** is obtained (Equation 9). A similar procedure has been used by Schrock and Osborn[34] for the preparation of the corresponding Ph_3P complex. The $^{31}P\{^1H\}$-NMR spectrum features a doublet at δP = 24.41 [$J(^{103}Rh$-$^{31}P)$ = 155.7 Hz] and a septet at δP = 142.97 [$J(^{31}P$-$^{19}F)$ = 707.8 Hz] for the PF_6^- ion. An analogous reaction with the bidentate ligand **3h** affords complex **10** as a mixture of three diastereoisomers (Equation 10), two of them giving rise to a simple doublet in the $^{31}P\{^1H\}$-NMR spectrum {symmetrical isomers, δP = 7.73 [$J(^{103}Rh$-$^{31}P)$ = 143.9 Hz], 7.48 [$J(^{103}Rh$-$^{31}P)$ = 146.1 Hz]}. The unsymmetrical diastereoisomer with non-equivalent phosphorus atoms (AB part of an ABX spin system, A, B = ^{31}P, X = ^{103}Rh) gives rise to eight lines (δP(A) = 5.62 {$J[^{103}Rh$-$^{31}P(A)]$ = 145.9 Hz}; δP(B) = 7.37 {$J[^{103}Rh$-$^{31}P(B)]$ = 145.9 Hz, $J[^{31}P(A)$-$^{31}P(B)]$ = 52.32 Hz})

Experimental Section

General: For experimental details, see Part 10 of this series.[1] – NMR spectra were recorded on a Bruker AMX 400 or a Bruker AC 250 instrument. – Mass spectra were obtained on a Varian MAT 311 A. – Racemic and (*R*)-(+)-glycidol (2,3-epoxy-1-propanol), 3-iodoaniline, phenylboronic acid, (*S*)-(+)-2,2-dimethyl-4-hydroxymethyl-1,3-dioxolane were purchased from Aldrich GmbH and used without further purification. 1,5-Cyclooctadiene dichloro palladium(II),[35] norbornadienechlororhodium(I) dimer,[36] (*R*)-(−)-2,3-*O*-isopropylideneglycerol tosylate **3**,[37] and $Pd(Ph_3P)_4$[19] were prepared according to literature methods. 3-Iodophenyl guanidine (**1e**)[5b,18] and sodium *p*-iodobenzenesulfonate[24] were prepared according to methods that we have described previously.

Preparation of *rac*- and (*R*)-(−)-2,3-Dihydroxypropyl-1-diphenylphosphane [*rac*-1a and (*R*)-(−)-1a]: 2.0 g (11.0 mmol) or 12.6 g (67.5 mmol) of diphenylphosphane was added to a suspension of 0.83 g (13.0 mmol) or 4.90 g (77.0 mmol) of KOH powder (88%) in 10 or 50 mL of dimethyl sulfoxide (DMSO). The reaction mixture was stirred for 1 h at ambient temperature. On addition of 0.90 g (12.0 mmol) of *rac*-glycidol or 5.0 g (68.0 mmol) of (*R*)-(+)-glycidol, the orange color of the solution disappeared. 10 mL of water was then added and thereafter the solvents were removed in vacuo (70°C, 0.01 mbar). The remaining residue was redissolved in 10 or 50 mL of ethanol and the solution was neutralized with conc. HCl. The precipitate of KCl formed was filtered off and the solvent was stripped off in vacuo (80°C, 0.01 mbar) leaving the phosphanes *rac*-**1a** (2.4 g, 84%) and (*R*)-(−)-**1a** (14.8 g, 84%) as colorless oily liquids. They were purified by distillation in vacuo (oil bath temperature 180°C, 0.01 mbar). – (*R*)-(−)-**1a**: $C_{15}H_{17}O_2P$ (260.3):

calcd. C 69.22, H 6.63; found C 69.14, H 6.63. – MS: *m/z* (%): 260 (32) [M^+], 243 (18) [$M^+ - OH$], 229 (4) [$M^+ - CH_2OH$], 199 (100) [$M^+ - C_2H_3(OH)_2$], 183 (65) [$M^+ - C_6H_5$]. – ^{1}H NMR (C_6D_6): δ = 2.21–2.43 (2 H), 3.55–3.72 (2 H), 3.92 (1 H), 4.1 (2 H, OH), 7.04–7.19, 7.46–7.55 (10 H). – $^{13}C\{^1H\}$ NMR (C_6D_6): δ = 33.49 (14.2), 67.51 (9.2), 70.60 (16.3), 128.63 (9.2), 128.75, 128.83 (6.1), 133.03 (18.3), 133.45 (19.3), 139.18 (13.2), 139.49 (12.2). – $^{31}P\{^1H\}$ NMR (C_6D_6): δ = −21.22. – $[\alpha]_D^{20}$ = −19.4° (*c* = 1.3, CH_2Cl_2).

Preparation of [(*R*,*S*)$_P$,*R*$_C$]-2,3-Dihydroxypropyl-1-phenylmethylphosphane (1b): 1.05 g (16.5 mmol) of KOH, 1.8 g (14.5 mmol) of Ph(Me)PH, and 1.07 g (14.5 mmol) of (*R*)-(+)-glycidol were reacted according to the same procedure as described for **1a**. Yield: 2.33 g (81%). – *rac*-**1b**: $C_{10}H_{15}O_2P$ (198.2): calcd. C 60.60, H 7.63; found C 59.98, H 7.67. – MS: *m/z* (%): 198 (29) [M^+], 181 (17.6) [$M^+ - OH$], 138 (100) [$M^+ - C_2H_2(OH)_2$]. – ^{1}H NMR (CD_3OD): δ = 1.33 (3.4, 3 H), 1.35 (3.1, 3 H), 1.74–1.97 (2 H), 3.32–3.71 (1 H), 4.15 (OH), 7.36, 7.54 (5 H). – $^{13}C\{^1H\}$ NMR (CD_3OD): δ = 12.56 (13.4), 13.24 (13.0), 36.68 (13.5), 37.08 (12.6), 67.81 (8.5), 68.19 (9.2), 71.26 (13.0), 71.89 (14.8), 129.44 (6.1), 132.54 (18.3), 132.64 (19.3), 141.84 (13.2), 129.55, 129.64. – $^{31}P\{^1H\}$ NMR (CD_3OD): δ = −39.13, −40.95.

Preparation of *rac*- or [(*R*,*S*)$_P$,*R*$_C$]-2,3-Dihydroxypropyl-1-phenylphosphane (1c): 2.0 g (18.2 mmol) or 1.5 g (13.5 mmol) of phenylphosphane was reacted with 1.4 g (22.0 mmol) or 1.0 g (15.7 mmol) of KOH and 1.48 g (20.0 mmol) or 1.1 g (14.8 mmol) of *rac*- or (*R*)-(+)-glycidol according to the same procedure as described for **1a**. 2.78 g (83%) of *rac*-**1c** and 1.98 g (80%) of [(*R*,*S*)$_P$,*R*$_C$]-**1c** were obtained as oily liquids. – *rac*-**1c**: $C_9H_{13}O_2P$ (184.2): calcd. C 58.69, H 7.11; found C 58.43, H 6.89. – MS: *m/z* (%): 184 (34) [M^+], 167 (7) [$M^+ - OH$], 153 (7) [$M^+ - CH_2OH$], 125 (100) [$M^+ - C_2H(OH)_2$], 109 (84) [PhPH]. – ^{1}H NMR (C_6D_6): δ = 1.74–2.22 (2 H), 3.46–3.64, 3.72–3.94 (3 H), 4.38 (211.4, 1 H), 4.34 (211.3, 1 H), 7.05–7.19, 7.45–7.51 (5 H). – $^{13}C\{^1H\}$ NMR (C_6D_6): δ = 27.92 (14.2), 27.97 (13.2), 67.35 (8.1), 67.40 (6.1), 71.00 (8.1), 71.30 (9.2), 128.34, 128.44, 128.72, 128.77 (2.0), 134.00 (16.3), 134.08 (16.3), 135.68 (10.2), 135.75 (10.2). – $^{31}P\{^1H\}$ NMR (C_6D_6): δ = −3.28 (212), −3.05 (212). – ^{31}P NMR (C_6D_6): δ = −63.05 (212), −63.39 (212).

Preparation of *rac*- or (*R*,*R*)-(−)-Bis(2,3-dihydroxypropyl)-1-phenylphosphane [*rac*-1d and (*R*,*R*)-(−)-1d]: Reaction of 64 g (0.1 mol) or 2.1 g (33 mmol) of KOH and 4.62 g (42.0 mmol) or 1.5 g (13.6 mmol) of $PhPH_2$ with 6.88 g (92.8 mmol) or 2.22 g (30.0 mmol) of *rac*- or (*R*)-(+)-glycidol using the same procedure as described for **1a**, although at a higher temperature (80°C). Yields: 8.35 g (77%) of *rac*-**1d**, 2.6 g (74%) of (*R,R*)-(−)-**1d**. – (*R,R*)-(−)-**1d**: $C_{12}H_{19}O_4P$ (258.3): calcd. C 55.80, H 7.42; found C 55.40, H 7.18. – MS: *m/z* (%): 258 (17) [M^+], 241 (28) [$M^+ - OH$], 227 (18) [$M^+ - CH_2OH$], 198 (18) [$M^+ - C_2H_2(OH)_2$], 184 (21) [$M^+ - C_3O_2H_6$], 138 (100) [$M^+ - 2\,C_2H_2(OH)_2$]. – $^{31}P\{^1H\}$ NMR ([D$_6$]DMSO): δ = −35.2. – $[\alpha]_D^{20}$ = −11.0° (*c* = 10, MeOH) or −25.7° (neat).

Preparation of *rac*-2,3-Dihydroxypropyl-1-phenyl-1-[3-(*N*,*N*-dimethylguanidino)phenyl]phosphane (*rac*-1g): A solution of 2.5 g (8.6 mmol) of 3-iodophenyl guanidine and 1.6 g (8.6 mmol) of *rac*-**1d** in 10 mL of acetonitrile was heated to 60°C and then 0.2 g (2 mol-%) of $Pd(Ph_3P)_4$ was added. After stirring for 3 h, the solvent was removed in vacuo (60°C, 0.01 mbar) and the remaining residue was redissolved in 20 mL of *n*-hexanol. The precipitate (**1f**; $^{31}P\{^1H\}$ NMR: δ = −18.6, −19.2) deposited following the addition of 150 mL of diethyl ether was filtered off and dried in vacuo. It was then treated with excess aqueous KOH and the resulting solution was extracted three times with 30 mL of dichloromethane. After evaporation of the solvent from the combined extracts, **1g** was obtained as a cream-colored powder. Yield: 1.8 g (55%). – *rac*-**1g**: $C_{18}H_{24}N_3O_2P \cdot 2.5\,H_2O$ (390.4): calcd. C 55.45, H 7.37, N 10.78; found C 55.70, H 7.20, N 10.62. – MS: *m/z* (%): 345 (39) [M^+], 289 (66) [$M^+ - HNCNMe$], 274 (19) [$M^+ - HNCNMe_2$]. – $^{13}C\{^1H\}$ NMR ($CDCl_3$): δ = 32.72 (14.3), 37.48, 66.88 (6.7), 66.94 (7.6), 69.81 (10.5), 69.94 (9.5), 124.06, 124.30, 126.42 (21.4), 126.68 (21.4) 127.38 (17.3), 127.73 (17.3), 128.21 (6.1), 128.27 (7.1), 129.28 (6.1), 129.35 (6.1), 130.28, 130.61, 132.32 (18.3), 132.63 (18.3), 138.57 (12.2), 138.61 (13.2), 138.86 (11.2), 138.93 (11.2), 149.91 (12.2), 149.98 (12.2), 152.29, 152.72, 153.17, 153.19. – $^{31}P\{^1H\}$ NMR ($CDCl_3$): δ = −21.54, −21.73.

Preparation of *rac*- or (*R*)-(+)-(2-Phenyl-1,3,2-dioxaborolano-4-methyl)diphenylphosphane [*rac*-2a, (*R*)-(+)-2a] and *rac*- or (*R*,*R*)-(−)-Bis(2-phenyl-1,3,2-dioxaborolano-4-methyl)phenylphosphane [*rac*-2b, (*R*,*R*)-(−)-2b]: To a suspension of 0.9 g (3.5 mmol) or 1.47 g (5.6 mmol) of racemic or (*R*)-(−)-**1a** in 20 mL of dichloromethane, a CH_2Cl_2 solution of 0.42 g (3.46 mmol) or 0.7 g (5.6 mmol) of benzeneboronic acid was added with stirring. After 1 h, all volatiles were removed from the clear solution leaving a colorless solid, which was recrystallized from ethanol for further purification. Yields: 0.90 g (74%) of *rac*-**2a**, 1.49 g (77%) of (*R*)-(+)-**2a**. – *rac*-**2a**: $C_{21}H_{20}BO_2P$ (346.2): calcd. C 72.85, H 5.82, P 8.95; found C 72.52, H 5.92, P 9.30. – MS: *m/z* (%): 346 (32) [M^+], 199 (100) [$M^+ - C_2H_3O_2B(Ph)$], 183 (44) [$M^+ - C_3H_5O_2B(Ph) - H_2$], 121 (23) [$M^+ - C_2H_3O_2B(Ph) - Ph$], 108 (22) [$M^+ - C_3H_5O_2B(Ph) - Ph$]. – ^{1}H NMR ($C_6D_6$): δ = 1.98–2.03 (2 H), 2.45–2.50 (2 H), 3.82–3.86 (2 H), 3.99–4.04 (2 H), 4.37–4.46 (1 H), 7.07–8.12 (15 H). – $^{13}C\{^1H\}$ NMR (C_6D_6): δ = 36.40 (15.26), 71.96 (10.18), 75.82 (19.33) 128.11, 128.68 (4.1), 128.74, 128.80 (4.1), 128.90, 131.69, 133.10 (20.4), 133.19 (19.3), 135.43, 138.50 (13.2), 138.93 (13.2). – $^{31}P\{^1H\}$ NMR (C_6D_6): δ = −22.8. – (*R*)-(+)-**2a**: $C_{21}H_{20}BO_2P$ (346.2): calcd: C 72.85, H 5.82, P 8.95; found C 72.37, H 5.90, P 9.13. – $[\alpha]_D^{20}$ = +9.0° (*c* = 2, $CHCl_3$).

rac-**2b** and (*R,R*)-(−)-**2b** were prepared in a manner analogous to that described for *rac*-**2a** and (*R*)-(+)-**2a** employing 3.58 g (13.9 mmol) or 1.06 g (4.1 mmol) of **1c** [*rac* or (*R*)-(+) form] and 3.38 g (27.7 mmol) or 1.0 g (8.2 mmol) of benzeneboronic acid. Yields: 4.6 g (77%) of *rac*-**2b**, 1.4 g (80%) of (*R*)-(−)-**2b**. – *rac*-**2b**: $C_{24}H_{25}B_2O_4P$ (430.0): calcd. C 67.03, H 5.96; found C 66.59, H 6.07. – MS: *m/z* (%): 430 (6.2) [M^+], 312 (12) [$M^+ - OCH_2B(Ph)$], 284 (7) [$M^+ - C_2H_2O_2B(Ph)$], 270 (6) [$M^+ - C_3H_4O_2B(Ph)$], 138 (100) [$M^+ - 2\,C_2H_2O_2B(Ph)$]. – $^{13}C\{^1H\}$ NMR (C_6D_6): δ = 36.0 (15.3), 36.28 (16.3), 36.47 (14.2), 37.10 (15.3), 71.84 (8.1), 71.95 (10.2), 72.12 (9.2), 72.16 (9.2), 75.56 (15.3), 75.70 (14.2), 76.21 (19.3), 76.24 (19.3). – $^{31}P\{^1H\}$ NMR (C_6D_6): δ = −36.46, −37.42, −39.60. – (*R,R*)-(−)-**2b**: $C_{24}H_{25}B_2O_4P$ (430.0): calcd. C 67.03, H 5.96; found C 66.59, H 6.07. – $^{13}C\{^1H\}$ NMR (C_6D_6): δ = 36.28 (16.3), 36.45 (14.2), 71.95 (9.2), 72.11 (9.2), 75.68 (15.3), 76.20 (18.3), 128.11, 128.15, 128.76 (7.1), 129.46, 131.70, 131.75, 133.01 (21.4), 135.36, 137.78 (13.2). – $^{31}P\{^1H\}$ NMR ($CDCl_3$): δ = −37.39. – $[\alpha]_D^{20}$ = −13.8° (*c* = 1.68, C_6H_6).

Preparation of *rac*- and (*R*)-(+)-2,3-*O*-Isopropylideneglycerol-1-diphenylphosphane [*rac*-3a, (*R*)-(+)-3a]: To a suspension of 1.9 g (29.6 mmol) or 1.0 g (14.7 mmol) of KOH powder (88%) in 30 mL of DMSO, 5.5 g (29.6 mmol) or 2.5 g (13.4 mmol) of diphenylphosphane was added at ambient temperature. 7.7 g (27.0 mmol) or 3.85 g (13.4 mmol) of *rac*- or (*R*)-(−)-2,3-*O*-isopropylideneglycerol-1-tosylate was then added to the intensely red-colored reaction mixture within a period of 30 min. After stirring for 8 h, 20 mL of water was added and the reaction mixture was extracted with toluene (3 × 50 mL). The combined toluene phases were dried with

$MgSO_4$ and the solvent was evaporated in vacuo (20°C, 0.01 mbar). The remaining oily residue was dried in vacuo (80°C, 0.01 mbar). Yields: 6.5 g (80%) of *rac*-**3a**, 3.1 g (77%) of (*R*)-(+)-**3a**. For further purification, the products were distilled in vacuo (oil bath temperature 180°C, 0.01 mbar). – (*R*)-(+)-**3a**: $C_{18}H_{21}O_2P$ (300.3): calcd. C 71.98, H 7.05, P 10.31; found C 71.71, H 6.65, P 9.76. – MS: *m/z* (%): 300 (32) [M^+], 285 (7) [$M^+ - CH_3$], 242 (7) [$M^+ - C_3H_6O$], 199 (47) [$M^+ - C_2H_3O_2C_3H_6$], 186 (100) [Ph_2PH]. – ^1H NMR (C_6D_6): δ = 1.28 (3 H), 1.42 (3 H), 2.15, 2.54 (2 H), 3.56, 3.88 (2 H), 4.19 (1 H), 7.08–7.44 (10 H). – $^{13}C\{^1H\}$ NMR (C_6D_6): δ = 26.01, 27.26, 33.87 (15.3), 70.34 (9.2), 74.31 (20.3), 108.94, 128.69 (7.1), 128.79 (9.2), 133.00 (18.3), 133.20 (19.3), 138.89 (13.2), 139.20 (14.2). – $^{31}P\{^1H\}$ NMR (C_6D_6): δ = −21.66. – $[\alpha]_D^{20}$ = +14.5° (*c* = 1, C_6H_6).

Preparation of (*R*,*R*)-(+)-Bis[2,3-*O*-isopropylideneglycerol]-1-phenylphosphane [(*R*,*R*)-(+)-3b]: 2.16 g (33.9 mmol) of KOH, 1.64 g (14.9 mmol) of $PhPH_2$, and 8.53 g (29.8 mmol) of (*R*)-(−)-2,3-*O*-isopropylideneglycerol-1-tosylate were reacted according to the same procedure as described for **3a**. Yield: 4.1 g (81%) of **3b**. – (*RR*)-(+)-**3b**: $C_{18}H_{27}O_4P$ (338.4): calcd. C 63.89, H 8.04; found C 63.55, H 7.81. – MS: *m/z* (%): 338 (29) [M^+], 323 (2) [$M^+ - CH_3$], 280 (6) [$M^+ - C_3H_6O$], 222 (18) [$M^+ - 2\ C_3H_6O$], 166 (100) [$M^+ - C_6H_{10}O_2 - C_3H_6O$]. – ^1H NMR (C_6D_6): δ = 1.21, 1.26 (6 H), 1.37 (6 H), 1.65–1.71, 1.85–1.92, 2.01–2.07 (4 H), 3.26–3.30, 3.59–3.64 (6 H), 7.08–7.16, 7.39–7.44 (5 H). – $^{13}C\{^1H\}$ NMR (C_6D_6): δ = 25.99, 26.01, 27.19, 27.23, 33.80 (15.3), 34.31 (13.2), 70.21 (9.2), 70.52 (8.1), 74.18 (16.3), 74.75 (20.3), 108.88, 108.89, 128.68 (7.1), 129.36, 132.96 (20.3), 138.48 (14.2). – $^{31}P\{^1H\}$ NMR (C_6D_6): δ = −35.57. – $[\alpha]_D^{20}$ = +32.8 (neat).

Preparation of [(*R*,*S*)$_P$,*R*$_C$]-2,3-*O*-Isopropylideneglycerol-1-phenylphosphane (3c) and [(*R*,*S*)$_P$,*R*$_C$]-2,3-*O*-Isopropylideneglycerol-1-phenylmethylphosphane (3d): These ligands were prepared in an analogous manner as (*R,R*)-(+)-**3b**, employing 5.04 g (45.8 mmol) of $PhPH_2$ or 1.08 g (8.7 mmol) of Ph(Me)PH, 3.20 g (50.3 mmol) or 0.63 g (9.6 mmol) of KOH, and 13.1 g (45.8 mmol) or 2.49 g (8.7 mmol) of (*R*)-(−)-2,3-*O*-isopropylideneglycerol tosylate. Yields: 6.7 g (65%) of **3c**, 1.48 g (71%) of **3d**. Purification of **3c** and **3d** was achieved by vacuum distillation (**3c**: 74–76°C, 0.01 mbar, **3d**: 104°C, 0.01 mbar). – **3c**: $C_{12}H_{17}O_2P$ (224.2): C 64.27, H 7.64; found C 63.83, H 7.67. – MS: *m/z* (%): 224 (7.4) [M^+], 209 (11.2) [$M^+ - CH_3$], 166 (83.9) [$M^+ - C_3H_6O$], 125 (100) [$M^+ - C_5H_8O_2$], 110 (46.4) [$PhPH_2$]. – ^1H NMR (C_6D_6): δ = 1.24, 1.25, 1.35, 1.37 (6 H), 1.62–1.70, 1.75–1.91, 2.08–2.15 (2 H), 3.28–3.38, 3.63–3.84, 3.91–4.05, 4.32–4.47 (4 H), 7.03–7.38 (5 H). – $^{13}C\{^1H\}$ NMR (C_6D_6): δ = 25.84, 25.98, 27.23, 27.27, 28.27 (15.3), 28.30 (14.3), 70.00 (5.2), 70.02 (5.1), 74.83 (10.2), 74.92 (8.1), 108.86, 109.13, 128.24, 128.65 (5.1), 128.70 (4.1), 133.84 (16.3), 134.08 (16.3), 135.29 (11.2), 135.33 (11.2). – $^{31}P\{^1H\}$ NMR (C_6D_6): δ = −62.94 (211.1), −63.44 (208.6). – **3d**: $C_{13}H_{19}O_2P$ (238.3): C 65.53, H 8.04; found C 65.25, H 7.91. – MS: *m/z* (%): 238 (20.7) [M^+], 223 (80) [$M^+ - CH_3$], 138 (45.8) [$M^+ - C_5H_8O_2$], 124 (100) [PhMePH]. – ^1H NMR (C_6D_6): δ = 1.15 (4.1), 1.20 (3.6, 3 H), 1.28, 1.32, 1.41, 1.42 (6 H), 1.64–1.74, 1.81–2.04 (2 H), 3.33–4.16 (3 H), 7.07–7.71 (5 H). – $^{13}C\{^1H\}$ NMR (C_6D_6): δ = 12.49 (14.3), 12.82 (15.3), 26.05, 27.26 (4.1), 35.57 (16.3), 36.56 (15.3), 70.29 (9.2), 70.67 (9.2), 74.23 (15.3), 74.94 (18.3), 108.85, 128.60 (7.1), 128.61 (7.1), 128.73, 128.76, 131.89 (19.3), 140.56 (14.2), 140.95 (14.2). – $^{31}P\{^1H\}$ NMR (C_6D_6): δ = −38.96, −41.22.

Preparation of 2,3-*O*-Isopropylideneglycerol-1-[3-(*N*,*N*-dimethylguanidinium)phenyl]phosphane Iodide (3e): 0.55 g (2.45 mmol) of [(*R*,*S*)$_P$,*R*$_C$]-**3c** and 0.71 g (2.45 mmol) of 3-iodophenylguanidine were dissolved in 10 mL of acetonitrile and 2.8 mg (1.0 mol-%) of the catalyst $Pd(Ph_3P)_4$ was added. After stirring the reaction mixture at 60°C for 5 h, all volatiles were removed in vacuo. [(*R*,*S*)$_P$,*R*$_C$]-**3e** was obtained as an off-white powder, which was recrystallized from acetone. Yield: 1.13 g (90%). – [(*R*,*S*)$_P$,*R*$_C$]-**3e**: $C_{21}H_{29}IN_3O_2P$ (513.3): calcd. C 49.13, H 5.69, N 8.19; found C 49.81, H 5.57, N 7.77. – ^1H NMR ([D$_6$]acetone): δ = 1.23, 1.24, 1.31, 1.33 (6 H), 3.30 (6 H), 2.47–2.55, 3.58–3.66, 3.92–4.10, 4.15–4.22 (5 H). – $^{13}C\{^1H\}$ NMR ([D$_6$]acetone): δ = 26.72, 27.86, 34.27 (11.2), 41.26, 71.21 (10.2), 71.31 (10.2), 75.18 (19.3), 109.88, 109.86, 126.19, 126.27, 129.59 (3.8), 129.76 (5.7), 130.01 (6.7), 130.03 (7.6), 130.99, 131.07, 131.94 (20.3), 132.28 (22.4), 134.38 (19.1), 134.64 (20.4), 134.88 (20.3), 137.86 (7.1), 137.92 (6.1), 139.22 (13.2), 139.35 (13.2), 142.17 (15.3), 142.45 (16.3), 157.34, 157.36. – $^{31}P\{^1H\}$ NMR ([D$_6$]acetone): δ = −20.68, −20.87.

Preparation of (2,3-*O*-Isopropylideneglycerol)[4-(sodiumsulfonato)-phenyl]phenylphosphane (3f): 0.73 g (3.25 mmol) of the secondary phosphane [(*R*,*S*)$_P$,*R*$_C$]-**3c** and sodium *p*-iodobenzenesulfonate were dissolved in 15 mL of methanol and 0.36 g (3.58 mmol) of NEt_3 was added. After the addition of 38.0 mg (1.0 mol-%) of the catalyst $Pd(Ph_3P)_4$, the reaction mixture was heated to 60°C and stirred for 24 h. The solvent was then removed in vacuo and the remaining residue was extracted with 25 mL of dichloromethane. On concentration of the combined extracts to dryness, **3f** was obtained as a pale-yellow powder. Yield: 1.3 g (99%). The sample was found to contain a small amount of $HNEt_3I$, which could not be completely removed by extraction. – **3f**: $C_{18}H_{20}NaO_5PS$: (402.4): calcd C 53.73, H 5.01; found C 53.09, H 5.51. – ^1H NMR (D_2O): δ = 1.14, 1.24 (6 H), 2.14–2.36 (2 H), 3.36–3.49, 3.77–4.02 (3 H), 7.02–7.94 (9 H). – $^{13}C\{^1H\}$ NMR (D_2O): δ = 27.41, 28.59, 34.50 (14.2), 34.55 (13.2), 71.76 (9.2), 75.92 (18.3), 111.48, 127.93, 131.07 (6.1), 131.52, 131.71, 134.75 (19.3), 135.04 (20.3), 135.24 (19.4), 135.58 (20.4), 139.05 (11.2), 143.99 (13.2), 144.11 (13.2), 145.66, 145.83. – $^{31}P\{^1H\}$ NMR (D_2O): δ = −22.1, −22.5.

Preparation of (*S*,*S*)-2,3-*O*-Isopropylidene-2,3-dihydroxy-1,4-bis[(*R*,*R*)-2′,3′-*O*-isopropylideneglycerol-1-phenylphosphano]butane (3g), Diastereomeric Mixture: To a solution of 0.36 g (11.0 mmol) of KOH in 10 mL of DMSO, 1.11 g (4.95 mmol) of **3c** was added and the solution was stirred for 1 h. A solution of 1.16 g (2.47 mmol) of (*R*,*R*)-(+)-1,4-di-*O*-*p*-toluolsulfonyl-2,3-isopropylidene-D-threitol in 20 mL of DMSO was then added and the mixture was stirred for 10 h. After the addition of 15 mL of water, the mixture was extracted with 50 mL of CH_2Cl_2. Evaporation of all volatiles in vacuo (20°C, 0.01 mbar) left **3g** as an off-white solid, which was dried in vacuo at 80°C. Yield: 1.32 g (93%). – **3g**: $C_{31}H_{44}O_6P_2$ (574.6): calcd. C 64.79, H 7.72; found C 65.20, H 7.63. – MS: *m/z* (%): 574 (<1) [M^+], 559 (2) [$M^+ - CH_3$], 558 (4) [$M^+ - CH_3 - H$], 459 (100) [$M^+ - C_6H_{11}O_2$], 351 (29) [$M^+ - C_6H_{11}O_2 - C_6H_5P$]. – ^1H NMR (C_6D_6): δ = 1.17–1.41 (18 H), 1.78–2.30 (8 H), 3.31–4.24 (8 H), 7.11–7.53 (10 H) – $^{31}P\{^1H\}$ NMR (C_6D_6): δ = −33.50 (isomer A), −37.50 (isomer B), −33.81, −37.24 (1.5) (isomer C).

Preparation of 1,3-Bis[(*R*,*R*)-2,3-*O*-isopropylideneglycerol-1-phenylphosphano]propane (3h), Diastereomeric Mixture: 1.84 g (8.2 mmol) of [(*R*,*S*)$_P$,*R*$_C$]-**3c** was added to a suspension of KOH powder (88%) in 20 mL of DMSO. 0.83 g (4.1 mmol) of 1,3-dibromopropane was added and the reaction mixture was stirred at ambient temperature for 8 h. The product was then extracted with dichloromethane (3 × 20 mL). The extracts were pooled and dried with $MgSO_4$. After removing the solvent in vacuo, **3h** was obtained as a colorless oily liquid. Yield: 1.56 g (78%). – **3h**: $C_{27}H_{38}O_4P_2$ (488.5): calcd. C 66.38, H 7.84; found C 66.28, H 7.86. – MS: *m/z* (%): 488 (2)

[M^+], 473 (15) [$M^+ - CH_3$], 374 (100) [$M^+ - C_6H_{10}O_2$], 373 (92) [$M^+ - C_6H_{11}O_2$], 259 (18) [$M^+ - 2\ C_6H_{11}O_2 + H$], 258 (18) [$M^+ - 2\ C_6H_{11}O_2$]. – $^{31}P\{^1H\}$ NMR (C_6D_6): δ = −29.81 (isomer A), −31.46 (isomer B), −29.68, −31.32 (1.0) (isomer C).

Syntheses of the Complexes L_2PdCl_2 (L = 1a, 2a, 3a) (4−6): The ligands **1a** (1.46 g, 5.6 mmol), **2a** (0.42 g, 1.2 mmol), and **3a** (0.5 g, 1.66 mmol) were dissolved in 10 mL aliquots of dichloromethane and stirred with 0.80 g (2.8 mmol) or 0.17 g (0.6 mmol) or 0.24 g (0.83 mmol) of 1,5-cyclooctadiene dichloropalladium(II) for 3 h. After evaporation of the solvent in vacuo, the complexes were obtained as yellow or cream-colored solids. Yields: 1.92 g (98%) of **4**, 0.43 g (83%) of **5**, 0.62 g (96%) of **6**. – Bis[(*R*)-(−)-2,3-dihydroxypropyl-1-diphenylphosphane]dichloropalladium(II) (**4**): $C_{30}H_{34}Cl_2O_4P_2Pd$ (697.9): calcd. C 51.63, H 4.91; found C 50.99, H 5.24. – $^{13}C\{^1H\}$ NMR (CD_3OD): δ = 38.31 (*N* = 35.5 Hz), 66.37 (*N* = 14.9 Hz), 72.84, 127.75 (*N* = 58.0 Hz), 129.87 (*N* = 11.2 Hz), 130.19 (*N* = 11.2 Hz), 132.65, 132.67, 133.72 (*N* = 11.2 Hz), 135.85 (*N* = 11.2 Hz). – $^{31}P\{^1H\}$ NMR (CD_3OD): δ = 26.38 (*trans*), 43.02 (*cis*). – Bis[(*R*)-(+)-1,3,2-dioxaborolano-4-methyl-2-phenyldiphenylphosphane]dichloropalladium(II) (**5**): $C_{42}H_{40}B_2Cl_2O_4P_2Pd$ (869.7): calcd. C 58.00, H 4.64; found C 57.82, H 4.58. – $^{13}C\{^1H\}$ NMR ($CDCl_3$): δ = 32.91 (*N* = 27.8 Hz), 72.37, 74.01, 127.68, 128.21 (*N* = 10.7 Hz), 128.31, 128.44 (*N* = 10.2 Hz), 129.1 (*N* = 47.8), 129.9 (*N* = 47.3 Hz), 130.69, 130.75, 131.42, 133.55 (*N* = 12.2 Hz), 134.39 (*N* = 13.2 Hz), 134.88. – $^{31}P\{^1H\}$ NMR: ($CDCl_3$): δ = 13.63 (*trans*), 30.95 (*cis*). – Bis[(*R*)-(+)-2,3-*O*-isopropylideneglycerol-1-diphenylphosphane]dichloropalladium(II) (**6**): $C_{36}H_{42}Cl_2O_4P_2Pd$ (778.0): calcd. C 55.58, H 5.44; found C 55.31, H 5.28. – $^{13}C\{^1H\}$ NMR (C_6D_6): δ = 25.56, 25.81, 26.82, 26.95, 30.77 (*N* = 28.5 Hz), 32.76 (*N* = 33.6 Hz), 70.22, 70.35, 72.25, 73.01, 108.90, 109.31, 128.18 (*N* = 10.5 Hz), 128.34 (*N* = 11.5 Hz), 128.49 (*N* = 9.5 Hz), 128.64 (*N* = 11.5 Hz), 130.40, 130.49, 131.55, 133.75 (*N* = 10.5 Hz), 134.14 (*N* = 12.4 Hz), 134.19 (*N* = 9.5 Hz), 134.49 (*N* = 12.4 Hz). – $^{31}P\{^1H\}$ NMR (C_6D_6): δ = 13.63 (*trans*), 28.13 (*cis*).

Preparation of Bis[(*R*)-(−)-2,3-dihydroxypropyl-1-diphenylphosphane]palladium(II) Diperchlorate (7): 0.22 g (1.06 mmol) of silver(I) perchlorate (in 5 mL of toluene) was added to a solution of 0.17 g (0.24 mmol) of **4** in 15 mL of toluene and the reaction mixture was stirred for 2 h. The solvent was then removed in vacuo and the remaining residue was extracted with 20 mL of CH_2Cl_2. The combined extracts were concentrated in vacuo to a volume of 10 mL. The precipitate formed on addition of 10 mL of diethyl ether was filtered off and the filtrate was concentrated to dryness in vacuo. Yield: 0.18 g (92%). – **7**: $C_{30}H_{34}Cl_2O_{12}P_2Pd$ (825.9): calcd. C 43.63, H 4.15; found C 43.65, H 3.87. – $^{13}C\{^1H\}$ NMR ([D_6]acetone): δ = 37.04 (*N* = 32.4 Hz), 65.27 (*N* = 15.0 Hz), 75.72, 123.10 (*N* = 60.0 Hz), 125.28 (*N* = 62.1 Hz), 130.86 (*N* = 11.2 Hz), 131.30 (*N* = 13.2 Hz), 134.61 (*N* = 11.2 Hz), 135.0, 135.34, 136.49 (*N* = 13.2 Hz). – $^{31}P\{^1H\}$ NMR ([D_6]acetone): δ = 51.50 (*cis*).

Preparation of (Bicyclo[2.2.1]hepta-2,5-diene)chloro[(*R*)-(−)-2,3-dihydroxypropyl-1-diphenylphosphane]rhodium(I) (8): To a suspension of 0.49 g (1.06 mmol) of bicyclo[2.2.1]hepta-2,5-dienechlororhodium(I) dimer in 8 mL of methanol, a solution of 0.55 g (2.12 mmol) of **1a** was added and the reaction mixture was stirred for 2 h. After removal of the solvent, **8** was obtained as an orange powder. Yield: 0.98 g (94%). – **8**: $C_{22}H_{25}ClO_2PRh$ (490.8): calcd. C 53.84, H 5.13; found C 53.32, H 5.11. – ^1H NMR ($CDCl_3$): δ = 1.39 (2 H), 3.63, 3.65, 3.77 (6 H), 2.39−2.47 (2 H), 2.61−2.69 (2 H), 4.16−4.25 (1 H), 7.30−7.69 (10 H). – $^{13}C\{^1H\}$ NMR ($CDCl_3$): δ = 33.29 (23.4), 63.81 (3.1), 67.18 (12.2), 67.77, 128.30 (9.2), 128.46 (9.2), 129.89 (2.0), 130.43 (2.0), 131.19 (41.7), 132.19 (42.7), 132.50 (10.2), 133.66 (11.2 Hz). – $^{31}P\{^1H\}$ NMR ($CDCl_3$): δ = 23.54 [^1J(Ph−P) = 168.7 Hz].

Preparation of (Bicyclo[2.2.1]hepta-2,5-diene)bis[(*R*)-(+)-2,3-*O*-isopropylideneglycerol-1-diphenylphosphane]rhodium(I) Hexafluorophosphate (9): 1.0 g (3.33 mmol) of **3a** and 0.38 g (0.83 mmol) of bicyclo[2.2.1]hepta-2,5-dienechlororhodium(I) dimer were dissolved in 15 mL of acetone. After addition of 0.31 g (1.67 mmol) of KPF_6, the reaction mixture was stirred for 12 h at ambient temperature and then concentrated in vacuo to a volume of 5 mL. The precipitate deposited on addition of 20 mL of diethyl ether was filtered off and dried in vacuo. Yield: 1.5 g (96%). – **9**: $C_{43}H_{50}F_6O_4P_3Rh$ (940.7): calcd. C 54.90, H 5.36; found C 54.06, H 5.33. – $^{13}C\{^1H\}$ NMR ([D_6]acetone): δ = 26.64, 26.74, 31.60 (*N* = 23.4 Hz), 54.49, 69.14, 71.81 (*N* = 10.9 Hz), 74.71, 93.1 (*N* = 92.4 Hz), 110.92, 130.20, 130.26, 132.10, 132.19 (*N* = 42.7 Hz), 132.62 (*N* = 44.8 Hz), 132.68, 134.38 (*N* = 10.2 Hz), 135.22 (*N* = 11.2 Hz). – $^{31}P\{^1H\}$ NMR ([D_6]acetone): δ = 24.4 (155.7); PF_6^-: δ = −142.97 [^1J(P−F) = 707.8 Hz]. – $[\alpha]_D^{20}$ = −78° (*c* = 5, CH_3CN).

Preparation of (Bicyclo[2.2.1]hepta-2,5-diene)-[1,3-bis{(*R*,*R*)-2,3-*O*-isopropylideneglycerol-1-phenylphosphano}propane]rhodium(I) Hexafluorophosphate (10): 0.79 g (1.62 mmol) of **3e**, 0.39 g (0.84 mmol) of bicyclo[2.2.1]hepta-2,5-dienechlororhodium(I) dimer, and 0.31 g (1.68 mmol) of KPF_6 were reacted according to the same procedure as described for **9**. The complex **10** was obtained as an orange powder. Yield: 1.32 g (98%). – **10**: $C_{34}H_{46}F_6O_4P_3Rh$ (828.6): calcd. C 49.29, H 5.60; found C 49.10, H 5.58. – $^{31}P\{^1H\}$ NMR ([D_6]acetone): δ = 7.48 [J(^{103}Rh−^{31}P) = 146.1 Hz] (isomer A), 7.72 [J(^{103}Rh−^{31}P) = 143.9 Hz] (isomer B), 5.62 [P(A)], 7.37 [P(B)] {J[^{31}P(A)−^{31}P(B)] = 52.3 Hz, J[^{103}Rh−^{31}P(A)] = 145.9 Hz, J[^{103}Rh−^{31}P(B)] = 145.9 Hz}.

Crystal Structure Analysis of (*R*)-$Ph_2P-CH_2-C^aH-O-B(Ph)-O-C^bH_2$ [*C^a-C^b*]: A crystal of (*R*)-(+)-**2a** was mounted in a glass capillary. X-ray data were collected using a Siemens P3 diffractometer equipped with a graphite monochromator and employing Cu-K_α radiation. The structure was solved by direct methods and refined on F^2 by full-matrix least-squares techniques using all unique data with all non-hydrogen atoms anisotropic and hydrogen atoms positioned geometrically. The value of the absolute

Table 1. Experimental data relating to the X-ray structure of **2a**

formula weight	346.2
temperature	293(2) K
crystal system	monoclinic
space group	$P2_1$
unit cell dimensions	*a* = 11.6050(11) Å
	b = 12.3033(13) Å
	c = 13.177(2) Å
	β = 98.769(8)°
V	1859.6(3) Å^3
Z	4
$D_{calcd.}$	1.236 Mg/m^3
absorption coefficient	1.383 mm^{-1}
crystal size	0.20 × 0.33 × 0.54 mm
θ range	3.4 to 57.2°
reflections collected	2807
independent reflections	2674
observed reflections [$I > 2\sigma(I)$]	1956
absorption correction	semiempirical
max. and min. transmission	0.690−0.354
data/restraints/parameters	2674/1/452
final *R* indices [$I > 2\sigma(I)$]	*R*1 = 0.0465, *wR*2 = 0.1064
R indices all data	*R*1 = 0.0660, *wR*2 = 0.1150
largest diff. peak and hole	0.24/−0.18 eÅ^{-3}

structural parameter, −0.03(4), shows that the configurations of C(14) and C(14a) had been determined correctly. Crystal data and refinement details are given in Table 1. The program SHELX-93 was used for the refinement.[38]

Acknowledgments

This work was supported by the Bundesministerium für Bildung, Wissenschaft, Forschung und Technologie and the Fonds der Chemischen Industrie. The Celanese GmbH (Hoechst AG) and Aventis (Hoechst AG) are thanked for financial support.

[1] P. Machnitzki, T. Nickel, O. Stelzer, C. Landgrafe, *Eur. J. Inorg. Chem.* **1998**, 1029.
[2] B. Cornils, W. A. Herrmann, in: *Applied Homogeneous Catalysis with Organometallic Compounds*, vol. 2 (Eds.: B. Cornils, W. A. Herrmann), VCH Verlagsgesellschaft, Weinheim, **1996**, p. 575.
[3] W. A. Herrmann, C. W. Kohlpaintner, *Angew. Chem*. **1993**, *105*, 1588; *Angew. Chem. Int. Ed. Engl*. **1993**, *32*, 1524; B. Cornils, W. A. Herrmann, in: *Aqueous-Phase Organometallic Catalysis* (Eds.: B. Cornils, W. A. Herrmann), Wiley-VCH, Weinheim, New York, Chichester, Brisbane, Singapore, Toronto, **1998**, p. 57.
[4] [4a] M. Hingst, M. Tepper, O. Stelzer, *Eur. J. Inorg. Chem*. **1998**, 73; M. Tepper, O. Stelzer, T. Häusler, W. S. Sheldrick, *Tetrahedron Lett*. **1997**, *38*, 2257. – [4b] M. Peuckert, W. Keim, *Organometallics* **1983**, *2*, 594.
[5] [5a] B. Mohr, D. M. Lynn, R. H. Grubbs, *Organometallics* **1996**, *2*, 4317. – [5b] A. Heßler, O. Stelzer, H. Dibowski, K. Worm, F. P. Schmidtchen, *J. Org. Chem*. **1997**, *62*, 2362; O. Stelzer, F. P. Schmidtchen, A. Heßler, M. Tepper, H. Dibowski, H. Bahrmann, M. Riedel, DE 19701245 (Celanese GmbH) 16. 1. 1997.
[6] [6a] J. Holz, M. Quirmbach, A. Börner, *Synthesis* **1997**, 983. – [6b] G. Muller, D. Sainz, *J. Organomet. Chem*. **1995**, *495*, 103. – [6c] Y. G. Shermolovich, A. V. Solovev, N. P. Kolesnik, L. N. Markowski, *Zh. Obshch. Khim*. **1990**, *60*, 1243. – [6d] M. G. Finn, K. B. Sharpless, in: *Asymmetric Synthesis*, vol. 5, *Chiral Catalysis* (Ed.: J. D. Morrison), Academic Press, New York, **1985**, p. 247; J. G. Hill, K. B. Sharpless, C. M. Exon, R. Regenye, *Org. Synth*. **1984**, *63*, 66. – [6e] H. Brunner, A. Sicheneder, *Angew. Chem*. **1988**, *100*, 730; *Angew. Chem. Int. Ed. Engl*. **1988**, *27*, 718.
[7] [7a] K. Issleib, H. R. Roleff, *Chem. Ber.* **1965**, *98*, 2091; K. Issleib, F. Ungvary, *Z. Naturforsch.* **1967**, *22b*, 1238; K. L. Marsi, M. E. Co-Sorno, *J. Org. Chem.* **1977**, *42*, 778. – [7b] H. Fujimoto, I. Hataue, N. Koga, T. Yamasaki, *Tetrahedron Lett*. **1984**, 5339; S. Harder, J. H. van Lenthe, N. J. R. van Eikema Hommes, P. von Ragué-Schleyer, *J. Am. Chem. Soc*. **1994**, *116*, 2508.
[8] D. Enders, T. Berg, *Synlett* **1996**, 796; D. Enders, T. Berg, G. Raabe, J. Runsink, *Liebigs Ann./Recueil* **1997**, 345.
[9] H. B. Kagan, M. Tahar, J. C. Fiaud, *Tetrahedron Lett.* **1991**, *32*, 5959.
[10] [10a] N. Mitchell, K. Heesche-Wagner, *J. Organomet. Chem*. **1992**, *436*, 43. – [10b] M. Beller, J. G. Krauter, A. Zapf, *Angew. Chem*. **1997**, *109*, 793; *Angew. Chem. Int. Ed. Engl*. **1997**, *36*, 793.
[11] W. Keim, *Angew. Chem*. **1990**, *102*, 251; *Angew. Chem. Int. Ed. Engl*. **1990**, *29*, 235; A. Baader, E. Lindner, *Coord. Chem. Rev.* **1991**, *108*, 27; M. Swamamura, Y. Ito, *Chem. Rev.* **1992**, *92*, 857.
[12] [12a] A. Börner, J. Ward, K. Kortus, H. B. Kagan, *Tetrahedron: Asymmetry* **1993**, *10*, 2219. – [12b] P. Pellon, *Tetrahedron Lett.* **1992**, *33*, 4451.
[13] K. P. Langhans, O. Stelzer, J. Svara, N. Weferling, *Z. Naturforsch*. **1990**, *45b*, 203; E. N. Tsvetkov, N. A. Bondarenko, I. G. Malakova, M. I. Kabachnik, *Synthesis* **1986**, 198.
[14] [14a] W. Gee, R. A. Shaw, B. C. Smith, *Inorg. Synth*. **1967**, *9*, 19. – [14b] N. K. Roberts, S. B. Wild, *J. Am. Chem. Soc*. **1979**, *101*, 6254. – [14c] F. Pass, H. Schindlbaur, *Monatsh. Chem.* **1959**, *90*, 148.
[15] A. J. Robertson, *Phosphorus and Sulfur* **1987**, *30*, 265.
[16] [16a] O. Herd, K. P. Langhans, O. Stelzer, N. Weferling, W. S. Sheldrick, *Angew. Chem*. **1993**, *105*, 1097; *Angew. Chem. Int. Ed. Engl*. **1993**, *32*, 1058; O. Herd, A. Heßler, K. P. Langhans, O. Stelzer, N. Weferling, W. S. Sheldrick, *J. Organomet. Chem.* **1994**, *475*, 99; F. Bitterer, O. Herd, A. Heßler, M. Kühnel, K. Rettig, O. Stelzer, W. S. Sheldrick, S. Nagel, N. Rösch, *Inorg. Chem*. **1996**, *35*, 4103. – [16b] O. Herd, A. Heßler, M. Hingst, M. Tepper, O. Stelzer, *J. Organomet. Chem.* **1996**, *522*, 69.
[17] O. Herd, A. Heßler, M. Hingst, P. Machnitzki, M. Tepper, O. Stelzer, *Catalysis Today* **1998**, *42*, 413.
[18] P. Machnitzki, M. Tepper, K. Wenz, O. Stelzer, E. Herdtweck, to be published.
[19] D. R. Coulson, *Inorg. Synth*. **1972**, *13*, 121.
[20] L. B. Fields, E. N. Jacobsen, *Tetrahedron: Asymmetry* **1993**, *4*, 2229.
[21] [21a] H. Brunner, H. Leyerer, *J. Organomet. Chem.* **1987**, *334*, 369; H. Brunner, K. Kramler, *Synthesis* **1991**, 1121. – [21b] W. J. Kerr, G. G. Kirk, D. Middlemiss, *J. Organomet. Chem.* **1996**, *519*, 93.
[22] H. Brunner, T. Rückert, *Monatsh. Chem.* **1998**, *129*, 339.
[23] M. Baacke, O. Stelzer, V. Wray, *Chem. Ber*. **1980**, *113*, 1356; S. Hietkamp, T. Lebbe, G. U. Spiegel, O. Stelzer, *Z. Naturforsch*. **1987**, *42b*, 177.
[24] I. Lukaschewisch, *Dokl. Akad. Nauk SSSR, Ser. Khim*. **1957**, *112*, 872.
[25] J. J. Daly, *J. Chem. Soc.* **1964**, 3799; B. J. Dunne, A. G. Orpen, *Acta Cryst.* **1991**, *C47*, 345.
[26] B. J. Dunne, R. B. Morris, A. G. Orpen, *J. Chem. Soc., Dalton Trans.* **1991**, 653; F. H. Allen, O. Kennard, D. G. Watson, L. Brammer, A. G. Orpen, *J. Chem. Soc., Perkin Trans. 2* **1987**, 1.
[27] H. Shimanouchi, N. Saito, Y. Sasada, *Bull. Chem. Soc. Jpn*. **1969**, *42*, 1239.
[28] [28a] S. O. Grim, R. L. Keiter, *Inorg. Chim. Acta* **1970**, *4*, 56. – [28b] B. E. Mann, B. L. Shaw, R. M. Slade, *J. Chem. Soc.(A)* **1971**, 2976. – [28c] G. Balimann, H. Motschi, P. S. Pregosin, *Inorg. Chim. Acta* **1977**, *23*, 191.
[29] T. Bartik, T. Himmler, *J. Organomet. Chem*. **1985**, *293*, 343.
[30] J. W. Emsley, J. Feeney, L. H. Suttcliffe, *High Resolution Nuclear Magnetic Resonance Spectroscopy*, vol. 1, Pergamon Press, Oxford, London, New York, Toronto, Sydney, Paris, Braunschweig, **1966**, p. 280; H. J. Bernstein, J. A. Pople, C. W. Schneider, *Can. J. Chem*. **1957**, *35*, 65.
[31] N. W. Alcock, A. W. G. Platt, P. G. Pringle, *Inorg. Chim. Acta* **1987**, *128*, 215; *J. Chem. Soc., Dalton Trans.* **1989**, 139.
[32] A. W. G. Platt, P. G. Pringle, *J. Chem. Soc., Dalton Trans.* **1989**, 1193.
[33] N. W. Alcock, A. W. G. Platt, P. G. Pringle, *J. Chem. Soc., Dalton Trans.* **1987**, 2273.
[34] R. R. Schrock, J. A. Osborn, *J. Am. Chem. Soc.* **1971**, *93*, 2397.
[35] J. Chatt, L. M. Vallarino, L. M. Venanzi, *J. Chem. Soc*. **1957**, 3413.
[36] E. W. Abel, M. A. Bennett, G. Wilkinson, *J. Chem. Soc.* **1959**, 3178.
[37] E. Baer, H. O. L. Fischer, *J. Am. Chem. Soc.* **1948**, *70*, 609; Y. Tsuda, Y. Okada, M. Tanaka, N. Shigematsu, Y. Hori, *Chem. Pharm. Bull.* **1991**, *39*, 607.
[38] Further details of the crystal structure investigation are available from the Cambridge Crystallographic Data Centre, 12 Union Road, Cambridge CB2 1EZ, U.K. [Fax: (internat.) +44(0)1223/336033; E-mail: deposit@ccdc.cam.ac.uk] on quoting the depository number CCDC-133697.

Received April 4, 1999
[I99115]

Solution Equilibria in YbDOTMA, a Chiral Analogue of One of the Most Successful Contrast Agents for MRI, GdDOTA

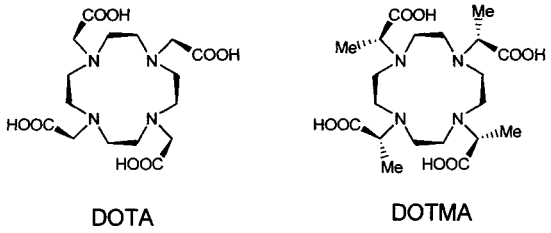
Lorenzo Di Bari,[a] Guido Pintacuda,[b] and Piero Salvadori*[a]

Keywords: Macrocyclic ligands / Conformational equilibria / EXSY spectroscopy / Lanthanide-induced shifts / Solution structure

The structure and the conformational equilibria in aqueous and methanolic solutions of YbDOTMA (DOTMA = (1*R*,4*R*,7*R*,10*R*)-α,α′,α′′,α′′′′-tetramethyl-1,4,7,10-tetraazacyclododecane-1,4,7,10-tetraacetic acid) are investigated and the dynamics studied by means of NMR methods. The presence of two isomeric forms in slow exchange is confirmed and quantitatively characterized by EXSY. The exchange peaks are assigned to the inversion of the conformation of the macrocycle ring. No evidence is obtained of a reorientation of the methyl acetate substituents. The protons switch between positions with the same geometrical factors, i.e. positions that would have the same pseudocontact shifts were it not for the different magnetic susceptibility anisotropies of the two species; steady-state NOE spectra on the major form allow unequivocal assignment of the conformations of the two isomers.

Introduction

Macrocyclic octadentate ligands derived from a tetraazacyclododecane (cyclen) ring have received attention from several research groups as a result of their ability to form stable and nonlabile complexes with metal, mainly lanthanide, cations. In particular, one of the most successful ligands, DOTA[1] (Scheme 1), whose Gd^{III} complex is widely used as a contrast agent in MRI and in biomedical applications, has been thoroughly investigated through the whole *f* transition.[2−9]



Scheme 1

More recently, chiral nonracemic derivatives and homologues of DOTA have also been synthesized and studied.[10−14] Among them, DOTMA (Scheme 1) is one of the most promising ligands because of the high relaxivity of its Gd complex.[15] Its crystal structure has been solved and some data reported, but the full set of coordinates is not yet available.[15] To our knowledge, no comprehensive study of the dynamics in solution of DOTMA complexes has so far appeared in the literature although a preliminary report on YbDOTMA can be found in a MRI/MRS context.[14][16]

Chiral Ln^{3+} complexes are expected to show optical activity of the lanthanide *f*−*f* transitions owing to the dissymmetrical crystal field the cation experiences. Indeed, preliminary results from a near-infrared (980 nm) circular-dichroism study of Yb complexes has been reported.[17] To understand the electronic spectroscopy of the lanthanide transitions, it is essential to have a clear picture of the structure in solution, particularly regarding the coordination polyhedron. Also, all the conformational rearrangements occurring at ordinary temperatures must be fully characterized. We undertook a thorough conformational and dynamical investigation of this molecule, making profit of a preliminary study due to Brittain and Desreux[10] and of the huge amount of work on DOTA-like molecules.[2−9]

The solid-state X-ray characterization of Ln^{3+} complexes with DOTA analogues reveals that the eight coordination sites, four nitrogens and four oxygens, provided by these ligands, are arranged in two parallel squares, tilted by an angle φ (Figure 1). According to the value of this angle the coordination polyhedron can range from a perfect antiprism (φ = 45°) to a prism (φ = 0°). Neither limiting case has been observed so far in the crystal structures and most known geometries cluster around two values: φ = 15° and 30°. For example, LnDOTA (Ln = Eu,[3] Gd,[5] Lu[7]) and the Eu-phenylethyl amide synthesized by Parker[11] belong to the latter group; to the former can be assigned La-DOTA,[9] LaDOTAM,[18] EuTHP,[19] $YDOTPBz_4$[20] and Parker's Eu-naphthylethyl amide.[12]

These two structures actually correspond to two main internal degrees of freedom. One, concerning the conformation of the ring (Figure 1a), can assume two forms referred to as (δδδδ) and (λλλλ),[21] which are in enantiomeric relation. The other involves the rotation about the $N-C^{\alpha}$ bond (Figure 1b), switching the substituent residue between

[a] Centro di Studio del CNR per le Macromolecole Stereoordinate ed Otticamente Attive,
Dipartimento di Chimica e Chimica Industriale,
Via Risorgimento 35, I-56126 Pisa, Italy
Fax: (internat.) + 39(050) 918260
E-mail: psalva@dcci.unipi.it
[b] Scuola Normale Superiore,
Piazza dei Cavalieri 7, I-56126 Pisa, Italy

Supporting information for this article is available on the WWW under http://www.wiley-vch.de/home/eurjic or from the author.

 © WILEY-VCH Verlag GmbH, D-69451 Weinheim, 2000 1434−1948/00/0101−0075 $ 17.50+.50/0

two *gauche* conformations. This induces a sign change in the distortion of the coordination polyhedron, named as Δ or Λ.

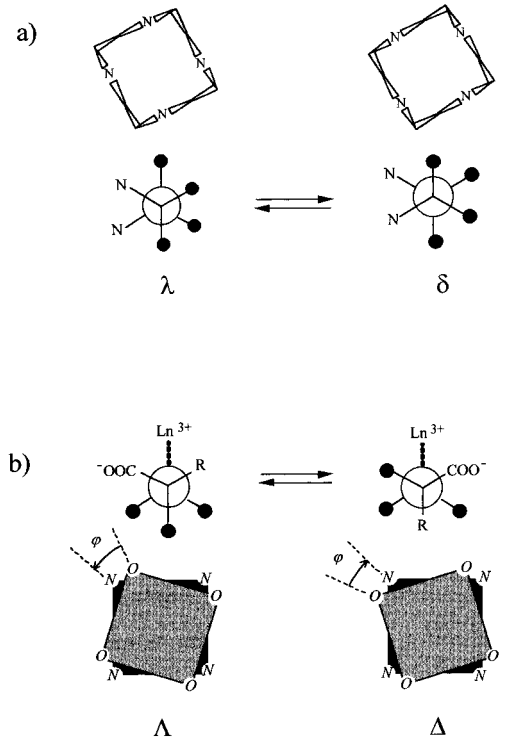
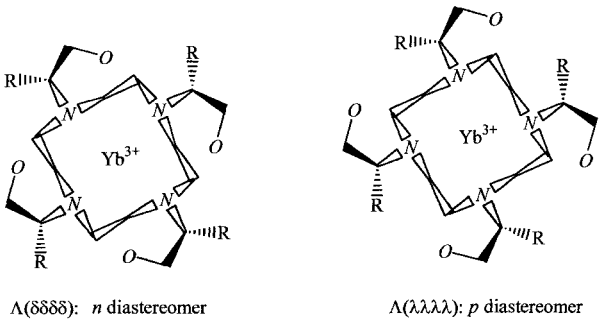


Figure 1. a) Equilibria between the δ and γ forms of the cyclen ring. The Newmann projection is referred to the bond connecting two ethilenic carbons of the macrocycle; the black circles represent the hydrogen atoms; b) equilibria between the Δ and Λ conformation of the cyclen side-arms in the DOTA-type complexes with $Ln^{(III)}$. The Newmann projection refers to the bond between the acetate C^{α} and the nitrogen; the black circles represents the hydrogen atoms and R = H, Me (DOTA and DOTMA, respectively). On the bottom, a schematic representation of the coordination polyhedron is depicted: at the corners of the light gray squares are the oxygens and at the corners of the dark ones the nitrogen atoms (the water molecule possibly axially coordinated is not indicated).

The two descriptors can be alike or different, e.g. Λ(λλλλ) or Λ(δδδδ), giving rise to a diastereomeric pair *p* or *n,* respectively (Scheme 2, *R* = H, Me).[22] A further relevant parameter to take into account is the orientation of the carboxylate bond, which is less accessible to experimental determination via NMR spectroscopy.



Scheme 2

The two diastereoisomeric forms *n* and *p* show a different arrangement of the oxygen atoms, in order to preserve the Ln−O distances at a value of about 2.4 Å. Accordingly, a less distorted (φ = 15°) coordination polyhedron corresponds to the *p* diastereomer, while the *n* diastereomer has a much more distorted (φ = 30°) structure.[4][8]

Most complexes have also been structurally characterized in solution, often using the paramagnetic character of the metal centre.[2−4,6,8,10] While in most cases there is no evidence of structural equilibria and X-ray geometries possibly reflect the most likely conformation in solution, the complexes of DOTA reveal an intriguing network of solution equilibria, which have been studied by various NMR techniques, with reference to limiting crystal geometries. In particular, Aime and co-workers pointed out that the ratio of populations of *n* and *p* types varies along the lanthanide series[4] and that superimposed on the conformational change, there is a hydration−dehydration equilibrium,[8] whose position depends on the size of the central ion.[4]

The pseudocontact shifts of YbDOTA[10] reveal that the two sets of signals for the two forms are proportional. This means that the sets of geometrical factors of the protons in the two forms are equal. This does not necessarily mean that *each* proton occupies a position characterized by the *same* geometrical factor in the two forms, since there can be a pairwise proton-swap between equivalent sites. In 1992, Aime and co-workers[4] assigned the two spectra to two *different* structures, corresponding to the diastereomeric pair *p* and *n*. Indeed, they demonstrated the occurrence of such a rearrangement through EXSY measurements, as discussed in ref.[4] and ref.[6] and below. However, no positive evidence of the assignment of the *n* structure to the major component of YbDOTA in solution can be found in the pseudocontact shifts. In the present work, to our knowledge for the first time, we use such a simple experiment as a monodimensional NOE measurement to assign unequivocally the structure of the major isomer.

The presence of a stereogenic centre on the side arm in DOTMA complicates the equilibrium network, since, for instance, the two forms Λ(λλλλ) and Δ(δδδδ) are no longer equivalent. The intrinsic chirality of the ligand is shown to induce a preference in the distortion of the coordination polyhedron, which in the present work is demonstrated to be Λ. This finding is essential in understanding the chiroptical properties of YbDOTMA.

Results

The spectrum of YbDOTMA in water, as discussed by Brittain and Desreux,[10] shows that the complex is present in solution in two forms ′D′ and ′d′ in slow exchange, characterized by different anisotropy factors D_D and D_d and different signal intensities, by analogy with YbDOTA.[4] However, unlike in DOTA, here the less populated form has the larger value of the *D* factor. We can observe that the spectra of the two forms are exactly proportional (isomorphic), as demonstrated in Figure 2, and

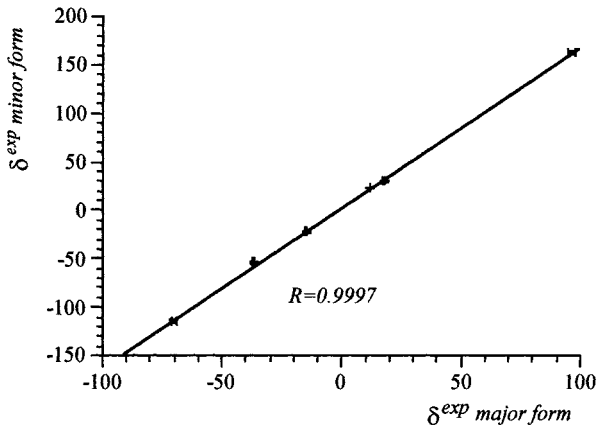


Figure 2. Correlation plot between the experimental δ^{exp} values of the major (D) and minor (d) forms of YbDOTMA in D_2O.

only the large difference between the anisotropy factors, D_D and D_d, justifies the appearance of two distinct sets of signals for the two isomers. It follows that, at least in principle, the two spectra can be associated with the same molecular structure. Alternatively, two conformations must be found bearing the protons in positions characterized by very similar geometrical factors.

Following Brittain and Desreux,[10] a set of suitable parameters for the spectral assignment can be produced from the coordinates of GdDOTA[5] [we chose to start from the Λ(δδδδ) form]. Since the spectrum is compatible with a C_4 symmetry, the analysis of the pseudocontact shifts involves only a linear fitting of one parameter (of the anisotropy D). The geometry factors for sets of equivalent protons were averaged in order to compensate for the lower symmetry of the crystal structure.[23] The pro-*R* hydrogen on each acetate arm was replaced by a methyl group with standard bond lengths and angles. The methyl acetate arm was then systematically rotated around the N−C^{α} bond to obtain the best agreement[24] between the geometrical factors and the observed pseudocontact shifts, finding an optimal value of the torsion angle YbNC^{a}M of about 167° (which corresponds to a coordination geometry of Λ-type). The carboxylate was then rotated to restore the distance Yb−O of 2.4 Å, but this had no effect on the proton geometrical factors.

In such a way, a full set of satisfactory geometrical parameters and the relative structure were obtained. It should be observed that the solution of this optimization is unique, which excludes a rotation of the methyl acetate as the origin of the two forms, in agreement also with other findings on similar structures.[13]

An equivalent set was provided by the following stereochemical operations on these structures: (i) mirror image (inversion) of the whole complex; (ii) epimerization of the four C^{α} stereocentres (these operations must be followed again by the carboxylate rotation). The result was once more a (*RRRR*)-YbDOTMA, but the arrangement of the macrocyclic ring is opposite. In other words, the tetraazacyclododecane shifts from a (λλλλ) to a (δδδδ) conformation. Obviously, starting from the Δ(λλλλ) form of GdDOTA, one would obtain first the Λ(λλλλ) isomer and, after the formal inversion and epimerization, the other. The two sets of geometrical factors for the cyclen ring are obviously equal. For the methyl group and for the CH such equality does not follow by necessity; however, the difference between the geometrical factors calculated for the two forms is less than 10%. Any attempt to use this small difference for structural assignment is nullified by the proportionality of the spectra of the two species. Furthermore, smaller geo-

Table 1. Experimental and calculated lanthanide-induced NMR shifts (δ, in ppm) of the major and minor YbDOTMA species in D_2O and MeOD (T = 25°C). The factors in the second column are calculated on a structure derived, as described in the text, from GdDOTA[5] (see also Table 4); induced chemical shifts are relative to diamagnetic LuDOTA (as far as it concerns the ring protons and the acetate one) and to a value of δ = 0.9 for the case of the methyl resonance.

		major form (m-type, *p* diastereomer)					minor form (M-type, *n* diastereomer)				
			D_2O		MeOD			D_2O		MeOD	
proton	$\frac{(3\cos^2\theta_i - 1)}{r_i^3} \cdot 10^2$		δ^{exp}	δ^{calc}	δ^{exp}	δ^{calc}		δ^{exp}	δ^{calc}	δ^{exp}	δ^{calc}
axial$_1$	3.09	A_1	94.3	94.0	109.9	109.8	a_1	160.9	159.9		179.9
axial$_2$	−0.942	A_2	−38.9	−35.1	-41.1	−38.2	a_2	−55.9	−53.9	−61.0	−60.5
equatorial$_1$	0.502	E_1	10.5	11.1	14.5	14.8	e_1	22.2	22.7	25.8	25.6
equatorial$_2$	0.652	E_2	16.3	15.9	20.5	20.3	e_2	28.7	30.6	32.8	34.6
acetate[c]	−2.16	C	−72.5	−74.2	-81.8	−82.9	c	−117.4	−118.5	−133.9	−133.1
methyl[c]	−0.407	M	−16.0	−18.0	-16.8	−18.6	m	−23.2	−25.6	−25.6	−28.6
R[a] %			3		2			2		2	
$\mathcal{D}$[b]			3200±90		3700±50			5300±100		6000±150	

[a] Nonweighted agreement factor; see ref.[23] – [b] Magnetic anisotropy factor, in units of [ppm Å^3]. – [c] Average between the values found in the two forms obtained as described in the text, (−2.09 and −2.23 for C; −0.423 and −0.391 for M in the major and minor form, respctively).

metrical adjustments[4] may account for minor improvements of the agreement factors.

In such a way, a full set of satisfactory geometrical parameters and two relative structures were obtained (see Table 1 and Figure 3).[25] The coordination geometry is of Λ type in both cases, with the same torsion angles around the N−C$^{\alpha}$ bond; only the arrangement of the macrocycle is opposite.

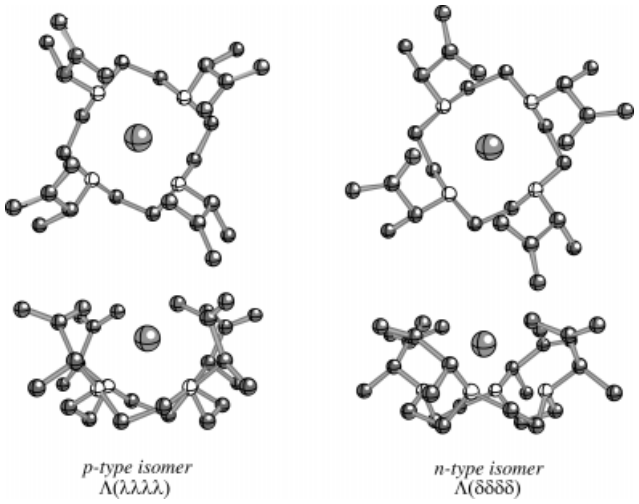


Figure 3. Two isomeric structures of YbDOTMA compatible with the observed proton paramagnetic shifts. On the left a Λ(λλλλ) conformation is displayed, on the ringt a Λ(δδδδ) one. They have been assigned to the major and minor form, respectively.

In order to determine the thermodynamic parameters for the isomerization equilibrium, a variable-temperature study was undertaken. On increasing the temperature, the signals of the minor form become comparatively smaller, which indicates a negative enthalpy for this process. We recorded the spectra in methanol as well, in order to cover a broader temperature range. Indeed, the spectrum in this solvent is very similar to that in water reported in Table 1; once more two forms are present, whose resonances can be predicted with the same geometrical factors used above. The two anisotropy factors are of the same order of magnitude as those found in water and their ratio seems solvent independent. Furthermore, in methanol the minor form is slightly more populated at room temperature than in water (D/d = 14.2 and 20, respectively). The main difference between the two solvents is that in MeOD the resonances of the counterion, *N*-methylglucammonium, which are strongly concentration and temperature dependent, are clearly visible, downfield shifted. Therefore, we can conclude that the cation is at least partly bound in methanol, while it is not in D_2O. The downfield shift shows that it lies axially above or below the metal centre, similar to recently reported for phosphonate systems.[26]

On recording variable temperature spectra in MeOD between −80 and 60°C one observes a migration of all the signals according to the variation of *D*, predicted by Bleaney.[27] Unfortunately, the values collected in Table 2 do not allow $1/T$ and $1/T^2$ dependences to be unambiguously distinguished. Furthermore, at low temperature, all the lines become broader, owing to faster transverse relaxation.

Table 2. Temperature variation of the anisotropy susceptivity parameter *D* of the major form of YbDOTMA and of the equilibrium constant *K* between the two isomers.

temperature (°C)	$\mathcal{D}$ (±100)	$\frac{[d]}{[D]}$ %
60	3180	6.55
25	3490	7.0
0	3770	8.1
-25	4025	9.6
-50	4450	12.0
-80	5070	14.2

The persistence of signals of the minor form up to 60°C could be observed, although at this temperature they appear very broadened. In fact, they start to coalesce with those of the major form, because of the faster equilibrium and of the smaller spectral width, which implies more stringent requirements for the slow exchange limit.

Integration of the signals of the methyl in the two forms afforded an estimation of the temperature dependence of the equilibrium constant, *K*, shown in Table 2. This gave the thermodynamic parameters in methanol: $\Delta H_s^0(M) = -4.0 \pm 0.9$ kJ mol^{-1} and $\Delta S_s^0(M) = -35.4 \pm 0.5$ J K^{-1} mol^{-1}. In D_2O, the temperature range that can be covered goes from 0 to 50°C, because above this limit the signals of the minor form become exceedingly broad. In water, the following values were found: $\Delta H_s^0(W) = -8 \pm 2$ kJ mol^{-1} and $\Delta S_s^0(W) = -50 \pm 10$ J K^{-1}mol^{-1}.

The dynamics of the interconversion between the two forms has been investigated through two-dimensional exchange spectra (EXSY) at variable mixing time in water and in methanol at 25°C.

From inspection of Figure 4, we observe the following equilibria, with reference to the notation of Table 1:

$$M \rightleftharpoons m$$
$$E \rightleftharpoons a$$
$$A \rightleftharpoons e$$

while there is no evidence of exchange within the major or the minor form [e.g., E ⇌ A], either between equatorial or axial protons of the two forms [e.g., E ⇌e]. Therefore, we can conclude that the isomerization process involves a ring inversion, exchanging the macrocycle hydrogens between positions characterized by pairwise equal geometrical factors. Such an observation is in perfect agreement with the structure pair determined above and depicted in Figure 3. Unfortunately, following their construction, it is impossible to assign either of the two to the major or minor component.

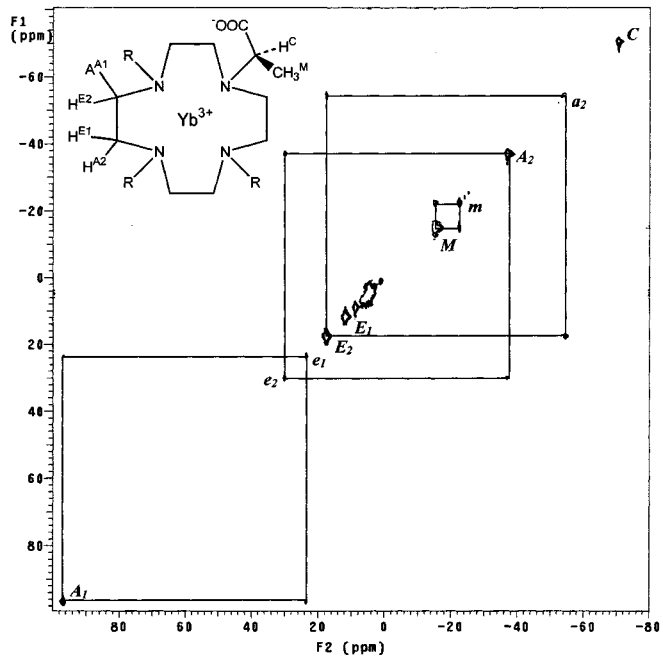


Figure 4. Proton labelling and EXSY spectrum of YbDOTMA at 25°C in D_2O (within −80 and 100 ppm). Upper and lower case letters refer to the major and minor forms resonances, respectively.

To this end, steady-state NOE[28] spectra were recorded between selected protons of the molecule (see Supporting Material). When the resonance at δ = −70.4, due to the methyl acetate methyn proton C, is irradiated, an intense enhancement of E_2 is observed, while no effect is detected on E_1; at the same time, on saturating A_2, C is enhanced. The interpretation of these data is discussed in the next section.

A quantitative evaluation of EXSY spectra at variable mixing time, τ_m, allowed us to assess the dynamic constant for the observed kinetic process. Direct analysis, as described by Perrin and Gipe,[29] of the integrated intensity matrix, $\mathbf{A}(\tau_m)$ for a given τ_m gives the dynamic matrix, **L**,

$$\mathbf{L} = \frac{1}{\tau_m}\ln(\mathbf{P}^{-1}\mathbf{A}) = \frac{1}{\tau_m}\mathbf{U}^{-1}\ln(\mathbf{\Lambda})\,\mathbf{U} \quad (1)$$

where **U** is the matrix of eigenvectors and the diagonal matrix **Λ** contains the eigenvalues, $\{\mathbf{\Lambda}\}_{ii}$, of $\mathbf{P}^{-1}\mathbf{A}$. The diagonal matrix **P** contains the relative populations of the exchanging species,[30] so that the elements of $\mathbf{P}^{-1}\mathbf{A}$ are the normalized amplitudes of the peaks.

We repeated the experiment with different mixing times, ranging from 5 to 30 ms, and we measured the integral of the methyl signals in the two forms and of the cross peaks between them, as reported in Table 3.

Cross relaxation gives only a negligible contribution to the cross-peak amplitudes at the very short τ_m used in our experiments, hence the off-diagonal elements of **L** are $L_{ij} = -k_{ij}$, where k_{ij} is the first-order rate constant for the exchange from site *i* to site *j*. Equation (1) then gives the rates, also shown in Table 3, whose average value is 6.3 ± 0.8 s^{-1} for the D → d process and 136 ± 16 s^{-1} for the reverse in water, whereas, for the same processes in methanol one finds 6.9 ± 0.6 s^{-1} and 93 ± 4 s^{-1}, respectively.[31] These values seem to be quite reliable, since the ratio between the two constants in water [k_{dD}/k_{Dd} = 21.6] is in agreement with the relative concentrations of the two isomers (major/minor = 20 under our experimental conditions) and the same holds true in methanol, as well. We can observe that the dynamics in the two solvents are very similar, which justifies our extrapolation of the thermodynamic data obtained in methanol to water.

Discussion

The possible solution equilibria in YbDOTMA can be represented, by analogy with YbDOTA,[8] as in Figure 5.

Table 3. Integrated intensity matrix for the exchange of the signals of the methyl group in water and in methanol. The index 1 represents the resonance frequency of M and 2 the one of m, so that I_{11} and I_{22} are the intensities of the diagonal peaks of the forms D and d, while I_{12} and I_{21} are the intensities of the cross-peaks, all normalized to I_{11} = 100.

D_2O:		τ = 5ms	τ = 10ms	τ = 20ms	τ = 30ms
	$\begin{pmatrix} I_{11} & I_{12} \\ I_{21} & I_{22} \end{pmatrix}$	$\begin{pmatrix} 100 & 2.26 \\ 2.27 & 2.78 \end{pmatrix}$	$\begin{pmatrix} 100 & 4.40 \\ 4.70 & 1.72 \end{pmatrix}$	$\begin{pmatrix} 100 & 4.19 \\ 4.73 & 0.69 \end{pmatrix}$	$\begin{pmatrix} 100 & 4.72 \\ 5.32 & 0.33 \end{pmatrix}$
	k_{mM} ($M^{-1}s^{-1}$)	6.00	7.47	5.32	6.38
	k_{Mm} ($M^{-1}s^{-1}$)	120.89	159.28	120.11	143.93

MeOD:		τ = 10ms	τ = 20ms	τ = 30ms
	$\begin{pmatrix} I_{11} & I_{12} \\ I_{21} & I_{22} \end{pmatrix}$	$\begin{pmatrix} 100 & 5.1 \\ 6.4 & 5.4 \end{pmatrix}$	$\begin{pmatrix} 100 & 6.7 \\ 6.6 & 1.5 \end{pmatrix}$	$\begin{pmatrix} 100 & 7.8 \\ 8.4 & 1.4 \end{pmatrix}$
	k_{mM} ($M^{-1}s^{-1}$)	6.33	7.69	6.61
	k_{Mm} ($M^{-1}s^{-1}$)	98.17	93.61	88.08

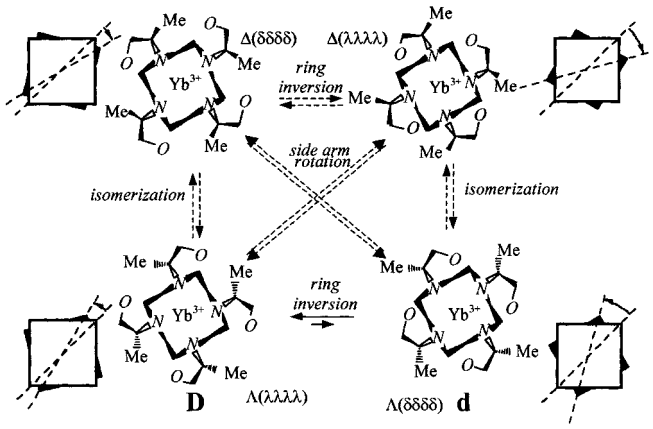


Figure 5. Schematic representation of the structure and dynamics of the diastereomers of YbDOTMA complexes. The conformation of the chelate systems and the coordination polyhedron are depicted. Following the interconversion between the major and minor forms, a different distortion of the coordination polyhedron is forced in the two forms, as discussed in the text.

The exchange processes in the rows are due to an inversion of the macrocyclic ring, while those on diagonals rely upon a rotation of the methyl acetate arms. In the columns, the two motions occur simultaneously (and possibly concertedly). On the left the *p* diastereomers are presented, on the right the *n*. In the case of DOTA, the two forms along each column are optical antipodes, whereas for DOTMA, the presence of the stereogenic centres at the C^{α} makes them diastereomers. Although this is only a crude representation, it shows that in the two rows the coordination polyhedra are distorted antiprisms with opposite tilt angles. Clearly, since DOTA is achiral, the sign of such a distortion is irrelevant (it cannot be defined on a macroscopic level).

The populations of all the four DOTMA structures must be expected to be different. Indeed, only two species could be identified in the one-dimensional ^{1}H-NMR spectrum, in largely different amounts; both have Λ conformation of the side arm, bearing the methyl group *anti* with respect to $N-Yb^{III}$. The excellent agreement of the chemical shifts with geometrical factors derived from a crystal structure rules out any fast motion and confirms the substantial rigidity of the chelate systems already reported in the literature.[4] We have observed that there is no evidence of a rotation of the methyl acetate arm, which amounts to saying that only one of two rows of Scheme 1 is populated and therefore that only one equilibrium is present in solution for YbDOTMA, between the Λ(λλλλ) and Λ(δδδδ) forms.

On the basis of the paramagnetic shifts (as well as the Yb-proton distances and therefore of Curie relaxation rates) it is not possible to assign either of the two conformations to the minor or major isomer; in contrast, the NOE spectra allow one to assign unequivocally the structure of the major isomer to one of the two conformations. In effect, the neat NOE between the C and E_2 protons cannot be justified for an *n*-type structure, since the two protons are far apart (3.35 Å). On the contrary, in the *p*-type the interproton distance is only 2.55 Å.[32] We can conclude that the Λ(δδδδ) conformation must be assigned to the minor isomer and the Λ(λλλλ) to the major one, as depicted in Figure 3; the relevant parameters of such geometries are shown in Table 4. It must be stressed that, in reverse analogy with YbDOTA, the metal ion is more buried in the major form in the case of YbDOTMA.

Table 4. Conformation and relevant atomic distances [Å] and angles in the two isomers of YbDOTMA. The geometries were obtained from the X-ray data of GdDOTA (ref.[5]), according to the procedure descibed in the text.

	major form	minor form
	Λ(λλλλ)	Λ(δδδδ)
O-O	3.07	3.19
N-N	2.97	2.97
Yb-O	2.48	2.48
Yb-plane(O_4)	1.01	0.72
Yb-N	2.66	2.66
Yb-plane(N_4)	1.63	1.63
twist angle (φ)	17°	40°
YbNC$^{\alpha}$Me	167°	167°
NC$^{\alpha}$CO	324°	324°

The kinetic rates are of the same order of magnitude of those reported for YbDOTA by Jacques and Desreux.[6] In the present case, however, only one process is observed, linked to the inversion of the macrocyclic ring. Apparently, the rotation of the methyl acetate arm is strongly hindered, by analogy with what observed in some LnDOTA analogues.[13][33] The detailed comparison with the kinetic rates of DOTA is not straightforward, owing to the different molar ratios of the forms in the two complexes. The averages of the direct to reverse rates of ring inversion at 25°, weighted for the two populations, gives 44.8 s^{-1} for YbDOTA[8][21] and 12.5 s^{-1} for YbDOTMA. The dynamics of the latter is probably slowed down by the crowding due to the presence of the methyl on the side branches.

The thermodynamic data for the interconversion process show both negative enthalpy and entropy. Apparently, the minor form is slightly more stable and only entropically unfavoured. The loss of entropy in the process D → d indicates that in this conversion the order of the system increases, which is compatible with a different coordination number of the central cation, that should be larger for the minor form. Aime et al.[8] reported that on going from the major to the minor form of YbDOTA, $\Delta H^{\circ} = +17.5$ kJ mol^{-1} and $\Delta S^{\circ} = +45$ J K^{-1} mol^{-1} and they attributed the large and *positive* entropy change to the release of a water molecule, axially coordinated in the former. This hypothesis is also strongly supported by variable-pressure NMR. Since the reaction entropy is rather similar to that found for the conversion m′→ M in DOTA,[8] it seems quite reasonable to extrapolate this result to DOTMA, where the major form should be eight coordinate and the minor form should be hydrated and nine coordinate; this further con-

sideration is in agreement with the assignment of an M-type structure (*n* diastereomer) to the minor isomer, where the metal ion is less hindered.

Conclusions

Pseudocontact shifted ^{1}H-NMR spectra of YbDOTMA have demonstrated that in solution two forms are present which exchange slowly and are, in principle, both compatible with the same set of geometrical factors for the protons. Two-dimensional EXSY spectra, on the other side, show that the two forms correspond to different conformations of the macrocyclic ring, in diastereomeric relation, as *p* or *n* forms. This is in close analogy with DOTA derivatives.[8][33] Only steady-state NOE spectra, however, indicate the geometry of the major isomer, thus finally solving the problem of the structural assignment of this molecule in solution in a fully consistent way and without reference to crystal structures. While three different equilibria could be observed for YbDOTA, in the temperature range examined in this work only one has been detected between the two YbDOTMA species, since the presence of the methyl group in the acetate side arms enhances the conformational homogeneity of the chelate system, constraining the arrangement of the pendant groups and favouring one conformation of the cycle ethylene groups.

The steric hindering affects the kinetic parameters, too, and quantitative EXSY measurements show that the ring inversion is slowed down with respect to the corresponding process in YbDOTA. The thermodynamic parameters of the equilibrium indicate that the structural rearrangement may be accompanied by a hydration process. The relative populations of the two forms and the hydration−dehydration dynamics are in reverse analogy with YbDOTA.[33]

It is noteworthy that the two species in equilibrium are Λ(λλλλ) and Λ(δδδδ), thus characterized by the same helicity about the metal cation. One can therefore conclude that, by analogy with other chiral ligands,[11−13] YbDOTMA shows a transfer of chirality from a local stereogenic element to the overall structure. This is a key point in understanding the stereochemistry and consequently the chiroptical properties of these complexes

Experimental Section

General: The anionic homochiral and enantiopure YbDOTMA complex as a methylglucammonium salt was a gift from Bracco Italy S.p.A. and was dissolved in D_2O (21.8 mg in 0.5 mL, 52.80 mM) and MeOD (6.95 mg in 0.5 mL, 16.83 mM). The NMR spectra were recorded on a Varian VXR 300 Spectrometer operating at 7.1 T, equipped with a VT unit stable within 0.1°C. Where not otherwise specified, the temperature was 25°C. The 90° pulse length was 14.5 μs. The recycle delay in all experiments was above 0.5 s, largely exceeding 5 T_1 of all YbDOTMA proton resonances and ensuring instrumental recovery. − Steady-state NOE spectra were recorded with 4096 transients after 0.5 s with cw presaturation of the relevant signals. − EXSY spectra were recorded with the standard NOESY sequence, using the hypercomplex method to obtain phase sensitivity in both dimensions. Since zero quantum coherences have an antiphase character, they cannot contribute neither in integrated nor in point amplitude in systems with a linewidth largely exceeding the scalar couplings; thus no attempt was made to suppress them. 2048 points were collected for each of the 512 t_1 increments, covering a spectral window of 50000 Hz in two dimensions. The matrices were zero-filled to 2 K × 2 K and weighted by Lorentz-to-Gauss functions in both dimensions. Since all quantitative analyses were performed only on the methyl resonances (within 12000 Hz from the transmitter), no correction for finite pulse length was used. No baseline correction was applied and the 1- and 2-dimensional integrals were evaluated with the VNMR software with reference to the area immediately adjacent to each peak. The pseudocontact shifts were calculated with reference to the data reported for LuDOTA.[4] The geometric factors for the protons were calculated with the aid of standard molecular modelling software.[23] In the first place, only the four cyclen-proton resonances were considered: a tentative value for *D* was obtained, through which starting values for the geometric factors of the acetate and the methyl protons were assessed. The dihedral angle about the N−C$^\alpha$ bond was systematically varied in order to approach those values. This procedure revealed that only one minimum could be found. Thereupon, for values of the dihedral YbNC^{a}M between 165° and 170°, all the geometric factors and pseudocontact shifts were included in the linear fitting, seeking for the best agreement factor.[24] − ^{1}H-NMR spectrum at 300 MHz of YbDOTMA in D_2O and in MeOD (Figure S1), correlation plot between the experimental δ^{exp} values and the geometrical factors calculated for YbDOTMA in D_2O (Figure S2), variable temperature behavior (from 25 to −80°C) of the methyl resonances of YbDOTMA (Figure S3), NOE difference spectra of YbDOTMA obtained upon saturation of the acetate C resonance of the major form (Figure S4) are available as supporting Information.

Acknowledgments

We thank Bracco Italy S.p.A. for a generous gift of YbDOTMA.

[1] Abbreviated names for this and the other compounds are DOTA = 1,4,7,10-tetraazacyclododecane-1,4,7,10-tetraacetic acid, DOTMA = (1*R*,4*R*,7*R*,10*R*)-α,α′,α′′,α′′′-tetramethyl-1,4,7,10-tetraazacyclododecane-1,4,7,10-tetraacetic acid, DOTAM = 1,4,7,10-tetrakis(2-carbamoylethyl)-1,4,7,10-tetraazacyclododecane, THP = 1,4,7,10-tetrakis(2-hydroxypropyl)-1,4,7,10-tetraazacyclododecane, DOTPBz$_4$ = 1,4,7,10-tetraazacyclododecane tetrakis(methylenebenzylphosphinic acid), DO3MA = (1*R*,4*R*,7*R*)-α,α′,α′′-trimethyl-1,4,7,10-tetraazacyclododecane-1,4,7-triacetic acid, Parker′s phenylethylamide = 1,4,7,10-tetrakis[(*R*)-1-(phenyl)ethylcarbamoylmethyl]-1,4,7,10-tetraazacyclododecane, Parker′s naphtylethylamide = 1,4,7,10-tetrakis[(*R*)-1-(1-naphtyl)ethylcarbamoylmethyl]-1,4,7,10-tetraazacyclododecane.

[2] J. F. Desreux, *Inorg. Chem.* **1980**, *19*, 1319−1324.
[3] M. R. Spirlet, J. Rebizant, J. F. Desreux, M. F. Loncin, *Inorg. Chem.* **1984**, *23*, 359−363.
[4] S. Aime, M. Botta, G. Ermondi, *Inorg. Chem.* **1992**, *31*, 4291−4299.
[5] J.-P. Dubost, M. Legar, D. Meyer, M. Schaefer, *C. R. Acad. Sci. Paris, Ser. 2* **1991**, *312*, 349−354.
[6] V. Jacques, J. F. Desreux, *Inorg. Chem.* **1994**, *33*, 4048−4053.
[7] S. Aime, A. Barge, M. Botta, M.Fasano, J. D. Ayala, G. Bombieri, *Inorg. Chim. Acta* **1993**, *246*, 423−429.
[8] S. Aime, M. Botta, M. Fasano, M. P. M. Marques, C. F. G. C. Geraldes, D. Pubanz, A. E. Merbach, *Inorg. Chem.* **1997**, *36*, 2059−2068.
[9] S. Aime, A. Barge, F. Benetollo, G. Bombieri, M. Botta, F. Uggeri, *Inorg. Chem.* **1997**, *36*, 4287−4289.

[10] H. G. Brittain, J. F. Desreux, *Inorg. Chem.* **1984**, *23*, 4459−4466.
[11] R. S. Dickins, J. A. K. Howard, C. W. Lehmann, J. Moloney, D. Parker, R. Peacock, *Angew. Chem. Int. Ed. Engl.* **1997**, *36*, 521−523.
[12] R. S. Dickins, J. A. K. Howard, J. Moloney, D. Parker, R. Peacock, G. Siligardi, *J. Chem. Soc., Chem. Commun.* **1997**, 1747−1748.
[13] J. A. K. Howard, A. M. Kenwright, J. M. Moloney, D. Parker, M. Port, M. Navet, O. Rousseau, M. Woods, *J. Chem. Soc., Chem. Commun.* **1998**, 1381−1382.
[14] S. Aime, M. Botta, M. Fasano, E. Terreno, P. Kinchesh, L. Calabi, L. Paleari, *Magn. Reson. Med.* **1996**, *35*, 648−651.
[15] M. F. Tweedle, K. Kumar, R. B. Shukla, R. Ranganathan, S. Aime, M. Botta, J. Di Marco, Z. Gougoutas, *Book of Abstracts, 23th International Symposium on Macrocyclic Chemistry*, Turtle Bay, Hawaii, **1998**.
[16] S. Aime, M. Botta, G. Ermondi, P. L. Anelli, F. Fedeli, F. Uggeri, *Proceedings, SMR, 2nd Annual Meeting,* San Francisco, **1994**.
[17] L. Di Bari, G. Pintacuda, P. Salvadori, *Book of abstracts, 6th International Conference on Circular Dichroism,* Pisa, Italy, **1997**; L. Di Bari, G. Pintacuda, P. Salvadori, *Book of abstracts, 24h FGIPS Meeting in Inorganic Chemistry*, Corfu, Greece, **1997**; G.Pintacuda, L. Di Bari, P. Salvadori, *Book of abstracts, 23th International Symposium on Macrocyclic Chemistry*, Turtle Bay, Hawaii, **1998**.
[18] J. R. Morrow, S. Amin, C. H. Lake, M. R. Churchill, *Inorg. Chem.* **1993**, *32*, 4566−4572.
[19] K. O. A. Chin, J. R. Morrow, C. H. Lake, M. R. Churchill, *Inorg. Chem.* **1994**, *33*, 656−664.
[20] S. Aime, A. S. Batsanov, M. Botta, J. A. K. Howard, D. Parker, K. Senanayake, G. Williams, *Inorg. Chem.* **1994**, *33*, 4696−4706.
[21] S. Hoeft, K. Roth, *Chem. Ber.* **1993**, *126*, 869−873.
[22] We prefer to borrow the stereochimical descriptors *n* and *p*, which clarify the diastereomeric nature of the rearranged forms, and avoid reference to the major form of YbDOTA. Indeed, the structures of the predominant form in solution depend on the nature of the ligand and on the size of the central ion.
[23] All the operations on the structures described can be performed with a standard molecular modelling package, such as *Hyperchem* (Hypercube Inc.) or *CS ChemDraw Pro* (CambridgeSoft Corporation).
[24] The agreement factor *R* between calculated, δ_s(calcd., *i*), and experimental, δ_s(exp., *i*), pseudocontact shifts, defined as:

$$R^2 = \frac{\sum_i (\delta_i^{calc} - \delta_i^{exp})^2}{\sum_i (\delta_i^{exp})}$$

is reported in Table 1, as well. We can observe that, even if the *R* value for the major isomer is slightly lower, the agreement is very good for both structures. Variation of the torsion around the $N-C^{\alpha}$ bond by 5° about the optimal value does not imply a relevant increase of the factor, *R* (about 10% higher when the angle is 170°).
[25] The geometrical factors calculated on the basis of the published of GdDOTA (ref.[5]) lead to the assignment shown in ref.[6], featuring the two protons on each macrocycle carbon bearing different numbers. This is in agreement with that reported by several authors (ref.[6][21]), but in contrast with Aime and coworkers (ref.[4][15]).
[26] S. Aime, M. Botta, S. Geminiatti Crich, E. Terreno, P. L. Anelli F. Uggeri, *Chem. Eur. J.* **1999**, *5*, 1261−1266.
[27] B. Bleaney, *J. Magn. Reson.* **1972**, *8*, 91−100.
[28] For a general reference on the NMR of paramagnetic molecules, see: I. Bertini, C. Luchinat, *Coord. Chem. Rev.* **1996**, *150*, 1−296.
[29] C. L. Perrin, R. K. Gipe, *J. Am. Chem. Soc.* **1984**, *106*, 4036−4038.
[30] E. W. Abel, T. P. J. Coston, K. G. Orrell, V. Sik, D. Stephenson, *J. Magn. Reson.* **1986**, *70*, 34−53.
[31] The errors on these values were estimated through their dispersion for the various experiments.
[32] The NOE between A_2 and C is not diagnostic, since in both structures Λ(δδδδ) and Λ(λλλλ) the two protons are nearby. Furthermore, it is very difficult to detect, owing to the large relaxation rates of the two nuclei, which sit close to the paramagnetic centre.
[33] S. Aime, M. Botta, G. Ermondi, E. Terreno, P. L. Anelli, F. Fedeli, F. Uggeri, *Inorg. Chem.* **1996**, *35*, 2726−2736.

Received April 22, 1999
[I99141]

Reactions of Cadmium(II) Acetate with Acetoacetanilide and Methylacetoacetate Thiosemicarbazones: A Cyclization Process Leading to a Pyrazolone − The Molecular and Crystal Structures of the Free Ligands and the Complex [CdL_2Py] (HL = 2-[Amino(thioxo)methyl]-5-methyl-2,3-dihydro-1*H*-3-pyrazolone, Py = Pyridine)

José S. Casas,[a] María V. Castaño,*[a] Eduardo E. Castellano,[b] María S. García-Tasende,[a] Agustín Sánchez,[a] María L. Sanjuán,[a] and José Sordo[a]

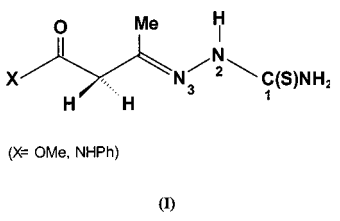
Keywords: Cadmium(II) pyrazolonates / Thiosemicarbazones / Cyclizations / 2-[Amino(thioxo)methyl]-3-pyrazolone / ^{1}H-, ^{13}C-, ^{113}Cd-NMR spectra

Acetoacetanilide- and methylacetoacetate thiosemicarbazones (HTSC^1 and HTSC^2, respectively) react with cadmium(II) acetate in methanol, giving complexes containing the ligand 2-[amino(thioxo)methyl]-5-methyl-2,3-dihydro-1*H*-3-pyrazolonate (L^-). An X-ray diffraction study of the structures of HTSC^1, HTSC^2, HL, and [CdL_2Py], identified the main structural changes in the cyclization process. Additionally, the coordination of the metal in the complexes [CdL(AcO)] · 2 MeOH and [CdL_2] · 3 H_2O was analyzed using IR spectroscopy in the solid state and ^{1}H-, ^{13}C-, and ^{113}Cd-NMR spectroscopy in solution. On reaction with aqueous trifluoroacetic acid, both complexes releases the free pyrazolone, which can be easily isolated.

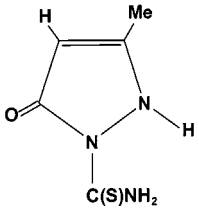
Cadmium is an environmental pollutant of worldwide concern. In most studies of its interaction with natural or man-made chelating agents, the products, complexes with a wide range of coordination spheres[1] and stabilities,[2] have shown no regiochemical modification of the ligand. We report here two cases of complexation involving cyclization of the ligand.

In spite of the frequent use of thiosemicarbazones (HTSCs) as ligands, mainly with transition metals,[3] only six complexes of HTSCs with cadmium have been fully identified by X-ray diffraction: namely, five adducts of cadmium with neutral HTSC and halide ligands[4] and the complex [$Cd(TSC)_2$] (TSC^- = pyridine-2-carbaldehyde thiosemicarbazonate).[4a] These six compounds exhibit a surprising range of coordination numbers (4, 5, 6, and 7) and coordination polyhedra (tetrahedral, bipyramidal trigonal, highly distorted octahedral and distorted bipyramidal pentagonal).[4]

As part of our work in this field, we recently prepared some HTSCs derived from β-keto esters and β-keto amides (**I**) and reacted them with cadmium(II) acetate in methanol solution. In view of the previous work of Jayasree and Aravindakshan,[5] we expected to obtain cadmium(II) complexes of the mono- or bi-deprotonated ligands, with or without an accompanying acetate ligand. Instead, we obtained new Cd^{II} compounds containing, in deprotonated form, the ligand 2-[amino(thioxo)methyl]-5-methyl-2,3-dihydro-1*H*-3-pyrazolone (HL, **II**).



(I)



(II)

The new pyrazolonate complexes [CdL(OAc)] · 2 MeOH and [CdL_2] · 3 H_2O are interesting for at least two reasons. Firstly, under acidic conditions they release the free pyrazolone; thus, reaction of this type of HTSC with Cd^{II} acetate and subsequent acidification, constitutes a means of obtaining good yields of compounds that are of great interest in organic, biological, pharmaceutical, analytical and agricultural chemistry.[6] Secondly, these cadmium(II) pyrazolonates appear to be the first to have been characterized by X-ray diffraction. In this paper we suggest a plausible reaction pathway and describe the structural characterization of the complexes in the solid state and in solution.

Results

Synthesis of the Complexes

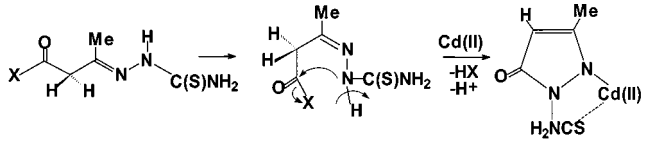
The analytical, spectroscopic, and structural data (vide infra) suggest that the HTSC molecules may be transformed into the final pyrazolonate ligand (L^-) via the reaction

[a] Departamento de Química Inorgánica,
Universidade de Santiago de Compostela,
15706 Santiago (A Coruña), Spain
E-mail: qitoyi@usc.es
[b] Instituto de Física de Sao Carlos, Universidade de Sao Paulo
Caixa Postal, 369, CEP 13.560, Sao Carlos, SP, Brazil
E-mail: pino@ifqsc.sc.usp.br

 © WILEY-VCH Verlag GmbH, D-69451 Weinheim, 2000 1434−1948/00/0101−0083 $ 17.50+.50/0

pathway shown in Scheme 1. This pathway is similar to that described by Katrizky et al.[7] for the condensation of a β-ketoester with hydrazine (Knorr′s synthesis of 2,4-dihydro-3*H*-pyrazol-3-ones).

The cyclization, with concomitant elimination of HX (= aniline in HTSC[1] and methanol in HTSC[2]) seems to be favoured by the Cd^{II} cation, possibly because the cadmium(II) thiosemicarbazonate is formed first, deprotonating N(2) and so favouring nucleophilic attack by N(2) on the −C(O)X group.



Scheme 1. Proposed cyclization mechanism

This reaction is related to those investigated by S.A. Samath et al.,[8] who found that β-ketoester complexes of Cu^{II} incorporated phenylhydrazine into the coordination sphere of the metal after a condensation/elimination reaction with the β-ketoester, and that cyclization to pyrazolones occurred upon subsequent demetallation with H_2S. In the reaction of HTSC[1] and HTSC[2] with Cd^{II}, the elimination/cyclization processes is so favoured that no thiosemicarbazonate intermediates were isolated at room temperature. The cadmium(II)-induced process is also related to previously described cyclizations of aldehyde thiosemicarbazones,[9] but differs from these latter examples in that it seems to involve no change in the oxidation state of the metal.

Structures of the Ligands

The numbering scheme used for the ligands are shown in Figure 1, and selected bond lengths and angles are listed in Table 1.

The bond lengths in the thiosemicarbazone ligands indicate the double bond character of C(5)−O [C(5)−O(2) in HTSC[2]], C(2)−N(3), and C(1)−S. In accordance with the canonical forms associated with the TSC chain[10] this also suggests some multiplicity in C(1)−N(2) and C(1)−N(1). In HTSC[1] the SC(1)N(1)N(2)N(3)C(2)C(3)C(4) and C(6)C(7)C(8)C(9)C(10)C(11)N(4) moieties are both planar (Rms. = 0.028 and 0.010, respectively) and form a dihedral angle of 67.9°; C(5) and O lie outside these planes. In HTSC[2] too, most atoms lie in one of two, almost orthogonal planes (dihedral angle 85.8°), one containing the TSC backbone [SN(1)C(1)N(2)N(3)C(2), Rms. = 0.019] and the other containing the non-thiosemicarbazone moiety C(4)C(5)O(1)O(2)C(6) (Rms. = 0.007); in this case C(3) lies outside these planes. In both HTSC[1] and HTSC[2], the configuration of the thiosemicarbazone chain is, as usual in this type of compound, (*E*) with respect to the C(2)−N(3) (aldimine) bond, and the thioamide S and N(3) atoms are mutually *trans* with respect to the C(1)−N(2) bond. This latter arrangement allows the formation of a strong intra-

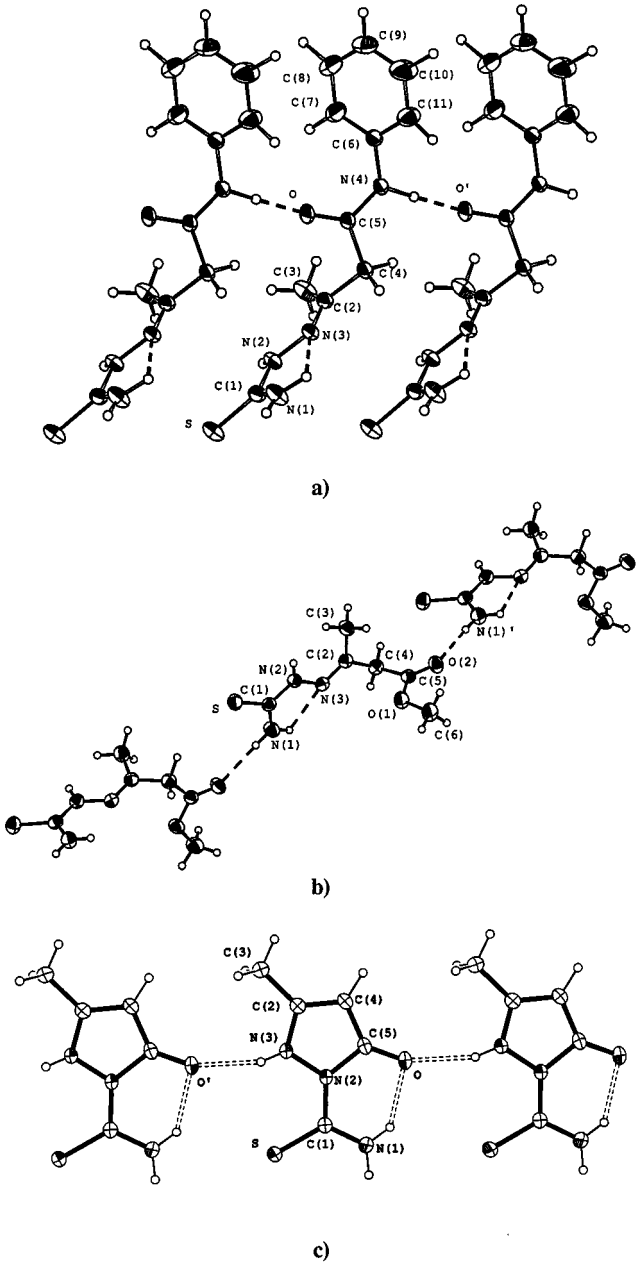


Figure 1. Crystal structures (with 30% probability ellipsoids) of a) HTSC[1], b) HTSC[2] and c) HL, showing intra- and intermolecular hydrogen bonds

molecular hydrogen bond between N(1)−H and N(3) (Figure 1, Table 1), which must aid the partial multiplicity of C(1)−N(1) bond in restricting rotation of the $-NH_2$ group in solution (vide infra NMR data). As Figure 1 and Table 1 show, there is also an intermolecular hydrogen bond between the carbonyl oxygen and N(4) (in HTSC[1]) or N(1) (in HTSC[2]), and this links the molecules in the lattice.

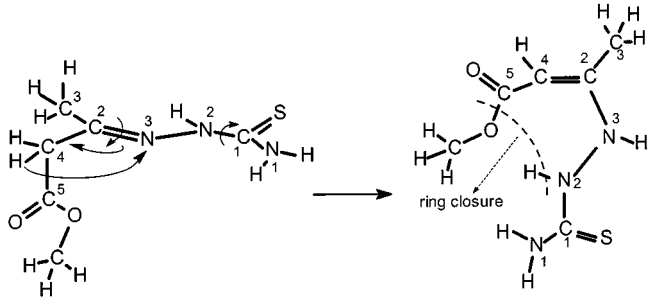
The formation of HL from these HTSC ligands implies that significant structural rearrangement occurs. The steps hypothesized are (Scheme 2): i) a 180° rotation about the C(1)−N(2) bond (as usually occurs when thiosemicarbazonates coordinate to a metal ion);[11] ii) a rotation about the C(2)−N(3) bond (by 67.9 and 85.8° in HTSC[1] and

Table 1. Selected bond lengths [Å] and angles [°]

Atom 1	Atom 2	Atom 3	HTSC[1]	HTSC[2]	HL	CdL_2Py[a]
S	C(1)		1.689(5)	1.685(3)	1.670(2)	1.698(4)/1.703(4)
N(1)	C(1)		1.311(7)	1.325(4)	1.318(3)	1.314(5)/1.306(5)
C(1)	N(2)		1.354(6)	1.341(4)	1.382(2)	1.369(5)/1.368(5)
N(2)	N(3)		1.387(5)	1.383(3)	1.376(2)	1.383(5)/1.390(5)
N(3)	C(2)		1.272(6)	1.268(4)	1.377(3)	1.324(6)/1.329(6)
C(2)	C(4)		1.502(7)	1.507(4)	1.376(3)	1.393(7)/1.378(7)
C(4)	C(5)		1.527(6)	1.517(4)	1.409(3)	1.382(7)/1.377(7)
C(5)	O[b]		1.216(6)	1.191(4)	1.240(2)	1.258(5)/1.265(5)
C(1)	N(2)	N(3)	117.2(4)	118.8(2)	121.77(15)	122.0(3)/122.1(3)
N(2)	N(3)	C(2)	117.7(4)	119.0(2)	108.6(2)	105.0(3)/104.7(3)
N(3)	C(2)	C(4)	115.6(4)	116.0(3)	109.8(2)	112.5(4)/112.6(4)
N(1)	N(3)		2.594(4)	2.617(4)		
O(1)	N(1)				2.669(3)	2.625/2.618
N(4)	O[i,c]		2.861(5)			
O(1)	N(1)[ii]			3.012(4)		
O(1)	N(3)[iii]				2.778(2)	
N(1)	O(2)[iv]					2.822
N(4)	O(1)[v]					2.821

[a] Values for the two L^- ligands. – [b] Carbonyl group distance. – [c] Symmetry operation: i) $x-1, y, z$; ii) $x+1, 1.5-y, z-0.5$; iii) $x-1, y, z$; iv) $-x, 0.5+y, 0.5-z$; v) $0.5+x, 1.5-y, -z$.

$HTSC^2$, respectively) so as to make the TSC and non-TSC moieties almost coplanar; iii) displacement of the double bond from C(2)−N(3) to C(2)−C(4) with simultaneous proton transfer from C(4) to N(3); and iv) deprotonation of N(2)−H, elimination of HX, and ring formation. This sequence of changes is in keeping with the following observed changes in bond lengths and bond angles: a) shortening of the C(2)−C(4) bond (which formally becomes a double bond), shortening of the C(4)−C(5) bond [which probably becomes involved in charge delocalization between O and C(5)] and lengthening of the C(2)−N(3) bond (which formally changes from double to single); b) narrowing of the [N(2)−N(3)−C(2)] and [N(3)−C(2)−C(4)] angles and widening of the [C(1)−N(2)−N(3)] angle, which are all affected by ring closure; and c) narrowing of the N(1)−C(1)−N(2) angle, possibly due to the strong intramolecular hydrogen bond −NH···O=C that is present in the cyclic compound (see Table 1). An intermolecular hydrogen bond between the carbonyl oxygen and the N(3)−H group of a neighbouring molecule is also shown in Figure 1 and Table 1.



Scheme 2. Hypothesized rearrangement of $HTSC^2$ under cyclization

Structure of the Complex $[CdL_2Py]$

Recrystallization of $[CdL(OAc)] \cdot 2\,MeOH$ from pyridine afforded monocrystals of $[CdL_2Py]$ (see Figure 2 for the numbering scheme used). In this complex, the deprotonated ligand coordinates to Cd^{II} via N(3) and the exocyclic S atom, as is usual in thiosemicarbazonates. According to Addison et al's τ-criterion,[12] the value $\tau = 0.63$ means that the coordination polyhedron is closer to a trigonal bipyramid (theoretical $\tau = 1$), with N(3) and N(6) in the apical positions [N(3)−Cd−N(6) = 170.3°], than to a square pyramid ($\tau = 0$). The bond lengths in the $[CdN_3S_2]$ kernel ($Cd-N_{Py}$ = 2.312 Å, average Cd−S = 2.554 Å, average $Cd-N_{TSC}$ = 2.293 Å) are shorter than in all the other cadmium(II) thiosemicarbazone derivatives studied so far,[4] including those in which the pyridine ring is part of the coordinated ligand [Cd^{II}-pyridine-2-carbaldehyde thiosemicarbazones[4a] and Cd^{II}-2,6-diacetylpyridine monothiosemicarbazone[4b]]. The bond lengths in this kernel are also clearly shorter than those reported for bis(benzothiazole-2-thiolato-*N,S*)bis(pyridine)cadmium(II) $[Cd(C_7H_4NS_2)_2(Py)_2]$,[13] which like $[CdL_2Py]$ contains two N,S-bound rings and coordinated pyridine (although it must be borne in mind that $[Cd(C_7H_4NS_2)_2(Py)_2]$ contains two mol of Py and its cadmium has a coordination number of six). In fact, the $Cd-N_{Py}$ distance is close to the minimum value found in the CSD[14] for Cd-pyridine compounds (2.300 Å), and is well below the mean, 2.355 Å. These data suggest strong metal-ligand interaction.

As in the free ligand, the pyrazolone rings are planar [Rms. = 0.009 and 0.010 for N(2)N(3)C(2)C(3)C(4)-C(5)O(1) and N(5)N(6)C(7)C(8)C(9)C(10)O(2), respectively] but upon coordination undergo certain structural changes that are worth mentioning. The C−S bond lengthens, though the fact that the lengthening is less than in the Cd^{II} complex of deprotonated pyridine-2-carbaldehyde

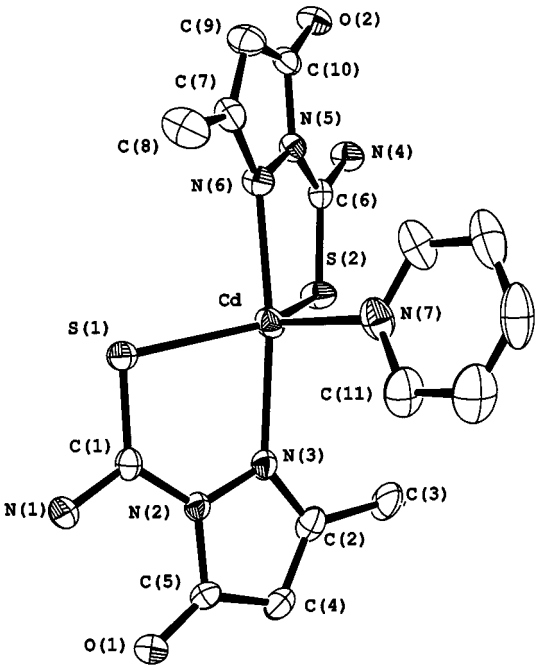


Figure 2. Molecular structure of $[CdL_2Py]$ (with 30% probability ellipsoids); selected bond lengths [Å] and angles [°]: Cd−S(1) 2.5546(11), Cd−S(2) 2.5540(11), Cd−N(3) 2.294(3), Cd−N(6) 2.292(3), Cd−N(7) 2.312(4), S(1)−Cd−S(2) 132.43(5), S(1)−Cd−N(3) 77.50(9), S(1)−Cd−N(6) 98.59(9), S(1)−Cd−N(7) 113.74(10), S(2)−Cd−N(3) 98.48(9), S(2)−Cd−N(6) 77.53(9), S(2)−Cd−N(7) 113.83(11), N(3)−Cd−N(6) 170.35(13), N(3)−Cd−N(7) 95.0(2), N(6)−Cd−N(7) 94.7(2)

thiosemicarbazone[4a] shows that there is less thione-to-thiol evolution in the pyrazolone compound. The associated shortening of the C(1)−N(2) bond is correspondingly slight, suggesting that the multiplicity of this bond increases only slightly upon coordination of the ligand to cadmium. The evolution of the bond lengths in the O(1)−C(5)−C(4)−C(2) and O(2)−C(10)−C(9)−C(7) pyrazolonato moieties [shortening of the C(4)−C(5)/C(9)−C(10) bonds and lengthening of the O(1)−C(5)/O(2)−C(10) and C(2)−C(4)/C(7)−C(9) bonds] is indicative of π-charge delocalization in this part of the ring upon metallation of nitrogen.

In $[CdL_2Py]$ the intramolecular $-NH_2\cdots O$ hydrogen bond is somewhat shorter than in the free ligand (2.625 Å). Four intermolecular hydrogen bonds involving the $-NH_2$ groups and the carbonyl O atoms connect the molecules of the complex in a three-dimensional network.

IR Spectroscopy

The significant IR bands of $HTSC^1$ and $HTSC^2$ (Experimental Section) were identified on the basis of previous data.[4a,5,15,16] Bands due to the $-N(H)C_6H_5$ and $-OCH_3$ groups were lost upon cyclization (this is more evident for $HTSC^1$ than $HTSC^2$, the $-OCH_3$ bands of which overlap those of the thiosemicarbazone fragment).

The N,S-coordination of the ligand L^- in $[CdL_2Py]$, shown by X-ray diffraction (vide supra), does not significantly shift the ring bands from their positions in the spectrum of free HL, but does shift the low-energy ν(C=S) band to lower wavenumbers and suppresses the high-energy band. The C=O group is non-coordinated, but is strongly involved in hydrogen bonds, which, together with the electronic reordering consequent on deprotonation and *N*-metallation, shift ν(C=O) to lower wavenumbers than in the spectrum of HL.

The positions of the main ring bands and ν(C=S) suggest that L^- is also N(3),S-coordinated in $[CdL(OAc)]\cdot 2\,MeOH$ and $[CdL_2]\cdot 3\,H_2O$. However, the larger shift in ν(C=O) suggests that this group is also Cd-coordinated in these two compounds. This would reduce the involvement of the −C=O group in strong hydrogen bonds with the NH_2 group, and might therefore explain why ν(N−H) lies at higher wavenumbers than for $[CdL_2Py]$. It thus seems reasonable to hypothesize that both $[CdL_2]\cdot 3\,H_2O$ and $[CdL(OAc)]\cdot 2\,MeOH$ have polymeric structures, with Cd hexacoordinated in an $N_2S_2O_2$ kernel in $[CdL_2]\cdot 3\,H_2O$, and pentacoordinated in an NSO_3 kernel in $[CdL(OAc)]\cdot 2\,MeOH$. The acetate anion in the latter complex is likely to be bidentate (it is difficult to draw this conclusion with certainty from the difference between ν_{as}(COO) and ν_s(COO) because of the breadth of the bands at 1602 and 1399 cm^{-1}, to which ν_{as}(COO) and ν_s(COO) must contribute[17]).

NMR Spectroscopy

The ^1H NMR spectra of $HTSC^1$ and $HTSC^2$ show two groups of signals for each of the groups $-N(1)H_2$, $-N(2)H$, $-C(2)H_3$, and $-C(4)H$, indicating that there is probably more than one conformer in solution (only signals for the major conformer are indicated in the Experimental Section). Signals for $-OCH_3$ and $-HNC_6H_5$ are also observed. The ^1H-NMR spectrum of HL differs markedly from those of its precursors: the signals of $-N(H)C_6H_5$ and $-OCH_3$ are missing, the −NH and $-CH_3$ protons are more deshielded, and there is a new signal at δ = 5.16 corresponding to the $-C(4)H$ group left upon loss of a proton by $-C(4)H_2$ in the cyclization process.

The ^1H-NMR spectra of the Cd^{II} complexes obtained by reaction of $HTSC^1$ and $HTSC^2$ with Cd^{II} acetate provided the first evidence of the cyclization of these ligands. They show no $-N(H)C_6H_5$ or $-OCH_3$ signals, and instead show a new signal at about δ = 4.7 which corresponds to the −CH signal latter observed at δ = 5.16 in the spectrum of HL. In view of this, the reaction was followed spectroscopically at room temperature by running spectra of a 2:1 $HTSC^1/Cd(OAc)_2$ mixture in DMSO. The spectrum of the freshly prepared mixture shows signals suggesting the initial formation of the complex $[Cd(TSC^1)_2]$, since only the signal of the −N(2)H proton is missing. The spectrum recorded 12 h later contains signals corresponding to $[Cd(TSC^1)_2]$ and $[CdL_2]$, and also signals for free aniline [at δ = 7.01(t), 6.57(t), 6.49(d), and 4.99(s)].

Comparison of the ^{1}H-NMR spectra of HL and its Cd^{II} complexes shows that coordination led to deprotonation of the ligand, as indicated by loss of the N(3)H signal.

In the ^{13}C-NMR spectrum, the main effects of coordination are a shielding of C(4) by about 5.5 ppm and a deshielding of C(2) and C(5) by about 4 ppm (Table 2). C(3) is deshielded by about 2 ppm, while the C(1) signal is hardly shifted. These data show that coordination causes only small modifications in the electronic charge distribution of the N(3)−N(2)−C(1)SNH_2 fragment, but major modifications in the fragment C(3)−C(2)−C(4)−C(5)−O, in accordance with the X-ray data for [CdL_2Py] in the solid state. This suggests that the solid−state coordination mode persists in [D_6]DMSO. The virtually constant position of the C(1) signal is attributable to slight shielding [due to some evolution from an N(2)−C(1)=S towards an N(2)=C(1)−S configuration] being offset by the deshielding inductive effect of the metal−sulfur bond.

The ^{113}Cd-NMR spectrum of [CdL_2] · 3 H_2O shows a single signal at δ = 281 (Table 2), which indicates greater shielding than is expected in an [S_2N_2] kernel.[18] In fact, even though the shielding of the ^{113}Cd nucleus generally increases with its coordination number,[19] the signal is even further upfield than in the complex [Cd(TSC)$_2$] (HTSC = pyridine 2-carboxyaldehyde thiosemicarbazone)[4a] which has an [S_2N_4] kernel. This probably indicates an increase in coordination number due to coordination to DMSO oxygen atoms. The fact that the ^{113}Cd chemical shift of [CdL_2Py] is exactly the same as that of [CdL_2] · 3 H_2O, showing Cd to have the same chemical environment in both, therefore suggests that in the former the Py ligand is replaced by molecules of solvent.

Table 2. ^{13}C- and ^{113}Cd-NMR chemical shifts (in ppm)

Compound	δC(1)	δC(2)	δC(3)	δC(4)	δC(5)	δ(^{113}Cd)
HTSC^1	178.8	148.8	16.8	46.5	167.3	
HTSC^2	178.9	147.2	16.8	43.7	170.1	
HL	175.8	152.7	12.1	91.4	163.3	
[CdL(AcO)] · 2 MeOH	176.3	157.3	14.7	85.7	167.0	156 286
[CdL_2] · 3 H_2O	176.2	156.8	14.7	86.0	166.7	281
[CdL_2Py]	176.1	156.8	14.4	85.9	166.7	281

[a] CH_3COO^-: 22.1 (Me), 178.0 (COO^-).

The ^{113}Cd-NMR spectrum of [CdL(OAc)] · 2 MeOH shows signals at both δ = 156 and 286 (area ratio 5:1). This suggests the existence of an equilibrium involving at least two species, in which the cadmium atom has different environments. Assuming that the replacement of S and N atoms by O atoms increases shielding,[20] the signal at δ = 156 can probably be assigned to the primary complex [CdL(OAc)], in which the Cd coordination sphere comprises pyrazolone N and S atoms (one each) together with O atoms from the OAc ligand and, probably, from the solvent. The signal at δ = 286, which lies very close to that of [CdL_2], may be due to a small amount of the later species being formed upon dissolution of [CdL(OAc)] · 2 MeOH in DMSO. The evolution of [CdL(OAc)] · 2 MeOH to [CdL_2] is also supported by the FAB mass spectrum of the former complex, in which the [CdL_2] peak is clearly observed, and by [CdL_2Py] having been isolated from a pyridine solution of [CdL(OAc)] · 2 MeOH (vide supra). The fact that the ^{113}Cd spectrum of [CdL(OAc)] · 2 MeOH shows no separate signal for the $Cd(OAc)_2$ that must be formed if the bispyrazolonate species is the result of symmetrization of [CdL(OAc)], may be due to the $Cd(AcO)_2$ signal being very broad.

Concluding Discussion

When acetoacetanilide and methylacetoacetate thiosemicarbazones (HTSC^1 and HTSC^2, respectively) react with cadmium(II) acetate in methanol, an elimination/cyclization process leads to the complexes [CdL(OAc)] · 2 MeOH and [CdL_2] · 3 H_2O (HL = 2-[amino(thioxo)methyl]-5-methyl-2,3-dihydro-1*H*-3-pyrazolone). In the case of HTSC^1, ^{1}H-NMR monitoring in [D_6]DMSO at room temperature suggests that the probable course of the reaction is initial formation of [Cd(TSC^1)$_2$] followed by gradual release of aniline and concomitant cyclization. Determination of the structures of the ligands HTSC^1, HTSC^2, and HL by X-ray diffraction showed the structural changes involved in this process.

Recrystallization of the complex [CdL(OAc)] · 2 MeOH from pyridine gave the new compound [CdL_2Py] which was also studied by X-ray diffraction. The structural parameters of the trigonal bipyramidal coordination sphere suggest that the N,S-bound L^- ligand and the pyridine ligand both form very strong bonds with the cadmium(II) ion. The coordination modes present in [CdL_2] · 3 H_2O and [CdL(OAc)] · 2 MeOH were diagnosed on the basis of their solid state IR spectra and ^{1}H-, ^{13}C-, and ^{113}Cd-NMR spectra in [D_6]DMSO: in solid state, both appear to have polymeric structures, with Cd hexacoordinate in [CdL_2] · 3 H_2O and pentacoordinate in [CdL(OAc)] · 2 MeOH. In [D_6]DMSO, solvent molecules appear to be included in the coordination sphere of the metal.

On reaction with aqueous trifluoroacetic acid both [CdL_2] · 3 H_2O and [CdL(OAc)] · 2 MeOH release the free pyrazolone, which can be easily isolated

Experimental Section

Thiosemicarbazide (Merck), acetoacetanilide (Merck), acetylacetoacetate (Aldrich), and cadmium acetate (Probus) were used as received. The HTSCs were obtained by the method of Jayasree and Aravindakshan.[5]

HTSC^1: M.p. 161°C. − $C_{11}H_{13}N_4OS$,: calcd. C 52.78, H 5.43, N 22.39, S 12.82; found C 52.75, H 5.60, N 22.54, S 12.74. − IR (KBr): $\tilde{\nu}$ = 3428 (s), 3268 (vs, b) 3155 (s), [ν(N−H)], 1655 (s), [ν(C=O)], 1595 (vs), [ν(C=N)], 1545 (s), 1248 (m), [ν[−N(H)C_6H_5], 1090 (s), 872 (m), [ν(C=S)]. − ^{1}H NMR (DMSO): δ = 10.17 [s, 1 H, N(4)*H*], 10.05 [s, 1 H, N(2)*H*], 8.16 [s, 1 H, N(1)H_2), 7.62 [s, 1 H, N(1)H_2], 7.03 [t, 1 H, C_6H_5(*Hp*)], 7.28 [t, 2 H, C_6H_5(*Hm*)], 7.57 [d, 2 H, C_6H_5(*Ho*)], 3.32 [s, 2 H, C(4)H_2], 1.98 [s, 3 H, C(3)H_3].

HTSC^2: M.p. 120°C. − $C_6H_{11}N_3O_2S$,: calcd. C 38.08, H 5.86, N 22.20, S 16.95; found C 38.25, H 6.05, N 22.10, S 17.60. − IR (KBr): $\tilde{\nu}$ = 3402 (vs), 3277 (vs), 3169 (s), [ν(N−H)], 1719 (vs), [ν(C=O)], 1599 (vs), [ν(C=N)], 1440 (m), [δ(−OCH_3)], 1246 (s), [ν(C−O)], 1090 (s), 853 (m), [ν(C=S)]. − ^{1}H NMR (DMSO): δ = 10.15 [s, 1 H, N(2)*H*], 8.54 [s, 1 H, N(1)H_2], 7.60 [s, 1 H, N(1)H_2], 3.33 [s, 2 H, C(4)H_2], 1.94 [s, 3 H, C(3)H_3].

The cyclic ligand **2-[amino(thioxo)methyl]-5-methyl-2,3-dihydro-1*H*-3-pyrazolone (HL)** was originally obtained serendipitously as a by-product of the synthesis of acetoacetanilide thiosemicarbazone; the solid formed when the reaction mixture was refluxed for 7 h recrystallizing from methanol as a mixture of HTSC^1 and HL. Diffraction and spectroscopic studies were performed using HL crystals separated by hand under a stereoscopic microscope. Later (vide infra) HL was also obtained by acidification of cadmium(II) complexes. − M.p. 185°C. − $C_5H_7N_3OS$: calcd. C 38.21, H 4.49, N 26.73, S 20.40, found C 38.5, H 4.5, N 26.5, S 21.6. − IR (KBr): $\tilde{\nu}$ = 3269 (vs), 3164 (vs), [ν(N−H)], 1654 (vs), [ν(C=O)], 1592 (vs), 1550 (vs), 1507 (m), [ν(ring)], 1093 (s), 875 (m), [ν(C=S)]. − ^{1}H NMR (DMSO): δ = 11.98 [s, 1 H, N(3)*H*], 10.36 [s, 1 H, N(1)H_2], 9.66 [s, 1 H, N(1)H_2], 5.16 [s, 1 H, C(4)*H*], 2.17 [s, 3 H, C(3)H_3].

Analytical data were obtained with a Fisons Instruments EA1108CHNS-O microanalyzer. − ^{1}H- and ^{13}C-NMR spectra were recorded on a Bruker WM-250 or a Bruker AMX-300, and ^{113}Cd-NMR spectra on a Bruker AMX-500. Chemical shifts are quoted on the δ scale (downfield shifts positive) relative to tetramethylsilane (^{1}H and ^{13}C NMR) or 0.1 M $Cd(ClO_4)_2$ (^{113}Cd NMR). The ^{13}C-NMR spectra of the thiosemicarbazone ligands HTSC^1 and HTSC^2 were interpreted on the basis of the chemical shifts, the multiplicity of the signals in the non-proton-decoupled spectra and DEPT-135 experiments, and that of HL on the basis of previous assignments for similar rings.[6] − Infrared spectra were recorded using KBr discs in Mattson Cygnus 100 and Bruker IFS66V spectrometers. − Mass spectra were recorded on a Kratos MS50TC spectrometer. − Melting points were determined in a Büchi apparatus.

Synthesis of [CdL(OAc)]·2 MeOH: A solution of HTSC^1 (0.50 g, 2 mmol) in methanol (15 mL) was added to a hot solution of $Cd(OAc)_2 \cdot 2\,H_2O$ (0.53 g, 2 mmol) in the same solvent (5 mL). After 4 days stirring, the pale yellow solid formed was filtered out and dried under reduced pressure. − M.p. 198°C. − $C_9H_{17}N_3O_5SCd$: calcd. C 27.6, H 4.3, N 10.7; found C 27.5, H 4.5, N 10.5. − MS (FAB, nitrobenzyl alcohol); *m*/*z* (%): 424 (76) [CdL_2], 328 (35) [M − 2 MeOH], 270 (60) [$C_5H_7N_3OSCd$], 140 (97) [$C_5H_7N_3S$], 99 (100) [$C_2H_2N_3S$]. − IR (KBr): $\tilde{\nu}$ = 3410 (m, br), [ν(OH)], 3236 (s, br), [ν(N−H)], 1602 (vs, br), [ν(C=O)], 1602 (vs, br) 1497 (m), [ν(ring)], 757 (m, br), [ν(C=S)]. − ^{1}H NMR (DMSO): δ = 11.72 [s, 1 H, N(1)H_2], 9.72 [s, 1 H, N(1)H_2], 4.67 [s, 1 H, C(4)*H*], 4.10 (c, 2 H, CH_3OH), 3.11 (d, 6 H, CH_3OH), 2.10 [s, 3 H, C(3)H_3], 1.83 (s, 3 H, CH_3COO).

Synthesis of [CdL_2]·3 H_2O: A solution of methylacetoacetate thiosemicarbazone (HTSC^2, 0.50 g, 2.64 mmol) in methanol (30 mL) was added to a methanolic solution (15 mL) of $Cd(OAc)_2 \cdot 2\,H_2O$ (0.70 g, 2.64 mmol). The mixture was refluxed for 2 h and stirred for a further 12 h. The white solid formed was filtered out and dried under reduced pressure; it decomposed before melting. − $C_{10}H_{18}N_6S_2O_5Cd$: calcd. C 25.1, H 3.8, N 17.6; found C 25.3, H 3.3, N, 17.4. − MS (FAB, nitrobenzyl alcohol); *m*/*z* (%): 425 (32) [M − 3 H_2O], 309 (31) [$C_6H_6N_4S_2Cd$], 270 (55) [$C_5H_8N_3OSCd$], 99 (91) [$C_2H_2N_3S$]. − IR (KBr): $\tilde{\nu}$ = 3550 (m), [ν(OH)], 3390 (m), 3223 (m, brs), [ν(N−H)], 1600 (vs, br), [ν(C=O)], 1600 (vs, br) 1498 (m), [ν(ring)], 752 (m, br), [ν(C=S)]. − ^{1}H NMR (DMSO): δ = 11.73 [s, 1 H, N(1)H_2], 9.70 [s, 1 H, N(1)H_2], 4.67 [s, 1 H, C(4)*H*], 1.97 [s, 3 H, C(3)H_3]. A small part of the product was recrystallized from pyridine and X-ray measurements and spectral studies were performed on the crystalline product so obtained, [CdL_2Py]: IR (KBr): $\tilde{\nu}$ = 3097 (s, br), 2959 [s, br, ν(N−H)], 1629 (vs, br), [ν(C=O)], 1600 (s), 1490 (m), [ν(ring)], 752

Table 3. Selected Crystallographic data for HTSC^1, HTSC^2, HL, and CdL_2Py.

Compound	HTSC^1	HTSC^2	HL	CdL_2Py
Empirical formula	$C_{11}H_{14}N_4OS$	$C_6H_{11}N_3O_2S$	$C_5H_7N_3OS$	$C_{15}H_{17}CdN_7O_2S_2$
Formula weight	250.32	189.24	157.20	503.88
Wavelenght [Å]	0.71073	0.71073	1.54184	1.54056
Crystal system	Triclinic	Monoclinic	Triclinic	Orthorhombic
Spacegroup	*P*-1 (n° 2)	$P2_1/c$ (n° 14)	*P*-1 (n° 2)	$P2_12_12_1$ (n° 19)
a [Å]	4.817(1)	7.5943(12)	6.1552(8)	12.1905(6)
b [Å]	8.696(1)	11.6146(13)	7.721(2)	12.1915(6)
c [Å]	15.469(2)	10.473(2)	8.1904(11)	13.3466(6)
α [°]	97.18(1)	90	82.55(2)	90
β [°]	97.351(1)	91.037(9)	71.18(2)	90
γ [°]	103.21(1)	90	70.80(2)	90
Volume [Å^3]	617.6(3)	923.7(2)	347.81(11)	1983.6(2)
Z	2	4	2	4
D_{calc} [g cm^{-3}]	1.820	1.361	1.501	1.687
Absortion coeffic. [mm^{-1}]	0.25	0.317	3.592	11.014
F(000)	264	400	164	1008
Crystal size [mm]	0.35_{max}, 0.26_{min}	0.12 × 0.06 × 0.07	0.1 × 0.15 × 0.25	0.20 × 0.25 × 0.30
Theta range for data collection [°]	1−26	3−30	6−70	5−74
Index ranges	−5,5; −10,10; 0,19	0,5; 0,16; −14,14	−7,7; −9,0; −9,9	−13,15; 0,15; −16−0
Reflections collected	2499	2061	1419	4665
Independent reflections	2406	1884	1315	3236
R_{int}	0.0158	0.0355	0.0123	0.0187
Reflections observed	1468	1389	1177	3134
Criterion for observation	$I > 2\sigma(I)$	$I > 2\sigma(I)$	$I > 2\sigma(I)$	$I > 2\sigma(I)$
R_1	0.0443	0.0596	0.0396	0.0270
R_w	0.1433	0.1553	0.1042	0.0700
Largest diff. peak and hole	0.274 and −0.373 e·Å^{-3}	0.309 and −0.372 e·Å^{-3}	0.243 and −0.306 e·Å^{-3}	0.390 and −0.663 e·Å^{-3}

(m, br), [ν(C=S)]. – ^{1}H NMR (DMSO): δ = 11.74 [s, 2 H, N(1)H_2], 9.70 [s, 2 H, N(1)H_2], 8.56 [d, 2 H, C_5H_5N (*Ho*)], 7.76 [t, 1 H, C_5H_5N (*Hp*)], 7.37 [t, 2 H, C_5H_5N (*Hm*)], 4.68 [s, 2 H, C(4)*H*], 2.10 [s, 6 H, C(3)H_3].

X-ray Crystal Structure Determinations: Data were collected on an Enraf–Nonius CAD-4 diffractometer. The structures were solved using the Patterson method for HTSC[1] and [CdL_2Py] and direct methods for HTSC[2]and HL, followed by normal difference Fourier techniques. The H atoms were introduced in calculated positions with fixed C–H distances and isotropic thermal parameters (C–H 0.95 Å; B_{iso} = 4 Å^2). The structures were refined by the full-matrix least-squares method (anisotropically for the non-H atoms). Atomic scattering factors were those included in SHELX93.[21] Other programs used were SHELX76[22]and, ORTEP.[23] Crystal and refinement data are listed in Table 3.[24]

Reactivity of Complexes in Acidic Media: Preliminary experiments exploring the behaviour of [CdL(AcO)] · 2 MeOH and [CdL_2] in acidic aqueous suspensions were performed using F_3CCOOH(aq) as proton source. The complexes released free HL, which precipitated and was easily isolated.

Acknowledgments

Support of these investigations by the Ministerio de Educación y Cultura (Spain) is gratefully acknowledged.

[1] C. E. Holloway, M. Melnik, *Main Group Met. Chem.,* **1995**, *18*, 451.
[2] D. G. Archer, *J. Phys. Chem. Ref. Data*, **1998**, *27*, 915 and ref. therein.
[3] D. X. West, S. B. Padhye, P. B. Sonawane, *Struct. Bonding*, **1991**, *76*, 4.
[4] [4a] J. S. Casas, M. V. Castaño, M. S. García-Tasende, I. Martínez-Santamarta, J. Sordo, E. E. Castellano, J. Zukerman-Schpector, *J. Chem. Res.(S)* **1992**, 234. – [4b] J. S. Casas, E. E. Castellano, M. S. García-Tasende, A. Sánchez, J. Sordo, J. Zukerman-Schpector, *Z. Anorg. Allg. Chem.* **1997**, *623*, 825 and refs. therein. – [4c] Y. Tian, C. Duan, C. Zhao, X. You, T. C. W. Mak, Z. Zhang, *Inorg. Chem.* **1997**, *36*, 1247. – [4d] C.-Y. Duan, Y.-P. Tian, C.-Y. Zhao, X.-Z. You, T. C. W. Mak, *Polyhedron* **1997**, *16*, 2857.
[5] S. Jayasree, K. K. Aravindakshan, *Trans. Met. Chem.* **1993**, *18*, 85; Ibid., *Polyhedron* **1993**,*12*, 1187.
[6] O. A. Attanasi, L. D. Crescenti, P. Filippone, E. Foresti, R. Galeazzi, I. Ghiviriga, A. R. Katritzky, *Tetrahedron* **1997**, *53*, 5617.
[7] A. R. Katrizky, P. Barczynski, D. L. Ostercamp, *J. Chem. Soc., Perkin Trans. 2,* **1987**, 969.
[8] S. A. Samath, K. Jeyasubramanian, S. Thanbidural, S. Kamardeen, S. K. Ramalingam, *Polyhedron* **1993**, *12*, 1265.
[9] M. Gruttadauria, P. Lo Meo, R. Noto, G. Werber, *Gazz. Chim. Ital.* **1997**, *127*, 277 and refs. therein.
[10] R. Restivo, G. I. Palenik, *Acta Cryst.*, **1970**, *B 26*, 1397.
[11] J. S. Casas, E. E. Castellano, A. Macías, M. C. Rodríguez-Argüelles, A. Sánchez, J. Sordo, *J. Chem. Soc., Dalton Trans.* **1993**, 353.
[12] A. W. Addison, T. N. Rao, J. Reedijk, J. Van Rijn, G. C. Verschoor, *J. Chem. Soc., Dalton Trans.* **1984**, 1349.
[13] R. Baggio, M. T. Garland, M. Perec, *J. Chem. Soc., Dalton Trans.* **1993**, 3367.
[14] F. H. Allen, O. Kennard, R. Taylor, *Acc. Chem. Res.* **1983**, *16*, 146.
[15] A. K. El-Sawat, D. X. West, F. A. El-Saied, R. M. El-Bahnasawy, *Synth. React. Inorg. Met-Org. Chem*. **1997**, *27*, 1127.
[16] N. B. Colthup, C. H. Daly, S. E. Wiberly, *Introduction to Infrared and Raman Spectroscopy,* 3th ed., Academic Press, London, **1990**, pp. 301, 321.
[17] K. Nakamoto, *Infrared and Raman Spectra of Inorganic and Coordination Compounds*, 5th ed., part B, John Wiley, New York, **1997**, p. 60.
[18] R. A. Santos, E. S. Gruff, S. A. Koch, G. S. Harbison, *J. Am. Chem. Soc.* **1990**, *112,* 9257.
[19] P. G. Mennitt, M. P. Shatlock, V. J. Bartuska, G. E. Maciel, *J. Phys. Chem.* **1981**, *85*, 2087.
[20] P. S. Marchetti, S. Bank, T. W. Bell, M. A. Kennedy, P. D. Ellis, *J. Am. Chem. Soc*. **1989**, *111*, 2063.
[21] G. M. Sheldrick, *SHELX93*. Program for crystal structure refinement. Univ. of Göttingen, **1993**.
[22] G. M. Sheldrick, *SHELX76*. Program for crystal structure determination. Univ. of Cambridge, **1976**.
[23] C. K. Johnson, *ORTEP.* Report ORNL-3794. Oak Ridge National Laboratory, Tennessee, USA, **1965**.
[24] Crystallographic data (excluding structure factors) for the structures reported in this paper have been deposited with the Cambridge Crystallographic Data Centre as CCDC-118936 (HTSC[1]), -118937 (HTSC[2]), -118938 (HL), -118939 ([CdL_2Py]). Copies of the data can be obtained free of charge on application to CCDC, 12 Union Road, Cambridge CB2 1EZ, UK [Fax: internat. + 44 (0)1223/336-033; E-mail: deposit@ccdc.cam.ac.uk].

Received April 29, 1999
[I99154]

Photocatalyzed Oxidation of Cyclohexene and Cyclooctene with $(n\mathrm{Bu_4N})_4W_{10}O_{32}$ and $(n\mathrm{Bu_4N})_4W_{10}O_{32}$/$Fe^{III}$[*meso*-Tetrakis(2,6-dichlorophenyl)-porphyrin] in Homogeneous and Heterogeneous Systems

Alessandra Molinari,[a] Rossano Amadelli,[a] Vittorio Carassiti,[a] and Andrea Maldotti*[a]

Keywords: Photocatalysis / Polyoxotungstates / Catalytic oxidations / Iron porphyrins

Photoexcitation of $(n\mathrm{Bu_4N})_4W_{10}O_{32}$ is a suitable mean of oxidizing cyclohexene and cyclooctene with O_2 at room temperature and pressure. This process can be carried out in homogeneous solution as well as using the decatungstate in a dispersed form after its heterogenisation on silica. Cyclohexene and cyclooctene are mainly oxidized to the corresponding hydroperoxides as a consequence of primary photoprocesses which lead to the formation of allylic radicals. The presence of the Fe^{III}[*meso*-tetrakis(2,6-dichlorophenyl)porphyrin] chloride as cocatalyst strongly affects the photocatalytic properties of $(n\mathrm{Bu_4N})_4W_{10}O_{32}$, playing a key role in the allylic-hydroperoxide dependent oxidation of the cycloalkenes. In the photooxidation of cyclohexene, the porphyrin increases the photocatalytic efficiency of the decatungstate in terms of total turnover number and catalyses the decomposition of cyclohexenyl hydroperoxide with the selective formation of cyclohex-2-en-1-ol. On the other hand, its presence during the photoinduced oxidation of cyclooctene favours the formation of cyclooctene epoxide by addition of ROO· and RO· radicals to the double bond. In the case of cyclooctene, the heterogenisation of the decatungstate on the solid support also affects the chemoselectivity of the photocatalytic process in the absence of the iron porphyrin complex.

Introduction

The catalytic oxidation of hydrocarbons at room temperature and atmospheric pressure using environmentally friendly reagents, such as O_2, is an important goal both in fine and industrial chemistry.[1] In this challenging field, a number of groups are investigating polyoxometallates as catalysts with a noticeable activity in the oxidation of numerous organic compounds.[2] Their heterogenisation with solid matrices is attracting more and more interest[3] because the support makes them more easily handled and recycled than in homogeneous solution and, moreover, it can play a fundamental role in controlling both the efficiency and the selectivity of the catalytic process. In this framework, we have recently reported that photoexcitation of $(n\mathrm{Bu_4N})_4W_{10}O_{32}$ supported on silica induces the oxidation of cyclohexane by O_2.[4] In particular we pointed out that the $(n\mathrm{Bu_4N})_4W_{10}O_{32}/SiO_2$ system is a very promising photocatalyst for synthetic purposes, because its efficiency is comparable to that of the semiconductor TiO_2, with the advantage that it does not cause any oxidative mineralisation of the substrate.

We examine here the photocatalytic properties of $(n\mathrm{Bu_4N})_4W_{10}O_{32}$ **1** and $(n\mathrm{Bu_4N})_4W_{10}O_{32}/SiO_2$ **2** in the oxidation of cyclohexene and cyclooctene. We have chosen these two substrates as representative unsaturated hydrocarbons which are expected to present different oxidation mechanisms under aerobic conditions.[5] As part of our continuing interest in composite systems based on the use of polyoxotungstates and iron porphyrins,[6] we have also investigated the photocatalytic properties of **1** and **2** in the presence of Fe^{III}[*meso*-tetrakis(2,6-dichlorophenyl)porphyrin] chloride [Fe(TDCPP)Cl] as cocatalyst. In this case, we are interested in verifying the possible role of the porphyrin complex in governing the oxidation product distribution through its well-known mechanisms.[7] The bulky substituents in the *ortho* positions of the porphyrin *meso*-aryl groups provide a steric protection of the aromatic ring against a rapid oxidative degradation of the complex during both thermal[8] and photochemical catalytic processes.[9]

Results and Discussion

EPR Spin Trapping Investigation

In this section we report the results obtained during photoexcitation of **1** and **2** in the presence of phenyl *tert*-butyl nitrone, which is known to trap radicals to give more stable nitroxides.[10] Although the trapping process is not quantitative, in many instances the captured radical can be identified by the parameters obtained from the EPR spectrum. Using this technique, we revealed the radical species formed during the oxidation of cyclohexane[6a] and cyclohexylamine[11] photocatalysed by complex **1**.

Both **1** and **2** were irradiated in a CH_3CN/cyclohexene (6:1) mixture containing phenyl *tert*-butyl nitrone (1×10^{-3} mol·dm^{-3}) inside the cavity of an EPR spectrometer. The spectrum obtained is shown in Figure 1. It consists of a triplet of doublets with hyperfine coupling constants (a_N =

[a] Dipartimento di Chimica, Centro di Studio su Fotoreattività e Catalisi del CNR,
Via Luigi Borsari 46, I-44100 Ferrara, Italy
Fax: (internat.) + 39-0532/240709
E-mail: mla@dns.unife.it

 © WILEY-VCH Verlag GmbH, D-69451 Weinheim, 2000 1434−1948/00/0101−0091 $ 17.50+.50/0

13.7 G and a_H = 2.1 G) which can be assigned to the adducts between the spin trap and cyclohexenyl radicals.[10] This spectrum remained the same even when an analogous irradiation was performed under anaerobic conditions. We can therefore conclude that it is not due to the trapping of cyclohexenylperoxo radicals, which are known to form a paramagnetic adduct with very similar hyperfine coupling constants.[12] The trapping of cyclohexenyl radicals is in agreement with the results of other authors who proposed that the dimeric species obtained in analogous experiments under anaerobic conditions originated from the coupling of these allylic radicals.[13]

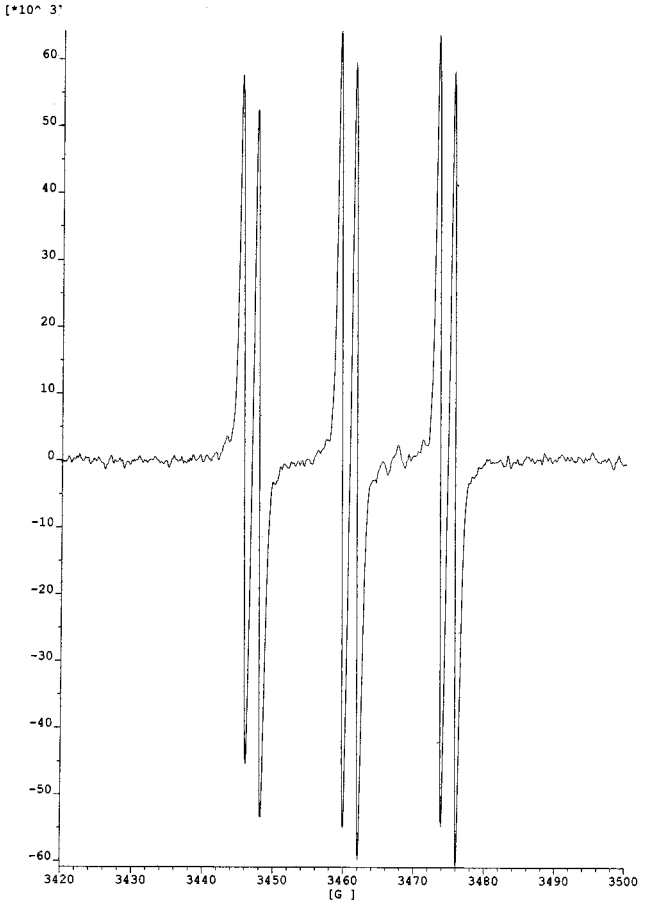
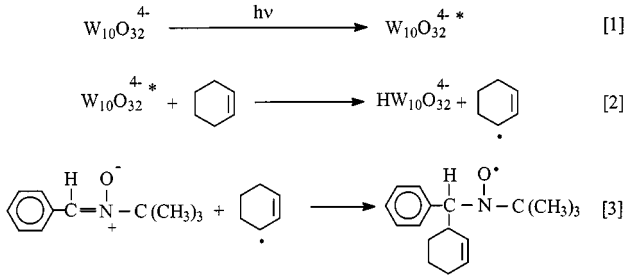


Figure 1. EPR spectrum obtained during irradiation ($\lambda > 320$ nm) of an aerated cyclohexene/CH_3CN (1:6 v/v) solution of $W_{10}O_{32}^{4-}$ (1×10^{-3} mol·dm^{-3}) in the presence of phenyl *tert*-butyl nitrone (1×10^{-3} mol·dm^{-3})

The detection of allylic radicals indicates that the photoinduced oxidation of cyclohexene occurs according to the mechanisms already proposed for the oxidation of other hydrocarbons and alcohols.[14] In particular, compound **1** in the photogenerated excited state is able to abstract a hydrogen from the cycloalkene to produce allylic radicals according to Equations 1 and 2. These radical species can be trapped by phenyl *tert*-butyl nitrone giving a paramagnetic nitroxide stable enough to be detected by EPR spectroscopy (Equation 3).

We failed to detect any EPR signals on irradiating **1** or **2** in CH_3CN/cyclooctene (6:1), indicating that the photoinduced oxidation of cyclooctene (Equation 2), although possible, does not give a steady state concentration of allylic radicals that is sufficiently high to obtain an observable paramagnetic adduct with phenyl *tert*-butyl nitrone. The different behaviour of the two investigated cycloalkenes can be explained by taking into account that cyclooctene is much less reactive than cyclohexene in hydrogen-abstraction processes. In particular, the relative rate constants differ by a factor of 17, depending mainly on the degree of reorganization required to give a planar allylic radical.[5]



Photocatalyzed Oxygenations with $(n\mathrm{Bu_4N})_4W_{10}O_{32}$ and $(n\mathrm{Bu_4N})_4W_{10}O_{32}/SiO_2$

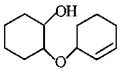
The EPR experiments show that under photolytic conditions, the decatungstate is able to initiate the oxidation of cyclohexene through allylic hydrogen abstraction (Equations 1 and 2). It is clear that for efficient catalytic cycles to be observed, the polyoxotungstate in its original form should be easily restored after the primary photoreduction. It has already been reported that **1** and **2** in their oxidised states can be regenerated by O_2, which, in turn, undergoes a reductive activation process[14c,15] with a pseudo first-order rate constant of about 150 s^{-1}.[6b] On this basis, we have investigated the possibility of inducing the photocatalytic oxidation of cyclohexene to stable products in the presence of O_2.

In typical experiments, **1** (2×10^{-4} mol·dm^{-3}) was irradiated in a CH_3CN/cyclohexene (6:1) mixture saturated with O_2, and **2** (20 g·dm^{-3}) as a powder suspension in the same dispersing medium. The selected excitation wavelength range ($300 < \lambda < 370$ nm) and the amounts of photocatalysts were chosen so that the maximum absorption of the incident light was the same in the two systems. Table 1 reports the distribution of the oxidation products and the overall turnover values after two hours irradiation.

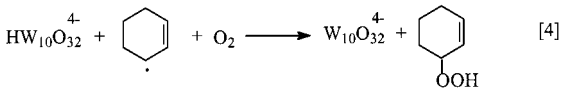
Photoexcitation of **1** in the homogeneous phase leads to the oxidation of cyclohexene to the corresponding allylic hydroperoxide as the main product (about 90% of the overall oxidized cycloalkene). In agreement with literature data on the photocatalysed oxidation of alkanes in the presence of decatungstates and O_2, we propose that the hydroperoxide is formed according to Equation 4.[14c]

In agreement with previous evidence,[16] we also observed the formation of cyclohex-2-en-1-ol and cyclohex-2-en-1-one during irradiation. On the basis of literature data regarding alkane photooxidation with **1**,[6,14c] we propose that

Table 1. Photocatalytic properties[a] of $(n\mathrm{Bu_4N})_4W_{10}O_{32}$ **1** and $(n\mathrm{Bu_4N})_4W_{10}O_{32}/SiO_2$ **2** in CH_3CN/cyclohexene (6/1), in the presence of 760 Torr of O_2, with and without Fe(TDCPP)Cl

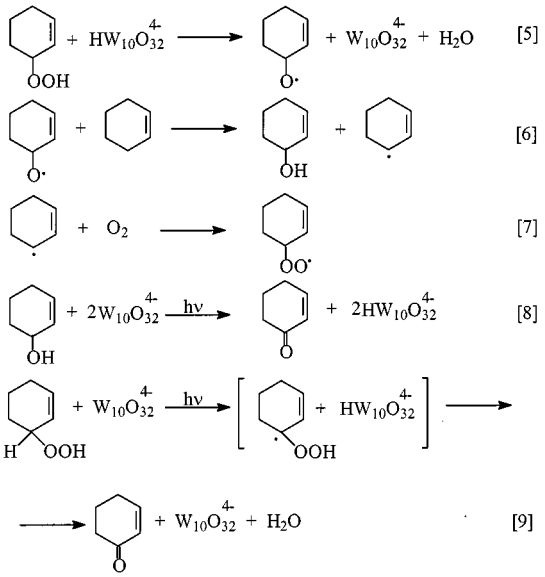
Photocatalyst	Total turnover [b]	 [c] (%)	 [f] (%)	 [f] (%)	 (%)	 (%)
1+ hν	123	89	7.5	1.8	0.7	1.0
1/Fe(TDCPP)Cl + hν [d]	185	59	24	15	0.9	1.1
1/Fe(TDCPP)Cl + hν + dark [e]	215	40	27	30	1.2	1.8
2 + hν [g]	25	89	6.4	1.9	1.2	1.5
2/Fe(TDCPP)Cl + hν [d, g]	43	73	16	9	0.8	1.2
2/Fe(TDCPP)Cl + hν + dark [e]	52	48	29	20	1.4	1.6

[a] 3 ml of CH_3CN/cyclohexene 6:1 containing **1** ($2x10^{-4}$ mol· × dm^{-3}, 0.6 μmol of irradiated polyoxotungstate) or **2** (20 g·dm^{-3}, 1.93 μmol of irradiated polyoxotungstate) were irradiated for 120 minutes at 22 ± 1°C. Excitation wavelengths: 300<λ<370 nm. Light intensity: 15 mW × cm^{-2}. The error calculated on the basis of the obtained concentration data is ±5%. – [b] μmol of oxidised cyclohexene/μmol of decatungstate. – [c] Total peroxides are determined with the iodometric method; however, considering that cyclohexene exhibits a higher reactivity than acetonitrile and on the basis of literature data,[14c] we can approximate that the allylic hydroperoxide is the main component. – [d] Initial concentration of Fe(TDCPP)Cl: 2 × 10^{-5} mol × dm^{-3}. – [e] 180 minutes after light interruption. – [f] The reported values are corrected for the thermal decomposition of hydroperoxide inside the chromatographic column (see Experimental section). – [g] The photocatalyst has been used for four consecutive cycles, leading to similar values within the experimental error.



[4]

the formation of these products occurs mainly according to Equations 5–9 which involve the decatungstate both in its excited state and in its photoreduced form.



The possibility that the allylic hydroperoxide undergoes a secondary disproportionation or reactions with the cycloalkene without the involvement of the photoexcited decatungstate can be excluded since the total turnover number and the product distribution did not show any appreciable change when irradiation is interrupted. This statement is in agreement with the conclusion of a previous paper concerning the oxidation of cyclohexene by hydroperoxides in the presence of polyoxoanions.[17] Another possible reaction leading to the formation of allylic oxidation products is the well-known direct photochemistry of hydroperoxides.[18] However this possibility can be ruled out by taking into account the fact that the chosen amount of decatungstate avoids any possible light absorption by the hydroperoxide. Finally, we have to consider that some possible autooxidation reactions may give the observed traces of cyclohexene epoxide. Thus, the hydroxy ether reported in the last column of Table 1 can originate from the opening of the epoxide ring as a consequence of a nucleophilic attack by cyclohex-2-en-1-ol, favoured by the presence of protons. Despite a significant reduction in the turnover values, the use of the heterogeneous photocatalyst **2** does not cause any significant change in the nature and distribution of the oxidation products of cyclohexene.

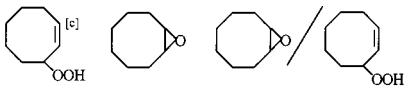
The absence of any EPR signals during irradiation of **1** or **2** in the presence of cyclooctene is in agreement with the low tendency of this cycloalkene to release allylic hydrogen atoms and, therefore, to form hydroperoxides according to Equation 4. On the other hand, even small amount of hydroperoxides are sufficient to initiate radical chain processes under aerobic conditions leading to the autooxidation of cyclooctene. This process is well-known to occur via addition of ROO· or RO· radicals to the double bond and is largely responsible for cyclooctene epoxide formation.[5]

In line with the above accepted mechanism, Table 2 shows that irradiation of **1** or **2** in a CH_3CN/cyclooctene mixture (6:1) saturated with O_2 leads to the formation of allylic hydroperoxide and cyclooctene epoxide, although with turnover values significantly lower than those obtained during the photooxidation of cyclohexene. It is worth not-

ing that, contrary to what was observed with cyclohexene, heterogenisation of the decatungstate on the solid support affects the chemoselectivity of the photocatalytic process by increasing the epoxide/hydroperoxide concentration ratio.

tive moiety of both the integrated systems **1/**Fe(TDCPP)Cl and **2/**Fe(TDCPP)Cl. The presence of Fe(TDCPP)Cl induces the following main effects on the photocatalytic properties of **1** in the oxidation of cyclohexene (Table 1): (i)

Table 2. Photocatalytic properties[a] of $(n\mathrm{Bu_4N})_4W_{10}O_{32}$ **1** and $(n\mathrm{Bu_4N})_4W_{10}O_{32}/SiO_2$ **2** in CH_3CN/cyclooctene (6:1), in the presence of 760 Torr of O_2, with and without Fe(TDCPP)Cl

Photocatalyst	Turnover [b] 		
1 + hν	5.8	1.9	0.3
1/Fe(TDCPP)Cl + hν [d]	3	4.9	1.6
1/Fe(TDCPP)Cl + hν + dark [e]	1	8.1	8.1
2 + hν [f]	1	2.3	2.3
2/Fe(TDCPP)Cl + hν [d, f]	0.1	4.0	40
2/Fe(TDCPP)Cl + hν + dark [e]	<0.03	4.2	>140

[a] 3 ml of CH_3CN/cyclooctene (6:1) containing **1** (2×10^{-4} mol·dm^{-3}, 0.6 μmol of irradiated polyoxotungstate) or (**2**) (20 g·dm^{-3}, 1.93 μmol of irradiated polyoxotungstate) were irradiated for 120 minutes at 22 ± 1°C. Excitation wavelengths: 300<λ<370 nm. Light intensity: 15 mW × cm^{-2}. Reported values are ±5%. – [b] μmoles of formed product/μmoles of irradiated decatungstate. – [c] Because of the lower reactivity of cyclooctene, we were forced to verify the amount of peroxide, deriving from CH_3CN, formed during irradiation. We observed that it was negligible with respect to that obtained from cyclooctene. – [d] Initial concentration of Fe(TDCPP)Cl: 2×10^{-5} mol × dm^{-3}. – [e] 180 minutes after light interruption. – [f] The photocatalyst has been used for four consecutive cycles, leading to similar values within the experimental error.

A confirmation that the overall oxidation process is initiated by a hydrogen abstraction process from the cycloalkene comes from some additional experiments in which the decatungstate was irradiated in the presence of styrene which, under our photocatalytic conditions, is not oxidised at all.

Since we observe that the oxidation of both cyclohexene and cyclooctene does not continue when irradiation is interrupted, we can conclude that the photoreduced decatungstate plays a key role in the oxidation mechanism. In particular, it could participate in the formation of RO· and ROO· according to Equations 5–7.

As a final note on the use of the heterogeneous photocatalyst **2**, we should point out that it presents the important characteristic of not suffering irreversible modification, except a negligible release of the polyoxotungstate into solution (less than 2%). Moreover, it could be reused several times without any significant loss of photocatalytic activity. These features make **2** a very promising system in heterogeneous catalysis, where the advantages deriving from a higher ease of employment and recycling of the photocatalyst are often priority objectives.

Photocatalyzed Oxygenations with $(n\mathrm{Bu_4N})_4W_{10}O_{32}$ and $(n\mathrm{Bu_4N})_4W_{10}O_{32}/SiO_2$ in the Presence of Fe(TDCPP)Cl

Irradiation of **1** and **2** was also carried out in the presence of Fe(TDCPP)Cl (2×10^{-5} mol·dm^{-3}) as cocatalyst. Since the decatungstate absorbs more than 95% of the selected incident light, it can be considered the photochemically active moiety of both the integrated systems **1/**Fe(TDCPP)Cl and **2/**Fe(TDCPP)Cl. The presence of Fe(TDCPP)Cl induces the following main effects on the photocatalytic properties of **1** in the oxidation of cyclohexene (Table 1): (i) the efficiency in terms of total turnover increases; (ii) a lower amount of allylic hydroperoxide is obtained; (iii) the sum of the alcohol and the ketone represents 40% of the overall oxidised cycloalkene; (iv) the ketone to alcohol concentration ratio decreases (from 4.1 to 1.6). Table 1 also shows that the presence of the iron porphyrin has the additional effect of inducing a residual catalytic activity after irradiation is interrupted. This activity changes the product distribution by converting the allylic hydroperoxide mainly to cyclohex-2-en-1-ol, whose concentration increases to almost 100%.

Fe(TDCPP)Cl also affects the catalytic properties of **2** during irradiation as well as in the dark. In these cases, the effects are similar to those observed in the homogeneous phase, but appear less evident. This could be due to the fact that the iron porphyrin complex preferably remains in solution, thereby reducing its interactions with the supported photocatalyst and the reactive species photogenerated in the neighbours.

As far as the stability of the porphyrin complex is concerned, we do not observe any appreciable bleaching of its UV/Vis spectrum in the wavelength range from 350 to 700 nm thus indicating that it does not undergo any significant degradation during the irradiation. This fact represents an important improvement with respect to both the photocatalytic activity of the iron porphyrins alone[19] and the same composite system used in the photooxidation of cyclohexane.[6b]

The possibility that the photoreduced decatungstate can transfer one electron to the iron(III) porphyrin,[20] so creating a ferrous complex able to induce the reductive acti-

vation of O_2, can be ruled out, since the reoxidation of $W_{10}O_{32}^{5-}$ by O_2 is known to be the kinetically favoured process under aerobic conditions.[6b,6c] Therefore, we consider that the iron porphyrin in its oxidised form plays a dominant role in the overall oxidation mechanism. In particular, an iron-porphyrin-mediated decomposition of allylic hydroperoxides to give the corresponding alcohols according to Equations 10−13 can be proposed on the basis of intensive studies on halogenated iron porphyrins.[21] The great significance of this reaction pathway in the overall oxidation mechanism is demonstrated by the residual reactivity observed after irradiation. In fact, under these conditions, cyclohex-2-en-1-ol cannot undergo photoinduced oxidation by the decatungstate (Equation 8) and so has the possibility to reach concentrations higher than those of cyclohex-2-en-1-one.

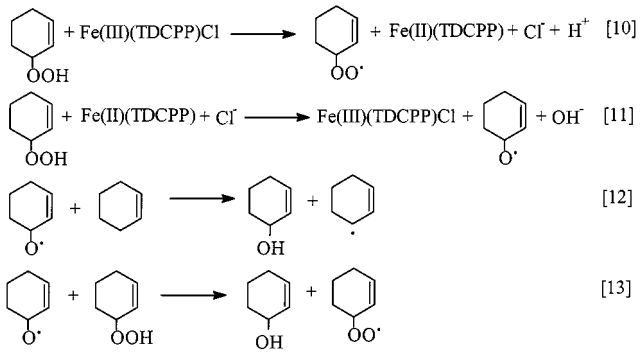


Table 2 shows that the iron porphyrin also affects the chemoselectivity of the oxidation of cyclooctene, significantly increasing the epoxide/hydroperoxide concentration ratio. Its main effect is likely to be that it favours the decomposition of the allylic hydroperoxide to give ROO· and RO· radicals following reactions similar to those shown in Equations 10 and 11 for cyclohexene. In agreement with previous evidence, these species are able to epoxidize cyclooctene by addition to the double bond.[5]

On the basis of the bleaching of the iron porphyrin during the photoinduced cyclooctene oxidation we conclude that about 300 equivalents of allylic hydroperoxide and cyclooctene epoxide were formed per equivalent of consumed iron porphyrin.

Conclusion

Photoexcitation of $(n\text{Bu}_4\text{N})_4\text{W}_{10}\text{O}_{32}$ is a suitable means of performing the catalytic oxidation of cycloalkenes by O_2 at room temperature and pressure. This process can be carried out in homogeneous solution as well as by using the decatungstate in a dispersed form after its heterogenisation on silica. Cyclohexene and cyclooctene are mainly oxidized to allylic hydroperoxides as a consequence of allylic hydrogen abstraction both in homogeneous solution and in the heterogeneous system. In the case of cyclooctene, the heterogenization of the decatungstate on the solid support affects the epoxide/hydroperoxide concentration ratio. The EPR spin trapping investigation has revealed for the first time the formation of cyclohexenyl radicals during the photocatalytic process.

The Fe(TDCPP)Cl complex can increase the efficiency of the photocatalytic process and affects its chemoselectivity. In particular, the iron porphyrin can catalyse the decomposition of allylic hydroperoxides giving, exclusively, the allylic alcohol from cyclohexene. On the contrary, this process induces the formation of epoxide from cyclooctene.

The possibility of obtaining allylic hydroperoxides in the presence of metalloporphyrins with molecular oxygen and light as reagents can open new perspectives for the development of new, clean processes of interest in oxidative syntheses.

Experimental Section

General: IR: Nicolet 510P FTIR instrument in KBr, fitted with a Spectra-Tech collector diffuse reflectance accessory (range from 4000 to 200 cm^{-1}). − EPR: X-band Bruker 220 SE, calibrated with α-α′-diphenylpicrylhydrazyl. − UV/Vis: Kontron Uvikon 940. − GC: Dani 8521, equipped with a FID detector and a packed column (Carbowax, 20 M, 5% on Chromosorb W-AW). − Irradiation: medium-pressure Hanau Q-400 mercury lamp.

Compound **1** and Fe(TDCPP)Cl were synthesised following literature procedures.[22] CH_3CN was a commercial spectroscopic grade solvent (Carlo Erba), used as received. Cycloalkenes were purchased from Fluka and employed after distillation. Phenyl *tert*-butyl nitrone was purchased from Aldrich and employed without any further purification.

Procedures: Heterogenisation of **1** on silica, leading to **2**,[4] was performed by dissolving 0.1 g of the decatungstate in CH_3CN and adding 1 g of colloidal silica (0.012 μm, Strem Chemicals). Subsequently, the suspension was continuously shaken at room temperature for two hours. The excess CH_3CN was evaporated at 80°C, and the sample was then dried at 100°C for 24 hours. UV/Vis spectra indicated that after this treatment the powder photocatalysts were stable and did not release the decatungstate in CH_3CN. IR spectra of the solid sample **2** have shown the characteristic bands for tetraalkylammonium cations [$\tilde{\nu}$ = 2963 and 2875 cm^{-1} (-CH_3 and -CH_2), 1481 (C−H of CH_3, C−H of CH_2), 1383 (C−H of CH_3)] and for $W_{10}O_{32}^{4-}$ [$\tilde{\nu}$ = 958, 890, 802 cm^{-1}].[23]

EPR spin-trapping experiments were carried out by irradiating (λ > 320 nm), directly in the EPR cavity, an aerated solution of **1** (1×10^{-3} mol·dm^{-3}) in CH_3CN and cycloalkene (6:1) containing phenyl *tert*-butyl nitrone (5×10^{-3} mol·dm^{-3}). A flat quartz cell was used as the reaction vessel. Signals of significant intensity were not observed in the absence of the polyoxoanion, or cycloalkene or light. Analogous experiments were carried out with **2** (20 g·dm^{-3}) dispersed in the same mixed solvent.

Continuous irradiations were performed with a Hg medium pressure lamp, selecting a wavelength range from 300 to 370 nm with a chemical-optical filter made from a Corning glass filter and a cuvette with a path length of 1 cm containing a $NiSO_4$ solution (0.8 g·cm^{-3}). The amounts of irradiated photocatalysts have been chosen in order to have the maximum absorption of incident light in any case. A 3 mL solution of **1** (2×10^{-4} mol·dm^{-3}, 0.6 μmol of decatungstate) in CH_3CN and cycloalkene (6:1) mixed solvent was irradiated for 120 minutes under an O_2 pressure of 760 Torr at 22 ± 1°C. The same procedure has been followed for **2** (20 g·dm^{-3}, 1.93 μmol of decatungstate). Catalyst **2** was kept in suspension by

magnetic stirring. The UV/Vis spectrum of the CH_3CN/cycloalkene mixture after the photocatalytic experiment with **2** indicated that between 1% or 2% of decatungstate had been lost from the silica-supported catalyst. When needed, Fe(TDCPP)Cl (2×10^{-5} mol·dm^{-3}) was added before irradiation.

The reaction products were determined by GC analysis comparing their retention times with those of authentic samples, and with iodobenzene as internal standard. No oxidation products were observed when blank experiments were run in the dark.

The determination of hydroperoxides was performed by a spectrophotometric standard method reported in the literature.[24] The concentrations of the allylic oxidation products obtained from cyclohexene could not be determined by GC analysis of the irradiated sample because the allylic hydroperoxide is thermally unstable and is expected to decompose inside the chromatographic column to give a mixture of cyclohex-2en-1ol and cyclohex-2-en-1-one.[14c] On the other hand, it was possible to perform the GC analysis of the ketone in the irradiated sample, after a complete reduction of the allylic hydroperoxide to the corresponding alcohol by an excess of iodide; control experiments showed that the ketone is not reduced to the corresponding alcohol by iodide. The difference between the alcohol concentration obtained in this last experiment and that of the allylic hydroperoxide obtained by the spectrophotometric method represents the amount of alcohol formed during the photocatalytic experiment. On this basis, we could also calculate the amounts of alcohol and ketone formed inside the chromatographic column: the allylic hydroperoxide was decomposed by 45% to give a mixture of the corresponding alcohol and ketone in the concentration ratio 1:2.

Acknowledgments

We thank Dr. Battioni and Dr. Mansuy of the Laboratoire de Chimie et Biochimie Pharmacologique and Toxicologique, URA 400 CNRS, Université Paris V, for their work in the synthesis of the iron porphyrin complex used in this study. Financial support from the MURST (Ministero della Università e della Ricerca Scientifica e Tecnologica) and the CNR (Consiglio Nazionale delle Ricerche, project 95/95−5%) is gratefully acknowledged.

[1] [1a] A. Bielanski, J. Haber, in *Oxygen in Catalysis*, Marcel Dekker, **1991**. − [1b] A. Kroty, J. P. Kingsley, *Chemtech.*, **1996**, 39−46.
[2] [2a] M. T. Pope, in *Heteropoly and Isopoly Oxometallates*, Springer Verlag, Berlin, Heidelberg, New York, Tokyo, **1993**. − [2b] C. L. Hill, C. M. Prosser-McCartha, in *Photosensitization and Photocatalysis using Inorganic and Organometallic Compounds*, Kluwer Academic Publishers, The Netherlands, **1993**. − [2c] R. Neumann, M. Dahan, *Nature,* **1997**, *388,* 353−355. − [2d] C. L. Hill, C. M. Prosser-McCartha, *Coord. Chem. Rev.,* **1995**,*143*, 407−455.
[3] [3a] N. Mizuno, M. Misono, *Chem. Rev.* **1998**, *98*, 199−217. − [3b] L. K. Kolkova, E. S. Rudakov, V. P. Tretyakov, *Kinet. Katal.*, **1996**, *37*, 540−546. − [3c] R. Neumann, H. Miller, *J. Chem. Soc., Chem. Commun*. **1995**, 2277−2278.
[4] A. Molinari, R. Amadelli, L. Andreotti, A. Maldotti, *J. Chem. Soc., Dalton Trans.* **1999**, 1203−1204.
[5] D. E. Van Sickle, F. R. Mayo, R. M. Arluck, *J. Am. Chem. Soc.* **1965**, *87*, 4824−4832.
[6] [6a] A. Maldotti, R. Amadelli, V. Carassiti, A. Molinari *Inorg. Chim. Acta*, **1997**, *256*, 309−312. − [6b] A. Maldotti, A. Molinari, P. Bergamini, R.Amadelli, P. Battioni, D. Mansuy, *J. Mol. Catal*. **1996**, *113*, 147−157. − [6c] A. Molinari, A. Maldotti, R. Amadelli, A. Sgobino, V. Carassiti, *Inorg. Chim. Acta*, **1998**, *272*, 197−203.
[7] [7a] T. J. McMurry, J. T. Groves in *Cytochrome P-450, Structure, Mechanism and Biochemistry*, P. R. Ortiz de Montellano ed., Plenum Press, New York and London **1986**. − [7b] B. Meunier *Chem. Rev.* **1992**, *92*, 1411−1456.
[8] [8a] P. S. Traylor, D. Dolphin, T. G. Traylor *J. Chem. Soc., Chem. Commun*. **1984**, 279−280. − [8b] T. G. Traylor, S. Tsuchiya *Inorg. Chem*. **1987**, *26*, 1338−1339.
[9] C. Bartocci, A. Maldotti, G. Varani, P. Battioni, V. Carassiti, D. Mansuy, *Inorg. Chem*. **1991**, *30*, 1255- 1259.
[10] G. R. Buettner, *Free Radical Biology & Medicine* **1987**, *3*, 259−303.
[11] A. Maldotti, R. Amadelli, G. Varani, S. Tollari, F. Porta *Inorg. Chem.*, **1994**, *33*, 2968−2973.
[12] E. Niki, S. Yokoi, J. Tsuchiya, Y. Kamiya, *J. Am. Chem. Soc.* **1983**, *105*, 1498−1503.
[13] T. Yamase, T. Usami, *J. Chem. Soc., Dalton Trans.* **1988**, 183−190.
[14] [14a] R. F. Renneke, M. Pasquali, C. L. Hill, *J. Am. Chem. Soc.* **1990**, *112*, 6585−6594. − [14b] D. C. Duncan, T. L. Netzel, C. L. Hill, *Inorg. Chem.* **1995**, *34*, 4640- 4646. − [14c] L. P. Ermolenko, C. Giannotti, *J. Chem. Soc., Perkin Trans.* **1996**, 1205−1210.
[15] [15a] A. Hiskia, E. Papaconstantinou *Inorg. Chem.* **1992**, *31*, 163−167. − [15b] D. C. Duncan, C. L. Hill *J. Am. Chem. Soc.* **1997**, *119*, 243−244. − [15c] C. Tanielan, K. Duffy, A. Jones *J. Phys. Chem. B* **1997**, 101, 4276−4282.
[16] R. C. Chambers, C. L. Hill, *Inorg. Chem.* **1989**, *28*, 2509−2511.
[17] R. Neumann, M. Dahan, *J. Chem. Soc., Chem. Commun.* **1995**, 171−172.
[18] J. G. Calvert, J. N. Pitts in *Photochemistry* J. Wiley and Sons, Inc., **1966**, chapter 5, pp. 447−450.
[19] [19a] A. Maldotti, C. Bartocci, G. Varani, A. Molinari, P. Battioni, D. Mansuy, *Inorg. Chem.* **1996**, *35*, 1126−1131. − [19b] A. Maldotti, A. Molinari, L. Andreotti, M. Fogagnolo, R. Amadelli, *Chem. Commun.* **1998**, 507−508. − [19c] A. Maldotti, L. Andreotti, A. Molinari, V. Carassiti, *J. Biol. Inorg. Chem.* **1999**, *4*, 154−161.
[20] [20a] T. Yamase, N. Takabayashi, M. Kaji, *J. Chem. Soc., Dalton Trans.* **1984**, 793−799. − [20b] K. M. Kadish, *Prog. Inorg. Chem.* **1986**, *34*, 435−605.
[21] M. W. Grinstaff, M. G. Hill, J. A. Labinger, H. B. Gray, *Science* **1994**, *264*, 1311−1313.
[22] [22a] M. Filowitz, R. K. C. Ho, W. G. Klemperer, W. Shun, *Inorg. Chem.* **1979**, *18*, 93−103. − [22b] P. Battioni, J. P. Renaud, J. F. Bartoli, J. F. Reina-Artiles, M. Fort, D. Mansuy, *J. Am. Chem. Soc.* **1988**, *110*, 8462−8470.
[23] A. Chemseddine, C. Sanchez, J. Livage, J. P. Launay, M. Fournier, *Inorg. Chem.* **1984**, *23,* 2609−2613.
[24] R. D. Mair, A. J. Graupner, *Anal. Chem.* **1964**, *36*, 194−204.
Received May 14, 1999
[I99171]

Structural Studies of MCM-48 Derivatized with (1,1′-Ferrocenediyl)dimethylsilane

Paula Ferreira,[a] Isabel S. Gonçalves,[a] Fred Mosselmans,[b] Martyn Pillinger,[a] João Rocha,*[a] and Alan Thursfield[a]

Keywords: Mesoporous materials / MCM-48 / Immobilization / (1,1′-Ferrocenediyl)dimethylsilane / ^{13}C and ^{29}Si solid-state NMR / Sandwich-complexes

The walls of the cubic mesoporous silicate MCM-48 have been grafted with ferrocenyl end groups by a ring-opening reaction of the *ansa*-bridged ferrocene [Fe{(η-C_5H_4)$_2$SiMe_2}], carried out in a pentane solution at room temperature. The orange product has been characterized by elemental analysis, powder X-ray diffraction, ^{13}C and ^{29}Si solid-state NMR, N_2 adsorption measurements, and Fe K-edge EXAFS. A high loading has been obtained (8.18 mass % Fe) and, as a result of the inclusion of the organometallic moiety, the N_2 adsorption isotherm exhibits a lower uptake. Direct structural evidence for the surface attachment of both single ferrocenyl and short chain oligo(ferrocenyl) fragments has been obtained.

Introduction

Interest in the inclusion chemistry of mesoporous oxides has accelerated since the report in 1992 by researchers at the Mobil Corporation of the discovery of a new generation of liquid crystal surfactant templated aluminosilicates,[1] distinguished by having highly ordered structures with high surface areas (1000 $m^2\ g^{-1}$), high pore volumes (1 $cm^3\ g^{-1}$), and very narrow pore-size distributions, tuneable in the range 20−100 Å. The so-called M41S family includes the thermally stable hexagonal MCM-41 and cubic MCM-48 phases. Their unique properties have stimulated research in areas that include sorption and phase transitions in confined spaces, ion exchange, the formation of intrachannel metal, metal oxide, and semiconductor clusters, and inclusion of metal complexes and other guests.[2] Like the commonly used silica and alumina supports, the inner surfaces of these mesoporous hosts contain pendant Si−OH groups (silanols) that enable covalent anchoring of functional groups to the channel walls. Potential applications include heterogeneous catalysis and photocatalysis involving bulky grafted catalysts and/or the conversion of large substrates, separation, removal of heavy metals, and chromatography. Our objective is the immobilization of relevant complexes on the surfaces of these mesoporous supports.

Much of the published work to date has been centred on MCM-41 as the mesoporous host. In contrast, little has been reported regarding MCM-48 which has a very different lattice. The pore system in MCM-41 is simple and consists of a hexagonal arrangement of parallel one-dimensional channels. MCM-48 possesses a complex pore architecture consisting of two mutually intertwined but unconnected three-dimensional nets. It is assumed that the silica interface resembles a minimal surface of the gyroid type.[3] Recently, O′Brien et al. showed that the walls of MCM-41 may be functionalized with ferrocenyl end groups by a ring-opening reaction with the strained metallocenophane [Fe{(η-C_5H_4)$_2$SiMe_2}].[4] We have followed up this work and now wish to report structural studies on MCM-48 functionalized with (1,1′-ferrocenediyl)dimethylsilane. The results are compared with MCM-41. All materials have been fully characterized by elemental analysis, powder X-ray diffraction, N_2 adsorption, magic-angle spinning (MAS) NMR (^{13}C, ^{29}Si) and Fe K-edge EXAFS spectroscopies.

Results and Discussion

Synthesis and Spectroscopic Characterization

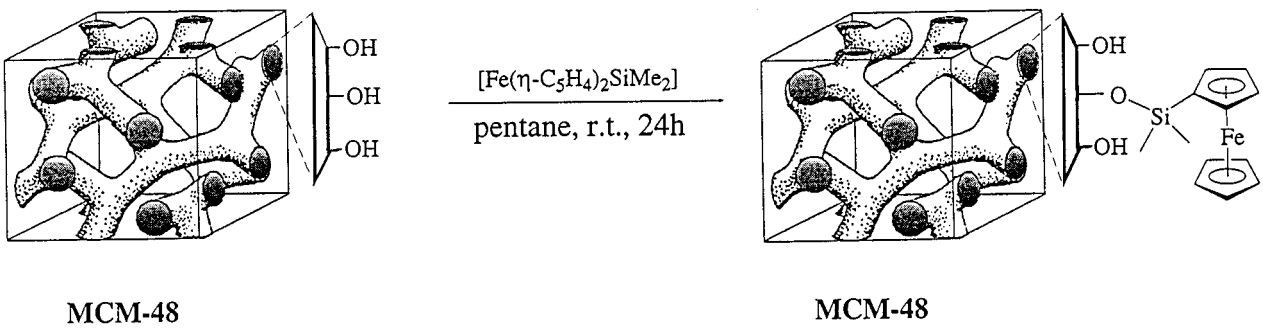
The synthesis and some reaction chemistry of (1,1′-ferrocenediyl)dimethylsilane and other derivatives have been reported, and it was found that [1]ferrocenophanes are susceptible to nucleophilic attack by ROH.[5] This ring-opening reaction is responsible for the persistent attachment of the [Fe{(η-C_5H_4)$_2$SiMe_2}] unit to surfaces. Like silica and alumina supports, MCM-48 should be capable of surface reactions via terminal silanol groups.

Mixing of a suspension of MCM-48 with excess of the organometallic (1,1-ferrocenediyl)dimethylsilane in pentane at room temperature for 24 hours gives an orange solid MCM-48/[Fe{(η-C_5H_4)$_2$SiMe_2}] (**1**, Scheme 1). The air-stable powder was washed with pentane to remove a small portion of converted ferrocene and some unchanged [Fe{(η-C_5H_4)$_2$SiMe_2}].

Elemental analysis indicated that a high loading of [Fe{(η-C_5H_4)$_2$SiMe_2}] in the material had been achieved (8.18% mass Fe). The powder X-ray diffraction pattern of

[a] Department of Chemistry, University of Aveiro, 3810-193 Aveiro, Portugal
Fax: (internat.) + 351-34/370-084
E-mail: ROCHA@DQ.UA.PT
[b] CLRC Daresbury Laboratory, Warrington, Cheshire, WA4 4AD, UK

 © WILEY-VCH Verlag GmbH, D-69451 Weinheim, 2000 1434−1948/00/0101−0097 $ 17.50+.50/0



Scheme 1. Functionalization of MEM-48 with $[Fe(\eta\text{-}C_5H_4)_2SiMe_2]$

parent MCM-48 (Figure 1) can be indexed on a cubic unit cell (using the strongest reflection, d_{211}, a = 88.616 Å). The pattern of functionalized MCM-48 is consistent with retention of the cubic mesoporous structure. The strongest peak shifts slightly (a = 86.559 Å). In addition, the observed slight decrease in peak intensities does not necessarily reflect a decrease in the order of the structure but could instead be due to a decrease in the scattering contrast between the silica framework and the pores as a result of inclusion of the ferrocenyl groups.[6]

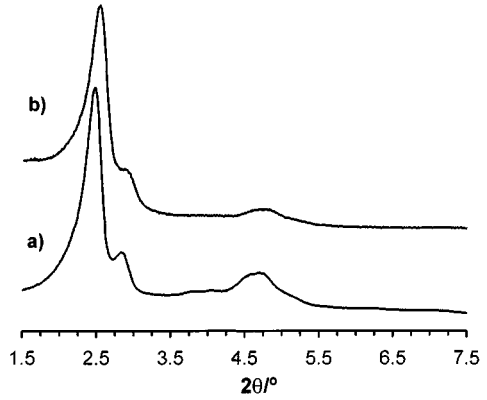


Figure 1. Powder X-ray diffraction patterns of a) as-synthesized and b) functionalized MCM-48

Solid-State NMR Studies

The ^{29}Si-CP MAS NMR spectrum of functionalized MCM-48 (Figure 2) exhibits two broad overlapping peaks $\delta = -108.8$ and -101.5, assigned to the Q_4 and Q_3 units of the silica framework, respectively. A small amount of Q_2 environments (faint peak at $\delta = -91.2$) is also present [$Q_n = Si(OSi)_n(OH)_{4-n}$]. Both the ^{29}Si CP MAS and MAS NMR spectra clearly show that upon functionalization the intensity of the Q_3 (and Q_2) peak decreases considerably. This result is consistent with the observed large decrease in the intensity of the IR absorption-band associated with OH groups on the silica surface [ν(OH) = 3742 cm^{-1}].[7] Functionalized MCM-48 also displays two strong resonances at high-frequency. The peak at δ = 6.5 may be assigned to Si−O−**Si**Me_2Fc environments (Fc = ferrocenyl group),[4] and the signal at $\delta = -6.4$ has been previously assigned to the bridging silicon atoms in small oligomeric units of poly(ferrocenylsilane), the first unit of which is bound to the channel wall.[8] A third faint peak is seen at $\delta = -2.3$. At present, we are unable to assign this resonance.

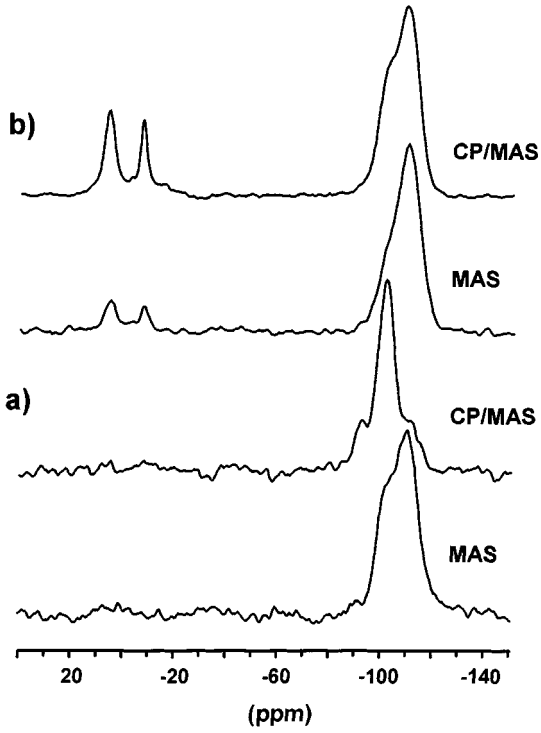


Figure 2. ^{29}Si-CP MAS and MAS NMR spectra of a) as-synthesized and b) functionalized MCM-48

The solid-state ^{13}C-CP MAS NMR spectrum of MCM-48/[Fe{(η-$C_5H_4)_2SiMe_2$}] (**1**) is shown in Figure 3. The spectrum exhibits three resonances at δ = 72.3, 68.6 and 0.1, attributed to C_5H_4Si, C_5H_5, and $SiMe_2$, respectively. The unusually high-field resonance at δ = 33.5, for the cyclopentadienyl carbon attached to silicon in the [Fe{(η-$C_5H_4)_2SiMe_2$}], shifted to a more conventional value δ = 72.3 in the spectrum of the material **1**.

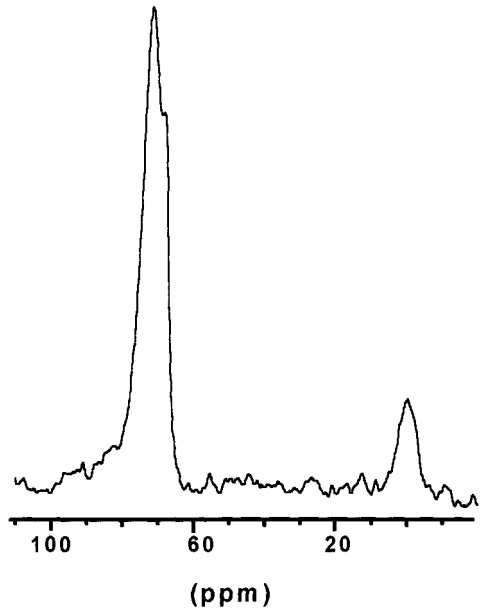


Figure 3. ^{13}C CP MAS spectrum of functionalized MCM-48

N_2 Adsorption Studies

The calcined MCM-48 sample gave a type IV N_2 adsorption isotherm (Figure 4) as designated in the IUPAC classification,[9] which is typical of a mesoporous solid and is comparable to that reported by other workers for cubic mesoporous MCM-48.[10] A well-defined step, and sharp inflection between relative pressure $P/P_o = 0.3$ and 0.4 corresponds to capillary condensation and suggests a rather narrow pore size distribution. The calcined MCM-41 sample also gave a type IV N_2 adsorption isotherm.

BET surface areas were calculated with the average area occupied by a N_2 molecule in the monolayer taken as 16.2 Å^2. Values of 770 m^2 g^{-1} and 970 m^2 g^{-1} were obtained for MCM-48 and MCM-41, respectively. The N_2 adsorption isotherms of the functionalized MCMs are quite different from those of the parent materials, demonstrating a lower uptake. Diffusion of N_2 through the pore system of the functionalized MCM-41 material was found to be extremely slow, hence the isotherm presented is produced from nonequilibrium points, but it serves to indicate the greatly reduced uptake. These results indicate that the free pore volume of the materials has been reduced as a result of immobilization of ferrocenyl fragments on the internal surface of the mesoporous hosts. In support of this conclusion, the BET surface areas decreased to 500 m^2 g^{-1} for MCM-48 and 270 m^2 g^{-1} for MCM-41, although of course the latter value is based on nonequilibrium data but again serves as a general indicator.

EXAFS Studies

The Fe K-edge EXAFS of MCM-41 and MCM-48 derivatized with [Fe{(η-C_5H_4)$_2$SiMe_2}] were analysed by beginning with a model of ferrocene for the Fe centre, and therefore selecting a single shell of ten carbon atoms (fit A). Refinement gave very similar theoretical fits to both EXAFS spectra and very similar structural parameters with an average Fe−C bond length of 2.06−2.07 Å and a Debye-Waller factor of 0.011−0.012 Å^2 (Table 1).

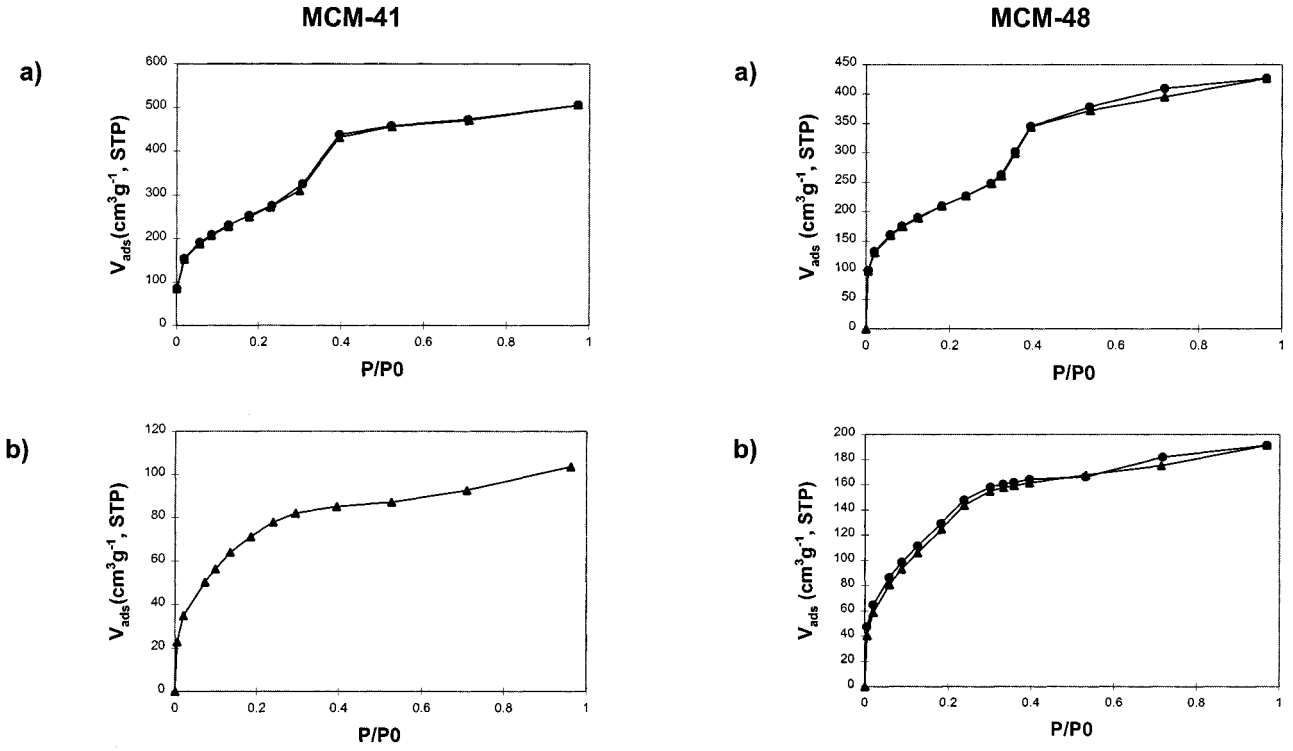


Figure 4. N_2 adsorption isotherms of a) as-synthesized and b) functionalized MCM materials

Table 1. The Fe K-edge EXAFS-derived structural parameters for [Fe{(η-$C_5H_4)_2SiMe_2$}], MCM-41/[Fe{(η-$C_5H_4)_2SiMe_2$}] and MCM-48/[Fe{(η-$C_5H_4)_2SiMe_2$}]

	fit	T[a]	N[b]	r[c]/Å	$2\sigma^2$[d]/Å^2	$E°$/eV	R (%)[e]
[Fe{(η-$C_5H_4)_2SiMe_2$}]	A	C	10	2.019(7)	0.0242(20)	−1.2	52.7
	B	C	4.3(3)	2.053(3)	0.0069(12)	−9.1	27.6
MCM-41/[Fe{(η-$C_5H_4)_2SiMe_2$}]	A	C	10	2.064(3)	0.0115(9)	−8.7	31.3
	B	C	8.5(7)	2.068(3)	0.0089(8)	−9.7	30.1
MCM-48 /[Fe{(η-$C_5H_4)_2SiMe_2$}]	A	C	10	2.070(4)	0.0109(9)	−9.7	29.0
	B	C	8.5(7)	2.075(3)	0.0084(8)	−10.9	26.9

[a] T = Atom type. − [b] N = Coordination number. Note that the errors in EXAFS-derived coordination numbers for well-defined shells are generally accepted to be of the order 20%. − [c] r = interatomic distance (standard deviations in parentheses). The systematic errors in bond lengths arising from data collection and analysis procedures are ± 0.02−0.03 Å for well-defined coordination shells. − [d] Debye−Waller factor; σ = root-mean-square deviation of interatomic distance about r. − [e] R factor = $(\Sigma|\chi^{calc} - \chi^{exp}| k^3 dk / \Sigma|\chi^{exp}| k^3 dk) \times 100\%$.

These results are comparable to those reported by O'Brien et al. for MCM-41 modified with the same complex (10 carbons at 2.045 Å, $2\sigma^2$ = 0.007 Å^2).[4] The coordination number for this shell was subsequently refined, and in both cases the best fits were obtained with a value of about 8.5 (fit B, Figure 5). It may be concluded therefore that the structural integrity of the ferrocenyl units has remained intact in the functionalid MCMs, given that errors in EXAFS-derived coordination numbers for well defined shells are generally accepted to be of the order of 20%. Additional shells in the model for nonbonded silicon or carbon atoms were not reliable as either the resulting structural parameters were poorly defined (high statistical errors) or the decrease in the fit index was not statistically significant.

In the fit to the Fe K-edge EXAFS of (1,1-ferrocenediyl)-dimethylsilane (fit A, 10 carbon atoms), the refined Fe−C bond length was slightly shorter (2.02 Å) and the Debye−Waller factor was significantly higher (0.024 Å^2) than the corresponding values obtained for the derivatized MCMs (Table 1). Overall the fit was much poorer (R-factor 52.7%). The high Debye−Waller factor is indicative of high thermal and/or static disorder in the Fe−C bond. In this *ansa*-bridged ferrocene, the cyclopentadienyl rings are tilted with respect to one another by an angle of 20.8°, the compound is appreciably strained and there is significant departure from planarity at the *ipso* carbon atom.[12] These factors are responsible for the compounds reactivity to ring-opening polymerizations. The iron lies closer to the *ipso* carbon and the two carbons adjacent to it than the two opposite it. The resulting wide and nonsymmetric distribution in Fe−C bond lengths (1.99−2.07 Å) explains the high EXAFS-derived Debye−Waller factor and the inadequate fit to the EXAFS. Attempts to fit more than one shell for bonded carbon atoms were unsuccessful. In contrast the shell of ten carbon atoms in fit A for the MCM-supported materials was well-defined and this is good evidence that the ring strain in the organometallic guest molecule has been released, i.e., that a ring-opening reaction has occurred and the cyclopentadienyl ligands are parallel, resulting in a narrower and more symmetric distribution in Fe−C bond lengths.

An attempt was made to improve the model for [Fe{(η-$C_5H_4)_2SiMe_2$}] by including a shell for nonbonded silicon, expected at 2.69 Å. This resulted in a modest improvement in the fit and a reasonable value for the distance but the statistical errors for the structural parameters of this shell

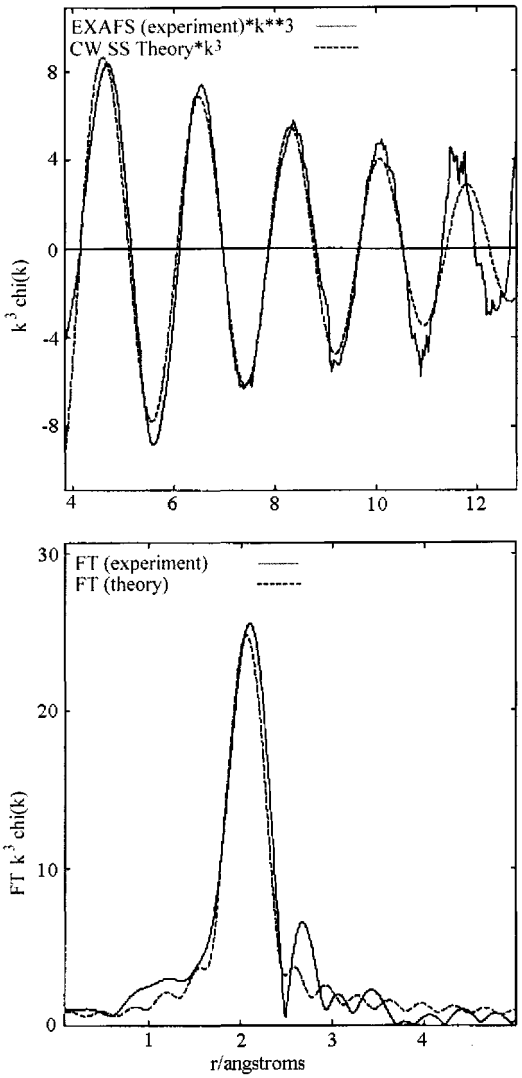


Figure 5. Fe K-edge k^3-weighted EXAFS spectrum and Fourier transform, phase-shift corrected for carbon (—— experimental; ------- curved wave theory, fit B in Table 1) of functionalized MCM-48 at 298 K.

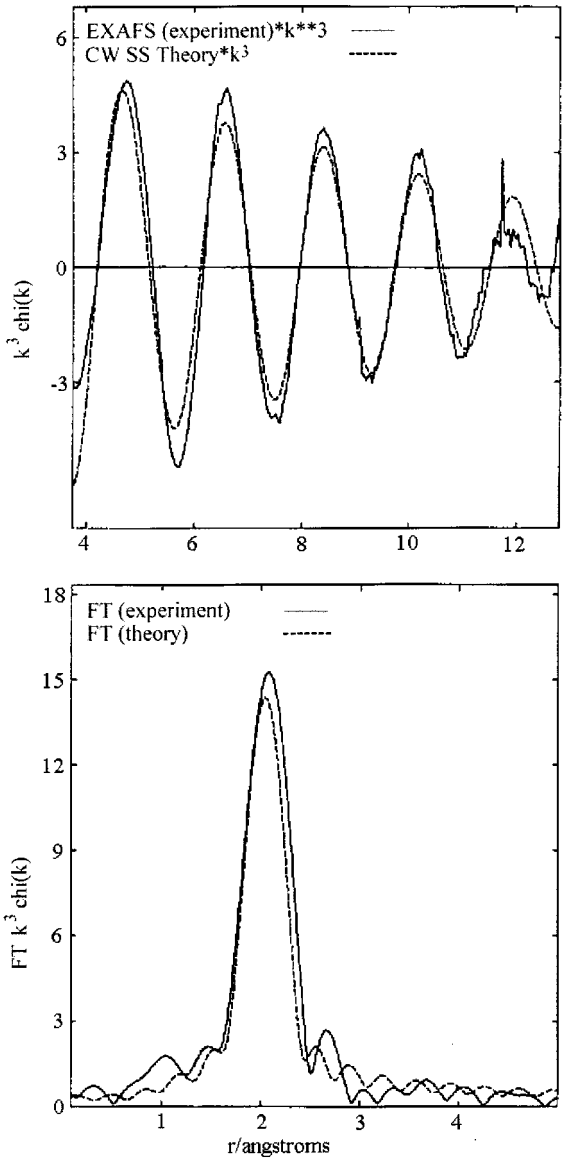


Figure 6. Fe K-edge k^3-weighted EXAFS spectrum and Fourier transform, phase-shift corrected for carbon (—— experimental; ------- curved wave theory, fit B in Table 1), of [Fe{(η-$C_5H_4)_2SiMe_2$}] at 298 K

were very large: R factor 45.5%, $E°$ −1.8 eV, r(Fe−C) 2.023(5) Å, 2 σ^2 0.0236(17) Å^2, r(Fe···Si) 2.736(33) Å, 2 σ^2 0.0176(83) Å^2. A better fit to the experimental data was obtained by starting from fit A and refining the coordination number (fit B, Table 1, Figure 6). The final value was 4.3 but the error in this value must be much higher than 20% for the reasons outlined above.

Conclusion

The pore walls of mesoporous siliceous MCM-48 have been successfully derivatized with (1,1′-ferrocenediyl) dimethylsilane. The organometallic complexes react with the MCM-48 surface silanols (particularly of the Q^3 type) to give a $C_5H_4SiMe_2$−O linkage to the silica surface. Despite the fact that MCM-48 and MCM-41 possess very different mesoporous surfaces, this process strongly resembles the process previously reported for the functionalization of the latter by strained ferrocenophanes.

Experimental Section

General: All preparations and manipulations were performed using standard Schlenk techniques under an oxygen-free and water-free argon atmosphere. Pentane was dried by reflux over Na/benzophenone ketyl, distilled under argon, and kept over 4-Å molecular sieves. − Powder X-ray diffraction (XRD) data were collected on a Philips Xpert diffractometer using Cu-K_α radiation filtered by Ni. − Microanalyses were performed at the TU Munich. − Infrared spectra were recorded on a Unican Mattson Mod 7000 FTIR spectrophotometer using KBr pellets and/or solutions. − ^{29}Si- and ^{13}C-NMR spectra were recorded at 79.49 and 100.62 MHz, respectively, on a (9.4 T) Bruker MSL 400P spectrometer. ^{29}Si-MAS NMR spectra were recorded with 40° pulses, spinning rates of 5.0−5.5 kHz, and 60 s recycle delays. ^{29}Si-CP MAS NMR spectra were recorded with 5.5 μs pulses, a spinning rate of 5.0 kHz and 5 s recycle delays. Chemical shifts are quoted in parts per million relative to TMS. ^{13}C-CP MAS NMR spectra were recorded with 4.5 μs pulses, a spinning rate of 8 kHz, and a 4 s recycle delay. Chemical shifts are quoted in ppm relative to TMS. − Nitrogen adsorption isotherms were recorded using a CI electronics MK2-M5 microbalance connected to a vacuum manifold line. The as-made MCM samples (typically around 0.02 g) were dehydrated overnight at 723 K to an ultimate pressure of 10^{-4} mbar, and then cooled to room temperature prior to adsorption. Extra care with the functionalized materials was necessary and so the samples were dehydrated at 423 K to prevent the destruction of the functionalities. Nitrogen isotherms were then recorded at 77 K. Equilibration of each data point was monitored using CI electronics Labweigh software, and the pressure monitored using an Edwards Barocel pressure sensor. Specific surface areas, A_{BET}, were determined from the linear part of the BET equation (P/P_o = 0.05−0.3). − Fe K-edge X-ray absorption spectra were collected at room temperature in transmission mode on station 9.2 [double crystal Si(220) order-sorting monochromator, 50% harmonic rejection] of the Synchrotron Radiation Source at the Daresbury Laboratory, operating at 2 GeV in single bunch mode, with typical currents of 13−19 mA. Solid samples, diluted if necessary with boron nitride, were held between layers of mylar film in 0.5 mm thick aluminium plates. Two spectra were recorded for each sample and summed using the program EXCALIB, available on the Daresbury computer XRSSERV1. The program EXBACK was used to extract the raw EXAFS, $\chi^E(k)$, and curve-fitting analyses, by least-squares refinement of the non-Fourier filtered k^3-weighted EXAFS data, were carried out within EXCURVE (version EXCURV98[13]) using spherical wave methods.[14] Phase shifts were calculated using Von Bart ground state and H. Lundqvis exchange potentials.

[Fe{(η-$C_5H_4)_2SiMe_2$}] was prepared by the method reported by Wrighton[15] and purified by sublimation under vacuum.

MCM-41 was synthesized according to the literature employing [($C_{14}H_{29}$)NMe_3]Br as a templating agent.[16] After calcination (540 °C/6 h) and dehydration (200 °C under a vacuum 10^{-4} Torr for 8 h) the material was characterized by XRD, N_2 adsorption and IR spectroscopy.

MCM-41/[Fe{(η-$C_5H_4)_2SiMe_2$}] was prepared as described in the literature.[4] Elemental analysis indicated 8.33 mass-% Fe. − IR

(KBr, $\tilde{\nu}$, cm^{-1}): 3574 vs, 3096 m, 2963 m, 1645 s, 1365 m, 1234 vs, 1169 vs, 901m, 816 s, 798 s, 667 m. – (^1H, ^{13}C, ^{29}Si) NMR data are in agreement with ref.[4]

MCM-48 was synthesized according to the literature employing $[(C_{16}H_{33})NMe_3]Cl$ as a templating agent.[17,10b] After calcination (540°C/6 h) and dehydration (220°C under a vacuum 10^{-4} Torr for 6 h) the material was characterized by XRD, N_2 adsorption and IR spectroscopy.

Preparation of MCM-48/[Fe{(η-$C_5H_4)_2SiMe_2$}]: A suspension of MCM-48 (0.5 g) in pentane (15 mL) was treated with a solution of [Fe{$C_5H_4)_2SiMe_2$}] (0.35 g) in pentane. After 24 h at room temperature, the resulting suspension was filtered off and the remaining orange solid was washed several times with pentane, and dried under an oil-pump vacuum. The pentane washings contained trace amounts of the starting material [Fe{(η-$C_5H_4)_2SiMe_2$}] and ferrocene, identified by solution ^1H-NMR spectroscopy. – Elemental analysis indicated 8.18 mass-% Fe. – IR (KBr, $\tilde{\nu}$ cm^{-1}): 3454 vs, 3103 m, 2960 m, 1637 s, 1423 m, 1234 vs, 1169 vs, 1081 vs, 968 m, 900m, 822 s, 798 s, 667 m, 453 s.

Acknowledgments

We thank PRAXIS XXI and FEDER for partial funding. P. Ferreira (BD) thanks PRAXIS XXI for a grant. I.S.G. wants to thank the CRUP (Acções Integradas Programme) for generous support.

[1] J. S. Beck, J. C. Vartuli, W. J. Roth, M. E. Leonowicz, C. T. Kresge, K. D. Schmitt, C. T.-W. Chu, D. H. Olson, E. W. Sheppard, S. B. McCullen, J. B. Higgins, J. L. Schlenker, *J. Am. Chem. Soc.* **1992**, *114*, 10834.
[2] [2a] K. Moller, T. Bein, *Chem. Mater.* **1998**, *10*, 2950. – [2b] T. Maschmeyer, *Curr. Opin. Solid State Mater. Sci.* **1998**, *3*, 71.
[3] V. Alfredsson and M. Anderson, *Chem. Mater.* **1996**, *8*, 1141.
[4] [4a] S. O'Brien, J. Tudor, S. Barlow, M. J. Drewitt, S. J. Heyes, D. O'Hare, *Chem. Commun.* **1997**, 641. – [4b] S. O'Brien, J. M. Keates, S. Barlow, M. J. Drewitt, B. R. Payne, D. O'Hare, *Chem. Mater.* **1998**, *10*, 4088.
[5] I. Manners, *Adv. Organomet. Chem.* **1995**, *37*, 131.
[6] B. Marler, U. Oberhagemann, S. Vortmann, H. Gies, *Microporous Mater.* **1996**, *6*, 375.
[7] X. S. Zhao, G. Q. Lu, A. K. Whittaker, G. J. Millar, H. Y. Zhu, *J. Phys. Chem. B.* **1997**, *101*, 6525.
[8] D. A. Foucher, R. Ziembinski, B.-Z. Tang, P. M. Macdonald, J. Massey, C. R. Jaeger, G. J. Vansco, I. Manners, *Macromolecules* **1993**, *26*, 2878.
[9] K. S. W. Sing, D. H. Everett, R. A. W. Houl, L. Moscou, R. A. Pierotti, J. Rouquerol, T. Siemieniewska, *Pure Appl. Chem.* **1985**, *57*, 603
[10] [10a] A. A. Romero, M. D. Alba, W. Zhou, J. Klinowski, *J. Phys. Chem. B.* **1997**, *101*, 5294. – [10b] J. Xu, Z. Luan, H. He, W. Zhou, L. Kevan, *Chem. Mater.* **1998**, *10*, 3690.
[11] R. Schmidt, M. Stöcker, E. Hansen, D. Akporiaye, O. H. Ellestad, *Microporous Mater.* **1995**, *3*, 443.
[12] W. Finckh, B.-Z. Tang, D. A. Foucher, D. B. Zamble, R. Ziembinski, A. Lough, I. Manners, *Organometallics* **1993**, *12*, 823.
[13] N. Binsted, (**1998**) EXCURV98: CCLRC Daresbury Laboratory computer program.
[14] S. J. Gurman, N. Binsted, I. Ross, *J. Phys. Chem.* **1984**, *17*, 143.
[15] A. B. Fischer, J. B. Kinney, R. H. Staley, M. S. Wrighton, *J. Am. Chem. Soc.* **1979**, *101,* 6501.
[16] C. T. Kresge, M. E. Leonowicz, W. J. Roth, J. C. Vartuli, J. S. Beck, *Nature* **1992**, *359*, 710.
[17] A. Monnier, F. Schüth, Q. Huo, D. Kumar, D. Margolese, R. S. Maxwell, G. D. Stucky, M. Krishnamurty, P. Petroff, A. Firouz, M. Janicke, B. F. Chmelka, *Science* **1993**, *261*, 1299.

Received June 2, 1999
[I99200]

Calculated Properties and Ring-Chain Rearrangements of Triphosphirane (P_3H_3)

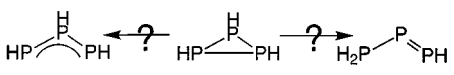
Minh Tho Nguyen,*[a] Alk Dransfeld,[a] Luc Landuyt,[a] Luc G. Vanquickenborne,[a] and Paul v. R. Schleyer[b]

Keywords: Ab initio calculations / Ionization potentials / Phosphorus / Heterocycles / Small ring systems

Ab initio quantum chemical calculations have been used to explore the P_3H_3 potential energy surface focussing on the ring-chain rearrangements of the three-membered ring in $(PH)_3$ (**1**), the parent triphosphirane. Relative energies between stationary points were estimated using the QCISD(T)/6–311G(d,p) method based on MP2/6–31G(d,p) geometries and corrected for zero-point contributions. Ring strain, proton affinities, ionization and excitation energies and heats of formation have been evaluated using larger basis sets, e.g. 6–311++G(3df,2p). The cyclic *trans*-triphosphirane (**1a**) is the most stable P_3H_3 isomer and lies about 40 kJ/mol below the open-chain phosphanyldiphosphene (H_2P–P=PH). The decrease of ring strain in three-membered rings when CH_2 is replaced by PH is confirmed. Triphosphirane **1a** is a virtually strain-free ring and even gains some stabilization relative to three separate P–P single bonds. The reduced ring strain also helps diminish the phosphorus inversion barrier to 224 kJ/mol compared to the monocyclic isomers of $(CH_2)(PH)_2$ and $(CH_2)_2(PH)$. Compound **1a** follows a pure ring-opening or a 1,2-hydrogen shift rather than a combined motion pathway, in fundamental contrast with corresponding processes of diphosphirane and phosphirane. This is due to the existence of an open-chain P_3H_3 phosphorane intermediate stabilized by allylic conjugation. The pericyclic ring-opening of **1a** is the most favored process but the energy barrier in the gas phase is about 180 kJ/mol high. Electron density is largely delocalized within the three-membered P_3 ring not only in the C_{3v}-symmetric **1b** (all-*cis*) but also in **1a** (C_s). The proton affinity of **1a** is similar to that of PH_3. The proton affinities decrease with n in *cyclo*-$(CH_3)_{3-n}(PH)_n$ and their values were obtained: PA(**1a**) = 777 ±10, PA(diphosphirane) = 799 ±10 and PA(phosphirane) = 802 ±10 kJ/mol. Heats of formation are evaluated as follows ($\Delta H°_{f0}$ at 0 K in kJ/mol): **1a**, 70 ±10; *cyclo*-$(PH)_2(PH_2)^+$ (protonated **1a**), 821 ±10; diphosphirane, 85 ±10; *cyclo*-$(CH_2)(PH)(PH_2)^+$ (protonated diphosphirane), 814 ±10; phosphirane, 86 ±10; and protonated phosphirane, 812 ±10 kJ/mol. All P rings remain cyclic following ionization to the radical cations. Adiabatic ionization energies (IE_a) are estimated as: **1a** and diphosphirane, 9.3 ±0.3 eV and phosphirane 9.5 ±0.3 eV. The first UV absorption band shifts toward the longer wavelength region on going from phosphirane to **1a**. The GIAO/B3LYP computed magnetic shieldings for **1a** and related molecules reveal a clear relationship between the narrow bond angles in the rings and their unusually strong magnetic shielding. The similarity of the predicted ^{31}P-NMR signals in **1a** and its heteroanalog diphosphirane, $(CH_2)(PH)_2$, can be rationalized in terms of a compensation of the carbon-substituent effect (downfield shift) and the bond-bending effect imposed by the ring (upfield shift).

Introduction

Phosphorus, in a similar way to carbon, is able to form stable open-chain and cyclic compounds with homonuclear bonds.[1] While the five-membered nitrogen ring (pentazole) could only be postulated as an intermediate at −50 °C,[2][3] the corresponding phosphorus ring in pentaphosphaphosphol was identified[4] at room temperature. An impressive number of polyphosphorus compounds have thus been prepared by different groups.[5−11] A simple example illustrates the close similarity between the chemistries of phosphorus and carbon: The experimentally known monocyclic P_5^- ion[4] is analogous to the cyclopentadienyl anion.[12] In general, the existence of polyphosphorus compounds as rings or chains depends on the number of P atoms involved. The simplest polyphosphane, which may have a ring and a chain isomer, was detected in 1972.[13] While many substituent-stabilized three-membered phosphorus homocycles (called triphosphiranes or cyclotriphosphanes) have been synthesized since,[11,13,14] the corresponding open-chain isomers are rare. The triphosphorus hydride, P_3H_3, has been positively identified by mass-spectrometric techniques,[13] but no information on its molecular structure is available. The ^{31}P-NMR-chemical shifts of three-membered rings comprising tricoordinate phosphorus cannot be described with substituent increments.[15][16] The question arises as to whether there are relationships between the NMR-chemical



Scheme 1. Alternative ring-chain rearrangments of triphosphirane

[a] Department of Chemistry, University of Leuven, Celestijnenlaan 200F, B-3001 Leuven, Belgium
Fax: (internat.) + 32-16/327992
E-mail: minh.nguyen@chem.kuleuven.ac.be
[b] Institute of Organic Chemistry, University of Erlangen-Nürnberg, Henkestraße 42, D-91054 Erlangen

 © WILEY-VCH Verlag GmbH, D-69451 Weinheim, 2000 1434−1948/00/0101−0103 $ 17.50+.50/0

shifts and geometric or electronic parameters in the parent three-membered compounds with 1−3 endocyclic phosphorus atoms and the related acyclic molecules. The tendency of phosphorus to accommodate cyclic structures easily is well established;[17] the competition between ring and chain often turns in favor of the former. However, the rare observation of open-chain P_3R_3 compounds raises the question about their thermodynamic and kinetic stabilities.

Previous theoretical studies[18−23] on the P_3H_3 model system were mainly confined to the electronic structure, ring strain and inversion barriers of the cyclic triphosphirane. The ring-chain conversion of the simplest parent triphosphirane, *cyclo*-$(PH)_3$, has not been investigated before. As part of our theoretical study on the structure and reactivity of P-containing three-membered rings,[24−27] we examine here the P_3H_3 potential energy surface by means of ab initio molecular orbital methods. In particular, the molecules with open-chain structures and their thermodynamic stability were investigated. The computed molecular properties of triphosphirane are discussed in the context of its organic heteroanalogs (diphosphirane and phosphirane).

Computational Details

Ab initio molecular orbital calculations were performed with the Gaussian 94 series of programs.[28] To facilitate comparison with our previous studies on phosphirane and diphosphirane,[24][26] we provide data derived with the same theoretical method. Higher-level computational results are included in the discussion. Each stationary point was characterized by harmonic vibrational analysis. Furthermore, the identity of each transition structure was determined by intrinsic reaction coordinate (IRC) calculations. Transition structures are designated by the **X/Y** notation where **X** and **Y** are the equilibrium structures connected by the TS. Geometrical parameters of the relevant equilibrium and TS were optimized using second-order Møller-Plesset perturbation theory, MP2/6-31G(d,p), which partly incorporates electron correlation. Based on these MP2/6-31G(d,p) geometries, the relative energies of the points on the (P_3H_3) energy surface have been estimated by single-point electronic energy computations using the quadratic configuration interaction method, QCISD(T), and the 6-311G(d,p) basis set. Improved estimates for thermochemical quantities were obtained by calculations with the larger 6-311++G(d,p) and 6-311++G(3df,2p) basis sets. The GIAO approach[29] was used to calculate magnetic shieldings at B3LYP/6-311G(d) //MP2/6-31G(d,p) level. Electron distributions (Mulliken) and the Wiberg bond indices, WBI,[30] were evaluated at the same level. For the open-shell systems, correlated wavefunctions were constructed using unrestricted Hartree-Fock (UHF) references. Throughout this paper, bond lengths are given in Ångstrøms, bond angles in degrees, magnetic shieldings in ppm, total energies in hartrees, zero-point vibrational and relative energies, unless otherwise noted, in kJ/mol.

Results and Discussion

Before examining the various chemical properties of triphosphirane and the related three-membered rings, the P_3H_3 potential energy surface will be first presented in order to establish the thermochemical and kinetic stabilities of the possible isomers.

The P_3H_3 Potential Energy Surface

Selected optimized structural parameters of the relevant stationary points considered at the MP2/6−31G(d,p) level of accuracy are given in Figures 1 and 2. The calculated total and zero-point vibrational energies are recorded in Table 1 while the relative energies are summarized in Table 2. The potential energy profiles are illustrated schematically in Figures 3 and 4. In general, the same energy ordering between the P_3H_3 structures considered was found at all levels employed. The discussion in this section is based on QCISD(T)/6−311G(d,p) //MP2/6−31G(d,p) + scaled ZPE/HF/6−31G(d,p) //HF/6−31G(d,p) energies. Triphosphirane can exist in the *trans* (**1a**) and the *cis* (**1b**) form. The endocyclic P−P distances (2.210 to 2.225 Å, Figure 1) are slightly longer than in diphosphane (2.209 Å, H_2P-PH_2). As expected, **1a** is more stable than **1b** [E_{rel}(*cis*) = 17 kJ/mol]. In **1b** the P atom environments remain strongly pyramidal; the phosphorus inversion barrier of **1a** is 217 kJ/mol via the TS **1a/1a**. This is far larger than the inversion barrier in PH_3, which is only 148 kJ/mol at the same level of theory (a more accurate estimate is discussed below). As seen in Table 2, **1a** is the P_3H_3 global minimum lying well below the open-chain isomers **2**, **3** and **4**. The cyclic form **5**, with a formal P=P double bond and a tetracoordinate P atom, is a high energy isomer that lies 137 kJ/mol above **1a**. Of the three different types of open-chain species, phosphanyldiphosphenes **2** are the more stable, followed by phosphoranes **4** and then phosphanylphosphinidenes **3**. Each of these species exhibits several conformations and configurations; here we present only the most stable and representative structures. The symmetrical conformer **2b** (C_s) of phosphanyldiphosphene is marginally more stable, by 1 kJ/mol, than **2a** (C_1), which is 42 kJ/mol less stable than **1a**. The preference of the phosphanyl group for a symmetrical configuration is similar to that in analogous phosphapropenes[31] where an interaction between the P lone pair and π electrons is weak.[32] Among the phosphoranes with allyl conjugation of the π system on the phosphorus backbone structure, **4a** is most stable [E_{rel} (**4b**) = 9 kJ/mol relative to **4a**]. Nevertheless, **4a** is 115 and 73 kJ/mol less stable than **1a** and **2a**, respectively. Stabilization by allylic conjugation is more pronounced (P−P = 2.06 Å) in **4a** than in the corresponding acyclic $P(PH)_2^-$ anion[11] (P−P = 2.09 Å). In contrast to the formal Lewis description of the central phosphorus atom in these molecules as pentavalent, the sum of Wiberg bond indexes, ΣWBI, is only four (one single P−H and two allylic, 1.5 fold, bonds; ΣWBI is 3.8 for **4a**; in "CH_2=PH=PH" ΣWBI is 3.9). Therefore, σ^3,λ^4-P is the

best characterization[8] of the allyl-type phosphorus valence.

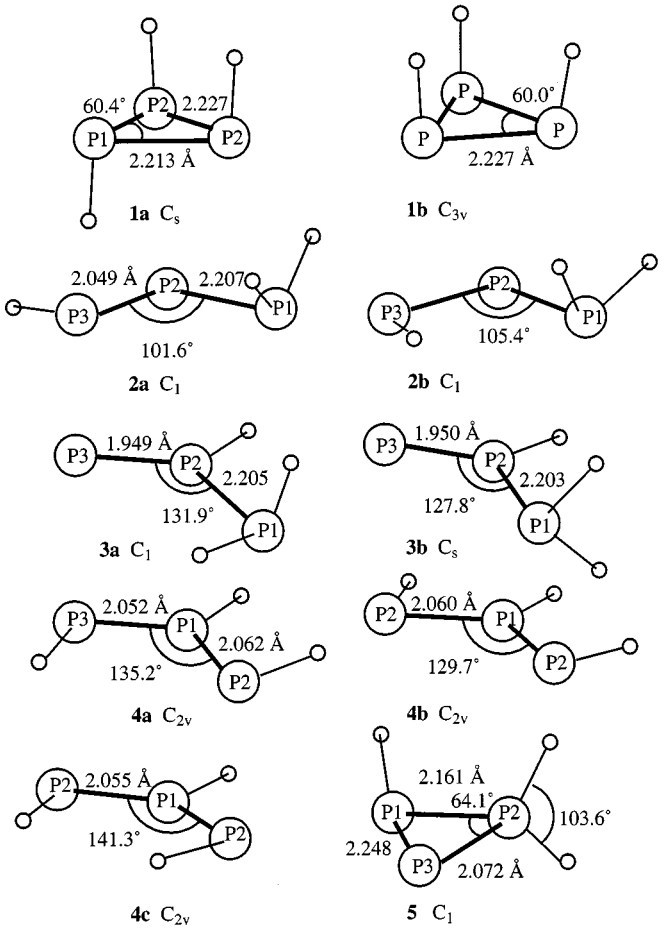


Figure 1. Minimum structures of P_3H_3 optimized at RMP2(fc) /6−31G(d,p)

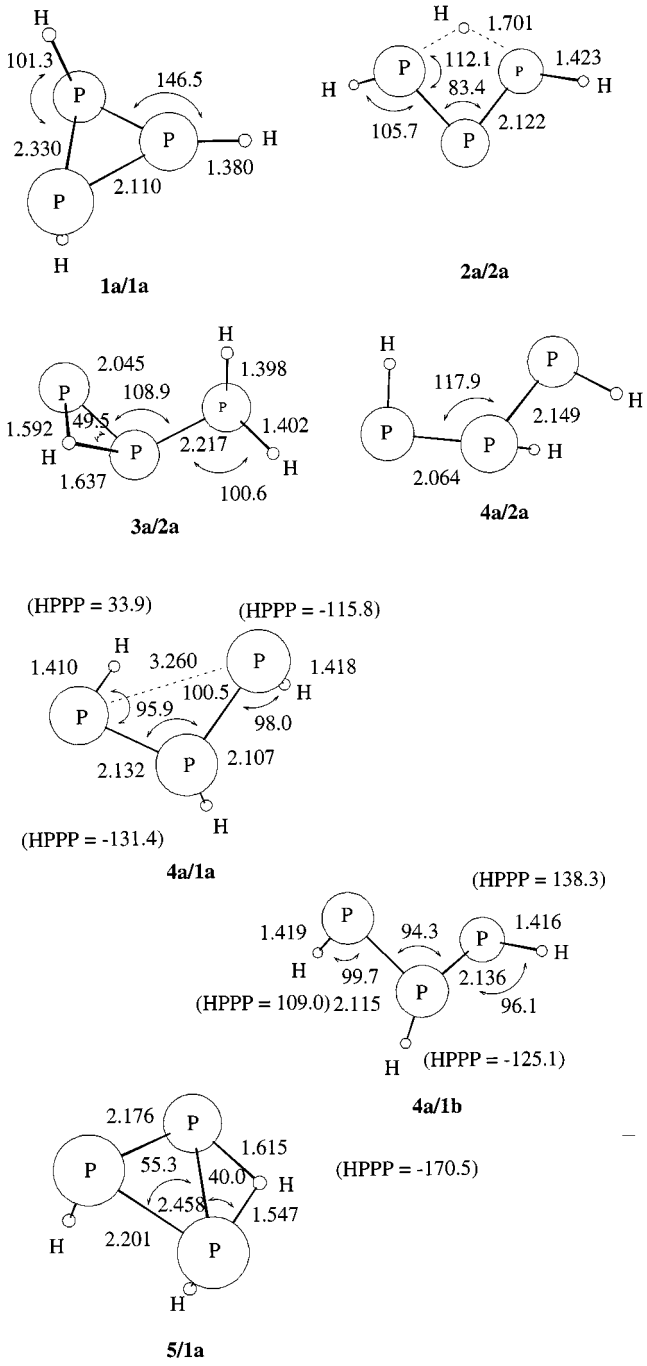


Figure 2. Transition structures of P_3H_3 optimized at RMP2(fc) /6−31G(d,p)

The singlet phosphanylphosphinidenes **3** represent the least stable open-chain isomers. As in $P-PH_2$, i.e. the unsubstituted case,[33−35] the central P atom has a planar configuration (**3b**; approximately planar in **3a**). The staggered conformer **3a** is slightly more stable than the C_s-symmetrical conformer **3b** with the phosphorus lone pair in the plane of the phosphinidine π bond. Conformer **3a** is 141 kJ/mol above **1a** and 99 kJ/mol above **2a**. Compared with the parent tautomers,[35] RHP=P/RP=PH with R=H, the phosphanyl group in **3a** ($R = PH_2$) has little effect on the relative energy of the tautomers. Accordingly, the P−P distances in **2**, as well as in **3**, remain almost unaffected upon replacing H in the parent by PH_2. It is well known that phosphinidenes usually have a triplet electronic ground state.[36][37] For the simplest phosphanylphosphinidene (H_2P-P), the triplet state with C_s symmetry was shown to lie about 28 kJ/mol below the corresponding closed-shell singlet state (see our previous study at the same level of accuracy).[35] In contrast, for **3a** calculations indicate that the triplet state is not clearly preferred (lowest-lying singlet is only 6.6 kJ/mol higher in energy than the triplet). While the π-donor effect of the PH_2 group is negligable for the P2−P3 bond in **2** and triplet **3**, it shifts electron density into the phosphinidine bond (P2−P3 is polarized towards δ^1-P in singlet **3**). As a result the energy of the singlet **3a** relative to the triplet is distinctly reduced.

Overall, successive replacement of the CH_2 in cyclopropane by PH tends to reinforce the thermodynamic stability of the cyclic isomer. In the all-phosphorus case considered here, the ring is by and large the most stable form. Whether it is also the kinetically most stable isomer will be examined in the following section.

Table 1. Total energies at different levels of MP2 and QCI theory,[a−c] of P_3H_3 structures and zero-point vibrational energies[d]

Structure[a]	MP2[b]	MP2[c]	QCISD[c]	QCISD(T)[c]	ZPE[d]
1a, C_s	−1024.26821	−1024.30886	−1024.35494	−1024.37143	77
1b, C_{3v}	−1024.26027	−1024.30136	−1024.34817	−1024.36465	76
1a/1a, C_2	−1024.18281	−1024.22414	−1024.26967	−1024.28685	72
2a, C_1	−1024.24884	−1024.28917	−1024.33633	−1024.35407	73
2b, C_s	−1024.24816	−1024.28879	−1024.33647	−1024.35413	72
2a/2a, C_2	−1024.19355	−1024.23750	−1024.27358	−1024.29682	64
3a, C_1	−1024.20946	−1024.25100	−1024.29843	−1024.31578	72
3b, C_s	−1024.20750	−1024.24946	−1024.29777	−1024.31475	72
3a/2a, C_1	−1024.17300	−1024.21460	−1024.26427	−1024.28124	65
4a, C_s	−1024.22371	−1024.26337	−1024.30515	−1024.32579	72
4b, C_s	−1024.22051	−1024.26010	−1024.30197	−1024.32253	72
4a/1a, C_1	−1024.18705	−1024.22751	−1024.27167	−1024.29618	69
4b/1b, C_1	−1024.18974	−1024.23020	−1024.27573	−1024.30001	69
4a/2a, C_1	−1024.17114	−1024.21451	−1024.25809	−1024.28250	65
5, C_1	−1024.21969	−1024.25872	−1024.30229	−1024.31939	77
5/1a, C_1	−1024.18216	−1024.22813	−1024.27379	−1024.29121	68

[a] Based on MP2/6−31G(d,p)-geometries. Core orbitals are frozen. Point groups of the geometries (see Figures 1 and 2) obtained without symmetry constraint. − [b] Using full sets of MOs for the 6−31G(d,p) basis set. − [c] Using the 6−311G(d,p) basis set. − [d] Zero point vibration energy, ZPE, in kJ/mol obtained at HF/6−31G(d,p) and scaled by 0.9 to account for systematic overestimation.

Table 2. Relative energies in kJ/mol of P_3H_3 structures[a] at different levels of theory[a−c]

Structure[a]	MP2[b]	MP2[c]	QCISD[c]	QCISD(T)[c]	CI+ZPE[d]
1a	0.0	0.0	0.0	0.0	0.0
1b	20.9	19.7	17.8	17.8	16.8
1a/1a	224.4	222.6	224.0	222.2	217.2
2a	50.9	51.7	48.9	45.6	41.6
2b	52.7	52.7	48.5	45.5	40.5
2a/2a	196.2	187.5	213.8	196.0	183.0
3a	154.4	152.0	148.5	146.2	141.2
3b	159.5	156.1	150.2	148.9	143.9
3a/2a	250.0	247.6	238.2	237.0	225.0
4a	116.9	119.5	130.8	119.9	114.9
4b	125.2	128.0	139.2	128.5	123.5
4a/1a	213.2	213.7	218.8	197.7	189.7
4b/1b	206.2	206.7	208.1	187.6	179.6
4a/2a	255.0	247.9	254.5	233.6	221.6
5	127.5	131.7	138.3	136.7	136.7
5/1a	226.1	212.1	213.2	210.8	201.8

[a] Transition structures, are designated by the **X/Y** notation where **X** and **Y** are the equilibrium structures connected by the TS (see Figures 1 and 2). −[b] Using the 6−31G(d,p) basis set. − [c] Using the 6−311G(d,p) basis set. − [d] QCISD(T)/6−311G(d,p) + ZPE/HF/6−31G(d,p).

Interconversions Between the P_3H_3 Isomers

As shown in Figures 3 and 4, **1a** can undergo a ring-opening simply by breaking an endocyclic P−P bond to give phosphorane **4**. This opening, via **4a/1a**, is not accompanied at all by a hydrogen shift from one P center to another. Despite extensive searches, a single-step pathway connecting **1a** either to diphosphene **2a** or to phosphinidene **3a** could not be located. The behavior of **1a** thus differs basically from that of its homologous phosphirane and diphosphirane.[24] The pure ring openings in the latter molecules require activation energies that are much larger than those for pathways where hydrogen transfer is involved. This is presumably due to the fact that the TS **4a/1a** profits from the allyl delocalization, which stabilizes triphosphorane **4a**. The ring opening of the *cis*-triphosphirane (**1b**) through **4b/1b** is an even more facile process. This implies that a *cis*-triphosphirane might be formed kinetically upon ring-closure of a triphosphorane like **4b**. A 1,2-shift of the hydrogen between two ring atoms via **5/1a** is also possible, without ring opening, to yield the cyclic compound **5**. The energy barrier for transformation of **1a** to **5** is somewhat larger than that for ring-opening but slightly smaller than that for inversion. The energy diagram in Figure 3 demonstrates the peculiar feature of **1a**, which prefers either a pure ring opening or a 1,2-shift but does not undergo combined motions.

Chain-chain rearrangements are summarized in Figure 4. The isomers **2**, **3** and **4** are related to each other by a single 1,2- or 1,3-hydrogen shift. Structure **2a/2a** is the TS for an antarafacial 1,3-hydrogen shift between the two terminal P atoms of the diphosphene **2a**. The energy barrier of 141 kJ/mol relative to **2a** is rather low for this type of process.[31] The corresponding barrier for 1,3-H shift in diphosphapropene ($H_2P-CH=PH \rightarrow HP=CH-PH_2$) has been calculated to be 163 kJ/mol at the same level of accuracy. Again the reduced ring strain in **2a/2a** facilitates this isomerization. Two observations are worth noting: (i) a TS for a suprafacial migration could not be located, in contrast to the situation in phosphapropenes,[31] and the high stability of **4** renders this migrating mode inoperative; (ii) experimental results have shown that 1,3-shifts in P compounds are thermally accessible unimolecular processes.[38] The rearrangement via **2a/2a** is therefore quite a realistic connection. Both 1,2-H shift TSs **4a/2a** and **3a/2a** have similar energies but lie above the TS **2a/2a** for 1,3-H shift and **4a/1a** for ring opening. Ring-closure of phosphorane **4a** is favored over isomerization to another acyclic isomer. The connection between **1a** and the most stable open-chain phosphanyldiphosphene, **2a**, takes place in two steps through the intermediate **4a**. The most energy-demanding step is the 1,2-H shift (**4a/2a**). While the reaction barriers in the triphosphorus system differ fundamentally from those con-

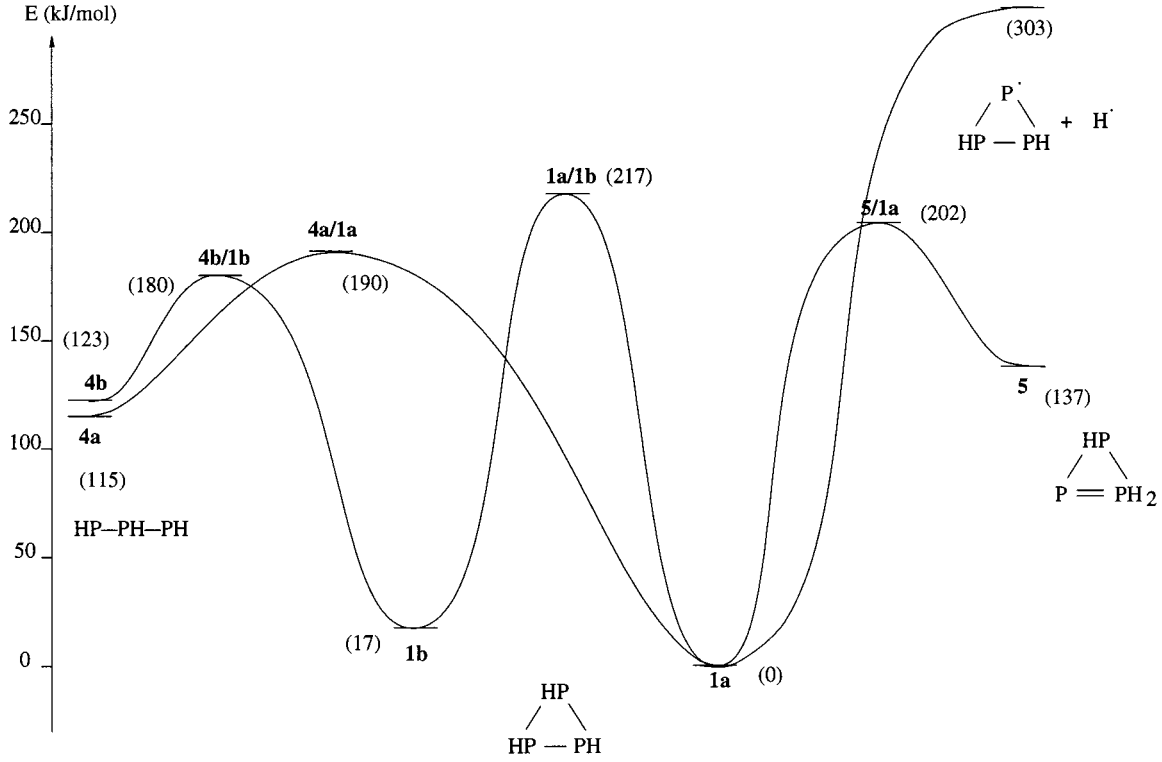


Figure 3. Relative energies calculated at QCISD(T) /6−311G(d,p) + ZPE/HF/6−31G(d,p) of TS and intermediate products of P_3H_3 ring isomerization in kJ/mol

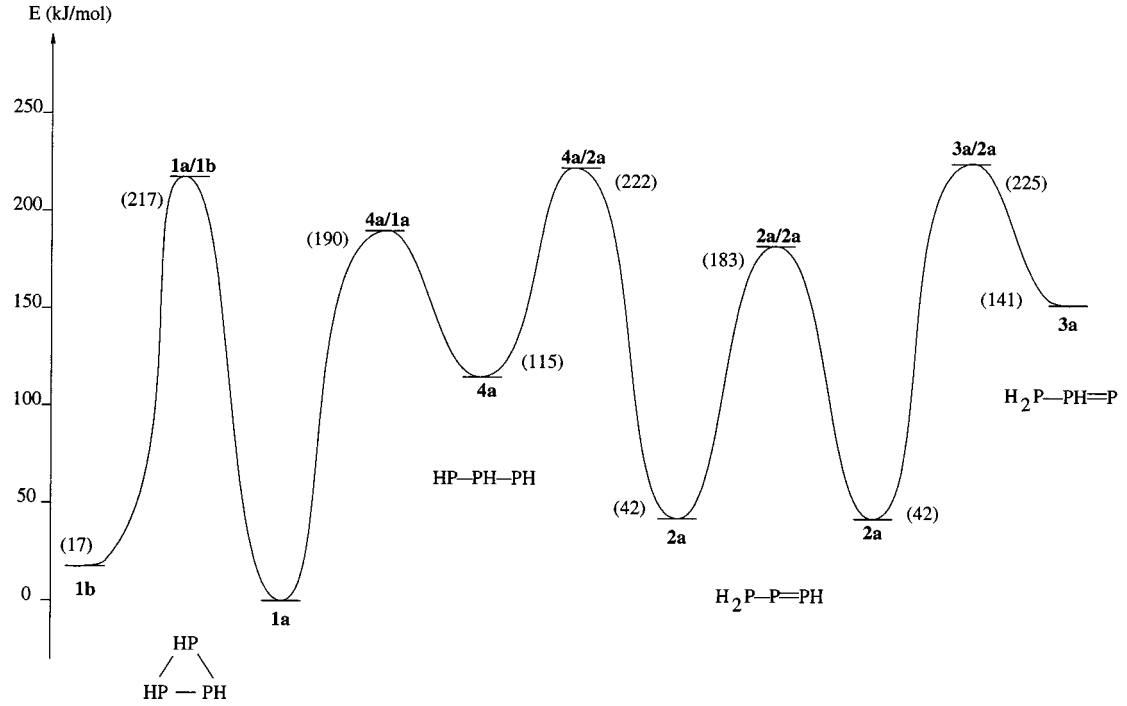


Figure 4. Relative energies calculated at QCISD(T) /6−311G(d,p) + ZPE/HF /6−31G(d,p) of TS and intermediate products of the rearrangements of acyclic P_3H_3 isomers in kJ/mol

taining only one P atom, physical properties differ only gradually.

Comparison of Triphosphirane Properties with Those of $(CH_2)_{3-n}(PH)_n$ with $n < 3$

Having established that the triphosphirane **1a** is the most stable form among P_3H_3 isomers, we now discuss some of its molecular properties and compare them with those of other three-membered rings built from PH and/or CH_2 groups (diphosphirane, phosphirane and cyclopropane).

Barrier of Inversion at Phosphorus

The inversion process at phosphorus in acyclic and cyclic molecules has been examined previously.[24,39,40] The semi-empirical finding that "the barrier in $(PH)_3$ is smaller than that in PH_3"[9][20] is a misleading artifact of the MNDO method. Our ab initio calculated inversion barriers, $\Delta_{inv}E$, are compiled in Table 3. The listed $\Delta_{inv}E$ values confirm that the phosphorus inversion barrier is about 100 kJ/mol larger in three-membered rings than in the corresponding acyclic molecules.[40] In the $(CH_2)_{3-n}(PH)_n$ series the barrier decreases with n (when σ^4-C is replaced by σ^3-P). How can this be explained? While "normal" (not T-shaped) TSs of σ^3-P have bond angles at phosphorus of around 120°, the three-membered ring only allows a Y-shaped TS with an endocyclic angle of around 60°. This bond-angle constraint rationalizes the pronounced destabilization of the $TS_{inv,P}$ in the rings relative to the related acyclic molecule [e.g. $(PH)_3$ vs. $HP(PH_2)_2$, cf. Table 3]. As the endocyclic bond angle at the inversion center increases (53° for phosphirane, 60° for diphosphirane, and 68° in the $TS_{inv,P}$ of **1a**) the phosphorus inversion barrier decreases.

Table 3. Inversion barriers at phosphorus in kJ/mol of σ^3-phosphorus in $(CH_2)_{3-n}(PH)_n$ rings (triphosphirane, $n = 3$; diphosphirane, $n = 2$; phosphirane, $n = 1$) and PH_3 calculated at different levels of theory[a]

Method[a]	$n = 1$	$n = 2$	$n = 3$	PH_3
MP2/6−31G(d,p)[a]	291	258	224	148
CISD/6−31G(d,p)	296	260	227	151
QCISD(T)/6−311G(d,p)[a]	280[c]	250	217	148
Experiment[b]				132

[a] Based on MP2(fc)/6−31G(d,p) geometries and corrected for zero-point energies. − [b] Estimated[51] experimental phosphorus inversion barrier. − [c] A. Göller and T. Clark (*Chem Commun.* **1997**, 1033) reported a value of 278 kJ/mol at CCSD(CT)/6-31+G(d)//MP2 /6-31+G(d) with C_s symmetry.

Ring Strain

The strain in a cyclic species arises from the enforced deformation of bond angles from their normal values in acyclic systems. To estimate the ring strain, different isodesmic reactions using reference molecules that are as strain-free as possible can be employed.[41][42] Here, simple bond separation reactions (Table 4) provide reasonable measures for ring strains. These values are somewhat sensitive to the computational methods. For cyclopropane, where experimental heats of formation are available, the calculated value using MP4SDTQ/6−311++G(3df,2p) + ZPE calculations compares quite well with the experimental data. From the results in Table 4, two important points can be concluded: (i) the ring strain decreases consistently on going from cyclopropane to triphosphirane; for each replacement of a CH_2 by a PH the ring strain is reduced by about 25 kJ/mol; (ii) for **1a**, variation of the calculated value with respect to the methods employed suggests that the isodesmic reaction considered might be slightly endothermic. The endothermicity obtained at MP4 is particularly interesting as lower level calculations[19,43,44] consistently predicted a small but significant exothermicity for reaction (1) (Table 4). In contrast to the conventional wisdom, corrections for zero-point vibration energies are found to be important: They change the energies of reactions (1) to (4) by up to 20 kJ/mol. The smaller ring strain in cyclophosphanes, relative to cyclopropane, is often interpreted as arising from two main factors; namely (i) the inherent ability of σ^3 phosphorus to form small rings owing to its sp^3 hybridization[9] and (ii) a larger concentration of its s electrons in the lone pair coupled with a greater use of its p electrons to form ring bonds.[19] In other words, formation of stronger ring-P bonds results in a partial compensation of the inherent destabilization due to bond angle deformation. Another question regards whether the endocyclic bond angle also has an effect on the ability of the lone pair of phosphorus to bind a proton.

Proton Affinities of Phosphorus

Table 5 lists the calculated proton affinities (PA) of related cyclic and acyclic phosphorus-containing molecules. A number of observations are worth mentioning: (i) Accurate calculations of PA with an absolute error of ±5 kJ/mol could only be achieved by using fairly large basis sets; for PH_3, the experimental value can be reproduced by calculations with the 6−311++G(3df,2p) basis set with either the MP4 or the QCISD(T) method. (ii) The relative trend in PAs can, however, be well established using lower level calculations; the difference in PAs between PH_3 and $PH(CH_3)_2$ is computed to be 112 ± 5 kJ/mol at the QCISD(T)/6−311G(d,p) + ZPE level whereas the experimental[45] difference is 113 kJ/mol. (iii) Comparison of calculated as well as experimental[45] PAs of PH_3, CH_3PHCH_3 and H_2PPHPH_2 shows that methyl substituents tend to increase the PA; the phosphanyl group also exerts a similar effect but to a lesser extent; while the PA is increased by 112 kJ/mol by two CH_3 groups (R = CH_3 in HPR_2), two PH_2 groups make it only 75 kJ/mol larger than in PH_3. (iv) In contrast, PAs in polyphosphaphosphiranes are quite close to each other; their PAs are around 800 kJ/mol, irres-

Table 4. Ring strain in kJ/mol of three-membered rings calculated from bond separation reactions[a]

	Reaction		CI[a,b]	CI[a,c]	MP4[a,d]	Exptl.[e]
cyclo-$(PH)_3$ (Triphosphirane)	+ 3 PH_3 → 3 H_2P-PH_2 (C_2)	(1)	−3.6	−0.5	6.2	
cyclo-$(CH_2)(PH)_2$ (Diphosphirane)	+ CH_4 + 2 PH_3 → 2 H_3C-PH_2 + H_2P-PH_2	(2)	−25.5	−24.7	−23.0	
cyclo-$(CH_2)_2(PH)$ (Phosphirane)	+ 2 CH_4 +3 PH_3 → 2 H_3C-PH_2 + H_3C-CH_3	(3)	−55.2	−54.5	−50.7	
cyclo-$(CH_2)_3$ (Cyclopropane)	+ 3 CH_4 → 3 H_3C-CH_3	(4)	−85.4	−83.1	−74.6	−75.7

[a] Based on MP2/6−31G(d,p) geometries and including ZPE correction. − [b] QCISD(T) /6−311G(d,p). − [c] QCISD(T) / 6−311++G(d,p). − [d] MP4SDTQ /6−311++G(3df,2p). − [e] Based on experimental heats of formation at 0 K (kJ/mol): cyclopropane, 70.9; CH_4, −66.8 and CH_3-CH_3, −68.4 from the literature.[50]

pective of the number of P atoms within the ring. (v) Comparing PA($H_3C-PH-CH_3$) with PA(phosphirane) on the one hand and PA($H_2P-PH-PH_2$) with PA(triphosphirane, **1a**)[46] on the other hand, clearly emphasizes that the strong effect of methyl and the weaker effect of the phosphanyl groups on PA is virtually offset in the cyclic structures. It is remarkable that the PA value of **1a** is very near to that of PH_3. The behavior of phosphirane toward protonation thus differs from that of aziridine, its nitrogen analog, which has a much larger PA (about 70 kJ/mol) than NH_3.[47][48] It is also worth noting that a stable phosphiranium cation has been isolated and characterized recently.[46][49]

Table 5. Calculated proton affinities of cyclic, $(CH_2)_n(PH)_{3-n}$, and acyclic, $H-(CH_2)_n(PH)_{3-n}-H$, molecules with $n < 4$

Compound	QCISD(T)[a,b]	MP4SDTQ[a,c]	Exptl[e]
Phosphirane	813	802	
Diphosphirane	811	799	
Triphosphirane	803	777	
PH_3	800	778[d]	782
$H_3C-PH-CH_3$	912		895
$H_2P-PH-PH_2$	875		

[a] Proton affinities based on MP2/6−31G(d,p)-optimized geometries (see Figure 5) and corrected for ZPE. − [b] Used basis set: 6−311G(d,p). − [c] Used basis set: 6−311++G(3df,2p). − [d] At QCISD(T)[a] /6−311++G(3df,2p) the PA is 777. − [e] Taken from ref.[38]

Heats of Formation

At the present time, accurate thermochemical data on phosphorus compounds are rather scarce. Heats of formation of small low-coordinated P species have been determined mainly by quantum-chemical calculations.[47] Therefore, it would be useful to evaluate this quantity for the three-membered rings and their protonated forms. Table 6 records our estimates for heats of formation at 0 K of neutral species, using heats of isodesmic reactions (1), (2) and (3) listed in Table 4 in conjunction with experimental[50] and theoretical values evaluated for the reference molecules. Heats of formation of the protonated species were determined from the data for neutral counterparts and proton affinities given in Table 5. At the level of theory considered, namely MP4SDTQ /6−311++G(3df,2p) + ZPE, absolute errors of about ±10 kJ/mol in heats of formation can be expected. We note that our estimate for phosphirane, $\Delta H°_{f0}$(phosphirane) = 86 ±10 kJ/mol, differs somewhat from the experimental value at 298 K (69 ± 2 kJ/mol; in the compilation of Lias et al.[50]).

Table 6. Heats of formation of polyphosphaphosphiranes, *cyclo*-$(CH_2)_n(PH)_{3-n}$ (with n = 1, 2, and 3), and their protonated forms ($\Delta H°_{f0}$ at 0 K in kJ/mol)

Molecule considered	$\Delta H°_{f0}$[a]	Reference molecule	$\Delta H°_{f0}$[b]
Triphosphirane	70 ± 10	PH_3	13.3
Triphosphirane − H^+	821 ± 10	H_3C-PH_2	−8.1
Diphosphirane	85 ± 10	H_2P-PH_2	38.7
Diphosphirane − H^+	814 ± 10	H^+	1528.0
Phosphirane	86 ± 10		
Phosphirane − H^+	812 ± 10		

[a] Based on heats of isodesmic reactions (1), (2) and (3) listed in Table 4 and proton affinities given in Table 5 obtained from MP4SDTQ /6−311++G(3df,2p) + ZPE calculations. − [b] Values from the literature.[50][52]

Ionization and Excitation Energies

The vertical excitation energies as well as the geometries of the ionized structures give additional insight into the electronic structure of these rings. In contrast to cyclopropane, where the ring opens after ionization, the radical cation minimum of **1a** is cyclic **1a**$^{+\cdot}$ (Figure 5). The lengths of the P−P bonds that are *trans*-substituted are only slightly longer in **1a**$^{+\cdot}$ than in **1a**. In contrast, the *cis*-substituted P−P distance is clearly (0.103 Å) shorter in the radical cation. This can be rationalized by the reduced repulsion of the less populated *cis*-oriented phosphorus lone pairs, which form a 3-electron/2-center π bond in **1a**$^{+\cdot}$. The en-

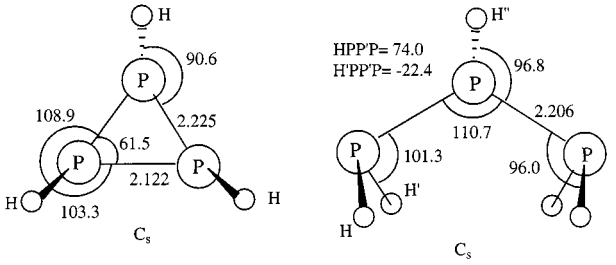


Figure 5. Minimum structure of the *cyclo*-$(PH)_3$ radical cation optimized at UMP2(fc) /6−31G(d,p) and and of the best triphosphane, $PH_2-PH-PH_2$, minimum structures at RMP2(fc) /6−31G(d,p)

ergy decrease due to geometrical relaxation, measured by the difference between vertical and adiabatic ionization energies, is only 0.25 eV in **1a**$^{+\cdot}$.

Separate calculations on some simple phosphanes indicate that IE_as calculated at QCISD(T)/6−311++G(d,p) + ZPE level are consistently underestimated by about 0.3 eV. Taking this correction into account, we estimate the values: IE_a = 9.3 ±0.3 eV for both **1a** and diphosphirane and IE_a = 9.5 ±0.3 eV for phosphirane (Table 7). The latter value agrees well with the available experimental estimate of 9.4 ±0.1 eV.[50] Thus, adiabatic ionization energies of three-membered P rings are rather independent of the number of P atoms. Note that the IE_a = 9.87 eV of PH_3[50] is somewhat larger than for the polyphosphaphosphiranes. The first vertical electronic excitation energies of P rings are listed in Table 7. CIS/6−311++G(d,p) calculations, which include only singly excited configurations, provide only upper bounds for this property; usually, an overestimation of 0.5 eV relative to the experimental value is expected.[26] More realistic estimates assume a systematic correction of 0.5 eV to CIS values. With the basis set employed, no Rydberg states could be identified. It is apparent that the first transition energy decreases with increasing number of P atoms. A shift of the absorption bands toward longer wavelength region is noticeable.

Table 7. Calculated adiabatic ionization energies and vertical excitation energies of polyphosphaphosphiranes (eV)

Molecule	First ionization energies[a]	First vertical excitation energies[b]
Triphosphirane	8.97	5.5 (f = 0.010)[d] (9.3 ±0.3) ($^1A'' \leftarrow {}^1A'$)
Diphosphirane	9.00	5.7 (f = 0.320) (9.3 ±0.3) ($^1B \leftarrow {}^1A$)
Phosphirane	9.18	6.4 (f = 0.015) (9.5 ±0.3) ($^1A'' \leftarrow 1A'$)

[a] Calculated values from QCISD(T)/6−311++G(d,p) + ZPE level based on MP2/6−31G(d,p) geometries. In parentheses are corrected IE_a; see text. − [b] Experimental value.[50] − [c] Calculated values from CIS/6−311++G(d,p) level and corrected by −0.5 eV for overestimation; see text. − [d] In parenthesis are oscillator strengths.

NMR Properties of Triphosphirane and Related Molecules

Table 8 shows, for the $PH(PH_2)_{2-n}(CH_3)_n$ molecules with n = 0, 1, and 2, that the magnetic shielding, $\sigma(^{31}P)$, decreases with decreasing electron density around the ^{31}P nucleus. This is in agreement with a more general study.[16] Since the range of the phosphorus valence in this set of molecules, characterized by the sum of Wiberg bond indices, ΣWBI(P), is small (2.8−3.1), no significant correlation with $\sigma(^{31}P)$ can be established. The bond-angle sum at phosphorus, Σα, ranges from 236.5° in phosphirane, $(PH)(CH_2)_2$, to 303.5° in $(PH)_3$. In contrast to the atomic charges, which do not correlate with the chemical shifts in these cyclic molecules, the bond angles are roughly related to $\sigma(^{31}P)$. The square of the correlation coefficient is 0.82 for the σ − Σα and 0.74 for the σ − α(P) relationship. Despite the fact that these relationships are rough, they indicate that the unusually large ^{31}P shieldings in the small rings are due to the small bond angles at σ^3-P. The similarity of $\sigma(^{31}P)$ of the two symmetry equivalent atoms in **1a** and the phosphorus atoms in diphosphirane can therefore be rationalized by compensation of two effects: (i) the more electronegative endocyclic substituents reduce $\sigma(^{31}P)$ (charge changes from −0.06 to +0.11) and (ii) the contracted endocyclic bond angle, which increases magnetic shielding [angle α(P) changes from 59.8° to 53.3°].

Table 8. Absolute NMR isotropic magnetic shielding, σ[a] charges, q[b] valence,[c] and coordination[d] of phosphorus in optimized[e] geometries

Molecule[e]		σ[a]	q[b]	val[c]	Σα[d]	α(P)[d]
1a, P1	C_s	570	−0.06	3.01	249.3	60.4
1a, P2	C_s	599	−0.06	3.01	251.9	59.8
$(\mathbf{P}H)_2(CH_2)$ ring	C_2	599	0.11	2.94	242.6	53.3
$(\mathbf{P}H)(CH_2)_2$ ring	C_s	636	0.20	2.87	236.5	46.9
PH_3	C_{3v}	561	−0.17	2.99	283.7	99
$H\mathbf{P}(PH_2)_2$	C_s	457	−0.11	3.01	303.4	110.4
$H\mathbf{P}(CH_3)PH_2)$	C_1	423	0.11	2.97	297.7	104.1
$H\mathbf{P}(CH_3)_2$	C_s	403	0.29	2.91	294.5	99.7

[a] Magnetic shielding at phosphorus, σ, computed at GIAO / B3LYP /6−311G(d) //RMP2(fc) /6−31G(d,p). Details at http://www.ccc.uni-erlangen.de/sharc/ in NMR-SHARC format. The corresponding NMR chemical shifts, δ, can be derived with δ(X) = δ(PH_3, reference) − [σ(PH_3) − σ(X)], using σ(PH_3) = 561 from the table. − [b] Charge at phosphorus from Mulliken population analysis. − [c] Sum of Wiberg bond indexes at B3LYP /6−31G(d,p). − [d] Bond angle sum of the phosphorus bonds, Σα, and endocyclic (HPH and CPC, respectively) bond angle at phosphorus, α(P). − [e] NMR properties, population analysis and geometric properties for global minimum structures at RMP2(fc) /6−31G(d,p); see Figures 1 and 5.

Summary and Conclusions

We explored the P_3H_3 potential energy surface by ab initio methods, MP2/6−31G(d,p), with particular focus on ring-chain rearrangements of triphosphirane **1**. Further-

more, molecular properties of **1** are compared with those of other polyphosphaphosphiranes and cyclopropane. A number of conclusions emerge from this theoretical study: (i) The cyclic *trans*-triphosphirane (**1a**) is by far the most stable P_3H_3 isomer; the most stable open-chain isomer is phosphanyldiphosphene, which lies about 42 kJ/mol above **1a**. The cyclic form is increasingly favored upon successive replacement of C by P in polyphosphaphosphiranes, $(CH_2)_{3-n}(PH)_n$ (n = 1−3). (ii) The energy ordering of P_3H_3 isomers is (in kJ/mol): **1a** (0) > phosphanylphosphene (42) > phosphorane (115) > cyclic PH−P=PH_2 (137) > phosphanylphosphinidene (141). (iii) Isomer **1a** is almost a strain-free ring; it even exhibits a small stabilization relative to three separated P−P single bonds. In contrast to cyclopropane, ring strain in phosphirane has essentially vanished. (iv) As the ring strain decreases from phosphirane to triphosphaphosphirane, the phosphorus inversion barrier, $\Delta_{inv}E$, also decreases. $\Delta_{inv}E$ of *cyclo*-$(PH)_3$ is only 224 kJ/mol. (v) Isomer **1a** has a proton affinity, PA, that is almost identical to that of PH_3, PA(**1a**) = 777 ±10 kJ/mol. The values for diphosphirane (799 ±10 kJ/mol) and phosphirane (802 ±10 kJ/mol) are somewhat larger, but they are far smaller than the corresponding values of their open-chain counterparts. This reduced PA appears to be due to the bonding characteristics of the three-membered rings. (vi) Another special feature of the carbon−phosphorus triangles is that the calculated adiabatic ionization energies, IE_a, are rather similar for all polyphosphaphosphiranes (IE_a = 9.5 ±0.3 eV for phosphirane; 9.3 ±0.3 eV for diphosphirane and **1a**). The first UV absorption band shifts toward shorter wavelength on going from phosphirane to triphosphirane. (vii) The heats of formation are computed to be ($\Delta H°_{f0}$ at 0 K in kJ/mol): 70 ± 10 *trans*-triphosphirane, 821 ± 10 protonated triphosphirane, 85 ± 10 *trans*-diphosphirane, 814 ± 10 protonated diphosphirane, 86 ± 10 phosphirane, and 812 ±10 protonated phosphirane. (viii) The ^{31}P-NMR-chemical shifts of the C_s-symmetric *trans*-triphosphirane are predicted to be at δ = −249 for one phosphorus and δ = −278 for the two *cis*-substituted nuclei. (ix) In contrast to phosphirane, triphosphirane undergoes preferentially either a ring-opening by P−P bond breaking or a 1,2-hydrogen shift, but not a combined motion. Ring-opening is, in the gas phase, the more favored reaction path but the energy barrier for this process is still rather large [213; at QCISD(T)/6−311G(d,p) //RMP2(fc)/6−31G(d,p) 190 kJ/mol]. The TS of ring-opening profits from stabilization by a three-center π bond completely formed in triphosphaallyl, PH=PH=PH. For the parent triphosphirane the conversion into the open-chain phosphanyldiphosphene is a two-step process in which the 1,2-H shift is the most energy-demanding step.

Acknowledgments

The authors are indebted to the Fund for Scientific Research Flanders (FWO) and the KULeuven Research Council (GOA program) for continuing support.

[1] M. Baudler, *Angew. Chem. Int. Ed. Engl.* **1982**, *21*, 492.
[2] R. Huisgen, I. Ugi, *Angew. Chem.* **1956**, *68*(2), 705.
[3] K. O. Christe, W. W. Wilson, J. A. Sheehy, J. A. Boatz, *Angew. Chem. Int. Ed. Engl.* **1999**, *38*, 2004.
[4] M. Baudler, S. Akpapoglou, D. Ouzounis, F. Wasgestian, B. Meinigke, H. Budzikiewicz, H. Münster, *Angew. Chem. Int. Ed. Engl.* **1988**, *27*, 288.
[5] M. Baudler, *Angew. Chem. Int. Ed. Engl.* **1987**, *26*, 419.
[6] M. Yoshifuji, I. Shima, N. Inamoto, K. Hirotso, T. Higuchi, *J. Am. Chem. Soc.* **1981**, *103*, 4587.
[7] A. Baceiredo, G. Bertrand, J. P. Majoral, G. Sicard, J. Jaud, J. Galy, *J. Am. Chem. Soc.* **1984**, *106*, 6088.
[8] M. Regitz, O. J. Scherer, *Multiple Bonds and Low Coordination in Phosphorus Chemistry*, Georg Thieme Verlag: Stuttgart, **1990**.
[9] M. Baudler, K. Glinka, *Chem. Rev.* **1993**, *93*, 1623.
[10] E. Niecke, D. Gudat, *Angew. Chem. Int. Ed. Engl.* **1991**, *30*, 217.
[11] N. Wiberg, A. Wörner, H.-W. Lerner, K. Karaghiosoff, D. Fenske, G. Baum, A. Dransfeld, P. v. R. Schleyer, *Eur. J. Inorg. Chem.* **1998**, *1*, 833.
[12] A. Dransfeld, L. Nyulászi, P. v. R. Schleyer, *Inorg. Chem.* **1998**, *37*, 4413.
[13] M. Baudler, H. Ständeke, M. Kemper, *Z. Anorg. Allg. Chem.* **1972**, *388*, 125.
[14] M. Baudler, J. Hahn, E. Clef, *Z. Naturforsch.* **1984**, *39b*, 438.
[15] J. Hahn, M. Baudler, C. Krüger, Y.-H. Tsay, *Z. Naturforsch.* **1982**, *37b*, 797.
[16] A. Dransfeld, P. v. R. Schleyer, *Magn. Reson. Chem.* **1998**, *36*, 29.
[17] M. Baudler, G. Reuschenbach, J. Hahn, *Chem. Ber.* **1983**, *116*, 847.
[18] R. Gleiter, W. Schäfer, M. Baudler, *J. Am. Chem. Soc.* **1985**, *107*, 8043.
[19] W. W. Schoeller, V. Staemmler, P. Rademacher, E. Niecke, *Inorg. Chem.* **1986**, *25*, 4382.
[20] W. W. Schoeller, *J. Mol. Struct. (Theochem)* **1986**, *137*, 341.
[21] M. Yoshifuji, N. Inamoto, K. Ito, S. Nagase, *Chem. Lett.* **1985**, 437.
[22] S. Inagaki, K. Yoshikawa, Y. Hayano, *J. Am. Chem. Soc.* **1993**, *115*, 3706.
[23] S. Inagaki, Y. Ishitani, T. Kalefu, *J. Am. Chem. Soc.* **1994**, *116*, 5954.
[24] M. T. Nguyen, L. Landuyt, L. G. Vanquickenborne, *J. Chem. Soc., Faraday Trans.* **1994**, *90*, 1770.
[25] M. T. Nguyen, H. Vansweevelt, L. G. Vanquickenborne, *Chem. Ber.* **1992**, *125*, 923.
[26] M. T. Nguyen, E. Van Praet, L. G. Vanquickenborne, *Inorg. Chem.* **1994**, *33*, 1153.
[27] N. J. Fitzpatrick, D. F. Brougham, P. J. Groarke, M. T. Nguyen, *Chem. Ber.* **1994**, *127*, 969.
[28] M. J. Frisch, G. W. Trucks, H. B. Schlegel, P. M. W. Gill, B. G. Johnson, M. A. Robb, J. R. Cheeseman, T. Keith, G. A. Petersson, J. A. Montgomery, K. Raghavachari, M. A. Al-Laham, V. G. Zakrzewski, J. V. Ortiz, J. B. Foresman, J. Cioslowski, B. B. Stefanov, A. Nanayakkara, M. Challacombe, C. Y. Peng, P. Y. Ayala, W. Chen, M. W. Wong, J. L. Andres, E. S. Replogle, R. Gomperts, R. L. Martin, D. J. Fox, J. S. Binkley, D. J. Defrees, J. Baker, J. P. Stewart, M. Head-Gordon, C. Gonzalez, J. A. Pople, *GAUSSIAN 94*, Gaussian Inc., Pittsburgh PA, U.S.A. 1995.
[29] J. R. Cheeseman, G. W. Trucks, T. A. Keith, M. J. Frisch, *J. Chem. Phys.* **1996**, *104*, 5497.
[30] K. B. Wiberg, *Tetrahedron* **1968**, *24*, 1083.
[31] M. T. Nguyen, L. Landuyt, L. G. Vanquickenborne, *Chem. Phys. Lett.* **1993**, *212*, 543.
[32] C. Schade, P. v. R. Schleyer, *J. Chem. Soc., Chem. Commun.* **1987**, 1399.
[33] M. T. Nguyen, *Chem. Phys.* **1986**, *109*, 277.
[34] M. T. Nguyen, T.-K. Ha, *Chem. Phys. Lett.* **1989**, *158*, 135.
[35] M. T. Nguyen, A. Van Keer, T.-K. Ha, L. G. Vanquickenborne, *J. Mol. Struct. (Theochem)* **1994**, *130*, 125.
[36] D. Gonbeau, G. Pfister-Guillouzo, *Inorg. Chem.* **1987**, *26*, 1799.
[37] F. Mathey, *Angew. Chem. Int. Ed. Engl.* **1987**, *26*, 275.
[38] F. Mercier, C. Huegel-Le Goff, F. Mathey, *Tetrahedron Lett.* **1989**, *30*, 2397.
[39] W. Egan, R. Tang, G. Zon, K. Mislow, *J. Am. Chem. Soc.* **1971**, *93*, 6205.
[40] A. Dransfeld, Dissertation Thesis, Erlangen, **1998**.
[41] W. W. Schoeller, *J. Mol. Struct. (Theochem)* **1993**, *284*, 61.
[42] V. I. Minkin, M. N. Glukhovtsev, B. Ya. Simkin, *Aromaticity*

and Antiaromaticity − Electronic and Structural Aspects, John Wiley & Sons Ltd., New York, **1994**.
[43] H. Schiffer, R. Ahlrichs, M. Häser, *Theor. Chim. Acta* **1989**, *75*, 1.
[44] B. M. Gimarc, M. Zhao, *Phosphorus Sulfur Silicon* **1994**, *93*, 231.
[45] S. Ikuta, P. Kebarle, *Can. J. Chem.* **1982**, *61*, 97.
[46] H. Heydt, J. Hoffmann, A. Göller, T. Clark, M. Regitz, *Synthesis* **1998**, *2*, 175.
[47] M. T. Nguyen, A. Van Keer, L. G. Vanquickenborne, *J. Org. Chem.* **1996**, 7077.
[48] O. Mo, J. L. G. De Paz, M. Yanez, *J. Phys. Chem.* **1987**, *91*, 6484.
[49] D. C. R. Hockless, M. A. McDonald, M. Pabel, S. B. Wild, *J. Chem. Soc., Chem. Commun.* **1995**, 257.
[50] S. J. Lias, J. E. Bartmess, J. F. Liebmann, J. M. Holmes, R. D. Levin, W. G. Mallard, *J. Phys. Chem. Ref. Data* **1988**, *17*, Suppl. 1
[51] P. Schwerdtfeger, L. Laakkonen, P. Pyykkö, *J. Chem. Phys.* **1992**, *96*, 6807.
[52] G. Leroy, D. R. Temsamani, C. Wilante, J. P. Dewispelaere, *Theochem* **1994**, *309*, 113.

Received June 7, 1999
[I99206]

Electrochemical and Spectroscopic Properties of Cyclometallated and Non-Cyclometallated Ruthenium(II) Complexes Containing Sterically Hindering Ligands of the Phenanthroline and Terpyridine Families

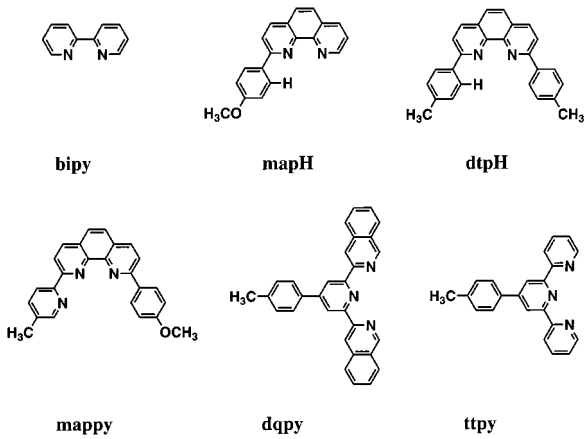
Francesco Barigelletti,*[a] Barbara Ventura,[a] Jean-Paul Collin,*[a] Robert Kayhanian,[a] Pablo Gaviña,[a][+] and Jean-Pierre Sauvage[a]

Keywords: Ruthenium / Phenanthroline / Luminescence / Sterically hindered ligands / Terpyridine / Cyclometallation

Two series of cyclometallated and noncyclometallated ruthenium(II) complexes incorporating mono- or disubstituted 1,10-phenanthroline- and 2,2′:6′,2″-terpyridine-type ligands have been synthesized and characterized. An X-ray crystal structure for one of the complexes, Ru(ttpy)(mapH)(Cl)(PF_6), has been obtained (mapH = 2-*p*-anisyl-1,10-phenanthroline; ttpy = 4′-tolyl-2,2′:6′,2″-terpyridine). Distinct electrochemical and photophysical properties have been observed for the two series: a remarkable feature is the observation of relatively long-lived MLCT excited states (from 70 to 106 ns at room temperature in CH_3CN) for three of the cyclometallated complexes. A discussion is given on the role of factors like sigma donation by the cyclometallating ligands, interligand steric hindrance and interligand π-π interactions that affect the electrochemical and spectroscopic properties.

Introduction

The photophysical behavior of transition metal polypyridine complexes is of prime importance in molecular devices based on photoinduced electron and energy transfer reactions.[1] Numerous studies on complexes exhibiting luminescence from metal-to-ligand charge-transfer (MLCT) excited states have shown the determining effects of different factors on the excited state properties.[2] Among others, the energy level of the low-lying states (energy gap law),[3] the electron delocalization on the acceptor ligand,[4] as related to its structure and rigidity[5] have been correlated with parameters like absorption and luminescence wavelengths, lifetime and quantum yield. With the aim of developing new approaches to the tuning of excited-states properties, we have prepared a series of ruthenium(II) complexes incorporating cyclometallated and noncyclometallated sterically hindering ligands. In these complexes, the electron density distribution associated with the presence of cyclometallating positions may result in improved luminescence properties, as illustrated below for some of the compounds investigated. We also show that the interligand interactions between hindering ligands can play a non-negligible role in determining the luminescence properties[6] provided that the steric constraint does not distort excessively the octahedral coordination. The schematic structures of the relevant ligands are illustrated in Scheme 1. A preliminary report of some properties of compounds **4**, **7**, and **9** has been published previously.[7]



Scheme 1

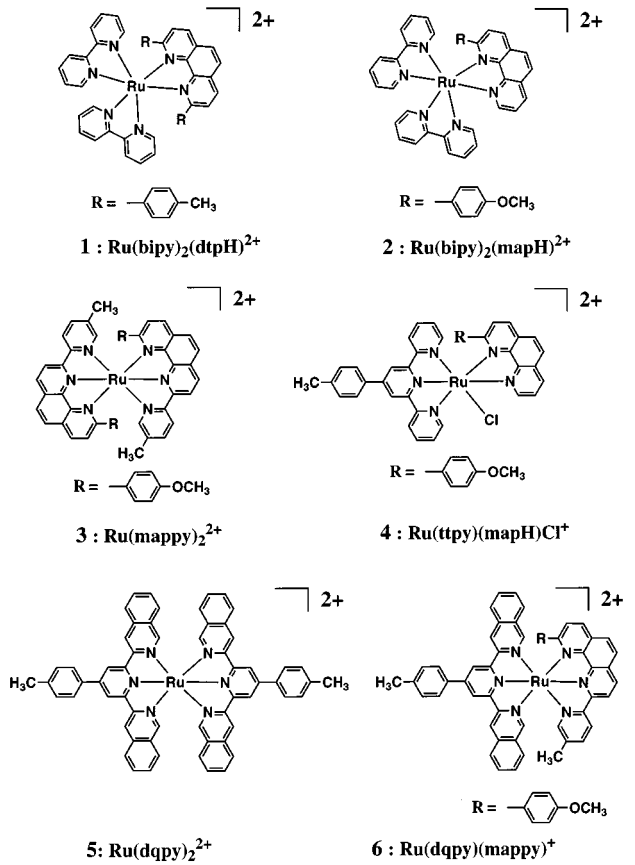
Results and Discussion

The ruthenium complexes synthesized and studied are represented in Scheme 2 (**1**−**6**: noncyclometallated compounds) and Scheme 3 (**7**−**10**: cyclometallated compounds). Cyclometallated ruthenium(II) complexes involving ligands that contain a phenyl group adjacent to a nitrogen donor atom are relatively easy to obtain.[8] Depending on the potential donor atoms implied and the experimental conditions, the complexation reaction leads to the normal N_6 coordination sphere or to the N_5C set.[9] The reaction of paramagnetic ruthenium(III) species ($RuLCl_3$; L = ttpy, dqpy or mappy) with one equivalent of hindering phenanthroline (mapH, dtpH or mappy) in refluxing glacial acetic acid in the presence of a mild reducing agent (*N*-ethylmorpholine) gave the complexes **3** to **10**. In the case of

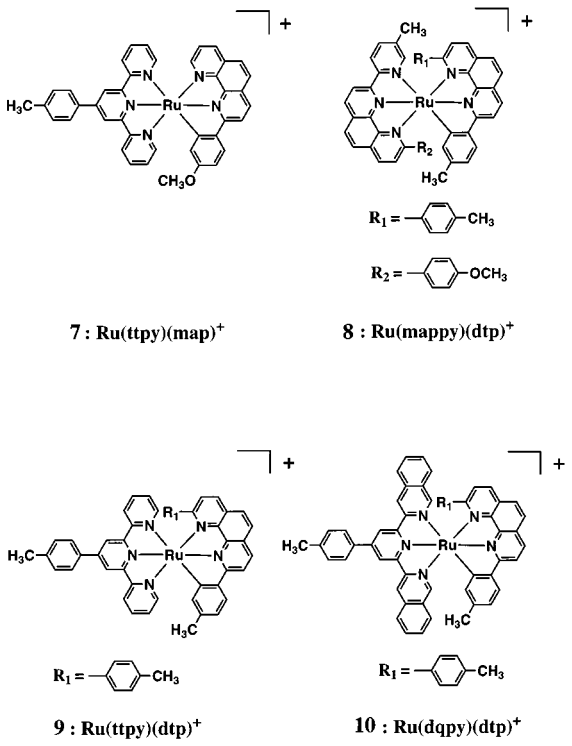
[a] Istituto FRAE-CNR,
via P. Gobetti 101, I-40129 Bologna, Italy
[b] Laboratoire de Chimie Organo-minérale, Institut Le Bel, Université Louis Pasteur,
4 rue Blaise Pascal, F-67070 Strasbourg, France
E-mail: sauvage@chimie.u-strasb.fr
[+] Present address: Departament de Quimica Orgànica, Universitat de València, Facultat de Farmàcia,
Av. Vicent Andrés Estellés s/n, E-16100 Burjassot (València), Spain

 © WILEY-VCH Verlag GmbH, D-69451 Weinheim, 2000 1434−1948/00/0101−0113 $ 17.50+.50/0

complexes **1** and **2**, the ruthenium precursor was Ru(bipy)$_2$Cl$_2$. All the compounds were characterized by ^{1}H-NMR and FAB-MS spectra and these data are in full agreement with their postulated structures.



Scheme 2



Scheme 3

The X-ray structures of **7** and **9** have already been reported.[7] Single crystals of **4** were obtained by crystallization from a mixture acetonitrile and benzene. The ORTEP diagram of **4** is shown in Figure 1. Selected bond lengths and bonds angles are presented in Table 1. For comparison purposes some data concerning **7** and **9** are also given.

The ruthenium ligand environment exhibits a distorted octahedral geometry with the terpyridine ligand coordinated in meridional configuration. The phenanthroline plane is orthogonal to the terpyridine mean plane whereas the anisyl substituent is in a stacking position with the central pyridine of the terpyridine (the angle between these rings is 4.2° and the distance between planes is around 3.4 Å). The chloride ion is directed from the N2 nitrogen atom of the phenanthroline. The Ru−Cl bond length of 2.391 Å is very similar to that reported for other ruthenium terpyridine chloro complexes, such as 2.405 Å for Ru(terpy)(bpz)Cl$^+$[10] (bpz = 2,2′-bipyrazine) and 2.400 Å for [Ru(terpy)(CO)$_2$Cl]Cl.[11] The terpyridine ligand affords two almost identical Ru−N bond lengths of ca. 2.05 Å (Ru−N3 and Ru−N5) whereas the distance Ru−N4 is shorter for the central pyridine (1.950 Å). The two side pyridines bind to ruthenium at angles of 79.3° (N3−Ru−N4) and 79.8° (N4−Ru−N5) and these angles also show that terpyridine is constrained such that it cannot fit with an ideal (90°) geometry.

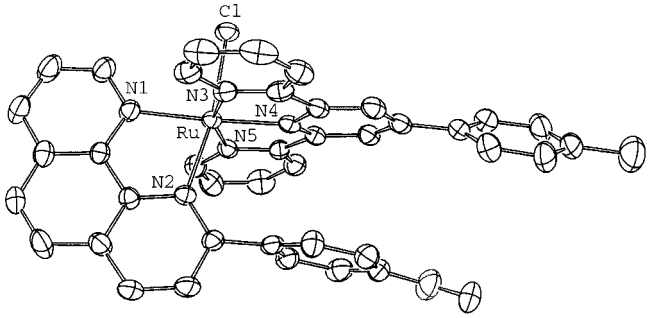


Figure 1. ORTEP representation of the X-ray structure of **4**. The hydrogen atoms and PF_6 anion have been omitted for clarity. Thermal ellipsoids are scaled to enclose 30% of the electronic density

Contrary to what was observed in compound **7** and **9**[7] the Ru−N1 and Ru−N2 bond lengths are in agreement with the usual coordination of the substituted phenanthroline to the ruthenium. In fact, for **7** and **9**, the unusually long Ru−N1 (for **7**) and Ru−N2 (for **9**) bond lengths (2.198 Å and 2.256 Å, respectively) could be the consequence of a *trans* effect (due to the carbon atom in the *trans* position) as well as the constrained geometry inherent in terpyridine-type chelate.

The electrochemical data for the noncyclometallated (**1** to **6**) and cyclometallated (**7** to **10**) ruthenium complexes are presented in Table 2. Oxidations are metal-centered and reductions are ligand-centered processes respectively. Reversible monoelectronic waves are observed for almost all

Table 1. Selected bond lengths and bond angles for **4**, **7** and **9** (numbers in parentheses are estimated standard deviations in the least significant digits)

	Bonds lengths [Å]		Bonds angles [°]	
4	Ru−Cl	2.3917(8)	Cl−Ru−N1	91.89(8)
	Ru−N1	2.078(3)	N1−Ru−N2	79.2(1)
	Ru−N2	2.087(3)	N1−Ru−N3	100.8(1)
	Ru−N3	2.067(3)	N1−Ru−N4	176.6(1)
	Ru−N4	1.953(2)	N3−Ru−N4	79.3(1)
	Ru−N5	2.043(3)	N4−Ru−N5	79.8(1)
7	Ru−N1	2.198(6)	N1−Ru−N2	76.9(2)
	Ru−N2	2.009(6)	N1−Ru−C18	156.0(3)
	Ru−C18	2.030(8)	N1−Ru−N3	93.7(2)
	Ru−N3	2.050(5)	N1−Ru−N4	105.4(2)
	Ru−N4	1.961(6)	N1−Ru−N5	91.5(2)
	Ru−N5	2.062(5)	N2−Ru−C18	79.1(3)
9	Ru−N1	2.010(2)	N1−Ru−N2	76.6(1)
	Ru−N2	2.256(3)	N1−Ru−C18	78.3(1)
	Ru−N3	2.031(3)	N1−Ru−N3	100.6(1)
	Ru−N4	1.942(3)	N3−Ru−N4	79.8(1)
	Ru−N5	2.052(2)	N4−Ru−C18	93.5(1)
	Ru−C18	2.037(4)	N2−Ru−N4	111.5(1)

redox couples. As expected, compounds **1**, **2** and **3** display redox processes typical of the well-known bipyridine, phenanthroline, and terpyridine complexes.[1] In compound **4**, due to the coordinated chloride ion, the ruthenium is easier to oxidize (by 500 mV as compared to **3**) and one ligand is more difficult to reduce. In compounds **5** and **6**, the presence of electron-withdrawing quinoline ligands provides a slightly higher acceptor character to these complexes than the classical bis(terpyridine) compound.

Table 2. Redox potentials (vs SCE) measured by cyclic voltammetry. Conditions: CH_3CN (nBu$_4$NBF$_4$ = 0.1 M), v = 100 mVs^{-1}, room temperature.

	$Ru^{III/II}$	$L^{0/-}$	$L^{-/2-}$	$L^{2-/3-}$
1	1.27	−1.33	−1.60	
2	1.27	−1.33	−1.52	
3	1.29	−1.16	−1.42	−1.91
4	0.77	−1.50	−1.85[b]	
5	1.14	−1.36	−1.52	
6	1.08	−1.19	−1.56	−1.82
7	0.54	−1.54	[a]	
8	0.57	−1.47	[a]	
9	0.54	−1.57	[a]	
10	0.44	−1.63	−1.83	2.08[b]

[a] Large cathodic current occurs without distinctive peak. − [b] Irreversible.

For complexes **7** to **10**, the effect of the cyclometallation on the stability of the Ru^{III} state is illustrated by a cathodic shift of 750 mV. This behavior demonstrates the strong σ-donating character of the anionic (map^- or dtp^-) ligands. The ligand-centered reduction is also strongly affected by the presence of the cyclometallating ligand. In fact, the first reduction in these compounds occurs at around −1.6 V while it occurs around −1.3 V for **1** and **2**.

The absorption maxima, the molar absorption coefficients and the luminescence properties in acetonitrile and in butyronitrile are collected in Table 3 and representative absorption spectra in the series are shown in Figure 2.

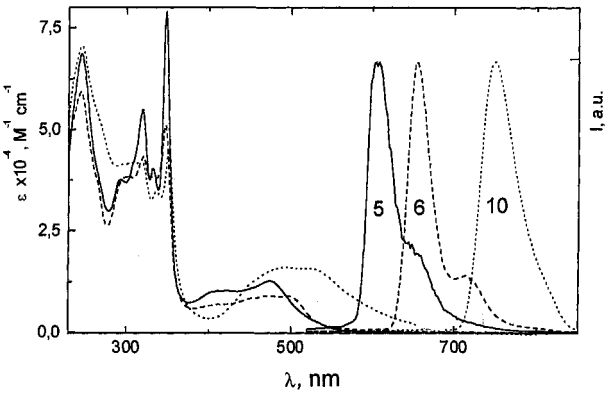


Figure 2. Absorption spectra (acetonitrile, room temperature) and normalized luminescence spectra (butyronitrile, 77 K) of complexes **5**, **6**, and **10**

The absorption bands in the UV region are ascribed to ligand-centered transitions (^{1}LC) and those occurring in the visible part, with ε around 10^4 M^{-1} cm^{-1}, correspond to ^{1}MLCT transitions.[1a] In the case of the cyclometallated complexes (**7**−**10**) the absorption bands occurring at low energy (495 to 527 nm) could be attributed to MLCT transitions involving the LUMO of the noncyclometallating ligand, i.e. ttpy (case of **7**, **9**, **10**) or mappy (case of **8**). Actually, as has already been established,[12] the level of the LUMO for the cyclometallated (anionic) ligand is expected to be higher in energy than that of an isoelectronic but neutral polypyridine ligand.

All the ruthenium complexes exhibit an intense luminescence at 77 K in butyronitrile (Table 3). The luminescence band maxima for the cyclometallated complexes are bathochromically shifted with respect to the noncyclometallated compounds. At room temperature, in CH_3CN, a more distinct behavior appears between the two series. Whereas compounds **1** and **3**−**6** are nonluminescent, as found for many tpy-containing derivatives,[1c] the cyclometallated complexes **8**, **9** and **10** luminesce and display relatively long-lived excited states (from 70 to 106 ns). This behavior can be understood in terms of the interplay of MLCT and metal-centered (MC) excited states, as discussed below.

In the case of ruthenium terpyridine-type complexes the distorted octahedral geometry induces a relatively weak ligand field at the metal center.[1c] As a consequence, effective pathways for deactivation of the ^{3}MLCT state are established by population of thermally accessible upper-lying ^{3}MC states. This effect is likely to be enhanced by the presence of bulky substituents in the α-position with respect to the N atom (case of **3** and **6**). This type of argument also could be used to explain the behavior of **1**, in which 2,9-bis-*p*-tolyl-1,10-phenanthroline is associated with a Ru(bipy)$_2$ core. In contrast, if the coordination sphere of the metal is less constrained as in **2**, a sizable luminescence can be observed.

Table 3. Spectroscopic properties[a]

	Absorption λ_{max}[nm] (ε [M^{-1} cm^{-1}])			Luminescence					
				λ_{max} [nm]	293 K τ [ns]	293 K Φ	293 K λ_{max} [nm]	77 K τ[μs]	77 K
1			452 (10200)	288 (46000)	–	–	–	602	6.6
2		448 (10500)	288 (44000)	267 (39000)	618	3.4	5.6×10^{-3}	586	6.2
3	503 (9100)	344 (36000)	300 (41200)	246 (44600)	–	–	–	646	9.3
4		508 (13400)	285 (48500)	269 (55700)	–	–	–	790	0.8
5		473(12700)	348 (79000)	245 (69000)	–	–	–	605	17.2
6	495 (8900)	474 (9000)	347 (51000)	245 (59300)	–	–	–	655	11.3
7	518 (17800)	355 (26500)	309 (39000)	286 (49600)	–	–	–	704	3.6
8	523 (8600)	440 (6700)	314 (35000)	252 (49000)	816	106	1.9×10^{-3}	814	2.3
9	527 (16300)	388 (12000)	316 (43000)	290 (46500)	802	95	2.0×10^{-2}	778	2.6
10	520 (15700)	493 (16000)	351 (44000)	246 (70500)	778	70.5	2.8×10^{-4}	750	3.4

[a] Acetonitrile solvent at room temperature, butyronitrile at 77 K.

In the case of cyclometallated ruthenium complexes it has already been recognized[13] that the strong ligand field provided by σ-donation at the carbon coordination increases the energy gap between the lowest-lying ^{3}MLCT levels (which involve the noncyclometallating ligand) and the upper-lying ^{3}MC states. This increase is basically due to a loading of electron density at the metal center, which results both in destabilization of the ^{3}MC level and stabilization of the ^{3}MLCT level (as indicated by the values of the luminescence band maxima at 77 K, Table 3). It is noteworthy that, according to the ″energy-gap law″, the latter effect is expected to enhance the nonradiative processes from the emitting state.[3] In the case of **8**, **9** and **10**, the balance of these effects results in sizable luminescence at room temperature, which is not the case for most of the terpyridine-containing ruthenium complexes.[1c] We noticed that, for **8**, **9**, and **10**, large ligand fragments undergoing interligand π-π interactions are present,[7] which can assist an extended electron delocalization for the MLCT states and result in the known beneficial effects noted in the case of large rigid ligands.[4] By contrast, the Ru(ttpy)(map)$^+$ (**7**) complex, which is necessarily devoid of such interligand interactions, does not luminesce at room temperature (Table 3).

Experimental Section

Physical Measurements: ^{1}H NMR: Bruker WP200 SY (200 MHz). – UV/Vis: Kontron Uvikon 860. – MS: VG ZAB-HF, Thomson THN 208. – Cyclic voltammetry data: PAR model 273A potentiostat, Pt disk as working electrode, CH_3CN solution, 0.1 M Bu_4NBF_4 as supporting electrolyte, Pt wire as auxiliary electrode, SCE as reference electrode.

Photophysical Measurements: Absorption spectra were determined with a Perkin–Elmer Lambda 5 spectrometer. – Uncorrected luminescence spectra were obtained from a Spex Fluorolog II fluorimeter equipped with a Hamamatsu R928 phototube. Uncorrected band maxima are used throughout the text. The luminescence quantum yields, Φ, were obtained from dilute solutions (the absorbance at the selected excitation wavelength was < 0.1)[20a] by analysing spectra that were corrected for the photomultiplier response and by comparison with the spectrum of Ru(bpy)$_3^{2+}$ (Φ = 0.028 in aerated water).[20b] Luminescence lifetimes were obtained with an IBH single photon apparatus employing a lamp filled with N_2; the decays were found to follow a single exponential behavior in each case. Further details were given elsewhere.[21] The experimental uncertainties were estimated to be 2 nm for the absorption and luminescence spectra, 20% for the luminescence intensities and 10% for the luminescence lifetimes.

Materials and General Procedures: The following chemicals were prepared according to literature procedures: 2-*p*-anisyl-1,10-phenanthroline (**mapH**);[14] 2,9-bis(*p*-tolyl)-1,10-phenanthroline (**dtpH**);[15] 4′-tolyl-2,2′,6′,2″-terpyridine (**ttpy**);[16] Ru(bp)$_2$Cl$_2$·2H$_2$O;[17] Ru(ttpy)Cl$_3$.[18]

2-*p*-Anisyl-9-(4-methyl-2-pyridyl)-1,10-phenanthroline (mappy): To a degassed solution of 2-bromo-5-methylpyridine (0.757 g, 4.4 mmol) in dry ether (15 mL) at −78°C was added dropwise *n*BuLi (soln. in hexane approx. 1.3 m, 3.7 mL, 4.84 mmol). The resulting red solution was warmed to −40°C and stirred at this temperature, under Ar, for 30 min. The organolithic solution was then transferred, by cannula, to a degassed solution of 2-*p*-anisyl-1,10-phenanthroline (1.145 g, 4.0 mmol) in dry ether (35 mL) at 0°C. The mixture was stirred under argon for 3 h at 0°C and then for a further 3 h at 10°C. After hydrolysis at 0°C with water (15 mL), the organic layer was decanted and the aqueous layer extracted with dichloromethane. The combined organic layers were rearomatized by succesive additions of MnO_2 (3 × 3 g, 3 g each 20 min), dried over $MgSO_4$ and filtered. After evaporation of the solvent the crude product was purified by column chromatography on alumina, with dichloromethane as eluent. The product, **mappy**, was obtained as a pale yellow solid (0.89 g, 59%). The solid crystallized from ethanol to give pale yellow crystals (m.p. 243.5–245.0°C). – ^{1}H NMR (200 MHz, $CDCl_3$): δ = 9.00 (d, *J* = 8.2 Hz, 1 H, H$^{3'}$), 8.82 (d, *J* = 8.4 Hz, 1 H, H^3), 8.58 (d, *J* = 2.2 Hz, 1 H, H$^{6'}$), 8.45 (d, *J* = 8.9 Hz, 2 H, 2 H^o), 8.36 (d, *J* = 8.4 Hz, 1 H, H^4), 8.29 (d, *J* = 8.5 Hz, 1 H, H^7), 8.11 (d, *J* = 8.5 Hz, 1 H, H^8), 7.81 (dd, *J* = 8.2 and 2.2 Hz, 1 H, H$^{4'}$), 7.79 (s, 2 H, H^{5,6}), 7.13 (d, *J* = 8.9 Hz, 2 H, 2 H^m), 3.94 (s, 3 H), 2.46 (s, 3 H). – Anal. calcd. for $C_{25}H_{19}N_3O$ (377.45): C 79.55, H 5.07, N 11.13; found: C 79.30, H 5.26, N 11.17.

3-Acetylisoquinoline: To sodium ethoxide (0.27 g, 0.012 mol) in dry benzene (40 mL) was added, with stirring, a mixture of methyl 3-isoquinoline carboxylate (1.8 g, 9.6 mmol) and anhydrous ethyl acetate (1.14 g, 15.8 mmol) in benzene (35 mL). The mixture was allowed to reflux with stirring for 24 h. The mixture was allowed to cool to room temperature and poured into a solution of sodium hydroxide (0.40 g, 0.01 mol) in water (7 mL). The light yellow solid that separated on the addition of the base was filtered off and water

(20 mL) was added to the filtrate. After decantation of the phases, the benzene layer was washed with water and the combined aqueous layer was extracted with ether (3 × 30 mL). The combined organic layers were evaporated and combined with the light yellow solid. To this was added concentrated hydrochloric acid and the mixture was heated to reflux for 2 h. On cooling, the mixture was made basic with sodium carbonate, the organic layer was extracted with ether (2 × 40 mL) and dried over sodium sulfate. Removal of the ether and purification on silica (dichloromethane/hexane 80:20) gave 1.23 g (75%) of 3-acetyl-isoquinoline. − ^{1}H NMR (200 MHz, $CDCl_3$): δ = 9.26 (s, 1 H), 8.45 (s, 1 H), 8.05−7.94 (m, 2 H), 7.79−7.67 (m, 2 H), 2.80 (s, 3 H). − MS (EI); *m*/*z*: 171.

2,6-Diisoquinolyl-(4-tolyl)pyridine (dqpy): To a dried sample of 3-acetyl-isoquinoline (1.23 g, 7.19 mmol), ammonium acetate (3.6 g, 46.7 mmol) and acetamide (5.54 g, 93.8 mmol) was added *p*-tolualdehyde (0.37 g, 3.11 mmol). The mixture was heated with stirring to 170°C under solvent-free conditions under an atmosphere of argon for 3 h. After this time the temperature of the reaction mixture was lowered to 120°C and the mixture was added to a solution of sodium hydroxide (2.8 g, 0.07 mol) in water (10 mL), a process that resulted in a brownish oil. The mixture was left at this temperature for a further 2 h. The dark brown oil and the yellow hot solution was poured into a beaker and, after cooling, the brown oil solidified. The solid was dissolved in acetic acid (10 mL) and refluxed for 2 h. 47% hydrobromic acid (10 mL) was then added and the mixture was left to stir at room temperture for a further 2 h. After this time, addition of a 5 N solution of potassium hydroxide (20 mL) resulted in the formation of a precipitate. The organic layer was extracted with dichloromethane (3 × 60 mL) and the combined organic layers were washed with sodium hydrogen carbonate and dried over magnesium sulfate. After column chromatography on alumina (hexane/ether; 8:2), dqpy was obtained as a white material (1.3 g, 43%). − ^{1}H NMR (300 MHz, $CDCl_3$): δ = 9.36 (s, 2 H), 9.08 (s, 2 H), 8.83 (s, 2 H), 8.08 (d, 2 H, *J* = 7.29 Hz), 8.03 (d, 2 H, *J* = 8.04 Hz), 7.87 (d, 2 H, *J* = 8.22 Hz), 7.74 (td, 2 H, *J* = 1.28 Hz), 7.63 (td, 2 H, *J* = 1.10 Hz), 7.33 (d, 2 H, *J* = 7.86 Hz), 2.43 (s, 3 H). − MS (EI); *m*/*z*: 423.2.

Ru(mappy)Cl$_3$: To absolute ethanol (30 mL) in a 100 mL round-bottomed flask was added $RuCl_3 \cdot 3H_2O$ (0.042 g, 0.132 mmol) and mappy (0.050 g, 0.132 mmol). The mixture was heated at reflux for 3 h with vigorous stirring. After this time, the reaction mixture was cooled to room temperature and the fine brown powder was collected by vacuum filtration, washed with cold absolute ethanol (3 × 30 mL) followed by Et_2O (3 × 30 mL) and dried under vacuum to give 0.065 g (84%) of Ru(mappy)Cl_3.

Ru(dqpy)Cl$_3$: This compound was prepared in the same manner as for the analogous compound, Ru(mappy)Cl_3, in almost quantitative yield. The insoluble brown-red product obtained was used without further purification.

General Workup Procedure for the Complexes 1 to 10: After reaction, the solvent was removed under reduced pressure and the colored solid was redissolved in methanol. The colored solution was filtered to remove any trace of unchanged starting complex and the filtrate obtained was added to an aqueous solution of KPF_6 (0.5 g in 50 mL of water) to give a solid. This solid was purified by silica gel chromatography, eluting with a mixture of CH_2Cl_2/CH_3OH (95:5) for all the complexes excepted for **5**, where the elution was performed with a CH_3CN/H_2O/saturated KNO_3 mixture (100:10:1).

Ru(bipy)$_2$(dtpH)(PF$_6$)$_2$ (1): A suspension of $Ru(bipy)_2Cl_2 \cdot 2H_2O$[17] (0.065 g, 0.13 mmol) and dtpH (0.046 g, 0.13 mmol) in acetic acid (10 mL) with 2−3 drops of *N*-ethylmorpholine was refluxed under argon for 3 h. Yield 0.033 g (24%). − ^{1}H NMR (200 MHz, CD_2Cl_2): δ = 8.56 (d, 2 H, *J* = 8.22 Hz), 8.28 (s, 2 H), 8.25 (d, 2 H, *J* = 8.22 Hz), 8.09 (td, 2 H, *J* = 6.21 Hz, *J* = 1.47 Hz), 7.82 (d, 2 H, *J* = 8.21 Hz), 7.78 (d, 2 H, *J* = 5.49 Hz), 7.70 (d, 2 H, *J* = 8.24 Hz), 7.52−7.39 (m, 4 H), 7.02 (br, 2 H), 6.65−6.61 (m, 7 H), 5.96 (br, 3 H), 2.16 (s, 6 H). − MS (FAB-MS) (nitrobenzyl alcohol matrix); *m*/*z* (%): 919 (20) [M − PF_6^-], 774 (10) [M − 2PF_6^- + e^-], 617 (12) [M − 2PF_6^- − bipy + e^-].

Ru(bipy)$_2$(mapH)(PF$_6$)$_2$ (2): A suspension of $Ru(bp)_2Cl_2 \cdot 2H_2O$ (0.050 g, 0.096 mmol) and mapH (0.026 g, 0.09 mmol) in acetic acid (7 mL) with 2−3 drops of *N*-ethylmorpholine was refluxed under argon for 4 h. Yield 0.065 g (68%). − ^{1}H NMR (200 MHz, CD_2Cl_2): δ = 8.62 (d, 1 H, *J* = 8.4 Hz), 8.56 (dd, 1 H, *J* = 8.4 Hz, *J* = 1.29 Hz), 8.40 (d, 1 H, *J* = 7.86 Hz), 8.34 (d, 1 H, *J* = 7.50 Hz), 8.31−8.22 (m, 4 H), 8.07 (td, 1 H, *J* = 7.86 Hz, *J* = 8.01 Hz), 7.99−7.94 (m, 4 H), 7.91 (d, 1 H, *J* = 5.49 Hz), 7.74−7.62 (m, 4 H), 7.49−7.31 (m, 6 H), 7.29 (br, 1 H), 7.07 (d, 1 H, *J* = 5.67 Hz), 6.93 (t, 1 H, *J* = 7.11 Hz), 3.70 (s, 3 H). − MS (FAB-MS) (nitrobenzyl alcohol matrix); *m*/*z* (%): 845 (50) [M − PF_6^-], 700 (35) [M − 2PF_6^- + e^-].

Ru(mappy)$_2$(PF$_6$)$_2$ (3): A suspension of Ru(mappy)Cl_3 (0.060 g, 0.10 mmol) and mappy (0.039 g, 0.10 mmol) was heated to reflux for 3 h in glacial acetic acid (6 mL) with 2−3 drops of *N*-ethylmorpholine. Yield 0.10 g (87%). − ^{1}H NMR (200 MHz, CD_2Cl_2): δ = 8.77 (d, 2 H, *J* = 8.6 Hz), 8.63 (d, 2 H, *J* = 8.6 Hz), 8.44 (t, 4 H, *J* = 8.06 Hz), 8.24 (s, 4 H), 7.69 (dd, 2 H, *J* = 8.20 Hz, *J* = 1.2 Hz), 7.36 (d, 2 H, *J* = 8.34 Hz), 6.23−6.19 (br, 2 H), 6.15 (s, 2 H), 5.93−5.63 (m, 6 H), 3.76 (s, 6 H), 1.89 (s, 6 H). − MS (FAB-MS) (nitrobenzyl alcohol matrix); *m*/*z* (%): 1001 (15) [M − PF_6^-], 856 (24) [M − 2PF_6^- + e^-].

Ru(ttpy)(mapH)(Cl)(PF$_6$) (4) and Ru(ttpy)(map)(PF$_6$) (7): Ru(ttpy)Cl_3 (0.10 g, 0.19 mmol) and mapH (0.054 g, 0.19 mmol) were heated to reflux for 3 h in glacial acetic acid (6 mL) with 2−3 drops of *N*-ethylmorpholine. Yield: 0.042 g (35%) of the cyclometallated product [Ru(ttpy)(map)PF_6] (**7**) and 0.060 g (31%) of the noncyclometallated product [Ru(ttpy)(mapH)(Cl)PF_6] (**4**). **Noncyclometallated complex (4):** ^{1}H NMR (200 MHz, CD_3CN): δ = 8.88 (s, 2 H), 8.54 (d, 2 H, *J* = 7.78 Hz), 8.49 (d, 1 H, *J* = 8.86 Hz), 8.32 (dd, 1 H, *J* = 8.19 Hz), 8.22 (d, 1 H, *J* = 8.23 Hz), 8.08 (d, 2 H, *J* = 8.34 Hz), 7.85 (d, 1 H, *J* = 8.88 Hz), 7.93−7.86 (m, 2 H), 7.77 (d, 1 H, *J* = 1.62 Hz), 7.74 (d, 1 H, *J* = 1.62 Hz), 7.69 (d, 1 H, *J* = 1.65 Hz), 7.52 (d, 2 H, *J* = 8.06 Hz), 7.34−7.25 (m, 3 H), 6.92 (td, 2 H, *J* = 7.24 and 1.34 Hz), 6.36 (dd, 1 H, *J* = 5.92 Hz), 5.34 (d, 1 H, *J* = 2.42 Hz), 3.39 (s, 3 H), 2.50 (s, 3 H). − MS; *m*/*z* (%): 891 (35) [M − PF_6^-], 746 (100) [M − 2PF_6^- + e^-].

Compound 7: ^{1}H NMR (200 MHz, CD_2Cl_2): δ = 8.75 (dd, 1 H, *J* = 6.72 Hz, *J* = 1.56 Hz), 8.32 (d, 1 H, *J* = 8.86 Hz), 8.34−8.17 (m, 5 H), 8.10 (s, 2 H), 7.87 (dd, 2 H, *J* = 7.8 Hz, *J* = 1.45 Hz), 7.79 (d, 2 H, *J* = 8.32 Hz), 7.47 (d, 2 H, *J* = 8.06 Hz), 7.37 (dd, 2 H, *J* = 5.38 Hz, *J* = 1.36 Hz), 7.17 (d, 2 H, *J* = 8.34 Hz), 7.11−7.09 (m, 2 H), 6.45 (d, 2 H, *J* = 8.88 Hz), 6.07 (d, 2 H, *J* = 8.60 Hz), 3.52 (s, 3 H), 2.52 (s, 3 H). − MS (FAB-MS) (nitrobenzyl alcohol matrix); *m*/*z* (%): 855 (40) [M^+], 710 (100) [M − PF_6^-].

Ru(dqpy)$_2$(PF$_6$)$_2$ (5): A suspension of Ru(dqpy)Cl_3 (0.070 g, 0.11 mmol) and dqpy (0.049 g, 0.12 mmol) was heated to reflux for 6 h in glacial acetic acid (8 mL) with 2−3 drops of *N*-ethylmorpholine. Yield 0.040 g (30%). − ^{1}H NMR (200 MHz, CD_2Cl_2): δ = 9.09 (d, 8 H, *J* = 7.88 Hz), 8.24 (d, 8 H, *J* = 10.08 Hz), 8.07 (4 H, *J* = 8.12 Hz), 7.79 (d, 1 H, *J* = 1.48 Hz), 7.75 (t, 2 H, *J* = 1.72 Hz), 7.71 (d, 1 H, *J* = 1.72 Hz), 7.68−7.54 (m, 8 H), 2.56 (s, 6 H). − MS (FAB-MS) (nitrobenzyl alcohol matrix); *m*/*z* (%): 1093 (15) [M − PF_6^-], 948 (35) [M − 2PF_6^- + e^-].

Ru(dqpy)(mappy)(PF_6)$_2$ (6): A suspension of Ru(dqpy)Cl_3 (0.08 g, 0.13 mmol) and mappy (0.048 g, 0.13 mmol) was heated to reflux for 5 h in glacial acetic acid (12 mL) with 2−3 drops of *N*-ethylmorpholine. Yield 0.076 g (49%) of **6** as a dark violet solid. − ^{1}H NMR (300 MHz, CD_2Cl_2): δ = 9.06−8.90 (m, 3 H), 8.70 (s, 2 H), 8.54 (d, 1 H, *J* = 8.76 Hz), 8.39 (d, 2 H, *J* = 8.22 Hz), 8.32 (d, 1 H, *J* = 8.97 Hz), 8.24−8.18 (m, 5 H), 7.83 (td, 3 H, *J* = 1.11 Hz, *J* = 1.26 Hz, *J* = 1.08 Hz), 7.76 (s, 2 H), 7.67−7.52 (m, 7 H), 7.36 (d, 1 H, *J* = 8.22 Hz), 6.60 (d, 2 H, *J* = 8.79 Hz), 6.11 (d, 2 H, *J* = 8.58 Hz), 3.51 (s, 3 H), 2.60 (s, 3 H), 1.96 (s, 3 H). − MS (FAB-MS) (nitrobenzyl alcohol matrix); *m*/*z* (%): 1047 (80) [M − PF_6^-], 902 (100) [M − 2PF_6^- + e^-], 451 (55) [(M − 2PF_6^-)/ 2].

Ru(mappy)(dtp)(PF_6) (8): A suspension of Ru(mappy)Cl_3 (0.060 g, 0.10 mmol) and dtpH (0.039 g, 0.10 mmol) was heated to reflux for 3 h in glacial acetic acid (6 mL) with 2−3 drops of *N*-ethylmorpholine. Yield 0.040 g (41%).. − ^{1}H NMR (200 MHz, CD_3CN): δ = 8.57 (d, 1 H, *J* = 2.68 Hz), 8.39−8.27 (m, 4 H), 8.20 (d, 1 H, *J* = 8.86 Hz), 8.09 (d, 1 H, *J* = 8.84 Hz), 7.99 (d, 2 H, *J* = 6.71 Hz), 7.92 (d, 1 H, *J* = 6.2 Hz), 7.82 (d, 2 H, *J* = 7.8 Hz), 7.50 (d, 1 H, *J* = 9.68 Hz), 7.34−7.18 (m, 2 H), 6.59−6.52 (m, 2 H), 6.32 (d, 1 H, *J* = 8.32 Hz), 6.12 (d, 2 H, *J* = 8.31 Hz), 5.87−5.76 (br, 3 H), 5.70 (d, 2 H, *J* = 8.32 Hz), 5.04 (s, 1 H), 3.66 (s, 3 H), 2.08 (s, 3 H), 1.82 (s, 3 H), 1.64 (s, 3 H). − MS (FAB-MS) (nitrobenzyl alcohol matrix); *m*/*z* (%): 838 (100) [M − PF_6^-]

Ru(ttpy)(dtp)(PF_6) (9): A mixture of Ru(ttpy)Cl_3 (0.070 g, 0.13 mmol) and dtpH (0.047 g, 0.13 mmol) was heated to reflux for 3 h in glacial acetic acid (6 mL) with 2−3 drops of *N*-ethylmorpholine. Yield 0.042 g (35%). − ^{1}H NMR (200 MHz, CD_2Cl_2): δ = 8.39 (s, 2 H), 8.31 (d, 1 H, *J* = 8.32 Hz), 8.24 (d, 2 H, *J* = 7.80 Hz), 8.48−8.20 (m, 4 H), 8.05 (d, 1 H, *J* = 8.86 Hz), 7.96 (d, 2 H, *J* = 8.06 Hz), 7.74 (d, 1 H, *J* = 7.78 Hz), 7.73 (td, 2 H, *J* = 1.48 Hz, *J* = 6.72 Hz), 7.53 (d, 2 H, *J* = 7.8 Hz), 7.30 (d, 2 H, *J* = 8.32 Hz), 7.24 (d, 1 H, *J* = 1.22 Hz), 6.94 (dd, 1 H, *J* = 11.56 Hz, *J* = 1.34 Hz), 6.93 (t, 1 H, *J* = 1.62 Hz), 6.68 (d, 2 H, *J* = 7.8 Hz), 6.57 (dd, 1 H, *J* = 6.72 Hz, *J* = 1.30 Hz), 5.97 (d, 2 H, *J* = 7.8 Hz), 2.53 (s, 3 H), 2.02 (s, 3 H), 1.78 (s, 3 H). − MS (FAB-MS) (nitrobenzyl alcohol matrix); *m*/*z* (%): 784 (100) [M − PF_6^-].

Ru(dqpy)(dtp)(PF_6) (10): A suspension of Ru(dqpy)Cl_3 (0.070 g, 0.11 mmol) and dtpH (0.041 g, 0.11 mmol) was heated to reflux for 3 h in glacial acetic acid (10 mL) with 2−3 drops of *N*-ethylmorpholine. Yield: 0.072 g (64%) of **10** as a dark purple solid. − ^{1}H NMR (300 MHz, CD_2Cl_2): δ = 8.59 (s, 3 H), 8.52 (d, 1 H, *J* = 8.76 Hz), 8.44 (s, 3 H), 8.38 (d, 1 H, *J* = 8.76 Hz), 8.29 (d, 1 H, *J* = 6.96 Hz), 8.26 (d, 1 H, *J* = 6.39 Hz), 8.02 (t, 7 H, *J* = 8.76 Hz, *J* = 7.14 Hz), 7.79 (d, 2 H, *J* = 8.04 Hz), 7.68 (t, 2 H, *J* = 6.93 Hz, *J* = 8.22 Hz), 7.58 (d, 2 H, *J* = 7.86 Hz), 7.50 (td, 2 H, *J* = 1.11 Hz, *J* = 1.11 Hz, *J* = 1.08 Hz), 7.37 (d, 2 H, *J* = 8.4 Hz), 6.75 (d, 2 H, *J* = 7.68 Hz), 6.54 (d, 1 H, *J* = 6.57 Hz), 6.09 (d, 2 H, *J* = 7.86 Hz), 2.61 (s, 3 H), 2.29 (s, 3 H), 2.08 (s, 3 H). − MS (FAB-MS) (nitrobenzyl alcohol matrix); *m*/*z* (%): 1029 (5) [M^+], 884(100) [M − PF_6^-].

X-ray Data Collection: Details concerning the crystal structure are given in Table 4. For all computations the MolEN package was used.[19] Crystallographic data (excluding structure factors) for the structure reported in this paper have been deposited with the Cambridge Crystollographic Data Centre as supplementary publication no. CCDC-119759. Copies of the data can be obtained free of charge on application to CCDC, 12 Union Road, Cambridge CB21EZ, UK [Fax: (internat.) +44(1223)336-033; E-mail: deposit@ccdc.cam.ac.uk].

Table 4. X-ray experimental data of Ru(ttpy)(mapH)(Cl)(PF_6) (**4**)

Formula	$C_{41}H_{31}N_5OClRu{\cdot}PF_6$
Molecular mass	891
Color	red
Crystal system	monoclinic
a [Å]	15.378(4)
b [Å]	13.263(3)
c [Å]	20.306(6)
β [deg]	90.54(2)
Volume [Å^3]	4141.4
Z	4
$D_{calcd.}$ [g cm^{-3}]	1.553
Wavelength [Å]	1.5418
m [cm^{-1}]	47.206
Space group	$P2_1/c$
Diffractometer	Philips PW1100/16
Crystal dimensions [mm]	0.30 × 0.20 × 0.10
Temperature [°C]	−100
Radiation (monochromated)	Cu-K_α graphite
Mode	q/2q flying step-scan
Scan speed [deg^{-1}]	0.020
Step width [deg]	0.05
Scan width [deg]	1.10 + 0.14*tg(q)
Octants	±*h*+*k*+*l*
$q_{min/max}$ [deg]	3/54
Number of data collected	5459
Number of data with *I* > 3s(*I*)	4247
Number of variables	559
$Abs_{min/max}$	0.89/1.11
R(*F*)	0.037
$R_w(F)$	0.062
P	0.08
Largest peak in final diff. [e·Å^{-3}]	0.07
GOF	1.434

Acknowledgments

This work was performed with financial support from the CNRS (France), CNR (Italy), and the HCM Research Network (Contract no. ERBCH RXCT930145). We thank André De Cian, Nathalie Kyritsakas and Jean Fischer for the X-ray structure and Patrice Staub for his technical assistance.

[1] [1a] A. Juris, V. Balzani, F. Barigelletti, S. Campagna, P. Belser, A. Von Zelewsky, *Coord. Chem. Rev.* **1988**, *84*, 85−277. − [1b] V. Balzani, F. Scandola, *Supramolecular Photochemistry*; Ellis Horwood; Chichester, **1991**. − [1c] J.-P. Sauvage, J.-P. Collin, J.-C. Chambron, S. Guillerez, C. Coudret, V. Balzani, F. Barigelletti, L. De Cola, L. Flamigni, *Chem. Rev.* **1994**, *94*, 993−1019.

[2] [2a] F. Barigelletti, A. Juris, V. Balzani, P. Belser, A. Von Zelewsky, *Inorg. Chem.* **1983**, *22*, 3335−3339. − [2b] R. S. Lumpkin, E. M. Kober, L. A. Worl, Z. Murtaza, T. J. Meyer, *J. Phys. Chem.* **1990**, *94*, 239−243. − [2c] P. A. Anderson, G. F. Strousse, J. A. Treadway, F. R. Keene, T. J. Meyer, *Inorg. Chem.* **1994**, *33*, 3863−3864. − [2d] M. Maestri, N. Armarolio, V. Balzani, E. C. Constable, A. M. W. Cargill Thompson, *Inorg. Chem.* **1995**, *34*, 2759−2767.

[3] T. J. Meyer, *Pure Appl. Chem.* **1986**, *58*, 1193− 1206.

[4] [4a] C. R. Hecker, A. K. I. Gushurst, D. R. McMillin, *Inorg. Chem.* **1991**, *30*, 538−541. − [4b] A. C. Benniston, V. Grosshenny, A. Harriman, R. Ziessel, *Angew. Chem. Int. Ed. Engl.* **1994**, *33*, 1884−1885. − [4c] G. F. Strousse, J. R. Schoonover, R. Duesing, S. Boyde, W. E. Jones Jr., T. J. Meyer, *Inorg. Chem.* **1995**, *34*, 473−487. − [4d] N. H. Damauer, T. R. Boussie, M. Devenney, J. K. McCusker, *J. Am. Chem. Soc.* **1997**, *119*, 8253−8268. − [4e] L. Hammarstrøm, F. Barigelletti, L. Flamigni, M. T. Indelli, N. Armaroli, G. Calogero, M. Guardigli, A. Sour, J.-P. Collin, J.-P. Sauvage, *J. Phys. Chem.* **1997**, *101*, 9061−9069.

[5] J. A. Treadway, B. Loeb, R. Lopez, P. A. Anderson, F. R. Keene, T. J. Meyer, *Inorg. Chem.* **1996**, *35*, 2242−2246.

[6] A. P. Zipp, L. A. Sacksteder, J. Streich, A. Cook, J. N. Demas, B. A. DeGraff, *Inorg. Chem.* **1993**, *32*, 5629−5632.

[7] J.-P. Collin, R. Kayhanian, J.-P. Sauvage, G. Calogero, F. Barigelletti, A. De Cian, J. Fischer, *J. Chem. Soc., Chem. Commun.* **1997**, 775−776.
[8] [8a] P. Reveco, J. H. Medley, A. R. Garber, N. S. Bhacca, J. Selbin, *Inorg. Chem.* **1985**, *24*, 1096−1099. − [8b] E. C. Constable, J. M. Holmes, *J. Organomet. Chem*. **1986**, *301*, 203−208.
[9] E. C. Constable, M. J. Hannon, *Inorg. Chim. Acta* **1993**, *211*, 101−110.
[10] A. Gerli, J. Reedijk, M. T. Lakin, A. L. Spek, *Inorg. Chem.* **1995**, *34*, 1836−1843.
[11] G. B. Deacon, J. M. Patrick, B. W. Skelton, N. C. Thomas, A. H. White, *Aust. J. Chem.* **1984**, *37*, 929−945.
[12] M. Beley, S. Chodorowski, J.-P. Collin, J.-P. Sauvage, L. Flamigni, F. Barigelletti, *Inorg. Chem.* **1994**, *33*, 2543−2547.
[13] J.-P. Collin, M. Beley, J.-P. Sauvage, F. Barigelletti, *Inorg. Chim. Acta* **1991**, *186*, 91−93.
[14] S. Chardon-Noblat, J.-P. Sauvage, *Tetrahedron* **1991**, *47*, 5123−5132.
[15] C. O. Dietrich-Buchecker, J. F. Nierengarten, J.-P. Sauvage, N. Armaroli, V. Balzani, L. De Cola, *J. Am. Chem. Soc.* **1993**, *115*, 11237−11244.
[16] J.-P. Collin, S. Guillerez, J.-P. Sauvage, F. Barigelletti, L. De Cola, L. Flamigni, V. Balzani, *Inorg. Chem.* **1991**, *30*, 4230−4238.
[17] B. P. Sullivan, D. J. Salmon, T. J. Meyer, *Inorg. Chem.* **1978**, *17*, 3334−3341.
[18] B. P. Sullivan, J. M. Calvert, T. J. Meyer, *Inorg. Chem.* **1980**, *19*, 1404−1407.
[19] C. K. Fair In *MolEN*, *An interactive Intelligent System for Crystal Structure Analysis*, Nonius, Delft, The Netherlands, **1990**.
[20] [20a] J. N. Demas, G. A. Crosby, *J. Phys. Chem.* **1971**, *75*, 991. − [20b] K. Nakamaru, *Bull. Chem. Soc. Jpn.* **1982**, *55*, 2697.
[21] F. Barigelletti, L. Flamigni, M. Guardigli, A. Juris, M. Beley, S. Chodorowski-Kimmes, J.-P. Collin, J.-P. Sauvage, *Inorg. Chem*. **1996**, *35*, 136−142.

Received June 11, 1999
[I99210]

Two Examples of Novel and Unusual Double-Layered, Two-Dimensional Cu^{II} Compounds with Bridging 1,3-Bis(1,2,4-triazol-1-yl)propane

Gerard A. van Albada,*[a] Reinier C. Guijt,[a] Jaap G. Haasnoot,[a] Martin Lutz,[b] Anthony L. Spek,[b] and Jan Reedijk*[a]

Keywords: Polymeric copper complexes / Group–subgroup relationships / 2D-sheets

The synthesis and characterisation of two new polymeric Cu^{II} complexes is described, i.e. $\{[Cu(btp)_2(CH_3CN)(H_2O)](CF_3SO_3)_2\}_n$ (**1**) and $\{[Cu(btp)_2(CH_3CN)_2](ClO_4)_2\}_n$ (**2**), in which btp = [1,3-bis(1,2,4-triazol-1-yl)propane]. Compound **1** crystallizes in space group $P2_1/c$ with a = 11.9337(15) Å, b = 20.108(6) Å, c = 12.748(6) Å, β = 92.247(14)°, and Z = 4. Compound **2** crystallizes in space group $Pna2_1$ with a = 18.770(8) Å, b = 12.648(8) Å, and c = 12.019(8) Å. The structures refined to $R1$ values of 0.0683 for **1** and 0.0846 for **2**. In both structures the Cu^{II} ions are linked by the bridging ligands, resulting in two-dimensional networks. Two such curved layers are arranged on top of each other with center-to-center of layer distances of 2.12 Å in **1** and 1.98 Å in **2**. Such double layers are separated from each other by 10.05 Å in **1** and 9.385 Å in **2**. The space between the double layers is occupied with interstitial anions. No significant interaction between Cu^{II} ions is observed by EPR and magnetic susceptibility measurements. The compounds form a new class of a lattice engineered system held together by the Cu^{II} ions. – The coordination geometry of the copper ions is distorted octahedral, with the equatorial plane formed by the N4 nitrogens of the four triazole groups and the axial sites occupied by solvent molecules; acetonitrile and water in structure **1** and two acetonitrile molecules in structure **2**. The two structures are related by a group–subgroup relationship, which appears to be the first such case in supramolecular chemistry. – The Cu–N vibrations in the FIR region are found at 274 cm^{-1} for **1**, and at 276 cm^{-1} for **2**. The ligand-field maxima are observed at about $16{\cdot}10^3$ cm^{-1}, with a shoulder at about $12{\cdot}10^3$ cm^{-1}. The ν_{CN} stretching vibrations of the acetonitrile molecules are found at 2303 and 2261 cm^{-1} for **1**, and at 2313, 2294, 2278, and 2260 cm^{-1} for **2**.

Introduction

Metal complexes with supramolecular features in their structure have recently aroused much interest as materials with potentially new electronic, optical, magnetic, or catalytic properties.[1] Given the strong preference of Cu^{II} for square-planar based geometries, bridging ligands would be almost ideally suited for building a square 2-dimensional lattice. Well-known classical cases are structures like $(cation)_2CuCl_4$[2] (cation = organic substituted ammonium). Such 2D systems also allow the coordination of weak axial ligands, like in some clathrate compounds.[3]

When bridging ligands are large, cavities result which need to be filled to form a stable lattice. and This can be accomplished by, for instance, the counter anions and/or guest molecules, or by the formation of interpenetrating lattices.[1a] With proper vertical stacking of such 2D systems, supramolecular systems with channels might result, in which the anions and/or guest molecules could move or migrate. A totally different way of packing would be a case where layers occur in pairs, and be organized in such a way that a corner of a lattice grid in one 2D lattice cell, lies above the cavity of the other cell, filling it up with its axial ligand. In such a case double-layers of 2D lattices result, which as such can be separated by counter anions and solvent/guest molecules. Such systems, when properly stabilized with strongly bridging ligands, would have the axial ligand sites of the copper ions accessible for ligand exchange and/or − more importantly − catalytic reactions, with the reagents transported through the spaces [slabs] between the double-layers.

For Cu^{II} a number of 2D and 3D frameworks are already known with *N,N′*-bidentate spacers.[4] In most cases the spacer molecules are rigid heterocyclic ligands;[4a,5] however, only a few structures are known in which the 2D or 3D frameworks consist of two heterocyclic donors linked by spacers of variable length, like in the compound Cu^{I}[(1,4-bis(4-pyridyl)butadiyne],[4b] and Cu^{II} and Mn^{II} compounds with [(1,2-bis(imidazol-1′-yl)alkane] ligands.[6]

Recently, a new class of ligands, [bis(1,2,4-triazol-1-yl)-alkanes], was developed in our laboratories and characterised by X-ray diffraction. A variety of new types of polymeric 2D and 3D frameworks with Fe^{II} and Mn^{II} were found.[7]

We now wish to report the first case of two examples of such lattice-engineered systems using Cu^{II}, and generating double layers of a 2D system. By the using the ligand [1,3-bis(1,2,4-triazol-1-yl)propane] (abbreviated btp), we synthe-

[a] Leiden Institute of Chemistry, Gorlaeus Laboratories, Leiden University,
P. O. Box 9502, NL-2300 RA Leiden, The Netherlands
E-mail: reedijk@chem.leidenuniv.nl
[b] Bijvoet Center for Biomolecular Research, Departement of Crystal and Structural Chemistry, Utrecht University,
Padualaan 8, NL-3584 CH Utrecht, The Netherlands

Supporting information for this article is available on the WWW under http://www.wiley-vch.de/home/eurjic or from the author: http://www.cryst.chem.uu.nl/structures/s1725a/s1725a.html

 © WILEY-VCH Verlag GmbH, D-69451 Weinheim, 2000 1434−1948/00/0101−0121 $ 17.50+.50/0

sized two compounds, i.e. $Cu(btp)_2(CH_3CN)(H_2O)](CF_3SO_3)_2$ (**1**) and $[Cu(btp)_2(CH_3CN)_2](ClO_4)_2$ (**2**), from which crystal structures were obtained.

Results and Discussion

Description of the Crystal Structures

The structures of both compounds are depicted in Figures 1 and 2, respectively, together with the numbering scheme and relevant bond length and bond angle information. In both structures, the coordination polyhedra of the Cu^{II} ions are distorted octahedra, in which the equatorial plane is formed by the N4 nitrogens of the triazole groups, with Cu−N distances of 2.009(4)−2.020(3) Å in **1** and 1.974(12)−2.039(12) Å in **2**. The axial positions in the octahedra are occupied by weaker ligands, i.e. solvent molecules, acetonitrile and water in **1**, and two acetonitrile molecules in **2**. The axial distances in **1** are 2.399(4) Å for Cu−N and 2.462(4) Å for Cu−O. In **2** the axial Cu−N distances are 2.260(15) and 2.665(15) Å, the latter at a semi-coordination distance.

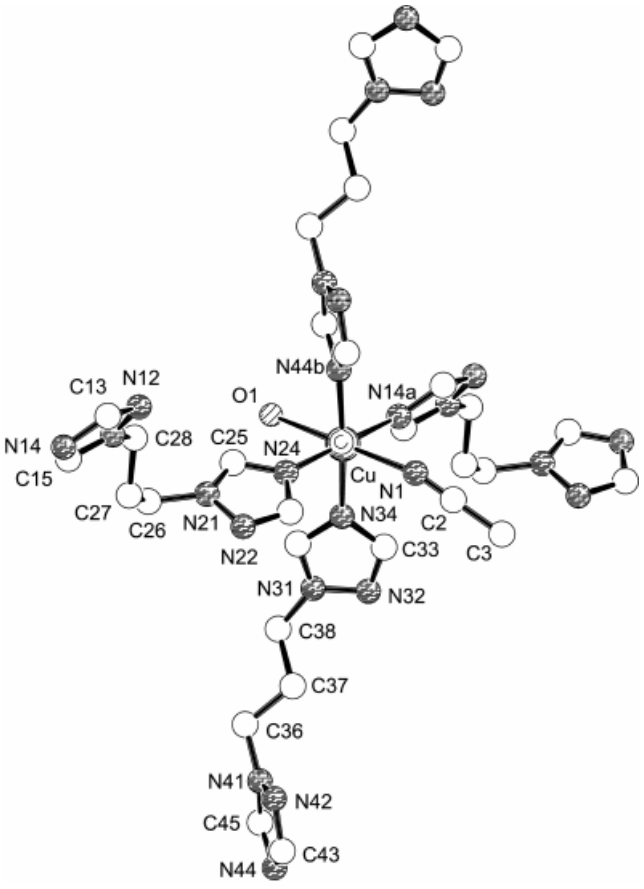


Figure 1. Coordination environment of the Cu atom in $\{[Cu(btp)_2(CH_3CN)(H_2O)](CF_3SO_3)_2\}_n$ (Structure **1**) with atom-labelling scheme. Hydrogen atoms and triflate anions are omitted for clarity. Symmetry operations: $a = x - 1, y, z$; $b = x, y, z - 1$. Bond length [Å] and angles [°]: Cu−O1 2.462(4); Cu−N1 2.399(4); Cu−N14a 2.013(3); Cu−N34 2.020(3); Cu−N44b 2.011(3); Cu−N24 2.010(3); N24−Cu−N44b 91.05(13); N24−Cu−N14a 178.51(14); N44b−Cu−N14a 90.04(13); N24−Cu−N34 89.11(13); N44b−Cu−N34 175.17(15); N14a−Cu−N34 89.72(13); N24−Cu-N1 91.93(14); N44b−Cu−N1 93.12(14); N14a−Cu−N1 89.02(14); N34−Cu−N1 91.70(14); N24−Cu−O1 90.43(14); N44b−Cu−O1 88.44(13); N14a−Cu−O1 88.59(13); N34−Cu−O1 86.73(13); N1−Cu−O1 177.14(13).

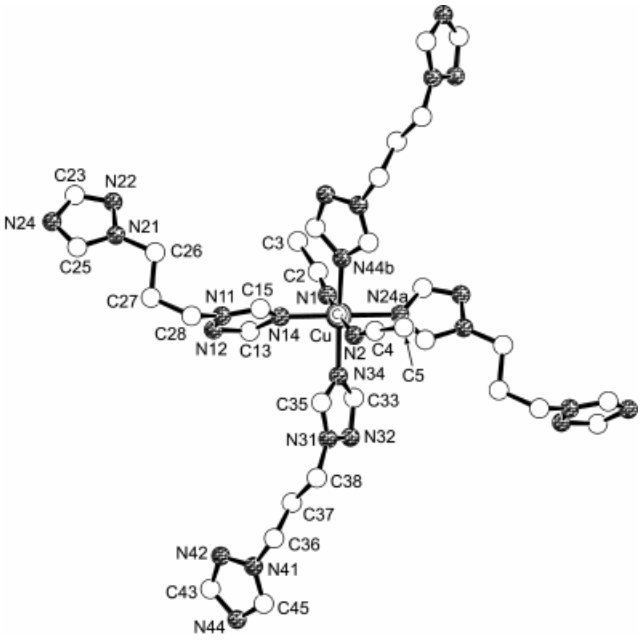


Figure 2. Coordination environment of the Cu atom in $\{[Cu(btp)_2(CH_3CN)_2](ClO_4)_2\}_n$ (structure **2**) with atom-labelling scheme. Hydrogen atoms and perchlorate anions are omitted for clarity. Only one configuration of the disordered acetonitrile (N1−C3) is shown. Symmetry operations: $a = x, y, z + 1$; $b = x, y + 1, z$. Bond length [Å] and angles [°]: Cu−N1 2.261(15); Cu−N14 1.974(13); Cu−N34 2.029(14); Cu−N24a 2.040(13); Cu−N44b 2.009(14); Cu−N2 2.665(15); N14−Cu−N44b 90.6(5); N14−Cu−N34 89.9(5); N44b−Cu−N34 169.0(5); N14−Cu−N24a 178.0(5); N44b−Cu−N24a 89.1(5); N34−Cu−N24a 90.1(5); N14−Cu−N1 90.1(5); N44b−Cu−N1 92.7(6); N34−Cu−N1 98.3(6); N24a−Cu−N1 91.9(5); N14−Cu−N2 91.0(5); N44b−Cu−N2 84.5(5); N34−Cu−N2 84.5(5); N24a−Cu−N2 87.0(5); N1−Cu−N2 177.0(5).

In both structures, the Cu^{II} ions are linked by the btp ligands, building up polymers to a two-dimensional network. In **1**, this 2D sheet is situated parallel to the crystallographic *a,c* plane. A second layer with no bonding interaction to the first one, is situated 2.12 Å above it. So in fact these two layers, shown in Figure 3, should be considered as a double layer. The double layers are stacked in the crystallographic *b* direction with a distance of $b/2 = 10.054$ Å. The space between the sets of double layers is filled up with the triflate anions as shown in Figure 4. The crystal structure of **1** is further stabilized by H-bonding between the water molecule and oxygens of the triflate anion [O1···O2 2.780(6) Å and O1···O5 2.855(5) Å].

The situation in **2** is quite similar. Here the 2D sheets are located parallel to the crystallographic *b,c* plane, and stacked in the *a* direction. The distance within the double layer is even smaller (1.98 Å). Because perchlorate anions are smaller than triflate anions the distance between the double layers is shortened to 9.385 Å ($= a/2$).

The cell parameters of both structures differ slightly, which must be caused by the different anions. The reason

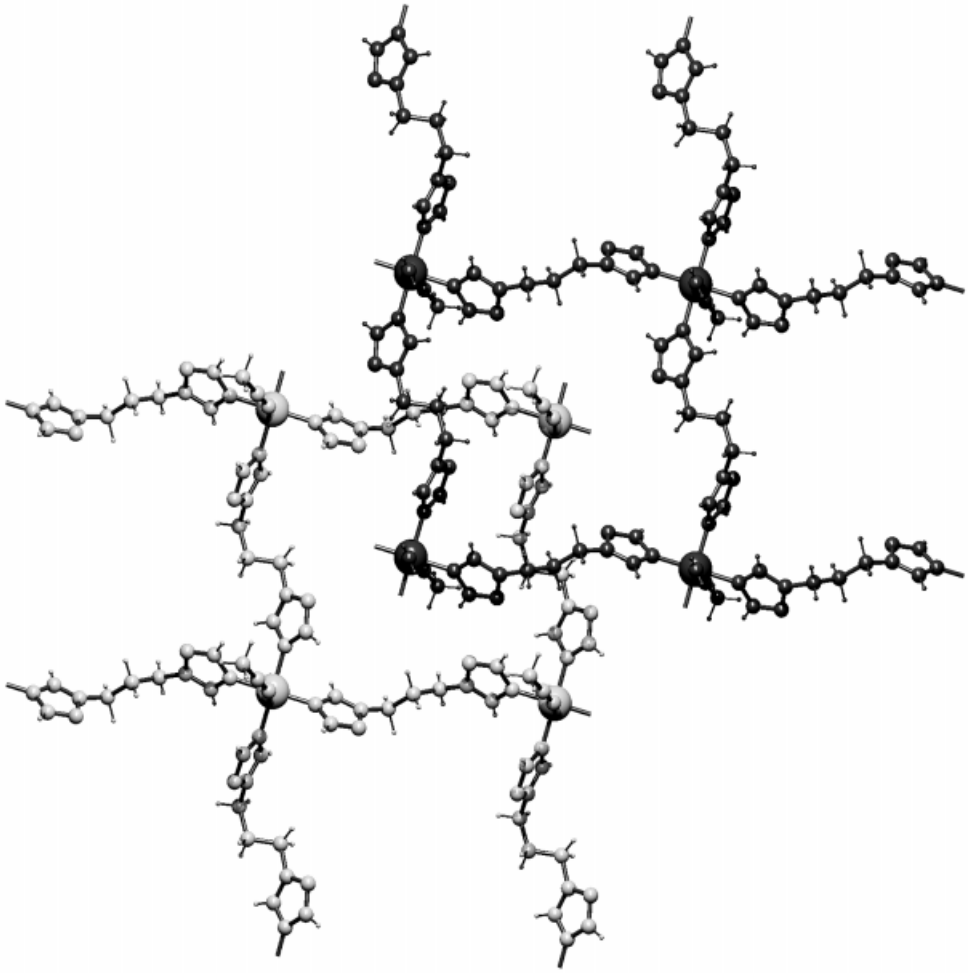


Figure 3. View along the crystallographic b-axis on one double layer in structure **1**

for changing the orientations of the unit cell in **1** and **2** was to achieve the standard setting of the space groups. The space groups $P2_1/c$ for **1** and $Pna2_1$ for **2** are both subgroups of the same super-group; *Pnma.* While such "family tree" relations are well-known in other areas of inorganic chemistry, such as in perovskite-like structures,[8] to our knowledge, this is the first case of such a group−subgroup relationship in supramolecular coordination chemistry.

The shortest Cu−Cu distances are 8.753(3) Å in **1** and 8.946(4) Å in **2**. These distances are shorter than observed in $[(Cu(bim)_{2,5})(ClO_4)_2 \cdot 2\ MeOH]$ [bim = 1,2-bis(imidazol-1′-yl)ethane],[6a] one of the few compounds that also have an alkane chain as a spacer, in which the Cu−Cu distance is 12.55 Å. In fact, this confirms the importance of this family of ligands in adjusting the metal-metal distance. With other metals like Fe^{II} and Mn^{II}, this type of ligand [bis(1,2,4-triazol-1-yl)alkanes] leads to a variety of 2D and 3D structures.[7]

Ligand Field Spectra

The d-d transitions in the UV-Vis-NIR absorption spectra for both Cu compounds are found at about $16{\cdot}10^3$ cm^{-1}, with a shoulder at about $12{\cdot}10^3$ cm^{-1} (See Table 1). These values agree with ligand field transitions for copper square-planar or square-planar based CuN_4 or a CuN_4X_2 chromophore.[9]

EPR and Magnetic Properties

The EPR measurements on **1** and **2** reveal the normal parameters (see Table 1) for a Cu^{II} isolated spin $S = {}^1/_2$,[9a] as almost no Cu−Cu interaction is present due to the large distances between the Cu centres. The $A_{//}$ value of ca. 17 mT (measured as a frozen solution at 77 K) is consistent with a $CuN_4(X)_{1-2}$ (X = N,O) geometry around the copper ion.[9] Magnetic susceptibility data recorded down to 40 K indicate a magnetic moment of 1.8 B.M., below which a slight decrease is observed down to 5 K, which is at best in agreement with a very weak exchange coupling.

Infrared Spectra

In the infrared spectrum the vibrations of the acetonitrile molecules are found at 2261 and 2303 cm^{-1} for compound

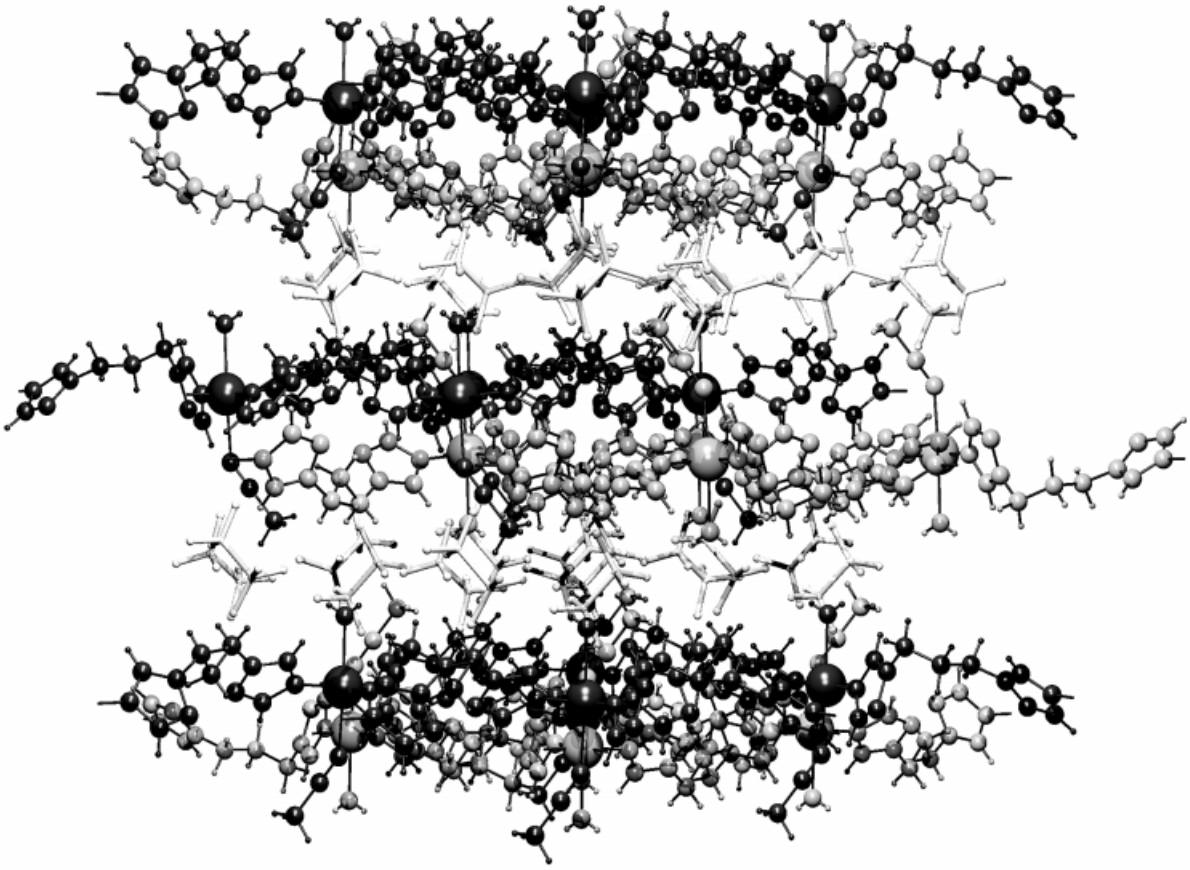


Figure 4. Stacking of the double layers in structure **1** in the direction of the crystallographic *b* axis. The double layers are separated by the triflate anions. (View along [1.0.1])

Table 1. UV-VIS-NIR, EPR, and FIR spectral data[a] for Cu^{II} compounds with btp

Compound	UV-VIS-NIR [10^3 cm^{-1}]	EPR values, (powder, room temp.) $g_\perp$, $g_{//}$	EPR values, 77 K[b] $g_\perp$, $g_{//}$, $A_{//}$ [mT]	MIR [cm^{-1}] ν_{CN}	FIR [cm^{-1}] ν_{Cu-N}
1, $\{[Cu(btp)_2(CH_3CN)(H_2O)](CF_3SO_3)_2\}_n$	ca.12.0 (sh) 16.1	2.07, ca.2.4 (vw)	2.06, 2.27, 17.3	2303 (w), 2261 (m)	274
2, $\{[Cu(btp)_2(CH_3CN)_2](ClO_4)_2\}_n$	ca.12.0 (sh) 16.8	2.07, ca.2.4 (vw)	2.06, 2.30, 16.4	2313 (w), 2278 (m) 2294 (vw), 2260 (m,sh)	276

[a] Abbreviations: vbr = very broad, vw = very weak, sh = shoulder. – [b] Frozen solution in DMSO/MeOH (1:1)

1, which contains only one coordinated acetonitrile molecule. In compound **2**, which has two acetonitrile molecules, with one short distance of 2.260(15) Å and one long Cu–N distance of 2.665(15) Å, the vibrations are found at 2313 and 2278 cm^{-1} for the first and at 2294 and 2260 cm^{-1} for the second acetonitrile molecule. In each case, the bands at lower frequencies are assigned to the C≡N stretching vibration and those at higher frequencies to the $\nu_3+\nu_4$ combination band mixed with C≡N stretch.[10] In the far-infrared region, the Cu–N vibrations are clearly visible as strong broad peaks at 274 cm^{-1} for **1** and at 276 cm^{-1} for **2**, which is comparable with Cu–N vibrations given in the literature.[11]

In summary, the compounds presented herein are a first step in a new series of supramolecular compounds, and we are currently working on the use of metal ions other than Cu^{II}, as well as changing the anions and axial ligands to synthesizing materials that can be used as host/guest molecules and can be active in catalytic processes.

Experimental Section

General: C, H, N, and Cu determinations were performed by the Microanalytical Laboratory of University College, Dublin, Ireland. – Ligand field spectra were obtained on a Perkin–Elmer Lambda 900 spectrophotometer using the diffuse reflectance technique, with MgO as a reference. – X-band EPR spectra were obtained on a Jeol RE2x electron spin resonance spectrometer using DPPH (g = 2.0036) as a standard. – FTIR spectra were obtained on a Bruker 113v infrared spectrophotometer as KBr disks (4000–400 cm^{-1},

mirror velocity 0.166 cm/s, resolution 2 cm^{-1}), or as polyethylene mulls (600−100 cm^{-1}, mirror velocity 0.099 cm/sec, resolution 2 cm^{-1}, Mylar 3.5 μ beam splitter). − Magnetic susceptibilities were measured in the temperature range 5−300 K with a Manics DSM-8 susceptometer. Data were corrected for magnetization of the sample holder and for diamagnetic contributions, which were estimated from the Pascal constants.

Synthesis of the Ligand. − 1,3-Bis(1,2,4-triazol-1-yl)propane: A modified literature procedure[12] was followed. To a solution of 0.5 mol 1*H*-1,2,4-triazole in 200 mL of absolute ethanol, an equimolar amount of metallic sodium was added in small portions, while cooling in ice and stirring vigorously. When the formation of sodium triazolate was completed, 0.22 mol of 1,3-dichloropropane was added, while still cooling and stirring. The solution was then heated under reflux for 7 days. After cooling to room temperature the precipitate of sodium chloride was filtered off. The ethanol filtrate was evaporated to a small volume, while the desired product separated. The compound was recrystallized from absolute ethanol (yield 64%). − ^{1}H NMR data ([D$_6$]DMSO, TMS as a standard): δ = 2.29 (q, 2 H), 4.18 (t, 4 H), 7.97 (s, 2 H), 8.52(s, 2 H).

Compounds 1 and 2: 1.2 mmol of hydrated Cu^{II} salt and 1.2 mmol of the ligand were each dissolved in 10 mL of water/acetonitrile (1:1). The Cu^{II} salt solution was then added slowly to the ligand solution and filtered to remove any undissolved material. After a few days the blue-green products separated and were isolated by filtration and dried in air (yield 70%). − Elemental analysis: for $Cu(btp)_2(CH_3CN)(H_2O)](CF_3SO_3)_2$: found (calc) (%) 27.82 (28.73) C, 3.24 (3.24) H, 22.43 (21.81) N, 14.67 (14.66) F, 8.18 (8.34) Cu. For $[Cu(btp)_2(CH_3CN)_2](ClO_4)_2$: found (calc) (%) 29.25 (30.84) C, 3.59 (3.74) H, 27.21 (27.98) N, 10.22 (10.12) Cl, 9.24 (9.07) Cu.

X-ray Data Collection and Structure Determination: The single crystal X-ray diffraction work was done at 150 K on an Enraf−Nonius CAD4T diffractometer with rotating anode and Mo-*Kα* radiation (graphite monochromator, λ = 0.71073 Å). Unit cell parameters were determined from a least-squares treatment of the SET4 setting angles of 25 reflections and were checked for the presence of higher lattice symmetry. No absorption correction was considered necessary. The structures were solved with automated Patterson methods and subsequent phase refinement techniques (DIRDIF[13a]). Refinement was done with SHELXL97.[13b] In **1** the non-hydrogen atoms of the acetonitrile molecule were refined as a rigid group; the hydrogens of the water molecule were refined freely with isotropic displacement parameters. All other hydrogens were located in the difference map and were not refined. In **2** the copper and chlorine were refined with anisotropic displacement parameters. All other non-hydrogen atoms were refined freely with isotropic displacement parameters; one of the acetonitrile molecules is disordered. The hydrogen atoms were in calculated positions and not refined. All other calculations were performed with the PLATON package.[13c] Crystallographic data and information about the structure determination are given in Table 2.

Colour pictures of Figures 3 and 4 are available as supplementary material (also on http://www.cryst.chem.uu.nl/structures/s1725a/s1725a.html)

Tables with atomic coordinates of all atoms, anisotropic thermal parameters, bond lengths and angles, and tables of observed and calculated structure factors are available from one of the authors (A.L.S.)

Crystallographic data (excluding structure factors) for the structure in this paper have been deposited with the Cambridge Crystallographic Data Centre as supplementary publication no. CCDC-115865 for structure **1** and CCDC-115866 for structure **2**. Copies of the data can be obtained free of charge on application to CCDC, 12 Union Road, Cambridge CB2 1EZ, UK [Fax: (internat.) +44(1223)336−033, E-mail: deposit@ccdc.cam.ac.uk].

Table 2. Crystal data and details of the structure determination

Crystal data	**1**	**2**
Formula	$C_{18}H_{25}CuF_6N_{13}O_7S_2$	$C_{18}H_{26}Cl_2CuN_{14}O_8$
Formula weight	777.17	700.97
Crystal system	monoclinic	orthorhombic
Space group	$P2_1/c$ (No. 14)	$Pna2_1$ (No. 33)
a [Å]	11.9337(15)	18.770(8)
b [Å]	20.108(6)	12.648(8)
c [Å]	12.748(6)	12.019(8)
β [°]	92.247(14)	90
V [Å^3]	3056.7(17)	2853(3)
Z	4	4
$D_{calcd.}$ [g cm^{-3}]	1.689	1.632
F(000)	1580	1436
μ [mm^{-1}]	0.95	1.02
Crystal size [mm]	0.65 × 0.23 × 0.23	0.15 × 0.10 × 0.10
Crystal colour	blue	blue
$(\sin\nu/\lambda)_{max}$	0.649	0.572
Refl.collected/ uniques	16416/7015	4595/2358
Restraints	0	32
Parameters	432	208
Goodness-of-fit on F^2	1.032	0.976
Final *R*1, *wR*2 [$I > 2\sigma(I)$]	0.0683, 0.1722	0.0846, 0.1860
Final *R*1, *wR*2 [all data]	0.0992, 0.1920	0.1707, 0.2189
Max. diff. peak and hole [e/Å^3]	2.483, −0.868	0.719, −0.755

Acknowledgments

This work was supported in part (M.L. and A.L.S.) by the Council for Chemical Sciences of the Netherlands Organization for Scientific Research (CW-NWO). The work described in the present paper has been supported by the Leiden University Study group WFMO (Werkgroep Fundamenteel Materialen Onderzoek). The authors are indebted to the EU for a grant as Host Institute in the EU Programme Human Capital and Mobility (1994−1997). Use of the services and facilities of the Dutch National NWO/SURF Expertise Center CAOS/CAMM, under grant numbers SON 326−052 and STW NCH99.1751, is gratefully acknowledged.

[1] [1a] S. R. Batten, R. Robson, *Angew. Chem. Int. Ed.* **1998**, *37*, 1460−1494; *Angew. Chem.* **1998**, *110,* 1558−1595. − [1b] S. Kawata, S. Kitagawa, H. Kumagai, S. Iwabuchi, M. Katada, *Inorg. Chim. Acta* **1998**, *267*, 143−145 and references cited therein. − [1c] D. Braga, F. Grepioni, G. R. Desiraju, *Chem. Rev.* **1998**, *98*, 1375−1405. − [1d] K. N. Power, T. L. Hennigar, M. J. Zaworotko, *New J. Chem.* **1998**, 177−181. − [1e] S. Decurtins, H. Schmalle, R. Pellaux, *New J. Chem.* **1998**, 117−121. − [1f] M. J. Zaworotko, *Angew. Chem. Int. Ed.* **1998**, *37*, 1211−1213; *Angew. Chem.* **1998**, *110,* 1269−1271. − [1g] B. Olenyuk, A. Fechtenkötter, P. J. Stang, *J. Chem. Soc., Dalton Trans.* **1998**, 1707−1728.

[2] J. P. Steadman, R. D. Willett, *Inorg. Chim. Acta* **1970**, *4*, 367−371.

[3] [3a] W. Zhang, J. R. Jeitler, M. M. Turnbill, C. P. Landee, M. Wei, R. D. Willett, *Inorg. Chim. Acta* **1997**, *256*, 183−198. − [3b] E. Ruiz, S. Alvarez, R. Hoffmann, J. Bernstein, *J. Am. Chem. Soc.* **1994**, *116*, 8207−8221. − [3c] X.-M. Chen, M.-L. Tong, Y.-L. Luo, Z.-N. Chen, *Aust. J. Chem.* **1996**, *49*, 835−838. − [3d] C. Janiak, *J. Chem. Soc., Chem. Comm.* **1994**, 545−547. − [3e] K. N. Power, T. L. Hannigar, M. J. Zaworotko, *Chem. Comm.* **1998**, 595−596.

[4] [4a] M.-L. Tong, X.-M. Chen, X.-L. Yu, T. C. W. Mak, *J. Chem. Soc., Dalton Trans.* **1998**, 5−6 and references cited therein. − [4b] A. J. Blake, N. R. Champness, A. Khlobystov, D. A. Lemenovskii, W.-S. Li, M. Schröder, *Chem. Comm.* **1997**, 2027−2029 and references citied therin.

[5] [5a] S. Kawata, S. R. Breeze, S. Wang, J. E. Greedan, N. P. Raju, *Chem. Comm.* **1997**, 717−718. − [5b] H. Zhang, D. Fu, F. Ji, G. Wang, K. Yu, T. Yao, *J. Chem. Soc., Dalton Trans.* **1996**, 3799−3803. − [5c] P. Chaudhuri, I. Karpenstein, M. Winter, M. Lengen, C. Butzlaff, E. Bill, A. X. Trautwein, U. Flörke, H.-J. Haupt, *Inorg. Chem.* **1993**, *32*, 888−894.

[6] [6a] L. P. Wu, Y. Yamagiwa, T. Kuroda-Sowa, T. Kamikawa, M. Munakata, *Inorg. Chim. Acta* **1997**, *256*, 155−159. − [6b] P. C. M. Duncan, D. M. L. Goodgame, S. Menzer, D. J. Williams, *Chem. Comm.* **1996**, 2127−2128.

[7] J. J. A. Kolnaar, Ph. D. Thesis, Leiden University, The Netherlands, **1998**.

[8] Y. Billiet, *Acta Crystallogr.* **1978**, *A34*, 1023−1025.

[9] [9a] B. J. Hathaway, in: *Comprehensive Coordination Chemistry*, (Eds.: G. Wilkinson, R. D. Gill, J. A. McCleverty), Pergamon Press, Oxford, **1987**, Vol.5. − [9b] A. B. P. Lever, *Inorganic Electronic Spectroscopy*, 2nd. Ed, Elsevier, Amsterdam, **1984**. − [9c] J. E. Bol, W. L. Driessen, J. Reedijk, *J. Chem. Soc., Chem. Comm.* **1995**, 1365−1366. − [9d] P. J. van Koningsbruggen, J. G. Haasnoot, R. A. G. de Graaff, J. Reedijk, *Inorg. Chim. Acta* **1995**, *234*, 87−94. − [9e] S. Myllyviita, R. Sillanpää, J. J. A. Kolnaar, J. Reedijk, *J. Chem. Soc., Dalton Trans.* **1995**, 2209−2213. − [9f] W. L. Driessen, R. M. de Vos, A. Etz, J. Reedijk, *Inorg. Chim. Acta.* **1995**, *235*, 127−133.

[10] J. Reedijk, A. P. Zuur, W. L. Groeneveld, *Recl. Trav. Chim.* **1967**, *86*, 1127−1137.

[11] [11a] C.-C. Su, T.-T. Hwang, O. Y.-P. Wang, S.-L. Wang, F.-L. Liao, *Trans. Met. Chem.* **1992**, *17*, 91−96. − [11b] J. Server-Carrió, E. Escrivà, J.-V. Folgado, *Trans. Met. Chem.* **1996**, *21*, 541−545. − [11c] G. A. van Albada, M. T. Lakin, N. Veldman, A. L. Spek, J. Reedijk, *Inorg. Chem.* **1995**, *34*, 4910−4917. − [11d] G. A. van Albada, W. J. J. Smeets, A. L. Spek. J. Reedijk, *Inorg. Chim. Acta* **1999**, *288*, 220−225. − [11e] S. Amani Komaei, G. A. van Albada, I. Mutikainen, U. Turpeinen, J. Reedijk, *Polyhedron* **1999**, *18*, 1991−1997.

[12] M. R. Atkinson, J. B. Polya, *J. Chem. Soc.* **1954**, 141−145.

[13] [13a] P. T. Beurskens, G. Admiraal, G. Beurskens, W. P. Bosman, S. Garcia-Granda, R. O. Gould, J. M. M. Smits, C. Smykalla, *The DIRDIF program system.* Technical report of the Crystallography Laboratory. University of Nijmegen, The Netherlands, **1996**. − [13b] G. M. Sheldrick, SHELXL97. *Program for Crystal Structure Refinement.* University of Göttingen, Göttingen, Germany, **1997**. − [13c] A. L. Spek, PLATON, *A multipurpose crystallographic tool.* Utrecht University, Utrecht, The Netherlands, **1998**.

[14] The angles around the Cu^{II} ions are only slightly deviating from a perfect octahedron [N14−Cu−N24b = 178.51(12) and N34−Cu−N44b = 175.17(14)° for **1**; N14−Cu−N24c −178.0(6) and N34−Cu−N44d = 169.0(5)° for **2**]. The octahedron can therefore be considered as extended along the C_4 axis or as tetragonally distorted.

Received June 14, 1999
[I99211]

Synthesis and Structural Characterization of Tin(IV) *N*-nitroso-*N*-phenylhydroxylaminato Complexes: Crystal Structures of $Sn(O_2N_2Ph)_4$, $Ph_2Sn(O_2N_2Ph)_2$ and $[Me_2Sn(O_2N_2Ph)_2]_2$

Andrea Deák,[a,b] Monica Venter,[b] Alajos Kálmán,*[a] László Párkányi,[a] Lajos Radics,[a] and Ionel Haiduc*[b]

Keywords: Coordination chemistry / Inorganic rings / O ligands / Structure elucidation / Tin

Reaction of cupferron [NH_4L, L = PhN(O)NO$^-$] with tin(IV), diphenyltin(IV) and dimethyltin(IV) halides yields the cupferronato complexes SnL_4 (**1**), Ph_2SnL_2 (**2**) and $[Me_2SnL_2]_2$ (**3**). All were characterized by FT-IR, FT-Raman, NMR (^{1}H, ^{13}C and ^{119}Sn) spectroscopic methods and X-ray structural analysis. An almost ideal, very rare dodecahedral geometry is found in the structure of **1**. The hexacoordinated tin center exhibits a bicapped tetrahedral geometry in complex **2**. The tin centers are heptacoordinated in a pentagonal bipyramidal geometry in the dimeric complex **3**. These complexes incorporate five-membered SnO_2N_2 and four-membered Sn_2O_2 inorganic rings. Vibrational spectral data are consistent with the structures determined. The ^{119}Sn NMR spectra indicate that in solution **1** retains its octacoordinated nature; in compound **2** the tin atom is hexacoordinated, while in **3** the tin atom is pentacoordinated.

Introduction

We became interested in tin and organotin(IV) *N*-nitroso-*N*-phenylhydroxylaminato (cupferronato) complexes since many organotin compounds are known to display antitumor activity.[1] In addition, the biological activity of cupferron [NH_4L, L = PhN(O)NO$^-$] has also been investigated, carcinogenic, genotoxic, mutagenic and DNA-damaging effects being observed.[2] The knowledge of the coordination chemistry of cupferron could provide more information about the interaction modes of nitric oxide with metal centers of biologically important species (e.g. hemes or heme models) and could help to elucidate the mechanism of activation of the NO-receptor enzyme guanylate cyclase.[2] Moreover, a large structural diversity of cupferronato complexes is expectable due to the ability of tin to exhibit various coordination geometries[3] and to the diverse coordination patterns of cupferronato anion.[4] In order to accumulate precise structural data concerning the binding modes of *N*-nitroso derivative with tin we prepared tin and diorganotin(IV) cupferronato complexes: $Sn(O_2N_2Ph)_4$ (**1**), $Ph_2Sn(O_2N_2Ph)_2$ (**2**) and $[Me_2Sn(O_2N_2Ph)_2]_2$ (**3**) which were investigated by FT-IR, FT-Raman, multinuclear (^{1}H, ^{13}C and ^{119}Sn) NMR as well as X-ray diffraction analysis.

[a] Institute of Chemistry, Chemical Research Center of the Hungarian Academy of Sciences,
P. O. Box 17, H-1525 Budapest, Hungary
Fax: (internat.) + 36-1/325-7554
E-mail: akalman@cric.chemres.hu
[b] Chemistry Department, Babes-Bolyai University,
RO-3400 Cluj-Napoca, Romania
Fax: (internat.) + 40-64/190-818
E-mail: ihaiduc@chem.ubbcluj.ro

Results and Discussion

Reaction of cupferron [NH_4L, L = PhN(O)NO$^-$] with SnI_4 in chloroform (Equation 1) results in the formation of **1**.

$$SnI_4 + 4\,NH_4L \xrightarrow{CHCl_3} \underset{\mathbf{1}}{SnL_4} + 4\,NH_4I \quad (1)$$

In similar manner, cupferron reacts with diorganotin dichlorides R_2SnCl_2 (R = Ph and Me) in acetone or dried MeOH (Equation 2) to give **2** and **3**.

$$n\,R_2SnCl_2 + 2\,n\,NH_4L \xrightarrow[\text{or MeOH}]{\text{acetone}} \underset{\begin{array}{c}\mathbf{2}\text{: n = 1, R = Ph}\\ \mathbf{3}\text{: n = 2, R = Me}\end{array}}{[R_2SnL_2]_n} + 2\,n\,NH_4Cl \quad (2)$$

All the complexes **1**−**3** are stable and are soluble in $CHCl_3$ and *n*-heptane.

Structures in the Solid State

Vibrational Behavior

The FT-IR and Raman spectra were recorded for the complexes **1**−**3** in the 3500−100 cm^{-1} spectral range. As was expected all these new compounds display ν(N−N), ν(N=O) and δ(ONNO) absorption bands typical for the $PhN_2O_2^-$ ligand.[4] Taking into account the coordination of the anionic cupferronato ligand to the metal centers through the oxygen atoms, the Sn−O stretching vibration

 © WILEY-VCH Verlag GmbH, D-69451 Weinheim, 2000 1434−1948/00/0101−0127 $ 17.50+.50/0

was also characteristic.[4] Selected bands and assignments are listed in Table 1.

Table 1. Selected FT-IR/Raman data and vibrational assignments for complexes **1**–**3**

1		2		3		Assign-
IR	Raman	IR	Raman	IR	Raman	ment
1356 s	1361 w	1344 ms	1345 m	1351 ms 1336 ms	1353 mw	ν(N–N)
1205 ms	–	1214 w	–	1216 s	1218 w	ν(N=O)
1168 ms	1167 w	1181 s	–	1180 ms	1199 w	
949 s	940 m	926 s	930 m	923 s	929 mw	δ(ONNO)
401 s	–	400 s	–	401 vs	–	ν(Sn–O)

w: weak, m: medium, ms: medium strong, mw: medium weak, s: strong, vs: very strong.

X-ray Crystallographic Studies

The molecular structures of compounds **1**, **2** and **3** are shown in Figures 1–3, respectively. Selected bond lengths and angles are listed in Table 2 and Table 4.

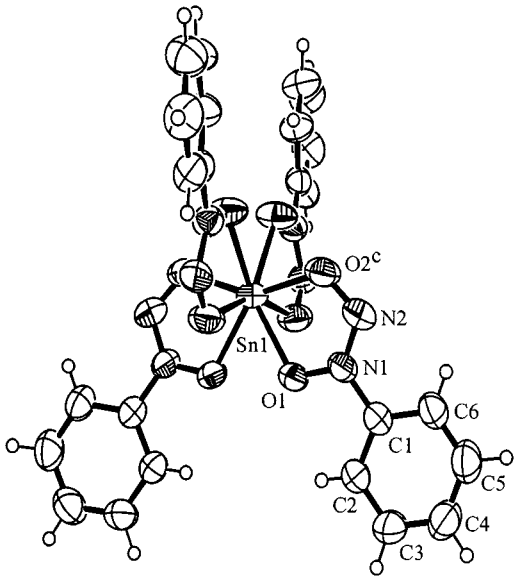


Figure 1. Molecular structure of **1**

The molecular structure of **1** provides a new example of an octacoordinated Sn^{IV} species in an almost perfect dodecahedral geometry of the metal center coordination environment defined by eight oxygen atoms from the four cupferronato ligands. Hitherto, only four Sn^{IV} complexes with octacoordinated tin centers have been characterized by X-ray crystallography: tin tetranitrate,[5] stannic phthalocyanine,[6] tin tetraacetate,[7] and tetrakis(tropolonato)tin.[8] The distortion of the idealized dodecahedron towards the bicapped trigonal prism and/or square antiprism can be described by δ and φ parameters.[9] As shown in Table 3, the four δ (29.5°) and two φ (0°) values are identical in an ideal dodecahedron, while this equality becomes more or less changed for the bicapped trigonal prism and square antiprism. The δ and φ values observed for **1** reveal an almost perfect dodecahedral geometry around the tin atom.

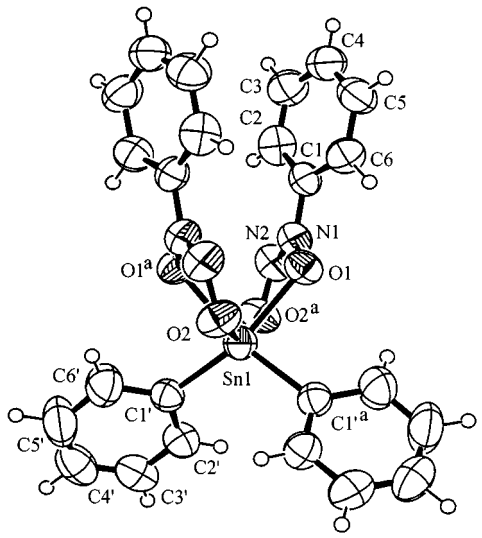


Figure 2. Molecular structure of **2**

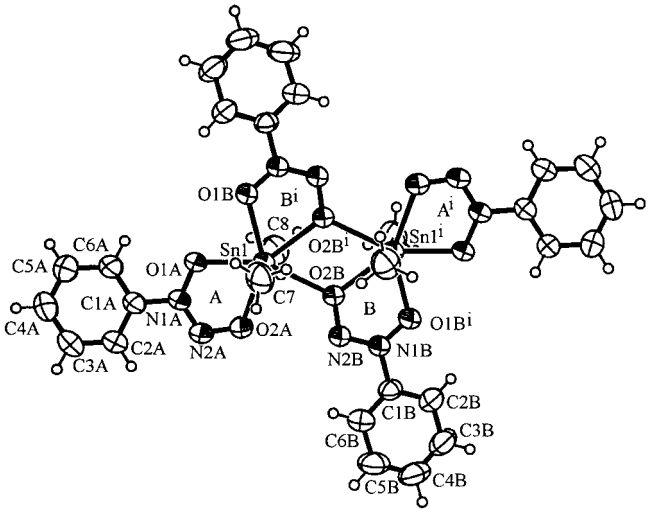


Figure 3. Molecular structure of **3**

The cupferronato anions are bound to the Sn^{IV} center in a bidentate chelating fashion leading to five-membered carbon-free chelate rings SnO_2N_2 with an O(1)–Sn(1)–O(2)^c bite angle of 70.1(1)°. The Sn–O(2) bond length is slightly shorter (by 0.041 Å) than that of Sn–O(1), and somewhat longer than the ideal value of 2.14 Å.[3] The average Sn–O bond length of 2.164 Å is, however, consistent with tin-oxygen distances observed in other octacoordinated tin(IV) species, such as $Sn(NO_3)_4$ (average Sn–O = 2.161 Å)[5] and the recently reported Sn(tropolonato)$_4$ (average Sn–O = 2.168 Å).[8]

The crystal lattice is built up from infinite one-dimensional C–H···O interactions, C(3)–H(3)···O(2) [C–H = 0.94 Å; H···O = 2.45 Å; C···O = 3.37 Å; C–H···O = 165.8°] that extends through (x, 0.5 − y, −0.5 − z). This hydrogen-bonding interaction has no significant impact on the adoption of the almost ideal dodecahedral geometry.

Table 2. Selected interatomic bond lengths (Å), bond angles (°) and torsion angles (°) for **1** and **2**

	1	**2**
Sn(1)−O(1)	2.185(1)	2.206(2)
Sn(1)−O(2)^{i}	2.144(1)	2.158(2)
O(2)^{i}−N(2)	1.303(2)	1.306(4)
O(1)−N(1)	1.309(2)	1.314(3)
N(1)−N(2)	1.278(2)	1.287(4)
C(1)−N(1)	1.428(2)	1.445(5)
Sn(1)−C(1′)	−	2.132(3)
O(1)−Sn(1)−O(2)^{i}	70.1(1)	69.7(1)
Sn(1)−O(1)−N(1)	112.8(1)	108.7(2)
O(1)−N(1)−N(2)	122.0(2)	122.8(3)
N(1)−N(2)−O(2)^{i}	113.2(2)	112.1(3)
N(2)−O(2)^{i}−Sn(1)	119.1(1)	116.3(2)
C(1′)−Sn(1)−O(2)	−	108.2(1)
C(1′)−Sn(1)−C(1′)^{i}	−	107.7(2)
O(1)−N(1)−N(2)−O(2)^{i}	1.8(2)	3.3(5)

Equivalent atoms (i) generated for **1** by c = (x, −y + 0.5,−z + 0.5), and for **2** by a = (−x, y, −z + 0.5).

Table 3. Ideal and observed δ (°) and φ (°) for octacoordinated complexes

Complex	δ				φ	
dodecahedron[9]	29.5	29.5	29.5	29.5	0	0
bicapped trigonal prism[9]	0	21.7	48.2	48.2	16.1	16.1
square antiprism[9]	0	0	52.5	52.5	10.8	10.8
1	28.4	28.4	25.7	25.7	−1.9	1.1

In the class of hexacoordinated tin(IV) compounds the octahedral geometry is predominant.[3] Distorsions in the solid state can be attributed to a compromise between the close packing and the ideal shape of the molecules.[9] In complex **2** the hexacoordinated metal center surrounded by two carbon atoms of two phenyl groups and four oxygen atoms of the chelating cupferronato anions exhibits a slightly distorted bicapped tetrahedral arrangement.[10] In this arrangement the capping ligand atoms O(1) and O(1)^{a} are located in the middle of two faces of the nearly regular tetrahedron C(1′)^{a}···C(1′)···O(2)···O(2)^{a}. The basic tetrahedral geometry around the tin center is retained with angles C(1′)^{a}−Sn(1)−C(1)′ of 107.74(2)°, C(1)′−Sn(1)−O(2) and symmetry equivalent C(1′)^{a}−Sn(1)−O(2)^{a} of 108.2(1)°, and these values are close to the ideal tetrahedral value. The Sn(1)−C(1)′, Sn1−C(1′)^{a} and Sn(1)−O(2), Sn(1)−O(2)^{a} distances belonging to the tetrahedral core are almost equal. Otherwise, the Sn(1)−O(2) distances are close to the ideal value for a normal covalent bond 2.14 Å, while the Sn(1)−O(1) distances are somewhat longer. The O(1)−Sn(1)−O(2)^{a} bite angle of 69.7(1)° is comparable to the bite angle measured in **1** and depends partially on the strain in the five-membered inorganic SnO_2N_2 ring.

The ligand hydrogens in the *para* position interact with the π system of the phenyl rings (1 − x, y, 1.5 − z) bound directly to the tin atom via weak C−H···π interactions [C(4)···π = 3.84 Å, H(4)···π = 3.09 Å, C(4)−H(4)···π = 139.4°].

Table 4. Selected interatomic bond lengths (Å), bond angles (°) and torsion angles (°) for **3**

	3	
	L = A; X = 7	L = B; X = 8
Sn(1)−O(1L)	2.198(2)	2.247(1)
Sn(1)−O(2L)	2.274(2)	2.440(1)
Sn(1)−O(2L)^{i}	−	2.395(1)
O(2L)−N(2L)	1.294(3)	1.303(2)
O(1L)^{i}−N(1L)	1.321(2)	1.306(2)
N(1L)−N(2L)	1.280(2)	1.284(2)
C(1L)−N(1L)	1.433(2)	1.436(2)
Sn(1)−C(X)	2.092(3)	2.103(3)
O(1L)−Sn(1)−O(2L)^{i}	69.5(1)	65.5(1)
O(1A)−Sn(1)−O(1B)	77.4(1)	
O(2B)−Sn(1)−O(2A)	83.9(1)	
O(2B)−Sn(1)−O(2B)^{i}	63.7(1)	
Sn(1)^{i}−O(1L)^{i}−N(1L)	113.8(1)	116.7 (1)
O(1L)^{i}−N(1L)−N(2L)	123.7(2)	124.2(2)
N(1L)−N(2L)−O(2L)	114.5(2)	112.2(1)
N(2L)−O(2 L)−Sn(1)^{i}	116.7(1)	117.4(1)
C(7)−Sn(1)−C(8)	173.6(1)	
O(1 L)^{i}−N(1 L)−N(2 L)−O(2 L)	−1.7(4)	1.0(3)

Equivalent atoms (i) generated for L = B by (−x, −y, −z).

According to the X-ray data compound **3** is represented by the centrosymmetric dimeric structure $[Me_2Sn(O_2N_2Ph)_2]_2$. Both tin(IV) centers are heptacoordinated. The nearly pentagonal bipyramidal coordination is achieved by one bidentate chelating (A and its symmetry equivalent, A^{i}) and two triconnective bridging cupferronato ligands (B and its symmetry equivalent B^{i}) lying in the equatorial plane, and two methyl groups occupying the axial positions. This arrangement with five equatorial oxygen atoms is similar to those reported for the bridged binuclear and polynuclear pentagonal bipyramidal dimethyltin(IV) complexes of aminocarboxylate and aminopolycarboxylate ligands.[11−14] In the majority of these structures,[11−13] while the methyl groups are invariably in the axial position, one oxygen is replaced by a nitrogen atom. There is an additional case where two oxygen atoms are replaced by two nitrogen atoms.[14]

A notable feature in the structure of **3** is the occurrence of a central planar [torsion angle: O2(B)^{i}−Sn(1)^{i}−O(2B)−Sn(1) = 0.(0)°] four-membered Sn_2O_2 ring. In this ring, the two pairs of Sn−O distances [Sn(1)−O(2B)^{i} and Sn(1)−O(2B)] are unequal, and the bridging oxygen atoms [O(2B) and O(2B)^{i}] participate in two additional, planar, five-membered SnO_2N_2 rings resulting in a Sn···Sn separation of 4.108 Å. Distannoxanes generally form dimeric ladder-type structures that also contain a planar four-membered Sn_2O_2 ring,[3][15] a feature which can be found in the bridged binuclear and polynuclear pentagonal bipyramidal dimethyltin(IV) complexes discussed.[11−14] The Sn(1)−O(2B)^{i} bond length in the triconnective bridging ligand seems to be significantly longer by 0.121 Å than the corresponding distance of 2.274(2) Å for the chelating ligand. The O(1B)−Sn(1)−O(2B)^{i} bite angle in ligand B deviates by ca 4° from the bite angle of the chelating ligands.

There are weak intramolecular hydrogen bonds such as C−H···O [C(6A)···O(1A) 2.69 Å, H(6A)···O(1A) 2.35 Å, C(6A)−H(6A)···O(1A) 100.8°] between the phenyl hydrogens and the ONNO group.

In the crystal lattice the symmetry-related dimeric molecules interact along the *a* axis *via* weak C−H···π interactions [C(6B)···π 3.56, H(6B)···π 3.30 Å, C(6B)−H(6B)···π 98.8°].

Structures in Solution

^{1}H, ^{13}C and ^{119}Sn NMR spectra were recorded (in $CDCl_3$) to gain some insight into the solution structure of the complexes. For proton-containing groups directly attached to the Sn atom (Me, Ph), proton spectra exhibited ^{119}Sn (and ^{117}Sn) satellite signals due to $^{2}J(^{119}Sn-^{1}H)$ or $^{3}J(^{119}Sn-^{1}H)$ couplings. In a similar fashion, resonances due to the carbon atoms in groups attached to tin exhibited ^{119}Sn (and ^{117}Sn) satellites arising from one-bond and multiple bond $^{n}J(^{119}Sn-^{13}C)$ spin−spin couplings. The relationship[16,17] $|^{1}J(^{119}Sn-^{13}C)| > |^{3}J(^{119}Sn-^{13}C)| > |^{2}J(^{119}Sn-^{13}C)| > |^{4}J(^{119}Sn-^{13}C)|$ was used to assign the ^{13}C resonances of the phenyl moiety. All the ^{1}H and ^{13}C chemical shifts have the values normally expected and can be found in the Experimental Section.

The chemical shift values of the ^{119}Sn resonance signals of similar tin(IV) complexes are known to reflect the coordination of the Sn atoms in the solution state.[17] Thus in **1**, the observed −747.9 ppm, falls within the range observed in chloroform solutions of other octacoordinated tin(IV) compounds such tetrakis(tropolonato)tin(IV) [$\delta(^{119}Sn)$ = −793.10 ppm][8] and tetrakis(1-pyrrolecarbodithioato)-tin(IV) [$\delta(^{119}Sn)$ = −729.2 ppm].[18]

The magnitude of the vicinal Sn−H coupling, $|^{3}J(^{119}Sn-^{1}H)|$ = 77 Hz exhibited by the resonance due to the *ortho* protons of the Sn−Ph rings in **2** reflects the (equilibrium) rotational angle of the aromatic ring in liquid state.[17] The angle C−Sn−C calculated from the available relationships with the $|^{1}J(^{119}Sn-^{13}C)|$ coupling[19] indicates an increase in C−Sn−C angle from 107.7° in the solid to 176.4° in solution, which is consistent with octahedral Sn^{IV} units with two phenyl groups in *trans* positions.[19]

Lockhart and Manders noticed that the $|^{2}J(^{119}Sn-^{1}H)|$ coupling constant is a function of coordination number of dimethyltin(IV) compounds, ranging between 64 and 79 Hz for pentacoordinated compounds.[20] For **3** the $|^{2}J(^{119}Sn-^{1}H)|$ coupling constant of 76.8 Hz indicates pentacoordination in chloroform solution. A single resonance at −159.2 ppm observed in the ^{119}Sn NMR spectra is compatible with the pentacoordinated geometry proposed for the structure in solution. Comparison with ^{119}Sn chemical shifts (−126, −129, −121, and −133 ppm, respectively) of pentacoordinated dimethyltin(IV) alkoxides $Me_2Sn(OR)_2$ (R = Et, ^{n}Pr, ^{i}Bu and ^{n}Bu) serves to confirm this interpretation.[21] These data, combined with the $|^{1}J(^{119}Sn-^{13}C)|$ coupling constants, tend to confirm that this compound has a pentacoordinated geometry in solution.[19]

Conclusion

A noteworthy trend has been observed in the bonding pattern of the O-donor cupferronato anion in the $[R_nSnL_{4-n}]_m$ series of tin(IV) cupferronate complexes. The nature of the organic moieties attached to tin produces significant changes in coordinational behavior of the ligand: bridging coordination,[4][22] bridging-chelating and chelating coordination patterns are observed. The bonding mode of the ligand to tin is reflected in the length of the Sn−O bonds and in the O(1)−Sn(1)−O(2) bite angles (Table 2 and 4). The Sn(1)−O(1) bond lengths in complexes **1**−**2** are significantly longer than Sn(1)−O(2), while the opposite was observed for **3** and for the tetrameric trimethyltin(IV) cupferronate $[Me_3SnL]_4$, which contains an unprecedented inorganic metallamacrocycle $Sn_4O_8N_8$.[22] For the chelating ligands the O(1)−Sn(1)−O(2) bite angles lie in the narrow range 69−70° while for the triconnective bridging and bridging ligands[22] this angle tends to close up by approximately 4−5°. In spite of the varied coordination behavior of the nitrosohydroxylaminato [N(O)NO] group in the cupferronato tin complexes, a comparison of the corresponding structural data does not reveal major differences. The N(O)NO moiety is essentially planar. The N(1)−N(2) bond length is shorter than an N−N single bond (1.45 Å) and is closer to an N=N double bond (1.21 Å).[23] The N(1)−O(1) and N(2)−O(2) bond length is between single (1.40 Å) and double bonds (1.21 Å).[23] These data reveal the same electron delocalization along the nitrosohydroxylaminato group in all tin compounds investigated here.

Experimental Section

General Methods: The preparation and purification of the complexes were carried out in the open air, or in dry atmosphere, with anhydrous organic solvents. Organic solvents for reactions and recrystallization were distilled from appropriate drying agents prior to use. The SnI_4 reagent was prepared by a published method.[24] All other starting materials were obtained from commercial sources as pure compounds.

Microanalyses (C, H and N) of the complexes were performed by the Microanalytical Service of the Department of Chemistry, University of Santiago de Compostela (Spain). FT-IR spectra were recorded with a Perkin−Elmer 2000 spectrometer. FT-Raman spectra were recorded with a Bruker FT Raman spectrometer (IFS model 66). Solution NMR data were recorded on a Varian Unity Inova 400 spectrometer in $CDCl_3$, using TMS as internal standard for ^{1}H and ^{13}C, and $SnMe_4$ for ^{119}Sn as external reference.

Preparation of Tetrakis(*N*-nitroso-*N*-phenyl-hydroxylaminato)tin-(IV), Sn[PhN(O)NO]$_4$, (1): The ammonium salt NH_4[PhN(O)NO] (0.50 g, 3.25 mmol) was added to a solution of SnI_4 (0.51 g, 0.81 mmol) in 15 mL chloroform. The NH_4I promptly precipitated and the mother liquor became colorless. After stirring for 20 minutes at room temperature, the precipitate was filtered off and the liquid was evaporated. Recrystallization from *n*-heptane gave the product as colorless crystals. Yield 0.22 g, 40%, melting point 168−172°C (decomp.). − FT-IR (KBr): $\tilde{\nu}$ = 1486 cm^{-1}(Ph) (m), 1465 (Ph) (m), 1356 (N−N) (s), 1300 (vs), 1205 (N=O) (ms), 1168 (N=O) (ms), 949 (ONNO) (s), 758 (Ph) (s), 696 (Ph) (s), 684

(OSnO) (m, sh), 410 (s), 401 (Sn−O) (s), 237 (C−H) (vs). − FT-Raman: $\tilde{\nu}$ = 1590 cm^{-1}(C−H) (m), 1487 (C−H) (w), 1361 (N−N) (w), 1314 (vs), 1167 (N=O) (w), 1004 (Ph) (m), 940 (ONNO) (m), 112 (m). − ^{1}H NMR ($CDCl_3$, 399.92 MHz, 30°C): δ = 7.97 (m, 2 H, Ph-H2, -H6), 7.43 (m, 3 H, Ph-H3, -H4, -H5). − ^{13}C NMR ($CDCl_3$, 100.6 MHz, 30°C): δ = 140.0 (s, Ph-C1), 130.3 (s, Ph-C4) ppm; 129.1 (s, Ph-C3, -C5), 119.6 (s, Ph-C2, -C6). − ^{119}Sn NMR ($CDCl_3$, 149.106 MHz, 30°C): δ = −747.9 (s). − $C_{24}H_{20}N_8O_8Sn$ (667.17): calcd. C 43.2, H 3.0, N 16.8; found C 43.1, H 3.3, N 16.8.

Preparation of Diphenylbis(*N*-nitroso-*N*-phenyl-hydroxylaminato)-tin(IV), $Ph_2Sn[PhN(O)NO]_2$ (2): The salt NH_4[PhN(O)NO] (0.20 g, 1.29 mmol) was added to a solution of Ph_2SnCl_2 (0.22 g, 0.64 mmol) in 15 mL acetone. The NH_4Cl promptly precipitated. After stirring for one hour at room temperature, the precipitate was filtered off and the mother liquor was concentrated to low volume, and 5−10 mL *n*-heptane was added. This solution was placed in the refrigerator overnight to yield **2** as a pale yellow solid. Recrystallization from *n*-heptane gave the product as colorless crystals. Yield 0.21 g, 60%, melting point 87−88°C. − FT-IR (KBr): $\tilde{\nu}$ = 1483 cm^{-1} (Ph) (m), 1463 (Ph) (m), 1429 (m), 1344 (N−N) (ms), 1294 (vs), 1214 (N=O) (w), 1181 (N=O) (s), 1156 (s), 926 (ONNO) (s), 762 (Ph) (s), 733 (s), 696 (Ph) (s), 686 (OSnO) (m, sh), 400 (Sn−O) (s), 267 (vs), 122(w). − FT-Raman: $\tilde{\nu}$ = 1591 cm^{-1} (C−H) (s), 1486 (C−H) (w), 1465 (C−H) (vw), 1345 (N−N) (m), 1307 (vs), 1158 (C−H) (mw), 1070 (C−H) (vw), 1025 (C−H) (w), 1005 (Ph) (s), 998 (s), 930 (ONNO) (m), 168 (m), 110 (ms). − ^{1}H NMR ($CDCl_3$, 399.92 MHz, 30°C): δ = 7.97 (m, 2 H, Ph-H2, -H6), 7.72 [m, ^3J (^{119}Sn−^{1}H) = 77 Hz, 2 H, Ph_A-H2, -H6], 7.46−7.36 (m, 6 H). − ^{13}C NMR ($CDCl_3$, 100.6 MHz, 30°C): δ = 145.6 [m, ^1J(^{119}Sn, ^{13}C) = 908.3 Hz, Ph_A-C1], 140.0 (s, 1, Ph-C1), 135.6 [m, ^2J (^{119}Sn−^{13}C) = 58.8 Hz, Ph_A-C2, -C6], 130.6 (s, Ph-C4), 129.5 [m, Ph_A-C4, ^4J(^{119}Sn−^{13}C) = 17.2 Hz], 129.2 (s, Ph-C3, -C5), 128.6 [m, ^3J(^{119}Sn−^{13}C) = 85.0 Hz, Ph_A-C3, -C5], 119.7 (s, Ph-C2, C6). − ^{119}Sn NMR ($CDCl_3$, 149.106 MHz, 30°C): δ = −327.2 (b, s). − $C_{24}H_{20}N_4O_4Sn$ (547.13): calcd. C 52.7, H 3.7, N 10.2; found C 52.5, H 3.4, N 10.2.

Preparation of Dimethylbis(*N*-nitroso-*N*-phenyl-hydroxylaminato)-tin(IV), $[Me_2Sn(PhN(O)NO)_2]_2$ (3): The salt NH_4[PhN(O)NO] (0.40 g, 2.58 mmol) dissolved in 15 mL MeOH was added to a solution of Me_2SnCl_2 (0.28 g, 1.27 mmol) in 15 mL MeOH. The NH_4Cl promptly precipitated. After stirring for one hour at room temperature, the solution was concentrated to low volume and cooled in a refrigerator for 24 hours. The microcrystalline product deposited was filtered, dried in an anhydrous atmosphere and recrystallized from *n*-heptane as colorless crystals. Yield 0.31 g, 57%, melting point 112−114°C. − FT-IR (KBr): $\tilde{\nu}$ = 1488 cm^{-1} (Ph) (m), 1465 (Ph) (ms), 1351 (N−N) (ms), 1336 (N−N) (ms), 1294 (vs), 1216 (N=O) (s), 1180 (N=O) (ms), 1156 (s), 923 (ONNO) (s), 756 (Ph) (s), 693 (Ph) (s), 683 (OSnO) (ms sh), 545 (Sn−C) (m), 401(Sn−O) (vs), 217 (C−H) (s), 189 (C−H) (s). − FT-Raman: $\tilde{\nu}$ = 1592 cm^{-1} (C−H) (s), 1489 (C−H) (w), 1353 (N−N) (mw), 1298 (vs), 1218 (N=O) (w), 1199 (N=O) (w), 1005 (Ph) (m), 929 (ONNO) (mw), 546 (Sn−C) (w), 517 (SnC_2) (m), 112 (m). − ^{1}H NMR ($CDCl_3$, 399.92 MHz, 30°C): δ = 7.93 (m, 2 H, Ph-H2, -H6), 7.45 (m, 3 H, Ph-H3, -H4, -H5), 0.77 [s, ^2J(^{119}Sn−^{1}H) = 76.8 Hz, ^2J(^{117}Sn−^{1}H) = 73.4 Hz, ^1J(^{13}C−^{1}H) = 132.6 Hz, 3 H, Sn−CH_3]. − ^{13}C NMR ($CDCl_3$, 100.6 MHz, 30°C): δ = 140.0 (s, Ph-C1), 130.3 (s, Ph-C4), 129.1 (s, Ph-C3, -C5), 119.6 (s, Ph-C2, -C6), 7.8 [m, ^1J(^{119}Sn, ^{13}C) = 647.7 Hz, Sn−CH_3]. − ^{119}Sn NMR ($CDCl_3$, 149.106 MHz, 30°C): δ = −159.2 (b, s). − $C_{28}H_{32}N_8O_8Sn_2$ (846.04): calcd. C 39.8, H 3.8, N 13.2; found C 39.8, H 4.0, N 13.2.

X-ray Structure Determination for 1−3

Crystal data and refinement parameters are summarized in Table 5. Intensity data were collected on an Enraf−Nonius CAD-4 diffractometer with graphite monochromated Mo-K_α radiation (λ = 0.71073 Å) using the ω-2θ scan technique. Three standard reflections were monitored every hour; these remained constant within

Table 5. Summary of X-ray diffraction data for **1−3**

	1	**2**	**3**
Empirical formula	$C_{24}H_{20}N_8O_8Sn$	$C_{24}H_{20}N_4O_4Sn$	$C_{28}H_{32}N_8O_8Sn_2$
Formula mass	667.17	547.13	846.04
Crystal size [mm]	0.3 × 0.25 × 0.2	0.40 × 0.15 × 0.15	0.60 × 0.40 × 0.20
Color	colorless	colorless	colorless
Crystal system	tetragonal	orthorhombic	triclinic
Space group	$P4_2/n$	*Pbcn*	$P\bar{1}$
θ range for data collection (°)	2.27 ≤ θ ≤ 31.97	2.32 ≤ θ ≤ 25.97	2.42 ≤ θ ≤ 34.99
a [Å]	12.702(2)	13.258(1)	9.417(2)
b [Å]	12.702(2)	11.683(1)	9.458(1)
c [Å]	8.500(2)	14.973(1)	10.738(1)
α [°]	90.00	90.00	76.17(1)
β [°]	90.00	90.00	64.27(1)
γ [°]	90.00	90.00	78.24(1)
V [Å^3]	1371.4(4)	2319.2(3)	831.1(2)
Z	2	4	1
d_{calc} [Mg/m^3]	1.616	1.567	1.681
μ [mm^{-1}]	0.994	1.140	1.453
F(000)	668	1096	420
Index ranges (°)	$-18 \le h \le 18$	$0 \le h \le 16$	$-15 \le h \le 15$
	$0 \le k \le 18$	$0 \le k \le 14$	$-15 \le k \le 15$
	$0 \le l \le 12$	$0 \le l \le 18$	$-17 \le l \le 17$
No. of reflections collected	5254	4549	15581
No. of indep. reflns./R_{int}	2376/0.021	2231/0.020	7253/0.012
No. of obsd. reflections, $I > 2\sigma(I)$	1312	1133	4828
No. of parameters	99	160	210
GOOF	0.879	0.779	0.977
*R*1 (obsd. data)	0.0283	0.0280	0.0305
*wR*2 (all data)	0.0734	0.0622	0.0831
Largest diff. peak/hole (eÅ^{-3})	0.348/−0.369	0.488/−0.332	1.337/−0.452

experimental error. The structure was solved by direct methods (SHELXS-97)[25a] and refined by full-matrix least-squares (SHELXL-97).[25b] All non-hydrogen atoms were refined anisotropically. Hydrogen atomic positions were generated from assumed geometries. The riding model was applied for the hydrogen atoms. Crystallographic data (excluding structure factors) for the structures reported in this paper have been deposited with the Cambridge Crystallographic Data Center as supplementary publication nos. CCDC-125074 (**1**), CCDC-125075 (**2**) and CCDC-125076 (**3**). Copies of the data can be obtained free of charge on application to CCDC, 12 Union Road, Cambridge CB2 1EZ, UK [Fax: (internat.) + 44−1223/336−033; E-mail: deposit@ccdc.cam.ac.uk].

Acknowledgments

We thank Prof. Agustin Sanchez (Department of Inorganic Chemistry, University of Santiago de Compostela, Spain) for facilitating the analytical, FT-IR, FT-Raman measurements. This work was supported by the National Council of Academic Research (Bucharest) under Grant No. 108/82/1999.

[1] I. Haiduc, C. Silvestru, *Organometallics in Cancer Chemotherapy*, Vol. 1., Main Group Metal Compounds, CRC Press, Boca Raton, Florida, **1989**.
[2] G. B. Yi, M. A. Khan, G. B. Richter-Addo, *Inorg. Chem.* **1995**, *34*, 5703−5704.
[3] B. Y. K. Ho, J. J. Zuckerman, *J. Organomet. Chem.* **1973**, *49*, 1−84.
[4] L. Párkányi, A. Kálmán, A. Deák, M. Venter, I. Haiduc, *Inorg. Chem. Commun.* **1999**, *2*, 265−268.
[5] C. D. Garner, D. Sutton, S. C. Wallwork, *J. Chem. Soc. (A)* **1967**, 1949−1954.
[6] W. E. Bennett, D. E. Broberg, N. C. Baenziger, *Inorg. Chem.* **1973**, *12*, 930−936.
[7] [7a] N. W. Alcock, V. L. Tracy, *J. Chem. Soc., Dalton Trans.* **1976**, 2246−2249. − [7b] N. W. Alcock, V. L. Tracy, *Acta Crystallogr.* **1979**, *B35*, 80−83.
[8] M. Kira, L. C. Zhang, C. Kabuto, H. Sakurai, *Organometallics* **1998**, *17*, 887−892.
[9] E. L. Muetterties, L. J. Guggenberger, *J. Am. Chem. Soc.* **1974**, *96*, 1748−1756.
[10] R. Hoffmann, J. M. Howell, A. R. Rossi, *J. Am. Chem. Soc.* **1976**, *98*, 2484−2492.
[11] F. L. Lee, E. J. Gabe, L. E. Khoo, W. H. Leong, G. Eng, F. E. Smith, *Inorg. Chim. Acta* **1989**, *166*, 257−261.
[12] F. Huber, H. Preut, E. Hoffmann, M. Gielen, *Acta Crystallogr.* **1989**, *C45*, 51−54.
[13] S. Aizawa, T. Natsume, K. Hatano, S. Funahashi, *Inorg. Chim. Acta* **1996**, *248*, 215−224.
[14] T. P. Lockhart, F. Davidson, *Organometallics* **1987**, *6*, 2471−2478.
[15] D. Dakternieks, K. Jurkschat, S. van Dreumel, E. R. T. Tiekink, *Inorg. Chem.* **1997**, *36*, 2023−2029.
[16] H. O. Kalinowski, S. Berger, S. Braun, *Carbon NMR spectroscopy*, Wiley, Chichester, U. K., **1988**, p 313.
[17] B. Wrackmeyer, *Ann. Rep. NMR Spectrosc.* **1985**, *16*, 73−186.
[18] N. Seth, V. D. Gupta, H. Nöth, M. Thomann, *Chem. Ber.* **1992**, *125*, 1523−1528.
[19] W. F. Howard, R. W. Creely, W. H. Nelson, *Inorg. Chem.* **1985**, *24*, 2204−2208.
[20] T. P. Lockhart, W. F. Manders, *Inorg. Chem.* **1986**, *25*, 892−895.
[21] J. D. Kennedy, *J. Chem. Soc., Perkin Trans. 2* **1977**, 242−248.
[22] A. Deák, I. Haiduc, L. Párkányi, M. Venter, A. Kálmán, *Eur. J. Inorg. Chem.* **1999**, 1593−1596.
[23] J. E. Huheey, E. A. Keiter, R. L. Keiter, *Inorganic Chemistry: Principles of Structure and Reactivity*, Harper Collins, New York, **1993**, p. A31.
[24] Z. Szafran, R. M. Pike, M. M. Singh, *Microscale Inorganic Chemistry. A Comprehensive Laboratory Experience*, John Wiley & Sons, New York, **1991**, p. 181.
[25] [25a] G. M. Sheldrick, *SHELXS97-Program for Crystal Structure Determination* and [25b] *SHELXL97-Program for the Refinement of Crystal Structures*, Universität Göttingen (Germany), **1997**.

Received June 14, 1999
[I99216]

Ionic Silver Amino Complexes Displaying Liquid Crystalline Behavior Close to Room Temperature

Ana C. Albéniz,[a] Joaquín Barberá,[b] Pablo Espinet*,[a] M. Carmen Lequerica,[a] Anne M. Levelut,[c] F. Javier López-Marcos,[b] and José L. Serrano*[a]

Keywords: Metallomesogens / Liquid crystals / Silver / N ligands / Amines

The liquid crystalline properties of a series of ionic silver complexes $[Ag(NH_2n\text{-}C_nH_{2n+1})_2]X$ (X = NO_3, n = 6, 8, 10, 12, 14; X = BF_4, n = 8, 10, 12, 14), derived from silver nitrate or tetrafluoroborate and aliphatic amines, have been investigated by optical microscopy, DSC, and X-ray diffraction. The materials exhibit a birefringent fluid phase identified as a smectic A mesophase by optical microscopy and X-ray diffraction. Some of the complexes are liquid crystalline at temperatures close to room temperature. The X-ray results are consistent with the existence in the mesophase of a bilayer organization. The silver cations adopt a U-shape, which allows for the adoption of this bilayer arrangement, with alternating ionic and apolar regions and a short-range square-planar array inside the cationic sublayers. The thermodynamic parameters suggest that the melting transition clearly involves only disorder (melting) of the chains, whereas the clearing transition implies breaking the anion-cation arrangement.

Introduction

Metallomesogens (metal complexes that are formed with organic ligands and exhibit liquid crystalline behavior) have considerably enhanced the field of liquid crystals.[1] The vast majority of metallomesogens reported so far have a rod- or disk-shaped rigid core (usually with aryl rings) bearing long hydrocarbon tails. Ionic amphiphilic metal complexes have been reported less frequently.[2]

In this paper we report the synthesis and liquid crystalline properties of two series of ionic silver complexes, both of which are based on apparently simple coordination compounds $[Ag(NH_2n\text{-}C_nH_{2n+1})_2]X$ (X = NO_3, n = 6, 8, 10, 12, 14; X = BF_4, n = 8, 10, 12, 14). These compounds appear to be deceptively simple as they are similar in stoichiometry and metal coordination to other compounds based on 4-substituted pyridines {$[AgL_2]X$; L = 4-substituted pyridine; X = alkyl sulfate, BF_4, CF_3SO_3, NO_3, PF_6}.[3] In fact they turn out to be structurally very different: the cation, which lacks rigid rings, has a flexible aliphatic structure that is able to adopt any shape, whereas in the pyridine derivatives previously reported, the cation has, by necessity, an extended central rigid rod-like geometry. In this respect the complexes reported here are more similar to the U-shaped structures found for *trans*-$[PdCl_2\{PEt_2(O\text{-}chl)\}_2]$ (chl = cholesteryl)[4] and for the silver complexes [AgL]X with the macrocyclic ligand 1,10-bis[4-(dodecyloxy)-benzoyl]-1,10-diaza-4,7,13,16-tetrathiacyclooctadecane.[5]

[a] Departamento de Química Inorgánica, Facultad de Ciencias, Universidad de Valladolid,
E-47005 Valladolid, Spain
E-mail: espinet@qi.uva.es
[b] Química Orgánica, Facultad de Ciencias-ICMA, Universidad de Zaragoza-CSIC,
E-50009 Zaragoza, Spain
[c] Laboratoire de Physique des Solides, Bâtiment 510, Université Paris-Sud,
F-91405 Orsay Cédex, France

Thus the complexes reported in this paper combine a number of unusual features: (i) their mesogenic behavior appears at rather low temperatures; (ii) the metal is included in the promesogenic cation; (iii) X-ray characterization of their mesophases supports a bilayer structure reminiscent of that observed in classical lyotropic bilayer mesophases, with the cation adopting a U-shaped geometry comparable to that observed in phospholipid-based lyotropic derivatives.

Results and Discussion

Synthesis

The complexes were prepared by the stoichiometric reaction of the appropriate silver salt, AgX, and the corresponding alkylamine in acetonitrile (Equation 1), and were isolated as crystalline solids. They are light-sensitive and their preparation and handling must be carried out in the dark. However, they can survive moderately long exposure to light, such as the periods required for the microscopy studies.

$$AgX + 2\ NH_2n\text{-}C_nH_{2n+1} \rightarrow [Ag(NH_2n\text{-}C_nH_{2n+1})_2] \quad (1)$$

Microscopy Studies

Optical microscopy with polarized light revealed that the solids melt, upon heating, to a fluid phase exhibiting a dark homeotropic texture with some elongated bright birefringent regions. At a higher temperature the texture disappears, with the fluid phase becoming isotropic. Upon cooling the resultant isotropic liquid, some *bâtonnets* are formed at the transition point to the mesophase, but they immediately disappear to leave a homeotropic texture consisting of dark areas scattered, in some cases, with small

 © WILEY-VCH Verlag GmbH, D-69451 Weinheim, 2000 1434−1948/00/0101−0133 $ 17.50+.50/0

focal-conic domains and Maltese crosses. This behavior is typical of a fluid lamellar (S_A) mesophase.[6] All the compounds studied underwent some decomposition when exposed to air and visible light in the isotropic state. Therefore extended heating and repeated heating-cooling cycles are to be avoided.

DSC Studies

The DSC data are collected in Table 1. The thermograms show two endothermic peaks on heating (exothermic on cooling) corresponding to the solid-to-mesophase and the mesophase-to-liquid transitions. Occasionally, small endothermic peaks were observed in the first heating scan at temperatures below the melting point (crystal-crystal transitions or pre-melting phenomena) but these were not usually observed in subsequent cooling or reheating scans. The existence of the liquid crystal phase at very low temperatures (compared to common metallomesogens) for the short chain derivatives is noteworthy. The mesophases of some complexes can be supercooled to below room temperature.

In the two series of complexes (nitrates and tetrafluoroborates) the melting temperatures increase steadily with the number of carbon atoms in the hydrocarbon chains (Table 1). The clearing temperatures increase with the number of carbon atoms for short chains, reach a maximum, and decrease for the longer chains. In each series the melting molar enthalpy $(\Delta H_M)_{melt}$ and entropy $(\Delta S_M)_{melt}$ values increase steadily with the number of carbon atoms in the aliphatic amine (Table 1), and are very different from one series (NO_3^-) to the other (BF_4^-). In contrast, the clearing molar enthalpy and entropy values, $(\Delta H_M)_{clear}$ and $(\Delta S_M)_{clear}$, decrease steadily upon increasing the number of carbon atoms in the aliphatic chain. A closer examination can be made by means of a crude but informative linear plot of these values against number of carbon atoms in the chain.

Table 1. Optical, thermal and thermodynamic data of $[Ag(NH_2\text{-}C_nH_{2n+1})_2]X$ complexes (C: crystal; S_A: smectic A mesophase; I: isotropic liquid).

X	*n*	Transition	T [°C]	ΔH [kJ·mol^{-1}]	ΔS [J·K^{-1}·mol^{-1}]
NO_3	6	C−S_A	37.8	14.6	47.0
		S_A−I	118.2	4.3	11.0
NO_3	8	C−S_A	54.8	19.9	60.7
		S_A−I	141.3	4.0	9.7
NO_3	10	C−S_A	67.0	25.2	74.1
		S_A−I	141.3	3.3	8.0
NO_3	12	C−S_A	76.7	31.7	90.6
		S_A−I	138.6	2.7	6.6
NO_3	14	C−S_A	79.7	36.6	103.7
		S_A−I	131.9	2.3	5.7
BF_4	8	C−S_A	39.5	38.3	122.5
		S_A−I	113.5	3.8	9.8
BF_4	10	C−S_A	53.4	49.1	150.4
		S_A−I	129.8	3.5	8.7
BF_4	12	C−S_A	59.9	62.1	186.5
		S_A−I	137.4	2.8	6.8
BF_4	14	C−S_A	67.0	68.2	200.5
		S_A−I	131.7	2.5	6.2

The fitting of the lines for $(\Delta H_M)_{melt}$ is remarkably good for both series (Figure 1). The slope affords the contribution to the melting enthalpy per carbon atom in the cation and the values are $(\Delta H_C)_{melt} = 1.395$ kJ·mol^{-1} for the NO_3^- series and 2.568 kJ·mol^{-1} for the BF_4^- series. The fit for $(\Delta S_M)_{melt}$ is also quite good and affords values of $(\Delta S_C)_{melt} = 3.583$ J·K^{-1}·mol^{-1} for the NO_3^- series and 6.753 J·K^{-1}·mol^{-1} for the BF_4^- series. The $(\Delta H_M)_{melt}$ and $(\Delta S_M)_{melt}$ values extrapolated for $n = 0$ (even though they lack a rigorous physical meaning are in all cases very small compared to the value $2n(\Delta H_C)_{melt}$ or $2n(\Delta S_C)_{melt}$, even for the shortest chains. This indicates that the melting enthalpy and melting entropy values almost exclusively arise due to the chains and, hence, the melting transition mainly involves melting of the chains, whereas the anion-cation interactions seem to be hardly affected. The nature of the anion, however, clearly affects the ΔH_C and ΔS_C values, which are almost twice as high for the BF_4^- series than for the NO_3^- series. In a purely ionic anion-cation interaction no difference should be expected, thus this effect is a reflection of some covalent donor interaction from the anion to the silver center. Such an interaction would be expected to be higher from the O atoms of the NO_3^- than from the F atoms of the BF_4^-.[7] Consequently, the silver atom becomes less of an acceptor towards the amine when the anion is NO_3^-, the chain is less polarized, and the chain interactions diminish, as is observed.

The fitting of the lines for $(\Delta H_M)_{clear}$ and $(\Delta S_M)_{clear}$ is also acceptable for both series (Figure 2). The slopes in this case are small and negative. The intercepts at $n = 0$ are comparatively high and are similar for both anions: about 5.9 kJ·mol^{-1} for $(\Delta H_M)_{clear}$ and 15.0 J·K^{-1}mol^{-1} for $(\Delta S_M)_{clear}$. This suggests that the clearing transition is mainly due to the melting of the anion-cation arrangement. The actual values are tuned by the size of the cation, with the transition becoming easier for the bulkier the cation.

X-ray Studies

X-ray diffraction experiments were carried out on magnetically oriented mesophases of three nitrate complexes (hexylamine, octylamine, and decylamine derivatives) and one tetrafluoroborate complex (octylamine derivative).

Two regions can be distinguished in the X-ray patterns {Figure 3 shows the pattern of $[Ag(octylamine)_2]BF_4$ at 50 °C}. In the low angle region a set of sharp arcs (labelled A), which extend over ±20° around the magnetic field direction, correspond to lattice spacing ratios 1, 1/2, 1/3, etc., and are characteristic of a lamellar system. The layer periodicity *d* is 18.8 Å, 22.5 Å, and 27.0 Å for the hexylamine, octylamine, and decylamine nitrate complexes, respectively, and 21.9 Å for the octylamine tetrafluoroborate complex (Table 2). In the wide-angle region the long-exposure time patterns exhibit two diffuse rings, both showing a large azimuthal spreading. The intensity maxima correspond to mean distances $l/(2\sin\theta) = 2\pi \cdot q^{-1}$ that are equivalent to 6.3−6.4 Å (labelled B) and 4.5 Å (labelled C).

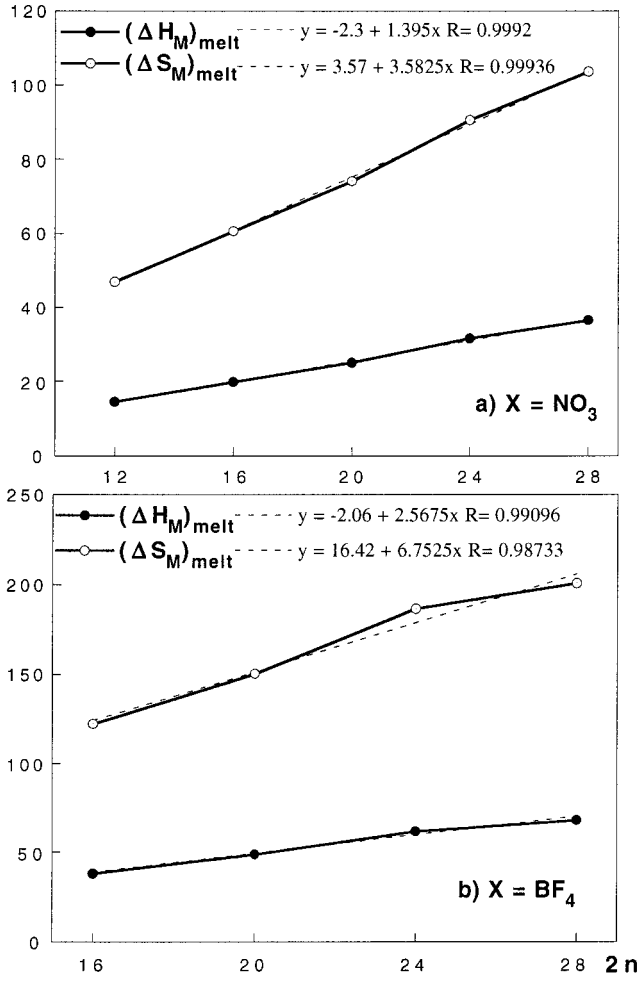


Figure 1. Plot of melting molar enthalpy $(\Delta H_M)_{melt}$ and entropy $(\Delta S_M)_{melt}$ values versus the total number of carbon atoms in the complex, $2n$, for: (a) $[Ag(NH_2n\text{-}C_nH_{2n+1})_2]NO_3$; (b) $[Ag(NH_2n\text{-}C_nH_{2n+1})_2]BF_4$.

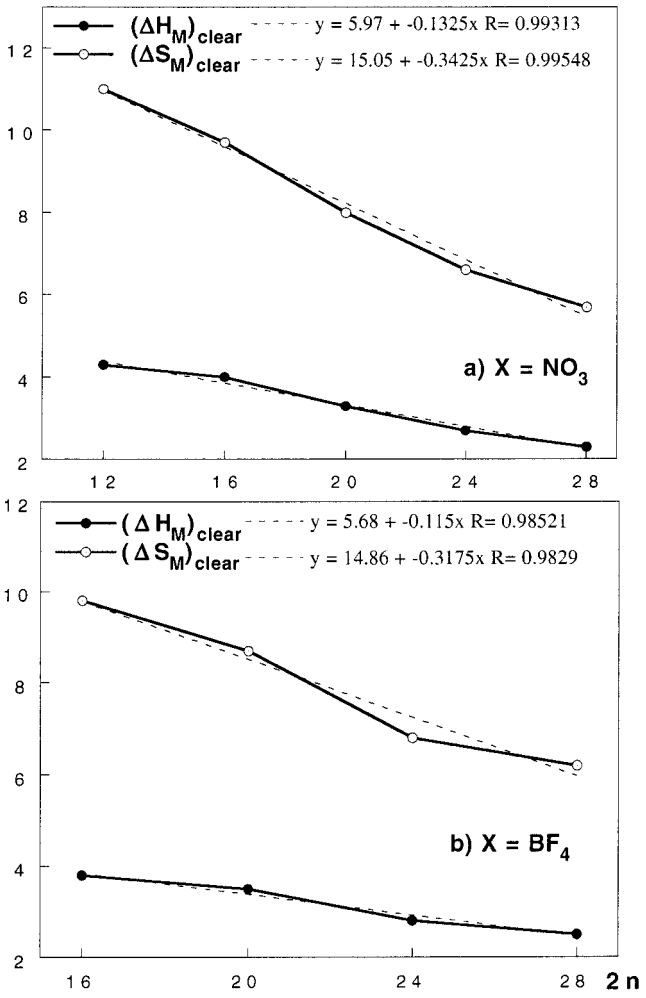


Figure 2. Plot of clearing molar enthalpy $(\Delta H_M)_{clear}$ and entropy $(\Delta S_M)_{clear}$ values versus the total number of carbon atoms in the complex, $2n$, for: (a) $[Ag(NH_2n\text{-}C_nH_{2n+1})_2]NO_3$; (b) $[Ag(NH_2n\text{-}C_nH_{2n+1})_2]BF_4$.

The only set of sharp reflections observed corresponds to the lamellar structure and therefore there is no periodic intra-lamellar order. Moreover, this set of arcs is aligned along the magnetic field and confirms the existence of a smectic A mesophase. The number of observed reflections on the layer planes is higher than usual for thermotropic smectic phases, although the intensities of these reflections decrease monotonically as the scattering vector is increased. Therefore the heavy components of the complex, namely the silver atom and the anion, are located in a thin slab of the smectic layer. Moreover, it is possible to give an estimation of the positional fluctuations of the heavy components of the layer from the Debye−Waller factor, $\exp(-2q\langle u^2\rangle)$. If this factor is equal to 10^{-6} for the fourth order ($q = 4 \times 2\pi/d$), the average extension of the heavy sublayer will be equal to a tenth of the total layer thickness d.

The diffuse ring at 4.5 Å is characteristic of a molten paraffinic medium. The mosaic spread of the smectic planes is large and consequently it is not possible to determine the degree of orientational order of the chains. However, since

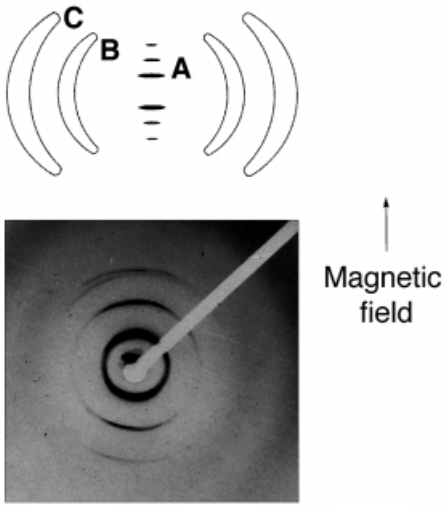


Figure 3. X-ray diffraction pattern of the magnetically aligned mesophase of $[Ag(NH_2n\text{-}C_8H_{17})_2]BF_4$ (at 50°C) along with a schematic interpretation of the pattern.

Table 2. Distances [Å] in $[Ag(NH_2n\text{-}C_nH_{2n+1})_2]X$ complexes measured in the mesophase by X-ray diffraction

X	n	d_A	d_B	d_C
NO_3	6	18.8	6.3	4.5
NO_3	8	22.5	–	–
NO_3	10	27.0	–	–
BF_4	8	21.9	6.4	4.5

the ring is nearly isotropic, the chains are likely to be poorly oriented. The second diffuse ring at 6.4 Å reveals that the intralayer ordering is more complex than for usual rod-like smectogenic molecules. The fact that 6.4 Å $\sqrt{4.5} \approx 2$ Å is consistent with a short range square array. However, it is important to note that, given the intensity of the diffuse ring at 4.5 Å, it cannot be simply considered as a second order maximum arising from a local square primitive cell with a lattice constant of 6.4 Å. It rather suggests that the equatorial scattering pattern results from the superposition of two different lattices, the area of one (approximately 6.4 Å × 6.4 Å = 41 Å^2) being twice as much as the area of the other (approximately 4.5 Å × 4.5 Å = 20 Å^2). It is important to note that an area of 41 Å^2 corresponds to twice the cross-sectional area of a hydrocarbon chain in an quasiextended conformation.[8]

The results described above, as well as density criteria, are consistent with the presence of two $[AgL_2]X$ units in the tetragonal cell that are arranged in such a way that the chain-to-chain distance is about 4.5 Å and the mean distance of 6.4 Å describes the ordering of the polar head groups. All these requirements can only be fulfilled if the silverdiamine cations adopt a U-shape and arrange themselves in a bilayer structure (Figure 4). The silver atoms form a square-planar local array of 6.4 Å size, and the aliphatic chains extend on each side of a central slab containing the polar groups in such a way that the two hydrocarbon chains belonging to the same cation point in the same direction. This arrangement is adequate to fill space efficiently and accommodate the anions between these layers, where a good anion-cation electrostatic interaction (with some covalent component for the nitrate series, as discussed above) can be obtained. Figure 5 and Figure 6 show a space-filling model of this kind of arrangement. Clearly the intralayer order in the mesophase must be lower and also just local. This structure is comparable to the L_δ phase observed in phospholipid-based lyotropic systems.[6] A bilayer organization of U-shaped cations has also been found in some thermotropic ionic metallomesogens based on macrocyclic N,S-containing ligands.[5] However, in that case the in-plane order does not correspond to a local square lattice but to a periodic undulation of the ionic sublayer.

It is important to note that the scattering factors of a silver atom (47) and the anions (31 for NO_3^-, or 40 for BF_4^-) are quite similar. Consequently, these two components must be close to each other, both in the plane perpendicular to the director and in the direction parallel to the director, in order to make a contribution to the intensity scattered in the Bragg reflections and in the 6.4 Å and 4.5 Å rings. Assuming that the silver atoms in the proposed arrangement lie at the corners of the two-dimensional square lattice and the anions lie at the center of the square, the 4.5 Å ring would arise from chain-chain and cation-anion interferences, and the 6.4 Å ring from cation-cation and anion-anion interferences.

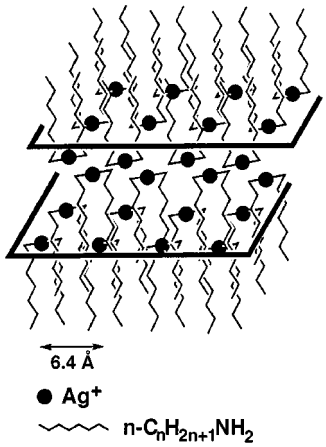


Figure 4. Model of a bilayer in the liquid crystal phase of $[Ag(NH_2n\text{-}C_nH_{2n+1})_2]X$ complexes (anions omitted).

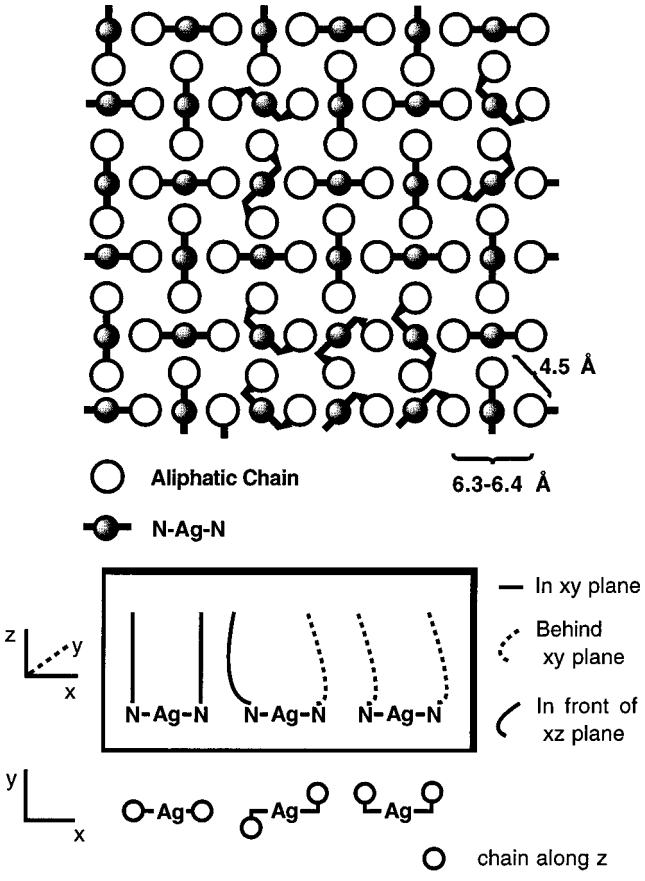


Figure 5. Sketch of the arrangement of the cations in the mesophase viewed along the director (perpendicular to the layer plane). The flexibility of the aliphatic chains allows different arrangements with respect to the N–Ag–N bond, which are a source of disorder and are illustrated in the lower part of the figure.

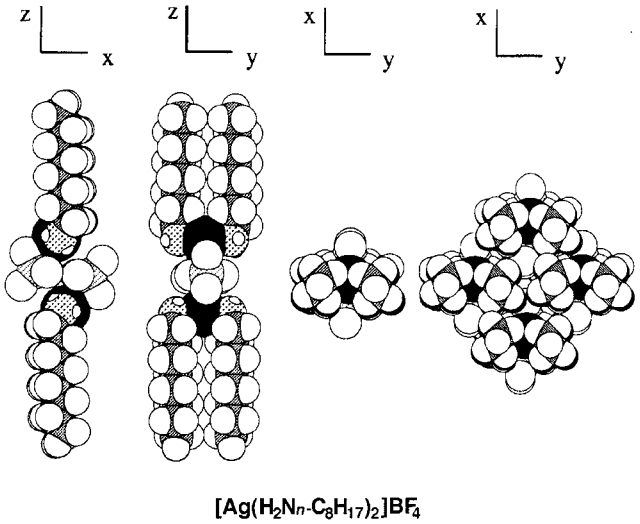


Figure 6. Space-filling model proposed for the complexes (X = BF_4). Left: possible arrangement of two anions and two cations (as the building block of the bilayers) viewed along the three axis. Right: packing of eight anions and eight cations (four up and four down) viewed along the z axis. Note that the overall packing results in a cylindrical cluster that should be able to rotate quite freely, thus introducing additional disorder. (Ag = black solid; N = large dots; B = small dots; C = shadow, H and F = white).

An alternative structural model could be proposed in which the local tetragonal unit cell contains one $[AgL_2]X$ unit per local cell. In this model the silverdiamine cation would sit at the four corners of the cell in an extended (rod-like) conformation parallel to the four-fold axis and the anions would be at the center of the cell. In this model the 4.5 Å ring would arise from anion-cation interferences and the 6.4 Å ring from anion-anion and cation-cation interferences. However, a tetragonal cell of width 6.4 Å and length *d* (Table 2) containing only one $[AgL_2]X$ unit would lead to very inefficient packing. Indeed, the density associated with this model would be too low (approximately 0.8 g cm^{-3}), and the average area per chain would be too large (S = 6.4 Å × 6.4 Å = 41 $Å^2$). Moreover, the intensity ratio of the two diffuse rings should be the reverse of that actually observed. Therefore this array, based on extended (rod-like) silverdiamine cations, is not consistent with the X-ray data and must be discounted. A similar structure with interdigitated layers would be consistent with the observed local order, but should lead to a layer thickness twice as small as that experimentally measured.

The bilayer model contains two molecules per unit cell, leading to a reasonable estimated density (approximately 1.6 g cm^{-3}), and fits all the X-ray data. The surface available for each paraffinic chain is about 20.0−20.5 $Å^2$ (S = 6.4 Å × 6.4 Å/2). Unfortunately we have not been able to grow single crystals of the complexes, but further support for the bilayer model comes from powder X-ray experiments carried out at room temperature on the decylamine nitrate complex. The powder pattern corresponds to a three-dimensional triclinic phase with parameters a = 5.03 Å, b = 8.84 Å, c = 27.2 Å, α = 93.0°, β = 93.3°, γ = 92.3°, with two molecules per unit cell. Parameter c is almost identical to the interlayer spacing (27.0 Å) found for the mesophase of the same compound (see Table 2). The fact that in the crystalline structure there are two molecules in a pseudo-rectangular section of approximately 5.0 Å × 8.8 Å = 44 $Å^2$ proves that is it possible for two molecules to be located in the two-dimensional square lattice of 41 $Å^2$ proposed for the mesophase. The calculated density of the crystal packing is 1.33 g cm^{-3}, whereas the density estimated for the mesophase is about 1.6 g cm^{-3}. This high value can be explained because it has been calculated on the basis of the diffraction data from the locally ordered areas in the mesophase. In fact, the square array has a short correlation range, and the presence of some rod-shaped molecules in with the U-shaped molecules cannot be ruled out. In addition, the orientational order of the chains is weak and the angle between the two chains of a molecule is widely fluctuating.

Finally, it is interesting to note that there are indications that the silverdiamine cations with long aliphatic primary amines may also adopt a U-shape in aqueous solution. In fact it has been reported that the values of ΔH^0 and ΔS^0 for the coordination of *n*-butyl- and *n*-pentylamine to Ag^+ are anomalous when compared with the values for the corresponding protonation reactions. It has been suggested that "a possible explanation for these anomalies is that there may be some hydrophobic interaction between the two ends of the hydrophobic chains". Clearly, although not explicitly stated, this implies the adoption of a U-shape.[9]

Conclusions

In summary, these simple silver coordination compounds reveal that metal cations can induce thermotropic behavior in non-mesogenic ligands, even if these ligands lack rigid cores and have only short aliphatic chains. Moreover, very low transition temperatures are obtained. The diffraction data support a bilayer model based on the packing of U-shaped silverdiamine cations. The thermodynamic parameters suggest that the melting transition involves only disorder (melting) of the chains, whereas the clearing transition involves breaking the anion-cation arrangement

Experimental Section

General: All compounds were satisfactorily characterized by IR spectroscopy and elemental microanalysis. − IR spectra were recorded on a Perkin−Elmer 1600 (series FTIR) spectrometer. − Microanalyses were performed with a Perkin−Elmer 240 B microanalyzer. − The optical textures of the mesophases were studied with a Meiji polarizing microscope equipped with a Mettler FP8 hot stage and an FP80 central processor. − The transition temperatures and enthalpies were measured by differential scanning calorimetry with a Perkin−Elmer DSC-7 instrument operated at a scanning rate of 10°C/min on heating. The apparatus was calibrated with indium (156.6°C; 28.4 $J \cdot g^{-1}$) as a standard. − X-ray diffraction experiments were carried out on magnetically aligned samples held in Lindemann glass capillary tubes of 1 mm diameter. The capillary tube, containing the sample, was set in an oven placed

between the poles of a magnet (magnetic field 0.3 T). The sample was irradiated with a point-focused X-ray beam (Cu-K_α radiation, $\lambda = 1.541$ Å) perpendicular to the magnetic field. The camera was evacuated in order to suppress air scattering. The diffraction patterns were collected on a flat film perpendicular to the X-ray beam. Powder experiments were carried out in a Guinier diffractometer (Huber 644) operating with a Cu-$K(\alpha_1)$ beam ($\lambda = 1.5405$ Å) issued from a germanium monochromator. The samples were held in rotating Lindemann glass capillaries (0.5 mm diameter) and the diffraction patterns were registered with a scintillation counter.

Preparation of $[Ag(NH_2n\text{-}C_nH_{2n+1})_2]NO_3$ ($n = 6$ and 8): A solution of $AgNO_3$ (0.255 g, 1.5 mmol) and amine (3.0 mmol) in acetonitrile (ca. 10 mL) was stirred at room temperature for 2 h. The resulting solution was concentrated under vacuum until crystallization began. Diethyl ether was added and the suspension was cooled in the freezer overnight. The white needles obtained were collected by filtration, washed with ether and dried under vacuum. Yield: 65% ($n = 6$) and 75% ($n = 8$). − Analytical data: ***n* = 6**: calcd. C 38.72, H 8.12, N 11.29); found C 38.31, H 8.25, N 11.30. −***n* = 8**: calcd. C 44.86, H 8.94, N 9.81; found C 44.74, H 9.31, N 9.79.

Preparation of $[Ag(NH_2n\text{-}C_nH_{2n+1})_2]NO_3$ ($n = 10$, 12 and 14): A suspension of $AgNO_3$ (0.221 g, 1.3 mmol) and amine (2.6 mmol) in acetonitrile (ca. 15 mL) was stirred at room temperature for 6 h. The resulting white suspension was concentrated under vacuum. Diethyl ether was added and the suspension was cooled in the freezer overnight. The crystallized product was collected by filtration, washed with ether and dried under vacuum. Yield: 70−90%. If necessary, the products can be further purified by recrystallization from acetonitrile/diethyl ether. − Analytical data ***n* = 10:** calcd. C 49.58, H 9.57, N 8.67; found C 49.79, H 10.04, N 8.63. − ***n* = 12:** calcd. C 53.32, H 10.07, N 7.77; found C 53.23, H 10.36, N 7.80. − ***n* = 14**: calcd. C 56.36, H 10.47, N 7.04; found C 56.51, H 10.50, N 6.93.

Preparation of $[Ag(NH_2n\text{-}C_nH_{2n+1})_2]BF_4$: A suspension of $AgBF_4$ (0.234 g, 1.2 mmol) and amine (2.4 mmol) in acetonitrile (ca. 10 mL) was stirred at room temperature under nitrogen for 6 h. The resulting solution ($n = 8$) or white suspension ($n = 10$, 12, 14) was concentrated under vacuum and cooled in the freezer overnight. The crystallized white product was collected by filtration, washed with ether and dried under vacuum. Yield: 60−75%. If necessary, the products can be further purified by recrystallization from acetonitrile/diethyl ether. − Analytical data ***n* = 8:** calcd. C 42.41, H 8.45, N 6.18; found C 42.61, H 8.83, N 6.30. − ***n* = 10:** calcd. C 47.17, H 9.10, N 5.50; found C 47.27, H 9.30, N 5.54. − ***n* = 12**: calcd. C 50.99, H 9.63, N 4.95; found C 51.40, H 10.01, N 4.91. − ***n* = 14**: calcd. C 54.11, H 10.06, N 4.51; found C 54.35, H 10.20, N 4.37.

Acknowledgments

This work was financed by the Comisión Interministerial de Ciencia y Tecnología (Spain, Projects MAT96-0708 and MAT97-0968-C02) and the Junta de Castilla y León (Project VA23/97).

[1] Reviews: A. M. Giroud-Godquin, P. M. Maitlis, *Angew. Chem.* **1991**, *103*, 370; *Angew. Chem. Int. Ed. Engl.* **1991**, *30*, 375; P. Espinet, M. A. Esteruelas, L. A. Oro, J. L. Serrano, E. Sola, *Coord. Chem. Rev.* **1992**, *117*, 215; D.W. Bruce in *Inorganic Materials* (Eds.: D. Bruce, D. O′Hare), Wiley, Chichester, **1992**, chapter 8; S. A. Hudson, P. M. Maitlis, *Chem. Rev.* **1993**, *93*, 861; *Metallomesogens. Synthesis, Properties and Applications* (Ed.: J. L. Serrano), VCH, Weinheim, **1996**; A. M. Giroud-Godquin in *Handbook of Liquid Crystals* (Eds.: D. Demus, J. Goodby, G. W. Gray, H.W. Spiess, D. V. Vill), Wiley-VCH, Weinheim, **1988**, Vol 2B, chapter 14.

[2] For a review of ionic metallomesogens see: F. Neve, *Adv. Mater.* **1996**, *8*, 277.

[3] D. W. Bruce, D. A. Dunmur, E. Lalinde, P. M. Maitlis, P. Styring, *Nature (London)* **1986**, 323, 791; D. W. Bruce, D. A. Dunmur, P. M. Maitlis, P. Styring, M. A. Esteruelas, L. A. Oro, M. B. Ros, J. L. Serrano, E. Sola, *Chem. Mater.* **1989**, *1*, 479; M. Marcos, M. B. Ros, J. L. Serrano, M. A. Esteruelas, E. Sola, L. A. Oro, J. Barberá, *Chem. Mater.* **1990**, *2*, 748; D. W. Bruce, D. A. Dunmur, S. A. Hudson, E. Lalinde, P. M. Maitlis, M. P. McDonald, R. Orr, P. Styring, A. S. Cherodian, R. M. Richardson, J. L. Feijoo, G. Ungar, *Mol. Cryst. Liq. Cryst.* **1991**, *206*, 79; H. Adams, N. A. Bailey, D. W. Bruce, S. C. Davis, D. A. Dunmur, P. D. Hempstead, S. A. Hudson, S. Thorpe, *J. Mater. Chem.* **1992**, *2*, 395; D. W. Bruce, S. A. Hudson, *J. Mater. Chem.* **1994**, *4*, 479; D. W. Bruce, B. Donnio, S. A. Hudson, A. M. Levelut, S. Megtert, D. Petermann, M. Veber, *J. Phys. II France* **1995**, *5*, 289; D. W. Bruce, S. Estdale, D. Guillon, B. Heinrich, *Liq. Cryst.* **1995**, *19*, 301.

[4] P. Verdagué, J. Courtieu, H. Adams, N. A. Bailey, P. M. Maitlis, *J. Chem. Soc., Chem. Commun.* **1994**, 1589.

[5] F. Neve, M. Ghedini, G. De Munno, A. M. Levelut, *Chem. Mater.* **1995**, *7*, 688.

[6] V. Luzzati in *Biological Membranes* (Ed.: D. Chapman), Academic Press, London, **1968**, Chap. 3; J. Charvolin, A. Tardieu in *Solid State Physics, Supplement 14* (Ed.: L. Liébert), Academic Press, New York, **1978**, pp. 209−257.

[7] Covalent interactions are found, for instance, in the X-ray structure of the pyrazine complex $[Ag(N_2C_4H_8)]_n(NO_3)_n$: R. G. Vranka, E. Lamma, *Inorg. Chem.* **1966**, *5*, 1020.

[8] A. A. Schaerer, C. J. Busso, A. E. Smith, L. B. Skinner, *J. Am. Chem. Soc.* **1955**, *77*, 2017.

[9] L. D. Hansen, D. J. Temer, *Inorg.Chem.* **1971**, *10*, 1439.

Received June 14, 1999
[I99218]

Molecular and Electronic Structure of Two Linear Thiophenolate-Bridged Heterotrinuclear Complexes $[LFeRuFeL]^{2+/3+}$ (L = 1,4,7-Tris(4-*tert*-butyl-2-mercaptobenzyl)-1,4,7-triazacyclononane)

Belen Albela,[a] Eckhard Bill,[a] Oliver Brosch,[a] Thomas Weyhermüller,[a] and Karl Wieghardt*[a]

Keywords: Thiolato-bridged complexes / Iron / Ruthenium / Mixed-valent compounds / Mössbauer spectroscopy

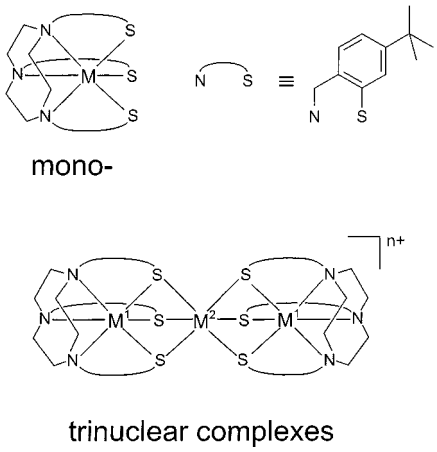
The reaction of $[Fe^{III}L]$ with $[Ru^{II}Cl_2(dmso)_4]$ in methanol under argon, affords, upon addition of $NaPF_6$, brown crystals of $[LFeRuFeL](PF_6)_2 \cdot 3\ CH_3OH$ (**1**). Its one-electron oxidation product $[LFeRuFeL](PF_6)_3$ (**2**) [L = 1,4,7-(4-*tert*-butyl-2-mercaptobenzyl)-1,4,7-triazacyclononane] was generated by using one equivalent of $[NO]BF_4$. The crystal structure determination of $[LFeRuFeL](BPh_4)_2 \cdot CH_3CN \cdot 3\ (CH_3)_2CO$ shows that **1** contains a trinuclear, face-sharing thiolato-bridged dication. Mössbauer spectroscopy established that the oxidation state distribution of **1** can best be described by $Fe^{2.5}Ru^{III}Fe^{2.5}$ and **2** by $Fe^{III}Ru^{III}Fe^{III}$. Complex **1** possesses a diamagnetic (S_t = 0) and **2** an S_t = 1/2 ground state. The electronic structures of **1** and **2** are rationalized by an MO picture involving Fe–Ru metal-metal bonds of bond order 0.5 in both species. Complex **1** is formally a mixed valence compound with complete delocalization of the "excess electron" (class III).

Introduction

In a series of papers[1−6] we have recently shown that mononuclear complexes of the type $[M^{III}L]$ (where L represents the trianionic ligand 1,4,7-tris(4-*tert*-butyl-2-mercaptobenzyl)-1,4,7-triazacyclononane and M = Fe, Ru) readily form homo- or heterotrinuclear complexes $[LM^1M^2M^1L]^{n+}$ with metal ions. These cations are isostructural, containing three face-sharing octahedra, namely two terminal $[M^1L]$ units comprising a *cis*-N_3S_3 donor set and a central MS_6 moiety. The three thiolato pendant arms of L form μ_2-thiolato bridges (Scheme 1). Complexes of this type have been shown to possess a rich redox chemistry where the isostructural tetra-, tri-, di- and monocationic species of a given transition metal ion combination are accessible via simple one-electron transfer steps. Thus it is possible to study magnetic exchange phenomena in paramagnetic species in a well-defined ligand matrix as a function of the local d^n electron configuration of the respective metal ion.

We have recently studied the complexes $[LFeFeFeL]^{2+/3+}$ [3] and their homologs $[LRuRuRuL]^{2+/3+}$.[5] It was shown that the two isoelectronic dications display an S_t = 1 ground state in the case of the tri-iron species but an S_t = 0 ground state for the triruthenium species. In contrast, both trications have an S_t = 1/2 ground state. In order to obtain a better understanding of their electronic structure, we decided that it would be of value to investigate the isoelectronic *hetero*trinuclear analogs $[LFeRuFeL]^{2+/3+}$. Here we report the synthesis, the molecular and electronic structures, and spectroscopic characterizations of these cations.

[a] Max-Planck-Institut für Strahlenchemie,
Stiftstrasse 34−36, D-45470 Mülheim an der Ruhr, Germany
Fax: (internat.) + 49(0)208/306-3952



Scheme 1. Schematic structures of ML and $[\{M^1L\}_2M^2]^{n+}$ complexes

Results

Preparation of Complexes

Reaction of the mononuclear species $[Fe^{III}L]$[1][2] with $[Ru^{II}Cl_2(dmso)_4]$ (dmso = dimethyl sulfoxide) in the ratio 1:1 in methanol, under argon, at elevated temperatures, produced a clear, dark brown solution from which, upon addition of $NaPF_6$, brown microcrystals of $[LFeRuFeL](PF_6)_2 \cdot 3\ CH_3OH$ (**1**) were obtained. Recrystallization of this material from acetone/acetonitrile (1:1) and addition of $Na[BPh_4]$ afforded single crystals of $[\{LFe\}_2Ru](BPh_4)_2 \cdot CH_3CN \cdot 3\ (CH_3)_2CO$.

When the above reaction mixture was cooled, treated with one equivalent of $[NO]BF_4$, and stored at 4°C, brown microcrystals of $[LFeRuFeL](PF_6)_3$ (**2**) were obtained after addition of $NaPF_6$. Complex **2** is the one-electron oxidized form of **1**.

 © WILEY-VCH Verlag GmbH, D-69451 Weinheim, 2000 1434−1948/00/0101−0139 $ 17.50+.50/0

Electronic spectra of solutions **1** and **2** in CH_3CN are displayed in Figure 1. The spectrum of **1** shows absorption maxima λ_{max} (ε, $L \cdot mol^{-1} \cdot cm^{-1}$) at 365 sh (ca. $9.5 \cdot 10^3$), 475 ($4.1 \cdot 10^3$), 670 sh ($2.0 \cdot 10^3$), 830 ($1.9 \cdot 10^3$), 1320 nm ($3.6 \cdot 10^3$); for **2** these values are at ca. 420 sh ($1.2 \cdot 10^4$), ca. 550 sh ($4.7 \cdot 10^3$), ca. 620 sh ($3.2 \cdot 10^3$), 750 sh ($2.0 \cdot 10^3$). Clearly, the intense band at 1320 nm in the spectrum of **1** is an intervalence charge transfer band (see below) since it is absent in the spectrum of **2**.

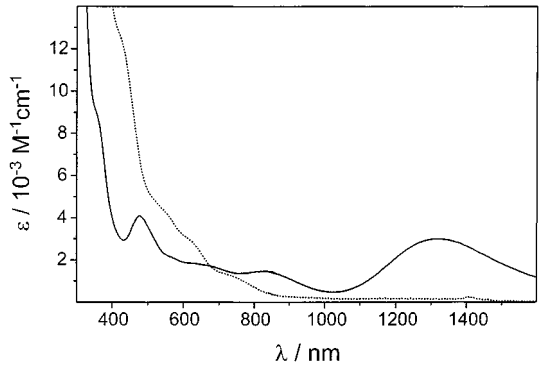


Figure 1. Electronic spectra of **1** (−) and **2** (---) in CH_3CN

The cyclic and square-wave voltammograms of **1** and **2** measured in CH_3CN (0.10 M $[N(nBu)_4]PF_6$) at 293 K are identical and are shown in Figure 2. Three reversible one-electron transfer processes are observed at $E^1_{1/2} = 1.09$ V vs ferrocenium/ferrocene (Fc^+/Fc), $E^2_{1/2} = -0.07$ V vs Fc^+/Fc, and $E^3_{1/2} = -1.07$ V vs Fc^+/Fc which are assigned as depicted in Equation 1.

$$[LFeRuFeL]^{4+} \underset{+e}{\overset{-e}{\rightleftharpoons}} [LFeRuFeL]^{3+} \underset{+e}{\overset{-e}{\rightleftharpoons}} [LFeRuFeL]^{2+} \underset{+e}{\overset{-e}{\rightleftharpoons}} [LFeRuFeL]^{1+} \quad (1)$$

Reduction of the dication to the monocation is only reversible on the time-scale of a CV experiment; it decomposes to $[Fe^{II}L]^-$ and (probably) $[Ru^{II}(NCCH_3)_6]^{2+}$ at slower scan rates. The small peaks at −0.75 V and +0.60 V vs Fc^+/Fc correspond to the [FeL]/$[FeL]^-$ and $[Ru^{III}(NCCH_3)_6]^{3+/2+}$ couple, respectively.

Magnetic Susceptibility and EPR Spectroscopy

Temperature-dependent magnetic-susceptibility measurements in the range 2−298 K were performed on a SQUID magnetometer in a field of 1 T. The raw data were corrected for underlying diamagnetism by using Pascal's tabulated constants. Temperature-independent paramagnetism (TIP), χ_{TIP}, is a fit parameter.

Figure 3 shows the calculated effective magnetic moments as a function of the temperature for **1** (top) and **2** (bottom). For complex **1**, μ_{eff} varies from 0.59 μ_B at 2 K to 1.97 μ_B at 290 K, which is predominantly due to TIP ($\chi_{TIP} \approx 2.0 \cdot 10^{-3}$ cm^3 mol^{-1}). Thus **1** has a diamagnetic $S_t = 0$ electronic ground state. A small amount of a paramagnetic impurity (< 2%) is also present in the sample of **1**.

The temperature-dependence of the effective magnetic moment of **2** was satisfactorily modeled for an $S_t = 1/2$ ground state with the following parameters: $g = 2.11$; $\chi_{TIP} = 1380 \cdot 10^{-6}$ cm^3 mol^{-1}. Note that large TIP values have been found for all trinuclear complexes of the type $[LFeMFeL]^{n+}$ (M = Cr, Co, Fe, Ni).[3−6]

The $S_t = 1/2$ ground state of **2** has been confirmed by its X-band EPR spectrum in CH_3CN solution at 10 K, which is shown in Figure 4. An axial signal with $g_\perp = 2.31$ and $g_\parallel = 1.86$ has been observed. The average $g^{av} = 2.16$ is

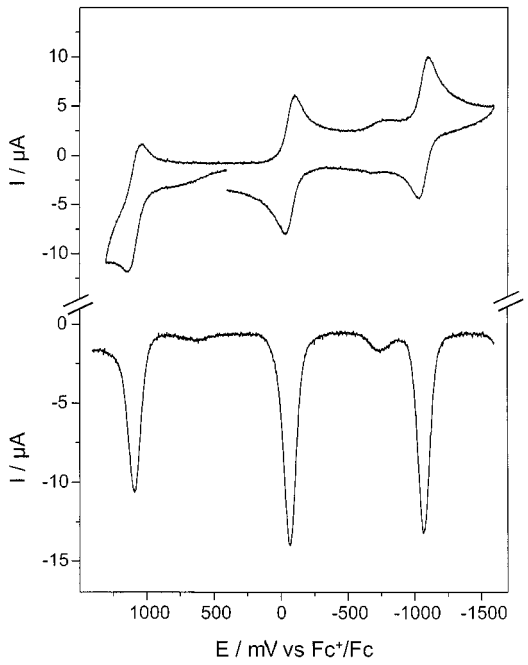


Figure 2. Cyclic (top) and square-wave (bottom) voltammogram of **1** at 298 K in CH_3CN (0.10 M $[N(nBu)_4]PF_6$, glassy carbon electrode, scan rate *cv* 100 mV s^{-1}; pulse height *sw* 25 mV, frequency 30 Hz)

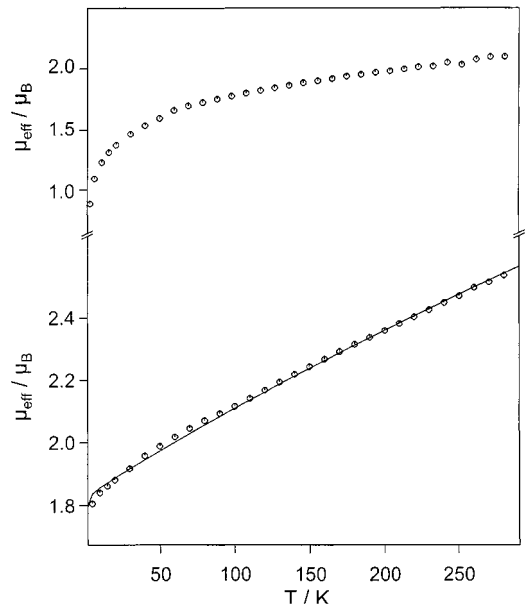


Figure 3. Temperature-dependence of the magnetic moment μ_{eff}/μ_B of solid **1** (top) and **2** (bottom); the solid line represents a fit; see text for parameters

in good agreement with that obtained from susceptibility measurements. Complex **1** is EPR-silent.

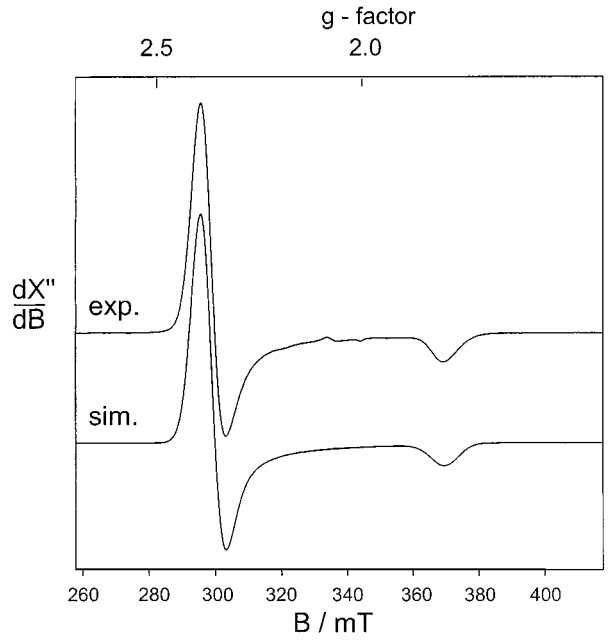


Figure 4. X-band EPR spectrum of **2** in frozen CH_3CN at 10 K and simulation (frequency 9.64 GHz; power 0.05 mW; modulation amplitude 11.4 G; modulation frequency 100 kHz)

Crystal Structure Determination

Crystals of $[LFeRuFeL](BPh_4)_2 \cdot CH_3CN \cdot 3\,(CH_3)_2CO$ consist of well-separated dications $[LFeRuFeL]^{2+}$ and tetraphenylborate anions together with acetonitrile and acetone molecules of crystallization. Figure 5 shows different views of the dication and Table 1 summarizes bond lengths and angles of the trinuclear core. The dication consists of three face-sharing thiolato-bridged octahedra with two terminal iron ions and a central ruthenium ion. The stereochemistry of these trinuclear cations, $[\{LM^1\}_2M^2]^{n+}$, has been discussed previously.[3,5,6] The staggered configuration of the six tertiary butyl groups (looking down the Fe···Ru···Fe axis) in the achiral stereoisomer $\Delta(\lambda\lambda\lambda)\cdots\Lambda(\delta\delta\delta)$ yields a stable structure which has been observed in all cases where the M1···M2 distance is >2.9 Å. Only in $[LRuRuRuL](PF_6)_2 \cdot H_2O$ has the $\Delta(\lambda\lambda\lambda)\cdots\Delta(\lambda\lambda\lambda)$ [and its enantiomer $\Lambda(\delta\delta\delta)\cdots\Lambda(\delta\delta\delta)$] diastereomer been observed.[5] In this case, the six tertiary butyl groups are eclipsed and the Ru−Ru distance is at 2.775 Å. The dication in **1** adopts the achiral $\Delta(\lambda\lambda\lambda)\cdots\Lambda(\delta\delta\delta)$ configuration. The ruthenium ion is located on a crystallographic inversion center. The average Fe−N and Fe−S bond lengths at 2.061(4) and 2.251(4) Å are indentical to those observed in all other structure containing an $[LFeMFeL]^{n+}$ cation.[1−6] Interestingly, the three crystallographically independent Ru−S distances of the central RuS_6 moiety are not quite equivalent. There are two longer Ru−S distances at 2.368(1) Å and a shorter one at 2.350(1) Å (tetragonally compressed octahedron). The Fe···Ru distance at 2.804(1) Å is short and may indicate the onset of direct metal−metal bonding. In $[LRuRuRuL]^{2+}$ the Ru−Ru distance is found at 2.775(1) Å[5] and in $[LFeFeFeL]^{2+}$ the Fe···Fe distance is 2.848(1) Å.[3]

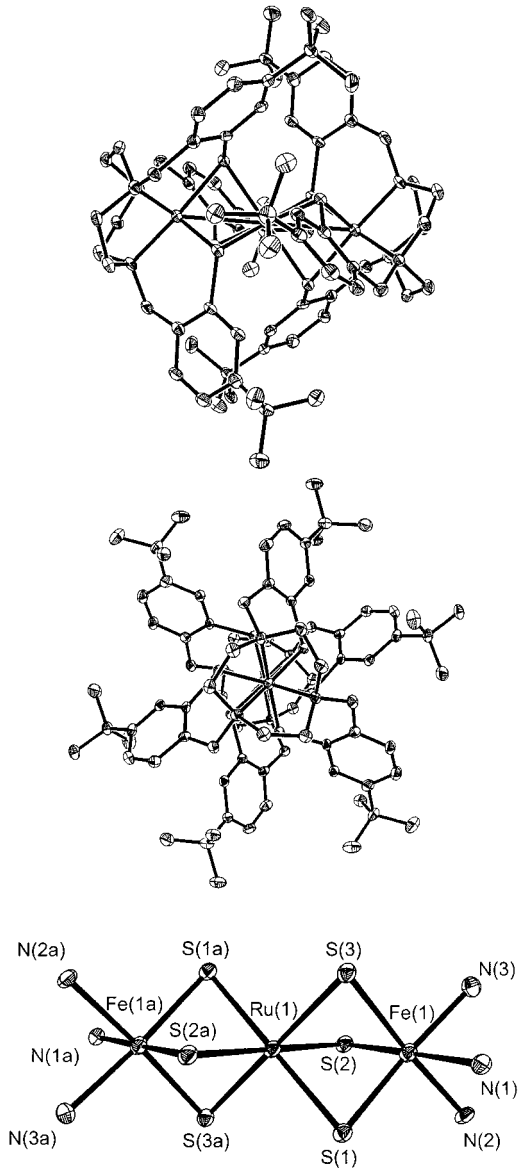


Figure 5. Structure of the dication in crystals of $[LFeRuFeL](BPh_4)_2 \cdot CH_3CN \cdot 3\,(CH_3)_2CO$: a) side-view, b) view down the Fe···Ru···Fe axis, and c) view of the core structure with atom labels

Mössbauer Spectroscopy

Complexes **1** and **2** have been studied by ^{57}Fe-Mössbauer spectroscopy in zero and applied fields. For both compounds, the zero-field spectra recorded on solid material at 80 K are single quadrupole doublets that could be fitted with Lorentzian lines as shown in Figure 6. The two local iron sites in **1** and **2** are indistinguishable; the parameters are summarized in Table 2. Since the same behavior is

Table 1. Selected bond lengths [Å] and angles [deg] for $[LFeRuFeL](BPh_4)_2 \cdot CH_3CN \cdot 3\,(CH_3)_2CO$ (**1**)

Ru(1)−S(1)	2.3502(12)	Fe(1)−N(1)	2.065(4)
Ru(1)−S(2)	2.3661(12)	Fe(1)−N(2)	2.059(4)
Ru(1)−S(3)	2.3696(14)	Fe(1)−N(3)	2.060(4)
Ru(1)−Fe(1)	2.8038	Fe(1)−S(1)	2.247(2)
		Fe(1)−S(2)	2.249(2)
		Fe(1)−S(3)	2.256(2)
S(1)−Ru(1)−S(2)	84.46(4)	N(2)−Fe(1)−N(3)	84.1(2)
S(1)−Ru(1)−S(2)′	95.54(4)	N(2)−Fe(1)−N(1)	84.7(2)
S(1)′−Ru(1)−S(3)	94.80(5)	N(3)−Fe(1)−N(1)	84.5(2)
S(2)′−Ru(1)−S(3)	96.88(5)	N(2)−Fe(1)−S(1)	93.21(12)
S(1)′−Ru(1)−S(3)′	85.20(5)	N(1)−Fe(1)−S(1)	91.40(12)
S(2)′−Ru(1)−S(3)′	83.12(5)	N(2)−Fe(1)−S(2)	92.65(12)
S(1)′−Ru(1)−S(2)′	84.46(5)	N(3)−Fe(1)−S(2)	94.30(12)
S(1)′−Ru(1)−S(2)	95.54(4)	S(1)−Fe(1)−S(2)	89.69(5)
S(1)−Ru(1)−S(3)	85.20(5)	N(3)−Fe(1)−S(3)	92.28(12)
S(2)−Ru(1)−S(3)	83.12(5)	N(1)−Fe(1)−S(3)	94.16(11)
S(1)−Ru(1)−S(3)′	94.80(5)	S(1)−Fe(1)−S(3)	90.39(5)
S(2)−Ru(1)−S(3)′	96.88(5)	S(2)−Fe(1)−S(3)	88.44(5)

found for the measurements at liquid helium temperatures, we can exclude the possibility of dynamic processes like valence detrapping playing a role. The ^{57}Fe-Mössbauer parameters of **1** and **2** clearly show that the redox states of the complexes are related to the iron oxidation states. The higher isomer shift and the lower quadrupole splitting of **1** indicates the more ferrous character of iron in **1** than in **2**. The iron ions in both **1** and **2** are low-spin.

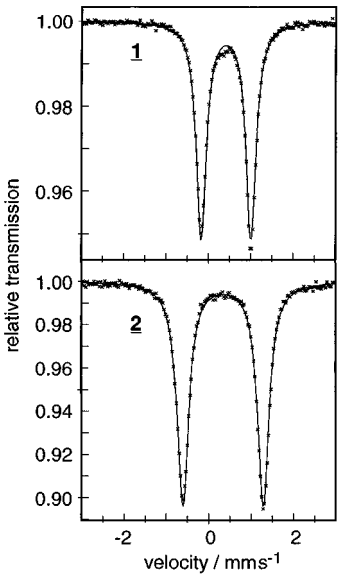


Figure 6. Zero-field Mössbauer spectra of crystalline samples of **1** and **2** measured at 80 K. The solid lines are a fit with Lorentzian lines with isomer shift, quadrupole splitting and line width (fwhm) of (**1**: $\delta = 0.41$ mm s^{-1}, $\Delta E_Q = 1.18$ mm s^{-1}, $\Gamma = 0.33$ mm s^{-1}) and (**2**: $\delta = 0.34$ mm s^{-1}, $\Delta E_Q = 1.83$ mm s^{-1}, $\Gamma = 0.33$ mm s^{-1}). The small difference in isomer shift relative to the 4.2 K values given in Table 2 originates from the second-order Doppler shift

The Mössbauer parameters of **1** and **2** fit perfectly in a $\delta/\Delta E_Q$ correlation diagram (Figure 7A) that we have previously established for a series of isostructural complexes with the same $[FeMFe]^{n+}$ core where M is Cr, Fe, or Co. The terminal iron sites thus have variable formal oxidation states, which depend on the cluster oxidation state and on

Table 2. Mössbauer parameters for complexes **1** and **2**

Complex Complex	δ[a] [mm s^{-1}]	ΔE_Q,[b] [mm s^{-1}]	η[c]	S_t[d]	$\bar{\bar{A}}/\mu_N g_N$ [T][e]
1	0.43	+1.23	0.3	0	−
2	0.34	+1.83	0.2(1)	1/2	−3.07, −3.07, +1.76

[a] Isomer shift (4.2 K). − [b] Quadrupole splitting (4.2 K). − [c] Asymmetry parameter. − [d] Spin ground state. − [e] Magnetic hyperfine tensor.

the degree of valence delocalization mediated via the central MS_6 unit.[3] If we take these compounds as a reference series (Table 3) we can determine the iron valences of **1** and **2**. In particular, the Mössbauer isomer shift is a sensitive parameter for this purpose because it is a measure of the charge density at the iron nucleus. The apparently linear correlation of oxidation state and isomer shift shown in Figure 7B reveals an iron oxidation state of 2.9 for **2** (≈ +III) and an intermediate value of 2.5 for the reduced analogue **1**. Therefore the central ruthenium ion in this system must be persistently close to the trivalent state (+III) and

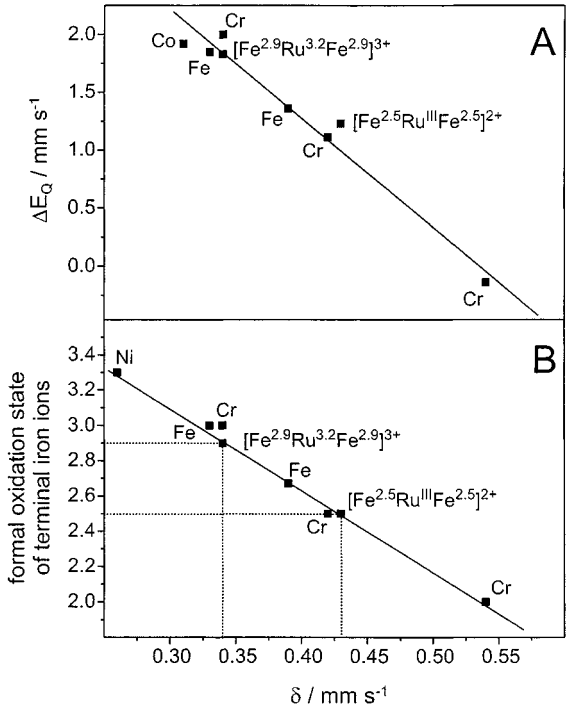


Figure 7. (A) Plot of the quadrupole splitting and ^{57}Fe-Mössbauer isomer shift for **1** and **2** together with the values of related complexes with the $[FeMFe]^{n+}$ core, M = Cr, Fe, Co, Ni taken from ref.[3][6] − (B) Correlation of the formal oxidation state and isomer shift for the same set of compounds. The dotted lines show the determination of this oxidation state for the iron ions in **1** and **2**, respectively

is not affected by the 2+/3+ redox transition of the cluster.

For diamagnetic compound **1**, the sign of V_{zz}, the main component of the electric field gradient (efg), and the asymmetry parameter η of the efg were determined from the Mössbauer spectrum, measured from a crystalline sample

Table 3. Summary of Mössbauer Parameters (4.2 K) of Complexes $[LFeMFeL]^{n+}$

Complex	ref.	δ[a] mm s^{-1}	ΔE_Q[b] mm s^{-1}	S_t[c]	Oxidation state of terminal iron ions
$[FeRuFe]^{2+}$	this work	0.43	+1.23	0	2.5
$[FeRuFe]^{3+}$	this work	0.34	+1.83	1/2	3.0
$[FeCrFe]^{1+}$	[3]	0.54	−0.14	$^3/_2$	2.0
$[FeCrFe]^{2+}$	[3]	0.42	+1.11	2	2.5
$[FeCrFe]^{3+}$	[3]	0.34	+2.00	1/2	3.0
$[FeCoFe]^{3+}$	[3]	0.31	+1.92	1	3.0
$[FeFeFe]^{2+}$	[3]	0.39	+1.36	1	2.67
$[FeFeFe]^{3+}$	[3]	0.33	+1.85	1/2	3.0
$[FeNiFe]^{3+}$	[6]	0.31	+0.52	1/2	3.0
$[FeNiFe]^{4+}$	[6]	0.26	+1.85	0	3.3

[a] Isomer shift of the terminal iron ions. − [b] Quadrupole splitting of the terminal iron ions. − [c] Electronic ground state of the trinuclear cation.

with an applied field of 7 T at 4.2 K (Figure 8). The spectrum could be readily simulated with the usual nuclear Hamiltonian[7][8] for the external field and a vanishing internal field. The sign of V_{zz} is found to be positive with η = 0.3. The parameters are summarized in Table 2.

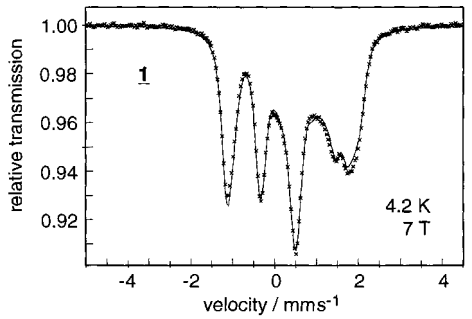


Figure 8. Magnetically perturbed Mössbauer spectrum of **1** measured at 4.2 K with a field B = 7 T applied perpendicular to the γ-rays. The solid line is a simulation for a diamagnetic system (zero internal field); the parameters are given in Table 2

Figure 9 shows the magnetic Mössbauer spectra of solid complex **2** recorded with applied fields of 4 T and 7 T at 4.2 K and 120 K. The spin ground state S_t = 1/2 of complex **2** is well separated from the excited states and the limit of strong coupling ($J >> \mu_B B$, kT) is valid even at 120 K according to the static magnetic susceptibility measurement. We have therefore used an effective spin Hamiltonian for the description of the magnetic Mössbauer spectra.[3] At liquid helium temperatures the spectra were simulated in the slow relaxation limit whereas at 120 K fast relaxation prevails. To limit the number of free parameters the g factors were fixed to the values determined from EPR. The sign of V_{zz} is unambiguously positive, as is clearly shown by the 120 K measurement, and the asymmetry parameter is 0.2(1). This result discloses the order of the 1e and a_1 iron 3d orbitals in the trigonal symmetry (t_{2g} in O_h symmetry).[3][9] The positive V_{zz} is consistent with a large positive valence electron contribution to the efg which is expected for an $(1e)^4(a_1)^1$ electron configuration if the 1e orbital set is lower in energy than the a_1 orbital.

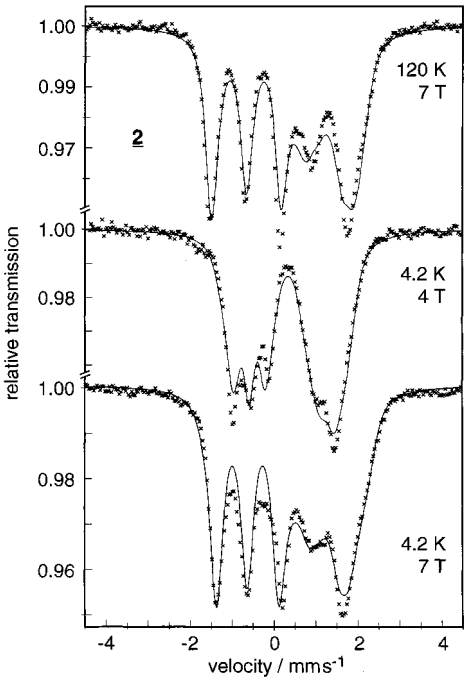


Figure 9. Magnetically perturbed Mössbauer spectrum of **2** measured at 4.2 K and 120 K with the indicated fields applied perpendicular to the γ-rays. The solid lines are a simulation for a system spin S_t = 1/2; the parameters are given in Table 2

Surprisingly, the fits required a finite value of the asymmetry parameter η = 0.2(1), and an Euler angle β = 22° which orients the principal z'-axis of the efg off from the principal z'-axis of the g and A tensors. The deviation is in contrast to the anticipated C_{3v} symmetry of the complex. A close inspection of the molecular structure shows a small distortion of the local iron sites in the crystal. There are two slightly longer Fe−S bonds [Fe(1)−S(3) and Fe(1)−S(3)′] and the RuS_6 octahedron shows a tetragonal compression with two shorter Ru−S bonds [Ru(1)−S(1) and Ru(1)−S(1)′].

The internal magnetic field induced by the total spin (S_t = 1/2) of the complex has a relatively small isotropic contribution and large anisotropy as shown by the trace and the components of the hyperfine coupling tensor given in Table 2 ($1/3\mathrm{Tr}(A)/g_N\beta_N$ = −1.46 T). This closely resembles the magnetic properties of iron in the corresponding $[FeFeFe]^{3+}$ complex.[3] The asymmetry owes its origin to significant spin-dipolar contributions to the A tensor, due to spin-orbit interaction in the $3d^5$ configuration of the low-spin Fe^{III}. The sign of the isotropic contribution to A is negative as it is for usual mononuclear iron compounds. This demonstrates that the local spins of the iron ions are parallel to the cluster spin, whereas the Ru^{III} spin is antiparallel, giving rise to the $|S_t = 1/2, S^* = 1>$ ground state. The A-tensor components given with respect to the total spin can be converted into local values related to the iron spin by using the spin projection factor derived from an application of the Wigner-Eckart theorem: $A_{(S_t=1/2)} = 2/3\ a_{S=1/2}$.

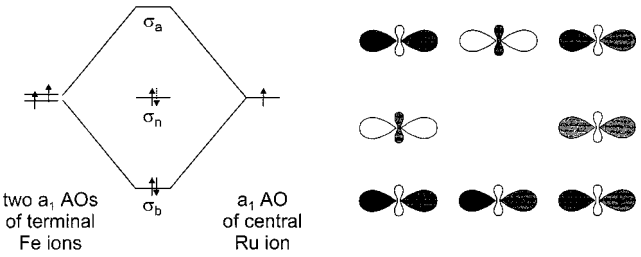
The obtained local values are $a_{S = 1/2}/g_N\mu_N$ = (−4.61, −4.61, +2.65) T.

In summary, Mössbauer spectroscopy allows one to experimentally determine the formal oxidation state of the iron ions in $[LFeMFeL]^{n+}$ complexes. As shown in Figure 7A, the isomer shift and the quadrupole splitting parameters of all complexes of this type reported to date are linearly correlated, and the corresponding data of **1** and **2** are in excellent agreement with this correlation. We have conclusively shown[3] that the iron ions in $[LFeCr^{III}FeL]^{3+}$ are purely low-spin ferric ions (oxidation state +III), whereas in $[LFeCr^{III}FeL]^{1+}$ they are low-spin ferrous (+II) and in $[LFeCr^{III}FeL]^{2+}$ are a mixed valent species with delocalized electronic structure (two $Fe^{2.5}$ ions). A plot of the corresponding ^{57}Fe-isomer shift vs the formal oxidation state is again linear, as displayed in Figure 7B. Using this correlation, an oxidation state of 2.9 (≈ +III) for **2** and of 2.5 for **1** is determined for the respective iron ions. Thus, **1** may be described as a $[LFe^{2.5}Ru^{III}Fe^{2.5}L]^{2+}$ and **2** as a $[LFe^{III}Ru^{III}Fe^{III}L]^{3+}$ species. In this manner we have established that the reduction of **2** by one-electron, yielding **1**, affects only the iron ions, and that both **1** and **2** contain a central Ru^{III} ion. Furthermore, the observation in the ^{57}Fe-Mössbauer spectrum of **1** of only a single iron site − even at 4.2 K − renders the dication a mixed valent species with a completely delocalized "excess" electron (class III according to Robin and Day[10]); the alternative formulation of **1** as a $[LFe^{III}Ru^{II}Fe^{III}L]^{2+}$ species is clearly ruled out by its Mössbauer spectra.

Discussion

In the preceding section it has been experimentally established that the cation $[LFeRuFeL]^{3+}$ in complex **2** contains two low-spin ferric ions with an $(1e)^4(a_1)^1$ local electron configuration and a central low-spin Ru^{III} ion, probably also with an $(1e)^4(a_1)^1$ configuration. The S_t = 1/2 ground state can then be rationalized by a MO description invoking two weak Fe−Ru bonds. The formation of three-center MOs by overlap of metal t_{2g} orbitals (specifically the a_1 orbitals) having lobes along the threefold symmetry axis, yields a bonding σ_b, a nonbonding σ_n, and an antibonding σ_a molecular orbital.[11][12] There are three electrons to occupy these MOs, σ_b^2 and σ_n^1, yielding an S_t = 1/2 ground state (Scheme 2). In the structurally characterized species $[Ru_3Cl_8(PEt_3)_4][SbF_6]$[13] a Ru−Ru distance at 2.91 Å has been found and a formal Ru−Ru bond order of 0.5 has been proposed. Analogously, an Fe−Ru bond of bond order 0.5 can be envisaged in $[LFeRuFeL]^{3+}$ (as in its previously described isoelectronic homotrinuclear species $[LRu^{III}Ru^{III}Ru^{III}L]^{3+}$).[5]

It is interesting that the isoelectronic species $[LFe^{III}Fe^{III}Fe^{III}L]^{3+}$ containing a low-spin central and two low-spin terminal ferric ions also possesses an S_t = 1/2 ground state.[3] The Fe···Fe distance has been determined at 2.86(2) Å by EXAFS spectroscopy or 2.79(2) Å from a low-quality X-ray crystal structure. The observed very strong antiferromagnetic coupling (J_a < −400 cm^{-1}) has been rationalized as originating from direct exchange between local a_1-orbitals and the onset of metal−metal bonding.

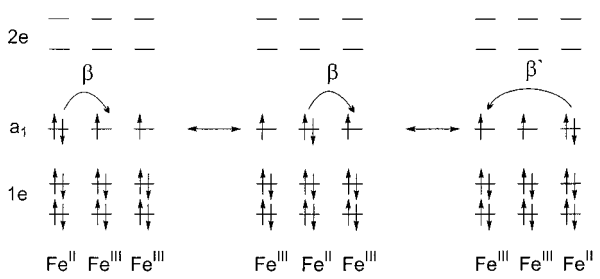


Scheme 2. Schematic MO representation for $[\{LFe\}_2Ru]^{2+/3+}$

Mössbauer spectroscopy unequivocally demonstrates that one-electron reduction of **2** to **1** affects only the two terminal iron ions which are on the time scale of this spectroscopy equivalent: $[LFe^{2.5}Ru^{III}Fe^{2.5}L]^{2+}$. The Ru−Fe distance at 2.804(1) Å is in the range where direct metal−metal bonding is certainly a possibility. The MO scheme (Scheme 2) immediately implies that the "excess" electron occupies the σ_n MO, giving rise to an electron configuration $\sigma_b^2\sigma_n^2$ where the Fe−Ru bonds also have a BO of 0.5 and the dication adopts a diamagnetic ground state. Similarly, $[LRuRuRuL]^{2+}$ has been shown to possess an S_t = 0 ground state and a relatively short Ru−Ru distance at 2.775(1) Å.[5]

On the other hand, isoelectronic $[LFeFeFeL]^{2+}$ possesses an S_t = 1 ground state[3] with no thermally accessible excited spin states. The Fe···Fe distance has been determined to be 2.848(2) Å which is slightly, but significantly, longer than in **1** or $[LRuRuRuL]^{2+}$. From Mössbauer spectroscopy, a fractional oxidation state of +2.67 for each of the three iron ions has been determined. The positive sign of the quadrupole splittings indicated that the local a_1-orbitals are the magnetic orbitals. The origin of the S_t = 1 ground state has been rationalized by a double exchange mechanism over three metal centers (Scheme 3). Only parallel alignment of the three respective local spins allows the excess electron to be transferred over all *three* metal centers. The negative sign of the effective Mössbauer hyperfine coupling constants A_i^{iso} indicates positive spin density at the central *and* terminal centers, thereby corroborating the above picture.[3] In this instance Fe···Fe metal bonding does not play a significant role, but delocalization of the excess electron via a double exchange mechanism enforces the above triplet ground state.

Finally, for the isoelectronic species $[LFe^{III}Co^{III}Fe^{III}L]^{3+}$, the observed S_t = 1 ground state[3] is thought to be attained via strong intramolecular ferromagnetic exchange coupling between two localized low-spin ferric ions which is mediated by a low-spin Co^{III} ion. For a detailed discussion of this rather surprising result see ref.[3][4] Interestingly, $[LRu^{III}Co^{III}Ru^{III}L]^{3+}$ also possesses an S_t = 1 ground state.[14] In both low-spin cobalt(III) containing species no metal-metal bonding is anticipated to play a role due to the



Scheme 3. Electron delocalization in $[\{LFe\}_2Fe]^{2+}$

small size of a cobalt(III) ion (the overlap of a_1 orbitals is very poor).

In the isoelectronic series $[LRuRuRuL]^{2+}$, **1**, $[LFeFeFeL]^{2+}$, $[LRu^{III}Co^{III}Ru^{III}L]^{3+}$, and $[LFe^{III}Co^{III}Fe^{III}L]^{3+}$, each containing 16 valence electrons, the actual ground state correlates with the extent of direct metal−metal bonding, which is significant only in the first two cases, where it yields an $S_t = 0$ ground state. In $[LFeFeFeL]^{2+}$ delocalization of an excess electron over all three iron sites enforces a triplet ground state via double exchange, whereas in $[LRu^{III}Co^{III}Ru^{III}L]^{3+}$ and $[LFe^{III}Co^{III}Fe^{III}L]^{3+}$ there is no metal-metal bonding and the $d^5d^6d^5$ electron configuration is *localized*. Intramolecular spin exchange (ferromagnetic in nature) yields the observed triplet ground state

Experimental Section

Syntheses: The ligand $H_3L \cdot 3\,HPF_6$ was prepared by following the published procedure for $H_3L \cdot 3\,HCl$ by using an HPF_6 solution (ether) instead of HCl in the last step. The synthesis of the mononuclear species $[Fe^{III}L]$ has been described previously.[1]

$[LFeRuFeL](PF_6)_2 \cdot 3\,CH_3OH$ (1): A degassed solution of [FeL] (0.30 g; 0.42 mmol) and $[Ru^{II}Cl_2(dmso)_4]$ (0.20 g; 0.42 mmol) in CH_3OH (50 mL) were heated to reflux under argon for 3 h. To the cooled (20°C) dark brown solution an excess of $NaPF_6$ (1.0 g) dissolved in degassed CH_3OH (25 mL) was added. Within a few hours at 4°C a brown microcrystalline precipitate formed which was collected by filtration (Yield: 0.19 g; 50%). Recrystallization of this material from an acetone-acetonitrile mixture (1:1) produced, after addition of $Na[BPh_4]$, single crystals of $[LFeRuFeL](BPh_4)_2 \cdot CH_3CN \cdot 3\,(CH_3)_2CO$ suitable for X-ray crystallography. − $C_{78}H_{108}N_6S_6RuFe_2(PF_6)_2 \cdot 3\,CH_3OH$: calcd. C 50.95, H 6.30, N 4.37, S 10.01; found C 51.5, H 6.1, N 4.2, S 10.3. − LSIMS *m/z* $[\{LFe\}_2Ru]^+$ 1535; $\{[\{LFe\}_2Ru](PF_6)\}^+$ 1679.6; $[\{LFe\}_2Ru]^{2+}$ 768.3.

$[LFeRuFeL](PF_6)_3$ (2): A degassed solution of [FeL] (0.30 g; 0.42 mmol) and $[RuCl_2(dmso)_4]$ (0.20 g; 0.42 mmol) in CH_3OH (50 mL) was heated to reflux under argon for 3 h. To the cooled (20°C) solution $[NO]BF_4$ (0.05 g; 0.42 mmol) was added and then stirred at 45°C for 3 h. Upon addition of $NaPF_6$ (0.3 g; 1.8 mmol) dissolved in CH_3OH (25 mL) and storage at 4°C for a few hours, a brown precipitate formed (0.15 g). Recrystallization of this material from CH_3CN afforded brown microcrystals of **2**. − $C_{78}H_{108}N_6S_6RuFe_2 \cdot (PF_6)_3$: calcd. C 47.56, H 5.53, N 4.27, S 9.77; found: C 47.2, H 5.5, N 4.1, S 9.5. − ESI (pos. ion) mass spectrometry: $[\{(LFe)_2Ru\}(PF_6)_2]^+$ 1824.2; $[\{(LFe)_2Ru\}(PF_6)]^+$ 1679; $[\{(LFe)_2Ru](PF_6)]^{2+}$ 839.3; $[(LFe)_2Ru]^{2+}$ 766.8.

X-ray Structure Determination: A brown single crystal of $[LFeRuFeL](BPh_4)_2 \cdot CH_3CN \cdot 3\,(CH_3)_2CO$ was mounted on an Enraf−Nonius CAD4 diffractometer in a glass capillary sealed under argon. Graphite-monochromated Mo *Kα* radiation (λ = 0.71073 Å) was used. Cell constants were obtained from a least-squares fit of the setting angles of 25 carefully centered reflections. Intensity data were collected at 100(2) K by using the ω-2θ scan technique, corrected for Lorentz and polarization effects, but no absorption correction was carried out due to the small absorption coefficient.

The Siemens ShelXTL software package[15] was used for solution, refinement, and artwork of the structure which was readily solved and refined by direct methods and difference Fourier techniques. All non-hydrogen atoms were refined anisotropically except the methyl carbon atoms of one disordered acetonitrile and acetone molecule which were isotropically refined on two sites (with occupancy factors 0.5 for each atom). All hydrogen atoms were placed at calculated positions and refined as riding atoms with isotropic displacement parameters. $C_{137}H_{169}B_2Fe_2N_7O_3RuS_6$, M = 2388.54 g mol^{-1}, crystal dimensions 0.49 × 0.35 × 0.21 mm, monoclinic, $Z = 2$, space group $P2_1/c$, a = 12.926(4), b = 15.613(4), c = 31.467(9) Å, β = 90.24(3)°, V = 6350(3) Å^3, $\rho_{calcd.}$ = 1.249 g cm^{-3}, T = 100(2) K, 2θ range = 5.6 to 50.0°, 11387 measured reflections, 11167 unique reflections, 6958 observed reflections [$I > 2\sigma(I)$], 710 parameters, $R_1 = 0.056$, $wR_2 = 0.135$. Further details of the crystal structure determination have been deposited with the Cambridge Crystallographic Data Centre as supplementary publication no. CCDC−125733. Copies of the data can be obtained free of charge on application to CCDC, 12 Union Road, Cambridge CB2 1EZ [Fax: +44 (0)1223/336-033; E-mail: deposit@ccdc.cam.ac.uk].

Physical Measurements: UV/Vis/near-IR spectra of CH_3CN solutions of **1** and **2** were measured on a Perkin−Elmer Lambda 19 spectrophotometer in the range 210−3200 nm at ambient temperature. − Cyclic and square-wave voltammetric and coulometric measurements were performed on EG & G equipment (potentiostat/galvanostat model 273A) on Ar-flushed acetonitrile solutions of samples containing 0.10 M $[N(nBu)_4]PF_6$ as supporting electrolyte at a glassy carbon working electrode and a $Ag/AgNO_3$ reference electrode. Ferrocene (Fc) was added as internal standard; all potentials are referenced vs the Fc^+/Fc couple. − Temperature-dependent magnetic susceptibilities of powdered samples were measured by using a SQUID magnetometer (Quantum Design) at 1.0 T (2.0−300 K). For calculations of the molar magnetic susceptibility, χ_M, the experimental susceptibilities were corrected for the underlying diamagnetism of the sample by using tabulated Pascal's constants. The temperature-independent paramagnetism (χ_{TIP}) was obtained by a fitting procedure. − The X-band EPR spectrum of a frozen solution of **2** was recorded on a Bruker ESP 300E spectrometer equipped with a helium flow cryostat (Oxford Instruments ESR 910). The X-band resonator was a dual-mode cavity (Bruker ER 4116 DM/95). − The Mössbauer spectra were recorded on an alternating constant-acceleration spectrometer. The minimal linewidth was 0.24 mm s^{-1} (full width at half-height). The sample temperature was maintained constant in either an Oxford Variox or an Oxford Mössbauer-Spectromag cryostat. The latter is a split-pair superconducting magnet system for applied fields up to 8 T where the temperature of the sample can be varied in the range 1.5−250 K. The field at the samples is oriented perpendicular to the γ-beam. The $^{57}Co/Rh$ source (1.8 GBq) was positioned at room temperature inside the gap of the magnet system at a zero-field position. Isomer shifts are referenced relative to α-iron metal at 295 K. Details of the analysis within the usual spin Hamiltonian

formalism are given in ref.[3] The depicted fits are the results of an optimization applied simultaneously to the whole series of experimental spectra.

Acknowledgments

We thank the Fonds der Chemischen Industrie for financial support. B. A. is grateful to the Ministry of Education and Culture of Spain for a fellowship.

[1] T. Beissel, K.-S. Bürger, G. Voigt, K. Wieghardt, C. Butzlaff, A. X. Trautwein, *Inorg. Chem.* **1993**, *32*, 124.
[2] T. Beissel, T. Glaser, F. Kesting, K. Wieghardt, B. Nuber, *Inorg. Chem.* **1996**, *35*, 3936.
[3] T. Glaser, T. Beissel, E. Bill, T. Weyhermüller, V. Schünemann, W. Meyer-Klaucke, A. X. Trautwein, K. Wieghardt, *J. Am. Chem. Soc.* **1999**, *121*, 2193.
[4] T. Glaser, K. Wieghardt, in: *Spectroscopic Methods in Bioinorganic Chemistry* (Eds. E. I. Solomon, K. O. Hodgson), ACS Symposium Series, Vol. *692*, 314 (**1998**).
[5] B. Albela, E. Bothe, O. Brosch, K. Mochizuki, T. Weyhermüller, K. Wieghardt, *Inorg. Chem.*, in press.
[6] T. Glaser, F. Kesting, T. Beissel, E. Bill, T. Weyhermüller, W. Meyer-Klaucke, K. Wieghardt, *Inorg. Chem.* **1999**, *38*, 722.
[7] P. Gütlich in: *Mössbauer Spectroscopy*, U. Gonser, Ed., Springer Verlag: Berlin, Heidelberg, New York, 1975.
[8] A. X. Trautwein, E. Bill, E. L. Bominaar, H. Winkler, *Struct. Bonding* **1991**, *78*, 1.
[9] U. Bossek, D. Nühlen, E. Bill, T. Glaser, K. Wieghardt, A. X. Trautwein, *Inorg. Chem.* **1997**, *36*, 2834.
[10] M. B. Robin, P. Day, *Adv. Inorg. Chem. Radiochem.* **1967**, *10*, 247.
[11] A. Bino, F. A. Cotton, *J. Am. Chem. Soc.* **1980**, *102*, 608.
[12] B. E. Bursten, F. A. Cotton, A. Fang, *Inorg. Chem.* **1983**, *22*, 2127.
[13] F. A. Cotton, R. C. Torralba, *Inorg. Chem.* **1991**, *30*, 3293.
[14] O. Brosch, K. Wieghardt, unpublished results.
[15] *ShelXTL V.5*, Siemens Analytical Instruments, Inc., **1994**.

Received June 15, 1999
[I99219]

[(Ethylenediamine)Pt(uracilate)]$_4$ – A Metal Analogue of Calix[4]arene: Coordination Chemistry of Its 1,3-Alternate Conformer towards First-Row Transition-Metal Ions

Jorge A. R. Navarro,[a] Eva Freisinger,[a] and Bernhard Lippert*[a]

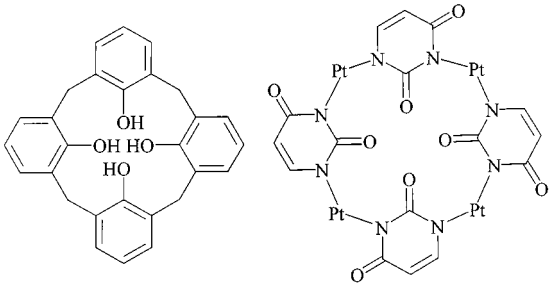
Keywords: Platinum / Uracil / Nucleobase / Host-guest chemistry

The open "molecular box" [(en)Pt(U-N^1,N^3)]$_4$ (**1**) (where en = ethylenediamine, U = uracil dianion) is able to act as an efficient ligand for additional metal ions. Reactions of the 1,3-alternate conformer of **1** with divalent metal ions result in the formation of octanuclear compounds of the general formula [(en)Pt(U-N^1,N^3,O^2,O^4)M]$_4$X$_8$ [M = Cu^{2+}, X = Cl (**2a**), X = $(SO_4)_{0.5}$ (**2b**), and M = Co^{2+} (**3**), Ni^{2+} (**4**), Zn^{2+} (**5**) with X = $(SO_4)_{0.5}$], in which the heterometals are bound at the exocyclic oxygen atoms of the uracil nucleobases. The structurally characterized heteronuclear compounds show a 1,3-alternate arrangement of the uracil nucleobases. Pt–M contacts are in the range 2.743(2)–2.804(2) Å; the Pt atoms act as weak σ donors to the heterometals. In spite of the high degree of positive charge associated with compounds **2a**–**5**, they do not behave as hosts for anions. This is a consequence of the orientation of the four nucleobases which, in contrast to a cone arrangement, does not produce a sufficiently large cavity for the incorporation of anions.

Introduction

Calixarenes and related cyclic compounds are presently the subject of considerable attention owing to their versatility as hosts for inclusion complexation.[1] In addition to their host-guest chemistry, calixarenes can also act as efficient ligands for metal ions, either through their basic oxo surfaces[2][3] or through the arene π electrons.[4] Analogous macrocyclic coordination compounds are likewise also the focus of considerable research efforts as they may also exhibit host-guest chemistry, which might ultimately be combined with the intrinsic magnetic, optical, catalytic, and structural properties of metal ions.[5]

[(en)Pt(U-N^1,N^3)]$_4$ (**1**) (where en = 1,2-diaminoethane, U = uracil dianion) shows structural similarities to calix[4]-arenes (Scheme 1) and is an interesting example of a macrocyclic coordination compound that combines receptor properties analogous to those of classical calixarenes[6] with versatility as a ligand for metal ions.[7]



1

Scheme 1

[a] Fachbereich Chemie, Universität Dortmund,
Otto-Hahn-Straße 6, D-44221 Dortmund, Germany
Fax: (internat.) + 49-(0)231/755-3797
E-mail: lippert@pop.uni-dortmund.de

In a previous report, we showed **1** to be a very efficient ligand towards metal ions, leading to various stoichiometries depending on the nature of the metal ion and the original conformation of the metallocalixarene.[6] A frequently encountered problem in the structural characterization of such heteronuclear compounds stems from the large number of anions present. Due to anion disorder problems, it proved impossible, in spite of a well-characterized octanuclear cation, to report complete X-ray crystallographic characterizations. Only in one case, namely that of [(en)Pt(U-N^1,N^3,O^2,O^4)Pt$(NH_3)_2]_4(NO_3)_8$, was a complete structure determination achieved.[7c] In this communication, we report on the coordination chemistry of **1** towards first row divalent transition metal ions, which has led to the generation of a series of octanuclear compounds having sulfate or chloride anions. In three cases, it has been possible to obtain X-ray quality crystals. In addition, the potential of these compounds to act as anion receptors has been studied.

Results

Reaction of a solution of freshly prepared **1** with 4 equiv. of a divalent transition metal salt at pH = 5−6 results in an immediate color change of the solution (other than in the case of Zn^{2+}), which is accompanied by a drop in the pH by 2−3 units. In the case of Zn^{2+}, addition of the metal salt leads to a significant downfield shift (+0.33 ppm) of the H^5 resonance of uracil in the ^{1}H-NMR spectrum, as well as an upfield shift (−0.10 ppm) of the H^6 resonance, indicating the formation of a thermodynamically stable species. In all other cases (compounds **2a**−**4**), the aforementioned immediate color change of the solution, to green (Cu^{2+}), purple (Co^{2+}), and yellow-green (Ni^{2+}), indicates rapid complexation of the heterometal by **1**. In each case,

 © WILEY-VCH Verlag GmbH, D-69451 Weinheim, 2000 1434−1948/00/0101−0147 $ 17.50+.50/0

four metal ions are incorporated in the resulting compound, giving [(en)Pt(U-N^1,N^3,O^2,O^4)CuCl$(H_2O)_2]_4Cl_4$ (**2a**) and [(en)Pt(U-N^1,N^3,O^2,O^4)M$(H_2O)_3]_4(SO_4)_4$ (M = Cu, **2b**; Co, **3**; Ni, **4**; Zn, **5**). The structures of **2a**, **2b**, and **5** have been fully resolved by X-ray crystallography. The compounds consist of octanuclear cations of approximate S_4 molecular symmetry (see Figures 1 and 2), four chloride (**2a**) or sulfate (**2b**, **5**) counterions, and water molecules of hydration.

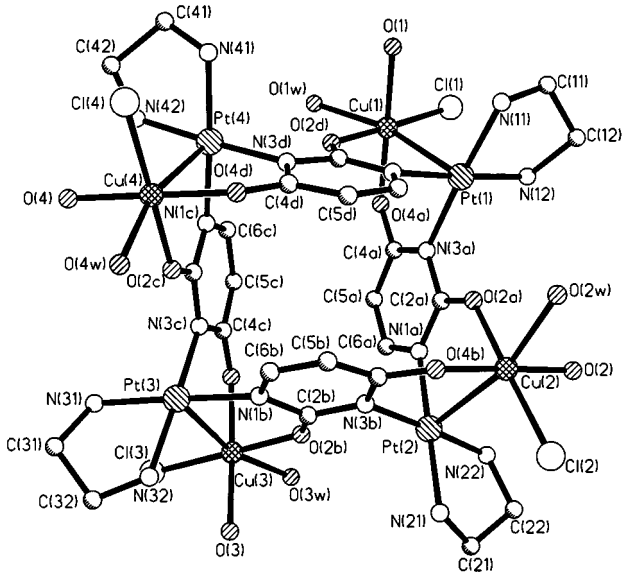


Figure 1. View of the cation [(en)Pt(U-N^1,N^3,O^2,O^4)CuCl$(H_2O)_2]_4^{4+}$ in **2a**

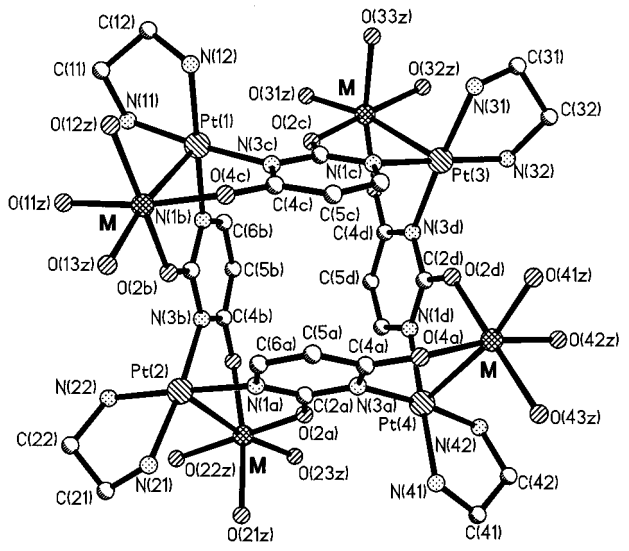


Figure 2. Perspective view of the isomorphous cations of type [(en)Pt(U-N^1,N^3,O^2,O^4)M$(H_2O)_3]_4^{8+}$ in **2b** (M = Cu^{2+}) and **5** (M = Zn^{2+})

The structures of the cations are similar to that of the original cyclic [(en)PtHU(N^1,N^3)$]_4^{4+}$ framework of **1**, with the uracil N^1 and N^3 sites platinated and a 1,3-alternate arrangement of the uracil nucleobases. There is little variation in the dimensions of the box between the complexes, the starting **1**, and the octanuclear compound [(en)Pt(U-N^1,N^3,O^2,O^4)Pt$(NH_3)_2]_4(NO_3)_8$.[7c] The mean separation between the platinum centers, which define the sides of the box, is ca. 5.8 Å, while the diagonal measures ca. 8.2 Å. In addition to the four platinum centers, four $[CuCl(H_2O)_2]^+$, $[Cu(H_2O)_3]^{2+}$, or $[Zn(H_2O)_3]^{2+}$ entities are strongly bound to pairs of exocyclic O^2 and O^4 donor atoms of uracil in **2a**, **2b**, and **5**, respectively. The spatial disposition of the four heterometals in the molecular box is 1,3-alternate, with a displacement of ca. 1.9 Å from the plane defined by the four platinum centers (mean deviation ca. 0.05 Å). The four copper ions in both compounds **2a** and **2b** reside in tetragonally distorted octahedral [4+1+1] environments (see Table 1). In the case of **5**, the zinc centers have distorted octahedral [5+1] environments.

Table 1. Metal−metal separations and average Pt^{2+} and M^{2+} environments (Å) in **2a**, **2b**, and **5**

	2a	**2b**	**5**
Pt−M	2.764(2)	2.804(3)	2.743(1)
	2.760(2)	2.790(3)	2.788(1)
	2.778(2)	2.767(3)	2.777(1)
	2.770(2)	2.789(3)	2.778(1)
M−O2	1.978(8)	1.95(1)	2.008(5)
M−O4	1.950(8)	1.97(1)	2.048(5)
M−Cl	2.307(4)	−	−
M−O[a]	1.98(1)	2.01(1)	2.103(5)
M−O[b]	2.31(1)	2.31(1)	2.082(5)
Pt−N1	2.02(1)	2.00(2)	2.031(6)
Pt−N3	2.04(1)	2.02(2)	2.027(6)

[a] Water molecules placed in *cis* position to the Pt center. − [b] Water molecule placed in *trans* position to the Pt center.

In **2a**, the equatorial positions of the copper coordination spheres are occupied by uracil O^2 and O^4 donor atoms, a water molecule, and a chloride ion, while the axial positions are occupied by water molecules and Pt^{2+} centers. In **2b** and **5**, the heterometals have coordination environments analogous to those in **2a**, differing only in that the equatorial chloride anion is replaced by a water molecule. The Pt−M separations [2.743(2)−2.804(3) Å, see Table 1] are very similar to those found in related di-[8] or trinuclear[9] complexes containing bridging 1-methyluracilato ligands and *cis*-Pt$(NH_3)_2$ entities, where distances of 2.684(1) Å and 2.765(3) Å have been observed. These distances are significantly longer than those found in heteronuclear complexes derived from *trans*-Pt$(NH_3)_2$,[10] where Pt−M distances as short as 2.49 Å have been found as a consequence of a particularly favourable interaction between the occupied d_{z^2} orbital of Pt^{2+} and the $d_{x^2-d y^2}$ orbitals of Cu^{2+} or Pd^{2+} centers.[11] Nevertheless, the Pt^{2+} centers in **2a**−**5** probably also act as weak σ-donors, as is the situation with other first row transition metals.[12] The weakness of the Pt−M interaction is highlighted by the fact that in compound **5** the axial water ligand is more closely bound to the Zn^{2+} center than the equatorial water ligand, whereas in the case of the copper compounds the tetragonal distortion is always found along the Pt−Cu axis with longer Cu^{2+}−axial water ligand separations. Taking into account the fact that the d^{10}

Zn^{2+} is not subject to a Jahn−Teller effect, in contrast to the d^9 Cu^{2+} ion, it is tentatively concluded that the Pt−Cu interaction is as weak as the Pt−Zn interaction. The tendency of Zn^{2+} to form octanuclear complexes and the weakness of the Pt−Zn donation may be offset by a stronger Zn^{2+}−axial water ligand interaction. The close structural similarities of related di- and trinuclear PtM and Pt_2M complexes (M = Pt^{2+}, Pd^{2+}, Cu^{2+}, Zn^{2+}, etc.) containing bridging uracil nucleobases suggest that the octanuclear frameworks in compounds **3** and **4** may be analogous.[13]

No unusual packing features are observed in **2a**, **2b**, and **5**. Octanuclear cations do not interact directly but are rather separated by counterions and water molecules. Multiple H-bonding interactions are seen between the Cl^- or SO_4^{2-} anions and the amino and water ligands coordinated to the metal centers of the cations, although none of these are unusual.

It has previously been reported that compound **1** displays interesting behaviour in solution, with two main species being present, namely the 1,3-alternate and cone conformers. Depending on the experimental conditions, either of the two main species can be stabilized.[7] It is interesting to note that compound **1** in its cone conformation has been shown to be able to incorporate either four[7c] or only one additional metal ion,[6] instead of always four in the case of the 1,3-alternate conformer. Therefore, it may be concluded that the 1,3-alternate form is a much more efficient ligand for divalent metal ions as a result of a more favorable orientation of the exocyclic donor groups of the uracil nucleobases.

The ability of **5** to include anions in its cavity has been studied by means of ^{1}H-NMR spectroscopy using a series of sulfonate anions (see Experimental Section). However, in contrast to the anion host-guest chemistry exhibited by some of the metallated species of the cone conformer of **1**,[6] we found that **5** is unable to include anions in spite of its high positive charge. In fact, the ^{1}H-NMR spectrum of **5** remains unaltered following the addition of anions. Moreover, X-ray analysis results prove beyond doubt that neither chloride (**2a**) nor sulfate anions (**2b**, **5**) are included in the cavity of the compounds. Space-filling representations of the compounds with the 1,3-alternate conformation clearly reveal that the cavity is too small to permit the inclusion of an anion (Figure 3).

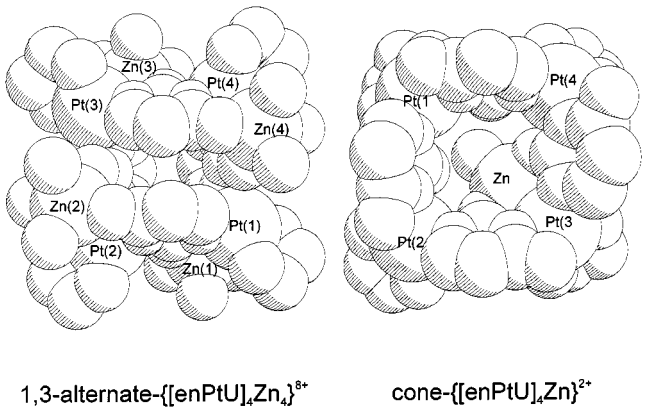


Figure 3. Space-filling representation of the 1,3-alternate-{(en)PtU]$_4$Zn$_4$}$^{8+}$ cation in **5** from the present work and the cone-{(en)PtU]$_4$Zn}$^{2+}$ cation in compound **2b** from ref.[6]

The opening of the cavity, as estimated from the separation between two opposite C^5 atoms of the uracil nucleobases, measures just ca. 3.5 Å in **5** compared to ca. 8.2 Å in cone-{(en)PtU]$_4$Zn(H$_2$O)}$^{2+}$.[6] Since the metal ions bound to the exocyclic oxygen atoms prevent a 1,3-alternate → cone conversion, this situation does not change with time.

Experimental Section

Materials: enPtCl$_2$,[14] (en)PtCl(UH-N^1)]Cl,[15] and [(en)Pt(UH-N^1,N^3)]$_4$(NO$_3$)$_4$ (**1**)[7b] were prepared from K$_2$PtCl$_4$, ethylenediamine, and uracil (Sigma) as appropriate. Sodium *p*-toluenesulfonate (TS) was purchased from Merck; sodium 3-[tris(methylsilyl)]-1-propanesulfonate (TSP), sodium 1-propanesulfonate (PS), sodium ethylsulfonate (ES), and sodium methylsulfonate (MS) from Aldrich.

Synthesis of [(en)Pt(U-N^1,N^3,O^2,O^4)CuCl(H$_2$O)$_2$]$_4$Cl$_4$ · *n* H$_2$O (2a): A freshly prepared solution of **1** (150 mg) in 10 mL of H$_2$O was passed through an anion-exchange column in its Cl^- form. The eluate was concentrated to a volume of 1 mL in a stream of dry N$_2$ and then CuCl$_2$ (30 mg) in 1 mL of H$_2$O was added. An immediate color change from pale-green to brown-green was observed. After storage of the solution for a week, brown-green crystals of **2** could be collected. Yield 46 mg (20%). − C$_{24}$H$_{80}$Cl$_8$Cu$_4$N$_{16}$O$_{28}$Pt$_4$ (2359.13): calcd. C 12.22, H 3.42, Cl 12.02, N 9.50; found C 11.8, H 3.3, Cl 11.6, N 9.2.

Synthesis of [(en)Pt(U-N^1,N^3,O^2,O^4)M(H$_2$O)$_3$]$_4$(SO$_4$)$_4$ · *n* H$_2$O (2b, 3, 4, 5): The general procedure used for the synthesis of the complexes was as follows: a freshly prepared solution of **1** (0.059 mmol) in 3 mL of H$_2$O (pH = 4.9) was mixed with a solution of the metal salt (0.24 mmol) in 1 mL of H$_2$O. Following the addition of the metal salt, the pH value of the respective solutions dropped to 2.5−3 and some turbidity appeared, which was removed by centrifugation. Storage of the resulting solutions (**2a**, green; **3**, purple; **4**, green; **5**, colorless) led to the deposition of crystalline precipitates of the resulting complexes within one day. − **2a:** green, yield 50 mg (34%). − C$_{24}$H$_{80}$Cu$_4$N$_{16}$O$_{44}$Pt$_4$S$_4$ (2459.75): calcd. C 11.72, H 3.28, N 9.11; found C 11.9, H 3.3, N 9.3. − **3:** purple, yield 37 mg (25%). − C$_{24}$H$_{80}$Co$_4$N$_{16}$O$_{44}$Pt$_4$S$_4$ (2441.19): calcd. C 11.81, H 3.30, N 9.18; found C 11.9, H 3.0, N 9.7. − **4:** yellow-green, yield 50 mg (34%). − C$_{24}$H$_{80}$N$_{16}$Ni$_4$O$_{44}$Pt$_4$S$_4$ (2440.38): C 11.81, H 3.30, N 9.18; found C 11.8, H 3.1, N 9.3. − **5:** colorless, yield 50 mg (34%). − C$_{24}$H$_{80}$N$_{16}$O$_{44}$Pt$_4$S$_4$Zn$_4$ (2467.11): calcd. C 11.68, H 3.27, N 9.08; found C 11.9, H 3.1, N 9.6. − ^{1}H NMR (200 MHz, D$_2$O, pH* = 6.5): δ = 2.75 (s, 4 H, CH$_2$), 5.67 (d, *J* = 7.0 Hz, 1 H, 5-H), 7.69 (d, *J* = 7.0 Hz, 1 H, 6-H).

Instrumentation: IR spectra (in KBr pellets) were recorded with a Bruker IFs 113v FT-IR spectrometer. − ^{1}H-NMR spectra were recorded with a Bruker AC 200 FT NMR spectrometer in D$_2$O solution using NMe_4^+ (δ = 3.18 relative to TMS) as an internal standard.

NMR Titrations: Stock solutions ($1\cdot10^{-2}$ M) of the 1,3-alternate conformer of **1** were prepared in D$_2$O. To a 0.40-mL sample of this solution in a 5-mm NMR tube at pH* = 6.5 was added 4 equiv. of 0.2 M ZnSO$_4$ solution, followed by increasing aliquots of (0.4 M

Table 2. Crystallographic data for compounds **2a**, **2b**, and **5**

Compound	**2a**	**2b**	**5**
Empirical formula	$C_{24}H_{71.8}Cl_8Cu_4N_{16}O_{23.9}Pt_4$	$C_{24}H_{86}Cu_4N_{16}O_{47}Pt_4S_4$	$C_{24}H_{86}N_{16}O_{47}Pt_4S_4Zn_4$
M_r	2285.29	2513.85	2521.17
Crystal system	triclinic	triclinic	triclinic
Space group	$P-1$	$P-1$	$P-1$
a [Å]	16.232(3)	14.256(3)	14.177(3)
b [Å]	16.324(3)	14.187(3)	14.221(3)
c [Å]	16.367(3)	17.895(4)	17.903(4)
α [°]	117.37(3)	92.80(3)	83.58(3)
β [°]	110.49(3)	95.36(3)	86.88(3)
γ [°]	90.87(3)	90.36(3)	89.89(3)
V [Å^3]	3526(1)	3599(1)	3581(1)
Z	2	2	2
ρ(calcd.) [Mg/m^{-3}]	2.153	2.320	2.338
μ(Mo-K_α) [mm^{-1}]	9.459	9.126	9.322
F(000)	2166	2420	2428
Crystal color	green-yellow	green-yellow	colorless
Crystal size [mm]	0.63 × 0.56 × 0.44	0.38 × 0.13 × 0.09	0.63 × 0.15 × 0.14
$2\theta_{max}$[°]	47.3	42	54
Index ranges	$0 \le h \le 18$ $-18 \le k \le 18$ $-18 \le l \le 16$	$0 \le h \le 14$ $-14 \le k \le 14$ $-17 \le l \le 17$	$0 \le h \le 18$ $-18 \le k \le 18$ $-19 \le l \le 19$
Reflns. collected	9862	48399	14410
Independent reflns.	9862	7254	14410
Obsd. reflns. [$I > 2\sigma(I)$]	5755	3783	10336
Parameters refined	808	533	889
R_1[a] (obsd. data)	0.0404	0.0466	0.0372
wR_2[b] (obsd. data)	0.0889	0.0962	0.0940
Goodness of fit (obsd. data)	1.119	1.115	1.118
Residuals [eÅ^{-3}]	0.809/−1.638	1.999/−0.923	1.550/−1.763

[a] $R_1 = \Sigma||F_o| - |F_c||/\Sigma|F_o|$. − [b] $wR_2 = [\Sigma w(F_o^2 - F_c^2)^2/\Sigma w(F_o^2)^2]^{1/2}$.

or 4 M) solutions of NaX (X = TSP, TS, PS, ES, MS) (pH* indicates uncorrected pH meter reading). ^{1}H-NMR spectra were recorded for ten different mixtures and the shifts of the H^5 and H^6 resonances of uracil were analyzed as described previously[6] in order to evaluate the association constants.

X-ray Crystallography: Intensity data for **2a**, **2b**, and **5** were collected with an Enraf−Nonius KappaCCD diffractometer[16] (Mo-K_α, λ = 0.71069 Å, graphite monochromator) with sample-to-detector distances of 30.7, 32.7, and 25.7 mm, respectively. The whole sphere of reciprocal space was covered by measurement of 360 frames rotating about ω in steps of 1° with scan times of 13, 230, and 40 s per frame. Preliminary orientation matrices and unit cell parameters were obtained from the peaks of the first ten frames and were then refined using the whole data set. Frames were integrated and corrected for Lorentz and polarization effects using DENZO.[17] The scaling and the global refinement of crystal parameters were performed by SCALEPACK.[17] Reflections that were partly measured on previous and following frames were used to mutually scale these frames. Merging of redundant reflections partly eliminates absorption effects and, if present, also takes crystal decay into account.

The structures were solved by standard Patterson methods[18] and refined by full-matrix least squares based on F^2 using the SHELXTL-PLUS[19] and SHELXL-93 programs.[20] The atom scattering factors were taken as those given in the SHELXTL-PLUS program. Transmission factors were calculated using SHELXL-97.[21] Hydrogen atoms were placed in calculated positions and refined with a common isotropic temperature factor. In the case of **2a**, only two of the positions of the chloride counterions were found to be fully occupied. For the remaining two anions, seven positions were assumed, as represented by the seven strongest peaks showing a reasonable H-bonding pattern. The residual peaks were assigned to positions fully or partly occupied by water molecules. All non-hydrogen atoms were refined anisotropically, with the exception of a few disordered chloride anions and water molecules. In **2b**, only the heavy atoms, the oxygens of one sulfate, and seven of the eleven water molecules could be anisotropically refined because of the poor reflections-to-parameters ratio. In compound **5**, part of the water molecules and the disorder shown by the oxygens of two sulfate counterions could only be calculated isotropically. Crystal data and data collection parameters are summarized in Table 2.

Crystallographic data (excluding structure factors) for the structures reported in this paper have been deposited with the Cambridge Crystallographic Data Centre as supplementary publication nos. CCDC-101632, -127613, and -127614. Copies of the data can be obtained free of charge on application to the CCDC, 12 Union Road, Cambridge CB2 1EZ, U.K. [Fax: (internat.) + 44-1223/336-033; E-mail: deposit@ccdc.cam.ac.uk].

Acknowledgments

This work was supported by the Deutsche Forschungsgemeinschaft and the Fonds der Chemischen Industrie. JARN thanks the University of Granada for a Postdoctoral Fellowship.

[1] [1a] C. D. Gutsche, *Calixarenes*, Royal Society of Chemistry, Cambridge, **1989**. − [1b] V. Böhmer, *Angew. Chem. Int. Ed. Engl.* **1995**, *34*, 713−745. − [1c] A. Ikeda, S. Shinkai, *Chem. Rev.* **1997**, *97*, 1713−1734.

[2] Some examples of metallated species: [2a] L. Giannini, A. Caselli, E. Solari, C. Floriani, A. Chiesi-Villa, C. Rizzoli, N. Re, A. Sgamellotti, *J. Am. Chem. Soc*. **1997**, *119*, 9198−9210. − [2b] V. C. Gibson, C. Redschaw, W. Clegg, M. R. J. Elsegood, *J.*

Chem. Soc., Chem. Commun. **1995**, 2371−2372. − [2c] G. E. Hofmeister, E. Alvarado, J. A. Leary, D. I. Yoon, S. F. Pedersen, *J. Am. Chem. Soc*. **1990**, *112*, 8843−8851. − [2d] J. A. Acho, T. Ren, J. W. Yun, S. J. Lippard, *Inorg. Chem*. **1995**, *35*, 5226−5532. − [2e] S. R. Dubberley, A. J. Blake, P. Mountford, *Chem. Commun.* **1997**, 1603−1604. − [2f] M. G. Davidson, J. A. K. Howard, S. Lamb, C. W. Lehmann, *Chem. Commun*. **1997**, 1607−1608.

[3] Review: C. Wieser, C. B. Dieleman, D. Matt, *Coord. Chem. Rev.* **1997**, *165*, 93−161.

[4] [4a] M. Staffilani, K. S. B. Hancock, J. W. Steed, K. T. Holman, J. L. Atwood, R. K. Juneja, R. S. Burkhalter, *J. Am. Chem. Soc*. **1997**, *119*, 6324−6335. − [4b] J. W. Steed, R. K. Juneja, J. L. Atwood, *Angew. Chem. Int. Ed. Engl*. **1994**, *33*, 2456−2457. − [4c] H. Iki, T. Kikuchi, S. Shinkai, *J. Chem. Soc., Perkin Trans. 2* **1993**, 205−208. − [4d] A. Ikeda, S. Shinkai, *J. Am. Chem. Soc.* **1994**, *116*, 3102−3110.

[5] [5a] K. Yamanari, I. Fukuda, T. Kawamoto, Y. Kushi, A. Fuyuhiro, N. Kubota, T. Fukuo, R. Arakawa, *Inorg. Chem*. **1998**, *37*, 5611−5618. − [5b] M. Fujita, J. Yazaki, K. Ogura, *Tetrahedron* **1991**, *32*, 5589−5592. − [5c] R. V. Slone, D. I. Yoon, R. M. Calhoun, J. T. Hupp, *J. Am. Chem. Soc*. **1995**, *117*, 11813−11814. − [5d] R. Bakthiar, H. Chen, S. Ogo, R. H. Fish, *Chem. Commun*. **1997**, 2135−2136. − [5e] V. L. Pecoraro, A. J. Stemmler, B. R. Gibney, J. J. Bodwin, H. Wang, J. W. Kampf, A. Barwinski, *Prog. Inorg. Chem.* **1996**, *45*, 83−178. − [5f] J. A. Hafen, J. J. Bodwin, V. L. Pecoraro, *Inorg. Chem.* **1998**, *37*, 5416−5417.

[6] [6a] J. A. R. Navarro, M. B. L. Janik, E. Freisinger, B. Lippert, *Inorg. Chem*. **1999**, *38*, 426−432. − [6b] J. A. R. Navarro, B. Lippert, *Coord. Chem. Rev.* **1999**, *185−186*, 653−657.

[7] [7a] H. Rauter, E. C. Hillgeris, B. Lippert, *J. Chem. Soc., Chem. Commun.* **1992**, 1385−1386. − [7b] H. Rauter, E. C. Hillgeris, A. Erxleben, B. Lippert, *J. Am. Chem. Soc*. **1994**, *116*, 616−624. − [7c] H. Rauter, I. Mutikainen, M. Blomberg, C. J. L. Lock, P. Amo-Ochoa, E. Freisinger, L. Randaccio, E. Zangrando, E. Chiarparin, B. Lippert, *Angew. Chem. Int. Ed.* **1997**, *36*, 1296−1301.

[8] [8a] D. Neugebauer, B. Lippert, *J. Am. Chem. Soc.* **1982**, *104*, 6596−6601. − [8b] H. Schöllhorn, U. Thewalt, B. Lippert, *Inorg. Chim. Acta* **1985**, *107*, 77−81.

[9] I. Mutikainen, O. Orama, A. Pajunen, B. Lippert, *Inorg. Chim. Acta* **1987**, *137*, 189−193.

[10] G. Fusch, E. C. Fusch, A. Erxleben, J. Hüttermann, H.-J. Scholl, B. Lippert, *Inorg. Chim. Acta* **1996**, *252*, 167−178 and references cited therein.

[11] C. Mealli, F. Pichierri, L. Randaccio, E. Zangrando, M. Krumm, D. Holthenrich, B. Lippert, *Inorg. Chem.* **1995**, *34*, 3418−3424.

[12] [12a] D. M. L. Goodgame, R. W. Rollins, B. Lippert, *Polyhedron* **1985**, *4*, 829−839. − [12b] D. M. L. Goodgame, M. A. Hitchman, B. Lippert, *Inorg. Chem.* **1986**, *25*, 2191−2194. − [12c] D. M. Duckworth, D. M. L. Goodgame, M. A. Hitchman, B. Lippert, *Inorg. Chem.* **1987**, *26*, 1823−1825.

[13] [13a] B. Lippert, *Prog. Inorg. Chem.* **1989**, *37*, 1−98. − [13b] E. Zangrando, L. Pichierri, L. Randaccio, B. Lippert, *Coord. Chem. Rev.* **1996**, *156*, 275−332.

[14] F. Basolo, J. C. Bailar, Jr., *J. Am. Chem. Soc.* **1950**, *72*, 2433−2438.

[15] B. Lippert, *Inorg. Chem*. **1981**, *20*, 4326−4343.

[16] NONIUS B.V., *KappaCCD Package*, Röntgenweg 1, P. O. Box 811, NL-2600 AV Delft, The Netherlands.

[17] Z. Otwinowsky, W. Minor, "Processing of X-ray Diffraction Data Collected in Oscillation Mode", *Methods in Enzymology* (Eds.: C. W. Carter, Jr., R. M. Sweet), Academic Press, **1996**, p. 276.

[18] G. M. Sheldrick, *Acta Crystallogr.* **1990**, *A46*, 467−473.

[19] G. M. Sheldrick, *SHELXTL-PLUS (VMS)*, Siemens Analytical X-ray Instruments, Inc., Madison WI, **1990**.

[20] G. M. Sheldrick, *SHELXL-93, Program for Crystal Structure Refinement*, University of Göttingen, Germany, **1993**.

[21] G. M. Sheldrick, *SHELXL-97, Program for the Refinement of Crystal Structures*, University of Göttingen, Germany **1997**.

Received June 25, 1999
[I99231]

Syntheses of Chiral, Intramolecularly Coordinated Aluminum Bromides

Jens Müller,*[a] Ralf Schröder,[b] and Ruimin Wang[b]

Keywords: Aluminum / Ab initio calculations / Isomers / Intramolecular donor–acceptor systems

Three aluminum compounds Ar*$AlBr_2$ (**1**), Ar*AlBr*t*Bu (**2**), and Ar*$_2$AlBr (**3**), incorporating the chiral ligand Ar* = 2-[1-(*S*)-$Me_2NCH(Me)]C_6H_4$, have been synthesized by salt metathesis reactions and have been characterized by multinuclear NMR (^{1}H, ^{13}C, and ^{27}Al), mass spectrometry, and elemental analysis. The molecular structure of compound **3** has been determined by a single-crystal X-ray analysis (space group $P2_12_12_1$). Alane **2** exists as a temperature-independent equilibrium mixture of two diastereomers in solution (ratio 45:55); results of NOE experiments on **2** are discussed. Only one isomer was found for compound **3** in solution and its dynamic behavior has been investigated by variable-temperature NMR methods; a ΔH of 56.6(4) kJ mol^{-1} and a ΔS of –0.79(1) J K^{-1}mol^{-1} were deduced from band-shape analysis of the ^{1}H-NMR signals of the *N*-bound methyl groups.

Introduction

The first organometallic compound with an intramolecular donor group was described by Bähr and Müller in 1955.[1] The authors synthesized the two intramolecularly coordinated alanes $[EtO(CH_2)_4]AlEt_2$ and $[Et_2N(CH_2)_3]AlEt_2$, which contain five- and six-membered rings, respectively. According to cryoscopic measurements, these air- and moisture-sensitive substances are monomeric in benzene solution.[1] Since this investigation, many more intramolecularly coordinated organometallic compounds of the Group 13 elements have been synthesized.[2] One of the driving forces behind these investigations is the need for volatile, non-pyrophoric precursors for chemical vapor deposition (CVD). Recently, it has been shown that Group 13 nitrides, which are promising materials for new microelectronic and optoelectronic devices,[3] can be grown by CVD of intramolecularly coordinated Group 13 azides.[4]

When we started our investigations of aluminum compounds, intramolecularly coordinated with the commonly used 2-[(dimethylamino)methyl]phenyl ligand, the diethyl derivative $[2\text{-}(Me_2NCH_2)C_6H_4]AlEt_2$[5] was the only known example. We investigated the tetracoordinated alanes $[2\text{-}(Me_2NCH_2)C_6H_4]AlRR'$ [R/R′ = Me/Me, Cl/Cl, Cl/Me, Cl/*t*Bu, and Cl/$C(SiMe_3)_3$] and the pentacoordinated alanes $[2\text{-}(Me_2NCH_2)C_6H_4]_2AlCl$, $[2\text{-}(Me_2NCH_2)C_6H_4]_2AlMe$, and $[2\text{-}(Me_2NCH_2)C_6H_4]AlCl_2(L)$ (L = H_2N*i*Pr, thf).[6] In the same year, Cowley et al. published the structures of the bromide $[2\text{-}(Me_2NCH_2)C_6H_4]AlBr_2$ and the hydride $[2\text{-}(Me_2NCH_2)C_6H_4]AlH_2$, which is a dimer in the solid state.[7]

A trigonal-bipyramidal complex with two bidentate ligands and one monodentate ligand with an idealized C_2-symmetry exists as Λ and Δ enantiomers (Figure 1). In the case of the alanes $[2\text{-}(Me_2NCH_2)C_6H_4]_2AlCl$ and $[2\text{-}(Me_2NCH_2)C_6H_4]_2AlMe$, we found a rapid equilibration between the Δ and Λ isomers with respect to the ^{1}H-NMR time scale.[6] In order to ascertain whether a cleavage of the Al−N donor bonds is involved in this process, we synthesized some novel aluminum compounds intramolecularly coordinated through a chiral, one-armed phenyl ligand, namely 2-[1-(*S*)-(dimethylamino)ethyl]phenyl. The main advantage of this chiral ligand is illustrated by Figure 2. If we assume a fast envelope inversion of the five-membered ring in compound **A**, this species exhibits C_s point-group symmetry, i.e. the two *N*-bound methyl groups are equivalent and thus give rise to one resonance in the ^{1}H- and ^{13}C-NMR spectra. Similar spectra are obtained for compound **A** when the N donor atom is not coordinated to the acceptor M. Compound **B**, which incorporates the chiral phenyl ligand, shows no symmetry (C_1 point group) and therefore two resonances for the NMe_2 group are to be expected. However, if the N donor atom is not coordinated to the acceptor M, pyramidal inversion at the N atom renders the attached methyl groups equivalent on the NMR time scale, thus resulting in only one resonance. Consequently, the chiral, one-armed phenyl ligand is an ideal substituent for probing whether the amino group is coordinated to the acceptor M. This chiral ligand has previously been used in main group chemistry for similar purposes.[8]

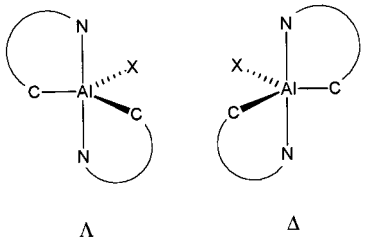


Figure 1. Λ and Δ enantiomers of a trigonal-bipyramidal complex

[a] Anorganische Chemie II, Ruhr-Universität Bochum, D-44780 Bochum, Germany
[b] Institut für Anorganische Chemie der RWTH Aachen, Professor-Pirlet-Straße 1, D-52056 Aachen, Germany
Fax: (internat.) +49 (0)234/321-4174
E-mail: jens.mueller@aci.ruhr-uni-bochum.de

 © WILEY-VCH Verlag GmbH, D-69451 Weinheim, 2000 1434−1948/00/0101−0153 $ 17.50+.50/0

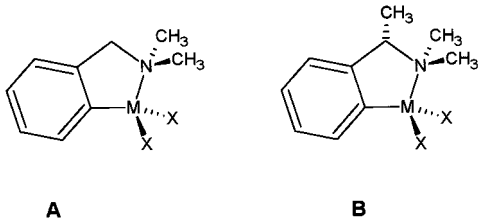
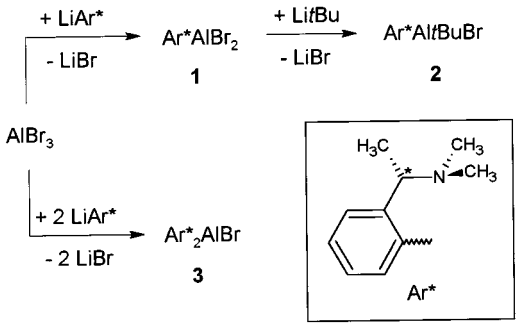


Figure 2. Complexes incorporating the achiral (**A**) and the chiral (**B**), one-armed phenyl ligand

In this paper, we report on the syntheses and properties of three chiral, intramolecularly coordinated alanes.

Results and Discussion

The intramolecularly coordinated alanes **1**, **2**, and **3**, which are accessible in high yields by salt metathesis reactions (Scheme 1), have been characterized by multinuclear NMR, mass spectrometry, and elemental analyses.



Scheme 1. Syntheses of compounds **1**, **2**, and **3**

It is known that the chemical shifts of ^{27}Al nuclei are very sensitive to the number of coordinated ligands.[9] Thus, the tetracoordination of the Al atom in compound **1** can be deduced from the ^{27}Al-NMR shift of $\delta = 129$; a similar value of $\delta = 127$ has been found for the dichloride [2-(Me_2NCH_2)C_6H_4]$AlCl_2$ incorporating the achiral, one-armed phenyl ligand.[6][10] The ^{1}H- and ^{13}C-NMR spectra of **1** each show one set of signals, in accordance with a C_1-symmetrical species having an intramolecularly coordinated dimethylamino group.

Five-membered rings, such as that in **1**, usually exist in an envelope conformation with the nitrogen atom displaced out of the AlC_3 plane. In the case of **1**, this could result in two diastereomers depending on the bending direction of the nitrogen atom. We were interested in assessing whether an envelope conformation could be "frozen" and therefore we examined compound **1** by variable-temperature ^{1}H-NMR spectroscopy. Between +80 and −80°C, the NMR spectra show only one set of signals for the chiral chelating ligand; coalescence was not observed. This means that either the inversion of the five-membered ring is fast at −80°C with respect to the NMR time scale, or that this inversion is slow but one isomer is very much favored over the other. In order to distinguish between these two alternatives, we investigated the structure of **1** by ab initio methods. Figure 3 shows the optimized geometries of the two diastereomers at the HF/6-31G(d) level of theory.[11]

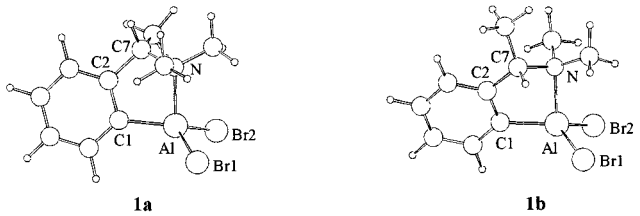
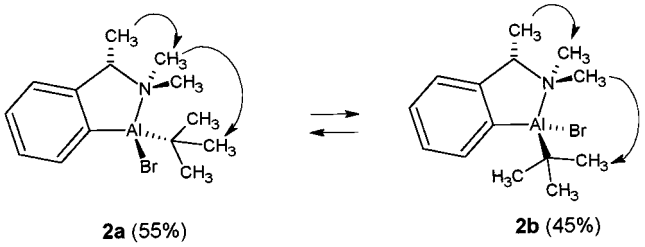


Figure 3. Calculated structures of compound **1** [HF/6-31G(d) level]; selected bond lengths [pm], angles and torsion angles [°] for **1a** (**1b**): Al−N 205.9 (205.2), Al−Br1 228.6 (229.2), Al−Br2 229.2 (228.3), Al−C1 195.6 (195.4); N−Al−C1 86.7 (86.8), N−Al−Br1 107.7 (106.2), N−Al−Br2 108.1 (107.8), C1−Al−Br1 119.6 (116.2), C1−Al−Br2 118.4 (121.6), Br1−Al−Br2 111.9 (113.0); Al−C1−C2−C7 5.8 (−3.3), C1−C2−C7−N −30.2 (−32.8)

In isomer **1a**, the H atom bound to the chiral carbon center is staggered with respect to the Me_2N group, whereas in **1b** the methyl group of the chiral carbon atom occupies this position. The difference between the calculated Gibbs free energies of **1a** and **1b** at −80°C is only 1.1 kJ/mol, which corresponds to an equilibrium mixture of **1a**/**1b** in the ratio 2:1.[12][13] Of course, too much importance should not be attached to the absolute magnitude of the ΔG value; the calculation merely shows that the two isomers **1a** and **1b** are very similar in energy. This means that the envelope inversion in **1** is not frozen at −80°C in solution, otherwise two sets of signals would be seen in the ^{1}H-NMR spectrum.

One bromide ligand in compound **1** can readily be substituted by a *tert*-butyl group to form the alane **2** in 84% isolated yield (Scheme 1). The tetracoordination of the Al atom in **2** is evident from the ^{27}Al-NMR shift of $\delta = 149$; a similar value has been found for [2-(Me_2NCH_2)C_6H_4]-Al*t*Bu ($\delta = 145$).[6] Compound **2** consists of the two isomers **2a** and **2b** (Scheme 2), as revealed by two complete sets of signals in the ^{1}H- and ^{13}C-NMR spectra.



Scheme 2. Equilibrium between the two isomers **2a** and **2b**; arrows correspond to intense signals in the NOE experiment (see text for details)

Within experimental error, the ratio of 55:45 found for **2a**/**2b** at ambient temperature does not change over the temperature range from −80 to +80°C, which means that the transformation between **2a** and **2b** is thermally neutral ($\Delta H \approx 0$ kJ/mol). That the two species do indeed exist in equilibrium was proven by NMR methods. We did not observe coalescence of any of the signals in the ^{1}H-NMR spectra of compounds **2a**/**2b** over the temperature range from +80 to −80°C, but an NOE experiment clearly showed that

an exchange between the two isomers occurs. If one nitrogen-bound methyl group of a particular isomer, e.g. **2a**, is irradiated, there is a magnetization transfer to the two nitrogen-bound methyl groups of **2b**. This can be rationalized by assuming a cleavage of the Al−N bond, followed by a 180° rotation about the Al−C bond and re-formation of the Al−N bond. Furthermore, when the N atom is not coordinated to the Al center, a rotation about the N−C* bond, N inversion, and re-formation of the Al−N bond result in an exchange of the two *N*-bound methyl groups of one particular isomer. Because of the dynamic behavior, the signals detected in the NOE experiment are caused by magnetization transfer and NOE. However, an unambiguous assignment of the two sets of signals to the respective isomer is possible; e.g. for both isomers there is an intense NOE from the methyl group bound to the chiral carbon to one nitrogen-bound methyl group, but the *tert*-butyl ligand shows an intense NOE to this NMe group in isomer **2a** and to the other NMe group in isomer **2b** (see arrows in Scheme 2).

In order to study the dynamic behavior of compound **2** in detail, we conducted 2D EXSY experiments, which we envisaged as possibly being an appropriate NMR technique.[14] Unfortunately, however, the intensities of the cross-peaks were too low for the desired evaluation (see Experimental Section).

The alane **3** was obtained in 72% yield as a pure substance (Scheme 2), which was found to crystallize in the space group $P2_12_12_1$ (Figure 4).

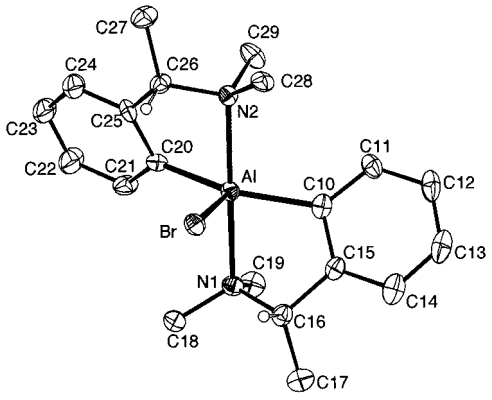


Figure 4. Molecular structure of **3** (PLATON,[20] thermal ellipsoids drawn at a 30% probability level); selected bond lengths [pm], angles and torsion angles [°]: Al−N1 217.9(7), Al−N2 216.8(7), Al−Br 239.6(2), Al−C10 202.6(8), C10−C15 140(1), C15−C16 154(1), C16−N1 150(1), C16−C17 154(1), Al−C20 199.2(8), C20−C25 142(1), C25−C26 152(1), C26−N2 150.0(9), C26−C27 1.52(1); N1−Al−N2 177.0(3), N1−Al−Br 91.7(2), N1−Al−C10 79.7(3), Al−N1−C16 103.8(5), N2−Al−Br 91.2(2), N2−Al−C20 80.0(3), Al−N2−C26 102.7(4), Br−Al−C10 105.3(2), Br−Al−C20 107.5(2), C10−Al−C20 147.2(3), C18−N1−C19 108.5(6), C28−N2−C29 108.5(6); Br−Al−N1−C18 55.5(5), Br−Al−N1−C19 177.7(4), Br−Al−N2−C28 52.9(5), Br−Al−N2−C29 175.6(5), Al−C10−C15−C16 10.8(8), Al−C20−C25−C26 5.5(8)

The aluminum atom in **3** is distorted trigonal-bipyramidally coordinated, with N1 and N2 in axial positions and C10, C20, and Br in the equatorial plane. The N1−Al−N2 axis is almost linear [N1−Al−N2 = 177.0(3)°] and the sum of the three angles in the equatorial plane is 360°. The deviation from ideal trigonal-bipyramidal geometry is manifested in an angle of 100.3(2)° between the least-squares plane comprising N1, Al, N2, and Br and the equatorial plane. Similar angles have been found in [2-(Me_2NCH_2)-C_6H_4]$_2$AlMe (101°)[6] and [2-(Me_2NCH_2)C_6H_4]$_2$Al(N_3) (101°)[4a] incorporating the achiral one-armed phenyl ligand. Clearly, these deviations from ideal trigonal-bypyramidal geometry can be attributed to the steric requirements of the two chelating ligands. Al−N donor bond lengths are known to vary over a wide range. The Al−N bond lengths of 217.9(7) pm for Al−N1 and 216.8(7) pm for Al−N2 in compound **3** are comparable with those found in five-fold coordinated alanes having similar chelating ligands and one electronegative substituent, e.g. 216.8(5) and 220.9(4) pm in [2-(Me_2NCH_2)C_6H_4]$_2$Al(N_3), 218.9(2) and 221.0(2) pm in [$Me_2N(CH_2)_3$]$_2$AlCl, and 216.7(2) and 219.9(2) pm in [$Me_2N(CH_2)_3$]$_2$Al(N_3).[4a]

As mentioned in the introduction, a trigonal-bipyramidal complex with two bidentate ligands and one monodentate ligand with an idealized C_2 symmetry exists as Λ and Δ enantiomers (Scheme 1). In the case of compound **3**, each of the chelating ligands incorporates an (*S*)-configured carbon atom, hence the Λ and Δ forms constitute a pair of diastereomers. Furthermore, five-membered rings such as those in **3** exist in envelope conformations with the nitrogen atoms being the "flap" atoms; e.g. N1 and N2 in **3** are displaced out of the respective AlC_3 planes by 79 and 81 pm. Because compound **3** contains two fused five-membered rings, three isomers for each of the Λ and Δ diastereomers are possible, depending on the "bending directions" of the nitrogen "tips". In the case of compound **3**, we found the Δ isomer with both N atoms bent in the same direction, giving an idealized C_2-symmetrical molecule.

The alane **3** shows a resonance at δ = 95 in its ^{27}Al-NMR spectrum, which is in the typical range for five-fold coordinated aluminum;[9] a similar chemical shift has been found for [2-(Me_2NCH_2)C_6H_4]$_2$AlCl (δ = 96).[6] The ^{27}Al resonance is unchanged over the temperature range from −40 to +80°C, which means that, time-averaged, the aluminum remains pentacoordinated. However, at high temperatures, the ^{1}H-NMR spectra show only one set of signals for the two chelating ligands with only *one* singlet for the four *N*-bound methyl groups. With decreasing temperature, the resonance of the NMe_2 groups get broader and finally resolves into *two* sharp singlets at −80°C. These findings are in accord with a C_2-symmetrical compound and we assume that the geometry of the molecule in solution corresponds to that found in the crystalline state. The coalescence of the NMe_2 signals indicates that the two methyl groups of each amino group undergo rapid positional interchange with respect to the NMR time scale. This can be rationalized if one assumes that the NMe_2 group is detached from the Al atom, undergoes a subsequent 180° rotation about the C* −N bond, then N inversion, and finally a re-formation of the N−Al donor bond. From band-shape analyses of the ^{1}H-NMR signals of the NMe_2 groups, we deduced a ΔH of

56.6(4) kJ mol^{-1} and a ΔS of $-0.79(1)$ J K^{-1} mol^{-1} for this dynamic process.[15]

As mentioned in the introduction, the chiral one-armed phenyl ligand has previously been used in main group chemistry, in particular for the Group 13 elements indium[8d] and thallium[8c] by van Koten et al. They investigated Ar*InMe$_2$, Ar*$_2$InCl, Ar*TlCl$_2$, and Ar*$_2$TlCl {Ar* = 2-[1-(*S*)-Me$_2$NCH(Me)]C$_6$H$_4$} and found that in all cases the N atom is coordinated to the In or Tl atom at low temperatures in solution; for all species, a process involving cleavage and re-formation of the nitrogen−element donor bond was found by NMR methods. As in the case of the alane **3**, for the pentacoordinated species Ar*$_2$InCl and Ar*$_2$TlCl only one diastereomer was detected by NMR spectroscopy at low temperatures.

Experimental Section

General Remarks: All procedures were carried out under a dry nitrogen atmosphere using standard Schlenk techniques. Solvents were dried by standard procedures, distilled, and stored under nitrogen over molecular sieves (4 Å). $AlBr_3$ (> 98%, Aldrich) was sublimed prior to use; 2-[(*S*)-1-(dimethylamino)ethyl]phenyllithium was synthesized as described in the literature.[16] *t*BuLi (1.7 M in pentane) was purchased from Aldrich. − NMR: Varian Unity 500 (ambient temp.; 499.843, 130.195, and 125.639 MHz for ^{1}H, ^{27}Al, and ^{13}C, respectively); spectra were calibrated against residual protons of the deuterated solvents. ^{1}H- and ^{13}C-NMR chemical shifts are reported relative to TMS and ^{27}Al-NMR shifts relative to the external standard [Al(acac)$_3$] in C$_6$D$_6$. As a result of the electric quadrupole moment of the ^{27}Al nucleus, the carbon atoms bound to aluminum could not be detected in the ^{13}C-NMR measurements. The assignments of the ^{1}H- and ^{13}C-NMR signals were made either with the aid of ^{1}H/^{13}C-HMQC and NOE experiments or according to the literature.[6] The 2D EXSY ^{1}H-NMR experiments on compound **2** were performed with a Bruker DRX 500 instrument (5 mm ^{1}H probe head) over the temperature range 20−45°C. The NOESYTP pulse program, with mixing times between 0.4 and 1.2 s, was used. − Elemental analyses (C, H, N): Carlo Erba elemental analyzer, Model 1106. − MS: Finnigan MAT 95.

Band-shape analyses of nine ^{1}H-NMR spectra (−20 to +80°C) of compound **3** were performed with the program *DNMR − Sim (Version 1.0)*.[15a] The ΔH and ΔS values were calculated using the equation $\ln(k/T) = -\Delta H/RT + \Delta S/R + \ln(k_B/h)$.[15b] The standard error limits quoted for ΔH and ΔS are based on the linear regression.

Dibromo{2-[(*S*)-1-(dimethylamino)ethyl]phenyl}aluminum (1): 3.65 g (23.5 mmol) of 2-[(*S*)-1-(dimethylamino)ethyl]phenyllithium was added to a solution of 6.28 g (23.5 mmol) of $AlBr_3$ in 150 mL of toluene at −78°C. After 30 min, the cooling bath was removed and the reaction mixture was stirred at ambient temperature for 16 h. The mixture was then filtered and the solvent was removed under high vacuum. Sublimation (100°C; ca. 10^{-3} mbar) yielded 6.30 g (80%) of compound **1**. − ^{1}H NMR: δ = 0.94 (d, *J* = 6.9 Hz, 3 H, CHC*H*$_3$), 1.84 (s, 3 H, NCH$_3$), 2.05 (s, 3 H, NCH$_3$), 3.48 (q, *J* = 6.9 Hz, 1 H, C*H*CH$_3$), 6.76 (m, 1 H, 3-H), 7.08/7.14 (2 m, 2 H, 4-,5-H), 7.60 (m, 1 H, 6-H). − ^{13}C NMR: δ = 14.48 (s, CH*C*H$_3$), 39.19 (s, NCH$_3$), 45.33 (s, NCH$_3$), 67.71 (s, *C*HCH$_3$), 124.17/127.80/129.72 (3 s, 3 C, C-3/4/5), 136.32 (s, C-6), 148.31 (s, C-2). − ^{27}Al NMR: δ = 129 ($h_{1/2}$ = 1800 Hz). − HRMS: *m*/*z*: calcd. for [M$^+$] 334.9288; found 334.9289. − MS: *m*/*z* (%) = 335 (13) [M$^+$], 320 (21) [M$^+$ − CH$_3$], 230 (100) [M$^+$ − C$_8$H$_9$], 134 (48) [C$_9$H$_{12}$N$^+$], 105 (20) [C$_8$H$_9^+$], 72 (58) [C$_4$H$_{10}$N$^+$]. − C$_{10}$H$_{14}$AlBr$_2$N (335.02): calcd. C 35.85, H 4.21, N 4.18; found C 35.13, H 4.20, N 4.04.

Bromo(*tert*-butyl){2-[(*S*)-1-(dimethylamino)ethyl]phenyl}aluminum (2): A 1.7 M solution of *t*BuLi in pentane (8.1 mL, 13.8 mmol) was slowly added to a solution of 4.61 g (13.8 mmol) of **1** in 100 mL of toluene at −78°C. After 15 min, the cooling bath was removed and the reaction mixture was stirred at ambient temperature for 16 h. The mixture was then filtered and the solvent was removed under high vacuum. Sublimation (115°C, ca. 10^{-3} mbar) yielded 3.61 g (84%) of a 55:45 mixture of two isomers (**2a** and **2b**). − ^{1}H NMR: Isomer **2a** (55%): δ = 0.77 (d, *J* = 6.8 Hz, 3 H, CHC*H*$_3$), 1.22 (s, 9 H, C$_4$H$_9$), 1.53 [s, 3 H, N(CH$_3$)$_2$], 2.19 [s, 3 H, N(CH$_3$)$_2$], 3.96 (q, *J* = 6.8 Hz, 1 H, C*H*CH$_3$), 6.76 (m, 1 H, 3-H), 7.10 (m, 2 H, 4-,5-H), 7.65 (m, 1 H, 6-H); isomer **2b** (45%): δ = 1.04 (d, *J* = 6.8 Hz, 3 H, CHC*H*$_3$), 1.16 (s, 9 H, C$_4$H$_9$), 1.88 [s, 3 H, N(CH$_3$)$_2$], 1.96 [s, 3 H, N(CH$_3$)$_2$], 3.31 (q, *J* = 6.8 Hz, 1 H, C*H*CH$_3$), 6.74 (m, 1 H, 3-H), 7.10 (m, 2 H, 4-,5-H), 7.68 (m, 1 H, 6-H). − ^{13}C NMR: Isomer **2a** (55%): δ = 8.62 (s, 1 C, CH*C*H$_3$), 29.97 (s, 3 C, C$_4$H$_9$), 36.33 [s, 1 C, N(CH$_3$)$_2$], 43.92 [s, 1 C, N(CH$_3$)$_2$], 65.50 (s, 1 C, *C*HCH$_3$), 123.69 (s, 1 C, C-3), 127.18/128.71 (2 s, 2 C, C-4/5), 136.59 (s, 1 C, C-6), 147.94 (s, 1 C, C-2); isomer **2b** (45%): δ = 16.26 (s, 1 C, CH*C*H$_3$), 29.58 (s, 3 C, C$_4$H$_9$), 41.12 [s, 1 C, N(CH$_3$)$_2$], 44.90 [s, 1 C, N(CH$_3$)$_2$], 70.20 (s, 1 C, *C*HCH$_3$), 123.69 (s, 1 C, C-3), 127.32/128.71 (2 s, 2 C, C-4/5), 137.26 (s, 1 C, C-6), 149.53 (s, 1 C, C-2). − ^{27}Al NMR: δ = 149 ($h_{1/2}$ = 4400 Hz). − MS: *m*/*z* (%) = 311 (0.3) [M$^+$], 254 (100) [M$^+$ − C$_4$H$_9$], 211 (29) [C$_8$H$_9$AlBr$^+$], 134 (81) [C$_9$H$_{12}$N$^+$], 105 (15) [C$_8$H$_9^+$], 72 (19) [C$_4$H$_{10}$N$^+$]. − C$_{14}$H$_{23}$AlBrN (312.23): calcd. C 53.86, H 7.43, N 4.49; found C 52.72, H 7.48, N 4.37.

Bromobis{2-[(*S*)-1-(dimethylamino)ethyl]phenyl}aluminum (3): 2.18 g (14.0 mmol) of 2-[(*S*)-1-(dimethylamino)ethyl]phenyllithium was added to 1.87 g (7.0 mmol) of $AlBr_3$ in 40 mL of toluene at −78°C. After 10 min, the cooling bath was removed and the mixture was stirred for 64 h. All volatile components were then removed under high vacuum and the residue was extracted with 120 mL of hexane in a soxhlet apparatus. Removal of the hexane under high vacuum afforded 2.05 g (72%) of compound **3**. Single crystals of compound **3** were obtained from the hexane solution in the soxhlet apparatus. − ^{1}H NMR (60°C): δ = 1.12 (d, *J* = 6.4 Hz, 6 H, CHC*H*$_3$), 2.35 [br. s, 12 H, N(CH$_3$)$_2$], 4.70 (br. s, 2 H, C*H*CH$_3$), 7.02 (m, 2 H, 3-H), 7.20 (m, 4 H, 4-,5-H), 7.80 (m, 2 H, 6−H); (−60°C): δ = 0.82 (d, *J* = 6.7 Hz, 6 H, CHC*H*$_3$), 1.91 [s, 6 H, N(CH$_3$)(C*H*$_3$)], 2.45 [s, 6 H, N(C*H*$_3$)(CH$_3$)], 4.81 (q, 2 H, C*H*CH$_3$), 7.02 (m, 2 H, 3-H), 7.26 (m, 4 H, 4-,5-H), 7.79 (m, 2 H, 6-H); $T_{coal.}$: 22°C [Δν = 270 Hz, N(CH$_3$)$_2$]. − ^{13}C NMR: δ = 9.19 (br. s, 2 C, CH*C*H$_3$), 37.12 [br. s, 2 C, N(CH$_3$)$_2$], 43.43 [br. s, 2 C, N(CH$_3$)$_2$], 63.27 (s, 1 C, *C*HCH$_3$), 124.77/125.73/127.76 (3 s, 6 C, C-3/4/5), 147.34 (br. s, 2 C, C-6), 151.81 (s, 2 C, C-2). − ^{27}Al NMR: δ = 95 ($h_{1/2}$ = 5500 Hz). − MS: *m*/*z* (%) = 387 (19) [M$^+$ − CH$_3$], 323 (15) [M$^+$ − Br], 254 (30) [M$^+$ − C$_{10}$H$_{14}$N], 134 (100) [C$_9$H$_{12}$N$^+$], 105 (27) [C$_8$H$_9^+$], 72 (64) [C$_4$H$_{10}$N$^+$]. − C$_{20}$H$_{28}$AlBrN$_2$ (403.34): calcd. C 59.56, H 7.00, N 6.95; found C 59.20, H 7.09, N 7.00.

Ab initio Calculations: The GAUSSIAN-94 package,[11] run on a cluster of workstations (Rechenzentrum der RWTH Aachen), was employed for all ab initio calculations. The vibrational analyses of compounds **1a** and **1b** were performed at the HF/6-31G(d) level. The total energies E_h [HF/6-31G(d) in Hartrees] and the ZPVE (in kJ mol^{-1}; in parentheses) are as follows: **1a**: −5823.185119 (634.14); **1b**: −5823.184664 (634.27).

Single Crystal X-ray Structure Determination of 3: C$_{20}$H$_{28}$AlBrN$_2$, Enraf−Nonius CAD4 diffractometer; Mo-K_α radiation, λ =

0.71073 Å, graphite monochromator; data collection by ω scans at 243 K; colorless crystal, 0.20 × 0.28 × 0.36 mm, orthorhombic space group $P2_12_12_1$ (No. 19); a = 9.452(2), b = 10.937(3), c = 19.225(4) Å, U = 1987(2) Å^3, Z = 4, ρ_{calcd} = 1.35 g/cm^3, μ(Mo-K_α) = 20.95 cm^{-1}; 3924 reflections were collected in the scan range $2 < \theta < 25°$. After Lorentz and polarization corrections, an empirical absorption correction on the basis of azimuthal scans[17] (min. trans. 0.765, max. trans. 1.000) was applied prior to averaging symmetry related intensity data. 2752 independent observations with $I > \sigma(I)$ were used in the structure solution by direct methods;[18] refinement with the SDP program system[19] for 217 variables; all non-hydrogen atoms were refined with anisotropic displacement parameters; hydrogen atoms were included as a riding model [C−H = 98 pm, U_{iso}(H) = 1.3 U_{iso}(C)]. R = 0.069, R_w = 0.057, $w^{-1} = \sigma^2(F_o)$, GoF = 1.134. Max. residual electron density: 0.786 eÅ^{-3}.

Crystallographic data (excluding structure factors) for the structure reported in this paper have been deposited with the Cambridge Crystallographic Data Centre as supplementary publication no. CCDC-127942. Copies of the data can be obtained free of charge on application to the CCDC, 12 Union Road, Cambridge CB2 1EZ, U.K. [Fax: (internat.) +44 (0)1223/336033; E-mail: deposit@ccdc.cam.ac.uk].

Acknowledgments

We are grateful to the Deutsche Forschungsgemeinschaft and to the Fonds der Chemischen Industrie for generous financial support. We would also like to thank Prof. B. Wrackmeyer (Bayreuth) for performing the 2D EXSY experiments on compound **2**, and B. Rußbüldt for growing suitable crystals of **3**.

[1] G. Bähr, G. E. Müller, *Chem. Ber.* **1955**, *88*, 251−264.
[2] G.-J. M. Gruter, G. P. M. van Klink, O. S. Akkerman, F. Bickelhaupt, *Chem. Rev.* **1995**, *95*, 2405−2456.
[3] [3a] D. A. Neumayer, J. G. Ekerdt, *Chem. Mater.* **1996**, *8*, 9 and references therein. − [3b] A. C. Jones, P. O′Brien, *CVD of Compound Semiconductors*, VCH, Weinheim, **1997**.
[4] [4a] J. Müller, R. A. Fischer, H. Sussek, P. Pilgram, R. Wang, H. Pritzkow, E. Herdtweck, *Organometallics* **1998**, *17*, 161−166. − [4b] R. A. Fischer, A. Miehr, H. Sussek, H. Pritzkow, E. Herdtweck, J. Müller, O. Ambacher, T. Metzger, *J. Chem. Soc., Chem. Commun.* **1996**, 2685−2686. − [4c] A. Miehr, M. R. Mattner, R. A. Fischer, *Organometallics* **1996**, *15*, 2053−2059. − [4d] A. Miehr, O. Ambacher, W. Rieger, T. Metzger, E. Born, R. A. Fischer, *Chem. Vap. Deposition* **1996**, *2*, 51−55. − [4e] R. A. Fischer, A. Miehr, E. Herdtweck, M. R. Mattner, O. Ambacher, T. Metzger, E. Born, S. Weinkauf, C. R. Pulham, S. Parsons, *Chem. Eur. J.* **1996**, *2*, 1353−1358. − [4g] R. A. Fischer, A. Miehr, T. Metzger, E. Born, O. Ambacher, H. Angerer, R. Dimitrov, *Chem. Mater.* **1996**, *8*, 1356−1359.
[5] H. Schumann, U. Hartmann, W. Wassermann, A. Dietrich, F. H. Görlitz, L. Pohl, M. Hostalek, *Chem. Ber.* **1990**, *123*, 2093−2099.
[6] J. Müller, U. Englert, *Chem. Ber.* **1995**, *128*, 493−497.
[7] H. S. Isom, A. H. Cowley, A. Decken, F. Sissingh, S. Corbelin, R. J. Lagow, *Organometallics* **1995**, *14*, 2400−2406.
[8] [8a] G. van Koten, J. T. B. H. Jastrzebski, J. G. Noltes, W. M. G. F. Pontenagel, J. Kroon, A. L. Spek, *J. Am. Chem Soc.* **1978**, *100*, 5021−5028. − [8b] A. F. M. J. van der Ploeg, C. E. M. van der Kolk, G. van Koten, *J. Organomet. Chem.* **1981**, *212*, 283−290. − [8c] A. F. M. J. van der Ploeg, G. van Koten, K. Vrieze, *J. Organomet. Chem.* **1981**, *222*, 155−174. − [8d] J. T. B. H. Jastrzebski, G. van Koten, D. G. Tuck, H. A. Meinema, J. G. Noltes, *Organometallics* **1982**, *1*, 1492−1495. − [8e] R. J. P. Corriu, *J. Organomet. Chem.* **1990**, *400*, 81−106. − [8f] J. T. B. H. Jastrzebski, J. Boersma, G. van Koten, *J. Organomet. Chem.* **1991**, *413*, 43−53. − [8g] H. Suzuki, T. Murafuji, Y. Matano, N. Azuma, *J. Chem. Soc., Perkin Trans. 1* **1993**, 2969−2973. − [8h] F. Carré, C. Chuit, R. J. P. Corriu, P. Monforte, N. K. Nayyar, C. Reyé, *J. Organomet. Chem.* **1995**, *499*, 147−154. − [8i] S. Attar, J. H. Nelson, J. Fischer, *Organometallics* **1995**, *14*, 4776−4780.
[9] R. Benn, E. Janssen, H. Lehmkuhl, A. Rufinska, *J. Organomet. Chem.* **1987**, *333*, 155−168.
[10] The ^{27}Al-NMR shift of $ArAlBr_2$ is not mentioned in ref.[7]
[11] Gaussian 94, M. J. Frisch, G. W. Trucks, H. B. Schlegel, P. M. W. Gill, B. G. Johnson, M. A. Robb, J. R. Cheeseman, T. Keith, G. A. Petersson, J. A. Montgomery, K. Raghavachari, M. A. Al-Laham, V. G. Zakrzewski, J. V. Ortiz, J. B. Foresman, J. Cioslowski, B. B. Stefanov, A. Nanayakkara, M. Challacombe, C. Y. Peng, P. Y. Ayala, W. Chen, M. W. Wong, J. L. Andres, E. S. Replogle, R. Gomperts, R. L. Martin, D. J. Fox, J. S. Binkley, D. J. Defrees, J. Baker, J. P. Stewart, M. Head-Gordon, C. Gonzalez, J. A. Pople, Gaussian, Inc., Pittsburgh PA, **1995**.
[12] ZPVE scaled by 0.89.
[13] J. B. Foresman, M. J. Frisch, *Exploring Chemistry with Electronic Structure Methods*, 2nd ed., Gaussian Inc., Pittsburgh PA, **1996**.
[14] C. L. Perrin, T. J. Dwyer, *Chem. Rev.* **1990**, *90*, 935−967.
[15] [15a] G. Hägele, R. Fuhler, *DNMR-SIM simulation program for dynamic NMR spectra, Version 1.0*, University of Düsseldorf, **1994**. − [15b] J. Sandström, *Dynamic NMR Spectroscopy*, Academic Press, London, **1982**, chapter 7.
[16] G. van Koten, J. T. B. H. Jastrzebski, *Tetrahedron* **1989**, *45*, 569−578.
[17] A. C. T. North, D. C. Phillips, F. S. Mathews, *Acta Crystallogr.* **1968**, *A24*, 351.
[18] G. M. Sheldrick, *SHELXS-86: Program for Structure Solution*, University of Göttingen, Göttingen, Germany, **1986**.
[19] ENRAF-Nonius, SDP Version 5.0, Delft, The Netherlands, **1989**.
[20] L. A. Spek, *PLATON-94*, University of Utrecht, **1994**.

Received July 7, 1999
[I99245]

Different Reactivity Patterns in Dinuclear Pyrazolate-Bridged Complexes: Stereoselective Formation of Ketonic Carbonyls

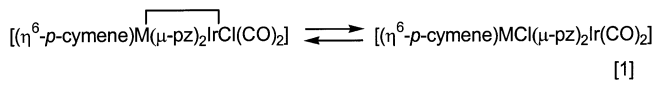
Daniel Carmona,*[a] Joaquina Ferrer,[a] José Miguel Arilla,[a] Josefa Reyes,[b] Fernando J. Lahoz,[a] Sergio Elipe,[a] Javier Modrego,[a] and Luis A. Oro*[a]

Keywords: Pyrazolato complexes / Dinuclear complexes / Ketonic carbonyls / Ruthenium / Osmium / Rhodium / Iridium

The metal–metal bonded dicarbonyl compounds [(η^6-*p*-cymene)M(μ-pz)$_2$IrCl(CO)$_2$](*M–Ir*) react stereospecifically with PPh_3 to yield an enantiomeric pair of ketonic carbonyl compounds [(η^6-*p*-cymene)M(μ-CO)(μ-pz)$_2$IrCl(CO)(PPh_3)] [M = Ru (**1**), Os (**2**)] in which the chloride ligand is *trans* to the bridging ketone group. However, the non metal–metal bonded isomers [(η^6-*p*-cymene)MCl(μ-pz)$_2$M′(CO)$_2$], under similar conditions, eliminate CO forming the monosubstitution products [(η^6-*p*-cymene)MCl(μ-pz)$_2$M′(CO)(PPh_3)] [M = Ru; M′ = Ir (**3**), Rh (**4**). M = Os; M′ = Rh (**5**)]. Removal of the chloride ligand in **1** affords [RuIr(η^6-*p*-cymene)(CO)$_2$(PPh_3)(pz)$_2$]BPh_4 as two isomers, **6a**,**b**. The related OsIr compound [(η^6-*p*-cymene)Os(μ-CO)(μ-pz)$_2$Ir(CO)(PPh_3)]BPh_4 (**9**) has been prepared from [(η^6-*p*-cymene)Os(CO)(μ-pz)$_2$Ir(CO)$_2$]BPh_4 (**7**) and PPh_3. Again, the OsRh tricarbonyl related to **7** [(η^6-*p*-cymene)Os(CO)(μ-pz)$_2$Rh(CO)$_2$]BPh_4 (**8**) reacts differently with PPh_3 affording [(η^6-*p*-cymene)Os(CO)(μ-pz)$_2$Rh(CO)(PPh_3)]BPh_4 (**10**).

Introduction

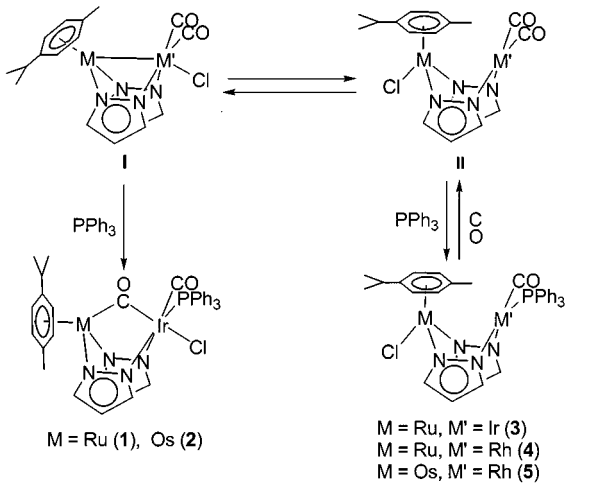
Heterodinuclear complexes are promising candidates for new stoichiometric and catalytic reactions.[1] Synergism between the metal centres is believed to be responsible for the improved activity of these heterodimetallic catalysts.[2][3] We have previously described an unusual isomerization equilibrium between heteronuclear pyrazolato complexes implying a chlorotropic shift and the reversible cleavage and formation of M−Ir bonds (M = Ru, Os)[4] according to Equation 1.



[1]

We now report on the reaction of the above-mentioned complexes towards triphenylphosphane. This reaction is remarkable because it allows the synthesis of new heterodimetallic complexes that contain bridging ketonic carbonyls supported by unusual *cis* frameworks.[5] Furthermore, according to the structural parameters (see below), the reaction implies the oxidation of the iridium from +1 to +3; from theoretical calculations,[6] the ketonic carbonyl group could be envisaged as a CO^{2-} ligand.

[a] Departamento de Química Inorgánica, Instituto de Ciencia de Materiales de Aragón,
Universidad de Zaragoza-CSIC, E-50009 Zaragoza, Spain
E-mail: dcarmona@posta.unizar.es
[b] Departamento de Química Inorgánica, Centro Politécnico Superior,
Instituto de Ciencia de Materiales de Aragón, Universidad de Zaragoza-CSIC,
E-50015 Zaragoza, Spain



Scheme 1. Reaction of isomers **I** and **II** with PPh_3

Results and Discussion

Complexes **1** and **2** were prepared in good yield by treating the metal−metal bonded compounds **I** with triphenylphosphane in dichloromethane (Scheme 1). The IR spectra of **1** and **2** showed two strong absorptions in the 2000 and 1650 cm^{-1} regions attributable to ν(CO) stretching modes. The first one is assignable to a terminal metal carbonyl whereas the lower frequency band, in the range expected for organic carbonyls, is typical for ketonic carbonyl ligands.[5] The addition of phosphane caused the molecule to become chiral and, consequently, the ^1H NMR spectra of the complexes showed six resonances, each integrating for one proton, attributable to six inequivalent C−H pyrazolate protons, and two AB systems and two doublets assignable to the aromatic and isopropyl methyl

 © WILEY-VCH Verlag GmbH, D-69451 Weinheim, 2000 1434−1948/00/0101−0159 $ 17.50+.50/0

protons of the *p*−cymene ligand, respectively.[7] The molecular structure of complex **1** was determined by an X-ray crystallographic study (Figure 1). Complex **1** has the ruthenium and iridium atoms triply bridged by two *exo*-bidentate nitrogen-bonded pyrazolates and one CO ligand. The ruthenium atom completes its coordination sphere with an η^6-bonded *p*-cymene ring. The iridium displays a distorted octahedral geometry typical for Ir^{III} complexes and is also linked to a chloride, *trans* to the carbon atom of the bridging carbonyl [Cl−Ir−C(17) = 167.95(18)°], to a terminal carbonyl and to the triphenylphosphane ligand. The six-membered ring formed by the metals and the pyrazolate nitrogen atoms adopts the usual boat conformation.[8] The Ru···Ir distance observed, 3.4089(5) Å, excludes any significant metal−metal interaction. The structural parameters of the bridging CO ligand [C(17)−O(1) = 1.177(8) Å, Ru−C(17)−Ir = 109.8(3), Ru−C(17)−O(1) = 128.1(6), and Ir−C(17)−O(1) = 121.3(5)°] compare well with those found for ketonic carbonyls[5] suggesting an sp^2 hybridization for the carbon atom. The Ir−N distances, 2.095(6) and 2.069(6) Å, are in the range described for other Ir^{III} complexes with bridging pyrazolate ligands.[8] It is interesting to point out the high stereoselectivity of this reaction; only the enantiomeric pair in which the ketonic carbonyl is *trans* to the chlorine atom has been detected among the three possible geometrical isomers (in the other two the ketonic group would be *trans* to the terminal CO or to the PPh_3 ligand).

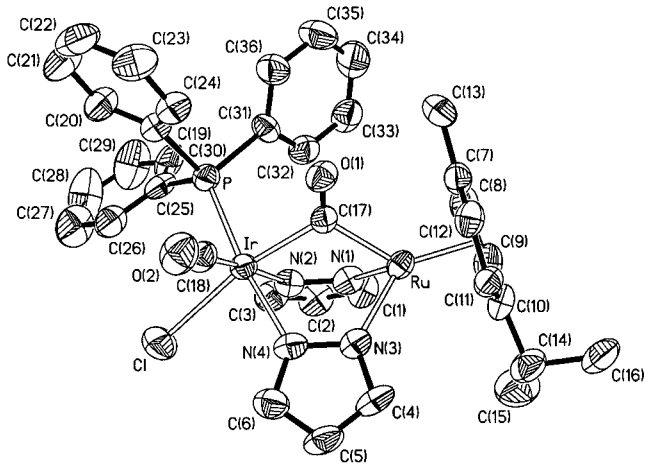


Figure 1. Molecular structure of **1** together with the atom numbering scheme used

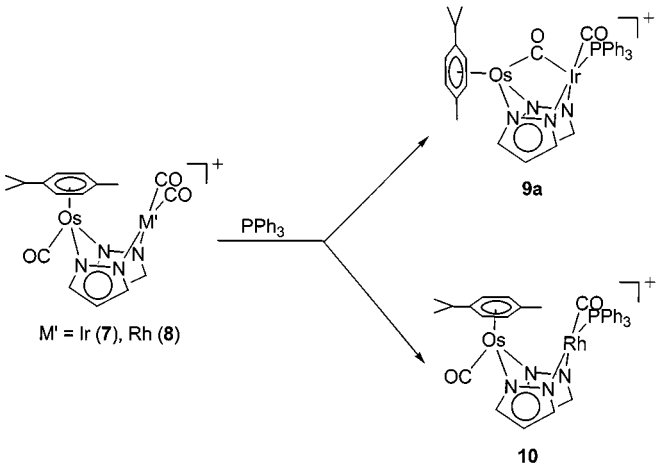
On the other hand, the non metal−metal bonded isomers **II** (Scheme 1) reacted with PPh_3 with apparent elimination of CO affording the monocarbonyls **3−5**. Their IR spectra showed a unique strong band at ca. 2000 cm^{-1} corresponding to the ν(CO) stretching mode. The substitution of one of the CO groups by the phosphane also caused the molecules to become chiral as revealed by their ^1H NMR spectra (see Experimental Section). As expected, the ^{31}P NMR spectra of the M−Rh complexes **4** and **5** consist of a doublet due to the coupling to ^{103}Rh, whereas a singlet at 1.8 ppm was observed for the Ru−Ir species **3**. The proposed structure for complexes **3−5** is that depicted in Scheme 1 (only one enantiomer has been drawn). The above reaction is reversible: treatment of compounds **3** and **5** with CO afforded the corresponding dicarbonyl species **II**. However, for the RuIr complex, the final isolated product was **1**, because of the chlorotropic equilibrium which operates between **I** and **II**. In fact, complex **3** has only been detected by IR and ^{31}P NMR spectroscopy in the reaction of the appropriate compound **II** with PPh_3.

The chloride ligand in **1** can easily be removed by treatment with $NaBPh_4$ in methanol, giving a 45:55 mixture of

Table 1. Selected bond distances (Å) and angles (deg) for the complexes [(η^6-*p*-cymene)Ru(μ-CO)(μ-pz)$_2$IrCl(CO)(PPh_3)] (**1**) and [(η^6-*p*-cymene)Os(μ-CO)(μ-pz)$_2$Ir(CO)(PPh_3)]BPh_4 (**9**)

	1 (M = Ru)	**9** (M = Os)		**1** (M = Ru)	**9** (M = Os)
M−N(1)	2.095(6)	2.112(13)	Ir−N(2)	2.069(6)	2.087(11)
M−N(3)	2.097(6)	2.106(12)	Ir−N(4)	2.095(6)	2.113(12)
M−G[a]	1.749(8)	1.741(16)	Ir−Cl	2.586(2)	−
M−C(7)	2.240(8)	2.294(17)	Ir−P	2.339(2)	2.324(4)
M−C(8)	2.197(8)	2.213(15)	Ir−C(17)	2.105(7)	2.184(14)
M−C(9)	2.302(8)	2.232(16)	Ir−C(18)	1.874(8)	1.893(16)
M−C(10)	2.334(7)	2.253(13)	C(17)−O(1)	1.177(8)	1.144(17)
M−C(11)	2.193(7)	2.231(16)	C(18)−O(2)	1.127(8)	1.094(18)
M−C(12)	2.195(7)	2.275(15)	N(1)−N(2)	1.357(8)	1.381(16)
M−C(17)	2.060(7)	2.084(15)	N(3)−N(4)	1.374(8)	1.346(16)
N(1)−M−N(3)	86.2(2)	83.5(5)	N(2)−Ir−N(4)	85.1(2)	85.0(5)
N(1)−M−C(17)	86.8(3)	88.1(5)	N(2)−Ir−C(17)	88.3(3)	90.4(5)
N(1)−M−G[a]	128.9(3)	130.8(7)	N(2)−Ir−C(18)	174.3(3)	176.6(6)
N(3)−M−C(17)	81.6(2)	86.3(5)	N(4)−Ir−P	172.45(18)	173.6(4)
N(3)−M-G[a]	130.2(3)	128.6(6)	N(4)−Ir−C(17)	82.9(2)	85.3(5)
C(17)−M-G[a]	127.2(3)	124.8(7)	N(4)−Ir−C(18)	89.3(3)	91.7(6)
M−C(17)−O(1)	128.1(5)	138.5(12)	P−Ir−C(17)	90.95(18)	99.6(4)
Ir−C(17)−O(1)	121.3(5)	116.2(11)	P−Ir−C(18)	95.1(2)	92.4(5)
M−C(17)−Ir	109.8(3)	105.3(6)	Cl−Ir−C(17)	167.95(18)	−
Ir−C(18)−O(2)	173.5(7)	175.2(15)	Cl−Ir−C(18)	89.8(2)	−

[a] G represents the centroid of the *p*-cymene ring.



Scheme 2. Reaction of compounds **7** and **8** with PPh_3

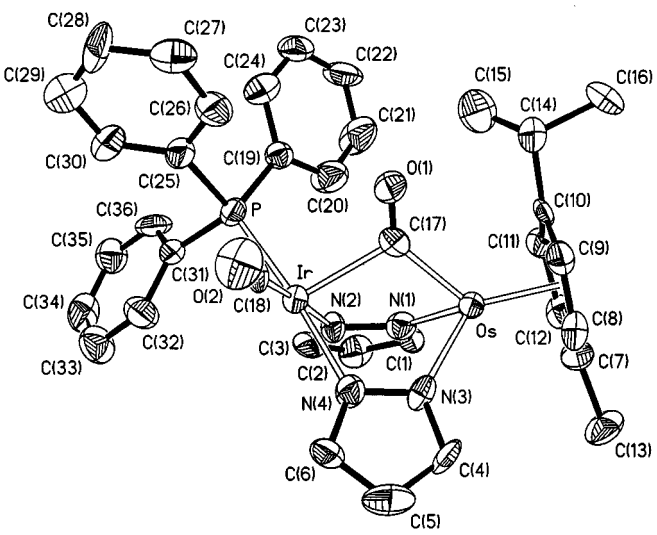


Figure 2. Molecular representation of the dinuclear cation of compound **9** with the atom labelling scheme

two isomers of stoichiometry $[RuIr(\eta^6\text{-}p\text{-cymene})(CO)_2(PPh_3)(pz)_2]BPh_4$ (**6a,b**). According to ^1H NMR spectroscopic data the minor isomer is chiral while the major is achiral. The IR spectrum of the mixture revealed the presence of both terminal (2035 cm^{-1}) and ketonic (1780 cm^{-1}) CO groups. In this context, it is interesting to mention that the related tricarbonyl compound $[(\eta^6\text{-}p\text{-cymene})Os(CO)(\mu\text{-}pz)_2Ir(CO)_2]BPh_4$ (**7**)[9] reacts with PPh_3 to yield, by CO elimination, the ketonic OsIr complex $[(\eta^6\text{-}p\text{-cymene})Os(\mu\text{-}CO)(\mu\text{-}pz)_2Ir(CO)(PPh_3)]BPh_4$ (**9**) whilst the homologous OsRh compound $[(\eta^6\text{-}p\text{-cymene})Os(CO)(\mu\text{-}pz)_2Rh(CO)_2]BPh_4$ (**8**)[9] yields, under similar conditions, the non-ketonic dicarbonyl compound $[(\eta^6\text{-}p\text{-cymene})Os(CO)(\mu\text{-}pz)_2Rh(CO)(PPh_3)]BPh_4$ (**10**) (Scheme 2).

The structures of complexes **9** and **10** have been determined by X-ray diffraction methods. For compound **9**, the molecular structure of the dinuclear cation closely resembles that of **1**, after the loss of the terminal chloride ligand (Figure 2). Thus, complex **9** contains the two metal atoms, osmium and iridium, triply bridged by one CO and two pyrazolate ligands. As in **1**, the osmium atom completes its coordination sphere with an η^6-bonded *p*-cymene ring. In this case, however, the iridium centre displays a distorted square-based pyramidal geometry with the carbon atom of the bridging carbonyl ligand occupying the apical position, and with the terminal carbonyl, the triphenylphosphane ligand and the pyrazolate nitrogen atoms forming the polyhedron base. The osmium−iridium separation is very similar to that reported in **1**, 3.3941(12) Å, and excludes any intermetallic interaction. The structural parameters of the bridging carbonyl group serve again to confirm the ketonic nature of this ligand (see Table 1). Unfortunately, in the case of **10**, only very small and weakly diffracting crystals were obtained. Although the data collected for these crystals were of reduced quality, they allowed us to verify the dinuclear framework and, in particular, the absence of any bridging CO group between the two metals.

In conclusion, it is worthwhile to point out the remarkable stereoselectivity encountered in the preparation of **1** and **2** from **I** and in the isolation of **9** from **7**. Furthermore, the different reactivity towards PPh_3 that has been found for species **I** and **II**, and for **7** and **8**, is also noteworthy. Most probably, the greater tendency of iridium(I) compared to that of rhodium(I) to pentacoordination and to be oxidised to M^{3+} would explain the obtained results.

Experimental Section

General: All solvents were dried and distilled before use. All reactions were performed under nitrogen. − IR: Perkin−Elmer 783. CH_2Cl_2 as solvent. − NMR: Varian XL (300.0 MHz and 121.4 MHz, for ^1H and ^{31}P, respectively). For ^1H NMR, TMS as internal standard; for ^{31}P NMR, $CDCl_3/CHCl_3$, (1:1, v/v) as solvent.

$[(\eta^6\text{-}p\text{-cymene})Ru(\mu\text{-}CO)(\mu\text{-}pz)_2IrCl(CO)(PPh_3)]$ (1): Triphenylphosphane (60 mg, 0.23 mmol) was added to a solution of $[(\eta^6\text{-}p\text{-cymene})Ru(\mu\text{-}pz)_2IrCl(CO)_2]$ (150 mg, 0.23 mmol) in dichloromethane (25 mL). After stirring for 12 h the solution was reduced in volume to 0.5 mL under vacuum. Slow addition of diethyl ether led to the precipitation of orange **1** (149 mg, 71%), which was filtered off, washed with diethyl ether and dried under vacuum. Complex **2** was similarly prepared from the corresponding OsIr dicarbonyl. Complexes **4−5** were similarly prepared starting from the corresponding species **II**. The reaction time was 2 h.

1: $C_{36}H_{35}ClIrN_4O_2PRu$ (915.43): calcd. C 47.23, H 3.85, N 6.12; found C 46.72, H 3.91, N 6.02. − IR: $\tilde{\nu}$ = 2050, 1650 cm^{-1} (CO). − ^1H NMR ($CDCl_3$): δ = 8.03 (d, 1 H, H_5 pz), 7.76 (d, 1 H, H_5 pz), 7.65 (t, 1 H, H_3 pz), 7.11 (d, 1 H, H_3 pz), 6.09 (q, $^3J_{H3H4} = {}^3J_{H5H4} = {}^4J_{PH}$ = 2.1 Hz, 1 H, H_4 pz), 5.92 (t, $^3J_{H3H4} = {}^3J_{H5H4}$ = 2.1 Hz, 1 H, H_4 pz), 5.51, 4.88 (AB system, J_{AB} = 6.4 Hz, C_6H_4 *p*-cymene), 5.03, 4.66 (AB system, J_{AB} = 5.9 Hz, C_6H_4 *p*-cymene), 2.72 (sp, 1 H, C*H*Me_2 *p*-cymene), 1.81 (s, 3 H, Me *p*-cymene), 1.19 (d, $^3J_{HH}$ = 6.9 Hz, 3 H, CH*Me p*-cymene), 1.10 (d, $^3J_{HH}$ = 6.8 Hz, 3 H, CH*Me p*-cymene). − ^{31}P NMR: δ = −14.7 (s).

2: $C_{36}H_{35}ClN_4O_2PRuOs$ (1004.59): calcd. C 43.05, H 3.48, N 5.58; found C 42.65, H 2.80, N 5.34. − IR: $\tilde{\nu}$ = 2050, 1640 cm^{-1} (CO). − ^1H NMR ($CDCl_3$): δ = 7.98 (br. s, 1 H, H_5 pz), 7.75 (br. s, 1 H,

H_5 pz), 7.64 (br. s, 1 H, H_3 pz), 7.03 (d, 1 H, H_3 pz), 5.98 (br. s, 1 H, H_4 pz), 5.81 (br. s, 1 H, H_4 pz), 5.51, 4.92 (AB system, J_{AB} = 5.1 Hz, C_6H_4 *p*-cymene), 5.07, 4.68 (AB system, J_{AB} = 5.7 Hz, C_6H_4 *p*-cymene), 2.62 (sp, 1 H, C*H*Me$_2$ *p*-cymene), 1.91 (s, 3 H, Me *p*-cymene); 1.10 (d, $^3J_{HH}$ = 6.6 Hz, 3 H, CH*Me* *p*-cymene), 1.05 (d, $^3J_{HH}$ = 6.9 Hz, 3 H, CH*Me* *p*-cymene). − ^{31}P NMR: δ = −13.8 (s).

3: IR: ν̃ = 1970 cm^{-1} (CO). − ^{31}P NMR (δ): 1.8 (s).

4: $C_{35}H_{35}ClN_4OPRhRu$ (798.11): calcd. C 52.68, H 4.43, N 7.04; found C 52.43, H 4.91, N 6.92. − IR: ν̃ = 1980 cm^{-1} (CO). − ^{1}H NMR ($CDCl_3$) δ = 7.71 (br. s, 1 H, $H_{3/5}$ pz), 7.62 (br. s, 1 H, $H_{3/5}$ pz), 6.67 (d, 1 H, $H_{5/3}$ pz), 6.18 (br. s, 1 H, H_4 pz), 5.80 (t, $^3J_{H3H4}$ = $^3J_{H5H4}$ = 1.8 Hz, 1 H, H_4 pz), 6.13, 5.14 (AB system, J_{AB} = 5.5 Hz, C_6H_4 *p*-cymene), 5.86, 5.00 (AB system, J_{AB} = 5.8 Hz, C_6H_4 *p*-cymene), 2.55 (sp, 1 H, C*H*Me$_2$ *p*-cymene), 1.77 (s, 3 H, Me *p*-cymene), 1.22 (d, $^3J_{HH}$ = 6.8 Hz, 3 H, CH*Me* *p*-cymene), 1.05 (d, $^3J_{HH}$ = 7.0 Hz, 3 H, CH*Me* *p*-cymene). − ^{31}P NMR: δ = 41.9 (d, $^1J_{RhP}$ = 153 Hz).

5: $C_{35}H_{35}ClN_4OOsPRh$ (887.27): calcd. C 47.39, H 3.94, N 6.31; found C 46.63, H 3.64, N 6.06. − IR: ν̃ = 1980 cm^{-1} (CO). − ^{1}H NMR ($CDCl_3$): δ = 7.65 (br. s, 1 H, $H_{3/5}$ pz), 7.57 (br. s, 1 H, $H_{3/5}$ pz), 6.54 (br. s, 1 H, $H_{5/3}$ pz), 6.09 (br. s, 1 H, H_4 pz), 5.74 (br. s, 1 H, H_4 pz), 6.57, 5.45 (AB system, J_{AB} = 5.1 Hz, C_6H_4 *p*-cymene), 6.10, 5.22 (AB system, J_{AB} = 5.1 Hz, C_6H_4 *p*-cymene), 2.45 (sp, 1 H, C*H*Me$_2$ *p*-cymene), 1.77 (s, 3 H, Me *p*-cymene); 1.20 (d, $^3J_{HH}$ = 6.9 Hz, 3 H, CH*Me* *p*-cymene), 1.02 (d, $^3J_{HH}$ = 6.9 Hz, 3 H, CH*Me* *p*-cymene). − ^{31}P NMR: δ = 42.3 (d, $^1J_{RhP}$ = 154 Hz).

[RuIr(η^6-*p*-cymene)(CO)$_2$(PPh$_3$)(pz)$_2$]BPh$_4$ (6a,b): To a solution of [(η^6-*p*-cymene)Ru(μ-CO)(μ-pz)$_2$IrCl(CO)(PPh$_3$)] (**1**) (100 mg, 0.11 mmol) in methanol (40 mL) was added $NaBPh_4$ (79 mg, 0.23 mmol). An orange solid precipitated which, after stirring for 15 h, was filtered off and washed with cold methanol (79 mg, 60%). − $C_{60}H_{55}BIrN_4O_2PRu$ (1199.21): calcd. C 60.11, H 4.62, N 4.69; found C 60.19, H 4.92, N 4.76. − ^{1}H NMR ($CDCl_3$): δ = 6.48 (br. s, pz), 6.20 (br. s, pz), 6.01 (pt, pz), 5.98 (pt, pz), 5.94 (pt, pz), 5.29 (s, C_6H_4 *p*-cymene), 5.13 (br. s, C_6H_4 *p*-cymene), 4.89 (br. s, C_6H_4 *p*-cymene), 2.40 (m, C*H*Me$_2$ *p*-cymene), 1.81 (s, Me *p*-cymene), 1.79 (s, Me *p*-cymene), 1.13 (d, ^3JHH = 6.7 Hz, CH*Me* *p*-cymene), 0.94 (d, $^3J_{HH}$ = 6.3 Hz, CH*Me* *p*-cymene), 0.94 (d, $^3J_{HH}$ = 6.3 Hz, CH*Me* *p*-cymene). − ^{31}P{^{1}H} NMR: δ = −12.3 (s), 1.2 (s).

[(η^6-*p*-cymene)Os(μ-CO)(μ-pz)$_2$Ir(CO)(PPh$_3$)]BPh$_4$ (9): To a solution of [(η^6-*p*-cymene)Os(CO)(μ-pz)$_2$Ir(CO)$_2$]BPh_4 (100 mg, 0.09 mmol) in dichloromethane (20 mL) was added PPh_3 (25 mg, 0.09 mmol). After stirring for 1 h the solution was evaporated to *ca.* 0.5 mL under vacuum. Slow addition of diethyl ether led to a yellow precipitate (107 mg, 88%), which was filtered off, washed with diethyl ether and dried under vacuum. Complex **10** was similarly prepared from the corresponding OsRh tricarbonyl parent compound.

9: $C_{60}H_{55}BIrN_4O_2OsP$ (1288.37) calcd. C 55.95, H 4.27, N 4.35; found C 55.40, H 4.01, N 4.13. − IR: ν̃ = 2045, 1745 cm^{-1} (CO). − ^{1}H NMR [$(CD_3)_2CO$]: δ = 8.07 (m, 1 H, $H_{3/5}$ pz), 6.17 (br. s, 1 H, $H_{3/5}$ pz), 6.05 (br. s, 1 H, H_4 pz), 5.96 (br. s, 1 H, H_4 pz), 6.64, 6.29 (AB system, J_{AB} = 6.3 Hz, C_6H_4 *p*-cymene), 5.95, 5.76 (AB system, J_{AB} = 5.7 Hz, C_6H_4 *p*-cymene), 2.89 (sp, 1 H, C*H*Me$_2$ *p*-cymene), 2.40 (s, 3 H, Me *p*-cymene), 1.30 (d, $^3J_{HH}$ = 6.6 Hz, 3 H, CH*Me* *p*-cymene), 1.06 (d, $^3J_{HH}$ = 6.6 Hz, 3 H, CH*Me* *p*-cymene). − ^{31}P NMR (δ): 1.5 (s).

10: $C_{60}H_{55}BN_4O_2OsPRh$ (1199.05): calcd. C 60.12, H 4.59, N 4.67; found C 59.98, H 4.62, N 4.58. − IR: ν̃ = 2019, 1998 cm^{-1} (CO). − ^{1}H NMR [$(CD_3)_2CO$]: δ = 6.60 (br. s, 1 H, $H_{3/5}$ pz), 6.25 (br. s, 1 H, H_4 pz), 5.91 (br. s, 1 H, H_4 pz), 6.12 (AB system, J_{AB} = 6.0 Hz, C_6H_4 *p*-cymene), 5.99 (AB system, J_{AB} = 6.6 Hz, C_6H_4 *p*-cymene), 2.60 (sp, 1 H, C*H*Me$_2$ *p*-cymene), 1.93 (s, 3 H, Me *p*-cymene), 1.17 (d, $^3J_{HH}$ = 6.6 Hz, 3 H, CH*Me* *p*-cymene), 1.10 (d, $^3J_{HH}$ = 6.9 Hz, 3 H, CH*Me* *p*-cymene). − ^{31}P NMR: δ = 41.3 (d, $^1J_{RhP}$ = 154 Hz).

X-ray Crystal Structure Analysis: Crystal data for **1**: $C_{36}H_{35}ClIrN_4O_2PRu{\cdot}CHCl_3$, M = 1034.79, orange irregular block (0.35 × 0.29 × 0.19 mm), monoclinic, space group $P2_1/n$, Z = 4, a = 10.8933(7), b = 17.8179(15), c = 20.0620(14) Å, β = 94.908(7)°, V = 3879.7(7) Å^3, D_c = 1.772 g cm^{-3}, μ = 4.171 mm^{-1}, *F(000)* = 2024. Intensity data were collected at 293 K on a Siemens-Stoe AED2 diffractometer with graphite-monochromated Mo-*K*α radiation (λ = 0.71073 Å) using a ω/2θ scan. The structure was solved by Patterson method (SHELXS-97)[11] and refined on F^2 by full-matrix least-squares (532 parameters, 106 restraints; SHELXL-97[11]). Static disorder was observed for the isopropyl group of the *p*-cymene and for a phenyl ring of the phosphane ligand; a chloroform solvent molecule was also found disordered. Anisotropic adps were used for nondisordered non-hydrogen atoms. A total of 6871 unique reflections were obtained from 7257 measured reflections [R_{int} = 0.0236; 4534 with $I > 2\sigma(I)$]. Final agreement factors *R1* = 0.0420, *wR2* = 0.0965 and S = 0.904. The final Fourier difference map showed residual peaks in the range 1.57 to −1.86 e/Å^3; the most intense were close to the iridium atom. Crystal data for **9**: $C_{60}H_{55}BIrN_4O_2OsP{\cdot}(CH_3)_2CO$, M = 1346.34, yellow irregular block (0.32 × 0.17 × 0.08 mm), triclinic, space group $P\bar{1}$, Z = 2, a = 9.623(2), b = 16.991(3), c = 18.605(4) Å, α = 71.390(10), β = 85.13(2), γ = 76.01(2)°, V = 2797.3(10) Å^3, D_c = 1.598 g cm^{-3}, μ = 4.723 mm^{-1}, *F(000)* = 1328. Intensity data were collected at 200 K on a Siemens P4 diffractometer with graphite-monochromated Mo-*K*α radiation (λ = 0.71073 Å) using a θ/2θ scan. The structure was solved by direct methods (SIR92)[12] and refined as described for **1** (SHELXL-97)[11] from 696 parameters and 65 restraints. Disorder was observed for the isopropyl group and for the acetone solvent molecule. 9619 unique reflections from a total of 12234 collected reflections [R_{int} = 0.0825; 6184 with $I > 2\sigma(I)$]. Final refinement with *R1* = *0*.0690, *wR2* = *0*.1821 and S = 1.037. The final Fourier difference map showed residual extrema in the range 1.84 to −0.98 e/Å^3; those positive over 1 e/Å^3 where localised close to the metal atoms. Crystallographic data for the structures reported in this paper have been deposited at the Cambridge Crystallographic Data Centre as supplementary publication numbers CCDC-131460 (**1**) and CCDC-131461 (**9**). Copies of the data can be obtained free of charge on application to CCDC, 12 Union Road, Cambridge CB2 1EZ, UK (E-mail: deposit@ccdc.cam.ac.uk).

Acknowledgments

We thank the *Dirección General de Investigación Científica y Técnica* for financial support (Projects PB96/0845 and PB95/1186). S. E. thanks the *DGICYT* for a fellowship.

[1] R. D. Adams, F. A. Cotton, *Catalysis by Di- and Polynuclear Metal Complexes,* VCH, New York, **1998**.
[2] R. D. Adams, T. S. Barnard, *Organometallics* **1998**, *17*, 2885−2890.
[3] [3a] M. A. Esteruelas, M. P. García, A. M. López, L. A. Oro, *Organometallics* **1991**, *10*, 127−133. − [3b] M. P. García, A. M. López, M. A. Esteruelas, F. J. Lahoz, L. A. Oro, *J. Chem. Soc., Dalton Trans.* **1990**, 3465−3472.
[4] [4a] D. Carmona, J. Ferrer, A. Mendoza, F. J. Lahoz, J. Reyes, L. A. Oro, *Angew. Chem. Int. Ed. Engl.* **1991**, *30*, 1171−1173.

– [4b] D. Carmona, J. Ferrer, L. A. Oro, S. Trofimenko, *Gazz. Chim. Ital.* **1994**, *124*, 35–42.
[5] D. Carmona, J. Ferrer, F. J. Lahoz, L. A. Oro, J. Reyes, M. Esteban, *J. Chem. Soc., Dalton Trans.* **1991**, 2811–2820, and refs. therein.
[6] D. M. Hoffman, R. Hoffmann, *Inorg. Chem.* **1981**, *20*, 3543–3555.
[7] [7a] M. A. Bennett, J. P. Ennett, Organometallics **1984**, *3*, 1365–1374. – [7b] D. Carmona, J. Ferrer, J. Reyes, L. A. Oro, *Organometallics* **1993**, *12*, 4241–4243. – [7c] M. Esteban, A. Pequerul, D. Carmona, F. J. Lahoz, A. Martín, L. A. Oro, *J. Organomet. Chem.* **1991**, *204*, 421–434. The assignment of the signals within each heterocyclic ring was made by double resonance decoupling experiments. Furthermore, the resonance of the H_4 proton of the pyrazolate *trans* to the phosphorus ligand could be identified because of its multiplicity: a long range $^5J_{HP}$ coupling constant,[10] of similar value to $^3J_{H4H3}$ and $^3J_{H4H5}$, was observed. Finally, the H_3 and H_5 protons could also be unambiguously assigned from its $^4J_{H3P}$ coupling constant.
[8] [8a] L. A. Oro, D. Carmona, M. P. Puebla, M. P. Lamata, C. Foces-Foces, F. H. Cano, *Inorg. Chim. Acta* **1986**, *112*, L11–L13. – [8b] D. Carmona, M. P. Lamata, J. Ferrer, J. Modrego, M. Perales, F. J. Lahoz, R. Atencio, L. A. Oro, *J. Chem. Soc., Chem. Commun.*, **1994**, 575–576.
[9] D. Carmona, J. Ferrer, J. M. Arilla, J. Reyes, F. J. Lahoz, S. Elipe, J. Modrego, L. A. Oro, unpublished results.
[10] P. P. Deutsch, R. Eisenberg, *J. Am. Chem. Soc.* **1990**, *112*, 714–721.
[11] G. M. Sheldrick, *SHELX-97. Program for Crystal Structure solution and refinement*, University of Göttingen, Germany, **1997**.
[12] A. Altomare, G. Cascarano, C. Giacovazzo, A. Guagliardi, *J. Appl. Cryst.* **1994**, *27*, 435–436.

Received July 19, 1999
[I99265]

A New Route to Iminoarsanes

Christian Kruppa,[a] Martin Nieger,[a] Bernd Ross,*[a] and Inka Väth[a]

Keywords: Arsenic / Imino compound / Hydrazinoiminoarsane / Aminoiminoarsane

Dehydrohalogenation of (2,4,6-tri-*tert*-butylphenylamino)chloro[tris(trimethylsilyl)hydrazino]arsane **(3)** or [*tert*-butyl(trimethylsilyl)amino]chloro(2,4,6-tri-*tert*-butylphenylamino)arsane **(4)** with DBU yields novel stable compounds containing an As–N double bond, (2,4,6-tri-*tert*-butylphenylimino)[tris(trimethylsilylhydrazino]arsane) **(5)** and [*tert*-butyl(trimethylsilyl)amino]-(2,4,6-tri-*tert*-butylphenylimino)arsane **(6)**. The structure of **5** was confirmed by an X-ray structure determination.

Introduction

In contrast to the well-known iminophosphanes[1] little is known about the corresponding compounds containing an As−N double bond.[2−4] The first compound in which an As−N double bond was clearly proven by X-ray structural analysis was (2,4,6-tri-*tert*-butylphenylamino)(2,4,6-tri-*tert*-butylphenylimino)arsane prepared by Lappert et al. in 1986.[5] It is an example for an aminoiminoarsane, in which the As−N (p-p)π-bond is stabilized by both steric and electronic effects. Ten years later Roesky et al. described the synthesis and X-ray structural characterization of *As,N*-bis[2,4,6-tris(trifluoromethyl)phenyl]iminoarsane,[6] an iminoarsane which is only kinetically stabilized by its bulky organyl groups. Herein we report the preparation of hydrazino- and aminoiminoarsanes using a new method to generate the As−N (p-p)π-bond.

Results and Discussion

Synthesis

The Lappert and Roesky methods for the synthesis of iminoarsanes are based on generation of the As−N (p-p)π-bond by alkali metal chloride elimination from *N*-metalated aminochloroarsanes, produced by substituting an H-atom of the amino group with lithium or potassium amide. Our method of synthesis is distinct from these syntheses as it uses the principle of direct base-induced dehydrohalogenation of aminochloroarsanes to iminoarsanes. Bisaminochloroarsanes suitable for the dehydrohalogenation to aminoiminoarsanes were obtained by successively substituting two chlorine atoms of $AsCl_3$ by treatment with lithium organyl amides. The introduction of two amino groups in a stepwise sequence with isolation of the primary formed aminodichloroarsane allows the synthesis of bisaminochloroarsanes and corresponding aminoiminoarsanes with differently substituted N atoms (Scheme 1).

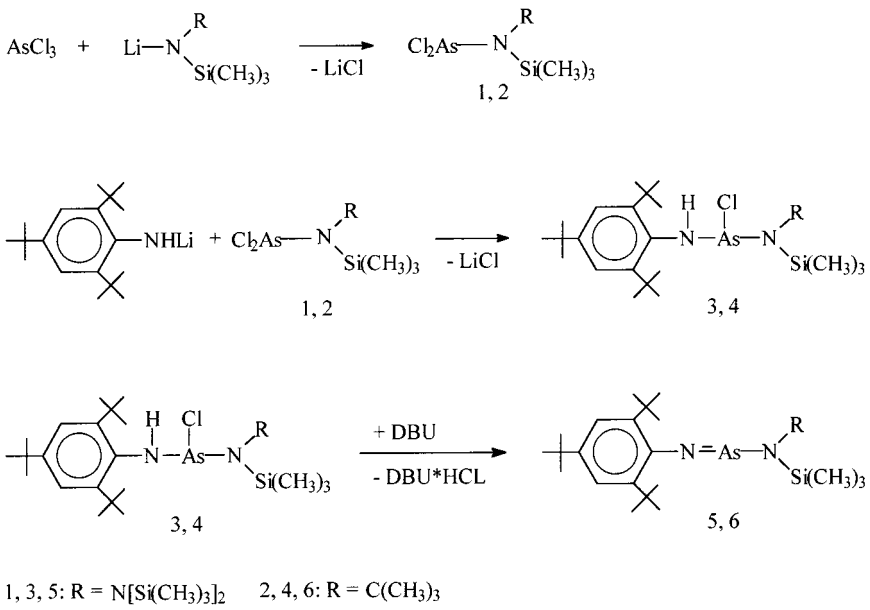
Treatment of $AsCl_3$ with lithium tris(trimethylsilyl)hydrazide or lithium trimethylsilyl(*tert*-butyl)amide, yielded the hydrazinodichloroarsane **1** or the aminodichloroarsane **2**, respectively. These compounds react with lithium (2,4,6-tri-*tert*-butylphenyl)amide to give the hydrazinoaminochloroarsane **3** and the bisaminochloroarsane **4**. All precursors were isolated in good yield and have not yet been described, except for compound **1**.[4b] Compounds **3** and **4** were dehydrohalogenated by reaction with 1,8-diazabicyclo(5.4.0)undec-7-ene (DBU) to give the hydrazinoiminoarsane **5** and the aminoiminoarsane **6** in good yields. Compound **6** is a red-orange amorphous solid and compound **5** is a red crystalline solid from which crystals suitable for X-ray structural analysis could be isolated. Under dry, oxygen-free argon both these novel compounds are stable indefinitely.

X-ray Crystal Structure of 5

A suitable crystal for data collection was obtained from toluene at room temperature. The molecular structure is shown in Figure 1 and selected bond lengths and angles are given in the legend. The As−N double bond of compound **5** has an (*E*)-configuration and a bond length of 170.8(3) pm. This bond length is comparable to those found for the aminoiminoarsane [171.4(7) pm] synthesized by Lappert et al.[5] and the iminoarsane [170.7(2) pm] prepared by Roesky et al.[6] The As1−N2 distance [182.2(2) pm] is shorter than the calculated value (187 pm) for an As−N single bond.[7] Therefore it is likely that there is some conjugation of the hydrazino nitrogen (N2) lone pair with the As−N (p-p)π-bond system, which one would expect because of the sp^2-hybridization of the planar coordinated N2 atom (sum of angles at N2 = 360°). The N2−N3 distance of 148.0(3) pm lies within the range expected for N−N single bonds (147 pm).[8] The nitrogen (N3) lone pair is not available for conjugation effects because of the perpendicular arrangement of the nitrogen lone pairs at N2 and N3. The plane formed by the phenyl ring occupies a vertical position to the central π-system. For that reason there is no conjugation between the two π-systems.

[a] Institut für Anorganische Chemie der Universität Bonn, Gerhard-Domagk-Straße 1, D-53121 Bonn, Germany
E-mail: ross@snchemie1.chemie.uni-bonn.de

 © WILEY-VCH Verlag GmbH, D-69451 Weinheim, 2000 1434−1948/00/0101−0165 $ 17.50+.50/0



Scheme 1. Synthesis of aminoiminoarsanes

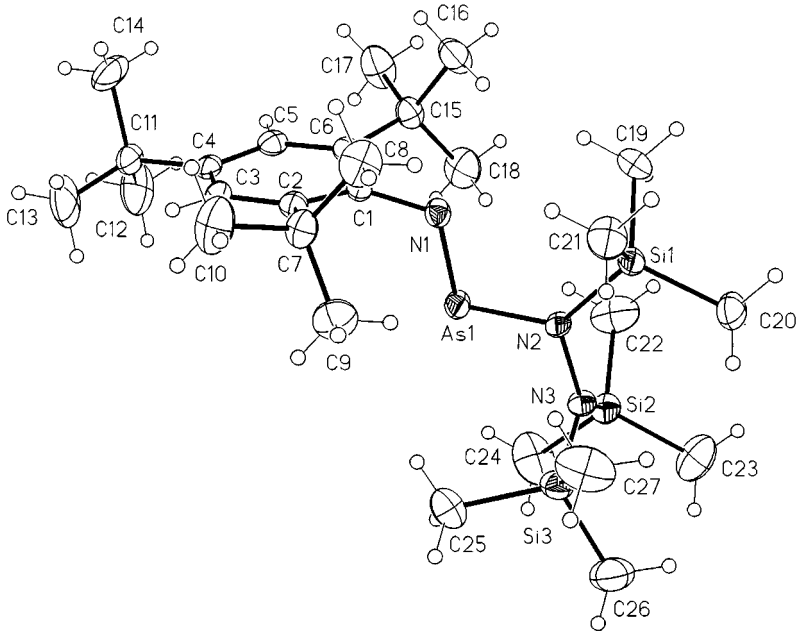


Figure 1. Moleculare structure of 5 (50% probabillity level, only one orientation of the disordered group is shown); selected bond lengths [pm], angles [°] and torsion angles [°]: As(1)−N(1) 170.8(3), As(1)−N(2) 182.3(2), N(2)−N(3) 147.9(4), N(1)−C(1) 144.5(4); As(1)−N(1)−C(1) 111.9(2), N(1)−As(1)−N(2) 104.0(1); C(1)−N(1)−As(1)−N(2) −178.5(2)

Experimental Section

General Remarks: All investigations were carried out in the absence of air and moisture under dry, oxygen-free argon. − ^{1}H NMR: Varian EM 360 (60 MHz) or Bruker WH 90 (90 MHz), standards used: residual solvent or TMS. − ^{13}C NMR: Bruker WH 90 (22 MHz), standard used: solvent. − ^{29}Si NMR: Bruker AMX 300 (59.63 MHz), external standard TMS. − Mass spectra: Kratos MS 50. − IR spectra: Bruker FT IR IFS 113 V. − Microanalyses were performed by the microanalytical laboratory E. Pascher, Remagen-Bandorf. − Trimethylsilyl(*tert*-butyl)amine[9] and tris(trimethylsilyl)hydrazine[10] were prepared as reported in the literature.

Dichloro[tris(trimethylsilyl)hydrazino]arsane (1): Tris(trimethylsilyl)hydrazine (13 g, 52.4 mmol), dissolved in diethyl ether (120 mL), was treated with *n*BuLi (34 mL of a 1.6 M solution in *n*-hexane, 52.4 mmol) at room temperature and stirred for 1 h. This solution was then added dropwise at −78°C to $AsCl_3$ (9.5 g, 52.4 mmol), dissolved in diethyl ether (40 mL). Stirring was continued for another hour whilst allowing the mixture to warm to room tempera-

ture. Thereafter the solvent was removed under reduced pressure, and the residue was extracted with *n*-hexane (40 mL). Lithium chloride was filtered off and cooling at −24°C over two days yielded **1**. Yield: 14.4 g (70%), colourless solid, M.p. 130°C (slow decomposition). − ^{1}H NMR (C_6D_6): δ = 0.13 [s, 18 H, N(Tms)$_2$], 0.41 [s, 9 H, NTms]. − ^{13}C NMR (C_6D_6): δ = 2.51 [s, N(Tms)$_2$], 2.70 [s, NTms]. − MS (EI): *m*/*z* (%) = 392 (0.1) [M$^+$], 377 (3) [M$^+$ − CH_3], 357 (10) [M$^+$ − Cl], 247 (100) [M$^+$ − $AsCl_2$], 73 (95) [Tms$^+$] and other fragments.

[*tert*-Butyl(trimethylsilyl)amino]dichloroarsane (2): Trimethylsilyl(*tert*-butyl)amine (7.25 g, 50 mmol), dissolved in diethyl ether (20 mL), was mixed with *n*BuLi (31.5 mL of a 1.6 M solution in *n*-hexane, 50 mmol) at 0°C. Following 1 h stirring at room temperature the solution of the lithium salt was added dropwise to $AsCl_3$ (9.1 g, 50 mmol), dissolved in diethyl ether (20 mL), at −78°C during 30 mins. The mixture was then warmed slowly to room temperature, lithium chloride was filtered off and the solvent was removed under reduced pressure. Distillation of the remaining yellow-brown oil yielded **2**. Yield: 11.79 g (81%), Bp. 78°C/1 mbar. − ^{1}H NMR ($CDCl_3$): δ = 0.43 [s, 9 H, Tms], 1.53 [s, 9 H, *t*Bu]. − ^{13}C NMR ($CDCl_3$): δ = 6.05 [s, Si(*C*H$_3$)$_3$], 33.86 [s, C(*C*H$_3$)$_3$], 61.92 [s, *C*(CH$_3$)$_3$]. − MS (EI): *m*/*z* (%) = 289 (1) [M$^+$], 274 (33) [M$^+$ − CH_3], 254 (5) [M$^+$ − Cl], 218 (15) [M$^+$ − CH_3 − isobutene], 198 (21) [M$^+$ − Cl − isobutene], 166 (100) [M$^+$ − TmsCl − CH_3], 73 (80) [Tms$^+$], 57 (92) [*t*Bu$^+$] and other fragments.

(2,4,6-Tri-*tert*-butylphenylamino)chloro[tris(trimethylsilyl)hydrazino]arsane (3): 2,4,6-Tri-*tert*-butylphenylamine (1.25 g, 4.8 mmol), dissolved in diethyl ether (10 mL), was treated with *n*BuLi (3 mL of a 1.6 M solution in *n*-hexane) at room temperature. After stirring for 30 mins. the solution of the lithium salt was added dropwise to dichloro[tris(trimethylsilyl)hydrazino]arsane **(1)** (1.88 g, 4.8 mmol), dissolved in diethyl ether (50 mL). Stirring was continued for 30 mins. and the solvent was removed under reduced pressure. The residue was extracted with *n*-hexane (10 mL) and lithium chloride was filtered off. Crystallization from the filtrate at −78°C yielded **3**. Yield: 1.5 g (50%), light rose solid, M.p. 81−83°C. − ^{1}H NMR (C_6D_6): δ = 0.26 [s, 9 H, N(Tms)$_2$], 0.34 [s, 9 H, N(Tms)$_2$], 0.42 [s, 9 H, AsNTms], 1.28 [s, 9 H, *p*-*t*Bu], 1.56 [s, 18 H, *o*-*t*Bu], 5.82 [s, 1 H, NH], 7.49 [s, 2 H, Aryl]. − ^{13}C NMR (C_6D_6): δ = 3.80 [s, N{Si(*C*H$_3$)$_3$}$_2$], 3.86 [s, N{Si(*C*H$_3$)$_3$}$_2$], 3.98 [s, AsNSi(*C*H$_3$)$_3$], 30.48 [s, *p*-*C*(CH$_3$)$_3$], 31.71 [s, *p*-C(*C*H$_3$)$_3$], 34.55 [s, *o*-C(*C*H$_3$)$_3$], 36.71 [s, *o*-*C*(CH$_3$)$_3$], 124.08 [s, C3, C5], 138.13 [s, C4], 141.02 [s, C2, C6], 143.19 [s, C1]. − ^{29}Si NMR (C_6D_6): δ = 11.37 [N(Tms)$_2$], 12.37 [N(Tms)$_2$], 16.06 [NTms]. − MS (EI): *m*/*z* (%) = 617 (2) [M$^+$], 602 (0.4) [M$^+$ − CH_3], 581 (5) [M$^+$ − HCl], 509 (0.4) [M$^+$ − TmsCl], 357 (100) [M$^+$ − Mes*NH], 334 (54) [M$^+$ − HCl − N_2Tms_3], 247 (75) [$Tms_3N_2^+$], 73 (82) [Tms$^+$], 57 (20) [*t*Bu$^+$] and other fragments.

[*tert*-Butyl(trimethylsilyl)amino]chloro(2,4,6-tri-*tert*-butylphenylamino)arsane (4): 2,4,6-Tri-*tert*-butylphenylamine (3 g, 11.5 mmol), dissolved in diethyl ether (130 mL), was treated with *n*BuLi (9.3 mL of a 1.6 M solution in *n*-hexane) at room temperature. After stirring for 30 mins. the solution of the lithium salt was added dropwise at −78°C to [*tert*-butyl(trimethylsilyl)amino]dichloroarsane **(2)** (3.32 g, 11.5 mmol), dissolved in diethyl ether (20 mL). The mixture was warmed slowly to room temperature and stirring was continued for 1 h. The solvent was removed under reduced pressure and the residue was extracted with *n*-hexane (15 mL). Lithium chloride was filtered off and cooling of the filtrate at −78°C for three weeks yielded **4**. Yield: 3.6 g (60%), colourless solid, M.p. 90−92°C. − ^{1}H NMR (C_6D_6): δ = 0.47 [s, 9 H, Tms], 1.33 [s, 9 H, *p*-*t*Bu], 1.40 [s, 9 H, N−*t*Bu], 1.66 [s, 18 H, *o*-*t*Bu], 6.03 [s, 1 H, NH], 7.55 [s, 2 H, Aryl]. − ^{13}C NMR (C_6D_6): δ = 6.26 [s, Si(*C*H$_3$)$_3$], 30.41 [s, *p*-*C*(CH$_3$)$_3$], 31.58 [s, *p*-C(*C*H$_3$)$_3$], 33.78 [s, NC(*C*H$_3$)$_3$], 34.10 [s, *o*-C(*C*H$_3$)$_3$], 36.82 [s, *o*-*C*(CH$_3$)$_3$], 59.54 [s, N*C*(CH$_3$)$_3$], 124.05 [s, C3, C5], 138.20 [s, C4], 144.67 [s, C1], 145.03 [s, C2, C6]. − MS (EI): *m*/*z* (%) = 514 (6) [M$^+$], 479 (2) [M$^+$ − Cl], 260 (90) [Mes*NH$^+$], 254 (20) [M$^+$ − Mes*NH], 246 (100) [Mes*H$^+$], 198 (84) [TmsNHAsCl$^+$] and other fragments.

(2,4,6-Tri-*tert*-butylphenylimino)[tris(trimethylsilyl)hydrazino]-arsane (5): DBU (0.39 g, 2.55 mmol), dissolved in *n*-hexane (5 mL), was added dropwise to (2,4,6-tri-*tert*-butylphenylamino)chloro[tris-(trimethylsilyl)hydrazino]arsane **(3)** (1.5 g, 2.43 mmol), dissolved in *n*-hexane (10 mL), at room temperature. The solution immediately turned red. Stirring was continued for 1 h, DBU·HCl was filtered off and crystallization from the filtrate at −26°C yielded **5**. Yield: 1.08 g (77%), red crystalline solid, M.p. 164−170°C. − ^{1}H NMR (CCl_4/TMS): δ = 0.2 [s, 18 H, N(Tms)$_2$], 0.5 [s, 9 H, NTms], 1.34 [s, 9 H, *p*-*t*Bu], 1.44 [s, 18 H, *o*-*t*Bu], 7.27 [s, 2 H, Aryl]. − ^{13}C NMR (C_6D_6): δ = 2.67 [s, Si(*C*H$_3$)$_3$], 30.41 [s, *p*-*C*(CH$_3$)$_3$], 32.06 [s, *p*-C(*C*H$_3$)$_3$], 33.82 [s, *o*-C(*C*H$_3$)$_3$], 36.73 [s, *o*-*C*(CH$_3$)$_3$], 121.77 [s. C3, C5], 137.05 [s, C2, C6], 142.20 [s, C4], 149.29 [s, C1]. − ^{29}Si (C_6D_6): δ = 10.96 [N(Tms)$_2$], 15.68 [NTms]. − MS (EI): *m*/*z* (%) = 581 (52) [M$^+$], 566 (5) [M$^+$ − CH_3], 334 (100) [M$^+$ − N_2(Tms)$_3$], 247 (92) [(Tms)$_3N_2^+$], 73 (65) [Tms$^+$], 57 (28) [*t*Bu$^+$] and other fragments. − IR (KBr): ṽ = 2956 (vs), 2904 (s), 2856 (s), 1595 (m), 1478 (m), 1460 (m), 1413 (s), 1389 (m), 1360 (s), 1253 (vs), 1213(s), 1191 (m), 1146 (m), 1021 (m), 925 (vs), 880 (vs), 842 (vs), 768 (s), 747 (m), 681 (m), 655 (m), 640 (w), 610 (w), 572 (m) cm^{-1}. − $C_{27}H_{56}AsN_3Si_3$ (581.94): calcd. C 55.73 H 9.70 N 7.22; found C 56.22 H 9.81 N 7.01

[*tert*-Butyl(trimethylsilyl)amino](2,4,6-tri-*tert*-butylphenylimino)arsane (6): [*tert*-Butyl(trimethylsilyl)amino]chloro(2,4,6-tri-*tert*-butylphenylamino)arsane **(4)** (1.6 g, 3.1 mmol), dissolved in *n*-hexane (10 mL), was treated with DBU (0.5 g, 3.3 mmol), dissolved in *n*-hexane (3 mL). The solution immediately turned red. Stirring was continued for 1 h, DBU·HCL was filtered off and cooling of the filtrate at −26°C yielded **6**. Yield: 1.1 g (75%), red solid, M.p. 87−90°C. − ^{1}H NMR (CCl_4/TMS): δ = 0.39 [s, 9 H, Tms], 1.32 [s, 9 H, *p*-*t*Bu], 1.37 [s, 18 H, *o*-*t*Bu], 1.80 [s, 9 H, N−*t*Bu], 7.24 [s, 2 H, Aryl]. − ^{13}C NMR (C_6D_6): δ = 5.93 [s, Si(*C*H$_3$)$_3$], 30.48 [s, *p*-*C*(CH$_3$)$_3$], 32.10 [s, *p*-C(*C*H$_3$)$_3$], 33.31 [s, *o*-C(*C*H$_3$)$_3$], 33.47 [s, NC(*C*H$_3$)$_3$], 36.63 [s, *o*-*C*(CH$_3$)$_3$], 60.97 [s, N*C*(CH$_3$)$_3$], 121.63 [s, C3, C5], 138.23 [s, C2, C6] 142.17 [s, C4], 150.16 [s, C1]. − ^{29}Si NMR (C_6D_6): δ = 5.99. − MS (EI): *m*/*z* (%) = 478 (30) [M$^+$], 463 (6) [M$^+$ − CH_3], 421 (12) [M$^+$ − *t*Bu], 334 (100) [M$^+$ − N(Tms)*t*Bu], 278 (50) [M$^+$ − N(Tms)*t*Bu − isobutene], 73 (90) [Tms$^+$], 57 (50) [*t*Bu$^+$] and other fragments. − IR (KBr): ṽ = 2963 (vs), 2903 (m), 2864 (m), 1621 (w), 1596 (w), 1479 (m), 1436 (m), 1409 (s), 1388 (m), 1360 (s), 1253 (s) 1234 (w), 1215 (s) 1179 (m), 1116 (s), 1034 (m), 958 (s), 917 (w), 847 (vs), 761 (m), 739 (m), 678 (s), 632 (m), 534 (w), 485 (m), 416 (w) cm^{-1}.

Crystal Data for 5: $C_{27}H_{56}AsN_3Si_3$, M = 581.9, monoclinic, space group $P2_1/n$ (No. 14), red crystals, dimensions 0.10 × 0.15 × 0.35 mm, a = 9.865(3), b = 34.578(2), c = 10.035(1) Å, β = 98.80(2)°, V = 3.383(1) Å^3, D_c = 1.14 Mg m^{-3}, Z = 4, μ (CuKα) = 2.5 mm^{-1}, T = 208(2) K, F(000) = 1256; 5328 reflection were collected on an Enraf−Nonius CAD4 diffractometer ($2\theta_{max}$ = 120°, $-11 \le h \le 0$, $0 \le k \le 38$, $-11 \le l \le 11$), 5008 symmetry independent reflections (R_{int} = 0.027) were used for the structure solution (direct methods)[11] and refinement (full matrix least-squares on F^2,[12] 302 parameters, 60 restraints), non-hydrogen atoms were refined anisotropically, H atoms localized by difference electron density and refined using a riding model; $wR2$ = 0.108 [R_1 = 0.039 for 3969 $I > 2\sigma(I)$]. An empirical absorption correction on the basis of

ψ-scans was applied (min./max. transmission 0.190/0.764). The *p*-*t*Bu-group is disordered.

Crystallographic data (excluding structure factors) for the structure reported in this paper have been deposited with the Cambridge Data Centre as supplementary publication no. CCDC-132004. Copies of the data can be obtained free of charge on application to CCDC, 12 Union Road, Cambridge CB2 1EZ, UK [Fax: (internat.) + 44-1223/336-033; E-mail: deposit@ccdc.cam.ac.uk].

[1] E. Niecke, D. Gudat, *Angew. Chem*. **1991**, *103*, 251−270; *Angew. Chem. Int. Ed. Engl*. **1991**, *30*, 217
[2] G. I. Kokorev, F. D. Yambushev, Sh. Kh. Badrutdinov, *Zh. Obshch. Khim*. **1986**, *56(9)*, 2058−2061 *Chem. Abstr.* **1987**, *107*, 59134c.
[3] [3a] H. G. Ang, F. K. Lee, *Polyhedron* **1989**, *8*, 1461−1462. − [3b] H. G. Ang, F. K. Lee, *Polyhedron* **1989**, *8*, 2331−2332.
[4] [4a] S. K. Vasisht, M. Sood, P. K. Verma, T. Kaur, K. Usha, *Phosphorus, Sulfur, Silicon* **1990**, *47*, 349−355. − [4b] S. K. Vasisht, T. P. Kaur, K. Usha, J. Kaushal, K. Bandhu, *Phosphorus, Sulfur, Silicon* **1995**, *107*, 189−195.
[5] P. B. Hitchcock, M. F. Lappert, A. K. Rai, H. D. Williams, *J. Chem. Soc., Chem. Commun*. **1986**, 1633−34.
[6] J.-T. Ahlemann, A. Künzel, H. W. Roesky, M. Noltemeyer, L. Markovskii, H.-G. Schmidt, *Inorg Chem* **1996**, *35*, 6644−6645.
[7] V. Schomaker, D. P. Stevenson, *J. Am. Chem. Soc*. **1941**, *63*, 37−49.
[8] P. A. Giguère, V. Schomaker, *J. Am. Chem. Soc* **1943**, *65*, 2025−2029.
[9] I. Schumann-Ruidisch, W. Kalk, R. Brüning, *Z. Naturforsch*. **1968**, *B 23*, 307−312
[10] K. Witke, P. Reich, H. Kriegsmann, *J. Organomet. Chem*. **1968**, *15*, 37−41
[11] G. M. Sheldrick, SHELXS-86, *Acta Crystallogr*. **1990**, *A46*, 467−473.
[12] G. M. Sheldrick, SHELXL-97, University of Göttingen, **1997**.

Received July 20, 1999
[I99268]

Controlled Thiolate Coordination and Redox Chemistry: Synthesis, Structure, Axial-Binding, and Electrochemistry of Dinickel(II) Dithiolate Macrocyclic Complexes

Sally Brooker,*[a] Paul D. Croucher,[a] Tony C. Davidson,[a] Geoffrey S. Dunbar,[a] Corina U. Beck,[b] and S. Subramanian[c]

Keywords: Macrocycles / Nickel / Redox chemistry / Schiff bases / S ligands

A single crystal X-ray analysis of $[Ni_2L1](ClO_4)_2 \cdot MeCN \cdot 1/4\ H_2O$, **1a** [formed directly from a mixture of nickel(II) template ions, 2,6-diformyl-4-methyl-thiophenolate, and 1,4-diaminobutane] reveals that the nickel(II) ions are in square-planar N_2S_2 environments and that the four "bowed" dinickel macrocycles in the asymmetric unit pack around a single central perchlorate template ion encapsulating it to form "star" clusters of stoichiometry $\{[Ni_2L1]_4(ClO_4)\}^{7+}$. These "stars" stack together, via π–π-stacking interactions, to form two-dimensional sheets, which are separated from one another by layers of the remaining perchlorate anions and solvent molecules. Reduction, by $NaBH_4$, of the four imine bonds in $[Ni_2L2](ClO_4)_2$ **2a** (analogous to **1a** but formed from 1,3-diaminopropane not 1,4-diaminobutane) or $[Ni_2L2](CF_3SO_3)_2$ **2b** to amine bonds produces the corresponding tetra-amine complex, $[Ni_2L3](ClO_4)_2$ **3**. These complexes are shown to contain diamagnetic nickel(II) ions by a combination of magnetic, NMR and UV/Vis spectroscopic results. The ^1H NMR spectra of **1–3** run in $[D_3]MeNO_2$ and in $[D_3]MeCN$ are consistent with increasing axial binding ability in the order: **3** < **2** < **1**. Thiocyanate ion binding studies reveal that **1** and **2** are able to coordinate two thiocyanate ions, forming $[Ni_2L1(NCS)_2]$ **4** and $[Ni_2L2(NCS)_2]$ **5** respectively, whereas **3** does not. Single crystal X-ray analyses of complexes **4** · 2 MeCN and **5** · MeCN show that adjacent square-planar and octahedral nickel(II) ions result. Two one-electron oxidations *and* two one-electron reductions are a feature of the electrochemistry of **1–3** in MeCN: curiously, the potentials for the oxidation processes are almost invariant whereas those for the reduction processes vary as anticipated. EPR spectroscopy shows that the first one-electron reduction process and the first one-electron oxidation process are metal centred. Spectroelectrochemical studies and redox titrations indicate that a purplish-coloured complex is produced by one-electron oxidation of **2** (λ = 870 nm, ε = 1320 L mol cm^{-1}). The synthesis of a phenolate analogue, $[Ni_2L'(MeCN)_4](ClO_4)_2$ (**6**), of the thiophenolate complex **2a** is also detailed. Complex **6** undergoes two one-electron oxidations in MeCN, but, in contrast to the thiophenolate complexes **1–3**, these occur at much higher potentials. Only a single one-electron reduction process is observed and this occurs at a more negative potential than for any of **1–3**.

Introduction

There is intense interest in modelling nickel thiolate metalloprotein active sites including the [Ni,Fe] hydrogenases mixed metal active site which is responsible for catalysing the reversible oxidation of dihydrogen, $H_2 = 2\,H^+ + 2\,e^-$.[1–4] Many dinickel thiolate-bridged complexes have been reported although the number which have been fully characterised (ie. structure and physical properties including redox chemistry) is still relatively small.[5] As a result of these biologically-inspired studies much is being learnt about fundamental thiolate coordination chemistry. Gaining an understanding of the nature of the redox products of polynuclear thiolate complexes is a considerable and fascinating challenge.[6–9]

Robson and co-workers investigated the coordination chemistry of some acyclic ligands prepared from the thiolate-precursor (*S*)-(2,6-diformyl-4-methylphenyl)dimethyl thiocarbamate.[10–13] We,[14–19] and others[20–24] have subsequently prepared a range of Schiff-base macrocycles from this thiolate-precursor: most of these macrocycles can be templated by nickel(II) ions thus giving direct access to the complexes of interest. By using *macrocyclic* ligands the many problems typically encountered when working with transition metal thiolates are minimised and the resulting thiolate coordination chemistry can be explored in a relatively controlled way.[25] The investigation of the dinickel(II) thiolate macrocyclic complexes $[Ni_2Lj]X_2$ **1–3** (j = 1–3 and X = ClO_4^- for complexes **1a**, **2a**, and **3** respectively, j = 1–2 and X = $CF_3SO_3^-$ for complexes **1b** and **2b** respectively) and $[Ni_2Lj(NCS)_2]$ **4** and **5** (j = 1 for complex **4** and j = 2 for complex **5**), shown in Figure 1, is presented.

[a] Department of Chemistry, University of Otago, P. O. Box 56, Dunedin, New Zealand
Fax: (internat.) +64-3/479-7906
E-mail: sbrooker@alkali.otago.ac.nz
[b] School of Chemistry, University of Sydney, Sydney, NSW 2006, Australia
[c] Department of Chemistry, University of Victoria, Victoria, B.C., Canada

 © WILEY-VCH Verlag GmbH, D-69451 Weinheim, 2000 1434–1948/00/0101–0169 $ 17.50+.50/0

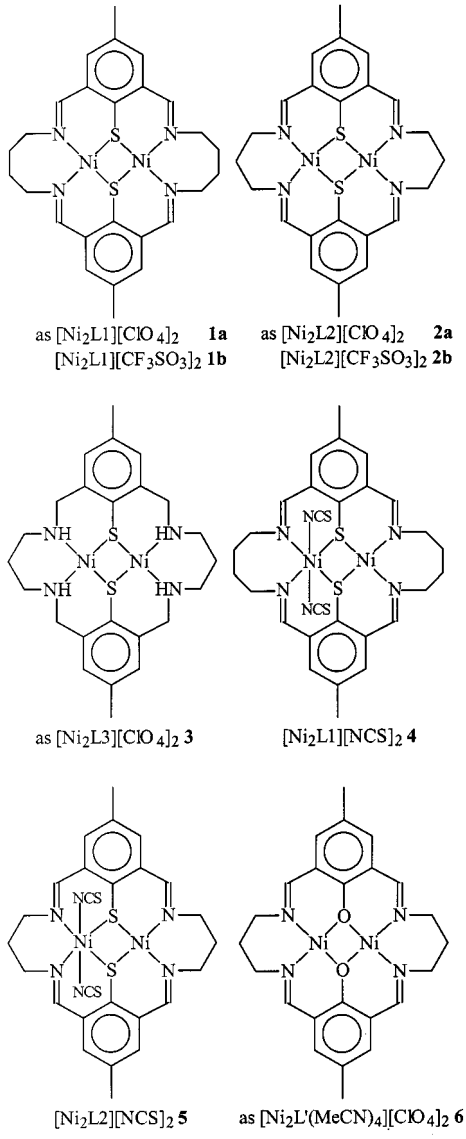


Figure 1. Macrocyclic dinickel(II) complexes **1**−**6**

Results and Discussion

Synthesis

The red complexes $[Ni_2L1](ClO_4)_2 \cdot MeCN \cdot 1/4\ H_2O$, **1a**, $[Ni_2L1](CF_3SO_3)_2 \cdot H_2O$, **1b**, and $[Ni_2L2](CF_3SO_3)_2$, **2b**, were prepared in acceptable yields. The sodium borohydride reduction of the tetra-imine analogue **2b**, to produce the red tetra-amine complex $[Ni_2L3](ClO_4)_2$ **3**, in excellent yield (80%), was carried out according to the method described by Curtis.[26] The ability of this complex to resist protonation during the acidic workup is remarkable and indicates that there is no remaining nucleophilicity associated with the bridging thiolate suphur atoms. The red-black complexes $[Ni_2L1(NCS)_2]$ **4** and $[Ni_2L2(NCS)_2]$ **5** were prepared by the addition of a solution of 2.2 equivalents of NaSCN to acetonitrile solutions of **1** and **2**, respectively. Complex **4** is obtained in excellent yield (83%) in marked contrast to **5** (19%). No change occurred on addition of 2.2 equivalents of NaSCN to a red acetonitrile solution of **3** whereas an excess of NaSCN caused the solution to turn green and deposit, over time, a green oily solid. The IR spectrum of this impure complex indicated that the nickel ions had been removed from the ligand and formed a simple salt. This was not pursued further. We found the direct preparation of the previously reported[21] phenolate complex, $[Ni_2L'(MeCN)_4](ClO_4)_2$ **6**, non-trivial. Therefore the dichloride analogue[27] was prepared and reacted with silver perchlorate[28] to give a green powder which was then recrystallised from MeCN by vapour diffusion of diethyl ether to give **6**.

In the case of the tetra-imine macrocyclic complexes **1a**, **1b**, **2b**, and **6** IR spectroscopy showed imine formation (1615, 1614, 1623, 1639 cm^{-1}, respectively) and that no unchanged carbonyl or primary amine functional groups were present. The IR spectrum of the perchlorate complex **1a** did not show bands consistent with the very small amount of lattice water present (1/4 H_2O per macrocyclic complex) whereas for the triflate complex **1b** the IR spectrum was consistent with the presence of lattice water[29] (bands were observed at 3526, 3462, and 1623 cm^{-1}) and this was subsequently confirmed by microanalysis (one H_2O per macrocyclic complex). In contrast, the triflate complex **2b** did not have these IR bands and microanalysis gave no evidence for the presence of any waters of crystallisation. The IR spectra of **4** and **5** are consistent with retention of the imine macrocycle (1628 and 1621 cm^{-1} respectively), loss of the perchlorate anions and gain of thiocyanate anions (2081 and 2075 cm^{-1}, respectively). The brown powder formed as the major by-product in the low yielding reaction to form **5** has a shoulder at ca. 1652 cm^{-1} in the IR spectrum indicating that it is a ring-opened complex. This presumably results from imine hydrolysis relieving the strain of encircling a, larger, high spin nickel(II) ion.

Satisfactory elemental analyses were obtained for all of the new complexes, $[Ni_2L1](ClO_4)_2 \cdot MeCN \cdot 1/4\ H_2O$ **1a**, $[Ni_2L1](CF_3SO_3)_2 \cdot H_2O$ **1b**, $[Ni_2L2](CF_3SO_3)_2$ **2b**, $[Ni_2L1(NCS)_2]$ **4**, $[Ni_2L2(NCS)_2]$ **5**, and $[Ni_2L'(MeCN)_4](ClO_4)_2$ **6**. The red complexes **1**−**3** were found to be diamagnetic ($\mu = 0.0$ BM in all cases) which is consistent with a square planar nickel(II) formulation. The red-black complex **4** has a magnetic moment of 2.8 BM per complex which is consistent with the presence of a single high-spin nickel(II) ion per complex.

Crystal Structures

The structures of **2a** and **3** have been reported previously.[16][19] Red crystals of **1a** suitable for X-ray crystal structure analysis were grown from acetonitrile solutions by vapour diffusion of diethyl ether. The structure determination reveals that the asymmetric unit contains *four* dinickel(II) dithiolate macrocycles which, despite lacking crystallographic symmetry, are reasonably similar to each other and form a "star" which is templated on a perchlorate ion (Figure 2, Tables 1 and 2). Each nickel atom is square

planar, as predicted, and is located within 0.05 Å of the mean plane through the N_2S_2 donors provided by the respective macrocycle. Bonds between these donors and the nickel atoms are typical for square planar nickel(II).[16][30] In each macrocycle one of the two nickel atoms interacts very weakly with the central perchlorate ion (Figure 2, Ni···O 3.34−3.36 Å). The mean planes of the two N_2S_2 donor sets within each macrocycle intersect at angles of 137.6° [for Ni(7), Ni(8)] to 140.0° [for Ni(5), Ni(6)]. In addition, each of the macrocycles is bent such that the two aromatic rings are inclined almost at right angles (84.2−97.0°) to each other. The tetrahedrally-distorted bridging-thiolate sulfur donors (Ni−S−Ni 92.3−93.6, Ni−S−C 97.4−108.4°) facilitate this folding of the macrocycles and in doing so reveal their geometrical flexibility.[31−33]

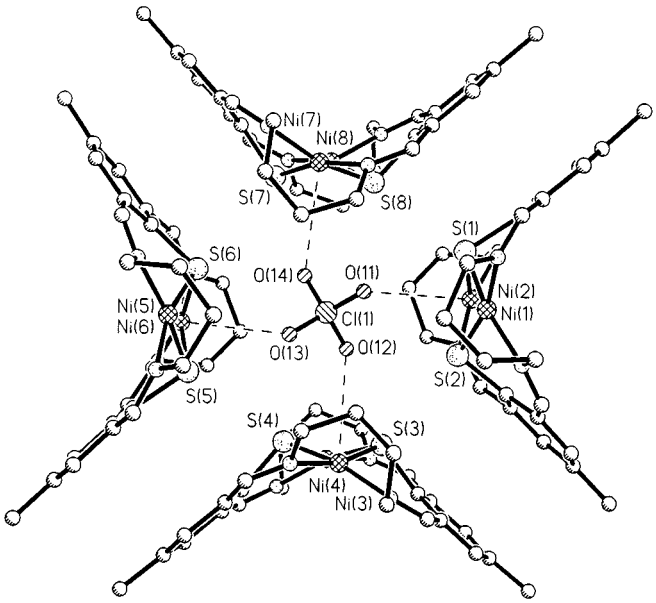


Figure 2. Perspective view of the four $[Ni_2L1]^{2+}$ cations and one of the perchlorate ions, Cl(1), in the asymmetric unit of **1a** (hydrogen atoms, solvent molecules, and remaining perchlorate ions omitted for clarity)

The folding is optimal for the formation of a large number of favourable π−π interactions both between phenyl rings within the asymmetric unit [Figure 2, pairs of π-stacked aromatic rings intersect at 7.8(7)−10.2(7)° and are 3.17(3)−3.65(1) Å apart] and between symmetry generated units [Figure 3, pairs of parallel, π-stacked aromatic rings are 3.43−3.53 Å apart]. Both edge-on ("T") and offset face-to-face π−π interactions[34] are observed and these result in the formation of sheets of dinickel macrocyclic cations, between which lie layers of counter ions and solvent molecules [with the exception of perchlorate Cl(1) which is at the centre of the four macrocycles in the asymmetric unit (Figure 2)].

Differences in the coordination environment of the square planar nickel(II) ions in $L1^{2-}$ compared to those in $L2^{2-}$ are revealed by an examination of the dihedral angles between the respective NiN_2 and NiS_2 planes: the longer alkyl chain in **1a** has caused some buckling and tetrahedral

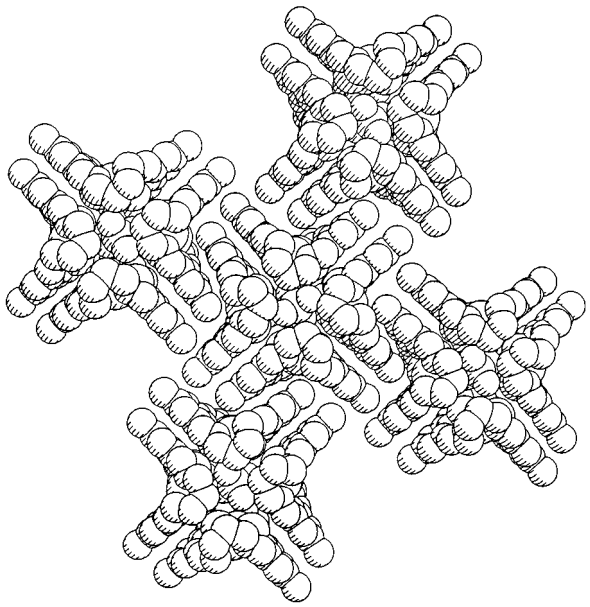


Figure 3. Space-filling diagram of part of a sheet of π−π-stacked $[Ni_2L1]^{2+}$ cations of **1a** [hydrogen atoms, anions, and solvent molecules omitted for clarity, with the exception of the central perchlorate ion, Cl(1)]

distortion away from square planar (15.4−18.9°), whereas an almost planar (slightly folded) arrangement is found in **2a** (2.3−6.1°).[16] A series of related mononickel acyclic complexes has been studied and a wide variation in properties was found depending on the degree of distortion.[30] To probe the significance of this distortion binding studies were undertaken and led to the formation and characterisation of **4**.

Red-black crystals of **4** · 2 MeCN suitable for X-ray crystal structure analysis were grown from the acetonitrile reaction solutions on standing. The structure determination (Figure 4, Tables 1 and 2) reveals that the thiocyanate anions are indeed coordinated to nickel(II). Interestingly both thiocyanate ions bind to one nickel atom, Ni(2), giving it a distorted octahedral geometry overall [Ni(2) is 0.010(2) Å out of the $N(macro)_2S_2$ plane] whilst the remaining nickel atom, Ni(1), remains square planar [Ni(1) is 0.036(2) Å out of the N_2S_2 plane]. Bond lengths to Ni(1) are in the usual range observed for square planar nickel(II) complexes and the corresponding bond lengths involving Ni(2) are ca. 0.2 Å longer as is typical of octahedral (high spin) nickel(II) complexes.[16,35,36]

Complex **4** is folded in the same way as complex **1a**: the two $N(macro)_2S_2$ planes intersect at 140.2(1)° and the two phenyl ring planes at 86.7(1)° in **4** compared to averages of 138.8(2)° and 85.3(4)°, respectively, for **1a**. Slightly larger S···S [2.79−2.83 in **1a** vs. 2.979(2) Å in **4**] and Ni···Ni separations [3.12−3.14 in **1a** vs. 3.2935(8) Å in **4**] are observed in **4**. The three-dimensional packing arrangements of **1a** and **4** are different as a result of the differences in anion template effects. Rather than the anion templating the packing together of the macrocyclic complexes, as is the case with the perchlorate ion in **1a**, the thiocyanate ions block the formation of all but one set of π−π interactions.

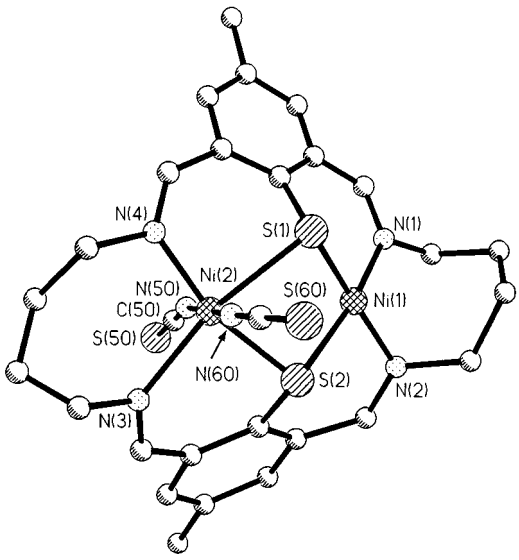


Figure 4. Perspective view of $[Ni_2L1(NCS)_2]$ **4** (hydrogen atoms and solvent molecules omitted for clarity)

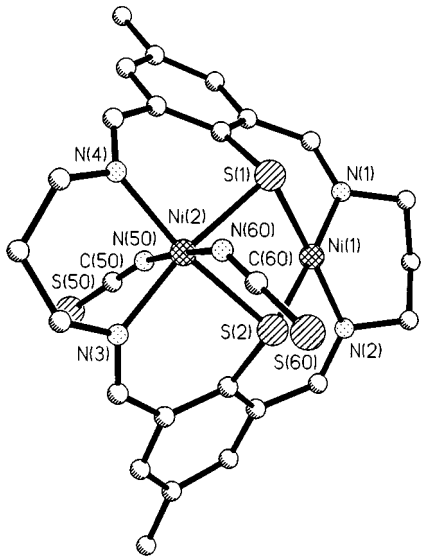


Figure 5. Perspective view of $[Ni_2L2(NCS)_2]$ **5** (hydrogen atoms and solvent molecule omitted for clarity)

The successful formation of **4** prompted us to test whether or not the analogous reaction could be carried out with the less tetrahedrally distorted, macrocyclic complex of the smaller ring $L2^{2-}$, $[Ni_2L2](ClO_4)_2$ **2b**. Red-black crystals of **5** · MeCN suitable for X-ray analysis were obtained, in low yield, from the reaction of **2b** with 2.2 equivalents of NaSCN in MeCN. A similar overall structure to that of **4** is revealed by the structure determination: one nickel atom remains square planar [Ni(1) is 0.003(1) Å out of the N_2S_2 plane] whilst the other is distorted octahedral [Ni(2) is 0.026(1) Å out of the $N(macro)_2S_2$ plane] and coordinated to both thiocyanate ions (Figure 5, Tables 1 and 2). The bond lengths to Ni(1) and Ni(2) are similar to those found in **4** and reflect the respective low spin and high spin configurations of these atoms. The smaller ring size of $L2^{2-}$ is still sufficient to accommodate the high-spin nickel(II) ion. However, there is sufficient ring strain induced by the change in spin state to promote Schiff-base hydrolysis (by traces of moisture) and ring opening, as the major product of the reaction with NaSCN is shown by IR spectroscopy to be a ring opened product (see above).

Comparison of the structure of the perchlorate derivative **2a** with the thiocyanate derivative **5** leads to similar trends to those obtained from the comparison of the corresponding $L1^{2-}$ analogues **1a** and **4**. Complex **5** is folded with the $N(macro)_2S_2$ planes intersecting at 142.21(6)° and the two phenyl ring planes, almost at right angles to one another, intersecting at 91.17(9)° [av. 146.4(2) and 102.4(4)° respectively in **2a**]. Slightly larger S···S [av. 2.839(5) in **2a** vs. 3.011(1) Å in **5**] and Ni···Ni separations [av. 3.146(2) in **2a** vs. 3.244(1) Å in **5**] are observed in **5**. Again the coordinated thiocyanate ions block all but one set of π-π interactions.

Complexes with adjacent square planar and octahedral nickel(II) ions have been reported previously.[14,18,35,37–39] Of these one of the most closely related examples is **A1**, a dinickel(II) complex derived from a "three-quarter" amine thiolate ligand (Figure 6).[39] In this complex both of the thiocyanate ions coordinated to the nickel ion which was bound to the secondary, as opposed to the primary, amine groups due to the slightly weaker field strength exerted by them. However, in complexes **4** and **5** the differing nickel(II) geometries have resulted despite the provision of potentially identical metal ion binding sites and this situation is much less common. We have observed this situation before for the macrocyclic thiolate complex **A2** (Figure 6), where the macrocycle provided potentially identical N(imine)N(amine)SO donor sites,[14][18] but the isolation of complexes **4** and **5** is an important extension of the series of dinickel thiolate complexes produced to date[11,14,16,18–21,25,39–43] as, until recently, it was thought that the $N(imine)_2S_2$ systems exclusively formed square planar complexes.

Table 1. Selected bond lengths (Å) in $[Ni_2L1](ClO_4)_2(MeCN)\cdot 1/4\,H_2O$ **1a**, $[Ni_2L1(NCS)_2]$ **4**, and $[Ni_2L2(NCS)_2]$ **5**

Bond lengths	**1a**	**4**	**5**
Ni(1)−N(1)	1.929(10)	1.944(3)	1.924(2)
Ni(1)−N(2)	1.928(10)	1.926(3)	1.935(2)
Ni(1)−S(1)	2.157(4)	2.1732(12)	2.2009(10)
Ni(1)−S(2)	2.152(3)	2.1987(12)	2.1836(10)
Ni(2)−N(3)	1.920(10)	2.073(3)	2.037(2)
Ni(2)−N(4)	1.939(9)	2.078(3)	2.024(2)
Ni(2)−S(1)	2.147(3)	2.3849(13)	2.3738(10)
Ni(2)−S(2)	2.167(3)	2.4080(12)	2.3608(11)
Ni(2)···O(11)	3.340(9)	−	−
Ni(2)−N(50)	−	2.071(4)	2.096(3)
Ni(2)−N(60)	−	2.065(4)	2.112(3)
Ni(1)···Ni(2)	3.115(2)	3.2935(8)	3.2437(11)
S(1)···S(2)	2.828(4)	2.979(2)	3.0112(12)

Table 2. Selected bond angles (°) in $[Ni_2L1](ClO_4)_2(MeCN)\cdot 1/4\ H_2O$ **1a**, $[Ni_2L1(NCS)_2]$ **4**, and $[Ni_2L2(NCS)_2]$ **5**

Bond angles	**1a**	**4**	**5**
N(1)−Ni(1)−N(2)	96.6(4)	94.97(14)	94.44(10)
N(1)−Ni(1)−S(2)	165.5(4)	167.23(11)	176.11(8)
N(1)−Ni(1)−S(1)	88.8(3)	94.28(10)	89.36(7)
S(2)−Ni(1)−N(2)	95.0(3)	86.80(11)	89.44(7)
S(2)−Ni(1)−S(1)	82.04(13)	85.90(4)	86.75(3)
N(2)−Ni(1)−S(1)	165.3(3)	167.88(11)	176.16(7)
N(3)−Ni(2)−N(4)	97.1(4)	106.46(13)	99.08(9)
N(3)−Ni(2)−S(2)	89.0(3)	87.71(9)	90.84(7)
N(4)−Ni(2)−S(2)	165.4(3)	165.51(10)	170.03(7)
N(3)−Ni(2)−S(1)	165.6(3)	164.30(9)	169.66(7)
N(4)−Ni(2)−S(1)	94.4(3)	89.12(10)	91.07(7)
S(2)−Ni(2)−S(1)	81.91(13)	76.85(4)	78.99(3)
N(60)−Ni(2)−N(50)	−	177.75(15)	175.80(9)
N(60)−Ni(2)−N(3)	−	90.81(13)	89.54(10)
N(50)−Ni(2)−N(3)	−	88.03(13)	86.30(9)
N(60)−Ni(2)−N(4)	−	88.58(13)	92.61(10)
N(50)−Ni(2)−N(4)	−	89.91(13)	88.54(9)
N(60)−Ni(2)−S(1)	−	91.51(11)	91.99(7)
N(50)−Ni(2)−S(1)	−	90.13(10)	92.02(7)
N(60)−Ni(2)−S(2)	−	88.15(10)	88.48(7)
N(50)−Ni(2)−S(2)	−	93.73(10)	91.08(7)
Ni(1)−S(1)−Ni(2)	92.73(13)	92.41(4)	90.23(4)
C(1)−S(1)−Ni(1)	97.7(4)	109.32(14)	102.77(10)
C(1)−S(1)−Ni(2)	107.3(4)	102.39(15)	98.68(10)
C(14/13)−S(2)−Ni(1)	105.7(4)	98.25(14)	104.23(10)
C(14/13)−S(2)−Ni(2)	97.4(4)	100.40(14)	101.20(10)
Ni(1)−S(2)−Ni(2)	92.32(13)	91.16(4)	91.00(3)

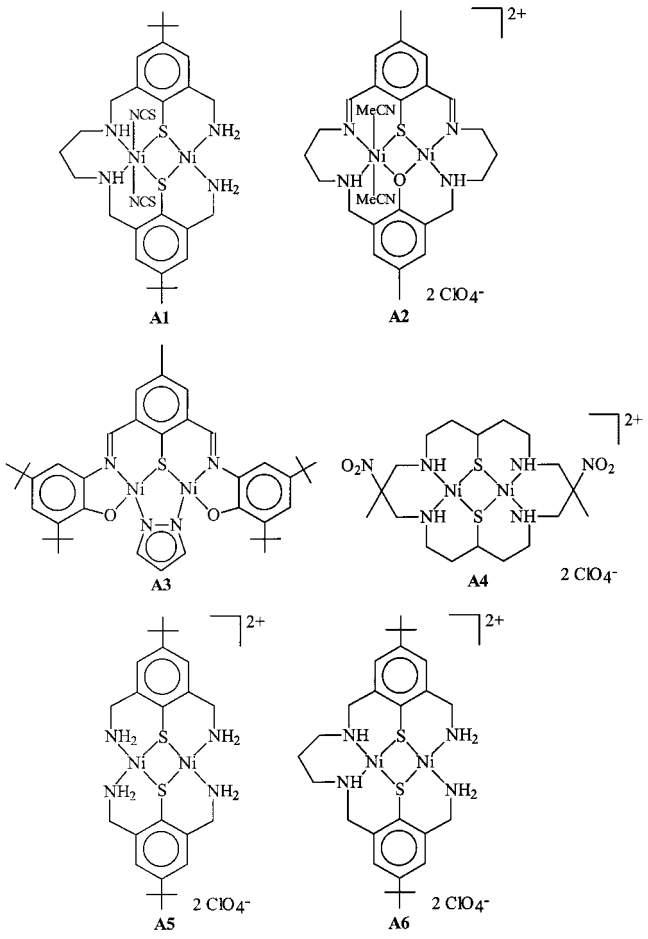


Figure 6. Dinickel(II) thiolate complexes **A1**−**A6**

NMR Studies

In the non-coordinating solvent $[D_3]MeNO_2$ **1**−**3** all gave easily assigned diamagnetic ^1H- and ^{13}C-NMR spectra. In coordinating solvents such as $[D_3]MeCN$ and $[D_7]DMF$ complexes **1**−**3** have some tendency to coordinate solvent molecules in the otherwise vacant axial sites leading to traces of paramagnetic species in solution. The ^1H-NMR spectrum obtained at elevated temperatures for **2** in $[D_3]MeCN$ could be assigned but that obtained for **1** was too broad over the temperature range studied (253 to 333 K). In contrast, **3**, the amine analogue of **2**, gave a reasonably sharp ^1H-NMR spectrum at ambient temperature showing that this complex remains close to diamagnetic even in acetonitrile solution. The amine proton signal for complex **3** has now been correctly identified[19] via a NH/ND exchange experiment: a few drops of a $[D_3]MeOD/D_2O$ (95:5) mixture was added to a solution of **3** in $[D_3]MeNO_2$ which caused the signal at 3.58 ppm to disappear over a period of days. In $[D_7]DMF$ no ^1H-NMR spectrum was obtained for complexes **1** and **2** whilst complex **3** gave a very broad spectrum. Consistent with this, an axial interaction with a DMF molecule was observed in the crystal structure of the hexafluorophosphate salt of **2**.[20]

The NMR data, in both $[D_3]MeNO_2$ (**1**−**3**) and $[D_3]MeCN$ (**2**, **3**), indicate that the macrocycles remain intact in these solvents.

Cyclic Voltammetry Studies

Of particular interest in this series of compounds are the effects of (a) increasing the size of the macrocyclic cavity, $L1^{2-}$ vs. $L2^{2-}$, (b) changing the nature of the nitrogen donors, from imine groups in **2** to amine groups in **3**,[19] and (c) changing from thiophenolate donors in **2** to phenolate donors in **6**. Representative cyclic voltammograms for compounds **1**−**3** and **6** in MeCN are presented in Figure 7 and the potentials of the four well-separated (> 0.2 V) one-electron redox processes for **1**−**3** are provided in Table 3. The three well-separated (> 0.2 V) one-electron redox processes for **6** occur at -1.40^{I}, $+1.05^{QR}$, and $+1.26^{I}$ V (referenced to 0.01 M $AgNO_3/Ag$ and recorded at 200 mV s^{-1}). The redox processes are considered to be predominantly metal centred (vide infra) and the following discussion is made in light of this assignment.

Intriguingly the $[Ni_2Lj]^{2+/3+}$ and $[Ni_2Lj]^{3+/4+}$ potentials ($j = 1-3$) show relatively small shifts upon quite large changes in the ligation of the nickel centres. The peak separation, ΔE, for the first process in all three systems was comparable to that of ferrocene indicating that this is a reversible process in each case, a conclusion that is further supported by analysis of the ratio of peak currents and scan rate dependence.[44]Like the $[Ni_2Lj]^{2+/3+}$ process the position of the $[Ni_2Lj]^{3+/4+}$ process shifts very little from $j = 1$ to $j = 3$. However in each case the peak separation for this second process is larger than that observed for the first process, and the ratio of the peak currents differs significantly from unity, indicating that the $[Ni_2Lj]^{3+/4+}$ couple is a

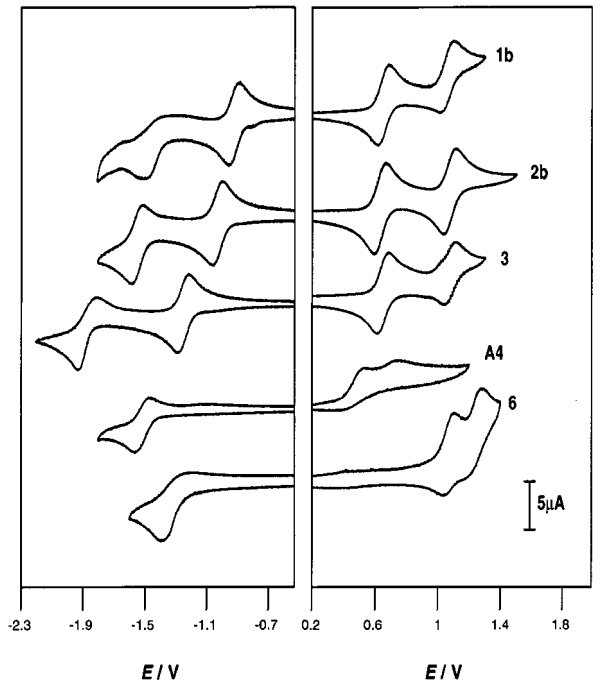


Figure 7. Cyclic voltammograms of complexes (listed from top to bottom) **1b**, **2b**, **3**, **A4**, and **6** in MeCN (200 mV s^{-1}, 0.1 M NEt_4ClO_4, platinum electrode, vs. 0.01M $AgNO_3$/Ag)

Table 3. Potentials ($E_{1/2}$, V) and E (V) for the dinickel complexes $[Ni_2Lj]^{2+}$, (j = 1−3,′). All data were referenced to 0.01 M $AgNO_3$/Ag and recorded at 200 mV s^{-1}. In all cases the Fc/Fc^+ couple, added as an internal reference, occurred at +0.13 V with ΔE = 0.07 V

Complex	$[Ni_2Lj]^{0/+}$	$[Ni_2Lj]^{+/2+}$	$[Ni_2Lj]^{2+/3+}$	$[Ni_2Lj]^{3+/4+}$
1b[a]	−1.45 (0.16)^{I}	−0.92 (0.07)^{R}	+0.64 (0.06)^{R}	+1.05 (0.08)^{QR}
2b[a]	−1.46 (0.07)^{R}	−1.01 (0.06)^{R}	+0.63 (0.08)^{R}	+1.07 (0.08)^{QR}
3[a]	−1.86 (0.10)^{QR}	−1.18 (0.08)^{R}	+0.69 (0.08)^{R}	+1.10 (0.08)^{QR}
1b[b]	−1.49 (0.09)^{QR}	−0.95 (0.09)^{R}	+0.50^{I}	–
2b[b]	−1.49 (0.07)^{R}	−1.03 (0.07)^{R}	+0.40 (0.08)^{R}	+0.82 (0.10)^{I}
3[b]	−1.86 (0.09)^{QR}	−1.21 (0.08)^{QR}	+0.41 (0.11)^{QR}	+0.61^{I}
2b[c]	−1.42^{I}	−1.10^{I}	–	–
6[a]	–	−1.40^{I}	+1.05 (0.10)^{QR}	+1.26^{I}

[a] Solvent = MeCN, [b] solvent = DMF, [c] solvent = $MeNO_2$. ^{R} reversible, ^{QR} quasireversible, ^{I} irreversible (hence in this case E_{pc} or E_{pa} is quoted not $E_{1/2}$); these assignments were made on the basis of peak separation ΔE (cf. ferrocene), analysis of the ratio of peak currents and scan rate dependence of $E_{1/2}$.[44] Electron counts (in MeCN): **1b** $[Ni_2L1]^{2+} \rightarrow [Ni_2L1]^{+}$ 0.87 e-equivalent; **2b** $[Ni_2L2]^{2+} \rightarrow [Ni_2L2]^{3+}$ 0.95 e-equivalent and $[Ni_2L2]^{3+} \rightarrow [Ni_2L2]^{4+}$ 0.88 e-equivalent; **3** $[Ni_2L3]^{2+} \rightarrow [Ni_2L3]^{3+}$ 0.98 e-equivalent.

quasi-reversible process in all three cases.[44] Thiolate donors are known to stabilise high metal ion oxidation states[45] so the fact that the two one-electron oxidation processes observed for the phenolate analogue, complex **6**, occur at much more positive potentials is consistent with expectations.[46−48] Changes to the ligand, either by increasing the macrocyclic cavity size or by changing from imines to amines, usually has a much larger effect on the potentials than is the case here.[49][50]

In contrast, the peak positions for the $[Ni_2Lj]^{2+/+}$ and $[Ni_2Lj]^{+/0}$ processes (j = 1−3) are very sensitive to the changes in the macrocyclic ligand. The $[Ni_2Lj]^{2+/+}$ processes are reversible for all three complexes **1**−**3**. The $[Ni_2Lj]^{2+/+}$ process occurs at −1.01 V for $[Ni_2L2]^{2+}$ while the complex with the larger macrocyclic cavity, $[Ni_2L1]^{2+}$, is easier to reduce, by 90 mV, and the complex of the tetra-amine macrocycle, $[Ni_2L3]^{2+}$, is harder to reduce, by 170 mV. Only a single one-electron irreversible reduction process is observed for the phenolate analogue, complex **6**, and it occurs at a significantly more negative potential, as is expected[45] (although not *always* observed)[11] due to the presence of the harder phenolate donors. In only one of the three systems was the $[Ni_2Lj]^{+/0}$ process truly reversible, namely the $[Ni_2L2]^{+/0}$ couple. The $[Ni_2L1]^{+/0}$ process is irreversible whilst the $[Ni_2L3]^{+/0}$ process is quasi-reversible. These $[Ni_2Lj]^{+/0}$ processes shift in the same direction as the shifts observed for the $[Ni_2Lj]^{2+/+}$ processes. The $[Ni_2L2]^{+/0}$ and $[Ni_2L1]^{+/0}$ processes occur at a similar potentials (−1.46 and −1.45 V, respectively) whereas the $[Ni_2L3]^{+/0}$ process is 370 mV more negative {ie. $[Ni_2L3]^{+}$ is harder to reduce}. No second reduction process was observed for **6**.

Overall the $[Ni_2Lj]^{2+/+}$ and $[Ni_2Lj]^{+/0}$ potentials for the complexes of the tetra-imine-containing ligands $L1^{2-}$ and $L2^{2-}$, **1** and **2**, are significantly less negative than those for the complex of the tetra-amine-containing ligand $L3^{2-}$, **3**. The imine-containing ligands stabilise the reduced metal centre(s) more effectively than the amine-containing ligand (which has no imine π* orbital).[49][50] It had been hoped that conversion of the hydrolytically unstable imine bonds to relatively stable amine bonds would make the reductive electrochemistry more reversible as decomposition via, for instance, water attack of the adjacent imine bond would no longer be possible. However these redox processes are actually less reversible than those of the tetra-imine analogue **2**.

A study of a large number of mono nickel(II) tetra-aza macrocycles has shown that there is a correlation between the size of the macrocycle cavity and the potentials, with the larger cavities stabilising the nickel(I) oxidation state.[49] This has been interpreted as indicating that the d^9 nickel(I) ion is larger than the d^8 nickel(II) ion and is therefore better accommodated by a larger ring, resulting in a less negative potential for the $Ni^{2+/+}$ process.[49][51] Our results are consistent with this correlation.

As the NMR studies (above) indicated that some solvent coordination is occurring in MeCN and DMF solutions but not in $MeNO_2$, cyclic voltammograms were also run in DMF and $MeNO_2$. The results for **2** are shown in Figure 8 and Table 3. In DMF and MeCN, the $[Ni_2L2]^{2+/+}$ and $[Ni_2L2]^{+/0}$ processes are relatively insensitive to the change in solvent indicating that the formally $Ni^{II}Ni^{I}$ and Ni^{I}_2 species coordinate solvent molecules only weakly, if at all. However, in DMF, the $[Ni_2L2]^{3+/4+}$ process is a substantial 230 mV less positive {$[Ni_2L2]^{3+}$ is easier to oxidise in DMF than in MeCN}. This shift is to be expected as the Ni^{III} ion will be stabilised by axial coordination of solvent molecules,[11][51] and DMF has a greater tendency to bind axially than MeCN.[48] The results obtained in the non-coordi-

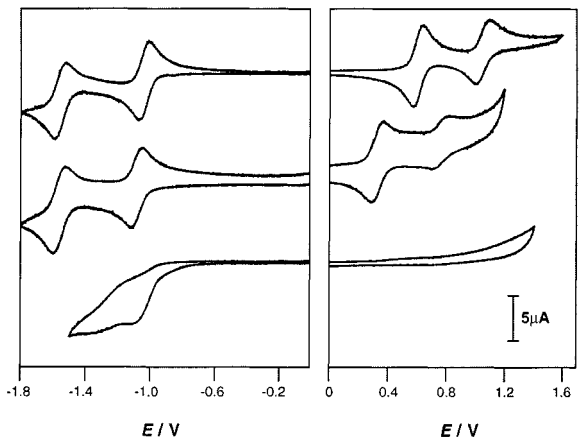


Figure 8. Solvent dependence of cyclic voltammograms of **2b**: comparison of cyclic voltammograms obtained in MeCN (top), DMF (middle), and $MeNO_2$ (bottom) (200 mV s^{-1}, 0.1 M NEt_4ClO_4, platinum electrode, vs. 0.01M $AgNO_3$/Ag)

nating solvent, $MeNO_2$ (Figure 8, Table 3), are consistent with this explanation. No oxidation processes are observed for **2** within the $MeNO_2$ solvent window: two reduction processes are observed but they are irreversible so a meaningful comparison of the potentials is not possible. These observations are consistent with the processes being largely metal centred.

The results of this solvent dependence study are also consistent with those obtained for an acyclic dinickel thiophenolate complex **A3** (Figure 6):[11] the reduction processes varied only slightly with solvent (CH_2Cl_2, acetone, THF, PrCN, and DMF) indicating that there was little or no solvent coordination to the nickel(I) centres whereas the first oxidation process was less positive in DMF than in the other solvents investigated [ie. CH_2Cl_2 (where the processes became reversible), acetone, and THF], which was attributed to solvent coordination to the nickel(III) centres.

As expected, the cyclic voltammetry results for complex **2b** in MeCN are consistent within experimental error with those reported for the perchlorate salt **2a**[16,52] and for the hexafluorophosphate salt of **2**.[22] To date no electrochemical properties have been reported for the other Schiff base macrocyclic di- and tetra-nickel(II) complexes derived from the 2,6-diformylthiophenolate head unit.[23][24] The cyclic voltammogram we obtained in MeCN for the dark orange dinickel(II) aliphatic-thiolate macrocyclic complex **A4** (Figure 6) is shown for comparison in Figure 7.[25] The relatively electron-rich aliphatic-thiolate donors stabilise Ni^{III} and destabilise Ni^{I} relative to the aromatic-thiolate donors in Lj^{2-}, $j = 1-3$. Changing the ligation around the nickel(II) ions from two separate tridentate ligands, complex **A5**, to one "three-quarter" hexadentate ligand, complex **A6** (Figure 6), results in improved reversibility of the two one-electron, metal centred, reductions in DMF.[39] As expected, on completely encircling the nickel ions with a hexadentate *macrocyclic* ligand, as in complexes **1**–**3**, the reversibility improves still further.

In summary, in these three macrocyclic dinickel(II) thiolate systems, $[Ni_2Lj]^{2+}$ where $j = 1-3$, the two one-electron oxidation processes are relatively insensitive to the changes made to the ligand but are sensitive to changes in solvent (MeCN vs. DMF vs. $MeNO_2$). As we believe the oxidation processes, $[Ni_2Lj]^{2+/3+}$ and $[Ni_2Lj]^{3+/4+}$, are primarily metal centered (vide infra) it seems likely that the relatively invariant value of the potentials for $j = 1-3$ for a particular solvent is largely due to the consistent supply of an axial donor (either N of MeCN or O of DMF). In contrast the $[Ni_2Lj]^{2+/+}$ and $[Ni_2Lj]^{+/0}$ processes, which are also believed to be primarily metal centred, are significantly influenced by changes to the ligand but are relatively insensitive to changes in solvent (MeCN vs. DMF). As expected, a change in the nitrogen donors from imines to amines made the potentials more negative, while increasing the size of the macrocyclic cavity made the potentials slightly less negative. The formally nickel(I) centres are expected to be square planar hence the lack of solvent dependence.

EPR Spectra

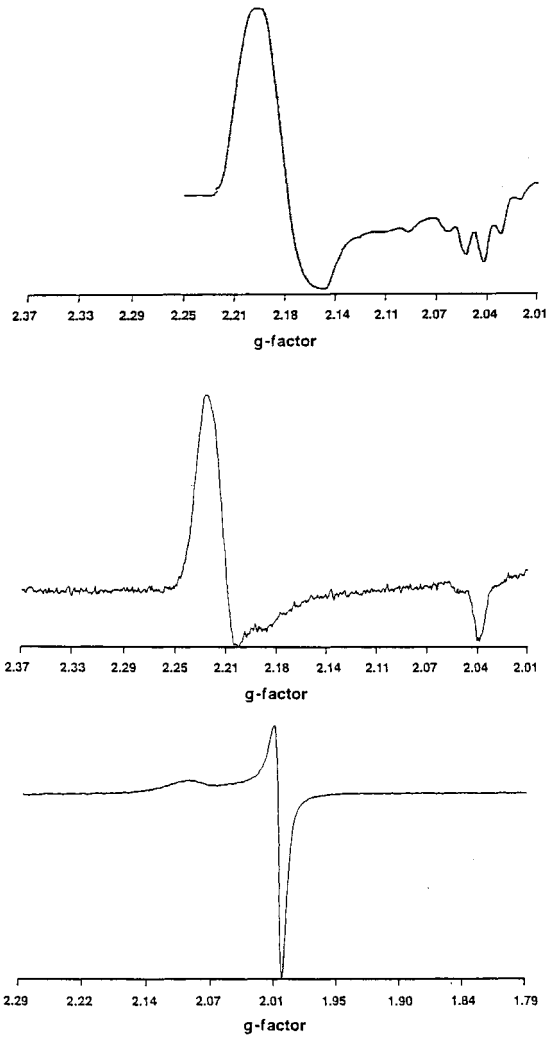


Figure 9. EPR spectra of 10^{-4} mol L^{-1} chemically generated $[Ni_2L2]^{3+}$ (top, 10 mW, 9.142 GHz), electrochemically generated $[Ni_2L2]^{3+}$ (middle, 0.816 mW, 9.284 GHz), and $[Ni_2L3]^{+}$ (bottom, 0.766 mW, 9.284 GHz), in MeCN at 77 K

Due to the instability of the majority of the redox products on a time scale of minutes (cf. the cyclic voltammetry time scale) EPR spectroscopic studies were limited to the oxidation products (both electrochemically and chemically generated) of complexes **2** and **3**, and the reduction products (electrochemically generated) of complexes **1** and **3**.

The EPR spectrum of the purple solution obtained by one electron electrochemical oxidation of **2b** at 1.0 V vs Ag wire is shown in Figure 9. The spectrum is characteristic of the presence of an axial Ni^{III} centre, with $g_{||} = 2.04$ and $g_{\perp} = 2.22$, indicating the presence of a mixed valent Ni^{II}-Ni^{III} centre.[51] Similar EPR behaviour was observed for the purple, electrochemically generated $[Ni_2L3]^{3+}$ species.

Chemical oxidation of an MeCN solution of **2a** with aqueous Co^{III} in 1 M $HClO_4$ yielded a purple solution which again gave an EPR spectrum typical of an axial Ni^{III} centre, with $g_{||} = 2.04$ and $g_{\perp} = 2.17$. The $g_{||}$ feature shows hyperfine splitting associated with two axially coordinated MeCN solvent molecules.

The reduction products of complex **2** were not stable enough to be studied by EPR, however, those of complexes **1** and **3** were investigated (Figure 9). The orange-brown one-electron reduction products of **1** and **3** showed very similar EPR behaviour consistent with a metal-centred reduction to a d^9 Ni^{I} centre ($g_{||} = 2.11$, $g_{\perp} = 2.00$).[51]

These results are consistent with both the first one-electron oxidations and reductions being largely metal based with little delocalisation onto the ligand. Importantly there is no evidence for the presence of organic radicals. The nature of the formally Ni^{I}_2 and Ni^{III}_2 species could not be established due to the low stability of these products.

Electronic Spectra

In $MeNO_2$, MeCN, and DMF the red dinickel(II) complexes **1**−**3** all have an absorption band in the range 490−520 nm (ε = 900−1800 L mol^{-1} cm^{-1}) which is assigned as a ligand-to-metal charge transfer (LMCT) transition, S$\pi \rightarrow$ Ni.[5][39] This band occurs at slightly higher energy in the case of the amine complex **3** (490 nm) than in the imine analogue **2** (510 nm) leading to the former being somewhat more red in colour than the latter. In DMF, in addition to the 490−520 nm band, some further low intensity bands/shoulders are observed at longer wavelengths which are presumably due to axial solvent coordination to least one of the two nickel atoms.[39] Only in the case of complexes **1** and **3** can distinct bands be clearly identified: the lowest energy band, $^3A_{2g} \rightarrow {}^3T_{2g}$, occurs at 990 nm (80 L mol^{-1} cm^{-1}) for **3** and at 860 nm (25 L mol^{-1} cm^{-1}) for **1**. This corresponds to a smaller Δ_O for **3** (10,101 cm^{-1}) than for **1** (11,630 cm^{-1}), consistent with the NMR finding that **3** is less able to bind solvent molecules axially than **1**. In all cases further bands are observed at higher energy, below 380 nm, due to intraligand transitions. Over a period of weeks both the $MeNO_2$ and DMF solutions of **1**−**3** slowly decolorise whereas the acetonitrile solutions remain red.

The instability of the majority of the redox products on a time scale of minutes limited the UV/Vis studies to the oxidation products (both electrochemically and chemically generated) of complex **2** and the one-electron reduction product (electrochemically generated) of complex **1**.

Complex **1b** was electrochemically reduced in MeCN at −1.10 V vs. 0.01 M $AgNO_3$/Ag (87% of one-electron equivalent) resulting in an orange solution: the 510 nm band diminishes in absorbance and an isobestic point is observed at 495 nm (Figure 10). This mixed valent complex, $[Ni_2L1]^+$, is reasonably stable at ambient temperature under argon but attempts to further reduce it by one electron were unsuccessful.

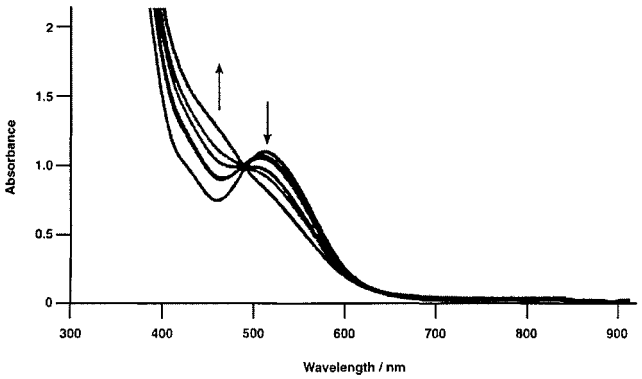


Figure 10. Electrochemical one electron reduction of **1b** in MeCN followed by UV/Vis spectroscopy

Controlled potential electrolysis of **2b** in MeCN at +0.90 V vs. 0.01 M $AgNO_3$/Ag removes one-electron (97%) giving a purplish-coloured solution: a new band develops at approximately 870 nm (isobestic point at ca. 390 nm). This mixed valent complex, $[Ni_2L2]^{3+}$, is reasonably stable at ambient temperature under argon. When a second electron is removed from this sample, by holding the potential at +1.40 V vs. 0.01 M $AgNO_3$/Ag, a dark green solution results, and the 870 nm band bleaches out. Nickel(III) complexes are typically green in colour.[53] Removal of the second electron to form $[Ni_2L2]^{4+}$ is nontrivial due to the low stability of this fully oxidised species.

Complex **2a** was also chemically oxidised by titrating with CAN [ammonium cerium(IV) nitrate]. The titration with the first equivalent of CAN (Figure 11) resulted in a new absorption band at 870 nm. When the titration was continued with the second equivalent of CAN (Figure 11) a dark green solution resulted. During this second stage of the titration the feature at 870 nm decreased in absorbance, as did all of the other bands. Due to the instability of this fully oxidised species it is not possible to determine whether the 870 nm band (11,494 cm^{-1}, ε = 1,320 L mol cm^{-1}) observed for the mixed valent $[Ni_2L1]^{3+}$ complex is due to a ligand to nickel(III) charge transfer transition or to a Class II intervalence charge transfer transition (the bandwidth at half height is approximately 5400 cm^{-1} which is greater than the calculated value of 5153 cm^{-1}).[54]

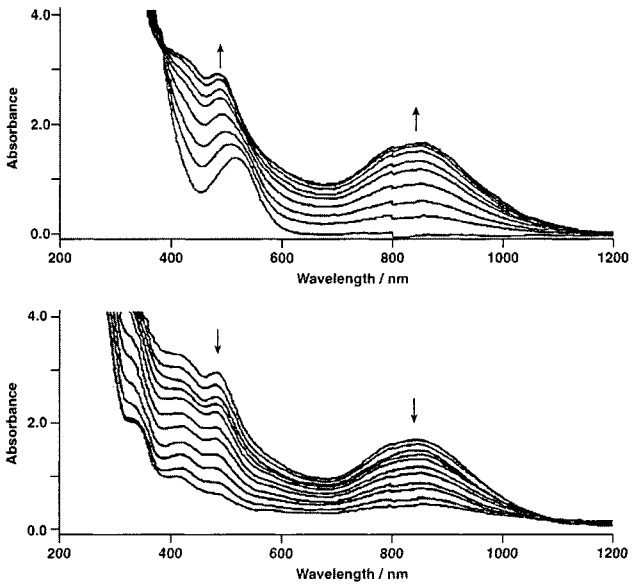


Figure 11. Titration of a 2.7 mL aliquot of a 6.34×10^{-4} mol L^{-1} MeCN solution of **2a**, firstly with one (top) and then with a second (bottom) equivalent of CAN (0.0785 mol L^{-1}, aliquots of 2 μL per scan)

Conclusion

The nickel coordination chemistry of $L1^{2-}$ and $L2^{2-}$ has produced a range of attractive and interesting products, including rare examples of adjacent N_2S_2 and N_4S_2 nickel(II) ions despite the provision of potentially equivalent binding sites. The aim of increasing the degree of tetrahedral distortion over that found in the macrocycle $L2^{2-}$ by increasing the macrocycle cavity size, despite the strong preference of the nickel ions to be square planar in this donor environment, has been achieved with $L1^{2-}$. This increased tetrahedral distortion confers a greater tendency for dinickel(II) complexes of $L1^{2-}$ to bind molecules axially. The ability to manipulate and control the environments of the nickel(II) ions in this way is important with respect to developing model complexes suitable for binding/reactivity studies, and is facilitated by the wide range of geometries which the bridging thiolate donors can adopt.

Experimental Section

Measurements were carried out as previously described,[16] with the exception of most of the NMR spectra which, where noted, were obtained on a Varian 500 MHz spectrometer. Magnetic moments were obtained on a Johnson Matthey Alfa Products Mk1 magnetic susceptibility balance. Electrochemical experiments were performed using a PAR 273A potentiostat/galvinostat in a 3-electrode cell (design by Dr. E. Bothe and Prof. K. Wieghardt, MPI für Strahlenchemie) using Pt working and counter electrodes and a $Ag/AgNO_3$ reference electrode. *tert*-Butyl ammonium perchlorate (recrystallised twice from H_2O and dried in vacuo at room temperature) was used as the supporting electrolyte. All solutions were degassed thoroughly with argon and an argon atmosphere was maintained during the experiments. (*S*)-(2,6-Diformyl-4-methylphenyl)dimethylthiocarbamate[16] and $[Ni_2L'Cl_2]$[27] were prepared according to the literature procedures. Isopropanol (IPA) was stored over CaO, then decanted and distilled. HPLC grade MeCN and DMF were distilled from CaH_2 (DMF in vacuo) immediately before use. Reactions were carried out using Schlenk techniques.

CAUTION: *Perchlorate salts are potentially explosive and should therefore be handled with appropriate care.*

$[Ni_2L1](ClO_4)_2 \cdot MeCN \cdot 1/4\ H_2O$ (1a): (*S*)-(2,6-Diformyl-4-methylphenyl)dimethylthiocarbamate (0.251 g, 1.00 mmol) in IPA (80 cm^3) was brought to reflux. NaOH (0.040 g, 1.00 mmol) was added, the resulting orange solution refluxed for 5 hours, then $Ni(ClO_4)_2 \cdot 6\ H_2O$ (0.365 g, 1.00 mmol) in IPA (20 cm^3) and 1,4-diaminobutane (0.088 g, 1.00 mmol) in IPA (20 cm^3) were added. After 4 hours the mixture was filtered hot to obtain **1a** as an impure red-brown solid. Repeated fractional recrystallisation from MeCN by vapour diffusion of diethyl ether gave $[Ni_2L1](ClO_4)_2(MeCN) \cdot 1/4\ H_2O$ **1a** as large red crystals suitable for X-ray structural analysis. The sample was washed with H_2O to give analytically pure **1a** (0.170 g, 42%). (Found: C 40.6, H 4.2, N 9.0, S 8.0, Cl 8.6. $C_{28}H_{33.5}Cl_2N_5Ni_2O_{8.25}S_2$ requires C 40.8, H 4.1, N 8.5, S 7.8, Cl 8.6%); λ_{max}/nm (MeCN) (ε/L mol^{-1} cm^{-1}) 510 (1 800); $\tilde{\nu}/cm^{-1}$ (KBr disk, inter alia) 1624, 1090, 623; Λ_m(MeCN) = 268 mol^{-1} cm^2 Ω^{-1} (c.f. 220−300 mol^{-1} cm^2 Ω^{-1} for a 2:1 electrolyte in MeCN);[55] FAB mass spectrum *m*/*z* 578 $[Ni_2L1]^+$.

$[Ni_2L1](CF_3SO_3)_2 \cdot H_2O$ (1b): The reaction was performed as for $[Ni_2L1](ClO_4)_2$ but nickel(II) trifluoromethansulfonate hexahydrate (0.465 g, 1.00 mmol) was used instead of nickel(II) perchlorate hexahydrate. In contrast to $[Ni_2L1](ClO_4)_2$ the reaction solution became clear red-brown on addition of the amine and after two hours at reflux the solution was reduced in volume in vacuo to ca. 30 cm^3. From this solution red single crystals of $[Ni_2L1](CF_3SO_3)_2 \cdot H_2O$ were grown by vapour diffusion of diethyl ether (0.171 g, 38%). (Found C 37.7, H 4.0, N 6.1, S 13.9. $C_{28}H_{32}F_6N_4Ni_2O_7S_4$ requires C 37.5, H 3.6, N 6.3, S 14.3%); $\tilde{\nu}/cm^{-1}$ (KBr disk, inter alia) 3526, 3462, 1623, 1614, 1257, 1026, 636; δ_H (500 MHz, CD_3NO_2, 298 K): 8.03 (4 H, s), 7.60 (4 H, s), 3.97, 3.65 (4 H, t; 4 H, d), 2.39 (6 H, s), 3.45, 2.25 (4 H, d; 4 H,q) δ_C (125 MHz, CD_3NO_2, 298 K): 169.4, 141.8, 140.5, 136.2, 121.7, 61.7, 27.5, 20.9; λ_{max}/nm (MeCN) (ε/L mol^{-1} cm^{-1}) 510 (1800), ($MeNO_2$) 515 (1410), (DMF) 520 (900), 860 (25); Λ_m(MeCN) = 280 mol^{-1} cm^2 Ω^{-1} (c.f. 220−300 mol^{-1} cm^2 Ω^{-1} for a 2:1 electrolyte in MeCN);[55] FAB mass spectrum *m*/*z* 578 $[Ni_2L1]^+$; μ = 0.0 BM.

$[Ni_2L2](ClO_4)_2$ (2a): A slight modification of the synthesis reported previously:[16] (*S*)-(2,6-Diformyl-4-methylphenyl)dimethylthiocarbamate (0.251 g, 1.00 mmol) in IPA (80 cm^3) was brought to reflux. NaOH (0.040 g, 1.00 mmol) was added, the resulting orange solution refluxed for 5 hours. Nickel(II) perchlorate hexahydrate (0.365 g, 1.00 mmol) in IPA (20 cm^3) was then added. To the dark red-brown mixture was added 1,3-diaminopropane (0.074 g, 1.00 mmol) in IPA (20 cm^3). The mixture was refluxed for five hours and then filtered whilst hot. The resulting red-brown solid was repeatedly recrystallised from MeCN by vapour diffusion of diethyl ether to remove the brown impurity yielding $[Ni_2L2](ClO_4)_2$ as large red single crystals (0.161 g, 43%). (Found: C 38.4, H 3.7, N 7.4, S 8.0, Cl 9.8. $C_{24}H_{26}Cl_2N_4Ni_2O_8S_2$ requires C 38.4, H 3.5, N 7.5, S 8.5, Cl 9.4%); $\tilde{\nu}/cm^{-1}$ (KBr disk, inter alia) 1615, 1084, 622; δ_H (300 MHz, CD_3CN, 343 K) reference external TMS: 9.48 (4 H, s), 7.54 (4 H, s), (ca. 4.50, ca 4.31) (4 H, t, br; 4 H, t, br), 2.46 (6 H, s), (2.24, 1.64) (2 H, d; 2 H, s). λ_{max}/nm (MeCN) (ε/L mol^{-1} cm^{-1}) 510 (1600), Λ_m(MeCN) = 265 mol^{-1} cm^2 Ω^{-1} (c.f. 220−300 mol^{-1} cm^2 Ω^{-1} for a 2:1 electrolyte in MeCN);[55] FAB mass spectrum *m*/*z* 550 $[Ni_2L2]^+$.

$[Ni_2L2](CF_3SO_3)_2$ (2b): The reaction was performed as for $[Ni_2L2](ClO_4)_2$ but nickel(II) trifluoromethansulfonate hexahydrate (0.465 g, 1.00 mmol) was used instead of nickel(II) perchlorate hexahydrate. In contrast to $[Ni_2L2](ClO_4)_2$ the reaction solution became clear red-brown on addition of the amine. After two hours at reflux the solution was reduced in volume in vacuo to ca. 5 cm^3, 10 cm^3 of MeCN added and red crystals of $[Ni_2L2](CF_3SO_3)_2$ obtained by vapour diffusion of diethyl ether (0.14 g, 33%). (Found: C 36.4, H 3.5, N 6.3, S 14.8. $C_{26}H_{26}F_6N_4Ni_2O_6S_4$ requires C 36.7, H 3.1, N 6.6, S 15.1%); $\tilde{\nu}/cm^{-1}$ (KBr disk, inter alia) 1615, 1259, 1026, 637; δ_H (500 MHz, CD_3NO_2, 298 K): 7.93 (4 H, s), 7.56 (4 H, s), 4.38, 3.80 (4 H, t,; 4 H, d), 2.37 (6 H, s), 2.30, 1.60 (2 H, d; 2 H,q) δ_C (125 MHz, CD_3NO_2, 298 K): 167.9, 141.6, 140.1, 135.9, 123.0, 63.1, 29.3, 20.8. λ_{max}/nm (MeCN) (ε/L mol^{-1} cm^{-1}) 510 (1500), ($MeNO_2$) 510 (1480), (DMF) 510 (1040); Λ_m(MeCN) = 265 mol^{-1} cm^2 Ω^{-1} (c.f. 220−300 mol^{-1} cm^2 Ω^{-1} for a 2:1 electrolyte in MeCN);[55] FAB mass spectrum *m*/*z* 550 $[Ni_2L2]^+$; μ = 0.0 BM.

$[Ni_2L3](ClO_4)_2$ (3): To an ice-cold, fine particulate suspension of $[Ni_2L2](CF_3SO_3)_2$ **2b** (0.13 g, 0.18 mmol) in methanol (40 cm^3), was added $NaBH_4$ (0.030 g, 0.77 mmol) in water (2 cm^3). The reaction mixture was allowed to warm to room temperature, stirred for one hour and then refluxed for a further two hours. Then 5% $HClO_{4(aq)}$ (20 cm^3) was added and the mixture refluxed for one hour before being filtered whilst hot to remove $[Ni_2L3](ClO_4)_2$ as a red powder. Further crops were obtained by slow evaporation of the reaction filtrate (0.106 g, 80%). (Found C 37.5, H 4.8, N 7.2, S 8.7, Cl 9.3. $C_{24}H_{34}Cl_2N_4Ni_2O_8S_2$ (**3**) requires C 38.0, H 4.5, N 7.4, S 8.5, Cl 9.3%); $\tilde{\nu}/cm^{-1}$ (KBr disk, inter alia) 3220, 1603, 1096, 622; δ_H (500 MHz, CD_3NO_2, 298 K) 7.20 (4 H, s), 3.68 (4 H, d), 3.59 (4 H, d), 3.58 (4 H, s), 2.92 (4 H, td), 2.51 (4 H, dt), 2.25 (6 H, s), 2.02 (2 H, m), 1.85 (2 H, m); δ_C (125 MHz, CD_3NO_2, 298 K) 140.3, 135.6, 134.2, 121.7, 56.2, 50.4, 27.1, 21.1; λ_{max}/nm (MeCN) (ε/L mol^{-1} cm^{-1}) 490 (1500), ($MeNO_2$) 490 (1430), (DMF) 490 (900), 990 (80); Λ_m(MeCN) = 280 mol^{-1} cm^2 Ω^{-1} (c.f. 220−300 mol^{-1} cm^2 Ω^{-1} for a 2:1 electrolyte in MeCN);[55] FAB mass spectrum *m*/*z* 558 $[Ni_2L3]^+$; μ = 0.0 BM.

$[Ni_2L1(NCS)_2]$ (4): Complex **1b** (0.040 g, 0.046 mmol) was dissolved in MeCN (2 cm^3) to give a deep red solution. To this was added, in a dropwise fashion, a colorless solution of sodium thiocyanate (0.0085 g, 0.103 mmol) in MeCN (3 cm^3). Over time the solution became colorless and red-black crystals of **4** developed. These were filtered off and dried under vacuum (0.027 g, 83%). (Found: C 48.2, H 4.5, N 12.4, S 18.1. $C_{28}H_{30}N_6Ni_2S_4$ (**4**) requires C 48.3, H 4.3, N 12.1, S 18.4%); $\tilde{\nu}/cm^{-1}$ (KBr disk, inter alia) 2081, 1628; λ_{max}/nm (MeCN) (ε/L mol^{-1} cm^{-1}) 340 (2960); Λ_m(freshly prepared solution in DMF) = 50 mol^{-1} cm^2 Ω^{-1} (c.f. 65−90 Ω^{-1} mol^{-1} cm^{-1} for a 1:1 electrolyte in DMF);[55] FAB mass spectrum *m*/*z* 636 $[Ni_2(L1)(SCN)]^+$; 578 $[Ni_2(L1)]^+$; μ = 2.8 BM.

$[Ni_2L2(NCS)_2]$ (5): A colourless MeCN solution (4 cm^3) of sodium thiocyanate (0.0128 g, 0.154 mmol) was layered on top of a deep red MeCN solution (1 cm^3) of **2b** (0.060 g, 0.071 mmol). On standing, red-black crystals of **5** formed, along with a brown precipitate, leaving a light yellow solution. The crystals were physically separated from the powder, washed with MeCN and dried in vacuo (0.009 g, 19%). (Found: C 47.2, H 3.6, N 13.0, S 19.7. $C_{26}H_{26}N_6Ni_2S_4$ (**5**) requires C 46.8, H 3.9, N 12.6, S 19.2%); $\tilde{\nu}/cm^{-1}$ (KBr disk, inter alia) 2075, 1621; λ_{max}/nm (MeCN) (ε/L mol^{-1} cm^{-1}) 335 (2820); Λ_m(DMF) = 70 Ω^{-1} mol^{-1} cm^{-1} (c.f. 65−90 Ω^{-1} mol^{-1} cm^{-1} for a 1:1 electrolyte in DMF);[55] FAB mass spectrum *m*/*z* 550 $[Ni_2L2]^+$.

$[Ni_2L'(MeCN)_4](ClO_4)_2$ (6): $[Ni_2L'Cl_2]$ (0.120 g, 0.17 mmol) was dissolved in a 1:1 mixture of MeCN:water (10 cm^3). To this green solution was added $AgClO_4$ (0.072 g, 0.35 mmol) and the resulting off-white precipitate filtered off.[28] Overnight a dark green crystalline solid formed in the filtrate. This was collected and recrystallised from MeCN by vapour diffusion of diethyl ether to give **6** as large dark green blocks (0.115 g, 76%). (Found: C 43.3, H 4.6, N 12.5, $C_{32}H_{38}Cl_2N_8Ni_2O_{10}$ requires C 43.5, H 4.3, N 12.7%); $\tilde{\nu}/cm^{-1}$ (KBr disk, inter alia) 1639, 1083, 625; λ_{max}/nm (MeCN) (ε/L^{-1} mol^{-1} cm^{-1}) 375 (12800); Λ_m(DMF) = 180 mol^{-1} cm^2 Ω^{-1} (c.f. 130−170 Ω^{-1} mol^{-1} cm^{-1} for a 2:1 electrolyte in DMF);[55] FAB mass spectrum *m*/*z* 617 $[Ni_2(L')(ClO_4)]^+$; 518 $[Ni_2L']^+$.

X-ray Crystallography: Data were collected, on **1a** at 153 K with a Siemens P4 four circle diffractometer and on **5** and **6** at 158 K with a Bruker SMART diffractometer, using graphite-monochromated Mo-*K*α radiation (λ = 0.71013 Å). The data were corrected for Lorentz and polarisation effects and empirical absorption corrections were applied. Hydrogen atoms were inserted at calculated positions and rode on the atoms to which they are attached (including isotropic thermal parameters which were equal to 1.2 times the equivalent isotropic displacement parameter for the attached non-hydrogen atom).

Crystal data for **1a** ($C_{28}H_{33.5}Cl_2N_5Ni_2O_{8.25}S_2$): M_r = 412.3, red block, 0.50 × 0.50 × 0.40 mm, triclinic, space group *P*-1, *a* = 18.174(4), *b* = 18.997(9), *c* = 23.121(8) Å, α = 70.56(3), β = 69.58(3), γ = 77.78(2)°, *V* = 7013(4) $Å^3$, *Z* = 8, μ = 1.40 mm^{-1}, ρ_{calc} = 1.562 g cm^{-3}. A total of 18709 reflections were collected in the range 4 < 2θ < 45°, and the 18013 independent reflections were used in the structural analysis after a semi-empirical absorption correction had been applied (T_{min} = 0.41, T_{max} = 0.50). The structure, four independent macrocyclic complexes in the asymmetric unit, was solved by direct methods (SHELXS-86)[56][57] and refined against all F^2 data (SHELXL-93)[58] to *R1* = 0.083 [for 10954 $F > 4\sigma(F)$; *wR2* = 0.239 and GOF = 1.04 for all 18013 F^2; 1370 parameters; all Ni, S/N/alkyl-C atoms of the macrocycles, O/N/Cl of the full occupancy solvents and perchlorates, Cl(8) and Cl(9) of the partial occupancy perchlorates, anisotropic; 2 (of 8) perchlorates and 2 (of 4) acetonitriles disordered; +1.77/−1.11 e$Å^{-3}$].

Crystal data for **4** · 2 MeCN ($C_{32}H_{36}N_8Ni_2S_4$): M_r = 778.4, red-black rectangular plate, 0.80 × 0.20 × 0.03 mm, triclinic, space group *P*-1, *a* = 10.134(2), *b* = 11.273(2), *c* = 16.112(4) Å, α = 83.957(3), β = 82.082(3), γ = 73.049(3)°, *V* = 1739.7(6) $Å^3$, *Z* = 2, μ = 1.36 mm^{-1}, ρ_{calc} = 1.486 g cm^{-3}. A total of 11118 reflections were collected in the range 5 < 2θ < 53°, and the 6468 independent reflections were used in the structural analysis after a semi-empirical absorption correction had been applied (T_{min} = 0.43, T_{max} = 1.00). The structure was solved by direct methods (SHELXS-97)[56][57] and refined against all F^2 data (SHELXL-97)[58] to *R1* = 0.0446 [for 4250 $F > 4\sigma(F)$; *wR2* = 0.1220 and GOF = 0.92 for all 6468 F^2; 419 parameters; all non-hydrogen atoms anisotropic; +0.79/−0.61 e$Å^{-3}$].

Crystal data for **5** · MeCN ($C_{28}H_{29}N_7Ni_2S_4$): M_r = 709.2, red-black rectangular plate, 0.60 × 0.30 × 0.03 mm, monoclinic, space group $P2_1/c$, *a* = 12.466(5), *b* = 14.267(5), *c* = 17.226(6) Å, β = 93.792(5)°, *V* = 3056.9(19) $Å^3$, *Z* = 4, μ = 1.54 mm^{-1}, ρ_{calc} = 1.541 g cm^{-3}. A total of 32103 reflections were collected in the range 5 < 2θ < 53°, and the 6244 independent reflections were used in the structural analysis after a semi-empirical absorption correction had been applied (T_{min} = 0.76, T_{max} = 1.00). The structure was solved by direct methods (SHELXS-97)[56][57] and refined against all F^2 data (SHELXL-97)[58] to *R1* = 0.0328 [for 3601 $F > 4\sigma(F)$; *wR2* = 0.0612 and GOF = 0.79 for all 6244 F^2; 373 parameters; all non-hydrogen atoms anisotropic; +0.51/−0.49 e$Å^{-3}$].

Crystallographic data (excluding structure factors) for the structures reported in this paper have been deposited with the Cambridge Crystallographic Data Centre as supplementary publication numbers CCDC-125078, CCDC-125079 and CCDC-125080. Copies of the data can be obtained free of charge on application to CCDC, 12 Union Road, Cambridge CB2 1EZ, UK [Fax: (+44) 1223/336-033; E-mail: deposit@ccdc.cam.ac.uk].

Acknowledgments

This work was supported by grants from the University of Otago. We are grateful to Professor W. T. Robinson and Dr. J. Wikaira (University of Canterbury) for the X-ray data collections, B. M. Clark (University of Canterbury) for the FAB mass spectra, Dr. M. Thomas (University of Otago) for obtaining the NMR spectra, and to V. Camplin and R. Cooke (University of Otago) for their help. The help and advice given to us by Professor A. McAuley (University of Victoria), particularly regarding the interpretation of the EPR spectra run by CB and SS, is greatly appreciated. We thank Dr. E. Bothe and Professor K. Wieghardt (MPI für Strahlenchemie) for providing us with details of their spectroelectrochemical cell design and gratefully acknowledge the glass blowing skills of J. Wells (University of Otago) which allowed construction of this cell.

[1] R. Cammack, *Nature* **1999**, *397*, 214.
[2] M. Frey, *Struct. Bond.* **1998**, *90*, 97.
[3] J. C. Fontecilla-Camps, *Struct. Bond.* **1998**, *91*, 1.
[4] A. Volbeda, M. H. Charon, C. Piras, E. C. Hatchikian, M. Frey, J. C. Fontecilla-Camps, *Nature* **1995**, *373*, 580.
[5] M. A. Halcrow, G. Christou, *Chem. Rev.* **1994**, *94*, 2421.
[6] G. Musie, P. J. Farmer, T. Tuntulani, J. H. Reibenspies, M. Y. Darensbourg, *Inorg. Chem.* **1996**, *35*, 2176.
[7] C. H. Lai, J. H. Reibenspies, M. Y. Darensbourg, *Angew. Chem.* **1996**, 108, 2551; *Angew. Chem. Int. Ed. Engl.* **1996**, *35*, 2390.
[8] T. Beissel, F. Birkelbach, E. Bill, T. Glaser, F. Kesting, C. Krebs, T. Weyhermuller, K. Wieghardt, C. Butzlaff, A. X. Trautwein, *J. Am. Chem. Soc.* **1996**, *118*, 12376.
[9] T. Glaser, F. Kersting, T. Beissel, E. Bill, T. Weyhermueller, W. Meyer-Klaucke, K. Wieghardt, *Inorg. Chem.* **1999**, *38*, 722.
[10] P. Illiopoulos, K. S. Murray, R. Robson, J. Wilson, G. A. Williams, *J. Chem. Soc., Dalton Trans.* **1987**, 1585.
[11] A. M. Bond, M. Haga, I. S. Creece, R. Robson, J. C. Wilson, *Inorg. Chem.* **1988**, *27*, 712.
[12] A. M. Bond, M. Haga, I. S. Creece, R. Robson, J. C. Wilson, *Inorg. Chem.* **1989**, *28*, 559.
[13] B. F. Hoskins, C. J. McKenzie, R. Robson, Z. R. Lu, *J. Chem. Soc., Dalton Trans.* **1990**, 2637.
[14] S. Brooker, P. D. Croucher, *J. Chem. Soc., Chem. Commun.* **1995**, 2075.
[15] S. Brooker, P. D. Croucher, *J. Chem. Soc., Chem. Commun.* **1995**, 1493.
[16] S. Brooker, P. D. Croucher, F. M. Roxburgh, *J. Chem. Soc., Dalton Trans.* **1996**, 3031.
[17] S. Brooker, T. C. Davidson, *Chem. Commun.* **1997**, 2007.
[18] S. Brooker, P. D. Croucher, *Chem. Commun.* **1997**, 459.
[19] S. Brooker, P. D. Croucher, T. C. Davidson, G. S. Dunbar, A. J. McQuillan, G. B. Jameson, *Chem. Commun.* **1998**, 2131.
[20] A. J. Atkins, A. J. Blake, M. Schroder, *J. Chem. Soc., Chem. Commun.* **1993**, 1662.
[21] A. J. Atkins, D. Black, A. J. Blake, A. Marin-Becerra, S. Parsons, L. Ruiz-Ramirez, M. Schroder, *Chem. Commun.* **1996**, 457.
[22] N. D. J. Branscombe, A. J. Blake, A. Marin-Becerra, W. S. Li, S. Parsons, L. Ruiz-Ramirez, M. Schroder, *Chem. Commun.* **1996**, 2573.
[23] A. Christensen, H. S. Jensen, V. McKee, C. J. McKenzie, M. Munch, *Inorg. Chem.* **1997**, *36*, 6080.
[24] P. E. Kruger, V. McKee, *Chem. Commun.* **1997**, 1341.
[25] G. A. Lawrance, M. Maeder, T. M. Manning, M. A. O'Leary, B. W. Skelton, A. H. White, *J. Chem. Soc., Dalton Trans.* **1990**, 2491.
[26] N. F. Curtis, *J. Chem. Soc.* **1965**, *169*, 924.
[27] N. H. Pilkington, R. Robson, *Aust. J. Chem.* **1970**, *23*, 2237.
[28] H. Okawa, private communication.
[29] K. Nakamoto, *Infrared and Raman Spectra of Inorganic and Coordination Compounds, Wiley, New York*, **1997**, *Part B*, 53.
[30] H. Frydendahl, H. Toftlund, J. Becher, J. C. Dutton, K. S. Murray, L. F. Taylor, O. P. Anderson, E. R. T. Tiekink, *Inorg. Chem.* **1995**, *34*, 4467.
[31] I. G. Dance, *Polyhedron* **1986**, *5*, 1037.
[32] J. R. Dilworth, J. Hu, *Adv. Inorg. Chem.* **1993**, *40*, 411.
[33] G. Aullon, G. Ujaque, A. Lledos, S. Alvarez, *Chem. Eur. J.* **1999**, *5*, 1391.
[34] C. A. Hunter, *Chem. Soc. Rev.* **1994**, *23*, 101.
[35] M. D. Glick, R. L. Lintvedt, T. J. Anderson, J. L. Mack, *Inorg. Chem.* **1976**, *15*, 2258.
[36] M. P. Suh, *Adv. Inorg. Chem.* **1997**, *44*, 93.
[37] A. McAuley, K. Beveridge, S. Subramanian, T. W. Whitcombe, *J. Chem. Soc., Dalton Trans.* **1991**, 1821.
[38] X. Chen, S. Zhan, C. Hu, Q. Meng, J. Shun, *Inorg. Chim. Acta.* **1997**, *260*, 95.
[39] B. Kersting, G. Steinfeld, J. Hausmann, *Eur. J. Inorg. Chem.* **1999**, 179.
[40] B. Kersting, D. Siebert, *Inorg. Chem.* **1998**, *37*, 3820.
[41] B. Kersting, *Eur. J. Inorg. Chem.* **1998**, 1071.
[42] B. Kersting, G. Steinfeld, J. Hausmann, *Eur. J. Inorg. Chem.* **1999**, 179.
[43] B. Kersting, D. Siebert, *Eur. J. Inorg. Chem.* **1999**, 189.
[44] T. J. Kemp (Ed.), *Southampton Electrochemistry Group: Instrumental Methods in Electrochemistry*, Ellis Horwood Ltd, Chichester, **1985**.
[45] H. J. Kruger, R. H. Holm, *Inorg. Chem.* **1987**, *26*, 3645.
[46] Y. Aratake, M. Ohba, H. Sakiyama, M. Tadokoro, N. Matsumoto, H. Okawa, *Inorg. Chim. Acta.* **1993**, *212*, 183.
[47] K. K. Nanda, R. Das, K. Venkatsubramanian, P. Paul, K. Nag, *J. Chem. Soc., Dalton Trans.* **1993**, 2515.
[48] K. K. Nanda, A. W. Addison, N. Paterson, E. Sinn, L. K. Thompson, U. Sakaguchi, *Inorg. Chem.* **1998**, *37*, 1028.
[49] D. H. Busch, E. S. Gore, F. V. Lovecchio, *J. Am. Chem. Soc.* **1974**, *96*, 3109.
[50] T. Yamamura, M. Tadokoro, K. Tanaka, R. Kuroda, *Bull. Chem. Soc. Jpn.* **1993**, *66*, 1984.
[51] A. G. Lappin, A. McAuley, *Adv. Inorg. Chem.* **1988**, *32*, 241.
[52] P. Delahay, C. W. Tobias, *Advances in Electrochemistry and Electrochemical Engineering*, Wiley, New York, **1970**, *7*, 77.
[53] R. I. Haines, A. McAuley, *Coord. Chem. Rev.* **1981**, *39*, 77.
[54] M. B. Robin, P. Day, *Adv. Inorg. Chem. Radiochem.* **1967**, *10*, 247.
[55] W. J. Geary, *Coord. Chem. Rev.* **1971**, *7*, 81.
[56] G. M. Sheldrick, *Acta Crystallogr., Sect. A* **1990**, *46*, 467.
[57] G. M. Sheldrick, *Methods Enzymol.* **1997**, *276*, 628.
[58] G. M. Sheldrick, T. R. Schneider, *Methods Enzymol.* **1997**, *277*, 319.

Received August 17, 1999
[I99304]

Pyrazolato Metal Complexes: Synthesis, Characterization and X-ray Crystal Structures of Polynuclear Organometallic Re–Mn Derivatives

G. Attilio Ardizzoia,*[a][+] Girolamo LaMonica,[a][+] Angelo Maspero,[a] Massimo Moret,[b] and Norberto Masciocchi*[b][+]

Keywords: Pyrazolato ligands / Rhenium / Manganese / Crystal structure / Heterometallic complexes

By reacting $[Re(CO)_3(Hpz)_2(pz)]$ (Hpz = pyrazole) with $[Mn(CO)_5Br]$ in toluene in the presence of Et_3N, the dinuclear complex $[(CO)_3Re(pz)_3Mn(CO)_3](Et_3NH)$ (**1**) was obtained. The reaction of **1** with molecular oxygen affords the tetranuclear compound $[(CO)_3Re(pz)_3Mn(O)_3Mn(pz)_3Re(CO)_3](Et_3NH)_2$ (**3**) or the trinuclear compound $[(CO)_3Re(pz)_3Mn(pz)_3Re(CO)_3](Et_3NH)_2$ (**5**) depending on the experimental conditions. Complexes **1**, **3** and **5** were characterized in the solid state by single crystal X-ray diffraction analysis and were showed to contain Re···Mn interactions linked by and tris-μ_2-pyrazolato bridges. In **5**, a short [2.397(4) Å] tris(μ_2-oxo)bridged Mn^{IV}–Mn^{IV} contact is found, leading to strong antiferromagnetic coupling of the d^3 ions. The homometallic species $[(CO)_3Mn(pz)_3Mn(CO)_3](Et_3NH)$ (**2**) was also prepared and found to be isostructural with **1**.

Introduction

The formation of polynuclear complexes whose atoms are kept at nearly fixed distances by ancillary ligands is a strict requirement for multicentred catalysis; in particular, when specific synthetic routes to heteropolymetallic species can be devised, complexes where the synergic effects of metals of different nature, geometry or oxidation state are present can be prepared.[1]

In a recent paper we have demonstrated that the organometallic complex $[(CO)_3Re(Hpz)_2(pz)]$,[2] once deprotonated, can act as a multidentate ligand toward the metals of group 11 in the +I oxidation state.[3] The proposed analogy of this ligand with the trispyrazolylborate anion was, however, partially obscured by the observation that "tripod-like" coordination of group 11 metal atoms did not occur, probably because of their peculiar electronic and steric requirements which favour low-coordination numbers. Therefore, in order to substantiate our hypothesis, we decided to react $[(CO)_3Re(Hpz)_2(pz)]$ with molecular fragments prone to hexacoordination. For this we have chosen $[Mn(CO)_5Br]$ which, upon removal (and substitution) of three ligands, can easily afford stable 18-electron Mn^I species. Accordingly, in this paper we report the synthesis and chemical reactivity of polynuclear Re−Mn species which contain metal-metal interactions linked by rare tris(μ_2-pyrazolato) bridges, along with their spectroscopic, magnetic and structural characterization.

[a] Dipartimento di Chimica Inorganica, Metallorganica e Analitica, Università di Milano e Centro CNR,
Via Venezian, 21−20133 Milano, Italy
[b] Dipartimento di Chimica Strutturale e Stereochimica Inorganica, Università di Milano e Centro CNR,
Via Venezian, 21−20133 Milano, Italy
[+] On leave from: Dipartimento di Scienze Chimiche, Fisiche e Matematiche, Università dell'Insubria,
Via Lucini, 3−22100 Como, Italy

Results and Discussion

The pyrazole/pyrazolate derivative compound $[(CO)_3Re(Hpz)_2(pz)]$ reacts with $[Mn(CO)_5Br]$ in the presence of Et_3N leading to the dinuclear ionic derivative $[(CO)_3Re(pz)_3Mn(CO)_3](Et_3NH)$ **(1)** according to Equation 1.

$$[(CO)_3Re(Hpz)_2(pz)] + [Mn(CO)_5Br] \longrightarrow [(CO)_3Re(pz)_3Mn(CO)_3](Et_3NH) \quad (1)$$

The IR spectrum of **1** in toluene shows four strong carbonyl stretching absorptions at 2023, 2008, 1915 and 1901 cm^{-1}, respectively. The latter two (broad) bands are due to the superimposition of the E vibration modes expected for a facial coordination of the carbonyl ligands bonded to the metal centres,[4] later confirmed by the X-ray diffraction study reported below, while the first two absorptions are assigned to the A_1 mode of carbonyls coordinated to the manganese(I) and rhenium(I) centres, respectively.

In order to draw useful structural and spectroscopic comparisons, we tried to synthesize the homometallic dirhenium derivative $[(CO)_3Re(pz)_3Re(CO)_3](Et_3NH)$, by reacting $[(CO)_3Re(Hpz)_2(pz)]$ with a stoichiometric amount of $[Re(CO)_5Br]$ in the presence of Et_3N. Unfortunately, all attempts to reach this goal failed, unreacted $[(CO)_3Re(Hpz)_2(pz)]$ being always recovered. In contrast to this, when $[Mn(CO)_5Br]$ was reacted with pyrazole in the presence of triethylamine, the homobimetallic manganese(I) derivative $[(CO)_3Mn(pz)_3Mn(CO)_3](Et_3NH)$ **(2)** could be easily prepared in high yields. The proposed structure of complex **2**, originally prepared and spectroscopically characterized by Trofimenko[5] as its tetraethylammonium salt, is here confirmed by means of a X-ray powder diffraction study (see Experimental Section).

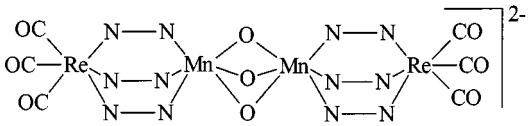
The ^1H NMR spectrum of **1**, measured in $[D_6]$acetone at −80°C, shows only one set of signals for each pyrazolate proton, revealing the equivalence of the three pyrazolate

 © WILEY-VCH Verlag GmbH, D-69451 Weinheim, 2000 1434−1948/00/0101−0181 $ 17.50+.50/0

groups; on the other hand, bridging of two different metal centres causes the splitting of the H(3)/H(5) proton signals [two doublets at δ = 7.81 (J = 2.19 Hz) and δ = 7.79(J = 1.75 Hz) and a *pseudo*-triplet centred at δ = 6.15]. Moreover, the signals attributable to the triethylammonium cation are also clearly detected [δ = 1.41 (t, J = 6.29 Hz, CH_3), δ = 3.40 (q, J = 6.29 Hz, CH_2), δ = 4.00 (br, N*H*)]. For the sake of comparison, in the related homometallic species $[(CO)_3Mn(pz)_3Mn(CO)_3](Et_3NH)$ **(2)** due to the equivalence of the H(3) and H(5) protons, only one doublet (δ = 7.79, J = 2.19 Hz), a triplet at δ = 6.15 and the signals attributable to the Et_3NH^+ cation are found. On the basis of the observed values of the $J_{4,(3,5)}$ coupling constants, we tentatively attribute the downfield doublet in the ^{1}H NMR spectrum of **1** to the H protons leaning out over the manganese(I) centre.

Reactivity of 1 With O_2

Complex **1** reacts with molecular oxygen leading, depending on the experimental conditions, to different species. When CH_2Cl_2 solutions of **1** are exposed to an O_2 atmosphere, a pronounced colour change of the solution from pale yellow to dark red occurs, and the formation of a brick-red precipitate takes place. An X-ray structure analysis (see later) revealed this species to be the tetranuclear rhenium(I)/manganese(IV) $[Re_2Mn_2(CO)_6(O)_3(pz)_6](Et_3NH)_2$ complex, **(3)**, where two $[(CO)_3Re(\mu\text{-}pz)_3Mn]$ sub-units are connected together through three μ_2-oxo bridges.



Therefore, the complete reaction leading to **3** can be written as:

$$2\,[(CO)_3Re(pz)_3Mn(CO)_3](Et_3NH) + 3/2\,O_2 \rightarrow [Re_2Mn_2(CO)_6(O)_3(pz)_6](Et_3NH)_2 + 6\,CO \quad (2)$$

The IR spectrum of solid **3** shows the typical pattern of carbonyl absorptions for a *fac* geometry around the rhenium(I) centre [2053(s) and 1903(br) cm^{-1}]; moreover, two strong, broad bands in the 1800−1600 cm^{-1} region are present and can be attributed to H-bonds between the triethylammonium protons and the oxo bridges, as found by the crystallographic study.

Depicting the organometallic residue $\{(CO)_3Re(pz)_3\}^{2-}$ as {L} and, hence, **3** as $[\{L\}Mn(O)_3Mn\{L\}]^{2-}$, it is easy to show that **3** belongs to the relatively large class of dinuclear face-sharing octahedral complexes of the $[L_nM(X)_3ML_n]^{m-}$ type, containing d^3-d^3 metals.[6] For this class of derivatives, it has been shown[6a] that the spin-exchange interaction is independent of the type of bridging ligand (X = O^{2-}, OH^-, RO^-, Cl^-, Br^-, I^-) and also of the nature of the metal centre [M = Mn^{IV}, Cr^{III}, V^{II}], the only relevant parameter being the metal−metal distance. A plot of ln(J) versus the M−M distance D_{M-M} (J being the spin-exchange coupling constant) is linear, leading to a phenomenological equation of the type $J = B\cdot\exp(-\varepsilon D_{M-M})$.[6a] The species which allowed the determination of this law contain d^3 ions with intermetallic distances in the 2.3−4.0 Å range depending on the type of the bridging ligands; consequently, many different values of spin interactions could be found, with 2J estimates ranging from 0 to −780 cm^{-1}, equivalent to μ_{RT} values in the 3.9−0.5 BM (per metal centre) range.[6a] For complex **3** we measured a μ_{RT} value of 0.99 BM, revealing a strong antiferromagnetic interaction between the two manganese(IV) centres, in agreement with the short Mn−Mn separation [2.394(3) Å, vide infra] and with that predicted on adopting the aforementioned equation.[7]

According to the strong antiferromagnetic coupling between the Mn^{IV} centres, the ^{1}H NMR spectrum of complex **3** shows well resolved signals, without substantial band broadening or paramagnetic shifts. Its spectral features are quite similar to those of the parent compound $[(CO)_3Re(pz)_3Mn(CO)_3](Et_3NH)$ **(1)**. In the pyrazolate proton region two doublets, centred at δ = 7.81 and 7.76 (J = 2.01 and 1.83 Hz) and assigned to the H(3) and H(5) protons leaning out over the rhenium and manganese centres are present. The pyrazolate protons in the 4-position give rise to a pseudo-triplet centred at δ = 6.10. The spectral features do not change significantly upon changing the temperature, revealing the high rigidity of the $M(\mu\text{-}pz)_3M'$ core.

Complex **3** can be easily protonated to the neutral oxo/dihydroxo species $[(CO)_3Re(pz)_3Mn(OH)_2(O)Mn(pz)_3Re(CO)_3]$ **(4)** by employing stoichiometric amounts of aqueous HBF_4. In complex **4**, the ν(CO) absorptions are found at 2037 and 1926 cm^{-1}, slightly shifted with respect to the parent compound **3**; moreover, a broad band attributable to ν(OH) is found at about 3500 cm^{-1}. Such a reaction can be quantitatively reversed by treating **4** with Et_3N. Interestingly, excess HBF_4 does not lead to the formation of the cationic $[(CO)_3Re(pz)_3Mn(OH)_3Mn(pz)_3Re(CO)_3]^+$ species.

When $[(CO)_3Re(pz)_3Mn(CO)_3](Et_3NH)$ **(1)** was reacted with O_2 in the presence of free pyrazole [or when the mother liquors of reaction (1) were exposed to air], the trinuclear species $[(CO)_3Re(pz)_3Mn(pz)_3Re(CO)_3](Et_3NH)_2\cdot H_2O$ **(5)** was isolated in low yields (see Experimental Section) and crystallographically characterized. The IR spectrum of **5** shows two bands attributable to ν(CO) at 2018 (sharp) and 1901 (broad) cm^{-1}, in agreement with the facial geometry about the rhenium(I) centres. This latter reaction is accompanied by the formation of noncarbonylic manganese species. IR evidence suggests that, most probably, hydroxo/pyrazole derivatives of Mn^{II} are formed, but their real nature still remains unclear. Work is in progress in order to identify these species, which could not be easily isolated by standard chemical or chromatographic techniques.

Crystal Structures of 1, 3 and 5

All these compounds are ionic species, containing $[Et_3NH]^+$ cations and organometallic polynuclear anions; in addition, crystals of **5** contain clathrated water molecules. ORTEP drawings of the complex anions are shown in Fig-

ures 1, 2 and 3, respectively; a summary of chemically relevant bond lengths is presented in Table 1.

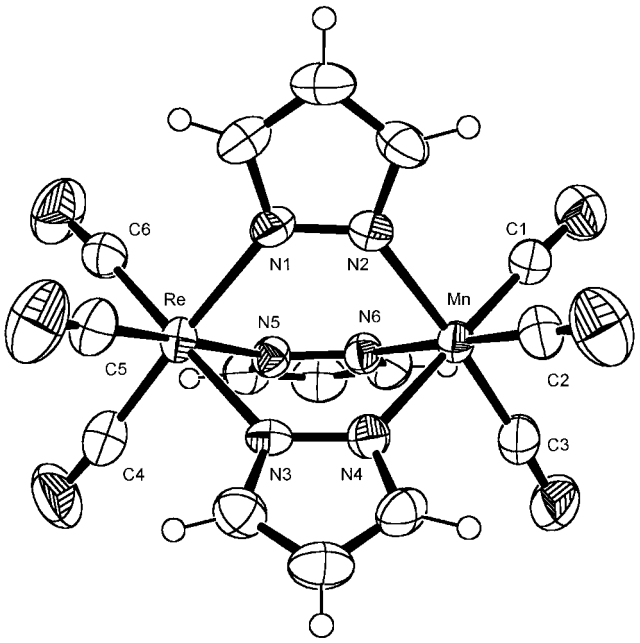


Figure 1. ORTEP drawing of the $[(CO)_3Re(pz)_3Mn(CO)_3]^-$ anion in **1**, with partial labelling scheme; thermal ellipsoids are drawn at the 30% probability level; hydrogen atoms are given arbitrary radii

Table 1. Synoptic collection of relevant bond lengths (e.s.d.'s in parentheses)

Compound	**1**[a]	**3**[b]	**5**[b]
Metals	Re^I-Mn^I	Re^I-Mn^{IV}	Re^I-Mn^{II}
Re−Mn	3.905(1)	3.897(2)	3.854(2)
Mn−Mn	−	2.394(3)	−
Re−C	1.874(9)	1.906(4)	1.89(1)
	1.889(9)	1.907(3) (2 ×)	1.90(2)
	1.906(8)	−	1.91(2)
<Re−C>	1.89	1.91	1.90
Mn−C	1.811(9)	−	−
Mn−C	1.811(9)	−	−
Mn−C	1.818(8)	−	−
<Mn−C>	1.81	−	−
Re−N	2.157(6)	2.156(8)	2.150(8)
Re−N	2.143(5)	2.162(3) (2 ×)	2.169(9)
Re−N	2.134(5)	−	2.174(9)
<Re−N>	2.14	2.16	2.16
Mn−N	2.086(6)	2.047(8)	2.030(9) (2 ×)
Mn−N	2.090(6)	2.029(5) (2 ×)	2.021(9) (2 ×)
Mn−N	2.110(6)	−	2.012(9) (2 ×)
<Mn−N>	2.09	2.03	2.02
Mn−O	−	1.835(7)	−
Mn−O	−	1.849(4) (2 ×)	−
<Mn−O>	−	1.84	−

[a] These values may be slighly affected by the Re/Mn disorder discussed in the text. − [b] The anion in **3** possesses crystallographically imposed *mm2* symmetry, while that of **5** lies on an inversion centre.

All three species contain "terminal" *fac*-$M(CO)_3$ (M = Re or Mn) fragments, connected by a tris-pyrazolato bridge (tpb) or longer (linear) spacers, i.e. [(tpb)Mn(μ−O)$_3$Mn(tpb)] in **3** and [(tpb)Mn(tpb)] in **5**. Therefore, the nature of the metal atoms in **1**, **3** and **5** can be easily depicted by the Re^I-Mn^I, $Re^I-Mn^{IV}-Mn^{IV}-Re^I$ and $Re^I-Mn^{II}-Re^I$ sequences, respectively.

Only a few polynuclear complexes bearing tris-pyrazolato bridges are known, the only structurally characterized species being $[(ON)Ni(tpb)Ni(NO)]^-$ (containing a tris-3,5-dimethylpyrazolato bridge),[8] $[Cu_3(fpz)_5]$ [Hfpz = 3,5-bis(trifluoromethyl)pyrazole],[9] $[(C_5Me_5)Ir(tpb)Rh(OOH)(dppe)]^+$,[10] $[(C_5Me_5)Ir(tpb)Ni(R_3BH)]$ and [(*p*-cymene)-Ru(tpb)Ni(R_3BH)] (HR = 4-bromo-3-isopropylpyrazole).[11] In such species, as well as in compounds **1**, **3**, and **5**, the rare M(tpb)M fragment mimics structural features which are usual for tris(pyrazolyl)borato metal complexes. Indeed, the trispyrazolylborato derivatives of **1** and **3**, as well as a bis(μ$_2$-oxo) analogue of **5**, obtained by formally replacing the organometallic $(CO)_3Re(pz)_3$ fragment with the $HB(pz)_3$ tripod, have been known for a long time.[12] Differently, heterobridged metals possessing a $(\mu\text{-}pz)_a(\mu\text{-}X)_b$ (a + b = 2, 3) core are quite common.[13] In addition, several triazolato and tetrazolato complexes of this kind are present in the Cambridge Crystallographic Database but, since the vast majority are not organometallic species, they will not be discussed any further; however, these observations show that the M(tpb)M fragments should not be rare at all and, as confirmed by the present study, that they can easily be prepared if the proper synthons are used.[14]

As expected, in complexes **1**, **3** and **5**, the M−C distances of the *fac*-$M(CO)_3$ [average values (Å): Re−C 1.89 (in **1**), 1.90 (**3** and **5**); Mn−C 1.81 (**1**)] reflect the larger atomic radius of Re vs. Mn; analogously, Re^I-N bond lengths are about 0.1 Å larger than the Mn^I-N ones.[15] However, if compared to those found in the mononuclear precursors (for which, typically, Re^I-N ca. 2.19 Å),[2] a relevant shortening of the M−N bonds is evident; this effect can possibly be related to the Mn−N−N angles of the (tpb)$Mn(CO)_3$, (tpb)Mn(μ-O)$_3$Mn(tpb) and (tpb)Mn(tpb) fragments which are wider (>126°) than those found in the known species $[Re(CO)_3(Hpz)_2(pz)]$, $[Re(CO)_3(Hpz)(pz)(py)]$ and $[(CO)_3Re\{(pz)_2Br\}Re(CO)_3]^-$ (ca. 124°)[2]; indeed, overlap between the metal d orbital(s) and the nitrogen lone-pairs is most effective for Re−N vectors bisecting the $N_{ipso}-N-C_{ipso}$ angles (ca. 108°), i.e. for Re−N−N angles close to (360 − 108)/2 = 126°. The slightly divergent nature of the pyrazolato ligands in **1**, **3** and **5** is also confirmed by comparing the theoretical Re−Mn distances [$(Re-N_{avg.} + Mn-N_{avg})\cdot\sin(36°) + N-N_{avg.} = 3.85$, 3.83 and 3.83 Å] to the observed values [3.905(1), 3.897(2) and 3.854(2) Å, respectively]. For the sake of comparison, a dimanganese(I) species, structurally similar to **1** but bearing 5-fluoromethyltetrazolates (Hftz), $[(CO)_3Mn(ftz)_3Mn(CO)_3]^-$, shows an Mn−Mn interaction of 3.79 Å.[16]

Since each tpb fragment binds through six donor nitrogen atoms, all metals in **1**, **3** and **5** are octahedrally coordinated: the manganese atoms of **3** are bound to three pyrazolates and three oxo-bridges, while Mn^{II} in **5** is bound to six different pyrazolates. Rather surprisingly, and in disagreement with Shannon's radii for octahedrally coordi-

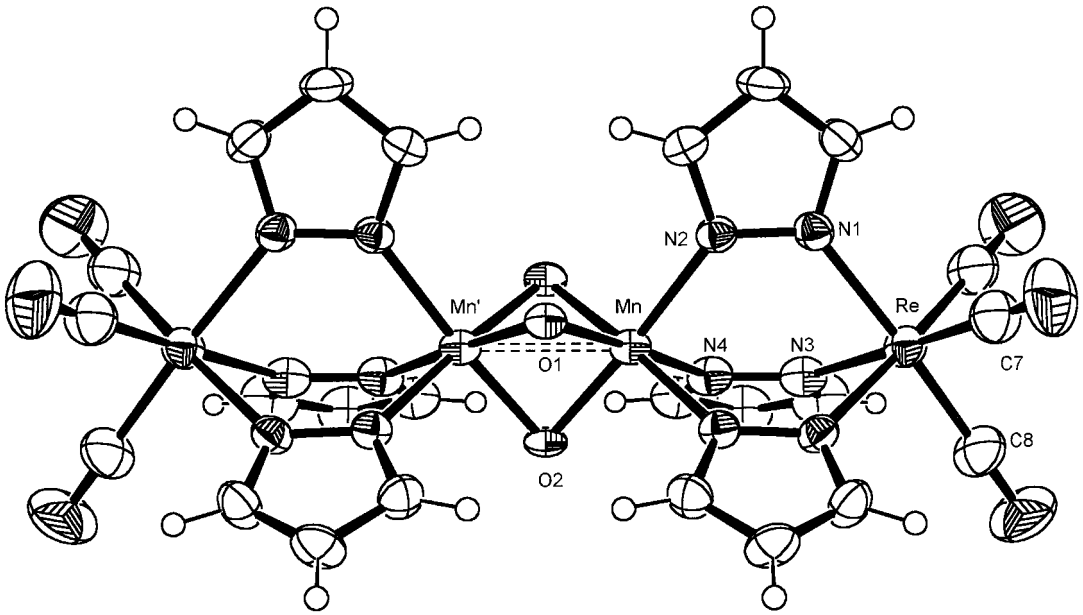


Figure 2. ORTEP drawing of the $[(CO)_3Re(pz)_3Mn(O)_3Mn(pz)_3Re(CO)_3]^{2-}$ anion in **3**, with partial labelling scheme; the dashed bond links Mn^{IV} ions which are 2.394(3) Å apart; thermal ellipsoids are drawn at the 50% probability level, hydrogen atoms are given arbitrary radii

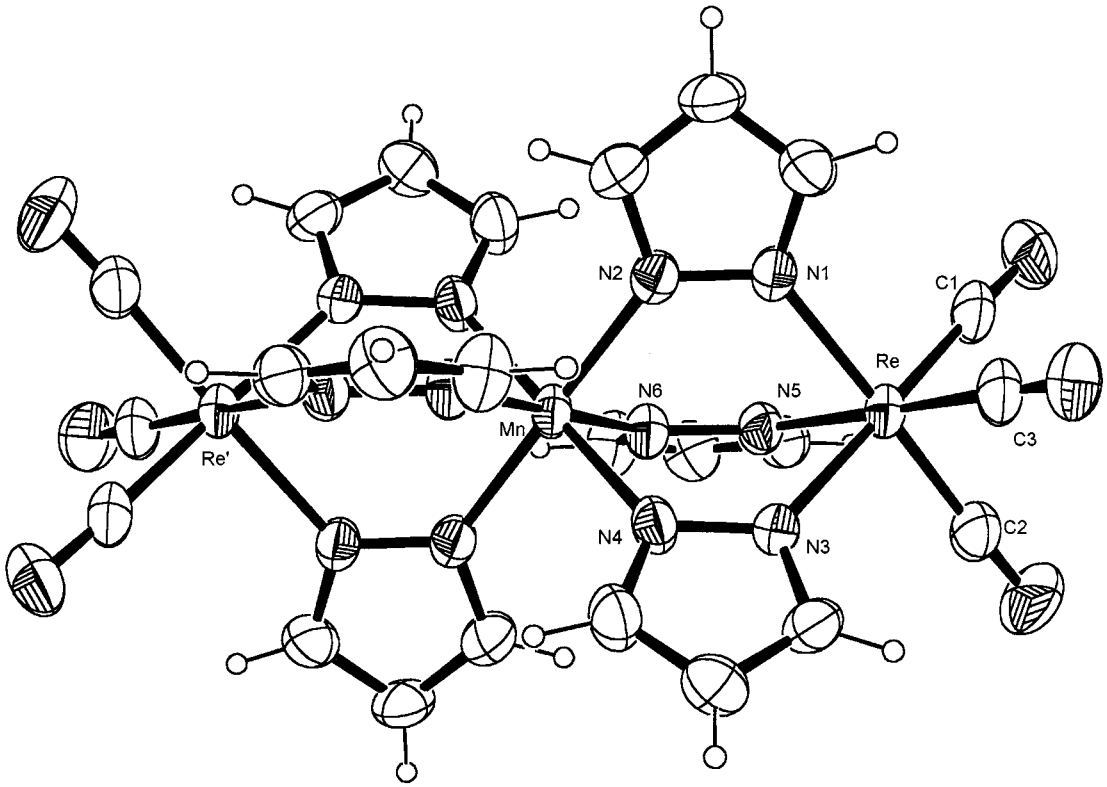


Figure 3. ORTEP drawing of the $[(CO)_3Re(pz)_3Mn(pz)_3Re(CO)_3]^{2-}$ anion in **5**, with partial labelling scheme; thermal ellipsoids are drawn at the 50% probability level; primed atoms are symmetry-equivalents; hydrogen atoms are given arbitrary radii

nated atoms,[17] Mn^{II} (probably a high-spin d^5 ion) in **5** shows bond lengths comparable with those found in tetravalent (d^3) Mn in **3** (see Table 1). This effect needs further comments: owing to the very short Mn···Mn interaction [2.394(3) Å],[18] and in agreement with the observed magnetic response of powders of **3**, a rather profound interaction occurs between the two d^3 ions, making each Mn atom formally seven- rather than six-coordinate; in addition, the very narrow Mn−O−Mn angles (ca. 81°) are also a consequence of this "incipient" bond.

Interestingly, a similar trioxo bridge with a very short M···M distance [M = Tc, a Mn congener, Tc···Tc = 1.867(4) Å] was extensively discussed in experimental[19] and theoretical[20] reports, but was eventually found to be a pure artifact stemming from poor structural analysis of a misinterpreted rhenium species, i.e. solid $(C_5Me_5)ReO_3$, which affords rare two-dimensional polytypes.[21] With these aspects in mind, and suspecting a similar behaviour, we also formulated a crystal disorder of the hypothetical $Re^{I}-Mn^{VII}$ $[(CO)_3Re(tpb)MnO_3]^-$ species, which was easily discarded on the basis of packing considerations, chemical and spectroscopic analyses and much poorer agreement factors. However, since it has been shown here that species such as tris-pyrazolylborates and their organometallic analogue $[(CO)_3Re(tpb)]^{2-}$ have similar coordinating capabilities, and thanks to the well-recognized similarity of the cyclopentadienyl and $[HB(pz)_3]^-$ fragments,[22] it is likely that the still elusive $[(CO)_3Re(tpb)MnO_3]^-$ may exist.

Conclusions

The present work has demonstrated that organometallic analogues of the tris-pyrazolylborato ligands can be successfully employed in building heterometallic species. In addition, selective oxidation of one of the metals was easily attained, opening the way to the synthesis of polynuclear species containing metals in different, and tunable, oxidation states, which may be of interest in multimetal-centred homogeneous catalysis. Accordingly, tris-pyrazolato-bridged $Re^{I}-Mn^{I}$, $Re^{I}-Mn^{II}$ and $Re^{I}-Mn^{IV}$ species were prepared. Also, preliminary results on analogous oxidation reactions of **2** revealed the formation of $Mn^{I}-Mn^{IMnII}-Mn^{I}$ and $Mn^{I}-Mn^{III}-Mn^{I}$ links, but their complete characterization will be reported in a forthcoming paper.

In addition, in the light of our continuous interest in the chemistry of coordination polymers containing metal−diazolato links,[23] the formation of {M(tpb)M} and {M(tpb)M(μ-O)$_3$M} fragments opens the way, at least in principle, to the preparation of robust species containing linear chains of metals and displaying a variety of physical properties such as interesting electrical, magnetic and optical effects.[24]

Experimental Section

Solvents were dried and purified by standard methods. Pyrazole and $[Mn(CO)_5Br]$ (Aldrich Chemical Co.) were used as supplied, $[Re(CO)_5Br]$[25] and $[Re(CO)_3(Hpz)_2(pz)]$[2] were prepared according to literature procedures. Infrared spectra were measured on a BIO RAD FTIR 7 instrument, ^1H NMR spectra were acquired on a Bruker AC-300 FT spectrometer operating at 300.13 MHz. Magnetic data were achieved employing a Sherwood Scientific magnetic susceptibility balance. Elemental analyses were performed at the Microanalytical Laboratory of this University (C, H, N). All reactions were carried out using standard Schlenk techniques.

$[(CO)_3Re(pz)_3Mn(CO)_3](Et_3NH)$ (1): $[(CO)_3Re(Hpz)_2(pz)]$ (360 mg, 0.761 mmol) was dissolved in 8 mL of toluene and solid $[Mn(CO)_5Br]$ (216 mg, 0.785 mmol) was added with stirring. Deoxygenated Et_3N (0.5 mL) was then added and the solution kept at 45°C for 4 h. During this time, evolution of CO from the reaction medium was accompanied by the formation of a pale yellow precipitate. The solid was then filtered, washed with water and dried under vacuum (481 mg, 89% yield) − $C_{21}H_{25}MnN_7O_6Re$ (712): calcd. C 35.39, H 3.51, N 13.76; found C 35.25, H 3.55, N 13.87. Crystals suitable for X-ray structure analysis were obtained by slow diffusion of *n*-hexane into a dichloromethane solution of **1**.

$[(CO)_3Mn(pz)_3Mn(CO)_3](Et_3NH)$ (2): $[Mn(CO)_5Br]$ (300 mg, 1.09 mmol) was added to a solution of pyrazole (134 mg, 1.97 mmol) in toluene (10 mL) kept at 60°C. Et_3N (0.5 mL) was then added and the formation of a yellow precipitate observed. After 6 h, the suspension was cooled to room temperature, and 10 mL of *n*-hexane were added to the reaction medium in order to reduce the solubility of **2**. The solid was then filtered, washed with water and dried under vacuum (550 mg, 86% yield). − $C_{21}H_{25}Mn_2N_7O_6$ (581): calcd. C 43.37, H 4.30, N 16.87; found C 43.01, H 4.21, N 16.41.

$[(CO)_3Re(pz)_3Mn(O)_3Mn(pz)_3Re(CO)_3](Et_3NH)_2$ (3): A solution of **1** (160 mg, 0.225 mmol) in CH_2Cl_2 (5 mL) was stirred under a dioxygen atmosphere for 6 h. During this time a brick-red solid formed. The solid was then filtered off, washed with diethyl ether and dried under vacuum (232 mg, 79% yield). − $C_{36}H_{50}Mn_2N_{14}O_9Re_2$ (1304): calcd. C 33.13, H 3.83, N 15.03; found C 33.22, H 3.45, N 14.67. Crystals suitable for X-ray structure analysis were obtained by slow diffusion of *n*-hexane into an acetone solution of **3**.

$[(CO)_3Re(pz)_3Mn(OH)_2(O)Mn(pz)_3Re(CO)_3]$ (4): Complex **3** (200 mg, 0.153 mmol) was dissolved in acetone (5 mL) and aqueous HBF_4 (48% wt, solution in water, 60 μL) was added. The colour of the solution turned from red to violet. After 15 min. stirring, the solution was evaporated to dryness and the solid was extracted with CH_2Cl_2 (in order to remove the formed $Et_3NH{\cdot}BF_4$). The violet solution was then evaporated to dryness and the residue was triturated with diethyl ether, filtered off and dried under vacuum. (115 mg, 68% yield). − $C_{24}H_{20}Mn_2N_{12}O_9Re_2$ (1102): calcd. C 26.13, H 1.82, N 15.25; found C 26.22, H 2.15, N 15.37.

$[(CO)_3Re(pz)_3Mn(pz)_3Re(CO)_3](Et_3NH)_2{\cdot}H_2O$ (5): To a solution of pyrazole (160 mg, 1.17 mmol) in CH_2Cl_2 (10 mL) was added complex **1** (200 mg, 0.281 mmol) with stirring. The solution was maintained overnight under a dioxygen atmosphere. During this time, the colour of the solution turned from yellow to deep red. The solution was evaporated to dryness and the solid treated with water, filtered and dried under vacuum. The crude product was then dissolved in acetone (3 mL) and *n*-hexane (15 mL) was allowed to diffuse into the solution. Complex **5** was isolated as well-shaped red crystals. (92 mg, 27% yield). − $C_{36}H_{52}MnN_{14}O_7Re_2$ (1219): calcd. C 35.44, H 4.27, N 16.08; found C 35.28, H 4.31, N 15.97.

Crystallography. − Single Crystal Data Collection and Reduction: Crystals of **1**, **3**, **5** were mounted, in air and at room temperature, on the tip of a glass fiber and optically centred in the X-ray beam with the aid of goniometer heads. For **1** and **5**, a CAD4 Enraf−Nonius diffractometer, equipped with graphite monochromated Mo-*Kα* radiation (λ = 0.71073 Å) was used, and the HV generator set at 50 kV and 30 mA. Cell parameters were determined by least-squares on the basis of the setting angles of 25 reflections having $10 < \theta < 14°$. The data collections were performed by the ω-technique with constant scan speed but variable scan range. The crystal stabilities under diffraction conditions were checked by monitoring three standard reflections every 180 minutes: relative decay values of about 6.5 and 20.4% were observed. Analytical absorption cor-

rections were applied, using ψ-scans of three suitable reflections having χ near 90°. The measured intensities were corrected for decay, Lorentz, polarization and background effects and reduced to F_o^2. The crystal of **3** was measured on a SMART Bruker diffractometer, equipped with a CCD area detector and graphite monochromatized Mo-*Kα* radiation (generator setting: 40 kV, 45 mA). Initial cell parameters were determined on the basis of the angular settings of 34 unique reflections. A full hemisphere of data (1350 frames, ω scan, Δω = 0.3°, *t* = 50s) was collected; integration by SAINT[26] and absorption correction by SADABS[27] lead to a total of 18908 F_o^2 values.

Single Crystal Structure Solution and Refinement: All three structures have been solved by direct methods (SIR97[28]) and difference Fourier methods, and subsequently refined by full-matrix least-squares against F_o^2 using all reflections and the program SHELX[29] on an IBM compatible PC. Scattering factors for neutral atoms (including dispersion corrections) were taken from the internal library of SHELX. Owing to the very similar packing environment of the $Mn(CO)_3$ and $Re(CO)_3$ fragments in **1**, a partial disorder [refined values 0.773(1):0.227(1)] is observed for Re/Mn substitution, which has been modeled using the EXYZ and EADP options of SHELX97; this disorder is also reflected by the presence of a few weak reflections which violate the systematic absences conditions. The very small size of the acicular crystal of **3** (10 × 10 × 200 μm) and the larger sphere of data collected are reflected by rather poor estimates of the integrated intensities of the weak reflections (see *R*1 and R_{int} in Table 2); a parallel refinement, performed only with intense data [$I > 10\sigma(I)$], resulted in much better agreement factors (*R*1 = 0.027 and *wR*2 = 0.048 for the same structural model). Apart from the cation and water oxygen atoms in **5** (which experience very large thermal motion or unrationalized static disorder, leading to poor(er) agreement factors), all remaining non-H atoms have been treated anisotropically. Hydrogen atoms were ultimately included in calculated positions and refined isotropically riding on the atoms to which they are attached. A list of crystal data, refinement parameters and final agreement factors can be found in Table 2.[30]

X-ray Powder Diffraction: The light yellow powders of **2** were gently ground in an agate mortar and then deposited on the clean surface of a Si(511) monocrystal with the aid of a thin layer of silicone grease. XRPD data were collected in the step-scan θ:2θ mode on a Rigaku D-III/Max horizontal-scan diffractometer equipped with parallel (Soller) slits and a graphite monochromator (Cu-*Kα* λ = 1.5418 Å) in the diffracted beam. Generator set at 40 kV and 40 mA; Slits used: DS = 1.0°; AS = 1.0°; RS = 0.3 mm. Δ2θ = 0.02°, t = 5 s; the sample was rotated at about 60 rpm about the scattering axis in order to minimize preferred orientation effects. A whole pattern profile fitting performed by the Le Bail method[31]

Table 2. Summary of X-ray single-crystal data and structure refinement parameters

Compound	**1**	**3**	**5**
Formula	$C_{21}H_{25}MnN_7O_6Re$	$C_{36}H_{50}Mn_2N_{14}O_9Re_2$	$C_{36}H_{52}MnN_{14}O_7Re_2$
Formula weight	712.62	1305.17	1220.26
Crystal system	Monoclinic	Orthorhombic	Triclinic
Space group	$P2_1/n$	*Pnmm*	*P*-1
a [Å]	9.807(1)	7.926(1)	11.003(2)
b [Å]	16.376(2)	17.524(1)	11.067(2)
c [Å]	16.095(3)	17.120(1)	12.619(5)
α [°]	–	–	65.64(2)
β [°]	92.33(1)	–	88.77(2)
γ [°]	–	–	60.12(2)
V [Å^3]	2582.7(6)	2377.9(2)	1171.0(6)
Z	4	2	1
F(000)	1392	1272	597
D(calcd.) [g cm^{-3}]	1.833	1.823	1.730
Temperature [K]	293(2)	293(2)	293(2)
Diffractometer	CAD4	SMART	CAD4
Radiation [Å]	0.71073	0.71073	0.71073
Absorption coeff [mm^{-1}]	5.22	5.65	5.48
Crystal size [mm]	0.30×0.15×0.10	0.01 × 0.01 × 0.20	0.05 × 0.05 × 0.08
Scan method	ω	ω	ω
Scan interval [°]	0.9+0.35tanθ	0.3[a]	0.8+0.35tanθ
Max time per refl [s]	60	50[a]	50
θ range [°]	3.0–25.0	1.7–30.7	3.0–25.0
Index ranges	$-11 \le h \le 11$, $0 \le k \le 19$ $0 \le l \le 19$	$-11 \le h \le 11$, $-25 \le k \le 16$ $-24 \le l \le 24$	$-13 \le h \le 13$, $-11 \le k \le 13$ $0 \le l \le 14$
Reflections collected	4515	18371	4094
Independent reflections	4515 [R_{int} = 0.00]	3825 [R_{int} = 0.121]	4094 [R_{int} = 0.000]
Crystal decay	6.4%	none	20.5
Absorption correction	Ψ-scan	Sadabs	Ψ-scan
Min. transmission factor	0.62	0.89	0.93
Obsd. reflection criterion	–	all reflections	–
Refinement method	[full matrix	least-squares	on F_o^2]
Data/restraints/parameters	4515/0/329	3825/0/154	4094/0/229
Goodness–of–fit[b] on F_o^2	1.173	1.228	1.005
*R*1, *wR*2 indices[c] [$F_o > 4\sigma(F_o)$]	0.0419, 0.1013	0.1046, 0.0845	0.0543, 0.1067
*R*1, *wR*2 indices (all data)	0.0541, 0.1067	0.1801, 0.0962	0.1090, 0.1270
Largest diff. peak and hole [eÅ^{-3}]	1.02, −0.96	0.84, −1.11	1.28, −0.87
Weighting scheme,[d] *a*, *b*	0.0426, 9.54	0.0184, 2.57	0.0590, 0

[a] Frame width and exposure time per frame. – [b] GOF = $[\Sigma w(F_o^2 - F_c^2)^2/(n-p)]^{1/2}$ where *n* is the number of reflections and *p* is the number of refined parameters. – [c] $R1 = \Sigma||F_o|-|F_c||/\Sigma|F_o|$, $wR2 = [\Sigma w(F_o^2 - F_c^2)^2/\Sigma wF_o^4]^{1/2}$. – [d] $w = 1/[\sigma(F_o^2) + (aP)^2 + bP]$ where $P = (F_o^2 + 2F_c^2)/3$.

using GSAS[32] afforded the following lattice parameters (a = 9.774; b = 16.286, c = 16.002 Å, β = 92.09°), indicating the strict isomorphous character of the powders of **2** with compound **1**. Since these two unit cells are very similar, they probably share atoms with similar fractional coordinates: indeed a Rietveld refinement for fixed, isotropic atoms, whose coordinates are taken from **1** (with the obvious replacement of Re by Mn), rapidly converged to R_p = 0.083 and R_F = 0.085, demonstrating the validity of such a structural model (see Figure 4); however, since powder diffraction is known to afford only approximate bonding parameters, no further refinements were performed in the search for better powder data fitting by the customary (for single-crystal data) independent atom model.

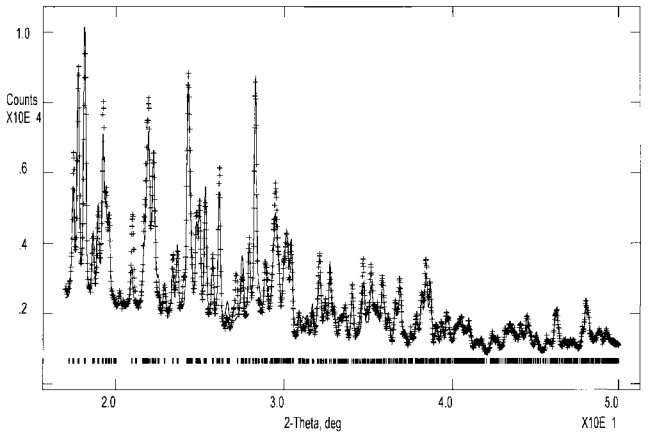


Figure 4. Rietveld refinement plot for $[(CO)_3Mn(pz)_3Mn(CO)_3](Et_3NH)$ (**2**) in the 17 < 2θ < 50° range, with peak markers at the bottom

Acknowledgments

This work was supported by the Ministero dell'Università e della Ricerca Scientifica e Tecnologica (MURST) and by the Italian Consiglio Nazionale delle Ricerche (CNR). The technical support of Mr. Gianni Mezza is also acknowledged.

[1] R. Poilblanc, *Inorg. Chim. Acta*, **1982**, 62, 75−86.
[2] G. A. Ardizzoia, G. La Monica, A. Maspero, M. Moret, N. Masciocchi, *Eur. J. Inorg. Chem.* **1998**, 1503−1511.
[3] G. A. Ardizzoia, G. La Monica, A. Maspero, M. Moret, N. Masciocchi, *Eur. J. Inorg. Chem.* **1999**, 1301−1307.
[4] R. J. Angelici, F. Basolo, A. J. Poe, *J. Am. Chem. Soc.* **1963**, *86*, 2215−2219.
[5] S. Trofimenko, *J. Am. Chem. Soc.* **1969,** 91**,** 5410−5411.
[6] [6a] A. Niemann, U. Bossek, K. Wieghardt, B. Nuber, *Angew. Chem. Int. Ed. Engl.* **1992**, *31*, 311−313. *Angew. Chem.* **1992**, *104*, 345−347. − [6b] J. H. Koek, S. W. Russel, L. van der Wolf, R. Hage, J. B. Warnaar, A. L. Spek, J. Kerschner, L. DelPizzo, *J. Chem. Soc., Dalton Trans.,* **1996**, 353−362.
[7] Having no easy access to facilities to perform cryomagnetic studies in order to estimate the coupling constant J, using the literature data of ref.[6a] we have evaluated the dependence of the room temp. magnetic moment (μ_{RT}) vs. D_{M-M}, modelled by the $\ln(\mu_{RT}) = a\cdot[1-b\cdot\exp(-cD_{M-M})]$ relashionship [with a = 1.366, $b = 1.88 \times 10^4$ and c = 4.09].
[8] K. S. Chong, S. J. Rettig, A. Storr, J. Trotter, *Can. J. Chem.*, **1979**, *57*, 3099−3106
[9] M. K. Ehlert, A. Storr, D. A. Summers, R. C. Thompson, *Can. J. Chem*., **1997**, *75*, 491−498
[10] D. Carmona, M. P. Lamata, J. Ferrer, J. Modrego, M. Perales, F. J. Lahoz, R. Atencio, L. A. Oro, *J. Chem. Soc., Chem. Comm.* **1994**, 575−576.
[11] D. Carmona, F. J. Lahoz, R. Atencio, A. J. Edwards, L. A. Oro, M. P. Lamata, M. Esteban, S. Trofimenko, *Inorg. Chem.*, **1996**, *35*, 2549−2557.
[12] [12a] J. E. Joachim, C. Apostolidis, B. Kanellakopulos, R. Maier, N. Marques, D. Meyer, J. Muller, A. P. de Matos, B. Nuber, J. Rebizant, M. L. Ziegler, *J. Organomet. Chem.*, **1993**, *448*, 119−129. − [12b] M. K. Chan, W. H. Armstrong, *Inorg. Chem*., **1989**, *28*, 3777−3779. − [12c] J. E. Sheats, A. L. Rheingold, M. B. Allen, Personal Communication 1996.
[13] G. La Monica, G. A. Ardizzoia, *Prog. Inorg. Chem.* **1997**, *46*, 151−238.
[14] A unique M−M link quadruply bridged by μ_2-pyrazolato ligands is also known: A. R. Barron, G. Wilkinson, M. Motevalli, M. B. Hursthouse, *Polyhedron* **1985**, *4*, 1131−1134.
[15] Note, however, that the slight Re/Mn disorder discussed in the Experimental Section in **1** significantly smoothes this difference.
[16] E. O. John, R. D. Willet, B. Scott, R. L. Kirchmeier, J. M. Shreeve, *Inorg. Chem.* **1989**, *28*, 893−897.
[17] R. D. Shannon, *Acta Crystallogr.* **1976**, *A32*, 751−767.
[18] For comparison, Mn−Mn distances in the metal (α-phase) lie in the 2.26−2.93 Å range, while the metallic radius of 12-coordinated Mn has been estimated to be 1.37 Å (A. F. Wells, *Structural Inorganic Chemistry*, Oxford Science Publications, **1995**, p. 1306)
[19] [19a] B. Kanellakopulos, B. Nuber, K. Raptis, M. Ziegler, *Angew. Chem. Int. Ed. Engl.* **1989**, *28*, 1055. *Angew. Chem.* **1989,** *101,* 1055. − [19b] A. K. Burrell, F. A. Cotton, L. M. Daniels, V. Petricek, *Inorg. Chem*. **1995**, *34*, 4253−4255.
[20] A. W. E. Chan, R. Hoffmann, S. Alvarez, *Inorg. Chem*. **1991**, *30*, 1086−1093.
[21] N. Masciocchi, P. Cairati, F. Saiano, A. Sironi, Inorg. Chem. **1996**, *35*, 4060−4063.
[22] A. Shaver, in *Comprehensive Coordination Chemistry* (Eds.: G. Wilkinson, R. D. Gillard, J. A. McCleverty), Pergamon, Oxford, **1987**, vol. 2, p. 247.
[23] [23a] N. Masciocchi, M. Moret, P. Cairati, A. Sironi, G. A. Ardizzoia, G. La Monica, *J. Am. Chem. Soc.* **1994**, *116*, 7668−7676. − [23b] N. Masciocchi, M. Moret, P. Cairati, A. Sironi, G. A. Ardizzoia, G. La Monica, *J. Chem. Soc., Dalton Trans.* **1995**, 1671−1675. − [23c] N. Masciocchi, E. Corradi, M. Moret, G. A. Ardizzoia, A. Maspero, G. La Monica, A. Sironi, *Inorg. Chem.* **1997**, *36*, 5648−5650. − [23d] N. Masciocchi, G. A. Ardizzoia, G. La Monica, A. Maspero, A. Sironi, *Angew. Chem. Int. Ed. Engl.,* **1998**, *37*, 3366−3369. *Angew. Chem.* **1998**, *110*, 3561−3564. − [23e] N. Masciocchi, G. A. Ardizzoia, A. Maspero, G. La Monica, A. Sironi, *Inorg. Chem.* **1999**, *38*, 3657−3664.
[24] [24a] J. E. Mark, H. R. Alcock, R. West, *Inorganic Polymers*, Prentice Hall, Englewood Cliffs, **1992**. − [24b] *Inorganic and Organometallic Polymers II* (Eds.: P. Wisian-Neilson, H. R. Alcock, K. J. Wynne), ACS Symposium Series 572, American Chemical Society, Washington, **1994**.
[25] M. O. Albers, E. Singleton, N. J. Coville, *Inorg. Synth.* **1990**, *28*, 160−165.
[26] SAINT, **1994**, Bruker AXS Inc., Madison, Wisconsin.
[27] G. M. Sheldrick, unpublished results.
[28] A. Altomare, M. C. Burla, M. Camalli, G. L. Cascarano, C. Giacovazzo, A. Guagliardi, A. G. G. Moliterni, G. Polidori, R. Spagna, *J. Appl. Crystallogr.* **1999**, *32*, 115−119.
[29] G. M. Sheldrick, SHELXL-97: *Program for structure refinement*, University of Göttingen, Germany, **1997**.
[30] Crystallographic data (excluding structure factors) for the structures in this paper have been deposited with the Cambridge Crystallographic Data Centre as supplementary publication no. CCDC-132468 (**1**), CCDC-132469 (**3**) and CCDC-132470 (**5**). Copies of the data can be obtained, free of charge, on application to CCDC, 12 Union Road, Cambridge CB2 1EZ, UK, [Fax: (internat.) + 44-1223/336-033; E-mail: deposit@ccdc.cam.ac.uk].
[31] A. Le Bail, H. Duroy, J. L. Fourquet, *Mat. Res. Bull.* **1988**, *23*, 447−452.
[32] A. C. Larson, R. B. Von Dreele, *Lansce, Ms-H805*, Los Alamos National Laboratory, Los Alamos, New Mexico, **1990**.

Received August 26, 1999
[I99313]

The Interaction between Amminehalocobalt(III) Cations and Polythionate Anions: Hydrogen-Bonding Patterns and S–S Bond Cleavage Reactions

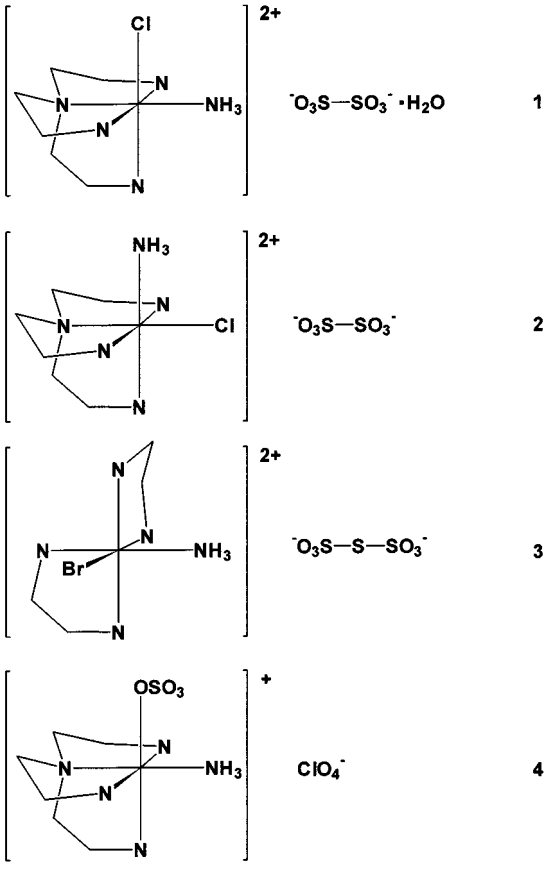
Hyungphil Chun,[a] W. Gregory Jackson,[b] Josephine A. McKeon,[b] Fernando B. Somoza, Jr.,[a] and Ivan Bernal*[a]

Keywords: Cobalt(III) / Dithionate / Trithionate / Sulfato ligand

Crystal structures of amminehalocobalt(III) compounds with di- or trithionate anions have been determined in order to know whether they interact to adopt specific molecular packing patterns and whether di- and trithionate anions undergo the S–S bond cleavage reactions as has been found for the $S_4O_6^{2-}$ ion. In the structures of *p*-[Co(tren)(NH_3)Cl]-S_2O_6•H_2O (**1**) and *t*-[Co(tren)(NH_3)Cl]S_2O_6 (**2**), the configurational differences in the cations dictate the hydrogen-bonding pattern with the dithionate anion to lead to racemic structures. *cis*-[Co(en)$_2$(NH_3)Br]S_3O_6 (**3**) also crystallizes in a racemic space group $P2_1/c$ in which the ions form a macrocyclic hydrogen-bonded network. Aqueous solutions of $S_3O_6^{2-}$ and *p*-[Co(tren)(NH_3)Cl]$^{2+}$ produce *p*-[Co(tren)(NH_3)(OSO_3)]ClO_4 (**4**) which is believed to be derived from the hydrolytic cleavage of S–S bond in the trithionate anion. These results reinforce our previous observation of the S–S cleavage reactions for the tetrathionate anion.

In the course of investigating crystallization behavior of Werner-type cobalt(III) compounds, Bernal et al. reported that the *cis*-[Co(en)$_2$(NH_3)Br]$^{2+}$ cation spontaneously resolves into its optical antipodes when crystallized with the $S_4O_6^{2-}$ ion.[1] And, in a recent study, we reported that when the $S_4O_6^{2-}$ ion was used to crystallize the *cis*-α-[Co(trien)(NH_3)Cl]$^{2+}$ ion, an unexpected cleavage at a S−S bond, followed by a disproportionation, occurs to give *cis*-α-[Co(trien)(NH_3)Cl]S_5O_6.[2] Also reported in that paper was the crystal structure of K[Co(tren)(NH_3)(OSO_3)]-S_4O_6·2H_2O produced by the same cleavage reaction of $S_4O_6^{2-}$ ion. These observations led us to further investigate the hydrogen-bonding modes of amminehalocobalt(III) cations with polythionate anions and the specificity of S−S bond cleavage reactions.

In this study, we discuss the crystal structures of *p*-[Co(tren)(NH_3)Cl]S_2O_6·H_2O (**1**), *t*-[Co(tren)(NH_3)Cl]S_2O_6 (**2**), *cis*-[Co(en)$_2$(NH_3)Br]S_3O_6 (**3**) and *p*-[Co(tren)(NH_3)-(OSO_3)]ClO_4 (**4**). Although the cations of **1** and **2** differ only in the position of the NH_3 ligand with respect to the tertiary nitrogen atom of the tren ligand, their molecular packing structures show totally different hydrogen-bonding patterns leading to the racemic structures. The crystal structure of **3** is interesting in that the cation crystallizes as a conglomerate with a tetrathionate anion[1] but as a racemate with two bromide ions and two water molecules of crystallization.[3] Compound **3** also is interesting when viewed against the fact that the $S_3O_6^{2-}$ ion underwent a hydrolytic cleavage reaction while the chloro ligand of the *p*-[Co(tren)(NH_3)Cl]$^{2+}$ ion was replaced to produce compound **4**.



Although both *p* and *t* isomers of the [Co(tren)(NH_3)Cl]$^{2+}$ ion and their related compounds have been studied extensively by Buckingham and co-workers,[4−6] their crystal

[a] Department of Chemistry, University of Houston
Houston, TX 77204−5641, USA
Fax: (internat.) + 1-713/743−2709
E-mail: ibernal@uh.edu
[b] School of Chemistry, University College, The University of New South Wales, Australian Defence Force Academy
Campbell, ACT, Australia 2600

 © WILEY-VCH Verlag GmbH, D-69451 Weinheim, 2000 1434−1948/00/0101−0189 $ 17.50+.50/0

structures have not been reported in the CSD[7] except for a few compounds with an *N*-methylated tren ligand.[8] Also it is noted that Asakura et al. reported a chiral autocatalysis reaction leading to the preparation of an optically pure form of the cation of **3** as a bromide salt without water molecules of crystallization.[9]

Results and Discussion

As described by Buckingham and co-workers,[4] the red compound *p*-[Co(tren)(NH_3)Cl]Cl·ClO_4 was prepared by ligand substitutions of four ammine groups with the tren ligand followed by acidic cleavage (HCl) of the peroxo bridge of [Co(NH_3)$_5$(O_2)(NH_3)$_5$Co](NO_3)4·2H2O and then converted into a dithionate salt to give compound **1**. Its molecular structure is shown in Figure 1.

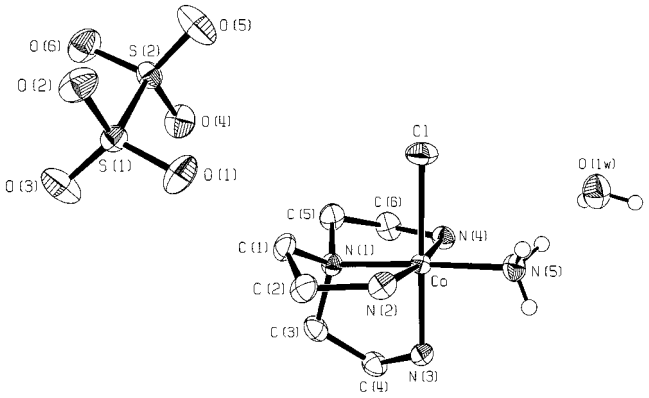


Figure 1. ORTEP diagram of **1** drawn at 50% probability level; hydrogen atoms of the tren ligand have been omitted for clarity; selected bond lengths and angles: Co−N(1) 1.964(2), Co−N(2) 1.967(2), Co−N(3) 1.930(2), Co−N(4) 1.963(2), Co−N(5) 1.959(2), Co−Cl 2.2783(9), S(1)−S(2) 2.1357(9) Å; N(1)−Co−N(5) 177.33(10), N(2)−Co−N(4) 171.32(9), N(3)−Co−Cl 178.70(7)°

In the geometry of the cobalt cation, the largest deviation from a regular octahedron is the angle N(2)−Co−N(4) [171.32(9)°]and N(5)−Co−Cl [87.21(8)°]. The former is a consequence of the geometrical features of the tren ligand and the latter is attributed to the weak the internal hydrogen bonds between Cl and hydrogen of the ammine ligand. For the anion, two S−O bond lengths, S(1)−O(1), 1.435(2) Å and S(2)−O(5), 1.436(2) Å, are significantly shorter than the other four [average 1.452(2) Å] and the two oxygen atoms do not participate in any hydrogen bond shorter than 2.5 Å.

When [Co(tren)Cl_2]Cl is stirred in a warm methanolic ammonia solution, the other isomer *t*-[Co(tren)(NH_3)Cl]Cl_2 is isolated as a reddish purple microcrystalline precipitate with a reasonable yield (> 50%) and then converted into a dithionate salt to give compound **2**. In the structure shown in Figure 2, the crystallographic asymmetric unit contains the cobalt cation and two $-SO_3$ fragments of a dithionate anion in different positions.

The fragment generates the other half when an inversion symmetry operation is performed. The structural parameters for the cation and anion show the same trends as those

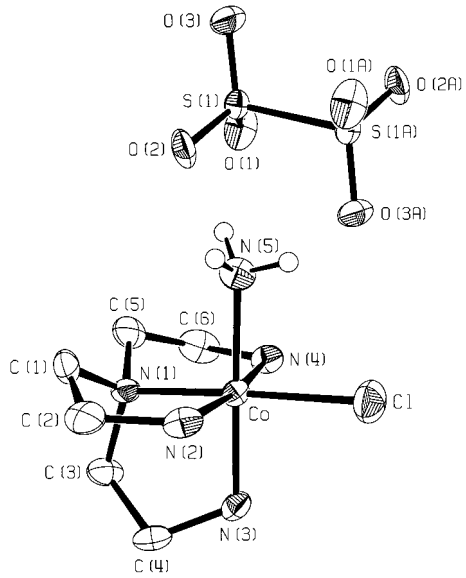


Figure 2. Molecular structure of **2**; hydrogen atoms of the tren ligand have been omitted for clarity; selected bond lengths and angles: Co−N(1) 1.949(4), Co−N(2) 1.959(5), Co−N(3) 1.939(5), Co−N(4) 1.946(5), Co−N(5) 1.976(5), Co−Cl 2.247(2), S(1)−S(1A) 2.114(3) Å; N(2)−Co−N(4) 171.5(2), N(3)−Co−N(5) 178.3(2), N(1)−Co−Cl 176.56(13)°

of **1** described above. **3** was prepared by adding an aqueous solution of $K_2S_3O_6$ to a saturated solution of *cis*-[Co($en)_2$(NH_3)Br]Br_2 and its molecular structure is shown in Figure 3.

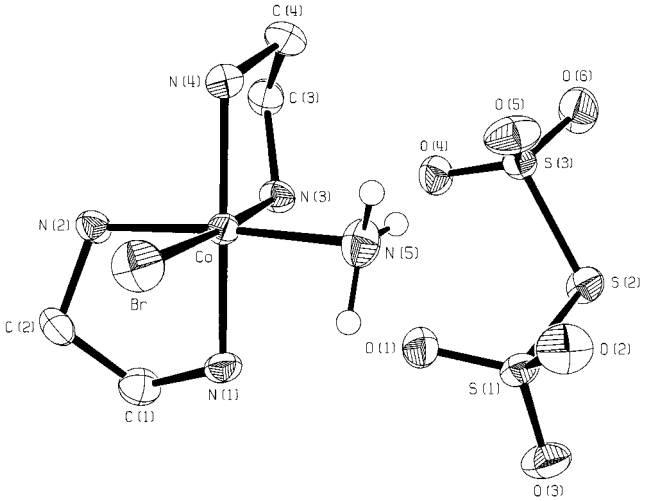


Figure 3. Molecular structure of **3**; hydrogen atoms of the en ligands have been omitted for clarity; selected bond lengths and angles: Co−N(1) 1.945(3), Co−N(2) 1.958(3), Co−N(3) 1.961(3), Co−N(4) 1.962(3), Co−N(5) 1.960(4), Co−Br 2.3915(10), S(1)−S(2) 2.1120(13), S(2)−S(3) 2.092(2) Å; N(1)−Co−N(4) 176.81(14), N(2)−Co−N(5) 174.7(2), N(3)−Co−Br 176.42(11), S(1)−S(2)−S(3) 102.71(7)°

In the structure, the two S−S bonds of the trithionate anion are not equal in distances [2.1120(13) and 2.092(2) Å] and the six S−O lengths fall within their 3σ ranges with the average of 1.443(3) Å.

For compound **4**, a solution mixture of *p*-[Co(tren)(NH_3)Cl]Cl·ClO_4 and $K_2S_3O_6$ did not yield any

crystalline product, unlike the compounds **1** and **2**, which began to crystallize almost immediately after mixing the two reactants. Instead, a white powdery precipitate was slowly deposited on the bottom of the beaker as the solvent evaporated. When the solution was concentrated, it was divided into four portions. Three of them were used for liquid diffusion with acetone, ethanol and acetonitrile and from the fourth the solvent was allowed to evaporate slowly. Only the one with ethanol produced a small amount of red crystals after standing for several weeks. A suspicion for the integrity of the trithionate thus entered our mind and was later proved to be true when we solved the structure. The structure and geometrical parameters of the cation shown in Figure 4 are very similar to the one produced by hydrolytic cleavage of the $S_4O_6^{2-}$ anion.[2]

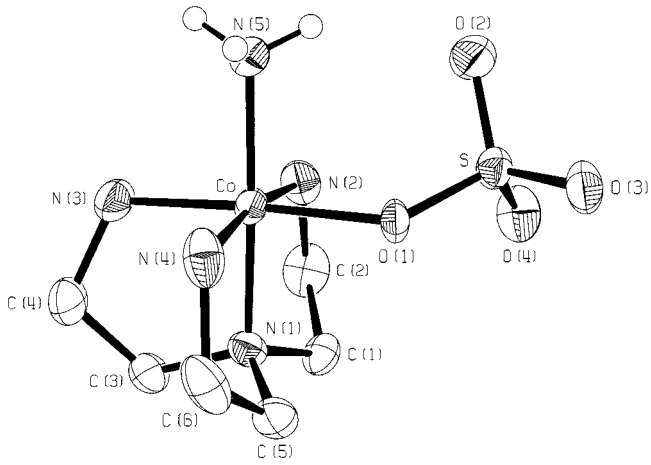


Figure 4. View of the cation of **4**; hydrogen atoms of the tren ligand have been omitted for clarity; selected bond lengths and angles: Co−N(1) 1.962(4), Co−N(2) 1.935(5), Co−N(3) 1.926(5), Co−N(4) 1.974(5), Co−N(5) 1.955(5), Co−O(1) 1.958(3), S−O(1) 1.510(4), S−O(2) 1.460(4), S−O(3) 1.464(4), S−O(4) 1.476(4) Å; N(1)−Co−N(5) 178.1(2), N(2)−Co−N(4) 170.8(2), N(3)−Co−O(1) 175.1(2), Co−O(1)−S 131.3(2)°

In the packing structure of **1**, shown in Figure 5, a dithionate anion displays hydrogen bonds with a cation in a side-on fashion.

Such one-to-one side-on contacts are possible because the ammine ligand is *cis* to all three hydrogen-bearing nitrogen atoms of the tren ligand. That is, the so-called *p* configuration of the cation allows the hydrogen atoms of N-donor atoms to be arranged around two trigonal faces of an octahedron. The closest hydrogen bond found was between the oxygen atom of a water molecule and a hydrogen atom of the ammine ligand [2.005(42) Å].

The apparently complicated packing structure of **2**, shown in Figure 6, can be best understood by realizing that the three hydrogen-bearing nitrogen atoms of the tren and the NH_3 ligands are lying on the same plane.

As a consequence, four dithionate anions are arranged around a tetragonal basal plane of an octahedron to form hydrogen bonds with hydrogen atoms of tren and of the NH_3 ligand. Since the anions are positioned on crystallographic inversion centers, as mentioned above, the two cobalt cations connected to $-SO_3$ ends of a dithionate anion by hydrogen bonds are a racemic pair.

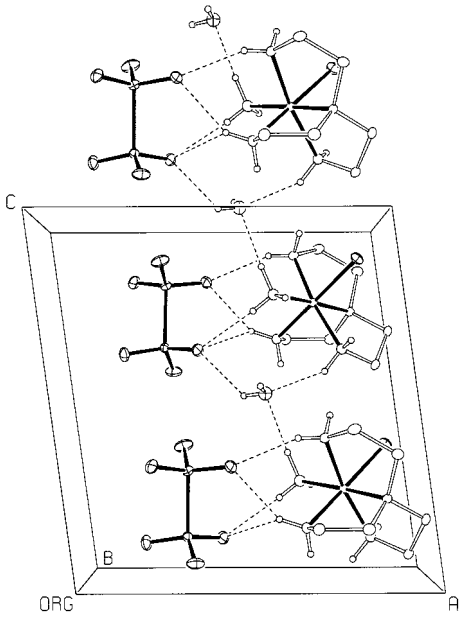


Figure 5. Packing of ions and water molecules of crystallization of **1**; the molecules shown are related by *c*-glide plane symmetry; hydrogen bonds shorter than 2.5 Å are shown as dotted lines

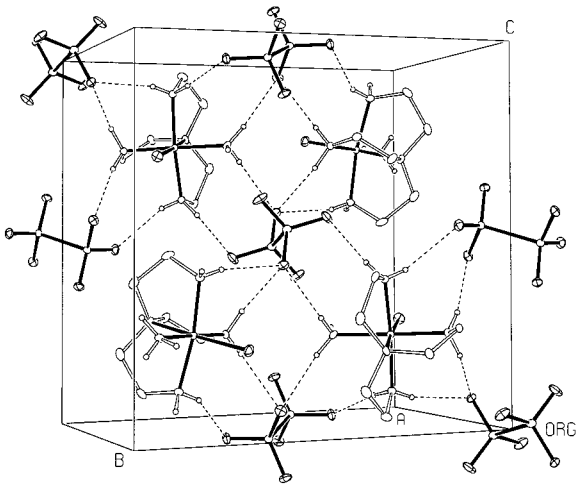


Figure 6. Packing diagram of **2** showing hydrogen-bonded interactions; note that dithionate anions are positioned on crystallographic inversion centers.

Figure 7 depicts the packing of *cis*-$[Co(en)_2(NH_3)Br]^{2+}$ ions with trithionate anions in **3**.

In the structure, an $-SO_3$ end of a trithionate ion bridges two neighboring cations to form a macrocyclic hydrogen-bonded network made of four molecules. Meanwhile, the $-SO_3$ moieties, which are not involved in forming the network, have contacts with other cations located along the *a* axis of the unit cell, and those cations form the macrocyclic networks again.

Trithionate ($S_3O_6^{2-}$) has been known to thermally decompose to produce SO_4^{2-}, SO_2 and S in aqueous solution.[10] And as the preparation and structure of **3** implies, the divalent anion is perfectly stable in aqueous solutions

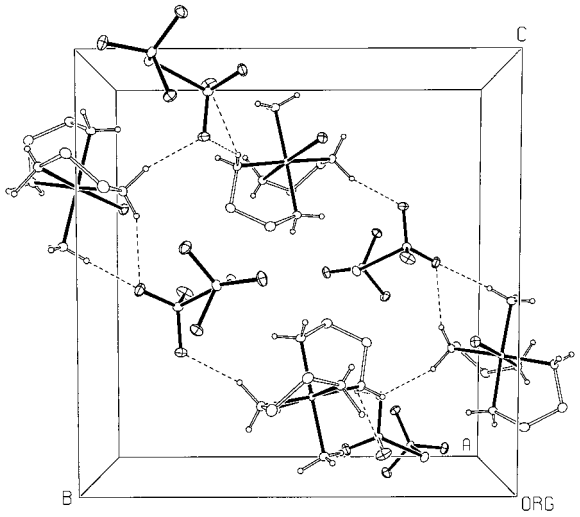


Figure 7. Macrocyclic hydrogen-bonded network structure of **3**; dotted lines represent hydrogen bonds shorter than 2.5 Å

at room temperature for the relatively short period of time required for crystallization. However, the production of compound **4**, in conjunction with our previous report,[2] might suggest the ability of $[CoN_4(NH_3)X]^{n+}$ ions [where N_4 is tren or trien, but not $(en)_2$] to apparently promote the cleavage reactions of S−S bonds in a series of polythionates. Dithionate, which has no reduced form of sulfur atoms, however, does not readily cleave its single S−S bond (although it does in strong acid, albeit slowly).

The trien and especially the tren complexes are slow to hydrolyze by the spontaneous pathway, but are very base-sensitive, and base-catalyzed hydrolysis of bound Cl^- or Br^- is the major contribution to the hydrolysis rate even at pH = 7−8. Certainly, color changes consistent with formation of $[CoN_4(NH_3)(OH_2)]^{3+}$ are observed for solutions of these ions in water, in the presence or absence of polythionates, over periods of hours. Thus, for tren and trien complexes where the time scale for the crystallization are long (days to weeks), sulfato complexes are formed, and sulfur, free sulfate and polythionates of different stoichiometry are also formed by hydrolysis and disproportionation of the original polythionate (be it $S_4O_6^{2-}$ or $S_3O_6^{2-}$). Slow anation of the aquametal complex by sulfate logically accounts for the formation of the sulfato complex, and it preferentially crystallizes from solution simply because it is less soluble than the other components. We also note that the crystalline potassium polythionate salts have a finite shelf life, $K_2S_4O_6$, $K_2S_5O_6$ and $K_2S_6O_6$ in particular, such that fresh solutions of aged salts (months to years) can lead to the immediate crystallization of unexpected polythionates. Moreover, we note that the published syntheses[11] of the penta- and hexathionates are not particularly reproducible.

Activation to hydrolysis through metal ion coordination of amino acid esters and peptides have long been known and well documented,[12,13] and a similar mechanism for $S_nO_6^{2-}$ merits consideration. For example, polythionate complexes $[Co(N)_4(NH_3)O_3S(S)_nSO_3]^+$ might be formed

Table 1. Summary of data collection and refinements

	1	**2**	**3**	**4**
Empirical formula	$C_6H_{23}ClCoN_5O_7S_2$	$C_6H_{21}ClCoN_5O_6S_2$	$C_4H_{19}BrCoN_5O_6S_3$	$C_6H_{21}ClCoN_5O_8S$
Molecular mass	435.79	417.78	468.26	417.72
λ [Å]	0.71073	0.71073	0.71073	0.71073
Crystal system	monoclinic	monoclinic	monoclinic	monoclinic
Space group	$P2_1/c$	$P2_1/n$	$P2_1/c$	$P2_1/c$
a [Å]	11.310(2)	8.640(2)	8.207(1)	12.875(4)
b [Å]	11.602(6)	13.356(4)	13.356(2)	8.675(4)
c [Å]	11.958(2)	13.103(4)	13.543(1)	14.234(5)
β [°]	97.96(2)	91.88(3)	93.54(9)	111.51(3)
V [Å^3]	1553.9(9)	1511.2(8)	1482.8(3)	1479.2(9)
Z	4	4	4	4
$D_{calcd.}$ [g/cm^3]	1.863	1.836	2.098	1.876
μ [mm^{-1}]	1.586	1.622	4.305	1.531
$F(000)$	904	864	944	864
Crystal size [mm]	0.48 × 0.46 × 0.23	0.50 × 0.12 × 0.11	irregular fragment	0.64 × 0.47 × 0.35
θ_{max} [°]	25.00	24.97	27.56	25.98
Index ranges (h,k,l)	±13, +12, +14	±10, +15, +15	±10, +17, +17	±15, +10, +17
Total reflections	2803	2761	3570	3025
Independent (R_{int})	2668 (0.0274)	2647 (0.0337)	3436 (0.0534)	2900 (0.0352)
Observed [$I > 2\sigma(I)$]	2165	1407	2509	1405
Absorption correction	ψ scans	ψ scans	ψ scans	ψ scans
T_{max}/T_{min}	0.9950/0.8277	0.9730/0.9111	0.9996/0.5920	0.9991/0.8898
Refinement method	Full-matrix least-squares on F^2	Full-matrix least-squares on F^2	Full-matrix least-squares on F^2	Full-matrix least-squares on F^2
Data/parameters	2668/291	2647/274	3436/257	2900/202
GOF on F^2	1.072	0.958	0.981	0.981
Final R indices [$I > 2\sigma(I)$]	R_1 = 0.0264 wR_2 = 0.0707	R_1 = 0.0404 wR_2 = 0.0801	R_1 = 0.0393 wR_2 = 0.1035	R_1 = 0.0454 wR_2 = 0.1205
R indices (all data)	R_1 = 0.0380 wR_2 = 0.0741	R_1 = 0.1223 wR_2 = 0.0924	R_1 = 0.0626 wR_2 = 0.1117	R_1 = 0.1380 wR_2 = 0.1388
Largest diff. peak and hole [e/Å^3]	0.375 and −0.403	0.500 and −0.410	1.314 and −0.911	0.546 and −0.419

from the aqua complex by anation, and cleaved at the S−S bond nearest the polarizing Co^{III} center by activated hydrolysis, thereby providing the sulfato complex. We have as yet not performed the appropriate control experiments to either support or discount this mechanism, but note that the synthesis of even the simplest polythionate complex, $[Co(NH_3)_5O_3SSO_3]^+$, has so far eluded us. Chelated polythionates are likely to be more viable, and we are presently investigating potential 5- and 6-membered ring systems derived from $S_2O_6^{2-}$ and $S_3O_6^{2-}$, respectively, in the *cis*-$[Co(en)_2X_2]^+$ system.

In summary, di- and trithionate anions do not show a specific hydrogen-bonding pattern with amminehalocobalt(III) cations; according to the geometrical arrangement of hydrogen atoms around the coordination sphere, they show a one-to-one side-on pattern or play end-on bridging roles. Sulfur−sulfur bonds in polythionates other than $S_2O_6^{2-}$ seem to be prone to slow hydrolytic cleavage reactions at room temperature.

Experimental Section

General: *p*-$[Co(tren)(NH_3)Cl]Cl{\cdot}ClO_4$ and *t*-$[Co(tren)(NH_3)Cl]Cl_2$ were prepared by known methods[4] except for chromatographic procedures. *cis*-$[Co(en)_2(NH_3)Br]Br_2$ was prepared by the method reported earlier.[3] $Na_2S_2O_6{\cdot}2H_2O$ (Fisher Scientific Company) was used as received. Elemental analyses were carried out by the Galbraith laboratories.[14]

$K_2S_3O_6$: Each of the two methods described in Brauer's book[11] was used. A set of X-ray data was collected for a single crystal to confirm its structure. The structure is known[15]: orthorhombic, *Pmnb*, $a = 5.751(6)$, $b = 9.810(1)$, $c = 13.700(3)$, $Z = 4$ and $R = 0.0381$ for 672 observed reflections [$> 2\sigma(I)$]. − $K_2S_3O_6$ (270.37): calcd. S 35.57; found S 35.73.

***p*-$[Co(tren)(NH_3)Cl]S_2O_6{\cdot}H_2O$ (1):** A solution of partly dissolved *p*-$[Co(tren)(NH_3)Cl]Cl{\cdot}ClO_4$ (1.97 g, 5 mmol) in 40 mL of water was filtered directly into a 50-mL aqueous solution containing $Na_2S_2O_6{\cdot}2H_2O$ (7.27 g, 30 mmol) so that the two solutions formed layers. Dark red crystals began to grow within 30 min. − $C_6H_{23}ClCoN_5O_7S_2$ (435.79): calcd. C 16.54, H 5.33, Cl 8.13, Co 13.52, N 16.08, S 14.71; found C 16.24, H 5.52, Cl 8.20, Co 14.03, N 15.79, S 15.10.

***trans*-$[Co(tren)(NH_3)Cl]S_2O_6$ (2):** 0.40 g(1.2 mmol) of *t*-$[Co(tren)(NH_3)Cl]Cl_2$ was dissolved in 5 mL of water and added to a 10-mL aqueous solution of 0.50 g (2.1 mmol) of $Na_2S_2O_6{\cdot}2H_2O$. Purple crystals were formed immediately and collected the next day (0.21 g, 41%). − $C_6H_{21}ClCoN_5O_6S_2$ (417.77): calcd. C 17.25, H 5.07, N 16.76; found C 17.31, H 5.08, N 16.35.

***cis*-$[Co(en)_2(NH_3)Br]S_3O_6$ (3):** To a saturated solution of *cis*-$[Co(en)_2(NH_3)Br]Br_2$ in water was added an aqueous solution of $K_2S_3O_6$. Crystals suitable for X-ray work were grown from water by the same method but using more dilute solutions. − $C_4H_{19}BrCoN_5O_6S_3$ (468.24): calcd. C 10.29, H 4.09, N 14.96; found C 10.28, H 4.16, N 14.85.

***p*-$[Co(tren)(NH_3)(OSO_3)]ClO_4$ (4):** This compound was prepared by the same method used for **1** except for using $K_2S_3O_6$ instead of $Na_2S_2O_6{\cdot}2H_2O$. The solution was frequently filtered off in order to remove a white powdery precipitate, most likely S and $KClO_4$. A small amount of single crystals were obtained by liquid diffusion with ethanol after 2 months.

Crystallography: For all four compounds, the intensity data were collected with an Enraf−Nonius CAD-4 diffractometer at room temperature and SHELXS-86[16] and SHELXL-93[17] were used to solve and refine the structures. All the hydrogen atoms of **1**, **2** and **3** were located from difference maps and refined isotropically; those of **4** were placed in their geometrically ideal positions with isotropic temperature factors 1.2 times those of the attached non-hydrogen atoms. In the refinement of **3**, relatively large residual electron densities found in the final difference map were ignored since they are too close to cobalt and bromide (< 1 Å). The structures of **2** and **4**, for which many weak reflections were collected, yielded *R* factors a little higher than the other two. Parameters for data collection and structure refinements are summarized in Table 1. Crystallographic data (excluding structure factors) for the structures reported in this paper have been deposited with the Cambridge Crystallographic Data Centre[7] as supplementary publication no. CCDC-118583 to -118586. Copies of the data can be obtained free of charge on application to CCDC, 12 Union Road, Cambridge CB2 1EZ, UK [Fax: int. code + 44-1223/336-033; E-mail: deposit@ccdc.cam.ac.uk].

Acknowledgments

We thank the Robert A. Welch Foundation for support of this research (Grant E-592 to I. B.) and for a fellowship granted to H. C. Financial support from the Australian Research Council (to W. G. J.) is gratefully acknowledged, and also, I. B. thanks the National Science Foundation for the funds used in purchasing the diffractometer.

[1] I. Bernal, J. Cetrullo, W. G. Jackson, *Inorg. Chem.* **1993**, *32*, 4098.
[2] H. Chun, I. Bernal, *Eur. J. Inorg. Chem.* **1999**, 717.
[3] I. Bernal, J. Cetrullo, W. G. Jackson, *J. Coord. Chem.* **1993**, *28*, 89.
[4] D. A. Buckingham, P. J. Creswell, A. M. Sargeson, *Inorg. Chem.* **1975**, *14*, 1485.
[5] M. J. Gaudin, C. R. Clark, D. A. Buckingham, *Inorg. Chem.* **1986**, *25*, 2569.
[6] D. A. Buckingham, C. R. Clark, W. S. Webley, *Aust. J. Chem.* **1980**, *33*, 263.
[7] Cambridge Crystallographic Data Centre, 12 Union Road, Cambridge, CB2 1EZ, UK.
[8] D. A. Buckingham, J. D. Edwards, G. M. McLaughlin, *Inorg. Chem.* **1982**, *21*, 2770.
[9] K. Asakura, K. Kobayashi, Y. Mizusawa, T. Ozawa, S. Osami, S. Yoshikawa, *Physica D* **1995**, *84*, 72.
[10] W. G. Palmer, *Experimental Inorganic Chemistry*, Cambridge University Press, **1954**, p. 372.
[11] F. Fehér in *Handbook of Preparative Inorganic Chemistry*, 2nd ed. (Ed.:G. Brauer), Academic Press, New York, **1967**, vol. 1, p. 398.
[12] R. W. Hay, P. J. Morris in *Metal Ions in Biological Systems* (Ed.: H. Sigel), vol. 5, Basel, New York, **1976**, p. 224.
[13] P. A. Sutton, D. A. Buckingham, *Acc. Chem. Res.* **1987**, *20*, 357.
[14] Galbraith Laboratories, Inc., P. O. Box 51610, Knoxville, TN, 37950−1610, USA.
[15] J. M. Stewart, J. T. Szymanski, *Acta Crystallogr.* **1979**, *B35*, 1967.
[16] G. M. Sheldrick, *Acta Crystallogr.* **1990**, *A46*, 467.
[17] G. M. Sheldrick, *SHELXL-93, A program for crystal structure determination*, University of Göttingen, **1993**.

Received April 27, 1999
[I99148]

Synthesis, Crystal Structures, and Solution Properties of *N*-Methylene(phenyl)phosphinic Acid Derivatives of Cyclen and Cyclam

Jan Rohovec,[a] Mojmír Kývala,[a] Pavel Vojtíšek,[a] Petr Hermann,[a] and Ivan Lukeš*[a]

Keywords: Acid derivatives / Cyclen and cyclam derivatives / Phosphinic acid / Potentiometry / Protonation and stability constants / ^{31}P-NMR titration / Hydrogen bonding

Two phenylphosphinic acid derivatives of tetraaza macrocycles, (1,4,7,10-tetraazacyclododecanetetrayl)tetrakis(methylene)tetrakis(phenylphosphinic acid)] (H_4L^1) and (1,4,8,11-tetraazacyclotetradecanetetrayl)tetrakis(methylene)tetrakis(phenylphosphinic acid)] (H_4L^2), were synthesised and the crystal structures of H_4L^2 and its bis(1-adamantylammonium) salt were determined. In both the structures, the ring conformation is virtually the same and is stabilised by hydrogen bonds. Protonation constants of the acids and stability constants of their Zn^{2+} and Cd^{2+} complexes were determined pH-metrically at 25 °C and at an ionic strength of 0.1 mol dm^{-3} (KNO_3). The pK_A values found for both the compounds are lower than those for their carboxylic analogues and correspond to the expected electron-withdrawing ability of the –P(Ph)O_2H moiety. The value pK_1 of the last dissociation constant of H_4L^1 is surprisingly high. The complexes of Zn^{2+} and Cd^{2+} with $(L^1)^{4-}$ and $(L^2)^{4-}$ are less stable than those with other similar ligands, which is in accordance with lower overall basicity of H_4L^1 and H_4L^2. A pronounced drop in the stability of the complexes of H_4L^2 can be explained by partial coordination of the ligand to the metal ions. The solution properties of the ligands were also investigated by ^{31}P-NMR spectroscopy. The spectra observed suggest stable (on the NMR time scale) conformations of the protonated ligands in solution. A comparison of NMR spectra in solution and CP/MAS-NMR spectra indicates that the structures of the conformers roughly correspond to the structures observed in the solid state. The conformations are stabilised by intramolecular hydrogen bonds and by hydrophobic interactions of phenylphosphinic moieties. The conformers are stable even at 90 °C, but not in the presence of complexing metal ions.

A large number of derivatives of 12- and 14-membered tetraazamacrocycles, "cyclen" and "cyclam", have been described. The macrocycles are usually substituted on the nitrogen atoms by four identical pendant groups. The selectivity of complexation (i.e. the stability of the complexes) of such ligands towards various metal ions can be tuned by adjusting the ring size, the number or kind of coordinating atoms in the ring and the type of side chain.[1] Tetraazacycles with acetate side chains and their complexes are the most thoroughly studied substances of this kind.[2] They form thermodynamically very stable complexes, the most stable being generally those formed with di- and trivalent metals.[1][2] Some of the complexes formed are kinetically inert; e.g. with lanthanides.[3] These complexes have been widely tested because of their use, e.g. as contrast substances in MRI,[4] for labelling antigenic antibodies using metal radioisotopes[4c,5] for both diagnostic and therapeutic purposes, and also as catalysts for the splitting of nucleic acids.[6]

Some years ago, a study of aza cycles with side chains containing a methylenephosphonic[7–9] ($-CH_2-PO_3H_2$) or methylenephosphinic[7a,10–16] [$-CH_2-P(R)O_2H$] groups was begun, in a search for ligands with properties different from those containing acetic acid groups. Variation of the R group should also contribute to a change in the ion selectivity and properties of the macrocyclic compounds. Therefore, we studied the influence in a series of simple aminomethylphosphinic acids $H_2NCH_2P(R')O_2$ H, where R′ = H, methyl, phenyl, or *tert*-butyl.[17] Changes in complexing properties of the simple acids were surprisingly large, the formation constants increasing from phenyl to methyl, *tert*-butyl and hydrogen substituents. Except for R′ = H, the order follows that of the increasing basicity of the acids. Thus, we focused on the study of the influence of the methylene(phenyphosphinic acid) substituent on complexing properties of the 12- and 14-membered tetraazacycles. We have reported on the synthesis of 1,4,7-triazacyclononane and 1,4,7,10-tetraazacyclododecane functionalised with methylenephosphinic pendant groups [R = $-CH_2-P(H)O_2H$].[18] In the present paper, we report the synthesis, structure and solution properties of two polyazamacrocycle ligands; the previously described[19] (1,4,7,10-tetraazacyclododecanetetrayl)tetrakis(methylene)tetrakis(phenylphosphinic acid)] (H_4L^1), and the new ligand (1,4,8,11-tetraazacyclotetradecanetetrayl)tetrakis(methylene)tetrakis(phenylphosphinic acid)] (H_4L^2). The formulae of both the ligands studied, together with those of analogous ligands known from the literature and mentioned in the discussion, are shown in the following scheme.

Results and Discussion

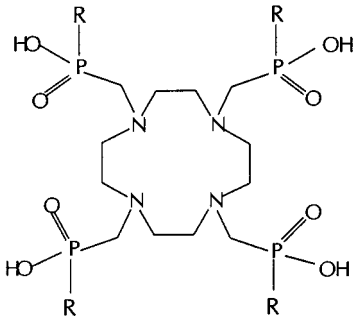
Synthesis

Compounds H_4L^1 and H_4L^2 were synthesised by the Mannich reaction of 1,4,7,10-tetraazacyclododecane tetra-

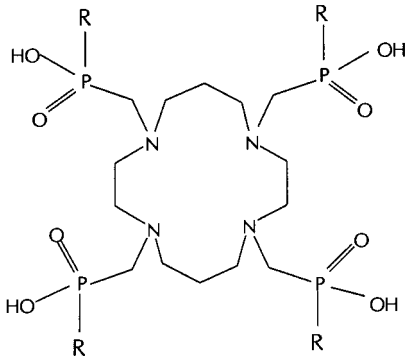
[a] Department of Inorganic Chemistry, Universita Karlova (Charles University),
Albertov 2030, 128 40 Prague 2, Czech Republic

Supporting information for this article is available on the WWW under http://www.wiley-vch.de/home/eurjic or from the author.

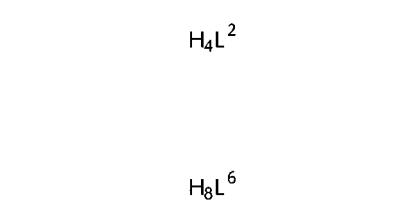
 © WILEY-VCH Verlag GmbH, D-69451 Weinheim, 2000 1434–1948/00/0101–0195 $ 17.50+.50/0



R = Ph H_4L^1
R = H H_4L^3
R = Et H_4L^4
R = OH H_8L^5



H_4L^2



H_8L^6

hydrochloride and 1,4,8,11-tetraazacyclotetradecane tetrahydrochloride, respectively, with paraformaldehyde and phenylphosphinic acid in aqueous HCl. The reaction conditions, i.e. concentration of HCl, rate of the addition of paraformaldehyde and temperature in the range 50−110 °C, were optimised for both the syntheses and the best conditions are described in the Experimental Section. The ligand H_4L^2 precipitated from the reaction mixture as $H_4L^2 \cdot n\,HCl$ ($n = 3-4$) and was purified by recrystallisation from methanol containing propylene oxide to give the free acid. The ligand H_4L^1 was isolated as an oily ammonium salt after ion-exchange chromatography of the reaction mixture and was subsequently converted into the free acid by acidification. In some cases, the acid contained traces of HCl, which were usually removed in high vacuum over KOH. Samples of the ligands for potentiometric measurements were recrystallised from MeOH solution containing propylene oxide to remove any traces of HCl. Elemental analysis, thin layer chromatography, ^{31}P-CP/MAS-NMR spectra of the bulk materials, and X-ray analysis of H_4L^2 indicate that both the compounds were obtained in the pure form.

Synthesis of phosphinic acid derivatives of azamacrocycles by the Mannich reaction in acid aqueous solution seems to be a convenient reaction; however, the reaction conditions for each phosphinic acid and azamacrocycle have to be optimised to reduce *N*-methylation of the cycle.[20] In accordance with the literature,[20][21] we can confirm that the side reactions are suppressed by a lower temperature, higher acidity, higher concentration of reagents than is usually recommended and by the use of paraformaldehyde, instead of an aqueous solution of formaldehyde, and its slow addition.

Structure

In solving the structure of $H_4L^2 \cdot 4\,H_2O$ we wanted to confirm the protonation and conformation of the $(H_2L^2)^{2-}$ anion. Only bis(1-adamantylammonium) salt $(AdNH_3)_2(H_2L^2) \cdot 6\,H_2O$ was found to form crystals suitable for X-ray analysis. Structures of both the compounds are shown with the numbering scheme in Figures 1 and 2. Tables 1 and 2 list selected bond lengths and angles. Superposition of the molecular structures of H_4L^2 and $(H_2L^2)^{2-}$ is projected in Figure S1 (see Supplementary Material).

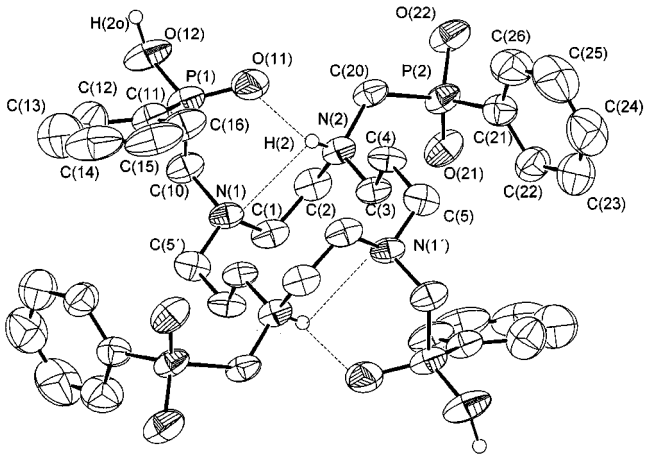


Figure 1. View of $H_4L^2 \cdot 4\,H_2O$ with the atom numbering scheme. The hydrogen bonds are denoted with primed lines

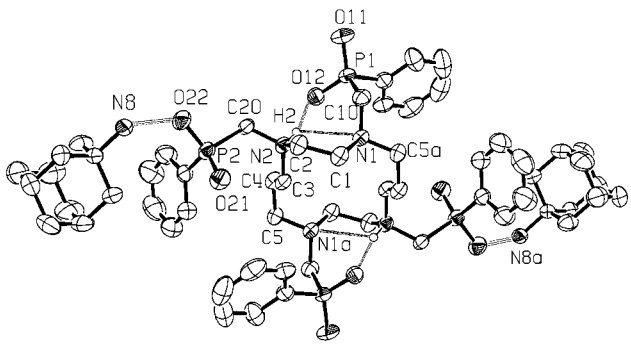


Figure 2. View of $(AdNH_3)_2(H_2L^2) \cdot 6\,H_2O$ with the atom numbering scheme. The hydrogen bonds in the structure of the $(H_2L^2)^{2-}$ anion are denoted with primed lines

Table 1. Selected bond lengths [Å], bond angles [°], and structure of $H_4L^2 \cdot 4\ H_2O$

The geometry of phosphorus atoms		
P(1)−O(11) 1.491(2)	O(11)−**P(1)**−O(12) 117.3(1)	O(12)−**P(1)**−C(11) 108.4(1)
P(1)−O(12) 1.520(2)	O(11)−**P(1)**−C(10) 108.8(1)	C(11)−**P(1)**−C(12) 109.3(1)
P(1)−C(10) 1.801(2)	O(11)−**P(1)**−C(11) 108.1(1)	
P(1)−C(11) 1.785(3)	O(12)−**P(1)**−C(10) 104.8(1)	
P(2)−O(21) 1.478(2)	O(21)−**P(2)**−O(22) 115.3(1)	O(22)−**P(2)**−C(21) 107.8(1)
P(2)−O(22) 1.527(2)	O(21)−**P(2)**−C(20) 112.9(1)	C(21)−**P(2)**−C(22) 107.6(1)
P(2)−C(20) 1.819(3)	O(21)−**P(2)**−C(21) 110.5(1)	
P(2)−C(21) 1.788(3)	O(22)−**P(2)**−C(20) 102.3(1)	
The geometry of atoms C(10) and C(20)		
C(10)−P(1) 1.801(3)	P(1)−**C(10)**−N(1) 112.0(2)	P(1)−**C(10)**−**N(1)**−C(1) 124.2(2)
C(10)−N(1) 1.480(3)		P(1)−**C(10)**−**N(1)**−C(5)[a] −10.4(2)
C(20)−P(2) 1.819(3)	P(2)−**C(20)**−N(2) 119.6(2)	P(2)−**C(20)**−**N(2)**−C(2) 71.7(3)
C(20)−N(2) 1.502(3)		P(2)−**C(20)**−**N(2)**−C(3) −59.6(3)
The geometry of the symmetrically independent part of the macrocyclic ring		
N(1)−C(1) 1.460(3)	C(5)[a]−**N(1)**−C(1) 111.7(2)	C(5)[a]−**N(1)**−**C(1)**−C(2) −170.6(2)
C(1)−C(2) 1.504(4)	N(1)−**C(1)**−C(2) 113.5(2)	N(1)−**C(1)**−**C(2)**−N(2) 46.1(3)
C(2)−N(2) 1.506(3)	C(1)−**C(2)**−N(2) 113.3(2)	C(1)−**C(2)**−**N(2)**−C(3) 59.7(3)
N(2)−C(3) 1.492(3)	C(2)−**N(2)**−C(3) 113.4(2)	C(2)−**N(2)**−**C(3)**−C(4) −166.8(2)
C(3)−C(4) 1.509(3)	N(2)−**C(3)**−C(4) 112.2(2)	N(2)−**C(3)**−**C(4)**−C(5) 179.1(2)
C(4)−C(5) 1.514(3)	C(3)−**C(4)**−C(5) 112.7(2)	C(3)−**C(4)**−**C(5)**−N(1)[a] −68.2(3)
C(5)−N(1)[a] 1.460(3)	C(4)−**C(5)**−N(1)[a] 115.0(2)	C(4)−**C(5)**−**N(1)**[a]−C(1)[a] −75.7(3)
The geometry of the hydrogen bonds		
O(12)−O(22)[b]	2.402(4)	O(12)−H(20)−O(22)[b] 165(2)
N(2)−O(11)	2.675(4)	N(2)−H(2N)−O(11) 160(2)
N(2)−N(1)	2.888(3)	N(2)−H(2N)−N(1) 116(1)
O(8)−O(12)	2.795(6)	O(8)−H(81 W)−O(12) 156(2)

[a] $-x+1, -y+1, -z+2$. − [b] $-x, -y+1, -z+1$.

Table 2. Selected bond lengths [Å], bond angles [°], and structure of $(AdNH_3)_2 \cdot (H_2L^2) \cdot 6\ H_2O$

The geometry of phosphorus atoms		
P(1)−O(11) 1.491(1)	O(11)−**P(1)**−O(12) 118.77(8)	O(12)−**P(1)**−C(11) 108.96(8)
P(1)−O(12) 1.508(1)	O(11)−**P(1)**−C(10) 107.80(9)	C(11)−**P(1)**−C(12) 105.75(8)
P(1)−C(10) 1.825(2)	O(11)−**P(1)**−C(11) 107.98(9)	
P(1)−C(11) 1.805(2)	O(12)−**P(1)**−C(10) 106.85(8)	
P(2)−O(21) 1.466(1)	O(21)−**P(2)**−O(22) 119.12(8)	O(22)−**P(2)**−C(21) 108.94(8)
P(2)−O(22) 1.486(1)	O(21)−**P(2)**−C(20) 109.95(7)	C(21)−**P(2)**−C(22) 5.48(8)
P(2)−C(20) 1.842(2)	O(21)−**P(2)**−C(21) 108.62(8)	
P(2)−C(21) 1.810(2)	O(22)−**P(2)**−C(20) 103.87(8)	
The geometry of atoms C(10) and C(20)		
C(10)−P(1) 1.825(2)	P(1)−**C(10)**−N(1) 112.6(1)	P(1)−**C(10)**−**N(1)**−C(1) 127.3(1)
C(10)−N(1) 1.474(2)		P(1)−**C(10)**−**N(1)**−C(5)[a] −105.9(1)
C(20)−P(2) 1.842(2)	P(2)−**C(20)**−N(2) 117.3(1)	P(2)−**C(20)**−**N(2)**−C(2) 71.3(2)
C(20)−N(2) 1.505(2)		P(2)−**C(20)**−**N(2)**−C(3) −56.9(2)
The geometry of the symmetrically independent part of the macrocyclic ring		
N(1)−C(1) 1.459(2)	C(5)[a]−**N(1)**−C(1) 111.8(1)	C(5)[a]−**N(1)**−**C(1)**−C(2) −170.8(2)
C(1)−C(2) 1.519(2)	N(1)−**C(1)**−C(2) 112.8(1)	N(1)−**C(1)**−**C(2)**−N(2) 45.2(2)
C(2)−N(2) 1.509(2)	C(1)−**C(2)**−N(2) 113.4(1)	C(1)−**C(2)**−**N(2)**−C(3) 63.3(2)
N(2)−C(3) 1.495(2)	C(2)−**N(2)**−C(3) 112.9(1)	C(2)−**N(2)**−**C(3)**−C(4) −171.4(1)
C(3)−C(4) 1.512(2)	N(2)−**C(3)**−C(4) 112.7(1)	N(2)−**C(3)**−**C(4)**−C(5) 177.5(1)
C(4)−C(5) 1.524(2)	C(3)−**C(4)**−C(5) 111.9(1)	C(3)−**C(4)**−**C(5)**−N(1)[i] −66.2(2)
C(5)−N(1)[a] 1.467(2)	C(4)−**C(5)**−N(1)[a] 114.0(1)	C(4)−**C(5)**−**N(1)**[a]−C(1)[a] −73.5(2)
The geometry of the hydrogen bonds		
N(2)−O(12)	2.702(3)	N(2)−H(2)···O(12) 166(1)
N(8)−O(11)[b]	2.691(5)	N(8)−H(81)···O(11)[b] 162(2)
N(8)−O(22)	2.800(4)	N(8)−H(82)···O(22) 170(2)
N(8)−O(99)[c]	2.913(5)	N(8)−H(83)···O(99)[c] 165(3)
O(97)−O(22)[d]	2.917(4)	O(97)−H(972)···O(22)[d] 174(3)
O(98)−O(21)[d]	2.711(4)	O(98)−H(981)···O(21)[d] 170(4)
O(98)−O(12)[a]	2.794(4)	O(98)−H(982)···O(12)[a] 170(3)
O(99)−O(22)	2.922(4)	O(99)−H(991)···O(22) 175(2)
O(99)−O(98A)[e]	2.479(5)	O(99)−H(992)···O(98A)[e] 148(4)
O(99)−O(98)[e]	2.729(5)	O(99)−H(992)···O(98)[e] 171(4)

[a] $-x, -y, -z$. − [b] $-x, -y+1, -z$. − [c] $-x+1, -y+1, -z$. − [d] $-x+1, -y, -z$. − [e] $x, y-1, z$.

In the crystalline state, both the compounds exist as zwitterions with two protonated nitrogen atoms in the rings and their structures contain the centres of symmetry. A comparison of bond lengths and angles in the rings shows that the ring conformation is virtually the same for both structures. This is also evident from the superposition of the two molecules, as shown in Figure S1 in the Supplementary Material available (see footnote on the first page). The ring conformations are stabilised by hydrogen bonds N2−H2···O11 (2.67 Å) in $H_4L^2 \cdot 4\ H_2O$ and N2−H2···O12 (2.70 Å) in $(AdNH_3)_2(H_2L^2) \cdot 6\ H_2O$. The bond lengths of N2−N1 are 2.88 Å and 2.89 Å respectively, which would point to additional hydrogen bonds, although the angles N2−H2.N1 are about 110° and, hence, we assume only a weak interaction.

The coordination around the P atoms significantly departs from the regular tetrahedron. In both the structures, the P−O distances are strongly influenced by hydrogen bonds and in $H_4L^2 \cdot 4\ H_2O$ also by protonation. In the structure of $H_4L^2 \cdot 4\ H_2O$, the molecules are linked through a very short hydrogen bond (2.4 Å) between P(1)−O(12)−H(20)···O(22)−P(2) to give a polymeric struc-

ture with the P−O distances virtually the same due to the strong hydrogen bond. The P(1)−O(11) and P(2)−O(21) distances are also very similar and are linked by hydrogen bonds with an H_2O molecule [P(2)−O(21)] or with the N(2)−H(2) bond [P(1)−O(11)]. In the structure of $(AdNH_3)_2(H_2L^2) \cdot 6\,H_2O$ the P−O distances are shorter than in $H_4L^2 \cdot 4\,H_2O$. All oxygen atoms are linked through hydrogen bonds of 2.8−2.9 Å with the nitrogen of adamantylammonium or with molecules of water (Table 2). The changes in the geometry on C10 and C20 atoms also correspond to the protonation of phosphinic acid groups. The longest C−P and the shortest C−N distance was found for N1−C10−P1 (the phosphinic acid group is protonated) in H_4L^2.

Comparing the structure of $H_4L^2 \cdot 4\,H_2O$ with structures of $H_4teta \cdot 6\,H_2O$[22] (H_4teta = 1,4,8,11-tetraazacyclotetradecane-1,4,8,11-tetraacetic acid) and $H_4dotp \cdot 7\,H_2O$[23] (H_4dotp = 1,4,8,11-tetraazacyclotetradecane-1,4,8,11-tetrapropionic acid), it is clear that orientation of the acetic groups in H_4teta is completely different from that of phosphinic acid groups in H_4L^2 and the conformations of both the rings also show small differences. On the other hand, the molecular structure of H_4dotp is very similar to that of H_4L^2, and that of $Na_2H_2dotp \cdot 16\,H_2O$[24] is similar to $(AdNH_3)_2(H_2L^2) \cdot 6\,H_2O$. In the structures, the orientation of two pendant arms towards protonated nitrogen atoms of the ring and formation of the same motif of hydrogen bonds and conformation were found. The similarity of H_4dotp to H_4L^2 probably results from better flexibility of the propionic acid arms in contrast to the short acetic acid moiety.

Differences in protonation of both phosphinate groups and amine of the ring were also observed in ^{31}P-CP/MAS-NMR spectra. In the spectrum of $H_4L^2 \cdot 4\,H_2O$, two signals at δ = 33.2 and 20.4 were observed and in the spectrum of $(AdNH_3)_2(H_2L^2) \cdot 6\,H_2O$, signals at δ = 23.5 and 15.6 were observed. From the solution NMR titration curves of (aminoalkyl)phosphinic[25−27] and (aminoalkyl)phosphonic[28] acids, it is known that the minimum of the curve corresponds to a system with protonated amine and deprotonated phosphorus acid groups. Therefore, in the ^{31}P-CP/MAS-NMR spectrum of $H_4L^2 \cdot 4\,H_2O$ the signal at δ = 33.2 should correspond to $N-CH_2-P(Ph)O_2H$ and that at δ = 20.4 to $NH^+-CH_2-P(Ph)O_2^-$ moieties, while in the spectrum of $(AdNH_3)_2(H_2L^2) \cdot 6H_2O$ the signal at δ = 23.5 corresponds to $N-CH_2-P(Ph)O_2^-$ and that at δ = 15.6 to $NH^+-CH_2-P(Ph)O_2^-$ moieties. The value of the chemical shift of the $NH^+-CH_2-P(Ph)O_2^-$ system is higher for H_4L^2 than for $(H_2L^2)^{2-}$ and this is probably due to the strong intermolecular hydrogen bond mentioned previously. The assignment of phosphorus signals confirms the values found in the ^{31}P-CP/MAS-NMR spectra of a simple (aminomethyl)(phenyl)phosphinic acid $H_3N^+CH_2P(Ph)O_2^-$ (δ = 20.8) and its sodium salt (δ = 27.8). In the spectrum of the solid H_4L^1, two phosphorus signals at δ = 24.0 and 26.7 were also observed, and thus a similar way of protonation is assumed.

Potentiometry

The calculated values of the protonation and stability constants are given in Table 3. The computed standard deviations seem to be inadequately small. This fact mainly points to a high precision and good reproducibility of the measurements, the use of a suitable calibration function with many degrees of freedom and also to a large number of experimental points. However, the real accuracy is substantially lower (and the real standard deviations are substantially larger). According to the conclusions of several inter-laboratory tests the real standard deviations of the determined protonation and stability constants are at least 0.05−0.1 units on the logarithmic scale,[29] which is discussed in the Supplementary Materials.

A comparison of pK_A values determined for H_4L^1 and H_4L^2 with the values for cyclen, cyclam and their acetic acid, methylenephosphinic acid, and methylenephosphonic acid derivatives is shown in Table 4. From the comparison, it is clear that the protonation scheme of both the acids H_4L^1 and H_4L^2 corresponds to the protonation of the other ligands. The first two protonations occur in the alkaline region and reflect protonations of two opposite nitrogen atoms of the ring. On the basis of protonation of $H_4L^2 \cdot 4\,H_2O$ and $(AdNH_3)_2(H_2L^2) \cdot 6\,H_2O$ in the solid state and on comparison of the constants in Table 4, we assume that the next protonations occur on phosphinic moieties.

Table 3. Protonation constants of H_4L^1 and H_4L^2 and stability constants of their Zn^{2+} and Cd^{2+} complexes at 25°C and I = 0.1 mol dm^{-3} (KNO_3); the values in parentheses are standard deviations given by the programme

Ion	Species	$\log \beta_{pqr}$ H_4L^1	H_4L^2
H^+	HL^{3-}	11.436(7)	9.85(1)
	H_2L^{2-}	18.71(1)	19.793(5)
	H_3L^-	21.46(2)	21.639(9)
	H_4L	22.91(2)	
Zn^{2+}	ZnH_2L	21.06(5)	21.92(5)
	$ZnHL^-$	18.61(4)	
	ZnL^{2-}	15.92(1)	9.79(1)
	Zn_2L	18.32(5)	
	$Zn(H_{-1}L)^{3-}$	4.16(2)	
	$Zn_2(H_{-2}L)^{2-}$	3.45(2)	−3.24(3)
	$Zn_2(H_{-4}L)^{4-}$		−26.11(4)
Cd^{2+}	CdH_2L		22.05(5)
	$CdHL^-$	20.96(2)	
	CdL^{2-}	18.24(2)	9.91(2)
	Cd_2L	21.32(3)	12.99(4)

The last dissociation constant (pK_1) of H_4L^1 is unexpectedly higher than the values for H_4L^3 and H_4L^4, probably due to steric hindrance and hydrophobic interactions, which are discussed in the NMR section, and is not as strongly influenced by the electron-withdrawing $-P(R)O_2^-$ group[17] as the next protonation steps. The values for the other steps (pK_2, pK_3) indicate that the $-P(Ph)O_2^-$ group is more electron-withdrawing than $-CO_2^-$ and $-PO_3^{2-}$, as was expected from the well-known order observed for simple aminophosphinic, phosphonic, and carboxylic acids.[17]

Table 4. Comparison of the protonation constants and of H_4L^1 and H_4L^2 and of the stability constants of their complexes with the constants of their analogues

		cyclen[a]	H_4dota[b]	H_4L^1[g]	H_4L^3[c]	H_4L^4[d]	H_8L^5[e]	cyclam[f]	H_4teta[b]	H_4L^2[g]	H_8L^6[e]
$\log \beta_1$	pK_1	10.6	12.6	11.44	10.41	10.94	13.7	11.29	10.52	9.85	13.4
$\log \beta_2 - \log \beta_1$	pK_2	9.6	9.70	7.27	6.84	8.24	12.2	10.19	10.17	9.94	12.8
$\log \beta_3 - \log \beta_2$	pK_3	(1.5)	4.50	2.75	1.97	3.71	9.28	1.61	4.09	1.85	8.82
$\log \beta_4 - \log \beta_3$	pK_4	(0.7)	4.14	1.45			8.09	1.91	3.35		7.75
$\log \beta_5 - \log \beta_4$	pK_5		2.32				6.12				6.25
$\log \beta_6 - \log \beta_5$	pK_6						5.22				5.42
Zn^{2+} $\log \beta_{101}$		16.2	21.10	15.92	14.60	15.8		15.5 [a]	16.40	9.79	
Cd^{2+} $\log \beta_{101}$		14.3	21.31	18.24	17.34	16.65		11.7 [a]	18.02	9.91	

[a] Ref.[39] – [b] Refs.[2a,2b] (0.1 M NMe_4Cl or NMe_4NO_3). – [c] Ref.[18] (0.1 M KNO_3). – [d] Ref.[11] (0.1 M KNO_3). – [e] Refs.[8,9a] (0.1 M NMe_4NO_3). – [f] Ref.[30] (0.1 M KCl). – [g] This work.

In comparison with the phosphinic acid derivatives of cyclen, we can also observe an influence of the substituent on the phosphorus atom. The values increase in the order $H_4L^3 < H_4L^1 < H_4L^4$, i.e. from H to phenyl and ethyl substituents. The same order was observed for phosphinic analogues of glycine.[17] The pK_A values of H_4L^1 and other phosphinic acids were also reported in a short communication[26] and were discussed for similar azacyclic phosphinic acid ligands in ref.[27] We agree with Sherry's[27] opinion; therefore, the pK_A values found for H_4L^1 from potentiometry and NMR titration published previously[26] are incorrect. A reverse order of pK_1 and pK_2 found for H_4L^2 is discussed in the Supplementary Material.

Systems with the diamagnetic metal ions Zn^{2+} and Cd^{2+} were also studied in order to obtain information on whether solution conformations influence of the coordination ability of the ligands (see NMR section). Results are presented in Table 3 and are compared with the constants of the related ligands in Table 4. In the system with Zn^{2+}, H_4L^1 forms species $[ZnH_2L^1]$, $[ZnHL^1]^-$, $[ZnL^1]^{2-}$, $[Zn_2L^1]$, $[ZnH_{-1}L^1]^{3-}$ and $[Zn_2H_{-2}L^1]^{2-}$. The protonated species were found at a pH of around 3 with a low abundance. The anion $[ZnL^1]^{2-}$ is the predominant species in the neutral region (molar ratio M/L = 1:1). In the alkaline region, hydroxo complexes $[ZnH_{-1}L^1]^{3-}$ (molar ratio M/L = 1:1) and $[Zn_2H_{-2}L^1]^{2-}$ (molar ratio M/L = 2:1) were observed. In the system with Cd^{2+}, H_4L^1 forms species $[CdHL^1]^-$, $[CdL_1]^{2-}$ and $[Cd_2L^1]$. Hydroxo complexes were not found.

In contrast to H_4L^1, H_4L^2 forms species $[ZnH_2L^2]$, $[ZnL^2]^{2-}$, $[Zn_2H_{-2}L^2]^{2-}$, and $[Zn_2H_{-4}L^2]^{4-}$ in the system with Zn^{2+} and $[CdH_2L^2]$, $[CdL^2]^{2-}$, and $[Cd_2L^2]$ in the system with Cd^{2+}. The species $[MH_2L^2]$ have the same number of protons as $(H_2L^2)^{2-}$ and, thus, evidence for their existence can be provided by potentiometry only indirectly; however, its inclusion into the chemical model significantly improved the goodness of fit. For the protonated complexes, we suggest protonation of two nitrogen atoms of the ring. The almost simultaneous deprotonation of both the nitrogen atoms is similar to the process observed for the free H_4L^2. Interactions of the metal ions with the ligands in the acid region were confirmed by NMR measurements (see below).

As expected, the stability constant values of H_4L^1 with Zn^{2+} and Cd^{2+} (15.92 and 18.24) are lower than those of H_4dota (21.10 and 21.31) due to the lower overall basicity of the ligand caused by the electron-withdrawing effect of the phosphinic acid group. On the other hand, the stability constant of H_4L^1 with Cd^{2+} is higher than that for Zn^{2+}, probably due to the larger size of the cadmium ion, which may enable coordination of more pendant arms than for Zn^{2+}, in an analogous way to that observed for 1,4,8,10-tetraazacyclododecane-1,4,8,10-tetrakis(acetamide).[31] Azacycles with methylenephosphinic acid pendant arms seem to be selective to larger ions.[18] For $[ML^1]^{2-}$, we can assume coordination of all nitrogen atoms of the ring as is the case in other cyclene derivatives (e.g. H_4dota). The pK_A values of the $[MHL^1]^-$ for both the metal ions (2.69 for Zn^{2+} and 2.72 for Cd^{2+}) are close and could be attributed to protonation of phosphinic acid pendant arms.

In contrast to H_4L^1 systems, the stability constant values of H_4L^2 for complexes with both of the cations (9.79 for Zn^{2+} and 9.91 for Cd^{2+}) are much lower (Table 4) than the values for H_4teta (16.40 and 18.02, respectively). These lower values could result from differences in the size of the ring for H_4L^1 and H_4L^2, from the lower overall basicity of H_4L^2 in comparison with other ligands and, mainly, from a different bonding mode of the ligand. If we compare the stability constant values for H_4L^2 and H_4teta, we can see that the values for H_4L^2 are about half (on the logarithmic scale) that for H_4teta. This points to the fact that only a part of H_4L^2 is coordinated in $[ML^2]^{2-}$ complexes. The suggestion could be supported by formation of complexes with the ratio M/L = 2:1.

NMR Spectroscopy

Contrary to our expectation, extremely broad signals in the ^{1}H-NMR spectra of both the compounds and the presence of several signals in the ^{31}P-NMR spectra were found, and these roughly correspond to the spectra of the compounds in the solid state. Some ^{31}P-NMR spectra of both the compounds in dependence on pD are shown in Figure 3. From Figure 3, it is evident that coalescence of the signals occurs only in the strong alkaline region after full deprotonation of the compounds. The coalescence of the signals in the neutral region does not occur, even at a temperature of 90°C. In our opinion, the hydrophobic phenyl

groups surround protonated amines in H_4L^1 or H_4L^2 molecules and thus protect them against attack by bulk water. Consequently, the hydrogen bonds N(2)−H(2)···O(11) in H_4L^2 and in $(H_2L^2)^{2-}$ and analogous hydrogen bonds in $(H_2L^1)^{2-}$ are stable in solution and, therefore, can stabilise some ligand conformations. After complete deprotonation, the structures are not stabilised by hydrogen bonds, fast conformation changes occur and only one sharp signal is observed in ^{31}P-NMR spectra. The conformations can also be stabilised by hydrophobic interactions between phenyl groups and/or phenyl-propylene/ethylene chains. Analogous changes in the ^{31}P-NMR spectra were observed for 1,2-diaminoethane-*N*,*N*,*N*′,*N*′-tetrayl-tetramethylene-tetrakis-(phenylphosphinic acid).[25a] Two peaks in the ^{31}P-NMR spectrum at low temperature were also observed in a solution of H_8L^5, which is in accordance with the molecular structure of the compound in the solid state.[32]

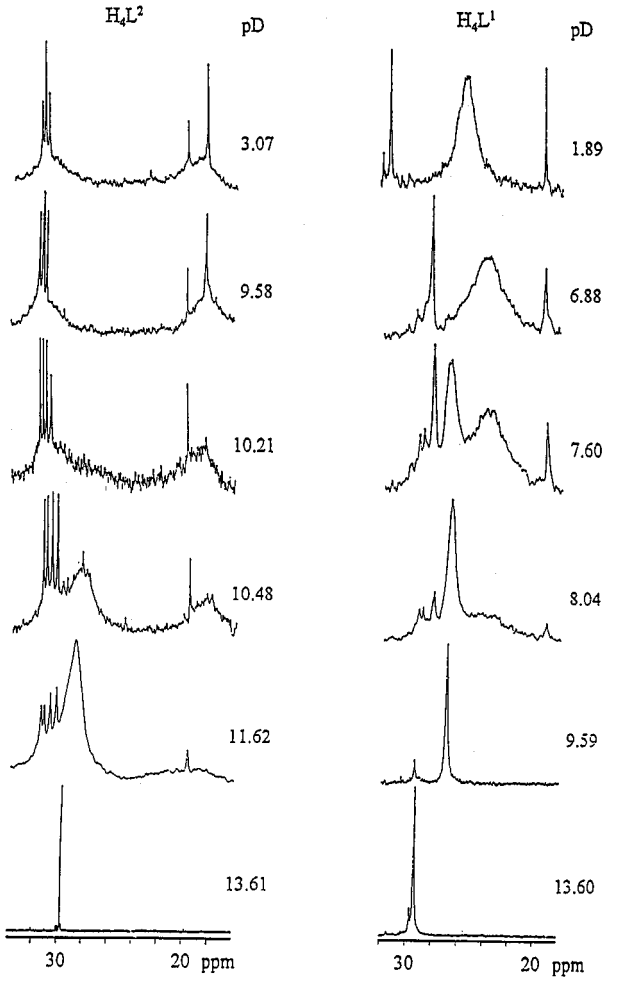


Figure 3. The ^{31}P-NMR spectra of H_4L^1 (right) and H_4L^2 (left) in dependence on pD

The ^{31}P-NMR spectra of H_4L^1 show the same features as the spectra of H_4L^2; however, the conformation of $(H_2L^1)^{2-}$ does not seem to be as rigid as that of $(H_2L^2)^{2-}$. In the spectra in the region of pD = 1.89−6.88 (pH ≈ 2.6−6.5), two sharp signals at δ = 19 corresponding to the pendant arm with the protonated amine and at δ = 30 corresponding to the pendant arm with the deprotonated amine were observed. In addition to the signals at δ = 19 and 30, the spectrum contains a broad signal at about δ = 25. Fast protonation of a phosphinic acid pendant arm occurs, as can be illustrated by the changes in the chemical shifts of the peaks in the acid region. The broad signal probably reflects a number of conformers in which all phosphorus atoms are equivalent with respect to the site of protonation. On the other hand, the sharp signals belong to a conformer with nonequivalent phosphorus atoms. The sharp peak at δ = 30 changes its position with pD significantly whereas the other one changes only negligibly. Thus, it is evident that the former peak corresponds to a phosphinic group where the third protonation takes place. Near the pD value corresponding to the pK_2 = 7.27 (pD = 7.6, pH ≈ 7.2), a strong sharp signal at about δ = 27 appears and reflects the $(HL^1)^{3-}$ species. The spectrum looks like a superposition of the spectra at lower and higher pD values. This is a consequence of a slow exchange (dissociation) of protons in $(H_2L^1)^{2-}$ and differences in the structure of conformers belonging to $(H_2L^1)^{2-}$ and $(HL^1)^{3-}$species. The signal at δ = 27 is dominant in the spectra over the range of pD 7.5−10.5. With the last deprotonation (pD = 10.9−13.6), the signal becomes increasingly sharp and continuously moves to δ = 29, which confirms the fast proton exchange in the $(HL^1)^{3-}$ anion.

The acid pK's determined from the ^{31}P-NMR titration in the range of −log[H^+] 1.0−2.5 under the conditions of the potentiometric titrations correspond to the values found from potentiometry. The changes in the ^{31}P-NMR spectra indicate the unsymmetrical protonations of phosphinic acid groups as the peaks at about δ = 19 and 30 are shifted to different pH values.

H_4L^2 exhibits virtually the same spectrum in the range of pD 3.07−9.58. This range of pD corresponds to conformers of a species $(H_2L^2)^{2-}$ in which two nitrogen atoms are protonated [see the crystal structure of $(AdNH_3)_2(H_2L^2)\cdot 6\,H_2O$]. As mentioned above, the ^{31}P-NMR titration curves of (aminoalkyl)phosphinic and (aminoalkyl)-phosphonic acids point to the fact that the minimum of the curve corresponds to a system with protonated amine and deprotonated phosphorus groups.[25−27] Therefore, signals in the region δ = 18−20 reflect $NH^+-CH_2-PPhO_2^-$ pendant arms and signals in the region δ = 30−32 reflect $N-CH_2-PPhO_2^-$ pendant arms bound by hydrogen bonds to the other nitrogen atoms of the ethylenediamine chains (see the crystal structure of the adamantylammonium salt). The broad peak observed in the spectrum of H_4L^1 at about δ = 25 was not found in the spectrum of H_4L^2, probably due to the presence of propylene chains in H_4L^2 dividing the molecule into two almost independent parts each stabilised by the hydrogen bond. The spectra in the region above pD 10.21, i.e. pH 9.8, (Figure 3) reflect the first and second deprotonations of the ring. A new signal at δ = 28 is seen and this belongs to $(HL^2)^{3-}$ and $(L^2)^{4-}$ species in almost fast conformation changes with the fast deprotonation of the last proton as indicated by a continuous change of the chemical shift from δ = 28 to 30 and by a sharpening of

the signal. At pD = 13.61, the deprotonation is complete and only one sharp signal is observed in the spectrum. Unfortunately, full interpretation of all observed changes in the ^{31}P-NMR spectra of the ligand is more complicated than for H_4L^1.

We wanted to know whether the ligand conformations are influenced by the presence of complexing ions and thus ^{31}P-NMR spectra of both the ligands in the presence of Zn^{2+} or Cd^{2+} were measured. The NMR spectra are very sensitive to complexation. Only one sharp signal at about δ = 27 is observed in the spectra of the solutions containing H_4L^1 with Zn^{2+} or Cd^{2+} in the L:M molar ratio 1:1 in the wide region of pH from 1.8 to 12. The signal is observed even in the acid region where formation of protonated complexes starts. Similarly, H_4L^2 in the M/L ratio 1:1 gives a sharp peak (δ = 26) in the neutral region and a very broad unresolved peak (δ = 18−32) in acidic solution (pH 2.0). This behaviour confirms the presence of metal ion/ligand interactions and, therefore, complexes $[MH_2L^2]$ should be present in acidic solutions. We assume that nitrogen atoms are protonated in the species and metal ion/ligand interactions occur through phosphinic acid groups. These results indicate a fast exchange of a metal ion between ligand molecules. On the other hand, H_4L^1 or H_4L^2 in the presence of noncoordinating ions such as Li^+ or K^+ (concentration of LiCl or KCl solutions was about 3 mol·dm^{-3}) in the neutral region give virtually the same spectra as the solutions with a low ionic strength. These results suggest that complexation of metal ions with ligands through phosphinic acid group(s) and/or nitrogen atom(s) breaks the system of hydrogen bonds that stabilise conformations of free ligands.

Experimental Section

Chemicals: Cyclen hydrochloride[33] and cyclam hydrochloride[34] were synthesised using known procedures. Other chemicals used were from commercial sources and were of the best quality available.

Crystallography: Crystals of $H_4L^2 \cdot 4\,H_2O$ and $(AdNH_3)_2(H_2L^2) \cdot 6\,H_2O$ suitable for X-ray diffraction were obtained from methanol/water solutions. For unit-cell and space-group determinations and for data collections, crystals of both the compounds were mounted at random orientations on glass fibres using an epoxy glue and were coated with a thin paraffin film. An Enraf−Nonius CAD4 diffractometer was used for measurements at 293(2) K with Mo-K_α radiation (λ = 0.71073 Å). Unit-cell dimensions were determined from angular settings of every twenty-five high-order (θ from 14 to 15° and from 13.5 to 14.5°, respectively) reflections using the CAD4 centring routines. Selected crystallographic and other relevant data for both compounds are listed in Table 6.

Intensities were collected using variable scan speeds to assure constant statistical precision. Three standard reflections measured every hour were used to confirm the stability of the crystal and of the experimental conditions. The orientation of the crystal was checked by measuring five standards every 100 reflections. The data were corrected for Lorenz polarisation, but not for absorption. The extinction correction was applied only in the case of $(AdNH_3)_2(H_2L^2) \cdot 6\,H_2O$ using the procedure included in SHELXL97.[35] The structure was solved by a combination of Patterson and Fourier methods (SHELXS86,[36] SHELXL97) and refined by full-matrix least-squares techniques (SHELXL97). Scattering factors for neutral atoms used were included in the program SHELXL97. The hydrogen atoms were found (with the exception of two hydrogen atoms of the water molecules in the structure of H4L2···4 H_2O) on the difference maps and refined isotropically. The partially disordered water molecules in the crystal lattice of H4L2···4 H_2O were described as two oxygen atoms [O(8) and O(8A)] in two close positions [distance O(8)···O(8A) 0.81(1) Å]. The refined total occupancy of this water molecule converged to unity within experimental error and the final relative ratio of the individual position was 0.69:0.31.

Table 6. Experimental data for the X-ray diffraction studies

Parameter	$(AdNH_3)_2\,H_2L^2 \cdot 6\,H_2O$	$H_4L^2 \cdot 4\,H_2O$
Empirical formula	$C_{58}H_{86}N_6O_8P_4 \cdot 6\,H_2O$	$C_{38}H_{52}N_4O_8P_4 \cdot 4\,H_2O$
M	1227.30	888.78
T/K	293(2)	293(2)
λ/Å	0.71073	0.71073
Crystal system	triclinic	monoclinic
Space group	$P\bar{1}$ (no. 2)	$P2_1/c$ (no. 14)
a/Å	8.6179(7)	8.5729(8)
b/Å	14.0002(7)	24.449(3)
c/Å	14.9305(10)	10.873(3)
α /°	67.892(5)	−
β /°	79.452(6)	108.38(1)
γ /°	85.790(6)	−
V/Å^3	1640.7(2)	2162.7(7)
Z	1	2
D_c/g•cm^{-3}	1.242	1.365
μ/mm^{-3}	0.179	0.239
F(000)	660	944
Crystal habit and colour	plate, colourless	rod, colourless
Crystal size/mm	0.6 ± 0.9 ± 0.2	0.35 ± 0.3 ± 0.7
Scan mode	$\omega - 2\theta$	$\omega - 2\theta$
θ range for data collection/°	1.49−24.98	1.67−27.22
Index ranges	$-10 \le h \le 10$ $-15 \le k \le 16$ $0 \le l \le 17$	$0 \le h \le 11$; $0 \le k \le 31$; $-13 \le l \le 13$
Reflections collected	5773	5117
Reflections observed [$I \ge 2\sigma(I)$]	4907	3403
Independent reflections	5773	4809 (R_{int} = 0.0335)
Coefficients in weighting scheme[a]	0.0541; 0.4778	0.0757; 1.0441
Data, restrains, parameters	5773; 0; 577	4809; 0; 388
Goodness-of-fit on F^2	1.076	1.043
Final R, R' indices [$I \ge 2\sigma(I)$][b]	0.0365; 0.0978	0.0510; 0.1380
Maximum shift/e.s.d.	0.008 (H atom)	0.065 (H atom)
Largest differ. peak and hole /eÅ^{-3}	0.43; −0.40	0.35; −0.43

[a] $R = \Sigma|F_o - F_c|/\Sigma|F_c|$ $R' = [\Sigma w(F_o^2 - F_c^2)^2/\Sigma w(F_o^2)^2]^{1/2}$ (SHELXL97; ref.[35]). − [b] $w = 1/[\sigma^2(F_o^2) + (A \bullet P)^2 + B \bullet P]$ (SHELXL97, see ref.[36])

Crystallographic data (excluding structure factors) for the structures reported in this paper have been deposited with the Cambridge Crystallographic Data Centre as supplementary publication no. CCDC-118658 $[(AdNH_3)_2(H_2L^2) \cdot 6\,H_2O]$ and -118659 $(H_4L^2 \cdot 4\,H_2O)$. Copies of the data can be obtained free of charge on application to CCDC, 12 Union Road, Cambridge CB21EZ, UK [Fax: (internat.) +44(1223)336-033; E-mail:deposit@ccdc.cam.ac.uk].

Chemicals and Stock Solutions for Potentiometric Titrations: Stock solutions of the individual metal cations were prepared by dissolving appropriate nitrates recrystallised from aqueous solutions. The

metal contents in the solutions were determined by titration with Na_2H_2edta solution. Nitric acid was prepared by passing aqueous potassium nitrate solution through a Dowex 50 W-8 column in the H^+ form because of traces of NO and NO_2 present in the concentrated acid. KOH solution was standardised against potassium hydrogen phthalate and HNO_3 solution against the KOH solution. Stock solutions of the ligands were prepared by dissolving solids in a standard KOH solution (≈ 1.8 equivalents) followed by addition of water. Analytical concentrations of the ligands were determined by pH-metric end-point titrations. Four protons of H_4L^1 in the presence of an equivalent amount of $Cu(NO_3)_2$ and two protons of H_4L^2 were titrated using a potassium hydroxide solution of known analytical concentration.

Potentiometric Titrations: Titrations were carried out in a vessel thermostatted at 25±0.1°C, at an ionic strength of I (KNO_3) = 0.1 mol·dm^{-3} and in the presence of an excess of HNO_3 in the region $-\log[H^+] = 1.8-12$ [except for the titrations where precipitation of $Zn(OH)_2$ and $Cd(OH)_2$ was detected] using a PHM 240 pH-meter, a 2 cm^3 capacity Radiometer ABU 900 automatic piston burette and a GK 2401B combined electrode (Radiometer). The initial volume was 5 cm^3 and concentration of both the ligands was 0.002 mol.dm^{-3} due to their low solubility in the acid region. The metal:ligand ratios were 2:1, 1:1 and 1:2. Titration for each ratio was carried out at least three times. Each titration consisted of about 40 points. An inert atmosphere was ensured by constant passage of argon saturated with the solvent vapor during measurements. The stability constants for $M^{2+} - OH^-$ systems included in the calculations and $pK_w = 13.78$ were taken from the literature.[37] The protonation and stability constants β_{pqr} are concentration constants and are defined by $\beta_{pqr} = [M_pH_qL_r]/[M]^p\cdot[H]^q\cdot[L]^r$. The constants and the analytical concentrations were calculated using the program OPIUM.[38] The program minimises the criterion of the generalised least squares method using the calibration function where the additive term E_0 contains standard potentials of the electrodes used and contributions of inert ions to the liquid-junction potential, S corresponds to the Nernstian slope, the value of which should be close to the theoretical value and $j_1[H^+]$ and $j_2[OH^-]$ terms are contributions of the H^+ and OH^- ions to the liquid-junction potential. It is clear that j_1 and j_2 cause deviation from a linear dependence between E and $-\log[H^+]$ only in strongly acidic and strongly alkaline solutions.

$$E = E_0 + S\cdot\log[H^+] + j_1[H^+] + j_2(K_W/[H^+])$$

NMR Spectra: NMR spectra were obtained with a Varian Inova Plus instrument, ^{1}H (400 MHz) at 25°C with sodium 4,4-dimethyl-4-silapentane-1-sulfonate as an internal standard, $^{31}P\{^1H\}$ (161,.9 MHz) with 85% H_3PO_4 as an external standard. The ^{31}P-NMR titration experiments were performed in D_2O at concentrations of the ligands of 0.01 mol·dm^{-3} and at room temperature. The pD values (pD = pH + 0.40; electrode calibration in pH scale using standard buffers) were adjusted by addition of KOD or DCl solutions. Solutions for ^{31}P-NMR titrations in the acidic region ($-\log[H^+] = 1.0-2.5$) and the measurements in the presence of metals were run under the same conditions as the potentiometric measurements in H_2O with D_2O in the coaxial capillary for the lock. ^{31}P-CP/MAS-NMR spectra were measured at 161.9 MHz, spinning 4 kHz, contact time 0.5 ms and repetition time 8 s with $CaHPO_4$ as external standard.

Synthesis of $H_4L^1 \cdot 4\,H_2O$: To a stirred suspension of cyclen hydrochloride (1.0 g, 3.14 mmol) and phenylphosphinic acid (2.75 g, 19.3 mmol) in 20 mL of aqueous HCl (1:1, v/v) was added paraformaldehyde (0.85 g, 28.3 mmol) in portions at 100°C over 7 h. A clear solution was formed after addition of the first portion of paraformaldehyde [***Caution:*** Formation of carcinogenic $(ClCH_2)_2O$ cannot be excluded, work in an efficient fumehood]. The reaction mixture was held at the same temperature for 2.5 h. The volatiles were removed using a rotary evaporator and the resulting yellow oily residue was co-distilled three times with water. The residue was dissolved in an H_2O/EtOH mixture (1:1, v/v) and loaded onto Dowex 50 W8 cation exchange resin in the H^+ form. The resin was washed with H_2O and the product was subsequently eluted with 10% aqueous NH_3. Fractions containing H_4L^1 as its ammonium salt were evaporated. The oily product obtained was dissolved in 7 mL of an H_2O/EtOH mixture (1:1, v/v) and acidified with 1 mol dm^{-3} HCl to pH ≈ 1. H_4L^1 started to crystallise after scratching of the flask wall and standing overnight. The product was filtered off, washed with water, and dried at 100°C over solid KOH under vacuum (1.33 kPa). The solution was filtered (S4), evaporated, and the product precipitated by addition of water. Yield 1.7 g (65%). M.p. 200−203°C (dec.). Elemental analysis: found (calcd.) C 50.2 (50.2); H 6.1 (6.5); N 6.6 (6.5). − ^{1}H NMR (0.1 M KOD/D_2O): δ = 2.51 (s, 16 H, NCH_2), 2.91 (d, 8 H, $^2J_{PH}$ = 6.4 Hz, NCH_2P), 7.5−7.9 (m, 20 H, aryl H). − $^{31}P\{^1H\}$ NMR (0.1 M KOD/D_2O): δ = 29.38. A sample used for potentiometric measurements was recrystallised from refluxing MeOH containing propylene oxide.

Synthesis of $H_4L^2 \cdot 4\,H_2O$: To a stirred suspension of cyclam hydrochloride (0.8 g, 1.9 mmol) and phenylphosphinic acid (2.0 g, 14 mmol) in 7.5 mL of aqueous HCl (1:1, v/v) was added paraformaldehyde (0.9 g, 30 mmol) in portions at 65°C over 2 h [***Caution:*** Formation of carcinogenic $(ClCH_2)_2O$ cannot be excluded, work in an efficient fumehood]. A clear solution formed during addition of paraformaldehyde and a white precipitate of the product began to separate after addition of approximately half of the amount. The mixture was stirred for 3 h at 65°C to complete the reaction. A white precipitate of $H_4L^2 \cdot n$ HCl (n = 3−4) was filtered off, washed with 5% aqueous HCl, acetone, and dried over KOH. The hydrochloride was converted into H_4L^2 by dissolution in a large volume of boiling methanol and addition of an excess of propylene oxide (2 mL) to trap HCl. The solution was concentrated to about 1/4 volume and crystallisation started after addition of water. The isolated product was dried to constant weight under vacuum (1.33 kPa) over KOH at 100°C in an Abderhalden apparatus. Yield 1.3 g (75%). M.p. 221−224°C (dec.). − Elemental analysis: found (calcd.) C 51.6 (51.4); H 6.6 (6.8); N 6.5 (6.3). − ^{1}H NMR (0.1 M KOD/D_2O): δ = 0.82 (bp, 4 H, $CH_2CH_2CH_2$), 1.87 (s, 8 H, NCH_2CH_2N), 2.07 (bt, 8 H, $NCH_2CH_2CH_2N$), 2.32 (d, 8 H, NCH_2P, $^2J_{PH}$ = 9.4 Hz), 7.3−7.5 (m, 20 H, aryl H). − $^{31}P\{^1H\}$ NMR (0.1 M KOD/ D_2O): δ = 29.8, s.

Synthesis of $(AdNH_3)_2(H_2L^2) \cdot 6\,H_2O$: To a stirred MeOH/$H_2O$ (1:1, v/v, 10 mL) solution of $H_4L^2.4H_2O$ (0.89 g, 1 mmol) was added a methanolic solution (10 mL) of 1-adamantylamine (0.30 g, 2 mmol). The product crystallised from the solution during a few days. Yield 0.65 g (53%). M.p. 207−209°C (dec.). Elemental analysis: found (calcd.) C 56.9 (56.7), H 7.8 (8.0), N 6.9 (6.8).

Acknowledgments

This work was supported by the Grant Agency of the Czech Republic, Project 203/97/0252 and by the Ministry of Education of the Czech Republic, grant No. VS96140.

[1] [1a] M. Meyer, V. Dahaoui-Gindrey, C. Lecomte, R. Guilard, *Coord. Chem. Rev.* **1998**, *178−180*, 1313−1405. − [1b] K. P. Wainwright, *Coord. Chem. Rev.* **1997**, *166*, 35−90. − [1c] S. F. Lincoln, *Coord. Chem. Rev.* **1997**, *166*, 255−289. − [1d] R. D.

Hancock, H. Maumela, A. S. De Sousa, *Coord. Chem. Rev.* **1996**, *148*, 315−347. − [1e] A. E. Martell, R. J. Motekaitis, E. T. Clarke, R. Delgado, Y. Sun, R. Ma, *Supramol. Chem*. **1996**, *6*, 353−363.

[2] [2a] L. Burai, I. Fabián, R. Király, E. Szilágyi, E. Brücher, *J. Chem. Soc., Dalton Trans.* **1998**, 243−248. − [2b] S. Chaves, R. Delgado, J. J. R. Frausto Da Silva, *Talanta* **1992**, *39*, 249−254. − [2c] E. T. Clarke, A. E. Martell, *Inorg. Chim. Acta* **1991**, *190*, 27−36.

[3] [3a] S. Aime, M. Botta, M. Fasano, M. B. M. Marques, C. F. G. C. Geraldes, D. Pubanz, A. E. Merbach, *Inorg. Chem.* **1997**, *36*, 2059−2068 and references cited therein. − [3b] V. Jacques, D. Gilsoul, V. Comblin, J. F. Desreux, *J. Alloys Compd.* **1997**, *249*, 173−177.

[4] [4a] S. Aime, M. Botta, M. Fasano, E. Terreno, *Chem. Soc. Rev.* **1998**, *27*, 19−29. − [4b] K. Kumar, *J. Alloys Compd.* **1997**, *249*, 163−172. − [4c] V. Alexander, *Chem. Rev.* **1995**, *95*, 273−342.

[5] [5a] P. A. Schubiger, R. Alberto, A. Smith, *Bioconjugate Chem.* **1996**, *7*, 165−179. − [5b] D. Parker, *Chem. Br*. **1994**, 818−822. − [5c] S. Jurisson, D. Berning, W. Jia, D. D. Ma, *Chem. Rev.* **1993**, *93*, 1137−1156. − [5d] D. Parker, *Chem. Soc. Rev.* **1990**, 271−291.

[6] L. L. Chappell, D. A. Voss Jr., W. de Horrocks Jr., J. R. Morrow, *Inorg. Chem.* **1998**, *37*, 3989−3998 and references cited therein.

[7] [7a] A. D. Sherry, *J. Alloys Compd*. **1997**, *249*, 153−157. − [7b] F. I. Belskii, Y. M. Polikarpov, M. I. Kabachnik, *Usp. Khim.* **1992**, *61*, 415−455.

[8] R. Delgado, L. C. Siegfried, T. A. Kaden, *Helv. Chim. Acta* **1990**, *73*, 140−148.

[9] [9a] A. D. Sherry, J. Ren, J. Huskens, E. Brücher, E. Tóth, C. F. G. C. Geraldes, M. M. C. A. Castro, W. P. Cacheris, *Inorg. Chem*. **1996**, *35*, 4604−4612. − [9b] J. Ren, A. D. Sherry, *Inorg. Chim. Acta* **1996**, *246*, 331−341.

[10] D. Parker, J. A. G. Williams, *J. Chem. Soc., Dalton Trans.* **1996**, 3613−3628.

[11] I. Lázár, A. D. Sherry, R. Ramasamy, E. Brücher, R. Király, *Inorg. Chem.* **1991**, *30*, 5016−5019.

[12] C. J. Broan, E. Cole, K. J. Jankowski, D. Parker, K. Pulukkody, B. A. Boyce, N. R. A. Beeley, K. Miller, A. J. Millican, *Synthesis* **1992**, 63−69.

[13] S. Aime, M. Botta, R. S. Dickins, C. L. Maupin, D. Parker, J. P. Richl, J. A. G. Williams, *J. Chem. Soc., Dalton Trans.* **1998**, 881−892 and references cited therein.

[14] J. Huskens, A. D. Sherry, *J. Chem. Soc., Dalton Trans.* **1998**, 177−184 and references cited therein.

[15] [15a] T. J. Norman, F. C. Smith, D. Parker, A. Harrison, L. Royle, C. A. Walker, *Supramol. Chem.* **1995**, *4*, 305−308. − [15b] T. J. Norman, D. Parker, L. Royle, A. Harrison, P. Antoniw, D. J. King, *J. Chem. Soc., Chem. Commun.* **1995**, 1877−1878. − [15c] T. J. Norman, D. Parker, F. C. Smith, D. J. King, *J. Chem. Soc., Chem. Commun.* **1995**, 1879−1880.

[16] [16a] E. Huskowska, C. L. Maupin, D. Parker, J. A. G. Williams, J. P. Richl, *Enantiomer* **1997**, *2*, 381−395. − [16b] D. Parker, P. Senanayake, J. A. G. Williams, *J. Chem. Soc., Perkin Trans. 2* **1998**, 2129−2139.

[17] J. Rohovec, I. Lukeš, P. Vojtíšek, I. Císarová, P. Hermann, *J. Chem. Soc., Dalton Trans.* **1996**, 2685−2691.

[18] K. Bazakas, I. Lukeš, *J. Chem. Soc., Dalton Trans.* **1995**, 1133−1137.

[19] K. P. Pulukkody, T. J. Norman, D. Parker, L. Royle, C. J. Broan, *J. Chem. Soc., Perkin Trans. 2* **1993**, 605−620.

[20] I. Lázár, A. D. Sherry, *Synthesis* **1995**, 453−457.

[21] D. Redmore, *J. Org. Chem.* **1978**, *43*, 992−996.

[22] [22a] M. R. Spirlet, J. Rebizant, P. D. Barthélemy, J. F. Desreux, *J. Chem. Soc., Dalton Trans.* **1991**, 2477−2481. − [22b] M. R. Maurya, E. J. Zaluzec, S. F. Pawkovic, A. W. Herlinger, *Inorg. Chem.* **1991**, *30*, 3657−3662.

[23] V. Dahaoui, C. Lecomte, H. Chollet, A. K. Mishra, C. Mehadji, R. Guilard, *New J. Chem.* **1995**, *19*, 839−850.

[24] V. Dahaoui-Gindrey, S. Dahaoui, C. Lecomte, F. Barbette, R. Guilard, *Acta Crystallogr. Sect. C* **1997**, *53*, 1797−1799.

[25] [25a] I. Lukeš, P. Hermann, P. Pech, *Collect. Czech. Chem. Commun.* **1989**, *54*, 653−662. − [25b] I. Lukeš, K. Bazakas, P. Hermann, P. Vojtíšek, *J. Chem. Soc., Dalton Trans.* **1992**, 939−944.

[26] E. Cole, D. Parker, G. Ferguson, J. F. Gallagher, B. Kaitner, *J. Chem. Soc., Chem. Commun*. **1991**, 1473−1475.

[27] J. Huskens, A. D. Sherry, *J. Am. Chem. Soc.* **1996**, *118*, 4396−4404.

[28] [28a] T. G. Appleton, J. R. Hall, A. D. Harris, M. A. Kimlin, I. J. McMahon, *Aust. J. Chem*. **1984**, *37*, 1833−1840. − [28b] K. Sawada, T. Araki, T. Suzuki, *Inorg. Chem.* **1987**, *26*, 1199−1204. − [28c] T. Ichikawa, K. Sawada, *Bull. Chem. Soc. Jpn.* **1997**, *70*, 829−835.

[29] [29a] W. A. E. MacBryde, *IUPAC Chemical data Series No. 17*, Pergamon, Oxford, **1979**. − [29b] G. Anderegg, *IUPAC Chemical Data Series No. 14*, Pergamon, Oxford, **1977**.

[30] R. D. Hancock, R. J. Motekaitis, J. Mashishi, I. Cukrowski, J. H. Reibenspies, A. E. Martell, *J. Chem. Soc., Perkin Trans. 2* **1996**, 1925−1929.

[31] H. Maumela, R. D. Hancock, L. Carlton, J. H. Reinbenspies, K. P. Wainwright, *J. Am. Chem. Soc.* **1995**, *117*, 6698−6707.

[32] I. Lázár, D. C. Hrncir, N. D. Kim, G. E. Kiefer, A. D. Sherry, *Inorg. Chem.* **1992**, *31*, 4422−4424.

[33] D. W. Swinkels, J. P. H. Duynhoven, C. W. Hilbers, G. I. Tesser, *Recl. Trav. Chim. Pays-Bas* **1991**, *110*, 124−129.

[34] E. K. Barefield, F. Wagner, A. W. Herlinger, A. R. Dahl, *Inorg. Synth.* **1976**, *16*, 220−225.

[35] G. M. Sheldrick, *SHELXL97, Program for Crystal Structure Refinement from Diffraction Data*, University of Goettingen, Goettingen **1997**.

[36] G. M. Sheldrick, *Acta Crystallogr. Sect. A,* **1990**, *46*, 467.

[37] C. F. Baes Jr., R. E. Mesmer, *The Hydrolysis of Cations*, Wiley, New York **1976**.

[38] M. Kývala, I. Lukeš, *Chemometrics '95*, International Conference, Pardubice, Czech Republic, **1995**, Book of Absracts, p. 63.

[39] R. M. Smith, A. E. Martell, *Critical Stability Constants*, Vols 1−6, Plenum Press, New York, **1974**−**1989**.

Received April 27, 1999
[I99149]

Synthesis, Spectroscopic, and Electrochemical Properties of Rare Earth Double-Deckers with Tetra(*tert*-butyl)-2,3-naphthalocyaninato Ligands

Jianzhuang Jiang,*[a,b] Wei Liu,[a] Ka-Wo Poon,[c] Daming Du,[a] Dennis P. Arnold[b] and Dennis K. P. Ng*[c]

Keywords: Rare earth complexes / Naphthalocyaninato ligand / Double-decker complexes

A series of rare earth(III) double-deckers RE[Nc(*t*Bu)$_4$]$_2$ [RE = La, Ce, Pr, Nd, Eu, Gd, Tb, Y, Er; Nc(*t*Bu)$_4$ = dianion of tetra(*tert*-butyl)-2,3-naphthalocyanine] (**1**–**9**) have been prepared by treating RE(acac)$_3$ · *n* H$_2$O (acac = acetylacetonate) with 6-*tert*-butylnaphthalonitrile in refluxing *n*-octanol in the presence of 1,8-diazabicyclo[5.4.0]undec-7-ene (DBU). These novel sandwich-type complexes have been spectroscopically characterized. The electrochemical studies show that the first oxidation and the first reduction potentials increase with the size of the central metal ions with a relatively small separation (0.28–0.33 V), reflecting the narrow HOMO–LUMO gap.

Introduction

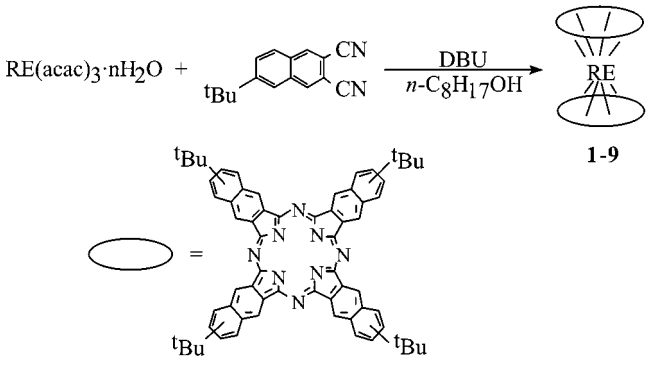
Sandwich-type phthalocyaninato metal complexes, in which the large conjugated π systems are held in close proximity by metal ions, have found widespread applications in materials science.[1] The lutetium complex Lu(Pc)$_2$ (Pc = dianion of phthalocyanine), for example, is the first intrinsic molecular semiconductor with a conductivity of $5\cdot10^{-5}$ $\Omega^{-1}cm^{-1}$ in thin films,[2] and shows promising electrochromic[3] and gas-sensing properties.[4] As the bulk characteristics of a molecular material are largely related to the properties of individual molecules, various modifications have been made on these sandwich compounds with the goal of improving their performance as advanced materials.

Long alkyl side chains[5] and crown-ether units[6] are two common functionalities added to the macrocycles to facilitate the formation of various mesophases and supramolecular structures. Another rational modification involves the replacement of the Pc ring with a naphthalocyaninato (Nc) ligand. Having more delocalized π systems, the resulting sandwich complexes should have distinct electronic and electrical properties. This has been demonstrated by L′Her et al. who show that the energy gap between the highest and lowest molecular orbitals (HOMO and LUMO) is much narrower for these Nc complexes than for the Pc counterparts.[7] Although these Nc-containing sandwich compounds appear to be promising, only a few lutetium Nc complexes have been known so far.[2,7,8] We have recently extended this series of compounds by reporting the first heteroleptic europium complexes having mixed Nc and porphyrinato ligands.[9] In this paper, we describe a new series of homoleptic Nc double-decker complexes of various rare earth metals. By changing the size of the metal center, the ring-to-ring separation can be altered, thereby providing another method of fine tuning the electronic properties of this novel class of complexes.

[a] Department of Chemistry, Shandong University,
Jinan 250100, P. R. China
Fax: (internat.) +86 (0)531/856-5211
E-mail: jzjiang@sdunetnms.sdu.edu.cn
[b] Centre for Instrumental and Developmental Chemistry,
Queensland University of Technology,
GPO Box 2434, Qld. 4001, Australia
[c] Department of Chemistry, The Chinese University of Hong Kong,
Shatin, N.T., Hong Kong, P. R. China
Fax: (internat.) +852/2603-5057
E-mail: dkpn@cuhk.edu.hk

Results and Discussion

All the double-deckers **1**–**9** were prepared by base-promoted cyclization of 6-*tert*-butylnaphthalonitrile in refluxing *n*-octanol in the presence of 0.25 equiv. of RE(acac)$_3\cdot n$ H$_2$O (RE = La, Ce, Pr, Nd, Eu, Gd, Tb, Y, Er) and DBU (Scheme 1). The use of additional naphthalonitrile also gave a significant amount of metal-free 2,3-naphthalocyanine H$_2$[Nc(*t*Bu)$_4$]$_2$ as a side product, as in the case of phthalocyanines,[10] which complicated the purification process. Changing the solvent to *n*-pentanol, *n*-hexanol, 1,2,4-trichlorobenzene, or 1-chloronaphthalene did not give the desired products, indicating that solvent is a critical factor for these reactions.



Scheme 1. Synthesis of rare earth double-deckers

The lutetium analog Lu[Nc(*t*Bu)$_4$](Pc) was reported previously, but only very few characterizing data were given.[11]

 © WILEY-VCH Verlag GmbH, D-69451 Weinheim, 2000 1434–1948/00/0101–0205 $ 17.50+.50/0

As is the case in the Pc complexes,[10] these reactions afforded the protonated species $REH[Nc(tBu)_4]_2$ or the monoanions $\{RE[Nc(tBu)_4]_2\}^-$ as the initial products, which underwent oxidation in air to give the corresponding one-electron ring-oxidized complexes $RE[Nc(tBu)_4]_2$. The UV/Vis spectra of the dark-brown sandwich intermediates and the dark-blue/violet oxidized products were very different (see below), so the course of the reactions could be monitored by electronic absorption spectroscopy. The rate of conversion depended on the size of the metal center. Intermediates with a smaller metal center (heavy lanthanide) were more susceptible to oxidation than those with a larger metal ion (light lanthanide) which is consistent with the electrochemical data as described below. The oxidation was also found to be accelerated by the acidity of silica gel; only the ring-oxidized species **1**−**9** were isolated after chromatographic purification. It is worth noting that the yield of these double-deckers increases gradually with the size of the central metal ion (Table 1). This is in line with the $RE(Por)_2$ series (Por = dianion of *meso*-tetraphenylporphyrin or octaethylporphyrin),[12] but in contrast with the trend observed for $RE(Pc)_2$[13] and $RE[Pc(OC_8H_{17})_8]_2$,[14] showing that bis(phthalocyaninato) complexes are easier to obtain and more stable with the smaller rare earth cations.

All these double-deckers, after being purified by column chromatography and recrystallization, were essentially pure, as shown by thin-layer chromatography. However, satisfactory analytical data could not be obtained which might be due to the presence of traces of impurities, which could not be completely removed by conventional purification methods.[15] The compounds, however, were unambiguously characterized with a range of spectroscopic methods. The matrix-assisted laser desorption/ionization time-of-flight (MALDI-TOF) mass spectra of all these double-deckers [except RE = Gd (**6**)] showed prominent signals attributed to the molecular ions, whose isotopic patterns were in good agreement with the respective simulated spectra (Table 1).

The electronic absorption spectra of **1**−**9** were recorded in $CHCl_3$/EtOH (1:1) and the data are summarized in Table 1. The spectral features resembled those of bis(phthalocyaninato) rare earth complexes (except RE = Ce),[10,16] except that all absorption bands were significantly red-shifted in the Nc series due to the extended conjugation. The spectra could thus be interpreted in a similar manner.

Figure 1 gives the UV/Vis spectra of the La, Eu, and Er double-deckers. It can be seen from this figure and Table 1, that while the B band (328−334 nm) remains relatively unshifted, both the Q band (767−799 nm) and the π-radical anion band (593−648 nm) are shifted to the red as the ionic radius of the tervalent metal cation increases from Er to La. A similar trend was also observed for the broad near-IR band (1818−2346 nm) which is characteristic of sandwich compounds having an unpaired electron in one of the rings. Similar to the Pc[17] and Por analogs,[12b,18] a linear correlation could be established between the wavenumbers of these absorptions and the RE^{III} ionic radii (Figure 2).[19] All the observation shows that as the ring-to-ring separation increases with the size of the metal ion, the π-π interactions between the Nc rings become weaker. Another interesting feature for these spectra is the intensities of the two visible bands in ca. 600−700 nm which are generally higher for sandwich compounds with a larger metal center.

Among these complexes, the Ce double-decker **2** is particularly interesting. To our knowledge, the metal center in all known Ce double-deckers including $Ce(Por)_2$,[20] $Ce(Pc)_2$,[21] and Ce(Pc)(Por)[22] is tetravalent. The presence of π-radical anion bands and the near-IR absorptions in the spectra of **2**, however, strongly suggests that the cerium center, like all the other rare earth ions, is tervalent and one of the Nc rings exists as a π-radical anion, i.e. $Ce^{III}\{[Nc(tBu)_4]^{2-}\}\{[Nc(tBu)_4]^{\bullet-}\}$. The electronic environment imposed by the Nc ligands seems to be unique to stabilize the Ce^{III} state and allow a facile one-electron ring-oxidation.

Upon addition of $NaBH_4$ to solutions of **1**−**9** in $CHCl_3$/EtOH (1:1), the absorption spectra were remarkably changed and the resulting spectra could be attributed to the monoanions $\{RE[Nc(tBu)_4]_2\}^-$ in which both macrocycles are dianionic. The spectral data for these anions are summarized in Table 2, and the spectra for the La, Eu, and Er double-deckers, after being treated with $NaBH_4$, are displayed in Figure 3.

It is interesting to note that while the B band (328−333 nm) is virtually unshifted upon reduction, the Q

Table 1. Reaction yields and spectral data for $RE[Nc(tBu)_4]_2$ (**1**−**9**)

Compound	Yield (%)	Mass (m/z)[a]	ν ($Nc^{\bullet-}$) (cm^{-1})	λ_{max} (nm)[b]							
$La[Nc(tBu)_4]_2$ (**1**)	69	2014	1314	334	437 (sh)	648	694	799	1052		2346
$Ce[Nc(tBu)_4]_2$ (**2**)	71	2015	1313	332	435 (sh)	640	691	790	1055		2190
$Pr[Nc(tBu)_4]_2$ (**3**)	63	2015	1316	331	437 (sh)	637	691	786	1057		2129
$Nd[Nc(tBu)_4]_2$ (**4**)	56	2019	1317	332	438 (sh)	633	690	783	1062	1681	2041
$Eu[Nc(tBu)_4]_2$ (**5**)	48	2027	1324	331	440 (sh)	627	689	776	1071	1674	1928
$Gd[Nc(tBu)_4]_2$ (**6**)	52	—[c]	1324	328	439 (sh)	596	688	774	1072	1674	1883
$Tb[Nc(tBu)_4]_2$ (**7**)	47	2034	1327	331	438 (sh)	622	687	772	1073	1671	1864
$Y[Nc(tBu)_4]_2$ (**8**)	43	1963	1329	330	443 (sh)	597	686	769	1081	1666	1822 (sh)
$Er[Nc(tBu)_4]_2$ (**9**)	35	2042	1329	330	448 (sh)	593	685	767	1084	1646	1818 (sh)

[a] Mass corresponding to the most abundant isotopic peak of the molecular ion. − [b] Recorded in $CHCl_3$/EtOH (1:1). − [c] The molecular ion peak could not be detected.

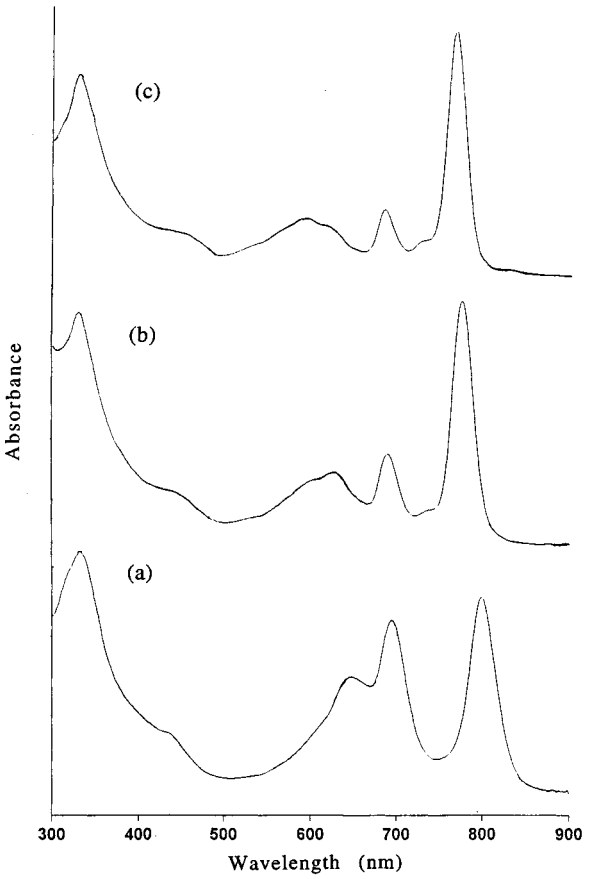


Figure 1. UV/Vis spectra of (a) La[Nc(*t*Bu)$_4$]$_2$ (**1**), (b) Eu[Nc(*t*Bu)$_4$]$_2$ (**5**), and (c) Er[Nc(*t*Bu)$_4$]$_2$ (**9**) in $CHCl_3$/EtOH (1:1)

band is split for these anions (except RE = La) giving an intense and blue-shifted band at 715−729 nm together with a weak band at 782−821 nm. The energy difference between these Q bands, or the extend of splitting, increases as the metal center becomes smaller, reflecting the degree of HOMO-HOMO interactions of the two Nc rings. This fully

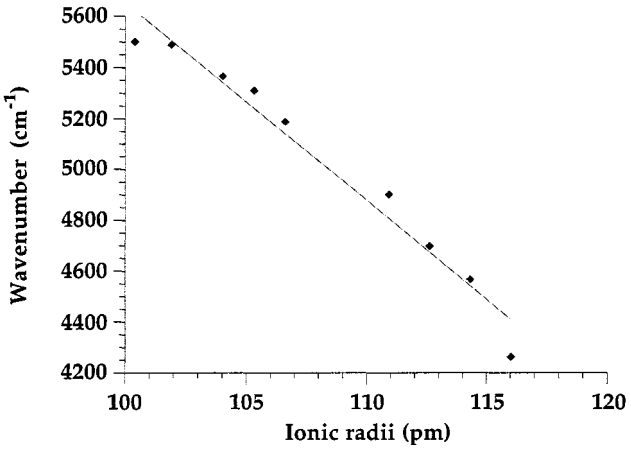


Figure 2. Plot of wavenumber of the near-IR bands of RE[Nc(*t*Bu)$_4$]$_2$ (**1**−**9**) as a function of the ionic radius of the RE^{III} ions[19]

Table 2. UV/Vis data for {RE[Nc(*t*Bu)$_4$]$_2$}$^-$ generated by adding $NaBH_4$ to **1**−**9** in $CHCl_3$/EtOH (1:1)

Compound	λ_{max} [nm]				
{La[Nc(*t*Bu)$_4$]$_2$}$^-$	333	400 (sh)	663	729	
{Ce[Nc(*t*Bu)$_4$]$_2$}$^-$	330	410 (sh)	658	727	782 (sh)
{Pr[Nc(*t*Bu)$_4$]$_2$}$^-$	328	417 (sh)	662	726	783 (sh)
{Nd[Nc(*t*Bu)$_4$]$_2$}$^-$	333	419 (sh)	659	725	787 (sh)
{Eu[Nc(*t*Bu)$_4$]$_2$}$^-$	332	413 (sh)	654	721	799
{Gd[Nc(*t*Bu)$_4$]$_2$}$^-$	329	418 (sh)	649 (sh)	719	802
{Tb[Nc(*t*Bu)$_4$]$_2$}$^-$	332	405 (sh)	654 (sh)	718	808
{Y[Nc(*t*Bu)$_4$]$_2$}$^-$	332	401 (sh)	657 (sh)	719	821
{Er[Nc(*t*Bu)$_4$]$_2$}$^-$	333	400 (sh)	647 (sh)	715	821

agrees with that which is observed for the analogous Pc anions.[23]

As expected, the characteristic near-IR band was not seen for these anions, showing that the single-hole species **1**−**9** underwent a one-electron ring-reduction. It is also worth noting that the time for complete spectral changes again depends on the size of the metal center ranging from a few minutes (for RE = La, Ce) to more than one hour (for RE = Y, Er). This is in accord with our previous observation that the intermediates REH[Nc(*t*Bu)$_4$]$_2$ or {RE[Nc(*t*Bu)$_4$]$_2$}$^-$ with a smaller metal center are easier to undergo oxidation than those with a larger metal ion.

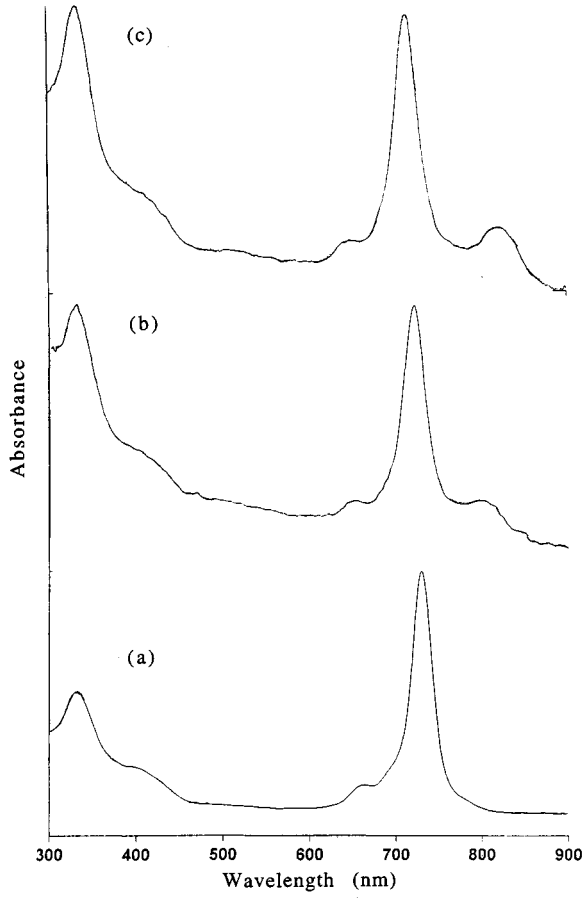


Figure 3. UV/Vis spectra of (a) La[Nc(*t*Bu)$_4$]$_2$ (**1**), (b) Eu[Nc(*t*Bu)$_4$]$_2$ (**5**), and (c) Er[Nc(*t*Bu)$_4$]$_2$ (**9**) in $CHCl_3$/EtOH (1:1) after the addition of $NaBH_4$

It is well-documented that all $RE^{III}(Pc)_2$ complexes show a strong IR band at ca. 1310 cm^{-1} which is a diagnostic band for the Pc π radical anion ($Pc^{\bullet -}$).[24] This band was also seen in this Nc series with the exact position (1313−1329 cm^{-1}) depending on the metal center (Table 1). It suggests that, due to the similar structure, the Nc π radical anion ($Nc^{\bullet -}$) also gives a marker IR band at roughly the same position as for $Pc^{\bullet -}$.

The electrochemical properties of the Nc double-deckers **1**−**9** in CH_2Cl_2 were studied by cyclic voltammetry (CV) and differential pulse voltammetry (DPV). The voltammograms generally displayed three quasi-reversible couples at 0.1−0.24, −(0.07−0.23), and −(1.18−1.24) V, all vs. the saturated calomel electrode (SCE), which could be assigned to the first one-electron oxidation and the first two one-electron reductions of the sandwich compounds, respectively. Additional couples could be revealed for some complexes, usually by DPV. Figure 4 gives the voltammograms of $Y[Nc(tBu)_4]_2$ (**8**) for exemplification and the results are tabulated in Table 3.

Similar to what is observed with the Pc analogs [cation][$RE(Pc)_2$] (cation = NBu_4,[25] Li[23]), the first oxidation and the first reduction potentials are linearly dependent on the ionic radius of the metal center (Figure 5), while the other redox processes are rather insensitive to the metal ions. The separation between these two potentials (0.28−0.34 V), which reflects the HOMO−LUMO gap of the complexes, is comparable with that reported for Lu(2,3-Nc)$_2$ (0.29 V) and Lu(1,2-Nc)$_2$ (0.33 V),[7] but significantly smaller than that for the Pc counterparts (ca. 0.40 V).[10]

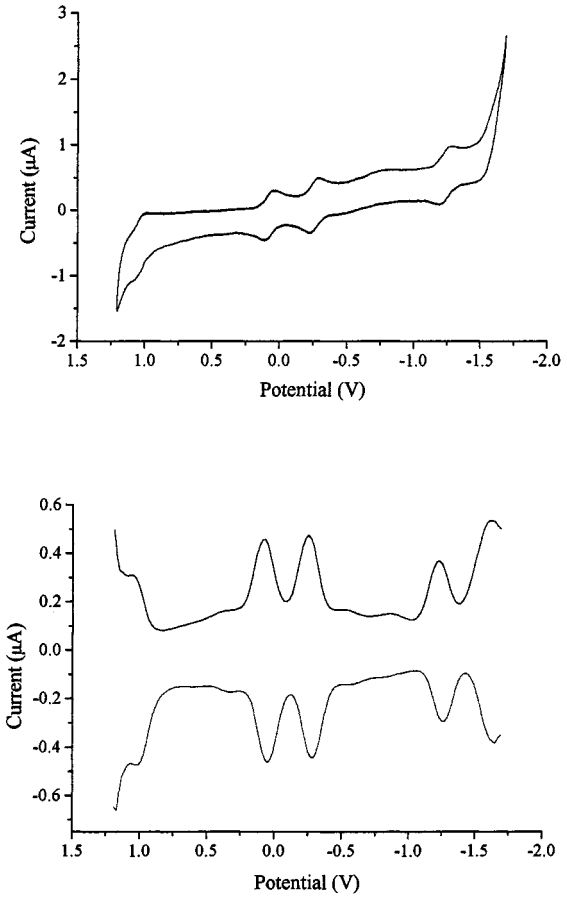


Figure 4. Cyclic voltammogram (upper) and differential pulse voltammogram (lower) of $Y[Nc(tBu)_4]_2$ (**8**) in CH_2Cl_2 containing 0.1 M $[Bu_4N][ClO_4]$ at a scan rate of 100 mV s^{-1}

Table 3. Electrochemical data for $RE[Nc(tBu)_4]_2$ (**1**−**9**)[a]

Compound	*E* (oxd.2)	*E* (oxd.1)	*E* (red.1)	*E* (red.2)	*E* (red.3)
$La[Nc(tBu)_4]_2$ (**1**)	−	0.24	−0.07	−1.20[b]	−1.59[b]
$Ce[Nc(tBu)_4]_2$ (**2**)	0.87[b,c]	0.20	−0.08	−1.18	−1.50
$Pr[Nc(tBu)_4]_2$ (**3**)	1.06[b]	0.18	−0.12	−1.19	−
$Nd[Nc(tBu)_4]_2$ (**4**)	1.10	0.17	−0.14	−1.21	−1.51
$Eu[Nc(tBu)_4]_2$ (**5**)	−	0.13	−0.21	−1.24	−
$Gd[Nc(tBu)_4]_2$ (**6**)	−	0.16	−0.15	−1.18	−1.50[b]
$Tb[Nc(tBu)_4]_2$ (**7**)	1.13[b]	0.13	−0.20	−1.19	−1.54[b]
$Y[Nc(tBu)_4]_2$ (**8**)	1.05[b]	0.07	−0.25	−1.23	−1.62[b]
$Er[Nc(tBu)_4]_2$ (**9**)	−	0.10	−0.23	−1.19	−

[a] Recorded with $[Bu_4N][ClO_4]$ as electrolyte in CH_2Cl_2 (0.1 M) at ambient temperature. Potentials were obtained by cyclic voltammetry with a scan rate of 100 mV s^{-1}, and are expressed as half-wave potentials ($E_{1/2}$) in volts relative to SCE, unless otherwise stated. − [b] By differential pulse voltammetry. − [c] May also contain the Ce^{III}/Ce^{IV} couple.

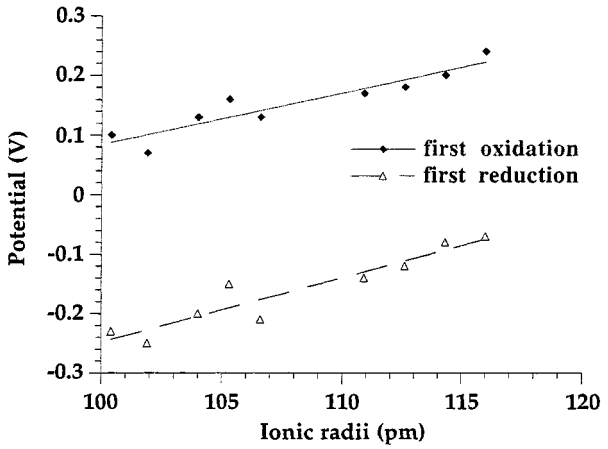


Figure 5. Redox potentials of $RE[Nc(tBu)_4]_2$ (**1**−**9**) as a function of the ionic radius of the RE^{III} ions[19]

The electrochemical behavior of $Ce[Nc(tBu)_4]_2$ (**2**) is of particular interest, as the Ce^{III} metal center may also undergoes an oxidation to Ce^{IV}. However, apart from the ring-based redox couples, no additional couple could be observed. As the peak to peak separation (ΔE) for the second oxidation of **2** was large (270 mV), as shown in its cyclic voltammogram, and the differential pulse voltammogram showed that the peak was broad and slightly split, it is likely that the Ce^{III}/Ce^{IV} couple is also embedded at this position. It has been found that the reversibility of the Ce^{III}/Ce^{IV} couple for sandwich-type compounds is usually poor, probably because the electron exchange between the electrode and the Ce center is retarded by the bulky ligands, which also participate in the electron transfer.[26] Our assignment thus seems to be in line with the previous findings.

Experimental Section

n-Octanol was distilled from sodium. The electrolyte $[Bu_4N][ClO_4]$ was recrystallized from dry acetone three times prior to use. All other reagents and solvents were of reagent grade and used as received. 6-*tert*-Butylnaphthalonitrile[27] and $RE(acac)_3 \cdot n\ H_2O$[28] were prepared by previously described methods. – UV/Vis: Hitachi U-3300. – Near-IR: Hitachi U-3100. – IR: Perkin–Elmer 1600. – MALDI-TOF-MS: Bruker BIFLEX III, α-cyano-4-hydroxycinnamic acid as matrix. – Electrochemical measurements were carried out with a BAS CV-50 W voltammetric analyzer. The cell comprised inlets for a platinum-sphere working electrode, a silver-wire counter electrode and an $Ag/AgNO_3$ (0.1 M in MeCN) reference electrode which was connected to the solution by a Luggin capillary whose tip was placed close to the working electrode.[29] Typically, a 0.1 M solution of $[Bu_4N][ClO_4]$ in CH_2Cl_2 containing the sample was purged with nitrogen for 20 min, then the voltammograms were recorded at ambient temp. Potentials were referenced to the Ag/Ag^+ couple in MeCN, which was taken as +0.31 V vs. SCE as determined for this system previously using ferrocene as an internal standard.[30]

General Procedure for the Preparation of $RE[Nc(tBu)_4]_2$ (1–9): A mixture of $RE(acac)_3 \cdot n\ H_2O$ (0.10 mmol), 6-*tert*-butylnaphthalonitrile (93 mg, 0.40 mmol), and DBU (40 mg, 0.26 mmol) in *n*-octanol (2 mL) was refluxed overnight (> 18 h) under a slow stream of nitrogen. The dark brown mixture was cooled to room temperature and the volatiles were removed under reduced pressure. The residue was purified by column chromatography on a silica gel, with $CHCl_3$ as eluent to develop a blue band containing the desired double-decker. The product obtained by this method was further purified by the same chromatographic procedure, followed by recrystallization from a mixture of $CHCl_3$ and MeOH to give a dark blue/violet powder.

Acknowledgments

Financial support from the Natural Science Foundation of China (Grant No. 29701002), The Ministry of National Educational Division of China, The Science Committee of Shandong Province, Shandong University, State Key Laboratory of Rare Earths, Peking University, The Hong Kong Research Grants Council, The Chinese University of Hong Kong, and the Queensland University of Technology is gratefully acknowledged.

[1] [1a] D. K. P. Ng, J. Jiang, *Chem. Soc. Rev.* **1997**, *26*, 433–442. – [1b] J. W. Buchler, D. K. P. Ng, in: *The Porphyrin Handbook* (Eds.: K. M. Kadish, K. M. Smith, R. Guilard), Academic Press, San Diego, **2000**, vol 3, chapter 20.
[2] M. Passard, J. P. Blanc, C. Maleysson, *Thin Solid Films* **1995**, *271*, 8–14.
[3] [3a] M. M. Nicholson, in: *Phthalocyanines: Properties and Applications* (Eds.: C. C. Leznoff, A. B. P. Lever), VCH, New York, **1993**, vol. 3, pp. 71–117. – [3b] R. Jones, A. Krier, K. Davidson, *Thin Solid Films* **1997**, *298*, 228–236.
[4] [4a] M. Trometer, R. Even, J. Simon, A. Dubon, J.-Y. Laval, J. P. Germain, C. Maleysson, A. Pauly, H. Robert, *Sensors Actuators B* **1992**, *8*, 129–135. – [4b] R. E. Clavijo, D. Battisti, R. Aroca, G. J. Kovacs, C. A. Jennings, *Langmuir* **1992**, *8*, 113–117. – [4c] M. L. Rodriguez-Mendez, R. Aroca, J. A. De-Saja, *Chem. Mater.* **1993**, *5*, 933–937.
[5] [5a] J. Simon, C. Sirlin, *Pure Appl. Chem.* **1989**, *61*, 1625–1629. – [5b] T. Komatsu, K. Ohta, T. Fujimoto, I. Yamamoto, *J. Mater. Chem.* **1994**, *4*, 533–536. – [5c] T. Komatsu, K. Ohta, T. Watanabe, H. Ikemoto, T. Fujimoto, I. Yamamoto, *J. Mater. Chem.* **1994**, *4*, 537–540.
[6] [6a] N. Ishikawa, Y. Kaizu, *Chem. Lett.* **1998**, 183–184. – [6b] F. Steybe, J. Simon, *New J. Chem.* **1998**, 1305–1306.
[7] [7a] F. Guyon, A. Pondaven, P. Guenot, M. L′Her, *Inorg. Chem.* **1994**, *33*, 4787–4793. – [7b] F. Guyon, A. Pondaven, J.-M. Kerbaol, M. L′Her, *Inorg. Chem.* **1998**, *37*, 569–576.
[8] [8a] M. Bouvet, J. Simon, *Chem. Phys. Lett.* **1990**, *172*, 299–302. – [8b] N. Ishikawa, O. Ohno, Y. Kaizu, *Chem. Phys. Lett.* **1991**, *180*, 51–56. – [8c] N. Ishikawa, O. Ohno, Y. Kaizu, *J. Phys. Chem.* **1993**, *97*, 1004–1010. – [8d] M. Bouvet, P. Bassoul, J. Simon, *Mol. Cryst. Liq. Cryst.* **1994**, *252*, 31–38. – [8e] M. Passard, A. Pauly, J. P. Germain, C. Maleysson, *Synth. Met.* **1996**, *80*, 25–28.
[9] J. Jiang, D. Du, M. T. M. Choi, J. Xie, D. K. P. Ng, *Chem. Lett.* **1999**, 261–262.
[10] J. Jiang, R. C. W. Liu, T. C. W. Mak, T. W. D. Chan, D. K. P. Ng, *Polyhedron* **1997**, *16*, 515–520.
[11] N. B. Subbotin, L. G. Tomilova, E. V. Chernykh, N. A. Kostromino, E. A. Luk′yanets, *Zh. Obshch. Khim.* **1986**, *56*, 232–233.
[12] [12a] J. W. Buchler, J. Hüttermann, J. Löffler, *Bull. Chem. Soc. Jpn.* **1988**, *61*, 71–77. – [12b] J. W. Buchler, P. Hammerschmitt, I. Kaufeld, J. Löffler, *Chem. Ber.* **1991**, *124*, 2151–2159.
[13] C. Clarisse, M. T. Riou, *Inorg. Chim. Acta* **1987**, *130*, 139–144.
[14] J. Jiang, unpublished results.
[15] J. Jiang, F. Furuya, W. Liu, D. Du, N. Kobayashi, *Inorg. Chem.* submitted.
[16] [16a] D. Markovitsi, T.-H. Tran-Thi, R. Even, J. Simon, *Chem. Phys. Lett.* **1987**, *137*, 107–112. – [16b] K. Takahashi, Y. Tomita, Y. Hada, K. Tsubota, M. Handa, K. Kasuga, K. Sogabe, T. Tokii, *Chem. Lett.* **1992**, 759–762.
[17] G. Ostendorp, H. Homborg, *Z. Anorg. Allg. Chem.* **1996**, *622*, 1222–1230.
[18] J. W. Buchler, K. Elsässer, M. Kihn-Botulinski, B. Scharbert, S. Tansil, *ACS Symp. Ser.* **1986**, *321*, 94–104.
[19] R. D. Shannon, *Acta Cryst.* **1976**, *A32*, 751–767. The radii of the metal ions at the coordination number 8 were taken.
[20] [20a] J. W. Buchler, A. De Cian, J. Fischer, P. Hammerschmitt, J. Löffler, B. Scharbert, R. Weiss, *Chem. Ber.* **1989**, *122*, 2219–2228. – [20b] O. Bilsel, J. Rodriguez, D. Holten, *J. Phys. Chem.* **1990**, *94*, 3508–3512.
[21] M. S. Haghighi, C. L. Teske, H. Homborg, *Z. Anorg. Allg. Chem.* **1992**, *608*, 73–80.
[22] [22a] M. Lachkar, A. De Cian, J. Fischer, R. Weiss, *New J. Chem.* **1988**, *12*, 729–731. – [22b] T.-H. Tran-Thi, T. A. Mattioli, D. Chabach, A. De Cian, R. Weiss, *J. Phys. Chem.* **1994**, *98*, 8279–8288.
[23] A. Iwase, C. Harnoode, Y. Kameda, *J. Alloys Comp.* **1993**, *192*, 280–283.
[24] K. M. Kadish, G. Moninot, Y. Hu, D. Dubois, A. Ibnlfassi, J.-M. Barbe, R. Guilard, *J. Am. Chem. Soc.* **1993**, *115*, 8153–8166.
[25] H. Konami, M. Hatano, N. Kobayashi, T. Osa, *Chem. Phys. Lett.* **1990**, *165*, 397–400.
[26] J. W. Buchler, B. Scharbert, *J. Am. Chem. Soc.* **1988**, *110*, 4272–4276.
[27] E. I. Kovshev, V. A. Puchnova, E. A. Luk′yanets, *Zh. Org. Khim.* **1971**, *7*, 369–371.
[28] J. G. Stites, C. N. McCarty, L. L. Quill, *J. Am. Chem. Soc.* **1948**, *70*, 3142–3143.
[29] D. T. Sawyer, A. Sobkowiak, J. L. Roberts, Jr., *Electrochemistry for Chemists*, 2nd ed., Wiley, New York, **1995**, chapter 6.
[30] Y.-L. Wong, J.-F. Ma, W.-F. Law, Y. Yan, W.-T. Wong, Z.-Y. Zhang, T. C. W. Mak, D. K. P. Ng, *Eur. J. Inorg. Chem.* **1999**, 313–321.

Received May 20, 1999
[I99184]

Exchange Coupling Parameters and Energy Levels for Cyclic Metal-Radical Complexes of Bis(hexafluoroacetylacetonato)manganese(II) with 5-*tert*-Butyl-1,3-phenylenebis(*N*-*tert*-butylaminoxyl) and (4-*N*-*tert*-Butyl-*N*-oxyamino)pyridine

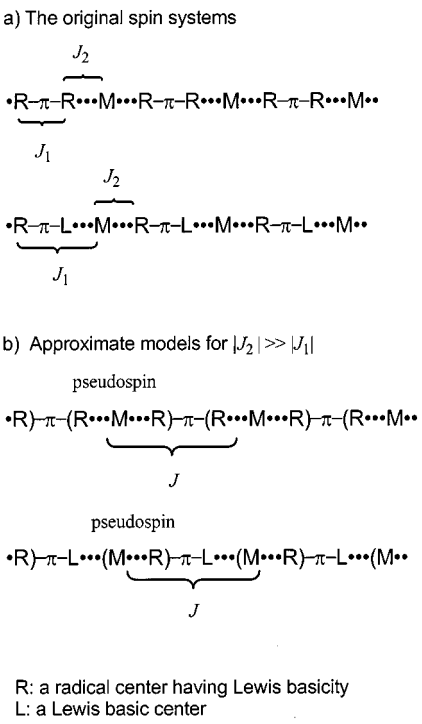
Pierre Rabu,*[a] Marc Drillon,[a] Hiizu Iwamura,*[b,e] Gunter Görlitz,[b] Tetsuji Itoh,[b] Kenji Matsuda,[b] Noboru Koga,[c] and Katsuya Inoue[d]

Keywords: Manganese / Radicals / Cyclic dimer complexes / Exchange coupling parameters / Spin states

Temperature-dependent paramagnetic susceptibility data for two cyclic dimer complexes of bis(hexafluoroacetylacetonato)manganese(II) with 5-*tert*-butyl-1,3-phenylenebis(*N*-*tert*-butylaminoxyl) and 4-(*N*-*tert*-butyl-*N*-oxyamino)pyridine have been analyzed to obtain two sets of two intramolecular exchange coupling parameters J_1 and J_2. A previous model, based on one of these interactions being much weaker than the other, could not be explicitly correlated to these actual exchange-coupling parameters. However, the energy levels of the low-lying spin states were found to be reproduced reasonably well by the approximate method.

Introduction

Coordination polymers $(R-\pi-R-M)_n$ and $(R-\pi-L-M)_n$, consisting of magnetic metal ions M and basic free radicals R−π−R and R−π−L with two ligating sites, constitute recent highlights in molecular-based magnets since they afford samples exhibiting high Curie temperatures in the range 3.4−46 K.[1] It is very often the case that there are two or more kinds of exchange pathways in such systems (Scheme 1) and, therefore, the temperature dependence of the paramagnetic susceptibility data is not simple to analyze rigorously.[2] As a first approximation, such spin systems may be analyzed by assuming a model in which one of the interactions is much stronger than the other. Then high-temperature susceptibility data would be regarded as governed by the stronger interaction, and lower temperature data would be approximated by the development of the weaker interactions between the pseudo-spins already established at the high temperature.[3−6] The physical meaning of the effective exchange coupling thus obtained is not understood straightforwardly. We have attempted to make the physical meaning of such effective exchange coupling clearer by taking advantage of the cyclic units in which the numbers of the spins are finite and rigorous solutions of the spin Hamiltonian are feasible.



Scheme 1. Schematic presentation of the spin systems

Results and Discussion

Cyclic Coordination Complex of Bis(hexafluoroacetylacetonato)manganese(II) with {5-*tert*-Butyl-1,3-phenylenebis(*N*-*tert*-butylaminoxyl)} (1)

The 1:1 complex $[Mn(hfac)_2\mathbf{1}]_2$ was obtained by reaction of bis(hexafluoroacetylacetonato)manganese(II) [Mn(hfac)$_2$]

[a] Groupe des Matériaux Inorganiques, Institut de Physique et Chimie des Matériaux de Strasbourg,
Unité Mixte CNRS − ULP − ECPM (UMR 7504),
23, rue du Loess, F-67037 Strasbourg Cedex, France
[b] Institute for Fundamental Research in Organic Chemistry, Kyushu University,
Fukuoka 812−8581, Japan
[c] Faculty of Pharmaceutical Sciences, Kyushu University,
Fukuoka 812−8582, Japan
[d] Division of Applied Molecular Science, Institute for Molecular Science,
Okazaki 444−8585, Japan
[e] Present address: National Institution for Academic Degrees,
4259 Nagatsuta, Midori-ku, Yokohama 226−0026 Japan
Fax: (internat.) + 81-45/923-0258
E-mail: iwamura@niad.titech.ac.jp

 © WILEY-VCH Verlag GmbH, D-69451 Weinheim, 2000 1434−1948/00/0101−0211 $ 17.50+.50/0

with the diradical 5-*tert*-butyl-1,3-phenylenebis(*N*-*tert*-butylaminoxyl) **(1)**.[3] Its crystal structure (Figure 1) shows that it is a cyclic analog of previously described 1-D complex polymers made up of similar components without ring *tert*-butyl groups or with halogen substituents in their place.[1b,1e] The molecule consists of two Mn^{II} ions ($S = 5/2$) and four aminoxyl radicals ($S = 1/2$) arranged in a ring as shown in Scheme 2.

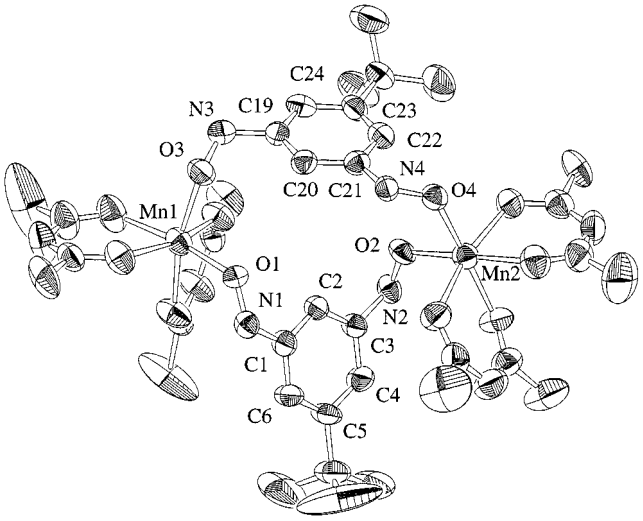
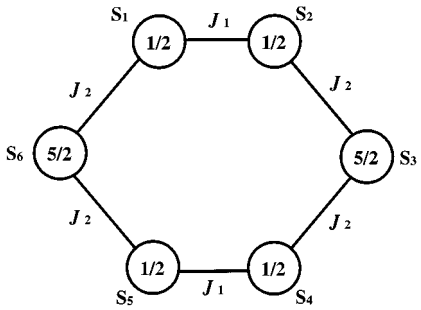


Figure 1. Structure of the cyclic complex $[Mn(hfac)_2\mathbf{1}]_2$; fluorine atoms, *N*-*tert*-butyl groups and hydrogen atoms are omitted for clarity; thermal ellipsoids are drawn at the 50% probability level



Scheme 2. A cyclic arrangement of the spins in $[Mn(hfac)_2{\cdot}\mathbf{1}]_2$

$S = 3/2$ pseudo-spins [5/2 − (2 × 1/2)], obtained by assuming a predominant antiferromagnetic (AF) coupling (J_2) between the manganese(II) ions and the two coordinated radicals. This high-spin ground state is stabilized with respect to the upper energy levels by a few hundred wavenumbers, as deduced from the decrease of χT upon increasing temperature. A decrease of χT at the lowest temperatures may be analyzed in terms of intermolecular AF coupling.

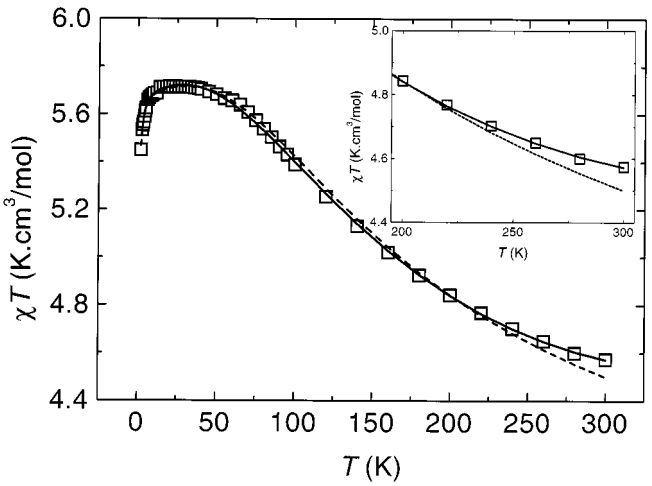
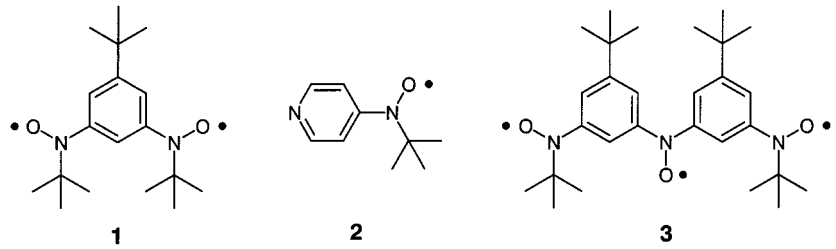


Figure 2. Dependence of the χT product on temperature T for the $[Mn(hfac)_2\mathbf{1}]_2$ complex; full and broken curves correspond to the best-fit theoretical curves based on the exact and approximate solutions, respectively (see text); the high-temperature region is expanded and shown in Inset

On this basis, the experimental data were fitted in a previous paper[7] by using a model of dimers of $S = 3/2$ pseudo-spins, with the exchange constant J and a molecular field contribution to account for the weak inter-dimer interactions. Note that the high temperature value of 4.57 Kcm^3mol^{-1} is significantly higher than that expected for two isolated $S = 3/2$ spins, suggesting a strong ferromagnetic coupling. The best agreement between theory and experiment was found for $J = +68.6$ K (±0.6 K), a Weiss constant of $\theta = -0.10$ K, and a Lande factor g = 2.002,



The molar paramagnetic susceptibility χ of the complex was investigated in the temperature range 2−300 K. The χT values exhibit a continuous increase from room temperature down to ca 50 K, reaching a plateau at 5.71 Kcm^3mol^{-1} (Figure 2). This value agrees well with the theoretical spin-only value for a $S = 3$ spin ground state, which can be explained from a ferromagnetic (F) interaction between two taking into account a scaling factor of 0.954 related to sample quality, errors in sample weighing, etc.[3] However, above 220 K, the calculated data are somewhat lower than the experimental data points (see broken curve in Figure 2). Similar analysis of a chain polymer consisting of bis(hexafluoroacetylacetonato)manganese(II) and *m*-phenylenebis(*N*-*tert*-butylaminoxyl) in a 1:1 ratio gives a ferro-

magnetic exchange constant $J = +23$ K (± 5 K) for repeating $S = 3/2$ units.[4] In these analyses, J is an "effective" interaction between pseudo-spins, and it is assumed that the Mn−aminoxyl AF interaction J_2 is much more efficient than the F intraligand aminoxyl−aminoxyl one (J_1).

Clearly, such a description may be improved by considering the rigorous spin Hamiltonian of the magnetic system:

$$\mathbf{H} = -J_1(S_1S_2 + S_4S_5) - J_2(S_2S_3 + S_3S_4 + S_5S_6 + S_6S_1) - g\mu_B H\sum S_i \quad (1)$$

corresponding to the sum of the exchange (H_{ex}) and field dependent contributions. In this expression, J_1 and J_2 are the exchange constants defined above, $S_i = 5/2$ for $i = 3$, (6 manganese(II) ions) and $S_i = 1/2$ for the others (aminoxyl radicals). The g factor is assumed to be 2.0 for both spin carriers (isotropic spins).

The energy levels of H_{ex} were determined by using as basis functions $|F_i>$ the direct products of the individual spin states $|m_{si}>$ quantified through their z component. Owing to the values of the m_{si} components, the total number of basis functions is $6^2 \times 2^4 = 576$. Taking into account the spin space symmetry, the size of the largest block to be diagonalized is reduced to 84×84.

The energy levels of the magnetic system are given by the eigenvalues of the exchange matrix whose coefficients are given by the products $<F_i|H_{ex}|F_j>$. They are obtained numerically by diagonalization of the matrix $[H_{ij}]$ (see Experimental Section); the temperature dependence of the magnetic susceptibility χ is then deduced from the usual expression:[8]

$$\chi = \frac{Ng^2\mu_B^2\sum M_{S_i}^2 \exp(-E_i/kT)}{kT\sum(2S_i+1)\exp(-E_i/kT)} \quad (2)$$

For comparison with the experimental data, this expression has been modified by taking the molecular field contribution into account with the Curie-Weiss law. The best result, illustrated in Figure 2 for the parameters $J_1 = +1005$ K (± 11 K), $J_2 = -539$ K (± 19 K), and Weiss constant $\theta = -0.10$ K (± 0.01 K), with a scaling factor 0.954,[9] gives a very good description of the experimental data over the whole temperature range. Simulation of the high-temperature values was very much improved: from 4.50 to 4.57 Kcm^3mol^{-1} for the observed value of 4.58 Kcm^3mol^{-1} at 300 K (see solid curve in Figure 2). It thus appears that the pseudo-spin approximation is not valid to determine the actual interactions. Indeed, unlike the assumption made previously, the radical-radical interaction (J_1) is found to be stronger than the manganese(II)−radical one (J_2). Furthermore, the value of J_1 is about 30 times greater than that refined in the pseudo-spin approximation. Let us recall that the "efficiency" of the exchange interaction depends also on the spin values; the energy is actually governed by $\approx JS^2$. As a result, the aminoxyl−aminoxyl and Mn−aminoxyl interaction energies are shown to be $1005 \times (1/2)(1/2) = 251$ K and $-539 \times (5/2)(1/2) = -674$ K, respectively. The latter remains stronger but does not justify the neglect of J_1 with respect to J_2. This result is in agreement with the fact that the room temperature value of χT is significantly higher than that expected for two independent $S = 3/2$ pseudo-spins.

Using the refined values of J_1 and J_2, the energy levels obtained for the above system are plotted in Figure 3 for the different spin S. It appears that the low lying levels correspond to S ranging from 3 to 0, according to the energy scheme expected for a ferromagnetic dimeric unit of $S = 3/2$ spins. These energy levels are contrasted in Figure 4 with those of the $S = 3/2$ dimer exhibiting an exchange constant $J = +68.6$ K, as reported above. A clear similarity between the two diagrams explains why the dimer approximation gives quite a satisfactory fit to the experimental data. Indeed, the energy gap between the $S = 3$ and $S = 2$ levels in the dimer model is shown to be $3J = +205.8$ K which is similar to that obtained for the real system, $\Delta E = f(J_1, J_2) \approx 190$ K.

Within the present model, all the energy levels of the hexamer system are taken into account for the calculation of $\chi T = f(T)$, while only 4 levels are involved in the dimer approximation. Thus, as the higher energy levels are neglected, the experimental susceptibility is not well reproduced at high temperature (dashed curve in Figure 2).

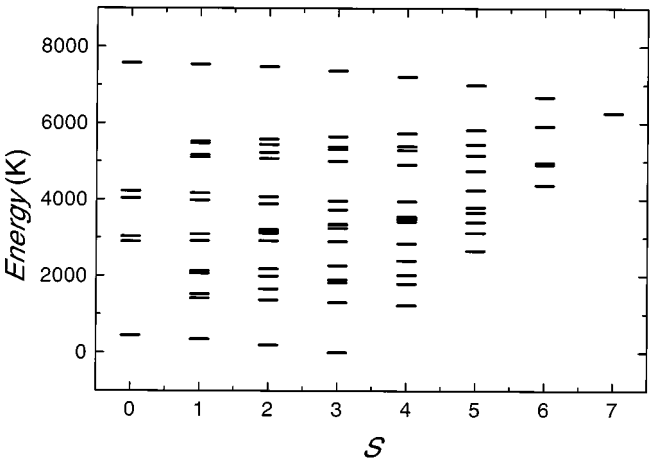


Figure 3. An energy level diagram calculated for the magnetic hexamer with the refined values of J_1 and J_2

Cyclic Coordination Complex of Bis(hexafluoroacetylacetonato)manganese(II) with 4-(*N*-*tert*-Butyl-*N*-oxyamino)pyridine (2)

The complex $[Mn(hfac)_2\mathbf{2}]_2$ was obtained by reaction of bis(hexafluoroacetylacetonato)manganese(II) with the radical 4-(*N*-*tert*-butyl-*N*-oxyamino)pyridine **(2)** in a 1:1 ratio.[5] The crystal structure (Figure 5) shows that it consists of two Mn^{II} ions ($S = 5/2$) and two aminoxyl radicals ($S =$

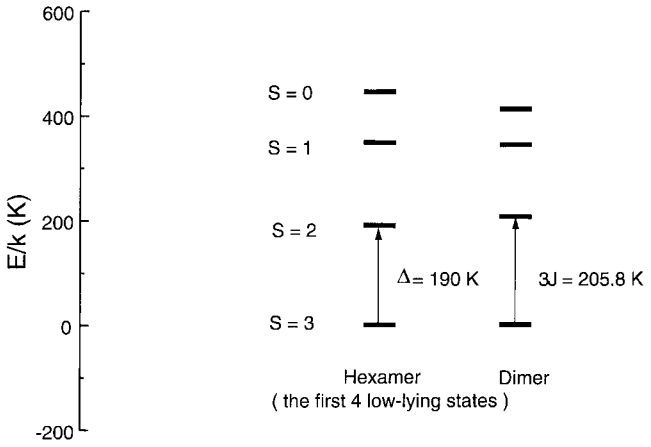


Figure 4. Comparison between the low-lying energy levels as obtained from the hexamer model and the dimer approximation for $[Mn(hfac)_2\mathbf{1}]_2$

1/2) forming a four-spin ring as illustrated in Scheme 3. The manganese atoms are coordinated to the pyridyl nitrogen atom on one side and the aminoxyl radical ligand, through the oxygen, on the other. Thus, two different exchange constants J_1 and J_2 have to be considered.

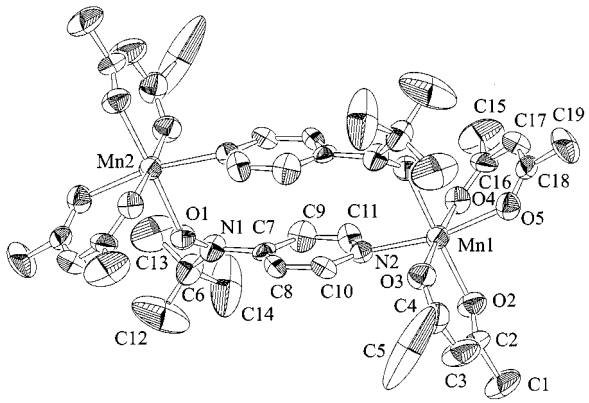
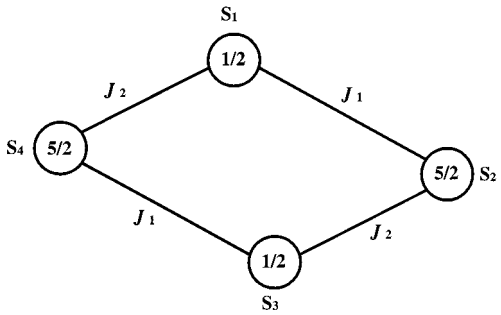


Figure 5. ORTEP view of the cyclic complex $[Mn(hfac)_2\mathbf{2}]_2$ at 30% probability; hydrogen atoms are omitted for clarity



Scheme 3. A cyclic arrangement of the spins in $[Mn(hfac)_2\cdot\mathbf{2}]_2$

The magnetic susceptibility has been investigated in the range 2.5−300 K (Figure 6). The χT versus T plot shows a continuous increase from 6.4 Kcm^3mol^{-1} at 300 K to 9.97 Kcm^3mol^{-1} at 2.5 K. The high temperature value is close to that expected for two noninteracting $S = 2$ spins, whereas the low temperature behavior agrees with that of an $S = 4$ ground state ($g = 2$). In reference to the previous Mn^{II}−radical complex, the magnetic behavior of this system may be described as ferromagnetic dimers of $S = 2$ pseudo-spins, arising from strong AF interactions between the directly bonded manganese(II) and aminoxyl centers. The experimental data, tentatively fitted to the dimer model by assuming two $S = 2$ pseudo-spins, are well reproduced for the effective interaction $J = +8.70$ K and $g = 1.97$ (see broken curve in Figure 6).

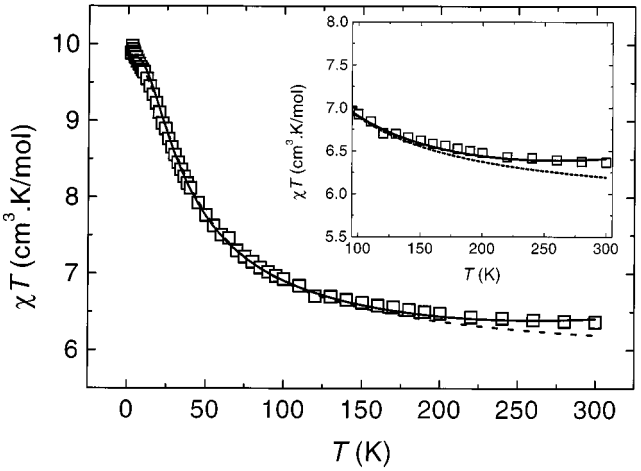


Figure 6. Variation of the χT vs T for the $[Mn(hfac)_2\mathbf{2}]_2$ complex; full and broken curves correspond to the best-fit theoretical curves based on the exact and approximate solutions, respectively (see text); the high-temperature region is expanded and shown in Inset

In the same way as above, and in order to compare the Mn−NO interactions in both systems, the actual spin Hamiltonian for the cyclic array of four spins, expressed as:

$$\mathbf{H} = -J_1(S_1S_2 + S_3S_4) - J_2(S_2S_3 + S_4S_1) - g\mu_B H\Sigma S_i \quad (3)$$

has been solved exactly. In this expression, J_1 and J_2 now stand for the exchange pathways between the Mn^{II} and NO through the pyridine ring and the direct coordination bond, respectively (Scheme 3). This model gives a very good agreement between theoretical and experimental susceptibility data, especially in the high temperature region (Figure 6), for the refined parameters $J_1 = -22.6$ K (±0.1 K), $J_2 = -372$ K (±9 K) and a scaling factor of 0.980. All the exchange couplings are antiferromagnetic, and a ferrimagnetic ground-state is stabilized. Note that the former value is in good agreement with the exchange constant of −24.8 K[9] between Mn^{II} and aminoxyl radical through the 4-pyridyl unit in the mononuclear 1:2 complex [Mn(hfac)2**2**2].[5] In this complex, the Mn^{II} ion is only coordinated to the pyridyl nitrogen atoms.

The energy scheme, corresponding to the refined values of J_1 and J_2, is contrasted to that for the $S = 2$ dimer in Figure 7. The energy gap between the ground state and the first excited state is shown to be $4J = +34.8$ K in the dimer limit, in very good agreement with that obtained for the exact model based on Equation 3 (34.8 K).

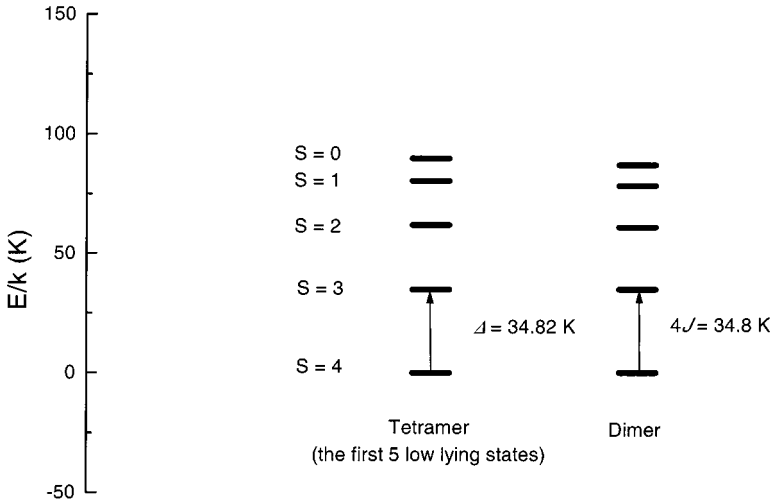


Figure 7. Comparison between the low-lying energy levels as obtained by using the tetramer model and the dimer approximation for $[Mn(hfac)_2\mathbf{2}]_2$

The Exchange Coupling Parameters J_1 and J_2 Obtained by Exact Solution

These are summarized in Table 1. The intraligand NO−NO interaction (J_1) obtained for $[Mn(hfac)_2\mathbf{1}]_2$ is as large as 10^3 K. From a classical-classical and quantum-classical chain model, Markosyan and co-workers obtained $J_1 \geq 350$ K for a 3-D complex of $[Mn(hfac)_2]$ with the tris(-aminoxyl) triradical **3** which has a *m*-phenylene connectivity.[4] The χT values for the free ligand **1** stay constant at 1 Kcm^3mol^{-1} between 4 K and room temperature, confirming that the corresponding J_1 value should be much larger than 300 K.[10] The intraligand NO−NO coupling in the neat triradical **3** is 480 K.[10][11] The value obtained in this study serves as the first example in which the magnitude of the ferromagnetic coupling parameter in *m*-phenylenebis(aminoxyl) compounds has been determined rigorously. The ferromagnetic J_1 values in these compounds originate from the in-phase spin polarization of the π-electrons on the *m*-phenylene rings due to their topology. The limited data available seem to suggest that the magnitude of such F coupling increases upon complexation with magnetic metal ions. Accumulation of more data is necessary before such a conclusion is confirmed.

It should be noted that all the direct Mn^{II}−NO exchange interactions through coordination bonds represented by J_2 are of the same order: −539, −372, and −520 K for $[Mn(hfac)_2\mathbf{1}]_2$, $[Mn(hfac)_2\mathbf{2}]_2$, and $[\{Mn(hfac)_2\}_3\mathbf{3}_2]_2$, respectively. Gatteschi et al. obtained similar AF coupling values ranging from −210 to −430 K for the coupling of Mn^{II} with 2-substituted 4,4,5,5-tetramethyl-4,5-dihydro-3-oxylimidazol-1-oxides, so called Ullman′s nitronyl nitroxides. The AF interactions derive from the pairing of the unpaired electrons in the dπ metal and pπ ligand orbitals.

Finally, we note that the indirect Mn^{II}−NO exchange coupling through the 4-pyridyl unit is AF: −22.6 and −24.8 K for cyclic $[Mn(hfac)_2\mathbf{2}]_2$ and mononuclear 1:2 complex $[Mn(hfac)_2\mathbf{2}_2]$, respectively.[5][10] The π-electrons on the pyridine ring should be polarized in such a way that the 3- and 5-carbons and the ring nitrogen atom carry positive spin which in turn overlap with the π-type d-orbital of the magnetic Mn^{II} ion attached to the pyridyl nitrogen atom. The reduced AF interaction is reasonable considering the Mn^{II} complex of bis(4-pyridyl)carbene.[13]

Table 1. Comparison of the related exchange coupling parameters

Radical or metal-radical complex	J_1/K intraligand NO - NO	J_1/K Mn(II) - NO via the 4-pyridyl unit	J_2/K directly coordinated Mn(II) - NO
$[Mn(hfac)_2\bullet\mathbf{1}]_2$	1005 ± 11		-539 ± 19
1	>300		
$[\{Mn(hfac)_2\}_3\bullet\mathbf{3}_2]$	>350		-520
3	480 ± 40		
$[Mn(hfac)_2\bullet\mathbf{2}]_2$		-22.6 ± 0.1	-372 ± 9
$[Mn(hfac)_2\bullet\mathbf{2}_2]$		-24.8 ± 0.2	
$[Mn(acac)_2\bullet\mathbf{2}_2]$		-20.4 ± 0.1	

Conclusion

Is there a merit in the pseudo-spin model for analyzing the temperature-dependence of the magnetic susceptibility of complex magnetic systems? Note that, whereas the energy values of the spin states are directly proportional to J in the dimer units, they are nonlinear combinations of J_1 and J_2 in the polymeric complexes investigated. As a result, J is an "effective" interaction with no physical meaning, and cannot be related to the actual interactions (even the sign may differ) in the latter, except when one interaction is negligible. Finally, let us point out that the use of such pseudo-spin models has an important merit of giving an insight into the splitting of the low lying spin-states. The information obtained here should be useful,[14][15] for the comparison of the exchange interactions in extended heterospin systems and for the design of such new systems.

Experimental Section

Preparation of the Complexes: The cyclic dimer complexes $[Mn(hfac)_2\mathbf{1}]_2$[3] and $[Mn(hfac)_2\mathbf{2}]_2$[5] were prepared by mixing bis(hexafluoroacetylacetonato)manganese(II) with radical ligands **1** and **2** in a 1:1 ratio as described previously.

X-ray Structures: The structures and magnetic data for cyclic complexes $[Mn(hfac)_2\mathbf{1}]_2$[3] and $[Mn(hfac)_2\mathbf{2}]_2$[5] have already been reported. Crystallographic data (excluding structure factors) for the structures $[Mo(hfac)_2\mathbf{1}]_2$ and $[Mo(hfac)_2\mathbf{2}]_2$ reported in this paper have been deposited with the Cambridge Crystallographic Data Centre as supplementary publications no. CCDC-114418 and -135189, respectively. Copies of the data can be obtained free of charge on application to CCDC, 12, Union Road, GB-Cambridge CB2 1EZ, UK [Fax: int. code + 44/1223/336-033; E-mail: deposit@ccdc.cam.ac.uk]..

Magnetic Measurements: Fine crystalline samples were mounted in a capsule (Japan Pharmacopoeia No. 5, o. d. 4.5 × 11 mm) and measured on a Quantum Design MPMS-5S SQUID susceptometer at 500 G. Corrections for the diamagnetic contribution of the samples were made by using Pascal′s constants. The diamagnetic contribution of sample capsules and holding straws used was in the range -3.7×10^{-5} – -6.7×10^{-5} emu.G.

Theoretical/Computational Analysis of the Magnetic Susceptibility Data: *SPIN*, a computer program for calculation and analysis of the magnetic properties of low dimensional systems, was employed.[16] An optimized diagonalization vectorial subroutine was used, from the library of the French institute for development and means in computer science, IDRIS (Orsay, France); the MINUIT function minimization program of the CERN library (CERN, Geneva, Switzerland) was used as a minimization subroutine.

Acknowledgments

This work is a part of the research project No. 980626 supported by the French institute for development and means in computer science, IDRIS, Orsay, France. The work was also supported by Grant-in-Aid for COE Research "Design and Control of Advanced Molecular Assembly Systems" (No. 08CE2005) from the Ministry of Education, Science, Sports, and Culture, Japan. P. R. and T. I. are thankful to the Japanese Society for the Promotion of Science for a Visiting Grant and a Postdoctoral Fellowship, respectively.

[1] [1a] K. Inoue, H. Iwamura, *J. Am. Chem. Soc.* **1994**, *116*, 3173−3174. − [1b] K. Inoue, H. Iwamura, *J. Chem. Soc., Chem. Commun.* **1994**, 2273−2274. − [1c] K. Inoue, H. Iwamura, *Synth. Met.* **1995**, *71*, 1791−1794. − [1d] K. Inoue, T. Hayamizu, H. Iwamura, *Mol. Cryst. Liq. Cryst.* **1995**, *273*, 67−80. − [1e] K. Inoue, T. Hayamizu, H. Iwamura, *Chem. Lett.* **1995**, 745−746. − [1f] T. Mitsumori, K. Inoue, N. Koga H. Iwamura, *J. Am. Chem. Soc.* **1995**, *117*, 2467−2478. − [1g] K. Inoue, T. Hayamizu, H. Iwamura, D. Hashizume, Y. Ohashi, *J. Am. Chem. Soc.* **1996**, *118*, 1803−1804. − [1h] K. Inoue, H. Iwamura, *Adv. Mater.* **1996**, *8*, 73−76. − [1i] D. C. Oniciu, K. Matsuda, H. Iwamura, *J. Chem. Soc., Perkin II* **1996**, 907−913. − [1j] H. Iwamura, K. Inoue, T. Hayamizu, *Pure Appl. Chem.* **1996**, *68*, 243−252. − [1k] K. Inoue, H. Iwamura, *Mat. Res. Soc. Symp. Proc.* **1996**, *413*, 313−320. − [1l] A. S. Markosyan, T. Hayamizu, H. Iwamura, K. Inoue, *J. Phys.*: *Condens. Matter* **1998**, *10*, 2323−2337. − [1m] H. Iwamura, *New J. Chem*. **1998**, 201−210.

[2] J. C. Bonner, M. E. Fisher, *Phys. Rev.* **1964**, A *135*, 640−658. E. Coronado, M. Drillon, R. Georges, *Resaerch Frontiers in Magnetochemistry* (Ed.: C. J. O′Connor), World Scientific Publishing Co. Plc. Ltd., **1993**, pp 27−66; O. Kahn, *Molecular Magnetism*, VCH Publishers, Inc., New York, **1993**, Chapt. 11.

[3] G. Görlitz, T. Hayamizu, T. Itoh, K. Matsuda, H. Iwamura, *Inorg. Chem.* **1998**, *37*, 2083−2085.

[4] A. S. Markosyan, K. Inoue, T. Hayamizu, H. Iwamura, to be published in *Coord. Chem. Rev.*

[5] M. Kitano, Y. Ishimaru, K. Inoue, N. Koga, H. Iwamura, *Inorg. Chem.* **1994**, 33, 6012−6019.

[6] P. Rey, D. Luneau, A. Cogne, *Magnetic Molecular Materials*, (Eds.: D. Gatteschi, O. Kahn, J. S. Miller, F. Palacio), Kluwer, Dordrecht, The Netherlands, **1991**, pp 203−214.

[7] Strictly speaking it is J/k_B rather than J itself which is given in the unit of K; 1 K corresponds to 0.695 cm^{-1}.

[8] R. L. Carlin, *Magnetochemistry*, Springer-Verlag, **1986**.

[9] Scaling factors employed here contains all the errors due to the sample purity, weighing the samples, calibration of SQUID susceptometer, etc. in addition to the deviation of the g factor from 2.00 as assumed in this study. If the last term is predomiant, $f = g2$ and, therefore, $f = 0.954$ corresponds to a g factor of 1.95 ($= 2 \times \sqrt{0.954}$).

[10] Since spin Hamiltonian $H = -2J(S_1S_M + S_MS_2)$ is used in ref.[5][10] the actual exchange constant is $2J$.

[11] T. Ishida, H. Iwamura *J. Am. Chem. Soc.* **1991**, *113*, 4238−4241.

[12] A. Caneschi, D. Gatteschi, R. Sessoli, P. Rey, *Acc. Chem. Res.* **1989**, *22*, 392−398.

[13] S. Karasawa, Y. Sano, T. Akita, N. Koga, T. Itoh, H. Iwamura, P. Rabu, M. Drillon, *J. Am. Chem. Soc*. **1998**, *120*, 10080−10087.

[14] Similar data for the copper(II) complexes are also available.

[15] P. Rey. D. Luneau, *Magnetism: A Supramolecular Function* (Ed.: O. Kahn), NATO ASI Series, Kluwer Academic Pub., Dordrecht, **1996**, pp. 431−451.

[16] Written by P. Legoll, M. Drillon, P. Rabu, F. Maingot.

Received February 16, 1999
[I99054]

Mechanisms of Cyclopalladation Reactions in Acetic Acid: Not So Simple One-Pot Processes

Montserrat Gómez,[a] Jaume Granell,[a] and Manuel Martinez*[a]

Keywords: Reaction mechanisms / Cyclopalladation / Acetic acid / Pd–C bond stability / Polynuclear species / Palladium

The processes operating during the synthetic cyclopalladation reactions of imines in acetic acid have been studied from a kinetico-mechanistic point of view. These reactions include a fast initial coordination to the palladium through the N-donor atom of the imine, followed by the proper C–H bond activation to produce the acetato bridged dimeric species. At this point, the lability of the bridging acetato groups, the hydrolysis of the C–Pd bonds, and/or the hydrolysis of C=N *exo* bonds contribute to the generation of dark red polynuclear compounds. The processes occurring after the C–H activation have been followed kinetically, both from palladium acetate plus imine, and the synthetically pure isolated acetato dimers as starting materials. The kinetic and activation parameters have been found identical within experimental error whatever the starting material was ($k^{323} = 1.5 \times 10^{-4}$ s^{-1}; $\Delta H^{+} = 51$ kJ mol^{-1}; $\Delta S^{+} = -163$ JK^{-1} mol^{-1} $\Delta V^{+} = +19$ cm^3 mol^{-1} for the 4-ClC_6H_4–CH=N–CH_2–C_6H_5 imine derivative **1a**). Acidolysis of C–Pd bonds has been found to occur in these polynuclear species. When alternative monomeric $C_{benzylic}$–Pd bond-containing complexes are possible follow ups of the reactions produce them as final dead-end complexes ($k^{323} = 2.2 \times 10^{-5}$ s^{-1}; $\Delta H^{+} = 61$ kJ mol^{-1}; $\Delta S^{+} =$ JK^{-1} mol^{-1} $\Delta V^{+} \approx 0$ cm^3 cm^{-1} for the [2,4,6-$(CH_3)_3$]C_6H_2–CH=N–CH_2-[2-$(CH_3)C_6H_4$] imine derivative **3d**). The same study has been carried out with primary amines in order to check the validity of the data if C=N bond hydrolysis is taking place in the imine derivatives with *exo* C=N bonds. For complexes with similar type of metallacycles, the results agree reasonably well with the proposed mechanism [$k^{323} = 1.2 \cdot 10^{-4}$ s^{-1}, $\Delta H^{+} = 46$ kJ·mol^{-1}, $\Delta S^{+} = -180$ J·K^{-1}mol^{-1}, $\Delta V^{+} = -16$ cm^3·mol^{-1} for the polynuclear formation of the C_6H_5–CH_2–NH_2 derivative **4e**; $k^{323} = 3.0 \cdot 10^{-4}$ s^{-1}, $\Delta H^{+} = 55$ kJ·mol^{-1}, $\Delta S^{\ddagger} = -147$ J·K^{-1}mol^{-1}, $\Delta V^{+} = -24$ cm^3·mol^{-1} for the polynuclear formation of the C_6H_5–CH_2–N=CH–2,3,6-$(CH_3)_3C_6H_2$ derivative **2c**].

Introduction

Cyclometallation reactions were one of the first known examples of C–H bond activation and cyclometallated compounds of a wide variety of ligands (containing N, P, As, O, or S as heteroatoms) have been described.[1] The cyclopalladation of N-donor ligands has been extensively studied by a number of research groups, and this reaction has acquired great interest because of the applications of metallacycles in many areas including organic synthesis,[2] homogeneous catalysis,[3] the design of new metallomesogenes,[4] and antitumor drugs.[5] The factors that influence the ease and mode of cyclopalladation of N-donor ligands are not entirely understood, but in general the following trends are accepted: intramolecular electrophilic attack of "Pd^{2+}" at the carbon atom, strong tendency to form five-membered metallacycles, and preferential activation of aromatic versus benzylic C–H bonds.[1]

There are few studies on these reactions dealing with kinetico-mechanistic information for the cyclopalladation of N-donor ligands like tertiary amines,[6] imines,[7] 2-phenylpyridines,[8] or triamines.[9] For these reactions, a highly ordered transition state has been proposed, in which the leaving proton is accepted by a base. Recently, the formal relationship that may be established between the cyclometallation reaction and the protonation of σ M–C bonds of d^8 organometallic species has been pointed out, as well as the possible role of arenonium ions in both processes.[10]

Very little information is available about the nature of the species existing in these reaction solutions. It is generally assumed that cyclopalladated compounds maintain their dimeric structure in solution, but recently it has been shown by ^{1}H-NMR spectroscopy that compounds like [Pd(μ-Br){$C_6H_4CH(CH_3)NH_2$}]$_2$ and [Pd{1-CH_2-2-(CH=$NCH_2C_6H_4$)-3,5-$(CH_3)_2C_6H_2$}(CH_3COO)]$_2$ adopt mononuclear structures in acetone[11] and acetic acid respectively.[7a]

Following our research on the cyclopalladation of N-donor ligands[12] and the mechanisms operating on organometallic reactions involving the activation of C–H and C–X bonds,[13] we present, in this paper, the study of the process that occurs between imines and palladium acetate in an acetic acid solution, both from a kinetic and a synthetic point of view. The imines have been selected to allow comparison of the behaviour of *endo*- and *exo*-metallacycles containing $C_{arom.}$–Pd or $C_{benz.}$–Pd bonds. As an extension of this work, the action of palladium acetate on primary amines has also been investigated.

Results and Discussion

The processes taking place when imines ***a***, ***b***, ***c***, and ***d*** (Scheme 1) are treated stoichiometrically with palladium acetate in acetic acid have been studied both from a synthetic and from a kinetic point of view. Although the for-

[a] Departament de Química Inorgànica, Universitat de Barcelona, Martí i Franquès 1–11, E-08028 Barcelona, Spain

 © WILEY-VCH Verlag GmbH, D-69451 Weinheim, 2000 1434–1948/00/0101–0217 $ 17.50+.50/0

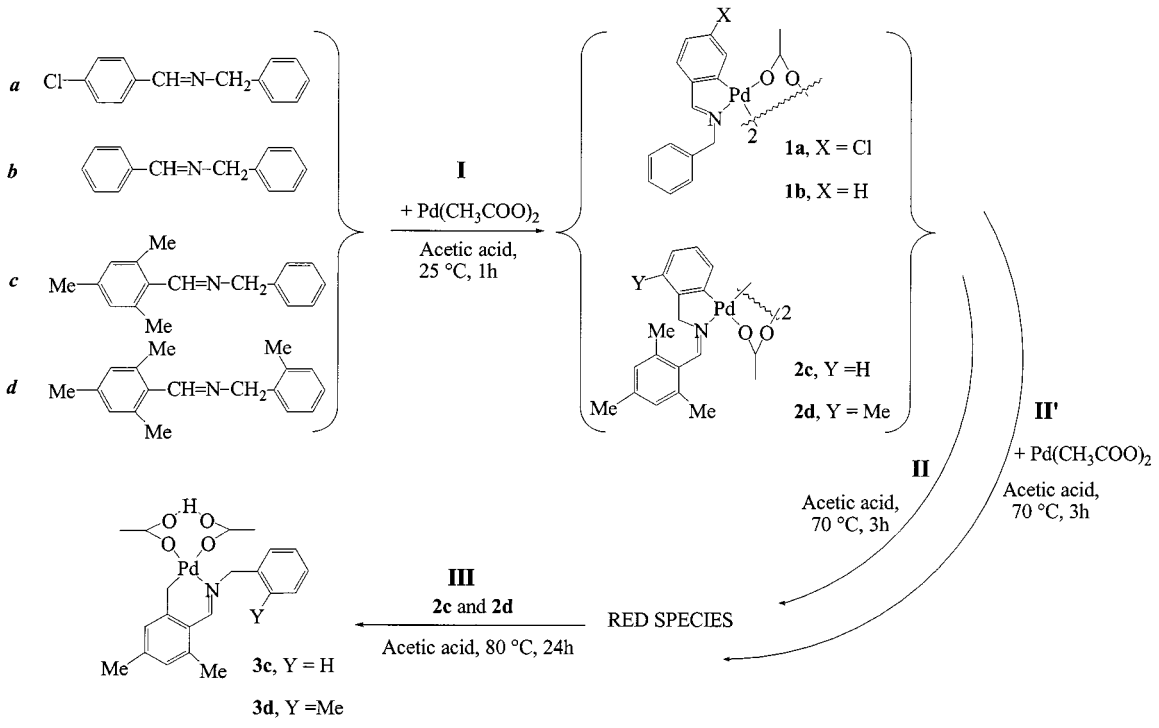
mation of cyclopalladated compounds is a well-established reaction, and even kinetico-mechanistic studies have been carried out by us[7] and other groups,[6] when the compounds are prepared in an acetic acid solution, important quantities of undefined material appear, and reduced yields are evident, compared with the reactions carried out in toluene (20% yield in acetic acid versus 60% in toluene for compounds **2c** and **2d**).[7a,12a] The available kinetic studies carried out in acetic acid also show the presence of further processes, once the main C−H electrophilic bond activation has taken place.[7a] Previous studies have indicated that the isolated acetato-bridged cyclopalladated complexes have significant differences when considered in acetic acid or in toluene. Furthermore, even though the nature of the complexes in solution is also dependent on the nature of the activated C−H bond (benzylic in **3c** and **3d**, versus aromatic in **2c** and **2d**), differences in behaviour for *endo*, **1a** and **1b**, versus *exo*, **2c** and **2d**, compounds are not so certain. In any case, it is clear that the lability of protonated bridging or terminal acetato groups plays a key role in the overall process.

Scheme 1 shows a simplified view of the reactivity involved in these cyclopalladation reactions. Discussion of Scheme 1 has to be carried out very cautiously. Any of the processes depicted (i.e. **I**, **II**, and **III**) does not necessarily have to be a single reaction; in fact, most of them have to be considered as rather complex reactions. Consequently, any rate constants and activation parameters discussed are ***apparent*** values that can only be considered as such, despite the fact that can be very informative about the equivalence of processes between different systems.

Examination of Scheme 1 gives a very good viewpoint of the cyclopalladation process. Reaction **I** takes place by the initial fast formation of a 1:1 coordination compound in stoichiometric conditions, followed by the proper C−H bond activation.[19] Kinetic measurements both in toluene and acetic acid are available at variable temperature and pressure, and the results have already been published.[7a]

The crude yellow acetato-bridged complexes isolated from the reaction **I**, **1a** and **1b**, are stable for days in the solid state, but when dissolved in acetic acid a deep red solution is formed; the process (**II**) is complete after 3 h at 70°C. Kinetic studies at variable temperature and pressure have been carried out. Table 1 collects the available data together with those for all the other processes depicted in Scheme 1. Despite the similar reactivity, the values determined for the volume of activation indicate a dramatic difference between the mechanism for the *endo*, **1a** and **1b**, and *exo*, **2c** and **2d**, complexes. Although in both cases an induction period exists, for the *exo* complexes this period is much better defined.

Where possible, spectroscopic and kinetic measurements for the initiation have been made (Table 1). If the reaction is carried out in the presence of palladium acetate (**II′**) the intensity of the red colour increases with its concentration, and the induction period decreases. The kinetic results agree with those of the experiments carried out in the absence of $Pd(CH_3COO)_2$, that is, the palladium acetate concentration does not affect the rate constant, only its extent. The deep red reaction mixture formed when the reaction was carried out with *exo* complexes, **2c** and **2d**, contains free aldehyde, as detected by ^{1}H-NMR spectroscopy. For the *endo* com-



Scheme 1. Reactivity involved in the cyclopalladation reactions of imines in acetic acid

Table 1. Available kinetic data for the processes depicted in Scheme 1. Apparent thermal activation parameters are obtained from 4−5 measures in a range of at least 35 degrees and apparent pressure activation parameters from 5−6 measures in a range of 1500 atm. Parameters indicated for process labeled as **I** + **II** correspond to the process following the C−H bond activation, i.e. process **II**, under synthetic conditions starting from imine plus palladium acetate mixtures

Imine[a]	Process	k^{323} s^{-1}	$\Delta H^{\neq}$ $kJ{\cdot}mol^{-1}$	$\Delta S^{\neq}$ $J{\cdot}K^{-1}mol^{-1}$	$\Delta V^{\neq}$ $cm^3{\cdot}mol^{-1}$
a	**I** + **II**	$1.5{\cdot}10^{-4}$	51	−163	+19
	II	$1.4{\cdot}10^{-4}$	id **I** + **II**	id **I** + **II**	
	II′[b]	$8.5{\cdot}10^{-5}$	id **I** + **II**	id **I** + **II**	
b	**I** + **II**	$1.7{\cdot}10^{-4}$	78	−74	+11
c	**II**	$3.0{\cdot}10^{-5}$	55	−147	−24
	III	$1.5{\cdot}10^{-5}$	70	−123	*ca.* 0
d	**I** + **II**	$1.0{\cdot}10^{-4}$	id **II**	id **II**	
	II	$9.7{\cdot}10^{-5}$	70	−108	−25
	II initiation[c]	$3.7{\cdot}10^{-3}$	66	−89	[d]
	I + II	$2.2{\cdot}10^{-5}$	61	−149	*ca.* 0

[a] Only compounds with the best spectroscopic handles are included. − [b] $[Pd(CH_3COO_2)_2]$ in the 5−15% range from that of the cyclometallated complex. − [c] Initial fast process corresponding to the appearance of aldehyde (see text). − [d] Reaction with too small spectroscopic changes to be measured.

plexes, **1a** and **1b**, the amount of aldehyde is less important, and appears after longer periods. Furthermore, practically no free or metallated amine is found by NMR spectroscopy, indicating that most of it remains coordinated to the palladium through the N atom. The presence of polynuclear species in the red reaction mixture has been detected by FAB and ion-spray (IS) mass-spectrometry. While mass spectra for the isolated yellow material (**1a**, **1b**, **2c**, and **2d**) indicate molecular peaks corresponding to the formulated dimer complexes, the isolated red material following process **II** has peaks at masses that correspond to species containing further acetato and palladium groups.

The IS mass spectrum of the red solid obtained from the reaction between palladium acetate and imine ***a*** shows peaks up to 1121, while the molecular weight of the dinuclear compound **1a** is 786. Furthermore, proton NMR spectroscopy of this red material shows an extremely complicated pattern in the 2.0 ppm zone, indicating that many different types of acetato ligands are present in the material, as should correspond to an undefined polynuclear compound. Further confirmation of our assumptions comes from the fact that in spite of pure dinuclear acetato bridged compounds usually being obtained in solid state after a purification process (recrystallization or column chromatography), the action of palladium acetate on 2-dimethylaminotoluene in acetic acid affords a trinuclear species, of general formula $[Pd_3(C-N)_2(\mu_2\text{-}O_2CCH_3)_4]$ (C−N≡metallated amine), as a mixture of *cis* and *trans* isomers [in relation to the $Pd_3(CH_3COO)_4$ moiety].[14] In addition, the formation of trinuclear species containing acetato bridges, isostructural to palladium acetate, has recently also been described for ligands containing C,S donor atoms.[15]

Process **I** + **II** corresponds, *de facto*, to the standard synthetic procedure in acetic acid. Under these conditions, besides cyclometallated complexes, the red coloured solution is always observed to some extent. Purification of the obtained product by column chromatography produces the final acetato-bridged dimer plus some quantities of an unidentified red material. The existence, in the acetic acid reaction medium, of palladium acetate and the final cyclometallated complex should enable the formation of polynuclear species according to reaction sequence **I** and **II′**. Kinetic measurements at variable temperature and pressure are available for this reaction sequence starting from imine and palladium acetate. Table 1 collects the data corresponding to the process that follows the C−H bond activation already described in previous studies.[7] The results agree with those obtained from the reactions carried out with the crude isolated yellow acetato dimers, **1a**, **1b**, **2c**, and **2d** (processes **II** and **II′**).

Figure 1 collects all the spectroscopic changes observed in the UV/Vis spectrum for the sequence **I** + **II**. For the reactions carried out with *exo* compounds, **2c** and **2d**, keeping these intense red solutions for 24 h at 80°C produces the light yellow *endo* monomeric complexes, **3c** and **3d**, as indicated by NMR experiments in deuterated acetic acid (process **III**).[7a] Kinetic measurements at variable temperature and pressure are available for this process starting from the isolated *exo* dimers, and these are also collected in Table 1. These *endo*, $C_{benz.}-Pd$ bond containing, complexes seem to be the dead-end of the whole process given their stability over very long periods in acetic acid.

The results, although difficult to interpret unequivocally, can be rationalized by taking into account the different stabilities in acid medium of the $C_{benz.}-Pd$ and $C_{arom.}-Pd$ bonds, as well as the reactivity of the labile acetato bridging groups. From the results presented, it is evident that, while the $C_{arom.}-Pd$ bond-containing complexes can be hydrolyzed in acetic acid, the stability of the metallacycles containing $C_{benz.}-Pd$ bond is much higher. This stability can be related both to the nature of the C−Pd bond, and to the final form of the complex in acetic acid (dimeric or polynuclear in the case of $C_{arom.}-Pd$ bond-containing complexes and monomeric for the $C_{benz.}-Pd$ bond-containing complexes). The presence of monomeric cyclometallated complexes containing $C_{benz.}-Pd$ bonds in acetic acid that do not evolve during long periods indicate that these are the most thermodynamically favourable compounds under these conditions. These results can be related with the ligand exchange reaction of N-donor ligands on cyclopalladated compounds. It has been shown that Pd^{II} effectively migrates to the ligand, forming the palladacycle less susceptible to acidolysis.[16]

As for the details of the reactivity, from the kinetic and activation parameters data, *endo* and *exo* cyclometallated $C_{arom.}-Pd$ bond-containing complexes present dramatic differences in their reaction mechanism. This can be attributed to the greater ease of Pd−C acidolysis of *exo*-metallacycles[16c] and the hydrolysis of the C=N imine bond, as seen by NMR spectroscopy. Given the fact that the reaction mixture contains "all the necessary ingredients", and that the cyclopalladated amine derivatives react with benzaldehydes to form imine *endo*-metallacycles (see below), long

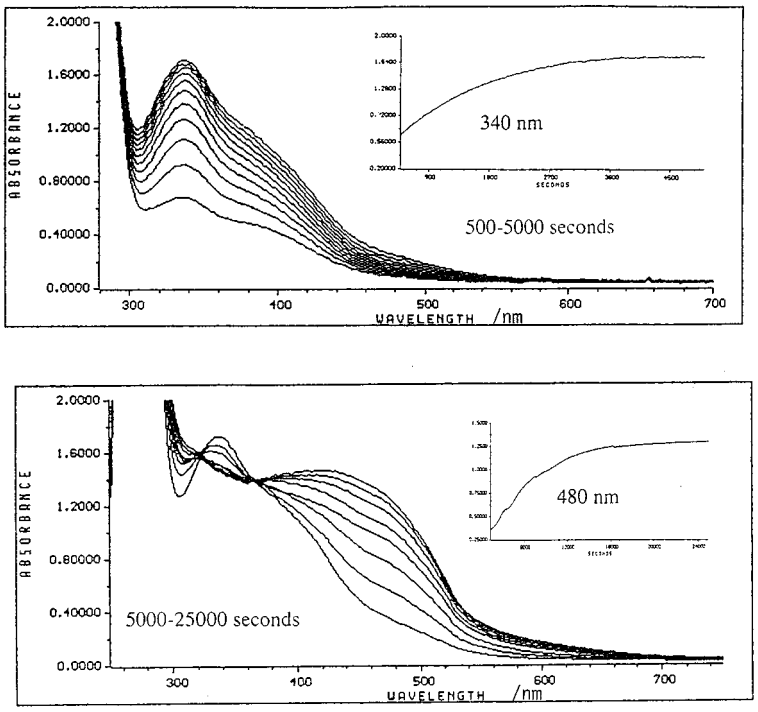
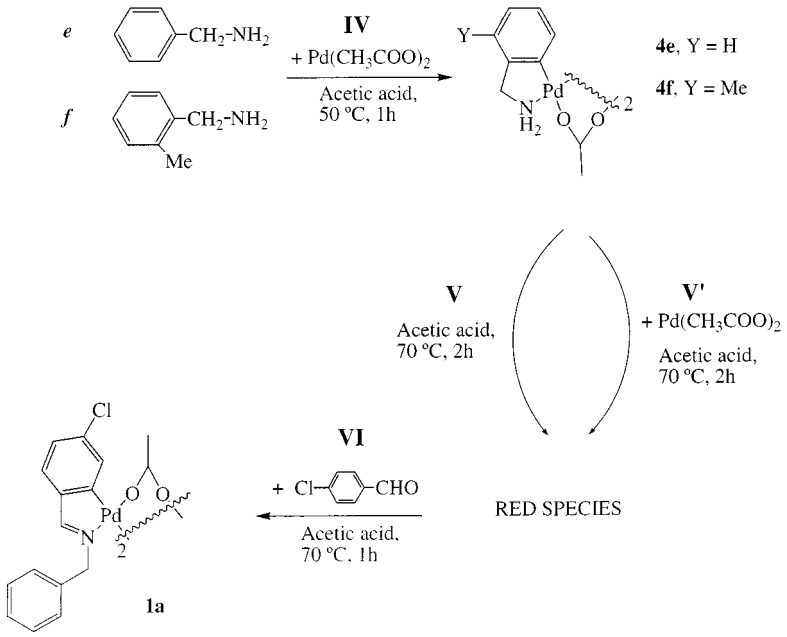


Figure 1. UV/Vis spectroscopic changes for the synthetic process, **I** + **II**, at 50°C between palladium acetate ($1\cdot10^{-3}$ M) and imine ***a*** ($1\cdot10^{-3}$ M) depicted in Scheme 1; above, metallation process (**I**); below, polynuclear formation process (**II**)

standing periods at high temperature of these red solutions produce the final dead-end monomeric *endo* $C_{benz.}-Pd$ bond-containing complex. On the other hand, the induction period for the *endo* metallacycle for the same process has to be the formation of palladium acetate via the initial $C_{arom.}-Pd$ *endo* bond hydrolysis, given the fact that the presence of palladium acetate seems to somehow reduce this induction period. From then on, the complex reaction to produce polynuclear red material (and a certain degree of decomposition) takes place with kinetic and activation parameters independent of the presence of palladium acetate in the reaction medium. The pressure activation parameters derived for the processes agree with this differentiation. While the activation volume for the polynuclear formation process for the ***a*** and ***b*** imines *endo* $C_{arom.}-Pd$ bond-containing complexes is positive, in spite of the extremely negative activation entropy, the value measured for the process that takes place for the *exo* $C_{arom.}-Pd$ bond-containing complexes is very negative. Kinetic factors seem to be dominant in the differentiation of these two processes as seen for the inverse cyclometallation reaction already studied.

In view of the interest of the processes labeled as **II** and **III** for **2c** and **2d**, the action of palladium acetate on primary amines has also been studied. It is generally accepted that primary amines are inert towards cyclometallation reactions, but they can undergo cyclopalladation if experimental conditions are appropriate. The action of $AgClO_4$ on coordination compounds $[PdCl_2L_2]$ (L=primary amine), or the action of palladium acetate on the amines in a 1:1 ratio leads to the cyclopalladation of primary amines with good yields. These results have been explained by the generation of coordinatively unsaturated species that experience the metallation.[11][17] The cyclopalladated derivative of benzylamine was prepared by refluxing a 1:1 mixture of palladium acetate and the amine in acetonitrile, as has been reported,[17e] and the cyclopalladation of the 2-methylbenzylamine was accomplished under the same reaction conditions. The dimeric compound obtained in this latter case $[Pd(CH_3COO)(3\text{-}CH_3C_6H_3CH_2NH_2)]_2$ (**4f**) was characterized by elemental analyses and NMR spectra. The monomeric triphenylphosphane complex $[PdBr(3\text{-}CH_3C_6H_3CH_2NH_2)(PPh_3)]$ (**5f**) was prepared by reaction of the acetate bridged derivative with LiBr and PPh_3 in acetone.

The action of palladium acetate on these primary amines in acetic acid was also studied; in this case the addition of deuterated pyridine to a deuterated chloroform solution of the compounds obtained, shows the formation of the $[Pd(CH_3COO)(C-N)([D_5]py)]$ (C−N ≡ ***e*** or ***f*** metallated amine, see Scheme 2) derivatives, indicating that the metallation of these ligands can take place even in acetic acid. The proton NMR spectra of the compounds obtained in absence of deuterated pyridine show, in addition to the signals of the dimeric derivatives, new signals at $\delta = 2.2-1.7$ suggesting that, under these reaction conditions, polynuclear acetato bridged complexes are also formed. This fact has been confirmed by mass spectra. The overall process depicted in Scheme 2 and its study from a kinetic point of view has also been carried out. Again, reaction **IV** takes place by the initial fast formation of the 1:1 coordination



Scheme 2. Reactivity involved in the cyclopalladation reactions of amines in acetic acid

compound in stoichiometric conditions, followed by the $C_{arom.}-H$ bond activation.

The metallation process has been studied kinetically in toluene solution at variable temperature and pressure. Table 2 collects the kinetic and thermal and pressure activation parameters for this process together with relevant comparative data; the results in solution agree with those obtained for the already published[7] metallation reactions. For the reactions studied in acetic acid solution, the activation parameters show important differences with respect to the systems already published. These observations can be explained by the fact that the metallation product obtained in acetic acid, although containing the palladacycle depicted in Scheme 2, does not correspond to that isolated according to literature procedures. As in the processes depicted in Scheme 1, the isolated solid dimer prepared according to the literature procedure is stable indefinitely, but when dissolved in acetic acid evolves to produce intense red coloured solutions. This reaction has been studied, both in neat acetic acid and in an acetic acid solution of palladium acetate, on the crude isolated acetato dimer (processes **V** and **V′** respectively). After an induction period, the formation of an intense red coloured solution takes place; the kinetic and activation parameters determined for this process are the same, within experimental error, in both cases and are characterized by extremely negative activation entropies and a negative volume of activation. Table 3 collects these data together with those for all the processes depicted in Scheme 2.

The induction period can be detected spectrophotometrically, although it implies very small absorbance changes; the kinetic and thermal activation parameters associated indicate dramatic changes with respect to the other processes involved in the overall reaction scheme. As seen in Table 3, the activation enthalpy is extremely large and the

Table 2. Kinetic and activation parameters for the cyclometallation reaction of palladium acetate with the amines ***e*** and ***f*** indicated in Scheme 2 in toluene and acetic acid solutions (process **IV**); literature data from the related imines ***c*** and ***d*** from Scheme 1 are also included.[7]

Ligand	Solvent	10^4k^{323} s^{-1}	ΔH^{+} $kJ\cdot mol^{-1}$	ΔS^{+} $J\cdot K^{-1}mol^{-1}$	ΔV^{+} $cm^3\cdot mol^{-1}$
e	Toluene	2.6	73	−91	−16
	Acetic acid[a]	76	100	+3	−11
f	Toluene	2.5	55	−145	−20
c	Toluene	70	67	−100	−12
	Acetic acid	13[b]	49	−138	−13
d	Toluene	9.2	62	−120	−17
	Acetic acid	2.2[b]	69	−91	−13

[a] In acetic acid solution process **IV** cannot be completely separated from process **V**, consequently the kinetic and activation parameters indicated have a limited reliability (see text). – [b] Measured at 298 K.

Table 3. Available kinetic data for the processes depicted in Scheme 2. Apparent thermal activation parameters are obtained from 4−5 measures in a range of at least 35 degrees and apparent pressure activation parameters from 5−6 measures in a range of 1500 atm. Parameters indicated for process labeled as **IV + V** correspond to the process following the C−H bond activation, *i.e.* process **V**, under synthetic conditions starting from amine plus palladium acetate mixtures

Amine[a]	Process	k^{323} s^{-1}	ΔH^{+} $kJ\cdot mol^{-1}$	ΔS^{+} $J\cdot K^{-1}mol^{-1}$	ΔV^{+} $cm^3\cdot mol^{-1}$
e	**IV + V**	$2.5\cdot10^{-4}$	82	−63	+14
	V initiation[b]	$3.4\cdot10^{-3}$	121	80	>>0
	V	$1.2\cdot10^{-4}$	46	−180	−16
	V′ initiation[b,c]	id **V** initiation[b]			
	V′[c]	id **V**			

[a] Only compounds with the best spectroscopic handles are included. – [b] Initial fast process (see text). – [c] $[Pd(CH_3COO_2)_2]$ in the 5−15% range from that of the cyclometallated complex.

value found for the activation entropy is very positive. As for the activation volume, an extremely large positive value is estimated from the experiments. Its determination has not been possible due to the fact that there is an important pressure retardation of the initiation process with small spectroscopic changes implied, and that the above mentioned process has a large pressure acceleration with important differences in the spectra. The presence of polynuclear species in the red reaction mixture is clearly indicated in solid state by mass spectrometry, as well as in solution (^{1}H-NMR spectroscopy). Peaks up to 757 are observed in the FAB mass spectrum of the red solid obtained from the reaction of palladium acetate and amine ***e***. The molecular weight of the dinuclear compound **4e** is 543. From gas chromatography analysis of the crude red solution small quantities of free amine are also detected. Under synthetic conditions in acetic acid solution (process **IV** + **V**) the final red coloured solution is always observed. Kinetic measurements have been carried out at variable temperature and pressure for the reaction following the C−H bond activation process; the results obtained for both thermal and pressure activation parameters and collected in Table 3. When *para*-chlorobenzaldehyde is added to the crude deep red solution in acetic acid, condensation with the amine takes place, producing the *endo* cyclometallated compound, **1a**, derived from the corresponding imine as detected by NMR spectroscopy.

The results from the data in Scheme 2 have to be interpreted together with those for the imine derivatives. It is noteworthy to indicate that the behaviour of the cyclometallated amine has to be directly related to the reactivity of the *exo* cyclometallated complexes, **2c** and **2d**, containing $C_{arom.}$−Pd bonds, once the initial C=N bond hydrolysis has taken place (see above). The fact that formation of an intense red coloured solution is observed, both in synthetic conditions in acetic acid and by further treatment of the isolated acetato dimers in neat acetic acid or acetic acid solutions of palladium acetate, is a clear indication that the reactivity is related to the acidolysis of the $C_{arom.}$−Pd bond in the complexes. Again mass spectra indicate that important amounts of polynuclear species are present in the isolated red material. Nevertheless, even in these intense red polynuclear containing solutions, the presence of cyclometallated complexes is always detected, no full decomposition of the cyclopalladated compound is taking place.

Reaction of these red solutions with the corresponding aldehyde produces solutions where the *endo* cyclometallated complex **1a**, already described, is detected. We assume that the presence of the free amine in the polynuclear material solutions allows for the amine-aldehyde condensation;[20] thereafter the cyclometallation process, already described for the imine derivatives, takes place. As for the kinetic and activation parameters measured, an interesting fact is that those related to reaction **V** are in perfect agreement with those measured for the appearance of the polynuclear-containing red solutions for the reactions of the *exo* imine derivative complexes, **II**. In both cases, an initiation reaction is detected, while for the *exo* imine complexes it has been proven to be partly due to the hydrolysis reaction of the C=N bond, for compounds **4e** and **4f** this reaction has to be related solely to the hydrolysis of the main $C_{arom.}$−Pd bond. It is also interesting to note that, although in the presence of palladium acetate in the acetic acid solution medium this initiation also exists, it involves smaller spectral changes. It seems evident that the initiation process in this reaction needs the presence of $Pd(CH_3COO)_2$ in order to start the formation of the red polynuclear material. In this respect, the values measured for the activation parameters (specially the activation volume) for the synthetic process **IV** + **V**, have to be looked into more carefully. Given the fact that the $C_{arom.}$−H bond activation of the amines (process **IV**) is much slower (see Table 2) than the fast initiation process of reaction **V**, detected when the isolated acetato dimer **4e** is dissolved in acetic acid (see Table 3), the values determined for the polynuclear formation process starting from amine and palladium acetate mixtures, probably also contain a contribution from the C−H bond activation reaction, **IV**.

Conclusions

In summary, our mechanistic studies have shown that the reaction between imines and palladium acetate, in acetic acid solution, is a rather complex process in which several different reactions, such as acidolysis of Pd−C and C=N bonds, and substitution on the acetato bridging positions take place. It has also been found that cyclopalladated amine compounds react with benzaldehydes to afford the corresponding metallated imines in the *endo* form. Even the structures generally assumed for all these complexes are not so simple and they strongly depend on the reaction conditions. Under smooth conditions (25°C, 1 h), dimeric species containing five-membered metallacycles in *endo* (**1a** and **1b**) and *exo* (**2c** and **2d**) conformations, are formed and can be isolated as yellow solids in good yields. Longer reaction periods or higher temperatures induce the formation of polynuclear red materials due to the reactivity of the acetato bridging groups, as well as the reactivity of the C−Pd and C=N bonds. Obviously these more drastic reaction conditions favour the formation of the more thermodynamically stable metallacyclic species (*endo* six-membered monomeric cycles versus *exo* five-membered dimeric cycles, for ligands ***c*** and ***d***). In any case, the reaction mixture contains polynuclear species that can be detected, both in solution by NMR spectroscopy and in solid state by mass spectrometry. The cyclometallation of amines ***e*** and ***f*** in acetic acid has also been accomplished for the first time; in an analogous way, dimeric cyclopalladated compounds are initially formed, but the existence of dynamic processes affords some final polynuclear species.

Deeper interpretation of the kinetic and activation data available would be speculative at this point, given the multitude of steps taking place in any of the processes depicted in the reaction schemes. Further detailed studies for some of these systems are currently under way in order to establish a better kinetic understanding.

Experimental Section

General: ^{1}H- and ^{31}P{^{1}H}-NMR spectra were recorded on a Varian XL-200 (200 MHz) or Bruker 250 DRX (101.25 MHz) spectrometer. Chemical shifts (in ppm) are relative to $SiMe_4$ for ^{1}H and to 85% H_3PO_4 for ^{31}P spectra. The solvents used were $CDCl_3$ for ^{1}H spectra and $CHCl_3$ for ^{31}P spectra. − IR spectra were recorded as KBr disks on a Nicolet 520 FT-IR spectrometer. − GC analyses were performed on a Hewlett-Packard 5890 Series II gas chromatograph (50-m Ultra 2 capillary column 5% phenylmethylsilicone and 95% dimethylsilicone) with a FID detector. − Microanalyses were performed by the Institut de Química Bio-Orgànica de Barcelona (CSIC) and by the Serveis Científico-Tècnics de la Universitat de Barcelona. − Mass spectra (FAB and IS) were recorded on a Micromass VG-Quattro spectrometer; the samples were introduced in a matrix of 2-nitrobenzyl alcohol for FAB spectra and a mixture of water/acetonitrile was used as eluent for ion-spray spectra. − Imines **a**−**d** and cyclopalladated compounds **1a**, **1b**, **2c**, **2d**, and **4e** were prepared according to literature procedures.[12a,17e,18]

[Pd(CH$_3$COO)$_2$(4-ClC$_6$H$_4$CH=NCH$_2$C$_6$H$_5$)$_2$]: 0.100 g ($0.45\cdot10^{-3}$ mol) of palladium acetate and 0.21 g of **a** ($0.90\cdot10^{-3}$ mol) were dissolved in 10 cm^3 of toluene and stirred at room temperature for 2 hours, affording a pale yellow precipitate. The solid was filtered off and washed successively with toluene and diethyl ether, and dried under reduced pressure. Yield: 0.24 g (80%). − $C_{32}H_{30}Cl_2N_2O_4Pd$ (683.91): calcd. C 56.22, H 4.42, N 4.10; found C 56.26, H 4.48, N 4.38. − ^{1}H NMR: δ = 9.06 (br. s, 1 H, C*H*=N), 7.70−7.10 (m, 9 H, aromatic), 5.39 (s, 2 H, CH_2N), 1.60 (s, 3 H, CH_3).

Synthesis of 1a: 0.080 g of **4e** ($0.15\cdot10^{-3}$ mol) and 0.082 g of 4-chlorobenzaldehyde ($0.60\cdot10^{-3}$ mol) were treated with 5 cm^3 of acetic acid at 75°C overnight. The solution was filtered over celite, and the solution was concentrated under reduced pressure. After addition of diethyl ether, a yellow solid was precipitated. The solid **1a** was filtered off and washed successively with hexane and diethyl ether, and dried in vacuo.

[Pd(CH$_3$COO)(3-CH$_3$C$_6$H$_3$CH$_2$NH$_2$)]$_2$ (4f): 0.3 g ($0.25\cdot10^{-3}$ mol) of 2-methylbenzylamine, ***f***, were treated with palladium acetate ($0.25\cdot10^{-3}$ mol, 0.55 g) in acetonitrile at reflux for 4 h and then filtered. The solution was concentrated in vacuo, and the solid, obtained after addition of diethyl ether was recrystallised from chloroform/diethyl ether to obtain **4f** in 60% yield (0.4 g). Anal. [found (calcd. for $C_{20}H_{26}N_2O_4Pd_2$ (571.24): C 42.3 (42.05), H 4.7 (4.59), N 5.0 (4.90)%. − ^{1}H NMR: δ = 7.25 (m, 1 H, aromatic), 6.80 (br m, 2 H, aromatic), 4.00 (br m, 2 H), 3.05 (br. s, 2 H), 2.05 (br. s, 6 H, CH_3−C$_6$H$_3$, CH_3COO). ^{1}H NMR (**4f**+[D$_5$]py): δ = 7.15 (m, 1 H, aromatic), 7.05 (br m, 1 H, aromatic), 6.0 (br d, 1 H, aromatic), 4.62 (br. s, 2 H, NH_2), 4.42 (s, 2 H, CH_2N), 2.26 (s, 3 H, CH_3), 1.98 (s, 3 H, CH_3COO).

[PdBr(3-MeC$_6$H$_3$CH$_2$NH$_2$)(PPh$_3$)] (5f): 0.15 g ($0.25\cdot10^{-3}$ mol) of **4f** were treated with PPh_3 ($0.50\cdot10^{-3}$ mol, 0.14 g) and LiBr ($0.5\cdot10^{-3}$ mol, 0.046 g) in acetone at room temperature for 45 min and then filtered. The solution was concentrated in vacuo, and the solid, obtained after addition of diethyl ether was recrystallized from chloroform to obtain **5f** in 80% yield (0.23 g). − $C_{26}H_{25}BrNPPd$ (568.77): calcd. C 54.91, H 4.43, N 2.46; found C 54.5, H 4.5, N 2.60. − ^{1}H NMR: δ = 7.90−7.70 (m, 6 H, aromatic),7.60 7.40 (m, 9 H, aromatic), 6.75 (d, 7.2 Hz, 1 H, aromatic), 6.46 (t, 7.2 Hz, 1 H, aromatic), 6.36 (br t, 1 H, aromatic), 4.46 (s, 2 H, CH_2N), 4.05 (br. s, 2 H, NH_2), 2.35 (s, 3 H, CH_3). − ^{31}P{^{1}H} NMR: δ = 41.5 (s).

Kinetics: The reactions at atmospheric pressure were followed by UV/Vis spectroscopy in the full 750−300 nm range on a HP8542A instrument equipped with a multicell transport, thermostated (±0.1°C) with a circulation bath. Observed rate constants were derived from the absorbance versus time traces at the wavelengths where a maximum increase or decrease of absorbance was observed. The general kinetic technique is that previously described.[13] The concentration range for the different compounds used in this work is the same as that in previous papers;[7] no dependence on the different concentrations has been found for any of the rate constants in the $0.7-1.3\cdot10^{-3}$ M range. For runs at high pressure, a previously described pressurizing system and high pressure cell were used.[7][13] In these cases, the absorbance versus time traces were recorded on a J&M TIDAS instrument. Rate constants were derived from exponential least-square fitting by the standard routines. Least-square errors for the rate constants were always in the range of 10−15% of the calculated value. All post-run fittings to rate laws were done by standard, commercially available fitting programmes.

Acknowledgments

We acknowledge financial support from the DGICYT (Projects PB97−0407-C05−04, PB96-0164, PB97-0914), CIRIT and the Direcció General d'Universitats (Generalitat de Catalunya). Helpful comments from Drs. Joan Albert and Margarita Crespo are gratefully acknowledged.

[1] [1a] M. I. Bruce, *Angew. Chem. Int. Ed. Engl.* **1977**, *16*, 73. − [1b] G. R. Newkome, W. E. Puckett, W. K. Gupta, G. E. Kiefer, *Chem. Rev.* **1986**, *86*, 451. − [1c] I. Omae, *Coord. Chem. Rev.* **1988**, *83*, 137. − [1d] V. Dunina, O. A. Zalevskaya, V. M. Potatov, *Russ. Chem. Rev.* **1988**, *57*, 250.
[2] [2a] A. D. Ryabov, *Synthesis* **1985**, 233. − [2b] M. Pfeffer, *Recl. Trav. Chim. Pays Bas.* **1990**, *109*, 567.
[3] [3a] M. Camargo, P. Dani, J. Dupont, R. F. de Souza, M. Pfeffer, I. Tkatchenko, *J. Mol. Catal.* **1996,** *109*, 127. − [3b] R. Navarro, E. P: Urriolabeitia, C. Cativiela, M. D. Diaz de Villegas, M. P. López, E. Alonso, *J. Mol. Catal.* **1996**, *105*, 111.
[4] P. Espinet, M. A. Esteruelas, L. A. Oro, J. L. Serrano, E. Sola, *Coord. Chem. Rev.* **1992**, *117*, 215.
[5] C. Navarro-Ranninger, I. López-Solera, J. M. Pérez, J. R. Masaguer, C. Alonso, *Appl. Organomet. Chem.* **1993**, *7*, 57
[6] [6a] A. D. Ryabov, *Chem. Rev.* **1990**, *90*, 403. − [6b] A. D. Ryabov, I. K. Sakodinskaya, A. K. Yatsimirsky, *J. Chem Soc., Dalton Trans.* **1985**, 2629.
[7] [7a] M. Gómez, J. Granell, M. Martinez, *J. Chem. Soc., Dalton Trans.* **1998**, 37. − [7b] M. Gómez, J. Granell, M. Martinez, *Organometallics* **1997**, *16*, 2539.
[8] R. P. Thummel, Y. Jahng, *J. Org. Chem.* **1987**, *52*, 73.
[9] T. Yagyu, S. Iwatsuki, S. Aizawa, S. Funahashi, *Bull. Chem. Soc. Jpn.* **1998**, *71*, 1857.
[10] A. J. Canty, G. van Koten, *Acc. Chem. Res.* **1995**, *28*, 406.
[11] J. Vicente, I. Saura-Llamas, P. G. Jones, *J. Chem. Soc., Dalton Trans.* **1993**, 3619.
[12] [12a] J. Albert, R. M. Ceder, M. Gómez, J. Granell, J. Sales, *Organometallics* **1992,** *11*, 1536. − [12b] J. Albert, J. Granell, J. Sales, M. Font-Bardía, X. Solans, *Organometallics* **1995**, *14*, 1393. − [12c] J. Albert, A. González, J. Granell, R. Moragas, X. Solans, M. Font-Bardía, *J. Chem. Soc., Dalton Trans.* **1998**, 1781.
[13] [13a] M. Crespo, M. Martinez, J. Sales, X. Solans, M. Font-Bardia, *Organometallics* **1992**, *11*, 1288. − [13b] M. Crespo, M. Martinez, J. Sales, *Organometallics* **1993**, *12*, 4297. − [13c] G. González, P. Lahuerta, M. Martinez, M. Sanau, E. Peris, *J. Chem. Soc.*, *Dalton Trans.* **1994**, 545. − [13d] F. Estevan, P. Lahuerta, E. Peris, M. A. Ubeda, S. García-Granda, F. Gómez-Beltrán, E. Pérez Carreño, G. González, M. Martinez, *Inorg. Chim. Acta* **1984**, *218*, 189. − [13e] F. Estevan, G. González, P. Lahuerta, M. Martinez, E. Peris, R. van Eldik, *J. Chem. Soc., Dalton Trans.* **1996**, 1045.

[14] M. Pfeffer, E. Wehman, G. van Koten, *J. Organomet. Chem.* **1985**, *282*, 127.
[15] M. Basato, C. Bertani, M. Zena, A. Grassi, G. Valle, *J. Organomet. Chem.* **1999**, *575*, 163.
[16] [16a] A. D. Ryabov, *Inorg. Chem.* **1987**, *26*, 1252. – [16b] A. D. Ryabov, A. K. Yatsimirky, *Inorg. Chem.* **1984**, *23*, 789. – [16c] R. M. Ceder, M. Gómez, J. Sales, *J. Organomet. Chem.* **1989**, *361*, 391. – [16d] J. Granell, D. Sainz, J. Sales, X. Solans, M. Font-Altaba, *J. Chem. Soc., Dalton Trans.* **1986**, 1785.
[17] [17a] A. Avshu, R. D. O′Sullivan, A. W. Parkins, N. W. Alcock, R. M. Countryman, *J. Chem. Soc., Dalton Trans.* **1983**, 1619. – [17b] Y. Fuchita, H. Tsuchiya, A. Miyafuji, *Inorg. Chim. Acta*, **1995**, *233*, 91. – [17c] J. Vicente, I. Saura-Llamas, M. G. Palin, P. G. Jones, *J. Chem. Soc., Dalton Trans.* **1995**, 2535. – [17d] J. Albert, J. Granell, A. Luque, J. Mínguez, R. Moragas, M. Font-Bardía, X. Solans, *J. Organomet. Chem.* **1986**, *522*, 87. – [17e] J. Vicente, I. Saura-Llamas, M. Palin, P. G. Jones, M. C. Ramírez de Arellano, *Organometallics* **1997**, *16*, 826.
[18] J. Albert, J. Granell, J. Sales, *J. Organomet. Chem.* **1984**, *273*, 393.
[19] Formation of *bis*-coordination complexes, $[Pd(CH_3COO)_2(imine)_2]$, has also been achieved by precipitation from toluene solution when a 1:2 Pd/imine ratio is used. in addition, further treatment of $[Pd(CH_3COO)_2(\boldsymbol{a})_2]$ in acetic acid for 3 h at 70 °C produces mainly mono-cyclometallated acetato dimer plus free imine.
[20] The direct condensation of ***e*** plus *p*-clorobenzaldehyde in acetic acid yields quantitatively imine ***a***. In addition, after 3 hours in refluxing acetic acid only a 3% of decomposition of imine ***a*** is observed as monitored by GC chromatography.

Received May 27, 1999
[I99195]

Novel Organometallic Derivatives of Thioesters of the Trivalent Phosphorus Acids: Synthesis and Structure

Vasily A Milyukov,[a] Alexander V. Zverev,[a] Sergey M. Podlesnov,[a] Dmitry B. Krivolapov,[a] Igor A. Litvinov,[a] Aidar T. Gubaidullin,[a] Olga N. Kataeva,*[a] Allan G. Ginzburg,[b] and Oleg G. Sinyashin[a]

Keywords: Thiophosphites / X-ray diffraction, / Manganese / Iron / Phosphorus

Thioesters of the phosphorous acid containing cymantrenyl and ferrocenyl substituents at sulfur were obtained for the first time from the reaction of organometallic disulfides with white phosphorus. According to an X-ray diffraction study tricymantrenyl trithiophosphite adopts an unusual asymmetric *cis*, *gauche*, *trans* conformation along the P–S bonds with respect to the phosphorus lone electron pair. Tri-ferrocenyl trithiophosphate possesses a classical propeller-like structure in the solid state which is different from its oxygen analogue.

Introduction

The chemistry of the thioesters of the trivalent phosphorus acids is a topic of great current interest and has experienced significant advances in recent years.[1] Surprisingly, the synthesis and structure of organometallic thioesters of the trivalent phosphorus acids has not been previously reported. The synthesis of such compounds provides a promising approach to obtain novel bi- and polynuclear complexes of transition metals, the coordination ability of trithiophosphites being promoted by their conformational flexibility due to internal rotation around the P−S bonds.[2−6]

In this paper we report the method of synthesis and the structure of novel thioesters of the trivalent phosphorus acids containing cymantrenyl and ferrocenyl fragments at the sulfur atoms.

Results and Discussion

Syntheses

Three general methods for the preparation of the thioesters of the trivalent phosphorus acids are known. The first one[7] involves the phosphorylation of mercaptans by chlorides of the trivalent phosphorus acids. This reaction can proceed both in the presence or absence of the hydrogen chloride acceptors (R, R′ = alkyl or aryl):

$$RSH + R'_{3-n}PCl_n \longrightarrow R'_{3-n}P(SR)_n + HCl \quad (1)$$

Following this method we have synthesised *S*-cymantrenyldiphenylthiophosphinite, the first compound belonging to the class of organometallic thioesters of the trivalent phosphorus acids.[8] This compound was obtained from the reaction of cymantrenylmercaptan with diphenylchlorophosphane in boiling dichloromethane. However, it appears that this method has significant limitations and does not allow us to obtain organometallic thioesters of phosphorous or phosphoric acid, though oxygen analogues − triferrocenyl phosphite and the corresponding phosphate − were prepared by Max Herberhold and co-workers[9] by the interaction of ferrocenol with PCl_3.

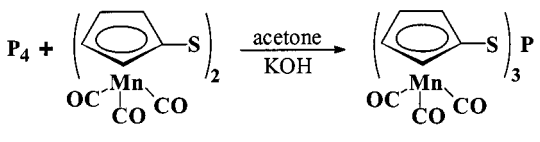
The second method[10] involves the phosphorylation of mercaptides of alkali metals by chlorides of the trivalent phosphorus acids:

$$RSNa + R'_{3-n}PCl_n \longrightarrow R'_{3-n}P(SR)_n + NaCl \quad (2)$$

The most simple and convenient way to obtain trithiophosphites[11] is by the treatment of dialkyl (diaryl) disulfides with white phosphorus, this reaction also being used[12] to synthesise triseleno- and tritellurophosphites:

$$6(RS)_2 + P_4 \longrightarrow 4(RS)_3P \quad (3)$$

This reaction proceeds under mild conditions in aprotic solvents in the presence of a small amount of 15N KOH. In order to introduce a metal-containing thio-group at the phosphorus atom, for example cymantrenyl or ferrocenyl, the corresponding organometallic disulfides can be used as precursors to give tricymantrenyl and triferrocenyl trithiophosphites. Tricymantrenyl trithiophosphite was obtained in one step at room temperature in high yield by the reaction of white phosphorus with dicymantrenyl disulfide (**1**) in acetone solution.

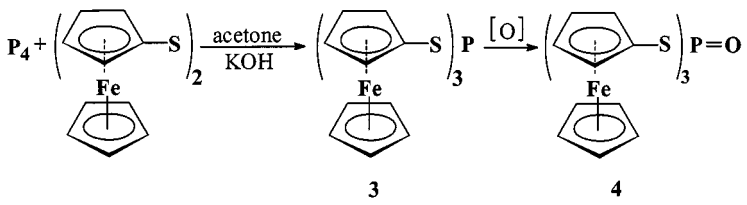


1 **2**

Scheme 1. Synthesis of tricymantrenyl trithiophosphite

[a] A. E. Arbuzov Institute of Organic and Physical Chemistry, Russian Academy of Sciences,
A. E. Arbuzov str. 8, Kazan 420088, Russia
Fax: (internat.) + 7-8432/76-7424
[b] A. N. Nesmeyanov Institute of Organoelement Compounds, 28, Vavilov str., Moscow 117334, Russia

 © WILEY-VCH Verlag GmbH, D-69451 Weinheim, 2000 1434−1948/00/0101−0225 $ 17.50+.50/0



Scheme 2. Synthesis of triferrocenyl trithiophosphite and trithiophosphate

The identity of trithiophosphite **2** was unequivocally determined by ^{1}H, ^{31}P NMR and IR spectroscopy as well as by X-ray single crystal diffraction.

A similar method was used to obtain triferrocenyl trithiophosphite (**3**) from diferrocenyl disulfide and white phosphorus. Its structure was proved by ^{1}H and ^{31}P NMR spectroscopy.

Compound **3** did not form single crystals suitable for X-ray analysis, but was easily oxidized to give triferrocenyltrithiophosphate (**4**) which was studied by X-ray single crystal diffraction.

Structures

Tricymantrenyl trithiophosphite has nine axes of internal rotation: three P−S bonds, three C−S bonds and three Mn−cyclopentadienyl axes. Rotation around the P−S bonds results in a totally asymmetric structure with three cymantrenylthio-groups exhibiting different orientations towards the phosphorus lone electron pair: *cis* around the P−S3 bond (torsion angle −7.2°), *gauche* around the P−S2 bond (−31.0°) and *trans* (178.1°) around the P−S1 bond (Figure 1). The torsion angles around the S−C bonds vary within smaller limits with an almost orthogonal orientation of the P−S bonds with respect to the cyclopentadienyl planes and the largest deviation from the perpendicular arrangement of 16° for the *cis* cymantrenylthiogroup (S3−C31). As for the third set of axes, the rotational flexibility of the cymantrenyl substituents leads to large thermal displacement parameters of the carbonyl groups and their variable orientation respective to the cyclopentadienyl rings in the three cymantrenyl moieties.

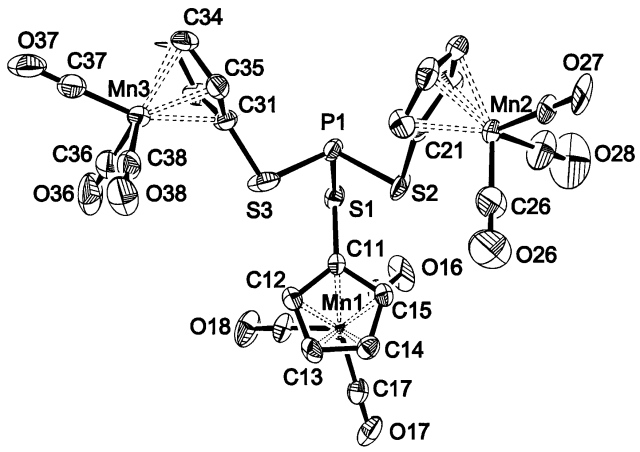


Figure 1. Molecular structure of compound **2** and atomic numbering

The carbonyl groups in the cymantrenyl substituents are staggered with respect to the C−S bonds and nearly eclipsed with respect to the C−H bonds, with torsion angles O=C···C−H of between 7 and 23°. The asymmetry of the structure accounts for an appreciable difference between the corresponding geometrical parameters in this molecule (Table 1). The P1−S1−C11 valence angle, 104.6(1)°, is 7° bigger than the angles at the two other sulfur atoms due to steric repulsion between the cyclopentadienyl ring (C11−C15) and the S2 and S3 atoms. Two short C−H···O intermolecular contacts, which meet the crystallographic criteria for weak hydrogen bonds are observed in the crystals of **2** with participation of the hydrogen atoms of the "trans"-cyclopentadienyl ring: C12−H12···O27′ (1 + *x*, 1/2 − *y*, −1/2 + *z*), C12−H12 0.88(3) Å, H12···O27′ 2.58 Å, ∠C12−H12−O27′ 158(2)°; C15−H15···O38′′ (*x*, 1/2 − *y*, 1/2 + *z*), C15−H15 0.96(3) Å, H15···O38′′ 2.59 Å, ∠C15−H15−O38′′ 153(2)°.

In comparison with thiophosphites which do not contain a metal atom, tricymantrenyl trithiophosphite **2** has a rather unusual structure, although the geometry of its central inorganic part is very close to that of non metal containing derivatives, in particular triphenyl trithiophosphite.[13] In the crystal, a propeller-like conformation (C_3-symmetry) was observed for most of the phosphorus compounds containing three identical SR groups studied regardless of the phosphorus coordination number.[13−15] A *cis*-orientation of the SR group relative to the phosphorus lone electron pair is also unusual even in the liquid and gaseous phases, with a mixture of several conformers with *gauche* and *trans* orientations of the alkylthio or phenylthio groups relative to the phosphorus lone electron pair or phosphoryl (thiophosphoryl) bonds being found normally.[2−6] Thus, several factors might be responsible for the unusual structure of **2** in the crystalline phase: the bulkiness of the cymantrenyl groups, their irregularity caused by the respective rotation of the carbonyl moieties and cyclopentadienyl rings, the ability of the carbonyl groups to participate in intermolecular interactions with the C−H bonds. In a series of reviews[16−19] it was shown that such weak interactions can significantly influence the observed conformations of molecules and are responsible for their crystal packing.

In order to compare the structure of the cymantrenylthio fragment in trithiophosphite **2** and in disulfides, we have carried out an X-ray study of the dicymantrenyldisulfide **1**. Its molecular structure is shown in Figure 2. The orientation of the five-membered rings with respect to the carbonyl groups is identical for both cymantrenyl fragments in

the molecule. Two cymantrenylthio groups are twisted around the central S−S bond by 103.3(1)° with the S−S bond being perpendicular to both cyclopentadienyl rings. The same perpendicular arrangement around the central S−S bond is observed in the chloro-substituted derivative of dicymantrenyl disulfide[20] and in bis[2-(1-dimethylaminoethyl)ferrocenyl]disulfide.[21] In general the structures of **1** and its chloro derivative are very similar and the values of the S−S and S−C bonds and valence angles at the sulfur atoms are the same within experimental error (Table 1). The substitution of one of the sulfur atoms in dicymantrenyl disulfide by phosphorus does not significantly effect the geometry of the cymantrenylthio moieties in **2**. The orientation of the S−P bonds relative to the cyclopentadienyl rings is perpendicular in trithiophosphite, as is the orientation of the S−S bond in **1**.

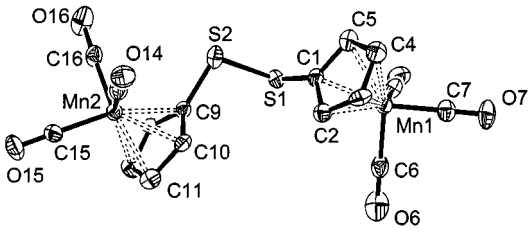


Figure 2. Molecular structure of compound **1** and atomic numbering

Table 1. Selected geometrical parameters[a]

Parameter	**2**	**4**
Bond lengths, Å		
P=O	–	1.453(6)
P1−S1	2.107(1)	2.077(3)
P1−S2	2.120(1)	2.080(4)
P1−S3	2.121(2)	2.090(4)
S1−C11	1.760(4)	1.76(1)
S2−C21	1.766(4)	1.781(9)
S3−C31	1.759(4)	1.75(1)
Bond angles, deg.		
S1−P1−S2	98.88(6)	100.6(1)
S1−P1−S3	103.38(7)	101.8(2)
S2−P1−S3	102.57(7)	102.3(2)
S1−P1−O1	–	117.1(3)
S2−P1−O1	–	117.3(3)
S3−P1−O1	–	115.3(3)
P1−S1−C11	104.6(1)	100.9(3)
P1−S2−C21	98.5(1)	103.0(3)
P1−S3−C31	98.3(1)	99.9(4)

[a] Selected parameters for compound **1**: Bond lengths S1−S2 2.066(1), S1−C1 1.764(3), S2−C9 1.757(3) Å; bond angles S2−S1−C1 102.1(1), S1−S2−C9 102.8(1)°.

An X-ray study of triferrocenyl trithiophosphate (Figure 3) showed that this molecule, in contrast to tricymantrenyl trithiophosphite, adopts a classical propeller-like conformation with *gauche* orientations of all three ferrocenylthio groups relative to the P=O bond. Three C−S−P=O torsion angles in this molecule are equal to −54.2, −45.9, and −46.5°. The respective orientation of the ferrocenyl moieties and the P−S bonds is slightly different. It is perpendicular around the C1−S1 and C11−S2 bonds and slightly skewed around the C21−S3 bond with ∠ P−S3−C21−C22 = 75.6°. An almost symmetrical conformation results in equal (within experimental error) P−S, O=PS and PSC bond angles in the molecule (Table 1). The ferrocenyl substituents have the symmetrical structure of ferrocene with planar and nearly parallel cyclopentadienyl rings. The dihedral angles between the rings in the ferrocene moieties are 0.9 (Fc^1), 0.7 (Fc^2) and 2.5° (Fc^3). The angles δ at iron between the two cyclopentadienyl ring centers are 178.9 (Fc^1), 178.0 (Fc^2) and 178.7° (Fc^3). The geometry of the ferrocenyl substituents in **4** is the same as in its oxygen analogue triferrocenyl phosphate,[9] although the conformations of the two molecules are totally different. Unlike the thio derivative, triferrocenyl phosphate adopts an asymmetrical conformation in the crystal with *cis*, *gauche* and *trans* (∠O=P−O−C = −27.8, −73.4, 178.7°) orientations of the ferrocenyloxo groups with respect to the P=O bond. The dihedral angles between the P−O bonds and the cyclopentadienyl rings are also different, being equal to 40.2, −77.3 and −2.7° for the three ferrocenyl substituents. Thus, the organometallic thioester and ester of phosphoric acid have completely different structures. One of the reasons for this difference is the presence of several intermolecular C−H···O short contacts observed in the crystal of the oxygen derivative

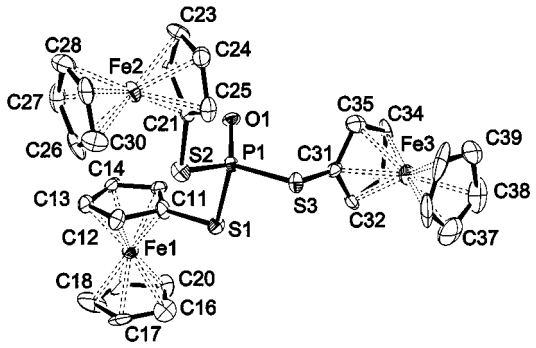


Figure 3. Molecular structure of compound **4** and atomic numbering

Experimental Section

All syntheses were performed using standard Schlenk techniques under an argon atmosphere using pre-dried solvents saturated with argon. The initial organometallic disulfides were obtained following refs.[22][23] IR spectra were measured on an UR-20 spectrometer. ^{1}H and ^{31}P NMR spectra were recorded on the NMR-FT spectrometers MSL-400 and WM-250 (Bruker) with deuteriated solvents (C_6D_6, $CDCl_3$).

Tricymantrenyl Trithiophosphite (2): To a solution of dicymantrenyl disulfide (0.75 g, 1.6 mmol) in acetone (30 mL) were added white phosphorus (0.037 g, 0.28 mmol) and KOH (0.02 mL 15N KOH). The reaction mixture was stirred at ambient temperature for one hour. The solvent was then evaporated and the residue was recrystallized twice from a mixture of benzene/hexane (1:1) to give yellow-green crystals of **2** (0.7 g, 90%), m.p. 125°C. – ^{1}H NMR(C_6D_6): δ = 4.21 (m, 2 H_α), 4.56 (m, 2 H_β). – ^{31}P ($CDCl_3$): δ = 128. – IR (hexane): $\nu_{C=O}$ = 1945, 2025 cm^{-1}. – $C_{24}H_{12}Mn_3O_9PS_3$ (736.34): calcd. C 39.15, H 1.64, P 4.21, S 13.06; found C 38.94, H 1.62, P 4.00, S 13.25.

Triferrocenyl Trithiophosphite (3): To a solution of diferrocenyldisulfide (1.1 g, 2.5 mmol) in acetone (30 mL) were added white phosphorus (0.052 g, 0.4 mmol) and 0.2 mL 15N KOH. The reaction mixture was stirred at room temperature for one hour. The solvent was then evaporated and the residue was recrystallized twice from a mixture of benzene/hexane (1:1) to give dark-orange crystals of **3** (0.93 g, 81%), m.p. 200−203°C. − ^{1}H NMR(C_6D_6): δ = 4.35 (m, 2 H_α), 4.52 (m, 2 H_β), 4.50 (s, 5 H). − ^{31}P ($CDCl_3$): δ = 131. − $C_{30}H_{27}Fe_3PS_3$ (760.37): C 52.82, H 3.99, P 4.54, S 14.09; found C 52.74, H 3.95, P 4.25, S 14.15.

Triferrocenyl Trithiophosphate (4): A solution of triferrocenyltrithiophosphite (2.1 g, 3 mmol) in benzene (20 mL) was boiled with the constant bubbling of air through it during one hour. The solvent was evaporated and the residue was recrystallized from a mixture of benzene/hexane (2:1) to give dark-orange crystals of **4** (1.77 g, 85%), m.p. 230°C. − ^{1}H NMR(C_6D_6): δ = 4.3 (m, 2 H_α), 4.45 (m, 2 H_β), 4.52 (s, 5 H). − ^{31}P ($CDCl_3$): δ = 47.7. − $C_{30}H_{27}Fe_3OPS_3$ (776.37): C 51.60, H 3.89, P 4.44, S 13.77; found C 51.67, H 3.87, P 4.31, S 14.25.

X-ray Structure Determination: The X-ray diffraction data were collected on a CAD4 Enraf−Nonius automatic diffractometer with the graphite monochromated Mo K_α radiation (λ = 0.71073 Å) in the ω-scan mode.

Crystal Data for 1: $C_{16}H_8Mn_2O_6S_2$, formula weight 470.24, (yellow prism, crystal dimensions 0.1 × 0.2 × 0.3 mm), space group $P2_1/n$, a = 6.495(1), b = 12.141(2), c = 22.509(2) Å, β = 93.27(2)°, V = 1772.1(4) Å^3 at 20°C, Z = 4, ρ = 1.76 (g·cm^{-3}), μ = 16.24 cm^{-1}, total number of reflections measured 6041, number of observed reflections with $I > 3\sigma(I)$ 2714, number of variables 267, final R/R_w = 0.032/0.030.

Crystal Data for 2: $C_{24}H_{12}Mn_3O_9PS_3$, formula weight 736.34, (crystal dimensions 0.4 × 0.25 × 0.2 mm), space group $P2_1/c$, a = 10.519(3), b = 21.598(6), c = 12.788(2) Å, β = 98.32(1)°, V = 2875(1) Å^3 at 20°C, Z = 4, ρ = 1.70 (g·cm^{-3}), μ = 15.58 cm^{-1}, total number of reflections measured 9262, number of observed reflections with $I > 3\sigma(I)$ 3520, number of variables 409, final R/R_w = 0.038/0.044.

Crystal Data for 4: $C_{30}H_{27}Fe_3OPS_3 \cdot C_6H_6$, formula weight 776.37, (crystal dimensions 0.4 × 0.1 × 0.04 mm), space group $C2/c$, a = 25.353(3), b = 10.873(3), c = 23.147(4) Å, β = 103.04(1)°, V = 6212(2) Å^3 at 20°C, Z = 8, ρ = 1.66 (g·cm^{-3}), μ = 16.58 cm^{-1}, total number of reflections measured 14329, number of observed reflections with $I > 3\sigma(I)$ 3669, number of variables 363, final R/R_w = 0.058/0.057. The stability of the crystals and the experimental conditions was checked every two hours by measuring three control reflections, while the orientation was monitored every 200 reflections by centering two standards. No significant decay was observed. Corrections for Lorentz and polarization effects were applied. An empirical absorption correction based on ψ-scans was applied for all crystals. The structures were solved by direct methods and difference Fourier syntheses using the MolEN package.[24] All non-hydrogen atoms were refined anisotropically, H-atoms, located in ΔF maps, were refined isotropically for **1** and **2**; for **4** H-atoms were placed into calculated positions and included into structure factor calculations with fixed positional and thermal parameters. It should be noted that crystals of **4** are stabilized by solvate benzene molecules, in which four carbon atoms are disordered.

Crystallographic data (excluding structure factors) for the structures reported in this paper have been deposited with the Cambridge Crystallographic Data Centre as supplementary publication no. CCDC 130650−130652 (**1, 2, 4**). Copies of the data can be obtained free of charge on application to CCDC, 12 Union Road, Cambridge CB2 1EZ, UK [Fax: (internat.) + 44−1223/336−033; E-mail: deposit@ccdc.cam.ac.uk].

Acknowledgments

The grants of the Russian Foundation for Basic Research 98−03−32777 and 98−03−33074 are gratefully acknowledged.

[1] A. N. Pudovik, E. S. Batyeva, O. G. Sinyashin, *Thioesters of the Trivalent Phosphorus Acids*, Moscow "Nauka", **1990**, 176 (in Russian).
[2] I. I. Pazanovsky, E. A. Ishmaeva, A. B. Remizov, F. S. Bilalov, E. N. Ofizerov, A. N. Pudovik, *Dokl. Akad. Nauk SSSR*, **1980**, 254, 414−417, *Chem. Abstr.* **1981**, *94*, N2, 9437w.
[3] V. A. Naumov, O. N. Kataeva, O. G. Sinyashin, Zhurn. Strukt. Khimii **1984**, 25, no. 3, 79−84, *Chem. Abstr.* **1984,** *101*, W19, 171377m.
[4] O. N. Kataeva, V. A. Naumov, Zhurn. Strukt. Khimii **1987**, 28, no. 5, 153−155, *Chem. Abstr.* **1988**, *108*, W8, 62885z.
[5] E. A. Filippova, S. A. Kazyuba, R. R. Shagidullin, O. G. Sinyashin, *Zhurn. Prikladnoi Spektroskopii* **1987**, 46, 761−766, *Chem. Abstr.* **1987**, *107*, N23, 217742f.
[6] M. Korn, H. Oberhammer, R. Minkwitz, *J. Mol. Struct*. **1993**, 300, 61−72.
[7] A. Michaelis, G. L. Linke, *Chem. Ber*. **1907**, 40, 3419−3425.
[8] V. A. Milyukov, A. V. Zverev, S. M. Podlesnov, A. G. Ginzburg, V. I. Sokolov, O. G. Sinyashin, *XI International Conference on Chemistry of Phosphorus Compounds*, Abstracts. Kazan **1996**, p.244.
[9] M. Herberhold, A. Hofmann, W. Milius, F. F. de Biani, P. Zanello, *Inorg. Chim. Acta* **1998**, 273, 24−30.
[10] R. A. N. McLean, *Inorg. Nucl. Chem. Letters* **1969**, 5, 745−747.
[11] C. Wu, *J. Am. Chem*. Soc. **1965**, 87, 2522.
[12] L. Maier, *Helv. Chim. Acta* **1976**, 59, 252−256.
[13] V. A. Alfonsov, I. A. Litvinov, O. N. Kataeva, D. A. Pudovik, S. A. Kazyuba, *Zh. Obsch. Khimii* **1995**, 65, 1129−1133, *Chem. Abstr.* **1996**, *124*, N18, 246835v.
[14] R. K. Shibao, N. L. Keder, H. Eckert, *Acta Crystallogr.* **1992**, C48, 1525−1527.
[15] A.-F. Shihada, F. Weller, *J. Organometal. Chem*. **1988**, 342, 177−183.
[16] D. Braga, F. Grepioni, G. R. Desiraju, *Chem. Rev.* **1998**, 98, 1375−1405.
[17] G. R. Desiraju, *Acc. Chem. Res.* **1991**, 290−296.
[18] G. R. Desiraju, *Acc. Chem. Res.* **1996**, 441−449.
[19] T. Steiner, W. Saenger, *J. Am. Chem. Soc*. **1992**, 114, 10146−10154.
[20] K. Sünkel, A. Blum, *Chem. Ber*. **1992**, 125, 1605−1608.
[21] Y. Nishibayashi, J. D. Singh, S. Fukuzawa, S. Uemura, *J. Chem. Soc. Perkin Trans. 1* **1995**, 2871−2876.
[22] H. Egger, A. Nikiforov, *Monatsch. Chem*. **1969**, 100, 1069−1076.
[23] G. R. Knox, P. L. Pauson, *J. Chem. Soc*. **1958**, 692−696.
[24] L. Straver, A. J. Schierbeek, *MolEN Structure Determination System*, Nonius B. V, **1994**, Vol. 1.2.

Received July 14, 1999
[I99258]

Dipolar and Non-Dipolar Pyridine and Bipyridine Metal Complexes for Nonlinear Optics

Hubert Le Bozec*[a] and Thierry Renouard[a]

Keywords: Pyridine derivatives / Bipyridine derivatives / Metal complexes / Chromophores / Nonlinear optics

Metal complexes of pyridine and bipyridine-type ligands represent an important class of nonlinear optical (NLO) materials: (i) They can incorporate a variety of functionalised ligands with a wide range of metals which can give rise to tuneable NLO properties; (ii) they are generally associated with intense low-lying charge-transfer excitations such as metal to ligand charge-transfer (MLCT) or intraligand charge-transfer (ILCT); (iii) bipyridyl ligands are also good building blocks that allow the construction of octupolar complexes with a defined geometry and symmetry. This review describes the recent developments in the design of such dipolar and octupolar chromophores for second-order nonlinear optics.

Contents

1. Introduction
2. Background
3. Dipolar Complexes
3.1. Dipolar Complexes with Metal-to-Ligand Charge-Transfer Transitions
3.2. Dipolar Complexes with Intraligand Charge-Transfer Transitions
4. Non-Dipolar Complexes
4.1. Octupolar Complexes with Metal-to-Ligand Charge-Transfer Transitions
4.2. Octupolar Complexes with Intraligand Charge-Transfer Transitions
4.2.1. Octahedral Complexes
4.2.2. Tetrahedral Complexes
5. Concluding Remarks

[a] UMR 6509 CNRS-Université de Rennes 1,
Université de Rennes 1,
Campus de Beaulieu, F-35042 Rennes Cedex, France
E-mail: lebozec@univ-rennes1.fr

1. Introduction

The search for new molecular materials with large second-order nonlinear optical properties (NLO) is currently the subject of considerable investigations due to their potential applications in photonic devices such as frequency doublers and electrooptic modulators.[1] Organic and met-



Hubert Le Bozec was born in Brittany, France. He entered the CNRS in 1978 and received his "Doctorat d'Etat" in 1981 from the University of Rennes 1, working under the supervision of Prof. Pierre Dixneuf. After a postdoctoral period in 1982 at the University of North Carolina (Chapel Hill, USA) with Prof. Thomas Meyer, he returned to Rennes and was promoted "Directeur de Recherche" in 1994. His research interests concern the coordination chemistry of bipyridyl metal complexes and their application in nonlinear optics as well as the chemistry of group-6 and group-8 carbene metal complexes.



Thierry Renouard was born in 1971 in Saint Brieuc, France. He studied Chemistry at the University of Rennes 1 and obtained his Ph. D. in 1998, under the supervision of Dr. Hubert Le Bozec. In the same year, he joined the group of Prof. Michael Grätzel at the Swiss Federal Institute of Technology in Lausanne as a Post-Doctoral fellow. His current research interest concerns the synthesis of novel sensitizers for photovoltaic cells.

MICROREVIEWS: This feature introduces the readers to the authors' research through a concise overview of the selected topic. Reference to important work from others in the field is included.

 © WILEY-VCH Verlag GmbH, D-69451 Weinheim, 2000 1434–1948/00/0202–229 $ 17.50+.50/0

allo-organic materials are of particular interest because of their large NLO susceptibilities and fast response times; they also provide good architectural flexibility to tailor their molecular structures and maximize the optical nonlinearity.[2−4] Thus, extensive efforts are now directed towards the design and synthesis of efficient chromophores which can be incorporated into macroscopic assemblies such as polymers, to form materials exhibiting large NLO responses.[5−7]

Traditionally, chromophores possessing large molecular hyperpolarisability β responses contain donor and acceptor substituents linked through a π-backbone. A great deal of work has been carried out over the past 20 years toward the synthesis of noncentrosymmetric dipolar (or "push-pull") molecules such as functionalised benzene, stilbene, polyene or azobenzene derivatives.[8−12] Moreover, a comprehensive understanding of the design of dipolar organic molecules with optimised molecular hyperpolarisability β has been established − recent computational and experimental studies have introduced several concepts such as bond-length alternation (BLA),[13−16] reduced aromaticity in the ground state,[17] as well as the criterion of electron deficiency or excessivity[18] to establish structure-property relationships for nonlinear optical molecules.

Beyond this classical dipolar approach, a new concept of octupolar nonlinearities has been recently proposed on the basis of group theoretical and quantum mechanical studies.[19][20] The molecular hyperpolaribility β can be reduced into two irreducible components $\beta_{J=1}$ (dipolar part) and $\beta_{J=3}$ (octupolar part). For molecules belonging to purely octupolar space groups such as D_3, D_{3h}, T_d, and D_2, the vector part of β is canceled out and only the octupolar contribution of β remains. The advantages of using nondipolar chromophores include easier noncentrosymmetric arrangements and an improved nonlinearity/transparency trade-off. An increasing number of two- and three-dimensional (2D and 3D) octupolar molecules has appeared in the literature[21] with the development of the Hyper Raleigh Scattering technique (see Background). For example, research on octupolar structures has recently focused on organic molecules with threefold symmetry such as triamino-trinitrobenzenes derivatives,[22] crystal violet cation,[23] trisubstituted amines[24] and cyanine salts.[25]

In the late 1980s, the field of molecular materials for nonlinear optics was extended to organometallic and coordination compounds.[11][26] One reason is that they offer a wide range of metals with different oxidation states and ligands which can give rise to tuneable electronic properties. In addition many complexes are known to possess low-lying charge-transfer states which can be associated with large nonlinearities. Non-centrosymmetric structures can also be achieved by coordination of different ligands to a metal centre. For example, there has been considerable interest in using metallocenes, especially ferrocene derivatives, as donor groups since the pioneering work of Green and co-workers in 1987 who reported a second-harmonic generation (SHG) efficiency 62 times that of the urea standard for the compound (*Z*)-1-ferrocenyl-2-(4-nitrophenyl)ethene.[27][28] Metal complexes of nitrogen-heterocyclic ligands, such as pyridines and oligopyridines, represent another important class of NLO chromophores which have received increasing attention over the last ten years. These ligands, which can be easily functionalized, are among the most widely studied in coordination chemistry resulting in a wide choice of stable complexes.[29] They are generally associated with intense low-energy metal to ligand charge-transfer (MLCT) or intraligand charge-transfer (ILCT) [also known as ligand-centred (LC)] excitations. In addition, bipyridyl ligands are excellent building blocks for the construction of octupolar metal complexes like $[M(bpy)_3]^{n+}$ of D_3 symmetry and $[M(bpy)_2]^{n+}$ of D_{2d} symmetry. This microreview highlights the recent developments in the design of pyridyl- and bipyridyl-metal complexes for nonlinear optics. The first part is concerned with dipolar chromophores whereas the second part will deal with the more recent and promising field of octupolar metal complexes. In each section we have gathered the chromophores into two categories: (i) complexes in which the NLO response is dictated by a MLCT transition, and (ii) complexes with ligands bearing π-donor substituents in which the main charge-transfer governing the NLO response is an ILCT transition.

2. Background

The second-order nonlinear effect is correlated with quadratic (or first molecular) hyperpolarisability β. The dipole moment μ induced in a molecule by an intense external electric field E can be expressed by the relationship of Equation 1, where α is the linear polarisability, and β and γ the first and second molecular hyperpolarisability, respectively.

$$\mu = \alpha \cdot E + \beta \cdot E^2 + \gamma \cdot E^3 + \cdots \quad (1)$$

The coefficient β governs the magnitude of the second-order response, and vanishes in a centrosymmetric medium.

The experimental determination of β can be carried out by using the Electric-Field-Induced Second Harmonic generation (EFISH) method.[30−32] A high-voltage electric pulse breaks the centrosymmetry of the liquid by a dipolar orientation of the molecules. This technique allows determination of $\gamma + \mu \cdot \beta/5kT$, where γ is the cubic hyperpolarisability of the molecule, μ its dipole moment, and β the vectorial projection of the first hyperpolarisability tensor along the dipole direction. By neglecting the third order contribution, β can be evaluated. The ground state dipole moment can be measured independently by a classical method based on the Guggenheim law.[33] Modelling the dispersion of β for a two-level system according to Equation 2 enables us to extract a frequency-independent nonresonant $\beta(0)$ value.[31][34]

$$\beta = \frac{3e^2\hbar^2}{2mW^3} F(W,\omega) f \Delta\mu \quad (2)$$

With respect to Equation 2, W is the energy of the CT transition, ω the fundamental frequency, f the oscillator strength of the charge-transfer band, $\Delta\mu = \mu_{exc} - \mu_g$ the

difference between excited- and ground-state moments, and F the dispersion factor, which is defined by Equation 3; β is related to the static hyperpolarisability coefficient $\beta(0)$ by $\beta = \beta(0) \cdot F(W,\omega)$.

$$F(W,\omega) = \frac{W^4}{\left[W^2 - (\hbar\omega)^2\right]\left[W^2 - (2\hbar\omega)^2\right]} \quad (3)$$

The experimental determination of β can also be carried out with the Hyper-Raleigh Scattering (HRS), also termed Harmonic Light Scattering (HLS), method.[35][36] This is a unique technique for β measurement of nondipolar and/or ionic molecules. For such molecules the EFISH experiment is not possible as it requires uncharged species and a non-zero ground state dipole moment. The HRS method is based on an incoherent scattering of the second harmonic originating from the fluctuation of optically induced microscopic dipoles. The HRS harmonic response can be expressed as in Equation 4, where $I^{2\omega}$ is the scattered SHG intensity, I^{ω} is the intensity of the fundamental wave, G is a geometrical factor, N_1 (N_2) is the molecular density of the solute (solvent) and $<\beta_1^2>$ ($<\beta_2^2>$) is the orientational average of the square of the first hyperpolarisability of the solute (solvent).

$$I^{2\omega} = G(N_1<\beta_1^2> + N_2<\beta_2^2>)\,(I^{\omega})^2 \quad (4)$$

The HLS technique also allows us to determine the individual components of the β tensor.[37] In the case of nondipolar molecules, the static hyperpolarisability $\beta(0)$ at zero-frequency may be calculated using a three-level model.[38] The dispersion factor is similar to that of a two-level system (Equation 3).

3. Dipolar Complexes

3.1 Dipolar Complexes with Metal-to-Ligand Charge-Transfer Transitions

In 1986, Frazier and co-workers[39] investigated for the first time the second-harmonic powder efficiencies of the 4-substituted group-6 metal carbonyl pyridyl complexes **1** (Figure 1). However, only very weak SHG efficiencies, from 0 to 1 relative to ammonium dihydrogen phosphate (ADP), were obtained. Presumably most of these complexes crystallise in centrosymmetric space groups. The first examples of metal-bipyridine complexes possessing second-order polarisabilities were reported by Calabrese and Tam in 1987.[40] They studied the macroscopic SHG powder efficiencies by the Kurtz technique at 1.06 μm. The rhenium(I) complexes (bpy)Re(CO)$_3$X (**2**) [X = Cl, CF_3SO_3] were found to crystallise in a noncentrosymmetric space group and gave SHG efficiencies from 1.6 to 3 times that of urea. Other complexes such as (4-Y-pyridine)$_2$Re(CO)$_3$Br (**3**) [Y = H, styryl], (bpy)MCl_4 (**4**) [M = Pd, Pt] and (bpy)M(CO)$_4$ (**5**) [M = Cr, Mo, W] showed rather small SHG efficiencies ranging from 0.1 to 1.2 times that of urea (Figure 1). The first EFISH studies on metal pyridine and bipyridine (or phenanthroline) complexes were described by Cheng et al.[41][42] They measured the molecular hyperpolarisability β of (4-Y-pyridine)W(CO)$_5$ (**1a**), (4-Y-stilbazole)W(CO)$_5$ (**1b**) and (5-Y-1,10-phenanthroline)W(CO)$_5$ (**6**) (Figure 1). Their optical nonlinearities, ranging from -2 to -20×10^{-30} esu, were significantly enhanced relative to that of the free ligands. The negative values of β are consistent with the negative solvatochromism observed for such complexes by Wrighton and co-workers.[43] The use of 4-substituted pyridines with electron-acceptor groups led to a bathochromic shift of the MLCT transition energy and to larger β values. These trends can be explained by the lowering of the π*-acceptor orbital of the pyridine (phenanthroline) ligands and a decrease in the energy gap of the MLCT transition. Respectable nonlinearities were observed for complexes containing nitro-substituted ligands such as (4-NO_2-stilbazole)W(CO)$_4$ [$\beta = -20 \times 10^{-30}$ esu] and (5-Y-1,10-phenanthroline)W(CO)$_5$ [$\beta = -18 \times 10^{-30}$ esu].[41]

A ZINDO-SOS computational study of the related (4-Y-pyridine)Cr(CO)$_5$ (**1a**) and (4-Y-stilbazole)Cr(CO)$_5$ (**1b**) has more recently been described by Ratner, Marks and co-workers.[44] The computed molecular hyperpolarisabilities were in good agreement with the experimental values. These calculations also showed that the NLO response is dictated by the MLCT transition, that the pyridine ring is the primary charge acceptor and that the calculations also predicted the negative sign of β and an increase of the NLO response when electron-accepting groups are attached to the pyridine ring.

Thompson et al.[45] investigated the second-order NLO properties of iron(III) compounds Fe(SALEN)(4-Y-pyridyl)X (**7**), where X is a halide or an azide (Figure 2). The Kurtz powder test gave a sizeable SHG efficiency twice that of urea when X = N_3, whereas weak SHG intensities were found for the other complexes (0−0.2 × urea). The nonlinearity finds its origin in charge-transfer transitions in both the SALEN ligand and pyridyl-iron system. Attempts to measure the molecular hyperpolarisability β by EFISH in chloroform failed due to low solubility and dissociation of the pyridyl ligand. Thompson and co-workers also described the preparation of an interesting polymer chain **8** from the reaction of Mn(SALEN)Br and 4-pyridyl glycinate ligands or 4-(pyridylthio)acetic acid (Figure 2).[46] The polymers consisted of metal centres bridged by 4-pyridyl ligands. The crystal structures showed a head-to-tail alignment of adjacent dipoles along the polymer backbone. Unfortunately, adjacent polymer chains were antiparallel, so no NLO effects were observed.

Large molecular hyperpolarisabilities have recently been observed by Coe et al.[47] in donor-acceptor ruthenium(II) complexes. They reported the synthesis of a series of *trans*-$[Ru(NH_3)_4(L^A)(L^B)]^{n+}$ complexes **9**, where L^A and L^D are acceptor/donor-substituted pyridyl ligands (Figure 2). All these complexes show highly solvatochromic low energy $d\pi(Ru) \rightarrow \pi^*(L^A)$ metal-to-ligand charge-transfer bands in the visible region. Using the HRS technique at 1.064 μm, large β values in the range $230-790 \times 10^{-30}$ esu were found, especially for complexes **9b−9d** containing *N*-meth-

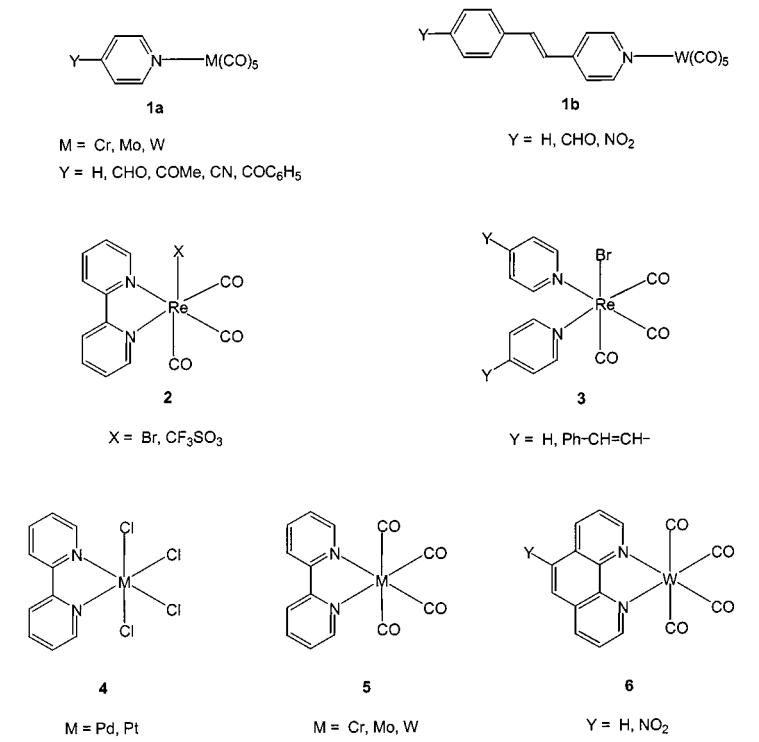


Figure 1. Dipolar complexes with MLCT transitions

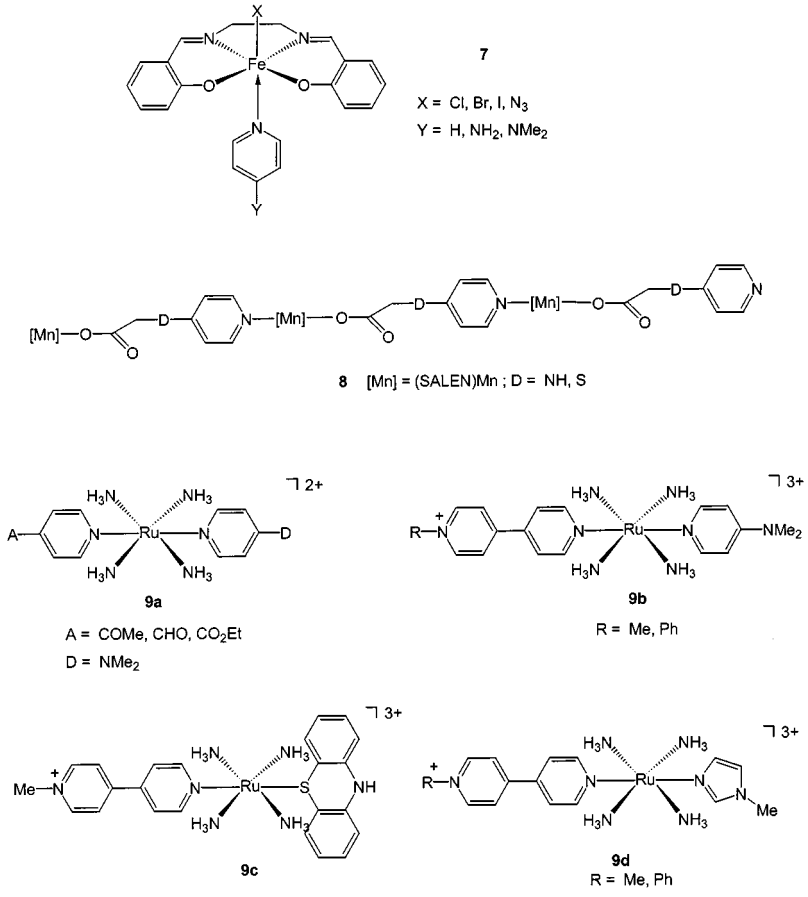


Figure 2. Dipolar complexes with MLCT transitions

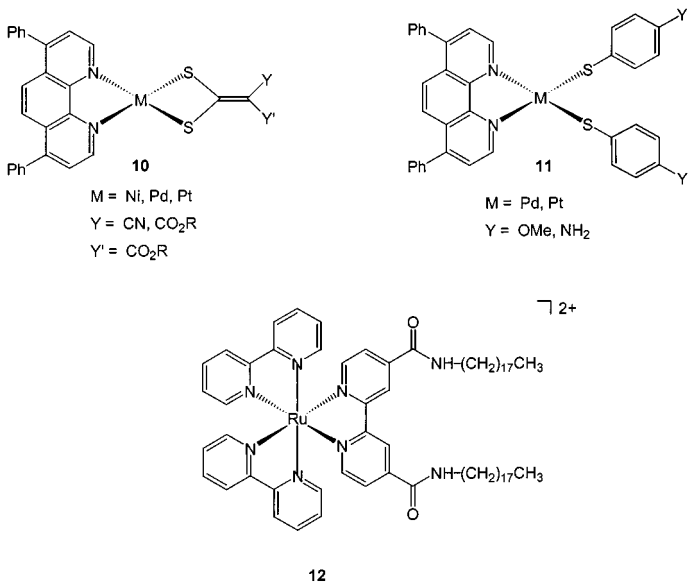


Figure 3. Dipolar diimine metal complexes with MLCT transitions

yl- and *N*-phenyl-4,4′-bipyridinium (MQ^+) as electron-acceptor ligands. As these complexes absorb in the region of the second harmonic (0.532 μm), the large β values were attributed in part to resonance enhancement. Static hyperpolarisabilities $\beta(0)$ were also calculated and ranged from 10 to 266×10^{-30} esu.

Eisenberg and co-workers[48] prepared a series of mixed-ligand transition-metal diimine dithiolate complexes **10−11** (diimine = phenanthrolines, bipyridines; metal = Ni, Pd, Pt) and studied their NLO properties by EFISH at 1.91 μm. Some examples of complexes are displayed in Figure 3. Their lowest-energy excited states involve a HOMO which is a mixture of M(d)- and dithiolate-orbital character and a LUMO which is a π* orbital of the diimine ligands. This transition has been termed by the authors as "charge-transfer-to-diimine."[49][50] The role of the metal ion, dithiolate and diimine ligands in the tuning of the optical and nonlinear optical properties was investigated. Negative β values in the range 0 to -40×10^{-30} esu were found. Larger values of β were observed with Pt^{II} metal ions and dithiolate ligands containing electron-donating substituents such as in **11**. In contrast, complexes **10** with dithiolate ligands containing electron-withdrawing groups exhibited reduced β values: a decrease of the electron-donating strength of the dithiolate and the presence of another charge-transfer-to-dithiolate, which is vectorially opposed to the charge-transfer-to-diimine, were proposed to explain the lowering of the molecular hyperpolarisability.

Matsuo and co-workers[51] studied the second-harmonic generation of the amphiphilic tris(2,2′-bipyridyl)ruthenium(II) complex **12** in a Langmuir-Blodgett film (Figure 3). Amide groups were introduced at the 4,4′-position of one bipyridine ligand in order to increase the vectorial properties of the MLCT. The absorption spectrum of the LB film showed a typical MLCT band at 450 nm and another at 480 nm which was assigned to the MLCT transition to the 4,4′-diamide-2,2′-bipyridine ligand. The β value was estimated to be 70×10^{-30} esu. Second harmonic generation was also observed from ultrathin polyvinyl chloride films impregnated with the same tris(bipyridyl)ruthenium(II) complex.[52]

3.2 Dipolar Complexes with Intraligand Charge-Transfer Transitions

In the first phase of our work on bipyridyl metal complexes for nonlinear optics, we developed the synthesis of the 4-alkenyl-2,2′-bipyridines **13−14** bearing π-donor substituents (Figure 4).[53][54] These ligands are easily available from 4,4′-dimethyl-2,2′-bipyridine.[55] The optical UV/Vis absorption spectra of **13** showed a characteristically intense solvatochromic intramolecular charge-transfer transition, whereas that of the metallocenylvinyl bipyridines **14** exhibited two less intense bands assigned to MLCT and π−π* transitions, respectively.[28b,56] The EFISH measurements of **13** and **14** at 1.34 μm[57] indicated moderate β values ranging from 4 to 14×10^{-30} esu; the most efficient donor group was, as expected, dibutylaminophenyl [4-$Bu_2N-C_6H_4$- >> 4-RO−C_6H_4- ≈ $(C_5H_5)Fe(C_5H_4$-) > $(C_5H_5)Ru(C_5H_4$-)]. These ligands were coordinated to acceptor organometallic fragments, and two types of complexes were prepared: octahedral rhenium(I) carbonyl complexes of general formula *fac*-(bpy)$Re(CO)_3X$ (**15**) and tetrahedral zinc and mercury complexes of general formula $(bpy)MX_2$ (**16**) (Figure 4).[53][57] A selection of optical and nonlinear optical data are displayed in Table 1. We observed a red shift of the ILCT transition ($\Delta\lambda \approx 40-70$ nm) which was sensitive to the nature of both the organometallic moiety and the conjugated donor group. For a given donor group (for example Bu_2N), the relative ordering of the acceptor strength was: $Re(CO)_3Br$ > $ZnCl_2$ > $Zn(OAc)_2$ >

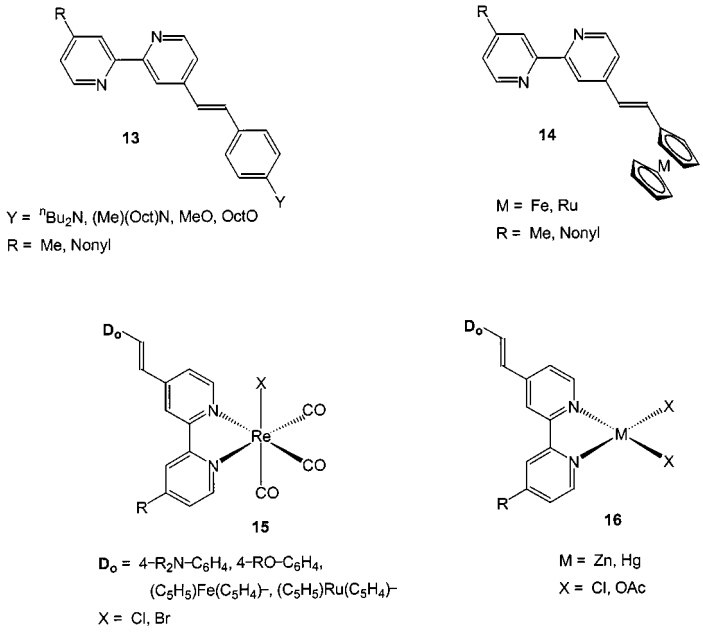


Figure 4. Dipolar bipyridine metal complexes with ILCT transitions

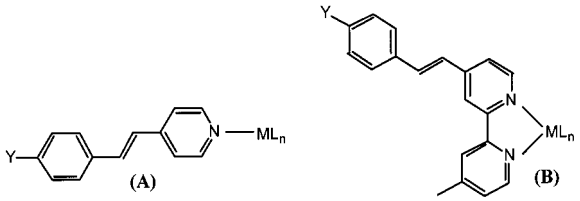
$HgCl_2 > Hg(OAc)_2$. In addition to the ILCT band, each of the rhenium complexes also exhibited a less intense absorption near 380 nm, which was assigned to a $d\pi(Re) \rightarrow \pi^*$ (bpy) transition. Upon coordination, the β values were found to increase by a factor ranging from 2 to 11 (Table 1). The inductive acceptor strength of the ML_n fragment contributes mainly to the enhancement of the NLO response. A conformational change of the bipyridine ligand upon chelation [trans $\rightarrow$ cis] could also play a non negligible role. The ordering of the β values followed that found for the relative energies of the ILCT bands, with the exception of the rhenium complexes **15** which were less efficient than the corresponding zinc complexes **16**: The presence of two vectorially opposed charge-transfer axes (MLCT and ILCT) in **15** could contribute to the decrease in β. The largest static response was found for compound **16** with dibutylaminophenyl as the electron donor and zinc dichloride as the electron acceptor [$\beta(0) = 71 \times 10^{-30}$ esu]; its molecular nonlinearity $\mu\cdot\beta(0)$ [$\mu\cdot\beta(0) = 831 \times 10^{-48}$ esu], which is the relevant parameter for poled polymer applications, compared well with that of the prototypical chromophore disperse red 1 [$\mu\cdot\beta(0) = 450 \times 10^{-48}$ esu].[58]

Molecular quadratic hyperpolarisabilities of donor-substituted stilbazole complexes have also been recently studied by several groups. Bruce and Thornton[59] prepared mesogenic 4-alkoxystilbazole complexes of Rh^I and Ir^I **17** (Figure 5). A chiral alkoxy chain such as (*S*)-(+)-2-methylbutoxy was used in order to promote noncentrosymmetric packing in the solid state. A bathochromic shift ($\Delta\lambda \approx 20-30$ nm) was observed upon complexation of the ligand to the $[MCl(CO)_2]$ fragment. The complexation also resulted in enhanced values of μ by a factor of ca. 2, and $\beta(0)$ by a factor of ca. 1.5 (Table 1). Ratner, Marks and co-workers[44] studied the experimental and computed NLO properties of [4-(dimethylamino)stilbazole]$M(CO)_5$ complexes **18** (M = Cr, W). The EFISH studies at 1.064 μm indicated an increase in β of two times the organic stilbazole ligand. The calculated β [65×10^{-30} esu] was in excellent agreement with the observed experimental molecular hyperpolarisability [61×10^{-30} esu]. It is noteworthy that this response is larger and of an opposite sign to the (4-acceptorstilbazole)$M(CO)_5$ derivatives **1b**. As for the donor substituted bipyridine metal complexes **15**, the NLO response is here dictated by an ILCT transition and the role of the metal fragment is that of an inductive acceptor. ZINDO calculations were used to study the difference in electronic populations between ground state and excited state: The study showed that the MLCT excitation is of secondary importance since only 0.14 electrons are transferred from $M(CO)_5$.[44]

Marder et al.[60] have recently examined the NLO properties of the same 4-donorstilbazoles and their Lewis acidic borane adducts **19** (Figure 5). The β values of the free stilbazole ligands were found to be larger than those of the related 4-alkoxy- or 4-aminostyryl-2,2′-bipyridine (**13**) (Table 1).[57] This difference could be explained by the transoid conformation of the bipyridine ligands and thus to the presence of opposed charge-transfer excited states which are expected to reduce the magnitude of β. The red shift ($\Delta\lambda \approx 40-90$ nm) of the intramolecular charge-transfer transition upon coordination of the Lewis acidic boranes was more pronounced than when the same ligands were complexed to $W(CO)_5$[44] or $[M(CO)_2Cl]$.[59] Enhanced molecular hyperpolarisabilities β by a factor > 2 were found in all cases. The largest value was found for the dimethylaminostilbazole adduct with $B(C_6F_5)_3$. Its molecular nonlinearity $\mu\cdot\beta(0)$ [724×10^{-48} esu] was found to be similar to that of our bipyridine zinc complexes **16** (Table 1).

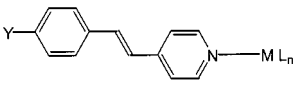
The NLO properties of several donor-vinylpyridine metal complexes, containing an organometallic fragment as the donor group, have recently been reported in the literature.

Table 1. Selected linear and nonlinear optical data for 4-donor-substituted stilbazoles, styrylbipyridines and complexes



	Y	ML$_n$	λ_{max} [nm]	μ [D]	β [10^{-30} esu]	$\beta(0)$ [10^{-30} esu]	$\mu\cdot\beta(0)$ [10^{-48} esu]	Ref.
	OMe		326	6	24[a]	17.2	103	[60]
	$OCH_2CH(Et)(Me)$		335	3.8	15.8[b]	13.4	51	[59]
	NMe_2		368	10	45[a]	29	291	[60]
	OMe	BF_3	364	7.3	48[a]	31.3	229	[60]
	OMe	$B(C_6F_5)_3$	376	6.4	48[a]	30.3	195	[60]
(A)	$OCH_2CH(Et)(Me)$	$Rh(CO)_2Cl$	355	7.4	20.1[b]	16.7	124	[59]
	$OCH_2CH(Et)(Me)$	$Rh(CO)_2Br$	357	7.7	23.9[b]	19.8	153	[59]
	$OCH_2CH(Et)(Me)$	$Ir(CO)_2Cl$	364	6.9	24.4[b]	20.0	138	[60]
	NMe_2	$W(CO)_5$	421	14.9[c]	61[d]	19.2	286	[44]
	NMe_2	BF_3	438	11.8	129[a]	66	721	[60]
	NMe_2	$B(C_6F_5)_3$	458	10	155[a]	72.5	724	[60]
	OOct		329	6.5	4[a]	3	20	[57]
	NBu_2		388	5.1	14[a]	8	41	[57]
	OOct	$Re(CO)_3Br$	367	11.6	11[a]	7	81	[57]
	OOct	$Hg(OAc)_2$	360	10.4	18[a]	12	125	[57]
(B)	OOct	$HgCl_2$	361	10.7	18[a]	12	128	[57]
	OOct	$Zn(OAc)_2$	358	10	19[a]	13	130	[57]
	NBu_2	$Re(CO)_3Br$	475	9.9	71[a]	31	307	[57]
	NBu_2	$HgCl_2$	442	11.7	65[a]	32	374	[57]
	NBu_2	$Zn(OAc)_2$	447	7.9	116[a]	57	450	[57]
	NBu_2	$ZnCl_2$	160	11.7	152[a]	71	831	[57]

[a] EFISH at 1.34 μm in $CHCl_3$. – [b] EFISH at 1.907 μm in $CHCl_3$. – [c] Calculated. – [d] EFISH at 1.064 μm in dioxane.



17 Y = $OCH_2CH(Me)(Et)$; M L_n = $Rh(CO)_2Cl$, $Ir(CO)_2Cl$
18 Y = NMe_2 ; M L_n = $Cr(CO)_5$, $W(CO)_5$
19 Y = OMe, NMe_2 ; M L_n = BF_3, $B(C_6F_5)_3$

Figure 5. 4-Donor stilbazole complexes

The heterobimetallic ferrocenyl(vinylpyridine)ML$_n$ compounds **20** were simultaneously prepared by Mata et al.[61] and by Lee et al.,[62] and their NLO responses measured by the HRS technique at 1.064 μm (Figure 6). Quite different β values were found for identical complexes by the two groups [for example, ML$_n$ = $W(CO)_5$: $\beta = 101 \times 10^{-30}$ esu[61] and 282×10^{-30} esu[62]]. Surprisingly, large β values were obtained, especially for cationic complexes [ML$_n$ = $Re(CO)_5^+$, $\beta_{1.06}$ (HRS) = 712×10^{-30} esu[62]], in comparison with that for our heterobimetallic ferrocenyl-bipyridine rhenium complexes **15** [$\beta_{1.34}$ (EFISH) = 17×10^{-30} esu]. However, since they absorbed relatively close to the frequency doubled scattered light ($\lambda/2$ = 532 mm), these values were substantially resonance enhanced. Gimeno, Persoons and co-workers[63] described the synthesis and HRS measurements of the novel enynylruthenium(II)–chromium(0) or –tungsten(0) bimetallic complexes **21** (Figure 6). The efficiencies of the half sandwich indenylbis(triphenylphosphane)ruthenium–alkynyl donor moiety was demonstrated by large hyperpolarisabilities, particularly when the pyridine ligand was coordinated to $W(CO)_5$ [λ_{max} = 462 nm; $\beta_{1.06} = 535 \times 10^{-30}$ esu; $\beta(0) = 71 \times 10^{-30}$ esu].

4. Non-Dipolar Complexes

4.1 Octupolar Complexes with Metal-to-Ligand Charge-Transfer Transitions

The quadratic nonlinear susceptibility of octupolar metal complexes was first demonstrated by Zyss et al[64] for the tris(bipyridine)- and tris(phenanthroline)ruthenium(II) cations **22** and **23** (Figure 7). These complexes have attracted intense interest over the past twenty years due to their luminescence properties and capacity for electron- and energy-transfer processes.[65] They possess D_3 symmetry and exhibit intense absorption transitions near 450 nm assigned to $d\pi(Ru) \rightarrow \pi^*$(bpy or phen) MLCT transitions. Large β_{HRS} values of 210×10^{-30} and 170×10^{-30} esu were found at 1.064 mm for **22** and **23**, respectively. However, the first hyperpolarisability of $Ru(bpy)_3^{2+}$ **22** was recently reexamined by Morrison et al,[66] and estimated to be 25×10^{-30} esu. The large β value appeared to be mainly due to a two-photon excited luminescence, and a typical red emission with a luminescence lifetime of 210 ns was observed by exciting with the harmonic frequency at 532 nm.

To achieve enhanced optical nonlinearities by extension of the π-electron system and introduction of strong ac-

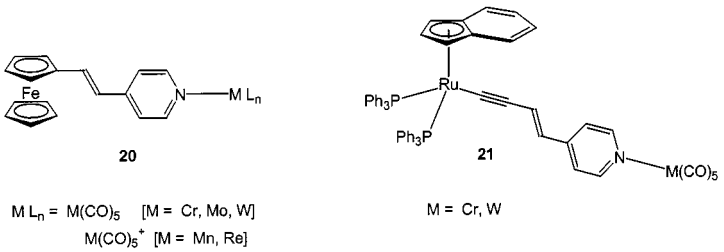


Figure 6. Dipolar heterobimetallic complexes

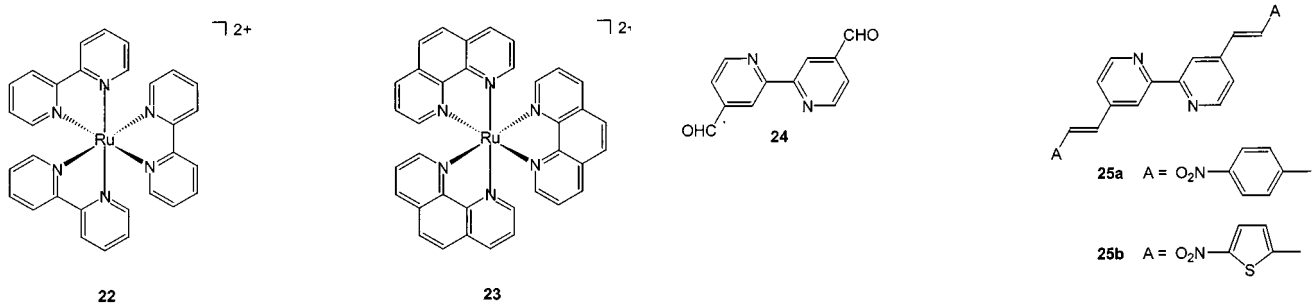


Figure 7. Octupolar diimine complexes with MLCT transitions

ceptor groups, we prepared the 4,4′-dialkenyl-2,2′-bipyridines **25a**,**b** containing nitrophenyl and nitrothienyl substituents.[67] To this end we have developed a convenient method for the preparation of the precursor 4,4′-diformyl-2,2′-bipyridine (**24**), based on the enamination of 4,4′-dimethyl-2,2′-bipyridine. Ligands **25a**,**b** were readily obtained from **24** by a classical Wittig-Horner reaction (Figure 8). The synthesis of tris(bipyridyl)ruthenium(II) (**26b**) was achieved by treating **25b** with ruthenium trichloride (Figure 8).[68] As expected from the presence of strong acceptors, the MLCT transition [λ_{max} (acetone) = 508 nm] was significantly red-shifted with respect to Ru(bpy)$_3^{2+}$. Unfortunately, very poor solubility precluded its β measurement by the HRS technique.

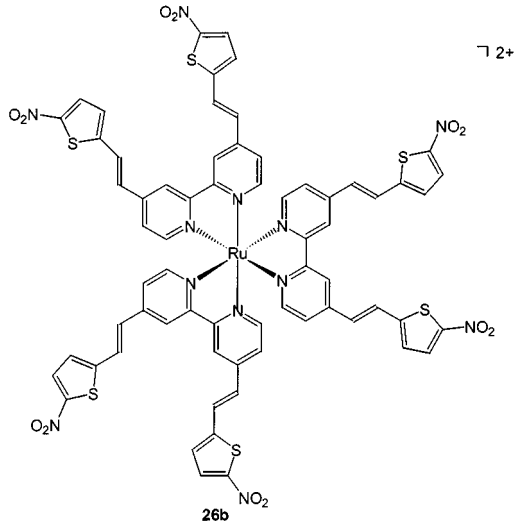


Figure 8. 4,4′-Dialkenyl-2,2′-bipyridines containing acceptor substituents, and corresponding octupolar ruthenium complexes

4.2 Octupolar Complexes with Intraligand Charge-Transfer Transitions

4.2.1. Octahedral Complexes

To design octupolar tris(bipyridyl)ruthenium(II) with a multidirectional intraligand charge-transfer as the main transition responsible for the NLO response, we developed the synthesis of a series of 4,4′-dialkenyl-2,2′-bipyridine ligands **27** bearing π-donor substituents (dialkylaminophenyl and alkoxyphenyl) by the same route employed for the preparation of bipyridines **19** (Figure 9).[54] The corresponding complex [Ru(**27**)$_3$](PF$_6$)$_2$ (**28**) showed characteristically intense charge-transitions ($\varepsilon \approx 120000-150000$) which were sensitive to the nature of the donor group.[68][69] For complexes **28a**,**b** [D = NBu$_2$, N(Me)(Oct)], a very broad ILCT band was observed at ca. 500−510 nm; the MLCT transition, expected at ca. 450−480 nm, was hidden by the more intense ILCT band. For **28c** (D = OOct) two maxima could be easily identified, the main ILCT transition at 380 nm and the less intense MLCT transition at 482 nm. The first HRS measurement of **28a** at 1.34 μm in chloroform gave an exceptionally high β value of 2200×10^{-30} esu.[69] This value was recently found to be overestimated due to some two-photon excited luminescence, and new measurements gave reduced, but still high, hyperpolarisabilities [**28a**: $\beta_{HRS} = 1130 \times 10^{-30}$ esu; **28b**: $\beta_{HRS} = 1000 \times 10^{-30}$ esu[70]]. The alkoxy derivative **28c** gave a smaller β value [$\beta_{HRS} = 490 \times 10^{-30}$ esu] but displayed a better nonlinearity-transparency trade-off. The ordering of the β values was the same as that found from the relative energies of the ILCT bands i.e. **28a** > **28b** >> **28c**.

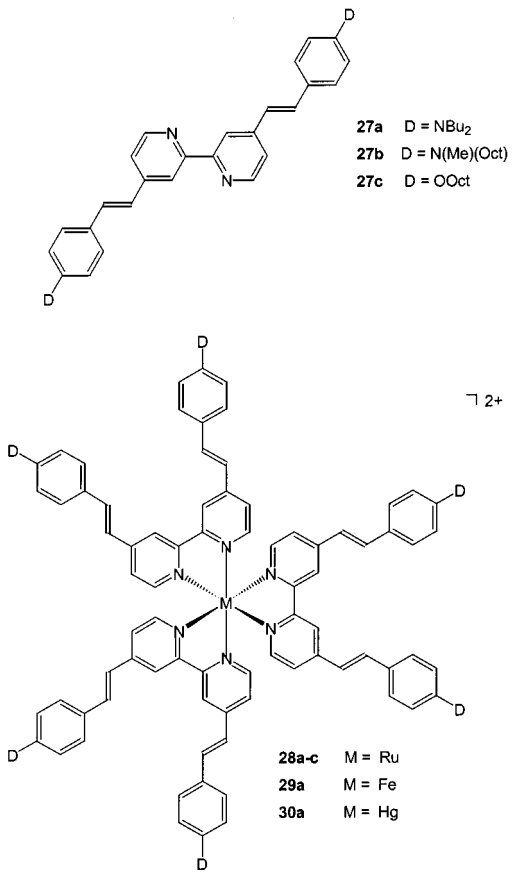


Figure 9. 4,4′-Dialkenyl-2,2′-bipyridines bearing π-donor substituents and corresponding octahedral complexes

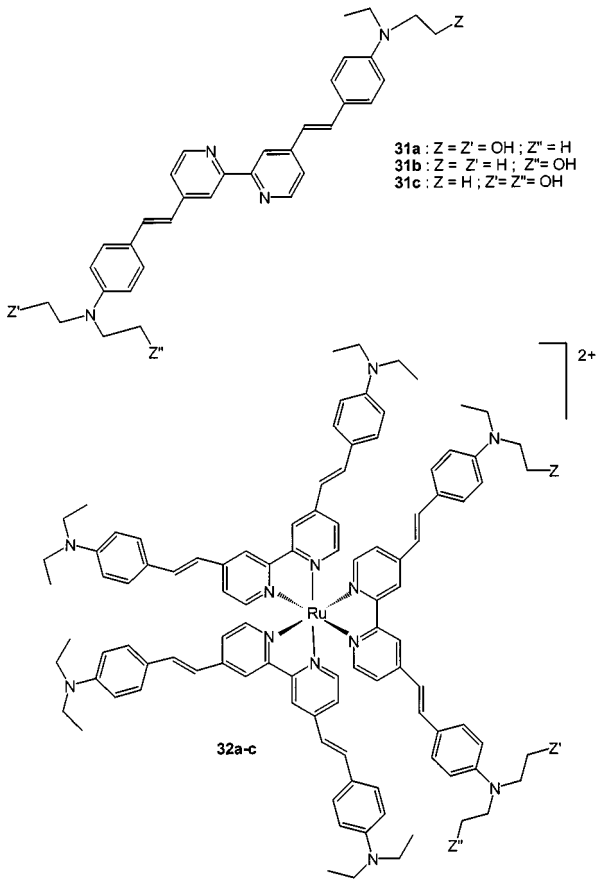


Figure 10. Hydroxy-functionalised bipyridines and corresponding octahedral complexes

The influence of the metal on the linear and nonlinear optical properties was also investigated.[68] For example, the iron derivative **29a** exhibited two absorption bands, the more intense ILCT transition blue-shifted with respect to the ruthenium derivative **28a** [λ_{max} = 467 nm] and the less intense blue-shifted MLCT transition [λ_{max} = 593 nm]. The mercury(II) derivative **30a** showed only the absorption band at λ_{max} = 438 nm, attributable to the ILCT transition, and the antagonist MLCT transition was nonexistent as expected from the high third ionisation potential of mercury. Smaller β values were obtained for such complexes [**29a**: $\beta_{HRS} = 260 \times 10^{-30}$ esu; **30a**: $\beta_{HRS} = 515 \times 10^{-30}$ esu], showing that the nonlinearity-transparency compromise can be fine-tuned by changing the metallic centre.

A current approach for the design of NLO materials is the covalent attachment of NLO-phores to a polymer backbone. As this approach usually requires the introduction of appropriate reactive functionalities at the electron-donating site of the chromophore, we have performed the synthesis of the mono- and dihydroxy-substituted 4,4′-bis(dialkylaminostyryl)-2,2′-bipyridines (**31**) (Figure 10).[71] The synthetic methodology for the preparation of the corresponding ruthenium complexes **32** was based on the sequential coordination of the "parent" 4,4′-bis(*p*-diethylaminostyryl)-2,2′-bipyridine and of the appropriate hydroxy-functionalised bipyridine **31**. Thus, macroscopic organisation of such octupoles in noncentrosymmetric assemblies can be envisaged from the new optical poling method.[72]

4.2.2. Tetrahedral Complexes

In comparison to D_{3h} and D_3 compounds, only a few examples of nondipolar tetrahedral chromophores have been investigated for nonlinear optics.[72−75] Bipyridine- or phenanthrolinecopper(I) complexes with substituents α to the nitrogen atoms are known to give stable tetrahedral molecules of D_{2d} symmetry.[76] Thus, we designed the new 4,4′-diaminostyryl-6,6′-dimethyl-2,2′-bipyridines (**33**); the corresponding copper(I) complexes **34** were simply obtained by treatment of the ligand with $Cu(CH_3CN)_4^+$ (Figure 11).[77] The UV/Vis spectra displayed the characteristic ILCT transition at $\lambda_{max} \approx 420$ nm, which was considerably blue-shifted relative to the corresponding ruthenium(II) complexes **28**. The MLCT transition was typically observed at ca. 480 nm as a shoulder of the more intense ILCT band.

Their molecular hyperpolarisabilities, measured by means of the HRS technique at 1.34 μm, revealed large β values, especially with the most effective electron-donating dialkylamino group [NRR′ = N*n*Bu$_2$ $\beta_{HRS} = 144 \times 10^{-30}$ esu]. Compared to the octahedral tris(bipyridyl)ruthenium(II) complex **28a**, the copper(I) derivatives **32** showed reduced values, as expected from the higher energy of the ILCT ex-

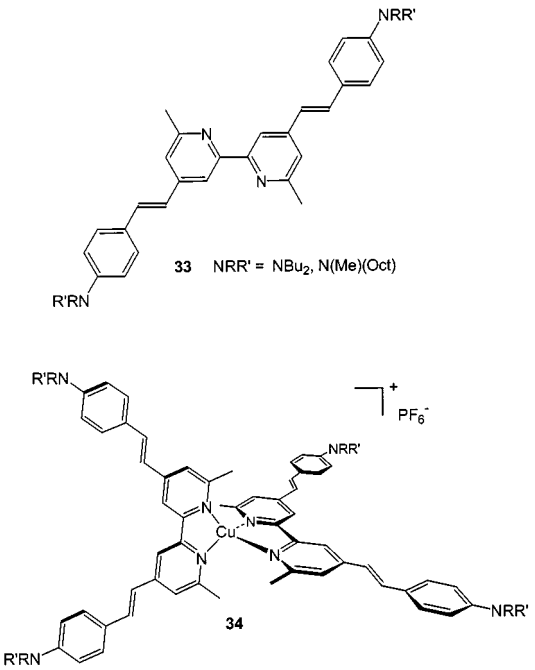


Figure 11. Tetrahedral octupolar copper(I) complexes

cited state. However, these complexes represent a new class of nondipolar NLO organometallic chromophores combining good transparencies and large nonlinearities.

5. Concluding Remarks

Studies on pyridyl- and bipyridylmetal complexes for nonlinear optics have been extensively developed since the first report of Frazier in 1986.[39] In such complexes, the NLO response can be dictated by either a MLCT or ILCT transition and the pyridine ring plays the role of the primary acceptor. Many strategies have emerged that allow access to new NLO chromophores. The most widely studied systems are still dipolar compounds, and versatile synthetic methodologies allow the design and synthesis of efficient second-order nonlinear materials. Octupolar bipyridyl metal complexes remain an emerging field of research. However, as the geometry can be imposed by the nature of the metallic centre and its oxidation state, many other polypyridyl metal derivatives can be potentially used in the construction of NLO compounds with the required 3D octupolar symmetry. Finally, the ability to substitute the pyridine rings with various functional groups offers the possibility of easily incorporating such types of chromophores into polymers. Development of these polymetallic materials will be an interesting challenge in the forthcoming years.

The experimental work reported from our group was performed by Manuel Bourgault, Thierry Renouard, Thomas Le Bouder, Barbara Lognoné, Philippe Dupau and Philippe Massiot. The EFISH and HRS studies were performed by Dr. Zyss′s group (ENS Cachan). We are grateful to all of them.

[1] P. N. Prasad, D. J. Williams, *Introduction of Nonlinear Optical Effects in Molecules and Polymers*, J. Wiley and Sons, New York, **1991**.
[2] D. S. Chemla, J. Zyss, *Nonlinear Optical Properties of Organic Molecules and Crystals*, Academic Press, New York, **1987**, vol. 1, 2.
[3] *Organic Materials for Nonlinear Optics II* (Eds.: R. A. Hahn, D. Bloor), Spec. Publ. No. 69, The Royal Society of Chemistry, Cambridge, **1991**.
[4] D. J. Williams. *Angew. Chem. Int. Ed. Engl.* **1984**, *23*, 690.
[5] D. M. Burland, R. Miller, C. A. Walsh. *Chem. Rev.* **1994**, *94*, 31.
[6] T. J. Marks, M. A. Ratner, *Angew. Chem. Int. Ed. Engl.* **1994**, *34*, 155.
[7] K. J. Drost, A. K.-Y. Jen, V. P. Rao, *Chem. Tech.* **1995**, 16.
[8] L.-T. Cheng, W. Tam, S. H. Stevenson, G. R. Meredith, G. Rikken, S. R. Marder, *J. Phys. Chem.* **1991**, *95*, 10631.
[9] L.-T. Cheng, W. Tam, S. R. Marder, A. E. Stiegman, G. Rikken, C. W. Spangler, *J. Phys. Chem.* **1991**, *95*, 10643.
[10] S. R. Marder, J. W. Perry, *Adv. Mater.* **1993**, *5*, 804.
[11] T. Verbiest, S. Houbrechts, M. Kauranen, K. Clays, A. Persoons, *J. Mater. Chem.* **1997**, *7*, 2175.
[12] P. N. Prasad, B. A. Reinhardt, *Chem. Mater.* **1990**, *2*, 660.
[13] C. B. Gorman, S. R. Marder, *Proc. Natl. Acad. Sci. USA* **1993**, *90*, 11297.
[14] S. R. Marder, C. B. Gorman, F. Meyers, J. W. Perry, G. Bourhill, J.-L. Bredas, B. M. Pierce, *Science* **1994**, *265*, 632.
[15] F. Meyers, S. R. Marder, B. M. Pierce, J.-L. Bredas, *J. Am. Chem. Soc.* **1994**, *116*, 10703.
[16] M. Barzoukas, A. Fort, M. Blanchard-Desce, *New. J. Chem.* **1997**, *21*, 309.
[17] S. R. Marder, D. N. Beratan, L.-T. Cheng, *Science* **1991**, *252*, 103.
[18] I. D. L. Albert, T. J. Marks, M. A. Ratner, *J. Am. Chem. Soc.* **1997**, *119*, 6575.
[19] J. Zyss, *Nonlinear Opt.* **1991**, *1*, 3.
[20] J. Zyss, I. Ledoux, *Chem. Rev.* **1994**, *94*, 77.
[21] J. J. Wolff, R. Wortmann, *J. Prakt. Chem.* **1998**, *340*, 99.
[22] [22a] J. Ledoux, J. Zyss, J. S. Siegel, J. Brienne, J. M. Lehn, *Chem. Phys. Lett.* **1990**,*172*, 440. – [22b] T. Verbiest, K. Clays, C. Semyr, J. Wolff, D. Reihoudt, A. Persoons, *J. Am. Chem. Soc.* **1994**, *116*, 9320. – [22c] J.-L. Bredas, F. Meyers, B. M. Pierce, J. Zyss, *J. Am. Chem. Soc.* **1992**, *114*, 4928. – [22d] R. Wortmann, C. Glana, P. Krämer, R. Matschiner, J. J. Wolff, S. Kraft, B. Treptow, E. Barbu, D. Längle, G. Gölitz, *Chem. Eur. J.* **1997**, *3*, 1765.
[23] J. Zyss, T. Chauvan, C. Dhenaut, I. Ledoux, *Chem. Phys.* **1993**, *177*, 281.
[24] S. Stadler, Ch. Bräuchle, S. Brandl, R. Gompper, *Chem. Mater.* **1996**, *8*, 414.
[25] S. Stadler, Ch. Bräuchle, S. Brandl, R. Gompper, *Chem. Mater.* **1996**, *8*, 676.
[26] For recent reviews see: [26a] H. S. Nalwa, *Appl. Organomet. Chem.* **1991**, *5*, 349. – [26b] S. R. Marder, in *Inorganic Materials* (Eds.: D. W. Bruce and D. O′Hare), Wiley, Chichester, **1992**, p. 115. – [26c] D. R. Kanis, M. A. Ratner, T. J. Marks, *Chem. Rev.* **1994**, *94*, 195. – [26d] N. J. Long, *Angew. Chem. Int. Ed. Engl.* **1995**, *34*, 21. – [26e] G. De La Torre, P. Vasquez, F. Agullo-Lopez, T. Torres, *J. Mater. Chem.* **1998**, *8*, 1671. – [26f] I. R. Whitall, A. M. Mc Donagh, M. G. Humphrey, M. Samoc, *Adv. Organomet. Chem.* **1998**, *42*, 291.
[27] M. L. H. Green, S. R. Marder, M. E. Thompson, J. A. Bondy, D. Bloor, P. V. Kolinsky, R. J. Jones, *Nature* **1987**, *330*, 660.
[28] [28a] D. R. Kanis, M. A. Ratner, T. J. Marks, *J. Am. Chem. Soc.* **1990**, *112*, 8205. – [28b] J. C. Calabrese, L.-T. Cheng, J. C. Green, S. R. Marder, W. Tam, *J. Am. Chem. Soc.* **1991**, *113*, 7227. – [28c] S. R. Marder, J. W. Perry, B. J. Tiemann, W. P. Schaefer, *Organometallics* **1991**, *10,* 1896. – [28d] D. R. Kanis, M. A. Ratner, T. J. Marks, *J. Am. Chem. Soc.* **1992**, *114,* 10338.
[29] J. Reedijk, in *Comprehensive Coordination Chemistry* (Eds.: G. Wilkinson, R. D. Gillard, J. A. McCleverty), Pergamon Press, Oxford, **1987**, vol. 2, pp. 73−98 and references therein.
[30] B. F. Levine, C. G. Bethea, *J. Chem. Phys.* **1975**, *63*, 2666.
[31] J. L. Oudar, *J. Chem. Phys.* **1977**, *67*, 446.
[32] I. Ledoux, J. Zyss, *J. Chem. Phys.* **1982**, *73*, 203.
[33] E. A. Guggenheim, *Trans. Faraday. Soc.* **1949**, *645*, 203.
[34] J. L. Oudar, D. S. Chemla, *J. Chem. Phys.* **1977**, *66*, 2664.
[35] R. W. Terhune, P. D. Maker, C. M. Sauvage, *Phys. Rev. Lett.* **1965**, *61*, 681.

[36] [36a] K. Clays, A. Persoons, *Phys. Rev. Lett.* **1991**, *66*, 2980. – [36b] K. Clays, A. Persoons, *Rev. Sci. Instrum.* **1992**, *63*, 3285.
[37] [37a] S. G. Cyvin, J. E. Rauch, J. C. Decius, *J. Chem. Phys.* **1965**, *43,* 4083. – [37b] J. Zyss, *J. Chem. Phys.* **1993**, *98*, 6583.
[38] M. Joffre, D. Yaron, R. J. Silbey, J. Zyss, *J. Chem. Phys.* **1992**, *97,* 5607.
[39] C. C. Frazier, M. A. Harvey, M. P. Cockerhan, H. M. Hand, E. A. Chauchard, C. H. Lee, *J. Phys. Chem.* **1986**, *90*, 5703.
[40] J. C. Calabrese, W. Tam, *Chem. Phys. Lett.* **1987**, *133*, 244
[41] L.-T. Cheng, W. Tam, D. F. Eaton, *Organometallics* **1990**, *9*, 2856.
[42] L-T. Cheng, W. Tam, G. R. Meredith, S. R. Marder, *Mol. Cryst. Liq. Cryst.* **1990**, *189*, 137.
[43] M. S. Wrighton, H. B. Abrahamson, D. L. Morse, *J. Am. Chem. Soc.* **1976**, *98*, 4105.
[44] D. R. Kanis, P. G. Lacroix, M. A. Ratner, T. J. Marks, *J. Am. Chem. Soc.* **1994**, *116*, 10089.
[45] W. Chiang, D. Vanegen, M. E. Thompson, *Polyhedron* **1996**, *15*, 2369.
[46] W. Chiang, D. M. Ho, D. Van Engen, M. E. Thompson, *Inorg. Chem.* **1993**, *32*, 2886.
[47] [47a] B. J. Coe, M. C. Chamberlain, J. P. Essex-Lopresti, S. Gaines, J. C. Jeffery, S. Houbrechts, A. Persoons, *Inorg. Chem.* **1997**, *36*, 3284. – [47b] B. J. Coe, J. P. Essex-Lopresti, J. A. Harris, S. Houbrechts, A. Persoons, *Chem. Commun.* **1997**, 1645. – [47c] B. J. Coe, S. Houbrechts, I. Asselberghs, A. Persoons, *Angew. Chem. Int. Ed.* **1999**, *38*, 366.
[48] S. D. Cummings, L.-T. Cheng, R. Eisenberg, *Chem. Mat.* **1997**, *9*, 440.
[49] J. A. Zuleta, J. M. Bevilacqua, J. M. Rehm, R. Eisenberg, *Inorg. Chem.* **1992**, *31*, 1332.
[50] S. D. Cummings, R. Eisenberg, *J. Am. Chem. Soc.* **1996**, *118*, 1949.
[51] H. Sakaguchi, H. Nakamura, T. Nagamura, T. Ogawa, T. Matsuo, *Chem. Lett.* **1989**, 1715.
[52] T. Matsuo, H. Nakamura, T. Nakao, M. Kawazu, *Chem. Lett.* **1992**, 2363.
[53] M. Bourgault, C. Mountassir, H. Le Bozec, I. Ledoux, G. Pucetti, J. Zyss, *J. Chem. Soc., Chem. Commun.* **1993**, 1623.
[54] M. Bourgault, T. Renouard, B. Lognone, C. Mountassir, H. Le Bozec, *Can. J. Chem.* **1997**, *75*, 318.
[55] [55a] P. K. Gosh, T. G. Spiro, *J. Am. Chem. Soc.* **1980**, *102*, 5543. – [55b] A. Juris, S. Campagna, I. Bidd, J.-M. Lehn, R. Ziessel, *Inorg. Chem.* **1988**, *27*, 4007.
[56] V. Alain, A. Fort, M. Barzoukas, C.-T. Cheng, M. Blanchard-Desce, S. R. Marder, J. W. Perry, *Inorg. Chim. Acta*, **1996**, *242*, 43.
[57] M. Bourgault, K. Baum, H. Le Bozec, G. Pucetti, I. Ledoux, J. Zyss, *New. J. Chem.* **1998**, 517.
[58] K. D. Singer, J. E. Sohn, L. A. King, H. M. Gordon, H. E. Katz, C. W. Dirk, *J. Opt. Soc. Am. B* **1989**, *6*, 1339.
[59] D. W. Bruce, A. Thornton, *Mol. Cryst. Liq. Cryst.* **1993**, *231*, 253.
[60] M. J. G. Lesley, A. Woodward, N. J. Taylor, T. B. Marder, I. Cazenobe, I. Ledoux, J. Zyss, A. Thornton, D. W. Bruce, A. K. Kakker, *Chem. Mater.* **1998**, *10*, 1355.
[61] J. Mata, S. Uriel, E. Peris, R. Llusar, S. Houbrechts, A. Persoons, *J. Organomet. Chem.* **1998**, *562*, 197.
pf1[62 I. S. Lee, S. S. Lee, Y. K. Cheung, D. Kim, N. W. Song, *Inorg. Chim. Acta* **1998**, *279*, 243.
[63] S. Houbrechts, K. Clays, A. Persoons, V. Cadernio, M. Pilar Gamasa, J. Gimeno, *Organometallics* **1996**, *15*, 5266.
[64] J. Zyss, C. Dhenaut, T. Chauvan, I. Ledoux, *Chem. Phys. Lett.* **1993**, *206*, 409.
[65] A. Juris, V. Balzani, F. Barigelletti, S. Campagna, P. Belser, A. Von Zelewski, *Coord. Chem. Rev.* **1988**, *84*, 85.
[66] I. D. Morrison, R. G. Denning, W. M. Laidlaw, M. A. Stammers, *Rev. Sci. Instrum.* **1996**, *67*, 1445.
[67] P. Dupau, T. Renouard, H. Le Bozec, *Tetrahedron Lett.* **1996**, *37*, 7503.
[68] T. Renouard, Ph. D. Thesis, University of Rennes, **1998**.
[69] C. Dhenaut, I. Ledoux, I. D. F. Samuel, J. Zyss, M. Bourgault, H. Le Bozec, *Nature* **1995**, *374*, 339.
[70] J. Zyss, C. Dhenaut, S. Brasselet, I. Ledoux, unpublished results.
[71] T. Le Bouder, P. Massiot, H. Le Bozec, *Tetrahedron Lett.* **1998**, *39,* 6869.
[72] C. Fiorini, F. Charra, J.-M. Nunzi, I. D. Samuel, J. Zyss, *Opt. Lett.* **1995**, *20,* 2469.
[73] M. Lequan, C. Branger, J. Simon, T. Thami, E. Chauchard, A. Persoons, *Adv. Mater.* **1994, 6**, 851.
[74] C. Lambert, E. Schmälzlin, K. Meerholz, C. Bräuchle, *Chem. Eur. J.* **1998, 4,** 512.
[75] M. Blanchard-Desce, J.-B. Baudin, O. Ruel, L. Julien, S. Brasselet, J. Zyss, *Opt. Mater.* **1998, 9,** 276.
[76] P. J. Burke, D. R. McMillin, W. R. Robinson, *Inorg. Chem.* **1980**, *19*, 1211.
[77] T. Renouard, H. Le Bozec, S. Brasselet, I. Ledoux, J. Zyss, *Chem. Commun*. **1999**, 871.

Received January 18, 1999
[I99011]

Reactivity of Silyl-Substituted Heterobimetallic Iron–Platinum Hydride Complexes towards Unsaturated Molecules, I Alkyne Insertions into the Platinum-Hydride Bond, Phosphane-Induced σ-Alkenyl–μ-Vinylidene Rearrangements and Formation of μ-Isonitrile Complexes

Michael Knorr*[a][+] and Carsten Strohmann[b]

Dedicated to Professor Helmut Werner on the occasion of his 65th birthday

Keywords: Heterobimetallics / Hydride complexes / Alkenyl complexes / μ-Isonitrile complexes / Silicon / Iron / Platinum

The heterobimetallic hydride complexes [(OC)$_3$Fe{Si(OMe)$_3$}(μ-Ph$_2$PXPPh$_2$)Pt(H)(PR$_3$)] (**1a**: X = CH$_2$, PR$_3$ = PPh$_3$; **1b**: X = NH, PR$_3$ = PPh$_3$; **1c**: X = CH$_2$, PR$_3$ = PMePh$_2$) have been prepared by the oxidative addition of [(OC)$_3$Fe(H){Si(OMe)$_3$}(η^1-Ph$_2$PXPPh$_2$)] to [Pt(H$_2$C=CH$_2$)(PPh$_3$)$_2$] or by reaction of K[(OC)$_3$Fe{Si(OMe)$_3$}(η^1-dppm)] with *trans*-[Pt(Cl)(H)(PPh$_3$)$_2$]. The solid-state structure of compound **1b** has been determined by single-crystal X-ray diffraction. 1-Alkynes such as methylpropiolate or phenylacetylene insert in a regiospecific manner into the Pt–H bond of **1** to yield the σ-alkenyl complexes [(OC)$_3$Fe{μ-Si(OMe)$_2$(OMe)}(μ-Ph$_2$PXPPh$_2$)Pt{C(R)=CH$_2$}] (**2a**: X = CH$_2$, R = CO$_2$Me; **2b**: X = NH, R = CO$_2$Me; **3a**: X = CH$_2$, R = Ph). Addition of the Pt–H bond of **3a** across the triple bond of [D$_1$]phenylacetylene affords [(OC)$_3$Fe{μ-Si(OMe)$_2$(OMe)}(μ-dppm)Pt{C(Ph)=C(D)H}] (**3a***) having the deuteron *trans* to platinum (*cis* addition). This insertion reaction is accompanied by dissociation of the platinum-bonded PR$_3$ ligand and saturation of the vacant coordination site by a dative μ-η^2-Si–O→Pt interaction. When **3** is treated with PR$_3$ again, a subsequent phosphane-induced rearrangement leading to vinylidene-bridged complexes [(OC)$_3$Fe{μ-C=C(H)R′}(μ-Ph$_2$PXPPh$_2$)Pt(PR$_3$)] (**4a**: X = CH$_2$, R′ = Ph, PR$_3$ = PPh$_3$; **4b**: X = NH, R′ = Ph, PR$_3$ = PPh$_3$; **4c**: X = CH$_2$, R′ = Ph, PR$_3$ = PMePh$_2$; **4d**: X = CH$_2$, R′ = *p*-tolyl, PR$_3$ = PPh$_3$) occurs. Upon purging a solution of **3a** with carbon monoxide, the labile CO adduct [(OC)$_3$Fe{Si(OMe)$_3$}(μ-dppm)-Pt(CO){C(Ph)=CH$_2$}] **5a** is formed, addition of 2,6-xylyl isocyanide to **2a** and **3a** affords the isonitrile adducts [(OC)$_3$Fe{Si(OMe)$_3$}(μ-dppm)Pt(CNxylyl){C(R)=CH$_2$}] (**5b**: R = CO$_2$Me; **5c**: R = Ph), respectively. When hydride complex **1a** is allowed to react with stoichiometric amounts of aromatic isonitriles, formal elimination of HSi(OMe)$_3$ occurs, yielding the heterodinuclear isonitrile-bridged complexes [(OC)$_3$Fe(μ-C=N-R)(μ-dppm)Pt(PPh$_3$)] (**6a**: R = 2,6-xylyl; **6b**: R = *o*-anisyl; **6c**: R = *p*-anisyl; **6d**: R = *p*-C$_6$H$_4$NH$_2$) and the bis(isonitrile) complexes [(OC)$_2$(RN≡C)Fe(μ-C=N–R)(μ-dppm)Pt(PPh$_3$)] (**7a**: R = 2,6-xylyl; **7b**: R = *p*-anisyl). Single-crystal X-ray diffraction studies perfomed on **6a** and **6b** reveal that the molecular structures of these μ-isonitrile complexes closely resemble the μ-vinylidene complexes **4**. The two metal centers are bridged in a symmetric manner by strongly bent CNR ligands, the aromatic groups R being oriented towards the Fe(CO)$_3$ moiety. Electrophilic addition of HBF$_4$ to the basic nitrogen atom of the μ-CNR ligand transforms **6** to the cationic μ-aminocarbyne complexes [(OC)$_3$Fe{μ-CN(H)R}(μ-dppm)Pt(PPh$_3$)][BF$_4$] (**8a**: R = 2,6-xylyl; **8b**: R = *p*-anisyl; **8c**: R = *p*-C$_6$H$_4$NH$_2$).

Introduction

The insertion of small molecules such as CO, CO$_2$, CNR, olefins, and alkynes into the metal−hydride bond of mononuclear transition metal complexes represents a fundamental reaction in organometallic chemistry, which is also of great relevance for homogenous catalysis.[1] The olefin insertion leading to transition metal alkyl complexes (as well as the reverse reaction, the β-elimination), has especially been the subject of numerous experimental and theoretical studies.[2] The insertion of alkynes into the metal−hydride bond, affording vinyl or alkenyl complexes, is very much related to the olefin insertion. In general, it is assumed that alkene and alkyne insertions proceed in most cases via a cyclic four-membered transition state. The insertion of acetylenes and isonitriles R−N≡C (which also possess a reactive triple bond) across the Pt−H bond of mononuclear platinum complexes has been examined in detail by Clark and co-workers.[3][4]

In the course of our investigations into the insertion and activation of small molecules by heterobimetallic complexes, we were interested in studying the insertion of such molecules into the Pt−H bond of heterodinuclear systems of the type L$_n$M−Pt(H)L$_2$, containing two *different* metal centers linked by a metal−metal bond. The influence of

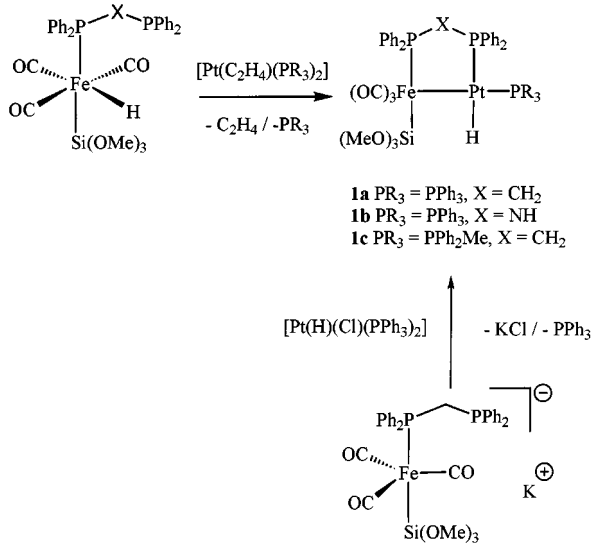
[a] Institut für Anorganische Chemie der Universität des Saarlandes,
Postfach 151150, D-66041 Saarbrücken, Germany
[b] Institut für Anorganische Chemie der Universität Würzburg, Am Hubland, D-97074 Würzburg, Germany
[+] New address: Laboratoire de Chimie et Electrochimie Moléculaire, Université de Franche-Comté, Faculté des Sciences et des Techniques
16, Route de Gray, F-25030 Besançon Cédex, France
E-mail: michael.knorr@rz.univ-fcomte.fr

 © WILEY-VCH Verlag GmbH, D-69451 Weinheim, 2000 1434−1948/00/0202−241 $ 17.50+.50/0

the second adjacent metal center close to a square planar platinum(II) moiety on the regio- and site selectivity of this important reaction was of special interest. Here we report on the reactivity of 1-alkynes and aromatic isonitriles towards heterobimetallic iron−platinum hydride complexes and their transformation into σ-alkenyl, μ-vinylidene, and μ-isonitrile complexes, respectively.

Results and Discussion

For our studies on the reactivity of heterometallic hydride complexes towards unsaturated molecules, the alkoxysilyl-substituted dinuclear complex $[(OC)_3Fe\{Si(OMe)_3\}(\mu\text{-dppm})Pt(H)(PPh_3)]$ **1a** appeared to be a promising system. Compound **1a** has been previously prepared by oxidative addition of the hydrido-silyl complex $[(OC)_3Fe(H)\{Si(OMe)_3\}(\eta^1\text{-dppm})]$ to the Pt^0 complex $[Pt(H_2C{=}CH_2)(PPh_3)_2]$.[5] Alternatively, this starting material can also be synthesized by the reaction of the metallate $K[(CO)_3Fe\{Si(OMe)_3\}(\eta^1\text{-dppm})]$[6a] with *trans*-$[Pt(Cl)(H)(PPh_3)_2]$ in 86% isolated yield (Scheme 1). In order to fine-tune the steric and electronic environment around the square-planar platinum center, we also prepared the bis(diphenylphosphanylamine)-bridged derivatives $[(OC)_3Fe\{Si(OMe)_3\}(\mu\text{-dppa})Pt(H)(PPh_3)]$ **1b** and $[(OC)_3Fe\{Si(OMe)_3\}(\mu\text{-dppm})Pt(H)(PMePh_2)]$ **1c** as precursors for reactivity studies (Scheme 1). All derivatives of **1** can be handled in the solid state in air without significant decomposition. They show only moderate solubility in aromatic solvents, but are fairly soluble in $CHCl_3$ and CH_2Cl_2.



Scheme 1

Comparative IR studies indicate that the dppa-backbone of **1b** slightly reduces the electron density of the bimetallic system, whereas due to the better σ-donor capacity of PPh_2Me relative to PPh_3, a slight shift of the ν(CO) frequencies to lower wavenumbers is noticeable for **1c**. A weak absorption band observed at 2119 cm^{-1} is assigned to the ν(PtH) stretch. The pattern of the hydride resonances in the ^{1}H-NMR spectra are virtually identical for all derivatives of **1** and consistent with a terminal platinum-bonded hydride ligand. For example, in the spectrum of **1b**, a doublet of triplets is observed at δ = −4.09 due to a strong P_{trans}-H coupling of ^2J = 209 Hz and an accidentally identical P_{cis}-H and P-H coupling of ^2J and ^{3+4}J = 16 Hz. In addition, the hydride signal is flanked by platinum satellites with a Pt-H coupling of ^1J = 662 Hz. For all new dppa-spanned compounds presented in this paper, a pronounced downfield shift is observed for the dppa phosphorus nuclei in the $^{31}P\{^1H\}$-NMR spectra compared to those of the dppm-spanned analogues. Thus, the AMX-type spectrum of **1b** consists of three mutually coupled phosphorus resonances. The doublet of doublets due to the dppa-phosphorus on iron at δ = 119.7 is strongly coupled [$^{2+3}J(P^1\text{-}P^2)$ = 138 Hz] to the dppa-phosphorus on platinum, whose resonance is found at δ = 81.7. Further splitting results from the platinum-bonded PPh_3 ligand at δ = 29.9 with couplings of 12 and 63 Hz, respectively. All resonances are flanked by ^{195}Pt satellites, the Pt-P couplings of which (J = 87, 2884, and 3503 Hz) are also evident in the ^{195}Pt-NMR spectrum giving rise to a doublet of doublets of doublets centered at δ = −2999.

Crystal Structure of $[(OC)_3Fe\{Si(OMe)_3\}(\mu\text{-dppa})Pt(H)(PPh_3)]$

The molecular structure of the dinuclear hydride complex **1b** including the atom numbering scheme is shown in Figure 1. Suitable crystals were obtained by slow diffusion of hexane into a saturated dichloromethane solution of **1b**. The iron and platinum centers are linked by a dppa bridge and a metal−metal bond. The Fe−Pt separation of 2.670(2) Å is almost identical to that observed in the trifluorosilyl-substituted complex $[(OC)_3Fe(SiF_3)(\mu\text{-dppm})Pt(H)(PPh_3)]$ [2.661(1) Å].[7] The coordination geometry around the Fe atom may be viewed as a distorted octahedral, consistent with a formal $Fe(d^7)$−$Pt(d^9)$ situation. The silyl ligand, which is situated *trans* to P(1) [Si−Fe−P(1) 167.71(4)°] has a Fe−Si bond length of 2.298(2) Å, which is in the typical range found for other heterometallic systems having a terminal $Si(OMe)_3$ unit. For example, a Fe−Si bond length of 2.271(4) Å has been found in $[(OC)_3Fe\{Si(OMe)_3\}(\mu\text{-dppm})Cu(PPh_3)]$.[6] Three meridianal arranged carbonyl ligands complete the environment of the iron center. The square-planar coordination geometry around the platinum center involves the Fe atom, two phosphorus atoms (one from the dppa-bridge [Pt−P(2) 2.304(2) Å], the second one from the PPh_3 ligand [Pt−P(3) 2.228(2) Å] and a hydride ligand [Pt−H(1) 1.544(4) Å]. The root mean square deviation from the plane passing through Fe, P(2), P(3), and H(1) amounts to 0.102 Å. Due to the good data set collected for **1b**, some electron density could successfully be refined as a *terminal* hydride position. This is consistent with the other spectroscopic results obtained (see above). The hydride ligand is quite close to one of the oxygen atoms of the $Si(OMe)_3$ group [d(O(6)···H(1)) 2.45(4) Å]. Similiar

close contacts were already observed for $[(OC)_3Fe(SiF_3\}(\mu\text{-}dppm)Pt(H)(PPh_3)]$,[7] where a weak intramolecular interaction between the hydride ligand and two F atoms of the SiF_3 ligand (bifurcated hydrogen bond with H···F 2.39(7) and 2.50(6) Å] was even retained in solution. As noticed for the latter hydride complex, the Pt−P(2) bond length of **1b** [2.304(2) Å] is significantly longer than that of Pt−P(3) [2.228(2) Å], which might reflect the high *trans* influence of the hydride ligand.

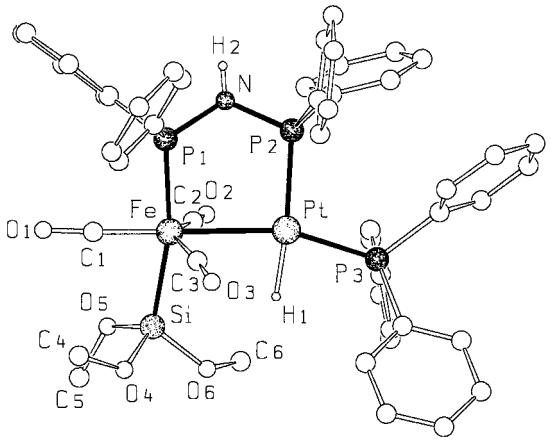
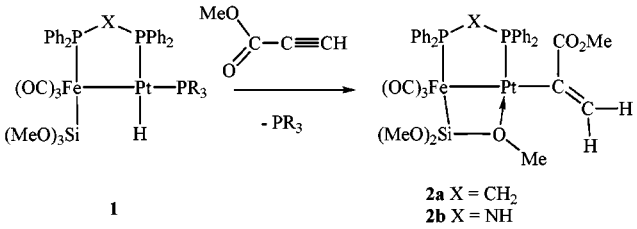


Figure 1. View of the crystal structure of **1b** showing the atom numbering scheme; selected bond lengths [Å] and angles [°]: Fe−Pt 2.670(2), Fe−Si 2.298(2), Fe−P(1) 2.203(2), Pt−P(2) 2.304(2), Pt−P(3) 2.228(2), Fe−C(1) 1.746(1), Fe−C(2) 1.756(4), Fe−C(3) 1.757(4), C(1)−O(1) 1.44(4), C(2)−O(2) 1.47(4), C(3)−O(3) 1.153(4), P(1)−N 1.684(3), P(2)−N 1.681(3), N−H(2) 0.81(4); Si−Fe−P(1) 167.71(4), H(1)−Pt−Fe 80.5(13), H(1)−Pt−P(3) 79.8(13), Fe−Pt−Si 100.61(6), C(1)−Fe−Si 80.11(13), C(2)−Fe−Si 85.85(12), C(3)−Fe−Si 86.01(13), O(1)−C(1)−Fe 177.6(3), O(2)−C(2)−Fe 177.3(3), O(3)−C(3)−Fe 175.2(4), C(1)−Fe−P(1) 87.67(13), C(2)−Fe−P(1) 96.68(12), C(3)−Fe−P(1) 99.79(13), C(1)−Fe−Pt 179.28(12), C(2)−Fe−Pt 72.47(13), C(3)−Fe−Pt 68.85(13), P(1)−Fe−Pt 91.61(6), P(2)−Pt−P(3) 105.60(6), Fe−Pt−P(2) 93.86(6), Fe−Pt−P(3) 157.68(3), P(1)−N−P(2) 119.8(2)

Reactivity towards 1-Alkynes

Upon addition of a threefold excess of methyl propiolate to a CH_2Cl_2 solution of **1a**, quantitative insertion into the platinum−hydride bond occurred within 4 h at ambient temperature leading to the heterobimetallic σ-alkenyl complex $[(OC)_3Fe\{\mu\text{-}Si(OMe)_2(OMe)\}(\mu\text{-}dppm)Pt\{C(CO_2Me)=CH_2\}]$ **2a** (Scheme 2). Elemental analyses and spectroscopic data showed that the alkyne insertion is accompanied by dissociation of the platinum-bonded PR_3 ligand. The vacant coordination site on the platinum center is electronically saturated by a dative interaction of a methoxy group of the trimethoxysilyl ligand, forming a four-membered Fe−Si−O→Pt cycle. This feature has been studied in detail, both in solution and in the solid state.[5,8,9] The σ-alkenyl complex **2a** is also formed using the Ph_2MeP-substituted derivative **1c** as starting material. In an analogous manner, the dppa-bridged insertion product $[(OC)_3Fe\{\mu\text{-}Si(OMe)_2(OMe)\}(\mu\text{-}dppa)Pt\{C(CO_2Me)=CH_2\}]$ **2b** is formed after addition of methyl propiolate to **1b**. Elemental analyses and spectroscopic data indicated that a triphenylphosphane oxide ligand, which stems from partial oxidation of the liberated PPh_3, is probably bonded by a hydrogen bond to the N−H group of the dppa ligand of **2b**. In all the cases, insertion occurs in a regioselective manner, affording the isomer with the ester group attached on the α-carbon. The new yellow compounds, which were moderately soluble in diethyl ether, were stable in solution for longer periods and thus permitted extensive multinuclear NMR measurements to be made (see Experimental Section).

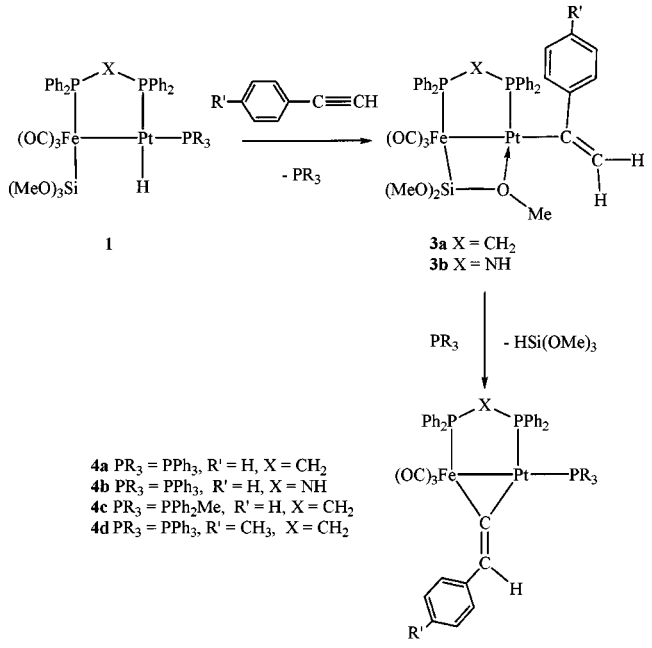


Scheme 2

A more complicated reaction occurred, when **1a** was treated with the less reactive phenylacetylene. ^{31}P-NMR monitoring of the course of the reaction revealed that 40 min after addition of 10 equivalents of phenylacetylene to **1a**, a ca. 60:40 mixture of unchanged **1a** and insertion product $[(OC)_3Fe\{\mu\text{-}Si(OMe)_2(OMe)\}(\mu\text{-}dppm)Pt\{C(Ph)=CH_2\}]$ **3a** was formed. The latter gave rise to an AX-type spectrum consisting of a doublet at $\delta = 61.2$ due to the phosphorus on iron, which is coupled to the platinum-bonded phosphorus at $\delta = 6.9$ with $^{2+3}J(P^1\text{-}P^2) = 41$ Hz. The latter resonance shows a very large ^1J coupling of 5010 Hz to the ^{195}Pt nucleus, whereas the former displays a small ^{2+3}J(Pt-P) coupling of 61 Hz. In addition, a broad signal centered at $\delta = -4.2$ due to the liberated PPh_3 is observed. After several hours, the intensity of the signals due to **3a** grows, whereas that of the hydride complex **1a** diminishes. In addition, a third set of signals emerges consisting of three mutually coupled resonances centered at $\delta = 63.0$, 43.6, and 22.2, whose chemical shifts and couplings are identical to those of the vinylidene-bridged complex $[(OC)_3Fe\{\mu\text{-}C=C(H)Ph\}(\mu\text{-}dppm)Pt(PPh_3)]$ **4a**. Compound **4a** has been prepared recently by the reaction of the vinylidene-bridged complex $[(OC)_3Fe\{\mu\text{-}C=C(H)Ph\}(\mu\text{-}dppm)Pt(CO)]$ with triphenylphosphane and was structurally characterized by an X-ray diffraction study.[10] Within 24 h, compound **1a** had been completely consumed and only the ^{31}P resonances of **3a** and **4a** were detected in a ca. 10:90 ratio. The quantitative transformation of the intermediate **3a** to **4a** may have been prevented by partial oxidation of the liberated PPh_3, since a singlet at $\delta = 29.5$ due to minor amounts of $O=PPh_3$ was also detected in the ^{31}P-NMR spectrum.

In a similar manner, phenylacetylene inserted into the Pt−H bond of **1b** to yield first the dppa-bridged σ-alkenyl complex $[(OC)_3Fe\{\mu\text{-}Si(OMe)_2(OMe)\}(\mu\text{-}dppa)Pt\{C(Ph)=CH_2\}]$ **3b** as an intermediate, which was characterized only

in solution [^{31}P δ = 111.2 P(Fe), 45.5 P(Pt), ^{2+3}J(P^1-P^2) = 45 Hz; ^{195}Pt δ = −2345, dd, ^1J(Pt-P) = 5524 Hz, ^{2+3}J(Pt-P) = 55 Hz]. The latter was finally transformed in situ to the new stable μ-vinylidene complex [(OC)$_3$Fe{μ-C=C(H)Ph}(μ-dppa)Pt(PPh$_3$)] **4b** after reaction with PPh$_3$. The derivatives [(OC)$_3$Fe{μ-C=C(H)Ph}(μ-dppm)Pt(PMePh$_2$)] **4c** and [(OC)$_3$Fe{μ-C=C(H)*p*-tolyl}(μ-dppm)Pt(PPh$_3$)] **4d** were prepared according to Scheme 3 by reaction of **1c** and **1a** with phenylacetylene and *p*-tolylacetylene, respectively.

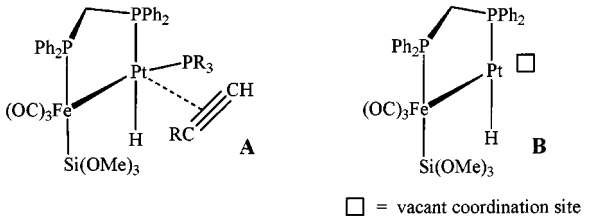


Scheme 3

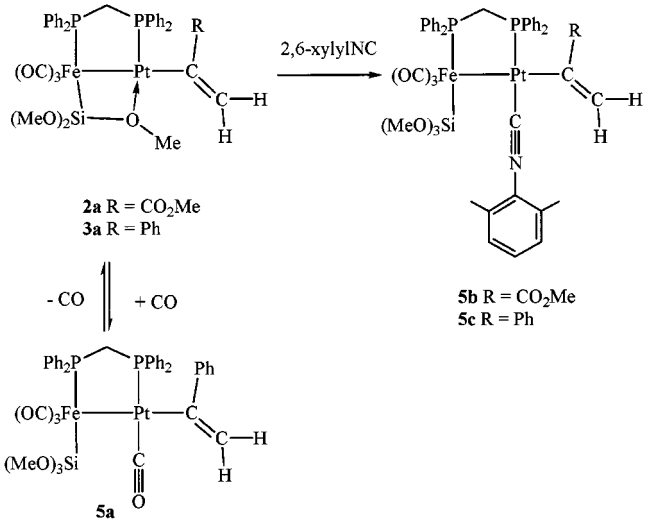
In order to assign the stereochemistry of the alkenyl group of **3a** unambiguously, we isolated this complex by stopping the reaction before all of **3a** had been converted into **4a**. Due to its solubility in an ether/hexane mixture, the alkenyl complex could be separated from unchanged **1a** and the final product **4a** by extraction. The geminal position of the alkenyl hydrogen atoms can be deduced from the ^{1}H-NMR spectrum, which shows no resolved coupling between these two protons. The broadened singlet at δ = 5.96 is assigned to the (*E*)-proton in a *trans* position to the platinum center, since it displays a strong Pt-H coupling of ^3J = 108 Hz, whereas the (*Z*)-proton signal at δ = 5.09 shows a coupling constant of *J* = 58 Hz only. Similar magnitudes and coupling patterns have been reported for mononuclear complexes of the type [L$_n$Pt(C(R)=CH$_2$}].[11] For regioisomer [L$_n$Pt{(*E*)-C(H)=CH(Ph)}], a *trans* coupling ^3J(H-H) of ca. 17 Hz should be expected, while regioisomer [L$_n$Pt{(*Z*)-C(H)=CH(Ph)}] should exhibit a *cis* coupling ^3J(H-H) of ca. 10 Hz.[11] Consistent with a rigid Fe−Si−O→Pt unit, two distinct signals in a 2:1 ratio at δ = 3.76 and 3.65 due to different methoxy groups are also observed. Employing [D$_1$]phenylacetylene (98%) as substrate, only the resonance of the (*Z*)-vinyl proton is observed in the ^{1}H-NMR spectrum of the deuterated complex **3a***. The resonance of the (*E*)-vinyl deuteron is found in the ^{2}H-NMR spectrum at δ = 6.07. This isotopic labeling experiment proves that insertion of [D$_1$]phenylacetylene occurred in a *cis* manner. The ^{13}C{^{1}H} NMR recorded at 268 K (see Experimental Section) further corroborates our structural proposal for **3a** possessing the same stereochemistry at the alkenyl group as [(OC)$_3$Fe{μ-Si(OMe)$_2$-(OMe)}(μ-Ph$_2$PXPPh$_2$)Pt{C(CO$_2$Me)=CH$_2$}] **2**.

The subsequent σ-alkenyl−μ-vinylidene rearrangement in the presence of PR$_3$, observed for the alkenyl complexes [(OC)$_3$Fe{μ-Si(OMe)$_2$(OMe)}(μ-Ph$_2$PXPPh$_2$)Pt{C(R)=CH$_2$}], seemed to depend in a sensitive manner on the electronic behaviour of the organic group R at the α-carbon atom of the alkenyl ligand. When [(OC)$_3$Fe{μ-Si(OMe)$_2$(OMe)}(μ-dppm)Pt{C(CO$_2$Me)=CH$_2$}], possessing a strong electron-withdrawing CO$_2$Me group, was treated with two equivalents of PPh$_3$ or PMePh$_2$, no σ-alkenyl−μ-vinylidene rearrangement was observed even after several hours. However, this transformation could be induced by addition of PPh$_3$ to **3**a. In an NMR experiment, performed in CDCl$_3$ solution, **3a** was gradually converted into the μ-vinylidene complex **4a** within 5 h after addition of three equivalents of PPh$_3$. A somewhat related phosphane-induced transformation has recently been studied on heterodinuclear acyl complexes of the type [(OC)$_3$Fe{μ-Si(OMe)$_2$(OMe)}(μ-dppm)Pt{C(=O)R}] (R = Me, Et). The latter acyl complexes were converted into μ-silyloxycarbene complexes [(OC)$_3$Fe{μ-C(R)OSi(OMe)$_3$}(μ-dppm)-Pt(PR′$_3$)] after addition of phosphanes or phosphites; the rate of the rearrangement depended on the basicity of PR′$_3$.[12] In the case of **3a**, the phosphane-promoted rearrangement occurs with concomitant reductive elimination of HSi(OMe)$_3$, as proved by NMR monitoring. Trimethoxysilane elimination has previously been observed upon treatment of the hydrido complex [(OC)$_3$Fe{μ-Si(OMe)$_2$(OMe)}(μ-dppm)Rh(H)(Cl)] with carbon monoxide and during the reaction of [(OC)$_3$Fe(H){Si(OMe)$_3$}(η^1-dppm)] with *fac*-[Re(CO)$_3$((THF)(μ-Br)]$_2$ affording the bromide-bridged complex [(OC)$_3$Fe(μ-Br)(μ-dppm)Re-(CO)$_3$].[13] Mechanistically, this alkenyl−vinylidene rearrangement probably involves intramolecular migration of a hydrogen atom from the β-carbon to the α-carbon of the alkenyl ligand, which forms the β-carbon of the vinylidene bridge after rearrangement. Related hydridovinylidene−alkenyl rearrangement involving α-hydrogen shifts have been investigated experimentally and theoretically in mononuclear tantalum and ruthenium complexes.[14] It should be noted that in the latter example, phenylacetylene has been inserted into the Ru−H bond of [RuHX(H$_2$)(PR$_3$)$_2$], leading to an alkenyl intermediate [L$_n$Ru−C(H)=C(H)Ph)] bearing the phenyl group on the β-carbon atom.[14b] An open question remains as to whether alkyne coordination on platinum prior to insertion into the Pt−H bond is associative or dissociative (Scheme 4). Both the initial formation of a penta-coordinated intermediate **A** or the initial dissociation of a ligand like PPh$_3$ (creating a vacant coordination site as in **B**) are well established pathways for migratory insertion reactions occurring in platinum com-

plexes.[15] We performed the reaction of **1a** with phenylacetylene in the presence of three equivalents of PPh_3 to investigate the role of the phosphane concentration on the acetylene insertion rate. Unfortunately, progressive fragmentation of the Fe−Pt bond occurred, leading to several mononuclear species, among them *trans*-$[Fe(CO)_3(PPh_3)_2]$.



Scheme 4

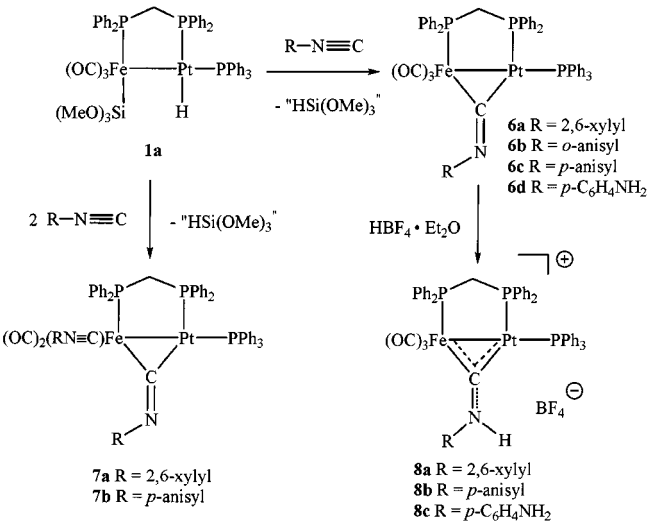


Scheme 5

We have recently shown that CO instantaneously reacts with dinuclear alkyl complexes of the type $[(OC)_3Fe\{\mu\text{-}Si(OMe)_2(OMe)\}(\mu\text{-dppm})PtR]$ (R = Me, Et, norbornyl) to give, by opening of the $\mu\text{-}\eta^2\text{-Si}-O$ bridge, the CO adducts $[(CO)_3Fe\{Si(OMe)_3\}(\mu\text{-dppm})Pt(CO)R]$. These intermediates rearrange due to a CO migratory insertion reaction into the Pt−C bond to the stable acyl complexes $[(OC)_3Fe\{\mu\text{-}Si(OMe)_2(OMe)\}(\mu\text{-dppm})Pt\{C(=O)R\}]$.[8] However, no spectroscopic change was noticed upon purging a solution of **2a** with a gentle stream of CO for 2 h. In contrast, **3b** afforded the CO adduct $[(OC)_3Fe\{Si(OMe)_3\}(\mu\text{-dppm})Pt(CO)\{C(Ph)=CH_2\}]$ **5a**, as evidenced by the appearance of a new ν(CO) vibration due to the Pt-bonded carbonyl ligand at 2088 cm^{-1} in the IR spectrum, and the emergence of a new AX pattern in the ^{31}P-NMR spectrum centered at δ = 60.8 and 15.0 with a P-P coupling constant of ^{2+3}J = 78 Hz and a P-Pt coupling constant of ^{1}J = 3414 Hz. Since **5a** readily lost the carbonyl ligand under reduced pressure regenerating **3a**, this complex could not be isolated. In the presence of stoichiometric amounts of 2,6-xylyl isocyanide, the dative Pt−OMe bond was instantaneously broken and the isonitrile adducts $[(OC)_3Fe\{Si(OMe)_3\}(\mu\text{-dppm})Pt(CNxyly)\{C(R)=CH_2\}]$ (**5b**: R = CO_2Me; **5c**: R = Ph) were isolated as stable yellow solids. In addition to the three ν(CO) stretches of the $Fe(CO)_3$ unit, the IR spectra of **5b/5c** displayed a strong vibration at 2181/2176 cm^{-1}, consistent with a terminal bonding mode of the isonitrile ligand at the platinum center.

Reactivity of 1 towards Isonitriles

The insertion of isonitriles into the Pt−H bond of platinum hydrido complexes leading to formimidoyl complexes $[L_nPt\{C(H)=NR\}]$ is a well established reaction.[3a,16] With the anticipation of inserting isonitriles C≡N−R into the Pt−H bond of **1**, we reacted **1a** with a stoichiometric amount of aromatic isonitriles in CH_2Cl_2 to yield heterodinuclear formimidoyl complexes.[17a] Surprisingly, no formyimidoyl complexes were isolated. Instead, the isonitrile-bridged bimetallic complexes $[(CO)_3Fe(\mu\text{-}C=NR)(\mu\text{-dppm})Pt(PPh_3)]$ (**6a**: R = 2,6-xylyl, **6b**: R = *o*-anisyl, **6c**: R = *p*-anisyl, **6d**: R = *p*-aminophenyl) were obtained as stable orange-yellow solids (Scheme 6). The NMR spectra of **6** resemble those of the structurally related dppm-bridged μ-vinylidene complexes **4a** and **4c**. Indicative of a bridging bent isonitrile ligand are the IR spectra of **6**, which displayed a broadened ν(C=N) vibration of medium intensity in the range between 1667−1669 cm^{-1}.



Scheme 6

Crystal Structures of $[(OC)_3Fe(\mu\text{-}C=N-R)(\mu\text{-dppm})Pt(PPh_3)]$

In heterobimetallic μ-isonitrile complexes $M(\mu\text{-}C=N-R)M'$ possessing a bent C=N−R arrangement, two isomeric forms are a priori conceivable, which differ in the relative orientation of R towards M or M′. In order to elucidate unambiguously the orientation of R and the degree of inclination, the molecular structure of

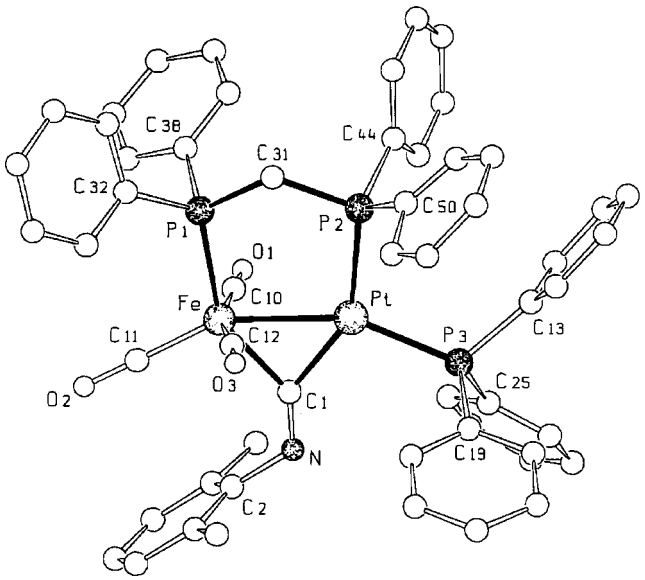


Figure 2. View of the crystal structure of **6a** showing the atom numbering scheme; selected bond lengths [Å] and angles [°]: Fe−Pt 2.522(4), Fe−P(1) 2.212(5), Pt−P(2) 2.297(5), Pt−P(3) 2.243(3), Pt−C(1) 1.994(8), Fe−C(1) 1.988(8), Fe−C(10) 1.768(9), Fe−C(11) 1.761(11), Fe−C(12) 1.836(11), C(1)−N 1.202(11), C(2)−N 1.425(14), C(10)−O(1) 1.138(12), C(11)−O(2) 1.129(13), C(12)−O(3) 1.066(12), P(1)−C(31) 1.851(9), P(2)−C(31) 1.831(9); C(1)−N(1)−C(2) 122.1(8), Pt−C(1)−Fe 78.6(3), Fe−Pt−C(1) 50.6(2), C(1)−Fe−Pt 50.8(2), C(1)−Fe−P(1) 147.7(3), C(1)−Pt−P(2) 147.7(2), C(1)−Pt−P(3) 105.7(3), P(1)−Fe−Pt 97.20(14), P(2)−Pt−P(3) 106.4(2), Fe−Pt−P(3) 155.94(9), P(1)−C(31)−P(2) 114.3(5)

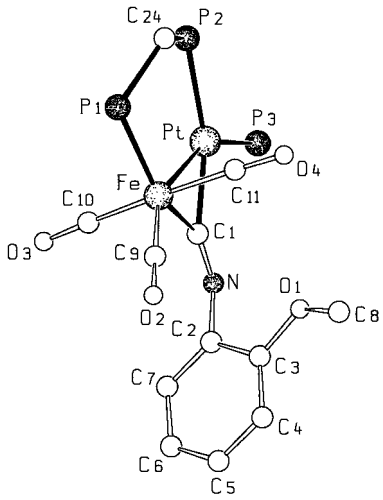


Figure 3. Perspective view of the core structure of **6b** along the Fe−Pt axis showing the atom numbering scheme. The phenyl groups are omitted for clarity; selected bond lengths [Å] and angles [°]: Fe−Pt 2.522(2), Fe−P(1) 2.226(3), Pt−P(2) 2.313(3), Pt−P(3) 2.259(3), Pt−C(1) 2.013(10), Fe−C(1) 1.991(10), Fe−C(10) 1.772(14), Fe−C(11) 1.789(13), Fe−C(9) 1.777(13), C(1)−N 1.92(12), C(2)−N 1.406(14), C(9)−O(2) 1.113(14), C(10)−O(3) 1.16(2), C(11)−O(4) 1.143(14), P(1)−C(24) 1.832(9), P(2)−C(24) 1.839(9); C(1)−N(1)−C(2) 127.2(9), Pt−C(1)−Fe 79.2(4), Fe−Pt−C(1) 50.0(3), C(1)−Fe−Pt 50.8(3), C(1)−Fe−P(1) 143.4(3), C(1)−Pt−P(2) 148.4(3), C(1)−Pt−P(3) 102.0(3), C(1)−Fe−C(9) 106.3(4), C(1)−Fe−C(10) 82.3(5), C(1)−Fe−C(11) 88.7(4), P(1)−Fe−Pt 93.63(8), P(2)−Pt−P(3) 109.61(10), Fe−Pt−P(3) 151.84(8), P(1)−C(24)−P(2) 112.4(5)

6a · 1.5 CH_2Cl_2 shown in Figure 2 has been determined by a single-crystal X-ray diffraction study. Suitable crystals were obtained by layering a saturated dichloromethane solution with Et_2O. The iron and platinum centers are linked by a dppm bridge and a metal−metal bond, whose Fe−Pt separation of 2.552(4) Å is almost identical to that of the vinylidene complex [$(OC)_3$Fe{μ-C=C(H)Ph}(μ-dppm)Pt(PPh_3)] [2.5503(8) Å].[10] Also, the other structural features are very reminiscent of the molecular structure of the latter compound. The bridging isonitrile ligand is symmetrically situated between the metals, with Fe−C(1) and Pt−C(1) distances of 1.988(8) and 1.994(8) Å, respectively. The length of the C(1)−N double bond of 1.20(1) Å is comparable to that of the W−Pt complex [$(OC)_4$W(μ-C=NCH_2SO_2−*p*-tolyl)(μ-dppa)Pt(PPh_3)] [1.229(12) Å][17b,17d] and to those reported for some homobimetallic isonitrile-bridged systems.[19] The C(1)−N−C(2) angle is extremely bent [122.1(8)°], the xylyl group being oriented towards the Fe$(CO)_3$ moiety. A comparable inclination with an average C−N−C angle of 123.1°, was found for the μ-C=N−Et ligands of [$(EtNC)_3$Fe−μ-CNEt)$_3$Fe(C-NEt)$_3$],[18d] whereas for most structurally characterized bent μ-CNR systems, C−N−C angles in the range between 130−133° have been documented.[18] For example, a C−N−C angle of 131.7(3)° has been determined for the bridging xylyl isocyanide ligands of the dinuclear compound *trans*-[η^5-CpFe(CN−2,6-xylyl)(μ-CN−2,6-xylyl)]$_2$.[18g] An unusual, widened C−N−C angle of 149.4(23) Å has been observed recently in a Pd(μ-CN*t*Bu)(μ-SiR_2)Pd complex.[18l,18m] We believe that this strong bending observed in **6a** may be caused by electronic factors, since the π-acceptor capacity of bridging isonitrile ligands is correlated to the degree of inclination.[19] Because the isonitrile complexes **6** represent electron-rich systems due to the presence of two metal centers in low oxidation states with three phosphorus donors as ligands, a strongly bent isonitrile bridge behaving as a good π-acceptor can at least partially compensate for the high electron density by back-bonding into π*-orbitals. Note that a bridging vinylidene unit, as encountered in **4**, also behaves as an efficient π-acceptor ligand.[20][21] As already discussed for the molecular structures of the μ-vinylidene complex **4a**[10] and the cationic μ-aminocarbyne complex [$(OC)_3$Fe(μ-CN(H)*o*-anisyl)(μ-dppa)Pt(PPh_3)],[17c,17d] the orientation towards the carbonyl fragment is imposed by the *steric bulk* of the triphenylphosphane ligand on platinum, which would otherwise interfere unfavorably with the 2,6-xylyl group.

As can be seen from Figure 3, which shows the core structure of **6b** along the Fe−Pt axis, the structural features of the *o*-anisyl isocyanide bridged derivative **6b** are similar to those of **6a**. As found in **6a**, the aromatic group of the isonitrile bridge is bent and aligned parallel to the Pt−Fe axis [C(2)−N−C(1)−Fe 4.14°]. Compared to **6a**, the C(1)−N−C(2) angle is somewhat widened and amounts to 127.2(9)°. At present we cannot state, whether this widening is due to a substituent effect on the phenyl group or caused by packing effects. The two mean planes defined by Fe−P(1)−P(2)−Pt and Fe−C(1)−Pt are nearly coplanar,

the angle between them being 6.20°. The rms deviation from the mean plane passing through Pt, C(1), P(2), P(3), and Fe is quite small and has been determined to be 0.025 Å (0.051 Å for **6a**). As in **6a**, a distorted square planar description seems to be appropriate for the coordination geometry around the platinum center.

In order to obtain compounds **6a–c** in satisfactory yields (ca 65–75%), slow stoichiometric addition of the corresponding isonitrile is important. When **1a** was directly mixed with a stoichiometric quantity of CNR, the isolation of pure **6** was hampered by competing formation of the bis(isonitrile) complexes $[(OC)_2(RN{\equiv}C)Fe(\mu\text{-}C{=}N{-}R)(\mu\text{-}dppm)Pt(PPh_3)]$ (**7a**: R = 2,6-xylyl; **7b**: R = *p*-anisyl) and separation from unchanged starting material **1a**. Compounds **7**, possessing both a bridging and a terminal iron-bonded CNR ligand, were formed as the sole species, when **1a** was allowed to react with 2 equivalents of the corresponding isonitrile for 8 h at ambient temperature. The coordination of the terminal CNR ligand in an orthogonal position relative to the metal–metal bond can be deduced from the IR spectra, which showed two ν(CO) stretches of approximate equal intensities. This pattern is only consistent with a *cis* arrangement of the two carbonyl ligands of the $Fe(CO)_2$ unit.[22] In addition, two ν(CN) vibrations due to the terminal and bridging isonitrile ligands were found in the IR spectra of **7a** and **7b** at 2089/2092 and 1655/1653 cm^{-1}, respectively. Compared to complexes **6**, the position of the latter absorption is shifted by ca. 16 wavenumbers to lower frequencies. This is probably due to the additional electron-donating effect of the second terminal CNR ligand, which is partially compensated by back-bonding in π* orbitals of the μ-CNR ligand, thus weakening the C=N bond.

At first glance, the formation of **6** and **7** seems to involve a simple reductive elimination of $HSi(OMe)_3$ as encountered in the σ-alkenyl–μ-vinylidene conversion of **2** into **4**. However, no evidence for the formation of trimethoxy silane was obtained. IR and ^{31}P-NMR monitoring revealed that one hour after the addition of two equivalents of CNR, breaking of the metal–metal bond occurred. A doublet of doublets found in the ^{31}P-NMR spectrum and an intense ν(CO) stretch at 1828 cm^{-1} indicated the formation of the metallate $[(OC)_3Fe\{Si(OMe)_3\}(\eta^1\text{-}dppm)]^-$.[6] The nature of the cationic fragment remains speculative. The observation of a very broad resonance in the ^{31}P-NMR spectrum at δ = 13.1 and a terminal ν(CN) stretch at 2185 cm^{-1} could be consistent with the existence of cationic species of the type $[Pt(H)(CNR)_2(PPh_3)]^+$, similar to the known complexes *trans*-$[Pt(H)(CN\textit{p}\text{-}tol)(PEt_3)_2]^+$, $[Pt(H)(CN\textit{p}\text{-}anisyl)(PEt_3)_2]^+$, and $[Pt(H)(PPh_3)_3]^+$.[3a,23] This assumption is further corroborated by the observation of a new broad and unresolved hydride resonance in the ^1H-NMR spectrum at δ = −6.27 exhibiting a Pt-H coupling constant of ^1J = 804 Hz. The mechanism of this reaction affording the μ-isonitrile complexes **6** and **7** has not been investigated further, since in the meantime more rational syntheses for complexes $[(OC)_3Fe(\mu\text{-}C{=}N{-}R)(\mu\text{-}Ph_2PXPPh_2)Pt(PPh_3)]$ have been developed by us.[17b–17d]

N-Protonation of $[(OC)_3Fe(\mu\text{-}CNR)(\mu\text{-}dppm)Pt(PPh_3)]$

As already described for $[(OC)_3Fe(\mu\text{-}CNR)(\mu\text{-}dppa)Pt(PPh_3)]$,[17c,17d] electrophilic addition of H^+ to the basic nitrogen atom of the μ-(CNR) ligand of **6** led instantaneously in a quantitative manner to stable cationic μ-aminocarbyne complexes $[(OC)_3Fe(\mu\text{-}CN(H)R)(\mu\text{-}dppm)Pt(PPh_3)][BF_4]$ (**8a**: R = 2,6-xylyl; **8b**: R = *p*-anisyl; **8c**: R = *p*-$C_6H_4NH_2$) (Scheme 5). According to the FAB^+ mass spectrum of the *p*-$C_6H_4NH_2$-substituted derivative **8c**, which displayed an intense peak at *m*/*z* 1100 (55%) for the cation, only monoprotonation occurred, despite the use of excess $HBF_4 \cdot Et_2O$. Characteristic NMR features of these *N*-protonated species are given for **8a** as an example. In the $^{13}C\{^1H\}$-NMR spectrum, the resonance of the μ-carbyne carbon is found downfield (doublet of doublets at δ = 313.7 with P–C couplings of ^2J = 77 and 11 Hz; in the ^1H-NMR spectrum, the N–H signal gave rise to a broad unresolved multiplet at δ = 9.18. Compared to the neutral precursors **6a**, the P^1-P^2 coupling in the $^{31}P\{^1H\}$-NMR spectrum was substantially reduced to ^{2+3}J = 89 Hz. Furthermore, a upfield shift of the dppm resonances of ca. 14 ppm results from the *N*-protonation, whereas the position of the PPh_3 ligand remains nearly unchanged. The doublet of doublets of doublets pattern at δ = − 2456 observed in the ^{195}Pt-NMR spectrum of **8a** is shifted downfield relative to the signal of **6a** (−2586), the Pt-P^3 coupling constant being reduced from ^1J = 4264 Hz (**6a**) to ^1J = 3739 Hz. The similar $^{31}P\{^1H\}$-NMR spectrum of derivative **8b**, showing the three mutually coupled phosphorus nuclei together with the coupling to the ^{195}Pt nucleus (33% natural abundance), is depicted in Figure 4.

A consequence of the positive charge, combined with the strong π-acceptor capacity of the μ-aminoarbyne ligand, is the IR shift of the ν(CO) vibrations to higher frequencies. Due to the decrease of the bond order of the C–N bond, the ν(CN) absorption is now detected at 1527 cm^{-1}. These spectroscopic data indicate that the aminocarbyne complexes **8** are also structurally closely related to the μ-vinylidene complexes **4** presented above.

Conclusion

These investigations have shown that the alkoxysilyl-substituted dinuclear hydride complexes **1** possess an interesting reactivity towards unsaturated molecules, which in most cases is difficult to predict. Whereas 1-alkynes insert in a regioselective manner into the Pt–H bond of **1** to yield σ-alkenyl complexes, reaction with aromatic isonitriles affords the RNC-bridged Fe–Pt complexes **6** and **7**. The phosphane-induced σ-alkenyl–μ-vinylidene rearrangement leading to $[(OC)_3Fe(\mu\text{-}C{=}C(H)R)(\mu\text{-}Ph_2PXPPh_2)Pt(PR_3)]$ and the formation of the μ-isonitrile complexes $[(OC)_3Fe(\mu\text{-}C{=}N\text{-}R)(\mu\text{-}dppm)Pt(PPh_3)]$ complement our previous studies on phosphane- and CO-induced silyl migrations resulting in μ-silyloxycarbene complexes $[(OC)_3Fe\{\mu\text{-}C(R)OSi(OMe)_3\}(\mu\text{-}dppm)Pt(PR_3)]$ and $[(OC)_3Fe\{\mu\text{-}C(Me)OSi\text{-}$

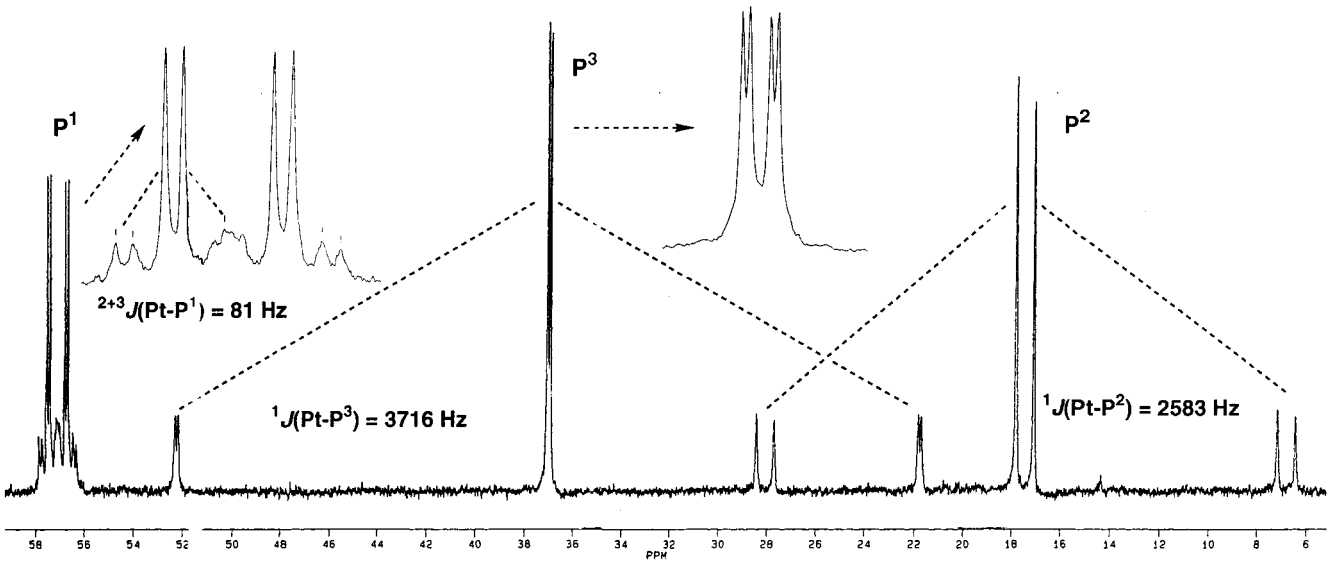


Figure 4. $^{31}P\{^1H\}$-NMR spectrum of $[(OC)_3Fe(\mu\text{-}CN(H)p\text{-anisyl})(\mu\text{-dppm})Pt(PPh_3)][BF_4]$ **8b** showing the three mutually coupled phosphorus nuclei together with the ^{195}Pt couplings

$(OSiMe)_3\}(\mu\text{-dppm})Pd(CO)]$.[12] The formation of these structurally closely related heterobimetallics underlines the tendency of these electron-rich systems to adopt a Fe(μ-C)M (M = Pd, Pt) core structure, bridged by μ-vinylidene, μ-isonitrile, μ-aminocarbyne, and μ-silyloxycarbene units behaving as efficient π-acceptor ligands. Our findings concerning the migratory insertion of activated alkynes such as DMAD or hexafluorobutyne into the Pt−H bond of **1**, as well as the molecular structures of the insertion products and their chemistry will be the subject of a forthcoming paper.[17e]

Experimental Section

All reactions were performed in Schlenk-tube flasks under purified nitrogen. Solvents were dried and distilled under nitrogen before use, toluene and hexane from sodium, dichloromethane from P_4O_{10}. Nitrogen was passed through BASF R3−11 catalyst and molecular sieve columns to remove residual oxygen and water. − Elemental C, H, and N analyses were performed on a Leco Elemental Analyzer CHN 900. − The ^1H-, $^{31}P\{^1H\}$-, ^{29}Si-INEPT and $^{13}C\{^1H\}$ NMR spectra were recorded at 200.13, 81.01 39.76, and 50.32 MHz, respectively, on a Bruker ACP 200 instrument. Phosphorus chemical shifts were referenced to 85% H_3PO_4 in H_2O with downfield shifts reported as positive. ^{195}Pt chemical shifts were measured with a Bruker ACP 200 instrument (42.95 MHz) and externally referenced to K_2PtCl_4 in water with downfield chemical shifts reported as positive. NMR spectra were recorded in pure $CDCl_3$, unless otherwise stated. The presence and amount of CH_2Cl_2 and Et_2O retained in **3a**, **3c**, **6a**, **8a**, and **8b** was determined from the ^1H-NMR spectra. − The reactions were generally monitored by IR spectroscopy in the ν(CO) region. − The acetylenes and 2,6-xylyl isocyanide were obtained from Aldrich and Fluka and were used as received. $[Pt(Cl)(H)(PPh_3)_2]$, $[Pt(H_2C{=}CH_2)(PPh_3)_2]$, dppa, dppm, and anisyl isocyanide were prepared as described in the literature.[24−28] $[(OC)_3Fe(H)\{Si(OMe)_3\}(\eta^1\text{-dppa})]$ was prepared as described for $[(OC)_3Fe(H)\{Si(OMe)_3\}(\eta^1\text{-dppm})]$.[6]

Preparation of $[(OC)_3Fe\{Si(OMe)_3\}(\mu\text{-dppm})Pt(H)(PPh_3)]$ (1a): To a solution of $[Pt(H)(Cl)(PPh_3)_2]$ (756 mg, 1.0 mmol) in CH_2Cl_2 (10 mL), 1 equiv. of $K[(OC)_3Fe\{Si(OMe)_3\}(\eta^1\text{-dppm})]$ (685 mg, 1.0 mmol) was added. After stirring for 4 h at ambient temperature, the yellowish solution was filtered and concentrated. Compound **1a** was precipitated by slow addition of hexane and washed with Et_2O. The resulting crude off-white product, which was sufficiently pure for further reactions, was then dried in vacuo. Yield: 949 mg (86%). For ^1H- and ^{31}P-NMR data see ref.[5] − IR (KBr): $\tilde{\nu}$ = 2149 cm^{-1} (w) ν(PtH); 1952 (s), 1885 (vs), 1865 (vs) ν(CO). − $^{195}Pt\{^1H\}$ NMR: δ = −2916 [ddd, $^{2+3}J(Pt\text{-}P^1)$ = 87, $^1J(Pt\text{-}P^2)$ = 2074, $^1J(Pt\text{-}P^3)$ = 3544 Hz]. − ^{29}Si-INEPT NMR: δ = 10.6 [dt, $^3J(P^2\text{-}Si)$ = 7, $^3J(P^3{-}Si)$ = 7, $^2J(P^1\text{-}Si)$ = 38 Hz]. − $C_{49}H_{48}FeO_6P_3PtSi$ (1104.84): calcd. C 53.27, H 4.38; found C 52.50, H 4.09.

Preparation of $[(OC)_3Fe\{Si(OMe)_3\}(\mu\text{-dppa})Pt(H)(PPh_3)]$ (1b): To a solution of $[Pt(H_2C{=}CH_2)(PPh_3)_2]$ (748 mg, 1.0 mmol) in toluene (10 mL), 1 equiv. of $[(OC)_3Fe(H)\{Si(OMe)_3\}(\eta^1\text{-dppa})]$ (647 mg, 1.0 mmol) was added. After stirring for 30 min at ambient temperature, the orange-red solution was concentrated and **1b** was precipitated by slow addition of hexane and washed with Et_2O. The resulting crude off-white product, which was sufficiently pure for further reactions, was then dried in vacuo. Yield: 905 mg (82%). Analytically pure **1b** was obtained in the form of colorless crystals by recrystallization from CH_2Cl_2/hexane. − IR (KBr): $\tilde{\nu}$ = 2119 cm^{-1} (w) ν(PtH); 1961 (s), 1896 (vs), 1887 (vs) ν(CO). − ^1H NMR: δ = −4.09 [dt, 1 H, PtH, $^2J(P_{trans}\text{-}H)$ = 209, $^2J(P_{cis}\text{-}H) \approx {}^3J(P\text{-}H)$ = 16, $^1J(Pt\text{-}H)$ = 662 Hz], 3.58 [s, 9 H, SiOMe], 4.51 [m, br., NH, $^3J(Pt{-}H)$ = 61.0 Hz], 7.10−7.45 (m, 35 H, phenyl). − $^{31}P\{^1H\}$ NMR: δ = 119.7 [dd, P^1(Fe), $^{2+3}J(P^1\text{-}P^2)$ = 138, $^{3+4}J(P^1\text{-}P^3)$ = 12, $^{2+3}J(Pt\text{-}P)$ = 87 Hz], 81.7 [dd, P^2(Pt), $^1J(Pt\text{-}P)$ = 2284 Hz], 29.9 [dd, P^3(Pt), $^2J(P^2\text{-}P^3)$ = 63, $^1J(Pt\text{-}P)$ = 3503 Hz]. − $^{195}Pt\{^1H\}$ NMR: δ = −2999 [ddd, $^{2+3}J(Pt{-}P^1)$ = 87, $^1J(Pt{-}P^2)$ = 2884, $^1J(Pt{-}P^3)$ = 3503 Hz]. − $C_{48}H_{47}FeNO_6P_3PtSi$ (1104.80): calcd. C 52.18, H 4.28, N 1.27; found C 52.23, H 4.04, N 1.31.

Preparation of $[(OC)_3Fe\{Si(OMe)_3\}(\mu\text{-dppm})Pt(H)(PMePh_2)]$ (1c): To a solution of $[Pt(H_2C{=}CH_2)(PMePh_2)_2]$ (624 mg, 1.0 mmol) in toluene (10 mL), 1 equiv. of $[(OC)_3Fe(H)\{Si(OMe)_3\}(\eta^1\text{-dppm})]$ (646 mg, 1.0 mmol) was added. After stirring for 30 min at ambient temperature, the orange-red solution was concentrated and **1c** was

precipitated by slow addition of hexane. The resulting crude off-white product, which was sufficiently pure for further reactions, was then dried in vacuo. Yield: 854 mg (82%). − IR (KBr): $\tilde{\nu}$ = 2114 cm^{-1} (w) ν(PtH); 1952 (s), 1880 (vs), 1860 (vs) ν(CO). − ^{1}H NMR: δ = −4.23 [dt, 1 H, PtH, $^2J(P_{trans}$-H) = 188, $^2J(P_{cis}$-H) ≈ ^3J(P-H) = 14, ^1J(Pt-H) = 693 Hz], 2.11 [d, 3 H, PCH_3, ^2J(P-H) = 10 Hz], 3.46 [t, br., 2 H, CH_2, ^2J(P-H) = 12 Hz], 3.63 [s, 9 H, Si-OMe], 6.90−7.65 (m, 25 H, phenyl)]. − ^{31}P{^{1}H} NMR: δ = 70.2 [dd, P^1(Fe), $^{2+3}J(P^1$-$P^2)$ = 128, $^{3+4}J(P^1$-$P^3)$ = 12, ^{2+3}J(Pt-P) = 84 Hz], 28.5 [dd, P^2(Pt), ^1J(Pt-P) = 2068 Hz], 28.0 [t, P^3(Pt), $^2J(P^2$-$P^3)$ = 12, ^1J(Pt-P) = 3571 Hz]. − ^{195}Pt{^{1}H}NMR: δ = −2933 [ddd, $^{2+3}J(Pt$-$P^1)$ = 84, $^1J(Pt$-$P^2)$ = 2068, $^1J(Pt$-$P^3)$ = 3571 Hz]. − $C_{44}H_{45}FeO_6P_3PtSi$ (1041.78): calcd. C 50.73, H 4.35; found C 51.13, H 4.78.

Preparation of [(OC)$_3$Fe{μ-Si(OMe)$_2$(OMe)}(μ-dppm)Pt-{C(CO$_2$Me)=CH$_2$}] (2a): To a solution of **1a** (552 mg, 0.5 mmol) in CH_2Cl_2 (10 mL), 3 equiv. of methyl propiolate was added. After stirring for 4 h at ambient temperature, the orange-red solution was concentrated and **2a** was precipitated by slow addition of hexane. The resulting crude orange-yellow product, which was sufficiently pure for further reactions, was then dried in vacuo. Yield: 905 mg (79%). An analytically pure sample was obtained by recrystallization from toluene/pentane. − IR (KBr): $\tilde{\nu}$ = 1971 (s), 1909 (vs), 1879 (s), 1687 (m) ν(CO). − ^{1}H NMR: δ = 3.41 [s, 3 H, CO_2Me], 3.65 [d, 3 H, Pt−OCH_3, ^4J(Pt-H) = 2 Hz], 3.78 [s, 6 H, $SiOCH_3$ (PCH_2P resonances obscured by the signals for the methoxy groups], 5.08 [d, 1 H, (*Z*)-vinyl-H, ^4J(P-H) = 2 Hz, ^3J(Pt-H) = 62 Hz], 6.56 [s, 1 H, (*E*)-vinyl-H, ^3J(Pt-H) = 118 Hz], 7.17−7.92 (m, 20 H, phenyl). − ^{13}C{^{1}H} NMR: δ = 216.4 [d, 2 CO, ^2J(P−C) = 17 Hz], 212.4 [d, 1 CO, ^2J(P-C) = 13 Hz], 171.7 [s, *C*(=O)OCH_3], 156.6 [d, $C_α$, ^2J(P-C) = 8 Hz], 120.3−138.2 (m, phenyl and $C_β$), 55.1 (s, Pt−*O*CH_3), 51.0 [s, C(=O)*O*CH_3], 50.7 (s, Si-*O*CH_3), 45.4 [dd, P*C*P, ^1J(P-C) = 22, ^1J(P-C) = 39 Hz]. − ^{31}P{^{1}H} NMR: δ = 59.8 [d, P^1(Fe), $^{2+3}J(P^1$-$P^2)$ = 41, ^{2+3}J(Pt-P) = 61 Hz], 5.6 [d, P^2(Pt), ^1J(Pt-P) = 5010 Hz]. − ^{195}Pt{^{1}H} NMR: δ = −2317 [dd, $^{2+3}J(Pt$-$P^1)$ = 61, $^1J(Pt$-$P^2)$ = 5010 Hz]. − ^{29}Si-INEPT NMR: δ = 17.0 [dd, $^3J(P^2$-Si) = 5, $^2J(P^1$-Si) = 35 Hz] − $C_{35}H_{36}FeO_8P_2PtSi \cdot 0.25\ C_7H_8$ (925.63 + 22.81): calcd. C 46.53, H 4.04; found C 46.58, H 3.70.

Preparation of [(OC)$_3$Fe{μ-Si(OMe)$_2$(OMe)}(μ-dppa)Pt-{C(CO$_2$Me)=CH$_2$}] (2b): This complex was prepared as described for **2a**. Yield: 678 mg (70%). An analytically pure sample of **2b** containing triphenylphosphane oxide (see text) was obtained in small amounts after two weeks at −25° C from a CH_2Cl_2/pentane mixture. − IR (KBr): $\tilde{\nu}$ = 1975 (s), 1909 (vs), 1890 (s), 1687 (m) ν(CO). − ^{1}H NMR: δ = 3.33 [s, 3 H, CO_2Me], 3.69 [s, 3 H, Pt−OCH_3], 3.75 [s, 6 H, $SiOCH_3$], 4.79 [m, br., NH, ^3J(Pt-H) = 108 Hz], 5.33 [s, 1 H, (*Z*)-vinyl-H, ^3J(Pt-H) = 67 Hz], 6.82 [s, 1 H, (*E*)-vinyl-H, ^3J(Pt-H) = 122 Hz], 7.16−7.86 (m, 20 H, phenyl). − ^{31}P{^{1}H} NMR: δ = 109.5 [d, P^1(Fe), $^{2+3}J(P^1$-$P^2)$ = 45, ^{2+3}J(Pt-P) = 50 Hz], 44.7 [d, P^2(Pt), ^1J(Pt-P) = 5299 Hz], 28.8 [s, $OPPh_3$]. − ^{195}Pt{^{1}H} NMR: δ = −2350 [dd, $^{2+3}J(Pt$-$P^1)$ = 50, $^1J(Pt$-$P^2)$ = 5299 Hz]. − ^{29}Si-INEPT NMR: δ = 16.1 [dd, $^3J(P^2$-Si) = 5, $^2J(P^1$-Si) = 38 Hz]. − $C_{34}H_{35}FeNO_8P_2PtSi \cdot O{=}PPh_3$ (1204.91): calcd. C 51.84, H 4.18, N 1.16; found C 50.36, H 3.96, N 1.29.

Preparation of [(OC)$_3$Fe{μ-Si(OMe)$_2$(OMe)}(μ-dppm)Pt-{C(Ph)=CH$_2$}] (3a): To a solution of **1a** (1105 mg, 1.0 mmol) in CH_2Cl_2 (20 mL), 10 equivalents of phenylacetylene were added. After stirring for 5 h at ambient temperature, all volatiles were removed in vacuo. The oily red−brown residue was rinsed with 40 mL of a ether/hexane mixture (75:25) to extract **3a** from unchanged **1a** and **4a**. On concentration of the extract, crude **3a** precipitated as an ochre solid. Analytically pure **3a** was obtained by redissolving the solid in 3 mL of CH_2Cl_2 and precipitation with cold pentane (15 mL). Yield: 158 mg (16%). − IR (CH_2Cl_2): $\tilde{\nu}$ = 1962 (s), 1999 (vs), 1870 (vs) ν(CO); 1588 (w) ν(C=C). − ^{1}H NMR: δ = 3.54 [t, 2 H, PCH_2P, ^2J(P-H) = 10.8 Hz], 3.65 [d, 3 H, Pt−OCH_3, ^4J(Pt-H) = 2.4 Hz], 3.76 [s, 6 H, $SiOCH_3$], 5.09 [s, 1 H, (*Z*)-vinyl-H, ^3J(Pt-H) = 58 Hz], 5.96 [s, 1 H, (*E*)-vinyl-H, ^3J(Pt-H) = 108 Hz], 6.86−7.67 (m, 25 H, phenyl). − ^{13}C{^{1}H} NMR (268 K): δ = 217.0 [d, 2 CO, ^2J(P-C) = 18 Hz], 212.7 [d, 1 CO, ^2J(P-C) = 13 Hz], 166.5 [dd, $C_α$, ^2J(P-C) = 6, ^3J(P-C) = 2 Hz]. 120.3−138.2 (m, phenyl), 117.0 (s, br, $C_β$), 54.8 (s, Pt−*O*CH_3), 50.7 (s, Si*O*CH_3), 44.6 [dd, P*C*P, ^1J(P-C) = 22, ^1J(P-C) = 39 Hz]. − ^{31}P{^{1}H} NMR: δ = 61.2 [d, P^1(Fe), $^{2+3}J(P^1$-$P^2)$ = 41, ^{2+3}J(Pt-P) = 60 Hz], 6.9 [d, P^2(Pt), ^1J(Pt-P) = 5246 Hz]. − ^{195}Pt{^{1}H}NMR: δ = −2308 [dd, $^{2+3}J(Pt$-$P^1)$ = 60, $^1J(Pt$-$P^2)$ = 5246 Hz]. − ^{29}Si-INEPT NMR: δ = 17.9 [dd, $^3J(P^2$-Si) = 4, $^2J(P^1$-Si) = 34 Hz]. − $C_{39}H_{38}FeO_6P_2PtSi \cdot 0.5\ CH_2Cl_2$ (943.69 + 42.47): calcd. C 48.11, H 3.99; found C 48.46, H 4.08.

Preparation of [(OC)$_3$Fe{μ-C=C(H)Ph}(μ-dppa)Pt(PPh$_3$)] (4b): To a solution of **1b** (551 mg, 0.5 mmol) in CH_2Cl_2 (15 mL), 10 equiv. of phenylacetylene was added. After stirring for 2 d at 35°C, the color of the solution had changed to red−brown. All volatiles were removed in vacuo, the residue redissolved in CH_2Cl_2 (5 mL) and layered with hexane (15 mL). After 3 d at 5°C, yellow microcrystals were formed. Yield: 367 mg (68%). − IR (KBr): $\tilde{\nu}$ = 3295 w ν(NH); 2007 (m), 1942 (vs), 1916 (m) ν(CO); 1585 (w) ν(C=C). − ^{1}H NMR: δ = 5.22 [m, br., NH, ^3J(Pt-H) = 89.0 Hz], 6.60−8.25 [m, 41 H, phenyl and vinylidene proton]. − ^{13}C{^{1}H} NMR (263 K): δ = 238.8 [dd, μ-Cα, ^2J(P-C) = 72, ^2J(P-C) = 12 Hz], 217.3 [d, 1 CO, ^2J(P-C) = 6 Hz), 213.8 (dd, 2 CO, ^2J(P-C), ^3J(P-C) = 5 Hz], 117.9−138.4 [m, phenyl]. − ^{31}P{^{1}H} NMR: δ = 107.9 [dd, P^1(Fe), $^{2+3}J(P^1$-$P^2)$ = 132, $^{3+4}J(P^1$-$P^3)$ = 14, ^{2+3}J(Pt-P) = 62 Hz], 80.4 [dd, P^2(Pt), ^1J(Pt-P) = 2778 Hz], 42.7 [dd, P^3(Pt), $^2J(P^2$-$P^3)$ = 33, ^1J(Pt-P) = 4101 Hz]. − ^{195}Pt{^{1}H}NMR: δ = −2308 [ddd, $^{2+3}J(Pt$-$P^1)$ = 62, $^1J(Pt$-$P^2)$ = 2777 $^1J(Pt$-$P^3)$ = 4101 Hz]. − $C_{53}H_{42}FeNO_3P_3Pt$ (1084.78): calcd. C 58.68, H 3.90, N 1.29; found C 58.29, H 3.61, N 1.20.

Preparation of [(OC)$_3$Fe{μ-C=C(H)Ph}(μ-dppm)Pt(PMePh$_2$)] (4c): This complex was prepared in an NMR tube experiment by addition of excess phenylacetylene to a solution of **1c** (26 mg, 0.025 mmol) in $CDCl_3$ (0.7 mL) and was only characterized spectroscopically. − IR (KBr): $\tilde{\nu}$ = 1990 (m), 1925 (vs), 1904 (s) ν(CO); 1592 (w) ν(C=C). − ^{31}P{^{1}H} NMR: δ = 62.2 [dd, P^1(Fe), $^{2+3}J(P^1$-$P^2)$ = 116, $^{3+4}J(P^1$-$P^3)$ = 14, ^{2+3}J(Pt-P) = 78 Hz], 40.9 [t, P^3(Pt), $^2J(P^2$-$P^3)$ = 15, ^1J(Pt-P) = 4056 Hz], 21.4 [dd, P^2(Pt), ^1J(Pt-P) = 2462 Hz].

Preparation of [(OC)$_3$Fe{μ-C=C(H)−*p*-tol}(μ-dppm)Pt(PPh$_3$)] (4d): This complex was prepared as described for **4b** by mixing **1a** (551 mg, 0.5 mmol) in CH_2Cl_2 (15 mL) with 8 equiv. of *p*-tolylacetylene. Yield: 374 mg (61%). − IR (KBr): $\tilde{\nu}$ = 1987 (m), 1921 (vs), 1903 (s) ν(CO); 1581 (w) ν(C=C). − ^{1}H NMR: δ = 2.26 [s, 3 H, tolyl-CH_3], 4.03 [t, br., 2 H, CH_2, ^2J(P-H) = 9.8, ^3J(Pt-H) = 38.3 Hz], 6.58−7.0 [m, 40 H, phenyl and vinylidene proton]. − ^{31}P{^{1}H} NMR: δ = 62.9 [dd, P^1(Fe), $^{2+3}J(P^1$-$P^2)$ = 117, $^{3+4}J(P^1$-$P^3)$ = 15, ^{2+3}J(Pt-P) = 79 Hz], 43.3 [dd, P^3(Pt), $^2J(P^2$-$P^3)$ = 19, ^1J(Pt-P) = 4023 Hz], 21.8 [dd, P^2(Pt), ^1J(Pt-P) = 2477 Hz]. − ^{195}Pt{^{1}H}NMR: δ = −2703 [ddd, $^{2+3}J(Pt$-$P^1)$ = 79, $^1J(Pt$-$P^2)$ = 2477, $^1J(Pt$-$P^3)$ = 4023 Hz]. − $C_{55}H_{45}FeO_3P_3Pt \cdot 1.5\ CH_2Cl_2$ (1097.81 + 127.40): calcd. C 55.39, H 3.95; found C 55.13, H 4.16.

Preparation of [(OC)$_3$Fe{Si(OMe)$_3$}(μ-dppm)Pt(CN−2,6-xyly)-{C(CO$_2$Me)=CH$_2$}] (5b): 2,6-Xylyl isocyanide (26 mg, 0.2 mmol) was added to a stirred solution of **2a** (190 mg, 0.2 mmol) in CH_2Cl_2

(7 mL). The orange−red solution was stirred for 10 min at ambient temperature, then the volume was reduced to ca. 2 mL. After addition of pentane, the product precipitated in the form of an orange−red solid. Yield: 199 mg (94%). − IR (KBr): $\tilde{\nu}$ = 2181 (s) ν(C≡N); 1959 (s), 1892 (vs), 1865 (vs), 1691 (m) ν(CO). − ^{1}H NMR: δ = 2.45 [s, 6 H, xylyl-CH_3], 3.29 [s, 3 H, CO_2Me], 3.59 [s, 9 H, $SiOCH_3$ (PCH_2P resonances obscured by the methoxy groups], 5.27 [s, 1 H, (*Z*)-vinyl-H, ^3J(Pt-H) = 80 Hz], 6.79 [s, 1 H, (*E*)-vinyl-H, ^3J(Pt-H) = 142 Hz], 7.03−7.87 (m, 23 H, phenyl). − $^{31}P\{^1H\}$ NMR: δ = 62.9. [d, P^1(Fe), $^{2+3}J(P^1\text{-}P^2)$ = 84, ^{2+3}J(Pt-P) = 38 Hz], 13.4 [d, P^2(Pt), ^1J(Pt-P) = 3182 Hz]. − $^{195}Pt\{^1H\}$NMR: δ = −2698 [d, br, ^{2+3}J(Pt-P^1) not resolved, $^1J(Pt\text{-}P^2)$ = 3182 Hz]. − $C_{44}H_{45}FeNO_8P_2PtSi$ (1056.81): calcd. C 50.01, H 4.29, N 1.32; found C 50.48 H 4.68, N 1.10.

Preparation of [(OC)$_3$Fe{Si(OMe)$_3$}(μ-dppm)Pt(CN−2,6-xyly)-{C(Ph)=CH$_2$}] (5c): 2,6-Xylyl isocyanide (13 mg, 0.1 mmol) was added to a stirred solution of **3a** (99 mg, 0.1 mmol) in CH_2Cl_2 (5 mL). The orange−red solution was stirred for 10 min at ambient temperature, then the volume was reduced to ca. 2 mL. After addition of pentane, the product precipitated in the form of an orange−red solid, which was dried in vacuo for 2 h. Yield: 76 mg (71%). − IR (KBr): $\tilde{\nu}$ = 2176 (s) ν(C≡N); 1955 (s), 1889 (vs), 1858 (vs) ν(CO). − ^{1}H NMR: δ = 2.34 [s, 6 H, xylyl-CH_3], 3.50 [m, 1 H, PCH_2P], 3.57 [s, 9 H, $SiOCH_3$], 3.80 [m, 1 H, PCH_2P], 5.08 [s, 1 H, (*Z*)-vinyl-H, ^3J(Pt-H) = 77 Hz], 6.16 [s, 1 H, (*E*)-vinyl-H, ^3J(Pt-H) = 141 Hz], 6.89−7.69 (m, 28 H, phenyl). − $^{31}P\{^1H\}$ NMR: δ = 63.5. [d, P^1(Fe), $^{2+3}J(P^1\text{-}P^2)$ = 87, ^{2+3}J(Pt-P) = 34 Hz], 14.0 [d, P^2(Pt), ^1J(Pt-P) = 3313 Hz]. − $C_{48}H_{47}FeNO_6P_2PtSi$ (1074.81): calcd. C 53.64, H 4.41, N 1.30; found C 53.37, H 4.10, N 1.12.

Preparation of [(OC)$_3$Fe(μ-C=N−xylyl)(μ-dppm)Pt(PPh$_3$)] (6a): 2,6-Xylyl isocyanide (131 mg, 1 mmol) was added in several portions over 30 min to a stirred solution of **1a** (1105 mg, 1.0 mmol) in CH_2Cl_2 (20 mL). The orange−red solution was stirred for 1 d at ambient temperature, then reduced to ca. 5 mL and layered with Et_2O. After 3 d at 5° C, orange crystals of **6a** containing 1.5 molecules of solvated CH_2Cl_2 were formed. These crystals rapidly lost 0.5 molecules of solvated CH_2Cl_2 in vacuo. Yield: 910 mg (76%). − IR (CH_2Cl_2): $\tilde{\nu}$ = 1994 (m), 1926 (vs), ν(CO); 1667 (m, br) ν(C=N). − ^{1}H NMR: δ = 2.18 [s, 6 H, xylyl-CH_3], 3.69 [t, 2 H, CH_2, ^2J(P-H) = 9.0, ^3J(Pt-H) = 37.0 Hz], 6.83−7.48 [m, 38 H, phenyl]. − $^{31}P\{^1H\}$ NMR: δ = 73.6 [dd, P^1(Fe), $^{2+3}J(P^1\text{-}P^2)$ = 152, $^{3+4}J(P^1\text{-}P^3)$ = 5, ^{2+3}J(Pt-P) = 75 Hz], 42.0 [dd, P^3(Pt), $^2J(P^2\text{-}P^3)$ = 27, ^1J(Pt-P) = 4264 Hz], 32.7 [dd, P^2(Pt), ^1J(Pt-P) = 2527 Hz]. − $^{195}Pt\{^1H\}$NMR: δ = −2586 [ddd, $^{2+3}J(Pt\text{-}P^1)$ = 75, $^1J(Pt\text{-}P^2)$ = 2527, $^1J(Pt\text{-}P^3)$ = 4264 Hz]. − $C_{55}H_{46}FeNO_3P_3Pt \cdot CH_2Cl_2$ (1112.83 + 84.93): calcd. C 56.15, H 4.04, N 1.17; found C 55.70, H 4.08, N 1.14.

Preparation of [(OC)$_3$Fe(μ-C=N−*o*-anisyl)(μ-dppm)Pt(PPh$_3$)] (6b): This complex was prepared as described for **6a** by adding *o*-anisyl isocyanide (133 mg, 1 mmol) (dissolved in 5 mL CH_2Cl_2) dropwise to a solution of **1a** (1105 mg, 1 mmol) in CH_2Cl_2 (15 mL). Yield: 825 mg (74%). − IR (CH_2Cl_2): $\tilde{\nu}$ = 1998 (m), 1929 (vs) ν(CO); 1668 (m, br) ν(C=N). − ^{1}H NMR: δ = 3.86 [s, 3 H, OCH_3], 3.88−4.00 [CH_2, partially hidden by the methoxy resonance], 6.80−7.58 [m, 39 H, phenyl]. − $^{31}P\{^1H\}$ NMR: δ = 73.6 [dd, P^1(Fe), $^{2+3}J(P^1\text{-}P^2)$ = 152, $^{3+4}J(P^1\text{-}P^3)$ = 5, ^{2+3}J(Pt-P) = 69 Hz], 42.0 [dd, P^3(Pt), $^2J(P^2\text{-}P^3)$ = 27, ^1J(Pt-P) = 4188 Hz], 30.2 [dd, P^2(Pt), ^1J(Pt-P) = 2527 Hz]. − $^{195}Pt\{^1H\}$NMR: δ = −2594 [ddd, $^{2+3}J(Pt\text{-}P^1)$ = 69, $^1J(Pt\text{-}P^2)$ = 2527, $^1J(Pt\text{-}P^3)$ = 4188 Hz]. − $C_{54}H_{44}FeNO_4P_3Pt$ (1114.81): calcd. C 58.18, H 3.99, N 1.26; found C 58.00, H 3.81, N 1.14.

Preparation of [(OC)$_3$Fe(μ-C=N−*p*-anisyl)(μ-dppm)Pt(PPh$_3$)] (6c): This complex was prepared as described for **6a** by adding *p*-anisyl isocyanide (133 mg, 1 mmol) (dissolved in 5 mL CH_2Cl_2) dropwise to a solution of **1a** (1105 mg, 1 mmol) in CH_2Cl_2 (15 mL). Yield: 825 mg (74%). − IR (CH_2Cl_2): $\tilde{\nu}$ = 1996 (m), 1928 (vs) ν(CO); 1669 (m, br) ν(C=N). − ^{1}H NMR: δ = 3.81 [s, 3 H, OCH_3], 3.79 [t, 2 H, CH_2, ^2J(P-H) = 10.0, ^3J(Pt-H) = 39.0 Hz] 6.57−7.77 [m, 39 H, phenyl]. − $^{31}P\{^1H\}$ NMR: δ = 71.2 [dd, P^1(Fe), $^{2+3}J(P^1\text{-}P^2)$ = 153, $^{3+4}J(P^1\text{-}P^3)$ = 4, ^{2+3}J(Pt-P) = 67 Hz], 41.7 [dd, P^3(Pt), $^2J(P^2\text{-}P^3)$ = 29, ^1J(Pt-P) = 4196 Hz], 30.2 [dd, P^2(Pt), ^1J(Pt-P) = 2490 Hz]. − $C_{54}H_{44}FeNO_4P_3Pt$ (1114.81): calcd. C 58.18, H 3.99, N 1.26; found C 58.09, H 4.35, N 1.47.

Preparation of [(OC)$_3$Fe(μ-C=N−*p*-C$_6$H$_4$NH$_2$)(μ-dppm)Pt(PPh$_3$)] (6d): This complex was prepared as described for **6a** by adding *p*-aminophenyl isocyanide (118 mg, 1 mmol) (dissolved in 5 mL CH_2Cl_2) dropwise to a solution of **1a** (1105 mg, 1 mmol) in CH_2Cl_2 (15 mL). Yield: 715 mg (65%). − IR (CH_2Cl_2): $\tilde{\nu}$ = 1995 (m), 1927 (vs) ν(CO); 1668 (m, br) ν(C=N). − ^{1}H NMR: δ = 3.421 [s, br, 2 H, NH_2], 3.80 [t, CH_2, ^2J(P-H) = 9.8, ^3J(Pt-H) = 40.0 Hz], 6.78−7.72 [m, 39 H, phenyl]. − $^{31}P\{^1H\}$ NMR: δ = 71.3 [dd, P^1(Fe), $^{2+3}J(P^1\text{-}P^2)$ = 154, $^{3+4}J(P^1\text{-}P^3)$ = 4, ^{2+3}J(Pt-P) = 66 Hz], 42.0 [dd, P^3(Pt), $^2J(P^2\text{-}P^3)$ = 29, ^1J(Pt-P) = 4012 Hz], 30.3 [dd, P^2(Pt), ^1J(Pt-P) = 2556 Hz]. − $C_{53}H_{43}FeN_2O_3P_3Pt$ (1099.79): calcd. C 57.88, H 3.94, N 2.55; found C 57.90, H 4.21, N 2.47.

Preparation of [(OC)$_2$(xylylNC)Fe(μ-C=N−xylyl)(μ-dppm)-Pt(PPh$_3$)] (7a): 2,6-Xylyl isocyanide (131 mg, 1 mmol) was added to a stirred solution of **1a** (552 mg, 0.5 mmol) in CH_2Cl_2 (10 mL). The orange−red solution was stirred for 8 h at ambient temperature, then reduced to ca. 5 mL and layered with hexane. After 2 d at 5° C, yellow crystals of **7a** were formed. Yield: 383 mg (63%). − IR (CH_2Cl_2): $\tilde{\nu}$ = 2089 (m) ν(C≡N); 1940 (s), 1902 (s), ν(CO); 1655 (m, br) ν(C=N). − ^{1}H NMR (238 K): δ = 1.69 [s, 6 H, xylyl-CH_3], 1.97 [s, 3 H, xylyl-CH_3], 2.23 [s, 3 H, xylyl-CH_3], 3.41 [m, 1 H, PCH_A], 4.21 [m, 1 H, PCH_B], 6.58−7.46 [m, 41 H, phenyl]. − $^{31}P\{^1H\}$ NMR: δ = 73.7 [dd, P^1(Fe), $^{2+3}J(P^1\text{-}P^2)$ = 163, $^{3+4}J(P^1\text{-}P^3)$ = 4, ^{2+3}J(Pt-P) = 69 Hz], 41.7 [dd, P^3(Pt), $^2J(P^2\text{-}P^3)$ = 35, ^1J(Pt-P) = 4024 Hz], 31.8 [dd, P^2(Pt), ^1J(Pt-P) = 2586 Hz]. − $^{195}Pt\{^1H\}$ NMR: δ = −2586 [ddd, $^{2+3}J(Pt\text{-}P^1)$ = 75, $^1J(Pt\text{-}P^2)$ = 2527, $^1J(Pt\text{-}P^3)$ = 4264 Hz]. − $C_{63}H_{55}FeN_2O_2P_3Pt$ (1216.0): calcd. C 62.23, H 4.56, N 2.30; found C 62.28, H 4.08, N 2.23.

Preparation of [(OC)$_2$(*p*-anisylNC)Fe(μ-C=N−*p*-anisyl)(μ-dppm)-Pt(PPh$_3$)] (7b): *p*-Anisyl isocyanide (133 mg, 1 mmol) was added to a stirred solution of **1a** (552 mg, 0.5 mmol) in CH_2Cl_2 (10 mL). The orange−red solution was stirred for 8 h at ambient temperature, then reduced to ca. 5 mL and layered with hexane. Yield: 454 mg (81%). − IR (CH_2Cl_2): $\tilde{\nu}$ = 2092 (m) ν(C≡N); 1942 (s), 1902 (s), ν(CO); 1653 (m, br) ν(C=N). − ^{1}H NMR (243 K): δ = 3.77 [s, 3 H, OCH_3], 3.80 [s, 3 H, OCH_3], 3.48 [m, vbr, not resolved, 1 H, PCH_A], 4.25 [m, vbr, not resolved, 1 H, PCH_b], 6.29−7.69 [m, 43 H, phenyl]. − $^{31}P\{^1H\}$ NMR: δ = 71.5 [dd, P^1(Fe), $^{2+3}J(P^1\text{-}P^2)$ = 162, $^{3+4}J(P^1\text{-}P^3)$ = 5, ^{2+3}J(Pt-P) = 65 Hz], 41.7 [dd, P^3(Pt), $^2J(P^2\text{-}P^3)$ = 35, ^1J(Pt-P) = 4059 Hz], 30.3 [dd, P^2(Pt), ^1J(Pt-P) = 2427 Hz]. − $C_{61}H_{51}FeN_2O_4P_3Pt$ (1219.94): calcd. C 60.06, H 4.21, N 2.30; found C 60.09, H 4.35, N 2.55.

Preparation of [(OC)$_3$Fe(μ-CN(H)xylyl)(μ-dppm)Pt(PPh$_3$)][BF$_4$] (8a): This complex was prepared by adding excess $HBF_4 \cdot Et_2O$ to a solution of **6a** (119 mg, 0.1 mmol) in CH_2Cl_2 (5 mL) at 253 K. After warming to ambient temperature, all volatiles were removed under reduced pressure. The orange−red residue was rinsed with Et_2O (3 mL) and dried in vacuo. Yield: 133 mg (97%). − IR (CH_2Cl_2): $\tilde{\nu}$ = 2036 (m), 1981(vs), 1969 (vs) ν(CO); 1527 (w) ν(CN). − ^{1}H NMR: δ = 2.18 [s, 6 H, CH_3], 4.41 [t, 2 H, CH_2,

^2J(P-H) = 10.0, ^3J(Pt-H) = 39.5 Hz], 6.89−7.69 [m, 38 H, phenyl], 9.18, [s, br, 1 H, NH]. − $^{13}C\{^1H\}$ NMR: δ = 313.7 [dd, μ-C, ^2J(P-C) = 77, ^2J(P-C) = 11 Hz], 209.7 [d, 3 FeCO, ^2J(P-C) = 19 Hz), 128.1−134.2 [m, phenyl], 49.4 [m, unresolved, P*C*P], 18.1 [s, xylyl-*C*H$_3$]. − $^{31}P\{^1H\}$ NMR: δ = 60.6 [dd, P^1(Fe), ^{2+3}J(P^1-P^2) = 89, ^{3+4}J(P^1-P^3) = 13, ^{2+3}J(Pt-P) = 79 Hz], 37.4 [dd, P^3(Pt), ^2J(P^2-P^3) = 4, ^{3+4}J(P^1-P^3) = 12, ^1J(Pt-P) = 3739 Hz], 19.6 [dd, P^2(Pt), ^1J(Pt-P) = 2600 Hz]. − $^{195}Pt\{^1H\}$NMR: δ = −2456 [ddd, ^{2+3}J(Pt-P^1) = 79, ^1J(Pt-P^2) = 2600, ^1J(Pt-P^3) = 3739 Hz]. − $C_{55}H_{47}BF_4FeNO_3P_3Pt \cdot 2\ CH_2Cl_2$ (1200.64 + 169.86): calcd. C 49.95, H 4.08, N 0.79; found C 49.40, H 3.99, N 0.97.

Preparation of [(OC)$_3$Fe(μ-CN(H)−*p*-anisyl)(μ-dppm)Pt(PPh$_3$)][BF$_4$] (8b): This complex was prepared by adding excess $HBF_4 \cdot Et_2O$ to a solution of **6c** (111 mg, 0.1 mmol) in CH_2Cl_2 (5 mL) at 253 K. After warming to ambient temperature, all volatiles were removed under reduced pressure. The orange−red residue was rinsed with Et_2O (3 mL) and dried in vacuo. Yield: 115 mg (96%). − IR (CH_2Cl_2): $\tilde{\nu}$ = 2036 (m), 1977 (vs) ν(CO); 1532 (w) ν(CN). − ^{1}H NMR: δ = 3.84 [s, 3 H, OCH$_3$], 4.44 [t, 2 H, CH$_2$, ^2J(P-H) = 10.8, ^3J(Pt-H) = 40.0 Hz], 6.81−7.79 [m, 39 H, phenyl], 9.45, [m, br, 1 H, NH]. − $^{13}C\{^1H\}$ NMR: δ = 306.8 [dd, μ-C, ^2J(P-C) = 76, ^2J(P-C) = 10 Hz], 209.8 [d, 3 FeCO, ^2J(P-C) = 18 Hz), 115.2−159.8 [m, phenyl], 55.7 [s, O*C*H$_3$], 49.3 [m, unresolved, P*C*P], 55.7 [s, O*C*H$_3$]. − $^{31}P\{^1H\}$ NMR: δ = 57.2 [dd, P^1(Fe), ^{2+3}J(P^1-P^2) = 89, ^{3+4}J(P^1-P^3) = 14, ^{2+3}J(Pt-P) = 81 Hz], 37.1 [dd, P^3(Pt), ^2J(P^2-P^3) = 4, ^{3+4}J(P^1-P^3) = 14, ^1J(Pt-P) = 3716 Hz], 18.0 [dd, P^2(Pt), ^1J(Pt-P) = 2583 Hz]. − $C_{54}H_{45}BF_4FeNO_4P_3Pt$ (1202.61): calcd. C 53.93, H 3.72, N 1.17; found C 53.60, H 3.45, N 1.07.

Preparation of [(OC)$_3$Fe(μ-CN(H)−*p*-C$_6$H$_4$NH$_2$)(μ-dppm)Pt(PPh$_3$)][BF$_4$] (8c): This complex was prepared by adding excess $HBF_4 \cdot Et_2O$ to a solution of **6d** (110 mg, 0.1 mmol) in CH_2Cl_2 (5 mL) at 253 K. After warming to ambient temperature, all volatiles were removed under reduced pressure. The orange−red residue was rinsed with Et_2O (3 mL) and dried in vacuo. Yield: 102 mg (93%). − IR (CH_2Cl_2): $\tilde{\nu}$ = 2036 (m), 1977 (vs) ν(CO). − ^{1}H NMR: δ = 2.35 [s, 2 H, NH$_2$], 4.45 [t, 2 H, CH$_2$, ^2J(P-H) = 10.0, ^3J(Pt-H) = 39.0 Hz], 6.90 −7.95 [m, 39 H, phenyl], 9.45 [s, br, 1 H, NH]. − $^{31}P\{^1H\}$ NMR: δ = 57.8 [dd, P^1(Fe), ^{2+3}J(P^1-P^2) = 87, ^{3+4}J(P^1-P^3) = 15, ^{2+3}J(Pt-P) = 81 Hz], 37.9 d, P^3(Pt), ^{3+4}J(P^1-P^3) = 15, ^1J(Pt-P) = 3689 Hz], 17.9 [d, P^2(Pt), ^1J(Pt-P) = 2581 Hz]. − MS: (FAB$^+$/diglyme matrix): 1100 M$^+$ (55%). − $C_{53}H_{44}BF_4FeN_2O_3P_3Pt \cdot Et_2O$ (1187.60 + 74.12): calcd. C 54.26, H 4.31, N 2.22; found C 54.14, H 4.33, N 2.09.

Collection of the X-ray Data and Structure Determination: For **1b**, **6a**, and **6b** data were collected with a Siemens Stoe AED2 four-circle diffractometer using graphite-monochromated Mo-K_α radiation (λ = 0.71073 Å). The final unit cell parameters were obtained by least squares on the setting angles for 20 reflections with 2Θ = 20−23°. Data were corrected semiempirically for absorption correction using Ψ scans. SHELXS-97 and SHELXL-97 computer programs were used.[29] Crystallographic data (excluding structure factors) for the structures reported in this paper have been deposited with the Cambridge Crystallographic Data Centre as supplementary publication no. CCDC-114806−114808. Copies of the data can be obtained free of charge on application to CCDC, 12 Union Road, Cambridge CB2 1EZ, UK [Fax: (internat.) + 44-1223/336-033; E-mail: deposit@ccdc.cam.ac.uk].

Crystal Structure Determination of 1b: Collection of crystallographic data: intensity data were collected using the Ω/2Θ scan mode at 293 K. $C_{48}H_{46}FeNO_6P_3PtSi$ (1104.80): colorless crystals with approximate dimensions 0.3 × 0.2 × 0.2 mm, monoclinic, space group $P2_1/n$; a = 10.069(9), b = 18.475(10), c = 24.71(2) Å, β = 101.12(6)°, V = 4.510(6) Å^3, Z = 4, $\rho_{calcd.}$ = 1.627 g cm^{-3}, F(000) = 2208; 9351 independent reflections in the scan range 1.68° < 2θ < 53.0°, of which 9351 with $I > 2\sigma(I)$ were used in the structure solution and refinement for 734 parameters; $R1 = \Sigma|F_{o-Fc}|/\Sigma|F_o| = 0.0247$ [$I > 2\sigma(I)$], $wR2 = [\Sigma w(F_o^2 - F_c^2)^2/\Sigma wF_o^4]^{1/2} = 0.0603$ (all data), GoF = 1.034; anisotropic refinement for non-hydrogen atoms; hydrogen atoms in idealized geometries, except for H(1) and H(2), which were refined isotropically. Highest residual electron density 1.105 eÅ^{-3}.

Crystal Structure Determination of 6a: Collection of crystallographic data: intensity data were collected using the Ω/2Θ scan mode at 293 K. $C_{56.5}H_{49}Cl_3FeNO_3P_3Pt$ (1240.17): orange crystals with approximate dimensions 0.2 × 0.3 × 0.4 mm, triclinic, space group $P-1$; a = 12.08(2), b = 13.54(3), c = 18.60(3) Å, α = 101.86(14)°, β = 100.72(13)°, γ = 111.81(12)°, V = 2646(8) Å^3, Z = 2, $\rho_{calcd.}$ = 1.557 g cm^{-3}, F(000) = 1238; 9172 independent reflections in the scan range 1.90° < 2θ < 50.0°, of which 8179 with $I > 2\sigma(I)$ were used in the structure solution and refinement for 604 parameters; $R1 = \Sigma|F_{o-Fc}|/\Sigma|F_o| = 0.0673$ [$I > 2\sigma(I)$], $wR2 = [\Sigma w(F_o^2 - F_c^2)^2/\Sigma wF_o^4]^{1/2} = 0.1871$ (all data), GoF = 1.075; anisotropic refinement for non-hydrogen atoms; hydrogen atoms in idealized geometries. Highest residual electron density 2.653 eÅ^{-3}.

Crystal Structure Determination of 6b: Collection of crystallographic data: intensity data were collected using the Ω/2Θ scan mode at 293 K. $C_{54}H_{44}FeNO_3P_3Pt$ (1114.75): orange crystals with approximate dimensions 0.4 × 0.4 × 0.3 mm, monoclinic, space group $P2_1/n$; a = 18.727(4), b = 12.668(3), c = 20.706(4) Å, β = 109.19(3)°, V = 4639(2) Å^3, Z = 4, $\rho_{calcd.}$ = 1.596 g cm^{-3}, F(000) = 2224; 6968 independent reflections in the scan range 1.79° < 2θ < 48.0°, of which 6866 with $I > 2\sigma(I)$ were used in the structure solution and refinement for 578 parameters; $R1 = \Sigma|F_{o-Fc}|/\Sigma|F_o| = 0.0488$ [$I > 2\sigma(I)$], $wR2 = [\Sigma w(F_o^2 - F_c^2)^2/\Sigma wF_o^4]^{1/2} = 0.1466$ (all data), GoF = 1.200; anisotropic refinement for non-hydrogen atoms; hydrogen atoms in idealized geometries. Highest residual electron density 2.621 eÅ^{-3}.

Acknowledgments

The Deutsche Forschungsgemeinschaft and the Fonds der Chemischen Industrie is gratefully thanked for habilitation grants and financial support to M. K. and C. S. We are also indebted to Prof. M. Veith and Dr. P. Braunstein for their support and for providing the institute's facilities.

[1] [1a] C. Elschenbroich, A. Salzer, *Organometallchemie*, Teubner, Stuttgart, **1988**. − [1b] *Transition Metal Hydrides* (Ed.: A. Dedieu), VCH Publishers, Weinheim, New York, **1991**. − [1c] *Modern Acetylene Chemistry* (Eds.: P. J. Stang, F. Diederich), Wiley-VCH, Weinheim (Germany), **1995**.

[2] [2a] D. L. Thorn, R. Hoffmann, *J. Am. Chem. Soc.* **1978**, *100*, 2079−2090. − [2b] N. M. Doherty, J. E. Bercaw, *J. Am. Chem. Soc.* **1985**, *107*, 2670−2682. − [2c] N. Koga, S.-Q. Jin, K. Morokuma, *J. Am. Chem. Soc.* **1988**, *110*, 3417−3425. − [2d] P. E. M. Siegbahn, *J. Am. Chem. Soc.* **1993**, *115*, 5803−5812. − [2e] W. R. Rocha, W. B. De Almeida, *Organometallics* **1998**, *17*, 1961−1967.

[3] [3a] D. F. Christian, H. C. Clark, R. F. Stepaniak, *J. Organomet. Chem.* **1976**, *112*, 209−225. − [3b] H. C. Clark, C. R. Jablonski, C. S. Wong, *Inorg. Chem.* **1975**, *14*, 1332−1335. − [3c] T. G. Attig, H. C. Clark, C. S. Wong, *Can. J. Chem.* **1977**, *55*, 189−198. − [3d] H. C. Clark, G. Ferguson, A. B. Goel, E. G. Janzen, H. Ruegger, P. Y. Siew, C. S. Wong, *J. Am. Chem. Soc.* **1986**, *108*, 6961−6972.

[4] For further examples of olefin and alkyne insertions into Pt−H bonds see: [4a] J. Chatt, B. L. Shaw, *J. Chem. Soc.* **1962**, *21*, 5075−5084. − [4b] R. Puddephatt, M. A. Thomson, *Inorg. Chem.* **1982**, *21*, 725−730. − [4b] C. Wieser, D. Matt, J. Fischer, A. Harriman, *J. Chem. Soc., Dalton Trans.* **1997**, 2391−2402. − [4c] L. M. Venanzi, in: *20 Int. Conf. Coord. Chem.*, *1979* (Ed.: D. Banjera), Pergamon, Oxford **1980**, pp. 99−105. − [4d] W. R. Meyer, L. M. Venanzi, *Angew. Chem. Int. Ed. Engl.* **1984**, *23*, 529−531. − [4e] R. Ros, R. A. Michelin, R. Bataillard, R. Roulet, J. *Organomet. Chem.* **1979**, *165*, 107−116. − [4f] C. M. Lukehart, W. R. True, *Organometallics* **1988**, *7*, 2387−2393. − [4g] A. C. Dema, X. Li, C. M. Lukehart, M. D. Owen, *Organometallics* **1991**, *10*, 1197−1200. − [4h] M. Gomez, G. Muller, D. Sainz, J. Sales, X. Solans, *Organometallics* **1991**, *10*, 4036−4045. − [4i] L.-B. Han, M. Tanaka, *J. Am. Chem. Soc.* **1996**, *118*, 1571−1572. − [4j] L.-B. Han, N. Choi, M. Tanaka, *Organometallics* **1996**, *118*, 3259−3261. − [4k] A. Furiani, M. V. Russo, A. Chiesi Villa, A. G. Manfredotti, *J. Chem. Soc., Dalton Trans.* **1977**, 2154−2160. −
For further examples of alkyne insertions into M−H bonds of heterobimetallic hydride complexes see: [4l] B. T. Sterenberg, R. McDonald, M. Cowie, *Organometallics* **1997**, *16*, 2297−2312. − [4m] T. Sterenberg, R. W. Hilts, G. Moro, R. McDonald, M. Cowie, *J. Am. Chem. Soc* **1995**, *117*, 245−258. − [4n] T. Yasuda, A. Fukuoka, M. Hirano, S. Komiya, *Chem. Lett.* **1998**, 29−30.

[5] P. Braunstein, M. Knorr, A. Tiripicchio, M. Tiripicchio-Camellini, *Angew. Chem.* **1989**, *101*, 1414−1416; *Angew. Chem. Int. Ed. Engl.* **1989**, *28*, 1361−1363.

[6] [6a] P. Braunstein, M. Knorr, U. Schubert, M. Lanfranchi, A. Tiripicchio, *J. Chem. Soc., Dalton Trans.* **1991**, 1507−1514. − [6b] J. Blin, P. Braunstein, J. Fischer, G. Kickelbick, M. Knorr, X. Morise, T. Wirth *J. Chem. Soc., Dalton Trans.* **1999**, 2159−2169.

[7] P. Braunstein, E. Colomer, M. Knorr, A. Tiripicchio, M. Tiripicchio-Camellini, *J. Chem. Soc., Dalton Trans* **1992**, *5*, 903−909.

[8] P. Braunstein, T. Faure, M. Knorr, T. Stährfeldt, A. De Cian, J. Fischer, *Gazz. Chim. Ital.* **1995**, *125*, 35−50.

[9] P. Braunstein, M. Knorr, C. Stern, *Coord. Chem. Rev.* **1998**, *178−180*, 903−965.

[10] M. Knorr, C. Strohmann, P. Braunstein, *Organometallics* **1996**, *15*, 5653−5663.

[11] [11a] B. E. Mann, B. L. Shaw, N. I. Tucker, *J. Chem. Soc. A* **1971**, 2103−2108. − [11b] P. J. Stang, Z. Zhong, M. Kowalski, *Organometallics* **1990**, *9*, 833−838. − [11c] C. J. Cardin, D. J. Cardin, M. F. Lappert, *J. Chem. Soc., DaltonTrans.* **1977**, 767−778.

[12] [12a] M. Knorr, P. Braunstein, A. De Cian, J. Fischer, *Organometallics* **1995**, *14*, 1302−1309. − [12b] M. Knorr, P. Braunstein, A. Tiripicchio, F. Ugozzoli, *Organometallics* **1995**, *14*, 4910−4919.

[13] [13a] P. Braunstein, M. Knorr, E. Villarroya, A. De Cian, J. Fischer, *Organometallics* **1991**, *10*, 3714−3722. − [13b] M. Knorr, P. Braunstein, A. Tiripicchio, F. Ugozzoli, *J. Organomet. Chem.* **1996**, *526*, 105−116.

[14] [14a] A. van Asselt, B. J. Burger, V. C. Gibson, J. E. Bercaw, *J. Am. Chem. Soc.* **1986**, *108*, 5357−5349. − [14b] M. Olivan, E. Clot, O. Eisenstein, K. G. Caulton, *Organometallics* **1998**, *17*, 3091−3100.

[15] [15a] P. E. Garrou, R. F. Heck, *J. Am. Chem. Soc*. **1976**, *98*, 4115−4127. − [15b] G. K. Anderson, R. J. Cross, *Acc. Chem. Res.* **1984**, *17*, 67−74.

[16] [16a] M. Ciriano, M. Green, D. Gregson, J. A. K. Howard, J. L. Spencer, F. G. A. Stone, P. Woodward, *J. Chem. Soc., Dalton Trans.* **1979**, 1294−1300. − [16b] N. W. Alcock, J. M. Brown, T. D. MacLean, *J. Chem. Soc., Chem. Commun*. **1984**, 1689−1691. − [16c] G. Facchin, P. Uguagliati, R. A. Michelin, *Organometallics* **1984**, *3*, 1818−1822.

[17] [17a] A part of this work has already been communicated: M. Knorr, T. Faure, P. Braunstein, *J. Organomet. Chem*. **1993**, *447*, C4. − [17b] M. Knorr, C. Strohmann, *Organometallics* **1999**, *18*, 248−257. − [17c] M. Knorr, C. Strohmann, *Eur. J. Inorg. Chem.* **1998**, 495−499. − [17d] M. Knorr, C. Strohmann, Poster abstract 98, *4th Anglo/German Inorganic Chemistry Meeting*, University of Marburg, **1997**. − [17e] M. Knorr, *Abstract B 32 Chemiedozententagung*, Universität GH Essen, **1998**.

[18] [18a] E. Singleton, H. E. Oosthuizen, *Adv. Organomet. Chem.* **1983**, *22*, 209−310. − [18b] D. Lentz, *Angew. Chem.* **1994**, *106*, 1377−1393; *Angew. Chem. Int. Ed. Engl.* **1994**, *33*, 1315−1331. − [18c] K. S. Ratliff, P. E. Fanwick, C. P. Kubiak, *Polyhedron* **1990**, *9*, 2651−2653. − [18d] J. M. Basset, G. K. Barker, M. Green, J. A. K. Howard, F. G. A. Stone, W. C. Wolsey, *J. Chem. Soc., Dalton Trans.* **1981**, 219 −227. − [18e] W. P. Fehlhammer, A. Mayr, W. Kehr, *J. Organomet. Chem.* **1980**, *197*, 327−334. − [18f] W. P. Fehlhammer, A. Schröder, W. Sperber, J. Fuchs, *Chem. Ber.* **1992**, *125*, 1087−1 092. − [18g] M. O. Albers, A. A. Chalmers, G. J. Kruger, D. C. Liles, H. E. Oosthuizen, E. Singleton, N. J. Coville, *J. Organomet. Chem.* **1986, 306**, 385−394. − [18h] S. Bordoni, L. Busetto, M. C. Cassani, V. Zanotti, V. G. Albano, M. Monari, F. Prestopino, P. Sabatino, *Gazz. Chim. Ital*. **1995**, *125*, 57−62. − [18i] R. D. Adams, F. A. Cotton, *Inorg. Chem.* **1974**, *13*, 249−253. − [18j] F. A. Cotton, B. A. Frenz, *Inorg. Chem.* **1974, 13**, 253−256. − [18k] M. Ennis, R. Kumar, A. R. Manning, J. A. S. Howell, P. Mathur, A. J. Rowan, F. S. Stephens, *J. Chem. Soc., Dalton Trans.* **1981**, 1251−1259. − [18l] M. Suginome, Y. Kato, N. Takeda, H. Oike, Y. Ito, *Organometallics* **1998**, *17*, 495−497. − [18m] Note that μ-CNR ligands may also adopt a linear CN−R arrangement: Y. Yamamoto, H. Yamazaki, *Inorg. Chem.* **1986**, *25*, 3327−3329.

[19] J. A. Howell, J. Y. Saillard, A. L. Beuze, G. Jaouen, *J. Chem. Soc., Dalton Trans.* **1982**, 2533−2537.

[20] N. M. Kostic, R. F. Fenske, *Organometallics* **1982**, *1*, 974−982.

[21] [21a] M. I. Bruce, *Chem. Rev.* **1991**, *91*, 197−257. − [21b] A. B. Antonova, A. A. Johansson, *Russ. Chem. Rev.* **1989**, *58*, 693−710. − [21c] A. B. Antonova, A. A. Johansson, N. A. Deykhina, E. D. Korniyets, N. I. Pavlenko, G. V. Burmakina, A. I. Rubaylo, A. G. Ginzburg, P. V. Petrovskii, *J.Oganomet. Chem.* **1996**, *524*, 81−85. − [21d] H. Werner, Angew. Chem. **1990**, *102*, 1109−1121; *Angew. Chem. Int. Ed. Engl.* **1990**, *29*, 1077.

[22] P. S. Braterman, *Metal Carbonyl Spectra*, Academic Press, London, New York, **1975**.

[23] [23a] M. J. Church, M. J. Mays, *J. Chem. Soc. A* **1968**, 3074−3078. − [23b] K. Thomas, J. T. Dumler, B. W. Renoe, D. M. Roundhill, *Inorg. Chem.* **1972**, *11*, 1795−1799.

[24] J. C. Bailar, H. Itatani, *Inorg. Chem.* **1965**, *4,* 1618−1620.

[25] U. Nagel, *Chem. Ber.* **1982**, *115*, 1998−1999.

[26] H. Nöth, E. Meinel, *Z. Anorg. Allg. Chem.* **1967**, 349, 225 −240.

[27] K. Sommer, *Z. Anorg. Chem.* **1970**, *376*, 37−43.

[28] I. Ugi, R. Meyr, *Chem. Ber.* **1960**, *93*, 239−246.

[29] G. M. Sheldrick, *SHELXL-97*, *SHELXS-97*, Universität Göttingen, Germany, **1997**.

Received March 1, 1999
[I99070]

"Crowned" Fe_4S_4 Clusters as Electrochemical Metal Ion Sensors

Robertus J. M. Klein Gebbink,[a] Stephen I. Klink,[a] Martinus C. Feiters,*[a] and Roeland J. M. Nolte*[a]

Keywords: Iron-sulfur clusters / Crown ethers / Electrochemical devices / Host-guest chemistry

A series of Fe_4S_4 cluster compounds, **I**, **III**, and **V**, in which the cuboidal cluster core is appended with four crown ether thiolate ligands, and **II** and **IV**, bearing thiolate ligands without crown ether parts, has been synthesized and characterized. The spectroscopic and electrochemical properties of these compounds are determined by the electronic nature of the thiolate ligands. Only in the case of **III**, where a very short α-thioacetyl linker was used to connect the crown ether ligands to the cluster core, was a restricted conformational freedom of the ligand observed. A detailed electrochemical study of the influence of alkali and earth alkali metal ions (Li^+, Na^+, K^+, Mg^{2+}, and Ba^{2+}) on the reversible $2^-/3^-$ reduction of the cluster compounds was performed. In the case of the crown ether appended clusters **I**, **III**, and **V**, the addition of these metal ions resulted in an anodic shift, i.e. in positive direction, of the reduction potential (modulation effect) and to larger current responses (promotion effect). The magnitude of the modulation effects is determined by the binding affinity of the metal ions in the crown ether ligands, and by the distance between bound metal ions and the redox active cluster core. Variation of the linker between the cluster core and the metal ion binding site resulted in cluster compounds with almost inverse selectivities for e.g. K^+ and Ba^{2+} in the case of **I** and **III**. For the large effects found for compound **I** a lariat binding mode is proposed.

Introduction

Iron sulfur clusters play various roles as prosthetic groups in proteins. Their main function is to catalyze electron transfer reactions, e.g. to another redox active prosthetic group within a protein, or from one protein to another.[1] In a biological environment, tetranuclear Fe_4S_4 clusters generally exist in oxidation states that are designated as $3^-/2^-/1^-$ when the charges on the cysteinyl ligands are considered together with the core charge.[2] Synthetic thiolate clusters of this type show a somewhat richer redox chemistry; they can exist in four distinct oxidation states, $4^-/3^-/2^-$ and 1^-.[3] Early studies on biological and synthetic systems have shown that the potentials at which these states interconvert are strongly influenced by the environment of the cluster. Factors such as hydrogen bonding to the cluster, electron-donating or -accepting properties of the thiolate ligands, hydrophobicity of the ligands, and solvent polarity are all important in determining the actual values of the redox potentials.[4] In general, it can be said that the (partial) electron delocalization in the clusters is the reason why these systems are easily influenced by polarizing forces.

One of the challenges in the field of electrochemical sensory devices is to develop molecular systems that selectively recognize metal ions in general, and alkali and alkaline earth metal ions in particular.[5] Many of these systems are based on transition metal complexes, because they have a rich and well-understood electrochemistry. In these systems a binding site for the above-mentioned metal ions is located closely to a transition metal ion. Upon binding of a metal ion the redox potential of the transition metal complex is changed. This can be caused either by through-space electrostatic interactions or communication via various bond linkages between the binding site and the redox-active center. In the latter case the connector between the binding site and the redox-active site should be conducting in order to achieve the desired effect, whereas in the former case this is not required. In either case, the transition metal ion should be easily polarized to undergo a change in its redox potential. Two examples of such polarizable systems are ferrocene and $[Ru(bipy)_3]^{2+}$, which have both been frequently used in electrochemical devices.[5]

Fe_4S_4 thiolate clusters can also be considered as suitable building blocks for this purpose, as (i) they have a rich and well-defined electrochemistry, (ii) their redox potentials are highly sensitive to polarizing effects, (iii) they can be relatively easily functionalized, and (iv) four ligands can be used to influence one redox center. For these reasons, we decided to study thiolate clusters as the redox-active site for the recognition of alkali and alkaline earth metal ions. As mentioned earlier, these clusters bear a 2− or 3− overall negative charge in their most stable forms, whereas most other systems used for this purpose are neutral or positively charged. These clusters are therefore expected to lack repulsive Coulomb forces that disturb the interaction with metal ions; instead, one can take advantage of attractive Coulomb forces to favour it.

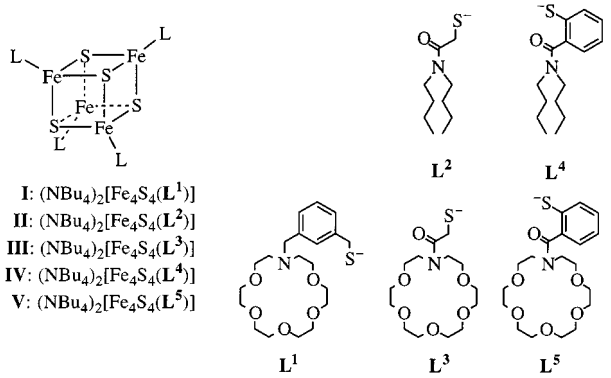
In this paper, the synthesis, characterization, and properties as electrochemical devices of a small series of crown ether substituted clusters will be presented. A simple aza crown ether compound, 1-aza-4,7,10,13,16-pentaoxacyclooctadecane (monoaza-18-crown-6), was used as the metal ion binding unit because of its ease of functionalization,

[a] Department of Organic Chemistry, NSR Center, University of Nijmegen, Toernooiveld, NL-6525 ED Nijmegen, The Netherlands
Fax: (internat.) + 31-24/365-2676
E-mail: mcf@sci.kun.nl

 © WILEY-VCH Verlag GmbH, D-69451 Weinheim, 2000 1434−1948/00/0202−253 $ 17.50+.50/0

and its well-documented binding properties towards metal ions.[6] The binding selectivity of this crown ether is mainly determined by its size compatibility with a metal ion guest, and increases in the order $Li^+ \approx Mg^{2+} < Na^+ < K^+ \approx Ba^{2+}$.

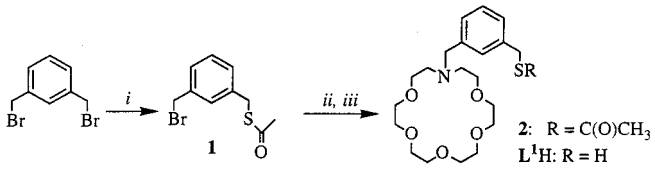
First of all, three cluster compounds **I**, **III**, and **V** were synthesized with different crown ether thiol ligands. The actual binding unit is not changed in this small series, but the spacer units and the nature of the thiol groups are. In addition, two cluster compounds **II** and **IV** were synthesized and to some extent studied, as these cluster compounds lack the crown ether moieties and can therefore be considered as model compounds.



Results and Discussion

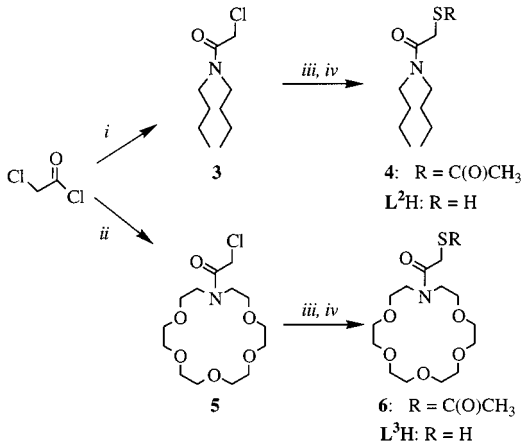
Ligand Synthesis

The synthesis of ligand $\mathbf{L^1}$H is depicted in Scheme 1. Starting from α,α′-dibromo-*m*-xylene, one of the bromide substituents was replaced by a thioacetyl group using a procedure described by Kellogg and co-workers[7] in which freshly distilled thioacetic acid was treated with K_2CO_3 to obtain the thioacetate nucleophile. After purification, the desired monobromide **1** was coupled to monoaza-18-crown-6 in DMF in the presence of base. The final step involved the hydrolysis of the thioacetyl function to the desired thiol. This reaction proceeded smoothly under acidic conditions in methanol (3% HCl) and under an inert gas.[8] Due to the presence of an internal base, i.e. the tertiary amine group, $\mathbf{L^1}$H is prone to dimerize under aerobic conditions. This compound was, therefore, kept strictly under N_2 during workup and storage. The overall yield of $\mathbf{L^1}$H was 41%.



Scheme 1. Synthesis of ligand $\mathbf{L^1}$H: (*i*) K_2CO_3, $CH_3C(O)SH$, DMF; (*ii*) monoaza-18-crown-6, K_2CO_3, DMF; (*iii*) 3% HCl/MeOH

In the synthesis of ligand $\mathbf{L^2}$H and $\mathbf{L^3}$H, the spacer unit was added to the respective secondary amines, di-*n*-butylamine and monoaza-18-crown-6, prior to introduction of the protected thiol functionality, as is shown in Scheme 2. The respective secondary amines were acylated at the nitrogen position by treatment with freshly distilled α-chloroacetyl chloride, followed by substitution of the halide by a thioacetyl group as discussed above. The desired thiols were then isolated after hydrolytic deprotection of the thioacetate by treatment with 3% HCl in methanol. Overall yields were 16 and 52% for $\mathbf{L^2}$H and $\mathbf{L^3}$H, respectively. Because these compounds lack an internal base, they are less sensitive to oxidative dimerization than $\mathbf{L^1}$H.

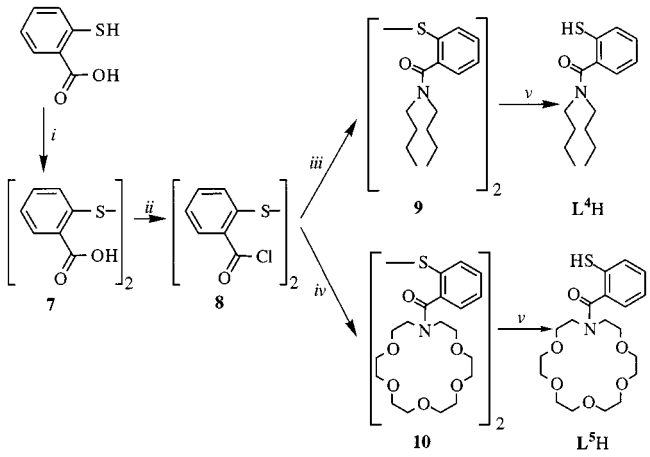


Scheme 2. Synthesis of ligands $\mathbf{L^2}$H and $\mathbf{L^3}$H: (*i*) di-*n*-butylamine, K_2CO_3, DMF; (*ii*) monoaza-18-crown-6, K_2CO_3, toluene; (*iii*) K_2CO_3, $CH_3C(O)SH$, DMF; (*iv*) 3% HCl/MeOH

A different strategy was used for the synthesis of $\mathbf{L^4}$H and $\mathbf{L^5}$H (Scheme 3). In the first step, 2-thiosalicylic acid was protected as its disulfide, which was then converted into the corresponding diacid chloride by treatment with thionyl chloride. Acylation of secondary amines with this diacid chloride proceeded smoothly in the presence of triethylamine as a base. The final step, cleavage of the disulfide bond to yield two identical thiols, was performed in a water/dioxane mixture with triphenylphosphane as the nucleophile, under acidic conditions.[9] Pure samples of $\mathbf{L^4}$H and $\mathbf{L^5}$H could be obtained by column chromatography. The overall yields were 48 and 52% for $\mathbf{L^4}$H and $\mathbf{L^5}$H, respectively.

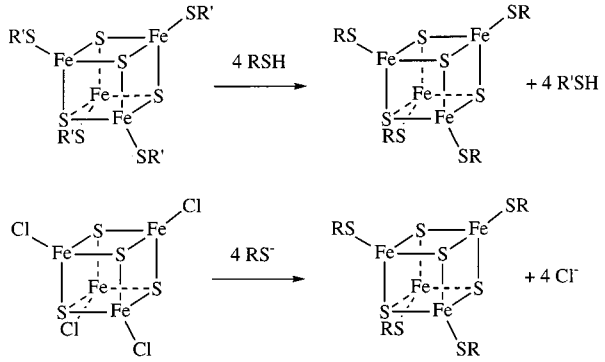
Synthesis and Characterization of Substituted Fe_4S_4 Clusters

Cluster compounds **I**−**V** were synthesized by ligand exchange reactions (Scheme 4),[10] and were isolated as dianionic species with either tetraalkylammonium or tetraphenylphosphonium counter ions. In one approach, these exchange reactions are based on an acid-base equilibrium, in which a more acidic thiol replaces a more basic thiolate ligand from an $Fe_4S_4(SR)_4$ cluster.[11] By making use of volatile thiols as the leaving group, e.g. tertiary butyl thiol, the equilibrium is easily driven to one desired product by



Scheme 3. Synthesis of ligands $\mathbf{L^4}$H and $\mathbf{L^5}$H: (*i*) H_2O_2, KOH, water; (*ii*) $SOCl_2$; (*iii*) di-*n*-butylamine, TEA, CH_2Cl_2; (*iv*) monoaza-18-crown-6, TEA, CH_2Cl_2; (*v*) PPh_3, dioxane/water/HCl

applying a "dynamic" vacuum. The other approach makes use of an Fe_4S_4 cluster that bears good leaving groups such as Cl^- ligands. The thiol used in these reactions is first deprotonated in order to make it a better nucleophile and to prevent the formation of HCl. Both methods were applied in the syntheses of clusters **I**−**V** since each of them has its advantages. The first method proceeds under very mild conditions without the need of any additive, whereas the second method is much faster but suffers from the fact that a base has to be added which may lead to counter ion scrambling.



Scheme 4. Preparation of Fe_4S_4 cluster compounds by ligand exchange reactions

Prior to the synthesis of the cluster compounds, test reactions were performed in situ in an electrochemical cell, and followed by differential pulse voltammetry (DPV). With this procedure, the quality of the freshly prepared thiols was tested, and an indication of the electrochemical characteristics of the final cluster compounds was obtained. On a preparative scale, the desired cluster compounds **I**−**V** were isolated as black oils after filtration of the crude reaction mixtures, followed by repeated precipitations from solution, and in vacuo removal of residual solvent.

Initial spectroscopic characterization of the isolated cluster compounds was performed by means of UV/Vis spectroscopy. Their UV/Vis characteristics closely matched the properties of related cluster compounds[12][13] and confirmed the integrity of the cubane core in these newly synthesized compounds (see Experimental Section). Further characterization was performed by NMR spectroscopy and electrochemical techniques (vide infra). NMR showed that all isolated cluster compounds contained residual solvent. In spite of the above workup procedures, and after several crystallization attempts and washings of the isolated products with various nonsolvents, it was not possible to remove these solvent traces. Elemental analyses of the isolated cluster compounds were therefore not performed.

NMR spectra of Fe_4S_4 cluster compounds in general are characterized by large chemical shifts of nuclei close to the cluster core and by broadened signals, due to the thermal accessibility of paramagnetic excited states at ambient temperature.[14] These two features can be observed in Figure 1, which shows the ^{1}H-NMR spectrum of cluster **III** in [D_7]DMF solution. In Table 1, the isotropic shifts are listed for the protons closest to the cluster core in clusters **I**−**V**. These shifts are defined as the difference in chemical shift for a given nucleus in the free ligand and in the cluster compound. For clusters **I**−**III** the shifts all have a negative sign, whereas for clusters **IV** and **V** some have a positive sign. The latter observation is a characteristic feature of aryl thiolate-substituted clusters and is correlated to the sign of spin density at the respective carbon atom in the aromatic ring. For aliphatic ligands, the sign has been shown to be non-alternative; its magnitude depends strongly on the distance between the metal center and the hydrogen nucleus.[14]

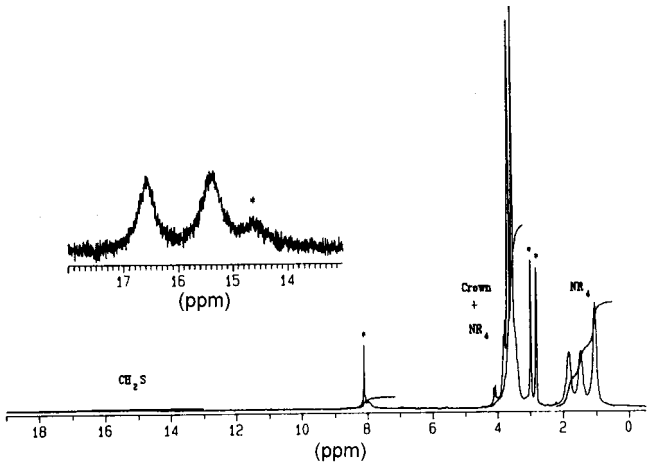


Figure 1. ^{1}H-NMR spectrum of cluster compound **III** in [D_7]DMF (the asterisks denote unassigned peaks and residual solvent peaks)

These general features were also found in temperature-dependent NMR studies on clusters **III** and **IV**, in the temperature range 298−350 K. The experiments showed that the isotropic shifts for these cluster compounds changed in magnitude upon increase of the temperature, due to a higher occupation of the first excited state, whereas their sign did not change. The temperature dependencies of the isotropic shifts are listed in Table 1, and were analyzed as linear relationships. Similar linear dependencies have been

Table 1. Isotropic shifts of ligand protons in cluster compounds **I**−**V**, together with their temperature dependence (temperature range: 300−340 K; solvent: [D_7]DMF or [D_6]DMSO, see Experimental Section)

Compound		Ligand δ [ppm]	Cluster δ [ppm]	ΔH_{iso} [ppm]	$\Delta H_{iso}/T$ [Hz/K]
I	CH_2S	3.62	15.08	−11.46	n.d.[a]
II	CH_2S	3.36	13.83	−10.47	n.d.[a]
III	CH_2S	3.76	15.35	−11.59	−3.32
			16.58	−12.82	−3.32
IV	*p*ArH	7.25	3.73	3.52	0.43
	*o*ArH	″	5.32	1.93	0.31
	*m*ArH	″	7.97	−0.72	−0.20
	*m*ArH	″	8.28	−1.03	−0.27
V	*p*ArH	7.25	n.o.[b]	−	−
	*o*ArH	″	5.29	1.96	n.d.[a]
	*m*ArH	″	7.96	−0.71	n.d.[a]
	*m*ArH	″	8.39	−1.14	n.d.[a]

[a] n.d.: not determined. − [b] n.o.: not observed.

observed for other cluster compounds in the same temperature range.[14][15]

An interesting feature from Figure 1 is the fact that the CH_2−S hydrogen signals in cluster **III** appeared as two singlets with approximately equal intensity. Apparently, the ligands in **III** have a restricted rotational freedom, which results in nonequivalent methylene hydrogen atoms due to the angular dependence of their isotropic shifts. Similar observations have been made for the cysteinyl methylene hydrogenatoms in iron-sulfur proteins and in oligopeptide model compounds.[16][17] For cluster **II**, only one signal was observed for the CH_2−S protons, suggesting that in **III** the crown ethers play a determining role in restricting the conformation of the ligands.

The electrochemical properties of **I**−**V** were studied by means of cyclic voltammetry (CV) and differential pulse voltammetry (DPV) in DMF. This solvent was chosen because both R_4N and Ph_4P salts of iron-sulfur clusters are soluble in it. Numerical data of the study are presented in Table 2.

Table 2. Electrochemical data for the 2−/3− reduction of cluster compounds **I**−**V** in DMF[a]

	CV			DPV	
	$E_{1/2}$ [V][b]	i_b/i_f	ΔE_p	E_p [V][b]	$W_{1/2}$
I	−1.74	0.68	85	−1.74	160
II	−1.65	0.86	221	−1.66	100
III	−1.58	0.80	213	−1.58	150
IV	−1.52	0.56	170	−1.50	140
V	−1.50	0.49	270	−1.48	284

[a] For conditions see Experimental Section. Pt working electrode. − [b] Potentials are given relative to the Fc/Fc^+ redox couple in the same solvent.

The halfwave potentials ($E_{1/2}$) for the 2−/3− reduction of clusters **I**, **IV**, and **V** compare well with values for simple, related thiolate clusters. For $[Fe_4S_4(SCH_2Ph)_4]^{2-}$ and $[Fe_4S_4(SPh)_4]^{2-}$ the $E_{1/2}$ values have been reported to be −1.74 and −1.52 V, respectively.[18] The corresponding $E_{1/2}$ for cluster **II** has an intermediate value; this reflects the fact that the thiolate ligands in this compound have relatively strong electron-accepting properties. The halfwave potentials of these cluster compounds are therefore solely determined by the electronic properties of the thiolate ligands. In contrast, the $E_{1/2}$ value of cluster **III** was found to be 70 mV more positive than that of cluster **II**. This is probably caused by the crown ethers, which are in close proximity of the cluster core due to the short acetyl spacers. The exact nature of the influence of the crown ethers on the reduction potential is not yet understood. NMR experiments showed that the ligands in **III** have restricted conformations (vide supra).

For all cluster compounds, the peak separations (ΔE_p) in the cyclic voltammograms and the peak widths at half peak height ($W_{1/2}$) in the differential pulse voltammograms were larger than the theoretical values of 59 mV and 90.4 mV, respectively. These deviations indicate that the electron-transfer rate between the electrode and the cluster compound is slow on the experimental time scale. A reason for the electrochemically quasi-reversible redox processes, in the case of the crown ether-functionalized compounds, could be the shielding of the cluster core from the electrode. Direct contact between the electrode and the redox-active species is desirable, as diminished contact delays the velocity of electron-transfer between the redox active moiety and the electrode, resulting in large peak separations. In addition, the ratio of the peak currents for the backward and the forward processes (i_b/i_f) in CV did not approach the value of 1 in most cases.

To obtain insight into the factors that govern the electrochemical properties of the above-mentioned cluster compounds, a more elaborate study was undertaken for compounds **IV** and **V**. First of all, scan rate dependent CV experiments were performed. The $E_{1/2}$ values of both clusters were found to be independent of the scan rate, whereas ΔE_p increased considerably with increasing scan rate. A linear relationship was found between the cathodic peak current ($i_{p,c}$) and the square root of the scan rate ($\upsilon^{1/2}$), suggesting that the mass transport of redox-active species toward the Pt electrode was diffusion-controlled. In addition, it was found that at higher scan rates the 2−/3− reduction was chemically more reversible. The 2−/3− reductions can therefore be described as chemically quasi-reversible, which implies that the reduction of the cluster core is followed by a chemical reaction that is fast enough to influence the voltammetric analysis (EC mechanism). This can either be due to the coordinating properties of the solvent, which would lead to diminished stability of the generated 3− cluster, or to ligand reactivity.

For cluster compound **IV**, the solvent and the type of electrode in the electrochemical experiments were varied. In solvents with relatively high ε, the $E_{1/2}$ values of **IV** were similar to those of $[Fe_4S_4(SPh)_4]^{2-}$, i.e. −1.52 V and −1.40 V in DMF and acetonitrile, respectively. In dichloromethane, the $E_{1/2}$ for **IV** was found to be 100 mV more negative than for $[Fe_4S_4(SPh)_4]^{2-}$. This might be the result of ion pair formation or (diminished) interactions of the cluster with the solvent. The electrochemical reversibility was im-

proved in acetonitrile. The best results were obtained, however, when a pyrolytic graphite-edge (PGE) electrode was used. With this electrode, also in DMF, a rather fast electron transfer was observed, together with a somewhat higher chemical reversibility. Compared to Pt electrodes PGE electrodes are chemically less inert, i.e. due to surface oxidation, interactions between electrode and redox-active species are more plausible.

In conclusion, it appears that the relatively large organic ligands influence the electrochemical behaviour of cluster compounds **I**−**V** to some extent. Due to shielding of the negatively charged cluster core by the large organic ligands, which apparently slows down the electron transfer from electrode to cluster core, the observed electrochemical processes were not always ideal. By varying the circumstances under which the compounds were studied, however, it was shown that these clusters inherently undergo reversible redox transitions.

Electrochemical Recognition of Alkali and Alkaline Earth Metal Ions

The effects of alkali and alkaline earth metal ions on the $E_{1/2}$ for the 2−/3− transition of cluster compounds **I**, **III**, **IV**, and **V**, were investigated by performing DPV experiments in the presence of varying amounts of perchlorate salts of lithium, sodium, potassium, magnesium, and barium. The use of the DPV technique has the advantage that very small amounts of material can be used. This technique also has a higher resolution compared to CV. Figure 2 shows the changes in the differential pulse voltammograms of cluster compound **I** and of **V** upon the addition of Ba^{2+} ions. The peak potentials for the reduction of both compounds shift to more positive values, i.e. the clusters are more easily reduced to the 3− form. Compound **I** exhibited so-called multi-wave behaviour, whereas **V** showed a continuous shift of its E_p (vide infra). Similar titrations were performed with the cluster compounds **III** and **IV**.

In all cases, a change in E_p occurs in an anodic, i.e. in a positive direction (Table 3). The magnitude of this change depends on the cluster compounds as well as on the metal ions. For example, Ba^{2+} ions give a shift in E_p of 190 mV with **I**, but only 20 mV with **IV**. The crown ether parts in the ligands thus appear to be essential to give large changes in the electrochemical properties of the Fe_4S_4 core upon addition of metal ions. A more detailed investigation of the effect of the crown ether ligands on the electrochemical behaviour toward alkali and alkaline earth metal ions was performed with compounds **I**, **IV**, and **V**, and is described below.

Table 3. Changes in E_p for the reduction of compounds **I**, **III**, **IV**, and **V** upon addition of 10 equivalents of metal ion[a]

	I	III	IV	V
Li^+	90 (120)	(0)	0 (0)	0 (10)
Na^+	30 (n.d.)[b]	–	0 (10)	50 (60)
K^+	40[c] (n.d.)[b]	–	0 (10)	50 (60)
Mg^{2+}	190[d] (290)[e]	(130)	30 (90)	70 (110)
Ba^{2+}	190[d] (210)	(120)	20 (50)	30 (50)

[a] In parentheses the E_p change when a large excess (100 equivalents) of metal ion is added. − [b] n.d. = not determined. − [c] Reached after 2 equivalents had been added. − [d] Reached after 4 equivalents had been added. − [e] Small additional peak observed.

Promotion and Modulation Effects

First of all, it is worthwhile to explain the difference between promotion and modulation effects on the electrochemical properties of redox active species. In general, promotion effects involve an improvement of both current response and electrochemical reversibility of a redox process, and in addition often involve an increase of peak currents after repetitive CV scans. Modulation effects involve changes in the potential of a redox process. The electrochemistry of large biomolecules often suffers from very poor current responses due to slow electron transfer from the redox active entity, embedded in the protein core, to the electrode.[19] Addition of a promoter increases the electron-transfer rate either by improving the protein-electrode interaction or by mediating electron transfer. Generally, promoters are polar or charged compounds that bear coordinating groups. Sometimes the use of a promoter also results in an altered $E_{1/2}$. In that case this compound behaves as a

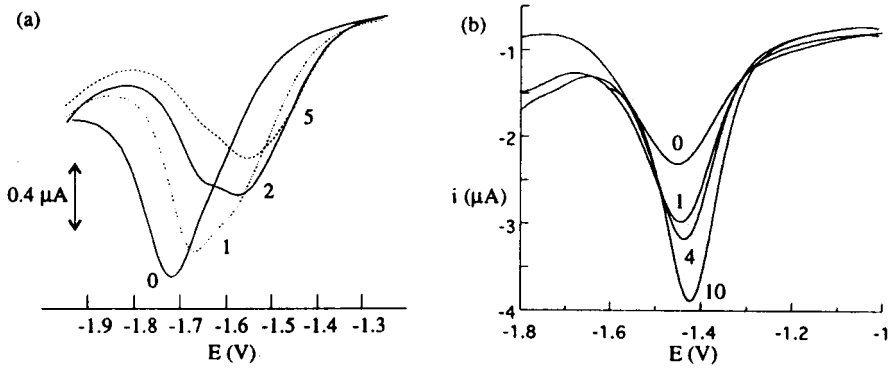


Figure 2. Changes in E_p upon addition of Ba^{2+} ions for the reduction of (a) compound **I** (prepared in situ) and (b) compound **V**, followed by DPV; numbers correspond to the amount of metal ion added (mol. equiv.)

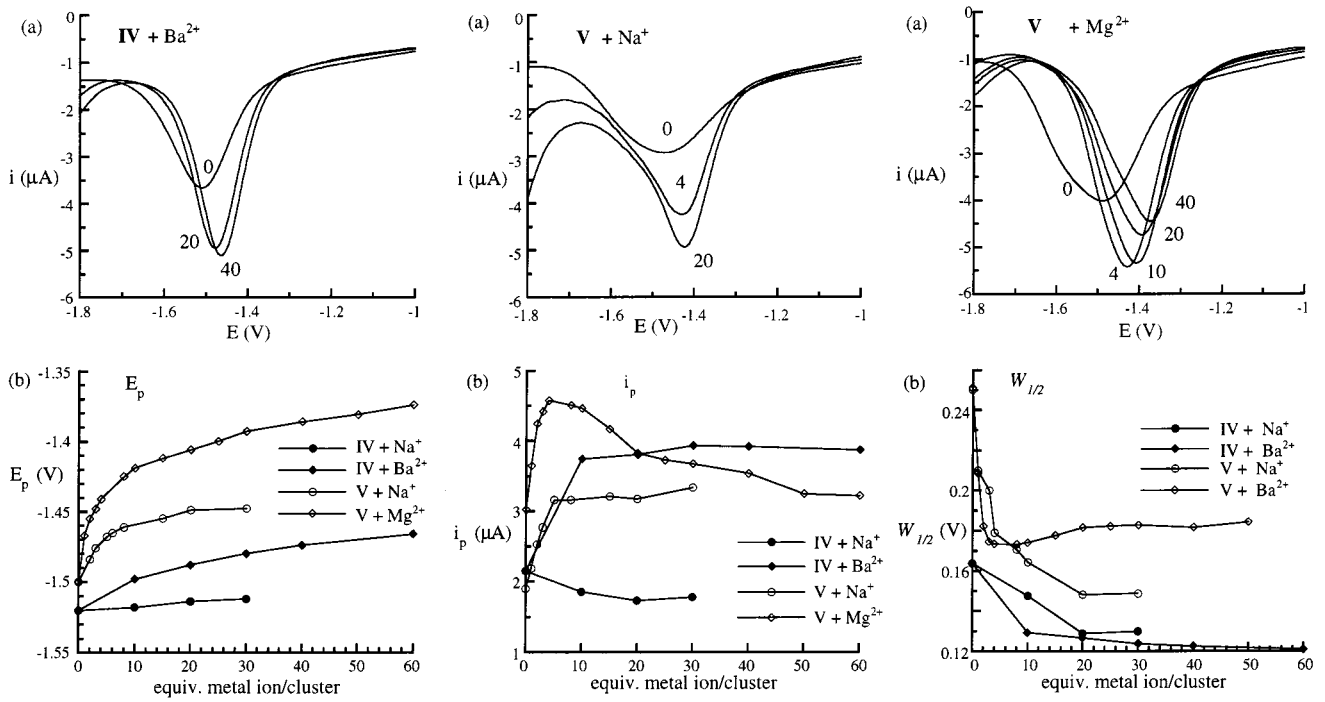


Figure 3. (a) DPV titrations of compound **IV** with Ba^{2+} ions, and compound **V** with Na^+ and Mg^{2+} ions, numbers correspond to the amount of metal ion added; (b) corresponding titration curves (including those for compound **IV** and Na^+) in which E_p, i_p, and $W_{1/2}$ are plotted as a function of the amount of metal ion added

modulator as well. Promoter/modulator effects similar to those observed for proteins have also been observed for semi-encapsulated, synthetic cluster compounds.[20][21]

Overlays of subsequent differential pulse voltammograms in the titration of cluster compounds **IV** with Ba^{2+} ions, and **V** with Na^+ and Mg^{2+} ions are shown in Figure 3a. Figure 3b shows the titration curves in which i_p, and $W_{1/2}$ (and also E_p, see below) are plotted as a function of the amount of metal ion added per cluster. The curves derived from the titration of **IV** with Na^+ ions are also shown. For compound **IV**, a small decrease in current response (i_p) was observed upon the addition of monovalent alkali metal ions. The addition of divalent metal ions clearly resulted in an increase in i_p as well as in the electrochemical reversibility of the redox process (decreased $W_{1/2}$ value). The i_p and $W_{1/2}$ values of **V** improved considerably upon the addition of monovalent as well as divalent metal ions, except in the case of Li^+ for which only minor improvements were observed (not shown).

The fact that divalent metal ions have an influence on the electrochemical properties of **IV** indicates that the overall negative charge of **IV** to some extent hampers a clean redox process. Divalent metal ions are assumed to form a layer of positive charges on a negatively charged electrode, thereby facilitating the reduction of negatively charged species, while monovalent metal ions do not give this effect.[22] This phenomenon can be explained by the larger polarizing strength of the divalent alkaline earth metal ions as compared to the monovalent alkali metal ions.

The addition of metal ions to cluster compound **V**, with the exception of Li^+, resulted in an improvement of the current response and in smaller $W_{1/2}$ values (vide supra). The titration curves in Figure 3b indicate that changes in these parameters are directly related to the amount of metal ion that is added to **V**. These promotion effects were already observed upon addition of less than four equivalents of metal ions per cluster. Binding of more than two monovalent metal ions by **V** converts this compound from an overall negatively to an overall positively charged species, resulting in a more favourable interaction with the negatively charged electrode. This observation is in sharp contrast to the large excess of $Ba(ClO_4)_2$ which is required to promote the electrochemistry of metalloproteins and the earlier mentioned semi-encapsulated cluster compounds.[19–21] This strongly suggests that specific binding of metal ions in the crown ether rings causes the observed effects. In addition, compound **IV**, having no specific metal ion binding sites, was only affected at metal ion concentrations approaching the millimolar range.

The promoter effects observed for cluster compound **I** were in line with those obtained for **V**, albeit less pronounced (not shown). Apparently, the larger flexibility of the crown ether ligands in **I** as compared to **V** results in a better electrochemical behaviour even without the addition of metal ions.

Changes in the peak potentials of compounds **IV** and **V** vary from 0 for Li^+ to 70 mV for Mg^{2+} after the addition of 10 equivalents of these ions per cluster compound (Table 3). In general, the changes of the E_p of **IV** are very small; a maximum modulation of 20–30 mV for divalent metal ions is observed. This small change may be the result of a weak coordination of the metal ions to the amide function

in the ligand, or may be caused by changes in the electrode surface as pointed out above. At very high metal ion concentration, larger effects were observed with Mg^{2+} and Ba^{2+}, suggesting that either of the two factors became more important in the modulation process.

For compound **V**, the modulation effects are more pronounced than for **IV**. The titration curves in Figure 3b show that the largest effect is achieved after the addition of several equivalents of Na^+. For Ba^{2+}, the major effect is achieved after the addition of approximately 20 equivalents (not shown). After the addition of an excess of modulator, minor additional changes in E_p were observed. These additional changes closely match the effects found for compound **IV** at low modulator concentrations.

In Figure 2a, an overlay of sequential voltammograms for the titration of compound **I** with Ba^{2+} is depicted (vide supra). Figure 4 presents the changes in E_p for this compound upon the addition of Ba^{2+}, Na^+, and K^+ ions. Due to the multi-wave behaviour observed in the Ba^{2+} titration and problems with the deconvolution, the Ba^{2+} curve in Figure 4 deviates from an ideal titration curve. Nevertheless it can be concluded that the effect of Ba^{2+} ions is much larger than the effects of K^+ and Na^+ ions. The addition of very small amounts of both Ba^{2+} and K^+ results in a steep rise in E_p, whereas for Na^+ this is not observed. In accordance with the observations for compound **V**, it is likely that the binding of ions in the crown ether ligands of the cluster contributes most to the observed changes in E_p. The fact that multi-wave behaviour is observed with Ba^{2+}, as well as with Li^+ and Mg^{2+} ions, points to a strong binding of these metal ions by compound **I**.

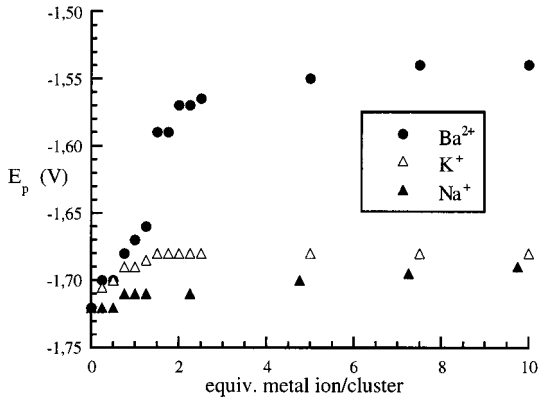


Figure 4. Changes in E_p upon titration of compound **I** with Na^+, K^+, and Ba^{2+} ions

Rationalization of the Modulator Effects

The different changes in E_p upon the addition of stoichiometric amounts of metal ions to cluster compounds **I** and **V** probably arise from the fact that the affinities of the crown ether ligands of the host compounds for the metal ions are different. As was mentioned in the introduction, the binding of metal ions in the monoaza-18-crown-6 ligands of **I** is expected to follow the trend $Li^+ \approx Mg^{2+} < Na^+ < K^+ \approx Ba^{2+}$, which is based on size complementarity. From the point of view of charge stabilization, the divalent metal ions are expected to bind more strongly than the monovalent metal ions.[6] The binding constants for the ligands of **V** were anticipated to be lower than those of the ligands of **I**. The acyl functions on the nitrogen centers in the aza crown ether rings of **V** lead to a host molecule which is a less efficient metal ion binder. This modification could explain the generally smaller changes in E_p found for **V**. However, these rules of thumb do not explain the trends in responses of compounds **I** and **V**.

Figure 5 shows the dependence of the modulation of the E_p of compound **I** on the charge density of the metal ion that causes the modulation. Metal ions bearing a high charge density give rise to a larger change in the reduction potential than metal ions bearing a low charge density. In other words, the higher the polarizing strength of the metal ion, the larger the modulation of the redox properties of the polarizable Fe_4S_4 core in **I**. It is likely therefore that this modulation is governed by electrostatic forces. In this way, metal ions with similar binding constants or ionic radii such as K^+ and Ba^{2+}, but different polarizing effects, bring about different modulations. Similar observations have been made by Hall et al. for their ferrocene based cryptates.[23]

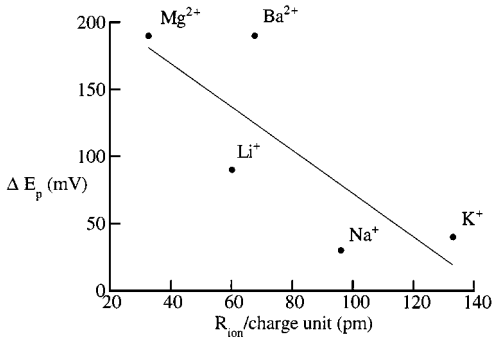


Figure 5. Dependence of the metal ion induced change in $E_{p,red}$ of compound **I** on the charge density of the metal ion

The multi-wave behaviour that is observed for **I** in combination with Ba^{2+}, Li^+, and Mg^{2+} ions, and the magnitude of the modulations, suggests that the binding of these metal ions by **I** is strong. Since the connection between the binding site and redox site in **I** is not conducting, the metal ions should be bound in very close proximity to the redox active center in order to be able to affect the redox potential to the observed extent. It is proposed therefore, that compound **I** binds metal ions in a lariat-ether fashion,[24] with the oxygen and nitrogen atoms of the crown ether ring and the negatively charged thiolate sulfur atom, which coordinates to the cluster, as donor atoms (see Figure 6). In this way the interaction between the binding site and the redox site would be through-bond instead of through-space and the overall negative charge of the cluster compounds would contribute to its interaction with metal ions. Similar lariat

interactions have been proposed before by Gokel et al. in nitrobenzene pivoted crown ethers.[25]

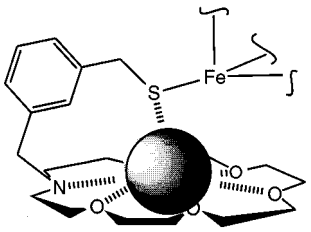
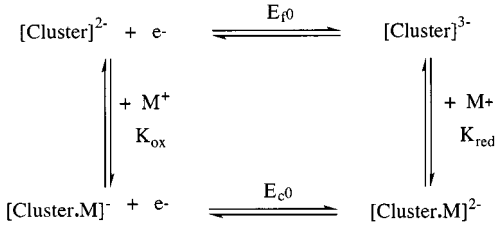


Figure 6. Proposed mode of metal ion binding by compound **I**

Due to conformational restrictions, the host-guest interaction in **V** is not expected to be similar to that of **I**. As in cluster compound **I**, there is no conducting connection between the redox center and the binding site in this compound. An effective impact on the redox potential of the cluster core should, therefore, arise via through-space interactions. The more rigid ligand connection in **V** compared to **I** is likely to result in a less favourable approach of the metal ion to the redox active center, which could explain that, in general, smaller modulation effects and no multiwave behaviour were observed for compound **V**. Combining the values from Table 3 with the curves in Figure 3b, and taking into account the metal ion charge densities, one can conclude that the binding constants in **V** roughly follow the trend $Li^+ < Ba^{2+} < Mg^{2+} < Na^+ < K^+$. In particular, acylation of the aza crown ether rings seems to influence the binding of metal ions with a high charge density in a negative sense. The modulation effects observed for **V** can then be explained by combining the known trend in binding constants with the polarizing strength of the metal ions.

Another way of dealing with the observed modulation effects is presented in Scheme 5, which is taken from earlier papers by Kaifer et al.[26] Starting from a redox-active host compound (an Fe_4S_4 cluster in this case) and an uncomplexed guest, there are two ways to come to a reduced host-guest complex. In one way, the guest is bound by the host compound in the first step, resulting in a facilitated reduction of the redox active center. In the second way, the redox-active center is first reduced, which in turn results in an enhanced binding of the guest.



Scheme 5. Pathways for metal ion complexation in an Fe_4S_4 cluster compound; E_c^0 and E_f^0 are the midpoint potentials for the complex and the free ligand, respectively

For the respective reduction potentials and binding constants Equation 1 can be derived.[26]

$$E_p^{complex} - E_p^{free} = - RT/n\mathrm{F}\ [\ln K_{red}/K_{ox}] \quad (1)$$

In words, the ratio of the binding constants of a guest in the reduced and oxidized host is given by the change in E_p brought about by the binding of the guest. In this model, the modulations that are observed for the cluster compounds reflect the enhanced binding of metal ions by these compounds upon reduction of the cluster core. Comparison of the modulations brought about by the different metal ions will then involve more than just the comparison of binding constants of the oxidized host. Equation 1 has been shown by Kaifer to be valid for systems with $K_{ox} > 10^4$. For systems with $1 < K_{ox} < 10^4$, which is expected to be the range for our compounds, the increase in binding constant is underestimated by this Equation.[26] The results of application of the above-mentioned analysis to the effects found for **I** and **V** are presented in Table 4.

Table 4. Ratio of K_{red} and K_{ox} for binding of different metal ions in compounds **I** and **V**[a]

	I	**V**
Li^+	33 (13)	–
Na^+	3 (1)	7 (3)
K^+	5 (2)	7 (3)
Mg^{2+}	1600 (650)	5 (2)
Ba^{2+}	1600 (650)	2 (1)

[a] Determined after the addition of 4 equivalents of metal ion. Estimated errors are given in parenthesis.

The titration curves presented in Figure 4 indicate that more than 2 and possibly 4 metal ions are bound to the crown ether cluster compounds. From our experiments it could not be determined whether the four binding sites behaved independently from each other, in terms of equal binding constants for every site, or that these sites influenced each other, e.g. by diminishing the binding of every next metal ion. It should be noted that applying Equation 1 might lead to overestimated values in the latter case. The numbers in Table 4 should therefore not be treated as absolute values but merely as representing trends in metal ion affinities of the cluster compounds.

Conclusion

A number of new thiolate-functionalized iron-sulfur cubane clusters **I**–**V** were prepared and characterized. In **I**, **III**, and **V**, the cluster cores are appended with binding sites for metal ions, viz. crown ether ligands. Electrochemical studies show that the large crown ether ligands hamper, to some extent, the electrochemical analysis of the cluster compounds. Only in the case of cluster compound **III** does the presence of the relatively large ligands have a pronounced effect on the $E_{1/2}$ value. Here, the ligands are believed to have a restricted conformational freedom, resulting in a more effective shielding of the cluster core.

Examination of the promotion and modulation effects of metal ions on cluster compounds **I**, **IV**, and **V** reveals that

the largest effects occur in the case of the crown ether functionalized cluster compounds **I** and **V**. Addition of stoichiometric amounts of metal ions leads to large changes in the electrochemical characteristics of the cluster reduction, implying that metal ions are bound in the crown ether ligands. Smaller changes arise from electrode modification, which facilitates the reduction of the negatively charged cluster compounds, as was shown for compound **IV**. Reduction of the cluster compounds enhances their affinity for alkali and alkaline earth metal ions. A lariat-binding mode is proposed for the complexation of metal ions to compound **I**, resulting in a more or less through-bond interaction between the redox site and the crown ether bound metal ion. In this way, binding of metal ions by this compound is favoured by the negative charge of its redox center. Such a favourable interaction was ruled out, however, for compound **V** due to restrictions in the conformation of its ligands; probably related to the lack of rotational freedom of the amide bonds. The modulations observed for compound **V** seem to take place via through-space interactions. Overall, the characteristic features of the modulations measured for the novel cluster compounds were shown to be governed by the interplay of crown ether selectivity, ligand flexibility, and electrostatic forces. As a result, the modulations observed for compounds **I** and **V** are in sharp contrast to each other. Whereas **I** shows a strong response towards Ba^{2+} ions and hardly any response towards K^+, compound **V** displays much smaller effects and an opposite selectivity.

The results presented here show that crown ether-functionalized iron-sulfur clusters can serve as electrochemically active host compounds, and can in principle be applied as building blocks for the construction of electrochemical sensory devices which are able to display selective responses towards charged species

Experimental Section

General Procedures: All chemicals were commercial products and were used as received. α-Chloroacetyl chloride was synthesized using a literature procedure.[27] Di-*n*-butylamine and thioacetic acid were distilled under reduced pressure. Diethyl ether was distilled from sodium metal/benzophenone, hexane was distilled from sodium metal, and dichloromethane and chloroform were distilled from $CaCl_2$. Pyridine and triethylamine were distilled from CaH_2. DMF used for electrochemical experiments was stored over BaO for at least one day, after which it was distilled under reduced pressure. Ethyl acetate used for flash chromatography was distilled from K_2CO_3/Na_2CO_3. Hexane used for the same purpose was distilled once using a rotary evaporator. All other solvents were used as received. Manipulations involving thiol compounds were performed under N_2 unless stated otherwise. Glassware used in thiol handling was left overnight in a hypochlorite solution to prevent stench. Manipulations involving iron-sulfur clusters were performed using standard Schlenk techniques. − Flash chromatography was performed on Silica Gel (60 H) purchased from Merck, or on neutral alumina purchased from Across. Prior to use, neutral alumina was activated to activity III, according to the Brockman scale.[28] − TLC analyses were performed on silica 60 F_{254} coated glass plates from Merck. Thiol compounds were detected by treatment of the TLC plates with a nitroprusside reagent.[29] − FT-IR spectra were recorded with a BioRad FTS 25 instrument. − UV/Vis spectra were recorded with a Perkin−Elmer Lambda 5 instrument. − ^{1}H-NMR spectra were recorded with Bruker WF-90, Bruker AC-100, Bruker WM-200, Bruker AC-300, or Bruker AM-400 instruments (internal standards: $CDCl_3$ as solvent TMS, δ_H = 0.00; [D_6]DMSO as solvent, δ_H = 2.50; [D_7]DMF as solvent, δ_H = 2.94). − Mass spectra were obtained from a VG 7070E instrument [FAB$^+$ (3-nitrobenzyl alcohol), EI$^+$]. − Elemental analyses were performed with a Carlo Erba EA 1180 instrument. − Melting points were measured with a Reichert−Jung Hotstage 600 instrument (uncorrected values). − Electrochemical analysis (CV, DPV) were performed with an EG & G Princeton Applied Research Model 273 Electrochemistry System equipped with Model 270 Electrochemical Analysis Software 200. Reference electrodes: Ag/AgCl (0.1 M LiCl) in DMF, Ag/AgI (0.02 M Bu_4NI/0.1 M Bu_4NPF_6) in CH_2Cl_2, and Ag/Ag$^+$ (0.1 M $AgNO_3$) in CH_3CN. Supporting electrolyte: 0.1 M tetrabutylammonium hexafluorophosphate (TBAH). All measurements were performed under an inert gas, using a conventional three-electrode electrochemical cell equipped with either platinum or PGE working and Pt auxiliary electrodes. PGE electrodes were polished with 0.3 μm alumina, rinsed with water, and sonicated in water for 10 min before use. Before every session, the experimental setup was tested using ferrocene and $[Fe_4S_4(S\mathit{t}Bu)_4](NBu_4)_2$. Halfwave and peak potentials are given against the reversible Fc/Fc$^+$ couple. Scan rates were 100 mV/s (CV) and 10 mV/s (DPV) unless stated otherwise. Concentrations of electroactive species were between 0.01 mM and 1 mM.

α-Bromo-α′-thioacetyl-*m*-xylene (1): To a solution of K_2CO_3 (1.05 g, 7.6 mmol) in 4 mL of DMF was slowly added a solution of freshly distilled thioacetic acid (1.14 g, 15 mmol) in 2 mL of DMF. After CO_2 formation had ceased, the resulting yellow solution was diluted with the same amount of DMF. This diluted solution was added dropwise to a solution of α,α′-dibromo-*m*-xylene (4.0 g, 15.2 mmol) in 20 mL of DMF, and the resulting mixture was stirred overnight under the exclusion of light. These manipulations were all performed under N_2. After filtration and removal of the solvent in vacuo, the resulting residue was dissolved in 100 mL of diethyl ether, washed with water (3×), dried with $MgSO_4$, filtered, and concentrated in vacuo. Purification by flash chromatography (silica, ethyl acetate/hexane = 1:10, v/v) yielded 2.1 g (54%) of **1** as a yellow oil. − ^{1}H NMR (90 MHz, $CDCl_3$): δ = 2.36 [s, 3 H, C(O)CH_2], 4.11 (s, 2 H, ArCH_2S), 4.45 (s, 2 H, ArCH_2Br), 7.29 (m, 4 H, Ar*H*). − EI-MS; *m*/*z*: 260 [M]$^+$. − $C_{10}H_{11}BrOS$ (259.2): calcd. C 46.35, H 4.28, S 12.37; found C 46.50, H 4.39, S 11.85.

1-(α-Thioacetyl-*m*-xylyl)-4,7,10,13,16-pentaoxa-1-azacyclooctadecane (2): A solution of **1** (390 mg, 1.51 mmol) in 5 mL of DMF was added dropwise to a solution of 4,7,10,13,16-pentaoxa-1-azacyclooctadecane (400 mg, 1.51 mmol) in 15 mL of DMF which contained some K_2CO_3 as a base. The reaction mixture was stirred overnight at 40°C under N_2, after which the solvent was removed under reduced pressure. The resulting oil was dissolved in 40 mL of dichloromethane, washed twice with a saturated aqueous $NaHCO_3$ solution, dried with $MgSO_4$, filtered, and concentrated in vacuo. Purification by flash chromatography (silica, $CHCl_3$/MeOH/TEA = 97:2:1, v/v) yielded 530 mg (80%) of **2** as a viscous yellow oil. − ^{1}H NMR (90 MHz, $CDCl_3$): δ = 2.36 [s, 3 H, C(O)CH_3], 2.78 (t, *J* = 6.6 Hz, 4 H, NCH_2CH$_2$O), 3.62 (m, 22 H, OCH_2, ArCH_2N), 4.11 (s, 2 H, ArCH_2S), 7.24 (m, 4 H, Ar*H*). − FAB-MS; *m*/*z*: 442 [M + 1]$^+$. − $C_{22}H_{35}NO_6S$ (441.6): C 59.84, H 7.99, N 3.17, S 7.26; found C 59.63, H 8.05, N 3.22, S 7.36.

1-(α-Mercapto-*m*-xylyl)-4,7,10,13,16-pentaoxa-1-azacyclooctadecane (L^{1}H): A solution of **2** (200 mg, 0.45 mmol) in 5 mL of 3%

HCl in methanol was stirred at ambient temperature for 3 d. At this point, TLC analysis showed one spot that was positive in a sodium nitroprusside test. To the reaction mixture were then added 20 mL of dichloromethane and 10 mL of water. The layers were neutralized using a saturated aqueous $NaHCO_3$ solution, after which the organic layer was washed once again with water. After drying with $MgSO_4$, filtration, and removal of the solvent under reduced pressure, 170 mg (95%) of **L^{1}H** was obtained as a yellowish oil. − ^{1}H NMR (90 MHz, $CDCl_3$): δ = 1.75 (t, *J* = 7.3 Hz, 1 H, *SH*), 2.78 (t, *J* = 6.0 Hz, 4 H, N*CH*$_2$CH$_2$O), 3.62 (m, 22 H, O*CH*$_2$, Ar*CH*$_2$N, Ar*CH*$_2$S), 7.24 (m, 4 H, Ar*H*). − $C_{20}H_{33}NO_5S$ (399.5): calcd. C 60.28, H 8.09, N 3.51, S 8.09; found C 60.44, H 8.24, N 3.67, S, 8.18.

(α-Chloroacetyl)di-*n*-butylamine (3): To a solution of di-*n*-butylamine (1.06 g, 7.8 mmol) in CH_2Cl_2 (75 mL) which contained 1.1 mL of triethylamine as a base, was added dropwise a solution of α-chloroacetyl chloride (875 mg, 7.75 mmol) in 25 mL of CH_2Cl_2. The reaction mixture was stirred overnight at ambient temperature and subsequently washed (3×) with a saturated aqueous $NaHCO_3$ solution, and dried with $MgSO_4$. Flash chromatography (silica, $CHCl_3$/MeOH = 98.5:1.5, v/v) gave **3** as a colourless oil in 26% yield. − ^{1}H NMR (90 MHz, $CDCl_3$): δ = 0.82−1.04 (m, 6 H, *CH*$_3$), 1.14−1.70 (m, 8 H, *CH*$_2$*CH*$_2$CH$_3$), 3.20−3.43 (m, 4 H, N*CH*$_2$), 4.07 (s, 2 H, *CH*$_2$Cl). − EI-MS; *m*/*z*: 205 $[M]^+$. − $C_{10}H_{20}ClNO$ (205.7): calcd. C 58.38, H 9.80, N 6.81; found C 57.95, H 10.17, N 6.87.

[α-(Thioacetyl)acetyl]di-*n*-butylamine (4): Under N_2, 299 mg (2.15 mmol) of K_2CO_3 was allowed to react with 155 μL of thioacetic acid in a minimum amount of DMF. The resulting solution was added dropwise to a solution of **3** (446 mg, 2.16 mmol) in DMF, and this mixture was stirred overnight under the exclusion of light. After removal of the solvent under reduced pressure, the residue was dissolved in CH_2Cl_2 and washed twice with brine and once with water. The organic layer was dried with $MgSO_4$. Flash chromatography (silica, $CHCl_3$/MeOH = 99:1, v/v) yielded **4** as a yellow oil in 65% yield (345 mg). − ^{1}H NMR (90 MHz, $CDCl_3$): δ = 0.84−1.05 (m, 6 H, CH$_2$CH$_2$*CH*$_3$), 1.19−1.73 (m, 8 H, *CH*$_2$*CH*$_2$CH$_3$), 2.39 [s, 3 H, C(O)*CH*$_3$], 3.22−3.43 (m, 4 H, N*CH*$_2$), 4.37 (s, 2 H, *CH*$_2$S). − FT-IR (KBr, cm^{-1}): $\tilde{\nu}$ = 2959, 2932, 2874 (CH_2, CH_3), 1695 (C=OCH$_3$), 1647 (C=O), 1428, 1377 (CH_2, CH_3), 1355 (C=OCH$_3$), 733 (CH_2). − EI-MS; *m*/*z*: 245 $[M]^+$. − $C_{12}H_{23}NO_2S$·0.5MeOH (260.4): calcd. C 57.44, H 9.64, N 5.36, S 12.26; found C 57.46, H 9.49, N 5.68, S 12.07.

(α-Mercaptoacetyl)di-*n*-butylamine (L^{2}H): To a solution of **4** (130 mg, 0.53 mmol) in 3 mL of CH_2Cl_2 was added 3 mL of 6% HCl in MeOH. The resulting mixture was stirred overnight. At this point, TLC analysis revealed a single spot that turned red when treated with nitroprusside. The reaction mixture was diluted with CH_2Cl_2 and neutralized with saturated aqueous $NaHCO_3$, washed once with water and dried with $MgSO_4$. Removal of the solvent in vacuo yielded 108 mg (100%) of **L^{2}H** as a brownish-yellow oil. − ^{1}H NMR (200 MHz, $CDCl_3$): δ = 0.99−0.89 (m, 6 H, CH$_2$CH$_2$*CH*$_3$), 1.26−1.37 (m, 4 H, CH$_2$*CH*$_2$CH$_3$), 1.49−1.61 (m, 4 H, *CH*$_2$CH$_2$CH$_3$), 2.17 (t, *J* = 7.43 Hz, 1 H, *SH*), 3.20−3.36 (m, 6 H, N*CH*$_2$CH$_2$, CH$_2$S). − FT-IR (KBr, cm^{-1}): $\tilde{\nu}$ = 2958−2863 (CH_2, CH_3), 2554 (SH), 1642 (C=O), 1454, 1430, 1376 (CH_2, CH_2). − EI-MS; *m*/*z*: 203 $[M]^+$. − No reproducible analysis could be obtained for this compound.

1-(α−Chloroacetyl)-4,7,10,13,16-pentaoxa-1-azacyclooctadecane (5): To a solution of 4,7,10,13,16-pentaoxa-1-azacyclooctadecane (300 mg, 1.14 mmol) in 15 mL of toluene, containing some solid K_2CO_3 as a base, a solution of α-chloroacetyl chloride (150 mg, 1.3 mmol) in 2 mL of toluene was added dropwise. The reaction mixture was stirred overnight at ambient temperature, after which the solvent was removed in vacuo. The resulting residue was dissolved in 50 mL of dichloromethane; this solution was washed twice with a saturated aqueous $NaHCO_3$ solution, dried with $MgSO_4$, and filtered. After removal of the solvent under reduced pressure, 350 mg (90%) of **5** was obtained. − ^{1}H NMR (90 MHz, $CDCl_3$): δ = 3.82 (m, 24 H, O*CH*$_2$, N*CH*$_2$), 4.24 (s, 2 H, *CH*$_2$Cl). − FT-IR (KBr, cm^{-1}): $\tilde{\nu}$ = 3003, 2872 (br, CH_2), 1648 (C=O), 1455, 1353 (CH_2), 1121 (COC), 712 (CH_2). − EI-MS; *m*/*z*: 340 $[M]^+$. − $C_{14}H_{26}ClNO_6$ (339.8): calcd. C 49.54, H 7.73, N 4.13; found C 49.45, H 7.84, N 4.09.

1-[α-(Thioacetyl)acetyl]-4,7,10,13,16-pentaoxa-1-azacyclooctadecane (6): To prepare this compound, a similar procedure as described for the synthesis of **4** was used. A DMF solution of potassium thioacetate, prepared from K_2CO_3 (100 mg, 0.72 mmol) and thioacetic acid (100 mg, 1.3 mmol), was added to a DMF solution containing **5** (350 mg, 1.03 mmol). After workup using dichloromethane and flash chromatography (silica, $CHCl_3$/MeOH = 98:2, v/v) compound **6** (250 mg, 61%) was obtained as a viscous, yellow oil. − ^{1}H NMR (300 MHz, $CDCl_3$): δ = 2.38 (s, 3H, *CH*$_3$), 3.50−3.81 (m, 24 H, O*CH*$_2$, N*CH*$_2$), 3.98 (s, 2 H, *CH*$_2$S). − ^{13}C NMR (75 MHz, $CDCl_3$): δ = 30.5 (CH_3), 32.5 (SCH_2), 48.0 (NCH_2), 70.0−71.5 (m, OCH_2), 168.5 (NC=O), 196.0 (SC=O). − FT-IR (KBr, cm^{-1}): $\tilde{\nu}$ = 2867 (br, CH_2, CH_3), 1691 (SC=O), 1656, 1648 (C=O), 1468, 1450 (CH_2, CH_3), 1353 ($COCH_3$), 1120 (COC), 732 (CH_2). − EI-MS; *m*/*z*: 379 $[M]^+$. − No reproducible analysis could be obtained for this compound.

1-(α-Mercaptoacetyl)-4,7,10,13,16-pentaoxa-1-azacyclooctadecane (L^{3}H): This compound was prepared using the procedure described for compound **L^{2}H**. Starting from **6** (100 mg, 0.24 mmol), 77 mg (95%) of ligand **L^{3}H** was isolated. − ^{1}H NMR (300 MHz, $CDCl_3$): δ = 2.17 (t, *J* = 7.52 Hz, 1 H, *SH*), 3.40−3.76 (m, 26 H, O*CH*$_2$, N*CH*$_2$, S*CH*$_2$). − ^{13}C NMR (75 MHz, $CDCl_3$): δ = 27.0 ($HSCH_2$), 47.83 (NCH_2), 70.03−71.78 (m, OCH_2), 171.1 (NC=O). − FT-IR (KBr, cm^{-1}): $\tilde{\nu}$ = 2867 (br, CH_2), 2546 (SH), 1654 (C=O), 1448, 1421 (CH_2), 1119 (br, COC). − EI-MS; *m*/*z*: 338 $[M]^+$. − No reproducible analysis could be obtained for this compound.

2,2′-Dithiobisbenzoic Acid (7):[30] To a solution of thiosalicylic acid (8 g, 51.9 mmol) and NaOH (6.4 g, 160 mmol) in 60 mL of water was added very slowly, by means of a dropping funnel, 25 mL of a solution of 15% H_2O_2 in water. During the addition the reaction mixture was cooled on ice. After the addition was completed the mixture was slowly allowed to come to ambient temperature. Finally, it was stirred overnight at 60°C. The mixture was again cooled on ice, and neutralized with aqueous 2N HCl, which resulted in the formation of a white precipitate. The product was filtered off, washed with cold ethanol and cold water, and dried in vacuo. This procedure yielded 6.3 g (80%) of **7** as a white powder, m.p. 298−299°C. − ^{1}H NMR (90 MHz, [D$_6$]DMSO): δ = 7.39 (m, 2 H, Ar*H*$^{4,4'}$), 7.62 (m, 4 H, Ar*H*$^{5,5'}$, Ar*H*$^{6,6'}$), 8.04 (m, 2H, Ar*H*$^{3,3'}$). − FT-IR (KBr, cm^{-1}): $\tilde{\nu}$ = 3500−2500 (OH), 1673 (C=O), 735 (ArH). − FAB-MS; *m*/*z*: 306 $[M]^+$. − $C_{14}H_{10}O_4S_2$·0.25EtOH (317.8): calcd. C 56.20, H 3.74, S 20.69; found C 56.20, H 3.36, S 20.81.

***N*,*N*,*N*′,*N*′-Tetra-*n*-butyl-2,2′-dithiobisbenzoylamine (9):** A suspension of **7** (410 mg, 1.33 mmol) in 10 mL of $SOCl_2$ was heated under reflux overnight, yielding a clear solution. After removal of the excess of $SOCl_2$ in vacuo, the resulting residue, **8**, was dissolved in 5 mL of dichloromethane. This solution was then added dropwise to a solution of di-*n*-butylamine (387 mg, 3.0 mmol) and of triethylamine (220 μL) in 50 mL of dichloromethane. The reaction mixture

was stirred overnight at ambient temperature, after which it was washed (3×) with a saturated aqueous $NaHCO_3$ solution. The organic layer was dried with $MgSO_4$, filtered, and concentrated. After purification by flash chromatography (alumina, CH_2Cl_2/EtOH = 99:1, v/v) compound **9** (650 mg, 82%) was obtained as a yellowish, viscous oil. − ^{1}H NMR (90 MHz, $CDCl_3$): δ = 0.90 (m, 12 H, $CH_2CH_2CH_3$), 1.50 (m, 16 H, $CH_2CH_2CH_3$), 3.10 (t, *J* = 8.2 Hz, 4 H, NCH_2CH_2), 3.52 (t, *J* = 7.4 Hz, 4 H, NCH_2CH_2), 7.24 (m, 6 H, Ar*H*$^{4,4'}$, Ar*H*$^{5,5'}$, Ar*H*$^{6,6'}$), 7.67 (m, 2 H, Ar*H*$^{3,3'}$). − FAB-MS; *m*/*z*: 529 $[M + H]^+$. − No reproducible analysis could be obtained for this compound.

***N*,*N*-Di-*n*-butyl-2-mercaptobenzoylamine (L^4H):** A solution of **9** (528 mg, 1.0 mmol) and triphenylphosphane (263 mg, 1.0 mmol) in a mixture of aqueous 37% HCl (2.5 mL), water (7.5 mL), and dioxane (40 mL) was stirred overnight at 40 °C. The organic solvent was removed under reduced pressure and 100 mL of dichloromethane was added to the residue. The organic layer was washed (3×) with a saturated aqueous $NaHCO_3$ solution, dried with $MgSO_4$, filtered, and concentrated. Purification by means of flash chromatography (alumina, CH_2Cl_2/EtOH = 99:1, v/v) yielded 420 mg (80%) of L^4H as a viscous oil. − ^{1}H NMR (90 MHz, $CDCl_3$): δ = 0.90 (m, 6 H, $CH_2CH_2CH_3$), 1.50 (m, 8 H, $CH_2CH_2CH_3$), 3.10 (t, *J* = 8.0 Hz, 2 H, NCH_2CH_2), 3.52 (t, *J* = 8.0 Hz, 2 H, NCH_2CH_2), 4.74 (s, 1 H, *SH*), 7.25 (m, 4 H, Ar*H*). − FT-IR (KBr, cm^{-1}): $\tilde{\nu}$ = 3055 (Ar), 2958, 2932, 2872 (CH_2, CH_3), 2519 (SH), 1628 (C=O), 1462, 1425, 1377 (CH_2, CH_3), 773, 747 (ArH). − EI-MS; *m*/*z*: 265 $[M]^+$. − $C_{15}H_{23}NOS{\cdot}0.5EtOH$ (288.4): calcd. C 66.62, H 9.09, N 4.86, S 11.11; found C 66.71, H 8.64, N 5.31, S 11.01.

***N*,*N*′-(2,2′-Dithiobenzoyl)bis(4,7,10,13,16-pentaoxa-1-azacyclooctadecane) (10):** To prepare this compound, a similar procedure as described for **9** was used. Starting from 4,7,10,13,16-pentaoxa-1-azacyclooctadecane (395 mg, 1.5 mmol), 478 mg (80%) of **10** was obtained as a yellowish, viscous oil after flash chromatography (alumina, CH_2Cl_2/EtOH = 95:5, v/v). − ^{1}H NMR (90 MHz, $CDCl_3$): δ = 3.71 (m, 24 H, OCH_2, NCH_2), 7.39 (m, 2 H, Ar*H*$^{4,4'}$), 7.62 (m, 4 H, Ar*H*$^{5,5'}$, Ar*H*$^{6,6'}$), 8.04 (m, 2 H, Ar*H*$^{3,3'}$). − FAB-MS; *m*/*z*: 835 $[M + K]^+$, 819 $[M + Na]^+$, 797 $[M + H]^+$. − $C_{38}H_{56}N_2O_{12}S_2{\cdot}0.5EtOH$ (831.2): calcd. C 56.81, H 7.31, N 3.44, S 7.88; found C 57.14, H 7.04, N 3.71, S 7.55.

2-Mercaptobenzoyl-4,7,10,13,16-pentaoxa-1-azacyclooctadecane (L^5H): This compound was prepared in a similar way as ligand L^4H. Starting from **10** (200 mg, 0.25 mmol) and triphenylphosphane (66 mg, 0.25 mmol), compound L^5H was obtained in 75% yield (150 mg) after flash chromatography (alumina, CH_2Cl_2/EtOH = 95:5, v/v). − ^{1}H NMR (90 MHz, $CDCl_3$): δ = 3.50−3.63 (m, 24 H, OCH_2, NCH_2), 3.86 (s, 1 H, *SH*), 7.25 (m, 4 H, Ar*H*). − EI-MS; *m*/*z*: 399 $[M]^+$. − No reproducible analysis could be obtained for this compound.

Synthesis of Cluster Compounds: In situ synthesis of cluster compounds **I**−**V** for initial electrochemical characterization was performed by the stepwise addition of 4−6 equivalents of thiol ligand and 4−6 equivalents of base to the appropriate amount of $(PPh_4)_2[Fe_4S_4Cl_4]$ in DMF. A stock solution of 0.081 M of $[Bu_4N]OH$ in methanol was used as the base. Differential pulse voltammograms were recorded after the addition of each equivalent ligand and base, and after equilibration. Typically, 1.8 mg (1.54 μmol) of $(PPh_4)_4[Fe_4S_4Cl_4]$ was used in these experiments. Quantitative synthesis of the cluster compounds for detailed characterization was performed by using either the chloro cluster reaction starting from $(PPh_4)_2[Fe_4S_4Cl_4]$, or the ligand exchange reaction starting from $(Bu_4N)_2[Fe_4S_4(StBu)_4]$. The starting materials, $(PPh_4)_2[Fe_4S_4Cl_4]$[31] and $(Bu_4N)_2[Fe_4S_4(StBu)_4]$[32] were synthesized using published methods.

$(Bu_4N)_2[Fe_4S_4(L^1)_4]$ (I): To a stirred solution of $(PPh_4)_2[Fe_4S_4Cl_4]$ (38.2 mg, 0.033 mmol) in 15 mL of DMF was added a solution of L^1H (65 mg, 0.163 mmol, 5 equiv.) in 5 mL DMF. After this addition was completed, 2 mL of 0.081 M $[Bu_4N]OH$ in methanol was added dropwise to the reaction mixture. After stirring for several hours, the reaction mixture was filtered and then concentrated in vacuo, followed by the addition of Et_2O to induce precipitation of the desired product. Storage at −20 °C overnight resulted in the formation of the tetrabutylammonium salt **I**, which was isolated as a black oil after decanting the supernatant and drying in vacuo (yield not determined). − ^{1}H NMR (90 MHz, $[D_6]$DMSO): δ = 0.81−1.10 [m, br., 24 H, CH_3 (NBu_4)], 1.19−1.81 [m, br., 32 H, $CH_2CH_2CH_3$ (NBu_4)], 2.68 (NCH_2, the structure of this peak is obscured by the solvent peak), 3.02−3.36 [m, 16 H, NCH_2 (NBu_4)], 3.36−3.75 (m, 104 H, OCH_2, NCH_2, NCH_2Ar), 7.20 [m, br., 4 H, Ar*H*], 7.49−7.90 (m, 12 H, Ar*H*), 15.08 [ds, br, 8 H, SCH_2]. − UV/Vis (DMF): λ_{max} (nm) = 300 (sh), 420.

$(Bu_4N)_2[Fe_4S_4(L^2)_4]$ (II): To a solution of the thiol ligand L^2H (55 mg, 0.27 mmol) in 5 mL of DMF was added dropwise a solution/suspension of $(Bu_4N)_2[Fe_4S_4(StBu)_4]$ (54.6 mg, 0.056 mmol) in 10 mL of DMF. The resulting black solution was stirred for several hours under dynamic vacuum, and overnight under N_2. After filtration, the volume was reduced in vacuo to about 1 mL and a large amount of Et_2O was added. The Schlenk vessel was placed at −20 °C overnight, which resulted in the precipitation of a black powder. The product was finally isolated by decantation of the supernatant, washing with Et_2O, and drying under vacuum. This procedure gave **II** as a black oil in 91% yield (84 mg). − ^{1}H NMR (200 MHz, $[D_6]$DMSO): δ = 0.87−0.97 (m, 48 H, CH_3), 1.29−1.56 (m, 64 H, CH_2CH_3, NCH_2CH_2), 3.18−3.33 (m, 32 H, NCH_2), 13.83 [s, br, 8 H, SCH_2]. − UV/Vis (DMF): λ_{max} (nm) = 301, 415, 620 (sh).

$(Bu_4N)_2[Fe_4S_4(L^3)_4]$ (III): This compound was prepared using the procedure described for compound **II**. Starting from L^3H (98.4 mg, 0.29 mmol, 5 equiv.) and $(Bu_4N)_2[Fe_4S_4(StBu)_4]$ (69.6 mg, 0.058 mmol), a black oil was obtained. The yield was not determined. − ^{1}H NMR (200 MHz, $[D_7]$DMF): δ = 1.05 [s, br, 24 H, CH_3 (NBu_4)], 1.49 [s, br, 16 H, CH_2CH_3 (NBu_4)], 1.85 [s, br, 16 H, NCH_2CH_2 (NBu_4)], 3.40−4.13 [m, 112 H, OCH_2, NCH_2, NCH_2 (NBu_4)], 15.35, 16.58 [d, br, 8 H, SCH_2]. − UV/Vis (DMF): λ_{max} (nm) = 300, 410, 660 (sh).

$(Bu_4N)_2[Fe_4S_4(L^4)_4]$ (IV): This compound was prepared using the procedure described for compound **II**, using L^4H (18.5 mg, 0.7 mmol, 5.8 equiv.) and $(Bu_4N)_2[Fe_4S_4(StBu)_4]$ (14.3 mg, 0.12 mmol). THF was used as the nonsolvent in the isolation of the black oil, **IV** (yield was not determined). Inspection of the ^{1}H-NMR spectrum showed that this compound was contaminated with some free ligand L^4H. − ^{1}H NMR (200 MHz, $[D_6]$DMSO): δ = 0.64−1.57 (m, 112 H, $CH_2CH_2CH_3$), 2.95−3.45 [m, 32 H, NCH_2, NCH_2 (NBu_4)], 3.73 [s, br, 4 H, *p*Ar*H*], 5.32 [s, br., 4 H, *o*Ar*H*], 7.97 [s, br., 4 H, *m*Ar*H*], 8.28 [s, br, 4 H, *m*Ar*H*]. − UV/Vis (DMF): λ_{max} (nm) = 307 (sh), 458.

$(Bu_4N)_2[Fe_4S_4(L^5)_4]$ (V): This compound was prepared using the procedure described for compound **II**. Amounts used were: 32 mg (0.08 mmol, 6.3 equiv.) of L^5H and 15.18 mg (0.013 mmol) of $(Bu_4N)_2[Fe_4S_4(StBu)_4]$. The yield of the black oil, **V**, was not determined. − ^{1}H NMR (90 MHz, $[D_6]$DMSO): δ = 0.79−1.09 [m, 24 H, CH_3 (NBu_4)], 1.09−1.78 [m, 32 H, $CH_2CH_2CH_3$ (NBu_4)], 3.01−3.94 [m, 114 H, NCH_2, OCH_2, *p*Ar*H*, NCH_2 (NBu_4)], 5.29

[s, br, 4 H, *o*Ar*H*], 7.96 [s, br, 4 H, *m*Ar*H*], 8.39 [s, br, 4 H, *m*Ar*H*]. – UV/Vis (DMF): λ_{max} (nm) = 307 (sh), 452.

Acknowledgments

This work was supported by the Dutch Foundation for Chemical Research (SON) with financial aid from the Dutch Foundation for Scientific Research (NWO). The authors would like to thank Dr. J. G. M. van der Linden for fruitful discussions and Mrs. A. M. Roelofsen for help with electrochemical experiments. In addition, R. Fokkens of the Institute for Mass Spectrometry at the University of Amsterdam is acknowledged.

[1] [1a] R. Cammack, *Adv. Inorg. Chem.* **1992**, *38*, 281–322. – [1b] H. Beinert, R. H. Holm, E. Münck, *Science* **1997**, *277*, 653–659.
[2] Only recently was evidence provided for an all-ferrous Fe_4S_4 cluster in biology, viz. in the Fe protein of *Azotobacter vinelandii* nitrogenase. The structure of this cluster has not been determined yet. See: [2a] H. C. Angove, S. J. Yoo, B. K. Burgess, E. Münck, *J. Am. Chem. Soc.* **1997**, *119*, 8730–8731. – [2b] K. B. Musgrave, H. C. Angove, B. K. Burgess, B. Hedman, K. O. Hodgson, *J. Am. Chem. Soc.* **1998**, *120*, 5325–5326.
[3] R. H. Holm, S. Ciurli, J. A. Weigel, *Prog. Inorg. Chem.* **1990**, *38*, 1–74.
[4] J. M. Berg, R. H. Holm in *Iron Sulfur Clusters* (Ed.: T. G. Spiro), J. Wiley & Sons, New York, **1983**, pp. 1–66.
[5] P. D. Beer, *Adv. Inorg. Chem.* **1992**, *39*, 79–157.
[6] [6a] R. M. Izatt, K. Pawlak, J. S. Bradshaw, R. L. Bruening, *Chem. Rev.* **1991**, *91*, 1721–2085. – [6b] R. M. Izatt, J. S. Bradshaw, S. A. Nielsen, J. D. Lamb, J. J. Christensen, D. Sen, *Chem. Rev.* **1985**, *85*, 271–339.
[7] B. Strijtveen, R. M. Kellogg, *J. Org. Chem.* **1986**, *51*, 3664–3671.
[8] H. Okuno, K. Uoto, T. Tomohiro, Y. Youinou, *J. Chem. Soc., Dalton Trans.* **1990**, 3375–3381.
[9] L. Overman, S. Smoot, J. D. Overman, *Synthesis* **1974**, 59–60.
[10] L. Que, Jr., M. A. Bobrik, J. A. Ibers, R. H. Holm, *J. Am. Chem. Soc.* **1974**, *96*, 4168–4177.
[11] Kinetic studies on this type of exchange reaction have been performed by Henderson et al. They showed that in the absence of acid a thiolate ligand first dissociates from the cluster, leaving one iron center with a vacant coordination site, followed by nucleophilic attack at this center of a second thiolate. In the presence of acid, the dissociation of the first thiolate is facilitated by protonation. See: R. A. Henderson, K. E. Oglieve, *J. Chem. Soc., Dalton Trans.* **1993**, 1467–1472.
[12] B. V. DePamphilis, B. A. Averill, T. Herskovitz, L. Que, Jr., R. H. Holm, *J. Am. Chem. Soc.* **1974**, *96*, 4159–4167.
[13] See for example: S. Ciurli, M. Carrié, J. A. Weigel, M. J. Carney, T. D. P. Stack, G. C. Papaefthymiou, R. H. Holm, *J. Am. Chem. Soc.* **1990**, *112*, 2654–2664.
[14] R. H. Holm, W. D. Philips, B. A. Averill, J. J. Mayerle, T. Herskowitz *J. Am. Chem. Soc.* **1974**, *96*, 2109–2117.
[15] J. G. Reynolds, E. J. Laskowski, R. H. Holm, *J. Am. Chem. Soc.* **1978**, *100*, 5315–5322.
[16] See for example: I. Bertini, F. Briganti, C. Luchinat, A. Scozzafava, M. Sola, *J. Am. Chem. Soc.* **1991**, *113*, 1237–1245.
[17] See: A. Nakamura, N. Ueyama, *Adv. Inorg. Chem.* **1989**, *33*, 39–67, and references cited therein.
[18] H. L. Blonk, Ph. D. Dissertation, Univ. of Nijmegen, **1991**.
[19] [19a] A. M. Bond, H. A. O. Hill in *Metal Ions in Biological Systems*, vol. 27 (Ed.: H. Siegel, A. Siegel), Marcel Dekker, Inc., New York, **1991**, p. 432–494. – [19b] F. A. Armstrong, H. A. Heering, J. Hirst, *Chem. Soc. Rev.* **1997**, *26*, 169–179.
[20] [20a] C. F. Martens, M. M. G. Bongers, P. J. A. Kenis, R. Czajka, M. C. Feiters, J. G. M. van der Linden, R. J. M. Nolte, *Chem. Ber./Recueil* **1997**, *130*, 23–33. – [20b] C. F. Martens, H. L. Blonk, T. Bongers, J. G. M. van der Linden, G. Beurskens, P. T. Beurskens, J. M. M. Smits, R. J. M. Nolte, *J. Chem. Soc., Chem. Commun.* **1991**, 1623–1625.
[21] [21a] G. P. F. van Strijdonck, J. A. E. H. van Haare, P. J. M. Hönen, R. C. G. M. van der Schoor, M. C. Feiters, J. G. M. van der Linden, J. J. Steggerda, R. J. M. Nolte *J. Chem. Soc., Dalton Trans.* **1997**, 449–461. – [21b] G. P. F. van Strijdonck, J. A. E. H. van Haare, J. G. M. van der Linden, J. J. Steggerda, R. J. M. Nolte, *Inorg. Chem.* **1994**, *33*, 999–1000.
[22] F. A. Armstrong, P. A. Cox, H. A. O. Hill, V. J. Lowe, B. N. Oliver, *J. Electroanal. Chem.* **1987**, *217*, 331–366.
[23] C. D. Hall, N. W. Sharpe, I. P. Danks, Y. P. Sang, *J. Chem. Soc., Chem. Commun*. **1989**, 419–421.
[24] For a review on lariat ethers, see: G. W. Gokel, *Chem. Soc. Rev.* **1992**, 41–47.
[25] A. E. Kaifer, D. A. Gustowski, L. Echegoyen, V. J. Gatto, R. A. Schultz, T. P. Cleary, C. R. Morgan, D. M. Golli, A. M. Rios, G. W. Gokel, *J. Am. Chem. Soc.* **1985**, *107*, 1958–1965.
[26] S. R. Miller, D. A. Gustowski, Z. Chen, G. W. Gokel, L. Echegoyen, A. E. Kaifer, *Anal. Chem.* **1988**, *60*, 2021–2024.
[27] R. Adams, L. H. Ulich, *J. Am. Chem. Soc.* **1920**, *42*, 599–611.
[28] H. Brockman, H. Schodder, *Ber. Dtsch. Chem. Ges.* **1941**, *74B*, 73–78.
[29] G. Tonnies, J. J. Kolb, *Anal. Chem.* **1951**, *23*, 823–826.
[30] Although this compound is commercially available, its purity was not sufficient for our purposes.
[31] G. Christou, C. D. Garner, *J. Chem. Soc., Dalton Trans.* **1979**, 1093–1094.
[32] G. B. Wong, M. A. Bobrik, R. H. Holm, *Inorg. Chem.* **1978**, *17*, 578–584.

Received March 11, 1999
[I99094]

$[Hg_7As_4I_3](SnI_3)$: Trapping the SnI_3^{1-} Anion in the Cavities of the Unprecedented Mercury-Arsenic-Iodine Network

Andrei V. Olenev,[a] Alexei I. Baranov,[b] Andrei V. Shevelkov,*[a] and Boris A. Popovkin[a]

Keywords: Host–guest compounds / Tin / Mercury / Pnictide halides

A novel host–guest compound $[Hg_7As_4I_3](SnI_3)$ has been prepared by a standard ampoule technique and its crystal structure was determined. It crystallizes in a cubic system [space group $P2_13$, a = 13.110(1) Å, Z = 4] with a unique structure type. The crystal structure comprises two parts: the three-dimensional $[Hg_7As_4I_3]^{1+}$ host network, and the SnI_3^{1-} guest anions encapsulated in the cavities of the network. The network is built from the As_2Hg_7 bitetrahedra and As_2Hg_6 octahedra, which share corners, and contains an additional iodine atom connected to one of the mercury vertices. The SnI_3^{1-} anion has the shape of a pyramid with the tin atom in a vertex. According to the quantum-chemistry calculations, the geometry of the anion deviates substantially from the equilibrium one, and is influenced by the distant mercury atoms of the host network.

Introduction

The rapidly developing field of inorganic supramolecular chemistry covers a large diversity of compounds, and classes of compounds, the important feature of which is a weak interaction between host and guest units.[1] In most cases, electrically neutral hosts and guests constitute supramolecular compounds, and their interaction is normally limited to van der Waals forces. However, in compounds where hosts and guests are electrically charged, weak electrostatic host−guest interaction is expected. The "weakness" of such an interaction is sometimes illustrated by the positional and/or rotational disorder of small guest anions encapsulated in host structures, but perfectly ordered structures are not rare cases.[2]

A number of inorganic supramolecular compounds containing linearly coordinated mercury in the host substructures has been reported in the literature.[3−10] Apart from $2HgS{\cdot}SnBr_2$,[3] a unique one-dimensional host−guest compound, all mercury-based supramolecular compounds comprise charged guests and hosts. Hg_2VO_4 is the exception and contains the Hg_2^{2+} cations in the host network.[4] In all other compounds, hosts are three-dimensional cationic networks, based on divalent mercury atoms linearly coordinated by Group-15 elements. Two principal types of networks can be distinguished in these compounds according to the dimension of the voids. Channels are the characteristic feature of the Millon′s base salts[5][6] and their phosphorus and arsenic analogs,[7][8] while closed cavities form in highly symmetric mercury pnictide halides, such as $[Hg_6As_4](HgCl_6)Hg_{0.4}$ and related cases.[9][10] Different types of positional disorder of guest anions are frequently observed in both types of compounds, indicating the weakness of the host−guest interaction.[5,8−10]

The structure of host networks and the size of the voids are primarily controlled by the nature and coordination demands of the elements composing the network. In all mercury/pnicogen networks, linearly coordinated mercury atoms alternate with tetrahedrally coordinated pnicogen atoms. Pnicogens, other than nitrogen, adopt a tetrahedral coordination in any oxidation state, and at least two of them, −2 and −3, are displayed in supramolecular mercury pnictide halides.[7−10] In the −2 oxidation state, pnicogens form Z_2^{4-} dumbbells, which substantially influence the size of the voids; the greater the number of dumbbells, the smaller the size.[8] Therefore, the size of the voids does not necessarily increase on going from nitrogen to antimony. The second factor that controls the size of the voids is the nature and the size of the guest. The latter can serve as a template, and the network forms around it in the course of the synthesis. In recent work[8] we have shown that decreasing the size of the tetrahedral anion ZnX_4^{2-} from X = I to X = Cl leads to the Hg/As networks with decreasing size of the voids; and the adjustment of the network dimensions to the size of the anions occurs through a formation of the As−As bonds.

In the course of our research, aimed at the preparation of new host−guest compounds based on a mercury−pnicogen framework, we attempted the synthesis of $[Hg_6As_4](SnI_6)Hg$. Taking into account the ease of suppressing the Sn^{II} lone electron pair in the iodine environment,[11] we expected to obtain an ordered analog of a supramolecular compound $[Hg_6As_4](HgCl_6)Hg_{0.4}$.[10] The latter possesses a 3D cationic network, $[Hg_6As_4]^{4+}$, with voids of different sizes. The larger cavities are filled with regular octahedral anions $(HgCl_6)^{4-}$, while the smaller cavities are partially (40%) filled by zero-valent mercury atoms. Surprisingly, another new compound, $[Hg_7As_4I_3](SnI_3)$, having a unique crystal structure, but the same overall composition as the target phase, was obtained. In this article we report

[a] Inorganic Synthesis Laboratory, Department of Chemistry, Moscow State University,
Leninskie Gory, Moscow 119899, Russia
Fax: (internat.) + 7-095/939-4788
E-mail: shev@inorg.chem.msu.ru
[b] High School for Material Sciences, Moscow State University

 © WILEY-VCH Verlag GmbH, D-69451 Weinheim, 2000 1434−1948/00/0202−265 $ 17.50+.50/0

the synthesis and crystal structure of a novel supramolecular compound $[Hg_7As_4I_3](SnI_3)$. The influence of the charged host network on the geometry of the guest $(SnI_3)^{1-}$ anion is analyzed based on the quantum-chemistry ab initio calculations.

Results and Discussion

Synthesis and X-ray Study

$[Hg_7As_4I_3](SnI_3)$ was obtained from a stoichiometric mixture of mercury, arsenic, tin, and mercury diiodide by a standard two-step ampoule synthesis at 670 K over 10 d. The almost single-phase product appears as a black polycrystalline, air-stable bulk sample, dark-brown after fine grinding. After accounting for the weak admixture reflections, an X-ray pattern taken from the sample was indexed in a primitive cubic cell with a unit cell edge $a = 13.1117(6)$ Å (Guinier data). Single crystals suitable for the structure determination were prepared by annealing the starting materials mixed in a 2:2:1:2 ratio at 670 K for 1 week in a sealed silica ampoule. The crystal structure was refined based on single-crystal X-ray data (Table 1). The refinement confirms both crystal system and composition.

Table 1. Data collection and structure refinement parameters for $[Hg_7As_4I_3](SnI_3)$

Empirical formula	$As_4Hg_7I_6Sn$
Space group	$P2_13$ (No. 198)
Cell parameter a [Å]	13.110(1)
V [Å^3]	2253.2(3)
Z	4
Density (calcd.) [g cm^{-3}]	7.617
μ [1/mm]	62.624
Crystal size [mm]	0.25 × 0.10 × 0.05
Radiation, λ [Å]	Mo-K_α, 0.71069
Data collection range [°]	$2.20 < \theta < 25.97$
Reflections collected	2715
Independent refl.	1013 ($R_{int} = 0.1444$)
Parameters refined	56
R_1,[a] wR_2[b] [$F_o > 4\sigma(F_o)$]	0.0464, 0.0940
R_1, wR_2 (all data)	0.0668, 0.1020
Largest diff. peak and hole [e/Å^3]	2.208, −2.392
G.o.f. on F^2	1.079

[a] $R1 = \Sigma||F_o| - |F_c||/\Sigma|F_o|$. – [b] $wR_2 = [\Sigma w(F_o^2 - F_c^2)^2/\Sigma w(F_o^2)^2]^{1/2}$, $w = [\sigma^2(F_o^2) + 0.0310\,(F_o^2 + 2F_c^2)/3]^{-1}$.

Description of the Crystal Structure

Atomic positions, equivalent isotropic displacement parameters, and selected bond lengths and valence angles are summarized in Tables 2 and 3. Two parts of the crystal structure of $[Hg_7As_4I_3](SnI_3)$ can be subtracted: a $[Hg_7As_4I_3]^{1+}$ positively charged framework and $(SnI_3)^{1-}$ anions, which are encapsulated in the cavities of the framework (Figure 1). The $(SnI_3)^{1-}$ anion comprised of the unique tin and I(2) atoms has a shape of a trigonal pyramid with the tin atom at the vertex, the Sn−I distances and I−Sn−I angles being 2.95 Å and 90.97°, respectively. Surprisingly, we have not found any data on such an anion in literature, although the analogous $(SnCl_3)^{1-}$ anion with the same shape has been observed in various compounds.[12]

Table 2. Atomic parameters for $[Hg_7As_4I_3](SnI_3)$

Atom	Wykoff	x/a	y/b	z/c	U_{eq}[a] 10^{-4}
Hg(1)	*4a*	0.0342(1)	0.0342(1)	0.0342(1)	25(1)
Hg(2)	*12b*	0.0930(1)	0.0726(1)	0.3143(1)	23(1)
Hg(3)	*12b*	0.5677(1)	−0.0007(1)	0.2488(1)	25(1)
I(1)	*12b*	0.9696(2)	0.2585(2)	0.8181(2)	25(1)
I(2)	*12b*	0.1856(2)	0.0543(2)	0.7889(2)	21(1)
Sn	*4a*	0.7671(2)	0.7671(2)	0.7671(2)	26(1)
As(1)	*4a*	0.9258(2)	0.9258(2)	0.9258(2)	12(1)
As(2)	*4a*	0.1428(2)	0.1428(2)	0.1428(2)	11(1)
As(3)	*4a*	0.4315(2)	0.4315(2)	0.4315(2)	10(1)
As(4)	*4a*	0.5370(2)	0.5370(2)	0.5370(2)	11(1)

[a] U_{eq} is defined as one third of the trace of the orthogonalized U_{ij} tensor.

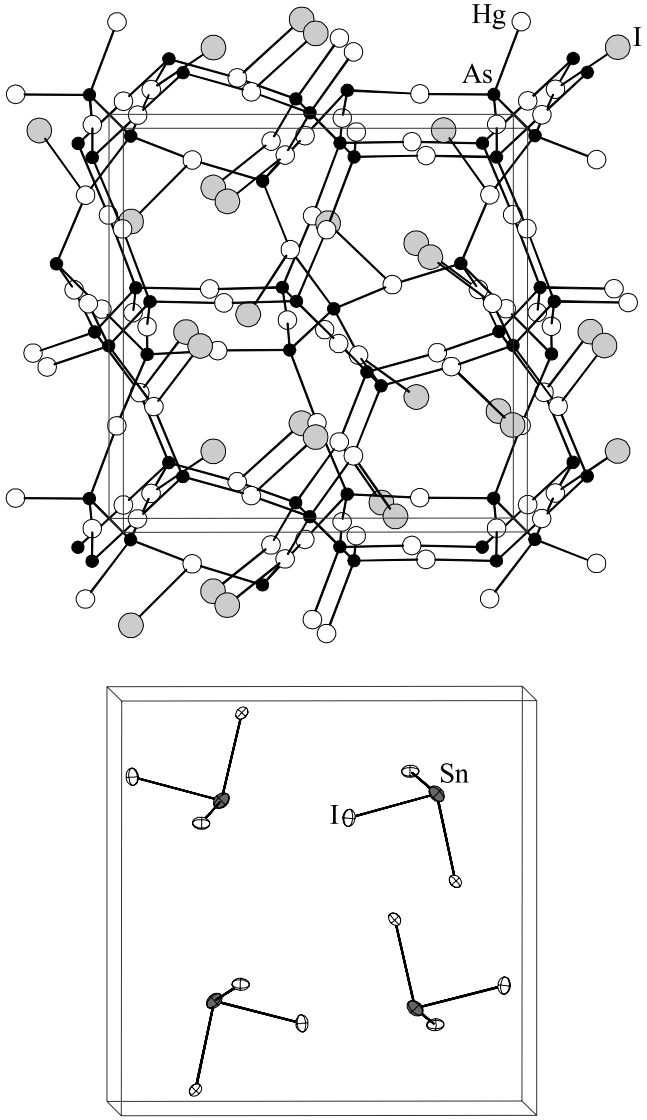


Figure 1. Building units of the crystal structure of $[Hg_7As_4I_3](SnI_3)$; a fragment of the $_\infty{}^3[Hg_7As_4I_3]^{1+}$ framework (top) and a distribution of the $(SnI_3)^{1-}$ within the unit cell (bottom)

The 3D cationic net is built of the arsenic, mercury, and one of two nonequivalent iodine atoms. Three independent mercury atoms have almost the same linear coordination of two arsenic atoms. While the coordination of the Hg(1) atom is regular, the As−Hg−As angle deviates from 180° for the Hg(2) and Hg(3) atoms. Clearly, a rather distant (3.16 Å) iodine neighbor, the I(1) atom, which we consider to belong to the cationic net, causes the departure from linearity in the case of the Hg(2) atom. The Hg−I separation of 3.16 Å is noticeably longer than the covalent interactions in all three forms of HgI_2 (2.62−2.78 Å),[13] but is only slightly longer than the Hg−I distances in various mercury pnictide iodides (3.03−3.14 Å).[14]

Four independent arsenic atoms have a tetrahedral coordination of two different types. The As(1) and As(2) atoms are surrounded by four mercury atoms. These two tetrahedra are connected through the common Hg(1) atom, forming a bitetrahedral As_2Hg_7 unit (Figure 2). The As(3) and As(4) atoms are joined in an As−As dumbbell, and each of them completes its tetrahedral coordination with three mercury atoms. Six mercury atoms thus surround the dumbbell, forming an As_2Hg_6 octahedron (Figure 2). The bitetrahedra and octahedra share vertices to compose the cationic net, the polyhedral presentation of which is drawn in Figure 3. It should be mentioned that the analogous building blocks, the P_2Hg_6 octahedra and P_2Hg_7 bitetrahedra, are found in $Hg_9P_5I_6$,[15] which, however, possesses another type of crystal structure.

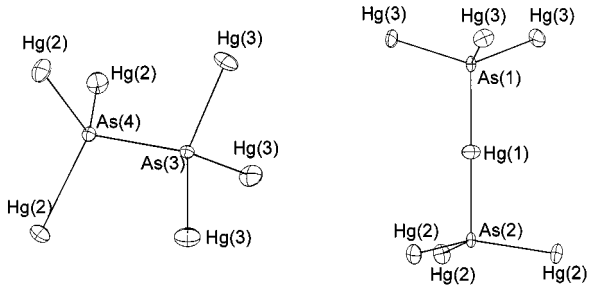


Figure 2. Coordination of the arsenic atoms in $[Hg_7As_4I_3](SnI_3)$ (50% probability ellipsoids)

The As−As separation of 2.40 Å is usual for numerous pnictide halides containing As_2^{4-} anions.[8,10,16,17] It falls in the range of 2.37−2.43 Å, where the shortest and longest distances refer to $Hg_4As_2Br_3$[10] and $Hg_{19}As_{10}Br_{18}$,[17] respectively. The As−Hg distances (2.46−2.53 Å) are also typical for the mercury arsenide halides,[8,10,17] and do not depend much on the formal oxidation state of the arsenic atoms, −3 for As(1) and As(2), and −2 for As(3) and As(4). The absence of the Hg−Hg bonds indicates that the oxidation state +2 can be assigned to the mercury atoms, and hence the crystallographic formula $[(Hg^{2+})_7(As^{3-})_2(As_2^{4-})(I^{1-})_3](SnI_3)^{1-}$ can be derived for the title compound. The formula reflects an unusual composition of the cationic network. To our knowledge, it is the second example of the mercury-based supramolecular compound, which has a halogen atom as a part of the cationic net. A host−guest compound $[Hg_9As_4Br_2](Bi_2Br_{10})$ has been reported[18] to contain two bromine atoms per network formula.

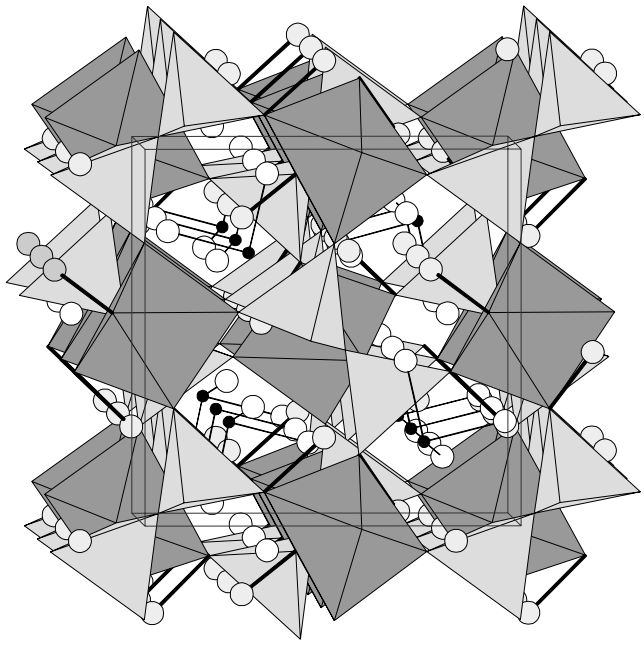


Figure 3. A polyhedral presentation of the crystal structure of $[Hg_7As_4I_3](SnI_3)$; polyhedra: As_2Hg_6 octahedra, dark gray; As_2Hg_7 bitetrahedra, light gray; atoms: tin, filled circles; I(1), shaded circles; I(2), open circles

Theoretical Study of SnI_3^{1-}

The SnI_3^{1-} anion encapsulated in the closed cavities of the three-dimensional network exhibits a geometry well predicted by the Gillespie-Nyholm rules.[19] Qualitatively, one can expect a pseudo-tetrahedral arrangement of three iodine atoms and one lone electron pair around the Sn^{2+} cation in an isolated $(SnI_3)^{1-}$ anion, with I−Sn−I angles being lower than regular tetrahedral ones. The Extended Hückel[20] calculations, performed on the anion having the geometry found from the structure refinement, show (Figure 4) that the $4a_1$ orbital, the HOMO, has the greatest contribution from the tin 5s and $5p_z$ atomic orbitals. These orbitals interact slightly with the iodine 5p orbitals (namely, $5p_z$ orbitals if each iodine atom resides on its local coordinate system with z axis pointing to the tin atom). The resulting orbital, the HOMO, can be considered as a lone electron pair, as visualized in Figure 5.

The anion trapped in the 3D cationic net, however, may feel the influence of the charged net. While the Sn−I(1) separation is rather distant (3.63 Å), the I(2) atom, which belongs to the anion, lies not very far from three mercury atoms, which belong to the cationic framework. The respective distances of 3.36−3.43 Å significantly exceed the sum of the respective covalent radii, but are even shorter than the longest Hg−I separation of 3.51 Å observed in the structure of the yellow modification of HgI_2.[13] Thus, a slight "host−guest" interaction is expected to affect the geometry of the anion under consideration. To obtain the

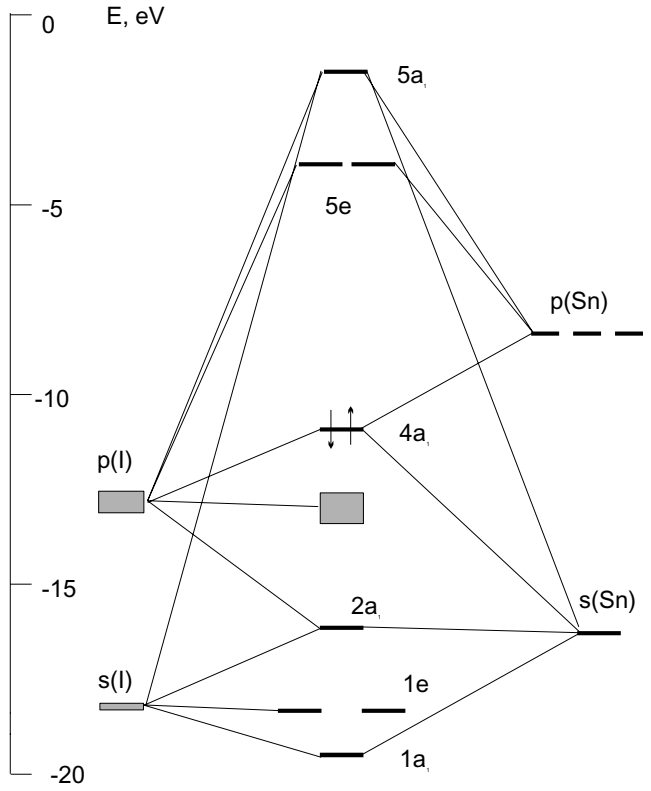


Figure 4. The Extended Hückel molecular orbital diagram for the $(SnI_3)^{1-}$ anion in $[Hg_7As_4I_3](SnI_3)$; mainly nonbonding orbitals in the energy range of −13.3 to −12.5 eV, localized on the iodine atoms, are shown as a dashed box

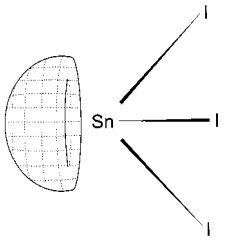
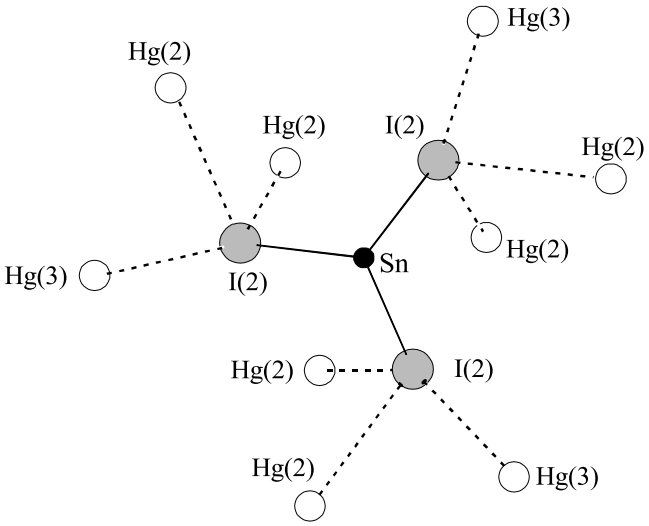


Figure 5. The shape of the $4a_1$ orbital (HOMO) of the isolated $(SnI_3)^{1-}$ anion from the Extended Hückel calculations

equilibrium geometry of $(SnI_3)^{1-}$, quantum-chemistry ab initio RHF calculations[21] were performed. The geometry of the $(SnI_3)^{1-}$ anion was optimized with both Sn−I bond lengths frozen at d(Sn−I) = 2.95 Å (C_{3v} symmetry) and without any constraints (C_{3v} and C_s symmetries). Constraint-free calculations converged at 2.900 Å Sn−I bond length and 99.18° I−Sn−I bond angle. These values deviate significantly from 2.952(3) Å and 90.9(1)° found from the structure refinement. Only marginal geometry differences were encountered between anions optimized in the C_s and C_{3v} point groups. Optimization with the frozen Sn−I bond length resulted in less than 0.2° I−Sn−I angle difference with the fully optimized ion. The results of the calculations can be explained with the help of Figure 6, which shows the arrangement of the distant mercury atoms of the network around the $(SnI_3)^{1-}$ anion. The observed $(SnI_3)^{1-}$ anion exhibits a Sn−I bond length 0.05 Å longer than the equilibrium bond length, and such an elongation indicates a slight bonding interaction of the iodine atoms with the mercury atoms. Evidently, the almost 9° difference in the I−Sn−I bond angle is also caused by the same I−Hg interaction, since the optimization with the Sn−I distance frozen at 2.95 Å gives the same I−Sn−I angle as the full optimization. Therefore, the observed I−Sn−I bond angle value of 90.9° is obviously a result of the "combined influence" (a vector sum) of nine mercury atoms on the anion under consideration.



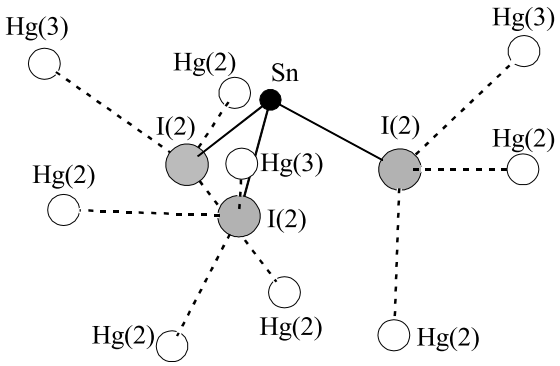


Figure 6. Arrangement of the distant mercury atoms around the $(SnI_3)^{1-}$ anion in the structure of $[Hg_7As_4I_3](SnI_3)$: a) a view along the 3-fold axis; b) a side-view almost along a (011) direction of the unit cell

Conclusions

$[Hg_7As_4I_3](SnI_3)$ is a novel host−guest compound possessing two interesting structural features. Firstly, the cationic network is composed not only of mercury and arsenic, but also iodine atoms. Secondly, the closed cavities are filled with the $(SnI_3)^{1-}$ anions, which have never been observed as guest units in supramolecular compounds. The positions

of the SnI_3^{1-} anions within the unit cell are accurately determined; no sign of positional and/or rotational disorder has been observed during the structure refinement. Together with deviation of the observed anion geometry from that at equilibrium, this indicates the existence of a weak host−guest interaction in the title compound, the nature of which was not investigated in this work. However, such an interaction seems to be very important in the formation of compounds. Evidently, being isolated from each other in the closed cavities of the 3D network, the anions cannot exhibit ion exchange, nor can they enter the well-formed net. The net itself carries a positive charge, and hence cannot exist without anionic guests. Consequently, the title compound can only form spontaneously during the synthesis through a self-assembly process.

Experimental Section

Synthesis: Liquid mercury, gray arsenic, tin powder and mercury diiodide (all > 99.9% purity) were mixed in a 4:4:1:3 molar ratio. The mixture (1 g) was vacuum-sealed in a silica tube and annealed for 10 d at 670 K with intermediate grinding. An X-ray analysis (Guinier FR-552, Nonius) of the product revealed traces of unchanged starting materials, while most reflections belonged to a new phase. The corresponding reflections were indexed in a cubic system with a unit cell parameter a = 13.1117(6) Å. For the single-crystal preparation, the starting materials were mixed in a molar ratio 2:2:1:2 and vacuum-sealed in a silica tube, 60 mm in length and 7 mm inner diameter. The ampoule was placed in a vertical furnace, heated slowly (30°/h) to 670 K and exposed to this temperature for 1 week. After cooling to room temperature at 30°/h, well-formed black crystals were found all over the ampoule. The crystals were separated mechanically, and an X-ray analysis confirmed them to be the desired phase.

Crystal Structure Determination: A suitable single crystal (0.25 × 0.1 × 0.05 mm) was selected from the sample and mounted on a CAD-4 (Nonius) goniometer head for structure investigation. A cubic unit cell parameter a = 13.110(1) Å was refined based on 24 well-centered reflections in the angular range 10.56° < θ < 13.47°. Data were collected at ambient temperature in the ω-2θ scan mode with data collection parameters listed in Table 1. A semi-empirical absorption correction was applied to data based on ψ-scans of 6 reflections having their χ angles close to 90°. Analysis of systematic reflection conditions showed that two space groups $P2_13$ (No. 198) and $P4_232$ (No. 208) were the possibilities. The refinement was successful in the lower symmetry space group $P2_13$. Positions of mercury, tin and iodine atoms were found by direct methods. Arsenic atoms were localized by a sequence of Δρ(xyz) syntheses and least square cycles. The final anisotropic refinement on F^2 led to R_1 = 0.0464 and wR_2 = 0.0939. All calculations were carried out using SHELX97 programs.[22] Further details of the crystal structure determination may be obtained from Fachinformationszentrum Karlsruhe, D-76344 Eggenstein-Leopoldshafen, Germany, on quoting the depository number CSD-410814.

Computational Aspects: Extended Hückel calculations were carried out on the $(SnI_3)^{1-}$ anion, with the geometry found from the crystal structure refinement (Table 3) using CACAO program.[23] Atomic orbital parameters were taken from the literature.[24] Ab initio RHF calculations were performed using GAMESS-US program. SBKJC effective core potentials applied to all atoms and SBKJC basis set[25] implemented in GAMESS were used. Starting geometry of the $(SnI_3)^{1-}$ was taken from the crystal structure refinement. Geometry optimizations were performed by the quasi-Newton algorithm[26] implemented in GAMESS. The followed Hessian computation and normal vibration analysis showed all stationary points located to be minima.

Table 3. Selected interatomic distances and bond angles for $[Hg_7As_4I_3](SnI_3)$

	Distances [Å]
Sn−I(2)	2.952(3) × 3
As(1)−Hg(1)	2.462(6)
As(1)−Hg(3)	2.520(2) × 3
As(2)−Hg(1)	2.466(6)
As(2)−Hg(2)	2.515(2) × 3
As(3)−Hg(3)	2.526(2) × 3
As(4)−Hg(2)	2.530(2) × 3
As(3)−As(4)	2.397(7)
Hg(2)−I(1)	3.160(3)
Hg(3)−I(1)	3.308(3)
Hg(2)−I(2)	3.362(2)
Hg(2)−I(2)	3.431(2)
Hg(3)−I(2)	3.435(2)
	Angles [°]
I(2)−Sn−I(2)	90.87(11) × 3
Hg(1)−As(1)−Hg(3)	106.69(12) × 3
Hg(3)−As(1)−Hg(3)	112.11(11) × 3
Hg(1)−As(2)−Hg(2)	98.91(13) × 3
Hg(2)−As(2)−Hg(2)	117.65(7) × 3
Hg(3)−As(3)−Hg(3)	109.40(12) × 3
Hg(2)−As(4)−Hg(2)	112.26(11) × 3
As(3)−As(4)−Hg(2)	106.51(12) × 3
As(4)−As(3)−Hg(3)	109.54(12) × 3
As(1)−Hg(1)−As(2)	180.0(3)
As(2)−Hg(2)−As(4)	166.29(15)
As(1)−Hg(3)−As(3)	176.84(14)

Acknowledgments

Authors wish to thank Dr. A. N. Kuznetsov for helpful discussion. This work was supported by the state program "Universities of Russia".

[1] A. Müller, H. Reuter, S. Dillinger, *Angew. Chem. Int. Ed. Engl.* **1995**, *34*, 2328; *Angew. Chem.* **1995**, *107*, 2505.
[2] [2a] P. N. W. Baxter, J.-M. Lehn, B. O. Kneisel, G. Baum, D. Fenske, *Chem. Eur. J.* **1999**, *5*, 113. − [2b] P. N. W. Baxter, J.-M. Lehn, G. Baum, D. Fenske, *Chem. Eur. J.* **1999**, *5*, 102. − [2c] W. Schnick, J. Lücke, *Angew. Chem. Int. Ed. Engl.* **1992**, *31*, 213; *Angew. Chem.* **1992**, *104*, 208.
[3] R. Blachnik, K. Lytze, H. Reuter, *J. Solid State Chem*. **1996**, *126*, 95.
[4] A. L. Wessel, W. Jeitschko, *J. Solid State Chem.* **1996**, *125*, 140.
[5] W. Ruedorf, K. Brodersen, *Z. Anorg. Allg. Chem.* **1953**, *274*, 223.
[6] L. Nijssen, W. N. Lipscomb, *Acta Crystallogr.* **1954**, *7*, 103.
[7] A. V. Shevelkov, M. Yu. Mustyakimov, E. V. Dikarev, B. A. Popovkin, *J. Chem. Soc., Dalton Trans.* **1996**, *1*, 147.
[8] A. V. Olenev, A. V. Shevelkov, B. A. Popovkin, *Zh. Neorg. Khim.*, in press.
[9] A. V. Shevelkov, E. V. Dikarev, B. A. Popovkin, *J. Solid State Chem.* **1992**, *98*, 133.
[10] A. V. Shevelkov, E. V. Dikarev, B. A. Popovkin, *J. Solid State Chem.* **1996**, *126*, 324.
[11] [11a] R. A. Howie, W. Moser, I. C. Trevena, *Acta Crystallogr. B.* **1972**, *28*, 2965. − [11b] K. Yamada, S. Funabiki, H. Horimoto,

T. Matsui, T. Okuda, S. Ishiba, *Chem. Lett.* **1991**, 801. – [11c] H. P. Beck, W. Thiel, M. Schuster, *Z. Anorg. Allg. Chem.* **1993**, *619*, 221.
[12] For example, see [12a] $CsSnCl_3$: F. R. Poulsen, S. E. Rasmussen, *Acta Chem. Scand.* **1970**, *24*, 150. – [12b] $[Co(CO)_4]SnCl_3$: P. Klüfers, *Z. Naturforsch. B* **1991**, *46*, 187.
[13] A. F. Wells, *Structural Inorganic Chemistry*, 5th ed., Oxford, Clarendon Press, **1984**, chapter 26.
[14] [14a] P. Labbé, M. Ledésert, B. Raveau, A. Rebbah, *Z. Kristallogr.* **1989**, *187*, 117. – [14b] A. V. Shevelkov, E. V. Dikarev, B. A. Popovkin, *J. Solid State Chem.* **1991**, *93*, 331. – [14c] A. V. Shevelkov, E. V. Dikarev, B. A. Popovkin, *Z. Anorg. Allg. Chem.* **1994**, *620*, 389.
[15] M. Ledésert, A. Rebbah, Ph. Labbé, *Z. Kristallogr.* **1990**, *192*, 223.
[16] A. Rebbah, J. Yazbeck, A. Leclaire, A. Deschanvres, A. Leclaire, A. Deschanvres, *Acta Crystallogr. B* **1980**, *36*, 771.
[17] A. V. Shevelkov, E. V. Dikarev, B. A. Popovkin, *Zh. Neorg. Khim.* **1995**, *40*, 1496; *Chem. Abstr.* **1995**, *123*, 905020e.
[18] H. Puff, M. Grönke, B. Kilger, P. Möltgen, *Z. Anorg. Allg. Chem.* **1984**, *518*, 120.
[19] R. J. Gillespie, I. Hargittai, *The VSEPR Model of Molecular Geometry*, Allyn and Bacon, Boston, **1991**.
[20] J. H. Ammeter, H. B. Bürgi, J. C. Thibeaut, R. Hoffmann, *J. Am. Chem. Soc.* **1978**, *100*, 3686.
[21] M. W. Schmidt, K. K. Baldridge, J. A. Boatz, S. T. Elbert, M. S. Gordon, J. H. Jensen, S. Koseki, N. Matsunaga, K. A. Nguyen, S. J. Su, T. L. Windus, M. Dupuis, J. A. Montgomery, *J. Comput. Chem.* **1993**, *14*, 1347.
[22] [22a] G. M. Sheldrik, *SHELXS-97*, *Program for crystal structure solution*, University of Göttingen, Germany, **1997**. – [22b] G. M. Sheldrik, *SHELXL-97*, *Program for crystal structure refinement*, University of Göttingen, Germany, **1997**.
[23] C. Mealli, D. M. Proserpio, *J. Chem. Educ.* **1990**, *67*, 3399.
[24] P. Pyykkoe, L. L. Lohr, Jr., *Inorg. Chem.* **1981**, *20*, 1950.
[25] [25a] W. J. Stevens, H. Basch, M. Krauss, *J. Chem. Phys.* **1984**, *81*, 6026. – [25b] W. J. Stevens, H. Basch, M. Krauss, P.Jasien, *Can. J. Chem.* **1992**, *70*, 612. – [25c] T. R. Cundari, W. J. Stevens, *J. Chem. Phys.* **1993**, *98*, 5555.
[26] J. Baker, *J. Comput. Chem.* **1986**, *7*, 385.

Received June 6, 1999
[I99214]

Transition Metal Complexes with Sulfur Ligands, 139[+]

Synthesis and Exchange Reactions of Sulfur-Rich Nickel and Palladium [M(L)('S_3')] Complexes ['S_3'$^{2-}$ = Bis(2-mercaptophenyl)sulfide(2–)]

Dieter Sellmann,*[a] Franz Geipel,[a] and Frank W. Heinemann[a]

Dedicated to Professor Egon Uhlig on the occasion of his 70th birthday

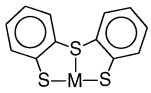
Keywords: Nickel complexes / Palladium complexes / S ligands / Exchange reactions / Azide / Sulfinylimide

In order to obtain suitable precursors for nickel and palladium complexes that model the reactivity of the active sites of hydrogenases and CO dehydrogenases, a series of [M(L)('S_3')] complexes has been synthesized [M = Ni^{II}, Pd^{II}; 'S_3'$^{2-}$ = bis(2-mercaptophenyl)sulfide(2–)]. X-ray structure determinations of [Ni('S_3')]$_3$ (**1**) and [Pd('S_3')]$_3$ (**2**) have revealed that the [M('S_3')] fragments trimerize to give six-membered [MS]$_3$ rings, which exhibit chair conformations with alternating M^{II} centers and thiolate bridging atoms. Reactions of the parent complex [Ni('S_3')]$_3$ (**1**) with nucleophiles L, such as thiolates SR^- (R = *t*Bu, Cy, Me, Ph), phosphanes PR_3 (R = Cy, Ph), chloride, or azide, have been found to yield the corresponding anionic or neutral [Ni(L)('S_3')] complexes, which were isolated as (NBu_4)[Ni(SR)('S_3')] [R = *t*Bu (**3**), Cy (**4**), Me (**5**), Ph (**6**)], [Ni(PR_3)('S_3')] [R = Cy (**7**), Ph (**8**)], (NBu_4)[Ni(Cl)('S_3')] (**9**), and (NBu_4)[Ni(N_3)('S_3')] (**10**). When treated with Me_3SiX, the S*t*Bu$^-$ ligand in (NBu_4)[Ni(S*t*Bu)('S_3')] (**3**) was exchanged to give (NBu_4)[Ni(X)('S_3')] [X = Cl^- (**9**), N_3^- (**10**), NCS^- (**11**), NSO^- (**12**)]. The palladium complex [Pd('S_3')]$_3$ (**2**) could also be cleaved with S*t*Bu$^-$, but the resulting (NBu_4)[Pd(S*t*Bu)('S_3')] (**13**) proved inert towards exchange reactions with Me_3SiX. All the mononuclear complexes have been characterized by standard spectroscopic techniques and by elemental analysis. The molecular structures of **3**, **4**, **6**, **7**, **8**, **9**, and **13** have been determined by X-ray crystallography. The [MS_3L] core geometries of all the complexes are non-planar, exhibiting a considerable tetrahedral distortion.

Introduction

Much of the current interest in nickel thiolate−thioether complexes stems from the discovery that nickel in sulfur-rich coordination spheres forms the active centers of enzymes such as hydrogenases[1] and CO dehydrogenases.[2] In the quest for model compounds of these enzymes, a considerable number of new nickel complexes with different donor sets and geometries has been synthesized.[3,4,5] However, complexes exhibiting structural (Ni−S coordination) and functional (catalysis of enzyme reactions) features of the enzymes have remained extremely rare. Our search for such compounds has recently yielded complexes containing [M('S_3')] fragments (M = Ni, Pt) with the tridentate ligand 'S_3'$^{2-}$ = bis(2-mercaptophenyl)sulfide(2−).[6]

The [M('S_3')] fragments with d^8 electron metal(II) centers were anticipated to have an accessible site for the coordination and activation of substrates. With regard to hydrogenases, dihydrogen and hydride are, of course, the substrates of primary interest. Unfortunately, however, all attempts to coordinate these species to [Ni('S_3')] fragments have to date been unsuccessful,[6] despite the fact that NMR spectroscopic investigations have yielded conclusive evidence for the formation of [Pt(H)('S_3')]$^-$.[6] Further experiments showed that a favored reaction of [M('S_3')] fragments is oligomerization to give either dinuclear [Ni('S_3')]$_2$ or trinuclear [Pt('S_3')]$_3$. These complexes contain thiolate bridges, which block the fourth coordination site at the metal centers. As a consequence, they are extremely sparingly soluble in all common solvents such that homogeneous phase reactions are prevented. The thiolate bridges in [Ni('S_3')]$_2$ or [Pt('S_3')]$_3$ may be cleaved by nucleophiles such as PMe_3 or cyanide. The resulting mononuclear [M(L)('S_3')] derivatives are much more soluble than the parent complexes, but the coligands L proved to be inert.[6] Thus, the aim of the work described herein was to obtain [M(L)('S_3')] species with exchangeable coligands L and thus a readily accessible coordination site.



[+] Part 138: D. Sellmann, D. Häußinger, F. W. Heinemann, *Eur. J. Inorg. Chem.* **1999**, 1715−1725.

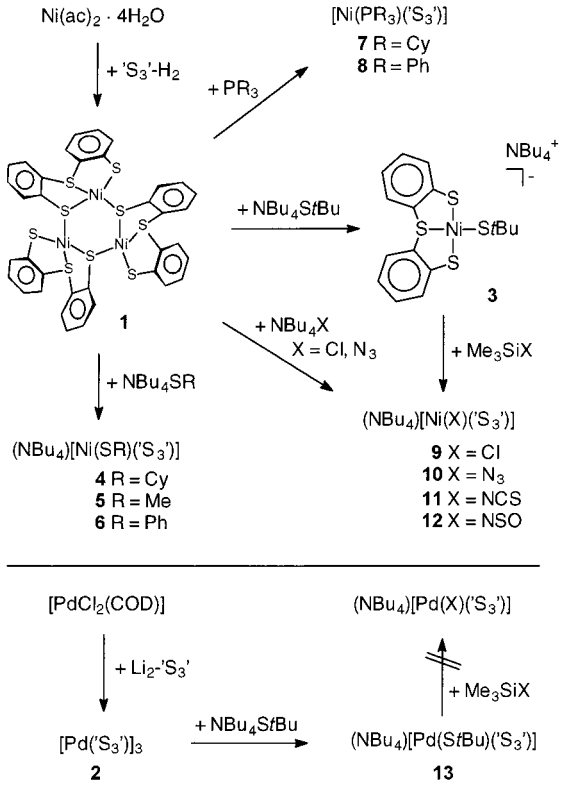
[a] Institut für Anorganische Chemie der Universität Erlangen-Nürnberg,
Egerlandstraße 1, D-91058 Erlangen, Germany
Fax: (internat.) + 49-(0)9131/852-7367
E-mail: sellmann@anorganik.chemie.uni-erlangen.de

 © WILEY-VCH Verlag GmbH, D-69451 Weinheim, 2000 1434−1948/00/0202−271 $ 17.50+.50/0

Results

Cleavage of [Ni('S_3')]$_3$ and Substitution Reactions of [Ni(L)('S_3')] Complexes (L = PR_3, SR^-)

The extremely insoluble [Ni('S_3')]$_2$ parent complex has previously been obtained from $Ni(ac)_2 \cdot 4\,H_2O$ and 'S_3'-H_2.[6] A solvothermal recrystallization from hot DMF (175°C) in a sealed ampoule yielded single crystals, X-ray structure analysis of which showed the product to contain dinuclear [Ni('S_3')]$_2$. On repeating the synthesis, we have now obtained single crystals from the mother liquor of the reaction solution at room temperature. An X-ray structure determination of these crystals revealed that they consisted of the trinuclear [Ni('S_3')]$_3$ (**1**). Complex **1** is structurally analogous to [Pt('S_3')]$_3$ and shows that the crystallization conditions can influence the trimerization vs. dimerization of [Ni('S_3')] fragments. These results prompted us to synthesize [Pd('S_3')]$_3$ (**2**) as well (for the sake of completeness). Complex **2** was obtained from 'S_3'-Li_2 and [$PdCl_2$(COD)] (Scheme 1).



Scheme 1. Synthesis and reactions of [Ni('S_3')] and [Pd('S_3')] complexes

In order to achieve an all-sulfur coordination of the nickel center, we first examined reactions of [Ni('S_3')]$_3$ with thiolates. Both small and sterically demanding thiolates, such as SMe^- and SCy^-, gave essentially the same results. When black-brown THF suspensions of [Ni('S_3')]$_3$ (**1**) were treated with MeOH solutions of the respective NaSR salts at room temperature, dark-brown solutions resulted. Addition of NBu_4OH and subsequent workup yielded the dark-brown to black salts (NBu_4)[Ni(SR)('S_3')] with R = *t*Bu (**3**), Cy (**4**), Me (**5**), and Ph (**6**). These salts were found to be readily soluble in THF, acetone, MeOH, and CH_2Cl_2, but insoluble in Et_2O and *n*-hexane. The molecular structures of (NBu_4)[Ni(S*t*Bu)('S_3')] (**3**), (NBu_4)[Ni(SCy)('S_3')] (**4**), and (NBu_4)[Ni(SPh)('S_3')] (**6**) were determined by X-ray diffraction analysis.

Reactions with the bulky phosphanes PCy_3 and PPh_3 were then investigated in order to probe the lability of the phosphanes and the potential for formation of agostic C−H···Ni interactions in [Ni(PR_3)('S_3')] complexes. The [Ni(PR_3)('S_3')] complexes with R = Cy (**7**), Ph (**8**) were readily formed from THF suspensions of [Ni('S_3')]$_3$ and the respective phosphanes. They were fully characterized but proved as inert to substitution as [Ni(PMe_3)('S_3')]. No agostic C−H···Ni interactions could be detected, neither by X-ray structure determinations nor by ^{1}H-NMR spectra.

Halides and Pseudohalides as Nucleophiles

Initial attempts to cleave [Ni('S_3')]$_3$ with weak nucleophiles such as chloride from NMe_4Cl to give the [Ni(Cl)('S_3')]$^-$ anion invariably proved unsuccessful. However, this anion was readily formed when the S*t*Bu derivative (NBu_4)[Ni(S*t*Bu)('S_3')] (**3**) was treated with Me_3SiCl. The resulting (NBu_4)[Ni(Cl)('S_3')] (**9**) has been fully characterized and its molecular structure has been determined by X-ray diffraction analysis.

Since these results proved the viability of [Ni(Cl)('S_3')]$^-$, we repeated the attempts to cleave [Ni('S_3')]$_3$ directly with chloride, but employed NBu_4Cl instead of NMe_4Cl. Indeed, when suspensions of [Ni('S_3')]$_3$ in THF were treated with equimolar amounts of NBu_4Cl at room temperature, (NBu_4)-[Ni(Cl)('S_3')] (**9**) was formed in yields in excess of 70%. Analogously, (NBu_4)[Ni(N_3)('S_3')] (**10**) was obtained first from (NBu_4)[Ni(S*t*Bu)('S_3')] (**3**) and Me_3SiN_3 and subsequently from the direct reaction between [Ni('S_3')]$_3$ and NBu_4N_3. Syntheses of (NBu_4)[Ni(NCS)('S_3')] (**11**) and (NBu_4)[Ni(NSO)('S_3')] (**12**) required the "silylating" procedure. Thus, complexes **11** and **12** were obtained from (NBu_4)[Ni(S*t*Bu)('S_3')] (**3**) using Me_3SiNCS and Me_3Si-NSO, respectively. The driving force behind these syntheses is presumably the formation of Me_3SiS*t*Bu. Attempts to obtain (NBu_4)[Ni(NCO)('S_3')] using either of the aforementioned two methods proved unsuccessful.

The palladium complex [Pd('S_3')]$_3$ (**2**) could also be cleaved with S*t*Bu$^-$ to yield (NBu_4)[Pd(S*t*Bu)('S_3')] (**13**). Exploratory experiments showed the S*t*Bu$^-$ ligand in **13** to be inert. For example, treatment of **13** with Me_3SiX (X = Cl, N_3, NCS, or NSO) did not yield the corresponding [Pd(X)('S_3')]$^-$ ions.

Characterization of Complexes and Monitoring of Reactions

All the complexes are diamagnetic and have been characterized by standard spectroscopic techniques and elemental

analysis. Several of the complexes have also been characterized by X-ray structure analysis. In contrast to the extremely insoluble starting complexes [M('S_3')]$_3$, all [M(L)('S_3')] derivatives with phosphane or anionic coligands L proved sufficiently soluble in THF, acetone, or CH_2Cl_2 to allow recording of their NMR spectra. The solutions are black-brown (**3**−**6**), orange (**12**), red (**7**, **8**, **11**, **13**), or violet (**9**, **10**).

The ^{1}H-NMR splitting pattern of the aromatic protons is a typical feature of the [M('S_3')] fragment and can be used as a "fingerprint" of the individual complexes since

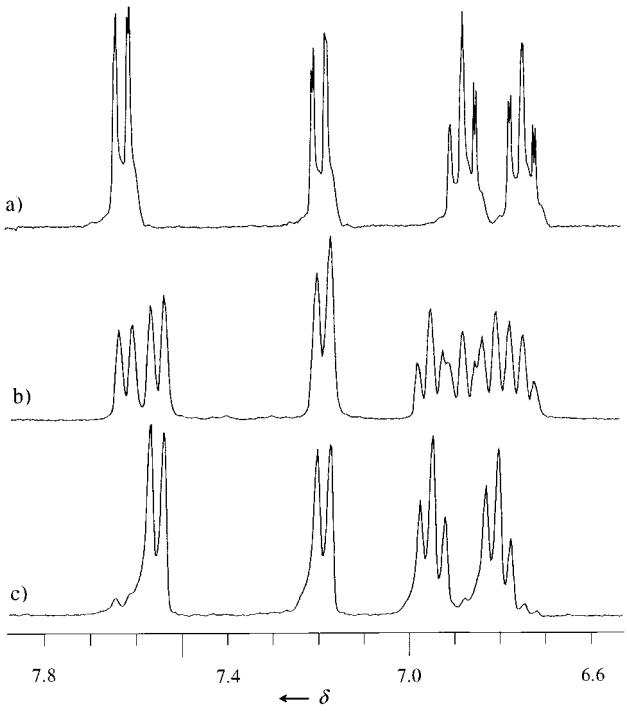


Figure 1. Aromatic region of the ^{1}H-NMR spectra of (a) (NBu_4)[Ni(S*t*Bu)('S_3')] in [D_8]THF, (b) 2 h after addition of Me_3SiN_3, and (c) after 12 h and almost complete formation of (NBu_4)[Ni(N_3)('S_3')]

the multiplet shifts specifically depend on the coligands L.

Figure 1 illustrates the ^{1}H-NMR spectroscopic monitoring of the reaction between (NBu_4)[Ni(S*t*Bu)('S_3')] (**3**) and Me_3SiN_3. The clean aromatic multiplets demonstrate that complex **3** is converted into the azido complex **10** without the formation of any other complexes as by-products. This is further corroborated by the IR spectrum and, in particular, the UV/Vis spectrum of the reaction solution, which shows two isosbestic points (Figure 2). In all cases, the ^{13}C{^{1}H}-NMR spectra of the mononuclear complexes exhibit six ^{13}C signals for the twelve aromatic C atoms of the 'S_3' ligand, in accordance with the twofold symmetry of the [M('S_3')] fragments. Strong and characteristic bands in the IR spectra are well suited for identifying the complexes **10** (2037 cm^{-1}), **11** (2105 cm^{-1}), and **12** (1230, 1030 cm^{-1}).

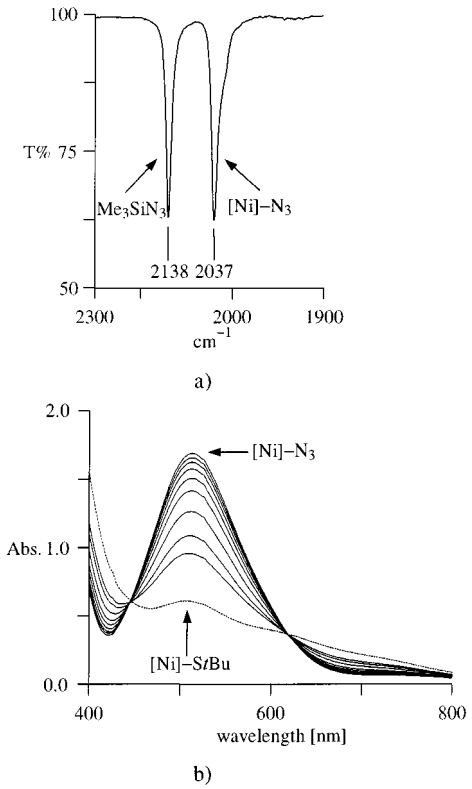


Figure 2. (a) IR spectrum of the reaction solution containing (NBu_4)[Ni(S*t*Bu)('S_3')], Me_3SiN_3, and the resulting (NBu_4)[Ni(N_3)('S_3')], (b) UV/Vis monitoring of the reaction between (NBu_4)[Ni(S*t*Bu)('S_3')] and Me_3SiN_3 in THF

X-ray Structure Determinations

Several of the complexes were obtained in the form of single crystals suitable for X-ray structure analysis. Figure 3 depicts the mononuclear structures, showing different views of the individual species. Table 1 lists selected distances and angles.

All the complexes were found to consist of discrete molecules or ions. The [M('S_3')] fragments invariably exhibit the characteristic butterfly-shape, which arises from the rigid 'S_3' topology and sp^3 hybridization of the central S(thicether) donor.[6] The 'S_3' topology is also responsible for the tetrahedral distortion of the [MS_3L] cores, which are not planar as might have been expected for low-spin four-coordinate d^8 electron metal(II) centers. Figure 4 illustrates this tetrahedral distortion in [Ni(Cl)('S_3')]$^-$.

Distances and angles show no anomalies. It has been pointed out previously that the M−S(thiother) distances are invariably shorter than the corresponding M−S(thiolate) distances and are practically unaffected by the *trans* ligands L. Because the ligands used here range from "hard" chloride, through "soft" σ-π donating thiolates, to σ-donor/π-acceptors such as phosphanes, the [M('S_3')] fragments evidently also exhibit the structural invariance that has previously been noted as a typical feature of [MS_x] centers.[7] The molecular structure of the PCy_3 complex [Ni(PCy_3)('S_3')] (**7**) differs from those of all the other complexes in that it has crystallographic C_S symmetry.

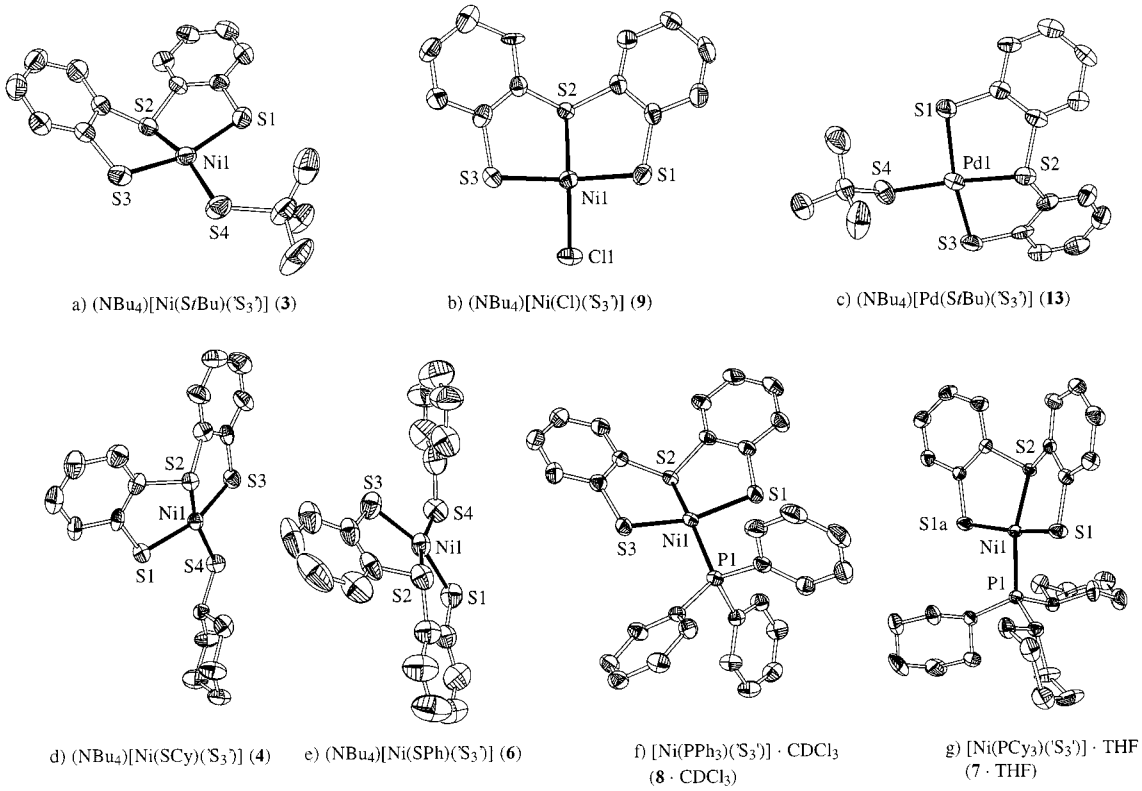


Figure 3. ORTEP plots of (a) $(NBu_4)[Ni(StBu)('S_3')]$ (**3**), (b) $(NBu_4)[Ni(Cl)('S_3')]$ (**9**), (c) $(NBu_4)[Pd(StBu)('S_3')]$ (**13**), (d) $(NBu_4)[Ni(SCy)('S_3')]$ (**4**), (e) $(NBu_4)[Ni(SPh)('S_3')]$ (**6**), (f) $[Ni(PPh_3)('S_3')] \cdot CDCl_3$ (**8** · $CDCl_3$), and (g) $[Ni(PCy_3)('S_3')] \cdot THF$ (**7** · THF); 50% probability ellipsoids; hydrogen atoms, solvent molecules and counterions omitted for the sake of clarity; different projections were chosen to illustrate the tetrahedral distortion of the $[M('S_3')]$ fragments

Table 1. Selected distances [pm] and angles [°] in $(NBu_4)[Ni(StBu)('S_3')]$ (**3**), $(NBu_4)[Ni(SCy)('S_3')]$ (**4**), $(NBu_4)[Ni(SPh)('S_3')]$ (**6**), $[Ni(PCy_3)('S_3')] \cdot THF$ (**7** · THF), $[Ni(PPh_3)('S_3')] \cdot CDCl_3$ (**8** · $CDCl_3$), $(NBu_4)[Ni(Cl)('S_3')]$ (**9**), and $(NBu_4)[Pd(StBu)('S_3')]$ (**13**)

Compound	[Ni]−S*t*Bu (**3**)	[Ni]−SCy (**4**)	[Ni]−SPh (**6**)	[Ni]−PCy_3 (**7**)	[Ni]−PPh_3 (**8**)	[Ni]−Cl (**9**)	[Pd]−S*t*Bu (**13**)
M1−S1	217.2(2)	218.3(2)	217.5(1)	217.6(1)	217.5(1)	217.0(1)	229.1(1)
M1−S2	214.2(1)	211.9(2)	211.5(1)	213.3(1)	213.1(1)	211.4(2)	226.0(2)
M1−S3	221.2(2)	216.8(2)	218.0(1)	217.6(1)[a]	215.8(1)	219.5(2)	231.0(1)
M1−L	219.2(2)	219.2(2)	220.0(1)	220.9(1)	219.7(1)	220.6(2)	233.3(2)
S1−M1−S2	90.86(6)	89.47(6)	90.00(5)	88.72(3)	89.14(3)	91.05(7)	88.44(5)
S1−M1−S3	160.88(7)	160.09(6)	159.78(5)	163.66(5)[a]	159.73(4)	161.31(6)	164.04(6)
S2−M1−S3	86.66(6)	89.73(6)	89.46(5)	88.72(3)[a]	89.85(3)	87.86(7)	86.96(5)
S1−M1−L	100.68(6)	97.40(7)	96.89(6)	94.01(3)	91.64(3)	92.32(7)	95.72(6)
S2−M1−L	164.04(7)	163.70(6)	164.95(5)	159.55(5)	164.11(3)	166.90(6)	175.72(5)
S3−M1−L	85.91(6)	88.75(6)	88.64(5)	94.01(3)[a]	94.81(3)	92.93(7)	89.30(6)

[a] S3 = S1a (symmetry code: x, $-y - {}^1/_2$, z).

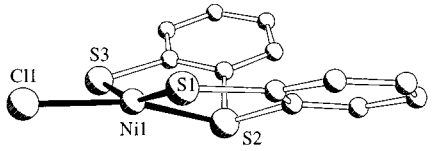


Figure 4. View showing the tetrahedral $[NiClS_3]$ core distortion in $[Ni(Cl)('S_3')]^-$

Figure 5 depicts views of the two trinuclear $[M('S_3')]_3$ complexes **1** and **2** from different angles, while Table 2 lists selected distances and angles. Like the previously described $[Pt('S_3')]_3$ complex,[6] the trinuclear $[Ni('S_3')]_3$ (**1**) and $[Pd('S_3')]_3$ (**2**) exhibit a cyclohexane-like $[M^{II}S]_3$ six-membered ring with a chair conformation that leads to a characteristic propeller-like twist of the three $[M('S_3')]$ units (Figure 5b). Related structures have been found for $[Ni('\mu\text{-}S_2C_3Me_2')]_3$,[5e] $[Ni('t BuS_4')]_3$,[8] and $[Pd(SC_2H_4SC_2H_4S)]_3$.[9]

Concluding Discussion

The trinuclear complex $[Ni('S_3')]_3$ (**1**) has been characterized. Complex **1** and the similarly new $[Pd('S_3')]_3$ (**2**) now complete the series of $[M('S_3')]_3$ complexes with Ni^{II}, Pd^{II}, and Pt^{II}. The extremely sparingly soluble $[Ni('S_3')]_3$ (**1**) gave

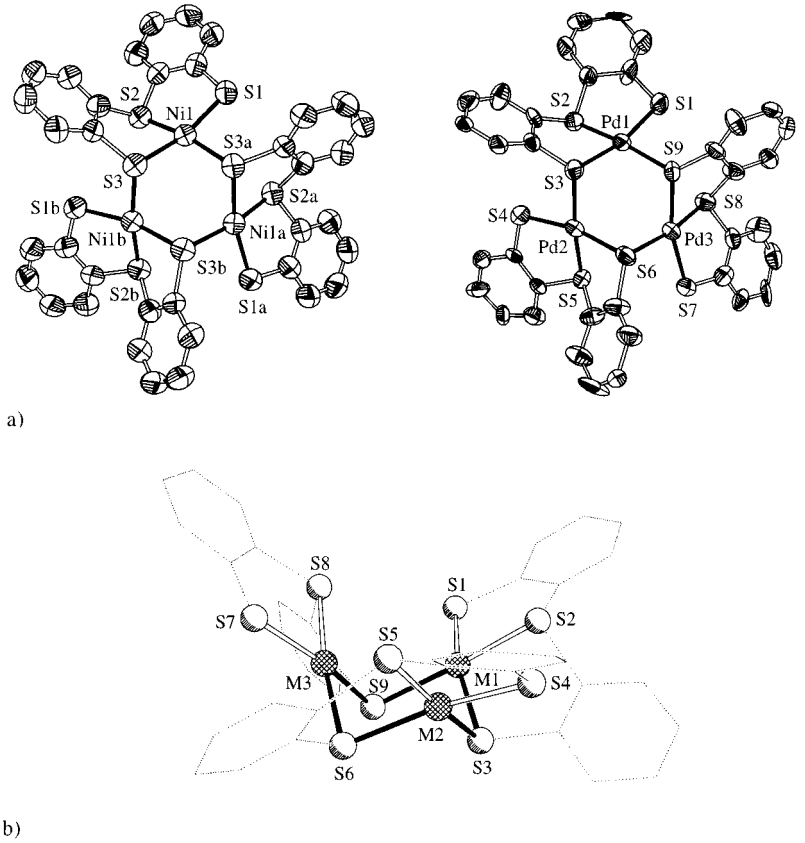


Figure 5. (a) Molecular structures of the $[M('S_3')]_3$ complexes (**1**·3 THF·6 MeOH) (M = Ni), and (**2**·2 CH_2Cl_2) (M = Pd); 50% probability ellipsoids; hydrogen atoms and solvent molecules omitted for the sake of clarity; (b) view showing the chair conformation of the $[MS]_3$ rings

Table 2. Selected distances [pm] and angles [°] in $[Ni('S_3')]_3 \cdot 3$ THF · 6 MeOH (**1** · 3 THF · 6 MeOH), and $[Pd('S_3')]_3 \cdot 2\ CH_2Cl_2$ (**2** · 2 CH_2Cl_2)

Compound	$[Ni('S_3')]_3$ (**1**)		$[Pd('S_3')]_3$[c] (**2**)	
M1−S1	214.2(2)	229.0(7)	226.3(7)[d]	226.6(7)[e]
M1−S2	213.4(2)	226.6(7)	225.7(7)	226.4(7)
M1−S3	221.4(2)	236.1(7)	232.6(7)	234.3(7)
M1−L	218.4(2)[a]	233.8(7)[f]	229.7(7)[g]	229.8(7)[h]
M1···M2	333.6(2)[b]	337.9(4)	355.3(4)[i]	340.9(4)[j]
S3···L	311.0(4)[a]	337.8(9)[f]	325.6(9)[h]	333.3(9)[k]
S1−M1−S2	90.7(1)	88.2(3)	89.2(3)	87.5(3)
S1−M1−S3	163.5(1)	166.7(2)	164.8(3)	166.2(3)
S2−M1−S3	87.7(1)	86.1(2)	86.7(2)	87.4(2)
S1−M1−L	94.4(1)[a]	95.2(3)[f]	96.4(3)[g]	94.7(3)[h]
S2−M1−L	169.6(1)[a]	172.6(2)[f]	170.8(3)[g]	172.9(3)[h]
S3−M1−L	90.0(1)[a]	91.9(3)[f]	89.6(2)[g]	91.9(2)[h]
M1−S3−M2	98.7(1)[b]	93.0(3)	100.4(3)[l]	93.5(2)[m]

[a] L = S3a (symmetry code: $-y-1, x-y-1, z$). − [b] M2 = Ni1b (symmetry code: $-x+y, -x-1, z$). − [c] Three independent $[Pd('S_3')]$ units. − [d] Pd2−S4. − [e] Pd3−S7. − [f] L = S9. − [g] L = S3. − [h] L = S6. − [i] Pd2−Pd3. − [j] Pd3−Pd1. − [k] S6−S9. − [l] Pd2−S6−Pd3. − [m] Pd3−S9−Pd1.

mononuclear $[Ni(L)('S_3')]$ complexes with L = thiolates, phosphanes, halides, and pseudohalides, which proved to be much more soluble than **1**. The chloro ligand in $(NBu_4)[Ni(Cl)('S_3')]$ (**9**) and the S*t*Bu$^-$ ligand in $(NBu_4)[Ni(S\mathit{t}Bu)('S_3')]$ (**3**) were found to be labile, making **3** and **9** suitable starting materials for the synthesis of other $[Ni(L)('S_3')]$ complexes that had previously been found to be inaccessible by direct reaction of $[Ni('S_3')]_3$ and the respective L. It is noteworthy that $(NBu_4)[Ni(N_3)('S_3')]$ (**10**) represents one of the few azido complexes in which a hard azide ligand is bound to a sulfur-rich metal complex fragment.[10] Very few such NSO complexes have been reported[11] and, to the best of our knowledge, $(NBu_4)[Ni(NSO)('S_3')]$ (**12**) represents the first NSO complex with an $[MS_x]$ center.

Experimental Section

General Methods: Unless noted otherwise, all reactions and operations were carried out under nitrogen using standard Schlenk techniques. Solvents were dried and distilled prior to use. − As far as possible, reactions were monitored by IR or NMR spectroscopy. Spectra were recorded on the following instruments: IR (KBr discs or CaF_2 cuvettes, solvent bands were compensated): Perkin−Elmer 983, 1620 FT-IR, and 16PC FT-IR. − NMR: Jeol JNM-GX 270, EX 270, and Lambda LA 400 with the residual protio-solvent signal used as an internal reference. Chemical shifts are quoted on the δ scale (downfield shifts are positive) relative to tetramethylsilane (^1H, $^{13}C\{^1H\}$ NMR) or 85% H_3PO_4 ($^{31}P\{^1H\}$ NMR); spectra were recorded at 25°C. − UV/Vis: Shimadzu UV3101 PC spectrophotometer. − Mass spectra: Jeol MSTATION 700 spectrometer. − Elemental analyses: Carlo Erba EA 1106 or 1108 analyzer. − Me_3SiCl, Me_3SiN_3, Me_3SiNCS, NBu_4Cl, and PR_3 were purchased from either Aldrich or Fluka;

'S_3'-H_2,[6] [$PdCl_2$(COD)],[12] and Me_3SiNSO[13] were prepared according to literature methods.

[Ni('S_3')]$_3$ (1): A solution of 'S_3'$-H_2$ (4.327 g, 17.28 mmol) in THF (70 mL) was added dropwise to $Ni(ac)_2 \cdot 4\ H_2O$ (4.300 g, 17.28 mmol) in MeOH (10 mL) and the resulting brown suspension was refluxed for 4 h. The black-brown precipitate was then separated by filtration, washed with THF (50 mL), and dried in vacuo. A second batch of the product was obtained in the form of single crystals on slow evaporation of the solvent from the filtrate at room temperature. Yield: 5.093 g of **1**·THF (89%). − $C_{40}H_{32}Ni_3OS_9$ (993.41): calcd. C 48.36, H 3.25, S 29.05; found C 48.01, H 3.03, S 30.58.

[Pd('S_3')]$_3$ (2): A solution of 'S_3'$-H_2$ (1.327 g, 5.3 mmol) in THF (30 mL) was combined with *n*BuLi (4.24 mL, 10.6 mmol) at −50°C and the mixture was subsequently allowed to warm to room temperature. Addition of [$PdCl_2$(COD)] led to a dark-red reaction mixture, which was stirred at room temperature overnight and then stored at −30°C for 24 h. A brown solid precipitated, which was separated, washed with MeOH/THF, and dried in vacuo. Yield: 1.536 g of **2** · THF (77%). − $C_{40}H_{32}OPd_3S_9$ (1136.48): calcd. C 42.28, H 2.84, S 25.39; found C 42.29, H 2.71, S 24.79.

(NBu$_4$)[Ni(SR)('S_3')], where R = *t*Bu (3), Cy (4), Me (5), Ph (6) − General Procedure: The appropriate thiol was first deprotonated in MeOH by the addition of one equivalent of NaOMe or LiOMe. The resulting solution was then combined with a black-brown suspension of [Ni('S_3')]$_3$ (**1**) in THF and the mixture was stirred until all the solid material had dissolved (ca. 30 min). One equivalent of NBu_4OH in MeOH was then added and all volatile components were removed in vacuo. The residue obtained was taken up in THF (ca. 20 mL), undissolved material was removed by filtration, and the filtrate was concentrated to one-third of its original volume. On layering with Et_2O or *n*-hexane, black crystals precipitated, which were separated after 4 d, washed with Et_2O (60 mL), and dried in vacuo.

(NBu$_4$)[Ni(S*t*Bu)('S_3')] (3): 1.685 g (1.83 mmol) of **1**; 5.1 mL (5.61 mmol) of a 1.1 M solution of NaS*t*Bu in MeOH; 6.9 mL (5.52 mmol) of a 0.8 M solution of NBu_4OH in MeOH; 30 mL of THF. Yield: 1.858 mg (53%). − $C_{32}H_{53}NNiS_4$ (638.71): calcd. C 60.18, H 8.36, N 2.19, S 20.08; found C 60.14, H 8.81, N 2.29, S 19.47. − ^{1}H NMR (269.6 MHz, [D_6]acetone): δ = 7.67 (d, 2 H, C_6H_4), 7.22 (d, 2 H, C_6H_4), 6.94 (m, 2 H, C_6H_4), 6.82 (m, 2 H, C_6H_4), 3.48 (t, 8 H, NCH_2), 1.77 (m, 8 H, NCH_2CH_2), 1.50 (s, 9 H, $SCCH_3$), 1.37 [m, 8 H, $N(CH_2)_2CH_2$], 0.90 [t, 12 H, $N(CH_2)_3CH_3$]. − ^{13}C{^{1}H} NMR (100.4 MHz, [D_6]acetone): δ = 158.0, 134.3, 129.8, 128.2, 128.0, 121.0 (C_6H_4), 59.4 (NCH_2), 40.1 ($SCCH_3$), 37.5 ($SCCH_3$), 24.6, 20.3 [$NCH_2(CH_2)_2$], 13.9 [$N(CH_2)_3CH_3$].

(NBu$_4$)[Ni(SCy)('S_3')] (4): 1.365 g (1.48 mmol) of **1**; 8.84 mL (4.42 mmol) of a 0.5 M solution of NaSCy in MeOH; 4.44 mL (4.44 mmol) of a 1.0 M solution of NBu_4OH in MeOH; 50 mL of THF. Yield: 2.508 g (85%). − $C_{34}H_{55}NNiS_4$ (664.78): calcd. C 61.43, H 8.34, N 2.11, S 19.29; found C 61.35, H 8.45, N 2.19, S 18.68. − ^{1}H NMR (269.6 MHz, [D_6]acetone): δ = 7.65 (d, 2 H, C_6H_4), 7.20 (d, 2 H, C_6H_4), 6.94 (m, 2 H, C_6H_4), 6.82 (m, 2 H, C_6H_4), 3.49 (t, 8 H, NCH_2), 2.43−1.10 [m, 27 H, $NCH_2(CH_2)_2$, SC_6H_{11}], 0.90 [t, 12 H, $N(CH_2)_3CH_3$]. − ^{13}C{^{1}H} NMR (67.8 MHz, [D_6]acetone): δ = 157.2, 134.7, 129.8, 128.4, 128.1, 121.2 (C_6H_4), 69.3, 59.5, 39.9, 29.6, 29.4, 24.7, 20.4, 14.1 (SC_6H_{11}, $NC_{16}H_{36}$).

(NBu$_4$)[Ni(SMe)('S_3')] (5): 369 mg (0.41 mmol) of **1**; 12.32 mL (1.23 mmol) of a 0.1 M solution of LiSMe in MeOH; 1.50 mL (1.20 mmol) of a 0.8 M solution of NBu_4OH in MeOH; 20 mL of THF. Yield: 494 mg (69%). − $C_{29}H_{47}NNiS_4$ (596.63): calcd. C 58.38, H 7.94, N 2.35, S 21.49; found C 58.11, H 8.27, N 2.39, S 21.39. − ^{1}H NMR (269.6 MHz, [D_6]acetone): δ = 7.66 (d, 2 H, C_6H_4), 7.21 (d, 2 H, C_6H_4), 6.96 (m, 2 H, C_6H_4), 6.84 (m, 2 H, C_6H_4), 3.50 (t, 8 H, NCH_2), 1.78 (m, 8 H, NCH_2CH_2), 1.59 (s, 3 H, SCH_3), 1.38 [m, 8 H, $N(CH_2)_2CH_2$], 0.90 [t, 12 H, $N(CH_2)_3CH_3$]. − ^{13}C{^{1}H} NMR (67.7 MHz, [D_6]acetone): δ = 156.9, 134.9, 129.8, 128.4, 128.2, 121.2 (C_6H_4), 59.5, 24.6, 20.4, 13.9, 11.1 (SCH_3, $NC_{16}H_{36}$).

(NBu$_4$)[Ni(SPh)('S_3')] (6): 845 mg (0.92 mmol) of **1**; 5.52 mL (2.76 mmol) of a 0.5 M solution of NaSPh in MeOH; 3.50 mL (2.80 mmol) of a 0.8 M solution of NBu_4OH in MeOH; 20 mL of THF. Yield: 1.400 g (77%). − $C_{34}H_{49}NNiS_4$ (658.70): calcd. C 61.99, H 7.50, N 2.13, S 19.47; found C 62.03, H 7.47, N 2.14, S 19.57. − ^{1}H NMR (269.6 MHz, CD_2Cl_2): δ = 7.70 (d, 2 H, C_6H_5), 7.55 (d, 2 H, C_6H_4), 7.21 (d, 2 H, C_6H_4), 7.02−6.84 (m, 7 H, C_6H_5, C_6H_4), 3.18 (t, 8 H, NCH_2), 1.50 (m, 8 H, NCH_2CH_2), 1.29 [m, 8 H, $N(CH_2)_2CH_2$], 0.87 [t, 12 H, $N(CH_2)_3CH_3$]. − ^{13}C{^{1}H} NMR (67.7 MHz, CD_2Cl_2): δ = 155.0, 140.3, 133.8, 134.4, 129.4, 128.1, 127.7, 127.2, 122.6, 121.4 (C_6H_5, C_6H_4), 59.4, 24.6, 20.3, 13.9 ($NC_{16}H_{36}$).

[Ni(PR$_3$)('S_3')], where R = Cy (7), Ph (8) − General Procedure: The appropriate PR_3 was added as a solid to a stirred black-brown THF suspension of [Ni('S_3')]$_3$ (**1**). In the course of few seconds, a deep-red solution formed, which was filtered. Upon dropwise addition of MeOH (ca. 20 mL), a dark-red solid precipitated, which was separated, washed with MeOH (ca. 50 mL), and dried in vacuo.

[Ni(PCy$_3$)('S_3')] (7): 665 mg (0.72 mmol) of **1**; 841 mg (3.00 mmol) of PCy_3; 10 mL of THF. Yield: 1.16 g (91%). − $C_{30}H_{41}NiPS_3$ (587.50): calcd. C 61.33, H 7.03, S 16.37; found C 61.47, H 7.29, S 16.23. − IR (KBr): $\tilde{\nu}$ = 1099 cm^{-1}, δ(PCH). − ^{1}H NMR (270.6 MHz, $CDCl_3$): δ = 7.70 (d, 2 H, C_6H_4), 7.40 (d, 2 H, C_6H_4), 7.10 (m, 2 H, C_6H_4), 7.00 (m, 2 H, C_6H_4), 2.20−1.20 [m, 33 H, $P(C_6H_{11})_3$]. − ^{13}C{^{1}H} NMR (67.7 MHz, $CDCl_3$): δ = 152.4 (d, $^3J_{P,C}$ = 10.2 Hz), 132.2, 129.7, 128.2, 127.0, 122.2 (C_6H_4), 34.0 (d, $^1J_{P,C}$ = 20.2 Hz), 30.0, 27.6 (d, $J_{P,C}$ = 10.1 Hz), 26.4 [$P(C_6H_{11})_3$]. − ^{31}P{^{1}H} NMR (109.4 MHz, $CDCl_3$): δ = 28.3 [s, $P(C_6H_{11})_3$]. − MS (FD, THF); *m/z*: 587 [Ni(PCy_3)('S_3')]$^+$.

[Ni(PPh$_3$)('S_3')] (8): 500 mg (0.54 mmol) of **1**; 525 mg (2.00 mmol) of PPh_3; 5 mL of THF. Yield: 894 mg (97%). − $C_{30}H_{23}NiPS_3$ (569.36): calcd. C 63.29, H 4.07, S 16.89; found C 63.47, H 4.17, S 16.51. − IR (KBr): $\tilde{\nu}$ = 1094 cm^{-1}, δ(PCH). − ^{1}H NMR (269.6 MHz, $CDCl_3$): δ = 7.82 (m, C_6H_5), 7.72 (d, 2 H, C_6H_4), 7.46 (m, C_6H_5), 7.28 (d, 2 H, C_6H_4), 7.07 (m, 2 H, C_6H_4), 7.01 (m, 2 H, C_6H_4). − ^{13}C{^{1}H} NMR (67.7 MHz, CD_2Cl_2): δ = 152.8 (d, $^3J_{P,C}$ = 5.7 Hz), 134.9 (d, $J_{P,C}$ = 12.2 Hz), 132.6, 131.3, 130.0 (d, $^1J_{P,C}$ = 48.0 Hz), 129.7, 129.0, 128.6 (d, $J_{P,C}$ = 10.8 Hz), 127.8, 123.0 [C_6H_4, $P(C_6H_5)_3$]. − ^{31}P{^{1}H} NMR (109.4 MHz, $CDCl_3$): δ = 30.4 [s, $P(C_6H_5)_3$].

(NBu$_4$)[Ni(Cl)('S_3')] (9): [Ni('S_3')]$_3$ (**1**) (1.660 g, 1.80 mmol) and NBu_4Cl (1.550 g, 5.41 mmol) were combined in THF (20 mL) and the mixture was stirred at room temperature for 24 h to give a violet suspension. This suspension was then cooled to −30°C, and the precipitate was filtered off, washed with THF, and dried in vacuo. Yield: 2.311 g (73%). − $C_{28}H_{44}ClNNiS_3$ (584.99): calcd. C 57.49, H 7.58, N 2.39, S 16.44; found C 56.98, H 7.68, N 2.36, S 16.54. − ^{1}H NMR (269.7 MHz, [D_8]THF): δ = 7.63 (d, 2 H, C_6H_4), 7.18 (d, 2 H, C_6H_4), 6.94 (m, 2 H, C_6H_4), 6.77 (m, 2 H, C_6H_4), 3.53 (t, 8 H, NCH_2), 1.75 (m, 8 H, NCH_2CH_2), 1.38 [m, 8 H, $N(CH_2)_2CH_2$], 0.90 [t, 12 H, $N(CH_2)_3CH_3$]. − ^{13}C{^{1}H} NMR

(67.7 MHz, [D$_6$]acetone): δ = 153.9, 138.2, 131.7, 129.4, 129.0, 122.3 (C_6H_4), 59.4, 24.8, 20.7, 14.1 ($NC_{16}H_{36}$).

(NBu_4)[Ni(N_3)('S_3')] (10): A 1.0 M THF solution of NBu_4N_3 (3.0 mL, 3.00 mmol) was added to a black-brown suspension of [Ni('S_3')]$_3$ (**1**) (900 mg, 0.97 mmol) in THF (10 mL). The reaction mixture was stirred overnight at room temperature to give a violet solution, which was then filtered. Layering of the filtrate with (iPr)$_2$O (10 mL) led to the precipitation of black-violet microcrystals, which were separated, washed with (iPr)$_2$O, and dried in vacuo. Yield: 1.364 g (79%). − $C_{28}H_{44}N_4NiS_3$ (591.55): calcd. C 56.85, H 7.50, N 9.47, S 16.26; found C 56.87, H 8.47, N 9.17, S 16.36. − IR (KBr): $\tilde{\nu}$ = 2035 cm^{-1}, ν(N_3). − ^{1}H NMR (269.7 MHz, [D$_8$]THF): δ = 7.56 (d, 2 H, C_6H_4), 7.19 (d, 2 H, C_6H_4), 6.96 (m, 2 H, C_6H_4), 6.81 (m, 2 H, C_6H_4), 3.49 (t, 8 H, NCH_2), 1.75 (m, 8 H, NCH_2CH_2), 1.39 [m, 8 H, $N(CH_2)_2CH_2$], 0.89 [t, 12 H, $N(CH_2)_3CH_3$]. − ^{13}C{^{1}H} NMR (67.8 MHz, [D$_8$]THF): δ = 154.9, 134.7, 129.7, 128.5, 128.3, 121.6 (C_6H_4), 59.6, 25.0, 20.7, 14.2 ($NC_{16}H_{36}$).

(NBu_4)[Ni(X)('S_3')] from 3 and Me_3SiX, where X = Cl^- (9), N_3^- (10), NCS^- (11), NSO^- (12) − General Procedure: The appropriate Me_3SiX was added to a black-brown THF solution of (NBu_4)[Ni(StBu)('S_3')] (**3**). A color change was observed within a period of time ranging from 5 min up to 48 h depending on the Me_3SiX compound. All volatile components were then removed in vacuo, and the residue obtained was extracted with Et_2O (ca. 10 mL), separated, washed with Et_2O, and dried in vacuo.

(NBu_4)[Ni(Cl)('S_3')] (9): 250 mg (0.39 mmol) of **3**; 0.10 mL (1.07 mmol) of Me_3SiCl; 3 mL of THF; volatile components were removed after 30 min.; violet powder.

(NBu_4)[Ni(N_3)('S_3')] (10): 275 mg (0.43 mmol) of **3**; 0.15 mL (1.47 mmol) of Me_3SiN_3; 15 mL of THF; volatile components were removed after 24 h; violet powder.

(NBu_4)[Ni(NCS)('S_3')] (11): 125 mg (0.20 mmol) of **3**; 0.07 mL (0.47 mmol) of Me_3SiNCS; 3 mL of THF; volatile components were removed after 5 min; dark-red powder. Yield: 114 mg (94%). − $C_{29}H_{44}N_2NiS_4$ (607.61): calcd. C 57.33, H 7.30, N 4.61, S 21.11; found C 56.82, H 7.33, N 4.78, S 20.12. − IR (KBr): $\tilde{\nu}$ = 2105 cm^{-1}, ν(NCS). − ^{1}H NMR (269.6 MHz, [D$_6$]acetone): δ = 7.66 (d, 2 H, C_6H_4), 7.21 (d, 2 H, C_6H_4), 7.06 (m, 2 H, C_6H_4), 6.92 (m, 2 H, C_6H_4), 3.47 (t, 8 H, NCH_2), 1.81 (m, 8 H, NCH_2CH_2), 1.45 [m, 8 H, $N(CH_2)_2CH_2$], 0.95 [t, 12 H, $N(CH_2)_3CH_3$]. − ^{13}C{^{1}H} NMR (67.7 MHz, [D$_6$]acetone): δ = 153.3 (C_6H_4), 140.6 (NCS), 133.2, 129.3, 129.0, 128.0, 122.4 (C_6H_4), 59.2, 24.4, 20.2, 13.8 ($NC_{16}H_{36}$).

(NBu_4)[Ni(NSO)('S_3')] (12): 1.00 g (1.57 mmol) of **3**; 500 mg (3.70 mmol) of Me_3SiNSO; 20 mL of THF; volatile components were removed after 2 d; orange powder. Yield: 824 mg (86%). − $C_{28}H_{44}N_2NiOS_4$ (611.60): calcd. C 54.99, H 7.25, N 4.58, S 20.97; found C 54.75, H 7.22, N 4.21, S 20.28. − IR (KBr): $\tilde{\nu}$ = 1230 cm^{-1}, ν_{asym}(NSO), 1030 cm^{-1}, ν_{sym}(NSO). − ^{1}H NMR (269.6 MHz, [D$_8$]THF): δ = 7.59 (d, 2 H, C_6H_4), 7.19 (d, 2 H, C_6H_4), 6.95 (m, 2 H, C_6H_4), 6.81 (m, 2 H, C_6H_4), 3.41 (t, 8 H, NCH_2), 1.65 (m, 8 H, NCH_2CH_2), 1.35 [m, 8 H, $N(CH_2)_2CH_2$], 0.85 [t, 12 H, $N(CH_2)_3CH_3$]. − ^{13}C{^{1}H} NMR (67.8 MHz, [D$_8$]THF): δ = 155.8, 134.1, 129.9, 128.4, 128.2, 121.5 (C_6H_4), 59.6, 25.0, 20.7, 14.2 ($NC_{16}H_{36}$).

(NBu_4)[Pd(StBu)('S_3')] (13): A 1.1 M MeOH solution of NaStBu (0.74 mL, 0.81 mmol), NBu_4Cl (220 mg, 0.80 mmol), and [Pd('S_3')]$_3$ (**2**) (290 mg, 0.27 mmol) were combined in THF (10 mL). The resulting mixture was stirred at room temperature for 24 h to give a red solution. Undissolved material was removed by filtration, and the red filtrate was concentrated to one-third of its original volume. Layering with Et_2O led to the precipitation of red crystals, which were separated after 4 d, washed with Et_2O (10 mL), and dried in vacuo. Yield: 452 mg (81%). − $C_{32}H_{53}NPdS_4$ (686.44): calcd. C 55.99, H 7.78, N 2.04, S 18.68; found C 53.37, H 8.36, N 1.98, S 18.05. − ^{1}H NMR (269.7 MHz, [D$_6$]acetone): δ = 7.64 (d, 2 H, C_6H_4), 7.25 (d, 2 H, C_6H_4), 6.97 (m, 2 H, C_6H_4), 6.85 (m, 2 H, C_6H_4), 3.41 (t, 8 H, NCH_2), 1.73 (m, 8 H, NCH_2CH_2), 1.46 (s, 9 H, $SCCH_3$) 1.38 [m, 8 H, $N(CH_2)_2CH_2$], 0.90 [t, 12 H, $N(CH_2)_3CH_3$]. − ^{13}C{^{1}H} NMR (100.4 MHz, [D$_6$]acetone): δ =

Table 3. Selected crystallographic data for [Ni('S_3')]$_3$ · 3 THF · 6 MeOH (**1** · 3 THF · 6 MeOH), [Pd('S_3')]$_3$ · 2 CH_2Cl_2 (**2** · 2 CH_2Cl_2), (NBu_4)[Ni(StBu)('S_3')] (**3**), (NBu_4)[Ni(SCy)('S_3')] (**4**), and (NBu_4)[Ni(SPh)('S_3')] (**6**)

Compound	**1** · 3 THF · 6 MeOH	**2** · 2 CH_2Cl_2	**3**	**4**	**6**
Formula	$C_{54}H_{72}Ni_3O_9S_9$	$C_{38}H_{28}Cl_4Pd_3S_9$	$C_{32}H_{53}NNiS_4$	$C_{34}H_{55}NNiS_4$	$C_{34}H_{49}NNiS_4$
M_r [g/mol]	1329.79	1234.14	638.70	664.74	658.69
Crystal system	trigonal	triclinic	monoclinic	orthorhombic	monoclinic
Space group	*P*3(bar)	*P*1(bar)	$P2_1/n$	*Pbca*	*C*2/*c*
a [pm]	1851.0(7)	951.6(6)	1059.1(3)	1005.4(2)	4474.6(9)
b [pm]	1851.0(7)	1462.7(10)	1931.8(3)	1608.9(9)	1024.3(2)
c [pm]	983.2(8)	1593.7(12)	1717.8(5)	4352.5(9)	1590.4(3)
α [°]	90	88.47(6)	90	90	90
β [°]	90	77.90(5)	103.20(3)	90	107.70(3)
γ [°]	120	82.01(5)	90	90	90
V [nm^3]	2.917(3)	2.148(3)	3.422(2)	7.041(4)	6.944(2)
Z	2	2	4	8	8
$d_{calcd.}$ [g/cm^3]	1.514	1.908	1.240	1.254	1.260
μ [cm^{-1}]	13.34	19.59	8.32	8.12	8.22
Cryst. size [mm^3]	0.5 × 0.4 × 0.4	0.3 × 0.2 × 0.1	0.7 × 0.5 × 0.4	0.4 × 0.4 × 0.1	0.8 × 0.4 × 0.2
ω-scan [°/min]	8.0	10.0	10.0	3.0−30.0	3.0−30.0
2θ range [°]	4.0−54.0	3.8−52.0	4.1−52.0	6.1−54.0	4.0−50.1
Measured refl.	5423	9400	8330	5453	8680
Independent refl.	4145	8436	6710	5453	6136
Observed refl.	1083	1487	3625	1024	2776
ref. parameters	228	487	344	361	361
$R1$[a]; $wR2$ [%]	6.4; 17.5	7.4; 20.0	6.5; 19.5	2.9; 7.5	4.7; 10.7

[a] [$I > 2\sigma(I)$].

Table 4. Selected crystallographic data for [Ni(PCy$_3$)('S$_3$')] · THF (**7** · THF), [Ni(PPh$_3$)('S$_3$')] · CDCl$_3$ (**8** · CDCl$_3$), (NBu$_4$)[Ni(Cl)('S$_3$')] (**9**), and (NBu$_4$)[Pd(S*t*Bu)('S$_3$')] (**13**)

Compound	**7** · THF	**8** · CDCl$_3$	**9**	**13**
Formula	$C_{34}H_{49}NiOPS_3$	$C_{31}H_{23}Cl_3DNiPS_3$	$C_{28}H_{44}ClNNiS_3$	$C_{32}H_{53}NPdS_4$
M_r [g/mol]	659.59	689.72	584.98	686.39
Crystal system	orthorhombic	monoclinic	monoclinic	orthorhombic
Space group	*Pnma*	$P2_1/c$	$P2_1/n$	*Pbca*
a [pm]	2275.1(7)	1731.1(2)	953.8(4)	1952.2(2)
b [pm]	1713.1(4)	922.5(1)	1660.4(7)	1666.1(3)
c [pm]	859.8(3)	1883.4(3)	1891.2(6)	2116.0(2)
α [°]	90	90	90	90
β [°]	90	95.4(1)	90.01(4)	90
γ [°]	90	90	90	90
V [nm^3]	3.351(2)	2.994(1)	2.995(2)	6.882(2)
Z	4	4	4	8
$d_{calcd.}$ [g/cm^3]	1.307	1.530	1.297	1.325
μ [$^{-1}$]	8.39	12.00	9.63	8.03
Cryst. size [mm^3]	0.5 × 0.5 × 0.3	0.6 × 0.6 × 0.6	0.5 × 0.3 × 0.1	0.4 × 0.3 × 0.1
ω-scan [°/min]	3.0−30.0	3.0−30.0	3.0−30.0	3.0−30.0
2θ range [°]	4.0−54.0	4.0−54.0	4.2−55.2	4.2−52.0
Measured refl.	6237	6810	9724	8097
Independent refl.	3787	6593	6922	6766
Observed refl.	1882	4317	3644	2310
ref. parameters	190	352	309	350
$R1$[a]; $wR2$ [%]	3.4; 7.4	3.6; 8.9	4.1; 11.0	4.0; 7.9

[a] [$I > 2\sigma(I)$].

158.0, 134.2, 131.2, 129.6, 128.5, 121.4 (C_6H_4), 59.4 (NCH_2), 41.7 ($SCCH_3$), 37.6 ($SCCH_3$), 24.6, 20.4 [$NCH_2(CH_2)_2$], 13.9 [$N(CH_2)_3CH_3$].

X-ray Structure Analyses of [Ni('S$_3$')]$_3$ · 3 THF · 6 MeOH (1 · 3 THF · 6 MeOH), [Pd('S$_3$')]$_3$ · 2 CH$_2$Cl$_2$ (2 · 2 CH$_2$Cl$_2$), (NBu$_4$)[Ni(S*t*Bu)('S$_3$')] (3), (NBu$_4$)[Ni(SCy)('S$_3$')] (4), (NBu$_4$)[Ni(SPh)('S$_3$')] (6), [Ni(PCy$_3$)('S$_3$')] · THF (7 · THF), [Ni(PPh$_3$)('S$_3$')] · CDCl$_3$ (8 · CDCl$_3$), (NBu$_4$)[Ni(Cl)('S$_3$')] (9), and (NBu$_4$)[Pd(S*t*Bu)('S$_3$')] (13): Black hexagons of **1** · 3 THF · 6 MeOH were grown by slow evaporation of the solvent at room temperature from the THF/MeOH mother liquor resulting from the synthesis of [Ni('S$_3$')]$_2$.[6] Black single crystals of **2** · 2 CH$_2$Cl$_2$ were formed upon layering a CH$_2$Cl$_2$ solution of **2** with Et$_2$O. Black-red plates of **3**, **4**, **6**, and **13** were obtained directly from the respective reaction solutions. Orange plates of **7** · THF were grown by layering a THF solution of **7** with MeOH. Red-brown blocks of **8** · CDCl$_3$ were similarly grown by layering the CDCl$_3$ solution of **8** that had been used for NMR measurements with MeOH. Black plates of **9** were grown by layering a THF solution of **9** with Et$_2$O. In all cases, suitable single crystals were sealed in glass capillaries under N$_2$. Data were collected at 200 K (**1** · 3 THF · 6 MeOH, **3**, **4**, **6**, **7** · THF, **8** · CDCl$_3$, **9**, **13**) or 298 K (**2** · 2 CH$_2$Cl$_2$) on a Siemens P4 or a Nicolet R3 m/V (**2** · 2 CH$_2$Cl$_2$) diffractometer using graphite-monochromated Mo-K_α radiation (λ = 71.073 pm) by the ω-scan technique. In the case of **2** · 2 CH$_2$Cl$_2$ and **3**, an absorption correction was applied on the basis of ψ-scans. The structures were solved by direct methods (SHELXTL-PLUS[14a] or SHELXTL 5.03[14b]). Full-matrix least-squares refinement was carried out on F^2 (SHELXL-93[14c] or SHELXTL 5.03[14b]). All non-hydrogen atoms were refined anisotropically. The positions of the hydrogen atoms in **3**, **4**, **6**, **7** · THF, **8** · CDCl$_3$, and **9** were taken from the difference Fourier map and were kept fixed with a common isotropic displacement parameter. In the case of **1** · 3 THF · 6 MeOH, **2** · 2 CH$_2$Cl$_2$, and **13**, the hydrogen atoms were geometrically positioned with isotropic displacement parameters fixed at 1.5 times the U(eq) of the adjacent carbon atom. One *n*-butyl group (C40−C43) in the cation of **3** is evidently disordered, but no well-separated sites could be refined. In the case of complex **9**, the crystal under study proved to be a pseudomerohedral twin. The twin component ratio was refined to give 0.694(1) and 0.306(1), respectively. Selected crystallographic data are listed in Tables 3 and 4.[15]

Acknowledgments

Support of these investigations by the Deutsche Forschungsgemeinschaft and the Fonds der Chemischen Industrie is gratefully acknowledged.

[1] [1a] E. G. Graf, R. K. Thauer, *FEBS Lett.* **1981**, *136*, 165−169. − [1b] J. R. Lancaster, *FEBS Lett.* **1980**, *115*, 285−288.
[2] [2a] A. S. W. Ragsdale, J. E. Clark, G. Ljungdahl, L. L. Lundie, H. L. Drake, *J. Biol. Chem.* **1983**, *258*, 2364−2369. − [2b] R. B. Diekert, M. Ritter, *FEBS Lett.* **1983**, *151*, 41−44.
[3] [3a] M. A. Halcrow, G. Christou, *Chem. Rev.* **1994**, *94*, 2421−2481. − [3b] A. F. Kolodziej, *Progr. Inorg. Chem.* **1994**, *41*, 493−598. − [3c] M. J. Maroney, C. B. Allan, B. S. Chohan, S. B. Choundhury, Z. Gu, in: *Redox Metalloenzymes Featuring S-Donor Ligands: Hydrogenase − A Case Study* (Eds.: E. I. Stiefel, K. Matsumoto), *ACS Symposium Series*, Washington DC, **1996**, *653*, 74−100. − [3d] C. A. Grapperhaus, M. Y. Darensbourg, *Acc. Chem. Res.* **1998**, *31*, 451−459.
[4] [4a] S. Fox, Y. Wang, A. Silver, M. Millar, *J. Am. Chem. Soc.* **1990**, *112*, 3218−3220. − [4b] J. D. Franolic, W. Y. Wang, M. Millar, *J. Am. Chem. Soc.* **1992**, *114*, 6587−6588. − [4c] H. J. Krüger, R. H. Holm, *Inorg. Chem.* **1989**, *28*, 1148−1155. − [4d] H. J. Krüger, G. Peng, R. H. Holm, *Inorg. Chem.* **1991**, *30*, 734−742. − [4e] P. Stavropoulos, M. C. Muetterties, M. Carrié, R. H. Holm, *J. Am. Chem. Soc.* **1991**, *113*, 8485−8492. − [4f] N. Baidya, M. Olmstead, P. K. Mascharak, *Inorg. Chem.* **1991**, *30*, 929−937.
[5] [5a] D. Sellmann, S. Fünfgelder, G. Pöhlmann, F. Knoch, M. Moll, *Inorg. Chem.* **1990**, *29*, 4772−4778. − [5b] D. Sellmann, S. Fünfgelder, F. Knoch, M. Moll, *Z. Naturforsch.* **1991**, *46b*, 1601−1608. − [5c] D. Sellmann, H. Schillinger, F. Knoch, M. Moll, *Z. Naturforsch.* **1992**, *47b*, 748−753. − [5d] D. Sellmann, W. Prechtel, F. Knoch, M. Moll, *Inorg. Chem.* **1993**, *32*, 538−546. − [5e] D. Sellmann, D. Häußinger, F. Knoch, M. Moll, *J. Am. Chem. Soc.* **1996**, *118*, 5368−5374. − [5f] D. Sellmann, C. Allmann, F. W. Heinemann, F. Knoch, J. Sutter, *J. Organomet. Chem.* **1997**, *541*, 291−305.

[6] D. Sellmann, D. Häußinger, F. W. Heinemann, *Eur. J. Inorg. Chem.*, **1999**, 1715−1725.
[7] D. Sellmann, J. Sutter, *Acc. Chem. Res.* **1997**, *30*, 460−469.
[8] D. Sellmann, H. Schillinger, F. Knoch, M. Moll, *Z. Naturforsch.* **1992**, *47b*, 645−655.
[9] G. A. Barclay, E. M. McPartlin, N. C. Stephenson, *Inorg. Nucl. Chem. Lett.* **1967**, *3*, 397−402.
[10] [10a] D. Sellmann, T. Gottschalk-Gaudig, F. W. Heinemann, *Inorg. Chim. Acta* **1998**, *269*, 63−72. − [10b] D. Sellmann, T. Hofmann, F. Knoch, *Inorg. Chim. Acta* **1994**, *224*, 61−71. − [10c] D. Sellmann, M. Geck, M. Moll, *Z. Naturforsch.* **1992**, *47b*, 74−78.
[11] [11a] H. W. Roesky, K. K. Panday, B. Krebs, M. Dartmann, *J. Chem. Soc., Dalton Trans.* **1984**, 2271−2273. − [11b] H. Plenio, H. W. Roesky, M. Noltemeyer, G. M. Sheldrick, *J. Chem. Soc., Chem. Commun.* **1987**, 1483−1484. − [11c] R. Short, M. B. Hursthouse, T. G. Purcell, J. D. Woollins, *J. Chem. Soc., Chem. Commun.* **1987**, 407−408. − [11d] M. Herberhold, F. Neumann, G. Süss-Fink, U. Thewalt, *Inorg. Chem.* **1987**, *26*, 3612−3615. − [11e] H. Plenio, H. W. Roesky, F. T. Edelmann, M. Noltemeyer, *J. Chem. Soc., Chem. Commun.* **1989**, 1815−1818.
[12] D. Drew, J. R. Doyle, *Inorg. Synth.* **1972**, *13*, 52−53.
[13] [13a] O. J. Scherer, P. Hornig, *Angew. Chem. Int. Ed. Engl.* **1966**, *5*, 729−730. − [13b] E. Parkes, J. D. Woollins, *Inorg. Synth.* **1989**, *25*, 48−49.
[14] [14a] *SHELXTL-PLUS for Siemens Crystallographic Research Systems*, Release 421/V, Siemens Analytical X-ray Instruments Inc., Madison WI, **1990**. − [14b] *SHELXTL 5.03 for Siemens Crystallographic Research Systems*, Copyright **1995** by Siemens Analytical X-ray Instruments Inc., Madison WI, U.S.A. − [14c] G. M. Sheldrick, *SHELXL-93, Program for the Refinement of Crystal Structures*, University of Göttingen, **1993**.
[15] Crystallographic data (excluding structure factors) for the structures reported in this paper have been deposited with the Cambridge Crystallographic Data Centre as supplementary publication nos. CCDC-128896 (**1** · 3 THF · 6 MeOH), -128897 (**2** · CH_2Cl_2), -128898 (**3**), -128899 (**4**), -128900 (**6**), -128901 (**7** · THF), -128902 (**8** · $CDCl_3$), -128903 (**9**), -128904 (**13**). Copies of the data can be obtained free of charge on application to The Director, CCDC, 12 Union Road, Cambridge CB2 1EZ, U.K. [fax: (internat.) +44 (0)1223/336033, E-mail: deposit@ccdc.cam.ac.uk].

Received July 9, 1999
[I99250]

Aluminium Coordinations in Zeolite Mordenite By ^{27}Al Multiple Quantum MAS NMR Spectroscopy

Tie-Hong Chen,[a] Bart H. Wouters,[a] and Piet J. Grobet*[a]

Keywords: NMR spectroscopy / Zeolites / Al-coordination / Mordenite

^{27}Al 3Q MAS NMR spectroscopy has been applied to study the coordination state of the species giving the 30 ppm Al NMR signal in the ^{27}Al MAS NMR spectrum of activated mordenite materials. From the ^{27}Al 3Q MAS NMR measurements it is evident that the broad peak at 30 ppm in the ^{27}Al NMR spectrum of the mordenite calcined at temperatures up to 600 °C comes mainly from the distorted four-coordinated Al. By simulation a quadrupolar coupling constant of 5.8 MHz was estimated for the distorted tetrahedral Al. For samples calcined at 650 and 700 °C, a small amount of pentacoordinated Al emerges. The majority of the signal, however, arises from distorted tetrahedral Al. A two-step calcination results in a significant contribution of the pentacoordinated Al to the signal at 30 ppm. From the simulated line-shape, a quadrupole coupling constant of 6.2 MHz is obtained for the latter signal. These data show that during the calcination of the mordenite, the coordination environment at the Al centre gradually becomes distorted to give rise to the shoulder at 30 ppm. With the increase of the calcination temperature, pentacoordinated Al species form

Introduction

Since the discovery of the ultrastabilisation process of zeolites, the relationship between the structure and the properties of these materials has puzzled many scientists. ^{27}Al and ^{29}Si solid-state NMR spectroscopy has significantly contributed to unraveling the structural changes accompanying the ultrastabilisation.[1] Although ^{27}Al MAS NMR is nowadays routinely applied in this field of research,[2][3] some questions regarding the interpretation of the spectra still need to be answered due to the interaction of the quadrupolar aluminium nucleus with the surrounding electric field. This not only broadens the spectral lines but also results in a quadrupole-induced chemical shift of the NMR signals.[4]

In the ^{27}Al MAS NMR spectrum of hydrothermally activated zeolites, signals centred at 60, 30 and 0 ppm can easily be observed. The signal at 60 ppm is attributed to tetrahedrally coordinated Al species whereas that at 0 ppm is assigned to octahedrally coordinated species. The interpretation of the signal at 30 ppm, however, needs further discussion. In literature reports on the ultrastable Y zeolite (USY) several assignments are reported for the latter signal: four-coordinated Al species shifted upfield due to the quadrupolar induced chemical shift,[5][6] pentacoordinated Al[7][8] or an overlap of both four- and five-coordinated Al species.[9]

The activation conditions cannot be overlooked in any discussion about the coordination number of the different aluminium species in the activated zeolites. Several studies indicate key differences in the Al speciation due to the method of activation.[5,6,9] Owing to the ability to average out the second-order quadrupolar interaction of the Al nucleus, some improvement regarding the assignment of the signal at 30 ppm was obtained by the technique of Double Rotation (DOR) NMR spectroscopy.[10] In a sample of single thermally treated zeolite Y a signal was observed at 47.5 ppm due to tetrahedrally coordinated Al, while in the doubly hydrothermally treated sample, the signal at 30 ppm was assigned to the pentacoordinated Al species. However, because of the low spinning rates of the inner rotor, spinning side bands can overlap with actual resonance lines.[11] Some ambiguity therefore remains in the assignments.

With the development of two-dimensional multiple quantum MAS NMR spectroscopy a powerful tool for the study of quadrupolar nuclei is available.[12][13] This method can refocus the second-order anisotropic broadening of the half-integer quadrupolar nuclei by selecting the multiple-quantum transition (3Q or 5Q) and transferring it to the single-quantum signal over two time domains. Isotropic resolution can be obtained, while problems with overlapping spinning side bands are avoided because of the high spinning rate of the MAS rotor.

Here we report ^{27}Al 3Q MAS NMR spectroscopic experiments on the activated zeolite mordenite, for which a signal at 30 ppm in the ^{27}Al MAS NMR spectrum has been reported.[14] The focus of this paper will be on the coordination state of the Al species giving rise to this signal.

Results and Discussion

Figure 1 shows the ^{27}Al MAS NMR spectra of the parent and the 550 to 700°C calcined H-mordenite samples after hydration, as well as the two-step activated mordenite. The signal at 55 ppm in the spectrum of parent H-mordenite (Figure 1a) is assigned to the framework tetrahedrally coordinated Al atoms, while that at 0 ppm results from extra-framework Al atoms in an octahedral environment.[14]

[a] Centrum voor Oppervlaktechemie en Katalyse,
Departement Interfasechemie, K.U. Leuven,
Kardinaal Mercierlaan 92, B-3001 Heverlee (Leuven), Belgium
Fax: (internat.) + 32-16/321-998
E-mail: Piet.Grobet@agr.kuleuven.ac.be

 © WILEY-VCH Verlag GmbH, D-69451 Weinheim, 2000 1434–1948/00/0202–281 $ 17.50+.50/0

Some framework-related octahedrally coordinated Al may appear at 0 ppm as was recently reported for the HY.[15] The small signal that can be seen at 30 ppm is probably due to activation at 400°C and the subsequent acid washing that was performed to prepare the acid form of the sample (Figure 1).

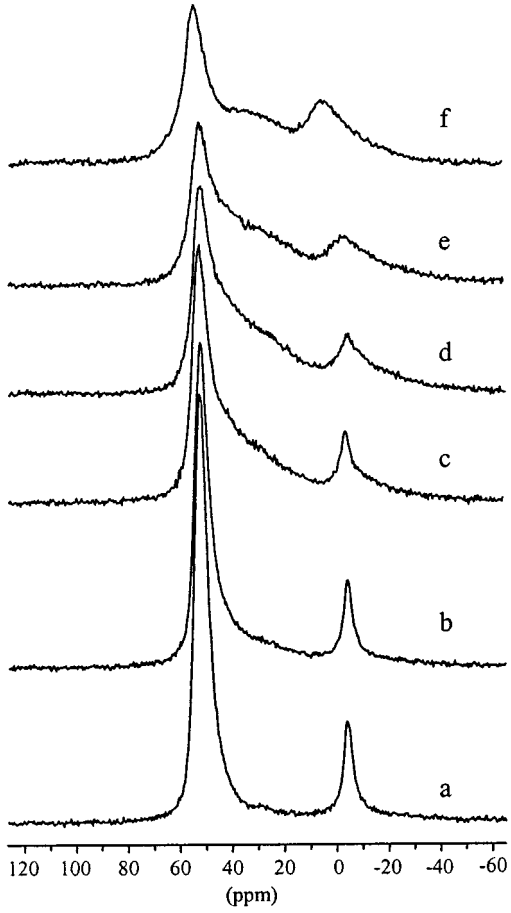


Figure 1. ^{27}Al MAS NMR spectra of zeolite mordenite; (a) parent mordenite, (b) 550°C calcined, (c) 600°C calcined, (d) 650°C calcined, (e) 700°C calcined and (f) the two-step calcination

In the spectra of the calcined samples (Figure 1, b−f), besides the peaks at 55 and 0 ppm, a broad line gradually emerges at around 30 ppm, with increasing calcination temperature, while the 0 ppm signal broadens. Furthermore, the total Al intensity within the spectra decreases. For the sample calcined at 700°C, an intensity loss of 15−20% was found relative to the parent sample. The formation of "NMR-invisible Al" at high calcination temperatures is in agreement with the measurements of Grobet et al. for the zeolite Y.[5] Because of this "NMR-invisible Al", quantification of the Al content from the ^{27}Al MAS NMR spectrum is not possible, in contrast to the statement of Barras et al.[14]

By application of the two-dimensional ^{27}Al 3Q MAS NMR technique the resolution of the ^{27}Al MAS NMR spectra of the calcined mordenite samples is enhanced, as shown in Figure 2. In these spectra the position of the lines in the MAS-dimension corresponds to the conventional ^{27}Al MAS NMR measurements, while isotropic resolution is obtained in the second dimension. In the spectrum of the parent H-mordenite (Figure 2a) a strong signal (A) originating from the framework Al and a signal (B) due to the octahedrally coordinated Al are seen. Furthermore a small signal (C) appears near the four-coordinated Al (signal A). From the projection on the MAS-axis signal C can be correlated with the small signal at 30 ppm in the 1D ^{27}Al MAS NMR spectrum (Figure 1a). Artificial peaks along the isotropic dimension near signal (A) can be observed due to the truncation of the NMR signal in the *t1* time domain (see Experimental Section).

After calcination at 550°C (Figure 2b), signals A and B are still present, while the intensity of signal C is increased. This process continues until 600°C (Figure 2c). From its position in the isotropic-dimension of the 3Q MAS NMR spectrum, signal C should also be regarded as arising from four-coordinated aluminium species. Pentacoordinated species are expected to be found between signals A and B. From both the centre of gravity and the tailing of the signal in the MAS-dimension a significantly higher quadrupolar coupling constant (QCC) than that of the tetrahedral signal A is expected.

A slice through signal C, parallel to the MAS-dimension, of the sample calcined at 600°C is shown in Figure 3a. From the fitting of a theoretically calculated powder pattern to this slice the quadrupole parameters can be obtained.[16] Due to the high dispersion which is typical of zeolite samples,[17] only average values can be obtained for both the chemical shift and the quadrupolar parameters. Several authors have published quadrupolar coupling constants for the signal at 30 ppm in the ^{27}Al MAS NMR spectrum of an activated zeolite Y. Ray and Samoson estimated a QCC of 6.2 MHz for a single thermally dealuminated Y sample.[10] Coster et al. indicate that nonframework Al debris in the USY are consists of two species contributing to the signal in 30 ppm region. The first has an isotropic chemical shift of about 58 ppm and a QCC of 6 MHz, the second an isotropic shift of 40 ppm and a slightly lower QCC.[17] For the simulated powder pattern of Figure 3b a quadrupolar constant of 5.8 MHz and an asymmetry parameter (η) of 0.4 were used. These values agree well with those reported in the literature. A Gaussian line broadening of 50 Hz was introduced to the theoretical line shape to account for the dispersion of the chemical shift. The dispersion of the quadrupolar parameters was not taken into account and this may explain the rudimentary nature of the fit. The isotropic chemical shift determined by the simulated pattern is at 59 ppm, giving further evidence that signal C originates from four-coordinated Al as expected from the position of this line in the isotropic dimension. From the high quadrupolar coupling constant, and the consequent dispersion in the 2D MQ spectrum, a highly distorted site is expected. The broad band at 30 ppm in the corresponding 1D spectra (Figure 1a−c) arises from this kind of distorted Al species.

If the temperature of calcination is further increased to 650°C, an additional signal (D) appears in the ^{27}Al 3Q

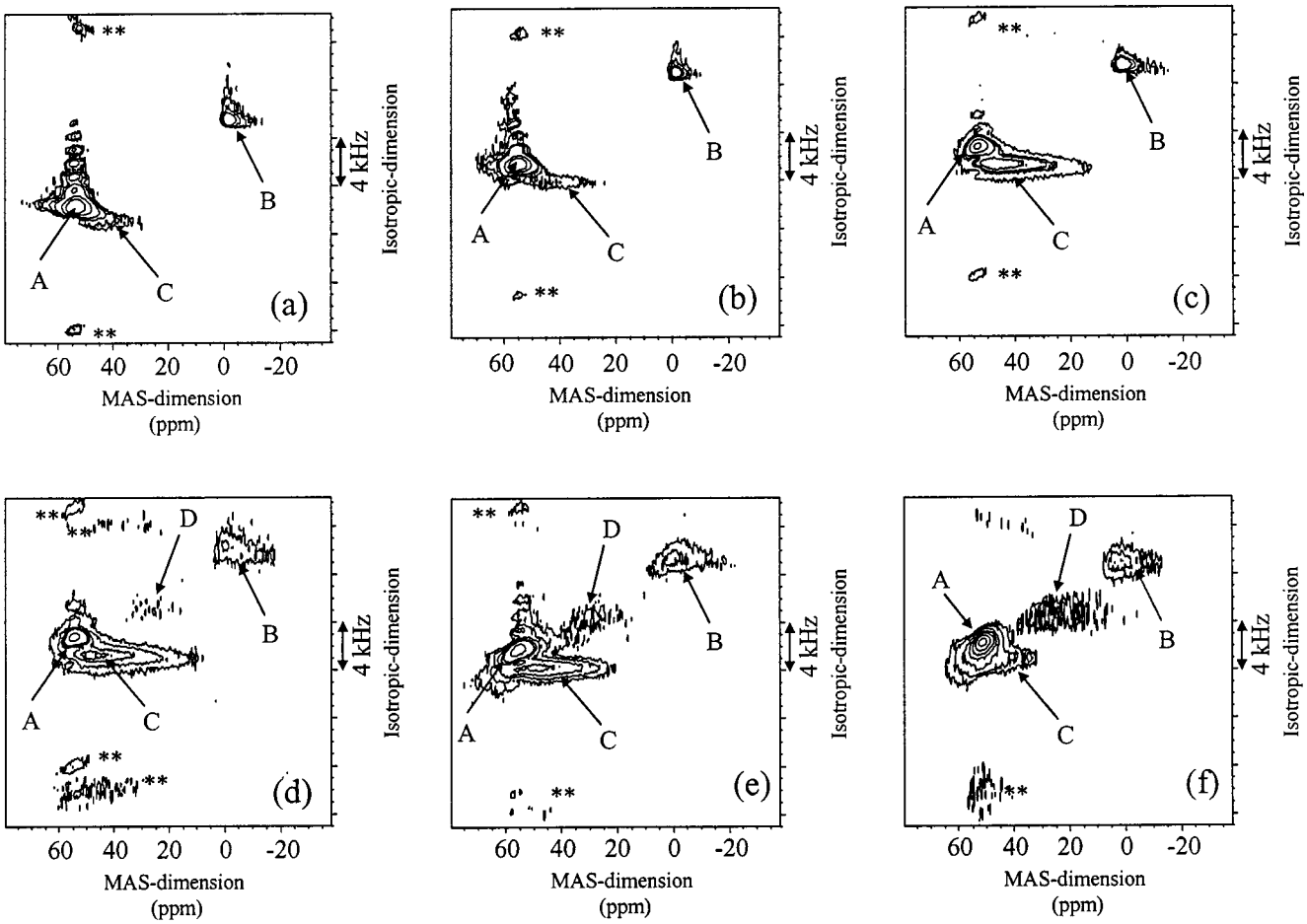


Figure 2. ^{27}Al 3Q MAS NMR spectra of zeolite mordenite; (a) parent sample, (b) 550°C calcined, (c) 600°C calcined, (d) 650°C calcined, (e) 700°C calcined and (f) the two-step calcination; ** denote spinning side bands

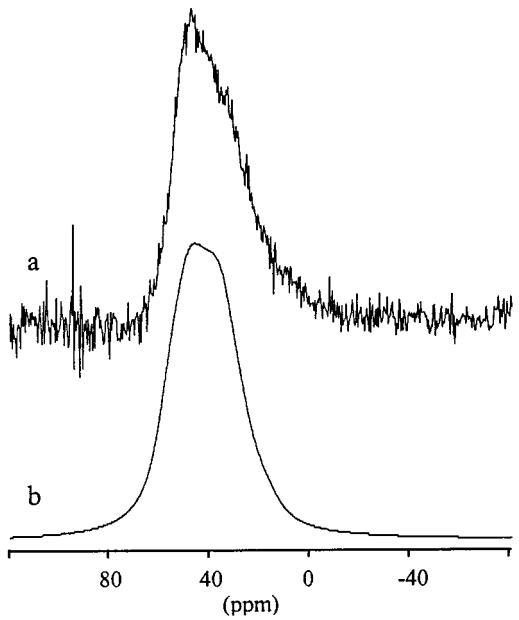


Figure 3. (a) Slice through signal (C) in Figure 2c, (b) simulation with a calculated quadrupolar powder pattern, QCC = 5.8 MHz, η = 0.4, and δ^{cs}_{iso} = 59

MAS NMR spectrum (Figure 2d). The intensity of signal D is weak but becomes more pronounced after calcination at 700°C (Figure 2e). The much lower intensity of signal D relative to signal C in Figures 2d and 2e can either be explained by the low quantity of the former species or by differences in the excitation efficiency of the multiple quantum transition under our experimental conditions. From the position of signal D in the ^{27}Al 3Q MAS NMR spectra, which is between those expected for tetrahedral and octahedral coordination, the Al species giving rise to signal D should be pentacoordinated.

From the 3Q MAS NMR spectra it can be observed that signal B gradually broadens in both the MAS and isotropic dimension, implying that its QCC and its isotropic chemical shift became more dispersed. The properties of signal C do not change as the calcination temperature increases from 600 to 700°C.

Spin-lattice relaxation measurements on the USY revealed that the signal at 30 ppm is not due to a single Al site but results from a mixture of different Al species, which are believed to be in a nonframework environment.[18] From the projection of signals C and D on the MAS-dimension, it is clear that both contribute to the broad hump at 30 ppm in the 1D spectrum.

After the two-step activation of the mordenite (Figure 2f), a significant contribution of the pentacoordinated Al species (signal D) to the signal at 30 ppm is encountered. By simulation of a slice through signal D, a quadrupolar coupling constant of 6.2 MHz is estimated (Figure 4), which is slightly higher than the value obtained for the distorted tetrahedral Al after a single activation. However, for the two-step calcination of zeolite Y, Ray et al. found a lower QCC for the pentacoordinated Al species than for the distorted Al sites seen after a single hydrothermal treatment.[10] On the other hand, Rocha et al. indicate an increase of the QCC in zeolite Y with increasing degree of dealumination of the sample.[9] These differences may result from the activation conditions applied by the authors.

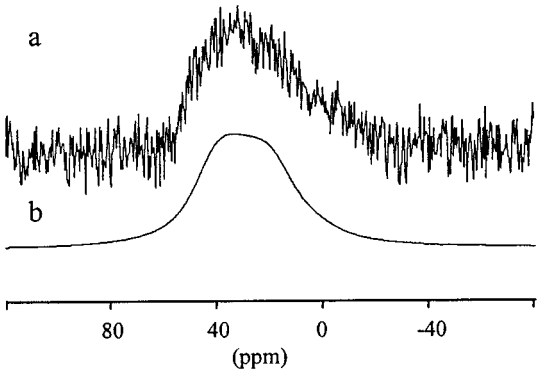


Figure 4. (a) Slice through signal (D) in Figure 2f, (b) simulation with a calculated quadrupolar powder pattern, QCC = 6.2 MHz, $\eta = 0.5$, and $\delta^{cs}_{iso} = 44$

For both the distorted tetrahedral Al sites and the pentacoordinated aluminium similar QCC′s are observed. Therefore the excitation efficiency, which is dependent on the QCC, is not responsible for the low intensity of the pentacoordinated Al species observed in the spectra of samples calcined above 600°C. This implies that only a small amount of the latter species is formed. The signal at 30 ppm in the ^{27}Al MAS NMR spectrum can thus mainly be assigned to distorted tetrahedral Al. Only after a second activation step does a significant part of this signal result from five-coordinate Al.

Conclusion

In the ^{27}Al MAS spectra of the parent, 550, 600, 650, 700°C calcined zeolite mordenite, three signals are observed at 55, 30 and 0 ppm, respectively. The 55 ppm signal is related to tetrahedrally coordinated Al species while the 0 ppm line is related to octahedrally coordinated Al. A broad 30 ppm signal gradually appears when the calcination temperature is increased. From the ^{27}Al 3Q MAS NMR experiments it can be concluded that during the calcination of mordenite, tetrahedral Al species gradually undergo distortion. Due to the second order quadrupolar broadening, these species give rise to the 30 ppm shoulder in the 1D spectrum. Further increase of the calcination temperature to 650°C and above results in the formation of pentacoordinated Al. These species contribute to the 30 ppm signal although the majority of this band remains related to distorted tetrahedral Al. After a second calcination the formation of pentacoordinated aluminium species is more pronounced.

Experimental Section

Samples: Commercially available H-mordenite with a Si/Al ratio of 6.2, referred to as the parent sample, was subjected to different calcination treatments. This parent sample was heated in a muffle furnace for 2 hours at temperatures of 550, 600, 650 and 700°C. All the calcined samples were placed in a desiccator to hydrate over a saturated NH_4Cl solution for at least one week. After hydration, the sample calcined at 650°C was calcined a second time at 500°C for two hours and was subsequently equilibrated in a desiccator. This latter sample will be referred to as the two-step activated mordenite.

NMR Measurements: ^{27}Al NMR spectra were measured on a Bruker MSL-400 spectrometer at 104.26 MHz. The MAS spin rate was 12.5 kHz. ^{27}Al MAS NMR spectra were recorded with a short 0.6 μs pulse (corresponding to π/18 flip angle). A "split-*t1*" 3Q pulse sequence was applied for the triple-quantum MAS NMR experiments to obtain a sheared spectrum without further treatment of the 2D data.[19] The three pulses of 100 kHz had a length of 3.5, 1.2 and 0.6 μs. 200 FID′s for each experiments were accumulated with a time increment of 5 μs. 1920 scans were accumulated for each FID. The TPPI method was used in the 2D data acquisition and processing. ^{27}Al chemical shifts were referenced to a 0.5 M $Al(NO_3)_3$ solution.

Acknowledgments

T.-H. C. and P. J. G. acknowledge the Research Council of the Catholic University of Leuven for a postdoctoral fellowship and the FWO-Vlaanderen for a research position, respectively.

[1] J. Klinowski, J. M. Thomas, C. A. Fyfe, G. C. Gobbi, *Nature* **1982**, *296*, 533−536.
[2] G. Engelhardt, D. Michel, *High-Resolution Solid-State NMR of Silicates and Zeolites,* John Wiley & Sons, Chichester, **1987**.
[3] J. Klinowski, *Chem. Rev.* **1991**, *91*, 1459−1479.
[4] A. P. M. Kentgens, *Geoderma* **1997**, *80*, 271−306.
[5] P. J. Grobet, H. Geerts, M. Tielen, J. A. Martens and P. A. Jacobs in *Zeolites as Catalysts, Sorbents and Detergent Builders* (Ed.: H. G. Karge, J. Weitkamp), Elsevier Science Publishers B. V., Amsterdam, **1989**.
[6] A. Samoson, E. Lippmaa, G. Engelhardt, U. Lohse, H.-G. Jerschkewitz, *Chem. Phys. Lett.* **1987**, *134*, 589−592.
[7] J.-P. Gilson, G. C. Edwards, A. W. Peters, K. Rajagopalan, R. F. Wormsbecher, T. G. Roberie, M. P. Shatlock, *J. Chem. Soc., Chem. Commun.* **1987**, 91−92.
[8] L. Kellberg, M. Linsten, H. J. Jakobsen, *Chem. Phys. Lett.* **1991**, *182*, 120−126.
[9] J. Rocha, S. W. Carr, J. Klinowski, *Chem. Phys. Lett.* **1991**, *187*, 401−408.
[10] G. J. Ray, A. Samoson, *Zeolites* **1993**, *13*, 410−413.
[11] G. W. Haddix, M. Narayana, W. D. Gillespie, M. B. Georgellis, Y. Wu, *J. Am. Chem. Soc.* **1994**, *116*, 672−674.
[12] L. Frydman, J. S. Harwood, *J. Am. Chem. Soc.* **1995**, *117*, 5367−5368.
[13] C. Fernandez, J. Amoureux, *Chem. Phys. Lett*. **1995**, *242*, 449−454.

[14] J. Barras, J. Klinowski, D. W. McComb, *J. Chem. Soc., Faraday Trans.* **1994**, *90*, 3719−3723.
[15] B. H. Wouters, T. H. Chen, P. J. Grobet, *J. Am. Chem. Soc.* **1998**, *120*, 11419−11425.
[16] D. Massiot, B. Touzo, D. Trumeau, J. P. Coutures, J. Virlet, P. Florian, P. J. Grandinetti, *Solid State Nucl. Magn. Reson.* **1996**, *6*, 73−83.
[17] D. Coster, A. L. Blumenfeld, J. J. Fripiat, *J. Phys. Chem.* **1994**, *98*, 6201−6211.
[18] X. Yang, *J. Phys. Chem.* **1995**, *99*, 1276−1280.
[19] S. P. Brown, S. Wimperis, *J. Magn. Reson.* **1997**, *128*, 42−61.
Received July 19, 1999
[I99262]

Enantioselective Organic Syntheses With Chiral Transition Metal Complexes, 11[+]

Chiral Ruthenium–Sulfene Complexes – Synthesis and C–C Coupling Reactions

Wolfdieter A. Schenk,*[a] Jürgen Bezler,[a] Nicolai Burzlaff,[a] Michael Hagel,[a] and Bernhard Steinmetz[a]

Keywords: Enolates / Nucleophilic additions / Ruthenium / S ligands / Sulfenes

Reaction of the chiral racemic complex [CpRu(mppe)-(SO_2)]PF_6 (**1**, mppe = $Me_2PC_2H_4PPh_2$) with diazomethane or -ethane gave the sulfene complexes [CpRu(mppe)(RHC=SO_2)]PF_6 (R = H, **2a**; R = Me, **2b**). Treatment of **2a** with prochiral enamines or deprotonated β-oxo esters yielded C–C coupling products with 32–60% de. An analog of **2a**, [NmcpRu(mppe)(H_2C=SO_2)]PF_6 (**8**, Nmcp = neomenthylcyclopentadienyl) was prepared in a four-step synthesis starting from LiNmcp and [$RuCl_2(PPh_3)_3$]. Repeated crystallization of the intermediate [NmcpRu(mppe)Cl] (**6**) provided diastereomerically pure **6′** which added methylene stereospecifically to give diastereomerically pure **8′**. Compound **8** turned out to be much less reactive towards nucleophiles than **2a**, but still added deprotonated ethyl 2-methyl-3-oxobutanoate with 44% de. The chiral, enantiomerically pure sulfur dioxide complex [CpRu(chir)(SO_2)]PF_6 [**10**, chir = (*S*,*S*)-$Ph_2PCHMeCHMePPh_2$] was synthesized from [CpRu(chir)Cl] and SO_2 and was characterized by X-ray crystallography. Reaction of **10** with diazomethane gave the enantiomerically pure sulfene complex [CpRu(chir)(H_2C=SO_2)]PF_6 (**11**). Addition reactions of **11** with *N*-(1-cyclopentenyl)morpholine, as well as with various enolates derived from β-oxo esters or 1,3-diesters proceeded with high yields and 20–90% de. The structure of a diastereomerically pure addition product, [CpRu(chir)(SO_2CH_2C(Me){C(O)Me}{C(O)O*t*Bu}] (**13d′**), was determined crystallographically and was shown to have (*R*) configuration at the quaternary carbon atom. After alkylation of one of the S=O functions, the sulfinate ligand was cleaved from the metal center by ligand substitution with acetonitrile, and the resulting acetonitrile complex **15** was converted back into **10** by treatment with SO_2.

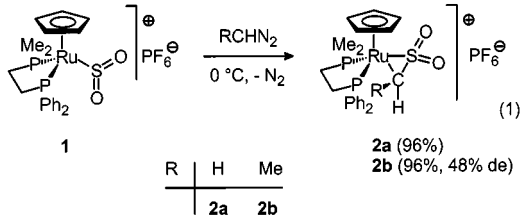
In previous publications we described the synthesis of ionic sulfene complexes of the type [$Cp(R_3'P)_2Ru(RHC$=SO_2)]PF_6 (R = H, Me) by methylene addition to sulfur dioxide complexes.[1–3] Through the coordination to a transition metal atom, the sulfene molecule experiences considerable stabilization as well as umpolung. The latter was demonstrated by addition reactions with a number of heteroatom and carbon nucleophiles, which occurred exclusively at carbon.[2][3]

The use of chiral transition metal complexes as diastereodirecting auxiliaries in stoichiometric reactions is a topic of long-standing interest.[4][5] In the majority of the work, complexes of the types [$CpMo(CO)_2(L-L^*)$],[6] [$CpM(NO)(PPh_3)L$] (M = Mn,[4] Re[7]), [$CpFe(CO)(PPh_3)L$][8][9] and [$CpRu(L-L^*)L$][10] (L–L* = chiral bidentate ligand) were employed. If L is a coordinated alkene, such complexes may undergo nucleophilic additions with remarkable diastereoselectivity.[5,7,11] In this context it seemed promising to carry out C–C coupling reactions with chirally modified sulfene complexes.

Results

Complexes with Metal-Centered Chirality

Reaction of the chiral racemic sulfur dioxide complex **1**[12] with diazomethane or -ethane gave the sulfene complexes **2a** and **2b** as colorless, crystalline, and thermally quite sensitive materials (Equation 1).



(1)

1

2a (96%)
2b (96%, 48% de)

Compound **2a** was obtained as a single isomer with the CH_2 group *cis* to the PPh_2 group of the $Me_2PC_2H_4PPh_2$ (mppe) ligand. A strong NOE upon irradiation of the Cp resonance allowed the identification of the *exo*-H of the sulfene as well as the *exo*-CH_3 of the diphosphane ligand. Due to the small dihedral angle H–C–Ru–P,[2] the *endo*-H is strongly coupled to the *cis*-phosphorus atom,[13] which was shown by selective ^{31}P decoupling to be that of the PPh_2 group. Four different rotamers/diastereoisomers are possible for **2b**, of which only two were observed in a 74:26

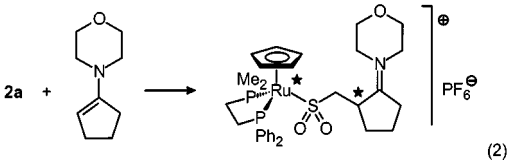
[+] Part 10: B. Steinmetz, M. Hagel, W. A. Schenk, *Z. Naturforsch., B*, **1999**, *54*, 1265–1271.

[a] Institut für Anorganische Chemie der Universität, Am Hubland, D-97074 Würzburg, Germany
Fax: (internat.) + 49-(0)931/888-4605
E-mail: wolfdieter.schenk@mail.uni-wuerzburg.de

 © WILEY-VCH Verlag GmbH, D-69451 Weinheim, 2000 1434–1948/00/0202–287 $ 17.50+.50/0

ratio. The major isomer **2b′** has the structure shown in Equation 1, as evidenced again by the large coupling of the *endo*-H with the PPh_2 group. The relative configurations of the two stereocenters are thus $R_{Ru},R_C/S_{Ru},S_C$. Unfortunately, the resonance of the sulfene-H of the minor isomer **2b″** could not be detected due to extensive signal overlap. In view of the fairly low diastereoselectivity of the addition reaction described below, it is reasonable to assume that **2b″** is the ($R_{Ru},S_C/S_{Ru},R_C$) diastereomer but we have no way of distinguishing between the two possible rotamers.

Cationic sulfene complexes readily undergo C−C coupling reactions with enamines.[3] Thus, treatment of **2a** with *N*-(1-cyclopentenyl)morpholine gave the immonium salt **3** in 76% yield and 60% de (Equation 2).

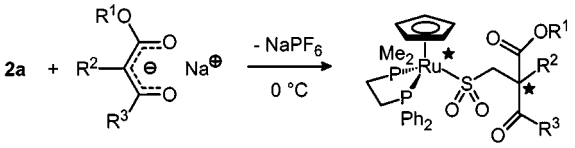


(2)

3 (76%, 60% de)

Immonium salt **3** is a colorless crystalline compound whose constitution was readily inferred from its spectroscopic data. Particularly characteristic is the AB system of the methylene group at sulfur and the downfield signal of the immonium carbon at $\delta = 203.4$. The shift differences in the NMR spectra of the two diastereoisomers are rather small due to the large spatial separation of the two stereocenters.

Reaction of **2a** with deprotonated β-oxo esters gave the neutral addition products **4a**−**c** in fair yields and diastereoselectivities (Equation 3).



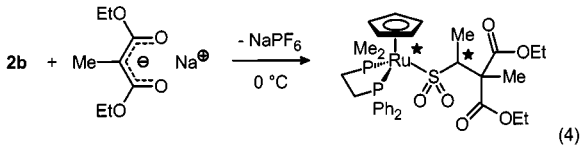
(3)

R^1	Et	*t*-Bu	Et
R^2, R^3	Me, Me	Me, Me	$-CH_2CH_2CH_2-$
	4a	**4b**	**4c**

4a (54%, 42% de)
4b (60%, 48% de)
4c (63%, 32% de)

Through chromatography and crystallization the major diastereoisomers could be enriched. The stereochemical course of enolate reactions is strongly influenced by the nature of the counter cation.[14] Therefore, the reaction of **2a** with deprotonated ethyl 2-oxocyclopentanecarboxylate was carried out on a small scale in the presence of various salts. Upon addition of $LiClO_4$, $MgBr_2$, or $ZnCl_2$ to the reaction mixture, the diastereoselectivity disappeared almost completely. However, the coupling product **4c** was formed with 81% de when the sodium enolate was first converted into a titanium enolate and then added to **2a**. Unfortunately, we were unable in this case to separate **4c** without its decomposition from the titanium-containing side products. Nevertheless, it appears that, with the choice of suitable reagents, highly stereoselective addition reactions can be performed.

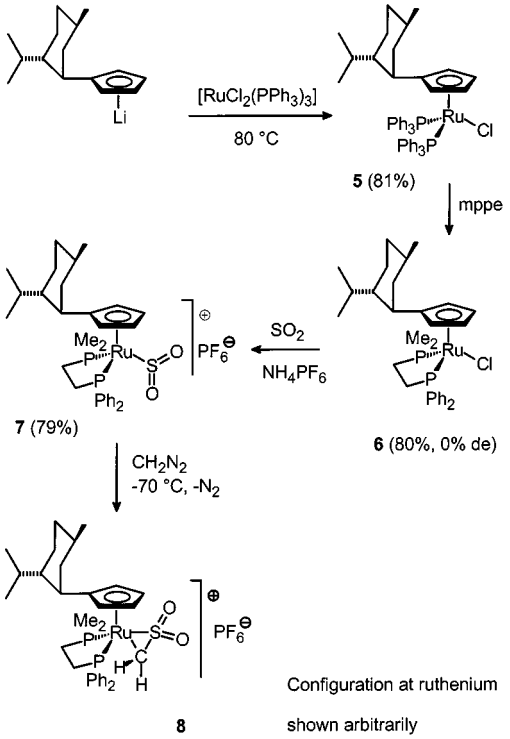
Nucleophilic additions on **2b** should be stereospecific with respect to the configuration at the sulfene carbon atom. Still, the addition of the sodium enolate of diethyl methylmalonate produced **4d** in somewhat lower de than expected (Equation 4). This is certainly due to competing decomposition which may affect both diastereoisomers of the thermolabile starting material **2b** at slightly different rates.



(4)

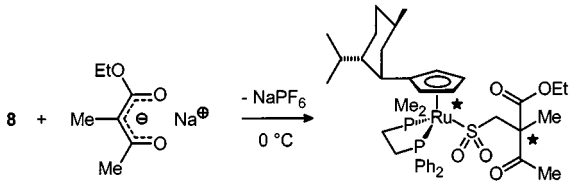
4d (71%, 26% de)

Although the results obtained so far were not overly promising we set out to synthesize enantiomerically pure analogs of **1** and **2a** (Scheme 1). Reaction of neomenthylcyclopentadienyllithium with $[RuCl_2(PPh_3)_3]$ gave **5** in high yield as a yellow crystalline compound which, unlike its C_5H_5 analog, is readily soluble even in aliphatic hydrocarbons. Notable spectroscopic features are four separated NMR signals of the protons on the cyclopentadienyl ring, and a narrow AB system in the ^{31}P NMR spectrum. Phosphane exchange with mppe gave **6** in high yield as a 50:50 mixture of diastereoisomers. Through repeated crystallizations a small amount of diastereomerically pure **6′** was obtained as orange-yellow crystals. Treatment of **6** with sulfur dioxide at room temperature gave the SO_2 complex **7** in high isolated yield as a yellow crystalline material. Similarly, **6′** gave **7′** as a single diastereoisomer, which to our knowledge is the first chiral, enantiomerically pure complex of sulfur dioxide.



Scheme 1. Synthesis of diastereoisomeric neomenthylcyclopentadienyl ruthenium complexes

The reaction of **7** or **7′** with diazomethane produced the expected sulfene complex either as the 50:50 mixture **8** or in its diastereomerically pure form **8′** (Scheme 1), both of which are brownish-white semisolid materials. Disappointingly, **8** and **8′** turned out to be even more labile than **2a**, to preclude the isolation of analytically pure samples and to hamper their use in further reactions considerably. In the next experiments, **8** was therefore generated in situ. The reaction with *N*-(1-cyclopentenyl)morpholine resulted only in complete decomposition of the sulfene complex. Enolate addition, however, gave the expected product **9**, after workup in 47% yield, as a 72:28 mixture of two diastereoisomers (Equation 5).

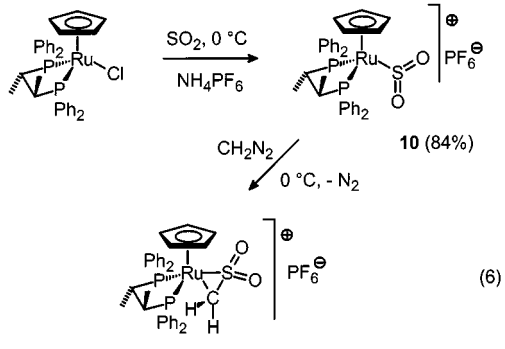


9 (47%, 44% de) (5)

Since this reaction is not expected to proceed with significantly higher diastereoselectivity than that described in Equation 3, we have to assume that the two remaining stereoisomers were lost during workup. Although **9** is a stable compound, neomenthylcyclopentadienyl complexes do not tend to crystallize well, therefore making it impossible to obtain analytically pure samples or achieve any further diastereoisomer enrichment.

Complexes with Ligand-Centered Chirality

We recently found that ligand-centered reactions of [CpRu(chir)L] complexes [chir = (*S*,*S*)-2,3-bis(diphenylphosphanyl)butane] proceed with remarkably high diastereoselectivity.[15−19] For example, the oxidation of coordinated thioethers routinely gave de values greater than 80% and up to 98%.[16−18] Thus, besides avoiding the tedious diastereoisomer separation step, we also expected improved selectivities for the C−C coupling reactions of sulfene complexes containing this chiral diphosphane ligand. The enantiomerically pure sulfur dioxide complex **10** was obtained as a yellow solid in high yield from [CpRu(chir)Cl] and SO_2 (Equation 6).



(6)

Diffusion of hexane into a dichloromethane solution gave crystals of **10**·$2CH_2Cl_2$ suitable for X-ray structure determination. Figure 1 shows a view of the cation. The structure may be described as distorted octahedral, in which the C_5H_5 ligand occupies three sites. As expected,[20][21] the SO_2 ligand aligns itself in the pseudo mirror plane of the $CpRu(PR_3)_2$ complex fragment. The two P−Ru−S angles differ by 5.3° as a result of the asymmetric nature of the chiral diphosphane ligand. The geometry around sulfur is perfectly planar, with the sum of the bond angles being 359.9°.

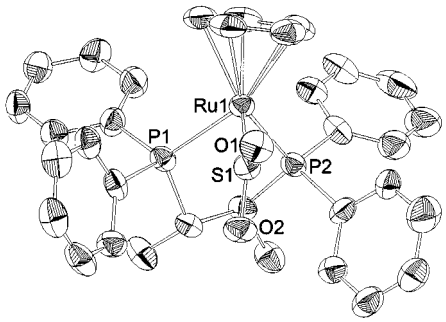
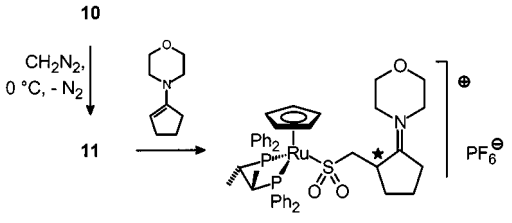


Figure 1. Molecular structure of [CpRu(chir)(SO_2)]PF_6·2 CH_2Cl_2 (**10**·$2CH_2Cl_2$) (hydrogen atoms, anion, and solvent molecules omitted); selected distances [pm] and angles [°] (standard deviations in parentheses): Ru(1)−P(1) 232.9(2), Ru(1)−P(2) 232.2(2), Ru(1)−S(1) 212.8(2), S(1)−O(1) 143.2(6), S(1)−O(2) 145.8(6), S(1)−Ru(1)−P(1) 88.48(8), S(1)−Ru(1)−P(2) 93.81(9), P(1)−Ru(1)−P(2) 83.41(8), Ru(1)−S(1)−O(1) 120.9(3), Ru(1)−S(1)−O(2) 125.1(3), O(1)−S(1)−O(2) 113.9(4)

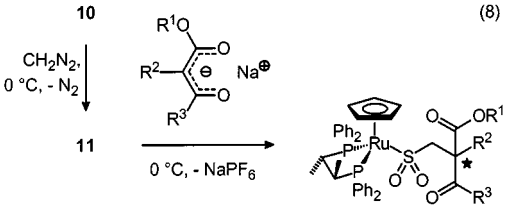
The reaction of **10** with diazomethane at −70°C gave the enantiomerically pure sulfene complex **11** in almost quantitative yield (Equation 6). Sulfene complex **11** is a colorless, crystalline compound which decomposes in solution at 20°C. NMR spectra taken at −60 °C revealed that **11** exists as a single rotamer. The two sulfene protons give signals at δ = 0.85 and 2.31, the latter of which was shown by NOE to arise from the proton *syn* to the Cp ligand.

In the following experiments the sulfene complex **11** was produced in situ and was treated with carbon nucleophiles. Thus, treatment of the solution with *N*-(1-cyclopentenyl)-morpholine gave **12** in 81% yield and 64% de (Equation 7). Apparently, the chir ligand does not introduce excessive steric hindrance that would inhibit the nucleophilic addition at the sulfene ligand. Furthermore, the diastereoselectivity achieved here represents some improvement over the analogous reaction of the racemic mppe complex **2a** (Equation 2).



12 (81%, 64% de) (7)

Reactions of **11** with deprotonated diethyl methylmalonate or deprotonated β-oxo esters gave the expected addition products **13a**−**e** in good yields (Equation 8). Complexes **13b** and **13d** were formed with considerably higher diastereoselectivity than their mppe analogs **4a** and **4b**.



(8)

R^1	Et	Et	Et	*t*-Bu	Et
R^2, R^3	Me, OEt	Me, Me	Me, Ph	Me, Me	-$CH_2CH_2CH_2$-
	13a	**13b**	**13c**	**13d**	**13e**
Yield (%)	79	84	76	81	76
de (%)	-	62	36	90	20

After recrystallization, the major diastereoisomer of **13d** was obtained pure and was subjected to an X-ray structure determination. A view of the molecule is shown in Figure 2.The geometry around ruthenium is very similar to that of **10**. The addition of an organic group to the SO_2 ligand results in a slight decrease of the Ru−P bond lengths and a sizeable increase of the Ru−S distance by 17.4 pm. The latter is due to the combined effects of raising the coordination number at sulfur from three to four and occupying the vacant b_2 orbital at sulfur, which is responsible for the carbene-type π-backbonding in η^1-planar SO_2 complexes.[20] Nevertheless, the Ru−S bond is still shorter than expected for a single bond, but this is commonly observed for electron-rich sulfinato complexes.[22] The difference of the P−Ru−S angles has increased to 8.8° as a result of the repulsions encountered between the organic groups of the sulfinate ligand and the chiral chelate phosphane. The configuration at the former enolate carbon atom C72 is (*R*).

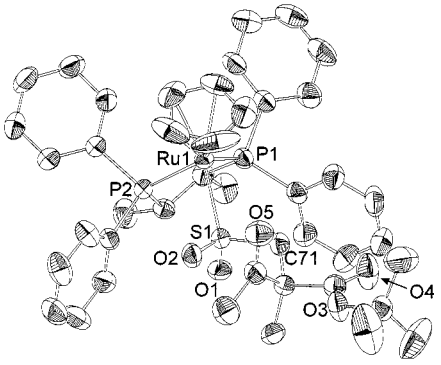
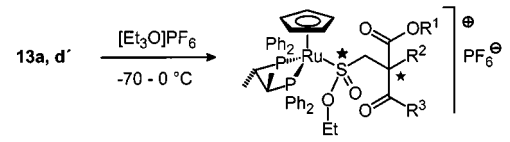


Figure 2. Molecular structure of [CpRu(chir){SO_2CH_2C(Me){C(O)Me}[C(O)O*t*Bu}}] (**13d′**) (hydrogen atoms omitted); selected distances [pm] and angles [°] (standard deviations in parentheses): Ru(1)−P(1) 228.0(2), Ru(1)−P(2) 228.3(2), Ru(1)−S(1) 230.2(2), S(1)−O(1) 146.7(3), S(1)−O(2) 146.8(4), S(1)−C(71) 182.7(5), S(1)−Ru(1)−P(1) 94.10(5), S(1)−Ru(1)−P(2) 85.28(5), P(1)−Ru(1)−P(2) 84.95(5), Ru(1)−S(1)−O(1) 115.3(2), Ru(1)−S(1)−O(2) 109.7(2), O(1)−S(1)−O(2) 113.4(2), Ru(1)−S(1)−C(71) 110.7(2)

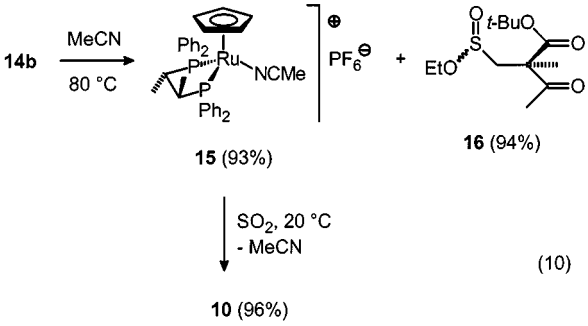
Electron-rich sulfinato complexes may be readily alkylated at one of the S=O functions.[3][23] Thus, reaction of **13a** or diastereomerically pure **13d′** with triethyloxonium hexafluorophosphate gave the sulfinic acid ester complexes **14a**, **b** in almost quantitative yields and, in the case of **14a**, good diastereoselectivity (Equation 9).



R^1	Et	*t*-Bu	
R^2, R^3	Me, OEt	Me, Me	
	14a	**14b**	
			14a (92%, 62% de)
			14b (94%, 6% de)

(9)

Sulfinic acid esters are weak donors which may readily be released from the metal.[3] Thus, heating **14b** in acetonitrile under reflux gave the acetonitrile complex **15** along with the diastereomeric ester **16**. Compound **15** may be converted back into the SO_2 complex **10** by treatment with sulfur dioxide (Equation 10).



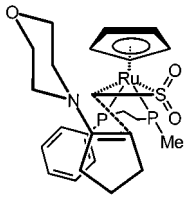
(10)

Discussion

In the symmetrical complex [CpRu(dppe)(CH_2=SO_2)]PF_6, the sulfene ligand rotates rapidly on the NMR timescale.[3] Therefore, we have to assume that in the similar sulfene complexes **2a**, **2b**, and **11**, the different rotamers are in thermodynamic equilibrium, dictated solely by steric requirements. Thus, for **2a** only one rotamer is found, in which the small CH_2 group is positioned *cis* to the large PPh_2 end of the chelate diphosphane. In **2b** the major (R_{Ru},R_C/S_{Ru},S_C) diastereoisomer has an analogous geometry with the methyl group in an *exo* position. The second isomer is most likely to be the opposite diastereomer. Both may even be in a slow equilibrium via an η^2-(S=O) bonded intermediate similar to the recently characterized sulfur trioxide complex [Cp*Ru(PMe_3)$_2$(η^2-O=SO_2)]-PF_6.[24]

Of the nucleophilic additions of **2a**, the reaction with the enamine (Equation 2) stands out for its fairly large diastereoselectivity. In this case, a prediction of the stereochemical course may be warranted. Simple molecular models suggest that the approach of (*R*)-**2a** on the *re* side of the enamine is favored, since this avoids any close contact

between the morpholino substituent and the *P*-phenyl group protruding into the space around the sulfene ligand (Scheme 2).



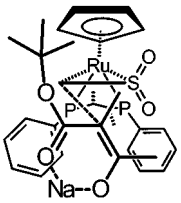
Scheme 2. Diastereoselective approach of *N*-(1-cyclopentenyl)morpholine to sulfene complex **2a**

The main product of the reaction (Equation 2) should thus be the (R_{Ru},R_C/S_{Ru},S_C) diastereoisomer. A remarkable gain in the diastereoselectivity of formation of **4c** was achieved when a titanium enolate was used. Such effects are often observed[14] but are difficult to interpret, since Ti^{IV} complexes of β-dicarbonyl compounds in solution invariably exist as mixtures of different monomers and dimers.[25] Precoordination of titanium to one of the sulfene oxygens may also have an influence.

Knowing that reactions at [NmcpRu(CO)$_2$X] proceed with rather low diastereoselectivity,[26][27] we had expected that the reactivity of the neomenthylcyclopentadienyl sulfene complex **8** would be quite similar to that of its C_5H_5 analog **2a**. Indeed, the de values of the formation of **4a** (Equation 3) and **9** (Equation 5) are almost the same. Nevertheless, the neomenthyl substituent does introduce considerable steric hindrance, as is seen in the lack of any reactions of **8** with enamines. An inspection of the molecular structures of [NmcpRu(CO)(PPh$_3$)I],[26] [NmcpRu(dppe)IEt]OTf,[27] and [NmcpRu(dppe)Cl][28] shows that the substituents at phosphorus force the Nmcp ligand into a rotational arrangement which places the neomenthyl group in close proximity to the site of the sulfene ligand and thus impedes nucleophilic additions. In view of the combined difficulties − low reactivity of the sulfene complex, unsatisfactory diastereoselectivity, and inefficient diastereoisomer separation − we finally abandoned the concept of chirality-at-the-metal.

The synthesis of the chiral, enantiomerically pure sulfene complex **11** posed no challenge at all. At low temperature, **11** is present as a single rotamer with the sulfene ligand oriented in such a way that the SO_2 group is placed into the largest void of the [CpRu(chir)] complex fragment.[17] The stereochemical course of the enamine addition (Equation 7) should therefore be again as outlined by Scheme 2, that is, the major diastereomer of **12** is expected to have (*R*) configuration at the newly created stereocenter. Unfortunately, we were unable to grow crystals of **12** suitable for an X-ray structure determination.

In the case of the enolate addition product **13d**, the (*R*) configuration at carbon was corroborated crystallographically. The outcome of the reaction would thus suggest a transition state as shown in Scheme 3, in which the large *tert*-butoxy group of the β-oxo ester is placed in the vicinity of the Cp ligand, which is less bulky than the PPh_2 groups of the chelate diphosphane. The solvated Na^+ cation is too far removed to interfere with the ruthenium complex.



Scheme 3. Diastereoselective approach of deprotonated β-oxo ester to sulfene complex **11**

Enantiomerically pure esters of sulfinic acids are important starting materials for the stereoselective synthesis of chiral sulfoxides.[29] It was, therefore, quite gratifying that the alkylation of **13a** (Equation 9) proceeded with good stereoselectivity. Inspection of the molecular structure of **13d′** or the closely related achiral sulfinate complex [CpRu(dppm)(SO_2Et)][22] shows that the SO_2R ligand in halfsandwich complexes is always oriented so that one of the two S=O groups is nested between the phenyl groups of the chelate diphosphane while the other one is accessible from the direction of the Cp ligand. For a chiral sulfinate complex with a fixed rotational arrangement of the SO_2R ligand such as **13a**, this means that the formation of the (R_S) ester complex will be favored. In the alkylation of **13d′**, the low de is then probably the result of a mismatch situation caused by the stereocenter at the quaternary carbon atom.

Conclusions

Chiral ruthenium halfsandwich complexes combine two interesting and potentially quite useful properties, the stabilization of otherwise short-lived unsaturated species, and the asymmetric induction in ligand-based reactions. The enantiomerically pure fragment $[CpRu(chir)]^+$ in particular stands out for its ready accessibility and excellent crystallization of almost all of its complexes. A promising potential in synthetic applications can thus be easily foreseen

Experimental Section

General Remarks: All experiments were carried out in Schlenk tubes under nitrogen in suitably purified solvents. The crystallization of oily products was often conveniently induced by immersing the Schlenk tube in a small ultrasonic cleaning bath. − IR: Perkin−Elmer 283, Bruker IFS 25. − ^{1}H NMR: Bruker AMX 400, δ values relative to TMS; diastereotopic methylene protons of ethoxy groups in most cases gave well-resolved ABX_3 spectra with ^2J(H,H) = 9−11 Hz and ^3J(H,H) = 7.2 Hz; for the sake of simplicity they are denoted in the following as "res. m" (resolved multiplet). − ^{13}C NMR: Bruker AMX 400, δ values relative to TMS; assignments were routinely checked by DEPT; in some cases the ^{13}C NMR signals of quaternary carbon atoms were too weak to be detected. ^{31}P NMR: Bruker AMX 400, δ values relative to 85% H_3PO_4. The ^{1}H and ^{13}C NMR signals of the phosphane ligands and the ^{31}P NMR signal of the PF_6^- ion are very similar for all compounds and have therefore been omitted from the lists of spectral data. − Elemental analyses: Analytical Laboratory of the Insti-

tut für Anorganische Chemie. − The following starting materials were obtained as described in the literature: [CpRu(mppe)(-SO_2)]PF_6 (**1**),[12] diazomethane, diazoethane,[30] neomenthylcyclopentadiene,[31] $[RuCl_2(PPh_3)_3]$,[32] [CpRu(chir)Cl].[33] Enolates were obtained from the corresponding 1,3-dicarbonyl compounds by deprotonation with sodium bis(trimethylsilyl)amide. All other reagents were used as purchased.

[CpRu(mppe)(CH_2=SO_2)]PF_6 (2a): To a solution of **1** (89 mg, 0.14 mmol) in dichloromethane (15 mL), a solution of diazomethane in diethyl ether (0.6 mL, 0.2 mmol) was added at −70 °C. Gas evolution and a rapid color change to pale yellow were observed. The mixture was allowed to warm to 0 °C, and was concentrated rapidly to 2 mL. Hexane (15 mL) was added to precipitate the tan-colored microcrystalline product. Yield 87 mg (96%), m.p. 98 °C (dec.). − ^{1}H NMR (400 MHz, CD_2Cl_2, 20 °C): δ = 0.20 [dd, ^2J(H,H) = 4.4 Hz, ^3J(P,H) = 16.1 Hz, 1 H, SO_2=CH_2], 2.41 [d, ^2J(H,H) = 4.4 Hz, SO_2=CH_2], 5.68 (s, 5 H, C_5H_5). − ^{13}C NMR (100 MHz, CD_2Cl_2, 20 °C): δ = −19.1 [d, ^2J(P,C) = 6 Hz, SO_2=CH_2], 95.1 (s, C_5H_5). − ^{31}P NMR (162 MHz, CD_2Cl_2, 20 °C): δ = 66.4 [d, J(P,P) = 18 Hz, PMe_2], 78.3 [d, J(P,P) = 18 Hz, PPh_2]. − IR (Nujol): $\tilde{\nu}$ = 1236, 1104 cm^{-1} (S=O). − $C_{22}H_{27}F_6O_2P_3RuS$ (663.5): calcd. C 39.83, H 4.10; found C 39.97, H 4.00.

[CpRu(mppe)(CHMe=SO_2)]PF_6 (2b): This compound was prepared from **1** (146 mg, 0.22 mmol) and diazoethane (0.25 mmol) as described above except that the product was isolated at −30 °C by addition of precooled hexane. Yield 146 mg (96%), m.p. 129 °C (dec.). − Major diastereoisomer (74%): ^{1}H NMR (400 MHz, CD_2Cl_2, 20 °C): δ = 0.68 [dq, ^3J(H,H) = 6.4 Hz, ^3J(P,H) = 16.4 Hz, 1 H, SO_2=CH], 1.50 [d, ^3J(H,H) = 6.4 Hz, 3 H, CH_3], 5.61 (s, 5 H, C_5H_5). − ^{13}C NMR (100 MHz, CD_2Cl_2, 20 °C): δ = 2.1 [d, ^2J(P,C) = 5 Hz, CH=SO_2], 18.6 (s, CH_3), 95.9 (s, C_5H_5). − ^{31}P NMR (162 MHz, CD_2Cl_2, 20 °C): δ = 67.6 [d, J(P,P) = 19 Hz, PMe_2], 77.6 [d, J(P,P) = 19 Hz, PPh_2]. − Minor diastereoisomer (26%): ^{1}H NMR (400 MHz, CD_2Cl_2, 20 °C): δ = 1.74 [d, ^3J(H,H) = 6.4 Hz, 3 H, CH_3], 5.46 (s, 5 H, C_5H_5). − ^{13}C NMR (100 MHz, CD_2Cl_2, 20 °C): δ = 91.4 (s, C_5H_5). − ^{31}P NMR (162 MHz, CD_2Cl_2, 20 °C): δ = 64.6 [d, J(P,P) = 15 Hz, PMe_2], 85.8 [d, J(P,P) = 15 Hz, PPh_2]. − IR (Nujol): $\tilde{\nu}$ = 1220, 1117 cm^{-1} (S=O). − $C_{23}H_{29}F_6O_2P_3RuS$ (677.5): calcd. C 40.77, H 4.31, S 4.73; found C 41.08, H 4.51, S 4.45.

[CpRu(mppe)$SO_2CH_2(C_9H_{15}NO)$]PF_6 (3): To a solution of **2a** (73 mg, 0.11 mmol) in dichloromethane (10 mL), a solution of *N*-(1-cyclopentenyl)morpholine in diethyl ether (0.5 mL, 0.12 mmol) was added at −70 °C. The solution was allowed to warm to 20 °C and stirred for an additional hour at this temperature. The mixture was then concentrated to 2 mL and the colorless product was precipitated by adding diethyl ether. Yield 68 mg (76%), m.p. 127 °C (dec.). − Major diastereoisomer (80%): ^{1}H NMR (400 MHz, CD_2Cl_2, 20 °C): δ = 1.61−2.19 (m, 4 H, 2 × CH_2), 2.31 [dd, ^2J(H,H) = 13.6 Hz, ^3J(H,H) = 7.2 Hz, 1 H, SO_2CH], 2.44 [dd, ^2J(H,H) = 13.6 Hz, ^3J(H,H) = 7.2 Hz, 1 H, SO_2CH], 2.77−2.96 (m, 4 H, 2 × OCH_2), 3.72−3.99 (m, 4 H, 2 × NCH_2), 4.97 (s, 5 H, C_5H_5). − ^{13}C NMR (100 MHz, CD_2Cl_2, 20 °C): δ = 21.0 (s, C-4), 31.7 (s, C-3), 35.6 (s, C-5), 43.2 (s, C-2), 58.9 (s, NCH_2), 61.9 (s, NCH_2), 64.3 (s, OCH_2), 66.0 (s, OCH_2), 70.5 (s, SO_2CH_2), 84.0 (s, C_5H_5), 203.4 (s, C=N). − ^{31}P NMR (162 MHz, CD_2Cl_2, 20 °C): δ = 51.7 [d, J(P,P) = 28 Hz, PMe_2], 85.2 [d, J(P,P) = 28 Hz, PPh_2]. − Minor diastereoisomer (20%): ^{1}H NMR (400 MHz, CD_2Cl_2, 20 °C): δ = 1.61−2.19 (m, 4 H, 2 × CH_2), 2.77−2.96 (m, 4 H, 2 × OCH_2), 3.72−3.99 (m, 4 H, 2 × NCH_2), 4.92 (s, 5 H, C_5H_5). − ^{13}C NMR (100 MHz, CD_2Cl_2, 20 °C): δ = 22.3 (s, C-4), 32.4 (s, C-3), 35.1 (s, C-5), 39.7 (s, C-2), 65.6 (s, OCH_2), 67.0 (s, OCH_2), 74.1 (s, SO_2CH_2), 84.1 (s, C_5H_5). − ^{31}P NMR (162 MHz, CD_2Cl_2, 20 °C): δ = 51.8 [d, J(P,P) = 26 Hz, PMe_2], 85.3 [d, J(P,P) = 26 Hz, PPh_2]. − IR (Nujol): $\tilde{\nu}$ = 1678 cm^{-1} (C=N), 1132, 1017 cm^{-1} (S=O). − $C_{31}H_{42}F_6NO_3P_3RuS$ (816.7): calcd. C 45.59, H 5.18, N 1.72; found C 44.95, H 5.08, N 1.57.

Addition of Enolates to 2a: To a solution of Na[$N(SiMe_3)_2$] (40 mg, 0.22 mmol) in THF (5 mL), an equimolar amount of the respective C−H acidic compound was added at −70 °C. The resulting slurry was then added to a solution of **2a** (135 mg, 0.20 mmol) in THF (20 mL). The mixture was allowed to warm to 20 °C and stirred for 2 h. The solvent was removed under vacuum, the oily residue was taken up in dichloromethane and chromatographed (neutral alumina, activity grade I, acetone/dichloromethane, 5:1). A broad, pale-yellow band containing the product was collected. The solvent was evaporated and the colorless product was recrystallized from benzene/hexanes.

4a: Yield 72 mg (54%), m.p. 115 °C (dec.). − Major diastereoisomer (71%): ^{1}H NMR (400 MHz, $CDCl_3$, 20 °C): δ = 1.13 [t, ^3J(H,H) = 7.1 Hz, 3 H, CH_3], 1.49 (s, 3 H, CH_3), 2.18 [d, ^2J(H,H) = 13.5 Hz, 1 H, SO_2CH_2], 2.26 (s, 3 H, CH_3), 3.46 [d, ^2J(H,H) = 13.5 Hz, 1 H, SO_2CH_2], 3.98 (res. m, OCH_2), 4.89 (s, C_5H_5). − ^{13}C NMR (100 MHz, $CDCl_3$, 20 °C): δ = 13.9 (s, CH_3), 20.3 (s, CH_3), 27.8 (s, CH_3), 57.8 (s, C_{quat}), 60.9 (s, OCH_2), 74.7 (s, SO_2CH_2), 84.3 (s, C_5H_5), 171.9 (s, CO), 207.1 (s, CO). − ^{31}P NMR (162 MHz, $CDCl_3$, 20 °C): δ = 53.3 [d, J(P,P) = 28 Hz, PMe_2], 87.0 [d, J(P,P) = 28 Hz, PPh_2]. − Minor diastereoisomer (29%): ^{1}H NMR (400 MHz, $CDCl_3$, 20 °C): δ = 1.22 [t, ^3J(H,H) = 7.1 Hz, 3 H, CH_3], 1.37 (s, 3 H, CH_3), 1.81 (s, 3 H, CH_3), 2.19 [d, ^2J(H,H) = 13.6 Hz, 1 H, SO_2CH_2], 3.21 [d, ^2J(H,H) = 13.6 Hz, 1 H, SO_2CH_2], 4.17 (res. m, OCH_2), 4.92 (s, C_5H_5). − ^{13}C NMR (100 MHz, $CDCl_3$, 20 °C): δ = 14.0 (s, CH_3), 18.5 (s, CH_3), 24.8 (s, CH_3), 59.3 (s, C_{quat}), 61.1 (s, OCH_2), 71.6 (s, SO_2CH_2), 84.1 (s, C_5H_5), 172.0 (s, CO), 204.4 (s, CO). − ^{31}P NMR (162 MHz, $CDCl_3$, 20 °C): δ = 53.5 [d, J(P,P) = 27 Hz, PMe_2], 86.8 [d, J(P,P) = 27 Hz, PPh_2]. − IR (Nujol): $\tilde{\nu}$ = 1738, 1706 cm^{-1} (CO), 1187, 1150, 1000 cm^{-1} (S=O). − $C_{29}H_{38}O_5P_2RuS$ (661.7): calcd. C 52.64, H 5.79, S 4.85; found C 51.82, H 5.76, S 4.89.

4b: Yield 83 mg (60%), m.p. 160 °C (dec.). − Major diastereoisomer (74%): ^{1}H NMR (400 MHz, $CDCl_3$, 20 °C): δ = 1.30 (s, 9 H, *t*Bu), 1.42 (s, 3 H, CH_3), 2.13 (s, 3 H, CH_3), 2.10 [d, ^2J(H,H) = 13.6 Hz, 1 H, SO_2CH_2], 3.45 [d, ^2J(H,H) = 13.6 Hz, 1 H, SO_2CH_2], 4.89 (s, 5 H, C_5H_5). − ^{13}C NMR (100 MHz, $CDCl_3$, 20 °C): δ = 20.7 (s, CH_3), 27.5 (s, CH_3), 27.7 (s, *t*Bu), 31.7 (s, CH_3), 58.6 (s, C_{quat}), 74.5 (s, SO_2CH_2), 80.9 (s, C_{quat}), 84.2 (s, C_5H_5), 170.6 (s, CO), 206.7 (s, CO). − ^{31}P NMR (162 MHz, $CDCl_3$, 20 °C): δ = 53.3 [d, J(P,P) = 28 Hz, PMe_2], 87.0 [d, J(P,P) = 28 Hz, PPh_2]. − Minor diastereoisomer (26%): ^{1}H NMR (400 MHz, $CDCl_3$, 20 °C): δ = 1.23 (s, 9 H, *t*Bu), 1.41 (s, 3 H, CH_3), 2.15 (s, 3 H, CH_3), 2.40 [d, ^2J(H,H) = 13.7 Hz, 1 H, SO_2CH_2], 3.07 [d, ^2J(H,H) = 13.7 Hz, 1 H, SO_2CH_2], 4.91 (s, 5 H, C_5H_5). − ^{13}C NMR (100 MHz, $CDCl_3$, 20 °C): δ = 18.8 (s, CH_3), 27.8 (s, CH_3), 29.3 (s, *t*Bu), 59.9 (s, C_{quat}), 71.8 (s, SO_2CH_2), 83.7 (s, C_{quat}), 84.1 (s, C_5H_5), 170.9 (s, CO), 204.7 (s, CO). − ^{31}P NMR (162 MHz, $CDCl_3$, 20 °C): δ = 53.5 [d, J(P,P) = 28 Hz, PMe_2], 86.9 [d, J(P,P) = 28 Hz, PPh_2]. − IR (Nujol): $\tilde{\nu}$ = 1727, 1700 cm^{-1} (CO), 1139, 1025 cm^{-1} (S=O). − $C_{31}H_{42}O_5P_2RuS$ (689.8): calcd. C 53.98, H 6.14; found C 53.28, H 6.38.

4c: Yield 85 mg (63%), m.p. 177 °C (dec.). − Major diastereoisomer (66%): ^{1}H NMR (400 MHz, $CDCl_3$, 20 °C): δ = 1.14 [t, ^3J(H,H) = 7.1 Hz, 3 H, CH_3], 2.34 [d, ^2J(H,H) = 13.8 Hz, 1 H, SO_2CH_2], 3.31 [d, ^2J(H,H) = 13.8 Hz, 1 H, SO_2CH_2], 3.96 (res. m, 2 H, OCH_2), 4.90 (s, 5 H, C_5H_5). − ^{13}C NMR (100 MHz, $CDCl_3$, 20 °C): δ =

14.0 (s, CH_3), 19.8 (s, CH_2), 30.8 (s, CH_2), 37.5 (CH_2), 58.6 (s, C_{quat}), 60.9 (s, OCH_2), 72.5 (s, SO_2CH_2), 84.5 (s, C_5H_5), 170.8 (s, CO), 215.5 (s, CO). − ^{31}P NMR (162 MHz, $CDCl_3$, 20°C): δ = 53.3 [d, J(P,P) = 28 Hz, PMe_2], 86.9 [d, J(P,P) = 28 Hz, PPh_2]. − Minor diastereoisomer (34%): ^{1}H NMR (400 MHz, $CDCl_3$, 20°C): δ = 1.21 [t, ^3J(H,H) = 7.1 Hz, 3 H, CH_3], 1.63 [d, ^2J(H,H) = 13.5 Hz, 1 H, SO_2CH_2], 3.15 [d, ^2J(H,H) = 13.5 Hz, 1 H, SO_2CH_2], 4.13 [q, ^3J(H,H) = 7.1 Hz, 2 H, OCH_2], 4.94 (s, 5 H, C_5H_5). − ^{13}C NMR (100 MHz, $CDCl_3$, 20°C): δ = 19.1 (s, CH_2), 19.5 (s, CH_3), 30.4 (s, CH_2), 37.0 (s, CH_2), 59.8 (s, C_{quat}), 61.2 (s, OCH_2), 69.0 (s, CH_2SO_2), 84.2 (s, C_5H_5), 169.2 (s, CO), 213.7 (s, CO). − ^{31}P NMR (162 MHz, $CDCl_3$, 20°C): δ = 53.4 [d, J(P,P) = 28 Hz, PMe_2], 86.7 [d, J(P,P) = 28 Hz, PPh_2]. − IR (Nujol): $\tilde{\nu}$ = 1742, 1721 cm^{-1} (CO), 1150, 1121, 1024, 1011 cm^{-1} (S=O). − $C_{30}H_{38}O_5P_2RuS$ (673.7): calcd. C 53.48, H 5.69; found C 52.62, H 5.44.

4c by Titanium Enolate Addition: Ethyl 2-oxocyclopentanecarboxylate (35 mg, 0.22 mmol) was deprotonated as described above and then treated at −30°C with $TiCl(OiPr)_3$. After addition of **2a** (135 mg, 0.20 mmol), the mixture was allowed to warm to 20°C and was stirred for 2 h. The solvent was removed under vacuum, and the oily residue was taken up in CD_2Cl_2 and analysed by ^{1}H and ^{31}P NMR, which indicated the formation of **4c** with 81% de. Attempted workup by hydrolysis and chromatography, however, resulted in an intractable mixture from which **4c** could not be separated in pure form.

[CpRu(mppe){$SO_2CH(Me)(C_8H_{13}O_4)$}] (4d): To a solution of $Na[N(SiMe_3)_2]$ (103 mg, 0.56 mmol) in THF (20 mL), diethyl methylmalonate (87 mg, 0.50 mmol) was added at −70°C. In a separate reaction, a solution of **1** (325 mg, 0.50 mmol) in dichloromethane (25 mL) was treated with a solution of diazoethane in diethyl ether (2.0 mL, 0.51 mmol) at −70°C and stirred at this temperature for 5 min. The two solutions were combined at −70 °C, and the resulting mixture was allowed to warm to 20 °C and was stirred for an additional hour. The solvent was then removed under vacuum and the oily residue was taken up in dichloromethane and chromatographed (neutral alumina, activity grade I, acetone/dichloromethane, 2:1). A broad, pale-yellow band containing the product was collected. The solvent was evaporated and the product was recrystallized from benzene/hexanes. Yield 251 mg (71%), m.p. 106°C (dec.). − Major diastereoisomer (63%): ^{1}H NMR (400 MHz, $CDCl_3$, 20°C): δ = 0.19 [d, ^3J(H,H) = 7.2 Hz, 3 H, CH_3], 1.14 [t, ^3J(H,H) = 7.2 Hz, 3 H, CH_3], 1.17−1.26 (m, 3 H, CH_3), 1.46 (s, 3 H, CH_3), 3.45 [q, ^3J(H,H) = 7.2 Hz, 1 H, SO_2CH], 3.98−4.28 (m, 4 H, 2 × OCH_2], 4.84 (s, 5 H, C_5H_5). − ^{13}C NMR (100 MHz, $CDCl_3$, 20°C): δ = 9.7 (s, CH_3), 14.0 (s, CH_3), 14.1 (s, CH_3), 14.5 (s, CH_3), 58.0 (s, C_{quat}), 60.8 (s, OCH_2), 61.0 (s, OCH_2), 74.2 (s, SO_2CH), 83.5 (s, C_5H_5), 171.1 (s, CO), 171.2 (s, CO). − ^{31}P NMR (162 MHz, $CDCl_3$, 20°C): δ = 61.0 [d, J(P,P) = 16 Hz, PMe_2], 85.9 [d, J(P,P) = 16 Hz, PPh_2]. − Minor diastereoisomer (37%): ^{1}H NMR (400 MHz, $CDCl_3$, 20°C): δ = 1.16 [t, ^3J(H,H) = 7.2 Hz, 3 H, CH_3], 1.17−1.26 (m, 3 H, CH_3), 1.24 [d, ^3J(H,H) = 8.0 Hz, 3 H, CH_3], 1.45 (s, 3 H, CH_3), 3.70 [q, ^3J(H,H) = 8.0 Hz, 1 H, SO_2CH], 3.98−4.28 (m, 4 H, 2 × OCH_2], 5.00 (s, 5 H, C_5H_5). − ^{13}C NMR (100 MHz, $CDCl_3$, 20°C): δ = 12.5 (s, CH_3), 14.0 (s, CH_3), 15.1 (s, CH_3), 29.4 (s, CH_3), 56.9 (s, C_{quat}), 61.0 (s, OCH_2), 61.2 (s, OCH_2), 71.7 (s, SO_2CH), 83.3 (s, C_5H_5), 171.1 (s, CO), 171.2 (s, CO). − ^{31}P NMR (162 MHz, $CDCl_3$, 20°C): δ = 51.6 [d, J(P,P) = 29 Hz, PMe_2], 81.5 [d, J(P,P) = 29 Hz, PPh_2]. − IR (Nujol): $\tilde{\nu}$ = 1731 cm^{-1} (CO), 1165, 1051 cm^{-1} (S=O). − $C_{31}H_{42}O_6P_2RuS$ (705.8): calcd. C 52.76, H 6.00, S 4.54; found C 53.01, H 6.01, S 4.54.

[NmCpRu(PPh_3)$_2$Cl] (5): To a solution of (+)-neomenthylcyclopentadiene (1.94 g, 9.49 mmol) in diethyl ether (50 mL) was added, at 0°C, a solution of methyllithium in diethyl ether (6.25 mL, 10.0 mmol). The mixture was allowed to warm to room temperature and was stirred overnight. A white precipitate was formed, which was washed thoroughly with diethyl ether; the resulting solution was dried under vacuum. The lithium neomenthylcyclopentadienide (84 mg, 0.40 mmol) was added to a solution of [$RuCl_2(PPh_3)_3$] (336 mg, 0.35 mmol) in benzene (30 mL). The mixture was heated under reflux for 1 h, causing a color change to orange. The solvent was removed under vacuum and the residue was chromatographed (silica gel, acetone/dichloromethane, 10:1). A broad orange band containing the product was collected and concentrated to dryness. The residue was taken up in hexane and treated with ultrasound whereupon the product separated out as an orange crystalline powder. Yield 212 mg (70%), m.p. 125°C (dec.). − ^{1}H NMR (400 MHz, $CDCl_3$, 20°C): δ = 0.74 [d, ^3J(H,H) = 6.4 Hz, 3 H, CH_3], 0.89 [d, ^3J(H,H) = 6.4 Hz, 3 H, CH_3], 0.91 [d, ^3J(H,H) = 6.4 Hz, 3 H, CH_3], 1.01−1.77 (m, 7 H, Nm), 2.43−2.51 (m, 2 H, Nm), 2.88−2.96 (m, 1 H, Nm), 3.05, 3.62, 3.91, 4.02 (4 × s, 4 × 1 H, C_5H_4Nm). − ^{13}C NMR (100 MHz, $CDCl_3$, 20°C): δ = 21.3 (s, CH_3), 22.4 (s, CH_3), 22.7 (s, CH_3), 24.9 (s, CH_2), 28.0 (s, CH), 28.6 (s, CH), 34.3 (s, CH), 35.4 (s, CH_2), 38.1 (s, CH_2), 50.2 (s, CH), 73.5, 76.1 (2 × s, 2 × C_5H_4), 78.7, 80.4 [2 × d, ^2J(P,C) = 9 Hz, 2 × C_5H_4], 115.9 [d, ^2J(P,C) = 5 Hz, C_5H_4]. − ^{31}P NMR (162 MHz, $CDCl_3$, 20°C): δ = 39.9 [d, ^2J(P,P) = 41 Hz], 40.8 [d, ^2J(P,P) = 41 Hz]. − $C_{51}H_{53}ClP_2Ru$ (864.5): calcd. C 70.86, H 6.18; found C 70.81, H 6.19.

[NmCpRu(mppe)Cl] (6): A solution of **5** (425 mg, 0.49 mmol) and mppe (137 mg, 0.50 mmol) in benzene (100 mL) was heated under reflux for 20 h. The solvent was evaporated and the red oily residue was taken up in dichloromethane and chromatographed (silica gel, dichloromethane/acetone, 1:10). A broad, orange band containing the product was collected and the orange crystalline product was isolated as described above for **5**. Yield 242 mg (80%), m.p. 144°C (dec.). − Diastereoisomer **6′** (50%): ^{1}H NMR (400 MHz, $CDCl_3$, 20°C): δ = 0.75 [d, ^3J(H,H) = 6.6 Hz, 3 H, CH_3], 0.82 [d, ^3J(H,H) = 6.2 Hz, 3 H, CH_3], 0.93 [d, ^3J(H,H) = 6.6 Hz, 3 H, CH_3], 0.95−1.95 (m, 7 H, Nm), 2.10−2.25 (m, 2 H, Nm), 2.80−2.88 (m, 1 H, Nm), 3.33, 3.97, 4.73, 5.07 (4 × s, 4 × 1 H, C_5H_4). − ^{13}C NMR (100 MHz, $CDCl_3$, 20°C): δ = 20.6 (s, CH_3), 22.4 (s, CH_3), 23.1 (s, CH_3), 24.4 (s, CH_2), 28.6 (s, CH), 29.6 (s, CH), 35.2 (s, CH), 35.9 (s, CH_2), 40.6 (s, CH_2), 48.5 (s, CH), 63.9, 77.4 (2 × s, 2 × C_5H_4), 81.5 [d, ^2J(C,P) = 8 Hz, C_5H_4], 85.4 [d, ^2J(C,P) = 8 Hz, C_5H_4], 106.6 [d, ^2J(C,P) = 8 Hz, C_5H_4]. − ^{31}P NMR (162 MHz, $CDCl_3$, 20°C): δ = 51.8 [d, J(P,P) = 30 Hz, PMe_2], 84.3 [d, J(P,P) = 30 Hz, PPh_2]. − Diastereoisomer **6′′** (50%): ^{1}H NMR (400 MHz, $CDCl_3$, 20°C): δ = 0.96 [d, ^3J(H,H) = 6.6 Hz, 3 H, CH_3], 0.92−1.95 (m, 13 H, Nm), 2.10−2.25 (m, 2 H, Nm), 2.93−2.99 (m, 1 H, Nm), 3.48, 3.95, 4.45, 4.98 (4 × s, 4 × 1 H, C_5H_4Nm). − ^{13}C NMR (100 MHz, $CDCl_3$, 20°C): δ = 20.5 (s, CH_3), 22.3 (s, CH_3), 22.8 (s, CH_3), 24.3 (s, CH_2), 27.1 (s, CH), 29.4 (s, CH), 35.1 (s, CH), 35.7 (s, CH_2), 40.5 (s, CH_2), 48.4 (s, CH), 71.3 [d, ^2J(P,C) = 11 Hz, C_5H_4], 73.1 (s, C_5H_4), 77.5 [d, ^2J(P,C) = 8 Hz, C_5H_4], 87.8 [d, ^2J(P,C) = 6 Hz, C_5H_4], 106.5 [d, ^2J(P,C) = 6 Hz, C_5H_4]. − ^{31}P NMR (162 MHz, $CDCl_3$, 20°C): δ = 51.8 [d, J(P,P) = 29 Hz, PMe_2], 81.7 [d, J(P,P) = 29 Hz, PPh_2]. − $C_{31}H_{43}ClP_2Ru$ (614.2): calcd. C 60.62, H 7.06; found C 60.84, H 7.39. − A sample of diastereomerically pure **6′** was obtained from **6** (5.00 g) by four cycles of slow crystallization from toluene/hexane. Yield 0.45 g (18%).

[NmCpRu(mppe)(SO_2)]PF_6 (7): A pressure tube equipped with a teflon needle valve was charged with **6** (210 mg, 0.34 mmol), NH_4PF_6 (73 mg, 0.45 mmol), and dichloromethane (20 mL). After this solution was cooled to −70°C, an excess of sulfur dioxide (ca

1 mL) was condensed into it. The mixture was stirred at 20°C for 15 h, during which a color change to yellow occurred. The excess SO_2 was removed under vacuum and the solution was filtered through Celite. After this solution was concentrated to dryness, the residue was recrystallized from dichloromethane/pentane to obtain a yellow crystalline powder. Yield 212 mg (79%), m.p. 153°C (dec.). − Diastereoisomer **7′** (50%): ^{1}H NMR (400 MHz, [D$_6$]acetone, 20°C): δ = 0.76 [d, ^3J(H,H) = 6.4 Hz, 3 H, CH$_3$], 0.93 [d, ^3J(H,H) = 6.4 Hz, 3 H, CH$_3$], 0.99 [d, ^3J(H,H) = 6.4 Hz, 3 H, CH$_3$], 1.05−2.05 (m, 7 H, Nm), 2.50−2.68 (m, 2 H, Nm), 2.88−3.02 (m, 1 H, Nm), 4.62, 5.12, 5.32, 5.89 (4 × s, 4 × 1 H, C$_5$H$_4$). − ^{13}C NMR (100 MHz, [D$_6$]acetone, 20°C): δ = 20.5 (s, CH$_3$), 22.4 (s, CH$_3$), 23.1 (s, CH$_3$), 24.4 (s, CH$_2$), 28.6 (s, CH), 29.6 (s, CH), 35.8 (s, CH), 36.0 (s, CH$_2$), 45.9 (s, CH$_2$), 49.2 (s, CH), 79.2 (s, C$_5$H$_4$), 95.1 [d, ^2J(C,P) = 4 Hz, C$_5$H$_4$], 96.4 [d, ^2J(C,P) = 6 Hz, C$_5$H$_4$], 122.76 (s, C$_5$H$_4$). − ^{31}P NMR (162 MHz, [D$_6$]acetone, 20°C): δ = 55.7 [d, J(P,P) = 20 Hz, PMe$_2$], 77.9 [d, J(P,P) = 20 Hz, PPh$_2$]. − Diastereoisomer **7′′** (50%): ^{1}H NMR (400 MHz, [D$_6$]acetone, 20°C): δ = 0.80 [d, ^3J(H,H) = 6.4 Hz, 3 H, CH$_3$], 0.81 [d, ^3J(H,H) = 6.4 Hz, 3 H, CH$_3$], 1.01 [d, ^3J(H,H) = 6.4 Hz, 3 H, CH$_3$], 1.05−2.05 (m, 7 H, Nm), 2.50−2.68 (m, 2 H, Nm), 3.16−3.28 (m, 1 H, Nm), 5.12, 5.27, 5.84, 6.29 (4 × s, 4 × 1 H, C$_5$H$_4$). − ^{13}C NMR (100 MHz, [D$_6$]acetone, 20°C): δ = 20.8 (s, CH$_3$), 22.5 (s, CH$_3$), 22.8 (s, CH$_3$), 24.7 (s, CH$_2$), 28.8 (s, CH), 30.4 (s, CH), 35.6 (s, CH), 35.9 (s, CH$_2$), 43.7 (s, CH$_2$), 48.2 (s, CH), 83.2, 87.9 (2 × s, 2 × C$_5$H$_4$), 94.4 [d, ^2J(C,P) = 2 Hz, C$_5$H$_4$], 95.0 [d, ^2J(C,P) = 4 Hz, C$_5$H$_4$], 122.81 (s, C$_5$H$_4$). − ^{31}P NMR (162 MHz, [D$_6$]acetone, 20°C): δ = 55.5 [d, J(P,P) = 21 Hz, PMe$_2$], 74.8 [d, J(P,P) = 21 Hz, PPh$_2$]. − IR (Nujol): $\tilde{\nu}$ = 1282, 1016 cm^{-1} (S=O). − $C_{31}H_{43}F_6O_2P_3RuS$ (787.7): calcd. C 47.27, H 5.50; found C 48.64, H 5.79. − From the same procedure, diastereomerically pure **7′** was obtained from pure **6′**.

[NmCpRu(mppe)(CH$_2$=SO$_2$)]PF$_6$ (8′): This compound was prepared from diastereomerically pure **7′** and diazomethane as described above for **2a**. Attempted crystallization at 0°C yielded only a pale-brown semi-solid product which was identified spectroscopically. − ^{1}H NMR (400 MHz, CD$_2$Cl$_2$, 20°C): δ = 0.39 [dd, ^2J(H,H) = 4.4 Hz, ^3J(P,H) = 16.8 Hz, 1 H, SO$_2$=CH$_2$], 0.91 [d, ^3J(H,H) = 6.4 Hz, 3 H, CH$_3$], 0.94 [d, ^3J(H,H) = 6.1 Hz, 3 H, CH$_3$], 1.04 [d, ^3J(H,H) = 6.3 Hz, 3 H, CH$_3$], 4.81, 5.31, 5.61, 5.98 (4 × s, 4 ×1 H, C$_5$H$_4$); due to sample decomposition, the remaining signals could not be assigned with certainty. − ^{31}P NMR (162 MHz, CD$_2$Cl$_2$, 20°C): δ = 67.6 [d, J(P,P) = 16 Hz, PMe$_2$], 80.0 [d, J(P,P) = 16 Hz, PPh$_2$].

[NmCpRu(mppe){SO$_2$CH$_2$(C$_7$H$_{11}$O$_3$)}] (9): A solution of **7** (0.24 g, 0.30 mmol) in dichloromethane (20 mL) was treated consecutively with diazomethane and the sodium enolate of ethyl 2-methyl-3-oxobutanoate, as described above for the synthesis of **4d**. Chromatographic workup gave a yellow oil which could not be induced to crystallize. Yield 112 mg (47%) − Major diastereoisomer (72%): ^{1}H NMR (400 MHz, CDCl$_3$, 20°C): δ = 0.71 [d, ^3J(H,H) = 6.4 Hz, 3 H, CH$_3$], 0.82 [d, ^3J(H,H) = 6.0 Hz, 3 H, CH$_3$], 0.97 [d, ^3J(H,H) = 6.4 Hz, 3 H, CH$_3$], 1.12 [t, ^3J(H,H) = 7.0 Hz, 3 H, CH$_3$], 1.54 (s, 3 H, CH$_3$), 2.11 [d, ^2J(H,H) = 13.6 Hz, 1 H, SO$_2$CH$_2$], 2.45 (s, 3 H, CH$_3$), 2.92−2.95 (m, 1 H, CH), 3.44 [d, ^2J(H,H) = 13.6 Hz, 1 H, SO$_2$CH$_2$], 3.87−4.01 (m, 2 H, OCH$_2$), 4.33, 4.78, 5.15, 5.40 (4 × s, 4 × 1 H, C$_5$H$_4$). − ^{13}C NMR (100 MHz, CDCl$_3$, 20°C): δ = 13.9 (s, CH$_3$), 27.8 (s, CH), 29.5 (s, CH), 36.0 (s, CH$_2$), 36.5 (s, CH), 42.3 (s, CH$_2$), 48.8 (s, CH), 57.7 (s, C$_{quat}$), 60.8 (s, OCH$_2$), 74.6 (s, SO$_2$CH$_2$), 75.1, 77.7, 88.0 (3 × s, 3 × C$_5$H$_4$), 98.6 [d, ^2J(P,C) = 4 Hz, C$_5$H$_4$], 106.8 [d, ^2J(P,C) = 10 Hz, C$_5$H$_4$], 172.0 (s, CO), 207.6 (s, CO). − ^{31}P NMR (162 MHz, CDCl$_3$, 20°C): δ = 48.8 [d, J(P,P) = 28 Hz, PMe$_2$], 88.3 [d, J(P,P) = 28 Hz, PPh$_2$]. − Minor diastereoisomer (28%): ^{1}H NMR (400 MHz, CDCl$_3$, 20°C): δ = 0.10 [d, ^3J(H,H) = 6.4 Hz, 3 H, CH$_3$], 0.88 [d, ^3J(H,H) = 6.0 Hz, 3 H, CH$_3$], 1.11 [t, ^3J(H,H) = 7.0 Hz, 3 H, CH$_3$], 1.51 (s, 3 H, CH$_3$), 2.24 (s, 3 H, CH$_3$), 2.29 [d, ^2J(H,H) = 13.6 Hz, 1 H, SO$_2$CH$_2$], 2.96−3.01 (m, 1 H, CH), 3.42 [d, ^2J(H,H) = 13.6 Hz, 1 H, SO$_2$CH$_2$], 3.87−4.01 (m, 2 H, OCH$_2$), 4.15, 5.03, 5.05, 5.14 (4 × s, 4 × 1 H, C$_5$H$_4$). − ^{13}C NMR (100 MHz, CDCl$_3$, 20°C): δ = 13.9 (s, CH$_3$), 34.5 (s, CH), 36.0 (s, CH$_2$), 41.8 (s, CH$_2$), 48.8 (s, CH), 57.8 (s, C$_{quat}$), 60.8 (s, OCH$_2$), 74.6, (s, SO$_2$CH$_2$), 75.2, 78.1, 87.9 (3 × s, 3 × C$_5$H$_4$), 94.3 [d, ^2J(P,C) = 4 Hz, C$_5$H$_4$], 105.9 [d, ^2J(P,C) = 10 Hz, C$_5$H$_4$], 171.9 (s, CO), 206.9 (s, CO). − ^{31}P NMR (162 MHz, CDCl$_3$, 20°C): δ = 52.4 [d, J(P,P) = 26 Hz, PMe$_2$], 86.3 [d, J(P,P) = 26 Hz, PPh$_2$]. − IR (Nujol): $\tilde{\nu}$ = 1732, 1712 cm^{-1} (CO), 1136, 1025 cm^{-1} (S=O).

[CpRu(chir)(SO$_2$)]PF$_6$ (10): This compound was prepared from [CpRu(chir)Cl] (0.26 g, 0.42 mmol), NH_4PF_6 (88 mg, 0.54 mmol) and SO_2 as described above for **7**. Yield 0.28 g (84%), m.p. 160°C (dec.). − ^{1}H NMR (400 MHz, CD$_2$Cl$_2$, 20°C): δ = 5.36 (s, 5 H, C$_5$H$_5$). − ^{13}C NMR (100 MHz, CD$_2$Cl$_2$, 20°C): δ = 92.2 (s, C$_5$H$_5$). − ^{31}P NMR (162 MHz, CD$_2$Cl$_2$, 20°C): δ = 69.3 [d, J(P,P) = 34 Hz], 74.2 [d, J(P,P) = 34 Hz]. − IR (Nujol): $\tilde{\nu}$ = 1296, 1118 cm^{-1} (S=O). − $C_{33}H_{33}F_6O_2P_3RuS$ (801.7): calcd. C 49.44, H 4.15, S 4.00; found C 49.34, H 4.17, S 3.94.

[CpRu(chir)(SO$_2$=CH$_2$)]PF$_6$ (11): This compound was prepared from **10** (80 mg, 0.10 mmol) and diazomethane as described above for **2a**. Yield 78 mg (96%), m.p. 157°C (dec.). − ^{1}H NMR (400 MHz, CD$_2$Cl$_2$, 20°C): δ = 0.85 [dd, ^2J(H,H) = 4.3 Hz, ^3J(H,P) = 16.7 Hz, 1 H, SO$_2$CH$_2$], 2.31 [dt, ^2J(H,H) = 4.3 Hz, ^3J(H,P) = 1.6 Hz, 1 H, SO$_2$CH$_2$], 5.21 (s, 5 H,C$_5$H$_5$). − ^{13}C NMR (100 MHz, CD$_2$Cl$_2$, 20°C): δ = −17.7 [d, ^2J(P,C) = 3 Hz, SO$_2$CH$_2$], 97.9 (s, C$_5$H$_5$). − ^{31}P NMR (162 MHz, CD$_2$Cl$_2$, 20°C): δ = 62.0 [d, J(P,P) = 42 Hz], 77.4 [d, J(P,P) = 42 Hz]. − IR (Nujol): $\tilde{\nu}$ = 1245, 1104 cm^{-1} (S=O). − $C_{34}H_{35}F_6O_2P_3RuS$ (815.7): calcd. C 50.06, H 4.33, S 3.93; found C 50.25, H 4.56, S 4.08.

{CpRu(chir)[SO$_2$=CH$_2$(C$_9$H$_{15}$NO)]}PF$_6$ (12): A solution of **10** (88 mg, 0.11 mmol) in dichloromethane (10 mL) was treated consecutively with diazomethane and *N*-(1-cyclopentenyl)morpholine as described above for the synthesis of **3**. Yield 86 mg (81%), m.p. 141°C (dec.). − Major diastereoisomer (82%): ^{1}H NMR (400 MHz, CD$_2$Cl$_2$, 20°C): δ = 4.62 (s, 5 H, C$_5$H$_5$); due to extensive signal overlap the remaining resonances could not be assigned with certainty. − ^{13}C NMR (100 MHz, CD$_2$Cl$_2$, 20°C): δ = 21.0 (s, CH$_2$), 32.0 (s, CH$_2$), 35.6 (s, CH$_2$), 43.2 (s, CH), 54.7 (s, NCH$_2$), 65.3 (s, OCH$_2$), 66.6 (s, OCH$_2$), 68.5 (s, SO$_2$CH$_2$), 86.3 (s, C$_5$H$_5$), 202.9 (s, CN). − ^{31}P NMR (162 MHz, CD$_2$Cl$_2$, 20°C): δ = 67.3 [d, J(P,P) = 35 Hz], 85.4 [d, J(P,P) = 35 Hz]. − Minor diastereoisomer (18%): ^{1}H NMR (400 MHz, CD$_2$Cl$_2$, 20°C): δ = 4.61 (s, 5 H, C$_5$H$_5$); due to extensive signal overlap the remaining resonances could not be assigned with certainty. − ^{13}C NMR (100 MHz, CD$_2$Cl$_2$, 20°C): δ = 21.9 (s, CH$_2$), 31.3 (s, CH$_2$), 34.5 (s, CH$_2$), 44.0 (s, CH), 52.5 (s, NCH$_2$), 64.7 (s, OCH$_2$), 65.6 (s, OCH$_2$), 69.8 (s, SO$_2$CH$_2$), 86.5 (s, C$_5$H$_5$), 201.7 (s, CN). − ^{31}P NMR (162 MHz, CD$_2$Cl$_2$, 20°C): δ = 65.4 [d, J(P,P) = 36 Hz], 86.0 [d, J(P,P) = 36 Hz]. − IR (Nujol): $\tilde{\nu}$ = 1666 cm^{-1} (CN), 1087, 995 cm^{-1} (S=O). − $C_{43}H_{50}F_6NO_3P_3RuS$ (968.9): calcd. C 53.30, H 5.20, N 1.45; found C 53.04, H 5.55, N 1.45.

Addition of Enolates to 11: A solution of **10** (0.16 g, 0.20 mmol) in dichloromethane (15 mL) was treated at −70°C with diazomethane and a suspension of the respective sodium enolate as described above for **4a−c**.

13a: Yield 133 mg (79%), m.p. 130°C (dec.). − ^{1}H NMR (400 MHz, CDCl$_3$, 20°C): δ = 1.15 [t, ^3J(H,H) = 7.1 Hz, 3 H,

CH_3], 1.18 [t, ^3J(H,H) = 7.1 Hz, 3 H, CH_3], 1.23 (s, 3 H, CH_3), 1.90 [d, ^2J(H,H) = 12.0 Hz, 1 H, SO_2CH_2], 3.07 [d, ^2J(H,H) = 12.0 Hz, 1 H, SO_2CH_2], 3.93−4.19 (m, 4 H, 2 × OCH_2), 4.53 (s, 5 H, C_5H_5). − ^{13}C NMR (100 MHz, $CDCl_3$, 20°C): δ = 13.9 (s, 2 × CH_3), 19.4 (s, CH_3), 53.1 (s, C_{quat}), 60.9 (s, 2 × OCH_2), 69.8 (s, SO_2CH_2), 86.4 (s, C_5H_5), 171.2 (s, CO), 171.5 (s, CO). − ^{31}P NMR (162 MHz, $CDCl_3$, 20°C): δ = 65.0 [d, J(P,P) = 34 Hz], 86.5 [d, J(P,P) = 34 Hz]. − IR (Nujol): $\tilde{\nu}$ = 1734 cm^{-1} (CO), 1148, 1025 cm^{-1} (S=O). − $C_{42}H_{48}O_6P_2RuS$ (843.9): calcd. C 59.78, H 5.73; found C 59.50, H 5.99.

13b: Yield 137 mg (84%), m.p. 220°C (dec.). − Major diastereoisomer (81%): ^{1}H NMR (400 MHz, $CDCl_3$, 20°C): δ = 1.19 [t, ^3J(H,H) = 7.2 Hz, 3 H, CH_3], 1.49 (s, 3 H, CH_3), 1.89 (s, 3 H, CH_3), 1.88 [d, ^2J(H,H) = 13.4 Hz, 1 H, SO_2CH_2], 3.00 [d, ^2J(H,H) = 13.4 Hz, 1 H, SO_2CH2], 4.13 (res. m, 2 H, OCH_2), 4.65 (s, 5 H, C_5H_5). − ^{13}C NMR (100 MHz, $CDCl_3$, 20°C): δ = 13.9 (s, CH_3), 18.6 (s, CH_3), 25.2 (s, CH_3), 59.3 (s, C_{quat}), 61.1 (s, OCH_2), 69.9 (s, SO_2CH_2), 86.5 (s, C_5H_5), 172.0 (s, CO), 204.8 (s, CO). − ^{31}P NMR (162 MHz, $CDCl_3$, 20°C): δ = 65.3 [d, J(P,P) = 35 Hz], 86.4 [d, J(P,P) = 35 Hz]. − Minor diastereoisomer (19%): ^{1}H NMR (400 MHz, $CDCl_3$, 20°C): δ = 1.14 [t, ^3J(H,H) = 7.2 Hz, 3 H, CH_3], 1.61 (s, 3 H, CH_3), 1.81 [d, ^2J(H,H) = 13.6 Hz, 1 H, SO_2CH_2], 2.24 (s, 3 H, CH_3), 3.28 [d, ^2J(H,H) = 13.6 Hz, 1 H, SO_2CH_2], 3.97 (res. m, 2 H, OCH_2) 4.53 (s, 5 H, C_5H_5). − ^{13}C NMR (100 MHz, $CDCl_3$, 20°C): δ = 13.9 (s, CH_3), 20.4 (s, CH_3), 27.6 (s, CH_3), 57.8 (s, C_{quat}), 60.9 (s, OCH_2), 72.6 (s, SO_2CH_2), 86.6 (s, C_5H_5), 171.9 (s, CO), 207.3 (s, CO). − ^{31}P NMR (162 MHz, $CDCl_3$, 20°C): δ = 65.2 [d, J(P,P) = 36 Hz], 86.6 [d, J(P,P) = 36 Hz]. − IR (Nujol): $\tilde{\nu}$ = 1712 cm^{-1} (CO), 1144, 1022 cm^{-1} (S=O). − $C_{41}H_{46}O_5P_2RuS$ (813.9): calcd. C 60.51, H 5.70; found C 60.33, H 5.72.

13c: Yield 133 mg (76%), m.p. 121°C (dec.). − Major diastereoisomer (68%): ^{1}H NMR (400 MHz, $CDCl_3$, 20°C): δ = 1.04 [t, ^3J(H,H) = 7.2 Hz, 3 H, CH_3], 1.23 (s, 3 H, CH_3), 2.07 [d, ^2J(H,H) = 13.6 Hz, 1 H, SO_2CH_2], 3.16 [d, ^2J(H,H) = 13.6 Hz, 1 H, SO_2CH_2], 3.96−4.15 (m, 2 H, OCH_2), 4.50 (s, 5 H, C_5H_5). − ^{13}C NMR (100 MHz, $CDCl_3$, 20°C): δ = 13.7 (s, CH_3), 20.5 (s, CH_3), 57.4 (s, C_{quat}), 61.2 (s, OCH_2), 71.0 (s, SO_2CH_2), 86.3 (s, C_5H_5), 172.4 (s, CO), 198.0 (s, CO). − ^{31}P NMR (162 MHz, $CDCl_3$, 20°C): δ = 65.2 [d, J(P,P) = 36 Hz], 86.6 [d, J(P,P) = 36 Hz]. − Minor diastereoisomer (32%): ^{1}H NMR (400 MHz, $CDCl_3$, 20°C): δ = 1.07 [t, ^3J(H,H) = 7.2 Hz, 3 H, CH_3], 1.22 (s, 3 H, CH_3), 2.10 [d, ^2J(H,H) = 13.4 Hz, 1 H, SO_2CH_2], 3.35 [d, ^2J(H,H) = 13.4 Hz, 1 H, SO_2CH_2], 3.96−4.15 (m, 2 H, OCH_2), 4.25 (s, 5 H, C_5H_5). − ^{13}C NMR (100 MHz, $CDCl_3$, 20°C): δ = 13.8 (s, CH_3), 21.2 (s, CH_3), 56.9 (s, C_{quat}), 61.1 (s, OCH_2), 71.7 (s, SO_2CH_2), 86.2 (s, C_5H_5), 172.5 (s, CO), 199.2 (s, CO). − ^{31}P NMR (162 MHz, $CDCl_3$, 20°C): δ = 65.0 [d, J(P,P) = 36 Hz], 86.3 [d, J(P,P) = 36 Hz]. − IR (Nujol): $\tilde{\nu}$ = 1680 cm^{-1} (CO), 1143, 1020 cm^{-1} (S=O). − $C_{46}H_{48}O_5P_2RuS$ (876.0): calcd. C 63.07, H 5.52; found C 62.94, H 5.84.

13d: Yield 136 mg (81%), m.p. 164°C (dec.). − Major diastereoisomer (95%): ^{1}H NMR (400 MHz, $CDCl_3$, 20°C): δ = 1.38 (s, 9 H, *t*Bu), 1.47 (s, 3 H, CH_3), 1.95 (s, 3 H, CH_3), 2.21 [d, ^2J(H,H) = 13.6 Hz, 1 H, SO_2CH_2], 2.88 [d, ^2J(H,H) = 13.6 Hz, 1 H, SO_2CH_2], 4.56 (s, 5 H, C_5H_5). − ^{13}C NMR (100 MHz, $CDCl_3$, 20°C): δ = 19.0 (s, CH_3), 25.8 (s, CH_3), 27.8 (s, *t*Bu), 59.8 (s, C_{quat}), 70.9 (s, SO_2CH_2), 80.8 (s, C_{quat}), 86.5 (s, C_5H_5), 170.8 (s, CO), 205.4 (s, CO). − ^{31}P NMR (162 MHz, $CDCl_3$, 20°C): δ = 66.8 [d, J(P,P) = 35 Hz], 86.6 [d, J(P,P) = 35 Hz]. − Minor diastereoisomer (5%): ^{1}H NMR (400 MHz, $CDCl_3$, 20°C): δ = 1.86 (s, 3 H, CH_3), 2.33 [d, ^2J(H,H) = 13.4 Hz, 1 H, SO_2CH_2], 4.89 (s, 5 H, C_5H_5); remaining signals obscured by major diastereoisomer. − ^{31}P NMR (162 MHz, $CDCl_3$, 20°C): δ = 65.0 [d, J(P,P) = 36 Hz]; second doublet obscured by major diastereoisomer. − IR (Nujol): $\tilde{\nu}$ = 1732, 1701 cm^{-1} (CO), 1145, 1025 cm^{-1} (S=O). − $C_{43}H_{50}O_5P_2RuS$ (842.0): calcd. C 61.34, H 5.99; found C 61.85, H 6.26. − Recrystallization from benzene/hexane gave the major diastereoisomer **13d′** in pure form.

13e: Yield 125 mg (76%), m.p. 150°C (dec.). − Major diastereoisomer (60%): ^{1}H NMR (400 MHz, $CDCl_3$, 20°C): δ = 1.18 [t, ^3J(H,H) = 7.2 Hz, 3 H, CH_3], 1.70−2.22 (m, 4 H, CH_2CH_2), 1.99 [d, ^2J(H,H) = 13.3 Hz, 1 H, SO_2CH_2], 3.07 [d, ^2J(H,H) = 13.3 Hz, 1 H, SO_2CH_2], 3.38−3.57 (m, 2 H, CH_2), 4.10 (res. m, 2 H, OCH_2), 4.56 (s, 5 H, C_5H_5). − ^{13}C NMR (100 MHz, $CDCl_3$, 20°C): δ = 14.0 (s, CH_3), 19.5 (s, CH_2), 30.8 (s, CH_2), 37.2 (s, CH_2), 59.7 (s, C_{quat}), 61.2 (s, OCH_2), 67.8 (s, SO_2CH_2), 86.6 (s, C_5H_5), 169.4 (s, CO), 214.1 (s, CO). − ^{31}P NMR (162 MHz, $CDCl_3$, 20°C): δ = 65.8 [d, J(P,P) = 35 Hz], 86.3 [d, J(P,P) = 35 Hz]. − Minor diastereoisomer (40%): ^{1}H NMR (400 MHz, $CDCl_3$, 20°C): δ = 1.14 [t, ^3J(H,H) = 7.2 Hz, 3 H, CH_3], 1.39 [d, ^2J(H,H) = 13.6 Hz, 1 H, SO_2CH_2], 1.70−2.22 (m, 4 H, CH_2CH_2), 2.99 [d, ^2J(H,H) = 13.6 Hz, 1 H, SO_2CH_2], 3.38−3.57 (m, 2 H, CH_2), 3.97 (res. m, 2 H, OCH_2), 4.53 (s, 5 H, C_5H_5). − ^{13}C NMR (100 MHz, $CDCl_3$, 20°C): δ = 14.0 (s, CH_3), 20.0 (s, CH_2), 29.7 (s, CH_2), 37.6 (s, CH_2), 58.6 (s, C_{quat}), 60.9 (s, OCH_2), 70.2 (s, SO_2CH_2), 86.7 (s, C_5H_5), 170.9 (s, CO), 215.2 (s, CO). − ^{31}P NMR (162 MHz, $CDCl_3$, 20°C): δ = 66.0 [d, J(P,P) = 35 Hz], 86.5 [d, J(P,P) = 35 Hz]. − IR (Nujol): $\tilde{\nu}$ = 1793, 1714 cm^{-1} (CO), 1146, 1021 cm^{-1} (S=O). − $C_{42}H_{46}O_5P_2RuS$ (825.9): calcd. C 61.08, H 5.61; found C 60.83, H 5.95.

***O*-Alkylation of the Sulfinato Complexes:** To a solution of the sulfinato complex (0.1 mmol) in dichloromethane (10 mL), a solution of triethyloxonium hexafluorophosphate (25 mg, 0.1 mmol) in the same solvent was added at −70°C. After being allowed to warm to room temperature, the mixture was concentrated to a volume of 1 mL and the product was precipitated by the addition of pentane.

14a: Yield 92 mg (92%), m.p. 121°C (dec.). − Major diastereoisomer (81%): ^{1}H NMR (400 MHz, [D_6]acetone, 20°C): δ = 0.81 [t, ^3J(H,H) = 7.2 Hz, 3 H, CH_3], 1.11 [t, ^3J(H,H) = 7.2 Hz, 3 H, CH_3], 1.19 [t, ^3J(H,H) = 7.2 Hz, 3 H, CH_3], 1.36 (s, 3 H, CH_3), 2.65 [dq, ^2J(H,H) = 9.7 Hz, ^3J(H,H) = 7.2 Hz, S(O)OCH], 2.87 [dq, ^2J(H,H) = 9.7 Hz, ^3J(H,H) = 7.2 Hz, S(O)OCH_2], 3.10 [d, ^2J(H,H) = 16.0 Hz, 1 H, SO_2CH_2], 3.68 [d, ^2J(H,H) = 16.0 Hz, 1 H, SO_2CH_2], 3.91−4.21 (m, 4 H, 2 × OCH_2), 4.98 (s, 5 H, C_5H_5). − ^{13}C NMR (100 MHz, [D_6]acetone, 20°C): δ = 14.0 (s, CH_3), 14.1 (s, CH_3), 14.3 (s, CH_3), 19.0 (s, CH_3), 54.4 (s, C_{quat}), 60.9 (s, OCH_2), 62.0 (s, OCH_2), 62.4 (s, OCH_2), 72.6 (s, SO_2CH_2), 88.9 (s, C_5H_5), 170.0 (s, CO), 170.1 (s, CO). − ^{31}P NMR (162 MHz, [D_6]acetone, 20°C): δ = 55.7 [d, J(P,P) = 38 Hz], 76.2 [d, J(P,P) = 38 Hz]. − Minor diastereoisomer (19%): ^{1}H NMR (400 MHz, [D_6]acetone, 20°C): δ = 3.46 [d, ^2J(H,H) = 14.7 Hz, 1 H, SO_2CH_2], 4.98 (s, 5 H, C_5H_5); remaining signals obscured by major diastereoisomer. − ^{13}C NMR (100 MHz, [D_6]acetone, 20°C): δ = 19.0 (s, CH_3), 54.5 (s, C_{quat}), 60.9 (s, OCH_2), 62.1 (s, OCH_2), 62.6 (s, OCH_2), 70.9 (s, SO_2CH_2), 88.7 (s, C_5H_5). − ^{31}P NMR (162 MHz, [D_6]acetone, 20°C): δ = 55.8 [d, J(P,P) = 37 Hz,], 77.4 [d, J(P,P) = 37 Hz]. − IR (Nujol): $\tilde{\nu}$ = 1735 cm^{-1} (CO), 1155 cm^{-1} (S=O). − $C_{44}H_{53}F_6O_6P_3RuS$ (1017.9): calcd. C 51.92, H 5.25, S 3.15; found C 52.19, H 5.05, S 3.06.

14b: Yield 95 mg (95%), m.p. 137°C (dec.). − Major diastereoisomer (53%): ^{1}H NMR (400 MHz, [D_6]acetone, 20°C): δ = 0.81 [t, ^3J(H,H) = 7.2 Hz, 3 H, CH_3], 1.27 (s, 3 H, CH_3), 1.32 (s, 9 H, *t*Bu), 1.95 (s, 3 H, CH_3), 2.55 [d, ^2J(H,H) = 15.2 Hz, 1 H, SO_2CH_2],

2.89 (res. m, 1 H, OCH_2), 3.70 (res. m, 1 H, OCH_2), 3.42 [d, ^2J(H,H) = 15.2 Hz, 1 H, SO_2CH_2], 4.98 (s, 5 H, C_5H_5). − ^{13}C NMR (100 MHz, [D$_6$]acetone, 20°C): δ = 14.0 (s, CH_3), 18.5 (s, CH_3), 26.5 (s, CH_3), 27.8 (s, *t*Bu), 60.9 (s, OCH_2), 61.1 (s, C_{quat}), 71.2 (s, SO_2CH_2), 82.8 (s, C_{quat}), 88.8 (s, C_5H_5), 169.2 (s, CO), 201.9 (s, CO). − ^{31}P NMR (162 MHz, [D$_6$]acetone, 20°C): δ = 55.6 [d, *J*(P,P) = 37 Hz], 77.1 [d, *J*(P,P) = 37 Hz]. − Minor diastereoisomer (47%): ^{1}H NMR (400 MHz, [D$_6$]acetone, 20°C): δ = 0.74 [t, ^3J(H,H) = 7.1 Hz, 3 H, CH_3], 1.41 (s, 3 H, CH_3), 1.42 (s, 9 H, *t*Bu), 2.11 (s, 3 H, CH_3), 2.62 (res. m, 1 H, OCH_2), 2.99 [d, ^2J(H,H) = 15.2 Hz, 1 H, SO_2CH_2], 3.48 (res. m, 1 H, OCH_2), 3.73 [d, ^2J(H,H) = 15.2 Hz, 1 H, SO_2CH_2], 4.99 (s, 5 H, C_5H_5). − ^{13}C NMR (100 MHz, [D$_6$]acetone, 20°C): δ = 14.8 (s, CH_3), 19.1 (s, CH_3), 25.2 (s, CH_3), 27.5 (s, *t*Bu), 60.6 (s, OCH_2), 65.8 (s, C_{quat}), 72.6 (s, SO_2CH_2), 83.2 (s, C_{quat}), 88.7 (s, C_5H_5), 170.0 (s, CO), 203.0 (s, CO). − ^{31}P NMR (162 MHz, [D$_6$]acetone, 20°C): δ = 55.9 [d, *J*(P,P) = 37 Hz], 76.2 [d, *J*(P,P) = 37 Hz]. − IR (Nujol): $\tilde{\nu}$ = 1715 cm^{-1} (CO), 1148 cm^{-1} (S=O). − $C_{45}H_{55}F_6O_5P_3RuS$ (1016.0): calcd. C 53.20, H 5.46; found C 53.43, H 5.75.

Liberation of the Sulfinic Acid Ester 16: 14b (0.22 g, 0.22 mmol) was dissolved in acetonitrile (10 mL) and heated under reflux for 15 h. Thereafter, the mixture was concentrated to dryness, and the resulting residue was suspended in diethyl ether. Upon ultrasonic treatment, complex **15** separated as a yellow powder, which was filtered off, washed with diethyl ether, and dried. The filtrate was concentrated to dryness, leaving the ester **16** as a colorless, spectroscopically pure oil.

15: Yield 0.16 g (93%), m.p. 113°C (dec.). − ^{1}H NMR (400 MHz, [D$_6$]acetone, 20°C): δ = 1.78 (s, 3 H, CH_3), 4.70 (s, 5 H, C_5H_5). − ^{13}C NMR (100 MHz, [D$_6$]acetone, 20°C): δ = 3.2 (s, CH_3), 83.2 [t, ^2J(P,C) = 2 Hz, C_5H_5], 127.5 (s, CN). − ^{31}P NMR (162 MHz, [D$_6$]acetone, 20°C): δ = 75.7 [d, *J*(P,P) = 40 Hz], 85.4 [d, *J*(P,P) = 40 Hz]. − $C_{35}H_{36}F_6NP_3Ru$ (778.7): calcd. C 53.99, H 4.66, N 1.80; found C 53.70, H 4.90, N 2.08.

16: Yield 58 mg (94%). − Major diastereoisomer (53%): ^{1}H NMR (400 MHz, $CDCl_3$, 20°C): δ = 1.32 [t, ^3J(H,H) = 7.1 Hz, 3 H, CH_3], 1.46 (s, 9 H, *t*Bu), 1.50 (s, 3 H, CH_3), 2.20 (s, 3 H, CH_3), 3.13 [d, ^2J(H,H) = 13.8 Hz, 1 H, SO_2CH_2], 3.28 [d, ^2J(H,H) = 13.8 Hz, 1 H, SO_2CH_2], 3.97−4.13 (m, 2 H, OCH_2). − ^{13}C NMR (100 MHz, $CDCl_3$, 20°C): δ = 15.8 (s, CH_3), 19.6 (s, CH_3), 22.5 (s, CH_3), 27.7 (s, *t*Bu), 58.0 (s, C_{quat}), 62.7 (s, CH_2), 65.1 (s, SO_2CH_2), 83.3 (s, C_{quat}), 169.7 (s, CO), 203.2 (s, CO). − Minor diastereoisomer (47%): ^{1}H NMR (400 MHz, $CDCl_3$, 20°C): δ = 1.33 [t, ^3J(H,H) = 7.1 Hz, 3 H, CH_3], 1.45 (s, 9 H, *t*Bu), 1.50 (s, 3 H, CH_3), 2.19 (s, 3 H, CH_3), 3.16 [d, ^2J(H,H) = 13.8 Hz, 1 H, SO_2CH_2], 3.30 [d, ^2J(H,H) = 13.8 Hz, 1 H, SO_2CH_2], 3.97−4.13 (m, 2 H, OCH_2). − ^{13}C NMR (100 MHz, $CDCl_3$, 20°C): δ = 15.7 (s, CH_3), 19.7 (s, CH_3), 25.8 (s, CH_3), 27.7 (s, *t*Bu), 58.1 (s, C_{quat}), 62.7 (s, CH_2), 64.9 (s, SO_2CH_2), 83.2 (s, C_{quat}), 169.8 (s, CO), 203.3 (s, CO).

X-ray Structure Determination of [CpRu(chir)(SO$_2$)]PF$_6$·2CH$_2$Cl$_2$ (10·2CH$_2$Cl$_2$): $C_{33}H_{33}F_6O_2P_3RuS{\cdot}2CH_2Cl_2$: molecular mass 971.49, crystal size 0.6 × 0.4 × 0.35 mm, obtained by diffusion of pentane into a concentrated dichloromethane solution; orthorhombic crystal system, space group $P2_12_12_1$ (No. 19), a = 12.6062(13), b = 16.025(2), c = 19.614(3) Å; V = 3962.3(9) Å^3, Z = 4, $d_{calcd.}$ = 1.629 g cm^{-3}; μ(Mo-K_α) = 9.00 cm^{-1}. Data were collected at 193 K in the range 2° < Θ < 25° from slightly more than one-eighth of the reflection sphere (index range $0 \le h \le 14$, $-3 \le k \le 19$, $-3 \le l \le 23$, Enraf−Nonius CAD4 diffractometer, graphite monochromator, Mo-K_α radiation, λ = 0.71073 Å). Of the 5595 measured reflections, 5128 were symmetry-independent and 4117 were classified as observed [$I_0 > 2\sigma(I_0)$]. An empirical absorption correction based on Ψ-scans was applied (average transmission 89.3%). The structure was solved by Direct Methods using the program package SHELXS-93[34] with hydrogen atoms included in their calculated positions. Refinement with the program package SHELXL-96[35] gave R_1 = 0.0545, wR_2 = 0.1214. The five highest maxima of a final difference Fourier map were below 0.78 e/Å^3. Further details of the structure determination may be obtained from the Cambridge Crystallographic Data Centre on quoting the depository number CCDC-132910.

X-ray Structure Determination of [CpRu(chir){SO$_2$CH$_2$C(Me)-{C(O)Me}[C(O)O*t*Bu]}] (13d′): $C_{43}H_{50}O_5P_2RuS$: molecular mass 841.90, crystal size 0.4 × 0.3 × 0.25 mm, obtained by diffusion of heptane into a concentrated benzene solution; tetragonal crystal system, space group $P4_32_12$ (No. 96), a = 16.389(2), b = 16.389(2), c = 29.607(5) Å; V = 7952(2) Å^3, Z = 8, $d_{calcd.}$ = 1.406 g cm^{-3}; μ(Mo-K_α) = 2.07 cm^{-1}. Data were collected at 293 K in the range 2° < Θ < 27° from one-eighth of the reflection sphere (index range $0 \le h \le 20$, $0 \le k \le 20$, $0 \le l \le 37$, Enraf−Nonius CAD4 diffractometer, graphite monochromator, Mo-K_α radiation, λ = 0.70930 Å). Of the 9400 measured reflections, 8646 were symmetry-independent and 5906 were classified as observed [$I_0 > 2\sigma(I_0)$]. An empirical absorption correction based on the counts of nine reflections was applied. The structure was solved by the Patterson method, with the program package SHELXS-86,[36] with hydrogen atoms included in their calculated positions. Refinement with the program package SHELXL-93[37] gave R_1 = 0.0444, wR_2 = 0.07128. The five highest maxima of a final difference Fourier map were below 0.30 e/Å^3. Further details of the structure determination may be obtained from the Cambridge Crystallographic Data Centre on quoting the depository number CCDC-132859.

Acknowledgments

This work was supported by the Deutsche Forschungsgemeinschaft (SFB 347, "Selektive Reaktionen Metall-aktivierter Moleküle").

[1] W. A. Schenk, P. Urban, *J. Organomet. Chem.* **1991**, *411*, C27−C31.
[2] W. A. Schenk, P. Urban, E. Dombrowski, *Chem. Ber.* **1993**, *126*, 679−684.
[3] W. A. Schenk, J. Bezler, *Eur. J. Inorg. Chem.* **1998**, 605−611.
[4] H. Brunner, *Adv. Organomet. Chem.* **1980**, *18*, 152−206.
[5] S. Blystone, *Chem. Rev.* **1989**, *89*, 1663−1679.
[6] H. Brunner, *Top. Curr. Chem.* **1975**, *56*, 67−90.
[7] J. A. Gladysz, B. J. Boone, *Angew. Chem.* **1997**, *109*, 566−602; *Angew. Chem. Int. Ed. Engl.* **1997**, *36*, 551−583.
[8] S. G. Davies, *Pure Appl. Chem.* **1988**, *60*, 13−20.
[9] H. Brunner, *Angew. Chem.* **1991**, *103*, A310−A313.
[10] G. Consiglio, F. Morandini, *Chem. Rev.* **1987**, *87*, 761−778.
[11] M. Rosenblum, *J. Organomet. Chem.* **1986**, *300*, 191−218.
[12] W. A. Schenk, U. Karl, M. R. Horn, *Z. Naturforsch., B* **1989**, *44*, 1513−1518.
[13] J. I. Seeman, S. G. Davies, *J. Chem. Soc., Chem. Commun.* **1984**, 1019−1021.
[14] A. ur−Rahman, Z. Shah, *Stereoselective Synthesis in Organic Chemistry,* Springer, New York, **1993**, pp. 217−242.
[15] W. A. Schenk in: *Stereoselective Reactions of Metal−Activated Molecules, Part 2* (Eds.: H. Werner, J. Sundermeyer), Vieweg, Frankfurt, **1995**, pp. 195−200.
[16] W. A. Schenk, J. Frisch, W. Adam, F. Prechtl, *Angew. Chem.* **1994**, *106*, 1699−1701; *Angew. Chem. Int. Ed. Engl.* **1994**, *33*, 1609−1611.
[17] W. A. Schenk, J. Frisch, M. Dürr, N. Burzlaff, D. Stalke, R. Fleischer, W. Adam, F. Prechtl, A. K. Smerz, *Inorg. Chem.* **1997**, *36*, 2372−2378.
[18] W. A. Schenk, M. Dürr, *Chem. Eur. J.* **1997**, *3*, 713−716.
[19] W. A. Schenk, J. Kümmel, I. Reuther, N. Burzlaff, A. Wuzik, O. Schupp, G. Bringmann, *Eur. J. Inorg. Chem.* **1999**, 1745−1756.

[20] W. A. Schenk, *Angew. Chem.* **1987**, *99*, 101−112; *Angew. Chem. Int. Ed. Engl.* **1987**, *26*, 98−109.
[21] E. Lindner, M. Haustein, R. Fawzi, M. Steinmann, P. Wegner, *Organometallics* **1994**, *13*, 5021−5029.
[22] W. A. Schenk, P. Urban, T. Stährfeldt, E. Dombrowski, *Z. Naturforsch., B* **1992**, *47*, 1493−1500.
[23] C. A. Poffenberger, A. Wojcicki, *Inorg. Chem.* **1980**, *19*, 3795−3803.
[24] E. Dombrowski, W. A. Schenk, *Angew. Chem.* **1995**, *107*, 1098−1099; *Angew. Chem. Int. Ed. Engl.* **1995**, *34*, 1008−1009.
[25] R. J. Errington, J. Ridland, W. Clegg, R. A. Coxall, J. M. Sherwood, *Polyhedron* **1998**, *17*, 659−674.
[26] E. Cesarotti, A. Chiesa, G. Ciani, A. Sironi, R. Vefghi, C. White, *J. Chem. Soc., Dalton Trans.* **1984**, 653−661.
[27] D. D. Pathak, H. Adams, C. White, *J. Chem. Soc., Chem. Commun.* **1994**, 733−734.
[28] M. Dürr, Dissertation, Universität Würzburg, **1997**.
[29] K. K. Anderson in: *The Chemistry of Sulfones and Sulfoxides* (Eds.: S. Patai, Z. Rappoport, C. Stirling), Wiley, New York, **1988**, pp. 55−94.
[30] T. H. Black, *Aldrichim. Acta* **1983**, *16*, 3−10.
[31] E. Cesarotti, H. B. Kagan, R. Goddard, C. Krüger, *J. Organomet. Chem.* **1978**, *162*, 297−309.
[32] P. S. Hallman, T. A. Stephenson, G. Wilkinson, *Inorg. Synth.* **1970**, *12*, 237−240.
[33] G. Consiglio, F. Morandini, F. Bangerter, *Inorg. Chem.* **1982**, *21*, 455−457.
[34] G. M. Sheldrick, *SHELXS-93, Program for Crystal Structure Solution,* Universität Göttingen, Germany, **1993**.
[35] G. M. Sheldrick, *SHELXL-96, Program for Crystal Structure Refinement,* Universität Göttingen, Germany, **1996**.
[36] G. M. Sheldrick, *SHELXS-86, Program for Crystal Structure Solution,* Universität Göttingen, Germany, **1986**.
[37] G. M. Sheldrick, *SHELXL-93, Program for Crystal Structure Refinement,* Universität Göttingen, Germany, **1993**.

Received August 10, 1999
[I99298]

Nickel Chelate Complexes of 2-Alkylphenylphosphanylphenolates: Synthesis, Structural Investigation and Use in Ethylene Polymerization

Joachim Heinicke,*[a] Manuela Koesling,[a] Robert Brüll,[b] Wilhelm Keim,[b] and Hans Pritzkow[c]

Keywords: Phosphanylphenolate / Cyclopentadienylnickel complexes / Chelates / Ethylene polymerization / Crystal structure / Polymerizations

2-Diphenylphosphanyl- and 2-alkylphenylphosphanyl-4-methylphenols **1** or their silyl ethers **2** and equimolar amounts of nickelocene react in benzene preferably to give orange-brown diamagnetic cyclopentadienylnickel chelate complexes [η-CpNi(P⌒O)] (**3**). Addition of a second equivalent of **1** or **2** affords (*RR*) and (*SS*) diastereoisomers of *cis*-bis(P⌒O-chelates) **4a–c** (R = Ph, Me, *i*Pr) or the unsymmetrical *cis*-bis(P⌒O-chelate) **5**, whereas with bulkier substituted derivatives **1d** or **2d** (R = *t*Bu) the second step is hindered or retarded. The reactivity of **1d** remains high towards nickel salts in polar solvents, but in contrast to **1a–c**, yielding **4**, a sparingly soluble green *trans*-bis(P–O-chelate) nickel complex **6d** is formed. Complexes formed in situ from **1** or **2** and $Ni(COD)_2$ in toluene catalyze the polymerization of ethylene. The cyclopentadienyl (P⌒O) complexes **3**, however, are too stable to be active in this process. The crystal and molecular structure of **3c** and **4c** are described.

Introduction

Functionalized phosphanes containing hard and soft donor centers allow various coordination modes with transition metals in high or low oxidation states and thus have attracted considerable interest in complex chemistry and homogenous catalysis. Tertiary 2-phosphanylphenolates[1−3] prefer bis(P⌒O-chelate) transition-metal complexes;[2,4] these are remarkably stabilized, are formed even by dealkylation of 2-phosphanylphenyl-alkyl ether complexes[5] and are able to undergo *O*,*O*′-coordination with a second hard metal ion.[6] Furthermore, monophosphanylphenolate chelate complexes bearing an additional phosphane molecule,[7] a solely *P*-coordinate 2-phosphanylphenol or a cyclopentadienyl ligand[2,8,9] are known. Very recently, phenylnickel diphenylphosphanylphenolate phosphane complexes were reported.[10] In view of the crucial role of mono(P⌒O-chelate) species in the industrially important homogenous nickel-catalyzed oligomerization of ethene (Shell Higher Olefin Process, SHOP),[11] we investigated complex chemical reactions of various *P*-substituted 2-phenylphosphanyl-4-methylphenols **1a−d** and their *O*-trimethylsilyl ethers **2a−d** with nickelocene in toluene, some nickel salts or complexes in more polar solvents and the polymerization with catalysts obtained from phosphanylphenols and $Ni(COD)_2$. The influence of substituents on the polymerization will be reported separately.

Results and Discussion

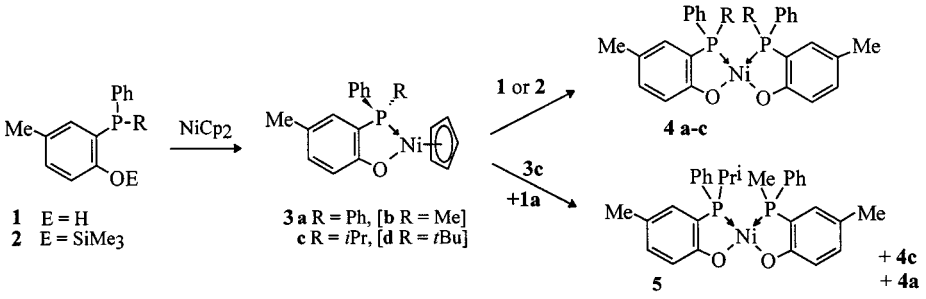
Reactions

2-Diphenylphosphanyl-4-methylphenol (**1a**) and an equimolar amount of nickelocene in benzene afford the cyclopentadienyl(P⌒O-chelate)nickel complex **3a** ($\delta^{31}P$ = 37.8; $\Delta\delta$ = 65 ppm) and a small amount of *cis*-$(P\text{-}O)_2Ni$ (**4a**) ($\delta^{31}P$ = 34.4; $\Delta\delta$ = 61.6 ppm) (Scheme 1). 2-Isopropylphenylphosphanyl-4-methylphenol (**1c**) exhibits a higher selectivity for monosubstitution and is isolated as pure orange-brown **3c** ($\delta^{31}P$ = 50.5; $\Delta\delta$ = 80.3 ppm) from a benzene solution at 20°C. Contamination by **4c** is observed if the complex is precipitated by ether or, markedly increased, on heating solutions of **1c** or **2c** with nickelocene. The silyl ethers **2** are less reactive than **1** and the higher temperatures required favor contamination by **4**. Reactions of the methyl- (**1b**, **2b**) or *tert*-butyl derivatives (**1d**, **2d**) with nickelocene (1:1) in benzene furnish brown diamagnetic substances, which are highly soluble in benzene, THF, CH_2Cl_2 or chloroform. NMR spectra of the products give evidence of monosubstitution of the *tert*-butyl derivatives, whereas disubstitution to **4b** is preferred for the sterically less demanding methyl species. This is seen in the ^{1}H-NMR spectra by pseudotriplets for the *P*-methyl protons. A side product with $\delta^{31}P$ = 26.4 (ca. 15%) in the reaction with **2b**, which could not be isolated, is tentatively assigned to **3b**. Like the other η^5-cyclopentadienyl(P⌒O-chelate)nickel complexes, it exhibits modest larger values of the typical downfield coordination shift of five-membered chelate complexes[12] than the *cis*-bis(phosphanylphenolato)nickel com-

[a] Institut für Chemie und Biochemie, Ernst-Moritz-Arndt-Universität Greifswald,
Soldmannstr. 16, D-17487 Greifswald, Germany
Fax: (internat.) + 49(0)3834/86-4319
E-mail: heinicke@mail.uni-greifswald.de
[b] Institut für Technische Chemie und Petrolchemie, Rheinisch-Westfälische Technische Hochschule Aachen,
Worringer Weg 1, D-52056 Aachen, Germany
[c] Anorganisch-Chemisches Institut, Universität Heidelberg,
Im Neuenheimer Feld 270, D-69120 Heidelberg, Germany
Supporting information for this article is available on the WWW under http://www.wiley-vch.de/home/eurjic or from the author.

 © WILEY-VCH Verlag GmbH, D-69451 Weinheim, 2000 1434−1948/00/0202−299 $ 17.50+.50/0

plexes **4** with O^- donors *trans* to the phosphorus atoms (Table 1).



Scheme 1. Reactions of **1** or **2** with nickelocene

Table 1. ^{31}P chemical shifts of **1a−d**, **3a−d**, **4a−c**[a] and **6d** and coordination chemical shifts Δδ

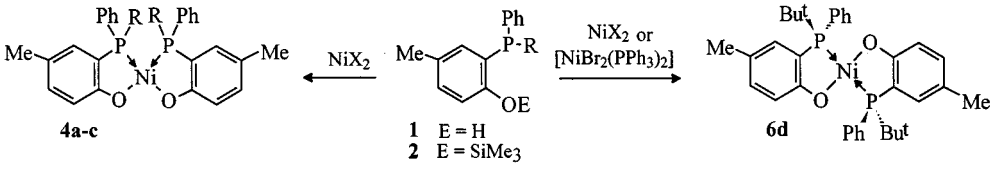
R	δ (**1**)	δ (**3**)	Δδ (**3−1**)	δ (**4a−c**) [δ (**6d**)]	Δδ (**4−1**) [Δδ (**6d−1d**)]
a Ph	−27.2	37.8	65	34.4	61.6
b Me	−50.9	26.4[b]	77.3	21.9[c]	72.8
c iPr	−29.8	50.5	80.3	45.3	75.1
d tBu	−18.7	57.1[b]	75.8	[24.4][d]	[43.1][d]

[a] Spectra in $CDCl_3$. − [b] Substance not isolated, tentative assignment. − [c] ^{31}P resonance of a minor isomer at δ = 20.0. − [d] Solid-state NMR data.[19]

The reaction of nickelocene with two equivalents of **1a−c** or **2a−c** in benzene smoothly gives *cis*-bis(P−O-chelate)nickel complexes **4a−c,** indicating an easy replacement of the second cyclopentadienyl ligand in the 18-valence-electron complexes **3**. Similarly, addition of **1b** to **3c** yields the unsymmetrical *cis*-[Ni(P⌒O)(P′⌒O)] chelate complex **5**. Contamination by **4c** and to a smaller amount by **4b** (ratio roughly 60:30:10) provides evidence that ligand substitution is not limited to the cyclopentadienyl anion but involves also the (P⌒O-chelate) group. The reaction of nickelocene with two equivalents of the *tert*-butyl-substituted 2-phosphanylphenol derivatives **1d** or **2d** in benzene does not proceed completely. Neither **4d** nor **6d** can be detected. It is assumed that the conversion in benzene is hindered or slowed for steric reasons. In polar solvents, however, the ligand exchange is much faster, and bis(P⌒O)nickel complexes are formed with **1a−c** or **2a−c** as well as with **1d** or **2d**. The reason is the high driving force for the bis(phosphanylphenolato)nickel complexes which are also the usual products in reactions with nickel acetylacetonate, with aqueous nickel salts in methanol, or anhydrous nickel salts in THF if a sufficient amount of base or buffer is added. Similarly, attempts to prepare [(Ph*t*BuP⌒O)NiBr(PPh$_3$)$_n$] by reacting **1d(Li)** with $NiBr_2 \cdot 2PPh_3$ in ether in an equimolar ratio failed in favor of the bis(P⌒O)nickel complex (Scheme 2). The bulkier *tert*-butyl derivatives react differently to the others, forming brown solutions of **4a−c**, by precipitation of a diamagnetic green *trans*-bis(P⌒O-chelate)nickel complex **6d** which is insoluble or sparingly soluble in all common organic solvents.

Catalysis

The organonickel phosphanylphenolates **3** are structurally related to organonickel phosphanylenolates,[9,13-15] which form the catalytically active species in the Shell Higher Olefin Process.[10] Attempts to oligomerize ethylene by using the cyclopentadienylnickel complex **3c** at 40 bar and 140°C failed, however. The reason is, that despite the easy replacement of the cyclopentadienyl group by **1** or **2**, the semisandwich complexes **3** are thermally very stable and are unable to form catalytically active η^1-CpNi- or NiH-(PO-chelate) complexes. DTA of **3c** indicates loss of cyclopentadiene only at 190−210°C (endothermic). Complete decomposition of the Ni(P⌒O-chelate) structure occurs at 280−340°C. For comparison, the thermal degradation of **4c** proceeds in the same temperature range (280−340°C) after an exothermic process at 271°C, whereas **5d** starts to decompose at even higher temperature (310−340°C). The importance of the loss of the cyclopentadienyl group for catalytic activity was demonstrated for the less stable related



Scheme 2. Reactions of **1** or **2** with nickel salts

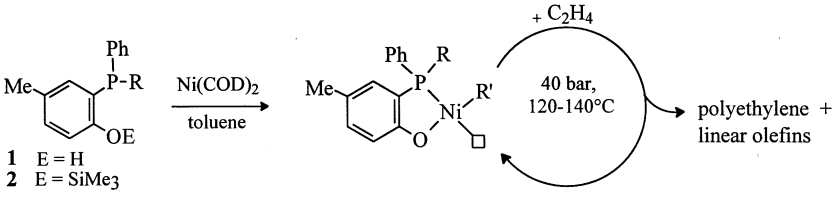
phosphanylenolate complex [Ni(η^5-Cp){Ph_2PCH=C(Ph)O}] (decomp. at 130°C) which like other nickel enolate complexes becomes active at the decomposition temperature and thus gives evidence that the remaining (phosphanylenolato)nickel hydride represents the starting catalyst.[11,13b] That less stable organonickel complexes obtained from phosphanylphenols and $Ni(COD)_2$ catalyze the polymerization or oligomerization of ethylene was first claimed by Singleton.[16] A catalyst prepared from *o*-diphenylphosphanylphenol and $Ni(COD)_2$ was found to convert ethylene in high yield (95%) to linear polyethylene and a lower amount of linear oligomers whereas a catalyst prepared with 2-diethylphosphanylphenol was found to be much less active (conversion 3.5%) and shows high preference for lower oligomers (C_4 68%, C_6 24%, C_8 4.3%). The recently reported phenylnickel phosphanylphenolate phosphane complexes[10] and an immobilized [$PhNi(PPh_3)$(2-Ph_2P-6-HO-$C_6H_3O^-$)] (P⌒O-chelate) complex[17] were found to oligomerize ethylene. We observed that complex solutions prepared from the alkylarylphosphanylphenol **1c** or its silyl ether **2c** and equimolar amounts of Ni(1,5-COD)$_2$ form catalysts for the formation of polymers and smaller amounts of oligomers of ethylene with high selectivity for linear structures (Scheme 3). Toluene was used as the solvent to avoid conversion into the catalytically inactive bis(phosphanylphenolato)nickel complex **4c,** which as seen above, is strongly favored in more polar solvents. Indeed, no catalytic activity was observed if the reaction was run in ethanol. In toluene, at 50 bar/160°C, the oligomer-to-polymer ratio was 15%:85%. The oligomer portion consisted of linear olefins, mainly from C_6 to C_{26} with a flat maximum at C_{16}/C_{18}. The polymer exhibits sharp absorptions for vinyl end groups at 909 and 991 cm^{-1} ($\tilde{\nu}_{C=C}$ 1641 cm^{-1}) and a small band for CH_3 at 1368 cm^{-1} but only weak bands for the *trans*-CH=CH or C=CH_2 groups and no indications of branching.[18] X-ray powder diffraction revealed high crystallinity. A molar mass distribution with M_w = 9310 $gmol^{-1}$ (corresponding to n = 330) and M_n = 6087 $gmol^{-1}$ was determined. The results with **1c** and **2c** are similar and can be attributed to the easy formation of (P⌒O-chelates) in both cases, as was also found in the reaction with nickelocene.

Structure Investigations

Compounds **3**–**5** are sparingly soluble in hexane or ether but easily soluble in benzene, CH_2Cl_2, chloroform or THF, allowing structure elucidation by multinuclear NMR spectra. **6d**, obtained as powder or microcrystals, was not sufficiently soluble for solution-NMR studies, and therefore was structurally characterized in comparison with **4c** by a solid-state ^{31}P-NMR investigation which is reported separately.[19] The solid-state structures of **3c** and **4c** were determined by single-crystal X-ray structure analysis.

^{13}C-NMR data of **3c** indicate unambiguously the semi-sandwich arrangement by a doublet for the cyclopentadienyl group and typical doublet or singlet signals for the phosphanylphenolate ligand with $J(^{31}P^{13}C)$, depending on the position towards the phosphorus atom. Proton, CH-COSY and phosphorus-NMR data of **3c** support the proposed structure. The assignment of the proton signals of **3a**, **3b** and **3d** was done by comparison with those of **3c**. In the solid state, **3c** crystallizes in the centrosymmetric space group $P\bar{1}$ with two independent molecules in the asymmetric unit, which show no significant deviations. The molecular structure of **3c** (Figure 1) shows a perpendicular arrangement of the Cp^- moiety and the planar (P⌒O) chelate ring (89.1 and 88.5°), with the Ni atom only slightly distorted from this plane. The distance from Ni to the cyclopentadienyl carbon atom (C21 and C39, respectively) placed in the *trans* position to the oxygen atom, are significantly shorter than are the Ni–C distances to the remaining cyclopentadienyl carbon atoms. This indicates a stabilization of the Ni–C bond by the phenolate *trans* coordination which for related catalytically active organonickel phosphanylphenolate species is important for the chain growth in the polymerization or oligomerization of ethylene. The C–P–C angles are typical for tetracoordination at the phosphorus atom, whereas the small P–Ni–O and C_{aroxy}–P–Ni angles result from geometric factors of the rigid five-membered ring and the bond lengths. The slight increase of the P–Ni–O angle (by 2–3°) in comparison to (diphenylphosphanylenolato)-[13–15] and (diphenylphosphanylalkoxido)nickel complexes[20,21] is consistent with a shorter P–Ni bond length (ca. 5 pm) within the ring.

In solution ^{1}H- and ^{13}C-NMR spectra of **4**, various nuclei show "triplets" or other multiplets representing the A_n or A_nA_n' part of A_nXX' or $A_nA'_nXX'$ spin systems by coupling with two ^{31}P nuclei (X, X′) and hence, reveal the bis(P⌒O-chelate) nature of **4**. The appearance depends on the relative magnitudes and signs of all coupling constants in the spin system.[22,23] Whereas the *cis* geometry of **5** is deduced from $^2J_{PP}$ = 80 Hz, which is much smaller than $^2J_{PP}$ in *trans*-methylnickel(phosphanylphenolato)PMe_3 complexes (ca. 316 Hz),[24] the geometry of **4** cannot easily be derived from the NMR data. In the proton spectrum



Scheme 3

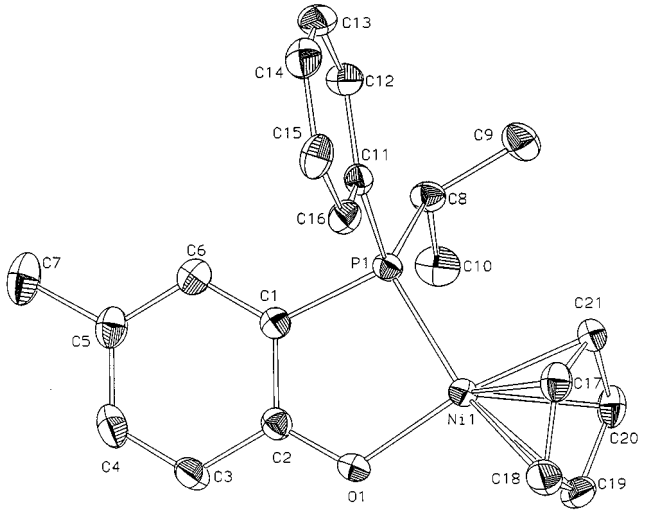


Figure 1. ORTEP plot of **3c**; selected bond lengths [Å] and angles [°], corresponding data for the second independent molecule are given in brackets: Ni1−P1 2.126(2) [2.132(2)], Ni1−O1 1.889 (3) [1.885(3)], Ni1−C21 2.048(4) [2.048(4)], Ni1−(C17−20) 2.144(4)−2.155(4) [2.146−2.162(4)], P1−C1 1.807(4) [1.807(4)], P1−C11 1.819(4) [1.823(4)], P1−C8 1.840(3) [1.850(3)]; O1−Ni1−P1 89.49(11) [89.56(12)], Ni1−P1−C1 98.90(13) [98.48(14)], C2−C1−P 111.9(2) [112.3(2)], C2−O1−Ni1 118.3(1) [118.1(2)], O1−C2−C1 121.5(3) [121.5(3)], C1−P1−C11 105.7 (2) [107.4(2)], C1−P1−C8 107.0(2) [106.2(2)]

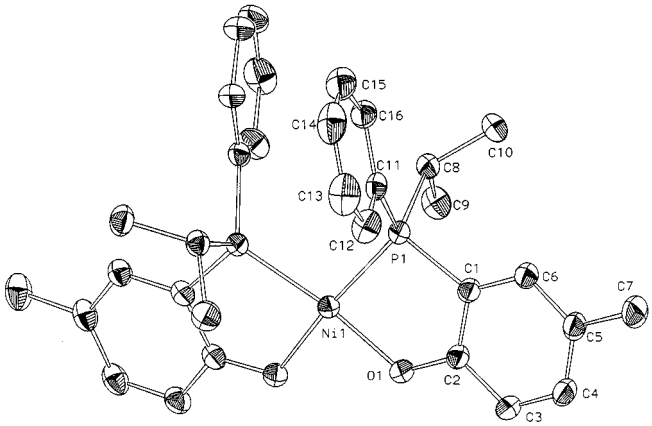


Figure 2. ORTEP plot of **4c**; selected bond lengths [Å] and angles [°]: Ni1−P1 2.1423 (13), Ni1−O1 1.885 (2), P1−C1 1.800 (2), P1−C11 1.814 (3), P1−C8 1.844 (3); P1−Ni1−P£1 97.93 (7), O1−Ni1−O£1 87.50 (11), O1−Ni1−P1 87.50 (8), Ni1−P1−C1 99.22 (10), C2−C1−P1 110.9 (2), C2−O1−Ni1 118.7 (2), O1−C2−C1 121.6 (2), C1−P1−C11 107.16 (12), C1−P1−C8 109.55 (12); symmetry transformation used to generate equivalent atoms: £1: $-x$, y, $-z + 1/2$)

of **4c** multiplets are observed for the diastereotopic methyl groups of $PCHMe_2$ resembling a "doublet of a doublet" and a "filled-in doublet" with doublet splitting of the external lines. Pseudotriplets by coupling with two ^{31}P nuclei ($|J_{XX'}| > |J_{AX} - J_{AX'}|$) are observed in the proton spectra of **4b** (PMe) or **6d** ($PCMe_3$) as well as in the ^{13}C-NMR spectra of **4b**,**c**. The two external lines in the five-line pattern in the A part (^{13}C) depend significantly on $^2J_{PP}$ and should allow an assignment of the geometry. However, the intensity of these lines is too low, even for the resonances of C2 or C_i(Ph), which exhibit the largest $^{31}P-^{13}C$ couplings and should display the most intensive external lines. As mentioned above, the geometry of **4c** was determined by solid-state investigations.[19] From the ^{31}P-CP/MAS NMR study, a two-bond coupling constant $^2J_{PP}$ of ca. 75 Hz was determined, thus indicating *cis* geometry. Detailed structural information is provided by the single-crystal X-ray structure analysis indicating a slightly distorted square-planar *cis* configuration of **4c** (Figure 2). The molecule has a crystallographic two-fold axis through the Ni atom yielding the (*RR*) or (*SS*) configuration. The P−Ni−O and P′−Ni−O′ planes are twisted by 7.1°. The distances and angles within the five-membered rings are similar to those in **3c** (P−Ni−O less by 2°). The O−Ni−O′ angle (87.5°) is somewhat smaller than 90° whereas the P−Ni−P′ angle is considerably widened in order to reduce steric repulsion of the P substituents. For the sterically less hindered methyl derivative **4a,** we observe characteristic ^{31}P- and ^1H-NMR signals of a second nickel atom bis(P⌒O-chelate) (B) (about 15%), which gives evidence of the existence of *rac* and *meso* isomers of **4a**.

The bulkier nickel bis(2-*tert*-butylphenylphosphanyl-4-methylphenolate) (**6d**), resembling *trans*-[Ni(tBu$_2$P−C$_6$H$_4$O)$_2$][2a] and *trans*-[Ni($Ph_2PCH_2R_2O)_2$] (R = CF_3)[20] in its unusual green color and low solubility, prefers an (*RS*)/(*SR*)-*trans* configuration with an inversion center at the nickel atom, as established by the high symmetry found in the solid-state ^{31}P-NMR investigation.[19] The low coordination shift of $\Delta\delta(^{31}P)$ = 43 ppm for **6d** as compared to $\Delta\delta(^{31}P)$ = 61−75 ppm for **4a−c** may be indicative for the different geometry but the lack of data for comparison needs further investigations to establish such a dependence.

Conclusion

(P⌒O-chelate)nickel(II) complexes **3−6** containing phosphanylphenolato ligands may be obtained by reaction of phosphanylphenols **1** or their silyl ethers **2** with nickelocene or nickel salts. Monochelates are formed with nickelocene in benzene. Small substituents, addition of polar solvents or increased temperature favor formation of bis(P⌒O-chelate)nickel complexes. Complexes formed in situ from **1c** or **2c** and equimolar amounts of $Ni(COD)_2$ in toluene were found to catalyze the formation of linear polymers and a smaller amount of oligomers of ethylene. From the slower formation of catalytically inactive **6d** from **1d** and nickelocene in benzene or toluene, it may be concluded that bulkier organonickel 2-phosphanylphenolate (P⌒O-chelate) complexes form interesting catalysts for olefin oligomerization or polymerization. The strengthening of the Ni−C bond in the *trans* position to the oxygen atom, as observed in **3c**, suggests a strong influence of donor properties at the O^- site on the chain length of polyethylene. A more detailed study on the influence of steric and electronic effects of substituents at the phosphorus atom and the aroxy group on polymerization or oligomerization of ethylene is in progress.

Experimental Section

General: All reactions were carried out under argon, using Schlenk techniques and freshly distilled dry solvents. Synthesis, properties and structures of the *P*-tertiary *o*-phosphanylphenols have been described elsewhere.[3b] Thermal analyses were carried out with a TGDTA92 (SETARAM) instrument. UV-Vis spectra were recorded with a Lambda19 spectrometer (Perkin−Elmer), mass spectra with a single-focussing mass spectrometer AMD40 (Intectra). NMR spectra were measured in $CDCl_3$ (unless indicated otherwise), using a multinuclear FT-NMR spectrometer ARX300 (Bruker) at 300.13 (^{1}H), 75.47 (^{13}C), and 121.49 (^{31}P) MHz. Shift references are tetramethylsilane for ^{1}H and ^{13}C, and H_3PO_4 (85%) for ^{31}P. For resonances which are part of a A_nX_2 spin system (X = ^{31}P) vc denotes "virtual coupling", τ the usual triplet appearance of the A resonance (n = 1) and $N = |J + J'|$.

Reactions of 1 and 2 with Nickelocene in Equimolar Ratio. − Cyclopentadienyl(2-diphenylphosphanyl-4-methylphenolato)nickel (3a): A solution of **1a** (900 mg, 3.08 mmol) in benzene (10 mL) was added to a solution of nickelocene (580 mg, 3.07 mmol) in benzene (10 mL) and stirred for 2 h. Most of the solvent (ca. 18 mL) was removed in vacuo and ether (5 mL) was added to give 1.15 g of an orange-brown precipitate, consisting of **3a** and **4a** (ca. 70%:30%, d^{31}P = 37.8, 34.5). Column chromatography on silica gel yielded 0.7 g (55%) of pure **3a** by elution with $CHCl_3$/acetone (10:1). − ^{1}H NMR: δ = 2.13 (s, 3 H, 4-Me), 5.31 (s, 5 H, Cp), 6.63 (d, $^3J_{HH}$ = 7−8, $^4J_{PH}$ = 5.5 Hz, 1 H, 6-H), 6.87 (d, $^3J_{HH}$ = 7−8 Hz, 1 H, 5-H), 6.87 (d, $^3J_{PH}$ = 10 Hz, 1 H, 3-H), 7.35−7.55 (m, 6 H, *m,p*-H), 7.65−7.8 (m, 4 H, *o*-H). − $C_{24}H_{21}NiOP$ (415.10): calcd. C 69.44, H 4.80; found C 69.62, H 4.95.

Cyclopentadienyl(2-isopropylphenylphosphanyl-4-methylphenolato)-nickel (3c): (a) A solution of **1c** (274 mg, 1.06 mmol) in benzene (10 mL) was added to nickelocene (200 mg, 1.06 mmol) in benzene (10 mL). After 1 d, about 80% of the solvent was removed. Within 3 d, 216 mg (53%) of orange-brown **3c** crystallized, m.p. 184°C. − UV/Vis [MeOH; λ_{max}/nm (ε/M^{-1}cm^{-1})]: 454 (880), 301 (1700), 267 (1500), 226 (sh, 2600). − ^{1}H NMR and CH COSY (C_6D_6): δ = 0.99 (dd, $^3J_{PH}$ = 18.5, $^3J_{HH}$ = 7.0 Hz, 3 H, Me_A), 1.17 (dd, $^3J_{PH}$ = 16.8, $^3J_{HH}$ = 6.9 Hz, 3 H, Me_B), 2.04 (m, 1 H, CH), 2.07 (s, 3 H, 4-Me), 5.18 (s, 5 H, Cp), 6.81 (d, $^3J_{HH}$ = 8.5, 1 H, 5-H), 6.97 (dd, $^3J_{HH}$ = 8.5, $^4J_{PH}$ = 5.5 Hz, 1 H, 6-H), 7.07 (s, 1 H, 3-H), 6.94 (m, 1 H, *p*-H), 7.06 (m, 2 H, *m*-H), 7.66 (m, *o*-H). − ^{13}C NMR (C_6D_6): δ (J_{PC}) = 18.2 (d, 1.9 Hz, Me_B), 18.8 (d, 5.6 Hz, Me_A), 20.4 (s, Me-4), 27.4 (d, 31.0 Hz, CH), 91.4 (d, 1.8 Hz, Cp), 117.9 (d, 51.1 Hz, C_q-2), 119.3 (d, 9.9 Hz, C-6), 121.9 (d, 7.0 Hz, C_q-4), 128.9 (d, 10.4 Hz, 2 C-*m*), 129.9 (d, 2.6 Hz, C-3), 130.5 (s, C-*p*), 131.9 (d, 10.3 Hz, 2 C-*o*), 134.1 (d, 1.7 Hz, C-5), 134.2 (d, 43.3 Hz, *i*-C), 176.1 (d, Hz, C_q-1). − ^{31}P {^{1}H} NMR: δ = 50.4. − $C_{21}H_{23}NiOP$ (381.1): calcd. C 66.19 H 6.08 P 8.13; found C 66.26 H 6.48 P 7.76. − (b) 965 mg of **2c** (2.9 mmol) in benzene (10 mL) was added to nickelocene (545 mg, 2.9 mmol) in benzene (10 mL). No visible reaction took place within 5 d at 20°C, but on reflux (24 h) a dark brown solution was formed. Work up as above afforded 750 mg (70%) of **3c**, m.p. 185°C. A trace of **4c** was formed besides **3c**. The proportion increased up to 1:3 in larger runs and on precipitation with ether from the benzene solution. Single crystals of **3c** and of **4c** were grown from benzene/nitromethane (ca. 1:1) solution.

Reactions of Nickelocene with Two Equivalents of 1 or 2. − *cis*-Bis(2-isopropylphenylphosphanyl-4-methylphenolato)nickel (4c): (a) Nickelocene (831 mg, 4.4 mmol) in benzene (10 mL) was added to **1c** (2.27 g, 8.8 mmol) in benzene (10 mL). The color turned from green to brown within 1 h, and an orange-brown precipitate was formed after refluxing for 30 min. After removing a part of the solvent, the suspension was filtered, **4c** was washed with a little benzene and dried at 10^{-2} Torr (8 h) affording 1.65 g (65%) of an orange powder, m.p. 278−280°C. − ^{1}H NMR and CH COSY: δ = 0.98 (dd, $^3J_{PH}$ = 12.7, $^3J_{HH}$ = 6.8 Hz, 6 H, Me_A), 1.24 (m, 2 H, C*H*Me_2), 1.41 (vc, $^3J_{HH} \approx$ 7 Hz, 6 H, Me_B) 2.08 (s, 6 H, 4-Me), 6.42 (vc, 2 H, 3-H), 6.88 (dτ, $^3J_{HH}$ = 8.6, N = 5.2 Hz, 2 H, 6-H), 7.02 (br. d, $^3J_{HH}$ = 8.6 Hz, 2 H, 5-H), 7.40 (m, 4 H, *o*-H), 7.51 (m, 4 H, *m*-H), 7.60 (m, 2 H, *p*-H). − ^{13}C NMR: δ (N_{PC}) = 16.6 (τ, N = 8.2 Hz, Me_B), 19.4 (τ, N = 6.8 Hz, Me_A), 20.0 (s, Me-4), 23.0 (τ, N = 28.1 Hz, CH), 112.9 (τ, N = 54 Hz, C_q-2), 118.2 (τ, N = 13.8 Hz, C-6), 123.5 (τ, N = 6.9 Hz, C_q-4), 128.8 (τ, N = 10.0 Hz, C-*m*), 129.2 (τ, N = 46.3 Hz, C-*i*), 131.0 (s, C-*p*), 131.4 (s, C-3), 132.1 (τ, N = 8.3 Hz, C-*o*), 135.2 (s, C-5), 175.1 (τ, N = 16.6 Hz, C_q-1). − ^{31}P {^{1}H} NMR: δ = 45.3. − $C_{32}H_{36}NiO_2P_2$ (573.27): calcd. C 67.05 H 6.33 Ni 10.24 P 10.81; found C 66.76 H 6.66 Ni 10.56 P 10.27. (b) A solution of nickelocene (493 mg, 2.6 mmol) and **2c** (1.73 g, 5.2 mmol) in benzene (30 mL) was refluxed for 3 d to afford a brown solution. Most of the benzene was removed by distillation. From the residual suspension (ca. 3 mL) the solid was separated by filtration and washed with cold benzene (1 mL) yielding 319 mg (21%) of **4c**, m.p. 285°C. − ^{31}P NMR: δ = 45.3.

Reaction of 1b with 3c: A solution of **3c** (0.95 g, 2.5 mmol) in benzene (10 mL) was added to **1b** (0.57 g, 8.8 mmol) in benzene. About 12 mL of benzene was distilled off. 1.1 g of a brown precipitate was separated from the resulting viscous solution and analyzed by ^{31}P NMR ($CDCl_3$). The precipitate was found to be a mixture of the unsymmetrical *cis*-bis(P⌒O-chelate) **5** and the symmetrical *cis*-bis-(P⌒O-chelates) **4c** and **4b** (intensity ratio roughly 60:30:10). − ^{31}P{^{1}H} NMR of **5**: δ = 46.4 (d), 21.7 (d), $^2J_{PP}$ = 80 Hz.

Reactions of 1 or 2 with Nickel Salts or Complexes. − *cis*-Bis(2-diphenylphosphanyl-4-methylphenolato)nickel (4a): $NiCl_2 \cdot 6H_2O$ (650 mg, 2.74 mmol) was dissolved in hot methanol (20 mL), and a solution of **1a** (1.6 g, 5.48 mmol) in methanol (5 mL) was added. A rapid color change to orange started on addition of Et_3N of which a total of 1.1 g (10.9 mmol, ca. 100% excess) was added. After removing the solvent, the solid residue was crystallized from MeOH/CH_2Cl_2 (1:1) and dried for 2 h at 10^{-2} Torr to yield 1.4 g (80%) of orange-brown **4a** containing a small amount of water. − ^{1}H NMR: δ = 2.04 (s, 6 H, 4-Me), 3.50 (s, 2 H, H_2O), 6.47 (vc to br. τ, 2 H, 3-H), 6.89 (dτ, $^3J_{HH}$ = 8.7, N = 5.5 Hz, 2 H, 6-H), 7.02 (br. d, $^3J_{HH}$ = 8.7 Hz, 2 H, 5-H), 7.42 (m, 4 H, *o*-H), 7.10 (τ, $^3J \approx$ 7.4−7.6 Hz, 4 H, *m*-H), 7.32 (τ, $J \approx$ 7.3−7.5 Hz, 2 H, *p*-H). − ^{31}P{^{1}H} NMR: δ = 34.4. − $C_{38}H_{32}NiO_2P_2 \cdot H_2O$ (659.32): calcd. Ni 8.90; found Ni 8.85.

***cis*-Bis(2-methylphenylphosphanyl-4-methylphenolato)nickel (4b):** (a) A solution of **1b** (103 mg, 0.45 mmol) in ethanol (5 mL) was added to a warm solution of nickel acetate · 4 H_2O (57 mg, 0.23 mmol) in ethanol (10 mL), affording a yellow solution which slowly turned brown. The solvent was removed in vacuo (after 3 d), the remainder was extracted with CH_2Cl_2 and dried with Na_2SO_4. Hexane was added and a part of the solvent (mainly CH_2Cl_2) was evaporated in vacuo to yield a brown precipitate which was dried for 2 h at 10^{-2} Torr. 70 mg (59%) of two isomers of **4b** were obtained, isomer ratio (A)/(B) ca. 85%:15% with δ(^{31}P) = 21.9, 20.0. − ^{1}H NMR: (A): δ = 1.09 (τ, N = 11.7 Hz, 6 H, PMe), 2.06 (s, 6 H, 4-Me), 6.43 (br. τ, N = 8−9 Hz, 2 H, 3-H), 6.87 (m, 2 H), 6.98 (m, 2 H), 7.4−7.6 (m, 10 H, Ph); (B): δ = 1.87 (τ, N = 11.1 Hz, PMe), other signals superimposed. − ^{13}C NMR: δ (N_{PC}) = 9.1 (τ, N = 32 Hz, PMe), 20.0 (Me-4), 118.3 (τ, C-6), 124.6 (τ, C-4), 128.9 (C-*p*), 129.1 (τ, N = 10.6 Hz, C-*m*), 131.4 (τ, N = 10.6 Hz, C-*o*), 135.3 (C-5); weak intensities of C-1, C-2, C-*i* signals. − $C_{28}H_{28}NiO_2P_2$ (517.17): calcd. Ni 11.35; found Ni 11.08. − (b) An equimolar mixture of

2b (647 mg, 2.14 mmol) and nickel acetylacetonate (550 mg, 2.14 mmol) was refluxed for 8 h in benzene (30 mL) to give, after removal of 2/3 of the solvent, 188 mg (34%) of the bis(phosphanylphenolate) **4b**, m.p. 216−218°C. − UV/Vis [MeOH, λ_{max}/nm (ε/$M^{-1}cm^{-1}$)]: 403(400), 347 (1.300), 293 (sh), 281 (14.000), 220 (sh, 17.000). − $^{31}P\{^1H\}$ NMR: δ = 21.8.

***cis*-Bis(2-isopropylphenylphosphanyl-4-methylphenolato)nickel (4c):** **2c** (193 mg, 0.59 mmol) and nickel acetylacetonate (54 mg, 0.21 mmol) were refluxed for 8 h in benzene (20 mL) to give, after removal of the bulk of the solvent, 88 mg (73%) of **4c**, NMR data as above.

***trans*-Bis(2-isopropylphenylphosphanyl-4-methylphenolato)nickel (6d):** (a) 160.8 mg (0.735 mmol) of $NiBr_2$ and 170 μL of HBr (48%, 1.51 mmol) were dissolved in warm methanol and two equivalents of **1d** (400 mg, 1.47 mmol) in methanol (7 mL) were added. A transient brown color was observed in the mixing area, indicating an equilibrium with dominance of octahedral Ni^{2+} complexes in solution [λ_{max}/nm: 398 (st), 730 (w), 660 (sh)]. On buffering with excess sodium acetate the solution turned brown and 265 mg (60%) of green **6d** precipitated. − (b) A solution of **1d** (588 mg, 2.16 mmol) in THF (15 mL) was added to a suspension of $NiBr_2$·1.1DME (337 mg, 1.09 mmol) in 15 mL of THF. On addition of LiO*i*Pr (2.3 mmol) the solution turned brown and a total of 415 mg (63%) of green **6d** precipitated. The reaction of $NiBr_2$·1.1DME with **2d** proceeded similarly. − (c) The best variant yielding microcristalline **6d** was the following: Butyllithium in hexane (9.6 mmol) was added at −5°C to 3.26 g (9.46 mmol) of **2d** in THF (20 mL). A solution of $NiBr_2$·$2Ph_3P$ (3.52 g, 4.73 mmol) in THF (40 mL) was added dropwise, forming a brown solution and, after 5−10 min, a green precipitate. The reaction was complete within 20−30 min and gave 2.06 g (73%) of microcrystalline, diamagnetic **6d**, m.p. 312−317°C (DTA 327.5°C with dec.). Above 120°C **6d** exhibited a reversible gradual color change via olive-green to yellow. The solubility in acetonitrile, nitromethane, methanol, acetone, benzene or hexane was very low and in THF, $CHCl_3$ or CH_2Cl_2 was just sufficient for UV/Vis spectra. − UV/Vis [THF; λ_{max}/nm, (relative intensities in satd. soln.)]: 611 (10), 434 (100), 391 (500), 320 st, 284 st, 275 st. − Solid-state NMR investigation see ref.[19] − $C_{34}H_{40}NiO_2P_2$ (601.3): calcd. C 67.92, H 6.70, Ni 9.76, P 10.30; found C 67.36, H 6.83, Ni 9.63, P 10.26. − X-ray powder diffraction data and density (in ethanol) = 0.89−0.95 gcm^{-3} fit best with a triclinic crystal system with unit cell dimensions of a_o = 10.126 Å, b_o = 17.630 Å, c_o = 12.184 Å, α = 89.44°, β = 90.55°, γ = 89.98°, Z = 2.

Thermal Analysis: DTA/TG analyses of **3c**, **4c** and **6d** were performed under nitrogen. **3c**: mass lost at 190−210°C, Δm_{210} = 17%, corresponding to cleavage of cyclopentadiene (endothermic); further continously increasing mass lost at 280−340°C, $\Delta m_{350} \approx$ 70%, endothermic peak at 309°C. **4c**: mass lost at 280−340°C, Δm_{350} = 66−72%, exothermic peak at 271°C, endothermic at 290°C. **6d**: mass lost at 310−340°C, Δm_{350} = 72%, endothermic peak at 328°C.

Catalysis Experiments: **1c** (56.8 mg, 0.22 mmol) or **2c** (72.6 mg, 0.22 mmol) in toluene (10 mL) were added at 0°C to a solution of $Ni(COD)_2$ (0.22 mmol) in toluene (10 mL). After stirring for 30 min, the solution was transferred into an autoclave, ethylene added until the pressure was 40 bar and heated for 12 h while stirring with a teflon-coated magnetic stirrer. **2c** was used first. At 60°C no conversion of ethylene occurred, at 120°C the pressure (8.7 g C_2H_4) decreased to 29 bar and polyethylene (3.65 g, 88% of converted ethylene) and a lower portion of linear olefins (C_4 to C_{26}) with a flat maximum at C_{16}/C_{18} was isolated. The TON was 666. X-ray powder diffraction and IR revealed high crystallinity and low branching of the PE. Use of a catalyst prepared from **1c** and $Ni(COD)_2$ and 8.7 g of C_2H_4 at 140°C led similarly to PE (TON = 698; 3.64 g of HDPE, 85% of converted ethylene), m.p. 121°C; DTA (5 K/min): 131.8°C (up), 117.2°C (down). M_w = 9310 $gmol^{-1}$, M_n = 6087 $gmol^{-1}$. Ethylene (40 bar) heated with a solution of **3c** (37.3 mg) in toluene (20 mL) for 12 h at 140°C was not converted. A more detailed study of ethylene polymerization and oligomerization with varied phosphanylphenols is in progress and will be described elsewhere.

Crystal Structure Analysis: Crystal data are presented in Table 2, selected bond angles and bond lengths are given in the captions of Figures 1 and 2. − Data collection: The crystals were mounted on a glass fiber in inert oil and transferred to the cold gas stream (−55°C) of the diffractometer (Siemens-Stoe AED2). Data were collected in the ω-scan mode using monochromated Mo-K_α radiation (0.71073 Å). − Solution and refinement: The structures were solved by direct methods (G.M. Sheldrick, *SHELXS-86*, Univ. Göttingen, **1986**) and were refined by the least-squares method based on F^2 with all measured reflections (G. M. Sheldrick, *SHELXL-93*, Univ. Göttingen, **1993**) using anisotropic temperature factors for all non-hydrogen atoms. Hydrogen atoms were included in calculated positions or as part of a rigid group (methyl). Only an isotropic temperature factor for each type of hydrogen atom was refined. − Crystallographic data (excluding structure factors) for the structure reported in this paper have been deposited with the Cambridge Crystallographic Data Centre as supplementary publication no. CCDC-114167 (**3c**) and -114168 (**4c**). Copies of the data can be obtained free of charge on application to CCDC, 12 Union Road, Cambridge CB2 1EZ, UK [Fax: (internat.) + 44-1223/336-033; E-mail: deposit@ccdc.cam.ac.uk].

Acknowledgments

Financial support by the Deutsche Forschungsgemeinschaft and the Fond der Chemischen Industrie is gratefully acknowledged. We thank Dr. M. K. Kindermann and B. Witt for NMR experiments, P. Engler for thermal analyses, Prof. Dr. Fink (Mülheim) for determination of the molar mass distribution and Dr. H. Wulff for powder X-ray diffraction measurements.

[1] H.-G. Henning, W. Wild, *J. Prakt. Chem.* 1976, *318*, 69.
[2] [2a] H. D. Empsall, B. L. Shaw, B. L. Turtle, *J. Chem. Soc., Dalton Trans.* **1976**, 1500. − [2b] T. B. Rauchfuss, *Inorg. Chem.* **1977**, *16*, 2966. − [2c] J. Heinicke, R. Kadyrov, M. Koesling, U. Jux, *Phosphorus Sulfur Silicon* **1996**, *109−110*, 501.
[3] [3a] J. Heinicke, E. Nietzschmann, A. Tzschach, *J. Organomet. Chem.* **1983**, *243*, 1. − [3b] J. Heinicke, R. Kadyrov, M. K. Kindermann, M. Koesling, P. G. Jones, *Chem. Ber.* **1996**, *129*, 1547. − [3c] O. Herd, A. Heßler, M. Hingst, M. Trepper, O. Stelzer, *J. Organomet. Chem.* **1996**, *522*, 69.
[4] [4a] S. B. Sembiring, S. B. Colbran, D. C. Craig, *Inorg. Chem.* **1995**, *34*, 761. − [4b] H. Luo, I. Setyawati, S.J. Rettig, C. Orvig, *Inorg. Chem.* **1995**, *34*, 2287.
[5] [5a] C. E. Jones, B. L. Shaw, B. L. Turtle, *J. Chem. Soc., Dalton Trans.* **1974**, 992. − [5b] R. Mason, K. M. Thomas, H. D. Empsall, S. R. Fletcher, P. N. Heys, E. M. Hyde, C. E. Jones, B. L. Shaw, *J. Chem. Soc., Chem. Commun.* **1974**, 612. − [5c] H. D. Empsall, E. M. Hyde, B. L. Shaw, *J. Chem. Soc., Dalton Trans.* **1975**, 1690. − [5d] K. R. Dunbar, J. H. Matonic, V. P. Saharan, *Inorg. Chem.* **1994**, *33*, 25.
[6] [6a] K. R. Dunbar, A. Quillevéré, *Organometallics* **1993**, *12*, 618. − [6b] D. Weiß, A. Schier, H. Schmidbaur, *Z. Naturforsch.* **1998**, *53b*, 1307.
[7] [7a] S. Park, M. Pontier-Johnson, D. M. Roundhill, *Inorg. Chem.* **1990**, *29*, 2689. − [7b] H.-F. Klein, A. Brand, G. Cordier, *Z. Naturforsch.* **1998**, *53b*, 307.

[8] [8a] M. Canestrari, B. Chaudret, F. Dahan, Y.-S. Huang, R. Poilblanc, T.-C. Kim, M. Sanchez, *J. Chem. Soc., Dalton Trans.* **1990**, 1179. – [8b] L. Miquel, M. Basso-Bert, R. Choukroun, R. Madhouni, B. Eichhorn, M. Sanchez, M.-R. Mazieres, J. Jaud, *J. Organomet. Chem*. **1995**, *490*, 21. – [8c] J. Pietsch, L. Dahlenburg, A. Wolski, H. Berke, I. L. Eremenko, *J. Organomet. Chem*. **1995**, *495*, 113. – [8d] C. A. Willoughby, R. R. Duff, W. M. Davis, S.L. Buchwald, *Organometallics* **1996**, *15*, 472.

[9] A. Lankes, Dissertation, Aachen, **1994**

[10] J. Pietsch, P. Braunstein, Y. Chauvin, *New J. Chem*. **1998**, 467.

[11] [11a] W. Keim, *J. Mol. Catal.* **1989**, *52*, 19. – [11b] W. Keim, *Angew. Chem. Int. Ed. Engl*. **1990**, *29*, 235. – [11c] W. Keim, *New J. Chem*. **1994**, *18*, 93.

[12] P. Garrou, *Chem. Rev.* **1981**, *81*, 229.

[13] [13a] W. Keim, F.H. Kowaldt, R. Goddard, C. Krüger, *Angew. Chem*. **1978**, *90*, 493, *Angew. Chem., Int. Ed. Engl*. **1978**, *17*, 466. – [13b] W. Keim, A. Behr, B. Gruber, B. Hoffmann, F. H. Kowaldt, U. Kürschner, B. Limbäcker, F. P. Sistig, *Organometallics* **1986**, *5*, 2356.

[14] [14a] D. Matt, M. Huhn, J. Fischer, A. DeCian, W. Kläui, I. Tkatchenko, M. Bonnet, *J. Chem. Soc., Dalton Trans.* **1993**, 1173. – [14b] P. Braunstein, Y. Chauvin, S. Mercier, L. Saussine, A. DeCian, J. Fischer, *J. Chem. Soc., Chem. Commun.* **1994**, 2203. – [14c] J. Andrieu, P. Braunstein, Y. Dusausoy, N. E. Ghermani, *Inorg. Chem*. **1996**, *35*, 7174.

[15] K.A. Ostoja-Starzewski, L. Born, *Organometallics* **1992**, *11*, 2701.

[16] [16a] D. M. Singleton (Shell Oil Comp.), US 4,472,522; *Chem. Abstr*. **1985**, *102*, 46405. – [16b] D. M. Singleton (Shell Oil Comp.), US 4,472,525; *Chem. Abstr*. **1985**, *102*, 85118.

[17] G. A. Nesterov, G. Fink, V.A. Zakharov, W. Frenzl, *J. Mol. Catal*. **1991**, *69*, 129.

[18] K. A. Ostoja-Starzewski, J. Witte, K. H. Reichert, G. Vasiliou, *Transition Metals and Organometallics as Catalysts for Olefin Polymerization* (Eds.: W. Kaminski, H. Sinn), Springer Verlag, Heidelberg, **1988**, p. 349.

[19] J. Heinicke, E. Klaus, M. Koesling, H. Pritzkow, A. Sebald, *Solid State Nucl. Magn. Reson*., in press.

[20] R. T. Boeré, C. D. Montgomery, N. C. Payne, C. J. Willis, *Inorg. Chem*. **1985**, *24*, 3680.

[21] U. Müller, W. Keim, C. Krüger, P. Betz, *Angew. Chem. Int. Ed. Engl*. **1989**, *28*, 1011.

[22] P. L. Corio, *Structure of High-Resolution NMR Spectra*, Academic Press, New York, **1966**.

[23] P. S. Pregosin, R. W. Kunz, ^{31}P and ^{13}C NMR of Transition Metal Phosphine Complexes, NMR Basic Principles and Progress (Eds.: P. Diehl, E. Fluck, R. Kosfeld), vol. 16, Springer Verlag, Berlin, **1979**.

[24] J. Heinicke, M. He, H.-F. Klein, A. Dal, O. Hetche, W. Keim, H.-J. Haupt, U. Flörke, to be published.

Received February 3, 1999
[I99035]

Synthesis, Crystal Structure, Spectroscopic and Magnetic Properties of an Unprecedented Three-Dimensional Cu^{II} Coordination Compound of 1,2-Bis(1,2,4-triazol-4-yl)ethane

Yann Carcia,*[a] Petra J. van Koningsbruggen,*[a] Huub Kooijman,[b] Anthony L. Spek,[b] Jaap G. Haasnoot,[c] and Olivier Kahn†[a][+]

Keywords: Copper / Magnetic properties / Supramolecular chemistry / Three-dimensional architecture

A novel three-dimensional copper(II) compound of the formula $[Cu_3(btre)_5(H_2O)_2](ClO_4)_6\cdot H_2O$ (btre = 1,2-bis(1,2,4-triazol-4-yl)ethane) has been synthesized. The structure has been solved at 150 K by single-crystal X-ray analysis. The compound $[C_{30}H_{44}Cu_3N_{30}O_2\cdot 6(ClO_4)\cdot H_2O]$ crystallizes in the triclinic space group $P\bar{1}$ with a = 12.488(1), b = 13.195(1), c = 19.756(2) Å, α = 78.959(8), β = 84.553(8), γ = 63.869(7)°, V = 2868.4(5) Å^3, Z = 2 (trinuclear Cu^{II} units), 6484 reflections [$I > 4\sigma(I)$], R_F = 0.0581, wR_2 = 0.1214. The structure of this coordination polymer consists of a three-dimensional network built up from linear trinuclear Cu^{II} cations of formula $[Cu_3(btre)_5(H_2O)_2]^{6+}$. This crystallographically independent unit comprises a linear array of three Cu^{II} ions linked by triple N1,N2-1,2,4-triazole bridges, yielding Cu1–Cu2 = 3.893(1) Å and Cu2−Cu3 = 3.889(1) Å. These linear trinuclear Cu^{II} units are linked by various pathways involving tridentate and tetradentate bridging btre ligands, which yields an unprecedented three-dimensional network. The Cu^{II} ions are weakly antiferromagnetically coupled with J = –1.01(2) cm^{-1} (based on the Hamiltonian: $\mathbf{H} = -J[S_{Cu1}\cdot S_{Cu2} + S_{Cu2}\cdot S_{Cu3}]$ using the expression for the molar magnetic susceptibility S = 1/2 of a linear trinuclear system). The nature and the magnitude of the antiferromagnetic exchange have been discussed on the basis of the structural features.

Introduction

Polynuclear coordination compounds containing derivatives of 1,2,4-triazole have been of increasing interest during the last decade. Several studies have dealt with the search for magneto-structural correlations for transition metal(II) compounds containing N1,N2-1,2,4-triazole bridges.[1−10] On the other hand, polynuclear (1,2,4-triazole)iron(II) compounds have been found to yield spin-crossover materials exhibiting cooperative behavior.[11−33]

The capability of the 1,2,4-triazole ligand to form a bridge between metal(II) ions by establishing the N1,N2 coordination mode makes them very useful for obtaining polynuclear coordination compounds in which the (paramagnetic) transition metal(II) ions are maintained at relatively short distances. Substituents have been attached to the N4 of the 1,2,4-triazole in order to prevent coordination at this position. Consequently, in coordination compounds, the ligand will be incorporated in its neutral form. Earlier studies dealt with 4-amino-1,2,4-triazole, of which mostly linear chain compounds have been obtained, where the metal(II) ions are linked by triple N1,N2-1,2,4-triazole bridges.[11b,12,13,16−20,23−29] This has been confirmed by an X-ray crystallographic study for $[Cu(4\text{-amino-}1,2,4\text{-triazole})_3](ClO_4)2\cdot 0.5H_2O$.[34] Using alkyl[21,30,31,35] or hydroxyalkyl substituents[8,22,32,33] of different sizes, this triply bidentate N1,N2 bridging of the 4-substituted 1,2,4-triazole ligand has again uniquely been found. In the absence of coordinating anions, this yields linear trinuclear compounds[21,30,31,35] or infinite linear chains.[8,21,22,32,33] On the other hand, taking 4-phenyl-substituted derivatives under the same experimental conditions only led to the formation of linear trinuclear species having triple N1,N2-1,2,4-triazole bridges.[36]

Surprisingly, with 4,4′-bis(1,2,4-triazole) (abbreviated as btr) this N1,N2 bridging coordination mode has not yet been observed. Instead, the ligand has been found to link transition metal(II) ions using N1 and N1′ − the nitrogen atoms originating from the two different 1,2,4-triazole rings − resulting in one-,[37] two-,[38−41] and three-dimensional[42] networks. The occurrence of solely this N1,N1′ bidentate coordination mode may be related to the observation that this coordination of btr is possible while keeping its geometric conformation close to that what has been found for the free ligand, i.e. with fairly perpendicular 1,2,4-triazole rings.[43] Furthermore, charge distribution efficiency considerations may favor a wide separation of the twofold positively charged transition metal(II) ions, which is indeed realized by this N1,N2′ bidentate coordination.

The purpose of this study is to investigate the way in which a more flexible linkage between the 1,2,4-triazole moieties, as compared to the direct N4−N4′ bond in btr, will influence the coordination mode of the ligand, and thus the type of compound to be formed. Therefore, we have

[a] Laboratoire des Sciences Moléculaires, Institut de Chimie de la Matière Condensée de Bordeaux,
UPR CNRS No 9048, F-33608 Pessac, France
E-mail: kahn@icmcb.u-bordeaux.fr
[b] Bijvoet Center for Biomolecular Research, Crystal and Structural Chemistry, Utrecht University,
Padualaan 8, NL-3584 CH Utrecht, The Netherlands
[c] Leiden Institute of Chemistry, Gorlaeus Laboratories, Leiden University,
P. O. Box 9502, NL-2300 RA Leiden, The Netherlands
[+] We are very sad that Olivier suddenly passed away on December 8, 1999. We will never forget him and dedicate this paper to him.

 © WILEY-VCH Verlag GmbH, D-69451 Weinheim, 2000 1434−1948/00/0102−0307 $ 17.50+.50/0

selected 1,2-bis(1,2,4-triazol-4-yl)ethane (abbreviated as btre). In this paper we describe the structure of a new type of polynuclear copper(II) compound together with its spectroscopic and magnetic properties.

Results and Discussion

Description of the Structure of $[Cu_3(btre)_5(H_2O)_2](ClO_4)_6 \cdot H_2O$

The structure of this coordination polymer consists of a three-dimensional network built up from linear trinuclear Cu^{II} cations of formula $[Cu_3(btre)_5(H_2O)_2]^{6+}$ (see Figure 1). This crystallographically independent unit comprises a linear array of three Cu^{II} ions linked by triple N1,N2-1,2,4-triazole bridges. Ligands labeled 3 and 4 have an inversion center at the middle of the ethylene linkage. One noncoordinating water molecule, as well as six free perchlorate anions complete the asymmetric unit. Selected bond lengths and bond angles are given in Tables 1 and 2. These linear trinuclear Cu^{II} units are linked via various pathways involving tridentate (ligands marked 1, 2, 5 and 6) and tetradentate (ligands marked 3 and 4) bridging btre ligands, yielding an unprecedented three-dimensional network (see Figure 2). The structure is additionally stabilized by hydrogen bonding involving coordinating as well as noncoordinating water molecules.

Table 1. Bond lengths [Å] for $[Cu_3(btre)_5(H_2O)_2](ClO_4)_6 \cdot H_2O$; estimated standard deviations in the last significant digits are given in parentheses

Cu1−O1	2.449(5)
Cu1−N101	1.994(6)
Cu1−N202	2.369(5)
Cu1−N301	2.070(6)
Cu1−N511[a]	1.997(6)
Cu1−N111[b]	2.020(6)
Cu2−N102	2.359(5)
Cu2−N201	2.015(6)
Cu2−N302	1.996(5)
Cu2−N401	1.988(5)
Cu2−N501	2.045(5)
Cu2−N601	2.454(5)
Cu3−O2	2.557(5)
Cu3−N402	2.056(6)
Cu3−N502	2.279(5)
Cu3−N602	1.986(6)
Cu3−N211[c]	1.985(7)
Cu3−N611[d]	2.030(6)

Marked atoms are generated by symmetry operations: [a] $-1 + x, y, z$. − [b] $1 - x, 1 - y, 2 - z$. − [c] $1 + x, y, z$. − [d] $2 - x, -y, 1 - z$.

Within the trinuclear Cu^{II} unit, three btre ligands link each pair of adjacent copper(II) ions via nitrogen atoms N1 and N2. The central ion, Cu2, is in a strongly distorted octahedral environment formed by six N-donating btre ligands. The coordination plane is formed by four nitrogen donor atoms at 1.988(5)−2.045(5) Å, whereas two btre li-

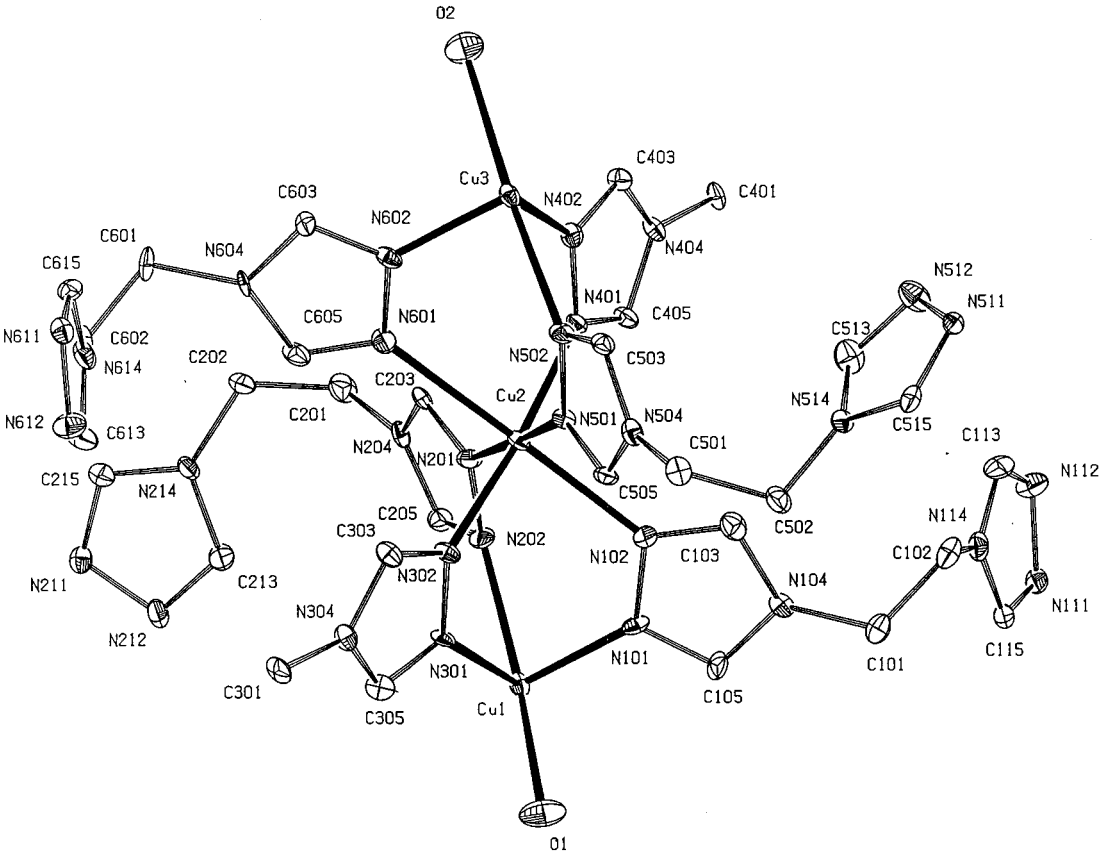


Figure 1. Atomic displacement ellipsoid drawing[57] (50% probability level) and atomic labeling system showing the asymmetric unit of $[Cu_3(btre)_5(H_2O)_2](ClO_4)6 \cdot H2O$; hydrogen atoms, noncoordinating counter ions, and water molecules have been omitted for clarity

Table 2. Bond angles [°] for $[Cu_3(btre)_5(H_2O)_2](ClO_4)_6 \cdot H_2O$; estimated standard deviations in the last significant digits are given in parentheses

O1−Cu1−N101	89.2(2)	O2−Cu3−N402	84.3(2)
O1−Cu1−N202	163.2(2)	O2−Cu3−N502	171.1(2)
O1−Cu1−N301	78.4(2)	O2−Cu3−N602	90.9(2)
O1−Cu1−N511[a]	89.0(2)	O2−Cu3−N211[c]	87.2(2)
O1−Cu1−N111[b]	93.7(2)	O2−Cu3−N611[d]	89.9(2)
N101−Cu1−N202	87.2(2)	N102−Cu2−N201	89.3(2)
N101−Cu1−N301	92.5(2)	N102−Cu2−N302	88.8(2)
N101−Cu1−N511[a]	175.8(2)	N102−Cu2−N401	96.0(2)
N101−Cu1−N111[b]	89.8(2)	N102−Cu2−N501	92.6(2)
N202−Cu1−N301	85.4(2)	N102−Cu2−N601	179.3(2)
N202−Cu1−N511[a]	95.6(2)	N202−Cu1−N111[b]	102.7(2)
N301−Cu1−N511[a]	90.9(2)	N201−Cu2−N401	88.0(2)
N301−Cu1−N111[b]	171.7(2)	N201−Cu2−N501	178.1(2)
N511[a]−Cu1−N111[b]	86.6(2)	N201−Cu2−N601	90.0(2)
N402−Cu3−N502	86.9(2)	N302−Cu2−N401	174.4(2)
N402−Cu3−N602	92.8(2)	N302−Cu2−N501	90.7(2)
N402−Cu3−N211[c]	88.0(2)	N302−Cu2−N601	90.9(2)
N402−Cu3−N611[d]	173.2(2)	N401−Cu2−N501	91.9(2)
N502−Cu3−N602	90.1(2)	N401−Cu2−N601	84.3(2)
N502−Cu3−N211[c]	88.0(2)	N501−Cu2−N601	88.1(2)
N502−Cu3−N611[d]	98.9(2)	N602−Cu3−N211[c]	177.8(2)
N602−Cu3−N611[d]	90.7(2)	N211[b]−Cu3−N611[d]	88.3(2)
Cu1−N101−N102	126.9(4)	Cu2−N501−C505	129.3(4)
Cu1−N101−C105	125.3(5)	Cu3−N502−N501	127.0(4)
Cu2−N102−N101	123.1(4)	Cu3−N502−C503	126.2(4)
Cu2−N102−C103	129.8(4)	N512−N511−Cu1[c]	120.1(4)
C115−N111−Cu1[b]	129.2(4)	C515−N511−Cu1[c]	131.8(5)
N112−N111−Cu1[b]	121.4(4)	Cu2−N602−N601	123.3(4)
Cu2−N201−N202	125.9(4)	Cu2−N601−C603	128.5(4)
Cu2−N201−C203	126.4(4)	N612−N611−Cu3[d]	121.4(4)
Cu1−N202−N201	121.6(4)	Cu1−N202−C205	129.3(4)
N212−N211−Cu3[a]	117.1(4)	C615−N611−Cu3[d]	126.8(4)
C215−N211−Cu3[a]	134.9(4)	Cu1−N301−N302	128.7(4)
Cu1−N301−C305	125.3(4)	Cu2−N302−N301	127.3(3)
Cu2−N302−C303	124.2(4)	Cu2−N401−N402	129.2(3)
Cu2−N401−C405	123.3(4)	Cu3−N402−N401	127.6(4)
Cu3−N402−C403	125.1(4)	Cu2−N501−N502	123.5(4)

Marked atoms are generated by symmetry operations: [a] $-1 + x, y, z$. − [b] $1 - x, 1 - y, 2 - z$. − [c] $1 + x, y, z$. − [d] $2 - x, -y, 1 - z$.

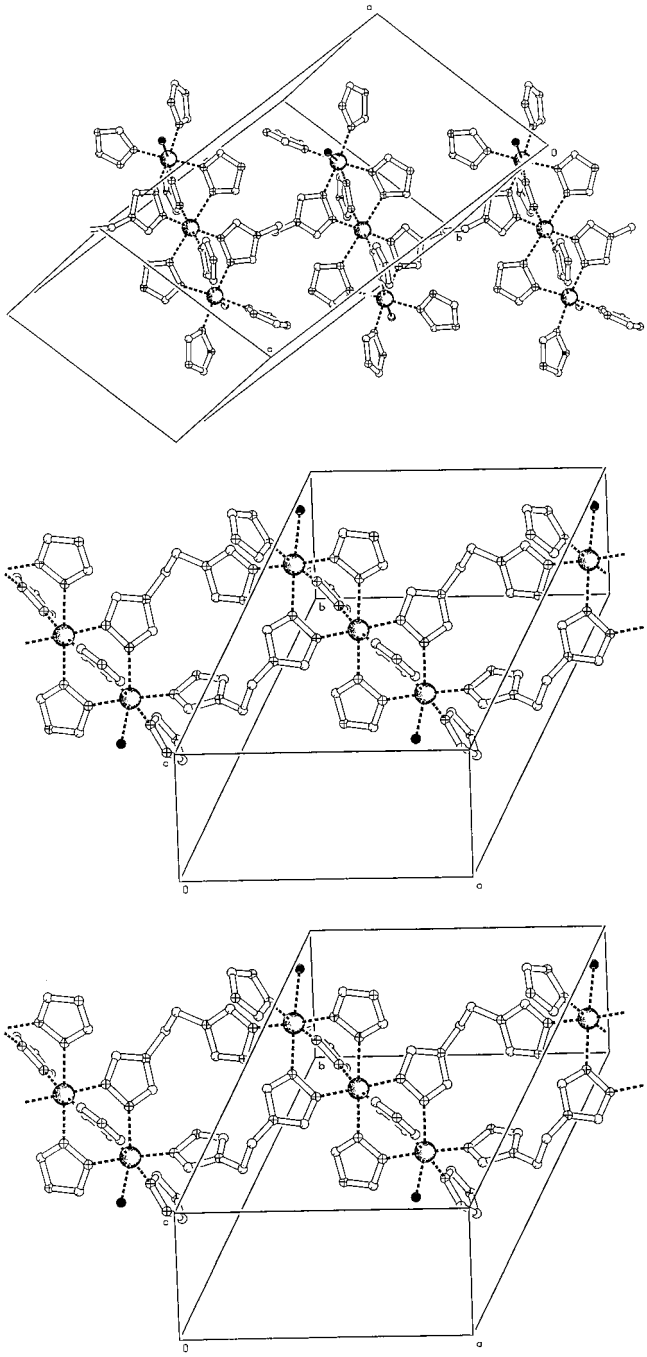


Figure 2. PLUTON[57] drawing showing the structure of $[Cu_3(btre)_5(H_2O)_2](ClO_4)_6 \cdot H_2O$: (a) (1 −1 1) chain of trinuclear Cu units linked by ligands 3 and 4; (b) (1 0 0) chain of trinuclear Cu units linked by ligands 2 and 5; (c) (1 −1 −1) chain of trinuclear Cu units linked by ligands 1 and 6

gands coordinate at significantly longer distances [2.359(5) and 2.454(5) Å to N102 and N601, respectively]. The coordination geometry about this Cu^{II} ion very closely resembles those of the Cu^{II} ions in the linear chain compounds $[Cu(4\text{-amino-}1,2,4\text{-triazole})_3](ClO_4)_2 \cdot 0.5H_2O$[34] and $[Cu(hyetrz)_3](ClO_4)_2 \cdot 3H_2O$ [hyetrz = 4-(2-hydroxyethyl)-1,2,4-triazole].[8] It is, however, in contrast to the geometry of the central Cu^{II} ion in the linear trinuclear compound $[Cu_3(metz)_6(H_2O)_4](CF_3SO_3)_6(H_2O)_4$ (metz = 3-methyl-4-ethyl-1,2,4-triazole),[42][44] where it appears that the dynamic Jahn−Teller distortion results in a completely regular octahedral coordination about the Cu^{II} ion octahedron, with six relatively short Cu−N distances of 2.14(5) Å.

The terminal copper(II) ions, Cu1 and Cu3, are linked to Cu2 via triple N1,N2-1,2,4-triazole bridges, resulting in a Cu1−Cu2 distance of 3.893(1) Å and a Cu2−Cu3 distance of 3.889(1) Å. This compares rather well to the Cu−Cu distances of 3.853(2) Å and 3.829(2) Å encountered in $[Cu(hyetrz)_3](ClO_4)_2 \cdot 3H_2O$.[8] However, it should be noted that the Cu−Cu distances observed in the present coordination polymer are significantly longer than the 3.719(7) Å for Cu^{II} ions linked by triple μ-N1,N2-1,2,4-triazole bridges in the linear trinuclear compound $[Cu_3(metz)_6(H_2O)_4](CF_3SO_3)_6(H_2O)_4$.[42][44] This may be related to the dynamic Jahn−Teller effect involving the central Cu^{II} ion in the metz compound.

As has also been observed in $[Cu(hyetrz)_3](ClO_4)_2 \cdot 3H_2O$,[8] that in order to establish the linkage of Cu^{II} ions in Jahn−

Teller-distorted octahedra by triple μ-N1,N2-1,2,4-triazole bridges, the geometric disposition of the ligands becomes such that important deviations from the ideal threefold axis running through the Cu^{II} ions are required. Also in the present compound, the N1,N2 bridging mode of all btre ligands involve unequal Cu−N distances, as well as Cu−N−N angles. The torsion angles Cu−N−N−Cu involving ligands 1, 2, 3, 4, 5, and 6 are 9.7(7)°, 20.7(7)°, 7.9(7)°, 4.9(8)°, −0.1(7)°, and 7.3(7)°, respectively.

The coordination octahedra around Cu1 and Cu3 are completed by two N-donating btre ligands and a coordinating water molecule, yielding an N_5O chromophore. For both terminal Cu^{II} ions, the axial coordination is formed by a water molecule and an N-donating btre ligand. The coordination plane of Cu2 [N201, N302, N401, N501] makes an angle of 68.3(2)° with the coordination plane of Cu1 [N101, N301, N511 ($-1 + x, y, z$), N111 ($1 - x, 1 - y, 2 - z$)], whereas the angle with the least-squares plane through the equatorial coordination sphere of Cu3 [N402, N602, N211 ($1 + x, y, z$), N611 ($2 - x, -y, 1 - z$)] is 61.4(2)°.

All 1,2,4-triazole rings are fairly planar: The maximum deviation of an atom from the least-squares plane through the ring atoms is 0.011(7) Å. The three-dimensional structure consists of three chains of trinuclear Cu units running in directions (1 −1 1), (1 0 0) and (1 1 −1). Each chain is formed by two ligands: 3 and 4, 2 and 5, and 1 and 6, respectively.

The btre ligands which are located on a crystallographic inversion center have N4−C1−C2−N4′ torsion angles of 180° and act as tetradentate ligands, linking two pairs of Cu^{II} ions originating from two different trinuclear units. Ligand 3 uses its N1 and N2 to link Cu1 and Cu2, and N1′ and N2′ to establish a bridge between Cu1 (symmetry operation: $1 - x, 1 - y, 1 - z$) and Cu2 ($1 - x, 1 - y, 1 - z$). Ligand 4 bridges Cu2 and Cu3 and links Cu2 ($2 - x, -y, 2 - z$) and Cu3 ($2 - x, -y, 2 - z$) by its symmetry-related counterpart. The resulting Cu−Cu distances are in the range 10.742(2)−11.460(2) Å. In this way, a chain of trinuclear units running along the $x, -y, z$ direction is formed (see Figure 2a). In fact, this doubly bridging coordination mode of btre involves an inversion lying on the middle of the ethylene bridge. Consequently, it may be more correct to describe this as a twisted chain of trinuclear entities.

The four other btre molecules are tridentate ligands, which have a bent conformation, as is illustrated by the values for the N4−C1−C2−N4′ torsion angles involving the N4,N4′ ethylene linkage. These angles are −79.5(7)°, −86.1(7)°, 75.5(7)° and 63.0(7)° for the ligands marked 1, 2, 5 and 6, respectively. The tridentate coordination is established by forming both a long and a rather short Cu−N bond length within the N1,N2 bridging triazole, together with a short Cu−N distance involving the second triazole ring. Ligand 2 and ligand 5 establish an N1,N2 bridge between two Cu^{II} ions within the asymmetric unit, and they coordinate with N1 of the second 1,2,4-triazole ring to a terminal Cu^{II} of a symmetry-related trinuclear entity. Ligand 2 establishes an N1,N2 bridge between Cu1 and Cu2, while coordinating with its triazole counterpart to Cu3 ($-1 + x, y, z$); while ligand 5 links Cu2 and Cu3 via its μ-N1,N2 coordination mode, and binds to Cu1 ($1 + x, y, z$). The resulting Cu−Cu distances are: Cu1−Cu3 ($-1 + x, y, z$) = 9.053(2) Å, Cu2−Cu3 ($-1 + x, y, z$) = 10.243(2) Å and Cu2−Cu1 ($1 + x, y, z$) = 10.136(2) Å. This yields a chain running along the x direction (Figure 2b).

A chain of trinuclear Cu^{II} entities along the $x, -y, -z$ direction is formed through the tridendate coordination of ligand 1 and ligand 6. Like ligands 2 and 5, these ligands also form a μ-N1,N2-1,2,4-triazole bridge between Cu^{II} ions within the asymmetric unit, together with the coordination of a nitrogen atom of the second 1,2,4-triazole ring to a symmetry-related Cu^{II} ion of another trinuclear unit. Ligand 1 links Cu1 and Cu2 via the N1,N2 bridging mode, and coordinates with N1′ to Cu1 ($1 - x, 1 - y, 2 - z$). Ligand 6, which establishes an N1,N2 bridge between Cu2 and Cu3, binds to Cu3 ($2 - x, -y, 1 - z$). The shortest Cu−Cu distances resulting from this coordination pathway are Cu1−Cu1 ($1 - x, 1 - y, 2 - z$) = 9.262(2) Å and Cu3−Cu3 ($2 - x, -y, 1 - z$) = 8.595(1) Å (Figure 2c).

The difference between the chains formed by ligands 2 and 5 and that formed by ligands 1 and 6 is that in the former chain, the link between each pair of adjacent tricopper units is formed by one ligand 2 and one ligand 5. In the latter chain, the links between adjacent tricopper units are formed by either two molecules of ligand 1 or two molecules of ligand 6.

In the present compound, the perchlorate anions are noncoordinating and some are involved in hydrogen bonding interactions with the btre ligands, as well as with the lattice water molecules. The noncoordinated nitrogen atoms of the tridentate ligands 1 and 2 are involved in hydrogen bonding. N112 ($2 - x, -y, 2 - z$) is hydrogen-bonded to water oxygen atom O2, which is in turn coordinated to Cu3. N212 accepts an (intermolecular) hydrogen bond from the noncoordinated water molecule O3. Details of the hydrogen bonds are listed in Table 3. The shortest "intermolecular" Cu−Cu distance is formed through hydrogen bond links. Cu1−O1−H···O2 ($-1 + x, 1 + y, z$) − Cu3 ($-1 + x, 1 + y, z$) gives a Cu−Cu distance of 6.784(1) Å.

Table 3. Selected interatomic distances [Å] and angles [°] for the hydrogen bonding interactions in $[Cu_3(btre)_5(H_2O)_2](ClO_4)_6 \cdot H_2O$; estimated standard deviations in parentheses

D−H···A	D−H	H···A	D···A	D−H···A
O1−H1A···O2[a]	0.81(5)	1.99(6)	2.729(7)	151(7)
O1−H1B···O21[b]	0.81(7)	2.15(7)	2.900(9)	154(7)
O2−H2A···N112[c]	0.81(4)	2.23(7)	2.931(8)	146(7)
O2−H2B···O31[d]	0.80(9)	2.02(9)	2.828(9)	178(8)
O2−H2B···O33[d]	0.80(9)	2.59(8)	3.057(9)	119(7)
O3−H3A···O13[b]	0.82(6)	2.29(6)	3.060(8)	157(7)
O3−H3A···O14[b]	0.82(6)	2.36(7)	3.046(8)	142(6)
O3−H3B···N212	0.81(7)	2.11(7)	2.913(8)	168(7)

Marked atoms are generated by symmetry operations: [a] $-1 + x, 1 + y, z$. − [b] $1 - x, 1 - y, 1 - z$. − [c] $2 - x, -y, 2 - z$. − [d] $1 - x, -y, 1 - z$.

Spectroscopic Properties

The UV/Vis spectrum shows a broad asymmetric band with a maximum situated at 11.6×10^3 cm^{-1} and a shoulder at 9.3×10^3 cm^{-1}, which is in agreement with the presence of both CuN_6 and CuN_5O chromophores, as well as with the tetragonal distortion of the Cu^{II} octahedra.[45]

There is no evidence for a strong deviation from T_d symmetry for the noncoordinating perchlorate anions, as is indicated by the strong ν_3 absorption at 1102 cm^{-1} and the ν_4 at 623 cm^{-1} observed in the infrared spectrum.[46]

Magnetic Measurements

The magnetic behavior of $[Cu_3(btre)_5(H_2O)_2](ClO_4)_6 \cdot H_2O$ is shown in Figure 3 in the form of a $\chi_M T$ vs. T plot, χ_M being the molar magnetic susceptibility and T the temperature. At 296 K the $\chi_M T$ value is 1.278 cm^3 mol^{-1} K, which is about the value expected for three uncoupled copper(II) ions. The value of $\chi_M T$ decreases upon cooling, reaching a value of 0.732 cm^3 mol^{-1} K at 2 K. This behavior is characteristic for compounds with an overall antiferromagnetic interaction between the metal(II) ions. The structure indicates the presence of interconnected linear trinuclear Cu^{II} units, these trinuclear entities being magnetically isolated. Therefore, the magnetic data have been interpreted using the expression for the molar magnetic susceptibility of a linear trinuclear system with S = 1/2.[11a,47]

$$\chi_M T = (N\beta^2 g^2/4k)[(1 + e^x + 10e^{3x/2})/(1 + e^x + 2e^{3x/2})] \quad (1)$$

in which $x = J/kT$. J is the energy gap defined by the phenomenological spin Hamiltonian with quantum spin operators $\mathbf{S}_{Cu1}$, $\mathbf{S}_{Cu2}$, and $\mathbf{S}_{Cu3}$ where Cu1, Cu2 and Cu3 refer to nearest neighbor ions:

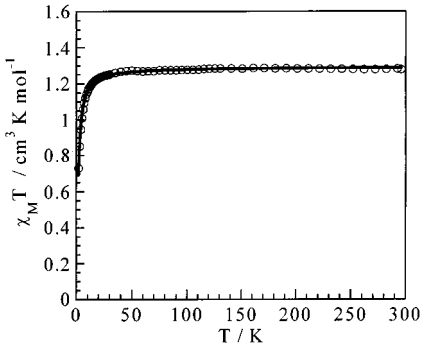


Figure 3. Observed (o) and calculated [—; $J = -1.01(2)$ cm^{-1}, $g = 2.14(1)$] $\chi_M T$ vs. T curves for $[Cu_3(btre)_5(H_2O)_2](ClO_4)_6 \cdot H_2O$

$$\mathbf{H} = -J[S_{Cu1} \cdot S_{Cu2} + S_{Cu2} \cdot S_{Cu3}] \quad (2)$$

The assumption of negligible magnetic exchange between second neighbor copper(II) ions is justified in view of the study of the triply N1,N2-1,2,4-triazole bridged $Fe^{II}-Fe^{II}-Fe^{II}$[30] and $Co^{II}-Co^{II}-Co^{II}$[48] trinuclear clusters, where the central metal ion is diamagnetic, and no magnetic interactions could be detected between the paramagnetic terminal metal ions. In Equation 1, N, g, β, k, and T have their usual meanings. The g factor must be considered as an average value of the local Zeeman factors, and intercluster exchange interactions were supposed to be negligible. A good fit has been obtained for the parameters $g = 2.14(1)$ and $J = -1.01(2)$ cm^{-1} (see Figure 3).

The spectrum of the (S,S′) low-lying spin states, where S and S′ are the quantum numbers associated with the **S** and **S**′ operators:

$$\mathbf{S} = \mathbf{S}_{Cu1} + \mathbf{S}_{Cu2} + \mathbf{S}_{Cu3}$$

$$\mathbf{S}' = \mathbf{S}_{Cu1} + \mathbf{S}_{Cu3}$$

consists of a ground doublet (1/2, 1), an excited doublet (1/2, 0) at the energy $-J$, and an excited quartet at the energy $-3J/2$. This excited spin quartet state is further split into two Kramers doublets, which to a first approximation can be labeled as $M_S = \pm 1/2$ and $\pm 3/2$.

The X-band powder EPR spectra for $[Cu_3(btre)_5(H_2O)_2](ClO_4)_6 \cdot H_2O$ have been recorded at 298 K and 4 K. The spectrum at 4 K is shown in Figure 4. It exhibits features around $g = 2$ that can be assigned to the envelop of the three resonances within the $M_S = \pm 1/2$ Kramers doublets, as well as a smaller feature around $g = 5.6$ that may be assigned to the resonance within the $M_S = \pm 3/2$ Kramers doublet. It should be noticed that, due to the low symmetry of the Cu^{II} triad, the $M_S = \pm 1/2$ and $M_S = \pm 3/2$ Kramers doublets states arising from the spin quartet are somewhat mixed.

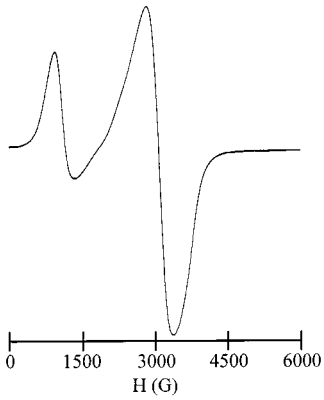


Figure 4. X-band powder EPR spectrum ($\nu = 9.46780$ GHz) of $[Cu_3(btre)_5(H_2O)_2](ClO_4)_6 \cdot H_2O$ recorded at 4 K

Concluding Remarks

The btre ligand has been shown to be a powerful tool in preparing supramolecular architectures. The structure of $[Cu_3(btre)_5(H_2O)_2](ClO_4)_6 \cdot H_2O$ represents an unprecedented architecture of a three-dimensional compound. Recently, a polynuclear Cu^{II} compound of a bis(imidazole) ligand has been reported. $[Cu(bim)_{2.5}](ClO_4)_2 \cdot 2CH_3OH$ [bim = 1,2-bis(imidazole-1-yl)ethane][49] contains Cu^{II} ions

in a distorted square-based pyramidal coordination environment. The neutral ligands in the $a-b$ plane bind to four Cu^{II} ions in a *trans* mode, leading to a two-dimensional sheet arrangement. The resulting Cu−Cu distances are 7.05 Å and 11.43 Å in this $a-b$ plane. Furthermore, the axially coordinating neutral bim ligand has a bent, *cis* conformation, and alternatively links the $a-b$ plane to sheets above and below. The closest inter-sheet Cu−Cu separation is 12.55 Å.

Upon using the btre ligand, a larger versatility in coordination is anticipated due to the presence of the additional nitrogen atom within the 1,2,4-triazole ring compared to the imidazole. In fact, in $[Cu_3(btre)_5(H_2O)_2](ClO_4)_6 \cdot H_2O$ btre acts as a spacer between three and even four Cu^{II} ions. The tridentate ligands are bent, as is illustrated by the values for the N4−C1−C2−N4′ torsion angles involving the N4,N4′ ethylene linkage. These angles are −79.5(7)°, −86.1(7)°, 75.5(7)° and 63.0(7)° for the ligands marked 1, 2, 5 and 6, respectively. On the other hand, the N4−C1−C2−N4′ torsion angles of the tetradentate ligands 3 and 4 are restricted by crystallographic symmetry to a value of 180°.

Interestingly, the coordination mode of btre shows features already observed in coordination compounds of 3- or 4-substituted 1,2,4-triazoles where the well-known triply bidentate N1,N2 bridging of the 1,2,4-triazole ring has been found to result in linear trinuclear species.[21,30,31,35,50] In those cases, the chain growth is blocked by monodentately coordinated 1,2,4-triazole ligands and/or by water molecules. In fact, the trinuclear cation $[Cu_3(btre)_5(H_2O)_2]^{6+}$ can be regarded as a linear, trinuclear Cu^{II} compound of this type, in which the coordination environment about the terminal Cu^{II} ions is completed by two monodentate 1,2,4-triazole ligands and a water molecule. On the other hand, the btr ligand was originally designed in order to force a tetradentate coordination mode.[21] However, exclusively the N1,N1′ bidentate mode has been observed so far,[37−42] which may be due to charge distribution efficiency considerations, or more likely, may be ascribed to the fact that even in coordination compounds the btr ligand favors a conformation close to the one observed in the free ligand,[43] i.e. with fairly perpendicular 1,2,4-triazole nuclei. The more flexible nature of the ethylene linkage in the present btre ligand overcomes these problems, and indeed the tetradentate coordination has been achieved for some of the ligand molecules present. Furthermore, it could well be that this type of rigid tetradentate spacer allows a crystal packing of the trinuclear Cu^{II} units with distances close to those found in the compounds containing nonconnected trinuclear units of this type. Moreover, the bent, *cis*-btre ligands allows us to satisfactorily maintain these trinuclear entities, which are further stabilized by a network of hydrogen bonds.

In the present polynuclear Cu^{II} compound, a relatively small antiferromagnetic interaction [$J = -1.01(2)$ cm^{-1}] has been found between adjacent metal(II) ions. It may be proposed that the linear trinuclear Cu^{II} cations represent the magnetic entities responsible for this magnetic interaction. Indeed, the magnetic data could satisfactorily be interpreted using the theoretical expression for linear trinuclear S = 1/2 units. The low J value can be explained on the basis of the superexchange pathway and the geometry around Cu^{II}. The unpaired electron for the d^9 ion clearly resides in the $d(x^2 - y^2)$ orbital, with hardly any density in the direction of the axially coordinating 1,2,4-triazole ligands. The magnitude of the antiferromagnetic interaction between Cu^{II} ions can therefore be explained by the superexchange pathway involving the σ orbitals of the N1,N2 diazine moiety of the bridging triazole network.[1−10] It should be noted that the magnetic orbitals located on the Cu^{II} ion are only favorably oriented to yield a considerable overlap on the 1,2,4-triazole ligand, linking the metal(II) ions with rather short Cu−N distances. Consequently, the main pathway for the superexchange only proceeds through one triazole ligand, i.e. ligand 3 between Cu1 and Cu2, and ligand 4 between Cu2 and Cu3. However, the bridging geometry of these ligands is slightly asymmetric, involving unequal Cu−N−N angles. Furthermore, the 1,2,4-triazole tends to twist slightly out of the equatorial plane formed by the two Cu^{II} ions involved, which is illustrated by the torsion angles of 7.9(7)° and 4.9(8)° involving ligands 3 and 4, respectively. These features lead to a rather inefficient propagation of the superexchange via this bridging network, which explains the rather low isotropic interaction parameter. This compares very well to the $J = -1.18(2)$ cm^{-1} (based on the Hamiltonian: $\mathbf{H} = -J [\Sigma_i S_i \cdot S_{i+1}]$) observed for the linear chain compound $[Cu(hyetrz)_3](ClO_4)_2 \cdot 3H_2O$, having triple N1,N2-1,2,4-triazole bridges of comparable geometry.[8]

Only one linear trinuclear Cu^{II} compound containing triple N1,N2-1,2,4-triazole bridges has so far been structurally characterized. A detailed comparison with the magnetic data of $[Cu_3(metz)_6(H_2O)_4](CF_3SO_3)_6(H_2O)_4$ is not possible, since no accurate data are available as yet.[42][44]

We have shown that this first member of a new class of *N*,*N*′-bis(1,2,4-triazol-4-yl)alkane ligands leads to the creation of a unique new supramolecular Cu^{II} compound. Preliminary studies have already indicated that polynuclear Fe^{II} spin-crossover materials could be obtained using ligands of this family.

Experimental Section

Physical Measurements: Elemental analyses were performed by the Service Central d′Analyse (CNRS) in Vernaison, France. − Infrared spectra were carried out with a Perkin−Elmer Paragon 1000 FTIR spectrophotometer using KBr pellets. − UV/Vis spectra were recorded with a CARRY 5E spectrophotometer using the diffuse reflectance technique, with polytetrafluoroethylene as a reference. − X-band powder EPR spectra were obtained with a Bruker ESP 300 E electron spin resonance spectrometer. − Magnetic susceptibilities were carried out in the temperature range 300−2 K with a quantum design MPMS-5S SQUID magnetometer. − Magnetic data were corrected for diamagnetic contributions, which were estimated from the Pascal constants and were fitted to theoretical expressions by means of a Simplex routine. All parameters (J, g) were varied independently during the fitting procedure. This routine minimizes the function $R = |\Sigma|\chi_{obs} - \chi_{calc}|^2/|\Sigma|\chi_{obs}|^2|^{1.2}$.

Starting Materials: Commercially available solvents, monoformylhydrazine, triethyl orthoformate, ethylenediamine, and copper(II) perchlorate hexahydrate were used without further purification.

Synthesis of 1,2-Bis(1,2,4-triazol-4-yl)ethane (btre): The ligand btre was prepared from monoformylhydrazine, triethyl orthoformate, and ethylenediamine according to the general method described by Bayer et al.[51] Yield: 30%. M.p. > 260°C. – ^{1}H NMR (200 MHz, D_2O): δ = 2.67 (s, CH_2), 6.40 (s, trz–H), – IR: $\tilde{\nu}$ = 675 and 642 cm^{-1} (out-of-plane ring torsion vibrations of the 1,2,4-triazole), 887 cm^{-1} [C–H out of plane vibration (γ_{C-H})]. – $C_6H_8N_6$: calcd. C 43.90, H 4.91 N 51.19; found C 44.07, H 4.39, N 50.00.

Synthesis of $[Cu_3(btre)_5(H_2O)_2](ClO_4)_6\cdot H_2O$: $Cu(ClO_4)_2\cdot 6H_2O$ (0.48 mmol, 0.18 g), dissolved in 20 mL of water, was added to btre (1.52 mmol, 0.25 g), dissolved in 20 mL of water. The reaction mixture was diluted to 100 mL with water, and heated to give a clear solution. The compound precipitated upon cooling. The precipitate formed was left in the solution. Then, after a couple of days, well-shaped single crystals could be collected after slow evaporation of a part of the solvent at room temperature. Crystals were washed with water, and air-dried. Yield: 12.4%. – $C_{30}H_{46}Cl_6Cu_3N_{30}O_{27}$: calcd. C 21.68, H 2.79, Cl 12.80, Cu 11.47, N 25.28, O 25.99; found C 22.22, H 2.60, Cl 12.80, Cu 11.35, N 25.09, O 25.55.

Crystal Structure Determination of $[Cu_3(btre)_5(H_2O)_2](ClO_4)_6\cdot H_2O$: A blue, needle-shaped crystal of approximate dimensions 0.05 × 0.1 × 0.4 mm was mounted in a Lindemann glass capillary and transferred into the cold nitrogen stream on an Enraf–Nonius CAD4-T diffractometer on a rotating anode. Accurate unit-cell parameters and an orientation matrix were determined by least-squares fitting of the setting angles of 24 well-centered reflections (SET4[52]) in the range 10.0° < θ < 13.9°. The unit-cell parameters were checked for the presence of higher lattice symmetry.[53] Crystal data and details on data collection are presented in Table 4. Data were collected in ω scan mode with scan angle Δω = 0.73 + 0.35tanθ. Intensity data were collected up to θ = 26.5°. Intensity data of 11106 reflections were measured, 10579 of which were independent (R_{int} = 0.0665). Data were corrected for Lp effects and for 2% linear instability of the three periodically measured reference reflections during 50 h of X-ray exposure time, but not for absorption. The structure was solved by automated direct methods (SHELXS86[54]). Refinement on F^2 was carried out using full-matrix least-squares techniques (SHELXL-97[55]). Hydrogen atoms were included in the refinement on calculated positions riding on their carrier atoms, except for the water hydrogen atoms, which were located in a difference Fourier map. Their coordinates were included as parameters in the refinement. All nonhydrogen atoms were refined with anisotropic thermal parameters. The hydrogen atoms were included in the refinement with a fixed isotropic thermal parameter related to the value of the equivalent isotropic displacement parameter of their carrier atoms by a factor of 1.5 for the water hydrogen atoms and 1.2 for the other hydrogen atoms. Final refinement included 318 parameters and final weights were $w^{-1} = \sigma^2(F_o^2) + (0.0365P)^2 + 2.98P$, where $P = [(F_o^2, 0)_{max} + 2F_c^2]/3$. No residual density was found outside –0.66 and 0.95 e $Å^{-3}$. Neutral atom scattering factors and anomalous dispersion corrections were taken from the International Tables for Crystallography.[56] Geometrical calculations and illustrations were performed with PLATON.[57] Crystallographic data (excluding structure factors) for the structure reported in this paper has been deposited with the Cambridge Crystallographic Data Centre as supplementary publication no CCDC-124884. Copies of the data can be obtained free of charge on application to CCDC, 12 Union Road, Cambridge CB2 1EZ, UK [Fax: (internat) + 44-1223/336-033; E-mail: deposit@ccdc.cam.uk].

Table 4. Crystallographic data for $[Cu_3(btre)_5(H_2O)_2](ClO_4)_6\cdot H_2O$

Empirical formula	$C_{30}H_{44}Cu_3N_{30}O_2\cdot 6(ClO_4)\cdot H_2O$
Molecular mass	1662.23
T [K]	150
Space group	$P\bar{1}$ (No. 2)
Crystal system	triclinic
a [Å]	12.488(1)
b [Å]	13.195(1)
c [Å]	19.756(2)
α [°]	78.959(8)
β [°]	84.553(8)
γ [°]	63.869(7)
V [Å^3]	2868.4(5)
Z	2
$\rho_{calcd.}$ [g/cm^3]	1.925
μ (Mo-K_α) [cm^{-1}]	15.0
Radiation [Å]	0.71073 (Mo-K_α, graphite monochromator)
$R(F)$[a]	0.058 [for 6484 $F_o > 4\sigma(F_o)$]
wR_2[b]	0.1214
GoF	1.012

[a] $R(F) = \Sigma||F_o| - |F_c||/\Sigma|F_o|$. – [b] $wR2 = \{\Sigma[w(F_o^2 - F_c^2)^2]/\Sigma[w(F_o^2)^2]\}^{1/2}$.

Acknowledgments

This work was supported in part (A. L. S.) by the Council for Chemical Sciences of the Netherlands Organization for Scientific Research (CW–NWO).

[1] R. Prins, P. J. M. W. L. Birker, J. G. Haasnoot, G. C. Verschoor, J. Reedijk, *Inorg. Chem*. **1985**, *24*, 4128.
[2] A. Bencini, D. Gatteschi, C. Zanchini, J. G. Haasnoot, R. Prins, J. Reedijk, *Inorg. Chem.* **1985**, *24*, 2812.
[3] W. M. E. Koomen-van Oudenniel, R. A. G. de Graaff, J. G. Haasnoot, R. Prins, J. Reedijk, *Inorg. Chem*. **1989**, *28*, 1128.
[4] P. J. van Koningsbruggen, J. G. Haasnoot, R. A. G. de Graaff, J. Reedijk, S. Slingerland, *Acta Crystallogr.* **1992**, *C48*, 1923.
[5] P. M. Slangen, P. J. van Koningsbruggen, K. Goubitz, J. G. Haasnoot, J. Reedijk, *Inorg. Chem*. **1994**, *33*, 1121.
[6] P. M. Slangen, P. J. van Koningsbruggen, J. G. Haasnoot, J. Jansen, S. Gorter, J. Reedijk, H. Kooijman, W. J. J. Smeets, A. L. Spek, *Inorg. Chim. Acta* **1993**, *212*, 289.
[7] P. J. van Koningsbruggen, J. G. Haasnoot, H. Kooijman, J. Reedijk, A. L. Spek, *Inorg. Chem*. **1997**, *36*, 2487.
[8] Y. Garcia, P. J. van Koningsbruggen, G. Bravic, P. Guionneau, D. Chasseau, G. V. Cascarano, J. Moscovici, K. Lambert, A. Michalowicz, O. Kahn, *Inorg.Chem*. **1997**, *36*, 6357.
[9] P. J. van Koningsbruggen, M. W. Gluth, V. Ksenofontov, D. Walcher, D. Schollmeyer, G. Levchenko, P. Gütlich, *Inorg. Chim. Acta* **1998**, *273*, 54.
[10] P. J. van Koningsbruggen, J. G. Haasnoot, H. Kooijman, J. Reedijk, A. L. Spek, *J. Chem. Soc., Dalton Trans.*, submitted.
[11] [11a] O. Kahn, *Molecular Magnetism*, VCH Publishers, New York, **1993**. – [11b] O. Kahn, C. Jay-Martinez, *Science* **1998**, *79*, 44.
[12] O. Kahn, E. Codjovi, Y. Garcia, P. J. van Koningsbruggen, R. Lapouyade, L. Sommier, in *Molecule-Based Magnetic Materials* (Eds.: M. M. Turnbull, T. Sugimoto, L. K. Thompson), ACS Symposium Series No. 644, American Chemical Society, Washington DC, **1996**, p. 298.
[13] O. Kahn, J. Kröber, C. Jay, *Adv. Mater.* **1992**, *4*, 718.
[14] C. Jay, F. Grolière, O. Kahn, J. Kröber, *Mol. Cryst. Liq. Cryst*. **1993**, *234*, 255.
[15] J. Kröber, J.-P. Audière, R. Claude, E. Codjovi, O. Kahn, J. G. Haasnoot, F. Grolière, C. Jay, A. Bousseksou, J. Linarès, F. Varret, A. Gonthier-Vassal, *Chem. Mater.* **1994**, *6*, 1404.

[16] J. Kröber, E. Codjovi, O. Kahn, F. Grolière, C. Jay, *J. Am. Chem. Soc*. **1993**, *115*, 9810.
[17] L. G. Lavrenova, V. N. Ikorskii, V. A. Varnek, I. M. Oglezneva, S. V. Larionov, *Koord. Khim*. **1986**, *12*, 207; *Chem. Abstr.* **1986**, *104*, 218034b.
[18] L. G. Lavrenova, V. N. Ikorskii, V. A. Varnek, I. M. Oglezneva, S. V. Larionov, *J. Struct. Chem*. **1993**, *34*, 960.
[19] L. G. Lavrenova, V. N. Ikorskii, V. A. Varnek, I. M. Oglezneva, S. V. Larionov, *Koord. Khim*. **1990**, *16*, 654; *Chem. Abstr.* **1991**, *114*, 34747m.
[20] L. G. Lavrenova, N. G. Yudina, V. N. Ikorskii, V. A. Varnek, I. M. Oglezneva, S. V. Larionov, *Polyhedron* **1995**, *14*, 1333.
[21] J. G. Haasnoot, in *Magnetism: A Supramolecular Functio* (Ed: O. Kahn), Kluwer Academic Publishers, Dordrecht, The Netherlands, **1996**, p. 299.
[22] Y. Garcia, P. J. van Koningsbruggen, E. Codjovi, R. Lapouyade, O. Kahn, L. Rabardel, *J. Mater. Chem*. **1997**, *7*, 857.
[23] N. V. Bausk, S. B. Érenburg, L. N. Mazalov, L. G. Lavrenova, V. N. Ikorskii, *J. Struct. Chem.* **1994**, *35*, 509.
[24] N. V. Bausk, S. B. Érenburg, L. G. Lavrenova, L. N. Mazalov, *J. Struct. Chem.* **1995**, *36*, 925.
[25] S. B. Érenburg, N. V. Bausk, N. A. Varnek, L. G. Lavrenova, *J. Magn. Magn. Mater.* **1996**, *157/158*, 595.
[26] S. B. Érenburg, N. V. Bausk, L. G. Lavrenova, V. A. Varnek, L. N. Mazalov, *Solid State Ionics* **1997**, *101−103*, 571.
[27] E. Codjovi, L. Sommier, O. Kahn, C. Jay, *New. J. Chem.* **1996**, *20*, 503.
[28] R. Bronisz, K. Drabent, P. Polomka, M. F. Rudolf, *Conference Proceedings*, *ICAME95* **1996**, *50*, 11.
[29] P. J. van Koningsbruggen, Y. Garcia, E. Codjovi, R. Lapouyade, L. Fournès, O. Kahn, L. Rabardel, *J. Mater. Chem*. **1997**, *7*, 2069.
[30] [30a] G. Vos, R. A. Le Fêbre, R. A. G. de Graaff, J. G. Haasnoot, J. Reedijk, *J. Am. Chem. Soc.* **1983**, *105*, 1682. − [30b] G. Vos, R. A. G. de Graaff, J. G. Haasnoot, A. M. van der Kraan, P. de Vaal, J. Reedijk, *Inorg.Chem.* **1984**, *23*, 2905.
[31] J. J. A. Kolnaar, G. van Dijk, H. Kooijman, A . L. Spek, V. Ksenofontov, P. Gütlich, J. G. Haasnoot, J. Reedijk, *Inorg. Chem.* **1997**, *36*, 2433.
[32] Y. Garcia, P. J. van Koningsbruggen, R. Lapouyade, L. Rabardel, O. Kahn, M. Wierczorek, R. Bronisz, Z. Ciunik, M. F. Rudolf, *C. R. Acad. Sci. Paris* **1998**, *IIc*, 523.
[33] Y. Garcia, P. J. van Koningsbruggen, R. Lapouyade, L. Fournès, L. Rabardel, O. Kahn, V. Ksenofonov, G. Levchenko, P. Gütlich, *Chem. Mater.* **1998**, *10*, 2426.
[34] V. P. Sinditskii, V. I. Sokol, A. E. Fogel′zang, M. D. Dutov, V. V. Serushkin, V. M. A. Porai-Koshits, B. S. Svetlov, *Russ. J. Inorg. Chem*. **1987**, *32*, 1149.
[35] G. Vos, A. J. de Kok, G. C. Verschoor, *Z. Naturforsch.* **1981**, *36b*, 809.
[36] M. Thomann, O. Kahn, J. Guilhem, F. Varret, *Inorg. Chem.* **1994**, *33*, 6029.
[37] M. Biagini−Cingi, A. M. Manotti-Lanfredi, F. Ugozzoli, J. G. Haasnoot, J. Reedijk, *Gazz. Chim. Ital*. **1994**, *124*, 509.
[38] W. Vreugdenhil, S. Gorter, J. G. Haasnoot, J. Reedijk, *Polyhedron* **1985**, *4*, 1769.
[39] W. Vreugdenhil, J. H. van Diemen, R. A. G. de Graaff, J. G. Haasnoot, J. Reedijk, A. M. van der Kraan, O. Kahn, J. Zarembowitch, *Polyhedron* **1990**, *24*, 2971.
[40] A. Ozarowski, Y. Shunzhong, B. R. McGarvey, A. Mislankar, J. E. Drake, *Inorg. Chem.* **1991**, *30*, 3167.
[41] W. Vreugdenhil, J. G. Haasnoot, R. A. G. de Graaff, H. A. Nieuwenhuis, D. Reefman, J. Reedijk, *Acta Crystallogr.* **1987**, *C43*, 1527.
[42] W. Vreugdenhil, Ph. D. Thesis, Leiden University, **1987**.
[43] P. Domiano, *Cryst. Struct. Commun*. **1977**, *6*, 503.
[44] W. Vreugdenhil, J. G. Haasnoot, J. Reedijk, J. S. Wood, *Inorg. Chim. Acta* **1990**, *167*, 109.
[45] B. J. Hathaway, D. E. Billing, *Coord. Chem. Rev.* **1972**, *5*, 143.
[46] K. Nakamoto, in *Infrared and Raman Spectra of Inorganic and Coordination Compounds*, 5th ed., Wiley, New York, **1997**.
[47] D. B. Brown, J. R. Wasson, J. W. Hall, W. E. Hatfield, *Inorg. Chem*. **1977**, *16*, 2526.
[48] L. Antolini, A. C. Fabretti, D. Gatteschi, A. Giusti, R. Sessoli, *Inorg. Chem.* **1991**, *30*, 4858.
[49] L. P. Wu, Y. Yamagiwa, T. Kuroda-Sowa, T. Kamikawa, M. Munakata, *Inorg. Chim. Acta* **1997**, *256*, 155.
[50] P. J. van Koningsbruggen, J. G. Haasnoot, W. Vreugdenhil, J. Reedijk, O. Kahn, *Inorg. Chim. Acta* **1995**, *239*, *5*.
[51] H. O. Bayer, R. S. Cook, W. C. von Meyer, U.S. Patent 3, 821, 376, 28/6/**1974**.
[52] J. L. de Boer, A. J. M. Duisenberg, *Acta Crystallogr.* **1984**, *A40*, C410.
[53] A. L. Spek, *J. Appl. Crystallogr*. **1988**, *21*, 578.
[54] G. M. Sheldrick, *SHELXS86, Program for crystal structure determination*, University of Göttingen, Germany, **1986**.
[55] G. M. Sheldrick, *SHELXL-97, Program for crystal structure refinement*, University of Göttingen, Germany, **1997**; *International Tables for Crystallography* (Ed.: A. J. C. Wilson), vol. C, Kluwer, Academic Publishers, Dordrecht, The Netherlands, **1992**.
[56] A. L. Spek, *Acta Crystallogr.* **1990**, *A46*, C34.

Received June 2, 1999
[I99201]

Mixed Linear (M,Sb) Chains in the New Antimonides $Hf_{10}M_{\delta}Sb_{6-\delta}$ (M = V, Cr, Mn, Fe, Co, Ni, Cu): Crystal and Electronic Structures, Phase Ranges, and Electrical and Magnetic Properties

Holger Kleinke,*[a,b] Christel Ruckert,[b] and Claudia Felser[c]

Keywords: Metal-rich antimonides / Magnetism / Structure and bonding / Conductivity / LMTO

The title compounds can be synthesized in quantitative yields by arc-melting of stoichiometric amounts of $HfSb_2$, Hf and one of the *3d* metals V, Cr, Mn, Fe, Co, Ni, and Cu. These antimonides crystallize in a substitution variant of the W_5Si_3 type, in which one position is statistically mixed, occupied by the *3d* metal atom M or the Sb2 atom in different ratios. Within the linear (M,Sb) chain, the M:Sb ratio may vary between 3:1 and 2:3. According to calculations of the electronic structures of $Hf_{10}M_{\delta}Sb_{6-\delta}$ with $\delta = 1$, these phases are metallic compounds stabilized by strong Hf–Hf, Hf–M, and Hf–Sb bonds, and to a smaller extent by bonding interactions within the linear (M,Sb) chain. The metallic character was confirmed by measurements of the electrical resistivity and the magnetism of selected samples. Whereas Pauli paramagnetism was observed experimentally for M = V, Co, and Ni, $Hf_{10}FeSb_5$ is apparently the only phase with localized magnetic moments and magnetic coupling. This is in agreement with the magnetic ground state obtained solely for the ordered structure model of $Hf_{10}FeSb_5$ with spin-polarized calculation within the local spin density approximation.

Introduction

The W_5Si_3 type is adopted by a variety of different phases, including mainly silicides, germanides and stannides of the valence electron-poor (so-called "early") transition metal atoms T.[1] In this structure type, linear chains of the T atoms run parallel to linear chains of main group elements E along [001] with the same interatomic distances in both chains. As a consequence a matrix effect, i.e. somewhat short T−T and long E−E distances or vice versa, may occur.

It is assumed that the W_5Si_3 structure type is basically limited to compounds of the third and fourth main group because the pnicogen and chalcogen atoms Q will most likely not form short Q−Q bonds in such metal-rich phases. Exceptions are the tellurides $M_xK_4Te_3$ (M = Ca, Sr)[2] which can be considered as electron-precise compounds $(M^{+2})_{0.5}(K^{+1})_4(Te^{-1})(Te^{-2})_2$, each Te^{-1} forming two one-electron-two-center bonds. However, one binary vanadium arsenide was described to crystallize in the W_5Si_3 structure type, the structure of which exhibits either a disordered As or a mixed (V,As) chain, thus reducing the As−As interactions.[3] Three examples based on antimony ($Zr_5M_{\delta}Sb_{3-\delta}$, M = Fe, Co, Ni, $\delta \approx 0.5$) are already known and show an incorporation of ca. 50% M atoms in the linear antimony chain.[4] Although alternating the M and Sb atoms within this chain would maximize the M−Sb bonds and prohibit the occurrence of Sb−Sb bonds, no long-range ordering was observed. This is probably a consequence of the gain in the configurational entropy. Note that each individual chain might be ordered, but in that case there could be no ordering between the chains, i.e. within the *a,b* plane.

In this paper, we present the results of our investigations of the Hf−M−Sb system with the *3d* metal atoms from titanium to copper. This includes different methods for the synthesis of the compounds $Hf_{10}M_{\delta}Sb_{6-\delta}$ (M = V, Cr, Mn, Fe, Co, Ni, and Cu), their crystal and electronic structures, phase ranges and magnetic properties. The phases $Hf_{10}M_{\delta}Sb_{6-\delta}$ are isostructural with the corresponding zirconium antimonides, which is not an obvious result, as investigations of ternary zirconium hafnium phosphides showed.[5−6]

Results and Discussion

Crystal Structure

The hitherto unknown antimonides $Hf_{10}M_{\delta}Sb_{6-\delta}$ (M = V, Cr, Fe, Mn, Co, Ni, Cu) occur in ternary variants of the W_5Si_3 structure type, the Hf atoms occupying the W sites and the M and Sb atoms replacing the Si atoms (Figure 1). Whereas the *8h* position is filled solely by antimony (Sb1), the *4a* site is occupied by mixtures of the M and Sb2 atoms without long-range ordering.

This comes along with a linear (M,Sb) chain with interatomic distances of approximately 280 pm which is surrounded by eight Hf2 atoms that form chains of face-condensed distorted square antiprisms (right part of Figure 2). The chains of Hf antiprisms, sheathed by the Sb2 atoms, are interconnected by Hf2−Hf2 bonds of ca. 320 pm to a

[a] Department of Chemistry, University of Waterloo, Waterloo, Ontario, Canada N2L 3G1
Fax: (internat.) + 1-519/746-435
E-mail: Kleinke@sciborg.uwaterloo.ca
[b] FB Chemie und Wissenschaftliches Zentrum für Materialwissenschaften der Philipps-Universität, Hans-Meerwein-Straße, D-35032 Marburg, Germany
[c] Institut für Anorganische Chemie und Analytische Chemie der J.-Gutenberg-Universität, Duesbergweg 10−14, D-55099 Mainz, Germany

 © WILEY-VCH Verlag GmbH, D-69451 Weinheim, 2000 1434−1948/00/0202−315 $ 17.50+.50/0

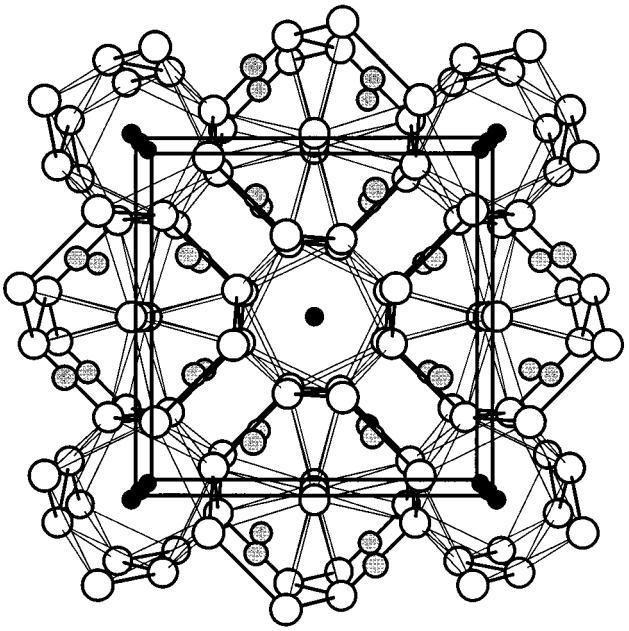


Figure 1. Structure of $Hf_{10}M_{\delta}Sb_{6-\delta}$ in a projection along the *c* axis; large, white circles: Hf; medium, gray: Sb; small, black: (M,Sb); Hf−Hf distances < 340 pm are indicated by bold lines

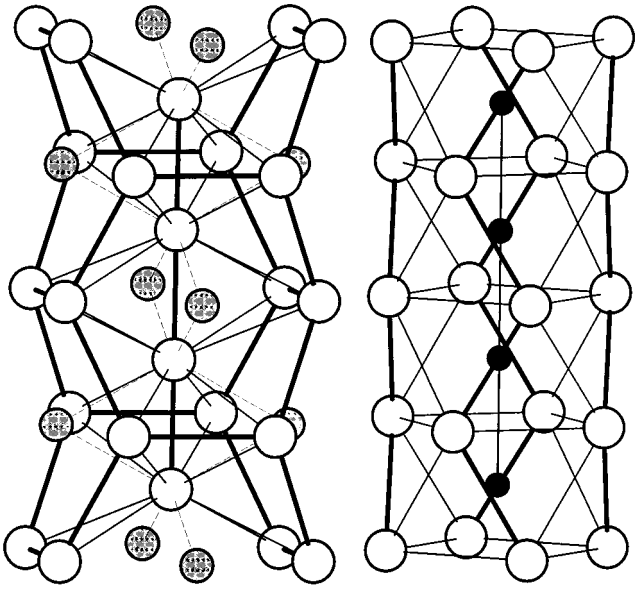


Figure 2. Columnar structure motifs of $Hf_{10}M_{\delta}Sb_{6-\delta}$; left: Chain of Hf1, surrounded by 8 Hf2 and 4 Sb1 atoms; the $Hf1Sb_4$ tetrahedra are indicated by dashed lines; right: chain of (M,Sb), situated in face-sharing $Hf2_8$ square antiprisms; Hf−Hf distances < 340 pm are indicated by bold lines

three-dimensional network surrounding linear chains of the Hf1 atoms ($d_{Hf1-Hf1} \approx 280$ pm). The Hf1 atoms are located in Sb_4 tetrahedra (left part of Figure 2), which are condensed via common vertices to form linear chains parallel to [001].

One can therefore divide the Hf−Hf distances into three classes. The first one includes the bonds within the linear Hf1 chain (ranging from $d = 277$ pm in $Hf_{10}Fe_{1.54}Sb_{4.46}$ to $d = 280$ pm in $Hf_{10}V_{0.80}Sb_{5.20}$ and $Hf_{10}V_{0.88}Sb_{5.12}$). The second one includes the distances of ca. 320−330 pm, and the third the longer ones of ca. 350 pm. These may be compared to elemental hafnium in its hexagonal modification with Hf−Hf distances of 313 and 320 pm, or to another Hf-rich antimonide, Hf_6NiSb_2, the structure of which exhibits Hf−Hf distances between 321 and 329 pm.[7] These comparisons reveal the extraordinary shortness of the bonds of class 1.

The Hf−Sb1 distances vary from 288 to 292 pm depending on the metal atom M and the δ parameter. The Hf−Sb2 bond lengths are somewhat shorter (between 278 and 289 pm); they are equal to the Hf−M distances by symmetry, which results in averaged values: since all M atoms are smaller than an Sb atom (e.g. the Pauling single bond radii: $r_V = 122$ pm, $r_{Ni} = 115$ pm, $r_{Cu} = 118$ pm, $r_{Sb} = 139$ pm[8]), the Hf−M distances are longer and the Hf−Sb2 distances shorter than in analogous compounds. This correlates well with the increase of the Hf2−(M,Sb2) distances with decreasing δ (Table 1), which range from 278 pm (δ = 1.54, M = Fe) to 289 pm (δ = 0.80 and 0.88, M = V). Correspondingly, the Hf−Sb distances of 296−297 pm in the structure of Hf_6NiSb_2 are much longer than the Hf−Ni bonds in the same structure (259 pm).[7]

The short Hf2−(M,Sb2) distance in the structure of $Hf_{10}Fe_{1.5}Sb_{4.5}$, i.e. in the case of the highest δ parameter (1.5), is reflected in a significant shift of the Hf2 atom towards the (M,Sb2) chain relative to all other examples with $0.80 \leq \delta \leq 1.18$ (see Table 2). This shift occurs with significantly smaller Hf2−Hf2 distances within the square antiprisms, but larger ones between the prisms (i.e. 334 pm vs. 320−321 pm) and between Hf1 and Hf2 (354 pm vs. 349−350 pm).

Electronic Structure

We successfully synthesized $Hf_{10}MSb_5$ with a variety of *3d* M atoms ranging from vanadium to copper. For a qualitative discussion of the influence of M on the electronic structure and thereby on the physical properties, the electronic structures were calculated for M = V and M = Ni, which are the most *d*-electron-poor and -rich examples, respectively (except for Cu). To model different possibilities of the ordering in the (M,Sb) chain, we calculated three hypothetical structures twice using the Extended Hückel approximation, i.e. in the Hf−V−Sb and in the Hf−Ni−Sb system. In model **I**, an ordering corresponding to the symmetry of space group *I*422 is assumed. In this case, M and Sb alternate in the two chains of the body-centered unit cell, with M of one chain being situated at the Sb position of the other chain, and thus exhibits the same *z* parameter. In model **II**, M and Sb also alternate within each chain, but the M atoms are located at the same positions in both chains of the body-centered unit cell. In model **III**, one chain consists only of M atoms and the other solely of Sb atoms. Models **II** and **III** can be described in the space groups *P*4/*nbm* and *P*4/*mcc*, respectively. In all cases, the stoichiometry remains the same, namely $Hf_{10}MSb_5$.

Table 1. Interatomic distances [pm] of $Hf_{10}M_{\delta}Sb_{6-\delta}$

	mult.	$Hf_{10}V_{0.80}Sb_{5.20}$	$Hf_{10}V_{0.88}Sb_{5.12}$	$Hf_{10}Mn_{1.16}Sb_{4.84}$	$Hf_{10}Fe_{1.54}Sb_{4.46}$	$Hf_{10}Ni_{1.18}Sb_{4.82}$
Hf1−Hf1	2 ×	279.08(5)	280.20(5)	277.6(1)	277.00(5)	279.45(5)
Hf1−Sb1	4 ×	289.7(1)	289.95(9)	289.5(3)	287.8(1)	289.7(1)
Hf1−Hf2	8 ×	350.00(9)	350.45(8)	349.2(2)	354.27(9)	350.36(9)
Hf2−X	2 ×	288.66(8)	288.72(7)	287.3(2)	277.50(8)	288.53(8)
Hf2−Sb1	1 ×	291.8(1)	291.7(1)	290.2(4)	288.8(2)	291.7(2)
Hf2−Sb1	1 ×	293.4(1)	293.5(1)	293.0(4)	292.7(1)	293.6(1)
Hf2−Hf2	1 ×	320.6(1)	320.9(1)	320.3(3)	334.1(1)	320.9(1)
Hf2−Sb1	2 ×	322.75(8)	323.81(7)	321.3(2)	324.67(9)	323.17(8)
Hf2−Hf2	2 ×	325.02(7)	326.00(7)	323.5(2)	319.78(7)	325.42(7)
Hf2−Hf1	2 ×	350.00(9)	350.45(8)	349.2(2)	354.27(1)	350.36(9)
Hf2−Hf2	2 ×	355.12(8)	355.75(7)	353.2(2)	346.27(8)	355.07(8)
Hf2−Hf2	2 ×	357.4(1)	357.0(1)	355.8(3)	340.1(1)	357.0(1)
Sb1−Hf1	2 ×	289.7(1)	289.95(9)	289.5(3)	287.8(1)	289.7(1)
Sb1−Hf2	2 ×	291.8(1)	291.7(1)	290.2(4)	288.8(2)	291.7(2)
Sb1−Hf2	2 ×	293.4(1)	293.5(1)	293.0(4)	292.7(1)	293.6(1)
Sb1−Hf2	4 ×	322.75(8)	323.81(7)	321.3(2)	324.67(9)	323.17(8)
Sb1−Sb1	2 ×	387.0(1)	387.8(1)	384.1(3)	382.2(1)	387.3(1)
X−X	2 ×	279.08(5)	280.20(5)	277.6(1)	277.00(5)	279.45(5)
X−Hf2	8 ×	288.66(8)	288.72(7)	287.3(2)	277.50(8)	288.53(8)

X = (M/Sb2) position.

Table 2. Atomic positions, equivalent displacement parameters and occupancy factors for $Hf_{10}M_{\delta}Sb_{6-\delta}$

Atom	site	*x*	*y*	*z*	$U_{eq}/(10^4 pm^2)$	occupancy
Hf1	*4b*	0	1/2	1/4	0.0105(3)	100%
Hf2	*16k*	0.07592(7)	0.21745(7)	1/2	0.0108(2)	100%
Sb1	*8h*	0.1636(1)	0.3364(1)	0	0.0091(3)	100%
V/Sb2	*4a*	0	0	1/4	0.013(1)	40(2)% V, 60% Sb
Hf1	*4b*	0	1/2	1/4	0.0058(3)	100%
Hf2	*16k*	0.07594(6)	0.21722(6)	1/2	0.0062(2)	100%
Sb1	*8h*	0.16362(9)	0.33638(9)	0	0.0044(3)	100%
V/Sb2	*4a*	0	0	1/4	0.0065(9)	44(2)% V, 56% Sb
Hf1	*4b*	0	1/2	1/4	0.0141(8)	100%
Hf2	*16k*	0.0759(2)	0.2171(2)	1/2	0.0113(5)	100%
Sb1	*8h*	0.1642(3)	0.3358(3)	0	0.0093(8)	100%
Mn/Sb2	*4a*	0	0	1/4	0.008(3)	58(5)% Mn, 42% Sb
Hf1	*4b*	0	1/2	1/4	0.0129(4)	100%
Hf2	*16k*	0.07357(7)	0.20887(8)	1/2	0.0105(2)	100%
Sb1	*8h*	0.1643(1)	0.3358(1)	0	0.0079(4)	100%
Fe/Sb2	*4a*	0	0	1/4	0.009(1)	77(3)% Fe, 23 Sb
Hf1	*4b*	0	1/2	1/4	0.0064(4)	100%
Hf2	*16k*	0.07600(7)	0.21718(7)	1/2	0.0072(3)	100%
Sb1	*8h*	0.1636(1)	0.3364(1)	0	0.0054(4)	100%
Ni/Sb2	*4a*	0	0	1/4	0.007(1)	59(3)% Ni, 41% Sb

For general considerations, we will discuss model **I** of $Hf_{10}MSb_5$ with M = V and Ni. The densities of states calculated with the Extended Hückel approach (Figure 3) exhibit some significant differences as well as common features. In both cases, a peak occurs between ca. −12 and −15 eV, which consists mainly of the *5p* states of antimony. (The *5s* states are located below the energy window shown.) The contributions of each of Hf, V, and Ni to this peak point to covalent character of the metal−Sb bonds. The different chemistry of the M atoms vanadium and nickel is reflected in some differences in the densities of states: whereas the *3d* states of nickel are located in a sharp peak at −10 eV (well below the Fermi level of −8.56 eV), the vanadium states are extended broadly from ca. −10 eV up to well above the Fermi level of −8.09 eV). In the latter case, the M states occur in basically the same energy area as the Hf states. It is concluded that the *d* orbitals of Ni are more or less completely filled, whereas the V and Hf *d* states are partly occupied. This occurs with a significant number of states filled at the Fermi level for both $Hf_{10}MSb_5$ phases, which is larger in the case of M = V.

For an evaluation of the bonding situations, the semiempirical Hf−Hf, Hf−M, and Hf−Sb COOP curves, summed over all interactions in the unit cell, are shown in Figure 4. Averaged over the first Brillouin zone, almost no antibonding states are filled. Almost no Hf−Sb states occur at the

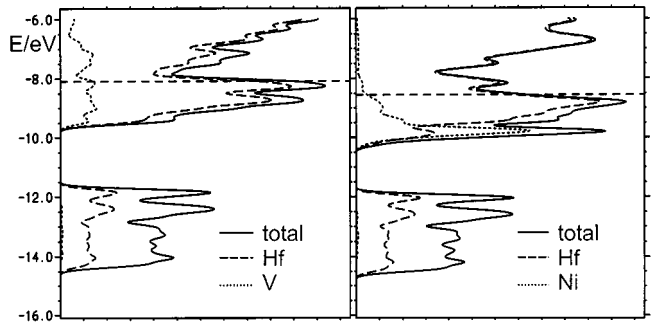


Figure 3. Calculated densities of states for $Hf_{10}MSb_5$ (EH approximation); left: M = V; right: M = Ni; horizontal lines: Fermi levels; solid line: total DOS; dashes: Hf contribution; dots: M contribution

Fermi level, which is dominated by bonding Hf−Hf interactions. Increasing the number of valence electrons would occur with more filled bonding Hf−Hf states, but with some filled antibonding Hf−M states in $Hf_{10}NiSb_5$. The Hf−V interactions are still bonding at the Fermi level (140 valence electrons), but become antibonding in character above −7.73 eV (ca. 151 valence electrons).

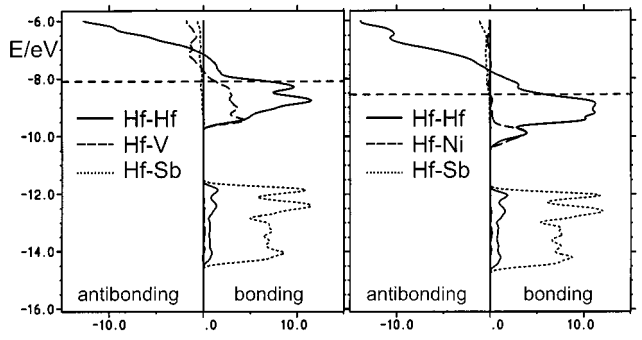


Figure 4. Selected summed COOP curves for $Hf_{10}MSb_5$; left: M = V; right: M = Ni; horizontal lines: Fermi levels; solid line: Hf−Hf interactions; dashed: Hf−M; dots: Hf−Sb; right parts of the diagrams: bonding interactions (+); left: antibonding (−)

After having considered some general features of the electronic structures, we focus now on the different structure models. In contrast to the model **III**, no homoatomic contacts occur in the (M,Sb) chains of models **I** and **II**. In model **I**, the M−Sb bonds of ca. 280 pm have net positive overlap populations although some antibonding states are filled in both cases (Figure 5). As a consequence of the filled *d* orbitals of nickel, antibonding Ni−Sb states occur above −10.5 eV, whereas fewer antibonding V−Sb states are filled. In addition to the differences in the antibonding states, the differences in the Mulliken overlap populations (*OP*) per bond (Ni−Sb: *OP* = 0.086; V−Sb: *OP* = 0.240) are also due to size effects (besides the dependence on the basis functions used): because of the smaller radius of nickel, a smaller overlap between the Ni and Sb orbitals is expected, which reflects itself in a smaller Pauling bond order *PBO* with $d(PBO) = d(1) - 60$ pm log *PBO*[8] [*PBO*(Ni−Sb): 0.38; *PBO*(V−Sb) = 0.48]. Since the differences in the (M,Sb) chains of models **I** and **II** arise solely from through-bond coupling between the chains, the interchain distance of 780 pm means that they are negligible. In model **III**, these bonds are replaced by homoatomic, namely M−M and Sb−Sb, interactions. They have definite bonding character in the case of $Hf_{10}VSb_5$ (V−V: *OP* = 0.24; Sb−Sb = 0.33), whereas the Ni−Ni interactions in $Hf_{10}NiSb_5$ are basically nonbonding (*OP* = 0.02), again because of the filled *d* orbitals. On the other hand, the Sb−Sb overlap populations in $Hf_{10}NiSb_5$ are of the same scale as in $Hf_{10}VSb_5$ (0.34 vs. 0.33). Comparable linear Sb−Sb chains were discussed recently:[9,10] in the structures of $(Zr,V)_{13}Sb_{10}$ and $(Zr,V)_{11}Sb_8$, the calculations revealed 1-electron 2-center *sigma* Sb−Sb bonds, which is in agreement with the values of the overlap populations of ca. 0.33 electrons per bond.

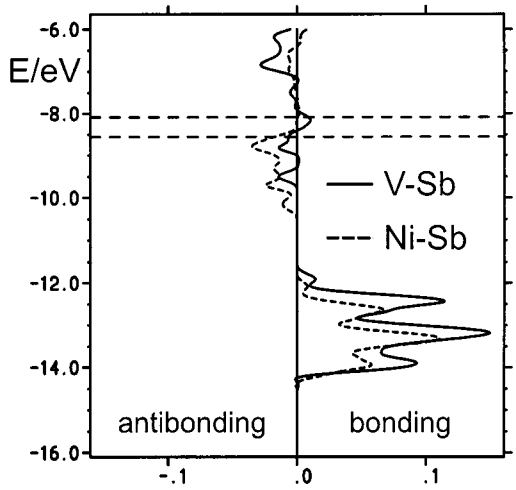


Figure 5. Averaged M−Sb COOP curves for $Hf_{10}MSb_5$; horizontal lines: Fermi levels; solid line: $Hf_{10}VSb_5$; dashed: $Hf_{10}NiSb_5$; right parts of the diagrams: bonding interactions (+); left: antibonding (−)

Based on the different Coulomb interactions one might expect that two M−Sb bonds are energetically favored relative to one M−M and one Sb−Sb bond. In the case of $Hf_{10}M_\delta Sb_{6-\delta}$, however, both M and Sb are somewhat negatively charged because of the more electropositive nature of hafnium, the major component of this phase. For example, the Pauling electronegativity values are 1.3 for hafnium, 1.6 for vanadium, 1.8 for nickel, and 1.9 for antimony. Correspondingly, the semiempirical Mulliken charges are −0.12 for vanadium and −0.49 for the Sb2 atom (Sb1: −0.67) in $Hf_{10}VSb_5$ (model **I**), and ≈0.00 for nickel and −0.43 for the Sb2 atom (Sb1: −0.49) in $Hf_{10}NiSb_5$ (model **I**). The metalloid antimony is obviously the most negatively charged atom, which renders reasonable the *antimonide* formulation for $Hf_{10}M_\delta Sb_{6-\delta}$. Furthermore, the Sb1 atom, being surrounded solely by Hf atoms, is more negatively charged than the Sb2 atom, which has two neighboring M atoms in model **I**. Both different kinds of Hf atoms show positive Mulliken charges, i.e. in the case of model **I** of $Hf_{10}VSb_5$ +0.17 for Hf1 and +0.38 for Hf2, and in the case of $Hf_{10}NiSb_5$ +0.06 for Hf1 and +0.29 for Hf2.

On the other hand, the charges of the M and Sb2 atoms obtained for model **III** differ significantly. The M atoms are

more and the Sb2 atoms less negatively charged in model **III** than in model **I** ($Hf_{10}VSb_5$: V −0.35 and Sb2 −0.07; $Hf_{10}NiSb_5$: Ni −0.22 and Sb +0.08). It is concluded that model **III** should exhibit a higher total energy because the Mulliken charges obtained are in direct contradiction to the trends expected based on electronegativity, especially for $Hf_{10}VSb_5$: the V atom exhibits a higher negative charge in model **III** than the Sb2 atom despite the lower electronegativity.

The entropy of an ordered structure generally differs from the disordered one by the configurational entropy. An estimation of the entropy of a completely disordered structure model $Hf_{10}MSb_5$, given by $\Delta S = -R\ \Sigma(X_i \ln X_i)$,[11] gives a value of 11.5 J/(molK). Since the free energy, ΔG, is determined by the equation $\Delta G = \Delta H - T\Delta S$, $T\Delta S$ is, besides the differences in the enthalpy, the factor which determines whether ordering occurs. According to our experiments, the minimum formation temperature of $Hf_{10}MSb_5$ is T = 1350°C, which corresponds to $T\Delta S = 0.2$ eV. Since this value is higher than the difference between the total energies of models **I** and **II** calculated with the LMTO method (0.02 eV in the case of $Hf_{10}NiSb_5$), one cannot expect complete (M,Sb) ordering from one chain to another.

The densities of states for the ordered structure model **I** of $Hf_{10}NiSb_5$, as obtained by the LMTO method, are shown in Figure 6. This shows that in contrast to the results of the Extended Hückel calculation, the peaks dominated by metal and antimony atoms do overlap. Furthermore, the overlap between the Hf and Ni states is more extensive than according to the EH calculations. The region around the Fermi level, however, is similar.

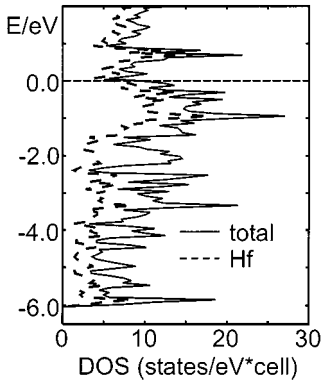


Figure 6. Calculated densities of states for $Hf_{10}NiSb_5$ (LMTO approach); DOS: Solid line: total DOS; dashes: Hf contribution

The significant densities of states at the Fermi level should occur with metallic properties, which is confirmed by several bands of $Hf_{10}NiSb_5$ crossing the Fermi level, as shown in Figure 7 which emphasizes the Ni centered bands with the fat band representation. The bands with a high Ni character occur about 2 eV below the Fermi level, which is reflected in a large Ni contribution to the densities of states in that energy area. Referring to the body-centered unit cell, two bands cross the Fermi level parallel to the c^* axis (symmetry lines ΓZ and XP), whereas no bands cross the Fermi level along the directions situated in the a^*,b^* plane, namely ΓX and PN. The latter is a consequence of the low dispersion of the Hf centered bands in the a,b plane, but does not imply one-dimensional metallic properties of all members of the $Hf_{10}M_{\delta}Sb_{6-\delta}$ series since the Fermi level depends on the number of valence electrons. The band structure of model **I** of $Hf_{10}VSb_5$ does not exhibit bands crossing the Fermi level along these symmetry lines, either, although that of $Hf_{10}FeSb_5$ does.

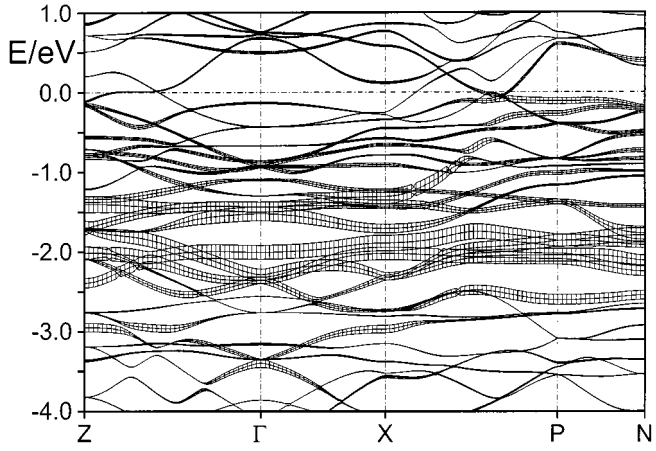


Figure 7. Band structure of $Hf_{10}NiSb_5$ (LMTO approach); fat bands projected on the Ni eigenvector contributions; symmetry points: Z = (−1/2, 1/2, 1/2); Γ = (0, 0, 0); X = (0, 0, 1/2); P = (1/4, 1/4, 1/4); N = (0, 1/2, 0) in units of the reciprocal primitive unit cell

Spin-polarized calculations within the local spin-density approximation were performed for the structure models containing the metal atoms Mn, Fe, Co, and Ni. Only in the case of $Hf_{10}FeSb_5$ was a magnetic ground state (0.6 μ_B) calculated. This occurred with a lowering of the total energy of just 4×10^{-5} eV relative to the non spin-polarized, and thus nonmagnetic, model calculation. The lower total energy is found to arise from a decrease in the number of states at the Fermi level, i.e. from 151 to 141 states/(eV × cell). The relatively small effects are a consequence of the small Fe content and the absence of any direct Fe−Fe interactions in $Hf_{10}FeSb_5$, while the difference between the energies of magnetic and (hypothetical) nonmagnetic α-Fe of 0.426 eV arises from a significant enhancement of Fe−Fe bonding.[12]

In order to check for a magnetic superstructure we carried out a spin-polarized self-consistent calculation of the tetragonal unit cell containing two (Fe,Sb) chains and thus two Fe atoms. The magnetic moments of the two Fe atoms were calculated to be +1.2 and −0.3 μ_B, respectively. Thus, the magnetic cell of $Hf_{10}FeSb_5$ in structure model **I** corresponds to the metric of the tetragonal unit cell in space group $P422$, with ferrimagnetic coupling between the Fe atoms of the two neighboring chains. However, different coupling of the magnetic moments of the Fe atoms resulted for the structure models **II** and **III**, namely ferromagnetic coupling with magnetic moments of 2.1 and 2.4 μ_B, respectively.

Physical Properties

The metal-rich composition, the presence of Hf−Hf contacts along all three directions, and the results of the electronic calculations discussed above strongly suggest metallic properties for all $Hf_{10}M_{\delta}Sb_{6-\delta}$ phases. The temperature dependence of the resistivity of a cold-pressed bar of the sample **II** (nominal composition $Hf_{10}CrSb_5$) is typical for a metallic sample (linearly increasing resistivity with increasing temperature), but the $\rho_{(10K)}/\rho_{(280K)}$ ratio of 0.94 is rather high. According to the Matthiesen rule $\rho(T) = \rho_i + \rho_L(T)$, the impurity contribution ρ_i to the measured resistivity $\rho(T)$ is basically independent of the temperature.[13] It is concluded that the contribution ρ_i is relatively large in this case, relative to the intrinsic lattice resistivity $\rho_L(T)$, thus leading to a small temperature dependence of the resistivity measured. This could be a consequence of either large grain boundaries or of an oxidation of the surface by oxygen, which we tried to minimize by working under an inert atmosphere in a glove-box as far as possible.

The metallic properties reflect themselves in the Pauli paramagnetism experimentally observed for the bulk samples of the initial compositions $Hf_{10}MSb_5$ with M = V, Co, and Ni (Figure 8). Aside from small Curie tails at low temperatures, the curves are basically temperature independent, indicating that no unpaired localized electrons are present in the samples investigated. On the other hand, the sample with the initial composition $Hf_{10}FeSb_5$ exhibits a slope typical of weak ferromagnetic or ferrimagnetic materials. This is in agreement with the results of the spin-polarized LMTO calculation, which yielded a magnetic moment only in the case of $Hf_{10}FeSb_5$.

Similar results were found experimentally for the antimonides Zr_5MSb_3 (Ti_5Ga_4 type): in the case of M = Fe ferromagnetic properties were observed, while Zr_5CoSb_3 and Zr_5NiSb_3 showed Pauli paramagnetism.[14]

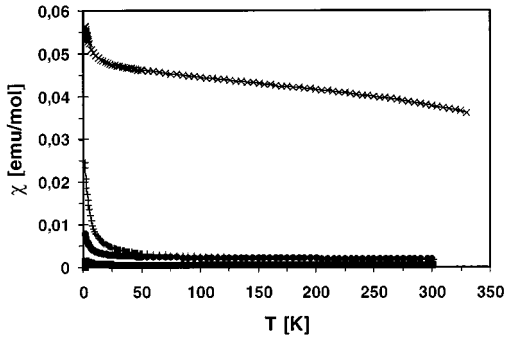


Figure 8. Temperature-dependence of the molar susceptibilities at 1 Tesla. ×: $Hf_{10}FeSb_5$; +: $Hf_{10}VSb_5$; filled circles: $Hf_{10}CoSb_5$; filled squares: $Hf_{10}NiSb_5$

To check for the ferromagnetic behavior, a field-dependent magnetization was measured at 5 Kelvin (Figure 9). Whilst the slope is familiar from ferromagnetic compounds, the hysteresis is almost zero, pointing to a very weak ferromagnetic material. The magnetic moment per Fe atom of 2 μ_B, as determined from an estimation of the saturation magnetization, suggests that the sample investigated consisted of different domains, i.e. a mixture of the different structure models, since the models **I**, **II** and **III** exhibit magnetic moments of 0.6, 2.1 and 2.4 μ_B, respectively (according to the LMTO calculations).

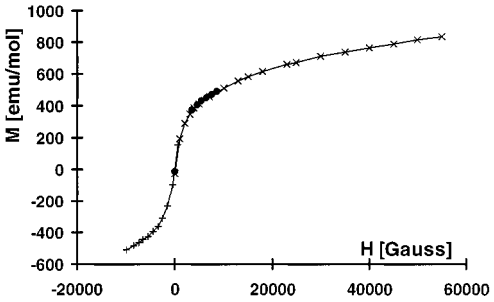


Figure 9. Field dependence of the magnetization *M* of $Hf_{10}FeSb_5$ at 5 Kelvin. +: 1. Series, *M* measured from 0 to 55000 Gauss; ×: 2. Series, field dropped rapidly from 55000 to 500 Gauss, then *M* measured from 500 Gauss to −10000 Gauss; filled circles: 3. Series, field increased rapidly to 0, then *M* measured from 0 to 8500 Gauss

Conclusions

The new antimonides $Hf_{10}M_{\delta}Sb_{6-\delta}$ (M = V, Cr, Mn, Fe, Co, Ni, Cu) were synthesized and subsequently characterized by single crystal structure studies, calculations of the electronic structures, and measurements of the magnetic and electrical properties of selected samples. The compounds $Hf_{10}M_{\delta}Sb_{6-\delta}$, exhibiting a phase range of at least $0.80(4) \leq \delta \leq 1.54(6)$, crystallize in the W_5Si_3 structure type. The X-ray experiments revealed no long-range ordering of the M/Sb atoms on the Si site. The calculations suggest that an ordering within a given (M,Sb) chain is likely to occur, but the correlation between the chains are too small for systematic ordering between the chains. The disordering can be explained by an increase of the configurational entropy, compared to the ordered structure model. The phases $Hf_{10}M_{\delta}Sb_{6-\delta}$ are metallic without localized magnetic moments, except for M = Fe, where weak ferromagnetic properties are detected experimentally, in agreement with theoretical calculations based on the spin-polarized LMTO method.

Experimental Section

Syntheses: In order to minimize the loss of antimony during the process of arc-melting, we first prepared $HfSb_2$ as the antimony source in a fused silica tube at 650°C, starting from the elements in the stoichiometric 1:2 ratio (Hf: STREM, powder, 99.6% (including up to 2.2% zirconium), Sb: MERCK, powder, 99.8%). The compounds $Hf_{10}MSb_5$ were synthesized by arc-melting of stoichiometric ratios of Hf, $HfSb_2$ and M on a water-cooled copper hearth under a flow of argon (3 L/min). With weight losses of typically between 1 and 4 weight-%, the yields can be optimized by adding a small excess of antimony. Attempts to synthesize $Hf_{10}MSb_5$ with different *3d* metals M (from vanadium to copper, all powder; V: ABCR, −45 micron, 99.7%; Cr: VENTRON, −50 mesh, 99.8%; Mn: VENTRON, −325 mesh, 99.9%; Fe: STREM, 99.999%; Co: ALFA, −50 mesh, 99.8%; Ni: VENTRON, −150 mesh, 99.9%; Cu:

Table 3. Selected reactions with Hf: (M + Sb) = 10: 6 (M = V, Cr, Mn, Fe, Co, Ni, Cu)

No.	M	M: Sb ratio	reaction conditions	main products
I	V	1: 5	arc-melting	$Hf_{10}V_{\delta}Sb_{6-\delta}$*
II	Cr	1: 5	arc-melting	$Hf_{10}Cr_{\delta}Sb_{6-\delta}$
III	Mn	1: 5	arc-melting	$Hf_{10}Mn_{\delta}Sb_{6-\delta}$
IV	Fe	1: 5	arc-melting	$Hf_{10}Fe_{\delta}Sb_{6-\delta}$
V	Co	1: 5	arc-melting	$Hf_{10}Co_{\delta}Sb_{6-\delta}$
VI	Ni	1: 5	arc-melting	$Hf_{10}Ni_{\delta}Sb_{6-\delta}$
VII	Cu	1: 5	arc-melting	$Hf_{10}Cu_{\delta}Sb_{6-\delta}$
VIII	V	1: 5	arc-melting, then annealing at 900 °C	$Hf_{10}V_{\delta}Sb_{6-\delta}$*
IX	Ni	1: 5	arc-melting,then annealing at 900 °C	$Hf_{10}Ni_{\delta}Sb_{6-\delta}$*
X	Mn	1: 5	annealing at 1350 °C	$Hf_{10}Mn_{\delta}Sb_{6-\delta}$*
XI	Fe	2: 4	arc-melting	$Hf_{10}Fe_{\delta}Sb_{6-\delta}$* + ?
XII	Fe	1.75: 4.25	arc-melting	$Hf_{10}Fe_{\delta}Sb_{6-\delta}$ + ?
XIII	Fe	1.5: 4.5	arc-melting	$Hf_{10}Fe_{\delta}Sb_{6-\delta}$
XIV	Fe	1.25: 4.75	arc-melting	$Hf_{10}Fe_{\delta}Sb_{6-\delta}$
XV	Fe	0.75: 5.25	arc-melting	$Hf_{10}Fe_{\delta}Sb_{6-\delta}$
XVI	Fe	0.5: 5.5	arc-melting	$Hf_{10}Fe_{\delta}Sb_{6-\delta}$ + Hf_5Sb_3
XVII	Fe	0.25: 5.75	arc-melting	$Hf_{10}Fe_{\delta}Sb_{6-\delta}$ + Hf_5Sb_3

*: Single crystal structure study.

Table 4. Lattice parameters of $Hf_{10}MSb_5$

No.	M	*a*/pm	*c*/pm	*V*/(10^6pm^3)
I	V	1095.54(9)	558.08(9)	669.8
II	Cr	1094.06(5)	556.54(1)	666.2
III	Mn	1093.70(4)	556.52(6)	665.7
IV	Fe	1091.5(1)	555.22(8)	661.5
V	Co	1091.3(1)	553.7(1)	659.4
VI	Ni	1092.6(1)	552.7(1)	659.8
VII	Cu	1093.74(5)	554.01(6)	662.7

VENTRON, 99.9%) were successful in all cases, according to the powder diagrams of all reaction products and EDX investigations on selected samples ($Hf_{10}VSb_5$ and $Hf_{10}NiSb_5$, numbers **I** and **VI** in Table 3). An analogous reaction using titanium (Ti: ALFA, −100 mesh, 99.4%) instead of hafnium resulted in the formation of Ti_5NiSb_3[15] as the main product. A reaction using titanium as the *3d* metal did not yield the hypothetically isostructural "$Hf_{10}TiSb_5$", but resulted in the formation of the hitherto unknown compound $(Hf,Ti)_7Sb_4$[16] as the main product. Table 4 lists the lattice parameters obtained from the ground samples with the Guinier technique (Cu-K_{α}, using silicon as internal standard).

A single crystal of the sample **I** was investigated on an IPDS diffractometer (STOE). Parts of **I** and **VI** were annealed over a period of three weeks at 900 °C in tantalum tubes, placed in fused silica tubes sealed under vacuum. No differences were observed between the powder diagrams obtained before and after the annealing procedure. Nevertheless, the annealed samples of the initial compositions $Hf_{10}VSb_5$ (**VIII**) and $Hf_{10}NiSb_5$ (**IX**) were investigated also

Table 5a. Crystallographic data for $Hf_{10}V_{0.80(4)}Sb_{5.20}$ and $Hf_{10}V_{0.88(4)}Sb_{5.12}$

Empirical formula	$Hf_{10}V_{0.80(4)}Sb_{5.20}$	$Hf_{10}V_{0.88(4)}Sb_{5.12}$
Synthesis	arc-melting	arc-melting + annealing
Molar mass	2458.8 g/mol	2453.1 g/mol
T. of data collection	295 K	295 K
Crystal size /mm^3	0.04 × 0.02 × 0.01	0.03 × 0.02 × 0.01
Space group	*I4/mcm*	*I4/mcm*
a/pm	1097.1(2)	1097.1(2)
c/pm	558.17(9)	560.4(1)
V/(10^6pm^3)	671.8(2)	674.5(2)
No. of f. u.; F(000)	2; 1003	2; 1002
Calculated density	12.15 g/cm^3	12.08 g/cm^3
Absorption coefficient	87.58 mm^{-1}	22.87 mm^{-1}
Range of 2θ	3° − 60°	3° − 60°
No. of independent reflections	298 (R_{int} = 0.083)	297 (R_{int} = 0.065)
No. of observed reflections (I>2σ(I))	232	214
No. of parameters	17	17
R(F), $R_w(F^2)$, GOF	0.028, 0.065, 1.05	0.023, 0.040, 0.97
Extinction coefficient	0.00009(5)	0.00035(4)
Absorption correction	numerical	numerical
Min., max. transmission	0.10, 0.67	0.09,0.37
Max., min. peak in final diff. map	2.42 e$^-$/(10^6pm^3), −2.94 e$^-$/(10^6pm^3)	2.50 e$^-$/(10^6pm^3), −2.94 e$^-$/(10^6pm^3)

Table 5b. Crystallographic data for $Hf_{10}Mn_{1.1(1)}Sb_{4.88}$, $Hf_{10}Fe_{1.54(6)}Sb_{4.46}$ and $Hf_{10}Ni_{1.18(6)}Sb_{4.82}$

Empirical formula	$Hf_{10}Mn_{1.16(10)}Sb_{4.84}$	$Hf_{10}Fe_{1.54(6)}Sb_{4.46}$	$Hf_{10}Ni_{1.18(6)}Sb_{4.82}$
Synthesis	annealing	arc-melting	arc-melting + annealing
Molar mass	2437.9 g/mol	2410.0 g/mol	2441.0 g/mol
T. of data collection	295 K	295 K	295 K
Crystal size /mm^3	0.02 × 0.02 × 0.01	0.03 × 0.02 × 0.02	0.01 × 0.01 × 0.005
Space group	*I4/mcm*	*I4/mcm*	*I4/mcm*
a/pm	1094.0(2)	1085.9(2)	1097.1(2)
c/pm	555.2(1)	554.0(1)	558.9(1)
V/(10^6 pm^3)	664.5(3)	653.2(2)	672.7(2)
No. of f. u.; *F*(000)	2; 996	2; 988	2; 999
Calculated density	12.19 g/cm^3	12.27 g/cm^3	12.05 g/cm^3
Absorption coefficient	88.35 mm^{-1}	89.68 mm^{-1}	87.80 mm^{-1}
Range of 2θ	3° − 60°	3° − 60°	3° − 60°
No. of independent reflections	292 (R_{int} = 0.196)	288 (R_{int} = 0.092)	298 (R_{int} = 0.088)
No. of observed reflections (*I*>2σ(*I*))	144	213	223
No. of parameters	17	17	17
R(*F*), $R_w(F^2)$, GOF	0.041, 0.082, 0.89	0.028, 0.058, 0.99	0.031, 0.069, 0.93
Extinction coefficient	0.00000(4)	0.00001(4)	0.00052(8)
Absorption correction	numerical	numerical	numerical
Min., max. transmission	0.12, 0.23	0.09, 0.37	0.14, 0.59
Max., min. peak in final diff. map	3.46 e$^-$/(10^6pm^3), −4.53 e$^-$/(10^6pm^3)	2.27 e$^-$/(10^6pm^3), −2.64 e$^-$/(10^6pm^3)	4.04 e$^-$/(10^6pm^3), −3.14 e$^-$/(10^6pm^3)

by single crystal structure analyses. Reactions starting from $HfSb_2$, Hf, and different M atoms, carried out in sealed tantalum tubes without previous arc-melting, did not result in the formation of the $Hf_{10}M_{\delta}Sb_{6-\delta}$ phases after annealing for six days at temperatures of 1300°C. At a reaction temperature of 1350°C, $Hf_{10}Mn_{\delta}Sb_{6-\delta}$ formed, and a single crystal study was also performed using a small crystal of this sample (**X**).

A study of the phase range was carried out in the Hf−Fe−Sb system by arc-melting different mixtures, corresponding to the starting compositions of "$Hf_{10}Fe_{\delta}Sb_{6-\delta}$" with δ = 2, 1.75, 1.5, 1.25, 0.75, 0.5 and 0.25. At δ = 2 and 1.75, the phase $Hf_{10}Fe_{\delta}Sb_{6-\delta}$ formed together with other unidentified products, and at δ = 0.5 and 0.25, the hitherto unknown binary antimonide Hf_5Sb_3[17] was detected, as well as $Hf_{10}Fe_{\delta}Sb_{6-\delta}$. It is concluded that the phase range is within $0.5 < \delta < 1.75$. Correspondingly, a single crystal study of the sample with δ = 2 (**XI**) yielded the formula $Hf_{10}Fe_{1.54(6)}Sb_{4.46}$, and thus δ = 1.54(6).

Single-Crystal Studies: All five data sets were collected with an IPDS diffractometer. The data were corrected for Lorentz and polarization effects. No superstructure reflections were observed in any of these data sets. The structure solutions and refinements were performed using SHELXS86 and SHELXL97.[18] The systematic extinction of $l = 2n + 1$ for all *0kl* reflections (in addition to the integral extinctions, namely $h + k + l = 2n + 1$) restricted the possible space groups to $I4/mcm$ (W_5Si_3), $I4cm$ and $I\bar{4}c2$. The *4a* position of *I*4/*mcm*, which is occupied by a mixture of M and Sb atoms, has the multitude of four in all three space groups. To check for ordering on this site, all five structure models were refined in the space group *I*4*22*, which allows alternating M and Sb atoms within the (M,Sb) chains by splitting the *4a* site of *I*4/*mcm* into *2a* and *2b*. No ordering was observed. Final refinements in the space group *I*4/*mcm* yielded, in all cases, different ratios of the M and Sb atoms in this chain, which were refined under the restriction of $f_M + f_{Sb} = 1$, i.e. 100% occupancy in the sum of the occupancies of the M and Sb atoms. The results are summarized in the Tables 2, 5a and 5b.[19]

Calculations of Electronic Structures: Semiempirical band-structure calculations were performed using the Extended Hückel approximation.[20−22] The metal parameters were optimized by alternating charge iterations until convergence using constant Sb parameters (Table 6). The tetragonal cell (80 *k* points) was chosen for all calculations for consistency, because not all models considered exhibited the body-centered symmetry (see main text).

More sophisticated electronic calculations were carried out with the self-consistent TB-LMTO-ASA program within the local-density approximation.[23−25] The integration in *k* space was performed by the tetrahedron method[26] on a grid of 1331 irreducible *k* points. The *5f* orbitals of hafnium and the *4f* orbitals of antimony were included by using a downfolding technique. The symmetry points of the band structure were chosen according to Bradley and Cracknell.[27]

Table 6. Parameters used for EH calculations

Orbital	H_{ii}/eV	ζ_1	c_1	ζ_2	c_2
Hf, 6s	−7.79[a]/−8.14[b]	2.21			
Hf, 6p	−4.27[a]/−4.57[b]	2.17			
Hf, 5d	−7.62[a]/−8.08[b]	4.36	0.6967	1.709	0.5322
V, 4s	−7.49	1.30			
V, 4p	−4.00	1.30			
V, 3d	−7.95	4.75	0.4755	1.70	0.5798
Ni, 4s	−7.63	1.925			
Ni, 4p	−3.58	1.925			
Ni, 3d	−9.55	5.75	0.5862	2.20	0.5845
Sb, 5s	−18.80	2.32			
Sb, 5p	−11.70	2.00			

[a] Values for the calculation on $Hf_{10}VSb_5$. − [b] Values for the calculation on $Hf_{10}NiSb_5$.

Transport Properties: Temperature dependent resistivity measurements were performed on a cold-pressed bar with the nominal composition $Hf_{10}CrSb_5$. The pellet was contacted at four points, which enables a measurement independent of the resistivities of the contacts.

Magnetic Properties: Magnetic data were obtained for the bulk samples of $Hf_{10}M_1Sb_5$ with M = Fe, V, Co, and Ni. Temperature-dependent measurements were made at 1 Tesla in the temperature range of 1.8−300 K on a Quantum Design MPMS SQUID magnetometer. The data were corrected for the diamagnetic atom cores.

Acknowledgments

The experimental work was carried out at the Department of Chemistry, University of Marburg. Financial support from the "Deutsche Forschungsgemeinschaft", the "Fonds der Chemischen Industrie" and the "Bundesministerium für Bildung, Wissenschaft, Forschung und Technologie" is gratefully acknowledged. Insightful discussions with Professor Dr. B. Harbrecht are appreciated.

[1] P. Villars, L. D. Calvert, *Pearson's Handbook of Crystallographic Data for Intermetallic Phases*, 2nd Edition, ASM, Materials Park, OH 1996.
[2] I. Schewe-Miller, P. Böttcher, *J. Alloys Compd.* **1992**, *183*, 98−108.
[3] R. Berger, *Acta Chem. Scand.* **1977**, *31A*, 223−226.
[4] Y.-U. Kwon, S. C. Sevov, J. D. Corbett, *Chem. Mater.* **1990**, *2*, 550−556.
[5] H. Kleinke, H. F. Franzen, *J. Solid State Chem.* **1998**, *136*, 221−226.
[6] L. Zeng, H. F. Franzen, *J. Alloys Compd.* **1998**, *270*, 119−122.
[7] H. Kleinke, *J. Alloys Compd.* **1998**, *270*, 136−141.
[8] L. Pauling, *The Nature of the Chemical Bond*, Cornell University Press, Ithaca, NY, 3rd ed., 1948.
[9] H. Kleinke, *Chem. Commun.* **1998**, 2219−2220.
[10] H. Kleinke, *J. Mater. Chem.* **1999**, *9*, 2703−2708.
[11] H. F. Franzen, J. A. Merrick, *J. Solid State Chem.* **1980**, *33*, 371−374.
[12] G. A. Landrum, R. Dronskowski, *Angew. Chem. Int. Ed.* **1999**, *38*, 1389−1393.
[13] C. Kittel, *Introduction to the Solid State Physics*, New York, Wiley, 7th ed., **1996**.
[14] E. Garcia, H. C. Ku, R. N. Shelton, J. D. Corbett, *Solid State Comm.* **1988**, *65*, 757−760.
[15] W. Rieger, E. Parthé, *Acta Crystallogr.* **1968**, *24B*, 456−458.
[16] H. Kleinke, *Inorg. Chem.* **1999**, *38*, 2931−2935.
[17] H. Kleinke, C. Felser, *J. Alloys Compd.* **1999**, *291*, 73−79.
[18] G. M. Sheldrick, *SHELXS86*, University of Göttingen, **1986**; *ibid.*, *SHELXL93*, **1993**.
[19] Further details of the crystal-structure investigations may be obtained from the Fachinformationszentrum Karlsruhe, D-76344 Eggenstein-Leopoldshafen, Germany, on quoting the depository numbers CSD-410803 − CSD-410807.
[20] R. Hoffmann, *J. Chem. Phys.* **1963**, *39*, 1397−1412.
[21] M.-H. Whangbo, R. Hoffmann, *J. Am. Chem. Soc.* **1978**, *100*, 6093−6098.
[22] Program EHMACC, adapted for use on a PC by M. Köckerling, Gesamthochschule Duisburg, 1997.
[23] L. Hedin, B. I. Lundqvist, *J. Phys.* **1971**, *C4*, 2064−2083.
[24] O. K. Andersen, *Phys. Rev.* **1975**, *B12*, 3060−3083.
[25] H. L. Skriver, *The LMTO Method*, Springer, Berlin, **1984**.
[26] O. Jepsen, O. K. Andersen, *Solid State Commun.* **1971**, *9*, 1763−1767.
[27] C. J. Bradley, A. P. Cracknell, *The Mathematical Theory of Symmetry in Solids*, Clarendon Press, Oxford, **1972**.

Received June 10, 1999
[I99220]

A Two-Step Palladium-Catalyzed Coupling Scheme for the Synthesis of Ferrocene-Labeled Amino Acids

Oliver Brosch,[a] Thomas Weyhermülle,r[a] and Nils Metzler-Nolte*[a]

Keywords: Amino acids / Alkynes / Ferrocene / Palladium / Catalysis / Bioorganometallic chemistry / Biosensors

This work describes a Pd-catalyzed coupling of ferrocene alkyne derivatives to iodo amino acids. Ferrocene carboxylic acid propargyl amides were easily obtained in high yield. The crystal structures of the propargyl amine derivative **3** and the 1,1-diethylpropargylamine derivative **4** have been determined by X-ray diffraction. Pd-catalyzed coupling to ***p***-iodoanilide amino acids gave the corresponding ferrocene-labeled amino acid derivatives, which were easily purified by diethyl ether extraction in the case of the 1,1-diethyl derivatives **8**. The coupling reaction did not require anhydrous solvents and tolerated a variety of functional groups present in peptides such as alcohols (**8a**, Ser), thioethers (**8b**, Met), disulfide bonds (cystine, **12**) esters (as in the *N*-labeled Leu derivative **10**) and of course amides. A minor by-product of the coupling reaction, namely the homo-dimer bis(ferrocene carboxylic acid propargylamide) **9**, was identified in the crude reaction mixtures by mass spectrometry and independently synthesized by oxidative coupling (Glaser and Eglington) of **3**. All new compounds were completely characterized spectroscopically, including ^{15}N- and 2D NMR spectroscopy, Mössbauer spectroscopy and electrochemistry. This work introduces a versatile procedure for a selective functionalization of amino acids with organometallics at the *C-terminus* which is expected to be of general applicability to peptide chemistry.

Introduction

We are exploring new ways of covalently linking organometallic compounds to biomolecules.[1−5] In these conjugates, the organometallic moiety serves as a sensitive probe for the detection of the biomolecule, e. g. electrochemically[6−8] or by IR spectroscopy.[9−18] The key issue in any of these assays is *chemoselectivity*:[12,18] No doubt is to remain about the number of attached organometallics nor their site of attachment to the biomolecule − which may even be, for example, a large enzyme[10,11,13] or peptide hormone like secretin.[19] Also, the reaction should be mild enough to comply with the possibly sensitive organometallic compounds and the variety of functional groups present in a peptide. We[1] and others[20,21] have suggested the use of a Pd-catalyzed two-step coupling reaction for this purpose. In the first step, an anchoring group is incorporated into the peptide. Secondly, a suitably-functionalized organometallic compound is reacted with that anchoring group to form the covalent link to the peptide. The prerequisite of this concept is that the anchoring group is left untouched under standard peptide chemistry conditions and vice versa the reaction that links the organometallic to the peptide may not affect any functionality present in the peptide other than the anchoring group. In compliance with this prerequisite, our group has recently reported the synthesis of alkynyl amino acids for the coupling with organometallic halides and demonstrated the viability of our approach by selectively labeling the *N*- and *C*-protected tripeptide Boc-Phe-Glu-Met-OMe at the C_γ of Glu with a ferrocene derivative.[1] However, derivatizing a peptide with alkynyl groups is not feasable in solid-state synthesis of peptides as the alkyne may not withstand the concentrated HF frequently used to cleave the peptide from the support. In an effort to circumvent this problem, this work reports the synthesis of alkynyl ferrocene derivatives and their Pd-catalyzed coupling to iodobenzene amino acids with different functional groups. Iodinated aromatic compounds were previously used as radio-labels for amino acids[22] and monoclonal antibodies[23] and as such were successfully employed in solid support peptide synthesis.[24] In this study, alternatively-functionalized amino acids were chosen as model compounds for peptides and ferrocene was selected owing to its potential in electrochemical detection.[3,8,25−31]

Results and Discussion

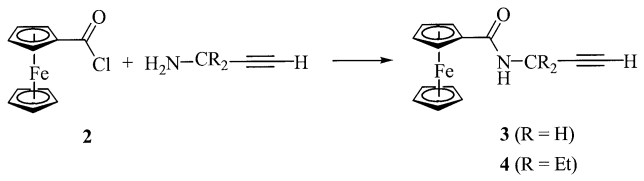
Synthesis

Ferrocene carboxylic acid chloride **2**, which was prepared in situ by heating ferrocene carboxylic acid **1** at reflux with oxalic acid chloride, reacts with propargyl amine and 1,1-diethylpropargyl amine to give the ferrocene amido alkynes **3** and **4** in >90% yield (Scheme 1). Both derivatives are orange, crystalline solids and their solid-state structures were determined by X-ray diffraction (vide infra).

In these preparations, ferrocene carboxylic acid anhydride was frequently found as a by-product. To avoid the formation of this anhydride, we explored other means of activating the organometallic acid. Kraatz et al. prepared ferrocene amino acids by activation of **1** with hydroxybenzotriazole and dicyclohexylcarbodiimide in >70% yield.[32] In our hands, however, yields for this coupling were usually much lower. Isobutyl chloroformate/*N*-methyl-

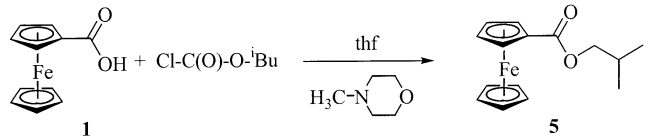
[a] Max-Planck-Institut für Strahlenchemie,
Stiftstrasse 34−36, D-45470 Mülheim/Ruhr, Germany.
Fax: (internat.) + 49-(0)208/306-3951
E-mail: nils@mpi-muelheim.mpg.de

 © WILEY-VCH Verlag GmbH, D-69451 Weinheim, 2000 1434−1948/00/0202−323 $ 17.50+.50/0



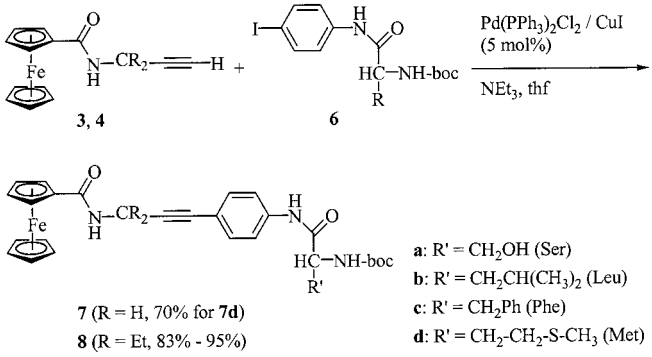
Scheme 1

morpholine in THF is an alternative well-established reagent for peptide coupling reactions in solution.[33] According to Scheme 2, ferrocene carboxylic acid isobutyl ester **5** could be prepared in 95% yield. However, 14 h of reflux were necessary to obtain **3** from **5** and propargyl amine. Unlike amino acids, which react with amines within minutes under comparable conditions,[34] ferrocene carboxylic acid is not easily activated by the most common reagents.



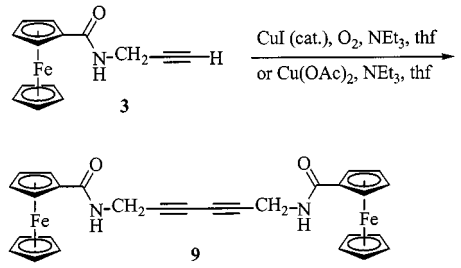
Scheme 2

Reaction of organometallic alkynes **3** and **4** with iodoarene amino acid derivatives **6** gave the desired ferrocene-labeled amino acids **7** and **8** in very good yield (Sonogashira coupling,[35–37] Scheme 3). By extracting the crude reaction products with diethyl ether, the diethyl derivatives **8** could be obtained as analytically pure solids. Owing to their reduced solubility, the simpler propargyl amine derivatives **7** were more difficult to separate from impurities. In fact, only the methionine derivative **7d** could be obtained analytically pure after extensive washing.



Scheme 3

The inability to obtain pure coupling products **7** prompted us to carry out a careful product analysis. Electron spray ionization mass spectrometry (ESI-MS) revealed the presence (< 5%) of an iron-containing by-product with m/z = 532. In addition, the ^{1}H-NMR spectrum of the crude reaction mixture contained a number of Cp signals, a signal for one amide proton and a further signal which was not assigned. Since we suspected that oxidative homo-coupling of **3** might have occurred, we set out to synthesize the dimer **9** by air oxidation of **3** with a catalytic amount of CuI (Glaser coupling,[38] 32% yield) or stoichiometric amounts of $Cu(OAc)_2$ under Ar (Eglington coupling,[38] 38% yield, Scheme 4). The bis-ferrocene-diyne **9** is an orange-coloured solid, which is stable both as a solid and in solution for prolonged periods of time.



Scheme 4

Characterization

Solid-State Structures of 3 and 4

Crystals of suitable quality for an X-ray structure analysis were obtained for the two alkynyl–ferrocene derivatives **3** and **4**. Both compounds crystallize in the orthorhombic space group *Pbca* with very similar unit cells and packing in the crystal lattice (see Table 1, Experimental Section). ORTEP plots of the molecular structures are shown in Figures 1 and 2, repectively. The amide groups are almost parallel to the plane of the neighbouring cyclopentadienyl ring (9° angle between amide and Cp least squares planes for **3** and 15.5° for **4**). The tilt of both cyclopentadienyl rings is 1.8° (**3**) and 2.5° (**4**) away from an eclipsed conformation (mean value of H/C–C–C–H dihedral angles) and the rings are almost parallel as shown by the centroid–Fe–centroid angle (179° and 177.8° for **3** and **4**, respectively). All these parameters compare well to related compounds.[32,39,40] Unlike ferrocene carboxylic acid, which forms dimers in the solid state,[40,41] both **3** and **4** form hydrogen bridges with their nearest neighbours through the amide bonds in the crystal lattice. By arranging in a "head-to-tail" fashion, the molecules form one-dimensional zigzag chains (Figure 3).

Spectroscopy and Discussion

The Sonogashira coupling has recently gained some attention for the synthesis of organometallic alkynes[42,43] and polymers.[44,45] Beck et al. have used *p*-ethynylphenylalanine, which is a potent inhibitor of tryptophan hydroxylase,[46] in Pd-catalyzed alkyne coupling reactions to obtain a variety of novel phenylalanine derivatives.[47–49] NMR spectroscopy provides an excellent handle to establish the constitution of all new compounds. The alkyne pro-

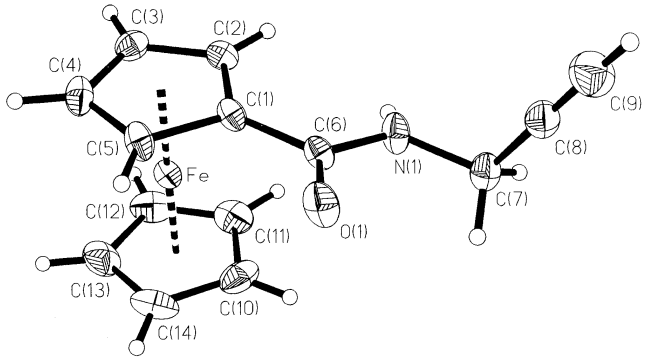


Figure 1. ORTEP drawing of **3**, indicating the numbering scheme. Selected bond lengths [Å] and angles eg.]: Fe−C_{Cp} (av.) 2.038, Fe−Cp(centroid) 1.647 and 1.647 (unsubstituted Cp), C(1)−C(6) 1.476(4), C(6)−O(1) 1.233(3), C(6)−N(1) 1.338(3), C(8)−C(9) 1.164(5), O(1)−C(6)−N(1) 121.2(3), N(1)−C(7)−C(8) 114.1(3)

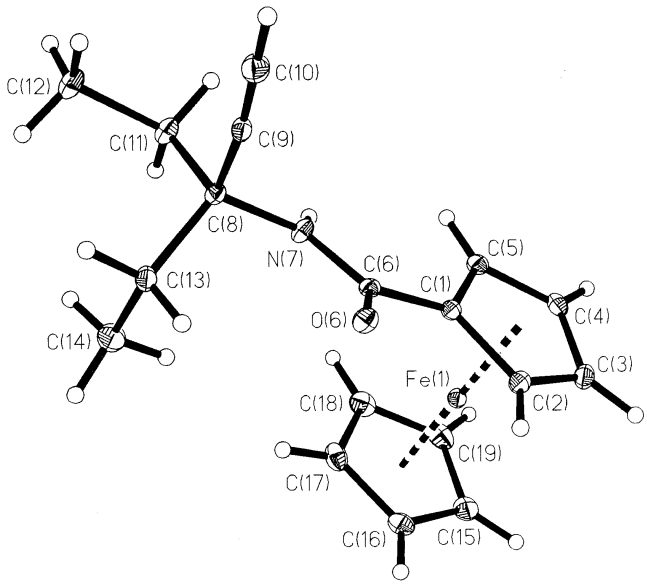


Figure 2. ORTEP drawing of **4**, indicating the numbering scheme. Selected bond lengths [Å] and angles eg.]: Fe−C_{Cp} (av.) 2.050, Fe−Cp(centroid) 1.652 and 1.653 (unsubstituted Cp), C(1)−C(6) 1.489(3), C(6)−O(6) 1.239(2), C(6)−N(7) 1.351(3), C(9)−C(10) 1.190(3), O(6)−C(6)−N(7) 122.3(2), N(7)−C(8)−C(9) 110.3(2)

ton in **3** and **4** is readily detected at ca. δ = 2.3 as a singlet (**4**) or a triplet with $^4J_{HH}$ = 2.6 Hz due to coupling with the methylene protons (**3**). The success of the Pd-catalyzed coupling can be immediately established by ^{1}H-NMR spectroscopy, especially by the disappearance of this signal of the terminal alkyne. In an earlier report on ferrocene carboxylic acid amides of amino acids,[32] two signals were observed for the *ortho* protons of the substituted Cp ring owing to the presence of a chiral centre. Even at 500 MHz, we were unable to detect more than one signal for these *ortho* protons, probably because of the large distance between the Cp ring and the chiral centre. From molecular modelling (Sybyl force field[50]) of the alanine derivative **7e** (R = H, R′ = CH_3), it follows that the C≡C triple bond, an aromatic ring and two amide groups enforce a minimum distance of >10 Å between the iron centre and the chiral

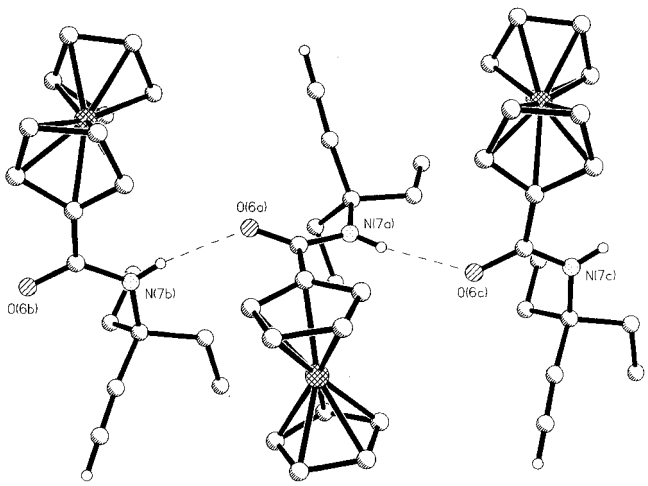


Figure 3. Part of the solid-state structure of **4**, showing the head-to-tail orientation of neighbouring molecules by means of hydrogen bridges. Distance N(7b)−O(6a) 2.998 Å

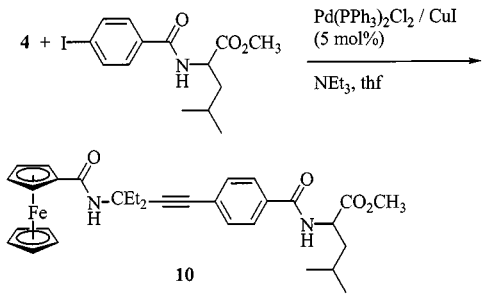
carbon atom C_α. There are also characteristic signals in the ^{13}C-NMR spectra of conjugates **7** and **8**, in particular for the two carbon atoms between which the new bond is formed. The alkyne carbon atom shifts downfield by about 13 ppm, whereas the signal of the aryl carbon atom, having been shielded by the iodine centre in **6** (ca. 87 ppm), is found at ca. 119 ppm in **7** and **8**. The alkyne ^{13}C-NMR signals for the diyne **9** are observed remarkably upfield (δ = 65.5 for the internal carbon atoms and δ = 76.7). These values are about 6 and 10 ppm higher than in a related phenylacetylene-chromium-tricarbonyl dimer[42] or in (ethynylcyclobutadiene)-cyclopentadienyl-cobalt dimer by Bunz and co-workers.[51] Since the NMR signals for all amide protons are readily detectable in aprotic solvents we used 2D indirect detection ^{1}H-^{15}N NMR spectroscopy to detect the ^{15}N-NMR signals of all nitrogen atoms in the new compounds. There are indeed characteristic ranges for ^{15}N-NMR shifts which will facilitate the identification of related coupling products in the future, namely δ_N = −275 for **7** and δ_N = −260 for **8**. The N_{Boc} signal is generally observed at δ_N = −290 and the anilide nitrogen atom at δ_N = −250.[52,53] All these chemical shifts are fairly insensitive to solvent changes, which indicates that intermolecular hydrogen bonds are broken up in solution for **7** and **8**. This notion is further substantiated by IR spectroscopy.

In the IR spectra of **3**, **4**, **7** and **8**, the C≡C stretching frequency is often too weak to be detected. It is, however, usually the strongest band in the RAMAN spectra. Upon substitution of the terminal proton, its frequency shifts by more than 100 cm^{-1} from 2121 cm^{-1} (**3**) and 2105 cm^{-1} (**4**) to about 2230 cm^{-1} (see Experimental Section). It is possible to distinguish between propargylamine compounds **7** and their 1,1-diethyl derivatives **8** on the basis of their RAMAN spectra alone since there is a difference of about 10 cm^{-1} in the respective stretching frequencies of the C≡C bond (ca. 2230 cm^{-1} in **8** and 2240 cm^{-1} in **7**), quite comparable to compounds **3** and **4**. Unfortunately, we were unable to obtain single crystals of the ferrocene amino acid

conjugates **7** or **8**. However, the IR spectrum of **7d** sheds some light on structural differences between the solid-state and solutions of **7** and **8**.[54,55] A broad band well below 3400 cm^{-1} for **7d** in a KBr pellet is indicative of hydrogen bonding involving the amide groups. These hydrogen bonds will govern the packing of molecules in the solid state[56] as described for **3** and **4**. In contrast, there is only one sharp amide band observed at 3428 cm^{-1} in CH_2Cl_2 solution, clearly showing that all hydrogen bonds are broken up even in aprotic solvents.[57]

Electrochemical detection − where applicable − is a useful tool in chromatography (HPLC-ECD) and the use of ferrocene derivatives in peptide chemistry has been explored by the group of Eckert.[6,7] Their approach of using activated acids of ferrocene derivatives was hampered by low yields in the coupling reactions or by precursors which were difficult to prepare. Using the methodology outlined in this work, we can easily prepare electrochemically active amino acid derivatives in high yield. To demonstrate the feasibility of ECD, compounds **7** and **8** were investigated electrochemically. Both groups of compounds show a reversible wave in the cyclic voltammogram (CV) at +173 mV (**7**) and between +187 and +197 mV (**8**) vs. ferrocene/ferrocenium. Similar values have previously been observed for ferrocene carboxylic acid amides.[32] A second, irreversible wave in the CV of **8d** is attributed to oxidation of the sulfur atom.

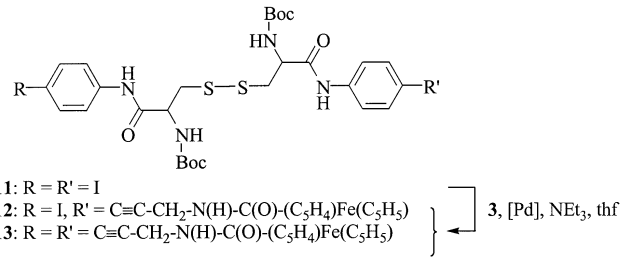
Compounds **7** and **8** demonstrate a general principle for the functionalization of the *C-terminus* of amino acids, which has not been achieved before. Naturally, this two-step procedure can also be applied to the labeling of the *N-terminus* of amino acids as shown in Scheme 5.



Scheme 5

An excess of *p*-iodobenzoic acid chloride is reacted with leucine methyl ester and subsequently coupled to **4** under Pd catalysis. The coupling product **10**, which is obtained analytically pure in 89% yield, is easily identified by its spectral features, namely the disappearance of the signal of the alkyne proton in the ^{1}H-NMR spectrum, characteristic changes in the ^{13}C-NMR spectrum as described above and a strong band at 2227 cm^{-1} in the RAMAN spectrum. Compounds **4** and **10** were also investigated by ^{57}Fe Mössbauer spectroscopy. The isomer shift (0.53 mm s^{-1} for **4** and 0.52 mm s^{-1} for **10**) and quadrupolar splitting [2.34 mm s^{-1} (**4**) and 2.32 mm s^{-1} (**10**)] are very similar to the values of ferrocene (0.53 mm s^{-1} and 2.37 mm s^{-1}).[58] This similarity indicates that attachment of an amino acid (**10**) or even functionalization of one Cp ring (**4**) has no significant influence on the field gradients of the iron nucleus. Significant deviations were observed only in compounds where the two Cp rings were no longer coplanar.[59]

Beck and co-workers have prepared a veritable number of stable Pd^{II} complexes of amino acids and peptides, in which the metal coordinates − usually in a chelating fashion − to the N, O, or S atoms of the amino acids.[5,60−65] Other authors reported the hydrolysis of amino acid esters by *ortho*-metallated Pd complexes.[66,67] In the light of their results, the success of the Pd-catalyzed coupling with amino acids is all the more surprising. A number of ubiquitous functional groups in peptide chemistry such as thio-ethers (**7d** and **8d**), alcohols (**8a**), esters (**10**), and of course amides is tolerated without notable loss of catalytic activity. Since disulfide bonds play a pivotal structural role in many enzymes,[68] and insertion reactions into disulfide bonds are well documented for Pt complexes,[69,70] the obvious question needs to be answered as to whether our coupling would work for cystine derivatives. The bis(*N*-Boc)-bis(*p*-iodo-anilined)-cystine **11** was prepared from activated *N*-protected cystine and two equivalents of *p*-iodo-aniline. Reaction with **3** under Pd-catalysis yielded the mono-ferrocene derivative **12** (Scheme 6).



Scheme 6

Using an excess of **3**, the bis-ferrocene derivative **13** could also be obtained but was impossible to purify. Regardless of the stoichiometry used, signals were detected for both **12** (*m*/*z* = 1004 for [**12** + Na]) and **13** (*m*/*z* = 1143 for [**13** + Na]) by ESI-MS in all preparations. We were able to obtain **12** in analytically pure form by liquid chromatography (HPLC). ^{1}H-NMR spectroscopy shows characteristic patterns for two AA′XX′ spin systems. In addition, the presence of eight ^{13}C NMR signals in the aromatic region is indicative of two different aromatic rings. A reversible oxidation occurs at a potential of +196 mV vs. Fc/Fc^+ for a solution of **12** in CH_2Cl_2. Controlled potential coulometry of this solution requires 89% of the charge calculated for *one* ferrocene unit. All these results taken together allow for the conclusion that the disulfide bridge in cystine derivatives does not interfere with the Pd-catalyzed alkyne coupling. Furthermore the two iodoarene rings are so far away from each other in **11** that it is impossible to control the

ratio of mono- to disubstitution during the Pd-catalyzed coupling to ferrocene derivative **3**.

Conclusion

We have demonstrated a general way of attaching amino acids to ferrocene derivatives by means of a Pd-catalyzed two-step procedure starting from the amino acid ester and ferrocene alkyne derivatives. Using this scheme, a selective labeling of the *C-terminus* of amino acids is possible.[13,21] A different approach for ferrocene functionalization of hemin was recently proposed by Ryabov et al. by means of activation of the propionic acid groups and reaction with ferrocene methylamine.[71] The disadvantage of their approach, i.e. unselective reaction of the activated acid with *any* primary amine, can only be resolved by employing different, "non-peptide" chemistry. The Pd-catalyzed Sonogashira coupling applied in this work tolerates a wide variety of functional groups often encountered in peptides and does not require dry solvents. In fact, Schmidtchen and coworkers have recently introduced water-soluble cationic phosphane ligands for Heck-type reactions in water.[72] It should be noted that the coupling reactions were usually carried out for 4 h at 80°C. Very similar yields and product purity were obtained by stirring for 24 h at room temperature, making this method suitable for the derivatization of more sensitive organometallic or biological compounds. Investigations along these lines are currently underway in our laboratory.

Experimental Section

General: All reactions were carried out in ordinary glassware and solvents without further precautions except where indicated. Chemicals were purchased from Aldrich-Sigma GmbH and Fluka AG and used as received, only enantiomerically pure L-amino acids were used. Ferrocene carboxylic acid chloride **1** was prepared by refluxing ferrocene carboxylic acid with oxalic chloride in CH_2Cl_2 for 1 h, followed by complete removal of all volatiles. The resulting red oil was handled under argon and used immediately. Iodoarene amino acids **6** were prepared from the pre-activated *N*-Boc-protected amino acids (isobutyl chloroformate and *N*-methylmorpholine) and *p*-iodoaniline in THF and recrystallized from hot heptane/THF (10:1).[73] − Melting points (uncorrected) were determined in a Tottoli apparatus (Büchi, Switzerland). − Elemental analysis were carried out by H. Kolbe, Analytisches Laboratorium, Mülheim. − IR spectra were recorded on a Perkin−Elmer System 2000 instrument as KBr disks, and additionally in CH_2Cl_2 solution where indicated. Frequencies $\tilde{\nu}$ are given in cm^{-1}. − RAMAN spectra were recorded on the same instrument as neat substances ($\tilde{\nu}$ in cm^{-1}). − UV/Vis spectra were recorded on a Perkin−Elmer Lambda 19 spectrometer, only the wavelengths of the highest-energy ferrocene transition is given in nm, ε ($dm^3mol^{-1}cm^{-1}$) in brackets. − Mass spectra were recorded by the mass spectrometry service group, Mülheim, on a MAT 8200 (Finnigan GmbH, Bremen) instrument (EI, 70 eV) or on a MAT95 (Finnigan GmbH, Bremen) instrument (ESI, CH_3OH solution, positive ion detection mode). Only characteristic fragments from EI spectra are given with relative intensities (%) in brackets. − HPLC separations were carried out on a Nucleosil-7-C_{18} column (Merck L6000 pump and Shimadzu SPD-2A UV detector operating at 260 nm), 4 mL min^{-1} flow rate with a methanol/water (5:1) mixture. − Cyclic voltammograms were obtained with a three-electrode cell and an EG&G Princeton Applied Research model 273A potentiostat. A $Ag/AgNO_3$ (0.01 mol L^{-1} in $AgNO_3$) reference electrode, a glass carbon disk working electrode of 2 mm diameter and a Pt wire counter electrode were used. CH_2Cl_2 solutions (ca. 10^{-4} mol L^{-1}) contained 0.1 mol L^{-1} Bu_4NPF_6 as supporting electrolyte. Potentials $E^{0\prime}$ were determined by square-wave voltammetry. As an internal standard, ferrocene was added in excess as a reference. − NMR spectra were recorded in $CDCl_3$ at room temp. on a Bruker ARX 250 (^1H at 250.13 MHz and ^{13}C), DRX 400 (^1H at 400.13 MHz, ^{13}C and 2D spectra) and DRX 500 (^1H at 500.13 MHz, ^{13}C, ^{15}N, 2D). ^1H and ^{13}C spectra were referenced to TMS, using the residual proton signals of the deuterated solvents (^1H) or solvent signals (^{13}C) as internal standards [$CDCl_3 \equiv 7.24$ (^1H) and 77.0 (^{13}C), DMSO ≡ 2.49 (^1H) and 39.5 (^{13}C), $CD_3OD \equiv 3.30$ (^1H) and 49.0 (^{13}C)]. Positive chemical shift values δ (in ppm) indicate a downfield shift from the standard, only the absolute values of coupling constants are given in Hz. ^{15}N spectra were referenced to the absolute frequency of 50.6969910 MHz, which was the resonance frequency of neat nitromethane under the same experimental conditions. All resonances were assigned by 2D NMR (H,H-COSY and ^1H,^{13}C-HMQC for ^1J and long-range couplings). ^{15}N chemical shifts were taken from the F1 projection of indirect detection ^1H,^{15}N-correlated 2D spectra with 1024/256 data points in F1/F2, processed after applying a matched cosine function and zero filling in both dimensions. − Mössbauer data were recorded on a spectrometer with alternating constant-accelaration and a ^{57}Co source in 6 μm Rh matrix. The minimum experimental line width was 0.24 mms^{-1} full width at half maximum. The sample temperature was maintained constant in an Oxford Instruments VARIOX cryostat. Isomer shifts are quoted relative to iron metal at 300 K.

X-ray Crystallographic Data Collection and Refinement: Transparent yellow-orange single crystals of 0.74 × 0.35 × 0.05 mm (**3**) and 0.47 × 0.20 × 0.03 mm (**4**) were sealed in glass capillaries and mounted on the diffractometer. Graphite monochromated Mo-*Kα* radiation (λ = 0.71073 Å) was used. For **3**, cell constants were obtained from a least square fit of the setting angles of 25 carefully centred reflections and intensities were collected by the usual ω/2θ scan technique and corrected for Lorentz and polarization effects. The Siemens ShelXTL software package (Siemens Analytical X-ray Instruments, Inc.) was used for solution and refinement of the structure. Neutral atom scattering factors were taken from the usual source.[74] All non-hydrogen atoms were refined anisotropically. H-atoms were placed at calculated positions and refined as riding atoms with isotropic displacement parameters. All crystallographic details are listed in Table 1. Crystallographic data (excluding structure factors) for the structures reported in this paper have been deposited with the Cambridge Crystallographic Data Centre and allocated the deposition numbers CCDC 119109 (**3**) and CCDC 119110 (**4**). Copies of the data may be obtained free of charge on application to CCDC, 12 Union Road, Cambridge CB2 1EZ, UK [Fax: (internat). +44 1223/33 60 33; E-mail: deposit@ccdc.cam.ac.uk].

Preparations: Ferrocene propargylamine derivatives **3** and **4**: Ferrocene carboxylic acid chloride was dissolved in CH_2Cl_2 (40 mL). Propargylamine [(0.36 g, 6.5 mmol) for **3**, 1,1-diethylpropargylamine (0.72 g, 6.5 mmol) in the case of **4**] and triethylamine (0.66 g, 6.5 mmol) were added at room temp. and the solution was stirred for 4 h. After removal of the triethylamine−hydrochloride the solvent was removed in vacuo. The residue was dissolved in chloro-

form, the organic phase washed three times with water and dried with Na_2SO_4. After filtration and removal of the solvent, virtually pure products were obtained which could be recrystallized to yield single crystals. **3** (1.51. g, 87%), recrystallized from warm ethyl acetate/methanol, m.p. 167°C. − ^{1}H NMR ($CDCl_3$): δ = 5.85 (br, 1 H, N*H*), 4.66 (pseudo-t, 2 H, H_{Cp}), 4.34 (pseudo-t, 2 H, H_{Cp}) 4.21 (s, 5 H, H_{Cp}), 2.25 (t, *J* = 2.6 Hz, 1 H, C≡C*H*). − ^{13}C NMR ($CDCl_3$): δ = 170.2 (*C*=O), 80.3 (*C*≡CH), 71.5 (C≡*C*H), 75.0, 70.7, 69.8, 68.2 (C_{Cp}), 29.2 (*C*H$_2$). − ^{15}N NMR ($CDCl_3$): δ = −276. − IR: ṽ (cm^{-1}) = 3281 (m), 3264 (m), 2121 (w), 1634 (s). − Raman: 2121 cm^{-1} (C≡C). CV: +187 mV. MS (EI, 70 eV): 267 (100), 213 (4), 186 (14). − $C_{14}H_{13}FeNO$ (267.11): calcd. C 63.0, H 4.9, N 5.2; found C 62.9, H 4.9, N 5.2. − **4** (1.91 g, 91%) recrystallized from methanol, m.p. 149°C. − ^{1}H NMR ($CDCl_3$): δ = 5.61 (br, 1 H, N*H*), 4.61 (pseudo-t, 2 H, H_{Cp}), 4.30 (pseudo-t, 2 H, H_{Cp}) 4.21 (s, 5 H, H_{Cp}), 2.38 (s, 1 H, C≡C*H*), 2.33−2.19 and 1.93−1.79 (mult., 2 H each, C*H*$_2$-CH$_3$), 1.03 (t, *J* = 7.4 Hz, 6 H, CH$_2$-C*H*$_3$). − ^{13}C NMR ($CDCl_3$): δ = 169.2 (*C*=O), 85.6 (*C*≡CH), 76.8 (C_{Cp}), 71.6 (C≡*C*H), 70.3, 69.7, 68.1 (C_{Cp}), 57.5 [*C*(Et)$_2$], 30.8 (*C*H$_2$), 8.8 (*C*H$_3$). − ^{15}N NMR ($CDCl_3$): δ = −263. − IR: ṽ (cm^{-1}) = 3304 (w), 3277 (m), 1631 (s). − Raman 2105. − CV: +182 mV. − MS (EI, 70 eV): 323 (100), 229 (40), 213 (32), 121 (19). − $C_{18}H_{21}FeNO$ (323.22): calcd. C 66.9, H 6.6, N 4.3; found C 67.2, H 6.5, N 4.3. − **5**: Ferrocene carboxylic acid (0.5 g, 2.17 mmol) was dissolved in THF (30 mL) at room temp. and neutralized with N-methylmorpholine (0.22 g, 2.17 mmol). Upon addition of isobutyl chloroformate (0.3 g, 2.17 mmol) a white precipitate rapidly formed. After stirring for one hour, the solution was filtered and the solvent was removed in vacuo. The residue was dissolved in chloroform, the organic phase washed three times with water and dried with Na_2SO_4. After filtration the solvent was removed to yield 0.57 g (79%) of **5. 5** can be recrystallized from *n*-pentane, m.p. 46°C. − ^{1}H NMR ($CDCl_3$): δ = 4.84 (pseudo-t, 2 H, H_{Cp}), 4.51 (pseudo-t, 2 H, H_{Cp}) 4.28 (s, 5 H, H_{Cp}), 4.08 (d, *J* = 6.6 Hz, 2 H, C*H*$_2$), 2.05 (mult., 1 H, C*H*), 0.98 (d, *J* = 6.7 Hz, 6 H, C*H*$_3$). − ^{13}C NMR ($CDCl_3$): δ = 166.5 (Fc-*C*=O), 149.9 (*C*=O), 75.4 (*C*H$_2$), 72.8, 70.9, 70.2, 67.7 (C_{Cp}), 27.7 (*C*H), 18.8 (*C*H$_3$). − IR: ṽ (cm^{-1}) = 3450 (br), 1793 (s), 1731 (s). − MS (EI, 70 eV): 330 (35), 230 (100), 213 (38), 185 (8), 138 (31). − $C_{16}H_{18}FeO_4$ (330.16): calcd. C 58.2, H 5.5; found C 58.4, H 5.5.

General Procedure for Pd Coupling Reactions: The iodoamino acid (1 mmol), bis(triphenylphosphane)palladium(II) dichloride (35 mg, 0.05 mmol), and copper(I) iodide (9.5 mg, 0.05 mmol) were dissolved at room temp. in a deoxygenated mixture of THF (40 mL) and triethylamine (10 mL). The alkyne (1 mmol), dissolved in THF (3 mL) was added dropwise at room temp. After complete addition, the reaction mixture was immediately heated at reflux under argon for 4 hours. After cooling to room temp., the dark suspension was filtered and the solvents were removed on a rotary evaporator. The resulting residue was redissolved in chloroform, the organic phase was washed three times with water and dried with Na_2SO_4. After filtration *n*-pentane was added until a light orange precipitate was formed. The precipitate was collected and dried in vacuo for several hours to yield 70−95% of light orange product. If necessary the product can be purified by redissolving the precipitate in ether, filtration and evaporation of the solvent. − **7d**, m.p. 105−108°C. − ^{1}H NMR ($CDCl_3$): δ = 8.78 (s,br, 1 H, N*H*$_{Ar}$), 7.42 (pseudo-d, 2 H, H_{Ar}), 7.29 (pseudo-d, 2 H, H_{Ar}), 6.14 (s, 1 H, N*H*-CH$_2$), 5.41 (d, *J* = 8 Hz, 1 H, N*H*$_{Boc}$), 4.72 (s, 2 H, H_{Cp}), 4.37 (mult., 1 H, C$_\alpha$*H*), 4.36 (mult., 2 H, C*H*$_2$-C≡C), 4.33 (s, 2 H, H_{Cp}), 4.20 (s, 5 H, H_{Cp}), 2.59−2.55 (mult., 2 H, C$_\gamma$*H*), 2.15−2.12 (mult., 1 H, C$_\beta$*H*), 2.07 (s, 3 H, S-C*H*$_3$), 1.99−1.96 (mult., 1 H, C$_\beta$*H*), 1.41 (s, 9 H, C(C*H*$_3$)$_3$). − ^{13}C NMR ($CDCl_3$): δ = 170.3 (*C*=O), 170.2 (C_{Fc} = O), 156.1 (C_{Boc} = O), 137.8, 132.4, 119.5, 118.3 (C_{Ar}), 85.2 (*C*≡C-CH$_2$), 82.8 (C≡*C*-CH$_2$), 80.7 [*C*(CH$_3$)$_3$], 75.1, 70.7, 69.8, 68.3, (C_{Cp}), 54.3 (C$_\alpha$), 31.2 (C$_\beta$), 30.3 (C$_\gamma$), 30.0 (C≡C-*C*H$_2$), 28.3 [C(*C*H$_3$)$_3$], 15.3 (S-*C*H$_3$). − ^{15}N NMR ($CDCl_3$): d = −291 (*N*H$_{Boc}$), −274 (*N*H), −249 (*N*H$_{Ar}$). − IR: ṽ (cm^{-1}) = 3315 (br, m), 1678 (br, m), 1636 (br, m), 1601 (m). − IR (CH_2Cl_2): 3428 (m), 1701 (s), 1660 (s), 1606 (m). − Raman: 2240 cm^{-1}. − MS (ESI): 590 (M + H), 612 (M + Na), 628 (M + K). − $C_{30}H_{35}FeN_3O_4S$ (589.54): calcd. C 61.1, H 6.0, N 7.1; found C 61.3, H 6.0, N 6.7. − **8a**, m.p. 114°C. − ^{1}H NMR ($CDCl_3$): δ = 8.89 (s, 1 H, N*H*$_{Ar}$), 7.46 (app. d, 2 H, H_{Ar}), 7.39 (app. d, 2 H, H_{Ar}), 5.70 (s, 1 H, N*H*-C(Et)$_2$), 5.65 (br, 1 H, N*H*$_{Boc}$), 4.64 (pseudo-t, 2 H, H_{Cp}), 4.31 (pseudo-t, 2 H, H_{Cp}), 4.25−4.21 (mult., 7 H, H_{Cp}, O*H*, C$_\alpha$*H*), 3.70 (mult., 1 H, C$_\beta$*H*), 3.01 (mult., 1 H, C$_\beta$*H*), 2.42−2.34 (mult., 2 H, C*H*$_2$-CH$_3$), 1.96−1.87 (mult., 2 H, C*H*$_2$-CH$_3$), 1.46 (s, 9 H, C(C*H*$_3$)$_3$), 1.12−1.06 (overlapping t, 6 H, CH$_2$-C*H*$_3$),. − ^{13}C NMR ($CDCl_3$): δ = 170.3 (*C*=O), 169.1 (C_{Fc} = O), 155.1 (C_{Boc} = O), 137.5, 132.6, 119.6, 118.8 (C_{Ar}), 90.4 [*C*≡C-C(Et)$_2$], 83.6 (C≡*C*-C(Et)$_2$), 81.1 (*C*(CH$_3$)$_3$), 76.0, 70.3, 69.7, 68.1 (C_{Cp}), 62.3 (C$_\beta$), 58.6 [C≡C-*C*(Et)$_2$], 55.9 (C$_\alpha$), 31.1 (*C*H$_2$-CH$_3$), 28.3 [C(*C*H$_3$)$_3$], 9.1 (CH$_2$-*C*H$_3$). − ^{15}N NMR ($CDCl_3$): δ = −295 (*N*H$_{Boc}$), −258 (*N*H), −252 (*N*H$_{Ar}$). − IR: ṽ (cm^{-1}) = 3235 (br, m), 1686 (m), 1643 (m). − Raman: 2227 cm^{-1}. − CV: +193 mV. − UV: 442 (400). − MS (EI, 70 eV): 601 (100), 572 (11), 501 (23), 385 (4), 229 (89), 213 (64), 185 (16). − $C_{32}H_{39}FeN_3O_5$ (601.52): calcd. C 63.9, H 6.5, N 7.0; found C 64.1, H 6.7, N 6.9. − **8b**, m.p. 100°C. − ^{1}H NMR ($CDCl_3$): δ = 7.55 (app. d, 2 H, H_{Ar}), 7.45 (s, 1 H, N*H*$_{Ar}$), 7.38 (app. d, 2 H, H_{Ar}), 6.19 (s, 1 H, N*H*-C(Et)$_2$), 4.85 (br, 1 H, N*H*$_{Boc}$), 4.76 (pseudo-t, 2 H, H_{Cp}), 4.41 (s, 2 H, H_{Cp}), 4.23 (s, 5 H, H_{Cp}), 4.00 (mult., 1 H, C$_\alpha$*H*), 2.32−2.26 (mult., 2 H, C*H*$_2$-CH$_3$), 1.84−1.80 (mult., 2 H, C*H*$_2$-CH$_3$), 1.67−1.62 (mult., 2 H, C$_\beta$*H* und C$_\gamma$*H*) 1.46−1.42 (mult., 1 H, C$_\beta$*H*), 1.42 [s, 9 H, C(C*H*$_3$)$_3$], 1.04−0.97 (overlapping t, 6 H, CH$_2$-C*H*$_3$), 0.94−0.90 (mult., 6 H, C$_\delta$*H*). − ^{13}C NMR ($CDCl_3$): δ = 171.3 (*C*=O), 168.6 (C_{Fc} = O), 155.7 (C_{Boc} = O), 138.2, 132.7, 119.2, 118.1 (C_{Ar}), 90.0 [*C*≡C-C(Et)$_2$], 83.5 [C≡*C*-C(Et)$_2$], 80.1 [*C*(CH$_3$)$_3$], 76.0, 71.0, 69.9, 68.3 (C_{Cp}), 58.6 (C≡C-*C*(Et)$_2$), 53.0 (C$_\alpha$), 40.9 (C$_\beta$), 30.3 und 30.9 (*C*H$_2$-CH$_3$), 28.3 [C(*C*H$_3$)$_3$], 24.8 (C$_\gamma$), 22.1 und 22.9 (C$_\delta$), 8.9 und 9.0 (CH$_2$-*C*H$_3$). − ^{15}N NMR ($CDCl_3$): δ = −289 (*N*H$_{Boc}$), −258 (*N*H), −254 (*N*H$_{Ar}$). − IR: ṽ (cm^{-1}) = 3421 (m), 3324 (m), 1701 (sh), 1654 (br, m). − Raman: 2228 cm^{-1}. − CV: +197 mV. − UV: 444 (400). − MS (EI, 70 eV): 627 (100), 571 (3), 553 (29), 385 (30), 213 (64), 185 (36), 129 (21). − $C_{35}H_{45}FeN_3O_4$ (627.60): calcd. C 67.0, H 7.2, N 6.7; found C 66.5, H 6.9, N 6.7. − **8c**. m.p. 194°C. − ^{1}H NMR ($CDCl_3$): δ = 7.85 (s,br, 1 H, N*H*$_{Ar}$), 7.39−7.20 (mult., 9 H, H_{Ar} and H_{Phe}) 5.70 (s, 1 H, N*H*$_{DEPA}$), 5.30 (br, 1 H, N*H*$_{Boc}$), 4.64 (pseudo-t, 2 H, H_{Cp}), 4.31 (s, 2 H, H_{Cp}), 4.40 (mult., 1 H, C$_\alpha$*H*), 4.21 (s, 5 H, H_{Cp}), 3.13 (d, *J* = 6.9 Hz, 2 H, C$_\beta$*H*), 2.43−2.35 (mult., 2 H, C*H*$_2$-CH$_3$), 1.95−1.87 (mult., 2 H, C*H*$_2$-CH$_3$), 1.40 (s, 9 H, C$_{Boc}$*H*$_3$), 1.12−1.06 (overlapping t, 6 H, CH$_2$-C*H*$_3$). − ^{13}C NMR ($CDCl_3$): δ = 169.6 (*C*=O), 169.1 (C_{Fc} = O), 155.8 (C_{Boc} = O), 137.4, 132.5, 119.5, 118.6 (C_{Ar}), 136.5, 129.3, 128.8, 127.8 (C_{Phe}), 90.6 [*C*≡C-C(Et)$_2$], 83.3 [C≡*C*-C(Et)$_2$], 80.7 [*C*(CH$_3$)$_3$], 76.0, 70.3, 69.7, 68.1 (C_{Cp}), 58.6 [*C*(Et)$_2$], 56.8 (C$_\alpha$), 38.3 (C$_\beta$), 30.3 und 31.1 (*C*H$_2$-CH$_3$), 28.2 [C(*C*H$_3$)$_3$], 9.24 and 9.11 (CH$_2$-*C*H$_3$). − ^{15}N NMR ($CDCl_3$): δ = −291 (*N*H$_{Boc}$), −262 (*N*H), −249 (*N*H$_{Ar}$). − IR: ṽ (cm^{-1}) = 3432 (br, m), 3310 (br, m), 1665 (br, s), 1601 (sh). − Raman: 2226 cm^{-1}. − MS (EI, 70 eV): 661 (100), 644 (28), 587 (53), 561 (33), 229 (85), 120 (52). − $C_{38}H_{43}FeN_3O_4$ (661.62): calcd. C 69.0, H 6.6, N 6.4; found C 68.7, H 6.5, N 6.3. − **8d**, m.p. 107°C. − ^{1}H NMR ($CDCl_3$): δ = 8.53 (s,br, 1 H, N*H*$_{Ar}$), 7.47 (app. d, 2 H, H_{Ar}), 7.38 (app. d, 2 H, H_{Ar}), 5.70 (s, 1 H, N*H*-C(Et)$_2$), 5.25 (d, *J* = 8 Hz, 1 H, N*H*$_{Boc}$), 4.63 (pseudo-t, 2 H, H_{Cp}), 4.40 (mult., 1 H, C$_\alpha$*H*), 4.30 (s, 2 H, H_{Cp}), 4.21 (s, 5 H, H_{Cp}), 2.63−2.57

(mult., 2 H, $C_\gamma H$), 2.41−2.36 (mult., 2 H, CH_2-CH_3), 2.20−2.13 (mult., 1 H, $C_\beta H$), 2.10 (s, 3 H, S-CH_3), 2.01−1.91 (mult., 3 H, $C_\beta H$ and CH_2-CH_3), 1.43 [s, 9 H, C(CH_3)$_3$], 1.10−1.06 (overlapping t, 6 H, CH_2-CH_3). − ^{13}C NMR ($CDCl_3$): δ = 170.3 (C=O), 169.1 (C_{Fc} = O), 155.9 (C_{Boc} = O), 137.8, 132.4, 119.4, 118.4 (C_{Ar}), 90.5 [C≡C-C(Et)$_2$], 82.4 [C≡C-C(Et)$_2$], 80.5 [$C(CH_3)_3$], 76.0, 70.3, 69.6, 68.0 (C_{Cp}) 58.5 [$C(Et)_2$], 54.2 (C_α), 31.3 (C_β), 31.34 und 31.01(CH_2-CH_3), 30.3 (C_γ), 28.3 [C(CH_3)$_3$], 15.3 (S-CH_3), 9.08 and 8.23 (CH_2-CH_3). − ^{15}N NMR($CDCl_3$): δ = −291 (NH_{Boc}), −262 (NH), −249 (NH_{Ar}). − IR: $\tilde{\nu}$ (cm^{-1}) = 3433 (br, m), 3316 (br, m), 1685 (br, s), 1648 (br, s). − Raman: 2229 cm^{-1}. − MS (ESI): 646 (M + H), 668 (M + Na), 684 (M + K). − $C_{34}H_{43}FeN_3O_4S$ (645.64): calcd. C 63.3, H 6.7, N 6.5; found C 62.9, H 6.7, N 6.2. − **10**, m.p. 132°C. − ^{1}H NMR ($CDCl_3$): δ = 7.72 (app. d, 2 H, H_{Ar}), 7.49 (app. d, 2 H, H_{Ar}), 6.49 (d, J = 8 Hz, 1 H, NH_{Leu}), 5.69 (s, 1 H, NH-C(Et)$_2$), 4.82 (mult., 1 H, $C_\alpha H$), 4.65 (pseudo-t, 2 H, H_{Cp}), 4.32 (s, 2 H, H_{Cp}), 4.21 (s, 5 H, H_{Cp}), 3.75 (s, 3 H, OCH_3), 2.41−2.32 (mult., 2 H, CH_2-CH_3), 2.00−1.91 (mult., 2 H, CH_2-CH_3), 1.78−1.63 (mult., 3 H, $C_\beta H_2$ and $C_\gamma H$), 1.13−1.07 (overlapping t, 6 H, CH_2-CH_3), 0.97−0.95 (overlapping t, 6 H, $C_\delta H$). − ^{13}C NMR ($CDCl_3$): δ = 173.6 (C=O), 169.1 (C_{Fc} = O), 166.3 (C_{OMe}=O), 133.2, 131.9, 127.0, 126.4 (C_{Ar}), 93.6 [C≡C-C(Et)$_2$], 82.8 [C≡C-C(Et)$_2$], 76.8, 70.3, 69.7, 68.1 (C_{Cp}), 58.2 [$C(Et)_2$], 52.4 (OCH_3), 51.2 (C_α), 41.8 (C_β), 31.0 (CH_2-CH_3), 25.0 (C_γ), 22.0 and 22.8 (C_δ), 9.0 (CH_2-CH_3). − ^{15}N NMR ($CDCl_3$): δ = −267 (NH_{Leu}), −263 (NH). − IR: $\tilde{\nu}$ (cm^{-1}) = 3313 (m), 1746 (m), 1637 (s), 1608 (w). − Raman: 2227 cm^{-1}. − CV: +197 mV. − UV: 444 (400). − MS (EI, 70 eV): 570 (100), 541 (4), 229 (34), 213 (35), 185 (9). − $C_{32}H_{38}FeN_2O_4$ (570.51): calcd. C 67.3, H 6.7, N 4.9; found C 67.5, H 6.8, N 4.8. − **9**: Compound **3** (267 mg, 1 mmol) was dissolved in methanol (30 mL). A solution of copper(II) acetate monohydrate (199.6 mg, 1 mmol) in a mixture of methanol (20 mL) and pyridine (10 mL) was added dropwise and the resulting solution was stirred at 60°C for one hour. After cooling to room temp., the solution was reduced to about one third of the initial volume and CH_2Cl_2 and water were added. The organic phase was separated, washed three times with water and dried with Na_2SO_4. After filtration, the solvent was removed on a rotary evaporator to yield 101 mg (38%) of light-orange product, m.p. 108°C. − ^{1}H NMR ($CDCl_3$): δ = 5.76 (br, 2 H, NH), 4.65 (pseudo-t, 4 H, H_{Cp}), 4.34 (pseudo-t, 4 H, H_{Cp}) 4.24−4.20 (mult., 14 H, H_{Cp} and CH_2). − ^{13}C NMR ([D$_6$]DMSO): δ = 169.0 (C=O), 76.7 (C≡C-C≡C), 75.3, 70.2, 69.3, 68.2 (C_{Cp}), 65.5 (C≡C-C≡C), 28.7 (CH_2). − IR: $\tilde{\nu}$ (cm^{-1}) = 3324 (br), 3306 (br), 1637 (s), 1533 (s). − MS (EI, 70 eV): 532 (100), 467 (19), 401 (14), 211 (15), 121 (19). − $C_{28}H_{24}Fe_2N_2O_2$ (532.20): calcd. C 63.2, H 4.6, N 5.3; found C 62.9, H 4.3, N 5.1. − **11**: Boc-protected cystine (10 mmol, 4.41 g) was dissolved in THF (100 mL) at room temp. and neutralized with *N*-methylmorpholine (2.02 g, 20 mmol). Isobutyl chloroformate (2.74 g, 20 mmol) was added and a white precipitate was rapidly formed. 4-iodoaniline (4.38 g, 20 mmol) was added and the solution was allowed to stir for one hour. The *N*-methylmorpholine hydrochloride was removed by filtration and the solvent was removed on a rotary evaporator. The resulting residue was redissolved in ether, the organic phase was washed three times with water and dried with Na_2SO_4. After filtration the solvent was removed to yield 7.1 g (84%) of **11**. **11** can be recrystallized from hot chloroform, m.p. 218°C. − ^{1}H NMR ([D$_6$]DMSO): δ = 10.14 (s, 2 H, NH), 7.61 and 7.42 (app. d, 4 H each, H_{Ar}), 7.20 (d, 2 H, $N_{Boc}H$, J = 7.6), 4.32 (mult., 2 H, $C_\alpha H$) 3.14 and 2.94 (mult., 2 H each, $C_\beta H_2$), 1.36 (s, 18 H, C(CH_3)$_3$). − ^{13}C NMR ([D$_6$]DMSO): δ = 169.3 (C=O), 155.2 (C_{Boc} = O), 138.5, 137.3, 121.7, 87.0 (C_{Phe}), 78.4 (C (CH_3)$_3$), 54.5 (C_α) 40.1 (C_β), 28.1 [C(CH_3)$_3$]. − ^{15}N NMR ([D$_6$]DMSO): δ = −290 (N_{Boc}), −249 (N_{Ar}). − IR: $\tilde{\nu}$ (cm^{-1}) = 3341 (m), 1685 (m), 1670 (s). − MS (EI, 70 eV): 842 (< 1%), 422 (9), 366 (32), 219 (46), 57 (88), 41 (100). − $C_{28}H_{36}I_2N_4O_6S_2$ (842.55): calcd. C 39.9, H 4.3, N 6.7; found C 40.0, H 4.4, N 6.6. − **12**, purified by HPLC: ^{1}H NMR ($CDCl_3$): δ = 9.32 (br, 2 H, NH_{Ar}), 7.61−7.54 (mult., 4 H, H_{Ar}), 7.38−7.36 (mult., 4 H, H_{Ar}), 5.84 (br, 1 H, NH-CH_2), 5.61 (br, 2 H, NH_{Boc}), 4.92 (mult., 2 H, $C_\alpha H$), 4.68 (pseudo-t, 2 H, H_{Cp}), 4.37−4.34 (mult., 4 H, H_{Cp} and CH_2), 4.21 (s, 5 H, H_{Cp}), 3.09−2.96 (mult., 4 H, $C_\beta H_2$), 1.45 [s, 18 H, C(CH_3)$_3$]. − ^{13}C NMR ($CDCl_3$): δ = 169.8 (C_{Fc} = O), 168.5 (C_{Cys}=O), 156.1 (C_{Boc} = O), 137.8, 137.2, 132.2, 122.6, 119.6, 120.4, 118.7, 85.3 (C_{Ar}), 88.2 (C≡C-CH_2), 82.8 (C≡C-CH_2), 80.5 [$C(CH_3)_3$], 75.1, 70.7, 69.8, 68.2 (C_{Cp}), 55.6 (C_α), 47.4 (C_β), 30.0 (CH_2), 28.4 [C(CH_3)$_3$]. − ^{15}N NMR ($CDCl_3$): δ = −292 (NH_{Boc}), −275 (NH), −250 (NH_{Ar}). − IR (CH_2Cl_2): 3420 (w), 3327 (w), 1683 (br, s), 1659 (sh). − MS (ESI, in CH_2Cl_2): 1004 [M + Na]. − $C_{42}H_{48}FeIN_5O_7S_2$ (981.76): calcd. C 51.4, H 4.9, N 7.1; found C 51.9, H 5.2, N 7.1. − **13**: Compound **13** could not be separated completely from **12**. Compounds **12** and **13** have virtually identical NMR spectra, except for the integration ratios. − MS (ESI, in CH_2Cl_2): 1043 [M + Na], 1160 [M + K].

Table 1. Crystallographic details

	3	**4**
Empirical formula	$C_{14}H_{13}FeNO$	$C_{18}H_{21}FeNO$
Formula weight	267.10	323.21
Temperature [K]	293 (2)	100 (2)
Crystal system, space group	orthorhombic, *Pbca*	orthorhombic, *Pbca*
Diffractometer used	Enraf−Nonius CAD4	Siemens SMART
Unit cell dimensions, l. s., on	25 reflections	8192 reflections
a [Å]	11.636(2)	11.844(2)
b [Å]	9.881(2)	9.962(1)
c [Å]	21.053(3)	25.770(4)
Volume [Å^3]	2420.6(7)	3040.6(8)
Z	8	8
Absorption coefficient [mm^{-1}]	1.227	0.990
Absorption correction	None	SADABS (G. Sheldrick, 1994)
θ range for data collection [°]	2.61 to 25.99	1.58 to 30.00
Reflections collected, Independent reflections	2376, 2376	28110, 4369
R_{int}	−	0.0767
Data/Restraints/ Parameters	2067/0/160	4054/0/195
Goodness-of-fit on F^2	1.050	1.039
Final R indices $[I > 2\sigma(I)]$[a]	R_1 = 0.0402, wR_2 = 0.1004	R_1 = 0.0465, wR_2 = 0.0895
R indices (all data)[a]	R_1 = 0.0701, wR_2 = 0.1137	R_1 = 0.0809, wR_2 = 0.1018
Largest diff. peak and hole [eA^{-3}]	0.656, −0.434	0.557, −0.561

[a] $R_1 = (\Sigma||F_o| - |F_c||/\Sigma|F_o|)$; $wR_2 = [\Sigma w(F_o^2 - F_c^2)^2/\Sigma wF_o^4]^{1/2}$.

Acknowledgments

The authors are grateful to Prof. K. Wieghardt for many scientific discussions and for his generous support of this work. The technical help of H. Schucht (X-ray), K. Sand and J. Bitter (NMR) is gratefully appreciated. Our thanks are also extended to Dr. E. Bill for recording the Mössbauer spectra.

[1] O. Brosch, T. Weyhermüller, N. Metzler-Nolte, *Inorg. Chem.* **1999**, *38*, 5308−5313.
[2] A. Hess, N. Metzler-Nolte, *J. Chem. Soc., Chem. Commun.* **1999**, 885−886.
[3] A. D. Ryabov, *Angew. Chem.* **1991**, *103*, 945−955; *Angew. Chem. Int. Ed. Engl.* **1991**, *30*, 931−941.
[4] G. Jaouen, A. Vessières, I. S. Butler, *Acc. Chem. Res.* **1993**, *26*, 361−369.
[5] K. Severin, R. Bergs, W. Beck, *Angew. Chem.* **1998**, *110*, 1722−1743; *Angew. Chem. Int. Ed. Engl.* **1998**, *37*, 1634−1654.
[6] H. Eckert, M. Koller, *Z. Naturforsch.* **1990**, *45b*, 1709−1714.
[7] H. Eckert, M. Koller, *J. Liq. Chromatogr.* **1990**, *13*, 3399−3414.
[8] T. Ihara, M. Nakayama, M. Murata, K. Nakano, M. Maeda, *J. Chem. Soc., Chem. Commun.* **1997**, 1609−1610.
[9] G. Jaouen, A. Vessières, S. Top, *J. Am. Chem. Soc.* **1985**, *107*, 4778−4780.
[10] M. Salmain, A. Vessières, I. S. Butler, G. Jaouen, *Bioconjugate Chem.* **1991**, *2*, 13−15.
[11] M. Savignac, A. Sasaki, P. Potier, G. Jaouen, *J. Chem. Soc., Chem. Commun.* **1991**, 615−617.
[12] A. Varenne, M. Salmain, C. Brisson, G. Jaouen, *Bioconjugate Chem.* **1992**, *3*, 471−476.
[13] M. Salmain, A. Vessières, P. Brossier, I. S. Butler, G. Jaouen, *J. Immun. Meth.* **1992**, *148*, 65−75.
[14] M. Salmain, M. Gunn, A. Gorfti, S. Top, G. Jaouen, *Bioconjugate Chem.* **1993**, *4*, 425−433.
[15] V. Philomin, A. Vessiéres, M. Gruselle, G. Jaouen, *Bioconjugate Chem.* **1993**, *4*, 419−424.
[16] M. Salmain, K. L. Malisza, S. Top, G. Jaouen, M.-C. Sénéchal-Tocquer, D. Sénéchal, B. Caro, *Bioconjugate Chem.* **1994**, *5*, 655−659.
[17] K. L. Malisza, S. Top, J. Vaissermann, B. Caro, M.-C. Sénéchal-Tocquer, D. Sénéchal, J.-Y. Saillard, S. Triki, S. Kahlal, J. F. Britten, M. J. McGlinchey, G. Jaouen, *Organometallics* **1995**, *14*, 5273−5280.
[18] D. Osella, M. Ravera, M. Vincenti, M. Salmain, G. Jaouen, *Organometallics* **1996**, *15*, 3037−3041.
[19] D. B. Grotjahn, C. Joubran, D. Combs, D. C. Brune, *J. Am. Chem. Soc.* **1998**, *120*, 11814−11815.
[20] P. Meunier, I. Ouattara, B. Gautheron, J. Tirouflet, D. Camboli, J. Besançon, *Eur. J. Med. Chem.* **1991**, *26*, 351−362.
[21] H. Dibowski, F. P. Schmidtchen, *Angew. Chem.* **1998**, *110*, 487−489; *Angew. Chem. Int. Ed. Engl.* **1998**, *37*, 476−478.
[22] G. Vaidyanathan, M. R. Zalutsky, T. R. DeGrado, *Bioconjugate Chem.* **1998**, *9*, 758−764.
[23] S. Garg, P. K. Garg, X. G. Zhao, H. S. Friedman, D. D. Bigner, M. R. Zalutsky, *Nucl. Med. Biol.* **1993**, *20*, 835−842.
[24] S. Garg, P. K. Garg, M. R. Zalutsky, *Bioconjugate Chem.* **1991**, *2*, 50−56.
[25] F. A. Armstrong, H. A. O. Hill, N. J. Walton, *Acc. Chem. Res.* **1988**, *21*, 407−413.
[26] W. Schuhmann, T. J. Ohara, H.-L. Schmidt, A. Heller, *J. Am. Chem. Soc.* **1991**, *113*, 1394−1397.
[27] A. D. Ryabov, A. M. Trushkin, L. I. Baksheeva, R. K. Gorbatova, I. V. Kubrakova, V. V. Mozhaev, B. B. Gnedenko, A. V. Levashov, *Angew. Chem.* **1992**, *104*, 788−790; *Angew. Chem. Int. Ed. Engl.* **1992**, *31*, 789−791.
[28] A. Riklin, E. Katz, I. Willner, A. Stocker, A. F. Bückmann, *Nature* **1995**, *376*, 672−675.
[29] S. O. Kelley, J. K. Barton, *Bioconjugate Chem.* **1997**, *8*, 31−37.
[30] P. D. Beer, M. G. B. Drew, D. K. Smith, *J. Organomet. Chem.* **1997**, *543*, 259−261.
[31] C. Chavigny, F. Le Bideau, C.-M. Pradier, S. Palacin, P. Brossier, G. Jaouen, *J. Chem. Soc., Chem. Commun.* **1998**, 1727−1728.
[32] H.-B. Kraatz, J. Lusztyk, G. D. Enright, *Inorg. Chem.* **1997**, *36*, 2400−2405.
[33] M. Bodanszky, *Principles of Peptide Synthesis*, Springer-Verlag, Berlin, **1984**.
[34] Y. S. Klausner, M. Bodansky, *Synthesis* **1972**, 453−463.
[35] K. Sonogashira, Y. Tohda, N. Hagihara, *Tetrahedron Lett.* **1975**, *50*, 4467−4470.
[36] N. Hagihara, K. Sonogashira, Y. Tohda, *Synthesis* **1977**, 777−778.
[37] N. Hagihara, S. Takahashi, Y. Kuroyama, K. Sonogashira, *Synthesis* **1980**, 627−630.
[38] G. Eglington, W. McCrae, *Adv. Org. Chem.* **1963**, *4*, 225−328.
[39] R. S. Herrick, R. M. Jarret, T. P. Curran, D. R. Dragoli, M. B. Flaherty, S. E. Lindyberg, R. A. Slate, L. C. Thornton, *Tetrahedron Lett.* **1996**, *30*, 5289−5292.
[40] L. Lin, A. Berces, H.-B. Kraatz, *J. Organomet. Chem.* **1998**, *556*, 11−20.
[41] F. A. Cotton, A. H. Reid Jr., *Acta Cryst. C* **1985**, *41*, 686−688.
[42] T. J. J. Müller, H. J. Lindner, *Chem. Ber.* **1996**, *129*, 607−613.
[43] T. J. J. Müller, M. Ansorge, H. J. Lindner, *Chem. Ber.* **1996**, *129*, 1433−1440.
[44] U. H. F. Bunz, *Pure Appl. Chem.* **1996**, *68*, 309−312.
[45] U. H. F. Bunz, *Synlett* **1997**, 1117−1127.
[46] A. H. Stokes, Y. Xu, H. Tamir, M. D. Gershon, P. Butkerait, B. Kayser, J. Altman, W. Beck, K. E. Vrana, *J. Neurochem.* **1998**, *70*, S29-S29.
[47] B. Kayser, J. Altman, W. Beck, *Tetrahedron* **1997**, *53*, 2475−2484.
[48] B. Kayser, J. Altman, H. Nöth, J. Knizek, W. Beck, *Eur. J. Inorg. Chem.* **1998**, 1791−1798.
[49] B. Kayser, J. Altman, W. Beck, *Chem. Eur. J.* **1999**, *5*, 754−758.
[50] Program *Spartan version 5.0*, **1997**, Wavefunction Inc., 18401 Von Karman Avenue, Suite 370, Irvine, CA; used on SGI Indigo^2.
[51] M. Altmann, V. Enkelmann, F. Beer, U. H. F. Bunz, *Organometallics* **1996**, *15*, 394−399.
[52] M. Witanowski, L. Stefaniak, *Annu. Rep. NMR Spectrosc.* **1986**, *18*, 1−761.
[53] M. Witanowski, L. Stefaniak, G. A. Webb, *Annu. Rep. NMR Spectrosc.* **1993**, *25*, 1−480.
[54] S. H. Gellman, G. P. Dado, G.-B. Liang, B. R. Adams, *J. Am. Chem. Soc.* **1991**, *113*, 1164−1173.
[55] K. y. Tsang, H. Diaz, N. Graciani, J. W. Kelly, *J. Am. Chem. Soc.* **1994**, *116*, 3988−4005.
[56] B. Schade, J.-H. Fuhrhop, *New J. Chem.* **1998**, 97−104.
[57] G.-B. Liang, G. P. Dado, S. H. Gellman, *J. Am. Chem. Soc.* **1991**, *113*, 3994−3995.
[58] N. N. Greenwood, T. C. Gibb, *Mössbauer Spectroscopy*, Chapman and Hall, London, **1971**.
[59] A. V. Lesikar, *J. Chem. Phys.* **1964**, *40*, 2746.
[60] Y. Zhou, B. Wagner, K. Polborn, K. Sünkel, W. Beck, *Z. Naturforsch. B* **1994**, *49*, 1193−1202.
[61] T. Hauck, K. Sünkel, W. Beck, *Inorg. Chim. Acta* **1995**, *235*, 391−396.
[62] D. Freiesleben, K. Polborn, C. Robl, K. Sünkel, W. Beck, *Canad. J. Chem.* **1995**, *73*, 1164−1174.
[63] R. Urban, R. Krämer, S. Mihan, K. Polborn, B. Wagner, W. Beck, *J. Organomet. Chem.* **1996**, *517*, 191−200.
[64] A. Böhm, K. Sünkel, K. Polborn, W. Beck, *J. Organomet. Chem.* **1998**, *552*, 237−246.
[65] J. Spencer, F. Maassarani, M. Pfeffer, A. DeCian, J. Fischer, *Tetrahedron Asym.* **1994**, *5*, 321−324.
[66] E. V. Krooglyak, G. M. Kazankov, S. A. Kurzeev, V. A. Polyakov, A. N. Semenov, A. D. Ryabov, *Inorg. Chem.* **1996**, *35*, 4804−4806.
[67] E. N. Korneeva, M. V. Ovchinnikov, N. M. Kosti′c, *Inorg. Chim. Acta* **1996**, *243*, 9−13.
[68] S. J. Lippard, J. M. Berg, *Principles of Bioinorganic Chemistry*, University Science Books, Mill Valley, California, **1994**.
[69] W. Weigand, G. Bosl, B. Vondielingen, K. Gollnick, *Z. Naturforsch. B* **1994**, *49*, 513−518.
[70] W. Weigand, R. Wunsch, *Chem. Ber.* **1996**, *129*, 1409−1419.
[71] A. D. Ryabov, V. N. Goral, L. Gorton, E. Csöregi, *Chem. Eur. J.* **1999**, *5*, 961−967.
[72] A. Hessler, O. Stelzer, H. Dibowski, K. Worm, F. P. Schmidtchen, *J. Org. Chem.* **1997**, *62*, 2362−2369.
[73] J. Meienhofer, *The Mixed Carbonic Anhydride Method of Peptide Synthesis*, Academic Press, London, **1979**.
[74] *International Tables for Crystallography*, Kynoch Press, Birmingham, **1974**.

Received June 17, 1999
[I99223]

Compared Reductive Chemistry of Molybdenocene and Indenyl-Substituted Complexes

Maria J. Calhorda,[a,b] Carla A. Gamelas,[a,c] Carlos C. Romão,*[a] and Luís F. Veiros[d]

Keywords: Indenyl complexes / Cyclopentadienyl complexes / Molybdenocene / Ring slippage / Molybdenum / DFT calculations

Reduction of [IndCpMo(L)Br]Br (L = **1a**, CO; **2**, NCMe) with Cp_2Co in the presence of two equivalents of the ligand L′ gives the ring-slipped neutral complexes [(η^3-Ind)CpMoL′$_2$] (L′ = **5**, CO; **6**, 1/2 dppe; **7**, PMe_3; **8**, $P(OMe)_3$; **9**, CN*t*Bu) in good yield. Products **7**, **8**, and **9**, but not [IndCpMoL′], are also formed in the presence of only 1 equivalent of L′ in modest yields. In the case of the reduction of [IndCpMo(L)Br]Br [L = **2**, NCMe; **3a**, CN*t*Bu; **4**, $P(OMe)_3$] mixtures of the complexes, [(η^3-Ind)CpMoL$_2$] (**8**, **9**) and [(η^5-Ind)CpMoL] [L = **11**, $P(OMe)_3$; **12**, CN*t*Bu] were obtained. The only product of formal type [(η^5-Ind)CpMoL] that could be prepared by these methods was the alkyne complex [(η^5-Ind)CpMo(η^2-PhC≡CPh)] (**10**). These results contrast with the well-known reductions of similar bis-cyclopentadienyl cations [Cp_2Mo(L)Br]$^+$, which produce [Cp_2MoL] complexes under the same conditions. The reduction of the dications [Cp_2MoL_2][BF_4]$_2$ [L = CO; $P(OMe)_3$] with Cp_2Co is now reported to afford the neutral complexes [CpMo(η^3-C_5H_5)(CO)$_2$] (**13**) and [Cp_2Mo($P(OMe)_3$)] (**14**), respectively, showing that the stability of the ring-slipped complexes is dependent on the other ligands. From DFT and EHMO calculations used to probe the bonding and the energetics of these ring slippage processes it is concluded that weak π acceptor ligands favour η^5-Ind → η^3-Ind slippage and disfavour η^5-Cp → η^3-Cp slippage at the $CpMoL_2$ fragment. Redox-induced ring slippages involve very similar energies for both indenyl and cyclopentadienyl complexes and should be able to produce more examples of the otherwise rare η^3-Cp coordination mode.

Introduction

We have recently reported the synthesis of a variety of indenyl analogues of molybdenocene and tungstenocene in the +4 oxidation state, [$IndCpMX_2$].[1] The chemistry of these complexes follows closely the chemistry of the corresponding metallocene derivatives, [Cp_2MX_2]. The most interesting reaction type observed so far is the facile, reversible, chemical and electrochemical reduction of several dications [$IndCpML_2$]$^{2+}$ to the ring-slipped neutral, 18e complexes [(η^3-Ind)CpML$_2$] (L = CO, dppe, PMe_3, bipy, CN*t*Bu).[2] Although the strictly parallel reductions of the corresponding metallocene dications [Cp_2ML_2]$^{2+}$ have never been reported, the general rule holding for the reductions of Cp_2M^{IV} complexes is the formation of Cp_2ML species, e.g. L = CO,[3] CNR,[4] (η^2-NCMe),[5] (η^2-C_2Ph_2),[3][6] (η^2-C_2H_4),[7] PR_3,[8] (η^2-CO_2).[9] Such species have played a central role in revealing the chemistry of the very reactive and electron-rich [Cp_2M^{II}] fragment (M = Mo, W). The only exception is the reduction of [Cp_2WCl(CO)]$^+$ under a CO atmosphere, to give [(η^3-Cp)CpW(CO)$_2$].[3b]

With the aim of continuing the comparative study of the chemistry of the [Cp_2Mo] and [IndCpMo] fragments, we set out to synthesize the Mo^{II} mixed-ring complexes [IndCpMoL] that might give access to the as yet unstudied [$IndCpMo^{II}$] fragment. As described in the present paper, in spite of the numerous different synthetic variations used, IndCpMo(η^2-C_2Ph_2) was the only such complex that we could isolate. Instead, the unexpectedly effective synthesis of ring-slipped complexes of type [(η^3-Ind)CpMoL$_2$] took place even at Mo/L = 1:1 ratios, suggesting that the electron-rich complexes [IndCpMoL] undergo facile ligand addition in contrast to their Cp_2MoL analogues. The comparison of the behaviour of the [IndCpMo] and [Cp_2Mo] fragments towards ring slippage was then studied by reduction of the corresponding cationic Mo^{IV} complexes under similar conditions. DFT and EHMO calculations were used to study these ring slippages and provide the energetic relationships between [(η^5-Cp′)CpMoL$_2$]$^{2+}$, [(η^3-Cp′)CpMoL$_2$], and [(η^5-Cp′)CpMoL] (Cp′ = Cp, Ind) complexes.

Results

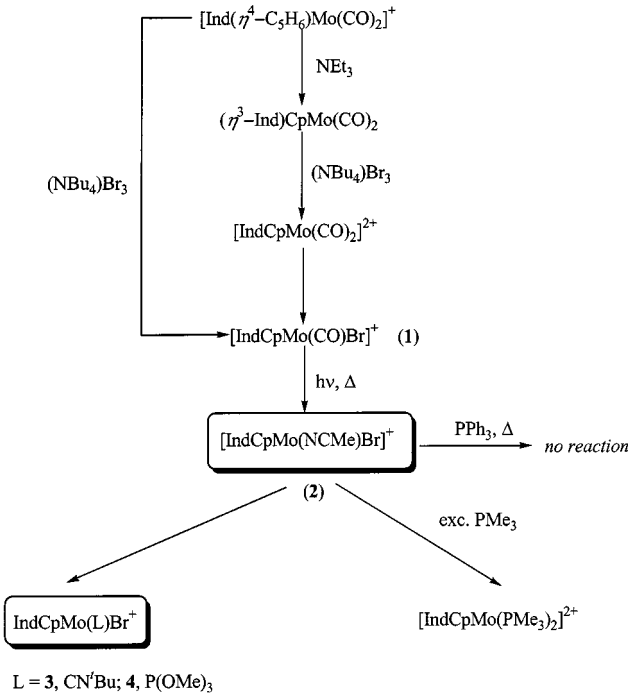
Chemical Studies

In order to prepare the target [IndCpMoL] complexes we considered the methods that are well established for the synthesis of [Cp_2MoL] complexes. From all these methods, reductive dehalogenation from [IndCpMo(L)Br]$^+$ [L = **1**, CO; **2**, NCMe; **3**, CN*t*Bu; **4**, $P(OMe_3)_3$] was selected as the most practical method since we improved a convenient syn-

[a] Instituto de Tecnologia Química e Biológica, Quinta do Marquês, EAN,
Apt 127, P-2781-901 Oeiras, Portugal
[b] Departamento de Química e Bioquímica, Faculdade de Ciências da Universidade de Lisboa,
P-1749-016 Lisboa, Portugal
[c] Escola Superior de Tecnologia, Instituto Politécnico de Setúbal, Vale de Estefanilha, P-2900 Setúbal, Portugal
[d] Centro de Química Estrutural, Instituto Superior Técnico, P-1096 Lisboa Codex, Portugal

 © WILEY-VCH Verlag GmbH, D-69451 Weinheim, 2000 1434−1948/00/0202−331 $ 17.50+.50/0

thesis of the appropriate starting halides **1** and **2**, whose congeners $[IndCpMo(L)X]^+$ (X = Cl, I) are known.[1] In fact, oxidation of $[(\eta^3\text{-Ind})CpMo(CO)_2]$ (**5**) with $(NBu_4)Br_3$ leads to the immediate precipitation of the white oxidation product $[IndCpMo(CO)_2]Br_2$, identified by comparison of its IR and ^{1}H-NMR spectra with those of an authentic sample;[1] further stirring of the suspension leads to substitution of one carbonyl ligand, affording [IndCpMo(CO)Br]Br (**1a**), as depicted in Scheme 1. The oxidation of $[IndMo(\eta^4\text{-}C_5H_6)(CO)_2]BF_4$ with $(NBu_4)Br_3$ is even better because it avoids the preparation of **5** and leads to $[IndCpMo(CO)Br]BF_4$ (**1b**) in 70% yield.



Scheme 1. Reaction sequence for the synthesis of the cationic $IndCpMo^{(IV)}$ derivatives

Refluxing **1a** in NCMe solution under visible light irradiation gave rise to complex **2** in 90% yield. Simple substitution of NCMe in **2** with CN*t*Bu and $P(OMe)_3$ afforded **3** and **4**. The characterization of these complexes was straightforward from their ^{1}H-NMR data and elemental analysis. The ^{1}H-NMR pattern of the indenyl ligand in **1**, **3**, and **4** is typical for η^5-coordination in asymmetric complexes, as resonances are doubled and occasionally superimposed, because the (normally equivalent) pairs of indenyl protons are now diastereotopic and, therefore, exhibit different chemical shifts. Complex **2**, on the other hand, shows only one resonance for protons $H^{1/3}$, probably due to a fast isomerization process in solution. This behaviour was also observed in the previously reported complex $[IndCpMo(NCMe)Cl]BF_4$.[1] Surprisingly, no reaction occurred between **2** and PPh_3, probably due to steric hindrance; the congener complex $[IndCpMo(PPh_3)Cl]BF_4$ has been prepared by the facile reaction of the dichloride $[IndCpMoCl_2]$ with PPh_3 in the presence of $TlBF_4$.[1] Reaction of **2** with PMe_3 under mild conditions readily gave the reported dication $[IndCpMo(PMe_3)_2]^{2+}$.[2]

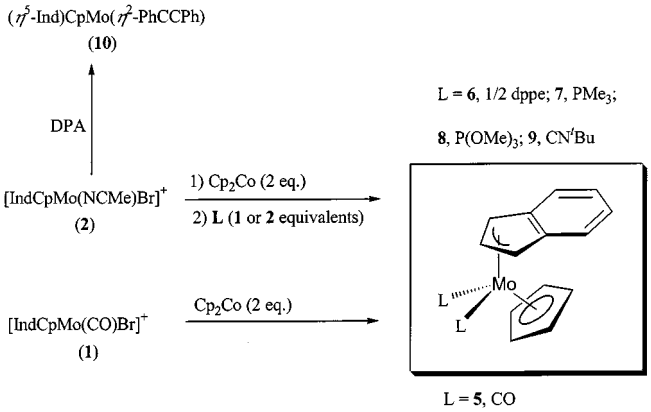
Reduction of [IndCpMo(CO)Br]Br with Cp_2Co gave a dark solution. The hexane-soluble extract is $[(\eta^3\text{-Ind})CpMo(CO)_2]$ (**5**), identified by comparison of its IR and ^{1}H-NMR spectra with those of an authentic sample.[1] The IR spectrum displays two characteristic stretching vibrations of the *cis* carbonyl ligands, at $\tilde{\nu}$ 1959 and 1888 cm^{-1}. We could not observe the formation of the intermediate complex IndCpMo(CO) and the yield of the reaction is relatively low (40%).

The metallocene fragments $[Cp_2M^{II}]$ (M = Mo, W) produce one of the most striking examples of side-on coordinated nitriles in complexes $[Cp_2M(\eta^2\text{-NCMe})]$.[5] These complexes are readily available by reduction of $[Cp_2MX_2]$ and provide one of the most useful starting materials for the preparation of other $[Cp_2ML]$ complexes, since the η^2-NCMe ligand is quite labile.[4][8]

We therefore attempted the reduction of $[IndCpMo(NCMe)Br]^+$ (**2**) with Cp_2Co in acetonitrile solvent. A brown-red solution was formed but, in spite of many attempts, we were unable to isolate any complex from the reaction mixture. Decomposition products were similarly obtained in the reduction of $[IndCpMoCl_2]$ with Na/Hg in NCMe, the method used for the synthesis of the $[Cp_2Mo(\eta^2\text{-NCMe})]$ analogues.

However, the chemical evidence described below points to the formation of some labile acetonitrile derivative of the fragment [IndCpMo], which can only be formulated as $[(\eta\text{-Ind})CpMo(NCMe)_x]$, that decomposes upon loss of NCMe solvent.

Treatment of the brown-red solutions of this compound with *one equivalent* of several ligands (L) affords the ring-slipped neutral complexes $[(\eta^3\text{-Ind})CpMoL_2]$ [**7**, L = PMe_3; **8**, L = $P(OMe)_3$; **9**, L = CN*t*Bu] instead of the intended congeners [IndCpMoL] (as depicted in Scheme 2). Compounds **7**–**9** are formed in < 50% yields (ca. 30%), as expected. In the case of PPh_3 no tractable product was obtained.



Scheme 2. Reductive reactions of the $IndCpMo^{(IV)}$ cations

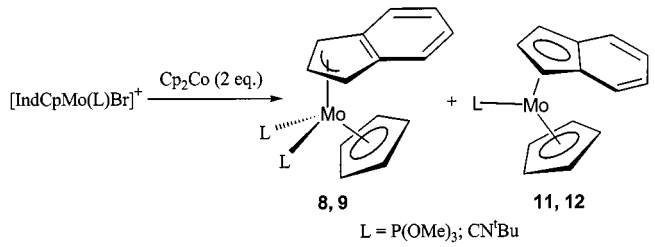
On the other hand, reaction with 1 equivalent of diphenylacetylene (DPA) produces $[(\eta^5\text{-Ind})CpMo(\eta^2\text{-PhC}\equiv\text{CPh})]$ (**10**) in 80% yield. The analytical and ^{1}H-NMR

data agree with a structure with η^5-indenyl and only one DPA molecule, which is the same type of structure present in the analogous $[Cp_2Mo(\eta^2\text{-PhC}{\equiv}CPh)]$.[10] In fact, **10** presents the ^{1}H-NMR chemical shift pattern expected for η^5-coordination of the indenyl ligand in a neutral complex, with two multiplets for benzenoid protons H^{5-8} (δ = 6.93−6.90 and δ = 6.75−6.72), a triplet for H^2 (δ = 5.53), a doublet for $H^{1/3}$ (δ = 3.85), and a singlet for the Cp ring (δ = 4.21). Another reaction leading to **10** is discussed below.

Of course, the yields of complexes **7** to **9** increase to much higher values (ca. 50−90%) when *two equivalents* of the ligand L are used. Reaction with dppe affords [(η^3-Ind)CpMo(dppe)] (**6**). In the case of P(^{i}Pr)$_3$ (2 equiv.) no tractable product was obtained.

Complexes **6**−**9** have been previously prepared by reduction of the respective dications $[IndCpMoL_2]^{2+}$ with Cp_2Co;[2][11] reported preparations of **6** and **8** also include deprotonation of the cyclopentadiene cations $[IndMo(\eta^4\text{-}C_5H_6)(dppe)]BF_4$ and $[IndMo(\eta^4\text{-}C_5H_6)(P(OMe)_3)_2]BF_4$ with NEt_3.[2][11]

Reduction of [IndCpMo(L)Br]Br complexes [L = **3a**, CN*t*Bu; **4**, P(OMe)$_3$] produced mixtures of the respective [(η^5-Ind)CpMoL] [L = **11**, P(OMe)$_3$; **12**, CN*t*Bu] and [(η^3-Ind)CpMoL$_2$] (**8** and **9**), as depicted in Scheme 3. All attempts to separate the two products were unsuccessful due to their similar solubility properties. However, their presence in the mixtures is easily recognized by ^{1}H-NMR spectroscopy; *trihapto* and *pentahapto* complexes present distinctly different patterns of chemical shifts.[2]



Scheme 3. Reduction of the cations $[IndCpMo(L)Br]^+$

Complex [(η^5-Ind)CpMo(CN*t*Bu)] (**12**) presents the expected ^{1}H-NMR pattern for η^5-coordination mode of the indenyl ligand in a neutral complex. Signals in the ^{1}H-NMR spectrum of the mixture in C_6D_6 related to complex [(η^3-Ind)CpMo(CN*t*Bu)$_2$] are in agreement with those of an authentic sample (see Experimental Section).[2] A similar assignment was made for the resonances in the mixture of **11** and **8** (see Experimental Section).

In order to be able to compare the properties of the Cp_2M and IndCpM complexes, the reduction of some dications $[Cp_2ML_2]^{2+}$ was carried out under the same conditions reported for the reduction of several mixed-ring dications $[IndCpML_2]^{2+}$.[2] Somewhat unexpectedly, the previously reported neutral complex [(η^3-Cp)CpMo(CO)$_2$][1] (**13**) was now obtained, in high yield (80%), upon reduction of $[Cp_2Mo(CO)_2]^{2+}$ with Cp_2Co. The reaction of $[Cp_2Mo(P(OMe)_3)_2]^{2+}$ under similar conditions affords [Cp_2Mo(P(OMe)$_3$)] (**14**), instead of [(η^3-Cp)CpMo(P(OMe)$_3$)$_2$]. This behaviour differs from that of the indenyl congener $[IndCpMo(P(OMe)_3)_2]^{2+}$, which is readily reduced to the neutral complex [(η^3-Ind)CpMo(P(OMe)$_3$)$_2$] (**8**).[11] The dication $[Cp_2Mo(CNtBu)_2]^{2+}$ (**15**) proved to be resistant to reduction by both Cp_2Co and Na/Hg.

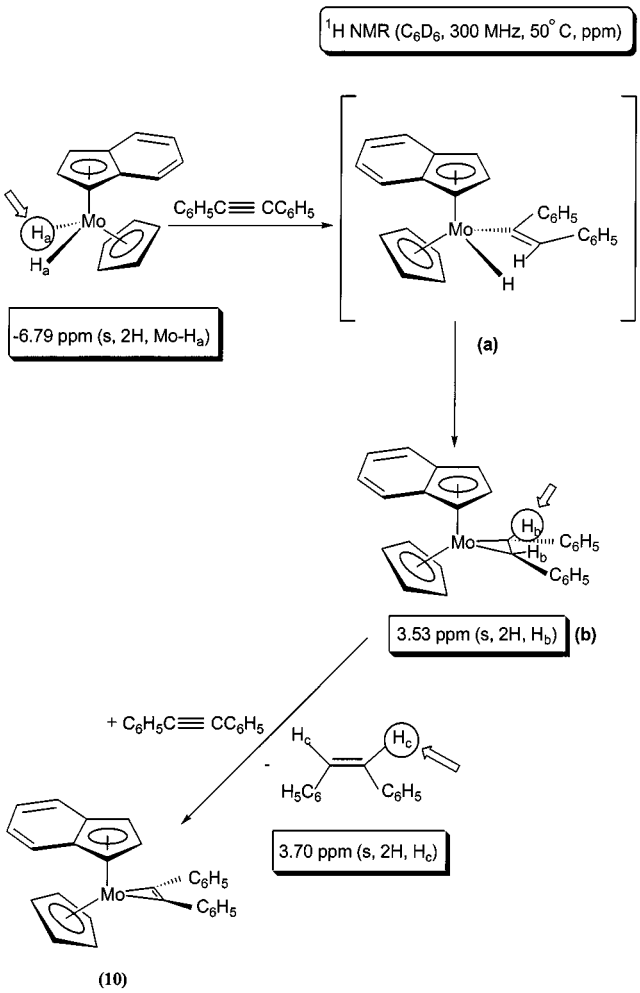
The complex [(η^5-Ind)CpMo(η^2-PhC≡CPh)] (**10**), the only one in which the stoichiometry [IndCpMoL] is preferred over the ring-slipped complexes of stoichiometry [(η^3-Ind)CpMoL$_2$], is the final product of DPA insertion across the Mo−H bonds in $[IndCpMoH_2]$. Nakamura and Otsuka,[12] as well as Herberich and Okuda,[13] studied the analogous reaction between DPA and $[Cp_2MoH_2]$. Assuming the same mechanism, Scheme 4 summarizes our observations and relevant chemical shifts for this experiment. Reaction of the dihydride and DPA in a 1:2 ratio was monitored by ^{1}H-NMR spectroscopy in C_6D_6. After 1 h at room temperature no reaction had occurred. At 50°C, the resonances corresponding to the protons of stilbene, both coordinated (H_b at δ = 3.53 in intermediate **b**; Scheme 4) and free (H_c at δ = 3.70), immediately appeared. The vinyl-hydride intermediate **a** could not be observed because of the very fast second insertion step. Signals at δ = 5.26 and δ = 4.21 can be ascribed to the Cp rings of **b** and **10**, respectively. After 3 h at 50°C neither $[IndCpMoH_2]$ nor the stilbene complex **b** were present (the former was monitored by its characteristic hydride signal at δ = − 6.79 and the latter by its resonance at δ = 3.53), revealing the presence of **10** and some free DPA.

Theoretical Studies

The previously described experiments indicate that the [IndCpMo] fragment produces only with difficulty the monoligand [IndCpMoL] derivatives, leading preferentially to the slipped [(η^3-Ind)CpMoL$_2$] species. On the other hand, for the [Cp_2MoL] complexes a different pattern is observed. [Cp_2MoL] complexes seem favoured over [(η^3-Cp)CpMoL$_2$], the only example of the latter being [(η^3-Cp)CpMo(CO)$_2$], which is easily accessible by reduction of its dicationic precursor.

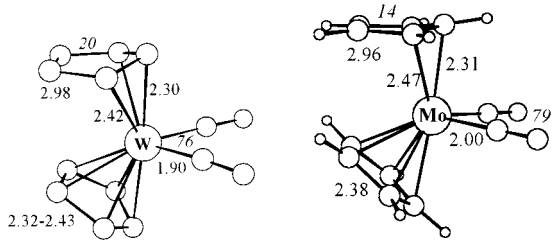
We therefore performed DFT calculations[14] in order to find out the relative stabilities of these types of compounds, both for the biscyclopentadienyl and the indenylcyclopentadienyl systems. We started the calculations for models with L = CO but, in order to understand the different reactivities of the systems as a function of the ligand, the same study was repeated for L = P(OMe)$_3$.

The geometry of the following six compounds was optimized: [(η^5-Ring)CpMo(CO)$_2$]$^{2+}$ (**I**), [(η^3-Ring)CpMo(CO)$_2$] (**II**) and [(η^5-Ring)CpMo(CO)] (**III**) (Ring = **a**, Ind; **b**, Cp). The indenyl derivatives **Ia** and **IIa** are studied in detail using DFT calculations in another work,[11] and the reliability of the theoretical approach has been checked by comparing the optimized geometries with the available structures of the indenyl derivatives.[1] The remaining indenyl complex



Scheme 4. Insertion of DPA across the Mo−H bonds

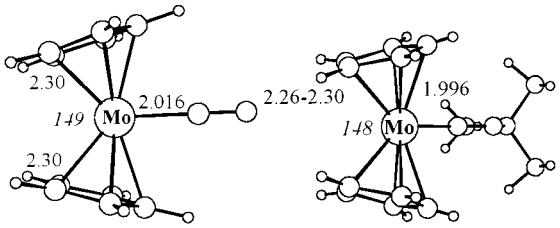
type (**IIIa**) has not been isolated and the optimized geometry cannot be compared with that of a known species. Concerning the biscyclopentadienyl complexes, there is a structure of the tungsten analogue of **IIb** [(η^3-Cp)CpW(CO)$_2$][15] and of the *tert*-Butylnitrile derivative of **IIIb** [$Cp_2Mo(CNtBu)$],[4] which can be used for comparison. The molybdenum and tungsten compounds are usually very similar as far as their geometric characteristics are concerned and therefore they can be compared. The main features of the geometry of [(η^3-Cp)CpW(CO)$_2$] and those of our optimized [(η^3-Cp)CpMo(CO)$_2$] are shown in Scheme 5 (left and right, respectively).



Scheme 5. Relevant distances and angles in [(η^3Cp)CpW(CO)$_2$] (left, exp.) and [(η^3Cp)CpMo(CO)$_2$] (right, calcd.)

The agreement is very good, both for distances and angles, except for the folding of the Cp ring, which is 6° less in the model than in the tunsgten compound. It should be remembered that, in the optimization procedure, the C−C and C−H distances of one Cp ring were kept fixed, with only the position of the ring being allowed to change. The second ring was totally optimized, in order to allow it to become η^3 if necessary (it always started as η^5).

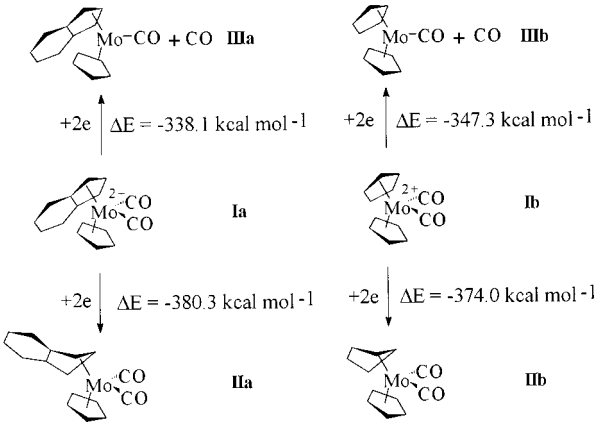
There is no carbonyl complex of type **III** structurally characterized, and the most similar to [$Cp_2Mo(CO)$] is [$Cp_2Mo(CNtBu)$],[4] the isonitrile ligand being also a π-acceptor. There are not so many parameters to compare in this situation, but the agreement between Mo−C distances and the Cp−Mo−Cp angle is acceptable, considering that it is not exactly the same species (Scheme 6).



Scheme 6. Relevant distances and angles in [$Cp_2Mo(CO)$] (left, calcd.) and [$Cp_2Mo(CNtBu)$] (right, exp.)

Finally, compound **I** $[Cp_2Mo(CO)_2]^{2+}$ has not been structurally characterized, but belongs to the large family of the [Cp_2MoL_2] complexes.[16] Both the Mo−C distances (ca. 2.35 Å), the C−Mo−C angle (139°) and the Cp−Mo−Cp angle (88°) fit in the general pattern.

The relative energies of the six compounds are given in Scheme 7, taking into account that to make the numbers directly comparable we added one molecule of free CO on going from **I** to **III**.



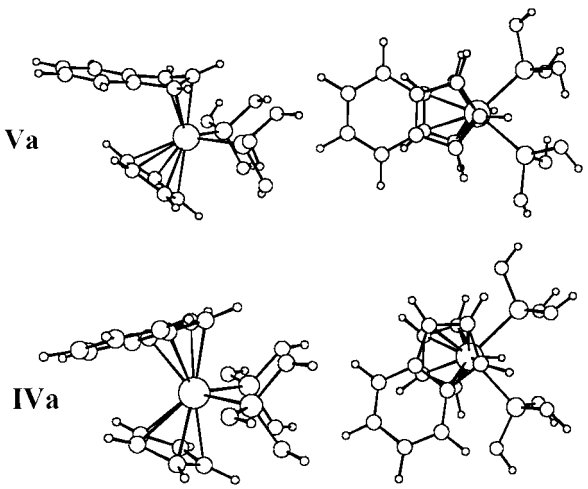
Scheme 7. Relative DFT energies of CO complexes

The energies of the final products are much lower for the η^3 species than for the monoligand derivative, both for Cp and Ind derivatives. Even taking into account the fact that

entropy should favour **IIIa** and **IIIb**, that difference is significant. Indeed, the experimental results show the formation of this species when the ligands are carbonyls, i.e. strong π-acceptors. When carbonyls are replaced by other ligands, such as phosphites, only the monoligand complex is formed for Ring = Cp and a mixture of both species is detected for the Ind system.

We therefore also performed DFT calculations for the corresponding phosphite complexes [L=P(OH)$_3$], [(η^5-Ring)CpMo(L)$_2$]$^{2+}$ (**IV**), [(η^3-Ring)CpMo(L)$_2$] (**V**), and [(η^5-Ring)CpMo(L)] (**VI**) (Ring = **a**, Ind; **b**, Cp), using P(OH)$_3$ instead of P(OMe)$_3$. The geometries of the six complexes were fully optimized.

The calculations on **IVa** and **Va** are also been discussed in another work, along with the description of the X-ray structures of the parent phosphite compounds.[11] It might be important to stress that the conformation of the indenyl ring in the η^3-coordination is different from that in the η^5-coordination. This is easily seen in Scheme 8, where the side and top views of [(η^5-Ind)CpMo(L)$_2$]$^{2+}$ (**IVa**) and [(η^3-Ind)CpMo(L)$_2$] (**Va**) are shown.

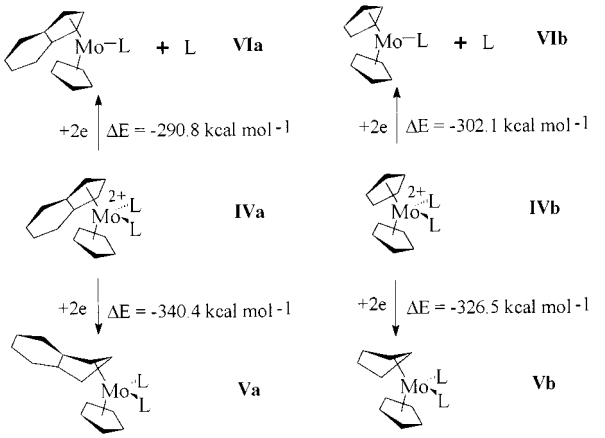


Scheme 8. Side (left) and top (right) views of the structures of complexes **Va** and **IVa**

For the η^3-Ind derivative, the ring is slipped away from the two L (phosphite) ligands and lies trans to them. The folding is plainly seen. The change of coordination to η^5 results in a planar ligand, so that the Ind ring approaches the Cp ring. Steric repulsion forces a rotation of the ring. This change in conformation of the ligand accompanying a change of hapticity has already been observed and analysed in another family of compounds.[17] The distances and angles in the geometries of the calculated complexes are within the range of expected values.

The relative energies of the six species are given in Scheme 9, the energy of **V** being adjusted with the energy of free P(OH)$_3$, as performed previously for the CO series of compounds.

The most striking feature is the similarity of Schemes 7 and 9, at first sight, and the very small difference of energy in the parallel redox processes that form [(η^3-Ind)CpMoL$_2$] and [(η^3-Cp)CpMoL$_2$] from their corresponding cations. A further comparison of these values is found in the Discussion. However, the understanding of the relative stability of the several species involved, namely, the reason why η^3-Ring derivatives are more stable for indenyl than Cp and why carbonyls stabilize η^3-Cp rings, can be traced qualitatively by extended Hückel calculations performed on the same models. The first important aspect when comparing Cp and Ind is that η^5-Cp binds more strongly than η^5-Ind. The calculated bonding energy (DFT calculation) between Cp$^-$ or Ind$^-$ and the CpMo(CO)$^+$ fragment is −237.5 and −221.4 kcal mol^{-1}, respectively. The reason is clearly seen on the molecular orbital diagram of Figure 1, where one compares the binding of each of the two rings to the CpMo(CO)$^+$ fragment.



Scheme 9. Relative DFT energies of P(OH)$_3$ complexes

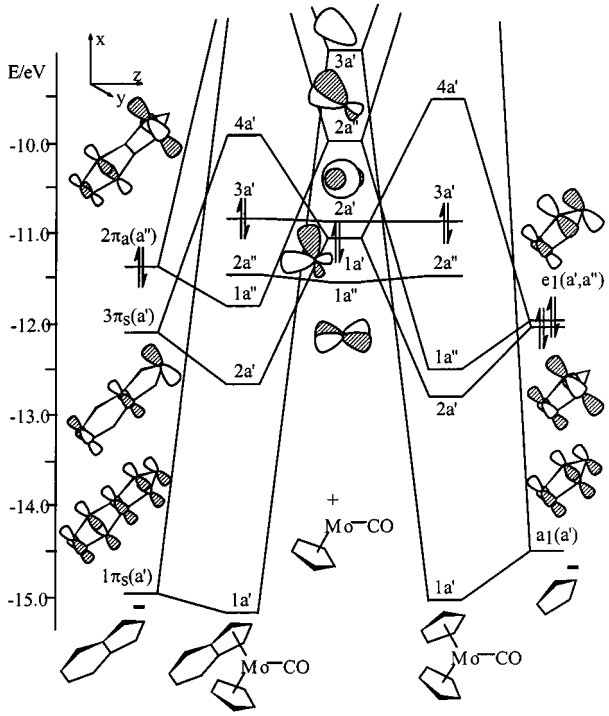
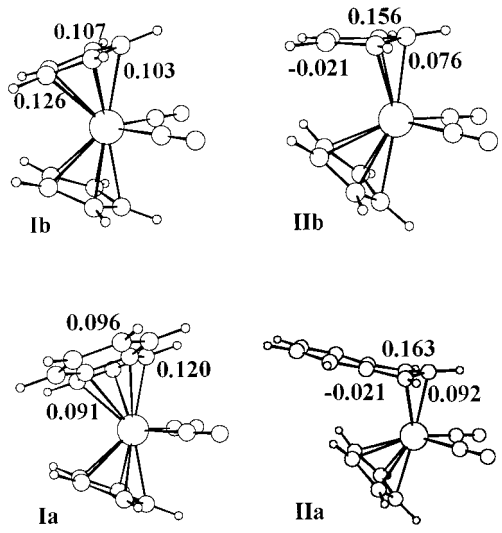


Figure 1. Molecular orbital diagram for the interaction between one η^5-Ind ring (left)/η^5-Cp (right) and the CpMo(CO)$^+$ fragment

Both rings formally donate three pairs of electrons into empty levels of the metal fragment. These electrons come from the lowest energy, totally symmetric a_1, and from the e_1 set in the Cp. The a_1 level is similar for the indenyl (lower energy, owing to the largest number of the carbon atoms and to bonding interactions), but those corresponding to the e_1 set are different, as not all the carbon atoms from the C_5 ring contribute to the orbital, and their contributions are smaller, as sketched on the left side of the drawing and discussed elsewhere.[18] As a result, the overlap between Ind−CpMo(CO) is smaller (0.45) than between Cp−CpMo(CO) (0.58) and the resulting bonding molecular orbitals have higher energies (1a″ is 18.5 kcal mol^{-1} higher and 2a′ is 2.3 kcal mol^{-1} higher for Ind, see diagram in Figure 1).

The same diagram can help us to understand why a η^3-coordination mode is more favorable for the indenyl ring. Upon bending, only three carbon atoms remain coordinated to the metal. For the Cp ring this is an effective loss of overlap, as the five carbon atoms were all strongly bound to the metal, while for the indenyl unit the two hinge atoms, which do not participate in all indenyl π orbitals, are much less affected by this distortion. This can be seen by the Mo−C overlap populations in Scheme 10, where we compare compounds **I** and **II**.



Scheme 10. Mo−C overlap populations (EHMO) in complexes **Ia,b** and **IIa,b**

The overlap populations between fragments lead us to the same conclusion, but in a different way. In fact, the Ring-[CpMo(CO)$_2$] overlap populations are 0.54 for Ring = η^5-Cp, 0.40 for Ring = η^5-Ind, 0.26 for Ring = η^3-Cp, and 0.30 for Ring = η^3-Ind. Another contribution to this behaviour is that the energy required to distort Cp is larger than that needed to distort Ind, as in the latter the orbitals of the resulting benzene ring are much stabilized relative to those of the ethylene formed from Cp. Brintzinger and co-workers attempted to understand these problems,[15c] but the lack of structural information at the time makes the results of their calculations difficult to compare.

When the carbonyl groups are replaced by other ligands, which are not (or are weaker) π-acceptors, the small stabilization provided to the bonding of the η^3-Cp ring by back-donation to the carbonyls is lost, and this explains the much higher energy of the comparable phosphite derivative. Other derivatives become more competitive.

Discussion

[Cp$_2$MoL] complexes are well known for being very electron-rich d^4 species. Their chemistry is, therefore, essentially characterized by oxidative addition reactions to the carbene-like metal fragment, as well as protonation and methylation with Mo−H and Mo−CH$_3$ formation, both of which reflect the nucleophilicity and basicity of the metal centre. Ligand substitution, L for L′, has also been reported for several complexes. Replacement of Cp by indenyl was expected to give 18e complexes with overall analogous reactivity since they would present the same type of high energy metal-based lone pairs. However, the results reported above point to the appearance of a new type of reactivity around [IndCpMoL] complexes. In fact, these complexes failed to be prepared by reductive methods analogous to those employed for [Cp$_2$MoL] and, even under stoichiometries favouring the formation of [IndCpMoL], ring-slipped [(η^3-Ind)CpMoL$_2$] complexes were always observed. The only exceptions were found for the diphenyl acetylene complex, [IndCpMo(η^2-C$_2$Ph$_2$)], *tert*-Butyl isocyanide and phosphite complexes [IndCpMo(CN*t*Bu)] and [IndCpMo(P(OMe)$_3$)], which are formed simultaneously with [(η^3-Ind)CpMo(CN*t*Bu)$_2$] and [(η^3-Ind)CpMo{P(OMe)$_3$}], respectively.

These results mean that the metal centre in [IndCpMoL] complexes readily accepts 2e donors according to the Equation (a).

$$[\text{IndCpMoL}] + \text{L} \rightleftharpoons [(\eta^3\text{-Ind})\text{CpMoL}_2] \quad \text{(a)}$$

In this equation the equilibrium seems to be shifted to the right hand side. For all that has been reported in the literature, the similar Equation (b) represents an equilibrium that is, in most cases, shifted to the left hand side.

$$[\text{Cp}_2\text{MoL}] + \text{L} \rightleftharpoons [(\eta^3\text{-Cp})\text{CpMoL}_2] \quad \text{(b)}$$

The only known exception is described in this work for L = CO. In general, these results are normal insofar as they fit in with the well established higher tendency of the indenyl ligand to undergo $\eta^5 \rightarrow \eta^3$ ring slippage when compared with the Cp ligand. However, the term tendency is qualitative and the very fact that there are unpredictable exceptions prompted us to attempt some quantification of the energetics involved in these ring slippages. The results of the

DFT calculations, which are summarized in schemes 7 and 9, can be written according to Equations (c)−(f).

$$[IndCpMo(CO)] + CO \rightleftharpoons [(\eta^3\text{-Ind})CpMo(CO)_2]\ \Delta E_1 = -42.2\ \text{kcal mol}^{-1} \quad (c)$$

$$[Cp_2Mo(CO)] + CO \rightleftharpoons [(\eta^3\text{-Cp})CpMo(CO)_2]\ \Delta E_2 = -26.7\ \text{kcal mol}^{-1} \quad (d)$$

$$[IndCpMo\{P(OH)_3\}] + P(OH)_3 \rightleftharpoons [(\eta^3\text{-Ind})CpMo\{P(OH)_3\}_2]\ \Delta E_3 = -49.6\ \text{kcal mol}^{-1} \quad (e)$$

$$[Cp_2Mo\{P(OH)_3\}] + P(OH)_3 \rightleftharpoons [(\eta^3\text{-Cp})CpMo\{P(OH)_3\}_2]\ \Delta E_4 = -24.4\ \text{kcal mol}^{-1} \quad (f)$$

From these energy differences, the following conclusions may be drawn:

(i) Both the indenyl and cyclopentadienyl ring slippages in Equations (a) and (b) are exothermic, but they are entropically disfavoured association processes (ΔE is negative in all equations).

(ii) The ring slippage of the indenyl complexes is more exothermic than that of the cyclopentadienyl congeners regardless of the nature of the ligand L ($|\Delta E_1| > |\Delta E_2|$; $|\Delta E_3| > |\Delta E_4|$).

(iii) Weaker π-acceptor ligands L favour the ring slippage of indenyl and disfavour the ring slippage of cyclopentadienyl, therefore widening the energy gap between the two similar transformations ($\Delta E_3 - \Delta E_4 = -25.1$ kcal mol^{-1}; $\Delta E_1 - \Delta E_2 = -15.4$ kcal mol^{-1}).

The last conclusion means that CO-containing fragments will level out the differences between indenyl and cyclopentadienyl slippage by facilitating the latter due to orbital stabilization of the η^3-Cp ligand, as shown in the EHMO studies. For the same reasons, indenyl slippages will be favoured in systems carrying weak π-acceptors and/or π-donors where the corresponding Cp slippages become strongly disfavoured. One might then set the value of ca. 15 kcal/mol as the lowest energy difference between a Cp and an indenyl ring slippage on the same fragment when it contains strong π-acceptor ligands. All other ligands will be less favourable for Cp ring slippage. This type of ligand dependence of the ring slippage has been experimentally observed and authenticated by DFT calculations for the reaction according to Equation (g) which takes place for L = NCMe but is thermodynamically forbidden for L = CNMe.[17]

$$[IndMo(CO)_2(L)_2]^+ + NCMe \rightleftharpoons [(\eta^3\text{-Ind})Mo(CO)_2(L)_2(NCMe)]^+ \quad (g)$$

Whereas the result of the second conclusion was largely expected due to the more facile ring slippages of indenyl relative to cylopentadienyl, the result of the first conclusion is not so obvious given the fact that the trihapto coordination of Cp has proven to be very difficult to achieve experimentally. We believe that one of the main difficulties is the need to overcome the entropy factor. The use of redox-induced ring slippage seems to be the most favourable method to achieve difficult ring slippages because it does not involve changes in the number of ligands in the coordination sphere. As a matter of fact, as depicted in Scheme 7, the reductions of the dications **Ia** and **Ib** to give the ring slipped products **IIa** and **IIb**, respectively, differ very little in energy (6.2 kcal mol^{-1}) and allow a simple synthesis of the thermally sensitive $[(\eta^3\text{-Cp})CpMo(CO)_2]$ complex. The mild conditions of the synthesis of $[(\eta^3\text{-Cp})CpW(CO)_2]$ by reduction of $[Cp_2W(CO)Cl]$ under a CO atmosphere (1 atm)[3b] are similar to our conditions and strongly contrast with the 100 atm of CO pressure necessary to prepare it from $[Cp_2W(CO)]$, according to Equation (b).[15b] Related observations were made for CO addition to $[Cp_2Cr(CO)]$.[15d] A classical example is the formation of the $[Ru(\eta^4\text{-}C_6R_6)(\eta^6\text{-}C_6R_6)]$ by reduction of its dicationic precursor $[Ru(\eta^6\text{-}C_6R_6)_2]$,[19a] but there are many other examples of these redox-induced slippages.[2][19] The formation of the ring slipped product **Vb** might appear likely from our calculations, as ΔE_4 is not too different from ΔE_2. The fact that such product has never been detected may be related to kinetic factors.

The examples reported in this work show the remarkable capacity of the $CpMo(CO)_2$ fragment to stabilize rather elusive trihapto-coordinated hydrocarbon ligands like η^3-Cp or the exocyclic-coordination of the fluorenyl ligand in $[(\eta^3\text{-}C_{13}H_9)(Ind)Mo(CO)_2]$.[20] The only examples of a different behaviour were the complexes $[IndCpMo(\eta^2\text{-}C_2Ph_2)]$ and the *tert*-Butyl isocyanide complex [IndCpMo(CN*t*Bu)]. We believe that the formation of the latter is favoured not only by the fact that CN*t*Bu is a good π-acceptor but also because $[(\eta^3\text{-Ind})CpMo(CNtBu)_2]$ is a rather bulky species. On the other hand, the coordination of the acetylene molecule may involve significant oxidative addition as in the analogous $[Cp_2Mo(\eta^2\text{-}C_2Ph_2)]$.[10] In this case the complex may be better considered as a Mo^{IV} species where no ring slippage is expected to occur.

Experimental Section

General: All experiments were carried out under dry nitrogen using Schlenk techniques. Solvents were dried by standard procedures (tetrahydrofuran, diethyl ether, toluene, and pentane over Na/benzophenone ketyl; dichloromethane, and acetonitrile with CaH_2), distilled under argon and kept over 4-Å molecular sieves (3 Å for NCMe). − Microanalyses were performed in our laboratories (ITQB). − ^{1}H NMR spectra were obtained with a Bruker AMX 300 spectrometer. − Infrared spectra were recorded with a Perkin−Elmer 457 and with a Unican Mattson Mod 7000 FTIR spectrophotometer using KBr pellets. − PMe_3,[21] $[(\eta^3\text{Ind})\text{-}CpMo(CO)_2]$, $[Ind(\eta^4C_5H_6)Mo(CO)_2]BF_4$, $[IndCpMo(NCMe)\text{-}Cl]BF_4$, $[IndCpMoH_2]$, $[Cp_2Mo(CO)_2][BF_4]_2$,[1] $[Cp_2Mo(P(OMe)_3)_2][BF_4]_2$[22] were prepared as described previously.

Preparation of [IndCpMo(CO)Br]Y (1). − Method (a): Treatment of a solution of $[(\eta^3\text{-Ind})CpMo(CO)_2]$ (0.45 g, 1.35 mmol) in CH_2Cl_2 with $(NBu_4)Br_3$ (0.65 g, 1.35 mmol) led to the immediate formation of a white precipitate of $[IndCpMo(CO)_2][Br]_2$. The mixture was stirred for 15 h and the purple precipitate of [IndCpMo(-CO)Br]Br (**1a**) was filtered off and washed with CH_2Cl_2. Yield: 60%. − **Method (b):** A solution of $[Ind(\eta^4\text{-}C_5H_6)Mo(CO)_2]BF_4$ (0.21 g, 0.50 mmol) in CH_2Cl_2 was treated with $(NBu_4)Br_3$ (0.24 g, 0.50 mmol) and stirred overnight. The violet precipitate of $[IndCpMo(CO)Br]BF_4$ (**1b**) was separated by filtration in 70% yield

and washed with CH_2Cl_2. – $C_{15}H_{12}Br_2MoO$ (464.01): calcd. C 38.82, H 2.61; found C 38.75, H 2.12. – Selected IR (KBr): $\tilde{\nu}$ = 3077, 2045 (*sv*, CO), 1539, 1413, 946, 856, 760 cm^{-1}. – ^1H NMR ([D_6]acetone, 300 MHz, room temp.): δ = 7.95 (m, 1 H, H^{5-8}), 7.74 (m, 2 H, H^{5-8}), 7.57 (m, 1 H, H^{5-8}), 7.12 (m, 1 H, H^{1-3}), 6.65 (t, 1 H, H^{1-3}), 6.45 (m, 1 H, H^{1-3}), 6.34 (s, 5 H, Cp).

Preparation of [IndCpMo(NCMe)Br]Br (2): A solution of [IndCpMo(CO)Br]Br (0.07 g, 0.15 mmol) in NCMe was refluxed and irradiated with a 60 Watt tungsten bulb for 5 h. The solution was evaporated to dryness and the residue efficiently extracted with CH_2Cl_2. The purple powder was obtained in 90% yield upon evaporation of the solvent. The product was purified by recrystallization from CH_2Cl_2/Et_2O. – $C_{16}H_{15}Br_2MoN$ (477.05): calcd. C 40.28, H 3.17, N 2.94; found C 40.48, H 3.49, N 3.32. – Selected IR (KBr): $\tilde{\nu}$ = 3100, 2317, 2278, 1427, 802, 758 cm^{-1}. – ^1H NMR (CD_3CN, 300 MHz, room temp.): δ = 7.35 [s (br), 4 H, H^{5-8}], 5.98 (t, 1 H, H^2), 5.83 (d, 2 H, $H^{1/3}$), 5.33 (s, 5 H, Cp), 2.12 (s, 3 H, CH_3).

Preparation of [IndCpMo($CNCMe_3$)X]Y (3). – Method (a): A solution of [IndCpMo(NCMe)Br]Br (0.11 g, 0.23 mmol) in CH_2Cl_2 was treated with excess CN*t*Bu (0.25 mL) and refluxed overnight. The solution was evaporated to dryness to afford the grey complex [IndCpMo($CNCMe_3$)Br]Br (**3a**) in 80% yield. This was recrystallized from CH_2Cl_2/Et_2O. – $C_{28}H_{39}Br_2MoN$ (645.38): calcd. C 52.11, H 6.09, N 2.17; found C 52.44, H 6.17, N 2.60. – Selected IR (KBr): $\tilde{\nu}$ = 3102, 2982, 2191, 1449, 1373, 1194, 1084, 845, 764 cm^{-1}. – ^1H NMR (CD_3CN, 300 MHz, room temp.): δ = 7.69–7.67 (m, 1 H, H^{5-8}), 7.56–7.54 (m, 2 H, H^{5-8}), 7.47–7.43 (m, 1 H, H^{5-8}), 6.02 (t, 1 H, H^{1-3}), 5.92 (t, 1 H, H^{1-3}), 5.75 [s (br), 1 H, H^{1-3}], 5.58 (s, 5 H, Cp), 1.60 (s, 9 H, CH_3). – **Method (b):** Treatment of a solution of [IndCpMo(NCMe)Cl]BF_4 (0.18 g, 0.40 mmol) in CH_2Cl_2 with excess CN*t*Bu (0.14 mL) at room temperature led to an immediate color change from green to dark violet. After stirring for 4 h the reaction mixture was concentrated to ca. 5 mL and Et_2O was added and caused the precipitation of the grey-violet complex [IndCpMo($CNCMe_3$)Cl]BF_4 (**3b**), which was recrystallized from CH_2Cl_2/Et_2O in 85% yield. – $C_{19}H_{21}BClF_4MoN$ (481.58): calcd. C 47.39, H 4.40, N 2.91; found C 47.48, H 4.25, N 3.41. – Selected IR (KBr): $\tilde{\nu}$ = 3095, 2982, 2193, 1449, 1373, 1194, 1084, 845, 764 cm^{-1}. – ^1H NMR ([D_6]acetone, 300 MHz, room temp.): δ = 7.89 (d, 1 H, H^{5-8}), 7.70–7.54 (m, 2 H, H^{5-8}), 7.40 (d, 1 H, H^{5-8}), 6.22 [s (br), 1 H, H^{1-3}], 5.97 (s, 1 H, H^{1-3}), 5.83 [s (br), 1 H, H^{1-3}], 5.79 (s, 5 H, Cp), 1.68 (s, 9 H, CH_3).

Preparation of [IndCpMo($P(OMe)_3$)Br]Br (4): A solution of [IndCpMo(NCMe)Br]Br (0.21 g, 0.43 mmol) in CH_2Cl_2 was treated with excess $P(OMe)_3$ (2.5 mL) and refluxed for 4 h. The solution was evaporated to dryness to afford the complex in 80% yield. The complex was recrystallized from CH_2Cl_2/Et_2O. – $C_{17}H_{21}Br_2MoO_3P$ (560.08): calcd. C 36.46, H 3.78; found C 36.65, H 3.49. – Selected IR (KBr): $\tilde{\nu}$ = 3082, 2942, 1425, 1541, 1134, 1042, 716 cm^{-1}. – ^1H NMR (CD_2Cl_2, 300 MHz, room temp.): δ = 7.45 (d, 1 H, H^{5-8}), 7.36–7.27 (m, 2 H, H^{5-8}), 7.21 (d, 1 H, H^{5-8}), 6.08 (m, 1 H, H^{1-3}), 5.72 (d, 1 H, H^{1-3}), 5.01 (t, 5 H, Cp), 4.50 [s (br), 1 H, H^{1-3}], 3.67 {d, 9 H, $P(OMe)_3$, [J_{PH} = 9.0 Hz]}.

Attempted Preparation of [IndCpMo(PMe_3)Br]Br: A solution of [IndCpMo(NCMe)Br]Br (0.20 g, 0.42 mmol) in CH_2Cl_2 was treated with excess PMe_3 (0.15 mL) and stirred for 3 h at room temperature. The pink precipitate of [IndCpMo(PMe_3)$_2$]Br_2 was filtered off and washed with CH_2Cl_2. Yield: 50%. – $C_{20}H_{30}Br_2MoP_2$ (588.16): calcd. C 39.91, H 5.02; found C 39.74, H 5.52. – Selected IR (KBr): $\tilde{\nu}$ = 3366, 3092, 2912, 1423, 1300, 965, 845, 779 cm^{-1}. – ^1H NMR (CD_3CN, 300 MHz, room temp.): δ = 7.72–7.68 (m, 4 H, H^{5-8}), 6.09 (m, 2 H, $H^{1/3}$), 5.48 (t, 1 H, H^2), 5.17 (t, 5 H, Cp, [$^3J_{PH}$ = 2.1 Hz]), 1.66–1.62 (t, 18 H, CH_3).

Preparation of Complexes [(η^3-Ind)CpMoL_2] (5–9): A suspension of [IndCpMo(L)Br]Br (L = **5**, CO; **6** to **9**, NCMe) in toluene (or NCMe) was treated with a solution of Cp_2Co (2 equiv.) in the same solvent at 0°C. Addition of the ligand (1 or 2 mol) caused an immediate change and after 2 h stirring at room temperature the solution was separated from [Cp_2Co]Br by filtration. The solvent was removed under vacuum and the residue extracted with Et_2O (3 × 30 mL). The product, which separated upon concentration and cooling of the extract, was identified by comparison of its IR and ^1H-NMR spectra with those of an authentic sample.[1,2,11]

Preparation of [(η^3-Ind)CpMo$(CO)_2$] (5): [IndCpMo(CO)Br]Br: 0.30 g, 0.65 mmol; Cp_2Co: 0.24 g, 1.29 mmol. Light protection. Purple microcrystalline complex (η^3-Ind)CpMo$(CO)_2$. Yield: 40%.

Preparation of [(η^3-Ind)CpMo(dppe)] (6): [IndCpMo(NCMe)Br]Br: 0.20 g, 0.42 mmol; Cp_2Co: 0.16 g, 0.84 mmol; dppe: 0.17 g, 0.42 mmol. Orange complex. Yield: 80%.

Preparation of [(η^3-Ind)CpMo$(PMe_3)_2$] (7). – (a) [IndCpMo(NCMe)Br]Br: 0.21 g, 0.44 mmol; Cp_2Co: 0.16 g, 0.87 mmol; PMe_3: 0.087 mL, 0.87 mmol. Orange complex. Yield, 90%. – **(b)** [IndCpMo(NCMe)Br]Br: 0.21 g, 0.44 mmol; Cp_2Co: 0.16 g, 0.87 mmol; PMe_3: 0.044 mL, 0.44 mmol. Orange complex. Yield: 45%.

Preparation of [(η^3-Ind)CpMo$(P(OMe)_3)_2$] (8). – (a) [IndCpMo(NCMe)Br]Br: 0.359 g, 0.752 mmol; Cp_2Co: 0.285 g, 1.504 mmol; $P(OMe)_3$: 2.5 mL, excess. Orange complex. Yield, 80%. – **(b)** [IndCpMo(NCMe)Br]Br: 0.179 g, 0.374 mmol; Cp_2Co: 0.142 g, 0.748 mmol; $P(OMe)_3$: 44 μL, 0.374 mmol. Orange complex. Yield: 40%.

Preparation of [(η^3-Ind)CpMo$(CNCMe_3)_2$] (9). – (a) [IndCpMo(NCMe)Br]Br: 0.27 g, 0.35 mmol; Cp_2Co: 0.13 g, 0.70 mmol; CN*t*Bu: 0.10 mL, excess. Reaction solvent: NCMe. Orange complex. Yield, 50%. – **(b)** [IndCpMo(NCMe)Br]Br: 0.27 g, 0.35 mmol; Cp_2Co: 0.13 g, 0.70 mmol; CN*t*Bu: 0.039 mL, 0.35 mmol. Reaction solvent: NCMe. Orange complex. Yield, 30%.

Preparation of [(η^5-Ind)CpMo(η^2-PhCCPh)] (10): A suspension of [IndCpMo(NCMe)Br]Br (0.20 g, 0.42 mmol) in toluene was treated with a solution of Cp_2Co (0.16 g, 0.84 mmol) in the same solvent at 0°C. Addition of DPA (0.075 mL, 0.42 mmol) caused an immediate change and after 2 h stirring at room temperature the solution was separated from [Cp_2Co]Br by filtration. The solvent was removed under vacuum and the residue extracted with Et_2O (3 × 30 mL). The garnet-like complex separated upon concentration and cooling of the extract to give 80% yield. – $C_{28}H_{22}Mo$ (454.43): calcd. C 74.01, H 4.88; found C 74.40, H 4.90. – Selected IR (KBr): $\tilde{\nu}$ = 3505, 3067, 1580, 1486, 1414, 1261, 824, 756 cm^{-1}. – ^1H NMR (C_6D_6, 300 MHz, room temp.): δ = 7.69 (d, Ph), 7.52–7.49 (m, Ph), 7.32 (t, Ph), 6.99–6.97 (m, Ph), 6.93–6.90 (m, 2 H, H^{5-8}), 6.75–6.72 (m, 2 H, H^{5-8}), 5.53 (t, 1 H, H^2), 4.21 (s, 5 H, Cp), 3.85 (d, 2 H, $H^{1/3}$).

Attempted Ppreparation of [(η^5-Ind)CpMoL] (11, 12) by Reduction of [IndCpMo(L)Br]Br: Treatment of a solution of [IndCpMo(L)Br]Br [L = $P(OMe)_3$, $CNCMe_3$] in NCMe with a solution of Cp_2Co (2 equiv.) in the same solvent, at 0°C, caused an immediate change. After 2 h stirring at room temperature the solvent was removed under vacuum and the residue extracted with toluene (3 × 30 mL). Upon evaporation of the solvent and washing of the residue with cold pentane, a mixture of two complexes, [(η^3-Ind)CpMoL_2] and [(η^5-Ind)CpMoL], was obtained. The previously

reported complexes [(η^3-Ind)CpMoL$_2$] were identified by comparison of the IR and ^{1}H-NMR spectra of the mixture with those of an authentic sample.[2][11]

Attempted Isolation of [(η^5-Ind)CpMo(P(OMe)$_3$)] (11): [IndCpMo{P(OMe)$_3$}Br]Br: 0.07 g, 0.125 mmol; Cp_2Co: 0.045 g, 0.25 mmol. Orange powder (mixture of two complexes). − Selected IR (KBr) $\tilde{\nu}$ = 3104, 2944, 1417, 1109, 1044, 1012, 808, 717 cm^{-1}. − ^{1}H NMR (C_6D_6, 300 MHz, room temp.); [(η^5-Ind)CpMo{P(OMe)$_3$}]: δ = 7.33−7.26 (m, 2 H, H$^{5-8}$), 7.06−7.00 (m, 2 H, H$^{5-8}$), 5.85 [t (br), 1 H, H^2], 5.71 (m, 2 H, H$^{1/3}$), 4.23 (d, 5 H, Cp, [J_{PH} = 1.8 Hz]), 3.76 {d, 9 H, P(OMe)$_3$, [J_{PH} = 10.8 Hz]}. − [(η^3-Ind)CpMo{P(OMe)$_3$}$_2$]: δ = 6.57−6.50 (m, 4 H, H$^{5-8}$), 4.58 (t, 5 H, Cp, [J_{PH} = 1.8 Hz]), 3.90−3.87 (m, 3 H, H$^{1-3}$), 3.24 {t, 18 H, P(OMe)$_3$, [J_{PH} = 10.8 Hz]}.

Attempted Isolation of [(η^5-Ind)CpMo(CNCMe$_3$)] (12): [IndCpMo(CNCMe$_3$)Br]Br: 0.09 g, 0.14 mmol; Cp_2Co: 0.052 g, 0.28 mmol; orange powder (mixture of two complexes). − Selected IR (KBr); [(η^5-Ind)CpMo(CNCMe$_3$)]: $\tilde{\nu}$ = 2934, 1934, 1728, 1456, 1198, 1036, 800, 737 cm^{-1}. − ^{1}H NMR (C_6D_6, 300 MHz, room temp.); [(η^5-Ind)CpMo(CNCMe$_3$)]: δ = 7.64−7.61 (m, 2 H, H$^{5-8}$), 6.93−6.90 (m, 2 H, H$^{5-8}$), 5.84 [s (br), 1 H, H^2], 5.65 [s (br), 2 H, H$^{1/3}$], 5.11 (s, 5 H, Cp), 1.22 (s, 9 H, CH_3). − [(η^3-Ind)CpMo(CNCMe$_3$)$_2$]: δ = 6.81 (t, 1 H, H^2), 6.64−6.61 (m, 2 H, H$^{5-8}$), 6.51−6.48 (m, 2 H, H$^{5-8}$), 4.80 (s, 5 H, Cp), 4.41 (d, 1 H, H$^{1/3}$), 1.04 (s, 18 H, CH_3).

Preparation of [(η^3-C_5H_5)CpMo(CO)$_2$] (13): A suspension of [Cp_2Mo(CO)$_2$][BF_4]$_2$ (0.27 g, 0.60 mmol) in toluene was treated with a solution of Cp_2Co (0.23 g, 1.21 mmol) in the same solvent at 0°C. After 3 h stirring at room temperature the solution was separated from [Cp_2Co]Br by filtration. The solvent was removed under vacuum and the residue extracted with hexane (3 × 30 mL). The green powder that separated upon concentration and cooling of the extract was identified by comparison of its IR and ^{1}H-NMR spectra with those of an authentic sample.[1] Yield, 80%.

Preparation of [Cp_2Mo(P(OMe)$_3$)] (14): A suspension of [Cp_2Mo{P(OMe)$_3$}$_2$][BF_4]$_2$ (0.34 g, 0.53 mmol) in NCMe was treated with a solution of Cp_2Co (0.23 g, 1.21 mmol) in the same solvent at 0°C. After 3 h stirring at room temperature the solvent was removed under vacuum and the residue extracted with Et_2O (3 × 30 mL). The brown powder was separated upon evaporation of the solvent. Yield: 30%. − $C_{13}H_{19}MoO_3P$ (350.21): calcd. C 44.59, H 5.47; found C 44.40, H 5.50. − Selected IR (KBr): $\tilde{\nu}$ = 3104, 2926, 1416, 1036, 866 cm^{-1}. − ^{1}H NMR (C_6D_6, 300 MHz, room temp.): δ = 4.14 (d, 10 H, Cp, [J_{PH} = 4.8 Hz]), 3.29 {t, 9 H, P(OMe)$_3$, [J_{PH} = 5.7 Hz]}.

Preparation of [Cp_2Mo(CNCMe$_3$)$_2$][BF_4]$_2$ (15): A solution of [Cp_2Mo(NCMe)$_2$][BF_4]$_2$ (0.34 g, 0.71 mmol) in CH_2Cl_2/NMF (2:1) was treated with excess CN*t*Bu (0.50 mL) and refluxed overnight. The solution was concentrated under vacuum (until the only remaining solvent was NMF) and Et_2O/EtOH (30:1) was added to precipitate the yellow complex. The compound was washed with CH_2Cl_2. Yield: 90%. − $C_{20}H_{28}B_2F_8MoN_2$ (566.01): calcd. C 42.44, H 4.99, N 4.95; found C 42.35, H 5.22, N 4.42. − Selected IR (KBr): $\tilde{\nu}$ = 3119, 3047, 2992, 2226, 2114, 1417, 1377, 1204, 1065, 872 cm^{-1}. − ^{1}H NMR (CD_3CN, 300 MHz, room temp.): δ = 5.92 (s, 10 H, Cp), 1.55 (s, 18 H, CH_3).

Molecular Orbital Calculations. − Extended Hückel Calculations: EH calculations were performed using the ICON8 program[23a,b] with modified H_{ij} values.[23c] The basis set for the metal atoms consisted of *n*s, *n*p and (*n* − 1)d orbitals. The s and p orbitals were described by single Slater-type wave functions, and the d orbitals were taken as contracted linear combinations of two Slater-type wave functions. The parameters used for Mo were [H_{ii} (eV), ζ]: 5s −8.77, 1.960; 5p −5.60, 1.900; 4d −11.06, 4.542, 1.901 (ζ_2), 0.5899 (C_1), 0.5899 (C_2). Standard parameters were used for other atoms. − The calculations were performed on model complexes with idealised geometries taken from the real structures quoted along the text. Thus, [(η^m-Ind)CpMo(CO)$_2$]$^{n+}$ (*m* = 3, *n* = 0 or *m* = 5, *n* = 2) and [(η^3-Cp)CpMo(CO)$_2$] complexes have a distorted tetrahedral geometry with C_s symmetry and Cp/Ind−Mo−Cp and CO−Mo−CO angles of 140° and 80°, respectively. The bis(η^5-Cp) model, [Cp_2Mo(CO)$_2$]$^{2+}$, has C_{2v} symmetry and the same L−Mo−L angles as mentioned above. The trihapto coordination mode of the indenyl and Cp ligands was accomplished by a 30° folding of those ligands. The mono-carbonyl models, [(Ind/Cp)CpMo(CO)], have a Cp/Ind−Mo−Cp angle of 140°, their symmetries being C_s for the Ind complex and C_{2v} for the Cp species. The bond lengths (Å) were as follows: M−(C_5 ring centroid) 2.00, M−C(CO) 2.00, C−O 1.15, C−C 1.40, C−H 1.08. − **DFT Calculations:** Density functional calculations[14] were carried out on model compounds based on the structures of the complexes described in the text, under C_s symmetry or no symmetry, using the Amsterdam Density Functional (ADF) program[24] developed by Baerends and co-workers.[25] The slipping, folding and position of the cyclopentadienyl and indenyl rings, the Mo−C(CO) distance and position of the carbonyl groups were optimized for the six carbonyl complexes. A full optimization was performed for the six phosphite complexes, using P(OH)$_3$ as a model for P(OMe)$_3$. Vosko, Wilk, and Nusair′s local exchange correlation potential was used,[26] with Becke′s nonlocal exchange[27] and Perdew′s correlation corrections.[28] The geometry optimization procedure was based on the method developed by Versluis and Ziegler,[29] using the nonlocal correction terms in the calculation of the gradients. The core orbitals were frozen for Mo ([1−4]s, [1−4]p, 3d) and C, N, O (1s), P (1s, 2s, 2p). Triple-ζ Slater-type orbitals (STO) were used for H 1s; C, N, O 2s and 2p; P 3s and 3p; Mo 5s, 5p, and 4d. One polarization function was added for H, C, N, O, and P.

Acknowledgments

This work was supported by PRAXIS XXI under projects 2/2.1/QUI/316/94, PBIC/C/QUI/2201/95 and PBIC/C/QUI/220/95. C. A. G. thanks PRAXIS XXI for a grant (BD).

[1] [1a] J. R. Ascenso, C. G. de Azevedo, I. S. Gonçalves, E. Herdtweck, D. S. Moreno, C. C. Romão, J. Zühlke, *Organometallics* **1994**, *13*, 429. − [1b] I. S. Gonçalves, C. C. Romão, *J. Organomet. Chem.* **1995**, *48*, 155. − [1c] J. R. Ascenso, C. G. de Azevedo, I. S. Gonçalves, E. Herdtweck, D. S. Moreno, M. Pessanha, C. C. Romão, *Organometallics* **1995**, *14*, 3901.
[2] C. A. Gamelas, E. Herdtweck, J. P. Lopes, C. C. Romão, *Organometallics* **1999**, *18*, 506.
[3] [3a] J. L. Thomas, H. H. Brintzinger, *J. Am. Chem. Soc.* **1972**, *94*, 1386. − [3b] L. G. Bell, H. H. Brintzinger, *J. Organomet. Chem.* **1977**, *135*, 173.
[4] A. M. Martins, M. J. Calhorda, C. C. Romão, C. Völkl, P. Kiprof, A. C. Filippou, *J. Organomet. Chem.* **1992**, *423*, 367.
[5] T. C. Wright, G. Wilkinson, M. Motevalli, M. B. Hursthouse, *J. Chem. Soc., Dalton Trans.* **1986**, 2017.
[6] J. Okuda, Ph.D. Dissertation, Technische Hochschule, Aachen, **1984**.
[7] F. W. S. Benfield, M. L. H. Green, *J. Chem. Soc., Dalton Trans.* **1974**, 1324.
[8] C. G. de Azevedo, M. A. A. F. de C. T. Carrondo, A. R. Dias, A. M. Martins, M. F. M. Piedade, C. C. Romão, *J. Organomet. Chem.* **1993**, *445*, 125.
[9] S. Gambarotta, C. Floriani, A. Chiesi-Villa, C. Guastini, *J. Am. Chem. Soc.* **1985**, *107*, 2985.

[10] A. de Cian, J. Colin, M. Schappacher, L. Ricard, R. Weiss, *J. Am. Chem. Soc.* **1981**, *103*, 1850.
[11] M. J. Calhorda, M. G. B. Drew, V. Félix, C. A. Gamelas, W. E. Geiger, I. S. Gonçalves, C. C. Romão, M. Stoll, L. F. Veiros, unpublished results.
[12] A. Nakamura, S. Otsuka, *J. Am. Chem. Soc.* **1972**, *92*, 1886.
[13] [13a] G. E. Herberich, B. Hessner, J. Okuda, *J. Organomet. Chem.* **1983**, *254*, 317. – [13b] G. E. Herberich, J. Okuda, *Chem. Ber.* **1984**, *117*, 3112.
[14] R. G. Parr, W. Yang, *Density Functional Theory of Atoms and Molecules*, Oxford University Press, New York, **1989**.
[15] [15a] G. Huttner, H. H. Brintzinger, L. G. Bell, P. Friedrich, V. Bejenke, D. Neugebauer, *J. Organomet. Chem.* **1978**, *145*, 329. – [15b] K. L. Tang Wong, H. Brintzinger, *J. Am. Chem. Soc.* **1975**, *97*, 5143. – [15c] H. H. Brintzinger, L. L. Lohr, Jr., K. L. Tang Wong, *J. Am. Chem. Soc.* **1975**, *97*, 5146. – [15d] E. U. van Raaij, H. H. Brintzinger *J. Organomet. Chem.* **1988**, *356*, 315.
[16] F. H Allen, J. E. Davies, J. J. Galloy, O. Johnson, O. Kennard, C. F. Macrae, D. G. Watson, *J. Chem. Inf. Comp. Sci.* **1991**, *31*, 204.
[17] M. J. Calhorda, C. A. Gamelas, I. S. Gonçalves, E. Herdtweck, C. C. Romão, L. F. Veiros, *Organometallics* **1998**, *17*, 2597.
[18] [18a] M. J. Calhorda, L. F. Veiros, *Coord. Chem. Rev.* **1999**, *185–186*, 37–51. – [18b] C. Bonifaci, A. Ceccon, S. Santi, C. Mealli, R. Zoellner, *Inorg. Chim. Acta* **1995**, *240*, 542.
[19] [19a] E. Fischer, C. Elschenbroich, *Chem. Ber.* **1970**, *103*, 162. – [19b] R. G. Finke, R. H. Voegeli, E. D. Laganis, V. Boekelheide, *Organometallics* **1983**, *2*, 347. – [19c] R. M. Nielson, M. J. Weaver, *Organometallics* **1989**, *8*, 1636. – [19d] W. J. Bowyer, J. W. Merkert, W. E. Geiger, A. L. Rheingold, *Organometallics* **1989**, *8*, 191. – [19e] G. A. Miller, M. J. Therien, W. C. Trogler, *J. Organomet. Chem.* **1990**, *383*, 279. – [19f] D. T. Pierce, W. E. Geiger, *J. Am. Chem. Soc.* **1992**, *114*, 6063. – [19g] S. Lee, S. R. Lovelace, N. J. Cooper, *J. Organomet. Chem.* **1995**, *14*, 1974.
[20] M. J. Calhorda, I. S. Gonçalves, E. Herdtweck, C. C. Romão, B. Royo, L. F. Veiros, *Organometallics* **1999**, *18*, 3956.
[21] W. Wollsberger, H. Schmidbauer, *Syn. React. Inorg. Metal. Org. Chem.* **1974**, *4*, 149.
[22] C. G. de Azevedo, M. J. Calhorda, M. A. A. F. de C. T. Carrondo, A. R. Dias, M. T. Duarte, A. M. Galvão, C. A. Gamelas, I. S. Gonçalves, F. M. Piedade, C. C. Romão, *J. Organomet. Chem.* **1997**, *544*, 257.
[23] [23a] R. Hoffmann, *J. Chem. Phys.* **1963**, *39*, 1397. – [23b] R. Hoffmann, W. N. Lipscomb, *J. Chem. Phys.* **1962**, *36*, 2179. – [23c] J. H. Ammeter, H.-J. Bürgi, J. C. Thibeault, R. Hoffmann, *J. Am. Chem. Soc.* **1978**, *100*, 3686.
[24] *Amsterdam Density Functional (ADF) program*, release 2.01; Vrije Universiteit, Amsterdam, The Netherlands, **1995**.
[25] [25a] E. J. Baerends, D. Ellis, P. Ros, *Chem. Phys.* **1973**, *2*, 41. – [25b] E. J. Baerends, P. Ros, *Int. J. Quantum Chem.* **1978**, *S12*, 169. – [25c] P. M. Boerrigter, G. te Velde, E. J. Baerends, *Int. J. Quantum Chem.* **1988**, *33*, 87. – [25d] G. te Velde, E. J. Baerends, *J. Comp. Phys.* **1992**, *99*, 84.
[26] S. H. Vosko, L. Wilk, M. Nusair, *Can. J. Phys.* **1980**, *58*, 1200.
[27] A. D. Becke, *J. Chem. Phys.* **1987**, *88*, 1053.
[28] [28a] J. P. Perdew, *Phys. Rev.* **1986**, *B33*, 8822. – [28b] J. P. Perdew, *Phys. Rev.* **1986**, *B34*, 7406.
[29] [29a] L. Versluis, T. Ziegler, *J. Chem. Phys.* **1988**, *88*, 322. – [29b] L. Fan, T. Ziegler, *J. Chem. Phys.* **1991**, *95*, 7401.

Received July 7, 1999
[I99249]

Mono and Dinuclear Tungsten Alkenyl-Carbyne Complexes Bridged by Cyanide and Diisocyanide Ligands: Synthesis, Electrochemical- and ^{183}W-NMR Studies

Lei Zhang,[a,b] M. Pilar Gamasa,[a] José Gimeno,*[a] Rodrigo J. Carbajo,[a] Fernando López-Ortiz,[a,c] M. Fátima C. Guedes da Silva,[b,d] and Armando J. L. Pombeiro*[b]

Keywords: Alkenylcarbynes / Dinuclear tungsten complexes / Electrochemistry / Tungsten NMR

Neutral *trans*-cyanide alkenylcarbyne complexes **2a** and **2b** have been prepared by reaction of the complex **1a** and **1b** with NaCN or $[Bu_4N]CN$. The reaction of complexes **2a** and **2b** with an equimolar amount of the acetonitrile complexes **1a** and **1b** in CH_2Cl_2 leads to the cationic cyanide-bridged bis(alkenylcarbyne) di-tungsten complexes **3a–d**. Diisocyanide-bridged bis(alkenylcarbyne) di-tungsten complexes **4a** and **4b** have been synthesized by the reaction of complexes **1a** and **1b** with 0.5 equivalents of the diisocyanide 1,4-$(CN)_2C_6H_4$. IR as well as ^{1}H-, ^{31}P{^{1}H}-, ^{13}C{^{1}H}-, and ^{183}W-NMR data are reported. The spectroscopic data show that in the dinuclear complexes **3a–d**, the bridging CN group and the alkenylcarbyne units are located in *trans* positions, while in the dinuclear complexes **4a** and **b**, the isocyanide groups of the bridging ligand 1,4-$(CN)_2C_6H_4$ and the two alkenylcarbyne moieties are *cis*. The ^{183}W chemical shifts of complexes **2a**, **2b**, **3a–d**, **4a**, and **4b** were obtained through two-dimensional indirect ^{31}P, ^{183}W NMR recording techniques. A downfield shifting of ^{183}W resonances of the cyanide-bridged dinuclear complexes **3a–d** with respect to the mononuclear ones, **2a** and **2b**, was observed. The δ^{183}W of isocyanide bridging dinuclear complexes **4a** and **4b** appear at higher field than those of the corresponding mononuclear cyanide **2a** and **2b** in accordance with the higher π-acceptor electron properties of the isocyanide ligand. The electrochemical behaviour of all the complexes has been investigated by cyclic voltammetry and controlled potential electrolysis in aprotic media and at a Pt (or vitreous C) electrode. Complexes **1**, **2**, or **3** undergo multi-electron irreversible oxidation processes involving anodically induced proton dissociation from the alkenylcarbyne ligands, and irreversible cathodic processes are also observed for all the complexes. The order of the redox potentials reflects that of the net electron π-acceptor/σ-donor character of the ligands and the ligating alkenylcarbynes are shown to behave as remarkably strong π-electron acceptors (even stronger than CO).

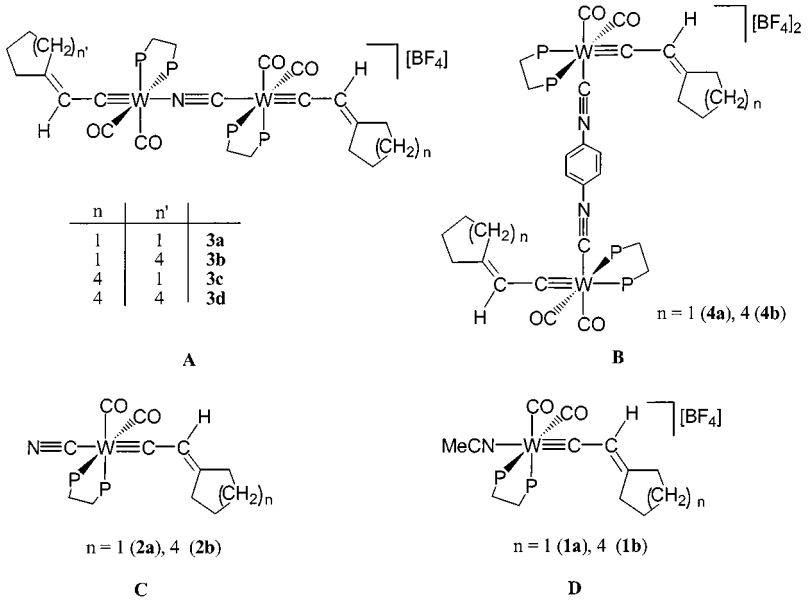
Introduction

Among the extensively studied chemistry of complexes with multiple metal−carbon bonds, that concerned with Fischer-type carbyne complexes of group 6 metals has remained a topic of interest during the last years.[1][2] However, it is now apparent that this chemistry is not as well developed as that of metal carbene derivatives. In particular, only a few carbyne complexes bearing α,β-unsaturated substituents have been described to date,[3] although the corresponding Fischer-type carbene derivatives have proven to be excellent substrates in modern organic synthesis. Even more rare derivatives are dinuclear complexes containing unsaturated carbyne groups.[4] Most of them are dimetallic species bearing a di-carbyne group acting as a bridging ligand: $[(\eta^5\text{-}C_5H_5)(CO)_2Cr{\equiv}C{-}CPh{=}CPh{-}C{\equiv}Cr(\eta^5\text{-}C_5H_5)(CO)_2]$,[5] {$[Br(CO)_4M{\equiv}C{-}(p\text{-}C_6H_4){-}C{\equiv}M(CO)_4Br]$ (M = Cr, W)},[6] {$[Tp'(CO)_2M{\equiv}C{-}CR{=}CR{-}C{\equiv}M(CO)_2Tp']$ (M = Mo; R = H. M = W; R = H, Me, CH_2Ph)}, {$[Tp'(CO)_2M{\equiv}C{-}C{\equiv}C{-}C{\equiv}M(CO)_2Tp']$ (M = Mo, W)}.[3c] Here we report the synthesis of ditungsten bis(alkenylcarbyne) complexes **A** and **B** along with the mononuclear complexes **C** (Scheme 1). Complexes of type **A** and **B** belong to a new type of α,β-unsaturated carbyne dimetallic derivatives in which the metal atoms are linked by a cyanide and diisocyanide bridging group.[7]

We have recently described[3b] the utility of the labile acetonitrile carbyne complexes **D** as excellent precursor of alkenylcarbyne and alkenylketenyl derivatives containing dithio ligands. In this work we report on an extension of this synthetic methodology which has led to the synthesis of dinuclear complexes of type **A** and **B**, obtained by the reaction of complexes **D** with the cyanide derivatives **C** and the diisocyanide ligand $C{\equiv}N{-}(1,4\text{-}C_6H_4){-}N{\equiv}C$, respec-

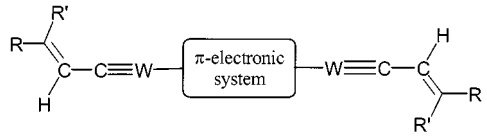
[a] Instituto Universitario de Química Organometálica "Enrique Moles" (Unidad Asociada al CSIC),
Departamento de Química Orgánica e Inorgánica, Facultad de Química, Universidad de Oviedo,
E-33071 Oviedo, Spain
Fax: (internat.) +34-98/510-3446
E-mail: jgh@sauron.quimica.uniovi.es
[b] Centro de Química Estrutural, Complexo I, Instituto Superior Técnico,
Av. Rovisco Pais, P-1049-001 Lisbon, Portugal
Fax: (internat.) +351-1/8414455
E-mail: pombeiro@alfa.ist.utl.pt
[c] Current address: Facultad de Ciencias Experimentales, Área de Química Orgánica,
Universidad de Almería, E-04120 Almería, Spain
[d] Universidade Lusófona de Humanidades e Tecnologias,
Av. Campo Grande 376, P-1749-024 Lisbon, Portugal

 © WILEY-VCH Verlag GmbH, D-69451 Weinheim, 2000 1434−1948/00/0202−341 $ 17.50+.50/0



Scheme 1. Alkenylcarbyne Fischer-type tungsten complexes

tively. Since the electrochemical investigation of complexes with multiple metal−carbon bonds is still a rather undeveloped field of research,[8−17] and has not been previously reported for alkenylcarbyne compounds, we have also studied the electrochemical behaviour of our novel alkenylcarbyne complexes. ^{183}W-NMR data of all the complexes are also reported.



Scheme 2. Two terminal unsaturated carbyne tungsten moieties linked by bridging ligands with π-electronic delocalized systems

Results and Discussion

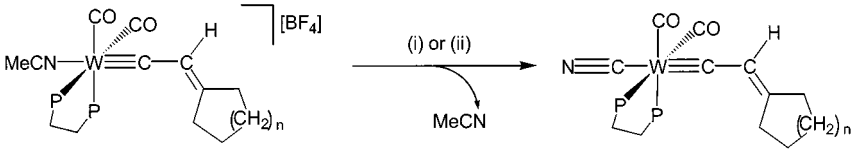
Mononuclear Cyanide Alkenylcarbyne Complexes 2a and 2b

The addition of NaCN to an orange solution of complexes**1a** and **1b** in methanol at room temperature led to the substitution of the acetonitrile ligand by the cyanide anion to afford the neutral alkenylcarbyne complexes **2a** and **2b** (90−95% yield) isolated as air stable orange solids (Equation 1). Complexes **2a** and **2b** are also formed by the treatment of **1a** and **1b** with $[NBu_4]CN$ in CH_2Cl_2.

IR spectra (CH_2Cl_2) show the typical pattern of *cis*-dicarbonyl complexes, of two ν(CO) absorptions at 1999 and 1931 (**2a**), and 1998 and 1930 (**2b**) cm^{-1}. As expected for the transformation of cationic to neutral complexes, a lowering in absorption frequencies (ca. 12 cm^{-1}) is observed. The presence of the terminal linear CN ligand is confirmed by the IR spectra (CH_2Cl_2 solution or KBr pellet) which show a very weak ν(CN) absorption at 2112 cm^{-1}.[18][19] The phosphorus resonances appear in the ^{31}P-NMR spectra (Table 1) as singlet signals, indicating the chemical equivalence of the phosphorus atoms of dppe, and are therefore in accordance with the *trans* carbyne-cyanide arrangement. The *J*(W-P) values (ca. 225.5 Hz) are similar to those found in analogous complexes

$$[(dppe)(CO)_2(X)W{\equiv}CCH{=}\overline{CCH_2CH_2(CH_2)_n}CH_2]$$

(X = Cl, Br, I) which also show a similar *trans* arrangement of phosphorus nuclei to the carbonyl ligands.[3a] The ^{1}H-NMR shows a broad signal for the alkenyl proton (≡C−CH=) at δ = 4.98 (**2a**) and 4.66 (**2b**). The carbyne carbon resonances of these complexes appear in the ^{13}C-NMR spectra as triplet signals at δ = 283.4 [^2J(P-C) ca. 10 Hz] (Table 2). These signals appear at a lower field with respect to those shown by the corresponding halide carbyne complexes [δ = 266.9−269.8, ^2J(P-C) ca. 10 Hz][3a] and at



(1)

n = 1 (**1a**), 4 (**1b**) n = 1 (**2a**), 4 (**2b**)

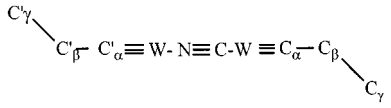
(i) NaCN, MeOH, rt, 2h. (ii) $[Bu_4N]CN$, CH_2Cl_2, rt, 2h.

Table 1. Selected IR[a] and $^{31}P\{^1H\}$- and ^1H-NMR[b] data for complexes **2a**, **2b**, and **3a−d**

	IR ν(CO)	ν(C≡N)	$^{31}P\{^1H\}$[c] 2 P, 2 P′	^1H CH_β	CH_β'
2a	1999 (vs), 1931 (vs)	2112 (vw)	39.8 s (225.7)	4.98 s,br	
2b	1998 (vs), 1930 (vs)	2112 (vw)	39.7 s (225.4)	4.66 s,br	
3a	2003 (vs), 1937 (vs)	2113 (vw), 2099 (vw)	39.5 s (229.0), 41.0 s (232.5)	4.67 s,br	4.58 s,br
3b	2004 (vs), 1938 (vs)	2113 (vw), 2100 (vw)	39.5 s (230.5), 41.0 s (233.0)	4.67 s,br	4.24 s,br
3c	2004 (vs), 1937 (vs)	2112 (vw), 2098 (vw)	39.4 s (228.7), 40.9 s (232.6)	4.31 s,br	4.58 s,br
3d	2003 (vs), 1937 (vs)	2112 (vw), 2098 (vw)	39.4 s (227.8), 41.0 s (234.0)	4.31 s,br	4.24 s,br

[a] Spectra recorded in CH_2Cl_2, ν(cm^{-1}). Abbreviations: s, strong; vs, very strong; vw, very weak. − [b] Spectra recorded in $CDCl_3$, δ in ppm, *J* in Hz. Abbreviations: s, singlet, br, broad. − [c] ^1J(W−P).

Table 2. Selected $^{13}C\{^1H\}$-NMR data for the complexes **2a**, **2b**, and **3a−d**[a]



	C_α	C_α'	C_γ	C_γ'	C≡N	2 *cis* CO, 2 *cis* CO′
2a	283.4 t (10.1)		166.0 t (3.2)[b]		140.2 t (10.7)	212.4 *vr.* dd (30.8, 7.0)
2b	283.4 t (10.2)		164.8 s		140.3 t (10.7)	212.6 *vr.* dd (31.4, 7.0)
3a	286.7 m	289.8 m	169.9 s	168.0 s	161.6 m	212.5 m
3b	286.7 t (9.5)	289.8 t (9.6)	169.7 s	166.1 s	161.9 m	211.4 *vr.* dd (29.9, 7.1)
3c	286.7 t (9.4)	289.5 t (9.6)	169.7 s	167.3 s	162.0 m	211.5 *vr.* dd (30.0, 7.1) 213.2 *vr.* dd (37.2, 7.2)
3d	286.8 m	289.7 m	169.2 s	166.3 s	162.1 m	211.6 *vr.* dd (30.1, 7.0) 213.2 *vr.* dd (36.5, 7.0)

[a] Spectra recorded in $CDCl_3$, δ in ppm, *J* in Hz. Abbreviations: s, singlet; d, doublet; t, triplet; dd, doublet of doublet; m, multiplet; *vr*, *virtual*. Within parenthesis ^2J(P-C). − [b] ^4J(P-C).

a higher field (ca. 8.5 ppm) than those of the cationic precursor complexes **1a** and **1b**. The resonances of the C_β atom of the alkenylcarbyne chain are assigned and distinguished by DEPT from the C_γ and the carbon atom of the cyanide group. The resonances of the *cis*-dicarbonyl ligands appear as doublet signals in the range of δ = 212.4−212.6 (Table 2) and are in accordance with the reported data for the similar alkenylcarbyne halide complexes.[3a]

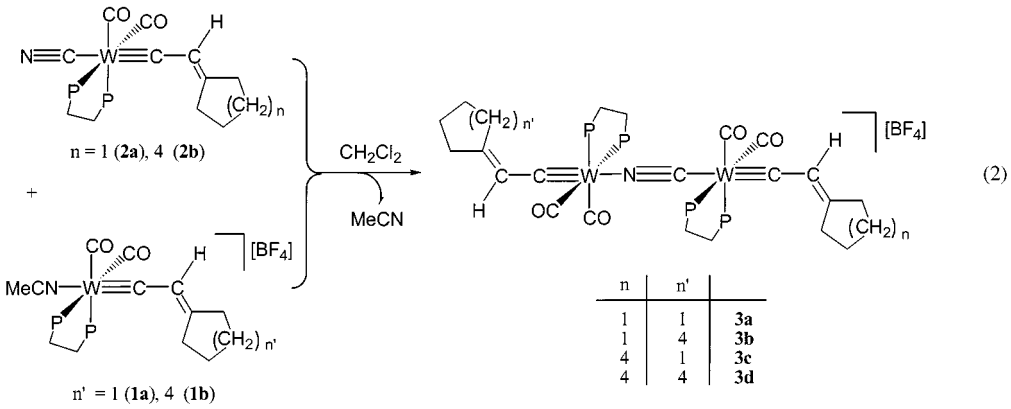
Cyanide Bridged Bis(alkenylcarbyne) Dinuclear Complexes 3a−d

The reaction of complexes **2a** and **2b** with an equivalent of **1a** and **1b** in dichloromethane at room temperature for 1 hour led to the displacement of the acetonitrile ligand to give the cationic bis(alkenylcarbyne) di-tungsten complexes **3a−d** (82−85% yield) in which the metal atoms are bridged by the cyanide group (Equation 2).

Complexes **3a** and **3d** have been also prepared in similar yields from the treatment of **1a** and **1b** in methanol with NaCN in a 2:1 molar ratio. The reaction probably proceeds through the formation of complexes **2a** and **b** as intermediates.

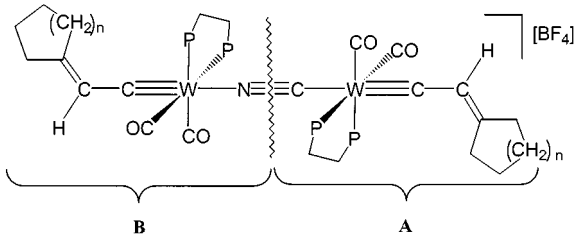
IR and NMR spectroscopic data show the molecular asymmetry of these dinuclear complexes even for **3a** ($n = n' = 1$) and **3d** ($n = n' = 4$) containing two identical metal carbyne moieties. Thus, IR spectra (CH_2Cl_2) show (Table 1) two weak ν(C≡N) absorptions[18][19] at 2112−2113 and 2098−2100 cm^{-1} and two very strong ν(CO) absorptions at 2003−2004 and 1937−1938 cm^{-1} which apparently indicate an overlapping of the absorptions expected for the two unsymmetrical *cis*-dicarbonyl pairs of each tungsten moiety. Since the ν(C≡N) absorptions at higher frequency appear at a similar energy to those of complexes **2a** and **b**, they may be assigned to the ν(N≡C−W) stretching (side A in Figure 1) while those at lower energy are assigned to the corresponding ν(W−N≡C) (side B in Figure 1).

NMR data of **3a−d** are in accordance with the linear −C≡W−(μ-N≡C)−W≡C− arrangement. Thus, the ^{31}P-NMR spectra (Table 1) show two singlets at δ = 39.4−39.5 [*J*(W-P) = 227.8−230.5 Hz] and 40.9−41.0 [*J*(W-P) = 232.5−234.0 Hz], which are expected for each equivalent pair of phosphorus nuclei of dppe *trans* to carbonyl groups in sides **A** and **B** (Figure 1). As discussed before, since the higher-field signals are at the same chemical shifts as those of **2a** and **2b** (0.3 ppm higher), they are assigned to the two equivalent phosphorus atoms at side **A**, while those at



(2)

n	n'	
1	1	3a
1	4	3b
4	1	3c
4	4	3d



Selected IR for 3a,d, ν(CN)

n =	A	B
1	2113	2098
4	2112	2098

Selected ^{1}H NMR for 3a,d, δ(C$_\beta$H)

n =	A	B
1	4.67	4.58
4	4.31	4.24

Figure 1. Selected IR and ^{1}H-NMR data for complexes **3a** and **3d**

lower-field are assigned to the phosphorus atoms of side **B**. We were not able to assign the proton and carbon resonances (Tables 1 and 2) for each moiety **A** and **B** using the conventional methods due to the similar values of chemical shifts. However, the spectroscopic characterisations have been performed through 2D ^{1}H,^{183}W- and ^{31}P,^{183}W-HMQC experiments, as will be discussed below (^{183}W-NMR studies). The alkenyl proton resonances appear in the ^{1}H-NMR spectra (Table 1) as two different broad singlets.

^{13}C-NMR spectra (Table 2) show two carbyne carbon resonances at δ = 286.7−289.8 [J(P-C) = 9.4−9.6 Hz]. For complexes **3b** and **3c**, bearing two different carbyne groups at each side of the bridge, the signals appear as two triplets, while for **3a** and **3d** these resonances are not well defined and appear as two multiplets. The assignments of these resonances for each moiety have been done through 2D ^{1}H,^{13}C-HMBC correlation experiments, on the basis of the previously known proton assignments. The carbon resonances of the cyanide group are shifted to lower field (> 20 ppm) (Table 2) appearing very close to those of the C$_\gamma$ atom of the alkenylcarbyne chain, indicating that a significant electron donation has occurred in the formation of the dinuclear species through the coordination of the [W]−CN moiety of complexes **2a** and **2b**. ^{13}C-NMR spectra also show carbonyl resonances which appear as virtual doublet-of-doublet signals at δ = 211.4−213.2 [^2J(P-C) = 7.0−7.2, 29.9−37.3 Hz] (Table 2) as expected for each unequivalent *cis*-dicarbonyl pair.

Diisocyanide-Bridged Bis(alkenylcarbyne) Dinuclear Complexes 4a and 4b

The reaction of **1a** and **1b** in dichloromethane with 1,4-CNC_6H_4NC (1:0.5 molar ratio) at room temperature for 2 hours afforded the diisocyanide bridged di-cationic bis(alkenylcarbyne) di-tungsten complexes **4a** (n = 1) and **4b** (n = 4) (75−80% yield) (Equation 3).

The reaction for the formation of complex **4a** was monitored by ^{31}P-NMR in CH_2Cl_2 (D_2O as external lock reference). However only the resonances due to the starting complex, along with those of the final product, are observed. Although the formation of an intermediate mononuclear complex is plausible, apparently the subsequent coordination of the uncoordinated isocyanide group is more favoured than the formation of the intermediate. All attempts to prepare the mononuclear complexes by using a 1:1 molar ratio failed, giving instead mixtures of the dinuclear complexes **4a** and **4b** and the mononuclear ones. even if a large excess of the ligand was used.

Elemental analyses, conductivity, and spectroscopic data support the dinuclear nature of the complexes and the proposed symmetric structure. The IR spectra of **4a** and **4b** (CH_2Cl_2) show two very strong and broad ν(CO) absorptions at 2006−2008 and 1960−1961 cm^{-1}, typical of a *cis* dicarbonyl arrangement for each tungsten centre. The spectra also show one ν(C≡N) absorption at 2130 and 2132 cm^{-1}, for **4a** and **4b**, respectively (Table 3).

The NMR spectra indicate that the two isocyanide groups occupy the *cis* positions with respect to the carbyne ligand of the corresponding metal centre. Thus, ^{31}P-NMR spectra of **4a** and **4b** display (Table 3) two singlet resonances at δ = 21.6 and 40.0, and δ = 21.9 and 40.1, respectively, indicating the chemical unequivalence of the phosphorus atoms of dppe. The J(W-P) values allow the assignment of the coordination sites. Thus, the lower-field signals with relatively large values [J(W-P) = 229.6 and 231.6 Hz] are typical of a mutually *trans* P−CO arrangement, while those of the higher-field signals [J(W-P) = 83.9−85.4 Hz] are characteristic of a phosphorus atom *trans* to carbyne ligands.[3a] This reflects the high *trans*-influence of the carbyne ligand,[3a,20] and it is also in accord with previous reported data for similar derivatives. The carbyne carbon resonances in the ^{13}C{^{1}H} NMR spectra (Table 4) which ap-

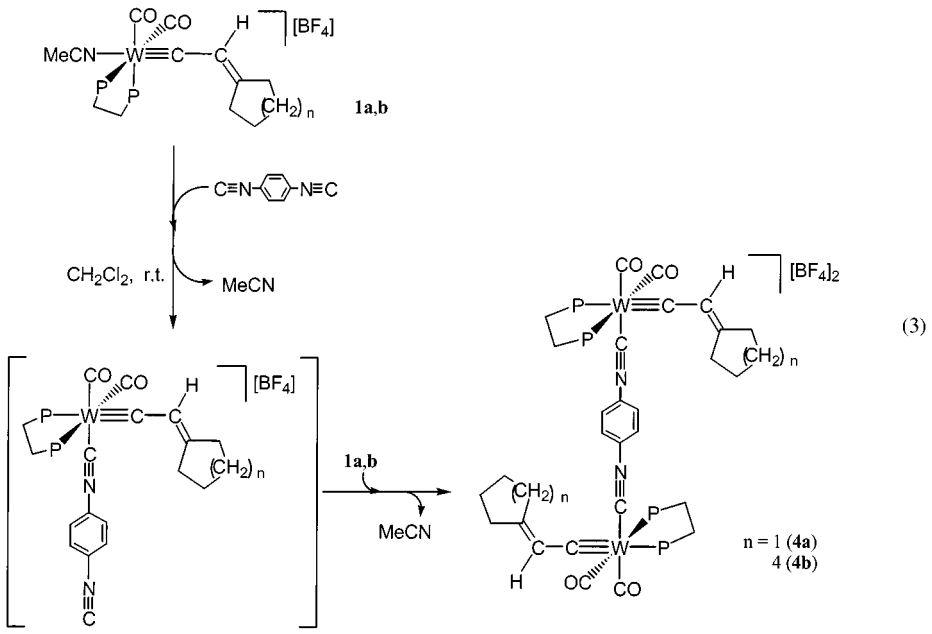


Table 3. Selected IR[a] and $^{31}P\{^1H\}$- and ^1H-NMR[b] data for complexes **4a**, and **4b**

	IR ν(CO)	ν(C≡N)	$^{31}P\{^1H\}$[c] 2 P *trans* to carbyne	2 P *trans* to carbonyl	^1H CH_β
4a	2008 (vs), 1961 (s)	2132 (m)	21.6 s (85.4)	40.0 s (231.6)	6.00 s,br
4b	2006 (vs), 1960 (s)	2130 (m)	21.9 s (83.9)	40.1 s (229.6)	5.92 s,br

[a] Spectra recorded in CH_2Cl_2, ν (cm^{-1}). Abbreviations: s, strong; vs, very strong; m, medium. – [b] Spectra recorded in $CDCl_3$, δ in ppm, *J* in Hz. Abbreviations: s, singlet, br, broad. – [c] within parenthesis *J*(W-P).

pear as a doublet of doublets at ca. δ = 298 [^2J(P-C) ca. 22, 10 Hz] are also consistent with the *trans* position of the carbyne groups with respect to one of the phosphorus atom of dppe. The chemical unequivalence of the carbonyl groups is also shown by the corresponding carbon resonances. Thus, those of carbonyl groups *trans* to the phosphorus atom of dppe appear as a double doublet signal at δ = 209.3 [^2J(P-C) = 7.3–8.6, 24.0–24.5 Hz] while those of the *cis* carbonyl ligands appear as an apparent triplet signal at δ = 207.5–207.9 [^2J(P-C) = 7.4–7.5 Hz] (Table 4). Furthermore, $^{13}C\{^1H\}$-NMR spectra also show resonances of the equivalent isocyanide groups at δ = 161.6 (**4a**) and 161.9 (**4b**) as apparent triplets [^2J(P-C) = 7.5–8.4 Hz] along with that of the C_γ atom of the alkenylcarbyne chain observed as a singlet at δ = 175.0 (**4a**) or 174.5 (**4a**).

^{183}W-NMR Studies

^{183}W-NMR data of complexes **2a**, **2b**, **3a–d**, **4a**, and **4b** are collected in Table 5. ^{183}W data were acquired by indirect detection through ^1H and/or ^{31}P, using standard HMQC pulse sequence.[21][22] For transition metal nuclei the chemical shift is dominated by the paramagnetic contribution to the total shielding, which can be approximated by Equation 4, where *r* represents the distance to the valence d electrons from the metal nucleus, ΔE is the average electronic excitation energy, and ΔQ_N is the angular imbalance of charge. The angular imbalance of charge can be considered as constant for complexes having the same d-electron configuration and symmetry. In this way we can rationalise the chemical shifts variations of the complexes studied accord-

Table 4. Selected $^{13}C\{^1H\}$-NMR data for complexes **4a** and **4b**[a]

	C_α	C_γ	$(W-CN)_2$	2 CO *cis* to P	2 CO *trans* to P
4a	298.4 dd (22.0, 10.0)	175.0 s	161.6 *vr.* t (8.4)	207.5 *vr.* t (7.4)	209.3 dd (24.0, 8.6)
4b	298.3 dd (23.2, 9.0)	174.5 s	161.9 *vr.* t (8.4)	207.9 *vr.* t (7.5)	209.3 dd (24.5, 7.3)

[a] Spectra recorded in $CDCl_3$, δ in ppm, *J* in Hz. Abbreviations: s, singlet; d, doublet; t, triplet; dd, doublet of doublet; m, multiplet; *vr*, *virtual*. Within parentheses, ^2J(P–C).

ing to the fluctuations of the r and ΔE terms, showing an upfield shift of the metal nucleus when r or ΔE increase, and consequently a deshielding when one of the terms becomes smaller.

$$\sigma_p \approx -\langle r^{-3}\rangle(\Delta E)^{-1}\Sigma Q_N \qquad (4)$$

Table 5. ^{183}W-NMR data for complexes **2−4**

	δ^{183}W		δ^{183}W	
			A	B
2a	−2116	**3a**	−2094	−1819
2b	−2100	**3b**	−2096	−1804
4a	−2127	**3c**	−2078	−1821
4b	−2108	**3d**	−2078	−1805

The ^{183}W-NMR spectra of **2a** and **2b** (δ = −2116, −2100, respectively) show that the substitution of the acetonitrile ligand of the starting material **1a** and **1b** (δ = −1786, −1775, respectively)[21] by the cyanide ligand produces a shielding of the tungsten nuclei by 330−325 ppm. This upfield shift effect is in agreement with the higher π-acceptor ability of CN^- compared to CH_3CN, which implies an increase in the ΔE term of Equation 4. The 16 ppm deshielding of **2b** with respect to **2a** is of the same order of the ^{183}W chemical shift difference between found in the starting carbyne complexes (**1a** and **1b**). This fact can be, and is explained, by the electronic and steric effects induced by the change in of the carbocyclic moiety size.[21]

The assignment of δ^{183}W for each moiety **A** and **B** of dinuclear complexes **3a−d** (Figure 1) is in accordance with the corresponding chemical shifts of precursor complexes **1a** and **1b**, and **2a** and **2b**. Thus, the δ^{183}W signals at higher field, which can be compared to those of cyanide complexes **2a** and **2b**, are assigned to the **A** moiety, while those at lower field, which resemble appear at analogous chemical shifts of the acetonitrile complexes **1a** and **1b**, are assigned to moiety **B**. When moving from the mononuclear complexes **2a** and **2b** to the dinuclear ones **3a−d**, a downfield shift of 20−22 ppm in the δ^{183}W of the **A** substructure is observed. The bidentate coordination of the CN^- group, acting as a bridging ligand, produces a reduction in its π-acceptor ability and consequently a decrease of the ΔE term. As observed before, an increase in the size of the carbocyclic moiety in either the **A** or **B** part of complexes **3a−d** leads to a deshielding of the metal by 15−18 ppm. It is worth mentioning that in complexes **3b** and **3c** the larger carbocyclic ring produces the expected deshielding of the tungsten nucleus bonded to the corresponding carbyne, but also a 2 ppm upfield shift to the signal of the other metal. Although $^5J(^{183}W\text{-}^1H)$[23] are observed within each moiety **A** and **B**, there are no cross peaks between the tungsten atom of the **A** moiety with the proton and phosphorus nuclei of **B** (and vice versa). Hereby, this small shift can be assigned to field or solvent effects.

As expected, the δ^{183}W of complexes **4a** and **4b** appear at higher field than those of the corresponding **2a** and **2b** (8 and 11 ppm, respectively) in accordance with the higher π-acceptor ability of diisocyanide ligand 1,4-$(CN)_2C_6H_4$ with respect to the cyanide group. The ^{183}W chemical shift of complex **4b** bearing two eight-membered rings is deshielded by 19 ppm with respect to **4a**, as is also shown in the spectra of complexes **2a**, **2b**, and **3a−d** (see above).

In addition, the ^{183}W-NMR spectra allow the assignment of the ^{1}H and ^{13}C resonances in compounds **3a−d**. Thus, the assignment of the alkenyl proton resonance in each moiety (H_β and H_β') was done through their correlations with the metal nuclei in the ^{1}H, ^{183}W HMQC spectra. On the basis of these assignments the rest of the ^{1}H and ^{13}C resonances were identified through the conventional ^{1}H,^{13}C-HMQC and -HMBC experiments.

Electrochemical Studies

The electrochemical behaviour of the alkenylcarbyne complexes has been investigated by cyclic voltammetry (CV) and controlled potential electrolysis (CPE) in aprotic medium (see Experimental Section).

With the exception of the dicationic complexes **4** (for which no anodic wave was detected, their oxidation conceivably occurring only at a potential above that of the onset of the solvent/electrolyte discharge), all the compounds exhibit irreversible anodic and cathodic waves by CV (Table 6). The oxidation peak potential of the first (I) anodic wave ($^IE_p^{ox}$) for the cyanide complexes **2** (ca. 1.1 V vs. SCE) is lower than those shown by the other complexes (ca. 1.3−1.4 V, for **1** and **3**) in agreement with the known[24] stronger net electron σ-donor minus π-acceptor ability of cyanide compared with a nitrile or an isocyanide ligand.

Table 6. Cyclic voltammetric data for complexes **1−4**[a]

Compound	$^IE_p^{ox}$	$^{II}E_p^{ox}$	$^IE_p^{red}$	$^{II}E_p^{red}$
1a	1.34	1.58	−1.58	–
1b	1.28	1.59	−1.65	–
2a	1.07	1.34	−1.89	–
2b	1.09	1.42	−1.88	
3a	1.30	1.38	−1.58	−1.89
3b[b]	1.38	1.50	−1.65	−1.90
3c[b]	1.26	1.37	−1.70	−1.94
3d[b]	1.28	1.43	−1.73	−1.96
4a	–	–	−1.25	−1.48
4b[c]	–	–	−1.20	−1.43
$[W(CO)_4(dppe)]$ [d]	1.02[e]	–	–	–

[a] Potentials in Volt ± 0.02 vs. SCE measured in 0.2 mol dm^{-3} $[NBu_4][BF_4]$/MeCN {CH_2Cl_2 for compounds **3a**, **4a**, and $[W(CO)_4(dppe)]$} at a scan rate of 0.2 V s^{-1} and at a Pt disc (d = 0.5 mm) electrode, unless stated otherwise. – [b] In vitreous C; at a Pt electrode, only one broad wave is observed at ca. 1.4 V. – [c] In vitreous C. – [d] Included for comparative purposes. – [e] Reversible wave ($\Delta E_{1/2}^{ox}$ value given).

Moreover, the values of oxidation potential for all the complexes are higher than that for $[W(CO)_4(dppe)]$ ($E_{1/2}^{ox}$ = 1.02 V) which was also measured for comparative purposes, indicating that the alkenylcarbyne ligands are behaving as even stronger net electron π-acceptors than CO, thus compensating for the stronger net electron donor ability of the nitrile, isocyanide, or cyanide ligand compared

with CO, which should result in a lowering of the oxidation potential of our complexes relative to that of $[W(CO)_4(dppe)]$. This is consistent with the reported[9] behaviour of the carbyne ligands in *trans*-$[ReX(\equiv CCH_2R)(dppe)_2][BF_4]$ (X = F or Cl; R = alkyl, aryl, or ester).

For the cyanide-bridged dinuclear complexes **3**, two close and extensively overlapped anodic waves are observed. Since these complexes can be viewed as the assembling of the tungsten moieties **A** (attached to a formal isocyanide ligand) and **B** (attached to a formal nitrile ligand) (Figure 1) it is expected that the tungsten atom of moiety **A** undergoes an oxidation process at a more anodic potential with respect to that of moiety **B**. Moreover, $^{I}E_p^{ox}$ values for these complexes are close to those of the acetonitrile precursors **1**. This is in accord with the ^{183}W chemical shifts for parts **A** and **B** of complexes **3** (see above).

In the cyclic voltammograms of complexes **1**, **2**, and **3**, the first anodic wave (I) is followed, at a slightly higher potential, by a second one (II), also irreversible and broad, that partially overlaps with the former wave. Although this precluded an accurate discrimination of the respective numbers of electrons, the overall involvement, by CPE, of multi-electron anodic processes with electron-induced proton liberation from the alkenylcarbyne ligand is evident.

In fact, exhaustive anodic CPE of those complexes, usually in acetonitrile, corresponds to an overall consumption (waves I + II) of ca. 3 (complexes **1** or **2**) or ca. 4 (complexes **3**) faradays/mol. The evolution of H^+ is indicated by the detection, by CV (cathodic sweep) of the electrolysed solution, at a Pt electrode, of an irreversible and broad cathodic wave at ca. −0.5 V, assigned to H^+ reduction. This wave shifts to a much lower potential upon replacement of the Pt by a vitreous carbon electrode, in accord with the expected large overpotential required for H^+ reduction at the latter electrode. The proton emission was also measured by acid-base titration of the electrochemically oxidised complex solutions: ca. 1 H^+/molecule for complexes **2**, ca. 3 H^+/molecule for complexes **1**, or ca. 4 H^+/molecule for complexes **3**. The higher numbers of protons for **1** and **3** relative to **2** are in accord with the expected stronger acidity of the carbyne ligand in the former complexes, as a result of the charge and the absence of the stabilising strong electron-donor mono-hapto cyanide ligand. Moreover, the highest number of protons lost for compounds **3** may also reflect their biscarbyne (dinuclear) character.

Proton dissociation can also occur during the time scale of CV, at a sufficiently low scan rate, since its cathodic wave (with the above features) is detected as well upon scan reversal following the anodic scan of a solution of an alkenylcarbyne complex.

Consistent with an anodic multi-electron process, at a sufficiently high time scale, involving electron-induced proton loss followed by further oxidation of the product(s), the following observations by CV are possible: the anodic current-functions $i_p^{ox}\ C^{-1}\cdot v^{-1/2}$ (i_p^{ox} − anodic peak current, C − concentration, v − scan rate) increase (i) with a decrease of the scan rate (e.g. by a factor of ca. 2 from v = 10 V s^{-1}, when it corresponds roughly to a single-electron process, to 50 $mV\cdot s^{-1}$ for complexes **1**) and (ii) with addition of a base such as pyridine, which enhances the deprotonation step.

The proton liberation at the anodic process, now reported for the first time for alkenylcarbyne ligands, indicates a promotion of their acidic character as a result of oxidation of the complexes, and parallels the anodically induced deprotonation observed for the aminocarbyne (CNH_2) and isocyanide (CNH) ligands in *trans*-$[ReCl(CNH_n)(dppe)_2][BF_4]_{n-1}$ (n = 2 or 1)[10] and *trans*-$[FeH(CNH)(dppe)_2][BF_4]$,[25] as well as for some aminocarbene complexes[11a] of Pd^{II} or Pt^{II}. However, the behaviour of the alkenylcarbyne ligands of this study contrasts with the stability, toward anodically-induced deprotonation, of the carbyne ligands $\equiv CCH_2R$ in the complexes *trans*-$[ReX(\equiv CCH_2R)(dppe)_2][BF_4]$,[9] which undergo a reversible single-electron oxidation by CV. This difference conceivably results from the higher acidity of the alkenyl proton ($\equiv C-CH=$) of our complexes compared to the alkyl protons ($\equiv C-CH_2R$) in the Re compounds, and/or the occurrence of anodically induced *ortho*-deprotonation of the ring. Hence, the anodic conversion of a ligating alkenylcarbyne into e.g., an allenylidene or a vinylidene ligand is plausible, but unfortunately we did not succeed in the identification of the products of the CPE or of the attempted chemical oxidations by oxidising agents such as the triarylaminium (Magic Blue) salt $[N(4\text{-}BrC_6H_4)_3][SbCl_6]$.

The alkenylcarbyne complexes of this study display, by CV, a single-electron irreversible cathodic wave (as shown by CPE) (Table 6), which for the dinuclear compounds (**3** and **4**), is followed by a second one at a lower potential, which involves a two-electron process for **4** (as measured by CPE). The observation of the two distinct cathodic waves for complexes **4** with two identical metal centres could suggest an interaction through a delocalized LUMO along the bridged aromatic diisocyanide, but the complexity of the cathodic processes prevents such an interpretation.

Conclusions

In this work, novel types of dinuclear **A** and **B** and mononuclear **C** alkenylcarbyne Fischer-type tungsten complexes are reported (Scheme 1). Complexes of type **A** and **B** belong to a new type of α,β unsaturated carbyne dimetallic derivatives, in which the metal atoms are linked by a cyanide and diisocyanide bridging group. These novel dinuclear complexes display a π-conjugated system consisting of two terminal unsaturated carbyne tungsten moieties linked by bridging ligands with π-electronic delocalized systems (Scheme 2). There is currently much research on this type of derivatives because they disclose appropriate molecular arrangements, with potential utility as precursors of mixed valence complexes and materials with enhanced electrical conductivities and nonlinear optical (NLO) properties.[26] Our study also allowed the investigation, for the first time, of the electrochemical behaviour of alkenylcarbyne com-

plexes, revealing that (i) the alkenylcarbyne ligands are activated, by oxidation of their complexes, towards heterolytic C−H bond cleavage (a behaviour which is of potential synthetic interest for the generation of other unsaturated multiple metal-carbon bonded species) and that (ii) the alkenylcarbyne ligands behave as even stronger π-electron acceptors than CO.

Experimental Section

Synthesis and Characterization of Alkenylcarbyne Complexes: The reactions were carried out under dry nitrogen using Schlenk techniques. All solvents were dried by standard methods and distilled under nitrogen before use. The precursor complexes **1a**, and **b** were prepared by the literature methods.[3a] NaCN, $[Bu_4N]CN$, and 1,4-$(CN)_2C_6H_4$ (Aldrich Chemical Co.) were used as received. − Infrared spectra were recorded on a Perkin−Elmer 1720-XFT spectrometer. − Mass spectra (FAB) were recorded using a VG-Autospec spectrometer, operating in the positive mode; 3-nitrobenzyl alcohol (NBA) was used as the matrix. − The conductivities were measured at room temperature, in ca. 10^{-3} mol dm^{-3} acetone solutions, with a Jenway PCM3 conductivimeter. − The C, H, and N analyses were carried out with a Perkin−Elmer 240-B microanalyzer. − NMR spectra were run on Bruker AC300 and AMX400 spectrometers. The parameters used for the indirect detection experiments ^1H,^{183}W 2D HMQC and ^{31}P,$^{183}W\{^1H\}$ 2D HMQC have been previously described.[3a,21] The spectral reference used for ^{183}W was Na_2WO_4. − Selected IR and ^1H-, $^{13}C\{^1H\}$-, $^{31}P\{^1H\}$-, and ^{183}W-NMR spectroscopic data for the novel carbyne tungsten complexes are collected in Tables 1−5.

Preparation of Mononuclear Cyanide Alkenylcarbyne Complexes 2a and 2b. − General Procedure: A small excess of NaCN solid was added to an orange solution of **1a** or **1b** (0.2 mmol) in 20 mL of methanol. The mixture was stirred at room temperature for 2 h. The resulting solution was filtered off and the filtrate was evaporated to dryness. The residue was extracted with CH_2Cl_2 and the filtrate was dried under vacuum to give an orange solid. Yield: **2a**, 90%; **2b**, 95%.

The complexes **2a** and **2b** were also prepared following the procedure below: An orange solution of **1a** or **1b** (0.2 mmol) and 1 equiv. of $[NBu_4]CN$ in 10 mL of CH_2Cl_2 was stirred at room temperature for 2 h. After evaporation of the solvent to dryness the residue was extracted with toluene and filtered of on Alox. Removal of the solvent and washing the resulting solid with diethyl ether (2 × 10 mL) and hexane (2 × 10 mL) and drying in vacuo gave an orange solid. Yields ca. 70%.

Spectral and Analytical Data for 2a: IR [KBr, ν(CN); ν(CO)] $\tilde{\nu}$ = 2111 (vw); 1987 (vs), 1917 (vs). − ^1H NMR (δ, $CDCl_3$) 1.48 (m, 4 H, 2 CH_2), 1.94 (m, 4 H, 2 CH_2), 2.60 [m, 2 H, $P(CH_aH_b)_2P$], 2.85 [m, 2 H, $P(CH_aH_b)_2P$], 7.36−7.75 (m, 20 H, 2 PPh_2). − $^{13}C\{^1H\}$ NMR (δ, $CDCl_3$) 25.5 (s, CH_2), 26.1 (s, CH_2), 28.5 [m, $P(CH_2)_2P$], 31.8 (s, CH_2), 34.7 (s, CH_2), 128.2−136.3 (m, $C_β$, 2 PPh_2). $-C_{36}H_{33}NO_2P_2W$: calcd C 57.1, H 4.4, N 1.8; found: C 57.5, H 4.2, N 1.9.

Spectral and Analytical Data for 2b: IR [KBr, ν(CN); ν(CO)] $\tilde{\nu}$ = 2112(vw); 1984 (vs), 1916 (vs). − ^1H NMR (δ, $CDCl_3$) 1.40 (m, 4 H, 2 CH_2), 1.44 (m, 2 H, CH_2), 1.53 (m, 2 H, CH_2), 1.70 (m, 2 H, CH_2), 1.82 (m, 2 H, CH_2), 2.31 (m, 2 H, CH_2), 2.58 [m, 2 H, $P(CH_aH_b)_2P$], 2.88 [m, 2 H, $P(CH_aH_b)_2P$], 7.36−7.88 (m, 20 H, 2 PPh_2). − $^{13}C\{^1H\}$ NMR (δ, $CDCl_3$) 25.5 (s, CH_2), 26.7 (s, CH_2), 26.9 (s, CH_2), 26.96 (s, CH_2), 27.02 (s, CH_2), 28.6 [m, $P(CH_2)_2P$], 31.9 (s, CH_2), 36.3 (s, CH_2), 128.3−136.2 (m, 2 PPh_2), 135.7 (s, $C_β$). − MS (FAB, *m/z*) $[M^+ - CN]$ = 773, $[M^+ - CO]$ = 771, $[M^+ - CN - CO]$ = 745, $[M^+ - 2\,CO]$ = 743. $-C_{39}H_{39}NO_2P_2W$: calcd. C 58.6, H 4.9, N 1.8; found: C 58.2, H 4.7, N 1.3.

Preparation of Cyanide-Bridged Bis(alkenylcarbyne) Ditungsten Complexes (3a−d): General Procedure: A mixture of complexes **2a** (0.2 mmol) and **1a** (0.2 mmol) in 20 mL of dichloromethane was stirred at room temperature for 1 h. The resulting orange-red solution was evaporated to dryness and the residue was washed with hexane (3 × 5 mL) to give an orange solid (**3a**). The complexes **3b−d** were prepared similarly. The complexes **3a** and **3d** were also prepared directly from the reaction of 2 equiv. of **1a** and **1b** with $[Bu_4N]CN$ in dichloromethane, or with NaCN in methanol, in the similar yields. Yield: 82−85%. − Conductivity (acetone, 20°C, $Ω^{-1}$ cm^2 mol^{-1}): **3a**, 123; **3b**, 120; **3c**, 115; **3d**, 118.

Spectral and Analytical Data for 3a: ^1H NMR (δ, $CDCl_3$) 1.40 (m, 8 H, 4 CH_2), 1.69 (m, 4 H, 2 CH_2), 1.85 (m, 4 H, 2 CH_2), 2.3−3.0 [m, 8 H, 2 $P(CH_2)_2P$], 7.18−7.70 (m, 40 H, 4 PPh_2). − $^{13}C\{^1H\}$ NMR (δ, $CDCl_3$) 25.2 (s, CH_2), 25.3 (s, CH_2), 25.9 (s, 2 CH_2), 28.0 [m, 2 $P(CH_2)_2P$], 31.4 (s, CH_2), 31.7 (s, CH_2), 34.4 (s, CH_2), 34.9 (s, CH_2), 128.2−136.4 (m, $C_β$, $C_β'$, 4 PPh_2). − $C_{71}H_{66}BF_4NO_4P_4W_2$: calcd. C 54.1, H 4.2, N 0.9; found: C 53.4, H 4.4, N 0.7.

Spectral and Analytical Data for 3b: IR [KBr, ν(CN); ν(CO); $ν(BF_4)$]: $\tilde{\nu}$ = 2110 (vw), 2099 (vw, sh); 1994 (vs, br), 1925 (vs, br); 1059 (m, br). − ^1H NMR (δ, $CDCl_3$) 1.30 (m, 12 H, 6 CH_2), 1.41 (m, 6 H, 3 CH_2), 1.69 (m, 2 H, CH_2), 2.10 (m, 2 H, CH_2), 2.3−2.9 [m, 8 H, 2 $P(CH_2)_2P$], 7.18−7.70 (m, 40 H, 4 PPh_2). − $^{13}C\{^1H\}$ NMR (δ, $CDCl_3$) 25.15 (s, CH_2), 25.23 (s, CH_2), 25.8 (s, CH_2), 26.4 (s, CH_2), 26.6 (s, CH_2), 26.7 (s, CH_2), 27.0−29.0 [m, CH_2, 2 $P(CH_2)_2P$], 31.4 (s, CH_2), 31.7 (s, CH_2), 34.8 (s, CH_2), 35.5 (s, CH_2), 128.3−136.4 (m, $C_β$, $C_β'$, 4 PPh_2). $-C_{74}H_{72}BF_4NO_4P_4W_2$: calcd. C 54.9, H 4.5, N 0.9; found: C 53.7, H 4.5, N 0.7.

Spectral and Analytical Data for 3c: IR [KBr, ν(CN); ν(CO); $ν(BF_4)$]: 2109 (vw, sh), 2098 (vw); 1993 (vs, br), 1924 (vs, br); 1056 (s, br). − ^1H NMR (δ, $CDCl_3$) 1.38 (m, 10 H, 5 CH_2), 1.69 (m, 4 H, 2 CH_2), 1.82 (m, 4 H, 2 CH_2), 2.07 (m, 4 H, 2 CH_2), 2.40- 3.0 [m, 8 H, 2 $P(CH_2)_2P$], 7.17−7.87 (m, 40 H, 4 PPh_2). − $^{13}C\{^1H\}$ NMR (δ, $CDCl_3$) 25.1 (s, CH_2), 25.8 (s, CH_2), 26.3 (s, CH_2), 26.6 (s, CH_2), 26.7 (s, CH_2), 26.8 (s, CH_2), 27.0 (s, CH_2), 28.0 [m, 2 $P(CH_2)_2P$], 31.2 (s, CH_2), 31.7 (s, CH_2), 34.2 (s, CH_2), 35.8 (s, CH_2), 127.9−136.6 (m, $C_β$, $C_β'$, 4 PPh_2). $-C_{74}H_{72}BF_4NO_4P_4W_2$: calcd. C 54.9, H 4.5, N 0.9; found: C 54.0, H 4.8, N 0.7.

Spectral and Analytical Data for 3d: ^1H NMR (δ, $CDCl_3$) 1.39 (m, 16 H, 8 CH_2), 1.68 (m, 4 H, 2 CH_2), 1.81 (m, 4 H, 2 CH_2), 2.09 (m, 4 H, 2 CH_2), 2.3−3.0 [m, 8 H, 2 $P(CH_2)_2P$], 7.17−7.68 (m, 40 H, 4 PPh_2). − $^{13}C\{^1H\}$ NMR (δ, $CDCl_3$) 25.3 (s, CH_2), 25.4 (s, CH_2), 26.6−27.1 (m, 8 CH_2), 28.2 [m, 2 $P(CH_2)_2P$], 31.8 (s, CH_2), 31.9 (s, CH_2), 35.6 (s, CH_2), 36.1 (s, CH_2), 128.2−135.6 (m, $C_β$, $C_β'$, 4 PPh_2). $-C_{77}H_{78}BF_4NO_4P_4W_2$: calcd. C 55.7, H 4.7, N 0.8; found: C 54.3, H 4.9, N 0.8.

Preparation of Diisocyanide-Bridged Bis(alkenylcarbyne) Ditungsten Complexes 4a and 4b: General Procedure: A mixture of complex **1a** or **1b** (0.2 mmol) and 0.5 equiv. of 1,4-phenylendiisocyanide (0.1 mmol) in 20 mL of dichloromethane was stirred at room temperature for 2 h. The resulting orange-red solution was evaporated to dryness and the residue was washed with diethyl ether (2 × 5 mL) and hexane (3 × 5 mL) to give an orange-red solid **4a** and **4b**. Yield: 75−80%. Conductivity (acetone, 20°C, $Ω^{-1}$ cm^2 mol^{-1}): **4a**, 200; **4b**, 195.

Spectral and Analytical Data for 4a: IR [KBr, ν(CN); ν(CO); ν(BF_4)]: $\tilde{\nu}$ = 2133 (m); 2000 (vs), 1947 (s); 1061 (s, br). − ^{1}H NMR (δ, $CDCl_3$) 1.76 (m, 8 H, 4 CH_2), 2.36 (m, 4 H, 2 CH_2), 2.56 (m, 4 H, 2 CH_2), 2.7−3.4 [m, 8 H, 2 $P(CH_2)_2P$], 6.42−7.78 [m, 44 H, $(CN)_2C_6H_4$, 4 PPh_2]. − $^{13}C\{^1H\}$ NMR (δ, $CDCl_3$) 25.4 (s, 2 CH_2), 25.5 (m, 2 $PC_aH_2C_bH_2P$), 26.0 (s, 2 CH_2), 27.3 (m, 2 $PC_aH_2C_bH_2P$), 33.2 (s, 2 CH_2), 35.6 (s, 2 CH_2), 125.7−133.5 [m, $C_β$, $C_β'$, $(CN)_2C_6H_4$, 4 PPh_2]. $-C_{78}H_{70}B_2F_8N_2O_4P_4W_2$: calcd. C 53.1, H 4.0, N 1.6; found: C 52.8, H 4.1, N 1.5.

Spectral and Analytical Data for 4b: IR [KBr, ν(CN); ν(CO); ν(BF_4)] $\tilde{\nu}$ = 2128 (m); 1997 (vs), 1944 (s); 1055 (s, br). − ^{1}H NMR (δ, $CDCl_3$) 1.50 (m, 12 H, 6 CH_2), 1.76 (m, 4 H, 2 CH_2), 1.82 (m, 4 H, 2 CH_2), 2.20 (m, 4 H, 2 CH_2), 2.63 (m, 4 H, 2 CH_2), 2.8−3.2 [m, 8 H, 2 $P(CH_2)_2P$], 6.36−7.79 [m, 44 H, $(CN)_2C_6H_4$, 4 PPh_2]. − $^{13}C\{^1H\}$ NMR (δ, $CDCl_3$) 25.6 (m, 2 $PC_aH_2C_bH_2P$), 25.5 (s, 2 CH_2), 26.5 (s, 2 CH_2), 26.7 (s, 2 CH_2), 27.2 (s, 2 CH_2), 27.5 (m, 2 $PC_aH_2C_bH_2P$), 27.8 (s, 2 CH_2), 33.0 (s, 2 CH_2), 37.1 (s, 2 CH_2), 125.7−133.6 [m, $(CN)_2C_6H_2$, 4 PPh_2], 136.4 [d, ^3J(C−P) = 16.7 Hz, $C_β$, $C_β'$]. − MS (FAB, *m*/*z*) 0.5 [M^+ − 2 × (BF_4) − $(CN)_2C_6H_4$] = 773. $-C_{84}H_{82}B_2F_8N_2O_4P_4W_2$: calcd. C 54.6, H 4.5, N 1.5; found: C 53.8, H 4.3, N 1.8.

Electrochemical Measurements: The electrochemical experiments were performed on an EG & G PARC 273 potentiostat/galvanostat connected to a PC computer through a GPIB interface (National Instruments PC-2A) or on an EG & G PARC 173 potentiostat/galvanostat and an EG & G PARC 175 Universal programmer. Cyclic voltammetry was undertaken in a two-compartment three-electrode cell, at a platinum- or vitreous carbon-disc working electrode (d = 0.5 or 1 mm, respectively), probed by a Luggin capillary connected to a silver-wire pseudo-reference electrode; a platinum auxiliary electrode was employed. Controlled potential electrolyses were carried out in a two-compartment three electrode cell with platinum gauze working and counter electrodes in compartments separated by a glass frit; a Luggin capillary, probing the working electrode, was connected to a silver wire pseudo reference electrode. The electrochemical experiments were performed in an inert atmosphere (N_2) at room temperature. The potentials were measured in 0.2 mol dm^{-3} [NBu_4][BF_4]/MeCN or CH_2Cl_2, and are quoted relative to the saturated calomel electrode (SCE) by using as internal reference the $[Fe(\eta^5\text{-}C_5H_5)_2]^{0/+}$ couple (E_{-}^{ox} = 0.45 or 0.53 V vs. SCE).

The acid-base potentiometric titrations of the electrochemically oxidised solutions were carried out by using a solution of NaOH in MeOH that was standardised by titration against benzoic acid in MeCN or CH_2Cl_2. The results have been corrected for background effects by also performing, in each case, the titration of a blank electrolyte solution which has been electrolysed under identical conditions to those used for the corresponding complex solution.

Acknowledgments

This work was supported by the Dirección General de Investigación Científica y Técnica (Project PB96-0558) and the EU (Human Capital Mobility Programme, Project ERBCHRXCT 940501). L. Z. is grateful to the Spanish Ministerio de Asuntos Exteriores (Agencia Española de Cooperación Internacional) for a doctoral grant and the Fundaçao para a Ciencia e a Tecnologia, PRAXIS XXI Programme (Portugal) for a post-doctoral grant (for doing the detailed electrochemical studies). R. J. C. thanks the Spanish Ministerio de Educación y Cultura for a predoctoral fellowship.

[1] For recent reviews on metal carbyne complexes see: [1a] P. F. Engel, M. Pfeffer, *Chem. Rev.* **1995**, *95*, 2281. − [1b] *Transition Metal Carbyne Complexes;* NATO ASI Series, Kluwer Academic Publishers, Dordrecht, **1993**.

[2] For applications of metal carbyne complexes in organic synthesis see: L. McElwee-White, *Synlett* **1996**, 806.

[3] For recent developments see: [3a] L. Zhang, M. P. Gamasa, J. Gimeno, R. J. Carbajo, F. López-Ortiz, M. Lanfranchi, A. Tiripicchio, *Organometallics* **1996**, *15*, 4274. − [3b] L. Zhang, M. P. Gamasa, J. Gimeno, A. Galindo, C. Mealli, M. Lanfranchi, A. Tiripicchio, *Organometallics* **1997**, *16*, 4099 and references therein. − [3c] B. E. Woodworth, P. S. White, J. L. Templeton, *J. Am. Chem. Soc.* **1997**, *119*, 828 and references therein. − [3d] D. E. Main, L. McElwee-White, *J. Am. Chem. Soc.* **1997**, *119*, 4551. − [3e] L. Weber, G. Dembeck, R. Boese, D. Bläser, *Chem. Ber. /Rec* **1997**, *130*, 1305. − [3f] B. E. Woodworth, D. S. Frohnapfel, P. S. White, J. L. Templeton, *Organometallics* **1998**, *17*, 1655.

[4] A few examples containing saturated di-carbyne bridging units are also known:[4a] $[Tp'(CO)_2M{\equiv}C{-}CH(R){-}CH(R){-}C{\equiv}M(CO)_2Tp']$ (M = Mo. R = H; M = W. R = Me, CH_2Ph, $CHMe_2$) (ref 3c). − [4b] $[Tp'(CO)_2M{\equiv}C{-}C{\equiv}W(CO)(PhC{\equiv}CPh)Tp']$ (M = Mo, W) B. E. Woodworth, P. S. White, J. L. Templeton, *J. Am. Chem. Soc.* **1998**, *120*, 9028. − [4c] $[Cp\{P(OMe)_3\}_2Mo{\equiv}C{-}C(H)tBu{-}C(H)tBu{-}C{\equiv}Mo\{P(OMe)_3\}_2Cp]$ R. G. Beevor, M. J. Freeman, M. Green, C. E. Morton, A. G. Orpen, *J. Chem. Soc., Chem. Commun.* **1985**, 68.

[5] N. A. Ustynyuk, V. N. Vinogradova, V. G. Andrianov, Y. T. Struchkov, *J. Organomet. Chem.* **1984**, *268*, 73.

[6] [6a] E. O. Fischer, W. Röll, N. H. T. Huy, K. Ackermann, *Chem. Ber.* **1982**, *115*, 2951. − [6b] N. O. Dao, H. Fevrier, M. Jouan, E. O. Fischer, W. Röll, *J. Organomet. Chem.* **1984**, *275*, 191.

[7] To the best of our knowledge only the following analogous complexes of this type are known: [7a] $[W_2(\mu\text{-}Cl)_2(\mu{-}Ph_2AsCH_2AsPh_2)(\equiv CPh)_2]$: E. O. Fischer, A. Ruhs, *Chem. Ber.* **1978**, *111*, 2774. − [7b] $[M(\equiv C{-}NEt_2)(CO)_3(\mu\text{-}L)]_2$ (M = Mo, W. L = Br, I, SPh, NCO, etc.): E. O. Fischer, D. Wittmann, D. Himmelreich, R. Cai, K. Ackermann, D. Neugebauer, *Chem. Ber.* **1982**, *115*, 3152.

[8] A. J. L. Pombeiro, J. A. McCleverty, *Molecular Electrochemistry of Inorganic, Bioinorganic, and Organometallic Compounds*, NATO ASI Series; Kluwer Academic Publishers, Dordrecht, The Netherlands, **1993**.

[9] S. S. P. R. Almeida, A. J. L. Pombeiro, *Organometallics*, **1997**, *16*, 4469.

[10] M. A. N. D. A. Lemos, M. F. C. Guedes da Silva, A. J. L. Pombeiro, *Inorg. Chim. Acta*, **1994**, *226*, 9.

[11] [11a] R. Bertani, M. Mozzon, R. A. Michelin, F. Benetollo, G. Bombieri, T. J. Castilho, A. J. L. Pombeiro, *Inorg. Chim. Acta*, **1991**, *189*, 175. − [11b] G. Facchin, M. Mozzon, R. A. Michelin, M. T. A. Ribeiro, A. J. L. Pombeiro, *J. Chem. Soc., Dalton Trans.,* **1992**, 2827. − [11c] R. Bertani, M. Mozzon, R. A. Michelin, T. J. Castilho, A. J. L. Pombeiro, *J. Organomet. Chem.*, **1992**, *431*, 117. − [11d] Y. Wang, A. J. L. Pombeiro, R. A. Michelin, M. Mozzon, R. Bertani, *Bull. Pol. Acad. Sci.,* **1994**, *42*, 307. − [11e] U. Belluco, R. Bertani, R. A. Michelin, M. Mozzon, M. F. C. Guedes da Silva, J. J. R. Fraústo da Silva, A. J. L. Pombeiro, Y. Wang, *Inorg. Chim. Acta,* **1995**, *235*, 397.

[12] N. G. Connelly, in: *Molecular Electrochemistry of Inorganic, Bioinorganic and Organometallic Compounds* (Eds.: A. J. L. Pombeiro, J. A. McCleverty), NATO ASI Series; Kluwer Academic Publishers, Dordrecht, The Netherlands, **1993**.

[13] M. K. Lloyd, J. A. McCleverty, J. A. Connor, M. B. Hall, I. H. Hillier, E. M. Jones, G. K. McEwen, *J. Chem. Soc., Dalton. Trans.,* **1973**, 1743.

[14] [14a] E. O. Fischer, M. Schluge, J. O. Besenhard, *Angew. Chem. Int. Ed. Engl.,* **1976**, *15*, 683. − [14b] E. O. Fischer, F. J. Gammel, J. O. Besenhard, A. Frank, D. Neugebauer, *J. Organomet. Chem.*, **1980**, *191*, 261. − [14c] E. O. Fischer, D. Wittmann, D. Himmerlreich, D. Neugebauer, *Angew. Chem. Int. Ed. Engl.,* **1982**, *21*, 444.

[15] [15a] I. Kovacik, O. Gevert, H. Werner, M. Schimittel, R. Sollner, *Inorg. Chim. Acta,* **1998**, *275−276,* 435. − [15b] R. D. Rieke, H. Kojima, K. Ofele, *Angew Chem., Int. Ed. Engl.,* **1980**, *19*, 538.

[16] [16a] P. J. Krusic, U. Klabunde, C. P. Casey, T. F. Block, *J. Am. Chem. Soc.*, **1976**, *98*, 2015. − [16b] C. P. Casey, L. D. Albin, M. C. Seaman, D. H. Evans, *Organomet. Chem.,* **1978**, *155*, C37.

[17] [17a] J. −P. Battioni, D. Lexa, D. Mansuy, J.-M. Savéant, *J. Am. Chem. Soc.,* **1983**, *105*, 207. − [17b] M. Lange, D. Mansuy, *Tetrahedron Lett.,* **1981**, *22*, 2561.
[18] K. Nakamoto, *Infrared and Raman Spectra of Inorganic and Coordination Compounds, 4th ed.*, Wiley-Interscience Publication: New York, **1986**, p.283.
[19] D. F. Shriver, S. A. Shriver, S. E. Anderson, *Inorg. Chem.* **1965**, *4*, 725.
[20] E. M. Shustorovich, M. A. Poraikoshits, Yu. A. Buslaev, *Coord. Chem. Rev.* **1975**, *17*, 1.
[21] R. J. Carbajo, L. Zhang, F. López-Ortiz, *Magn. Reson. Chem.* **1998**, *36*, 807.
[22] F. López-Ortiz, R. J. Carbajo, *Current Org. Chem.* **1998**, *2*, 97.
[23] $^{7}J(^{183}W\text{-}^{1}H)$ have been described in the literature: A. Macchioni, P. S. Pregosin, P. F. Engel, S. Mecking, M. Pfeffer, J.-C. Daran, J. Vaissermann, *Organometallics* **1995**, *14*, 1637.
[24] J. Chatt, C. T. Kan, G. J. Leigh, C. J. Pickett, D. R. Stanley, *J. Chem. Soc., Dalton Trans.*, **1980**, 2032.
[25] S. S. P. R. Almeida, M. F. C. Guedes da Silva, J. J. R. Fraústo da Silva, A. J. L. Pombeiro, *J. Chem. Soc., Dalton Trans.*, **1999**, 467.
[26] [26a] D. W. Bruce, D. O′Hare *Inorganic Materials,* Wiley, New York, **1992**. − [26b] M. H. Chisholm, *Angew. Chem. Int. Ed. Engl.* **1991***, 30*, 673.

Received July 7, 1999
[I99251]

Chiral 4-(Diphenylphosphanyl)-1-(dialkylamino)butane Ligands – Synthesis, Applications in Asymmetric Alkylation and Theoretical Study

Fabien Robert,[a] Françoise Delbecq,[b] Christelle Nguefack,[a] and Denis Sinou*[a]

Keywords: Aminophosphanes / Palladium / Alkylations / Enantioselectivity / Theoretical study

Various 4-(diphenylphosphanyl)-1-(dialkylamino)butane ligands were prepared from commercial (2*S*,3*S*)-2,3-*O*-isopropylidene-D-threitol. These ligands, associated with $Pd_2(dba)_3$, gave enantioselectivities of up to 75% in the alkylation of racemic 1,3-diphenylprop-2-enyl acetate with dimethyl malonate anion. A theoretical study shows the important role played by two factors in the alkylation reaction: steric control, leading to the formation of a unique diastereoisomer of the π-allylpalladium complex, and orbital control, which orients the attack of the nucleophile *trans* to the phosphorus atom.

Introduction

Asymmetric metal catalysis is one of the most powerful methods for the preparation of enantiomerically pure compounds.[1] An impressive number of chiral ligands have been prepared and used, among them P,P-, P,N- and N,N-based ligands. The phosphanyloxazolines, P,N-based ligands, induce high enantioselectivities, particularly in the palladium-catalyzed allylic substitution.[2] In comparison, P,N ligands with an sp^3 nitrogen atom have been used less in asymmetric catalysis. Hayashi et al. prepared chiral β-(aminoalkyl)phosphanes[3] and [(aminoalkyl)ferrocenyl]-phosphanes.[4] Chiral aminophosphanes, in which the chirality is on the substituents of the nitrogen atom through a pyrrolidine[5−6] or a naphthyl unit,[7] have also been described more recently. These ligands were successfully used in asymmetric hydrogenation, cross-coupling reactions and mainly allylic substitution.

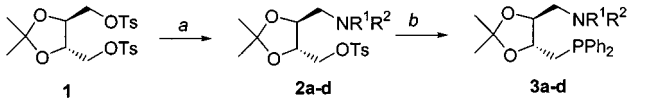
We recently reported, in a preliminary communication, the synthesis of chiral aminophosphanes derived from tartaric acid and their use in asymmetric alkylation.[8] We describe in this paper a full account of the synthesis of these new chiral ligands and their use as ligands in asymmetric alkylation, as well as a theoretical study concerning the nucleophilic attack on π-allyl(palladium) complexes associated with these ligands.

[a] Laboratoire de Synthèse Asymétrique, associé au CNRS,
CPE Lyon, Université Claude Bernard Lyon 1,
43, bd du 11 novembre 1918, F-69622 Villeurbanne Cedex, France
Fax: (internat.) + 33-4/72448160
E-mail: sinou@univ-lyon1.fr
[b] Institut de Recherches sur la Catalyse,
Groupe Théorie et Modélisation,
2, avenue Einstein, F-69626 Villeurbanne Cedex, France
Fax: (internat.) + 33-4/72445399
E-mail: delbecq@catalyse.univ-lyon1.fr

Results and Discussion

Synthesis of the P,N-Based Ligands

Ligands **3a**−**d**, bearing at least one aryl group at the nitrogen atom, were prepared from commercially readily available bis(tosylate) **1** (Scheme 1). Reaction of **1** at −17 °C in tetrahydrofuran with one equiv. of lithium diphenylamide, obtained by treating diphenylamine with *n*-butyllithium at −78 °C, gave diphenylamino tosylate **2a** in 26% yield. Subsequent treatment of compound **2a** with lithium diphenylphosphide in tetrahydrofuran led to the formation of the diphenylamino phosphane **3a** in 40% yield. Steric and electronic modifications of the substituents at the nitrogen atom were introduced with methyl(phenyl)-, *p*-methoxyphenyl(methyl)- and phenyl(α-naphthyl)amine instead of diphenylamine; the corresponding amino phosphanes **3b**, **3c**, and **3d** were obtained in 18%, 7%, and 21% yield, respectively, from compound **1**. All attempts to introduce the *p*-nitrophenyl(methyl)amino group failed, only the elimination product was observed.

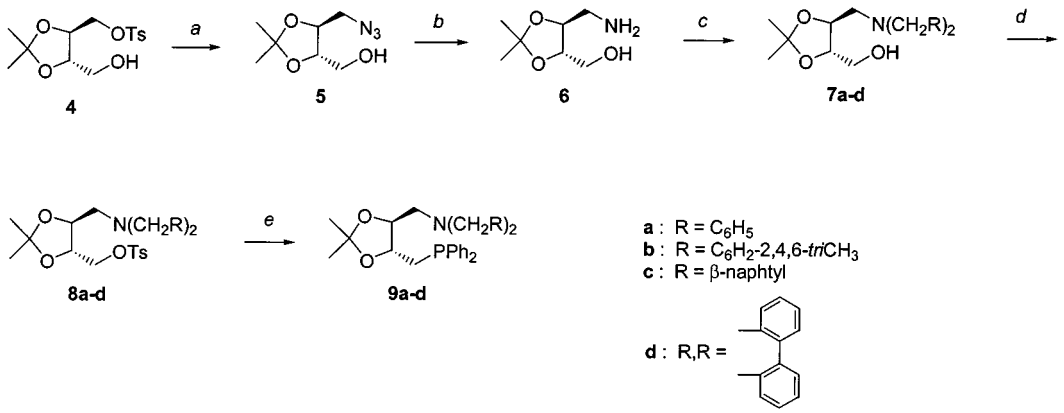


a : $R^1 = R^2 = C_6H_5$; **b** : $R^1 = C_6H_5$, $R^2 = CH_3$; **c** : $R^1 = C_6H_4$-*p*-OCH_3, $R^2 = CH_3$
d : $R^1 = C_6H_5$, R^2 = α-naphtyl

Scheme 1. a: $LiNR^1R^2$, THF, −17 °C; b: $LiPPh_2$, THF, 25 °C

Reaction of monotosylate **4**[9] with sodium azide in DMF gave the azido alcohol **5** in 95% yield (Scheme 2). Reduction of compound **5** with molecular hydrogen in the presence of 20% Pd/C led quantitatively to the amino alcohol **6**. Condensation of this amino alcohol **6** with two equiv. of benzyl bromide, 2,4,6-trimethylbenzyl bromide, 2-naphtylmethyl bromide or 2,2′-bis(bromomethyl)biphenyl in acetonitrile in the presence of potassium carbonate gave the bis(alkylamino) alcohols **7a**−**d** in 58−85% yield. Tosylation of these

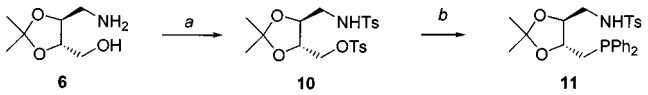
 © WILEY-VCH Verlag GmbH, D-69451 Weinheim, 2000 1434−1948/00/0202−351 $ 17.50+.50/0



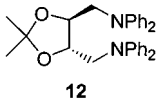
Scheme 2. a: NaN_3, DMF, 24 h, 95%; b: H_2, Pd/C, EtOH, 48 h, 100%; c: RCH_2Br (2 equiv.), K_2CO_3, CH_3CN, 30 min; d: $LiPPh_2$, THF, 25 °C

bis(alkylamino) alcohols **7** led to the bis(alkylamino) tosylates **8a**−**d**, whose treatment by lithium diphenylphosphide gave the desired bis(alkylamino) phosphanes **9a**−**d** in 40%, 45%, 20%, and 80% yield, respectively.

Reaction of amino alcohol **6** with two equiv. of tosyl chloride in pyridine gave the bis(tosylate) **10** in 65% yield (Scheme 3); tosylamino diphenylphosphane **11** was obtained in 73% yield by subsequent treatment of **10** with more than two equiv. of lithium diphenylphosphide. Finally, the bis(diphenyl)amino ligand **12** was obtained as a byproduct in the preparation of compound **2a**.

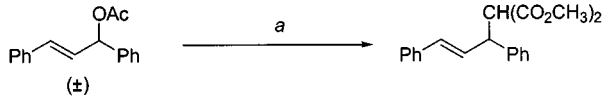


Scheme 3. a: TsCl, C_5H_5N, 25 °C, 65%; b: $LiPPh_2$, THF, 25 °C



Asymmetric Alkylation

The effectiveness of the above ligands in asymmetric allylic alkylation was tested in the reaction of racemic (*E*)-1,3-diphenylprop-2-enyl acetate with dimethyl malonate; an in situ catalyst prepared from $Pd_2(dba)_3$ and the chiral ligand in THF was used (Scheme 4).



Scheme 4. a: $CH_2(CO_2Me)_2$, base, cat. $Pd_2(dba)_3$, ligand

As a typical procedure, tris(dibenzylideneacetone)dipalladium and the amino phosphane were mixed in a solvent at room temperature under argon; *rac*-(*E*)-1,3-diphenylprop-2-enyl acetate was added, then the sodium salt of dimethyl malonate was added to the π-allylpalladium complex solution. The substituted product thus obtained was isolated by chromatography. The results are summarized in Table 1.

Table 1. Allylic alkylation of (±)-(*E*)-1,3-diphenylpropenyl acetate with dimethyl malonate, catalyzed by palladium complexes[a]

Entry	Ligand	Solvent	Conversion (%)[b]	ee (%)[b]
1	DIOP	THF	95	0
2	**12**	THF	90	0
3	**3a**	THF	97	50
4	**3b**	THF	94	68
5	**3c**	THF	96	63
6	**3d**	THF	93	69
7	**3d**	THF[c]	47	30
8	**3d**	CH_2Cl_2[d]	94	67
9	**3d**	CH_2Cl_2[c]	95	68
10	**3d**	Toluene[c]	4	8
11	**3d**	Toluene/CH_2Cl_2 (4:1)[d]	12	10
12	**9a**	THF	94	62
13	**9b**	THF	97	75
14	**9c**	THF	99	57
15	**9d**	THF	99	48
16	**11**	THF	49	39

[a] [acetate]/[malonate]/[NaH]/[$Pd_2(dba)_3$]/[ixgand] = 50:150:150:1:2; solvent: THF; 25 °C; 24 h. − [b] Determined by HPLC analysis with chiral stationary column Daicel Chiralcel OD−H (hexane/2-propanol 98:2); the configuration of the alkylated product was (*S*).[10] − [c] *N*,*O*-Bis(trimethylsilyl)acetamide (or BSA) and KOAc were used instead of NaH. − [d] *N*,*O*-Bis(trimethylsilyl)acetamide only was used instead of NaH.

It should first be noted that the use of ligands with C_2 symmetry, such as DIOP or ligand **12**, led to the formation of the racemic alkylated product (Entries 1−2). Ligands **3a**−**d** gave enantioselectivities up to 69% in THF as the solvent (Entries 3−6). Dissymmetrization at the nitrogen atom increased the enantioselectivity, although an enantioselectivity of 50% was observed with **3a** as the ligand; values of 68% and 69% were obtained in the presence of **3b** or **3d**, respectively. The presence of a methoxy group on the phenyl ring lowered the enantioselectivity (63% for **3c**). To increase the enantioselectivity, the alkylation was performed under various conditions, with **3d** as the ligand. While the use of BSA as the base in the presence of KOAc gave both lower yield and enantioselectivity (Entry 7), performing the reaction in CH_2Cl_2 gave almost the same e.e. (68%) in the

presence or absence of KOAc (Entries 8−9). The use of toluene (Entry 10) or a mixture of toluene/CH_2Cl_2 (Entry 11) as solvent again gave low yield and enantioselectivity. The use of ligands **9** in this alkylation reaction led to high chemical yields, with enantioselectivities depending on the nature of the aromatic ring. The highest enantioselectivity (75%) was obtained with ligand **9b**, which has 2,4,6-trimethylbenzyl substituents on the nitrogen atom. Finally, ligand **11** gave low yield (only 49%) and quite modest enantioselectivity (39%). To obtain more insight into the reasons behind the high enantioselectivities when these ligands are used, we undertook a theoretical study.

Theoretical Study

Some theoretical studies on η^3-allyl complexes of palladium have already been reported. In the past, semi-empirical methods have been used to study the nucleophilic attack on such complexes: Extended Hückel type (EHT) calculations were carried out to probe the effect of ligand asymmetry,[11] to distinguish between the central and the terminal carbon atoms,[12] to calculate the effect of the substituents on the regioselectivity,[13] and CNDO type calculations were carried out to determine the ligand effects.[14] The conclusions of these studies were that the nucleophilic attack on η^3-allylpalladium complexes is orbital-controlled rather than charge-controlled. More recently, studies using ab initio methods, both at the Hartree−Fock level and with the density functional theory (DFT), have begun to appear.[15−20]

In the present work we have used both types of methods, EHT and DFT. To determine the site of the nucleophilic attack, we have used the same method as in our previous work.[13] Since the reaction is frontier orbital controlled, we have focused first on the shape of the complex LUMO (Lowest Unoccupied Molecular Orbital) which interacts with the nucleophile HOMO (Highest Occupied Molecular Orbital). The larger the coefficient on one carbon atom in this orbital, the easier is the attack of the nucleophile on that carbon atom. Then we have put some nucleophiles at the same distance to both terminal carbon atoms and compared the overlap populations. These calculations are based on the EHT method. However, it is known from experiments that the presence of ligands of different natures on the palladium center induces a dissymmetry in the complex.[21−23] The EHT method does not allow the optimization of geometries. This is why we used a DFT method for these optimizations, to have reliable geometries for the EHT calculations.

Computational Methods

The parameters used for the EHT calculations are the usual ones[24][25] and the program is ICON version 8.0 from the group of R. Hoffmann at Cornell University.[26] The ab initio calculations are performed with Gaussian 94[27] with the DFT formalism. The chosen function is that of Perdew and Wang (BPW91). For palladium and phosphorus, the pseudopotentials of Hay and Wadt are used with the corresponding double ζ basis set of Dunning/Huzinaga (D95). A d polarization function is added to the palladium, nitrogen and carbon atoms. The ligands on the phosphorus center are modelled by PH_3 and NH_3 to save computational time. Since the allyl moiety is symmetrical with one phenyl group on each terminal carbon atom, we chose to model it in the first instance by the unsubstituted allyl group C_3H_5. By doing this, we obtained the electronic effects without taking into account the steric effects.

Results

The optimized geometry is shown in Figure 1. The most important information is that the Pd−$C_{trans\text{-}P}$ bond (2.23 Å) is longer than the Pd−$C_{trans\text{-}N}$ one (2.16 Å). This result can be explained by the *trans* effect of the phosphorus atom, which is greater than that of the nitrogen atom.[28] Experimentally, the same difference was observed,[15] although the nitrogen ligand was not of the same nature (sp^2 instead of sp^3). The C^1-C^2 and C^2-C^3 bond lengths are not equal either (1.417 and 1.432 Å, respectively). This means that the C^2-C^3 bond has a weaker double bond character. The carbon atoms C^1 and C^3 are 0.14−0.15 Å above the P−Pd−N plane, and the allyl plane makes an angle of 111° with the Pd−C^1−C^3 plane. Similar geometries were found experimentally.[22,23,29] The charge on carbon atoms C^1 and C^3 (0.55 e^-) is the same. As found in our previous EHT study, the LUMO is mainly the antibonding combination of the d_{xy} orbital of the metal center and the n-allyl orbital and the next unoccupied orbital is composed almost exclusively of the π*-allyl orbital.

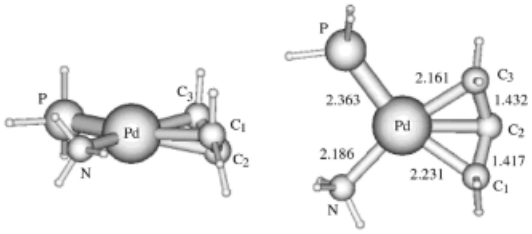


Figure 1. Optimized geometry for palladium complex Pd(NH_3)(PH_3)(η^3-allyl)

After this geometry optimization, we performed EHT calculations, following the method of our previous work.[13] We choose the same standard distances but we kept the difference between Pd−C^1 and Pd−C^3 bonds fixed (0.08 Å). The following geometry was used: Pd−P = 2.3 Å, Pd−N = 2.15 Å, Pd−C^1 = 2.20 Å, Pd−C^3 = 2.12 Å, $C^1-C^2 = C^2-C^3$ = 1.43 Å, P−Pd−N = 100°. For the sake of simplicity, the allyl plane was taken to be perpendicular to the P−Pd−N plane and to the bisector of the P−Pd−N angle. The hydrogen atoms on the carbon atoms C^1 and C^3 are bent away from the metal center by 15°. The projection on the *xy* plane is shown in Figure 2. The complex LUMO is also shown.

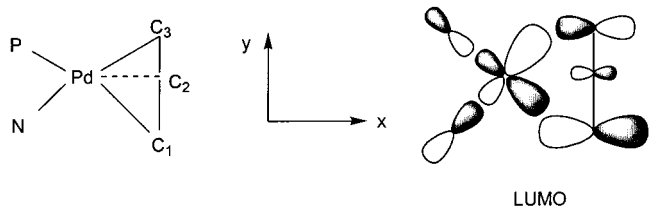


Figure 2. Projection of the model allyl−Pd complex on the *xy* plane and shape of its LUMO

We observe that the p_x coefficient is larger on the carbon atom C^1 than on C^3 (0.53 and 0.48, respectively). If the reaction is orbital-controlled, an incoming nucleophile will prefer to attack the carbon atom with the largest contribution in the LUMO. Hence it will preferentially attack C^1, *trans* to the phosphorus atom. Why is the LUMO dissymmetrical? The molecular orbital interaction diagram between the P−Pd−N and the allyl fragments shows that the LUMO, which is mainly antibonding between d_{xy} and the n-allyl orbital, also contains a small antibonding contribution of the π-allyl orbital and a small bonding contribution of the π*-allyl orbital, according to Equation 1.

$$\text{LUMO} = 0.80\ (\text{Pd}-\text{P}-\text{N LUMO}) - 0.69\ (\text{n}) - 0.04\ (\pi) + 0.08\ (\pi^*) \quad (1)$$

In fact, the LUMO of the P−Pd−N fragment is dissymmetric because the two ligands are different. This allows the mixing of the three allyl orbitals which are of different symmetry and they do not mix when the metal fragment is symmetrical (Figure 3).

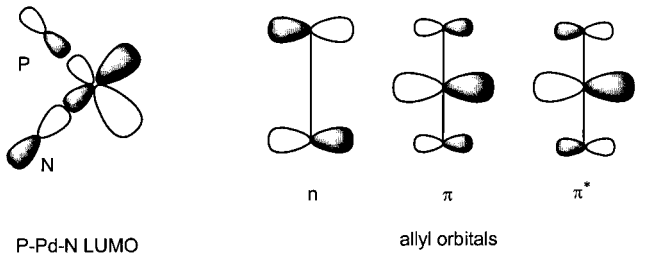


Figure 3. Shape of the LUMO of the P−Pd−N fragment and of the n, π and π* orbitals of the allyl fragment

However, we saw previously that other metal orbitals must be taken into account in the interaction with a nucleophile: for instance, the next LUMO and some occupied orbitals which have contributions to p_x of C^1 and p_x of C^3. Therefore, we tested the approach of some nucleophiles by putting them at the same distance to carbon atoms C^1 and C^3, and comparing the overlap population that represents the strength of the formed bond. To avoid too many steric repulsions, the allyl part is taken as being planar, this means that the hydrogen atoms are no longer bent away from the palladium center but are in the allyl plane (this looks like the transition state of an S_N2 reaction). We chose NH_3, $NHMe_2$ and the malonate anion $^-CH(CO_2Me)_2$ as nucleophiles, the latter of which is the nucleophile experimentally used in the present work. The amines and the malonate anion are put at 2 Å and 2.1 Å away from the carbon atoms, respectively. The best conformation of the nucleophile was searched for by rotating around the approach axis. The results are shown in Table 2. For all nucleophiles, the overlap population is larger with carbon atom C^1 than with C^3; this confirms that a nucleophile will preferentially attack at the carbon atom *trans* to the phosphorus atom, as long as only electronic interactions are taken into account. It is obvious that steric constraints, if for instance the carbon atoms are substituted, can reverse this trend.

Table 2. Overlap populations between a nucleophile and the terminal carbon atoms C^1 and C^3; energy in eV of the nucleophile HOMO

Nucleophile	HOMO	C^1	C^3
NH_3	−13.71	0.143	0.138
$NH(Me)_2$	−12.95	0.157	0.152
$^-HC(CO_2Me)_2$	−12.35	0.180	0.175

The interaction between the nucleophile and the allylic complex can be separated into terms of two-electron and four-electron interactions, by a simple perturbational treatment.[13][30] We consider the function f(x), which is the sum of the stabilizing interactions of the nucleophile HOMO with the vacant orbitals of the complex and the destabilizing interactions between the nucleophile HOMO and the occupied orbitals of the complex (Equation 2). The more positive f(x) is, the more the interaction is stabilizing.

$$f(x) = 0.75\Sigma(x + E_i)\ C_i^2 + \Sigma(0.875\ E_j - 0.125x)^2\ C_j^2/(E_j - x) \quad (2)$$

In Equation 2, x is the energy of the nucleophile HOMO, C_i and C_j are the coefficients of the p_x orbital of the attacked carbon atom in the occupied and vacant complex orbitals, respectively, and E_i and E_j are the energies of the corresponding complex orbitals; x was varied and f(x) was calculated for C_1 [$f_1(x)$] and C_3 [$f_3(x)$]. The difference $F(x) = f_1(x) - f_3(x)$ is drawn in Figure 4. If $F(x) < 0$, the nucleophile prefers carbon atom C^3, if $F(x) > 0$, the nucleophile prefers C^1. The attack preference depends on the HOMO of the nucleophile. For a high-lying HOMO (see Table 2), such as that of the malonate anion, carbon atom $C^{1\ trans}$ to the phosphorus atom is preferentially attacked; this agrees with the experimental results. The attractive two-electron interactions always favor the attack on $C_{trans\text{-}P}$ and, conversely, the repulsive four-electron interactions favor the attack on $C_{cis\text{-}P}$. Therefore, the site of attack depends on the balance between these two terms. The attractive term increases greatly with the HOMO energy. The repulsive term, being proportional to the sum of the interacting orbital energies (Equation 2), depends little on the HOMO position.

We therefore explained why the electronic interactions favor attack on carbon atom $C_{trans\text{-}P}$. We can predict that the use of a nucleophile with a higher HOMO than malonate, such as $^-C(CH_3)(CO_2Me)_2$, for example, would enhance the regioselectivity. How can the enantioselectivity be

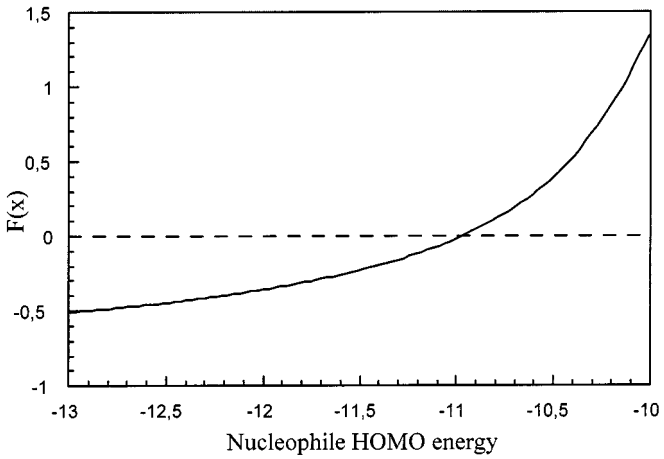


Figure 4. Plot of f(x) versus energy of the nucleophile HOMO

explained? For the π-allylpalladium complexes, two diastereoisomers are possible, *exo* and *endo* (Figure 5).

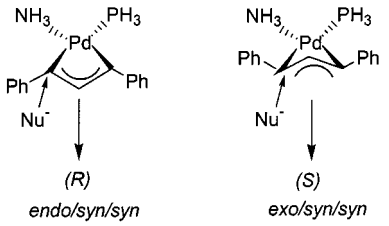


Figure 5. Most stable diastereoisomers of the model $(PH_3)(NH_3)$-(1,3-diphenylallyl)Pd complex

The phenyl rings may be positioned *syn* or *anti*, therefore eight diastereoisomers are possible. Using the EHT method, we calculated all of them and optimized the angle of the phenyl rings with the allyl plane. When the phenyl group is *syn*, it prefers to be in the allyl plane, when it is *anti*, it prefers to be perpendicular to this plane. This is in agreement with previous calculations.[5] The most stable isomers (by 13 kcal mol^{-1}) are those depicted in Figure 5 (*exo*/*syn*/*syn* and *endo*/*syn*/*syn*). With our model ligands PH_3 and NH_3, they are quasi isoenergetic, which cannot explain the enantioselectivity, since, by attack *trans* to the phosphorus atom, they each lead to one of the enantiomers (*S*) and (*R*). We therefore modeled the real catalyst by substituting the phosphorus and nitrogen atoms with phenyl and methyl groups, as shown in Figure 6. This corresponds to real catalysts [Pd/**3a**] and [Pd/**3b**], obtained by association of the palladium center with ligands **3a** and **3b**.

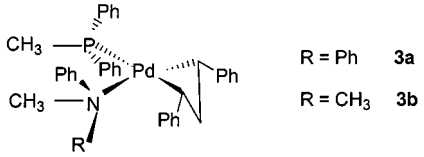


Figure 6. Modeling of the catalyst $Pd(CH_3PPh_2)(CH_3NPhR)(\eta^3$-1,3-diphenylallyl)

The substituents on the phosphorus and nitrogen atoms are disposed in a geometry that reproduced the X-ray structure of DIOP.[31] We calculated the *exo* and *endo* isomers for both [Pd/**3a**] and [Pd/**3b**]. For [Pd/**3b**] there are two *exo* and two *endo* isomers depending on the relative position (pseudo-axial or pseudo-equatorial) of the C_6H_5 and CH_3 substituents on the nitrogen atom. For [Pd/**3a**] the *exo* form is more stable by 30 kcal mol^{-1}. For [Pd/**3b**], the *exo* form is more stable by 18 kcal mol^{-1} when the methyl group is pseudo-axial and the *endo* form is more stable by 67 kcal mol^{-1} when the methyl group is pseudo-equatorial. However, the structure with the pseudo-equatorial methyl group is far less stable than that with the pseudo-axial one (47 kcal mol^{-1}). Therefore, of the four diastereoisomers of [Pd/**3b**], the most stable also has the *exo* geometry. The *exo* form of [Pd/**3a**] and [Pd/**3b**], attacked *trans* to the phosphorus atom, gives the (*S*) enantiomer, which is the one experimentally obtained. Despite the fact that the EHT method only gives qualitative results, the energy differences are large enough to be reliable. Hence, the enantioselectivity is explained by the existence of only one diastereoisomer of the complexes [Pd/**3a**] and [Pd/**3b**], regioselectively attacked *trans* to the phosphorus atom.

Conclusion

In conclusion, the new chiral amino phosphane ligands, easily obtained from tartaric acid, give enantioselectivities of up to 75% in the palladium-catalyzed alkylation of racemic 1,3-diphenylprop-2-enyl acetate with malonate anion. The calculations summarized in this paper allow the origin of the enantioselectivity in this asymmetric allylic alkylation to be understood. Two factors play an important role. The first one is steric control, which leads to the formation of a unique diastereoisomer (*exo*) of the η^3-allylpalladium complex. The second one is orbital control, which orients the nucleophile attack *trans* to the phosphorus atom; this is due to the dissymmetrical ligand. This is not the case for DIOP or ligand **12**. Our calculations also allow some predictions: To enhance the enantioselectivity, the HOMO of the nucleophile must be as high as possible. This means that the anion of $CH(CH_3)(CO_2Me)_2$ or of cyclopentanedione should be more efficient than the malonate anion $CH(CO_2Me)_2^-$

Experimental Section

General Remarks: ^{1}H NMR (200 or 300 MHz), ^{13}C NMR (50 or 75 MHz), and ^{31}P NMR (80 MHz) spectra were obtained with a Brüker AM 200 or AM 300 spectrometer. − Optical rotations were determined with a Perkin−Elmer 241 polarimeter. − GC analyses were recorded with a Shimadzu capillary gas chromatograph, equipped with a Chiraldex™ type B−PH (30 m × 0.32 mm) capillary column. − Reactions involving organometallic catalysis were carried out in Schlenk tubes under an inert gas. Tetrahydrofuran was distilled from sodium/benzophenone. (2*S*,3*S*)-2,3-*O*-Isopropylidene-1-*O*-*p*-toluenesulfonyl-D-threitol (**4**) was prepared according to a literature procedure.[9]

General Procedure for Preparation of Amino Tosylates 2: A solution of the lithium derivative of the secondary amine, obtained by mixing the amine (5 mmol) and butyllithium in hexane (5 mmol) in

THF (5 mL), was slowly added to a solution of ditosylate **1** (2.35 g, 5 mmol) in THF (5 mL) at −17°C. The solution was stirred for 1 h at −17°C, then 12 h at room temperature, and was finally treated with H_2O (50 mL). The organic compound was extracted with CH_2Cl_2 (3 × 50 mL). Evaporation of the solvent, followed by flash chromatography gave the amino tosylate **2**.

(2*S*,3*S*)-4-Diphenylamino-2,3-*O*-isopropylidene-1-*O*-tosylbutane-1,2,3-triol (2a): 26% yield; R_f = 0.5 (eluent: hexane/ethyl acetate, 4:1); $[\alpha]_D^{20}$ = +8.5 (*c* = 1.1, $CHCl_3$). − ^{1}H NMR (200 MHz, $CDCl_3$): δ = 1.29 (s, 3 H, CH_3), 1.38 (s, 3 H, CH_3), 2.43 (s, 3 H, CH_3), 3.90−4.05 (m, 5 H, CH_2N, CH_2O, CHO), 4.05−4.20 (m, 1 H, CHO), 6.90−7.10 (m, 6 H, H_{arom}), 7.15−7.30 (m, 6 H, H_{arom}), 7.71 (d, *J* = 8.3 Hz, 2 H, H_{arom}). − ^{13}C NMR (50 MHz, $CDCl_3$): δ = 21.6 (CH_3), 26.8 (CH_3), 27.2 (CH_3), 55.0 (d, CH_2N), 69.2 (CH_2O), 76.0 (CHO), 76.9 (CHO), 110.2 (CMe_2), 121.2, 121.9, 128.0, 129.4, 129.8, 132.5, 145.0 and 148.0 (C_{arom}). − $C_{26}H_{29}NO_5S$ (467.58): calcd. C 66.79, H 6.86; found C 66.65, H 6.57.

(2*S*,3*S*)-2,3-*O*-Isopropylidene-4-methyl(phenyl)amino-1-*O*-tosylbutane-1,2,3-triol (2b): 32% yield; R_f = 0.4 (eluent: hexane/ethyl acetate, 4:1); $[\alpha]_D^{20}$ = +24.6 (*c* = 1.1, $CHCl_3$). − ^{1}H NMR (200 MHz, $CDCl_3$): δ = 1.31 (s, 3 H, CH_3), 1.39 (s, 3 H, CH_3), 2.45 (s, 3 H, CH_3), 2.95 (s, 3 H, CH_3), 3.46 (dd, *J* = 15.0, 5.7 Hz, 1 H, CH_2N), 3.55 (dd, *J* = 15.0, 4.5 Hz, 1 H, CH_2N), 3.90−4.05 (m, 1 H, CHO), 4.05−4.20 (m, 3 H, CH_2O, CHO), 6.70 (m, 3 H, H_{arom}), 7.25 (m, 2 H, H_{arom}), 7.38 (d, *J* = 8.5 Hz, 2 H, H_{arom}), 7.76 (d, *J* = 8.5 Hz, 2 H, H_{arom}). − $C_{21}H_{27}NO_5S$ (405.51): calcd. C 62.20, H 6.71; found C 62.65, H 7.11.

(2*S*,3*S*)-2,3-*O*-Isopropylidene-4-*p*-methoxyphenyl(methyl)amino-1-*O*-tosylbutane-1,2,3-triol (2c): 25% yield; R_f = 0.55 (eluent: hexane/ethyl acetate, 3:1); $[\alpha]_D^{20}$ = +6.3 (*c* = 0.7, $CHCl_3$). − ^{1}H NMR (200 MHz, $CDCl_3$): δ = 1.30 (s, 3 H, CH_3), 1.40 (s, 3 H, CH_3), 2.88 (s, 3 H, CH_3), 2.89 (s, 3 H, CH_3), 3.40 (d, *J* = 5.2 Hz, 2 H, CH_2N), 3.78 (s, 3 H, CH_3), 3.90−4.05 (m, 1 H, CHO), 4.05−4.20 (m, 3 H, CH_2O, CHO), 6.60−7.00 (m, 4 H, H_{arom}), 7.20−7.40 (m, 2 H, H_{arom}). − $C_{22}H_{29}NO_6S$ (435.54): calcd. C 60.67, H 6.71; found C 61.82, H 6.40.

(2*S*,3*S*)-2,3-*O*-Isopropylidene-4-α-naphthyl(phenyl)amino-1-*O*-tosylbutane-1,2,3-triol (2d): 25% yield; R_f = 0.42 (eluent: hexane/ethyl acetate, 5:1); $[\alpha]_D^{20}$ = +21.6 (*c* = 0.8, $CHCl_3$). − ^{1}H NMR (200 MHz, $CDCl_3$): δ = 1.30 (s, 3 H, CH_3), 1.41 (s, 3 H, CH_3), 2.38 (s, 3 H, CH_3), 3.95−4.10 (m, 5 H, CH_2N, CH_2O, CHO), 4.15−4.25 (m, 1 H, CHO), 7.00−7.50 (m, 11 H, H_{arom}), 7.60−7.80 (m, 4 H, H_{arom}). − $C_{30}H_{31}NO_5S$ (517.64): calcd. C 69.61, H 6.04; found C 69.18, H 6.17.

(2*S*,3*S*)-4-Azido-2,3-*O*-isopropylidenebutane-1,2,3-triol (5): A mixture of (2*S*,3*S*)-2,3-*O*-isopropylidene-1-*O*-*p*-toluenesulfonyl-D-threitol (**4**)[9] (11.8 g, 37.5 mmol) and NaN_3 (3.5 g, 58 mmol) in DMF (95 mL) was heated at reflux for 24 h. After being cooled to room temperature, the solution was treated with H_2O (50 mL) and was then extracted with CH_2Cl_2 (3 × 50 mL). Evaporation of the solvent, followed by column chromatography (eluent: petroleum ether/ethyl acetate, 2:1) gave 6.6 g of compound **5** as an oil (95%); R_f = 0.3; $[\alpha]_D^{20}$ = −65.7 (*c* = 2.5, $CHCl_3$). − ^{1}H NMR (200 MHz, $CDCl_3$): δ = 1.36 (s, 3 H, CH_3), 1.41 (s, 3 H, CH_3), 2.84 (s, 1 H, OH), 3.34 (dd, *J* = 13.1, 4.6 Hz, 1 H, CH_2N), 3.55 (dd, *J* = 13.1, 3.7 Hz, 1 H, CH_2N), 3.74 (dd, *J* = 13.8, 3.9 Hz, 1 H, CH_2O), 3.86 (dd, *J* = 13.8, 4.0 Hz, 1 H, CH_2O), 4.02 (ddd, *J* = 11.4, 4.6, 3.7 Hz, 1 H, CHO), 4.07 (ddd, *J* = 11.4, 4.0, 3.9 Hz, 1 H, CHO). − $C_7H_{13}N_3O_3$ (187.20): calcd. C 44.91, H 6.00; found C 44.96, H 7.28.

(2*S*,3*S*)-4-Amino-2,3-*O*-isopropylidenebutane-1,2,3-triol (6): A solution of azido alcohol **5** (3 g, 16 mmol) in ethanol (20 mL) was hydrogenated at room temperature and atmospheric pressure in the presence of 20% Pd/C (300 mg). After 48 h, the solution was filtered and the solvent was evaporated to give 2.57 g of amino alcohol **6** as an oil (100%); $[\alpha]_D^{20}$ = −47.3 (*c* = 1.0, $CHCl_3$). − ^{1}H NMR (200 MHz, $CDCl_3$): δ = 1.32 (s, 3 H, CH_3), 1.38 (s, 3 H, CH_3), 2.20−2.50 (br. s, 3 H, NH_2, OH), 2.76 (dd, *J* = 12.6, 8.0 Hz, 1 H, CH_2N), 3.18 (dd, *J* = 12.6, 4.3 Hz, 1 H, CH_2N), 3.70−3.92 (m, 4 H, CH_2O, CHO). $C_7H_{15}NO_3$ (161.20): calcd. C 52.16, H 9.38; found C 51.76, H 9.16.

General Procedure for the Preparation of Amino Alcohols 7: The bromide (12.4 mmol) was slowly added to a mixture of amino alcohol **6** (1 g, 6.2 mmol) and K_2CO_3 (2,57 g, 18.6 mmol) in CH_3CN (6 mL), heated at reflux for 30 min. The reaction mixture was refluxed for 24 h, then cooled at room temperature, and treated with H_2O (10 mL). The solution was extracted with CH_2Cl_2 (3 × 30 mL). Evaporation of the solvent, followed by flash chromatography gave the corresponding dialkylated amino alcohol **7**.

(2*S*,3*S*)-4-Dibenzylamino-2,3-*O*-isopropylidenebutane-1,2,3-triol (7a): 85% yield; R_f = 0.3 (eluent: petroleum ether/ethyl acetate, 4:1); $[\alpha]_D^{20}$ = +32.1 (*c* = 0.8, $CHCl_3$). − ^{1}H NMR (200 MHz, $CDCl_3$): δ = 1.35 (s, 3 H, CH_3), 1.40 (s, 3 H, CH_3), 2.63 (s, 1 H, OH), 2.72 (d, *J* = 5.5 Hz, 2 H, CH_2N), 3.60−3.90 (m, 8 H, CH_2O, CHO, CH_2N), 7.30−7.50 (m, 10 H, H_{arom}). − $C_{21}H_{27}NO_3$ (341.45): calcd. C 73.87, H 7.97, N 4.10; found C 73.73, H 8.12, N 4.04.

(2*S*,3*S*)-4-Bis(2,4,6-trimethylbenzyl)amino-2,3-*O*-isopropylidenebutane-1,2,3-triol (7b): 76% yield; R_f = 0.4 (eluent: petroleum ether/ethyl acetate, 4:1); $[\alpha]_D^{20}$ = +10.2 (*c* = 1, $CHCl_3$). − ^{1}H NMR (200 MHz, $CDCl_3$): δ 1.35 (s, 3 H, CH_3), 1.41 (s, 3 H, CH_3), 1.65 (s, 1 H, OH), 2.23 (s, 6 H, CH_3), 2.26 (s, 12 H, CH_3), 2.58 (m, 2 H, CH_2N), 3.40−3.50 (m, 4 H, CH_2O), 3.49 (d, *J* = 12.5 Hz, 2 H, CH_2N), 3.69 (d, *J* = 12.5 Hz, 2 H, CH_2N), 3.80−4.00 (m, 2 H, CHO), 6.75 (s, 4 H, H_{arom}). − $C_{27}H_{39}NO_3$ (425.62): calcd. C 76.24, H 9.17; found C 76.21, H 9.34.

(2*S*,3*S*)-4-Bis(2-naphtylmethyl)amino-2,3-*O*-isopropylidenebutane-1,2,3-triol (7c): 82% yield; R_f = 0.34 (eluent: petroleum ether/ethyl acetate, 4:1); $[\alpha]_D^{20}$ = +14.0 (*c* = 0.65, $CHCl_3$). − ^{1}H NMR (200 MHz, $CDCl_3$): δ = 1.32 (s, 3 H, CH_3), 1.38 (s, 3 H, CH_3), 1.61 (s, 1 H, OH), 2.81 (d, *J* = 5.7 Hz, 2 H, CH_2N), 3.73 (d, *J* = 13.3 Hz, 2 H, CH_2N), 3.98 (d, *J* = 13.3 Hz, 2 H, CH_2N), 3.50−3.70 (m, 4 H, CH_2O), 4.00−4.20 (m, 2 H, CHO), 7.64 (m, 6 H, H_{arom}), 7.80−7.90 (m, 8 H, H_{arom}). − $C_{29}H_{31}NO_3$ (441.57): calcd. C 78.91, H 7.01; found C 80.15, H 7.06.

(2*S*,3*S*)-4-(6,7-Dihydro-5*H*-dibenzo[*c*,*e*]azepin-6-yl)-2,3-*O*-isopropylidenebutane-1,2,3-triol (7d): 58% yield; R_f = 0.20 (eluent: petroleum ether/ethyl acetate, 1:2). − ^{1}H NMR (200 MHz, $CDCl_3$): δ = 1.27 (s, 3 H, CH_3), 1.32 (s, 3 H, CH_3), 2.61 (dd, *J* = 12.7, 5.7 Hz, 1 H, CH_2N), 2.87 (s, 1 H, OH), 3.11 (dd, *J* = 12.7, 3.7 Hz, 1 H, CH_2N), 3.38 (d, *J* = 12.5 Hz, 2 H, CH_2N), 3.47 (d, *J* = 12.5 Hz, 2 H, CH_2N), 3.69 (dd, *J* = 9.4, 1.9 Hz, 1 H, CH_2O),), 3.87 (dd, *J* = 9.4, 3.4 Hz, 1 H, CH_2O), 3.90−4.15 (m, 2 H, CHO), 7.30−7.50 (m, 8 H, H_{arom}). − $C_{21}H_{25}NO_3$ (339.44): calcd. C 74.31, H 7.42; found C 74.24, H 7.27.

General Procedure for Preparation of Aminotosylates 8: p-Toluenesulfonyl chloride (1.13 g, 5.9 mmol, 1.1 equiv.) was added at 0°C to a solution of amino alcohol **7** (5.3 mmol) in pyridine (10 mL). After being stirred for 12 h, the solution was treated with cold H_2O (20 mL), and the organic product was extracted with CH_2Cl_2 (3 × 10 mL). Evaporation of the solvent gave a residue which was purified by flash chromatography to give the amino tosylate **8**.

(2*R*,3*S*)-4-Dibenzylamino-2,3-*O*-isopropylidene-1-*O*-tosylbutane-1,2,3-triol (8a): 91% yield; R_f = 0.35 (eluent: petroleum ether/ethyl

acetate, 4:1); $[\alpha]_D^{20} = -7.0$ ($c = 1.0$, $CHCl_3$). – ^1H NMR (200 MHz, $CDCl_3$): δ = 1.18 (s, 6 H, CH_3), 2.36 (s, 3 H, CH_3), 2.56 (d, $J = 5.5$ Hz, 2 H, CH_2N), 3.45 (d, $J = 13.5$, 2 H, CH_2N), 3.59 (d, $J = 13.5$ Hz, 2 H, CH_2N), 3.60−3.80 (m, 2 H, CH_2O), 3.85 (m, 1 H, CHO), 4.05 (m, 1 H, CHO), 7.10−7.30 (m, 12 H, H_{arom}), 7.66 (d, $J = 8.1$ Hz, 2 H, H_{arom}). – $C_{28}H_{33}NO_5S$ (495.64): calcd. C 67.85, H 6.71; found C 67.80, H 6.70.

(2*R*,3*S*)-4-Bis(2,4,6-trimethylbenzyl)amino-2,3-*O*-isopropylidene-1-*O*-tosylbutane-1,2,3-triol (8b): 65% yield; $R_f = 0.60$ (eluent: petroleum ether/ethyl acetate, 4:1); $[\alpha]_D^{20} = -10.2$ ($c = 1.1$, $CHCl_3$). – ^1H NMR (200 MHz, $CDCl_3$): δ = 1.19 (s, 3 H, CH_3), 1.22 (s, 3 H, CH_3), 2.23 (s, 6 H, CH_3), 2.24 (s, 12 H, CH_3), 2.45 (s, 3 H, CH_3), 2.56 (d, $J = 5.0$ Hz, 2 H, CH_2N), 3.50 (d, $J = 13.1$, 2 H, CH_2N), 3.58 (d, $J = 13.1$ Hz, 2 H, CH_2N), 3.60−3.71 (m, 4 H, CH_2O, CHO), 6.78 (s, 4 H, H_{arom}), 7.31 (d, $J = 8.1$ Hz, 2 H, H_{arom}), 7.70 (d, $J = 8.1$ Hz, 2 H, H_{arom}). – $C_{34}H_{45}NO_5S$ (579.80): calcd. C 70.43, H 7.82; found C 70.25, H 8.04.

(2*R*,3*S*)-4-Bis(2-naphtylmethyl)amino-2,3-*O*-isopropylidene-1-*O*-tosylbutane-1,2,3-triol (8c): 70% yield; $R_f = 0.40$ (eluent: petroleum ether/ethyl acetate, 4:1); $[\alpha]_D^{20} = -6.2$ ($c = 1.2$, $CHCl_3$). – ^1H NMR (200 MHz, $CDCl_3$): δ = 1.25 (s, 3 H, CH_3), 1.27 (s, 3 H, CH_3), 2.37 (s, 3 H, CH_3), 2.75 (d, $J = 5.9$ Hz, 2 H, CH_2N), 3.73 (d, $J = 13.1$, 2 H, CH_2N), 3.88 (d, $J = 13.1$ Hz, 2 H, CH_2N), 3.70−3.90 (m, 2 H, CHO), 4.00−4.20 (m, 2 H, CH_2O), 7.20 (d, $J = 8.1$ Hz, 2 H, H_{arom}), 7.50−7.70 (m, 6 H, H_{arom}), 7.62 (d, $J = 8.1$ Hz, 2 H, H_{arom}), 7.70−7.90 (m, 8 H, H_{arom}). – $C_{36}H_{37}NO_5S$ (595.76): calcd. C 72.58, H 6.26; found C 72.60, H 6.21.

(2*R*,3*S*)-4-(6,7-Dihydro-5*H*-dibenzo[*c*,*e*]azepin-6-yl)-2,3-*O*-isopropylidene-1-*O*-tosylbutane-1,2,3-triol (8d): Yield: 63%; $R_f = 0.65$ (eluent: petroleum ether/ethyl acetate, 1:1). – ^1H NMR (200 MHz, $CDCl_3$): δ = 1.38 (s, 3 H, CH_3), 1.44 (s, 3 H, CH_3), 2.42 (s, 3 H, CH_3), 2.66 (dd, $J = 13.1$, 4.8 Hz, 1 H, CH_2N), 2.85 (dd, $J = 13.1$, 6.5 Hz, 1 H, CH_2N), 3.34 (d, $J = 12.4$ Hz, 2 H, CH_2N), 3.46 (d, $J = 12.4$ Hz, 2 H, CH_2N), 3.96 (ddd, $J = 8.3$, 4.7, 3.9 Hz, 1 H, CHO), 4.10−4.30 (m, 12 H, CHO), 4.19 (dd, $J = 10.6$, 4.7 Hz, 1 H, CH_2O), 4.30 (dd, $J = 10.6$, 3.9 Hz, 1 H, CH_2O), 7.30−7.60 (m, 10 H, H_{arom}), 7.82 (d, $J = 8.2$ Hz, 2 H, H_{arom}). – $C_{28}H_{31}NO_5S$ (493.62): calcd. C 68.13, H 6.33; found C 68.47, H 6.90.

(2*S*,3*S*)-2,3-*O*-Isopropylidene-1-*O*-tosyl-4-tosylaminobutane-1,2,3-triol (10): 65% yield; $R_f = 0.7$ (eluent: petroleum ether/ethyl acetate, 1:1); $[\alpha]_D^{20} = +5.6$ ($c = 1.1$, $CHCl_3$). – ^1H NMR (200 MHz, $CDCl_3$): δ = 1.22 (s, 3 H, CH_3), 1.26 (s, 3 H, CH_3), 2.37 (s, 3 H, CH_3), 2.39 (s, 3 H, CH_3), 2.90−3.20 (m, 2 H, CH_2N), 3.80−4.10 (m, 6 H, CH_2O, CHO), 4.64 (t, $J = 6.5$ Hz, 1 H, NH), 710−7.30 (m, 5 H, H_{arom}), 7.60−7.80 (m, 5 H, H_{arom}), 7.71 (d, $J = 8.3$ Hz, 2 H, H_{arom}). – $C_{21}H_{27}NO_7S_2$ (469.57): calcd; C 53.72, H 5.80; found C 53.20, H 5.84.

General Procedure for Preparation of Amino Phosphanes 3 and 9: A solution of PPh_2Li, prepared under argon in THF (80 mL) at 0°C from $ClPPh_2$ (8.5 g, 38.5 mmol) and Li (10 equiv.), was slowly added to amino tosylate **2** or **8** (12.6 mmol), dissolved in THF (20 mL), until the red color of the solution remained. The solution was stirred for 2 h and was then hydrolyzed with H_2O (50 mL). The solvent was evaporated and the residue was treated with H_2O (50 mL) and CH_2Cl_2 (3 × 50 mL). Evaporation of the solvent, followed by flash chromatography gave the amino phosphane **3** or **9**.

(2*R*,3*S*)-1-Diphenylamino-4-diphenylphosphanyl-2,3-*O*-isopropylidenebutane-2,3-diol (3a): 40% yield; $R_f = 0.70$ (eluent: petroleum ether/ethyl acetate, 6:1); $[\alpha]_D^{20} = -11.3$ ($c = 1.0$, $CHCl_3$). – ^1H NMR (200 MHz, $CDCl_3$): δ = 1.33 (s, 3 H, CH_3), 1.39 (s, 3 H, CH_3), 2.35−2.45 (m, 2 H, CH_2P), 3.88 (dd, $J = 13.6$, 6.7 Hz, 1 H, CH_2N), 4.01 (d, $J = 13.6$, 4.4 Hz, 1 H, CH_2N), 4.00−4.20 (m, 2 H, CHO), 7.05−7.70 (m, 20 H, H_{arom}). – ^{31}P (80 MHz, $CDCl_3$): δ = −22.1. – $C_{31}H_{32}NO_2P$ (481.58): calcd. C 77.32, H 6.70; found C 76.90, H 6.76.

(2*R*,3*S*)-1-Diphenylphosphanyl-2,3-*O*-isopropylidene-4-methyl(phenyl)aminobutane-2,3-diol (3b): 55% yield; $R_f = 0.50$ (eluent: petroleum ether/ethyl acetate, 6:1)): $[\alpha]_D^{20} = -12.3$ ($c = 0.9$, $CHCl_3$). – ^1H NMR (200 MHz, $CDCl_3$): δ = 1.38 (s, 3 H, CH_3), 1.39 (s, 3 H, CH_3), 2.33 (dd, $J = 13.8$, 6.0 Hz, 1 H, CH_2P), 2.45 (dd, $J = 13.8$, 6.8 Hz, 1 H, CH_2P), 2.88 (s, 3 H, CH_3), 3.32 (dd, $J = 15.1$, 6.8 Hz, 1 H, CH_2N), 3.62 (d, $J = 15.1$, 4.2 Hz, 1 H, CH_2N), 3.86 (ddd, $J = 11.8$, 6.8, 6.0 Hz, 1 H, CHO), 4.11 (ddd, $J = 11.8$, 6.8, 4.2 Hz, 1 H, CHO), 6.70−6.85 (m, 3 H, H_{arom}), 7.20−7.40 (m, 12 H, H_{arom}). – ^{31}P (80 MHz, $CDCl_3$): δ = −23.8. – $C_{26}H_{30}NO_2P$ (419.51): calcd. C 74.44, H 7.21; found C 74.55, H 7.31.

(2*R*,3*S*)-1-Diphenylphosphanyl-2,3-*O*-isopropylidene-4-*p*-methoxyphenyl(methyl)aminobutane-2,3-diol (3c): 27% yield; $R_f = 0.34$ (eluent: petroleum ether/ethyl acetate, 10:1); $[\alpha]_D^{20} = -6.6$ ($c = 0.9$, $CHCl_3$). – ^1H NMR (200 MHz, $CDCl_3$): δ = 1.31 (s, 3 H, CH_3), 1.33 (s, 3 H, CH_3), 2.27 (dd, $J = 13.8$, 6.0 Hz, 1 H, CH_2P), 2.37 (dd, $J = 13.8$, 6.5 Hz, 1 H, CH_2P), 2.74 (s, 3 H, CH_3), 3.19 (dd, $J = 14.8$, 6.7 Hz, 1 H, CH_2N), 3.40 (d, $J = 14.8$, 4.2 Hz, 1 H, CH_2N), 3.71 (s, 3 H, CH_3), 3.82 (ddd, $J = 11.2$, 6.5, 6.0 Hz, 1 H, CHO), 4.01 (ddd, $J = 11.2$, 6.7, 4.2 Hz, 1 H, CHO), 6.74 (m, 4 H, H_{arom}), 7.50 (m, 10 H, H_{arom}). – ^{31}P (80 MHz, $CDCl_3$): δ = −23.7. $-C_{27}H_{32}NO_3P$ (449.53): calcd. C 72.14, H 7.18; found: C 72.16, H 6.23.

(2*R*,3*S*)-1-Diphenylphosphanyl-2,3-*O*-isopropylidene-4-α-naphthyl-(phenyl)aminobutane-2,3-diol (3d): 82% yield; $R_f = 0.5$ (eluent: petroleum ether/ethyl acetate, 6:1); $[\alpha]_D^{20} = -35.2$ ($c = 0.9$, $CHCl_3$). – ^1H NMR (200 MHz, $CDCl_3$): δ = 1.39 (s, 3 H, CH_3), 1.41 (s, 3 H, CH_3), 2.28 (dd, $J = 13.8$, 6.0 Hz, 1 H, CH_2P), 2.38 (dd, $J = 13.8$, 7.0 Hz, 1 H, CH_2P), 3.80−4.00 (m, 2 H, CH_2N), 4.00−4.20 (m, 2 H, CHO), 6.90−7.60 (m, 22 H, H_{arom}). – ^{31}P (80 MHz, $CDCl_3$): δ = −23.9. – $C_{35}H_{34}NO_2P$ (531.64): calcd. C 78.51, H 6.38; found C 78.54, H 6.50.

(2*R*,3*S*)-4-Dibenzylamino-1-diphenylphosphanyl-2,3-*O*-isopropylidenebutane-2,3-triol (9a): 40% yield; $R_f = 0.22$ (eluent: petroleum ether/ethyl acetate, 19:1); $[\alpha]_D^{20} = -21.8$ ($c = 0.9$, $CHCl_3$). – ^1H NMR (200 MHz, $CDCl_3$): δ = 1.19 (s, 3 H, CH_3), 1.29 (s, 3 H, CH_3), 2.16 (ddd, $J = 13.9$, 7.7, 1.4 Hz, 1 H, CH_2P), 2.22 (ddd, $J = 13.9$, 4.5, 1.9 Hz, 1 H, CH_2P), 2.47 (dd, $J = 13.7$, 5.5 Hz, 1 H, CH_2N), 2.60 (dd, $J = 13.7$, 4.3 Hz, 1 H, CH_2N), 3.46 (d, $J = 13.6$ Hz, 2 H, CH_2N), 3.61 (d, $J = 13.6$ Hz, 2 H, CH_2N), 3.60−3.75 (m, 1 H, CHO), 3.90−4.00 (m, 1 H, CHO), 7.10−7.30 (m, 20 H, H_{arom}). – ^{13}C NMR (50 MHz, $CDCl_3$): δ = 27.2 (CH_3), 27.3 (CH_3), 32.4 (d, $J = 15.0$ Hz, CH_2P), 54.8 (CH_2N), 59.0 (2 × CH_2N), 77.3 (d, $J = 13.1$ Hz, CHO), 80.7 (d, $J = 9.0$ Hz, CHO), 108.8 (CMe_2), 127.0−139.3 (C_{arom}). – ^{31}P (80 MHz, $CDCl_3$): δ = −23.1. – $C_{33}H_{36}NO_2P$ (509.63): calcd. C 77.78, H 7.12, N 2.75, P 6.08; found C 77.34, H 7.12, N 2.90, P 6.84.

(2*R*,3*S*)-4-Bis(2,4,6-trimethylbenzyl)amino-1-diphenylphosphanyl-2,3-*O*-isopropylidenebutane-2,3-triol (9b): 45% yield; $R_f = 0.6$ (eluent: petroleum ether/ethyl acetate, 9:1); $[\alpha]_D^{20} = -1.6$ ($c = 1.3$, $CHCl_3$). – ^1H NMR (200 MHz, $CDCl_3$): δ = 1.19 (s, 3 H, CH_3), 1.31 (s, 3 H, CH_3), 2.00−2.30 (m, 2 H, CH_2P), 2.23 (s, 6 H, CH_3), 2.25 (s, 12 H, CH_3), 2.45−2.60 (m, 2 H, CH_2N), 3.42 (d, $J = 12.4$ Hz, 2 H, CH_2N), 3.63 (d, $J = 12.4$ Hz, 2 H, CH_2N), 3.72−3.90 (m, 2 H, CHO), 7.30−7.70 (m, 10 H, H_{arom}). – ^{31}P (80 MHz, $CDCl_3$): δ = −23.6. – $C_{39}H_{48}NO_2P$ (593.79): calcd. C 78.89, H 8.15; found C 78.25, H 8.03.

(2*R*,3*S*)-4-Bis(2-naphtylmethyl)amino-1-diphenylphosphanyl-2,3-*O*-isopropylidenebutane-2,3-triol (9c): 20% yield; R_f = 0.22 (eluent: petroleum ether/ethyl acetate, 7:1); $[\alpha]_D^{20}$ = −28.6 (*c* = 0.6, $CHCl_3$). − ^{1}H NMR (200 MHz, $CDCl_3$): δ = 1.29 (s, 3 H, CH_3), 1.36 (s, 3 H, CH_3), 2.10−2.30 (m, 2 H, CH_2P), 2.71−2.80 (m, 2 H, CH_2N), 3.62 (d, *J* = 12.0 Hz, 2 H, CH_2N), 3.73 (d, *J* = 12.0 Hz, 2 H, CH_2N), 4.05−4.20 (m, 2 H, CHO), 7.20−7.80 (m, 24 H, H_{arom}). − ^{31}P (80 MHz, $CDCl_3$): δ = −23.5. − $C_{41}H_{40}NO_2P$ (609.75): calcd. C 80.76, H 6.61; found C 80.25, H 6.03.

(2*R*,3*S*)-4-(6,7-Dihydro-5*H*-dibenzo[*c*,*e*]azepin-6-yl)-1-diphenylphosphanyl-2,3-*O*-isopropylidenebutane-2,3-triol (9d): 80% yield, R_f = 0.32 (eluent: petroleum ether/ethyl acetate, 5:1). − ^{1}H NMR (200 MHz, $CDCl_3$): δ = 1.30 (s, 3 H, CH_3), 1.38 (s, 3 H, CH_3), 2.31 (m, 2 H, CH_2P), 2.72 (m, 2 H, CH_2N), 3.32 (d, *J* = 12.3 Hz, 2 H, CH_2N), 3.38 (d, *J* = 12.3 Hz, 2 H, CH_2N), 4.00−4.20 (m, 2 H, CHO), 7.20−7.60 (m, 18 H, H_{arom}). − ^{13}C NMR (50 MHz, $CDCl_3$): δ = 27.4 (CH_3), 27.5 (CH_3), 32.8 (d, *J* = 16.3 Hz, CH_2P), 55.9 (2 × CH_2N), 57.4 (CH_2N), 77.6 (d, *J* = 14.8 Hz, CHO), 80.7 (d, *J* = 7.8 Hz, CHO), 109.3 (CMe_2), 127.6−141.3 (C_{arom}). − ^{31}P (80 MHz, $CDCl_3$): δ = −23.8. − $C_{33}H_{34}NO_2P$ (507.62): calcd. C 78.08, H 6.75; found C 79.10, H 6.59.

(2*R*,3*S*)-1-Diphenylphosphanyl-2,3-*O*-isopropylidene-4-tosylaminobutane-2,3-diol (11): 73% yield; R_f = 0.25 (eluent: petroleum ether/ethyl acetate, 4:1); $[\alpha]_D^{20}$ = −4.2 (*c* = 0.3, $CHCl_3$). − ^{1}H NMR (200 MHz, $CDCl_3$): δ = 1.28 (s, 3 H, CH_3), 1.34 (s, 3 H, CH_3), 2.42 (s, 3 H, CH_3), 2.30−2.50 (m, 2 H, CH_2P), 3.00−4.20 (m, 2 H, CH_2N), 4.79 (t, *J* = 6.1 Hz, 1 H, NH), 3.80−4.20 (m, 2 H, CHO), 7.20−7.40 (m, 10 H, H_{arom}), 7.42 (d, *J* = 8.2 Hz, 2 H, H_{arom}), 7.83 (d, *J* = 8.2 Hz, 2 H, H_{arom}). − ^{31}P (80 MHz, $CDCl_3$): δ = −24.6. − $C_{26}H_{30}NSO_4P$ (483.57): calcd. C 64.58, H 6.25, N 2.89; found C 63.96, H 6.09, N 2.87.

(2*S*,3*S*)-1,4-Bis(diphenylamino)-2,3-*O*-isopropylidenebutane-2,3-diol (12): $[\alpha]_D^{20}$ = −5.2 (*c* = 0.8, $CHCl_3$). − ^{1}H NMR (300 MHz, $CDCl_3$): δ = 1.40 (s, 6 H, CH_3), 3.85 (d, *J* = 4.8 Hz, 4 H, CH_2), 4.20 (m, 2 H, CH), 6.90−7.02 (m, 12 H, H_{arom}), 7.18−7.32 (m, 8 H, H_{arom}). − ^{13}C NMR (75 MHz, $CDCl_3$): δ = 27.5 (CH_3), 55.7 (CH_2), 77.8 (s, CH), 109.7 (CMe_2), 121.5, 121.8, 129.4 and 148.2 (C_6H_5). − $C_{31}H_{32}N_2O_2$ (464.61): calcd. C 80.14, H 6.94, N 6.03; found C 80.08, H 6.85, N 6.15.

Asymmetric Alkylation. − Typical Procedure: A solution of the sodium salt of dimethyl malonate, prepared from dimethyl malonate (118.9 mg, 0.900 mmol) and sodium hydride in THF (2 mL) at room temperature, was added to a mixture of $Pd_2(dba)_3$ (55 mg, 6.10^{-3} mmol), ligand (12.10^{-3} mmol) and *rac*-(*E*)-1,3-diphenylprop-2-enyl acetate (75.7 mg, 0.300 mmol) in THF (2 mL). The solution was stirred for 24 h and was then quenched with a small amount of water. Evaporation of the solvent, followed by column chromatography gave the alkylated product. The conversion and enantiomeric purity was determined by HPLC with a chiral stationary phase column Chiraldex OD−H (hexane/2-propanol = 98:2). The absolute configuration was determined by polarimetry.[10]

Acknowledgments

R. F. thanks the MESRT and Région Rhône-Alpes for a fellowship.

[1] [1a] H. Brunner, W. Zettlmeier, *Handbook of Enantioselective Catalysis*, VCH, Weinheim, **1993**. − [1b] I. Ojima, *Catalytic Asymmetric Synthesis*, VCH, Weinheim, **1993**. − [1c] R. Noyori, *Asymmetric Catalysis in Organic Synthesis*, Wiley, New York, **1994**.
[2] [2a] A. Pfaltz, *Acc. Chem. Res.* **1993**, *26*, 339−345. − [2b] O. Reiser, *Angew. Chem*. **1993**, *105,* 576−578; *Angew. Chem. Int. Ed. Engl*. **1993**, *32*, 547−549. − [2c] B. M. Trost, D. L. Van Vranken, *Chem. Rev.* **1996**, *96*, 395−422. − [2d] J. M. J. Williams, *Synlett* **1996**, 705−710.
[3] T. Hayashi, M. Konishi, M. Fukushima, K. Kanehira, T. Hioki, M. Kumada, *J. Org. Chem*. **1983**, *48*, 2195−2202.
[4] [4a] T. Hayashi, M. Tajika, K. Tamao, M. Kumada, *J. Am. Chem. Soc.* **1976**, *98*, 3718−3719. − [4b] T. Hayashi, M. Konishi, M. Fukushima, T. Mise, M. Kagotani, M. Tajika, M. Kumada, *J. Am. Chem. Soc.* **1982**, *104*, 180−186.
[5] [5a] H. Kubota, K. Koga, *Tetrahedron Lett*. **1994**, *35*, 6689−6694. − [5b] H. Kubota, K. Koga, *Heterocycles* **1996**, *42*, 543−547.
[6] [6a] J. P. Cahill, F. M. Bohnen, R. Goddard, C. Krüger, P. J. Guiry, *Tetrahedron: Asymmetry* **1998**, *9*, 3831−3839. − [6b] J. P. Cahill, P. J. Guiry, *Tetrahedron: Asymmetry* **1998**, *9*, 4301−4306. − [6c] J. P. Cahill, A. P. Lighfoot, R. Goddard, J. Rust, P. J. Guiry, *Tetrahedron: Asymmetry* **1998**, *9*, 4307−4312.
[7] [7a] P. Wimmer, M. Widhalm, *Tetrahedron: Asymmetry* **1995**, *6*, 657−660. − [7b] P. Wimmer, M. Widhalm, *Monatsh. Chem*. **1996**, *127*, 669−681. − [7c] M. Boughida, M. Widhalm, *Tetrahedron: Asymmetry* **1998**, *9*, 1073−1083. − [7d] M. Widhalm, K. Mereiter, M. Bourghida, *Tetrahedron: Asymmetry* **1998**, *9*, 2983−2986.
[8] F. Robert, N. Gaillard, D. Sinou, *J. Mol. Catal*., in press.
[9] W. R. Jackson, C. G. Lovel, *Aust. J. Chem*. 1982, 35, 2069−2075.
[10] U. Leutenegger, G. Umbricht, C. Fahrni, P. von Matt, A. Pfaltz, *Tetrahedron* **1992**, *48*, 2143−2156.
[11] [11a] B. E. R. Schilling, R. Hoffmann, J. W. Faller, *J. Am. Chem. Soc*. **1979**, *101*, 592−598. − [11b] T. R. Ward, *Organometallics* **1996**, *15*, 2836−2838.
[12] M. D. Curtis, O. Eisenstein, *Organometallics* **1984**, *3*, 887−895.
[13] B. Bigot, F. Delbecq, *New J. Chem*. **1990**, *14*, 659−669.
[14] S. Sakaki, M. Nishikawa, A. Ohyoshi, *J. Am. Chem. Soc*. **1980**, *102*, 4062−4069.
[15] P. E. Blöchl, A. Togni, *Organometallics* **1996**, *15*, 4125−4132.
[16] K. J. Szabò, E. Hupe, A. L. E. Larsson, *Organometallics* **1997**, *16*, 3779−3785.
[17] [17a] K. J. Szabò, *J. Am. Chem. Soc.* **1996**, *118*, 7818−7826. − [17b] K. J. Szabo, *Chem. Eur. J.* **1997**, *3*, 592−600. − [17c] K. J. Szabo, *Organometallics* **1996**, *15*, 1128−1133.
[18] S. Sakaki, H. Satoh, H. Shono, Y. Ujino, *Organometallics* **1996**, *15*, 1713−1720.
[19] S. Sakaki, K. Takeuchi, M. Sugimoto, *Organometallics* **1997**, *16*, 2995−3003.
[20] A. Aranyos, K. J. Szabo, A. M. Castano, J. E. Bäckvall, *Organometallics* **1997**, *16*, 1058−1064.
[21] A. E. Smith, *Acta Crystallogr., Sect. A* **1969**, *25*, S161.
[22] R. Mason, D. R. Russel, *Chem. Commun*. **1966**, 26.
[23] S. Liu, J. F. K. Müller, M. Neuburger, S. Shaffner, M. Zehnder, *J. Organomet. Chem.* **1997**, *549*, 283−293.
[24] R. Hoffmann, *J. Chem. Phys.* **1963**, *39*, 1397−1412.
[25] O. Eisenstein and R. Hoffmann, *J. Am. Chem. Soc*. **1981**, *101*, 4308−4320.
[26] J. H. Ammeter, H. B. Burgi, J. C. Thibeault, R. Hoffmann, *J. Am. Chem. Soc.* **1978**, *100*, 3686.
[27] M. J. Frisch, G. W. Trucks, H. B. Schlegel, P. M. W. Gill, B. G. Johnson, M. A. Robb, J. R. Cheeseman, T. Keith, G. A. Peterson, J. A. Montgomery, K. Raghavachari, M. A. Al-Laham, V. G. Zakrzewski, J. V. Ortiz, J. B. Foresman, J. Cioslowski, B. B. Stefanov, A. Nanayakkara, M. Challlacombe, C. Y. Peng, P. Y. Ayala, W. Chen, M. W. Wong, J. L. Andres, E. S. Replogle, R. Gomperts, R. L. Martin, D. J. Fox, J. S. Binkley, D. J. Defrees, J. Baker, J. P. Stewart, M. Head-Gordon, C. Gonzalez, J. A. Pople, *Gaussian 94, Revision B.1*, Gaussian, Inc., Pittsburgh PA, **1995**.
[28] T. G. Appleton, H. C. Clark, L. E. Manzer, *Coord. Chem. Rev.* **1973**, *10*, 335−422.
[29] A. E. Smith, *Acta Crystallogr.* **1965**, *18*, 331−340.
[30] P. Sautet, O. Eisenstein, K. M. Nicholas, *Organometallics* **1987**, *6*, 1845−1849.
[31] S. Brunie, J. Mazan, N. Langlois, H. B. Kagan, *J. Organomet. Chem*. **1976**, *114*, 225−232.

Received July 26, 1999
[I99281]

Reduction of Metal-Stabilized α-CF_3-Carbenium Ion Complexes under Mild Conditions: Synthesis, Structures, and Reactivity

Michel Gruselle,*[a] Bernard Malézieux,[a] Román Andrés,[a] Hani Amouri,[a] Jacqueline Vaissermann,[a] and Gagik G. Melikyan[b]

Keywords: Radicals / Carbenium ions / Clusters / Cobalt / Molybdenum

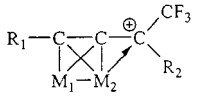
Complexed α-CF_3 propargyl alcohols of the general formula [(M_2L_6)\{μ-η^2,η^2-RC≡CCH(CF_3)(OH)\}] were prepared with M_2L_6 = $Co_2(CO)_6$, R = $CH_3(CH_2)_4$– (**1**), R = C_6H_5– (**2**); M_2L_6 = $Co_2(CO)_5P(C_6H_5)_3$, R = $CH_3(CH_2)_4$– (**3a**,**b**), R = C_6H_5– (**4a**,**b**); M_2L_6 = $Co_2(CO)_4$dppm, R = C_6H_5– (**5**); M_2L_6 = $Co(CO)_3$-MoCp$(CO)_2$, R = $CH_3(CH_2)_4$– (**6a**,**b**), R = C_6H_5– (**7a**,**b**). An X-ray molecular structure of the propargyl-alcohol complex [\{$Co_2(CO)_4$dppm\}\{μ-η^2,η^2-C_6H_5C≡CCH(CF_3)(OH)\}] (**5**) was also determined. The related carbenium ions [(M_2L_6)\{μ-η^2,η^3-RC≡CCH(CF_3)\}][BF_4] (**8–12**) were obtained from the parent propargyl alcohol complexes by direct protonation with HBF_4 · Et_2O in diethyl ether. These carbenium ions were reduced further by Zn in CH_2Cl_2 to give the alkyne adducts [(M_2L_6)\{μ-η^2,η^2-RC≡C$CH_2(CF_3)$\}] (**13–17**), as confirmed by the X-ray molecular structure of [$(Co_2(CO)_4$dppm)\{μ-η^2,η^2-C_6H_5-C≡C$CH_2(CF_3)$\}] (**17**). Treatment of the carbenium ion complex [\{$Co(CO)_3$MoCp$(CO)_2$\}\{μ-η^2,η^3-$CH_3(CH_2)_4$C≡CCH(CF_3)\}][BF_4] (**8**) with NaSMe unexpectedly afforded the reduced alkyne adduct [\{$Co(CO)_3$MoCp$(CO)_2$\}\{μ-η^2,η^2-$CH_3(CH_2)_4$C≡CCH_2-(CF_3)\}] (**13**), along with the alkyne-thioether diastereomers \{$Co(CO)_3$MoCp$(CO)_2$\}\{μ-η^2,η^2-$CH_3(CH_2)_4$C≡CCH(CF_3)(SMe)\}] (**18a**,**b**). Presumably, all the reduction reactions proceed primarily by the formation of the transient radical species, which are subsequently transformed into the reduced alkyne complexes by hydrogen abstraction from the solvent medium. Interestingly, in the case of the complexed alcohols [\{$Co_2(CO)_5P(C_6H_5)_3$\}\{μ-η^2,η^2-RC≡CCH(CF_3)(OH)\}] (**3a**,**b**) and (**4a**,**b**), the reduction process occurs in acidic medium in THF/CH_2Cl_2. An extensive study of the electronic and steric factors that influence the stability and reactivity of the carbenium ions were performed, which allowed us to explain the behavior of the related radical species in solution during the reduction process.

Introduction

Trifluoromethyl propargyl alcohols are easily available,[1] however their synthetic interest is still limited, due to the difficulty of preparing the related α-CF_3 carbenium ions prior to nucleophilic addition. Functionalization of the carbenium ion in the α-position relative to the CF_3 group is therefore a hard task.[2] Furthermore, the CF_3 function is a strong electron-withdrawing group and thus strengthens the C−O bond, which prevents the formation of a carbenium center (CF_3−C^+). In addition, the steric effects and electronic repulsion of the incoming nucleophiles with fluorine atoms of the α-CF_3 group decrease the reaction rate, and harsh conditions are often required.[3][4] To overcome such difficulties it is vital to stabilize the carbenium center (CF_3−C^+). This can be achieved by introducing a dinuclear cluster such as M_2L_6 = [−$Co_2(CO)_6$]; = [−$Cp_2Mo_2(CO)_4$] or a mixed dinuclear complex = [−$Co(CO)_3$MoCp$(CO)_2$] to the acetylenic unit of the trifluoromethyl propargyl alcohols. A direct metal···C^+ interaction with carbenium center therefore occurs, which stabilizes the whole complex and allows further functionalization to proceed under mild conditions.

Metal-stabilized carbon electron deficient systems of the type [(M_2L_6)(μ-η^2,η^3-RC≡CCR_2)]$^+$ have been the focus of several reviews.[5] The analogous carbon-radical complexes were also reported.[6] In the latter, coupling reactions were observed.[7] A synthetic application of this chemistry is the preparation of cyclic diacetylenic compounds promoted by recombination of [$Co_2(CO)_6$]$_2$ diacetylenic di-radicals.[8]

Pursuing our research investigations in this field we prepared a new class of α-CF_3-propargyl alcohol complexes, in which a dinuclear cluster of the type [$Co_2(CO)_6$], [Co_2-$(CO)_5P(C_6H_5)_3$], [$Co_2(CO)_4${$P(C_6H_5)_2$}$_2CH_2$], or heterobimetallic [$Co(CO)_3$MoCp$(CO)_2$] is coordinated to the acetylenic unit (−C≡C−) (Figure 1).



M_1 = M_2 = $Co_2(CO)_6$, R_1 = $(CH_2)_4CH_3$, R_2 = C_6H_5
M_1 = $Co(CO)_3$, M_2 = $MoCp(CO)_2$, R_1 = $(CH_2)_4CH_3$, R_2 = C_6H_5
M_1 = $Co(CO)_3$, M_2 = $MoCp(CO)_2$, R_1 = $(CH_2)_4CH_3$, R_2 = CH_3

Figure 1. General formula of metal-stabilized carbenium ion

In a preliminary communication,[9] we have shown that it is possible to obtain and isolate α-CF_3 methyl- or phenyl-substituted propargylium ions, when they are stabilized by

[a] Laboratoire de Chimie Inorganique et Matériaux Moléculaires, ESA 7071-CNRS, Université Pierre et Marie Curie,
4, place Jussieu, case 42, F-75252 Paris cedex 05, France
E-mail: gruselle@ccr.jussieu.fr
[b] Department of Chemistry, California State University-Northridge,
18111 Nordhoff Str., Northridge, CA 91330, USA

 © WILEY-VCH Verlag GmbH, D-69451 Weinheim, 2000 1434−1948/00/0202−359 $ 17.50+.50/0

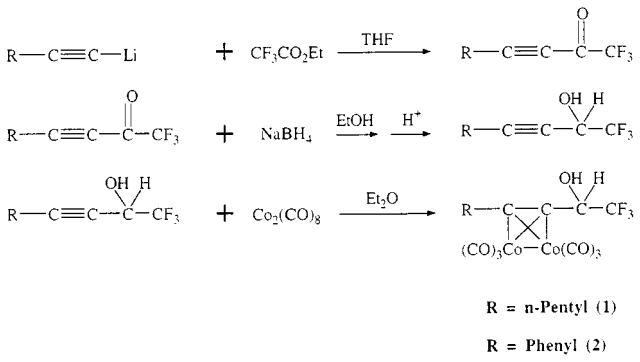
an adjacent bimetallic $[Co_2(CO)_6]$- or $[Co(CO)_3MoCp(CO)_2]$-acetylenic cluster. Through out the paper we will use the abbreviations $[Co_2]$ for $[Co_2(CO)_6]$, and [Co,Mo] for $[Co(CO)_3MoCp(CO)_2]$.

In this paper we describe the synthesis of bimetallic $[Co_2]$ and [Co,Mo] complexed acetylenic α-CF_3 alcohols and describe their ability to give carbenium ions in acidic medium. The capacity of these ions to be reduced, either directly from the complexed propargyl alcohols or starting from the related metal-stabilized carbenium ions, has also been investigated.

Results and Discussion

Synthesis, Structure, and Characterization of α-CF_3-Propargyl Alcohol Complexes $[(M_2L_6)\{\mu\text{-}\eta^2,\eta^2\text{-}RC{\equiv}CCH(CF_3)(OH)\}]$

The α-CF_3 propargyl alcohols were synthesized by treatment of the ethyltrifluoroacetate with the appropriate lithiated acetylenic compound: RC≡CLi [R = $CH_3(CH_2)_4-$; C_6H_5-]. The obtained ketones were then reduced by $NaBH_4$ in alcoholic medium, and the resulting alcohols are subsequently complexed by $Co_2(CO)_8$ leading to the alkyne complexes $[\{Co_2(CO)_6\}\{\mu\text{-}\eta^2,\eta^2\text{-}RC{\equiv}CC(OH)(CF_3)H\}]$ {R = $CH_3(CH_2)_4$-(**1**); R = C_6H_5-(**2**)} according to Scheme 1.



Scheme 1. Preparation of complexed $[Co_2(CO)_6]$propargyl alcohols

Substitution of a carbonyl ligand of complexes **1**−**2** by either a monophosphane $[P(C_6H_5)_3]$ or a chelating phosphane such as dppm = $[\{P(C_6H_5)_2\}_2CH_2]$ using standard methods[10] leads to the phosphane−$[Co_2]$-complexed alcohols **3a**, **3b**, **4a**, **4b**, and **5**. All compounds were completely characterized further, and the X-ray molecular structure of $[\{Co_2(CO)_4dppm\}\{\mu\text{-}\eta^2,\eta^2\text{-}C_6H_5C{\equiv}CCH(CF_3)(OH)\}]$ (**5**) was determined. This compound crystallizes in the monoclinic unit cell, space group *P*21/n. The bonding and molecular geometry of **5** are shown in a CAMERON[24] diagram in Figure 2. Crystallographic data and parameters for **5** are given in Table 4, selected bond lengths and angles are listed in Table 1. Complex **5** consists of a tetrahedral Co_2C_2 core with −C≡C− bond of the acetylene unit in a perpendicular orientation at a almost 90° angle relative to Co−Co bond. The metal-metal bond length of 2.473 Å conforms with previous literature values for a single Co−Co bond.[11] The coordination geometry of each Co center is a distorted octahedron occupied by the acetylene carbons, two carbonly ligands and a coordinated phosphane ligand of the bridged dppm unit.

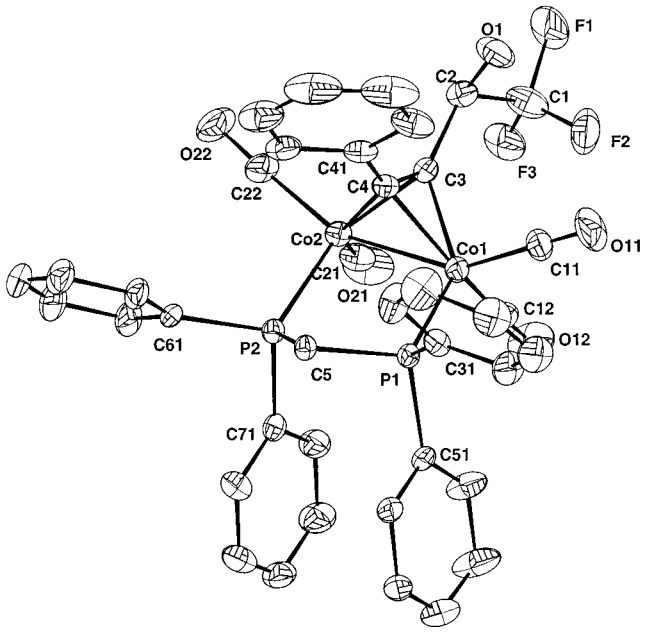


Figure 2. X-ray molecular structure of $[\{Co_2(CO)_4dppm\}\{\mu\text{-}\eta^2,\eta^2\text{-}C_6H_5C{\equiv}CCH(CF_3)(OH)\}]$ (**5**) with atom numbering system

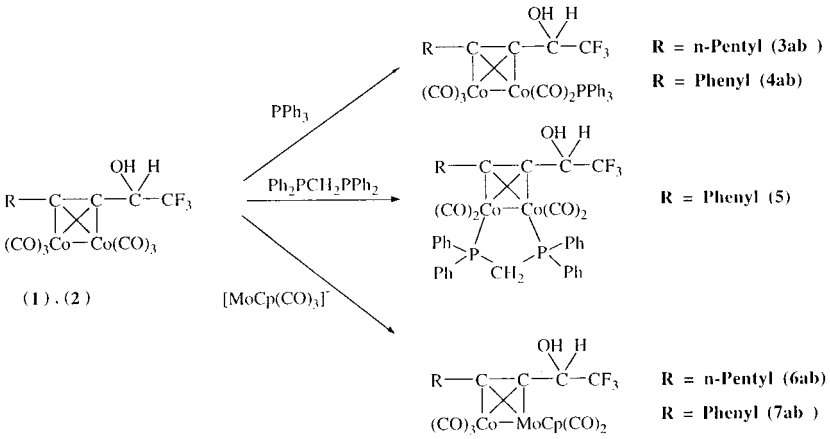
Table 1. Selected bond lengths [Å] and angles [°] for complex **5**

Co(1)−Co(2)	2.473(1)	Co(1)−P(1)	2.227(2)
Co(1)−C(3)	1.942(6)	Co(2)−P(2)	2.222(2)
Co(1)−C(4)	1.974(7)	Co(2)−C(3)	1.947(6)
Co(2)−C(4)	1.970(6)	C(3)−C(4)	1.357(9)
Co(1)−C(4)−Co(2)	77.7(2)	Co(1)−C(3)−Co(2)	79.0(2)
C(3)−C(4)−C(41)	141.5(6)	C(2)−C(3)−C(4)	126.6(7)

Furthermore, the α-CF_3-alcohol complexes **3a**, **b** and **4a**, **b** exist as a pair of diastereomers (Scheme 2). Starting from the $[Co_2]$-complexed alcohols **1**−**2**, the substitution of the metallic vertex $[Co(CO)_3]$ by the isolobal $[MoCp(CO)_2]$ leads to the hetero-bimetallic [Co,Mo]-complexed alcohols[12] obtained also as two diastereomers **6a**, **b** and **7a**, **b**, respectively. The complexed alcohols **1**−**7** thus obtained have the α-CF_3 substituent on the carbon atom bearing the hydroxyl function, while the C-4 acetylenic carbon is either substituted by an alkyl or an aryl substituent.

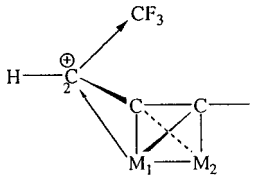
Mayr et al.[13] recently reported that alkyl or aryl substituents at C-4 do not affect the electronic density of the cluster unit, and consequently do not affect the electrophilicity of the corresponding $[Co_2]$−carbenium ions. The major differences among these complexed propargyl alcohols (**1**−**7**) therefore reside in the electronic nature of the bimetallic moieties coordinated to the acetylenic function.

It is well established that a cluster unit, or its electron donating ability, alleviates the positive charge of the adjacent α-carbenium center. It was previously shown by pK_R^+ measurements that the $[MoCp(CO)_2]$ vertex is much more



Scheme 2. Preparation of heterobimetallic [Co−Mo]- and [Co_2]-phosphane propargyl aclohols

efficient as an electron donating group than the [$Co_2(CO)_6$] unit[14][15] Consequently, the [Mo_2] or [Co,Mo] are much more stable and less reactive than the [Co_2]-complexed carbenium ions. Due to their low reactivity several X-ray structures of [Mo_2]- or [Co,Mo]-stabilized carbenium ions were reported in the literature.[1][5] However, very recently an X-ray structure of a [Co_2]−carbenium ion complex has been described. In this particular example, the carbenium center is flanked by two [Co_2] cluster units.[16] Spectroscopic results based on ^{1}H- and ^{13}C-NMR analysis and MO calculations on these metal-stabilized carbenium ions have shown that the electronic transfer occurs from the ligand to the carbon-deficient electronic center through the metal atom.[17] For instance, substituting a carbonyl ligand by a monophosphane or a diphosphane ligand has the dramatic effect of increasing the electronic density of the cluster core. This electronic density change is reflected on the ν_{CO} absorptions, which shift to low frequency.[18] Such behavior is illustrated by complex [{$Co_2(CO)_6$}{μ-η^2,η^2-$CH_3(CH_2)_4$-C≡CCH(CF_3)(OH)}] (**1**), which shows three ν_{CO} bands at 2097, 2057, and 2029 cm^{-1}. The related monophosphane complex [{$Co_2(CO)_5P(C_6H_5)_3$}{μ-η^2,η^2-$CH_3(CH_2)_2$-C≡CCH(CF_3)(OH)}] (**3**) exhibits ν_{CO} absorptions at 2063, 2015, 2005, 1987, and 1962 cm^{-1} (see Table 4). These results are in accord with those reported by Mayr et al,[13] which show that the carbenium ion complex [{$Co_2(CO)_5P(C_6H_5)_3$}{μ-η^2,η^3-HC≡CCH(C_6H_5)}]$^+$ is less electrophilic than the parent carbenium ion [$Co_2(CO)_6${μ-η^2,η^3-HC≡CCH(C_6H_5)}]$^+$. In summary, based on the literature data and our own experiments, we have classified the electron density on the cluster moieties of these α-CF_3-propargyl alcohols, in decreasing order as follows: [Co,Mo] > [Co_2P_2] > [Co_2P] > [Co_2]. As for carbenium ion complexes, it is noteworthy to remark that the carbenium center C-2 will be stabilized by the cluster unit, but to a different extent depending on the scale shown above. This should also overcome the withdrawing effect exerted by the α-CF_3 group. These two opposing effects (Figure 3) were examined by monitoring the reactivity of these carbenium ions in solution towards reduction. The results are presented in the next section.



[M_1-M_2] = [Co-Mo] = [$Co(CO)_3$-$MoCp(CO)_2$]
[Co_2] = [$Co_2(CO)_6$]
[Co_2P] = [$Co_2(CO)_5$ $P(Ph)_3$]
[Co_2P_2] = [$Co_2(CO)_4(P(Ph_2)_2CH_2$]

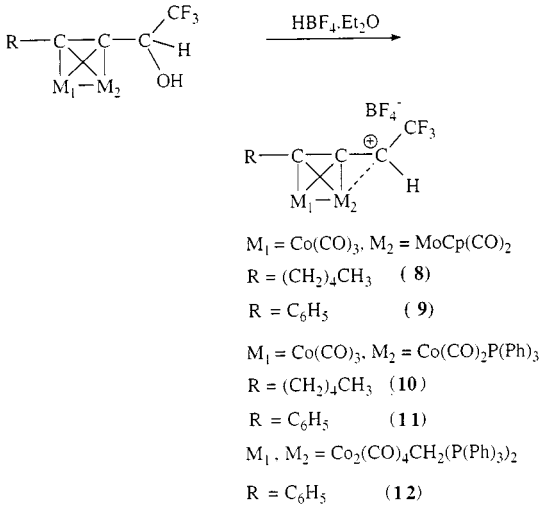
Figure 3. Schematic drawing showing two opposite interactions at the cabenium center: (a) metal-stabilized effect; (b) CF_3-distabilization attactive effect

Synthesis and Reduction of the Metal-Stabilized α-CF_3-Propargyl Carbenium Ion Complexes [(M_2L_6)-{μ-η^2,η^3-RC≡CCH(CF_3)}][BF_4]

Treatment of the propargyl alcohol complexes [{$Co_2(CO)_6$}{μ-η^2,η^2-RC≡CC(OH)(CF_3)H}] (**1−2**) by $HBF_4 \cdot Et_2O$ in ether did not afford any precipitate, as expected for the formation of the related carbenium ion salts. In contrast, the complexed alcohols **3−7** gave, under the same experimental conditions, the corresponding carbenium ions **8**, **9**, **10**, **11**, and **12**, respectively (Scheme 3). These results demonstrate that the electron donating effect of the [Co_2] cluster in Complexes (**1−2**) is not sufficient to overcome the α-CF_3 withdrawing effect. The ν_{CO} frequencies in the starting alcohols and their corresponding carbenium ions are listed in Table 3.

Furthermore, we noticed that protonation of the [Co_2P] complexed alcohols **3a**, **b** and **4a**, **b** by $HBF_4 \cdot Et_2O$ in a CH_2Cl_2/THF readily afforded the reduced complexes **15** and **16**, but not the related carbenium ion complexes

(Scheme 4). In the previous reaction the THF plays the role of the reducing agent, by acting as a mono-electron donor, as was previously reported.[19] Surprisingly, complexes **1**−**2**, were not reduced using CH_2Cl_2/THF as a solvent.



Scheme 3. Synthesis of the metal-stabilized carbenium ions (**8**−**12**).

It is also interesting to note that under the same experimental conditions the propargyl alcohols **5**−**7** afforded the carbenium ions **8**−**9** and **12**, therefore these compounds are very stable and cannot be reduced by the CH_2Cl_2/THF system. Carbenium ions **8**−**9** and **12** can readily be reduced, however, by using Zn/CH_2Cl_2 as reducing agent leading to compounds **13**−**14** and **17** (Scheme 5). The structures of these compounds were all identified by spectroscopic methods and elemental analysis (see Experimental Section), furthermore, the X-ray molecular structure of compound **17** was determined. The compound crystallizes with one molecule of acetone in the triclinic unit cell, space group *P*1. The bonding and molecular geometry of **17** are shown in a CAMERON[24] diagram in Figure 4. Crystallographic data and parameters for **17** are given in Table 4, selected bond lengths and angles are listed in Table 2. Complex **17** displays a tetrahedral Co_2C_2 core with -C≡C- bond of the acetylene unit in a perpendicular orientation at a almost 90° angle relative to Co−Co bond. The metal-metal bond length is 2.4876 Å, slightly longer than that of complex **5**.

The coordination geometry of each Co center is a distorted octahedron, occupied by the acetylene carbons, two carbonly ligands, and a coordinated phosphane ligand of the bridged dppm unit. Overall, the structure of **17** looks very similar to that of the parent molecule, **5**, and confirms its reduction since the hydroxyl group is now substituted by a hydrogen atom.

At this stage a few brief comments are required, since, according to our results, formation of a Co-complexed propargyl radical is only possible providing its related carbenium ion can be formed. This explains why the alcohol complexes **1**−**2** cannot be reduced by the THF/CH_2Cl_2 system. On the other hand, if the carbenium ion complex is strongly

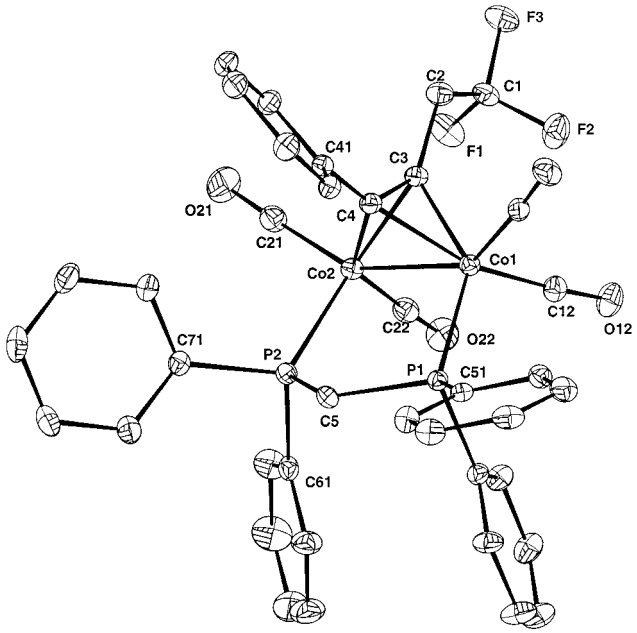


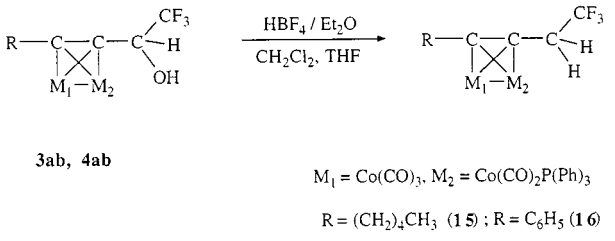
Figure 4. X-ray molecular structure of [{$Co_2(CO)_4$dppm}{μ-η^2,η^2-$C_6H_5C{\equiv}CCH_2(CF_3)$}] (**17**) with atom numbering system

Table 2. Selected bond lengths [Å] and angles [°] for complex **17**

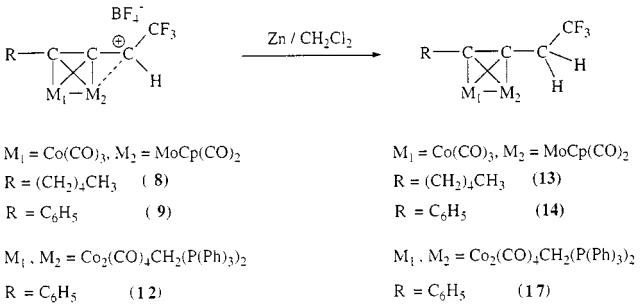
Co(1)−Co(2)	2.4876(7)	Co(1)−P(1)	2.227(1)
Co(1)−C(3)	1.950(4)	Co(2)−P(2)	2.225(2)
Co(1)−C(4)	1.939(4)	Co(2)−C(3)	1.934(4)
Co(2)−C(4)	1.967(4)	C(3)−C(4)	1.341(6)
Co(1)−C(4)−Co(2)	79.1(2)	Co(1)−C(3)−Co(2)	79.6(2)
C(3)−C(4)−C(41)	135.5(4)	C(2)−C(3)−C(4)	135.1(4)

Table 3. Comparison of ν(CO) (cm^{-1}) frequencies between the complexed alcohols and their corresponding carbenium ions

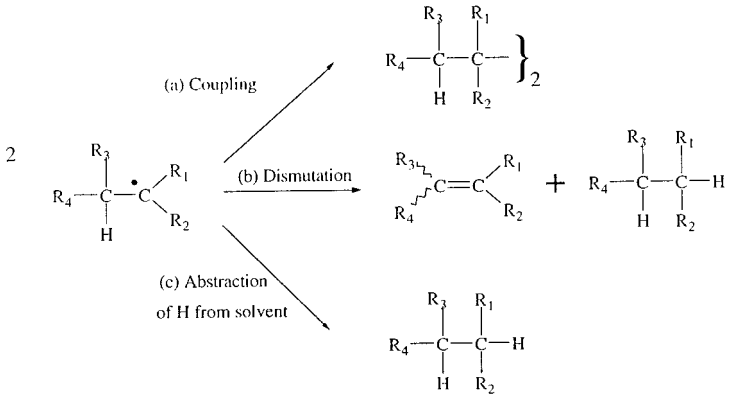
Alcohol	ν(CO) [cm^{-1}]	Cations	ν(CO) [cm^{-1}]
[Co_2]-(**1**)	2097, 2057, 2029		unstable, not isolated
[Co_2]-(**2**)	2048, 2050, 2020		unstable, not isolated
[Co_2P]-(**3**)	2063, 2015, 2005, 1987, 1967	**8**	2104, 2065, 2055, 2006, 1989
[Co_2P]-(**4**)	2068, 2018	**9**	2108, 2072, 2005
[Co_2P_2]-(**5**)	2066, 2029, 2001, 1974	**10**	2138, 2063, 2005
[Co,Mo]-(**6**)	2051, 2001, 1984, 1942	**11**	2123, 2071, 2022, 1973
[Co,Mo]-(**7**)	2057, 2002, 1949	**12**	2090, 2065, 2004, 1978



Scheme 4. Reduction of α-CF_3-propargyl alcohol complexes (**3**−**4**) using THF/CH_2Cl_2 in acidic medium



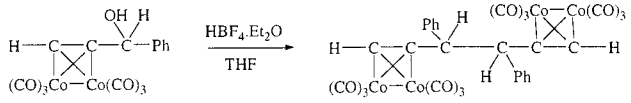
Scheme 5. Reduction of the metal-stabilized carbenium ions (**8**, **9**, and **12**) by Zn in CH_2Cl_2



Scheme 7. Possible reactions of carbon-centered radicals

stabilized by the bimetallic cluster, then the mono-electronic transfer from THF to the deficient electronic center is not possible, as shown by the alcohol complexes **5**−**7**, and the reaction stops at the carbenium ion stage. This hypothesis is also confirmed by the fact that the complex [{$Mo_2Cp_2(CO)_4$}{μ-η^2,η^2-HC≡CCH(C_6H_5)(OH)}], which is isolobal to the compound [{$Co_2(CO)_6$}{μ-η^2,η^2-HC≡CCH(C_6H_5)(OH)}], does not lead to coupling products. Finally, Co-stabilized carbenium ion exhibiting a stability between the two previous examples can be reduced by mono-electron transfer from THF to give the reduced compounds.

We would also like to outline that by either using the THF/CH_2Cl_2 system or by the action of Zn/CH_2Cl_2, our α-CF_3-propargyl alcohol complexes [{$Co_2(CO)_4L_2$}{μ-η^2,η^2-RC≡CC(OH)(CF_3)H}] (**3**−**7**) gave exclusively the reduction products, and never the coupling reaction products, which is the major product observed with [{$Co_2(CO)_6$}{HC≡CCH(C_6H_5)(OH)}] (Scheme 6).[19]



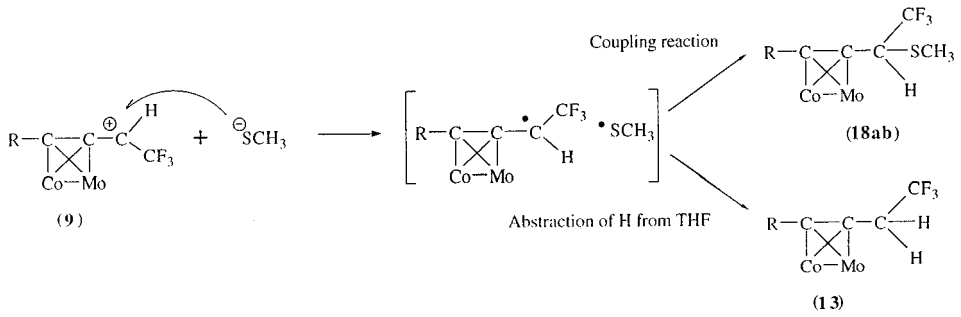
Scheme 6. Coupling reaction observed for a [CO_2]-complexed acetylenic alcohol in acidic medium

Generally, in carbon-centered radical reactions, the competition between coupling reactions, dismutation and abstraction of a hydrogen from the solvent, is a well documented area.[20](Scheme 7). For instance, primary carbon centered radical next to a hydrogen atom in the β position favors the dismutation reaction over the other reactions. Increasing the size of the substituents at the radical center favors the abstraction of a hydrogen from the solvent relative to recombination and dismutation. In our propargyl alcohol compounds, the presence of a CF_3 group in the alpha position to the carbon centered radical would impede the coupling reaction, due to electron repulsion, and hence abstraction of a proton from the solvent becomes the major reaction.

Another important feature of this chemistry was demonstrated when the carbenium ion complex [{$Co(CO)_3MoCp(CO)_2$}{μ-η^2,η^3-$CH_3(CH_2)_4$C≡CCH-(CF_3)}][BF_4] (**8**) was treated by NaSMe to give two compounds in 1:1 ratio. These compounds were identified, respectively, as the reduced compound [{$Co(CO)_3$-$MoCp(CO)_2$}{μ-η^2,η^2-$CH_3(CH_2)_4$C≡CCH(CF_3)H}] (**13**) and the substituted thio-ether complexes [{$Co(CO)_3$-$MoCp(CO)_2$}{μ-η^2,η^2-$CH_3(CH_2)_4$C≡CCH(CF_3)(SMe)}]-(**18a** and **b**) obtained as a pair of diastereomers. These results illustrate that the reaction between the isolated [Co,Mo] stabilized carbenium ion **9** and the methyl thiolato anion proceed through a radical pathway, whereby the transient radical pair species can either recombine in the solvent cage to give coupling reaction[21] as illustrated by formation of **18a**, **b** or, after diffusion from the solvent cage, would abstract a hydrogen atom from the solvent to afford the reduced alkyne adduct **13** (Scheme 8).

Conclusion

Co-complexed propargyl radicals may be formed during the reduction of α-CF_3 complexed acetylenic alcohols in acidic medium providing that their related carbenium ions are formed and are slightly stabilized. The stability of these carbenium ions depends on the electron donor ability of the bimetallic cluster. Our α-CF_3-complexed carbenium ions system seems to offer a new insight into, and the comprehension of the factors that allow certain cobalt-stabilized carbenium ions to undergo one electron reduction process rather than a substitution reaction. The present study shows that three classes of propargyl alcohol complexes can be distinguished. These classes could be defined as follows: class (a) − the parent alcohol complexes [{$Co_2(CO)_6$}{μ-η^2,η^2-RC≡CCH(CF_3)(OH)}] (**1**−**2**) cannot be reduced by THF/CH_2Cl_2 in acidic medium because the related [Co_2]-carbenium ions cannot be formed, class (b) − weakly stabilized carbenium ions such as [Co_2P] complexes **10** and **11** are easily reduced in acidic medium by THF/CH_2Cl_2, and class (c) − stable carbenium ions such as complexes **8**, **9**, and **12** can only be reduced when a strong reducing agent is used.

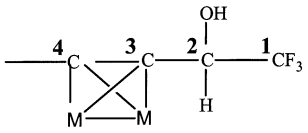


Scheme 8. Abstraction and coupling reactions occurring from a radical pair process

Experimental Section

General Methods: All reactions were carried out under an atmosphere of dry argon. Solvents were dried and distilled using standard techniques. Diethyl ether and THF were distilled from sodium benzophenone ketyl, dichloromethane and acetonitrile from sodium hydride, pentane was treated by sulfuric acid and distilled on sodium. Ethylrifluoroacetate, heptyne triphenylphosphane, Bis(diphenylphosphanyl)methane, $Mo_2Cp_2(CO)_6$, $Co_2(CO)_8$, HBF_4/Et_2O, aqueous 40% HBF_4, CD_2Cl_2, CD_3Cl, [D_6]acetone were used as purchased. − IR spectra were recorded on a Bio-rad FTS 165 spectrometer from KBr disks. All absorptions are expressed in wave numbers (cm^{-1}). − ^{1}H-, ^{13}C-, ^{19}F and ^{31}P-NMR spectra were recorded on a Bruker AM instrument, using standard programs for proton (299.MHz), carbon (75 MHz), fluoride (282 MHz) and phosphorus (124 MHz) spectra. NMR chemical shifts are reported in δ (ppm) relative to TMS (^{1}H, ^{13}C), $CFCl_3$ (^{19}F) or 85% H_3PO_4 (^{31}P); Data (^{13}C, ^{31}P) are proton decoupled. − Elemental analyses were performed by: "Centre régional de microanalyse-Université Pierre et Marie Curie".

Throughout the experimental section the carbon numbering system for the α-CF_3-propargyl alcohol complexes is shown on this diagram.



Synthesis of [{$Co_2(CO)_6$}-μ,η^2,η^2-(1,1,1-trifluoronon-3-yne-2-ol)] (1): To 1-heptyne (2.9 g, $3\cdot10^{-2}$ mol) in THF (40 mL) was added dropwise at 0°C, butyllithium (11.5 mL of a 2.5 M solution). After stirring 0.5 h, the mixture was cooled to −50°C and 2.48 g of ethyltrifluoroacetate ($2\cdot10^{-2}$ mol) were added dropwise. The mixture was stirred for 1 h and after attaining room temperature, 50 mL of NH_4Cl saturated aqueous solution were added. The organic phase was extracted by 3 × 25 mL of diethyl ether. The extracts were dried with $MgSO_4$ and the solvent removed under vacuum; The colorless oil was dissolved in 30 mL of ethanol and $NaBH_4$ (1.2 g) was added, progressively. The reaction was monitored by TLC on silica gel (eluent pentane/ether 5:1). The reaction was complete in one hour. After addition of water (50 mL) the organic phase was extracted by 3 × 25 mL of diethyl ether, dried ($MgSO_4$), and the solvent removed under vacuum to give a colorless oil (4.73 g). To the obtained oil in 50 mL of diethyl ether was added, at room temperature under argon, dicobalt octacarbonyl (1.2 g, 2.5 $.10^{-2}$ mol). The reaction was monitored by TLC on silica gel (eluent pentane/ether, 6:1). The reaction was complete in one hour. After adsorption of the crude product on silica gel, flash chromatography (pentane then pentane/ether, 10:1) leads to a dark red oil in 50% yield (5.1 g). − ^{1}H NMR ($CDCl_3$): δ = 5.12 (dq, J = 14.0 Hz, J = 7.2 Hz, 1 H, 2-H), 5.81 (t, J = 8.2 Hz, 2 H, 5-H), 2.53 (d, J = 7.2 Hz, 1 H, OH), 1.62 (m, 2 H, 6-H), 1.43 (m, 4 H, 7,8-H), 0.93 (t, J = 7.2 Hz, 3 H, 9-H). − ^{13}C NMR ($CDCl_3$): δ = 198.6 (CO), 123.2 (q, J = 282.0 Hz, C-1), 100.1 (C-3), 86.1 (C-4), 70.9 (q, J = 33.0 Hz, C-2), 32.9 (C-5), 31.3 (C-6), 31.0 (C-7), 22.0 (C-8), 13.5 (C-9). − ^{19}F NMR ($CDCl_3$): δ = −75.9 (d, J = 6.1 Hz). − IR ν(CO): $\tilde{\nu}$ = 2095, 2057, 2029 cm^{-1}. − $C_{15}H_{13}Co_2F_3O_7$ calcd. C 37.52, H 2.73; found C 37.70, H 2.81.

[{$Co_2(CO)_6$}-{μ-η^2,η^2-(1,1,1-trifluoro-4-phenylbut-3-yne-2-ol)] (2): The same synthetic procedure was used for the preparation of compound (**2**) as was used for (**1**). − ^{1}H NMR ($CDCl_3$): δ = 7.36 (m, 3 H, C_6H_5), 5.57 (m, 2 H, C_6H_5), 5.37 (dq, J = 13.5 Hz, J = 6.1 Hz, 1 H, 2-H), 2.86 (d, J = 6.1 Hz, 1 H, OH). − ^{13}C NMR ($CDCl_3$): δ = 198.3 (CO), 137.2, 129.5, 128.9, and 128.2 (C_6H_5), 124.1 (q, J = 283.0 Hz, C-1), 92.8 (C-3), 85.6 (C-4), 71.3 (q, J = 31.9 Hz). − ^{19}F NMR ($CDCl_3$): δ = −76.58 (d, J = 6.1 Hz). − IR ν(CO): $\tilde{\nu}$ = 2089, 2050, 2020 cm^{-1}. − $C_{16}H_7Co_2F_3O_7$ calcd: C 39.54,H 1.45; found C 40.41, H 1.65.

[{$Co_2(CO)_5P(C_6H_5)_3$}-μ-η^2,η^2-(1,1,1-trifluoronon-3-yne-2-ol)] (3a, 3b): To 0.58 g of (**1**) (1.21 mmol) in THF (15 mL) was added $P(C_6H_5)_3$ (0.40 g, 1.52 mmol) in THF (35 mL) and 2.3 mL of a 1 M solution of sodium/benzophenone in THF. The reaction was monitored by TLC (silica gel, eluent pentane/ether 4:1). The reaction was left for one hour at room temperature, then the mixture was purified by flash chromatography, giving the two diastereomers, which were separated in the order of increasing polarity (**3a**) then (**3b**), as red oils, 0.35 g and 0.06 g (40% and 7% yield, respectively).

Compound 3a: ^{1}H NMR ($CDCl_3$): δ = 7.56−7.31 (m, 15 H, C_6H_5), 3.96 (dq, J = 14 Hz, J = 8.0 Hz, 1 H, 2-H), 2.22 (m, 1 H, 5-H), 1.99 (d, J = 8.0 Hz, 1 H, OH), 1.72 (m, 1 H, 5-H), 1.51 (m, 2 H, 6-H), 1.25 (m, 4 H, 7,8-H), 0.89 (t, J = 7.1 Hz, 3 H, 9-H). − ^{13}C NMR ($CDCl_3$): δ = 206.2, 204.8, and 200.9 (CO), 134.3 (d, J = 53.4 Hz, $C_{ipso,}$ C_6H_5), 133.0 (d, J = 10.1 Hz, $C_{ortho,}$ C_6H_5), 130.8 ($C_{para,}$ C_6H_5), 129.0 (d, J = 9.5 Hz, $C_{meta,}$ C_6H_5), 123.0 (q, J = 283.5 Hz, C-1), 96.1 (C-3), 92.7 (C-4), 68.9 (q, J = 32.5 Hz, C-2), 31.7, 31.5, and 31.2 (C-5-6-7), 22.7 (C-8), 14.2 (C-9). − ^{19}F NMR ($CDCl_3$): δ = −76.5 (d, J = 6.1 Hz, CF_3). − ^{31}P NMR ($CDCl_3$): δ = 52.9 (broad). − IR ν(CO): $\tilde{\nu}$ = 2063, 2015, 2005, 1987, and 1962 cm^{-1}.

Compound 3b: ^{1}H NMR ($CDCl_3$): δ = 7.62−7.55 (m, 15 H, C_6H_5), 4.13 (dq, J = 14 Hz, J = 7.8 Hz, 1 H, 2-H), 2.36 (m, 1 H, 5-H), 2.04 (m, 1 H, 5-H), 1.86 (d, J = 7.8 Hz, 1 H, OH), 1.51 (m, 2 H, 6-H), 1.29 (m, 4 H, 7,8-H), 0.90 (t, J = 7.1 Hz, 3 H, 9-H). − ^{13}C NMR ($CDCl_3$): δ = 206.1−201.1 (CO), 134.6 (d, J = 39.6 Hz,C_{ipso}), 133.0 (d, J = 10.4 Hz,C_{ortho}), 130.7 (C_{para}), 128.9 (d,

J = 8.4 Hz,C_{meta}), 123.5 (q, J = 234.7 Hz, C-1), 98.8 (C-3), 79.9 (C-4), 71.5 (q, J = 32.0 Hz, C-2), 32.7, 31.9, and 22.7 (C-6-7-8), 14.1 (C-9). − ^{19}F NMR ($CDCl_3$): δ = −76.7.(d, J = 6.1 Hz, CF_3). − ^{31}P NMR ($CDCl_3$): δ = 51.3.(broad). − IR ν(CO): $\tilde{\nu}$ = 2062, 2015, 1998, 1963 cm^{-1}. − $C_{32}H_{28}Co_2F_3O_6P$ calcd: C 53.81, H 3.94; found C 55.65, H 4.14.

[{$Co_2(CO)5P(C_6H_5)_3$}-μ-η²,η²-(1,1,1-trifluoro-4-phenylbut-3-yne-2-ol)] (4a,4b): Compounds (**4a**) and (**4b**) were prepared in the same way described for **3a** and **3b**, and were isolated in 35% and 25% yield, respectively.

Compound 4a: ^{1}H NMR ($CDCl_3$): δ = 7.41−7.19 (m, 20 H, C_6H_5), 3.97 (qui, J = 14.0 Hz, J = 7.8 Hz 1 H, 2-H), 2.03 (d, J = 7.8 Hz, 1 H, OH). − ^{13}C NMR ($CDCl_3$): δ = 200.5 (CO), 138.8 ($C_{ipso,}$ C_6H_5), 133.9 (d, J = 40.3 Hz, $C_{ipso,}$ PC_6H_5), 133.2 (d, J = 11.6 Hz, $C_{ortho,}$ PC_6H_5), 130.7 ($C_{meta,}$ PC_6H_5), 130.4 (C_6H_5), 128.8 (C_6H_5), 128.7 (d, J = 9.7 Hz, $C_{meta,}$ C_6H_5), 128.2 (C_6H_5), 124.0 (q, J = 284.0 Hz, C-1), 85.7 (C-3), 82.4 (C-4), 70.0 (q, J = 31.8 Hz, C-2). − ^{19}F NMR ($CDCl_3$): δ = −75.77(d, J = 6.0 Hz, CF_3). − ^{31}P NMR ($CDCl_3$): δ = 48.27(broad). − IR ν(CO): $\tilde{\nu}$ = 2068, 2018 cm^{-1}.

Compound 4b: ^{1}H NMR ($CDCl_3$): δ = 7.41−7.18 (m, 20 H, C_6H_5), 3.97 (dq, J = 14.0 Hz, J = 7.8 Hz, 1 H, 2-H), 1.88 (d, J = 7.8 Hz, 1 H, OH). − ^{13}C NMR ($CDCl_3$): δ = 205.9−203.9−200.5 (CO), 139.5 ($C_{ipso,}$ C_6H_5), 133.8 (d, J = 41.1 Hz, $C_{ipso,}$ PC_6H_5), 133.3 (C_6H_5), 133.2 (d, J = 10.7 Hz, $C_{ortho,}$ PC_6H_5), 130.6 (C_6H_5), 130.5 (d, J = 10.4 Hz, $C_{meta,}$ PC_6H_5), 128.8 (C_6H_5), 128.7 (d, J = 8.2 Hz, $C_{para,}$ PC_6H_5), 128.2 (C_6H_5), 124.6 (q, J = 283 Hz, C-1), 88.1 (C-3), 79.6 (C-4), 70.3 (q, J = 30.5 Hz, C-2). − ^{19}F NMR ($CDCl_3$): δ = −76.34 (broad). − ^{31}P NMR ($CDCl_3$): δ = 48.29 (broad). − IR ν(CO): $\tilde{\nu}$ = 2068, 2018 cm^{-1}. − $C_{33}H_{22}Co_2F_3O_6P$ calcd: C 55.02, H 3.08; found C 56.22, H 3.06.

[{$Co_2(CO)_4$dppm}-μ-η²,η²-(1,1,1-trifluoro-4-phenylbut-3-yne-2-ol)] (5): To a solution of **2** (0.5 g, 1.27 mmol) in 50 mL of hexane was added dppm (0.5 g, 1.30 mmol). After 0.5 h of reflux, the reaction was completed. The mixture was purified by flash chromatography on silica gel, using pentane as eluent then using pentane/ether (1:4). Complex **5** was obtained in 58% yield (0.66 g). − ^{1}H NMR ($CDCl_3$): δ = 7.25−6.91 (m, 25 H, C_6H_5), 5.20 (dq, J = 14.0 Hz, J = 7.5 Hz, 1 H, 2-H), 3.22 (m, 2 H, PCH_2P), 2.34 (d, J = 7.5 Hz, 1 H, OH). − ^{13}C NMR ($CDCl_3$): δ = 205.8, 202.4, and 202.0 (CO), 141.7 ($C_{ipso,}$ C_6H_5), 130.7, 128.8, and 126.4 ($C_{o,m,p,}$ C_6H_5), 138.1, 134.1, 132.8, 130.2, 129.7, and 128.3 (m, PC_6H_5), 124.6 (q, J = 281.4 Hz, C-1), 93.9 (C-4), 91.7 (C-3), 72.4 (q, J = 31.6 Hz, C-2), 34.4 (t,.J = 21.7 Hz, PCH_2P). − ^{19}F NMR ($CDCl_3$): δ = −76.7 (d, J = 6.0 Hz, CF_3). − ^{31}P NMR ($CDCl_3$): δ = 37.7 (broad). − IR ν(CO): $\tilde{\nu}$ = 2066, 2029, 2001, 1974 cm^{-1}. − $C_{39}H_{29}F_3O_5P_2Co_2$ calcd: C 57.51, H 3.59; found C 54.37, H 3.54.

[{$Co(CO)_3MoCp(CO)_2$}-μ-η²,η²-(1,1,1-trifluoronon-3-yne-2-ol)] (6a, 6b): To 0.15 g (0.3 mmol) of **1** in 15 mL THF was added a solution of $NaMoCp(CO)_2$ in 15 mL THF, prepared from 0.15 g (0.3 mmol) of $Mo_2Cp_2(CO)_6$ and 0.014 g (0.6 mmol) of Na/1.4 g Hg [for the detailed preparation of $NaMoCp(CO)_3$ see reference[12]]. This mixture was stirred for 7 h at room temperature and monitored by TLC-silica gel using pentane/ether (2:1) as eluent. After chromatography on silica gel, two products were recovered, **2a** and **2b**, in the order of increasing polarity. Complexes **2a** and **2b** were obtained in 58.8% (0.10 g) and 35.3% (0.06 g) yield, respectively.

Compound 6a: ^{1}H NMR ($CDCl_3$): δ = 5.47 (s, 5 H, Cp), 5.07 (dq, J = 13 Hz, J = 5.8 Hz, 1 H, 2-H), 2.91 (t, J = 8.0 Hz, 2 H, 5-H), 2;39 (d, J = 5.8 Hz, OH), 1.75 (m, 1 H, 6-H), 1.60 (m, 1 H, 6-H), 1.40 (m, 4 H, 7,8-H), 0.92 (t, J = 6.8 Hz, 3 H, 9-H). − ^{13}C NMR ($CDCl_3$): δ = 203.0 (CO), 123.5 (q, J = 276.0 Hz, C-1), 105.2 (C-3), 90.3 (Cp), 79.8 (C-4), 73.4 (q, J = 32.0 Hz, C-2), 34.9 (C-5), 31.8 (C-6), 30.9 (C-7), 22.2 (C-8), 13.7 (C-9). − ^{19}F NMR ($CDCl_3$): δ = −75.9 (d, J = 6.1 Hz). − IR ν(CO): $\tilde{\nu}$ = 2051, 2001, 1984, 1942 cm^{-1}. − $C_{19}H_{18}CoF_3MoO_6$ calcd: C 41.17, H 3.27; found C 42.99, H 3.12.

Compound 6b: ^{1}H NMR ($CDCl_3$): δ = 5.42 (s, 5 H, Cp), 4.94 (dq, J = 13.0 Hz, J = 7.4 Hz, 1 H, 2-H), 2.96 (m, 2 H, 5-H), 2;19 (d, J = 7.4 Hz, 1 H, OH), 1.63 (m, 2 H, 6-H), 1.40 (m, 4 H, 7,8-H), 0.91 (t, J = 6.8 Hz, 3 H, 9-H). − ^{13}C NMR ($CDCl_3$): δ = 202.9 (CO), 124.0 (q, J = 281.0 Hz, C-1), 104.1 (C-3), 90.4 (Cp), 78.6 (C-4), 73.5 (q, J = 31.0 Hz, C-2), 35.1 (C-5), 31.9 (C-6), 30.9 (C-7), 22.2 (C-8), 13.8 (C-9). − ^{19}F NMR ($CDCl_3$): δ = −75.15(d, J = 6.5 Hz). − IR ν(CO): $\tilde{\nu}$ = 2052, 2003, 1987, and 1940 cm^{-1}. − $C_{19}H_{18}CoF_3MoO_6$ calcd: C 41.17, H 3.27; found C 43.11, H 3.16.

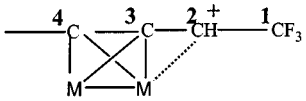
[{$Co(CO)_3MoCp(CO)_2$}-μ-η²,η²-(1,1,1-trifluoro-4-phenylbut-3-yne-2-ol)] (7a, 7b): A slightly modified procedure was used relative to that of (**6a**, and **6b**). A THF solution of **2** was heated under reflux for two hours with $NaMoCp(CO)_3$. The diastereomers **7a** and **7b** were separated by flash chromatography in the order of increasing polarity, and were obtained in 35% and 53% yield respectively (0.2 g) and (0.3 g).

Compound 7a: ^{1}H NMR ($CDCl_3$): δ = 7.43−7.33 (m, 5 H, C_6H_5), 5.46 (s, 5 H, Cp), 5.28 (dq, J = 13.0 Hz, J = 5.7 Hz, 1 H, 2-H), 2.27 (d, J = 5.7 Hz, 1 H, OH). − ^{13}C NMR ($CDCl_3$): δ = 225.6 (CO), 222.3 (CO), 202.7−202.3 (CO), 140.4 (C_{ipso}), 129.3 (C_{meta}), 128;6 (C_{ortho}), 127.6 (C_{para}), 124.7 (q, J = 282.2 Hz,C-1), 98.2 (C-3), 90.4 (Cp), 88.4 (C-4), 73.4 (q, J = 30.7 Hz, C-2). − ^{19}F NMR ($CDCl_3$): δ = −75.87 (d, J = 5.7 Hz). − IR ν(CO): $\tilde{\nu}$ = 2057, 2002, 1949 cm^{-1}.

Compound 7b: ^{1}H NMR ($CDCl_3$): δ = 7.43−7.32 (m, 5 H, C_6H_5), 5.46 (s, 5 H, Cp), 5.16 (dq, J = 13.0 Hz, J = 5.7 Hz, 1 H, 2-H), 2.34 (d, J = 5.7 Hz, 1 H, OH). − ^{13}C NMR ($CDCl_3$): δ = 225.4 (CO), 222.8 (CO), 203.0−201.8 (CO), 140.1 (C_{ipso}), 129.8 (C_{meta}), 128.5 (C_{ortho}), 127.9 (C_{para}), 124.9 (q, J = 283.0 Hz, C-1), 104.9 (C-3), 98.8 (C-4), 90.9 (Cp), 73.2 (q, J = 30.3 Hz, C-2). − ^{19}F NMR ($CDCl_3$): δ = −75.89 (d, J = 6.4 Hz). − IR ν(CO): $\tilde{\nu}$ = 2058, 1994, 1948 cm^{-1}. − $C_{20}H_{12}CoF_3MoO_6$ calcd: C 42.88, H 2.16; found C 43.90, H 2.54.

[{$Co(CO)_3MoCp(CO)_2$}-μ-η²,η³-(1,1,1-trifluoronon-3-yn-2-onium)] Tetrafluoroborate (8): To a solution of a mixture of (**6a**) and (**6b**) (0.277 g, 0.5 mmol) in 5 mL of ether was added HBF_4/Et_2O (0.25 mL). The red solution turns dark with the formation of an insoluble oil. The reaction was left for 1 h at room temperature, then the supernatant was removed and the oily material washed five times with diethyl-ether and finally dried under vacuum for several hours.

The carbon numbering system for the α-CF_3-carbenium complexes is illustrated by the following diagram:



^{1}H NMR (CD_2Cl_2): δ = 5.99 (s, 5 H, C_p), 5.94 (q, J = 7.2 Hz, 1 H, 2-H), 2.98 (m, 2 H, 5-H), 1.73 (m, 2 H, 6-H),1.38 (m, 4 H, 7,8-H), 0.93 (t, J = 6.6 Hz, 3 H, 9-H). − ^{13}C NMR (CD_3COCD_3): δ = 215.5, 209.2, and 198.2 (CO), 123.5 (q, J = 275.9 Hz, C-1), 107.3−84.7 (C-3,4), 94.0 (q, J = 36.9 Hz, C-2), 93.4 (s, Cp) (C-5), 35.7 (C-5), 32.6 (C-6), 31.4 (C-7), 22.4 (C-8), 13.9 (C-9). − ^{19}F

NMR (CD_2Cl_2): δ = −59.2 (broad). − IR ν(CO): $\tilde{\nu}$ = 2104, 2065, 2055, 2006, 1989, and 1947 cm^{-1}. − $C_{19}H_{17}BCoF_7MoO_5$ calcd: C 36.57, H 2.74; found C 34.88, H 3.00.

[{Co(CO)$_3$MoCp(CO)$_2$}-μ-η^2,η^3-(1,1,1-trifluoro-4-phenylbut-3-yn-2-onium)] Tetrafluoroborate (9): The same procedure was used as for compound **8**. − ^{1}H NMR (CD_2Cl_2): δ = 7.77 (m, 2 H, C_6H_5), 7.59 (m, 3 H, C_6H_5), 6.06 (q, *J* = 6.5 Hz, 1 H, C_6H_5), 7.43 (m, 2 H, C_6H_5), 7.35 (m, 3 H, C_6H_5), 6.06 (q, *J* = 6.5 Hz, 1 Hz), 6.04 (s, 5 H, Cp−Mo). − IR ν(CO): $\tilde{\nu}$ = 2108, 2072, 2005 cm^{-1}.

[{Co$_2$(CO)$_5$P(C$_6$H$_5$)$_3$}-μ-η^2,η^3-(1,1,1-trifluoronon-3-yne-2-onium)] Tetrafluoroborate (10): This compound hydrolyses rapidly in solution, therefore the ^{1}H-NMR spectrum could not be recorded, however the IR data are reminiscent of a cobalt−carbenium ion complex. − IR ν(CO): $\tilde{\nu}$ = 2138, 2063, and 2005 cm^{-1}.

[{Co$_2$(CO)$_5$P(C$_6$H$_5$)$_3$}-μ-η^2,η^3-(1,1,1-trifluoro-4-phenylbut-3-yne-2-onium)] Tetrafluoroborate (11): This compound hydrolyses rapidly in solution, therefore the ^{1}H-NMR spectrum could not be recorded. The infrared data are characteristic of a cobalt−carbenium ion complex. − IR ν(CO): $\tilde{\nu}$ = 2123, 2071, 2022 cm^{-1}.

[{Co$_2$(CO)$_4$dppm}-μ-η^2,η^3-(1,1,1-trifluoro-4-phenylbut-3-yne-2-onium)] Tetrafluoroborate (12): This complex hydrolyses rapidly in solution, therefore the ^{1}H-NMR spectrum could not be recorded. − IR ν(CO): $\tilde{\nu}$ = 2090, 2065, 2004, 1978 cm^{-1}. − $C_{39}H_{28}BCo_2F_7O_4P_2$ calcd: C 52.97, H 3.19; found C 52.52, H 3.85.

[{Co(CO)$_3$MoCp(CO)$_2$}-μ-η^2,η^2-(1,1,1-trifluoronon-3-yne)] (13): The carbenium ion complex **8** (0.11 mmol) was dissolved in CH_2Cl_2 (20 mL) and an excess of Zn powder (a small spatula portion) was added, and the reaction stirred for 20 minutes at room temperature then filtered, and the solvent removed under vacuum. The residue was purified by chromatography on silica gel using an Et_2O/pentane (10:90) mixture. Complex **13** was isolated as red-orange oily material in 85% yield (65 mg). − ^{1}H NMR ($CDCl_3$): δ = 5.37 (s, 5 H, C_p), 3.48 (oct, *J* = 10.6−4.3 Hz, 2 H, 2-H), 2.88 (t, *J* = 8.6 Hz, 2 H, 5-H), 1.61 (m, 2 H, 6-H),1.40 (m, 4 H, 7,8-H), 0.92 (t, *J* = 7.2 Hz, 3 H, 9-H).

[{Co(CO)$_3$MoCp(CO)$_2$}-μ-η^2,η^2-(1,1,1-trifluoro-4-phenylbut-3-yne)] (14): The preparation of this complex is similar to that of compound **13**. Thus, starting with 0.11 mmol of the carbenium ion complex **9** in CH_2Cl_2, the target compound **14** was isolated as a red-orange oily material in 80% yield (48 mg). − ^{1}H NMR (CD_3COCD_3): δ = 7.01 (m, 5 H, C_6H_5), 5.10 (s, 5 H, C_p), 3.37 (q, *J* = 9.75 Hz, 2 H, CH_2). − ^{13}C NMR ($CDCl_3$): δ = 233.1, 225.7, and 213.0 (CO), 141.2 ($C_{ipso,}$ C_6H_5), 128.9, 128.5, and 127.1 ($C_{o,m,p,}$ C_6H_5), 126.5 (q, *J* = 272 Hz, C-1), 91.4 (Cp), 95.5−90.8 (C-3, C-4), 39.2 (q, *J* = 29.3 Hz, C-2). − ^{19}F NMR ($CDCl_3$): δ = −64.43 (t, *J* = 9.8 Hz, CF_3). − IR ν(CO): $\tilde{\nu}$ = 2056, 2004, 1993, 1944 cm^{-1}. − Anal. for $C_{20}H_{12}CoF_3MoO_5$ calcd: C 44.14, H 2.22; found C44.26, H2.28.

[{Co$_2$(CO)$_5$P(C$_6$H$_5$)$_3$}-μ-η^2,η^2-(1,1,1-trifluoronon-3-yne)] (15): This complex was prepared by two different procedures:

Method A: This synthetic procedure is the same as the one described for complexes **13** and **14**. Complex **15** was obtained in 60% yield as red oily material (46 mg).

Method B: The alcohol starting materials **3a**, and **b** (100 mg, 0.142 mmol) were dissolved in 2 mL of CH_2Cl_2 in the presence of 31 μL of THF. The red solution was treated with $HBF_4 \cdot Et_2O$ (58 mL) at −5°C, and the reaction was left to attain room temperature. The solvents were removed and the residue was purified by chromatography on silica gel using Et_2O/pentane (10:90) as eluent. Complex **15** was isolated in 30% yield (30 mg). − ^{1}H NMR ($CDCl_3$): δ = 7.59−7.47 (m, 15 H, C_6H_5), 2.63 (q, *J* = 10.4 Hz, 2 H, 2-H), 2.20 (m, 1 H, 5-H), 2.04 (m, 1 H, 5-H), 1.60 (m, 1 H, 6-H), 1.47 (m, 1 H, 6-H), 1.31 (m, 4 H, 7,8-H), 0.91 (t, *J* = 6.4 Hz, 3 H, 9-H). − ^{13}C NMR ($CDCl_3$): δ = 206.4, 204.8, and 201.5 (CO), 134.6 (d, *J* = 40.2 Hz, $C_{ipso,}$ C_6H_5), 133.1 (d, *J* = 9.5 Hz, $C_{ortho,}$ C_6H_5), 130.7 (s, $C_{para,}$ C_6H_5), 128.9 (d, *J* = 7.3 Hz, $C_{meta,}$ C_6H_5), 125.9 (q,*J* = 279 Hz, C-1), 99.5−78.1 (C-3−4), 36.0 (q, *J* = 29 Hz, C-2), 32.1, 32.0, 31.4 (C-5, C-6, C-7), 22.7 (C-8), 14.2 (C-9). − ^{19}F NMR ($CDCl_3$): δ = −64.80.(t, *J* = 10.3 Hz, CF_3). − ^{31}P NMR ($CDCl_3$): δ = 52.84.(broad). − IR ν(CO): $\tilde{\nu}$ = 2059, 2010, 2005, 1997, 1987, and 1963 cm^{-1}. − $C_{32}H_{28}Co_2F_3O_5P$ calcd: C 55.02, H 4.04; found C 52.85 H 4.25.

[{Co$_2$(CO)$_5$P(C$_6$H$_5$)$_3$}-μ-η^2,η^2-(1,1,1-trifluoro-4-phenylbut-3-yne)] (16): This compound was also prepared by the two synthetic procedures outlined above: Method A: Complex **16** was obtained as red powder in 90% (70 mg). − Procedure B: Compound **16** was isolated in a lower yield of 27% (40 mg). − ^{1}H NMR ($CDCl_3$): δ = 7.36−7.19 (m, 20 H, C_6H_5), 2.87 (m, 1 H, 2-H), 2.28 (m, 1 H, 2-H). − ^{13}C NMR ($CDCl_3$): δ = 204.0 (CO), 200.7 (CO), 140.0 ($C_{ipso,}$ C_6H_5), 133.9 (d, $C_{ipso,\ J}$ = 41.1 Hz, PC_6H_5), 133.3 (d, $C_{ortho,\ J}$ = 10.5 Hz, PC_6H_5), 130.5, 129.8, 128.7 (s, $C_{ortho,\ meta,\ para}$), 128.6 (d, *J* = 9.8 Hz, $C_{meta,}$ PC_6H_5), 127.0 (s, $C_{para,}$ PC_6H_5), 126.1 (q, *J* = 281 Hz, C-1), 86.3 (C-3), 90.8 (C-4), 35.2 (q, *J* = 29.3 Hz, C-2). − ^{19}F NMR ($CDCl_3$): δ = −64.75.(t, *J* = 9.1 Hz, CF_3). − ^{31}P NMR ($CDCl_3$): δ = 49.53 (broad). − IR ν(CO): $\tilde{\nu}$ = 2065, 2013, and 1983 cm^{-1}. −$C_{33}H_{22}Co_2F_3O_5P$ calcd: C 56.27, H 3.15; found C 56.34, H 3.21.

[{Co$_2$(CO)$_4$dppm}-μ-η^2,η^2-(1,1,1-trifluoro-4-phenylbut-3-yne)] (17): In a similar manner to that described for complexes **13** and **14**, the reduced compound **17** was obtained from 0.11 mmol of the carbenium ion complex **12**, as a red-orange powder in 90% yield (79 mg). − ^{1}H NMR ($CDCl_3$): δ = 7.33−6.99 (m, 25 H, C_6H_5), 3.63 (m, 2 H, PCH_2P), 3.13 (m, 2 H, 2-H). − ^{13}C NMR ($CDCl_3$): δ = 205.9−202.6 (CO), 142.4 (s, $C_{ipso,}$ C_6H_5), 138.7, 134.4. and 132.8 (m, C_6H_5P), 132.7 (s, $C_{para,}$ C_6H_5), 130.7 (m, C_6H_5P), 130.4 ($C_{ortho,}$ C_6H_5), 128.6−128.2 (m, C_6H_5P), 125.9 (s, $C_{meta,}$ C_6H_5), 126.6 (q, *J* = 274.5 Hz, C-1), 93.8 (C-4), 88.9 (C-3), 39.1 (q, *J* = 28.9 Hz, C-2), 34.5 (t, *J* = 21.8 Hz, PCH_2P). − ^{19}F NMR ($CDCl_3$): δ = −64.90.(t, *J* = 10.49 Hz, CF_3). − ^{31}P NMR ($CDCl_3$): δ = 38.36 (s). − IR ν(CO): $\tilde{\nu}$ = 2027, 1999, 1969, 1959 cm^{-1}. − $C_{39}H_{29}Co_2F_3O_4P_2$ calcd: C 58.66, H 3.66; found C 56.67, H 3.70.

[{Co(CO)$_3$MoCp(CO)$_2$}-μ-η^2,η^2-(1,1,1-trifluoro-2-(methylthio)non-3-yne)] (18a, 18b) and [{Mo$_2$Cp$_2$(CO)$_4$}-μ-η^2,η^3-(prop-2-yn-1-onium)] Tetrafluoroborate (19): A mixture of the two alcohol diastereomers **6a**, and **b** (220 mg, 0.40 mmol) were dissolved in 10 mL of Et_2O. The red solution was protonated by 0.2 mL of $HBF_4 \cdot Et_2O$ at room temperature, affording a dark red oily precipitate. This material was isolated and washed 5 times with Et_2O. CH_2Cl_2 was then added (10 mL) and NaSMe (30 mg, 0.43 mmol.) was introduced, and the reaction was left to stir for 10 minutes. The solvent was removed and the residue was purified by chromatography on silica-gel using Et_2O/pentane 10:90 to yield inseparable mixture of the two diastereoisomer-substituted complexes **18a**, and **b** (1:1) in 35% yield (82 mg). The reduced complex **19** was obtained in 35% yield (74 mg).

Spectroscopic Data for 18a, and b: ^{1}H NMR ($CDCl_3$): δ = 5.44−5.40 (s, 5 H, C_p), 4.25 (m, 1 H, 2-H), 2.93 (m, 2 H, 5-H), 2.36−2.35 (s, 3 H, SCH_3), 1.7 (m, 2 H, 5-H), 1.65 (m, 2 H, 6-H), 1.42 (m, 4 H, 7,8-H), 0.92−0.93 (t, *J* = 6.3 Hz, 3 H, 9-H). − IR ν(CO): $\tilde{\nu}$ = 2051, 2000, 1985, 1939 cm^{-1}.

Table 4. Crystal data for compounds **5** and **17**

	Compound **5**	Compound **17**
Formula	$C_{39}H_{29}Co_2F_3O_5P_2$	$C_{39}H_{29}Co_2F_3O_4P_2 \cdot C_3H_6O$
mass	814.5	856.5
a [Å]	11.756(4)	11.099(5)
b [Å]	20.542(4)	11.712(2)
c [Å]	15.404(5)	15.575(7)
α [°]	90	87.57(3)
β [°]	96.98(3)	86.50(4)
γ [°]	90	76.26(4)
V [Å^3]	3692(2)	1962(1)
Z	4	2
Crystal system	monoclinic	triclinic
Space group	$P2_1/n$	*P*-1
Linear abs. coeff. μ [cm^{-1}]	10.4	9.8
Density ρ [g·cm^{-3}]	1.47	1.45
Diffractometer	CAD4 Enraf−Nonius	CAD4 Enraf−Nonius
Radiation	Mo-*K*α (λ = 0.71069 Å)	Mo-*K*α (λ = 0.71069 Å)
Scan type	ω /2θ	ω/2θ
Scan range [°]	0.8 + 0.345 tgθ	0.8 + 0.345 tgθ
θ Limits [°]	1−25	1−26
Temperature of measurement	295 K	223 K
Octants collected *h*; *k*; *l*	0,13; 0,24; −18,18	0,13; −14,14; −19,19
Decay%	<10	<10
No. of data collected	7041	8126
No. of unique data collect. (R_{int})	6483 (0.05)	7703 (0.03)
No. of unique data used for ref.	3057 (Fo)^2 > 3σ(Fo)^2	4787 (Fo)^2 > 3σ(Fo)^2
$R = \Sigma\|\|Fo\| - \|Fc\|\|/\Sigma\|Fo\|$	0.0506	0.0478
Rw* = [Σw(Fo − Fc)^2/Σw Fo ^{2}]$^{1/2}$	0.0597	0.0563
S	1.17	1.11
Extinction parameter	none	none
No. of variables	497	488
Δρmin [e·Å^{-3}]	−0.42	−0.48
Δρmax [e·Å^{-3}]	0.87	0.74

Spectroscopic Data for 19: ^{1}H NMR (CD_2Cl_2): δ = 7.39 (m, 5 H, C_6H_5), 7.15 (s, 1 H, 3-H), 7.00 (s, 1 H, 1-H), 5.38 (s, 5 H, Cp). − IR ν(CO): $\tilde{\nu}$ = 2052, 2006, 1993, 1907 cm^{-1}.

X-ray Structure Determination: Suitable crystals of [(Co_2(-CO)$_4$dppm)(μ-η^2,η^2-RC≡CCH(CF_3)(OH)] (**5**) were obtained by slow evaporation of a saturated solution in pentane/Et_2O (1:4), while complex [{Co_2(CO)$_4$dppm}{μ-η^2,η^2-C_6H_5C≡CCH_2(CF_3)}] (**17**) was obtained by slow evaporation of an acetone saturated solution. The selected crystal of complex **5** or **17** was glued on the top of a glass rod. Accurate cell dimensions and orientation matrix were obtained by least-squares refinements of 25 accurately centered reflections on a Nonius CAD4 diffractometer equipped with graphite-monochromated Mo-*K*α radiation. No significant variations were observed in the intensities of two checked reflections during data collection. The ψ-scan curve of **5** or **17** was flat, hence no absorption correction was applied. Complete crystallographic data and collection parameters for **5** and **17** are listed in Table 4. The data were corrected for Lorentz and polarization effects. Computations were performed by using the PC version of CRYSTALS.[22] Scattering factors and corrections for anomalous dispersion were taken from ref.[23] Complex **5** exhibited a disordered behavior for the CF_3−C−OH unit. A best structural resolution was achieved by considering two locations where the CF_3−C−OH fragment displayed occupation factor of (43%) and (57%). The asymmetric unit of complex **17** contains one molecule of solvated acetone, thus crystals of **17** decomposed at room temperature by loss of solvent and thus the X-ray data were recorded at low temperature. The structures of compounds **5** and **17** were refined by full-matrix least-squares with anisotropic thermal parameters for all non-hydrogen atoms. Hydrogen atoms were introduced in calculated positions in the last refinements and were allocated an overall refinable isotropic thermal parameter. Fractional parameters, anisotropic thermal parameters, and all bond lengths and angles are given in the Supporting Information for complexes **5** and **17**.

Acknowledgments

We would like to thank CNRS for supporting this work.

[1] G. K. S. Prakash, A. K. Yudin, *Chem. Rev.* **1997**, *97*, 757−786.
[2] A. D. Allen, T. T. Tidwell, in: *Advances in Carbocation Chemistry* (Ed.: X. Greary, JAI Press Inc. Greenwich, CT, **1989**, 1−44.
[3] T. Tsushima, K. Kawada, S. Ishihara, N. Uchida, O. Shiratori, J. Higaki, M Hirita, *Tetrahedron*, **1998**, *44*, 5375−5387.
[4] [4a] T. Hagiwara, K. Tanaka, T. Fuchikami, *Tetrahedron Lett.* **1996**, *37*, 8187−8190. − [4b] M. Neri, M. G. Brasca, A. Longo, W. Moretti, A. Panzeri, *Tetrahedron Lett.* **1997**, *38*, 4881−4884.
[5] [5a] H. Amouri, M. Gruselle, *Chem. Rev.* **1996**, *96*, 1077−1103. − [5b] M. J. Mc Glinchey, L. Girard, R. Ruffolo, *Coordination Chem. Rev.* **1995**, 143, 331−381. − [5c] K. M. Nicholas, Acc. Chem. Res. **1987**, *26*, 207 − [5d] G. G. Melikyan, K. M. Nicholas, "The Chemistry of Metal−Alkyne Complexes" in: *Modern Acetylene Chemistry* (Eds.: P. J. Stang, F. Diederich), VCH Publishers, **1995**, *4*, 99−138.
[6] [6a] M. R. Tirpak, C. A. Hollingsworth, J. H. Wotiz, *J. Organomet. Chem.* **1960**, *25*, 687−690. − [6b] S. Padmanabhan, K. M. Nicholas, *J. Organomet. Chem.* **1981**, *212*, 115−124. − [6c] G. G. Melikyan, O. Vostrowsky, W. Bauer, H. J. Bestmann, *J. Organomet. Chem.* **1992**, *423*, 24−27. − [6d] K. L. Salazar, M. A. Khan, K. M. Nicholas, *J. Am. Chem. Soc.* **1997**, *119*, 9053−9054.
[7] G. G. Melikyan, R. C. Combs, J. Lamirand, M. Khan, K. M. Nicholas, *Tetrahedron Lett.* **1994**, *35*, 363−366.
[8] G. G. Melikyan, M. A. Khan, K. M. Nicholas, *Organometallics*, **1995**, *14*, 2170−2172.

[9] M. A. Kondratenko, B. Malézieux, M. Gruselle, D. Bonnet-Delpon, J. P. Bégué, *J. Organomet. Chem.* **1995**, *487*, 15−17.
[10] [10a] M. F. D′Agostino, C. S. Frampton, M. J. Mc Glinchey, *Organometallics*, **1990**, *9*, 2972−2984. − [10b] D. H. Bradley, M. A. Khan, K. M. Nicholas, *Organometallics*, **1992**, *11*, 2598−2607.
[11] D. H. Braley, M. A. Khan, K. M. Nicholas, *Organometallics*, **1989**, *8*, 554−556.
[12] M. Gruselle, H. El Hafa, M. Nikolski, G. Jaouen, J. Vaissermann, L. Lijuan, M. J. Mc Glinchey, *Organometallics*, **1993**, *12*, 4917−4925.
[13] O. Kahn, D. Rau, H. Mayr, J. Am. Chem. Soc. **1998**, *120*, 900−907.
[14] R. E Connor, K. M. Nicholas, *J. Organomet. Chem.* **1997**, *125*, 45−48.
[15] M. Gruselle, C. Cordier, M. Salmain, H. Amouri, C. Guerin, J. Vaissermann, G. Jaouen, *Organometallics*, **1990**, *9*, 2993−2997.
[16] G. G. Melikyan, S. Bright, T. Monroe, K. I. Hardcastle, J. Ciurash, *Angew. Chem. Int. Ed. Engl.* **1998**, *37*, 161−164.
[17] C. Cordier, PhD Université Pierre et Marie Curie (France), **1991**.
[18] M. Gruselle, M. A. Kondratenko, H. Amouri, J. Vaissermann, *Organometallics*, **1995**, *14*, 5242−5250.
[19] G. G. Melikyan, A. Deravakian, S. Myer, S. Yadegar, K. I. Hardcastle, J. Ciurash, P. Toore, *J. Organomet. Chem.* **1999**, *544*, 143−145.
G. G. Melikyan, A. Deravakian, *J. Organomet. Chem.* **1997**, *578*, 68−75.
[20] J. Fossey, D. Lefort, J. Sorba, *Les radicaux libres en chimie organique*; Ed. Masson Paris, **1990**.
[21] [21a] R. Kaptein, in: *Chemically Induced Magnetic Polarisation*, Wiley-Interscience, New York **1973**. − [21b] M. Gruselle, *Tetrahedron*, **1975**, *31*, 2283−2287.
[22] D. J. Watkin, C. K. Prout, J. R. Carruthers, P. W. Betteridge; Crystal issue 10, *Chemical Crystallography Laboratory*: University of Oxford UK, **1996**.
[23] D. T. Cromer, International *Tables of X-ray Crystallography*; Kynoch Press Birmingham UK. **1974**; Vol. IV.
[24] L. J. Pearce and W. J. Watkin; *Chemical Crystallography Laboratory*, University of Oxford UK.

Received July 29, 1999
[I99282]

On the Electronic Properties of Substituted Phosphanylcarbenes

Wolfgang W. Schoeller[a]

Keywords: Phosphanylcarbenes / Substituent effects / Quantum chemical calculations

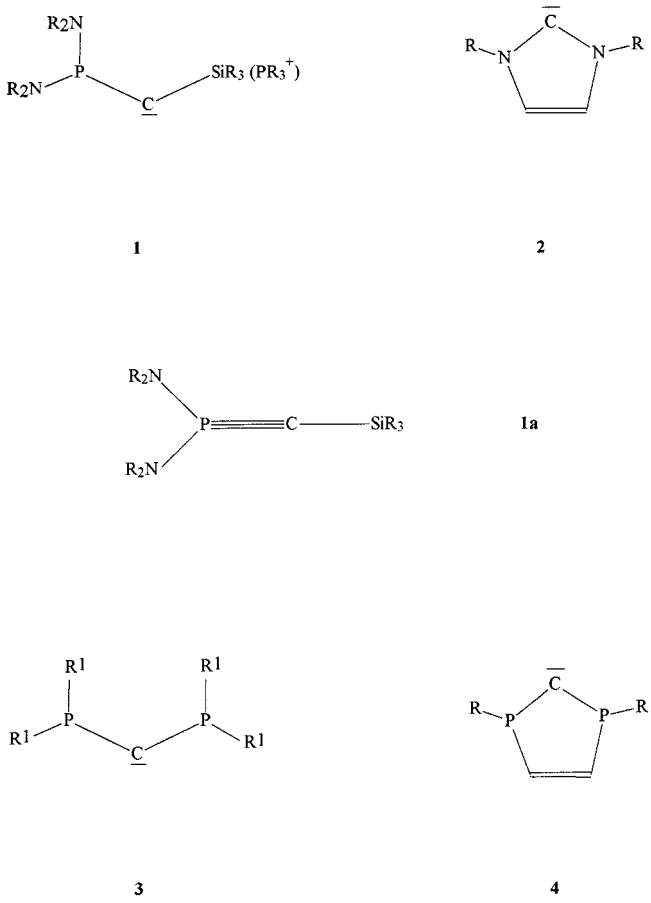
A phosphanyl group exerts much less π-conjugation properties than an amino group. On this basis, corresponding carbene structures exhibit much smaller singlet–triplet energy separations. Of the various structures investigated quantum-chemically the largest singlet–triplet energy separations are predicted for cyclic diphosphanylcarbenes, in which the two functional groups are incorporated into a ring system and the phosphorus atoms are substituted by phosphoraniminato groups. Then the singlet–triplet energy separations become essentially larger than for the Bertrand-type (push-pull) carbenes.

Introduction

Some time ago, Bertrand and co-workers reported in a series of pioneering investigations[1−9] the first syntheses of stable, isolable phosphanylcarbenes **1** (see Scheme 1). A prerequisite for the stability of the species is a substitution of the phosphanyl carbene with amino groups at phosphorus and an electron-withdrawing group (SiR_3, $PR_3^{(+)}$) at the carbon atom. The stabilizing effects of amino groups at the phosphorus and an electron-withdrawing group at the carbon atom have been rationalized by vinyl ylide structures, already suggested some time ago[1] for **1a** as a λ^5-phosphaalkyne structure. The assertion conforms with quantum-chemical calculations carried out later.[6] In other words, the positive charge at the phosphorus and the negative charge at the carbon atom are delocalized into the amino and the silyl (phosphonium) groups. It has been stated that the stabilities of the carbenes are often inversely proportional to the stability of the starting diazo compounds.[9]

Quantum-chemical calculations were first carried out on the singlet and triplet structural isomers of monophosphanylcarbene, H_2PCH.[10] An almost planar singlet state is predicted, with an inversion barrier of only 4 kcal mol^{-1}. It results in the electronic ground state, but only 3 kcal mol^{-1} lower in energy than the triplet state. The results are in agreement with more sophisticated calculations using the multiconfiguration-based unitary coupled electron pair approximation on parent phosphanyl carbenes.[11]

However, this study anticipates a somewhat larger energy difference (10 kcal mol^{-1}) between singlet and triplet states lowest in energy. While these two quantum chemical studies consider only a monophosphanyl-substituted carbene, a third study[12] examined the role of silicon substitution at the carbon (SiH_3) and of amino groups at the phosphorus atom. In essence, here the singlet−triplet energy separation is increased (13.9 kcal mol^{-1} in advantage to the singlet state, at PMP4 level) and the calculations indicate that this effect parallels an opening of the P−C−Si angle (135.7° predicted at MP2 level).



Scheme 1

Another representative of a stable carbene is the imidazol-2-ylidene **2** reported by Arduengo et al.[13][14] In this type of structure, the electron-deficient divalent carbon center is π-conjugated with two amino groups.[14][15] The carbenic nature and the question of their stabilities is presently under intensive debate, in particular the role of the heteroatom substituents.[16−22] To this end, a "mixed" car-

[a] Fakultät für Chemie der Universität,
Postfach 10 01 31, 33501 Bielefeld, Germany
E-mail: wolfgang@tc.uni-bielefeld.de

 © WILEY-VCH Verlag GmbH, D-69451 Weinheim, 2000 1434−1948/00/0202−369 $ 17.50+.50/0

bene which contains a phosphanyl and an amino group has been observed in transient formation recently.[23]

One of the major questions is an analysis of the electronic properties of carbene structures which combine both features: that of the types **1** and **2**. This will be discussed in the present quantum-chemical study. We evaluate the following aspects in detail: (1) Symmetrical, phosphanyl-substituted carbenes **3** and unsymmetrical, Bertrand-type carbenes **1** with various donors (acceptors) at the phosphorus (carbon) atom; and finally (2) the effect of incorporation of phosphanyl groups into ring systems, such as in **4** and related ring systems. We will show that a phosphoraniminato ligand ($-NPH_3$) is more effective than an amino group, to enhance the singlet−triplet energy separation in a phosphanylcarbene.

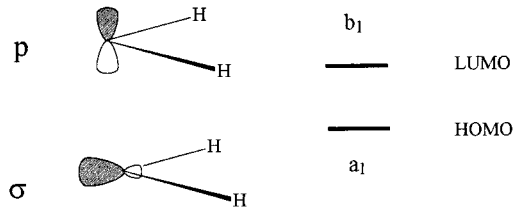
Theoretical Section

All calculations were performed with the Gaussian set of programs.[24] For the optimization of structures, double-ζ basis sets [6-31g(d,p)][25−28] were used. These basis sets include a single set of polarization functions at all atoms. In order to account for a proper electron correlation treatment, the optimization of structures was at times performed at a density functional level, utilizing the hybrid density function of Becke, Lee and Parr.[29] All structures were characterized by corresponding vibrational analysis, to identify these as energy minima on the corresponding electronic hypersurfaces. For some cases, the optimized geometries were energetically refined by single-point calculations at 6-311+g(d,p) basis set level[30][31] within the coupled cluster approximation, including single and double excitations from the ground state wavefunction, and triple excitation by corrections [CCSD(t)].[32][33] For the studied cases, the more elaborate CCSD(t) calculations parallel the results of the density functional (DFT) calculations at B3LYP level. As a consequence, general trends on singlet stabilities of carbenes can be explored on a large series of structures at the DFT level. The analysis of electron densities were performed within the Weinhold-Reed partitioning scheme.[34][35] Further investigations were also undertaken with Bader's method of "atoms in molecules" (AIM),[36] in order to analyze in more detail the nature of bonding in the corresponding structures.

Results and Discussion

a. Symmetrically Substituted Diphosphanylcarbenes

The frontier orbitals of a carbene, e.g. of the simplest representative methylene, are given as in Scheme 2. In the lowest energy singlet state, two electrons reside in the σ-orbital ($^1\sigma^2\rangle$, $^1A_1$ configuration) while in the lowest energy triplet state, one electron is in the σ and the other electron in the p orbital ($^3\sigma^1p^1\rangle$, $^3B_1$ configuration). It is the well-known picture of carbenes.[37−39] As a consequence, triplet carbenes possess widened R−C−R angles as relative to their singlet counterparts. One expects that in a carbene CR_2, the valence angle R−C−R increases with decreasing electronegativity of R.[40][41] For the methylene, the density functional calculations yield an energy difference of 12.2 kcal mol^{-1} between both electronic configurations [at B3LYP/6-31g(d,p) level], in favour of the triplet ($^1A_1$, CH = 1.119 Å, H−C−H = 100.0°; $^3B_1$, CH = 1.082 Å, H−C−H = 133.5°). This value may be compared to 9.0 kcal mol^{-1} obtained from the detailed experimental investigations.[42]



Scheme 2

In order to gain insight into the bonding of the phosphanylcarbenes, a variety of substituted carbenes were studied. A summary of symmetrically substituted species, CR_2 (R = phosphanyl unit) were calculated and the most important facets (singlet−triplet energy separations, relevant bonding parameters) are collected in Table 1.

Table 1. Relevant bonding parameters (bond lengths in Å, bond angles in °) and energy separations between singlet and triplet states of symmetrically substituted R_2C carbenes

Substituent	State	PC	∢PCP	Δ*E* (kcal mol^{-1})
PH_2	$^1A_1$	1.682	137.7	0.0 (0.0)
	^3B	1.765	137.7	8.4 (7.3)[a]
NH_2	$^1A_1$[b]	1.343	112.2	0.0
	^3B	1.392	122.5	51.1 (52.1), [58.5,[c] 50.7][d]
F	$^1A_1$[b]	1.313	104.1	0.0
	$^3B_1$[b]	1.325	120.1	52.1 (54.1) [56.6][c]
PF_2	^1A	1.651	154.2	0.0
	^3B	1.776	140.5	3.8
$P(NH_2)_2$	^1A	1.675	136.5	0.0
	^3B	1.761	139.9	0.6
$P(CH_3)_2$	^1A	1.672	141.7	0.0
	^3B	1.750	138.6	11.8
$P(SiH_3)_2$	^1A	1.696	138.6	0.0
	^3B	1.759	140.0	9.4
$PH(NPH_3)$	^1A	1.680	141.2	0.0
	^3B	1.740	135.6	16.0
$P(NPH_3)_2$	^1A (C_1)	1.622, 1.775	135.9	0.0
	^3B (C_2)	1.756	127.7	15.1

[a] In parentheses values with CCSD(t)/6-311+g(d,p)//B3LYP/6-31g(d,p) + zero-point vibrational energy correction. − [b] C_{2v} symmetry. − [c] Ref.[45] − [d] Ref.[44] − [e] S. Koda, *Chem. Phys.* **1982**, *66*, 383−390.

In most cases the species adopt a C_2 symmetry in their equilibrium structures (singlets and triplets). The matter may be illustrated for the parent diphosphanylcarbene, in

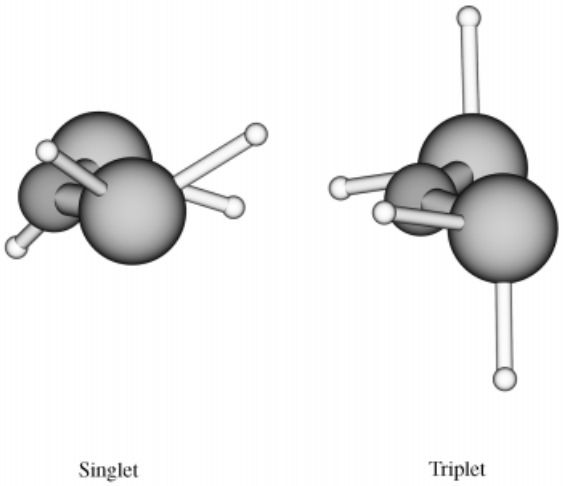


Figure 1. Molden plots of singlet and triplet diphosphanylcarbene

the Molden plots shown in Figure 1[43] of the singlet (left) and triplet (right) structures.

In the lowest energy singlet state (C_2 symmetry, P−C = 1.682 Å, P−C−P = 137.7°), the lone pairs at the phosphanyl groups tend to overlap with the empty p-orbital at the central carbon atom, so as to adopt π-conjugation, while in the lowest energy triplet state, the P−C bonds are elongated (1.765 Å, P−C−P = 137.7°) but the lone pairs at the phosphanyl substituents are almost perpendicularly oriented with respect to the central p-orbital. In both states the P−C−P angles are identical. Similar features were already predicted by previous quantum-chemical studies.[10]

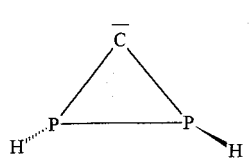
For comparison, we also included in our considerations the diaminocarbene. It adopts a planar (C_{2v} symmetry) structure in the singlet state, while the triplet state is confined to a twisted geometry (C_2 symmetry), in agreement with previous considerations.[44][45] For the diphosphanylcarbenes, the P−C distances are shorter in the singlet than in the triplet states. It indicates a stronger overlap in the former than in the latter. There is, however, an essential difference in the phosphanyl versus amino substitution. For R = NH_2 (diaminocarbene) in the singlet state the N−C−N valence angle is more acute than in the triplet state (112.2 vs. 122.5°). The trend is less unique for the various substituted diphosphanylcarbenes. The P−C−P angle is similar in both states [R = PH_2, $P(SiH_3)_2$, $P(CH_3)_2$, $P(NH_2)_2$], or even larger in the singlet relative to the triplet (R = PF_2) states.

Most of the singlet−triplet splitting is due to the height of the inversion barrier at the nitrogen or phosphorus atom. The large value for ΔE in the *N*-substituted carbenes is due to the low barrier at N (ca. 6 kcal mol^{-1} in NH_3)[46] which strongly stabilizes the singlet by allowing some back-donation into the vacant orbital. The much higher value for P (ca. 35 kcal mol^{-1} for PH_3)[46] leads to an inability of the P lone pair to stabilize the singlet and hence ΔE is much smaller. In addition, the more bent the phosphorus is compared to nitrogen (H−P−H in PH_3 is ca. 95° and H−N−H in NH_3 is ca. 109°), the more the triplet state will be stabilized as the lone pair at P is less repulsive than the lone pair on N when interacting with the single electron in the out-of-plane orbital on the carbene center. Since the C−N distance is much shorter than the C−P distance, the effects at the nitrogen are stronger than at the phosphorus atom. In accordance with Bent's rule,[47−49] within pyramidalization, the s-character of the lone pairs increases and the phosphorus atom utilizes more p-character in the formation of the σ-P−C bonds. It becomes a more electropositive substituent towards the central carbon atom. On this basis, it prefers a bonding situation in which the central carbon atom is expected to become more linear. At least this argument explains the essential difference in bonding between the singlet states of CR_2, R = PH_2 versus PF_2.

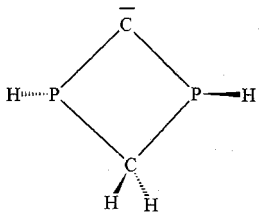
On the basis of these arguments, phosphanyl substituents with electronegative atoms [R = PF_2, $P(NH_2)_2$] possess small energy differences between singlet and triplet states lowest in energy. On the other hand, substituents which in general are known to decrease the inversion barrier in a phosphane [R = $P(CH_3)_2$, $P(SiH_3)_2$] increase the energy splitting. We have also studied the use of a phosphoraniminato group[50][51] [R = $P(PH(NPH_3)$] as a ligand at the phosphorus atom. The largest energy differences between singlet and triplet is obtained in this case. One may consider these substituents as extremely strong nucleophiles which increase the donor capability of a phosphanyl group. We have also probed the case of two phosphoraniminato ligands at the same phosphorus atom (see Table 1). It does not further increase the singlet−triplet energy gap. In the singlet state only one PR_2 (R = NPH_3) group is capable of interacting with the central carbon atom such as to maximize π-conjugation. The other PR_2 group is more strongly pyramidalized and avoids π-overlap with the central carbon atom. Overall, it causes reduction of the singlet equilibrium structure to C_1 symmetry. According to the population analysis in the investigated singlet structures (NBO and Laplacian of the electron densities), the carbon atom carries an excess negative charge (ca. −1.5 el), the phosphorus atoms are positively charged and the multiple bonding between the phosphorus and the carbon atom is weak (ca. 1.3 Wiberg bond indices).

Next we will discuss the bonding situation in diphosphanylcarbenes which are incorporated in a ring system. In these structures, a sharpened P−C−P angle is enforced which should be of more advantage to a singlet than to a triplet state. Various cases were studied and are collected in Table 2.

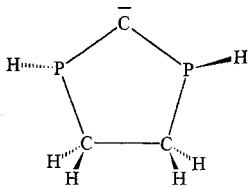
The singlet−triplet energy gap increases with increasing size of the ring system (Scheme 3). It is smallest for the 1.2-diphosphacyclopropenylidene (**5**, ΔE = 2.9 kcal mol^{-1}). The incorporation of a double bond in the five-membered ring system **4** (R = H) versus **7** slightly shortens the P−C bonds and concomitantly increases the singlet−triplet splitting. Compound **4** is the phosphorus analogue of the Arduengo carbene **2**.[15] We predict for the latter a sizeable energy splitting of 80.0 kcal mol^{-1} between lowest energy singlet and triplet states. Our findings are in agreement with previous calculations on this structure (ΔE = 79.3,[52]



5



6



7

Scheme 3

Table 2. Cyclic diphosphanylcarbenes (C_2 symmetry)

Compound	State	PC	∢PCP	ΔE(kcal mol^{-1})
5	^{1}A	1.775	72.1	0.0
	^{3}B	1.876	82.8	2.9 (3.6)
6	^{1}A	1.793	90.2	0.0
	^{3}B	1.817	101.2	8.0
7	^{1}A	1.759	106.6	0.0
	^{3}B	1.793	123.4	13.3
4 (R = H)	^{1}A	1.679	114.2	0.0
	^{3}B	1.808	120.0	17.3
4 (R =CH_3)	^{1}A	1.714	101.9	0.0
	^{3}B	1.784	121.8	20.1
4 (R = F)	^{1}A	1.697	98.6	0.0
	^{3}B	1.785	123.4	12.1
4 (R =Cl)	^{1}A	1.710	99.1	0.0
	^{3}B	1.783	122.8	9.1
4 (R = NH_2)	^{1}A	1.714	100.9	0.0
	^{3}B	1.793	122.7	15.9
4 (R = NPH_3)	^{1}A	1.712	101.6	0.0
	^{3}B	1.792	121.7	24.9
4 (R = PPH_3)	^{1}A	1.725	102.0	0.0
	^{3}B	1.775	121.7	19.2

84.5[45] kcal mol^{-1}). Similar aspects have been found for the singlet−triplet energy separation in the Arduengo carbene **2** versus its hydrogenated analogue[53] and have been attributed to the effect of additional divalent state stabilization energy (DSSE).[54] In other words, in the singlet and to a lesser extent in the triplet states, additional cyclic π-delocalization is gained. The incorporation of the phosphanyl units into the five-membered ring system considerably stabilizes the singlet state of the carbene.[45] According to our calculations the singlet can be further stabilized by introduction of a phosphoraniminato ligand at the phosphorus atom (**4**, R = NPH_3). Thus one expects that the phosphorus analogue of the Arduengo carbene is a rather stable species. The population analysis indicates similar electron distributions to the alicyclic congeners for the ring structures. However, the P−C bonds are strengthened, as witnessed by their shortening. We have also tested the phosphorus analogue of the phosphoraniminato ligand (R = PPH_3). It appears to be less effective in the singlet stabilization than the former ligand (R = NPH_3).

b. Asymmetrical Phosphanylcarbenes

Next we will discuss the cases in which only one phosphanyl group is attached to the electron-deficient carbene center. The most prominent example is the push−pull substituted carbene **1**, already well investigated by quantum chemical investigations.[6][12] These calculations indicate that electron-withdrawing substituents at the carbon atom possess a particular role in the stabilization of a singlet carbene.[12] However, a detailed investigation of related substituents has hitherto not been given. In this section we want to demonstrate the influence of various substituted phosphanyl groups on the singlet stability of the various substituted species. We record here in more detail the results of the unsymmetrically substituted carbenes $R^1R^2PCR^3$, with R^1 and R^2 being different substituents and with R^3 as various electron-withdrawing groups. The results of the quantum-chemical investigations are collected in Table 3.

Table 3. Singlet−triplet energy separations and relevant bonding parameters of asymmetrically substituted carbenes, $R^1R^2PCR^3$

R^1	R^2	R^3	State	PC	∢PCR^3	ΔE (kcal mol^{-1})
H	H	H	^{1}A	1.641	113.9	0.0
			^{3}A	1.764	131.9	6.5 (7.6)
H	H	CH_3	^{1}A	1.642	127.0	0.0
			^{3}A	1.770	135.5	3.0 (3.8)
H	H	CF_3	^{1}A	1.624	122.5	0.0
			^{3}A	1.767	132.3	5.7
H	H	SiH_3	^{1}A	1.607	133.5	0.0
			^{3}A	1.755	155.6	4.4 (6.2)
NH_2	NH_2	SiH_3	^{1}A	1.559	151.1	0.0
			^{3}A	1.749	156.5	11.1
NH_2	NH_2	$PH_3^{(+)}$	^{1}A	1.545	176.4	0.0
			^{3}A	1.745	136.3	26.1
NH_2	NH_2	CF_3	^{1}A	1.584	126.4	0.0
			^{3}A	1.760	133.3	11.8
H_3PN	H	H	^{1}A	1.616	120.7	0.0
			^{3}A	1.765	130.7	17.1
H_3PN	H	SiH_3	^{1}A	1.588	140.7	0.0
			^{3}A	1.746	180.0	21.8
H_3PN	H	$PH_3^{(+)}$	^{1}A	1.589	141.7	0.0
			^{3}A	1.760	135.1	31.8

In agreement with the previous considerations,[10][12] the singlet−triplet separation for the monophosphanylcarbene is fairly small. Given a diaminophosphanyl ligand, R^3 is most effective in the order $SiH_3 \approx CF_3 < PH_3^{(+)}$. Most

noticeable is again the fact that the phosphoraniminato ligand reveals a particular role in the stabilization of the carbene. The most stable carbene is predicted to be the case with one phosphoraniminato ligand and one phosphonium group at the carbon centre. Alternatively, stable carbenes require diamino substitution at the phosphorus atom. The Wiberg bond indices indicate a bond with almost double-bond character between the phosphorus and the carbon atom for these structures, superimposed by a strong charge separation between them. It is in conformity with previous considerations.[12] We note that recently a quantum-chemical study on parent phosphanylcarbene H_2PCH and related structures has been reported.[55] Regarding these findings, the reported structural details of H_2PCH are similar, while for the push−pull carbene $(H_2N)_2PCSiH_3$ the reported singlet−triplet energy separation is essentially larger (26.9 kcal mol^{-1}) than our value (11.1 kcal mol^{-1}, see Table 3).[56]

It is of interest also to examine the effect of push−pull substitution in the case of aminocarbene, H_2NCH. We calculate for it a singlet−triplet energy separation of 29.8 kcal mol^{-1} [B3LYP/6-31g(d,p) with ZPE correction]. The energy gap decreases to 20.6 kcal mol^{-1} when the hydrogen atom is replaced by a silyl group. In other words, a push−pull mechanism which is operative in the phosphanylcarbenes, does not hold true for the aminocarbene, the singlet−triplet energy gap is even considerably decreased. It is known that silyl groups tend to bring the triplet character of a carbene to the fore.[57][58] Finally, these values are related to the experimental results of the aminophosphanylcarbene.[23] We predict an energy gap in ΔE = 27.8 kcal mol^{-1}, almost similar in magnitude to the monoaminocarbene. The diaminocarbene resulted to ΔE = 51.1 kcal mol^{-1}, in agreement with previous quantum-chemical investigations (see Table 1).

Conclusions

The effect of various types of substituents on the singlet−triplet energy separations have been studied by density functional theory. The results of our investigations can be summarized as follows:

(1) The singlet−triplet energy separation in the diphosphanylcarbenes can be increased by suitable substitution at the phosphorus atom. In the parent compound, the energy gap is fairly small, but it increases by alkyl substitution or most effectively by substitution with a phosphoraniminato ligand.

(2) A considerable stabilization of the singlet species is observed by incorporation of the diphosphanyl ligand into a five-membered ring system, resulting in the phosphorus analogue of the Arduengo carbene. Again the singlet−triplet energy separation is increased by introduction of the phosphoraniminato ligand.

(3) Asymmetric phosphanylcarbenes are most stable in the case of the phosphorus atom being substituted by amino groups or alternatively by the phosphoraniminato ligand and the carbon atom in addition being attached to an electron-withdrawing substituent, such as a silyl or a phosphonium group.

Our theoretical analysis predicts new types of substitutent patterns which are effective in stabilizing singlet ground states of phosphanylcarbenes. Its verification may be a challenge to the experimental chemist. Further investigations will be dedicated to an investigation of the nucleophilic versus electrophilic character[37] of phosphanylcarbenes, towards cycloaddition reactions as well as to their transition metal complexation properties.

Acknowledgments

This work has been supported by the Fonds der Chemischen Industrie and by the Deutsche Forschungsgemeinschaft.

[1] R. Appel, J. Peters, R. Schmitz, *Z. Anorg. Allg. Chem*. **1981**, *475*, 18−26.
[2] A. Baceiredo, G. Bertrand, G. Sicard, *J. Am. Chem. Soc.* **1985**, *107*, 4781−4783.
[3] A. Igau, H. Grützmacher, A. Baceiredo, G. Bertrand, *J. Am. Chem. Soc*. **1988**, *110*, 6463−6466.
[4] G. Gillette, A. Baceiredo, G. Bertrand, *Angew. Chem*. **1990**, *102*, 1486−1488; *Angew. Chem. Int. Ed.* **1990**, *29*, 1429.
[5] G. Gillette, A. Igau, A. Baceiredo, G. Bertrand, *Nouv. J. Chim.* **1991**, *15*, 393−400.
[6] M. Soleilhavoup, A. Baceiredo, O. Treutler, R. Ahlrichs, M. Nieger, G. Bertrand, *J. Am. Chem. Soc.* **1992**, *114*, 10959−10961. O. Treutler, R. Ahlrichs, M. Soleilhavoup, *J. Am. Chem. Soc.* **1993**, *115*, 8788−8792.
[7] M. Soleilhavoup, G. Alcarez, R. Reau, A. Baceiredo, G. Bertrand, *Phosphorus Sulfur* **1993**, *76*, 49.
[8] G. Alcaraz, R. Reed, A. Baceiredo, G. Bertrand, *J. Chem. Soc., Chem. Comm*. **1993**, 1354−1355.
[9] G. Bertrand, R. Reed, Coord. *Chem. Rev.* **1994**, 137−355.
[10] M. T. Nguyen, M. A. McGinn, A. F. Hegarty, *Inorg. Chem*. **1986**, *25*, 2185−2190.
[11] M. R. Hoffmann, K. Kuhler, *J. Chem. Phys.* **1991**, *94*, 8029−8039.
[12] D. A. Dixon, K. D. Dobbs, A. J. Arduengo III, G. Bertrand, *J. Am. Chem. Soc*. **1991**, *113*, 8782−8785.
[13] A. J. Arduengo III, R. L. Harlow, M. Kline, *J. Am. Chem. Soc*. **1991**, *113*, 361−363.
[14] A. J. Arduengo III, H. V. R. Dias, R. L. Harlow, M. Kline, *J. Am. Chem. Soc.* **1992**, *114*, 5530−5534.
[15] A. J. Arduengo III, H. V. R. Dias, D. A. Dixon, R. L. Harlow, W. T. Klooster, T. F. Koetzle, *J. Am. Chem. Soc*. **1994**, *116*, 6812−6822.
[16] A. J. Arduengo III, R. Krafczyk, *Chem. Unserer Zeit* **1998**, *32*, 6−14.
[17] W. A. Hermann, C. Köcher, *Angew. Chem*. **1997**, *109*, 2256−2282; *Angew. Chem. Int. Ed.* **1997**, *36*, 2162−2187.
[18] R. Dagani, *Chem. Eng. News* **1991**, *69*, 19.
[19] M. Regitz, *Angew. Chem*. **1991**, *103*, 691−693; *Angew. Chem. Int. Ed.* **1991**, *30*, 674.
[20] R. Dagani, *Chem. Eng. News.* **1994**, *72*, 20.
[21] M. Regitz, *Angew. Chem.* **1996**, *108*, 791−794; *Angew. Chem. Int. Ed.* **1996**, *35*, 725.
[22] The role of heteroatom substitution is related to the discussion of cation stabilities and has been lucidly discussed recently: H. Grützmacher, C. M. Marchand, *Coord. Chem. Rev.* **1997**, *163*, 287−344; see also: J. Kapp, C. Schade, A. M. El-Nahasa, P. v. R. Schleyer, *Angew. Chem*. **1996**, *108*, 2373−2376; *Angew. Chem. Int. Ed*. **1996**, *35*, 2236−2238.
[23] S. Goumri, Y. Leriche, H. Gornitzka, A. Baceiredo, G. Bertrand, *Eur. J. Inorg. Chem.* **1998**, 1539−1542.
[24] M. J. Frisch, G. W. Trucks, H. B. Schlegel, G. E. Scuseria, M. A. Robb, J. R. Cheeseman, V. G. Zakrezewski, J. A. Montgomery, R. E. Stratmann, J. C. Burant, S. Dapprich, J. M. Millam, A. D. Daniels, K. N. Kudin, M. C. Strain, O. Farkas, J. Tomasi, V. Barone, M. Cossi, R. Cammi, B. Mennucci, C. Pomelli, C. Adamo, S. Clifford, J. Ochterski, G. A. Petersson, P. Y. Ayali, Q. Cui, K. Morokuma, D. K. Malick, A. D. Rabuck, K.

Raghavachari, J. B. Foresman, J. Cioslowski, J. V. Ortiz, B. B. Stefanov, G. Liu, A. Liashenko, P. Piskorz, I. Komaromi, R. Gomperts, R. L. Martin, D. J. Fox, T. Keith, M. A. Al-Laham, C. Y. Peng, A. Nanayakkara, C. Gonzalez, M. Challacombe, P. M. W. Gill, B. G. Johnson, W. Chen, M. W. Wong, J. L. Andres, M. Head-Gordon, E. S. Replogle, J. A. Pople, *Gaussian 98* (Revision A.1), Gaussian, Inc., Pittsburgh, PA, **1998**.
[25] R. Ditchfield, W. J. Hehre, J. A. Pople, *J. Chem. Phys.* **1972**, *56*, 2257−2261.
[26] P. C. Hariharan, J. A. Pople, *Mol. Phys.* **1974**, *27*, 209−214.
[27] P. C. Hariharan, J. A. Pople, *Theor. Chim. Acta* **1973**, *28*, 213−222.
[28] M. S. Gordon, *Chem. Phys. Lett.* **1980**, *76*, 163−168.
[29] [29a] A. D. Becke, *Phys. Rev. A* **1988**, *38*, 3098−3100. A. D. Becke, *J. Chem. Phys.* **1993**, *98*, 5648−5652. A. D. Becke, *J. Chem. Phys.* **1996**, *104*, 1040−1046. − [29b] J. K. Labanowski, J. W. Andzelm (Eds.), *Density Functional Methods in Chemistry*, Springer Verlag, New York, **1991**.
[30] A. D. McLean, G. S. Chandler, *J. Chem. Phys.* **1980**, *72*, 5639−5648.
[31] R. Krishnan, J. S. Binkley, R. Seeger, J. A. Pople, *J. Chem. Phys.* **1980**, *72*, 650−654.
[32] R. J. Bartlett, G. D. Purvis, *Int. J. Quant. Chem*. **1978**, *14*, 561−581.
[33] J. A. Pople, R. Krishnan, H. B. Schlegel, J. S. Binkley, *Int. J. Quant. Chem.* **1978**, *14*, 545−560.
[34] E. D. Glendening, A. E. Reed, J. E. Carpenter, F. Weinhold, *NBO Version 3.1*.
[35] A. E. Reed, L. A. Curtiss, F. Weinhold, *Chem. Rev.* **1988**, *88*, 899−926.
[36] R. F. W. Bader, *Atoms in Molecules: A Quantum Theory*, Oxford University Press, Oxford, **1990**.
[37] W. W. Schoeller, *Tetrahedron Lett.* **1980**, 1505−1508; *Tetrahedron Lett*. **1980**, 1509−1510.
[38] B. M. Gimarc, *Molecular Structure and Bonding*, Academic Press, New York, **1979**.
[39] W. W. Schoeller, *Angew. Chem*. **1981**, *93*, 685−686; *Angew. Chem. Int. Ed.* **1981**, *20*, 698.
[40] W. W. Schoeller, *J. Chem. Soc., Chem. Commun.* **1980**, 124−1250.
[41] L. Pauling, *J. Chem. Soc., Chem. Commun*. **1980**, 688−689.
[42] [42a] D. G. Leopold, K. K. Murray, A. E. S. Miller, W. C. Lineberger, *J. Chem. Phys.* **1985**, *83*, 4849−4865. − [42b] R. R. Bunker, T. J. Sears, *J. Chem. Phys.* **1985**, *83*, 4866−4876. For further references see therein.
[43] Program *Molden* written by G. Schaftonaar: www.caos.kun.nl/schaft/molden/molden.html
[44] D. Feller, W. T. Borden, E. R. Davidson, *Chem. Phys. Lett.* **1980**, *71*, 22−26.
[45] C. Heinemann, W. Thiel, *Chem. Phys. Lett*. **1994**, *217*, 11−16.
[46] [46a] J. M. Lehn, *Top. Curr. Chem.* **1970**, *15*, 311−377. − [46b] A. Rauk, L. C. Allen, K. Mislow, *Angew. Chem.* **1970**, *82*, 453−468; *Angew. Chem. Int. Ed.* **1970**, *9*, 400.
[47] H. A. Bent, *J. Chem. Educ.* **1960**, *37*, 616−624.
[48] H. A. Bent, *J. Chem. Phys.* **1960**, *33*, 1258, 1259, 1260−1261.
[49] H. A. Bent, *Chem. Rev.* **1961**, *61*, 275−311.
[50] K. Dehnicke, J. Strähle, *Angew. Chem.* **1981**, *93*, 451−464; *Angew. Chem. Int. Ed.* **1981**, *20*, 413.
[51] W. A. Nugent, J. M. Mayer, *Metal−Ligand Multiple Bonds*, Wiley, New York, **1988**.
[52] D. A. Dixon, A. J. Arduengo III, *J. Phys. Chem.* **1991**, *95*, 4180−4182.
[53] A. J. Arduengo III, J. R. Goerlich, W. J. Marshall, *J. Am. Chem. Soc.* **1995**, *117*, 11027−11028.
[54] R. S. Grev, H. F. Schaefer III, K. Baines, *J. Am. Chem. Soc.* **1990**, *112*, 9458−9467.
[55] L. Nyulászi, D. Szieberth, J. Réffy, T. Veszprémi, *J. Mol. Struct. (Theochem)* **1998**, *453*, 91−95.
[56] One possible reason for the discrepancy is the lack of the projection formalism (H. B. Schlegel, *J. Chem. Phys.* **1986**, *84*, 4530−4534) to the MP2 procedure in evaluating the triplet state (see also ref.[12]).
[57] W. T. Bordon, *Diradicals*, John Wiley Interscience, New York, **1982**.
[58] A more detailed analysis of this effect and its relation to other first-row substituents versus their higher element homologues will be presented elsewhere. W. W. Schoeller et al., manuscript in preparation.

Received April 13, 1999
[I99131]

Pentacoordination at Fluoro-Substituted Silanes by Weak Lewis Donor Addition

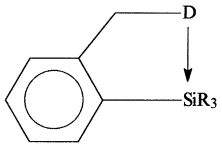
Wolfgang W. Schoeller*[a] and Alexander Rozhenko[a]

Keywords: Fluorine / Silicon / Ab initio calculations / Donor-acceptor systems

Quantum chemical calculations at the ab initio level indicate that Lewis donors such as amine or water form weak donor–acceptor complexes with fluoro-substituted silanes. The strength of the donor–acceptor formation increases with increasing degree of fluorine substitution. Amine and water form strong adducts only for tetrafluorosilane. The higher element homologues of Lewis donors, such as phosphane and sulfur dihydride, do not in essence coordinate. A considerable role in donor–acceptor formation is exerted by chelation effects which impose intramolecular interactions on functionalized ligands. The corresponding structures are explored.

Introduction

Corriu and co-workers have presented pioneering contributions in a series of experimental studies on the understanding of pentacoordination at silicon.[1−3] The results of these investigations further increased the knowledge of nucleophilic substitution at silicon.[4,5] For the extension of the coordination sphere at the silicon center aromatic ligands with a dimethylamino-functionalized side chain were mainly used, as indicated in Scheme 1. In this structure the Lewis donor is forced into close proximity to the substituted silane unit resulting in a D−A complex (D = donor, A = acceptor). Only a few species with other donor elements in the side chain are known.[5−11] Recently a structural investigation of an alkoxy-substituted pentacoordinated silicon compound has been reported (**1**, D = OCH_3)[13] (Scheme 1).



D = OR, NR_2

R = alkyl, aryl, F, OR

1

Scheme 1

Pentacoordination at silicon is usually monitored by ^{29}Si NMR spectroscopy[14] as the coupling to adjacent nuclei (^{19}F, ^{1}H) is influenced by pentacoordination.[15] This indicates that the stability of the pentacoordinated species is dictated by the electronegative fluorines at the silicon centre. Information about the varying strength of the donor-silicon interaction is also drawn from temperature-dependent NMR studies.[13] To this end an interesting 1,3-sigmatropic fluorine migration within a 2-phospha-1,3-disilaallyl derivative has been observed[16] thus indicating facile coordination at the silicon center with fluorine as a donor. One of the major questions is the magnitude of these bonding effects and how they are affected by the nature of the Lewis bases involved in the adduct formation.

Lewis bases can be classified into two categories, either as hard or soft donors, as discussed in detail in the pioneering work of Pearson et al.[17,18] In the present investigations we report quantum chemical calculations at an ab initio level which have a bearing on this problem. We will discuss the role of hard (NH_3, OH_2) and soft (PH_3, SH_2) donors for possible interaction with fluorosilanes. Fluorine atoms as substituents were chosen because they mimic best the effect of electronegative substituents attached to a silicon centre. In the experiment the coordination to a substituted silane is verified by intramolecular donor addition of an aromatic ligand functionalized with a donor side chain, e.g. compound **1**. Corresponding models will be explored in the last section of this publication. The details of the quantum chemical calculations are given in the Theoretical Section.

Results and Discussion

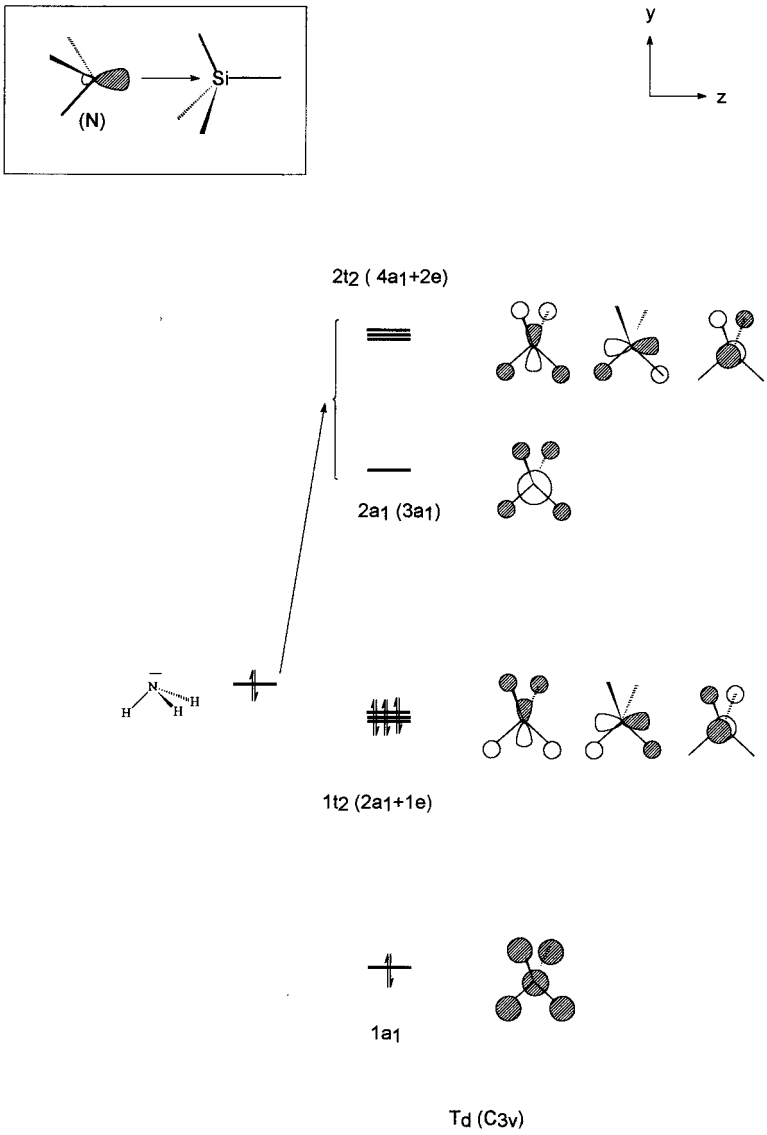
Qualitative Considerations

The donor−acceptor formation between an amine, phosphane, etc. and a silane is shown schematically in Scheme 2.

The parent silane possesses two sets of triply degenerate molecular orbitals (t_2 with T_d symmetry) constituted from the p-orbitals at the central silicon atom and the adjacent hydrogen atoms.[19] In addition, the s-orbital at the silicon atom forms a bonding and antibonding molecular orbital (a_1) with the neighbouring hydrogen atoms. Under the C_{3v} symmetry adopted in the donor−acceptor complex the t_2 orbitals reduce to (a_1 +e). A corresponding donor−acceptor interaction takes place by transfer of electron density from the n-orbital of the donor fragment (a_1) (lone pair

[a] Fakultät für Chemie der Universität,
Postfach 100131, D-33501 Bielefeld, Germany

 © WILEY-VCH Verlag GmbH, D-69451 Weinheim, 2000 1434−1948/00/0202−375 $ 17.50+.50/0



Scheme 2

orbital at NH_3, PH_3) into the antibonding orbitals (a_1) of the silane fragment. According to second-order perturbation theory[20–22] such a donor–acceptor interaction can be assumed to increase with the lowering of the ionization potential of the donor orbital, given the same acceptor. In other words PH_3 should be a better donor than NH_3 since the ionization potential of the former (9.9 eV) is smaller than that of the latter (10.9 eV); likewise OH_2 (12.6 eV) is a poorer donor than SH_2 (10.5 eV).[21] It is equivalent to the assignment that nitrogen is more electronegative than phosphorus. Thus within the concept of Pearson′s classification into hard and soft donors an amine is the harder donor than a phosphane.[23] Within the Klopman formulation of second-order perturbation theory[22] the interaction of the donor (nucleophile) and the acceptor (electrophile) is given according to Equation 1,

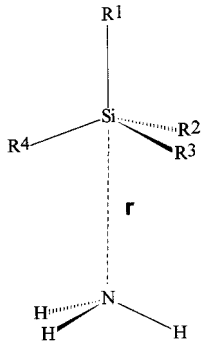
$$\Delta E = -\frac{Q_{nuc}Q_{elec}}{\varepsilon R} + \frac{2(c_{nuc}c_{elec}\beta)^2}{E_{HOMO(nuc)} - E_{LUMO(elec)}} \qquad (1)$$

with ε as the local dielectric constant (of the reaction medium), Q_{nuc} and Q_{elec} as the total charges at the overlapping atoms, E_{HOMO} and E_{LUMO} the molecular orbital energies of the donor (nucleophile) and the acceptor (electrophile) and ß as the overlap integral between the nucleophile and electrophile (for a detailed definition see ref.[22a]). The first term in this equation is simply the Coulombic repulsion or attraction. This term, which contains the total charge Q on each atom, is obviously important when ions or polar molecules are reacting together. The second term refers to the HOMO–LUMO interaction, as indicated schematically in the previous scheme. A priori one can differentiate between two extreme cases where either the coulombic term or the second term dominates. In the latter case one would expect that with decreasing ionization potential of the donor the adduct stability increases thus giving the opposite stability order, i.e. $OH_2 < NH_3$ for adduct formation. In general one assumes[20,21] that coulombic contributions are only important for interactions between charged species. This is not the case at hand as the Lewis donors and ac-

ceptors are neutral. From the qualitative discussion it is also clear that a possible HOMO−LUMO interaction, according to Equation (1), increases with the lowering of the LUMO energies of the silanes. This can be done by replacing the hydrogens with electronegative substituents. In this case at hand we have probed the effect on silanes successively substituted by fluorine. Such a situation is also observed experimentally,[15] where the shielding in the ^{29}Si NMR spectrum is changed by addition of amine to fluorine substituted silanes.

The Donor Adducts

In order to reveal the various factors which contribute to the overall donor-silicon stability we first determined the equilibrium structures for a selected variety of donor-adducts with NH_3, OH_2 and PH_3, SH_2 as donors, and with increasing fluorine substitution at the silicon center. In general the adducts tend to form a trigonal bipyramid, as shown in Scheme 3.



Scheme 3

The most relevant bonding parameter for the encounter complexes is given by r, the distance of the donor atom from the silicon center. Moreover, one has to differentiate between fluorine substitution at an equatorial (R^2, R^3, R^4) and/or an axial (R^1) position. The effect of substitution in both cases was investigated.

The binding energies (exothermic, in kcal/mol) of the various adducts together with the bonding parameter r (in Å) are collected in Table 1.

Overall the binding energies for the addition of an amine are fairly small. They increase with increasing fluorine substitution and are at a maximum for SiF_4. A fluorine in the axial position exerts a stronger acceptor effect towards the amine than in the corresponding equatorial position (e.g., structure 3 vs. 2 in Table 1) and the resulting adducts are slightly (ca. 2 kcal/mol) more stable. This reflects the well-known tendency that electronegative substituents in a trigonal bipyramid prefer the axial rather than the equatorial position, as already well rationalized on the basis of one-electron considerations.[19] We have also probed the results on the basis of more sophisticated calculations. By this we mean single point calculations on the equilibrium geometries with the CCSD(t)/6−311+g** method. The results

Table 1. Coordination of NH_3 (first entry) and OH_2 (second entry) at substituted silanes; D−A distances (in Å) and adduct energies (exothermic, in kcal/mol)

Structure	R^1	R^2	R^3	R^4	r [Å]	DZP[a]	TZP[b]
(1)	H	H	H	H	3.100	1.9	0.9
					3.264	1.9	0.9
(2)	H	F	H	H	2.839	3.6	2.2
					3.133	4.3	1.7
(3)	F	H	H	H	2.571	5.8	4.9
					2.76	4.1	3.1
(4)	H	F	F	H	2.588	4.2	2.6
					2.946	5.1	2.4
(5)	F	F	H	H	2.459	6.5	5.1
					2.748	5.6	3.6
(6)	F	F	F	H	2.275	7.1	5.2
					2.685	6.4	4.1
(7)	H	F	F	F	2.175	5.3	3.5
					2.838	4.0	2.2
(8)	F	F	F	F	2.114	10.2	8.5
					2.645	5.9	4.0

[a] MP2(fc)/6−31 g** plus zero-point vibrational energy correction. − [b] CCSD(t)/6−311+g**//MP2(fc)/6−31 g** plus zero-point vibrational energy correction, at level a).

thus obtained (see Table 1) are similar, although the adduct energies are somewhat smaller.

Our analysis indicates fairly small adduct energies for amine and water coordination. For addition to SiF_4 the strengths of the stabilities is in the order OH_2 (4.0 kcal/mol) < NH_3 (8.5 kcal/mol) [at the TZP level, see Table 1]. The latter donor possesses a lower ionization potential than the former.[20] In order to gain a more detailed understanding we have also evaluated adduct formation for the donors PH_3 and SH_2. The results of these investigations are summarized in Table 2.

Table 2. Donor−acceptor binding energies (exothermic, in kcal/mol) of SiF_4 with PH_3 and SH_2

Donor	r [Å]	DZP[a]	TZP[b]
SH_2	3.656	1.6	2.4
PH_3	3.741	1.9	2.4

[a] MP2(fc)/6−31 g** plus zero-point vibrational energy correction. − [b] CCSD(t)/6−311+g**//MP2(fc)/6−31 g** plus zero-point vibrational energy correction, at level a).

Only the tetrafluorosilane, which exerts the strongest acceptor properties, was examined. As before the binding energies of the various donors are fairly small. The energy results indicate that the coordination ability of the tetrafluoro-substituted silane is much smaller for these two donors i.e. they are negligibly small.

On the basis of the Klopman concept[21,22] it is apparent that the electrostatic interactions [first term in Equation (1)] are not the dominant contribution to the overall stability of the resulting adducts otherwise the donor OH_2 would form a stronger adduct towards SiF_4 than NH_3, which is not the case. Since the energy contributions for the binding of the donors are rather weak a further bisection into various con-

tributions was not attempted. The fact that the donors PH_3 and SH_2 form only very weak adducts is also in agreement with the recently explored dual-parameters equation for the stability of silylene adducts.[24] Accordingly, the resulting stability of a donor−acceptor complex depends on: (a) the donor ability (as measured by the ionization potential) and (b) the stability of a hypothetically covalent D(onor)−Si bond.[24] For the present system it means that a covalent D−Si bond is almost comparable for the series OH_2 and NH_3, or alternatively for SH_2 and PH_3. For the former two donors it is stronger than for the latter two donors, although the stabilities for all the investigated cases are fairly small.

The Chelation Effect

In the experiment the donor centre is coordinated intramolecularly to the silane unit, in structures such as **1**. The aromatic ligand exerts conformational rigidity which forces the donor fragment towards the silicon centre. This should enhance a possible donor−acceptor interaction. In order to reveal this aspect in more detail we performed quantum chemical calculations (MP2/6−31 g**) on **1** with the donors D = −OH, $-NH_2$, −SH, $-PH_2$. Only the results for the former two donor structures will be summarized here (Scheme 4).

The silicon center was substituted by three fluorine atoms which take up one axial and two equatorial positions. The substitution pattern was chosen in order to maximize the donor−acceptor interaction. For D = −SH and $-PH_2$ no coordination was observed. In other words for these cases the donor function rotates away from the silicon center. In general the D−Si distances for the intramolecularly coordinated cases are shorter (N−Si 2.176, O−Si 2.441 Å) than in the corresponding adducts for bimolecular addition (N−Si 2.275, O−Si 2.685 Å) for the trifluoro-substituted cases, see Table 1). Thus on this basis the chelation effect by intramolecular coordination of the donor to the silicon center seems slightly more strongly pronounced for oxygen than for nitrogen coordination. The D−Si bond ratios for intra- versus intermolecular donor coordination are: N (2.275/2.176 = 1.046, O 2.685/2.441 = 1.100). It must be noted that the actual D−Si distances in the intramolecular coordinated complexes are dependent on the substituents (alkyl, silyl) at the donor. In addition the D−Si bond energies are rather weak and therefore also depend on the chosen computational level.[25]

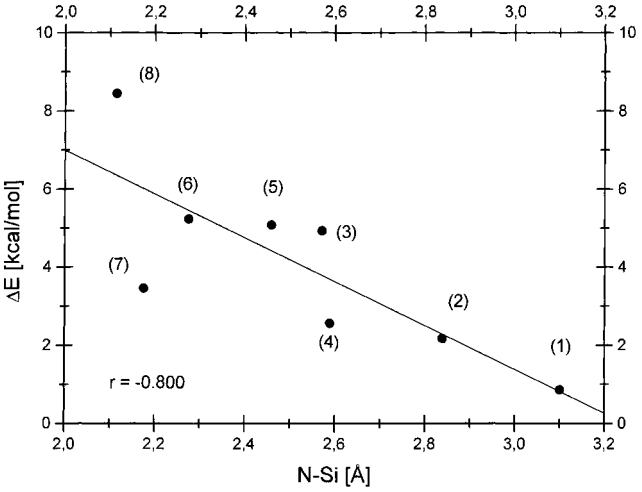


Figure 1. Linear correlation of N−Si distances (in Å) versus binding energies (negative, in kcal/mol) for amine coordination to substituted silanes

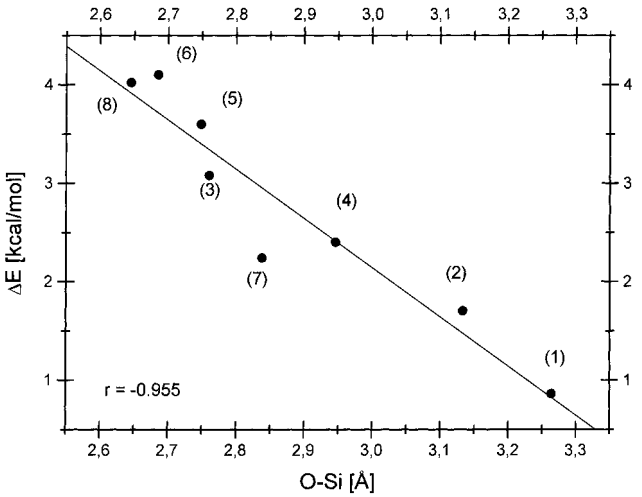
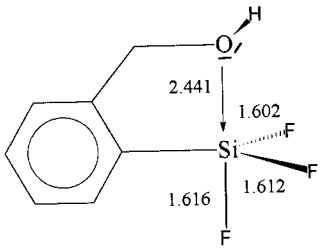
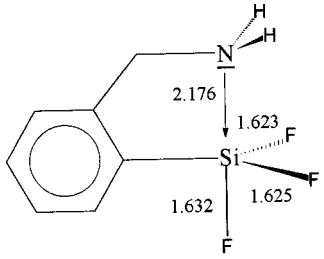


Figure 2. Linear correlation of O−Si distances (in Å) versus binding energies (negative, in kcal/mol) for water coordination to substituted silanes

To a first approximation the binding energies can be linearly related to the equilibrium bond lengths of the resulting donor−acceptor complexes. A rationale for this approach is given in the Experimental Section. A correspond-





Scheme 4

ing dependence of both quantities for amine and water addition is shown in Figure 1 (amine coordination) and Figure 2 (water coordination).

Accordingly, for both cases approximate linear relationships are apparent. It indicates that considerable changes in bond lengths (e.g. by 10%) cause only small changes in the resulting binding energies. On this basis it is evident that intramolecular coordination, such as in **1**, largely determines the actual equilibrium D−Si bond lengths, and, as we have seen, it is more pronounced for water than for amine coordination. Utilizing the linear relationship given in Figures 1 and 2 one can predict an extrapolation of the binding energies in the intramolecularly coordinated complexes **1**. They should be comparable and in the order of approx. 10 kcal/mol. Thus the binding energies are expected to be slightly larger than for the intermolecularly coordinated cases.

^{29}Si NMR Chemical Shifts

It is informative to analyze the effect of coordination on the chemical shifts of the silicon centers. We have calculated the corresponding ^{29}Si NMR chemical shifts for the cases of amine addition. A list of these values, obtained at the RHF and MP2 level of sophistication, are summarized in Table 3.

Table 3. d^{29}Si NMR shifts at RHF and MP2 level, with reference TMS

Compound	RHF[a,b]	MP2[a,b]	exp.[b]
TMS	0.0	0.0	0.0
$SiH_3^{(+)}$	280.4	303.7	(264)[c]
SiH_4	−92.3	−110.1	−93.1[d]
SiH_3F	−26.9	−24.1	−17.4[d]
SiH_2F_2	−35.3	−28.0	−28.5[d]
$SiHF_3$	−80.2	−73.7	−77.9[d]
SiF_4	−117.2	−109.0	−109.9[d]
H_4Si-NH_3	−89.1	−106.8	
$H_3SiF(eq)-NH_3$	−37.3	−35.8	
$H_3SiF(ax)-NH_3$	−63.3	−66.2	
$H_2SiF(eq)$-$F(eq)-NH_3$	−57.7	−51.0	
$H_2SiF(ax)$-$F(eq)-NH_3$	−69.9	−64.3	
$HSiF(ax)F(eq)$-$F(eq)-NH_3$	−112.1	−104.2	
$HSiF(eq)F(eq)$-$F(eq)-NH_3$	−114.0	−104.1	
SiF_4-NH_3	−145.6	−134.4	

[a] Basis set 6−311+g(2d,p). − [b] Chemical shifts relative to TMS: $\delta(^{29}Si) = \sigma(TMS) - \sigma(silane)$ [MP2 values]. σ(TMS) = 385.8 [367.2] ppm. − [c] C. Maerker, J. Kapp, P.v.R. Schleyer, in *Organosilicon Chemistry II*, Eds., N. Auner and J. Weis, VCH, 1996. − [d] Experimental values: H.C. Marsmann, *NMR Basic Principles and Progress, 17*, Springer, Berlin, **1981**.

For convenience we have also included here the values for tetramethylsilane (TMS) and the parent silyl cation. The results indicate a strong effect of electron correlation on the NMR chemical shifts only for the cases with low-lying empty orbitals, e.g., as the silyl cation, as seen by a comparison of the RHF versus MP2 values. For the other cases the computed chemical shifts at the RHF level are similar to those at the MP2 level. Is there a relationship between the changes in chemical shifts by coordination and adduct energies? In order to reveal a possible dependence between both quantities, we analyzed a linear relationship, as illustrated in Figure 3.

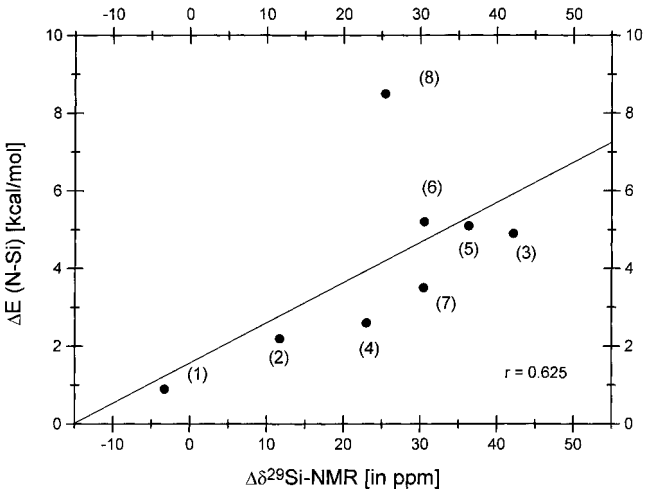


Figure 3. Linear correlation of amine adduct energies in (kcal/mol) versus differences in chemical shifts [$\Delta\delta^{29}Si = \delta^{29}Si$ (silane) − $d^{29}Si$ (silane−NH_3)]

We note that such a relationship is empirical, there is no theoretical justification for it. The difference in ^{29}Si NMR chemical shifts are given as the chemical shift of the amine-coordinated silane minus the chemical shift of the corresponding uncoordinated silane, at the MP2 level of sophistication (see Table 3). Our investigations indicate that a rough relationship between both quantities approximately exists, however the linear correlation is rather poor (r = 0.625).

Conclusions

The results of our investigations can be summarized as follows:

(1) Lewis donors, such as NH_3, PH_3, OH_2 and SH_2 form only weak donor−acceptor complexes with silanes. The effect of electronegative substituents was probed for fluorine. With increasing fluorine substitution the Lewis acidity is slightly increased.

(2) The donors NH_3 and OH_2 exert comparable donor properties, the former is slightly stronger than the latter whilst the higher element homologues PH_3 and SH_2 possess only negligible donor properties versus the substituted silane. The donor variety was studied for donation towards the best acceptor tetrafluorosilane. Within the Klopman concept one could describe the complexes by weak HOMO−LUMO interactions.

(3) For the intramolecular coordination shorter D−Si distances are observed than for intermolecular (bimolecular) coordination. Overall the resulting D−Si bonds are rather weak, in other words the chelating effects are dictating the equilibrium geometries

Experimental Section

Theoretical: The energy optimization of structures were performed using ab initio calculations with the valence double-ζ basis set, 6−31 g** of Pople et al.[26,27] Since donor−acceptor complexes are strongly determined by a superposition of covalent and ionic structures[28] all calculations were carried out at the MP2 level of optimization. Equilibrium geometries were identified by the corresponding vibrational analysis within the harmonic approximation. Further single-point calculations were done at the equilibrium geometries, utilizing the 6−311+g** basis set for first and second row elements.[29,30] This basis set has been considered of triple-zeta quality (TZP), since the 6−311 g basis set (triple split in the valence s- and p-shell) is augmented by one set of diffuse functions.[31] The basis sets utilized were augmented by a single set of polarization functions[32] at all atoms and the latter in addition by a set of diffuse functions.[33] Full details are given in the discussion. The NMR calculations were carried out with an enlarged basis set [6−311+g(2d,p)] at the optimized geometries. The isotropic shielding values were computed with the Gauge-Independent Atomic Orbital method (GIAO).[34,37] All calculations were performed with the Gaussian 98 set of programs.[38]

The Linear Bond Length-Bond Energy Relationship: Following the principal considerations of Pauling,[39] the energy of a bond as a function of the bond length is simply given by E(r) = A − B × ln (r), where A and B are constants and r the bond length. For small changes in the bond lengths this formula can be expanded in a Taylor series, resulting in an approximate linear relationship between the bond energy and the distance. Such an approximation holds true only for small changes in bond energies, as in the case at hand.

Acknowledgments

This work has been supported by the Deutsche Forschungsgemeinschaft and the Fonds der Chemischen Industrie.

[1] R. J. P. Corriu, C. Guerin, *J. Organomet. Chem*. **1980**, *198*, 231−320.
[2] R. J. P. Corriu, J. C. Young, in *The Chemistry of Organic Silicon Compounds* (Eds.: S. Patai and Z. Rappoport, John Wiley and Sons, New York, **1989**, 1241−1288.
[3] C. Chuit, R. J. P. Corriu, C. Reye, J. C. Young, *Chem. Rev*. **1993**, *93*, 1371−1448.
[4] R. R. Holmes, *J. Am. Chem. Soc*. **1984**, *106*, 3745−3750.
[5] J. A. Deiters, R. R. Holmes, *J. Am. Chem. Soc.* **1987**, *109*, 1686−1692; *ibid.* **1987**, *109*, 1692−1696.
[6] F. P. Boer, F. P. van Remoortere, *J. Am. Chem. Soc*. **1970**, *92*, 801−807.
[7] K. D. Onan, A. T. Mc Phail, C. H. Yoder, R. W. Hillyard, *J. Chem. Soc., Chem. Commun.* **1978**, 209−210.
[8] A. A. Macharashvili, V. E. Shklover, Yu. T. Struchkov, Yu. I. Baukov, E. P. Kramarova, G. I. Oleneva, *J. Organomet. Chem*. **1978**, *327*, 167−172.
[9] E. A. Zelbst, V. E. Shkloever, Yu. T. Struchkov, Yu. L. Frolov, A. A. Kashaev, L. I. Gubanova, V. M. D′yakov, M. G. Voronkov, *Zh. Strukt. Khim*. **1981**, *22*, 82.
[10] A. A. Macharasvili, V. E. Shklover, Yu. T. Struchkov, M. G. Voronkov, B. A. Gostevsky, I. D. Kalikhman, O. B. Bannikova, V. A. Pestunovich, *J. Organomet. Chem.* **1988**, *340*, 23−29.
[11] A. A. Macharasvili, V. E. Shklover, N. Yu. Chernikova, M. Yu. Antipin, Yu. T. Struchkov, Yu. I. Baukov, G. I. Oleneva, E. P. Kramarova, A. G. Shipov, *J. Organomet. Chem*. **1989**, *359*, 13−20.
[12] T. K. Prakasha, S. Srinivasan, A. Chandrasekaran, R. O. Day, R. R. Holmes, *J. Am. Chem. Soc.* **1995**, *117*, 10003−10009.
[13] A. Mix, U. H. Berlekamp, H.-G. Stammler, B. Neumann, P. Jutzi, *J. Organomet. Chem.* **1996**, *521*, 177−183.
[14] N. Auner, R. Probst, F. Hahn, E. Herdtweck, *J. Organomet. Chem*. **1993**, *459*, 25−41.
[15] R. J. P. Corriu, C. Guérin, B. Henner, Q. Wang, *Organometallics* **1991**, *10*, 2297−2303.
[16] M. Driess, S. Rell, H. Pritzkow, R. Janoscheck, *Angew. Chem.* **1997**, *109*, 1384−1387; *Angew. Chem. Int. Ed. Engl*. **1997**, *36*, 1326.
[17] R. G. Pearson, *J. Am. Chem. Soc.* **1963**, *85*, 3533−3539; R. G. Pearson, *Hard and Soft Acids and Bases Principles in Organic Chemistry*, Academic Press, New York, **1977**; R. G. Pearson, *Chemical Hardness*, Wiley-VCH, Weinheim **1977**.
[18] D. Bergmann, J. Hinze, *Angew. Chem*. **1996**, *108*, 162−176; *Angew. Chem. Int. Ed. Engl*. **1996**, *35*, 150−163.
[19] [19a] B. M. Gimarc, *Molecular Structure and Bonding*, Academic Press, New York, **1979**. − [19b] W. W. Schoeller, A. Sundermann, M. Reiher, *Inorg. Chem*. **1999**, *38*, 29−37.
[20] M. Klessinger, *Elektronenstruktur organischer Moleküle*, Verlag Chemie, Weinheim, **1982**.
[21] I. Fleming, *Frontier Orbitals and Organic Chemical Reactions*, John Wiley & Sons, London **1976**.
[22] [22a] L. Salem, *J. Am. Chem. Soc*. **1968**, *90*, 543−552; *ibid*. **1968**, *90*, 553−566. − [22b] G. Klopman, *J. Am. Chem. Soc*. **1968**, *90*, 223−234.
[23] According to Pearson[17] the hardness of the donor is defined as:

$$\lambda = \frac{1}{2}(I_p - E_a)$$

where I_p is the ionization potential and E_a the electron affinity of the donor or acceptor.
[24] W. W. Schoeller, R. Schneider, *Chem. Ber*. **1997**, *130*, 1013−1020.
[25] W. W. Schoeller, A. Rozhenko, unpublished results. A detailed discussion of this more computationally interesting aspect will be given elsewhere.
[26] R. Ditchfield, W. J. Hehre, J. A. Pople, *J. Chem. Phys.* **1971**, *54*, 724−728; W. J. Hehre, R. Ditchfield, J. A. Pople, *J. Chem. Phys.* **1972**, *56*, 2257−2261.
[27] P. C. Hariharan, J. A. Pople, *Mol. Phys.* **1974**, *27*, 209−214. P. C. Hariharan, J. A. Pople, *Theor. Chim. Acta*, **1973**, *28*, 213−222.
[28] R. S. Mulliken, *J. Am. Chem. Soc*. **1952**, *74*, 811−824; R. S. Mulliken, *J. Phys. Chem*. **1952**, *56*, 801−822; R. S. Mulliken, W. B. Person, *Molecular Complexes*, Wiley-Interscience, New York, **1969**.
[29] A. D. McLean, G. S. Chandler, *J. Chem. Phys.* **1980**, *72*, 5639−5648.
[30] R. Krishnan, J. S. Binkley, R. Seeger, J. A. Pople, *J. Chem. Phys.* **1980**, *72*, 650−654.
[31] R. S. Grev, H. F. Schaefer III, *J. Chem. Phys.* **1989**, *91*, 7305−7306.
[32] M. J. Frisch, J. A. Pople, J. S. Binkley, *J. Chem. Phys.* **1984**, *80*, 3265−3269.
[33] T. Clark, J. Chandrasekhar, G. W. Spitznagel, P. v. R. Schleyer, *J. Comput. Chem*. **1983**, *4*, 294.
[34] K. Wolinski, J. F. Hilton, P. Pulay, *J. Am. Chem. Soc*. **1990**, *112*, 8251−8260.
[35] K. Wolinski, A. J. Sadlej. *Mol. Phys.* **1980**, *41*, 1419−1430.
[36] R. Ditchfield, *Mol. Phys.* **1974**, *27*, 789−807.
[37] [37a] R. McWeeny, *Phys. Rev.* **1962**, *126*, 1028−1034. − [37b] F. London, *J. Phys. Radium, Paris* **1937**, *8*, 397.
[38] *Gaussian 98* (Revision A.1), M. J. Frisch, G. W. Trucks, H. B. Schlegel, G. E. Scuseria, M. A. Robb, J. R. Cheeseman, V. G. Zakrzewski, J. A. Montgomery, R. E. Stratmann, J. C. Burant, S. Dapprich, J. M. Millam, A. D. Daniels, K. N. Kudin, M. C.

Strain, O. Farkas, J. Tomasi, V. Barone, M. Cossi, R. Cammi, B. Mennucci, C. Pomelli, C. Adamo, S. Clifford, J. Ochterski, G. A. Petersson, P. Y. Ayala, Q. Cui, K. Morokuma, D. K. Malick, A. D. Rabuck, K. Raghavachari, J. B. Foresman, J. Cioslowski, J. V. Ortiz, B. B. Stefanov, G. Liu, A. Liashenko, P. Piskorz, I. Komaromi, R. Gomperts, R. L. Martin, D. J. Fox, T. Keith, M. A. Al-Laham, C. Y. Peng, A. Nanyakkara, C. Gonzalez, M. Challacombe, P. M. W. Gill, B. G. Johnson, W. Chen, M. W. Wong, J. L. Andres, M. Head-Gordon, E. S. Replogle and J. A. Pople, *Gaussian, Inc*. Pittsburgh PA, **1998**.

[39] L. Pauling, *The Nature of the Chemical Bond*, Cornell University Press, 3rd edition, **1960**.

Received April, 23
[I99144]

NMR Investigations of Restricted Rotations and Metallotropic Shifts in Rhenium(I) Tricarbonyl Halide Complexes of Pyridyl Carboxamide and Thioamide Ligands

Keith G. Orrell,*[a] Anthony G. Osborne,[a] Jade Ol Prince,[a] Vladimir Šik,[a] and Dionyssios K. Vellianitis[a]

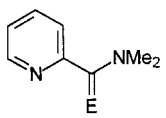
Keywords: Pyridyl carboxamides / Carbonyl complexes / Rhenium / Metallotropic shifts / MMR spectroscopy

A series of rhenium(I) tricarbonyl halide complexes of pyridyl mono- and di-carboxamides and -thioamides has been studied by dynamic NMR techniques. Oxygen coordination to Re^{I} of the carboxamide ligand reduced the energy barrier to C−N rotation by 2−13 kJ mol^{-1} whereas sulfur−Re^{I} coordination of the thioamide ligands led to a reduction of 28−33 kJ mol^{-1}. In the pyridyl dicarboxamide and -dithioamide metal chelate complexes metallotropic shifts occur between the three donor atoms, O, N, O or S, N, S, energies [$\Delta G^{\ddagger}$ (298.15 K)] being in the range 78−89 kJ mol^{-1}; these high values arise from the strong electron donating properties of the -NR2 (R = Me, Et) groups.

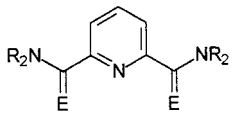
Introduction

As part of a research programme into the coordination properties of terdentate ligands and the molecular dynamics in solution of the metal complexes that are formed when the ligand is acting as a bidentate chelate ligand to a metal, we have previously investigated some metal complexes formed by ligands such as 2,2′:6′,2′′-terpyridine(terpy)[1] and 2,6-bis(pyrazol-1-yl)pyridine (bppy)[2] that present a N_3 donor set to the metal moieties. From these studies we have obtained quantitative information on the mechanisms and energetics of molecular motions such as 1,4-metallotropic shifts,[3] and metal-hurdling[4] fluxions. In order to investigate potential electronic and steric effects on the structures and dynamic behaviour in solution of related ligands and the corresponding metal complexes we have initiated an investigation into some complexes formed by pyridine-based terdentate ligands that present an ONO or a SNS donor set to a metal. In this paper we report our findings for the synthesis and studies by the methods of dynamic NMR spectroscopy on the carboxamide and thioamide ligands, *N*,*N*-dimethyl-2-pyridinecarboxamide (dmpc), *N*,*N*-dimethyl-2-pyridinethioamide (dmpt), *N*,*N*,*N*′,*N*′-tetramethyl-2,6-pyridinedicarboxamide (tmpdc), *N*,*N*,*N*′,*N*′-tetramethyl-2,6-pyridinedithioamide (tmpdt), *N*,*N*,*N*′,*N*′-tetraethyl-2,6-pyridinedicarboxamide (tepdc), *N*,*N*,*N*′,*N*′-tetraethyl-2,6-pyridinedithioamide (tepdt) and the metal complexes [$ReX(CO)_3L$] (X = Cl or Br; L = dmpc, dmpt, tmpdc, tmpdt or tepdc).

The dicarboxamide compounds have previously been used as ligands for complex formation with the lanthanide elements[5][6] and with cobalt(II), copper(II) and nickel(II) of the d-block metals.[7,8,9] In all the metal complexes studied previously the ligands are acting in a terdentate chelate mode that uses the pyridyl nitrogen and the two oxygen atoms as the donor set. To the best of our knowledge the thioamides have not been employed as ligands.



E = O dmpc
E = S dmpt



E = O, R = Me tmpdc
E = O, R = Et tepdc
E = S, R = Me tmpdt
E = S, R = Et tepdt

When the pyridyl dicarboxamide and dithioamide ligands act as bidentate chelates they may be described as hemilabile ligands.[10] Such ligands contain at least two different types of bonding group with different bonding strengths and these can lead to intramolecular ligand exchange processes ("fluxional shifts") and ligand displacement reactions. The coordination chemistry of such ligands has recently been reviewed.[11] This present work is a further contribution to this active area of chemistry.

Results

The carboxamide and thioamide ligands were prepared as described in the experimental section. The monofunctional ligands were air-stable oils and the difunctional ligands air-stable, crystalline solids. The rhenium(I) complexes of the ligands, namely *fac*-[$ReX(CO)_3L$] (X = Cl, L = tmpdc, tepdc, or tmpdt; X = Br, L = dmpc, tmpdc, tepdc, dmpt or tmpdt) were isolated in good yields as yellow or orange/red air-stable solids. The ligands and their Re^{I} complexes were characterised by melting point, IR and ^1H NMR spectroscopy, EI mass spectrometry, and, in the case of the metal complexes, by elemental analysis (Table 1).

In the metal carbonyl stretching region of the infrared spectra the complexes show three strong peaks (Table 1) consistent with a facial arrangement of the carbonyl groups.[1]

[a] School of Chemistry, The University, Exeter, Devon EX4 4QD, UK

 © WILEY-VCH Verlag GmbH, D-69451 Weinheim, 2000 1434−1948/00/0202−383 $ 17.50+.50/0

Table 1. Synthetic and analytical data for the Re^{I} complexes of pyridyl mono- and di-carboxamides and -thioamides

Complex	M.p./°C	% Yield[a]	$\tilde{\nu}$(CO)[b]/cm^{-1}	Analysis[c] (%)		
				C	H	N
[ReBr(CO)$_3$dmpc]	172 dec.	93	2026, 1917, 1895	26.6(26.4)	2.0(2.0)	5.6(5.6)
[[ReBr(CO)$_3$dmpt]	215 dec.	94	2027, 1933, 1900	25.8(25.6)	1.9(2.0)	5.4(5.4)
[ReCl(CO)$_3$tmpdc]	256 dec.	96	2027, 1920, 1901	32.2(31.9)	2.7(2.9)	7.9(8.0)
[ReBr(CO)$_3$tmpdc]	259 dec.	79	2028, 1921, 1901	29.4(29.4)	2.5(2.7)	7.1(7.4)
[ReCl(CO)$_3$tmpdt]	220 dec.	96	2028, 1930, 1908	30.9(30.1)	2.5(2.7)	7.4(7.5)
[ReBr(CO)$_3$tmpdt]	250 dec.	95	2028, 1931, 1906	28.4(27.9)	2.3(2.5)	6.9(7.0)
[ReCl(CO)$_3$tepdc]	218 dec.	67	2022, 1902, 1890	37.0(37.1)	3.8(3.9)	7.1(7.2)
[ReBr(CO)$_3$tepdc]	221 dec.	47	2010, 1905, 1880	34.4(34.5)	3.5(3.7)	6.4(6.7)

[a] Yield quoted relative to metal-containing reactant. – [b] Recorded as chloroform solution. – [c] Calculated values in parentheses.

This indicates that the pyridine-based ligands are acting as bidentate chelate ligands by substituting two equatorial carbonyl groups of the [ReX(CO)$_5$] compound. For the complexes derived from the dicarboxamide ligands two amide carbonyl stretching vibrations are observed in the infrared spectrum, one approximating to the free ligand value and the other 25–30 cm^{-1} lower. This observation indicates that the dicarboxamide ligands are bound to the metal in a bidentate chelate fashion via an ON donor set. This finding was confirmed by the ^{1}H NMR spectroscopic studies (see later).

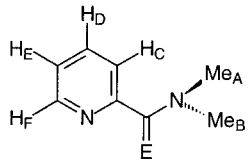
(i) Monoamide ligands, (L), dmpc, dmpt and Complexes [ReBr(CO)$_3$L]

The ^{1}H NMR spectra of dmpc and dmpt consisted of six signals (Table 2), the pairs of *N*-methyl shifts indicating severe restriction to rotation about the C–N bond of the carboxamide and thioamide functions. This is fully in accordance with previous studies of such systems and, in particular, on dmpc.[12] Distinction between the *N*-methyl signals was based on the results of the NOE difference experiments (carried out on the corresponding dicarboxamides tmpdc and tepdc, see later).

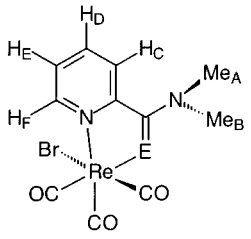
The energy barrier to rotation in dmpc was measured by obtaining ^{1}H NMR spectra in the temperature range 303–373 K. On increasing the temperature the two *N*-methyl signals broadened, coalesced (at 363 K) and then changed to a single, sharp signal. A bandshape analysis of signals in the range 323–373 K yielded an activation energy (see later) in good agreement with a previous study.[12] In contrast, variable temperature ^{1}H NMR spectra of the thioamide dmpt showed no signal broadening up to ca. 393 K, indicating that the rate of C(S)–N bond rotation was slow on the NMR timescale even at 393 K. The 2D-EXSY NMR method,[13–15] which is sensitive to slower exchange rates that are not accompanied by any line broadening, was therefore applied in the temperature range 353–393 K with mixing times 0.8 s (353 K), 0.1 s (373 K) and 0.02 s (393 K). Clear cross-peaks between the *N*-methyl signals were observed at these temperatures, from which first-order rate constants for the bond rotation process were computed with the authors' D2DNMR program.[27]

Coordination of dmpc and dmpt to form ReBr(CO)$_3$ complexes led to strikingly different room temperature ^{1}H NMR spectra. These are shown in Figure 1, where it will be noted that [ReBr(CO)$_3$dmpc] shows a clear chemical shift

Table 2. ^{1}H NMR spectroscopic data for the ligands dmpc, dmpt and the complexes [ReBr(CO)$_3$L] (L = dmpc, dmpt)



E = O, S



E = O, S

Compound	δ_A	δ_B	δ_C (J_{CD}/Hz)	δ_D (J_{CD}, J_{DE}/Hz)	δ_E (J_{DE}, J_{EF}/Hz)	δ_F (J_{EF}/Hz)
dmpc[a]	3.03 s	3.11 s	7.57 d (7.6)	7.35 t (7.6, 7.6)	7.80 dd (7.6, 5.0)	8.65 (broad)[c]
dmpt[b]	3.16 s	3.58 s	7.56 d (8.0)	7.22 t (8.0, 8.0)	7.70 dd (7.0, 4.0)	8.48 s (broad)[c]
[ReBr(CO)$_3$dmpc][a]	3.36 s	3.56 s	8.04 d (8.0)	7.70 t (8.0, 8.0)	8.14 dd (8.0, 6.6)	9.10 d (6.7)
[ReBr(CO)$_3$dmpt][b]	3.67 s	3.67 s	7.55 d (8.0)	7.47 t (8.0, 8.0)	7.98 dd (8.0, 6.2)	9.10 d (6.2)

[a] Measured in $(CDCl_2)_2$ at 303 K relative to Me_4Si (δ = 0). – [b] Measured in $CDCl_3$ at 303 K relative to Me_4Si (δ = 0). – [c] Due to ^{14}N quadrupole broadening. s = singlet, d = doublet, dd = doublet of doublets, t = 1:2:1 triplet.

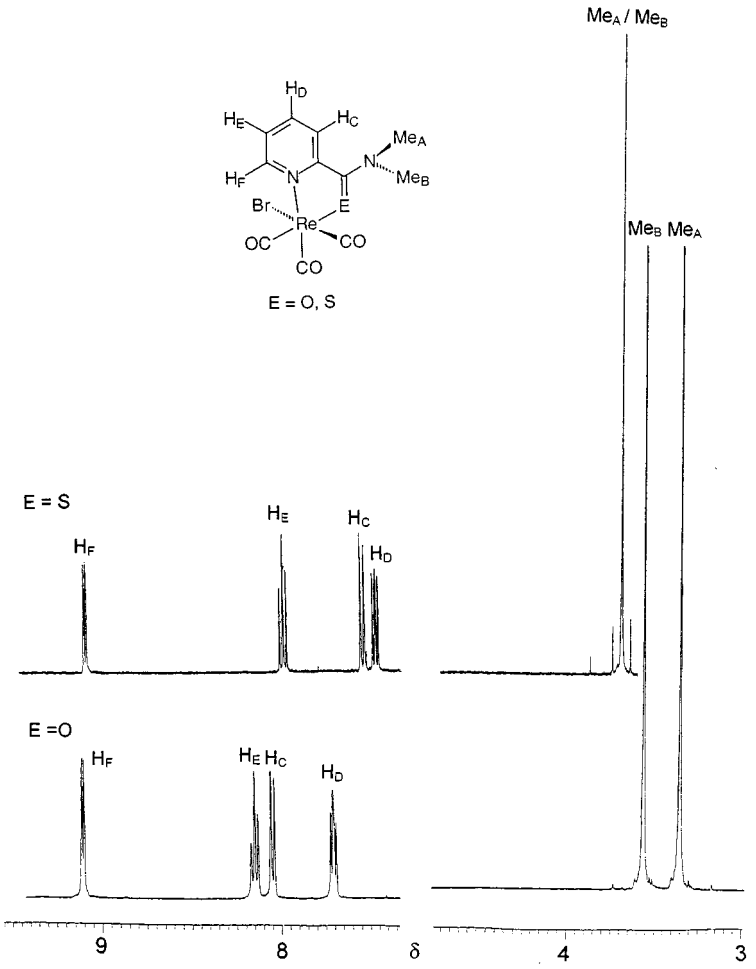
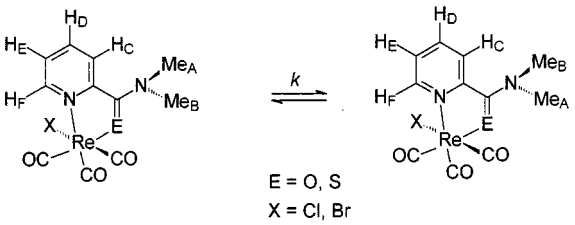


Figure 1. 400 MHz ^{1}H NMR spectra of [ReBr(CO)$_3$dmpc] and [ReBr(CO)$_3$dmpt] at 303 K in $(CDCl_2)_2$ and $CDCl_3$ respectively

distinction between the *N*-methyl signals, whereas [ReBr(CO)$_3$dmpt] does not, implying that C−N rotation in the carboxamide complex is slow on the NMR timescale at ambient temperatures whereas in the thioamide it is fast.

The temperature dependencies of these exchange rates, *k*, described according to Scheme 1, were measured by recording the ^{1}H NMR spectra of [ReBr(CO)$_3$dmpc] in the range 303−413 K and of [ReBr(CO)$_3$dmpt] in the range 223−303 K. Coalescences of the pairs of *N*-methyl signals in these two complexes occurred at ca. 363 K and ca. 268 K, respectively. Bandshape analyses in these temperature ranges enabled energy barriers for the C−N rotations to be evaluated (see later).



Scheme 1. Restricted rotation of the NMe_2 group in the monoamide ligand complexes

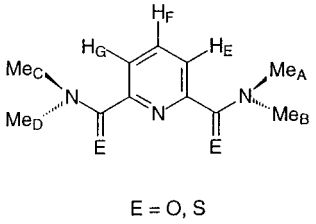
(ii) Diamide ligands (L) tmpdc, tmpdt, and Complexes [ReX(CO)$_3$L] (X = Cl, Br)

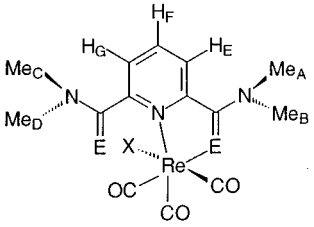
The ligands tmpdc and tmpdt exhibited ^{1}H NMR spectral features (Table 3) very similar to their monofunctional counterparts dmpc and dmpt. Thus, at ambient temperatures both ligands displayed chemical shift distinction within each of the *N*/*N*′-dimethyl pairs. Unambiguous assignments were made with the aid of Nuclear Overhauser Enhancement (NOE) difference experiments on tmpdc.

Irradiation of the lower frequency methyl signal at δ = 3.07 caused a positive NOE of the pyridyl $H_{E/G}$ signal whereas no such effect was observed on irradiating the signal at δ = 3.15. The NOE was small indicating that the NMe_2 groups are not coplanar with the ring but rotated such that the methyls Me_A/Me_C are in shielding zones associated with the aromatic ring current.

On warming, exchange broadening of the *N*-methyl signals occurred in the case of tmpdc, with coalescence being achieved at ca. 353 K, whereas no significant broadening occurred for tmpdt until ca. 393 K, which was near the high-temperature limit of the solvent $(CDCl_2)_2$. The 2D-EXSY method was therefore used for tmpdt, and good quality, rate-sensitive spectra achieved at temperatures 353,

Table 3. ^{1}H NMR spectroscopic data for the ligands tmpdc, tmpdt and the complexes [ReX(CO)$_3$L] (L = tmpdc, tmpdt; X = Cl, Br)





Compound	δ_A	δ_B	δ_C	δ_D	δ_E (J_{EF}/Hz)	δ_F (J_{EF}, J_{FG}/Hz)	δ_G (J_{FG}/Hz)
tmpdc[a]	3.07 s	3.15 s	3.07 s	3.15 s	7.65 d (7.7)	7.92 t (7.7, 7.7)	7.65 t (7.7)
tmpdt[b]	3.19 s	3.58 s	3.19 s	3.58 s	7.51 d (7.8)	7.77 t (7.8, 7.8)	7.51 d (7.8)
[ReCl(CO)$_3$tmpdc][a]	3.35 s	3.55 s	2.98 s	3.23 s	7.96 d (7.5)	8.18 t (7.9, 7.9)	7.65 d (7.5)
[ReBr(CO)$_3$tmpdc][a]	3.32 s	3.53 s	2.99 s	3.22 s	7.94 d (8.1)	8.19 t (7.9, 7.9)	7.65 d (8.0)
[ReCl(CO)$_3$tmpdt][b]	3.65 s	3.65 s	3.18 s	3.64 s	7.50 d (10.5)	8.02 t (10.5, 10.5)	7.38 d (10.5)
[ReBr(CO)$_3$tmpdt][b]	3.63 s	3.63 s	3.20 s	3.64 s	7.44 d (10.6)	7.95 t (10.6, 10.6)	7.31 d (10.5)

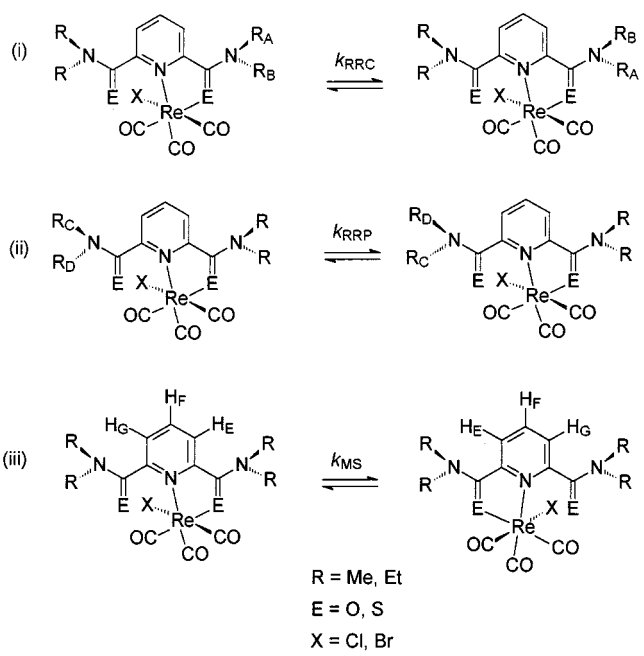
[a] Measured in $(CDCl_2)_2$ at 303 K. – [b] Measured in $CDCl_3$ at 303 K. s = singlet, d = doublet, t = triplet.

373 and 393 K, using mixing times of 0.5 s, 0.1 s and 0.01 s, respectively. The spectral characteristics of both these ligands indicate the very different degrees of restriction to C–N rotation in these species.

The ^{1}H NMR spectra of [ReX(CO)$_3$tmpdc] (X = Cl, Br) consisted of four separate *N*-methyl signals, the pair Me_A/Me_B associated with the coordinated carboxamide group being to high frequency of the other pair, Me_C/Me_D. On warming the $(CDCl_2)_2$ solution of the complex the signals of Me_A and Me_B began to broaden, coalescing at ca. 343 K and then sharpening to an averaged signal. The signals of Me_C and Me_D showed slight increases in bandwidth above ca. 323 K, indicating the onset of slow C–N rotation in the pendant – $C(O)NMe_2$ group as well as in the coordinated group. This broadening increased with increasing temperature until at ca. 403 K the Me_C/Me_D signals started to merge with the broad average Me_A/Me_B signal. By 413 K all signals had coalesced into a single broad signal. These changes are clearly indicative of the consecutive onset of (i) C–N rotation of the coordinated -$C(O)NMe_2$ group, (ii) C–N rotation of the pendant -$C(O)NMe_2$ group, and (iii) 1,4-metallotropic shifts which cause a loss of distinction between the coordinated and uncoordinated carboxamide functions. Further evidence for the 1,4-metallotropic shift was obtained from the signals of the pyridyl hydrogens at the 3- and 5-position (labelled H_E and H_G). These commenced broadening at 343 K and by 413 K had almost coalesced to a very broad band envelope with half-height width of ca. 100 Hz.

These spectral changes can be interpreted in terms of the exchanges depicted in Schemes 2 (i) – (iii) (E = O; R = Me).

Rate data for these schemes were obtained by bandshape analysis of the *N*-methyl region spectra in the temperature range 303–353 K for the C–N rotation rates (for coordinated and pendant groups) and the pyridyl hydrogen region spectra in the range 343–413 K for the 1,4-metallotropic shifts.



Scheme 2. Three types of internal dynamic process in the diamide ligand complexes

The room temperature ^{1}H NMR spectra of the complexes [ReX(CO)$_3$tmpdt] (X = Cl, Br) exhibited three *N*-methyl signals in the intensity ratio 6:3:3. The signal of intensity 6 was due to the *N*-methyl groups of the coordi-

nated thioamide group which rotates rapidly on the NMR timescale, while the signals of intensity 3 were due to the chemically distinct *N*-methyls of the uncoordinated -C(S)NMe_2 group where C−N rotation was slow on the NMR timescale, as was observed in the free ligand tmpdt. The rates of C−N rotation in the coordinated thioamide group were measured from spectra taken in the temperature range 263−313 K, with band coalescence occurring at ca. 288 K. Measurement of C−N rotation rates in the pendant -C(S)NMe_2 group required above-ambient temperature studies. Spectra measured in the range 383−413 K showed line broadenings but band coalescence was clearly above 413 K, the upper temperature limit of the solvent $(CDCl_2)_2$. Bandshape analysis of these line broadenings was dependent on the two rate constants k_{RRP} and k_{MS} (Scheme 2, E = S; R = Me); the latter, however, were most accurately measured from the effect of the metallotropic shifts on the H_E and H_G pyridyl hydrogens.

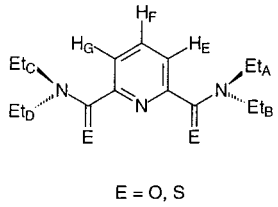
(iii) Ligands tepdc, tepdt and Complexes [ReX(CO)$_3$tepdc] (X = Cl, Br)

These ligands are the *N*,*N*,*N*′,*N*′-tetraethyl analogues of tmpdc and tmpdt and they behave in a very similar fashion. Their ^{1}H NMR characteristics are given in Table 4 where it will be observed that distinction within each of the pairs of *N*,*N*′-diethyl groups is seen in both the CH_2 and CH_3 signals.

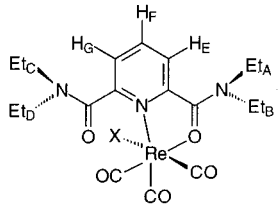
For tepdc unambiguous assignments of the CH_2 and CH_3 signals were made by NOE difference experiments. Irradiation of the CH_2 signal at δ = 3.35 caused a weak enhancement of the pyridyl hydrogens at the 3- and 5-positions whereas irradiation at the other CH_2 signal (δ = 3.55) caused no enhancement. The weakness of the enhancement indicated that the NEt_2 groups were considerably out of the pyridyl ring plane with the Et_A and Et_C groups shielded (relative to Et_B/Et_D) by the aromatic ring current. The NOEs of the methyl signals provided firm assignments of these signals also. It should be noted that all these assignments are rather at variance with those previously reported for tepdc[5] but in that study only a planar structure for this ligand was considered. However, molecular mechanics calculations on tepdc[8] have shown that the carbonyl groups of the carboxamide functions are twisted relative to the pyridine ring by ca. 64°. Such a twist accounts for the NOE effects between the methyl groups of Et_A and Et_C and the pyridyl hydrogens H_E and H_G being small, with these ethyl groups being shielded relative to Et_B and Et_D, since the latter are more remote from the effects of the pyridyl ring current. On raising the solution temperature of tepdc from 303 to 413 K, dynamic broadening occurs with coalescences at ca. 353 K (CH_3 signals) and ca. 360 K (CH_2 signals). Bandshape fittings of both sets of signals were made for six spectra in the temperature range 333−383 K, and provided reliable rate data.

The 2D-EXSY method had to be applied to the thioamide analogue tepdt to obtain rate data. Accordingly, 2D-EXSY spectra of tepdt were measured at 353, 373 and 393 K with mixing times of 0.8 s, 0.1 s and 0.01 s, respectively, and rate data obtained with the D2DNMR program.[27]

Table 4. ^{1}H NMR spectroscopic data for the ligands tepdc, tepdt and the complexes [ReX(CO)$_3$tepdc] (X = Cl, Br)



E = O, S



X = Cl, Br

Compound	δ(Et_A)		δ(Et_B)		δ(Et_C)		δ(Et_D)		δ_E	δ_F	δ_G
	CH_2	CH_3	CH_2	CH_3	CH_2	CH_3	CH_2	CH_3	(J_{EF}/Hz)	(J_{EF}, J_{FG}/Hz)	(J_{FG}/Hz)
tepdc[a]	3.35	1.16	3.55	1.27	3.35	1.16	3.55	1.27	7.62 (7.8)	7.91 (7.8, 7.8)	7.62 (7.8)
tepdt[a]	3.44	1.22	4.10	1.41	3.44	1.22	4.10	1.41	7.44 (7.8)	7.79 (7.8, 7.8)	7.44 (7.8)
[ReCl(CO)$_3$tepdc][b]	c	1.38	c	1.54	c	1.18	c	1.33	7.87 (7.8)	8.19 (7.9, 7.9)	7.62 (7.8)
[ReBr(CO)$_3$tepdc][b]	d	1.40	d	1.54	d	1.17	d	1.35	7.86 (7.9)	8.18 (8.0, 7.9	7.62 (7.8)

[a] Measured in $(CDCl_2)_2$ at 303 K. − [b] Measured in $(CDCl_2)_2$ at 273 K. − [c] Signals at δ = 4.25, 3.95*, 3.73*, 3.64*, 3.62*, 3.30, 3.27 and 3.08 (* coordinated side). − [d] Signals at δ = 4.24, 3.96*, 3.69*, 3.61*, 3.61*, 3.32, 3.29 and 3.08 (* coordinated side).

The ambient temperature ^{1}H NMR spectra of the complexes [ReX(CO)$_3$ tepdc] (X = Cl, Br) revealed some interesting features. Four distinct ethyl environments were identified as expected for a static bidentate chelate complex. These were represented by four methyl signals, two of which were sharp 1:2:1 triplets and two were broad, unsplit signals. On cooling to 273 K all four signals became sharp triplets (Figure 2).

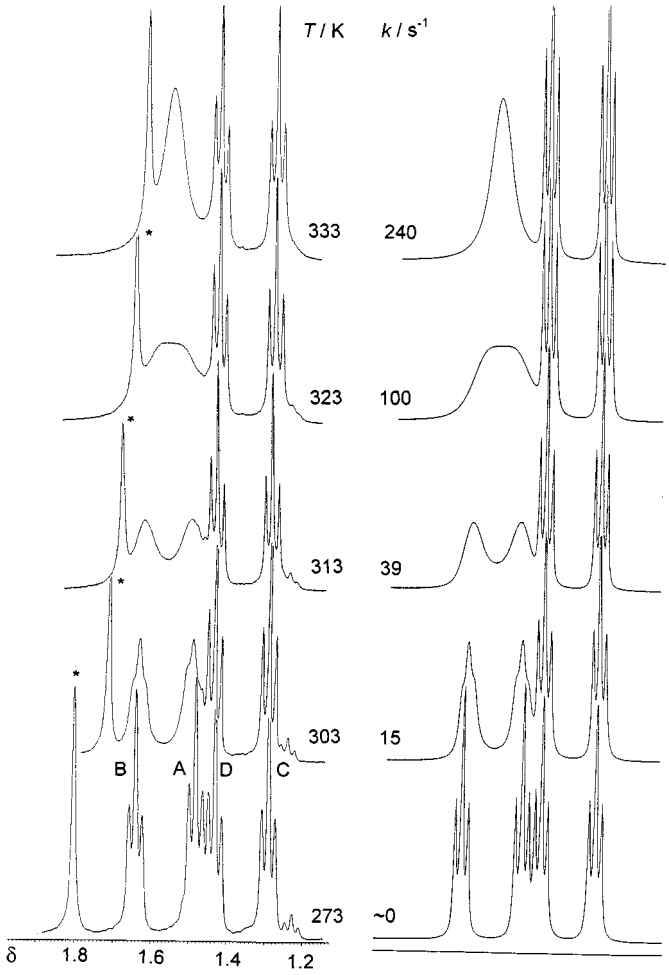


Figure 2. Variable temperature 400 MHz ^{1}H NMR spectra of [ReBr(CO)$_3$tepdc] in $(CDCl_2)_2$ showing the effects of restricted C−N rotation in the coordinated C(O)NEt$_2$ on the methyl signals; computer simulated spectra with "best-fit" rate constants are shown alongside. * solvent band

At 303 K the methylene hydrogens were represented by eight signals, four of which showed dynamic broadening and four which were sharp sextuplets. On cooling to 273 K all eight signals showed this same multiplet splitting which was interpreted as a combination of two-bond geminal methylene couplings and weaker three-bond couplings to the adjacent methyl hydrogens. The sextuplets resulting from partial overlap of the expected doublet of quadruplets had lines in the intensity ratio 1:3:4:4:3:1 and were the result of the $^2J_{HH}$ values being approximately twice the magnitude of the $^3J_{HH}$ values, (*viz*. $|^2J_{HH}| \approx 14$ Hz, $|^3J_{HH}| \approx 7$ Hz). The observation of spin-spin coupling between the geminal methylene hydrogens arises from the diastereotopic nature of these groups, which is not apparent in the free ligand.

The broadened signals in both the methyl and methylene regions of the spectra at room temperature are due to the ethyl environments A and B associated with the Re-coordinated -C(O)NEt$_2$ group. On warming, the broad methyl signals coalesced (at ca. 323 K for X = Br) and then the averaged signal sharpened. The four broadened methylene signals exhibited coalescences at ca. 313 K and 333 K, (X = Br). Bandshape analysis was performed on the methyl signals in the temperature range 273−373 K and excellent fits of experimental and theoretical spectra obtained (Figure 2), which led to activation energies for the restricted C−NEt$_2$ rotation on the metal-coordinated side.

On raising the temperature beyond 333 K additional dynamic broadenings involving all methyl and all methylene signals occurred. This was the result of fluxional shifts of the Re moiety between the N/O donor pairs and rotation of the NEt$_2$ group on the pendant side of the ligand. The relatively slow rates of magnetisation transfer arising from these processes were measured by 2D-EXSY as well as by 1D-bandshape analysis. The 2D-EXSY spectrum of [ReBr(CO)$_3$tepdc] at 343 K is shown in Figure 3.

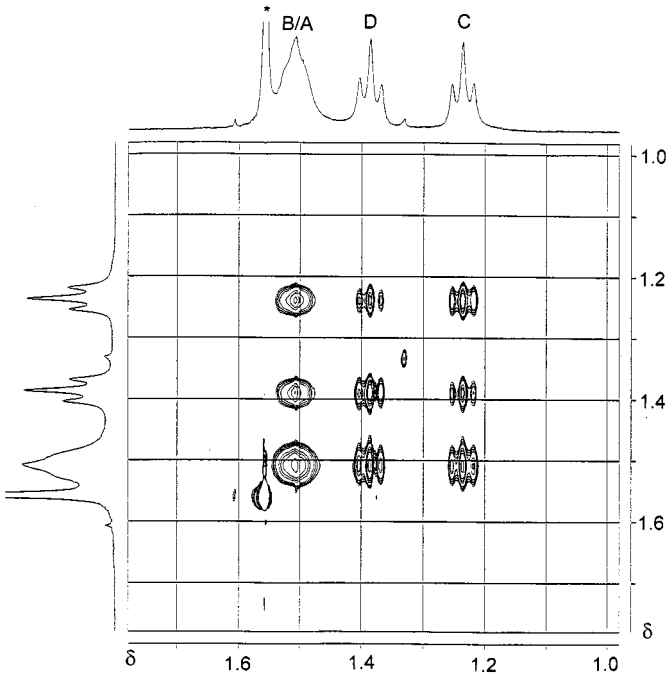


Figure 3. 400 MHz ^{1}H 2D-EXSY spectrum of [ReBr(CO)$_3$tepdc] at 343 K in $(CDCl_2)_2$ solution. Mixing time was 0.4 s. Cross peaks indicate restricted rotation in the pendant −C(O)NEt$_2$ group and 1,4-metallotropic shifts

At this temperature the methyl signals of the coordinated carboxamide moiety have coalesced, and cross peaks are observed between all three methyl signals. Cross peaks between the two lowest frequency signals (C and D) associated with the pendant carboxamide moiety, were due to restricted C−N rotation in this moiety, whereas the cross peaks between the signals C and D and the coalesced signal B/A was due to the metallotropic shift.

Table 5. Activation energy data for $C-NR_2$ restricted rotation in the pyridine-carboxamide and -thioamide ligands

Ligand	Temp range/K	Method[a]	$\Delta H^{\neq}$ /kJ mol^{-1}	$\Delta S^{\neq}$ /J K^{-1} mol^{-1}	$\Delta G^{\neq}$ [b] /kJ mol^{-1}
dmpc	323−373	BSA	81.2 ± 2.2	19.8 ± 6.7	75.3 ± 0.3[c]
tmpdc	333−373	BSA	72.7 ± 1.5	-7.3 ± 4.2	74.9 ± 0.2[d]
tepdc	333−383	BSA	108.5 ± 3.9	96.6 ± 6.6	79.8 ± 0.7
dmpt	353−393	EXSY	86.3 ± 0.2	-7.2 ± 0.5	88.4 ± 0.03
tmpdt	353−393	EXSY	107.8 ± 9.4	49.3 ± 25.3	93.2 ± 1.9
tepdt	353−393	EXSY	87.1 ± 0.5	-2.9 ± 1.3	88.0 ± 0.1

[a] BSA -^{1}H bandshape analysis, EXSY - ^{1}H exchange spectroscopy. − [b] At 298.15 K. − [c] Ref.[12] gives 74.9 kJ mol^{-1} (BSA); Ref.[16] gives 73.4 kJ mol^{-1} (coalescence 361 K).

Rate data for the restricted C−N rotation of the pendant -C(O)NEt$_2$ group (k_{RRP}) were obtained from the 2D-EXSY spectrum at 343 K and from the 1D spectra at 343, 353 and 363 K.

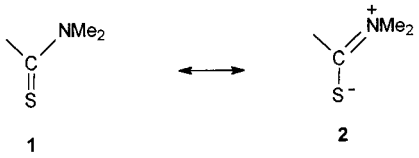
Rate constants for the metallotropic shifts (k_{MS}) were most accurately extracted from the 1D spectra of the pyridyl hydrogens, since this process interconverts the hydrogen atoms at the 3- and 5-position, but leaves that at the 4-position unaffected. Bandshape analysis of seven spectra in the temperature range 293−353 K provided reliable rate data for this fluxional process.

Discussion

Activation energy data for $C-NR_2$ restricted rotation in all six free ligands are collected in Table 5. Gibbs free energy values, $\Delta G^{\neq}$ (298.15 K), have the lowest associated uncertainties and it is most meaningful to make comparisons with this parameter. The 2-pyridine-carboxamide and 2,6-pyridine dicarboxamide, dmpc and tmpdc, have been studied previously, albeit rather less accurately in one case, and the present $\Delta G^{\neq}$ values of 75.3 and 74.9 kJ mol^{-1} are in moderately good agreement with the previous values of 74.9[12] and 73.4[16] kJ mol^{-1}.

These results imply that there is negligible electronic influence between the two amide groups in these systems. Replacement of the NMe_2 groups by NEt_2 appears to cause a slight rise in the C−N rotational barrier with the value for tepdc being 79.8 kJ mol^{-1}.

Replacement of the carbonyl oxygen of the amides by a sulfur atom in the thioamides causes a very significant increase in the C−N rotation barrier as can be seen by comparing $\Delta G^{\neq}$ data for the ligand pairs dmpc/dmpt, tmpdc/tmpdt and tepdc/tepdt, where increases of 13.1, 18.3 and 8.2 kJ mol^{-1}, respectively, occur. These increases are of similar magnitude to the increase of 9.6 kJ mol^{-1} which occurs on going from *N*,*N*-dimethylbenzamide[17] to the corresponding thioamide.[18] These increases may be attributed primarily to increased conjugation of the C−N bond(s) with the aromatic rings in the thioamide systems relative to the carboxamide systems, or alternatively to an increased contribution of the resonance form **2** below.



1 **2**

Such rationalisation is supported by the observation that in nonaromatic analogues such as *N*,*N*-dimethylcarbamoyl chloride $ClC(O)NMe_2$, and its thiocarbamoyl analogue $ClC(S)NMe_2$, the increase in the rotation energy barrier is only 5.4 kJ mol^{-1}.[19] However, recent ab initio calculations on formamide/thioformamide[20] and acetamide/thioacetamide[21] systems have implied that conjugation effects may not be the dominant contributors to C−N rotational barriers, but that the nitrogen lone pair may play a crucial role. For instance, a valence-bond study[20] suggests that the preferred orientation of the N lone pair perpendicular to the molecular plane may lead to resonance stabilisation of planar conformers which is responsible for about one half of the rotational barrier of formamide and two thirds of the barrier for thioformamide, the large magnitude of the latter being due to greater conjugation effects. An MO study[21] of acetamide and thioacetamide ascribes even greater importance to the N lone pair and the preference of the N atom for pyramidalization.

The full set of activation energy data for the various motional processes occurring in the $[ReX(CO)_3L]$ (X = Cl, Br) complexes is listed in Table 6.

For the complexes where L = tmpdc, tepdc and tmpdt, there appears to be no significant changes in the $\Delta G^{\neq}$ data for a change of halogen. The effect of Re coordination of the ligand on the C−N rotational characteristics of the $-C(E)NR_2$ groups is, however, particularly significant. This is highlighted in Table 7 where $\Delta G^{\neq}$ values for this process in both the coordinated and pendant portions of the complex are compared with the values for the free ligand.

Rhenium coordination of the amide oxygen reduces the -$C-NR_2$ rotation barriers by 2−13 kJ mol^{-1}, whereas coordination of the sulfur atom in the thioamide moieties greatly reduces the barrier by 28−33 kJ mol^{-1}. Metal σ-coordination acts as an electron drain on the carboxamide or thioamide functions, which will destabilise the zwit-

Table 6. Activation energy data for restricted C−NR_2 rotations and metallotropic shifts in [$ReX(CO)_3L$] (L = amide and thioamide ligands)

X	L	Temperature range /K	Motional process[a]	$\Delta H^{\ddagger}$/kJ mol^{-1}	$\Delta S^{\ddagger}$/J K^{-1} mol^{-1}	$\Delta G^{\ddagger}$/kJ mol^{-1}
Br	dmpc	313−373	RRC	80.2 ± 1.1	23.5 ± 3.1	73.2 ± 0.1
Br	dmpt	253−268	RRC	71.1 ± 3.6	34.3 ± 13.5	60.9 ± 0.5
Cl	tmpdc	303−353	RRC	66.9 ± 0.4	-10.9 ± 1.2	70.14 ± 0.03
		383−403	RRP	85.7 ± 1.3	-11.8 ± 3.3	89.2 ± 0.3
		343−413	MS	70.1 ± 3.7	-27.3 ± 10.0	78.3 ± 0.8
Br	tmpdc	313−353	RRC	61.4 ± 2.1	-26.3 ± 6.4	69.2 ± 0.2
		323−353	RRP	66.7 ± 9.2	-38.1 ± 27.1	78.0 ± 1.1
		343−413	MS	89.5 ± 1.6	19.2 ± 4.2	83.8 ± 0.4
Cl	tmpdt	263−333	RRC	70.1 ± 3.0	23.9 ± 10.3	62.93 ± 0.04
		383−413	RRP	92.7 ± 3.8	0.8 ± 9.6	92.4 ± 0.9
		383−413	MS	92.5 ± 2.5	14.6 ± 6.3	88.1 ± 0.6
Br	tmpdt	263−313	RRC	66.6 ± 1.07	20.9 ± 3.7	60.38 ± 0.02
		383−413	RRP	85.7 ± 9.3	-22.5 ± 23.3	92.4 ± 2.3
		383−413	MS	93.7 ± 1.4	14.9 ± 3.5	89.2 ± 0.3
Cl	tepdc	293−353	RRC	69.9 ± 1.7	8.9 ± 5.3	67.2 ± 0.1
		343−413	MS	73.5 ± 0.4	-13.4 ± 1.1	77.5 ± 0.1
Br	tepdc	293−353	RRC	71.4 ± 1.5	13.8 ± 3.2	67.3 ± 0.1
		343[b]	RRP	-	-	84.1
		343−363	RRP	78.9 ± 5.0	-0.2 ± 14.2	79.0 ± 0.8
		343−413	MS	78.2 ± 1.2	-1.7 ± 3.2	78.8 ± 0.3

[a] RRC = *r*estricted *r*otation on *c*oordinated side; RRP = *r*estricted *r*otation on *p*endant side; MS = *m*etallotropic *s*hift. − [b] 2D-EXSY value.

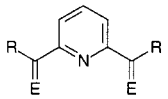
Table 7. Comparison of energy barriers for restricted C−N rotations for coordinated and uncoordinated amides −C(E)NR_2

Ligand, L	E	$\Delta G^{\ddagger}$/ (298.15 K)/kJ mol^{-1} Free ligand	[$ReBr(CO)_3L$]	$\Delta\Delta G^{\ddagger}$ [a]/ kJ mol^{-1}
dmpc	O	75.3	73.2 (coord)	−2.1
dmpt	S	88.4	60.9 (coord)	−27.5
tmpdc	O/O	74.9	69.2 (coord)	−5.7
			78.0 (pendant)	3.1
tepdc	O/O	79.8	67.3 (coord)	−12.5
			84.1 (pendant)	4.3
tmpdt	S/S	93.2	60.4 (coord)	−32.8
			92.4 (pendant)	−0.8

[a] $\Delta G^{\ddagger}$ (complex) − $\Delta G^{\ddagger}$ (free ligand).

Table 8. Activation energies of metallotropic shifts in [$ReBr(CO)_3L$] complexes

L =



R	E	$\Delta G^{\ddagger}$(298.15 K)/kJ mol^{-1}	Reference
Me_2N	O	83.8 ± 0.4	This work
Et_2N	O	78.8 ± 0.3	This work
Me_2N	S	89.2 ± 0.3	This work
Me	O	61.0 ± 0.05	[22]
H	O	Low[a]	[23]
^{t}Bu	O	63.5 ± 0.1	[23]
OMe	O	60.0 ± 0.1	[23]
OEt	O	60.3 ± 0.1	[23]

[a] Not measurable, complex thermally unstable.

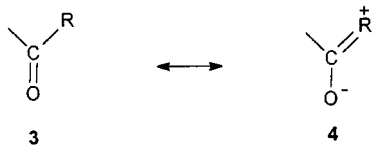
terionic form of the function leading to a decrease in the energy barrier to C−N rotation. This effect appears to be much stronger for the sulfur atom with its greater *p* electron complement compared to oxygen. Not unexpectedly, the barriers for the pendant portions of the ligands in the complex are of similar magnitude to those of the free ligand. For O coordination there is a small increase of 3−4 kJ mol^{-1} in the complex, and for S coordination there is a slight decrease of 0.8 kJ mol^{-1}.

Metallotropic shifts involving interchange of bidentate, chelate bonding between adjacent donor pairs in N_3 ligands have been reported for a variety of metal moieties, but data for the moiety $ReX(CO)_3$ where X is halogen, are most widely available. Much fewer data are available for metallotropic shifts in O, N, O and S, N, S ligands. However, Table 8 contains the activation energies [$\Delta G^{\ddagger}$ (298.15 K)] for a variety of complexes of general type [$ReBr(CO)_3L$] (L = 2,6-disubstituted pyridines where the substituents are either amides, thioamides, ketones or esters) from both published and unpublished work. $\Delta G^{\ddagger}$ values lie in the range 60−89 kJ mol^{-1}.

An increase in magnitude of ca. 5 kJ mol^{-1} on changing from a dicarboxamide to a dithioamide ligand mirrors somewhat the relative energies of C−N rotation of the analogous free ligands, and can again be related to increased conjugation of the -C=S function as opposed to the -C=O function with the pyridyl aromatic ring, thus increasing the donor strength of the S atoms.

Energy barriers for the -C(O)R groups also vary appreciably with the nature of R, being in the range 60−84 kJ mol^{-1}. The highest values, 79−84 kJ mol^{-1}, are associated with the strong electron donors NMe_2, NEt_2, and lower values, in the range 60−64 kJ mol^{-1}, with the weaker electron donors OMe, OEt, Me and *t*Bu. This can be rationalised in terms of the strength of the oxygen donor being increased by the extent to which its electron density is enhanced by donation from the R group, i.e. the extent to

which resonance form **4** (below) contributes to the overall structure.



3 **4**

The mechanism of 1,4 metallotropic shifts has been the subject of some controversy as to whether it has a dissociative or associative mechanism.[3] The present study does not provide further insight into this matter as no investigation was made into whether the rearrangement interchanged the equatorial carbonyl environments or not. This would have required variable temperature ^{13}C studies of the type performed on the E = O; R = Me complex.[22] This earlier study showed exchange broadening of the equatorial CO environments accompanying the metal fluxion, which lent support to an associative mechanism involving pairwise breaking and making of both metal coordinate bonds in a "windscreen wiper" or "tick-tock twist" process.[3] It would be surprising if the same mechanism was not operating in the present complexes

Experimental Section

Materials: The carboxamide ligands, *N*,*N*-dimethyl-2-pyridinecarboxamide (dmpc), *N*,*N*,*N*′,*N*′-tetramethyl-2,6-pyridinedicarboxamide (tmpdc) and *N*,*N*,*N*′,*N*′-tetraethyl-2,6-pyridinedicarboxamide (tepdc) were prepared by adapting literature methods.[8][24] The thioamides *N*,*N*-dimethyl-2-pyridinethioamide (dmpt), *N*,*N*,*N*′,*N*′-tetramethyl-2,6-pyridinedithioamide (tmpdt) and *N*,*N*,*N*′,*N*′-tetraethyl-2,6-pyridinedithioamide (tepdt) were prepared by treating the corresponding carboxamide with Lawesson′s reagent.[25]

Measurements: Elemental analyses were carried out by Butterworth Laboratories Ltd., Teddington, Middlesex, UK. − Melting temperatures were recorded on a Gallenkamp apparatus and are uncorrected. Infrared spectra were measured with a Nicolet Magna FT-IR instrument. − ^1H NMR spectra were recorded on a Bruker DRX400 instrument operating at 400.13 MHz. A standard B-VT2000 variable temperature unit was used to control the probe temperature, the calibration of this unit being checked periodically against a Comark digital thermometer. The temperatures are considered to be accurate to ±1 °C. Rate data were derived from band-shape analysis of the ^1H spectra using a version of the DNMR3 program,[26] or from 2D-EXSY spectra using volume integration data in the authors D2DNMR program.[27] − Activation parameters based on experimental rate data were calculated using the THERMO program.[28] − Two-dimensional exchange (EXSY) spectra were obtained using the standard Bruker program NOESY-PH.AU.

Synthesis of Complexes: All preparations were carried out using standard Schlenk techniques under purified nitrogen using freshly distilled and degassed solvents. Synthetic and analytical data are given in Table 1. The preparation of the complex [$ReBr(CO)_3$(dmpc)] is described by way of illustration.

Bromotricarbonyl(*N*,*N*-dimethyl-2-pyridinecarboxamide)rhenium(I): The compounds [$ReBr(CO)_5$] (0.23 g, 0.57 mmol) and dmpc (0.1 g, 0.67 mmol) were dissolved in benzene (15 cm^3) with gentle warming to produce a colourless solution. The solution was heated under reflux for 4 h and then hexane (20 cm^3) was added to the hot solution. After allowing the solution to stand at ambient temperature for 9 h the solvent was decanted off and the yellow solid washed with hexane (3 × 20 cm^3). The sample was then dried in vacuum for 7 h. Yield 0.27 g (93%).

Acknowledgments

The work carried out by one of us (D.K.V.) was in conjunction with the ERASMUS exchange scheme.

[1] E. W. Abel, K. G. Orrell, A. G. Osborne, H. M. Pain, V. Šik, M. B. Hursthouse, K. M. A. Malik, *J. Chem. Soc., Dalton Trans.* **1994**, 3441−3449, and refs. therein.
[2] M. A. M. Gąrcia, A. Gelling, D. R. Noble, K. G. Orrell, A. G. Osborne, V. Šik, *Polyhedron* **1996**, *15*, 371−379.
[3] A. Gelling, K. G. Orrell, A. G. Osborne, V. Šik, *J. Chem. Soc., Dalton Trans.* **1998**, 937−945.
[4] A. Gelling, M. D. Olsen, K. G. Orrell, A. G. Osborne, V. Šik, *Inorg. Chim. Acta* **1997**, *264*, 257−268.
[5] F. Renaud, C. Piguet, G. Bernardinelli, J-C. G. Bunzli, G. Hopfgartner, *Chem. Eur. J.* **1997**, *3*, 1646−1659.
[6] R. Jagannathan, S. Soundararajan, *Indian J. Chem*. **1979**, *18A,* 319−321.
[7] J. G. H. du Preez, B. J. A. M. van Brecht, *Inorg. Chim. Acta* **1989**, *162*, 49−56.
[8] J. Garcia-Lozano, M. A. Martinez-Lorente, E. Escrivá, R. Ballesteros, *Synth. React. Inorg. Met. Org. Chem*. **1994**, *24*, 365−376.
[9] J. Garcia-Lozano, L. Soto, J-V. Folgado, E. Escrivá, J-P. Legras, *Polyhedron* **1996**, *15*, 4003−4009.
[10] J. C. Jeffrey, T. B. Rauchfuss, *Inorg. Chem*. **1979**, *18*, 2658−2666.
[11] C. S. Slone, D. A. Weinberger, C. A. Mirkin, *Prog. Inorg. Chem*. **1999**, *48*, 233−350.
[12] F. G. Riddell, D. A. R. Williams, *J. Chem. Soc., Perkin Trans. II* **1973**, 587−588.
[13] R. Willem, *Prog. Nucl. Magn. Reson. Spectrosc.* **1987**, 20, 1−94.
[14] K. G. Orrell, *Prog. Nucl. Magn. Reson. Spectrosc*. **1990**, *22*, 141−208.
[15] C. L. Perrin, T. J. Dwyer, *Chem. Rev.* **1990**, *90*, 935−967.
[16] E. Buhleier, W. Wehner, F. Voegtle, *Chem. Ber*. **1979**, *112,* 559−566.
[17] L. M. Jackman, T. E. Kavanagh, R. C. Haddon, *Org. Magn. Reson*. **1969**, *1*, 109−123.
[18] G. Schwenker, H. Rosswag, *Tetrahedron Lett*. **1967**, 4237−4238.
[19] R. C. Neuman, Jr., D. N. Roark, V. Jonas, *J. Am. Chem. Soc.* **1967**, *89*, 3412−3416.
[20] D. Lauvergnat, P. C. Hiberty, *J. Am. Chem. Soc*. **1997**, *119*, 9478−9482.
[21] Y. K. Choe, G. I. Song, Y. S. Choi, C. J. Yoon, *Bull. Korean Chem. Soc*. **1997**, *18*, 1094−1099.
[22] K. G. Orrell, A. G. Osborne, V. Šik, M. Webba da Silva, *Polyhedron* **1995**, *14*, 2797−2802.
[23] M. L. Creber, K. G. Orrell, A. G. Osborne, V. Šik, unpublished work.
[24] H. Brunner, B. Nuber, M. Prommesberger, *J. Organomet. Chem.* **1996**, *523*, 179−185.
[25] S. Scheibye, B. S. Pedersen, S. O. Lawesson, *Bull. Soc. Chim. Belg.* **1978**, *87*, 229−238.
[26] D. A. Kleier, G. Binsch, DNMR3 Program 165, Quantum Chemistry Program Exchange, Indiana Uniyersity, IN, 1970.
[27] E. W. Abel, T. P. J. Coston, K. G. Orrell, V. Šik, D. Stephenson, *J. Magn. Reson*. **1986**, *70*, 34−53.
[28] V. Šik, Ph. D. Thesis, University of Exeter, 1979.

Received August 9, 1999
[I99291]

Substrate-Binding Ligand Approach in Chemical Modeling of Copper-Containing Monooxygenases, 1 Intramolecular Stereoselective Oxygen Atom Insertion into a Non-Activated C–H Bond

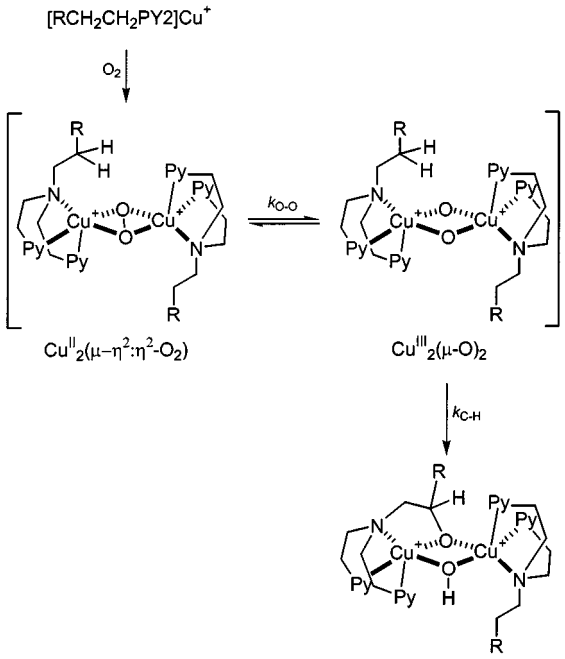
Ingrid Blain,[a] Michel Giorgi,[a] Innocenzo De Riggi,[b] and Marius Réglier*[a]

Keywords: Copper / Oxygenase / Copper–oxygen radical species / RPY2 ligand / Oxygenation

We describe the reactivity of new copper AlkylPY2 type complexes which react with dioxygen and thus hydroxylate an aliphatic C–H bond of the ligand in the same manner as copper-containing monooxygenases.

Introduction

Copper-containing monooxygenases[1] are involved in important biological reactions and copper-dioxygen chemistry has been the subject of important recent investigations.[2] It has been shown that copper(I) coordinated to tridentate ligands {HB(3,5-*i*Pr$_2$pz)$_3$,[3] RPY2,[4,5] P(2,4-*i*Pr$_2$im)$_3$[6] and *i*Pr$_3$tacn[7] leads to $[Cu^{II}_2(\mu\text{-}\eta^2\text{:}\eta^2\text{-}O_2)]^{2+}$ species upon reaction with dioxygen. More recently, Tolman et al.[8] reported that these species can exist in equilibrium with a bis(μ-oxo)dicopper species in a formal $[Cu^{III}_2(\mu\text{-}O)_2]^{2+}$ oxidation state. Whereas the structure of these copper-dioxygen adducts is now well documented, few examples of exogenous substrate oxidation mediated by these species are known.[4] In some cases, these peroxo species are capable of inserting an oxygen atom into a C−H bond of the ligand.[5−7,9,10] Taking advantage of this behavior, we described in previous papers,[10] the *substrate-binding ligand approach*, which involves the study of copper complexes derived from RPY2-type ligands. In these compounds a substrate is covalently bound to the ligand′s tertiary amino group in such a way that an intramolecular oxygen-atom transfer from the copper center to the ligand is favored. The chemio-, regio- and stereoselectivities of the oxygen atom transfer, as revealed by the structure of the hydroxylated ligands, are used to gain more information on the nature of the hydroxylating species and the exact oxidation mechanism. When using such complexes, benzylic hydroxylation (DBH functional model)[5,10c] and hydroxylation at the α-position of the amido group (PHM functional model)[10a] were described. Herein, we report the reactions of a new RPY2 ligand in which we chose to attach a propyl or cyclopentyl group as the substrate in order to find out if copper-oxygen species are capable of inserting an oxygen atom into a nonactivated C−H bond.



Scheme 1. Substrate-binding ligand approach

Results and Discussion

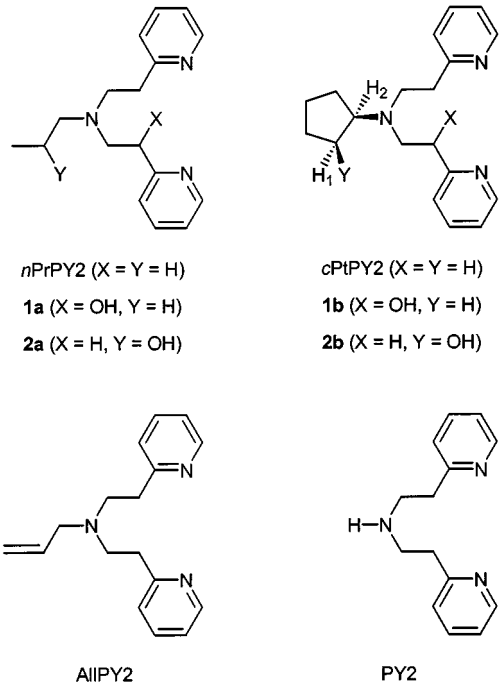
The new RPY2 ligands were synthesized from simple organic reactions. Thus, Michael addition of primary amines to freshly distilled 2-vinyl pyridine in a methanol/acetic acid mixture yielded the ligands *n*PrPY2 and *c*PtPY2. The copper(II) complexes [*n*PrPY2]Cu(OTf)$_2$ and [*c*PtPY2]Cu(OTf)$_2$ (OTf = OSO_2CF_3) were obtained in methanol in nearly quantitative yields by complexation of the corresponding ligands with Cu(OTf)$_2$. Recrystallization from dichloromethane using the diethyl ether vapor diffusion technique afforded blue crystals of [*n*PrPY2]Cu(OTf)$_2$ which were suitable for an X-ray diffraction analysis (Table 1, Figure 1).

[a] Chimie, Biologie et Radicaux Libres, UMR-CNRS 6517, case 432, Universités d'Aix-Marseille 1 et 3, Faculté des Sciences et Techniques de Saint Jérôme,
av. Escadrille Normandie-Niemen, F-13397 Marseille Cedex 20, France
Fax: (internat.) + 33-4/9198-3208
E-mail: marius.reglier@lbs.u-3mrs.fr
[b] ENSSPICAM, Université d′Aix-Marseille 3, Faculté des Sciences et Techniques de Saint Jérôme,
av. Escadrille Normandie-Niemen, F-13397 Marseille Cedex 20, France

 © WILEY-VCH Verlag GmbH, D-69451 Weinheim, 2000 1434−1948/00/0202−393 $ 17.50+.50/0

Table 1. Crystallographic data for [*n*PrPY2]Cu(OTf)$_2$·2H$_2$O

Crystal data	
Formula	$C_{19}H_{27}CuF_6N_3O_8S_2$
M_r	667.09
Crystal system	monoclinic
Space group	$P2_1/n$
a [Å]	8.899(1)
b [Å]	13.726(1)
c [Å]	22.980(1)
α [°]	90.000(1)
β [°]	100.598(1)
γ [°]	90.000(1)
V [Å^3]	2759.1(6)
D_{calc} [g cm^{-3}]	1.62
Z	4
F(000) [e]	1180
μ (Mo-K_α) [$^{-1}$]	10.299
Data collection	
T [K]	298
Scan mode	
ϕ scans	
Scan width [°]	2
$2\theta_{max}$ [°]	50−82
Measured refl.	5455
Unique refl.	5265
Refl. used for ref.	3321
Absorption correction	none
Extinction correction	none
Structure refinement	
Ref. parameters	418
H atoms	included not refined
R	0.047
R_w	0.054
w	$1/[\sigma^2F_0 + 0.03F_0^2]$
(shift/e.s.d.)$_{max}$	0.0653
Goodness of fit	1.783
$\Delta\rho_{fin}$(max/min) [eÅ^{-3}]	0.55/ −0.59



Scheme 2

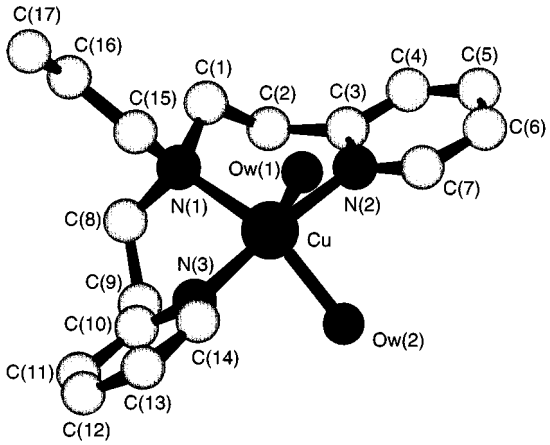


Figure 1. Perspective view of the copper(II) complex [*n*PrPY2]-Cu(OTf)$_2$ emphasizing the central coordination sphere; selected bond distances (Å): Cu−Ow(1), 2.224 (3), Cu−Ow(2), 2.045 (3), Cu−N(1), 2.088 (3), Cu−N(2), 1.994 (3), Cu−N(3), 1.990 (4); bond angles (°): Ow(1)−Cu−Ow(2), 102.8 (1), Ow(1)−Cu−N(2), 86.9 (2), Ow(1)−Cu−N(1), 106.8 (2), Ow(1)−Cu−N(3), 93.5 (2), Ow(2)−Cu−N(2), 87.8 (2), Ow(2)−Cu−N(1), 150.2 (2), Ow(2)−-Cu−N(3), 86.4 (2), N(2)−Cu−N(1), 96.4 (2), N(2)−Cu−N(3), 174.1 (2), N(1)−Cu−N(3), 89.1 (2).

The copper complex [*n*PrPY2]CuPF$_6$, was prepared in situ by interaction (under argon) of the corresponding ligand *n*PrPY2 with 1 equiv. of $(CH_3CN)_4CuPF_6$ in degassed dichloromethane. When it was placed in a dioxygen atmosphere the clear yellow solution rapidly turned green and a copper(II) complex was obtained. Demetallation with 35% aqueous ammonia and analysis of the organic products indicated the complete recovery of the starting ligand *n*PrPY2 with no products resulting from an oxygen-atom transfer to the ligand. More interesting were the results obtained by treatment of [*n*PrPY2]Cu(OTf)$_2$ with 2 equiv. of benzoin/NEt$_3$ in dichloromethane at 25°C. Under argon, reduction to a copper(I) state by 2 equiv. of benzoin/NEt$_3$ occurred in less than two hours. After exposure to a dioxygen atmosphere for 18 hours and demetallation with 35% aqueous ammonia, analysis of the organic products indicated the presence of compounds **1a**, **2a** and AllPY2 in addition to recovered ligand *n*PrPY2 and small amounts of secondary amine PY2 resulting from an *N*-dealkylation reaction (Table 2, entry 2).[11] A thorough analysis of the spectral data indicated that the main product **1a** was the result of hydroxylation at the benzylic position of one pyridine ring. This is clearly evident from the ^{13}C NMR spectra which show the splitting of all pyridine signals and the appearance of two new signals at δ = 61.5 and 70.8, attributable to the N−*C*H$_2$−*C*HOH−pyr sequence, and from the ^{1}H NMR spectra which show a doublet of doublets at δ = 4.75 corresponding to N−CH$_2$−C*H*OH−pyr. Compound **2a** as revealed by NMR analysis and confirmed by comparison with an authentic sample was the result of a β-hydroxylation of the *n*-propyl group.[12]

In order to study the stereoselectivity of the oxygen-atom transfer to the alkyl part of the ligand, we then studied the reactivity of *c*PtPY2-derived copper complexes. As already mentioned for [*n*PrPY2]CuPF$_6$, we did not observe any hydroxylation products by reaction of [*c*PtPY2]CuPF$_6$, prepared in situ, with dioxygen. However two equiv. of

Table 2. Reactions of [RPY2]Cu(OTf)$_2$ complexes with O_2/Benzoin/NEt_3 in CH_2Cl_2

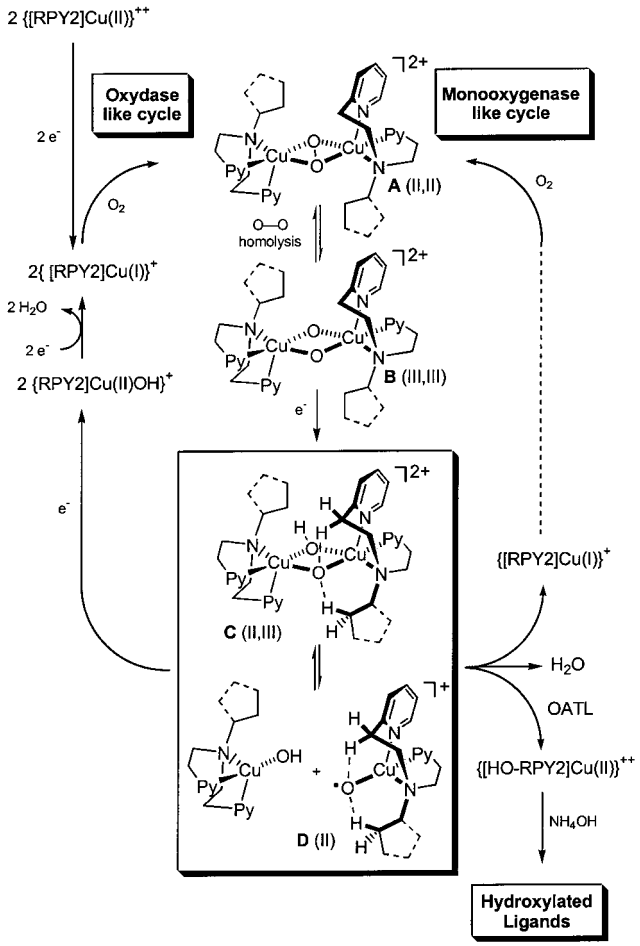
Entries	Ligands	Ratios Cu/Benzoin/NEt_3	Product Distributions[a]
1	*n*PrPY2	1/0/2	*n*PrPY2 (98%) + PY2 (2%)
2	*n*PrPY2	1/2/2	*n*PrPY2 (44%) + **1a** (37%) + **2a** (8%) + AllPY2 (2%) + PY2 (9%)
3	*n*PrPY2	1/2/4	*n*PrPY2 (37%) + **1a** (36%) + **2a** (6%) + AllPY2 (3%) + PY2 (18%)
4	*n*PrPY2	1/4/4	**1a** (64%) + **2a** (10%) + AllPY2 (6%) + PY2 (12%)
5	*c*PtPY2	1/2/2	*c*PtPY2 (35%) + **1b** (42%) + **2b** (13%) + PY2 (5%)

[a] Determined by HPLC (Ultrasphere C18 column, Beckmann) using H_2O/CH_3CN 90/10 containing 1% TFA as mobile phase, detection at 270 nm using diode array detector.

benzoin/NEt_3 in dichloromethane at 25°C transformed [*c*PtPY2]Cu(OTf)$_2$ into the hydroxylated compounds **1b** and **2b** (Table 2, entry 5). Compound **1b**, which showed the same spectroscopic features as **1a** (^{13}C NMR: splitting of all pyridine signals and appearance of two new signals at $\delta = 71$ and 59; ^{1}H NMR: dd at $\delta = 4.76$), was the result of a hydroxylation at a benzylic position. An NMR structural analysis of compound **2b** revealed that it was the result of a β-*cis* hydroxylation of the cyclopentane ring. The *cis* stereochemistry could be assigned by a two dimensional NOESY sequence showing a Nuclear Overhauser Effect (NOE) between protons H-2 and H-1.[13]

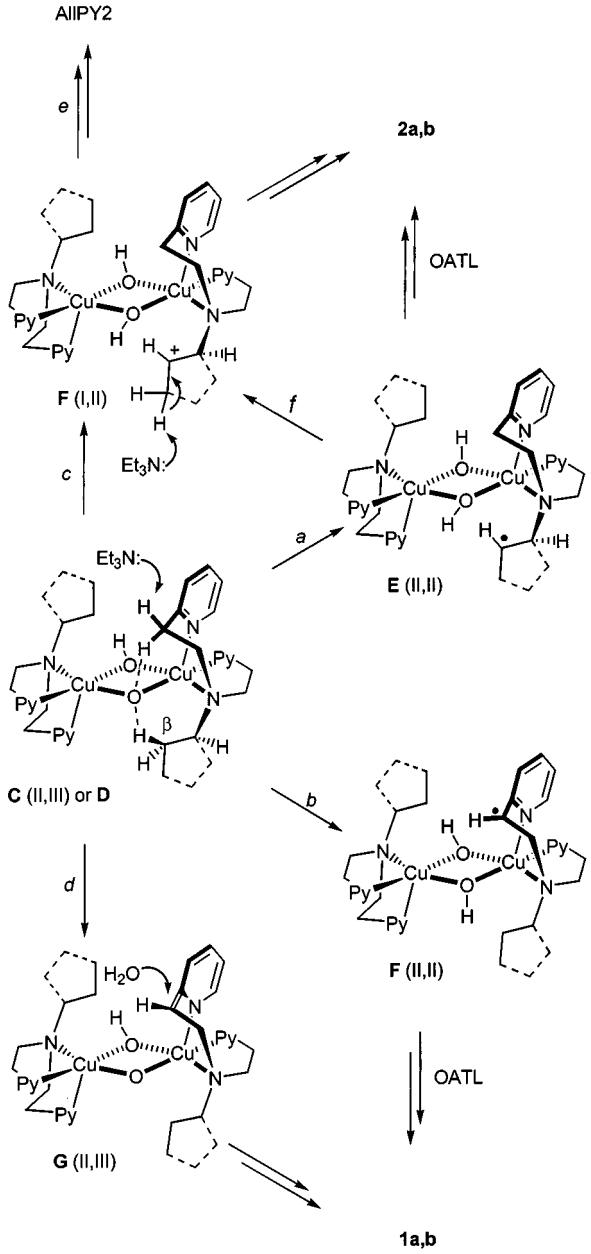
In one of our previous papers the higher deuterium kinetic isotope effect observed for reaction of [IndPY2]CuPF$_6$/O_2 relative to that of [IndPY2]Cu(OTf)$_2$/benzoin/NEt_3/O_2 (11 vs. 7.6) was rationalized as being due to the occurrence of two different copper-oxygen intermediates.[10c] The absence of Oxygen Atom Transfer to the Ligand (OATL) during the reaction of [RPY2]CuPF$_6$ with dioxygen confirms this suggestion. At this time it is difficult to provide any evidence for the oxygenated copper species responsible for the hydroxylation. Nevertheless, on the basis of the observed products we can formulate several hypotheses concerning the structure of the active oxygen species. Itho,[5] and more recently Karlin,[4a] with [PhenPY2]CuPF$_6$ and [MePY2]CuPF$_6$ complexes, respectively, have shown that such complexes lead to $\{[RPY2]Cu^{II}_2(\mu\text{-}\eta^2\text{:}\eta^2\text{-}O_2)\}^{2+}$ by oxygenation, and that a homolytic cleavage of the peroxy bond occurs (at least partially) to give, in the first step of the reaction, a $\{[RPY2]Cu^{III}_2(\mu\text{-}O_2)\}^{2+}$ species (Scheme 3). In this context, it is reasonable to assume the formation of species **A** and/or **B** upon reaction with dioxygen (Scheme 3). Except with complexes derived from PhenPY2 and IndPY2 ligands where activated benzylic hydrogen are present, such species do not transfer an oxygen atom to the AlkylPY2 ligand. In a recent study on pMMO, Chan et al. proposed that a $Cu^{III}_2(\mu\text{-}O_2)^{2+}$ species is not reactive enough to abstract a hydrogen atom from methane.[1d] Nevertheless, these authors suggested that transfer of an additional electron, probably from another copper atom, and the occurrence of the mixed valence $Cu^{II}Cu^{III}(\mu\text{-}O_2)^{2+}$ species,[14] may enhance the reactivity of the copper-oxygen core. This hypothesis is very attractive for the hydroxylation of complexes derived from an AlkylPY2 ligand, which only occurs when benzoin is present. Thus, we propose that benzoin acts in the monoelectronic reduction of **A** and/or **B** to give a mixed valence species **C** which, as suggested by Chan, could be active in transferring one oxygen atom to the ligand to give $\{[HORPY2]Cu^{II}\}^{2+}$. This process is accompanied by the formation of a copper(I) complex, which can participate again after reaction with dioxygen in a monooxygenase-like cycle.[15] According to this mechanism, the transformation of copper(II) complexes [RPY2]Cu(OTf)$_2$ in such a cycle needs two electrons (one equiv. of benzoin). We observed that the transformation of the original copper(II) complexes into the observed products consumed a four-fold excess of benzoin (Table 2, entry 4). Benzoin is a strong reducing agent that can participate in a second electron addition to **C** (and/or **D**) in a competitive reaction to give a different copper(II) species which is unreactive in the hydroxylation reaction (oxydase like cycle). The two competitive processes (oxydase vs. monooxygenase) may explain why the complete transformation of [RPY2]Cu(OTf)$_2$ needs more than one equiv. of benzoin.

The OATL mechanism needs some comments. Scheme 4 illustrates possible pathways whereby hydroxylation can occur *via* the dimeric species **C** (or monomer **D**). The first explanation for the formation of **1a** or **1b** is to consider that the electrophilic Cu^{III} core in **B** (or **C**) increases the acidity of the benzylic hydrogen of pyridine, thus facilitating the deprotonation with triethylamine (path *d*). This mechanism can be dismissed as increasing the amount of triethylamine did not increase the amount of **1a** in the [nPrPY2]Cu(OTf)$_2$/Benzoin/O_2 reaction (Table 2, entry 3). From our results two observations are in favor of a mechanism occurring in the coordination sphere of the copper core: (1) hydroxylation exclusively in the β position of the tertiary amino group, and (2) exclusive *cis* hydroxylation of the aminocyclopentane moieties of [*c*PtPY2]Cu(OTf)$_2$. While we cannot definitively exclude a concerted mechanism, several examples in the literature are in favor of a two step mechanism where the abstraction of a β hydrogen atom occurs in the partially rate determining step. Since AllPY2 is not the result of the dehydration of a copper(II) complex of [**2a**],[16] the isolation of AllPY2 can be considered as being indicative of a two-step mechanism where a carbenium ion is formed. The question which arises now is to know if this intermediate is formed directly by abstraction of a H^- by an electrophilic oxygen (path *c*) or by oxidation of the radical **E** (path *f*). At the moment, it is difficult to answer this fundamental question. More experiments are needed, notably using a radical clock fixed on the tertiary amino group



Scheme 3. Oxydase *vs.* monooxygenase-like cycles

of the ligand. However, initial radical formation from a hydrogen atom abstraction by the Cu−O core seems to be more reasonable since Mayer has recently shown that metal-oxo complexes oxidize hydrocarbons by a hydrogen-atom abstraction mechanism which is attributed to their thermodynamic affinity for a hydrogen atom (≡ $H^+ + e^-$).[17]



Scheme 4. Mechanism proposed for β-hydroxylations

Conclusion

While benzylic hydroxylation is the easier process, we have now demonstrated that copper-oxygen species are able to functionalise aliphatic C−H bonds probably *via* a two-step process. Once again, it is possible to show that the substrate binding ligand approach gives valuable information about the active species involved in the copper-dioxygen activation. This organic chemistry approach is complementary to that of inorganic chemists who are more interested in the structural study of copper-oxygen species

Experimental Section

General: Solvents were freshly distilled under argon: MeOH from Mg, Et_2O from sodium benzophenone ketyl and CH_2Cl_2 from P_2O_5. Deoxygenation of solvents and solutions was carried out by three vacuum/purge cycles. Standard Schlenk techniques were used in the preparation and handling of air-sensitive compounds. Commercial starting materials were used without further purification, except for 2-vinylpyridine, which was distilled prior to use. NMR spectra were recorded on Bruker AC-200 or AMX-400 spectrometers. Chemical shifts are reported in ppm as δ values downfield from an internal standard (TMS). Elemental analyses were obtained on a CHN Technicon microanalyser.

RPY2: To absolute MeOH were added freshly distilled 2-vinylpyridine, the primary amine and acetic acid. After refluxing for 2−5 days, MeOH and the excess 2-vinylpyridine were evaporated under vacuum. The crude product was dissolved in CH_2Cl_2, washed with a saturated solution of $NaHCO_3$ and dried over Na_2SO_4. Evaporation of CH_2Cl_2 under reduced pressure (18 Torr) and flash chro-

matography (Silica gel, CH_2Cl_2/MeOH 85/15) afforded ligands RPY2.

***n*PrPY2:** Yield: 610 mg (2.3 mmol, 38%) [from *n*-propylamine (354 mg, 6 mmol), 2-vinylpyridine (3.88 mL, 36 mmol), CH_3COOH (420 mL, 7.5 mmol), MeOH (8 mL), 2 day reflux]. − ^{1}H NMR (200 MHz, $CDCl_3$): δ = 0.83 (t, *J* = 7.5 Hz, 3 H), 1.52 (hex, *J* = 7.5 Hz, 2 H), 2.63−2.56 (m, 2 H), 3.00 (s, 8 H), 7.16−7.07 (m, 4 H), 7.57 (td, *J* = 7.5 and 1.7 Hz, 2 H), 8.51 (ddd, *J* = 4.8, 1.7 and 1 Hz, 2 H). − ^{13}C NMR (50.32 MHz, $CDCl_3$): δ = 11.47 (CH_3), 19.64 (CH_2), 34.99 (CH_2), 53.48 (CH_2), 55.46 (CH_2), 120.96 (CH), 123.18 (CH), 136.10 (CH), 148.82 (CH), and 159.86 (C).

***c*PtPY2:** Yield: 1.18 g (4 mmol, 40%) [*c*-pentylamine (850 mg, 10 mmol), 2-vinylpyridine (10 mL, 0.1 mol), CH_3COOH (2.3 mL, 40 mmol), MeOH (10 mL), 5 day reflux]. − ^{1}H NMR (200 MHz, $CDCl_3$): δ = 1.32−1.74 (m, 6 H), 1.75−1.85 (m, 2 H), 2.90−3.10 (m, 9 H), 7.00−7.10 (m, 4 H), 7.52 (td, *J* = 7.7 and 1.8 Hz, 2 H), 8.46 (dd, *J* = 4.8 and 0.9 Hz, 2 H). − ^{13}C NMR (50.32 MHz, $CDCl_3$): δ = 23.93 (CH_2), 30.10 (CH_2), 35.71 (CH_2), 51.80 (CH_2), 63.71 (CH), 121.11 (CH), 123.38 (CH), 136.27 (CH), 149.13 (CH), and 160.70 (C).

[RPY2]Cu(OTf)$_2$: To a solution of $Cu(OTf)_2$ (694 mg, 1.9 mmol) in CH_2Cl_2 (5 mL) was added dropwise a solution of ligand RPY2 (1.9 mmol) in CH_2Cl_2 (5 mL). The mixture was allowed to stir for 2 h, and Et_2O was added until precipitation. The precipitate obtained was centrifuged, washed with Et_2O and dried in vacuo to give [RPY2]Cu(OTf)$_2$.

[*n*PrPY2]Cu(OTf)$_2$: blue solid. − Yield: 1.10 g (1.66 mmol, 87%) − $C_{19}H_{23}CuF_6N_3O_6S_2$ (631.06): calcd. C 36.16, H 3.67, N 6.66; found C 35.16, H 3.88, N 6.47.

[*c*PtPY2]Cu(OTf)$_2$: blue solid. − Yield 1.23 g (1.78 mmol, 94%) − $C_{21}H_{25}CuF_6N_3O_6S_2$ (657.10): calcd. C 38.39, H 3.83, N 6.39; found C 37.36, H 4.03, N 6.22.

Oxidation of [RPY2]CuPF$_6$ With O$_2$: To a solution of $[CH_3CN]_4CuPF_6$ (0.1 mmol) in degassed CH_2Cl_2 (50 mL), was added dropwise a solution of RPY2 (0.1 mmol) in CH_2Cl_2 (50 mL). The mixture was stirred under argon for 1 h, and then exposed to an O_2 atmosphere for 24 h. The CH_2Cl_2 was subsequently evaporated in vacuo, Et_2O (50 mL) was added, and the precipitate thus obtained was filtered off, washed with Et_2O, and dried in vacuo to give a mixture of copper(II) complexes. This mixture was dissolved in CH_2Cl_2 (20 mL), washed with 35% NH_4OH (5 mL) and brine (3 × 5 mL), and dried over Na_2SO_4. Evaporation of the CH_2Cl_2 under reduced pressure (18 Torr) gave the crude product. Flash chromatography (SiO_2, CH_2Cl_2/MeOH, 90:10) afforded the recovered ligands RPY2.

Oxidation of [RPY2]Cu(OTf)$_2$ With O$_2$ in the Presence of Benzoin: To a solution of [RPY2]Cu(OTf)$_2$ in degassed CH_2Cl_2 were added benzoin (1 equiv.) and NEt_3 (1 equiv.). This mixture was stirred under argon for 2 h and then exposed to an O_2 atmosphere for 24 h. The CH_2Cl_2 was subsequently evaporated in vacuo and Et_2O was added. The precipitate thus obtained was filtered off, washed with Et_2O, dissolved in CH_2Cl_2, washed with 35% NH_4OH and brine, and dried over Na_2SO_4. Evaporation of the CH_2Cl_2 under reduced pressure (18 Torr) gave a mixture of recovered ligands RPY2 and compounds **1a**,**b**, **2a**,**b** and AllPY2 which were separated by flash chromatography (SiO_2, CH_2Cl_2/MeOH, 90:10).

1a: ^{1}H NMR (200 MHz, $CDCl_3$): δ = 0.75 (t, *J* = 7 Hz, 3 H), 1.4 (m, 2 H), 2.4−2.7 (m, 3 H), 3.1−2.85 (m, 5 H), 4.75 (dd, *J* = 9 and 3.4 Hz, 1 H), 6.95 (d, *J* = 7.5 Hz, 1 H), 7.2−7.05 (m, 4 H,), 7.4−7.7 (m, 3 H), 8.50 (m, 2 H). − ^{13}C NMR (50.32 MHz, $CDCl_3$): δ = 11.6 (CH_3), 20.0 (CH_2), 35.6 (CH_2), 54.1 (CH_2), 56.2 (CH_2), 61.5 (CH_2), 70.8 (CH), 121.4 (CH), 120.5 (CH), 123.4 (CH), 122.2 (CH), 136.7 (CH), 136.6 (CH), 149.1 (CH), 148.6 (CH), 162.1 (C), 160.2 (C).

1b: ^{1}H NMR (200 MHz, $CDCl_3$): δ = 1.20−1.80 (m, 8 H), 2.60 (dd, *J* = 13 and 10 Hz, 1 H), 2.90−3.08 (m, 5 H), 3.14−3.32 (m, 1 H), 4.76 (dd, *J* = 10 and 3 Hz, 1 H), 7.05−7.20 (m, 3 H), 7.50−7.72 (m, 3 H), 8.50 (m, 2 H). − ^{13}C NMR (50.32 MHz, $CDCl_3$): δ = 29.8 (CH_2), 27.6 (CH_2), 24.0 (CH_2), 23.9 (CH_2), 36.2 (CH_2), 52.3 (CH_2), 59.0 (CH_2), 63.5 (CH), 71.0 (CH), 121.3 (CH), 120.4 (CH), 123.4 (CH), 122.2 (CH), 136.7 (CH), 136.5 (CH), 149.0 (CH), 148.6 (CH), 162.4 (C), 160.3 (C).

2a: ^{1}H NMR (200 MHz, $CDCl_3$): δ = 1.08 (d, *J* = 6.2 Hz, 3 H), 2.35 (dd, *J* = 12.9 and 9.9 Hz, 1 H), 2.48 (dd, *J* = 12.9 and 3.1 Hz, 1 H), 2.70−3.10 (m, 8 H), 3.66 (dqd, *J* = 9.9, 6.2 and 3.1 Hz, 1 H), 4.09 (br. s, 1 H), 6.97 (d, *J* = 7.5 Hz, 2 H), 7.07 (ddd, *J* = 7.5, 5.1 and 1.0 Hz, 2 H), 7.51 (td, *J* = 7.5 and 1.7 Hz, 2 H), 8.48 (ddd, *J* = 5.1, 1.7 and 1.0 Hz, 2 H). − ^{13}C NMR (50.32 MHz, $CDCl_3$): δ = 19.5 (CH_3), 35.6 (CH_2), 53.9 (CH_2), 62.1 (CH_2), 63.5 (CH), 120.8 (CH), 123.9 (CH), 135.9 (CH), 148.7 (CH), 160.0 (C).

2b: ^{1}H NMR (200 MHz, $CDCl_3$): δ = 1.53−1.62 (m, 1 H), 1.78−1.90 (m, 4 H), 1.95 (br. t, *J* = 10 Hz, 1 H), 3.05−3.19 (m, 4 H), 3.23 (br. s, 1 H), 3.41−3.50 (m, 4 H), 4.35 (br. s, 1 H), 7.10 (ddd, *J* = 8, 5 and 2 Hz, 2 H), 7.58 (td, *J* = 8 and 2 Hz, 2 H), 7.16 (d, *J* = 8 Hz, 2 H), 8.38 (br. d, *J* = 5 Hz, 2 H). − ^{13}C NMR (50.32 MHz, $CDCl_3$): δ = 20.7 (CH_2), 26.6 (CH_2), 31.8 (CH_2), 32.5 (CH_2), 68.3 (CH), 51.0 (CH_2), 70.4 (CH), 121.9 (CH), 123.7 (CH), 137.0 (CH), 149.0 (CH), 158.5 (C). Two-dimensional NMR experiments were carried out on an AMX Bruker 400 MHz spectrometer. COSY gradient, HMQC and HMBC experiments were performed with 5 mm inverse broadband probehead incorporating a shielded z-gradient coil. These correlations allowed the total assignment of all the protons and carbon atoms of the compound **3b**. A 5 mm DUAL ^{1}H/^{13}C probehead was used to acquire the 2D phase-sensitive NOESY data.

AllPY2: ^{1}H NMR (200 MHz, $CDCl_3$): δ = 2.90 (br. s, 8 H), 3.25 (d, *J* = 6 Hz, 2 H), 5.10 (br. d, *J* = 10 Hz, 1 H), 5.18 (br. d, *J* = 17 Hz, 1 H), 5.80 (ddt, *J* = 17, 10 and 6 Hz, 1 H), 7.10−6.90 (m, 4 H), 7.50 (td, *J* = 8 and 2 Hz, 2 H), 8.50 (dt, *J* = 5 and 1 Hz, 2 H). − ^{13}C NMR (50.32 MHz, $CDCl_3$): δ = 35.7 (CH_2), 53.3 (CH_2), 58.8 (CH_2), 116.9 (CH_2), 120.7 (CH), 123.0 (CH), 135.5 (CH), 135.8 (CH), 146.8 (CH), 160.3 (C).

X-ray Structure Analysis: Crystal data for [*n*PrPY2]Cu(OTf)2 together with details of the X-ray diffraction experiment, are reported in Table 1. Crystallographic data for the structure reported in this paper has been deposited at the Cambridge Crystallographic Data Center as supplementary publication no. CCDC 113535. Copies of the data can be obtained free of charge on application to The Director, CCDC, 12 Union Road, Cambridge CB2 1EZ, UK [Fax: (internat.) + 44-1223/336-033, E-mail: deposit@ccdc.cam.ac. uk].

Acknowledgments

This research was supported by the CNRS and the French Ministry of Universities. The authors are grateful to Dr. A. Heumann for a number of enlightening discussions.

[1] [1a] General references on copper-containing enzymes: J. P. Klinman, *Chem. Rev.* **1996**, *96*, 2541−2561; W. Kaim. J. Rall, *Angew. Chem.* **1996**, *108*, 47−64; *Angew. Chem. Int. Ed. Engl.* **1996**, *35*, 43−60. − [1b] Dopamine β-hydroxylase (DBH),

benzylic hydroxylation of dopamine into noradrenaline: L. C. Stewart, J. P. Klinman, *Ann. Rev. Biochem.* **1988**, *57*, 551−592. − [1c] Peptidylglycine α-hydroxylating monooxygenase (PHM), neuropeptide amidation: S. T. Pridge, A. S. Kolhenar, B. A. Eipper, R. E. Mains, L. M. Amzel, *Science* **1997**, *278*, 1300−1305. − [1d] Particulate methane monooxygenase (pMMO), methane hydroxylation into methanol: S. J. Eliot, M. Zhu, L. Tso, H.-H. T. Nguyen, J. H.-K. Yip, S. I. Chan, *J. Am. Chem. Soc.* **1997**, *119*, 9949−9955.

[2] [2a] K. D. Karlin, S. Kaderli, A. D. Zuberbühler, *Acc. Chem. Res.* **1997**, *30*, 139−147. − [2b] W. B. Tolman, *Acc. Chem. Res.* **1997**, *30*, 227−237. − [2c] N. Kitajima, Y. Moro-Oka, *Chem. Rev.* **1994**, *94*, 737−757.

[3] N. Kitajima, K. Fujisawa, Y. Moro-Oka, K. Toriumi, *J. Am. Chem. Soc.* **1989**, *111*, 8975−8976.

[4] [4a] H. V. Obias, Y. Lin, N. N. Murthy, E. Pidcock, E. I. Solomon, M. Ralle, N. J. Blackburn, Y.-M. Neuhold, A. D. Zuberbühler, K. D. Karlin, *J. Am. Chem. Soc.* **1998**, *120*, 12960−12961. − [4b] M. A. Lockwood, T. J. Blubaugh. M. Coler, S. Lovell, J. M. Mayer, *Angew. Chem. Int. Ed.* **1999**, *38*, 225−227.

[5] S. Itho, T. Kondo, M. Komatsu, Y. Ohshiro, C. Li, N. Kanehisa, Y. Kai, S. Fukuzumi, *J. Am. Chem. Soc.* **1995**, *117*, 4714−4715; S. Itho, H. Nakao, L. M. Berreau, T. Kondo, M. Komatsu, S. Fukuzumi, *J. Am. Chem. Soc.* **1998**, *120*, 2890−2899.

[6] T. N. Sorrel, W. E. Allen, P. S. White, *Inorg. Chem.* **1995**, *34*, 952−960; W. E. Allen, T. N. Sorrell, *Inorg. Chem.* **1997**, *36*, 1732−1734.

[7] [7a] *S.* Mahapatra, J. A. Halfen, E. C. Wilkinson, L. Que, Jr., W. B. Tolman, *J. Am. Chem. Soc.* **1994**, *116*, 9785−9786. − [7b] S. Mahapatra, J. A. Halfen, E. C. Wilkinson, G. Pan, C. J. Cramer, L. Que Jr., W. B. Tolman, *J. Am. Chem. Soc.* **1995**, *117*, 8865−8866. − [7c] J. A. Halfen, V. G. Young Jr., W. B. Tolman, *J. Am. Chem. Soc.* **1996**, *118*, 10920−10921.

[8] J. A. Halfen, S. Mahapatra, E. C. Wilkinson, S. Kaderli, V. C. Young Jr., L. Que Jr., A. D. Zuberbühler, W. B. Tolman, *Science* **1996**, *271*, 1397−1400; S. Mahapatra, J. A. Halfen, E. C. Wilkinson, G. Pan, X. Wang, V. G. Young Jr., C. J. Cramer, L. Que Jr., W. B. Tolman, *J. Am. Chem. Soc.* **1996**, *118*, 11555−11574; S. Mahapatra, J. A. Halfen, W. B. Tolman, *J. Am. Chem. Soc.* **1996**, *118*, 11575−11586; C. J. Cramer, B. A. Smith, W. B. Tolman, *J. Am. Chem. Soc.* **1996**, *118*, 11283−11287; J. Cahoy, P. L. Holland, W. B. Tolman, *Inorg. Chem.* **1999**, *38*, 2161−2168.

[9] K. D. Karlin, J. C. Hayes, Y. Gultneh, R. W. Cruse, J. W. McKown, J. P. Hutchinson, J. Zubieta, *J. Am. Chem. Soc.* **1984**, *106*, 2121−2128.

[10] [10a] E. Amadéi, E. H. Alilou, F. Eydoux, M. Pierrot, M. Réglier, B. Waegell, *J. Chem. Soc., Chem. Commun.* **1992**, 1782−1784. − [10b] M. Réglier, E. Amadéi, E. H. Alilou, F. Eydoux, M. Pierrot, B. Waegell, *Bioinorganic Chemistry of Copper* (Eds.: K. D. Karlin, Z. Tiecklar), Chapman and Hall, **1993**, pp. 348−362. − [10c] I. Blain, P. Bruno, M. Giorgi, E. Lojou, D. Lexa, M. Réglier, *Eur. J. Inorg. Chem.* **1998**, 1297−1304.

[11] *N*-Dealkylation is a process already observed in the reaction of [BnPY2]$CuPF_6$ with dioxygen: I. Sanyal, M. Mahroof-Tahir, M. S. Nasir, P. Ghosh, Y. Gultneh, R. W. Cruse, A. Farooq, K. D. Karlin, S. Liu, J. Zubieta, *Inorg. Chem.* **1992**, *31*, 4322−4332.

[12] An authentic sample of compound **2a** was obtained by addition of 2-hydroxypropylamine to vinylpyridine in a methanol/acetic acid mixture.

[13] A sample of *trans*-**2b** was obtained by addition of PY2 to cyclopentene oxide and compared to the product obtained by β-hydroxylation.

[14] A. P. Cole, D. E. Root, P. Mukherjee, E. I. Solomon, T. D. P. Stack, *Science* **1996**, *273*, 1848−1850.

[15] Another possibility is to consider the occurrence of a mononuclear $Cu^{II}-O^{\bullet}$ ($\Leftrightarrow Cu^{III}-O^{-}$) species **D** that could result from a dissociation of **C**.

[16] The copper(II) complex of **2a** placed under O_2/Benzoin/NEt_3 does not produce any AllPY2 compound.

[17] [17a] K. Wang, J. M. Mayer, *J. Am. Chem. Soc.* **1997**, *119*, 1470−1471. − [17b] J. M. Mayer, *Acc. Chem. Res.* **1998**, *31*, 441−450.

Received June 4, 1999
[I99203]

Second Coordination Sphere Water Molecules and Relaxivity of Gadolinium(III) Complexes: Implications for MRI Contrast Agents

Mauro Botta[a]

Keywords: Relaxivity / Nuclear magnetic relaxation dispersion / Imaging agents / NMR spectroscopy / MRI contrast agents

Dipolar interaction between the metal ion and proximate water molecules represents an efficient mechanism for solvent relaxation in Gd^{3+} complexes currently employed as MRI contrast agents. Besides *inner sphere* (metal bound) and *outer sphere* hydration molecules, a well-defined second coordination shell may provide an additional mechanism for paramagnetic relaxation leading to a strong enhancement of the relaxivity of the complexes. Through a careful choice of hydrogen-bond-acceptor groups on the ligand we may: (1) promote the formation of a strong interaction; (2) increase the number of water molecules in the second hydration shell; (3) decrease their average distance from the paramagnetic metal center. These possibilities have been explored by considering complexes bearing phosphinate, phosphonate and carboxoamide pendant arms, by exploiting the formation of ion-pairs with cationic substrates and inclusion compounds of these adducts with β-cyclodextrin. Finally, the contribution of this relaxation mechanism to the relaxivity of the commercially available MRI contrast agents is discussed and the NMRD data reevaluated and compared with crystallographic data.

Introduction

The emergence of MRI as an important clinical tool has fostered the development of agents designed to enhance tissue differentiation.[1] These drugs, mainly complexes of Gd^{3+} and Mn^{2+}, are useful for increasing the image contrast between normal and diseased tissue and/or providing dynamic tissue function. Unlike the contrast agents (CAs) used in other clinical imaging studies, these paramagnetic complexes are not themselves directly imaged but rather enhance contrast indirectly by affecting the nuclear magnetic relaxation times of the water protons in surrounding tissues. Because Gd^{3+} has particularly favorable magnetic properties, complexes of this ion have been the primary focus for MRI contrast agent development.[2] The clinically approved CAs are stable, highly water soluble poly(aminocarboxylate) derived complexes (Gd^{3+} complexes with ligands **1–4**, Scheme 1). The requirements to design a practical, general, MRI CA can be summarized as follows:

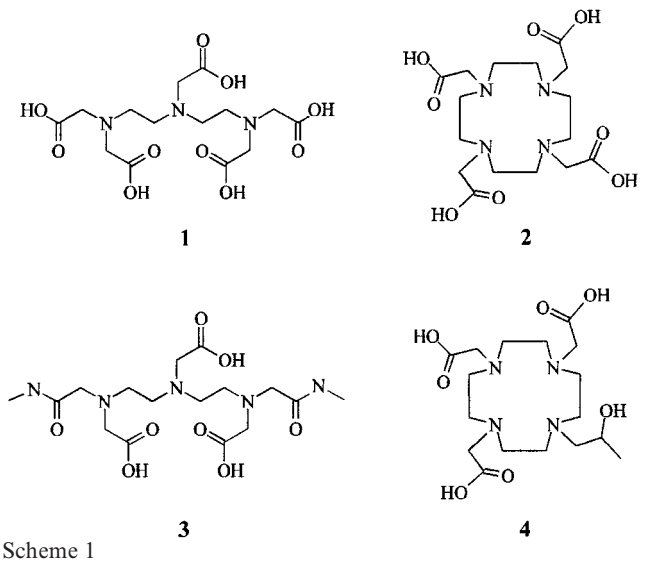
[a] Dipartimento di Scienze e Tecnologie Avanzate, Università del Piemonte Orientale "Amedeo Avogadro",
C.so Borsalino 54, 15100 Alessandria, Italy
Fax: (internat.) + 39-011/670-7524
E-mail: botta@ch.unito.it



Mauro Botta was born in Cuneo in 1958. He studied chemistry at the University of Torino where he received the Laurea degree in 1985. After three years spent as a research assistant in the Department of Chemistry working in the group of Prof. Silvio Aime, he held a tenure of Researcher (1990–1998) at the faculty of Pharmacy of the University of Torino and was nominated associate Professor (1998) at the University of Piemonte Orientale "Amedeo Avogadro." In 1998 he was awarded the Nasini Medal of the Inorganic Chemistry Division of the Italian Chemical Society. His research has mainly focused on the application of NMR spectroscopy to investigate solution and solid state properties of metal carbonyl clusters and coordination complexes for biomedical applications.

MICROREVIEWS: This feature introduces the readers to the authors' research through a concise overview of the selected topic. Reference to important work from others in the field is included.

 © WILEY-VCH Verlag GmbH, D-69451 Weinheim, 2000 1434–1948/00/0303–0399 $ 17.50+.50/0



Scheme 1

(1) *High stability.* The injection of gram amounts of gadolinium into patients presents some potential toxicity problems which requires strong metal complexation by the parent ligand.

(2) *Good water solubility and low osmolality of the solutions used clinically.* Injection of relatively small volumes of a fairly concentrated solutions of the metal complex is required. Neutral complexes have been developed with the goal of lessening the discomfort from injection of high osmolality salt solutions (Gd-**3** and Gd-**4**).

(3) *High relaxivity.* The relaxivity (r_{1p}) is an intrinsic property of a paramagnetic complex that characterize its ability to enhance the nuclear magnetic relaxation rates (R_i, i = 1,2) of nearby protons and is defined as the increase in R_i per millimolar concentration of the CA.[1–3]

The dependence of the relaxivity on structural features of the paramagnetic compounds has represented an important area of research in the field of inorganic chemistry over the last ten years. These studies have made significant contributions towards a rational design of MRI CAs, opened new perspectives in the use of paramagnetic complexes as diagnostic probes and increased our knowledge of the coordination chemistry of lanthanide ions. The general properties of MRI CAs,[1b] the determinants of the relaxivity,[2] the crucial role of the water exchange rate,[4] and the perspectives for attaining high relaxivities[5] have been recently reviewed. Here I will discuss recent results that have allowed us to pinpoint a direct role of the second coordination shell water molecules in determining the relaxivity of the paramagnetic complexes, the strategies used for optimizing this contribution and the implications for the analysis of relaxation data for MRI CAs.

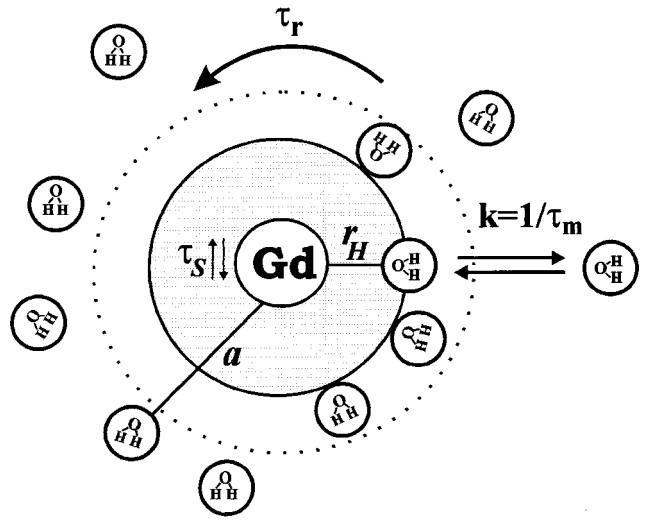


Figure 1. Schematic representation of the three types of hydration layers around a Gd^{3+} complex and the most relevant parameters of paramagnetic relaxation

Relaxivity: Contributions and Parameters

The relaxivity enhancement of water protons in aqueous solutions of Gd^{3+} complexes arises from time fluctuation of the dipolar coupling between the electron magnetic moment of the metal ion and the nuclear magnetic moment of the solvent nuclei.[6] This interaction is traditionally described with a model that considers two contributions (Figure 1): *inner sphere* (*IS*), due to water molecules present in number q in the coordination sites of the Gd^{3+} ion, and *outer sphere* (*OS*), which involves all the solvent molecules diffusing by the complex:

$$R_1^{obs} = R_{1p}^{IS} + R_{1p}^{OS} + R_1^W \quad (1)$$

where R_1^{obs} is the measured relaxation rate and R_1^W the relaxation rate of the solvent in the absence of the paramagnetic complex.

Inner Sphere

This term represents the most important contribution to r_{1p} and thus the efforts towards contrast agents of improved efficacy have been directed mainly towards its optimization. The large number of experimental data recorded over the last 15 years on small Gd^{3+} chelates have been interpreted on the basis of the Solomom-Bloembergen-Morgan approach,[7] and have provided a good understanding of the role played by the different relaxation parameters, of their mutual relationship, and of their dependence on the structural features of the complexes.[1–5,8] The relevant Equations are:

$$R_{1p}^{IS} = \frac{[M]q}{55.6}\frac{1}{T_{1M}+\tau_M} \quad (2)$$

$$\frac{1}{T_{1M}} = \frac{2}{15}\frac{\gamma_H^2 g^2 S(S+1)\beta^2}{r_H^6}\left[\frac{3\tau_{C1}}{1+\omega_H^2\tau_{C1}^2}+\frac{7\tau_{C2}}{1+\omega_S^2\tau_{C2}^2}\right] \quad (3)$$

$$\frac{1}{\tau_{Ci}} = \frac{1}{\tau_R} + \frac{1}{\tau_M} + \frac{1}{\tau_{Si}} \quad (4)$$

where M is the concentration of the CA, T_{1M} the longitudinal relaxation time of the bound water protons, S is the electron spin quantum number (7/2 for Gd^{3+}), γ_H is the proton nuclear magnetogyric ratio, β is the Bohr magneton, g is the Landè factor for the free electron, r_H is the distance between the metal ion and the bound water protons; ω_H and ω_S are the proton and electron Larmor frequencies, respectively, and τ_{Ci} (i = 1,2) are the correlation times of the modulation of the dipolar electron-proton coupling. The overall correlation times τ_{Ci} receive contributions from the reorientation of the paramagnetic species, τ_R, by the residence lifetime of the bound water protons, τ_M and by the electronic relaxation times of the metal ion, τ_S. A marked enhancement of r_{1p} at the magnetic fields currently employed clinically has been obtained primarily by slowing down the molecular tumbling (increasing τ_R) by different approaches.[9–15] However, the expected increase of r_{1p} has not been observed because of the limiting effect of the mean water residence lifetime τ_M.[2,4,11,12] A fine tuning of this parameter has emerged as a primary objective of the current research in this field, as only values around 30 ns would allow the full exploitation of the decrease of T_{1M} induced by the lengthening of τ_R.

Outer Sphere

This contribution accounts for about 40% of the relaxivity of monoaquo Gd^{3+} complexes at the imaging fields and arises from the modulation of the dipolar interaction by diffusion of the solvent molecules next to the paramagnetic center:

$$R_{1p}^{OS} = C^{OS}\left(\frac{1}{aD}\right)\left[7J(\omega_S) + 3J(\omega_H)\right] \quad (5)$$

$$J(\omega) = Re\left[\frac{1 + 1/4\left(i\omega\tau_d + \frac{\tau_d}{\tau_{Si}}\right)^{1/2}}{1 + \left(i\omega\tau_d + \frac{\tau_d}{\tau_{Sj}}\right)^{1/2} + 4/9\left(i\omega\tau_d + \frac{\tau_d}{\tau_{Sj}}\right) + 1/9\left(i\omega\tau_d + \frac{\tau_d}{\tau_{Sj}}\right)^{3/2}}\right] \quad (6)$$

$$with \quad j = 1,2; \quad \tau_d = \frac{a^2}{D}$$

where C^{OS} is a constant (5.8×10^{-13} s^{-2} M^{-1}) and the non-Lorentzian spectral density functions $J(\omega_i)$ contain the dependence on τ_S. At the magnetic fields of interest it depends primarily on the distance of closest approach a, related to the molecular dimension and charge distribution of the complex, and on the relative diffusion coefficient of solute and solvent D. It follows that r_{OS}^{1p} assumes a comparable value (above 10 MHz) for all the small gadolinium chelates of clinical interest.

Second Coordination Sphere: A Third Contribution to Relaxivity

In principle the outer sphere relaxivity can also receive contributions by another mechanism: fluctuation of the dipolar electron-nuclear coupling involving water molecules held in the second coordination shell of the paramagnetic ion by hydrogen bonding interactions with polar groups of the ligand (Figure 1). This term (2S) has to be distinguished from the traditional diffusion-controlled outer-sphere relaxivity only when the residence lifetime of the structured water in the second shell is longer than the diffusional correlation time τ_D ($\tau_D = a^2/D$). In this latter case the quantitative description of the effects on the relaxivity is analogous to that of the inner sphere water molecules (Equation 2), as clearly pointed out by Lauffer.[1b] Firm experimental evidence for the occurrence of this solvent/metal complex interaction is difficult to obtain and, in most cases, its consideration may only represent a negligible correction to the inner- and outer-sphere relaxivities in the traditional model. However, in several cases, a careful analysis of the relaxation rate of the solvent as a function of magnetic field, pH and temperature allowed the evaluation of this contribution and the extraction of more useful and correct information from the data analysis.

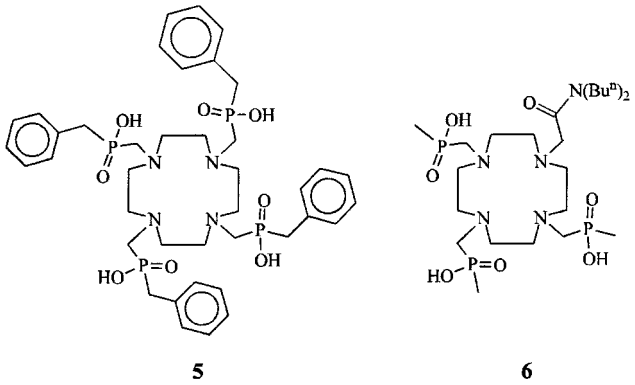
In 1981 Koenig et al. reported that replacement of the iron(III)-bound water molecule in methemoglobin by fluoride ion increases the relaxation rate drastically.[17] It was shown by variable temperature relaxivity data that the heme-iron-coordinated water molecule in met-Hb is kinetically inert as it is stabilized by a hydrogen bond with a proximate hystidine residue, and that the relaxivity enhancement upon fluoride binding can be attributed to a labile water molecule hydrogen bonded to the coordinated anion. Such structural arrangement brings a proton of this second sphere water molecule close enough to the paramagnetic center to be strongly relaxed. Recently this interpretation was confirmed by a crystallographic study that revealed the presence of a water molecule hydrogen bonded to the fluoride anion at a distance of 2.71 Å.[18] In 1984 Kushnir and Navon investigated the water relaxation-rate enhancement by Mn^{2+} bound to macromolecules and found the presence of an additional contribution to r_{1p}^{IS} which dominated the observed relaxivity at high fields and originated from outer sphere solvent molecules.[19] This additional contribution could not be explained on the basis of a spin-diffusion mechanism from the protein protons or of the usual dipolar interaction with the diffusing solvent molecules. A good quantitative account was obtained by considering water molecules bound outside the first hydration shell with an average lifetime of 0.3 ns.

The possible contribution of r_{1p}^{2S} to the overall relaxivity of small paramagnetic complexes has seldom been considered in the past. Oakes and Smith studied the proton relaxation properties of $[Mn(EDTA)(H_2O)]^{2-}$ and attributed the outer sphere contribution to the presence of

four water molecules hydrogen bonded to the four coordinated carboxylate groups.[20] The calculated Mn–H distance for these water molecules is 3.7 Å, a value that seems reasonable even though the validity of this very simple model is questionable, and it has not been checked by a magnetic field- and temperature-dependent study. More recently, Merbach et al. reported a detailed ^{17}O NMR and computer modeling study on the structure and dynamics of the second coordination shell water molecules around the Cr^{3+} hexaaqua ion.[21] In the case of this ion, which is endowed with a kinetically inert first hydration shell, where the bonding occurs through the O-atom of the water molecules, the authors were able to assess the presence of 13 water molecules in the second shell with an average lifetime of 128 ps. On the other hand no evidence was found for a well defined second shell in the case of a cation of larger ionic radius like Ln^{3+}.[22] It is worth noting that only in these latter two cases, characterized by an isotropic disposition of the ligand molecules around the metal ion, is the term "second sphere" strictly applicable. In the polyamminopolycarboxylate(-polyphosphonate) complexes considered here, the widely used definition of second sphere can be misleading as it refers exclusively to water molecules hydrogen-bonded to polar groups of the ligand present on the hydrophilic side of the metal complex.

Gd^{3+} Complexes

The lanthanide complexes with the macrocyclic tetrabenzylphosphinate ligand **5** (Scheme 2) have been characterized both in the solid state and in solution, where they are present as a single diastereoisomer with an inverted square antiprismatic coordination polyhedron.[23]



5 **6**

Scheme 2

Unlike the case of the carboxylate analogues, the higher steric bulk of the phosphinate groups prevents the access to the metal ion of the water molecules and the complexes have $q = 0$. Therefore, the relaxivity of [Gd-**5**]$^-$ does not present the complications of the inner sphere component and its NMRD (**N**uclear **M**agnetic **R**elaxation **D**ispersion, i.e. the magnetic field dependence of the relaxivity) profile is rather simple and characterized by a shape and an amplitude as predicted by the translational diffusion model of pure outer sphere relaxivity (Figure 2). Fitting of the data yields a value of 4.35 Å for the distance a of closest approach of the protons of the solvent molecules, in good agreement with the value estimated from the X-ray structure.[23]

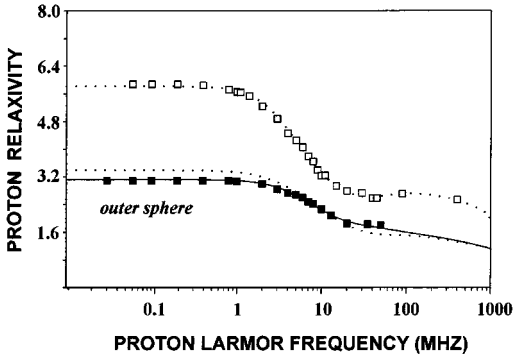


Figure 2. NMRD profiles (25 °C) of [Gd-**5**]$^-$ (filled squares) and Gd-**6** (open squares) and best-fit curves; the dotted line at the bottom is the calculated outer-sphere contribution for [Gd-**6**]$^-$

By substituting one phosphinate group with a less bulky carboxoamide **6** we obtain neutral Gd^{3+} complexes, of potential interest as low osmolality MRI CA, and furthermore we favor the access of water to the paramagnetic center by releasing part of the steric encumbrance.[24] The NMRD profile has the typical shape of $q = 1$ complexes such as [Gd-**1**]$^{2-}$, [Gd-**2**]$^-$ and Gd-**4**, but its magnitude is significantly lower. On the other hand, assuming $q = 0$ would imply for Gd-**6** either an a value shorter than the molecular radius or a dramatic change of the diffusional dynamics of its aqueous solution. The profile shows a small hump of relaxivity around 100 MHz, particularly evident at lower temperatures, which suggests a dependence of the relaxivity upon the rotational dynamics of the complex (τ_R), which substantiates the hypothesis of the presence of an "inner sphere" contribution. This increase in relaxivity observed on passing from pure outer-sphere complexes such as [Gd-**5**]$^-$ to Gd-**6** can be quantitatively explained on the basis of the presence of a tightly bound water molecule in the second coordination sphere of the metal ion at a distance of ca. 3.6 Å and with a sufficiently long lifetime. This interaction is likely to involve a hydrogen bond between the carboxoamide oxygen atom and a water molecule, which results in a metal–proton distance short enough to affect the solvent relaxation (Figure 3). Interestingly, a good correlation has been found in a series of related complexes between the r_H values derived from NMRD analysis and the average hydration state q ($0 < q < 1.3$) obtained by luminescence measurements on the Eu^{3+} derivatives.[24b]

This suggested the hypothesis that, besides the pure outer- ($q = 0$) and inner-sphere ($q = 1$) limiting cases, complexes with octadentate ligands may assume in solution any intermediate value depending on the number and nature of the hydrogen-bond acceptor groups of the ligand. In other words, this implies that fractional q values (and long r_H distances) can be correlated to the existence of a well-defined second hydration shell of the metal ion.[24b,25]

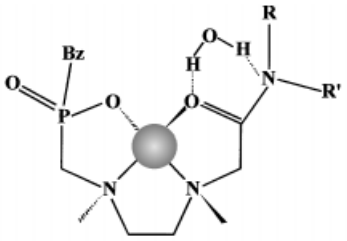
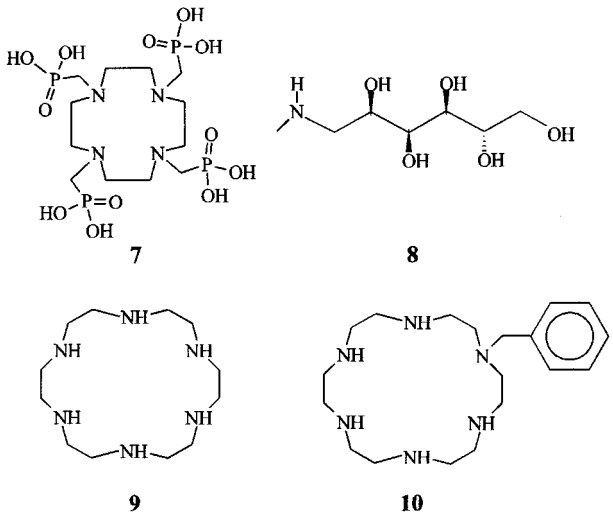


Figure 3. Schematic view of Gd-**6** showing the possible location of the second sphere water molecule

These results caused the reconsideration of the case of the anionic tetraphosphonate macrocyclic complex [Gd-**7**]$^{5-}$, whose solution structure is strictly related to that of the complexes [Ln-**5**]$^{-}$.[26] In recent years Ln^{3+} complexes of **7** (Scheme 3) have been extensively investigated as effective shift reagents for metal cations (Dy^{3+}, Tb^{3+} and Tm^{3+}), relaxation agents for MRI and probes of the charged regions of protein surfaces.



Scheme 3

The relaxation properties of [Gd-**7**]$^{5-}$ present unusual features whose interpretation has originated conflicting explanations: formation of oligomers,[27] fractional number q of coordinated waters (mixture of isomers differing in the q value),[27] one coordinated water molecule ($q = 1$) with an unusually long r_H distance.[28] The NMRD profile shows an anomalous behavior: on the basis of considerations of symmetry, rigidity and molecular dimension [Gd-**7**]$^{5-}$ is expected to show relaxivity values greater than the structurally similar [Gd-**2**]$^{-}$ over the entire frequency range. Nevertheless, the NMRD profile of [Gd-**7**]$^{5-}$ falls well below that of [Gd-**2**]$^{-}$ (but well above that of Gd-**6**) and the best-fitting analysis of the experimental data to the established theory of inner- and outer-sphere relaxivity components yielded a distance $r_H = 3.26$ Å for the inner sphere water molecule.[28] This value is significantly longer than that obtained by X-ray analysis of related macrocyclic Ln^{3+} complexes or derived from NMRD analysis and is therefore appears disputable. By considering that the phosphinate complexes of the type [Gd-**5**]$^{-}$ and Gd-**6** have $q = 0$ and that the high negative charge distributed over the eight uncoordinated oxygen atoms of the phosphonate groups may promote the formation of strong hydrogen bonds with the solvent molecules, we could interpret the relaxivity of [Gd-**7**]$^{5-}$ by considering a strong second-sphere contribution. By adopting values for a and D similar to those found for [Gd-**5**]$^{-}$ and Gd-**6**, and by allowing for the second-sphere water molecules an average distance in the range 3.3–4.0 Å, an excellent fit of the NMRD data is obtained for two solvent molecules localized at a distance of 3.89 Å. This result, although in good agreement with the available structural data for related complexes, represents only a rough estimation since there is probably an array of hydrogen-bonded solvent molecules characterized by different distances r_H and residence lifetimes τ_M. Moreover, these water molecules may present different rotational mobilities and the assumption of a single τ_R appears unlikely. What does seem reasonable is to attribute the nearly 50% increase of relaxivity of [Gd-**7**]$^{5-}$ versus [Gd-**5**]$^{-}$ to structured solvent molecules in the second coordination shell of the metal ion involved in a relatively strong bonding interaction with the oxygen atoms of the phosphonate groups. A strong support for this hypothesis was found by the measurement of the ^{17}O transverse relaxation rate (R_2^Q) as a function of temperature, a well-recognized method for obtaining information on the dynamics of the metal-bound water molecule(s). The profile of R_2^Q with temperature is typical of a $q = 0$ complex and thus confirms the absence of any *IS* water molecule for [Gd-**7**]$^{5-}$.[29] The case of [Gd-**7**]$^{5-}$ is particularly striking as it shows that a few solvent molecules held in the vicinity of the paramagnetic center through hydrogen-bonding interactions with polar groups on the ligand in a suitable geometrical arrangement provide a contribution to r_{1p} similar to that of a metal-bound water molecule. The second coordination sphere relaxation pathway depends on the same parameters as the *IS* term, and thus its efficacy is enhanced by slowing down the rotational mobility of the complex, as shown by the increase of r_{1p} by decreasing the temperature. There are some distinct features though that must be considered for optimizing r_{1p}^{2S}:

1) The value of τ_M for the currently used MRI CAs is about one or two orders of magnitude longer than the optimal value and this represents a serious obstacle to the achievement of the high relaxivity expected for dendrimeric or macromolecular derivatives and required by the new and emerging applications of MRI. Conversely, the mean lifetime of the interaction of the 2*S* water molecules, although only roughly estimated by relaxometry, is much shorter and can play a negative role in determining τ_C (Equations 3–4). Longer values of τ_M imply stronger interaction through a proper choice of the hydrogen-bond acceptor groups of the ligand and their suitable mutual spatial disposition on the Gd^{3+} complex;

2) The r_H values for *IS* water molecules show a negligible variation among Ln^{3+} chelates of different charge, coordination number and hydration state. The distance of 2*S* water molecules is a far more flexible parameter, which may assume values in the range 3.2 (*IS*) – 4.5(*OS*) Å. Because

of the $1/r_H^6$ dependence of r_{1p}, a control of this parameter, which is determined by the type and geometry of the interaction, would be of primary importance for attaining high relaxivities.

3) Unlike the *IS* case, the number of water molecules in the second shell can in principle be increased without altering the number of the donor atoms of the ligand and compromising the thermodynamic stability of the complex.

This latter possibility has been explored through the formation of ion-pair adducts between anionic Gd^{3+} chelates and positively charged organic bases. [Gd-**7**]$^{5-}$ was found to be particularly useful for this purpose: its negative charges localized on the oxygen atoms of the phosphonate groups directed outwards from the coordination cage favor multiple electrostatic interactions and formation of strong ion-pairs in solution with a variety of substrates.[29][30] It has been found that *N*-methyl-glucamine (**8**, Scheme 3) interacts with [Gd-**7**]$^{5-}$ and induces a marked relaxation enhancement of the bulk water protons that, at pH = 9 and 25 °C, is as large as 3.5 and corresponds to r_{1p} of about 15 $mM^{-1}s^{-1}$ (at 20 MHz), a value comparable to that of Gd^{3+} chelates linked to macromolecular substrates.[28] This effect was originally explained by a contribution of the exchangeable protons of the organic base maintained in the close proximity of the metal ion by the chelate-type structural organization of the substrate in the supramolecular adduct.[31] In light of the above considerations we can attribute the relaxivity gain to a high number of water molecules involved in a network of H-bonding interactions with the phosphonate groups of the complex and the hydroxyl groups of the substrate. Moreover, the coordination polyhedron of [Gd-**7**]$^{5-}$, an inverted square antiprism where the negative charges are localized about the O_4 square plane above the metal ion, suggests that the effects associated with the ion-pairing interaction could be further optimized by choosing polyammonium macrocycles of suitable size and charge as the anion receptor substrates. This hypothesis was verified in the case of exacyclen (**9**, Scheme 3). The large cavity size of **9** matches very well the square plane of [Gd-**7**]$^{5-}$ and results in a strong interaction ($K_A = 1 \times 10^4$ M; pH = 6) that is pH dependent as it depends on the protonation of both the anionic and cationic species. In the ion-pair adduct the average distance between the ring carbons of the macrocycle and the Gd^{3+} has been estimated to be 6.1 Å by ^{13}C NMR T_1 data, thus suggesting the possible presence of a number of water molecules sandwiched between the two planes, with the hydrogen atoms directed towards the paramagnetic center at a distance short enough for optimal relaxation effects (Figure 4).[29]

As pointed out above, the 2*S* relaxation mechanism is governed by the same type of parameters as *IS* and, in particular, depends strongly on rotation (τ_R). Thus, the increase of τ_R by increasing the molecular size of the complexes should provide a further relaxivity gain. This has been observed when a benzyl group is introduced into **9**. The substituted exacyclen (**10**, Scheme 3), interacts with [Gd-**7**]$^{5-}$ just as strongly but now the supramolecular adduct can be further involved in the formation of an inclusion compound

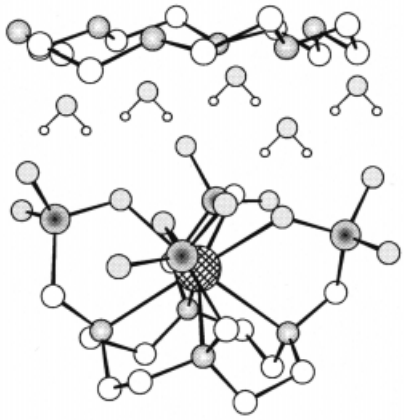


Figure 4. Model of the ion pair adduct between [Gd-**7**]$^{5-}$ and **9** showing the "sandwiched" water molecules of the second hydration shell

with β-cyclodextrin (β-CD), as shown in Figure 5. The noncovalent ternary complex presents a remarkably high relaxivity ($q = 0$!) of 18 $mM^{-1}s^{-1}$ at 20 MHz and 25 °C, which is entirely attributable to an optimized contribution of 2*S* hydration.[29]

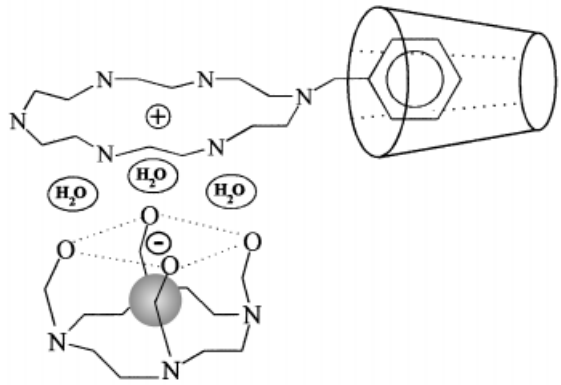
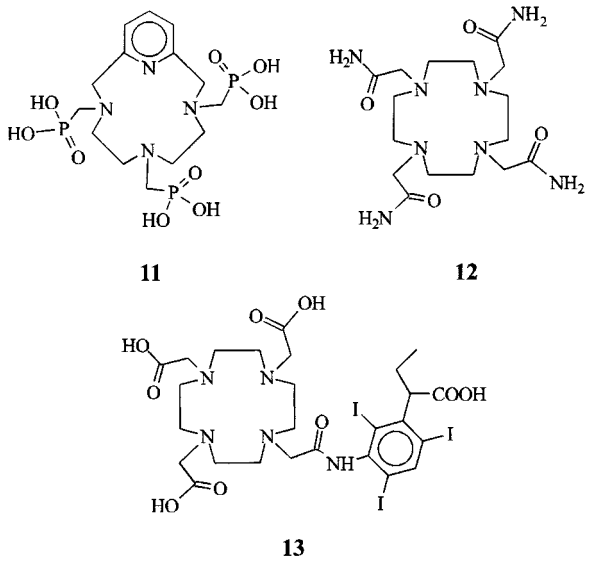


Figure 5. Schematic view of the noncovalent ternary complex between [Gd-**7**]$^{5-}$, **10** and β-cyclodextrin

From all these studies it appears evident that a very good candidate for a relaxation reagent of improved efficacy should be a complex where all the three relaxation mechanisms are operating, thus combining the properties of [Gd-**2**]$^-$ and [Gd-**7**]$^{5-}$. This interesting approach has been explored by investigating the relaxometric properties of the Gd^{3+} complex with **11**, a heptadentate macrocyclic ligand which features only three pendant arms bearing phosphonate groups (Scheme 4). As expected, the decreased denticity of the ligand allows a water molecule to occupy a coordination site of Gd^{3+}, and the relaxivity was measured to be as high as 7.7 $mM^{-1}s^{-1}$ (20 MHz, 25 °C).[32,33]

This high value of r_{1p}, about 50% higher than that of the commercial MRI CA, was shown to arise from comparable contributions of the three mechanisms: *OS*, *IS*, 2*S*. A quantitative analysis of the NMRD profile was performed under this hypothesis and an excellent fit of the data was obtained in the presence of a single *IS* water molecule at a distance of 3.06 Å from the metal ion. Moreover, in this octacoordinate complex, the exchange rate of the metal-



Scheme 4

bound water molecule is much faster than those found for enneacoordinated Gd^{3+} complexes. [Gd-**11**]$^{3-}$ represents the first example that clearly shows the feasibility and the potential of this strategy for relaxation enhancement.

Unusual, pH-dependent relaxation effects produced by second coordination shell water molecules have been observed also in the case of cationic Gd^{3+} complexes of macrocyclic tetraamide ligands such as **12** (Scheme 4).[34,35] The complexes are nine-coordinate, being bound to one water molecule, the four ring nitrogen and the amide carbonyl oxygen atoms, with a geometry corresponding to a monocapped square antiprism. At ambient pH and temperature the *IS* water exchange-lifetime, as determined by ^{17}O NMR spectroscopy, is long enough (19 μs) to strongly limit the *IS* contribution to r_{1p} and to allow a detailed study of the hydration structure and exchange dynamics. In the pH region above 7, despite the deprotonation of the bound water, which decreases the effective q value from 1 to 0.5, the relaxivity increases as a result of a base-catalyzed prototropic exchange taking place at the water coordination site. In fact, at high pH the rate of this process becomes faster than the rate of exchange of the whole water molecule, thus decreasing the effective τ_M and increasing the relaxivity. However, at pH 11, the relaxivity reaches a value (about 6 $mM^{-1}s^{-1}$) which is too high to be explained on the basis of prototropic exchange catalysis. This increase is associated with the deprotonation of the amide nitrogen (pK_a = 11.02 and 11.89) and has been shown to depend on the formation of a well-defined second hydration sphere consisting of water molecules bridging the amide group and the bound hydroxyl group through hydrogen-bond interactions (Figure 6). The profile of r_{1p} versus pH could be nicely fitted by considering two water molecules at a distance r_H = 3.6 Å.[35]

An analogous behavior was observed more recently in related macrocyclic tetra- and triamide derivatives.[36] Other examples of second coordination sphere water molecules tightly interacting with a negatively charged functional

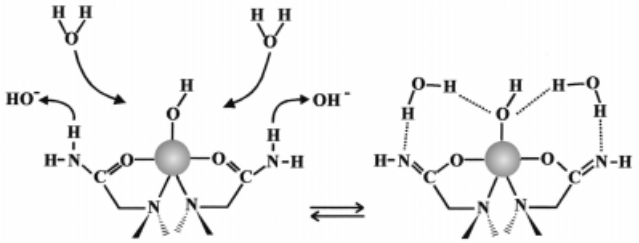


Figure 6. Deprotonation of the amide NH protons on [Gd-**12**]$^{3+}$ favors the formation of a second hydration sphere leading to a relaxivity enhancement

group of the ligand are the Gd^{3+} complexes with ligands **4** and **13** (Scheme 4). The monoaquo neutral complex [Gd-**4**] features a coordinated hydroxyl group that deprotonates at basic pH (pK_a = 11.36) with a concomitant structural rearrangement involving the loss of the coordinated water molecule. Surprisingly, this coordination equilibrium is not followed by a decrease of relaxivity which, at pH 12 (q = 0), assumes almost the same value as when measured at pH 7 (q = 1). It was concluded that the new contribution to r_{1p} measured at basic pH arises from a second coordination sphere water molecule hydrogen bonded to the alkoxide functional group whose protons were estimated to be at an average distance of 3.2 Å from Gd^{3+}.[4] Similarly, the monoamide neutral complex [Gd-**13**] presents a fairly acidic amidic proton ($pK_a \simeq 9$) and the profile of r_{1p} with pH is sensitive to this equilibrium: it passes from a value of 6.7 $mM^{-1}s^{-1}$ at pH 7 to 8.5 $mM^{-1}s^{-1}$ at pH > 10. This high relaxivity is again a consequence of the concomitant occurrence of all three relaxation mechanisms due to: one water coordinated to Gd^{3+} (*IS*) contributing about 50% of the overall relaxivity, one water molecule hydrogen bonded to the negatively charged nitrogen in the second coordination shell (2*S*, 20%), and the closely diffusing water molecules in the outer hydration sphere (*OS*, 30%).[4] It must be stressed that the relative contributions of the three mechanisms are not given as a direct result of experiments but rather derive from an analysis of the data based on a more plausible model, and therefore are to be considered as a qualitative interpretation.

Implications for MRI Contrast Agents

The relatively large body of data presented here clearly shows that 2*S* relaxation plays an important role in determining the relaxivity of aqueous solution of Gd^{3+} complexes bearing phosphonate or anionic groups next to the coordination sites of the metal ion. Can these effects be of more general importance and also partly affect the relaxivity of the currently available poly(aminocarboxylate) MRI CAs? Or can the contribution of 2*S* relaxation for these compounds be safely neglected as has so far been implicitly assumed? Some insights to correctly address these questions have recently been gained. Chen et al. have investigated the complexes of vanadyl (VO^{2+}) in order to exploit the absence of inner-sphere water molecules and analyze the re-

laxation data only in terms of *OS* and 2*S* contributions.[37–38] The rotational correlation times τ_R, one of the most important parameters for 2*S* relaxation, and τ_V were determined by ESR measurements and used to interpret the NMRD profiles. A large 2*S* contribution, predominant in the case of the DTPA complex, was found for all the compounds investigated. By making several assumptions the results from this study were then used to aid the interpretation of the NMRD profiles for the Gd^{3+} complexes with **1** and its ethoxybenzyl derivative. In the case of [Gd-**1**]$^{2-}$ the authors estimated a 2*S* contribution of roughly 25% to the overall relaxivity at the imaging fields. Though providing a qualitatively convincing interpretation of the relative role of inner-, outer- and second-sphere mechanisms to the relaxivity of the Gd^{3+}-based MRI CAs, the best-fitting procedure used yields poor values for the *IS* parameters τ_R (about two times larger than the value calculated for related complexes of similar molecular weight or estimated from ^{13}C T_1 data on diamagnetic derivatives), r_H (3.36, much longer than the values obtained from X-ray and ^{17}O NMR spectroscopic studies) and τ_M (20.9 ns, about one order of magnitude shorter than the value measured by a variable temperature ^{17}O $1/T_2$ data). We used a more direct approach to evaluate the 2*S* contribution of MRI CAs, involving a greatly reduced number of assumptions and fitting parameters, by taking advantage of a new X-ray crystal structure of [Yb-**1**]$^{2-}$ which clearly shows the three types of hydration shells of the complex.[39] In particular, a water molecule was located at a distance r_H = 3.28 Å from the ytterbium ion, strongly hydrogen bonded to the carboxylate oxygen atoms, and clearly belonging to the second coordination sphere. Six water molecules were also found in the outer coordination sphere surrounding the anionic complex, at an average r_H distance of 4.5 Å, a value in excellent agreement with that derived for the distance of closest approach *a* from NMRD analysis for the Gd^{3+} complexes with **5**, **6** and **7**. On the basis of the solid-state data we reanalyzed the NMRD profile of [Gd-**1**]$^{2-}$ on the basis of a model considering contributions from the water molecules in the three different environments (Figure 7).

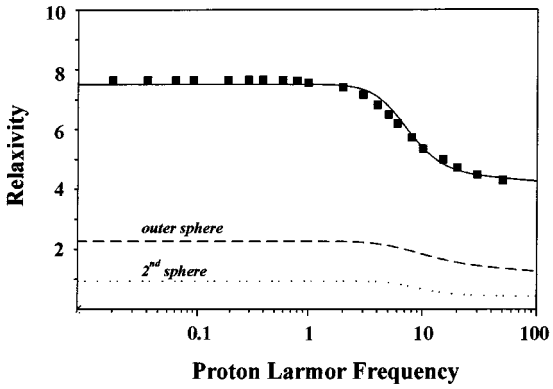


Figure 7. NMRD profile of [Gd-**1**]$^{2-}$ at 25 °C and pH = 7 showing the calculated outer- and second-sphere contributions

An excellent fitting of the relaxation data was obtained with relaxation parameters that are in very good agreement with crystallographic and NMR spectroscopic data and where: (1) the *IS* water molecule is located at 2.93 Å; (2) the 2*S* water molecule is hydrogen-bonded to the carboxylate oxygen atoms with a residence lifetime of 94 ps (at 25 °C) and at a distance of 3.28 Å, giving a contribution of about 10% to the total relaxivity at high fields; (3) the *OS* water molecules diffuse near the complex at a minimum distance of 4.5 Å.[39]

Conclusions

The qualitative picture which emerges from these data recognizes the importance of the structured water around the complexes and the potential of relaxometry to study the effects and test different hypotheses. 2*S* Solvation plays a small role in determining the relaxivity of the commonly used small poly(aminocarboxylate) Gd^{3+} chelates but its consideration is very important for a correct and more realistic interpretation of the relaxation data and for a better understanding of the structure-relaxivity relationship. Furthermore, large relaxation enhancements due to the 2*S* relaxation mechanism are possible through a careful ligand design and by exploiting strong interactions with suitable substrates (Figure 8).

Finally, the study of these effects has a direct implication in the understanding of the relaxivity changes occurring when a small Gd^{3+} chelate interacts with a macromolecule. We found that q = 0 complexes such as [Gd-**5**]$^{-}$, or its aryl methoxy-substituted derivatives, interact strongly with *bovine serum albumin* (BSA) leading to a marked relaxivity

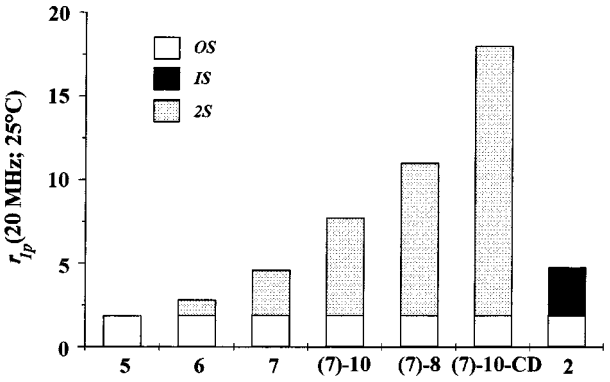


Figure 8. Plot of the relaxivity for some of the Gd^{3+} complexes discussed in this work showing the large relaxation enhancement achieved by exploiting the 2*S* mechanism

enhancement which cannot be accounted for either with an optimization of the outer sphere component of r_{1p} or with a change in the coordination number of the metal ion upon interaction with the protein.[23][40] Rather, it arises from exchangeable protons on the protein close to the interaction site of the complex and from a network of hydrogen-bonded water molecules in the second coordination sphere of Gd^{3+}. This contribution is only detected in the presence of the protein because of the reduced mobility of its well-structured hydration layer. A higher relaxation enhancement is observed in the case of the adduct of [Gd-**7**]$^{5-}$ with

BSA,[29,32] and the NMRD profile (Figure 9) is rather similar both in shape and in amplitude to those measured for $q = 1$ complexes, which shows that, even in this latter case, the 2*S* mechanism plays a major role, probably as a consequence of the limiting effect of the long τ_M value on r_{1p}^{IS}.

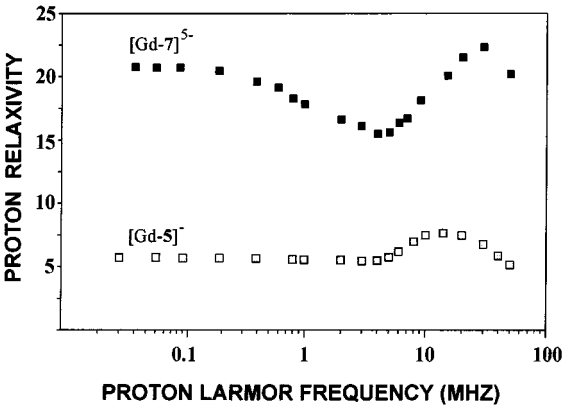


Figure 9. NMRD profiles of the non covalent adduct with BSA of [Gd-**5**]$^-$ (open squares) and [Gd-**7**]$^{5-}$ (filled squares) at 25 °C and pH = 7

Acknowlegdments

I am very grateful to Prof. Silvio Aime and his group (University of Turin) for the invaluable contribution given to the work presented here. I would also like to thank Prof. David Parker (University of Durham) for a fruitful and productive collaboration. Financial support from CNR (Legge 95/95) and a travel grant from the NATO Science Program are gratefully acknowledged.

[1] [1a] S. W. Young, *Magnetic Resonance Imaging: Basic Principles*, Raven Press, New Raven Press, New York, **1988**. – [1b] R. B. Lauffer, *Chem. Rev.* **1987**, *87*, 901–927. – [1c] M. F. Tweedle, in *Lanthanide Probes in Life, Chemical and Earth Sciences* (Eds: J.-C. Bunzli, G. R. Choppin), Elsevier, Amsterdam, **1989**, chapter 5. – [1d] B. L. Engelstad, G. L. Wolf, in *Magnetic Resonance Imaging* (Eds: D. D. Stark, W. G. Bradley, Jr.), The C. V. Mosby Company, St. Louis, **1988**, chapter 9.

[2] S. Aime, M. Botta, M. Fasano, E. Terreno, *Chem. Soc. Rev.* **1998**, *27*, 19–29.

[3] S. H. Koenig, R. D. Brown III, *Prog. NMR Spectrosc.* **1990**, *22*, 487–567.

[4] S. Aime, M. Botta, M. Fasano, E. Terreno, *Acc. Chem. Res.* **1999**, *32*, 941–949.

[5] S. Aime, M. Botta, M. Fasano, S. Geninatti Crich, E. Terreno, *Coord. Chem Rev.* **1999**, *185–186*, 321–333.

[6] [6a] L. Banci, I. Bertini, C. Luchinat, *Nuclear and Electron Relaxation*, VCH, Weinheim, **1991**. – [6b] I. Bertini, C. Luchinat, *NMR of Paramagnetic Molecules in Biological Systems*, The Benjamin/Cummings Publishing Company, Menlo Park, CA, **1986**. – [6c] L. Banci, I. Bertini, C. Luchinat, *Coord. Chem Rev.* **1996**, *150*, 1–296.

[7] [7a] I. Solomon, *Phys. Rev.* **1955**, *99*, 559. – [7b] N. Bloembergen, *J. Chem. Phys.* **1957**, *27*, 572. – [7c] N. Bloembergen, L. O. Morgan, *J. Chem. Phys.* **1961**, *34*, 842–850.

[8] J. A. Peters, J. Huskens, D. J. Raber, *Prog. NMR Spectrosc.* **1996**, *28*, 283–350.

[9] S. Aime, M. Botta, M. Panero, M. Grandi, F, Uggeri, *Magn. Reson. Chem.* **1991**, *29*, 923–927.

[10] S. Aime, L. Barbero, M. Botta, *Magn. Reson. Imag.* **1991**, *9*, 843–847.

[11] S. Aime, M. Botta, M. Fasano, S. Geninatti Crich, E. Terreno, *JBIC* **1996**, *1*, 312–319.

[12] E. Toth, D. Pubanz, S. Vauthey, L. Helm, A. E. Merbach, *Chem. Eur. J.* **1996**, *2*, 1607–1615.

[13] R. B. Lauffer, T. J. Brady, R. D. Brown III, C. Baglin, S. H. Koenig, *Magn. Reson. Med.* **1986**, *3*, 541–548.

[14] S. Aime, M. Botta, S. Geninatti Crich, G. Giovenzana, G. Palmisano, M. Sisti, *Bioconjugate Chem.* **1999**, *10*, 192–199.

[15] R. C. Brash, *Magn. Reson. Med.* **1991**, *22*, 282–287.

[16] J. H. Freed, *J. Chem. Phys.* **1978**, *68*, 4034–4039.

[17] [17a] S. H. Koenig, R. D. Brown III, T. R. Lindstrom, *Biophys. J.* **1981**, *34*, 397–408. – [17b] S. Aime, M. Fasano, S. Paoletti, A. Arnelli, P. Ascenzi, *Magn. Reson. Med.* **1995**, *33*, 827–831.

[18] S. Aime, M. Fasano, S. Paoletti, F. Cutruzzolà, A. Desideri, M. Bolognesi, M. Rizzi, P. Ascenzi, *Biophys. J.* **1996**, *70*, 482–488.

[19] T. Kushnir, G. Navon, *J. Magn. Reson*. **1984**, *56*, 373–379.

[20] J. Oakes, E. G. Smith, *J. Chem. Soc., Faraday Trans. 2* **1981**, *77*, 299–308.

[21] A. Bleuzen, F. Foglia, E. Furet, L. Helm, A. E. Merbach, J. Weber, *J. Am. Chem. Soc*. **1996**, *118*, 12777–12787.

[22] T. Kowall, F. Foglia, L. Helm, A. E. Merbach, *Chem. Eur. J.* **1996**, *2*, 285–294.

[23] S. Aime, A. S. Batsanov, M. Botta, J. A. K. Howard, D. Parker, K. Senanayake, G. Williams, *Inorg. Chem*. **1994**, *33*, 4696–4706.

[24] [24a] S. Aime, M. Botta, D. Parker, G. J. A. Williams, *J. Chem. Soc., Dalton Trans.* **1995**, 2259–2266. – [24b] S. Aime, M. Botta, D. Parker, G. J. A. Williams, *J. Chem. Soc., Dalton Trans.* **1996**, 17–23.

[25] D. Parker, G. J. A. Williams, *J. Chem. Soc., Dalton Trans.* **1996**, 3613–3628.

[26] [26a] C. F. G. C. Geraldes, A. D. Sherry, G. E. Kiefer, *J. Magn. Reson*. **1992**, *97*, 290–304. – [26b] E. S. Henriques, M. Bastos, C. F. G. C. Geraldes, M. J. Ramos, *Int. J. Quantum Chem.* **1999**, *73*, 237–248.

[27] C. F. G. C. Geraldes, R. D. Brown III, W. P. Cacheris, S. H. Koenig, A. D. Sherry, M. Spiller, *Magn. Reson. Med.* **1989**, *9*, 94–104.

[28] S. Aime, M. Botta, E. Terreno, P. L. Anelli, F. Uggeri, *Magn. Reson. Med.* **1993**, *30*, 583–591.

[29] M. Botta, First COST D1 European Workshop, Coimbra, **1995**, Abstract Book: p 24.

[30] R A. Carvalho, J. A. Peters, C. F. G. C. Geraldes, *Inorg. Chim. Acta* **1997**, *262*, 167–176.

[31] S. Aime, M. Botta, S. Geninatti Crich, E. Terreno, P. L. Anelli, F. Uggeri, *Chem. Eur. J.* **1999**, *5*, 1261–1266.

[32] S. Aime, M. Botta, S. Geninatti Crich, G. Giovenzana, R. Pagliarin, M. Piccinini, M. Sisti, E. Terreno, *JBIC* **1997**, *2*, 470–479.

[33] S. Aime, M. Botta, S. Geninatti Crich, G. Giovenzana, R. Pagliarin, M. Sisti, E. Terreno, *Magn. Reson. Chem*. **1998**, *36*, S200–S208.

[34] S. Aime, A. Barge, M. Botta, D. Parker, A. S. de Sousa, *J. Am. Chem. Soc*. **1997**, *119*, 4767–4768.

[35] S. Aime, A. Barge, J. I. Bruce, M. Botta, J. A. K. Howard, J. M. Moloney, D. Parker, A. S. de Sousa, M. Woods, *J. Am. Chem. Soc*. **1999**, *121*, 5762–5771.

[36] S. Aime, A. Barge, M. Botta, J. A. K. Howard, R. Kataky, M. P. Lowe, J. M. Moloney, D. Parker, A. S. de Sousa, *Chem. Commun*. **1999**, 1047–1048.

[37] J. W. Chen, F. P. Auteri, D. E. Budil, R. L. Belford, R. B. Clarkson *J. Phys. Chem.* **1994**, *98*, 13452–13459.

[38] J. W. Chen, R. L. Belford, R. B. Clarkson *J. Phys. Chem.* **1998**, *102*, 2117–2130.

[39] K. H. Hardcastle, M. Botta, M. Fasano, G. Digilio, *Eur. J. Inorg. Chem.*, in press.

[40] S. Aime, A. S. Batsanov, M. Botta, R. S. Dickins, S. Faulkner, C. E. Foster, A. Harrison, J. A. K. Howard, J. M. Moloney, T. J. Norman, D. Parker, L. Royle, J. A. G. Williams, *J. Chem. Soc., Dalton Trans.* **1997**, 3623–3636.

Received September 2, 1999
[O99316]

Reactions of Functional Groups at the Periphery of Group 4 Metallocene Frameworks: Selective Formation of a Cp-Bonded Azaboretidine Derivative by a Hydroboration Route

Doris Kunz,[a] Gerhard Erker,*[a] Roland Fröhlich,[a] and Gerald Kehr[a]

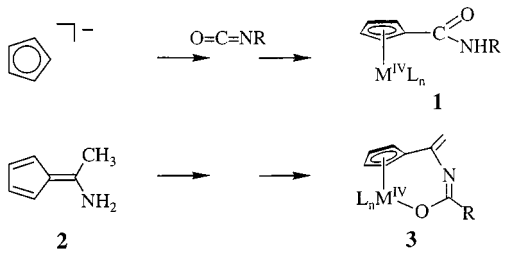
Dedicated to Professor Dirk Walther on the occasion of his 60th birthday

Keywords: Functionalized zirconocenes / Half-sandwich complexes / Hydroboration / Propene polymerization / Homogeneous catalysis

6-Amino-6-methylfulvene has been coupled with benzoic acid by treatment with 7-azahydroxybenzotriazole and DCC. Subsequent two-fold deprotonation, at the NH and 6-methyl groups, generated the vinylidene-bridged Cp/benzoylamido ligand **5**. Treatment of **5** with $ZrCl_4(THF)_2$ gave the *spiro*-metallocene complex **3a** (characterized by X-ray crystal structure analysis), while reaction of **5** with $(Et_2N)_2ZrCl_2(THF)_2$ yielded the bridged half-sandwich complex **3b**. Treatment of **3a** with two molar equivalents of the strongly electrophilic borane $HB(C_6F_5)_2$ resulted in hydroboration of the exocyclic C=C double bond with concomitant intramolecular N–B adduct formation to yield the azaboretidine-type systems **7** (three diastereoisomers, one of which has been characterized by X-ray diffraction analysis). Similarly, hydroboration of **3b** with $HB(C_6F_5)_2$ yielded the azaboretidine derivative **9**. Activation of the complexes **7** and **9** with methylalumoxane led to active homogeneous Ziegler-type propene polymerization catalysts.

Introduction

The chemistry of functional groups attached to Group 4 metallocene frameworks is important, e.g. for extending the structural scope of the "constrained geometry" Ziegler catalysts,[1] but as yet remains little developed. The introduction of functionalities typically used in organic chemistry is often difficult to accomplish by the conventional methods employed in organic synthesis due to the sensitivity of the organometallic Group 4 metal systems to hydrolytic conditions as well as to acidic or basic reaction environments. However, that increased efforts are being made to find suitable conditions and methods to overcome this apparent deficiency in the organic chemistry of Group 4 metallocenes is evident from recent literature.[2,3]



Scheme 1. Syntheses of functionalized Group 4 metal Cp-complexes

We have recently described several ways of introducing carboxamide-derived functional groups at the Cp rings of zirconocene or titanocene complexes (see Scheme 1).[4] A fulvene route has made functionalized systems such as **3** readily available.[5] It was conceivable that the azadiene moiety in **3**, the framework of which is perpendicularly oriented with respect to the metallocene backbone, could be used as a target for a hydrometallation reaction.[6] This posed the question as to whether the two parts of this conjugated metallocene side-chain would react independently or jointly with a suitable H–[M] reagent. Examples of zirconium complexes incorporating this ligand system have now been treated with the strongly electrophilic borane $HB(C_6F_5)_2$ (**6**, "Piers' borane"),[7] which has opened a simple route to novel organometallic azaboretidine derivatives exhibiting interesting structural and stereochemical properties as well as useful features in catalysis.

Results and Discussion

The synthesis of the ligand system used in this study started from 6-amino-6-methylfulvene (**2**), which, in turn, was prepared by amine exchange of 6-dimethylamino-6-methylfulvene by treatment with NH_3.[8] The aminofulvene **2** was then *N*-benzoylated. This was cleanly achieved by employing a coupling method used in peptide chemistry.[9] In a series of experiments it was found that benzoic acid was best activated for this purpose by treatment with 7-aza-hydroxybenzotriazole with subsequent addition of dicyclohexylcarbodiimide.[9b] The resulting active ester was then treated with 6-amino-6-methylfulvene **2** and triethylamine to cleanly afford the benzoylated product **4** in $> 60\%$ isolated yield. Double deprotonation of **4**, at the NH group and at the 6-CH_3 substituent,[5,10] was achieved by reaction with two molar equivalents of LDA in diethyl ether. The corresponding dianionic reagent **5** was not isolated but was

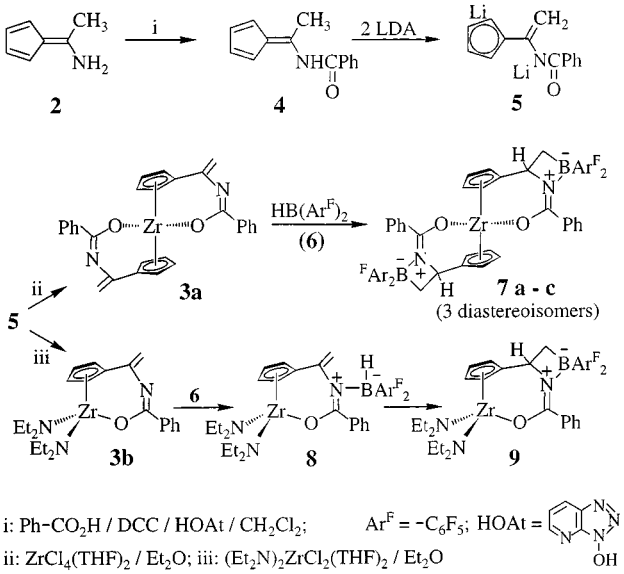
[a] Organisch-Chemisches Institut der Universität Münster, Corrensstraße 40, D-48149 Münster, Germany
Fax: (internat.) +49(0)251/8336503
E-mail: erker@uni-muenster.de

 © WILEY-VCH Verlag GmbH, D-69451 Weinheim, 2000 1434–1948/00/0303–0409 $ 17.50+.50/0

generated in situ and used directly for the preparation of the respective zirconium complexes.

Treatment of the dianion **5** with zirconium tetrachloride resulted in replacement of all four chloride ligands at the metal center with the formation of the *spiro*-metallocene product **3a**. In solution, complex **3a** shows the spectroscopic features of a C_2-symmetric, and hence chiral, framework. This leads to the observation of signals due to four pairs of diastereotopic cyclopentadienyl CH units in the ^{1}H- and ^{13}C-NMR spectra ([D$_6$]benzene, ^{1}H: δ = 5.74, 5.65, 5.61, 5.47; ^{13}C: δ = 120.9, 112.7, 108.3, 105.4). The ^{1}H-NMR signals of the *exo*-methylene group (C=CH$_2$) appear at δ = 5.38 and 5.00 (^2J = 1.1 Hz).

The organometallic *spiro*-complex **3a** was characterized by X-ray crystal structure analysis. It shows an approximately C_2-symmetric framework. Two monosubstituted η^5-Cp ligands and two imidato oxygen atoms are coordinated to zirconium in a pseudo-tetrahedral arrangement. The Zr–O bonds are rather long at 2.032(2) Å (Zr–O9) and 2.047(2) Å (Zr–O19). It would seem that the cyclic structure effectively prevents any pronounced metal–oxygen π-interaction.[11] The corresponding Zr–O9–C8 and Zr–O19–C19 angles are thus rather small [132.2(2)° and 134.2(2)°, respectively] for such a situation.[12] The adjacent C8–N7 bond length [1.277(5) Å] is in the appropriate range for a nitrogen–carbon double bond [C18–N17: 1.281(5) Å], while the adjacent C–O linkages [C8–O9: 1.327(4) Å; C18–O19: 1.335(4) Å] are in the typical C(sp^2)–O σ-bond range.[13] Characterization of **3a** as an *O*-bonded Zr-iminocarboxylate thus seems warranted (see Scheme 2 and Figure 1).



Scheme 2. Synthesis of the hydroboration compounds **7** and **9**

Treatment of the salt **5** with the reagent (Et$_2$N)$_2$ZrCl$_2$(THF)$_2$[14] resulted in selective replacement of the two chloride ligands to form the half-sandwich complex **3b**. The spectral data of **3b** indicate analogous bonding of the ligand system to zirconium as that seen in **3a**, i.e. through both the C$_5$H$_4$ moiety and the pendant imidato substituent, the latter being κ-*O*-bonded. The Cp–C(=CH$_2$)–N=C(Ph)–O ligand gives rise to characteristic NMR signals at δ = 160.7 (^{13}C of the imidato carbonyl carbon) and at δ = 5.38, 5.10 (^{1}H of the =CH$_2$ group, ^2J = 1.5 Hz). In complex **3b**, only two CH resonances of the monosubstituted Cp ligand are seen (^{1}H: δ = 5.97, 5.95; ^{13}C: δ = 110.64, 110.56). The complex is prochiral at the pseudotetrahedral zirconium center. Therefore, a single set of NCH$_2$CH$_3$ NMR resonances is observed, although the NCH$_2$ protons are diastereotopic.

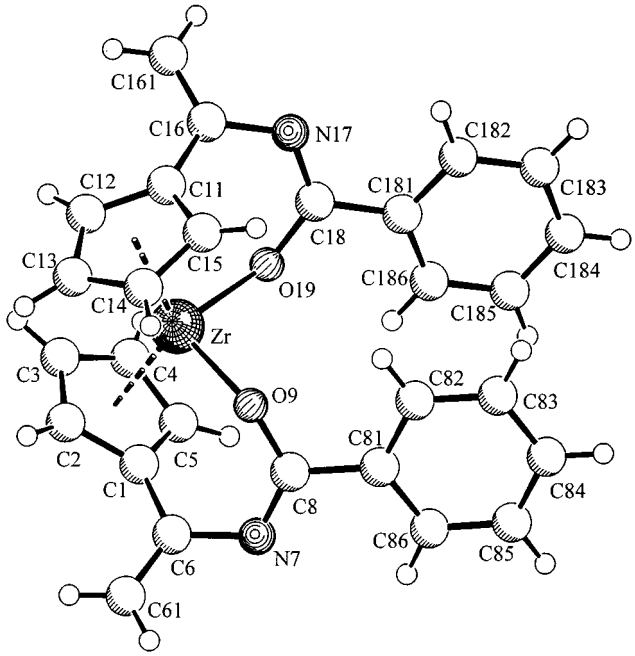


Figure 1. Molecular structure of **3a** showing the non-systematic atom numbering scheme; selected bond lengths [Å] and angles [°]: Zr–O9 2.032(2), Zr–O19 2.047(2), Zr–C$_{Cp(1-5)}$ 2.504(4), Zr–C$_{Cp(11-15)}$ 2.491(4), C8–O9 1.327(4), C18–O19 1.335(4), C8–N7 1.277(5), C18–N17 1.281(5), C8–C81 1.490(5), C18–C181 1.481(5), N7–C6 1.417(5), N17–C16 1.414(5), C6–C61 1.328(6), C16–C161 1.322(6), C1–C6 1.485(5), C11–C16 1.473(6); O9–Zr–O19 96.9(1), Zr–O9–C8 132.2(2), Zr–O19–C18 134.2(2), O9–C8–N7 125.9(3), O19–C18–N17 125.3(3), O9–C8–C81 114.0(3), O19–C18–C181 115.0(3), C81–C8–N7 120.0(3), C181–C18–N17 119.7(3), C8–N7–C6 117.1(3), C18–N17–C16 118.9(3), N7–C6–C61 120.0(4), N17–C16–C161 120.9(4), N7–C6–C1 117.2(3), N17–C16–C11 116.9(3), C1–C6–C61 122.7(4), C11–C16–C161 122.2(4)

The organometallic *spiro*-complex **3a** was treated with two molar equivalents of the electrophilic borane HB(C$_6$F$_5$)$_2$ in benzene solution. The reaction reached completion within 2 days at ambient temperature and a product fraction of low solubility (ca. 16%) precipitated from the reaction medium. Crystallization from [D$_6$]benzene gave single crystals of this material suitable for X-ray crystal structure analysis. This showed the crystals to be composed of a single isomerically pure 2:1 adduct of the borane with **3a**, resulting from addition of the borane to the exocyclic carbon–carbon double bonds of the pendant –C(=CH$_2$)–N=C(Ph)–O moiety. This hydroboration proceeded with complete *anti*-Markovnikov orientation, as is usual. Thus, the B(C$_6$F$_5$)$_2$ group was attached at the former olefinic methylene group, while the hydrogen was attached at C$_α$. The most remarkable structural feature of the hydroboration product **7a** is the strong coordination of the =N(R)

nitrogen atom to the adjacent electrophilic boron center.[15] This leads to the formation of two four-membered heterocycles in the approximately C_2-symmetric metallocene product. The corresponding bond lengths (in Å) at the substituted azaboretidine-type ring systems are 1.597(10) (B1–N13), 1.492(9) (N13–C14), 1.640(12) (B1–C20), 1.301(9) (N13–C12). The corresponding bond angles measure 83.9(5)° (C20–B1–N13), 92.0(5)° (B1–N13–C14), 126.8(6)° (C12–N13–C14), 138.7(6)° (C12–N13–B1), and 90.8(5)° (N13–C14–C20) (the approximately symmetry-equivalent second azaboretidine ring shows similar values, see Figure 2). The remaining bonding parameters of the framework of complex **7a** resemble those of its immediate precursor **3a**. In **7a**, the O11–Zr–O51 angle measures 98.3(2)°. The bond angles at the two oxygen atoms are 144.4(5)° (Zr–O11–C12) and 143.4(5)° (Zr–O51–O52) and the corresponding metal–oxygen bond lengths were determined as 2.041(5) Å (Zr–O11) and 2.043(5) Å (Zr–O51), respectively.

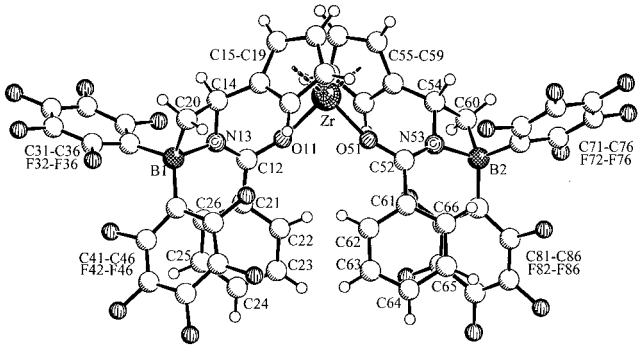


Figure 2. Molecular structure of **7a** showing the non-systematic atom numbering scheme; selected bond lengths [Å] and angles [°]; additional values are given in the text: Zr–O11 2.041(5), Zr–O51 2.043(5), Zr–$C_{Cp(15–19)}$ 2.485(8), Zr–$C_{Cp(55–59)}$ 2.479(8), C12–O11 1.300(8), C52–O51 1.305(7), C12–N13 1.301(9), C52–N53 1.278(8), C12–C21 1.473(10), C52–C61 1.493(9), N13–C14 1.492(9), N53–C54 1.493(8), C14–C20 1.548(10), C54–C60 1.539(10), C14–C15 1.483(10), C54–C55 1.498(9), N13–B1 1.597(10), N53–B2 1.602(9), C20–B1 1.640(12), C60–B2 1.647(11), B1–C31 1.634(12), B2–C71 1.617(11), B1–C41 1.621(11), B2–C81 1.619(11); O11–Zr–O51 98.3(2), Zr–O11–C12 144.4(5), Zr–O51–C52 143.4(5), O11–C12–N13 122.0(6), O51–C52–N53 123.4(6), O11–C12–C21 116.8(6), O51–C52–C61 114.7(6), C21–C12–N13 121.2(6), C61–C52–N53 121.8(6), C12–N13–C14 126.8(6), C52–N53–C54 126.9(5), N13–C14–C20 90.8(5), N53–C54–C60 91.8(5), N13–C14–C15 118.7(5), N53–C54–C55 118.2(5), C15–C14–C20 117.6(7), C55–C54–C60 117.7(7), C12–N13–B1 138.7(6) C52–N53–B2 141.2(5), C14–N13–B1 92.0(5), C54–N53–B2 90.7(5), C14–C20–B1 88.3(6), C54–C60–B2 87.4(6), N13–B1–C20 83.9(5), N53–B2–C60 84.2(5), N13–B1–C31 112.5(7), N53–B2–C71 110.8(6), N13–B1–C41 113.3(6), N53–B2–C81 113.4(6), C20–B1–C31 107.5(6), C60–B2–C71 107.4(6), C20–B1–C41 118.5(7), C60–B2–C81 118.2(7), C31–B1–C41 116.7(7), C71–B2–C81 117.9(6)

The stereochemistry of the complexes **7** is interesting. The *spiro*-metallocene framework of **7** (and also that of **3a**) is axially chiral. The hydroboration reaction introduced two new chiral centers at the carbon atoms α to the Cp rings (C14 and C54 in Figure 2). Therefore, a mixture of four chiral diastereomers could, in principle, have been formed (2^3 stereoisomers), each of course as a racemate. However, in the specific system **7** under consideration here, the two newly formed chiral carbon centers are topologically equivalent. Therefore, two of the four possible diastereomers are in fact identical. It thus remains that three diastereoisomers could possibly be formed upon hydroboration of the *spiro*-metallocene **3a**, their relative configurations being (a*R*,*S*,*S*)* (**7a**), (a*R*,*R*,*S*)* [**7b**, identical to (a*R*,*S*,*R*)*], and (a*R*,*R*,*R*)* (**7c**).[16] The single isomer found in the crystal conformed to the first case, i.e. the (a*R*,*S*,*S*)* diastereoisomer **7a** was characterized by X-ray diffraction analysis.

The hydroboration reaction of **3a** with $HB(C_6F_5)_2$ was, however, far from diastereoselective. Workup of the mother liquor after removal of the first batch of precipitated product gave a major fraction (ca. 40% yield) that was found to contain all three products **7a**, **7b**, and **7c** in a 2:10:3 ratio. This ratio may not accurately reflect the actual diastereoselectivity of the hydroboration reaction under the employed reaction conditions due to the separation of isomers during the workup, but it is rather close to the expected statistical ratio. This probably indicates that the two new stereogenic centers are formed independently of one another. The C_1-symmetric (a*R*,*R*,*S*)* isomer **7b** could readily be distinguished from its C_2-symmetric counterparts **7a** and **7c** by the characteristic splitting of the respective pairs of $^1H/^{13}C$-NMR resonances. For instance, complex **7b** shows a total of eight equally intense cyclopentadienyl methine proton ^1H-NMR signals (at δ = 7.16, 6.89, 6.60, 6.56, 6.51, 6.41, 6.29, 6.24 in [D_2]dichloromethane), whereas for **7a** and **7c** only four such resonances are seen in each case (**7a**: δ = 6.81, 6.55, 6.46, 6.37; **7c**: δ = 7.32, 7.27, 6.54, 6.19).

Hydroboration of the cyclic half-sandwich complex **3b** with $HB(C_6F_5)_2$ proceeds in a similar manner, but is of course stereochemically much simpler because, as expected, only a single isomerically pure product is obtained. H–[B] addition occurs cleanly (and regioselectively) at the *exo*-methylene functionality of the organometallic ring system, and the product **9** again contains a strong N–B interaction. This is evident from the characteristic ^{11}B-NMR shift at δ = –2.2 (**7a**: δ = –1.1). Moreover, ^{15}N-NMR data have proved very useful in characterizing the obtained structural type.[17] Complex **9** shows the ^{15}N-NMR resonance of the planar tricoordinate $=N^+$ nitrogen atom of the azaboretidine ring at δ = –205, very similar to the corresponding signal of complex **7a** (δ = –209). In contrast, the ^{15}N-NMR signals of the sp^2-hybridized dicoordinate nitrogen atoms in the starting materials **3a** and **3b** are seen at δ = –148 and δ = –145, respectively.

Complex **9** contains a single chiral center, i.e. at the tertiary carbon atom of the azaboretidine ring. Therefore, a set of four separated methine CH resonances due to the monosubstituted Cp ring are observed in the ^1H-NMR spectrum (at δ = 6.32, 6.15, 5.89, 5.82). The two metal-bonded $–N(CH_2CH_3)_2$ groups are diastereotopic, and thus give rise to two ^{15}N-NMR signals at δ = –171 and –187 and two ^1H-NMR methyl signals at δ = 0.85 and 0.73. The ethyl groups at each of the apparently trigonal-planar nitrogens behave homotopically, but the protons of each $–N(CH_2–)$ group are diastereotopic, giving rise to a total of four separated *AB*X_3 multiplets (at δ = 3.24, 3.04, 2.97, and 2.95 in [D_6]benzene at 298 K).

Under carefully controlled conditions, we were able to observe experimentally the formation of a 1:1 adduct (**8**) between the strongly electrophilic borane $HB(C_6F_5)_2$ and the metal complex **3b**. The addition product **8** was obtained in [D_8]toluene solution after mixing the two components at low temperature (–78 °C), allowing them to react briefly at ambient temperature (1 min), and then cooling the mixture to ca. 5 °C to record the NMR spectra. Under these conditions, complex **8** is relatively stable and is only slowly converted into the final product **9**. In **8**, the C=CH_2 double bond conjugated to the Cp ring remains intact [^{1}H NMR: δ = 5.41, 5.04; ^{13}C NMR: δ = 141.3, 109.6 (C=CH_2)]. The ^{13}C-NMR resonance of the C=N moiety is seen at δ = 177.5, i.e. downfield shifted relative to the starting material **3b** (δ = 160.7)[15] and no proton is attached to this carbon. The ^{15}N-NMR signal of **8** is found to be considerably shifted (**8**: δ = –204; **3b**: δ = –145). The broad ^{11}B-NMR signal at δ = –10.9 is indicative of the presence of a tetravalent borane adduct. The combined spectroscopic evidence indicates simple adduct formation between $HB(C_6F_5)_2$ and the imidato nitrogen atom of **3b** to give **8**. Complex **8** slowly undergoes conversion into the final hydroboration product **9**. Geometrically, this could take place by an intramolecular rearrangement process, since the large bending of the Cp–C(=CH_2)–N=C 2-azadiene unit from planarity [θ C61–C6–N7–C8 in the related system **3a** is –48.1(4)°] would probably allow H-transfer from boron to the trisubstituted sp^2 carbon. However, on electronic grounds, we regard it as more likely that the final hydroboration to give **9** may simply be preceeded by a reversible formation of the $HB(C_6F_5)_2$ adduct **8**.

The organometallic hydroboration products **7** and **9** are quite stable and can be used as homogeneous Ziegler-type catalyst precursors. Exploratory propene polymerization experiments were carried out by activating the respective catalyst precursors by treatment with a large excess of methylalumoxane (see Table 1).[18] Under the typical reaction conditions (for details, see the Experimental Section), the mixture of diastereomers **7a**–**c** gave a medium activity propene polymerization catalyst upon such MAO activation. A similar activity was obtained by employing the pure diastereoisomer **7a** as a precursor. It is clear that the Zr–O linkage in **7** must be cleaved during its conversion into an active catalyst. Consequently, pre-activation with excess MAO solution in toluene resulted in a slightly increased catalyst activity in these cases. Atactic polypropylene was generated in the experiments employing **7**.

Table 1. Propene polymerization experiments with the **3**, **7**, **9**/MAO systems

Precursor (mg/μmol)	Al/Zr ratio	PP[a]	activity[b]	σ[c]
3a (20/39)	0.82×10^3	[d]	–	–
3a (21/41)[e]	0.78×10^3	[d]	–	–
3b (23/52)	0.62×10^3	[d]	–	–
7 (20/17)	1.9×10^3	0.71	11	0.55
7 (15/12)[e]	2.6×10^3	0.71	14	0.57
7a (16/13)	2.4×10^3	0.66	12	0.50
7a (17/14)[e]	2.3×10^3	1.3	23	0.55
9 (20/25)	1.3×10^3	2.4	24	0.20

[a] g of polypropylene isolated. – [b] a in g polymer/mmol [Zr]·bar·h. – [c] Probability of obtaining an m diad under chain-end control. – [d] Traces. – [e] Pre-activation of the precursor with 2.5 mL of a 10% (1.6 M) methylalumoxane solution in toluene for 15 min.

The diethylamido ligands of **9** are seemingly more readily displaced during the activation process with MAO. Without pre-treatment, polypropylene was obtained with a medium activity (a = 24). In this case, the obtained polypropylene turned out to be slightly syndiotactic [with σ = 0.2 (where σ expresses the probability of having an m diad formed at the catalyst center by stereochemical chain-end control)], which probably just represents another example of an ordinary behavior of such a catalyst system in the high temperature regime.[19]

In contrast to **7** and **9**, similar treatment of their unsaturated precursors **3a** and **3b** did not produce active Ziegler-type catalysts for propene polymerization under the applied conditions. This may be due to the dominant role played by the nucleophilic imidato nitrogen center in these complexes, which renders them liable to form reasonably strong adducts with Lewis acidic reagents [for example, the $HB(C_6F_5)_2$ adduct described above]. One might speculate that such complex formation takes place preferentially upon treatment of **3a** or **3b** with the bulky MAO Lewis acid, leading to strong steric shielding of the potential catalytic centers in these adducts. On the basis of our observations, we conclude that hydroboration of these systems leading to azaboretidine formation very effectively inhibits the catalyst deactivation. We have thus, in effect, employed the $HB(C_6F_5)_2$ reagent as an organometallic protecting group that has facilitated conversion of the functionalized (CpX)Zr systems to active homogeneous Ziegler-type catalyst systems without complete loss of the pendant functional groups at the central organometallic framework. We are hopeful that the use of such protective groups might open ways of using a variety of functionalized Group 4 metal complexes in homogeneous Ziegler catalysis and related catalytic processes. Such studies are being actively pursued in our laboratory.

Experimental Section

All the described compounds (other than **4**) are air- and moisture-sensitive. They were thus prepared and handled under argon atmosphere using Schlenk-type glassware or in an argon-filled glovebox. Solvents (including deuterated solvents) were dried and distilled under argon prior to use. – NMR spectra were recorded on Varian Unity Plus, Bruker AMX 400, Bruker ARX 300, and Bruker AC 200 P-FT-NMR spectrometers. Spectroscopic characterization usually included ^{1}H,^{1}H GCOSY, ^{1}H,^{13}C (G)HMBC, and (G)HMQC experiments, even where not explicitly stated. – IR spectra were recorded on a Nicolet 5 DXC FT-IR spectrometer in KBr pellets or from films between NaCl plates. – Elemental analyses were carried out using a Foss Heraeus CHN-O-Rapid analyser, while DSC measurements were made on a Texas Instruments DSC 2010. – X-

ray crystal structure analyses: Data sets were collected with Enraf–Nonius CAD4 and Nonius KappaCCD diffractometers. Programs used: data collection: Express and Collect; data reduction: MolEN or Denzo-SMN; structure solution: SHELXS-86; structure refinement: SHELXL-93 and SHELXL-97; graphics: SCHAKAL.[20] – 7-Aza-hydroxybenzotriazole (HOAt),[9b] 6-amino-6-methylfulvene,[8] $ZrCl_4(thf)_2$,[21] $ZrCl_2(NEt_2)_2(thf)_2$,[14] and $HB(C_6F_5)_2$[7] were prepared according to literature procedures.

Preparation of 6-Amido-*N*-benzoyl-6-methylfulvene (4): To a yellow suspension of benzoic acid (2.44 g, 20.0 mmol) and 7-aza-hydroxybenzotriazole (2.72 g, 20.0 mmol) in dichloromethane (50 mL) at 0 °C was added dicyclohexylcarbodiimide (4.13 g, 20.0 mmol). The resulting suspension was stirred for 30 min at 0 °C until the active ester and dicyclohexylurea had been formed and the yellow colour of the suspension had turned to white. The suspension was then filtered into a cold (0 °C) solution of 6-amino-6-methylfulvene (2.14 g, 20.0 mmol) and triethylamine (7.0 mL, 50 mmol) in dichloromethane (30 mL). The filter cake was washed with 30 mL of dichloromethane and the filtrate was combined with the fulvenic solution. The resulting brown reaction mixture was allowed to warm to room temperature and then stirred for 3 days. It was subsequently washed with 5% aq. sodium bicarbonate solution (3 × 50 mL) and with water (3 × 30 mL). The organic phase was dried with magnesium sulfate and the solvent was removed in vacuo. The residual brown oil was purified by chromatography on silica gel 60, eluting with a mixture of diethyl ether/pentane (1:3), to which 1% (*v*/*v*) of *N*,*N*-dimethylethylamine had been added. Removal of the solvent in vacuo afforded 2.78 g (66%) of the product in the form of orange needles. DSC: 78 °C (m.p.), 131 °C (dec.). – $C_{14}H_{13}NO$ (211.26): calcd. C 79.59, H 6.20, N 6.63; found C 79.32, H 6.38, N 6.35. – IR (KBr): $\tilde{\nu}$ = 3304, 1659, 1633 cm^{-1}. – ^1H NMR (400.1 MHz, [D$_2$]dichloromethane, 300 K): δ = 8.62 (br. s, 1 H, NH), 7.87 (m, 2 H, *o*-Ph), 7.62 (m, 1 H, *p*-Ph), 7.53 (m, 2 H, *m*-Ph), 6.65, 6.53 (each m, each 1 H, α-Fulv), 6.49, 6.43 (each m, each 1 H, β-Fulv), 2.81 (s, 3 H, CH_3). – ^{13}C NMR (100.6 MHz, [D$_2$]dichloromethane, 300 K): δ = 166.0 (C=O), 146.4 (C-6), 135.1 (*i*-Ph), 133.3 (*p*-Ph), 130.8, 129.5 (β-Fulv), 130.3 (C-1), 129.7 (*m*-Ph), 128.0 (*o*-Ph), 122.6, 115.2 (α-Fulv), 15.9 (CH_3).

Preparation of Bis{η^5:κ*O*-1-(*N*-benzoylamido)ethenylcyclopentadienyl}zirconium (3a): Compound **4** (1.30 g, 6.15 mmol) and lithium diisopropylamide (1.32 g, 12.3 mmol) were weighed into a Schlenk vessel, which was subsequently cooled to –78 °C, whereupon diethyl ether (100 mL) was added. The cooling bath was removed and the suspension was stirred for 2 h while slowly warming to room temperature. The reaction was seen to be complete by the appearance of a light-yellow precipitate of the dilithium salt. The suspension was then cooled to –50 °C and a suspension of tetrachlorozirconium–bis(tetrahydrofuran) (1.16 g, 3.07 mmol) in diethyl ether (50 mL) was added. The cooling bath was removed once more, allowing the suspension to warm to room temperature, and stirring was continued for 12 h. The resulting yellow suspension was then concentrated to dryness and the remaining yellow powder was extracted with diethyl ether (5 × 100 mL). The ethereal solution was filtered and the filtrate was concentrated in vacuo. The product was isolated as a deep-yellow solid; yield 641 mg (41%). – DSC: 189 °C (m.p., followed by decomp.). – IR (KBr): $\tilde{\nu}$ = 1616, 1590, 1560 cm^{-1}. – ^1H NMR (599.9 MHz, [D$_6$]benzene, 298 K): δ = 8.31 (m, 4 H, *o*-Ph), 7.15 (m, 6 H, *m,p*-Ph), 5.74 (m, 2 H, 2-H), 5.65 (m, 2 H, 5-H), 5.61 (m, 2 H, 3-H), 5.47 (m, 2 H, 4-H), 5.38 (d, $^2J_{HH}$ = 1.1 Hz, 2 H, C=CH_2^{cis}), 5.00 (d, $^2J_{HH}$ = 1.1 Hz, 2 H, C=CH_2^{trans}). – ^{13}C NMR (gated decoupled) (150.8 MHz, [D$_6$]benzene, 298 K): δ = 162.9 (s, OC=N), 146.1 (s, *C*=CH_2), 135.6 (m, *i*-Ph), 130.8 (dm, $^1J_{CH}$ = 160 Hz, *p*-Ph), 128.9 (dm, $^1J_{CH}$ = 159 Hz, *o*-Ph), 128.3 (dm, $^1J_{CH}$ = 160 Hz, *m*-Ph), 120.9 (dm, $^1J_{CH}$ = 175 Hz, C-3), 112.7 (dm, $^1J_{CH}$ = 174 Hz, C-2), 108.3 (dm, $^1J_{CH}$ = 173 Hz, C-4), 105.4 (dm, $^1J_{CH}$ = 173 Hz, C-5), 104.8 (ps. t, $^1J_{CH}$ = 159 Hz, C=*C*H$_2$), the resonance of C-1 is obscured by the solvent signal. – ^{15}N,^1H GHMBC (60.8/599.9 MHz, [D$_6$]benzene): δ^{15}N/δ^{1}H = –148/5.38 (C=N/C=CH_2^{cis}), –148/5.00 (C=N/C=CH_2^{trans}).

X-ray Crystal Structure Analysis of 3a: Formula $C_{28}H_{22}N_2O_2Zr$, M_r = 509.70, yellow crystal, 0.35 × 0.25 × 0.10 mm, *a* = 23.282(2) Å, *b* = 11.318(1) Å, *c* = 17.345(3) Å, β = 96.11(1)°, *V* = 4544.5(10) Å^3, ρ_{calcd} = 1.490 g cm^{-3}, *F*(000) = 2080 e, μ = 5.12 cm^{-1}, empirical absorption correction based on ψ scan data (0.951 ≤ *C* ≤ 0.999), *Z* = 8, monoclinic, space group *C*2/*c* (No. 15), λ = 0.71073 Å, *T* = 223 K, 4771 reflections collected (±*h*, –*k*, +*l*), $[(\sin\theta)/\lambda]_{max}$ = 0.62 Å^{-1}, 4610 independent and 3377 observed reflections [$I \geq 2\sigma(I)$], 298 refined parameters, *R* = 0.037, wR^2 = 0.106, max. residual electron density 0.68 (–0.63) eÅ^{-3}.

Preparation of Bis{dimethylamido}{η^5:κ*O*-1-(*N*-benzoylamido)-ethenylcyclopentadienyl}zirconium (3b): Compound **4** (1.10 g, 5.21 mmol) and lithium diisopropylamide (1.12 g, 10.4 mmol) were weighed into a Schlenk vessel, which was then cooled to –78 °C, whereupon diethyl ether (100 mL) was added. The cooling bath was removed and the suspension was stirred for 2 h while slowly warming to room temperature. The suspension was then cooled to –50 °C, whereupon $(Et_2N)_2ZrCl_2(THF)_2$ (2.35 g, 5.21 mmol) in 50 mL of diethyl ether was added. The cooling bath was then removed once more, allowing the mixture to warm to room temperature, and stirring was continued for 12 h. The solvent was evaporated in vacuo from the resulting brown suspension and the residual brown oil was extracted with 150 mL of pentane. The light-brown suspension thus obtained was filtered and the filtrate was concentrated in vacuo to leave 1.88 g (81%) of a very viscous red-brown oil. – $C_{22}H_{31}N_3OZr$ (444.73): calcd. C 59.42, H 7.03, N 9.45; found C 58.92, H 6.93, N 9.39. – IR (NaCl): $\tilde{\nu}$ = 1609, 1591, 1558 cm^{-1}. – ^1H NMR (599.9 MHz, [D$_6$]benzene, 298 K): δ = 8.50 (m, 2 H, *o*-Ph), 7.23 (m, 2 H, *m*-Ph), 7.18 (m, 1 H, *p*-Ph), 5.97, 5.95 (each m, each 2 H, Cp), 5.38 (m, 1 H, C=CH_2), 5.10 (ps. d, $^2J_{HH}$ = 1.5 Hz, 1 H, C=CH'$_2$), 3.16 (ABX_3, $^{2/3}J_{HH}$ = 7.2 Hz, 4 H, C*H*$_2$CH$_3$), 3.12 (ABX_3, $^{2/3}J_{HH}$ = 6.6 Hz, 4 H, C*H'*$_2$CH$_3$), 0.89 (t, $^3J_{HH}$ = 6.9 Hz, 12 H, CH$_2$C*H*$_3$). – ^{13}C NMR (gated decoupled) (150.8 MHz, [D$_6$]benzene, 298 K): δ = 160.7 (t, $^3J_{CH}$ = 4 Hz, OC=N), 147.1 (s, *C*=CH_2), 136.6 (t, $^3J_{CH}$ = 7 Hz, *i*-Ph), 130.4 (dm $^1J_{CH}$ = 159 Hz, *p*-Ph), 129.0 (dm, $^1J_{CH}$ = 161 Hz, *o*-Ph), 128.1 (dm, $^1J_{CH}$ = 159 Hz, *m*-Ph), 126.0 (m, *i*-Cp), 110.64, 110.56 (each dm, each $^1J_{CH}$ = 171 Hz, Cp), 104.4 (ps. t, $^1J_{CH}$ = 159 Hz, C=*C*H$_2$), 44.1 (t, $^1J_{CH}$ = 131.7 Hz, N*C*H$_2$CH$_3$), 15.7 (qt, $^1J_{CH}$ = 125 Hz, $^2J_{CH}$ = 3 Hz, NCH$_2$*C*H$_3$). – ^{15}N,^1H GHMBC (60.8/599.9 MHz, [D$_6$]benzene, 298 K): δ^{15}N/δ^{1}H = –145/5.10 (C=*N*/C=C*H'*$_2$), –192/0.89 (*N*CH$_2$CH$_3$/C*H*$_2$CH$_3$).

Reaction of 3a with $HB(C_6F_5)_2$ – Formation of 7: Compound **3a** (255 mg, 500 μmol) and bis(pentafluorophenyl)borane (346 mg, 1.0 mmol) were weighed into a Schlenk vessel, which was then cooled to 0 °C, whereupon benzene (10 mL) was added. The resulting orange solution was allowed to warm to room temperature and stirred for 2 days. The yellow suspension obtained was filtered and the collected light-yellow precipitate was dried in vacuo yielding 102 mg (16%) of isomer **7a**. Concentration of the filtrate to dryness afforded a yellow powder (235 mg, 40% overall yield), which was found to contain the three diastereomers **7a**, **7b**, and **7c** in a ratio of 2:10:3.

Isomer 7a: $C_{52}H_{24}B_2F_{20}N_2O_2Zr \cdot C_6H_6$ (1279.70): calcd. C 54.44, H 2.36, N 2.19; found C 54.07, H 2.44, N 1.98. – DSC: 257 °C (m.p.), 267 °C (dec.). – ^1H NMR (599.9 MHz, [D$_2$]dichloromethane, 298 K): δ = 7.44 (ps. d, $^3J_{HH}$ = 7.78 Hz, 4 H, *o*-Ph), 7.34

(ps. t, $^3J_{HH}$ = 7.5 Hz, 2 H, *p*-Ph), 7.07 (m, 4 H, *m*-Ph), 6.81 (m, 2 H, Cp_β), 6.55 (m, 2 H, Cp_α), 6.46 (m, 2 H, Cp_α), 6.37 (m, 2 H, Cp_β), 5.20 (ps. t, $^3J_{HH}$ = 9.0 Hz, 2 H, NCH), 1.80 (ps. t, $^{2/3}J_{HH}$ = 10.5 Hz, 2 H, CH_2B), 1.67 (ps. t, $^{2/3}J_{HH}$ = 10.5 Hz, 2 H, CH'_2B). – ^{13}C NMR (gated decoupled) (150.8 MHz, [D$_2$]dichloromethane, 298 K): δ = 166.2 (s, OC=N), 136.6 [br. m, obscured by the carbon resonance of $B(C_6F_5)$, *i*-Cp], 133.1 (dt, $^1J_{CH}$ = 161 Hz, $^3J_{CH}$ = 8 Hz, *p*-Ph), 129.5 (d ps. t, $^1J_{CH}$ = 161 Hz, $^3J_{CH}$ = 7 Hz, *o*-Ph), 128.9 (t, $^3J_{CH}$ = 7 Hz, *i*-Ph), 128.1 (dd, $^1J_{CH}$ = 162 Hz, $^3J_{CH}$ = 7 Hz, *m*-Ph), 121.6 (dm, $^1J_{CH}$ = 175 Hz, Cp_β), 113.4 (dm, $^1J_{CH}$ = 175 Hz, Cp_α), 111.5 (dm, $^1J_{CH}$ = 175 Hz, Cp_β), 107.6 (dm, $^1J_{CH}$ = 174 Hz, Cp_α), 59.1 (d, $^1J_{CH}$ = 145 Hz, NCH), 27.2 (tm, $^1J_{CH}$ = 126 Hz, CH_2B). – ^{11}B NMR (64.2 Hz, [D$_2$]dichloromethane, 300 K): δ = –1.1 ($\nu_{1/2}$ = 670 Hz). – ^{15}N,^{1}H GHMBC (60.8 MHz/599.9 MHz, [D$_2$]dichloromethane, 298 K): $\delta^{15}N/\delta^1H$ = –209.3/5.20 (*N*C*H*), –209.3/1.67 (*N*CH/C*H'*$_2$B). – ^{19}F NMR (564.3 MHz, [D$_2$]dichloromethane, 298 K): δ = –133.3 [m, 2 F, *o*-$B(C_6F_5)$], –135.9 [m, 2 F, *o*-$B(C_6F_5)$'], –158.2 [t, $^3J_{FF}$ = 20.1 Hz, 1 F, *p*-$B(C_6F_5)$], 159.4 [t, $^3J_{FF}$ = 20.1 Hz, 1 F, *p*-$B(C_6F_5)$'], –164.5 [m, 2 F, *m*-$B(C_6F_5)$], –164.6 [m, 2 F, *m*-$B(C_6F_5)$'].

Isomer 7c: ^{1}H NMR (599.9 MHz, [D$_2$]dichloromethane, 298 K): δ = 7.51 (m, 4 H, *o*-Ph), 7.39 (m, 2 H, *p*-Ph), 7.32 (m, 2 H, Cp_β), 7.27 (m, 4 H, *m*-Ph), 6.54 (m, 2 H, Cp_α), 6.35 (m, 2 H, Cp_β), 6.19 (m, 2 H, Cp_α), 5.43 (ps. t, $^3J_{HH}$ = 9.1 Hz, 2 H, NCH), 1.88 (m, 2 H, CH_2B), 1.54 (m, 2 H, CH'_2B). – ^{1}H TOCSY (599.9 MHz, [D$_2$]dichloromethane, 298 K, irradiated at/response at): δ = 5.43 (NC*H*)/1.88 (C*H*$_2$B), 1.54 (C*H'*$_2$B). – ^{13}C NMR (gated decoupled) (150.8 MHz, [D$_2$]dichloromethane, 298 K): δ = 164.9 (s, OC=N), 132.7 (dm, $^1J_{CH}$ = 164 Hz, *p*-Ph), 131.1 (m, *i*-Cp), 124.3 (dm, $^1J_{CH}$ = 174 Hz, Cp_α), 116.9 (dm, $^1J_{CH}$ = 174 Hz, Cp_β), 109.6 (dm, $^1J_{CH}$ = 177 Hz, Cp_β), 109.1 (dm, $^1J_{CH}$ = 174 Hz, Cp_α), 59.2 (dm, $^1J_{CH}$ = 145 Hz, NCH), 27.3 (dm, $^1J_{CH}$ = 133 Hz, CH_2B) (signal obscured by those of the other isomers). The signals of the carbon atoms of the $B(C_6F_5)_2$ moiety are also obscured by those of the other isomers. The signals due to the phenyl carbon atoms cannot be distinguished from those due to the isomer **7b** and hence they are listed together. – ^{19}F NMR (564.3 MHz, [D$_2$]dichloromethane, 298 K): δ = –132.6 [m, 4 F, *o*-$B(C_6F_5)$], –136.2 [m, 4 F, *o*-$B(C_6F_5)$'], –158.2 [t, $^3J_{FF}$ = 20 Hz, 2 F, *p*-$B(C_6F_5)$], –159.9 [t, $^3J_{FF}$ = 20 Hz, 2 F, *p*-$B(C_6F_5)$'], –164.6 [m, 4 F, *m*-$B(C_6F_5)$'], –164.8 [m, 4 F, *m*-$B(C_6F_5)$].

Isomer 7b: ^{1}H NMR (599.9 MHz, [D$_2$]dichloromethane, 298 K): δ = 7.58 (m, 2 H, *o*-Ph), 7.42 (m, 2 H, *o*-Ph*), 7.41 (m, 1 H, *p*-Ph*), 7.40 (m, 1 H, *p*-Ph), 7.28 (m, 2 H, *m*-Ph), 7.27 (m, 2 H, *m*-Ph*), 7.16 (m, 1 H, Cp_β), 6.89 (m, 1 H, Cp_β*), 6.60 (m, 1 H, Cp_β*), 6.56 (m, 1 H, Cp_α*), 6.51 (m, 1 H, Cp_α*), 6.41 (m, 1 H, Cp_α), 6.29 (Cp_β), 6.24 (Cp_α), 5.51 (ps. t, $^3J_{HH}$ = 9.1 Hz, 1 H, NCH), 5.11 (ps. t, $^3J_{HH}$ = 9.0 Hz, 1 H, NCH*), 1.94 (m, 1 H, CH_2B), 1.91 (m, 1 H, CH_2B*), 1.52 (m, 1 H, CH'_2B*), 1.50 (m, 1 H, CH'_2B). – ^{1}H TOCSY (599.9 MHz, [D$_2$]dichloromethane, 298 K, irradiated at/response at): δ = 5.51 (NC*H*)/1.94 (C*H*$_2$B), 1.50 (C*H'*$_2$B); 5.11 (NC*H*)/1.91 (C*H*$_2$B*), 1.52 (C*H'*$_2$B*). – ^{13}C NMR (gated decoupled) (150.8 MHz, [D$_2$]dichloromethane, 298 K): δ = 166.7 (s, OC=N), 164.7 (s, OCN), 134.0 (m, *i*-Cp*), 133.0 (dm, $^1J_{CH}$ = 164 Hz, *p*-Ph*), 132.8 (dm, $^1J_{CH}$ = 164 Hz, *p*-Ph), 126.4 (m, *i*-Cp), 125.8 (dm, $^1J_{CH}$ = 175 Hz, Cp_α), 124.5 (dm, $^1J_{CH}$ = 175 Hz, Cp_β*), 116.2 (dm, $^1J_{CH}$ = 175 Hz, Cp_β), 112.4 (dm, $^1J_{CH}$ = 179 Hz, Cp_α*), 110.9 (dm, $^1J_{CH}$ = 174 Hz, Cp_α), 110.0 (dm, $^1J_{CH}$ = 175 Hz, Cp_β*), 109.1 (dm, $^1J_{CH}$ = 177 Hz, Cp_α*), 108.2 (dm, $^1J_{CH}$ = 177 Hz, Cp_β), 59. 6 (dm, $^1J_{CH}$ = 144 Hz, NCH), 59.0 (dm, $^1J_{CH}$ = 145 Hz, NCH*), 27.3 (tm, $^1J_{CH}$ = 133 Hz, CH_2B*), 27.0 (tm, $^1J_{CH}$ = 130 Hz, CH_2B). – ^{11}B NMR (64.2 MHz, [D$_2$]dichloromethane, 300 K): δ = –1.5 ($\nu_{1/2}$ = 920 Hz). – ^{15}N,^{1}H GHMBC (60.8 MHz/599.9 MHz, [D$_2$]dichloromethane, 298 K): $\delta^{15}N/\delta^1H$ = –208.6/5.51 (*N*C*H*), –208.6/1.50 (*N*CH/CH'$_2$B), –209.1/5.11 (*N*C*H**), –209.1/1.52 (*N*CH/C*H'*$_2$B*). – ^{19}F NMR (564.3 MHz, [D$_2$]dichloromethane, 298 K): δ = –132.1 [m, 2 F, *o*-$B(C_6F_5)$], –132.4 [m, 2 F, *o*-$B^*(C_6F_5)$], –136.7 [m, 2 F, *o*-$B(C_6F_5)$'], –137.3 [br. m, 2 F, *o*-$B^*(C_6F_5)$'], –158.0 [m, 1 F, *p*-$B(C_6F_5)$], –158.1 [m, 1 F, *p*-$B^*(C_6F_5)$], –159.8 [m, 1 F, *p*-$B^*(C_6F_5)$'], –159.9 [m, 1 F, *p*-$B(C_6F_5)$'], –164.2 [m, 2 F, *m*-$B^*(C_6F_5)$'], –164.6 [m, 2 F, *m*-$B(C_6F_5)$'], –164.7 [m, 2 F, *m*-$B(C_6F_5)$], –164.9 [m, 2 F, *m*-$B^*(C_6F_5)$].

X-ray Crystal Structure Analysis of 7a: Crystals from C_6D_6, formula $C_{62.5}H_{34.5}B_2F_{20}N_2O_2Zr$, M_r = 1338.26, light-yellow crystal, 0.25 × 0.20 × 0.20 mm, *a* = 12.621(2) Å, *b* = 14.907(2) Å, *c* = 15.900 (2) Å, α = 73.28(1)°, β = 80.74(1)°, γ = 83.67(1)°, *V* = 2821.2(7) Å^3, ρ_{calcd} = 1.575 g cm^{-3}, *F*(000) = 1339 e, μ = 3.09 cm^{-1}, empirical absorption correction based on SORTAV (0.927 ≤ *T* ≤ 0.941), *Z* = 2, triclinic, space group $P\bar{1}$ (No. 2), λ = 0.71073 Å, *T* = 198 K, 14406 reflections collected (±*h*, ±*k*, ±*l*), $[(\sin\theta)/\lambda]_{max}$ = 0.59 Å^{-1}, 8208 independent and 6373 observed reflections [$I \geq 2\sigma(I)$], 820 refined parameters, R = 0.088, wR^2 = 0.194, max. residual electron density 1.33 (–0.58) e Å^{-3}; the asymmetric unit contains two half-molecules of benzene and one three-quarter-molecule of benzene.

Reaction of 3b with $HB(C_6F_5)_2$. – Formation of 9: To a solution of compound **3b** (190 mg, 427 μmol) in toluene (20 mL) was added bis(pentafluorophenyl)borane (148 mg, 427 μmol). After stirring of the orange solution for 1 day, the solvent was removed in vacuo to provide 293 mg (87%) of the product as an orange solid. – DSC: 99 °C (dec.). – $C_{34}H_{32}BF_{10}N_3OZr$ (790.67): calcd. C 51.65, H 4.08, N 5.31; found C 51.64, H 4.34, N 4.46. – IR (KBr): $\tilde{\nu}$ = 1645, 1599, 1516 cm^{-1}. – ^{1}H NMR (599.9 MHz, [D$_6$]benzene, 298 K): δ = 7.69 (m, 2 H, *o*-Ph), 6.82 (m, 2 H, *m*-Ph), 6.77 (m, 1 H, *p*-Ph), 6.32 (m, 1 H, Cp_α), 6.15 (m, 1 H, Cp_β), 5.89 (m, 1 H, Cp_α), 5.82 (m, 1 H, Cp_β), 5.15 (ps. t, $^3J_{HH}$ = 9.1 Hz, 1 H, NCH), 3.24 (ABX_3, $^{2/3}J_{HH}$ = 7.0 Hz, 2 H, NCH_2CH_3), 3.04 (ABX_3, $^{2/3}J_{HH}$ = 7.0 Hz, 2 H, $N'CH_2CH_3$), 2.97 (ABX_3, $^{2/3}J_{HH}$ = 6.9 Hz, 2 H, NCH'_2CH_3), 2.95 (ABX_3, $^{2/3}J_{HH}$ = 7.0 Hz, 2 H, $N'CH'_2CH_3$), 2.22 (ps. t, $^{2/3}J_{HH}$ = 10.6 Hz, 1 H, CH_2B), 1.73 (ps. t, $^{2/3}J_{HH}$ = 10.3 Hz, 1 H, CH'_2B), 0.85 (t, $^3J_{HH}$ = 7.0 Hz, 6 H, $N'CH_2CH_3$), 0.73 (t, $^3J_{HH}$ = 6.9 Hz, 6 H, NCH_2CH_3). – ^{1}H TOCSY (599.9 MHz, [D$_6$]benzene, 298 K, irradiation at/response at): δ = 7.69 (o-Ph)/6.82 (*m*-Ph), 6.77 (*p*-Ph); 6.32 (Cp_α)/6.15 (Cp_β), 5.89 (Cp_α), 5.82 (Cp_β); 5.15 (NC*H*)/2.22 (C*H*$_2$B), 1.73 (C*H'*$_2$B); 3.24 (NCH_2CH_3)/2.97 (NCH'_2CH_3), 0.73 (NCH_2CH_3); 1.73 (C*H'*$_2$B)/5.15 (NC*H*), 2.22 (C*H*$_2$B); 0.85 ($N'CH_2CH_3$)/3.04 ($N'CH_2CH_3$), 2.95 ($N'CH'_2CH_3$); 0.73 (NCH_2CH_3)/3.24 (NCH_2CH_3), 2.97 (NCH'_2CH_3). – ^{13}C NMR (gated decoupled) (150.8 MHz, [D$_8$]toluene, 298 K): δ = 166.0 (s, OC=N), 149.0 (dm, $^1J_{CF}$ = 243 Hz) and 148.1 (dm, $^1J_{CF}$ = 238 Hz) [*o*-$B(C_6F_5)$, *o*-$B(C_6F_5)$'], 139.8 [ps. d, $^1J_{CF}$ = 247 Hz, *p*-$B(C_6F_5)$, *p*-$B(C_6F_5)$'], 137.7 (dm, $^1J_{CF}$ = 251 Hz) and 137.4 (dm, $^1J_{CF}$ = 251 Hz) [*m*-$B(C_6F_5)$, *m*-$B(C_6F_5)$'], 132.0 (dm, $^1J_{CH}$ = 161 Hz, *p*-Ph), 131.4 (s, *i*-Ph), 123.6, 118.8 [each m, *i*-$B(C_6F_5)_2$], 113.7 (dm, $^1J_{CH}$ = 171 Hz, Cp_α), 113.1 (dm, $^1J_{CH}$ = 174 Hz, Cp_β), 110.2 (dm, $^1J_{CH}$ = 171 Hz, Cp_α), 109.2 (dm, $^1J_{CH}$ = 172 Hz, Cp_β), 60.2 (d, $^1J_{CH}$ = 144 Hz, NCH), 44.0 (t, $^1J_{CH}$ = 132 Hz, $N'CH_2CH_3$), 43.3 (t, $^1J_{CH}$ = 132 Hz, NCH_2CH_3), 27.8 (tm, $^1J_{CH}$ = 134 Hz, CH_2B), 15.8 (q, $^1J_{CH}$ = 126 Hz, $N'CH_2CH_3$), 15.2 (t, $^1J_{CH}$ = 126 Hz, NCH_2CH_3). – ^{11}B NMR (64.2 MHz, [D$_6$]benzene, 300 K): δ = –2.4 ($\nu_{1/2}$ = 420 Hz). – ^{15}N,^{1}H GHMBC (60.8/599.9 MHz, [D$_6$]benzene, 298 K): $\delta^{15}N/\delta^1H$ = –171/0.85 (NCH_2CH_3), –187/0.73 ($N'CH_2CH_3$), –205/5.15 (*N*C*H*). – ^{19}F NMR (282.4 MHz, [D$_6$]benzene, 298 K): δ = –132.5 [m, 2 F, *o*-$B(C_6F_5)$], –136.4 [m, 2 F, *o*-$B(C_6F_5)$'], –158.2 [ps. t, $^3J_{FF}$ = 21 Hz,

1 F, *p*-B(C_6F_5)], –159.0 [ps. t, $^3J_{FF}$ = 21 Hz, 1 F, *p*-B(C_6F_5)'], –163.7 [m, 2 F, *m*-B(C_6F_5)'], –164.4 [m, 2 F, *m*-B(C_6F_5)].

Reaction of 3b with $HB(C_6F_5)_2$ at Low Temperature. – Generation of the Adduct 8: 30 mg (67 μmol) of **3b** was dissolved in [D_8]toluene (0.4 mL) and this solution was cooled to –78 °C and then added to an NMR tube containing a suspension of bis(pentafluorophenyl)borane (23 mg, 67μmol) in [D_8]toluene (0.1 mL) at –78 °C. While warming to room temperature, the NMR tube was shaken until all of the solid had dissolved. After 1 min under ambient conditions, the solution was cooled to 0 °C. Simultaneous formation of compound **9** could not be avoided. At 5 °C, however, the subsequent reaction to **9** is very slow and the adduct **8** could still be detected after 3 weeks. – ^{1}H NMR (599.8 MHz, [D_8]toluene, 273 K): δ = 7.55 (m, 2 H, *o*-Ph), 6.89 (m, 2 H, *m*-Ph), 6.83 (m, 1 H, *p*-Ph), 6.06, 5.77 (each m, each 2 H, Cp), 5.41 (ps. s, 1 H), 5.04 (d, $^2J_{HH}$ = 0.90 Hz, 1 H, C=CH_2), 2.95–2.86 (each m, each 4 H, N$CH_2$$CH_3$, N$CH'_2$$CH_3$), 0.63 (ps. t, $^3J_{HH}$ = 6.9 Hz, 12 H, NCH_2CH_3). – ^{13}C NMR (gated decoupled) (150.8 MHz, [D_8]toluene, 273 K): δ = 135.3 (t, $^2J_{CH}$ = 8 Hz, *i*-Cp), 130.6 (dm, $^1J_{HH}$ = 162 Hz, *p*-Ph), 127.1 (dm, $^1J_{HH}$ = 163 Hz, *o*-Ph), 111.5 (d, $^1J_{CH}$ = 175 Hz, Cp), 110.6 (d, $^1J_{CH}$ = 171 Hz, Cp), 43.6 (t, $^1J_{CH}$ = 130 Hz, NCH_2CH_3), 15.3 (q, $^1J_{HH}$ = 127 Hz, NCH_2CH_3); the *m*-Ph and *i*-Cp signals are obscured by those of the solvent. – ^{11}B NMR (64.2 MHz, [D_6]benzene, 300 K): δ = –11.6 (d, $^1J_{BH}$ = 60 Hz, $\nu_{1/2}$ = 390 Hz). – ^{15}N,^{1}H GHMBC (60.8/599.8 MHz, [D_8]toluene, 273 K): $\delta^{15}N/\delta^1H$ = –204/5.04 (OC=*N*/C=CH_2), –173/0.63 (*N*CH_2CH_3). – ^{19}F NMR (564.3 MHz, [D_6]benzene, 298 K): δ = –133.3 [br. ps. s, 4 F, *o*-B(C_6F_5)$_2$], –159.7 [ps. t, $^3J_{FF}$ = 20.6 Hz, 2 F, *p*-B(C_6F_5)$_2$], –164.8 [br. ps. s, 4 F, *m*-B(C_6F_5)$_2$].

Propene Polymerization Reactions. – General Procedure: A thermostated Büchi glass autoclave (25 °C) was charged with toluene (300 mL) and 20 mL of a 10% (1.6 M) methylalumoxane solution in toluene. Propene was introduced at a pressure of 2.0 bar. After 0.5 h, a solution of the organometallic catalyst precursor in 5 mL of toluene was added and the polymerization reaction allowed to proceed for 2.0 h. The system was then vented and its contents were quenched by treatment with aqueous HCl/CH_3OH (1:1). The layers were separated and the aqueous phase was extracted with toluene (3 × 100 mL). The combined organic layers were then washed with aqueous HCl (3 × 100 mL) and with water (3 × 100 mL) to remove inorganic salts. Evaporation of the solvent afforded the polymers as very viscous oils (see Table 1).

Acknowledgments

Financial support from the Fonds der Chemischen Industrie and the Deutsche Forschungsgemeinschaft is gratefully acknowledged.

[1] W. E. Piers, P. J. Shapiro, E. E. Bunel, J. E. Bercaw, *Synlett* **1990**, *2*, 74. J. C. Stevens, F. J. Timmers, D. R. Wilson, G. F. Schmidt, P. N. Nickias, R. K. Rosen, G. W. Knight, S. Lai, Eur. Patent Appl. EP 416815-A2, **1991** (Dow Chemical Co.). J. M. Canich, Eur. Patent Appl. EP 429436-A1, **1991** (Exxon Chemical Co.). J. M. Canich, G. G. Hlatky, H. W. Turner, PCT Appl. WO 92-00333, **1992**. P. J. Shapiro, W. D. Cotter, W. P. Schaefer, J. A. Labinger, J. E. Bercaw, *J. Am. Chem. Soc.* **1994**, *116*, 4623.

[2] W. P. Hart, D. W. Macomber, M. D. Rausch, *J. Am. Chem. Soc.* **1980**, *102*, 1196. M. D. Rausch, J. F. Lewison, W. P. Hart, *J. Organomet. Chem*. **1988**, *358*, 161. M. Ogasa, D. T. Mallin, D. W. Macomber, M. D. Rausch, R. D. Rogers, A. N. Rollins, *J. Organomet. Chem*. **1991**, *405*, 41. Review: D. W. Macomber, W. P. Hart, M. D. Rausch, *Adv. Organomet. Chem*. **1982**, *21*, 1. N. J. Coville, K. E. du Plooy, W. Pickl, *Coord. Chem. Rev.* **1992**, *116*, 1.

[3] M. Oberhoff, L. Duda, J. Karl, R. Mohr, G. Erker, R. Fröhlich, M. Grehl, *Organometallics* **1996**, *15*, 4005. K. Klaß, L. Duda, N. Kleigrewe, G. Erker, R. Fröhlich, E. Wegelius, *Eur. J. Inorg. Chem*. **1999**, 11.

[4] S. Knüppel, G. Erker, R. Fröhlich, *Angew. Chem.* **1999**, *111*, 2048; *Angew. Chem. Int. Ed. Engl*. **1999**, *38*, 1923. S. Knüppel, R. Fröhlich, G. Erker, *J. Organomet. Chem*. **1999**, *586*, 218. S.-D. Bai, X.-H. Wei, J.-P. Guo, D.-S. Liu, Z.-Y. Zhou, *Angew. Chem.* **1999**, *111*, 2051; *Angew. Chem. Int. Ed. Engl*. **1999**, *38*, 1926.

[5] L. Duda, G. Erker, R. Fröhlich, F. Zippel, *Eur. J. Inorg. Chem.* **1998**, 1153. A. Bertuleit, M. Könemann, L. Duda, G. Erker, R. Fröhlich, *Topics in Catalysis* **1999**, *7*, 37.

[6] R. E. v. H. Spence, W. E. Piers, *Organometallics* **1995**, *14*, 4617. See also: G. Erker, R. Aul, *Chem. Ber*. **1991**, *124*, 1301.

[7] [7a] Syntheses: D. J. Parks, R. E. v. H. Spence, W. E. Piers, *Angew. Chem.* **1995**, *107*, 895; *Angew. Chem. Int. Ed. Engl*. **1995**, *34*, 809. D. J. Parks, W. E. Piers, G. P. A. Yap, *Organometallics* **1998**, *17*, 5492. – [7b] Selected reactions: R. E. v. H. Spence, D. J. Parks, W. E. Piers, M.-A. MacDonald, M. J. Zaworotko, S. J. Retty, *Angew. Chem.* **1995**, *107*, 1337; *Angew. Chem. Int. Ed. Engl*. **1995**, *34*, 1230. Y. Sun, R. E. v. H. Spence, W. E. Piers, M. Parvez, G. P. A. Yap, *J. Am. Chem. Soc.* **1997**, *119*, 5132. R. E. v. H. Spence, W. E. Piers, Y. Sun, M. Parvez, L. R. MacGillivray, M. J. Zaworotko, *Organometallics* **1998**, *17*, 2459. Review: W. E. Piers, Y. Sun, L. W. M. Lee, *Topics in Catalysis* **1999**, *7*, 133.

[8] K. Hafner, G. Schultz, K. Wagner, *Chem. Ber*. **1964**, *768*, 539. K. Hafner, K. H. Vöpel, G. Ploss, C. König, *Org. Synth. Coll*. Vol. 5, Wiley, New York, **1973**, p. 431.

[9] [9a] M. Bodanszky, *Principles of Peptide Synthesis*, Springer, Berlin, **1993**. – [9b] D. A. Williamson, B. E. Bowler, *Tetrahedron* **1996**, *52*, 12357. Y. A. Avez, G. A. Mokrushina, I. Y. Postrovskii, Y. N. Sheinkov, O. S. Anisimova, *Chem. Heterocycl. Compds.* **1976**, 1172. L. A. Carpino, *J. Am. Chem. Soc.* **1993**, *115*, 4397. L. A. Carpino, A. El-Faham, C. A. Minor, F. Albericio, *J. Chem. Soc., Chem. Commun*. **1994**, 201. L. A. Carpino, A. El-Faham, F. Albericio, *Tetrahedron Lett.* **1994**, *35*, 2279.

[10] G. Erker, S. Wilker, C. Krüger, R. Goddard, *J. Am. Chem. Soc*. **1992**, *114*, 10983. G. Erker, S. Wilker, C. Krüger, M. Nolte, *Organometallics* **1993**, *12*, 2140.

[11] G. Erker, U. Dorf, C. Krüger, Y.-H. Tsay, *Organometallics* **1987**, *6*, 680.

[12] See, for comparison: G. Erker, K. Engel, J. L. Atwood, W. E. Hunter, *Angew. Chem*. **1983**, *95*, 506, *Angew. Chem. Int. Ed. Engl*. **1983**, *22*, 494.

[13] F. H. Allen, O. Kennard, D. G. Watson, L. Brammer, A. G. Orpen, R. Taylor, *J. Chem. Soc., Perkin Trans. 2* **1987**, S1.

[14] S. Brenner, R. Kempe, P. Arndt, *Z. Anorg. Allg. Chem*. **1995**, *621*, 2021.

[15] For related $B(C_6F_5)_3$ adducts, see e.g.: D. C. Bradley, M. B. Hursthouse, M. Motevalli, D. H. Zheng, *J. Chem. Soc., Chem. Commun.* **1991**, 7. X. Yang, C. L. Stern, T. J. Marks, *J. Am. Chem. Soc.* **1994**, *116*, 10015. D. J. Parks, W. E. Piers, *J. Am. Chem. Soc.* **1996**, *118*, 9440. D. C. Bradley, I. S. Harding, A. D. Keefe, M. Motevalli, D. H. Zheng, *J. Chem. Soc., Dalton Trans.* **1996**, 3931. D. Röttger, G. Erker, R. Fröhlich, S. Kotila, *J. Organomet. Chem*. **1996**, *518*, 17. D. J. Parks, W. E. Piers, M. Parvez, R. Atencio, M. J. Zaworotko, *Organometallics* **1998**, *17*, 1369. S. Döring, G. Erker, R. Fröhlich, O. Meyer, K. Bergander, *Organometallics* **1998**, *17*, 2183. H. Jacobsen, H. Berke, S. Döring, G. Kehr, G. Erker, R. Fröhlich, O. Meyer, *Organometallics* **1999**, *18*, 1724. Review: W. E. Piers, T. Chivers, *Chem. Soc. Rev.* **1997**, *26*, 345.

[16] E. L. Eliel, S. H. Wilen, *Stereochemistry of Organic Compounds*, Wiley, New York, **1994**, Chapter 14.

[17] [17a] S. Berger, S. Braun, H.-O. Kalinowski, *NMR Spektroskopie von Nichtmetallen, Vol. 2, ^{15}N-NMR Spektroskopie*, Thieme, New York, **1992**. – [17b] See, for comparison: H. G. Alt, K. Föttinger, W. Milius, *J. Organomet. Chem*. **1999**, *572*, 21. J. Pflug, A. Bertuleit, G. Kehr, R. Fröhlich, G. Erker, *Organometallics* **1999**, *18*, 3818.

[18] H. Sinn, W. Kaminsky, *Adv. Organomet. Chem*. **1980**, *18*, 99.

[19] G. Erker, C. Fritze, *Angew. Chem*. **1992**, *104*, 204, *Angew. Chem. Int. Ed. Engl*. **1992**, *31*, 199. See also: G. Erker, R. Nolte, Y.-H. Tsay, C. Krüger, *Angew. Chem.* **1989**, *101*, 642, *Angew. Chem. Int. Ed. Engl*. **1989**, *28*, 628.

[20] Programs used: [20a] Data collection: Express: Nonius B.V., **1994**. Collect: Nonius B.V., **1998**. – [20b] Data reduction: MolEN: K. Fair, Enraf–Nonius B.V., **1990**. Denzo-SMN: Z. Otwinowski, W. Minor, *Methods in Enzymology* **1997**, *276*, 307–326. – [20c] Absorption correction: MolEN: K. Fair, Enraf–Nonius B.V., **1990**; SORTAV: R. H. Blessing, *Acta Cryst*. **1995**, *A51*, 33–37; *J. Appl. Cryst*. **1997**, *30*, 421–426. – [20d] Structure solution: SHELXS-86 and SHELXS-97: G. M. Sheldrick, *Acta Cryst*. **1990**, *A46*, 467–473. G. M. Sheldrick, Universität Göttingen, **1997**. – [20e] Structure refinement: SHELXL-97: G. M. Sheldrick, Universität Göttingen, **1997**. – [20f] Graphics: SCHAKAL: E. Keller, Universität Freiburg, **1997**. – [20g] Crystallographic data (excluding structure factors) for the structures reported in this paper have been deposited with the Cambridge Crystallographic Data Centre as supplementary publications nos. CCDC-127619 and 127620. Copies of the data can be obtained free of charge on application to The Director, CCDC, 12 Union Road, Cambridge CB2 1EZ, U.K. [Fax: (internat.) +44 (0)1223 336033; E-mail: deposit@ccdc.cam.ac.uk].

[21] L. E. Manzer, *Inorg. Synth.* **1985**, *21*, 135.

Received July 26, 1999
[I99273]

2*H*-1,2-Azaphosphindoles – Synthesis and Characterization

Victorio Cadierno,[a] Bruno Donnadieu,[a] Alain Igau,[a] and Jean-Pierre Majoral*[a]

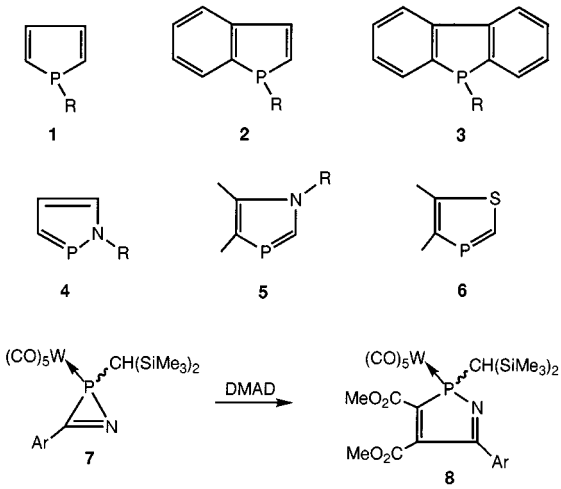
Keywords: Phosphorus / Benzynezirconocenes / Azazirconacyclopentenes / Exchange reactions / 1,2-Azaphosphindole

The first 1,2-azaphosphindoles **14a,b**, **15a,b** were obtained in a straightforward manner upon heating diphenylzirconocene in the presence of a cyanophosphane, which afforded azazirconacyclopentenes **11a,b** which can be reacted with various dichlorophosphanes. The use of the tetrachlorodiphosphane $Cl_2P(CH_2)_2PCl_2$ instead of a dichlorophosphane allowed the preparation of the bis(1,2-azaphosphindoles) **19**, **19′**. The monosulfur adduct of the azaphosphindole **14a**, i.e. **16a**, was characterized by X-ray structure analysis. Alkylation of **14a** or **16a** with methyltrifluoromethane sulfonate occurred selectively on the intracyclic phosphorus atom or on the sulfur atom, giving the salts **20** or **21**, respectively.

Introduction

Chemistry of 1*H*-phospholes **1** and of the corresponding fused-ring systems phosphindoles **2** (phosphorus analogs of indoles) and dibenzophospholes **3** has attracted considerable attention in the past two decades and is now well-documented.[1] The chemical behavior of these phosphorus heterocycles appeared to be quite different from that of the common heterocyclopentadiene systems such as furan, pyrrole and thiophene, and was the source of a rich and versatile chemistry.[1]

In marked contrast, synthesis and properties of analogous systems containing both phosphorus and one additional heteroatom are quite undeveloped and only a very few examples of 1*H*-1,2-azaphospholes **4**,[2a] 1*H*-1,3-λ^3-azaphospholes of type **5** or 1,3-λ^3-thiaphospholes of type **6** were reported.[2b,2c] Moreover, in all these derivatives the phosphorus atom is dicoordinated and not tricoordinated as in compounds **1–3**. Indeed, only recently was reported the formation of unique 2*H*-1,2-azaphosphole tungsten-complexes **8** by the thermal decomposition of 2*H*-azaphosphirene **7** in toluene at 75 °C in the presence of DMAD[3] (Scheme 1). However, such a method suffers from two main drawbacks: 2*H*-azaphosphirenes are not easy to prepare, and yields of isolated complexes **8** are poor (5–12%).

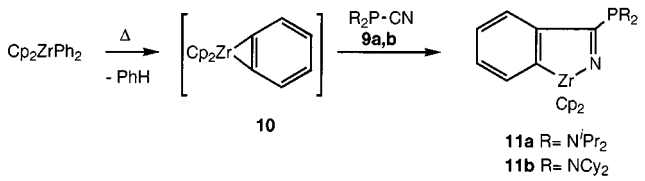


Scheme 1. Synthesis of 2*H*-1,2-azaphosphole tungsten complexes **8**

To our knowledge the preparation of free 1,2-azaphospholes and 1,2-azaphosphindoles has not yet been reported. We now present the facile synthesis of a number of azaphosphindoles, the X-ray characterization of an azaphosphindole, as well as preliminary studies concerning their reactivity.

Results and Discussion

Thermolysis of diphenylzirconocene in the presence of a wide variety of nitriles has previously been shown to generate azazirconacyclopentenes as dimers in the solid state in good to excellent yields.[4] A similar reaction was undertaken with the bisamino-cyanophosphanes **9a,b**[5] and diphenylzirconocene (Scheme 2). The transient zirconocene–benzyne complex **10** was trapped by **9a,b** to give the new azazirconacyclopentenes **11a,b** in 95% and 93% yield respectively. The reaction can be monitored by ^{31}P NMR spectroscopy, which shows the disappearance of the signal of the starting phosphane (**9a:** $\delta = 29.5$, **9b:** $\delta = 33.7$), which is replaced by a new signal at $\delta = 45.5$ (**11a**) or $\delta = 55.8$ (**11b**). Mass spectrometry (FAB) is in agreement with the expected compounds **11a** and **11b**.



Scheme 2. Synthesis of azazirconacyclopentenes **11a, b**

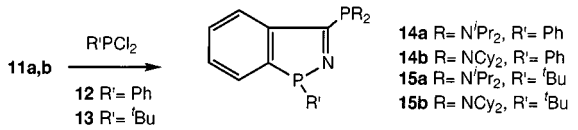
Infrared spectroscopy ($\tilde{\nu}_{C=N} = 1581–1583\ cm^{-1}$), and ^{13}C NMR [**11a:** $\delta_{C=N} = 191.3$ (d, $^1J_{CP} = 19.0$ Hz); **11b:** $\delta_{C=N} = 191.2$ (d, $^1J_{CP} = 19.5$ Hz)] corroborated the presence of an imino group. All the other NMR data are in agreement with the proposed azazirconacyclopentene structure.

Treatment of **11a** or **11b** with phenyldichlorophosphane **12** or *tert*-butyldichlorophosphane **13** at room temperature

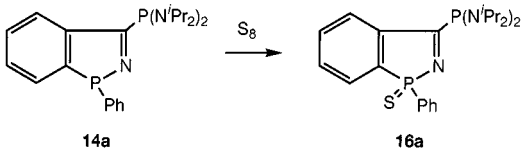
[a] Laboratoire de Chimie de Coordination, CNRS,
205 route de Narbonne, F-31077 Toulouse cedex 04, France
Fax: (internat.) + 33-5/61553003
E-mail: majoral@lcc-toulouse.fr

 © WILEY-VCH Verlag GmbH, D-69451 Weinheim, 2000 1434−1948/00/0303−0417 $ 17.50+.50/0

led to elimination of Cp_2ZrCl_2 to form the unprecedented 1,2-azaphosphindoles **14a,b** or **15a,b** as yellow solids obtained in 69–86% yield after workup (Scheme 3). The ^{31}P NMR spectrum exhibited, as expected, two doublets for compounds **14a**, **14b**, and **15b** {**14a:** δ = 41.1 [P(N*i*Pr$_2$)$_2$], 77.0 (PPh), J_{PP} = 6.7 Hz; **14b:** δ = 44.1 [P(NCy$_2$)$_2$], 76.5 (PPh), J_{PP} = 13.7 Hz; **15b:** δ = 44.9 [P(N*i*Pr$_2$)$_2$], 99.0 (P*t*Bu), J_{PP} = 6.5 Hz}; only two singlets were detected for **15a** at δ = 43.8 [P(N*i*Pr$_2$)$_2$] and at δ = 100.2 (P*t*Bu). Both 1,2-azaphosphindoles were further characterized by ^1H and ^{13}C NMR, IR, mass spectrometry and elemental analyses. Addition of sulfur to **14a** afforded selectively the monosulfide **16a** {δ = 39.8 (PN*i*Pr$_2$)$_2$ and 81.9 [P(S)Ph], J_{PP} = 6.5 Hz} (Scheme 4). Confirmation of the identity of **16a** and as a consequence of **14a** and the other 1,2-azaphosphindoles was achieved by a single-crystal X-ray study. The representation of the structure of **16a** is shown in Figure 1 , and the most representative bond lengths and angles are summarized.



Scheme 3. Synthesis of 1,2-azaphosphindoles **14a,b, 15a,b**



Scheme 4. Synthesis of the monosulfide adduct **16a**

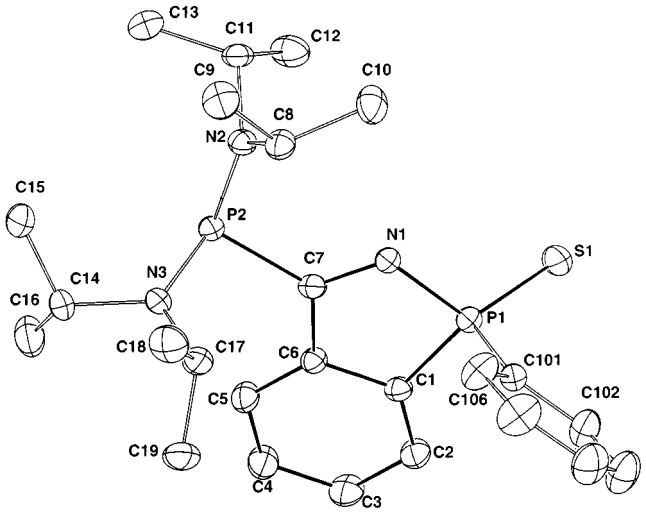
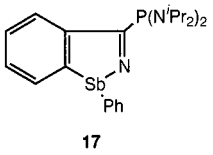
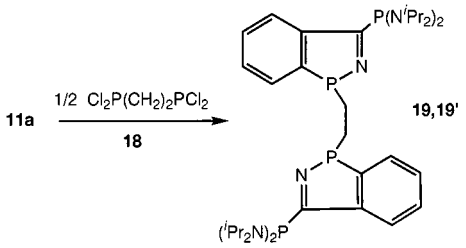


Figure 1. Molecular structure of **16a** with crystallographic numbering scheme; selected bond lengths (Å) and bond angles (°): P(1)–N(1) 1.702 (3), P(1)–C(1) 1.791 (4), C(7)–N(1) 1.300 (4), C(6)–C(7) 1.498 (5), C(6)–C(1) 1.393 (5), P(2)–N(3) 1.674 (3), N(1)–P(1)–C(1) 94.94 (15), C(7)–N(1)–P(1) 110.0 (2)

It appears therefore that such a one-pot reaction involving diphenylzirconocene, a cyanophosphane then by a dichlorophosphane, constitutes a very efficient method for the preparation of the first 3-phosphanyl-1,2-azaphosphindoles. A similar exchange reaction involving **11a** and phenyldichlorostilbene led to the formation of the corresponding 1,2-azastilbindole **17** obtained in 72% yield after workup. The ^{31}P chemical shift of **17** (δ = 83.8) as well as the $^1J_{CP}$ coupling constant of the imino carbon atom (J_{CP} = 0 Hz) differ notably from the values detected for the azaphosphindoles described above. However, such a variation of chemical shift and very small $^1J_{CP}$ values were already observed in different systems incorporating a bis(diisopropylamino)-phosphanyl group. Mass spectrometry (*m*/*z*: 532 [M + H]$^+$) and the other NMR data corroborate the proposed structure.

Such a methodology can be applied to the preparation of derivatives incorporating more than one 1,2-azaphosphindole unit. As an example, treatment of a solution of the complex **11a** in toluene with the phosphane $Cl_2P(CH_2)_2PCl_2$ **18** at 0 °C for 15 min afforded the expected bis 1,2-azaphosphindole in 91% yield as two diastereoisomers **19** and **19'** in a 2:1 ratio (Scheme 5). The formation of these two diastereoisomers can be detected mainly by ^{31}P NMR spectroscopy, where two singlets were observed for the P(N*i*Pr$_2$)$_2$ group at δ = 41.4 and 42.6.

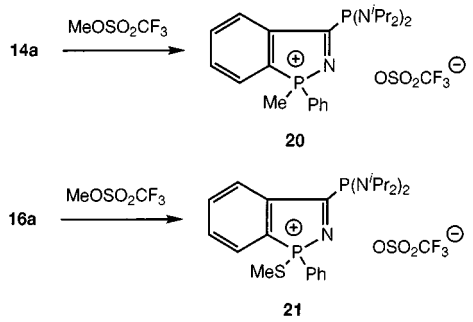




Scheme 5. Synthesis of bis(1,2-azaphosphindoles)

A preliminary study of the reactivity of these new phosphorus heterocycles was undertaken. Alkylation of **14a** by means of methyltrifluoromethane sulfonate selectively occurred on the intracyclic phosphorus atom leading to **20**. The signal of this phosphorus atom was deshielded ($\Delta\delta$ = 8.2) while the signal of the P(N*i*Pr$_2$)$_2$ unit was shielded ($\Delta\delta$ = 6.9). ^1H and ^{13}C NMR spectroscopy clearly indicated that the methyl group was linked to the P(Ph) group [^1H NMR: δ_{CH3} = 2.69 (d, J_{HP} = 14.6 Hz); ^{13}C NMR: δ_{CH3} = 8.7 (dd, J_{CP} = 61.0 Hz, J_{CP} = 4.0 Hz]. Alkylation of the sulfur adduct **16a** with methyltrifluoromethane sulfonate also took place selectively on sulfur, giving **21**

(Scheme 6). Alkylation did not occur on nitrogen or on the bis(diisopropylamino)phosphanyl group.



Scheme 6

Conclusion

In conclusion a simple and efficient way for the preparation of a new type of phosphorus heterocycles, namely 1,2-azaphosphindole, can be proposed through the thermolysis of benzynezirconocene in the presence of a cyanophosphane, followed by an exchange reaction involving the resulting azazirconacyclopentene and various dichlorophosphanes, or a tetrachlorodiphosphane. Taking into account the fascinating versatile chemistry of classical phospholes, azaphosphindoles should be reagents of choice to develop new applications of phosphorus heterocycles in different areas such as coordination and heterocyclic chemistry, and catalysis, to name a few. Such studies are under active investigation.

Experimental Section

General Remarks: All manipulations were conducted under a dry argon atmosphere using standard Schlenk techniques. All reagents were purchased from commercial suppliers and used without further purification. Solvents were dried by standard methods and distilled under argon before use. Nuclear magnetic resonance (NMR) spectra were recorded on Bruker AC-200, AM-250 or MSL 400 spectrometers. Chemical shifts are reported in ppm relative to $SiMe_4$ (^{1}H, ^{13}C) or H_3PO_4 (^{31}P). IR spectra were recorded on a Perkin–Elmer FT 1725x spectrometer. Mass spectrum analyses and elemental analyses were performed by the analytical service of the Laboratoire de Chimie de Coordination (LCC) of the CNRS.

General Procedure for the Synthesis of Compounds 11a,b: To a solution of Cp_2ZrPh_2 (0.410 g, 1.09 mmol) in toluene (5 mL) was added at room temperature the corresponding cyanophosphane $(R_2N)_2PC{\equiv}N$ [R = iPr (**9a**), Cy (**9b**)] (1.09 mmol). The mixture was heated at reflux for 45 min, and then evaporated to dryness. The resulting solid residue was washed with pentane (3 mL) to give compounds **11a**,**b** as red solids.

Compound 11a: 95% yield. – IR (KBr): $\tilde{\nu}_{(C=N)}$ = 1581 cm^{-1}. – ^{31}P{^{1}H} NMR (C_6D_6): δ = 45.5 (s). – ^{1}H NMR (C_6D_6): δ = 1.29 (d, J_{HH} = 2.2 Hz, 12 H, CH_3), 1.32 (d, J_{HH} = 2.4 Hz, 12 H, CH_3), 3.56 (m, 4 H, NCH), 5.94 (s, 10 H, CH_{Cp}), 6.95–7.12 (m, 3 H, CH_{arom}), 7.91 (m, 1 H, CH_{arom}). – ^{13}C{^{1}H} NMR (C_6D_6): δ = 24.7 (d, J_{CP} = 5.6 Hz, CH_3), 25.2 (d, J_{CP} = 6.5 Hz, CH_3), 48.9 (d, J_{CP} = 9.3 Hz, NCH), 111.6 (s, CH_{Cp}), 124.4, 126.5, 126.8 and 138.7 (s, CH_{arom}), 166.2 (d, J_{CP} = 51.7 Hz, ZrC*C*), 191.3 (d, J_{CP} = 19.0 Hz, C=N), 192.0 (d, J_{CP} = 7.7 Hz, ZrC). – MS (FAB.); *m*/*z*: 554 [M + H]$^+$, 453 [M – *i*Pr$_2$N]$^+$ – $C_{29}H_{42}N_3PZr$ (554.86): calcd. C 62.77, H 7.63, N 7.57; found C 62.68, H 7.59, N 7.65.

Compound 11b: 93% yield. – IR (KBr): $\tilde{\nu}_{(C=N)}$ = 1583 cm^{-1}. – ^{31}P{^{1}H} NMR (C_6D_6): δ = 55.8 (s). – ^{1}H NMR (C_6D_6): δ = 1.07–2.17 (m, 40 H, CH_2), 3.07 (m, 4 H, NCH), 6.02 (s, 10 H, CH_{Cp}), 7.00–7.33 (m, 3 H, CH_{arom}), 7.96 (d, J_{HH} = 7.1 Hz, 1 H, CH_{arom}). – ^{13}C{^{1}H} NMR (C_6D_6): δ = 26.7, 27.5 and 27.8 (s, CH_2), 35.7 (br s, CH_2), 58.4 (d, J_{CP} = 9.2 Hz, NCH), 59.2 (br s, NCH), 59.8 (d, J_{CP} = 9.1 Hz, NCH), 111.6 (s, CH_{Cp}), 124.2, 126.7 and 138.5 (s, CH_{arom}), 126.9 (d, J_{CP} = 8.6 Hz, CH_{arom}), 166.3 (d, J_{CP} = 50.8 Hz, ZrC*C*), 191.2 (d, J_{CP} = 19.5 Hz, C=N), 191.9 (d, J_{CP} = 7.8 Hz, ZrC). – MS (FAB.); *m*/*z*: 714 [M + H]$^+$. – $C_{41}H_{58}N_3PZr$ (715.13): calcd. C 68.86, H 8.17, N 5.87; found C 68.75, H 8.09, N 5.96.

General Procedure for the Synthesis of Compounds 14a,b: To a solution of the corresponding complex **11a**,**b** (0.364 mmol) in toluene (5 mL) was added at room temperature $PhPCl_2$ (**12**) (0.049 mL, 0.364 mmol). The mixture was stirred at room temperature for 30 min and then evaporated to dryness. The resulting solid residue was extracted with pentane (20 mL) and filtered. The volatiles were removed from the solution to give compounds **14a**,**b** as yellow solids.

Compound 14a: 86% yield. – IR (KBr): $\tilde{\nu}_{(C=N)}$ = 1571 cm^{-1} . – ^{31}P{^{1}H} NMR (C_6D_6): δ = 41.1 [d, J_{PP} = 6.7 Hz, P(N*i*Pr$_2$)$_2$], 77.0 (d, J_{PP} = 6.7 Hz, PPh). – ^{1}H NMR (C_6D_6): δ = 1.15 (d, J_{HH} = 6.4 Hz, 6 H, CH_3), 1.22 (d, J_{HH} = 6.6 Hz, 12 H, CH_3), 1.28 (d, J_{HH} = 6.7 Hz, 6 H, CH_3), 3.63 (m, 4 H, NCH), 6.97–7.58 (m, 8 H, CH_{arom}), 8.45 (m, 1 H, CH_{arom}). – ^{13}C{^{1}H} NMR (C_6D_6): δ = 24.6 (d, J_{CP} = 5.3 Hz, CH_3), 24.9 (d, J_{CP} = 6.8 Hz, CH_3), 48.6 (d, J_{CP} = 11.4 Hz, NCH), 49.1 (d, J_{CP} = 10.7 Hz, NCH), 126.2 (d, J_{CP} = 12.6 Hz, CH_{arom}), 127.8 and 128.3 (s, CH_{arom}), 128.6 (d, J_{CP} = 3.8 Hz, CH_{arom}), 129.1 (d, J_{CP} = 7.2 Hz, *o*-PPh), 130.2 (s, *p*-PPh), 132.7 (d, J_{CP} = 20.8 Hz, *m*-PPh), 135.6 (dd, J_{CP} = 18.7 Hz, J_{CP} = 4.5 Hz, *i*-PPh), 145.9 (dd, J_{CP} = 41.4 Hz, J_{CP} = 22.0 Hz, *C*CPPh), 154.0 (dd, J_{CP} = 17.0 Hz, J_{CP} = 3.8 Hz, CPPh), 187.5 (pt, J_{CP} = 15.5 Hz, J_{CP} = 15.5 Hz, C=N). – MS (DCI/NH$_3$); *m*/*z*: 442 [M + H]$^+$. – $C_{25}H_{37}N_3P_2$ (441.53): calcd. C 68.00, H 8.44, N 9.51; found C 67.91, H 8.58, N 9.70.

Compound 14b: 75% yield. – IR (KBr): $\tilde{\nu}_{(C=N)}$ = 1601 cm^{-1}. – ^{31}P{^{1}H} NMR (C_6D_6): δ = 44.1 [d, J_{PP} = 13.7 Hz, P(NCy$_2$)$_2$], 76.5 (d, J_{PP} = 13.7 Hz, PPh). – ^{1}H NMR (C_6D_6): δ = 0.97–2.06 (m, 40 H, CH_2), 3.21 (m, 4 H, NCH), 6.99–7.82 (m, 8 H, CH_{arom}), 8.50 (d, J_{HH} = 8.0 Hz, 1 H, CH_{arom}). – ^{13}C{^{1}H} NMR (C_6D_6): δ = 26.7 (d, J_{CP} = 4.3 Hz, CH_2), 27.2 (d, J_{CP} = 5.5 Hz, CH_2), 27.6 (d, J_{CP} = 2.7 Hz, CH_2), 35.6 (d, J_{CP} = 4.7 Hz, CH_2), 58.6 (d, J_{CP} = 7.8 Hz, NCH), 126.4 (d, J_{CP} = 10.3 Hz, CH_{arom}), 127.9 and 128.3 (s, CH_{arom}), 128.6 (d, J_{CP} = 2.8 Hz, CH_{arom}), 129.1 (d, J_{CP} = 6.5 Hz, *o*-PPh), 129.7 (s, *p*-PPh), 132.0 (d, J_{CP} = 18.1 Hz, *m*-PPh), 136.5 (dd, J_{CP} = 18.9 Hz, J_{CP} = 5.1 Hz, *i*-PPh), 145.8 (dd, J_{CP} = 40.7 Hz, J_{CP} = 22.2 Hz, *C*CPPh), 153.6 (dd, J_{CP} = 18.4 Hz, J_{CP} = 3.4 Hz, CPPh), 187.9 (dd, J_{CP} = 18.3 Hz, J_{CP} = 13.9 Hz, C=N). – $C_{37}H_{53}N_3P_2$ (601.79): calcd. C 73.84, H 8.87, N 6.98; found C 73.70, H 8.67, N 7.15.

General Procedure for the Synthesis of Compounds 15a,b: To a solution of the corresponding complex **11a,b** (0.673 mmol) in toluene (8 mL) was added at room temperature *t*BuPCl$_2$ (**13**) (0.107 g, 0.673 mmol). The mixture was stirred at room temperature for 8 h and then evaporated to dryness. The resulting solid residue was

extracted with pentane (20 mL) and filtered. The volatiles were removed from the solution to give compounds **15a,b** as yellow solids.

Compound 15a: 72% yield. – IR (KBr): 1571 cm^{-1} $\tilde{\nu}$(C=N). – $^{31}P\{^1H\}$ NMR (C_6D_6): δ = 43.8 [s, P(N*i*Pr$_2$)$_2$], 100.2 (s, P*t*Bu). – ^1H NMR (C_6D_6): δ = 1.09 (d, J_{HP} = 22.9 Hz, 9 H, CCH$_3$), 1.18 (d, J_{HH} = 6.6 Hz, 6 H, CHC*H*$_3$), 1.20 (d, J_{HH} = 8.3 Hz, 6 H, CHC*H*$_3$), 1.32 (d, J_{HH} = 4.4 Hz, 6 H, CHC*H*$_3$), 1.35 (d, J_{HH} = 4.3 Hz, 6 H, CHC*H*$_3$), 3.30–3.73 (m, 4 H, NCH), 6.99–7.24 (m, 2 H, CH$_{arom}$), 7.63 (d, J_{HH} = 7.4 Hz, 1 H, CH$_{arom}$), 8.44 (d, J_{HH} = 7.7 Hz, 1 H, CH$_{arom}$). – $^{13}C\{^1H\}$ NMR (C_6D_6): δ = 24.7 (d, J_{CP} = 6.5 Hz, CH*C*H$_3$), 25.0 (d, J_{CP} = 6.4 Hz, CH*C*H$_3$), 27.4 (d, J_{CP} = 12.6 Hz, C*C*H$_3$), 35.2 (dd, J_{CP} = 16.7 Hz, J_{CP} = 3.9 Hz, *C*CH$_3$), 48.7 (d, J_{CP} = 10.9 Hz, NCH), 126.2 (d, J_{CP} = 8.0 Hz, CH$_{arom}$), 127.7 (d, J_{CP} = 4.9 Hz, CH$_{arom}$), 127.9 and 128.2 (s, CH$_{arom}$), 146.4 (dd, J_{CP} = 41.8 Hz, J_{CP} = 19.2 Hz, *C*CP*t*Bu), 152.0 (dd, J_{CP} = 24.1 Hz, J_{CP} = 4.2 Hz, CP*t*Bu), 186.2 (pt, J_{CP} = 14.9 Hz, J_{CP} = 14.9 Hz, C=N). – $C_{23}H_{41}N_3P_2$ (421.54): calcd. C 65.53, H 9.80, N 9.96; found: C 65.60, H 9.77, N 10.10. – MS (DCI/NH_3); *m*/*z*: 422 $[M + H]^+$.

Compound 15b: 69% yield. – IR (KBr): $\tilde{\nu}_{(C=N)}$ = 1566 cm^{-1}. – $^{31}P\{^1H\}$ NMR (C_6D_6): δ = 44.9 [d, J_{PP} = 6.5 Hz, P(NCy$_2$)$_2$], 99.0 (d, J_{PP} = 6.5 Hz, P*t*Bu). – ^1H NMR (C_6D_6): δ = 0.88–1.93 (m, 49 H, CH$_2$ and CH$_3$), 3.30 (m, 4 H, NCH), 7.09–7.14 (m, 4 H, CH$_{arom}$). – $^{13}C\{^1H\}$ NMR (C_6D_6): δ = 25.0 (s, CH$_3$), 26.3, 26.7 and 27.5 (s, CH$_2$), 27.7 (d, J_{CP} = 6.0 Hz, CH$_2$), 34.7 (d, J_{CP} = 8.9 Hz, *C*CH$_3$), 35.6 (br s, CH$_2$), 57.7 (d, J_{CP} = 10.6 Hz, NCH), 58.6 (d, J_{CP} = 8.5 Hz, NCH), 59.8 (d, J_{CP} = 9.7 Hz, NCH), 126.2 (d, J_{CP} = 14.4 Hz, CH$_{arom}$), 127.6 (d, J_{CP} = 4.3 Hz, CH$_{arom}$), 127.8 and 129.8 (s, CH$_{arom}$), 146.6 (dd, J_{CP} = 41.7 Hz, J_{CP} = 20.1 Hz, *C*CP*t*Bu), 151.8 (dd, J_{CP} = 26.1 Hz, J_{CP} = 4.8 Hz, CP*t*Bu), 185.9 (pt, J_{CP} = 17.1 Hz,J_{CP} = 17.1 Hz, C=N). – $C_{34}H_{57}N_3P_2$ (569.79): calcd. C 71.67, H 10.08, N 7.37; found C 71.40, H 9.91, N 7.62.

Synthesis of Compound 16a: To a solution of compound **14a** (0.150 g, 0.339 mmol) in toluene (5 mL) was added at room temperature S_8 (0.128 g, 0.5 mmol). The mixture was stirred at room temperature for 2 h and then evaporated to dryness. The resulting solid residue was dissolved in THF (3 mL) and transferred to a silica gel chromatography column. Elution with pentane gave a yellow band from which compound **16a** was isolated after removal of the solvent (78% yield). – M.p. 121–122 °C (decomp.). – IR (KBr): $\tilde{\nu}_{(C=N)}$ = 1511 cm^{-1}. – $^{31}P\{^1H\}$ NMR (C_6D_6): δ = 39.8 [d, J_{PP} = 6.5 Hz, P(N*i*Pr$_2$)$_2$], 81.9 [d, J_{PP} = 6.5 Hz, P(S)Ph]. – ^1H NMR (C_6D_6): δ = 1.12 (d, J_{HH} = 6.6 Hz, 18 H, CH$_3$), 1.18 (d, J_{HH} = 6.6 Hz, 6 H, CH$_3$), 3.54 (m, 4 H, NCH), 6.95–7.17 (m, 5 H, CH$_{arom}$), 7.48 (m, 1 H, CH$_{arom}$), 7.88 (m, 2 H, CH$_{arom}$), 8.15 (d, J_{HH} = 7.6 Hz, 1 H, CH$_{arom}$). – $^{13}C\{^1H\}$ NMR (C_6D_6): δ = 24.5 (d, J_{CP} = 5.9 Hz, CH$_3$), 24.7 (d, J_{CP} = 7.5 Hz, CH$_3$), 25.0 (d, J_{CP} = 7.0 Hz, CH$_3$), 48.9 (d, J_{CP} = 11.2 Hz, NCH), 49.6 (d, J_{CP} = 10.3 Hz, NCH), 126.0 (pt, J_{CP} = 12.4 Hz, J_{CP} = 12.4 Hz, CH$_{arom}$), 128.8 (d, J_{CP} = 11.9 Hz, CH$_{arom}$), 128.9 [d, J_{CP} = 12.7 Hz, *o*-P(S)Ph], 131.5 [d, J_{CP} = 11.6 Hz, *m*-P(S)Ph], 131.8 (d, J_{CP} = 9.8 Hz, CH$_{arom}$), 132.2 [s, *p*-P(S)Ph], 132.6 (d, J_{CP} = 2.0 Hz, CH$_{arom}$), 142.3 [dd, J_{CP} = 82.0 Hz, J_{CP} = 2.6 Hz, CP(S)Ph], 144.3 [dd, J_{CP} = 43.9 Hz, J_{CP} = 37.3 Hz, *C*CP(S)Ph], 192.8 (pt, J_{CP} = 21.7 Hz, J_{CP} = 21.7 Hz, C=N). *i*-P(S)Ph not observed. – $C_{25}H_{37}N_3P_2S$ (473.59): calcd. C 63.40, H 7.87, N 8.87; found C 63.23, H 7.92, N 8.99.

Synthesis of Compound 17: To a solution of complex **11a** (0.345 g, 0.623 mmol) in toluene (5 mL) was added at room temperature $PhSbCl_2$ (0.168 g, 0.623 mmol). The mixture was stirred at room temperature for 15 min and then evaporated to dryness. The resulting solid residue was washed with pentane (3 × 20 mL) and diethyl ether (3 × 5 mL) to give compound **17** as a yellow solid (72% yield). – IR (KBr): $\tilde{\nu}_{(C=N)}$ = 1591 cm^{-1}. – $^{31}P\{^1H\}$ NMR (CD_2Cl_2): δ = 83.8 (s). – ^1H NMR (CD_2Cl_2): δ = 1.08 (d, J_{HH} = 5.9 Hz, 6 H, CH$_3$), 1.19 (d, J_{HH} = 6.9 Hz, 6 H, CH$_3$), 1.37 (d, J_{HH} = 6.9 Hz, 6 H, CH$_3$), 1.47 (d, J_{HH} = 6.9 Hz, 6 H, CH$_3$), 3.94 (m, 2 H, NCH), 4.25 (m, 2 H, NCH), 7.12–8.05 (m, 9 H, CH$_{arom}$). – $^{13}C\{^1H\}$ NMR (CD_2Cl_2): δ = 24.7 (br s, CH$_3$), 25.2 (br s, CH$_3$), 50.9 (d, J_{CP} = 6.3 Hz, NCH), 51.2 (d, J_{CP} = 6.5 Hz, NCH), 123.8, 127.4, 128.3, 128.6, 129.8, 136.3 and 141.7 (s, CH$_{arom}$), 134.0 (s, *i*-Ph), 144.7 (d, J_{CP} = 26.1 Hz, *C*CSbPh), 146.9 (d, J_{CP} = 10.3 Hz, *C*SbPh), 194.6 (s, C=N). – MS (DCI/CH_4); *m*/*z*: 532 $[M + H]^+$. – $C_{25}H_{37}N_3PSb$ (532.30): calcd. C 56.42, H 7.00, N 7.89; found C 56.30, H 7.11, N 7.95.

Synthesis of Compounds 19, 19': To a solution of complex **11a** (0.417 g, 0.753 mmol) in toluene (8 mL) was added at 0 °C $Cl_2PCH_2CH_2PCl_2$ (**18**) (0.056 mL, 0.376 mmol). The mixture was stirred at room temperature for 15 min and then evaporated to dryness. The resulting solid residue was extracted with pentane (15 mL) and filtered. The volatiles were removed from the solution to give a yellow solid containing an inseparable mixture of two diastereoisomers **19** and **19'** in a ratio of *ca.* 2:1 (91% yield). – IR (KBr): $\tilde{\nu}_{(C=N)}$ = 1566 cm^{-1}. – $^{31}P\{^1H\}$ NMR ($CDCl_3$): δ = 41.4 [s, P(N*i*Pr$_2$)$_2$ major isomer], 42.6 [s, P(N*i*Pr$_2$)$_2$ minor isomer], 81.5 (s, PCH$_2$). – ^1H NMR ($CDCl_3$): δ = 1.00–1.66 (m, 52 H, CH$_3$ and CH$_2$), 3.52 (m, 8 H, NCH), 7.25–7.65 (m, 6 H, CH$_{arom}$), 8.20 (m, 2 H, CH$_{arom}$). – $^{13}C\{^1H\}$ NMR ($CDCl_3$): δ = 23.0 (dd, J_{CP} = 28.5 Hz, J_{CP} = 3.9 Hz, CH$_2$), 23.9 (br s, CH$_3$), 24.1 (d, J_{CP} = 7.1 Hz, CH$_3$), 24.3 (d, J_{CP} = 7.2 Hz, CH$_3$), 47.9 (d, J_{CP} = 10.8 Hz, NCH), 48.3 (d, J_{CP} = 8.5 Hz, NCH), 48.4 (d, J_{CP} = 8.0 Hz, NCH), 125.5 (d, J_{CP} = 10.3 Hz, CH$_{arom}$), 126.5 (dd, J_{CP} = 14.9 Hz, J_{CP} = 10.7 Hz, CH$_{arom}$), 127.2 and 127.4 (s, CH$_{arom}$), 145.4 (dd, J_{CP} = 41.4 Hz, J_{CP} = 31.6 Hz, *C*CPCH$_2$), 151.7 (m, *C*PCH$_2$), 187.0 (pt, J_{CP} = 19.7 Hz, J_{CP} = 19.7 Hz, C=N). – $C_{40}H_{68}N_6P_4$ (756.91): calcd. C 63.47, H 9.05, N 11.10; found C 63.22, H 9.13, N 11.30.

Synthesis of Compound 20: To a solution of compound **14a** (0.115 g, 0.260 mmol) in dichloromethane (5 mL) was added at 0 °C CF_3SO_3Me (0.029 mL, 0.260 mmol). The mixture was stirred at room temperature for 15 min and then evaporated to dryness. The resulting solid residue was washed with pentane (3 × 15 mL) and dried in vacuo to give compound **20** as a red solid (81% yield). – IR (KBr): $\tilde{\nu}_{(C=N)}$ = 1631 cm^{-1}. – $^{31}P\{^1H\}$ NMR (CD_2Cl_2): δ = 49.2 [d, J_{PP} = 2.7 Hz, P(N*i*Pr$_2$)$_2$], 70.1 [d, J_{PP} = 2.7 Hz, P(Me)Ph]. – ^1H NMR (CD_2Cl_2): δ = 1.14–1.32 (m, 24 H, CH$_3$), 2.69 (d, J_{HP} = 14.6 Hz, 3 H, PCH$_3$), 3.60 (m, 4 H, NCH), 7.66–8.59 (m, 9 H, CH$_{arom}$). – $^{13}C\{^1H\}$ NMR (CD_2Cl_2): δ = 8.7 (dd, J_{CP} = 61.0 Hz, J_{CP} = 4.0 Hz, PCH$_3$), 23.9 (br s, CH$_3$), 49.5 (d, J_{CP} = 11.1 Hz, NCH), 49.6 (d, J_{CP} = 13.1 Hz, NCH), 117.8 [dd, J_{CP} = 93.3 Hz, J_{CP} = 5.0 Hz, *C*P(Me)Ph], 127.6 (pt, J_{CP} = 12.6 Hz, J_{CP} = 12.6 Hz, CH$_{arom}$), 130.3 (d, J_{CP} = 12.9 Hz, CH$_{arom}$), 131.8 [d, J_{CP} = 11.0 Hz, *o*-P(Me)Ph or CH$_{arom}$], 131.9 [d, J_{CP} = 8.9 Hz, *o*-P(Me)Ph or CH$_{arom}$], 133.5 [d, J_{CP} = 9.3 Hz, *m*-P(Me)Ph], 135.5 and 135.8 [s, CH$_{arom}$ and *p*-P(Me)Ph], 146.8 [dd, J_{CP} = 42.3 Hz, J_{CP} = 32.2 Hz, *C*CP(Me)Ph], 208.5 (dd, J_{CP} = 29.6 Hz, J_{CP} = 18.2 Hz, C=N). *i*-P(Me)Ph not observed. – $C_{27}H_{40}N_3O_3F_3P_2S$ (605.64): calcd. C 53.54, H 6.65, N 6.93; found C 53.42, H 6.59, N 7.10.

Synthesis of Compound 21: To a solution of compound **16a** (0.100 g, 0.211 mmol) in dichloromethane (5 mL) was added at room temperature CF_3SO_3Me (0.023 mL, 0.211 mmol). The mixture was stirred at room temperature for 15 min and then evaporated to dryness. The resulting solid residue was washed with pentane (2 × 15 mL) and dried in vacuo to give compound **21** as a red

solid (93% yield). – IR (KBr): $\tilde{\nu}_{(C=N)}$ = 1521 cm^{-1}. – $^{31}P\{^1H\}$ NMR (CD_2Cl_2): δ = 55.6 [s, $P(NiPr_2)_2$], 82.9 [s, P(SMe)Ph]. – ^1H NMR (CD_2Cl_2): δ = 1.28 (d, J_{HH} = 6.6 Hz, 12 H, CH_3), 1.34 (d, J_{HH} = 6.5 Hz, 12 H, CH_3), 2.21 (d, J_{HP} = 15.9 Hz, 3 H, SCH_3), 3.61 (m, 4 H, NCH), 7.44–8.50 (m, 9 H, CH_{arom}). – $^{13}C\{^1H\}$ NMR (CD_2Cl_2): δ = 18.4 (s, SCH_3), 23.6 (br s, CH_3), 47.9 (br s, NCH), 50.1 (br s, NCH), 117.2 [dd, J_{CP} = 96.3 Hz, J_{CP} = 4.0 Hz, *C*P(SMe)Ph], 128.3 (dd, J_{CP} = 14.6 Hz, J_{CP} = 9.6 Hz, CH_{arom}), 130.9 [d, J_{CP} = 14.1 Hz, *o*-P(SMe)Ph or CH_{arom}], 131.2 [d, J_{CP} = 9.9 Hz, *o*-P(SMe)Ph or CH_{arom}], 132.1 (d, J_{CP} = 10.5 Hz, CH_{arom}), 134.5 [d, J_{CP} = 10.1 Hz, *m*-P(SMe)Ph], 136.6 and 137.0 [s, CH_{arom} and *p*-P(SMe)Ph], 146.8 [dd, J_{CP} = 48.6 Hz, J_{CP} = 30.7 Hz, *C*CP(SMe)Ph], 210.2 (dd, J_{CP} = 28.5 Hz, J_{CP} = 23.4 Hz, C=N). *i*-P(SMe)Ph not observed. – $C_{27}H_{40}N_3O_3F_3S_2P_2$ (637.70): calcd. C 50.85, H 6.32, N 6.58; found C 50.91, H 6.40, N 6.71

X-ray Crystallographic Study of 16a: $C_{25}H_{37}N_3P_2S$. M=473.58; tetragonal, space group *P*, 42/*n*; *a* = 15.743(2) Å, *b* = 15.746(2) Å, *c* = 21.684(3) Å; *V* = 5375.4(12) $Å^3$; D_{calcd} = 1.170 g cm^{-3}; graphite-monochromated Mo-$K_($ radiation (λ = 0.71073 Å); μ = 0.256 mm^{-1}; *T* = 293(2) K. – Data collection was performed at room temperature on a STOE Imaging Plate Diffraction System (I.P.D.S) and corrected for Lorentz and polarisation effects: 3868 unique data in the range 2.05°< θ <23.26°, final unit cell parameters were obtained by a least-squares refinement on a set of 5000 reflections equally distributed in reciprocal space; crystal decay was monitored by measuring two hundred reflections per image. Any fluctuations in the intensity were observed over the course on the data collection. – Structure was solved by Direct Methods using (SIR92),[6] and refined by least-squares procedures on a F^2 with the aid of (SHELXL-97).[7] Final $R1 = \Sigma \| F_o | - | F_c \| / \Sigma | F_o | = 0.0441$ for 3868 $F_o > 4\sigma F_o$ and 0.1002 for all data, $wR2 = [\Sigma w(F_o^2 - F_c^2)^2 / \Sigma w(F_o^2)^2]^{1/2} = 0.0988$, 0.1238 for all data, G.O.F = $[\Sigma w(F_o^2 - F_c^2)^2 / (n-p)]^2 = 0.853$ for 289 parameters and with a Scheme of ponderation following: Weight = $1/[\sigma^2(F_o^2) + (0.0696P)^2]$ where $P = (F_o^2 + 2F_c^2)/3$. Residual electron density extrema are: 0.444 and –0.273e $Å^{-3}$. Drawing of molecules were performed using the program ZORTEP[8] with a 50% probability displacement ellipsoids for non-hydrogen atoms. – Crystallographic data for the structure reported in this paper have been deposited at the Cambridge Crystallographic Data Centre as supplementary information number CCDC-132612. Copies of the data can be obtained free of charge on application to CCDC, 12 Union Road, Cambridge CB2 1EZ, UK, E-mail: deposit@ccdc.cam.ac.uk.

Acknowledgments

Thanks are due to CNRS for financial support. V. C. thanks the Spanish Ministerio de Educación y Cultura for a postdoctoral fellowship.

[1] Review: F. Mathey, *Chem. Rev.* **1998**, *88*, 429.
[2] Review of aza- and thiaphosphindoles: [2a] K. Karaghiosoff, H. Klehr, A. Schmidpeter, *Chem. Ber.* **1986**, *119*, 410 – [2b] A. Schmidpeter, K. Karaghiosoff in *Multiple Bonds and Low Coordination Chemistry* (Eds.: M. Regitz, O. J. Scherer) Thieme Stuttgart **1990**, 258 – [2c] A. Schmidpeter in *Comprehensive Heterocyclic Chemistry II*, vol. 3 (Eds: A. R. Katritzky, C. W. Rees, E. F. V. Scriven), Pergamon, Oxford, **1996**, p. 709.
[3] [3a] R. Streubel, H. Wilkens, A. Ostrowski, C. Neumann, F. Ruthe, P. G. Jones, *Angew. Chem. Int. Ed. Engl.* **1997**, *36*, 1492 – [3b] H. Wilkens, F. Ruthe, P. G. Jones, R. Streubel, *Chem. Commun.* **1998**, 1529.
[4] S. L. Buchwald, A. Sayers, B. T. Watson, J. C. Dervan, *Tetrahedron Lett.* **1987**, *28*, 3245.
[5] C. Roques, M. R. Mazieres, J. P. Majoral, M. Sanchez, A. Foucaud, *J. Org. Chem.* **1989**, *54*, 5535.
[6] A. Altomare, G. Cascarano, G. Giacovazzo, A. Guagliardi, M. C. Burla, G. Polidori, M. Camalli, "SIR92 program for automatic solution of crystal structures by direct methods", *J. Appl. Crystallogr.* **1994**, *27*, 435.
[7] G. M. Sheldrick, *SHELXL97*, *Program for the refinement of Crystal Structures*, University of Göttingen, Germany, **1997**.
[8] L. Zolnaï, ZORTEP, *Graphical Program for X-ray Structures Analysis*, University of Heidelberg, Germany, **1998**.

Received July 26, 1999
[I99277]

Methyl(2-phosphanylphenolato[*P*,*O*])nickel(II) Complexes – Synthesis, Structure, and Activity as Ethene Oligomerization Catalysts

Joachim Heinicke,*[a] Mengzhen He,[a] Attila Dal,[a,b] Hans-Friedrich Klein,*[b] Olaf Hetche,[b] Wilhelm Keim,*[c] Ulrich Flörke,[d] and Hans-Jürgen Haupt[d]

Keywords: Methylnickel complexes / 2-Phosphanylphenolate / Chelates / Homogeneous catalysis / Oligomerization

Reactions of various substituted 2-phosphanylphenols **1a–f** with half-molar amounts of *cis*-[MeNi(μ-OMe)(PMe_3)]$_2$ have been found to yield square-planar methyl(2-phosphanylphenolato)(trimethylphosphane)nickel(II) complexes **2a–f**. $^2J_{PP}$ coupling constants of 305–316 Hz at low temperature indicate a *trans*-configuration for the products, while broad ^{31}P-NMR signals at room temperature can be attributed to rapid dissociation of PMe_3. Reaction with excess **1** gave rigid bis(2-phosphanylphenolato)nickel(II) complexes as exemplified by **3e**, whereas addition of PMe_3 to **2a** led to the pentacoordinate methyl(2-phosphanylphenolato)bis(trimethylphosphane)nickel(II) complex **4a**. Higher yields of **4a** and **4d** were obtained by reactions of **1a** and **1d** with $Me_2Ni(PMe_3)_3$. Single-crystal X-ray diffraction analyses of **3e** and **4a** have revealed the structures as square-planar *trans*-bis- and trigonal-bipyramidal mono(2-phosphanylphenolato)nickel(II) P∩O-chelate complexes, respectively. The methylnickel complexes **2** and **4** have been found to be effective one-component catalysts for the oligomerization of ethene. High conversions (> 96%) were achieved with the P-basic derivatives **2e**, **2f**, and **4d** bearing one or two branched alkyl groups (isopropyl, *tert*-butyl), whereas the diphenylphosphanyl derivatives were less active; **4d** gave shorter oligomers than **2e** or **2f**.

Introduction

P∩O-chelate complexes are of crucial importance in the oligomerization of ethene to give linear α-olefins by the Shell Higher Olefins Process.[1] In order to tune the catalyst properties, various P∩O-nickel complexes of varying ring sizes and bearing different functional groups have been investigated.[2,5] In early studies of the oligomerization of ethene, using in situ generated catalysts obtained from 2-diphenylphosphanylphenol and bis(1,5-cyclooctadiene)nickel or nickel salts in the presence of $NaBH_4$, mainly polymers were obtained.[6] Oligomers of ethene were, however, formed using phenyl(2-diphenylphosphanyl-4-hydroxyphenolato)(triphenylphosphane)nickel(II), obtained by phenyl migration from α-benzoyl phosphorus ylides.[2b,7] A recent study of the influence of various auxiliary phosphane ligands on the activity and selectivity of analogously prepared phenyl(2-diphenylphosphanylphenolato)(phosphane)nickel(II) catalysts established that high activity is seen with PPh_3, P(4-X–C_6H_4)$_3$ (X = Cl > Me > F), and PPh_2Me, whereas PCy_3 (Cy = cyclohexyl), which has a strong enhancing effect on the activity of the related phenyl(2-diphenylphosphanyl-1-phenylenolato)(phosphane)nickel(II) catalysts, induces only moderate activity. Generally, a marked tendency to produce higher oligomers, from $C_{10=}$ to $C_{90=}$, and only minor amounts of the desired $C_{4=}$ to $C_{10=}$ oligomers is observed. Exceptions are complexes with PMe_3 and $PPhMe_2$ ligands, which give α-olefins of low molecular weight ($C_{4=}$ to $C_{24=}$), although with lower catalytic activity.[3d] In view of the recently reported access to variously substituted 2-phosphanylphenols[8,9] and their high tendency to form P∩O-chelates,[8,10,11] we turned our attention to the synthesis of catalytically active (2-phosphanylphenolato[*P*,*O*])nickel(II) complexes and the tuning of their activity and selectivity by variation of substituents at the phosphorus and the phenolate group. We report here on methyl(2-phosphanylphenolato)nickel complexes, which differ from cyclopentadienyl(2-phosphanylphenolato)nickel(II) complexes[8b,11] in that they are active oligomerization catalysts.

[a] Institut für Chemie und Biochemie, Universität Greifswald,
Soldmannstraße 16, D-17487 Greifswald, Germany
Fax: (internat.) + 49(0)3834/864337
E-mail: heinicke@mail.uni-greifswald.de
[b] Institut für Anorganische Chemie, Technische Universität Darmstadt,
Petersenstraße 18, D-64285 Darmstadt, Germany
Fax: (internat.) + 49(0)6151/164173
E-mail: hfklein@hrz2.hrz.tu-darmstadt.de
[c] Institut für Technische Chemie und Petrolchemie, Rheinisch-Westfälische Technische Hochschule Aachen,
Worringer Weg 1, D-52056 Aachen, Germany
[d] Anorganische und Analytische Chemie, Universität-GH Paderborn,
Warburger Straße 100, D-33098 Paderborn, Germany
Fax: (internat.) + 49(0)5251/603423

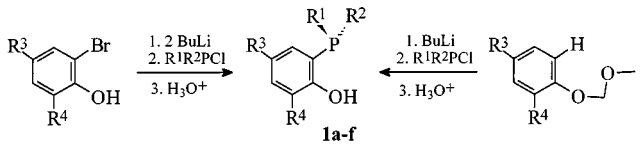
Results and Discussion

Synthesis

Selected 2-phosphanylphenols **1a**–**f** were synthesized either by dilithiation of 2-bromophenols, reaction with the respective chlorophosphane and acid workup,[9c,10i] or, in analogy to the procedure of Rauchfuß,[8b] by *ortho*-metallation of the corresponding phenolmethoxymethyl

 © WILEY-VCH Verlag GmbH, D-69451 Weinheim, 2000 1434−1948/00/0303−0431 $ 17.50+.50/0

ether with butyllithium, substitution with chlorophosphane, and subsequent acid ether cleavage (Scheme 1).



1	a	b	c	d	e	f
R^1	Ph	Ph	*i*Pr	*t*Bu	*i*Pr	*i*Pr
R^2	Ph	Ph	Ph	Ph	*i*Pr	*i*Pr
R^3	*t*Bu	*t*Bu	*t*Bu	*t*Bu	*t*Bu	F
R^4	*t*Bu	Me	*t*Bu	*t*Bu	*t*Bu	H

Scheme 1. Synthesis of 2-phosphanylphenols

The chosen substitution pattern, i.e. diphenyl, alkylphenyl, and dialkyl groups at phosphorus, 4,6-di-*tert*-butyl-, 4-methyl-6-*tert*-butyl-, and 4-fluoro-substituents at the phenoxy group, provided ligands with widely differing basicities at phosphorus and oxygen, allowing a qualitative appraisal of electronic effects on the oligomerization of ethene by the corresponding nickel P∩O-chelate complexes. Branched alkyl groups were selected since 2-isopropylphenylphosphanyl- and, in particular, 2-*tert*-butylphenylphosphanylcresol have been found to exhibit a lower tendency to form the thermodynamically preferred bis(P∩O-chelates) than 2-methylphenylphosphanyl- or 2-diphenylphosphanyl derivatives[11b] upon reaction with equimolar amounts of nickelocene in toluene. The 6-*tert*-butyl group stabilizes the P∩O-chelate complexes through its steric effect on the periphery, but does not significantly shield the metal center. The steric effect causes a bending of the substituents at oxygen towards the phosphorus, as is evident from the unusual formation of a 2-phosphanylphenolate P∩O-chelate complex with the hard titanium cation,[10h] an extremely increased $^4J_{PSn}$ in a 2-phosphanylphenolstannyl ether, and the presence of P···H–O hydrogen bonds in **1c** and **1d**.[9c] In **1e**, the presence of a P···H–O hydrogen bond is evident from a large $^4J_{PH}$ coupling constant of 12.4 Hz for the hydroxyl proton, whereas in **1f** this proton gives rise to a broad singlet. An X-ray structure analysis of single crystals of **1e**, performed at –100 °C, reveals a *trans*-eclipsed conformation (Figure 1), which means that the lone electron pair is also directed towards the hydroxyl group in the solid state. The lack of evidence for any such P···H–O hydrogen bond in **1f** underlines the role of the bulky 6-substituent in inducing such interactions.

Reactions of **1a–c** and **1f** with half-molar and of **1d** with equimolar amounts of $[NiMe(PMe_3)(\mu\text{-}MeO)]_2$ in diethyl ether, THF, or pentane solution proceeded via red intermediates and led to the yellow or red-brown methyl(2-phosphanylphenolato)(trimethylphosphane)nickel(II) complexes **2a–d** and **2f**. However, when the P-basic **1e** was used in slight excess relative to the half-molar amount of $[NiMe(PMe_3)(\mu\text{-}MeO)]_2$, the air-stable *trans*-bis(P∩O-chelate) complex **3e** was formed in high yield. This can be mainly attributed to the more facile dissociation of PMe_3 from **2e**.

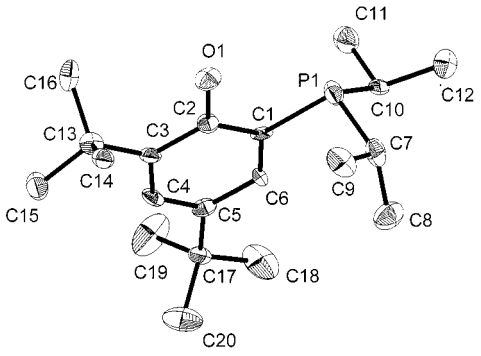
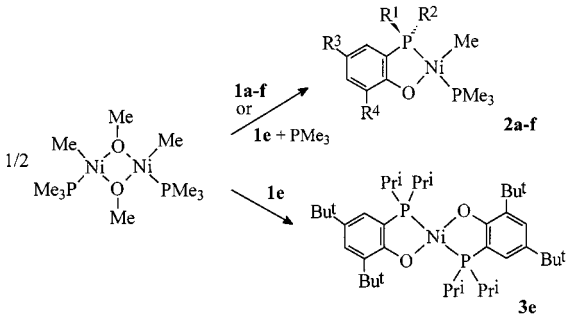


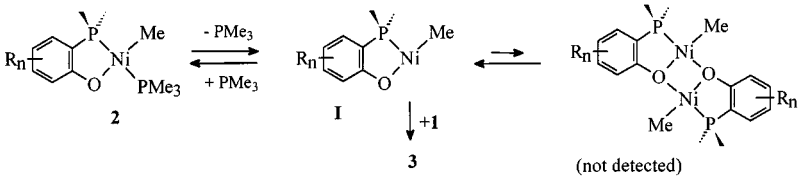
Figure 1. ORTEP plot of the molecular structure of **1e**; selected distances [Å] and angles [°]: P1–C2 1.847(9), P1–C7 1.877(10), P1–C10 1.838(10); P1–C1–C2 118.7(8), P1–C1–C6 122.1(8), O1–C2–C1 119.9(9), O1–C2–C3 116.9(10)

When the reaction was carried out in the presence of one equivalent of PMe_3, **2e** was isolated (Scheme 2). The complexes **2** were purified by fractional extraction of the crude products with pentane.

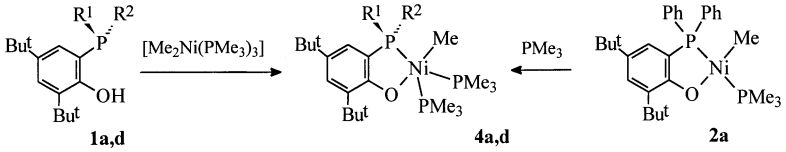


Scheme 2. Synthesis of the nickel complexes **2a**–**f** and **3e**

Whereas the room-temperature NMR spectra of *cis*- and *trans*-bis(2-phosphanylphenolato[*P,O*])nickel(II) chelate complexes **3** feature sharp signals and multiplets showing couplings to both phosphorus atoms for a number of ^1H as well as ^{13}C nuclei,[11,12] the room-temperature spectra of **2a–f** reveal couplings of the corresponding ^1H and ^{13}C nuclei to only one phosphorus atom, and in the ^{31}P-NMR spectra broad doublets or singlets are observed. At low temperature (–25 to –70 °C), the phosphorus signals of **2a–f** appear as sharp doublets with $^2J_{PP}$ couplings in the range 305–316 Hz, indicating a *trans* configuration. These values are similar to the $^2J_{PP}$ values of 245–290 Hz recently observed in phenylnickel-*o*-diphenylphosphanylphenolate phosphane complexes.[3d] The ^1H and ^{13}C signals of the NiMe groups in **2a**–**f** are split by couplings with both the phosphorus atoms, whereas the multiplicity of the ^1H and ^{13}C signals of the P∩O-ligand (at –25 to –30 °C) arises from coupling with the *o*-phosphorus nucleus only when PH or PC coupling is observed. These observations are indicative of rapid dissociation of the monodentate phosphane at room temperature, whereas exchange reactions of the P∩O-ligands, as indicated, e.g., by the different configurations of a bulky substituted bis(2-phosphanylphenolato)nickel complex in solution and in the solid state,[12] are slow on the NMR time scale. The decreased line-widths of the room-temper-



Scheme 3. Dissociation equilibria of **2**



Scheme 4. Syntheses of the nickel complexes **4a**, **d**

ature phosphorus resonances of the diisopropylphosphanyl complexes **2e** and **2f** and the lower temperature necessary for obtaining sharp doublets (–70 °C) indicate enhanced dissociation in the case of P$^{\frown}$O-ligands with increased donor and diminished acceptor strengths. The dissociation products, the tricoordinate 14-electron nickel intermediates **I**, undergo a rapid back-reaction with PMe_3 (Scheme 3). The presence of excess **1** disrupts this equilibrium by trapping **I**, thereby yielding the more stable bis(P$^{\frown}$O-chelates) **3**. The high reactivity of **I** prevents the observation of equilibrium concentrations. The concentrations of free trimethylphosphane and of dimers of **I** also fall below the limit of detection by NMR, suggesting a rapid association–dissociation equilibrium of PMe_3 with a small equilibrium constant. Dissociation of PMe_3 also seems to be responsible for the rapid aerial oxidation of solutions of **2a** since the solid material is stable in air for several hours.

In order to ascertain whether trimethylphosphane may be scavenged by the 16-electron complexes **2**, generation of the pentacoordinate complex **4a** was attempted by adding excess trimethylphosphane to **2a**. However, this method gave only a low yield (ca. 30%) of the red product. It was found that **4a** and **4d** could be obtained much more readily by reaction of **1a** and **1d**, respectively, with dimethyl tris(trimethylphosphane)nickel(II) in diethyl ether (Scheme 4). Complexes **4a** and **4d** were found to be stable under ambient conditions but lose trimethylphosphane on heating and decompose at around 106–109 °C. As expected for pentacoordinate nickel complexes, **4a** and **4d** are highly fluxional and exhibit two broad phosphorus singlets in their ^{31}P-NMR spectra, even at –30 °C, indicating rapid pseudo-rotation and dissociation of PMe_3. The ^{1}H and ^{13}C nuclei of the P$^{\frown}$O-ligand and the Ni methyl group only show coupling with the rigid chelate-bound phosphorus. As in the case of **2**, the dissociation equilibria account for the fact that solutions of **4** are rapidly oxidized, whereas the isolated complexes can be exposed to air for a short time.

Structural Aspects

In addition to the dynamic effects, the ^{1}H-, ^{13}C-, and ^{31}P-NMR chemical shifts and coupling constants of the rigid phosphanylphenolate ligands confirmed the configurations of **2**–**4**. Further structural information was provided by single-crystal X-ray structure analyses of **3e** and **4a**. In this regard, we will now discuss some trends by comparison of selected data (Table 1). The coordination chemical shifts of the *ortho*-phosphorus atoms (*o*-P) in complexes of types **4**, *cis*-**3**, and *trans*-**3** reveal a greater deshielding in the more highly alkylated P–alkyl$_n$Ph$_{2-n}$ derivative in each case, due to the lower acceptor strength. The same trend is observed for **2a** to **2d**, but the more P-basic diisopropylphosphanyl complexes **2e** and **2f** show smaller than expected values for $\Delta\delta$(*o*-P). Similarly, the coordination chemical shifts of PMe_3 in **2e** and **2f**, which approach those in **4a** and **4d**, are markedly lower than $\Delta\delta(PMe_3)$ in **2a**–**d**. This indicates a higher electron density at nickel(II) and an increased electron-repelling effect due to the lack of back bonding, which is also responsible for the noticeable high-field shifts of the NiMe carbon resonances in **2e** and **2f** as compared with those in **2a**–**d**, the lower $^{1}J_{PC2}$ and slightly lower $^{2}J_{PC1}$ coupling constants, and the aforementioned higher rate of dissociation in **2e** and **2f**. Comparison of the phosphorus coordination shifts of P$^{\frown}$O,P nickel complexes **2** with those of bis(P$^{\frown}$O-chelates) **3** having similar substitution patterns at phosphorus reveals smaller or slightly smaller $\Delta\delta$ values for the *trans* isomers of **3**, but significantly larger deshielding in *cis*-**3**. An even more clear-cut distinction of *cis* and *trans* isomers follows from the different $^{1}J_{PC2}$ (*Jcis* > *Jtrans*) and $^{2}J_{PC1}$ (*Jcis* < *Jtrans*) values, which indicate different electronic situations. The latter observation would suggest that substituent effects influence the configuration. Whereas this is true for the rigid bis(P$^{\frown}$O-chelates) **3**,[8a,11,12] monochelate P$^{\frown}$O,P nickel complexes **2** such as acyclic bis(phosphane)bis(phenolate)nickel complexes[13] always preferentially adopt a *trans* configuration. *cis*-Isomers of **2** would be expected to exhibit $^{2}J_{PNiP}$ coupling constants in the range 60–90 Hz.[11b,14,15] Such signals could not be detected, neither for P(R)–aryl nor for dialkylphosphanyl derivatives. Traces of impurities giving rise to sharp phosphorus doublets (J_{PP} = 14–16 Hz) were detected in the spectra of **2a**,**b**,**d**, the nature of which has not yet been established.

A single-crystal X-ray structure analysis of **3e** (Figure 2) confirmed the *trans* configuration and provided the first such data for a *trans*-bis(phosphanylphenolato[*P*,*O*])-nickel(II) complex. Like acyclic *trans*-bis(phosphane)bis-

Table 1. Selected ^{31}P- and ^{13}C-NMR data of **2–4** (nr = not resolved; $N = |J + J'|$)

Compound	$\Delta\delta(o\text{-}^{31}P)$	$\Delta\delta(^{31}PMe_3)$ at 25 °C (at T °C)		$\delta(Ni^{13}CH_3)$ at 25 °C ($^2J_{CP\text{-}2}$ [Hz])	$^1J_{PC1}$ [Hz]	$^2J_{PC2}$ [Hz]
2a	62.6	52.6	57.1 (–50)	–19.9 (25)	49.1	25.1
2b	61.9	55.9	57.7 (–50)	–20.3 (25.1)	48.6	25.8
2c	69.8[a]	55.3		–22.2 (nr)	(nr)	23.4
2d	66.8	55.3	56.8 (–28)	–21.1 (25)	44.5	23.4
2e	63.9	47.9		–24.9 (28.1)	41.2	22.0
2f	60.5	48.7	50.1 (–70)	–26.1 (26.8)	38.3	21.6
4a	56.7	34.8		–18.8 (br)[b]	45.8	28.1
4d	63.3	35.3		–20.7 (22.7)	43.0	24.9
cis-**3a** [12]	71.1	–	–	–	N = 61.2	N = 18.9
cis-**3c** [12]	77.5	–	–	–	N = 55.8	N = 17.7
trans-**3d** [12]	54.0	–	–	–	N = 46.8	N = 28.7
trans-**3e**	62.0	–	–	–	N = 42.6	N = 30.5

[a] Referred to δ(**1c**) at –15 °C, other peaks to **1** at 25 °C. – [b] At –30 °C, δ = –16.4 (19.6 Hz).

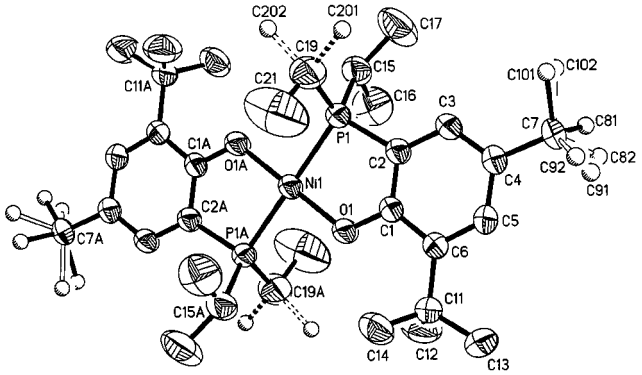


Figure 2. ORTEP plot of the molecular structure of **3e**; selected distances [Å] and angles [°]: Ni1–P1 = Ni1–P1A 2.1997(8), Ni1–O1 = Ni1–O1A 1.857(2), P1–C2 1.794(3), P1–C15 1.841(4), P1–C19 1.819(4), O1–C1 1.338(4), C1–C6 1.424(4); O1–Ni1–O1A 180.0, P1–Ni1–P1A 180.00(4), O1–Ni1–P1A = O1A–Ni1–P1 93.04(7), O1–Ni1–P1 = O1A–Ni1–P1A 86.96(7), C1–O1–Ni1 121.30(19), C2–C1–O1 120.8(3), P1–C2–C1 111.9(2), Ni1–P1–C2 98.80(11), P1–C2–C3 126.7(3), O1–C1–C6 120.4(3)

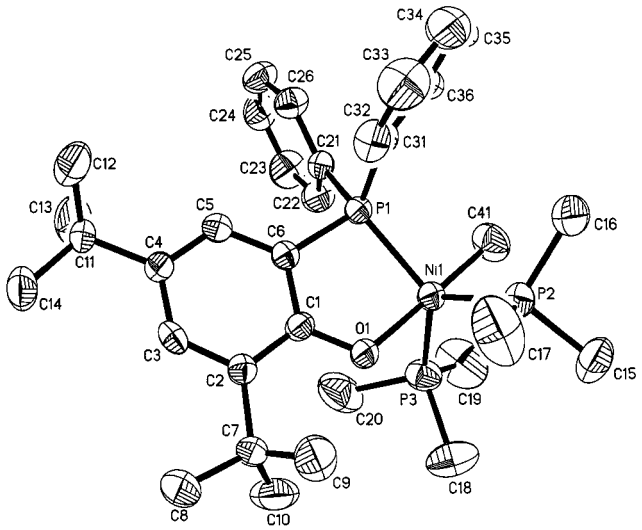


Figure 3. ORTEP plot of the molecular structure of **4a**; selected distances [Å] and angles [°]: Ni1–C41 1.981(5), Ni1–P1 2.191(2), Ni1–P2 2.245(2), Ni1–P3 2.224(2), Ni1–O1 1.984(3), P1–C6 1.797(5), O1–C1 1.332(5), C1–C6 1.411(6); C41–Ni1–O1 177.7(2), C41–Ni1–P1 92.6(2), C41–Ni1–P2 88.9(2), C41–Ni1–P3 91.7(2), P1–Ni1–P2 114.02(6), P1–Ni1–P3 125.16(6), P2–Ni1–P3 120.71(7), O1–Ni1–P1 86.35(10), C1–O1–Ni1 118.9(3), C6–C1–O1 120.1(4), P1–C6–C1 114.3(4), Ni1–P1–C6 99.2(2), P1–C6–C5 124.3(4), O1–C1–C2 122.1(4)

(phenolato)nickel(II) complexes,[13] **3e** possesses an almost ideal square-planar geometry about the nickel center, with O–Ni–O and P–Ni–P angles of 180°. This is in marked contrast to the distorted structures of *cis*-**3**, where O–Ni–O angles of 85.0 to 87.5° and P–Ni–P angles of 97.9 to 107.1° are found.[11b,12] The latter value relates to **3d**, which occurs in the *cis* form in the solid state, but in the kinetically preferred (*trans* effect) *trans* configuration in solution[12] and may thus represent the degree of steric congestion at the borderline of *cis*- and *trans*-bis(2-phosphanylphenolato)nickel(II) complexes. The Ni–P bond lengths in **3e** are somewhat longer [2.1997(8) Å] while the Ni–O [1.857(2) Å] distances are a little shorter as compared to the values in *cis*-bis(2-phosphanylphenolato)nickel(II) moieties, i.e. 2.1432(13) to 2.172(2) Å (the latter in *cis*-**3d**) and 1.869(10) to 1.889(3) Å, respectively. The angles within the chelate ring are as those in *cis*-**3** and underline the rigidity of the five-membered Ni–P∩O-chelate ring.

Although single crystals of *trans*-**2a**–**f** suitable for structure determinations could not be obtained, their structures are believed to be similar to those of phenyl(2-diphenylphosphanylenolato)(triphenylphosphane)nickel(II) complexes.[2a,3b] X-ray structure analysis of **4a** reveals an almost ideal trigonal-bipyramidal geometry with the three phosphorus atoms in equatorial positions and the oxygen and the methyl group in axial positions (Figure 3). The Ni–P(1) distance is markedly longer than the Ni–P bond lengths in *cis*-**3**, but is comparable to the corresponding distances in **3e** and phenyl(2-phosphanylenolato)(phosphane)nickel(II) complexes. The axial Ni–O bond is longer than Ni–O bonds in *cis*- and *trans*-**3**, but is comparable to the longer distances found in the (2-phosphanylenolato)(phosphane)nickel or pentacoordinate *o*-benzoyl(trimethylphosphane)nickel complexes.[16] The Ni–C(Me) and Ni–P(2) or Ni–P(3) distances fall in the usual ranges of bond lengths in methylnickel-trimethylphosphane complexes.[17]

Ethene Oligomerization

Toluene solutions of the methylnickel phosphane complexes **2c**,**e**,**f** and **4a**,**d** (ca. 0.1 mmol) were treated with

Table 2. Oligomerization of ethene (at 80 °C, 35 bar in 12 mL of toluene)

Oligomerization no.	I	II	III	IV	V
Catalyst, mg	**2c**, 56.0	**2e**, 58.0	**2f**, 47.9	**4a**, 67.7	**4d**, 70.8
(mmol)	(0.11)	(0.12)	(0.13)	(0.11)	(0.12)
Ethene, g (mmol)	7.7 (274)	7.6 (271)	7.8 (278)	7.5 (267)	7.7 (274)
Time [h]	10	6	6	10	10
Conv. of ethene g (%)	0.8 (10.4)	7.5 (98.7)	7.7 (98.7)	2.2 (29.3)	7.4 (96.1)
TON [mol/mol]	257	2174	2161	713	2218
Products[a]	C_4–C_{24}	C_4–C_{60}	C_4–C_{52}	oligomers[b]	C_4–C_{14}
% 1-olefins	99.0	95.1	93.2	[c]	95.9
K-value[c]	0.84	0.78	0.73	[c]	0.58

[a] Based on MS data. – [b] Oligomer mixture not analyzed. – [c] Calculated for oligomers > C4.

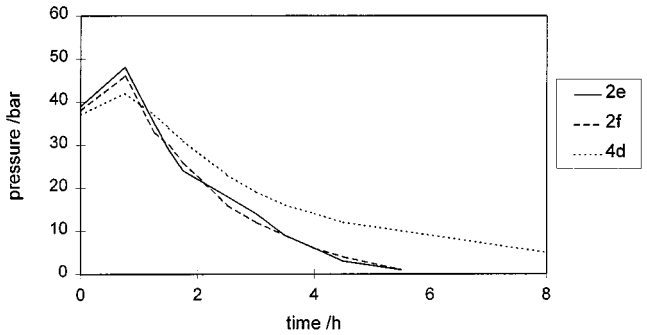
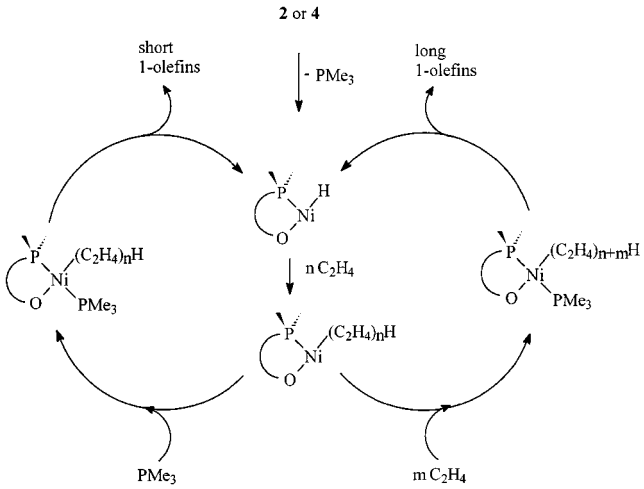


Figure 4. Conversion of ethene at 80 °C in the presence of **2e**, **2f**, and **4d**

ethene (ca. 7.7 g) at 80 °C in a 75 mL autoclave (Table 2). After an initial increase of the starting pressure (35 bar) to 45–50 bar during the induction period (about 30–45 min), the pressure fell at a rate that depended on the one-component catalyst (Figure 4). The bulk of the ethene reacted within ca. 4 h, whereas an almost quantitative conversion required 6 h in the case of **2e** and **2f**, and 10 h in the case of **4d**. The less P-basic diphenylphosphanyl- and alkylphenylphosphanyl representatives of **2** and **4** were much less active. This has a parallel in the low oligomerization activity of phenyl(2-diphenylphosphanylphenolato)(trimethylphosphane)nickel(II) as compared to phenylnickel complexes of this type with other, mainly P-arylated monodentate phosphane ligands.[3d] This is believed to be due to the greater stability of "push-pull" *trans*-diphosphane nickel complexes with a good donor on one side and a good acceptor ligand on the other as compared with the easily dissociating P-basic complexes **2e**, **2f**, and **4d** or phenyl(2-diphenylphosphanylphenolato)(triarylphosphane)nickel(II) species[3d] with similar phosphane ligands on either side.

The products of the catalytic conversion of ethene were oligomers (Scheme 5), mainly linear α-olefins (Table 3). The selectivity decreased somewhat with increasing chain length, from C4 to C12, as detected by GC. The unusually high content of a hexene isomer in II (11.5%) may be attributed to a competing reaction with 1-butene. With **4d**, lower oligomers with a Schultz–Flory distribution[18] and large amounts of 1-butene, 1-hexene, and octenes were observed. The mono-PMe_3 complexes form longer chain oligomers with broad, flat maxima in their molar weight distributions. In experiment I using the catalyst **2c**, the maximum was



Scheme 5. Proposed mechanism of oligomerization of ethene catalyzed by **2** or **4**

found in the range C10 to C14 by GC and C12 to C18 by mass spectrometry (based on abundance of $[M^+]$ using direct inlet). The most abundant oligomers (by GC) in experiments II and III using the diisopropylphosphanylphenolate catalysts **2e** and **2f** were 1-hexene and 1-octene, followed by either 1-decene (II/**2e**) or 1-butene (III/**2f**). Besides these, greater amounts of C14+ oligomers ($n > 7$) (33 and 51 mass%) were observed. Interestingly, the mass spectrum of the oligomer mixture of II revealed low abundance maxima due to the molecular ions of oligomers $n = 10$–12 and $n = 23$–25. The higher conversion and the occurrence of longer olefins using the diisopropylphosphanylphenolate catalysts **2e** and **2f** may be explained by the higher degree of dissociation allowing, over time, a proportionally faster uptake of ethene. Since diisopropylphosphanylphenolate catalysts, prepared in situ from **1e** or **1f** and $Ni(COD)_2$ and free of monodentate phosphanes, give higher polyethenes than diphenyl- or alkylphenyl-substituted species,[19] the lower-oligomer maxima seen in the catalysis using **2e** and **2f** might be induced by stronger promotion of β-hydride elimination in the alkyl(2-diisopropylphosphanylphenolato)(phosphane)nickel(II) intermediates than in intermediates formed using **2c**. This is in line with the higher electron density at nickel in **2e** and **2f** as compared with that in **2a**–**d**, which is reflected in a high-field shift of the methyl group ^{13}C resonance by ca. 4 ppm (Table 1). Coordination of an alkylphos-

Table 3. Composition of ethene oligomers obtained with **2c**,**e**,**f** and **4d**

Oligomerization (catalyst)	I (**2c**)	II (**2e**)	III (**2f**)	V (**4d**)
% C4 (% 1-olefin)	3.0	8.0 (100)	11.2 (100)	44.1 (100)
% C6 (% 1-olefin)	8.2 (90)	19.2 (99)	16.1 (87)	38.3 (99)
[% most abund. isoolefin]	[10]	[1]	[11.5]	
% C8 (% 1-olefin)	10.3	19.5 (99)	15.7 (94.4)	12.0 (85)
[% most abund. isoolefin]			[4]	
% C10 (% 1-olefin)	11.2	15.1 (85)	5.1 (91)	2.7 (79)
[% most abund. isoolefin]		[6]	[4.5]	
% C12	11.6	3.9 (79)	0.42	2.1 (69)
[% most abund. isoolefin]		[8]		
% C14	11.6	0.9	0.48	0.7
% C14+	[a]	33.3	51	

[a] C16 10.9%, C18 9.6%, C20 8.8%, C22 7.8%, C24 7%.

phane ligand will accelerate β-hydride transfer in the case of C_{2n}-alkyl chains at nickel. A small proportion of active centers, depending on the equilibrium concentration of PMe_3, may produce somewhat longer chains, promoted by a decreasing association of PMe_3 with increasing chain length.

Conclusions

Tertiary 2-phosphanylphenols **1** bearing phenyl and alkyl groups at phosphorus react with $[MeNi(\mu\text{-}OMe)(PMe_3)]_2$ to give 16-electron methyl(2-phosphanylphenolato)(trimethylphosphane)nickel(II) complexes **2** with *trans*-square-planar structures. Complex **2** reacts with excess **1** to give nickelbis(P$^\cap$O-chelates) **3** or adds PMe_3 to form 18-electron trigonal-bipyramidal methyl(2-phosphanylphenolato)bis(trimethylphosphane)nickel(II) complexes **4**. Higher yields of **4** are obtained from **1** and $Me_2Ni(PMe_3)_3$. Both **2** and **4** are fluxional molecules, particularly their dialkylphosphanyl derivatives. This is attributed to rapid dissociation–association equilibria; **4** may additionally undergo rapid pseudorotation. Both the expected unsaturated 14-electron species **I** (or dimers thereof) and free PMe_3 escape detection by NMR because of their low concentrations (low equilibrium constants). Nevertheless, alkylphenyl- or dialkylphosphanyl derivatives of **2** and **4** have proved to be effective one-component catalysts in the oligomerization of ethene. Since addition of ethene to **2** will be much less favorable than addition to **I**, and since electron-rich 2-dialkylphosphanylphenolates **2**, which bind trimethylphosphane in a *trans* fashion less tightly than 2-diphenylphosphanyl derivatives, form the more efficient catalysts, **I** can be regarded as the active species, which may even be formed by dissociation of **4**. The short chain lengths of the oligomers obtained with **2** as compared to those of the polymers produced with catalysts prepared in situ from **1** and $Ni(COD)_2$[6a,11b,19] and the even lower molecular weights of the oligomers formed with **4** suggest that β-hydride elimination is favored by coordination of PMe_3 at a free coordination site of the catalyst.

Experimental Section

General Procedures and Materials: All procedures were carried out under an atmosphere of purified argon using standard vacuum line or Schlenk techniques. Solvents (THF, diethyl ether, pentane) were dried with sodium (ketyls) and freshly distilled prior to use. $[NiMe(PMe_3)(\mu\text{-}OMe)]_2$,[16,17] *trans*-$Me_2Ni(PMe_3)_3$,[20] and the 2-phosphanylphenols **1a**,[9c] **1b**,[10i] and **1c**[9c] were prepared according to known procedures; iPr_2PCl was purchased from Aldrich and used without further purification. – IR spectra were recorded on a Nicolet Impact 400 FT-IR spectrometer. – NMR spectra were recorded on Bruker AM 200, WM 300, or ARX 300 multinuclear Fourier transform spectrometers and are referenced to tetramethylsilane for ^1H and ^{13}C and to H_3PO_4 (85%) for ^{31}P. The measuring temperature was 298 K unless otherwise stated. For resonances that are part of an AXX' spin system (X,X' = ^{31}P), vc and τ denote "virtual coupling" and the triplet appearance of the A resonance, respectively. – Melting points were determined in sealed capillaries (Büchi type 510) and are uncorrected. – Elemental analyses were carried out using CHN 240 A (Perkin–Elmer) or CHNS-932 (LECO) analyzers.

Ligand Preparation

4,6-Di-*tert*-butyl-2-(diisopropylphosphanyl)phenol (1e): At –40 °C, a hexane solution of *n*BuLi (21.0 mL, 1.6 N, 33.6 mmol) was slowly added to 2,4-di-*tert*-butylphenyl methoxymethyl ether (8.3 g, 33.2 mmol) in Et_2O (60 mL). After stirring for 4 h at 20 °C, chlorodiisopropylphosphane (5.0 g, 32.8 mmol) was rapidly added at 0 °C, the suspension was stirred for 1 h at room temperature, and then filtered. The filtrate was concentrated to dryness and the residue was treated with degassed 2 N HCl (200 mL) at 60 °C. After heating for 5 h, the volatiles were removed in vacuo and the residue was crystallized from methanol. Yield 7.8 g (73%) of **1e** as white crystals; m.p. 67–68 °C. – IR (Nujol): $\tilde{\nu}_{OH}$ = 3322 cm^{-1} s. – ^1H NMR (C_6D_6): δ = 0.86 (dd, $^3J_{PH}$ = 12.2, $^3J_{HH}$ = 6.9 Hz, 6 H, CH*Me*), 1.00 (dd, $^3J_{PH}$ = 16.5, $^3J_{HH}$ = 7.0 Hz, 6 H, CH*Me*), 1.34 (s, 9 H, CMe_3), 1.60 (s, 9 H, CMe_3), 1.94 (m, $^3J_{HH}$ = 7, $^2J_{PH}$ = ca. 3.5 Hz, 2 H, CH), 7.22 (ps. t, $^4J_{HH}$ = 2.4, $^3J_{PH}$ = ca. 2.6 Hz, 1 H, 3-H), 7.55 (d, $^4J_{HH}$ = 2.4 Hz, 1 H, 5-H), 7.76 (d, $^4J_{PH}$ = 12.4 Hz, 1 H, OH). – ^{13}C NMR (75.5 MHz, C_6D_6): δ = 18.6 (d, $^2J_{PC}$ = 7.0 Hz, CH*Me*), 20.0 (d, $^2J_{PC}$ = 17.9 Hz, CH*Me*), 23.1 (d, $^1J_{PC}$ = 6.9 Hz, C*H*Me), 29.8 (CMe_3), 31.8 (CMe_3), 34.5 (CMe_3), 35.4 (d, $^4J_{PC}$ = 2.0 Hz, CMe_3), 117.8 (d, $^1J_{PC}$ = 5.2 Hz, C-2), 125.6 (C-5), 127.1 (d, $^2J_{PC}$ = 1.1 Hz, C-3), 135.2 (d, $^3J_{PC}$ = 1.7 Hz, C-6), 141.2 (C-4), 158.1 (d, $^2J_{PC}$ = 18.8 Hz, C-1). – $^{31}P\{^1H\}$ NMR (121.5 MHz, C_6D_6): δ = –24.3. – MS (EI, 70 eV): *m/z*: 323 [M^+],

307 [$M^+ - CH_3$], 281 [$M^+ - C_3H_6$], 266 [$M^+ - t$Bu], 239 [$M^+ - 2\,C_3H_6$], 57 [tBu]. – $C_{20}H_{35}OP$ (322.47): calcd. C 74.49, H 10.94; found C 74.19, H 10.97.

4-Fluoro-2-(diisopropylphosphanyl)phenol (1f): At –40 °C, *n*BuLi (38.5 mL 1.6 N in hexane, 61.5 mmol) was added to 9.6 g (61.5 mmol) of 4-fluorophenyl methoxymethyl ether in Et_2O (100 mL) and the mixture was allowed to warm to room temperature. After 2 h, chlorodiisopropylphosphane (9.4 g, 61.6 mmol) was added. The resulting suspension was stirred for 1 h at 20 °C and then filtered. The filtrate was concentrated to dryness and the residue was treated with degassed aqueous 2 N HCl solution as above. After 5 h at 60 °C, the volatiles were removed in vacuo. The residue was crystallized from methanol to give 4.9 g (35%) of **1f** as white needles; m.p. 61–64 °C. – IR (Nujol): $\tilde{\nu}_{OH}$ = 3302 cm^{-1} s. – ^{1}H NMR (300.1 MHz, C_6D_6): δ = 0.70 (dd, $^3J_{PH}$ = 12.5, $^3J_{HH}$ = 6.9 Hz, 6 H, CH*Me*), 0.89 (dd, $^3J_{PH}$ = 16.5, $^3J_{HH}$ = 7.0 Hz, 6 H, CH*Me*), 1.68 (m, $^3J_{HH}$ = 7, $^2J_{PH}$ = ca. 3.5 Hz, 2 H, CH), 6.73 (m, $^3J_{HH}$ = 9.0, $^3J_{FH}$ = 8.1, $^4J_{HH}$ = 3.1 Hz, 1 H, 5-H), 6.82 (m, $^3J_{HH}$ = 9.0, $^4J_{FH}$ = 5.1, $^4J_{PH}$ = 3.9 Hz, 1 H, 6-H), 6.91 (m, $^3J_{FH}$ = 8.3, $^4J_{HH}$ $^3J_{PH}$ 2.8 Hz, 1 H, 3-H), 7.02 (br. s, 1 H, OH). – ^{13}C NMR (75.5 MHz, C_6D_6): δ = 19.3 (d, $^2J_{PC}$ = 7.6 Hz, CH*Me*), 20.5 (d, $^2J_{PC}$ = 18.0 Hz, CH*Me*), 23.8 (d, $^1J_{PC}$ = 7.7 Hz, *C*HMe), 117.2 (dd, $^3J_{FC}$ = 7.2, $^3J_{PC}$ = 1.7 Hz, C-6), 119.0 (dd, $^2J_{FC}$ = 21.1, $^2J_{PC}$ = 1.7 Hz, C-3), 119.0 (d, $^2J_{FC}$ = 23.1 Hz, C-5), 120.8 (dd, $^1J_{PC}$ = 4.5, $^3J_{FC}$ = 12.4 Hz, C-2), 157.6 (d, $^1J_{FC}$ = –239.7 Hz, C-4), 158.7 (dd, $^2J_{PC}$ = 18.7, $^4J_{FC}$ = 1.7 Hz, C-1). – ^{31}P{^{1}H} NMR (121.5 MHz, C_6D_6): δ = –21.8. – MS (EI, 70 eV): *m*/*z*: 228 [M^+], 186 [$M^+ - C_3H_6$], 144 [$M^+ - 2\,C_3H_6$], 111 [$M^+ - P$*i*Pr_2]. – $C_{12}H_{18}FOP$ (228.25): calcd. C 63.15, H 7.95; found C 63.01, H 7.91.

Preparation of Complexes

{4,6-Di-*tert*-butyl-2-(diphenylphosphanyl)phenolato[*P,O*]}methyl-(trimethylphosphane)nickel(II) (2a): At –78 °C, **1a** (649 mg, 1.66 mmol) was added to a solution of *cis*-[NiMe(PMe_3)(μ-OMe)]$_2$ (300 mg, 0.83 mmol) in Et_2O (60 mL). A rapid color change from yellow-brown to red was observed and after 3 h the mixture became orange. The solvent was then removed in vacuo and the residue was extracted with warm pentane, from which 580 mg (65%) of **2a** was obtained as yellow crystals; dec. at 162–163 °C. **2a** was found to be slightly contaminated with **3a**. – IR (Nujol): $\tilde{\nu}$ = 955 cm^{-1} s (ρ_1 PMe_3). – ^{1}H NMR (300 MHz, [D$_8$]THF): δ = –0.82 (d, $^3J_{PH}$ = 7.4 Hz, 3 H, NiMe), 1.15 (s, 9 H, PMe_3), 1.34, 1.38 (2 s, 18 H, 2 CMe_3), 6.95 (d, $^3J_{PH}$ = 8.0 Hz, 1 H, 3-H), 7.12 (s, 1 H, 5-H), 7.39 (m, 6 H, Ph), 7.65 (m, 4 H, Ph). – ^{13}C NMR (75.5 MHz, [D$_8$]THF): δ = –19.9 (d, $^2J_{PC}$ = 25 Hz, NiMe), 10.8 (d, $^1J_{PC}$ = 22.5 Hz, PMe_3), 27.9 (C*Me*$_3$), 30.3 (C*Me*$_3$), 32.6 (*C*Me$_3$), 33.9 (*C*Me$_3$), 115.9 (d, $^1J_{PC}$ = 49.1 Hz, C-2), 124.7 (C-5), 125.5 (C-3), 127.3 (d, $^3J_{PC}$ = 9.5 Hz, *m*-C), 128.6 (*p*-C), 132.2 (d, $^2J_{PC}$ = 11.4 Hz, *o*-C), 132.6 (C-4), 133.5 (d, $^1J_{PC}$ = 47.7 Hz, *i*-C), 135.9 (C-6), 173.6 (d, $^2J_{PC}$ = 25.1 Hz, C-1). – ^{31}P NMR (81 MHz, [D$_8$]THF): δ = –10.7 (br. s, PMe), 32.9 (br. s, 2-P). – Low-temperature NMR: ^{1}H NMR (200 MHz, [D$_8$]THF, 208 K): δ = –0.83 (m, 3 H, NiMe), 1.15 (s, 9 H, PMe_3), 1.35 (s, 9 H, CMe_3), 1.39 (s, 9 H, CMe_3), 7.00 (d, $^3J_{PH}$ = 8.6 Hz, 1 H, 3-H), 7.09 (s, 1 H, 5-H), 7.46 (m, 6 H, Ph), 7.64 (m, 4 H, Ph). – ^{31}P NMR (81 MHz, [D$_8$]THF, 223 K): **2a:** δ = –6.1 (d, $^2J_{PP}$ = 316 Hz, PMe), 32.7 (d, $^2J_{PP}$ = 316 Hz, 2-P); trace impurities: δ = 1.4 (d, J_{PP} = 15.9 Hz), 32.9 (d, J_{PP} = 15.9 Hz), 42.1 (**3a**). – $C_{30}H_{42}NiOP_2$ (539.30): calcd. C 66.81, H 7.85, P 11.49; found C 66.24, H 7.68, P 11.76.

{6-*tert*-Butyl-4-methyl-2-(diphenylphosphanyl)phenolato[*P,O*]}-methyl(trimethylphosphane)nickel(II) (2b): At –78 °C, **1b** (1.73 g, 4.97 mmol) was added to a solution of *cis*-[NiMe(PMe_3)(μ-OMe)]$_2$ (900 mg, 2.49 mmol) in Et_2O (80 mL), resulting in a color change to orange. After stirring for 3 h, the solvent was evaporated in vacuo and the residue was extracted with warm pentane. On cooling of the combined extracts, yellow crystals of **2b** were deposited. Yield 2.05 g (83%); dec. at 129 °C. – IR (Nujol): $\tilde{\nu}$ = 1166 s (NiMe), 956 cm^{-1} s (ρ_1 PMe_3). – ^{1}H NMR (300 MHz, [D$_8$]THF): δ = –0.82 (d, $^3J_{PH}$ = 7.4 Hz, 3 H, NiMe), 1.34 (s, 9 H, CMe_3), 1.37 (d, $^2J_{PH}$ = 8.6 Hz, 9 H, PMe_3), 2.07 (s, 3 H, 4-Me), 6.75 (d, $^3J_{PH}$ = 7.4 Hz, 1 H, 3-H), 6.85 (d, $^5J_{PH}$ = 1.7 Hz, 1 H, 5-H), 7.39 (m, 6 H, Ph), 7.65 (m, 4 H, Ph). – ^{13}C NMR (75.5 MHz, [D$_8$]THF): δ = –20.3 (d, $^2J_{PC}$ = 25.1 Hz, NiMe), 12.7 (d, $^1J_{PC}$ = 22.2 Hz, PMe_3), 20.7 (s, 4-Me), 29.7 (C*Me*$_3$), 35.4 (*C*Me$_3$), 118.3 (d, $^1J_{PC}$ = 48.6 Hz, C-2), 122.0 (d, $^3J_{PC}$ = 7.0 Hz, C-4), 129.1 (d, $^3J_{PC}$ = 9.2 Hz, *m*-C), 130.2 (C-5), 130.4 (*p*-C), 131.2 (C-3), 134.1 (d, $^2J_{PC}$ = 11.2 Hz, *o*-C), 134.5 (d, $^1J_{PC}$ = 47.0 Hz, *i*-C), 138.4 (d, $^3J_{PC}$ = 9.1 Hz, C-6), 173.8 (d, $^2J_{PC}$ = 25.8 Hz, C-1). – ^{31}P NMR (81 MHz, [D$_8$]THF): δ = –7.4 (br. d, $^2J_{PP}$ = 286 Hz, PMe), 32 (br. d, $^2J_{PP}$ = 259 Hz, *o*-P); trace impurity: δ = 0.5 (d, J_{PP} = 14.9 Hz, PMe), 32.3 (d, J_{PP} = 14.7 Hz, *o*-P). – Low-temperature NMR: ^{31}P NMR (81 MHz, [D$_8$]THF, 223 K): δ = –5.6 (d, $^2J_{PP}$ = 316 Hz, PMe), 32.1 (d, $^2J_{PP}$ = 316 Hz, *o*-P); trace impurity: δ = 2.0 (d, J_{PP} = 14.6 Hz, PMe), 32.0 (d, J_{PP} = 14.8 Hz, *o*-P). – $C_{27}H_{36}NiOP_2$ (497.22): calcd. C 65.22, H 7.30, P 12.46; found C 64.83, H 7.78, P 12.31.

{4,6-Di-*tert*-butyl-2-(isopropylphenylphosphanyl)phenolato[*P,O*]}-methyl(trimethylphosphane)nickel(II) (2c): At –78 °C, THF (80 mL) was condensed into a mixture of **1c** (0.90 g 2.52 mmol) and *cis*-[NiMe(PMe_3)(μ-OMe)]$_2$ (0.46 g, 1.27 mmol). On warming to room temperature the mixture became orange in color. The solvent was then replaced by pentane (60 mL). Crystallization furnished 0.28 g (22%) of yellow microcrystalline **2c**; m.p. 88–90 °C (dec.). An additional portion of orange, powdery **2c** was obtained by removal of the solvent from the mother liquor to give a total yield of 0.94 g (74%) of **2c**. – IR (Nujol): $\tilde{\nu}$ = 1138 m (NiMe), 953 cm^{-1} s (ρ_1 PMe_3). – ^{1}H NMR (200 MHz, [D$_8$]THF, 296 K): δ = –0.93 (d, $^3J_{PH}$ = 1.8 Hz, 3 H, NiMe), 0.98–1.24 (m, 12 H, CH*Me*$_A$, CMe_3), 1.30–1.45 (m, 21 H, CH*Me*$_B$, CMe_3, PMe_3), 2.67 (m, 1 H, CH), 6.93 (m, 1 H, 3-H), 7.13 (d, $^2J_{PH}$ = 2.4 Hz, 1 H, 5-H), 7.39 (m, 3 H, Ph), 7.64 (m, 2 H, Ph). – ^{13}C NMR (75.5 MHz, [D$_8$]THF): δ = –22.2 (m, NiMe), 10.8 (d, $^1J_{PC}$ = 22.2 Hz, PMe_3), 16.0 (br., Me), 17.6 (br., Me), 24.2 (d, $^1J_{PC}$ = 37.2 Hz, CH), 27.8 (C*Me*$_3$), 30.3 (C*Me*$_3$), 32.6 (*C*Me$_3$), 33.8 (*C*Me$_3$), 113.6 (m, C-2), 124.9 (C-5), 125.2 (C-3), 127.2 (d, 9.0 Hz, *m*-C), 128.1 (*p*-C), 131.2 (d, $^2J_{PC}$ = 9.0 Hz, *o*-C), 131.9 (C-4), ca. 133 (*i*-C), 135.6 (d, $^4J_{PC}$ = 9.0 Hz, C-6), 174.3 (d, $^2J_{PC}$ = 23.4 Hz, C-1). – ^{31}P NMR (81 MHz, [D$_8$]THF): δ = –8.0 (d, $^2J_{PP}$ = 310 Hz, PMe), 40.0 (d, $^2J_{PP}$ = 308 Hz, 2-P). – $C_{27}H_{44}NiOP_2$ (505.29): calcd. C 64.18, H 8.78, P 12.26; found C 63.64, H 8.55, P 12.56.

{4,6-Di-*tert*-butyl-2-(*tert*-butylphenylphosphanyl)phenolato[*P,O*]}-methyl(trimethylphosphane)nickel(II) (2d): At –78 °C, **1d** (1.13 g, 3.05 mmol) was added to a solution of [NiMe(PMe_3)(μ-OMe)]$_2$ (1.10 g, 3.04 mmol) in diethyl ether (80 mL). After stirring for 3 h at room temperature, the solvent was removed in vacuo from the dark-red solution and the residue was extracted with pentane. On cooling of the combined extracts, 1.15 g (73%) of **2d** was deposited as red-brown crystals; m.p. 78–79 °C. – IR (Nujol): $\tilde{\nu}$ = 1138 m (NiMe), 952 cm^{-1} s (ρ_1 PMe_3). – ^{1}H NMR (300 MHz, [D$_8$]THF): δ = –0.88 (d, $^3J_{PH}$ = 7.5 Hz, 3 H, NiMe), 1.24 (s, 9 H, CMe_3), 1.30 (br. s, 9 H, PMe_3), 1.39 (s, 9 H, CMe_3), 1.44 (d, $^3J_{PH}$ = 13.7 Hz, 9 H, $PCMe_3$), 7.01 (dd, $^3J_{PH}$ = 7.8, $^4J_{HH}$ = 2.5 Hz, 1 H, 3-H), 7.17 (d, $^4J_{HH}$ = 2.5 Hz, 1 H, 5-H), 7.43 (m, 3 H, Ph), 7.88 (m, 2 H, Ph). – ^{13}C NMR (75.5 MHz, [D$_8$]THF): δ = –21.1 (br. d, $^2J_{PC}$ = 25 Hz, NiMe), 12.8 (d, $^1J_{PC}$ = 20.4 Hz, PMe_3), 28.9 (d, $^2J_{PC}$ = 5.3 Hz, PC*Me*$_3$), 29.7 (C*Me*$_3$), 32.2 (C*Me*$_3$), 34.4 (*C*Me$_3$), 35.4 (d,

$^1J_{PC}$ = 21.1 Hz, P*C*Me$_3$), 35.7 (*C*Me$_3$), 117.2 (d, $^1J_{PC}$ = 44.5 Hz, C-2), 126.8 (C-5), 127.4 (C-3), 128.9 (d, $^3J_{PC}$ = 9 Hz, *m*-C), 129.9 (*p*-C), 133.0 (d, $^1J_{PC}$ = 33.2 Hz, *i*-C), 134.1 (d, $^2J_{PC}$ = 8.3 Hz, *o*-C), 134.6 (d, $^3J_{PC}$ = 6.1 Hz, C-4), 137.5 (d, $^3J_{PC}$ = 8.3 Hz, C-6), 175.3 (d, $^2J_{PC}$ = 23.4 Hz, C-1). – ^{31}P NMR (81 MHz, [D$_8$]THF): δ = –8.0 (br. d, $^2J_{PP}$ = 293.7 Hz, PMe), 47.8 (br. d, $^2J_{PP}$ = 307.7 Hz, 2-P); trace impurities: δ = –0.9 (d, J_{PP} = 13.9 Hz), 52.6 (d, J_{PP} = 13.6 Hz), 35.2 (**3d**). – Low-temperature NMR: ^{1}H NMR (200 MHz, [D$_8$]THF, 248 K): δ = –0.93 (dd, $^3J_{PH}$ = 11.2, $^3J_{P'H}$ = 7.6 Hz, 3 H, NiMe), 1.20 (s, 9 H, CMe$_3$), 1.31 (s, 9 H, PMe$_3$), 1.34 (s, 9 H, CMe$_3$), 1.38 (d, $^3J_{PH}$ = 13.8 Hz, 9 H, PCMe$_3$), 6.97 (dd, $^4J_{HH}$ = 2, $^3J_{PH}$ = 7.7 Hz, 1 H, 3-H), 7.11 (d, $^4J_{HH}$ = 2 Hz, 1 H, 5-H), 7.42 (m, 3 H, Ph), 7.83 (m, 2 H, Ph). – ^{31}P NMR (81 MHz, [D$_8$]THF, 245 K): δ = –6.5 (d, $^2J_{PP}$ = 308.3 Hz, PMe), 47.9 (d, $^2J_{PP}$ = 308.5 Hz, *o*-P); trace impurities: δ = 0.5 (d), 52.3 (d), 34.9 (**3d**). – $C_{28}H_{46}NiOP_2$ (519.31): calcd. C 64.76, H 8.93, P 11.93; found C 64.75, H 7.83, P 11.85.

{4,6-Di-*tert*-butyl-2-(diisopropylphosphanyl)phenolato[*O*,*P*]}-methyl(trimethylphosphane)nickel(II) (2e): At –78 °C, **1e** (1.42 g, 4.4 mmol) and PMe$_3$ (0.34 g, 4.4 mmol) were added to a solution of *cis*-[NiMe(PMe$_3$)(μ-OMe)]$_2$ (0.80 g, 2.2 mmol) in diethyl ether (50 mL). After stirring for 3 h at room temperature (color change through red to brown), the solvent was evaporated in vacuo and the residue was treated with a small volume of pentane, yielding 1.78 g (86%) of **2e** as red-brown crystals; m.p. 79–81 °C. – ^{1}H NMR (300.1 MHz, C$_6$D$_6$): δ = –0.66 (d, $^3J_{PH}$ = 7.4 Hz, 3 H, NiMe), 1.01 (d, 9 H, $^2J_{PH}$ = 8.1 Hz, PMe$_3$), 1.21 (dd, $^3J_{PH}$ = 13.7, $^3J_{HH}$ = 7.0 Hz, CH*Me*$_a$), 1.30 (dd, $^3J_{PH}$ = 15.6, $^3J_{HH}$ = 7.1 Hz, CH*Me*$_b$), 1.43 (s, 9 H, CMe$_3$), 1.65 (s, 9 H, CMe$_3$), 2.21 (m, 2 H, C*H*Me$_2$), 7.19 (d, $^4J_{HH}$ = 2.5 Hz, partly superimposed, 3-H), 7.54 (d, $^4J_{HH}$ = 2.5 Hz, 1 H, 5-H). – ^{13}C NMR (75.5 MHz, C$_6$D$_6$): δ = –24.9 (d, $^2J_{PC}$ = 28.1 Hz, 3 H, NiMe), 13.0 (d, $^1J_{PC}$ = 21.2 Hz, PMe$_3$), 18.8 (C*Me*$_a$), 19.7 (d, $^2J_{PC}$ = 4.8 Hz, C*Me*$_b$), 24.8 (d, $^1J_{PC}$ = 22.8 Hz, CH), 30.4 (C*Me*$_3$), 32.9 (C*Me*$_3$), 34.8 (*C*Me$_3$), 36.2 (*C*Me$_3$), 115.8 (d, $^1J_{PC}$ = 41.2 Hz, C-2), 125.4 (C-5), 127.4 (C-3), 135.2 (d, $^3J_{PC}$ = 5.3 Hz, C-4), 137.9 (d, $^3J_{PC}$ = 8.3 Hz, C-6), 176.2 (d, $^2J_{PC}$ = 22.0 Hz, C-1). – ^{31}P NMR (121.5 MHz, C$_6$D$_6$, 298 K): δ = –15.4 (br. s, PMe), 39.6 (br. s, 2-P); trace impurity: δ = 31.4 (br. s). – ^{31}P NMR (121.5 MHz, [D$_8$]toluene, 203 K): δ = –13.2 (d, $^2J_{PP}$ = 305 Hz, PMe), 39.6 (d, $^2J_{PP}$ = 305 Hz, 2-P). – MS (EI, 70 eV): *m*/*z* (%) = 470 (10) [M$^+$]. – $C_{24}H_{46}NiOP_2$ (471.27): calcd. C 61.17, H 9.84; found C 60.34, H 9.65.

{4-Fluoro-2-(diisopropylphosphanyl)phenolato[*O*,*P*]}-methyl(trimethylphosphane)nickel(II) (2f): At –78 °C, **1f** (0.23 g, 1.01 mmol) was added to a solution of *cis*-[NiMe(PMe$_3$)(μ-OMe)]$_2$ (0.21 g, 0.58 mmol) in pentane (30 mL) and the resulting mixture was stirred for 1 h at room temperature (color change through red to yellow). The solvent was then evaporated in vacuo and the residue was extracted with diethyl ether to afford 228 mg (60%) of yellow **2f**. – ^{1}H NMR (300.1 MHz, C$_6$D$_6$): δ = –0.73 (d, $^3J_{PH}$ = 7.9 Hz, 3 H, NiMe), 0.93 (d, $^2J_{PH}$ = 8.4 Hz, 9 H, PMe$_3$), 1.06 (dd, $^3J_{PH}$ = 13.8, $^3J_{HH}$ = 7.1 Hz, 6 H, CH*Me*$_a$), 1.21 (dd, $^3J_{PH}$ = 15.8, $^3J_{HH}$ = 7.1 Hz, 6 H, CH*Me*$_b$), 1.96 (m, 2 H, C*H*Me$_2$), 6.75 (dτ, $^3J_{HH}$ = 8.9, J_{PH} and J_{FH} = ca. 4.5–4.7 Hz, 1 H, 6-H), 6.87–6.98 (m, 2 H, 3-H, 5-H). – ^{13}C NMR (75.5 MHz, C$_6$D$_6$): δ = –26.1 (d, $^2J_{PC}$ = 26.8 Hz, 3 H, NiMe), 11.3 (d, $^1J_{PC}$ = 22.4 Hz, PMe$_3$), 17.9 (Me$_a$), 18.8 (d, $^2J_{PC}$ = 5.2 Hz, Me$_b$), 23.9 (d, $^1J_{PC}$ = 21.9 Hz, CH), 115.4 (d, $^1J_{PC}$ = 38.3 Hz, C-2), 115.8 (d, $^2J_{FC}$ = 21.7 Hz, C-5), 118.8 (ps. t, $^3J_{PC}$ and $^3J_{FC}$ = ca. 8 Hz, C-6), 120.0 (d, $^2J_{FC}$ = 23.4 Hz, C-3), 153.3 (dd, $^1J_{FC}$ = 230.8, $^3J_{PC}$ = 6.4 Hz, C-4), 176.0 (d, $^2J_{PC}$ = 21.6 Hz, C-1). – ^{31}P NMR (121.5 MHz, C$_6$D$_6$, 298 K): δ = –14.6 (s, PMe), 38.7 (s, 2-P). – $C_{16}H_{29}FNiOP_2$ (377.04).

***trans*-Bis{4,6-di-*tert*-butyl-2-(diisopropylphosphanyl)phenolato-[*O*,*P*]}nickel(II) (3e):** *cis*-[NiMe(PMe$_3$)(μ-OMe)]$_2$ (0.43 g, 1.19 mmol) was dissolved in THF (60 mL) and the solution was cooled to –50 °C. **1e** (0.98 g, 3.04 mmol) was then added, resulting in a color change from brown through orange to yellow-green. After stirring for 1 h at room temperature, the solvent was removed in vacuo. The residue was extracted with pentane (40 mL) and crystallized from this solvent yielding 0.84 g (79%) of **3e** as green crystals; m.p. 228–230 °C (with color change to brown), dec. at 234 °C. – ^{1}H NMR (300 MHz, C$_6$D$_6$): δ = 1.38 (s, 18 H, CMe$_3$), 1.35 (τd, *N* = 14.2, $^3J_{HH}$ = 7.0 Hz, 12 H, Me$_A$), 1.49 (s, 18 H, CMe$_3$), 1.64 (τd, *N* = 16.8, $^3J_{HH}$ = 7.4 Hz, 12 H, Me$_B$), 2.36 (m, 4 H, CH), 7.18 (τd, *N* 8, $^4J_{HH}$ = 2.3 Hz, 2 H, 3-H), 7.39 (d, $^4J_{HH}$ = 2.3 Hz, 2 H, 5-H). – ^{13}C NMR (75.5 MHz, C$_6$D$_6$): δ = 18.2 (s, C*Me*$_A$), 19.5 (τ, *N* = 6.0 Hz, C*Me*$_B$), 24.8 (τ, *N* = 22.0 Hz, CH), 29.8 (C*Me*$_3$), 32.1 (C*Me*$_3$), 34.0 (*C*Me$_3$), 35.3 (*C*Me$_3$), 113.1 (τ, *N* = 42.6 Hz, C-2), 125.3 (C-5), 126.9 (C-3), 136.2 (τ, *N* = 6.4 Hz, C-4), 138.5 (τ, *N* = 7.4 Hz, C-6), 175.2 (τ, *N* = 30.5 Hz, C-1). – ^{31}P NMR (121.5 MHz, C$_6$D$_6$): δ = 37.7. – MS (70 eV): *m*/*z* (%) = 701 (100) [M$^+$], 336 (24) [M – Lig – *i*Pr$^+$], 321 (31) [Lig – H$^+$], 280 (22) [Lig – *i*Pr$^+$] (Lig = **1e**-H$^+$). – $C_{40}H_{68}NiO_2P_2$ (701.62): calcd. C 68.48, H 9.77; found C 68.48, H 9.86.

{4,6-Di-*tert*-butyl-2-(diphenylphosphanyl)phenolato[*O*,*P*]}-methylbis(trimethylphosphane)nickel(II) (4a): At –78 °C, **1a** (945 mg, 2.42 mmol) was added to a solution of NiMe$_2$(PMe$_3$)$_3$ (800 mg, 2.52 mmol) in Et$_2$O (60 mL). On warming to room temperature and stirring for 3 h, the color of the mixture turned from yellow-brown to dark-red. Crystallization from diethyl ether containing PMe$_3$ furnished 1.06 g (71%) of **4a** as red crystals; m.p. 109 °C. – IR (Nujol): $\tilde{\nu}$ = 1159 m (NiCH$_3$), 937 cm^{-1} s (ρ$_1$ PMe$_3$). – ^{1}H NMR (300 MHz, [D$_8$]THF): δ = –0.69 (d, $^3J_{PH}$ = 8.8 Hz, 3 H, NiMe), 1.12 (s, 9 H, CMe$_3$), 1.15 (d, $^2J_{PH}$ = 3.3 Hz, 18 H, PMe$_3$), 1.34 (s, 9 H, CMe$_3$), 7.03 (br. d, $^3J_{PH}$ = 8.4 Hz, 1 H, 3-H), 7.09 (d, $^5J_{PH}$ = 2.3 Hz, 1 H, 5-H), 7.35 (m, 6 H, Ph), 7.62 (m, 4 H, Ph). – ^{13}C NMR (75.5 MHz, [D$_8$]THF, 293 K): δ = –18.8 (br., NiMe), 12.5 (d, $^1J_{PC}$ = 6.5 Hz, PMe$_3$), 28.1 (C*Me*$_3$), 30.3 (C*Me*$_3$), 32.6 (*C*Me$_3$), 34.0 (*C*Me$_3$), 117.1 (d, $^1J_{PC}$ = 45.8 Hz, C-2), 125.0 (C-5), 125.3 (C-3), 127.1 (d, $^3J_{PC}$ = 9.3 Hz, *m*-C), 128.0 (*p*-C), 132.0 (d, $^2J_{PC}$ = 11.7 Hz, *o*-C), 133.3 (d, $^3J_{PC}$ = 5.0 Hz, C-4), 134.5 (d, $^1J_{PC}$ = 36.5 Hz, *i*-C), 136.1 (d, $^3J_{PC}$ = 8.9 Hz, C-6), 173.3 (d, $^2J_{PC}$ = 28.1 Hz, C-1). – ^{31}P NMR (81 MHz, [D$_8$]THF): δ = –28.5 (br. s, PMe$_3$), 27.0 (br. s, *o*-P); trace impurity: δ = –15.9 (s), 41.4 (s). – Low-temperature NMR: ^{13}C NMR (75.5 MHz, [D$_8$]THF, 243 K): δ = –16.4 (d, $^2J_{PC}$ = 19.6 Hz, NiMe), 15.4 (d, $^1J_{PC}$ = 9.8 Hz, PMe$_3$), 30.2 (C*Me*$_3$), 32.2 (C*Me*$_3$), 34.5 (*C*Me$_3$), 35.9 (*C*Me$_3$), 120.4 (d, $^1J_{PC}$ = 43.0 Hz, C-2), 126.0 (C-5), 127.8 (C-3), 128.9 (d, $^3J_{PC}$ = 8.1 Hz, *m*-C), 129.3 (*p*-C), 133.5 (d, $^2J_{PC}$ = 11.9 Hz, *o*-C), 134.0 (br., C-4), 138.0 (d, $^3J_{PC}$ = 8.9 Hz, C-6), 138.6 (d, $^1J_{PC}$ = 30.0 Hz, *i*-C), 174.8 (d, $^2J_{PC}$ = 31.1 Hz, C-1). – $C_{33}H_{51}NiOP_3$ (615.38): calcd. C 64.41, H 8.35, P 15.10; found C 64.67, H 8.06, P 15.18.

{4,6-Di-*tert*-butyl-2-(*tert*-butylphenylphosphanyl)phenolato-[*O*,*P*]}methylbis(trimethylphosphane)nickel(II) (4d): At –78 °C, **1d** (945 mg, 2.55 mmol) was added to a solution of NiMe$_2$(PMe$_3$)$_3$ (800 mg, 2.52 mmol) in Et$_2$O (60 mL) and the mixture was stirred for 3 h at room temperature. The bulk of the solvent was then removed. Crystallization of the residue from diethyl ether containing PMe$_3$ furnished 1.07 g (71%) of **4d** as dark-red crystals; m.p. 106–109 °C. – IR (Nujol): $\tilde{\nu}$ = 1157 m (NiCH$_3$), 937 cm^{-1} s (ρ$_1$ PMe$_3$). – ^{1}H NMR (300 MHz, [D$_8$]THF): δ = –0.87 (d, $^3J_{PH}$ = 8.1 Hz, 3 H, NiMe), 1.22 (s, 9 H, CMe$_3$), 1.25 (br. s, 18 H, PMe$_3$), 1.34 (s, 9 H, CMe$_3$), 1.36 (d, $^3J_{PH}$ = 12.8 Hz, 9 H, PCMe$_3$), 7.06 (dd, $^3J_{PH}$ = 7.4, $^4J_{HH}$ = 2.5 Hz, 1 H, 3-H), 7.12 (d, $^4J_{HH}$ = 2.5 Hz, 1 H, 5-H),

7.37 (m, 3 H, Ph), 7.81 (m, 2 H, Ph). – ^{13}C NMR (75.5 MHz, [D$_8$]THF): δ = –20.7 (d, $^2J_{PC}$ = 22.7 Hz, NiMe), 15.1 (br. s, PMe_3), 28.5 (d, $^2J_{PC}$ = 5.3 Hz, PC*Me*$_3$), 29.3 (C*Me*$_3$), 31.7 (C*Me*$_3$), 33.9 (*C*Me$_3$), 35.0 (d, $^1J_{PC}$ = 20.4 Hz, P*C*Me$_3$), 35.2 (*C*Me$_3$), 117.3 (d, $^1J_{PC}$ = 43.0 Hz, C2), 125.9 (C-5), 127.2 (C-3), 128.3 (d, $^3J_{PC}$ = 8.3 Hz, *m*-C), 128.9 (*p*-C), 133.2 (d, $^2J_{PC}$ = 8.3 Hz, *o*-C), 133.6 (d, $^3J_{PC}$ = 5.3 Hz, C-4), 133.8 (d, $^1J_{PC}$ = 29.4 Hz, *i*-C), 137.1 (d, $^3J_{PC}$ = 9.1 Hz, C-6), 174.7 (d, $^2J_{PC}$ = 24.9 Hz, C-1). – ^{31}P NMR (81 MHz, [D$_8$]THF): δ = –28.0 (v br. s, PMe_3), 44.4 (br. s, *o*-P). – $C_{31}H_{55}NiOP_3$ (595.39): calcd. C 62.54, H 9.31, P 15.61; found C 62.06, H 9.11, P 15.31.

Complex-Catalyzed Oligomerization of Ethene. – General Procedure: A solution of the appropriate nickel complex **2** or **4** (ca. 0.1 mmol) in toluene (12 mL) was transferred at room temperature into an argon-filled stainless steel autoclave (75 mL) equipped with a magnetic stirrer. Ethene was introduced with stirring until the pressure remained constant at 35 bar (7.5–7.8 g by weight difference), then the valve was closed and the autoclave was heated at 80 °C for 6–10 h. After cooling to ca. 20 °C and weight control, the valve was opened and the gases were passed through a cooling trap (–60 °C) to condense gaseous butenes. The remaining material was flash distilled at 25–30 °C/10^{-2} Torr to separate volatile oligomers (condensed at –60 °C) and waxes. The former were analyzed by GC and in some cases by GC/MS. The results are summarized in Table 2 and 3.

Crystal Structure Analysis

1e: A crystal of **1e** was sealed under argon in a glass capillary, mounted on a Siemens R3m/V diffractometer, and examined using graphite-monochromated Mo-K^{α} radiation, λ = 0.71073 Å. Lattice parameters were determined from 25 selected reflections. The structure was solved by a full-matrix least-squares refinement (SHELXL-97). Non-hydrogen atoms were treated anisotropically, hydrogen atoms were fixed in idealized positions. Crystal data are presented in Table 4; selected bond lengths and angles are indicated in Figure 1.

3e: A green crystal of **3e** was sealed under argon in a capillary; data were collected as above on a Bruker P4 diffractometer. Lattice parameters were refined from 28 reflections in the range 15 ≤ 2Θ ≤ 40°. During data collection, 3 standard reflections were checked every 397 intensities and were found to show only random deviations. Lorentz and polarization corrections were applied, as well as an absorption correction based on psi-scans. The structure was solved by direct and conventional Fourier methods, with full-matrix least-squares refinement based on F^2. All atoms other than the H-atoms and disordered C-atoms were refined anisotropically. The *tert*-butyl group C7–C102 and the isopropyl group C19–C21 were each found to be disordered over two sites and were refined with a split model. Site occupancy factors were refined to 0.43(1) and 0.57(1) for the *tert*-butyl group and to 0.29(1) and 0.71(1) for the isopropyl group, respectively. Hydrogen atoms were refined at idealized positions with a riding model. Further crystallographic and refinement data are given in Table 4; selected bond lengths and angles are indicated in Figure 2.

4a: A red crystal of **4a** was sealed under argon in a glass capillary. Data collection was performed as described for **3e**. Lattice parameters were refined from 25 reflections in the range 17 ≤ 2Θ ≤ 34°. Standard reflections showed a decrease of 7%. Lorentz, polarization, and absorption corrections were applied as above. Structure solution and refinement and the positioning of the hydrogen atoms was as described above. Further crystallographic and refinement data are given in Table 4; selected bond lengths and angles are indicated in Figure 3.

Crystallographic data (excluding structure factors) have been deposited with the Cambridge Crystallographic Data Centre. Copies of the data [CCDC-136785 (**1e**)], [CCDC-135904 (**3e**)], [CCDC-135905 (**4a**)] can be obtained free of charge on application to the CCDC, 12 Union Road, Cambridge CB2 1EZ, U.K. [Fax: (internat.) +44 (0)1223/336033; E-mail: deposit@chemcrys.cam.ac.uk].

Table 4. Crystallographic data of compounds **1e**, **3e**, and **4a**

	1e	**3e**	**4a**
Empirical formula	$C_{20}H_{35}OP$	$C_{40}H_{68}NiO_2P_2$	$C_{33}H_{51}NiOP_3$
Molecular mass	322.47	701.59	615.36
Crystal size [mm^3]	0.49 × 0.56 × 0.39	0.58 × 0.55 × 0.50	0.35 × 0.21 × 0.10
Crystal system	Monoclinic	Orthorhombic	Triclinic
Space group	*P*21/*c*	Pbca	*P*-1
Unit cell dimensions			
a [Å]; α [°]	11.2190(4); 90	10.425(2); 90	9.646(2); 98.90(2)
b [Å]; β [°]	10.0580(6); 90.8(3)	18.611(2); 90	10.236(2); 95.86(2)
c [Å]; γ [°]	18.9040(8); 90	21.529(6); 90	18.837(4); 107.24(2)
V [Å^3]; *Z*	2132.93(17); 4	4177.0(15); 4	1733.2(6); 2
Density (calcd.) [Mg/m^3]	1.004	1.116	1.179
Temperature [K]	193	298(2)	293(2)
Absorption coefficient [mm^{-1}]	0.097	0.570	0.720
F(000)	712	1528	660
θ range for data collection [°]	2.00 to 17.50	2.38 to 27.50	2.22 to 25.00
Limiting indices	–9 *h* 9	–1 *h* 13	–12 *h* 12
	0 *k* 8	–1 *k* 24	–13 *k* 13
	0 *l* 15	–27 *l* 1	0 *l* 24
Reflections collected	3384	5889	6289
Independent reflections	1357	4788 (R_{int} = 0.0176)	6094 (R_{int} = 0.0564)
Absorption correction	–	Psi-scan	Psi-scan
Max./min. transmission		0.779/0.748	0.883/0.805
Data/restraints/parameters	1357/3/111	4788/332/203	3122/11/356
Goodness-of-fit on F^2	1.144	1.023	1.034
Final *R* indices [$I > 2\sigma(I)$]	*R*1 = 0.077; *wR*2 = 0.2364	*R*1 = 0.0599, *wR*2 = 0.1491	*R*1 = 0.0540, *wR*2 = 0.1093
R indices (all data)	*R*1 = 0.1018, *wR*2 = 0.2795	*R*1 = 0.1016, *wR*2 = 0.1732	*R*1 = 0.1423, *wR*2 = 0.1434
Largest diff. peak and hole	0.39/–0.41 eÅ^{-3}	0.566/–0.355 eÅ^{-3}	0.321/–0.348 eÅ^{-3}

Acknowledgments

Financial support from the Deutsche Forschungsgemeinschaft and the Fonds der Chemischen Industrie is gratefully acknowledged. We thank Dr. M. K. Kindermann and B. Witt for performing NMR experiments, and Dr. P. Lobitz, Dr. A. Müller, and W. Heiden, Institut für Chemie und Biochemie, Universität Greifswald, for GC and GC-MS measurements. We thank Prof. Dr. R. Kniep and G. Cordier, Institut für Anorganische Chemie, Technische Universität Darmstadt, for conducting low-temperature X-ray diffraction measurements.

[1] [1a] W. Keim, *J. Mol. Catal.* **1989**, *52*, 19. – [1b] W. Keim, *Angew. Chem. Int. Ed. Engl*. **1990**, *29*, 235. – [1c] W. Keim, *New J. Chem*. **1994**, *18*, 93.

[2] [2a] W. Keim, F. H. Kowaldt, R. Goddard, C. Krüger, *Angew. Chem*. **1978**, *90*, 493, *Angew. Chem. Int. Ed. Engl*. **1978**, *17*, 466. – [2b] W. Keim, A. Behr, B. Gruber, B. Hoffmann, F. H. Kowaldt, U. Kürschner, B. Limbäcker, F. P. Sistig, *Organometallics* **1986**, *5*, 2356. – [2c] A. Behr, U. Freudenberg, W. Keim, *J. Mol. Catal.* **1986**, *35*, 17. – [2d] K. Hirose, W. Keim, *J. Mol. Catal.* **1986**, *35*, 17. – [2e] W. Keim, R. P. Schulz, *J. Mol. Catal*. **1994**, *92*, 22. – [2f] M. C. Bonnet, F. Dahan, A. Ecke, W. Keim, R. P. Schulz, I. Tkatchenko, *J. Chem. Soc., Chem. Commun*. **1994**, 615. – [2g] I. Brassat, U. Englert, W. Keim, D. P. Keitel, S. Killat, G.-P. Suranna, R. Wang, *Inorg. Chim. Acta* **1998**, *280*, 150.

[3] [3a] D. Matt, M. Huhn, J. Fischer, A. DeCian, W. Kläui, I. Tkatchenko, M. Bonnet, *J. Chem. Soc., Dalton Trans.* **1993**, 1173. – [3b] P. Braunstein, Y. Chauvin, S. Mercier, L. Saussine, A. DeCian, J. Fischer, *J. Chem. Soc., Chem. Commun.* **1994**, 2203. – [3c] J. Andrieu, P. Braunstein, Y. Dusausoy, N. E. Ghermani, *Inorg. Chem*. **1996**, *35*, 7174. – [3d] J. Pietsch, P. Braunstein, Y. Chauvin, *New J. Chem*. **1998**, 467.

[4] [4a] K. A. Ostoja-Starzewski, J. Witte, *Angew. Chem. Int. Ed. Engl*. **1985**, *24*, 599. – [4b] K. A. Ostoja-Starzewski, J. Witte, *Angew. Chem. Int. Ed. Engl.* **1988**, *27*, 839. – [4c] K. A. Ostoja-Starzewski, L. Born, *Organometallics* **1992**, *11*, 2701.

[5] [5a] U. Klabunde, T. H. Tulip, D. C. Roe, S. D. Ittel, *J. Organomet. Chem*. **1987**, *334*, 141. – [5b] U. Klabunde, R. Mülhaupt, T. Herskovitz, A. H. Janowicz, J. Calabrese, S. D. Ittel, *J. Polym. Sci.: Polym. Chem*. **1987**, *25*, 1989.

[6] [6a] D. M. Singleton (Shell Oil Corp.), US 4,472,522; *Chem. Abstr*. **1985**, *102*, 46405. – [6b] D. M. Singleton (Shell Oil Corp.), US 4,472,525; *Chem. Abstr*. **1985**, *102*, 85118.

[7] G. A. Nesterov, G. Fink, V. A. Zakharov, W. Frenzl, *J. Mol. Catal*. **1991**, *69*, 129.

[8] [8a] H. D. Empsall, B. L. Shaw, B. L. Turtle, *J. Chem. Soc., Dalton Trans.* **1976**, 1500. – [8b] T. B. Rauchfuss, *Inorg. Chem*. **1977**, *16*, 2966.

[9] [9a] J. Heinicke, E. Nietzschmann, A. Tzschach, *J. Organomet. Chem*. **1983**, *243*, 1. – [9b] J. Heinicke, R. Kadyrov, *J. Organomet. Chem*. **1996**, *520*, 131. – [9c] J. Heinicke, R. Kadyrov, M. K. Kindermann, M. Koesling, P. G. Jones, *Chem. Ber*. **1996**, *129*, 1547. – [9d] M. K. Cooper, J. M. Downes, P. A. Duckworth, E. R. T. Tiekink, *Aust. J. Chem*. **1992**, *45*, 595. – [9e] O. Herd, A. Heßler, M. Hingst, M. Trepper, O. Stelzer, *J. Organomet. Chem*. **1996**, *522*, 69.

[10] [10a] S. Park, M. Pontier-Johnson, D. M. Roundhill, *Inorg. Chem*. **1990**, *29*, 2689. – [10b] M. Canestrari, B. Chaudret, F. Dahan, Y.-S. Huang, R. Poilblanc, T.-C. Kim, M. Sanchez, *J. Chem. Soc., Dalton Trans.* **1990**, 1179. – [10c] K. R. Dunbar, A. Quillevéré, *Organometallics* **1993**, *12*, 618. – [10d] S. B. Sembiring, S. B. Colbran, D. C. Craig, M. L. Scudder, *Inorg. Chem*. **1995**, *34*, 3731. – [10e] H. Luo, I. Setyawati, S. J. Rettig, C. Orvig, *Inorg. Chem*. **1995**, *34*, 2287. – [10f] L. Miquel, M. Bassoo-Bert, R. Choukroun, R. Madhouni, B. Eichhorn, M. Sanchez, M.-R. Mazieres, J. Jaud, *J. Organomet. Chem*. **1995**, *490*, 21. – [10g] J. Pietsch, L. Dahlenburg, A. Wolski, H. Berke, I. L. Eremenko, *J. Organomet. Chem*. **1995**, *495*, 113. – [10h] C. A. Willoughby, R. R. Duff, W. M. Davis, S. L. Buchwald, *Organometallics* **1996**, *15*, 472. – [10i] H.-F. Klein, A. Brand, G. Cordier, *Z. Naturforsch.* **1998**, *53b*, 307. – [10k] D. Weiß, A. Schier, H. Schmidbaur, *Z. Naturforsch*. **1998**, *53b*, 1307.

[11] [11a] J. Heinicke, R. Kadyrov, M. Koesling, U. Jux, *Phosphorus, Sulfur, and Silicon* **1996**, *109–110*, 501. – [11b] J. Heinicke, M. Koesling, R. Brüll, W. Keim, H. Pritzkow, *Eur. J. Inorg. Chem*. **2000**, 299–305.

[12] J. Heinicke, A. Dal, H.-F. Klein, O. Hetche, U. Flörke, H.-J. Haupt, *Z. Naturforsch.* **1999**, *54b*, 1235.

[13] H.-F. Klein, A. Dal, T. Jung, S. Braun, C. Röhr, U. Flörke, H.-J. Haupt, *Eur. J. Inorg. Chem*. **1998**, 621.

[14] H.-F. Klein, E. Auer, A. Dal, U. Lemke, M. Lemke, T. Jung, C. Röhr, U. Flörke, H.-J. Haupt, *Inorg. Chim. Acta* **1999**, *287*, 167.

[15] R. A. Palmer, D. R. Whitcomb, *J. Magn. Reson*. **1980**, *39*, 371.

[16] [16a] H.-F. Klein, A. Bickelhaupt, T. Jung, G. Cordier, *Organometallics* **1994**, *13*, 2557. – [16b] H.-F. Klein, A. Bickelhaupt, B. Hammerschmitt, U. Flörke, H.-J. Haupt, *Organometallics* **1994**, *13*, 2944.

[17] [17a] H.-F. Klein, H. H. Karsch, *Chem. Ber.* **1973**, *106*, 1433. – [17b] H.-F. Klein, H. H. Karsch, *Chem. Ber.* **1973**, *106*, 2438.

[18] G. Henrici-Olive, S. Olive, *Adv. Polym. Sci*. **1974**, *15*, 1.

[19] J. Heinicke, M. Köhler, W. Keim, unpublished results.

[20] H.-F. Klein, H. H. Karsch, *Chem. Ber*. **1972**, *105*, 2628.

Received August 16, 1999
[I99303]

Alcoholysis of Aluminum Alkyls Supported by Bulky Phenoxide Ligands: Synthesis, Characterization, and ε-Caprolactone Polymerization Activity of Two Dimeric Aluminum Isopropoxides

Insa Taden,[a] Hak-Chul Kang,[b] Werner Massa,[b] Thomas P. Spaniol,[a] and Jun Okuda*[a]

Keywords: Aluminum / Alkoxides / Lactone / Ring-opening / Polymerization

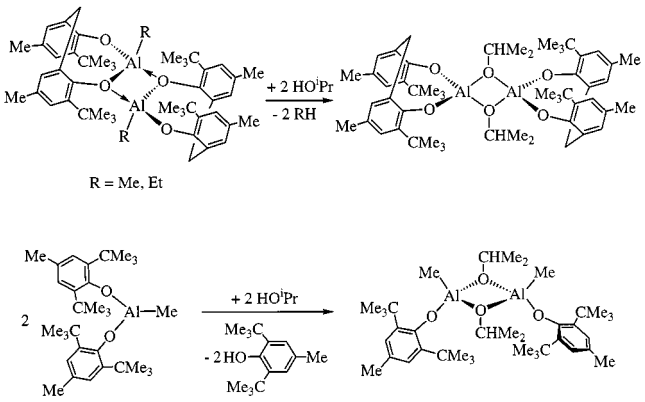
Reaction of trialkylaluminum Al_2R_6 (R = Me, Et) with 2,2′-methylenebis(6-*tert*-butyl-4-methylphenol) ($mbmpH_2$) gives the dimeric mono(alkyl) complex $[Al(mbmp)R]_2$ with bridging oxygen atoms. Reaction of $[Al(mbmp)R]_2$ with one equiv. of 2-propanol results in the formation of the dimeric isopropoxide $[Al(mbmp)(\mu\text{-O}i\text{Pr})]_2$. Single-crystal X-ray analysis shows a C_{2h}-symmetric structure with a planar Al_2O_2 core. Monomeric methylbis(2,6-di-*tert*-butyl-4-methylphenolato)aluminum, $AlMe(OC_6H_2\text{-}2,6\text{-}t\text{Bu}_2\text{-}4\text{-Me})_2$ (MAD), was found to react with one equiv. of 2-propanol to give a dimeric isopropoxide $[AlMe(OC_6H_2\text{-}2,6\text{-}t\text{Bu}_2\text{-}4\text{-Me})(\mu\text{-O}i\text{Pr})]_2$ in which the bulky phenolate, instead of the methyl group, has been displaced. According to the single-crystal X-ray structure analysis, the molecule contains a similar Al_2O_2 core, but the two 2,6-di-*tert*-butyl-4-methylphenolato ligands are *cis*- and orthogonally arranged to each other. ε-Caprolactone is polymerized at 50 °C in toluene in a controlled manner by $[Al(mbmp)(\mu\text{-O}i\text{Pr})]_2$, to give poly(ε-caprolactone) with high molecular weights and narrow molecular weight distributions ($M_w/M_n < 1.50$). The low efficiency values (number of polymer chains initiated per aluminum atom) imply that $[Al(mbmp)(\mu\text{-O}i\text{Pr})]_2$ exists in a monomer–dimer equilibrium. The polymerization of ε-caprolactone by $[AlMe(OC_6H_2\text{-}2,6\text{-}t\text{Bu}_2\text{-}4\text{-Me})(\mu\text{-O}i\text{Pr})]_2$ is faster, but somewhat less controlled.

Introduction

Aluminum tri(isopropoxide) is a readily available compound that, among various applications in organic synthesis, has been employed as an efficient initiator for the ring-opening polymerization of aliphatic cyclic esters such as ε-caprolactone.[1] In the crystalline state it is a tetranuclear aggregate in which one six-coordinate aluminum center is surrounded by three bridging $Al(O\textit{i}Pr)_4$ units.[2] In solution, several other species including a trimer are present and the thermodynamics as well as the kinetics of their interconversion evidently complicates the polymerization mechanism.[1d,e] We anticipated that a *monomeric* aluminum alkoxide supported by bulky phenoxide ligands[3] would furnish a structurally well-defined initiator for ring-opening polymerization, and be amenable to mechanistic investigation. By employing the mono(alkyl) complexes with the chelating mbmp ligand [mbmp: 2,2'-methylenebis(6-*tert*-butyl-4-methylphenolato)] and its nonchelating analog 2,6-di-*tert*-butyl-4-methylphenolato, we attempted the synthesis of mono(isopropoxide) complexes. We present here the somewhat unexpected outcome of the alcoholysis reactions as well as the reactivity of the resulting products.[4]

Results and Discussion

When the sterically demanding chelating bisphenol $mbmpH_2$ [2,2'-methylenebis(6-*tert*-butyl-4-methylphenol)] was treated with trimethylaluminum in hexane, vigorous evolution of methane was observed and the monomethyl complex $[Al(mbmp)Me]_2$ was formed in high yields as air- and moisture-sensitive colorless crystals. The aluminum-bound methyl group occurred as broad signals in the ^1H and ^{13}C NMR spectra at $\delta = -0.39$ and -7.36, respectively. The resonances of the mbmp ligand are all doubled, suggesting an unsymmetric structure in which the two halves of the mbmp ligand are inequivalent. We propose that a centrosymmetric dimer forms in which the Lewis-acidic aluminum center is coordinated to one phenoxy oxygen of the neighboring mbmp ligand (Scheme 1). By engaging in a bridging mode, for which the lone pair of the phenoxy oxygen is well suited, the coordinative unsaturation at the aluminum center is alleviated. Although, to the best of our knowledge, this bonding mode is unprecedented for the



Scheme 1

[a] Institut für Anorganische Chemie und Analytische Chemie, Johannes Gutenberg-Universität
Duesberg-Weg 10–14, D-55099 Mainz, Germany
[b] Fachbereich Chemie, Philipps-Universität Marburg, D-35032 Marburg, Germany

 © WILEY-VCH Verlag GmbH, D-69451 Weinheim, 2000 1434–1948/00/0303–0441 $ 17.50+.50/0

Table 1. Experimental Data for the Crystal Structure [Al(mbmp)(μ-O*i*Pr)]$_2$ and [AlMe(OC$_6$H$_2$-2,6-*t*Bu$_2$-4-Me)(μ-O*i*Pr)]$_2$

	[Al(mbmp)(μ-O*i*Pr)]$_2$	[AlMe(OC$_6$H$_2$–2,6-*t*Bu$_2$-4-Me)(μ-O*i*Pr)]$_2$
Crystal data		
Empirical formula	$C_{26}H_{37}AlO_3$	$C_{38}H_{66}Al_2O_4$
Molecular mass	424.54	640.87
Crystal color	colorless	colorless
Crystal size, mm	0.50 × 0.40 × 0.15	0.30 × 0.60 × 0.80
Crystal system	monoclinic	monoclinic
Space group	$P2_1/n$ (no. 14)	$P2_1/n$ (no. 14)
a [Å]	12.597(3)	9.7655(7)
b [Å]	16.762(3)	29.170(2)
c [Å]	16.029(3)	14.032(1)
β [deg]	108.23(3)	96.579(6)
V [Å^3]	3215(1)	3970.8(5)
Z	4	4
$\rho_{calc.}$ [g cm^{-3}]	0.877	1.072
μ [mm^{-1}] (Cu-K_α)	0.684	0.918
F(000)	920	1408
Wavelength	Cu-K_α (1.5418 Å)	Cu-K_α (1.5418 Å)
T [K]	173	296
θ-range [deg]	4–55	3–75
Index ranges	–13 *h* 13 –18 *k* 2 –17 *l* 17	–12 *h* 11 –14 *k* 36 –17 *l* 17
Solution and Refinement		
Number of reflections measured	8077	8170
Number of independent reflections	4034	8170
Number of observed reflections	2978	5030
ext coefficient	0.0006(2)	0.0021(2)
GOF	0.739	1.126
R [$I > 2\sigma(I)$]	0.0647	0.0588
wR_2 [$I > 2\sigma(I)$]	0.1802	0.1322
largest e-max, e-min, [eÅ^{-3}]	0.228, –0.341	0.294, –0.271

bulky bisphenolato ligand mbmp,[5] this type of bridging has been frequently observed in aluminum compounds with phenoxy[6] and chelating ligands in which at least one alkoxy function is present.[7] Addition of a Lewis base such as diethyl ether, THF, and pyridine, results in the formation of a mononuclear adduct with a four-coordinate aluminum center, as observed by NMR spectroscopy. The ethyl derivative [Al(mbmp)Et]$_2$ can be obtained in an analogous fashion from triethylaluminum, and isolated as colorless crystals. Due to the diastereotopicity, the methylene protons of the ethyl groups appear as a high-order multiplet, but give rise to a binomial quadruplet upon formation of the C_s-symmetric pyridine adduct [Al(mbmp)Et(py)]. The ethylene-linked bisphenol ebmpH$_2$[8] also forms a dimeric methyl complex [Al(ebmp)Me]$_2$ with NMR spectroscopic features similar to that of [Al(mbmp)Me]$_2$.

When precisely two equiv. of 2-propanol is added to an ethereal solution of the alkyl [Al(mbmp)R]$_2$ (R = Me, Et), the isopropoxide [Al(mbmp)(μ-O*i*Pr)]$_2$ is formed with concomitant alkane evolution and can be isolated as colorless crystals in 79% yield (Scheme 1). This compound can be independently prepared by reacting commercially available aluminum tri(isopropoxide) with one equiv. of mbmpH$_2$. The ^{1}H and ^{13}C NMR spectra indicate a molecule with a mirror plane bisecting the mbmp ligand, while the parent ion in the EI mass spectrum suggests a dimeric structure.

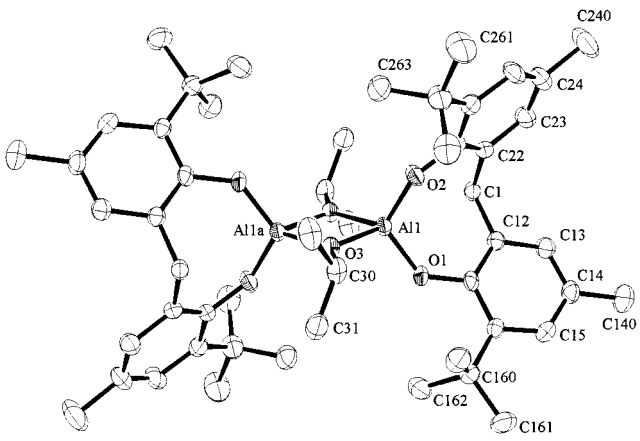


Figure 1. ORTEP diagram of the molecular structure of [Al(mbmp)(μ-O*i*Pr)]$_2$. Thermal ellipsoids are drawn at 50% probability level. Hydrogen atoms are omitted for the sake of clarity; selected bond lengths [Å] and angles [°]: Al1–O1 1.698(2), Al1–O2 1.694(3), Al1–O3 1.822(2), Al1–O3a 1.813(2); Al1–O1–C11 134.8(2), Al1–O2–C21 141.0(2), O1–Al1–O2 116.4(1), O1–Al1–O3 112.2(1), O3–Al1–O3a 81.1(1), Al1–O3–Al1a 99.0(1).

The single-crystal X-ray diffraction (Table 1, Figure 1) confirms the centrosymmetric dimeric structure with pseudo C_{2h} symmetry. The average Al–O bond lengths of 1.696(2) Å for the chelate is somewhat longer than those observed in AlMe(OC$_6$H$_2$-2,6-*t*Bu$_2$-4-Me)$_2$ (MAD) (1.686 Å), and the angles at the phenoxy oxygens of 134.8(2) and 141.0(2)° are

Table 2. Polymerization of ε-caprolactone (εCl) in toluene at 50 °C by [Al(mbmp)(μ-O*i*Pr)]$_2$ (run no. 1 to 4) and [AlMe(OC$_6$H$_2$–2,6-*t*Bu$_2$-4-Me)(μ-O*i*Pr)]$_2$ (run no. 5 to 10)

run no.	[εCl]/[Al]	time [h]	M_n(calcd.)	M_w(GPC)	M_n(GPC)	M_w/M_n	efficiency[a]
1	30	3.5	3424	9570	8820	1.09	0.39
2	50	3.0	5707	17010	16020	1.06	0.36
3	80	3.0	9132	39190	26140	1.50	0.35
4	150	3.5	17122	74850	53420	1.40	0.32
5	30	0.5	3424	48140	14660	3.28	0.23
6	50	0.5	5707	56270	31310	1.79	0.18
7	80	0.5	9132	84140	44970	1.87	0.20
8	100	0.5	11415	112900	60620	1.86	0.18
9	200	0.5	22829	163100	80700	2.02	0.28
10	500	0.5	57073	287000	155900	1.84	0.37

[a] Efficiency is defined as the fraction of active initiators, calculated from the observed number of polymer chains relative to the theoretical ones, assuming that each aluminum initiates one polymer chain.

smaller [average 143.6(2)° in MAD].[3a] These features may reflect the diminished double-bond character of the aluminum-oxygen bond within the mbmp chelate ring.[9] The two Al(mbmp) moieties with tetrahedrally-coordinated aluminum centers are linked by two isopropoxide groups. The geometry of the planar Al_2O_2 ring [average Al–O distance 1.818(2) Å; O–Al–O angle 81.1(1)°] corresponds to that of similar dimeric aluminum alkoxides such as [Al(OC$_6$H$_2$-2,4,6-*t*Bu$_3$)$_2$(μ−OEt)]$_2$ with Al–O distance of 1.845(2) Å and O–Al–O = 77.7(1)°,[10a] [AlH$_2$(μ−O*t*Bu)]$_2$ [Al–O = 1.810(3) Å and O–Al–O = 81.0(2)°],[10b] or [(η^1-C$_5$H$_5$)$_2$Al(μ-O-*i*Pr)]$_2$ [Al–O = 1.829(1) Å and O–Al–O = 80.85(1)°].[10c]

Molecular weight measurements in nonpolar solvents were inconclusive, probably due to the presence of a monomer–dimer equilibrium. As expected, molecular weight determination by vapor-pressure osmometry in THF indicated a mononuclear structure. By ^{1}H NMR spectroscopy, the formation of a 1:1 adduct with Lewis bases such as pyridine and γ-butyrolactone Al(mbmp)(O*i*Pr)(L) can be observed.

When monomeric AlMe(OC$_6$H$_2$-2,6-*t*Bu$_2$-4-Me)$_2$ is treated with 2-propanol, methane formation does not occur. Rather, under kinetic control, one equiv. of the bulky phenol HOC$_6$H$_2$-2,6-*t*Bu$_2$-4-Me is displaced to give [AlMe(OC$_6$H$_2$–2,6-*t*Bu$_2$-4-Me)(μ-O*i*Pr)]$_2$ as colorless crystals in high yields. The methyl group at the aluminum is recorded in the ^{1}H NMR spectrum at δ = –0.48. In the ^{13}C NMR spectrum the corresponding signal could not be detected, probably due to excessive broadening. Over the temperature range of +80 to –80 °C there is no significant change in the signal pattern. Molecular weight measurements in nonpolar solvents were inconclusive, but the dimeric structure can be inferred from the parent ion in the EI mass spectrum.

Single-crystal X-ray structural analysis (Table 1, Figure 2) showed a dimeric structure with two isopropoxo bridges and the ligands at the two aluminum centers arranged in a *cis* fashion. Metrical parameters such as Al–CH$_3$ [1.938(4), 1.945(4) Å] and Al–O distances of the phenoxy ligands [1.708(2), 1.698(2) Å] are within the expected ranges,[3a,10a,11] as are the values for the Al_2O_2 ring [average Al–O distance = 1.842(2) Å; O–Al–O angle = 99.1(1)°]. Most notably, the phenyl ring of one OC$_6$H$_2$-2,6-*t*Bu$_2$-4-Me ligand is turned in such a way as to bisect the plane formed by the Al_2O_2 lozenge [angle between the planes 82.4(1)°]. The other phenyl ring is in an almost orthogonal arrangement, the angle between the two aromatic rings amounting to 80.4(1)°. The two isopropyl groups of both of the bridging ligands are turned so that the methine hydrogens point toward the aluminum bearing the orthogonal aromatic ring. Evidently, the two aluminum fragments have to undergo substantial "gear-meshing" to alleviate the steric strain caused by the dimerization.

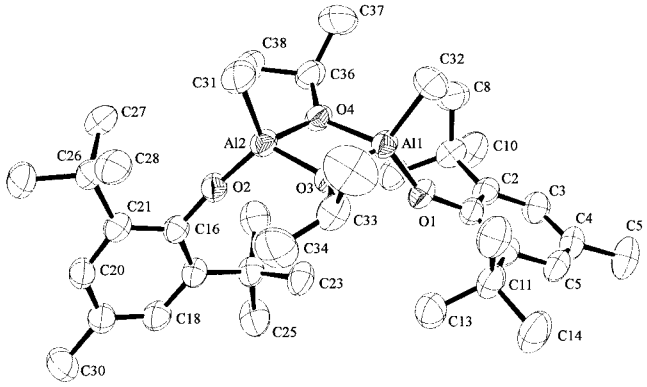


Figure 2. ORTEP diagram of the molecular structure of [AlMe(OC$_6$H$_2$–2,6-*t*Bu$_2$-4-Me)(μ-O*i*Pr)]$_2$. Thermal ellipsoids are drawn at 50% probability level. Hydrogen atoms are omitted for the sake of clarity; selected bond lengths [Å] and angles [°]: Al1–C32 1.938(4), Al1–O1 1.708(2), Al1–O3 1.839(2), Al1–O4 1.855(2), Al2–C31 1.945(4), Al2–O2 1.698(2), Al2–O3 1.837(2), Al2–O4 1.835(2); Al1–O1–C1 149.2(2), Al2–O2–C16 167.5(2), O1–Al1–C32 116.0(2), O1–Al1–O3 112.0(1), O3–Al1–O4 80.1(1), Al1–O3–Al2 99.3(1), Al1–O4–Al2 98.8(1), O2–Al2–C31 120.5(2), O2–Al2–O3 116.0(1).

Both the isopropoxo complexes are highly active initiators for the ring-opening polymerization of ε-caprolactone.[1] As summarized in Table 2, high molecular weights can be achieved in toluene at 50 °C, [AlMe(OC$_6$H$_2$–2,6-Bu$_2$-4-Me)(μ-O*i*Pr)]$_2$ being particularly active (complete conversion of a 2.0 M solution of monomer within 30 min). Moreover, the chelate complex [Al(mbmp)(μ-O*i*Pr)]$_2$ behaves in a controlled manner, as judged by the low molecular weight distribution values. The number-averaged molecular weights increase linearly with conversion, as well as with monomer to initiator ratio. Notably, since the effici-

ency, reflecting the number of chains started per aluminum, has a value of about 0.36 (run no. 1–4), we suggest that, under the conditions studied, the equilibrium between the dimer and the monomer Al(mbmp)(μ-O*i*Pr) is not completely on the side of the monomer.[12] The equilibrium constant for the dissociation in the presence of γ-butyrolactone as a nonpolymerizable lactone at 50 °C can be estimated to be K_{eq} = 0.15 mol L^{-1}. However, we cannot exclude the possibility that the dimeric species is also capable of initiating polymerization. Polymerization initiated by $[AlMe(OC_6H_2$–2,6-*t*Bu_2-4-Me)(μ-O*i*Pr)$]_2$ is noticeably less controlled, as can be judged by the higher molecular weight distribution values as well as by the rather erratic efficiencies. We suspect that initiation may occur both at the Al-Me and Al-O*i*Pr function.[13,14]

Experimental Section

General Considerations: All experiments were performed under argon using standard Schlenk or glovebox techniques. – THF, pentane, and hexane were purified by distillation from sodium/benzophenone ketyl. Toluene was distilled over sodium sand. ε-Caprolactone was dried over calcium hydride and distilled. Commercially available $mbmpH_2$ (Aldrich), trimethyl-, and triethylaluminum (WITCO) were used as received. $AlMe(OC_6H_2$–2,6-*t*Bu_2-4-Me$)_2$ was prepared according to a literature procedure.[3a] – NMR spectra were recorded on a Bruker DRX 400 spectrometer (^{1}H, 400 MHz; ^{13}C, 101 MHz) in $CDCl_3$ at 298 K, unless otherwise stated. Chemical shifts for ^{1}H and ^{13}C spectra were referenced internally using the residual solvent resonances and reported relative to tetramethylsilane. – Mass spectra were recorded on a Finnigan 8230 spectrometer. – Elemental analyses were performed by the microanalytical laboratory of this department. – Gel permeation chromatographic (GPC) analyses of the polymers were performed using a SpectraSeries P100 pump, a SDV 5μ 60 cm column, two 100 A 5 μ columns, with lengths of 5 cm and 30 cm, respectively, and a Shodex-RI-71 detector. THF was used as eluent; flow rate: 1 mL/min. – Molecular weights were corrected by universal calibration relative to polystyrene standards.

[Al(mbmp)Me]$_2$: To a suspension of $mbmpH_2$ (10.0 g, 29.5 mmol) in 40 mL of hexane was slowly added a 2.0 M solution of trimethylaluminum in hexane (14.75 mL, 29.5 mmol). Instantaneous and vigorous evolution of methane and heat was observed. Upon cooling the reaction mixture, a colorless precipitate formed that was filtered off, washed with cold hexane (2 × 10 mL), and dried in vacuo to give colorless microcrystals; yield 10.76 g (95%). – ^{1}H NMR: δ = –0.39 (s, 3 H, $AlCH_3$), 1.14 [s, 9 H, $C(CH_3)_3$], 1.28 [s, 9 H, $C(CH_3)_3$], 2.15 (s, 3 H, 4-CH_3), 2.24 (s, 3 H, 4-CH_3), 3.34 (d, $^2J_{HH}$ = 13.7 Hz, 1 H, CH_2), 4.27 (d, $^2J_{HH}$ = 13.7 Hz, 1 H, CH_2), 6.88 (d, $^4J_{HH}$ = 2.0 Hz, 1 H, 5-H), 6.91 (d, $^4J_{HH}$ = 2.0 Hz, 1 H, 5-H), 6.96 (d, $^4J_{HH}$ = 2.0 Hz, 1 H, 3-H), 7.01 (d, $^4J_{HH}$ = 2.0 Hz, 1 H, 3-H). – ^{13}C{^{1}H} NMR: δ = –7.4 ($AlCH_3$), 21.2, (4-CH_3), 21.3 (4-CH_3), 29.7 [$C(CH_3)_3$], 32.1 [$C(CH_3)_3$], 34.7 [$C(CH_3)_3$], 35.2 [$C(CH_3)_3$], 36.3 (CH_2), 126.6 (C-3), 127.5 (C-3'), 127.7 (C-5), 128.1 (C-5'), 130.7 (C-4), 130.9 (C-4'), 133.1 (C-2), 134.7 (C-2'), 138.1 (C-6), 141.3 (C-6'), 144.7 (C-1), 151.6 (C-1'). – EI MS; *m*/*z* (%): 760 (48) [M^+], 380 (100) [$M/2^+$], 57 (78) [$C_4H_9^+$]. – $C_{24}H_{33}AlO_2$ (380.5): calcd. C 75.76, H 8.74; found C 76.71, H 9.64.

[Al(mbmp)Et]$_2$: This compound was synthesized in a manner analogous to that described for $[Al(mbmp)Me]_2$ using triethylaluminum and isolated as colorless microcrystals in 86% yield. – ^{1}H NMR: δ = 0.42 (m, 2 H, $AlCH_2CH_3$), 0.84 (t, $^3J_{HH}$ = 7.0 Hz, 3 H, $AlCH_2CH_3$), 1.26 [s, 9 H, $C(CH_3)_3$], 1.36 [s, 9 H, $C(CH_3)_3$], 2.20 (s, 3 H, 4-CH_3), 2.31 (s, 3 H, 4-CH_3), 3.56 (d, $^2J_{HH}$ = 14.0 Hz, 1 H, CH_2-bridge), 4.56 (d, $^2J_{HH}$ = 14.0 Hz, 1 H, CH_2-bridge), 6.95 (d, $^4J_{HH}$ = 1.8 Hz, 1 H, 5-H), 7.09 (d, $^4J_{HH}$ = 1.8 Hz, 1 H, 3-H), 7.21 (d, $^4J_{HH}$ = 1.8 Hz, 1 H, 3-H). – ^{13}C{^{1}H} NMR: δ = 8.0 ($AlCH_2CH_3$), 21.3 ($AlCH_2CH_3$), 30.2, (4-CH_3), 30.3 (4'-CH_3), 32.3 [$C(CH_3)_3$], 35.0 [$C(CH_3)_3$], 35.6 [$C(CH_3)_3$], 35.9 (CH_2-bridge), 126.8 (C-3), 127.85 (C-3'), 128.3 (C-5), 129.9 (C-5'), 130.3 (C-4), 131.2 (C-4'), 133.5 (C-2), 134.9 (C-2'), 138.2 (C-6), 140.9 (C-6'), 152.9 (C-1). – EI MS; *m*/*z* (%): 788 (17) [M^+], 394 (74) [$M/2^+$]. – $C_{25}H_{35}AlO_2$ (394.5): calcd. C 76.11, H 8.94; found C 76.42, H 9.23.

Upon adding 10 equiv. of pyridine, the pyridine adduct Al(mbmp)Et(py) was formed. – ^{1}H NMR: δ = –0.41 (q, $^3J_{HH}$ = 6.4 Hz, 2 H, $AlCH_2CH_3$), 0.79 (t, $^3J_{HH}$ = 6.4 Hz, 3 H, $AlCH_2CH_3$), 1.13 [s, 18 H, $C(CH_3)_3$], 1.95 (s, 6 H, 4-CH_3), 3.08 (d, $^2J_{HH}$ = 14.0 Hz, 1 H, CH_2-bridge), 3.52 (d, $^2J_{HH}$ = 14.0 Hz, 1 H, CH_2-bridge), 6.42 (d, $^4J_{HH}$ = 1.6 Hz, 2 H, 5-H), 6.64 (d, $^4J_{HH}$ = 1.6 Hz, 2 H, 3-H), 6.98 (m, 2 H, py), 7.38 (m, 1 H, py), 8.33 (m, 2 H, py); – ^{13}C NMR: δ = 10.7 ($AlCH_2CH_3$), 16.1 ($AlCH_2CH_3$), 22.8 (4-CH_3), 31.9 [$C(CH_3)_3$], 35.4 [$C(CH_3)_3$], 36.8 (CH_2-bridge), 125.3 (C-3), 125.9 (py), 127.6 (C-5), 128.4 (py), 130.9 (C-4), 132.6 (C-2) 140.1 (C-6), 151.6 (py), 155.2 (C-1).

[Al(ebmp)Me]$_2$: This compound was synthesized in a manner analogous to that described for $[Al(mbmp)Me]_2$ and isolated as colorless microcrystals in 79% yield. – ^{1}H NMR: δ = –0.81 (s, 3 H, $AlCH_3$), 1.11 [s, 9 H, $C(CH_3)_3$], 1.43 [s, 9 H, $C(CH_3)_3$], 2.24 (s, 3 H, 4-CH_3), 2.31 (s, 3 H, 4'-CH_3), 2.71 (m, 3 H, CH_2CH_2), 3.27 (m, 1 H, CH_2CH_2), 6.81 (d, $^4J_{HH}$ = 1.8 Hz, 1 H, 5-H), 6.89 (d, $^4J_{HH}$ = 1.8 Hz, 1 H, 5-H), 6.93 (d, $^4J_{HH}$ = 1.8 Hz, 1 H, 3-H), 7.10 (d, $^4J_{HH}$ = 1.8 Hz, 1 H, 3-H). – ^{13}C NMR: δ = –5.5 ($AlCH_3$), 20.8 (4-CH_3), 20.9 (4-CH_3), 30.8 [$C(CH_3)_3$], 31.6 [$C(CH_3)_3$], 33.1 [$C(CH_3)_3$], 34.6 [$C(CH_3)_3$], 36.0 (CH_2-bridge), 37.9 (CH_2-bridge), 126.4 (C-6), 126.6 (C-3), 127.5 (C-6), 128.3 (C-4), 128.5 (C-4), 128.9 (C-4), 129.3 (C-5), 134.1 (C-2), 135.9 (C-2), 140.5 (C-1), 144.4 (C-1). – EI MS; *m*/*z* (%): 789 (100) [M^+], 774 (65) [$M^+ - C_4H_9$], 380 (24) [$M/2^+ - CH_3$]. – $C_{25}H_{35}AlO_2$ (394.5): calcd. C 76.11, H 8.94; found C 76.19, H 8.43.

[Al(mbmp)(μ-O*i*Pr)]$_2$: A suspension of $[Al(mbmp)Me]_2$ (4.66 g, 6.1 mmol) in 20 mL of diethyl ether was treated dropwise under vigorous stirring at room temperature with 2-propanol (0.9 mL, 12.1 mmol). After some minutes an exothermic gas evolution began. Upon cooling, a precipitate formed which was filtered, washed with hexane, and dried in vacuo; yield 4.07 g (79%) of colorless microcrystals. – ^{1}H NMR: δ = 1.39 [s, 18 H, $C(CH_3)_3$], 1.58 [d, $^3J_{HH}$ = 6.4 Hz, 6 H, $CH(CH_3)_2$], 2.18 (s, 6H, 4-CH_3), 3.69 (d, $^2J_{HH}$ = 14.0 Hz, 1 H, CH_2), 3.89 (d, $^2J_{HH}$ = 14.0 Hz, 1 H, CH_2), 4.66 [septet, $^3J_{HH}$ = 6.4 Hz, 1 H, $CH(CH_3)_2$], 6.97 (d, $^4J_{HH}$ = 2.0 Hz, 2 H, 5-H), 7.11 (d, $^4J_{HH}$ = 2.0 Hz, 2 H, 3-H). – ^{13}C{^{1}H} NMR: δ = 19.2 (4-CH_3), 23.4 [$CH(CH_3)_2$], 28.6 [$C(CH_3)_3$], 33.4 (CH_2), 69.7 [$CH(CH_3)_2$], 124.8 (C-3), 126.5 (C-5), 127.1 (C-4), 127.4 (C-6), 136.7 (C-2), 149.7 (C-1). – EI MS; *m*/*z* (%): 848 (6) [M^+]. – $C_{26}H_{37}AlO_3$ (424.6): calcd. C 73.55, H 8.78; found C 73.18, H 8.55.

Upon adding 10 equiv. of pyridine, the pyridine adduct Al(mbmp)(O*i*Pr)(py) was formed. – ^{1}H NMR: δ = 1.11 [d, $^3J_{HH}$ = 6.4 Hz, 6 H, $CH(CH_3)_2$], 1.56 [s, 18 H, $C(CH_3)_3$], 2.14 (s, 6 H, 4-CH_3), 3.31 (d, $^2J_{HH}$ = 14.1 Hz, 1 H, CH_2-bridge), 3.99 (d, $^2J_{HH}$ = 14.1 Hz, 1 H, CH_2-bridge), 4.81 [s, $^3J_{HH}$ = 6.4 Hz, 1 H, $CH(CH_3)_2$], 6.97 (d, $^4J_{HH}$ = 1.6 Hz, 2 H, 5-H), 7.18 (d, $^4J_{HH}$ = 1.8 Hz, 2 H, 3-H), 7.22 (m, 2 H, py), 7.62 (m, 1 H, py), 8.55 (m, 2

H, py). – ^{13}C NMR: δ = 21.3 (4-CH_3), 27.7 [$CH(CH_3)_2$], 30.4 [$C(CH_3)_3$], 34.2 (CH_2-bridge), 35.1 [$C(CH_3)_3$], 64.3 [$CH(CH_3)_2$], 125.3 (C-3), 126.0 (C-5), 126.2 (py), 129.4 (C-4), 130.7 (C-2), 138.21 (py), 40.1 (C-6), 149.9 (C-1), 153.8 (py).

[AlMe(OC$_6$H$_2$-2,6-*t*Bu$_2$-4-Me)(μ-O*i*Pr)]$_2$: To a suspension of MAD (2.63 g, 4.8 mmol) in 10 mL of diethyl ether was added over a period of 2 h 2-propanol (0.37 mL, 4.8 mmol) at room temperature. The reaction mixture was stirred overnight and the solvent volume reduced to half, resulting in a precipitate of a colorless solid. In order to complete the precipitation, hexane was added. The supernatant was filtered off, the precipitate washed with diethyl ether (2 × 10 mL), and dried in vacuo; yield 1.10 g (72%) of colorless crystals. – ^{1}H NMR: δ = –0.48 (s, 3 H, $AlCH_3$), 1.41 [s, 18 H, $C(CH_3)_3$], 1.44 [d, 6 H, $^3J_{HH}$ = 6.2 Hz, $CH(CH_3)_2$], 2.27 (s, 6 H, 4-CH_3), 4.93 [septet, $^3J_{HH}$ = 6.2 Hz, 1 H, $CH(CH_3)_2$], 7.03 (s, 2 H, C-3,5). – ^{13}C NMR: δ = 21.4 [$CH(CH_3)_2$], 25.3 (4-CH_3), 31.7 [$C(CH_3)_3$], 35.3 [$C(CH_3)_3$], 69.9 [$CH(CH_3)_2$], 126.5 (C-3,5), 126.9 (C-4), 139.0 (C-2,6), 153.4 (C-1). – EI MS; *m/z* (%): 640 (6) [M^+], 365 (61) [$Al(OC_{15}H_{24})(OC_3H_7)_2^+$]. – $C_{19}H_{33}AlO_2$ (320.4): calcd. C 71.21, H 10.38; found: C 71.19, H 10.43.

Polymerization of μ-Caprolactone: An appropriate amount of the initiator was dissolved in toluene (5 mL) and heated to 50 °C. ε-Caprolactone was added to give a ca. 2 M solution of the monomer, and the polymerization initiated. The reaction mixture was worked up after complete conversion by dropwise adding it to a tenfold volume of methanol. The poly(ε-caprolactone)s were filtered off and dried in vacuo until the weight remained constant.

X-Ray Crystal Structure Analysis of [Al(mbmp)(μ-O*i*Pr)]$_2$ and [AlMe(OC$_6$H$_2$–2,6-*t*Bu$_2$-4-Me)(μ-O*i*Pr)]$_2$: Relevant crystallographic data for [Al(mbmp)(μ-O*i*Pr)]$_2$ and [AlMe(OC$_6$H$_2$-2,6-*t*Bu$_2$-4-Me)(μ-O*i*Pr)]2 are summarized in Table 1. Single crystals suitable for X-ray crystal structure analysis were obtained by slow cooling of concentrated pentane solutions. Data collections were performed on an Enraf–Nonius CAD-4 diffractometer with graphite-monochromated Cu-K_α radiation. Data reductions were carried out using the program system XCAD4[15a] for [Al(mbmp)(μ-O*i*Pr)]$_2$ and MolEN[15b] for [AlMe(OC$_6$H$_2$-2,6-*t*Bu$_2$-4-Me)(μ-O*i*Pr)]$_2$. From the measured reflections, all independent reflections were used and the parameters were refined by full-matrix least-squares against all F_o^2 data (SHELXL-93).[15c] The structure was solved using direct methods (SHELXS-86)[15d] and difference-Fourier syntheses and refined with anisotropic thermal parameters for nonhydrogen atoms. The hydrogen atoms in [Al(mbmp)(μ-O*i*Pr)]$_2$ were calculated at their idealized positions, whereas those in [AlMe(OC$_6$H$_2$-2,6-*t*Bu$_2$-4-Me)(μ-O*i*Pr)]$_2$ were located and refined with isotropic parameters. Crystallographic data for the structures have been deposited with the Cambridge Crystallographic Data Centre as supplementary publication no. CCDC-104970 for [Al(mbmp)(μ-O*i*Pr)]$_2$ and –133689 for [AlMe(OC$_6$H$_2$-2,6-*t*Bu$_2$-4-Me)(μ-O*i*Pr)]$_2$. Copies of the data can be obtained free of charge from the Director, CCDC, 12 Union Road, Cambridge CB2 1EZ, UK [Fax: (internat.) + 44 (1223)336–033 or E-mail: deposit@ccdc.cam.ac.uk or http://www.ccdc.cam.ac.uk].

Acknowledgments

We thank the Volkswagen-Foundation and the Fonds der Chemischen Industrie for financial support. We are grateful to WITCO GmbH, Bergkamen, for the generous gift of the aluminum alkyls.

[1] [1a] J.-M. Vion, R. Jérôme, P. Teyssié, M. Aubin, R. E. Prud'homme, *Macromolecules* **1986**, 19, 1828. – [1b] H. R. Kricheldorf, M. Berl, M. Scharnagl, *Macromolecules* **1988**, *21*, 286. – [1c] N. Ropson, Ph. Dubois, R. Jérôme, P. Teyssié, *Macromolecules* **1993**, 26, 6378. – [1d] A. Löfgren, A.-C. Albertsson, Ph. Dubois, R. Jérôme, P. Teyssié, *Macromolecules* **1994**, 27, 5556. – [1e] A. Duda, S. Penczek, *Macromolecules* **1995**, *28*, 5981, and references therein.

[2] N. Ya. Turova, V. A. Kozunov, A. I. Yanovskii, N. G. Bokii, Yu. T. Struchkov, B. L. Tarnopolskii, *J. Inorg. Nucl. Chem.* **1979**, *41*, 5.

[3] Examples for three-coordinate aluminum alkoxides: [3a] A. P. Shreve, R. Mülhaupt, W. Fultz, J. Calabrese, W. Robbins, S. D. Ittel, *Organometallics* **1988**, *7*, 409. – [3b] R. Benn, E. Janssen, H. Lehmkuhl, A. Rufinska, K. Angermund, P. Betz, R. Goddard, C. Krüger, *J. Organomet. Chem.* **1991**, *411*, 37. – [3c] M. A. Petrie, M. M. Olmstead, P. P. Power, *J. Am. Chem. Soc.* **1991**, *113*, 8704. – Examples for four-coordinate Lewis base adducts: [3d] M. D. Healy, D. A. Wierda, A. R. Barron, *Organometallics* **1988**, *7*, 2543. – [3e] M. B. Power, S. G. Bott, D. L. Clark, J. L. Atwood, A. R. Barron, *Organometallics* **1990**, *9*, 3086.

[4] The reaction of AlMe(OC$_6$H$_2$-2,6-*t*Bu$_2$-4-Me)$_2$ (MAD) with 2-propanol was briefly mentioned before: M. Akatsuka, T. Aida, S. Inoue, *Macromolecules* **1994**, *27*, 2820.

[5] For examples of complexes for Lewis-acidic metals containing the mbmp ligand, see: C. Floriani, F. Corazza, W. Lesueur, A. Chiesi-Villa, C. Guastini, *Angew. Chem. Int. Ed. Engl.* **1989**, *28*, 66; P. J. Toscano, E. J. Schermerhorn, C. Dettelbacher, D. Macherone, J. Zubieta, *J. Chem. Soc., Chem. Commun.* **1991**, 933; J. Okuda, S. Fokken, H.-C. Kang, W. Massa, *Chem. Ber.* **1995**, *128*, 221, and references therein.

[6] R. Kumar, M. L. Sierra, S. J. de Mel, J. P. Oliver, *Organometallics* **1990**, *9*, 181; D. G. Hendershot, M. Barber, R. Kumar, J. P. Oliver, *Organometallics* **1991**, *10*, 3302.

[7] [7a] [*i*Bu$_2$Al(OCH$_2$-2-C$_5$H$_4$N]$_2$: M. R. P. van Vliet, P. Buysingh, G. van Koten, K. Vrieze, B. Kojic-Prodic, A. L. Spek, *Organometallics* **1985**, *4*, 1701. – [7b] [AlMe$_2$(μ−OCH$_2$CH$_2$OMe]$_2$: R. Benn, E. Janssen, H. Lehmkuhl, A. Rufinska, *J. Organomet. Chem.* **1987**, *333*, 155. – [7c] [AlMe$_2$(μ−OCHMeCH$_2$NMe$_2$]$_2$: K.-H. Thiele, E. Hecht, T. Gelbrich, U. Duemichen, *J. Organomet. Chem.* **1997**, *540*, 89. – [7d] J. Lewinski, J. Zachara, I Justyniak, *J. Chem. Soc., Chem. Commun.* **1997**, 1519.

[8] S. Fokken, T. P. Spaniol, J. Okuda, F. G. Sernetz, R. Mülhaupt, *Organometallics* **1997**, *16*, 4240.

[9] A. R. Barron, *Polyhedron* **1995**, *14*, 3197.

[10] [10a] S. Schulz, H. W. Roesky, M. Noltemeyer, H.-G. Schmidt, *J. Chem. Soc., Dalton Trans.* **1995**, 177. – [10b] M. Veith, S. Faber, H. Wolfanger, V. Huch, *Chem. Ber.* **1996**, *129*, 381. – [10c] A. Kunicki, R. Sadowski, J. Zachara, *J. Organomet. Chem.* **1996**, *508*, 249. – [10d] J. Lewinski, J. Zachara, E. Grabska, *J. Am. Chem. Soc.* **1996**, *118*, 6794. – [10e] For a review on compounds with Al_2O_2 ring, see: J. P. Oliver, R. Kumar, *Polyhedron* **1990**, *9*, 409. – [10f] For a compound with a puckered Al_2O_2 ring, see: O. Saied, M. Simard, J. D. Wuest, *Organometallics* **1996**, *15*, 2345.

[11] J. D. Fisher, P. J. Shapiro, P. M. H. Budzelaar, R. J. Staples, *Inorg. Chem.* **1998**, *37*, 1295.

[12] More precisely, the monomer concentration correspond to that of the ε-caprolactone adduct Al(mbmp)(μ-O*i*Pr)(ε-CL).

[13] We have evidence that the alkyls [Al(mbmp)R]$_2$ are also capable of initiation the polymerization of ε-caprolactone, albeit being much slower, I. Taden, Doctoral dissertation, University of Marburg, Germany, **1998**.

[14] A. Duda, Z. Florjanczyk, A. Hofman, S. Slomkowski, S. Penczek, *Macromolecules* **1990**, *23*, 1640; Ph. Dubois, P. Degee, R. Jérôme, P. Teyssié, *Macromolecules* **1993**, 26, 2730.

[15] [15a] K. Harms, XCAD4, University of Marburg, Germany, **1993**. – [15b] C. K. Fair, MolEN, An Interactive Structure Solution Procedure, Enraf–Nonius, Delft, **1990**. – [15c] G. M. Sheldrick, *SHELXL-93*, *Program for the Refinement of Crystal Structures*, University of Göttingen, Germany, **1993**. – [15d] G. M. Sheldrick, *SHELXS-86*, *Program for the Solution of Crystal Structures*, University of Göttingen, Germany, **1986**.

Received August 20, 1999
[I99309]

Effect of Substitution on the ESR Spectra and Electronic Ground State of ZnTPP Cation Radicals

Paresh C. Dave[a] and D. Srinivas*[b]

Keywords: Zinc / Metalloporphyrins / Porphyrins / Cations / Radicals / ESR

Zinc(II) complexes of substituted tetraphenylporphyrins, Zn[T(X–P)P], where X = H, *p*-F, *p*-Cl, *m*-Cl, *p*-CH_3O, and *m*-CH_3O, have been synthesized and characterized. Peripheral substitution shows marked changes in the chemical shifts of the phenyl proton resonances and $E_{1/2}$ values of the redox couples in the anodic region while the UV/Vis spectra are unaffected. The monocation radicals of these complexes are generated by chemical oxidation with bromine. The ESR spectra reveal the formation of two types of radical species, $Zn[T(X–P)P]^{+\cdot}Br^-$ (species **I**) and $Zn[T(X–P)(Br_n–P)]^{+\cdot}Br^-$ (species **II**): Species **I** at 298 K shows a spectrum, with well-resolved bromine hyperfine features, characteristic of a $^2A_{2u}$ electronic ground state while species **II**, except for the complex with X = *m*-CH_3O, shows a featureless, isotropic resonance attributable to a $^2A_{1u}$ state. $Zn[T(m\text{-}CH_3O–P)(Br_n–P)]^{+\cdot}Br^-$, on the other hand, exhibits nine resolved nitrogen hyperfine features corresponding to a $^2A_{2u}$ state. Variable temperature ESR spectra (77–298 K) indicate reduction in the bromine and nitrogen hyperfine coupling constants and an increase in the g value of species **I** from 2.0049 to 2.0060 with lowering temperature and suggest a labile electronic ground state for species **I**. The *p*-CH_3O substituted complex exhibits an electronic transformation from $^2A_{2u}$ to $^2A_{1u}$ while the remaining complexes, including *m*-CH_3O, show a transformation from $^2A_{2u}$ to an admixed $^2A_{1u}/^2A_{2u}$ state. The effect of substitution on the variable temperature ESR spectra are discussed.

Introduction

Porphyrin π-cation radicals play a crucial role in the mechanisms of various biocatalytic reactions, including oxygen activation by heme proteins,[1–9] and in the electron-transfer processes at the photosynthetic reaction centre.[10,11] Based on the electronic ground state, the π-cation radicals have been categorised into those possessing a $^2A_{1u}$ or a $^2A_{2u}$ ground state.[9] The two highest occupied molecular orbitals of metalloporphyrins (a_{1u} and a_{2u}) are nearly degenerate and their relative energies are dictated by many factors, including the nature and position of the porphyrin peripheral substitution, the central metal ion, the identity and disposition of the axial ligand, environment, temperature and symmetry of the molecule.[12–18] Compound **I** of catalase and chloroperoxidase enzymes belong to the former category of radicals.[7] The electronic ground state of compound **I** of horseradish peroxidase enzyme is still to be conclusively determined. ENDOR and magnetic circular dichroism studies have indicated a $^2A_{2u}$ ground state for HRP-I[19,20] while more recent NMR[21,22] and Resonance Raman (RR)[23,24] studies show a $^2A_{1u}$ state. A correlation between the electronic structure and functionality is interesting, but so far not conclusive and therefore needs further work.[2]

Generally, among the synthetic metalloporphyrins, the cation radicals of the octaethylporphyrins $M\{OEP\}^{+\cdot}$ possess a $^2A_{1u}$ ground state while those of the tetraphenylporphyrins $M\{TPP\}^{+\cdot}$ possess a $^2A_{2u}$ state ($M = Zn^{2+}$ and Mg^{2+}).[1,9,25,26] However, it was found that $Co\{OEP\}^{+\cdot}$ and $Ru\{OEP\}^{+\cdot}$ have a $^2A_{1u}$ ground state with Br^- as the counter ion and $^2A_{2u}$ with ClO_4^- as the counter ion.[21,27] The electron density is greater at the *meso* carbon atoms in the case of the $^2A_{2u}$ configuration, and hence electron-withdrawing substituents on the tetraphenyl groups of $M\{TPP\}^{+\cdot}$ affect the energetics of a_{2u} while a_{1u} is unaltered. On the other hand, for radicals with a $^2A_{1u}$ electronic ground state, the electron density is greater at the β carbon atoms of the pyrrole ring while the *meso* carbons lie in the nodal plane, and hence substitution on the pyrrole ring alters the position of the a_{1u} level while a_{2u} is hardly affected. Therefore, by a rational substitution it is possible, in principle, to design a molecule with a desired property.

Gross and co-workers have reported an admixed ground state for zinc complexes of halogen-substituted tetraphenylporphyrin cation radicals.[28,29] The quantum admixture of $^2A_{1u}$ and $^2A_{2u}$ states was also reported by Kalsbeck et al.[30] for $Zn[T(Cl_2–P)P]^{+\cdot}$ and $Mg\{T(Cl_2–P)P]^{+\cdot}$ radicals where $T(Cl_2–P)P$ = tetrakis(*o*-dichlorophenyl)porphyrin. Theoretical studies on the π-cation radicals of metalloporphyrins have shown that electron-withdrawing substituents in the *meso* position lead to a $^2A_{1u}$ ground state while electron-donating substituents result in a $^2A_{2u}$ state.[31] Density functional calculations have revealed that electron-withdrawing substituents in the *meta* and *para* positions should exert significantly stronger electronic effects than with *ortho* substitution.[32] Our recent studies using variable temperature ESR spectroscopy indicated, for the first time, a labile electronic ground state for $Zn[T(H–P)P]^{+\cdot}Br^-$ with a $^2A_{2u}$

[a] Sophisticated Analytical Instruments Laboratory, Central Salt Marine Chemicals Research Institute,
Gijubhai Badheka Marg, Bhavnagar 364 002, India
[b] Catalysis Division, National Chemical Laboratory,
Pune 411 008, India
Fax: (internat.) +91-20/589-3761
E-mail: srinivas@cata.ncl.res.in

 © WILEY-VCH Verlag GmbH, D-69451 Weinheim, 2000 1434–1948/00/0303–447 $ 17.50+.50/0

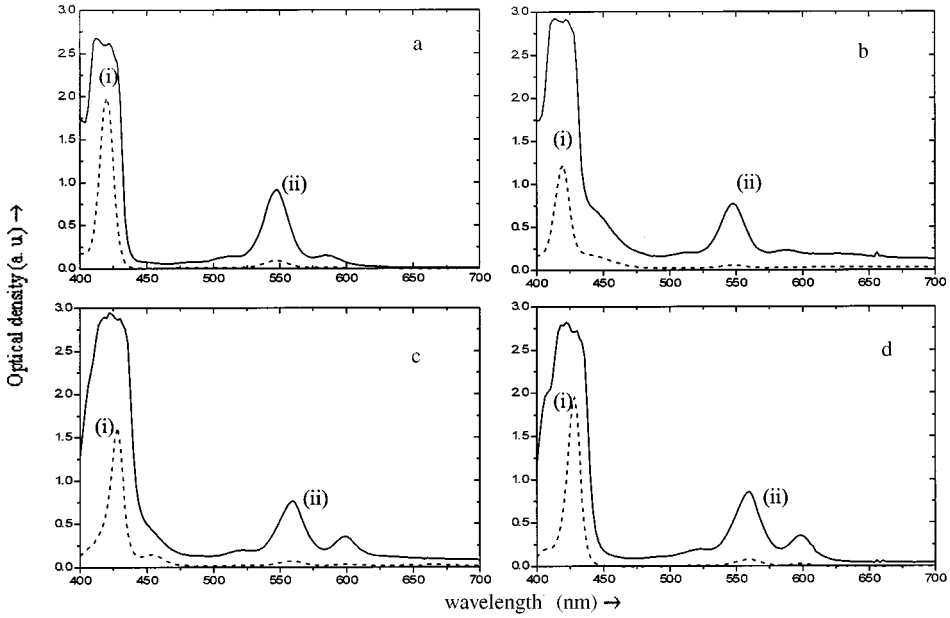


Figure 1. UV/Visible spectra for Zn[T(*m*-CH_3O–P)P] in CH_2Cl_2: (a) neutral species, (b) cation radical, (c) cation radical + pyrazine, and (d) neutral species + pyrazine; (i) spectrum for 10 times lower concentration and (ii) for higher concentrations; optical density is in units of mol·cm

ground state at 298 K changing to a $^2A_{1u}$ state at 77 K.[33] In the course of understanding the factors influencing the electronic structure and structure-reactivity correlations, we here report the effect of peripheral substitution (X) on the ESR spectral properties and ground state configuration of $Zn[T(X–P)P]^{+\cdot}Br^-$ radical cations generated by chemical oxidation with bromine. Two types of radical species viz., $Zn[T(X–P)P]^{+\cdot}Br^-$ (**I**) and $Zn[T(X–P)(Br_n–P)]^{+\cdot}$, $n = 8$ or 4 (**II** and **II'**, respectively) are observed on oxidation with bromine. Irrespective of the nature of the peripheral substitution (X = *p*-CH_3O, *p*-Cl, *p*-F, *m*-CH_3O, *m*-Cl), species **I** showed a labile electronic ground state ($^2A_{2u}$ at 298 K and $^2A_{1u}$ or admixed $^2A_{1u}/^2A_{2u}$ at 77 K). Species **II**, however, is $^2A_{1u}$ throughout the temperature range 77–298 K, although species **II'** exhibits ground state lability similar to that of species **I**. The changes in the electronic structure are proposed to be associated with the changes in the conformational geometry of the porphyrin skeleton. It is to be noted that the notations $^2A_{1u}$ and $^2A_{2u}$ assume D_{4h} symmetry for the porphyrin cores. These notations are used here only for simplicity as the porphyrin cores of the molecules studied in this work have a symmetry lower than D_{4h}.

Results and Discussion

A typical UV/Vis spectrum for Zn[T(*m*-CH_3O–P)P] is shown in Figure 1 a. Substituents have little effect and showed similar UV/Vis spectra for all the complexes. In strong donor solvents and in the presence of nitrogenous ligands, such as pyridine, imidazole and pyrazine (Figure 1 d), the Soret and Q-bands are red shifted indicating a change in molecular conformation, probably due to solvation and axial ligand coordination. The cation radicals of Zn[T(X–P)P], generated by chemical oxidation with bromine, showed a blue-shift and reduced intensity for the Soret band and broad, diffused, overlapping Q-bands in the region 500–700 nm (Figure 1 b). These spectral features are characteristic of a $^2A_{2u}$ ground state of the porphyrin cation radical.[25,26] Upon adding nitrogenous ligands to the radical solution, a spectrum typical of the neutral species was observed, indicating the instability of cation radicals in the presence of coordinating ligands (Figure 1 c). This agrees well with the RR results on some iron tetraphenylporphyrin cation radicals.[34]

The effect of substitution is clearly manifested on the chemical shifts of the phenyl proton resonances; the signals due to the β-protons are unaffected. These resonances were shifted up-field due to the substitution. This shift, with *para* substitution, was marginal for the *ortho* protons and varies in the sequence H < F < Cl < OCH_3 while it was significant for the *meta* protons where it varies in the order H < Cl < F < OCH_3. Similar trends were also observed with *meta* substitution. The ^{1}H-NMR spectroscopic data for all the complexes are listed in Table 1. The trends described for the chemical shifts are completely in line with what is expected for phenyl protons and simply show that there is practically no conjugation between the porphyrin and the phenyl groups, as they are probably perpendicular to one other.

Cyclic voltammograms (CVs) of the complexes showed two quasi-reversible redox couples in the range 0 to +2.0 V, corresponding to $Zn[T(X–P)P]^{+\cdot}/Zn[T(X–P)P]$ and $Zn[T(X–P)P]^{2+}/Zn[T(X–P)P]^{+\cdot}$, respectively. Representative CV and differential pulse voltammograms (DPV) for Zn[T(*m*-CH_3O–P)P] are shown in Figure 2 and the electrochemical data are provided in Table 2. Ferrocene was used as the reference. The $E_{1/2}$ values vary with the substituents in the order F > Cl > H > OCH_3. Electron donating

Table 1. ^{1}H NMR spectroscopic data for Zinc(II) complexes of substituted tetraphenylporphyrins Zn[T(X–P)P] in $CDCl_3$

X	Pyrrole	*o*-	*m*-	*p*-
H	8.95	8.27, 8.25, 8.18	7.78, 7.76, 7.72	–
p-OCH_3	8.85	8.15, 8.11	7.30, 7.2	4.07(OCH_3)
m-OCH_3	8.97	7.79, 7.77	7.33, 7.32, 7.29, 7.28	7.66, 7.62, 7.59, 3.95(OCH_3)
p-Cl	8.93	8.16, 8.12	7.78, 7.76, 7.72	–
p-F	8.93	8.20, 8.17, 8.16, 8.13	7.50, 7.45, 7.41	–
m-Cl	8.95	8.22, 7.82, 7.78	7.73, 7.69, 7.65	8.12, 8.09

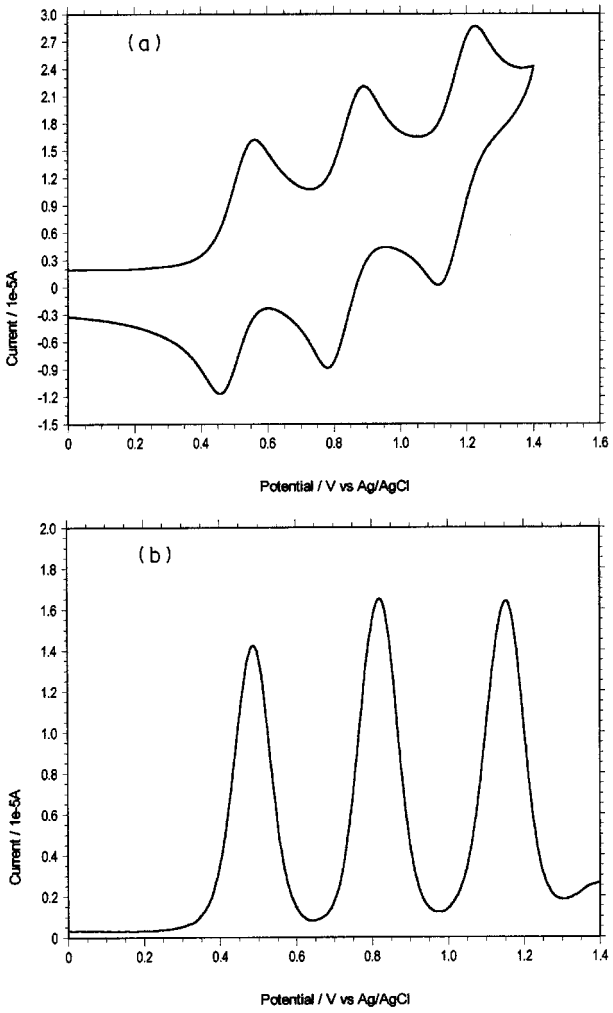


Figure 2. (a) CV (b) DPV of Zn[T(*m*-CH_3O–P)P] in CH_2Cl_2; working electrode: glassy carbon; reference electrode: Ag/AgCl; auxiliary electrode: Pt wire; supporting electrolyte: tetrabutylammonium hexafluorophosphate; scan rate: 100 mV/s; the first couple at $E_{1/2}$ = 0.51 V corresponds to the redox couple of ferrocene used as an internal reference

Table 2. Electrochemical data for 0.1 M Zn[T(X–P)P] in CH_2Cl_2

Compex	$E^1_{1/2}$	$E^2_{1/2}$
Zn[T(*p*-F–P)P]	0.95	1.42
Zn[T(*m*-Cl–P)P]	0.95	1.26
Zn[T(*p*-Cl–P)P]	0.93	1.2
Zn[T(H–P)P]	0.89	1.35
Zn[T(*m*-OCH_3–P)P]	0.84	1.17
Zn[T(*p*-OCH_3–P)P]	0.82	1.23

CH_3O substitution means that the oxidation is easier than with the electron-withdrawing halogen groups. The $E_{1/2}$ of the *meta*-substituted porphyrins is larger than that of the *para*-substituted porphyrins. The $E_{1/2}$ for couple **II**, $Zn[T(X–P)P]^{2+}/Zn[T(X–P)P]^{+\cdot}$ is more affected by the substitution than couple **I**, $Zn[T(X–P)P]^{+\cdot}/Zn[T(X–P)P]$. The trends in $E_{1/2}$ are as expected, as are the chemical shifts.

The ESR spectra of the cation radicals, in general, consist of four equally spaced resolved hyperfine (h.f.) features. The intensity of the third h.f. feature is greater than expected. Spectral simulations indicate the presence of two types of paramagnetic radical species; species **I** showing the characteristic four line h.f. pattern due to interaction of electron spin ($S = {}^1/_2$) with the nuclear spin (I) of ${}^3/_2$ and species **II** exhibiting an isotropic resonance. For species **I**, the coupling is due to coordinated bromide ion.[35] The intensity of the signal due to species **II** increased with excess bromine. Species **I** could be attributed to $Zn[T(X–P)P]^{+\cdot}Br^-$ and **II** to brominated cation radicals, $Zn[T(X–P)(Br_n–P)]^{+\cdot}Br^-$. Depending on the type of substitution (X) and its location (*para*/*meta*) the value of "*n*" can be 8 or 4.[36] Figure 3 shows a schematic representation of various oxidation products and their nomenclature. Two types of tetrabromotetraphenylporphyrin cation radicals (species **II'**) are possible, as shown in Figure 3 , one with one bromine substituent per pyrrole ring and the others with two bromine substituents on the two opposing pyrrole rings. ^{1}H-NMR spectroscopic studies by Crossley et al. favour the formation of the latter species with two bromine substituents on the two opposing pyrrole rings in the reaction of metal-free tetraphenylporphyrin with *N*-bromosuccinimide.[37]

The UV/Visible spectrum and the resolved h.f. coupling features of species **I** at ambient temperatures are characteristic of a $^2A_{2u}$ electronic ground state while the featureless isotropic signal for species **II** is characteristic of a $^2A_{1u}$ state. Upon sudden lowering of the temperature to 77 K, the h.f. features disappeared and, instead, only two overlapping isotropic resonances for species **I** and **II** or **II'** were visible. Representative spectra for the cation radicals of Zn[T(*p*-CH_3O–P)P] and Zn[T(*m*-CH_3O–P)P] at 298 and 77 K along with the simulated results are shown in Figure 4 and Figure 5 , respectively.

The spin Hamiltonian parameters for all the radicals are listed in Table 3. Except for Zn[T(*m*-CH_3O–P)P], the peak-to-peak linewidth (ΔH) increased from 5.5 to 8.0 G for species **II** while it decreased from 8.9 to 8.0 G for species **I** with lowering of the temperature. The g value increased from 2.0048 to 2.0057 and A_{Br} increased from 7.61 to 8.30

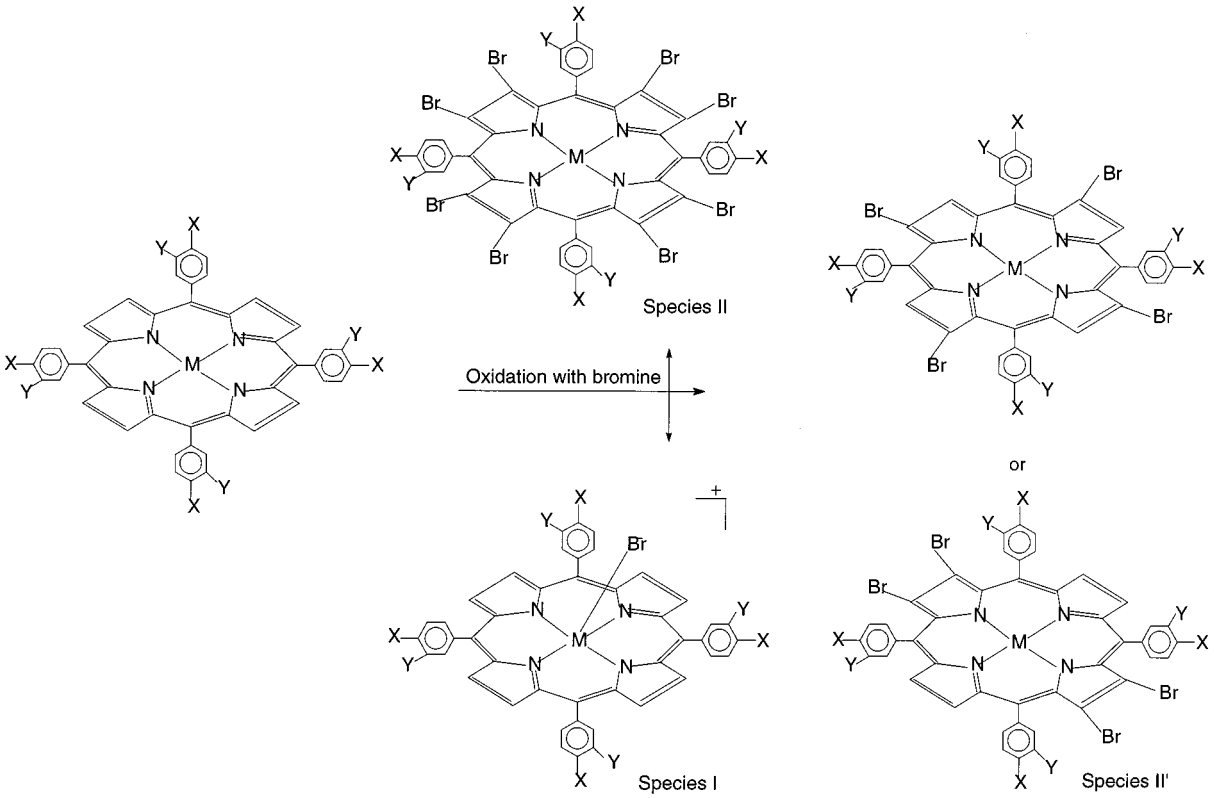


Figure 3. Schematic representation of various oxidation products of Zn[T(X–P)P]

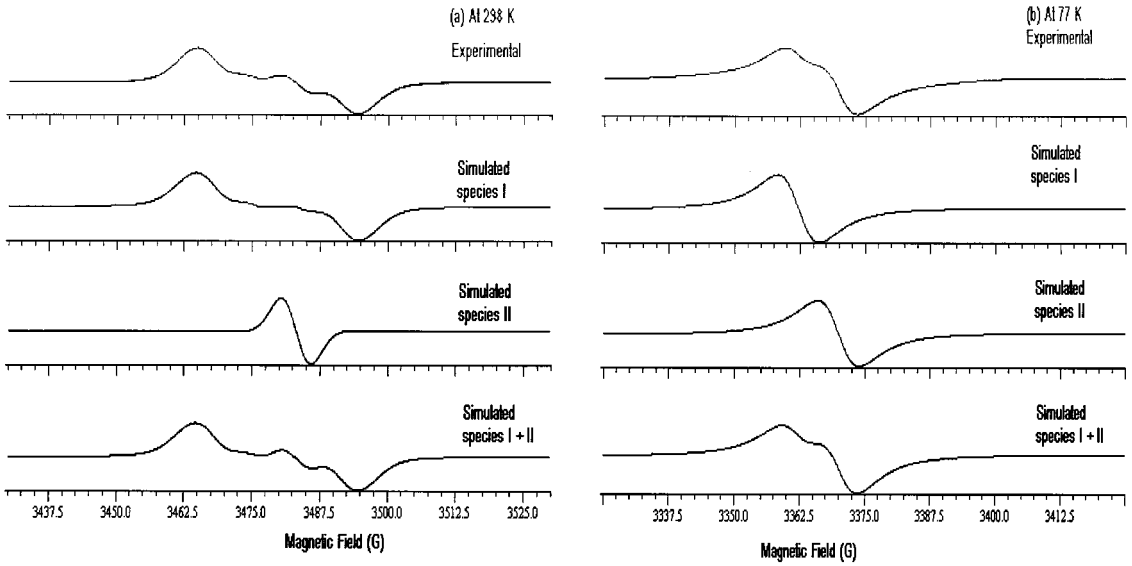


Figure 4. Experimental and simulated ESR spectra of Zn[T(*p*-CH_3O–P)P] in CH_2Cl_2 at 298 and 77 K; receiver gain = $5.02 \cdot 10^3$, modulation amplitude = 0.6 G, power = 2 mW, time constant = 81.92 ms, ν = 9.76 GHz (for 298 K) 9.46 GHz (for 77 K) and resolution in X = 1024

G with the increasing electron-withdrawing capacity of the substituent. The location of the substituent (*para* or *meta*) has a considerable effect on the A_{Br} value. This value increased from 7.61 to 8.20 for CH_3O substitution and decreased from 8.30 to 8.10 G for chloro substitution. The disappearance of the bromine h.f. coupling features at 77 K is attributed to a change in the electronic ground state from $^2A_{2u}$ to $^2A_{1u}$ for species **I**. A systematic variation of temperature in the range 298 K to 77 K, discussed below, for the cation radicals of Zn[T(*p*-CH_3O–P)P] and Zn[T(*m*-CH_3O–P)P], provides a deeper insight into the transition behaviour.

Figure 6 shows the variable temperature ESR spectra for the cation radicals of Zn[T(*p*-CH_3O–P)P] and Zn[T(*m*-CH_3O–P)P]. Bromine h.f. coupling constant (A_{Br}) for species **I** decreased gradually as the temperature was lowered

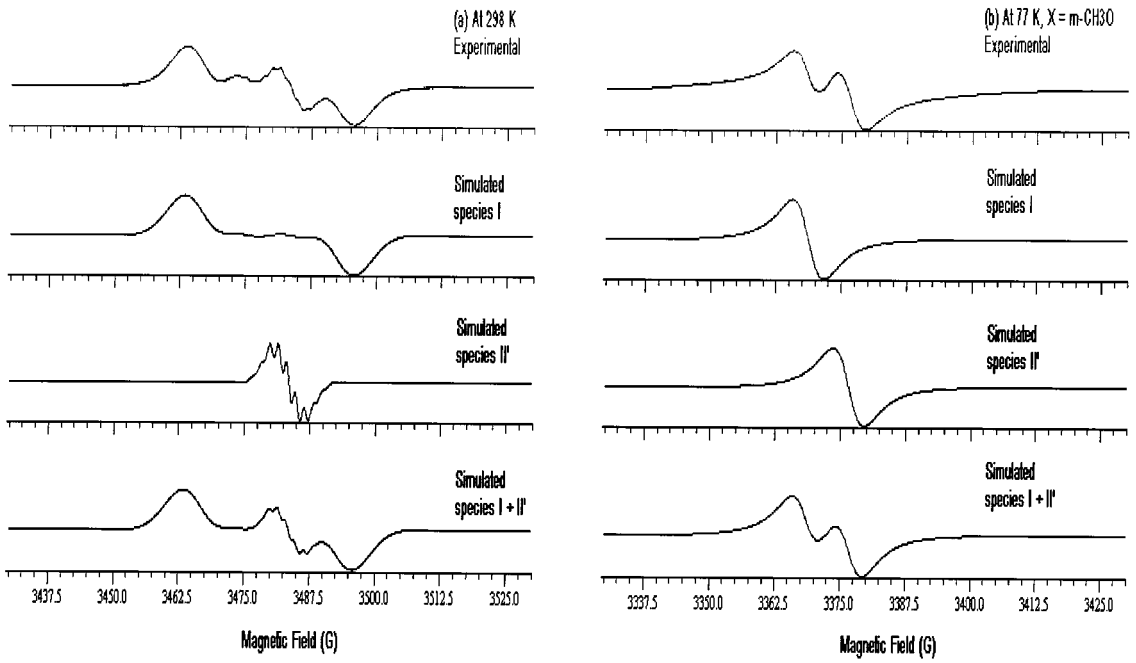


Figure 5. Experimental and simulated ESR spectra of Zn[T(*m*-CH_3O–P)P] in CH_2Cl_2 at 298 and 77 K; receiver gain = $5.02 \cdot 10^3$, modulation amplitude = 0.6 G, power = 2 mW, time constant = 81.92 ms, ν = 9.76 GHz (for 298 K) 9.46 GHz (for 77 K) and resolution in X = 1024

Table 3. Simulated EPR data for monocation radicals of Zinc(II) substituted tetraphenylporphyrins, $Zn[T(X–P)P]^{+\cdot}$, in $CHCl_3$

X	Temp. [K]	[g]	Species **I** A(Br) [G]	Δ*H* [G]	[g]	Species **II** Δ*H* [G]
p-CH_3O	298	2.0048	7.61	8.5	2.0028	5.5
	77	2.0075	–	8.0	2.0029	8.0
H	298	2.0050	8.15	8.8	2.0028	5.5
	77	2.0078	–	8.0	2.0019	8.0
p-F	298	2.0052	8.20	8.8	2.0030	5.5
	77	2.0080	–	8.0	2.0033	8.0
p-Cl	298	2.0055	8.30	8.9	2.0032	5.5
	77	2.0074	–	8.2	2.0037	8.1
m-CH_3O	298	2.0052	8.20	8.6	2.0030	1.50
	77	2.0080	–	6.0	2.0033	6.0
m-Cl	298	2.0057	8.10	8.25	2.0035	5.5
	77	2.0076	–	8.4	2.0039	7.4

from 298 to 190 K, in steps of 10 K and from then onwards showed a featureless isotropic resonance.

However, distinct changes were observed for species **II** with the *p*-CH_3O and *m*-CH_3O substituted complexes. The former, like the rest of the complexes, showed a featureless isotropic resonance throughout the temperature range, the latter complex with *m*-CH_3O substitution, on the other hand, showed nine well-resolved hyperfine features (Δ*H* = 1.70 G) due to interaction of the electron spin with the nuclear spin of four equivalent nitrogen atoms (*I* = 1). The spectral behaviour and the A_N value (1.56 G) are consistent with those of TPP radicals with ClO_4^- as the counterion.[26] Theoretical calculations for the $^2A_{2u}$ ground state revealed a larger electron density at the pyrrole nitrogen and meso carbon atoms and negligible electron density at the β pyrrole position. For the $^2A_{1u}$ ground state the pyrrole nitrogens and the meso carbons are in the nodal plane and the electron density is greater at the β-pyrrole position. Hence, a resolved, hyperfine-rich spectrum is observed for the cation radical with a $^2A_{2u}$ ground state while a featureless isotropic signal is observed for the $^2A_{1u}$ ground state. Variable temperature ESR results in the present study therefore indicate a $^2A_{2u}$ electronic ground state for species **II'** with *m*-CH_3O substitution and $^2A_{1u}$ for the rest of the complexes. As the temperature is lowered the h.f. resolution is lost. Figure 7 shows the variation of A_{Br} and $\Delta H/A_{Br}$ with temperature for Zn[T(*m*-CH_3O–P)P] cation radicals.

The former radical shows an abrupt change around 180 K while for the latter the bromine hyperfine coupling is reduced gradually up to 77 K. The rate of cooling has an effect on the nature of the spectrum. Sudden cooling to 77 K gives an overlapping two line spectrum for *p*-CH_3O substitution (Figure 5) whereas slow cooling shows a single resonance. However, such a behaviour is not observed for the complexes with X = *m*-CH_3O and H. These observations clearly indicate that the cation radical of Zn[T(*p*-CH_3O–P)P] (species **I**) undergoes an electronic transition from $^2A_{2u}$ to $^2A_{1u}$ at 180 K while the rest of the complexes exhibit a transition from $^2A_{2u}$ to an admixed $^2A_{1u}/^2A_{2u}$ state as the temperature is lowered. The reduction in the bromine hyperfine coupling constant at lower temperatures indicates a change in the degree of binding of the bromine ion in the $Zn[T(X–P)P]^{+\cdot}Br^-$ complex. Our earlier studies[33] revealed that the Zn–Br bond is labile and the Br^- could be replaced by ClO_4^-, PF_6^-, and BF_4^- ions. The perchlorato anion forms an axial coordination and shows a typical spectrum with a nine line hyperfine pattern due to interaction with the four equivalent nitrogen atoms of the pyrrole rings. With noncoordinating PF_6^- and BF_4^- ions, however, only a single line is observed.

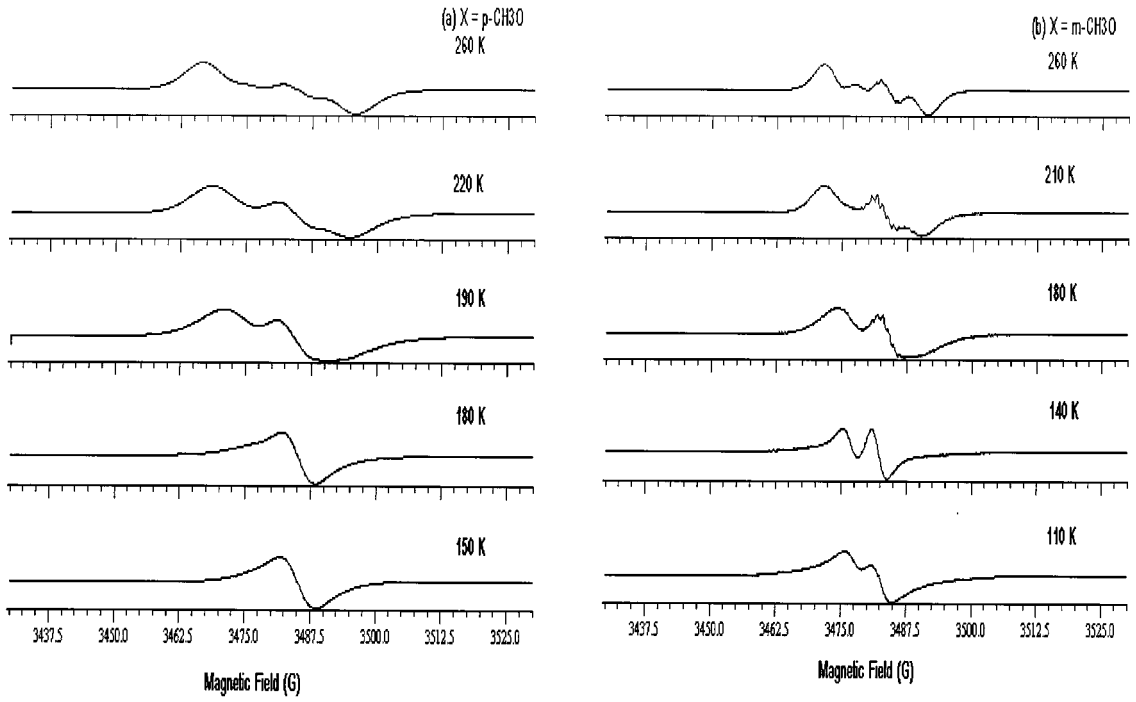


Figure 6. Variable temperature ESR spectra for (a) Zn[T(*p*-CH_3O–P)P] and (b) Zn[T(*m*-CH_3O–P)P] in CH_2Cl_2 showing the effect of substitution on the lability of the electronic ground state; species **II** shows resolved nitrogen hyperfine coupling for *m*-CH_3O (b) while a featureless signal is seen for *p*-CH_3O (a) substituted complexes; receiver gain = $5.02 \cdot 10^3$, modulation amplitude = 1.60 G, time constant = 163.84 ms, ν = 9. 46 GHz, resolution in X = 1024

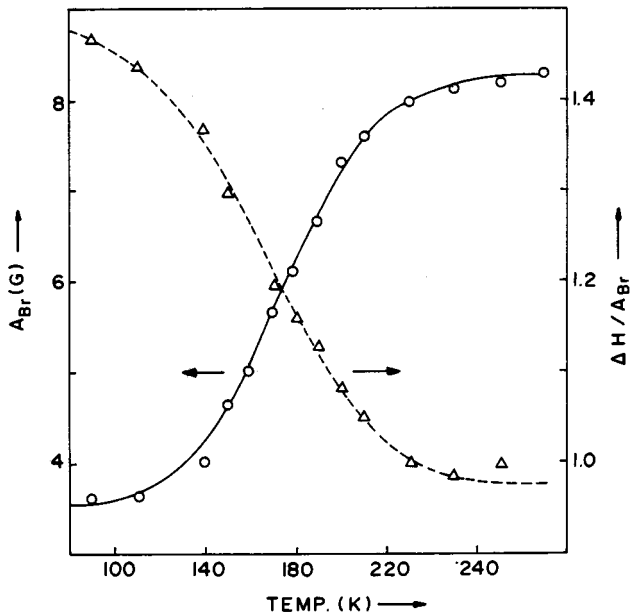


Figure 7. Variation of A_{Br}, $\Delta H/A_{Br}$ with temperature for Zn[T(*m*-CH_3O–P)P]$^{+\cdot}Br^-$

Species **II**, as mentioned earlier, is attributed to a brominated species, Zn[T(X–P)(Br_n –P)]$^{+\cdot}Br^-$.[36] The difference in the spectral features of the *m*-CH_3O substituted complex (showing resolved nitrogen hyperfine coupling) from the rest of the complexes is attributed solely to the location of the substituent and its electronic and steric effects. During chemical oxidation both the β-pyrrole positions can be brominated resulting in species **II**. However, bulkier CH_3O substitution in the *meta* position probably imposes a degree of steric hindrance and thereby forms a tetrabrominated cation radical (species **II'**) instead of the octabrominated species **II**. The former, with an electron-donating CH_3O group in the *meta* position and electron-withdrawing tetrabromo groups in the β-pyrrole position, stabilizes the $^2A_{2u}$ ground state while the rest of the substituted complexes with octabromo substitution in the β-pyrrole position stabilize the $^2A_{1u}$ state for species **II**. As for all the structures of the octabrominated tetraphenylporphyrin complexes studied so far, species **II** most probably possesses an S_4 symmetry and displays a saddle-shaped or ruffled conformation.[38] Such a nonplanar conformation probably stabilizes a $^2A_{1u}$ electronic ground state. As reported earlier,[38] the symmetry of the tetrabrominated cation radical (species **II'**) is expected to be, at least, C_i with slightly distorted chair-like conformation and such a geometry probably stabilizes a $^2A_{2u}$ state. With lowering of temperature, the conformational geometries of species **I** and **II'** change and this results in a transition in the electronic ground state from $^2A_{2u}$ to $^2A_{1u}$. Hence, it can be concluded that the lability in the electronic structure is associated with a change in the conformational geometry of the TPP moiety.

Conclusions

Chemical oxidation of zinc(II) substituted tetraphenylporphyrins with bromine generated two types of cation radicals, Zn[T(X–P)P]$^{+\cdot}Br^-$ (species **I**) and Zn[T(X–P)(Br_n–

P)]$^{+\cdot}$Br$^-$ (species **II** or **II'**). Species **I** for all the complexes exhibits a labile electronic ground state with a *p*-CH_3O substituted radical ion showing an electronic transition from $^2A_{2u}$ to $^2A_{1u}$ while the rest of the radical ions show a transition from $^2A_{2u}$ to an admixed $^2A_{1u}/^2A_{2u}$ state. Species **II** with octabromo substitution at β-pyrrole position possesses a $^2A_{1u}$ state throughout the temperature range (298–77 K), while the *m*-CH_3O complex with tetrabromo substitution (species **II'**) exhibits a labile $^2A_{2u}$ electronic state. The lability in the electronic state is associated with changes in the conformational geometry of the porphyrin macrocyclic moiety. Metal complexes with labile electronic ground states and flexible ligand geometries are potential materials for molecular devices. By and large the present study reveals that by incorporating an appropriate substitution into the porphyrin macrocycle it is possible to fine-tune the electronic structure to design a desired material.

Experimental Section

Materials: Aldehydes and other chemicals (E. Merck) were used as received. Solvents (A.R. grade) were purified and dried before use. Freshly distilled pyrrole (Aldrich) was used for the condensation.
Physical Measurements: Elemental (C,H,N) analysis was carried out on a Perkin–Elmer PE-2400 Series **II** analyzer. – FT-IR spectra were recorded as KBr pellets on a Biorad FTS 40 spectrophotometer. – Electronic spectra for solutions were measured on a HP 8452 Diode array UV/Visible spectrophotometer. – ^{1}H-NMR measurements were conducted on a Bruker DPX 200 MHz spectrometer using TMS as the internal standard. – Cyclic voltammetric studies were conducted on BAS CV-27 and CH 660 A USA instruments. Glassy carbon was used as a working electrode, Ag/AgCl as a reference electrode, Pt wire as an auxiliary electrode and 0.1 M tetrabutylammonium hexafluorophosphate as a supporting electrolyte. – ESR investigations were carried out on a Bruker EMX spectrometer (ν = 9.75 GHz) using 100 kHz field modulation. Frequency was monitored using a microwave frequency counter inbuilt in the Bruker ER 041 XD-G microwave bridge. DPPH was used a field marker (g = 2.0036). Temperature variation experiments were performed using a Bruker BVT-3000 set-up and liquid nitrogen temperature (77 K) measurements using a quartz inserting Dewar. – ESR spectral simulations were done using a Simfonia software package.

Synthesis: Zinc(II) tetraphenylporphyrin and its derivatives were prepared following the procedure of Adler et al.[39] Purification of the porphyrins was carried out by following the method of Barnett et al.[40] The π-cation radicals were generated by chemical oxidation of deoxygenated CH_2Cl_2 solutions of metalloporphyrins with 0.5 equivalents of bromine in carbon tetrachloride.[33]

The complexes were characterised by various physico-chemical techniques such as elemental analysis, UV/Visible, FT-IR, FT NMR, and ESR spectroscopy, and electrochemistry. The analytical data for the various complexes are as follows:

Zn[T(H–P)P]: $C_{44}H_{28}N_4Zn$: calcd. C 77.95, H 4.13, N 8.27; found C 77.20, H 3.99, N 8.00. – FT-IR: $\tilde{\nu}$ = 1486 (m, C–H bend), 1339 (s, C=N stretch), 1068 (s, *p*-subst. phenyl), 1002 (vs, C–H pyrrole rock), 798 (vs, C–H out-of-plane defor.), 717 (s, mono subst. C_6H_5) cm^{-1}. – UV/Vis: λ (ε), nm ($cm^{-1}\cdot mol^{-1}$): 420 (545000), 512 (3700), 548 (25200), 586 (4600).

Zn[T(*p*-CH_3O–P)P]: $C_{44}H_{36}N_4O_4Zn$: calcd. C 72.20, H 4.51, N 7.02; found C 69.54, H 5.33, N 6.75. – FT-IR: $\tilde{\nu}$ = 1490 (m, C–H bend), 1338 (s, C=N stretch), 1246 (vs, *p*-subst. C_6H_5), 1106 (s, *p*-subst. phenyl), 996 (vs, C–H pyrrole rock), 801 (vs, C–H out-of-plane defor.), 718 (s, mono subst. C_6H_5) cm^{-1}. – UV/Vis: λ (ε), nm ($cm^{-1}\cdot mol^{-1}$): 422 (368000), 514 (4200), 550 (22500), 590 (8100).

Zn[T(*m*-CH_3O–P)P] · CH_2Cl_2: $C_{45}H_{38}Cl_2N_4O_4Zn$: calcd. C 66.77, H 4.34, N 6.35; found C 67.39, H 5.07, N 8.10. – UV/Vis: λ (ε), nm ($cm^{-1}.mol^{-1}$): 420 (397200), 512 (2700), 548 (18300), 584 (3100).
Zn[T(*p*-Cl–P)P]: $C_{44}H_{24}N_4Cl_4Zn$: calcd. C 64.69, H 2.96, N 6.86; found C 62.03, H 3.36, N 7.88. – FT-IR: $\tilde{\nu}$ = 1480 (m, C–H bend), 1338 (s, C=N stretch), 1091(s, *p*-subst. phenyl), 1000 (vs, C–H pyrrole rock), 799 (vs, C–H out of plane defor.), 723 (s, mono subst. C_6H_5) cm^{-1}. – UV/Vis: λ (ε), nm ($cm^{-1}\cdot mol^{-1}$): 420 (431300). 512 (2200), 548 (16100), 586 (2800).

Zn[T(*m*-Cl–P)P]: $C_{44}H_{24}Cl_4N_4Zn$: calcd. C 64.69, H 2.96, N 6.86; found C 63.29, H 3.13, N 7.08. – UV/Vis: λ (ε), nm ($cm^{-1}\cdot mol^{-1}$): 420 (349800), 512 (3100), 548 (14300), 584 (2700).

Zn[T(*p*-F–P)P]: $C_{44}H_2F_4N_4Zn$: calcd. C 70.40, H 3.20, N 7.47; found C 69.80, H 3.85, N 8.31. – FT-IR: $\tilde{\nu}$ = 1489 (m, C–H bend), 1337 (s, C=N stretch), 1231 (vs, *p*-subst. C_6H_5), 1092 (s, *p*-subst. phenyl), 1003 (vs, C–H pyrrole rock), 793 (vs, C–H out of plane defor.), 720 (s, mono subst. C_6H_5) cm^{-1}. UV/Vis: λ (ε), nm ($cm^{-1}\cdot mol^{-1}$): 420 (453400), 512 (4600), 548 (24000), 586 (4600).

Acknowledgments

PCD thanks CSIR, New Delhi for providing Senior Research Fellowship. Financial support by The Department of Science Technology, New Delhi to DS is gratefully acknowledged.

[1] D. Dolphin, R. H. Felton, *Acc. Chem. Res.* **1974**, *7*, 26.
[2] J. H. Dawson, *Science* **1988**, *240*, 433.
[3] C. E. Schulz, R. Rutter, J. T. Sage, P. G. Debrunner, L. P. Hager, *Biochemistry* **1984**, *23*, 4743.
[4] W. R. Browett, M. J. Stillman, *Biochim. Biophys. Acta* **1981**, *660*, 1.
[5] W. R. Patterson, T. L. Poulos, D. B. Goodin, *Biochemistry* **1995**, *34*, 4342.
[6] C. E. Schulz, P. W. Devaney, H. Winkler, P. G. Debrunner, N. Doan, R. Chiang, R. Rutter, L. P. Hager, *FEBS Letts.* **1979**, *103*, 102.
[7] R. Rutter, L. P. Hager, H. Dhonau, M. Hendrich, M. Valentine, P. Debrunner, *Biochemistry* **1984**, *23*, 6809.
[8] M. J. Benecky, J. E. Frew, N. Scowen, P. Jones, B. M. Hoffman, *Biochemistry* **1993**, *32*, 11929.
[9] J. Fajer, M. S. Davis, in: *The Porphyrins*, Part B, Vol. 4, (Ed.: D. Dolphin), Academic Press, New York, p. 197, (**1979**).
[10] M. Bixon, J. Fajer, G. Feher, J. H. Freed, D. Gamliel, A. J. Hoft, H. Levanon, K. Mobius, R. N1achushtai, J. R. Norris, A. Scherz, J. L. Sessler, D. Stehlik, *Isr. J. Chem.* **1992**, *32*, 369.
[11] W. W. Parson, B. Ke, in: *Photosynthesis: Energy Conversion by Plants and Bacteria* (Ed.: Govindjee), Academic Press, New York, **1982**, Vol. I, Ch. 8.
[12] M. P. Gouterman in: *The Porphyrins* (Ed.: D. Dolphin), Academic Press, New York, **1978**, Vol. III, pp. 1–165.
[13] R. S. Czernuszewicz, K. A. Macor, X.-Y. Li, J. R. Kincaid, T. G. Spiro, *J. Am. Chem. Soc.* **1989**, *111*, 3860.
[14] W. A. Oertling, A. Salehi, C. K. Chang, G. T. Babcock, *J. Phys. Chem.* **1989**, *93*, 1311.
[15] A. G. Skillman, J. R. Collins, G. H. Loew, *J. Am. Chem. Soc.* **1992**, *114*, 9538.
[16] L. K. Hanson, C. K. Chang, M. S. Davis, J. Fajer, *J. Am Chem. Soc.* **1981**, *103*, 663.
[17] I. Fujita, L. K. Hanson, F. A. Walker, J. Fajer, *J. Am. Chem. Soc.* **1983**, *105*, 3296.
[18] M. W. Renner, R.-J. Cheng, C. K. Chang, J. Fajer, *J. Phys. Chem.* **1990**, *94*, 8508.

[19] J. E. Roberts, B. M. Hoffman, R. Rutter, L. P. Hager, *J. Biol. Chem.* **1981**, *256*, 2118.
[20] W. R. Browett, Z. Gasyne, M. J. Stillman, *J. Am. Chem. Soc.* **1989**, *110*, 3633.
[21] I. Morishima, Y. Takamuki, Y. Shiro, *J. Am. Chem. Soc.* **1984**, *106*, 7666.
[22] G. N. La Mar, V. Thanabal, R. D. Johnson, K. M. Smith, D. W. Parish, *J. Biol. Chem.* **1989**, *264*, 5428.
[23] J. R. Kincaid, Y. Zheng, J. Al-Mustafa, K. Czarnecki, *J. Biol. Chem.* **1996**, *271*, 28805.
[24] V. Palaniappan, J. Terner, *J. Biol. Chem.* **1989**, *264*, 16046.
[25] R. H. Felton, D. Dolphin, D. C. Borg, J. Jajer, *J. Am. Chem. Soc.* **1969**, *91*, 196.
[26] J. Fajer, D. C. Borg, D. Forman, D. Dolphin, R. H. Felton, *J. Am. Chem Soc*. **1970**, *92*, 3451.
[27] M. Satoh, Y. Ohba, S. Yamauchi, M. Iwaizumi, *Inorg. Chem*. **1992**, *31*, 298.
[28] Z. Gross, C. Barzilay, *Angew. Chem*. *Int. Ed. Engl.* **1992**, *31*, 1615.
[29] C. M. Brassily, S. A. Sibyl, T. G. Spire, Z. Gross, *Chem. Eur. J.* **1995**, *1*, 222.
[30] W. A. Kalsbeck, J. Seth, D. F. Bocian, *Inorg. Chem.* **1996**, *35*, 7935.
[31] A. G. Skillman, J. R. Collins, G. H. Loew, *J. Am. Chem. Soc.* **1991**, *114*, 9538.
[32] A. Ghosh, *J. Am. Chem. Soc*. **1995**, *117*, 4691.
[33] P. C. Dave, D. Srinivas, *J. Porphyrins and Phthalocyanines* **1998**, *2*, 243.
[34] K. Jayaraj, J. Terner, A. Gold, D. A. Roberts, R. N. Austin, D. Mandon, R. Weiss, E. Bill, M. Muther, A. X. Trautwein, *Inorg. Chem.* **1996**, *35*, 1632.
[35] A. Forman, D. C. Borg, R. H. Felton, J. Fajer, *J. Am. Chem. Soc.* **1971**, *93*, 2790.
[36] P. Bhyrappa, V. Krishnan, *Inorg. Chem*. **1991**, *30*, 239.
[37] M. J. Crossley, P. L. Burn, S. S. Chew, F. B. Cuttance, I. A. Newson, *J. Chem. Soc., Chem. Commun.* **1991**, 1564.
[38] P. Ochsenbein, K. Ayougon, D. Mandon, J. Fischer, R. Weiss, R. N. Austin, K. Jayaraj, A Gold, J. Terner, J. Fajer, *Angew. Chem. Int. Ed. Engl.* **1994**, *33*, 348.
[39] A. D. Adler, F. R. Longo, F. Kampas, J. Kim, *J. Inorg. Nucl. Chem.* **1979**, *32*, 2443.
[40] G. H. Barnett, M. F. Hudson, K. M. Smith, *J. Chem. Soc., Perkin Trans.I* **1975**, 1401.

Received May 3, 1999
[I99162]

Tetraazido Complexes of Aluminium, Gallium, and Indium

Harald Sussek,[a] Frank Stowasser,[a] Hans Pritzkow,[b] and Roland A. Fischer*[a]

Keywords: Aluminium / Gallium / Indium / Azide / Rietveld

The new tetraazido complexes of aluminium, gallium, and indium $[thf_2Na][thf_2Al(N_3)_4]$ (**1**), $[py_2Na][py_2In(N_3)_4]$ (**2**), and $Na[Ga(N_3)_4]$ (**3**) have been synthesized from MCl_3 and NaN_3 by salt metatheses and characterized by X-ray diffraction analysis. In compounds **1** and **2**, the Group 13 metal atom and the sodium atom are each hexacoordinated by four azido groups and two additional solvent molecules. The azido groups act as μ(1,3)-bridging ligands between the Group 13 metal and sodium, thereby forming network structures. In contrast, complex **3** is solvent-free and exhibits a tetracoordinated gallium centre and a heptacoordinated sodium atom. The structure of **3** has also been investigated by means of X-ray powder data and the Rietveld method and the results are compared with the single-crystal data.

Introduction

Organometallic and inorganic azide derivatives of the Group 13 metals (M = Al, Ga, In), including the compounds $[X_2Ga(N_3)]_3$ (R = Et, H, Cl),[1] $[(\mu\text{-}NMe_2)\text{-}Ga(N_3)(NMe_2)]_2$,[2] $(N_3)_aM[(CH_2)_3NMe_2]_{3-a}$ (M = Al, Ga, In; a = 1, 2), and $Ga(N_3)_3(L)$ (L = NMe_3, NEt_3)[3] have been studied as precursors of the respective Group 13 nitride materials. Gallium nitride, as well as the ternary alloys $Al_xGa_yIn_zN$ ($x + y + z = 1$), are wide-band-gap semiconductors that exhibit a unique combination of properties making them useful for a number of advanced applications in optoelectronics and various other fields.[4] The azido unit would appear to be an interesting choice for the introduction of the nitrogen component in metal nitride synthesis. The commonly used precursors, e.g. MR_3 and ammonia or alkylamines, contain M−C, C−H, N−H, and N−C bonds, fragmentation of which leads to the incorporation of impurities into the nitride material. However, a drawback to the use of metal azide derivatives as precursors of nitrides is their inherent tendency to undergo exothermic decomposition. Nitrogen-rich compounds such as $[H_2Ga(N_3)]_3$ and $Ga(N_3)_3L_n$ may even detonate under certain circumstances.[1][5] Intramolecular adduct formation has, however, proved to be a reliable method for stabilizing Group 13 metal azides against explosive decomposition.[3] In the context of potential applications as electronic materials, the purity of nonexplosive azide precursors with regard to contamination by dangerous explosive species is a very important issue. We were thus interested in characterizing all the possible species involved when Group 13 metal halides are treated with alkali azides, e.g. NaN_3. We report herein on the synthesis and structural chemistry of the previously unknown tetraazido complexes of aluminium, gallium, and indium, **1−3**.

[a] Lehrstuhl für Anorganische Chemie II, Ruhr Universität Bochum,
D-44780 Bochum, Germany
[b] Anorganisch Chemisches Institut, Ruprecht-Karls-Universität, Im Neuenheimer Feld 270, D-69120 Heidelberg, Germany

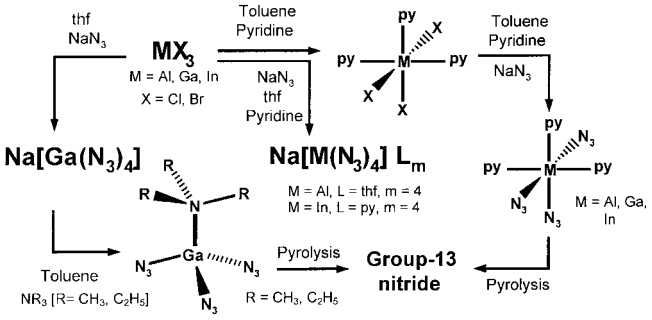
Syntheses and Properties

During the course of our investigations of Group 13 metal azide complexes containing various donor ligands $M(N_3)_3L_n$ (L = NR_3, n = 1; L = py, n = 3), the three new complexes of aluminium, gallium, and indium **1−3** have been isolated (Scheme 1). When the Group 13 chlorides MX_3 are treated with precisely stoichiometric amounts of sodium azide in a toluene/pyridine mixture, the tripyridine compounds $M(N_3)_3py_3$ are formed, which can be isolated in high yields.[3b,3c,3d,6] However, only use of a significant excess of sodium azide (> 5 equiv.) and an appropriate combination of solvent and additional ligands selectively gives **1−3**. A large excess of sodium azide is generally required in order to avoid halide contamination of Group 13 azide derivatives due to incomplete Cl^-/N_3^- exchange.[6] The donor-stabilized triazidogallium complexes $Ga(N_3)_3(NR_3)$ (**4**) are thus typically synthesized from compound **3** as an (isolated) intermediate. This intermediate is also important in the synthesis of the donor-free parent compound $[Ga(N_3)_3]_\infty$ (**5**), which can be extracted with toluene as an unstable thf adduct $Ga(N_3)_3(thf)_x$, in a similar manner as in the synthesis of compound **4**.[6] However, the isolation of the pure tetraazides **1−3** requires special precautions since they are explosive compounds and will detonate spontaneously when heated above 200°C at rates greater than 2 K/min, or when exposed to mechanical shock. The enthalpy of detonation of compound **2** was measured as 2.3 $MJ\cdot kg^{-1}$ (607 $kJ\cdot mol^{-1}$) using a special sealed calorimeter.[7] This value compares well with that of 1.54 $MJ\cdot kg^{-1}$ (450 $kJ\cdot mol^{-1}$) found for $Pb(N_3)_2$.

Crystal Structures

Different representations of the structure of **1** in the solid state, showing the coordination at the metal centres as well as the packing in the crystal, are given in Figures 1a−b. Compound **1** crystallizes from saturated thf solutions in the triclinic space group $P\bar{1}$. Each metal cation is octahedrally coordinated by four azido groups in equatorial positions

 © WILEY-VCH Verlag GmbH, D-69451 Weinheim, 2000 1434−1948/00/0303−0455 $ 17.50+.50/0



Scheme 1. Synthesis and chemistry of donor-stabilized triazido complexes and tetraazido complexes

and two apical thf molecules. The azido groups act as μ(1,3) bridging ligands between the aluminium and sodium octahedra, thereby forming a two-dimensional layer structure with the metal atoms and the azido groups in the *ab* plane of the unit cell. The thf molecules show a disordering, which could not be resolved. These positions were refined by assuming equivalent interatomic distances. The metal−O bond lengths were fixed at 201.3 pm for aluminium and at 235.9 pm for sodium. The Na−N bond lengths were found to be very similar to those in compound **3** and other related ionic sodium azides.[8][9] The $Na-N_\alpha-N_\beta$ angles were found to vary between 127.6(1)° (Na−N6−N5) and 150.0(2)° (Na−N3−N2). The corresponding values at the aluminium centre range from 129.3(1)° (Al−N1−N2) to 132.8(1)° (Al−N4−N5), which are similar to the angles found in other covalent metal azides and are thus indicative of sp^2 hybridization at the N_α atoms. An alternation of the N−N bond lengths, i.e. a longer $N_\alpha-N_\beta$ bond [119.7(2) pm and 119.2(2) pm] and a shorter $N_\beta-N_\gamma$ bond [114.2(2) pm and 114.7(2) pm] is found, which is a typical feature of covalent azides.[10a,10b] These features indicate the presence of a more covalently bonded tetraazidoaluminium moiety and a more ionic interaction with the sodium cation. Compound **1** consists of layers made up of sodium and aluminium atoms interconnected by azido groups, which are oriented parallel to each other in the *ab* plane of the unit cell.

Representations of the structure of compound **2** in the solid state, showing the coordination at the two metal centres as well as the packing in the crystal, are given in Figures 2a−c. Compound **2** is obtained from pyridine solution in the form of needles, which are monoclinic with space group *C*2/*c*. As in the case of **1**, the structure in the crystal resembles that of a coordination polymer. The metal centres are surrounded by four azido groups and two pyridine ligands in an octahedral arrangement. Each indium atom is connected to four sodium atoms through the terminal nitrogen atoms (N_α or N_γ) of the azido ($N_\alpha-N_\beta-N_\gamma$) groups and vice versa. At the indium centre, the azido groups occupy the *equatorial* positions and the pyridine ligands the *apical* positions. At the sodium centre, the pyridine ligands are *cis* orientated. The general features of the azide coordination and bonding properties compare well with the situation discussed for compound **2** and with the situations in

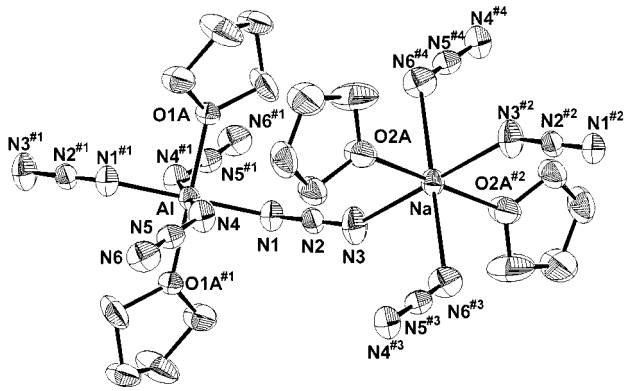


Figure 1a. Perspective view of the structure of **1** showing the coordination spheres of the aluminium and sodium atoms (ZORTEP[15] plot with 50% probability thermal ellipsoids); selected bond lengths [pm] and angles [°]: Al−N1 195.0(2), Al−N4 194.1(1), Al−O1A 201.3(9), Na−N3 249.9(2), $Na-N6^{\#3}$ 255.3(2), Na−O2A 235.9(1), N1−N2 119.7(2), N2−N3 114.2(2), N3−N4 119.2(2), N5−N6 114.7(2); Al−N1−N2 129.3(1), N1−N2−N3 175.3(2), Al−N4−N5 132.8(1), N4−N5−N6 176.0(2), $Na-N3-N2$ 150.0(2), $Na-N6^{\#3}-N5^{\#3}$ 127.7(1)

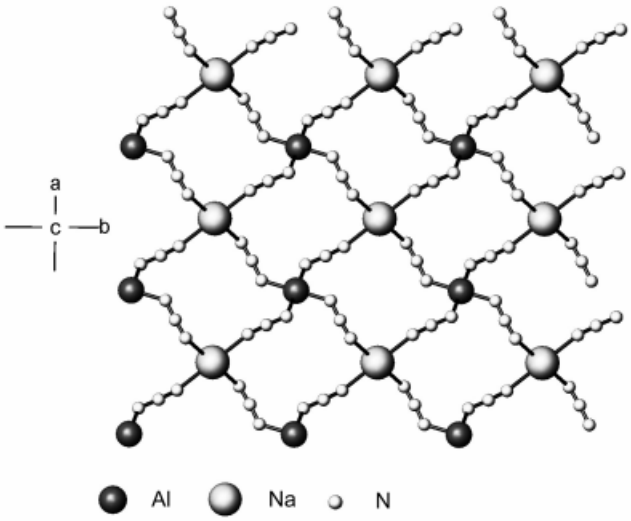


Figure 1b. Packing diagram of compound **1** in the solid state (projection along the *c* axis on the *ab* plane) showing an almost flat, two-dimensional network built-up of sodium and aluminium atoms interconnected by azido groups; the thf ligands, which are stacked between the metal azide layers, are omitted for the sake of clarity

other known covalent indium azides.[3b] The $M-N_{py}$ distances measure 230.7(2) pm for M = In and 247.5(2) pm for M = Na. The $In-N_{py}$ values are close to those in the related triazido compound $In(N_3)_3(py)_3$.[3b] The organic ligands do not show any unusually short intra- or intermolecular distances or any remarkable angles. Indeed, the structural parameters of compound **3** are rather similar to those of the isostructural compound $[(py)_2Na][(py)_2Cr(N_3)_4]$.[8] Because of the mutual *cis* orientation of the py ligands at the sodium atom, in contrast to the *trans* orientation of the thf ligands in the case of the related aluminium compound **1**, complex **2** forms a different type of coordination network. Whereas in **1** each metal atom in the layers parallel to the *ab* plane is interconnected through the

μ(1,3) azido groups (Figure 1b), in **2** the metal atoms in the layers parallel to the *ac* plane are only partly interconnected through μ(1,3) groups (Figure 2b). Every second sodium centre is connected through μ(1,3) azide bridges with the adjacent layers above and below (Figure 2c). Thus, a three-dimensional network is built-up. The py ligands occupy the holes in the packing in a similar fashion as the thf ligands of complex **1**.

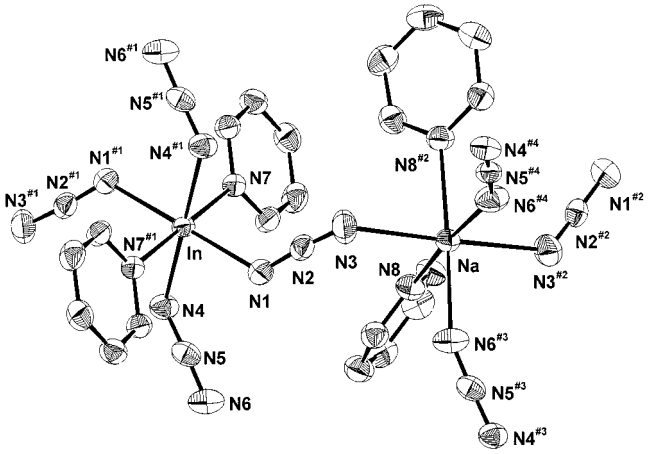


Figure 2a. A perspective view of the structure of **2** showing the coordination spheres of the indium and sodium atoms (ZORTEP plot with 50% probability thermal ellipsoids); selected bond lengths [pm] and angles [°]: In−N1 218.0(2), In−N4 222.6(2), In−N7 230.7(2), Na−N3 253.2(2), Na−N6 247.8(2), Na−N8 247.5(2), N1−N2 117.5(3), N2−N3 116.0(3), N3−N4 117.4(3), N5−N6 159.3(3); In−N1−N2 124.8(2), N1−N2−N3 176.2(2), Al−N4−N5 121.6(2), N4−N5−N6 176.5(2), Na−N3−N2 128.2(2), Na−N6−N5 151.6(2)

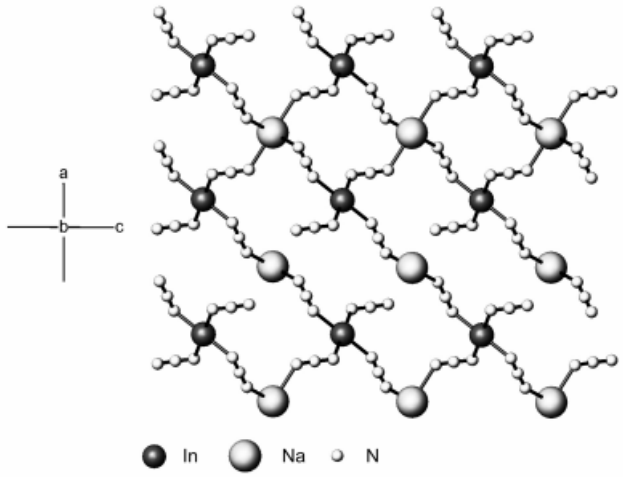


Figure 2b. Packing diagram of compound **2** in the solid state (projection along the *b* axis on the *ac* plane) showing a three-dimensional network with wave-like (in direction *b*) areas built-up of sodium and indium atoms interconnected by azido groups; the pyridine ligands, which are stacked between the metal azide layers, are omitted for the sake of clarity

Representations of the structure of **3** in the solid state, showing the coordination at the metal centres and the packing in the crystal, are given in Figures 3a−c. In contrast to **1** and **2**, compound **3** crystallizes from saturated THF solutions as a solvent-free complex in the orthorhombic

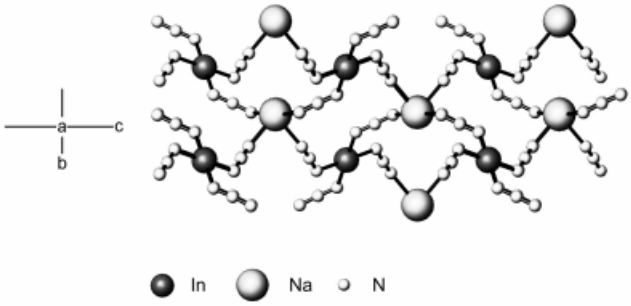


Figure 2c. Packing diagram of compound **2** in the solid state (projection along the *a* axis on the *bc* plane) showing the wave-like (in direction *b*) network built-up of sodium and indium atoms interconnected by azido groups; the pyridine ligands, which are stacked between the metal azide layers, are omitted for the sake of clarity

space group $P2_12_12_1$. The gallium atom is coordinated by azido groups in a tetrahedral fashion. Four of the six N−Ga−N angles are quite close to the ideal angle of 109°, while two show a stronger deviation [N10−Ga−N7: 93.7(1)°, N1−Ga−N7: 116.5(1)°]. The Ga−N bond lengths measure about 190(±2) pm, values that compare well with the bond lengths in other tetracoordinated gallium azides such as $(N_3)_2Ga[(CH_3)_3NMe_2]$ and $Ga(N_3)_3(NR_3)$.[5][6] The bending of the $Ga-N_\alpha-N_\beta$ units of 113.2(2)° (Ga−N1−N2) and 131.1(2)° (Ga−N7−N8) again indicates sp^2-hybridization at the N_α atom, which is typical for covalent metal azides. Three azido groups simultaneously bridge two different sodium atoms: one $Ga-N_\alpha-Na$ bridge and one head-to-tail $Ga-N_\alpha-N_\beta-N_\gamma-Na$ bridge. The azido group N10−N11−N12 is N_α-connected through N10 to the same sodium atom as N7. Interestingly, this azido group is *not* coordinated through the terminal atom N12, which is manifested in a higher temperature factor for this nitrogen. The sodium atoms are surrounded by seven azido groups, resulting in a rather asymmetric pentagonal bipyramid. Four azido groups bridge gallium and other sodium ions through their terminal nitrogen atom N_γ, while two azido groups are N_α-connected to gallium and N_γ-connected to other sodium ions. The N10−N11−N12 azide is only N_α bridged to gallium through N10. The $Na-N_{azide}$ bond lengths measure 250−260 pm, except for the Na−N7 bond, which is unusually long at 274.4(3) pm, probably as a result of steric requirements arising from the packing in the crystal. The series of $Na-N_\alpha-N_\beta$ angles are distinctly nonuniform and vary from 113.2(2)° (Na−N1−N2) to 170.5(3)° (Na−N6−N5), as expected for more ionic interactions. Each azido group exhibits the expected alternation in the N−N bond lengths, which is more pronounced than in the aluminium compound **1**, e.g. a short N2−N3 distance of 113.4(3) pm and a long N1−N2 distance of 122.9(3) pm. In this respect, the azide bonding to the gallium centre is rather similar to that in the covalent, neutral triazido congeners $Ga(N_3)_3(NR_3)$.[5][11] The packing of compound **3** (Figure 3c) can also be rationalized as a layer structure with cross-linking through μ(1,3) azido groups. The density of the packing is much higher than that in **1** and **2** due to the absence of the solvent ligands thf or py. As discussed above,

the N10−N11−N12 azide does not act as a μ(1,3) bridge. In the projection of Figure 3b, these groups point upwards and downwards along the *c* direction in an alternating fashion, into the empty space between the metal azide layers parallel to the *ab* plane.

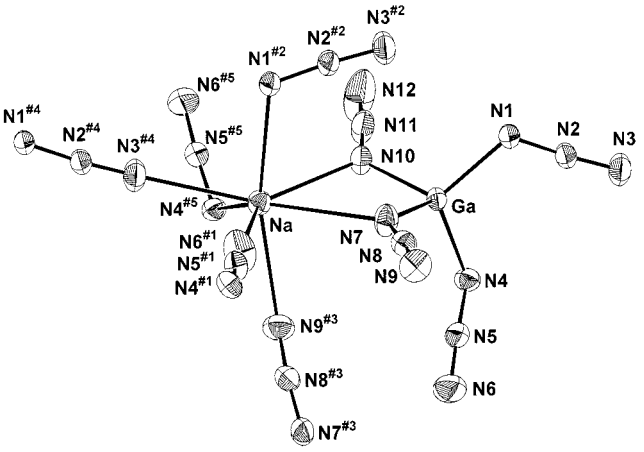


Figure 3a. A perspective view of the structure of **3** showing the coordination spheres of the gallium and sodium atoms (ZORTEP plot with 50% probability thermal ellipsoids); selected bond lengths [pm] and angles [°]: Ga−N1 189.6(2), Ga−N4 190.9(3), Ga−N7 190.9(2), Ga−N10 189.7(2); Ga−N1−N2 113.2(2), Ga−N4−N5 118.8(2), Ga−N7−N8 131.1(2), Ga−N10−N11 126.1(2); Na−$N1^{\#2}$ 251.8(3), Na−$N3^{\#4}$ 254.6(3), Na−$N4^{\#5}$ 258.5(3), Na−$N6^{\#1}$ 250.0(3), Na−$N9^{\#3}$ 252.3(3), Na−N7 274.4(3), Na−N10 258.9(3); N1−Ga−N4 110.1(1), N1−Ga−N7 116.5(1), N1−Ga−N10 112.6(1), N10−Ga−N4 111.6(1), N10−Ga−N7 93.7(1), N4−Ga−N7 111.5(1)

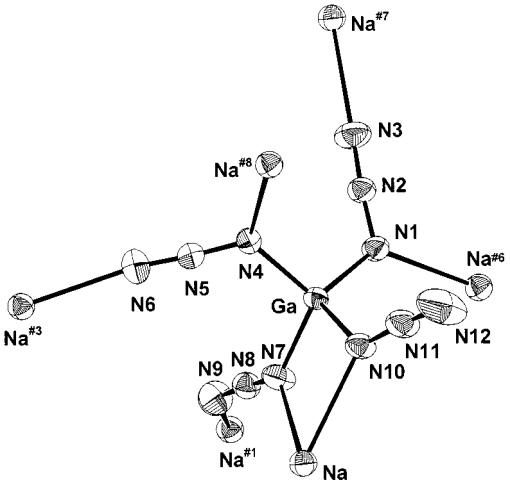


Figure 3b. A perspective view of the structure of **3** showing the interconnection between the sodium atoms and the azido groups (ZORTEP plot with 50% probability thermal ellipsoids); the azido group terminal atom N12 is not coordinated to any sodium atoms

X-ray Powder Diffraction and Rietveld Analysis of 3

As described above, compound **3** is a valuable intermediate in the synthesis of donor-stabilized gallium triazides $Ga(N_3)_3L_m$ (**4**) and other gallium azides, even for the parent

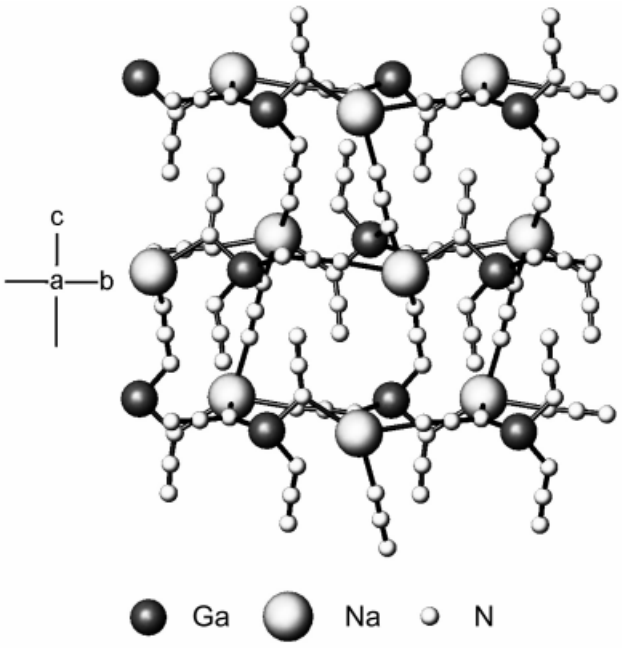


Figure 3c. Packing diagram of compound **3** in the solid state (projection along the *a* axis on the *bc* plane) showing a three-dimensional network built-up of sodium and gallium atoms interconnected by azido groups

compound $[Ga(N_3)_3]_\infty$ (**5**), which can all serve as percursors in the preparation of nanocrystalline GaN powders.[5] To verify the purity of the compounds **1−5**, it is necessary to check for the presence of sodium azide, gallium chloride, sodium chloride, and other possible inorganic impurities and side products. Reliable elemental analysis data are very difficult to obtain on a routine basis because of the explosive nature of the compounds. Consequently, we investigated X-ray powder diffraction patterns in detail using the Rietveld method so as to establish a routine tool to check the purities of **1−5** that could also be used for similar metal azide complexes and related problems. Compound **3** was selected for this study, because it is a likely and dangerous impurity in compounds of the type $Ga(N_3)_3L_m$ (**4**). Compound **3** is usually obtained as a microcrystalline powder. Figure 4 shows the measured and calculated XRD patterns. The difference curve exhibits only small deviations, thus indicating a very good agreement. The reflections induced by the beryllium window were fitted independently and have no influence on the overall structure refinement of the tetraazide. The general features of the structure of **3** are reproduced using the powder data, but details concerning bond lengths and angles differ to some extent. For example, the environment at the gallium centre shows a more marked deviation from tetrahedral in the case of the powder data and the obtained $Ga-N_{azide}$ bond lengths, which range from 201.4 pm to 216.2 pm, are longer. The $Ga-N_\alpha-N_\beta$ angles are close to the single-crystal data to within ±5°, with the exception of the Ga−N1−N2 angle where the powder data value of 130.5° is unusually large as compared with the single-crystal value of 113.2(2)°. Other deviations become apparent upon analyzing the bond lengths and angles in the

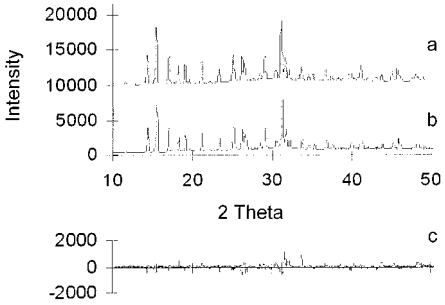


Figure 4. Detail of the X-ray patterns obtained for $NaGa(N_3)_4$ (**3**): (a) experimental data obtained with an aluminium sample holder and a beryllium window, (b) calculated data for the Rietveld structure refinement, (c) difference curve between observed and calculated data

plane containing the Na, Ga, N7, and N10 atoms. While the single-crystal data show the largest angle of 103.1(1)° located at N10 (Ga−N10−Na) and the smallest angle of 62.68(8)° at the Na atom (N7−Na−N10), the powder data show a largest angle of 106.3° for N7−Ga−N10 and a smallest angle of 81.3° at the Na centre (N7−Na−N10). Nevertheless, the constitution of the compound, the coordination features at the metal centres, and the packing mode in the crystal are reproduced quite well using X-ray powder diffraction analysis with Rietveld refinement. The deviations of the more specific structural parameters from the single-crystal reference (bond lengths and angles) are most likely attributable to the intrinsic limitations of the powder diffraction data. Moreover, the conditions of the two experiments were somewhat different. The powder data had to be collected at room temperature, while the single-crystal data were obtained at 203 K. Because of this difference in the conditions, a temperature-dependent phase transition also had to be taken into account. However, in view of the explosive nature of pure crystalline **3**, we decided not to pursue this matter further. Anyway, X-ray powder diffraction in combination with Rietveld analysis of the diffraction pattern constitutes a reliable method for establishing the identity and purity of compounds such as **3** and **4**, especially if single crystals are difficult to obtain. This is particularly true for $[Ga(N_3)_3]_\infty$ (**5**), the structure of which is still unknown due to the very poor X-ray powder diffraction data obtained to date. The work reported herein has shown that samples of **5** synthesized according to ref.[6] are essentially free of compound **3** and other likely by-products.

Experimental Section

General Procedures: All manipulations were performed using thoroughly oven-dried reaction vessels (Schlenk techniques) under an inert atmosphere of purified argon in a glove box (argon; O_2 and H_2O < 1 ppm). Solvents were dried and distilled according to standard procedures[12] and were stored over 4 Å molecular sieves (residual water < 1 ppm, Karl-Fischer). − The IR spectra were recorded in solution (thf, toluene, pyridine) using 0.1 mm CaF_2 or NaCl cells or freshly prepared KBr plates with a Perkin−Elmer 1650 FT-IR or a Bruker IFS-66 spectrometer. − Elemental analyses were provided by the Microanalytical Laboratory of the Chemical Institute at the University of Heidelberg. The metal content was determined by back-titration of excess EDTA solution (complexometric determination with Titriplex®, Merck KGaA, Darmstadt). − Melting points (uncorrected) were determined with a Gallenkamp hot-air melting point apparatus or a Seiko TG/DTA 6300

Table 1. Crystallographic data for the compounds **1**, **2**, and **3**

Compound	**1**	**2**	**3**
Empirical formula	$C_{16}H_{32}AlN_{12}NaO_4$	$C_{20}H_{20}InN_{16}Na$	$GaN_{12}Na$
Molecular mass [g mol^{-1}]	506.48	622.33	260.83
Crystal system	triclinic	monoclinic	orthorhombic
Space group (No.)	$P\bar{1}$ (2)	$C2/c$ (13)	$P2_12_12_1$(19)
a [Å]	7.728(4)	15.442(8)	7.011(4)
b [Å]	9.141(5)	10.432(5)	9.666(5)
c [Å]	9.169(5)	15.966(8)	12.320(6)
α [°]	75.34(5)	90	90
β [°]	88.90(5)	90.28(3)	90
γ [°]	89.16(5)	90	90
V [Å^3]	626.6(6)	2572.0(2)	834.9(8)
Z	2	4	4
$\rho_{calcd.}$ [g cm^{-3}]	1.343	1.607	2.075
Temperature [K]	203(2)	203(2)	203(2)
μ [mm^{-1}]	0.164	0.980	3.330
θ range for collection [°]	2.30−26.99	2.36−30.00	2.68−34.99
$h/k/l$ ranges	−9/9, −11/11, 0/1	−21/21, 0/14, 0/22	0/11, 0/15, 0/19
F(000)	268	1248	504
Crystal size [mm]	0.4 × 0.2 × 0.2	0.6 × 0.3 × 0.3	0.45 × 0.25 × 0.2
λ [Å]	0.71073	0.71073	0.71073
No. reflections collected	2748	3745	2107
No. independent reflections	2733 [R_{int} = 0.0408]	3745 [R_{int} = 0.0000]	2106 [R_{int} = 0.0000]
Transmission (min/max)	(0.766/0.998)	(0.881/1.000)	(0.862/0.999)
Refinement method	full-matrix least-squares on F^2		
Data/restraints/parameters	2732/42/247	3745/0/177	2106/0/128
Final R indices [$I > 2\sigma(I)$] $R1/wR2$	0.0390/0.01017	0.0275/0.0617	0.0275/0.0683
R indices [all data] $R1/wR2$	0.0496/0.1093	0.0426/0.0677	0.0368/0.0721
Goodness of fit on F^2	1.053	1.024	1.065
Residual electron density [eÅ^{-3}]	0.379/−0.204	0.348/−0.863	0.353/−0.794

SII thermobalance (DTA data). ***NOTE:*** Working with the described Group 13 azides requires strict adherence to special security precautions, i.e. the use of protective face shields, special gloves (metal net), and thick leather body protection. The compounds are shock-sensitive and detonate upon rapid heating (> 2 K/min) to temperatures above 200°C.

[Bis(tetrahydrofuran)sodium] [Tetraazidobis(tetrahydrofuran)aluminate], [thf_2Na][$thf_2Al(N_3)_4$] (1): A solution of anhydrous, freshly sublimed $AlCl_3$ (0.75 g, 5.63 mmol) in 25 mL of thf was slowly added to a suspension of sodium azide (1.45 g, 22.30 mmol) in 25 mL of THF at −78°C. After allowing the mixture to warm to room temperature, it was stirred for 15 h, then filtered, and the filtrate was concentrated to dryness in vacuo. The product was obtained in the form of colourless crystals. Yield: 2.43 g (4.8 mmol, 85.3% based on $AlCl_3$). − IR (KBr): $\tilde{\nu}(N_3)_{max}$ = 2122 cm^{-1} (vs), 2037 (vs), 1261 (w). − ***NOTE:*** The substance detonates vigorously on rapid heating (> 2 K/min) beyond 220°C! Decomposition at 200°C without melting. − $C_{16}H_{32}AlN_{12}NaO_4$ (506.48): calcd. Al 5.33; found Al 6.01. This large discrepancy may be attributed to evaporation of the coordinated thf and also to the very small amount of sample used for the analysis in view of the explosion risk.

[(Dipyridine)sodium] [Tetraazido(dipyridine)indate], [py_2Na][$py_2In(N_3)_4$] (2): A solution of anhydrous, freshly sublimed $InCl_3$ (1.0 g, 4.52 mmol) in 20 mL of pyridine was slowly added to a suspension of 1.3 g (20 mmol) of sodium azide in 10 mL of pyridine at −78°C. After allowing the mixture to warm to room temperature, it was stirred for 15 h, then filtered, and the filtrate was concentrated to dryness in vacuo. The product was obtained in the form of colourless crystals. Well-defined single crystals could be obtained by warming a saturated solution to 80°C and slowly cooling to room temperature. Yield: 2.43 g (3.93 mmol; 87% based on $InCl_3$). − IR (KBr): $\tilde{\nu}(N_3)_{max}$ = 2083 cm^{-1} (sh), 2067 (vs), 2037 (vs). − ***NOTE:*** The substance detonates vigorously on rapid heating (> 2 K/min) above 250°C! Decomposition at 200°C without melting. − $C_{20}H_{20}InN_{16}Na$ (622.33): calcd. C 38.60, H 3.24, N 36.01, In 18.45; found C 37.73, H 3.41, N 32.90, In 20.20.

Sodium Tetraazidogallate, Na[$Ga(N_3)_4$] (3): A solution of anhydrous, freshly sublimed $GaCl_3$ (1.05 g, 5.96 mmol) in 15 mL of thf was slowly added to a suspension of sodium azide (1.47 g, 22.61 mmol) in 25 mL of thf at −78°C. After allowing the mixture to warm to room temperature, 50 mL of toluene was added and the resulting solution was stirred for 15 h. It was then filtered and the filtrate was concentrated in vacuo. The product was obtained in the form of colourless crystals. Yield: 1.43 g (5.48 mmol; 92.0% based on $GaCl_3$). M.p. 122°C. − IR (KBr): $\tilde{\nu}(N_3)_{max}$ = 2094 cm^{-1} (sh), 2075 (s), 2064 (vs). − ***NOTE:*** The substance detonates vigorously on fast heating (> 2 K/min) above 150°C! − $GaN_{12}Na$ (260.83): calcd. Ga 26.73; found Ga 27.21.

X-ray Structure Determination: Experimental details relating to the X-ray crystal structure determinations of **1**, **2**, and **3** are listed in Table 1. Intensity data were collected with a Siemens−Stoe AED2 four-circle diffractometer using Mo-K_α radiation in ω-scan mode; an absorption correction was applied on the basis of φ scans. The structures were solved by direct methods (SHELXS-86)[13] and refined by full-matrix least-squares methods based on F^2 using all measured reflections (SHELXL-93)[13] with anisotropic temperature factors for all nonhydrogen atoms. X-ray powder diffraction data were collected with Cu-$K_{\alpha1/2}$ radiation employing a Siemens D500 instrument equipped with a secondary monochromator and a scintillation counter. In Table 2, the crystallographic data and parameters relating to the refinement are summarized. Data were collected in the Θ/2Θ mode with a step width of 0.02° and 15 s per step. The powder sample of **3** was carefully prepared in an aluminium sample holder for bulk measurements, which was covered by a beryllium window (0.25 mm) and sealed with epoxy resin to prevent decomposition by air or moisture. The measured data were refined using the program TOPAS.[14] The intensities were corrected for absorption by the beryllium window. The azido groups were defined as rigid bodies with five degrees of freedom (3 translation, 2 rotation). The isotropic temperature factors for sodium (0.5) and nitrogen (2.0) were fixed. The refined temperature factor for gallium was 0.3(1). The obtained R_{Bragg} factor of 3.2, which gives an indication of the refinement quality, is very good. Crystallographic data for the structures of **1**−**3** reported in this paper have been deposited with the Cambridge Crystallographic Data Centre as supplementary publication nos. CCDC-119351, -119352, and -119353. Copies of the data can be obtained free of charge on application to the CCDC, 12 Union Road, Cambridge CB2 1EZ, U.K. [Fax: (internat.) + 44-1223/336-033; E-mail: deposit@ccdc.cam.ac.uk].

Table 2. Crystallographic data and refinement parameters from XRD powder diffraction analysis of compound **3**

Compound	**3**
Empirical formula	$NaGaN_{12}$
Molecular mass [g mol^{-1}]	260.83
Temperature [K]	293(2)
Crystal system	orthorhombic
Space group (No.)	$P2_12_12_1$ (19)
a [Å]	7.0483(4)
b [Å]	9.6941(4)
c [Å]	12.2983(7)
V [$Å^3$]	840.31(5)
Z	4
2Θ range for collection [°]	10−90
λ [Å] Cu-$K_{\alpha1,2}$	1.540596/1.544410
R_{wp} (all data)	6.9
R_{exp} (all data)	3.2
Goodness of fit	2.2
R_{Bragg}	3.2

Acknowledgments

This work was supported by the DFG grant No. Fi 502/9−1.

[1] [1a] J. Kouvetakis, D. Beach, *Chem. Mater.* **1989**, *1*, 476−478. − [1b] J. McMurran, D. Dai, K. Balasubramanian, C. Steffek, J. Kouvetakis, J. L. Hubbard, *Inorg. Chem.* **1998**, *37*, 6638−6644. − [1c] J. McMurran, J. Kouvetakis, D. C. Nesting, D. J. Smith, J. L. Hubbard, *J. Am. Chem. Soc.* **1998**, *120*, 5233−5237. − [1d] J. Kouvetakis, J. McMurran, P. Matsunaga, M. O′Keefe, J. L. Hubbard, *Inorg. Chem.* **1997**, *36*, 1792−1797.
[2] D. A. Neumayer, A. H. Cowley, A. Decken, R. A. Jones, V. Lakhotia, J. G. Ekerdt, *J. Am. Chem. Soc.* **1995**, *117*, 5893−5894.
[3] [3a] R. A. Fischer, A. Miehr, O. Ambacher, W. Rieger, T. Metzger, E. Born, *Chem. Vap. Deposition* **1996**, *2*, 51−55. − [3b] R. A. Fischer, H. Sussek, A. Miehr, H. Pritzkow, E. Herdtweck, *J. Organomet. Chem.* **1997**, *548*, 73−82. − [3c] R. A. Fischer, A. Miehr, H. Sussek, H. Pritzkow, E. Herdtweck, J. Müller, O. Ambacher, T. Metzger, *J. Chem. Soc., Chem. Commun.* **1996**, 2685−2686. − [3d] C. J. Carmalt, A. H. Cowley, R. D. Culp, R. A. Jones, *J. Chem. Soc., Chem. Commun.* **1996**, 1453−1454.
[4] S. Nakamura, G. Fasol, *The Blue Laser Diode*, Springer, Berlin, **1997**.
[5] [5a] R. A. Fischer, A. C. Frank, F. Stowasser, H. Sussek, H. Pritzkow, C. Miskys, O. Ambacher, M. Giersig, *J. Am. Chem. Soc.* **1998**, *120*, 3512−3513. − [5b] R. A. Fischer, A. C. Frank,

Adv. Mater. **1998**, *10*, 961−964. − [5c] R. A. Fischer, A. C. Frank, F. Stowasser, O. Stark, H. T. Kwak, H. Sussek, A. Rupp, H. Pritzkow, O. Ambacher, M. Giersig, *Adv. Mater. Opt. Electron.* **1998**, *8*, 135−146.

[6] R. A. Fischer, A. Miehr, E. Herdtweck, M. R. Mattner, O. Ambacher, T. Metzger, E. Born, S. Weinkauf, C. R. Pulham, S. Parsons, *Chem. Eur. J.* **1996**, *2*, 1353−1358.

[7] A. C. Frank, Dissertation, *Fakultät für Chemie*, Heidelberg, **1998**.

[8] M. A. S. Goher, M. A. M. Abu-Youssef, F. A. Mautner, *Z. Naturforsch.* **1992**, *47b*, 139−143.

[9] U. Müller, *Struct. Bonding* **1973**, *14*, 141−172.

[10] [10a] T. M. Klapötke, I. C. Torniporth-Oetting, *Angew. Chem.* **1995**, *107*, 559−568; *Angew. Chem. Int. Ed. Engl.* **1995**, *34*, 511−520. − [10b] T. M. Klapötke, *Chem. Ber.* **1997**, *130*, 443−451.

[11] A. Devi, H. Sussek, H. Pritzkow, M. Winter, R. A. Fischer, *Eur. J. Inorg. Chem.*, in press.

[12] D. D. Perrin, W. L. F. Armarego, *Purification of Laboratory Chemicals*, Pergamon Press, London, **1988**.

[13] [13a] G. M. Sheldrick, "SHELXS-86", *Crystallographic Computing 3*, Oxford University Press, U.K., **1986**, p. 175−189. − [13b] G. M. Sheldrick, "SHELXL-93", *Program for Crystal Structure Refinement*, University of Göttingen, **1993**.

[14] [14a] R. W. Cheary, A. A. Coelho, *J. Appl. Crystallogr.* **1992**, *25*, 109−121. − [14b] R. W. Cheary, A. A. Coelho, *J. Appl. Crystallogr.* **1994**, *27*, 673−681.

Received May 10, 1999
[I99170]

Potentially Tridentate Hydrazonic Ligands in the Synthesis of Methyl and Acetyl Palladium(II) Complexes

Paolo Pelagatti,[a] Mauro Carcelli,[a] Francesca Franchi,[a] Corrado Pelizzi,*[a] Alessia Bacchi,[a] Andrea Fochi,[a] Hans-Werner Frühauf,[b] Kees Goubitz,[c] Kees Vrieze[b]

Keywords: Palladium / Insertion reactions / Tridentate ligands / Hydrazones

Potentially tridentate hydrazonic ligands of the type HNNO have been used in the synthesis of some methyl palladium(II) complexes. Depending on the applied experimental conditions two different kinds of complexes are obtained. Thus, the reactions between **HL1–HL5** and (COD)PdMeCl in diethyl ether led to the formation of bidentate methyl complexes of the type Pd(HNN)MeCl (**1–5**), where the ligands maintain a neutral character. However, in the presence of a base such as Et_3N or NaOMe, the ligands are deprotonated with the consequent formation of tridentate methyl complexes of the type Pd(NNO)Me (**7–10**). In solution, complexes **1–5** tend to lose the hydrazonic proton with elimination of methane and formation of a tridentate chloride complex Pd(NNO)Cl (**6**); this tendency can be correlated with the acidity of the free ligands, which has been determined. On bubbling carbon monoxide through solutions of **1–5**, the corresponding acetyl complexes Pd(HNN)[C(O)Me]Cl (**11–15**) are formed, in which both the *cis* and *trans* isomers are present. Their molar ratio is rationalised from the results of a molecular modelling study on the basis of electronic considerations. A remarkably different reactivity has been found in the carbonylation of the tridentate complexes **7–10**: they decompose rapidly and quantitatively to palladium black and an organic product corresponding to the ligand with an acetyl group bonded to the hydrazonic nitrogen. The X-ray structures of a methyl complex (**3**) and its corresponding acetyl (**13**) derivative have been determined.

Introduction

The use of potentially tridentate ligands in the synthesis of organometallic compounds has received much attention since tridentate metal complexes are expected to exhibit interesting catalytic properties, such as better stereoselective or chemoselective control of the reactions.[1] We have been interested in the study of the coordinating behaviour of tridentate hydrazonic ligands towards palladium(II) for some years,[2] and more recently our interest has been focused on the capability of the isolated complexes to activate a simple molecule like hydrogen.[3]

With the aim of studying the reactivity towards other simple molecules, we have investigated the insertion of CO into the Pd–C bond, this reaction being a key step in many palladium-mediated processes, such as the hydroxy- or alkoxycarbonylation of alkenes[4] and the copolymerisation of alkenes and CO.[5]

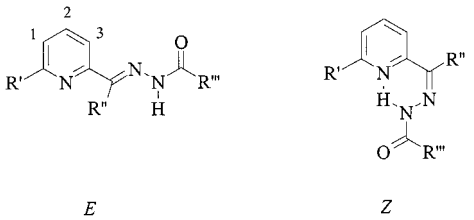
[a] Dipartimento di Chimica Generale ed Inorganica, Chimica Analitica, Chimica Fisica, Università degli Studi di Parma, Parco Area delle Scienze 17/A, 43100 Parma, Italy
Fax: (internat.) + 39-521/905-557
E-mail: Pelizzi@ipruniv.cce.unipr.it
[b] Anorganisch Chemisch Laboratorium, J. H. van't Hoff Research Instituut, Universiteit van Amsterdam, Nieuwe Achtergracht 166, NL-1018 WV Amsterdam, The Netherlands
[c] Laboratorium voor Kristallografie, J. H. van't Hoff Instituut, Universiteit van Amsterdam, Nieuwe Achtergracht 166, NL-1018 WV 166, The Netherlands

In this field much work has been done with both symmetrical[6] and unsymmetrical bidentate ligands.[7] Recently complexes with rigid bidentate nitrogen ligands showed faster CO and alkene insertion than those with flexible bidentate nitrogen ligands.[8] Moreover, as opposed to complexes containing phosphorous ligands, the insertion of CO into the Pd–Me bond was not prevented by either the flexible or the rigid tridentate nitrogen ligands,[9] and kinetic studies have shown that the insertion rate of CO and strained alkenes increases with increasing rigidity of the ligand.[10]

Asymmetric tridentate ligands have been scarcely studied in the synthesis of methyl and acetyl palladium(II) complexes and, importantly, only neutral ligands have been employed.[11] Although mechanistic details have not been reported, the rupture of a coordinative bond seems to be a prerequisite for CO coordination and insertion. The breaking of a Pd–N or Pd–O coordinating bond has been proposed also by us as a key step in the homogeneous hydrogenation of terminal alkenes and alkynes catalysed by palladium(II) complexes with tridentate ligands.[3] In the present work, we have prepared methyl palladium(II) complexes with acylhydrazones, HNNO (Scheme 1), which can behave as either neutral bidentate, or as anionic tridentate ligands, placing the metal in diverse electronic and steric environments.

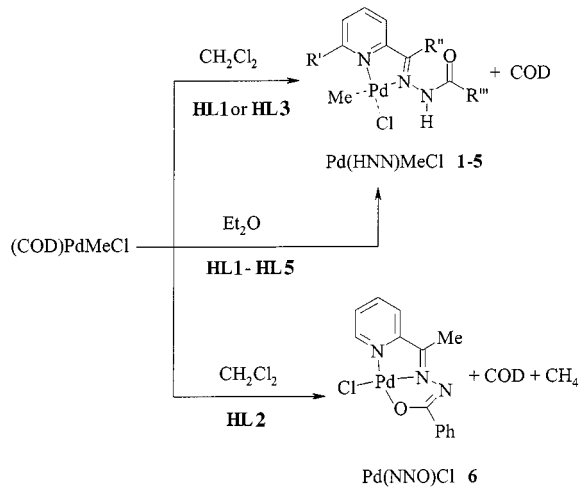
In relation to the experimental conditions, complexes with both coordination modes have been obtained, namely bidentate Pd(HNN)MeCl, and tridentate Pd(NNO)Me (see Scheme 2).

 © WILEY-VCH Verlag GmbH, D-69451 Weinheim, 2000 1434–1948/00/0303–0463 $ 17.50+.50/0



R′	R″	R‴	Ligand
H	Me	Me	**HL1**
H	Me	Ph	**HL2**
H	H	Ph	**HL3**
H	Et	Ph	**HL4**
Me	H	Ph	**HL5**

Scheme 1. The hydrazonic ligands **HL1–HL5**



Scheme 2. Synthesis of the complexes **1–6**

We now report on the synthesis and characterisation of these complexes, and on their reactivity towards CO insertion into the Pd–Me bond. The reactivity of the methyl complexes towards CO has also been investigated considering the coordination mode and steric hindrance of the ligand and, for the Pd(HNN)MeCl complexes, the acidity of the hydrazonic proton.

Results and Discussion

Synthesis and Characterisation of Ligands HL1–HL5

The acyl hydrazonic ligands **HL1–HL5** were obtained by condensation between a 2-pyridyl-carbonylic system and a hydrazide, in the presence of a catalytic amount of glacial acetic acid. All the ligands are colourless solids, readily soluble in common organic solvents. The N–H bond is visible in their IR spectra with a band at about 3200 cm^{-1}, whereas the C=O group gives rise to a strong band at about 1650 cm^{-1}. The hydrazonic chain is represented by two intense bands centred at about 1550 cm^{-1} and 1300 cm^{-1}, assigned to the AMIDE II and AMIDE III systems, respectively. With the exception of **HL5**, two different sets of signals are present in the ^{1}H-NMR spectrum of the ligands, showing the presence of both (*E*) and (*Z*) isomers (Scheme 1).[12]

Table 1. Selected ^{1}H-NMR ($CDCl_3$) data for ligands **HL1**–**HL5**

	δ[a] N–H	R′	H^1	H^2	H^3
HL1 (*E*)	8.89(s)	8.58(d)	7.26(t)	7.69(t)	8.07(d)
(*Z*)	9.04(s)	8.67(d)	7.32(t)	7.84(t)	7.51(d)
HL2 (*E*)	9.14(s)	8.59(d)	7.27(t)	7.70(t)	–[b]
(*Z*)	15.78(s)	8.71(d)	7.39(t)	7.91(t)	7.62(d)
HL3 (*E*)	11.15(s)	8.54(d)	7.33(t)	7.79(t)	8.13[b]
(*Z*)	15.48(s)	8.76(d)	7.41(t)	7.93(t)	8.02(d)
HL4 (*E*)	8.33(s)	8.59(d)	7.50(m)	7.68(t)	7.58(d)
(*Z*)	9.24(s)	8.75(d)	7.47(m)	7.93(t)	7.66(d)
HL5 (*E*)	9.67(s)	2.55(s)	7.13(d)	7.59(t)	7.88(d)

[a] For simplicity the coupling constants are not reported. – [b] Overlapping with other signals,

These can be distinguished from the signal of the hydrazonic proton (Table 1), which is more deshielded in the (*Z*) isomer, owing to the formation of an intramolecular hydrogen bond with the N_{py}.

Starting from the upper signal, the sequence shown by the pyridine protons of the (*E*) isomer is R′ > H^3 > H^2 > H^1, while in the (*Z*) isomer, and in the palladium complexes, the sequence becomes R′ > H^2 > H^3 > H^1. This indicates that the interaction between H^3 and the iminic nitrogen, present in the (*E*) form, is removed by rotation around the py–C(R″)N bond upon hydrogen-bond formation or coordination to the metal.[8a] Taking into account these observations, an initial predominance of the (*E*) isomer was established, with an (*E*/*Z*) ratio of about 1:0.3 for ligands **HL1**–**HL4**. After 24 hours in chloroform solution at room temperature, **HL2** and **HL3**, containing R‴ = Ph, showed a practically inverted ratio, whereas no change was observed for **HL1**, in agreement with the capacity of the phenyl group to support isomerisation around a C=N bond.[12a] For **HL5** the low deshielding of the hydrazonic proton and the sequence of the pyridinic signals are in favour of the *E* isomer and no changes were observed in a chloroform solution at room temperature after 24 hours.

Synthesis and Characterisation of the Bidentate Methyl Complexes Pd(HNN)MeCl (1–5)

Depending on the solvent, the ligands **HL1**–**HL5** showed a different reactivity towards (COD)PdMeCl. In dichloromethane, **HL1** and **HL3** gave the methyl complexes of formula Pd(HNN)MeCl (**1** and **3**), where the neutral ligand coordinates in a bidentate mode through the pyridinic and the iminic nitrogens, excluding the carbonyl oxygen from the coordination sphere (Scheme 2). The neutral character of the ligand is supported by both the IR and NMR spectra (presence of the N–H bond signals), whereas a strong IR band at about 1700 cm^{-1} indicates an uncoordinated C=O group. In the ^{1}H-NMR spectra of **1** and **3** (Table 2), the methyl group bonded to the metal gives rise to a singlet at 0.97 ppm and 1.01 ppm, respectively, which are typical values for a methyl group σ-bonded to palladium.[8a,c,9] The chemical shift of the R′ proton is useful in establishing the disposition of the methyl ligand with respect to the C=N

Table 2. Selected ^{1}H-NMR ($CDCl_3$) data for palladium complexes

	δ[a] N–H	R	H^1	H^2	H^3	Pd–Me
1 (*trans*)	9.53(s)	8.57(d)	7.56(t)	8.04(t)	7.78(d)	0.97(s)
2 (*trans*)	10.38(s)	8.59(d)	–[b]	8.08(td)	7.85(d)	0.98(s)
2 (*cis*)	9.78(s)	8.85(d)	7.43(t)	–[b]	–[b]	0.80(s)
3 (*trans*)[c]	11.15(s)	8.54(d)	7.64(d)	8.04(td)	7.73(d)	1.01(s)
4 (*trans*)	10.39(s)	8.64(d)	7.35(t)	8.08(t)	7.85(d)	1.01(s)
4 (*cis*)	10.66(s)	9.31(d)	7.37(t)	8.15(t)	7.66(d)	–[b]
5 (*cis*)	11.30(s)	2.75(s)	7.36(d)	7.83(t)	7.52(d)	1.18(s)
6	–	8.65(dd)	7.47(t)	7.91(td)	–[b]	–
7	–	8.53(d)	7.46(t)	7.99(t)	7.76(d)	0.69(s)
8[c]	–	8.38(d)	7.66(td)	8.03(td)	7.87(d)	0.24(s)
9	–	8.31(d)	7.34(td)	7.95(td)	7.68(d)	0.27(s)
10	–	2.93(s)	6.86(d)	7.37(m)[b]	7.15(d)	0.81(s)
11 (*trans*)	9.38(s)	8.50(d)	7.48(t)	8.04(t)	7.79(d)	2.59(s)
11 (*cis*)	10.80(s)	8.80(d)	7.48(t)	7.95(t)	7.82(d)	2.64(s)
12 (*trans*)	10.28(s)	8.57(d)	–[b]	–[b]	7.86(d)	2.62(s)
12 (*cis*)	11.66(s)	8.99(d)	–[b]	–[b]	7.86(d)	2.63(s)
13 (*trans*)	11.03(s)	8.54(d)	–[b]	8.08(td)	–[b]	2.67(s)
13 (*cis*)	12.40(s)	9.10(d)	–[b]	–[b]	–[b]	2.78(s)
14 (*trans*)	10.24(s)	8.60(d)	–[b]	–[b]	–[b]	2.62(s)
14 (*cis*)	11.44(s)	8.93(d)	–[b]	–[b]	–[b]	2.60(s)
15 (*trans*)	11.13(s)	2.76(s)	7.38(d)	7.83(t)	7.43(d)	2.70(s)

[a] For simplicity the coupling constants are not reported. – [b] Overlapping with other signals. – [c] Solvent: CD_2Cl_2.

bond. In fact when the alkyl group is *trans* to the C=N, R′ shows a resonance similar to that observed in the free ligand, while in a *cis* disposition, R′ resonates at higher ppm values as it is deshielded by the electron-withdrawing effect of the chlorine atom.[8a] On the basis of NMR spectroscopic data, a *trans* disposition was inferred for both **1** and **3**.

The assumed structures for **1** and **3** are confirmed by an X-ray analysis conducted on a single crystal of **3** obtained from a dichloromethane/diethyl ether mixture (1:1), as reported in the Crystallographic Section.

The reaction between **HL2** and (COD)PdMeCl in dichloromethane followed a different pathway (Scheme 2). No traces of the expected Pd(HNN)MeCl complex were observed, but only the formation of a tridentate chloride complex Pd(NNO)Cl (**6**). This reaction involves the deprotonation of the ligand with the consequent formation of methane. The loss of the hydrazonic proton forces the carbonylic oxygen to coordinate to the metal, as demonstrated by the disappearance of the stretching band of the C=O group in the IR spectrum.

The bidentate methyl complex **2** can be selectively obtained by addition of (COD)PdMeCl to an ethereal suspension of **HL2** (Scheme 2). The ^{1}H-NMR spectrum of **2** indicates the presence of both *cis* and *trans* isomers in a ratio of 0.07:1. The use of diethyl ether in the preparation of the Pd(HNN)MeCl complexes was extended to the synthesis of **1** and **3** with ligands **HL1** and **HL3**. The predominant *trans* configuration found in the Pd(HNN)MeCl complexes is probably due to steric factors, as previously reported.[8a,9b,13] In this way, the methyl ligand is kept far from the bulky hydrazonic chain. Furthermore, the *trans* configuration allows for the formation of a hydrogen bond between the chlorine atom and the hydrazonic proton, as shown by the molecular modelling study (see molecular modelling in the Crystallographic Section), and this may be considered as a further stabilising effect. This intramolecular interaction is clearly seen in the ^{1}H-NMR spectra of **2**, where the N–H signal of the *trans* isomer is more deshielded than that of the *cis* isomer (10.38 ppm for the *trans*, and 9.78 ppm for the *cis* isomer). As inferred from the molecular modelling study, the tendency to form the N–H···Cl hydrogen bond decreases with increasing bulkiness of R′′; with the aim of confirming this outcome, the reaction between **HL4** and (COD)PdMeCl in diethyl ether was carried out and, as expected, the resulting complex **4** showed a *cis*/*trans* ratio of 0.27:1, on the basis of the NMR integrals.

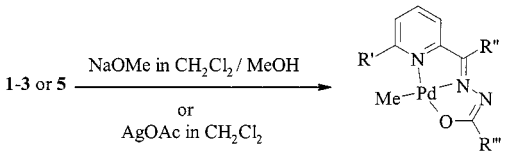
The different reactivity observed towards (COD)PdMeCl in dichloromethane for **HL2** relative to that of **HL1** and **HL3**, may be traced back to the different acidity of the hydrazonic proton, which was experimentally measured by spectrophotometric titration of the dissolved ligands with potassium hydroxide.[3b,e] These analyses established that **HL2** bears the most acidic proton and its acidity seems to be sufficient to cause the methane elimination in dichloromethane solution. On the other hand, when diethyl ether is used as solvent, complex **2** immediately precipitates, and deprotonation is prevented. On dissolution in deuteriochloroform, **2** appears to be rather unstable, and at room temperature its ^{1}H-NMR spectrum changes to that of the chloride complex **6** within a few hours. A similar behaviour was also found for complex **4**, whereas for complexes **1** and **3** only after several days was the transformation into the chloride complex complete (the full characterisation of the chloride complexes was not done, except for **6**).

One might suspect that the small amount of the *cis* isomer present in **2** and **4** could be responsible for their faster transformation into the chloride complexes, since the closeness of the methyl ligand to the hydrazonic proton should facilitate the methane formation. As this transformation happens in a quantitative way, an isomerisation around the metal centre would be required, whereby the methyl group shifts from a *trans* position to the more reactive *cis* one. In order to test this hypothesis, the reaction between the hindered ligand **HL5** and (COD)PdMeCl was carried out in diethyl ether. The presence of the methyl substituent on the aromatic ring forces the alkyl ligand to take a *cis* position,[8a,9b,14] so eventually favouring a faster methane elimination. Contrary to our expectations the stability of **5** in solution at room temperature was found to be higher than that of **2** under the same conditions; thus the acidity of the ligand must be considered decisive for the stability of complexes **1–5**. Furthermore, the ^{1}H-NMR spectra of **1–5** show very narrow resonance lines, indicating the absence of dynamic behaviour with respect to *cis*-*trans* isomerisation on the NMR time scale. Complexes **1–5** are stable in the solid state for months without releasing palladium black.

Synthesis and Characterisation of the Tridentate Methyl Complexes Pd(NNO)Me (7–10)

By adding an excess of a strong base like NaOMe to a solution of **1–3** or **5** at room temperature, or by stirring at

room temperature a dichloromethane solution of the same complexes in the dark overnight with a fivefold excess of silver acetate, the corresponding tridentate methyl complexes Pd(NNO)Me (**7–10** in Equation 1) were obtained as yellow-orange solids.

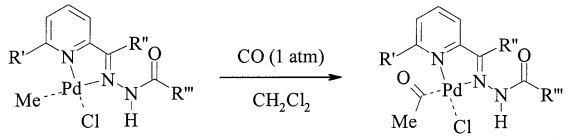


Pd(NNO)Me **7-10**

The addition of a base caused the deprotonation of the ligand and the consequent formation of a covalent Pd–O bond. Complexes **7–10** show a spectroscopic pattern similar to that of complex **6**, except for the presence of a Pd–Me resonance in the ^{1}H NMR spectra. This signal is generally more shielded than in the corresponding bidentate complexes (Table 2), owing to the increased electron density around the metal centre due to the higher chelating effect exerted by the tridentate ligands. A second significant difference with the ^{1}H-NMR spectrum of **6** is the stronger shielding of the R′ proton due to the absence of the electron-withdrawing effect of the chlorine atom; this proton, in fact, resonates at about 0.1–0.2 ppm lower (Table 2). To our knowledge these complexes represent the first example of methyl complexes where palladium is coordinated in a tridentate fashion by an anionic ligand; in fact the use of anionic chelating agents in this type of chemistry has so far been restricted to some bidentate systems.[15] Complexes **7–10** are stable for months in the solid state but only for some hours in solution, resulting in the formation of palladium black. The stability in solution of complex **10** is remarkably lower than that of complexes **7–9**, as expected from the encumbrance generated by the closeness of the alkyl ligand to the methyl substituent of the pyridine.

Carbonylation Reactions With Complexes Pd(HNN)MeCl

On bubbling CO for a few minutes through dichloromethane solutions of complexes **1** or **3–5** at room temperature, an insignificant amount of palladium black was formed. After filtration of the solution through celite and addition of an excess of *n*-hexane, the acetyl complexes Pd(HNN)[C(O)Me]Cl **11** and **13–15** were obtained in good yields (Equation 2).



1-5 Pd(HNN)(C(O)Me)Cl **11-15**

The CO insertion is clearly demonstrated in their ^{1}H-NMR spectra by the disappearance of the Pd–Me singlet in favour of a new singlet at about 3 ppm, a characteristic value for an acetyl group σ bonded to Pd.[8a,8c,9] The IR spectrum is not as helpful as usually reported in establishing the insertion as the stretching band of the carbonyl group of the ligand is partially overlapped by the same signal of the acetyl group bonded to palladium, and only a strengthening of the band at about 1700 cm^{-1} was observed. However, the persistence of the stretching band of the C=O group of the ligand, together with the IR and NMR signals of the N–H bond, indicates that the ligand behaviour in **11** and **13–15** is analogous to that in the methyl precursors. The ^{1}H NMR spectra of the four acetyl complexes show two sets of signals (Table 2), indicating the presence of the *cis* as well as the *trans* isomer.

Some difficulties have been found in the isolation of the acetyl complex of **2**. In fact by carrying out the reaction at room temperature in chloroform, dichloromethane or acetonitrile, the fast degradation of the complex to palladium black was observed. When the reaction was repeated in an NMR tube, the signals of the chloride complex **6** were found, together with other signals due to uncharacterised products. By bubbling CO into a dichloromethane solution of **2** at 0 °C, the decomposition was much slower, and two different acetyl isomers could be obtained, in good yields (**12**), where the ligand has the same chelating behaviour as observed in the other acetyl complexes. For **11–15** the separation of the two different isomers was not successful either by chromatographic techniques or by crystallisation. As already reported for the methyl complexes, no fluxional behaviour was found in their NMR spectra.

The amount of the *cis* isomer found in the acetyl complexes is much greater than that found in the methyl precursor. In fact, for complex **13** the *cis*/*trans* ratio is 0.41:1, but for **11**, **12** and **14** it becomes 1:0.57, 1:0.50, and 1:0.56, respectively. For complex **15** only the *cis* isomer was found which is in agreement with the encumbrance created in the coordination plane by a methyl R′ group. Usually an increase of the *cis*/*trans* ratio is observed from the methyl to the corresponding acetyl complexes,[8a,13] and this is generally justified by the tendency of the acetyl group to arrange itself perpendicularly to the coordination plane, thus reducing steric interactions. However the nature of the R′′ group also has a great deal of influence on the *cis*/*trans* ratio, as can be seen from the molecular modelling study (see Crystallographic Section). Thus whenever R′′ is an alkyl group (Me or Et) the *cis* isomer is the predominant one because of the formation of the N–H···O$_{acetyl}$ hydrogen bond; this intramolecular interaction is also corroborated by the deshielding of the hydrazonic proton in the ^{1}H NMR spectra (Table 2).

An X-ray diffraction analysis carried out on a crystal of **13**, showed that only the *trans* isomer is present in the crystalline state but, interestingly, in the ^{1}H-NMR spectrum of the same crystals both isomers were present in the same *cis*/*trans* ratio seen for the powdery product.

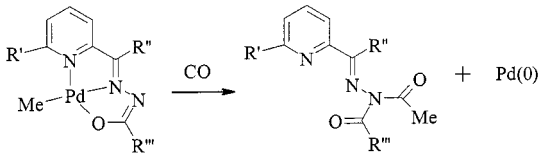
The fast formation of palladium black, observed when CO was bubbled into a solution of **2** at room temperature, can be related to the highly acidic character of the ligand, which is also responsible for the instability of **2** in solution.

The hydrazonic proton probably reacts with the acetyl ligand although, unfortunately, it was not possible to detect the presence of acetaldehyde by GC-MS or ^{1}H NMR analyses.

Owing to the high reaction rate, in no case could mechanistic information be obtained by monitoring the carbonylation reactions by ^{1}H NMR, even when conducting the reaction at –20 °C. At this temperature only the disappearance of the methyl resonance and the simultaneous appearance of the acetyl resonance was detected, without observing any signals attributable to an intermediate species. On the basis of literature data,[8a,16] we propose that the CO coordination occurs with the breaking of the Pd–py bond. The formation of both *cis* and *trans* isomers can be understood considering the possibility of rotation around the Pd–N_{iminic} bond after pyridine dissociation, a step which would involve a unidentate intermediate.

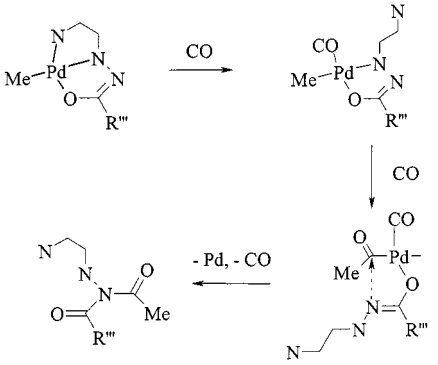
Carbonylation Reactions with Complexes Pd(NNO)Me

Contrary to what is usually reported in the literature for neutral tridentate ligands, the isolation of the tridentate acetyl palladium complexes of the type Pd(NNO)[C(O)Me] was unsuccessful owing to the fast formation of palladium black when CO was bubbled through a dichloromethane or THF solution of complexes **7–10** at 25, 0 or –40 °C. The formation of palladium black was accompanied by bleaching of the solutions. After removal of the metallic palladium, an MS analysis of the solution revealed the presence of a new organic species with a molecular weight corresponding to the acylated ligand. The spectroscopic data suggest that the acetyl group is bonded to the hydrazonic nitrogen, as depicted in Equation 3, giving rise to a bi(acyl) hydrazone derivative.



As a further confirmation, the same product i.e. 2-pyridylaldehyde *N*-acetylbenzoylhydrazone, was isolated by refluxing a mixture of **HL3** and acetylchloride in pyridine, following a known procedure.[17]

The course of the carbonylation reaction strongly resembles that of the palladium catalysed carbonylation of organic halides to form amides.[18] In this process an external nucleophile (usually a secondary amine in the presence of a base) directly attacks the acetyl group bonded to palladium or a pre-coordinated carbon monoxide molecule in a cationic intermediate.[19] Both pathways are followed by a reductive elimination step which leads to the formation of the amide and Pd^0. In our case, even if a plausible mechanism was not determined owing to the high reaction rate observed even at low temperatures, it is reasonable to suppose that the hydrazonic nitrogen acts as a nucleophile towards the acetyl group σ bonded to palladium, as depicted in Scheme 3; this attack is possible only if the formation of an oxygen-monodentate intermediate with a dangling ligand is supposed, the breaking of both Pd–N bonds being justified by the large excess of CO present in the reaction vessel.



Scheme 3. Proposed mechanism for the carbonylation with Pd(NNO)Me

In the attempt to isolate the tridentate acetyl complexes Pd(NNO)[C(O)Me] in the absence of CO, the corresponding bidentate acetyl complexes **11–15** were deprotonated by treatment with sodium methoxide in dichloromethane or THF. Rapid formation of palladium black was again observed and the ^{1}H-NMR spectra of the isolated product revealed the presence of the acylated ligand along with traces of the tridentate methyl complexes Pd(NNO)Me. This unexpected result can be rationalised by the presence of both *cis* and *trans* isomers in the solutions of **11–15**. In the case of the *cis* isomer it is plausible to suppose that, after deprotonation of the ligand, the hydrazonic nitrogen attacks the electrophilic acetyl group bonded to palladium, bringing about the formation of the acylated ligand, metallic palladium and NaCl. In the case of the *trans* isomer, the intramolecular nucleophilic attack is unlikely because of the distance of the acetyl group from the hydrazonic chain and, consequently, the deprotonation of the ligand may result only in the formation of the expected product Pd(NNO)-[C(O)Me]. This compound seems to lose CO rapidly, forming the corresponding tridentate methyl complex. A similar decarbonylation process undergone by the tridentate acetyl complexes has already been observed with tridentate ligands, both in solution and in the solid state.[9b,10,11b,11c]

Crystallographic Section

X-ray Crystal Structures of 13 and 3

In the neutral complex **13**, shown in Figure 1, the bidentate neutral ligand coordinates to the metal by the pyridinic and the iminic nitrogen atoms, while the carbonylic oxygen O1 does not participate in the chelation.

The square planar coordination around the palladium atom is completed by a chloride, *trans* to the pyridinic nitrogen, and by an acetyl group *trans* to the iminic nitrogen; the coordinated atoms are coplanar to the metal within 0.04 Å. A list of the most relevant bond lengths and angles is given in Table 3.

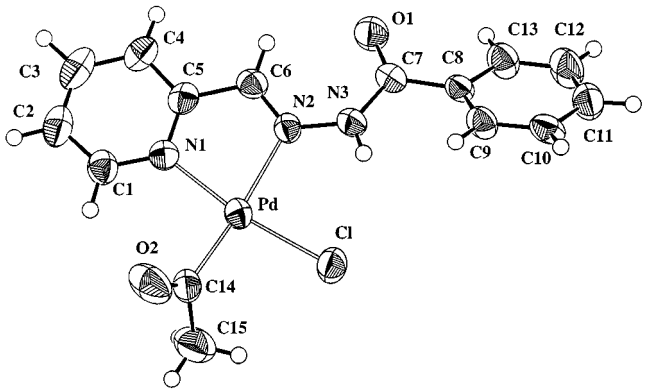


Figure 1. ORTEP view of **13**, with thermal ellipsoids at the 50% probability level

Table 3. Selected bond lengths [Å] and angles [°] with s.u.'s in parentheses for compound **13**

Bond Lengths		Bond Angles	
Pd–Cl	2.328(1)	C1–Pd–N1	1.70.52(1)
Pd–N1	2.090(3)	Cl–Pd–N2	92.8(1)
Pd–N2	2.166(3)	Cl–Pd–Cl4	92.4 (1)
Pd–C14	1.947(4)	N1–Pd–N2	77.8(1)
O1–C7	1.219(5)	N1–Pd–Cl4	97.0(2)
O2–C14	1.180(6)	N2–Pd–C14	174.8(2)
N1–C1	1.325(5)	Pd–N1–Cl	128.7(3)
N1–C5	1.357(6)	Pd–N1–C5	113.5(3)
N2–N3	1.366(4)	C1–N1–C5	117.7(4)
N2–C6	1.285(6)	Pd–N2–N3	121.7(2)
N3–C7	1.368(5)	Pd–N2–C6	115.2(3)
C1–C2	1.377(7)	N3–N2–C6	123.1(3)
C2–C3	1.373(9)	N2–N3–C7	129.1(3)
C3–C4	1.379(6)	N1–C1–C2	123.5(4)
C4–C5	1.391(7)	C1–C2–C3	118.9(5)
C5–C6	1.485(5)	C2–C3–C4	119.3(5)
C14–C15	1.492(7)	C2–C3–C4	119.3(5)
–	–	C3–C4–C5	118.6(4)
–	–	N1–C5–C4	122.1(4)
–	–	N1–C5–C6	118.0(4)
–	–	C4–C5–C6	119.9(4)
–	–	N2–C6–C5	115.4(4)
–	–	O1–C7–N3	122.2(4)
–	–	O1–C7–C8	123.3(4)
–	–	N3–C7–C8	114.4(3)
–	–	Pd–C14–O2	121.7(3)
–	–	Pd–C14–C15	117.1(3)
–	–	O2–C14–C15	121.2(4)

The entire ligand, with the exception of the terminal phenyl C8–C13, is coplanar within 0.22 Å, and the atoms which deviate most from this plane are the protonated hydrazonic N3 and the carbonyl O1, involved in the intramolecular hydrogen bonds N3–H···Cl [N3···Cl = 3.218(4) Å, H···Cl = 2.58(3)Å, N3–H···Cl = 145(3)°] and C6–H···O1 [C6···O1 = 2.806(5)Å, C6–H···O1 = 116(3)°]. The terminal phenyl C8–C13 makes a dihedral angle of 34° with the average molecular plane. The plane of the acetyl ligand is tilted by 63° with respect to the coordination plane. A search of the Cambridge Structural Database has shown that the corresponding values for acetyl groups coordinated to square-planar palladium or platinum atoms range from 68° to 90°. The bond Pd–C14 [1.947(3) Å] is the shortest ever observed among the seven palladium-acetyl complexes structurally characterised, whose bond lengths range between 1.948 and 2.001 Å. The influence of the acetyl group on the Pd–N bond lengths can be analysed by comparing **13** with acetyl(2,2′-bipyridine)chloropalladium[8a] and acetylchloro-[2-(*N*-isopropyl)carbaldiminopyridine]palladium.[8a] The coordination geometry of **13** is very close to that observed in the former (Pd–acetyl = 1.948, Pd–N1 = 2.067, Pd–N2 = 2.162 Å, with the acetyl group *trans* to N2). On the contrary, in acetylchloro[2-(*N*-isopropyl)carbaldiminopyridine]palladium the acetyl group is *trans* to the pyridine nitrogen, causing the elongation of the Pd–N1 bond (2.171 Å), while the bond length between palladium and the iminic nitrogen (2.062 Å), *trans* to a chloride, is shorter than in **13** and similar to the Pd–pyridine distances of **13** and acetyl(2,2′-bipyridine)chloropalladium.

The geometry of compound **3** (Figure 2) is identical to that of **13** (see Table 4); the coordinated atoms are coplanar with the metal within 0.06 Å. Also, the entire ligand is coplanar within 0.18 Å to the coordination plane. There are two intramolecular hydrogen bonds N3–H···Cl [N3···Cl =

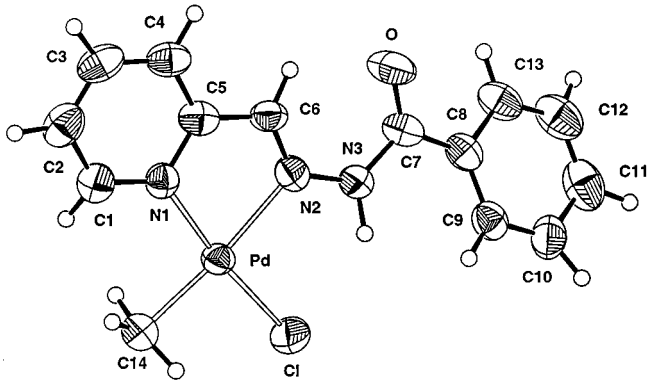
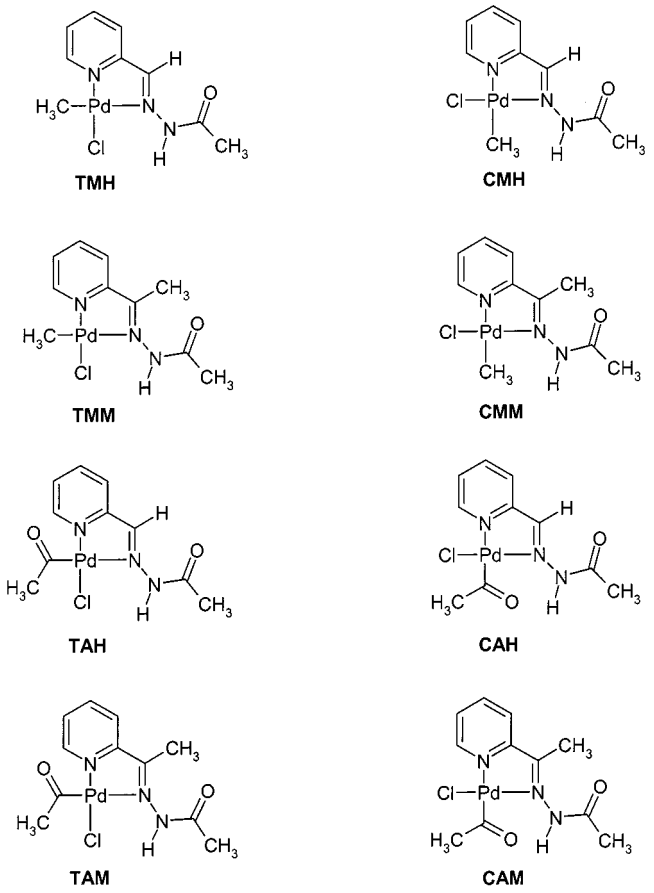


Figure 2. ORTEP view of **3**, with thermal ellipsoids at the 50% probability level

Table 4. Selected bond lengths [Å] and angles [°] with s.u.'s in parentheses for compound **3**; parameters in bold italic were not varied in the energy minimisation

Bond Lengths		Bond Angles	
Pd–Cl	***2.309(3)***	***Cl–Pd–N1***	***172.5(2)***
Pd–N1	***2.048(7)***	***Cl–Pd–N2***	***93.1(2)***
Pd–N2	***2.143(7)***	***Cl–Pd–C14***	***93.4(4)***
Pd–C14	***2.04(1)***	***N1–Pd–N2***	***79.8(3)***
O–C7	1.24(1)	***N1–Pd–C14***	***93.7(4)***
N1–C1	***1.35(1)***	***N2–Pd–C14***	***173.4(4)***
N1–C5	***1.38(1)***	***Pd–N1–C1***	***129.1(6)***
N2–N3	1.38(1)	***Pd–N1–C5***	***113.0(6)***
N2–C6	***1.31(1)***	***C1–N1***–C5	***117.8(8)***
N3–C7	1.38(1)	Pd–N2–N3	121.0(5)
C1–C2	***1.40(2)***	***Pd–N2–C6***	***112.2(6)***
C2–C3	***1.37(2)***	N3–N2–C6	126.8(7)
C3–C4	***1.40(2)***	N2–N3–C7	127.2(8)
C4–C5	***1.39(1)***	***N1–C1–C2***	***123.1(9)***
C5–C6	***1.45(1)***	***C1–C2–C3***	***119(1)***
–	–	***C2–C3–C4***	***119(1)***
–	–	***C3–C4–C5***	***120.3(9)***
–	–	***N1–C5–C4***	***120.8(8)***
–	–	***N1–C5–C6***	***117.1(8)***
–	–	***C4–C5–C6***	***122.1(8)***
–	–	***N2–C6–C5***	***117.9(7)***
–	–	O1–C7–N3	119.9(9)
–	–	O1–C7–C8	123.8(8)
–	–	N3–C7–C8	116.3(8)



Scheme 4. Molecular schemes of the compounds considered in the theoretical calculations; the numbering of the atoms follows that shown in Figure 1 and 2 for the crystal structures

3.183(8) Å, H···Cl = 2.43(12) Å, N3–H···Cl = 131(13)°] and C6–H···O [C6···O = 2.779(11) Å, C6–H···O = 118(6)°]. The terminal phenyl C8–C13 makes a dihedral angle of 27° with the average molecular plane.

Molecular Modelling

As shown by NMR spectroscopy, the proportion of *cis*/*trans* isomers in solution for compounds Pd(HL)(R)Cl (HL = **HL1–HL5**) [R = Me, C(O)Me] is related to the nature of the R group coordinated to the metal and to the steric hindrance of the substituent R′′ attached to the iminic carbon. Some factors that can affect the preference for one or the other forms involve the different *trans* influence of the pyridinic and iminic nitrogens, the steric hindrance of the ligand *cis* to the hydrazonic N–H group, and the repulsion between the carbonylic oxygen and the alkyl substituents on the iminic carbon. In order to elucidate the relative importance of these factors on the observed isomer distributions, we analysed the conformational energy of different model systems by semi-empirical calculations. The systems considered in the analysis are shown in Scheme 4: they comprise the *cis* and *trans* isomers, referring to the hydrazonic N–H, of methyl- and acetyl- derivatives of complexes containing the ligands **HL1** and **HL3′**. [**NB** The ligand HL3′ is modelled by replacing the terminal phenyl of HL3 with a methyl group (see Experimental Section)].

These differ in the presence of a hydrogen or a methyl on the iminic carbon. The simultaneous effect of the *cis* ligand and of the iminic substituent on the NH–C=O system has been studied by calculating the energetic profile for the rotation of the rigid terminal NH–C(O)Me group around the N–N single bond. The C6–N2–N3–C7 torsion angle (for labelling see Figure 1 and Figure 2) has been varied from –120° to +120°, in increments of 5°, and at each step the torsion angle has been held fixed, and the other parameters have been released to minimise the energy. Then, the most stable conformations have been found by minimising the energy of the molecular geometries close to the minima in the path.

Methyl Complexes

Figure 3 shows the energetic profile for molecules TMH, CMH, TMM, and CMM.

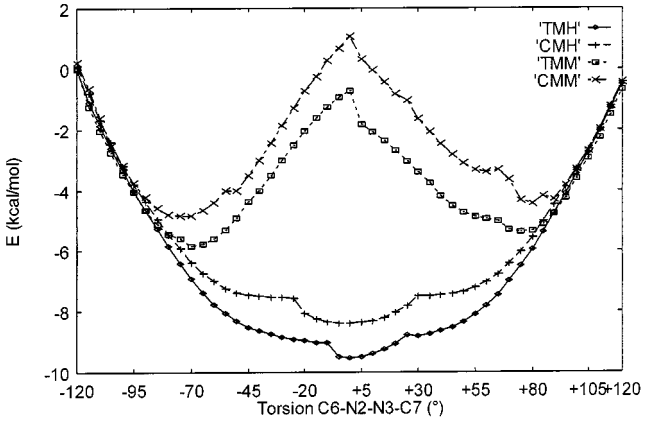


Figure 3. Energetic profiles for the rotation of the terminal NH(CO)–Me group around the N–N bond for methyl complexes TMH, CMH, TMM, and CMM; all energies have been rescaled referring to the value found for TMH at torsion = –120°

TMH and CMH do not present any steric obstacle for the carbonyl oxygen to lie in the ligand plane, and for both *cis* and *trans* isomers the conformation with minimum energy is planar, with the hydrazonic group practically coplanar to the coordination plane (C6–N2–N3–C7 = –19 and –11°, respectively), and the N–H group pointing towards the *cis* ligand. The *trans* form is about 1.2 kcal/mol more stable than the *cis* form due to the intramolecular hydrogen-bond N–H···Cl (H···Cl = 2.47 Å). This interaction is effective in the torsion angle window between –70° and +70° where the N–H dipole detects the stabilising attraction of the chloride, as shown by the fact that the curves for the two isomers coincide when the N–H group is oriented almost perpendicularly to the coordination plane (as for C6–N2–N3–C7 <–70° and >+70°). The introduction of a methyl group on the iminic carbon produces a remarkable destabilisation (about 9.3 kcal/mol) of the planar conformation, due to the repulsion between the carbonyl and the methyl (O···C = 2.76 and 3.15 Å for the most stable conformations of TMM and CMM, respectively). Two equivalent minima are found in the energy profile (Figure 3), corresponding to

torsion angles C6–N2–N3–C7 of –58° and +58° for TMM and –73° and +73° for CMM. Again, the molecule with the chloride *cis* to the N–H (TMM) is about 1 kcal/mol more stable than the molecule with the methyl close to the N–H (CMM), because of the N–H···Cl hydrogen bond (H···Cl = 2.52 Å), that can also explain the difference of about 15° between the positions of the energy minima for the two configurations. The optimisation of this interaction is favoured by a slight pyramidalisation of the bonding geometry for N3, expressed as the sum of the bond angles around it, which works out to 348.5° and 342.8° for TMM and CMM, respectively, whereas it is close to 360° for the sp^2-hybridized N3 in TMH and CMH (357.9° and 359.2°, respectively).

Acetyl Complexes

The oxygen of the acetyl group bound to the metal can compete with the chloride as a hydrogen-bond acceptor towards the N–H group. The acetyl complexes have an additional degree of freedom, represented by the orientation of the acetyl group around the Pd–C bond. The analysis of the energetic profile for the rotation shows that for the *trans* complex TAH there is a broad range of favoured orientations lying in a shallow minimum, with values of N1–Pd–C14–O2 ranging between –90° and +90°. For these conformations the acetyl oxygen is oriented towards the pyridine, and does not feel the repulsion of the negative charge localised on the chloride. Within this range two local minima are found, corresponding to –60° and +60°, as observed in the crystal structure of **13**, separated by a rotational barrier of about 5 kcal/mol, at N1–Pd–C14–O2 = 0° (with the acetyl in the square coordination plane). When the acetyl is bonded *cis* to the N–H group (CAH), the preferred orientations are situated in a shallow minimum with the torsion angle N2–Pd–C14–O2 ranging between –30° and +30° (Figure 4), which brings the acetyl oxygen close to the coordination plane and in proximity to the N3–H dipole.

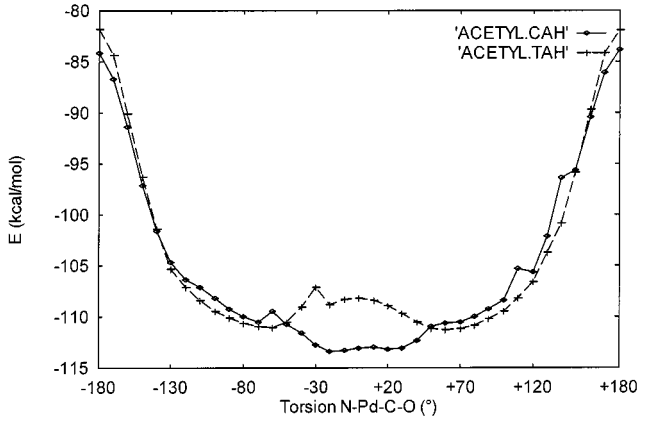


Figure 4. Energetic profiles for the rotation of the acetyl ligand around the Pd–C bond for TAH and CAH; torsion N–Pd–C–O refers to N2 for CAH and to N1 for TAH

These data suggest that the interaction between the acetyl and the N–H can stabilise the *cis* isomer. The relative stability of the *cis* and *trans* isomers when the steric hindrance on the iminic carbon is varied have been studied for compounds TAH, CAH, TAM, and CAM (Scheme 4), with the same procedure as in the case of the methyl complexes. The results are shown in Figure 5.

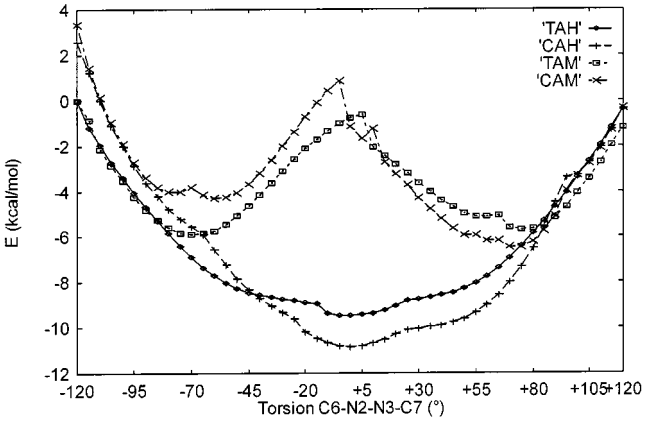


Figure 5. Energetic profiles for the rotation of the terminal NH(CO)–Me group around the N–N bond for acetyl complexes TAH, CAH, TAM, and CAM; all energies have been rescaled referring to the value found for TAH at torsion = –120°

As already observed for the methyl complexes, in the absence of steric hindrance for O1, for the most stable conformations the plane containing the NH–C(O)Me terminal group is coplanar with the metal coordination plane, and the N–H points towards the *cis* ligand (C6–N2–N3–C7 = –15° and –9° for TAH and CAH, respectively). However, the hydrogen-bond acceptor capabilities of the acetyl ligand produce a relevant inversion in the stability of the *cis* and *trans* isomers: when the terminal group is almost perpendicular to the coordination plane (C6–N2–N3–C7 < –50°) the *trans* isomer TAH is slightly more stable than the *cis* isomer CAH, but, as the N–H dipole enters in the range of interaction of the *cis* acetyl, at C6–N2–N3–C7 = –45°, the *cis* isomer CAH gains stability by the incipient formation of the N–H···O hydrogen bond (H···O = 1.80 Å at the minimum), which is much stronger than the N–H···Cl hydrogen bond present in the *trans* isomer TAH (H···Cl = 2.48 Å). The asymmetry of the profile relative to the *cis* isomer is due to the fact that the acetyl orientation is held fixed at N2–Pd–C14–O2 = –30°, meaning that at C6–N2–N3–C7 = –45° the N–H is on the opposite side of the acetyl oxygen with respect to the coordination plane, while at C6–N2–N3–C7 = +45° it is on the same side. The asymmetry of the energetic profile for the rotation of the torsion angle C6–N2–N3–C7 is even more significant for CAM and TAM, where the orientations with the hydrazonic group coplanar with the coordination plane are destabilised by the repulsion between O1 and C16 (Figure 5). Both molecules have two preferred conformations, as seen for CMM and TMM, but in the case of the acetyl complexes the *cis* complex CAM (with N2–Pd–C14–O2 = –30°) is about 1.9 kcal/mol less stable than the *trans* complex when the NH is oriented on the opposite side of the acetyl oxygen with respect to the coordination plane (C6–N2–N3–C7 = –56°). The stabilisation of TAM is due to the interaction N–H···Cl (H···Cl = 2.50Å), as found for TMM. The relative stability

of TAM and CAM is inverted when the torsion angle C6–N2–N3–C7 has positive values: in CAM the optimisation of the hydrogen bond to the *cis* group involves a gain of about 0.9 kcal/mol, relative to TAM, for the most stable conformation (C6–N2–N3–C7 = 66°, N2–Pd–C14–O2 = –31°, H···O = 1.79Å). This conformation is also the global minimum for CAM, and is about 2.0 kcal/mol more stable than the one with C6–N2–N3–C7 = –56°. For TAM the two minima are energetically equivalent, due to the local symmetry of the NH···Cl system with respect to the coordination plane.

These results show that the conformational preferences for compounds in Scheme 4 are mainly influenced by the hydrogen bond between the NH group and the *cis* ligand. When the choice is between Cl and Me, the hydrogen bond with the former is favoured in all cases (CMH, TMH, CMM, TMM). In TAH, CAH, CAM, TAM, the chloride must compete with the acetyl, and it has been seen that the latter is generally more suited to optimise the hydrogen bond, provided that it is correctly oriented.

Conclusions

We have shown that HNNO tridentate hydrazonic ligands can form two different kinds of methyl palladium(II) complexes, depending on the experimental conditions. Thus, in the absence of a basic medium, the ligands adopt a neutral bidentate HNN coordination, whereas in the presence of a base a tridentate NNO behaviour is preferred. In solution the bidentate complexes tend to eliminate methane in relation to the acidic character of the ligand. The reactivity towards CO of the bidentate and tridentate complexes is drastically different. The bidentate complexes form the corresponding acetyl complexes, where the ligand maintains a neutral bidentate HNN behaviour. On the contrary, the carbonylation of the tridentate complexes results in their fast and complete decomposition to palladium black together with the formation of the acylated ligand, the acetyl group being bonded to the hydrazonic nitrogen.

A molecular modelling study indicates that not only steric effects determine the isomeric *cis*/*trans* distribution observed in both bidentate methyl and acetyl complexes, but also that electronic considerations must be taken into account. Thus, for the methyl complexes the possibility of formation of a N–H···Cl hydrogen bond favours the *trans* isomer, whereas in the acetyl complexes the formation of a N–H···O_{acyl} hydrogen bond favours the *cis* isomer.

Experimental Section

General: All the manipulations were carried out under a purified dry nitrogen atmosphere, using standard Schlenk techniques. Solvents were dried prior to use and stored under nitrogen. 2-Acetylpyridine and 2-pyridinecarboxaldehyde were purchased (Aldrich), whereas 6-methyl-2-pyrdinecarboxaldehyde was synthesised by the oxidation of 6-methyl-2-pyridinemethanol with SeO_2 in dioxane.[20] The hydrazides were synthesised by reaction between the corresponding methyl or ethyl esters and hydrazine monohydrate (Fluka). (COD)PdMeCl was synthesised following literature methods.[11a] Silver acetate was purchased (Aldrich).

Proton NMR spectra were recorded on a Bruker 300 FT spectrometer, with $SiMe_4$ as internal standard, at 25 °C. IR spectra were obtained by a Nicolet 5PCFT-IR spectrophotometer in the 4000–400 cm^{-1} range with KBr disks. Mass spectra were recorded on a FINNIGAN SSQ 710 spectrometer. Elemental analysis (C,H,N) were performed by using a Carlo Erba Model EA 1108 apparatus. GC-MS spectra were obtained with a Hewlett–Packard 5890 series II gas chromatograph with a Gerstel CIS III temperature-controllable injector, an HP 5971A mass-selective detector with electron-impact ionisation at 70 eV, and an HP Ultra-2 column (25 m, 0.20 mm inner diameter, 0.33 μm film thickness).

Synthesis of Ligands HL1–HL4. – General Procedure: Ligands **HL1**–**HL4** were synthesised by refluxing a solution containing the ketone or the aldehyde (0.5 g) with a stoichiometric amount of the corresponding hydrazide, in the presence of a few drops of glacial acetic acid. The end of the reaction was determined by TLC, monitoring the disappearance of the stain corresponding to the pyridinic system. After concentration and cooling of the solution, the pure ligands crystallised as colourless needles which were washed with a few millilitres of diethyl ether and dried in vacuum.

Methyl 2-Pyridyl Ketone Acetylhydrazone (HL1): Yield: 0.571 g (78%). – M.p. 153 °C. – IR (cm^{-1}): ν(N–H) = 3198 m, ν(C=O) = 1678 vs, AMIDE II $\tilde{\nu}$ = 1580 s, AMIDE III = 1371 s. – ^{1}H NMR ($CDCl_3$): (*E*) isomer δ = 2.40 [s, 3 H, MeC(O)], 2.36 [s, 3 H, C(Me)=N]; (*Z*) isomer δ = 2.37 [s, 3 H, MeC(O)], 2.33 [s, 3 H, C(Me)=N]. – MS (C.I.): 178 [M^+ + 1]. – $C_9H_{11}N_3O$ (177.21): calcd. C 61.00, H 6.26, N 23.71; found C 60.88, H 6.23, N 23.81. – log β_1^H = 12.51(1).

Methyl 2-Pyridyl Ketone Benzoylhydrazone (HL2): Yield: 0.741 g (75%). – m.p.: 150–152 °C. – IR (cm^{-1}): ν(N–H) = 3180 br, ν(C=O) = 1654 vs, AMIDE II $\tilde{\nu}$ = 1544 s, AMIDE III = 1282 s. – ^{1}H NMR ($CDCl_3$): (*E*) isomer δ = 7.90 [d, 2 H, Ph *o*–C(O)], 7.51–7.46 [m, 4 H, H^3 + Ph *m* and *p*-C(O)], 2.49 [s, 3 H, C(Me)=N]; (*Z*) isomer δ = 7.95 [dd, 2 H, Ph *o*-C(O)], 7.52–7.43 [m, 3 H, Ph *m* and *p*-C(O)], 2.50 [s, 3 H, C(Me)=N]. – MS (C.I.): 240 [M^+ + 1]. – $C_{14}H_{13}N_3O$ (239.28): calcd. C 70.35, H 5.47, N 17.56; found C 70.36, H 5.67, N 17.86. – log β_1^H = 11.35(1).

2-Pyridyl Carboxaldehyde Benzoylhydrazone (HL3): Yield: 0.864 g (78%). – m.p.: 107–109 °C. – IR (cm^{-1}): ν(N–H) = 3193 w, ν(C=O) = 1662 vs, AMIDE II $\tilde{\nu}$ = 1553 vs, AMIDE III = 1286 vs. – ^{1}H NMR ($CDCl_3$): (*E*) isomer δ = 7.97 [d, 3 H, H^3 + Ph *o*-C(O)], 7.27 [s, 1 H, C(H)=N]; (*Z*) isomer δ = 8.02 [d, 3 H, H^3 + Ph *o*-C(O)], 7.61–7.50 [m, 5 H, Ph *m* and *p*-C(O)], 7.27 [s, 1 H, C(H)=N]. – MS (C.I.): 226 [M^+ + 1]. – $C_{13}H_{11}N_3O$ (225.25): calcd. C 69.32, H 4.92, N 18.66; found C 69.35, H 4.97, N 18.64. – log β_1^H = 11.48(1).

Ethyl 2-Pyridyl Ketone Benzoylhydrazone (HL4): Yield: 0.500 g (53%). – m.p.: 146 °C. – IR (cm^{-1}): ν(N–H) = 3174 m, ν(C=O) = 1653 vs, AMIDE II $\tilde{\nu}$ = 1548 s, AMIDE III = 1300 s. – ^{1}H NMR ($CDCl_3$): (*E*) isomer δ = 7.90 [d, 2 H, Ph *o*-C(O)], 7.53–7.48 [m, 3 H, Ph *m*- and *p*-C(O)], 3.04 (q, 2 H, Et), 1.25 (t, 3 H, Et). – (*Z*) isomer δ = 7.97 [d, 2 H, Ph *o*-C(O)], 7.49–7.45 [m, 3 H, Ph *m*- and *p*-C(O)], 2.94 (q, 2 H, Et), 1.31 (t, 3 H, Et). – MS (C.I.): 254 [M^+ + 1]. – $C_{13}H_{15}N_3O$ (229.28): calcd. C 71.13, H 5.97, N 16.59; found C 71.16, H 6.03, N 16.52.

Synthesis of Ligand HL5: The synthesis was carried out in situ introducing the correct amount of benzoylhydrazide into the solu-

tion coming from the synthesis of 6-methyl-2-pyridylcarboxyaldehyde. The solution was then refluxed for 30 minutes. After cooling a pale pink solid was filtered and washed with diethyl ether.

6-Methyl-2-pyridyl Aldehyde Benzoylhydrazone (HL5): Yield: 0.593 g (60%). – m.p.: 108 °C. – IR (cm^{-1}): ν(N–H) = 3187 m, ν(C=O) = 1653 vs, AMIDE II $\tilde{\nu}$ = 1560 s, AMIDE III = 1296 s. – ^1H NMR ($CDCl_3$): (*E*) isomer δ = 8.30 [s, 1 H, C(H)=N], 7.88 [d, 2 H, Ph *o*-C(O)], 7.45 [t, 2 H, Ph *m*-C(O)], 7.54 [t, 1 H, Ph *p*-C(O)]. – MS (C.I.): 240 [M^+ + 1]. – $C_{14}H_{13}N_3O$ (239.28): calcd. C 70.28, H 5.48, N 17.56; found C 70.31, H 5.53, N 17.60. – log β_1^H = 11.61(1).

Synthesis of the Bidentate Methyl Complexes Pd(HNN)MeCl 1–5. – General Procedure: To a vigorously stirred ethereal ligand suspension (0.100 g) was added a stoichiometric amount of (COD)PdMeCl. Instantaneously a pale yellow solid precipitated and the resulting mixture was stirred for two hours at room temperature. After filtration the isolated solid was repeatedly washed with diethyl ether and then dried in vacuum.

Complexes **1** and **3** can also be prepared with CH_2Cl_2 as solvent by the following procedure: 0.100 g of ligand are dissolved in 20 mL of CH_2Cl_2 and a stoichiometric amount of (COD)PdMeCl is added. The yellow solution is stirred at room temperature for two hours. Concentration of the solution and precipitation with *n*-hexane gives the desired products as a yellow powder, which is filtered off, washed with *n*-hexane and then dried under vacuum for several hours. The yields are lower then those obtained using diethyl ether (65%).

The yields reported below are those from the synthesis carried out in diethyl ether.

[PdMeCl(HL1)] (1): Yield: 0.106 g (92%). – IR (cm^{-1}): ν(N–H) = 3291 s, ν(C=O) = 1699 vs, AMIDE II $\tilde{\nu}$ = 1478 m, AMIDE III = 1374 m. – ^1H NMR ($CDCl_3$): δ = 2.26 [s, 3 H, MeC(O)], 2.20 [s, 3 H, C(Me)=N]. – $C_{10}H_{14}ClN_3OPd$ (334.09): calcd. C 35.95, H 4.22, N 12.58; found C 35.86, H 4.08, N 12.68.

[PdMeCl(HL2)] (2): Yield: 0.155 g (93%). – IR (cm^{-1}): ν(N–H) = 3195 w, ν(C=O) = 1673 vs, AMIDE II $\tilde{\nu}$ = 1499m–1460 s, AMIDE III = 1271 m. – ^1H NMR ($CDCl_3$): *trans* isomer δ = 7.99 [d, 2 H, Ph *o*-C(O)], 7.60–7.50 [m, 4 H, H^1 + Ph *m* and *p*-C(O)], 2.37 [s, 3 H, C(Me)=N]; *cis* isomer δ = 2.42 [s, 3 H, C(Me)=N]. – $C_{15}H_{16}ClN_3OPd$ (396.17): calcd. C 45.48, H 4.07, N 10.61; found C 45.51, H 4.01, N 10.60.

[PdMeCl(HL3)] (3): Yield: 0.153 g (91%). – IR (cm^{-1}): ν(N–H) = 3247 w, ν(C=O) = 1669 vs, AMIDE II $\tilde{\nu}$ = 1506vs–1485 s, AMIDE III = 1266 vs. – ^1H NMR (CD_2Cl_2): δ = 9.96 [s, 1 H, C(H)=N], 7.96 [d, 2 H, Ph *o*-C(O)], 7.52 [t, 3 H, Ph *m*- and *p*-C(O)]. – $C_{14}H_{14}ClN_3OPd$ (382.14): calcd. C 44.00, H 3.69, N 11.00; found C 43.99, H 3.53, N 10.85.

[PdMeCl(HL4)] (4): Yield: 0.115 g (91%). – IR (cm^{-1}): ν(N–H) = 3206 w, ν(C=O) = 1668 vs, AMIDE II $\tilde{\nu}$ = 1466 m, AMIDE III = 1268 m. – ^1H NMR ($CDCl_3$): *trans* isomer δ = 8.02 [d, 2 H, Ph *o*-C(O)], 7.50 [m, 3 H, Ph *m* and *p*-C(O)], 2.84 (q, 2 H, Et); *cis* isomer δ = 7.99 [d, 2 H, Ph *o*-C(O)], 2.89 (s, 2 H, Et). The triplets of the Et groups are fused in a multiplet centred at δ = 1.25 – $C_{16}H_{18}ClN_3OPd$ (410.19): calcd. C 46.85, H 4.42, N 10.24; found C 46.800, H 4.29, N 10.46.

[PdMeCl(HL5)] (5): Yield: 0.141 g (85%). – IR (cm^{-1}): ν(N–H) = 3234 w, ν(C=O) = 1674 vs, AMIDE II $\tilde{\nu}$ = 1483 m, AMIDE III = 1263 m. – ^1H NMR ($CDCl_3$): δ = 7.96 [d, 2 H, Ph *o*-C(O)], 7.60 [t, 1 H, Ph *p*-C(O)], 7.47 [t, 2 H, Ph *m*-C(O)], 9.96 [s, 1 H, C(H)=N]. – $C_{15}H_{16}ClN_3OPd$ (396.17): calcd. C 45.48, H 4.10, N 10.61; found C 45.45, H 4.08, N 10.46.

Synthesis of the Chloride Complex Pd(NNO)Cl 6: HL2 (0.020 g, 0.084 mmol) was dissolved in 30 mL of CH_2Cl_2 and (COD)PdMeCl (0.022 g, 0.084 mmol) was added. Immediately a yellow solution was formed from which a yellow solid precipitated within 20 minutes of stirring at room temperature. After two hours of reaction the solid was filtered, repeatedly washed with diethyl ether and then dried in vacuum.

[PdCl(L2)] (6): Yield: 0.260 g (82%). – IR (cm^{-1}) $\tilde{\nu}$: AMIDE II = 1498 s, AMIDE III = 1364 s. – ^1H NMR ($CDCl_3$): δ = 8.11 [d, 2 H, Ph *o*-C(O)], 7.38–7.30 [m, 4 H, H^3 + Ph *m*- and *p*-C(O)], 2.46 [s, 3 H, C(Me)=N]. $C_{14}H_{12}ClN_3OPd$ (380.12): calcd. C, 44.24, H 3.18, N 11.05; found C 44.43, H 2.99, N 11.12.

Synthesis of the Tridentate Methyl Complexes Pd(NNO)Me 7–10: i): Compound **1**, **2**, **3**, or **5** (0.050 g) was dissolved in 20 mL of THF together with a threefold excess of NaOMe. Soon after the base had been added, a colour change of the solution from yellow to orange was observed. The solution was then stirred at room temperature for two hours. The unchanged NaOMe and the formed NaCl were removed by filtration and the resulting solution was concentrated in vacuum. By adding *n*-hexane an orange powder precipitated which was filtered off and dried in vacuum for several hours. ii): Compound **1**, **2**, **3**, or **5** (0.050 g) was dissolved in 20 mL of CH_2Cl_2 and a fivefold excess of silver acetate was added. The resulting mixture was stirred in the dark overnight. After removal of the silver salts the solution was concentrated in vacuum and the product precipitated by adding diethyl ether. For both methods the yields vary from 55% to 75%.

[PdMe(L1)] (7): IR (cm^{-1}) $\tilde{\nu}$: AMIDE II = 1582 vs, AMIDE III = 1370 m. – ^1H NMR ($CDCl_3$): δ = 2.31 [s, 3 H, MeC(O)], 2.28 [s, 3 H, C(Me)=N]. $C_{10}H_{13}N_3OPd$ (297.63): calcd. C 40.35, H 4.40, N 14.12; found C 40.30, H 4.46, N 14.10.

[PdMe(L2)] (8): IR (cm^{-1}) $\tilde{\nu}$: AMIDE II = 1499 s, AMIDE III = 1365 s. – ^1H NMR (CD_2Cl_2): δ = 8.06 [d, 2 H, Ph *o*-C(O)], 7.30–7.26 [m, 3 H, Ph *m* and *p*-C(O)], 2.41 [s, 3 H, C(Me)=N]. $C_{15}H_{15}N_3OPd$ (359.70): calcd. C 50.09, H 4.20, N 11.68; found C 49.99, H 4.15, N 11.50.

[PdMe(L3)] (9): IR (cm^{-1}) $\tilde{\nu}$: AMIDE II = 1501 s, AMIDE III = 1380 s. – ^1H NMR ($CDCl_3$): δ = 9.21 [s, 1 H, C(H)=N], 8.19 [d, 2 H, Ph *o*-C(O)], 7.33–7.30 [m, 3 H, Ph *m* and *p*-C(O)]. $C_{14}H_{13}N_3OPd$ (345.68): calcd. C 48.64, H 3.79, N 12.16; found C 48.61, H 3.82, N 12.10.

[PdMe(L5)] (10): IR (cm^{-1}) $\tilde{\nu}$: AMIDE II = 1462 m, AMIDE III = 1366 vs. – ^1H NMR ($CDCl_3$): δ = 9.06 [s, 1 H, C(H)=N], 8.13 [d, 2 H, Ph *o*-C(O)], 7.41–7.33 [m, 3 H, H^2 + Ph *m* and *p*-C(O)].

Carbonylation Reactions of the Bidentate Methyl Palladium Complexes Pd(HNN)MeCl. General Procedure for the Preparation of Complexes 11, 13, 14, and 15: Compound **1**, **3**, **4**, or **5** (0.050 g) was placed in a 50 mL Schlenk tube and dissolved in about 10 mL of CH_2Cl_2; CO was then bubbled through this solution for about 5–10 minutes through a glass capillary. After filtration of the solution through celite the acetyl complexes were precipitated by addition of *n*-hexane.

{Pd[C(O)Me]Cl(HL1)} (11): Yield: 0.024 g (45%). – IR (cm^{-1}): ν(N–H) = 3174 s, ν(C=O) = 1692br, ν{Pd[C(O)Me]} = 1670 sh–1646 s, AMIDE II $\tilde{\nu}$ = 1501 s, AMIDE III = 1371 m. – ^1H NMR

($CDCl_3$): *trans* isomer δ = 2.28 [s, 3 H, MeC(O)], 2.20 [s, 3 H, C(Me)=N]; *cis* isomer δ = 2.48 [s, 3 H, MeC(O)], 2.19 [s, 3 H, C(Me)=N]. – $C_{11}H_{13}ClN_3O_2Pd$ (361.10): calcd. C 36.49, H 3.90, N 11.60; found C 36.43, H 3.54, N 11.43.

{Pd[C(O)Me]Cl(HL3)} (13): Yield: 0.043 g (80%). – IR (cm^{-1}): ν(N–H) = 3266 w, ν(C=O) + ν{Pd[C(O)Me]} = 1692 vs, AMIDE II $\tilde{\nu}$ = 1503 vs–1486 s, AMIDE III = 1250 s. – ^{1}H NMR ($CDCl_3$): *trans* isomer δ = 9.90 [s, 1 H, C(H)=N], 7.96 [d, 2 H, Ph *o*-C(O)], 7.67–7.51 [m, 5 H, H^1+H^3 + Ph *m* and *p*-C(O)]; *cis* isomer δ = 10.24 [s, 1 H, C(H)=N], 8.11 [d, 2 H, Ph *o*-C(O)]. – $C_{15}H_{14}ClN_3O_2Pd$ (410.15): calcd. C 43.93, H 3.44, N 10.24; found C 44.00, H 3.52, N 10.26.

{Pd[C(O)Me]Cl(HL4)} (14): Yield: 0.033 g (62%). – IR (cm^{-1}): ν(N–H) = 3206 m, ν(C=O) = 1692 vs, ν[Pd(C(O)Me)] = 1668 sh–1645 s, AMIDE II $\tilde{\nu}$ = 1462 s, AMIDE III = 1368 m. – ^{1}H NMR ($CDCl_3$): *trans* isomer δ = 2.92 (q, 2 H, Et); *cis* isomer δ = 2.98 (q, 2 H, Et). The low resolution of the spectrum does not allow a correct attribution of the signals of the pyridine and phenyl rings. For both isomers the Pd–Me signals are overlapped with the triplets generated by the methyl group of the R substituent in a multiplet centred at 1.27 ppm. – $C_{17}H_{18}ClN_3O_2Pd$ (438.20): calcd. C 47.14, H 3.03, N 9.70; found C 47.10, H 3.00, N 9.75.

{Pd[C(O)Me]Cl(HL5)} (15): Yield: 0.016 g (45%). – IR (cm^{-1}): ν(N–H) = 3234 m, ν(C=O) + ν(Pd(C(O)Me)] = 1700 vs, AMIDE II $\tilde{\nu}$ = 1509 s, AMIDE III = 1262 s. – ^{1}H NMR ($CDCl_3$): δ = 7.96 [d, 2 H, Ph *o*-C(O)], 7.61 [t, 1 H, Ph *p*-C(O)], 7.52 [t, 2 H, Ph *m*-C(O)], 6.94 [s, 1 H, C(H)=N]. – $C_{15}H_{16}ClN_3O_2Pd$ (412.16): calcd. C 45.31, H 3.80, N 9.91; found C 45.25, H 3.71, N 9.89.

Procedure for the Preparation of 12: Compound **2** (0.060 g, 0.150 mmol) was placed in a 50 mL schlenk tube and dissolved in 20 mL of cold CH_2Cl_2 (0 °C). The reactor was evacuated and filled with CO for three consecutive times. The solution was stirred for 15 minutes maintaining the temperature at 0 °C and then the solvent was removed in vacuum without varying the temperature. The solid residue was re-dissolved in CH_2Cl_2, filtered through celite and dried again in vacuum.

{Pd[C(O)Me]Cl(HL2)} (12): Yield: 0.042 g (78%). – IR (cm^{-1}): ν(N–H) = 3200 w, ν(C=O)+ν[Pd(C(O)Me)] = 1689 vs, AMIDE II $\tilde{\nu}$ = 1474 s, AMIDE III = 1261 s. – ^{1}H NMR ($CDCl_3$): *trans* isomer δ = 2.38 [s, 3 H, C(Me)=N]; *cis* isomer δ = 2.52 [s, 3 H, C(Me)=N]. In both isomers the residual protons are overlapped with other signals.

Carbonylation Reactions of the Tridentate Methyl Palladium Complexes Pd(NNO)Me. – General Procedure: Complexes **7–10** (0.020 g) were dissolved in 20 mL of CH_2Cl_2 in a 50 mL schlenk tube. CO was bubbled through the solution at room temperature for 5 minutes through a glass capillary. Immediately palladium black was formed. The solution was stirred under CO atmosphere until it was completely colourless and then filtered through celite. After evaporation of the solution a pale yellow solid was filtered off.

The characterisation of the formyl 2-pyridyl aldehyde *N*-acetyl benzoylhydrazone is reported: Yield: 0.015 g (complete conversion). – m.p: 116 °C. – IR (cm^{-1}) $\tilde{\nu}$: AMIDE II = 1459s–1421 m, AMIDE III = 1262 m. – ^{1}H NMR (CD_2Cl_2): δ = 8.63 (d, 1 H, R′), 7.78 (td, 1 H, H^2), 7.34 (td, 1 H, H^1), 7.88 [dd, 2 H, Ph *o*-C(O)], 7.55–7.43 [m, 4 H, H^3 + Ph *m* and *p*-C(O)], 7.02 [s, 1 H, C(H)=N], 2.33 [s, 3 H, C(O)Me]. – MS (CI): 268 (M^+ + 1). – $C_{15}H_{13}N_3O_2$ (267.29): calcd. C 67.41, H 4.90, N 15.72; found C 67.45, H 5.01, N 15.77.

Synthesis of Formyl 2-Pyridyl Aldehyde *N*-acetyl Benzoylhydrazone: Compound **HL3** (0.500 g, 2.220 mmol) was dissolved in 20 mL of pyridine under a nitrogen atmosphere. The obtained solution was stirred in an ice bath and acetyl chloride (0.871 g, 11.100 mmol) was added dropwise to the solution. Immediately pyridinium hydrochloride precipitated. The mixture was refluxed for 24 hours after which 30 mL of water was slowly added. From the solution a brown solid precipitated which was filtered off and dried in vacuum. Recrystallisation from ethanol gave 0.400 g (67%) of microcrystalline product.

X-ray Structure Determination of 13 and 3:[21] A single crystal of **13** suitable for X-ray analysis was glued to a glass fibre and mounted on a Philips PW100 diffractometer employing Mo-K_α radiation. The instrument was equipped with a graphite monochromator. Intensities were collected at room temperature, and corrected for absorption using the ψ-scan method. During data collection, no intensity decay was observed. Corrections for Lorenz and polarisation effects were applied. Relevant data collection and structure refinement parameters are summarised in Table 5.

Table 5. Crystal data and structure refinement for compounds **3** and **13**

Compound	**3**	**13**
Empirical formula	$C_{14}H_{14}ClN_3OPd$	$C_{15}H_{14}ClN_3O_2Pd$
Formula weight	382.1	410.15
Radiation, λ [Å]	Cu-K_α, 1.5418	Mo-K_α, 0.71069
Crystal system	monoclinic	monoclinic
Space Group	$P2_1/n$	$P2_1/c$
Unit cell dimensions [Å, °]	a = 5.9876(7)	a = 10.372(4)
	b = 12.776(2)	b = 7.146(3)
	c = 19.396(3)	c = 21.985(7)
	β = 96.20(1)	β = 102.83(2)
Volume [Å^3]	1475.1(4)	1589(1)
Z	4	4
Density (calculated) [g/cm^3]	1.72	1.71
F(000)	760	816
Crystal size [mm]	0.03 × 0.05 × 0.40	0.13 × 0.14 × 0.38
θ range [°]	4–75	3–30
Index ranges	$0 \le h \le 7$	$-14 \le h \le 14$
	$-15 \le k \le 0$	$-10 \le k \le 10$
	$-24 \le l \le 24$	$0 \le l \le 30$
Independent reflections	3277	4626
		R(int) = 0.0538
Observed reflections	2366 [$F_o > 2.5\sigma(F_o)$]	2308 [$F_o > 4\sigma(F_o)$]
Data/restraints/parameters	2366/14/238	2308/0/244
Goodness of fit	0.80	0.80
Final R indices [$I > 2\sigma(I)$]		
R_1[a]	0.052	0.038
R_w[b]	0.057	0.0906

[a] $R = \Sigma\| F_o | - | F_c \| / \Sigma | F_o |$. – [b] $R_w = \{\Sigma[w(F_o^2 - F_c^2)^2]/\Sigma [w(F_o^2)^2]\}^{1/2}$.

The phase problem was solved by direct methods employing SIR97.[22] Atom coordinates and anisotropic thermal parameters were refined for all non-hydrogen atoms by full-matrix least-squares on F^2 with the SHELXL97 program.[23] All hydrogen atoms were located in the difference Fourier maps and refined isotropically. The final geometry was analysed with the program PARST97.[24] The calculations were performed on a DIGITAL Alpha255 workstation at the "Centro di Studio per la Strutturistica Diffrattometrica del C.N.R." in Parma.

A wedge-shaped crystal of compound **3** was used for data collection on an Enraf–Nonius CAD-4 diffractometer with graphite-monochromated Cu-Kα radiation. Corrections for Lorentz and polarisation effects were applied. During data collection, no intensity decay was observed. The structure was solved by the PATTY op-

tion of the DIRDIF96 program system.[25] The hydrogen atoms were calculated and restrained so that the distance to their carrier remained constant at approximately 1.0 Å. Structure was refined by full-matrix least-squares on *F*, using anisotropic thermal parameters for non-hydrogen atoms and isotropic thermal parameters for hydrogen atoms. The DIFABS empirical absorption correction[26] was applied with coefficients in the range of 0.64–2.02. The secondary isotropic extinction coefficient[27] refined to $R = 70.(2)$. A final difference Fourier map revealed a residual electron density between –1.8 and 1.2 eÅ^{-3}, in the vicinity of the heavy atoms. Scattering factors were taken from Cromer and Mann,[28a] International Tables for X-ray Crystallography (1974).[28b] The anomalous scattering of Cl and Pd was taken into account.[29] The calculations were performed with XTAL.[30] All drawings were made with ZORTEP[31] an extensive use was made of the Cambridge Structural Database software.[32]

Molecular Energy Calculations: All the calculations were performed with the program MOPAC 6.00[33] running on a Pentium 200 MHz personal computer. The model compounds (Scheme 4) were built based on the geometry of the crystal structure of **3** (Figure 2, Table 4), which presented a *trans* configuration. In all cases the terminal phenyl has been replaced by an idealised methyl group. The atomic labelling refers to Figure 2. The acetyl derivatives were built by inserting the acetyl group on the metal, with geometry taken from the X-ray structure of **13**. The atomic labelling refers to Figure 1. The *cis* derivatives were built by exchanging the –R and –Cl ligands, preserving the original bond lengths. The iminomethyl molecules (TMM, CMM, TAM, CAM) have been built by substituting the H atom with an idealised methyl group. All hydrogen atoms were introduced in idealised geometry with the exception of the iminic and hydrazonic ones, which were taken from the crystal structure. The geometries of all models have been optimised by minimising the molecular energy using the PM3 Hamiltonian.[34] The metal was treated as a dummy bivalent cation, and the geometry of the molecular core around the metal was held fixed, as observed in the crystal (Table 4 indicates all the parameters which were not modified in the minimisation). The geometric parameters which were optimised are all the bond lengths, angles and torsions starting from the N2–N3 bond and proceeding towards the terminal methyl. The geometries of the iminic hydrogen and methyl, the NH group, and the rotation of the coordinated methyl and acetyl groups around the Pd–C bonds were also optimised.

The energetic profiles for the rotation of the terminal NH–C(O)–Me group around the N–N bond, and for the rotation of the acetyl around the Pd–C bond have been calculated by varying the torsion considered (C6–N2–N3–C7 for the former and N1–Pd–C14–O3 and N2–Pd–C14–O3 for the latter, *trans* and *cis*, respectively) in steps of 5° and 10°, respectively, and by optimising the rest of the molecule at each step, with the constraints described above. The acetyl was also constrained to remain planar during its rotation. In all cases a correction of 14*sin(τ) kcal/mol was applied to the rotational barrier for the N–C(O) bond, introducing an additional molecular mechanics energetic contribution due to the partial double-bond character of the amidic bond as implemented in MOPAC, depending on the torsion angle τ = C6–N2–N3–C7.

Acknowledgments

This work has been partially supported by a grant from C.N.R. (Rome). The C.I.M. (Centro Interfacoltà di Misure "Giuseppe Casnati") of the University of Parma is thanked for the technical support. Particular thanks are due to Prof. Mirco Costa for the helpful discussions.

[1] [1a] M. Alvarez, N. Lugan, R. Mathieu, *J. Chem. Soc., Dalton Trans.* **1994**, 2755–2761. – [1b] M. Ahmad, S. D. Perera, B. L. Shaw, M. Thornton-Pett, *J. Chem. Soc., Dalton Trans.* **1997**, 2607–2612. – [1c] P. Bhattacharyya, J. Parr, A. M. Z. Slawin, *J. Chem. Soc., Dalton Trans.* **1998**, 3609–3614.

[2] A. Bacchi, M. Carcelli, M. Costa, P. Pelagatti, C. Pelizzi, G. Pelizzi, *J. Chem. Soc., Dalton Trans.* **1996**, 4239–4244.

[3] [3a] A. Bacchi, M. Carcelli, M. Costa, P. Pelagatti, C. Pelizzi, G. Pelizzi, *Gazz. Chim. Ital.* **1994**, *124*, 429–435. – [3b] A. Bacchi, M. Carcelli, M. Costa, A. Leporati, E. Leporati, P. Pelagatti, C. Pelizzi, G. Pelizzi, *J. Organomet. Chem.* **1997**, *535*, 107–120. – [3c] P. Pelagatti, A. Venturini, A. Leporati, M. Carcelli, M. Costa, A. Bacchi, G. Pelizzi, C. Pelizzi, *J. Chem. Soc., Dalton Trans.* **1998**, 2715–2721. – [3d] P. Pelagatti, Ph.D. Dissertation, Univ. of Parma, Italy, **1998**. – [3e] P. Pelagatti, A. Bacchi, M. Carcelli, M. Costa, A. Fochi, P. Ghidini, E. Leporati, M. Masi, C. Pelizzi, G. Pelizzi, *J. Organomet. Chem.*, **1999**, *583*, 94–105.

[4] [4a] D. E. James, L. F. Hines, J. K. Stille, *J. Am. Chem. Soc.* **1976**, *98*, 1806–1809. – [4b] D. Milstein, *Acc. Chem. Res.* **1988**, *21*, 428. – [4c] G. Cavinato, L. Toniolo, *J. Organomet. Chem.* **1990**, *398*, 187–195.

[5] [5a] A. Sen, *Chemtech* **1986**, 48–51. – [5c] E. Drent, J. A. M. Broekhoven, M. J. Doyle, *J. Organomet. Chem.* **1991**, *417*, 235–251. – [5b] E. Drent, P. H. M. Budzelaar, *Chem. Rev.* **1996**, *96*, 663.

[6] [6a] G. P. C. M. Dekker, C. J. Elsevier, K. Vrieze, P. W. N. M. van Leeuwen, C. F. Roobeek, *J. Organomet. Chem.* **1992**, *430*, 357–372. – [6b] G. P. C. M. Dekker, C. J. Elsevier, K. Vrieze, P. W. N. M. van Leeuwen, *Organometallics* **1992**, *11*, 1598–1603. – [6c] B. A. Markies, D. Kruis, M. H. P. Rietveld, K. A. N. Verkerk, J. Boersma, H. Kooijman, M. T. Lakin, A. L. Spek, G. van Koten, *J. Am. Chem. Soc.* **1995**, *117*, 5263–5274.

[7] [7a] G. P. C. M. Dekker, A. Buijs, C. J. Elsevier, K. Vrieze, P. W. N. M. van Leeuwen, W. J. J. Smeets, A. L. Spek, Y. F. Wang, C. H. Stam, *Organometallics* **1992**, *11*, 1937–1948. – [7b] H. A. Ankersmit, N. Veldman, A. L. Spek, K. Eriksen, K. Goubitz, K. Vrieze, G. van Koten, *Inorg. Chim. Acta* **1996**, *252*, 203–219. – [7c] J. L. Hoare, K. J. Cavell, R. Hecker, B. W. Skelton, A. H. White, *J. Chem. Soc., Dalton Trans.* **1996**, 2197–2205. – [7d] L. Crociani, G. Bandoli, A. Dolmella, M. Basato, B. Corain, *Eur. J. Inorg. Chem.* **1998**, 1811–1820.

[8] [8a] R. E. Rülke, J. G. P. Delis, A. M. Groot, C. J. Elsevier, P. W. N. M. van Leeuwen, K. Vrieze, K. Goubitz, H. Schenk, *J. Organomet. Chem.* **1996**, *508*, 109–120. – [8b] J. H. Groen, J. G. P. Delis, P. W. N. M. van Leeuwen, K. Vrieze, *Organometallics* **1997**, *16*, 68–77. – [8c] J. G. P. Delis, J. H. Groen, K. Vrieze, P. W. N. M. van Leeuwen, N. Veldman, A. L. Spek, *Organometallics* **1997**, *16*, 551–562.

[9] [9a] R. E. Rülke, I. M. Han, C. J. Elsevier, K. Vrieze, P. W. N. M. van Leeuwen, C. F. Roobeek, M. C. Zoutberg, Y. F. Wang, C. H. Stam, *Inorg. Chim. Acta* **1990**, *169*, 5–8. – [9b] R. E. Rülke, V. E. Kaasjager, D. Kliphuis, C. J. Elsevier, P. W. N. M. van Leeuwen, K. Vrieze, K. Goubitz, *Organometallics* **1996**, *15*, 668–677.

[10] J. H. Groen, A. de Zwart, M. J. M. Vlaar, J. M. Ernsting, P. W. N. M. van Leeuwen, K. Vrieze, H. Kooijman, W. J. J. Smeets, A. L. Spek, P. H. M. Budzelaar, Q. Xiang, R. P. Thummel, *Eur. J. Inorg. Chem.* **1998**, 1129–1143.

[11] [11a] R. E. Rülke, J. M. Ernsting, A. L. Spek, C. J. Elsevier, P. W. N. M. van Leeuwen, K. Vrieze, *Inorg. Chem.* **1993**, *32*, 5769–5778. – [11b] H. A. Ankersmit, N. Veldman, A. L. Spek, K. Vrieze, G. van Koten, *Inorg. Chim. Acta* **1996**, *252*, 339–354. – [11c] R. E. Rülke, V. E. Kaasjager, P. Wehman, C. E. Elsevier, P. W. N. M. van Leeuwen, K. Vrieze, *Organometallics* **1996**, *15*, 3022–3031. – [11d] G. J. Britovsek, K. J. Cavell, M. J. Green, F. Gerhards, B. W. Skelton, A. H. White, *J. Organomet. Chem.* **1997**, *533*, 201–212.

[12] [12a] R. J. Cook, K. Mislow, *J. Am. Chem. Soc.* **1971**, *93*, 6703–6704. – [12b] J. L. Wong, M. F. Zady, *J. Org. Chem.* **1975**, *40*, 2512–2516. – [12c] R. Pichon, J. Le Saint, P. Courtot, *Tetrahedron* **1981**, *37*, 1517–1524. – [12d] R. N. Butler, S. M. Johnston, *J. Chem. Soc., Perkin Trans.* **1984**, 2109–2116.

[13] J. H. Groen, M. J. M. Vlaar, P. W. N. M. van Leeuwen, K. Vrieze, H. Kooijman, A. L. Spek, *J. Organomet. Chem.* **1998**, *551*, 67–79.

[14] J. G. P. Delis, M. Rep, R. E. Rülke, P. W. N. M. van Leeuwen,

K. Vrieze, J. Fraanje, K. Goubitz, *Inorg. Chim. Acta* **1996**, *250*, 87–103.
[15] [15a] H. Jin, K. J. Cavell, *J. Organomet. Chem.* **1991**, *419*, 259–268. – [15b] K. J. Cavell, H. Jin, B. W. Skelton, A. H. White, *J. Chem. Soc., Dalton Trans.* **1992**, 2923–2930. – [15c] H. Jin, K. J. Cavell, *J. Chem. Soc., Dalton Trans.* **1994**, 415–421. – [15d] H. Jin, K. J. Cavell, B. W. Skelton, A. H. White, *J. Chem. Soc., Dalton Trans.* **1995**, 2159–2169.
[16] [16a] J. L. Hoare, K. J. Cavell, R. Hecker, B. W. Skelton, A. H. White, *J. Chem. Soc., Dalton Trans.* **1996**, 2197–2205. – [16b] K. E. Frankcombe, K. J. Cavell, B. F. Yates, R. B. Knott, *Organometallics* **1997**, *16*, 3199–3206.
[17] D. B. Pendergrass Junior, I. C. Paul, D. Y. Curtin, *J. Am. Chem. Soc.* **1972**, *94*, 8730–8737
[18] [18a] B. Cornils, W. A. Herrmann, *Applied Homogeneous Catalysis with Organometallic Compounds*, VCH, Weinheim, **1996**, Vol. 1. – [18b] J. P. Collman, L. S. Hegedus, J. R. Norton, R. G. Finke, *Principles and Applications of Organotransition Metal Chemistry*, University Science Books, Mill Valley, CA, **1987**. – [18c] I. Tkatchenko, *Comprehensive Organometallic Chemistry* (Eds.: G. Wilkinson, F. G. A. Stone, E. W. Abel), Pergamon Press, Oxford, U.K., **1982**, Vol. 8.
[19] Y.-S. Li, A. Yamamoto, *Organometallics* **1998**, *17*, 3466–3478.
[20] S. Furukawa, Y. Kuroiwa, *Pharm. Bull. Japan* **1995**, *3*, 232–233.
[21] Crystallographic data (excluding structure factors) for the structures reported in this paper have been deposited with the Cambridge Crystallographic Data Centre as supplementary publication no. CCDC-125109 (**13**) and CCDC-125110 (**3**). Copies of the data can be obtained free of charge on application to CCDC, 12 Union Road, Cambridge CB2 1EZ, UK [Fax: (internat.) + 44–1223/336-033; E-mail:deposit@ccdc.cam.ac.uk].
[22] *SIR97*: *A New Program For Solving And Refining Crystal Structures*, A. Altomare, M.C. Burla, M. Camalli, G. Cascarano, C. Giacovazzo, A. Guagliardi, A. G. Moliterni, G. Polidori, R. Spagna, **1997**, Istituto di Ricerca per lo Sviluppo di Metodologie Cristallografiche C.N.R., Bari, Italy.
[23] G.M Sheldrick, *SHELXL97: Program for Structure Refinement*, University of Göttingen, Germany, **1997**.
[24] M. Nardelli, *PARST97*, updated version of *PARST95*, *J. Appl. Crystallogr.* **1995**, *28*, 659.
[25] P. T. Beurskens, G. Beuskens, W. P. Bosman, R. de Gelder, S. Garcia-Granda, R. O. Gould, R. Israël, J. M. M. Smits. The *DIRDIF-96* program system, Crystallography Laboratory, University of Nijmegen, The Netherlands, **1996**.
[26] N. Walker, D. Stuart, *Acta Cryst.* **1983**, *A39*, 158–166.
[27] [27a] W. H. Zachariasen, *Acta Cryst*. **1967**, *A23*, 558. – [27b] A. C. Larson, *The Inclusion of Secondary Extinction in Least-Squares Refinement of Crystal Structures. Crystallographic Computing* (Eds.: F.R. Ahmed, S.R. Hall, C.P. Huber), Munksgaard, Copenhagen, **1969**, 291–294.
[28] [28a] D. T. Cromer, J. B. Mann, *Acta Cryst*. **1968**, A24, 321–324; [28b] *International Tables for X-ray Crystallography*, Birmingham, Kynoch Press, **1974**, Vol. IV, p.55.
[29] D. T. Cromer, D. Liberman, *Journal of Chem. Phys.* **1970**, *53*, 1891.
[30] S. R. Hall, G. S. D. King, J. M. Stewart (Eds.), *XTAL3.4* User's Manual, University of Western Australia, Lamb, Perth, **1995**.
[31] L. Zsolnai, H. Pritzkow, *ZORTEP*, *ORTEP* original program modified for PC, University of Heidelberg, Germany, **1994**.
[32] F. H. Allen, O. Kennard, Cambridge Structural Database, *Chemical Design Automation News* **1993**, *8*, 1 and 31–37.
[33] J. J. P. Stewart, *MOPAC 6.0*, Frank J. Seiler Research Laboratory, United States Air Force Academy, CO 80840.
[34] J. J. P. Stewart, *J. Comp. Chem*. **1989**, *10*, 209.

Received June 15, 1999
[I99222]

Application of Photoelectron Spectroscopy to Molecular Properties, 55[±]

Low-Coordinate Arsenic Chemistry: Studies of Amino(iminoarsanes) Using UV Photoelectron Spectroscopy and Density Functional Theory

Karinne Miqueu,[a] J.-M. Sotiropoulos,[a] G. Pfister-Guillouzo,*[a] and V. Romanenko[b]

Keywords: Arsenic / UV photoelectron spectroscopy / Ab initio calculations

In this paper, we report the gas-phase characterization of two differently substituted amino(iminoarsanes), TmpAs=$NSiMe_3$ and $(SiMe_2tBu)_2NAs=N(SiMe_2tBu)$, by coupling flash vacuum thermolysis (FVT) with UV photoelectron spectroscopy (PES). Quantum chemical calculations, using the DFT method (B3LYP) with the basis set 6-311G(d,p), have also been carried out on the $R_1As=NR_2$ unit with R_1 = H, NH_2, $N(CH_3)_2$, $N(SiH_3)_2$ and R_2 = H, SiH_3, in order to study the effect of substitution on the electronic properties and the thermodynamic stability of the As=N skeleton. Similarities with phosphorus analogues are also discussed.

Introduction

In recent years, photoelectron spectroscopic (PES) investigation of multiple bond systems involving heavy main-group elements has been the subject of a great deal of experimental effort.[1] While low-coordinate phosphorus compounds have been extensively studied, the chemistry of related species containing dicoordinated arsenic remains practically unexplored. In parallel with the first studies of arsaalkenes,[2] we have envisaged the possibility of similarly characterizing the iminoarsanes. A small number of these compounds with bulky substituents have been unequivocally isolated and characterized.[3] To date, all their structures have been found to be *anti*, although only a few details concerning their geometrical parameters are as yet available.

A preliminary theoretical approach[4] showed that, as for iminophosphanes, the σ-push-pull substitution effect considerably modifies the structures and stabilities of the iminoarsanes. The As=N double-bond character is strengthened when the arsenic is substituted with an electron-withdrawing group (halogen) and the nitrogen with a σ-electron-releasing group (SiH_3). The substitution of arsenic with an amino group is more complex. In the present case, two effects operate concurrently: the electronegativity of the amino group nitrogen and the interactions of various kinds that depend on the orientation of the amino group.

The $\sigma^2\lambda^3$-iminophosphanes, in which a phosphorus atom is substituted with an amino group, represent an extensively studied[5] class of compounds. On the contrary, the preparation of amino(iminoarsanes) still represents a substantial challenge. Our purpose was to synthesize amino(iminoarsanes) bearing substituents of various degrees of bulkiness and to characterize them by UV photoelectron spectroscopy using our specially designed equipment to detect and analyse short-lived species by utilizing the band pattern as a "molecular fingerprint".[6] By generating these species by flash vacuum thermolysis in the proximity of the photoionization zone, we were able to avoid rearrangement and/or polymerization reactions. We have also carried out a theoretical study in order to define the stabilities of the isomers and rotamers, as well as to estimate the energies of the first two ionic states; considering the envisaged isomers or rotamers, these states were expected to be well-separated.

Results and Discussion

Our initial attempts to generate fully silylated amino(iminoarsane), $(Me_3Si)_2N–As=NSiMe_3$, by employing a synthetic approach similar to that used previously to synthesize its phosphorus analogue, met with little success. In accordance with preliminary results reported in the literature,[7] the decomposition of $\{[(Me_3Si)_2]_2N\}_2AsCl$ in the gas phase under flash vacuum thermolysis (FVT) conditions was found to commence at temperatures above 823 K and involves the elimination of $(Me_3Si)_3N$ instead of the expected Me_3SiCl. The PE spectrum observed is too complex to be interpreted.

In accordance with the hypothesis that on increasing the steric bulk of the substituent R in the R_2N ligand the elimination of R_2NSiMe_3 from the molecule $R_2NAs(Cl)N(SiMe_3)_2$ should become disfavoured compared to that of Me_3SiCl, we turned our attention to 2,2,6,6-tetramethylpiperidino (Tmp)-substituted chloroarsane $TmpAs(Cl)N(SiMe_3)_2$ (**1**). It is noteworthy that no *N*-

[±] Part 54: A. Chrostowska, S. Joanteguy, G. Pfister-Guillouzo, V. Lefevre, J. L. Ripoll, *Organometallics*, in press.

[a] Laboratoire de Physico-Chimie Moléculaire, CNRS UMR 5624, Université de Pau et des Pays de l'Adour, Avenue de l'Université, F-64000 Pau, France
Fax: (internat.) +33-5/59 80 83 44
E-mail: genevieve.pfister@univ-pau.fr
[b] Institute of Bioorganic Chemistry and Petrochemistry, National Academy of Sciences, Murmanskaya St. 1, 253660 Kiev 94, Ukraine

 © WILEY-VCH Verlag GmbH, D-69451 Weinheim, 2000 1434–1948/00/0303–477 $ 17.50+.50/0

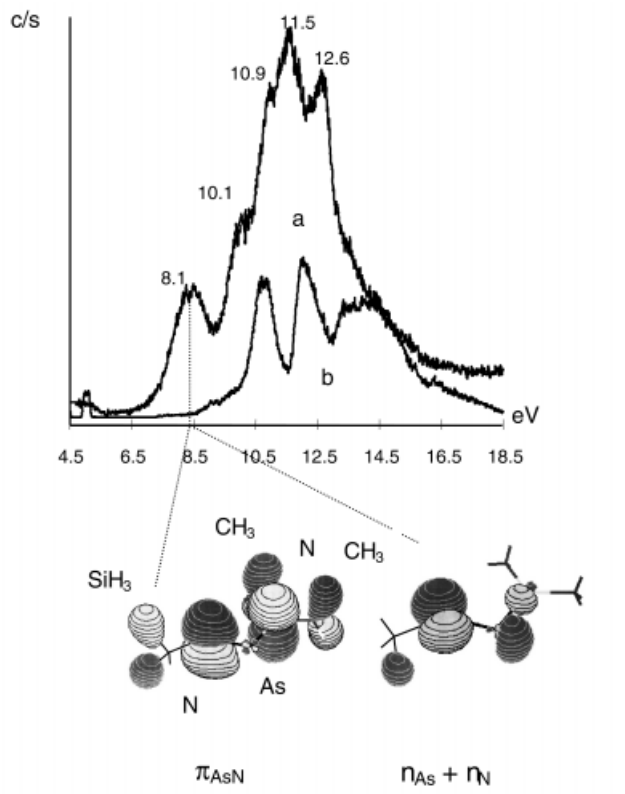


Figure 1. Photoelectron spectra at 813 K of (a) TmpAs=$NSiMe_3$ (**2**) with Me_3SiCl and (b) pure Me_3SiCl

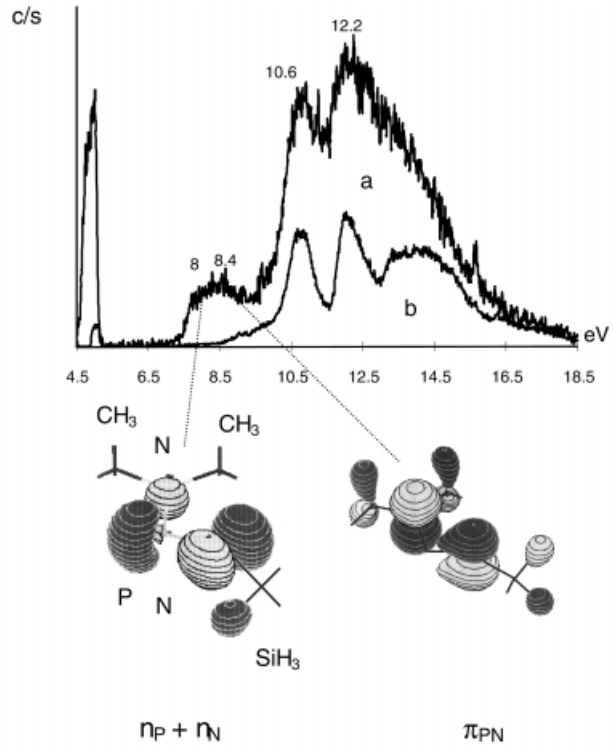


Figure 2. Photoelectron spectra of (a) TmpP=$NSiMe_3$ (**4**) and (b) Me_3SiCl

trialkylsilylated 2,2,6,6-tetramethylpiperidine has yet been characterized. The chloroarsenic precursor **1** was prepared by reaction of $TmpAsCl_2$ with $(Me_3Si)_2NLi$ and subjected to short-path internal FVT. As predicted, the replacement of one $(Me_3Si)_2N$ group in the compound $[(Me_3Si)_2N]_2$-AsCl by a Tmp substituent led to a different reaction pattern. The FVT/PES coupling indicated quite clearly that thermolysis of **1** at 813 K led to the formation of chlorotrimethylsilane and an arsenic species. The superposition of the spectra of Me_3SiCl and of the product obtained after thermolysis (see Figure 1) clearly shows the presence of a broad band centered at 8.1 eV. This band, which probably relates to two ionizations, could be assigned to TmpAs=$NSiMe_3$ (**2**). In order to confirm this hypothesis, a further experimental study was performed on the phosphorus analogue TmpP=$NSiMe_3$ (**4**). This species was obtained from $TmpPClN(SiMe_3)_2$ (**3**). The loss of Me_3SiCl was very rapid and did not require thermolysis, in contrast to $TmpAsClN(SiMe_3)_2$. This experimental observation can be attributed to the greater thermal stability of the precursor; its longer As–N and As–Cl bonds compared to their P–N and P–Cl counterparts retard the loss of Me_3SiCl.

The respective spectra obtained for TmpAs=$NSiMe_3$ and TmpP=$NSiMe_3$ (Figure 1 and Figure 2) show numerous similarities. The main ionization potentials (IP) are centered at 8.1 eV for **2** and at 8.0 eV and 8.4 eV for **4**.

In order to confirm that the bands observed at low energies (< 10 eV) in the PE spectra were indeed attributable to monomeric amino(iminoarsane), we studied the thermally induced decomposition of chlorobis(amino)arsane $\{[Me_2tBu)_2Si]_2N\}_2AsCl$ (**5**) bearing the sterically demanding Me_2tBuSi group. As in the case of the chloroarsane **1**, it was again hypothesized that the elimination of a silylamine from this arsane precursor would be sterically unfavorable. In fact, under FVT conditions (160–190 °C/0.5 Torr), compound **5** was found to decompose to furnish $Me_2tBuSiCl$ and the amino(iminoarsane) $(Me_2tBuSi)_2$-NAs=$NSiMe_2tBu$ (**6**), which proved sufficiently stable to be isolated by trapping at low temperature and subsequent revaporization. Moreover, in preparative experiments, we succeeded in high-vacuum redistillation of the product, which could then be immediately characterized by mass spectrometry. The spectrum of $(SiMe_2tBu)_2NAs=N(SiMe_2tBu)$ (Figure 3) features two characteristic bands at 8.4 eV and 9.5 eV.

Theoretical Results

Method Used

Ab initio calculations were performed using Gaussian 94/DFT.[8,9] The density functional theory method[10] was used in view of the non-trivial number of atoms present in the compounds under study. In this way, calculation times were shortened. Moreover, we have previously shown that this method correctly predicts the ionization energies of alkenes, alkynes, and heteroalkenes.[11] Nevertheless, we verified that the estimation of the first two ionic states of the *anti* form of MeP=NMe [A': 8.6 eV ($n_P + n_N$) and A": 10 eV ($\pi_{P=N}$), respectively] was indeed congruous with the spectrum observed by Elbel and Niecke for *t*BuP=N*t*Bu.[12] The calculations were performed using the hybrid Becke 3LYP

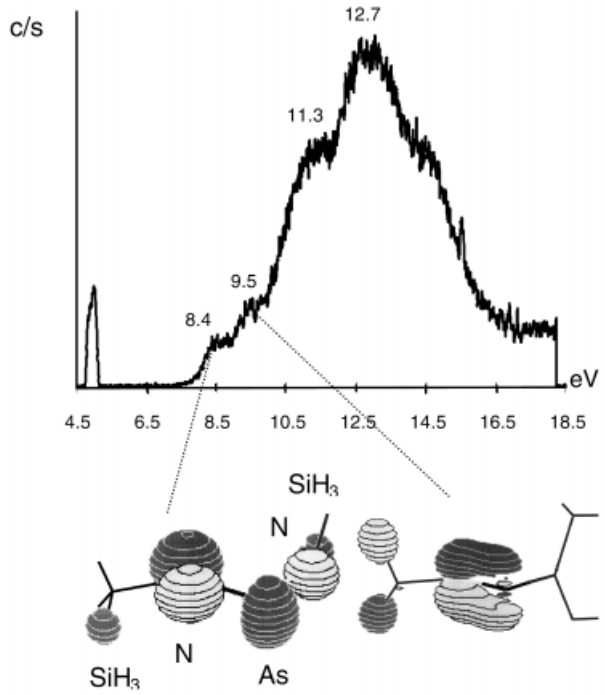


Figure 3. Photoelectron spectrum of (tBuMe$_2$Si)$_2$NAs=NSiMe$_2$$t$Bu (**6**)

functional[13] in conjugation with the basis set 6-311G(d,p). The structures were optimized at the resulting geometries and second-order derivatives were calculated in order to ascertain whether a minimum or a saddle point had been obtained. In order to calculate vertical ionization energies, the energy difference between the neutral molecule and the ion (both at the optimum geometry of the neutral molecule) was used. The obtained geometrical parameters are indicated in Figure 4.

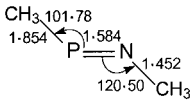


Figure 4. Geometrical parameters calculated for *anti*-CH$_3$P=NCH$_3$ [B3LYP, 6-311G(d,p)]; bond lengths in Å, bond angles in degrees

The experimental PE spectrum features two separated low-energy PE bands at 8.11 eV and 9.70 eV, attributable to ionizations from the bonding combination between the phosphorus and nitrogen lone pairs ($n_P + n_N$) and the $\pi_{P=N}$ orbital, respectively. Taking into account the destabilizing effect of the tBu group, the calculated data are in agreement with the experimentally determined ionizations. These observations encouraged us to use the latter method to carry out all the calculations on the As=N double bond systems that are described below.

Favoured Structures of the Amino(iminoarsanes) R$_1$As=NR$_2$ [R$_1$ = NH$_2$, N(CH$_3$)$_2$, N(SiH$_3$)$_2$; R$_2$ = H, SiH$_3$]

The *anti* form of the parent compound HAs=NH is slightly more stable than its *syn* form (by 0.4 kcal/mol). In both structures, the As=N bond length measures around 1.7 Å, but is slightly shorter in the *syn* isomer (1.712 Å: *syn*; 1.722 Å: *anti*), which is in agreement with the opening of the bond angles. The two bond angles H–As–N and As–N–H are larger in the *syn* conformation (103.37° and 113.41°, respectively) than in the *anti* form (H–As–N: 95.84° and As–N–H: 107.47°).

For the amino(iminoarsanes), two minima were found on the potential energy surface. These corresponded to the *syn* and *anti* isomers, in which the nitrogen of the amino group is sp^2 hybridized (except in the case of R$_1$ = H$_1$,H$_2$, where it is sp^3 hybridized in the favored *anti* isomer; ΣN = 341.51°) and is coplanar with the As=N moiety. The *anti* form is slightly favored compared to the *syn* form (Table 1).

Taking into account the electronegativity of silicon, the attachment of an SiH$_3$ group on the imino nitrogen gives the lone pair a considerable degree of p character. In fact, we observe an opening of the angle at nitrogen (imino), especially in the case of *syn*-(NH$_2$)As=NSiH$_3$ (140.48°) and *syn*-(CH$_3$)$_2$NAs=NSiH$_3$ (165.13°). This leads to a lowering of the inversion barrier (to around 2 kcal/mol vs. 14 kcal/mol for the non-silylated compounds). Only the *anti* isomer is found for (SiH$_3$)$_2$NAs=NSiH$_3$. The stabilization of the *anti* form can be rationalized in terms of electronic and repulsion energies. For NH$_2$As=NSiH$_3$, the weak nuclear energy governs the stability of the *anti* form, whereas for NH$_2$As=NH and N(CH$_3$)$_2$As=NSiH$_3$ it is the electronic energy (Table 1). It is interesting to note that for these two compounds the *syn* isomers have electronic energies lower than those of the *anti* forms, in spite of the more significant antiplanar stabilizing interactions (see NBO analysis, Table 2).[14] It is likely that highly destabilizing interactions involving four electrons counterbalance the stabilizing interactions.

In the two isomers of NH$_2$As=NSiH$_3$ and (CH$_3$)$_2$NAs=NSiH$_3$, as well as in (SiH$_3$)$_2$NAs=NSiH$_3$, the amino nitrogens are sp^2 hybridized and are coplanar with the AsNSi system, resulting in a maximized $n_N^{\pi}\,\pi^*_{As=N}$ interaction. In the course of the rotation process (Table 3), two saddle points are found (TS$_1$, TS$_2$), which correspond to an sp^3 hybridization of the amino nitrogen. For the *anti* isomer, the lower saddle point (TS$_2$) corresponds to the rotamer where the nitrogen sp^3 lone pair and that on arsenic are in a *syn* arrangement (Figure 5). In the particular case of (SiH$_3$)$_2$NAs=NSiH$_3$, the nitrogen remains sp^2 hybridized (one transition state), the barrier to rotation being 10.41 kcal/mol. For the *syn* isomers, substitution at the amino nitrogen reverses the nature of the lower saddle point (arsenic and nitrogen lone pairs antiperiplanar).

On analyzing the geometrical parameters presented in Table 1, it can be noted that a planar amino group at nitrogen makes the As=N double bond shorter as compared to that in the unsubstituted molecule. Comparison with the parent molecule also reveals a slight opening of the arsenic bond angle when this atom is substituted with an amino group (by up to 7°) and a more pronounced opening of the nitrogen bond angle (by up to 52°). This is understandable when the s character shown by natural bond orbital (NBO)

Table 1. Geometrical parameters for *syn* (s) and *anti* (a) $R_1As{=}NR_2$ [R_1 = H, NH_2, $N(CH_3)_2$, $N(SiH_3)_2$; R_2 = H, SiH_3] having a planar amino group coplanar with the $AsNR_2$ system, except * (sp^3 hybridization, nitrogen bond angle: 341.51° for the *anti* isomer); E_t, E_{elec}, E_{rep} in Hartrees; E_{inv} (in kcal/mol) = $E_{TS} - E_t$a

R_1	H		NH_2*		NH_2		$N(CH_3)_2$		$N(SiH_3)_2$	
R_2	H		H		SiH_3		SiH_3		SiH_3	
	s	a	s	a	s	a	s	a[d]	s	a
As=N[a]	1.712	1.722	1.697	1.711	1.683	1.693	1.672/–	1.696/*1.553*	–	1.695
R_1AsN[b]	103.37	95.84	109.21	98.98	108.47	100.93	109.16	102.59/*107.45*	–	99.16
% s [c]]	75.71	76.42	75.11	77.47	75.23	75.87	75.71/–	75.54	–	76.89
$AsNR_2$[b]	113.41	107.47	116.69	108.53	140.48	131.57	165.13/–	131.56/*142.82*	–	132.51
% p [c]	52.7	47.69	53.08	48.46	75.97	69.67	94.54	70.33	–	70.2
E_t	s: –2291.798154		s: –2347.196934		s: –2637.944169		s: –2716.575973		s: –	
	a: –2291.798797		a: –2347.198566		a: –2637.945110		a: –2716.579755		a: –3219.426802	
E_{elec}	s: –2387.205614		s: –2531.354918		s: –2971.106866		s: –3247.638271		s: –	
	a: –2387.165663		a: –2532.54915		a: –2970.683357		a: –3250.236252		a: –3944.274632	
E_{rep}	s: 95.407460		s: 184.157984		s: 333.124493		s: 531.062298		s: –	
	a: 95.366866		a: 185.350584		a: 332.738247		a: 533.658097		a: 724.847083	
E_{inv}	17.99		13.85		2.25		1.48		–	

[a] Bond lengths in Å. – [b] Bond angles in ° [B3LYP, 6-311G(d, p)]. – [c] From NBO analysis. – [d] Values in italics correspond to $(CH_3)_2NP{=}NSiH_3$.

Table 2. Main stabilization energies in kcal/mol for *syn* and *anti* $R_1As{=}NR_2$ [R_1 = H, NH_2, $N(CH_3)_2$, $N(SiH_3)_2$; R_2 = H, SiH_3] having a planar amino group coplanar with the $AsNR_2$ system, except * (sp^3 hybridization, nitrogen bond angle: 341.51° for the *anti* isomer) [B3LYP, 6-311G(d,p)] and *gauche* [*g*, for R_1 = $N(SiH_3)_2$ and R_2 = SiH_3]

R_1	H		NH_2*		NH_2		$N(CH_3)_2$		$N(SiH_3)_2$		
R_2	H		H		SiH_3		SiH_3		SiH_3		
	s	a	s	a	s	a	s	a	s	a	g
$n^{\sigma}_N \rightarrow \sigma^*_{AsR1}$	5.11	3.5	8.66	5.72	13.14	9.34	19.46	9.65	–	9.65	9.88
$n_{As} \rightarrow \sigma^*_{NR2}$	2.04	–	3.1	–	8.07	4.17	9.66	4.65	–	4.2	4.57
$n^{\pi}_N \rightarrow \pi^*_{AsN}$	–	–	24.70	–	27.8	26.89	28.41	28	–	21.63	–

Table 3. Calculated barriers associated with the rotation process in kcal/mol [B3LYP, 6–311G(d,p)]

form	molecules	ΔE_1 [a]	ΔE_2 [b]
anti	$H_2NAs{=}NH$	11.44	9.38
	$H_2NAs{=}NSiH_3$	13.78	11.24
	$(CH_3)_2NAs{=}NSiH_3$	18.64	15.64
	$(SiH_3)_2NAs{=}NSiH_3$		10.41
syn	$H_2NAs{=}NH$	7.67	8.63
	$H_2NAs{=}NSiH_3$	10.96	10.41
	$(CH_3)_2NAs{=}NSiH_3$	13.88	16.72

[a] $\Delta E_1 = E_{0°} - E_{min}$. – [b] $\Delta E_2 = E_{180°} - E_{min}$.

analysis is considered; in fact, it is almost identical for the arsenic lone pair in all these compounds, whereas for the nitrogen the sp^2 character changes considerably.

Comparison of the geometries of the iminoarsanes and iminophosphanes reveals the same features. Indeed, detailed quantum chemical calculations have shown that changing the substituents on phosphorus or nitrogen may lead to a considerable change in geometry. The P=N double bond shortens when the phosphorus is substituted with π-donors (e.g. NH_2),[15] due to the effect between n^{π}_N and π*; the σ-effect counteracts the π-effect.

Discussion of the Results: Interpretation of the Photoelectron Spectra

The Kohn–Sham energies and the two first ionization energies of the two forms (*syn* and *anti*) are presented in Table 4. For the *anti* isomer, the ionic state A' corresponds to the ejection of an electron from the orbital described as a bonding combination between the arsenic and nitrogen lone pairs, whereas for the *syn* conformation it corresponds to ionization from the antibonding combination orbital between these lone pairs.

When the arsenic atom was substituted with an amino group, the energy of the A'' ionic state clearly decreased compared to that of the parent molecule, in the same way for both the *syn* and *anti* isomers. The associated molecular orbital is seen to be strongly localized on the amino and imino nitrogens since it indicates an interaction between the amino lone pair and the $\pi_{As=N}$ and $\pi^*_{As=N}$ orbitals. This is shown in Figure 1 by means of the MOLDEN representations. X-ray analysis of $TmpP{=}NN(SiMe_3)_2$[16] reveals that the amino nitrogen is sp^2 hybridized (ΣN = 358.95°) and that the Tmp group is almost planar (dihedral angles $CN_{amino}PN_{imino}$ = 8.24° or 156.36°). Accordingly, it seems reasonable to use the fragments $(CH_3)_2NP{=}NSiH_3$ and $(CH_3)_2NAs{=}NSiH_3$ composed of an sp^2 hybridized amino nitrogen coplanar with As–N (or P–N) to model the experi-

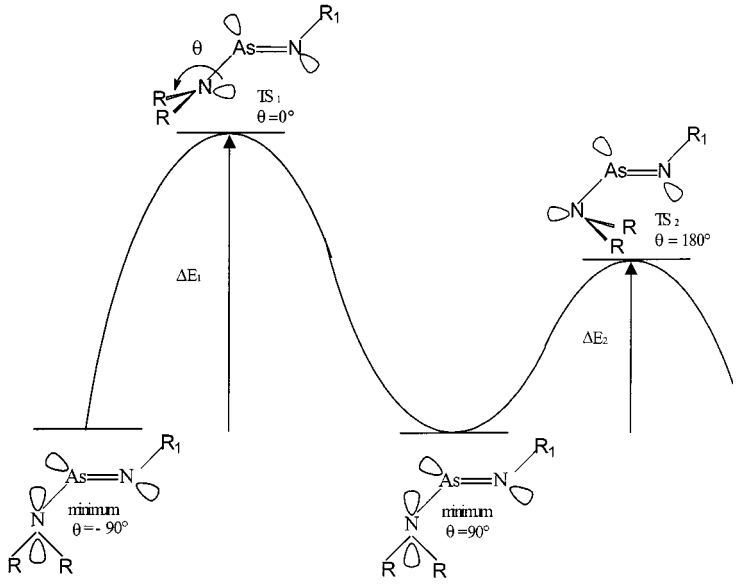


Figure 5. Profile of the rotation process about the nitrogen of the amino group in *anti*-$R_1As{=}NR_2$ with R_1 = NH_2, $N(CH_3)_2$, $N(SiH_3)_2$ and R_2 = H, SiH_3 [B3LYP, 6-311G(d,p)]

Table 4. Kohn–Sham energies (KS) in eV and ionization energies (IE) in eV for *syn* (s) and *anti* (a) $R_1As{=}NR_2$ having a planar amino group coplanar with the $AsNR_2$ system, except * (sp^3 hybridization, nitrogen bond angle: 341.51°) [B3LYP, 6-311G(d,p)]

R_1	H		NH_2*		NH_2		$N(CH_3)_2$		$N(SiH_3)_2$		
R_2	H		H		SiH_3		SiH_3		SiH_3		
	s	a	s	a	s	a	s	a [a]	s	a [a]	g
K.S.	–7.55	–6.95	–7.48	–6.74	–6.98	–6.67	–6.58	–6.61	–	–7.03	–7.03
							–	*–6.49*			
IE (A')	10.26	9.67	9.95	9.29	9.11	8.80	8.44	8.47	–	8.86	8.86
(n)							–	*8.49*		*8.80*	
K.S.	–8.26	–8.21	–6.78	–6.59	–6.99	–6.92	–6.41	–6.39	–	–7.28	–8.17
							–	*–6.68*			
IE(A'')	10.92	10.86	9.25	–	9.05	8.98	8.24	8.18	–	8.94	9.98
(π)							–	*8.58*		*9.27*	

[a] Italic values correspond to the phosphorus analogous.

mentally examined compounds. Taking into account the steric requirement of the Tmp substituent, the *syn* isomer can be excluded. Only calculations relating to the *anti* form may be used to interpret the PE spectra of $TmpAs{=}NSiMe_3$ and $TmpP{=}NSiMe_3$. For the two first ionic states of the respective systems $(CH_3)_2NAs{=}NSiH_3$ and $(CH_3)_2NP{=}NSiH_3$, we calculated a reverse order. The A' state, corresponding to a bonding combination between arsenic (phosphorus) and nitrogen lone pairs, was calculated at 8.47 eV (8.49 eV); the A'' state was calculated at 8.18 eV (ionization from the $\pi_{As=N}$ orbital) and 8.58 eV (ionization from the $\pi_{P=N}$ orbital). The values observed for $TmpP{=}NSiMe_3$ are similar to those described by Niecke[6] and we interpret them in the same way. The above result is interesting because it allows an interpretation of the different shapes of the two spectra (Figure 1 and Figure 2). The first broad band in the spectrum of $TmpAs{=}NSiMe_3$ is composed of two overlapping ionizations, the first associated with the A'' ionic state and the second with the A' state. For $TmpP{=}NSiMe_3$, the band at low energy corresponds to the A' ionic state and the broad feature at 8.4 eV is associated with the A'' ionic state.

The $2p_\pi$-$4p_\pi$ overlap is weaker than the $2p_\pi$-$3p_\pi$ overlap; it induces an energetic destabilization of the $\pi_{As=N}$ orbital as compared to the $\pi_{P=N}$ orbital as a result of the more diffuse character of the former. It also leads to a reduction in the contribution from the stabilizing $n^{\pi}_{Namino}\,\pi^{*}_{AsN}$ interaction. This difference between the phosphorus and arsenic derivatives is clearly apparent from the 3D MO plots shown in Figure 1 and Figure 2, which reveal more extensive delocalization for the phosphorus compound. The spectrum of $(SiMe_3)_2NP{=}NSiMe_3$ obtained by Niecke,[6] showed the first two ionizations at 8.10 eV (n) and 8.75 eV (π). The pronounced shift of the second ionization towards higher energy is due to the effect of the $SiMe_3$ group on the ionization energy of the lone pair of the amino nitrogen through its interaction with the π system. Considering the arsenic derivatives, calculations are indicative of the same tendency. Compared with a CH_3 substituent, the SiH_3 group stabilizes the $\pi_{As=N}$ orbital (0.76 eV) more than it does the n

orbital (0.31 eV). Ionic state energy calculations on $(SiH_3)_2NAs{=}NSiH_3$, in which the amino group is coplanar with the As=N system, show approximately the same values for the A''(π) and A'(n) states. The experimental spectrum observed for $(SiMe_2tBu)_2NAs{=}NSiMe_2tBu$ features two bands with a gap of 1 eV; it does not seem to correspond to an iminoarsane system having an sp^2 amino group interacting with the π system. The steric requirement of the $SiMe_2tBu$ substituent could modify the orientation of the amino group, as observed for *trans*-$(SiMe_2tBu)_2NP{=}PN(SiMe_2tBu)_2$, for which a bis-orthogonal conformation is seen[17] (the two amino groups are orthogonal to the π system). In contrast to the piperidino derivatives, in this case it seems possible to envisage a *gauche* form corresponding to a minimization of the steric demand.

The $(SiH_3)_2NAs{=}NSiH_3$ form, in which the amino group is orthogonal to the π system (to minimize steric hindrance), corresponds to TS_1. The relevant geometrical parameters are given in Figure 6. The first ionic state (A') is calculated at 8.87 eV. It is associated with an ionization from the bonding combination ($n_N + n_{As}$). The energy of the A'' state, corresponding to the ejection of an electron from the $\pi_{As=N}$ orbital, is calculated as 9.98 eV. Taking into account the destabilizing effect of the *tert*-butyl group as compared to a methyl group, the experimentally observed bands at 8.4 eV and 9.5 eV can be assigned to the amino(iminoarsane) $(SiMe_2tBu)_2NAs{=}N(SiMe_2tBu)$ with the amino group in a *gauche* orientation. In compound **6**, the steric effect leads to a rupture of the bond between the amino nitrogen lone pair and the $\pi_{As=N}$ system.

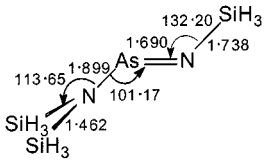


Figure 6. Geometrical parameters calculated for *anti*-$(SiH_3)_2NAs{=}NSiH_3$ [B3LYP, 6-311G(d,p)]; bond lengths in Å, bond angles in degrees

Conclusion

The study described in this paper represents the first effort to characterize amino(iminoarsanes). The diffuse character of the $\pi_{As=N}$ bonding, akin to that already known for iminophosphanes, made it difficult to isolate an As=N moiety that did not bear bulky substituents. Substitution at nitrogen by an electropositive SiR_3 group increases the s character of the As–N (P–N) bonding and induces stabilization of these reactive π systems through negative hyperconjugation. Likewise, for the σ skeleton, the attachment of an amino group at the arsenic strengthens the σ_{AsN} bond. The π electronic delocalization, induced by the coplanar amino group, would also lead to a stabilization of the system (interaction between the n_N^{π} and the $\pi_{P/AsN}^{\pi}$). Nevertheless, in spite of the non-existence of this delocalization, the attachment of a substituent with substantial steric bulk allows the isolation of amino(iminoarsanes) as a result of kinetic stabilization.

Experimental Section

General Remarks: All manipulations were carried out under nitrogen atmosphere using Schlenk techniques. Diethyl ether and pentane were distilled from sodium/benzophenone shortly prior to use. $TmpAsCl_2$, Tmp–P=$NSiMe_3$, and $(Me_2tBuSi)_2NH$ were prepared according to published methods.[18] – ^{1}H-NMR spectra were recorded on a Bruker AC80 spectrometer; chemical shifts are reported in ppm relative to Me_4Si as an external standard.

UV Photoelectron Spectra: The photoelectron spectra were recorded on a Helectros 0078 instrument equipped with a 127° cylindrical analyser and were monitored by means of a microcomputer supplemented with a digital analogue converter. The spectra were calibrated against the known autoionization of helium at 4.98 eV and nitrogen ionization at 15.59 eV. Our short-path thermolysis system has been described elsewhere.[19]

Chloro(2,2,6,6-tetramethylpiperidido)bis(trimethylsilyl)amidoarsenite (1): A freshly prepared solution of $(Me_3Si)_2NLi$ (20 mmol) [obtained by treatment of $(Me_3Si)_2NH$ in 25 mL of Et_2O with an equimolar amount of BuLi (1.6 M in hexane)] was added dropwise to a stirred solution of 2,2,6,6-tetramethylpiperidinodichloroarsenite (20 mmol) in pentane (20 mL) at 0 °C under nitrogen. The resulting mixture was stirred for 24 h and then the deposited LiCl was removed by filtration through a fine-pore glass frit under nitrogen. The filtrate was concentrated and the crude product was purified by low-temperature crystallization (–20 °C) from pentane. Yield 63%. – ^{1}H NMR ($CDCl_3$): δ = 0.36 (s, 18 H, Me_3Si), 1.45 (s, 12 H, CH_3), 1.25–1.48 (m, 6 H, CH_2). – $C_{15}H_{36}AsClN_2Si_2$: calcd. C 43.83, H 8.83; found C 49.19, H 8.65.

Chloro[bis(*tert*-butyldimethylsilyl)amido]arsenite (5): At 0 °C, a solution of $(Me_2tBuSi)_2NLi$ (15 mmol) in diethyl ether (35 mL) was added dropwise to a stirred solution of $AsCl_3$ (7.5 mmol) in diethyl ether (20 mL). The reaction mixture was stirred for a further 48 h and then the volatiles were removed in vacuo. Extraction of the residue with pentane, filtration of the extracts, concentration, and crystallization afforded the product as a colorless oil, which solidified on cooling. Yield 92%. – ^{1}H NMR ($CDCl_3$): δ = 0.21 (s, 24 H, Me), 1.15 (s, 36 H, *t*Bu). – $C_{24}H_{60}AsClN_2Si_4$: calcd. C 48.09, H 10.09; found C 48.45, H 10.61.

[Bis(*tert*-butyldimethylsilyl)amino][(*tert*-butyldimethylsilyl)imino]arsane (6): Vacuum distillation of chloroarsenite **5** obtained following short-path Arbusov FVT (160–190 °C, 0.5 Torr) gave 43% of crude **6** as a yellow oil. At this stage, the product was found to be contaminated with a small amount of $Me_2tBuSiCl$. Redistillation of the crude product afforded pure amino(iminoarsane) **6**; b.p. 130–135 °C (0.02 Torr). Yield 28%. – ^{1}H NMR (C_6D_6): δ = 0.31 (s, 18 H, Me_2Si), 0.93 (s, 27 H, *t*Bu). – $C_{18}H_{45}AsN_2Si_3$: calcd. C 48.18, H 10.10; found C 47.61, H 10.04. – EI-MS: *m*/*z* = 448 [M^+].

Acknowledgments

Financial support of this work by the CNRS (France) is gratefully acknowledged. We also thank the Institut du Developpement de Ressources en Informatique Scientifique (IDRIS, Orsay, France), administered by the CNRS, for providing access to the calculation facilities, and Dr. Gijs Schaftenaar for allowing us to use his graphics program Molden (ref.[20])

[1] [1a] *Multiple Bonds and Low Coordination in Phosphorus Chemistry* (Eds.: M. Regitz, O. J. Scherer), Georg Thieme Verlag, Stuttgart **1990**, p. 13–16. – [1b] E. Niecke, D. Gudat, *Angew. Chem. Int. Ed. Engl.* **1991**, *30*, 217–237.

[2] [2a] S. Lacombe, D. Gonbeau, J. L. Cabioch, B. Pellerin, J. M. Denis, G. Pfister-Guillouzo, *J. Am. Chem. Soc.* **1988**, *110*, 6964–6967. – [2b] N. P. C. Westwood, H. W. Kroto, J. F. Nixon, *J. Chem. Soc., Dalton Trans.* **1979**, 1405–1408. – [2c] V. Métail, A. Senio, L. Lassale, J. C. Guillemin, G. Pfister-Guillouzo, *Organometallics* **1995**, *14*, 4732–4735. – [2d] J. C. Guillemin, L. Lassale, P. Drean, G. Wlodarczak, J. Demaison, *J. Am. Chem. Soc.* **1994**, *116*, 8930–8936.

[3] [3a] P. Hitchcock, M. F. Lappert, A. K. Rai, H. D. Williams, *J. Chem. Soc., Chem. Commun.* **1986**, 1633–1636. – [3b] H. G. Ang, F. K. Lee, *Polyhedron* **1989**, *8*, 2331–2332. – [3c] S. K. Vasisht, M. Sood, P. K. Werma, T. Kaur, K. Usha, *Phosphorus, Sulfur, and Silicon* **1990**, *47*, 349–355. – [3d] J. Th. Ahlmann, A. Kunzel, H. W. Roesky, M. Noltemeyer, L. Markovskii, H. G. Schmidt, *Inorg. Chem.* **1996**, *35*, 6644–6645.

[4] K. Miqueu, J. M. Sotiropoulos, G. Pfister-Guillouzo, V. Romanenko, *Inorg. Chem.,* submitted.

[5] E. Niecke, T. Busch, W. W. Schoeller, R. Rademacher, *J. Chem. Soc., Faraday Trans.* **1994**, 2611–2616.

[6] H. Bock, B. Solouki, *Angew. Chem. Int. Ed. Engl.* **1981**, *20*, 427–444.

[7] E. Niecke, W. Bitter, *Syn. React. Inorg. Metal.-Org. Chem.* **1975**, *5*, 231–242.

[8] *Gaussian 94*, M. J. Frisch, G. W. Trucks, H. B. Schlegel, P. M. W. Gill, B. G. Johnson, M. A. Robb, J. R. Cheeseman, T. A. Keith, G. A. Petersson, J. A. Montgomery, K. Raghavachari, M. A. Al-Laham, V. G. Zakrzewski, J. V. Ortiz, J. B. Foresman, J. Cioslowski, B. B. Stefanov, A. Nanayakkara, M. Challacombe, C. Y. Peng, P. Y. Ayala, W. Chen, M. W. Wong, J. L. Andres, E. S. Replogle, R. Gomperts, R. L. Martin, D. J. Fox, J. S. Binkley, D. J. Defrees, J. Baker, J. P. Stewart, M. Head-Gordon, C. Gonzalez, J. A. Pople, *Gaussian 94, Revision C.3*, Gaussian Inc., Pittsburgh PA, **1995**.

[9] W. J. Hehre, L. Radom, P. v. R. Schleyer, J. A. Pople, *Ab Initio Molecular Orbital Theory*, John Wiley and Sons, New York, **1986**.

[10] R. G. Parr, W. Yang, in: *Functional Theory of Atoms and Molecules* (Eds.: R. Breslow, J. B. Goodenough), Oxford University Press, **1989**.

[11] S. Joantéguy, G. Pfister-Guillouzo, H. Chermette, *J. Chem. Phys.* **1999**, *103*, 3505–3511.

[12] S. Elbel, A. Ellis, E. Niecke, H. Egsgaord, L. Carlsen, *J. Chem. Soc., Dalton Trans.* **1985**, 879–884.

[13] [13a] A. D. Becke, *Phys. Rev.* **1988**, *38*, 3098. – [13b] A. D. Becke, *J. Chem. Phys.* **1993**, *98*, 5648–5652; C. Lee, W. Yang, R. G. Parr, *Phys. Rev. B37,* **1988**, 785–789.

[14] Natural bond orbital analysis, which represents ab initio molecular wavefunctions in terms of localized Lewis structures, was applied in order to provide a quantitative analytical framework for the interpretation of molecular orbital interactions. The NBO population analysis shows the presence of antiperiplanar stabilizing interactions between an occupied orbital (lone pair on arsenic and/or nitrogen) and a vacant one (σ^*_{AsR1}, σ^*_{NR2}); these are more important for the *syn* isomer (Table 2). – [14a] A. E. Reed, L. A. Curtiss, F. Weinhold, *J. Chem. Rev.* **1988**, *88*, 899–926. – [14b] J. P. Foster, F. Weinhold, *J. Am. Chem. Soc*. **1980**, *102*, 7211–7218.

[15] W. W. Schoeller, T. Busch, E. Niecke, *Chem. Ber.* **1990**, *123*, 1653–1654.

[16] U. Dressler, E. Niecke, S. Pohl, W. Saak, W. W. Schoeller, H. G. Schafer, *J. Chem. Soc., Chem. Commun*. **1986**, 1086–1087.

[17] E. Niecke, R. Ruger, M. Lysek, S. Pohl, W. W. Schoeller, *Angew. Chem. Int. Ed. Engl*. **1983**, *22*, 486–487.

[18] [18a] R. West, P. Boudjouk, *J. Am. Chem. Soc.* **1973**, *95*, 3987–3994. – [18b] V. D. Romanenko, A. V. Ruban, S. V. Iksanova, L. N. Markovskii, *Zh. Obshch. Khim.* **1984**, *54*, 313–325.

[19] [19a] F. Chuburu, S. Lacombe, G. Pfister-Guillouzo, A. Ben Cheik, J. Chuche, J. C. Pommelet, *J. Am. Chem. Soc.* **1991**, *113*, 1954–1960. – [19b] F. Chuburu, S. Lacombe, G. Pfister-Guillouzo, A. Ben Cheik, J. Chuche, J. C. Pommelet, *J. Org. Chem.* **1991**, *56*, 3445–3447.

[20] See: http://www-srs.caos.kun.nl/~schaft/molden

Received July 13, 1999
[I99255]

On the Nature of Arene η^6 Interactions in the Solid State and the Use of Cylindrophanes as Ligands for Sandwich Complexation of Metals with Longer-Range Interactions with the Benzene Ring

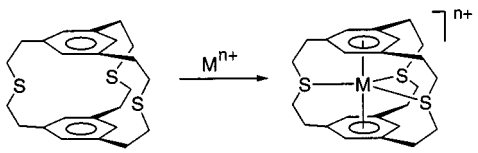
Mark Mascal,*[a] Jean-Luc Kerdelhué,[a] Alexander J. Blake,[a] Paul A. Cooke,[a] Roger J. Mortimer,[b] and Simon J. Teat[c]

Keywords: Coordination modes / Cyclophanes / Macrocycles / Sandwich complexes / Solid-state structures

A novel mode of containment for metal ions which participate in longer-range interactions with aryl rings (≥ 2.5 Å) is demonstrated in the preorganized cylindrical host **1**. Three equatorial sulfur atoms in **1** hold metals in a trigonal planar ligand field between two apical benzene centroids at an M–Ar distance of about 3 Å. Evidence of an interaction between the π electrons and the metals is gained by ^{1}H NMR spectroscopy of the complexes, and support for the general description of metal–arene contacts in the 2.5–3.5 Å range as "bonds" is derived from a statistical study of η^6-coordination in the solid state. Crystal structures of $[Ag(\mathbf{1})]BF_4$ and $[Cu(\mathbf{1})]BF_4$ confirm the first examples of arene Ag^I and Cu^I sandwich complexation and indeed the only structurally characterized Cu^I-aryl centroid interaction. The two isomeric *tris*-sulfoxides derived from **1** show less tendency to interact with metals ions.

Introduction

Since the discovery of ferrocene and transition metal-benzene complexes in the 1950's, there has been a constant fascination with the way metals interact with aromatic rings. The paradigmatic interaction involving neutral arenes is the η^6 mode of complexation, in which most group 3–10 metals participate.[1] We recently noted the bimodal nature of the arene–metal distance histogram generated from solid-state structures in the Cambridge Structural Database (CSD), which neatly divides this interaction into two categories, i.e. classic, short-range η^6 bonding, and longer-range aryl centroid–metal contact.[2] The *sym*-[5.5.5]trithiacyclophane macrobicycle **1**[3] was designed to take advantage of the fact that the mean value for the latter is around 3 Å (corresponding to the distance between the midpoint of the cavity and the center of each ring), which made possible the first structural characterization of the Ag^I and Cu^I arene sandwich complexes **2**. A divalent heteroatom (O, S) is required at the "equatorial" positions in ligands such as **1** because hydrogens occupy the cavity in the NH and hydrocarbon analogs,[4] but since the longer-range metal–arene interaction is weak, the complexes **2** owe their overall stability to the consequent trigonal-planar heteroatom ligand set. The analysis and reasoning which led to the design of "cylindrophane" **1**, and the subsequent preparation of novel cryptates **2**, are now presented in full.



1 **2**

Results and Discussion

Statistical Analysis of η^6-Metal Complexation

To appreciate the design principles behind **1**, it is first instructive to look in some detail at the nature of the interactions of metals with benzene rings. Although an account of η^6-benzene and arene complexes was included in Orpen et al.'s general analysis of coordination complexes in the CSD,[5] the study only tabulated data for 15 η^6-bonded *d*-block metals (vs. 29 in this analysis), with the longer-range noncovalent metal–arene contacts outside its remit.

The sampling of a cylindrical volume 0.5 Å in radius extending from the centroid of any benzene or aryl ring in the CSD was accomplished by constructing a query in QUEST3D[6] as follows: Three points were defined on a six-membered ring; point *x*, one C-atom of the ring; point *o*, the centroid of the ring; and point *y*, the centroid of one of the C–C bonds parallel to *xo* (Figure 1).

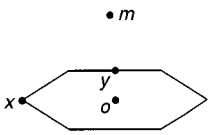


Figure 1. The QUEST3D query dialog used to generate parameters *om*, *xôm*, and *yôm*

Discrepancies in the 2D representation of arenes in the Database necessitates the use of both delocalized aromatic

[a] Department of Chemistry, University of Nottingham, Nottingham NG7 2RD, U.K.
Fax: (internat.) + 44–115/951–3564
E-mail: mark.mascal@nottingham.ac.uk
[b] Department of Chemistry, Loughborough University, Loughborough LE11 3TU, U.K.
[c] CLRC Daresbury Laboratory, Daresbury, Warrington, Cheshire WA4 4AD, U.K.

 © WILEY-VCH Verlag GmbH, D-69451 Weinheim, 2000 1434–1948/00/0303–0485 $ 17.50+.50/0

and "cyclohexatriene" arguments for the bonding in the ring. A metal atom at point *m* would have *x*,*y* coordinates $x_m = om \times \cos(x\hat{o}m)$ and $y_m = om \times \cos(y\hat{o}m)$. The radius of the cylinder (*r*) was defined by the relationship $x_m^2 + y_m^2 \leq r^2$, and the height of the cylinder was simply limited by constraining *om*. Choosing an arbitrary value of 5 Å for *om* produced a total of 2525 observations of metal atoms occupying this space. The *om* vs *xôm* scattergram (Figure 2a) reveals a massive data island centered around *om* = 1.7 Å corresponding to the plethora of η^6-complexes of the central transition metals. A discontinuity then precedes a second, more diffuse set of observations between ca. 2.5–3.5 Å. Subtracting the Bondi half-thickness of the benzene ring (1.77 Å) from this range of values gives a difference which is less than the van der Waals radius of the metal in most cases,[7] hence interactions of some description are indicated in this region (vide supra). Finally, the upward trend in the plot towards the 5 Å limit arises from the fixed

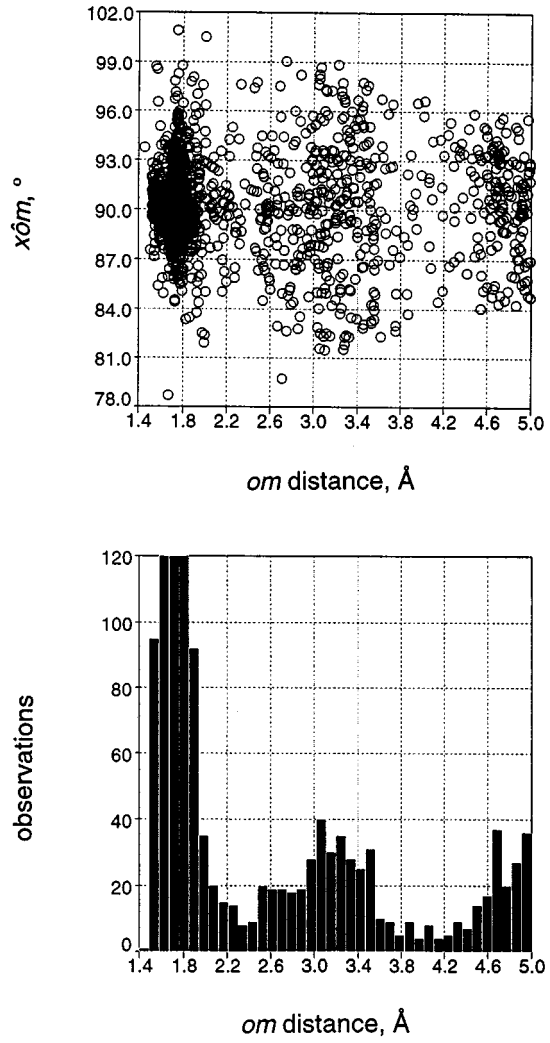


Figure 2. (a: top) *xôm* angle vs *om* distance scatterplot. (b: bottom) *om* distance histogram; the off-scale histogram bins between ca. 1.6–1.8 Å represent a total of 1648 observations

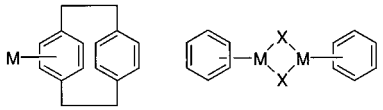


Figure 3. Increasing observations beyond 4.5 Å in the data presented in Figure 2 are due to relationships between metals and the *more distant* benzene rings in the above structures

relationships between metals and proximal rings in the numerous [2.2]paracyclophane η^6-metal complexes and μ-bridged bis(η^6-metal) species in the Database (Figure 3).

While statistical arguments are useful for generally characterizing the second maximum as a "bonding" region, individual cases are open to interpretation. Clearly, a sound basis for a cohesive electrostatic interaction can be derived from numerous gas phase studies between metal ions and aromatic systems, where bond energies on the order of 100 kJ mol^{-1} are typical.[8] Inspection of the datapoints individually gives valuable insights into the nature of the species involved. Analysis of both maxima by elemental composition, for example, leads to a reorganization of at least some of the data based on observed trends. Hence it becomes evident that the lanthanides and uranium, although formally in the second maximum in the plots in Figure 2, belong to the "short-range" bonding curve in the graphical representation of the data (Figure 4) taken from Tables 1 and 2. Likewise, some of the observations of Li–Ar contacts are contained within the first peak. After manual removal of redundant data arising from redeterminations, there are 1972 observations of short-range η^6 bonding to transition metals where the π-system can be counted in the valence electron set, and 328 other contacts which will simply be referred to as "longer-range."[9]

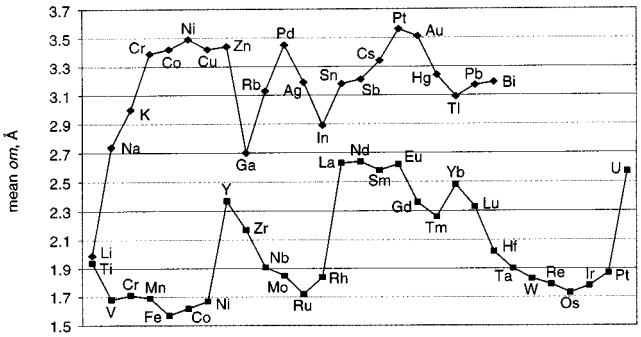


Figure 4. Mean longer-range (upper curve) and short-range (lower curve) Ar centroid–metal contact distances (*om*) by element with increasing atomic number

Certain elements appear to participate in both modes of complexation, i.e. divalent Cr, Co, Ni, and Pt, which in coordinatively unsaturated, square-planar complexes include a long-range arene contact over the vacant orbital. These, however, represent a total of only 18 observations and, in general, the longer-range complexes involve more-or-less exclusively main-group metals and some transition metals with filled *d*-shells. Indeed, apart from Ag^{I} and Hg^{II}, the case for including any transition metal among the longer-range complexes is debatable.

Table 1. Statistics for short-range Ar centroid–metal complexes

Metal	Observations	*om* Range	Mean *om*
Ti	25	1.74–2.11	1.94
V	24	1.59–1.87	1.68
Cr	728	1.52–1.82	1.71
Mn	38	1.55–1.77	1.69
Fe	116	1.46–2.18	1.57
Co	36	1.58–1.85	1.62
Ni	3	1.61–1.71	1.67
Y	5	2.26–2.53	2.37
Zr	33	1.98–2.37	2.17
Nb	24	1.82–2.02	1.91
Mo	55	1.72–1.95	1.85
Ru	672	1.58–2.01	1.72
Rh	41	1.76–1.90	1.84
La	2	2.54–2.72	2.63
Nd	5	2.58–2.71	2.64
Sm	8	2.52–2.67	2.58
Eu	5	2.55–2.68	2.62
Gd	2	2.22–2.51	2.36
Tm	2	2.16–2.36	2.26
Yb	2	2.48	2.48
Lu	1	2.33	*2.33*
Hf	12	1.91–2.33	2.02
Ta	3	1.83–1.94	1.90
W	32	1.74–2.00	1.83
Re	5	1.75–1.86	1.79
Os	56	1.61–1.83	1.73
Ir	24	1.72–1.89	1.78
Pt	1	1.87	*1.87*
U	12	2.54–2.60	2.57

Table 2. Statistics for longer-range Ar centroid-metal complexes

Metal	Observations	*om* Range	Mean *om*
Li	29	1.67–2.45	1.99
Na	29	2.29–3.56	2.74
K	73	2.69–3.27	3.00
Cr^{II}	1	3.39	3.39
Co^{II}	3	3.26–3.56	3.42
Ni^{II}	7	3.42–3.55	3.49
Cu^{II}	4	3.25–3.55	3.42
Zn	1	3.44	3.44
Ga^{I}	15	2.42–3.00	2.70
Rb	4	3.11–3.17	3.13
Pd^{II}	3	3.38–3.50	3.45
Ag^{I}	4	2.89–3.37	3.19
In^{I}	3	2.83–2.95	2.89
Sn^{II}	9	2.45–3.58	3.18
Sb^{III}	24	2.96–3.34	3.21
Cs	49	3.10–3.57	3.34
Pt^{II}	3	3.55–3.59	3.56
$Au^{I, III}$	2	3.48–3.55	3.51
Hg^{II}	11	3.05–3.52	3.24
Tl^{I}	24	2.85–3.52	3.09
Pb^{II}	6	2.78–3.43	3.17
Bi^{III}	24	2.67–3.56	3.19

Trends in the lower curve in Figure 4 are periodic and consistent with the electronic nature of the metals involved. The upper curve, on the other hand, shows the anticipated progression within the alkali metal series, although a conspicuous discontinuity occurs at gallium, indium, and thallium. This evidence of a comparatively strong interaction in these cases is consistent with the anomalous solubility of monovalent group 13 salts in aromatic hydrocarbons. This phenomenon was examined in detail by Schmidbaur in the 1980s and rationalized in terms of a particularly effective overlap of the empty LUMO set of *p*-orbitals on the metal with the HOMO of the arene.[10]

Since the issue at hand is sandwich complexation in **1**, the dataset for longer-range contacts was also scrutinized for other occurrences of this mode of assembly. Twenty three examples of metals simultaneously coordinated to two or more aryl rings are found, most involving the alkali and group 13 metals, but in all but a few cases the *o···m···o* angle was considerably less than 180°. One notable exception was $[Cs(p\text{-xylene})_2]^+$, with a mean *om* distance of 3.4 Å and $o\hat{m}o$ = 176.7°.[11] Also relevant here are the π-cation complexes between 1,3-alternate calix[4]arenes and metal ions, four examples of which meet the general search criteria set out in the present work, although again, $o\hat{m}o$ ranges from 138.8 to 159.8°.[12]

Finally, two examples of other purpose-designed, mixed π-heteroatom ligands also emerge in this search. In the first, a crown ether incorporates a single aromatic ring whose centroid is involved in longer-range bonding to either Tl^{I} (*om* = 2.96 Å)[13] or Ag^{I} (*om* = 2.89 Å).[14] The second involves a tripodal *tris*(pyrazoylmethyl)benzene ligand for ruthenium.[15]

Cylindrophane 1 and Complexes 2

As mentioned above, the utility of a receptor such as **1** derives from its Ar···Ar bisector distance, which coincides approximately with the second maximum of the histogram in Figure 2. This provides an opportunity to study metals residing in a trigonal planar heteroatom ligand field and their interactions with the apical benzene centroids. Although **1** was designed to possess a high degree of conformational stability, molecular dynamics simulations indicate an accordion-like flexibility along the axis which runs through the rings, which gives the ligand the potential to accommodate metals throughout a range of preferred *om* distances.[16]

Preorganization in cylindrophanes such as **1** is achieved through careful regard for the conformational preferences of chains which link aromatic rings together, and the structural arguments in the design of these molecules have been discussed in detail.[4] The synthesis of **1** was carried out as described[2] and the stable complexes $[Ag(\mathbf{1})]BF_4$ and $[Cu(\mathbf{1})]BF_4$ were prepared by simple mixing of **1** with the tetrafluoroborate salts of the respective metals. The ^{1}H-NMR spectra ($CDCl_3$) of the complexes indicated no loss of symmetry and gave evidence of a substantial interaction between the metals and the ligand by the marked shifts of the S–CH_2 signal (+0.6–0.7 ppm). Most interesting, however, was the downfield shift of the aromatic protons (+0.20 ppm in $[Ag(\mathbf{1})]BF_4$, 0.12 ppm in $[Cu(\mathbf{1})]BF_4$), supporting the view that the phenyl rings in $[M(\mathbf{1})]^+$ do not simply block the apical positions but actually coordinate to the metal center.

Final proof of the structure was gained by X-ray crystallography of the complexes. Because $[Ag(\mathbf{1})]BF_4$ and $[Cu(\mathbf{1})]BF_4$ are isostructural, only the latter is shown in Figure 5. Relevant angles and distances for each complex are presented in Table 3.[17] A mirror plane passes through the

metal and the three sulfur atoms which surround it with molecular C_3 symmetry. While trigonal planar coordination is unusual for Ag^I and Cu^I,[18] the bis(η^6)-complexation of the metals presented here is unique. Even simple η^6-coordination is unprecedented in the case of Cu^I, although this species is known to participate in η^1-complexation to arenes,[19] which is also the preferred mode of interaction for Ag^I.[20]

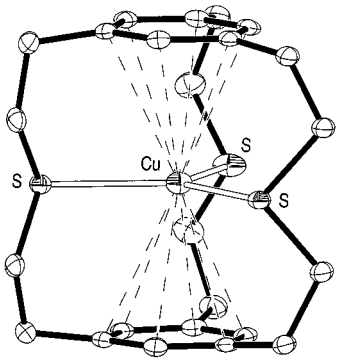


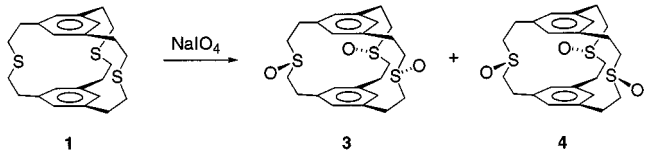
Figure 5. A view of the complex cation in the crystal structure of [Cu(**1**)]BF_4

Table 3. Selected geometric parameters for [Ag(**1**)]BF_4 and [Cu(**1**)]BF_4

	[Ag(**1**)]BF_4	[Cu(**1**)]BF_4
S–M, Å	2.577(2)	2.370(2)
	2.578(2)	2.380(3)
	2.631(2)	2.412(3)
S–M–S, °	117.72(5)	119.00(9)
	119.98(6)	119.91(9)
	122.31(5)	121.08(9)
M–centroid, Å	2.92	2.97
M–centroid–M, °	177.5	178.4

Cyclic voltammetry of [Cu(**1**)]BF_4 in $MeCN/CH_2Cl_2$ (1:1) gave a CV reminiscent of a metal deposition/stripping wave, with sharp oxidation and reduction peaks at E_{pa} = –0.61 V and E_{pc} = –0.87 V vs. Fc/Fc^+. When the solvent was switched to neat CH_2Cl_2, little if any current was measured up to the working limit of the platinum electrode. This result implied sufficient dissociation of the complex in the presence of acetonitrile to give a measurable concentration of electrochemically active, "free" Cu^I, whereas in the less-polar solvent system the cylindrophane effectively shields the metal and thus prevents redox activity. Analogous experiments with the silver complex had a similar outcome, with E_{pa} = –0.28 V and E_{pc} = –0.72 V and an irreversible anodic wave at 0.60 V vs Fc/Fc^+ in 1:1 $MeCN/CH_2Cl_2$.

Perhaps the most obvious modification of **1** is oxidation to the *tris*-sulfoxide. Modelling shows that in conformers where the three oxygens point into the cavity, the distance from these sites to the center of the trigonal plane they define is a convenient 2.3 Å, compared, for example, to 3.1 Å in the trioxa analog of **1**.[4] Thus, reaction of **1** with sodium periodate in aqueous THF provided the isomeric sulfoxides



Scheme 1. Synthesis of *tris*-sulfoxide cylindrophanes **3** and **4**

3 (12%) and **4** (62%) (Scheme 1). Even after chromatography, both of these compounds showed substantial $[M + Na]^+$ peaks in the FAB mass spectra, attributed to the presence of Na^+ in the oxidation reaction. However, sulfoxide **3** showed no noteworthy changes in the ^1H NMR spectrum during titration with a range of metal ions (in CD_3OD), while the unsymmetric **4** interacted only weakly and non-specifically with Na^+, Ag^+, and Cu^+.

Attempts to crystallize **3** or **4** in the presence of $NaBF_4$ led in one instance to the observation of very small crystals (of **4**), the structure of which could be determined using synchrotron radiation, but which did not include the metal (Figure 6). As might have been predicted, the sulfur lone pairs occupy the cavity in preference to the oxygens, which renders the complexation of metals in the cavity less favorable, despite the potentially more appropriate heteroatom-metal distance. The Ar···Ar separation in **4** is 5.66 Å in the crystal, i.e. slightly closer than in the metal complexes of **1** (cf. Table 3).

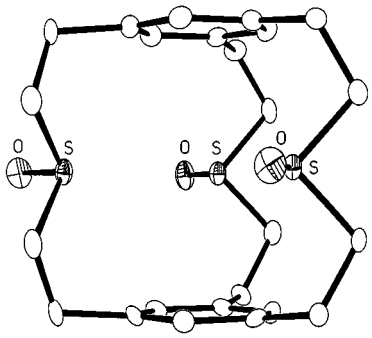


Figure 6. X-ray crystal structure of **4**

Conclusion

The encapsulation of metal ions in cylindrophane **1** provides a general approach to effective metal sandwich complexation in cases where longer (> 2.5 Å) aryl centroid–metal contacts are required. Two complexes, [Ag(**1**)]BF_4 and [Cu(**1**)]BF_4, have been prepared and characterized by NMR spectroscopy and X-ray crystallography. Together they constitute uncommon examples of Cu^I and Ag^I coordination in a trigonal-planar ligand field, a rare example of η^6-coordination to Ag^I, the first example of η^6-coordination to Cu^I, and, of course, the only examples of Cu^I and Ag^I sandwich complexes.[21] A detailed statistical analysis of metal-η^6 species in the solid state establishes a context for the study, and the population of metals in longer-range contact to the benzene ring supports the general characterization of such interactions as bonding. Although this me-

ans of association is energetically inferior to short-range η^6-complexation, this work nevertheless draws awareness to its availability as a noncovalent "design principle."

The metal–arene distances of ca. 3 Å in [Ag(**1**)]BF_4 and [Cu(**1**)]BF_4 invite speculation as to which other metals in Table 2 might give stable cylindrophane complexes, or indeed whether the lanthanides in Table 1, with metal–arene distances as great as 2.7 Å, might, as trivalent ions, complete their valence shell with the 18 electrons present in **1**. Basic modifications to the cylindrophane framework also suggest themselves, among them the use of phosphorus as the equatorial heteroatom, the transformation of which into the corresponding phosphane oxide would force the three O sites into the cavity between the rings (in preference certainly to any alkyl/aryl group on P). Work along these lines continues.

Experimental Section

[Ag(1)]BF_4: To a solution of the ligand **1** (51 mg, 0.12 mmol) in CH_2Cl_2 (5 mL) was added $AgBF_4$ (24 mg, 0.12 mmol) and the solution was stirred in the dark for 24 h. The solvent was evaporated and the residue dissolved in acetonitrile, preabsorbed onto silica and chromatographed (10% MeOH/$CHCl_3$) to give a white solid (48 mg, 64%), m.p. 270 °C (dec). – ^{1}H NMR (250 MHz, $CDCl_3$): δ = 2.95 (t, 12 H), 3.24 (m, 12 H), 6.93 (s, 6 H). – ^{13}C NMR (67.8 MHz, $CDCl_3$): δ = 34.0, 37.6, 127.4, 141.0; – MS (FAB): *m*/*z* 521 (23) [M^+]; elemental analysis calcd for $C_{24}H_{30}S_3AgBF_4$: C, 47.31, H, 4.96; found: C, 47.36, H, 4.90.

[Cu(1)]BF_4: To a solution of the ligand **1** (37 mg, 0.089 mmol) in a mixture of CH_2Cl_2 (1.5 mL) and MeCN (0.5 mL) was added [Cu(MeCN)$_4$]BF_4 (28 mg, 0.089 mmol) and the solution was stirred overnight. The solvent was evaporated and the residue chromatographed (5% MeOH/$CHCl_3$) to give a white solid (41 mg, 82%), m.p. 240 °C (dec). – ^{1}H NMR (250 MHz, $CDCl_3$): δ = 2.90 (t, 12 H), 3.16 (br s, 12 H), 6.85 (s, 6 H). – ^{13}C NMR (67.8 MHz, $CDCl_3$): δ = 33.4, 36.7, 126.3, 140.8. – HRMS (ES-TOF): *m*/*z* calcd. for $C_{24}H_{30}S_3Cu$: 477.0806; found 477.0780 (M^+).

***Tris*-sulfoxides 3 and 4:** To a solution of the sulfide **1** (274 mg, 0.661 mmol) in a mixture of THF (30 mL) and water (2 mL) was added sodium periodate (0.465 g, 2.17 mmol). The reaction was stirred for 12 h, filtered and the solvent evaporated. The residue was dissolved in methanol, preabsorbed onto silica gel, and chromatographed (12% MeOH/$CHCl_3$) to give **3** (37 mg, 12%) and **4** (190 mg, 62%), both as a white solids.

3: m.p. 300 °C (dec.). – ^{1}H NMR (250 MHz, $CDCl_3$): δ = 2.59–2.71 (m, 6 H), 2.92–3.15 (m, 18 H), 6.88 (s, 6 H). – ^{13}C NMR (67.8 MHz, $CDCl_3$): δ = 29.2, 55.7, 128.1, 139.4. – HRMS (FAB): *m*/*z* calcd. for $C_{24}H_{31}S_3O_3$: 463.1435; found: 463.1437 (M^+ + H).

4: m.p. 280 °C (dec.). – ^{1}H NMR (250 MHz, $CDCl_3$): δ = 2.47–2.63 (m, 7 H), 2.83–3.09 (m, 19 H), 6.73 (s, 2 H), 6.86 (s, 2 H), 7.02 (s, 2 H). – ^{13}C NMR (67.8 MHz, $CDCl_3$) δ = 28.2, 29.1, 54.1, 55.2, 55.4, 126.0, 127.9, 129.3, 139.7, 139.9, 140.5. – HRMS (FAB): *m*/*z* calcd. for $C_{24}H_{31}S_3O_3$ 463.1435; found: 463.1432 (M^+ + H).

Cyclic Voltammetry of [Ag(1)]BF_4 and [Cu(1)]BF_4: Cyclic voltammograms (CVs), 100 mV s^{-1}, were recorded at 22±2°C in the solvent indicated using an EG & G Princeton Applied Research (PAR) Model 173 potentiostat. The supporting electrolyte was tetraethylammonium tetrafluoroborate (0.2 M). A three-compartment electrochemical cell was employed using nitrogen-purged solutions, with a platinum wire working electrode, a platinum-mesh counter electrode, and a sodium chloride saturated calomel reference electrode. The platinum wire working electrode was pre-treated before measurements by anodisation, then cathodisation, (1 min each at 100 mA in 1 M sulfuric acid) followed by washing with deionised water, then acetonitrile and finally air dried.

Crystal Data for 4: Colorless needle from methanol, $C_{24}H_{30}O_3S_3$, M = 462.7, monoclinic, a = 8.891(2), b = 14.763(3), c = 17.928(4) Å, β = 100.695(6)°, U = 2312.3(9) Å^3, T = 150(2) K, space group $P2_1/c$ (no. 14), Z = 4, μ(Mo-$K\alpha$) = 0.344 mm^{-1}, 15450 reflections measured of which the 4904 unique to $2\theta_{max}$ 52° (R_{int} = 0.088) were used in all calculations. The final $wR(F^2)$ was 0.328, R_1 = 0.116. Data were collected on the Bruker SMART CCD area detector diffractometer on Station 9.8 at CLRC Daresbury Laboratory, using synchrotron radiation with a wavelength of 0.6917 Å. Crystallographic data (excluding structure factors) for the structure reported in this paper have been deposited with the Cambridge Crystallographic Data Centre as supplementary publication no. CCDC-132651. Copies of the data can be obtained free of charge on application to CCDC, 12 Union Road, Cambridge CB2 1EZ, UK [Fax: (internat.) + 44-1223/336-033; E-mail: deposit@ccdc.cam.ac.uk].

Acknowledgments

The financial support of the University of Nottingham and the use of the EPSRC's Chemical Database Service at Daresbury[6b] is acknowledged. We also thank the CLRC for the provision of beamtime on Station 9.8 of the SRS. The author is indebted to Dr. Richard Wheatley for helpful discussions and Mr. Neil Brooks for experimental assistance.

[1] With the apparent exception of Tc and Pd; scandium(0) η^6-complexes have been prepared (see F. G. N. Cloke, *Chem. Soc. Rev.* **1993**, *22*, 17–24), but do not appear in the present study since no X-ray crystal structures have been published.

[2] M. Mascal, J.-L. Kerdelhué, A. J. Blake, P. A. Cooke, *Angew. Chem.* **1999**, *111*, 2094–2096; *Angew. Chem. Int. Ed.* **1999**, *38*, 1968–1971.

[3] The term "macrobicycle" as applied here is used as an analogy to cryptand macrobicycles with aromatic rings counted as bridgeheads, and is not intended to be a formal description of the ring system.

[4] J. Hansen, A. J. Blake, W.-S. Li, M. Mascal, *J. Chem. Soc., Perkin Trans. 1* **1998**, 3371–3376.

[5] A. G. Orpen, L. Brammer, F. H. Allen, O. Kennard, D. G. Watson, R. Taylor, *J. Chem. Soc., Dalton Trans.* **1989**, S1–S83.

[6] [6a] O. Kennard, F. H. Allen, *Chem. Des. Autom. News* **1993**, *8*, 31–37. – [6b] D. A. Fletcher, R. F. McMeeking, D. Parkin, *J. Chem. Inf. Comput. Sci.* **1996**, *36*, 746–749.

[7] Van der Waals radius values for metals vary between 1.39 Å for zinc and 2.75 Å for potassium: A. Bondi, *J. Phys. Chem.* **1964**, *68*, 441–451.

[8] B. P. Pozniak, R. C. Dunbar, *J. Am. Chem. Soc.* **1997**, *119*, 10439–10445 and references therein.

[9] A generic Van der Waals cutoff limit of *om* < 3.6 Å applies to all longer-range contacts. Over 80% of the observations in this range involve intermolecular metal–arene contact, which mitigates against proximity imposed by bonded, intramolecular relationships between the metal and the ring.

[10] H. Schmidbaur, *Angew. Chem.* **1985**, *97*, 893–904; *Angew. Chem. Int. Ed. Engl.* **1985**, *24*, 893–904.

[11] J. L. Atwood, W. E. Hunter, R. D. Rogers, J. A. Weeks, *J. Inclusion Phenom.* **1985**, *3*, 113–123.

[12] [12a] A. Ikeda, H. Tsuzuki, S. Shinkai, *Tetrahedron Lett.* **1994**, *35*, 8417–8420. – [12b] P. D. Beer, M. G. B. Drew, P. A. Gale, P.

B. Leeson, M. I. Ogden, *J. Chem. Soc., Dalton Trans.* **1994**, 3479–3485. – [12c] X. Delaigue, M. W. Hosseini, N. Kyritsakas, A. de Cian, J. Fischer, *J. Chem. Soc., Chem. Commun.* **1995**, 609–610.

[13] F. Fages, J.-P. Desvergne, H. Bouas-Laurent, J. Hinschberger, P. Marsau, M. Petraud, *New J. Chem.* **1988**, *12*, 95–106.

[14] H. Andrianatoadndro, Y. Barrans, P. Marsau, J. P. Desvergne, F. Fages, H. Bouas-Laurent, *Acta Crystallogr., Sect. B* **1995**, *51*, 293–300.

[15] C. M. Hartshorn, P. J. Steel, *Angew. Chem.* **1996**, *108*, 2818–2820; *Angew. Chem. Int. Ed. Engl.* **1996**, *35*, 2655–2657.

[16] Molecular mechanics simulations performed with MACROMODEL version 5.5 with the MM2 force field: F. Mohamadi, N. G. J. Richards, W. C. Guida, R. Liskamp, M. Lipton, C. Caufield, G. Chang, T. Hendrickson, W. C. Still *J. Comp. Chem.* **1990**, *11*, 440–467.

[17] Full data for the crystal stucture determinations is given in reference 2.

[18] 9519 crystal structures in the Cambridge Structural Database contain Cu and 1734 contain Ag, of which 108 (1.1%) and 33 (1.9%), respectively, are found in a trigonal planar ligand field (i.e. trivalent with bond angles between 115° and 125°). It must be noted that it is not possible using the CSD's QUEST3D software to specify metal oxidation states, so the above figures for copper include both Cu^{I} and Cu^{II}.

[19] For example: M. Pasquali, C. Floriani, A. Gaetani-Manfredotti, *Inorg.Chem.* **1980**, *19*, 1191–1197.

[20] No less than 129 examples of Ag-η^1 and Ag-η^2 bonding with a mean Ag-arene distance of 2.82 Å are also found in the CSD. The nature of metal-η^1 and η^2 bonding will be the subject of a separate report (in preparation). See also K. Shelly, D. C. Finster, Y. J. Lee, W. R. Scheidt, C. A. Reed, *J. Am. Chem. Soc.* **1985**, *107*, 5955–5959.

[21] Although we report the first bis η^6-aryl Ag^{I} sandwich compound, an example of a bis η^2: η^2: η^2-cyclic triyne Ag^{I} sandwich has been described: J. D. Ferrara, A. Djebli, C. Tessier-Youngs, W. J. Youngs, *J. Am. Chem. Soc*. **1988**, *119*, 647–649.

Received July 26, 1999
[I99274]

Stabilization of Carbenium Ions Derived from Ethynylestradiol by Different Adjacent Organometallic Moieties. Implication in the Inactivation of the Estrogen Receptor

Domenico Osella,*[a] Mauro Ravera,[a] Carlo Nervi,[b] Giorgio Cavigiolio,[b] Marco Vincenti,[c] Anne Vessières,[d] and Gérard Jaouen*[d]

Keywords: Clusters / Steroids / Protonation / Carbocations / Immunoassay

The stabilization of carbenium ions by an adjacent organotransition metal moiety has been evaluated using the classical Deno's method as well as a new procedure based on DCI-MS spectrometry. The ability of transition metal clusters to enhance the stability of a proximate carbocationic center in 17α-alkynylestradiol–[OM] derivatives {[OM] = $Co_2(CO)_6$; $Co_2(CO)_4$(dppm); $Mo_2Cp_2(CO)_4$; $M_3(CO)_{10}$, M = Ru, Os; $HRu_3(CO)_9$} has been related to their capacity to inactivate the estrogen receptor (affinity marker properties).

The stabilization of carbenium ions by an adjacent organotransition metal moiety is a well documented phenomenon.[1,2] The study of the hexacarbonyldicobalt unit as a protecting group for the C≡C triple bond[3] led Nicholas et al. to discover the fast acid-promoted hydration/dehydration equilibrium, (Figure 1) which generates the $[(propargyl)Co_2(CO)_6]^+$ cation as an intermediate.[4]

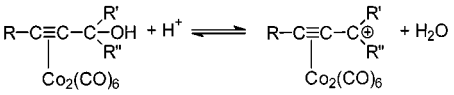


Figure 1. Hydration/dehydration equilibrium involving a $[(propargyl)Co_2(CO)_6]$-like compound

A large variety of propargyl cations coordinated to many different organometallic fragments have been investigated to date.[5–8] The major interest in these compounds is based on the possibility of employing them as electrophilic synthons. In this context, 17α-alkynylestradiol organometallic derivatives (Figure 2) may be regarded as analogous to the propargylic alcohol complexes.

Several examples of transition-metal carbonyl fragments, used as labeling agents for 17α-alkynylestradiol, have been reported in the literature {[OM] = $Co_2(CO)_6$; $Mo_2Cp_2(CO)_4$; $M_3(CO)_{10}$, M = Ru, Os}.[9] An appreciable

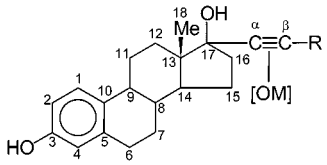


Figure 2. Conventional representation of the [OM]-steroidal ring system, showing the numbers used to identify the carbon atoms

recognition level for the receptor, evaluated in terms of the *relative binding affinity (RBA)*, is maintained even when relatively bulky groups are linked to a 17α-alkynylestradiol.[10] This particular labeling of steroids has been used in a new non-isotopic immunoassay (*carbonylmetalloimmunoassay, CMIA*) for assaying circulating hormones such as cortisol[9] or in receptorology for studying the interaction between the hormone and its receptor.

The synthesis of a large number of organometallic labeled hormones led to the discovery of a new family of *affinity markers* for the estrogen receptor, i.e. molecules able to bind irreversibly to the receptor, probably through a direct covalent bond. This unusual behavior may be attributed to the stability of the associated organometallic carbenium ion, as previously discussed. The 17β-OH group is essential for inactivation of the receptor.[11] The presence of cysteine acid residues near the association site of the receptor can account for the formation of the carbocation through an acid-promoted dehydration reaction on the OH group at the 17β position (Figure 3). Unfortunately, the recently published X-ray structure for the Ligand Binding Domain (LBD) of the α-estradiol receptor was obtained after chemical modification of the cysteines.[12] Therefore, this hypothesis cannot be proven for the moment, although these organometallic markers may help in the elucidation of the structure of the receptor binding site.[13,14,15]

[a] Dipartimento di Scienze e Tecnologie Avanzate, Università del Piemonte Orientale "Amedeo Avogadro,
Corso T. Borsalino, 54, I-15100 Alessandria, Italy
Fax: (internat.) +39-011/254410
[b] Dipartimento di Chimica IFM, Università di Torino,
Via P. Giuria, 7, I-10125 Torino, Italy
[c] Dipartimento di Chimica Analitica, Università di Torino,
Via P. Giuria, 5, I-10125 Torino, Italy
[d] Ecole Nationale Supérieure de Chimie de Paris, Laboratoire de Chimie Organométallique, UMR CNRS 7576,
11, rue Pierre et Marie Curie, F-75231 Paris Cedex 05, France

 © WILEY-VCH Verlag GmbH, D-69451 Weinheim, 2000 1434–1948/00/0204–0491 $ 17.50+.50/0

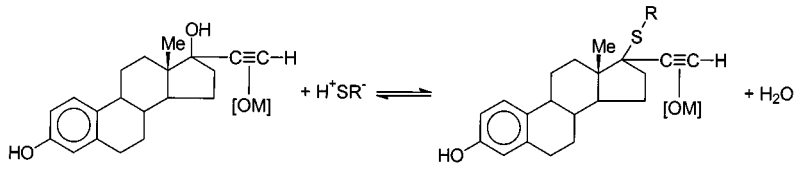
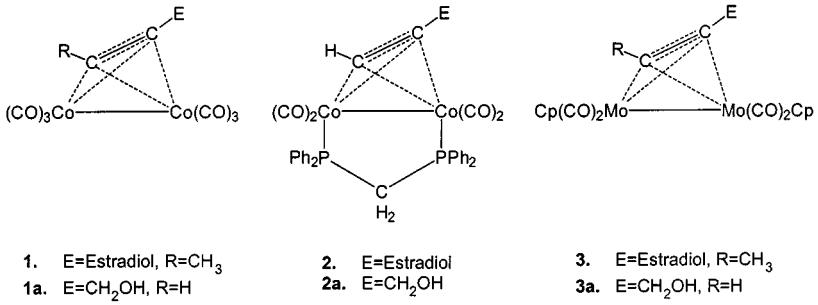


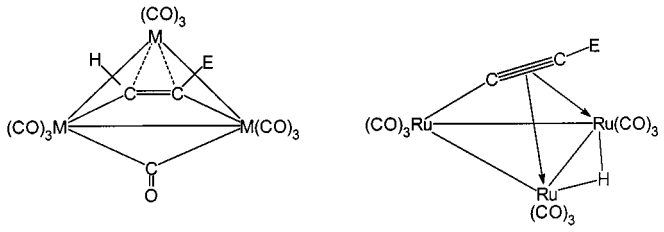
Figure 3. Proposed mechanism for the formation of the carbocation through an acid-promoted dehydration reaction on the 17β–OH group



1. E=Estradiol, R=CH_3
1a. E=CH_2OH, R=H

2. E=Estradiol
2a. E=CH_2OH

3. E=Estradiol, R=CH_3
3a. E=CH_2OH, R=H



4. M=Ru, E=Estradiol
4a. M=Ru, E=CH_2OH
5. M=Os, E=Estradiol
5a. M=Os, E=CH_2OH

6. E=Estradiol
6a. E=CH_2OH

Figure 4. Sketch of structures of complexes **1–6** and **1a–6a**

The aim of this work is to investigate both the relationship between the ability of transition metal clusters to enhance the stability of the neighboring carbocationic center in 17α-alkynylestradiol derivatives, and also to investigate their affinity marker properties. Breast cancers that retain estrogen receptor (ER) can usually be treated effectively by endocrine therapy, such as by the use of the antiestrogen tamoxifen. Moreover, by labeling estradiol with cytotoxic metal derivatives one could expect to synthesize a new family of anticancer drugs able to use the receptor system as a vector to reach the target cells and remain attached for a period sufficient to damage the cancerous tissue.

Results and Discussion

Several 17α-alkynylestradiol organometallic derivatives **1–6** and the corresponding propargylic model complexes **1a–6a** have been synthesized (Figure 4).

Compound **6a** [$HRu_3(CO)_9(–C{\equiv}CCH_2OH)$] was obtained in good yield by thermolysis of $Ru_3(CO)_{10}(HC{\equiv}CCH_2OH)$ (**4a**). In contrast, the direct reaction of $Ru_3(CO)_{12}$ and $HC{\equiv}CCH_2OH$ gave compound **6a** only in trace amounts; the major product was metallacyclopentadiene $Ru_2(CO)_6(alkyne)_2$.[16]

The relative binding affinities of these complexes for the ER were determined in a competition binding assay using lamb uterine cytosol as a source of ER, and [^{3}H]estradiol as the tracer. The values found range between 2.5 and 33% (estradiol itself being taken as 100%), indicating moderate recognition. Roughly, RBA values are inversely proportional to the steric bulk of the organometallic graft.

The possible existence of a covalent bond between the hormone derivatives and the receptor was investigated by receptor inactivation (RI) studies. The RI procedure involves a preliminary incubation of the organometallic tracer with the cytosol receptor after which the free organometallic tracer is removed by means of charcoal-dextran treatment. The remaining reversible estrogen binding activity of the tracer-receptor adduct is then measured by an exchange reaction of [^{3}H]estradiol with the organometallic tracer not covalently bound to the estrogen binding site. The quantification of the [^{3}H]estradiol specifically bound to the ER was then performed by protamine sulfate precipitation as previously described.[17] The residual radioactivity

on the precipitate is related to the remaining estrogen binding activity: the higher the radioactivity, the lower the receptor inhibition (RI% = 0 for estradiol itself).[18]

Carbenium ions can be generated in presence of strong acids. The pK_{R+} values for ionization of alcohols in aqueous sulfuric acid were determined spectrophotometrically. The position of the alcohol–carbenium ion equilibrium (Equation 1):

$$R^+ + H_2O \rightleftharpoons ROH + H^+ \quad (1)$$

was studied as a function of sulfuric acid concentration, using the empirical acidity function (C_0) proposed by Deno.[19] The Deno's method is a facile way of obtaining the thermodynamic stability of the carbenium ions, provided that a sharp change in the UV/Vis spectrum is produced upon acid addition. However, the strongly acidic conditions required by this method may induce rearrangements of the steroid skeleton to give several enyne complexes (Figure 5), a possibility proposed in a previous study.[6]

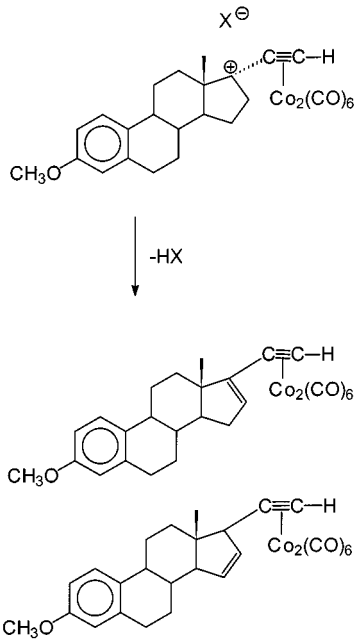


Figure 5. Proposed mechanism for the formation of enyne complexes through rearrangements of the steroid skeleton

Since the $[R^+]/[ROH]$ ratio is evaluated from the UV/Vis absorptions of both species, any chemical transformation of either is likely to alter the overall spectrum profile and, consequently, the pK_{R+} value. To prevent misinterpretations, several measurements have been carried out on the corresponding propargylic alcohol as models. This simplification is reasonable, as the pK_{R+} values measured for the propynylestradiol complexes **1** and **3** proved to be similar to those of the model propargyl complexes.[6]

To overcome the limitations inherent in the Deno's method, we propose an alternative gas phase procedure for evaluating carbocation stability with respect to the parent alcohol. This procedure utilizes chemical ionization mass spectrometry in combination with the fast thermal vaporization of the organometallic complex (DCI-MS). A relatively high pressure of reagent gas (i.e. isobutane) and a low pressure of analyte (M) are simultaneously present in the ionization chamber. The reagent gas is ionized by electron impact, and fragments in a conventional manner. Several collisions occur between ions and neutral isobutane molecules yielding the *tert*-butylcarbonium ion $[(CH_3)_3C]^+$ as a stable species. This may subsequently react with the analyte (M) by proton transfer to generate the quasi-molecular ion $[M + H]^+$. The facility of such a process, and thus the intensity of the quasi-molecular ion peak $[M + H]^+$, depends on the acid-base properties of the species involved in the equilibrium (Equation 2):

$$[(CH_3)_3C]^+ + M \rightleftharpoons (CH_3)C{=}CH_2 + [M{+}H]^+ \quad (2)$$

In the present case, the protonated ion $[M + H]^+$ can eliminate H_2O, provided the corresponding carbocation is sufficiently stable (Figure 6). Thus, the ratio, $[M - OH]^+/[M + H]^+$, between ion peak intensity represents a good estimate of the corresponding carbocation stability in the gas phase.

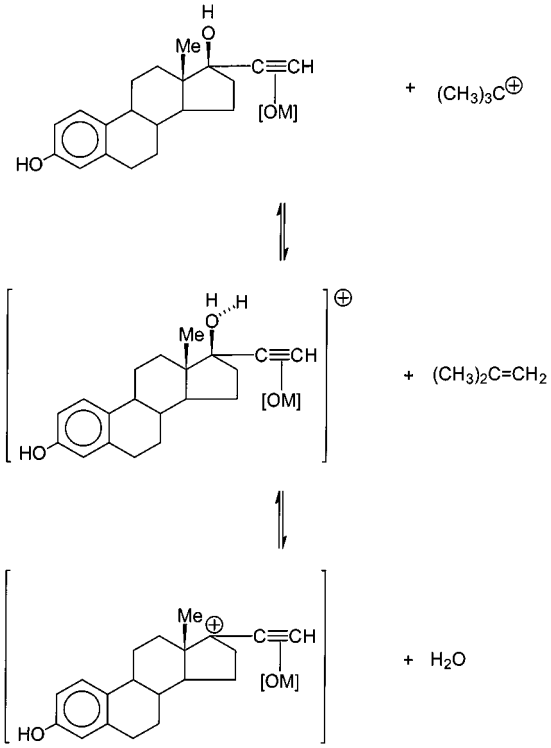


Figure 6. Water elimination reaction on the organometallic estradiol

The DCI method is experimentally simpler than the (chemical) Deno's method. Furthermore, the ionization process and ion detection is so rapid that elimination reactions on the carbenium ion do not occur, allowing a meaningful measure on real estradiol-organometallic derivatives.

The presence of the 17β-OH group is essential for carbocation formation; in fact, the DCI-MS spectrum of estrone (C=O group in lieu of the OH group) does not exhibit the $[M - OH]^+$ peak. The contribution of the phenolic OH in position 3 to the protonation-dehydratation process is negligible: $[M - OH]^+/[M + H]^+$ ratios of 17α-ethynylestradiol and 3-methoxy-17α-ethynylestradiol are identical, within error.

Compounds **4** and **5** show a fragmentation pathway different to all the other complexes. Since the major process is the loss of a CO ligand, a reaction previously found in solution,[20] the $[M + H]^+$ and $[M - OH]^+$ peaks are too small to be evaluated properly. For this reason, the mass ratio has been evaluated by the relative abundance of the daughter ions $[(M - CO) - OH]^+/[(M - CO) + H]^+$.

The DCI-MS data for the propargyl models **1a–6a** are similar to those of the estradiol homologues: the $[M - OH]^+/[M + H]^+$ ratios of the former are always higher than those of the latter. This result can be explained by postulating that the $[M + H]^+$ internal energy for estradiol derivatives is distributed over a much larger number of chemical bonds than for propargyl derivatives. Less energy is therefore available to induce the loss-of-water fragmentation process.

Complexes **1–6** may be separated into three categories:

(i) Complex **2** has a pK_{R+} value of –11 and a DCI-MS ratio of 0.87, indicating a highly unstable carbenium ion, and gives no alkylation of receptor at all (RI% = 0);

(ii) Compounds **1** and **4–6** have pK_{R+} values in the –6.0 to –1.4 range and DCI-MS ratios from 7.2 to 1.4, indicating the formation of moderately stable but still reactive carbocations; they efficiently inactivate the estradiol receptor ($80 < RI\% < 60$);

(iii) Complex **3** shows the highest pK_{R+} and DCI-MS values (+2.7 and 12.0, respectively) indicating a very stable but almost unreactive carbocation, associated with a low inactivation of the receptor (RI% = 22).

The best affinity marker was found to be compound **1**, which has a pK_{R+} around –6. With smaller or higher pK_{R+} values this phenomenon of receptor inactivation is not so apparent. Although 17α-propynylestradiol shows the same pK_{R+} value as **1**, it does not reveal any detectable RI effect. This implies that the C≡C triple bond in the α position is itself able to stabilize the adjacent carbocation, although the metal core should play a further active role in establishing a covalent bond with the receptor, for instance with the thiol groups of cysteine residues present in the LBD. In this context, it is known that cobalt carbonyls are able to react with thiol functionalities, giving rise to a plethora of compounds.[21]

Table 1. Relative binding affinity (RBA%) of the estradiol receptor, inactivation of the receptor (RI%), pK_{R+} and DCI-MS ($[M - OH]^+/[M + H]^+$) ratio

	Compound	RBA	RI%	pK_{R+}	$[M - OH]^+/[M + H]^+$
	estradiol (E–H)	100%[a]	0%[a]	–13.0[b]	0.3[b]
	17α-ethynylestradiol (E–C≡CH)	70%[b]	0%[b]	[d]	1.2[b]
	17α-propynylestradiol (E–C≡C–CH_3)	44%[b]	0%[b]	–6.4 [b]	1.6[b]
1	$Co_2(CO)_6(EC{\equiv}C{-}CH_3)$	18%[c]	80%[c]	–6.0[b]	7.2[b]
1a	$Co_2(CO)_6(HC{\equiv}CCH_2OH)$	–	–	–5.5[e]	16.0[b]
2	$Co_2(CO)_4(dppm)(EC{\equiv}CH)$	4.2%[b]	0%[b]	–11.0[b]	0.9[b]
2a	$Co_2(CO)_4(dppm)(HC{\equiv}CCH_2OH)$	–	–	[d]	1.3[b]
3	$Mo_2Cp_2(CO)_4(EC{\equiv}C{-}CH_3)$	33%[c]	22%[c]	+2.7[e]	12.0[b]
3a	$Mo_2Cp_2(CO)_4(HC{\equiv}CCH_2OH)$	–	–	+3.0[e]	12.3[b]
4	$Ru_3(CO)_{10}(EC{\equiv}CH)$	8%[c]	68% [c]	[d]	2.0[b,f]
4a	$Ru_3(CO)_{10}(HC{\equiv}CCH_2OH)$	–	–	–1.4[c]	2.0[b,f]
5	$Os_3(CO)_{10}(EC{\equiv}CH)$	2.5%[c]	65%[c]	[d]	1.4[b,f]
5a	$Os_3(CO)_{10}(HC{\equiv}CCH_2OH)$	–	–	–3.4[c]	1.6[b,f]
6	$HRu_3(CO)_9(-C{\equiv}CE)$	2.6%[c]	60%[c]	[d]	1.5[b]
6a	$HRu_3(CO)_9(-C{\equiv}CCH_2OH)$	–	–	[d]	2.8[b]

[a] Values by definition. – [b] This work. – [c] ref. [10]. – [d] No shape change in the UV/Vis spectrum occurred upon acid addition. This prevented the correct evaluation of pK_{R+} values. – [e] ref.[6] – [f] Calculated as the ratio $[(M–Co)–OH]^+/[(M–CO) + H]^+$.

The experimental results are summarized in Table 1.

There is a rough correlation between pK_{R+} and DCI-MS values, although the metallic grafts are very different throughout the series. Higher (less negative) pK_{R+} values correspond to higher DCI-MS ratios; both results point to a higher stabilization of the corresponding carbocations.

As previously mentioned, an approximate correlation exists between the affinity marker properties of estradiol organometallic derivatives (evaluated by their RI% value) and the carbenium ions stabilization (evaluated from both pK_{R+} and DCI-MS values).[9] However, the interactions in a sophisticated biological system are always more complex than in our simple model experiment.

As mentioned above, compound **1** shows the highest RI value (80%). Replacement of one carbonyl group on hexacarbonyldicobalt-coordinated propargyl cations by phosphane is expected to increase the stability, and hence the pK_{R+} values of these compounds. This would occur by increasing the electron density on the Co_2 moiety, in the manner qualitatively described by Nicholas.[22] Kuhn et al. quantified this effect in a kinetic study on the electrophilic reactivity of $[Co_2(CO)_5(PPh_3)(HC{\equiv}CPh)]^+$ cation.[23] Thus, the replacement of two carbonyls by diphosphanes in compound **1** (to give **2**) is expected to increase the carbocation

stability. Surprisingly, compound **2** gave a pK_{R+} value of –11 and a mass ratio of 0.87, both indicating a highly unstable cation. This unexpected behavior can be explained in terms of steric hindrance.

The build-up of a positive charge results in a shift of the cationic center towards one of the Co atoms. It has to be recognized that the mechanism of carbocation stabilization involves rearrangements on the overall skeleton which facilitate the metal–$C(17)^+$ interaction. Melikyan et al. resolved the structure of a $Co_2(CO)_6$-complexed propargyl cation showing that the C^+ atom is no longer equidistant from Co atoms.[24] The same behavior was observed in $\mathbf{3}^+$, where the organometallic moiety shifts below the estradiol D ring, enabling a Mo–$C(17)^+$ interaction to be established.[6] In the case of $\mathbf{3}^+$ this interaction is weaker than that reported for $\mathbf{3a}^+$, and interestingly, this difference has been attributed to the conformational constraints imposed by the bioligand.

In **2** the steric repulsion should be enhanced by the presence of two bulky diphosphane and the large steroidal skeleton. In order to investigate this hypothesis, we compared the size of **2** with respect to **1**, by representing them using the molecular modeling program PC Model.[25] The organometallic fragments were derived from the X-ray structure of $Co_2(CO)_6(PhC{\equiv}CPh)$[26] and $[Co_2(CO)_4(dppm)]_2[PhC{\equiv}C{-}C{\equiv}CPh]$.[27] The steroidal moiety structure was taken from the crystallographic data of the estradiol-propanol adduct.[28] The fragments were combined according to **1** and **2**. After adjusting the new bond distances to normal values, the resulting structures were energy-minimized by rotating the steroidal fragment around the C(17)–Cα bond (fixed at 1.50 Å). This procedure was repeated several times. Lastly, by allowing small oscillations of all atoms (except those in the organometallic moiety), the overall energy minimum was obtained. Although the approximation inherent to this procedure should be recognized (e.g. the organometallic fragment is considered as a frozen unit), this method provides a reasonable model of the overall molecular geometries of **1** and **2**. The molecular surfaces were obtained by simply considering the atomic radii of their constituents (CPK surface). The resulting space-filling models of **1** and **2** (Figure 7) suggest that the large size of the diphosphane ligand buries the cobalt metals and therefore hinders any $C(17)^+$–Co interaction, in the corresponding carbocation $\mathbf{2}^+$, that is responsible for carbocation stabilization.

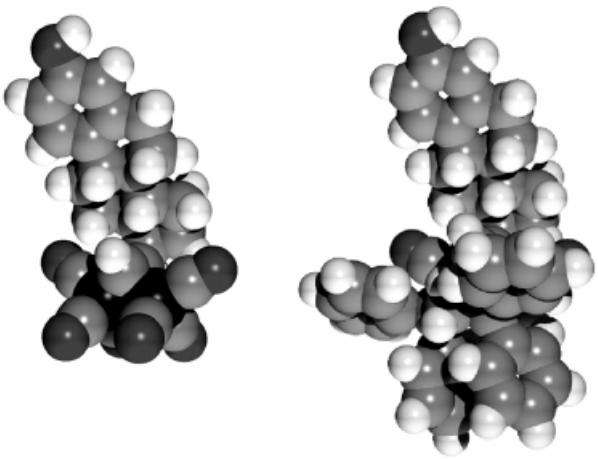


Figure 7. Space-filling models of **1** (left) and **2** (right). The picture was obtained by using molecular modeling program to graft the steroidal fragment onto the organometallic moiety

Experimental Section

General Chemical Procedures and Materials: All reactions were carried out under an atmosphere of dry nitrogen with standard Schlenk techniques. Solvents were distilled under nitrogen from appropriate drying agents. Published procedures were employed for the synthesis of 17α-propynylestradiol, **1** and **3**,[29] **4–6**,[10] and model complex **3a**.[30] Model complexes **1a**, **2a**, **4a**, and **5a** were synthesized by reaction of $Co_2(CO)_8$, $Co_2(CO)_6$(dppm),[31] or $M_3(CO)_{10}(NCCH_3)_2$,[32] (M = Ru for **7a** and Os for **8a**) with propargyl alcohol. Their purity was checked by IR, MS, and NMR spectroscopy. All elemental analyses are within ±0.5% of the theoretical values. Solution infrared spectra were recorded on a Bruker Equinox 55 in matched air-free cells with NaCl windows. ^{1}H-, ^{13}C-, and ^{31}P-NMR spectra were acquired on a JEOL EX-400 spectrometer operating at 400 MHz for ^{1}H, 100.6 MHz for ^{13}C, and 161.9 MHz for ^{31}P. Chemical shifts are reported downfield, positive with respect to the reference standard $SiMe_4$ (δ = 0) using the residual H signals as internal standard (^{1}H) or the characteristic resonances of the solvent nuclei (^{13}C); for ^{31}P, 85% H_3PO_4 was used as reference. ^{31}P and ^{13}C data are proton decoupled. DCI-MS spectra were recorded on a Finnigan-MAT 95Q instrument with magnetic and electrostatic analyzers. Isobutane was used as the reagent gas at 0.5 mbar pressure. The ion source temperature was kept at 50 °C, the electron emission current at 0.2 mA, and the electron energy at 200 eV. Positive ion spectra were collected. A computer program provides a digital readout of peak intensity and their comparison with the simulated isotopic pattern. The fit was excellent for all of the compounds under investigation.

Synthesis of $Co_2(CO)_4$(dppm)(EC≡CH) (2): Stoichiometric amounts of 17α-ethynylestradiol and $Co_2(CO)_6$(dppm), prepared according to the literature procedure,[33] were heated at reflux in benzene for 2 h, under nitrogen. The hot reaction mixture was filtered over a short silica column to remove any insoluble impurities and eluted with ethyl acetate/cyclohexane (40:60). The filtrate was dried under vacuum, and the complex was then purified by recrystallization from hexane/CH_2Cl_2 at –20 °C. Yields 60%. – IR (CH_2Cl_2): $\tilde{\nu}_{CO}$ = 2022 s, 1991 sh, 1989 vs, 1966 s cm^{-1}. – ^{1}H NMR ($CDCl_3$): δ = 8.12 (s, 1 H, C3–OH), 7.50–7.20 (m, 20 H, Ph), 7.10 (s, 1 H, C1–H), 6.62 (dd, 1 H, C2–H), 6.56 (d, 1 H, C4–H), 5.65 (t, ≡C21–H, $^3J_{HP}$ = 7.7 Hz), 4.69 (s, C17–OH), 3.62 and 3.22 (each m, 1 H, P–CH_2–P)[35], ca. 3.0–1.3 (all the remaining resonances heavily overlapped), 1.11 (s, 3 H, Me-18). – ^{13}C NMR ($CDCl_3$): δ = 204.42 (br, CO), 153.25 (C3), 138.34 (C5), 136–128 (Ph), 132.90 (C10), 126.42 (C1), 115.14 (C4), 112.51 (C2); 110.73 (C20), 85.04 (C17), 75.12 (C21), 48.21 (C13), 41.62 (t, P–CH_2–P, J_{CP} = 20.2 Hz), 42–20 (all the remaining resonances heavily overlapped); 15.73 (Me-18). – ^{31}P NMR ($CDCl_3$): δ = 42.5 (s).

Synthesis of $HRu_3(CO)_9$(–C≡C–CH_2OH) (6a): A solution of **6** in cyclohexane was heated at 75 °C under nitrogen for 45 min. The mixture was allowed to reach room temperature and purified by chromatography on a silica column. Cyclohexane first eluted some

adventitious $Ru_3(CO)_{12}$; pure CH_2Cl_2 then eluted the desired compound. Yield 50%. – IR (CH_2Cl_2): $\tilde{\nu}_{CO}$ = 2100 w, 2074 vs, 2054 vs, 2022 vs, 1989 m cm^{-1}. – ^1H NMR ($CDCl_3$): δ = 4.89 (d, 2 H, –CH_2–, J_{HH} = 6.1 Hz), 2.07 (t, 1 H, –OH), –21.03 (s, 1 H, hydride). – ^{13}C NMR ($CDCl_3$): δ = 197.15 and 188.19 (Ru–CO),[36] 160.58 (≡C–Ru), 102.64 (≡C–CH_2), 61.05 (CH_2).

pK_{R+}: Aliquots of a 10^{-3} M solution of the compound under investigation in acetonitrile (50 μL) were added to 450 μL of H_2SO_4/H_2O solutions of increasing acid concentration. The wavelength of maximum absorption was sought by scanning the 190–600 nm range and the approximate concentration of H_2SO_4 required to achieve 50% ionization of organometallic hormone determined by comparing the maximum UV/Vis absorbance for the different H_2SO_4/H_2O solutions.

A minimum of four aqueous H_2SO_4 solutions, whose concentrations were around the roughly estimated value, were prepared. Thirty minutes after the initial injection of acetonitrile solution into the acid solutions, a spectroscopic determination of the ratio [R^+]/[ROH] was performed. The final pK_{R+} value was calculated by use the following Equation (Equation 3):

$$pK_{R+} = C_0 + \log\frac{[R^+]}{[ROH]} \quad (3)$$

where C_0 is the Deno acidity function for H_2SO_4/H_2O solutions.[34]

Biochemical Materials and Methods: Estradiol, 17α-ethynylestradiol, charcoal (Norit A), and protamine sulfate (from salmon, grade X) were from Sigma. [6,7-^{3}H]Estradiol (specific activity 70 Ci/mmol) was purchased from C.E.A. (Saclay, France).

Preparation of Lamb Uterine Cytosol and Binding Assays: Lamb uteri, used as a source of estrogen receptor, were obtained from the slaughterhouse of Mantes-la-Jolie, France and kept frozen in liquid nitrogen until used. The lamb uteri were thawed, and the minced tissues homogenized with an Ultra-Turrax in buffer A (0.05 M Tris–HCl, sucrose 0.25 M, 0.1% 3β-mercaptoethanol, pH 7.4). The homogenate was centrifuged at 40,000 r.p.m. for 35 min in the TFT 65-13 rotor of a Kontron T-1160 ultracentrifuge. Aliquots (200 μL) of the supernatant (usually called cytosol) were incubated for 3 h at 0 °C with [^{3}H]estradiol ($6\cdot10^{-9}$ M) in presence of nine different concentrations (ranging from $1\cdot10^{-8}$ M to $1\cdot10^{-6}$ M) of the compound under investigation, acting as the competitor. An equivalent incubation, containing the same aliquots of cytosol and the same concentration of [^{3}H]estradiol, was prepared with nine different concentrations (ranging from $1\cdot10^{-8}$ M to $1\cdot10^{-6}$ M) of non-radioactive estradiol as the competitor. A blank (without competitors) was added to the incubation set to evaluate the maximum receptor binding capacity. At the end of the incubation, separation of the bound fractions of the steroids was achieved by using protamine sulfate precipitation.[17] The bound fractions were collected on glass fiber paper (Whatman GF/C) under a light vacuum and washed extensively with phosphate buffer (pH = 7.2). The filters were then transferred into a vial containing 10 mL of scintillation fluid (A.C.S., Amersham) and the radioactivity was measured in an LKB-1211 Rack-Beta scintillation counter. The percentage reduction in binding of [^{3}H]estradiol (Y) was calculated using the logit transformation of Y, where logit Y = ln(Y/1 – Y), vs. the log of the mass of competing steroid. The concentration of competitor required to displace 50% of the bound [^{3}H]estradiol was calculated for the compound under investigation (C_{50}) and for non-radioactive estradiol (C_{50e}); the result was expressed as the relative binding affinity [RBA = (C_{50e}/C_{50})×100].

Receptor Inactivation Assays: Aliquots (3 × 200 μL) of lamb uterine cytosol were first incubated for 2 h at 0 °C in the presence of $1\cdot10^{-8}$ M of compound under investigation (estradiol, 17α-ethynylestradiol**,** 17α-propynylestradiol, or **1–6)**, then [^{3}H]estradiol (final concentration $2.65\cdot10^{-9}$ M) was added to each fraction, which was again incubated for 1 h at 25 °C. At the end of this second incubation, the fraction of [^{3}H]estradiol specifically bound to its receptor was measured by protamine sulfate precipitation (vide supra). This value corresponds to the fraction of the estradiol receptor reversibly bound to the organometallic hormone in the first incubation. This value is compared to that of a control, i.e. aliquots of uterine cytosol (3 × 200 μL) incubated under the same conditions of time and temperature, but in the presence of tritiated estradiol only.

Acknowledgments

We thank Johnson Matthey Ltd. for a generous loan of $RuCl_3$ and OsO_4 and Ministero dell'Università e della Ricerca Scientifica e Tecnologica (MURST, Rome) for financial support (COFIN-98).

[1] K. M. Nicholas, R. F. Lockwood, *Tetrahedron Lett.* **1977**, *48*, 4163–4166.
[2] G. G. Melikyan, K. M. Nicholas, *Modern Acetylene Chemistry*, Weinheim, **1995**.
[3] K. M. Nicholas, R. Pettit, *Tetrahedron Lett.* **1971**, *37*, 3475–3478.
[4] K. M. Nicholas, R. Pettit, *J. Organomet. Chem.* **1972**, *44*, C21–C24.
[5] R. E. Connor, K. M. Nicholas, *J. Organomet. Chem.* **1977**, *44*, C45–C48.
[6] M. Gruselle, C. Cordier, M. Salmain, H. El Amouri, C. Guérin, J. Vaissermann, G. Jaouen, *Organometallics* **1990**, *9*, 2993–2997.
[7] K. M. Nicholas, *Acc. Chem. Res.* **1987**, *20*, 207–214.
[8] H. El Amouri, M. Gruselle, *Chem. Rev.* **1996**, *96*, 1077–1103.
[9] G. Jaouen, A. Vessières, I. S. Butler, *Acc. Chem. Res.* **1993**, *26*, 361–369.
[10] A. Vessières, S. Top, C. Vaillant, D. Osella, J.-P. Mornon, G. Jaouen, *Angew. Chem. Int. Ed. Engl.* **1992**, *31*, 753–755.
[11] D. Osella, G. C. Dutto, G. Jaouen, A. Vessières, P. R. Raithby, L. De Benedetto, M. J. McGlinchey, *Organometallics* **1993**, *12*, 4545–4552.
[12] A. M. Brzozowski, A. C. W. Pike, Z. Dauter, R. E. Hubbard, T. Bonn, O. Engström, L. Öhman, G. L. Greene, J. Gustafsson, M. Carlquist, *Nature* **1997**, *389*, 753–758.
[13] B. Cook, G. H. Beastall, *Steroid Hormones, A Practical Approach Series*, Oxford, U.K., **1987.**
[14] S. Aliau, D. El Garrouj, A. Yasri, B. S. Katzenellenbogen, J.-L. Borgna, *Biochemistry* **1997**, *36*, 5861–5867.
[15] K. W. Harlow, D. N. Smith, J. A. Katzenellenbogen, G. L. Greene, B. S. Katzenellenbogen, *J. Biol. Chem.* **1989**, *264*, 17476–17485.
[16] S. Aime, A. J. Deeming, *J. Chem. Soc., Dalton Trans.* **1981**, 828–832.
[17] A. Vessières, S. Top, A. A. Ismail, I. S. Butler, M. Louer, G. Jaouen, *Biochemistry* **1988**, *27*, 6659–6666.
[18] A. Vessières, C. Vaillant, M. Salmain, G. Jaouen, *J. Steroid Biochem.* **1989**, *34*, 301–305.
[19] K. England, P. C. Reeves, *J. Organomet. Chem.* **1987**, *319*, 355–360.
[20] S. Aime, R. Gobetto, L. Milone, D. Osella, L. Violano, A. J. Arce, Y. De Sanctis, *Organometallics* **1991**, *10*, 2854–2856.
[21] R. D. W. Kemmitt, D. R. Russell, in *Comprehensive Organometallic Chemistry,* ed. G. Wilkinson, F. G. A. Stone, E. W. Abel, Pergamon Press, Oxford, **1982**, Vol. 5, p. 43.
[22] D. H. Bradley, M. A. Khan, K. M. Nicholas, *Organometallics* **1992**, *11*, 2598–2607.
[23] O. Kuhn, D. Rau, H. Mayr, *J. Am. Chem. Soc.* **1998**, *120*, 900–907.
[24] G. G. Melikyan, S. Bright, T. Monroe, K. I. Hardcastle, J. Ciurash, *Angew. Chem. Int. Ed. Engl.* **1998**, *37*, 161–164.

[25] K. Gilbert, PCMODEL, Version June 1990, Serena Software, Bloomington, IN, **1990**, For more information, see: *Program MMP2*, N. L. Allinger, Y. H. Yuh, *QCPE* **1980**, 395. N. L. Allinger, H. L. Flanagan, *J. Comput. Chem.* **1983**, *4*, 399.
[26] D. Gregson, J. A. K. Howard, *Acta Crystallogr.* **1983**, *C39*, 1024.
[27] C. J. McAdam, N. W. Duffy, B. H. Robinson, J. Simpson, *Organometallics* **1996**, *15*, 3935–3943.
[28] B. Busetta, C. Courseille, S. Geoffe, M. Hospital, *Acta Crystallogr.* **1972**, *B28*, 1349.
[29] M. Savignac, G. Jaouen, C. A. Rodger, R. E. Perrier, B. G. Sayer, M. J. McGlinchey, *J. Org. Chem.* **1986**, *51*, 2328–2332.
[30] O. A. Reutov, I. V. Barinov, V. A. Chertkov, V. I. Sokolov, *J. Organomet. Chem.* **1985**, *297*, C25–C29.
[31] R. S. Dickson, P. J. Fraser, *Adv. Organomet. Chem.* **1974**, *12*, 323–377.
[32] S. R. Drake, R. Khattar, *Organomet. Syntheses* **1988**, *4*, 234–237.
[33] T. Fukumoto, Y. Matsumura, R. Okawara, *J. Organomet. Chem.* **1974**, *69*, 437–444.
[34] N. C. Deno, J. J. Jaruzelski, A. Schriesheim, *J. Am. Chem. Soc.* **1955**, *77*, 3044–3051.
[35] The CH_2 group shows two multiplets readily interpreted as an ABX_2 ($X = {}^{31}P$) system. This support an equatorial (pseudoaxial) coordination mode of the dppm ligand as found in the solid state structure of $Co_2(CO)_4$(dppm)(PhC≡CPh), see: P.H. Bird, A. R. Fraser, D. N. Hall, *Inorg. Chem.* **1977**, *16*, 1923–1930.
[36] These resonances, with an integrated intensities ratio of 1:2 from low to high field, are assigned to one axial and two equatorial carbonyl groups of the $Ru(CO)_3$ unit π-bonded to the alkyne; the remaining carbonyls are involved in a moderately fast exchange process at room temperature so that their resonances are too broad to be observed. They eventually merge in a single peak at higher temperature, see: D. Osella, O. Gambino, C. Nervi, M. Ravera, G. Jaouen, *Inorg. Chim. Acta* **1992**, *192*, 65–70.

Received July 29, 1999
[I99280]

Reactivity of 2-(Diphenylphosphanyl)thiophenol ($HSC_6H_4PPh_2$) with Ruthenium and Osmium Carbonyl Complexes; Breaking of $HSC_6H_4PPh_2$ into Sulfide, Phenyl and Diphenylphosphanyl Ligands on a Triruthenium Cluster

Javier A. Cabezza,*[a] M. Angeles Martínez-García,[a] Victor Riera,[a] Diego Ardura,[b] and Santiago García-Granda[b]

Keywords: Ruthenium / Osmium / Phosphane-thiolate ligands / C−P activation / C−S bond activation

2-(Diphenylphosphanyl)thiophenol ($HSC_6H_4PPh_2$) reacts with the carbonyl clusters $[Ru_3(CO)_{12}]$ and $[Os_3(CO)_{10}(MeCN)_2]$ to give mixtures of products, the composition of which depends upon the reaction conditions and the ratio of the reactants. The derivatives $[M_3(\mu\text{-}H)(\mu\text{-}\eta^2\text{-}SC_6H_4PPh_2)(CO)_9]$ (**1a**: M = Ru; **1b**: M = Os), $[Ru_3(\mu_3\text{-}S)(\mu\text{-}\eta^2\text{-}Ph)(\mu\text{-}PPh_2)(PPh_3)(CO)_6]$ (**2**), and $[Ru_2(\mu\text{-}\eta^2\text{-}SC_6H_4PPh_2)_2(CO)_4]$ (**3**) have been isolated. The $SC_6H_4PPh_2$ ligand of compounds **1a** and **1b** has the sulfur atom spanning the same M−M edge as the hydride ligand and the phosphorus atom attached to one of the bridged metal atoms. Compound **2**, which contains sulfide, phenyl, diphenylphosphanyl and triphenylphosphane ligands that arise from $HSC_6H_4PPh_2$, has the Ru_3 triangle capped by the sulfide and two Ru−Ru edges spanned by bridging phenyl and diphenylphosphanyl ligands. In complex **3**, the two $SC_6H_4PPh_2$ ligands have the same coordination behavior as in **1a** or **1b**; this binuclear complex is more conveniently prepared by treating $[Ru_2(\mu\text{-}\eta^2\text{-}MeCO_2)_2(CO)_4(MeCN)_2]$ with $HSC_6H_4PPh_2$.

Introduction

The reactivity of unfunctionalized arenethiols with ruthenium[1][2] and osmium[3−7] carbonyl clusters has been studied in detail. Most of these investigations have attempted to shed light on the fundamental steps of catalytic hydrodesulfurization (HDS) reactions[8] in which sulfur is removed from thiols and other organosulfur compounds in fossil fuels.[9] However, despite the widespread use of HDS processes and their economic and environmental significance, the nature of the interaction of the organosulfur compounds with the catalysts and the mechanisms of the catalytic processes are still far from being well-known.[9]

Both $[Ru_3(CO)_{12}]$ and $[Os_3(CO)_{12}]$ react with thiophenol to give $[M_3(\mu\text{-}H)(\mu\text{-}SPh)(CO)_{10}]$ (M = Ru,[2] Os[3]) as primary products. However, these compounds undergo facile C−S bond activation reactions, under thermal and/or photochemical conditions, leading to the sulfide derivatives $[M_3(\mu_3\text{-}S)(\mu_3\text{-}CO)(CO)_9]$ (M = Ru,[2] Os[4][5]), $[Os_3(\mu_3\text{-}S)_2(CO)_9]$,[3b,4,6] $[M_3(\mu\text{-}H)_2(\mu_3\text{-}S)(CO)_9]$ (M = Ru,[2] Os[4]), $[Ru_4(\mu_4\text{-}S)(\mu\text{-}CO)_2(CO)_9]$[2] $[Os_4(\mu_3\text{-}S)_2(CO)_{13}]$,[3b] $[Os_4(\mu_3\text{-}S)_2(CO)_{12}]$,[3b] and $[Os_6(\mu_4\text{-}S)_2(CO)_{17}]$.[5] It has also been reported that $[Os_3(CO)_{11}(MeCN)]$ reacts with *m*- and *p*-thiocresol to give $[Os_3(\mu\text{-}H)(\mu\text{-}SC_6H_4Me)(CO)_{10}]$ and that this reaction proceeds *via* the intermediate $[Os_3(CO)_{11}(HSC_6H_4Me)]$, in which both the sulfur and the hydrogen atoms of the thiol group interact with an osmium atom.[7]

Despite this interesting reactivity of thiophenols with ruthenium and osmium carbonyl clusters, only a limited number of studies involving functionalized thiophenols have been published. We have previously reported that 1,2-benzenedithiol reacts with $[Ru_3(CO)_{12}]$ and $[Os_3(CO)_{12}]$ to give the binuclear derivatives $[M_2(\mu\text{-}\eta^2\text{-}S_2C_6H_4)(CO)_6]$ (M = Ru, Os),[10] and that treatment of 2-aminothiophenol with $[Ru_3(CO)_{12}]$ gives $[Ru_3(\mu\text{-}H)(\mu\text{-}\eta^2\text{-}SC_6H_4NH_2)(CO)_9]$.[11] However, the reaction of 2-aminothiophenol with $[Os_3(CO)_{10}(MeCN)_2]$ gives $[Os_3(\mu\text{-}H)(\mu\text{-}SC_6H_4NH_2)(CO)_{10}]$,[12] in which the NH_2 group is not coordinated. It is also known that $[Os_3(CO)_{10}(MeCN)_2]$ reacts with 2-mercaptobenzoic acid to give the hexanuclear compound $[\{Os_3(\mu\text{-}H)(CO)_{10}\}_2(\mu\text{-}\eta^3\text{-}SC_6H_4CO_2)]$,[13] in which the $SC_6H_4CO_2$ ligand connects two triangles of osmium atoms through the thiolate and the carboxylate groups, each group bridging one edge of the corresponding trimetal fragment.

We report herein the reactivity of 2-(diphenylphosphanyl)thiophenol ($HSC_6H_4PPh_2$) with $[Ru_3(CO)_{12}]$ and $[Os_3(CO)_{10}(MeCN)_2]$.

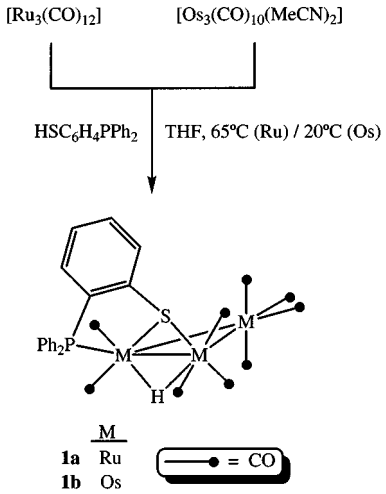
Results and Discussion

Treatment of a THF solution of $[Ru_3(CO)_{12}]$ with $HSC_6H_4PPh_2$, in a 1:1 ratio, at reflux temperature for 1.5 h gave $[Ru_3(\mu\text{-}H)(\mu\text{-}\eta^2\text{-}SC_6H_4PPh_2)(CO)_9]$ (**1a**) as the major component of a mixture of at least three products. The compound was isolated in 56% yield after a chromatographic workup. On the other hand, the osmium derivative $[Os_3(\mu\text{-}H)(\mu\text{-}\eta^2\text{-}SC_6H_4PPh_2)(CO)_9]$ (**1b**) was isolated in 48% yield after a chromatographic separation from a mixture of at least four compounds, formed from the reaction of $[Os_3(CO)_{10}(MeCN)_2]$ with $HSC_6H_4PPh_2$, in a 1:1 ratio, in THF at room temperature.

[a] Departamento de Química Orgánica e Inorgánica, Instituto de Química Organometálica "Enrique Moles," Universidad de Oviedo, E-33071 Oviedo, Spain
Fax: (internat.) + 34-985/103446
E-mail: jac@sauron.quimica.uniovi.es
[b] Departamento de Química Física y Analítica, Universidad de Oviedo, E-33071 Oviedo, Spain

 © WILEY-VCH Verlag GmbH, D-69451 Weinheim, 2000 1434−1948/00/0303−0499 $ 17.50+.50/0

In both cases, longer reaction times, higher temperatures or the use of larger amounts of $HSC_6H_4PPh_2$ resulted in lower yields of **1a** or **1b** and in the formation of complex mixtures. In the case of the ruthenium reactions, we managed to isolate and characterize some of these products (vide infra), but the osmium reactions did not allow the identification of more products, since they afforded a plethora of compounds in very small amounts as soon as the temperature was raised.



Scheme 1. Synthesis of compounds **1a** and **1b**

The structure depicted for compounds **1a** and **1b** in Scheme 1 is based on their analytical and spectroscopic data and on an X-ray diffraction study on the ruthenium derivative **1a**. Both compounds give molecular ions in their FAB MS corresponding to the proposed formulation. Their ^1H NMR spectra contain a hydride resonance as a doublet with a small J_{H-P} coupling constant (8.3 Hz for **1a** and 8.1 Hz for **1b**), which indicates a *cis* arrangement of the hydride and the phosphorus atom in the clusters.[14−16] All these data, in addition to their microanalyses and IR spectra, indicate that both compounds have analogous structures. In order to precisely assign the coordination of the $SC_6H_4PPh_2$ ligand to the clusters, the structure of the ruthenium derivative **1a** was determined by X-ray diffraction methods.

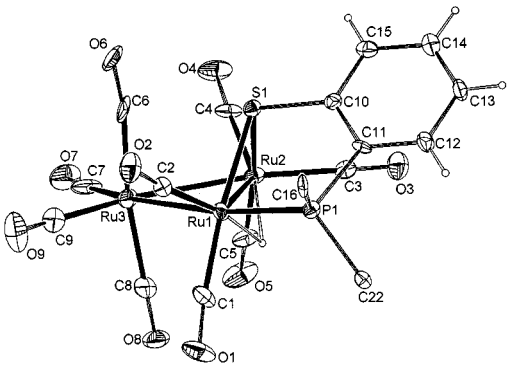


Figure 1. Molecular structure of complex **1a**; the atoms C(16) and C(22) are part of phenyl groups which have been omitted for clarity

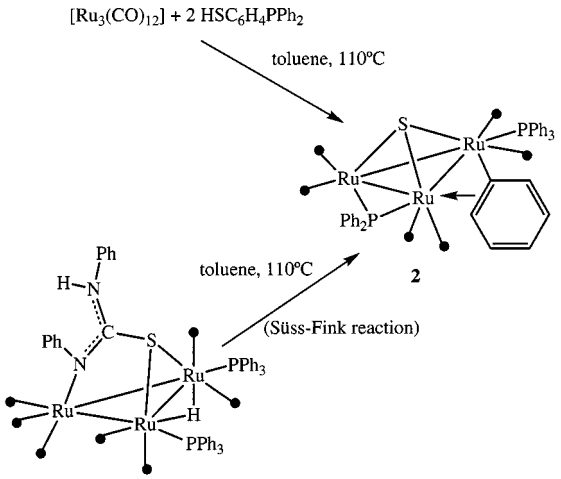
Table 1. Selected structural parameters of complex **1a**

Bond Lengths [Å]		Bond Angles [°]	
Ru(1)−Ru(2)	2.841(2)	C(1)−Ru(1)−P(1)	96.2(5)
Ru(1)−Ru(3)	2.824(2)	C(2)−Ru(1)−P(1)	99.1(6)
Ru(2)−Ru(3)	2.833(2)	C(1)−Ru(1)−S(1)	169.5(7)
Ru(1)−S(1)	2.381(4)	C(2)−Ru(1)−S(1)	98.2(6)
Ru(2)−S(1)	2.404(4)	P(1)−Ru(1)−Ru(3)	166.7(1)
Ru(1)−P(1)	2.309(4)	P(1)−Ru(1)−Ru(2)	107.1(1)
Ru(1)−C(1)	1.84(2)	P(1)−Ru(1)−S(1)	84.7(1)
Ru(1)−C(2)	1.90(2)	Ru(2)−Ru(1)−Ru(3)	60.01(6)
Ru(2)−C(3)	1.95(2)	C(3)−Ru(2)−S(1)	94.6(5)
Ru(2)−C(4)	1.91(2)	C(4)−Ru(2)−S(1)	94.9(5)
Ru(2)−C(5)	1.91(2)	C(5)−Ru(2)−S(1)	169.3(6)
Ru(3)−C(6)	1.93(2)	Ru(1)−Ru(2)−Ru(3)	59.70(5)
Ru(3)−C(7)	1.94(2)	Ru(1)−Ru(3)−Ru(2)	60.29(5)
Ru(3)−C(8)	1.94(2)	C(10)−S(1)−Ru(1)	105.2(6)
Ru(3)−C(9)	1.97(2)	C(10)−S(1)−Ru(2)	105.0(5)
		Ru(1)−S(1)−Ru(2)	72.8(1)

Figure 1 shows the molecular structure of compound **1a**. A selection of bond lengths and angles is given in Table 1. The cluster consists of an irregular triangle of ruthenium atoms in which the longest edge [Ru(1)−Ru(2) 2.841(2) Å], is spanned by the sulfur atom of a $SC_6H_4PPh_2$ ligand [Ru(1)−S(1) 2.381(4) Å, Ru(2)−S(1) 2.404(4) Å] and by a hydride ligand. The phosphorus atom of the $SC_6H_4PPh_2$ ligand is also attached to one of the ruthenium atoms of the same edge [Ru(1)−P(1) 2.309(4) Å] in a position approximately *trans* to the Ru(1)−Ru(3) edge [P(1)−Ru(1)−Ru(3) 166.7(1)°]. The cluster shell is completed by nine CO ligands, four of which are attached to Ru(3), three to Ru(2), and two to Ru(1). An analogous structure has been reported for the aminothiolate derivative $[Ru_3(\mu\text{-}H)(\mu\text{-}\eta^2\text{-}SC_6H_4NH_2)(CO)_9]$.[11] The structures of the ruthenium and osmium compounds $[M_3(\mu\text{-}H)(\mu\text{-}\eta^2\text{-}HNC_6H_4PPh_2)(CO)_9]$ (M = Ru,[15] Os[16]), derived from 2-(diphenylphosphanyl)aniline, have also been determined by X-ray diffraction methods and they are also similar to that of **1a**, although their bridged edges are shorter than the unbridged ones, in contrast to that of **1a**, probably as a consequence of the different sizes of the bridgehead atoms (N *vs* S).[17]

Treatment of THF or toluene solutions of $[Ru_3(CO)_{12}]$ with $HSC_6H_4PPh_2$, in 1:2 mol ratio, at reflux temperature, resulted in complex mixtures of products from which compounds **1a** and **2** could be separated by chromatographic means and subsequently identified. The best yield of complex **2** (13%) was obtained from a 1 h reaction in toluene at reflux temperature.

The structure depicted for compound **2** in Scheme 2 is based on an X-ray diffraction study, since little structural information was obtained from its analytical (microanalysis, FAB MS) and spectroscopic data (IR, ^1H and ^{31}P NMR). After having determined the structure, we found that Süss-Fink′s group had previously synthesized the same compound by thermolysis of $[Ru_3(\mu\text{-}H)(\mu\text{-}\eta^2\text{-}SCNHPhNPh)(CO)_7(PPh_3)_2]$ in refluxing toluene (Scheme 2), in the course of a study of the reactivity of $[Ru_3(CO)_{12}]$ with *N,N′*-disubstituted thioureas.[18] They also reported its



Scheme 2. Synthesis of compound **2**

X-ray structure. Consequently, we will not describe the structural details here.

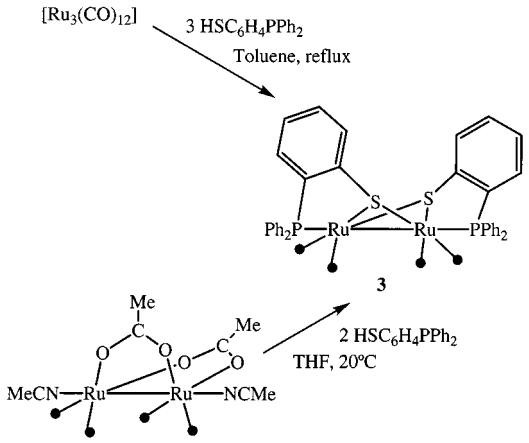
It should be noted that all the non-CO ligands of complex **2**, i.e. sulfide, phenyl, diphenylphosphanyl and triphenylphosphane, arise in our case from the degradation of 2-(diphenylphosphanyl)thiophenol, implying the cleavage of P−C, S−C, and S−H bonds and the formation of C−H bonds. To our knowledge, this is the first example in which such important processes occur in the same ligand in a metal complex.

As mentioned in the introduction, the reactions of arenethiols with carbonyl metal clusters often lead to stoichiometric desulfurization of the thiols, to give the arenes and sulfide-metal derivatives.[1−8] However, apart from compound **2**, few examples of cluster compounds containing phenyl ligands arising from the degradation of arylphosphane ligands have been reported, but in all of them the phenyl groups are η^1-coordinated in terminal[19] or bridging[20] modes. Cluster **2** is a rare example of a complex containing a bridging phenyl ligand which interacts in a monohapto manner with one metal atom and in a dihapto manner with the other metal atom. This type of coordination is frequently observed for bridging alkenyl ligands.

The reaction pathway by which complex **2** is formed appears to be quite intricate, since it involves the breaking and the formation of many bonds. The composition of **2** suggests that it may be formed from **1a** and two equivalents of $HSC_6H_4PPh_2$, but a sulfur atom is in excess from a stoichiometric point of view. This is in accordance with the fact that the formation of complex **2** is accompanied by the formation of other products which could not be characterized.

As a part of several attempts to shed light on the mechanism of formation of complex **2**, compound **1a** was thermolyzed in refluxing toluene for 1 h, both in the absence and presence of $HSC_6H_4PPh_2$. In the former case, a $^{31}P\{^1H\}$ NMR spectrum of the crude reaction mixture revealed the presence of **2**, in low yield, among many other products with high ^{31}P chemical shifts ($\delta > 200$). In the latter case, compound **2** was formed in a greater amount, being the major component (*ca.* 15%) of a mixture of many products ($^{31}P\{^1H\}$ NMR spectrum of the crude reaction mixture). These data suggest that compound **1a** may be an early intermediate in the formation of **2** from $[Ru_3(CO)_{12}]$ and $HSC_6H_4PPh_2$, although other possibilities excluding the intermediacy of **1a** cannot be ruled out.

In a further attempt to shed light on the mechanism of formation of complex **2**, $[Ru_3(CO)_{12}]$ was heated with three equivalents of $HSC_6H_4PPh_2$ in refluxing THF for 2 h. In this case, complex **2** was also formed in a small amount, but the major component of the mixture (*ca.* 20%) was a complex that could be separated by TLC and subsequently identified as the binuclear derivative $[Ru_2(\mu\text{-}\eta^2\text{-}SC_6H_4PPh_2)_2(CO)_4]$ (**3**). Similar results were obtained carrying out the reaction in refluxing toluene for 1 h.



Scheme 3. Synthesis of compound **3**

The microanalysis and FAB MS data of **3** support its binuclear formulation. Its $^{31}P\{^1H\}$ NMR spectrum, which only contains a singlet at $\delta = 75.3$, and its IR spectrum, which shows four absorptions in the carbonyl region, confirm the C_2 symmetry shown in Scheme 3 for this complex.

Complex **3** can be more efficiently prepared (45% yield) by treatment of the binuclear acetate dimer $[Ru_2(\mu\text{-}\eta^2\text{-}MeCO_2)_2(CO)_4(MeCN)_2]$[21] with $HSC_6H_4PPh_2$ (1:2 mol ratio) in THF at room temperature. The carboxylate bridges of $[Ru_2(\mu\text{-}\eta^2\text{-}RCO_2)_2(CO)_4(MeCN)_2]$ are labile in the presence of acids (HX) whose conjugate bases (X) are able to act as bridging ligands, the carboxylate bridge being released as the corresponding carboxylic acid. This synthetic method has previously been used to prepare some ligand-bridged diruthenium complexes, such as $[Ru_2(\mu\text{-}SR)_2(CO)_4(PPh_3)_2]$[22] or $[Ru_2(\mu\text{-}pz)_2(CO)_4(PPh_3)_2]$[23] (pz = pyrazolate). The preparation of complex **3** by this method, which starts from a binuclear precursor, also supports its binuclear nature.

In conclusion, the present work describes the synthesis of some bi- and trinuclear ruthenium and osmium carbonyl complexes derived from the reactions of $[Ru_3(CO)_{12}]$ and $[Os_3(CO)_{10}(MeCN)_2]$ with 2-(diphenylphosphanyl)thiophenol. We have shown that these reactions are not selec-

tive, since this thiol is very fragile once it is coordinated to a metal cluster, being liable to undergo a series of S−H, S−C and P−C bond cleavage reactions that often lead to mixtures of many products, as has been proven with the isolation and characterization of compound **2**

Experimental Section

General: Solvents were dried over sodium diphenyl ketyl (THF, diethyl ether, hydrocarbons) or CaH_2 (dichloromethane) and distilled under nitrogen prior to use. − Unless otherwise stated, the reactions were carried out under nitrogen, using standard Schlenk techniques, and were routinely monitored by solution IR spectroscopy (carbonyl stretching region) and by spot TLC on silica gel. − The compounds $[Ru_3(CO)_{12}]$,[24] $[Os_3(CO)_{12}]$,[25] $[\{Ru_2(\mu\text{-}\eta^2\text{-}MeCO_2)_2(CO)_4\}_n]$[21] and $HSC_6H_4PPh_2$[26] were prepared as described in the literature. Anhydrous Me_3NO was prepared by azeotropic distillation of a toluene solution of $Me_3NO{\cdot}2H_2O$ and was stored under nitrogen. $RuCl_3{\cdot}nH_2O$ and OsO_4 were purchased from Pressure Chemicals, all other reagents were purchased from Aldrich. − Microanalyses: University of Oviedo Analytical Service. − FAB MS (positive ion): Finnigan Mat-95 spectrometer, nitrobenzyl alcohol as matrix, cesium as bombarding gas. − IR: Perkin−Elmer FT 1720-X. − NMR: Bruker AC-200 and AC−300, 23°C, $SiMe_4$ (internal, for ^1H) or 85% H_3PO_4 (external, for ^{31}P) as standards ($\delta = 0$).

Synthesis of 1a: A solution of $[Ru_3(CO)_{12}]$ (100 mg, 0.156 mmol) and $HSC_6H_4PPh_2$ (50 mg, 0.158 mmol) in THF (15 mL) was stirred at reflux temperature for 1.5 h. The color changed from orange to deep red. After addition of neutral alumina (*ca.* 100 mg) to the solution, the solvent was removed under vacuum. The solid residue was poured on top of a column (2 × 15 cm) of neutral alumina (activity I) packed in hexane. Elution with dichloromethane/hexane (1:6) afforded to yellow bands. A dark residue remained uneluted at the top of the column. The second band was very weak and was discarded. The first band gave compound **1a**, as a yellow/orange solid, when the solvent was evaporated under vacuum. − Yield: 75 mg (56%). − $C_{27}H_{15}O_9PRu_3S$: calcd. C 38.17, H 1.78; found C 37.98, H 1.72. − IR (THF): ν(CO) = 2086 (m), 2050 (s), 2017 (m), 2005 (s), 1988 (m), 1961 (w), 1944 (w). − ^1H NMR ($CDCl_3$): δ = 7.86−7.10 (m, 14 H), −15.76 (d, J_{H-P} = 8.3 Hz, 1 H). − $^{31}P\{^1H\}$ NMR ($CDCl_3$): δ = 69.8 (s). − FAB MS: *m*/*z* = 850 $[M]^+$.

Synthesis of 1b: A solution of $[Os_3(CO)_{12}]$ (50 mg, 0.055 mmol) and anhydrous Me_3NO (10 mg, 0.14 mmol) in dichloromethane (15 mL) and acetonitrile (2 mL) was stirred at room temperature for 1 h. The resulting solution, containing the complex $[Os_3(CO)_{10}(MeCN)_2]$[27] (IR identification) was evaporated to dryness under vacuum. The residue was extracted into THF (10 mL) and was treated with $HSC_6H_4PPh_2$ (16 mg, 0.055 mmol). After stirring for 1 h at room temperature, the solution was concentrated to *ca.* 2 mL and was applied onto preparative silica gel TLC plates. Elution with dichloromethane/hexane (2:5) afforded four bands. The major band, yellow, was extracted with dichloromethane to give compound **1b**, as a yellow solid, after crystallization from dichloromethane/hexane. − Yield: 30 mg (48%). − $C_{27}H_{15}O_9Os_3PS$: calcd. C 29.03, H 1.35; found C 29.31, H 1.38. − IR (CH_2Cl_2): ν(CO) = 2110 (w), 2091 (m), 2052 (s), 2010 (s), 1990 (m), 1970 (w), 1951 (w). − ^1H NMR ($CDCl_3$): δ = 7.84−7.18 (m, 14 H), −17.42 (d, J_{H-P} = 8.1 Hz, 1 H). − $^{31}P\{^1H\}$ NMR ($CDCl_3$): δ = 43.8 (s). − FAB MS: *m*/*z* = 1117 $[M]^+$.

Synthesis of 2: A solution of $[Ru_3(CO)_{12}]$ (100 mg, 0.156 mmol) and $HSC_6H_4PPh_2$ (97 mg, 0.330 mmol) in toluene (20 mL) was stirred at reflux temperature for 1 h. The color changed from orange to deep red. The solution was concentrated to *ca.* 2 mL and the concentrate was applied onto preparative silica gel TLC plates. Elution with dichloromethane/hexane (2:5) afforded five bands and a residue at the base line. The major band, pink, was extracted with dichloromethane to give compound **2**, as a dark pink solid, after crystallization from dichloromethane/hexane. − Yield: 21 mg (13%). − $C_{42}H_{30}O_6P_2Ru_3S$: calcd. C 49.08, H 2.94; found C 49.03, H 2.87. − IR (THF): ν(CO) = 2002 (vs), 1977 (s), 1943 (m), 1927 (w). − ^1H NMR ($CDCl_3$): δ = 8.10 (d, J_{H-P} = 8.0 Hz, 1 H), 7.80−7.20 (m, 26 H), 7.06 (t, J_{H-P} = 8.0 Hz, 1 H), 6.52 (t, J_{H-P} = 8.0 Hz, 1 H), 6.09 (d, J_{H-P} = 8.0 Hz, 1 H) − $^{31}P\{^1H\}$ NMR ($CDCl_3$): δ = 215.1 (s, 1 P) 40.0 (s, 1 P). − FAB MS: *m*/*z* = 1028 $[M]^+$.

Synthesis of 3: A suspension of $[\{Ru_2(\mu\text{-}\eta^2\text{-}MeCO_2)_2(CO)_4\}_n]$ (100 mg, 0.231 mmol) was stirred in acetonitrile (20 mL) at reflux temperature for 15 min to give a yellow solution containing $[Ru_2(\mu\text{-}\eta^2\text{-}MeCO_2)_2(CO)_4(MeCN)_2]$[21] (IR identification). The solvent was removed under reduced pressure, and $HSC_6H_4PPh_2$ (136 mg, 0.463 mmol) and THF (20 mL) were added. The resulting solution was stirred at room temperature for 6 h. The color changed from orange to red. The solution was concentrated to *ca.* 2 mL and the concentrate was applied to preparative silica gel TLC plates. Elution with dichloromethane/hexane (1:5) afforded four bands. The first and major band, yellow, was extracted with dichloromethane to give compound **3**, as a yellow solid, after crystallization from dichloromethane/hexane. − Yield: 95 mg (45%). − $C_{40}H_{28}O_4P_2Ru_2S_2$: calcd. C 53.33, H 3.13; found C 53.71, H 3.33. − IR (hexane): ν(CO) = 1999 (w), 1978 (vs), 1940 (s), 1924 (w). − ^1H NMR ($CDCl_3$): δ = 7.84−7.06 (m) − $^{31}P\{^1H\}$ NMR ($CDCl_3$): δ = 75.3 (s). − FAB MS: *m*/*z* = 901 $[M]^+$.

Crystal Structure Determination of 1a: Crystal data and details of the structure determination are listed in Table 2. The unit cell dimensions were determined from the angular settings of 25 reflections with 10° < Θ < 15°. The orthorhombic space group *P*bca

Table 2. Crystallographic and refinement data for complex **1a**

formula	$C_{27}H_{15}O_9PRu_3S$
fw	849.63
cryst syst	orthorhombic
space group	*P*bca
a, *b*, *c* [Å]	30.282(7), 19.893(3), 10.195(3)
V [Å^3]	6142(3)
Z	8
F(000)	3296
D_{calcd} [g cm^{-3}]	1.838
μ [mm^{-1}]	1.625
cryst size [mm]	0.26 × 0.16 × 0.10
radiation (λ [Å])	Mo Kα (0.71073)
diffractometer	Enraf−Nonius CAD4
monochromator	graphite
temp [K]	293 (2)
scan method	ω−2θ
min/max *h, k, l*	0 /35, 0/23, 0/12
θ range [°]	1.34 to 24.98
data set	6243
unique data	5386 (R_{int} = 0.171)
data with $I>2\sigma(I)$	1304
restraints, parameters	0, 367
$R(F)_{I\geq 2\sigma(I)}$[a]	0.0487
$R_w(F^2)_{\text{all data}}$[b]	0.1342
GOF[c]	0.954
Δ/σ	0.001
max, min Δρ [e/Å^3]	0.500, −0.804

[a] $R(F) = \Sigma||F_o| - |F_c||/\Sigma|F_o|$. − [b] $R_w(F^2) = [\Sigma w(F_o^2 - F_c^2)^2/\Sigma w(F_o^2)^2]^{1/2}$. − [c] $GOF = [\Sigma w(F_o^2 - F_c^2)^2/(N - P)]^{1/2}$.

was determined from systematic absences and confirmed by the structure determination. The intensity was checked throughout data collection by monitoring three standard reflections every 60 min. Final drift correction factors were between 0.99 and 1.02. Profile analysis[28] was performed on all reflections. Lorentz and polarization corrections were applied and data were reduced to $|F_o|^2$ values.

The structure was solved by Patterson interpretation using the program DIRDIF92.[29] Anisotropic least-squares refinement, using a local version of SHELX,[30] was followed by an empirical absorption correction[31] (maximum and minimum correction factors 1.00 and 0.28, respectively). Full matrix anisotropic least squares refinement on F^2, using the program SHELXL92,[32] followed by a difference Fourier synthesis allowed the location of all the hydrogen atoms. Positional parameters and anisotropic thermal parameters of the nonhydrogen atoms were refined. All hydrogen atoms, except the bridging hydride ligand, were geometrically placed, and were isotropically refined. The function minimized was $\Sigma w(|F_o|^2-|F_c|^2)^2$, $w = 1/[\sigma^2(F_o^2) + (0.0236P)^2]$, with $\sigma(F_o)$ from counting statistics and $P = (F_o^2 + 2F_c^2)/3$. Atomic scattering factors were taken from the literature.[33] The plot in Figure 1 was made with the EUCLID package.[34] Geometrical calculations were made with PARST.[35] All computations were performed on an Alpha AXP3000 workstation.

Crystallographic data (excluding structure factors) for compound **1a** have been deposited with the Cambridge Crystallographic Data Centre as supplementary publication no. CCDC-133011. Copies of the data can be obtained free of charge on application to CCDC, 12 Union Road, Cambridge CB2 1EZ, UK [fax: (internat.) + 44-1223/336-033; E-mail: deposit@ccdc.cam.ac.uk; www: http://www.ccdc.cam.ac.uk].

Acknowledgments

Financial support from the Dirección General de Enseñanza Superior (Grants PB95−1042 and PB96−0558) is gratefully acknowledged.

[1] B. F. G. Johnson, D. R. Johnston, P. L. Josty, J. Lewis, I. G. Williams, *Nature* **1967**, *213*, 901.
[2] R. D. Adams, J. E. Babin, M. Tasi, *Inorg. Chem.* **1986**, *25*, 4514.
[3] [3a] G. R. Crooks, B. F. G. Johnson, J. Lewis, I. G. Williams, *J. Chem. Soc., A* **1969**, 797. − [3b] R. D. Adams, I. T. Hórvath, *Inorg. Synth.* **1989**, *26*, 303.
[4] R. D. Adams, L. W. Wang, *J. Am. Chem. Soc.* **1982**, *104*, 4115.
[5] R. D. Adams, I. T. Hórvath, S. H. Kim, *Organometallics* **1984**, *3*, 548.
[6] R. D. Adams, I. T. Hórvath, B. E. Segmüller, L. W. Wang, *Organometallics* **1983**, *2*, 1301.
[7] K. Kiriakidou, M. R. Plutino, F. Prestopino, M. Monari, M. Johansson, L. I. Elding, E. Valls, R. Gobetto, S. Aime, E. Nordlander, *Chem. Commun.* **1998**, 2721.
[8] For reviews on the use of molecular compounds as models for HDS processes, see: [8a] R. J. Angelici, *Acc. Chem. Res.* **1988**, *21*, 387. − [8b] R. J. Angelici, *Coord. Chem. Rev.* **1990**, *105*, 61. − [8c] T. B. Rauchfuss, *Prog. Inorg. Chem.* **1991**, *39*, 251. − [8d] R. Sánchez-Delgado, *J. Mol. Catal.* **1994**, *86*, 287. − [8e] C. Bianchini, A. Meli, *J. Chem. Soc., Dalton Trans.* **1996**, 801. − [8f] R. J. Angelici, *Polyhedron* **1997**, *16*, 3073.
[9] H. Topsøe, B. S. Clausen, F. E. Massoth, *Hydrotreating Catalysis*, in *Catalysis: Science and Technology* (Eds.: J. R. Anderson, M. Boudart), Vol. 11, Springer-Verlag, Berlin, **1996**.
[10] J. A. Cabeza, M. A. Martínez-García, V. Riera, D. Ardura, S. García-Granda, *Organometallics* **1998**, *17*, 1471.
[11] J. A. Cabeza, M. A. Martínez-García, V. Riera, S. García-Granda, J. F. Van der Maelen, *J. Organomet. Chem.* **1996**, *514*, 197.
[12] J. A. Cabeza, M. A. Martínez-García, V. Riera, S. García-Granda, D. Ardura, *J. Organomet. Chem.* **1996**, *525*, 133.
[13] E. A. Ainscough, A. M. Brodie, R. K. Coll, A. J. A. Mair, J. M. Waters, *J. Organomet. Chem.* **1996**, *509*, 259.
[14] [14a] P. L. Andreu, J. A. Cabeza, M. A. Pellinghelli, V. Riera, A. Tiripicchio, *Inorg. Chem*. **1991**, *30*, 4611. − [14b] P. L. Andreu, J. A. Cabeza, V. Riera, C. Bois, Y. Jeannin, *J. Chem. Soc., Dalton Trans.* **1990**, 3347.
[15] C. J. Adams, M. I. Bruce, P. A. Duckworth, P. A. Humphrey, O. Kühl, E. R. T. Tiekink, W. R. Cullen, P. Braunstein, S. Coco-Cea, B. W. Skelton, A. H. White, *J. Organomet. Chem.* **1994**, *467*, 251.
[16] E. A. Ainscough, A. M. Brodie, S. L. Ingham, J. M. Waters, *J. Organomet. Chem.* **1994**, *468*, 229.
[17] M. R. Churchill, R. A. Lashewycz, *Inorg. Chem.* **1979**, *18*, 3261.
[18] L. A. Hoferkamp, G. Rheinwald, H. Stoeckli-Evans, G. Süss-Fink, *Organometallics* **1996**, *15*, 704.
[19] [19a] P. Briard, J. A. Cabeza, A. Llamazares, L. Ouahab, V. Riera, *Organometallics* **1993**, *12*, 1006. − [19b] B. Delavaux, B. Chaudret, F. Dahan, R. Poilblanc, *Organometallics* **1985**, *4*, 935. − [19c] M. M. Harding, B. S. Nicholls, A. K. Smith, *J. Chem. Soc., Dalton Trans.* **1983**, 1479. − [19d] J. Jans, R. Naegeli, L. M. Venanzi, A. Albinati, *J. Organomet. Chem.* **1983**, *247*, C37. − [19e] N. J. Taylor, P. C. Chieh, A. J. Carty, *J. Chem. Soc., Chem. Commun.* **1975**, 448. − [19f] R. Bender, P. Braunstein, A. Tiripicchio, M. Tiripicchio-Camellini, *Angew. Chem. Int. Ed. Engl.* **1985**, *24*, 861.
[20] [20a] J. A. Cabeza, R. J. Franco, A. Llamazares, V. Riera, E. Pérez-Carreño, J. F. Van der Maelen, *Organometallics*, **1994**, *13*, 55. − [20b] L. J. Farrugia, A. D. Miles, F. G. A. Stone, *J. Chem. Soc., Dalton Trans.* **1984**, 2415. − [20c] C. W. Bradford, R. S. Nyholm, *J. Chem. Soc., Dalton Trans.* **1973**, 529. − [20d] S. E. Kabir, E. Rosenberg, J. Stetson, M. Yin, J. Ciurash, K. Mnatsakanova, K. I. Hardcastle, H. Noorani, N. Movsesian, *Organometallics*, **1996**, *15*, 4473.
[21] G. R. Crooks, B. F. G. Johnson, J. Lewis, J. Gamlen, *J. Chem. Soc., A* **1969**, 2761.
[22] J. Soler, J. Ros, M. R. Carrasco, A. Ruiz, A. Alvarez-Lorena, J. F. Piniella, *Inorg. Chem.* **1995**, *34*, 6211.
[23] S. J. Sherlock, M. Cowie, M. Singleton, M. M. de V. Stein, *J. Organomet. Chem.* **1989**, *361*, 353.
[24] M. I. Bruce, C. M. Jensen, N. L. Jones, *Inorg. Synth.* **1989**, *26*, 259.
[25] S. R. Drake, P. A. Loveday, *Inorg. Synth.* **1990**, *28*, 230.
[26] [26a] D. F. Garret, K. L. Cynthia, J. C. Martin, *J. Am. Chem. Soc.* **1989**, *111*, 654. − [26b] E. Block, G. Ofori-Okiai, J. Zubieta, *J. Am. Chem. Soc.* **1989**, *111*, 2327.
[27] J. N. Nicholls, M. D. Vargas, *Inorg. Synth.* **1990**, *28*, 232.
[28] [28a] M. S. Lehman, F. K. Larsen, *Acta Crystallogr.* **1974**, *A30*, 580. − [28b] D. F. Grant, E. J. Gabe, *J. Appl. Crystallogr.* **1978**, *11*, 114.
[29] P. T. Beurskens, G. Admiraal, G. Beurskens, W. P. Bosman, S. García-Granda, R. O. Gould, J. M. M. Smits, C. Smykalla, *The DIRDIF92 Program System*, University of Nijmegen, Nijmegen, The Netherlands, **1992**.
[30] J. F. Van der Maelen, Ph. D. Thesis, University of Oviedo, Oviedo, Spain, **1991**.
[31] S. Parkin, B. Moezzi, H. Hope, *J. Appl. Crystallogr.* **1995**, *28*, 53.
[32] G. M. Sheldrick, in *Crystallographic Computing 6*, (Eds.: H. D. Flack, L. Párkányi, K. Simon), International Union of Crystallography and Oxford University Press, Oxford, U. K., **1993**, p. 111.
[33] *International Tables for Crystallography*; vol. C, Kynoch Press, Birmingham, U. K., **1992** (present distributor: Kluwer Acad. Publ., Dordrecht, The Netherlands).
[34] A. L. Spek, in *Computational Crystallography* (Ed.: D. Sayre), Clarendon Press, Oxford, U. K., **1982**, p. 528.
[35] M. Nardelli, *Comput. Chem.* **1983**, *7*, 95.

Received August 2, 1999
[I99283]

Ion Chemistry in XH_4/Allene (X = Ge, Si) Gaseous Mixtures – Formation of X–C Bonds

Paola Benzi,[a] Lorenza Operti,*[a] and Roberto Rabezzana[a]

Keywords: Ion-molecule reactions / Mass spectrometry / Allene / Germanium / Silicon

The gas-phase ion chemistry of germane/allene and silane/allene mixtures has been studied, with the aim of obtaining information on the experimental conditions leading to the formation of clusters of increasing size containing Ge or Si bonded to carbon atoms. Mechanisms of ion/molecule reactions have been elucidated by ion-trap mass spectrometry using single and multiple isolation steps. Rate constants for the most important reactions have been determined experimentally and compared with collisional rate constants. The germane/allene mixtures display a low reactivity and the most abundant germanium and carbon containing ion is $GeCH_3^+$. However, chain propagation proceeds after the first nucleation step, even if rather slowly, with the formation of large clusters such as $Ge_4C_3H_3^+$ at low abundance. In contrast, the silane/allene mixtures are very reactive and many different processes are observed, with the formation of several silicon and carbon containing ions with appreciable efficiency. Chain propagation proceeds mainly through reactions of silicon-containing ions with allene molecules and the subsequent formation of large clusters such as $Si_3C_3H_5^+$ and $Si_4C_3H_7^+$.

Introduction

In the last few years, hydrogenated amorphous compounds of elements of the Group 14 have been extensively studied for their possible applications in electronic and optoelectronic devices.[1] Amorphous semiconductors based on germanium carbides, a-GeC:H, or silicon carbides, a-SiC:H, have recently been considered[2] in order to obtain collectors of wide range light.

The preparation of these materials is generally carried out by laser-assisted, X-ray-assisted, or other assisted chemical-vapour deposition (CVD) techniques, starting from suitable mixtures of gaseous hydrides containing germanium or silicon with hydrocarbons. It has been observed that the amount of Ge and C, or Si and C in the final solid is a function of the molar composition of the gaseous system, but it does not depend on it in a direct or predictable way. Therefore, it is very important to know which are the main processes taking place in the mixtures under examination, and which occur more rapidly, contributing to a larger extent to the growth of the polymer containing carbon bonded to germanium or silicon atoms. These results provide information on the relationship between the partial pressure of the gaseous reactants and the abundance of the corresponding elements in the solid material.

In previous studies, the mechanisms and kinetics of ionic reactions involved in radiolytically assisted CVD of volatile silicon and germanium hydrides in different mixtures (SiH_4/NH_3, SiH_4/PH_3, CH_3SiH_3/NH_3, CH_3SiH_3/PH_3, GeH_4/NH_3, GeH_4/PH_3, CH_3GeH_3/NH_3, CH_3GeH_3/PH_3) were determined by ion-trap mass spectrometry.[3] Germane or methylgermane/hydrocarbon mixtures, including GeH_4/allene and CH_3GeH_3/allene systems, were also studied by Fourier transform and chemical-ionisation mass spectrometry under different experimental conditions from the present work.[4] More recently, systems containing silane with propane or propene,[5] ethane or ethyne,[6] and ethene,[7] have been studied in an ion-trap instrument with the aim of investigating the formation of ion species containing Si–C bonds.

In this paper we report on the mechanisms of ion/molecule reactions in silane/allene and germane/allene mixtures studied by ion-trap mass spectrometry. Self-condensation processes in allene have also been investigated. The results are interesting both for fundamental and applied chemistry, as they give insights on pathways leading to the formation of silicon-carbon or germanium-carbon containing ions as possible precursors of amorphous silicon or germanium carbides.

The rate constants of the first steps of the chain propagation have been experimentally determined and compared with the collisional rate constants, calculated according to the Langevin theory.[8] A comparison can be also drawn on the gas-phase reactivity of germane and silane towards allene.

Results and Discussion

Tables 1–6 report experimental and collisional rate constants (Langevin theory) of the ion/molecule reactions taking place in the systems studied, and reaction efficiencies calculated as their ratio. When heats of formation were available,[9–17] enthalpies at 298 K were calculated to confirm the feasibility of the observed processes. The most

[a] Dipartimento di Chimica Generale ed Organica Applicata, Università di Torino,
Corso Massimo d'Azeglio 48, I-10125 Torino, Italy

 © WILEY-VCH Verlag GmbH, D-69451 Weinheim, 2000 1434–1948/00/0303–505 $ 17.50+.50/0

Table 1. Reactions of $C_2H_n^+$,$C_3H_n^+$, $C_4H_n^+$ and $C_5H_5^+$ ions in allene

Reactant Ions	Product Ions and Rate Constants (k_{exp})[a]	Σk_{exp}	k_L[b]	Efficiency[c]
$C_2H_2^+$	$C_3H_4^+$ (10), $C_3H_5^+$ (0.95)	11	13.76	0.80
$C_2H_3^+$	$C_3H_5^+$ (7.7)	7.7	13.60	0.57
$C_2H_4^+$	$C_2H_5^+$ (0.20), $C_3H_5^+$ (7.3), $C_3H_4^+$ (1.2), $C_3H_5^+$ (0.58)	9.3	13.46	0.69
C_3H^+	$C_2H_3^+$ (0.87), $C_3H_3^+$ (0.50), $C_4H_3^+$ (7.6)	9.0	12.46	0.72
$C_3H_2^+$	$C_3H_3^+$ (6.2), $C_4H_4^+$ (4.1), $C_6H_5^+$ (0.78)	11	12.37	0.90
$C_3H_3^+$	$C_4H_5^+$ (0.22), $C_6H_5^+$ (0.90)	1.1	12.29	0.090
$C_3H_4^+$	$C_3H_5^+$ (0.86), $C_6H_7^+$ (5.9)	6.8	12.21	0.56
$C_3H_5^+$	$C_4H_5^+$ (0.75), $C_6H_7^+$ (2.0), $C_6H_8^+$ (4.8)	7.6	12.14	0.63
$C_4H_3^+$	$C_5H_5^+$ (4.8)	4.8	11.54	0.42
$C_4H_4^+$	$C_5H_4^+$ (0.26), $C_7H_7^+$ (4.7)	5.0	11.49	0.44
$C_4H_5^+$	$C_6H_5^+$ (0.86), $C_7H_7^+$ (0.72), $C_7H_8^+$ (0.20)	1.8	11.44	0.16
$C_5H_5^+$	$C_5H_7^+$ (0.46), $C_6H_7^+$ (0.38)	0.84	10.98	0.076

[a] Rate constants are expressed as 10^{-10} $cm^3molecule^{-1}s^{-1}$; experiments were run at 333 K; uncertainty is within 20%. – [b] Rate constants have been calculated according to the Langevin theory calculating polarizability of C_3H_4 as in ref.[19] – [c] Efficiency has been calculated as the ratio $\Sigma k_{exp}/k_L$.

Table 2. Reactions of $C_2H_n^+$,$C_3H_n^+$ and $C_4H_n^+$ ions with germane and of GeH_n^+ ions with allene in a GeH_4/C_3H_4 mixture

Reactants	Product Ions and Rate Constants (k_{exp})[a]	Σk_{exp}	k_L[b]	Efficiency[c]
$C_2H_2^+ + GeH_4$	Ge^+ (2.0), GeH^+ (1.5), GeH_2^+ (1.6), GeH_3^+ (2.6), $GeCH_3^+$ (0.36), $GeC_2H_3^+$ (0.64)	8.7	11.83	0.74
$C_2H_3^+ + GeH_4$	GeH^+ (1.7), GeH_3^+ (2.6), $GeCH_3^+$ (0.78)	5.1	11.66	0.44
$C_2H_4^+ + GeH_4$	GeH^+ (0.81), GeH_2^+ (1.7), $GeCH_3^+$ (0.48)	3.0	11.51	0.26
$C_3H^+ + GeH_4$	Ge^+ (1.1), GeH^+ (1.8), $GeCH_3^+$ (0.94), $GeC_3H_3^+$ (0.72)	4.6	10.44	0.44
$C_3H_2^+ + GeH_4$	$GeCH_3^+$ (1.8)	1.8	10.34	0.17
$C_3H_3^+ + GeH_4$	$GeCH_3^+$ (0.40)	0.40	10.25	0.039
$C_3H_5^+ + GeH_4$	$GeCH_3^+$ (1.2)	1.2	10.08	0.12
$C_4H_3^+ + GeH_4$	$GeCH_3^+$ (0.96), $GeC_2H_3^+$ (0.92)	1.9	9.42	0.20
$C_4H_5^+ + GeH_4$	$GeCH_3^+$ (0.52)	0.52	9.31	0.056
$Ge^+ + C_3H_4$	$GeC_3H_3^+$ (2.8)	2.8	10.76	0.26
$GeH^+ + C_3H_4$	$GeCH_3^+$ (8.9)	8.9	10.73	0.83
$GeH_2^+ + C_3H_4$	$GeCH_2^+$ (0.65), $GeCH_3^+$ (0.84), $GeC_2H_3^+$ (1.1), $GeC_3H_3^+$ (1.1), $GeC_3H_5^+$ (1.2)	4.9	10.71	0.46

[a] Rate constants are expressed as 10^{-10} $cm^3molecule^{-1}s^{-1}$; experiments were run at 333 K; uncertainty is within 20%. – [b] Rate constants have been calculated according to the Langevin theory calculating polarizability of C_3H_4 as in ref.[19], and taking polarizability of GeH_4 from ref.[20] – [c] Efficiency has been calculated as the ratio $\Sigma k_{exp}/k_L$.

stable isomer for every species was considered in the calculations of the reaction enthalpies.

Allene Self-Condensation

The ion chemistry of allene has been previously studied by different mass spectrometric techniques.[18] Overall rate constants have been reported for reactions of the $C_3H_n^+$ (n = 1–4) ions with neutral allene,[18f] and are generally higher than those reported in the present paper (see Table 1). Such discrepancy is probably due to the different conditions of sample pressure at which the instruments operate, and to the presence of a buffer gas in the ion-trap mass spectrometric experiments, giving a lower population of excited ions with respect to other methods.

Ionisation of allene gives rise to the $C_3H_n^+$ (n = 1–4) and $C_2H_n^+$ (n = 2–4) ion families. Formation of $C_2H_3^+$ and $C_2H_4^+$ involves hydrogen migration before the fragmentation process. If stored for suitable periods of time, all the above-mentioned ions react with neutral allene to yield heavier ion species such as protonated allene ($C_3H_5^+$), $C_4H_n^+$ (n = 3–5), and $C_5H_5^+$ ions.

Many different reactions are observed (Table 1) taking place with elimination of different neutral moieties. Rather common paths involve loss of an ethyne molecule or, to a lesser extent, of an ethene molecule or a C_3H_3 fragment. Elimination of a hydrogen atom or molecule is also observed, but is limited to $C_3H_n^+$ (n = 2–5) and $C_4H_n^+$ (n = 4, 5) ions.

Efficiencies of reaction are rather high for all primary ions and protonated allene, except for $C_3H_3^+$, which reacts very slowly. Reactions of the $C_4H_n^+$ (n = 3–5) ion family show a lower efficiency, which further decreases for the stable $C_5H_5^+$ ion.

Germane/Allene Mixture

Table 2 reports the most significant ion/molecule reactions occurring in a germane/allene mixture. During ionisation, the GeH_n^+ (n = 0–3) ion family is formed, besides primary ions of allene as described above. The main reaction pathway shown by all the $C_2H_n^+$ (n = 2–4) ions, as well as C_3H^+, consists of charge transfer to GeH_4 with successive fragmentation to form ions of the GeH_n^+ (n = 0–3) family. It is worth noting that $GeCH_3^+$ ions are formed by almost all primary and secondary ions of allene, even if these processes are generally rather slow and only in two cases the reaction rate constants are in the 10^{-10} $cm^3molecule^{-1}s^{-1}$ order of magnitude. The exceptions are $C_3H_4^+$, $C_4H_4^+$, and

$C_5H_5^+$, which not only do not give the $GeCH_3^+$ product, but are unreactive towards germane.

Efficiencies of reaction of the primary $C_2H_n^+$ (n = 2–4) and $C_3H_n^+$ (n = 1–4) ion families decrease with increasing number of hydrogen atoms within the same family. Moreover, ions containing two carbon atoms are more efficient than the $C_3H_n^+$ species. Besides $GeCH_3^+$, which is unreactive under the experimental conditions used here, only two ion species, $GeC_2H_3^+$ and $GeC_3H_3^+$, contain Ge–C bonds and are interesting for the chain propagation towards germanium carbide. It is also worth noting that in previous studies on GeH_4/allene mixtures, performed by Fourier transform mass spectrometry, only these three Ge/C containing ions ($GeCH_3^+$, $GeC_2H_3^+$, and $GeC_3H_3^+$) were observed.[4a] Among the germane primary ions, GeH_3^+ is not included in the table as it is unreactive in the reaction times examined here. Germane self-condensation reactions are not reported as they have been already shown in previous papers.[3f,21] All reactions of GeH_n^+ (n = 0–2) ions with allene yield ion products containing germanium and carbon together. Again, $GeCH_3^+$, $GeC_2H_3^+$, and $GeC_3H_3^+$ ions are observed, together with $GeCH_2^+$ and $GeC_3H_5^+$, which are not formed from allene ions reacting with germane.

Unfortunately, mixed ions containing both Ge and C, as well as two-germanium containing ions, generally originate in very slow processes. It follows that, in the time range considered here, their abundance is too low to perform selective isolation with reproducible results. Moreover, as previously also observed in CH_3GeH_3/allene systems,[4b] in which $GeCH_3^+$ is a primary ion displaying a very high abundance, mixed Ge/C ions react very slowly and do not seem to be the precursors of higher order clusters. In particular, they do not react with germane in the reaction time considered, as all mixed ions show a unique germanium atom and up to six carbon atoms in high pressure chemical ionisation experiments.[4b]

However, as the main interest in these systems relies on the catenation of germanium and carbon atoms together to give mixed cluster ions of increasing size, experiments were carried out with isolation and reaction of the whole $Ge_2H_n^+$ (n = 2–4) ion family in the GeH_4/C_3H_4 ($4.7 \times 10^{-7}/1.9 \times 10^{-7}$ Torr) mixture. The mass spectra recorded immediately after the isolation (a), and after 0.5 s (b), 0.9 s (c), and 2 s (d) of reaction are reported in Figure 1. These data do not allow the calculation of the rate constants, nevertheless they give valuable information about $Ge_2H_n^+$ ions reactivity with allene.

At zero reaction time, signals in the mass spectra cover the range of m/z values due to $Ge_2H_2^+$, $Ge_2H_3^+$, and $Ge_2H_4^+$ germane secondary ions, the first one being the most abundant. Increase of the reaction time up to 2 s allowed us to detect several multiplets. Because of the low abundance of some signals, the identification of the number of hydrogen atoms contained in some of the ion species was not straightforward. Therefore, these ions are written with an 'x' as coefficient for hydrogen atoms. Anyway, it is interesting to note that with increasing reaction time the

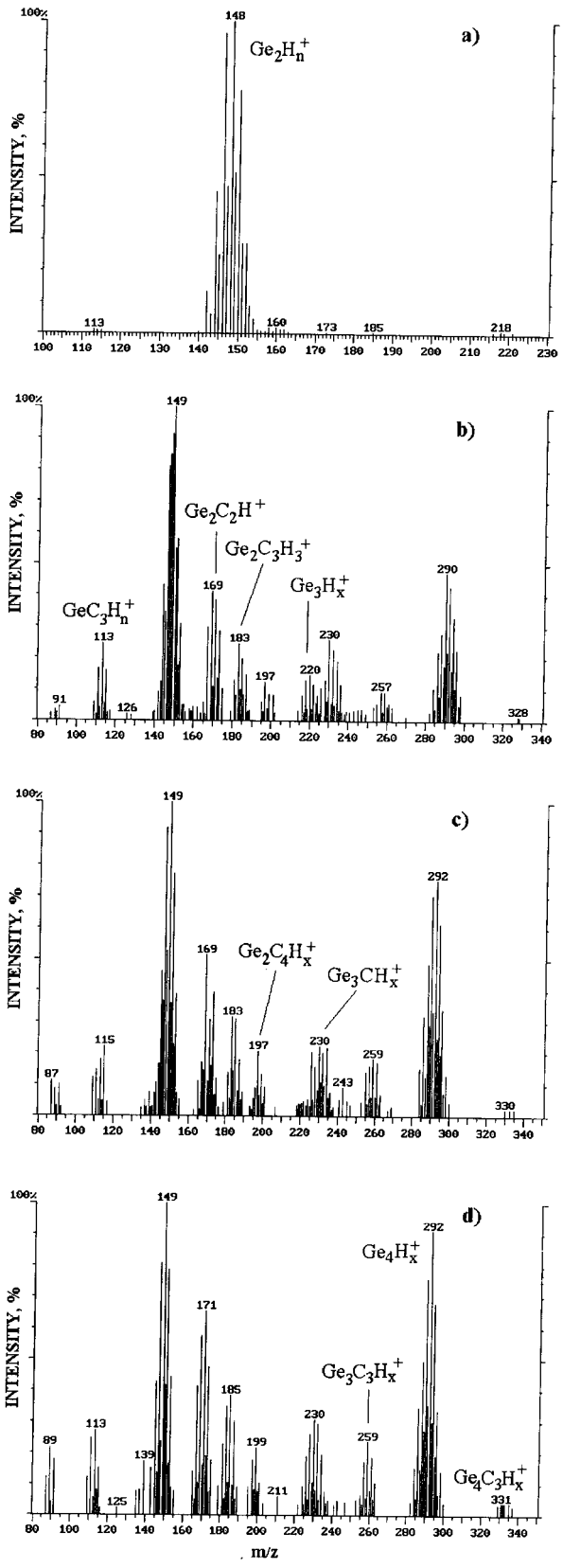


Figure 1. Mass spectra obtained after isolation of the $Ge_2H_n^+$ (n = 2–4) multiplet ions at 0 s (a), 0.5 s (b), 0.9 s (c), and 2 s (d) reaction times.

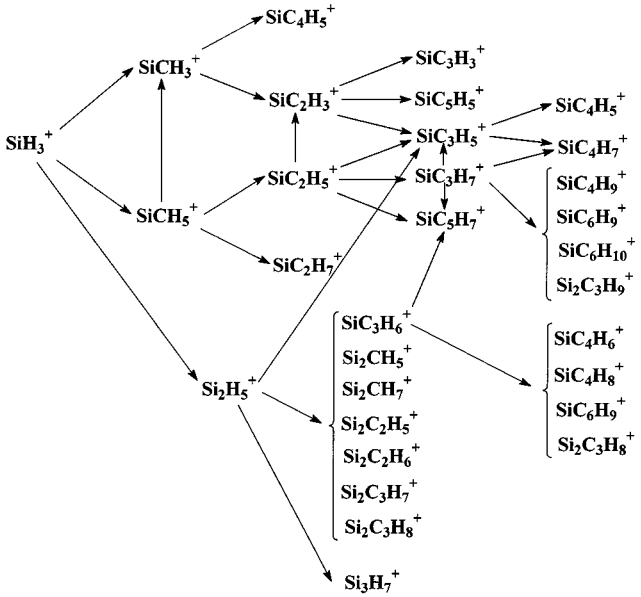
$Ge_2H_n^+$ multiplet reduces to the one corresponding to the $Ge_2H_3^+$ species only. It means that this ion is less reactive than the $Ge_2H_n^+$ (n = 2, 4) species, whose abundance decreases rapidly due to ion/molecule reactions occurring in the mixture. Therefore, the products observed are mainly formed from the $Ge_2H_2^+$ and $Ge_2H_4^+$ ion species reacting with allene, and in particular from $Ge_2H_2^+$, which is the most abundant ion at zero reaction time.

On the basis of the lower and upper limits and of the most intense signal of each multiplet in the spectra, $GeC_3H_n^+$ (n = 3–5), $Ge_2C_2H^+$, $Ge_2C_3H_3^+$, and $Ge_3H_x^+$ (x = 2 for the most abundant species in the multiplet) ion species are formed. Weak signals due to the $Ge_2C_4H_x^+$ (x = 5 for the most abundant species in the multiplet) ions are also observed. As it contains four carbon atoms, it cannot be directly formed from $Ge_2H_n^+$, but it can only originate from $Ge_2C_2H^+$ or $Ge_2C_3H_3^+$. After about 0.9 s reaction time, the signals due to the $Ge_3H_x^+$ ions almost disappear from the mass spectra, while the intensities of higher mass multiplets, assigned to the $Ge_3CH_x^+$ (x = 0 and 2 for the most abundant species in the multiplet), $Ge_3C_3H_x^+$ (x = 5 for the most abundant species in the multiplet), and $Ge_4H_x^+$ (x = 0 and 2 for the most abundant species in the multiplet) ion species, increase remarkably. If the reaction time is further increased, a weak multiplet due to the $Ge_4C_3H_x^+$ ions becomes detectable, the possible precursors being $Ge_3C_3H_x^+$ and $Ge_4H_x^+$ ions.

In separate and successive experiments, some of these ion families were in turn isolated and reacted, in order to determine their direct products. In particular, $Ge_2C_2H^+$ and $Ge_2C_3H_3^+$ ions were isolated together, and the main products of reaction observed after 2 s are $GeC_5H_x^+$ and $GeC_6H_x^+$. These ions were obtained by substitution of a Ge atom by two or three carbons. Moreover, small amounts of $Ge_2C_4H_x^+$ and $Ge_3H_x^+$ ions are also found. Isolation and reaction of the $Ge_3H_x^+$ ion family shows that it produces $Ge_3CH_x^+$ and $Ge_4H_x^+$ ions, but a partial contribution of other species, such as $Ge_2C_2H^+$ or $Ge_2C_3H_3^+$, cannot be ruled out. Finally, it was possible to isolate the $Ge_3CH_x^+$ multiplet, which leads to the formation of the $Ge_3C_3H_x^+$ ion species.

Silane/Allene Mixture

Three different mixtures were considered, which consist of silane and allene in the approximate ratios 1:5 ($1.8 \times 10^{-7}/8.5 \times 10^{-7}$ Torr), 1:1 ($5.0 \times 10^{-7}/4.6 \times 10^{-7}$ Torr), and 5:1 ($8.6 \times 10^{-7}/1.7 \times 10^{-7}$ Torr). Ionisation of the two reacting molecules again produces the allene primary ions and the SiH_n^+ (n = 0–3) ion species from silane. They are trapped in the cell of the mass spectrometer and react with both neutral species with increasing reaction times up to 2 seconds. During this time, several ion families are formed in successive reactions, and products that are obtained after four reaction steps are detected. As an example, Scheme 1 shows the paths of ion/molecule reactions starting from SiH_3^+ primary ion of silane, reacting with silane and allene neutral molecules.



Scheme 1. Paths of ion/molecule reactions starting from SiH_3^+ in a SiH_4/C_3H_4 mixture.

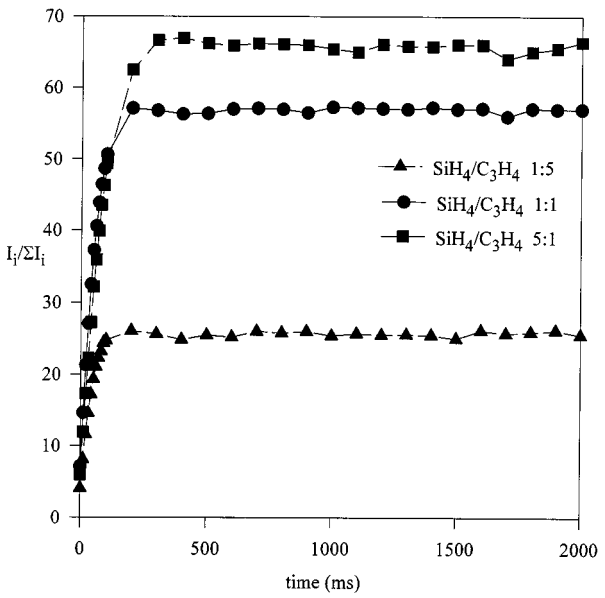


Figure 2. Variation of the total abundances of silicon and carbon containing ions as a function of reaction time for the 1:5, 1:1, and 5:1 silane/allene mixtures.

Figure 2 reports the variation of the total ion abundance of mixed ions as a function of reaction time for the three silane/allene mixtures. In all cases, the abundance rapidly increases to a maximum value, which remains constant up to two seconds of reaction. The highest yield is given by the SiH_4/C_3H_4 5:1 mixture, which is more than twice that of the 1:5 mixture. However, it is worth noting that the behaviour of the 1:1 silane/allene system is rather similar to that of the 5:1 one. Such a trend can be due to the involvement of allene as neutral reagent.

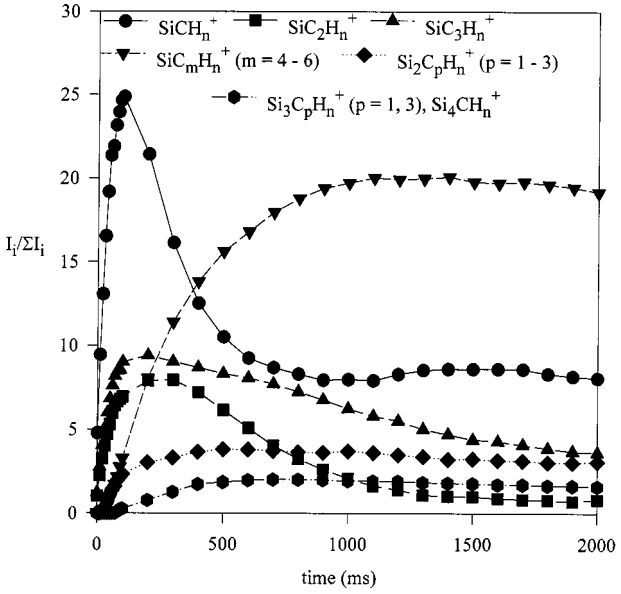


Figure 3. Variation of the abundances with reaction time of the $SiCH_n^+$, $SiC_2H_n^+$, $SiC_3H_n^+$, $SiC_mH_n^+$ (m = 4–6), $Si_2C_pH_n^+$ (p = 1–3), and $Si_3C_pH_n^+$ (p = 1, 3) with $Si_4CH_n^+$ ion families for the 1:1 silane/allene mixtures.

reason, Si^+ is not shown. Allene primary and secondary ions react with silane through different pathways, in which loss of small hydrocarbon molecules (C_2H_2, C_2H_4, C_3H_4), fragments (CH_3, C_2H_3), or H atom, with or without a molecule of hydrogen,occurs. Rate constants are generally low for all reaction paths considered. As observed for the germane/allene mixtures, efficiencies of reaction decrease with increasing number of hydrogen atoms in the families of primary $C_2H_n^+$ (n = 2, 3) and $C_3H_n^+$ (n = 1–4) ions.

Table 4 shows the ion/molecule reactions of the SiH_n^+ (n = 1–3) and $Si_2H_n^+$ (n = 2–5) ions with allene. Self-condensation reactions of silane are not reported, as already discussed in previous papers.[3a,21] Generally, many different products are detected and the reaction efficiencies are high. However, rate constants of single reactions are rather low and the high efficiencies are mainly due to the great number of pathways observed. The only two exceptions are the SiH^+ and SiH_3^+ ions, which yield $SiCH_3^+$with high rate constants, through loss of the stable neutrals, C_2H_2 and C_2H_4, respectively.

As a general remark, reactions with loss of hydrocarbon molecules are the most frequently observed paths. Addi-

Table 3. Reactions of $C_2H_n^+$, $C_3H_n^+$ and $C_4H_n^+$ ions with silane in a SiH_4/C_3H_4 mixture

Reactant Ions	Product Ions and Rate Constants (k_{exp})[a]	Σk_{exp}	k_L[b]	Efficiency[c]
$C_2H_2^+$	$SiCH_3^+$ (2.8), $SiC_2H_3^+$ (2.6), $SiC_2H_5^+$ (1.7)	7.1	12.85	0.55
$C_2H_3^+$	SiH_3^+ (2.6), $SiC_2H_5^+$ (0.77)	3.4	12.72	0.26
C_3H^+	$SiCH_3^+$ (5.3), $SiC_3H_2^+$ (1.8), $SiC_3H_3^+$ (2.4)	9.5	11.75	0.81
$C_3H_2^+$	$SiCH_3^+$ (1.6), $SiC_2H_3^+$ (1.3)	2.9	11.68	0.25
$C_3H_3^+$	$SiCH_3^+$ (0.47), $SiCH_5^+$ (0.89)	1.4	11.61	0.12
$C_3H_4^+$	$SiCH_4^+$ (0.38)	0.38	11.54	0.033
$C_3H_5^+$	$SiCH_5^+$ (3.0)	3.0	11.48	0.26
$C_4H_3^+$	$SiCH_3^+$ (0.40), $SiC_2H_3^+$ (0.56), $SiC_2H_5^+$ (0.89)	1.8	10.98	0.16
$C_4H_4^+$	$SiC_2H_4^+$ (0.38), $SiC_3H_5^+$ (0.26), $SiC_4H_7^+$ (0.34)	0.98	10.94	0.090

[a] Rate constants are expressed as 10^{-10} $cm^3molecule^{-1}s^{-1}$; experiments were run at 333 K; uncertainty is within 20%. – [b] Rate constants have been calculated according to the Langevin theory taking polarizability of SiH_4 from ref.[20] – [c] Efficiency has been calculated as the ratio $\Sigma k_{exp}k_L$.

Variation of the abundances of the $SiCH_n^+$, $SiC_2H_n^+$, $SiC_3H_n^+$, $SiC_mH_n^+$ (m = 4–6), $Si_2C_pH_n^+$ (p = 1–3), and $Si_3C_pH_n^+$ (p = 1–3) together with $Si_4CH_n^+$ ion families are reported in Figure 3 for the 1:1 silane/allene mixture. The total abundance of ions formed in the first reaction step ($SiCH_n^+$, $SiC_2H_n^+$, and $SiC_3H_n^+$) reaches a maximum value after about 100–200 ms of reaction, and then decreases to a rather constant value.

The other ion species show a slower increase, which is as high as 20% for the $SiC_mH_n^+$ ion family, whereas ions produced in successive reaction steps never exceed 4%. However, it is remarkable that the abundance of each ion family examined here does not change substantially after 1 s of reaction.

The rate constants of ion/molecule reactions occurring in the silane/allene system are displayed in tables 3–6. In Table 3, reactions of the $C_2H_n^+$ (n = 2, 3), $C_3H_n^+$ (n = 1–5), and $C_4H_n^+$ (n = 3, 4) ions with silane are listed. The $C_2H_4^+$ ion is not reported, as it has the same nominal mass of the Si^+ species formed from silane, and no experiment was possible that allowed its selection alone. For the same tions of C_3H_4 and losses of an atom of hydrogen together, or without a molecule of hydrogen are very frequent processes too, with rate constants that are generally lower than the previous ones. Every $Si_2H_n^+$ (n = 2–5) ion shows at least one process characterised by substitution of a neutral fragment containing only silicon and hydrogen by a moiety originating from allene. In fact, loss of a silyl radical is displayed by all the $Si_2H_n^+$ (n = 2–5) ions, except $Si_2H_3^+$, which loses a silylene group. The $Si_2H_n^+$ (n = 4, 5) ions also undergo substitution of a silane by an allene molecule.

In order to follow the growth of ions containing silicon and carbon already bonded together, reactions of the $SiCH_n^+$ (n = 2–5) ion family with both allene and silane are reported in Table 5. As already noticed for ions containing only silicon and hydrogen, reactions of the $SiCH_n^+$ (n = 2–5) species with allene proceed through loss of various neutral molecules (H_2, CH_4, C_2H_2, C_2H_4, and C_3H_6) or by elimination of a variety of hydrocarbon fragments or hydrogen atoms. In contrast, the reactivity of this ion family towards silane is remarkably low, as only $SiCH_2^+$ and $SiCH_4^+$ react

Table 4. Reactions of SiH_n^+ and $Si_2H_n^+$ ions with allene in a SiH_4/C_3H_4 mixture

Reactant Ions	Product Ions and Rate Constants (k_{exp})[a]	Σk_{exp}	k_L[b]	Efficiency[c]
SiH^+	$SiCH_3^+$ (14), $SiC_3H_3^+$ (0.50)	14	13.32	1.05
SiH_2^+	$SiCH_2^+$ (2.3), $SiCH_3^+$ (1.5), $SiCH_4^+$ (1.2), $SiC_2H_3^+$ (3.9), $SiC_3H_5^+$ (1.6)	10.5	13.19	0.80
SiH_3^+	$SiCH_3^+$ (7.4), $SiCH_5^+$ (2.4)	9.8	13.06	0.75
$Si_2H_2^+$	$SiC_3H_3^+$ (1.4), $Si_2CH_2^+$ (2.9), $Si_2C_2H_3^+$ (1.8), $Si_2C_3H_3^+$ (0.10), $Si_2C_3H_5^+$ (0.38)	6.6	11.22	0.59
$Si_2H_3^+$	$SiC_3H_5^+$ (0.38), $Si_2CH_3^+$ (1.4), $Si_2CH_5^+$ (0.46), $Si_2C_3H_3^+$ (0.25), $Si_2C_3H_5^+$ (0.38)	2.9	11.18	0.26
$Si_2H_4^+$	$Si_2H_2^+$ (0.23), $SiC_3H_4^+$ (0.28), $SiC_3H_5^+$ (2.8), $Si_2CH_4^+$ (1.5), $Si_2C_2H_5^+$ (1.1), $Si_2C_3H_6^+$ (0.39), $Si_2C_3H_7^+$ (0.79)	7.1	11.15	0.64
$Si_2H_5^+$	$Si_2H_3^+$ (0.65), $SiC_3H_5^+$ (1.1), $SiC_3H_6^+$ (0.76), $Si_2CH_5^+$ (2.3), $Si_2CH_7^+$ (0.31), $Si_2C_2H_5^+$ (0.36), $Si_2C_2H_6^+$ (0.40), $Si_2C_3H_7^+$ (0.53), $Si_2C_3H_8^+$ (0.21)	6.60	11.11	0.59

[a] Rate constants are expressed as 10^{-10} $cm^3molecule^{-1}s^{-1}$; experiments were run at 333 K; uncertainty is within 20%. – [b] Rate constants have been calculated according to the Langevin theory calculating polarizability of C_3H_4 as in ref.[19] – [c] Efficiency has been calculated as the ratio $\Sigma k_{exp}k_L$.

Table 5. Reactions of $SiCH_n^+$ ions with allene and silane in a SiH_4/C_3H_4 mixture

Reactants	Product Ions and Rate Constants (k_{exp})[a]	Σk_{exp}	k_L[b]	Efficiency[c]
$SiCH_2^+ + C_3H_4$	$SiCH_3^+$ (1.1), $SiC_2H_2^+$ (3.4), $SiC_2H_3^+$ (0.21), $SiC_3H_2^+$ (2.7), $SiC_3H_3^+$ (2.3), $SiC_4H_5^+$ (0.45)	10	12.06	0.84
$SiCH_2^+ + SiH_4$	$Si_2CH_4^+$ (1.5)	1.5	11.42	0.13
$SiCH_3^+ + C_3H_4$	$SiC_2H_3^+$ (1.4), $SiC_4H_5^+$ (1.0)	2.4	12.00	0.20
$SiCH_4^+ + C_3H_4$	$SiCH_3^+$ (1.0), $SiCH_5^+$ (2.3), $SiC_2H_4^+$ (1.3), $SiC_2H_6^+$ (0.52), $SiC_3H_5^+$ (1.3), $SiC_4H_6^+$ (0.58), $SiC_4H_7^+$ (0.84)	7.8	11.93	0.65
$SiCH_4^+ + SiH_4$	$Si_2CH_6^+$ (0.41)	0.41	11.30	0.036
$SiCH_5^+ + C_3H_4$	$SiCH_3^+$ (5.8), $SiC_2H_5^+$ (0.44), $SiC_2H_7^+$ (0.91)	7.2	11.87	0.60

[a] Rate constants are expressed as 10^{-10} $cm^3molecule^{-1}s^{-1}$; experiments were run at 333 K; uncertainty is within 20%. – [b] Rate constants have been calculated according to the Langevin theory calculating polarizability of C_3H_4 as in ref.[19], and taking polarizability of SiH_4 from ref.[20] – [c] Efficiency has been calculated as the ratio $\Sigma k_{exp}k_L$.

Table 6. Reactions of $Si_3H_5^+$, $Si_4H_7^+$,$SiC_2H_n^+$, and $SiC_3H_n^+$ ions with allene and silane in a SiH_4/C_3H_4 mixture

Reactants	Product Ions and Rate Constants (k_{exp})[a]	Σk_{exp}	k_L[b]	Efficiency[c]
$Si_3H_5^+ + C_3H_4$	$Si_3CH_5^+$ (0.93), $Si_3CH_9^+$ (0.90), $Si_3C_3H_5^+$ (2.6)			
4.4	10.38	0.43		
$Si_4H_7^+ + C_3H_4$	$Si_3C_3H_5^+$ (0.46), $Si_4CH_7^+$ (0.80), $Si_4CH_{11}^+$ (0.78), $Si_4C_3H_7^+$ (1.6)			
3.6	9.96	0.36		
$SiC_2H_3^+ + C_3H_4$	$SiC_3H_3^+$ (0.50), $SiC_3H_5^+$ (0.76), $SiC_5H_5^+$ (1.3)			
2.6	11.35	0.23		
$SiC_2H_5^+ + C_3H_4$	$SiC_2H_3^+$ (2.4), $SiC_3H_5^+$ (0.90), $SiC_3H_7^+$ (0.67), $SiC_5H_7^+$ (1.5)			
5.5	11.26	0.49		
$SiC_3H_5^+ + C_3H_4$	$SiC_4H_5^+$ (1.1), $SiC_4H_7^+$ (0.39)	1.5	10.85	0.14
$SiC_3H_6^+ + C_3H_4$	$SiC_4H_6^+$ (0.74), $SiC_4H_8^+$ (0.32), $SiC_5H_7^+$ (0.97), $SiC_6H_9^+$ (2.2)			
4.2	10.82	0.39		
$SiC_3H_6^+ + SiH_4$	$Si_2C_3H_8^+$ (0.95)	0.95	10.38	0.092
$SiC_3H_7^+ + C_3H_4$	$SiC_3H_5^+$ (0.15), $SiC_4H_7^+$ (1.6), $SiC_4H_9^+$ (0.66), $SiC_5H_7^+$ (1.1), $SiC_6H_9^+$ (1.3), $SiC_6H_{10}^+$ (0.25)			
5.1	10.80	0.47		
$SiC_3H_7^+ + SiH_4$	$Si_2C_3H_9^+$ (0.38)	0.38	10.36	0.037

[a] Rate constants are expressed as 10^{-10} $cm^3molecule^{-1}s^{-1}$; experiments were run at 333 K; uncertainty is within 20%. – [b] Rate constants have been calculated according to the Langevin theory calculating polarizability of C_3H_4 as in ref.[19], and taking polarizability of SiH_4 from ref.[20] – [c] Efficiency has been calculated as the ratio $\Sigma k_{exp}/k_L$.

with SiH_4 through loss of a hydrogen molecule with rather low rate constants.

The reaction of $SiCH_4^+$ to give $SiCH_5^+$ is an hydrogenation process which can involve both silane and allene as neutral reagent. Similarly, ions at nominal mass 58 and 59, could be formed by $SiCH_4^+$ reacting with both silane[5] ($Si_2H_2^+$ and $Si_2H_3^+$) and allene ($SiC_2H_6^+$ and $SiC_2H_7^+$). The hydrogenation process was observed in the SiH_4/C_3H_6 system previously studied,[5] and the use of a pulsed valve allowed us to state that both neutrals react with $SiCH_4^+$ to give $SiCH_5^+$. The procedure was repeated in this SiH_4/C_3H_4 system, isolating and reacting $SiCH_4^+$ in experiments with allene at a constant pressure and pulsing silane into the trap. In this way, it was found that the $SiCH_5^+$ ion is formed from $SiCH_4^+$ and allene, as well as $SiC_2H_6^+$ and $SiC_2H_7^+$ and the corresponding formation rate constants were calculated.

The propagation of the processes leading to cluster ions of increasing size was further studied and results are reported in Table 6. In this table, the reactions of the $Si_3H_5^+$,

$Si_4H_7^+$, $SiC_2H_n^+$ (n = 3, 5) and $SiC_3H_n^+$ (n = 5–7) ions with allene are shown, together with rate constants of reactions of $SiC_3H_n^+$ (n = 6, 7) with silane.

The $Si_3H_5^+$ and $Si_4H_7^+$ ions were chosen as an example of the behavior of tertiary and quaternary silane ions, as they are the most abundant within their corresponding families. Hence, it was possible to isolate and select them. Also the reactivity of the $Si_3H_4^+$ ion was studied, which reacts very slowly to give the $Si_3CH_4^+$ and $Si_3CH_8^+$ products. Unfortunately their abundance was too low to allow the determination of their formation rate constants. The $Si_3H_5^+$ and $Si_4H_7^+$ ions show a very similar behaviour towards allene.

The $SiC_2H_n^+$ (n = 3, 5) ions react only with allene with loss of hydrocarbon and H_2 molecules with rather low rate constants. A similar behaviour is displayed by the $SiC_3H_n^+$ (n = 5–7) ions. Within this family, the number of reactions with allene and the reaction efficiencies increase with increasing number of hydrogen atoms in the reacting ion. Only the $SiC_3H_n^+$ (n = 6, 7) ions react with silane and yield the large clusters $Si_2C_3H_{n+2}^+$ via loss of a hydrogen molecule characterised by low rate constants.

The present results may be compared with those obtained in the SiH_4/C_3H_8 and SiH_4/C_3H_6 systems previously studied.[5] The reactivity of the SiH_4/C_3H_8 system was found to be remarkably low, and hence the comparison may be limited to the SiH_4/C_3H_6 and SiH_4/C_3H_4 mixtures. Silane primary ions show a similar behaviour towards propene and allene. In fact, reaction efficiencies are quite high and the most favourable neutral losses are almost the same in the two systems. However, when allene is the neutral reagent, the number of different reaction paths is high. In contrast, reactions of the SiH_n^+ (n = 1–3) ions with propene proceed through a lower number of paths, but generally with higher rates. A similar trend is displayed by the $Si_2H_n^+$ (n = 2–5) ions in the comparison of the two systems. Because of the several different processes starting from silane ions, the number of Si, C, and H containing ion species formed in the SiH_4/C_3H_4 system is higher than in the SiH_4/C_3H_6 one. Among these, some ions are common to the two systems: $SiCH_n^+$ (n = 4, 5), $SiC_2H_5^+$ and $SiC_3H_7^+$. Their reactivity towards silane is supposed to be the same; nevertheless, reactions of $SiCH_5^+$ and $SiC_2H_5^+$ ions could not be studied in the SiH_4/C_3H_4 system, the reason being the lower abundance of the reacting ions in the SiH_4/C_3H_4 mixture. In fact, $SiCH_5^+$ is formed through fewer processes and with lower rate constants in the presence of allene than with propene. $SiC_2H_5^+$ has a higher number of precursors in the SiH_4/C_3H_4 system, but formation rate constants are remarkably low. Mixed ions, containing silicon, carbon and hydrogen, that are present in both the systems react with comparable efficiencies with allene and propene, the number of reaction paths being higher in the silane/allene mixture as already observed for silane ions. Finally, several hydrocarbon ions are common to the two mixtures: $C_2H_3^+$, $C_3H_n^+$ (n = 1–5), rate constants of their reactions with silane being in good agreement among the two systems.

Conclusions

In the comparison of the two mixtures studied in this paper, the great difference of reactivity between silane and germane towards allene is remarkable. In fact, neutral germane as well as ions originated by its ionisation are considerably less reactive than the corresponding silicon containing species. Primary and secondary ions of silane react with allene through many different paths and with appreciable reaction efficiencies to yield mixed ion clusters of growing size, such as $Si_4C_3H_7^+$ or $SiC_6H_{10}^+$. In contrast, germane primary ions react with allene to give only one product for each ion, the only exception being GeH_2^+ which gives several mixed ions but with low rate constants. Moreover, the distribution of the signal due to an ion species containing two Ge atoms and the consequent overlapping of different multiplets make the single selection procedures difficult. Anyway, the isolation of the whole $Ge_2H_n^+$ (n = 2–4) ion family and its reaction (with reaction times as long as 2 s) allowed the detection of mixed clusters, up to $Ge_4C_3H_x^+$ ions, although in low abundance.

Hydrocarbon ions, formed in self-condensation processes of allene, mainly reacted with germane by charge-exchange processes to give ion products containing Ge and H only, together with a few mixed ion clusters. To the contrary, allene ions react with silane to yield a great number of different products containing Si, C, and H atoms. These ion species react further, preferentially with allene, in successive steps, to give large clusters with increasing number of carbon atoms.

Finally, it appears clear that the cationic mechanism does not give a high contribution to the growth of materials, starting from gaseous mixtures in the GeH_4/C_3H_4 system, while it is more efficient in the SiH_4/C_3H_4 one. Moreover, in the silane/allene mixture, the largest cluster ions are generally formed in reactions of silicon containing ions with allene and the highest yield are observed in mixtures containing silane in excess.

Experimental Section

Allene and silane were commercially supplied in high purity and germane was prepared and purified as described in the literature.[22] Prior to use, each of the reagent gases was dried by means of anhydrous sodium sulfate. Helium was supplied at an extra-high degree of purity, and no further purification was necessary. The experiments were performed on a ITMS Finnigan mass spectrometer and the pressure was measured by a Bayard Alpert ionisation gauge. The read pressures were corrected for the relative sensitivity of the ion gauge with respect to different gases[23,24] and for a calibration factor, calculated as previously reported,[21] in order to get the real pressure in the trap. Helium buffer gas was admitted to the trap at a pressure of about 4×10^{-4} Torr (1 Torr = 133 Pa), and allene, germane and silane at pressures in the 2.0×10^{-7}–10.0×10^{-7} Torr range. The trap temperature was 333 K in order to avoid thermal decomposition of reagents and to obtain results comparable with systems studied previously. In all experiments, ions were detected in the mass range of 14–400 u . In order to prevent side

reactions with water background, the manifold and the lines for introduction of reagent gases and helium were frequently baked-out.

The scan modes used to isolate selected ion species or ranges of ions for the determination of reaction mechanisms and rate constants, as well as the procedures for calculations, were previously described in detail.[3,21,25] Ionic species that were selectively isolated from silane contained the ^{28}Si isotope, whereas those isolated from germane contained the ^{70}Ge (Ge^+, GeH^+) or ^{76}Ge (GeH_2^+, GeH_3^+) isotope. Selection of ions at a specific *m*/*z* value was performed by using dc voltages and by resonance ejection, as in previous studies.[25] The latter method, applying rf voltages only, is expected to cause a lower excitation of the selected ions with respect to the method in which a dc voltage is used. The rate constants obtained with the two different methods were very similar and this behaviour is consistent with the hypothesis that ions are thermalized by unreactive collisions with the buffer gas. The single exponential decays of the abundance of the reacting ions observed in the kinetic experiments further confirm this hypothesis.

Formation of ions was obtained with an electron beam at about 35 eV for ionisation times in the range 1–20 ms. A reaction time suitable to maximise the abundance of ions to be stored was applied after the ionisation event. Isolation of the selected ions, their reactions with neutrals present in the trap for convenient reaction times (50 ms for rate constants calculation and up to 2 s for mechanisms determination) and acquisition were the successive steps.

In the silane/allene mixture, where Si is isobaric with C_2H_4, some experiments were performed by introducing one reagent gas via a pulsed valve in order to determine the neutral species involved in the ion/molecule reaction under examination and, as a consequence, the composition of the product ion. A General Valve Corporation's Iota One pulse valve was used,[26] and the experimental procedures have been already described.[4] Briefly, the introduction into the ion trap of one of the reactants through a pulsed valve allows us to react selected ions with only the other gas which is continuously leaked into the trap. The pressure of the gas to be pulsed was set behind the valve to about 1×10^{-6} Torr, the valve opening time was 0.1 ms and the time required for the pressure of the pulsed gas to decrease to zero was about 1.5 s.

Acknowledgments

Authors wish to thank MURST and Università di Torino for financial support to this research.

[1] J. G. Ekerdt, Y.-M. Sun, A. Szabo, G. J. Szulczewski, J. M. White, *Chem. Rev.* **1996**, *96*, 1499.
[2] P. Hess, *Electron. Mat. Chem.* **1996**, *127*, 169.
[3] [3a] J.-F. Gal, R. Grover, P.-C. Maria, L. Operti, R. Rabezzana, G. A. Vaglio, P. Volpe, *J. Phys. Chem.* **1994**, *98*, 11978. – [3b] P. Antoniotti, L. Operti, R. Rabezzana, G. A. Vaglio, J.-F. Gal, R. Grover, P.-C. Maria, *J. Phys. Chem.* **1996**, *100*, 155. – [3c] L. Operti, R. Rabezzana, G. A. Vaglio, P. Volpe, *J. Organomet. Chem.* **1996**, *509*, 151. – [3d] G. Cetini, L. Operti, R. Rabezzana, G. A. Vaglio, P. Volpe, *J. Organomet. Chem.* **1996**, *519*, 169. – [3e] P. Benzi, L. Operti, R. Rabezzana, M. Splendore, G. A. Vaglio, *Int. J. Mass Spectrom. Ion Processes* **1996**, *152*, 61. – [3f] P. Antoniotti, L. Operti, R. Rabezzana, G. A. Vaglio, *Int. J. Mass Spectrom.* **1999**, *182*/*183*, 63.
[4] [4a] P. Benzi, L. Operti, G. A. Vaglio, P. Volpe, M. Speranza, R. Gabrielli, *Int. J. Mass Spectrom. Ion Processes* **1990**, *100*, 647. – [4b] L. Operti, M. Splendore, G. A. Vaglio, P. Volpe, M. Speranza, G. Occhiucci, *J. Organomet. Chem*. **1992**, *433*, 35.
[5] P. Antoniotti, L. Operti, R. Rabezzana, G. A. Vaglio, P. Volpe, *Int. J. Mass Spectrom.* **1999**, *190*/*191*, 243.
[6] P. Antoniotti, C. Canepa, L. Operti, R. Rabezzana, G. Tonachini, G. A. Vaglio, *J. Organomet. Chem.,* **1999**, *589*, 150.
[7] P. Antoniotti, C. Canepa, L. Operti, R. Rabezzana, G. Tonachini, G. A. Vaglio, *J. Phys. Chem. A* **1999**, *103*, 10945.
[8] M. T. Bowers, *Gas Phase Ion Chemistry,* Academic Press, New York, **1979**.
[9] S. G. Lias, J. E. Bartmess, J. F. Liebman, J. L. Holmes, R. D. Levin, W. G. Mallard, *J. Phys. Chem. ref. Data Suppl. 1* **1988**, *17*.
[10] B. Ruscic, M. Schwarz, J. Berkowitz, *J. Chem. Phys.* **1990**, *92*, 1865.
[11] R. Bakhtiar, C. M. Holznagel, D. B. Jacobson, *J. Phys. Chem.* **1993**, *97*, 12710.
[12] B. H. Boo, P. B. Armentrout, *J. Am. Chem. Soc.* **1991**, *113*, 6401.
[13] B. H. Boo, P. B. Armentrout, *J. Am. Chem. Soc.* **1987**, *109*, 3549.
[14] S. Wlodek, A. Fox, D. K. Bohme, *J. Am. Chem. Soc.* **1991**, *113*, 4461.
[15] B. H. Boo, J. L. Elkind, P. B. Armentrout, *J. Am. Chem. Soc.* **1990**, *112*, 2083.
[16] B. L. Kickel, E. R. Fisher, P. B. Armentrout, *J. Phys. Chem.* **1992**, *96*, 2603.
[17] S. K. Shin, R. R. Corderman, J. L. Beauchamp, *Int. J. Mass Spectrom. Ion Processes* **1990**, *101*, 257.
[18] [18a] J. J. Myher, A. G. Harrison, *J. Phys. Chem.* **1968**, *72*, 1905. – [18b] M. T. Bowers, D. D. Elleman, R. M. O'Malley, K. R. Jennings, *J. Phys. Chem.* **1970**, *74*, 2583. – [18c] A. Nato, M. Niwa, K. Honma, I. Tanaka, *Int. J. Mass Spectrom. Ion Phys.* **1980**, *34*, 287. – [18d] C. Lifshitz, Y. Gleitman, S. Gefen, U. Shainock, I. Dotan, *Int. J. Mass Spectrom. Ion Phys.* **1981**, *40*, 1. – [18e] C. Lifshitz, Y. Gleitman, *Int. J. Mass Spectrom. Ion Phys.* **1981**, *40*, 17. – [18f] V. G. Anicich, G. A. Blake, J. K. Kim, M. J. McEwan, W. T. Huntress Jr. *J. Phys. Chem.* **1984**, *88*, 4608. – [18g] D. Carrier, J. A. Herman, *Int. J. Mass Spectrom. Ion Processes* **1984**, *59*, 49.
[19] K. J. Miller, *J. Am. Chem. Soc.* **1990**, *912*, 8533.
[20] E. R. Lippincott, J. M. Stutman, *J. Phys. Chem.* **1964**, *68*, 2926.
[21] [21a] P. Benzi, L. Operti, G. A. Vaglio, P. Volpe, M. Speranza, R. Gabrielli, *J. Organomet. Chem.* **1988**, *354*, 39. – [21b] L. Operti, M. Splendore, G. A. Vaglio, A. M. Franklin, J. F. J. Todd, *Int. J. Mass Spectrom. Ion Processes* **1994**, *136*, 25.
[22] P. Benzi, M. Castiglioni, P. Volpe, L. Battezzati, M. Venturi, *Polyhedron* **1988**, *7*, 597.
[23] M. Decouzon, J.-F. Gal, P.-C. Maria, A. S. Tchinianga, *personal communication*.
[24] J. E. Bartmess, R. M. Georgiadis, *Vacuum* **1983**, *33*, 149.
[25] P. Antoniotti, L. Operti, R. Rabezzana, M. Splendore, G. Tonachini, G. A. Vaglio, *J. Chem. Phys.* **1997**, *107*, 1491.
[26] T. J. Carlin, B. S. Freiser, *Anal. Chem.* **1983**, *55*, 571.

Received July 30, 1999
[I99284]

Multinuclear 1D and 2D NMR Investigations on the Interaction between the Pyrimidic Nucleotides 5'-CMP, 5'-dCMP, and 5'-UMP and Diethyltin Dichloride in Aqueous Medium

Laurent Ghys,[a,b] Monique Biesemans,[b,c] Marcel Gielen,[c] Achilleas Garoufis,[d] Nick Hadjiliadis,[e] Rudolph Willem,*[b,c] José C. Martins[b]

Keywords: Tin / Nucleotides / NMR spectrometry / Mass spectroscopy

The interactions between diethyltin dichloride and 5′-CMP, 5′-dCMP, and 5′-UMP in aqueous solution were investigated by multinuclear 1D and 2D NMR techniques including ^{119}Sn, ^{15}N and ^{31}P nuclei. These studies were combined with electrospray mass spectrometry, infrared spectroscopy, solid state ^{13}C, ^{31}P and ^{117}Sn CP-MAS NMR, and elemental analysis. As demonstrated by ^{31}P-^{1}H HOESY spectroscopy, the diethyltin moiety interacts with the phosphate group of the pyrimidic mononucleotides in the pH range 0.5–3.5. Compound **8** (X = Cl), the solid isolated in this pH range from 5′-CMP, contains two tin atoms bridged by one oxygen and one chlorine atom, each tin atom being linked to the phosphate group of a nucleotide moiety. For 5′-UMP the solid isolated (**12**) has a dimeric structure with two different tin atoms; it can be formed by dimerization of compound **11** with the elimination of two water molecules. As demonstrated by ^{1}H-^{119}Sn HMQC correlation NMR data and the $^{2}J(^{119}\text{Sn–O–}^{117}\text{Sn})$ coupling constant of 156 Hz, the diethyltin moiety reacts with the O(2′) and O(3′) oxygen atoms of the nucleotides to form a dimeric diethyldioxastannolane at pH > 9.0. Between pH 5.0 and 9.0, no evidence for any interaction between the diethyltin moiety and the nucleotides was found.

Introduction

Many organometallic compounds exhibit interesting antitumoural activity against several human cancer cell lines.[1] The well-known complex cisplatin, $Pt(NH_3)_2Cl_2$, clinically used in cancer chemotherapy, proved to interact mainly with the N7 atoms of two adjacent guanines in the same DNA strand.[2–5] For several years, we have been interested in the synthesis and characterisation of organotin complexes which, in some cases, display higher antitumour activities in vitro than cisplatin.[6] In contrast to platinum compounds, very little is known about the origin of the antitumoural activity of organotin compounds although, as for cisplatin, DNA was proposed to be the target.[7] Some work has already been performed on the interactions between organotins and DNA or its precursors. Barbieri et al. have investigated the solid resulting from the reaction of ethanolic organotins [$SnR_2Cl_2(EtOH)_2$ and $SnR_3Cl(EtOH)$] with aqueous DNA or mononucleotide solutions. However, only ^{119}Sn Mössbauer spectroscopy was used.[8–10] The condensate was assumed to be a diorganotin species interacting with two vicinal phosphate groups of DNA. Li et al. have investigated the interaction of $(C_2H_5)_2SnCl_2$(phen) (phen = phenanthroline) with 5'-dGMP in aqueous medium using [*trans*-$en_2Os(\eta\text{-}H_2)](CF_3SO_3)_2$, a versatile ^{1}H NMR probe. They also studied solid mixtures of the same diethyltin dichloride complex with 5'-AMP, 5'-CMP, and 5'-GMP dissolved in DMSO, using ^{1}H and ^{31}P NMR and UV spectroscopy.[11a] More recently, Hadjiliadis et al.[11b] studied the interaction of the purine nucleotides 5'-IMP and 5'-GMP with Et_2SnCl_2 using various techniques, including ^{1}H, ^{13}C and ^{31}P 1D NMR and Mössbauer spectroscopy. Finally, a very recent paper described the investigation of the interaction between dimethyltin dichloride and 5'-GMP, 5'-ATP and 5'-$d(CGCGCG)_2$ by potentiometric titrations and ^{1}H and ^{31}P NMR spectroscopy.[11c] All these authors concluded that the organotin moiety reacts with the phosphate group of the nucleotides. However, these interactions have not been investigated further using spectroscopic techniques that provide more detailed structural data, such as ^{119}Sn NMR spectroscopy. Potentially, this technique is an ideal tool of investigation, comparable to ^{195}Pt NMR spectroscopy for platinum compounds.[12]

This study investigates the interaction between a diorganotin dichloride, Et_2SnCl_2, and pyrimidic nucleic acid precursors within a wide pH range in aqueous medium. The three mononucleotides investigated, cytidine-5'-monophosphate (5'-CMP), 2'-deoxycytidine-5'-monophosphate (5'-dCMP) and uridine-5'-monophosphate (5'-UMP), were selected on the basis of their increased solubility when they are complexed to tin (Figure 1).

First, we monitored the ^{31}P chemical shift of the mononucleotides in aqueous solution as a function of pH in the presence or absence of diethyltin dichloride and the ^{119}Sn chemical shift of a mixture of the latter with the mononu-

[a] Université Libre de Bruxelles, Service de Chimie Organique, Av. F. D. Roosevelt, 50, B-1050 Brussels, Belgium
[b] Vrije Universiteit Brussel, High Resolution NMR Centre, Pleinlaan, 2, B-1050 Brussels, Belgium
[c] Vrije Universiteit Brussel, Laboratory of General and Organic Chemistry, Pleinlaan, 2, B-1050 Brussels, Belgium
[d] Technological Institute of Athens, Department of Chemistry, Physics and Materials Technology, 12210 Egaleo, Greece
[e] University of Ioannina, Department of Chemistry, 45110 Ioannina, Greece

 © WILEY-VCH Verlag GmbH, D-69451 Weinheim, 2000 1434−1948/00/0303−0513 $ 17.50+.50/0

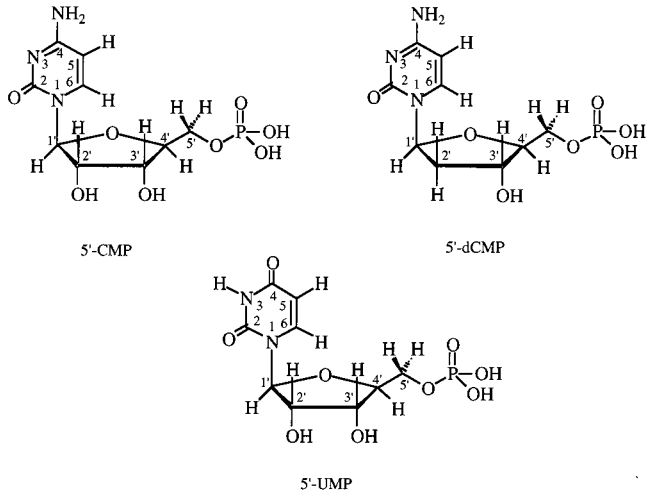


Figure 1. Structures and numbering scheme of the 5'-CMP, 5'-dCMP and 5'-UMP mononucleotides

cleotides. The differences in ^{31}P chemical shift titration profiles are used as indicators for an interaction between diethyltin dichloride and the mononucleotides. Subsequently, the structural features of the interaction are characterised by 1D and 2D NMR correlation techniques involving ^{1}H, ^{13}C, ^{15}N, ^{31}P and ^{119}Sn nuclei, completed by ^{35}Cl NMR data where appropriate. Proton detected ^{1}H-^{119}Sn HMQC[13–15] and phosphorus detected ^{31}P-^{1}H HOESY[16,17] have been reported to be very efficient for the characterisation of organotin complexes in solution.[18] Whenever precipitation occurs, the solid is isolated and characterised by solid state ^{13}C, ^{31}P, and ^{117}Sn CP-MAS NMR and IR spectroscopy as well as elemental analysis. None of the solids isolated provided crystals suitable for X-ray diffraction analysis.

Results and Discussion

Aqueous Chemistry of Diethyltin Dichloride

Figure 2 shows the different intermediates (in their monomeric form, for convenience) generated upon hydrolysis of Et_2SnCl_2 as mentioned in the literature.[19–21] The NMR data collected during this preliminary investigation are suitable references for the interpretation of data obtained in the presence of nucleotides.

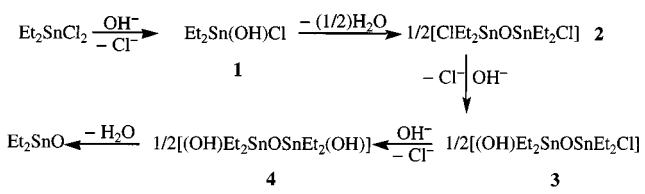
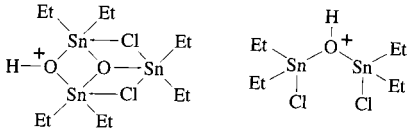


Figure 2. Different species formed under hydrolysis of Et_2SnCl_2 in aqueous solution

Table 1. Electrospray mass spectrometry data of a MeOH/H_2O (90/10) solution of Et_2SnCl_2 at pH 2.2



m/z	Assignment
653	**5** + H_3O^+
635	**5** + H^+
441	**2** + H^+
277	$[Et_2SnCl(CH_3OH)_2]^+$
245	$[Et_2SnCl(CH_3OH)]^+$

Table 2. Experimental elemental analysis data for the solid compound isolated from an aqueous solution of Et_2SnCl_2 at pH 2.8 as well as calculated data for the proposed structure

	%C	%H	%Cl	%Sn
Et_2SnCl_2 isolated at pH 2.8	21.8	4.3	14.0	52.2
$[ClEt_2SnOSnEt_2Cl]$ (**2**)	21.8	4.6	16.1	53.9

The pH of a 0.5 M aqueous solution of Et_2SnCl_2 is ca. 2.2. A precipitate is generated when the pH of the supernatant is raised above 2.2 with aqueous NaOH. Below pH 2.2, a clear solution is observed. An electrospray mass spectrum of a mixture obtained by adding methanol to an aqueous solution of Et_2SnCl_2 (pH 2.2) with a final MeOH/H_2O ratio of 90/10 reveals two species. On the basis of data from Dakternieks et al.[22a] these species can be assigned to compounds **5** and **2** (Table 1). The fragment detected at *m/z* 441 in the electrospray mass spectrum is the protonated form of intermediate **2** (Figure 2).

The other fragment ions correspond to $[Et_2SnCl]^+$ solvated by one or two methanol molecules or to hydrated **5** (Table 1). These results clearly indicate that in solution at pH 2.2 only one chloride anion dissociates from diethyltin dichloride.

The precipitate obtained at pH 2.8 was isolated. Its elemental analysis data (Table 2) indicate that it basically corresponds to compound **2**, probably contaminated by **3**, considering the slight chlorine deficit.

The ^{117}Sn NMR spectrum of this sample in $CDCl_3$ at 89.150 MHz displays eight resonances between $\delta = -87$ and $\delta = -182$. They can be divided into two pairs of equally intense resonances **B** and **C** and one set of four equally intense resonances **A**. Set **B** ($\delta = -91.7$ and -139.9) displays one pair of satellites with a coupling of 67 Hz. It is assigned to intermediate **2** which is described by Otera[22b] as a dimer for R = Me, Et and Bu with similar ^{119}Sn parameters for R = Et:[22b] $\delta(^{119}Sn1) = -140.6$; $\delta(^{119}Sn2) = -91.8$; $^{2}J(^{119}Sn–O–^{117/119}Sn) = 73$ Hz. Set **C** ($\delta = -157.0$ and -176.2) displays at least one pair of $^{2}J(^{117}Sn–O–^{117/119}Sn)$ satellites with a coupling of 212 Hz, others being unclear due to a low signal-to-noise ratio. The ^{117}Sn resonances of

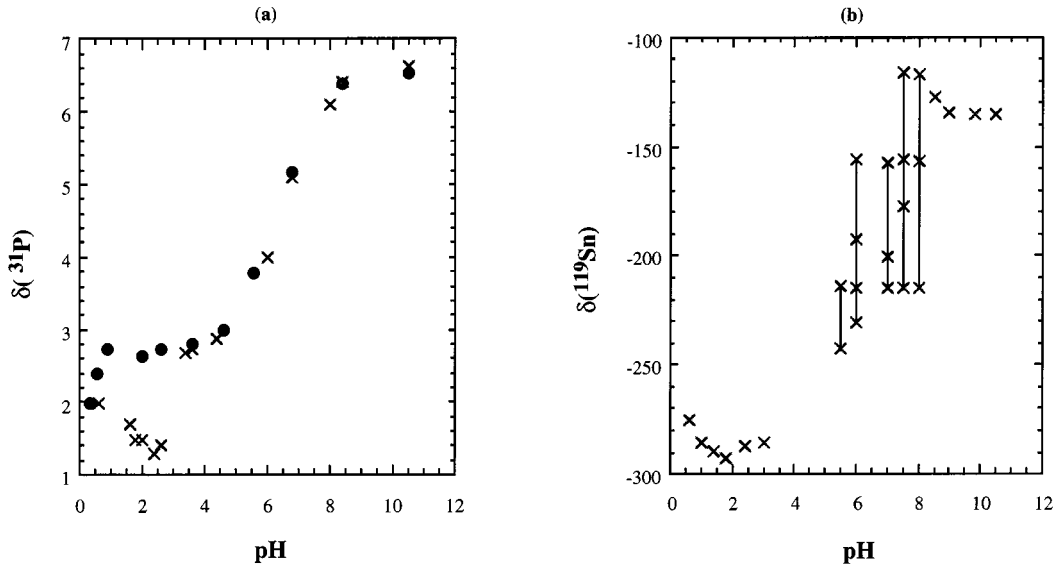


Figure 3. (a) ^{31}P NMR titration curve of 5'-CMP and a mixture of 5'-CMP and Et_2SnCl_2; full circles represent free 5'-CMP; crosses correspond to 5'-CMP/Et_2SnCl_2; (b) ^{119}Sn NMR titration curve for 5'-CMP/Et_2SnCl_2; multiple points related by straight lines for a given pH value account for the presence of multiple resonances

set **A** (δ = –87.9, –130.9, –151.8, and –181.8) display a pair of signals with a coupling constant of 98 Hz and another pair with a coupling constant of 175 Hz. Although the species generating **A** and **C** cannot be identified, these NMR data point to a mixture of intermediates including **3** and **4**, possibly aggregated to various degrees during hydrolysis of Et_2SnCl_2 depicted in Figure 2.

Interactions of Diethyltin Dichloride with the Nucleotides in Acidic Medium

Above pH 2.2, precipitation occurs from the solutions of the three 2:1 mixtures of 5'-CMP/Et_2SnCl_2, 5'-dCMP/Et_2SnCl_2, and 5'-UMP/Et_2SnCl_2. Consequently, samples for NMR experiments in solution are obtained from the supernatant of this precipitate. Because in acidic medium the three nucleotides behaved similarly in the presence of Et_2SnCl_2, only the mixture 5'-CMP/Et_2SnCl_2 is discussed in detail.

In the pH range 0.5–3.5, the addition of 0.5 equivalent of diethyltin dichloride to 5'-CMP, 5'-dCMP and 5'-UMP causes the ^{31}P resonance of the phosphate group of the nucleotides to shift to lower frequencies, with the maximum change in chemical shift in the pH range 2.0–2.5. The titration curve of the ^{31}P chemical shift is displayed in Figure 3a for 5'-CMP and 5'-CMP/Et_2SnCl_2.

This ^{31}P chemical shift modification can be traced back to an interaction of diethyltin dichloride with the phosphate group of the three nucleotides. ^{1}H-^{119}Sn, ^{1}H-^{31}P, ^{31}P-^{119}Sn, and ^{13}C-^{31}P HMQC experiments[23,24] performed on 5'-CMP/Et_2SnCl_2 at pH 2.2 failed to show any correlation peaks between the resonances of the organotin moiety and those of 5'-CMP. However, this does not formally exclude the interaction between diethyltin dichloride and the phosphate group of 5'-CMP. Indeed, the coupling can be very small or even nonexistent and undetectable depending on the bond strength.[25] The ^{31}P-^{1}H HOESY (^{31}P detected Heteronuclear Overhauser Spectroscopy) technique[16–18] which correlates nuclei through dipolar couplings was previously used by Barnham et al.[26] to characterise the Pt–NH···5'-phosphate intermolecular interaction in the complex [Pt(en)(5'-GMP–N7)$_2$]·9H_2O. This technique provided a 2D spectrum of 5'-CMP/Et_2SnCl_2 at pH 2.2 with four ^{31}P-^{1}H NOE cross-peaks, two from the CH_2 and CH_3 protons of diethyltin dichloride and two from the H5' and H6 protons of 5'-CMP. Similar results were obtained for the mixtures of the two other nucleotides with Et_2SnCl_2, i.e. 5'-dCMP/Et_2SnCl_2 and 5'-UMP/Et_2SnCl_2 at pH 2.2. With the ratio ($\gamma^1H/\gamma^{31}P$) > 2.38 in mind, the distances between the ethyl protons and the phosphorus atom of the three nucleotides cannot exceed 4 Å, proving that the tin moiety interacts with the phosphate group of the nucleotide. ^{31}P-^{1}H-NOE's are always positive, irrespective of the correlation time.[27] Hence, weak or missing NOE's cannot be assigned to a zero cross point of the NOE effect. The observed cross peak between the H6 proton and the ^{31}P nucleus of 5'-CMP, 5'-dCMP, and 5'-UMP arises from the *anti* conformation of the base relative to the sugar unit which is also known for free 5'-GMP.[28]

As assessed by the ^{119}Sn chemical shifts and the $^{1}J(^{13}C$–$^{119}Sn)$ values,[29,30] the tin atom is six-coordinated in all three mixtures, i.e. 5'-CMP/Et_2SnCl_2, 5'-dCMP/Et_2SnCl_2, and 5'-UMP/Et_2SnCl_2 at pH 2.2 (Table 3). Empirical correlations between C–Sn–C angles and coupling constants involving the ^{119}Sn nucleus[31] (Table 3) provide C–Sn–C angle values typically ranging from 150° to 170°, which are in agreement with distorted *trans*-octahedral, six-coordinate geometries at the tin atom.

As shown by ^{13}C, ^{31}P, and ^{117}Sn CP-MAS NMR, the solid isolated from the mixture 5'-CMP/Et_2SnCl_2 (2:1) at pH 2.2 contains both Et_2Sn and 5'-CMP moieties. The ^{31}P CP-MAS NMR spectrum exhibits 5'–CMP two resonances at δ = –11 and δ = –12 which are low frequency shifted

Table 3. ^{119}Sn chemical shifts (ppm) and coupling constants (Hz) determined at pH 2.2 for the three nucleotides in the presence of Et_2SnCl_2 in the molar ratio 2:1

	5'-CMP/Et_2SnCl_2	5'-dCMP/Et_2SnCl_2	5'-UMP/Et_2SnCl_2
$\delta(^{119}Sn)$ (D_2O)	–287	–278	–298
$\delta(^{117}Sn)$ (solid)	–274	*	–262 and –281
$^1J(^{13}C–^{119}Sn)$	850	834	876
$^2J(^1H–^{119/117}Sn)$	96	93	92
C–Sn–C angle[a]	172°	166°	163°
C–Sn–C angle[b]	152°	150°	154°
C–Sn–C angle[c]	160°	158°	162°

[a] Calculated from the empirical relationships of Howard et al.:[31a] Θ (deg) = 2.28 [$^2J(^1H–^{119}Sn)$] – 46.4. – [b] Lockhart et al.:[31b] Θ (deg) = 0.088 [$^1J(^{13}C–^{119}Sn)$] + 76.754. – [c] Holecek et al.:[31c] Θ (deg) = 0.1 [$^1J(^{13}C–^{119}Sn)$] + 74.675; * irreproducible, contaminated by Et_2SnO and other unidentified hydrolysis products.

with respect to the single one in solution at ca. $\delta = 1$. The assignment of the resonances in the ^{13}C CP-MAS spectrum is made by comparison with the solution ^{13}C chemical shifts of 5'-CMP/Et_2SnCl_2 at pH 2.2. In solution, ^{1}H-^{13}C HMBC and HMQC[23,24,32] spectra allowed the assignment of the ^{13}C and ^{1}H resonances that is further supported by literature data.[33]

Table 4. Comparison of the solid and solution state ^{13}C chemical shifts at pH 2.2 for the mixtures 5'-CMP/Et_2SnCl_2 (2:1) and 5'-UMP/Et_2SnCl_2 (2:1)

	5'-CMP/Et_2SnCl_2		5'-UMP/Et_2SnCl_2	
	solid	solution	solid	solution
C4	163.9	159.2	163.1	166.6
C2	154.0	148.5	152.2	152.2
C6	141.7	144.1	139.4	142.0
C5	98.9	95.3	102.3	103.0
			100.2	
C1'	87.2	89.8	93.1	89.3
	85.2			
C4'	83.4	83.4	84.4	83.5
			81.5	
C2'	76.2	74.2	75.2	74.3
	75.3			
C3'	72.9	69.2	71.8	70.1
	72.1		71.3	
C5'	68.0	63.8	67.6	65.1
CH_2	19.9	25.6	19.7	27.0
	18.4		19.0	
	17.8		17.2	
CH_3	9.2	9.2	9.7	9.8
			9.2	

Table 4 shows that some of the solid state ^{13}C resonances are duplicated, one is even triplicated; this is a result of the nucleotide moieties being nonequivalent, possibly because of chirality, packing effects, and/or polymorphism. The ^{13}C chemical shifts of the tin ethyl CH_2 group, the pyrimidic and the C5' carbons deviate most from those in the liquid state. For the pyrimidic carbons, this variation can be explained by a different H-bonding network in the solid state, as previously seen for several nucleotides by IR spectroscopy.[34] The ^{117}Sn NMR CP-MAS spectrum exhibits a single isotropic shift at $\delta = –274$ in the range typical for six-coordinate tin atoms in solution. These CP-MAS NMR data, combined with the solution NMR data, suggest that the tin environments in the solid and solution states are similar.

The vibrational data (Table 5) account exclusively for the existence of a tin–phosphate interaction, the ring vibration frequencies not being affected by the addition of Et_2SnCl_2. As suggested above for the variation of the pyrimidic ^{13}C chemical shifts, the shift of the ν(C(2)=O) frequency [$\Delta\nu$ = ν(5'-CMP/Et_2SnCl_2) – ν(5'-CMPNa_2) = 23 cm^{-1}] can be explained by different H-bonding networks.[34] The Raman spectrum displays two characteristic bands at 434 and 568 cm^{-1} that were tentatively assigned to the $\tilde{\nu}$(Sn–O–P) and $\tilde{\nu}$(Sn–O–Sn) vibration frequencies, respectively.[35–37]

On the basis of all previous data, four tin–phosphate complexes (Figure 4) are conceivable for the solid-state structure obtained from mixing 5'-CMP and Et_2SnCl_2. Unexpectedly, elemental analysis data from samples of the complex depend on the acid (HCl or HBr) used for the adjustment of the pH of the supernatant from which this solid precipitates; nevertheless, these data are self-consistent and reproducible (Table 6). With HCl, the chlorine detected originates not only from Et_2SnCl_2 but also, and even predominantly, from the excess HCl. However, chlorine is also detected when HBr is used in excess. In the latter case, the solid analysed contains two complexes, one only with bromine (ca. 80%) and one only with chlorine (ca. 20%). Structures **6**, **7** (X = Cl, OH), as well as structure **9** (X = OH) (Figure 4) can easily be rejected on the basis of the chlorine elemental analysis. Structure **8** (X = Cl) is favoured over structure **9** (X = Cl) because the calculated carbon and tin elemental data match the experimental data better for the former than for the latter (Table 6). A thermogravimetric analysis of the solid detects a weight loss of ca. 7% up to 170 °C, prior to a more substantial and continuous loss above 190 °C. The initial low weight loss is compatible with the expected loss of one equivalent of HCl and two equivalents of water, an observation which again matches structure **8** better than **9** (X = Cl). Structure **8** is proposed as a hydrochloric salt with a Sn–Cl–Sn bridge, which is known for various organotin oxides,[38,39] and a hydrogen bond between the chloride anion and the oxygen bridging the two

Table 5. IR data of free 5'-CMP and 5'-UMP as well as IR and Raman (*) data of the mixtures 5'-CMP/Et_2SnCl_2 and 5'-UMP/Et_2SnCl_2 in the solid state in KBr pellets (cm^{-1})

Tentative assignment	5'-CMPNa_2[a]	5'-CMP/Et_2SnCl_2[a]	5'-UMPNa_2[a]	5'-UMP/Et_2SnCl_2[a]
$\tilde{\nu}$(C2=O)	1653s	1730s, 1676s	1683s[b]	1708s, 1664m[b]
$\tilde{\nu}$(ring)	1540m	1540m	1472m	1466m
	1491m	1491m		
$\tilde{\nu}(PO_3)$asym + $\tilde{\nu}$[CO(sugar)]	1110s	1121s	1126s, 1091s	1120s, 1078m
	1082s	1075s		
$\tilde{\nu}(PO_3)$sym	978s	995m	976m	1009m, 1007m, 994m, 960w
		961m		
$\tilde{\nu}$(C–Sn)asym*	–	548m	–	548m
$\tilde{\nu}$(C–Sn)sym*	–	511s	–	511s
$\tilde{\nu}$(Sn–O–P)*	–	434w	–	436w
$\tilde{\nu}$(Sn–O–Sn)*	–	568w	–	568w

[a] s = strong, m = medium, w = weak, $\tilde{\nu}$ = stretching. – [b] $\tilde{\nu}$(C2=O) + $\tilde{\nu}$(C4=O).

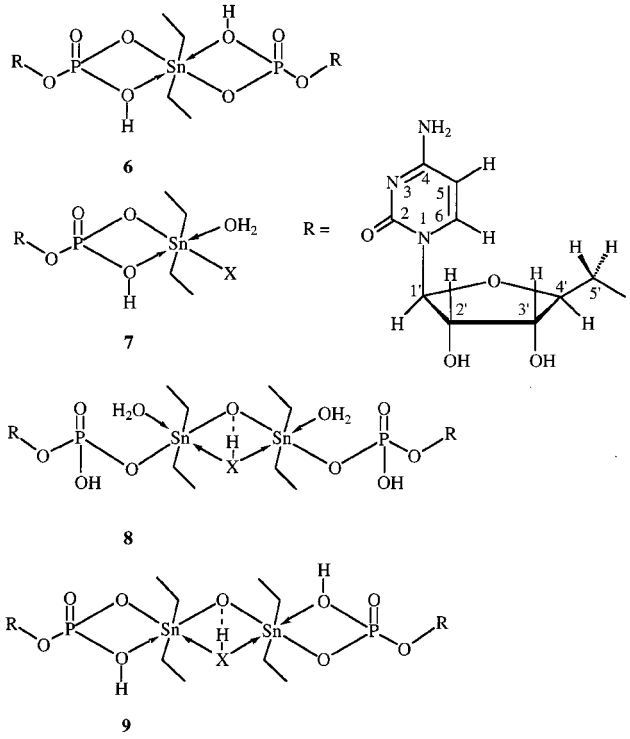


Figure 4. Potential structures for the solid isolated from the mixture 5'-CMP/Et_2SnCl_2 at pH 2.2 and assessed against the data (X = OH, Cl, or Br)

tin atoms. When prepared from the HBr solution, the compounds appear to be of type **8** with X being either Cl or Br.

As supported by similar ^{13}C and $^{117/119}Sn$ CP-MAS and solution NMR data, the environments of the tin atom in solution and in the solid state are proposed to be similar for 5'-CMP/Et_2SnCl_2. Thus, the structure of the complex in solution should be closely related to structure **8** (X = Cl), even if some differences between the solution and solid state ^{31}P and ^{13}C chemical shifts of the CH_2 group suggest local structure differences, possibly due to different H-bridge network or packing effects.

The ^{35}Cl solution NMR data of the supernatant shed some further, albeit indirect light on this proposal. It is well-known that the ^{35}Cl NMR signal of the chloride anion is very sharp and displays a chemical shift around $\delta = 0$.[40] In contrast, covalently bound chlorine generally fails to provide a useful ^{35}Cl signal since it is smeared out in the noise. The supernatant of the solid with proposed structure **8** falls into the latter category. Provided that **8** has identical structures in the supernatant and the solid, this structure implies that one chloride ion has been split off from the initial Et_2SnCl_2, while the second is covalently bound. The absence of any visible ^{35}Cl resonance in a solution of **8** implies the presence of covalently bound chlorine (as indicated by elemental analysis), necessarily being in fast exchange with the ionic chloride which must also be present.

Mixtures of Et_2SnCl_2 with the nonphosphorylated analogue of 5'-CMP, cytosine, also give rise to precipitates at pH 2–5; this occurs to an even larger extent than for 5'-CMP/Et_2SnCl_2. Indeed, the ^1H NMR spectra of the supernatants show that only small amounts of compounds containing a diethyltin moiety are present in solution, as assessed from a comparison of the integrations of the H6 and Et_2Sn protons. The precipitate was isolated; its ^{13}C CP-MAS NMR spectrum presents only ^{13}C resonances from the diethyltin moieties and none from the nucleobase. The ^{117}Sn CP-MAS NMR spectrum of the cytosine-derived

Table 6. Experimental elemental analysis data for the solid compounds isolated from 5'-CMP/Et_2SnCl_2 and 5'-UMP/Et_2SnCl_2 mixtures at pH 2.2 as well as calculated data for potential structures of Figures 4 and 5; the experimental data result from the average over three samples prepared independently with HCl or HBr; for 5'-UMP/Et_2SnCl_2, identical experimental results were obtained with HCl and HBr

	%C	%H	%N	%Cl	%Br	%P	%Sn
5'-CMP/Et_2SnCl_2[a]	28.4	4.7	7.5	3.1	–	5.6	21.2
5'-CMP/Et_2SnCl_2[b]	27.6	4.5	7.2	0.7	5.0	5.3	20.2
6	27.0	4.2	7.3	–	–	10.7	20.5
7 (X = Cl)	28.3	4.6	7.6	6.4	–	5.6	21.5
7 (X = OH)	29.2	4.9	7.9	–	–	5.8	22.2
8 (X = Cl)	28.7	4.7	7.7	3.3	–	5.7	21.9
8 (X = Br)	27.6	4.5	7.4	–	7.1	5.5	21.0
8 (X = OH)	29.2	4.9	7.9	–	–	5.8	22.2
9 (X = Cl)	29.7	4.5	8.0	3.4	–	5.9	22.6
9 (X = Br)	28.5	4.3	7.7	–	7.3	5.7	21.7
9 (X = OH)	30.2	4.7	8.1	–	–	6.0	23.0
5'-UMP/Et_2SnCl_2	31.0	4.3	5.5	–	–	5.9	23.0
10	29.2	4.7	5.2	–	–	5.8	22.2
11	30.2	4.5	5.4	–	–	6.0	23.0
12	30.7	4.4	5.5	–	–	6.1	23.4

[a] Prepared with HCl. – [b] Prepared with HBr.

Table 7. Experimental elemental analysis data for the solid compound isolated from cytosine/Et_2SnCl_2 at pH 2.2 as well as calculated data for the proposed structure

	%C	%H	%Cl
cytosine/Et_2SnCl_2	23.1	5.0	8.4
$[(OH)Et_2SnOSnEt_2Cl]$	22.8	5.0	8.4

sample displays two isotropic ^{117}Sn chemical shifts of comparable intensities at $\delta = -164$ and $\delta = -178$. In agreement with this, the elemental analysis data of this sample as well as the two equally intense ^{117}Sn resonances observed match the formula $[(OH)Et_2SnOSnEt_2Cl]$ (Table 7) that corresponds to intermediate **3** in the hydrolysis scheme of Figure 2. In line with Otera's finding on 3-chloro-1-hydroxytetraorganodistannoxanes (R = *n*Bu), this structure should be dimeric.[22b] In fact this compound, which is also soluble in $CDCl_3$, has a ^{117}Sn NMR spectrum which displays the same eight resonances as species A, B, and C, albeit with different relative populations, as in the sample isolated by precipitation at pH 2.8 from pure aqueous Et_2SnCl_2. Therefore, it probably includes intermediates **2**, **3** and **4**. Since essentially the same hydrolysis products are observed as with pure Et_2SnCl_2, it can be concluded that at least no peculiar interaction between the Et_2Sn moiety and cytosine occurs (Figure 2). In particular, this rules out any interaction between the Et_2Sn moiety and the nucleobase functionalities.

A solid was also isolated from a mixture of 5'-UMP and Et_2SnCl_2 at pH 2.2. The ^{31}P CP-MAS NMR spectrum exhibits two resonances at $\delta = -7$ and $\delta = -12$; they are shifted to low frequency with respect to the single one in solution at ca. 0.2 ppm. The ^{117}Sn CP-MAS NMR spectrum exhibits two isotropic resonances of equal intensity at $\delta = -262$ and $\delta = -281$ in the range corresponding to six-coordinate tin atoms. The vibrational data of 5'-UMP/Et_2SnCl_2 also unambiguously reflect a tin–phosphate interaction (Table 5). In contrast to 5'-CMP/Et_2SnCl_2, the elemental analysis data of 5'-UMP/Et_2SnCl_2 (Table 6) are independent of the acid used for adjusting the pH of the solution from which the solid originates, no chlorine or bromine being detected. These data are fairly consistent with structure **10** and even better for structure **11** (Table 6 and Figure 5). Unlike **8**, the thermogravimetric analysis of this solid does not indicate loss of H_2O or HCl, supporting structure **11** rather than **10**. However, the two different isotropic chemical shifts observed in the ^{117}Sn CP-MAS spectrum are in disagreement with both structures **10** and **11**; therefore, structure **12** can be proposed (Figure 5). It contains two different tin atoms and can be formed by dimerization of structure **11** with elimination of two water molecules. Among the three structures proposed, **12** agrees best with the elemental analysis data (Table 6) and is the only one to fit all the NMR data.

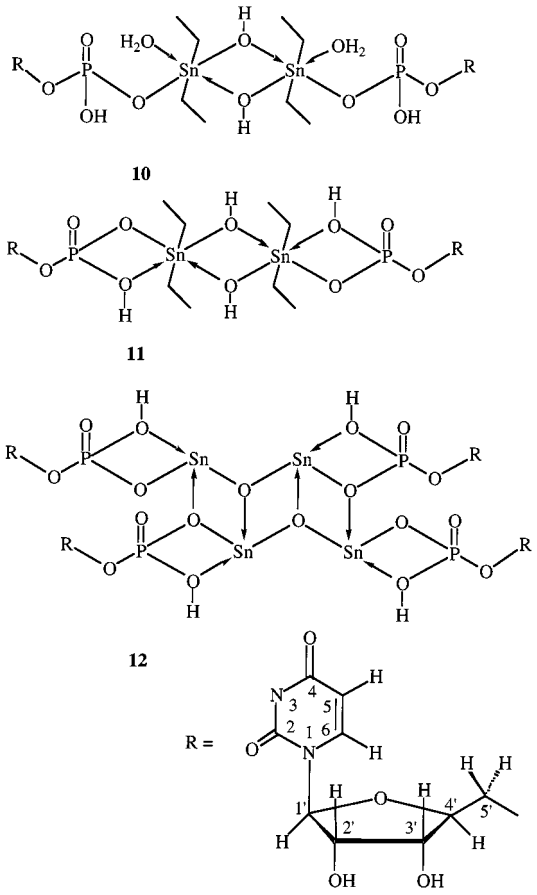


Figure 5. Potential structures for the solid isolated from the mixture 5'-UMP/Et_2SnCl_2 at pH 2.2 and assessed against the data; in structure **12**, the ethyl groups bonded to the tin atoms have been omitted for clarity

The tendency of the 5'-dCMP/Et_2SnCl_2 mixtures to precipitate is lower than that of 5'-CMP and 5'-UMP, with precipitation only occurring at higher pH's. Moreover, no reproducible elemental composition and solid state NMR data could be obtained as the solid appears to contain hydrolysis products of Et_2SnCl_2 as well as free and complexed 5'-dCMP with $\delta(^{31}P) = 0.6$ and –9.2.

Interaction of Diethyltin Dichloride with the Nucleotides at pH > 9.0

At pH 9.0, the 1D ^{119}Sn NMR spectrum of the mixture 5'-CMP/Et_2SnCl_2 (2:1) exhibits a single ^{119}Sn resonance at $\delta = -137$ (Figure 4), characteristic of R_2SnO_2 compounds in the presence of a donor giving rise to a five-coordinate tin.[31,41] The ^{13}C NMR spectrum exhibits a pair of signals for each carbon atom of the sugar unit, one ^{13}C resonance of each pair arising from free 5'-CMP. Upon addition of one more equivalent of diethyltin dichloride (5'-CMP/Et_2SnCl_2 = 1:1) the ^{13}C resonances corresponding to free 5'-CMP disappear but the 1D ^{119}Sn NMR spectrum displays a second very small ^{119}Sn signal at $\delta = -202$. The latter increases as the amount of Et_2SnCl_2 is further increased. The mixture 5'-UMP/Et_2SnCl_2 displays similar behaviour; in contrast, the mixture 5'-dCMP/Et_2SnCl_2 in any

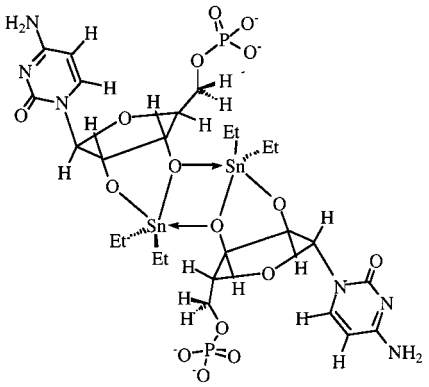


Figure 6. Structure proposed for the complex generated in mixture 5'-CMP/Et_2SnCl_2 at pH 10.5

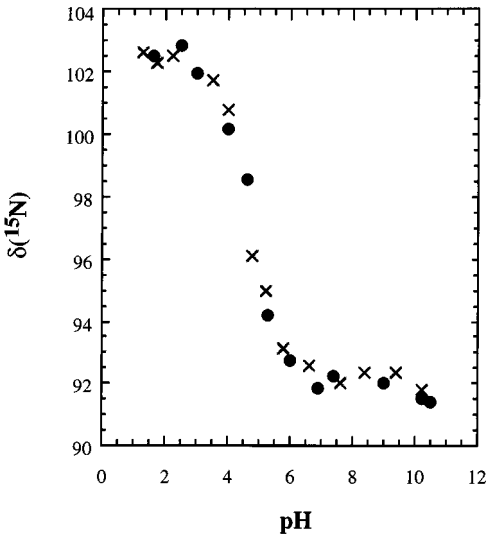


Figure 7. ^{15}N NMR titration curve as obtained for the N3 nitrogen atom of ^{15}N-enriched 5'-CMP and 5'-CMP/Et_2SnCl_2

Table 8. Chemical shifts (ppm) and coupling constants (Hz) for the three nucleotides studied at pH 10.5 in the presence of Et_2SnCl_2

	$\delta(^{119}Sn)$	$^1J(^{13}C–^{119/117}Sn)$	$^2J(^1H–^{119/117}Sn)$
5'-CMP/Et_2SnCl_2	–137	667	81
5'-dCMP/Et_2SnCl_2	–202	757	[a]
5'-UMP/Et_2SnCl_2	–137	665	79

[a] Nonobservable due to broad signal.

ratio exhibits a single ^{119}Sn resonance at δ = –202. Furthermore, the ^{119}Sn nuclei associated with the two ^{119}Sn resonances (δ = –137 and –202) are in chemical exchange, as demonstrated by the presence of intense cross-peaks in the 2D ^{119}Sn EXSY spectrum[42,43] recorded from the mixture 5'-CMP/Et_2SnCl_2. A 2D ^1H-^{119}Sn HMQC spectrum of this mixture reveals no correlations between the ^{119}Sn resonance at δ = –202 and the proton resonances of the 5'-CMP moiety. In contrast, the ^{119}Sn resonance at δ = –137 displays ^1H-^{119}Sn HMQC correlations with the H2' and H3' proton resonances of the sugar unit, as well as satellites corresponding to a $^2J(^{119}Sn–O–^{117/119}Sn)$ coupling constant of 156 Hz.

These ^1H-^{119}Sn HMQC correlations result from $^3J(^1H–^{119}Sn)$ couplings through the pathways H2'–C2'–O2'–Sn and H3'–C3'–O3'–Sn and can be traced to the formation of bonds between the tin atom and the O(2') and O(3') oxygen atoms of the sugar unit (Figure 6). The ^{119}Sn chemical shift of δ = –137, the $^1J(^{13}C–^{119}Sn)$ of 667 Hz (Table 8), and the $^2J(^{119}Sn–O–^{117/119}Sn)$ of 156 Hz, combined with the ^1H-^{119}Sn HMQC data, are consistent with a five-coordinate tin atom in a dimeric R_2SnO_2 diethyldioxastannolane as shown in Figure 6, one oxygen atom of the diol group of the sugar unit being tricoordinated.[41] Similarly, dimeric dibutylstannylene acetals have ^{119}Sn chemical shifts between δ = –115 and –150 in five-membered rings with pentacoordination at the tin atom (Table II of ref.[41b]).

A ^{35}Cl NMR spectrum of the mixture at pH 10.5 confirms that no covalently bonded chlorine is involved, as supported by the very narrow ^{35}Cl resonance at δ = 0[40] which indicates that this element is only present as a chloride anion. The ^{119}Sn resonance at δ = –202 starts appearing when the tin to nucleotide ratio exceeds 1:1 in a mixture of Et_2SnCl_2 with substrates which contain a diolic sugar unit, i.e. 5'-CMP, 5'-UMP, cytidine, and D-ribose. All of these substrates display a resonance around δ = –135 to –138, arising from the tin diolate complex being formed first. In contrast, the δ = –202 signal is the only resonance observed for a mixture of Et_2SnCl_2 with substrates which do not contain a diolic sugar unit, i.e. 5'-dCMP and cytosine. These observations unambiguously rule out that the second ^{119}Sn resonance at δ = –202 is due to any interaction between the tin moiety and functional groups of the pyrimidic unit, with or without a hydrogen bonding network. This is confirmed by ^{15}N NMR data obtained from ^{15}N enriched 5'-CMP/Et_2SnCl_2 mixtures (2:1, 1:1, 1:2) which did not reveal any deviation of the ^{15}N chemical shift of the N3, NH_2 or N1 atoms in the presence of diethyltin dichloride, with respect to free 5'-CMP. By way of an example, the titration curve of the $^{15}N3$ resonance of such a mixture is shown in Figure 7.

As in the acidic medium, the ^{119}Sn resonance at δ = –202 can only originate from some hydrolysed species on the hydrolysis pathway of Et_2SnCl_2 (Figure 2). Further evidence for this is the fact that the ^{119}Sn NMR spectrum of the supernatant of the mixture obtained from Et_2SnCl_2 in D_2O at pH 10.5 exhibits the very same resonance at δ = –202. By comparing the ^{117}Sn CP-MAS NMR spectrum with the one of pure Et_2SnO (δ = –166), the precipitate that was isolated from this mixture was identified as Et_2SnO (δ = –165), the anisotropy patterns being identical. As expected, the supernatant of this mixture exhibits a ^{35}Cl

resonance at a slightly higher chemical shift (δ = 4) than for completely anionic chloride (δ = 0, NaCl). This can originate from an equilibrium between intermediate **3**, with one chlorine atom covalently bonded to the tin atom, and intermediate **4**, from which chlorine can only be released as chloride. Compound **4** is the direct precursor of Et_2SnO which is indeed the solid detected; it can be formed directly by simple loss of a water molecule. Therefore, the species at δ = –202 is most likely intermediate **4** in the hydrolysis scheme of Et_2SnCl_2 (Figure 2).

Interaction of Diethyltin Dichloride with 5'-CMP, 5'-dCMP and 5'-UMP at pH 5.5–9.0

Several ^{119}Sn resonances appear in the ^{119}Sn NMR spectra of 5'-CMP/Et_2SnCl_2 in this pH range (Figure 3). These resonances are all very broad, needing a long acquisition time to obtain a reasonable signal-to-noise ratio. Due to the broadness of the resonances, ^1H-^{119}Sn HMQC correlations could not be detected between the proton resonances of the 5'-CMP moiety and the ^{119}Sn resonance. Attempts to reduce the line width of the ^{119}Sn resonances by recording a ^{119}Sn spectrum at lower temperatures failed, the resonances remaining still too broad. Likewise, 5'-CMP/Et_2SnCl_2 mixtures prepared in CD_3OD/D_2O (50:50) turned cloudy below 273 K.

Similar ^{119}Sn resonance frequencies, at least within experimental error, are found for all three nucleotides investigated in the pH range 5.5–9.0. For 5'-dCMP/Et_2SnCl_2, the ^{119}Sn resonance around δ = –202 is observed at pH 6.5.

These findings again suggest that all the ^{119}Sn resonances arise from hydrolysis products of Et_2SnCl_2, rather than from Et_2SnCl_2 interacting with the nucleotides. The broad ^{119}Sn resonances are in agreement with the associated species being in moderately slow exchange on the ^{119}Sn NMR time scale, since no evidence for multiple species was found in the ^1H and ^{13}C spectra (this indicates that these species, whatever they maybe, are in fast exchange on the ^1H and ^{13}C NMR time scales but in slow exchange on the ^{119}Sn NMR time scale). Unfortunately, 2D ^{119}Sn EXSY experiments which were aimed at supporting the presence of exchange were unsuccessful; this was due to broad linewidths and/or a low signal-to-noise ratio.

The solid isolated from the mixture 5'-CMP/Et_2SnCl_2 (1:1) around pH 7.0 mainly reveals a single isotropic ^{117}Sn chemical shift at δ = –167 in its CP-MAS spectrum. A comparison of its chemical shift anisotropy pattern with that of a pure sample of Et_2SnO reveals that this solid is the latter compound. However, a CP-MAS ^{117}Sn pattern from another unidentified minor species with much lower intensity (ca. 10%) is also observed at pH 7.0.

Conclusions

From pH 2.0–3.0, the Et_2Sn moiety from Et_2SnCl_2 is involved in bonding with the phosphate group of the three nucleotides studied. This interaction was characterised by a ^{31}P-^1H HOESY spectrum. At the same pH, the precipitated solid was isolated and structurally characterised. Among several possible structures, only one satisfied all data including the elemental analysis. This structure contains two tin atoms bridged by one oxygen and one chlorine atom, each tin atom being linked to the phosphate group of the nucleotide. Between pH 3.0 and 5.5 the absence of visible ^{119}Sn resonances precludes a conclusion.

Around neutral pH (5.5–9.0), no evidence for the Et_2Sn moiety interacting with the nucleotide was found, Et_2SnCl_2 giving rise to several hydrolysis products that are in mutual chemical exchange with one another.

In a 1:1 nucleotide/Et_2SnCl_2 mixture at pH > 9.0, Et_2SnCl_2 reacts with the O(2') and O(3') oxygen atoms of the sugar unit of the nucleotide as demonstrated by the presence of two HMQC cross-peaks H2'–Sn and H3'–Sn. With an excess of Et_2SnCl_2, a second ^{119}Sn resonance appears at δ = –202, which, however, does not correlate with any proton resonance of the nucleotides. This species is one of the hydrolysis products of Et_2SnCl_2, as further indicated by the absence of any ^{15}N chemical shift effect on the pyrimidic moieties that should have originated from the presence of a tin unit in the neighbourhood of nitrogen atoms.

The corresponding pH value limits for the interactions of the purine nucleotides 5'-IMP and 5'-GMP with Et_2SnCl_2 were: pH < 4 for the interaction through the phosphate group, pH > 9.5 for the interaction through the O(2') and O(3') oxygen atoms, and no observed interaction for pH 4–9.5.[11b]

These results are in contrast to the mode of interaction of cisplatin that interacts with the nitrogen atoms of purines (N7 of guanosine) and pyrimidines (N3 of cytidine).[44] However, they are similar to those reported for vanadium complexes which have been shown to interact with the phosphate group of mononucleotides at acidic pH, to hydrolyse at neutral pH and to react with the O(2') and O(3') oxygen atoms of the sugar unit of mononucleotides at basic pH.[45]

Experimental Section

Preparation of NMR Samples: The samples were typically prepared by dissolving the nucleotides (0.1 mmol) in D_2O (0.2 mL, 99.9% D, Aldrich). A solution of diethyltin dichloride (0.05 mmol) in D_2O (0.3 mL) was added dropwise. This resulted in a clear solution with a pH of approximately 6. The pH was adjusted by the dropwise addition of deuterated hydrochloric acid or sodium hydroxide solutions (0.1 M). Whenever generated, the precipitate was filtered and thoroughly washed with water and diethyl ether prior to drying in vacuum over P_2O_5 and further analysis (see Results and Discussion). The elemental analyses were performed by the "Laboratoire Central d'Analyse du CNRS", Vernaison, France. ^{15}N enriched (98% isotopic purity) 5'-CMP was purchased from CIL (MA).

NMR Experiments: All spectra were recorded at 303 K on a Bruker AMX500 spectrometer equipped with a digital lock and operating at 500.13, 202.46, 125.77, 186.50, 50.68, and 49.00 MHz for ^1H, ^{31}P, ^{13}C, ^{119}Sn, ^{15}N, and ^{35}Cl nuclei, respectively. ^{31}P chemical shifts were referenced to an aqueous solution of H_3PO_4 (85%). The ^{119}Sn chemical shifts were referenced to Ξ = 37.290665 MHz.[46a] The

^{35}Cl chemical shifts were referenced to a solution of NaCl (1 M, $\delta = 0$). The ^{15}N chemical shifts were referenced to $\Xi = 10.136767$ MHz.[46b]

Broad band ^{1}H-decoupled ^{13}C and ^{119}Sn spectra were recorded using the Bruker pulse sequences with standard delays. The 1D and 2D ^{1}H-^{119}Sn HMQC experiments consisted of gradient enhanced-versions of the standard HMQC pulse sequence processed in the magnitude mode and implemented as described elsewhere.[32] The 2D ^{31}P-^{1}H HOESY[16,17] experiments were performed by recording 128 FIDs of 1 K data points, 144 scans each, with an acquisition time of 0.2 s, a relaxation delay of 1.6 s and a mixing time of 1 s. The 2D ^{1}H-^{15}N HMQC spectra were typically obtained by recording 64 FIDs of 4 K data points, 32 scans each, with an acquisition time of 0.5 s and a relaxation delay of 1.5 s. The 2D ^{119}Sn EXSY spectra were typically obtained by recording 24 FIDs of 4 K data points, 3,200 scans each, with an acquisition time of 0.1 s, a relaxation delay of 1 s and a mixing time of 10 ms.

All CP-MAS NMR spectra[47] were recorded on a Bruker AC250 and, in later stages, on a Bruker DRX250 spectrometer operating at 101.26, 62.90, and 89.15 MHz for ^{31}P, ^{13}C, and ^{117}Sn nuclei, respectively. The spectrometer was equipped with a 7 or 4 mm MAS broad-band probe. The matching conditions for Hartmann-Hahn cross-polarization[47] (pulse length 5 μs) and the chemical shift reference for the ^{117}Sn nucleus were set with (*cyclo*-$C_6H_{11})_4Sn$ [$\delta = -97.35$ relative to $(CH_3)_4Sn$]. The ^{13}C chemical shift reference frequency was set with adamantane. The ^{117}Sn spectra were typically obtained by acquiring 32 K data points over a spectral width of 166.7 kHz, a 2 ms contact time and a relaxation delay of 2 s with 10,000 to 20,000 scans. The isotropic chemical shifts were identified by recording two spectra with sufficiently different spinning rates.[47] The ^{13}C CP-MAS spectra were obtained by acquiring 4 K data points over a spectral width of 17 kHz, a 2 ms contact time and a relaxation delay of 4 s with 1,000 to 10,000 scans. The ^{1}H-decoupled ^{31}P MAS spectra were obtained by acquiring 4 K data points over a spectral width of 20 kHz and a relaxation delay of 4 s with 100 to 1,000 scans.

Infrared Spectroscopy: Infrared spectra were acquired from KBr pellets in the Fourier transform mode from a Perkin–Elmer System 2000 FT-IR spectrometer. The Raman spectra were acquired in the Fourier-transform mode from a Perkin–Elmer System 2000 NIR FT-RAMAN spectrometer using a Raman dpy2 beam with 310 mW power.

Electrospray Mass Spectrometry: The electrospray mass spectra were recorded in the cationic and anionic modes on a Micromass Quattro II instrument coupled to a Masslynx system (ionisation in an electric field of 3.5 kV; source temperature 80 °C; source pressure 1 atm.; analyser pressure 10^{-5} mbar).[48] Cone voltages were 15 V. Calculated and experimental isotopic distributions were compared using the shareware program MassCluster v.2.1. for Apple Macintosh. The *m*/*z* ratios reported in Table 1 and Figure 3 correspond to the peak with the highest intensity of the isotopic distribution patterns.

Thermogravimetric Analysis: The thermogravimetric analysis was made on a Perkin–Elmer TGA-7 thermogravimetric analyser by heating the sample from 40 to 500 °C at 10 °C/min under a nitrogen atmosphere.

Acknowledgments

We thank Mrs I. Verbruggen for recording some of the NMR spectra, Dr. G. Laus and Mr. M. Desmet for recording the electrospray mass spectra, and Prof. Dr. Ir. B. Van Mele and Dr. Ir. H. Rahier for access to the IR, Raman and thermogravimetric analysis facilities. J. C. M. is a postdoctoral research associate of the Fund for Scientific Research Flanders (Belgium). The financial support by the "Bourse de la Fondation David et Alice Van Buuren" (L. G.), the Belgian "Fonds voor Kollektief Fundamenteel Onderzoek" (FKFO Grant N° 2.0094.94, R. W., M. B.), the Belgian "Nationale Loterij" (Grants N° 9.0006.93 and 9.0192.98, R. W., M. B.), the Fund for Scientific Research Flanders (Belgium, Grant N° G.0192.98, R. W, M. B.), and the Belgian "Nationaal Fonds voor Wetenschappelijk Onderzoek" (NFWO Grant N° G.0054.96, M. G.) is gratefully acknowledged.

[1] B. K. Keppler, *Metal Complexes in Cancer Chemotherapy*, VCH, Weinheim, **1993**.
[2] A. T. M. Marcelis, J. Reedijk, *Recl. Trav. Chim. Pays-Bas* **1983**, *102*, 121–129.
[3] S. J. Lippard, *Science* **1982**, *218*, 1075–1082.
[4] M. Bloemink, J. Reedijk, *Metal Ions in Biology* (Eds.: A. Sigel, H. Sigel), M. Dekker, New-York **1996**, *32*, p. 641.
[5] T. D. Tullius, S. J. Lippard, *J. Am. Chem. Soc.* **1981**, *103*, 4620–4622.
[6] M. Gielen, *Coord. Chem. Rev.* **1996**, *151*, 41–51.
[7] A. J. Crowe, *Drugs of the Future* **1987**, *12*, 255–275.
[8] R. Barbieri, A. Silvestri, *J. Inorg. Biochem.* **1991**, *41*, 31–35.
[9] V. Piro, F. Di Simone, G. Madonia, A. Silvestri, A. M. Giuliani, G. Ruisi, R. Barbieri, *Appl. Organomet. Chem.* **1992**, *6*, 537–542.
[10] R. Barbieri, A. Silvestri, A. M. Giuliani, V. Piro, F. Di Simone, G. Madonia, *J. Chem. Soc., Dalton Trans.* **1992**, 585–590.
[11] [11a] Q. Li, P. Yang, H. Wang, M. Guo, *J. Inorg. Biochem.* **1996**, *64*, 181–195. – [11b] Z. Yang, T. Bakas, A. Sanchez-Diaz, C. Charalambopoulos, J. Tsangaris, N. Hadjiliadis, *J. Inorg. Biochem.* **1998**, *72*, 133–140. – [11c] A. Jancso, L. Nagy, E. Moldrheim, E. Sletten, *J. Chem. Soc., Dalton Trans.* **1999**, 1587–1594.
[12] D. P. Bancroft, C. A. Lepre, S. J. Lippard, *J. Am. Chem. Soc.* **1990**, *112*, 6860–6871.
[13] F. Kayser, M. Biesemans, M. Gielen, R. Willem, *J. Magn. Reson.* **1993**, *A102*, 249–252.
[14] J. C. Martins, P. Verheyden, F. Kayser, M. Gielen, R. Willem, M. Biesemans, *J. Magn. Reson.* **1997**, *124*, 218–222.
[15] F. Kayser, M. Biesemans, M. Gielen, R. Willem, *Advanced Applications of NMR to Organometallic Chemistry* (Eds.: M. Gielen, R. Willem, B. Wrackmeyer), Wiley, Chichester, **1996**, chapter 3, 45–86.
[16] C. Yu, G. C. Levy, *J. Am. Chem. Soc.* **1983**, *105*, 6994–6996.
[17] C. Yu, G. C. Levy, *J. Am. Chem. Soc.* **1984**, *106*, 6533–6537.
[18] F. Ribot, C. Sanchez, R. Willem, J. C. Martins, M. Biesemans, *Inorg. Chem.* **1998**, *37*, 911–917.
[19] K. C. Molloy, *Chemistry of tin* (Ed.: P. J. Smith), Blackie Academic Professional, Thomson Science, London, **1998**, 2nd edition, p. 138.
[20] R. C. Poller, *J. Organomet. Chem.* **1965**, *3*, 321–329.
[21] A. G. Davies, *Organotin Chemistry*, VCH, Weinheim, **1997**, p. 144.
[22] [22a] D. Dakternieks, K. Jurkschat, S. van Dreumel, E. R. T. Tiekink, *Inorg. Chem.* **1997**, *36*, 2023–2029. – [22b] T. Yano, K. Nakashima, J. Otera, R. Okawara, *Organometallics* **1985**, *4*, 1501–1503.
[23] [23a] A. Bax, M. F. Summers, *J. Magn. Reson.* **1986**, *67*, 565–569. – [23b] A. Bax, R. H. Griffey, B. L. Hawkins, *J. Magn. Reson.* **1983**, *55*, 301–315.
[24] A. Bax, M. F. Summers, *J. Am. Chem. Soc.* **1986**, *108*, 2093–2094.
[25] F. Kayser, M. Biesemans, M. Bouâlam, E. R. T. Tiekink, A. El Khloufi, J. Meunier-Piret, A. Bouhdid, K. Jurkschat, M. Gielen, R. Willem, *Organometallics* **1994**, *13*, 1098–1113; 4126
[26] K. J. Barnham, C. J. Bauer, M. I. Djuran, M. A. Mazid, T. Rau, P. J. Sadler, *Inorg. Chem.* **1995**, *34*, 2826–2832.
[27] D. Neuhaus, M. Williamson, *The Nuclear Overhauser Effect in Structural and Conformational Ananlysis*, VCH Publishers, New-York, **1984**.

[28] H. Santos, A. V. Xavier, C. F. G. C. Geraldes, *Can. J. Chem.* **1983**, *61*, 1456–1464.
[29] T. P. Lockhart, W. F. Manders, E. M. Holt, *J. Am. Chem. Soc.* **1986**, *108*, 6611–6616.
[30] B. Wrackmeyer, *Annu. Rep. NMR Spectrosc.* **1985**, *16*, 71–184.
[31] [31a] W. H. Howard, R. W. Crecely, W. H. Nelson, *Inorg. Chem.* **1985**, *24*, 2204–2208. – [31b] T. P. Lockhart, W. F. Manders, *Inorg. Chem.* **1986**, *25*, 892–895. – [31c] J. Holecek, A. Lycka, *Inorg. Chim. Acta* **1986**, *118*, L15–L16.
[32] R. Willem, A. Bouhdid, F. Kayser, A. Delmotte, M. Gielen, J. C. Martins, M. Biesemans, B. Mahieu, E. R. T. Tiekink, *Organometallics* **1996**, *15*, 1920–1929.
[33] E. Breitmaier, W. Voelter, *Carbon-13 NMR Spectroscopy*, VCH Weinheim, **1987**.
[34] [34a] H. A. Tajmir-Riahi, T. Theophanides, *Can. J. Chem.* **1985**, *63*, 2065–2072. – [34b] H. A. Tajmir-Riahi, T. Theophanides, *Can. J. Chem.* **1983**, *61*, 1813–1822. – [34c] H. A. Tajmir-Riahi, T. Theophanides, *Inorg. Chim. Acta* **1983**, *80*, 183–190.
[35] F. K. Butcher, W. Gerrard, E. F. Mooney, R. G. Rees, H. A. Willis, A. Anderson, H. A. Gebbie, *J. Organomet. Chem.* **1964**, *1*, 431–434.
[36] H. Schumann, P. Jutzi, A. Roth, P. Schwabe, E. Schauer, *J. Organomet. Chem.* **1967**, *10*, 71–79.
[37] D. H. Lohmann, *J. Organomet. Chem.* **1965**, *4*, 382–391.
[38] B. Zobel, M. Schürmann, K. Jurkschat, *Organometallics* **1998**, *17*, 4096–4104.
[39] D. Dakternieks, K. Jurkschat, D. Schollmeyer, H. Wu, *Organometallics* **1994**, *13*, 4121–4123.
[40] J. W. Akitt, *Multinuclear NMR* (Ed.: J. Mason), Plenum Press, New-York, **1987**, p. 447.
[41] [41a] T. B. Grindley, R. E. Wasylishen, R. Thangarasa, W. P. Power, R. D. Curtis, *Can. J. Chem.* **1992**, *70*, 205–217. – [41b] T. B. Grindley, *Adv. Carbohydr. Chem. Biochem.* **1998**, *53*, 17–142.
[42] I. Pianet, E. Fouquet, M. Pereyre, M. Gielen, F. Kayser, M. Biesemans, R. Willem, *Magn. Reson. Chem.* **1994**, *32*, 617–623.
[43] R. Willem, *Progr. NMR Spectrosc.* **1987**, *20*, 1–94.
[44] B. Lippert, *Progress in Inorganic Chemistry* (Ed.: S. J. Lippard), John Wiley and Sons, New-York, **1989**, p. 1.
[45] [45a] L. Y. Kuo, A. H. Liu, T. J. Marks, *Metal Ions in Biology* (Eds.: A. Sigel, H. Sigel), M. Dekker, New-York **1996**, *33*, p. 641. –[45b] S. J. Angus-Dunne, R. J. Batchelor, A. S. Tracey, F. W. B. Einstein, *J. Am. Chem. Soc.* **1995**, *117*, 5292–5296. – [45c] G. Micera, A. Dessi, D. Sanna, *Inorg. Chem.* **1996**, *35*, 6349–6352.
[46] [46a] J. Mason, *Multinuclear NMR* (Ed.: J. Mason), Plenum Press, New York, **1987**, p. 627. – [46b] D. S. Wishart, C. G. Bigam, J. Yao, F. Abildgaard, H. J. Dyson, E. Oldfield, J. L. Markley, B. D. Sykes, *J. Biomol. NMR* **1995**, *6*, 135–140.
[47] F. A. Bovey, L. Jelinski, P. A. Mirau, *Nuclear Magnetic Resonance Spectroscopy*, Academic Press, San Diego, **1987**, 2nd edition, p. 399.
[48] [48a] G. Lawson, R. H. Dahm, N. Ostah, E. D. Woodland, *Appl. Organomet. Chem.* **1996**, *10*, 125–133. – [48b] G. Lawson, N. Ostah, *Appl. Organomet. Chem.* **1994**, *8*, 525–532. – [48c] W. Henderson, B. K. Nicholson, L. J. McCaffrey, *Polyhedron* **1998**, *17*, 4291–4313.

Received August 9, 1999
[I99292]

η^4-Coordination of Dienes and Heterodienes to the TripodCobalt(I) Template $[CH_3C(CH_2PPh_2)_3Co]^+$: Synthesis, Structure, and Dynamics

Rolf Rupp,[a] Axel Frick,[a] Gottfried Huttner,*[a] Peter Rutsch,[a] Ute Winterhalter,[a] Annette Barth,[a] Peter Kircher,[a] and Laszlo Zsolnai[a]

Dedicated to Prof. Dirk Walther on the occasion of his 60th birthday

Keywords: Tripol ligands / Dienes / Heterodienes / η^4-Coordination / Hindered rotation / Line-shape analysis

$CH_3C(CH_2PPh_2)_3CoCl$ (**1**) is easily accessible from $CH_3C(CH_2PPh_2)_3CoCl_2$ by reduction with activated zinc powder. Upon dehalogenation with $TlPF_6$, **1** reacts with dienes to give $[tripodCo^I\text{-}(\eta^4\text{-diene})]^+$ (**2**). The heterodienes acrolein and methyl vinyl ketone produce the analogous η^4-heterodiene compounds **3**. When crotonaldehyde is used as the potential η^4-diene ligand, decarbonylation is observed leading to $[tripodCo^I\text{-}(CO)_2]^+$ (**4**). Reaction of $[tripodCo_{aq}](BF_4)_2$ with allyl mercaptan produces $[tripodCo^I\text{-}(\eta^4\text{-thioacrolein})]^+$ (**3a**) through dehydrogenation of the ligand precursor. 1,2-Diketones such as benzil and phenanthrenequinone do not coordinate in a η^4 fashion but rather generate η^2-coordinate enediolato ligands by an electron-transfer process, resulting in compounds of the type $\{tripodCo^{III}\text{-}[\eta^2\text{-RC(O)=C(O)R}]\}^+$ (**5**). All the compounds have been characterized by standard analytical and spectroscopic techniques, including X-ray analysis in some cases. Compounds **4** and **5** show trigonal-bipyramidal coordination in the solid state, whereas the coordination polyhedra in compounds **2** and **3** are better described as square-pyramidal. While a minimum of two phosphorus resonances might be expected for each of these coordination geometries, only one time-averaged signal is normally observed. Only with the η^4-coordinated heterodienes acrolein, methyl vinyl ketone, and thioacrolein present in **3** is there a resolution of the signals of the three chemically distinct phosphorus nuclei at low temperatures. By ^{31}P-NMR line-shape analysis, the activation barriers for the rotational reorientation of the heterodienes are found to be around $\Delta H^{\neq} = 47$ kJmol^{-1} for all three compounds **3**.

Introduction

The chemistry of *tripod*cobalt templates $[CH_3C(CH_2Ph_2)_3Co]$ has been extensively studied. Largely due to the efforts of Sacconi and his group, the very special properties of this kind of template have been documented through the isolation of many types of compounds that are not accessible with any other type of $[L_3Co]$ template.[1] However, the chemistry of this highly valuable template $[CH_3C(CH_2PPh_2)_3Co]$ is hampered by the fact that the initial oxidation state of cobalt is generally Co^{II} and the [*tripod*Co] compounds are formed by addition of the *tripod* ligand and an appropriate coligand to the inorganic salt. The products of such reactions may well contain cobalt in the oxidation states of Co^I, Co^{II}, and Co^{III}, depending on the coligand and the reaction conditions.[2–4]

A systematic approach to the chemistry of the $[CH_3C(CH_2PPh_2)_3Co]^+$ template containing cobalt in the oxidation state (+I) has not yet been developed, even though a 14-electron species such as $[tripodCo]^+$ might be expected to provide a highly promising access to a novel type of coordination chemistry of the [*tripod*Co] entity. This expectation arises, in part, from consideration of the chemistry of the CpCo template, which has rapidly developed since the generation of this template by reductive decyclopentadienylation was reported by Jonas.[5][6] Moreover, since there are relatively few methods available for the generation of 14-electron species with late 3d transition metals, the development of suitable methods for the generation of a $[tripodCo]^+$ reagent would seem particularly worthwhile.

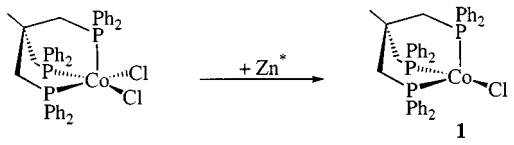
In this paper, we report on several methods for the in situ generation of $[tripodCo]^+$ and its reactions with unsaturated compounds.

Results and Discussion

Amongst the compounds containing the $[CH_3C(CH_2PPh_2)_3Co^I]$ template, the chloride $CH_3C(CH_2PPh_2)_3CoCl$ (**1**) appeared to be the most logical starting material for probing the chemistry of the $[CH_3C(CH_2PPh_2)_3Co]^+$ entity. **1** has been known for a long time and its preparation by $NaBH_4$ reduction of $CH_3C(CH_2PPh_2)_3CoCl_2$ has been reported by Sacconi et al.[2a] Its structure and its complicated equilibrium with respect to the starting material $CH_3C(CH_2PPh_2)_3CoCl_2$ have recently been described.[2b] While it is possible to prepare **1** by the method described by Sacconi et al., the accompanying formation of $\{[CH_3C(CH_2PPh_2)_3Co]_2H_3\}^+$ complicates this procedure and a simpler, cleaner preparation pathway remains desirable.[2a,2c,3a] We have found that $CH_3C(CH_2PPh_2)_3CoCl_2$ undergoes a clean reduction to **1** when treated with activated zinc powder in THF (Scheme 1).

[a] Anorganisch-Chemisches Institut der Universität Heidelberg, Im Neuenheimer Feld 270, D-69120 Heidelberg, Germany
Fax: (internat.) + 49-(0)6221/545707
E-mail: g.huttner@indi.aci.uni-heidelberg.de

 © WILEY-VCH Verlag GmbH, D-69451 Weinheim, 2000 1434–1948/00/0303–0523 $ 17.50+.50/0



Scheme 1

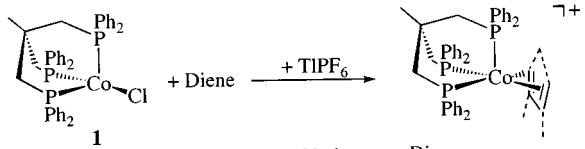
After filtration and evaporation of the THF, **1** is obtained as a microcrystalline beige powder in almost quantitative yield. While freshly prepared **1** dissolves in CH_2Cl_2 to produce a clear orange-brown solution, dissolution of samples of **1** left at room temperature for more than 6 h leads to green solutions, indicating different degrees of decomposition. The nature of the green products has not yet been established.

[TripodCo^{I}] Derivatives of Dienes

Freshly prepared **1** reacts with dehalogenating agents in the presence of 4-electron donors L_2 such as conjugated dienes to produce the corresponding [*tripod*Co^{I}-L_2]$^+$ species **2**. When **1** was treated with $(CH_3)_3SiOSO_2CF_3$, a colour change from orange-brown to red-brown was observed. Addition of 2,3-dimethyl-1,3-butadiene resulted in a colour change to orange and, after evaporation of the solvent, an orange microcrystalline powder was obtained. By comparison with authentic spectroscopic data for the corresponding compound [*tripod*Co^{I}-(η^4-2,3-dimethyl-1,3-butadiene)]$^+$ (**2b**; see below), the data obtained following this reaction clearly showed that the η^4-diene derivative had been formed. The product obtained this way was, however, found to be contaminated with some paramagnetic impurities, which could not be separated. While the ^{31}P-NMR spectrum of the product clearly showed the characteristic signals of **2b**, the ^{1}H-NMR spectrum featured only very broad signals, as befits the presence of some paramagnetic contamination. Mass spectra of the product showed the characteristic fragmentation pattern of **2b** as the dominant pattern, as well as the characteristic *m*/*z* peak of [*tripod*Co^{I}-(triflate)]. It is thus probable that the paramagnetic contamination was, in fact, due to [*tripod*Co^{I}-(triflate)] which, in analogy to [*tripod*Co^{I}-(formate)]$^+$, should be a 16-electron paramagnetic species.[2d] If this interpretation is correct, the coordinative power of the triflate anion is evidently still too high to allow for its complete exchange by the diene under the applied conditions.[7]

When a solution of **1** in CH_2Cl_2 was treated with an equimolar amount of $GaCl_3$, a colour change from orange-brown to red-brown was observed. When this solution was treated with 2,3-dimethyl-1,3-butadiene, a further colour change to orange was observed. Mass spectra showed the fragmentation pattern of **2b**. In contrast to the product obtained by dehalogenation with $(CH_3)_3SiOSO_2CF_3$ (see above), no paramagnetic contamination was apparent and both the ^{1}H- and ^{31}P-NMR spectra of the product were in complete agreement with those obtained for authentic **2b** (see below). While it is clear from these results that **2b** was indeed formed under the described conditions, elemental analysis data for the product were less than satisfactory. Carbon and hydrogen values were too low, indicating that the anionic part of the salt was not in fact $GaCl_4^-$, which had been assumed to constitute the counteranion.

$AgBF_4$ and $AgPF_6$, while also acting as dehalogenating agents, proved not to be appropriate for this reaction since they led to concomitant oxidation. The problems were finally overcome by using $TlPF_6$ as the dehalogenating agent (Scheme 2).



Nr.	Diene
2a	2-Methylbutadiene
2b	2,3-Dimethylbuta-1,3-diene
2c	Cyclopentadiene

Scheme 2

The orange PF_6 salts of **2a**−**2c** were obtained in good yields after purification by chromatography (Table 1, Table 4, Table 9). *Tripod*Co^{I} derivatives of conjugated dienes of type **2** are known.[2e] [*Tripod*Co^{I}-(η^4-butadiene)]$^+$, [*tripod*Co^{I}-(η^4-isoprene)]$^+$ (**2a**), [*tripod*Co^{I}-(η^4-1,3-cyclohexadiene)]$^+$, [*tripod*Co^{I}-(η^4-1,3,5,7-cyclooctatetraene)]$^+$, and [*tripod*Co^{I}-(η^4-1,3,5-cycloheptatriene)]$^+$ have previously been obtained by treating solutions of *tripod*Co^{II} precursors with propan-2-ol as the reductant in the presence of the appropriate olefinic ligand.[2e] A standard procedure for reactions of this type has not yet been established, nor have the products been completely characterized, although the structures of the products are known from a reported X-ray analysis of [*tripod*Co^{I}-(η^4-1,3,5-cycloheptatriene)]ClO_4.[2e] The type of coordination observed in this η^4-coordinated triene derivative remains essentially unchanged when dienes are coordinated to the [*tripod*Co]$^+$ entity. The general features already described by Sacconi et al. for the cycloheptatriene derivative apply equally well to the structure of **2c**, which has been determined in the case of its PF_6 salt (Figure 1, Figure 6; Table 5, Table 10).

The ^{31}P-NMR spectra of compounds **2**, besides the characteristic septet due to the PF_6 counteranion, show one sharp signal, the shape of which does not change significantly on cooling from 303 K to 193 K (Table 1). Irrespective of the specific coordination geometry (trigonal bipyramidal *vs.* square pyramidal), for a static structure arising from the combination of an entity with constitutional C_3-symmetry (*tripod*Co) and a coligand with at most C_{2v}-symmetry, a minimum of two different ^{31}P-NMR signals can be expected. This expectation is indeed borne out by the spectroscopic behaviour of the related compounds [L_3Co^{I}-(η^4-diene)]$^+$ (L = PMe_3, PMe_2Ph, PPh_2H) containing three isolated phosphane donors, where − depending on the symmetry of the diene coligand and the temperature of observation − up to three ^{31}P-NMR signals are observed.[8−10]

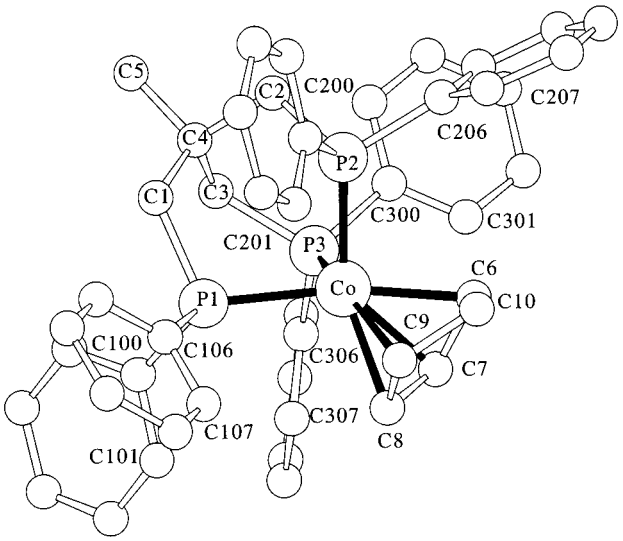


Figure 1. X-ray structure of **2c**

The fact that **2a**−**2c** show only one sharp signal for the three phosphorus nuclei of the coordinated ligand can only be rationalized by assuming that some dynamic process is operative, which renders the time-averaged environments of the phosphorus nuclei equivalent. This process must have a rather low activation energy, since not even a broadening of this ^{31}P-NMR signal is observed on cooling to 193 K. The most easily envisaged dynamic process is a tumbling of the diene coligands about the idealized C_3-axis of the [*tripod*Co] template. Such a tumbling motion would, of course, involve the transition of idealized square-pyramidal and idealized trigonal-bipyramidal coordination geometries. The ^{1}H-NMR spectra (Table 1) are in full agreement with the assigned constitutions, as are the mass spectra, which show the molecular ions as the most prominent peaks (Table 4). High-resolution mass spectra (**2a**−**2c**) and microanalytical data (**2b**) are also in agreement with the given formulae (Table 1).

When the procedure for the dehalogenation of **1** was performed in the presence of ethylene instead of a conjugated diene, $[tripodCo^{I}\text{-(ethylene)}_2]^+$ was formed, as was evident from the ^{31}P-NMR spectrum and mass spectroscopic data (see Experimental Section). However, it was not possible to purify the compound by chromatography, nor was it possible to obtain an analytically pure specimen by crystallization.

When non-conjugated dienes such as bicyclo[2.2.1]hepta-2,5-diene (2,5-norbornadiene) or 1,5-cyclooctadiene were used, PF_6 salts containing $[tripodCo^{I}\text{-(diene)}]^+$ as the cationic part were formed in high yields. Again, the compounds could not be purified by chromatography without significant decomposition (see Experimental Section). Even though the aforementioned compounds incorporating non-conjugated dienes or two ethylene ligands were invariably obtained with contamination by minor amounts of paramagnetic impurities, they were the only detectable products by ^{31}P-NMR and mass spectrometry. The species $[tripodCo^{I}\text{-(ethylene)}_2]^+$ is found to be thermodynamically far more stable than its isoelectronic equivalent CpCo(ethylene)$_2$.[5][6] While this latter compound starts to decompose at 323 K, [*tripod*Co(ethylene)$_2$]PF_6 is indefinitely stable at 343 K under an inert atmosphere.

On the other hand, the reactions of **1** described above show that, upon activation with $TlPF_6$, this compound constitutes a clean source for the intermediate generation of $[tripodCo]^+$. With regard to ease of handling, a method involving in situ reduction of $[tripodCo]^{2+}$ to $[tripodCo]^+$ would be desirable. It is in fact observed that a solution of $Co_{aq}(BF_4)_2$ and *tripod* in ethanol/CH_2Cl_2 reacts with conjugated dienes when treated with activated zinc powder in an ultrasonic bath. Compounds **2a**−**2c** are also accessible by this method (Scheme 3). They may be isolated as PF_6 salts by metathesis with KPF_6 in acetone following workup as described.

The yields of **2a**−**2c** achieved using this method were somewhat lower than those obtained starting from **1** (Table 9).

[TripodCo^{I}] Derivatives of Heterodienes

It has been observed that treatment of $Co_{aq}(BF_4)_2$ with 2-propene-1-thiol (allyl mercaptan) in the presence of $NaBPh_4$ and *tripod* produces the thioacrolein compound **3a** (Scheme 4).[2f]

In order to obtain this compound in a reproducible manner, it is necessary to keep the reaction mixture in a Schlenk tube sealed with a rubber stopper, presumably to keep the oxygen concentration at a very low but significant level. The BPh_4 salt of **3a** was obtained as a spectroscopically and analytically pure, dark-green, crystalline material consisting of single crystals suitable for X-ray analysis (Figure 2, Figure 5; Table 4, Table 5, Table 10).

When $Co_{aq}(BF_4)_2$ was treated with 2-propen-1-ol (allyl alcohol) instead of 2-propene-1-thiol (allyl mercaptan), a smooth colour change was again observed, leading to a red-brown solution. Evaporation of the solvent afforded a red-brown powder, the mass spectrum of which showed the molecular ion of the acrolein derivative **3b** as the most prominent peak. The ^{31}P-NMR data of the product were also identical with the data obtained for the analytically pure η⁴-acrolein compound **3b** (see below). However, it proved impossible to obtain an analytically pure compound using this reaction procedure.

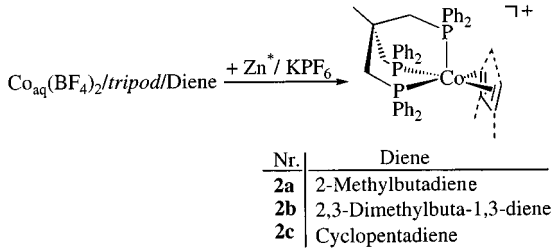
Based on the observation that **1** reacts with dienes in an almost quantitative manner, the procedure used for the activation of **1** in the presence of dienes was applied with heterodienes as the potential coligands. It was found that 2-propenal (acrolein) and its methylated derivative 3-buten-2-one (methyl vinyl ketone) became η⁴-coordinated at the $[tripodCo]^+$ template in the same way as observed for carbon-centred diene ligands (Scheme 5).

Compounds **3b** and **3c** were produced in yields comparable to those obtained in the synthesis of **2** (Table 9). Chromatographic workup of the PF_6 salts of **3b** and **3c** resulted in claret microcrystalline powders, which proved to be analytically and spectroscopically pure (Table 2, Table 4).

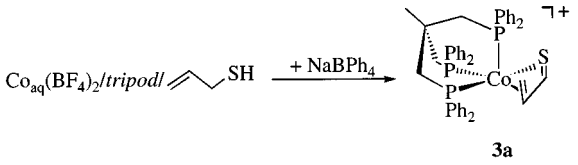
Table 1. Analytical data for compounds **2a** to **2c**

Compound	**2a**·PF_6^-	**2b**·PF_6^-	**2c**·PF_6^-
^{1}H NMR	CD_3NO_2	CD_2Cl_2	CD_2Cl_2
tripod-CH_3	1.17−1.95 m, 3 H	1.33−1.99 m, 3 H	1.93 br., 3 H
tripod-CH_2	2.74 br., 6 H	2.57 br., 6 H	2.62 br., 6 H
arom. H	7.26−7.61 m, 30 H	7.09−7.41 m, 30 H	7.16−7.78 m, 30 H
CH=CH_2	1.17−1.95 m, 2 H	−	−
C_q=CH_2	1.17−1.95 m, 2 H	1.33−1.99 m, 4 H	−
CH_2=CH	5.71 br., 1 H	−	−
ligand-CH_3	1.17−1.95 m, 3 H	1.33−1.99 m, 6 H	−
CH−CH_2	−	−	3.12 br., 2 H
CH=CH	−	−	6.70 br., 2 H
=CH−CH_2	−	−	2.62 br., 3.74 br., 2 H
^{31}P{^{1}H} NMR	CD_2Cl_2	CD_2Cl_2	CD_2Cl_2
PPh_2	22.2 s	19.1 s	25.9 s
PF_6	−144.2, $^1J_{PF}$ = 713 Hz	−144.2, $^1J_{PF}$ = 713 Hz	−144.2, $^1J_{PF}$ = 713 Hz
^{13}C{^{1}H} NMR[a]	CD_2Cl_2	CD_2Cl_2	CD_2Cl_2
tripod-CH_3	35.7 m	37.5 m	35.9 m
tripod-CH_2	34.5 m	35.4 m	34.4 m
tripod-C_q	37.5 s	37.7 s	37.6 s
arom. C	129.2−132.3	128.8−134.9	129.3−135.8
ligand-CH_3	20.3 s	18.2 s	−
CH=CH_2	42.0 s	−	−
C_q=CH_2	43.1 s	43.5 s	−
ligand-C_q	108.8	104.6	−
CH−CH_2	−	−	43.3 s
CH=CH	−	−	93.3 s
=CH−CH_2	−	−	150.9 s
elemental analysis: (calcd./found)	−[b]	C: 61.99/61.08 H: 5.42/5.64	−[b]
HR-FAB (m/z): (calcd./found)	751.2223/751.2236	765.2379/765.2394	749.2067/749.2039 748.1988/748.1973

[a] CH_3, CH_2, CH, and C carbons were assigned by means of a 135° DEPT experiment. − [b] Satisfactory microanalytical data could only be obtained for **2b**. The problems encountered with **2a** and **2c** may be traced to inappropriate handling of these air-sensitive compounds during microanalytical workup.



Scheme 3



Scheme 4

The reaction that was found to proceed cleanly in the case of acrolein and methyl vinyl ketone, leading to the η^4-coordinate heterodiene compounds **3b** and **3c**, could not be carried out with 2-butenal (crotonaldehyde) as the heterodiene. Reaction of this specific unsaturated aldehyde with **1** in the presence of $TlPF_6$ was found to produce the dicarbonyl compound **4** (Scheme 6).

The dicarbonyl compound **4** was isolated as its BPh_4 salt. **4** itself has previously been described by Ellermann et al. as the product of the reaction of *tripod* with $Co_2(CO)_8$.[2g] **4** could also be obtained from **1** in the presence of $TlPF_6$ and CO (see Experimental Section). The structure of **4**·$(BPh_4)^-$,

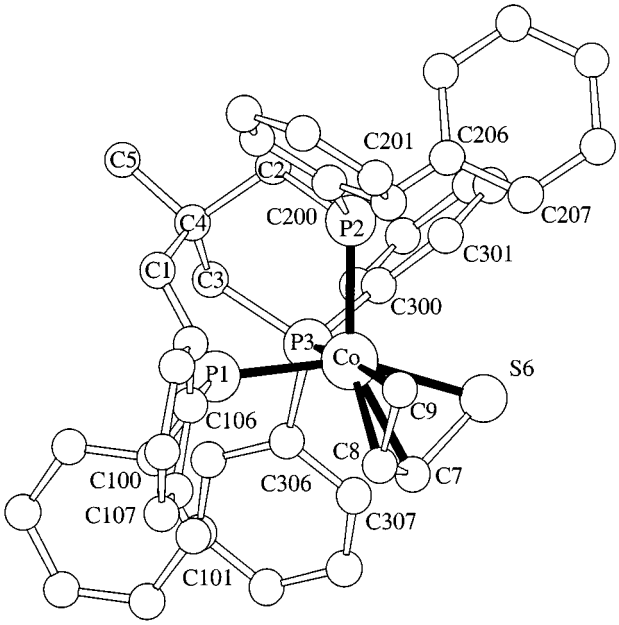
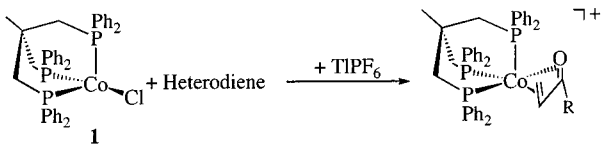
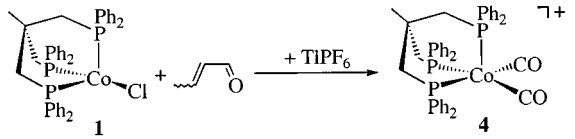


Figure 2. X-ray structure of **3a**; here, a consistent numbering scheme for all the compounds is used for the sake of easier comparison, which differs from that used for the deposited structure



Nr.	Heterodiene
3b	Acrolein
3c	Methyl vinyl ketone

Scheme 5



Scheme 6

as determined by X-ray analysis, is shown in Figure 3 (Table 6, Table 10).

The approximate idealized trigonal-bipyramidal coordination is evident from Figure 3, as well as from the data in Table 6.

In view of the clean reactions giving **3b** and **3c** as compounds with η⁴-coordinated heterodienes, the comparatively clean reaction of the linear C_4-heterodiene crotonaldehyde to produce the dicarbonyl compound **4** is remarkable. It appears that decarbonylation of α,β-unsaturated aldehydes is the predominant reaction pathway when allylic intermediates can be formed, which is possible by a simple hydrogen migration process with crotonaldehyde, thereby producing **4**, but cannot occur with the heterodienes leading to **3b** and **3c**.

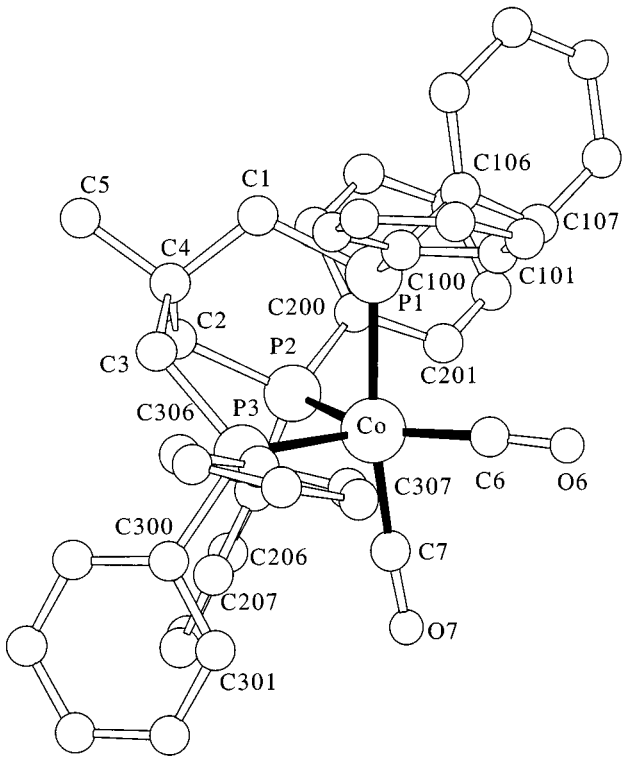


Figure 3. X-ray structure of **4**

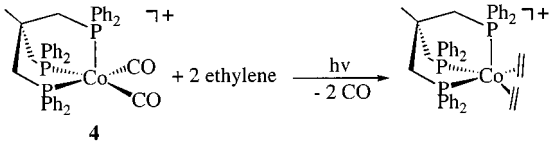
4 itself might represent a precursor for the generation of the [*tripod*Co]⁺ species if its carbonyl groups could be dis-

Table 2. Analytical data for compounds **3a** to **3c**

Compound	**3a**·BPh_4^-	**3b**·PF_6^-	**3c**·PF_6^-
^{1}H NMR	[D$_6$]acetone	CD_2Cl_2	CD_2Cl_2
tripod-CH_3	1.93 m, 3 H	1.99 br., 3 H	1.88 m, 3 H
tripod-CH_2	2.39−2.72 m, 6 H	2.39−2.96 m, 6 H	2.63−2.82 m, 6 H
arom. H	7.18−7.74 m, 50 H	7.08−7.91 m, 30 H	6.79−7.60 m, 30 H
ligand-CH_2-*i*[a]	1.45 m, 1 H	1.12 m, 1 H	1.24 m, 1 H
ligand-CH_2-*a*[a]	2.39−2.72 m, 1 H	2.39−2.96 m, 1 H	2.63−2.82 m, 1 H
CH_2=C*H*	6.24 s, 1 H	6.25 m, 1 H	5.88 m, 1 H
X=C*H*[d]	7.18−7.74 m, 1 H	8.57 br., 1 H	−
ligand-CH_3	−	−	2.34 m, 3 H
^{31}P{^{1}H} NMR[b]	CD_2Cl_2	CD_2Cl_2	[D$_8$]THF
PF_6	−	−144.2, $^1J_{PF}$ = 713 Hz	−144.2, $^1J_{PF}$ = 713 Hz
^{13}C{^{1}H} NMR[c]	CD_2Cl_2	CD_2Cl_2	CD_2Cl_2
tripod-CH_3	38.8 m	36.4 m	36.5 m
tripod-CH_2	34.3 m	31.6 m	32.6 m
tripod-C_q	37.9 s	37.3 s	38.4 s
arom. C	131.1−134.5	129.2−143.1	128.9−133.0
ligand-CH_2	54.0 s	45.7 s	44.4 s
ligand-CH_3	−	−	22.6 s
CH_2=*C*H	102.1 s	89.4 s	78.3 s
X=*C*[c,d,e]	108.9 s	129.2−143.1	153.7 s
elemental analysis (calcd./found)	−[f]	C: 59.74/59.33 H: 4.90/5.75	C: 60.14/59.16 H: 5.05/5.32
HR-FAB (m/z): (calcd./found)	755.1630/755.1679	−	−

[a] ligand-*i*: *endo*-H of the diene; ligand-*a*: *exo*-H of the diene. − [b] See also Table 7. − [c] CH_3, CH_2, CH, and C carbons were assigned by means of a 135° DEPT experiment. − [d] X = S: **3a**; X = O: **3b**, **3c**. − [e] In **3b**, this resonance appears in the aromatic region and is obscured by the arene carbon signals. − [f] Satisfactory microanalytical data could only be obtained for **3b** and **3c**. The sensitivity of **3a** coupled with the nature of the handling during microanalytical workup did not allow precise analysis.

placed. Considering the cationic [*tripod*Co]$^+$ template to which the carbonyl groups are coordinated, the cobalt−CO bonds should not be prohibitively strong. Indeed, the ν_{CO} IR absorptions of **4** are observed at rather high energies (2025 cm^{-1}, 1965 cm^{-1}; Table 4), indicating that the CO bond order is high with the consequence that the Co−C_{CO} bond order should be low. With this in mind, **4** was irradiated in the presence of ethylene, whereupon complete replacement of its CO groups by ethylene ligands was observed (Scheme 7).



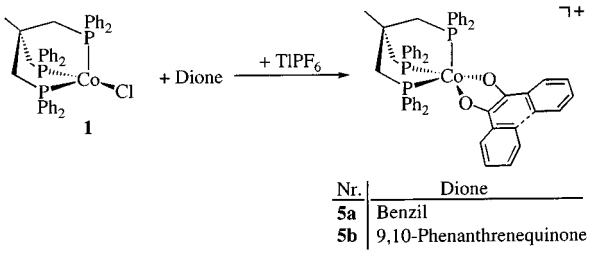
4

Scheme 7

Although the product formed in this reaction could not be obtained in analytically pure form, its mass spectrum and ^{31}P-NMR data leave no doubt as to its identity. The spectroscopic data obtained were in quantitative agreement with the data found for the same cation prepared from **1** (see Experimental Section).

The fact that not only carbon-centred dienes but also conjugated mono-heterodienes coordinate to the [*tripod*Co]$^+$ template in a η^4 fashion indicates that this template is ideally suited for the coordination of ligands containing a 4-centre 4π-system. In this respect, the template behaves as expected for an isoelectronic equivalent of $Fe(CO)_3$ and CpCo. The $Fe(CO)_3$ template is known to form stable derivatives with dienes, and is the only known template that also allows the η^4-coordination of heterodienes.[11−13] In fact, to the best of our knowledge, η^4-coordination of dienes and thioacrolein has hitherto only been achieved using this type of iron-centred template.[14]

By generating [*tripod*Co]$^+$ in the presence of 1,2-diketones, the question was addressed whether these 4-centre 4π-systems would bind in a η^4-coordination mode or whether, by electron-transfer processes, they would be transformed into η^2-coordinating enediolato-type ligands. The coordination of a dialdehyde to the Cp*Co template, in a fashion where at least one CO group of the ligand forms a π-bond with the other one acting as a σ-donor, has recently been reported by Brookhart et al., and hence the η^4-coordination of 1,2-diketones cannot a priori be excluded.[15] However, reaction of benzil or phenanthrenequinone with **1** in the presence of $TlPF_6$ produces the enediolato derivatives **5** (Scheme 8).



1

Nr.	Dione
5a	Benzil
5b	9,10-Phenanthrenequinone

Scheme 8

Formal oxidation of Co^I to Co^{III} thus took place, with a corresponding formal two-electron reduction of the diketones to produce enediolato ligands. It appears that the propensity of the [*tripod*Co]$^+$ template to acquire an 18-electron configuration − which it would have if the dione were to have bound as a η^4-diene ligand − is not sufficiently strong to counterbalance the formation of the stable five-membered cycles present in **5** accompanied by a 16-electron configuration at the cobalt centre. Many compounds showing the same type of bonding of 1,2-dioxo ligands as found in **5** are known, and an alternative synthesis of **5b** has been mentioned in the literature.[4a−4c] A characteristic feature of such compounds is that they show a prominent long-wavelength absorption at around 800 nm, which has been interpreted in terms of an LMCT band.[4c] This type of band is also seen for compounds **5** (Table 4). The η^4-binding mode of the dienes present in **2** and **3** gives rise to a distinctly different electronic absorption pattern (Table 4).

The η^2-bonding mode of the ligands in **5**, which, as outlined above, could be established on the basis of the electronic spectra, was further corroborated by the observation that the ^{13}C resonances of the carbon atoms in the 2,3-positions of the unsaturated ligands are at distinctly different δ values for the η^4-coordinated dienes (**2**, **3**) as compared to the corresponding shifts for the η^2-coordinated ligands in **5** (Table 1, Table 2, Table 3). Moreover, the ^{31}P resonances of **5** (Table 3) appear in a range characteristic of [*tripod*Co(diolato)]$^+$ compounds (δ = 30−36), which is again distinctly different from the range in which the corresponding resonances for the η^4-diene derivatives **2** and **3** are seen (Table 1, Table 2).[4a−4c]

Compounds **5** were obtained in microcrystalline form as the intense cornflower-blue PF_6 salt (**5a**) or as the blue-green BPh_4 salt (**5b**). The results of an X-ray structure analysis of single crystals of **5b** were in complete agreement with the constitution established on the basis of spectroscopic data, clearly showing the η^2-binding mode of the enediolato ligand (Figure 4; Table 6, Table 10).

Structure and Dynamics

While the structure of **5b** needs no further comment since it is in very good agreement with the many well-documented and discussed structures of the [*tripod*Co(enediolato)]$^+$ type, the structures of the compounds containing η^4-coordinated dienes merit further discussion.[4a−4c]

If the geometries of these compounds (Figure 1, Figure 2, Figure 5, Figure 6; Table 5) are described as square-pyramidal, then the axial Co−P bond lengths (Co−P2) might be expected to be different from the equatorial distances. However, it is found that in all the compounds mentioned in this paper, **2c**, **3a**, and in the literature, [*tripod*Co^I-(η^4-C_7H_8)]$^+$ (**A**, **B**, Figure 6; Table 5), [$(Me_3P)_3Co^I$-(η^4-C_7H_8)]$^+$ (**C**, Figure 6; Table 5), the Co−P bonds are of approximately equal length.[2e,10] In **2c**, the equatorial bond Co−P1 [228.5 (1) pm] is some 7 pm longer than the Co−P2 [221.2

Table 3. Analytical data for compounds **4** and **5**

	4·BPh_4^-	**5a**·PF_6^-	**5b**·BPh_4^-
^1H NMR	CD_2Cl_2	CD_3NO_2	CD_2Cl_2
tripod-CH_3	1.91 br., 3 H	1.94 br., 3 H	1.80 m, 3 H
tripod-CH_2	2.70 br., 6 H	2.81 br., 6 H	2.68 m, 6 H
arom. H	7.21−7.31 m, 50 H	7.15−7.93 m, 40 H	6.92−8.90 m, 38 H
$^{31}P\{^1H\}$ NMR	CD_2Cl_2	CD_3NO_2	CD_2Cl_2
PPh_2	23.8 s	32.7 s	36.8 s
PF_6	−	−144.2, $^1J_{PF}$ = 713 Hz	−
$^{13}C\{^1H\}$ NMR[a]	CD_2Cl_2	CD_3NO_2	CD_2Cl_2
tripod-CH_3	36.7 m	35.5 m	36.8 m
tripod-CH_2	33.7 m	30.9 m	32.0 m
tripod-C_q	37.4 s	38.2 s	38.6 s
arom. C	129.3−140.2	128.8−140.1	122.1−136.4
CO	206.1 s	172.1 s	165.0 s
elemental analysis[b]	C: 75.99/75.31	C: 63.59/62.83	C: 78.35/75.18
(calcd./found)	H: 5.62/5.55	H: 4.75/5.03	H: 5.58/5.78
HR-FAB (m/z):	739.1495/739.1497	893.2278/893.2316	891.2121/891.2157
(calcd./found)	711.1545/711.1562		

[a] CH_3, CH_2, CH, and C carbons were assigned by means of a 135° DEPT experiment. − [b] The rather poor data obtained for **5b**·BPh_4^- may be attributed to inappropriate handling of this sensitive compound during microanalytical workup. Moreover, with the equipment used, carbon values tend to be too low in the presence of boron.

(1) pm] and Co−P3 [221.4 (1) pm] bonds. An explanation for this difference might be found in the interaction between the phenyl groups at P1 and the cyclopentadiene ligand. A comparison of the structures shown in Figure 5 and Figure 6 shows that the orientation of these phenyl groups is distinctly different in **2c** (Figure 6) from the observed orientations in **3a** (Figure 5) and **A**, **B** (Figure 6). The torsion angles given in Table 5 quantify this difference. Comparing the positions of the diene ligands relative to the [*tripod*Co] entities in Figure 5 and Figure 6, it can be seen that the diene ligand in **2c** is positioned such as to reduce this interaction. In all the compounds examined (Figure 5, Figure 6; Table 5, Table 10), the cobalt−carbon bonds to the central carbon atoms of the diene systems are shorter than those to the terminal carbon atoms. This corresponds to a general rule.[9,10,16]

The cobalt−sulfur bond to the sulfur atom of the thioacrolein ligand in **3a** measures 231.3(4) pm. Since the heterodiene is approximately planar (C9−C8−C7−S6: 5°), this indicates a shift of the diene ligand relative to the [*tripod*Co] entity (Figure 5; Table 5, Table 10). The bond lengths within the diene ligands are as expected, as are the angles and torsion angles within the [*tripod*Co] cages (Table 5, Table 10).

The description of the compounds as idealized square-pyramidal is perhaps rather too simplistic. The rotational positions of the diene ligands relative to a pseudo C_3-axis of the [*tripod*Co] entity, vertical in relation to the P1−P2−P3 plane and centred at the cobalt atom, are rather

Table 4. Analytical data for compounds **2** to **5**

Compound	IR: $\tilde{\nu}$ [cm^{-1}]	UV/vis: nm [L $mol^{-1}cm^{-1}$][a]	CV potential[a]	MS (*m*/*z*)
2a·PF_6^-	PF: 837 vs	355 (1190); 440 (450)	$E_{1/2}$ = 888 mV, ΔE = 150 mV; E_p^A = 1680 mV; E_p^C = −1530 mV ΔE_{Fc} = 125 mV	FAB: 751 [M^+]; 683 [M^+ − isoprene]
2b·PF_6^-	PF: 839 vs	410 (1140); 460 (570)	$E_{1/2}$ = 885 mV, ΔE = 290 mV; E_p^C = −1770 mV ΔE_{Fc} = 120 mV	FAB: 765 [M^+]; 683 [M^+ − 2,3-dimethylbutadiene]
2c·PF_6^-	PF: 839 vs	340 (1190); 440 (310)	E_p^A = 900 mV; E_p^C = −1200 mV	FAB: 749 [M^+]; 748 [M^+ − H]; 683 [M^+ − cyclopentadiene]
3a·BPh_4^-		444 (1810); 590 (1230)	E_p^A = 360 mV; E_p^A = 1300 mV E_p^C = −830 mV	FAB: 755 [M^+]; 683 [M^+ − thioacrolein]
3b·PF_6^-	PF: 841 vs	420 (1105); 530 (890)	E_p^A = 1350 mV; E_p^C = −950 mV	FAB: 739 [M^+]; 683 [M^+ − acrolein]
3c·PF_6^-	PF: 841 vs	390 (1870); 580 (1250)	E_p^A = 1180 mV; E_p^C = −840 mV	FAB: 753 [M^+]; 683 [M^+ − methyl vinyl ketone]
4·BPh_4^-	CO: 1965, 2025 vs		$E_{1/2}$ = 1120 mV, ΔE = 155 mV[b] E_p^C = −1500 mV; ΔE_{Fc} = 125 mV	FAB: 739 [M^+]; 711 [M^+ − CO] 683 [M^+ − 2 CO]
5a·PF_6^-	PF: 837 vs	390 (2590); 590 (3140); 730 (2540)	E_p^C = −850 mV; E_p^A = 760 mV;	FAB: 893 [M^+]; 683 [M^+ − benzil] 683 [M^+ − benzil]
5b·BPh_4^-		390 (6920); 640 (5190); 810 (1380)	$E_{1/2}$ = −610 mV, ΔE = 110 mV; E_p^A = 840 mV; ΔE_{Fc} = 135 mV	FAB: 891 [M^+]; 683 [M^+ − phenanthrenequinone]

[a] All measurements were performed in CH_2Cl_2 solution at scan speeds of 200 mVs^{-1}. − [b] Quasi-reversible oxidation.

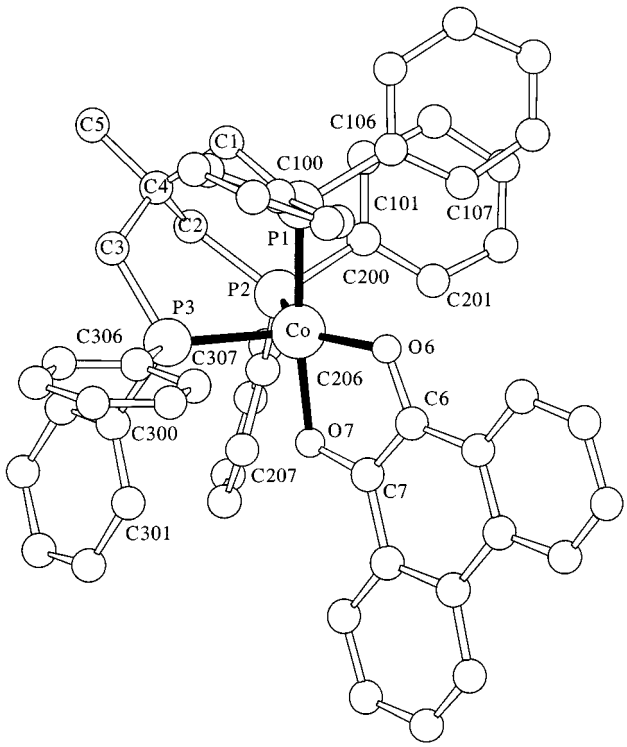


Figure 4. X-ray structure of **5b**

different. As a point of reference for describing this rotation with respect to the diene system, the midpoint of the central bond C7−C8 of this system was chosen. The point of reference with respect to the [*tripod*Co] template was chosen as P1. The angle φ describing the rotation of these reference points with respect to the pseudo axis was found to lie between 27° and 84° in the *tripod* derivatives and to be 40° in the PMe_3 derivative (Figure 5, Figure 6; Table 5, Table 10). It thus appears that the rotational position is rather flexible.

If the rotational positions were fixed, the phosphorus nuclei would reside in different environments even in solution, such that, depending on the symmetry of the arrangement, three or at least two different phosphorus signals could be expected to be observed by ^{31}P-NMR spectroscopy. In fact, it is observed that compounds **2** give rise to only one ^{31}P-NMR signal in CD_2Cl_2 solution, which shows no broadening even on cooling to 193 K. Since it is improbable that all three nuclei − given a static structure − are isochronous, it must be concluded that the all-carbon diene ligands in **2** are free to rotate even at low temperatures, such that a time-averaged ^{31}P-NMR signal is observed. This is in contrast to observations made for other compounds of the type $[L_3M(\eta^4\text{-diene})]$.[8−10,17] In these cases, the ligands L were non-chelating phosphorus donors. For compounds of this type, rotation − even at temperatures close to ambient − is generally sufficiently slow to result in resolution into dis-

Table 5. Bond lengths [pm], bond angles [°], and torsion angles [°] in **2c**, **3a**, **A**, **B**, and **C**

Compound[a]	**2c**·PF_6^-	**3a**·BPh_4^-	[*tripod*Co(η^4-C_7H_8)]$^+$ **A**, **B**[b,c]	[$(Me_3P)_3$Co(η^4-C_7H_8)]$^+$ **C**[b]
Co−P1	228.50(13)	221.4(4)	224.1(8)/223.1(8)	222.1(2)
Co−P2	221.23(12)	224.2(3)	223.7(7)/226.9(7)	223.4(2)
Co−P3	221.40(13)	224.4(3)	224.8(7)/226.0(8)	224.9(2)
Co−C6/Co−S6[d]	209.8(4)	231.3(4)	213(3)/208(2)	211.7(8)
Co−C7	205.6(5)	205.3(14)	213(3)/197(3)	203.9(8)
Co−C8	206.0(4)	206.9(12)	209(3)/204(2)	203.6(8)
Co−C9	212.4(4)	211.3(12)	224(2)/213(2)	213.6(9)
C7−C6/C7−S6[d]	141.2(6)	173.9(15)	150(4)/143(3)	142(1)
C7−C8	143.0(7)	138.2(2)	140(4)/140(3)	138(1)
C8−C9	139.8(7)	142.5(17)	148(4)/139(3)	143(1)
C8−C7−C6/S6[d]	106.5(4)	119.1(12)	114.6(26)/121.1(2)	119.2(8)
C7−C8−C9	106.9(4)	118.9(12)	126.2(25)/114.7(20)	120.3(8)
P1−Co−P2	93.71(5)	93.80(13)	95.5(3)/91.6(3)	100.87(8)
P2−Co−P3	89.12(5)	87.45(13)	90.8(3)/90.5(3)	95.49(9)
P1−Co−P3	91.71(5)	95.17(13)	872(3)/87.7(3)	97.91(9)
C9−C8−C7−C6/S6[d]	−1.1	5	−2.7/1.6	−0.3
C4−C1−P1−Co	34.4	36.3	18.3/28.8	−
C4−C2−P2−Co	32.9	32.7	14.8/32.6	−
C4−C3−P3−Co	29.6	21.8	−2.0/32.7	−
Hz−P1−C100−C101[e]	8.5	−14.6	24.6/−23.7	−
Hz−P1−C106−C107[e]	−6.2	−59.6	52.1/−53.6	−
Hz−P2−C200−C201[e]	−40.4	14.1	25.9/2.5	−
Hz−P2−C206−C207[e]	−62.7	7.7	65.8/−15.1	−
Hz−P3−C300−C301[e]	14.0	−68.1	33.3/−46.8	−
Hz−P3−C306−C307[e]	50.0	−23.3	28.6/−34.5	−
φ[f]	84	27	78/57	40

[a] Standard deviations in units of the least significant digit are given in each case. − [b] Here, a consistent numbering scheme for all the complexes is used for the sake of easier comparison, which differs from that used for the deposited structures. − [c] Two independent molecules. − [d] In **3a**, S6. − [e] In order to define the rotation of the phenyl groups with respect to the idealized C_3 axis of the [tripodCo] entity, the following procedure was adopted: a vector vertical in relation to the P1−P2−P3 plane and pointing towards the observer with respect to the projections shown in Figure 5 and Figure 6 was fixed at the individual phosphorus atoms. Its end point was designated as Hz. The given torsion angles refer to this convention. − [f] The rotational position of the diene systems was characterized by the torsion angle φ. φ is measured as the rotation about an axis vertical with respect to the P1−P2−P3 plane and fixed to the cobalt atom. As a fixed point in the diene system, the midpoint between the two central carbon atoms (C7−C8) was chosen. The torsion angle about the pseudo axis between P1 and this point is defined as φ.

Table 6. Bond lengths [pm], bond angles [°], and torsion angles [°] in **4** and **5b**

Compound	**4**·BPh_4^-[a]	**5b**·BPh_4^-[a]
Co−P1	222.57(8)	219.5(8)
Co−P2	223.47(6)	222.1(3)
Co−P3	226.02(7)	221.5(4)
Co−X1[b]	175.4(2)	185.7(8)
Co−X2[b]	177.6(2)	186.7(8)
X1−Y1[b]	115.5(3)	129.9(12)
X2−Y2[b]	113.7(2)	129.3(12)
X1−Co−X2[b]	86.94(9)	82.2(3)
P1−Co−P2	88.24(3)	91.26(12)
P2−Co−P3	96.01(3)	92.34(12)
P1−Co−P3	90.07(3)	91.57(13)
P1−Co−X1[b]	87.86(7)	88.0(3)
P2−Co−X1[b]	141.87(8)	136.5(3)
P3−Co−X1[b]	121.90(8)	131.2(3)
P1−Co−X2[b]	169.63(7)	169.9(3)
P2−Co−X2[b]	90.32(7)	97.6(3)
P3−Co−X2[b]	100.30(7)	93.0(3)
Co−X1−Y1[b]	175.54(18)	115.7(7)
Co−X2−Y2[b]	176.51(18)	113.3(8)
C4−C1−P1−Co	17.0	17.8
C4−C2−P2−Co	28.7	15.3
C4−C3−P3−Co	16.7	19.2
Hz−P1−C100−C101[c]	30.8	21.4
Hz−P1−C106−C107[c]	29.8	40.0
Hz−P2−C200−C201[c]	7.2	18.4
Hz−P2−C206−C207[c]	84.0	57.0
Hz−P3−C300−C301[c]	7.8	18.9
Hz−P3−C306−C307[c]	24.2	31.4

[a] Standard deviations in units of the least significant digit are given in each case. − [b] X, Y refer to the residues at the [*tripod*Co] template in the sequence Co−X−Y. For compound **4**, the meaning of these symbols is thus X1, X2 = C6, C7 and Y1, Y2 = O6, O7. For compound **5**, it is X1, X2 = O6, O7, and Y1, Y2 = C6, C7. − [c] In order to define the rotation of the phenyl groups with respect to the idealized C_3 axis of the [*tripod*Co] entity, the following procedure was adopted: a vector vertical in relation to the P1−P2−P3 plane and pointing towards the observer with respect to the projections shown in Figure 5 and Figure 6 was fixed at the individual phosphorus atoms. Its end point was designated as Hz. The given torsion angles refer to this convention.

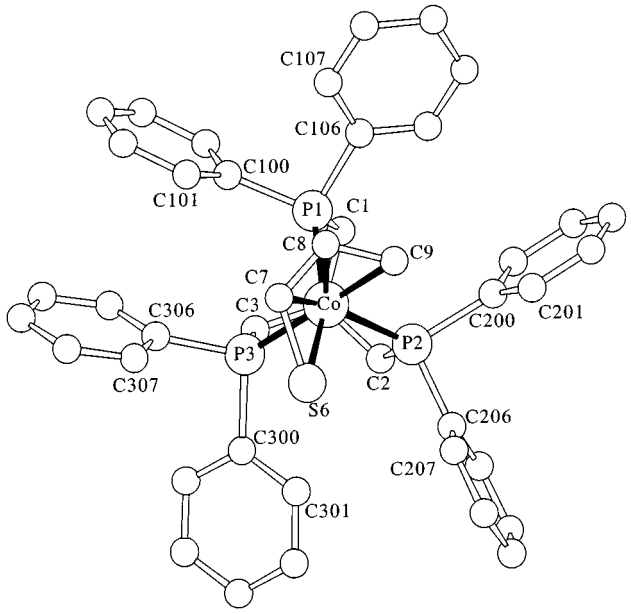


Figure 5. X-ray structure of **3a**; here, a consistent numbering scheme for all the compounds is used for the sake of easier comparison, which differs from that used for the deposited structure

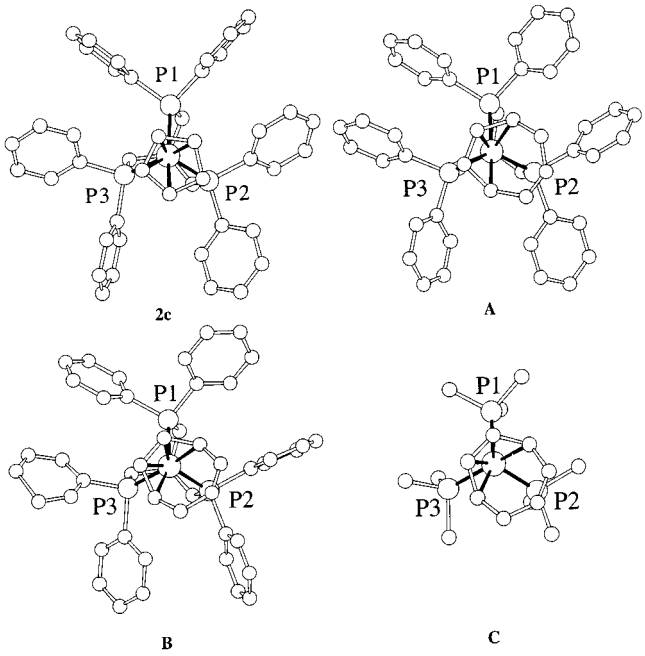


Figure 6. X-ray structures of compounds **2c**, **A**, **B**, and **C**; here, a consistent numbering scheme for all the compounds is used for the sake of easier comparison, which differs from that used for the deposited structures

crete signals in the ^{31}P-NMR spectra as well as in the ^{1}H-NMR spectra for the groups which are symmetrically non-equivalent in a static arrangement.[8−10,17]

At first glance, it is difficult to understand why this type of rotation of the diene ligands should have a lower associated activation energy in the [*tripod*Co] compounds as compared to the non-chelate $[L_3Co]$ derivatives. Comparing the structure of $[(Me_3P)_3Co^I\text{-}(\eta^4\text{-}C_7H_8)]^+$ (Figure 6; Table 5, Table 10) with those of the [*tripod*Co] compounds (Figure 5, Figure 6; Table 5, Table 10), it appears that the P−Co−P angles in the *tripod* derivatives are somewhat smaller than those in the $[(Me_3P)_3Co]$ compound. This would leave more space between the coordinated diene and the phosphorus nuclei in the *tripod* compounds as compared to that in the $[(Me_3P)_3Co]$ derivative (Figure 6; Table 5, Table 10). However, it would appear that the dominant repulsive interactions between the *tripod* ligand and the dienes are those between the substituents on phosphorus and the dienes and not those between the dienes and the phosphorus nuclei. Space-filling models of $[tripodCo^I\text{-}(\eta^4\text{-}C_7H_8)]^+$ (**A**) and $[(Me_3P)_3Co^I\text{-}(\eta^4\text{-}C_7H_8)]^+$ (**C**) are shown in Figure 7.[2e,9] For the *tripod* compound **A**, no ^{31}P-NMR data are available, but in view of the findings for compounds **2** it is probable that the diene ligand is free to rotate in this compound as well.[2e]

For $[(Me_3P)_3Co^I\text{-}(\eta^4\text{-}C_7H_8)]^+$, the NMR data reveal a static structure even at room temperature.[10] Figure 6 and Figure 7 suggest that the incorporation of methyl substituents at the phosphorus donors in $[(Me_3P)_3Co^I\text{-}(\eta^4\text{-}C_7H_8)]^+$ leads to a more congested steric situation than that in [*tri-*

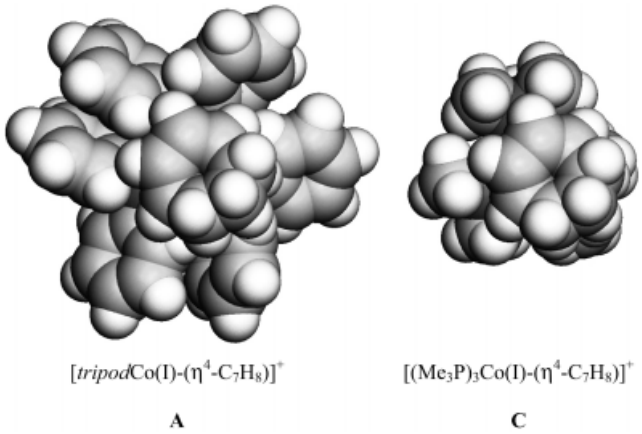


Figure 7. Space-filling models of **A** [*tripod*Co^{I}-(η^4-C_7H_8)]$^+$ and **C** [$(Me_3P)_3Co^{I}$-(η^4-C_7H_8)]$^+$

podCo^{I}-(η^4-C_7H_8)]$^+$, where a rotation of the phenyl groups may open up an almost unimpeded rotational pathway for the diene ligand.

The finding that there is still free rotation of the diene ligands in **2** at 193 K must mean that the electronic contribution to this barrier is rather low and hence the electronic preference for one orientation over the other must be small. This electronic contribution to the barrier might be expected to be higher with heterodiene ligands and indeed it is found that the heterodiene compounds **3** show three different phosphorus signals in their low-temperature ^{31}P-NMR spectra (Table 7). On warming to 303 K, exchange processes become apparent such that for **3a** and **3b** only one time-averaged ^{31}P-NMR signal is observed. In the case of **3c**, coalescence remains incomplete at 303 K. The spectra obtained at different temperatures have been analysed by line-shape analysis.[18] The quality of fit obtained by this procedure is shown for **3a** as a representative example, as is the Eyring plot obtained from the individual line-fitting procedures (Figure 8).

An activation enthalpy of 47 kJmol^{-1} was determined for **3a** (Table 8). The activation enthalpies similarly derived for **3b** and **3c** were 46 kJmol^{-1} and 48 kJmol^{-1} (Table 8).

The activation entropies were found to be negative throughout the series of compounds **3a**−**3c** (Table 8). While the entropy value derived for **3b** (−22 ± 6 Jmol^{-1}K^{-1}) was not too accurate, the activation entropy found for **3c** was definitely negative, more so than that determined for **3a** (Table 8). The entropy data thus suggest that the transition state associated with the rotational process is sterically more

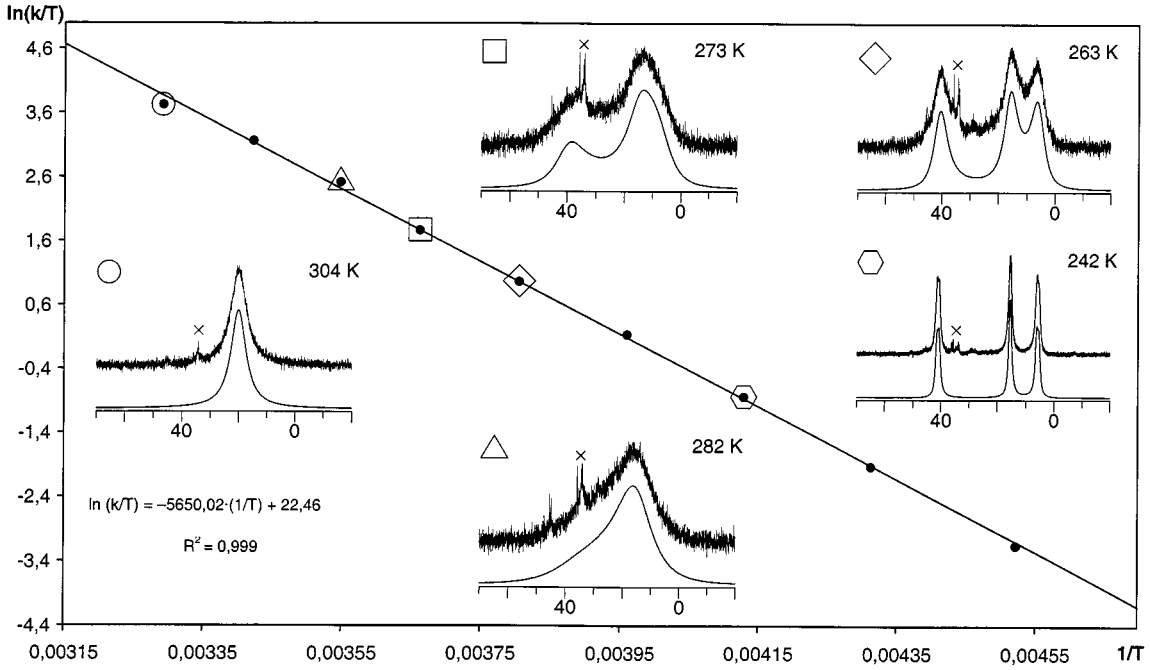


Figure 8. Eyring plot and examples of experimental (top) and simulated (bottom) spectra for compound **3a**; × denotes impurities

Table 7. ^{31}P-NMR data for compounds **3a** to **3c**

Compound	T [K]	P_a [ppm]	P_b [ppm]	P_c [ppm]	J_{ab} [Hz]	J_{ac} [Hz]	J_{bc} [Hz]
3a	221.13	41.1	15.3	6.2	16	64	8
	303.80	–	9.6	–			
3b	221.13	47.5	15.0	−3.0	10	68	6
	303.80	–	18.0	–			
3c	241.70	47.7	14.3	−3.4	16	67	13
	303.80	46.6	14.9	−3.9			

Table 8. Calculated rotational barriers and thermodynamic parameters from line-shape analysis

T [K]	**3a**; k [s^{-1}]	**3b**; k [s^{-1}]	**3c**; k [s^{-1}]
221.13	9.5	4	–
231.88	34	–	–
241.70	105	–	8
252.55	290	–	25
262.82	690	215	145
273.06	1600	–	320
281.83	3500	–	640
292.27	6900	–	1200
303.80	12600	5300	2700
Thermodynamic data[a]	$\Delta H^{\neq} = 47.0 \pm 0.5$ kJmol^{-1} $\Delta S^{\neq} = -11 \pm 2$ Jmol^{-1}K^{-1} $\Delta G^{\neq}_{298} = 50.2 \pm 0.5$ kJmol^{-1}	$\Delta H^{\neq} = 46.3 \pm 1.5$ kJmol^{-1} $\Delta S^{\neq} = -22 \pm 6$ Jmol^{-1}K^{-1} $\Delta G^{\neq}_{298} = 53.0 \pm 2.9$ kJmol^{-1}	$\Delta H^{\neq} = 47.9 \pm 0.7$ kJmol^{-1} $\Delta S^{\neq} = -27 \pm 3$ Jmol^{-1}K^{-1} $\Delta G^{\neq}_{298} = 56.0 \pm 0.1$ kJmol^{-1}

[a] Error estimates from linear regression; for a discussion concerning the estimation of the error in $\Delta G^{\neq}_{298}$, see ref.[24]

congested than the ground state. The activation enthalpies were found to be approximately equal for all three compounds **3a**–**3c**, despite the fact that the ligand in **3a** contains sulfur as the heteroatom while the ligands in **3b** and **3c** contain oxygen.

Conclusion

Simple and straightforward procedures for the synthesis of $[tripodCo^{I}\text{-}L_2]^+$ have been described, where L_2 is a diene (isoprene, 2,3-dimethylbuta-1,3-diene, cyclopentadiene) (**2**) or heterodiene (acrolein, methyl vinyl ketone, thioacrolein) (**3**), coordinated in a η^4 fashion. While the idealized square-pyramidal coordination geometry observed for **2** and **3** in the solid state might be expected to give rise to chemically different phosphorus nuclei, only one sharp time-averaged ^{31}P-NMR signal is observed for **2**. Only with **3** is the rotational reorientation process sufficiently slow to allow the observation of three different ^{31}P-NMR signals at low temperatures. Line-shape analysis has allowed the estimation of $\Delta H^{\neq}$ in these cases, for which values close to 47 kJmol^{-1} have been obtained for all the compounds analysed (**3a** thioacrolein, **3b** acrolein, **3c** methyl vinyl ketone).

Experimental Section

General Remarks: Unless noted otherwise, all manipulations were carried out under argon using standard Schlenk techniques. All solvents were dried by standard methods and distilled under argon.[19] The zinc powder (Merck) used in some of the reactions was activated by stirring it under argon by means of a magnetic bar for 12 h. The solvents CD_3NO_2, [D_6]acetone, [D_8]THF, and CD_2Cl_2 used for NMR spectroscopic measurements were degassed by three successive "freeze-pump-thaw" cycles and dried with 4 Å molecular sieves. – Photochemical reactions were carried out with a Hanau TQ high-pressure mercury lamp in a Duran glass 50 irradiation apparatus equipped with a cooling system. – NMR: Bruker Avance DPX 200 at 200.12 MHz (^{1}H), 50.323 MHz (^{13}C{^{1}H}), 81.015 MHz (^{31}P{^{1}H}); T = 303 K, unless stated otherwise; chemical shifts (δ) in ppm with respect to (residual protons in) CD_3NO_2 (^{1}H: δ = 4.33; ^{13}C: δ = 62.8), [D_6]acetone (^{1}H: δ = 2.05; ^{13}C: δ = 29.8, 206.2), [D_8]THF (^{1}H: δ = 1.72, 3.57; ^{13}C: δ = 25.3, 67.4), and CD_2Cl_2 (^{1}H: δ = 5.32; ^{13}C: δ = 53.8) as internal standards. ^{31}P chemical shifts (δ) in ppm with respect to 85% H_3PO_4 (^{31}P: δ = 0) as external standard. – IR: Bruker IFS-66; KBr discs. – UV/vis: Perkin–Elmer Lambda 19 – Fast-atom bombardment (FAB) MS: Finnigan MAT 8230; xenon atom beam; matrix: 4-nitrobenzyl alcohol. – HR-MS (FAB): JEOL JMS 700; matrix: 4-nitrobenzyl alcohol. – Elemental analyses: Microanalytical Laboratory of the Organisch-Chemisches Institut, Universität Heidelberg. – Melting points: Gallenkamp MFB-595 010; uncorrected values. – Cyclic voltammetry: Metrohm "Universal Meß- und Titriergefäß", Metrohm GC electrode RDE 628, platinum electrode, SCE electrode, Princeton Applied Research potentiostat model 273; 10^{-3} M substrate in 0.1 M nBu$_4$NPF$_6$/CH_2Cl_2.

Preparation of *Tripod*CoCl (1): 1 mmol (130 mg) of $CoCl_2$ and 1 mmol (624 mg) of $CH_3C(CH_2PPh_2)_3$ (*tripod*) were dissolved in 25 mL of THF to give a blue-green solution of *tripod*$CoCl_2$.[2b] An excess of activated zinc powder was then added to the solution, and the mixture was treated for 10 min. in an ultrasonic bath. When the reaction was complete, the mixture had become orange-beige in colour. The solvent was evaporated and the residue was redissolved in CH_2Cl_2. The solution was filtered to remove $ZnCl_2$ and excess zinc powder. The solvent was then evaporated once more to leave *tripod*CoCl (**1**) in analytically pure form. – $C_{41}H_{39}ClCoP_3$ calcd. C 68.48, H 5.47; found C 68.57, H 5.61.

A: General Procedure for the Synthesis of [*Tripod*Co^{I}-(η^4-diene)]$^+$ Complexes or [*Tripod*Co^{III}-diolato]$^+$ Compounds from 1,3-Dienes and Heterodienes [Diene = Isoprene (2a), 2,3-Dimethylbuta-1,3-diene (2b), Cyclopentadiene (2c), Acrolein (3b), Methyl Vinyl Ketone (3c), Benzil (5a), Phenanthrenequinone (5b)]: 1 mmol (718 mg) of freshly prepared *tripod*CoCl (**1**) and 1 mmol (349 mg) of $TlPF_6$ were suspended in 20 mL of THF to give a yellow solution, from which a fine white precipitate was deposited. 1 mmol of the appropriate ligand (Table 9) was then added to this suspension and the reaction mixture was treated in an ultrasonic bath for 10 min. During the course of this procedure, the reaction mixture underwent a colour change to orange in the case of the carbon-centred dienes, to claret in the case of acrolein and methyl vinyl ketone, to cornflower blue with benzil, and to blue-green with phenanthrenequinone. The solvent was subsequently evaporated in vacuo and the residue was redissolved in CH_2Cl_2. This solution was filtered to remove the TlCl produced. The solvent was then evaporated once more and the residue (except in the case of **5b**) was purified by chromatography on silica gel (ICN Biomedicals, 32–63 μm, 60 Å),

Table 9. Analytical data for compounds **2** to **5**

Compound	Coligand	Eluent mixture	Colour	Yield [%] (method)	m.p. [°C][a]
2a	68 mg (1 mmol) isoprene	Et_2O/CH_2Cl_2 (2:1)	orange	78 (A) 64 (B)	141 (dec.)
2b	82 mg (1 mmol) 2,3-dimethylbutadiene	Et_2O/CH_2Cl_2 (2:1)	orange	71 (A) 61 (B)	150 (dec.)
2c	66 mg (1 mmol) cyclopentadiene	Et_2O/CH_2Cl_2 (2:1)	orange	76 (A) 69 (B)	155 (dec.)
3a	108 mg (1.5 mmol) 2-propenethiol	–	brown-green	35	130 (dec.)
3b	56 mg (1 mmol) acrolein	Et_2O/CH_2Cl_2 (3:1)	claret	81	125 (dec.)
3c	70 mg (1 mmol) methyl vinyl ketone	Et_2O/CH_2Cl_2 (3:1)	claret	78	130 (dec.)
4	116 mg (2 mmol) 2-butenal	Et_2O/CH_2Cl_2 (3:1)	orange	76	175 (dec.)
5a	210 mg (1 mmol) benzil	Et_2O/CH_2Cl_2 (4:1)	cornflower blue	85	180 (dec.)
5b	208 mg (1 mmol) phenanthrenequinone	–	blue-green	91	185 (dec.)

[a] dec. = decomposition.

eluting with the solvent mixture indicated in Table 9, to afford the PF_6 salts of **2a**–**c**, **3b**, **3c**, and **5a**. In order to obtain the crystalline BPh_4 salt of **5b**, a solution of **5b**·PF_6 in THF was treated with a three-fold excess of $NaBPh_4$. The solvent was evaporated, the residue was redissolved in CH_2Cl_2, and this solution was filtered to remove $NaPF_6$ and excess $NaBPh_4$. Removal of the solvent afforded **5b**·BPh_4. For analytical data of the compounds, see Table 1, Table 2, Table 3, Table 4.

B: General Procedure for the Synthesis of [*Tripod*Co^I-(η^4-diene)]PF_6 Complexes [Diene = Isoprene (2a), 2,3-Dimethylbutadiene (2b), Cyclopentadiene (2c)]: 1 mmol (342 mg) of $Co_{aq}(BF_4)_2$ and 1 mmol (624 mg) of *tripod* were dissolved in 30 mL of CH_2Cl_2/ethanol (1:1) to give a brown-red solution. 1 mmol of the appropriate diene (Table 9) and a five-fold excess of zinc powder were then added. The reaction mixture was treated in an ultrasonic bath for 5 min. The solvent was then removed in vacuo, the residue was redissolved in CH_2Cl_2, and this solution was filtered to remove $ZnCl_2$ and excess zinc powder. The filtrate was then concentrated to dryness, the residue was redissolved in THF, and treated with a three-fold excess of KPF_6. The solvent was again removed in vacuo, the residue was redissolved in CH_2Cl_2, and this solution was filtered to remove excess KPF_6 and KBF_4. The filtrate was concentrated to dryness and the residue was purified by chromatography on silica gel (ICN Biomedicals, 32–63 μm, 60 Å), eluting with the solvent mixture indicated in Table 9. After workup of the appropriate fractions, the PF_6 salts of **2a**–**c** were obtained as microcrystalline powders. For analytical data of the compounds, see Table 1, Table 4.

Preparation of [*Tripod*Co^I-(η^4-thioacrolein)]BPh_4 (3a·BPh_4^-): 1 mmol (342 mg) of $Co_{aq}(BF_4)_2$ and 1 mmol (624 mg) of *tripod* were dissolved in 30 mL of THF/ethanol (1:1) to give a brown-red solution. Addition of 1.5 mmol (108 mg) of allyl mercaptan and 3 mmol (1026 mg) of $NaBPh_4$ led to an immediate colour change to dark brown. After filtration through silanized silica gel (Merck), the filtrate was concentrated in vacuo to a volume of 20 mL. The Schlenk tube was then flushed with argon and sealed with a rubber stopper. After 3 days, a brown-green precipitate had been deposited, which was washed with Et_2O (3 × 10 mL). The product, which could reproducibly be obtained, was identified as analytically and spectroscopically pure **3a**·BPh_4 (Table 2, Table 4).

Preparation of [*Tripod*Co^I-$(CO)_2$]BPh_4 (4·BPh_4^-): (a) From 2-Butenal: 1 mmol (718 mg) of freshly prepared *tripod*CoCl (**1**) and 1 mmol (349 mg) of $TlPF_6$ were suspended in 20 mL of THF to give a yellow solution, from which a fine white precipitate was deposited. 2 mmol (116 mg) of 2-butenal (commercial *E*/*Z* mixture) was added to this suspension and the reaction mixture was treated in an ultrasonic bath for 10 min. During the course of this procedure, the reaction mixture underwent a colour change to orange. The solvent was then evaporated in vacuo and the residue was redissolved in CH_2Cl_2. This solution was filtered to remove the TlCl produced. After concentration of the filtrate, the residue was redissolved in THF and this solution was treated with a three-fold excess of $NaBPh_4$. The solvent was evaporated, the residue was redissolved in CH_2Cl_2, and this solution was filtered to remove $NaPF_6$ and excess $NaBPh_4$. Concentration of the filtrate and purification of the residue by chromatography on silica gel (ICN Biomedicals, 32–63 μm, 60 Å), eluting with the solvent mixture indicated in Table 9, gave the BPh_4 salt of [*tripod*Co^I-$(CO)_2]^+$. For analytical data of the compound, see Table 3, Table 4.

(b) From CO: 1 mmol (718 mg) of freshly prepared *tripod*CoCl (**1**) and 1 mmol (349 mg) of $TlPF_6$ were suspended in 20 mL of THF to give a yellow solution, from which a fine white precipitate was deposited. CO was then bubbled through this solution for 10 min., leading to a colour change to orange. The solvent was then evaporated in vacuo and the residue was redissolved in CH_2Cl_2. This solution was filtered to remove the TlCl produced. After concentration of the filtrate, the residue was redissolved in THF and this solution was treated with a three-fold excess of $NaBPh_4$. The solvent was evaporated, the residue was redissolved in CH_2Cl_2, and this solution was filtered to remove $NaPF_6$ and excess $NaBPh_4$. Concentration of the filtrate and purification of the residue by chromatography on silica gel (ICN Biomedicals, 32–63 μm, 60 Å), eluting with the solvent mixture indicated in Table 9, gave the BPh_4 salt of [*tripod*Co^I-$(CO)_2]^+$. For analytical data of the compound, see Table 3, Table 4.

Preparation of [*Tripod*Co^I-(norbornadiene)]PF_6 and [*Tripod*Co^I-(1,5-cyclooctadiene)]PF_6: 1 mmol (718 mg) of freshly prepared *tripod*CoCl (**1**) and 1 mmol (349 mg) of $TlPF_6$ were suspended in 20 mL of THF to give a yellow solution, from which a fine white precipitate was deposited. 1 mmol of the appropriate ligand was then added to this suspension and the reaction mixture was treated in an ultrasonic bath for 10 min. During the course of this procedure, the reaction mixture underwent a colour change to brown-

Table 10. Crystal data for compounds **2c**, **3a**, **4**, and **5b**

Compound	**2c**·PF_6^-	**3a**·BPh_4^-	**4**·BPh_4^-	**5b**·BPh_4^-
Formula	$C_{46}H_{45}CoF_6P_4$	$C_{68}H_{63}BCoP_3S$	$C_{67}H_{59}BCoO_2P_3$	$C_{79}H_{67}BCoO_2P_3$
Molecular mass	894.630	1074.890	1058.790	1210.98
Crystal system	monoclinic	monoclinic	monoclinic	monoclinic
Space group	$P2_1/n$ (No. 14)[22]	$C2/c$ (No. 15)[22]	$P2_1/c$ (No. 14)[22]	$C2/c$ (No. 15)[22]
Lattice constants	a = 1051.7(2) pm b = 1745.5(4) pm c = 2239.9(5) pm β = 90.99(3)°	a = 3809(1) pm b = 909.0(2) pm c = 3277(1) pm β = 96.61(3)°	a = 1323.5(3) pm b = 2071.2(4) pm c = 1990.3(4) pm β = 98.50(3)°	a = 2450.8(5) pm b = 1620.3(4) pm c = 3652.0(7) pm β = 100.02(1)°
Cell volume	4111 × 10^6 pm^3	11564 × 10^6 pm^3	5396 × 10^6 pm^3	14281 × 10^6 pm^3
Molecular units per cell	Z = 4	Z = 8	Z = 4	Z = 8
Density (calculated)	1.445 g cm^{-3}	1.235 g cm^{-3}	1.303 g cm^{-3}	1.126 g cm^{-3}
Temperature	200 K	293 K	200 K	290 K
Measuring device	Nonius-Kappa CCD	Siemens Nicolet-Syntex	Nonius-Kappa CCD	SiemensNicolet-Syntex
No. reflns. for cell refinement	–	81	–	25
Scan range	3.6° < 2θ < 50.0°	4.2° < 2θ < 46.1°	2.9° < 2θ < 52.1°	3.6° < 2θ < 48.0°
Method	ω-scan, Δω = 1.0°	ω-scan, Δω = 0.75°	ω-scan, Δω = 1.0°	ω-scan, Δω = 0.54°
Scan speed	15 sec/frame	2.2 < dω/dt < 29.3° min^{-1}	25 sec/frame	12° min^{-1}
Measured reflections	16197	8166	126963	11305
Unique reflections	7247	8049	10664	11011
Observed reflections ($I \geq 2\sigma$)	5191	4383	8672	4632
No. of parameters refined	519	549	672	733
Max. residual electron density	2.89 × 10^{-6} e pm^{-3}	2.55 × 10^{-6} e pm^{-3}	0.93 × 10^{-6} e pm^{-3}	1.67 × 10^{-6} e pm^{-3}
Agreement factors (F^2 refinement)	R_1 = 0.058 R_w = 0.160	R_1 = 0.122 R_w = 0.328	R_1 = 0.038 R_w = 0.103	R_1 = 0.127 R_w = 0.406

orange. The solvent was evaporated in vacuo and the residue was redissolved in CH_2Cl_2. This solution was filtered to remove TlCl. Evaporation of the solvent from the filtrate afforded the PF_6 salts as dark-orange powders. – ^{31}P NMR (CD_2Cl_2): [*tripod*Co^I-(norbornadiene)]$^+$: δ = 23.8 (s), −144.2 (sept, $^1J_{PF}$ = 713 Hz); [*tripod*Co^I-(1,5-cyclooctadiene)]$^+$: δ = 24.1 (s), −144.2 (sept, $^1J_{PF}$ = 713 Hz). – IR (KBr): [*tripod*Co^I-(norbornadiene)]$^+$: ṽ (PF): 849 cm^{-1} vs; [*tripod*Co^I-(1,5-cyclooctadiene)]$^+$: ṽ (PF): 837 cm^{-1} vs. – FAB-MS: [*tripod*Co^I-(norbornadiene)]$^+$: *m*/*z* = 775 [M^+]; [*tripod*Co^I-(1,5-cyclooctadiene)]$^+$: *m*/*z* = 792 [M^+].

Preparation of [*Tripod*Co^I-(ethylene)$_2$]PF_6: 1 mmol (718 mg) of freshly prepared *tripod*CoCl (**1**) and 1 mmol (349 mg) of $TlPF_6$ were suspended in 20 mL of THF to give a yellow solution, from which a fine white precipitate was deposited. Ethylene was then bubbled through this solution for 15 min., leading to a colour change to brown-orange. The solvent was subsequently evaporated in vacuo and the residue was redissolved in CH_2Cl_2. This solution was filtered to remove the TlCl produced. Evaporation of the solvent from the filtrate afforded the PF_6 salt as a brown-orange powder. – ^{31}P NMR (CD_2Cl_2): δ = 22.5 (br. s), −144.2 (sept, $^1J_{PF}$ = 713 Hz). – IR (KBr): ṽ (PF): 839 cm^{-1} vs. – MS-FAB: *m*/*z* = 739 [M^+].

The BPh_4 salt of [*tripod*Co^I-(ethylene)$_2$]$^+$ could also be obtained by irradiation of [*tripod*Co^I-$(CO)_2$]BPh_4 (**4**) while bubbling ethylene through the reaction mixture for 1 h. – ^{31}P NMR (CD_2Cl_2): δ = 22.5 (br. s). – MS-FAB: 739 [M^+].

X-ray Crystallographic Study: The measurements were made on a Siemens P4 four-circle diffractometer (**3a** and **5b**) or on a Nonius-Kappa CCD diffractometer (**2c** and **4**), using graphite-monochromated Mo-K_α radiation throughout. In the case of the measurements on the Siemens P4 four-circle diffractometer, the intensities of three check reflections (measured every 100 reflections) remained constant throughout the data collection, thus indicating crystal and electronic stability. The data collected on this instrument were corrected in the usual manner, including an experimental absorption correction. The data from the Nonius-Kappa CCD device were processed using the standard Nonius software.[20] All calculations were performed using the SHELXT-PLUS software package. Structures were solved by direct methods using the SHELXS-97 program and refined with SHELXL-97.[21][22] Graphical handling of the structural data during solution and refinement was performed with XPMA.[23] Atomic coordinates and anisotropic thermal parameters of the non-hydrogen atoms were refined by full-matrix least-squares calculations. Data relating to the structure determinations are compiled in Table 10. Crystallographic data (excluding structure factors) for the structures reported in this paper have been deposited with the Cambridge Crystallographic Data Centre as supplementary publication nos. CCDC-127496 to CCDC-127498. Copies of data can be obtained free of charge on application to the CCDC, 12 Union Road, Cambridge CB2 1EZ, U.K. [Fax: (internat.) +44 (0)1223/336033; E-mail: deposit@ccdc.cam.ac.uk].

Acknowledgments

We are indebted to the Deutsche Forschungsgemeinschaft (SFB 247) and the Fonds der Chemischen Industrie for financial support. One of us (R.R.) is indebted to the Graduiertenkolleg "Selektivität in der organischen und metallorganischen Synthese und Katalyse" for a scholarship. The unselfish cooperation of Dr. J. Groß and Mr. T. Jannack (mass spectrometric measurements), Mr. D. Günauer (cyclic voltammetry), and Mrs. A. Dittes, Mrs. C. Vetter, Mrs. E. Weiß and Mr. F. Liebscher (elemental analysis) is gratefully acknowledged.

[1] L. Sacconi, F. Mani, *Trans. Met. Chem.* **1982**, *8*, 179.
[2] Cobalt(I): [2a] L. Sacconi, S. Midollini, *J. Chem. Soc., Dalton Trans.* **1972**, 1213–1216. – [2b] K. Heinze, G. Huttner, L. Zsolnai, P. Schober, *Inorg. Chem.* **1997**, *36*, 5457–5469. – [2c] V. Sernau, G. Huttner, J. Scherer. L. Zsolnai, T. Seitz, *Chem. Ber.* **1995**, *128*, 193–195. – [2d] V. Sernau, G. Huttner, J. Scherer, O. Walter, *Chem. Ber.* **1996**, *129*, 243–245. – [2e] C. Bianchini, P. Dapporto, A. Meli, L. Sacconi, *J. Organomet. Chem.* **1980**, *193*, 117–126. – [2f] A. Barth, Ph. D. Dissertation, Universität

Heidelberg, **1990**. – [2g] J. Ellerman, J. F. Schindler, *Z. Naturforsch*. **1975**, *30b*, 914–919. – [2h] J. Ellermann, J. F. Schindler, *Chem. Ber*. **1976**, *109*, 1095–1105. – [2i] J. Ellermann, J. F. Schindler, *J. Organomet. Chem.* **1975**, *94*, 201–212. – [2j] C. A. Ghilardi, C. Mealli, S. Midollini, V. I. Nefedov, A. Orlandini, L. Sacconi, *Inorg. Chem*. **1980**, *19*, 2454–2462. – [2k] D. L. DuBois, D. W. Meek, *Inorg. Chem*. **1976**, *15*, 3076–3088. – [2l] M. Di Vaira, L. Sacconi, *Angew. Chem*. **1982**, *94*, 338–351; *Angew. Chem. Int. Ed. Engl.* **1982**, *27*, 330. – [2m] A. Barth, G. Huttner, M. Fritz, L. Zsolnai, *Angew. Chem.* **1990**, *102*, 956–958; *Angew. Chem. Int. Ed. Engl.* **1990**, *29*, 929.

[3] Cobalt(II): see, for example ref.[1,2b,2f] – [3a] P. Dapporto, S. Midollini, L. Sacconi, *Inorg. Chem.* **1975**, *14*, 1643–1650. – [3b] S. Vogel, A. Barth, G. Huttner, T. Klein, L. Zsolnai, R. Kremer, *Angew. Chem*. **1991**, *103*, 325–327; *Angew. Chem. Int. Ed. Engl.* **1991**, *30*, 303. – [3c] S. Vogel, G. Huttner, C. Emmerich, *Z. Naturforsch*. **1993**, *48b*, 353–362.

[4] Cobalt(III): see, for example, literature cited in: [4a] C. Bianchini, D. Masi, C. Mealli, *Inorg. Chem*. **1987**, *26*, 3683–3693. – [4b] S. Vogel, G. Huttner, L. Zsolnai, *Z. Naturforsch*. **1993**, *48b*, 641–652. – [4c] K. Heinze, G. Huttner, L. Zsolnai, A. Jacobi, P. Schober, *Chem. Eur. J.* **1997**, *3*, 732–743.

[5] K. Jonas, C. Krüger, *Angew. Chem*. **1980**, *92*, 513–531; *Angew. Chem. Int. Ed. Engl.* **1980, 19**, 520.

[6] K. Jonas, *Angew. Chem*. **1985**, *97*, 292–307; *Angew. Chem. Int. Ed. Engl.* **1985**, *24*, 295.

[7] G. A. Lawrance, *Chem. Rev.* **1986**, *86*, 17–33.

[8] M. Bressan, R. Ettorre, P. Rigo, *J. Organomet. Chem*. **1978**, *144*, 215–223.

[9] L. C. A. de Carvalho, Y. Pérès, M. Dartiguenave, Y. Dartiguenave, A. L. Beauchamp, *Organometallics* **1985**, *4*, 2021–2028.

[10] L. C. A. de Carvalho, M. Dartiguenave, Y. Dartiguenave, *J. Organomet. Chem*. **1989**, *367*, 187–195.

[11] A. Guinot, P. Cadiot, *J. Organomet. Chem*. **1980**, *194*, 357–365.

[12] D. C. Dittmer, K. Takahashi, M. Iwanami, *J. Am. Chem. Soc*. **1976**, *98*, 2795–2803.

[13] R. L. Harlow, C. E. Pfluger, *Acta Cryst*. **1973**, *B29*, 2633–2635.

[14] STNeasy search 1 Jun 30, 07:49:04, **1999**.

[15] C. P. Lenges, M. Brookhart, P. S. White, *Angew. Chem*. **1999**, *111*, 535–538, *Angew. Chem. Int. Ed. Engl.* **1999**, *38*, 552.

[16] F. A. Cotton, V. W. Day, B. A. Frenz, K. I. Hardcastle, J. M. Troup, *J. Am. Chem. Soc.* **1973**, *95*, 4522–4528.

[17] S. Komiya, H. Minato, T. Ikariya, T. Yamamoto, A. Yamamoto, *J. Organomet. Chem*. **1983**, *254*, 83–88.

[18] [18a] G. Binsch, *J. Am. Chem. Soc.* **1969**, *91*, 1304–1309. – [18b] WIN-Dynamics 1.0 Release 951220, NMR Dynamic Spectra Simulation and Iteration, Bruker-Fanzen Analytik GmbH and K. Ill′yasow, O. Nedopekin, Bremen, Germany.

[19] *Organikum*, Deutscher Verlag der Wissenschaften, Berlin, **1990**.

[20] DENZO-SMN, Data processing software, Nonius **1998**; http://www.nonius.com.

[21] [21a] G. M. Sheldrick, *SHELXS-97, Program for Crystal Structure Solution*, University of Göttingen, **1997**; http://shelx.uni-ac.gwdg.de/shelx/index.html. – [21b] G. M. Sheldrick, *SHELXL-97, Program for Crystal Structure Refinement*, University of Göttingen, **1997**; http://shelx.uni-ac.gwdg.de/shelx/index.html.

[22] *International Tables for X-ray Crystallography*, vol. 4, Kynoch Press, Birmingham, U.K., **1974**.

[23] L. Zsolnai, G. Huttner, *XPMA, http://www.rzuser.uni-heidelberg.de/~v54/xpm.html*, Universität Heidelberg, **1994**.

[24] G. Binsch, H. Kessler, *Angew. Chem*. **1980**, *92*, 445–463; *Angew. Chem. Int. Ed. Engl.* **1980**, *92*, 440.

Received August 12, 1999
[I99300]

On the Spectral Similarities between 1,2,6,7-Tetracyano-3,5-dihydro-3,5-diiminopyrrolizinato Complexes and Phthalocyanines – X-ray Crystal and Molecular Structure of Two Mixed Monopyrrolizinato Nickel(II) Complexes with the 2,4-*tert*-Butylacetylacetonide Ligand

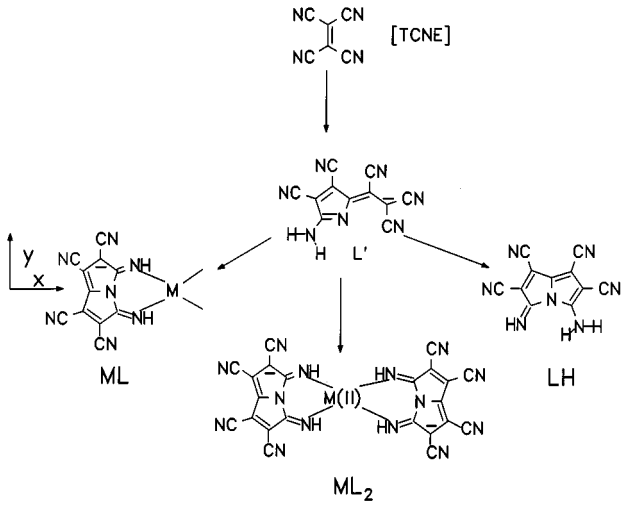
Alberto Flamini,*[a] Vincenzo Fares,*[a] and Augusto Pifferi[b]

Keywords: Pyrrolizinato complexes / Tetracyanoethylene / Phthalocyanines

Complexes of Ni^{II}, Cu^{II}, Zn^{II}, and Co^{III} containing the 1,2,6,7-tetracyano-3,5-dihydro-3,5-diiminopyrrolizinide (L) and the 2,4-*tert*-butylacetylacetonide (DPM) ligands have been synthesized and characterized. The absorption optical spectra of these species and of the corresponding ML_2 complexes in coordinating solvents are compared with those of metal-phthalocyanines (MPc) and hydrogen-phthalocyanine (H_2Pc), respectively. The comparison shows a close similarity, especially for the nickel-containing species, in the low-energy spectral region where the first $\pi\rightarrow\pi^*$ transitions occur (Q band). The Q band position of the pyrrolizinato complexes is much more dependant on the metal than is the case for MPc. For the same metal, the Q band position is also dependant on the M–N bond lengths in the molecular plane. For M = Ni, a reduction of this distance causes a red-shift of the Q band and a decrease of its maximum intensity. These conclusions are based on the X-ray molecular structure of the solvent-free NiL(DPM) complex and its pyridine solvate NiL(DPM)$(Pyr)_2 \cdot 2$ Pyr and on their solvatochromism. A symmetry-based correlation diagram between the frontier orbitals of the pyrrolizinato-complexes and the phthalocyanines is proposed.

Introduction

During the last ten years, we have been investigating the metal(II) complexes of the ligand (L) 1,2,6,7-tetracyano-3,5-dihydro-3,5-diiminopyrrolizinide, a derivative of tetracyanoethylene (TCNE) (Scheme 1). Our attention was mainly concentrated on the structurally characterized bis-pyrrolizinates ML_2 (ML_2 = Fe,[1] Co,[1] Ni,[2] Cu,[3] Zn,[4] and Pd[5]). An important feature of these species is the surprisingly strict similarity of their optical spectra (due to the $\pi\rightarrow\pi^*$ transitions), especially in the low-energy region (Q band), with those of metal-phthalocyanines (-tetraazatetrabenzoporphyrins, MPc). This allows ML_2 complexes to be used as spectroscopic models, potentially for better understanding the electronic structure of porphyrinic systems. This is in spite of the deep structural dissimilarities and differences in the number of π-orbitals and π-electrons between the two systems. Recently, the optical spectrum of FeL_2 was assigned in D_{2h} symmetry by using polarized specular reflectance measurements on single crystals of its tetrahydrofuran (THF) adduct, $FeL_2 \cdot 4$ THF.[6] Well-resolved solid-state optical spectra, in close agreement with the solution spectra, were obtained. Interestingly, it was found that the Q band in this system originates from four different electronic transitions [$Q_{(x)}$, $Q'_{(y)}$, $R_{(x)}$, $R'_{(y)}$]. So, it was concluded by analogy that the same band in the MPc's (D_{4h}) should be composed of two electronic transitions [$Q_{(x,y)}$, $R_{(x,y)}$]. This conclusion is in contrast with the widely accepted and supposedly well-established assignment, based on Gouterman's model, where the Q band in MPc's is due to a single electronic transition plus a vibronic component.[7–9] We sometimes also isolated a few monopyrrolizinates (ML), specifically [Cl_2PdL^-][10] and CH_3HgL,[11] but because of the lack of suitable single crystals, we were not able to characterize them using X-ray analysis. However, the optical spectrum of these species are also close to those of the corresponding MPc, even closer than the analogous ML_2. On these grounds, we were interested in synthesizing and characterizing a series of homologous monopyrrolizinates, and to compare their optical spectra with those of the series ML_2 and MPc in order to define



Scheme 1. Relationships between tetracyanoethylene and its derivatives L′, ML, LH, ML_2

[a] Istituto di Chimica dei Materiali del CNR, Area della Ricerca di Roma,
P. O. Box 10, 00016 Monterotondo Stazione (Roma), Italy
[b] Istituto di Strutturistica Chimica del CNR, Area della Ricerca di Roma,
P. O. Box 10, 00016 Monterotondo Stazione (Roma), Italy

 © WILEY-VCH Verlag GmbH, D-69451 Weinheim, 2000 1434–1948/00/0303–0537 $ 17.50+.50/0

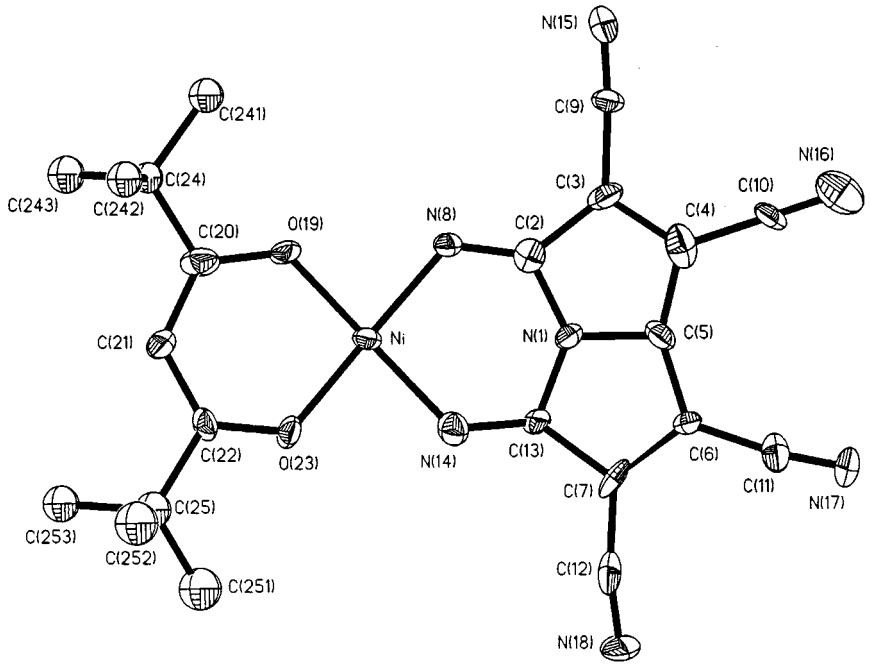


Figure 1. Molecular structure and labelling scheme of NiL(DPM). Thermal ellipsoids are at 30% of probability level

more precisely the significant spectral similarities within the ML series in comparison to the others and, at the same time, to provide further experimental data for an overall rationalization based on molecular orbital calculations. We then found that the acetylacetonide ligand (acac) may coexist with L in coordinating the same metal center for several metals (M = Co, Ni, Cu, Zn). More importantly, the 2,4-*tert*-butyl-derivative of acac (or dipivaloylmethanide, DPM) made it possible to isolate single crystals, suitable for the X-ray structure determination, of the complexes NiL(DPM) and the corresponding pyridine (Pyr) solvate NiL(DPM)$(Pyr)_2 \cdot 2$ Pyr. Furthermore, NiL(DPM) shows an exceptional solvatochromism in solution, varying the coordination properties of the solvent. The available structural data of these nickel complexes suggest that this phenomenon is due to a variation of the Q band in both energy and intensity, and is related to the variation of the Ni–N equatorial distances. We report here on all these findings.

Table 1. Selected bond lengths [Å] and angles [°] for compound **1**

Ni–N(8)	1.884 (8)	N(8)–Ni–N(14)	95.0(4)
Ni–N(14)	1.893 (9)	O(19)–Ni–O(23)	95.3(3)
Ni–O(19)	1.833 (7)	C(2)–N(1)–C(13)	132.2(7)
Ni–O(23)	1.848 (7)	N(1)–C(2)–N(8)	123.4(10)
N(1)–C(2)	1.376 (16)	Ni–N(8)–C(2)	122.1(7)
N(1)–C(5)	1.398 (8)	Ni–N(14)–C(13)	129.7(7)
N(1)–C(13)	1.382 (15)	N(1)–C(13)–N(14)	115.1(9)
C(2)–C(3)	1.468 (16)	Ni–O(19)–C(20)	127.5(7)
C(2)–N(8)	1.287 (13)	O(19)–C(20)–C(21)	121.5(11)
C(3)–C(4)	1.401 (16)	C(20)–C(21)–C(22)	126.0(9)
C(4)–C(5)	1.389 (18)	C(21)–C(22)–O(23)	123.9(10)
C(5)–C(6)	1.387 (16)	Ni–O(23)–C(22)	124.9(7)
C(6)–C(7)	1.396 (14)		
C(7)–C(13)	1.480 (14)		
N(14)–C(13)	1.290 (14)		
O(19)–C(20)	1.310 (15)		
C(20)–C(21)	1.378 (19)		
C(20)–C(24)	1.522 (18)		
C(21)–C(22)	1.376 (18)		
C(22)–O(23)	1.303 (13)		
C(22)–C(25)	1.517 (18)		

Results and Discussion

Synthesis and Structures of ML(DPM)

The monopyrrolizinates are readily formed from the reaction between LH and the bisacetylacetonates. This is not the case when using ML_2 as the pyrrolizinido source for the same reaction. Nevertheless, they are fairly stable towards the ligand metathesis, so that they could all be purified by recrystallization from hot saturated solutions. In any case, the pyrrolizinide moiety is planar and, with respect to DPM, either coplanar as in the Ni^{II} complexes (see later) or rotated by 90° as in ZnL(DPM) · 3 NAPH.[12] The complex CoL(DPM), if it exists, was not isolated. The reaction between LH and $Co(DPM)_2$, even under a rigorously controlled inert atmosphere, always gives a mixture of Co^{II} and Co^{III} complexes, characterized by a visible spectrum with two intense absorption maxima at 636 and 714 nm, respectively. Therefore, only the Co^{III} complex can be isolated as a pure species from the above reaction, provided that this is carried out under the appropriate conditions. A mild oxidizing agent (air) in a poorly Co^{II}-coordinating solvent (acetonitrile) was enough to achieve this. The complex $CoL(DPM)_2$ was therefore synthesized, and it could be recrystallized as a solvent-free species from hot toluene in air without decomposition.

X-ray Structure of the Solvent-Free NiL(DPM)

The molecular structure is shown in Figure 1. Selected bond lengths and angles are reported in Table 1. The nickel

atom is four-coordinate as NiN_2O_2 in a slightly distorted square-planar geometry with two imino-groups from the pyrrolizinido ligand (L) and two oxygen atoms from DPM. The Ni–N and Ni–O mean distances, of 1.889(8) and 1.840(9) Å respectively, are very close to the corresponding ones in the parent bis-chelate square-planar complexes NiL_2[13] and $Ni(DPM)_2$.[14] Also, the geometrical parameters within the two ligands L and DPM are similar to those of the above mentioned bis-chelates. This is different for the bis-pyrrolizinato NiL_2 complexes, in which two donor solvent molecules, doubly hydrogen-bonded to the chelating imino groups in the equatorial plane, are always present,[2,13] and no "equatorial adduct" is formed.

The NiL(DPM) molecule is essentially planar, the best plane being orthogonal to the (010) plane and is almost coincident with the crystallographic (–103) plane. The major molecular axis **x**, defined as the line passing through N(1), Ni, and C(21) atoms, makes angles of 35 and 62° with the *a* and *c* axes respectively, while the minor molecular axis **y**, normal to **x** through Ni in the plane, is parallel to *b*. The crystal structure of NiL(DPM) consists therefore of parallel, iso-oriented, solvent-free complex units, with only weak intermolecular interactions: symmetry-related molecular units weakly interact via –CN···HN– hydrogen bonds (N···H distances in the range 2.18–2.32 Å) developing along the *y* crystallographic direction.

X-ray Structure of NiL(DPM)(Pyr)$_2$ · 2 Pyr

The molecular structure is shown in Figure 2' and is strictly related to **1** decribed above. The nickel atom is in a distorted octahedral geometry NiN_4O_2, with two pyridine molecules axially coordinated at a distance Ni–N_{ax} of 2.117(9) Å (av.), whose planes are rotated 90° with respect to each other, bisecting the N(8)–Ni–N(14) and N(8)–Ni–O(19) angles, respectively. The Ni–N and Ni–O equatorial distances, of 2.084(12) and 2.004(11) Å respectively, are similar to those found in analogous octahedral nickel(II) complexes,[2,15] and longer by ca. 0.19 and 0.16 Å respectively than the corresponding values in the square-planar NiL(DPM). Also, the geometrical parameters of the two ligands L and DPM, although affected by high e.s.d.'s because of the presence of two interstitial solvent pyridine molecules in the asymmetric unit (each one disordered at two slightly different positions), are very similar to those found in **1** (see Table 2). As regards the crystal packing, it is noteworthy that the Ni–N_{ax} vector, the major molecular axis **x**, and the minor molecular axis **y** are parallel to *b*, *a*, and *c* respectively. Therefore, parallel iso-oriented molecular units are therefore also found, with weak intermolecular hydrogen-bonds (–CN···HN– in the range 2.56–2.64 Å) forming a monodimensional network along the *z* direction.

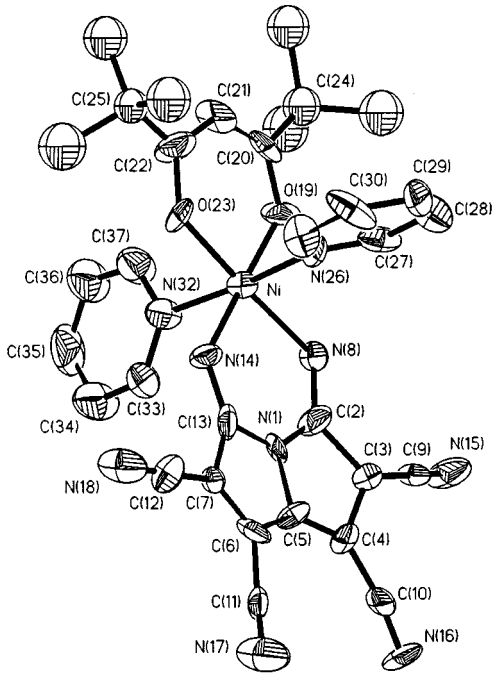


Figure 2. A perspective view of the complex NiL(DPM)(Pyr)$_2$ · 2 Pyr with the numbering scheme. The two disordered pyridine solvent molecules are not shown. Thermal ellipsoids are at 30% probability level

Table 2. Selected bond lengths [Å] and angles [°] for compound **2**

Ni–N(8)	2.089 (11)	N(8)–Ni–N(14)	91.0(4)
Ni–N(14)	2.079 (12)	O(19)–Ni–O(23)	91.4(4)
Ni–O(19)	2.007 (10)	N(26)–Ni–N(32)	176.2(6)
Ni–O(23)	2.001 (9)	C(2)–N(1)–C(13)	134.4(10)
Ni–N(26)	2.114 (8)	N(1)–C(2)–N(8)	124.6(13)
Ni–N(32)	2.120 (7)	N(1)–C(13)–N(14)	120.2(12)
N(1)–C(2)	1.369 (22)	Ni–N(14)–C(13)	126.3(10)
N(1)–C(5)	1.374 (16)	Ni–O(19)–C(20)	122.9(9)
N(1)–C(13)	1.372 (21)	O(19)–C(20)–C(21)	126.5(13)
C(2)–C(3)	1.451 (19)	C(20)–C(21)–C(22)	128.9(12)
C(2)–N(8)	1.291 (16)	C(21)–C(22)–O(23)	120.3(13)
C(3)–C(4)	1.412 (18)	Ni–O(23)–C(22)	129.0(9)
C(4)–C(5)	1.400 (23)		
C(5)–C(6)	1.412 (24)		
C(6)–C(7)	1.392 (21)		
C(7)–C(13)	1.440 (20)		
C(13)–N(14)	1.299 (15)		
O(19)–C(20)	1.302 (18)		
C(20)–C(21)	1.396 (23)		
C(20)–C(24)	1.502 (20)		
C(21)–C(22)	1.386 (22)		
C(22)–O(23)	1.299 (18)		
C(22)–C(25)	1.520 (20)		

We may note that both complexes **1** and **2**, because of their crystallographic features, are good candidates for a spectroscopic investigation using polarized light on single crystals in order to have valuable information on the electronic structure of porphyrins in addition to the data already known from $FeL_2 \cdot 4$ THF.[6]

Optical Spectra of ML(DPM)

These spectra (Figure 3 and Table 3) are characterized by intense bands due to $\pi \rightarrow \pi^*$ electronic transitions localized on the planar system formed by the pyrrolizinido moiety and the adjacent chelate ring including the metal. The low-energy portion of these spectra from the window centered at 500 nm is very similar to that of the corresponding MPc's spectra, except for an enhanced band intensity in the latter. In particular, the Q band profile is amanzingly alike for the

Table 3. Optical spectra [maxima in Kk and (log ε); shoulders in parentheses] of ML(DPM) and ML_2 complexes

NiL(DPM) in CH_2Cl_2	NiL(DPM) in THF	$CoL(DPM)_2$ in THF	CuL(DPM) in THF	ZnL(DPM) in THF	NiL_2 in CH_3OH	CoL_2 in THF	CuL_2 in THF	ZnL_2 in THF
13.19 (4.06)	14.90 (4.65)	14.14 (4.39)	15.08 (4.56)	15.13 (4.63)	15.29 (4.91)	15.72 (4.70)	15.31 (4.65)	14.97 (4.83)
14.60 (3.78)	[15.36] (4.17)	15.58 (3.96)	16.39 (4.18)	[15.58] (4.32)	16.26 (4.74)	16.61 (4.54)	16.13 (4.63)	15.36 (4.70)
[16.08] (3.46)	16.34 (4.11)	[17.04] (3.49)	[17.79] (3.63)	16.47 (4.17)	[16.81] (4.49)	[17.18] (4.30)	[16.67] (4.36)	16.31 (4.56)
[20.62] (3.99)	[17.04] (3.65)			[17.04] (3.86)	17.64 (4.16)	17.95 (4.01)	[17.54] (4.00)	[16.81] (4.30)
	[17.73] (3.46)			[17.86] (3.56)	[18.28] (3.93)			[17.70] (3.99)
								[18.35] (3.78)
22.47 (4.00)	24.45 (3.94)	24.39 (4.03)	25.38 (4.09)	25.44 (3.96)	24.45 (4.37)	25.25 (4.16)	25.38 (4.33)	25.19 (4.29)
[24.69] (3.81)	[25.84] (3.79)	[25.64] (3.91)	[26.67] (3.98)	[26.67] (3.83)	[25.84] (4.19)	[26.67] (4.01)	[26.67] (4.16)	[26.52] (4.15)
[29.24] (3.68)		[29.41] (3.97)						[28.82] (3.92)
[32.05] (4.01)	[32.05] (4.20)	34.48 (4.37)	[31.75] (4.26)	[32.79] (4.21)	[33.33] (4.25)	[32.05] (3.81)	[34.25] (4.34)	[33.33] (4.31)
[35.46] (4.13)	32.68 (4.21)		32.68 (4.34)	33.78 (4.38)	36.36 (4.41)	[33.90] (4.08)	36.76 (4.48)	36.36 (4.42)
39.06 (4.45)			36.76 (4.24)	36.76 (4.17)		36.90 (4.20)		

nickel-containing species. It is to be noted, however, that the Q band maximum in the monopyrrolizinates shows a comparatively large dependence on the nature of the metal ion, varying by 47 nm from ZnL(DPM) to $CoL(DPM)_2$. In fact, for MPc's such a trend is almost negligible, being at most 9 nm. More interestingly, in the monopyrrolizinato series, the effect on the Q band can be examined by varying the M–N bond length in the molecular plane for the same M, as detailed in the following section.

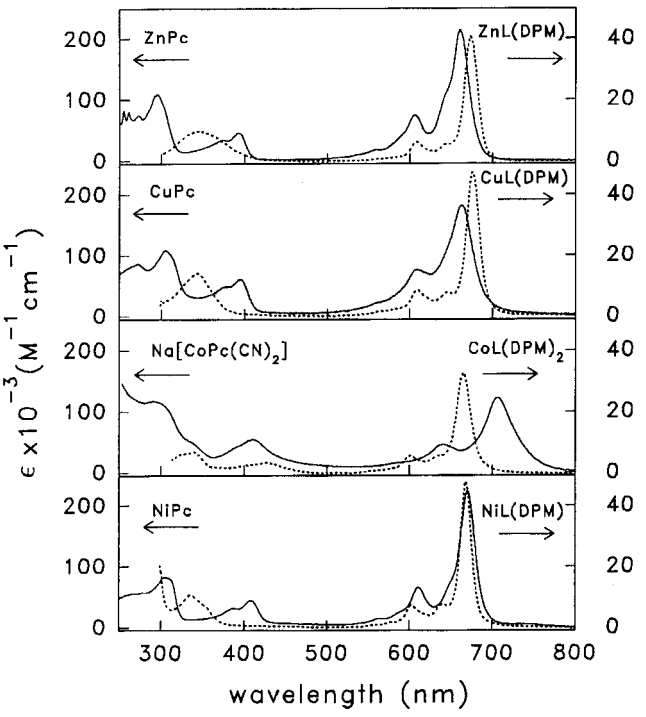


Figure 3. Solution optical spectra of the monopyrrolizinato metal complexes (—— in THF) and the corresponding metalphthalocyanines (- - - - NiPc and CuPc in 1,2,4-trichlorobenzene, Na-[$CoPc(CN)_2$] in acetone, ZnPc in dimethylacetamide)

Solvatochromism and Thermochromism of NiL(DPM)

NiL(DPM) shows an exceptional solvatochromism: its colour is pale-green in an uncoordinating solvent (CH_2Cl_2 or acetone) but becomes an intense blue in a coordinating solvent (THF) or on adding a coordinating species to the uncoordinating solvents, as for examples adding pyridine to CH_2Cl_2 or water to acetone. In Figure 4a, the pertinent spectral changes in question are reported for CH_2Cl_2/pyridine as a solvent system. These changes, being the same for the several solvent systems tested, can be interpreted as resulting from a perturbation of the frontier π orbitals of NiL(DPM) by axial coordination to the nickel atom. From the X-ray molecular structural parameters available, we can state that an elongation of the Ni–N bond in the molecular plane causes a sharpening, a blue shift, and an increase of the maximum intensity of the Q band. The change of the coordinating properties of the solvent also results in a different coordination geometry around the nickel ion, from square planar to octahedral, with an associated different optical metal d→d transition pattern.[16] However, such transitions are comparatively much weaker than the π→π* transitions, since their molar absorbitivities are in the range 1–100 $M^{-1}\cdot cm^{-1}$.[17] So, it can be concluded that the observed solvatochromism, which involves optical bands with molar absorbitivities in the range 10^4 $M^{-1}\cdot cm^{-1}$ (Table 3), originates from a conformational change of the π electron systems rather than by the difference in the metal coordination.

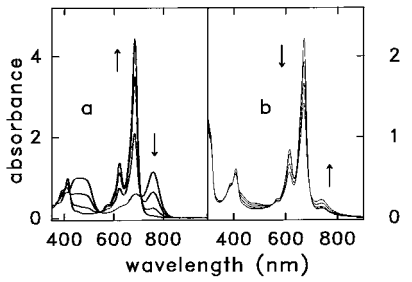


Figure 4. (**a**) Spectral changes of a dichloromethane solution of NiL(DPM) (3.0 mL, $C = 9.91\cdot10^{-5}$ M, pathlength = 1 cm) on adding increasing amounts (0.7, 1.7, 4.7 mL) of pyridine in CH_2Cl_2 (0.005 M). (**b**) Spectral changes of a THF solution of NiL(DPM) ($C = 6.03\cdot10^{-5}$ M, pathlength = 1 cm) on heating: 22, 40, 60, 75 °C. In both **a** and **b**, the arrows indicate the direction of the spectral changes

Moreover, NiL(DPM) in a coordinating solvent (e.g. THF) is thermochromic (Figure 4b). This phenomenon can be reasonably explained as solvatochromism. That is, by decreasing the temperature, the equilibrium in solution, NiL(DPM) · 2 THF $\rightleftarrows$ NiL(DPM) + 2 THF, shifts to the left. Therefore, the resulting spectral changes parallel those occurring on adding pyridine to NiL(DPM) in CH_2Cl_2.

For completeness, we ascertained that all other monopyrrolizinato complexes are neither solvatochromic nor thermochromic, including the isomorphous CuL(DPM). In this case, the reason for the absence of any solvatochromism, despite the well-known tendency of square-planar Cu^{II} complexes to increase the metal-coordination number, might be that the Cu–N_{eq} distances do not lengthen significantly, due to the large Jahn–Teller effect normally observed in these type of compounds,[3,18] on going from square-planar to tetragonally elongated hexa-coordination.

Optical Spectra of ML_2

We previously[1–4] reported the solution optical spectra of ML_2 complexes, but, for the reasons given below, most of these data actually referrred to ML species. Here, the correct spectra of the pertinent ML_2 species are presented for the first time (Figure 5 and Table 3). The resemblance of these spectra, particularly that of NiL_2, to the spectrum of H_2Pc is to be noted, within the limits already outlined in comparing ML(DPM) and MPc. This resemblance is now less surprising than in the previous interpretation, given that the two systems display the same symmetry (D_{2h}). We therefore conclude that the spectral changes occurring upon lowering the symmetry from D_{4h} to D_{2h} in tetraazatetrabenzoporphyrins are the same as those occurring when going from ML to ML_2, and that the resulting Q-band splitting is similar (0.8–1.0 Kk) in either case for M = Ni.

We now explain why the previously reported spectra of ML_2 were not interpreted correctly. Actually, the previous spectra were those of ML since they were recorded in solution with excess metal ion (M). Recently, we ascertained that an excess of free metal ion in solution in the presence of L' or ML_2 stabilizes the mono-pyrrolizinato species as a consequence of the reaction: ML_2 + M $\rightleftarrows$ 2 ML. The spectral changes associated with this reaction were recorded for M = Ni in methanol and methanol/THF as solvents. In both solvent systems, the initial and final spectra are the same, while the dynamics are different. The process is slower in methanol and can be easily followed at room temperature (Figure 6). From the presence of several isosbestic points it is clear that only one clean reaction occurs, and that the reaction product is the monopyrrolizinato-complex NiL, since the final spectrum is the same as that of NiL(DPM) (see Figure 3), except for the $\pi\rightarrow\pi^*$ electronic transitions (falling below 320 nm) localized on DPM in the latter.

Other noteworthy features of ML_2 spectra are, as in the ML(DPM) series, the dependence of the Q band maximum both on the metal ion (Table 3) and on the M–N bond length for constant M. Again, for M = Ni the consequent solvatochromism and thermochromism have been observed

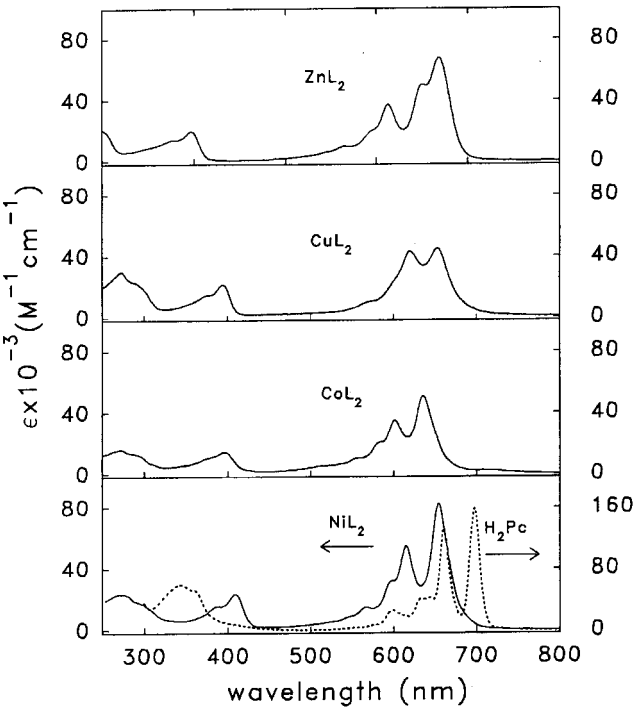


Figure 5. Solution optical spectra of bis-pyrrolizinato metal complexes (—— NiL_2 in CH_3OH, CoL_2, CuL_2, and ZnL_2 in THF) and of hydrogenphthalocyanine (- - - - in 1,2,4-trichlorobenzene)

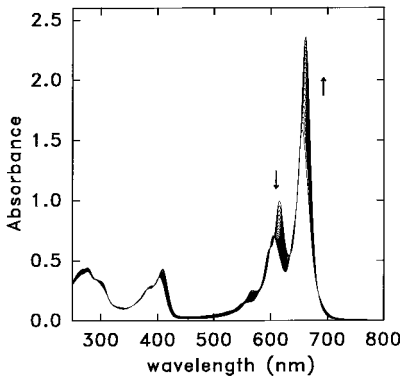


Figure 6. Spectral changes with time (every 5 min) undergone by a CH_3OH solution of NiL_2 (C = 1.96·10^{-4} M) after addition of 200 molar equivalents of $NiCl_2 \cdot 6\,H_2O$

in nitrobenzene/pyridine and ethyl acetate[19] as the solvent system, respectively.

Hypothesis on the Electronic Structure of ML Complexes

On the basis of the current solution spectral data, together with those from FeL_2, for which a close agreement between solution and solid state spectra was found, a correlation diagram of the frontier orbitals can be constructed for the MPc, H_2Pc, ML_2, and ML series, (Figure 7) and a reasonable hypothesis about the electronic structure of ML complexes can be put forward. This correlation diagram is presented in Figure 7. In ML_2 or H_2Pc (D_{2h}), four transitions give rise to the Q band. In MPc (D_{4h}) these transitions are reduced to two by symmetry.

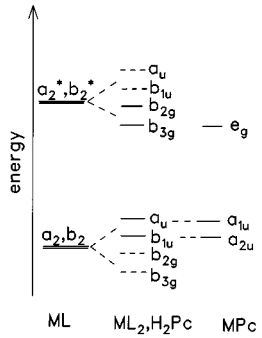


Figure 7. Qualitative scheme of the frontier orbitals for the systems ML, ML_2 or H_2Pc, and Mpc

Now, because of the similarity between ML and MPc, we must also suppose that the Q band is in ML is also composed of two electronic transitions involving MPc-like orbitals. In a C_{2v} molecule such as ML (Scheme 1), the π-molecular orbitals are of a_2 or b_2 symmetry and there is no forbidden π→π* transition, being $a_2 \rightarrow a_2$ or $b_2 \rightarrow b_2$ *x*-allowed and $a_2 \rightarrow b_2$ *y*-allowed. So, the frontier orbitals of ML could be two HOMO's (a_2, b_2) and two LUMO's (a_2^*, b_2^*), both nearly degenerate. The four excited electronic states, 2 A_1 and 2 B_1, originating from the transitions among these orbitals could be reduced to two after a configuration interaction: A_1 and B_1, consisting of the mixed configurations $a_2 \rightarrow a_2^*/b_2 \rightarrow b_2^*$ and $a_2 \rightarrow b_2^*/b_2 \rightarrow a_2^*$, respectively. Furthermore, this orbital pattern in ML is consistent with the frontier orbitals in ML_2. Here, the π-ligand orbitals can be considered as the symmetric and antisymmetric combinations of the corresponding orbitals of two ML weakly interacting fragments. As a matter of fact, the b_{3g} and a_u in D_{2h} are the symmetric and antisymmetric combination of a_2 in C_{2v}, while b_{1u} and b_{2g} are the corresponding combinations of b_2, respectively.

Conclusions

The optical spectra similarity between the pyrrolizinates and the phthalocyanines has been further studied: the spectra of ML_2 are similar to H_2Pc, and the increase of symmetry by switching from H_2Pc to MPc is spectrally equivalent to removing a pyrrolizinato moiety from ML_2. The origin of such similarity, in spite of the many differences between the two systems, still awaits an explanation and it will probably be accounted for only with appropriate molecular orbital calculations based mainly on the current experimental data. In the pyrrolizinates, the metal ion effect on the optical spectrum is much larger than in the phthalocyanines, so that the closest resemblance occurs for M = Ni and when Ni–N is relatively long (2.08 Å), in both ML and ML_2 series. The Ni-pyrrolizinates made it possible to see the effect on the electronic spectrum while varying the Ni–N bond length in the molecular plane. This effect is responsible for both the solvatochromism and the thermochromism in these species, while is not seen in the phthalocyanines because of the rigidity of the metal-coordinating hole size. Both title Ni–monopyrrolizinato species display a crystal structure suitable for spectroscopic investigation with polarized light, which is in progress. Therefore, additional experimental information on the electronic structure of these systems, valuable also for porphyrinic systems, will be available in the near future.

Experimental Section

Materials: Our procedures were followed for the synthesis of LH[20] and ML_2 (M = Co,[1] Ni,[2] Cu,[3] Zn[4]), while $M(DPM)_2$ (M = Co, Ni, Cu, Zn),[21] $Co(DPM)_3$[21] and $Na[CoPc(CN)_2]$[22] were prepared as described in the literature. Commercial H_2Pc, NiPc, CuPc, and ZnPc were purified by sublimation. Pyridine, CH_3CN, CH_3OH, THF, toluene, acetone, and CH_2Cl_2 were dried and freshly distilled before use. 1-Chloronaphthalene (NAPH) was used as received from Fluka.

General Procedures: Microanalyses were by Malissa and Reuter Analytische Laboratorien, Elbach, Germany, and by Servizio Microanalisi del CNR, Area della Ricerca di Roma. – Solution optical spectra were recorded on a Cary 5 and IR spectra on a Perkin–Elmer 16F PC FT spectrometer on Nujol mulls. – The magnetic measurements were carried out by using the Gouy method at room temperature. Molar susceptibilities were corrected for intrinsic diamagnetism estimated from Pascal's constants. – Suitable single crystals of ML for X-ray crystallography were grown in a sealed vial from a hot saturated solution of the sample in the appropriate solvent, followed by slow cooling, over several days, from the reflux temperature of the solvent down to room temperature (RT) in an ASCON M710 thermostatic oven.

Preparation of NiL(DPM): $Ni(DPM)_2$ (0.420 g, 0.985 mmol) was dissolved in methanol (60 mL) and LH (0.174 g, 0.746 mmol) added. After 1 h stirring a grey microcrystalline solid precipitated leaving a light-blue solution behind. After filtration, the solid was washed with methanol and dried in air. Yield 0.313 g (0.66 mmol, 88%). Diamagnetic: $\chi_M = -237 \cdot 10^{-6}$ e.m.u. – $C_{22}H_{21}N_7NiO_2$: calcd. C 55.73, H 4.46, N 20.68, Ni 12.38, O 6.75; found: C 56.77, H 4.30, N 21.10. Single crystals were obtained in a vial from a toluene/acetone (7:3) mixture, on cooling from 70 °C to room temp. over 15 d.

Crystal Growth of NiL(DPM)(Pyr)$_2$ · 2 Pyr: A suspension of NiL(DPM) (0.1 g) in a toluene/pyridine mixture (90:10, 30 mL) was heated under reflux, under N_2 for 30 min. The hot saturated solution was filtered and sealed in a vial under vacuum. On cooling the vial from 95 °C to room temp. over 20 h purple needle-like crystals of the NiL(DPM)–tetrapyridinate separated. This compound loses pyridine quite rapidly in air so that all the solid-state measurements on it were not reproducible, apart from the single crystal X-ray diffraction data, provided that the crystals were exposed to a saturated vapour of their mother liquor.

Preparation of CuL(DPM): $Cu(DPM)_2$ (1.930 g, 4.48 mmol) was dissolved in CH_3CN (80 mL) and LH (0.500 g, 2.15 mmol) added. An intense blue coloured solution was immediately formed. This solution was left 4 h at room temp. and then chilled down to –20 °C. A purple microcrystalline solid separated, which was filtered at low temperature and then dried in air. Yield 0.620 g, (1.29 mmol, 60%). Paramagnetic: $\mu_{eff} = 1.72\ \mu_B$. – $C_{22}H_{21}CuN_7O_2$: calcd. C 55.18, H 4.42, N 20.47, Cu 13.25, O 6.68; found: C 55.09, H 4.29,

N 21.51. Single crystals were obtained in a vial from a toluene/CH_3CN (7:3) mixture, on cooling from 90 °C to room temp. over 3 d and then leaving the sample at this temperature for another 10 d. This compound is isomorphous to the analogous NiL(DPM).[23]

Table 4. Crystallographic data for NiL(DPM) (**1**) and NiL(DPM)$(Pyr)_2 \cdot 2$ Pyr (**2**)

	1	**2**
Chemical formula	$C_{22}H_{21}N_7NiO_2$	$C_{42}H_{41}N_{11}NiO_2$
Molecular weight	474.2	790.6
Crystal size [mm]	1.0 × 0.1 × 0.01	0.3 × 0.3 × 0.3
X-ray source	HXD Elettra	Rotating anode
Data coll apparatus	Image Plate Area Det	Rigaku 4-circle Diffr
Data coll temp [K]	293	296
Crystal system	Monoclinic	Orthorhombic
Space group	$P2_1$ (No. 4)	$Pna2_1$ (No. 33)
Cell parameters [Å]	a = 5.901(3)	20.374(3)
	b = 18.275(9)	12.597(1)
	c = 10.288(4)	18.021(1)
	β = 96.81°	
V [Å^3]	1101.7(9)	4625.1(8)
Z	2	4
Density (calc.) [g cm^{-1}]	1.429	1.135
λ [Å]	0.75500	1.5418
Absorption coefficient [mm^{-1}]	0.915	0.958
No. collected data	9218	3444
No. unique reflections	2135	1948
R_{merge}[a]	0.075	0.070
No. observed reflections	1325[$F_o \geq 4\sigma(F_o)$]	1599 [$F_o \geq 6\sigma(F_o)$]
R indices[b]	R = 6.6%, R_w = 8.2%	R = 7.4%, R_w = 10.2%
GOF	1.09	1.04

[a] $R_{merge} = \Sigma_h \Sigma_i(\mid Ih,i - \langle Ih \mid \rangle)/\Sigma_h \Sigma_i Ih,i$ where Ih,i is the intensity value of the i^{th} measurement of h and $\langle Ih$ is the corresponding mean value of h for all i measurements of h. – [b] $R = \Sigma(\mid F_o - F_c \mid)/\Sigma|F_o|$. $R_w = [\Sigma_w(F_o - F_c)^2/\Sigma_w \mid F_o \mid ^2]^{1/2}$.

Preparation of ZnL(DPM) · 3 NAPH: $Zn(DPM)_2$ (1.119 g, 2.58 mmol) was dissolved in NAPH (40 mL). This solution was filtered and then LH (0.3 g, 1.29 mmol) added. After stirring the resulting suspension overnight under N_2, the microcrystalline solid in the reaction mixture changed colour from golden (LH) to purple. This solid was collected, washed with light petroleum and dried in air. It was then recrystallized from hot (120 °C) NAPH. The elemental analysis of this compound was not reproducibile, due to the partial loss of NAPH on drying it. Nevertheless, it was possible to ascertain its true composition by means of X-ray crystallography.[12]

Preparation of CoL(DPM)$_2$ $Co(DPM)_2$ (0.712 g, 1.67 mmol) was dissolved in CH_3CN (100 mL) and LH (0.400 g, 1.72 mmol) added. After stirring in air for 5 d at room temp., the resulting dark-green solution was evaporated to dryness. The residue was dissolved in boiling toluene. After filtration and cooling to room temp. the toluene solution afforded dark-green needle-like crystals. Yield 0.600 g (0.91 mmol, 55%). Diamagnetic: $\chi_M = -455 \cdot 10^{-6}$ e.m.u. – $C_{33}H_{40}CoN_7O_4$: calcd. C 60.27, H 6.13, N 14.91, Co 8.96, O 9.73; found: C 60.23, H 6.37, N 14.74, Co 9.02, O 9.95. Attempts to synthesize this compound from $Co(DPM)_3$ were unsuccessful due to the kinetic inertness of this species.

X-ray Crystallography of NiL(DPM) (1) and NiL(DPM)$(Pyr)_2 \cdot 2$ Pyr (2): Compound **1** crystallizes as dark-green needle-like platelets, stable in air, with one of the crystal dimensions being only some microns. In order to obtain a diffraction data set utilizable for an X-ray analysis, it was necessary to use high intensity synchrotron radiation. A well-formed crystal of dimensions 1.0 × 0.1 × 0.01 mm, fixed on a glass fiber, was therefore mounted on the Hard X-Ray Diffraction (HRD) beam-line of ELETTRA (Trieste).[24] Intensity data were collected by using a 16 keV radiation (λ = 0.775 Å) and a 180 mm MAR Image Plate Area Detector, and processed by DENZO[25] and CCP4[26] programs. Unit cell dimensions were determined by mounting the crystal on the Huber four-circle automated diffractometer of the same beam-line and refined from the setting angles of 15 selected high-angle reflections.

The crystals of **2** are unstable in air, leading to the loss of crystallization solvent: a selected crystal was therefore fixed inside a Lindemann capillary in the presence of the mother liquor. Data were collected on a rotating anode AFC5R Rigaku automated diffractometer (Cu-K_α radiation) with a graphite monochromator and corrected for absorption (psi-scan method), Lorentz and polarization effects. Cell constants were refined from setting angles of 22 reflections in the 2θ range 40–80°.

Both structures were solved by direct methods by using the SIR97 programs[27] and refined by full-matrix least-squares methods (248 and 405 variables segmented into two and four blocks for **1** and **2** respectively) by using the SHELXTL programs.[28]

Details of data collection and refinements are given in Table 42. Hydrogen atoms were included using a riding model.

Additional structural diagrams and tables listing atomic coordinates, bond lengths, bond angles, and anisotropic thermal parameters have been deposited with the Cambridge Crystallographic Data Centre under the numbers CCDC-130259 (**1**) and CCDC-130260 (**2**).Copies may be obtained without charge from: CCDC, 12 Union Road, Cambridge CB2 1EZ, UK [fax: +44-1223/336033, E-mail: deposit@ccdc.cam.ac.uk, www: http//www.ccdc.cam.ac.uk].

Acknowledgments

Dr. G. Pochetti for his help in the Image Plate data reduction process, Mr. M. Catricalà and Mr. C. Veroli for technical assistance.

[1] M. Bonamico, V. Fares, A. Flamini, N. Poli, *J. Chem. Soc., Dalton Trans.* **1992**, 3273–3280.
[2] M. Bonamico, V. Fares, A. Flamini, N. Poli, *Inorg. Chem*. **1991**, *30*, 3081–3087.
[3] M. Bonamico, V. Fares, A. Flamini, N. Poli, G. Mattei, *Polyhedron* **1993**, *12*, 1209–1214.
[4] V. Fares, A. Flamini, J. R. Jasin, R. L. Musselman, N. Poli, *J. Chem. Soc., Dalton Trans.* **1995**, 281–286.
[5] M. Bonamico, V. Fares, A. Flamini, N. Poli, *J. Chem. Soc., Dalton Trans.* **1993**, 2073–2074.
[6] C. B. Hoffman, V. Fares, A. Flamini, R. L. Musselman, *Inorg. Chem*. **1999**, *38*, 5742–5748.
[7] M. Gouterman, *J. Mol. Spectrosc*. **1961**, *6*, 138–163.
[8] M. Gouterman, in: *The Porphyrins* (Ed.: D. Dolphin), Academic Press, New York, **1978**, 1–166.
[9] M. Y. R. Wang, B. M. Hoffman, *J. Am. Chem. Soc*. **1984**, *106*, 4235−4240.
[10] A. Flamini, N. Poli, *Polyhedron* **1996**, *15*, 513–518.
[11] A. Flamini, G. Righini, L. Mannina, *Polyhedron* **1999**, *18*, 799–806.
[12] ZnL(DPM) · 3 NAPH crystallizes as dark violet prisms unstable in air. Diffraction data were collected on a selected crystal fixed in a capillary in the presence of mother liquor. Crystal data: monoclinic, $P2_1/c$, a = 10.737(4), b = 26.754(6), c = 17.840(5) Å, β = 102.16(4)°, V = 5009(2) Å^3, Z = 4, D (calc.) = 1.287 g·cm^{-3}. Although the presence of three inde-

pendent highly disordered NAPH molecules did not allow for obtaining accurate structural data, the X-ray analysis showed the Zn complex unit with the metal atom tetrahedrally coordinated to two nitrogen atoms from an L ligand and two oxygen atoms from a DPM ligand at Zn–N and Zn–O mean distances of 1.98 and 1.96 Å, respectively.

[13] M. Bonamico, V. Fares, A. Flamini, N. Poli, Y. Yamashita, K. Imaeda, *J. Chem. Soc., Dalton Trans.* **1993**, 3463–3470.
[14] F. A. Cotton, J. J. Wise, *Inorg. Chem*. **1966**, *5*, 1200–1207.
[15] L. Sacconi, F. Mani, A. Bencini, in: *Comprehensive Coordination Chemistry*, Pergamon Press, **1987**, *5*, 143.
[16] F. A. Cotton, G. Wilkinson, *Advanced Inorganic Chemistry*, 5th ed., Wiley, New York, **1988**, 744–752.
[17] E. Iwamoto, T. Kamamaru, Y. Sumitomo, Y. Suzuki, J. Nishimoto, *J. Chem. Soc., Faraday Trans.* **1995**, *91*, 627–630.
[18] M. Bonamico, V. Fares, A. Flamini, P. Imperatori, N. Poli, *Angew. Chem. Int. Ed. Engl*. **1989**, *28*, 1049–1050.
[19] A. Flamini, N. Poli, *Sensors and Materials*, **1995**, 7, 99–103.
[20] V. Fares, A. Flamini, N. Poli, *J. Am. Chem. Soc.* **1995**, *117*, 11580−11581.
[21] G. S. Hammond, D. C. Nonhebel, C. S. Wu, *Inorg. Chem*. **1963**, *2*, 73−76.
[22] J. Metz, M. Hanack, *J. Am. Chem. Soc*. **1983**, *105*, 828–830.
[23] Crystal data for CuL(DPM); monoclinic, $P2_1$, a = 5.878(1), b = 18.356(9), c = 10.307(5) Å, β = 95.45(3)°, V = 1107(1) Å^3.
[24] S. Bernstorff, E. Busetto, C. Gramaccioni, A. Lausi, L. Olivi, F. Zanini, A. Savoia, M. Colapietro, G. Portalone, M. Camalli, A. Pifferi, R. Spagna, L. Barba, A. Cassetta, *Rev. Sci. Instrum.* **1995**, *66*, 1661.
[25] Z. Otwinowski, W. Minor, in: *Methods in Enzymology* (Eds.: C. W. Carter Jr., R. M. Sweet, Academic Press, San Diego, CA, **1996**, vol. 276.
[26] Collaborative Computational Project, Number 4, *Acta Cryst.* **1994**, *D50*, 760–763.
[27] A. Altomare, M. C. Burla, C. Camalli, G. Cascarano, C. Giacovazzo, A. Guagliardi, A. G. G. Moliterni, G. Polidori, R. Spagna, *J. Appl. Cryst.* **1998**, in press.
[28] G. M. Sheldrick, *SHELXTL*; Siemens: Madison, WI, **1996**, vol 5.

Received August 9, 1999
[I99302]

Quantitative 2D EXSY and Dynamic ^{19}F-NMR Studies of the Dynamic Behaviour of the Bidentate Chelate Complex Ga(fox)$_3$ (fox = 5-fluoro-8-hydroxyquinoline)

Marina Gromova,[a] Olivier Jarjayes,[a] Sylvain Hamman,[a] Robert Nardin,[b] Claude Béguin,*[b] and Rudolph Willem[c]

Keywords: Coordination chemistry / Gallium(III) / Dynamik ^{19}F NMR / EXSY / Kinetics of ligand exchange / Bailar and Rây–Dutt mechanisms

The rates of intramolecular rearrangement of the *meridional* isomer of the metal *tris*-chelate complex [Ga(fox)$_3$, fox = 5-fluoro-8-hydroxyquinoline] in DMF solution were measured using 1D NMR line shape analysis and 2D EXSY spectra. The rates of exchange k_{ab}, k_{bc} and k_{ac} between the three non-equivalent ligands **a**, **b** and **c** were determined. The values of the activation parameters were obtained. ΔH^{+} was 70.6 kJ mol^{-1} for all the rate constants. ΔS^{+} was different in each of the three cases: ΔS^{+}_{ab}, ΔS^{+}_{bc} and ΔS^{+}_{ac} were 27.7, 28.5 and 34.6 J K^{-1} mol^{-1} respectively. The interpretation of these data was related to the discrimination of different twist processes (Bailar and Rây–Dutt) for intramolecular rearrangement of the *tris*-chelate complex.

Introduction

The elucidation of the mechanisms of intramolecular rearrangements of metal chelate complexes, especially those involving metal *tris*-chelate complexes, has been studied in depth but remains a problem of continuous significance in coordination chemistry.[1] *Tris*-chelate complexes with three identical unsymmetrical bidentate ligands can exist as two *facial* (*fac*) and *meridional* (*mer*) stereoisomers, each of which exists as enantiomers Δ and Λ. Changes in stereoisomers can be observed such as inversion or racemisation ($\Delta \rightleftarrows \Lambda$) and isomerisation (*fac* $\rightleftarrows$ *mer*). In the literature, two categories of intramolecular mechanism have been proposed, namely those involving temporary rupture of a metal-ligand bond and those that involve ligand twisting without any bond rupture. Among the different bond rupture mechanisms, Holm et al. showed that the most probable mechanism was the one with a square-pyramidal axial transition state.[2] For those processes with concerted non-bond-breaking geometrical changes, symmetry selection rules lead to the identification of four possible mechanisms named push-through, cross-over, Bailar (transition state with D_{3h} group of symmetry for symmetrical bidentate ligands) and Rây–Dutt (transition state with C_{2v} group of symmetry for symmetrical bidentate ligands).[3–7]

Several examples in the literature show that NMR spectroscopy is well adapted for kinetic measurements of such molecular rearrangements in complexes of appropriate metal cations:[1] chromium(III) complexes with the unsymmetrical bidentate (*S*)-tryptophan (^{1}H NMR),[7] ruthenium hydrides with triphenylphosphanes as other ligands (^{31}P NMR)[8] and several *tris*(unsymmetrical bidentate ligand)-metal(III) complexes of group 13 metals such as *tris*(trifluoroacetylacetonato)-Ga(III) complexes (^{19}F NMR),[9] *tris*-(substituted-tropolonato)metal(III) complexes (^{1}H NMR),[10] *tris*[2-(2'-hydroxyphenyl)-2-oxazolino]metal(III) complexes (^{1}H and ^{27}Al NMR),[11] *tris*(2-thienoyltrifluoroacetonato)metal(III) complexes (^{1}H and ^{19}F NMR),[12] *tris*(substituted-catecholato)metal(III) complexes (^{1}H NMR).[13]

Previously, we studied a new tripodal iron chelator, *O*-Trensox, based on 8-hydroxyquinoline.[14] Subsequently, we studied, as a model, the coordination chemistry of Ga(III) [the diamagnetic analogue of Fe(III)] with a fluorine-labelled sub-unit, the 5-fluoro-8-hydroxy-quinoline (fox).[15] The presence of only one fluorine atom per ligand leads to simplified ^{19}F-NMR studies. Recently, for the Ga(fox)$_3$ species, we were able to observe the minor *facial* isomer with its C_3 axis of symmetry and the more abundant *meridi-*

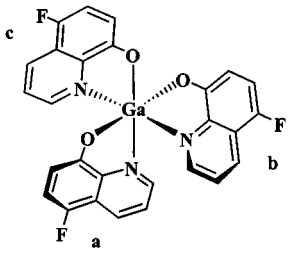


Figure 1. Structure and assignment of the sites for Ga(fox)$_3$ (fox = 5-fluoro-8-hydroxyquinoline)

[a] Laboratoire d'Etudes Dynamiques et Structurales de la Sélectivité, UMR CNRS 5616, Université Joseph Fourier, BP 53, F-38041 Cedex 9, Grenoble, France
Fax: (internat.) + 33-4/76 51 43 82
E-mail: Claude.Beguin@ujf-grenoble.fr
[b] Centre Grenoblois de Résonance Magnétique, CEA-Grenoble/CNRS/Université J. Fourier 17 rue des Martyrs, F-38054 Grenoble, France
[c] HNMR Centre, Organic Chemistry, Free University of Brussels, Plainlaan 2, B-1050 Brussels, Belgium
Fax: (internat.) + 32-2/629-3281
E-mail: rwillem@vub.ac.be

 © WILEY-VCH Verlag GmbH, D-69451 Weinheim, 2000 1434–1948/00/0303–0545 $ 17.50+.50/0

onal isomer with no elements of symmetry. In this case, the three ligands are chemically nonequivalent.[16] In addition, we were able to assign the three corresponding ^{19}F-NMR signals (using low temperature NOE experiments) as shown in Figure 1: **a** (the signal at higher frequency) assigned to the ligand perpendicular to the NGaN octahedral axis (or *antiperiplanar* to two oxygen atoms), **b** the signal at intermediate frequency, assigned to the ligand perpendicular to the OGaN axis, the first priority axis using Sloan's notation (or *antiperiplanar* to oxygen and nitrogen atoms), and **c** (the signal at lower frequency) assigned to the ligand perpendicular to the OGaO axis (second priority axis) (or *antiperiplanar* to two nitrogen atoms).[16,17]

The aim of this paper is to describe, very precisely, the stereochemical non-rigidity of the Ga(fox)$_3$ complex from the kinetic point of view and to analyse the nature of the intramolecular rearrangement mechanisms in dimethylformamide (DMF) solutions.

Results

The ^{19}F-NMR chemical shift values in ppm at low temperature (255 K, ^{1}H decoupled signals) in DMF for each fluorine of the ligands **a**, **b**, **c** in the *mer* complex were: $\delta_a = 22.80_5$, $\delta_b = 22.51_3$, $\delta_c = 21.83_8$. The corresponding chemical shift for the *fac* isomer was: $\delta = 22.28_9$.

1D Measurements versus Temperature

The line shapes of the ^{19}F Ga(fox)$_3$ signals at several temperatures are shown in Figure 2A. The exchange rates were determined by complete line shape analysis for a three-sites system (**a**, **b** and **c**). Calculated spectra are shown in Figure 2B.

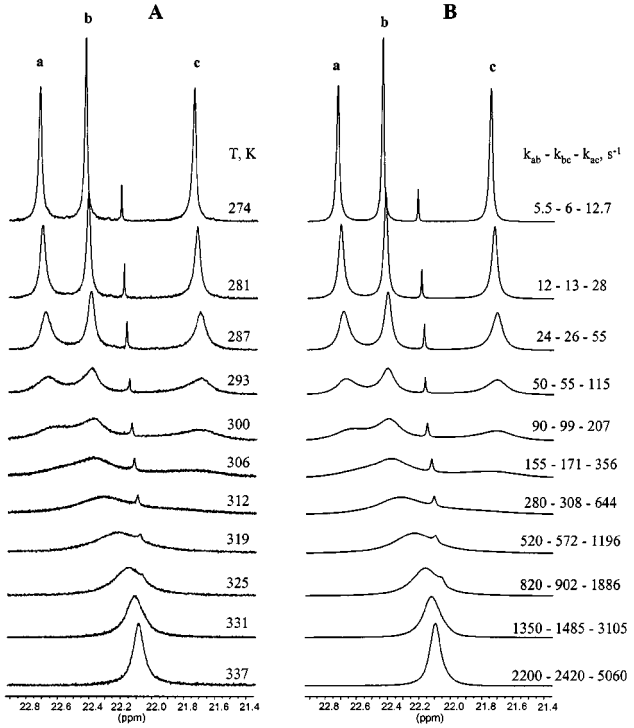


Figure 2. Variable temperature ^{19}F NMR spectra of Ga(fox)$_3$ in DMF (using ^{1}H decoupling): A – experimental, B – computer-simulated

A major problem for the refinement between experimental and calculated spectra is that the static NMR parameters were temperature dependent (chemical shifts and linewidths). Since the three populations for the different sites of exchange were equal and since all the coupling constants are suppressed, the temperature has no influence on these parameters. We also observed that the *fac* isomer intensity (5%) did not change in the explored temperature range.

(i) The temperature dependence of δ was not similar for the three signals **a**, **b** and **c**. We have recorded a set of spectra in a temperature range where the exchange effects were negligible. Assuming a linear variation of δ versus T we extrapolated the δ values at higher temperatures.

(ii) The linewidth was also an important parameter to determine in order to obtain accurate rate constants from the simulated spectra. The low temperature spectra allowed the determination of the relationship between the Ga(fox)$_3$ and C_6F_6 signals linewidth (lw). This ratio lw(*Ga(fox)$_3$*)/lw(*C_6F_6*) was approximately 1.6 in DMF. So, we evaluated the natural Ga(fox)$_3$ line from the C_6F_6 linewidth measured for each temperature, assuming that this pertinent ratio was constant for all the temperature range. We were comforted by the observation that the ratio between the width of the free ligand (fox) line and that of the C_6F_6 line was constant over the temperature range.

The exchange rates between the three ligands of the Ga(fox)$_3$ complex were determined by complete lineshape analysis for the 3-sites system through the " WIN-DYNAMICS " software (see Experimental Section). We differentiated three different exchange rates: k_{ab}, k_{bc} and k_{ac} corresponding to the **a** ⇄ **b**, **b** ⇄ **c** and **a**<->**c** ligand exchange respectively. The kinetics of exchange involving the *fac* isomer only occurred for temperatures higher than 319 K, so, its contribution in the main range was negligible. All the values are reported for the 262–350 K temperature range, along with their standard errors on the fit, in Table 1.

2D Measurements versus Temperature

2D EXSY experiments with appropriate mixing times were carried out. Figure 3 shows a contour plot of the spectra obtained in DMF at 273 K with $\tau_m = 30$ ms as a mixing time. From the volume of the cross-peaks, according to the methodology developed in the Experimental Section, we obtained a new set of reaction rates for three temperatures (249, 255 and 268 K). These values, with standard deviation higher than with 1D measurements, are also reported in Table 1. The aim of these experiments was to extend towards the low temperature range and to show clearly that the exchange rate k_{ac} was larger than the other rates, thus demonstrating the greater efficiency of the transfer of magnetization between **a** and **c**.

Table 1. Values of rate constants (s^{-1}) for exchange derived from 1D (lineshape analysis) and 2D EXSY ^{19}F-NMR spectra as a function of temperature (K)

T, K	k_{ab}, s^{-1}	k_{bc}, s^{-1}	k_{ac}, s^{-1}
249	0.17 (± 0.04)[a]	0.19 (± 0.04)[a]	0.39 (± 0.08)[a]
255	0.5 (± 0.05)[a]	0.55 (± 0.06)[a]	1.15 (± 0.1)[a]
262	1.2 (± 0.1)	1.3 (± 0.1)	2.8 (± 0.2)
268	2.5 (± 0.1)	2.75 (± 0.1)	5.75 (± 0.2)
268	2.7 (± 0.3)[a]	3 (± 0.3)[a]	6.2 (± 0.6)[a]
274	5.5 (± 0.4)	6 (± 0.4)	12.7 (± 0.8)
281	12 (± 1)	13 (± 1)	28 (± 2)
287	24 (± 1)	26 (± 1)	55 (± 2)
293	50 (± 4)	55 (± 4)	115 (± 9)
300	90 (± 4)	99 (± 4)	207 (± 8)
306	155 (± 5)	171 (± 5.6)	356 (± 11)
312	280 (± 9)	308 (± 10)	644 (± 21)
319	520 (± 14)	572 (± 16)	1196 (± 33)
325	820 (± 19)	902 (± 21)	1886 (± 45)
331	1350 (± 90)	1485 (± 104)	3105 (± 217)
337	2200 (± 170)	2420 (± 180)	5060 (± 380)
344	3600 (± 280)	3960 (± 315)	8280 (± 660)
350	7200 (± 650)	7920 (± 710)	16560 (± 150)

[a] 2D results.

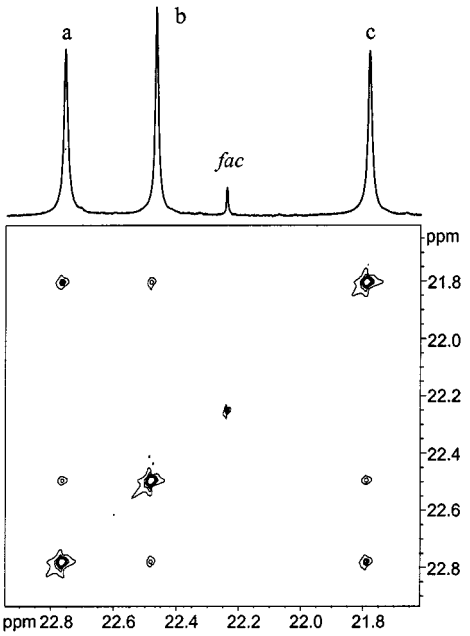


Figure 3. Contour plot of 2D EXSY ^{19}F NMR spectrum of $Ga(fox)_3$ in DMF obtained at 273 K with 30 ms as a mixing time

Rate Constants versus Temperature

For each temperature, the **a** ⇄ **b** exchange is the slowest, **b** ⇄ **c** is slightly faster and the **a** ⇄ **c** is the fastest (ratio of the rate constants k_{ab}, k_{bc} and k_{ac} were 1, 1.1 and 2.3 respectively).

The plots of $\log(kij/T)$ of these rate constants versus the reciprocal of temperature gave three straight lines (for the three lines, $r = 0.9997$) according to the Eyring formula (Figure 4):

$$\log(k/T) = \log(k_B/h) - \Delta H^{\#}/RT + \Delta S^{\#}/R$$

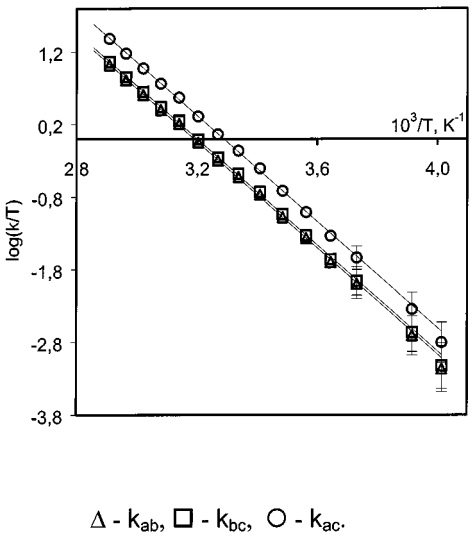


Figure 4. Eyring plot of $\log(k_{ij}/T)$ *versus* 1/T for ligand exchanges in $Ga(fox)_3$ in DMF

The activation parameters (enthalpy, entropy and free enthalpy at 293 K) are reported in Table 2.

Table 2. Activation parameters for the ligand exchanges for $Ga(fox)_3$ in DMF

Exchange	$\Delta H^{\#}$, kJ mol^{-1}	$\Delta S^{\#}$, J K^{-1} mol^{-1}	$\Delta G^{\#}$, kJ mol^{-1} (293 K)
a ⇄ b	70.6 ± 0.5	27.7 ± 2	62.3 ± 1.5
b ⇄ c	70.6 ± 0.5	28.5 ± 2	62.1 ± 1.5
a ⇄ c	70.6 ± 0.5	34.6 ± 2	60.2 ± 1.5

The slopes of the Eyring plot are, within the experimental errors, the same. The ratio ($k_{ac}/k_{ab} = 2.3$) between the fastest and the slowest rate constants can be described as an "extra" entropy effect of about 6.5 J mol^{-1} K^{-1}.

Discussion

The three main features of our kinetic results are:

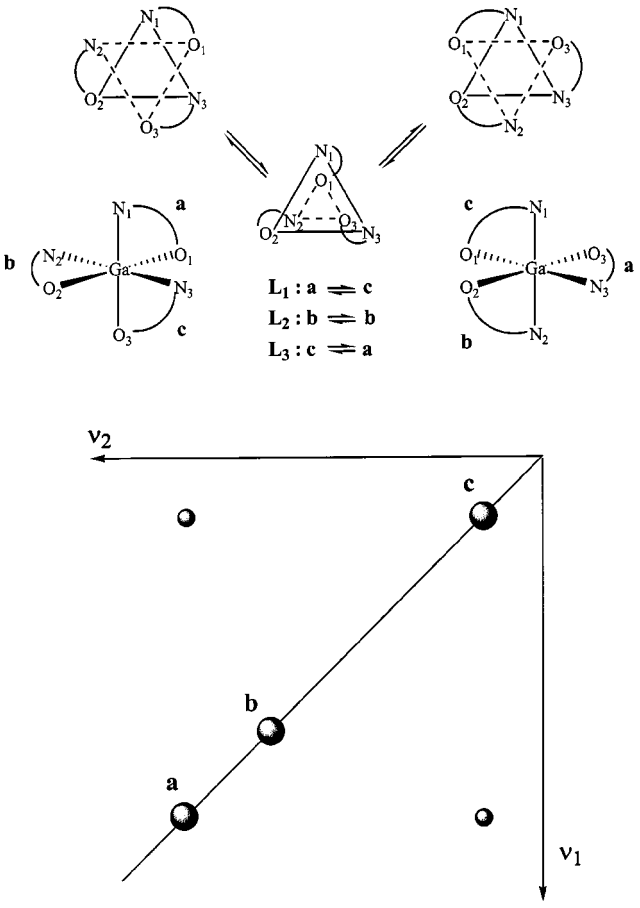
(i) For each temperature, the ratio of the exchange reaction rates between the three sites are 1:1.1:2.3 for $k_{ab}/k_{bc}/k_{ac}$ respectively. This effect is particularly clear as shown in Figure 3 where the cross-peak from the **a** and **c** signals was larger than the two others involving the ligand **b**.

(ii) The kinetics of exchange involving the *fac* isomer among the exchange between the three sites of the *meridional* isomers was negligible.

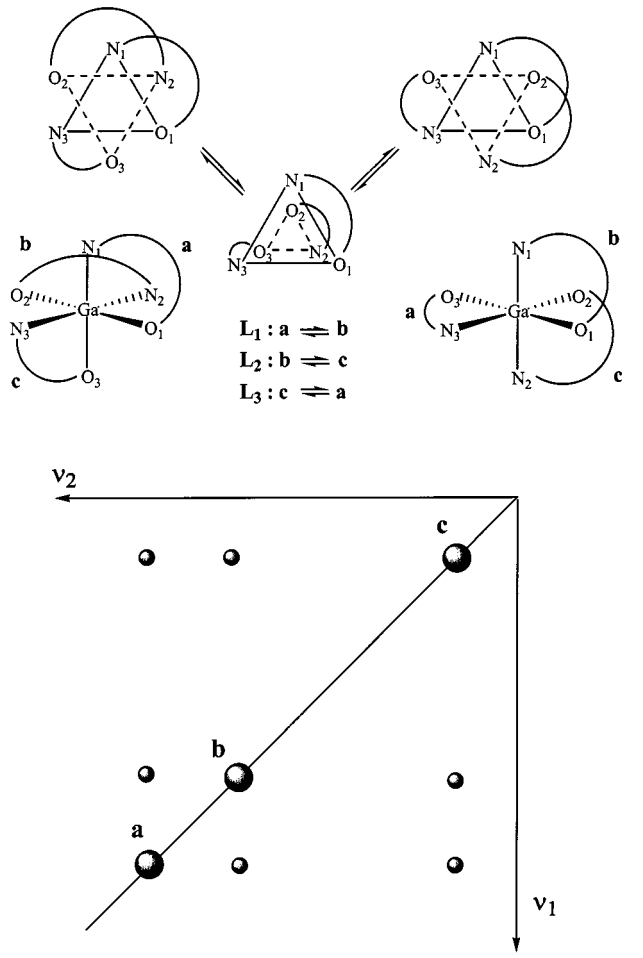
(iii) The enthalpies of activation are, within the experimental errors, the same (70.6 kJ mol^{-1}) and the value of k_{ac} in comparison of the k_{bc} and k_{ab} can be described as an "extra" entropy effect of about 6.5 J mol^{-1} K^{-1}.

The intramolecular rearrangement processes of the $Ga(fox)_3$ complex are described as an inversion without isomerisation. The inversion proceeds by two energetically favourable twist mechanisms that are easily discriminated through the structure of their transition state:[1]

(i) Bailar's transition state, which has a C_3 axis of symmetry (trigonal prismatic geometry, Scheme 1). There is only one such transition state, and



Scheme 1. Intramolecular rearrangement through a Bailar transition state and predicted cross-peak intensity in a 2D EXSY experiment



Scheme 2. Intramolecular rearrangement through a Rây–Dutt transition state and predicted cross-peak intensities in a 2D EXSY experiment

(ii) Rây–Dutt's transition state, which has no element of symmetry (the group of symmetry for the corresponding complex with a symmetrical bidentate ligand would be C_{2v} with the C_2 axis perpendicular to the ligand joining the two planes in Scheme 2). There are three such transition states depending on the nature of the ligand (1, 2 or 3) perpendicular to the plane of the drawing.

If the internal rearrangement only consisted of a Bailar-type mechanism then Scheme 1 shows that ligand 1 (with the heteroatoms N and O labelled as 1 in the starting structure), which has an environment **a** (from the electronic distribution in the neighbourhood and has a high frequency ^{19}F chemical shift named site **a**), is moving to give, in the final structure, the site **c**. From the same scheme, ligand 2 (site **b**) and ligand 3 (site **c**) move to sites **b** and **a** respectively. We can predict that the transfer of magnetization occurs only between **a** and **c** as shown in the bottom part of Scheme 1. If the internal rearrangement consisted only of a Rây–Dutt type mechanism, Scheme 2 shows that ligand 1 with the environment **a** (named site **a**) is moving to give, in the final structure, the site **b**. Similarly, from Scheme 2, sites **b** and **c** move to **c** and **a** sites respectively. We can predict that the transfer of magnetization occurs as a permutation between **a**, **b** and **c**. The same permutation occurs for the two other Rây–Dutt transition states. The prediction of the cross-peak intensities is shown in the lower part of Scheme 2. So, as we observe non-equal magnetization transfers between the three **a**, **b** and **c** signals, we suggest that two mechanisms for internal rearrangement occur: a Rây–Dutt mechanism giving equal magnetization transfers between the three signals (at the origin of the almost equal k_{ab} and k_{bc} reaction rates) and an almost equal contribution (1.3) by a Bailar mechanism, at the origin of the higher k_{ac} reaction rate value (~ 2.3 k_{ab}).

The activation parameters of the two mechanisms seem to be the same. The $\Delta H^{\neq}$ value was 70.6 kJmol^{-1}, which is of the same order of magnitude as values obtained in dipolar aprotic solvents and reported in the literature.[13] A positive moderate $\Delta S^{\neq}$ value (28.1 J K^{-1} mol^{-1}) for the two processes (Bailar and Rây–Dutt) implies more disorder in the transition states than in the initial states. The apparent increase of entropy of 6.5 J K^{-1} mol^{-1} is only due to the contribution of the two mechanisms ($2.2 = e^{6.5/8.32}$). The activation parameters for the two processes were almost the same as no predominance of one of the two mechanisms was evidenced at one of the edges of the temperature range.

This fact suggests that the bond modifications from the initial state to the transition state are almost the same around the C_3 axis for the Bailar twist or the *pseudo*-C_3 axis for the Rây–Dutt twists. The same types of interactions of the initial and transition states with the solvent are at the origin of the same activation entropy values. These facts also confirm that a bond-rupture mechanism with a pendant axial ligand did not occur, as the entropy of activation should not be the same for a mechanism with temporary rupture of a metal-ligand bond and those with twisting without any bond rupture.[4,12]

The relative importance of the Bailar mechanism can also be interpreted in relation with the metal-chelating heteroatom distances in the complex. We were unable to obtain sufficiently good crystals of $Ga(fox)_3$ for X-ray crystallography, but in the literature we have data for closely related complexes $Fe(ox)_3$ and $Ga(ox)_3$ (where ox is for 8-hydroxyquinoline or oxine).[18,19] Table 3 gives selected values of metal-oxygen, metal-nitrogen and oxygen-nitrogen bond lengths for these two complexes. We can see that the metal-nitrogen$_b$ bonds are the shortest in relation with the **b** site, which "sees" no change in the Bailar-type process. More precisely, as discussed in several papers,[4,7] the pertinent parameter for these studies is the bite size (also called the normalised bite), defined as the ratio of the distance between the donor atoms of the chelate ring divided by the metal-donor atom distance. When this value is less than 1.5, the Bailar twist is energetically preferred over a Rây–Dutt twist.[4,7] From literature data in Table 3, this bite value is included in 1.244 to 1.384 values for the gallium complex and 1.212 and 1.360 for the iron one. These values are calculated as: the higher ratio for gallium (1.384) was obtained as the ratio of the highest distance between the donor atoms (265.8 pm) divided by the smallest metal-donor atom distance (192.1 pm); the lowest ratio (1.244) was obtained as the ratio of the shortest distance between the donor atoms (263.3 pm) divided by the largest metal-donor atom distance (211.6 pm), and the same for the iron case. Arguments developed by Rodger and Johnson show that a Bailar twist was energetically preferred over a Rây–Dutt twist for bite values less than 1.5.[4] We suggest that both mechanisms are plausible because the bite values for our system are not too far from 1.5.

Table 3. Selected bond lengths (pm) for $M(ox)_3$ complexes [M = Ga(III) or Fe(III)] from the literature[18,19]

Bond	Distance (pm) for Ga[19]	Distance (pm) for Fe[18]
M–Oa	192.9	195.6
M–Ob	195.6	199.6
M–Oc	192.1	193.6
M–Na	211.6	216.6
M–Nb	206.7	212.5
M–Nc	209.1	217.2
Oa–Na	263.3	262.5
Ob–Nb	264.8	262.8
Oc–Nc	265.8	263.3

We were also able to undertake experiments on the same complex in methanol as a solvent instead of DMF. The data obtained were not as detailed, especially from evaluation of the experimental errors, as linewidths for the complex were not so easily related to those of C_6F_6 as they were in DMF. Nevertheless, we can make some comments on the data. Assignment of the fluorine signals is the same for site **c** but the reverse for sites **a** and **b**. The enthalpies of activation are almost the same ($\Delta H^{\neq} = 72.5$ kJ mol^{-1}) as in DMF, but the entropies of activation are much lower ($\Delta S^{\neq}$ about 22 J K^{-1} mol^{-1}) than for DMF as the reaction rates at the same temperatures were slower in methanol than in DMF. This smaller positive entropy value in methanol than in DMF can be related with closer interactions between the transition state and the highly ordered protic solvent methanol. More work has to be done using this solvent for more detailed analysis of the rate constants for exchange between the three sites.

Conclusion

To our knowledge, this work constitutes one of the first measurements of three different rates of exchange between the three sites **a**, **b** and **c** in this type of complex. We were able to discriminate, from the kinetic point of view, the different twist processes (Bailar and Rây–Dutt) for intramolecular rearrangement in *tris*-chelate complexes of metal cations such as Ga(III) in solution, using 1D NMR line shape analysis and 2D EXSY measurements.

Experimental Section

Preparation of $Ga(fox)_3$: To a solution of 5-fluoro-8-hydroxyquinoline (denoted fox) (0.05 g, 0.31 mmol) in methanol (10 mL) was added $Ga(NO_3).9\ H_2O$ (0.36 g, 0.088 mmol) in methanol/water (10:1), followed by slow addition of 3.3 equivalents of sodium hydroxide (1 M). The resulting mixture was stirred for 15 min and evaporated to dryness.

Apparatus: The 1D ^{19}F- and 2D phase-sensitive ^{19}F-EXSY-NMR spectra of $Ga(fox)_3$ in DMF were recorded at 376.42 MHz on a Bruker AM 400 spectrometer at various temperatures. The ^{19}F chemical shifts are expressed in ppm with respect to the C_6F_6 line used as the internal reference. The ^{19}F-NMR chemical shifts for ^1H decoupled signals at 255 K in DMF were: $\delta = 22.80_5$ (s, F_a), $\delta = 22.51_3$ (s, F_b), $\delta = 21.83_8$ (s, F_c), $\delta = 22.28_9$ (s, F_{fac}). The variable-temperature accessories were calibrated with methanol and ethylene glycol samples. The measurement was repeated three times for each point of calibration. The NMR tubes were left in the probe during at least 20 minutes in order to obtain an equilibrium and were not spinning.

1D ^{19}F-NMR Spectra: The temperature range variations were 224–368 K for DMF (with a variation of 6 K by step). The ^{19}F spectra of $Ga(fox)_3$ were acquired with ^1H decoupling in Waltz mode, using a spectral width of 11.6 kHz, 32 K memory size, 3.4 s total recycling delay and 256 scans. The series of spectra were realised at low temperatures (without chemical exchange effects) in order to study the chemical shift variations as a function of temperature. For the control of the magnetic field stability, an accurate measurement of the linewidth of the C_6F_6 signal was carried out for each temperature. We evaluated the $Ga(fox)_3$ linewidth from the measured C_6F_6

linewidth multiplied by the ratio lw($Ga(fox)_3$)/lw(C_6F_6) (approximately evaluated to be 1.6). The final spectra were obtained after Fourier transformation using "1D Win-NMR" software. The simulation of 1D NMR exchange spectra was performed using the Bruker "Win-Dynamics" software.[20] We treated the data with the model of three exchanging sites on only one non-coupled spin 1/2.

2D ^{19}F-EXSY Spectra: 2D ^{19}F-EXSY spectra were recorded in DMF at 258, 263 and 273 K using a conventional NOESY *90° – t1 – 90° – τ_m – 90° – acq* phase sensitive pulse sequence[21] with time-proportional phase incrementation (TPPI). The 90° pulse length was calibrated at low temperature. The following parameters were used: spectral width 1104 Hz, with a size of 512 × 1024 data points, 512 time incrementations, 56 scans, total recycling delay of 2.9 s. The used mixing times (τ_m) were 0.2, 0.4, 0.6, 0.8 and 1 s at 258 K; 40, 60, 80 ms at 263 K and 10, 20, 30, 40, 50 ms at 273 K. Each EXSY spectrum required approximately 20 h of accumulation. Both FID's were apodized by a shifted sine-bell window function, with a shift of 2 to minimise the truncature, and was zero filled in t_1 dimensions to build a 1024 × 1024 points matrix. The auto- and cross-peak volumes were determined using "2D Win-NMR" Bruker software after phase and baseline corrections in both dimensions. The calculations of matrix elements were performed with "Mathematica" software on a Unix computer.

Rate Constant Calculation for Treatment of 2D Data: To calculate the rate constants we used the method of Perrin, Gipe and Dwyer,[22,23] improved on several examples by Willem,[24,25] which consists of determining the matrix of exchange (**L**) from all peak volumes obtained from an experiment at a single mixing time: $\mathbf{L} = (1/\tau_m)\ln\mathbf{A} = (1/\tau_m)\mathbf{U}\ln\ \mathbf{U}^{-1}$, where the elements of the matrix **A** are defined as $A_{kj}(\tau_m) = V_{kj}(\tau_m)/x_j$ (**U** and λ are the matrices of the eigenvectors and eigenvalues of **A**). $V_{kj}(\tau_m)$ represents the integrated auto-peak (k = j) or cross-peak (k ≠ j) volume and x_j is the molar chemical equilibrium fraction of the species associated with resonance j (in our case of intramolecular exchange $x_a = x_b = x_c$). We prefer to use this method rather than the one with matrix $A_{kj}(\tau_m) = V_{kj}(\tau_m)/M_j^0$, where M_j^0 is the volume of the corresponding auto-peak for $\tau_m = 0$). The substitution of M_j^0 by x_j affects only the exchange matrix **L** diagonal part and leads to the loss of the information about the longitudinal relaxation rate (containing in L_{jj} diagonal elements calculated with M_j^0). This method, however, allows the avoidance of comparison between auto- and cross-peak volumes from different EXSY spectra with important error in the case of instrumental instabilities during the rather long times of experiments (instability accentuated by necessity of work at low temperature). The same calculations were performed with replacement of cross-peak volumes V_{kj} and V_{jk} in matrix **A** by symmetrical value $(V_{kj} + V_{jk})/2$ in order to "smooth out" experimental error.[24–26] The rate constant obtained for each temperature was averaged from the data obtained at different mixing time and given with its standard deviation.

Acknowledgments

We thank Bruker Ltd for access to " Win-Dynamics " program and Dr. Ursula Weber (Bruker) for fruitful discussions. We thank Marie-Françoise Foray and Claude Gey for help on treatment of the data from AM 400 Bruker spectrometer and Marie-Christine Brochier for help on the simulations (centre Grenoblois de Résonance Magnétique Nucléaire). We also thank the Chemistry Department of the C.N.R.S. for providing a position of associated researcher for one of us (M. G.).

[1] R. H. Holm in *Dynamic Nuclear Magnetic Resonance Spectroscopy*, L. M. Jackman and F. A. Cotton, Eds., Academic Press, New York, **1975**, Ch.9.
[2] I. R. Hutchinson, J. G. Gordon, R. H. Holm, *Inorg. Chem.* **1971**, *10*, 1004.
[3] A. Rodger, P. E. Schipper, *J. Chem. Phys.* **1987**, *91*, 189.
[4] A. Rodger, B. F. G. Johnson, *Inorg. Chem.* **1988**, *27*, 3061.
[5] J. C. Bailar, *J. Inorg. Nucl. Chem.* **1958**, *8*, 165.
[6] P. C. Rây, N. K. Dutt, *J. Indian Chem. Soc.* **1943**, *20*, 81.
[7] N. A. P. Kane-Maguire, T. W. Hanks, D. G. Jurs, R. M. Tollison, A. L. Heatherington, L. M. Ritzenthaler, L. M. McNulty, H. M. Wilson, *Inorg. Chem.* **1995**, *34*, 1121.
[8] G. E. Ball, B. E. Mann, *J. Chem. Soc., Chem. Commun*. **1992**, 561.
[9] R. C. Fay, T. S. Piper, *J. Am. Chem. Soc*. **1963**, *85*, 500.
[10] S. S. Eaton, G. R. Eaton, R. H. Holm, E. L. Muetterties, *J. Am. Chem. Soc*. **1973**, *95*, 1116.
[11] H. R. Hoveyda, V. Karunaratne, S. J. Rettig, C. Orvig, *Inorg. Chem.* **1992**, *31*, 5408.
[12] K. Kite, K. G. Orrell, V. Sik, Y. Roger, *Polyhedron* **1995**, *14*, 2711.
[13] B. Kersting, J. R. Telford, M. Meyer, K. N. Raymond, *J. Am. Chem. Soc*. **1996**, *118*, 5712.
[14] G. Serratrice, H. Boukhalfa, C. Béguin, P. Baret, C. Caris, J.-L. Pierre, *Inorg. Chem.* **1997**, *36*, 3898.
[15] O. Jarjayes, S. Hamman, F. Sarrazin, T. Benaïssa, C. G. Béguin, *New J. Chem.* **1998**, 361.
[16] O. Jarjayes, S. Hamman, M. C. Salon-Brochier, R. Nardin, C. Béguin, *Magn. Res. Chem.* accepted.
[17] T. S. Sloan's, *Top. Stereochem.* **1979**, *12*, 1.
[18] L. Pech, Y. Bankovsky, A. Kemme, J. Lejeis, *Acta Cryst.* **1997**, *C53*, 1043.
[19] O. Jarjayes, personal communication.
[20] U. Weber, H. Thiele in *NMR-Spectroscopy: Modern Spectral Analysis*, Wiley-VCH, Weinheim, **1998**, Chapter 5.
[21] J. Jeener, B. H. Meier, P. Bachmann, R. R. Ernst, *J. Chem. Phys.* **1979**, *71*, 4546.
[22] C. L. Perrin, R. K. Gipe, *J. Am. Chem. Soc*. **1984**, *106*, 4036.
[23] C. L. Perrin, T. J. Dwyer, *Chem. Rev.* **1990**, *90*, 935.
[24] R. Willem, M. Biesemans, K. Hallenga, G. Lippens, F. Malaisse-Lagae, W. J. Malaisse, *J. Biol. Chem*. **1992**, *267*, 210.
[25] R. Willem, *Prog. Nucl. Magn. Reson. Spectrosc*. **1987**, *20*, 1.
[26] I. Pianet, E Fouquet, H. Pereyre, M. Gielen, F. Kayser, M. Biesemans, R. Willem, *Magn. Reson. Chem.* **1994**, *32*, 617.

Received August 19, 1999
[I99307]

Structural Studies and Catalytic Activity of MCM-41 and MCM-48 Modified With the Titanocenophane $[SiMe_2(\eta^5\text{-}C_5H_4)_2]TiCl_2$

Paula Ferreira,[a] Isabel S. Gonçalves,[a] Fritz E. Kühn,[b] Martyn Pillinger,[a] João Rocha,*[a] Ana M. Santos,[b] and Alan Thursfield[a]

Keywords: Mesoporous materials / MCM-41 / MCM-48 / Immobilisation / Solid-state NMR / Heterogeneous catalysis / Titanium / Titanocenes

Titanium(IV)-grafted mesoporous silicas have been prepared by diffusion of an excess of the *ansa*-bridged titanocene $[SiMe_2(\eta^5\text{-}C_5H_4)_2]TiCl_2$ into the channels of hexagonal MCM-41 and cubic MCM-48 in dichloromethane or tetrahydrofuran at room temperature. The choice of solvent determines the course of the reaction and hence the activity of the resulting materials as catalysts in the catalytic epoxidation of cyclooctene with *tert*-butylhydroperoxide. Magic-angle spinning (MAS) NMR (^{13}C, ^{29}Si) spectroscopy was used to characterise the local environment of the surface-bound titanium active sites. When dichloromethane is used, the dominant species anchored to the surface are isolated *ansa*-bridged titanocene fragments. When THF is used, the $[SiMe_2(\eta^5\text{-}C_5H_4)_2]$ unit is lost with the concomitant formation of surface-bound Ti^{IV} species coordinated by THF molecules. These materials showed the best catalytic performance per Ti atom for the conversion of cyclooctene. All materials were further characterised by means of elemental analysis, powder X-ray diffraction (XRD), N_2 adsorption and FTIR spectroscopy.

Introduction

The confinement of redox-active metal centres on the surface of an inorganic oxide support matrix is a recognised route to heterogeneous catalysts for liquid-phase oxidations.[1] In the early Seventies the Shell Ti^{IV}/SiO_2 catalyst was developed for the epoxidation of propylene with ethylbenzene hydroperoxide.[2] An organic peroxide has to be used as the oxygen source in this process because the catalyst is sensitive to deactivation by water. This gives rise to toxic side products. A major step forward came with the discovery of titanium(IV) silicalite-I (TS-1),[3] obtained by the isomorphous substitution of titanium for silicon in the tetrahedral framework sites of silicalite-I, a hydrophobic molecular sieve possessing a three-dimensional system of intersecting elliptical pores with diameters of 5.3 × 5.5 and 5.1 × 5.5 Å. TS-1 is a catalyst for selective oxidations under very mild conditions with aqueous H_2O_2. Its remarkable activity is due to site isolation of Ti^{IV} centres in the hydrophobic pores of silicalite which allows for the simultaneous adsorption of the hydrophobic substrate and the oxidant. Site isolation is important because it prevents the oligomerisation of the Ti^{IV} centres to unreactive μ-oxo species.

TS-1 is a medium pore molecular sieve and its use is restricted to substrate molecules with kinetic diameters 5.5 Å. Thus, new materials with larger pore sizes and different coordination environments have always been sought. Examples include the hydrophilic Ti-doped zeolite β (pore diameter 7 × 7 Å),[4] and the recently discovered ETS-10 (Engelhard Corporation Titanium Silicate) containing tetrahedrally coordinated Si^{4+} and octahedrally coordinated Ti^{4+}.[5] A breakthrough into the mesoporous regime came with the discovery by researchers at the Mobil Corporation of a new generation of surfactant-templated (alumino)silicates (M41S) with very high surface areas (1000 $m^2\ g^{-1}$), high pore volumes (1 $cm^3\ g^{-1}$) and very narrow pore size distributions, tuneable in the range 16–100 Å.[6] The M41S family includes the thermally stable hexagonal MCM-41 and cubic MCM-48 phases. They have properties intermediate between those of SiO_2 and Al_2O_3, and microporous crystalline molecular sieves. Ti-substituted M41S, and related materials, have been prepared directly by either treating Ti alkoxides with silicon compounds, or mixing TiO_2 with silica.[7] One problem with these materials as catalysts is that access by the reactants to the Ti active centres is still somewhat limited as the latter are buried within the inner walls of the mesoporous solid.

An alternative strategy for the incorporation of redox-active metal centres into the internal surface of M41S materials is the covalent attachment of organometallic complexes by reaction with pendant silanol (Si–OH) groups.[1,8] Thomas and co-workers have prepared a heterogeneous titanium(IV) catalyst by diffusing a solution of Cp_2TiCl_2 in chloroform into the mesopores of MCM-41, followed by treatment with Et_3N to activate the Si–OH groups to form Si–O–Ti linkages.[9] The final catalyst is obtained by calcination to remove the organic ligands. An extension of this synthetic methodology comprises the functionalisation of the walls of MCM-41 with ferrocenyl end-groups by a ring-opening reaction of the strained metallocenophane $[Fe(\eta^5\text{-}C_5H_4)_2SiMe_2]$.[10] We followed up this work to show that

[a] Department of Chemistry, University of Aveiro,
3810–193 Aveiro, Portugal
Fax: (internat.) + 351-34/370-084
E-mail: ROCHA@DQ.UA.PT
[b] Anorganisch-chemisches Institut der Technischen Universität München,
Lichtenbergstraße 4, D-85747 Garching bei München, Germany

 © WILEY-VCH Verlag GmbH, D-69451 Weinheim, 2000 1434–1948/00/0303–0551 $ 17.50+.50/0

the organometallic complex reacts in a similar way with the surface silanols of MCM-48 to give a $C_5H_4SiMe_2$–O linkage.[11] We now wish to report studies on the derivatisation of MCM-41 and MCM-48 by direct reaction with the titanocenophane complex $[SiMe_2(\eta^5\text{-}C_5H_4)_2]TiCl_2$. All materials have been characterised by elemental analysis, powder XRD, N_2 adsorption and MAS NMR spectroscopy (^{13}C, ^{29}Si). The derivatised materials are catalysts for the epoxidation of cyclooctene.

Results and Discussion

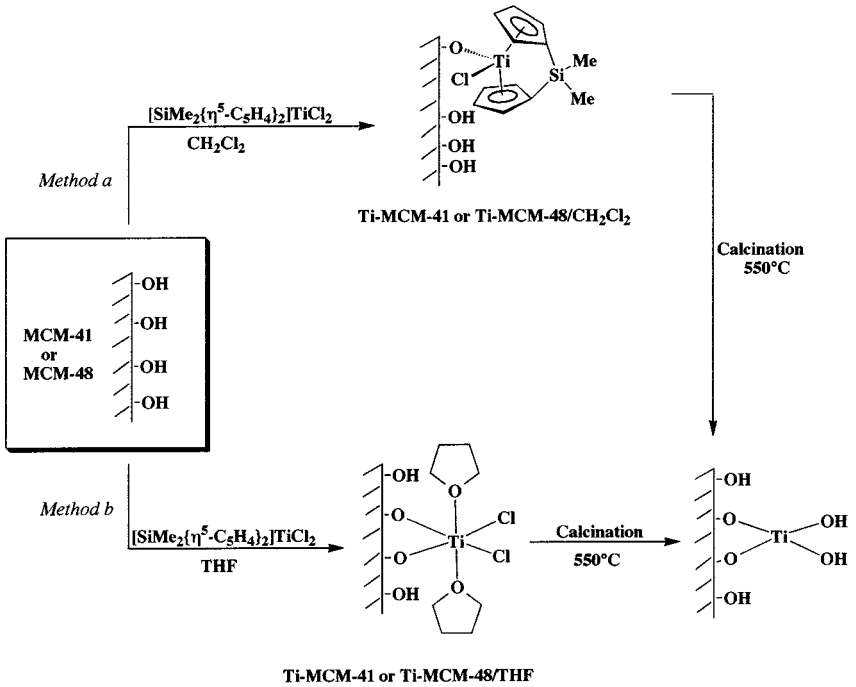
Synthesis and Spectroscopic Characterisation

The introduction of an interannular bridge in titanocene dichloride alters its reactivity considerably, particularly in relation to reduction. A comparison of the redox behaviour of Cp_2TiCl_2 and the dialkylsilyl-bridged derivatives $[SiR_2(\eta^5\text{-}C_5H_4)_2]TiCl_2$ showed that the bridged compounds exhibit a single one-electron reversible reduction whereas the unbridged compound exhibits several reduction waves.[12] The stability of the one-electron reduced d^1 Ti^{III} monoanion of the bridged compounds has been rationalised on the basis of the ability of the SiR_2 ligand to restrict the mobility of the Cp rings and to maintain their original canted arrangement. As mentioned above, titanocene dichloride grafted onto mesoporous MCM-41 is a precursor to an active and selective heterogeneous epoxidation catalyst. Detailed spectroscopic and computational studies have confirmed that $(\equiv Si\text{–}O)_3TiCp$ is more likely to form than $(\equiv Si\text{–}O)_2TiCp_2$.[13] To the best of our knowledge, no studies have yet been made of the effect of the presence of an interannular bridge on the anchoring process, or the catalytic properties, of the grafted product.

The Ti-modified mesoporous materials are designated as Ti-MCM-41/(CH_2Cl_2 or THF) and Ti-MCM-48/(CH_2Cl_2 or THF), and were prepared as depicted in Scheme 1. MCM-41 and MCM-48 were treated with an excess of $[SiMe_2(\eta^5\text{-}C_5H_4)_2]TiCl_2$ in either dichloromethane (method a) or THF (method b). The products were isolated by filtration and washed thoroughly with the relevant solvent to remove excess organometallic before drying in vacuo at room temperature.

Method a gave grey/dark-brown, air-sensitive products which transformed to light brown powders after exposure to air for several hours. The products from method b were pale pink/beige powders and not visibly air-sensitive. Elemental analysis indicated that the materials contained approximately 4.2 mass% Ti (method a) or 1.2 mass% Ti (method b). This is consistent with a coverage of titanium atoms of 8.8×10^{-25} mol/nm^2 (0.5 Ti atoms per nm^2) and 2.5×10^{-25} mol/nm^2 (0.15 Ti atoms per nm^2), respectively. The former value is similar to the concentration of surface silanol groups in parent calcined MCM-41, reported to be in the range 1 to 3 per nm^2.[14] Grafted samples were subsequently calcined in air at 550 °C for 10 hours to remove organic components.

After treatment of the mesoporous materials with the titanocenophane complex in CH_2Cl_2 or THF the infrared band of the OH groups at 3742 cm^{-1} was noticeably reduced in intensity. In addition the spectra of MCM-41/CH_2Cl_2 or MCM-48/CH_2Cl_2 show bands at 2962 and 2930 cm^{-1}, representing the asymmetric and symmetric CH_3 stretching vibrations. The IR spectra of these anchored materials and of the starting material show that the C=C stretching modes in the region of 1400 cm^{-1} are similar. The bands assigned to the Cp ring, appearing at 1456 cm^{-1} and



Scheme 1. Modification of MCM-41 and MCM-48 using $[SiMe_2(\eta^5\text{-}C_5H_4)TiCl_2]$

1375 cm^{-1} for the free organometallic, are not shifted to different frequency on anchoring, indicating a similar interaction between the titanium centre and the Cp_2SiMe_2 group.

The powder X-ray diffraction (XRD) patterns of the parent calcined MCM-41 and MCM-48 can be indexed on a hexagonal unit cell (using the strongest reflection, d_{100}, a = 40 Å) and cubic unit cell (using the strongest reflection, d_{211}, a = 88.62 Å), respectively. The data for the as-synthesised and calcined Ti-modified MCM materials are consistent with retention of the hexagonal and cubic mesoporous structures throughout the grafting and calcination process (Figure 1 and 2).

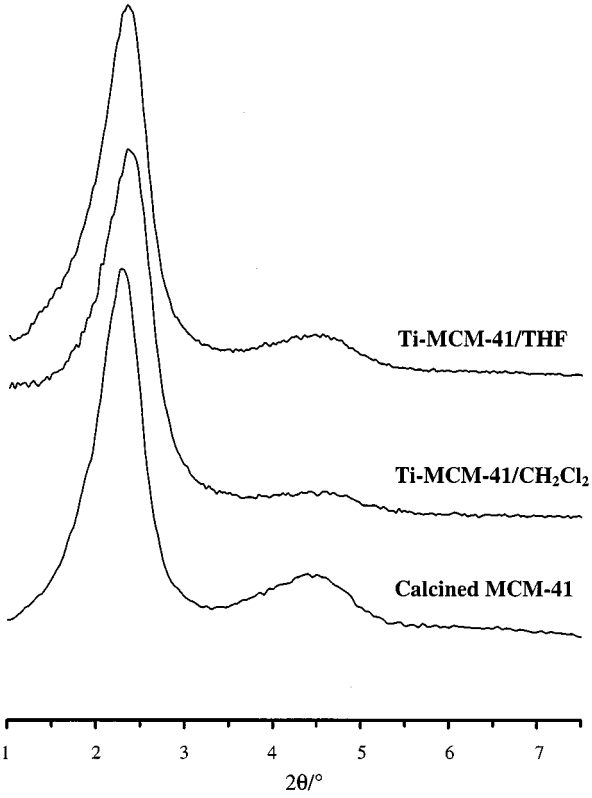


Figure 1. Powder XRD patterns of MCM-41 materials

Figure 3 and 4 show the ^{29}Si CP MAS and MAS NMR spectra for Ti-MCM-41 and Ti-MCM-48 prepared in dichloromethane, respectively. The ^{29}Si CP MAS NMR spectrum of Ti-MCM-41/CH_2Cl_2 exhibits two broad convoluted resonances, at δ = –108.4 and –100.3 assigned to Q^4 and Q^3 species, respectively [$Q^n = Si(OSi)_n(OH)_{4-n}$], together with a shoulder at δ = –92.8 ascribed to Q^2 species. The signal at δ = –3.8 can be assigned to asymmetric $[\mathbf{Si}Me_2(\eta^5\text{-}C_5H_4)_2]TiClO\text{–}Si$ in agreement with the ^{29}Si MAS NMR spectrum for $[\mathbf{Si}Me_2(\eta^5\text{-}C_5H_4)_2]TiCl_2$ (δ = –4.0). The other poorly defined broad resonances, at δ = 2.4 and δ = –16.2, are attributed to symmetric $[\mathbf{Si}Me_2(\eta^5\text{-}C_5H_4)_2]Ti(O\text{–}Si)_2$ species or to organic decomposition products. A similar result was obtained for Ti-MCM-48/CH_2Cl_2 (Figure 4). A comparison with the ^{29}Si CP MAS and MAS NMR spectra of the original mesoporous silicate showed that the intensity of the Q^2 and Q^3 species had decreased significantly.

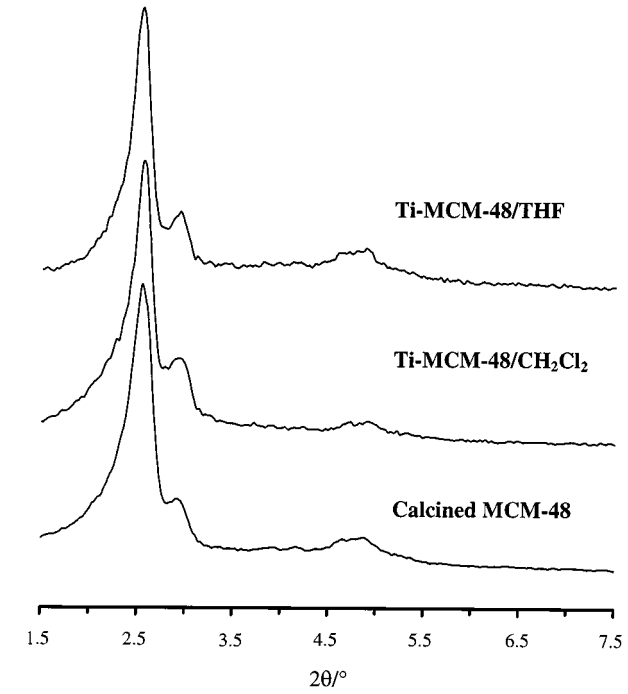


Figure 2. Powder XRD patterns of MCM-48 materials

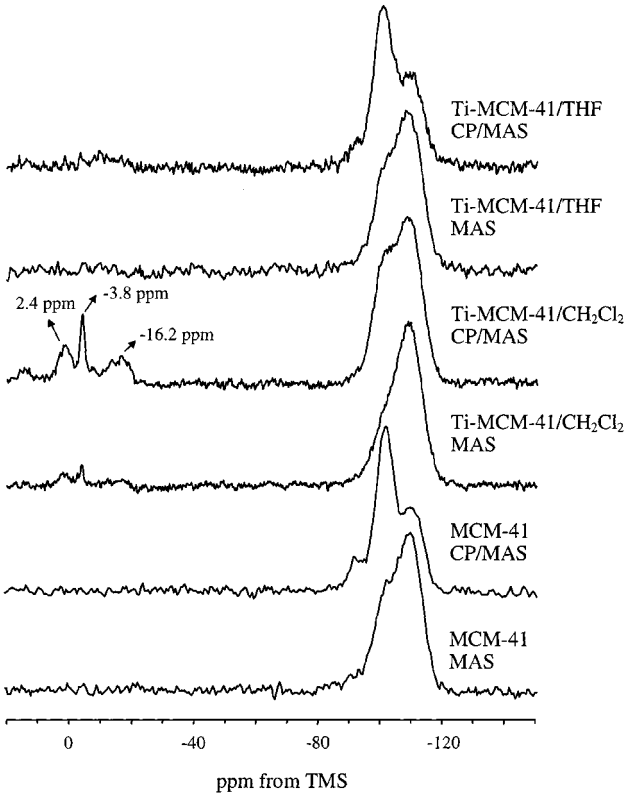


Figure 3. ^{29}Si CP MAS and MAS NMR at room temperature of MCM-41 materials

The ^{29}Si CP MAS NMR spectra of Ti-MCM-41/THF and Ti-MCM-48/THF only exhibited two broad, convo-

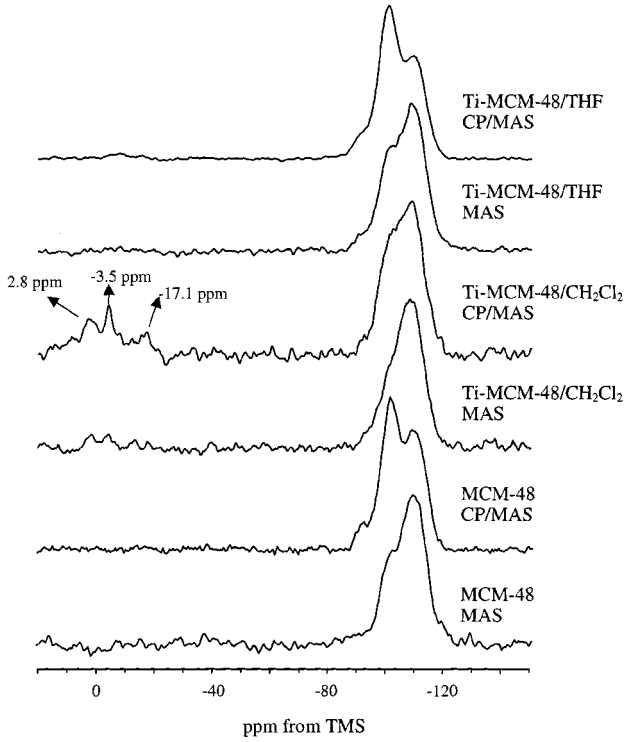


Figure 4. ^{29}Si CP MAS and MAS NMR at room temperature of MCM-48 materials

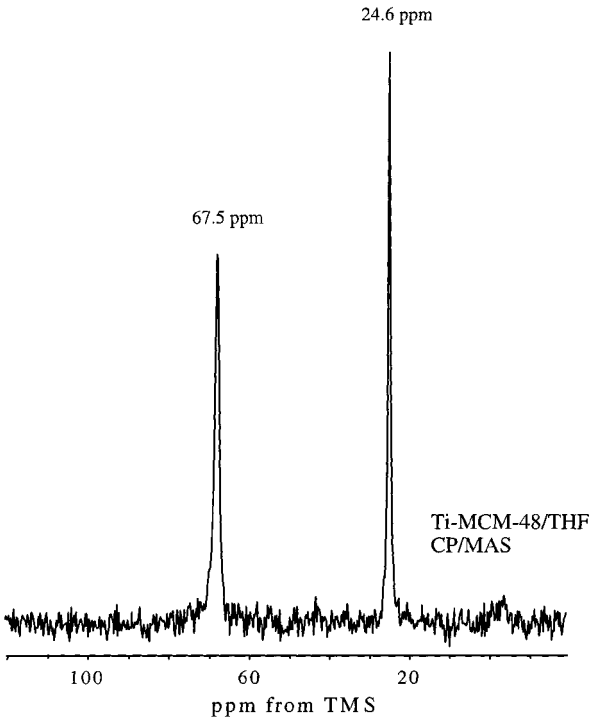


Figure 5. ^{13}C CP MAS NMR at room temperature

luted low-frequency resonances at δ –109.5 (Q^4) and at δ –101.0 (Q^3) together with a shoulder at δ –91 ppm (Q^2) (Figure 3 and 4). These results are consistent with the absence in the IR spectra of bands assignable to the Cp ring. Reaction of the organometallic with MCM-41 and MCM-48 in tetrahydrofuran replaces the Cp_2SiMe_2 group (Scheme 1). Alcohols are known to react with CpTi compounds with the replacement of the cyclopentadienyl group.[15]

Calcination of all these materials (Ti-MCM-41/CH_2Cl_2, Ti-MCM-48/CH_2Cl_2, Ti-MCM-41/THF, and Ti-MCM-48/THF) removes the organic ligand [$SiMe_2(\eta^5\text{-}C_5H_4)_2$ or THF] and these sites are probably occupied by an OH group (Scheme 1). After calcination all these materials give a similar ^{29}Si MAS NMR spectrum. Both the ^{29}Si CP MAS and MAS NMR spectra clearly show the diminished intensity of the Q^2 and Q^3 peaks relative to the Q^4 peak, indicating the esterification of the free hydroxyl groups. The presence of Ti-oxide species anchored to the silica surface is revealed by an IR absorption at around 950 cm^{-1} which has been assigned to the asymmetric stretching mode of Ti–O–Si groups.[7b]

The ^{13}C CP MAS NMR spectra of Ti-MCM-41/CH_2Cl_2 and Ti-MCM-48/CH_2Cl_2 are similar. The signals of the $SiMe_2$ and Cp ligands are slightly affected by immobilisation. Four broad resonances are observed, all of which are broader than those of the related crystalline titanocenophane [$SiMe_2(\eta^5\text{-}C_5H_4)_2$]$TiCl_2$. This broadening is due to the range of chemically different environments in which the molecules are located, giving rise to an envelope of peaks with very similar chemical shifts. The spectrum of Ti-MCM-41/CH_2Cl_2 exhibits four broad resonances at δ = 133.6, 120.6, 115.5 and –1.8 attributed to $(C_5H_4)_2Si$ and $SiMe_2$, respectively. These resonances can be compared with those given by the solid [$SiMe_2(\eta^5\text{-}C_5H_4)_2$]$TiCl_2$ (see Experimental Section). However, immobilisation takes place by elimination of one or more of the original chlorides with the hydrogen atoms from the silanol groups (Si–OH) in the MCM's and the spectrum appears more complicated. The low value of Cl/Ti suggests that the Ti–Cl bonds are involved in the reaction between the metallocene precursor and the MCM-41 or MCM-48 (Scheme 1). Analogous bipodal anchoring of the unbridged Cp_2Ti fragment has also been suggested for the very recently reported titanocene dichloride grafted ITQ-2,[16] a high surface area layered silica.

The ^{13}C MAS NMR spectra of Ti-MCM-41/THF and Ti-MCM-48/THF (Figure 5) only present two peaks at δ = 67.7 and 25.3 attributed to the THF coordinated to the titanium (Scheme 1).

N_2 Adsorption Studies

Figure 6 shows the N_2 isotherms of the parent and modified MCM-41 and -48 materials recorded at 77 K. The parent materials both gave a type IV isotherm with a small hysteresis, the A_{BET} specific surface areas were calculated to be 1035 m^2 g^{-1} for MCM-41 and 950 m^2 g^{-1} for MCM-48. The modified samples exhibit a lower uptake of N_2 than the parent solids as expected for successful incorporation of the organometallic within the pore systems. Adsorption of N_2 on the Ti-MCM-48/CH_2Cl_2 (Figure 6d) and Ti-MCM-41/THF (Figure 6e) samples was found to be very slow re-

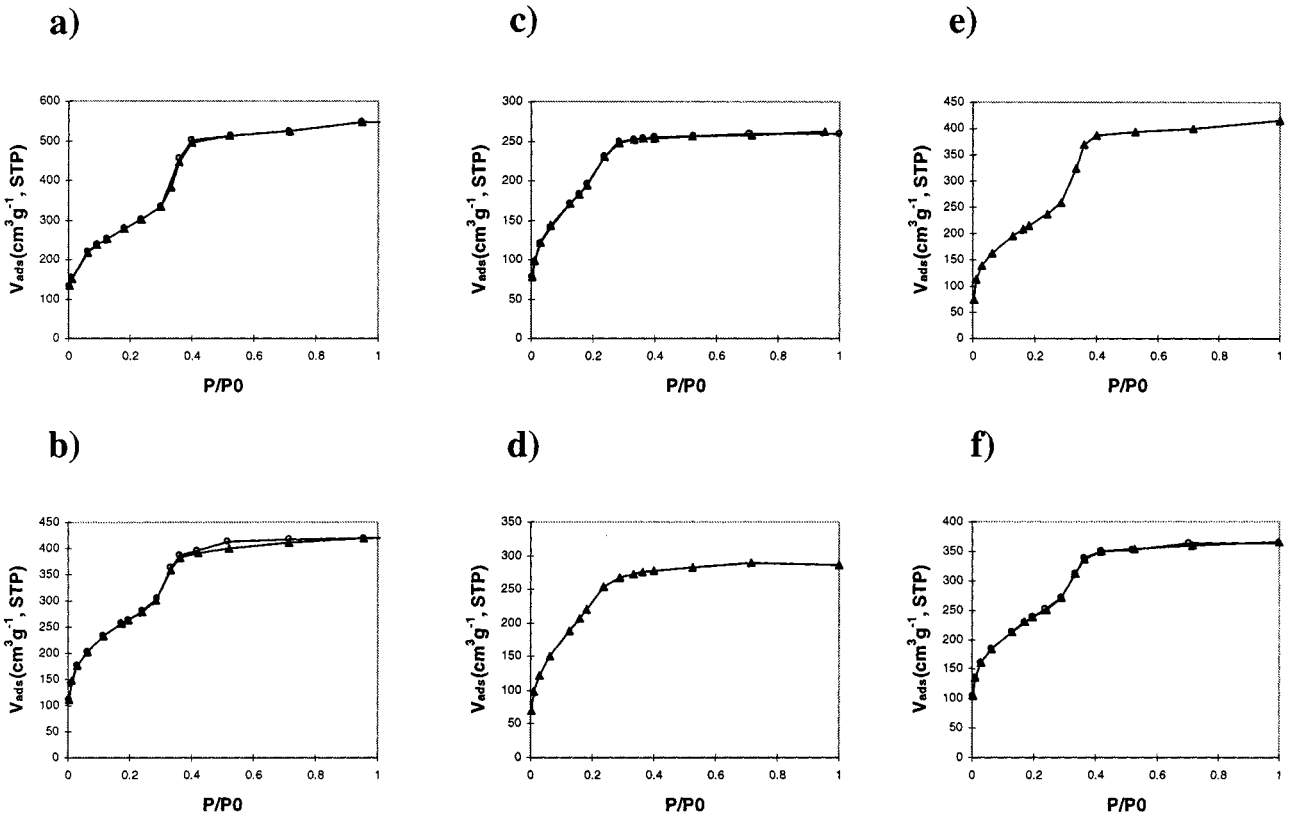


Figure 6. Isotherm of: (a) N_2 adsorption and desorption on MCM-41; (b) N_2 adsorption and desorption on MCM-48; (c) N_2 adsorption and desorption on Ti-MCM-41/CH_2Cl_2; (d) N_2 adsorption on Ti-MCM-48/CH_2Cl_2; (e) adsorption of N_2 on Ti-MCM-41/THF; (f) adsorption and desorption of N_2 on Ti-MCM-48/THF

sulting in nonequilibrium isotherms. The desorption part was not recorded for these two samples.

Inspection of the isotherms reveals that the materials produced using THF as the solvent exhibit a higher uptake of N_2 than those prepared using CH_2Cl_2 indicating that CH_2Cl_2 is superior in the task of promoting incorporation of the organometallic, in agreement with the elemental analysis results. The two samples produced using CH_2Cl_2 also have poorly defined capillary condensation regions as a result of the higher loadings. The incorporation of the organometallic appears to depend on the solvent employed and not on the pore system and pore diameters of the parent solids which are significantly different.

MCM-41 and MCM-48 Derivatives in Oxidation Catalysis

Reports have shown that Ti-MCM-41 materials are active and selective catalysts to perform the epoxidation of olefins by organic hydroperoxides.[7,9] Two distinct kinds of catalysts have been described, as mentioned above. The first accommodates the titanium ions within the walls of the mesoporous silica[7] and the second has the tetracoordinated Ti^{IV} ions grafted onto the inner surface of the mesoporous host.[9] The second catalyst is prepared via a titanocene dichloride-grafted precursor.[9] Surface-grafted Ti-MCM-41 catalysts have been shown to be more active than lattice-embedded Ti-MCM-41 materials in terms of activity per Ti centre, due to a large concentration of accessible, isolated and structurally well-defined active sites.[17]

The Ti-modified mesoporous silicas prepared in this work were screened as catalysts for the epoxidation of cyclooctene at 323 K with TBHP. The experimental details are given in the Experimental Section and results are shown in Figure 7.

It is evident that the materials prepared in CH_2Cl_2 show a higher conversion of cyclooctene after any given period than those prepared in THF. However, the materials prepared in THF are considerably more active in terms of conversion of cyclooctene per mol of titanium atoms. For example, after reacting for four hours, 55% conversion was observed for Ti-MCM-41/CH_2Cl_2 (25 mol cyclooctene per mol of titanium atoms) and 39% for Ti-MCM-41/THF (69 mol cyclooctene per mol of titanium atoms). Conversion was 88% for the former material after 24 h reacting.

As a general observation it can be concluded that $[SiMe_2(\eta^5\text{-}C_5H_4)_2]TiCl_2$ reacts in a similar way with the internal surfaces of MCM-41 and MCM-48 to give materials with similar titanium loadings, structurally similar monomeric Ti^{IV} species and similar catalytic activities. This is despite the fact that MCM-41 and MCM-48 possess very different mesoporous surfaces.

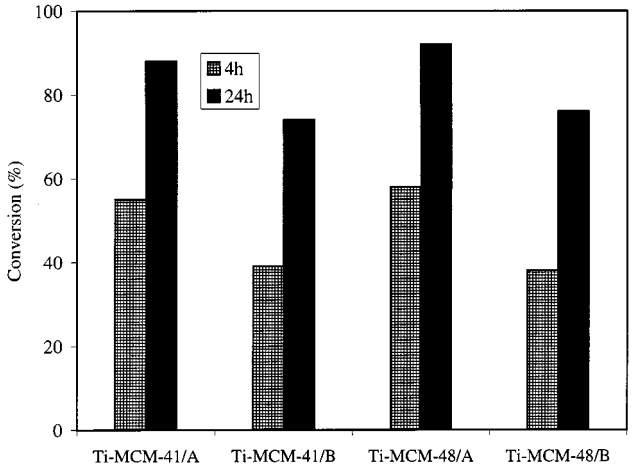


Figure 7. Conversion after 4 h and 24 h reacting in the catalytic oxidation of cyclooctene with TBHP on Ti-MCM materials (A, CH_2Cl_2); (B, THF); see text and Experimental Section for reaction details

Experimental

General: All preparations and manipulations were performed using standard Schlenk techniques under an oxygen- and water-free nitrogen atmosphere. Commercial grade solvents were dried and deoxygenated by refluxing for at least 24 h over appropriate drying agents under a nitrogen atmosphere and freshly distilled prior to use.

Powder X-ray diffraction (XRD) data were collected on a Phillips X'pert diffractometer using Cu-K_α radiation filtered by Ni. Microanalyses were performed at the TU Munich. Infrared spectra were recorded on a Unican Mattson Mod 7000 FTIR spectrophotometer using KBr pellets and/or solutions. ^{29}Si and ^{13}C NMR spectra were recorded at 79.49 and 100.62 MHz, respectively, on a (9.4 T) Bruker MSL 400P spectrometer. ^{29}Si magic-angle spinning (MAS) NMR spectra were recorded with 40° pulses, spinning rates 5.0–5.5 kHz and 60 s recycle delays. ^{29}Si CP MAS NMR spectra were recorded with 5.5 μs ^{1}H 90° pulses, 8 ms contact time, a spinning rate of 5.0 kHz and 4 s recycle delays. Chemical shifts are quoted in parts per million from TMS. ^{13}C CP MAS NMR spectra were recorded with a 4.5 μs ^{1}H 90° pulse, 2 ms contact time, a spinning rate of 8 kHz and 4 s recycle delays. Chemical shifts are quoted in ppm from TMS.

Nitrogen adsorption isotherms were recorded using a CI electronics MK2-M5 microbalance connected to a vacuum manifold line. The parent calcined MCM-41 and MCM-48 solids were dehydrated overnight at 723 K to an ultimate pressure of 10^{-4} mbar and then cooled to room temperature prior to adsorption. Extra care with the functionalised materials was necessary due to the possibility of aerial oxidation and therefore transfer to the balance and outgassing of the system was rapid. A lower dehydration temperature of 413 K was used with these samples to further minimise destruction of the functionalities. Nitrogen isotherms were then recorded at 77 K. Equilibration of each data point was monitored using CI electronics' Labweigh software and the pressure monitored using an Edwards Barocel pressure sensor. Specific surface areas, A_{BET}, were determined from the linear part of the BET plot (P/P_o = 0.05–0.3) assuming the average area occupied by a N_2 molecule in the monolayer to be 16.2 Å^2.

$[SiMe_2(\eta^5\text{-}C_5H_4)_2]TiCl_2$ was prepared as described previously.[12] ^{13}C CP MAS NMR (25 °C): δ = 132.6 [$(C_5H_4)_2Si$], 120.8 [$(C_5H_4)_2Si$], 116.2 [$(C_5H_4)_2Si$], –1.2 (SiMe_2). – ^{29}Si MAS NMR δ = –4.0 [$SiMe_2(\eta^5\text{-}C_5H_4)_2$]

The hexagonal channel host MCM-41 was synthesised from $[(C_{14}H_{29})NMe_3]Br$ according to published procedures.[18] After calcination (540 °C/6 h), the material was characterised by powder XRD, N_2 adsorption and FTIR spectroscopy.

The cubic channel host MCM-48 was synthesised from $[(C_{16}H_{33})NMe_3]Cl$ according to published procedures.[19] After calcination (540 °C/6 h), the material was characterised by powder XRD, N_2 adsorption and FTIR spectroscopy.

Preparation of Ti-MCM-41. Method A: Calcined MCM-41 (0.5 g) was activated at 180 °C under high vacuum for 2 hours and then treated with an excess of $[SiMe_2(\eta^5\text{-}C_5H_4)_2]TiCl_2$ in CH_2Cl_2 (20 mL). The mixture was stirred at room temperature for 4 days. The solution was filtered off and the grey solid washed three times with 15 mL portions of CH_2Cl_2 before drying under high vacuum at room temperature for several hours. Found: Ti 4.24, Cl 5.38, C 12.37, H 2.60. – IR (KBr): $\tilde{\nu}$ = 3428 vs, 2962 m, 2930 m, 2858 w, 1637 s, 1456 w, 1402 m, 1380 w, 1236 vs, 1172 w, 1080 vs, 955 m, 807 s, 586w, 453 s cm^{-1}. – ^{29}Si MAS NMR: δ = –108.6 (br.), –3.4 [$SiMe_2(\eta^5\text{-}C_5H_4)_2$], 3.1 (br.). – ^{29}Si CP MAS NMR: δ = –100.3 (br., Q^3), –108.4 (br., Q^4), –92.8 (weak, Q^2), –3.8 [$SiMe_2(\eta^5\text{-}C_5H_4)_2$], –16.2 (br.), 2.4 (br.). – ^{13}C CP MAS NMR (25 °C) δ = 133.6 [br., $(C_5H_4)_2Si$], 120.6 [br., $(C_5H_4)_2Si$], 115.5 [br., $(C_5H_4)_2Si$], –1.8 (br., SiMe_2).

Method B: Calcined MCM-41 (0.5 g) was activated at 180 °C under vacuum for 2 hours and then treated with an excess of $[SiMe_2(\eta^5\text{-}C_5H_4)_2]TiCl_2$ in THF (15 mL). The mixture was stirred at room temperature for 66 hours. The solution was filtered off and the pale pink solid washed three times with 10 mL portions of THF before drying under vacuum at room temperature for several hours. Found: Ti 1.10, Cl 2.00. – IR (KBr): $\tilde{\nu}$ = 3461 vs, 2976 w, 2932 w, 1637 s, 1383 w, 1235 vs, 1081 vs, 964 m, 801 m, 571 w, 458 s cm^{-1}. – ^{29}Si MAS NMR: δ = –107.9 (br.). – ^{29}Si CP MAS NMR: δ = –100.4 (br., Q^3), δ = –110.2 (br., Q^4), –91.0 (weak, Q^2). – ^{13}C MAS NMR (25 °C) δ = 67.7 (THF), 25.3 (THF).

Preparation of Ti-MCM-48. Method A: Calcined MCM-48 (0.5 g) was activated at 180 °C under vacuum for 3 hours and then treated with an excess of $[SiMe_2(\eta^5\text{-}C_5H_4)_2]TiCl_2$ in CH_2Cl_2 (20 mL). The mixture was stirred at room temperature for 4 days. The solution was filtered off and the grey solid washed three times with 15 mL portions of CH_2Cl_2 before drying under vacuum at room temperature for several hours. Found: Ti 4.10, Cl 5.20, C 11.33, H 2.70. – IR (KBr): $\tilde{\nu}$ = 3437 vs, 2965 m, 2929 m, 2858 m, 1636 s, 1457 w, 1395 m, 1375 w, 1238 vs, 1076 vs, 956 m, 807 s, 452 s cm^{-1}. – ^{29}Si MAS NMR: δ = –108.2 (br.), –3.6 [$SiMe_2(\eta^5\text{-}C_5H_4)_2$], 1.9 (br.). – ^{29}Si CP MAS NMR: δ = –101.6 (br., Q^3), –108.5 (br., Q^4), –91.9 (weak, Q^2), –3.5 [$SiMe_2(\eta^5\text{-}C_5H_4)_2$] –17.1 (br.), 2.8 (br.). – ^{13}C CP MAS NMR (25 °C) δ = 132.0 [br., $(C_5H_4)_2Si$], 124.5 [br., $(C_5H_4)_2Si$], 115.2 [br., $(C_5H_4)_2Si$], –2.0 (br., SiMe_2).

Method B: Calcined MCM-48 (0.5 g) was activated at 180 °C under vacuum for 2 hours and then treated with an excess of $[SiMe_2(\eta^5\text{-}C_5H_4)_2]TiCl_2$ in THF (20 mL). The mixture was stirred at room temperature for 66 hours. The solution was filtered off and the pale pink solid washed three times with 20 mL portions of THF before drying under vacuum at room temperature for several hours. Found: Ti 1.30, Cl 2.12. – IR (KBr): $\tilde{\nu}$ = 3481 vs, 1636 s, 1230 s, 1082 vs, 957 m, 804 m, 564 w, 455 s cm^{-1}. – ^{29}Si MAS NMR: δ = –101.2 (br., Q^3), δ = –108.2 (br., Q^4). – ^{29}Si CP MAS NMR: δ = –100.6 (br., Q^3), δ = –109.2 (br., Q^4). – ^{13}C CP MAS NMR (25 °C) δ = 67.5 (THF), 24.6 (THF).

Preparation of Calcined Samples: As-synthesised Ti-MCM-41 and Ti-MCM-48 were dried in air at 110 °C for 1 h prior to calcination in air at 550 °C for 10 h (heating rate 1 °C/min). The resultant materials have the same textural and structural characteristics as the parent calcined materials.[16]

Catalytic Reactions With Ti-MCM-41 and Ti-MCM-48: *cis*-Cyclooctene (800 mg, 7.3 mmol), *n*-dibutyl ether (800 mg, internal standard), Ti-MCM-41/(CH_2Cl_2 or THF) or Ti-MCM-48/(CH_2Cl_2 or THF) (180 mg) and 5.5 M *t*-butyl hydroperoxide in decane (2 mL) were added to a thermostated reaction vessel and stirred for 24 h at 50 °C. The course of the reaction was monitored by quantitative GC-analysis. Samples were taken every thirty minutes, diluted with dichloromethane, and chilled in an icebath. For the destruction of hydroperoxide and removal of water a catalytic amount of manganese dioxide and magnesium sulfate was added. After the gas evolution ceased the resulting slurry was filtered over a filter-equipped Pasteur pipette and the filtrate injected onto the GC column. The conversion of cyclooctene and formation of cyclooctene oxide was calculated from a calibration curve ($r^2 = 0.999$) recorded prior to the reaction course.

Acknowledgments

We thank PRAXIS XXI for partial funding. P. Ferreira (BD) thanks PRAXIS XXI for a grant. I.S.G. wants to thank the CRUP (Acções Integradas Programme) for generous support. A. M. S. is grateful to the Bayerische Forschungsstiftung for a fellowship and F. E. K. thanks Prof. W. A. Herrmann for his continous support.

[1] [1a] R. Murugavel, H. W. Roesky, *Angew. Chem. Int. Ed. Engl.* **1997**, *36*, 477–479. – [1b] R. A. Sheldon, I. W. C. E. Arends, H. E. B. Lempers, *Catalysis Today* **1998**, *41*, 387–407. – [1c] R. A. Sheldon, M. Wallau, I. W. C. E. Arends, U. Schuchardt, *Acc. Chem. Res.* **1998**, *31*, 485–493.

[2] [2a] R. A. Sheldon, in *Aspects of Homogeneous Catalysis* (Ed.: R. Ugo), Reidel, Dordrecht, The Netherlands, Vol. 4, **1981**, p. 1. – [2b] R. A. Sheldon, *J. Mol. Catal.* **1980**, *7*, 107–126.

[3] [3a] M. Taramasso, G. Perego, B. Notari (Enichem), US Pat. 4 410 501, **1983**. – [3b] B. Notari, *Stud. Surf. Sci. Catal.* **1987**, *37*, 413.

[4] [4a] T. Blasco, M. A. Camblor, A. Corma, J. Pérez-Pariente, *J. Am. Chem. Soc.* **1993**, *115*, 11806–11813. – [4b] M. A. Camblor, M. Constantini, A. Corma, L. Gilbert, P. Esteve, A. Martinez, S. Valencia, *Chem. Commun*. **1996**, 1339–1340.

[5] [5a] S. M. Kuznicki (Engelhard Corporation), US Pat. 4 938 939, **1990**. – [5b] US Pat. 4 853 202, **1989**. – [5c] M. W. Anderson, O. Terasaki, T. Ohsuna, A. Philippou, S. P. MacKay, A. Ferreira, J. Rocha, S. Lidin, *Nature* **1994**, *367*, 347–351.

[6] C. T. Kresge, M. E. Leonowicz, W. J. Roth, J. C. Vartuli, J. S. Beck, *Nature* **1992**, *359*, 710–712.

[7] [7a] P. T. Tanev, M. Chibwe, T. J. Pinnavaia, *Nature* **1994**, *368*, 321–323. – [7b] A. Corma, M. T. Navarro, J. Pérez-Pariente, *J. Chem. Soc., Chem. Commun*. **1994**, 147–148. – [7c] W. Zhang, J. Wang, P. T. Tanev, T. J. Pinnavaia, *Chem. Commun*. **1996**, 979–980. – [7d] W. Zhang, M. Froba, J. Wang, P. T. Tanev, J. Wong, T. J. Pinnavaia, *J. Am. Chem. Soc.* **1996**, *118*, 9164–9171.

[8] [8a] K. Moller, T. Bein, *Chem. Mater.*, **1998**, *10*, 2950–2963. – [8b] T. Maschmeyer, *Curr. Opin. Solid State Mater. Sci.* **1998**, *3*, 71–78.

[9] [9a] T. Maschmeyer, F. Rey, G. Sankar, J. M. Thomas, *Nature* **1995**, *378*, 159–162. – [9b] L. Marchese, E. Gianotti, V. Dellarocca, T. Maschmeyer, F. Rey, S. Coluccia, J. M. Thomas, *Phys. Chem. Chem. Phys.* **1999**, *1*, 585–592.

[10] [10a] S. O'Brien, J. Tudor, S. Barlow, M. J. Drewit, S. J. Heyes, D. O'Hare, *Chem. Commun.*, **1997**, 641–642. – [10b] S. O'Brien, J. M. Keates, S. Barlow, M. J. Drewit, B. R. Payne, D. O'Hare, *Chem. Mater.* **1998**, *10*, 4088–4099.

[11] P. Ferreira, I. S. Gonçalves, F. Mosselmans, M. Pillinger, J. Rocha, A. Thursfield, *Eur. J. Inorg. Chem*. **2000**, 97–102.

[12] C. S. Bajgur, W.R. Tikkanen, J. L. Petersen, *Inorg. Chem.*,**1985**, *24*, 2539–2546.

[13] P. E. Sinclair, G. Sankar, C. R. A. Catlow, J. M. Thomas, T. Maschmeyer, *J. Phys. Chem. B* **1997**, *101*, 4232–4237.

[14] X. S. Zhao, G. Q. Lu, A. K. Whittaker, G. J. Miller, H. Y. Zhu, *J. Phys. Chem. B* **1997**, *101,* 6525–6531.

[15] C. Blandy, R. Guerreiro, D. Gervais, *J. Organomet. Chem.* **1977**, *128,* 415–421.

[16] A. Corma, U. Díaz, V. Fornés, J. L. Jordá, M. Domine, F. Rey, *Chem. Commun.* **1999**, 779–780.

[17] R. D. Oldroyd, J. M. Thomas, T. Maschmeyer, P. A. MacFaul, D. W. Snelgrove, K. U. Ingold, D. D. M. Wayner, *Angew. Chem. Int. Ed. Engl.* **1996**, *35*, 2787–2790.

[18] J.S. Beck, J.C. Vartuli, W.J. Roth, M.E. Leonowicz, C.T. Kresge, K.D. Schmitt, C.T.-W. Chu, D.H. Olson, E.W. Sheppard, S.B. McCullen, J.B. Higgins and J.L. Schlenker, *J. Am. Chem. Soc.* **1992**, *114*, 10834–10843.

[19] [19a] A. Monnier, F. Schüth, Q. Huo, D. Kumar, D. Margolese, R. S. Maxwell, G. D. Stucky, M. Krishnamurty, P. Petroff, A. Firouz, M. Janicke, B. F. Chmelka, *Science* **1993**, *261*, 1299–1303. – [19b] J. Xu, Z. Luan, H. He, W. Zhou, L. Kevan, *Chem. Mater.* **1998**, *10*, 3690–3698.

Received September 20, 1999
[I99331]

Study of Copper(II) Polyazamacrocyclic Complexes by Electronic Absorption Spectrophotometry and EPR Spectroscopy

Carlos F. G. C. Geraldes,*[a] M. Paula M.Marques,[b] Baltazar de Castro,*[c] and Eulália Pereira[c]

Keywords: Macrocyclic ligands / Copper / EPR spectroscopy / Electronic spectrophotometry

Copper(II) mononuclear complexes with the polyazamacrocyclic ligands NOTA (1,4,7-triazacyclononane-*N*,*N*′,*N*″-triacetate), DOTA (1,4,7,10-tetraazacyclo-dodecane-*N*,*N*′,*N*″,*N*‴-tetraacetate), NOTP [1,4,7-triazacyclononane-*N*,*N*′,*N*″-tris(methylenephosphonate)] and DOTP [1,4,7,10-tetraazacyclododecane-*N*,*N*′,*N*″,*N*‴-tetrakis(methylenephosphonate)] were characterised in aqueous solution by electronic absorption spectrophotometry and electron paramagnetic resonance (EPR) spectroscopy. While two isomeric species were detected by EPR spectroscopy in frozen samples of the polycarboxylate complexes, only one complex form was found for the poly(methylenephosphonate) systems. The results obtained are in accordance with a six-coordinate pattern for the metal centre, yielding tetragonally distorted complexes in solution, in agreement with previously reported studies on Cu^{II} complexes, both in solution and in the solid state.

Introduction

In the past two decades there has been a growing interest in the study of metal complexes with macrocyclic polyfunctional ligands, as they have found use in a wide variety of applications, ranging from analytical chemistry[1–4] to biochemistry and medicine.[5–7] A knowledge of the conformational preferences of these systems in aqueous solution is thus of the utmost importance in predicting their coordination behaviour and understanding their mechanism of action.

Among the numerous macrocyclic ligands known, the coordination chemistry of many transition metal ions with the *N*-substituted polyazamacrocycles NOTA (1,4,7-triazacyclononane-*N*,*N*',*N*''-triacetate), DOTA (1,4,7,10-tetraazacyclododecane-*N*,*N*',*N*'',*N*'''-tetraacetate), NOTP [1,4,7-triazacyclononane-*N*,*N*',*N*''-tris(methylenephosphonate)] and DOTP [1,4,7,10-tetraazacyclododecane-*N*,*N*',*N*'',*N*'''-tetrakis(methylenephosphonate)] (Figure 1), due to their remarkable chelating properties, has been the object of numerous studies. Complexes of the above ligands with Cu^{II} are well characterised, but no studies by electron paramagnetic spectroscopy (EPR) have been reported to date on Cu^{II} complexes with the tri- and tetraaza-polyphosphonate ligands. Furthermore, even though there is a reported EPR study on the Cu^{II}/DOTA system,[8] the effect of the pH on the EPR pattern of these macrocyclic complexes in aqueous solution was never investigated.

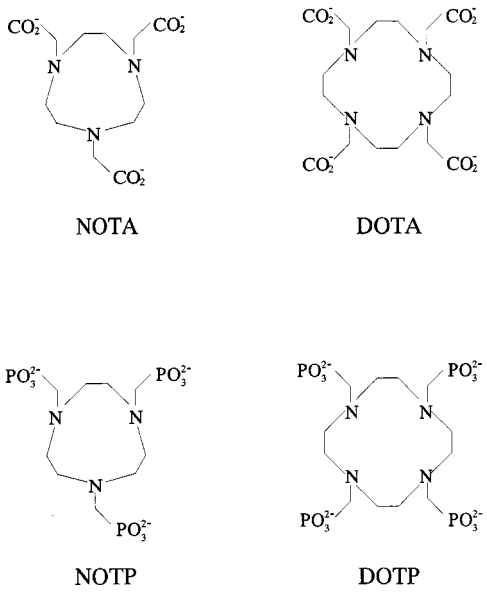


Figure 1. Schematic representation of the macrocyclic ligands investigated in this work

The solid-state structures of Cu^{II} complexes with NOTA,[9] NOTP,[10] DOTA,[11] and analogous tetraazamacrocyclic ligands,[12–20] have been obtained by X-ray diffractrometry. The NOTA complex in $Na[Cu(NOTA)] \cdot 2\,NaBr \cdot 8\,H_2O$ was found to have a distorted pseudoprismatic geometry, with the metal ion bound to all donor atoms of the ligand (three carboxylate oxygen atoms and three ring nitrogen atoms).[9] In the methylenephosphonate analogue Cu^{II}/NOTP the metal ion is bound to only two oxygen atoms from the pendant arms of the macrocycle and to the three ring nitrogen atoms in a dis-

[a] Centro de Neurociências da Universidade de Coimbra, and Dep. Bioquímica, Faculdade de Ciências e Tecnologia, Universidade de Coimbra, Ap. 3126, P-3049 Coimbra, Portugal
[b] Centro de Neurociências da Universidade de Coimbra, Unidade I D "Química-Física Molecular", Faculdade de Ciências e Tecnologia, Universidade de Coimbra, P-3049 Coimbra, Portugal
[c] CEQUP/Dep. Química, Faculdade de Ciências, Universidade do Porto, P-4169–007 Porto, Portugal

 © WILEY-VCH Verlag GmbH, D-69451 Weinheim, 2000 1434−1948/00/0303−0559 $ 17.50+.50/0

torted square-pyramidal structure; the axial position is occupied by a ring nitrogen atom, for which the usual long axial Cu–N bond length is observed.[10]

In the mononuclear Cu^{II} complex with the tetraaza ligand DOTA, the metal ion exists in a distorted octahedral geometry, coordinated to all ring nitrogen atoms and to two (opposite) carboxylate oxygen atoms; the other two carboxylate groups are protonated.[11] The two coordinated oxygen and two nitrogen atoms (in the *trans* positions in the macrocycle) occupy the equatorial positions, while the other two nitrogen atoms are axially bound. The axial bonds are elongated, as expected from the Jahn-Teller effect, but this elongation is not as pronounced as in other copper(II) complexes, probably as a consequence of steric constraints imposed by the cyclic structure of the ligand.

The stability constants in aqueous solution (at 298 K) of copper(II) complexes with polyaza ligands have been determined by several authors: NOTA, $\log K_{ML}$ = 21.63 (1 M $NaClO_4$);[21] DOTA, $\log K_{ML}$ = 22.25 [0.1 M $(CH_3)_4NNO_3$],[22–24] 22.72 (0.1 M KCl);[25] NOTP, $\log K_{ML}$ = 21.3 (1 M KNO_3);[26] DOTP, $\log K_{ML}$ = 25.4 (1 M KNO_3).[27] The presence of protonated species in aqueous solution (MH_nL, n is typically 1 or 2), along with the more stable nonprotonated form (ML), has been detected for some Cu^{II} macrocyclic chelates.[25,28,29] Although the formation of binuclear complexes (M_2L) has been observed in some cases in the solid state,[23] it appears to be negligible in solution.[20–22]

Most of the Cu^{II} tri- and tetraazamacrocyclic complexes present in aqueous solution are thus mononuclear and five- or six-coordinate, with the metal ion probably bound to all the nitrogen atoms of the macrocyclic ring and to two or three carboxylate oxygens of its pendant arms. These Cu^{II} complexes often display strong tetragonal distortions that normally result in a lengthening of the axial metal–ligand bonds and an associated compression of the four equatorial ones.

In the present work, Cu^{II} complexes with the polyazapolycarboxylate ligands NOTA and DOTA, and with the polyazapolymethylenephosphonate macrocycles NOTP and DOTP were studied in aqueous solution at different pH values and in the presence of distinct electrolytes, by electronic absorption spectrophotometry (visible region) and electron paramagnetic resonance spectroscopy (EPR). Whilst these techniques are not especially good indicators of the geometry of the copper(II) complexes, by taking into account the known solid-state structures of the NOTA, DOTA, and NOTP complexes, and those of other closely related compounds, it was possible to get some insight into the solution behaviour of these systems.[30]_[32]

Results and Discussion

Visible Spectrophotometry

The electronic absorption spectra (visible region) of the complexes studied exhibit an asymmetric band in the wavelength region between 500 and 850 nm (Table 1), with molar absorptivity coefficients that are typical of *d–d* transitions in highly symmetric Cu^{II} complexes with tetragonal Jahn–Teller distortion.[33] The cyclic nature of these chelating ligands, however, imposes limits on the extent of this distortion, and the difference in length between the axial and equatorial bonds to copper is smaller in Cu^{II} triaza and tetraazamacrocyclic chelates than in Cu^{II} complexes with noncyclic ligands.[34]

Table 1. Electronic transitions (visible region) for several Cu^{II} complexes with some polyazapoly-carboxylate/polymethylenephosphonate macrocycles, in aqueous solution at pH 7.0. The experiments were run at 298 K, for a sample concentration of $4 \cdot 10^{-3}$ mol·dm^{-3}

Complex	λ_{max}, nm (ε, dm^3·mol^{-1}·cm^{-1})
$Cu(H_2O)_6^{2+}$ [a]	833 (13)
Cu/NOTA	750 (75) 750 (72.2)[c]
Cu/DOTA	740 (95) 734 (100)[b]
$Cu(NOTP)^{4-}$	680 (110)
$Cu(DOTP)^{6-}$	640 (625)

[a] See ref. [33] – [b] See ref. [8], pH = 9.0, 298 K. – [c] See ref. [9], pH = 1.0–10.0, 298 K.

Cu/NOTA: Previous potentiometric and spectroscopic studies[21] have shown that two distinct complex species are present in aqueous solution. In the pH range 2.0 to 2.5, [Cu(HNOTA)] is present at concentrations higher than 60% of total copper, while for pH values above 3.5 the predominant form is $[Cu(NOTA)]^-$. These complexes exhibit different spectra: that of [Cu(HNOTA)] has a *d–d* band at 660 nm, which is bathochromically shifted to 750 nm in the deprotonated species.[21] The solid state geometry of $Na[Cu(NOTA)] \cdot 2\,NaBr \cdot 8\,H_2O$ is intermediate between pure octahedral and trigonal prismatic, and a distortion from octahedral geometry is expected to cause a decrease in ligand field strength and thus an increase in λ_{max}. Protonation of one of the carboxylate groups, and subsequent substitution by a solvent molecule, is accompanied by either a release of strain or a reorientation of the metal-to-ligand bonds, which leads to an increase in ligand field strength and thus explains the high energy for the *d–d* band in [Cu(HNOTA)]. These observations suggest that the ligand is five-coordinate in acidic solutions, but six-coordinate at high pH.

Cu/DOTA: Several copper complexes are present in solution: in the pH range 2.4 to 3.2, the fully protonated $[Cu(H_2DOTA)]$ complex is the most abundant, but at higher pH $[CuHDOTA]^-$ and $[Cu(DOTA)]^{2-}$ are also present in significant amounts, the former reaching its maximum concentration (ca. 30%, based on total Cu^{II} concentration) at pH 3.8, and the latter being the predominant form at pH higher than 4.6. However, the spectra now obtained were found to be insensitive to pH changes, thus suggesting that protonation does not impose severe structural changes in the coordination sphere. As the molecular struc-

ture of $[Cu(H_2DOTA)]$[11] reveals two nonbound carboxylate groups, deprotonation of these distant nonbonding carboxylate groups is not expected to exert a marked influence in the electronic structure of the metal complex. The spectrum of the crystalline form has one *d–d* band centred at 715 nm,[11] a value quite similar to that found in solution (Table 1); the small difference in band maxima is most probably due to solvation or solid-state effects. It should be noted that the energy of this *d–d* band is lower than that usually found for copper(II) complexes with tetragonally distorted octahedral geometry and an N_2O_2 equatorial plane. Nevertheless, the crystal structure shows that the tetragonal distortion is unusually small in this complex,[11] a consequence of the conformation adopted by the ligand, and this is expected to cause a decrease in the equatorial ligand field and thus in the energy of the *d–d* band. The similarity in the values of λ_{max} in the solid and in solution suggests that the ligand is mainly six-coordinate in solution.

Cu/NOTP: The band detected in the spectrum appears at energies similar to those of [Cu(HNOTA)][21] and $[Cu([9]aneN_3)(H_2O)_3]^{2+}$ in aqueous solution,[21,35] implying that the coordination mode of this macrocyclic polyphosphonate ligand is different from that of the similar complex, $[Cu(NOTA)]^-$. This is in accordance with the crystal structure reported for the NOTP complex, in which one of the phosphonate groups is not bound to the metal centre.[10] The distinct coordination behaviour of NOTP and NOTA may be attributed to their different charges. In fact, in Cu/NOTP a very high negative charge would be localised at the metal centre should the three available phosphonate groups bind to Cu^{II}, and thus NOTP is five-coordinate here.

Cu/DOTP: In this complex, the four nitrogen atoms of the cyclic structure are expected to be involved in bonding, leaving only two coordination sites of the metal centre available, either for pendant phosphonate groups or for solvent molecules. The spectra of the complexes with DOTP are significantly different from those with DOTA, implying distinct structures for these complexes in solution. However, the *d–d* band for Cu/DOTP is in the same energy range as that of the corresponding copper(II) complex with the ligand $[12]aneN_4$, which has a square-pyramidal geometry in solution, with the four ring nitrogen atoms defining the equatorial plane and one axial position occupied by a solvent molecule.[36] The present results support a similar structure for the Cu/DOTP complex, in which the axial position of the pyramid is probably occupied by an oxygen from one phosphonate side-arm, in analogy with the solid state geometry reported for the copper(II) complex with the similar ligand *N*,*N*',*N*'',*N*'''-tetrakis(2-diphenylphosphorylethyl)-1,4,7,10-tetraazacyclododecane.[37]

EPR Spectroscopy

The EPR spectra of frozen aqueous solutions (77 K) of the complexes under study are shown in Figures 2 and 3, and the corresponding anisotropic parameters are summarised in Table 2.

Cu/NOTA: The EPR spectrum of Cu/NOTA at pH 7 shows two different signals, corresponding to two distinct Cu^{II} complex species, in a 3:2 concentration ratio (Figure 2A, Table 2). Both signals are typical of Cu^{II} complexes in a tetragonal ligand field, with a $d(x^2 - y^2)$ ground state.[30] In order to check if the two species detected are pH dependent, EPR spectra were also recorded at pH 3 and pH 9. In alkaline solution the spectrum is identical to the one at pH 7, thus excluding the formation of hydroxo-complexes in this pH region. Under acidic conditions, however, it is possible to perceive at least one more Cu^{II} signal superimposed on the two signals observed at pH 7. Based on the stability constants reported in the literature[21] the additional signal detected at pH 3 must be due to [Cu(HNOTA)], while the other two signals observed in all the samples studied probably reflect the presence of two geometric isomers for $[Cu(NOTA)]^-$. Simulation of the spectrum obtained at pH 3 was unsuccessful, due to its poor resolution and to the existence of at least three different signals. To try to improve resolution, spectra were obtained in the presence of inert electrolytes: NaCl (1 M), $NaClO_4$ (0.1 and 1 M), and $(CH_3)_4NNO_3$ (0.1 M); however, no significant differences were obtained, either in resolution or in the overall signal pattern.

Several hypotheses concerning the occurrence of two isomeric forms of $[Cu(NOTA)]^-$, excluding protonation equilibria, may be advanced, but the large difference between the $g_\parallel$ and $A_\parallel$ values of the two signals observed at pH 7 clearly points to different coordination environments. The signal with $g_\parallel = 2.287$ and $A_\parallel = 149.5 \cdot 10^{-4}$ cm^{-1} is typical of a six-coordinate complex with a distorted octahedral structure similar to that observed in the solid state.[9] The smaller $g_\parallel$ and larger $A_\parallel$ values of the other signal, in turn, point to a significant decrease in the axial ligand field for the second isomer. This decrease in axial interaction may be caused either by substitution of one axial ligand by a solvent molecule, or simply by breaking of an axial ligand bond with formation of a five-coordinate square-pyramidal structure. The latter hypothesis is supported by the similarity between the EPR parameters of the system under discussion and those of Cu^{II} square-pyramidal complexes with the macrocyclic ligands $[12]aneN_4$,[36] 1,4,7,10-tetrabenzyl-2,5,8,11-tetraethyl-1,4,7,10-tetraazacyclododecane[39] and 7,11-bis(carboxymethyl)-1,4-dioxa-7,11-diazacyclotridecane.[40]

Cu/DOTA: The EPR spectrum of $[Cu(DOTA)]^{2-}$ in aqueous solution was previously obtained by other authors at pH 9 for a metal-to-ligand ratio of 1:2,[8] and the reported parameters are included in Table 2. The spectra obtained in the present work for a metal-to-ligand ratio of 1:1 and at pH 3, 7, and 9, are poorly resolved both at room temperature and in frozen solution (77 K). In order to improve spectral resolution several different electrolytes were added to the solutions; however, it was found that those electrolytes containing Na^+ interact with the copper(II) complexes studied (see below).

At pH 3 and in the absence of Na^+ ions, the spectra obtained either without electrolyte or in the presence of

Table 2. EPR parameters (X-band, 0.34 T, 9.5 GHz) for the Cu^{II} complexes with the polyazamacrocycles NOTA, DOTA, NOTP, and DOTP, in aqueous frozen solution (77 K), at pH 3.0 and 7.0

Complex[a]	pH		$g_{\parallel}$[b]	$g_{\perp}$[b]	$A_{\parallel}$ ($\times 10^4$) (cm^{-1})	$A_{\perp}$ ($\times 10^4$) (cm^{-1})[a,b]	$\kappa_{\parallel}$[c]	Population (%)[a]
Cu/NOTA	7.0[d]		2.233 2.287	2.051 2.063	179.0 149.5	30.0 15.0	0.46 0.57	60 40
Cu/DOTA	9.0		2.300[e]	2.062[e]	150.3[e]			
	7.0	no electrolyte	2.300	2.070	150.0			
	3.0	Na^+ (1 M)	2.278	2.063	169.0	< 5	–	100
	7.0[d]	Na^+ (1 M)	2.241	2.061	157.2	15.0	0.49	80
			2.301	2.058	150.0	10.0	0.61	20
Cu/NOTP	7.0		2.265	2.062	160.0	4.9	0.58	–
Cu/DOTP	7.0		2.210	2.035	165.0	4.4	0.49	–

[a] The experiments were run for a sample concentration of $1 \cdot 10^{-3}$ M. The reported values were obtained by simulation of the experimental spectra. – [b] Approximate value, as only one band is detected in this region of the spectrum. – [c] Calculated values using the spin-orbit coupling constant of the free Cu^{II} ion (-829 cm^{-1}) (ref.[38]) and the energy of the electronic transition band observed for each complex. – [d] Two different complexes in solution. – [e] From ref. [8], 9.28 GHz, pH 9.

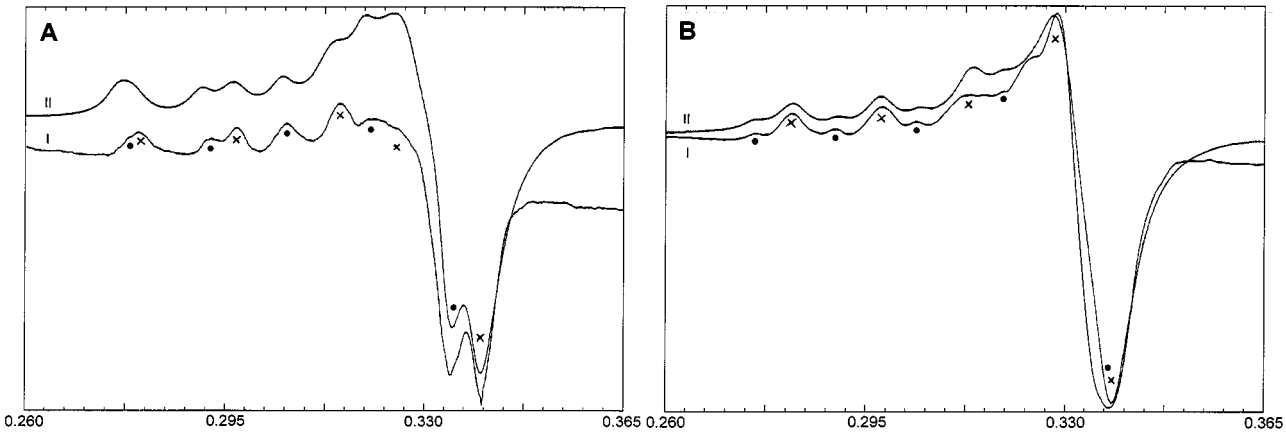


Figure 2. EPR spectra (X-band, 0.34 T, 9.5 GHz), at 77 K, of the Cu^{II} complexes (1:1) with the macrocyclic polyaza-polycarboxylate ligands NOTA (A) and DOTA (B), in aqueous solution at pH 7, in the presence of $1 \cdot 10^{-1}$ M Na^+: I – Experimental spectra; II – Simulated spectra; [complexes] = $1 \cdot 10^{-3}$ M; the symbols × and • refer to the major and minor complex species of each of the systems studied, respectively

$(CH_3)_4NNO_3$ (0.5 M) exhibit more than one signal but, due to their low resolution, no accurate EPR parameters could be obtained. Addition of $NaClO_4$ or NaCl caused significant spectral changes, namely the appearance of a new EPR signal superimposed on those observed for solutions without added electrolyte, and for $[Na^+] \geq 1$ M only this new signal was observed (see Figure 3).

Similar experiments were carried out for solutions at pH 7 and pH 9, but since the results obtained were identical for these two pH values they will be discussed together. In the absence of Na^+ the spectra, although poorly resolved, exhibit only one signal. Addition of NaCl or $NaClO_4$ induces clear changes in the spectra, with the appearance of a new copper(II) signal (Figure 2B). For these pH values, however, even for $[Na^+] = 1$ M, the new signal appears superimposed on the one detected without the electrolyte. The difference in EPR parameters for the two signals observed in solutions containing Na^+ is significant enough to indicate that the corresponding species have distinct coordination environments, thus implying that in the presence of high concentrations of Na^+ the Cu/DOTA complex undergoes a structural reorganisation.

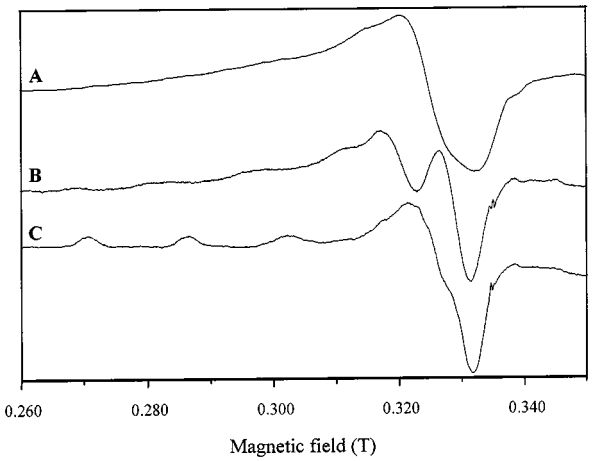


Figure 3. EPR spectra (X-band, 0.34 T, 9.5 GHz), at 77 K, of the Cu^{II} complex (1:1) with the macrocyclic polyaza-polycarboxylate ligand DOTA, in aqueous solution at pH 3, as a function of the concentration of Na^+ ion: A – $[Na^+] = 0$; B – $[Na^+] = 1 \cdot 10^{-1}$ M; C – $[Na^+] = 1$ M; [complex] = $1 \cdot 10^{-3}$ M

Analysis of the EPR parameters obtained in this work can yield additional information about the interaction of

the Cu/DOTA complex with Na^+. The signal obtained without added electrolyte at pH 7 was found to have unusual EPR parameters ($g_\perp = 2.10$, $g_\parallel = 2.30$ and $A_\parallel = 150 \cdot 10^{-4}$ cm^{-1}) for a tetragonally distorted octahedral chelate with a N_2O_2 equatorial plane, namely high $g_\parallel$ and low $A_\parallel$ values. These values can be accounted for by taking into consideration the crystallographic structure of this system,[11] that shows a small tetragonal distortion compared to what is usually found in other copper(II) complexes. A decrease in tetragonal distortion is expected to increase $g_\parallel$ and decrease $A_\parallel$, and also to decrease the anisotropy of the EPR spectra.[24] Thus, it is quite reasonable to assume that the spectrum observed at pH 7 without added Na^+ is due to $[Cu(DOTA)]^{2-}$, with a geometry similar to that observed in the solid state.

The new signals observed in the solutions containing Na^+, at both pH 3 and 7 are not significantly different. Comparison of the corresponding EPR parameters with those obtained from the spectrum at pH 7 in the absence of Na^+ shows that these new species have significantly lower $g_\parallel$ and higher $A_\parallel$ values. These values are similar to those commonly found for six-coordinate copper(II) complexes displaying a N_2O_2 equatorial plane. This seems to imply that these new complexes have a different structure, for which the steric constraints that impose a low axial distortion to copper coordination in $[Cu(DOTA)]^{2-}$ have been lost. This may be attributed either to partial solvolysis of $[Cu(DOTA)]^{2-}$ or to a rearrangement of the ligand around the metal, leading to a distinct coordination pattern. This structural reorganisation induced by Na^+ points to a strong interaction between the alkali metal ion and the copper(II) complex, either (a) by binding to the ligand free acetate groups, or (b) by competition of the sodium ions with Cu^{II} for the coordinated acetate side-arms.

A precedent for the former hypothesis is provided by noting that Na^+ binds to the free ligand ($\log K_{Na/DOTA} = 4.38$, $[(CH_3)_4NNO_3] = 0.1$ M).[16] However, against this it should be noted that if Na^+ only interacts significantly with the free acetate groups of the complex, its effect would be more important for negatively charged species; it was found that at pH 7 and $[Na^+] = 1$ M, where the predominant complex species would have a –2 charge, the presence of $[Cu(DOTA)]^{2-}$ is still detected, while at pH 3, where the Cu^{II} complexes are expected to be protonated, either neutral or with a +1 charge, only the signal due to the Na^+/Cu/DOTA complex was observed. Our results thus seem to support the second hypothesis, despite the large stability constants in aqueous solution of these Cu^{II} macrocyclic chelates. The observed pH dependence for the formation of Na^+/Cu/DOTA complexes may result from the lower stability of the protonated complexes, due to the smaller negative charge of the protonated ligand, which favours the release of at least one acetate group which would promptly bind to Na^+. It is worth noting, however, that the EPR signals detected at pH 3 and 7 (Figure 2 and Figure 3) in the presence of Na^+ are slightly different, which implies that they are not due to identical species but to structurally very similar complexes. These small differences are probably a consequence of differing degrees of protonation of the complex.

Analysis of the EPR parameters for the Na^+/Cu/DOTA system show that these new complexes seem to have very different structures to that of $[Cu(DOTA)]^{2-}$ in the solid state, an observation that also favours the hypothesis of release of at least one of the carboxylate pendant arms of the macrocyclic ligand, either yielding a five-coordinate complex or merely leading to substitution by a solvent molecule in the coordination sphere of the metal ion. In either case, breaking of one M−O(carboxylate) bond would release some of the steric strain imposed by the ligand, as present in the solid state, which would facilitate decoordination.

Cu/NOTP and Cu/DOTP: The frozen solution EPR spectra of Cu/NOTP and Cu/DOTP at pH 7 reflect the axial symmetry of these systems (with $g_\parallel >> g_\perp$). Hyperfine structure due to the copper nuclei (^{63}Cu and ^{65}Cu, $I = 3/2$) is detected in the parallel region (Table 2), whereas the perpendicular region is not sufficiently resolved to allow the observation of any such splitting. These data are typical of Cu^{II} complexes in a tetragonal field, with a $d(x^2 - y^2)$ ground state.[24] The band patterns at pH 3, 7, and 9 are very similar, which indicates that protonation of these complexes does not induce significant structural or electronic changes. This observation may be taken as an indication that protonation of these systems probably takes place at the unbound phosphonate side-arms.

The influence of added electrolytes [NaCl, $NaClO_4$, and $(CH_3)_4NNO_3$] was also checked, but no appreciable changes in the EPR spectra were detected, either in the overall signal pattern or in band width.

Based on the spectrophotometric results discussed above, a *trans* coordination of DOTP to the metal centre has been proposed, implying an N_4 equatorial plane. The EPR parameters obtained for this system support that hypothesis, although the $g_\parallel$ value is higher, and the $A_\parallel$ value smaller, than typical values found for other complexes with this coordination environment. These differences, however, may be a consequence of a strong axial bond with the oxygen atom of a phosphonate side-arm, similar to the one reported for the related complex with *N*,*N*',*N*'',*N*'''-tetrakis(2-diphenylphosphorylethyl)-1,4,7,10-tetraazacyclododecane.[37]

For Cu/NOTP, the $g_\parallel$ value is larger than that of DOTA, in agreement with the N_2O_2 equatorial plane expected for this complex. As in Cu/DOTP, the $A_\parallel$ value is smaller than expected for a square-pyramidal structure. This may also be rationalised by a strong axial metal–ligand interaction, since a low tetragonal distortion is expected in this case due to the facial coordination of the cycle, which imposes a short axial bond to the nitrogen atom.

Conclusion

One important result that emerged from the present study is that the polyphosphonate ligands NOTP and DOTP always coordinate to copper(II) in a pentadentate mode, although the corresponding complexes may be five- or six-coordinate by binding a solvent molecule. This behaviour is to be contrasted with that of the polycarboxylate

ligands NOTA and DOTA, which is more complex. Firstly, the coordination mode of the ligands was found to be pH dependent: (a) in copper(II) complexes with NOTA the ligand is five-coordinate in acidic solutions, through protonation of one carboxylate group, but at pH 7 two complexes were observed in solution, probably with the ligand being six- and five-coordinate; (b) in those complexes with DOTA, the ligand is essentially six-coordinate, although at low pH the possibility of protonation of one bound carboxylate group could not be ruled out. Secondly, the DOTA coordination mode was also found to be dependent on the presence of sodium ions in solution, which are capable of competing with Cu^{II} for coordinating carboxylates; in fact, with $[Na^+] = 1$ M and at pH 3 only complexes in which DOTA acts as a five-coordinate ligand could be detected by EPR, whereas at pH 7, two species – displaying a six-coordinate and five-coordinate DOTA – were observed. Once the presence of sodium ions was found not to affect the coordination equilibria of the other three macrocyclic ligands, it is likely that the steric constraint imposed by DOTA when acting in a six-coordinate mode eases by decoordination of one carboxylate group when in the presence of a large excess of sodium ions.

Experimental Section

General: The ligands were synthesised and purified as described elsewhere (NOTA,[41] DOTA,[23,42] NOTP and DOTP[43,44]). The purity of the ligands was checked by ^{1}H-NMR spectroscopy (Varian XL-200 and Varian Unity-500 spectrometers).

Preparation of Copper(II) Complexes: The concentration of the ligand solutions was determined by complexometric titration, using a copper chloride solution and murexide (5,5'-nitrilodibarbituric acid) as an indicator. The copper chloride solution was previously titrated with standard EDTA, with Black Sulphon F [1-hydroxy-8-(2-hydroxynaphthylazo)-2-(sulfonaphthylazo)-3,6-disulfonic acid] as an indicator. Stock aqueous solutions of the complexes ($1\cdot10^{-3}$ M) were prepared by adding stoichiometric amounts of the macrocyclic ligand to a solution of copper chloride (Aldrich). The pH of the solutions was adjusted with HCl and CO_2-free NaOH (using a Crison MicropH 2002 pH-meter with an Ingold 405-M5 combined electrode).

Spectroscopic Studies: The electronic spectra (visible region) were obtained in a double beam JASCO-7800 spectrometer (cell with 1 cm optical path). The experiments were run at 298 K, in the pH range between 2.0 and 10.0, for sample concentrations of $1\cdot10^{-3}$ and $1\cdot10^{-5}$ M. No changes in spectra were observed upon repeating the measurements one week after the first run.

The EPR spectra (X-band, 0.34 T, 9.5 GHz), were obtained in a continuous wave BRUKER ESP-300E spectrometer, with a microwave power of 15.9 mW and a modulation frequency of 100 kHz. The experiments were performed at pH 3.0, 7.0, and 9.0, both at 298 K and at 77 K (frozen samples). DPPH (2,2-diphenyl-1-picrylhydrazil radical) was used as an internal reference ($g = 2.0037$). Simulation of experimental EPR spectra, in order to obtain the corresponding anisotropic parameters, were performed using a modified version of the program developed by Pilbrow.[45] This program assumes a purely Lorentzian shape for the EPR bands, and does not account for changes in signal width with external magnetic field. The simulation was carried out ignoring the isotopic mixture of the copper nuclei and nuclear quadrupole effects.

Acknowledgments

Financial support from "Fundação para a Ciência e Tecnologia", Portugal, is gratefully acknowledged, through projects Praxis 2/2.1/SAU/1194/95 (CG), Praxis 2/2.1/QUI/316/94 (BC), and PBIC/C/QUI/2219/95 (MPM).

[1] M. Studer, T. A. Kaden, H. R. Mäcke, *Helv. Chim. Acta* **1990**, *73*, 149.
[2] G. L. DeNardo, G. R. Mirick, L. A. Kroger, R. T. O'Donnell, C. F. Meares, S. J. DeNardo, *J. Nucl. Med.* **1996**, *37*, 451.
[3] E. L. Hegg, J. N. Burstyn, *Inorg. Chem.* **1996**, *35*, 7474.
[4] E. L. Hegg, J. N. Burstyn, *J. Am. Chem. Soc.* **1995**, *117*, 7015.
[5] S. V. Deshpande, S. J. DeNardo, D. L. Kukis, M. K. Moi, M. J. McCall, G. L. DeNardo, C. F. Meares, *J. Nucl. Med.* **1990**, *31*, 473.
[6] C. F. G. C. Geraldes, A. D. Sherry, R. D. Brown III, S. H. Koenig, *Magn. Res. Med.* **1986**, *3*, 242.
[7] K. Kumar, M. F. Tweedle, *Pure Appl. Chem.* **1993**, *65*, 515, and refs. therein.
[8] R. Delgado, J. J. R. Fraústo da Silva, M. C. T. A. Vaz, *Talanta* **1986**, *33*, 285.
[9] K. Wieghardt, U. Bossek, P. Chanduri, W. Herrmann, B. C. Menke, J. Weiss, *Inorg. Chem.* **1982**, *21*, 4308.
[10] M. Y. Antipin, A. P. Baranov, M. I. Kabachnik, T. Y. Medved', Y. M. Polikarpov, Y. T. Struchkov, B. K. Shcherbakov, *Dokl. Akad. Nauk SSSR* **1986**, *287*, 130.
[11] A. Riesen, M. Zehnder, T. A. Kaden, *Helv. Chim. Acta* **1986**, *69*, 2067.
[12] K. Kumar, M. F. Tweedle, M. F. Malley, J. Z. Gougoutas, *Inorg. Chem.* **1995**, *34*, 6472.
[13] A. Riesen, M. Zehnder, T. A. Kaden, *Helv. Chim. Acta* **1986**, *69*, 2074.
[14] R. Clay, P. Murray-Rust, J. Murray-Rust, *Acta Cryst.* **1979**, *B35*, 1984.
[15] T. Sakurai, K. Kobayashi, A. Hasegawa, S. Tsuboyama, K. Tsuboyama, *Acta Cryst.* **1982**, *B38*, 107.
[16] R. E. DeSimeone, E. L. Blinn, K. F. Mucker, *Inorg. Nucl. Chem. Lett.* **1980**, *16*, 23.
[17] K. Kobayashi, T. Sakurai, A. Hasegawa, S. Tsuboyama, K. Tsuboyama, *Acta Cryst.* **1982**, *B38*, 1154.
[18] A. Riesen, M. Zehnder, T. A. Kaden, *J. Chem. Soc., Chem. Commun.* **1985**, 1336.
[19] A. Riesen, M. Zehnder, T. A. Kaden, *Acta Cryst.* **1988**, *C44*, 1740.
[20] F. P. Remoortere, F. B. Boer, E. C. Steiner, *Acta Cryst.* **1975**, *B31*, 1420.
[21] A. Bevilacqua, R. I. Gelb, W. B. Hebard, L. J. Zompa, *Inorg. Chem.* **1987**, *26*, 2699.
[22] H. Stetter, W. Frank, *Angew. Chem. Int. Ed. Engl.* **1976**, *15*, 686.
[23] R. Delgado, J. J. R. Fraústo da Silva, *Talanta* **1982**, *29*, 815.
[24] S. Chaves, R. Delgado, J. J. R. Fraústo da Silva, *Talanta* **1992**, *39*, 249.
[25] A. T. Clarke, A. E. Martell, *Inorg. Chim. Acta* **1991**, *190*, 27.
[26] I. M. Kabachnik, T. Y. Medved', Y. M. Polikarpov, B. K. Shcherbakov, F. I. Bel'skii, E. I. Matrosov, M. P. Pasechnik, *Bull. Acad. Sci. USSR* **1984**, *33*, 769.
[27] I. M. Kabachnik, T. Y. Medved', F. I. Bel'skii, S. A. Pisareva, *Bull. Acad. Sci. USSR* **1984**, *33*, 777.
[28] H. Z. Cai, T. A. Kaden, *Helv. Chim. Acta* **1994**, *77*,383.
[29] E. Hörmann, P. C. Riesen, M. Neuburger, M. Zehnder, T. A. Kaden, *Helv. Chim. Acta* **1996**, *79*, 235.
[30] B. J. Hathaway, *Coord. Chem. Rev.* **1983**, *52*, 87, and refs. therein.
[31] D. Kivelson, R. Neiman, *J. Chem. Phys.* **1961**, *35*, 149.
[32] J. Peisach, W. E. Blumberg, *Arch. Biochem. Biophys.* **1974**, *165*, 691.
[33] A. B. P. Lever, *Inorganic Electronic Spectroscopy*, Elsevier, Amsterdam **1968**.
[34] J. Gazo, I. B. Bersuker, J. Garaj, M. Kabesová, J. Kohout, H. Langfelderová, M. Melník, M. Serátor, F. Valach, *Coord. Chem. Rev.* **1976**, *19*, 253.
[35] R. Yang, L. J. Zompa, *Inorg. Chem.* **1976**, *15*, 1499.

[36] M. C. Styka, R. C. Smierciak, E. L. Blinn, R. E. DeSimone, J. V. Passariello, *Inorg. Chem.* **1978**, *17*, 82.
[37] M. Y. Antipin, A. P. Baranov, M. I, Kabachnik, S. A. Pisareva, Y. M. Polikarpov, E. I. Sinyasvskaya, Y. T. Struchkov, L. B. Tsimbal, *Heteroatom Chem.* **1996**, *7*, 229.
[38] A. Abragam, B. Bleaney, *Electron Paramagnetic Resonance of Transition Ions* (Eds.: W. Marshall, D. H. Wilkinson), Clarendon Press, Oxford **1970**.
[39] N. Azuma, Y. Kohno, F. Nemoto, Y. Kajirawa, K. Ishizu, T. Takakuwa, S. Tsubayama, K. Tsubayama, K. Kabayashi, T. Sakurai, *Inorg. Chim. Acta* **1994**, *215*, 109.
[40] S. Chaves, A. Cerva, R. Delgado, *Polyhedron* **1998**, *17*, 93.
[41] C. F. G. C. Geraldes, M. C. Alpoim, M. P. M. Marques, A. D. Sherry, M. Singh, *Inorg. Chem.* **1985**, *24*, 3876.
[42] J. F. Desreux, *Inorg. Chem.* **1980**, *19*, 1319.
[43] A. D. Sherry, C. R. Malloy, F. M. H. Jeffrey, W. P. Cacheris, C. F. G. C. Geraldes, *J. Magn. Res.* **1988**, *76*, 528.
[44] C. F. G. C. Geraldes, A. D. Sherry, W. P. Cacheris, *Inorg. Chem.* **1989**, *28*, 3336.
[45] J. R. Pilbrow, M. E. Winfield, *Mol. Phys.* **1973**, *25*, 1073.

Received April 29, 1999
[I99161]

Synthesis, Characterization and Electrochemistry of Complexes Derived from $[(1),2,3\text{-}P_2Mo_2W_{15}O_{61}]^{10-}$ and First Transition Metal Ions

Roland Contant,*[a] Mostefa Abbessi,[a][+] Jacqueline Canny,[a] Martine Richet,[a] Bineta Keita,[b] Abderrahmane Belhouari,[b] and Louis Nadjo*[b]

Keywords: Polyoxometalates / Heteropolyanions / Dawson-type structures / Transition metal cations / Electrochemistry

The complexes formed by $[(1)\text{-}2,3\text{-}P_2Mo_2W_{15}O_{61}]^{10-}$ with vanadium(IV), manganese(II), cobalt(II), nickel(II), copper(II), and zinc(II) were synthesized. They were characterized by elemental analysis, IR, UV/Vis and ^{31}P NMR spectroscopy. Their electrochemical studies are complemented by those of the previously synthesized iron(III)- and Mo(VI)-substituted complexes. Among the main conclusions from the electrochemistry of all these compounds, it can be pointed out that only the iron(III) and the copper(II) ions within the complexes are reducible in the same potential domain as the molybdenum(VI) moieties. In the case of the iron(III) complex, it has been possible to obtain a reversible overall three-electron process on the first wave of the oxometalate by varying the pH of the solution. In contrast, copper can be deposited from the corresponding complex. Substitution of $[(1)\text{-}2,3\text{-}P_2Mo_2W_{15}O_{61}]^{10-}$ with vanadium(IV), manganese(II), iron(III), cobalt(II), nickel(II), copper(II), zinc(II) and molybdenum(VI) gives a series of complexes in which the trimetallic moiety constituting one of the "caps" of the polyoxometalate contains cations different from the remaining tungsten skeleton. The electrochemical properties of these complexes are modulated by this particular constitution.

Introduction

In recent articles,[1,2] we described the syntheses, characterization and the electrochemical properties of some monoferro-heptadecatungsto-diphosphates and pentadecatungsto-dimolybdo-diphosphates. This work constitutes a first step in our systematic examination of parameters and combination of parameters which could favor or counteract the merging of the first several waves in heteropolyanion (HPA) electrochemistry. As a matter of fact, it turns out that most energetically favorable electro-reductive catalytic processes triggered by HPAs require more than one electron and are thus, usually accomplished at fairly negative potentials where the necessary number of electrons could be accumulated and delivered by the framework. In the above-mentioned articles from this group, three complexes of the present series have already been studied, with M = Mo^{VI}, V^{V}, Fe^{III}. The electrochemistry of $\alpha_2P_2Mo_3W_{15}$ has been described briefly.[2,3] In a pH = 2 medium, its cyclic voltammogram begins with three well-behaved one-electron diffusion waves. In contrast, with V^{V} as a substituent instead of Mo^{VI}, the molybdenum centers are easily reduced through an apparently direct two-electron process. Still more striking, the substitution by Fe^{III}, combined with pH effects, allows for an approach to an overall three-electron process on the first voltammetric wave of the corresponding complex in a pH = 2 medium. Such results stimulated the need for the present study. Furthermore, as another incentive, it is anticipated that the presence of two molybdenum atoms in the "cap" near the substituent heterocation might substantially influence the electronic communication between the various sites in this trimetallic moiety, especially during redox processes. In this context, we describe here the syntheses, characterization and electrochemical properties of the complexes formed by $[(1)\text{-}2,3\text{-}P_2Mo_2W_{15}O_{61}]^{10-}$ with some first transition metal ions and with the Zn dication.

[a] Laboratoire de Chimie Inorganique et Matériaux Moléculaires, UPRESA 7071, CNRS, Université Paris VI,
4, place Jussieu, 75252 Paris Cedex 05, France
Fax: (internat.)+33–1/44 27 38 41
[b] Laboratoire de Physicochimie des Rayonnements, UMR 8610, CNRS, Electrochimie et Photoélectrochimie, Université Paris-Sud,
Bâtiment 420, 91405 Orsay Cedex, France
Fax: (internat.)+33-1/69 15 43 28
[+] Permanent address: University of Annaba, Algeria

Results and Discussion

All the polyanions to be studied here can be considered as being primarily derived from $[\alpha P_2W_{18}O_{62}]^{6-}$, abbreviated as P_2W_{18}. In Figure 1, the tungsten atoms in αP_2W_{18} are

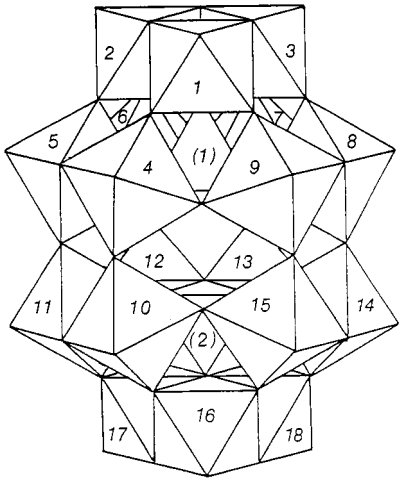


Figure 1. Numbering scheme of $\alpha\text{-}P_2W_{18}O_{62}^{6-}$ (Dawson structure)

 © WILEY-VCH Verlag GmbH, D-69451 Weinheim, 2000 1434–1948/00/0303–0567 $ 17.50+.50/0

Table 1. Selected IR data for $(M^{(x)}(H_2O)(P_2Mo_2W_{15}O_{61})^{10-x}$. The assignments follow from the results of references 9 through 11 (ν_{as}: $\nu_{asymmetric}$; vs.: very strong; s: strong; m: medium; sh: shoulder; w: weak).

	ν_{as} **PO$_a$**W	ν_{as} **PO$_a$**Mo	ν_{as}W**O$_d$**	ν_{as}Mo**O$_d$**
α-$K_6P_2W_{18}O_{62}$	1091(vs.)		959(s)	
	1021(w)		911(s)	
α2-$K_{10}P_2W_{17}O_{61}$	1084(vs.)		938(s)	
	1051(m)		910(m)	
	1014(m)		867(w)	
α-$Na_{12}P_2W_{15}O_{56}$	1131(s)		935(w)	
	1087(vs.)			
	1008(s)			
	977(w)		913(w)	
α2-$K_{10}P_2Mo_2W_{15}O_{61}$	1082(vs.)		936(vs.)	
	1022(w)	1047(m)	922(sh)	885(m)
α2-$K_8(VOP_2Mo_2W_{15}O_{61})$	1084(vs.)		945(vs.)	
	1016(m)	1062(w)	918(w)	888(w)
α3-$K_8(Mn(OH_2)P_2Mo_2W_{15}O_{61})$	1083(vs.)		939(m)	
	1012(m)	1054(m)	916(w)	896(sh)
α2-$K_8(Co(OH_2)P_2Mo_2W_{15}O_{61})$	1083(vs.)		941(vs.)	
	1010(m)	1060(w)	915(m)	892(sh)
α2-$K_8(Ni(OH_2)P_2Mo_2W_{15}O_{61})$	1083(vs.)		942(vs.)	
	1009(m)	1059(sh)	916(m)	893(sh)
α2-$K_8(Cu(OH_2)P_2Mo_2W_{15}O_{61})$	1083(vs.)		940(vs.)	
	1015(w)	1056(m)	918(w)	890(w)
α2-$K_8Zn(OH_2)P_2Mo_2W_{15}O_{61})$	1083(vs.)		940(vs.)	
	1014(m)	1055(m)	918(w)	890(sh)

numbered according to the IUPAC recommendations.[4] The two P atoms are numbered (1) and (2) for the upper and the lower halves of the molecule, respectively. Considering the upper half of the molecule and taking into account the numbering, the metal atoms in the "cap" occupy what will be termed α_2 positions and those in the "belt", α_1 positions. In the lacunary species, the vacancies (missing W atoms) are numbered in the same way and represented by □ in the formula of the anion. Any heterometal filling the vacancy will keep the same index.

Syntheses

The metal cation substituted species were elaborated under the same conditions as the iron(III)-substituted one. However, the ^{31}P NMR spectra have shown that there was an isomerically pure compound with V, Ni and Cu, but two compounds with Mn, Co and Zn. With heated Co sample, two main compounds and several isomeric impurities were observed. Such a behavior has been described by T. L. Jorris et al.[5] on metallo-heptadecatungsto-diphosphates. and was interpreted as $\alpha_2 \rightarrow \alpha_1$ isomerization. In our case the migration of molybdenum atoms may give numerous other isomers. The number and the nature and the ratio of isomers depend on preparation conditions. To obtain more than 90% of the α_2 isomer, the synthesis must be performed in acidic solution without heating.

UV/Vis and IR Characterization

The formation constants of the complexes have been measured. The logβ values are fairly large; they are shown in brackets for the various substituent metal cations: V^{IV} (>18); Mn^{II} (6.5); Fe^{III} (17.2); Co^{II} (7.4); Ni^{II} (7.5); Cu^{II} (7.9); Zn^{II} (7.5). The electrochemical behavior to be discussed in a subsequent section, has been studied essentially at pH 3 and 5 for all the complexes. Their stability in these media and, occasionally in others when necessary, has been checked by monitoring their UV/Vis spectra at least over a period of 24 h. The only slight instability was detected with the cobalt-substituted compound, which shows decreasing absorbance, even though the decrease is not fast enough to preclude an electrochemical study.

^{31}P NMR

The NMR study of paramagnetic elements containing HPAs was performed by Jorris et al.[5] on P_2W_{17}. They found no isomerically pure compound but a mixture of α_1 and α_2 isomers. They observed with the α_2 isomer that the chemical shifts of the P atom far from the paramagnetic elements were unaffected by the nature of the element. There is an exception: Co^{II}. The same observation, with the same exception, appears in Table 2 and in Figure 2. This

Table 2. ^{31}P NMR chemical shifts (from 85% H_3PO_4) and line widths of α_1- and α_2-monometallo-dimolybdo-pentadecatungsto-diphosphates at 298 K (0.01 M solutions of K^+ salts in LiCl 1 M, in 20% D_2O)

Species	δ(P1) ppm	Δν(P1) Hz	δ (P2) ppm	Δν(P2) Hz
$V^{IV}P_2Mo_2W_{15}$[a]	8.3	2500	–13.7	15
$Mn^{II}P_2Mo_2W_{15}$[a]	not observed		–13.0	150
$Fe^{III}P_2Mo_2W_{15}$[a]	ca. 900	ca.>30000	–13.6	100
$Co^{II}P_2Mo_2W_{15}$[a]	350	80	–17.7	6
$Ni^{II}P_2Mo_2W_{15}$[a]	ca. 230	1100	–14.1	80
$Cu^{II}P_2Mo_2W_{15}$[a]	–27.2	1100	–13.0	60
$Zn^{II}P_2Mo_2W_{15}$[a]	–6.3	3	–13.65	3
P_2Mo_2W15[b]	–4.93	2	–13.75	2
$P_2Mo_3W_{15}$[b]	–9.7	2	–12.24	2
$Mn^{II}P_2Mo_2W_{15}$[c] (α_1)	not observed		–4.1	200
$Co^{II}P_2Mo_2W_{15}$[c] (α_1)	300	100	–20.8	6
$Zn^{II}P_2Mo_2W_{15}$[c] (α_1)	–7.21	3	–13.6	2

[a] Pure isomer or main product. – [b] See ref.[4] – [c] Minor product.

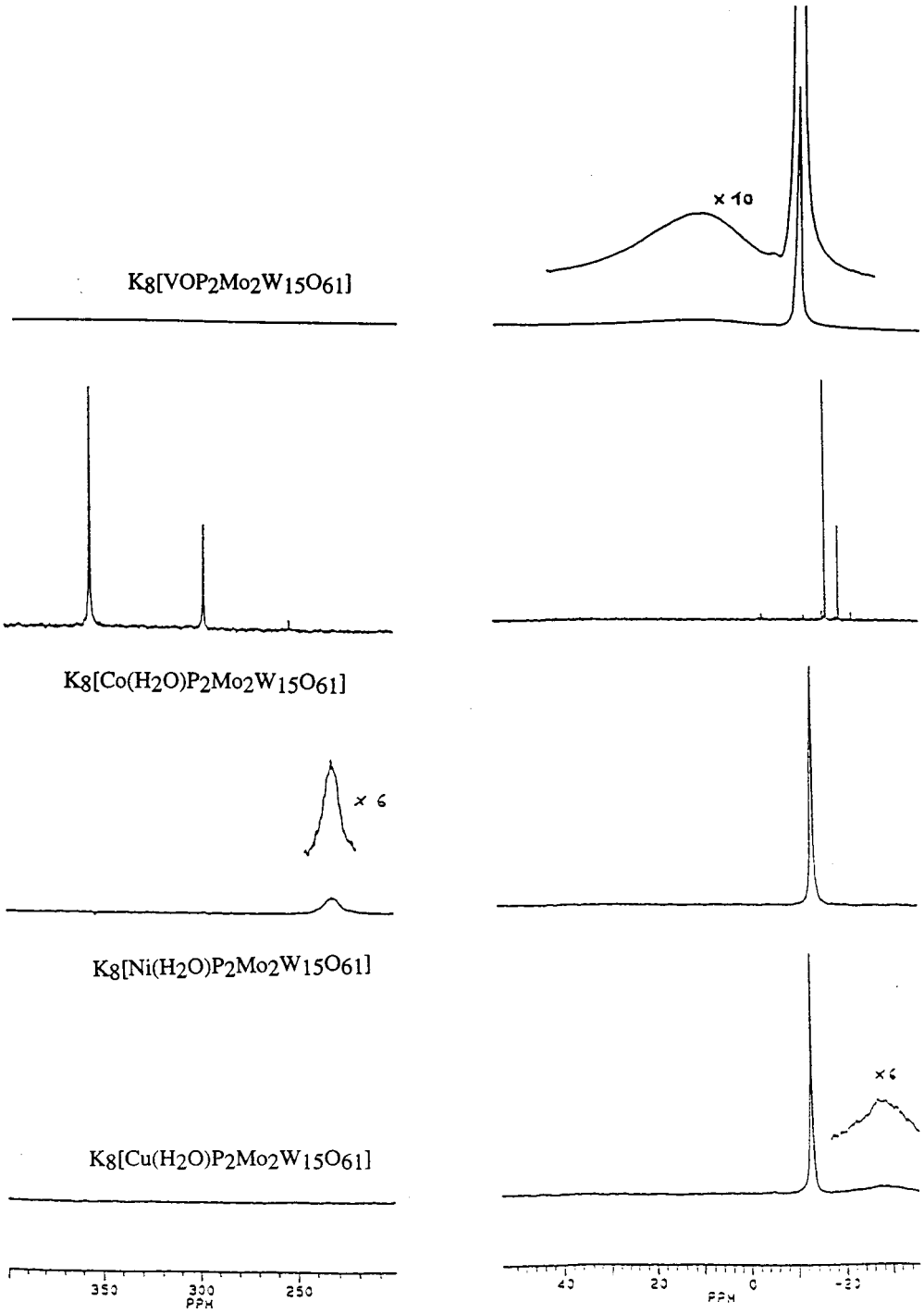


Figure 2. Selected representative ^{31}P NMR spectra. The appropriate compound formula is indicated on each spectrum

Figure shows spectra representative of the whole series. Such an observation confirms the stereospecificity of the syntheses. Under the same standard conditions used for all the other compounds, only one ^{31}P NMR line is observed for the V^{IV}-substituted species. Therefore, particular attention has been exercised to obtain a satisfactory ^{31}P NMR spectrum for this complex. A fairly concentrated solution of the lithium salt of this compound was prepared. With such a solution, it has been possible to observe the NMR line corresponding to the phosphorus atom in the close vicinity of the magnetic atom. This line appears at around $\delta = 8.3$ ppm and is roughly 2500 Hz broad.

Electrochemistry

The following studies are restricted either to the first or to the first few chemically reversible redox processes of the substituted complexes, and to their changes with pH. As a matter of fact, we are interested in controlling the number

of electrons which could be accumulated on the first wave of HPAs. This restriction also avoids any derivatization of the electrode surface as observed previously, albeit under different conditions.[9] In this study, the focus will be directed mainly on the reduction of molybdenum centers up to the first wave corresponding to the reduction of the tungsten framework. The redox behavior of the "substituent" metallic center will be considered simultaneously when it happens to appear in the potential domain of interest for the reduction of molybdenum centers. Otherwise, this behavior will be described separately.

Well-separated redox behaviors for the substituent cation and for the HPA framework: This situation is encountered with V^{IV}-, Mn^{II}-, Co^{II}-, Ni^{II}-, and Zn^{II}-substituted compounds. Figure 3 shows representative examples of the main features observed, throughout this work, for most of the complexes at pH = 3 and pH = 5. The Ni^{II} and V^{IV} complexes have been chosen. The cyclic voltammogram of the parent lacunary complex has been added for comparison. In Figure 3A, two well-behaved redox systems are observed. In line with previous work,[1,2,10] the first wave is assigned to the reduction of the molybdenum centers. Whatever the substituted complex, only very modest peak potential and peak current intensity variations are observed compared to the same parameters for the lacunary species, provided comparable concentrations are used. It must be concluded that for the pH = 3 medium, the Ni^{II}- and V^{IV}-substituted complexes behave in the same way as the lacunary compound, at least where the reduction of the molybdenum centers is concerned. No reduction of the substituent "heterometallic" cation has been detected in the potential domain studied. In Figure 3A, the wave corresponding to the reduction of the tungsten framework appears to be more discriminating among the complexes. Starting with the lacunary compound, the potential location of this "tungsten wave" is pushed to more and more negative values when passing to the Ni^{II}- and the V^{IV}-substituted complexes. It is worth noting that the trend is the same, but much more pronounced here than for the reduction of molybdenum centers. In this pH = 3 medium, exactly the same general behavior as observed for the Ni^{II}- and V^{IV}-substituted complexes is seen with Mn^{II}, Co^{II}, and Zn^{II} as substituents.

Figure 3B, obtained at pH = 5 for the lacunary species and for the Ni^{II}- and V^{IV}-substituted complexes displays more contrasted behaviors. We focus first on the cyclic voltammogram of the lacunary species. The cathodic pattern is composed of a system of drawn-out, presumably close-spaced two waves, followed by a well-defined two-electron wave. By continuity with the observations performed in the pH = 3 and the pH = 4 (not shown) media, the first system should be attributed to the reduction of molybdenum centers, while the last wave should feature the reduction of the tungsten framework. It is worth noting that on potential reversal, the respective anodic traces are well-behaved. In particular, a single anodic wave is observed for the reoxidation of the molybdenum centers. This result would suggest that no intrinsic electron-transfer "slowness" should actually exist for the reduction of molybdenum moieties. So, the

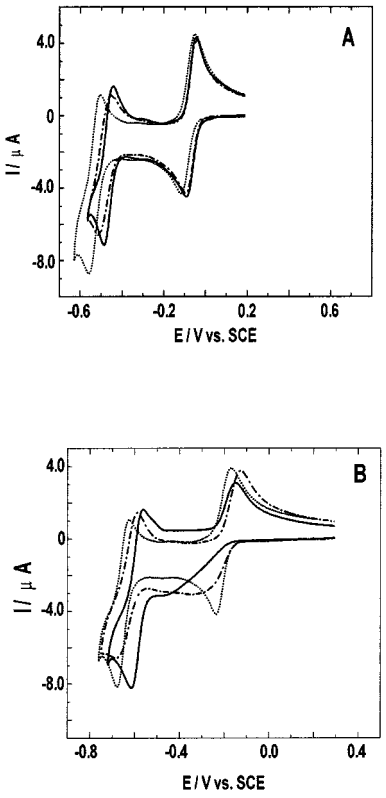


Figure 3. Comparison of the cyclic voltammograms observed for 5 × 10^{-4} M solutions of the lacunary heteropolyanion [(1)-2,3-$P_2Mo_2W_{15}O_{61}$]$^{10-}$ and the corresponding Ni^{II}- and V^{IV}-substituted complexes. Scan rate: 10 mV s^{-1} .(A) pH = 3 (0.2 M Na_2SO_4 + H_2SO_4): *solid line curve*: $P_2\square Mo_2W_{15}$; *dot and dash curve*: $P_2W_{15}Mo_2Ni$; *short dot curve*: $VP_2Mo_2W_{15}$. (B) pH = 5 (0.2 M CH_3COONa + CH_3COOH): *solid line curve*: $P_2\square Mo_2W_{15}$; *dot and dash curve*: $P_2W_{15}Mo_2Ni$; *short dot curve* $P_2VMo_2W_{15}$. For further details, see text.

observation might be traced to one or several of the following effects: condensation, pH and/or cation effects in the solution. The cyclic voltammetric patterns for Ni^{II}- and V^{IV}-substituted compounds can be considered as featuring a modulation, to different extents, of the observed sluggishness in the lacunary complex. For the V^{IV} complex, the first wave remains peak-shaped while a rather plateau current is obtained for the Ni^{II} complex. It must be noted that the "slowness" is less pronounced for these complexes than for the lacunary compound. Also, the tungsten wave can no longer be considered as a fingerprint to distinguish between the Ni^{II} and V^{IV} compounds, as their potential locations are now roughly the same.

The observations in the pH = 4 medium show a smooth transition of wave shapes and potential locations from the pH = 5 medium**.** The complexes substituted by the other metallic cations selected in this work, have also been examined in the same pH media. Due to the smooth evolution already mentioned, emphasis is put here only on the pH = 5 medium. The main qualitative difference is the extent of "slowness" observed from one complex to the next. In this series, it was found that the first wave of the V^{IV}-substituted complex has kept a sharp peak shape. All other complexes show plateau currents, with the same limiting current. For

this purpose, due care has been exercised concerning the reproducibility of the working electrode surface area and the concentrations of the complexes in solution. Incidentally, the results for pH = 3 prove that the diffusion coefficients remain very close to each other in these complexes. We arbitrarily chose the only well-defined peak potential value as the reference point for which the current intensities are measured for all the other complexes. Then, as no current crossing is observed between the various ''polarograms'' up to their common limiting value, the measured current intensities feature a qualitatively good index of the relative ''slowness'' among complexes. In the order of increasing slowness, the scale is then: V^{IV}(0.62), Ni^{II}(0.69), Co^{II}(0;72), Zn^{II}(0.74), Mn^{II}(0.80) and □, where this symbol represents the vacancy. Provisional crystal ionic radii of the various ions in Å are given in brackets.[11]

Considering all the results together, it becomes evident that a large number of parameters or combinations of parameters govern the electrochemical behaviors of the present complexes as revealed by cyclic voltammetry. Only qualitative aspects can be considered here as possible guidelines in an attempt at rationalization of the observed behaviors. Despite this really entangled situation, a simple electrostatic consideration might explain qualitatively the difference between the metal cation substituted complexes and the lacunary species. The substitution lowers the negative charge on the heteropolyanion and facilitates its reduction. Then, the differences between the potential locations of the various substituted complexes are more difficult to rationalize. As a matter of fact, it is probably more difficult to take several possible parameters into account. The size of each ion, its electronic configuration, its favorite geometry, should contribute to fix the extent of its penetration in the vacancy of the lacunary HPA. The possibility and extent of the Jahn–Teller effect should not be neglected. Furthermore, there is no change in the oxidation state of the heterometallic cation during the redox processes studied in this section, which could have modified the abovementioned considerations substantially. Also, it must be anticipated that the presence of the two MoO_6 octahedra next to the vacancy should render the latter more flexible than in a skeleton comprised totally of tungsten. The interplay of these various influences should determine the extent of ''effective'' lowering of the negative charge on the heteropolyanion due to substituent metallic cation, relative to the initial charge of the lacunary species. It should also determine, at least partly, the possibility and extent of electronic ''communication'' between neighbor redox centers in the complex, and, more specifically, between the heterometal substituent and the molybdenum moieties. A more important parameter in this last issue is the distribution of the redox potentials of the possibly interacting centers. Although no clear conclusions can be drawn, it is worth noting provisionally that it is now widely accepted that P_2W_{18} is initially reduced at one of the twelve equivalent tungsten atoms.[3,12,13] Here, the molybdenum centers, which are more easily reducible than the tungsten moieties, are situated in the "cap". On the basis of the foregoing discussion, no simple correlation is expected unless a single parameter overrides all others and/or several parameters show the same trend. However, the results in Figure 3B and the corresponding results for the other complexes would suggest that the ''slowness'' observed for the reduction of molybdenum centers is strictly larger as the crystal ionic radius of the substituent cation increases. But such an explanation would not include the results in Figure 3A, in which such a possible size effect could not be distinguished. Finally, in the present qualitative discussion, the pH appears as a decisive parameter. As a matter of fact, ECE-type mechanisms are known to intervene frequently in the redox behaviors of heteropolyanions.[14,15]

The redox behaviors of the substituent metal cations have been studied briefly. In the potential domains explored, no electrochemical activity has been detected for Ni^{II} or Zn^{II}. The Co^{II} center is oxidized to Co^{III}, with a peak potential observed at +1.120 V vs. SCE during the first positive potential scan. This wave disappears on subsequent runs. Even during the very first run, no reduction of Co^{III} back to Co^{II} is obtained. Such a behavior should be traced to the abovementioned lability of the cobalt-substituted complex rather than to an electrode material effect. In contrast, a well-behaved, reversible one-electron wave is observed for the oxidation of V^{IV} to V^{V} and the subsequent reduction of V^{V} to V^{IV} with E_0 around +0.412 V vs. SCE at pH = 5. This wave seems slightly pH-dependent. The case of Mn^{II} is more striking, as at least two fairly stable states are obtained, featuring the Mn^{II}/Mn^{III} and Mn^{III}/Mn^{IV} steps.

Mixed redox behaviors for the substituent cation and for the HPA framework: This situation, encountered with Fe^{III} and Cu^{II} as substituents in the present work, is the one likely to make the first wave of the corresponding HPAs involve *n* electrons (*n* □ 2). The case of the Fe^{III} complex has been described briefly,[1,2] and is mentioned here for completeness and for the sake of comparison with the Cu^{II} complex. Typically, the presence of the Fe^{III} cation in [$\alpha_2Fe(OH_2)P_2Mo_2W_{15}$]$^{7-}$, abbreviated as $\alpha_2FeP_2Mo_2W_{15}$, modifies substantially the electrochemical behavior of this heteropolyanion compared to the behavior of $\alpha_2P_2Mo_3W_{15}O_{62}^{6-}$·($\alpha_2P_2Mo_3W_{15}$). In a pH = 2 medium, the cyclic voltammogram of $\alpha_2P_2Mo_3W_{15}$ begins with three diffusion-controlled one-electron waves. In contrast, the iron(III)-substituted complex displays a cyclic voltammogram nearly identical in potential locations to that of the corresponding lacunary species. Comparison of current intensities as well as controlled potential coulometry indicate the consumption of roughly three electrons per molecule on the first wave of $\alpha_2FeP_2Mo_2W_{15}$. This result is consistent with the merging of the molybdenum and iron waves at pH = 2. The combined wave remains chemically reversible upon cycling. A study of this pattern as a function of pH allows the Fe^{III} wave to be separated from the molybdenum reduction, thus confirming the merging mechanism.

Figure 4 shows representative examples of the cyclic voltammograms obtained with the Cu^{II} substituted complex. In Figure 4A, the ''first'' wave of the system is displayed for pH = 3 and pH = 5. The pH-dependence is obvious for

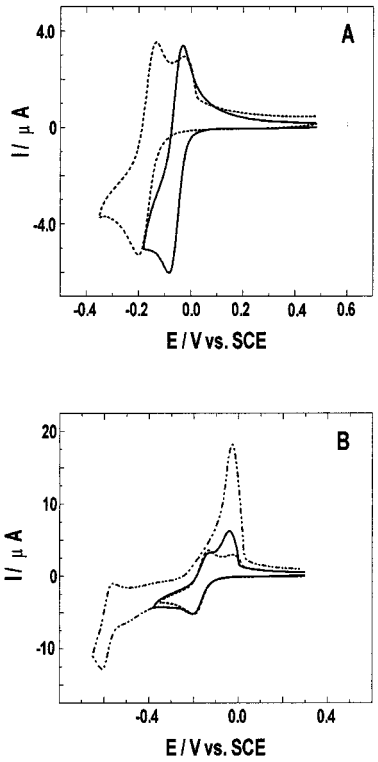


Figure 4. Cyclic voltammograms observed for [1,2,3-$P_2CuMo_2W_{15}$) under various conditions. Scan rate: 10 mV s^{-1}. – (A) *Solid line curve*: pH = 3 (0.2 M Na_2SO_4 + H_2SO_4). Use of an acetate medium does not modify the results. – *Short dot curve* pH = 5 (0.2 M CH_3COONa + CH_3COOH). The voltammograms are restricted to the "first" wave of the system. – (B) pH = 5 (0.2 M CH_3COONa + CH_3COOH): The negative going scan is reversed at different potential values.

the cathodic wave, concerning its potential location as well as its current intensity. A rough estimate would indicate a peak potential shift of 52 mV/pH-unit. These observations must be traced mainly to the electrochemical behavior of molybdenum centers. On potential reversal, two well-defined and well-separated oxidation peaks are observed at pH = 5. The same pattern is obtained at pH = 3, but with poorer separation. This result suggests that one of the two oxidation components is hardly pH-dependent, if at all. It has been checked that no splitting of the oxidation wave associated with the reduced molybdenum centers is observed at pH = 3 and at pH = 5 for the lacunary species α_2P_2 Mo_2W_{15}. A reasonable outcome is the hypothesis that the reduction of the Cu^{II} center mixes up, at least partly, with that of the molybdenum moieties. Support for such a possibility appears in Figure 4B. The well-behaved cathodic trace of the "molybdenum wave" is followed by an ill-defined series of waves. The potential excursion is reversed just past the first other well-behaved wave. Comparison of the cyclic voltammogram of Figure 4B with that of $\alpha_2P_2Mo_2W_{15}$ indicates that this last wave must be associated with the first tungsten-centered redox process of the heteropolyanion framework. The anodic trace associated with the ill-defined zone and the molybdenum wave is clearly composite. The more anodic wave of this composite trace is the larger and the sharper, the more cathodic is the value selected to reverse the potential during the negative going scan. In short, the anodic trace reveals the reduction of copper within the heteropolyanion. The electrochemical behavior of the Cu^{II} in $\alpha_2CuP_2Mo_2W_{15}$ deserves some comments. In the pH domain which could be explored in the present experiments, the copper reduction mixes up partly with the molybdenum reduction. A controlled potential coulometry is performed at E = –0.176 V vs. SCE, a potential just negative of the peak of the "molybdenum wave" in a pH = 3 medium, where no obvious reduction of Cu^{II} is observed on the cyclic voltammogram. Substantially more than two electrons per molecule of complex are consumed. Provisionally, it is worth noting that this electrolysis results in a red deposit, visible to the naked eye on the electrode surface. Preliminary XPS analyses indicate mainly the presence of copper in the deposit.

Concluding Remarks

One of the main ideas behind the present work is to take a further step in our systematic study of parameters which could favor several electron processes on the first wave of HPAs. The introduction of two molybdenum atoms in the "cap" of the framework of $\alpha P_2W_{18}O_{62}^{6-}$, with the possibility of varying the nature of the third metallic atom in the corresponding trimetallic moiety, has given interesting results. The molybdenum centers are reducible in a fairly positive potential domain, and their redox behaviors are pH-dependent. Another outcome worth noting is the importance of those heterometallic centers which are easily reduced in the same potential domain as the molybdenum centers. The Fe^{III}- and Cu^{II}-substituents appear to be two excellent illustrations of this conclusion. In the case of Fe^{III}, the interplay between the potential location of the iron-centered reduction and the pH effect on the potential location of the molybdenum moieties reduction, has permitted the observation of a three-electron first wave for $\alpha_2FeP_2Mo_2W_{15}$. For the Cu^{II} complex, a deposition process has been demonstrated, and further details are under scrutiny. For the other metallic cations used in this work, the comparison of their cyclic voltammograms with that of $\alpha_2P_2Mo_2W_{15}$ indicates unambiguously that the influence of all these substituents, in combination with the known pH effect, favors the two-electron reduction of the molybdenum centers. However, the first redox process of the corresponding heteropolyanion remains, at most, limited to the two-electron uptake of the molybdenum centers. Furthermore, some of the metallic substituents do not show any electrochemical activity within the heteropolyanion. Possibly, substitution at the α_1 position rather than at the α_2 position explored here, might be beneficial to circumvent some of the present difficulties. Work is in progress in this direction.

Experimental Section

Preparations: The potassium salt of [(1)-2,3-$P_2\square Mo_2W_{15}O_{61}$]$^{10-}$ was prepared by published methods.[1,3,16,17]

$K_8[VOP_2Mo_2W_{15}O_{61}]\cdot 16H_2O$: A sample of $K_{10}[P_2Mo_2W_{15}O_{61}]\cdot 19H_2O$ (9.4 g, 2 mmol) was dissolved in a stirred solution of LiCl (6.8 g), glacial acetic acid (3.7 mL) and lithium hydroxide (1.64 g) in water (220 mL). A sample of vanadyl sulfate, $VOSO_4\cdot 5H_2O$ (0.51 g, 2 mmol), was added and the whole solution was treated with saturated KCl solution (170 mL). After 30 min, the precipitate was filtered on a sintered glass frit, washed with ethanol and diethyl ether, and dried in air. $K_8[VOP_2Mo_2W_{15}O_{61}]\cdot 16H_2O$**:** calcd. K 6.72, V 1.10, Mo 4.12, W 59.2, H_2O 6.19; found: K 6.64, V 1.09, Mo 4.1, W 59.0, H_2O 6.25.

$K_8[Mn(H_2O)P_2Mo_2W_{15}O_{61}]\cdot 16H_2O$: To a stirred solution of $Mn(NO_3)_2\cdot 6H_2O$ (0.63 g, 2.2 mmol) in water (80 mL), acidified with HNO_3 (1 M, 0.5 mL), was added $K_{10}[P_2Mo_2W_{15}O_{61}]\cdot 19H_2O$ (9.4 g, 2 mmol). The solution was treated with saturated KCl solution (40 mL). The precipitate was filtered on a sintered glass frit, washed with ethanol and diethyl ether and air-dried. $K_8[Mn(H_2O)P_2Mo_2W_{15}O_{61}]\cdot 16H_2O$**:** calcd. K 6.71, Mn 1.18, Mo 4.12, W 59.2, H_2O 6.56; found: K 6.65, Mn 1.16, Mo 4.06, W 59.0, H_2O 6.49.

$K_8[CO(H_2O)P_2Mo_2W_{15}O_{61}]\cdot 15H_2O$: Prepared by the same method as the manganese(II) salt. $K_8[Co(H_2O)P_2Mo_2W_{15}O_{61}]\cdot 15H_2O$**:** calcd. K 6.73, Co 1.27, Mo 4.12, W 59.1, H_2O 6.20; found: K 6.60, Co 1.27, Mo 4.35, W 59.5, H_2O 6.19.

$K_8[Zn(H_2O)P_2Mo_2W_{15}O_{61}]\cdot 14H_2O$: Prepared by the same method as the manganese(II) salt. $K_8[Zn(H_2O)P_2Mo_2W_{15}O_{61}]\cdot 14H_2O$**:** calcd. K 6.75, Zn 1.41, Mo 4.12, W 59.2, H_2O 5.82; found: K 6.74, Zn 1.37, Mo 4.1, W 59.5, H_2O 5.71

$K_8[Ni(H_2O)P_2Mo_2W_{15}O_{61}]\cdot 15H_2O$: A sample of $Ni(NO_3)_2\cdot 6H_2O$ (0.73 g, 2.5 mmol) was added to water (80 mL) with stirring, and $K_{10}[P_2Mo_2W_{15}O_{61}]\cdot 19\ H_2O$ (9.4 g, 2 mmol) was added. The mixture was warmed up until dissolution occurred, and the solution was then left at 5 °C for a few hours. The pale yellow crystals were filtered off, washed with ethanol and diethyl ether, and then air-dried. $K_8[Ni(H_2O)P_2Mo_2W_{15}O_{61}].15H_2O$**:** calcd. K 6.73, Ni 1.25, Mo 4.12, W 59.2, H_2O 6.20; found: K 6.65, Ni 1.26, Mo 4.06, W 59.0, H_2O 6.12.

$K_8[Cu(H_2O)P_2Mo_2W_{15}O_{61}]\cdot 15.5H_2O$: Prepared by the same method as the nickel(II) salt. $K_8[Cu(H_2O)P_2Mo_2W_{15}O_{61}].15.5H_2O$**:** calcd. K 6.71, Cu1.36, Mo 4.12, W 59.2, H_2O 6.37; found: K 6.65, Cu 1.34, Mo 4.07, W 59.9, H_2O 6.34.

NMR, IR and UV Visible and Potentiometric Measurements: ^{31}P NMR spectra were recorded in 10 mm optical density tubes on a Bruker VM 250 apparatus operating at 101.2 MHz, in the Fourier transform mode. The ^{31}P chemical shifts were measured on 0.02 M solutions of the polyanions in aqueous 1 M LiCl (10% D_2O) solutions, and were referenced to external 85% H_3PO_4 by the substitution method. – IR spectra were recorded on a Bio-Rad FTS 165 FTIR spectrophotometer. – UV/Vis spectra were recorded on a 555 Perkin–Elmer spectrophotometer. – Potentiometric measurements were made on a Tacussel LPH 430T pH meter. The apparent formation constant β_{app} for the Fe^{III}-substituted compound was determined potentiometrically in 1M HNO_3, considering that in this medium, the lacunary polyoxometalates of this work do not complex Fe^{2+} ions.[1] The formation constant for the V^{IV}-substituted complex has been evaluated by comparison with the value obtained for the iron complex. For all the other compounds, a procedure derived from that described in detail for the stability constant measurements of Ce^{III} and Ce^{IV} complexes of both the α_1 and α_2 $[P_2W_{17}O_{61}]^{10-}$ isomers[18] was used. A detailed account of these measurements for each complex will be given elsewhere.[19] In the present work, the Co^{II} derivative of α_2 $[P_2W_{17}O_{61}]^{10-}$ was selected as the central species worked out in detail in an acid medium, and with which all the others are then compared. In an acid medium, the lacunary species is known[20] to be in the protonated form α_2 $[H_3P_2W_{17}O_{61}]^{7-}$. The determination of the three acidity constants of this species and that of the substituted complex are the main sources of error. An average estimation of the total error on the logβ values is in the range of ± 0.3.

Electrochemical Experiments; Chemicals, Equipment and Apparatus: Pure water was used throughout. It was obtained by passing through a Milli-RO_4 unit and subsequently through a Millipore Q water purification set. All the chemicals were of high-purity grade and were used as received. H_2SO_4, Na_2SO_4, CH_3COONa, CH_3COOH and NaOH were commercial products (Prolabo). The appropriate compositions of the various supporting electrolytes are indicated in the figure captions.

The solutions were purged thoroughly for at least 30 min. with pure argon and kept under a positive pressure of this gas during the experiments.

The source, mounting and polishing of the glassy carbon (GC, Tokai, Japan) electrodes has been described.[21] The glassy carbon samples had a diameter of 5 mm. The electrochemical set-up was an EG G 273 A driven by a PC with the 270 software. The data were recorded in the computer. Potentials are quoted against a saturated calomel electrode (SCE). The counter electrode was a platinum gauze of large surface area. Spectroelectrochemical experiments were performed in a three-compartment cell comprising a 1 cm optical path quartz cuvette. The working electrode was a sheet of glassy carbon (V25, Le Carbone Lorraine). The whole cell remained inserted in the spectrometer cavity and kept under continuous argon bubbling and stirring during the electrolysis. A second 1 cm quartz cell was matched with that of the electrochemical cell and served as a reference. The UV/Vis spectra were recorded with a Perkin–Elmer Lambda 19 spectrophotometer. All experiments were performed at the laboratory temperature.

Acknowledgments

This work was supported by the CNRS (UMR 8610 and UPRESA 7071) and the Universities Paris XI and Paris VI.

[1] R. Contant, M. Abbessi, J. Canny, A. Belhouari, B. Keita, L. Nadjo, *Inorg. Chem.* **1997**, *36*, 4961–4967.
[2] B. Keita, A. Belhouari, L. Nadjo, R. Contant, *J. Electroanal. Chem*. **1998**, *442*, 49–57.
[3] J. P. Ciabrini, R. Contant, J. M. Fruchart, *Polyhedron* **1983**, *2*, 1229–1233.
[4] Y. Jeannin, *Chem. Rev.* **1998**, *98*, 51–76.
[5] T. L. Jorris, M. Kozik, N. Casan-Pastor, P. J. Domaille, R. G. Finke, W. K. Miller, L. C. W. Baker, *J. Am. Chem. Soc.* **1987**, *109*, 7402–7408.
[6] C. Rocchiccioli-Deltcheff, R. Thouvenot, *Spectroscopy Letters* **1979**, *12*, 127–138.
[7] C. Rocchiccioli-Deltcheff, M. Fournier, R. Franck, R. Thouvenot, *Inorg. Chem.* **1983,** *22*, 207–216.
[8] R. Thouvenot, M. Fournier, R. Franck, C. Rocchiccioli-Deltcheff, *Inorg. Chem.* **1984**, *23*, 598–605.
[9] B. Keita, L. Nadjo, *Mater. Chem. Phys.* **1989**, *22*, 77–103.
[10] M. Abbessi, *Thesis*, **1989**, Université Paris VI, France.
[11] Handbook of Chemistry and Physics, 66th edition, p. F164.
[12] G. M. Varga, E. Papaconstantinou, M. T. Pope, *Inorg. Chem.* **1970**, *9*, 662–667.

[13] R. Acerete, S. Harmalker, C. F. Hammer, M. T. Pope, L. C. W. Baker, *J. Chem. Soc., Chem. Commun.* **1979**, 777–779.
[14] B. Keita, L. Nadjo, *Topics in Current Electrochem*. **1993**, *2*, 77–106.
[15] B. Keita, L. Nadjo, *J. Electroanal. Chem*. **1987**, *227*, 77–98.
[16] M. Abbessi, R. Contant, R. Thouvenot, G. Hervé, *Inorg. Chem*. **1991**, *30*, 1695–1702.
[17] R. Contant, *Inorg. Synth*. **1990**, *27*, 104–111.
[18] [18a] J. P. Ciabrini, R. Contant, *J. Chem. Res., Miniprint* **1993**, 2720. [18b] J. P. Ciabrini, R. Contant, *J. Chem. Res.,Synop.* **1993**, 391.
[19] R. Contant *et al., to be published*.
[20] [20a] R. Contant, J. P. Ciabrini, *J. Chem. Res., Miniprint* **1982**, 641–660. [20b] R. Contant, J. P. Ciabrini, *J. Chem. Res., Synop.* **1982**, 50–51.
[21] B. Keita, K. Essaadi, L. Nadjo, *J. Electroanal. Chem.* **1989**, *259*, 127–146.

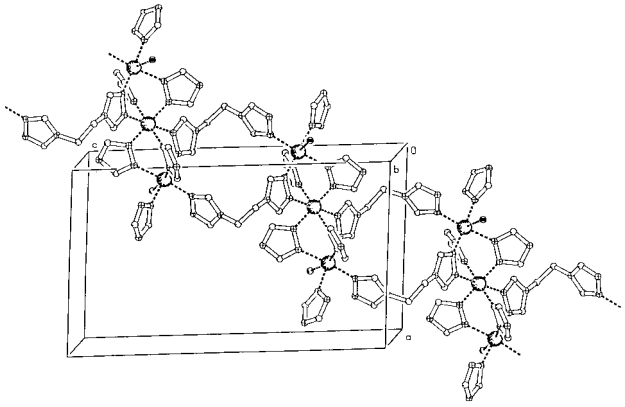
Received August 9, 1999
[I99293]

Synthesis, Crystal Structure, Spectroscopic and Magnetic Properties of an Unprecedented Three-Dimensional Cu^{II} Coordination Compound of 1,2-Bis(1,2,4-triazol-4-yl)ethane

Yann Garcia,* Petra J. van Koningsbruggen,* Huub Kooijman, Anthony L. Spek, Jaap G. Haasnoot, and Olivier Kahn†

Eur. J. Inorg. Chem. **2000**, 307−314

Due to a printing error the surname of the first author (Yann Garcia) was spelled wrong in the printed version. Furthermore, Figure 2b was inadvertently printed twice. The correct version of Figure 2c is reproduced below:



In the reference section references 55 and 56 were accidentally merged and reference 57 consequently renumbered. The correct references are as follows:

[55] G. M. Sheldrick, *SHELXL-97, Program for Crystal Structure Refinement*, University of Göttingen, Germany, **1997**.
[56] *International Tables for Crystallography* (Ed.: A. J. C. Wilson), vol. C, Kluwer, Academic Publishers, Dordrecht, The Netherlands, **1992**.
[57] A. L. Spek, *Acta Crystallogr.* **1990**, *A46*, C34.

Any correspondence relating to this article should be addressed to Dr. Garcia at his current address:

Institut für Anorganische und Analytische Chemie,
Johannes Gutenberg Universität Mainz,
Staudinger Weg 9, D-55099 Mainz, Germany
Fax: (internat.) + 49-6131/392-2990
E-mail: garcia@iacgu7.chemie.uni-mainz.de

We apologise to the authors and to our readers for any inconvenience.

The Editors
[I99201]

 © WILEY-VCH Verlag GmbH, D-69451 Weinheim, 2000 1434−1948/00/0303−0575 $ 17.50+.50/0

Structural Studies of MCM-48 Derivatized with (1,1′-Ferrocenediyl)dimethylsilane

Paula Ferreira, Isabel S. Gonçalves, Fred Mosselmans, Martyn Pillinger, João Rocha,* and Alan Thursfield

Eur. J. Inorg. Chem. **2000**, 97−102

Due to a printing error page 102 of this paper was not included in the printed journal. This page and its preceding page are reproduced on the following two pages. In the bound volume these pages will be inserted in the correct position. The electronic version on the Journal Web page is unaffected. We apologise to the authors and to our readers for any inconvenience.

The Editors
[I99200]

 © WILEY-VCH Verlag GmbH, D-69451 Weinheim, 2000 1434−1948/00/0303−0576 $ 17.50+.50/0

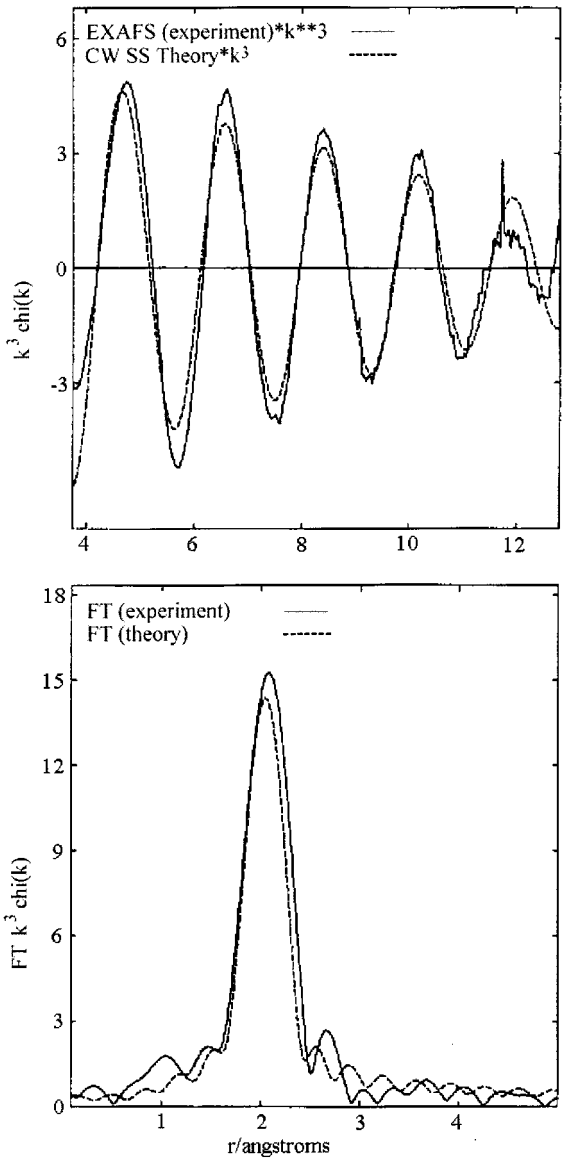


Figure 6. Fe K-edge k^3-weighted EXAFS spectrum and Fourier transform, phase-shift corrected for carbon (—— experimental; ------- curved wave theory, fit B in Table 1), of [Fe{(η-$C_5H_4)_2SiMe_2$}] at 298 K

were very large: *R* factor 45.5%, E° −1.8 eV, *r*(Fe−C) 2.023(5) Å, 2 σ^2 0.0236(17) Å^2, *r*(Fe···Si) 2.736(33) Å, 2 σ^2 0.0176(83) Å^2. A better fit to the experimental data was obtained by starting from fit A and refining the coordination number (fit B, Table 1, Figure 6). The final value was 4.3 but the error in this value must be much higher than 20% for the reasons outlined above.

Conclusion

The pore walls of mesoporous siliceous MCM-48 have been successfully derivatized with (1,1′-ferrocenediyl) dimethylsilane. The organometallic complexes react with the MCM-48 surface silanols (particularly of the Q^3 type) to give a $C_5H_4SiMe_2$−O linkage to the silica surface. Despite the fact that MCM-48 and MCM-41 possess very different mesoporous surfaces, this process strongly resembles the process previously reported for the functionalization of the latter by strained ferrocenophanes.

Experimental Section

General: All preparations and manipulations were performed using standard Schlenk techniques under an oxygen-free and water-free argon atmosphere. Pentane was dried by reflux over Na/benzophenone ketyl, distilled under argon, and kept over 4-Å molecular sieves. − Powder X-ray diffraction (XRD) data were collected on a Philips Xpert diffractometer using Cu-K_α radiation filtered by Ni. − Microanalyses were performed at the TU Munich. − Infrared spectra were recorded on a Unican Mattson Mod 7000 FTIR spectrophotometer using KBr pellets and/or solutions. − ^{29}Si- and ^{13}C-NMR spectra were recorded at 79.49 and 100.62 MHz, respectively, on a (9.4 T) Bruker MSL 400P spectrometer. ^{29}Si-MAS NMR spectra were recorded with 40° pulses, spinning rates of 5.0−5.5 kHz, and 60 s recycle delays. ^{29}Si-CP MAS NMR spectra were recorded with 5.5 μs pulses, a spinning rate of 5.0 kHz and 5 s recycle delays. Chemical shifts are quoted in parts per million relative to TMS. ^{13}C-CP MAS NMR spectra were recorded with 4.5 μs pulses, a spinning rate of 8 kHz, and a 4 s recycle delay. Chemical shifts are quoted in ppm relative to TMS. − Nitrogen adsorption isotherms were recorded using a CI electronics MK2-M5 microbalance connected to a vacuum manifold line. The as-made MCM samples (typically around 0.02 g) were dehydrated overnight at 723 K to an ultimate pressure of 10^{-4} mbar, and then cooled to room temperature prior to adsorption. Extra care with the functionalized materials was necessary and so the samples were dehydrated at 423 K to prevent the destruction of the functionalities. Nitrogen isotherms were then recorded at 77 K. Equilibration of each data point was monitored using CI electronics Labweigh software, and the pressure monitored using an Edwards Barocel pressure sensor. Specific surface areas, A_{BET}, were determined from the linear part of the BET equation (P/P_o = 0.05−0.3). − Fe K-edge X-ray absorption spectra were collected at room temperature in transmission mode on station 9.2 [double crystal Si(220) order-sorting monochromator, 50% harmonic rejection] of the Synchrotron Radiation Source at the Daresbury Laboratory, operating at 2 GeV in single bunch mode, with typical currents of 13−19 mA. Solid samples, diluted if necessary with boron nitride, were held between layers of mylar film in 0.5 mm thick aluminium plates. Two spectra were recorded for each sample and summed using the program EXCALIB, available on the Daresbury computer XRSSERV1. The program EXBACK was used to extract the raw EXAFS, $\chi^E(k)$, and curve-fitting analyses, by least-squares refinement of the non-Fourier filtered k^3-weighted EXAFS data, were carried out within EXCURVE (version EXCURV98[13]) using spherical wave methods.[14] Phase shifts were calculated using Von Bart ground state and H. Lundqvis exchange potentials.

[Fe{(η-$C_5H_4)_2SiMe_2$}] was prepared by the method reported by Wrighton[15] and purified by sublimation under vacuum.

MCM-41 was synthesized according to the literature employing [($C_{14}H_{29}$)NMe_3]Br as a templating agent.[16] After calcination (540 °C/6 h) and dehydration (200 °C under a vacuum 10^{-4} Torr for 8 h) the material was characterized by XRD, N_2 adsorption and IR spectroscopy.

MCM-41/[Fe{(η-$C_5H_4)_2SiMe_2$}] was prepared as described in the literature.[4] Elemental analysis indicated 8.33 mass-% Fe. − IR

(KBr): $\tilde{\nu}$ = 3574 vs cm^{-1}, 3096 m, 2963 m, 1645 s, 1365 m, 1234 vs, 1169 vs, 901m, 816 s, 798 s, 667 m. − (^1H, ^{13}C, ^{29}Si) NMR spectroscopic data are in agreement with ref.[4]

MCM-48 was synthesized according to the literature employing $[(C_{16}H_{33})NMe_3]Cl$ as a templating agent.[17,10b] After calcination (540°C/6 h) and dehydration (220°C at 10^{-4} Torr for 6 h) the material was characterized by XRD, N_2 adsorption and IR spectroscopy.

Preparation of MCM-48/[Fe{(η-C_5H_4)$_2$$SiMe_2$}]: A suspension of MCM-48 (0.5 g) in pentane (15 mL) was treated with a solution of [Fe{$(C_5H_4)_2SiMe_2$}] (0.35 g) in pentane. After 24 h at room temperature, the resulting suspension was filtered off and the remaining orange solid was washed several times with pentane, and dried under an oil-pump vacuum. The pentane washings contained trace amounts of the starting material [Fe{(η-C_5H_4)$_2$$SiMe_2$}] and ferrocene, identified by solution ^1H-NMR spectroscopy. − Elemental analysis indicated 8.18 mass-% Fe. − IR (KBr): $\tilde{\nu}$ = 3454 vs cm^{-1}, 3103 m, 2960 m, 1637 s, 1423 m, 1234 vs, 1169 vs, 1081 vs, 968 m, 900 m, 822 s, 798 s, 667 m, 453 s.

Acknowledgments

We thank PRAXIS XXI and FEDER for partial funding. P. Ferreira (BD) thanks PRAXIS XXI for a grant. I.S.G. wants to thank the CRUP (Acções Integradas Programme) for generous support.

[1] J. S. Beck, J. C. Vartuli, W. J. Roth, M. E. Leonowicz, C. T. Kresge, K. D. Schmitt, C. T.-W. Chu, D. H. Olson, E. W. Sheppard, S. B. McCullen, J. B. Higgins, J. L. Schlenker, *J. Am. Chem. Soc.* **1992**, *114*, 10834.
[2] [2a] K. Moller, T. Bein, *Chem. Mater.* **1998**, *10*, 2950. − [2b] T. Maschmeyer, *Curr. Opin. Solid State Mater. Sci.* **1998**, *3*, 71.
[3] V. Alfredsson and M. Anderson, *Chem. Mater.* **1996**, *8*, 1141.
[4] [4a] S. O′Brien, J. Tudor, S. Barlow, M. J. Drewitt, S. J. Heyes, D. O′Hare, *Chem. Commun.* **1997**, 641. − [4b] S. O′Brien, J. M. Keates, S. Barlow, M. J. Drewitt, B. R. Payne, D. O′Hare, *Chem. Mater.* **1998**, *10*, 4088.
[5] I. Manners, *Adv. Organomet. Chem.* **1995**, *37*, 131.
[6] B. Marler, U. Oberhagemann, S. Vortmann, H. Gies, *Microporous Mater.* **1996**, *6*, 375.
[7] X. S. Zhao, G. Q. Lu, A. K. Whittaker, G. J. Millar, H. Y. Zhu, *J. Phys. Chem. B.* **1997**, *101*, 6525.
[8] D. A. Foucher, R. Ziembinski, B.-Z. Tang, P. M. Macdonald, J. Massey, C. R. Jaeger, G. J. Vansco, I. Manners, *Macromolecules* **1993**, *26*, 2878.
[9] K. S. W. Sing, D. H. Everett, R. A. W. Houl, L. Moscou, R. A. Pierotti, J. Rouquerol, T. Siemieniewska, *Pure Appl. Chem.* **1985**, *57*, 603
[10] [10a] A. A. Romero, M. D. Alba, W. Zhou, J. Klinowski, *J. Phys. Chem. B.* **1997**, *101*, 5294. − [10b] J. Xu, Z. Luan, H. He, W. Zhou, L. Kevan, *Chem. Mater.* **1998**, *10*, 3690.
[11] R. Schmidt, M. Stöcker, E. Hansen, D. Akporiaye, O. H. Ellestad, *Microporous Mater.* **1995**, *3*, 443.
[12] W. Finckh, B.-Z. Tang, D. A. Foucher, D. B. Zamble, R. Ziembinski, A. Lough, I. Manners, *Organometallics* **1993**, *12*, 823.
[13] N. Binsted, (**1998**) EXCURV98: CCLRC Daresbury Laboratory computer program.
[14] S. J. Gurman, N. Binsted, I. Ross, *J. Phys. Chem.* **1984**, *17*, 143.
[15] A. B. Fischer, J. B. Kinney, R. H. Staley, M. S. Wrighton, *J. Am. Chem. Soc.* **1979**, *101,* 6501.
[16] C. T. Kresge, M. E. Leonowicz, W. J. Roth, J. C. Vartuli, J. S. Beck, *Nature* **1992**, *359*, 710.
[17] A. Monnier, F. Schüth, Q. Huo, D. Kumar, D. Margolese, R. S. Maxwell, G. D. Stucky, M. Krishnamurty, P. Petroff, A. Firouz, M. Janicke, B. F. Chmelka, *Science* **1993**, *261*, 1299.

Received June 2, 1999
[I99200]

Zwitterionic Organometallates

Remi Chauvin[a]

Keywords: Organometallate complexes / Zwitterionic states / Transition metals / Coordination modes / Electrostatic interactions / Ion pairs

Whereas ion-pairing has been long recognized as playing a key role in organometallic chemistry, the zwitterionic feature of organotransition metal complexes has only recently become an influential factor in the design of cationic metal catalysts. The prospective situation of reversed polarity, with metal fragments formally bearing an integral negative charge, may be envisaged. Besides the well-documented zwitterionic complexes derived from phosphonium ylides, other examples of zwitterionic organometallate complexes, formulated as such on the basis of structural, spectroscopic, or chemical evidence, have been reported in the recent literature and are reviewed here. They are classified according to the nuclearity of the anionic core and the nature of the cationic moiety, which can be a phosphonium, an ammonium, an iminium, a sulfonium, or a cationic organometallic fragment. The stabilization of the non-solvated charge separation is shown to arise from resonance and partial hapticity effects, hydrogen-type bonding, and tight intramolecular ion-pairing made possible by a back-folding of the ligand onto the metal center.

Introduction

Whereas dative bonds are generally assumed to govern the structures and reactivities of organometallic transition metal complexes as well as their catalytic properties, electrostatic interactions govern those of biochemical systems and enzymes. Of course, the borderline between the two realms is not quite so clear-cut. Indeed, metalloenzymes belong to the electrostatically-governed realm, whereas their models and biomimetic catalysts tend to rely on the auxiliary roles of dative interactions involving mainly electronegative atoms (O, N, S, etc.).[1] Conversely, electrostatic interactions play a definite albeit auxiliary role in organometallic complexes involving less electronegative atoms (C, P, H, etc.). Significantly, ion-pairing effects in organometallic species of both main group[2] and transition metals[3] have been widely studied. Nevertheless, intermolecular ion-pairing in solution remains a somewhat intangible phenomenon which is difficult to assess experimentally. In contrast, the intramolecular situation is chemically more relevant and is more easily appraised. Since the entropic effect is prone to favor rearrangements leading to the disappearance of the charge separation, the a priori fragile zwitterionic complexes merit special consideration. The purpose of this review is to classify a number of stable zwitterionic complexes selected from the recent literature, with particular emphasis on metallate species. In addition to the electrostatic energy of the intramolecular charge separation, the presence of a formal negative integral charge at an electropositive transition metal atom is apparently an intriguing feature of Lewis structures that are supposed to represent stable molecules (elusive zwitterionic excited states will not be discussed).[4] This misleading paradox can be rationalized by considering that the negative charge is actually more or less delocalized over the metal fragment and its auxiliary ligands (CO, X, Ph, etc.). Nevertheless, the *formal* presence of *integral* opposite charges linked through a path of covalent and dative bonds, located at the metal fragment and in a definite region of

[a] Laboratoire de Chimie de Coordination du CNRS, UPR 82421, lié par conventions à l'Université Paul Sabatier et à l'Institut National Polytechnique,
205 route de Narbonne, F-31077 Toulouse Cedex 4, France
Fax: (internat.) +33 (0)5/61 55 30 03
E-mail: chauvin@lcc-toulouse.fr



The author obtained his Ph. D. in 1988 under the supervision of Prof. H. B. Kagan in Orsay (France). He then pursued in the field of asymmetric organometallic synthesis and catalysis as a postodoctoral fellow with Prof. K. B. Sharpless at M.I.T. (Cambridge, MA), and then with Prof. A. Vasella at Zürich University (Switzerland). From 1991 to 1993 he worked as an organic chemist at the Roussel Uclaf Company in Romainville (France). He then moved back to academic research at the C.N.R.S. in Toulouse (France). In 1998, he was appointed as a Professor at Toulouse University, and launched new research axes ("carbomer" structures, and search for electrostatic effects in asymmetric catalysis). In the recent past, his general interests have focused on the problem of the quantification of chirality and on chiral organophosphorus complexes, especially chiral zwitterionic ones.

MICROREVIEWS: This feature introduces the readers to the authors' research through a concise overview of the selected topic. Reference to important work from others in the field is included.

 © WILEY-VCH Verlag GmbH, D-69451 Weinheim, 2000 1434–1948/00/0404–0577 $ 17.50+.50/0

the organic ligands, respectively, is explicitly emphasized as a peculiar feature by many authors: it is shown here to be a unifying feature of complexes designed for very different purposes.

Neglecting orbital components, the through-space electrostatic interaction corresponds to the energy of a formal point charge subjected to the isotropic electrostatic potential of the other. A number of cases may be distinguished depending on the relative positions of the formal charges. Firstly, if no non-zwitterionic connected Lewis structure can be drawn by resonance of the π-electrons, the complex will be classified as "mesoionic" or "truly zwitterionic". Secondly, if the opposite integral formal charges of the ion can be cancelled out by resonance in a non-zwitterionic mesomeric form, the complex will merely be partially zwitterionic. Three main situations are encountered:

(i) α-Dipole: This trivial situation corresponds to ionic ($M^{\pm}$,$X^{\mp}$) and semi-polar ($M^{\pm}$–$L^{\mp}$) bonds. It is trivially rendered degenerate by non-zwitterionic resonance forms (M–X, M=L, M↔L); the charge separation is thus weak and very formal.

(ii) β-Dipole: This situation can be mesoionic (M^{-}–X–Y^{+}) or otherwise ($M^{\pm}$=X–$Y^{\mp}$ ↔ M–X=Y) and corresponds to that of the well-studied derivatives of phosphonium ylide complexes M^{-}–CH_2–$^{+}PR_3$.[5]

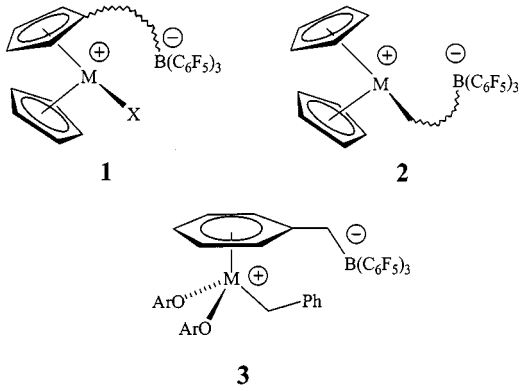
(iii) ω-Dipole: Here, the greater topological charge separation should a priori enhance the destabilization. Many push-pull transition metal complexes where the metal center plays the role of a donor or an acceptor have been prepared, particularly with a view to studying electron-transfer phenomena and to test their second-order nonlinear optical responses.[6] The ground states of such complexes can, however, essentially be described by the non-zwitterionic resonance form. In contrast, only zwitterionic complexes formulated by a main zwitterionic resonance form and stabilized by a secondary contribution from a non-zwitterionic resonance form will be dealt with here. Emphasis will be placed on stabilization stemming from inductive delocalization through σ-bonds, as well as from geometrical shortening of charge separation (back-folding of the ligand charge onto the metal charge).

After a brief overview of zwitterionic organometallic complexes of cationic metals that are currently the subject of growing interest for catalysis purposes, the review will then provide a survey of zwitterionic organometallic complexes exhibiting reversed polarity, i.e. with anionic transition metals, classified according to the nuclearity of the anionic fragment and the nature of the cationic terminus.

I. Zwitterionic Organometallic Complexes with Cationic Metals: A Brief Overview

Numerous neutral complexes containing a cationic transition metal center covalently bound to anions usually classified as weakly- or non-coordinating have been prepared, especially for catalysis purposes.

Catalysis in aqueous media is an active field of research of both industrial and academic relevance.[7] Water-soluble catalysts are obtained by tethering ionic functions to phosphane ligands of catalysts previously known to be effective in organic media. In this regard, the coordination sphere of the metal must be preserved, and the anion must be repelled at the periphery of the complex where it mainly interacts with the aqueous solvent. Although cationic functions such as ammonium can be used,[8] most water-solubilizing ligands bear anionic functions (carboxylate, sulfonate, etc.). Although the latter are often locally neutralized by a sodium cation, some cationic metal complexes such as the hydroformylation catalyst $Na_5[Co(CO)_3(P\{(CH_2)_nC_6H_4$-$p$-$SO_3\}_3)_2]$ can be formulated as zwitterionic.[9] Generally, however, the metal in the active species can be viewed as being formally neutral, ionicity being more important than zwitterionicity.

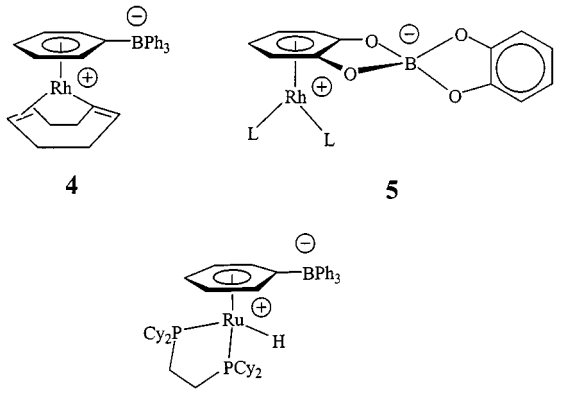


Besides water-solubilization effects, anionic end-groups can have more significant effects on catalytic activities. This is nicely illustrated by the design of efficient Group 4 metal catalysts for olefin polymerization. Since the pioneering work of Hlatky and Turner,[10] many research groups have focussed on the design of zwitterionic titanium, zirconium, and hafnium complexes bearing a borate functionality and acting as single-component polymerization catalysts. The state-of-the-art in cyclopentadienyl-containing zwitterionic catalysts (e.g. of types **1** or **2**) has periodically been reviewed.[11]

The active 14-electron cationic species must preserve its Lewis acidity as a target for the olefin, but as in the intermolecular situation, a sufficient degree of stabilization is required. Provided that it is allowed by the geometry, this is achieved by tight intramolecular $Zr^{+}\cdots H_2CB^{-}(C_6F_5)_3$ ion-pairing,[12] eventually assisted by α agostic interactions.[13] When the geometry enforces a large intramolecular charge separation, weak ArH→Zr^{+} or $^{-}$BArF:→Zr^{+} interactions serve to stabilize the structure. Zwitterionic complexes with a phenyl (instead of cyclopentadienyl) ancillary ligation (**3**) have also been reported, but proved to be poor polymerization catalysts owing to the π-donor properties of the aryloxy ligands.[14]

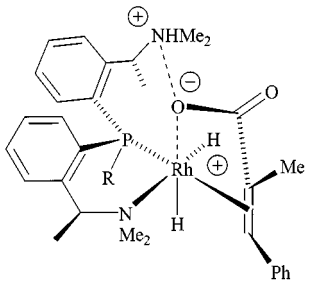
More generally, phenyl rings tethered to anionic borate centers can act as η^6-ligands towards other metals. Of par-

ticular relevance is Alper's zwitterionic rhodium(I) tetraphenylborate complex (**4**), which exhibits well-defined catalytic activity in various reactions (hydroformylation, hydrogenation, polymerization, etc.)[15] and, in particular, in the carbonylation of benzylic and allylic bromides under phase-transfer conditions.[16] Bis(catecholato)borate also acts as a η^6-coordinating anion in 18-electron cationic rhodium catalysts **5** for the hydroboration and diboration of alkenes.[17] Related hydridoruthenium complexes, such as **6**, have also been described, in which the boron atom of the η^6-tetraphenylborate ligand is even tilted away from the cationic ruthenium hydride.[18]



4 **5** **6**

The subtle effects of ion-pairing phenomena in catalysis have been the topic of several studies, e.g. in the case of palladium-catalyzed allylic alkylation,[19] and zwitterionic intermediates have been shown to play a key role in stereoselective catalysis. Thus, in order to achieve enantioselective hydrogenation of substituted acrylic acid derivatives, Yamagishi and co-workers designed rather oxophilic rhodium complexes of chiral ω-aminophosphane ligands: the non-chelating amino group acted as a basic center that could deprotonate the carboxylic group of the substrate.[20] A separation of three formal charges was assumed to occur in the cationic intermediate **7**, and the intramolecular electrostatic interaction was claimed to enhance the facial selectivity of the alkene coordination.



7

Similarly, Brunner et al. designed chiral rhodium complexes bearing chiral ligands where a ligand–substrate charge-transfer was found to control the stereoselectivity in asymmetric catalysis.[21]

Besides these applications in catalysis, the syntheses, structures, and properties of many zwitterionic organometallic complexes with cationic metal fragments have been studied. Consequently, the more rare situation of reversed polarity will now be considered in more depth.

II. Zwitterionic Organometallic Complexes with an Anionic Metal

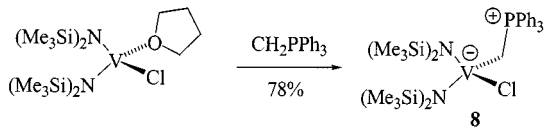
Among zwitterionic metallate complexes, a distinction can be made between mononuclear and dinuclear species.

II.1. Mononuclear Anionic Fragments

II.1.a. Phosphonium Complexes

Most zwitterionic representations of organometallic complexes with an anionic metal center encountered in the literature correspond to the coordination of a phosphonium ylide or a conjugated equivalent. In these complexes, the charge separation is weak and corresponds to a β-dipole (M^-–CH_2–$^+PR_3$). It is remarkable that the metal–phosphorus distance is non-bonding: despite the possibility of adopting a formally non-zwitterionic Lewis topology [phosphorane alkylidene complex M(η^2-CH_2=PR_3)], this limiting dative bonding resonance form (which might be called a "haptomer form" by reference to a limiting π bonding resonance form called a "mesomer form") makes a negligible or very low contribution to actual equilibrium ground-state structures. The M^-–(η^1-CH_2–P^+) sequence can be regarded as a homologue of the simple M^-–$^+PR_3$ semi-polar or M←PR_3 dative bond. Along the same lines, phosphoniocarbene metallate (M^-=CH–$^+PR_3$), phosphoniovinyl metallate (M^-–CH=CH–$^+PR_3$), and phosphonioacetylide metallate (M^-–C≡C–$^+PR_3$)[22a] structures are found to predominate over the non-zwitterionic mesomer forms in the descriptions of equilibrium ground-state complexes. Greater charge separations are also encountered in higher homologues of simple phosphane complexes M←PR_3. The chemistry of these complexes has been thoroughly reviewed on several occasions,[5] hence only a few recent illustrative examples will be outlined here.

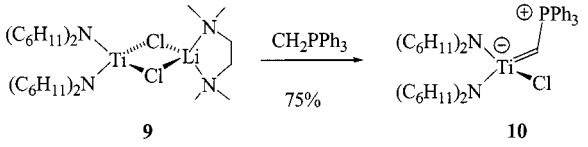
Phosphonium Ylide Complexes: The simplest method of preparation involves the substitution of a labile 2-electron ligand by the anionic end of an ylide. This is illustrated by the synthesis of the paramagnetic vanadium(III) zwitterionic complex **8** by substitution of a THF ligand by CH_2PPh_3 (Scheme 1).[22b] Despite the electrostatic attraction and the possibility of η^2-bonding, the V–C–P angle (128.6°) and the $V^-\cdots P^+$ distance (≈ 3.55 Å) are large. The analogous titanium(III) complex displays the same features.



8

Scheme 1

Phosphoniocarbene Metallate Complexes: The diamagnetic titanium(IV) complex **10** was obtained by oxidative coupling of an ylide with a titanium(III) complex **9** (Scheme 2).[22b] Analysis of the bond lengths by X-ray crystallography suggests that the non-zwitterionic phosphoranevinylidenyl limiting form $[(R_2N)_2(Cl)Ti–CH=PPh_3]$ makes only a minor contribution. This can be related to the pre-existence of a formal negative charge on the titanium atom in **9**, which can also be formulated as $[(R_2N)_2TiCl_2]^-[Li(NMe_2CH_2)_2]^+$.

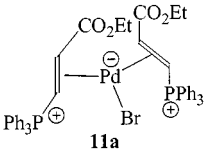


9 **10**

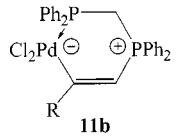
Scheme 2

Phosphoniovinyl Metallate Complexes: η^2-Phosphonioalkene complexes such as **11a**,[23a] and η^1-β-phosphoniovinyl complexes such as **11b**,[23b] **12**,[24] or **13**,[25] among many others, are stabilized by a non-polar resonance form and often adopt a *trans* configuration across the C=C bond.

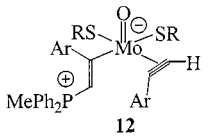
A *cis* configuration, as in **11b**, is enforced in metallacycles.[26] Stable 18-electron organometallic phosphonium zirconate complexes (**14**) have recently been described by Majoral and co-workers.[27] These were prepared by [3+2] cycloadditions of zirconaindene with alkynes (Scheme 3). The complexes were found to exhibit both an α- and a β-phosphonium configuration. Thus, several π-resonance paths can be envisaged, but the non-metallate resonance forms make only negligible contributions.



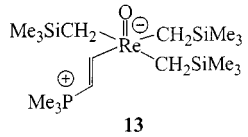
11a



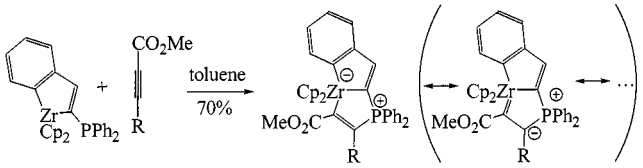
11b



12



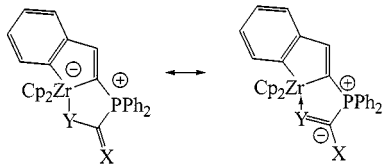
13



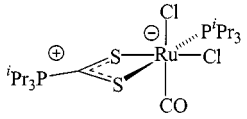
14

Scheme 3

This synthetic strategy has been extended to heteroallenes X=C=Y (X, Y = S, O, NR), leading to α-phosphoniovinyl complexes of type **15**.[28] Here, the Zr–Y bond lengths (Y = S, NR) were found to be longer than any known Zr–Y single bonds, thus indicating their dative character. A related type of covalent-dative zwitterionic ruthenate complex, **16**, has been obtained by insertion of CS_2 into a $iPr_3P\rightarrow Ru$ bond.[29]

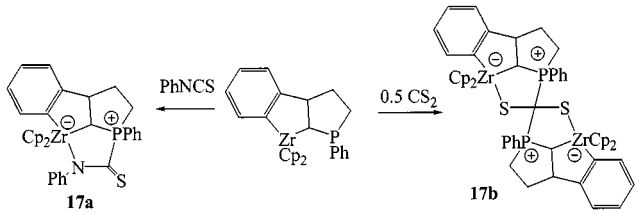


15 X = O, S; Y = S, NR



16

Finally, it must be pointed out that the phosphoniovinyl function is not necessary for stabilizing the zwitterionic structure. Reaction of X=C=S (X = S, NPh) with α-phospholane zirconaindane leads to either the tetracyclic phosphonium zirconate **17a** or to the spirocyclic bis-zwitterionic complex **17b** (Scheme 4).

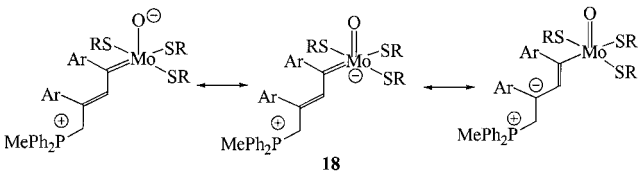


17a **17b**

Scheme 4

In all these cyclic phosphonium zirconate complexes, the $Zr^-\cdots P^+$ distances are in the typical range of 3.5–3.7 Å found in non-cyclic derivatives such as **8**.

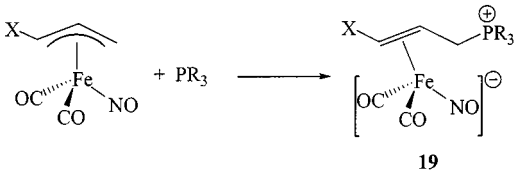
Other Phosphonium Metallates: Zwitterionic mononuclear phosphonium metallate complexes with a large intrinsic charge separation can be stabilized by resonance. This is illustrated by comparing the phosphonium carbene-molybdate complex **18** (where the shortness of the Mo–C bond length is indicative of strong alkylidene character) with the related **12**, which has neither non-zwitterionic nor α-ylide resonance forms.[24]



18

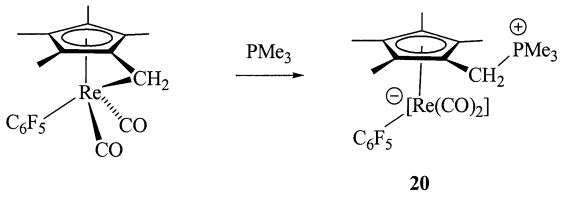
The γ-charge separation in allyl-type configurations is not greatly stabilized, as has previously been emphasized

for the η^2-allylphosphonium ferrate complexes **19**,[30] but many related complexes have been isolated (Scheme 5).



Scheme 5

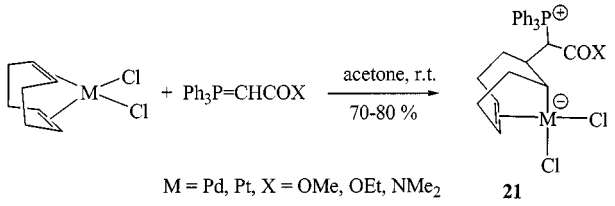
The principle of the above reaction (cleavage of a metal–CH_2 bond by a phosphane) can be applied to the preparation of zwitterionic phosphonium rhenate complexes,[31] e.g. **20** (Scheme 6), where the link between the charges contains a cyclopentadienyl ligand as in $[^{-}Cr(CO)_3\{\eta^5\text{-}C_5H_4(CH_2P^{+}Et_3)\}]$[32] or in the bimetallic complex $[Fe\{\eta^5\text{-}C_5H_4M^{-}(CO)_5\}(\eta^5\text{-}C_5H_4P^{+}Ph_2Me)]$.[33]



Scheme 6

In a similar process, cleavage of an Rh–C bond in a carborane-rhodium complex by nucleophiles leads to γ-zwitterionic phosphonium complexes.[34a] Owing to the fact that the $C_2B_9H_{11}^{2-}$ carborate is considered as an L_2X^{-} equivalent of the $C_5H_5^{-}$ ligand, the starting 18-electron Rh^{III} complex $[\{\sigma,\eta^5\text{-}10\text{-}[CH(p\text{-tol})]\text{-}7,9\text{-}C_2B_9H_{10}^{-}\}Rh^{+}(CO)(PPh_3)]$ is zwitterionic with a positive charge on the rhodium atom and a negative charge on the $C_2B_9H_{10}$ framework.[34b] Reductive cleavage by PEt_3 leads to the zwitterionic 18-electron Rh^{I} complex $[\{\eta^5\text{-}10\text{-}[Et_3P^{+}\text{–}CH(p\text{-tol})]\text{-}7,9\text{-}C_2B_9H_{10}^{-}\}Rh(CO)(PPh_3)]$, where no formal charge resides on the rhodium atom. The latter complex is therefore not a formal metallate.

Very recently, zwitterionic phosphonium organopalladate and organoplatinate complexes **21** with a δ non-conjugated charge separation were described. They were obtained through an unusual vinylogous nucleophilic attack of stabilized α-phosphonium ylides at a cyclooctadiene ligand in an *exo* fashion (Scheme 7).[35] Although the chloride ligands may be displaced by non-coordinating anions, the Pt–Cl 8distances in the crystal (2.3 or 2.4 Å depending on the *trans* effect of the facing ligand) are definitely bonding. IR and NMR data confirmed the formal zwitterionic nature of the complexes in solution.

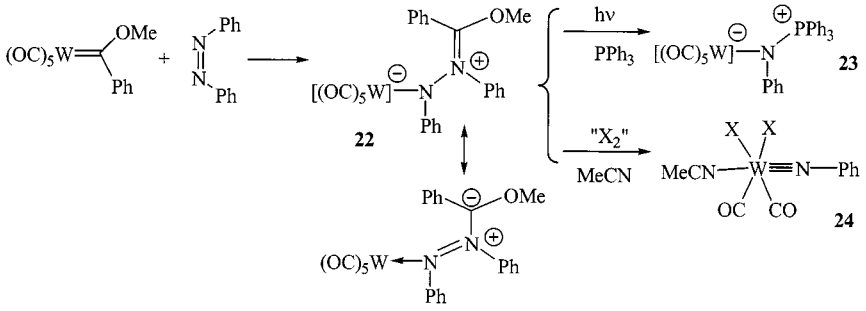


Scheme 7

II.1.b Mononuclear Ammonium and Iminium Metallate Complexes

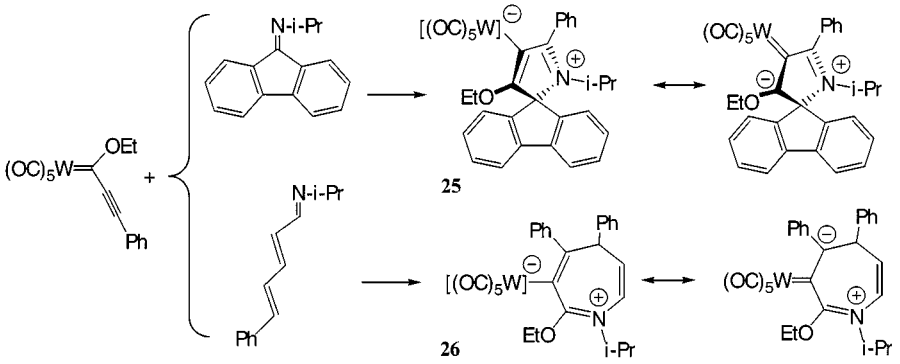
Interesting zwitterionic complexes, where the metal exhibits both a negative charge and a low formal oxidation state, are accessible from Fischer carbene complexes. This tendency is consistent with the analogy between the $(CO)_nM{=}C(R')\text{–}OR$ fragment and the ester $O{=}C(R')O\text{–}R$ fragment,[36] considering the resonance $O{=}C(R')O\text{–}R \leftrightarrow O^{-}\text{–}C(R'){=}{}^{+}OR$ to translate to $(CO)_nM{=}C(R')O\text{–}R \leftrightarrow (CO)_nM^{-}\text{–}C(R'){=}{}^{+}OR$. Such resonance arguments have been invoked to account for the α-CH acidities of Fischer-type carbene complexes $(CO)_5M{=}C(OR)(CH_2R')$.[37]

Unlike phosphonium ylides, "hydrazonium aza-ylides" are mesoionic. Their complexes have been prepared by formal metathesis of tungsten Fischer carbene complexes with *cis*-azobenzene.[38] The stereochemistry of complex **22** was deduced from its crystal structure, where the amido nitrogen atom was seen to be perfectly planar.[39] This planarity does not result from a p_π N:⇒W donation, but rather from steric constraints. The presence of the negative charge on the metal was supported by photochemical arguments, in particular by a shoulder in the UV/vis spectrum of the complex, which was interpreted as an MLCT transition. Under thermal or photochemical activation, complex **22** represents a source of the nitrene complex $(CO)_5W{=}NPh$, which can be trapped by PPh_3 to give the β-zwitterionic complex **23**, the zwitterionic (as opposed to apolar phosphinime) structure of which is suggested by its IR and ^{31}P-NMR data.[40] Under oxidative conditions, the zwitterionic amide complex **22** represents a precursor of imido tungsten complexes such as **24**, exhibiting various oxidation states.[41] The disappearance of the formal charge separation in the zwitterionic complex contributes to the driving force of the reaction (Scheme 8).



Scheme 8

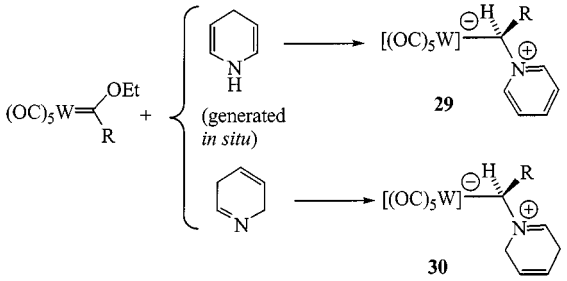
The formation of the zwitterionic amido complex **22** involves nucleophilic attack of the nitrogen atom of azobenzene at the carbenic center, followed by a 1,3-shift of the $W(CO)_5$ fragment. Zwitterionic chromium complexes have also been generated from chromium carbene electrophiles,[42] and from other nitrogen nucleophiles such as ketenimines.[43] α,β-Unsaturated Fischer carbene complexes are susceptible to 1,2- or 1,4-attack by nitrogen nucleophiles, and subsequent rearrangements lead to zwitterionic iminium carbonylmetallate complexes **25–28**.[44] When the nucleophile contains an imino but not an amino group, the final complexes **25** or **26** may be mesoionic, although not necessarily at the metal center: the metal fragment is indeed bonded to an sp^2 carbon atom and the negative charge can be delocalized by π-resonance from the metal to the organic ligand (Scheme 9).[45]



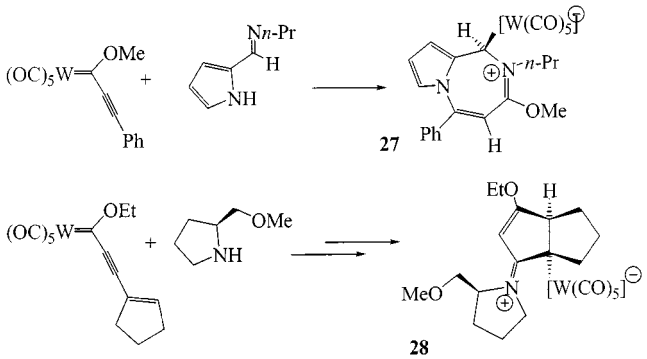
Scheme 9

In contrast, when the nucleophile contains a secondary amino group (Scheme 10), the metal in the iminium carbonylmetallate products **27** or **28** is bonded to an sp^3 carbon atom and the negative charge remains on the carbonyl-metal fragment (as reflected in the corresponding C–Cr^- or C–W^- and C=N^+ bond lengths in the crystal structures).[46][47] The zwitterionic complexes are readily formed at room temperature and exhibit an astonishing degree of hydrolytic and thermal stability. The $W^-\cdots N^+$ separation can involve two bonds (iminium ylide complexes) or three bonds, but the positive charge of the exocyclic or endocyclic nitrogen atom is stabilized by resonance with α,β-conjugated C=C bonds and α- or γ-C–OR bonds. Nonetheless, the charge localization in complexes of type **28** also requires the support of electron-donating substituents at the nitrogen atom. Analogous dialkylphospheniums are unstable and rearrange to non-zwitterionic tungsten vinylphosphane complexes.

Pyridinium ylide complexes of pentacarbonyltungsten, **29**, are true β-zwitterionic complexes where the metal fragment is bonded to an sp^3 carbon atom and retains its anionic charge in all possible π-resonance structures with the organic ligand. Such complexes are produced by the reaction of $(CO)_5M{=}C(OEt)R$ (M = Cr, W) with 1,4-dihydropyridine, formed in situ from 1-methoxycarbonyl-1,2-dihydropyridine and methyllithium (Scheme 11).[48] The stability of the zwitterionic complex might be ascribed to the aromaticity of the pyridinium product. However, non-aromatic 2,5-dihydropyridine analogues **30** have also been structurally characterized, demonstrating the presence of 2,5-dihydropyridine derivatives along with 1,4-dihydropyridine in the in situ formed reactant (Scheme 11).[49] The positive charge delocalization in **30** is restricted, and an X-ray analysis did not indicate any increased delocalization of the negative charge over the carbonyl ligand.

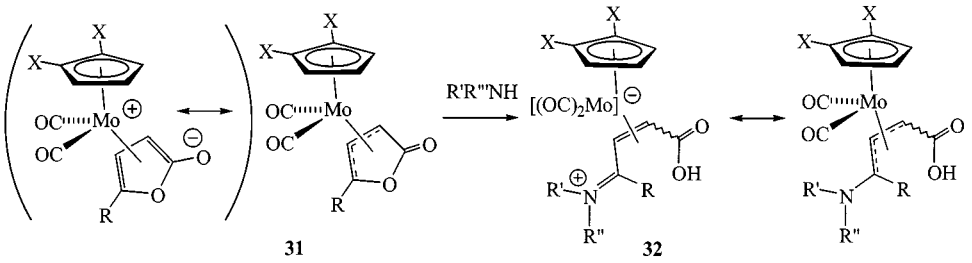


Scheme 11

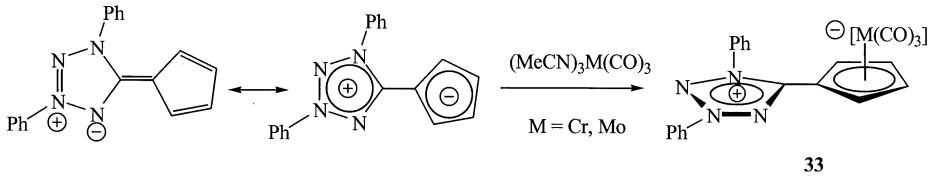


Scheme 10

In a reaction related to that leading to complex **19**, π-allyl ligands at $(CO)_2XMo^{II}$ centers undergo nucleophilic attack to afford zwitterionic intermediates.[50] In the case of η^3-lactonoyl ligands, despite the possible contribution of the reverse zwitterionic "haptomeric" structure in the electrophilic starting complex **31** (which has been explicitly invoked in related acyl π-allyl complexes),[51] the metal center is not directly attacked. The zwitterionic structure resulting from amine attack stabilizes by undergoing ring-opening (Scheme 12). According to IR spectroscopy and X-ray crystallography, the complexes **32** are better described by an iminium molybdate picture than by a non-zwitterionic structure.[52] The stability of **32** is somewhat surprising; the



Scheme 12

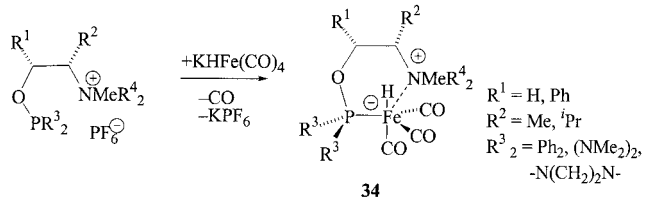


Scheme 13

anionic metal neither deprotonates the carboxylic acid function nor reacts with CH_3I.

Tetrazole is a cyclic imine that can act as an *N*-donor ligand in zwitterionic cationic metal tetrazolate complexes,[53] but it also provides the framework for a delocalized cationic moiety in zwitterionic complexes of reversed polarity (Scheme 13). The mesoionic character of olate, thiolate, selenolate, or cyclopentadienide 5-substituted tetrazolium can be transferred to zwitterionic Cr and Mo complexes **33**.[54] In the case of the cyclopentadienide derivative, the high-field shifts of the ^{1}H- and ^{13}C-NMR signals of the nuclei of the Cp ring and the decrease in the pivotal C–C stretching frequency in the IR spectrum upon complexation indicate that the resonance form with the shortest charge separation (N^+–N^-) tends to disappear in the complex. The latter is therefore truly zwitterionic. A similar conclusion can be drawn for olate, thiolate, and selenolate derivatives.

Zwitterionic metallate complexes with a positive charge completely localized at a quaternary ammonium center are not stabilized by resonance, but are less likely to lose the charge separation by a rearrangement of high-energy π-electrons. The intramolecular ion-pairing is thus expected to be very tight. Zwitterionic analogues of ammonium salts of phosphite and phosphinite hydridocarbonylferrates[55] have been studied in order to examine the possibility of a putative "chiral zwitterionic control strategy" in asymmetric reduction of prochiral ketones by chiral iron hydrides.[56] Chiral ammonium phosphinite ligands based on ephedrine or valinol skeletons ("ephosium", "valphosium", etc.) have thus been synthesized and reacted with $KHFe(CO)_4$ to give stable zwitterionic hydridotricarbonylferrate complexes **34** (Scheme 14).[57]



Scheme 14

An unusual *cis*-H–Fe–P arrangement was suggested by IR and NMR data in solution, and was confirmed in the crystal. It was proposed that this rare feature was dictated by a stabilizing electrostatic back-folding of the $[NMeR^4_2]^+$ terminus onto the $[FeH]^-$ center. Indeed, a precise intramolecular $N^+Me_3\cdots{}^-HFe$ van der Waals contact between hydrogen atoms of the two moieties has been observed in the crystal. For steric reasons (hindrance of the equatorial carbonyl ligands), this dative-electrostatic chelation is not possible in a *trans*-H–Fe–P isomer. The intramolecular pairing was shown to be retained in solution, by a ^{1}H-^{1}H NOE between NMe_3^+ and HFe^-, and by the variation of the $|^2J(H,P)|$ coupling constant with the dielectric constant of the solvent, which also increases with temperature.[58] The latter correlation was proposed to reflect the effect of the dielectric constant on the average opening of hemilabile electrostatic edge $[HFe]^-\cdots{}^+[N]$ in the equilibrium:

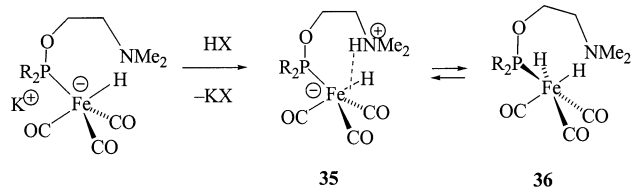
open-[$^+$N~PFeH$^-$···solvent] ⇄ *closed*-[~N$^+$···$^-$HFeP~] + solvent

Ammonium cations were shown to form intermolecular contact ion-pairs with $[HFe(CO)_3L]^-$ anions, and a multisite docking of Me_4N^+ onto the external $[HFe(CO)_3P]^-$ anion was proposed to occur in THF in the vicinity of the [FeCO] and the [Fe–H] sites.[59] An intramolecular contact of this type has been found in the solid-state structure of **34**. It is also entropically favored in solution, even in polar solvents such as acetonitrile and dimethyl sulfoxide.

In conclusion, the true zwitterionicity and the flexibility of these complexes allow for stabilization through the adoption of otherwise rare structural and dynamic features. The chiral zwitterionic complexes are capable of reducing activated ketones, but do not give significant enantiomeric excesses. Chiral phosphonium phosphanes ("diopium", "binapium") have been devised as alternative ligands, but their higher basicities have so far prevented the isolation of the corresponding zwitterionic hydridocarbonylferrate complexes.[60][61]

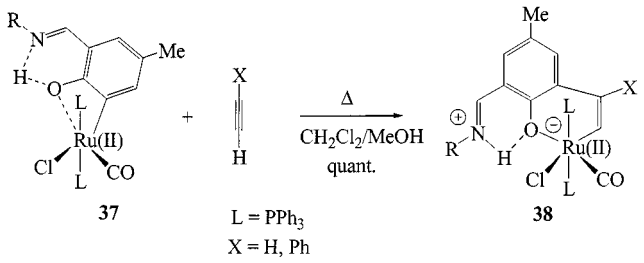
Hydrogen or dihydrogen bonds $A^{\delta'-}\cdots{}^{\delta+}HX^{\delta-}$ involving transition metal centers (X = N, O, F; A = M, MY, MH), although electrostatic in nature, do not generally involve

integral formal charges on both A and HX,[62] but some examples are worthy of mention. Transition metal complexes with a bond between a "proton" and a "hydride" $^{\delta-}$MH···HX$^{\delta+}$ are fascinating species corresponding to a heterolytic predissociation state of the dihydrogen molecule. In most cases, however, the charge on the metal is not formally –1 (the H ligands of neutral or even cationic transition metal hydrides are still refered to as "hydrides").[63] Protonation of an ω-aminophosphane hydridoferrate anion occurs at both nitrogen and iron sites (Scheme 15). In polar solvents at low temperatures, the zwitterionic structure **35** has been detected by ^{1}H-NMR, and measurements of the T_1 relaxation times for the NH$^+$ and FeH$^-$ ^{1}H nuclei at low temperatures allowed an estimation of the H···H distance of ca. 1.71 Å.[64] This value is typical for a dihydrogen bond, and was reproduced as the optimized distance in DFT calculations using the B3PW91 functional.[65] In less polar solvents and at higher temperatures, an equilibrium between the zwitterionic ammonium hydride structure **35** and the non-zwitterionic dihydride structure **36** was observed. DFT calculations showed the non-zwitterionic complex **36** to be more stable than **35** by 8 kcal mol^{-1} in vacuo, but that the order of stability is reversed on taking into account the dielectric constant of a polar solvent.



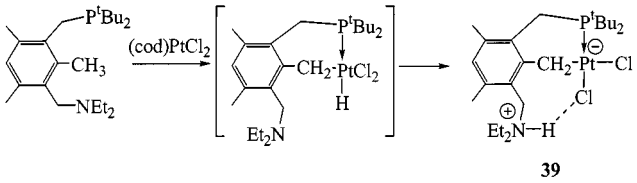
Scheme 15

More classically, hydrogen-type bonding can involve a halide or an oxygen atom instead of a hydride,[66] and occurs as a source of stabilization in truly zwitterionic complexes. The zwitterionic character of complex **38** arises from strain release following insertion into the four-membered metalla-oxetane ring of **37** (Scheme 16). Thus, the cyclic Ru–O bond in complex **37** is quite long (≈ 2.24 Å) and undergoes facile cleavage by ligands. The insertion of an alkyne into the adjacent Ru–C cyclic bond leads to a complex that features a much shorter Ru–O bond length (2.10 Å) with a definitely protonated nitrogen atom. This complex could be described by the zwitterionic structure **38**, featuring an NH···O hydrogen bond.[67]



Scheme 16

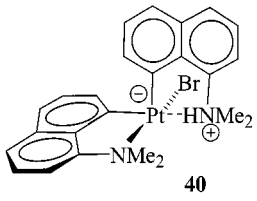
Milstein and co-workers reported that a non-zwitterionic Pt^{IV} complex produced by intramolecular C–H activation of a neutral Pt^{II} complex undergoes spontaneous stabilization through intramolecular proton-transfer to a pendant amino group to give the zwitterionic Pt^{II} complex **39** (Scheme 17).[68]



Scheme 17

The zwitterionic nature of **39** was established by X-ray crystallography. Thus, the chlorine atom involved in the hydrogen-bonding is tightly bound to the platinum atom (NH···ClPt ≈ 2.41 Å), the corresponding Pt–Cl bond being shorter (≈ 2.38 Å) than the others (≈ 2.41 Å).

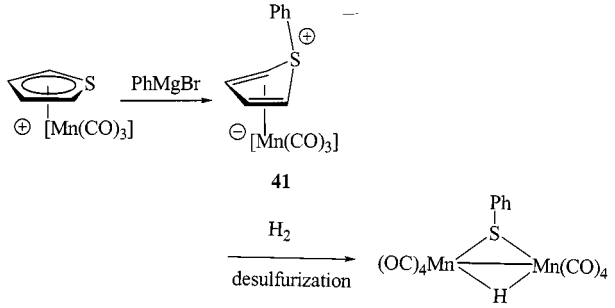
This coordination mode represents the alkylplatinum analogue of the zwitterionic arylplatinum complexes described by van Koten and co-workers.[69] The authors showed that ammonium protons of zwitterionic platinate complexes can interact with either a Pt–Br bond or the formally anionic platinum atom. In the latter situation, the formal charge separation is shorter, but is still present in the platinate(II) structure **40**. The non-zwitterionic hydridoplatinum(IV) structure was ruled out on the basis of NMR data (downfield shift of the proton resonance, small coupling constants between the *ortho*-aromatic protons of the ligand and ^{195}Pt) and by its X-ray crystal structure (N–H ≈ 0.88 Å, Pt···HN ≈ 2.11 Å >> classical Pt–H bond lengths). The stability of the zwitterionic structure of **40** is not only due to the hydrogen bonding, but also to steric shielding of both the platinate center (from strong electrophiles such as MeI) and the ammonium center (from D_2O exchange).



Borderline examples of zwitterionic ammonium metallate complexes are worthy of mention. Thus, zwitterionic 16-electron rhodium-carborate complexes have been prepared by substituting two 2-electron ligands of a neutral rhodium precursor {e.g. [RhBr(PPh$_3$)$_3$]} with a zwitterionic *nido*-carborate ligand (e.g. *nido*-7-*t*BuH$_2$N$^+$–7-CB$_{10}$H$_{10}^-$).[70] The product might a priori be formulated as an 18-electron rhodium(I) complex [(η^5-7-*t*BuH$_2$N$^+$–7-CB$_{10}$H$_{10}$)Rh$^-$Br(PPh$_3$)]. However, since the metallacarborane is not distorted from a triangular *closo*-icosahedral framework, the complex is actually a 16-electron cationic rhodium(III) complex [(η^5-7-*t*BuH$_2$N$^+$–7-CB$_{10}$H$_{10}^{2-}$)Rh$^+$Br(PPh$_3$)], in which both the Rh and N atoms are cationic and a double negative charge is delocalized over the carborane framework.

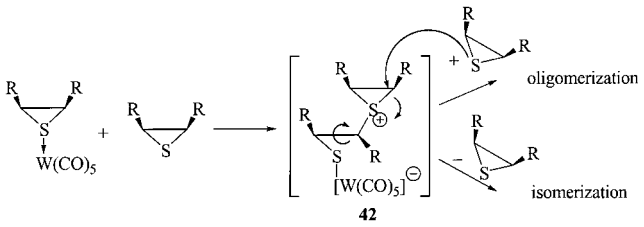
II.1.c. Sulfonium Metallate Complexes

Sulfonium metallate structures are of great relevance to the industrial challenge of petroleum desulfurization. Thus, thiophene derivatives can be hydrodesulfurized via zwitterionic sulfonium manganate(0) complexes **41** obtained by nucleophilic attack at the S atom of cationic η^5-thiophene species. A model of the above zwitterionic intermediate has been characterized by X-ray crystallography. Its structure reveals activation of both the manganese and sulfur atoms, which allows hydrogenolysis of the C–S^+ bonds (Scheme 18).[71]



Scheme 18

Zwitterionic sulfonium metallates occurring in catalytic processes cannot be isolated, but can be invoked as key intermediates. $W(CO)_5$(NCMe) and $W(CO)_5$(thiirane) complexes have been found to catalyze desulfurization, ring-opening oligomerization, and isomerization of thiiranes $S(CHR)_2$ (R = H, Me),[72] and the intermediacy of zwitterionic species **42** resulting from an S_N2 reaction of a free thiirane sulfur atom at a coordinated thiirane carbon atom has been postulated (Scheme 19).



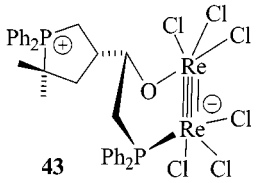
Scheme 19

II.1.d. Zwitterionic Oxonium Complexes

nido-Carborane complexes such as $[Mn(CO)_3\{\eta^5\text{-}7,8\text{-}C_2B_9H_{10}\text{–}10\text{-}O(CH_2)_4\}]$ have been described as zwitterionic. This representative complex has been characterized by X-ray crystallography, and has been shown to react with various nucleophiles to afford phosphonium and ammonium zwitterionic complexes with large charge separations. However, the dianion $C_2B_9H_{11}^{2-}$ is a complexing equivalent of the monoanion $C_5H_5^-$ and since the formally neutral manganese atom in $[Mn(CO)_3\{\eta^5\text{-}C_5H_5\}]$ obeys the 18-electron rule, the negative charge compensating the positive charge of the oxonium substituent is delocalized over the $C_2B_9H_{10}$ framework and not over the metal atom. Therefore, although the complex is indeed zwitterionic, it should not be regarded as a formal metallate species.[73]

II.2. Dinuclear Anionic Fragments

A negative charge can be delocalized over two or more metal fragments. Owing to the electropositivity of metals, this is a priori a destabilizing factor, but the metal–metal bond permits delocalization of the excess electron over twice as many auxiliary ligands (CO, Cl, etc.) on the anionic metals as in the corresponding mononuclear species. For example, in the nice zwitterionic complex of the chiral phosphonium ligand "isodiop", **43**,[74] the negative charge is delocalized through a quadruple rhenium–rhenium bond. Here, the X-ray crystal structure does not reveal any back-folding of the P^+ center onto the anionic metal.



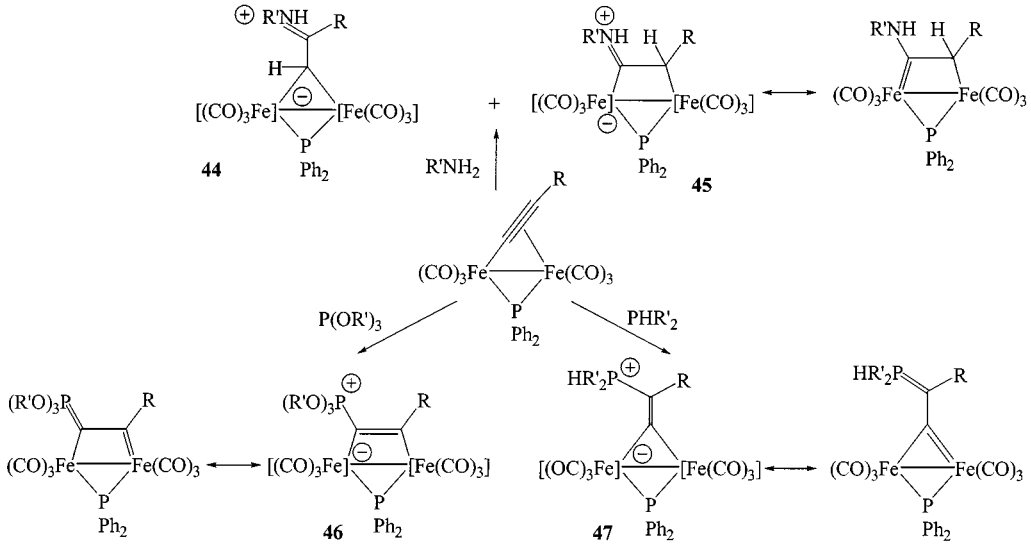
Homo- and heterobimetallic transition metal allenyl complexes with single metal–metal bonds provide frameworks for interesting zwitterionic organometallate complexes,[75] particularly in the case of diiron complexes. Nucleophilic additions at the μ-σ,π-acetylide ligand of $Fe_2(CO)_6(\mu\text{-}PPh_2)(\mu\text{-}C_2R)$ afford various kinds of zwitterionic complexes, in which a negative charge is delocalized over the two iron centers (Scheme 20).

Short β charge separations, also shadded off by minor contributions from non-dipolar resonance forms,[76] occur in **45**–**47**, but γ charge separation occurs in the truly zwitterionic complex **44**.[77] The negative charge can also reside on (and polarize) substituted $Fe_2(CO)_5P$ cores as in the C_β-phosphonio-phosphane complex **48**[78] (Scheme 21) or in related C_α-phosphonio-phosphane complexes.[79]

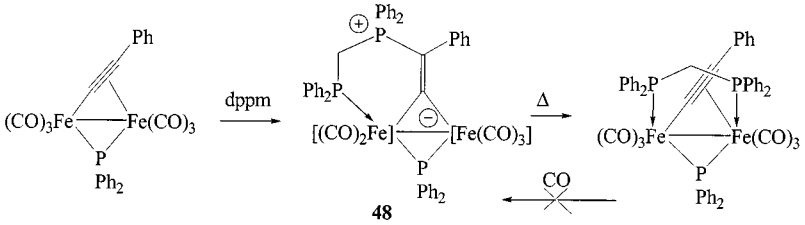
Related μ-σ,π-allenyl precursors generate similar phosphonium complexes,[80] but can also lead to a new type of mesoionic μ-η^2-propylene complex **49**,[81] which isomerizes to the non-dipolar complex **50** (Scheme 22).

Dinuclear phosphonium complexes with three-bond charge separation have long been characterized.[82] The X-ray crystal structure of complex **51** shows that the hydrocarbyl ligand adopts a μ-η^1:η^2 coordination mode (Scheme 23). The high-field shift of the ^{13}C-NMR signal of the C_α–Os center confirms the 18-electron rule and indicates that the osmium atom bears the negative charge which is no longer delocalized over the neutral 18-electron rhodium atom.[83]

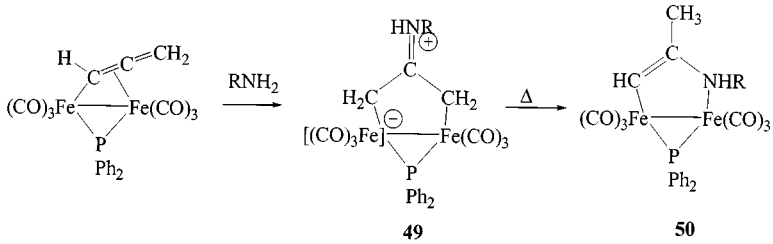
Among the Group 9 homodinuclear metallates, a complex of 2,3-bis(diphenylphosphanyl)maleic acid has been found to stabilize through formation of a zwitterionic cobaltate complex **52** at elevated temperatures (Scheme 24).[84] An 18-electron count for both the metal atoms indicates that the formal charges are separated by three bonds. This



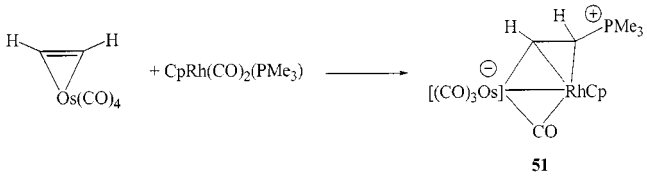
Scheme 20



Scheme 21

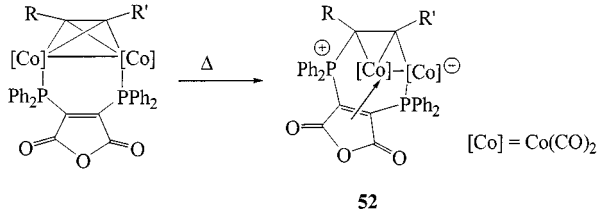


Scheme 22



Scheme 23

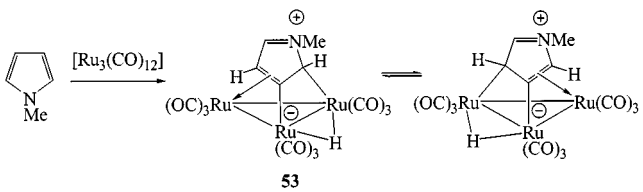
example does not represent a C-η^1-ylide complex, but rather a C,C-η^2-β-phosphoniovinyl complex, the non-coordinated analogue of which corresponds to complexes of types **12** and **13**.



Scheme 24

II.3. Trinuclear Anionic Fragments

Zwitterionic metallates of higher homonuclearity ($[Fe]^{-}_{3}$, $[Ti]^{-}_{3}$, $[Ru]^{-}_{3}$, etc.) have also been described, where the cationic charge is borne by either an appended metal fragment,[85] an iminium,[86] a phosphonium, or an ammonium group.[87] For example, the charge separation on the ruthenium cluster **53** has been evidenced by spectroscopy (ν_{CO} IR frequencies are lower than those found for classical non-zwitterionic related clusters) and by a strong solvent effect on the thermal stability the cluster. The charge delocalization over the three metal atoms also takes place dynamically in solution through rapid interconversion of isomers by

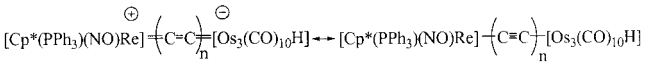


Scheme 25

concerted hydride shifts and small geometric displacements (Scheme 25).

III. Zwitterionic Complexes with both Anionic and Cationic Metals

Transition metals linked by a "wire" of sp carbon atoms are attracting a great deal of interest in the context of studies of electron-transfer between metals under various physicochemical stimuli. When the two metallic groups are different in electronegativity, a zwitterionic form can make a significant contribution to the ground state of the complex. For instance, in the rhenium–osmium bimetallic complex **54**, the zwitterionic cumulenic form is seen to make a significant contribution as opposed to the polyacetylenic form.[88]

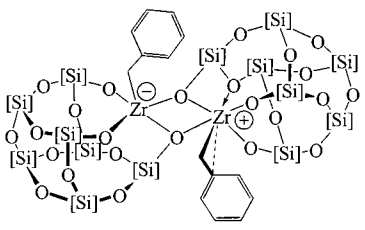


54

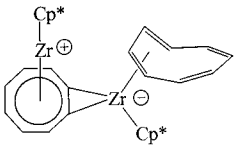
It is not the aim of this review to cover this large field; this section merely gathers together several examples of types of zwitterionic dinuclear complexes that can simply be described in terms of a static two-electron transfer from one metal to another on the basis of structural and spectroscopic data.

III.1. Zwitterionic Group 4 Metallates with an Appended Cationic Metal

It has previously been mentioned that both zwitterionic cationic zirconium and anionic zirconate complexes are known. The two charge states have been postulated as being present in the zirconium complexes **55a** and **55b**. Indeed, the dimeric silsesquioxane **55a** exhibits an asymmetric structure in the solid state.[89] A negative charge has been assigned to the zirconium atom bearing five oxygen ligands and one η^2-benzyl ligand. However, the comparable Zr–O bond lengths suggest that a non-zwitterionic limiting structure also contributes to the description of the complex. For the organo-bridged complex **55b**, the zwitterionic formulation was suggested by a reasonable electron count, showing two 16-electron Zr^{IV} and Zr^{II} atoms, and was confirmed by the diamagnetism of the complex.[90]



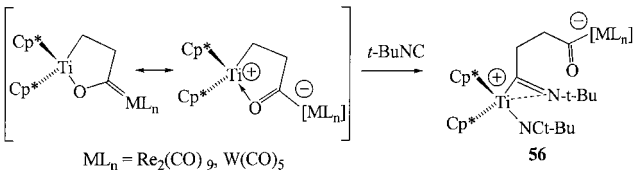
55a [Si] = c-C_5H_9Si



55b

III.2. Zwitterionic Group 5 Metallates with an Appended Cationic Metal

Alkyltitanium-rhenium and -tungstene complexes undergo insertion of *tert*-butylisocyanide to afford truly zwitterionic complexes of type **56**, in which the 18-electron metals are separated by a butanedioic bridge (Scheme 26). The reaction is favored by the existence of a zwitterionic resonance form of the starting complex.[91]



$ML_n = Re_2(CO)_9$, $W(CO)_5$

56

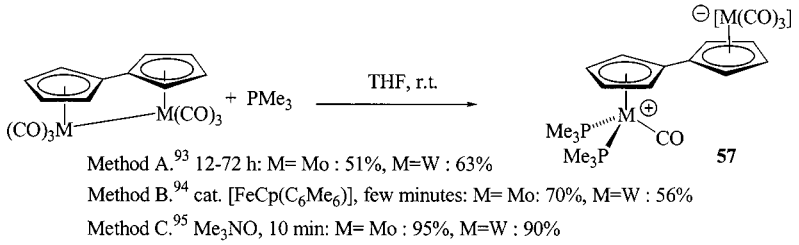
Scheme 26

1II.3. Zwitterionic Group 6 Metallates with an Appended Cationic Metal

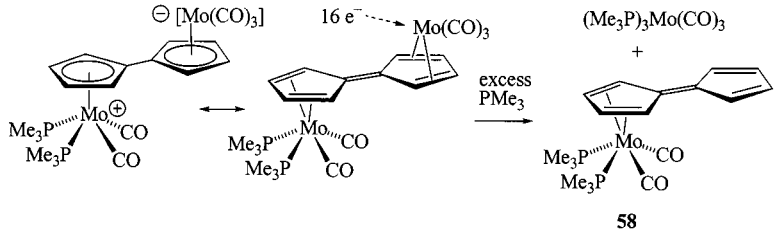
Besides metal-substituted (π-arene)chromium complexes polarized by subtle resonance and inductive effects (e.g. [{η^1:η^6-$C_6H_5(TiCp_2Cl)$}$Cr(CO)_3$]),[92] zwitterionic bimetallic complexes of Group 6 metals are found in the fulvalene series. Homodinuclear complexes, in which the metals exhibit different CO vs. phosphane substitution patterns, can be prepared by several methods (A,[93] B,[94] or C[95]) from (fulvalene)$Mo_2(CO)_6$ and basic phosphanes. After metal–metal bond cleavage, the steric repulsion between the metal centers overrides the electrostatic attraction and results in a 180° rotation of the cyclopentadienyl metal moieties, which, in turn, leads to a *trans* arrangement of the opposite charges with respect to the cyclopentadienyl plane. The zwitterionic nature of these complexes, e.g. **57**, is evident from comparisons of their IR and NMR spectroscopic data, X-ray crystal structures, and chemical reactivity with those of related separated anionic and cationic complexes (Scheme 27).

Most notably, the molybdenum zwitterionic complex undergoes ring-slippage to give the neutral mononuclear η^4-fulvalene complex **58**, probably via an intermediate in which one of the molybdenum atoms has a 16-electron configuration (Scheme 28). This intermediate structure might also be regarded as a non-zwitterionic "haptomer" form of the complex, accounting for its stability and the electron communication between the two metals.

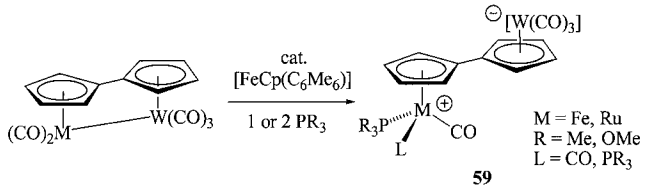
The use of electron-reservoir complexes such as [FeCp(arene)] can also serve to prepare heterodinuclear $^-$[Mo,W]–[Fe,Ru]$^+$-type zwitterions (**59**). Here, phosphane ligands selectively bind to the cationic Group 8 metal. The enhanced rate and selectivity of this reaction (Scheme 29) as compared with those of their homodinuclear counterparts can be rationalized in terms of the dissymmetry of the heterodinuclear system and has been verified by cyclic voltammetry experiments.



Scheme 27



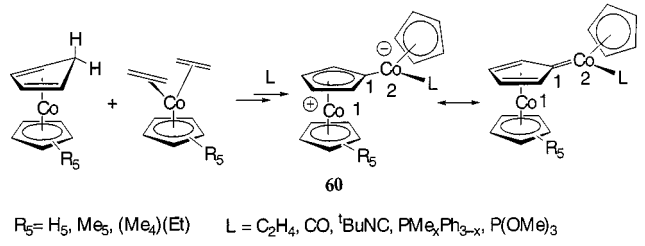
Scheme 28



Scheme 29

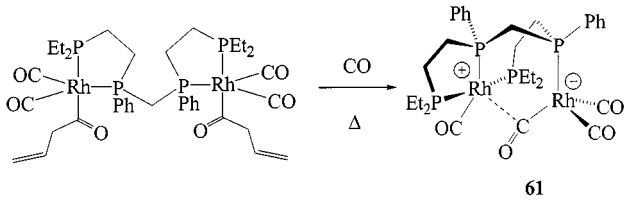
III.4. Zwitterionic Group 9 Metallates with an Appended Cationic Metal

Twofold C–H activation of the η^4-cyclopentadiene ligand in complexes by the homologous bis(ethylene) complex (Jonas' reagent) leads to dinuclear Co^{I}–Co^{III} complexes (**60**) (Scheme 30). X-ray crystal data ruled out the possibility of a metal–metal bond and the formal assignment of the oxidation states can be interchanged between the two metals by simple "haptomeric resonance". The relative contributions of these limiting structures have been carefully analyzed in terms of the π-acceptor vs. σ-donor character of the ligand L.[96] The C(1)–Co(2) distance is extremely short (average 1.87 Å) while the C(1)–Co(1) distance (average 2.20 Å) is longer than all the other (Cp)C–Co(1) distances (average 2.04 Å). Thus, although the occurrence of a cobaltocenium fragment is expected to be favored, the zwitterionic character is not pure. It nevertheless becomes quite important when L is an acceptor ligand.



Scheme 30

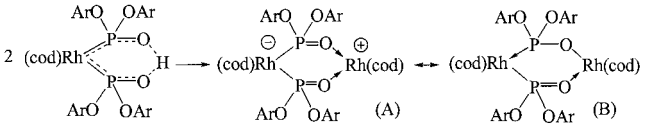
Potentially symmetrically bridged dinuclear complexes can exist as rearranged zwitterionic complexes. Thus, thermal activation of a symmetrical tetraphosphane diacyl dirhodium complex under CO pressure unexpectedly led to the disymmetrical dirhodium complex **61** (Scheme 31).[97] The zwitterionic character of **61** was ascertained by X-ray crystallography, which revealed a tetrahedrally coordinated anionic tricarbonylrhodium center facing a geometrically distorted cationic triphosphane rhodium center without an Rh–Rh bond. A semi-bridging carbonyl ligand accounts for the stability of the zwitterionic structure. This feature also results in an 18-electron count for both rhodium atoms in the $^{-}Rh{\approx}Rh^{+}$ structure without an Rh–Rh bond. The structure is also supported in solution by ν_{CO} IR and ^{31}P-NMR data.



Scheme 31

Dinuclear rhodium complexes can be formulated as zwitterionic on the basis of reactivity arguments. The acidic proton of a phosphito-phosphonato rhodium complex $[Rh^{I}]^{-}[H]^{+}$ can be removed by NaOH, but also by the basic Rh^{I} center of another identical molecule to give an intermediate $[Rh^{I}]^{-}[Rh^{III}H]^{+}$ salt, which reacts further to give the molecular salt $\{[Rh^{I}]^{-}[Rh^{I}]^{+}\}$, **62** (Scheme 32). The latter complex can therefore be regarded as a disymmetrical zwitterionic species, in which two "hard" oxygen atoms of the two equivalent phosphonate ligands point towards the hard cationic Rh atom, while the two "softer" phosphorus atoms point towards the softer anionic Rh atom. However, the

driving force of the reaction relates to the participation of two equivalent non-zwitterionic forms (B).

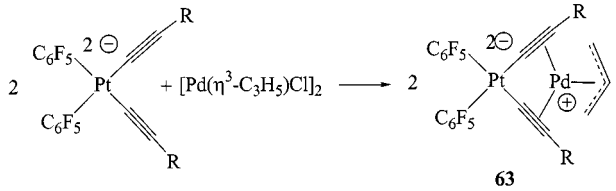


62

Scheme 32

III.5. Zwitterionic Group 10 Metallates with an Appended Cationic Metal

Cationic π-allyl complexes of palladium and platinum react with dianionic platinate to give stable anionic bimetallic complexes **63** with a 2–/+ charge separation (Scheme 33).[98] X-ray, IR, and NMR analyses indicate that the metals communicate through π-bonds.



63

Scheme 33

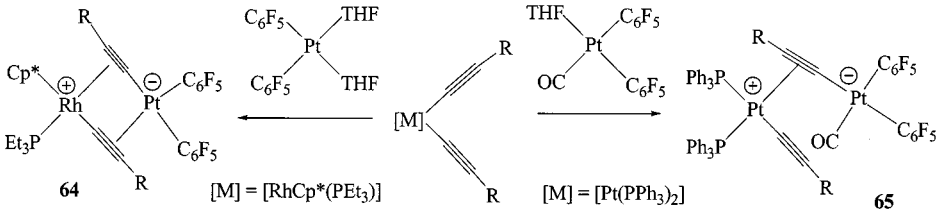
However, when the reactant is the twofold cationic $[Cp^*Ir(PEt_3)(acetone)_2]^{2+}$ complex, the expected 2–/2+ charge separation is unstable and a non-zwitterionic product results from a migration of the σ-alkynyl ligands to the iridium atom.[99] In contrast, migration of alkynyl ligands from neutral bis(alkynyl)platinum complexes to neutral platinum or rhodium reactants can occur in the presence of suitable ligands, thereby leading to charge separation in complexes **64**[100] and **65** (Scheme 34).[101]

A similar process of migration of a chlorine ligand between two neutral complexes leads to the trimetallic zwitterionic complex **66**, in which the positive charge is delocalized over a dimetallic core (Scheme 35).[102]

A zwitterionic monoanionic platinate complex with a cationic charge delocalized over a trinuclear platinum core has also been reported.[103] Trinuclear zwitterionic metallate complexes with a –2/+1/+1 charge separation on the metals may be prepared from a *trans*-dialkynylplatinate. The latter reacts with two equivalents of the cationic platinum reagent $[trans\text{-}PtH(PEt_3)_2]^+$ to give the neutral zwitterionic trinuclear complex **67**, in which the doubly negative platinate center acts as a bridging unit (Scheme 36). Although low stability in solution prevented characterization by ^{13}C-NMR, the zwitterionic nature could be ascertained from IR and X-ray diffraction data, although a contribution of a "haptomer" vinylidene structure has been suggested.[104]

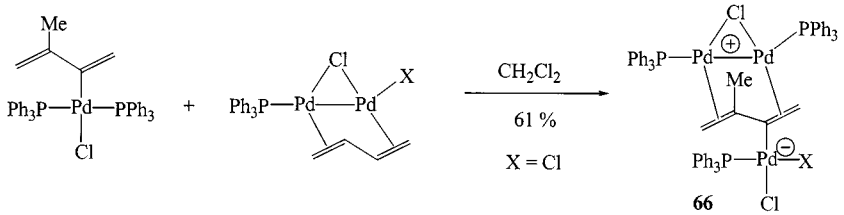
Conclusion

Besides the relative electronegativity of the formally charged fragments tuned by suitable auxiliary ligands, many complexes claimed to be zwitterionic are in fact stabilized by non-zwitterionic π-electron resonance or by partial hapticity. Although these forms have often been regarded



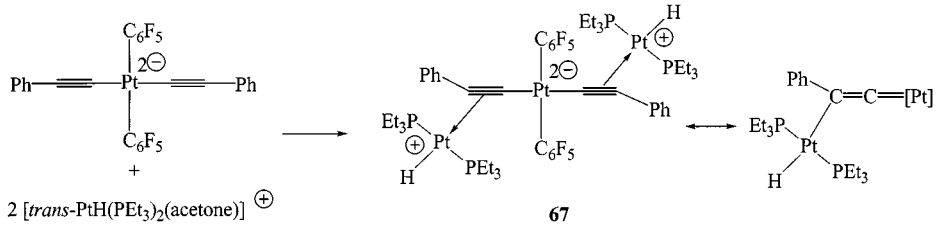
64 [M] = [RhCp*(PEt$_3$)] [M] = [Pt(PPh$_3$)$_2$] **65**

Scheme 34



66

Scheme 35



67

Scheme 36

as making only minor contributions, they play the role of a stabilizing force equilibrating the electrostatic destabilization due to charge separation. True zwitterionic complexes, in which the opposite charges are separated by two or more sp^3 carbon atoms (as in **28**, **34**, **35**, **39**, **43**, **56**), are less common, and multinuclear anionic cores and hydrogen-type bonding are found to be present as additional sources of stabilization.

The ''zwitterionic metallate'' feature may become a fundamental consideration in the design of mixed valence, push-pull or donor–acceptor complexes, for applications in nonlinear optics, molecular electronics, molecular conductivity, etc. Furthermore, just as zwitterionic cationic metal complexes are bringing new perspectives in catalysis, zwitterionic metallates might play a role in governing the activity or selectivity of catalytic reactions through specifically designed hybrid dative-electrostatic interactions in the coordination spheres of reduced metal centers.[56][57]

Acknowledgements

Thanks are due to Dr. Guy Lavigne for a critical reading and interesting discussions, and to Virginie Rouzaud for her help in correcting the proofs.

[1] A. E. Shilov, "*Metal Complexes in Biomimetic Chemical Reactions*", CRC Press, New York, **1997**. A. E. Shilov, *Structure and Bonding* **1997**, vol. *88–91*.
[2] C. Lambert, P. von Ragué Schleyer, *Angew. Chem. Int. Ed. Engl.* **1994**, *33*, 1129–1140.
[3] J. K. Kochi, T. M. Bockman, *Adv. Organomet. Chem.* **1991**, *33*, 51–124.
[4] See, for example: L. H. Gade, *Angew. Chem. Int. Ed. Engl.* **1995**, *34*, 547–549. D. J. Stufkens, N. P. Aarnts, J. Nijhoff, B. D. Rossenaar, A. Vlcek Jr., *Coord. Chem. Rev.* **1998**, *170–171*, 93–105.
[5] H. Schmidbaur, *Angew. Chem. Int. Ed. Engl.* **1983**, *22*, 907. U. Belluco, R. A. Michelin, M. Mozzon, R. Bertani, G. Facchin, L. Zanotto, L. Pandolfo, *J. Organomet. Chem.* **1998**, *557*, 37–68.
[6] I. R. Whitewall, A. M. McDonagh, M. G. Humphrey, M. Samoc, *Adv. Organomet. Chem.* **1998**, *42*, 291–362. S. R. Marder, *Inorganic Material* (Eds.: D. W. Bruce, D. O'Hare), chapt. 3, p. 122–169, Wiley, New York, **1996**.
[7] See, for example: P. Kalck, F. Monteil, *Adv. Organomet. Chem.* **1992**, *34*, 219–284. W. A. Herrmann, C. W. Kohlplaintner, *Angew. Chem. Int. Ed. Engl.* **1993**, *32*, 1524–1544. D. M. Roudhill, *Adv. Organomet. Chem.* **1995**, *38*, 155–188. I. T. Horvath (Ed.), *J. Mol. Cat. A* **1997**, *116*, ''Catalysis in Water''.
[8] See, for example: B. Mohr, D. M. Lynn, R. H. Grubbs, *Organometallics* **1996**, *15*, 4317–4325. I. Kovacs, M. C. Baird, *J. Organomet. Chem.* **1995**, *502*, 87–94. D. J. Brauer, J. Fischer, S. Kucken, K. P. Langhans, O. Stelzer, N. Weferling, *Z. Naturforsch. B. Chem. Sc.* **1994**, *49*, 1511–1524.
[9] T. Bartik, B. Bartik, I. Guo, B. E. Hanson, *J. Organomet. Chem.* **1994**, *477*, 15–21. C. Bianchini, A. Meli, V. Patinec, V. Sernau, F. Vizza, *J. Am. Chem. Soc.* **1997**, *119*, 4945–4954. H. Gulyas, P. Arva, J. Bakos, *Chem. Commun.* **1997**, 2385–2386.
[10] G. G. Hlatky, H. W. Turner, R. R. Eckman, *J. Am. Chem. Soc.* **1989**, *111*, 2728–2729.
[11] W. E. Piers, *Chem. Eur. J.* **1998**, 4, 13–18. M. Bochmann, *Topics Catal.* **1999**, *7*, 9–22. W. E. Piers, Y. Sun, L. W. M. Lee, *Topics Catal.* **1999**, *7*, 133–143.
[12] J. Karl, G. Erker, R. Fröhlich, F. Zippel, F. Bickelhaupt, M. Schreuder Goedheijt, O. S. Akkerman, P. Binger, J. Stannek, *Angew. Chem. Int. Ed. Engl.* **1997**, *36*, 2771–2774.
[13] H. van der Heijden, B. Hessen, A. G. Orpen, *J. Am. Chem. Soc.* **1998**, *120*, 1112–1113. A. H. Cowley, G. S. Hair, B. G. McBurnett, R. A. Jones, *Chem. Commun.* **1999**, 437–438.
[14] M. G. Thorn, Z. C. Etheridge, P. E. Fanwick, I. P. Rothwell, *Organometallics* **1998**, *17*, 3636–3638.
[15] See, for example: I. Amer, H. Alper, *J. Am. Chem. Soc.* **1990**, *112*, 3674–3676. J.-Q. Zhou, H. Alper, *Organometallics* **1994**, *13*, 1586–1591. Z. Zou, B. R. James, H. Alper, *Organometallics* **1995**, *14*, 4209–4212. Z. Zhou, G. Facey, B. R. James, H. Alper, *Organometallics* **1996**, *15*, 2496–2503. Y. Goldberg, H. Alper, *J. Chem. Soc., Chem. Commun.* **1994**, 1209–1210.
[16] S. Amaratunga, H. Alper, *J. Organomet. Chem.* **1995**, *488*, 25–28.
[17] S. A. Westcott, H. P. Blom, T. B. Marder, R. T. Baker, *J. Am. Chem. Soc.* **1992**, *114*, 8863–8869. C. Dai, T. B. Marder, E. G. Robins, D. S. Yufit, J. A. K. Howard, A. J. Scott, W. Clegg, *Chem. Commun.* **1998**, 1983–1984.
[18] R. F. Winter, F. M. Hornung, *Inorg. Chem.* **1997**, *36*, 6197–6204.
[19] B. M. Trost, R. C. Bunt, *J. Am. Chem. Soc.* **1998**, *120*, 70–79.
[20] I. Yamada, M. Ohkuchi, M. Yamaguchi, T. Yamagishi, *J. Chem. Soc., Perkin Trans. 1* **1997**, 1869–1873. I. Yamada, K. Fukui, Y. Aoki, S. Ikeda, M. Yamaguchi, T. Yamagishi, *J. Organomet. Chem.* **1997**, *539*, 115–120.
[21] H. Brunner, R. Störiko, F. Rominger, *Eur. J. Inorg. Chem.* **1998**, 771–781. H. Brunner, R. Störiko, *Eur. J. Inorg. Chem.* 783–788.
[22] [22a] See, for example: F. Rosche, G. Heckmann, E. Fluck, F. Weller, *Z. Anorg. Allg. Chem.* **1996**, *622*, 974–980; L. Dahlenburg, A. Weiss, M. Moll, *J. Organomet. Chem.* **1997**, *535*, 195–200. – [22b] P. Berno, S. Gambarotta, S. Kotila, G. Erker, *Chem. Commun.* **1996**, 779–780.
[23] [23a] J. P. Duan, F.-L. Liao, S.-L. Wang, C.-H. Cheng, *Organometallics* **1997**, *16*, 3934–3940. – [23b] A. Allen Jr., W. Lin, *Organometallics* **1999**, *18*, 2922–2925.
[24] S. A. Fairhurst, D. L. Hughes, K. Marjani, R. L. Richards, *J. Chem. Soc., Dalton Trans.* **1998**, 1899–1904.
[25] D. M. Hoffman, J. C. Huffman, D. Lappas, D. A. Wierda, *Organometallics* **1993**, *12*, 4312–4320.
[26] See also, for example, the zincate complex in: M. Steiner, H. Grützmacher, H. Pritzkow, L. Zsolnai, *Chem. Commun* **1998**, 285–286.
[27] Y. Miquel, A. Igau, B. Donnadieu, J.-P. Majoral, N. Pirio, P. Meunier, *J. Am. Chem. Soc.* **1998**, *120*, 3504–3505.
[28] V. Cardieno, M. Zablocka, B. Donnadieu, A. Igau, J.-P. Majoral, *Organometallics* **1999**, *18*, 1882–1886.
[29] H. Werner, M. A. Tena, N. Mahr, K. Peters, H.-G. von Schnering, *Chem. Ber.* **1995**, *128*, 41–47, and references therein.
[30] G. Cardaci, *J. Chem. Soc., Dalton Trans.* **1984**, 815–818.
[31] A. H. Klahn, B. Oelckers, F. Godoy, M. T. Garland, A. Vega, R. N. Perutz, C. L. Higgitt, *J. Chem. Soc., Dalton Trans.* **1998**, 3079–3086.
[32] O. Koch, F. Edelmann, U. Behrens, *Chem. Ber.* **1982**, *115*, 1313–1324.
[33] I. R. Butler, W. R. Cullen, F. W. B. Elnstein, A. C. Willis, *Organometallics* **1985**, *4*, 603–604.
[34] [34a] J. E. Goldberg, J. C. Jeffery, F. G. A. Stone, *J. Organomet. Chem.* **1993**, *462*, 353–363. – [34b] M. A. McWhannell, G. M. Rosair, A. J. Welch, F. Teixidor, C. Vinas, *J. Organomet. Chem.* **1999**, *573*, 165–170.
[35] J. Vincente, M.-T. Chicote, C. MacBeath, J. Fernandez-Baeza, D. Bautista, *Organometallics* **1999**, *18*, 2677–2682.
[36] K. H. Dötz, A. Tiriliomis, K. Harms, *Tetrahedron* **1993**, *49*, 5577–5597, and references therein.
[37] C. F. Bernasconi, W. Sun, *Organometallics* **1997**, *16*, 1926–1932.
[38] H. F. Sleiman, L. McElwee-White, *J. Am. Chem. Soc.* **1988**, *110*, 8700–8701.
[39] S. T. Massey, N. D. R. Barnett, K. A. Abboud, L. McElwee-White, *Organometallics* **1996**, *15*, 4625–4631.
[40] H. F. Sleiman, S. Mercer, L. McElwee-White, *J. Am. Chem. Soc.* **1989**, *111*, 8007–8009.
[41] N. D. R. Barnett, S. T. Massey, P. C. McGowan, J. J. Wild, K. A. Abboud, L. McElwee-White, *Organometallics* **1996**, *15*, 424–428. Y. He, P. C. McGowan, K. A. Abboud, L. McElwee-White, *J. Chem. Soc., Dalton Trans.* **1998**, 3373–3378.
[42] L. S. Hegedus, B. R. Lundmark, *J. Am. Chem. Soc.* **1989**, *111*, 9194–9198.
[43] H. Fischer, A. Schlageter, W. Bidell, A. Früh, *Organometallics* **1991**, *10*, 389–391.

[44] R. Aumann, H. Nienaber, *Adv. Organomet. Chem.* **1997**, *41*, 163–242.
[45] [45a] R. Aumann, Z. Yu, R. Fröhlich, F. Zippel, *Eur. J. Inorg. Chem.* **1998**, 1623–1629. – [45b] R. Aumann, Z. Yu, R. Fröhlich, *J. Organomet. Chem.* **1997**, *549*, 311–318.
[46] J. Barluenga, M. Tomas, E. Rubio, J. A. Lopez-Pelegrin, S. Garcia-Granda, M. Perez Priede, *J. Am. Chem. Soc.* **1999**, *121*, 3065–3071.
[47] R. Aumann, R. Fröhlich, J. Prigge, O. Meyer, *Organometallics* **1999**, *18*, 1369–1380.
[48] H. Rudler, M. Audouin, A. Parlier, B. Martin-Vaca, R. Goumont, T. Durand-Réville, *J. Am. Chem. Soc* **1996**, *118*, 12045–12058.
[49] H. Rudler, B. Martin-Vaca, M. Nicolas, M. Audouin, J. Vaissermann, *Organometallics* **1998**, 17, 361–366.
[50] D. A. Clark, D. L. Jones, R. J. Mawby, *J. Chem. Soc., Dalton Trans.* **1980**, 565–569.
[51] C. J. Beddows, M. R. Box, C. Butters, N. Carr, M. Green, M. Kursawe, M. F. Mahon, *J. Organomet. Chem.* **1998**, *550*, 267–282.
[52] C. Butters, N. Carr, R. J. Deeth, M. Green, S. M. Green, M. F. Mahon, *J. Chem. Soc., Dalton Trans.* **1996**, 2299–2308. L. Lee, D.-J. Chen, Y.-C. Lin, Y.-H. Lo, C. H. Lin, G.-H. Lee, Y. Wang, *Organometallics* **1997**, *16*, 4636–4644.
[53] K.-H. Chang, Y.-C. Lin, *Chem. Commun.* **1998**, 1411.
[54] S. Araki, Y. Butsugan, *Chem. Ber.* **1993**, *126*, 1157–1159.
[55] J.-J. Brunet, R. Chauvin, O. Diallo, F.-B. Kindela, P. Leglaye, D. Neibecker, *Coord. Chem. Rev.* **1998**, *178–179*, 331–351.
[56] J.-J. Brunet, R. Chauvin, G. Commenges, B. Donnadieu, P. Leglaye, *Organometallics* **1996**, *15*, 1752–1754.
[57] J.-J. Brunet, R. Chauvin, J. Chiffre, S. Huguet, P. Leglaye, *J. Organomet. Chem*. **1998**, *566*, 117–123.
[58] C. E. Ash, M. Y. Darensbourg, M. B. Hall, *J. Am. Chem. Soc.* **1987**, *109*, 4173–4180.
[59] M. Y. Darensbourg, J. M. Hanckel, *Organometallics* **1982**, *1*, 82–87. C. E. Ash, T. Delord, D. Simmons, M. Y. Darensbourg, *Organometallics* **1986**, *5*, 17–25.
[60] J.-J. Brunet, R. Chauvin, J. Chiffre, B. Donnadieu, S. Huguet, P. Leglaye, E. Mothes, *Inorg. Chim. Acta* **1999**, *291*, 300–310.
[61] P. Leglaye, B. Donnadieu, J.-J. Brunet, R. Chauvin, *Tetrahedron Lett.* **1998**, *39*, 9179–9182.
[62] E. S. Shubina, N. V. Belkova, L. M. Epstein, *J. Organomet. Chem.* **1997**, *536*, 17–29. R. H. Crabtree, O. Eisenstein, G. Sini, E. Peris, *J. Organomet. Chem.* **1997**, *567*, 7–11. R. H. Crabtree, *J. Organomet. Chem.* **1998**, *577*, 111.
[63] B. M. Trost, *Chem. Eur. J.* **1998**, *4,* 2405–2412.
[64] R. Chauvin, P. Leglaye, C. Lepetit, J.-J. Brunet, E. Mothes, *23th ICCC*, p. 455, Aug. 30 – Sept. 4, **1998**, Florence.
[65] C. Lepetit, R. Chauvin, B. Chaudret, *GSO 98 Meeting*, p. A701, Nov. 27, **1998**, Pau, and *5th FGIPS,* p. B25, Oct. 27–31, **1999**, Toulouse.
[66] R. Kuhlman, *Coord. Chem. Rev.* **1997**, *167*, 205–232.
[67] K. Ghosh, S. Pattanayak, A. Chakravorty, *Organometallics* **1998**, *17*, 1956–1960.
[68] M. Gandelman, A. Vigalok, L. J. W. Shimon, D. Milstein, *Organometallics* **1997**, *16*, 3981–3986.
[69] I. C. M. Wehman-Ooyevaar, D. M. Grove, H. Kooijman, P. van der Sluis, A. L. Spek, G. van Koten, *J. Am. Chem. Soc.* **1992**, *114*, 9916–9924.
[70] J. C. Jeffery, V. N. Lebedev, F. G. A. Stone, *Inorg. Chem.* **1996**, *35*, 2967–2976.
[71] C. A. Dullaghan, G. B. Carpenter, D. A. Sweigart, D. S. Choi, S. S. Lee, Y. K. Chung, *Organometallics* **1997**, *16*, 5688–5695.
[72] R. D. Adams, J. H. Yamamoto, *Organometallics* **1997**, *16*, 1430–1439.
[73] M. Gomez-Sazo, D. F. Mullica, E. Sappenfield, F. G. A. Stone, *Polyhedron* **1996**, *15*, 793–801, and references therein.
[74] J. D. Chen, F. A. Cotton, *J. Am. Chem. Soc*. **1991**, *113*, 2509–2512.
[75] S. Doherty, J. F. Corrigan, A. J. Carthy, E. Sappa, *Adv. Organomet. Chem.* **1995**, *37*, 39–130.
[76] Y. S. Wong, H. N. Paik, P. C. Chieh, A. J. Carty, *J. Chem. Soc., Chem. Commun.* **1975**, 309–310.
[77] A. J. Carty, G. N. Mott, N. J. Taylor, J. E. Yule, *J. Am. Chem. Soc.* **1978**, *100*, 3051.
[78] A. A. Cherkas, S. Doherty, M. Cleroux, G. Hogarth, L. H. Randall, S. M. Breckenridge, N. J. Taylor, A. J. Carthy, *Organometallics* **1992**, *11*, 1701–1711.
[79] G. Hogarth, S. A. R. Knox, B. R. Lloyd, K. A. Macpherson, D. A. V. Morton, A. G. Orpen, *J. Chem. Soc., Chem. Commun.* **1988**, 360–362.
[80] S. Doherty, M. R. J. Elsegood, W. Clegg, M. F. Ward, M. Waugh, *Organometallics* **1997**, *16*, 4251–4253.
[81] S. Doherty, G. Hogarth, M. R. J. Elsegood, W. Clegg, N. H. Rees, M. Waugh, *Organometallics* **1998**, *17*, 3331–3345.
[82] See, for example: J. Levisalles, F. Rose-Munch, H. Rudler, J.-C. Daran, Y. Dromzee, Y. Jeannin, *J. Chem. Soc., Chem. Commun.* **1980**, 685–687.
[83] J. Takats, J. Washington, *Organometallics* **1994**, *13*, 1078–1080.
[84] K. Yang, S. G. Bott, M. G. Richmond, *J. Organomet. Chem.* **1996**, *516*, 65–80.
[85] E. Louattani, J. Suades, K. Urtiaga, M. I. Arriortua, X. Solans, *Organometallics* **1996**, *15*, 468–471.
[86] R. Andrés, M. Galakhov, M. P. Gomez-Sal, A. Martin, M. Mena, C. Santamaria, *Chem. Eur. J.* **1998**, *4*, 1206–1213.
[87] A. J. Arce, R. Machado, Y. De Sanctis, M. V. Capparelli, R. Atencio, *Organometallics* **1997**, *16*, 1735–1742, and references[9] and [10] therein.
[88] S. B. Falloon, A. M. Arif, J. A. Gladysz, *Chem. Commun.* **1997**, 629.
[89] R. Duchateau, H. C. L. Abbenhuis, R. A. van Santen, A. Meetsma, S. K.-H. Thiele, M. F. H. van Tol, *Organometallics* **1998**, *17*, 5663–5673.
[90] P. J. Sinnema, A. Meetsma, J. H. Teuben, *Organometallics* **1993**, *12*, 184–189.
[91] K. Mashima, K. Jyodol, A. Hyoshi, H. Takaya, *Organometallics* **1997**, 6, 885.
[92] R. Meyer, M. Schindehütte, P. H. van Rooyen, S. Lotz, *Adv. Organomet. Chem.* **1994**, *33*, 3605.
[93] M. Tilset, K. P. C. Vollhardt, R. Boese, *Organometallics* **1994**, *13*, 3146-3169.
[94] D. S. Brown, M.-H. Delville-Desbois, R. Boese, K. P. C. Vollhardt, D. Astruc, *Angew. Chem. Int. Ed. Engl.* **1994**, 33, 661–663.
[95] C. Moreno, M. L. Marcos, M. J. Macazaga, R. M. Medina, D. H. Farrar, J. Gonzales-Velasco, S. Delgado, *Organometallics* **1998**, *17*, 4657–4665.
[96] H. Wadepohl, W. Galm, H. Pritzkow, A. Wolf, *Chem. Eur. J.* **1996**, *2*, 1453–1465.
[97] W. J. Peng, S. G. Train, D. K. Howell, F. R. Fronczek, G. G. Stanley, *Chem. Commun.* **1996**, 2607–2608.
[98] J. R. Berenguer, J. Fornies, E. Lalinde, F. Martinez, *J. Organomet. Chem.* **1994**, *470*, C15. J. R. Berenguer, J. Fornies, E. Lalinde, F. Martinez, *Organometallics* **1996**, *15*, 4537–4546.
[99] J. R. Berenguer, J. Fornies, E. Lalinde, F. Martinez, *J. Chem. Soc., Chem. Commun.* **1995**, 1227–1228.
[100] I. Ara, J. R. Berenguer, E. Eguizabal, J. Fornies, E. Lalinde, A. Martin, F. Martinez, *Organometallics* **1998**, *17*, 4578–4596.
[101] J. R. Berenguer, J. Fornies, E. Lalinde, F. Martinez, E. Urriolabeitia, A. J. Welch, *J. Chem. Soc., Dalton Trans.* **1994**, 1291–1299.
[102] T. Murahashi, H. Kurosawa, N. Kanehisa, Y. Kai, *J. Organomet. Chem*. **1997**, *530*, 187–189.
[103] J. R. Berenguer, E. Eguizabal, L. R. Favello, J. Fornies, E. Lalinde, A. Martin, *Organometallics* **1999**, *18*, 1653–1662.
[104] I. Ara, J. R. Berenguer, J. Fornies, E. Lalinde, M. T. Moreno, *Organometallics* **1996**, *15*, 1820–1825.

Received August 19, 1999
[I99305]

C_i Symmetric and Non-Centrosymmetric Crystalline Complexes of [60]Fullerene with Octakis(dimethylamino)porphyrazinato-Copper(II) and -Nickel(II)

Detlev H. Hochmuth,*[c] Sarah L. J. Michel,[b] Andrew J. P. White,[a] David J. Williams,[a] Anthony G. M. Barrett,*[a] and Brian M. Hoffman*[b]

Keywords: Porphyrazines / Fullerenes

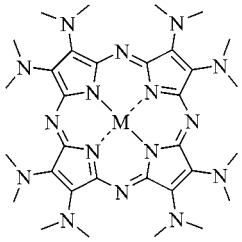
X-ray structural analysis of octakis(dimethylamino)porphyrazinato-metallo(II)·[60]fullerene complexes (M = Cu^{2+} and Ni^{2+}) surprisingly revealed two totally different supramolecular structures, the first exhibiting a C_i symmetric sandwich complex of two slightly dished porphyrazine units enclosing one fullerene sphere, the other featuring a noncentrosymmetric 1:1 complex with a strongly warped porphyrazine unit.

Introduction

In continuation of our previous studies[1] on charge-transfer complexes of porphyrazines we herein report on the syntheses and structures of two donor-acceptor crystals formed from [60]fullerene and metallated porphyrazines. These complexes are considered possible precursors for much sought-after three-dimensional molecular magnets[2] and possible structures with superconducting properties. For structurally related complexes see those of fullerenes with metallated octaethylporphyrines.[3,4]

Results and Discussion

The syntheses of octakis(dimethylamino)porphyrazinato-metallo(II) (Scheme 1, M-Pz, with M = Ni^{2+}, Cu^{2+}, $2H^+$) and of the $(2H\text{-}Pz)_2\text{-}C_{60}$ complex have been reported previously.[5] The complexes were synthesised by incubation of fullerene and excess of porphyrazine (M-Pz) under an argon atmosphere and subsequent isolation and purification by repeated extraction-evaporation-dissolution cycles. Slow evaporation of the benzene or toluene solution afforded nonconducting black needles which were subsequently handled in air.



Scheme 1. Oktakis(dimethylaminoporphyrazinato)-metal(II), the porphyrazine unit of the fullerene complexes **1**, **2**, and **3**; (M = Ni, Cu, 2H).

[a] Department of Chemistry, Imperial College of Science, Technology and Medicine, London SW7 2AY, UK
[b] Department of Chemistry, Northwestern University, Evanston, IL 60208–3113, USA
[c] Department of Chemistry, University of Hamburg, Martin-Luther-King-Platz 6, 20146 Hamburg, Germany

$(CuPz)_2\text{-}C_{60}$ (1)

The X-ray analysis of **1** (see Experimental Section) revealed the formation of a C_i symmetric 2:1 Cu(Pz):C_{60} complex (Figure 1) which at the molecular level is very similar to that formed between 2H-Pz and C_{60} (**3**), though in the latter the symmetry is C_2 and crystallisation occurred in a noncentrosymmetric space group. Here in **1**, each C_{60} molecule is sandwiched between pairs of dished Cu(Pz) units (Figure 1), the copper atom lying 0.06 Å out of the N_4 coordination plane, and 0.18 and 0.48 Å out of the planes of the four "pyrrole-linking" *meso*-N-atoms, and the eight peripheral dimethylamino N-atoms, respectively. The distance from the centroid of the C_{60} molecule to the N_4 coor-

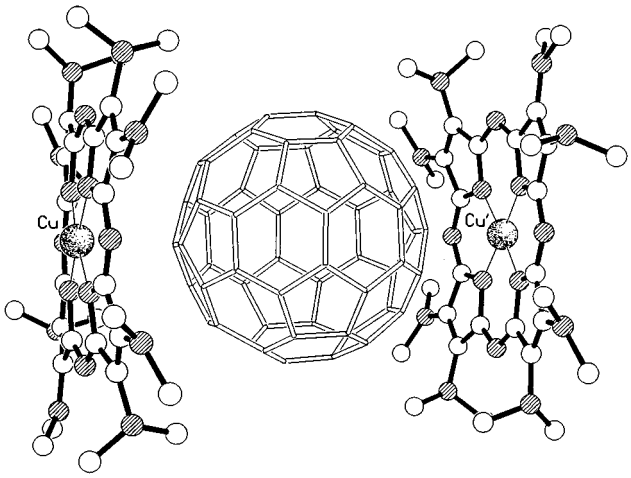


Figure 1. The 2:1 complex **1** formed between Cu(Pz) and C_{60}. The Cu–N distances are in the range 1.939(4) to 1.945(4) Å.

 © WILEY-VCH Verlag GmbH, D-69451 Weinheim, 2000 1434–1948/00/0404–0593 $ 17.50+.50/0

dination planes is 6.32 Å, (this parameter, and others given in this communication, refer to the low temperature structural determinations) a value identical to that observed in **3**. The copper atom lies 0.18 and 0.48 Å out of the planes of the four ''pyrrole-linking'' N-atoms, and the eight peripheral dimethylamino N-atoms, respectively. A feature of particular interest is a short approach of 2.89 Å between the copper and one of the C_{60} carbon atoms, the carbon being positioned almost directly above the centre of the copper coordination plane. Although, as in **3**, the crystals contain aromatic solvent molecules (S) positioned between C_{60} units, the overall supramolecular structure is distinctly different. The pattern of -Pz-C_{60}-Pz-Pz-C_{60}-Pz- and -C_{60}-S-C_{60}-S- sandwiches is retained (Figure 2), but in the third direction (into the plane of the paper in Figure 2) adjacent sheets are offset so that the linear -C_{60}-C_{60}-C_{60}- sequence seen (Figure 3) running horizontally in **3** is no longer present. The shortest inter-sheet $C_{60}\cdots C_{60}$ separation is 13.9 Å.

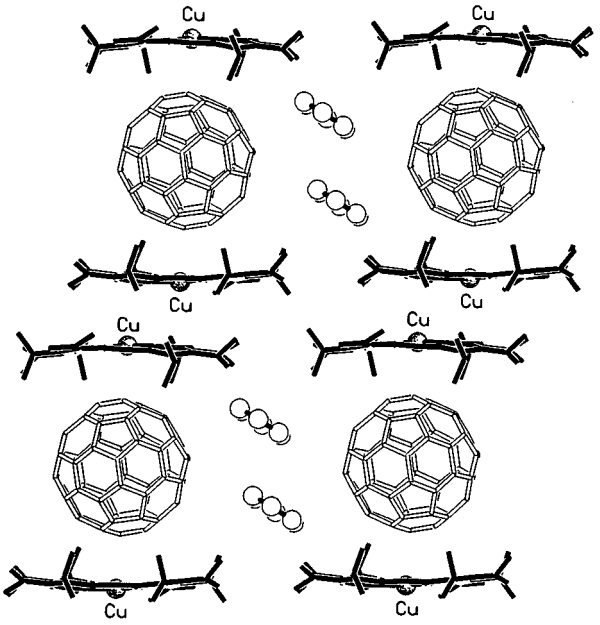


Figure 2. Part of one of the 2D sheets of C_{60}, Cu(Pz) and benzene solvent molecules in the structure of **1**. The back-to-back Cu···Cu separation is 4.67 Å, the lateral displacement being 3.31 Å. The interplanar separation between the Cu(Pz) units is ca. 3.4 Å. The lateral $C_{60}\cdots C_{60}$ distance is 15.1 Å.

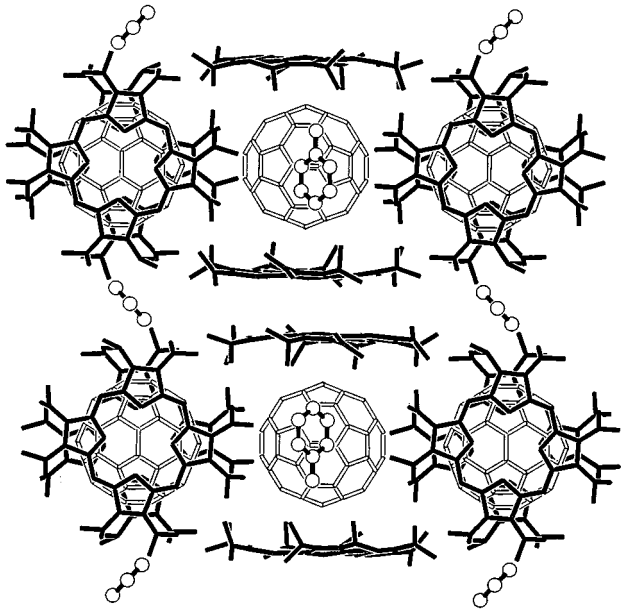


Figure 3. Part of the 3D network of Pz, C_{60} and toluene (S) molecules present in the structure of **3**. The centroids of the back-to-back Pz molecules are laterally displaced by 1.14 Å. The horizontal $C_{60}\cdots C_{60}$ centroid···centroid separation is 10.5 Å and the vertical and out of the plane $C_{60}\cdots S\cdots C_{60}$ distances are 15.9 Å.

NiPz-C_{60} (2)

Crystals of the complex formed between Ni(Pz) and C_{60} (**2**) (for crystal data see in the Experimental Section) were found to have a 1:1 stoichiometry and a totally different supramolecular structure. The Ni(Pz) unit has a distinctly warped conformation with the plane of diametrically opposite pyrrole rings being rotated by ca. 30° with respect to each other about their N···N vectors; the nickel and the four coordinated nitrogen atoms are coplanar to within 0.006 Å. In this complex each C_{60} unit lies within a cleft formed by

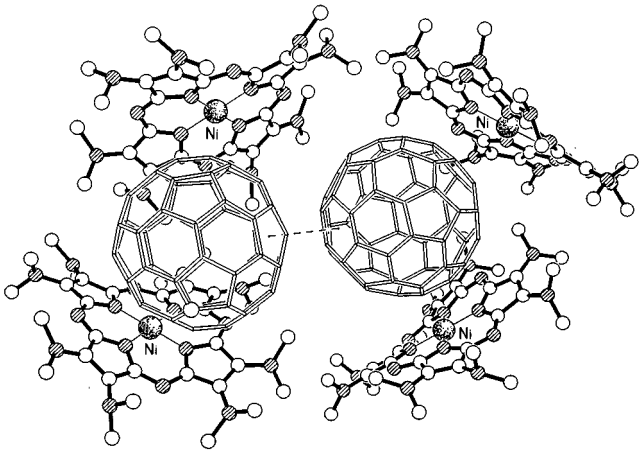


Figure 4. The partial encapsulation of a pair of π-stacked C_{60} units in the 1:1 Ni(Pz):C_{60} complex **2**. The Ni–N distances are in the range 1.859(4) to 1.870(4) Å. The N_4 plane···C_{60} centroid distances are 6.31 and 6.40 Å, and the $C_{60}\cdots C_{60}$ centroid···centroid separation is 9.95 Å.

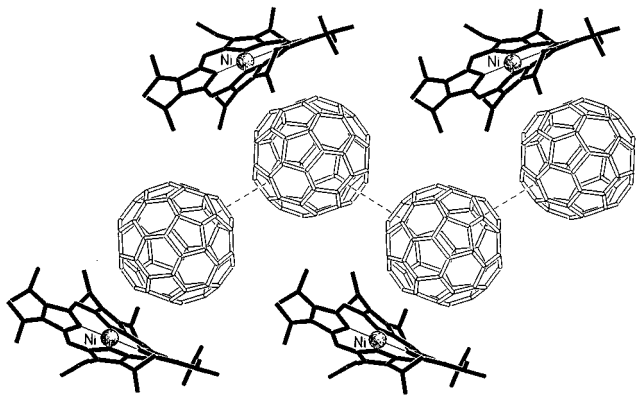


Figure 5. Part of one of the continuous zigzag chains of π-stacked, 2_1 screw related, C_{60} units in the structure of **2**. The $C_{60}\cdots C_{60}$ face-to-face and centroid···centroid separations are 3.39 and 9.95 Å respectively.

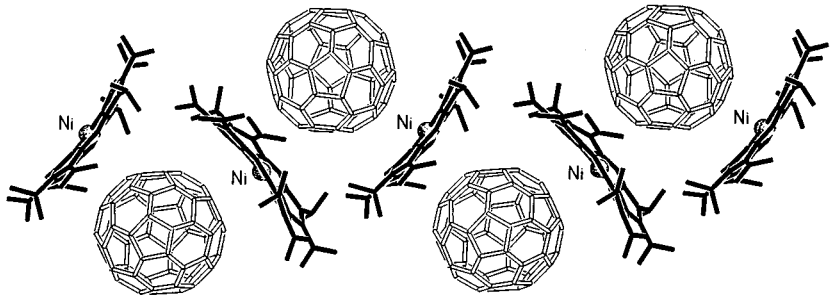


Figure 6. Part of one of the -C_{60}-Pz-C_{60}-Pz- zigzag chains in the structure of **2**.

two steeply inclined (by ca. 72°) Ni(Pz) molecules (Figure 4), the shortest Ni···C(C_{60}) distances being 3.29 and 3.64 Å. Two supramolecular features predominate; i) the formation in one direction of continuous zigzag chains of π-stacked, 2_1 screw related, C_{60} units (Figure 5) with a C_5···C_6 ring centroid···ring centroid separation of 3.39 Å, and ii) the formation in another direction of continuous -C_{60}-Pz-C_{60}-Pz- zigzag sandwiches (Figure 6). Perhaps the most important feature of interest of this 1:1 complex **2** is that, like **3**, crystallisation occurs in a noncentrosymmetric space group, thereby offering the potential for the complex to exhibit nonlinear optical properties.

Electron Paramagnetic Resonance

The electron paramagnetic resonance spectra at 77 K of the solid compound (**1**), and of the parent Cu(Pz) in dichloromethane solution are shown in Figure 7. The spectrum of this parent porphyrazine is characteristic of a monomeric square-planar Cu^{II} complex with axial g tensor ($g_\parallel = 2.15$, $g_\perp = 2.05$) and with ^{63,65}Cu hyperfine coupling of $A_\parallel = 210$ G.[6,7] Further hyperfine splittings from the four equivalent ligating ^{14}N are also resolvable both at $g_\parallel$ and $g_\perp$. The spectrum of **1** (Figure 7, inset) is characteristic of a binuclear triplet state ($S = 1$) species,[8,9] associated with the "back-to-back" Cu(Pz) pairs. The separation of the center fields of the two most intense peaks corresponding to $g_\perp$ in Figure 7 is 414 G and corresponds to $D_\perp$, the standard zero-field splitting parameter. Copper hyperfine splitting ($A_\parallel/2$) for the porphyrazine pairs is resolved for $g_\parallel$ as a seven-line pattern with a splitting half that for the porphyrazine monomer, which indicates that exchange coupling is larger than the Larmor energy. The expected "$\Delta M = 2$" transition at half field also is observed (not shown). If the system is treated with the point dipole model,[10,11] the Cu–Cu distances may be estimated as $R = (0.650 g_\perp^2/D_\perp\ [\mathrm{cm}^{-1}])^{1/3}$. The measured $D_\perp$ for the Cu(Pz)–C_{60} (**1**) complex gives $R =$ 4.3 Å. This approximates the crystal X-ray data of 4.78, the deviation likely arises from other contributions to $D_\perp$.[2]

Magnetic Properties

To determine the exchange coupling within the Cu "back to back" porphyrazine pairs, the molar magnetic susceptibility, χ_m, for **1** was measured over the temperature range of 2–300 K. Figure 8 plots $\chi_m T$ versus T with a plot of χ_m versus T as the inset. The value $\chi_m T = 0.71$–0.73 emu mol^{-1} K observed between 300 K and 10 K is expected from the Curie law for two uncoupled Cu porphyrazine pairs per mol of **1** (S = 1/2). The rapid decrease in $\chi_m T$ at temperatures below 10 K reflects antiferromagnetic coupling within the dimer. A least squares fit of the data

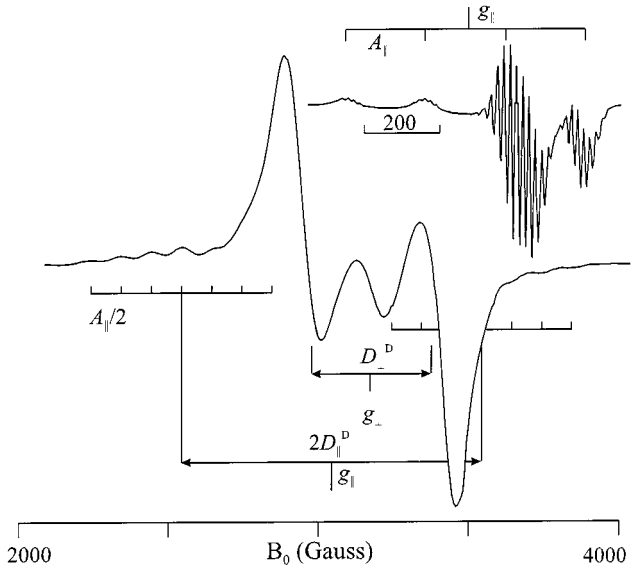


Figure 7. Electron paramagnetic resonance spectra of **1** and Cu(Pz).

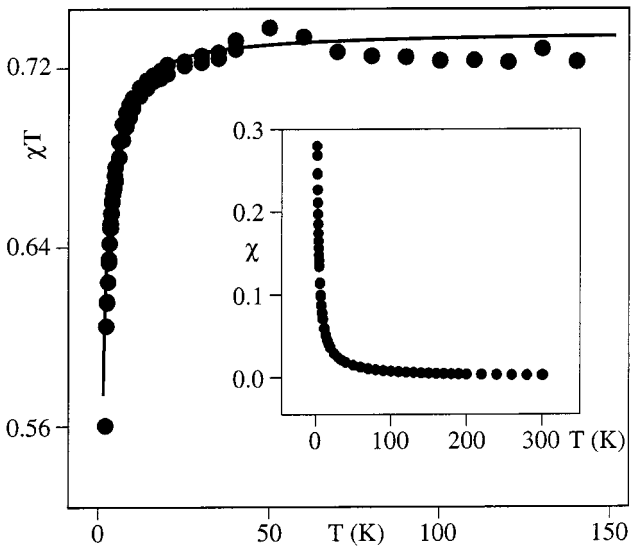


Figure 8. Susceptibility of **1**: *Main:* $\chi_m T$ vs. T for $T < 150$ K; fit as described in text with inclusion of 9.7% monomer. *Inset:* χ_m vs. T

to the Van Vleck Equation [$\chi_m T = [(2Ng^2\beta^2/3k)(3e^{-Jk/T}/(1+3e^{-J/kT})]$ for the thermally excited triplet state gave an exchange coupling of $J = 1.61$ cm^{-1}, such a small value being expected from the noncovalent nature of the intradimer interaction.

Conclusion

Two new octakis(dimethylaminoporphyrazinato)metal(II) fullerene complexes have been synthesised, their interesting different supramolecular structures have been investigated by X-ray crystallography, and the electromagnetic properties of the copper derivative have been characterised by EPR and SQUID measurements. Further investigations on the potential of the nonlinear optical properties of the nickel(porphyrazine) fullerene complex are being carried out.

Experimental Section

A toluene solution of three equivalents of M-Pz and one equivalent of [60]fullerene was incubated under argon in a sealed tube for 24 h at 130 °C. After evaporation of toluene the excess of M-Pz was washed out with pentane and the complex subsequently extracted with small amounts of benzene. After evaporation, the pentane-benzene extraction cycle was repeated three times. Slow evaporation of the benzene or toluene solution, respectively, afforded non-conducting black needles which were subsequently handled in air.

Crystal Data for 1 (173 K): $(C_{32}H_{48}N_{16}Cu)_2{\cdot}C_{60}{\cdot}2$ PhH, M = 2317.6, triclinic $P\bar{1}$ 1, (no. 2), a = 13.892(2), b = 14.229(2), c = 15.840(2) Å, α = 67.01(1), β = 83.60(1), γ = 65.08(1)°, V = 2608.6(6) Å^3, Z = 1 (C_i symmetry), D_c = 1.475 g cm^{-3}, μ(Cu-K_α) = 11.0 cm^{-1}, F(000) = 1206; 7948 independent reflections, F^2 refinement, R_1 = 0.068, wR_2 = 0.171, 6912 absorption corrected reflections with $F_o > 4\sigma(F_o)$, $2\theta \leq 124°$, 891 parameters. CCDC 135910.

Data for 1 (293 K): Triclinic $P\bar{1}$, (no. 2), a = 13.957(2), b = 14.320(1), c = 15.955(1) Å, α = 67.37(1), β = 83.75(1), γ = 65.03(1)°, V = 2662.7(4) Å^3, Z = 1 (C_i symmetry), D_c = 1.445 g cm^{-3}, μ(Cu-K_α) = 10.8 cm^{-1}, F(000) = 1206; 7972 independent reflections, F^2 refinement, R_1 = 0.054, wR_2 = 0.148, 6743 absorption corrected reflections with $F_o > 4\sigma(F_o)$, $2\theta \leq 124°$, 1041 parameters.

Crystal Data for 2 (123 K): $C_{32}H_{48}N_{16}Ni{\cdot}C_{60}$, M = 1436.2, orthorhombic, $P2_12_12_1$ (no. 19), a = 15.413(1), b = 18.337(1), c = 21.855(1) Å, V = 6177.0(6) Å^3, Z = 4, D_c = 1.544 g cm^{-3}, μ(Cu-K_α) = 10.3 cm^{-1}, F(000) = 2960; 6599 independent reflections, F^2 refinement, R_1 = 0.056, wR_2 = 0.154, 6154 absorption corrected reflections with $F_o > 4\sigma(F_o)$, $2\theta \leq 128°$, 999 parameters. The absolute structure was unambiguously determined by a combination of R factor tests [R_1^+ = 0.0563, R_1^- = 0.0589] and by use of the Flack parameter [x^+ = 0.00(4), x^- = 1.00(4)].

Data for 2 (293 K): Orthorhombic, $P2_12_12_1$ (no. 19), a = 15.480(2), b = 18.604(1), c = 22.025(1) Å, V = 6343.0(8) Å^3, Z = 4, D_c = 1.504 g cm^{-3}, μ(Cu-K_α) = 10.0 cm^{-1}, F(000) = 2960; 5791 independent reflections, F^2 refinement, R_1 = 0.061, wR_2 = 0.161, 4950 independent observed absorption corrected reflections with $F_o > 4\sigma(F_o)$, $2\theta \leq 128°$, 1000 parameters, R_1^+ = 0.0610, R_1^- = 0.0631, x^+ = –0.01(5), x^- = +1.01(5).

Crystallographic data for the structures reported in this paper have been deposited with the Cambridge Crystallographic Data Centre as supplementary publication no. CCDC-135910 and -135912 (**1**), CCDC-135911 and -135913 (**2**). Copies of the data can be obtained free of charge on applicaton to The Director, CCDC, 12 Union Road,m Cambridge CB2 1EZ, UK [Fax: (internat.) + 44 (1223) 336-033; E-mail: deposit@ccdc.cam.ac.uk].

Acknowledgments

D. H. H. thanks the European Commission for a Marie-Curie fellowship of the TMR programme (ERB4001GT970456). We gratefully acknowledge financial support from the National Science Foundation (B. M. H., A. G. M. B.; NSF CHE9727590) and the Materials Research Center of Northwestern University (NSF DMR9523228).

[1] D. M. Eichhorn, S Yang, W. Jarrell, T. F. Baumann, L. S. Beall, A. J. P. White, D. J. Williams, A. G. M. Barrett, B. M. Hoffman, *J. Chem. Soc., Chem. Commun.* **1995**, 1703.
[2] O. Kahn, *Molecular Magnetism*; VCH Publishers, New York, **1993**.
[3] M. M. Olmstead, D. A. Costa, K. Maitra, B. C. Noll, S. L. Phillips, M. M. Van Calcar, A. L. Balch, *J. Am. Chem. Soc.* **1999**, *121*, 7090.
[4] H. Maruyama, M. Fujiwara, K. Tanak, *Chem. Lett.* **1998**, 805.
[5] N. S. Mani, L. S. Beall, T. Miller, O. P. Anderson, H. Hope, S. R. Parkin, D. J. Williams, A. G. M. Barrett, B. M. Hoffman, *J. Chem. Soc., Chem. Commun.* **1994**, 2095.
[6] S. E. Harrison, J. M. Assour, *J. Chem. Phys.* **1964**, *40*, 365–370.
[7] T. G. Brown, J. L. Petersen, G. P. Lozos, J. R. Anderson, B. M. Hoffman, *Inorg. Chem.* **1977**, *16*, 1563–1565.
[8] J. P. Collman, C. M. Eliott, T. R. Hulbert, B. S. Tovrog, *Proc. Natl. Acad. Sci. U. S. A.* **1977**, *74*, 18–22.
[9] R. L. Belford, N. D. Chasteen, H. So, R. E. Tapscott, *J. Am. Chem. Soc.* **1969**, *91*, 4675–4680.
[10] N. D. Chasteen, R. L. Belford, *Inorg. Chem.* **1970**, *9*, 169–175.
[11] C. J. Schramm, B. M. Hoffman, *Inorg. Chem.* **1980**, *19*, 383–385.

Received November 16, 1999
[I99410]

How to Predict Activation Barriers − Conformational Transformations of Compounds $CH_3C(CH_2PPh_2)_{3-n}[CH_2P(oTol)_2]_nMo(CO)_3$ (n = 1−3): Force Field Calculations versus NMR Data

Stefan Beyreuther,[a] Axel Frick,[a] Johannes Hunger,[a] Gottfried Huttner,*[a] Björn Antelmann,[a] Peter Schober,[a] and Rainer Soltek[a]

Dedicated to Prof. Wolf-Peter Fehlhammer on the occasion of his 60th birthday

Keywords: *Tripod* molybdenum tricarbonyl compounds / Conformational analysis in solution / Dynamic NMR / Force field calculations / Activation barriers

Tripod metal entities *tripod*M are sterically congested systems. The conformations adopted by compounds $CH_3C(CH_2PPh_2)_{3-n}[CH_2P(oTol)_2]_nMo(CO)_3$ (n = 1: **1**, n = 2: **2**, n = 3: **3**) will thus be largely determined by the repulsive forces acting in these molecules. The steric demand of the *o*-tolyl groups impedes their free rotation and enantiomerization processes referring to the compounds as a whole are sufficiently slow to permit their analysis by NMR techniques. Through a combination of line-shape analysis, EXSY methods, and coalescence experiments, the $\Delta G^{\ddagger}$ values for these conformational enantiomerization processes have been determined as $\Delta G^{\ddagger}_{298K}$ = 54.3, 57.9, 65.5 kJ·mol^{-1} for compounds **1**, **2**, and **3**, respectively. By an exhaustive search on a force field generated hypersurface, activation energies of 53, 57 and 69 kJ·mol^{-1} have been calculated. Thus, the force field approach correctly reproduces the dependence of the activation energy on the degree of *o*-tolyl substitution. Moreover, the force field simulation also gives an insight into the individual microsteps of the enantiomerization pathways.

Introduction

In any attempt to understand the reactivity of molecules, the shape of the reactants will play an important role. Thus, as far as we know, the reactivity as well as the outstanding selectivity of biological catalysts can, to a large extent, be attributed to the specific shape of the pocket in which the reactive center is embedded. Given appropriate electronic conditions for bond making and bond breaking in a specific catalyst system, the surrounding of the reactive center determines whether or not a substrate will be transformed through its secondary interactions with the latter. In the study of coordination compounds with potential catalytic applications, the electronic situation may nowadays be understood in part by quantum mechanical methods.[1][2]

The secondary interactions, which govern the specific shape of the catalyst as well as of the reactive entity formed upon approach of the substrate at the active site, are not so easy to handle by quantum chemical methods, one problem still being the size of the aggregate formed by a real catalyst and a real substrate. As far as those secondary interactions that are usually referred to as "steric" are concerned, force field methods appear to offer a solution to this problem.[3−7]

There remains a problem, however, when these methods are applied to coordination compounds. Reliable parameters for modelling the interactions involving the metal are generally not available and the only way to obtain an appropriate set of parameters is to gather as much experimental information as possible. If it is desired to develop a force field approach for a specific family of compounds, the structures of the members of this family constitute a valuable piece of information, not only because this information is quite detailed but also because in most cases it is easy to obtain and amply available. It has been shown how this type of information may be systematically analyzed and how, by the application of a combination of statistical tools, including pattern recognition by neural networks, it may be shown for a given family of compounds that, even though the structures have been determined in the solid state, the conformations are almost exclusively determined by the inner molecular potential.[8][9] It has also been shown how this information relating to the molecular potential, intrinsically embedded in these structures, may be extracted in an unbiased way by the use of Genetic Algorithms.[10][11] It has been found that in the specific case of *tripod* metal templates [*tripod* = $RCH_2C(CH_2X)(CH_2Y)(CH_2Z)$; X, Y, Z = $PR'R''$] this two-step process − systematic analysis of the structural database and algorithmic extraction of force field parameters therefrom − makes the force field approach a reliable means of prediction as far as stationary structures are concerned.

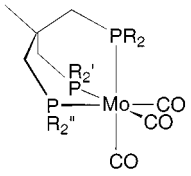
It has also been found that the properties of a conformational ensemble, as present for a specific *tripod* metal compound in solution, are adequately reproduced by such a force field approach, in so far as observed NOE distances

[a] Anorganisch-Chemisches Institut der Universität Heidelberg, Im Neuenheimer Feld 270, D-69120 Heidelberg, Germany
Fax: (internat.) + 49-(0)6221/54-5707
E-mail: INVERSION@indi.aci.uni-heidelberg.de

 © WILEY-VCH Verlag GmbH, D-69451 Weinheim, 2000 1434−1948/00/0404−0597 $ 17.50+.50/0

compare favorably with the values predicted on the basis of the force field model.[12] In order to predict NOE distances, a Boltzmann weighted sum has to be taken over all possible conformations and the fact that the observed distances are well reproduced by these model calculations would appear to be supportive of the notion that the relative energies as calculated by the model should be somehow on scale with the experimental reality. NOE measurements thus provide a further valuable piece of information in validating a force field approach.[12]

Experimental data more directly related to the relative energies would provide yet further information. If it were possible to measure the height of the barrier associated with transmutation of a pair of conformers of a given molecule into one another, this barrier height could be compared with the corresponding value calculated by the force field approach.



	R	R'	R"
1	*o*Tol	Ph	Ph
2	*o*Tol	*o*Tol	Ph
3	*o*Tol	*o*Tol	*o*Tol

Figure 1. Compounds **1**−**3**

This approach is taken in this paper: It is found that the three molecules $CH_3C(CH_2PPh_2)_{3-n}[CH_2P(oTol)_2]_nMo(CO)_3$, $n = 1$: **1**, $n = 2$: **2**, $n = 3$: **3** (Figure 1) exist in the form of two necessarily isoenergetic conformational enantiomers in solution. These conformers transform into each other by a process that is sufficiently slow to be energetically analyzed by NMR techniques and hence the activation barriers for this process are known for all three compounds. A force field approach, as developed previously,[10,11,12] is used to model these transformations and a highly satisfying agreement between the observed and the calculated energies is found.

Results and Discussion

NMR Analysis

Compounds **1**−**3** (Figures 2, 3, 4) were synthesized by procedures akin to those well-established for the preparation of compounds of this type (see Experimental Section).

Single crystals of sufficient quality could not be obtained for **1** and **2**, so that only the structure of **3** could be determined by X-ray crystallography.[10] NMR data for the compounds were obtained from solutions (**1**, **2**: CD_2Cl_2; **3**: $CDCl_3$) in sealed NMR tubes under argon. An almost complete assignment of all the protons and carbon atoms was achieved by a combination of one- and two-dimensional NMR techniques including DQF-COSY,[13] TOCSY,[14] NOESY,[15] HSQC,[16] and HMBC[17] experiments (Figure 20 and Tables 13 and 14) show the assignment of the

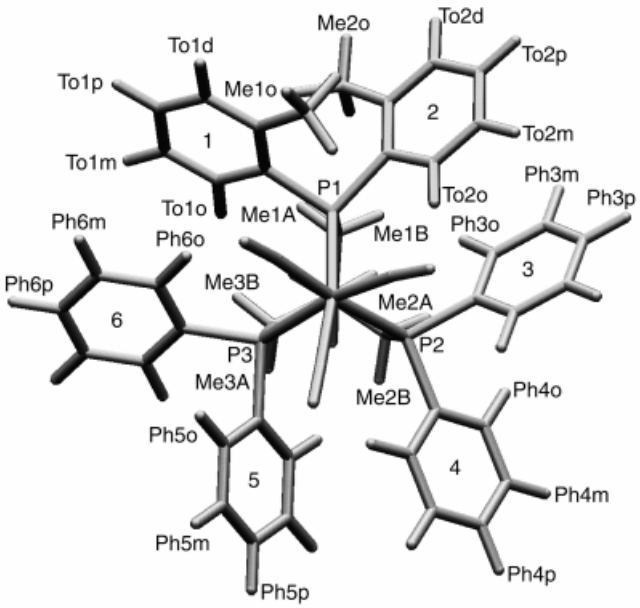


Figure 2. Projection of **1** onto the plane defined by its 3 P atoms; the numbering scheme given here is used throughout in the text

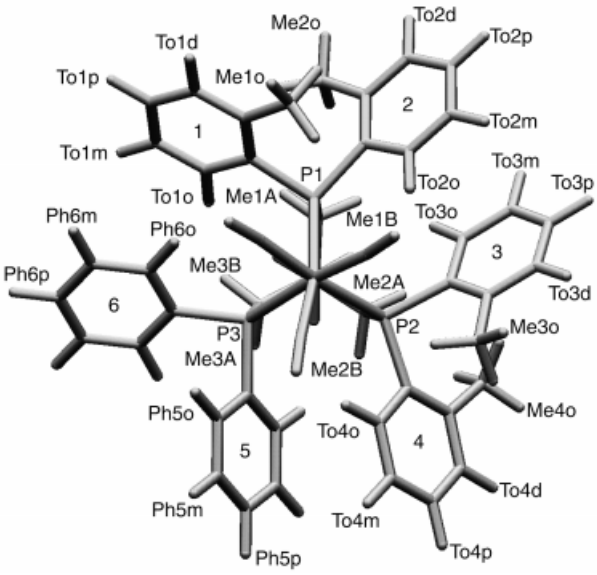


Figure 3. View of the structure of **2** in a projection onto the plane defined by the 3 P atoms; the numbering scheme given here is used throughout the text and tables

^1H and ^{13}C resonances as well as the NOESY, EXSY, and HMBC cross-peaks; see Experimental Section).

It is observed that the phenotype of the spectra changes with temperature. This is exemplified in Figure 5 by focussing on the phosphorus signals of **1** at a few selected temperatures.

At 313 K, only one triplet and one doublet are observed, in accord with the presence of one $P(oTol)_2$ group and two PPh_2 groups. At lower temperatures (Figure 5), a more complicated pattern evolves with the triplet transforming into a doublet of doublets and the doublet splitting into

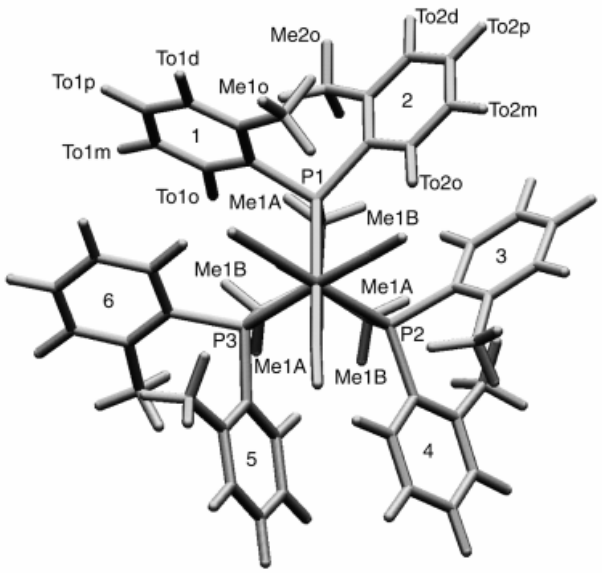


Figure 4. The structure of **3** as projected onto the plane of its 3 P atoms; according to the constitutional C_3 symmetry of the compound, only a subset of atom designators is given; designators for the symmetrically dependent atoms are defined through appropriate reference to the numbers assigned to the phosphorus atoms and the aryl rings as shown in this figure; this numbering scheme is used throughout in the text and tables

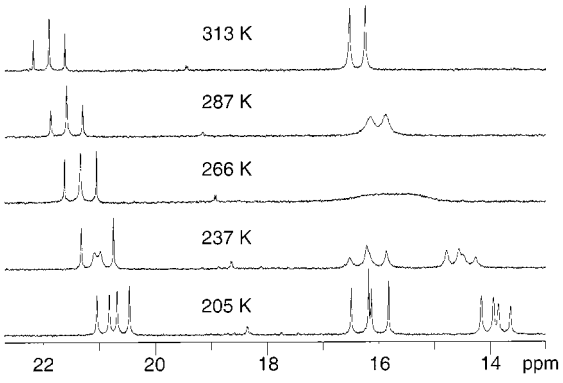


Figure 5. Temperature dependence of the $^{31}P\{^1H\}$-NMR spectrum of **1**; of the 21 spectra collected over the temperature range between 166 K and 313 K, only a few salient examples are shown in the figure; measuring frequency: 81.014 MHz

two such doublet of doublets patterns (Figure 5). The low-temperature spectrum is in accord with a structure of **1** where chiral differentiation between the two PPh_2 groups is static on the NMR time scale. With the shifts and coupling constants given for this type of structure in the legend of Figure 6, the spectrum at the low-temperature limit is correctly reproduced.

The NMR data thus show that there is only one compound present in solution at low temperatures. There remains, however, the possibility that this compound exists as a racemic mixture of two enantiomeric forms.

The ^{1}H-NMR spectra behave accordingly (Figure 7). While the methylene protons, for instance, give rise to a broad unresolved signal at around $\delta = 2.4$ at 293 K, this signal coalesces on cooling and reappears in the form of a

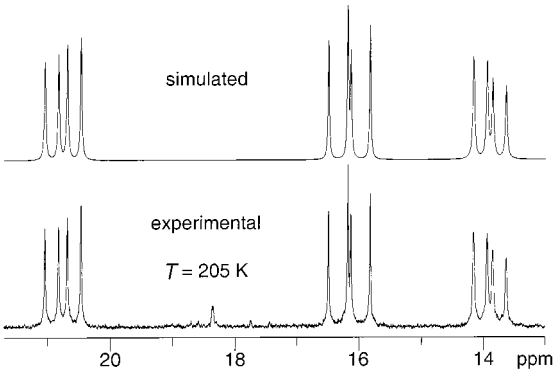


Figure 6. Experimental and simulated $^{31}P\{^1H\}$-NMR spectra of **1** at the low-temperature limit; experimental (bottom) and simulated (top) $^{31}P\{^1H\}$-NMR spectra of **1** at 205 K; $\delta(P1) = 20.75$, $\delta(P2) = 13.91$, $\delta(P3) = 16.15$, $^2J_{P1P2} = 17.8$ Hz, $^2J_{P1P3} = 29.0$ Hz, $^2J_{P2P3} = 25.0$ Hz

complicated multiplet between $\delta = 1.8$ and 2.8. Upon ^{31}P decoupling, this simplifies to a pattern with a minimum of 12 well-resolved lines (Figure 7).

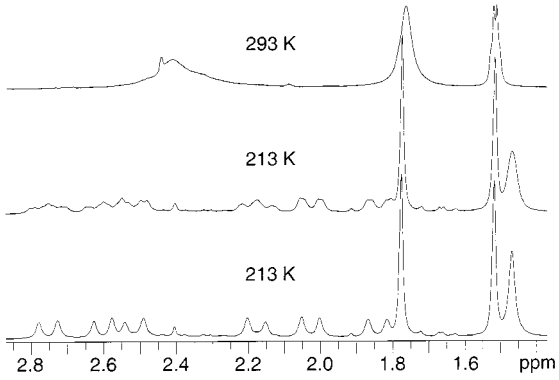


Figure 7. Temperature dependence of the aliphatic region of the ^{1}H-NMR spectrum of **1**; of the 21 spectra collected over the temperature range between 166 K and 313 K, only 3 are shown in the figure; measuring frequency: 300.13 MHz; ^{1}H-NMR spectrum of **1** at 293 K (top), 213 K (middle), and $^1H\{^{31}P\}$-NMR spectrum at 213 K (bottom)

The signal due to the *o*-tolylic methyl groups (Me1o, Me2o, Figure 2) appears as a singlet at around $\delta = 1.8$ at 293 K, which after coalescence is seen as two well-separated sharp singlets at 213 K (Figure 7; from the temperature dependence of these shifts, the center of these two lines can be placed at around $\delta = 1.65$ at 213 K). From this last finding, together with the aforementioned findings from the ^{31}P-NMR data, it is clear that the two methyl groups are in a chemically different environment in the low-temperature structure. Analogous observations have also been made for compounds **2** and **3**, with the different constitutional symmetries of the compounds leading to different appearances of the spectra, although clearly corresponding to the same phenomena. For instance, due to the constitutional equivalence of all three of its $P(o\text{Tol})_2$ groups the ^{31}P-NMR spectrum of **3** shows only one ^{31}P-NMR signal over the entire temperature range. On the other hand, the *o*-tolylic methyl groups as well as the methylene protons of **3** give rise to the

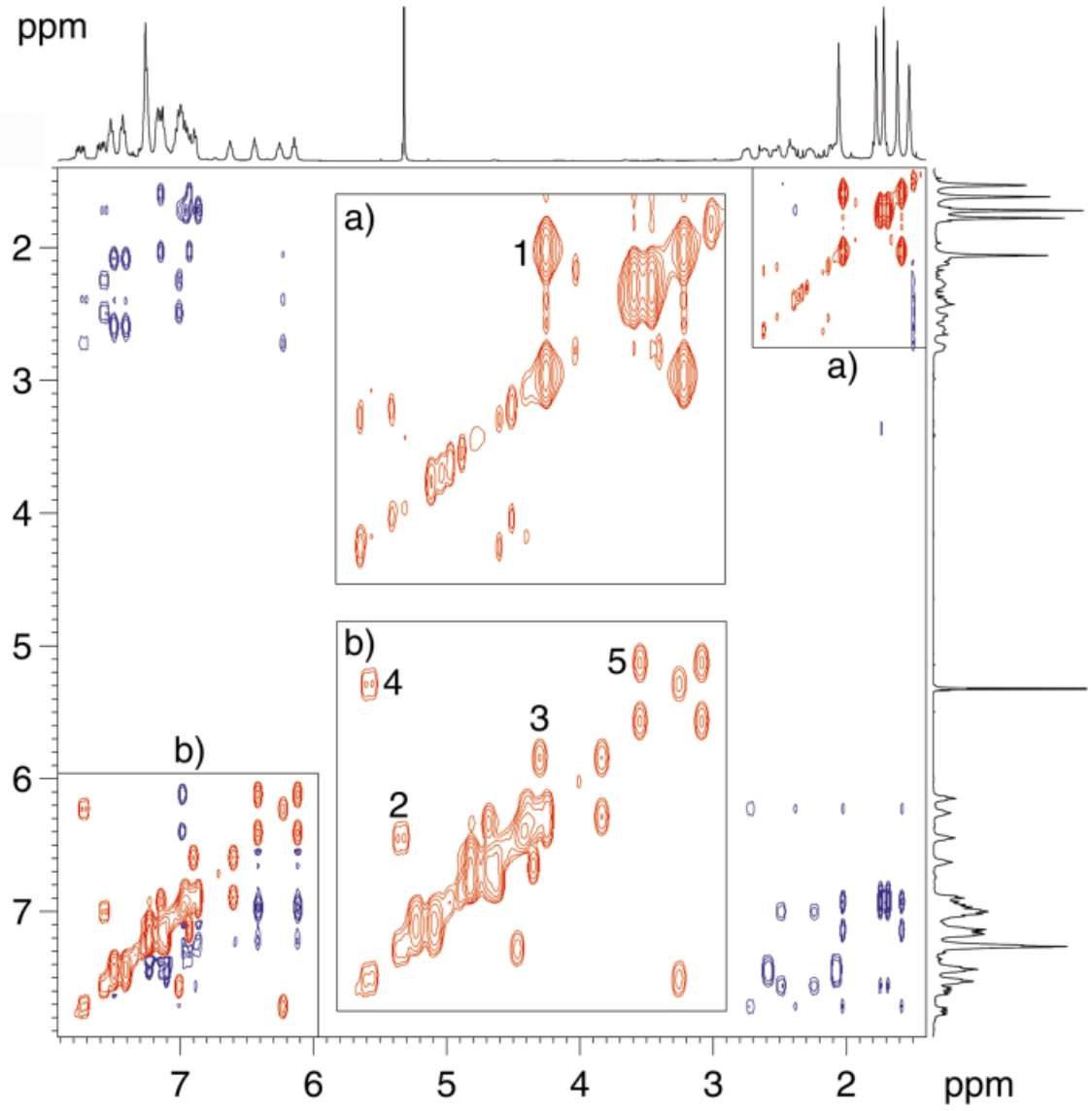


Figure 8. NOESY/EXSY spectrum of **2** at 246 K with a mixing time of 700 ms; measuring frequency: 500.13 MHz; NOESY peaks in blue, EXSY and autocorrelation peaks in red; EXSY peaks are apparent in the methyl, methylene, and arene regions; the EXSY parts of the spectrum between ca. $\delta = 1.5-2.8$ (a) and $\delta = 6.0-8.0$ (b) are shown as enlarged insets; the numbers in these insets refer to the following exchange polarization transfers: 1: Me1o−Me4o, 2: To4o−To1o, 3: To1m−To4m, 4: To2o−To3o, 5: To3m−To2m; designators are as given in Figure 3

same sequence of patterns as seen in the ^{1}H-NMR spectrum of **1**.

If the spectra of **1**−**3** are analyzed for cross-peaks due to dynamic exchange (EXSY) it is observed that the same type of exchange phenomena is present in all cases. This is exemplified by the case of **2** in Figure 8.

The EXSY cross-peaks observed for compounds **1**−**3** are given in Figure 20 and Tables 13 and 14 (see Experimental Section). It can be seen that the *o*-tolyl substituents of each P(*o*Tol)$_2$ group are involved in a mutual exchange. The protons of the CH_2 groups of the backbone of the chelate cage are likewise in a dynamic exchange.

The findings reported thus far show that in each case only one constitutional isomer is present. The observed exchange phenomena must therefore be due to a dynamic exchange between two conformational isomers such that in compound **3**, for instance, Me2o and Me1o as well as Me1A and Me1B etc. (Figures 4, 20) are interchanged in the two different conformeric forms. The most plausible process to account for these observations is a conformational racemization of the compounds, where the torsional arrangement of the aryl groups and the torsion of the chelate cage switch between the image and the mirror image. Figure 9 illustrates this kind of process for the compounds **1**−**3**.

The energy associated with this enantiomerization process has been deduced from relevant NMR observations by three different approaches: (i) Measurement of the coalescence temperature at different field strengths. (ii) Line-shape analysis at different temperatures and field strengths. (iii)

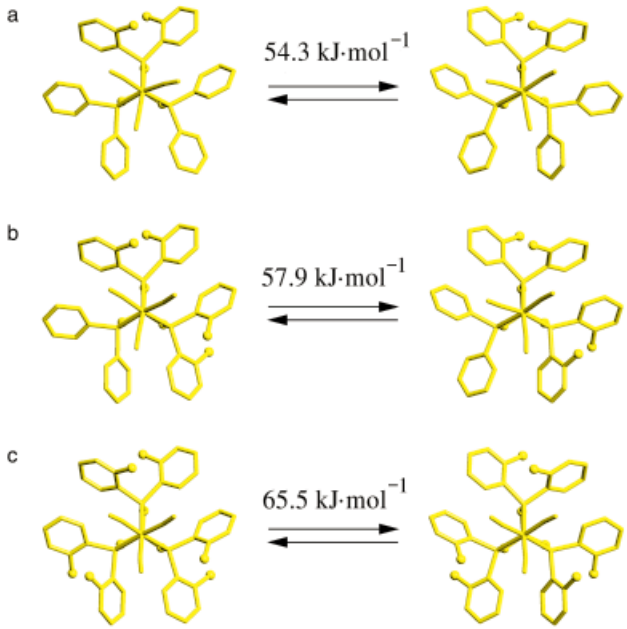


Figure 9. Inversion processes for compounds **1** (a), **2** (b), and **3** (c) and the corresponding experimental $\Delta G^{\neq}_{298K}$ values

Quantification of EXSY data at different temperatures and field strengths. Coalescence experiments have been performed for all three compounds **1**−**3**. Using the phosphorus nuclei as a probe, only **1** and **2** can be analyzed since only one ^{31}P signal is seen for **3** (see Table 12 in the Experimental Section). It is possible, however, to use the ^{1}H signal of the methyl groups of the *o*-tolyl substituents as the analytical tool for all three compounds (**1**−**3**) (Table 1).

Using the methyl protons as the probe, coalescence experiments were performed at various field strengths (Table 1), yielding closely similar results in terms of $\Delta G^{\neq}$ for all the independent experiments in each case (Table 1).

Line-shape analysis[18] of the ^{31}P-NMR data could only be performed for **1** and **2** for the reasons indicated above. As already evident from the case of compound **1** (Figure 5), the shifts are found to be strongly temperature dependent. In order to correct for this temperature dependence, a linear interpolation was used,[19] as is the usual practice. Only very minor additional corrections were found to be necessary for correcting the shift values during refinement.

The quality of fit obtained by the simulation procedure is shown in the insets of Figure 10 for compound **2** at two selected temperatures. The rate constants determined by this procedure should produce a linear plot in an $\ln(k/T)$ vs. $1/T$ diagram (Figure 10), with the slope of the line indicating $\Delta H^{\neq}$ and the abscissa value at $(1/T) = 0$ indicating the activation entropy $\Delta S^{\neq}$.[20] The $\Delta G^{\neq}$ values at 298 K were evaluated as 54.3 kJ·mol^{-1} for **1** ($\Delta H^{\neq}$ = 45.3 kJ·mol^{-1}, $\Delta S^{\neq}$ = −30 J·K^{-1}·mol^{-1}) and 57.9 kJ·mol^{-1} for **2** ($\Delta H^{\neq}$ = 51.8 kJ·mol^{-1}, $\Delta S^{\neq}$ = −20 J·K^{-1}·mol^{-1}) (Table 1).

EXSY spectroscopy constitutes yet another appropriate tool. The exchange phenomena observed pertain to the so-called "equally populated two-site exchange" case, which lends itself to a straightforward analysis by EXSY[15] methods if groups of signals are found which are related to each other solely by exchange and not by coupling.[21] The methyl signals of the *o*-tolyl groups give rise to such sets of signals, so that activation energies can also be derived from EXSY experiments.

If instead of the methyl signals Me1o−Me4o (1, Figure 8) the clearly resolved pairs of signals in the aromatic region e.g. To2m−To3m are used as a probe (5, Figure 8; signals labelled 2, 3, 4 in Figure 8 could also be used), the values

Table 1. Activation energies for the conformational isomerization of **1**−**3**; temperatures in K are given in brackets

Compound	Field [MHz]	$\Delta G^{\neq}_{C(31P)}$ [a] [kJ·mol^{-1}]	$\Delta G^{\neq}_{C(Me)}$ [b] [kJ·mol^{-1}]	$\Delta G^{\neq}_{C(Ar,CH2)}$ [c] [kJ·mol^{-1}]	$\Delta G^{\neq}_{EXSY}$ [d] [kJ·mol^{-1}]	$\Delta G^{\neq}_{LS(31P)}$ [e] [kJ·mol^{-1}]	$\Delta G^{\neq}_{mean}$ [f] [kJ·mol^{-1}]
1	500	54.2 (278)	54.0 (274)	53.9 (274)	52.9 (226)	54.3 (298)	54.4 (298)
	300	54.3 (274)	54.1 (269)	54.1 (269)	51.9 (212)		
	200	53.1 (266)	53.7 (263)	53.6 (263)	52.7 (221)		
2	500	57.8 (297)	58.0 (299)	58.0 (293)	54.8 (224)	57.9 (298)	57.9 (298)
			57.0 (276)				
	300	56.8 (287)	58.1 (293)	56.6 (281)	55.0 (218)		
			56.7 (268)				
	200	56.5 (282)	57.8 (287)	56.9 (277)	55.2 (227)		
			56.8 (261)				
3	200	–	66.6 (338)	65.8 (329)	67.0 (297)	–	65.5 (298)
				65.2 (317)	64.6 (268)		
					64.6 (261)		

[a] ^{31}P{^{1}H}-NMR spectra; coalescence data. − [b] ^{1}H-NMR spectra; coalescence data based on methyl protons. − [c] ^{1}H-NMR coalescence measurements based on arene (**1**−**3**) and CH_2 protons (**3**). − [d] EXSY measurements. − [e] ^{31}P{^{1}H}-NMR line-shape analysis data obtained at three different field strengths: **1**: R^2 = 0.998, $\Delta H^{\neq}$ = 45.3 ± 0.4 kJ·mol^{-1}, $\Delta S^{\neq}$ = −30 ± 1 J·K^{-1}·mol^{-1}; **2**: R^2 = 0.995, $\Delta H^{\neq}$ = 51.8 ± 0.7 kJ·mol^{-1}, $\Delta S^{\neq}$ = −20 ± 2 J·K^{-1}·mol^{-1}; the limits given refer to the estimated standard deviation σ in each case. − [f] Eyring plot constructed from coalescence, EXSY, and line-shape analysis data; **1**: R^2 = 0.995, $\Delta H^{\neq}$ = 45.7 ± 0.5 kJ·mol^{-1}, $\Delta S^{\neq}$ = −29 ± 2 J·K^{-1}·mol^{-1}; **2**: R^2 = 0.990, $\Delta H^{\neq}$ = 48.7 ± 0.7 kJ·mol^{-1}, $\Delta S^{\neq}$ = −31 ± 3 J·K^{-1}·mol^{-1}; **3**: R^2 = 0.986, $\Delta H^{\neq}$ = 59.3 ± 3.5 kJ·mol^{-1}, $\Delta S^{\neq}$ = −21 ± 12 J·K^{-1}·mol^{-1}; the limits given refer to the estimated standard deviation σ in each case; details are given in the Experimental Section.

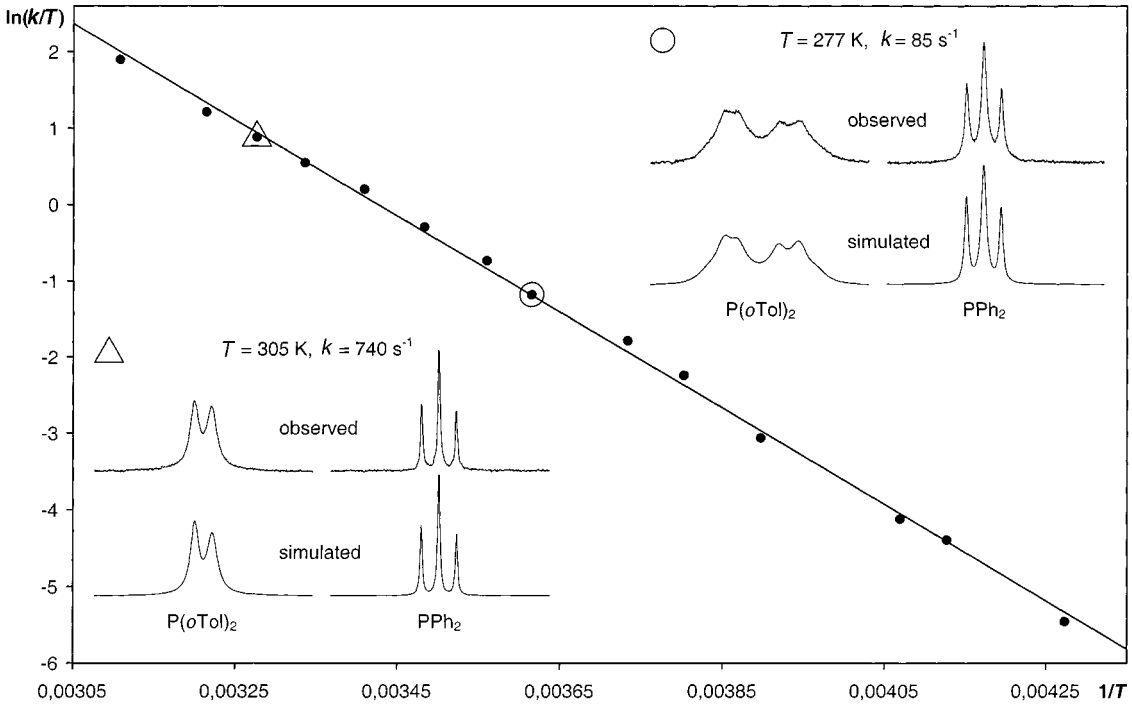


Figure 10. Eyring plot derived from line-shape analysis of compound **2**; the data shown refer to a series of $^{31}P\{^{1}H\}$-NMR measurements taken at 129.495 MHz (^{1}H: 300 MHz); the quality of fit as obtained by the line-shape analysis procedure at the two selected temperatures is indicated in the insets

calculated for the activation barriers remain unchanged as expected.

The activation barriers associated with the conformational enantiomerization of compounds **1**, **2**, **3** are found to increase in the sequence $\Delta H^{\neq} \approx 45,\ 52,\ 59\ kJ{\cdot}mol^{-1}$ (Table 1). On increasing the number of *o*-tolyl groups, the steric congestion increases, making the isomerization process more energy consuming. The activation entropies are found to be negative throughout (**1**: −30; **2**: −20; **3**: −21 $J{\cdot}K^{-1}{\cdot}mol^{-1}$; Table 1). Even though the determination of these activation entropies is based on an extrapolation to $1/T = 0$ in the Eyring diagrams and, owing to the long distance over which this extrapolation has to be taken, is subject to considerable uncertainty, the quality of the data collected suffices to show that the activation entropies are definitely negative. This indicates that the transition state conformations will be even more sterically congested than the ground state conformations. It definitely precludes the hypothesis that the conformational racemization process might occur through decoordination of one of the "legs" of the *tripod* ligand. If this hypothesis were to apply, positive activation entropies would necessarily be observed.

Force Field Model

The force field used to describe compounds **1**−**3** has been derived by global optimization of the relevant force field parameters on the basis of the molecular structures of ten different compounds *tripod*$Mo(CO)_3$ [*tripod* = $RCH_2C(CH_2X)(CH_2Y)(CH_2Z)$; X, Y, Z = PR′R″].[10][11] It has been shown that the conformations adopted by these molecules in the solid state are equilibrium conformations, which are not disturbed to any great extent by the crystal forces.[8][9] In order to derive the relevant force field parameters, those parameters involving contributions from the metal were varied such as to reproduce the observed conformations as local minima on the corresponding energy hypersurfaces. Scaling of the energy was implicitly achieved by using standard MM2* values for all those parameters to which the metal makes no direct contribution. It was not obvious from the outset whether or not the energy scale implicitly defined by the force field parameters would also be appropriate for making energy-based predictions. However, an indication that this is approximately so was provided by the observation that NOE distances are correctly predicted by using the force field generated energies in the exponential terms of a Boltzmann weighting scheme.[12] More direct evidence would be obtained if it were possible to calculate the activation barriers associated with the enantiomerization processes of **1**−**3** and if these values were then found to be close to those observed experimentally in each case.

The experimentally determined activation energies for the conformational racemization processes of compounds **1**−**3** do, in fact, allow a comparison of the energy scale intrinsic to the force field approach with the real world. To this end, a complete reconstruction of the molecular hypersurface by the force field is necessary in order to delineate the least-energy pathway and to finally calculate the activation barrier predicted by this model. Whereas the equilibrium struc-

ture of **3** is more reliable since it has been established by X-ray analysis,[10] the least-energy conformations of **1** and **2** have to be inferred from the force field calculations themselves. This does not, however, appear to be a serious drawback since the structure of **3** as determined by X-ray methods is well reproduced by the force field approach, even as the global minimum on the hypersurface,[10] and since other structures have been predicted with high accuracy by the force field approach taken here.[10] The minimum energy conformations calculated for **1** and **2** are shown in Figures 2 and 3, respectively.

Analysis of 3

With regard to the search for a global minimum on the hypersurface relating to **3**, a complete conformational search has already been carried out, the details of which have been described.[10] It was found that from a starting set of 1376 symmetrically independent conformers, only 262 survived as local minima after refinement based on the *mm2f* parameter set.[10] The conformational space used for the grid search was defined by the six rotations of the aryl groups about their respective P−C_{ipso} bonds.

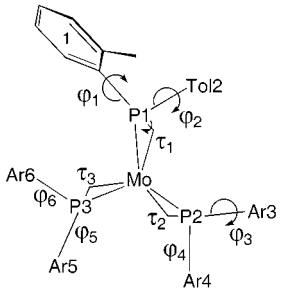


Figure 11. Definition of the six aryl rotations $\varphi_1-\varphi_6$ and the three cage torsions $\tau_1-\tau_3$ used to define the conformational space of compounds **1**−**3**; for the definition of $\varphi = 0°$ see Figure 14; $\tau = 0°$ means that the carbon atom of the bridging CH_2 group would be obscured by the Mo−P line in the diagram

The definition of these rotations denoted as φ is as shown in Figure 11 and is in accord with the definition used previously.[10] The technique used to set these rotations at the values defined by the grid points has also been described previously.[10] The torsion of the chelate cage as described by τ,[8] defined as indicated in Figure 11, was set at a uniform starting value of 20° for all three "legs" of the ligand and it was found that the strain imposed on it by the forced rotation of the aryl groups is sufficiently strong to produce negative as well as positive torsions after refinement.

The energies of the local minima obtained after refinement are distributed as shown in Figure 12a. There are only a few low-energy conformations in the energy band of 20−30 kJ·mol^{-1} above the global minimum. The three conformations with the lowest energy are qualitatively identical (the arrangement of the heavy atoms is designated as 3.1 in Figure 13); the main difference between them stems from a slightly different orientation of the methyl groups of the *o*-tolyl moieties and the energy difference between these almost identical conformers is correspondingly small.

The conformation at position four on the energy scale is already more than 10 kJ·mol^{-1} above the global minimum, with a geometry as shown in Figure 13 (designated as 3.2). This result is well in accord with the observation that in the solid state **3** adopts a conformation corresponding to the global minimum.[10]

The spread of the φ and τ values characterizing the conformations of the different energy minima has been analyzed in a global way. Cumulating all six independent φ values to obtain just one average representative as well as averaging the three individual τ values found for each conformer through the minimization process to a mean value of this torsion, the distributions shown in Figure 12b/c are obtained. There are clear preferences at around 40° and 140° for the rotational positions of the aryl groups and, of course, by the very symmetry of the problem, at around −40° and −140° (Figure 12b). The spread of the τ values is more uniform with a slight preference for torsions of around 0° and ±30° (Figure 12c). If the rotational positions of the aryl groups are analyzed individually, pronounced regularities are observed.[22]

The distinct types of mutual orientation at each specific P(*o*Tol)$_2$ group have been systematically labelled using the scheme shown in Figure 13. To describe the aforementioned regularities, the orientations are classified according to the direction in which the two methyl groups are pointing. If, for the sake of definition, "inward" means that in the projection shown (Figure 13) the methyl group lies within the sector defined by the two P−C_{ipso} bonds and outward means that it lies outside, then three classes of arrangements may be defined. Firstly, for an arrangement where both methyl groups point inward, we use the term "syn" (Figure

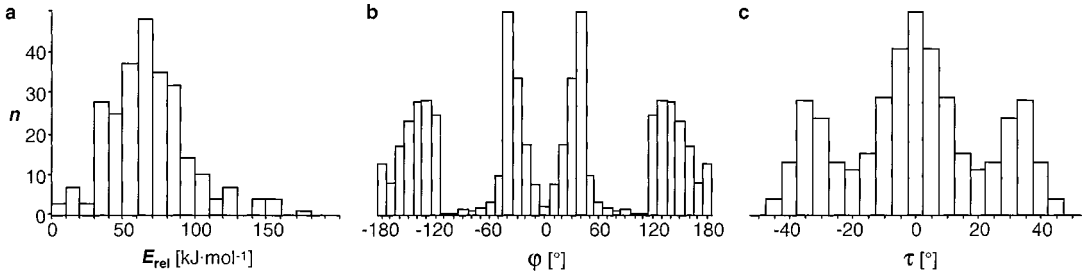


Figure 12. Histograms showing the distributions of the energies (a) and of the parameters φ (b) and τ (c) relating to the local minima found for compound **3**

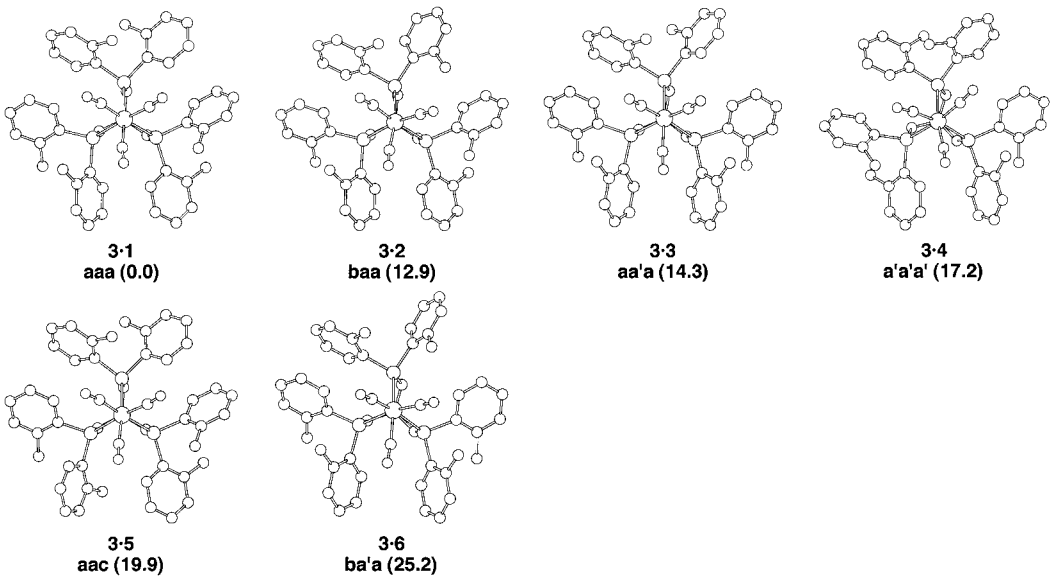


Figure 13. Conformations of **3** corresponding to local minima on the energetic hypersurface

13, 3.1). Secondly, where both methyl groups point outward, the arrangement shall be classified as "anti". The final arrangement, where one methyl group points inward and the other points outward, is referred to as "peri" (Figure 13, 3.2). For each class of orientation thus defined, there are further subclasses depending on whether a specific methyl group is on the left-hand or on the right-hand side and whether it points forwards or backwards. Designator *a* denotes a "syn" orientation with the left-hand *o*-tolyl group pointing forward and the right-hand one pointing backwards (Figure 13, 3.1). A "peri" arrangement of the methyl groups with both of them pointing forward is denoted as *b* (Figure 13, 3.2). Finally, a "peri" arrangement with both methyl groups pointing backwards is denoted as *c* (Figure 13, 3.5). These designators are combined to give the three-letter codes indicated in Figure 13, which describe the orientations adopted by the three P(*o*Tol)$_2$ groups in the sequence P1/P2/P3 (for the numbering scheme, see the definition in Figure 11). An orientation not shown in Figure 13, but referred to in Figure 14a and throughout the text, in which the left-hand methyl group points backwards and the right-hand one points forward while being in a mutual "anti" arrangement, is designated *d*.

For each of these local conformations, classified as *a*, *b*, *c*, or *d* as outlined above, an obverse conformation exists with forward and backward directions exchanged. These conformations are encoded by a prime (see, for instance, *a*′ in Figure 13, 3.4). The resulting eight designators suffice to characterize all the conformations up to calculated relative energies of around 60 kJ·mol^{-1}.

Analyzing the ensemble of conformers with respect to the specific classes to which their PAr$_2$ groups can be assigned, it is found that up to an energy of 27 kJ·mol^{-1} all these low-energy conformations have at least two local conformations

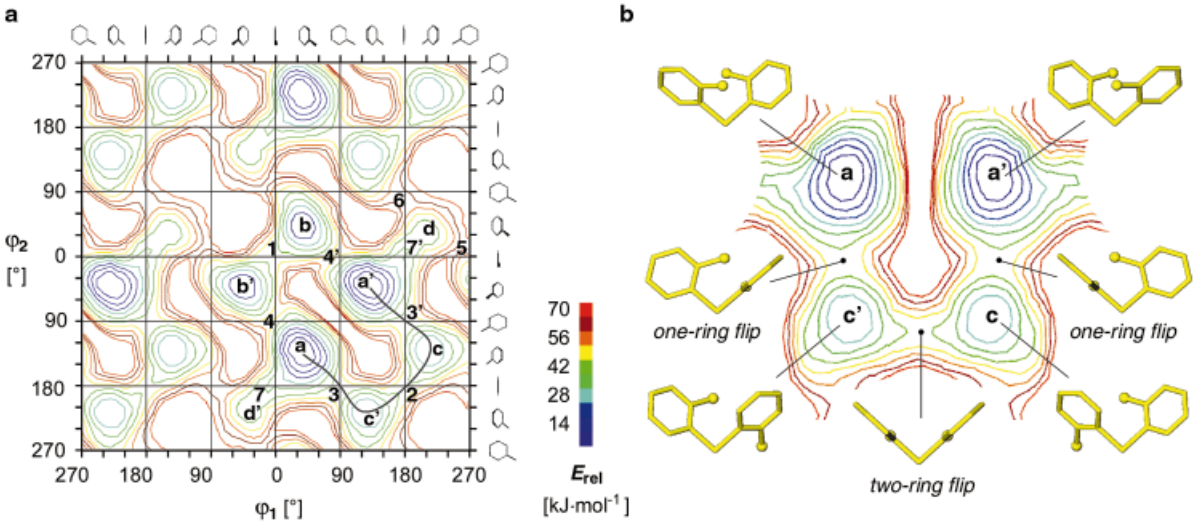


Figure 14. Contour diagram showing the enantiomerization pathway of **3**

corresponding to *a* or *a′* as defined above. This type of local orientation appears to be of peculiar stability.

The observation that conformations in which two of the P(*o*Tol)$_2$ groups remain in the orientation characterizing the arrangement of all three of these groups in the global minimum allows for a simplification of the conformational search. Selecting just one P(*o*Tol)$_2$ group and driving the rotational positions of its *o*-tolyl groups through the whole range of values from 0° to 360° should be sufficient to delineate the pathway of the overall isomerization process. The two remaining P(*o*Tol)$_2$ groups, which are not driven, will adopt the appropriate orientations during the minimization process. To allow for the torsional flexibility of the chelate scaffolding, these scans were made at two different settings of the torsion angle τ. To generate the starting conformations, all three torsion angles of one conformer were set at the same value and two complete scans of φ values were made, one at τ = 10° and the other at τ = 31°. These starting values were selected because analyses of similar compounds[8] have shown the τ values to cumulate around these values. The search was only performed with positive starting values of τ owing to the fact that all conformations must exist in isoenergetic enantiomeric pairs such that for every conformation with a given set of τ and φ values, an inverted conformation exists where the τ and φ values each have opposite signs. To allow for the torsional flexibility of the P(*o*-Tol)$_2$ groups that are not actively driven, the starting conformations of these groups were set according to the optimum arrangement (φ values) found to be characteristic for each value of τ. Initially, for small τ values an orientation as found for the global minimum (Figure 13, 3.1) was chosen, while for large τ values an orientation as shown in 3.4 (Figure 13) was used.

The subspace thus defined for the grid search has three dimensions; two aryl rotations φ_1 and φ_2 at the selected P(*o*Tol)$_2$ group and τ as a third dimension. While the τ space was only probed at two levels, the φ space was analyzed by a full rotation of both *o*-tolyl groups with an initial increment of 10°. To illustrate the result of these computations, a projection onto the subspace defined by the two aryl torsions φ_1 and φ_2 is shown in Figure 14.

Of the two energy values available at each grid point, resulting from the two values of τ assigned to it, the lower one was selected for this projection in each case. To generate the contour plot, we applied a symmetry expansion reflecting (i) the 360° translational symmetry along the φ axes, and (ii) the symmetry equivalence of enantiomeric pairs in each case. This second symmetry is evident from the diagram as a diagonal mirror plane from top left to bottom right (Figure 14).

There are three symmetrically independent energy minima apparent in this diagram. Position *a* (Figure 14; the designators *a*, *b*, *c*, *d* as used here are in accord with the definition given above in relation to Figure 13) corresponds to the global minimum. The minimum corresponding to the enantiomeric conformation is designated as *a′*. The local minima designated as *b*/*b′* correspond to an enantiomeric pair of conformations, as do the minima designated as *c*/*c′*. The positions *d*/*d′* correspond to another local minimum albeit a very flat one. The local minima *b*/*b′* (ca. 33 kJ·mol^{-1}) and *c*/*c′* (ca. 35 kJ·mol^{-1}) as well as the flat minimum *d*/*d′* (ca. 54 kJ·mol^{-1}) are all well above the energy of the global minimum *a*/*a′* (0.0 kJ·mol^{-1}). The diagram is thus consistent with the observation that only the enantiomeric conformations corresponding to the global minimum (*a*/*a′*) are seen in the NMR experiments. Although the local minima are relatively high in energy with respect to the equilibrium conformation *a*/*a′* and do thus not make a significant contribution to the conformational ensemble on thermodynamic grounds, the question still remains as to whether, once formed, they might survive due to the height of the relevant activation barriers. If this were to be the case, a thermodynamic equilibrium would not be established.

A rough estimate of the different activation barriers may be made simply by analyzing the diagram (Figure 14). The activation barriers associated with processes transforming *b′* back to *a* and *c′* back to *a* should be about 30 and 35 kJ·mol^{-1}, respectively, which are lower than those for the inverse processes, i.e. for transforming the conformation corresponding to the global minimum into the conformations characterizing the local minima *b′* and *c′*, respectively. A very rough estimate of the barriers associated with the latter transformations, as taken from the diagram, would be of the order of 50 kJ·mol^{-1} or higher. From these estimates of the relative energies of the activation barriers, it follows that the system as a whole should be in thermodynamic equilibrium under the conditions of the NMR experiments.

As far as the racemization process itself is concerned, only two plausible alternatives are suggested by the diagram: a trajectory along *a*−*b′*−*b*−*a′* or, alternatively, a transformation along *a*−*c′*−*c*−*a′*, which ever has the lower activation energy. By a more detailed analysis (see below), it is found that the latter pathway is in fact the important one.

The section of the diagram corresponding to this pathway is reproduced at the right-hand side of Figure 14 as an enlarged inset. Around this inset, the conformations characteristic of some selected points on the φ_1, φ_2 diagram are shown. It can be seen that following the pathway *a*−*c′*−*c*−*a′* corresponds to the transition of three saddle-points, which characterize one-ring, two-ring, and one-ring flip transitions in this sequence.[23]

In order to model the possible transformation pathways in a more accurate way, which would ultimately allow the extraction of reliable estimates of activation barriers, the following procedure was adopted. Starting with the ground state conformation, the P(*o*Tol)$_2$ group at P1 was selected for active rotation of its *o*-tolyl groups. A rotational increment of 2° was used throughout this analysis. The forward and backward rotations of these two *o*-tolyl groups have a different physical meaning due to the chirality of the system (this is even true at points in conformational space which, like the global minimum, correspond to C_3-symmetric arrangements).

To analyze the consequence of these rotations, each of these *o*-tolyl groups was actively driven and after each step the molecule as a whole was allowed to relax with the actively driven ring being fixed at the set position. It was found that − over a large range − the other *o*-tolyl group at P1 monotonically adopted its own rotational position in response to that of the driven group. Referring to the diagram in Figure 14, rotation of φ_1 in a negative direction, as well as independently starting with rotations of φ_2 in a positive direction, led to a route along the valley in the direction $a-b'$. Starting with φ_1 as the active rotator caused the system to follow the valley leading from *a* to *c'*. When the search was started by incrementing the rotation φ_1 in a negative sense, entry into a valley leading to *d'* was opened. Stepwise rotation in all four of these starting directions, with the appropriate relaxation after each step, led to the minima *b', c'*, and *d'* without further manipulation.

The saddlepoint 4 (Figure 14) was found at 79 kJ·mol^{-1}, irrespective, of course, of how it was arrived at. The saddlepoint 3 (Figure 14) connecting *a* and *c'* was found at 55.8 kJ·mol^{-1}, while that close to 7, separating *d'* from *a*, was found at 75 kJ·mol^{-1}.

With the analysis driven so far, a transformation following the direction *a* to *c'* is the most probable one and, as long as the saddlepoints separating *c'* from *c* and *c* from *a'* are lower in energy than the saddlepoints along the routes $a-b'$ or $a-d'$, this route is necessarily the best one. Accordingly, on driving φ_1 from its position at *c'* further in the positive direction, the local minimum *c* was reached without further interference. The saddlepoint between *c'* and *c* (2, Figure 14) was found at 52.1 kJ·mol^{-1}. If φ_1 was then further driven in a positive direction, a transition to the symmetry equivalent of *c'* was observed. Therefore, in order to delineate the route from *c* to *a'*, φ_2 was driven from this point on. In this way, *a'* was reached, the saddlepoint being found at 69.2 kJ·mol^{-1}. This is the maximum energy required for the conformational enantiomerization of the selected P(*o*Tol)$_2$ group along the route $a-c'-c-a'$. Since the saddlepoints separating *a* from *b'* as well as from *d'* are higher in energy, the routes via *b'* and *d'* do not need to be considered further.

The analysis described so far is not yet complete. There remain the other two P(*o*Tol)$_2$ groups, the rotational positions of which might, in principle, have a strong influence on the barrier height. During the optimization process described so far, the conformation at these groups remained essentially the same as in the starting conformation, with only minor undulations around the starting positions. On the one hand, this shows that coupling between neighboring P(*o*Tol)$_2$ groups is weak as compared to that dominating the interactions between two *o*-tolyl groups at one and the same phosphorus atom. Nevertheless, on the other hand, it has to be analyzed to ascertain whether any other rotational position of these neighboring P(*o*Tol)$_2$ groups would lead to a more favorable transition energy.

To simplify this problem, the following assumption was made. The lowest energy pathway for a rotational enantiomerization at each of these groups should be analogous to that already delineated for the group at P1. This assumption is well supported by the observation of almost decoupled behavior for the individual P(*o*Tol)$_2$ groups. To produce the analogous transitions, the rotations φ_3 (at P2) and φ_5 (at P3), respectively, were driven in a positive direction. This led directly to minima corresponding to *c'* with activation barriers of 73.6 kJ·mol^{-1} and 65.4 kJ·mol^{-1}. Due to the C_1 symmetry of the problem, the two routes are distinctly different and it is energetically more feasible to rotate the groups at P3 first. Driving φ_5 further in the positive direction led over a saddlepoint at 48.8 kJ·mol^{-1} to a minimum analogous to *c*. Driving φ_5 in the negative direction from this point on led to a minimum conformation locally enantiomeric to the starting conformation at P3 and thus analogous to *a'*. The saddlepoint for this last transition was found to be at 60.3 kJ·mol^{-1}. The same procedure was then applied to the rotation of the *o*-tolyl groups at P2. The saddlepoints in a sequence corresponding to the positions $a-c'-c-a'$ were found at 49.5, 44.7, and 43.6 kJ·mol^{-1}. Taking all the values together, it emerged that the energetically most costly step is the conformational enantiomerization of the first P(*o*Tol)$_2$ group (there is only one such "first" group due to the C_3 symmetry of the ground state conformation). Within the scope of the model, the value of 69.2 kJ·mol^{-1} (*mm2f*) or 61.1 kJ·mol^{-1} (*mm2t*) thus characterizes the activation energy for the racemization of the compound. The sequence of individual rotations taking place over the whole process is illustrated in Figure 15, which shows the conformations of all the minima encountered along this route.

The labels *a*,*a'* and *c*,*c'* correspond to the labels in Figure 13. The three-letter code refers to the local conformation at the phosphorus atoms P1, P2, and P3 in this sequence. The relative energies, together with the values quantifying the conformations, are given in Table 2, as are the energies calculated for the intervening saddlepoints. The energy profile given in Figure 16 summarizes the energetics of the pathway in a condensed form.

Analysis of 2

The structure of **2** is not known from crystallography. In order to model the low-energy structures, it was − in view of the knowledge already acquired with compounds of this type[12] − not considered necessary to carry out a full conformational search. Starting conformations, which should be close to the global minimum, were constructed either from low-energy conformations of $CH_3C(CH_2PPh_2)_3Mo(CO)_3$ by adding methyl groups at the appropriate positions to transform the phenyl groups into *o*-tolyl groups, or from low-energy conformations of $CH_3C[CH_2P(oTol)_2]_3Mo(CO)_3$ (**3**) by the reverse operation. Starting conformations with both types of helicity with respect to the arrangement of the aryl groups and with high (ca. 30°) and low (ca. 10°) values of the torsional arrangement of the chelate cage were analyzed. Refinement of all these conformations led to two analogous minima in each case. A con-

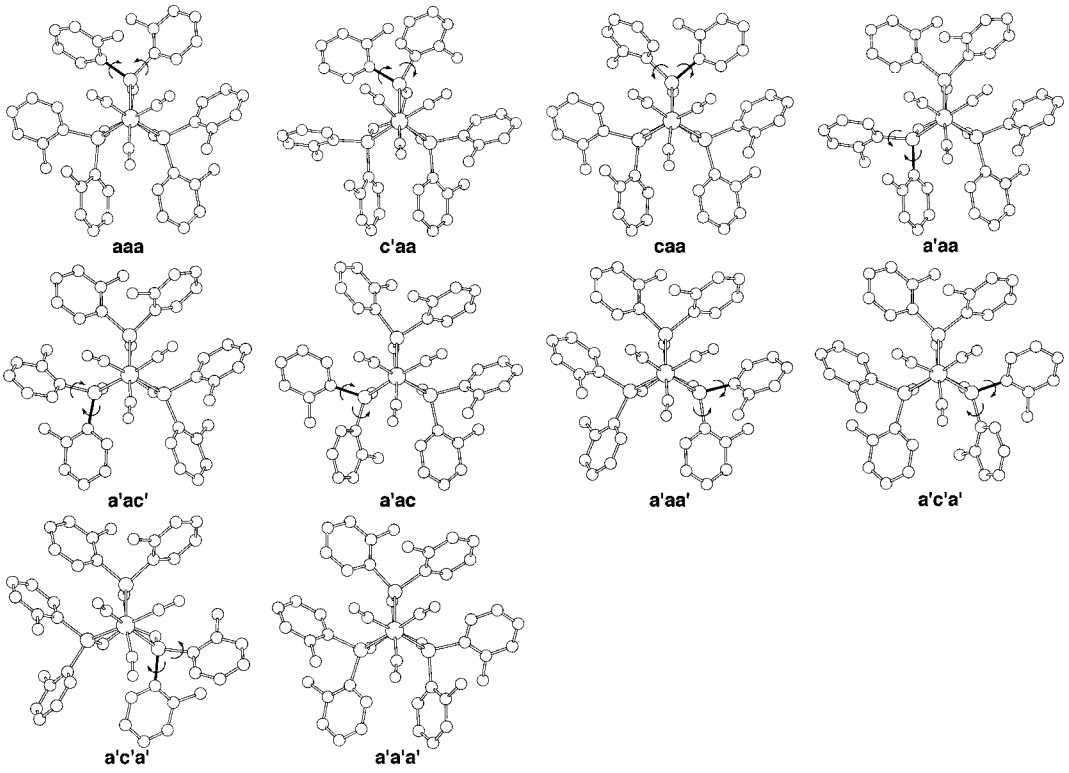


Figure 15. Sequence of rotational processes along the enantiomerization pathway of **3**

Table 2. Conformations of **3** characterized by their φ and τ values (*mm2f* parameter set)

i	*ring flip*	E_{rel}(TS) [kJ·mol^{-1}]	E_{rel} [kJ·mol^{-1}]	Codon[a] P1P2P3	φ_1 [°]	φ_2 [°]	φ_3 [°]	φ_4 [°]	φ_5 [°]	φ_6 [°]	τ_1 [°]	τ_2 [°]	τ_3 [°]
–	–	–	0.0	**aaa**	34	–127	34	–127	34	–127	10	10	10
1	1-r. f.	55.8	35.1	**c'aa**	118	128	33	–141	23	–160	27	10	31
1	2-r. f.	52.1	19.9	**caa**	–146	–127	34	–128	36	–125	5	6	3
2	1-r. f.	**69.2**	14.3	**a'aa**	123	–37	34	–130	32	–148	9	6	19
5	1-r. f.	**65.4**	38.9	**a'ac'**	128	–32	33	–143	125	147	5	9	–2
5	2-r. f.	48.8	38.9	**a'ac**	143	–33	32	–128	–147	–125	–9	–5	2
6	1-r. f.	60.3	14.3	**a'aa'**	130	–34	37	–123	148	–32	–6	–9	–19
3	1-r. f.	**59.5**	19.9	**a'c'a'**	128	–34	127	146	125	–36	–6	–5	–3
3	2-r. f.	54.7	35.1	**a'ca'**	141	–33	–128	–118	160	–23	–10	–27	–31
4	1-r. f.	43.6	0.0	**a'a'a'**	127	–34	127	–34	127	–34	–10	–10	–10

[a] For the meaning of the designators, see the text and Figure 15.

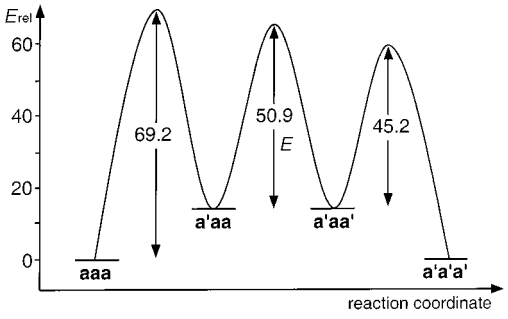


Figure 16. Energy profile along the enantiomerization pathway of **3**; E_{rel} in kJ·mol^{-1}; for the meaning of the designators, see Figure 15

formation with small τ values (Table 3) was found as the global minimum (this is shown as 2*sf* in Figure 17).

Table 3. Energies and conformational parameters of the two pairs of low-energy conformations of **1** and **2** for the parameter sets *mm2f* and *mm2t* (designators refer to Figure 17)

	Parameter	E_{rel} [kJ·mol^{-1}]	φ_1 [°]	φ_2 [°]	φ_3 [°]	φ_4 [°]	φ_5 [°]	φ_6 [°]	τ_1 [°]	τ_2 [°]	τ_3 [°]
1*sf*	*mm2f*	0.0	38	–135	35	50	37	49	7	11	9
1*st*	*mm2t*	8.8	29	–126	29	57	27	59	18	19	20
1*lf*	*mm2f*	2.1	118	–38	–36	–20	–48	–27	27	33	36
1*lt*	*mm2t*	0.0	118	–41	1	–14	–47	–29	29	36	39
2*sf*	*mm2f*	0.0	40	–135	38	–136	35	50	6	8	10
2*st*	*mm2t*	5.6	30	–126	30	–125	29	58	17	17	19
2*lf*	*mm2f*	5.9	120	–40	122	–38	–31	–21	29	23	35
2*lt*	*mm2t*	0.0	120	–39	121	–38	–3	–18	34	26	39

A conformation with relatively large τ values is only around 6 kJ·mol^{-1} higher in energy (Figure 17, *2lf*). It is predicted that one of these conformations (as quantified in Table 3) would be found if the structure of **2** were to be accessible to X-ray crystallography. This result was obtained using the *mm2f* parameter set.[10] On applying the *mm2t*[10] parameter set, qualitatively identical conformations were obtained (Figure 17, 2*st*, 2*lt*). With the force field approach *mm2t*, the conformation with the large values for the torsion angles of the cage was found at the absolute minimum, while the other one, corresponding to small cage torsions τ, was calculated to lie 6 kJ·mol^{-1} above it. The relative energies of the two lowest-energy conformations of **2**, as calculated by the two parameter sets, are

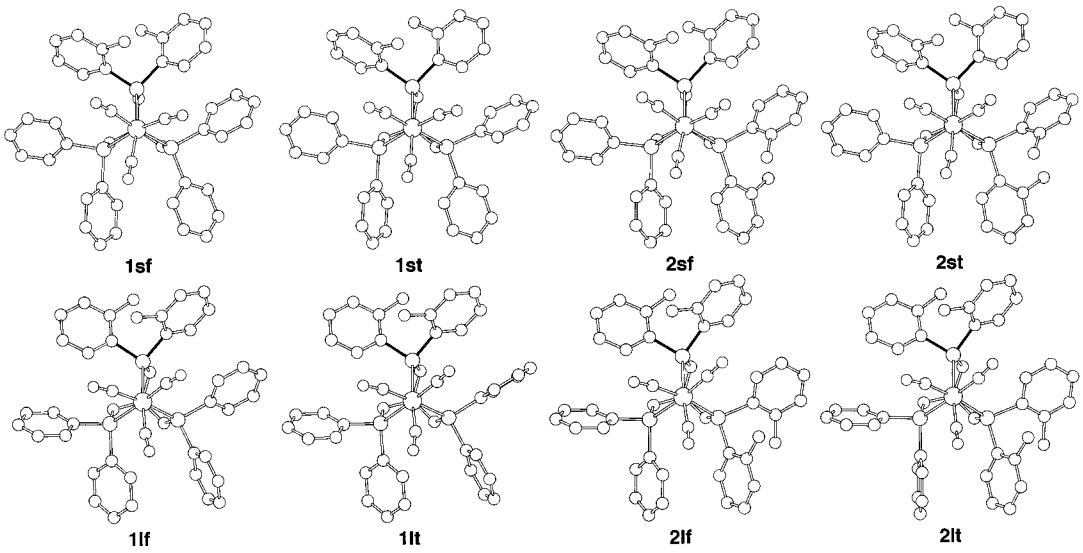


Figure 17. Lowest-energy conformations of **1** and **2** as calculated with the force field parameter sets *mm2f* and *mm2t*; the extensions *f* and *t* are used to designate the force field parameter set *mm2f* and *mm2t*, while the designators *s* and *l* refer to small and large torsions of the chelate cage

given in Table 3, together with the values quantifying these conformations.

Analysis of the racemization of the conformation corresponding to the global minimum was carried out in a similar manner as described in detail for compound **3**. The contour diagram obtained for the rotational inversion of the first P(*o*Tol)$_2$ group is very similar to that shown for **3** in Figure 14. The same types of minima and saddlepoints are observed. The energetic differentiation is, however, less pronounced than in the case of **3**. In the case of **2**, it is of relevance which of the two P(*o*Tol)$_2$ groups is selected as the first one to be subjected to the forced rotation process. Once one P(*o*Tol)$_2$ group is selected, its neighboring PAr$_2$ groups are no longer equivalent. The PPh$_2$ group is either on the left-hand or on the right-hand side of the selected fragment. This situation is reflected in the contour plot, which is no longer strictly symmetrical with respect to an idealized mirror plane lying along the diagonal.

The least-energy pathway from the global minimum coded as *aaa* in Figure 18 to its enantiomer *a′a′a′* traverses the local minima shown in Figure 18, where the meaning of the three-letter code is the same as that used for the description of **3**; due to the C_2 symmetry of the phenyl groups, only the two designators *a* and *a′* are necessary to describe the arrangement of the PPh$_2$ groups.

There is no need to actively rotate the phenyl groups; they are found to automatically orientate themselves during the minimization processes. Their reorientation is characterized by a two-ring flip transition (Figure 18, *aca*−*aa′a*). The relative energies of the corresponding minima, together with their corresponding conformational parameters and the energies of the saddlepoints en route from *aaa* to *a′a′a′* according to Figure 18, are given in Table 4.

The assignment of the individual transition processes in terms of one-ring and two-ring flip transitions given in Table 4 is also apparent from Figure 18. It is found that the highest barrier is associated with inversion of the second P(*o*Tol)$_2$ group; a barrier height of 56.5 kJ·mol^{-1} (*mm2f*) or 57.1 kJ·mol^{-1} (*mm2t*) is calculated for this step, which, within the model, characterizes the activation barrier.

Analysis of 1

The structure of **1** is not known experimentally. The low-energy conformations for **1** were calculated on a similar basis as discussed above in the case of **2**. Irrespective of the starting geometries, which were also refined as discussed for **2**, two low-energy conformations were found (*mm2f* [10]), energetically very close together (2.1 kJ·mol^{-1}) and structurally differentiated in the same way as described for **2**. These conformations were also found with *mm2t* as the force field, albeit with interchanged relative energies.

One of the calculated low-energy conformations of **1** has small torsions τ of the chelate cage and a left helical arrangement of the aryl groups (Figure 17, 1*sf*, 1*st*; Table 3). The other one has large τ values with the helicity of the aryl "propeller" being, in principle, right-handed (Figure 17, 1*lf*, 1*lt*; Table 3). The contour plot for the local enantiomerization of the P(*o*Tol)$_2$ group is again qualitatively similar to that shown for **3** and is of course symmetrical due to the mirror plane along the diagonal of this type of diagram. The calculated energies are somewhat lower than those obtained for **2**, which are in turn lower than those calculated for **3**. This is a consequence of the decreasing steric strain on descending the sequence **3**, **2**, **1**. Detailed analysis of the racemization pathway was performed as extensively as described for **3**. In contrast to the observations made for **2**, the phenyl groups do not completely adapt to the rearrangement at the P(*o*Tol)$_2$ group and have hence to be actively driven in the final step. The lowest-energy pathway for the racemization of **1** is qualitatively analogous to those described for **3** and **2**.

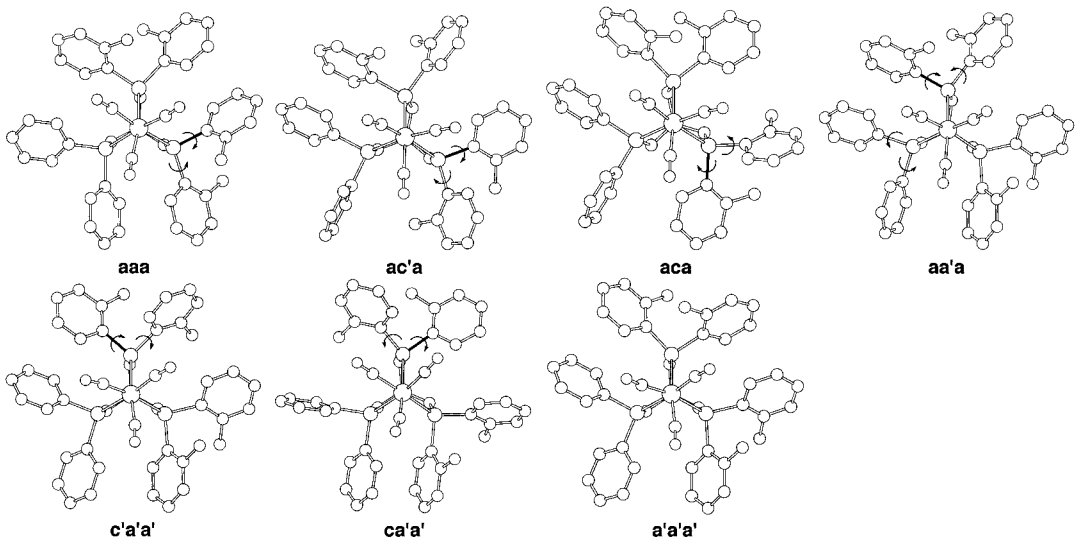


Figure 18. Sequence of rotational processes along the enantiomerization pathway of **2**

Table 4. Conformations of **2** characterized by their φ and τ values (*mm2f* parameter set)

i	*ring flip*	E_{rel}(TS) [kJ·mol^{-1}]	E_{rel} [kJ·mol^{-1}]	Codon[a] P1P2P3	φ_1 [°]	φ_2 [°]	φ_3 [°]	φ_4 [°]	φ_5 [°]	φ_6 [°]	τ_1 [°]	τ_2 [°]	τ_3 [°]
–	–	–	0.0	**aaa**	40	–135	38	–136	35	50	6	8	10
3	1-r. f.	53.8	28.5	**ac'a**	28	–154	118	130	10	32	24	12	2
3	2-r. f.	50.4	24.1	**aca**	36	121	–148	–117	15	25	–22	–30	–36
4	1-r. f.	50.3	11.4	**aa'a**	33	–143	124	–36	24	41	14	2	0
1	1-r. f.	**56.5**	21.7	**c'a'a'**	126	145	125	–37	–45	–36	–5	–3	–7
1	2-r. f.	51.3	28.5	**ca'a'**	–130	–118	154	–28	–32	–10	–12	–24	2
2	1-r. f.	52.5	0.0	**a'a'a'**	136	–38	135	–40	–50	–35	–8	–6	–10

[a] For the meaning of the designators, see the text and Figure 18.

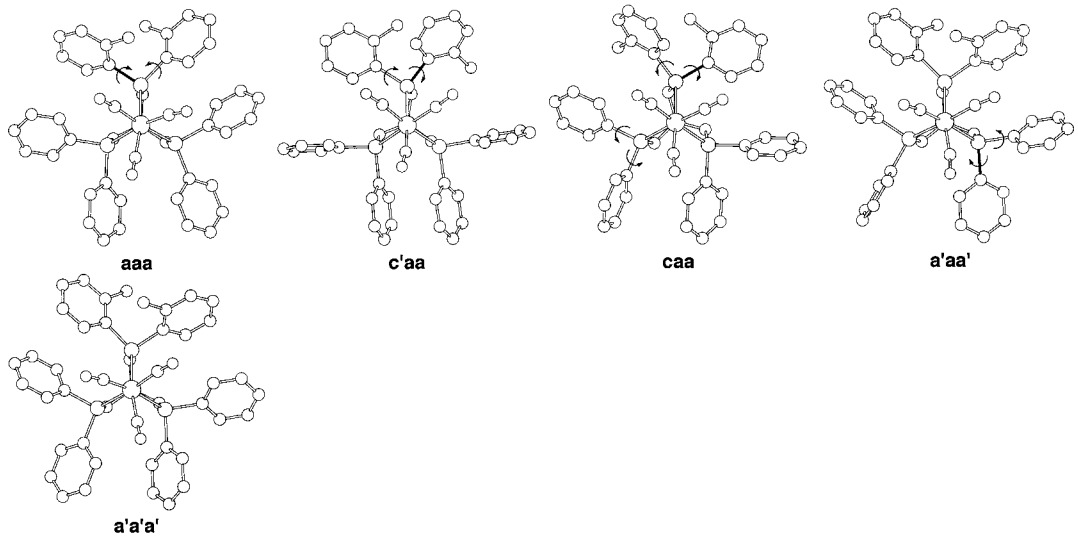


Figure 19. Sequence of rotational processes along the enantiomerization pathway of **1**

Figure 19 illustrates the local minima encountered along this pathway. The energies of these minima, together with those of the saddlepoints separating them, are given in Table 5. The highest barrier dominating the process as a whole is found at 53.1 kJ·mol^{-1} (*mm2f*) or 44.0 kJ·mol^{-1} (*mm2t*).

Table 5. Conformations of **1** characterized by their φ and τ values (*mm2f* parameter set)

i	*ring flip*	E_{rel}(TS) [kJ·mol^{-1}]	E_{rel} [kJ·mol^{-1}]	Codon[a] P1P2P3	φ_1 [°]	φ_2 [°]	φ_3 [°]	φ_4 [°]	φ_5 [°]	φ_6 [°]	τ_1 [°]	τ_2 [°]	τ_3 [°]
–	–	–	0.0	**aaa**	38	–135	35	50	37	49	7	11	9
1	1-r. f.	42.0	22.2	**c'aa**	116	128	9	27	20	6	16	3	27
2	2-r. f.	**53.1**	22.3	**caa**	–150	–116	21	42	19	41	–28	–37	–30
2	1-r. f.	42.9	3.4	**aaa'**	138	–36	30	64	–5	–21	–11	–18	–27
4	1-r. f.	9.6	0.0	**a'a'a'**	135	–38	–49	–37	–50	–35	–7	–9	–11

[a] For the meaning of the designators, see the text and Figure 19.

Table 6. Comparison between calculated and measured activation barriers for **1**–**3**

Compound	ΔH_{calc} [kJ·mol^{-1}] *mm2f*	ΔH_{calc} [kJ·mol^{-1}] *mm2t*	$\Delta G^{\neq}_{298K}$ [kJ·mol^{-1}] NMR	$\Delta H^{\neq}$ [kJ·mol^{-1}] NMR	$\Delta S^{\neq}$ [J·K^{-1}·mol^{-1}] NMR
1	53.1	44.0	54.3	45.3	–30
2	56.5	57.1	57.9	51.8	–20
3	69.2	61.1	65.5	59.3	–21

Comparison of Calculated and Measured Activation Barriers

Comparison of the calculated activation barriers with those observed for **1**–**3** provides a means of assessing the quality of the force field approach and especially of assessing the appropriateness of the energy scale produced by the force field approach.[24] It has previously been shown that the force field approach used is capable of correctly reproducing NOE distances in a series of compounds.[12] The best one can do in this respect is to use the energies calculated by the force field as the basis to produce a Boltzmann weighted average. Even though $\Delta G^{\neq}$ values would be necessary to make this approach a physically correct one, $\Delta H^{\neq}$ values, as obtained by the force field approach, are still the best and only choice one has. The fact that the NOE distances calculated by this approach are in close agreement with the observed values indicates that the calculated $\Delta H^{\neq}$ values are somehow on scale with the $\Delta G^{\neq}$ values.[12]

The results obtained for the activation energies of **1**–**3** using the force field approach appear highly satisfying in this respect (Table 6). Irrespective of the type of force field used (*mm2f*, *mm2t*), the activation energies are predicted to increase with increasing steric congestion on ascending the series **1**, **2**, **3**. The energies given by the force field approach do not contain entropy terms and thus have to be compared with the $\Delta H^{\neq}$ values as the experimental counterpart. Using the *mm2f* parameter set, the predicted energies are equal to the experimental values with a maximum deviation of 10 kJ·mol^{-1}; based on the *mm2t* set of parameters, the maximum deviation is only around 5 kJ·mol^{-1} (Table 6). With either parameter set, the ranking of the compounds in order of increasing activation barriers is correctly predicted. Indeed, the agreement between calculated and experimental values is as good as might be hoped for using a force field approach. This may be taken as a further confirmation of the validity of the approach taken to derive the force field parameters.

Conclusion

1. *Tripod* compounds $CH_3C(CH_2PPh_2)_{3-n}[CH_2P(o\text{-}Tol)_2]_nMo(CO)_3$ ($n = 1-3$) undergo conformational enantiomerization with activation barriers $\Delta H^{\neq}$ between 45 and 59 kJ·mol^{-1}. The barriers increase with increasing number of P(oTol)$_2$ groups present.

2. Using a force field approach, for which the force field parameters were derived by global optimization on the basis of all the structural information available,[10] reaction pathways for these enantiomerization processes have been delineated. The activation barriers predicted by this approach are in close agreement with the experimental values.

3. The approach of deriving force field parameters by global optimization over a complete basis of molecular structures[10][11] is capable of predicting conformations and conformational energy differences in agreement with experimental findings.

Experimental Section

General Remarks: All manipulations were carried out under an argon atmosphere at 20°C by means of standard Schlenk techniques, unless mentioned otherwise. All solvents were dried by standard methods and distilled under argon. The solvents used for the NMR spectroscopic measurements were degassed by three successive "freeze-pump-thaw" cycles and were dried over 4 Å molecular sieves. The silica gel (Kieselgel p.A. 0.06–0.02 mm, J. T. Baker Chemical B.V.) used for chromatography and the Kieselgur (Kieselgur, washed, heat-treated, Erg. B.6, Riedel de Haen AG) used for filtration were degassed at 1 mbar at 20°C for 48 h and then saturated with argon. – IR: Bruker FT-IR IFS-66; CaF_2 cells. – MS(EI): Finnigan MAT 8400. – Elemental analysis: Microanalytical laboratory of the Organisch-Chemisches Institut, Universität Heidelberg. Under the conditions employed, the carbon content is often found to be too low for molybdenum-containing compounds due to the formation of non-combustible molybdenum carbide. – Melting points: Gallenkamp MFB-595 010; uncorrected values. – All chemicals were obtained commercially and were used without further purification.

NMR: NMR spectra were recorded on Bruker NMR spectrometers operating at 200, 300, and 500 MHz, respectively. Two-dimensional spectra were recorded with quadrature detection in both dimensions; TPPI was used in F_1. All information about sizes and data points of the spectra is given in real points. ^{1}H- and ^{13}C-NMR spectra were calibrated internally using the residual solvent signals (CD_2Cl_2, $\delta_H = 5.32$, $\delta_C = 53.8$; $CDCl_3$, $\delta_H = 7.24$, $\delta_C = 77.0$) and tetramethylsilane (TMS, $\delta = 0$) as an external standard; ^{31}P-NMR chemical shifts are given in ppm relative to 85% H_3PO_4 ($\delta = 0$) as an external standard. Assignment of all the ^{1}H, ^{13}C, and ^{31}P resonances was accomplished by a combination of 1D and 2D NMR experiments (DQF-COSY,[13] TOCSY,[14] NOESY,[15] {^{1}H-^{13}C}-HSQC,[16] {^{1}H-^{13}C}-HMBC,[17] {^{1}H-^{31}P}-HMBC;[17] see Tables 12−14, Figure 20). For NMR analysis, saturated solutions of the compounds in CD_2Cl_2 (**1**, **2**) and $CDCl_3$ (**3**) were prepared in precision NMR tubes on a vacuum line; the tubes were flame-sealed after deoxygenation by repeated evacuation followed by readmission of argon (minimum of three freeze/pump/thaw cycles). The experimental set-ups for the various experiments are outlined in Tables 7 and 8. While compounds **1** and **2** were analyzed by a combination of all the available methods (Table 7), analysis of **3** had to be limited to a subset of these methods as indicated in Table 8.

The temperature was calibrated using a [D_4]methanol (99.8%) NMR thermometer[25] in the low-temperature range (−100°C to 30°C) and ethylene glycol at higher temperatures (20−180°C).[26] Temperatures were kept constant to within ±0.2 K (DRX500) and ±1 K (DRX300, DPX200, AC200). As judged from the calibration with [D_4]methanol, the actual sample temperatures were accurate to within approximately ±1 K. Various parameters relating to the equipment used and the experimental set-ups are given in Tables 9−11, while ^{31}P-NMR data of **1**−**3** are given in Table 12.

A matrix representation of the different types of cross-correlation signals observed for **3** is presented in Figure 20.

Tables 13 and 14 show ^{13}C- and ^{1}H-NMR data of **1** and **2**, together with the correlations used for assignment and analysis.

Experiments and Analyses: The assignments were made according to standard procedures, the salient details of which are given in Tables 12−14 and Figure 20. Rate constants were estimated using three different approaches, the most straightforward of these involving determination of the coalescence temperature. This type of experiment was performed at different field strengths and by using both ^{1}H- and ^{31}P-NMR spectroscopy (Tables 1 and 10). A somewhat more extended range of temperatures was covered by EXSY experiments based on exchange signals between pairs of different types of protons; these were also performed at different field strengths (Tables 1 and 11). The most extensive range of temperatures was covered by line-shape analysis of the ^{31}P-NMR signals. This type of experiment was, of course, limited to compounds **1** and **2** owing to the constitutional C_3 symmetry of **3**. Again, different field strengths were used for these experiments (Tables 1, 10, and 12). The quality of fit obtained is exemplified by the case of **2** in Figure 10. All the rate constants for **1** and **2** obtained by line-shape analysis were used to construct an Eyring plot in each case. Considering the error statistics, the enthalpy and entropy values obtained by this procedure would seem to be quite accurate (**1:** $R^2 = 0.998$, $\Delta H^{\neq} = 45.3 \pm 0.4$ kJ·mol^{-1}, $\Delta S^{\neq} = -30 \pm 1$ J·K^{-1}·mol^{-1}; **2:** $R^2 = 0.995$, $\Delta H^{\neq} = 51.8 \pm 0.7$ kJ·mol^{-1}, $\Delta S^{\neq} =$

Table 8. Set-up for 2D NMR experiments on **3**

	2D NMR experiment		
	DQF-COSY	TOCSY	NOESY
Pulse program[a]	cosyphdq.au	mlev17ph.au	noesyph.au
Temperature [K]	259	259	259
Instrument	AC200	AC200	AC200
Spectral width F_2 [Hz]	1639.34	1639.34	1639.34
Time domain F_2 [Word]	2 K	2 K	2 K
Size F_2 [Word]	2 K	2 K	2 K
Spectral width F_1 [Hz]	1639.34	1639.34	1639.34
Time domain F_1 [Word]	256	128	256
Size F_1 [Word]	512	512	1 K
Scans	32	48	48
Mixing time [ms]	-	170	400
Relaxation delay [s]	1.5	1.0	2.0

[a] The acronyms in this row refer to pulse sequences supplied under these names for the Bruker series of instruments.

Table 9. Equipment used for the DNMR experiments

Spectrometer	Temperature control unit	Cooling	NMR frequency [MHz]		
			^{1}H	^{31}P	^{13}C
DRX500	BVT3000	N_2 evaporator	500.130	202.456	125.758
DRX300	BVT3300	N_2 exchanger	300.130	121.495	75.468
DPX200	BVT3300	N_2 exchanger	200.130	81.014	50.323
AC200	BVT1000	N_2 evaporator	200.130	81.026	50.330

Table 7. Set-up for 2D NMR experiments on **1** and **2**

	2D NMR experiment											
	{^{1}H–^{13}C}-HSQC		{^{1}H–^{13}C}-HMBC		{^{1}H–^{31}P}-HMBC		DQF-COSY		TOCSY		NOESY	
Pulse program[a]	invigstp		inv4gslplrnd		inv4gslrnd		cosyphdq.au		mlev17ph.au		noesytp	
Compound	**1**	**2**	**1**	**2**	**1**	**2**	**1**	**2**	**1**	**2**	**1**	**2**
Temperature [K]	212	224	212	224	212	224	211	219	211	219	226	224
Instrument	DRX500	DRX300	DRX500	DRX300	DRX500	DRX300	AC200	AC200	AC200	AC200	DRX500	DRX500
Spectral width F2 [Hz]	3360.22	2042.48	3443.53	2069.54	3443.53	2069.54	1582.28	1683.50	1582.28	1683.50	3501.40	3415.30
Time domain F2 [Word]	4 K	2 K	4 K	2 K	4 K	4 K	2 K	2 K	2 K	2 K	1 K	4 K
Size F2 [Word]	2 K	2 K	2 K	1 K	2 K	2 K	4 K	4 K	2 K	2 K	1 K	2 K
Spectral width F1 [Hz]	2389.72[b]	4981.47[b]	16349.80	9811.69	1720.88	1032.71	1582.28	1683.50	1582.28	1683.50	3501.40	3415.30
Time domain F1 [Word]	256	256	512	512	128	128	512	256	256	256	128	128
Size F1 [Word]	1 K	1 K	1 K	1 K	1 K	1 K	1 K	1 K	512	1 K	1 K	1 K
Scans	32	38	30	24	24	24	32	48	32	48	32	24
Mixing time [ms]	-	-	70	50	60	60	-	-	125	200	600	200
Relaxation delay [s]	1.5	2.0	1.5	1.5	1.5	1.5	1.4	1.6	1.5	1.8	1.8	2.0

[a] The acronyms in this row refer to pulse sequences supplied under these names for the Bruker series of instruments. − [b] Folded in F1 dimension.

Table 10. Set-up for variable-temperature 1D NMR experiments on **1**−**3**

Compound	^{1}H NMR frequency	Temperature range [K] static[a]		dynamic[b]			^{31}P{^{1}H} NMR spectra[c]			^{1}H NMR spectra[c]		
							Spectral width	Time domain	Scans	Spectral width	Time domain	Scans
	[MHz]	T	(n)	T	(n)	[ΔT]	[Hz]	[Word]		[Hz]	[Word]	
1	500	206–226	(3)	270–300	(6)	[3/5/10]	10162.6	32 K	200	3472.2	32 K	16
	300	203–224	(3)	263–293	(5)	[5/10]	3655.0	16 K	200	2083.3	16 K	16
	200	165–206	(5)	216–313	(16)	[3/5/10]	2435.7	8 K	200	1436.8	16 K	16
2	500	206–241	(5)	270–307	(9)	[3/5]	10162.6	32 K	200	3472.2	32 K	16
	300	198–224	(4)	234–322	(14)	[5/10]	3655.0	16 K	200	2097.3	16 K	16
	200	221–253	(4)	258–304	(9)	[3/5/10]	5668.9	16 K	200	1398.2	16 K	16
3	200	158–261	(6)	278–343	(6)	[10]	8928.6	16 K	750	1639.4	32 K	64

[a] The number of spectra taken in the specified temperature range at intervals of ≈10 K is given in brackets (*n*). − [b] The number of spectra taken in the specified temperature range is given in brackets (*n*); square brackets: temperature increments used [Δ*T*]. − [c] A relaxation delay of 2 s was used throughout.

Table 11. Set-up for EXSY experiments on **1**−**3**

	Compound								
	1			**2**			**3**		
Frequency [MHz]	500	300	200	500	300	200	200	200	200
Temperature [K]	226.4	211.7	221.1	223.9	218.4	226.9	296.6	268.2	261.4
Spectral width F_1/F_2 [Hz]	3501.4	2042.5	1398.2	3415.3	2042.5	1388.9	1639.3	1639.3	1639.3
Time domain F_2 [Word]	1 K	2 K	1 K	4 K	2 K	2 K	2 K	2 K	2 K
Size F_2 [Word]	1 K	1 K	1 K	2 K	1 K	1 K	2 K	2 K	2 K
Time domain F_1 [Word]	128	128	128	128	128	128	256	256	256
Size F_1 [Word]	1 K	1 K	1 K	1 K	1 K	1 K	1 K	1 K	1 K
Scans	32	24	32	24	32	24	32	32	48
Mixing time [ms]	100/600	100–200[a]	10–300[b]	200	75/200	200	100	200	400
Relaxation Delay [s]	1.8	2.0	1.7	2.0	1.6	1.8	1.8	1.5	2.0

[a] 3 spectra were taken with mixing times of 100, 150, and 200 ms. − [b] 6 spectra were taken with mixing times of 10, 20, 50, 100, 200, and 300 ms.

-20 ± 2 J·K^{-1}·mol^{-1}; the limits given refer to the estimated standard deviation σ in each case; Table 1). Since ^{31}P-NMR line-shape analysis was not possible for **3**, the basis for estimating activation parameters was inferred from coalescence and EXSY data (Tables 1, 10, and 11). With only six available data points (Table 1), the statistical accuracy of the estimated parameter values is somewhat lower than those obtained for **1** and **2** on the basis of the data obtained by line-shape analysis (**3**: $R^2 = 0.986$, $\Delta H^{\neq} = 59.3 \pm 3.5$ kJ·mol^{-1}, $\Delta S^{\neq} = -21 \pm 12$ J·K^{-1}·mol^{-1}; limits refer to σ; Table 1). In order to get some appraisal of the mutual agreement between the data obtained by the three different techniques, the complete set of data obtained for **1** and **2**, irrespective of the acquisition procedure (line-shape analysis, EXSY spectroscopy, coalescence measurements) was also used to construct Eyring plots. Based on the complete set of data, $\Delta H^{\neq}$ and $\Delta S^{\neq}$ as estimated for **1** ($R^2 = 0.995$, $\Delta H^{\neq} = 45.7 \pm 0.5$ kJ·mol^{-1}, $\Delta S^{\neq} = -29 \pm 2$ J·K^{-1}·mol^{-1}; limits refer to σ; Table 1) are in excellent agreement with the values obtained from line-shape analysis alone (see above, Table 1). Apply-

Table 12. ^{31}P-NMR data for compounds **1**−**3**

Compound	*T* [K]	δ(P1)	δ(P2)	δ(P3)	$^2J_{P1P2}$ [Hz]	$^2J_{P1P3}$ [Hz]	$^2J_{P2P3}$ [Hz]
1	313[a]	21.91 t	—— 16.40 d ——		—— 22.79 ——		
	205	20.75 dd	16.15 dd	13.91 dd	29.04	17.76	25.04
2	322[a]	—— 21.79 d ——		16.06 t		—— 22.73 ——	
	198	19.67 dd	20.37 dd	13.99 dd	23.09	29.07	18.27
3	343	20.79 s					
	210	18.40 s					

[a] High-temperature limit, coalescence of **1**: P2/P3, **2**: P1/P2.

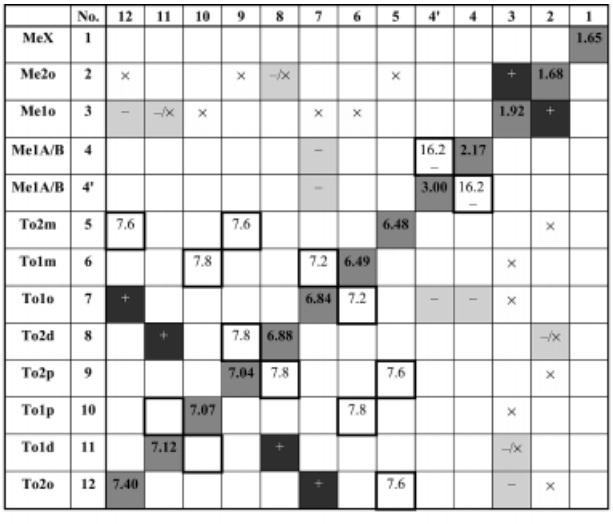


Figure 20. Matrix-type representation of the ^{1}H-NMR data of **3**; the meanings of the designators are as described for Figure 4; along the diagonal: chemical shifts; off-diagonal: H−H coupling constants (numbers); DQF-COSY cross-peaks bold framed, TOCSY cross-peaks (×), NOE cross-peaks light grey (−), EXSY cross-peaks dark grey (+); the data refer to a solution of **3** in $CDCl_3$ at 261 K (due to the low solubility and with the available equipment, exact ^{13}C-NMR data of **3** could not be obtained).

Table 13. ^{1}H- and ^{13}C{^{1}H}-NMR data of **2**; the meaning of symbols is as in Figure 3

	NMR Spectra			Correlations			Data for quaternary carbons		
No	Nucleus[a]	δ(^{13}C)[b]	δ(^{1}H)[c]	NOESY	EXSY	HMBC	No	Nucleus[a]	δ(^{13}C)[b]
1	**MeX**	40.13 q (9.6)	1.51 bs	Me1/2/3A/B		6/7/8/30	**30**	**Npq**	37.50 q (7.2)
2	**Me4o**	21.35[d] d (~2)	1.58 s	To4d/To3o/Me2B	Me1o	2/14/11//3238			
3	**Me2o**	21.22[d] d (~2)	1.70 s	Me1B/A/To2d		3/8/12/31/37	**31**	**Me2o$_{ipso}$**	132.10 dd (26.7/3.2)
4	**Me3o**	21.81[e] d (8.9)	1.74 s	To3d		4/9/10/15/34/39			
5	**Me1o**	21.58[e] d (9.5)	2.04 s	To1d/To2o	Me4o	5/13/21/33/40	**32**	**Me4o$_{ipso}$**	133.98 dd (27.1/4.4)
6'	**Me3B**	31.02 m (~10)	2.05 dd (16.0)[f]	Ph6o/Ph5o	Me3A	7/8/30//3536			
7'	**Me2B**	35.62 m (~10)	2.25 dd (15.6)[f]	Me4o/Me2A	Me1A	1/6/30/32	**33**	**Me1o$_{ipso}$**	134.06 dd (29.3/4.6)
8'	**Me1B**	34.33 m (~10)	2.41 dd (15.3)[f]	Me2o	Me2A	1/7/30/31			
8	**Me1A**	34.33 m (~10)	2.48 dd (15.3)[f]	Me2o/To1o/Ph6o	Me2B	6/7/30/31/33	**34**	**Me3o$_{ipso}$**	134.58 dd (32.8/4.7)
6	**Me3A**	31.02 m (~10)	2.64 dd (16.0)[f]	Ph5o/m/Me3B	Me3B	1/8/30/35			
7	**Me2A**	35.62 m (~10)	2.73 dd (15.6)[f]	To3o/Me2B	Me1B	6/8/30/32/34	**35**	**Ph5$_{ipso}$**	138.76 dd (26.5/5.9)
8	**To2m**	124.20 d (16.4)	6.11 pt (7.8/7.4)		To3m	3/12/16/29/31/37			
9	**To3o**	126.49 d (4.3)	6.22 pt (7.2)[f]	Me2A/Me4o	To2o	4/17/39	**36**	**Ph6$_{ipso}$**	139.88 d (2.9)
10	**To3m**	124.46 d (6.0)	6.41 pt (7.1/7.8)		To2m	9/15/17/34/39			
11	**To4m**	125.42 d (16.3)	6.60 pt (7.8/7.5)		To1m	2/14/20/28/32/38	**37**	**To2$_{ipso}$**	139.89 dd (32.5/5.9)
12	**To2d**	131.74 d (3.7)	6.86 d (7.6)	Me2o		3/8/31/37			
13	**To1m**	124.55 d (5.4)	6.89 m (7.4)[g]			21	**38**	**To4$_{ipso}$**	139.92 d (2.3)
14	**To4d**	131.44 bs	6.93 m (7.5)[g]	Me4o		2/11			
15	**To3d**	131.08 d (6.6)	6.95 m[g]	Me3o		4/10/34	**39**	**To3$_{ipso}$**	140.14 d (13.5)
16	**To2p**	129.41 s	6.97 m (7.4)[g]			29/37			
17	**To3p**	127.49 s	6.98 m (7.8)[g]			9/39	**40**	**To1$_{ipso}$**	141.10 d (14.3)
18	**To1o**	129.76 d (~2)	7.01 m[f][g]		To4o	24/40			
19	**Ph5m**	128.36 d (8.9)	7.10 m[g]			19/26/35			
20	**To4p**	129.59 s	7.14 m (7.5)[g]		To1p	14/28/38			
21	**To1d**	131.47 d (3.7)	7.14 m (7.2)[g]	Me1o		5/13/33			
22	**Ph6m**	128.10 d (9.2)	7.22 m (~7)[g]			36			
23	**Ph6p**	128.79 s	7.22 m (~7)[g]			36			
24	**To1p**	128.65 s	7.23 m (7.4/7.2)[g]		To4p	13/18/33/40			
25	**Ph5p**	128.96 s	7.24 m[g]			26/35			
26	**Ph5o**	130.80 d (12.9)	7.40 pt (7.8)[f]	Me3A/B	Ph6o	25/26/35			
27	**Ph6o**	130.22 d (12.3)	7.49 pt (6.8)[f]	Me3A/B/Me1A	Ph5o	23/27/36			
28	**To4o**	138.62 d (34.1)	7.57 dd (7.6)[f]		To1o	2/14/20/38			
29	**To2o**	138.98 d (35.3)	7.72 dd (7.8)[f]	Me1o	To3o	3/12/16/37			

[a] The numbering scheme refers to Figure 3 with the following addenda: MeX denotes the carbon atom of the methyl group on the ligand backbone; Npq refers to the quaternary carbon atom of the neopentane backbone; Meαo_{ipso} refers to the carbon atoms of the *o*-tolyl group α (α = 1−4) bearing the methyl substituent; Toα_{ipso} denotes the corresponding *ipso* carbon atom of the *o*-tolyl groups, while Phβ_{ipso} (β = 5−6) analogously denotes the *ipso* carbon atoms of the phenyl groups. − [b] $^nJ_{CP}$ in Hz is given in brackets. − [c] $^{2/3}J_{HH}$ in Hz is given in brackets. − [d] $^1J_{CH}$ = 127.1 Hz. − [e] $^1J_{CH}$ = 127.8 Hz. − [f] $^nJ_{HP}$ = 5.1 Hz (Me3B); 8.7 Hz (Me2B); 8.4 Hz (Me1B); 5.9 Hz (Me1A); 10.4 Hz (Me3A); 6.7 Hz (Me2A); 8.3 Hz (To3o); 7.7 Hz (To1o); 8.8 Hz (Ph5o); 7.9 Hz (Ph6o); 17.3 Hz (To4o); 17.5 Hz (To2o). − [g] Signals of individual groups overlap; $^3J_{HH}$ coupling constants were determined by DQF-COSY experiments.

ing an analogous procedure to the complete set of data for **2** leads to an estimate of $\Delta H^{\neq}$ (R^2 = 0.990, $\Delta H^{\neq}$ = 48.7 ± 0.7 kJ·mol^{-1}; limits refer to σ; Table 1) in satisfying agreement with the value derived from the line-shape analysis data alone. The estimated activation entropy, however, is about 10 J·K^{-1}·mol^{-1} more negative ($\Delta S^{\neq}$ = −31 ± 3 J·K^{-1}·mol^{-1}; limits refer to σ; Table 1) than that obtained by using data solely from the line-shape analysis (see above, $\Delta S^{\neq}$ = −20 ± 2 J·K^{-1}·mol^{-1}; limits refer to σ; Table 1). This discrepancy between the $\Delta S^{\neq}$ values estimated on the basis of the two different data sets (line-shape analysis data alone vs. augmented data set) is close to the three σ limit, which is conventionally used to discriminate between equality or inequality of the statistical distribution that two items are subject to. It is thus found that, within the appropriate confidence interval, the two different approaches used generate estimates which, as expected, can be taken as equal. As judged from the scatter of data, the activation parameters derived from line-shape analysis alone are the most reliable, and hence these data have been quoted for **1** and **2** wherever appropriate in the text; Table 1 contains both types of estimates. To sum up, it appears that the line-shape analysis produces the most reliable data. It is felt that the data derived from EXSY measurements are less reliable, where different types of biases may result from overlap of peaks along the diagonal, NOE contributions, and loss of polarization during different delays. Likewise, coalescence data do not appear to be as reliable as the data obtained from line-shape analysis in the specific cases studied. Estimating the coalescence temperature is a procedure which is subject to personal judgement. Coupling between the coalescing nuclei makes this process even more subject to human error.

Finally, it is felt that the NMR work reported herein has some importance beyond the specific chemistry studied in this paper since the utility and reliability of three NMR techniques for the assessment of rate constants have been compared in the analysis of one and the same problem.

Force Field Calculations: Programs and parameters have been described previously,[10] as have the protocols of the individual computational procedures.[12] Details relating to the scanning of the hypersurface are given explicitly in the text. All computations were performed on a Silicon Graphics Indigo^2 MIPS R4400 workstation, 200 MHz, 128 MB RAM, operating under IRIX 5.3. Graphical representations of hypersurfaces were obtained using the *plot2D* option of MacroModel.[27]

Synthetic Procedures

1-[Bis(*o*-tolyl)phosphanyl]-3-(diphenylphosphanyl)-2-(diphenylphosphanylmethyl)-2-methylpropane (1a): To a solution of 1.3 g (2.8 mmol) of 1-chloro-2-bis(diphenylphosphanylmethyl)propane[28] in DMSO (50 mL), 730 mg (3.4 mmol) of bis(*o*-tolyl)phosphane and 380 mg (3.4 mmol) of KO*t*Bu were added and the mixture was stirred for 3 h at 130°C. The reaction mixture was worked-up hydrolytically by adding water (50 mL) and then neutralizing

Table 14. ^{1}H- and ^{13}C{^{1}H}-NMR data of **1**; the meaning of symbols is as in Figure 2

	NMR spectra			Correlations			Data for quaternary carbons		
No	Nucleus[a]	δ(^{13}C)[b]	δ(^{1}H)[c]	NOESY	EXSY	HMBC	No	Nucleus[a]	δ(^{13}C)[b]
1	MeX	39.43 q (9.2)	1.46 bs			4/5/6/27	27	Npq	36.60 q (6.5)
2	Me2o	21.15[d] d (2.3)	1.51 s	To2d	Me1o	2/8/11/29/34			
3	Me1o	21.15[d] d (8.6)	1.77 s	To1d	Me2o	3/7/9/12/28/34	28	Me1o$_{ipso}$	133.52 dd (4.9/31.8)
4	Me3A	30.59 pt (12.5)	1.82 dd (15.6)[e]		Me2B	5/6/27/31/33			
5	Me2A	33.87 pt (12.3)	2.02 dd (14.9)[e]	Ph3o	Me3B	4/6/27/30/32	29	Me2o$_{ipso}$	134.13 dd (3.3/26.0)
6'	Me1B	34.38 pt (11.1)	2.17 pt (15.2)[e]		Me1A	1/4/27/29			
6	Me1A	34.38 pt (11.1)	2.51 dd (15.2)[e]	To1o	Me1B	4/5/27/28/29	30	Ph4$_{ipso}$	137.50 dd (4.0/26.7)
5'	Me2B	33.87 pt (12.3)	2.60 ddd (14.9)[e]		Me3A	1/6/27/30/32			
4'	Me3B	30.59 pt (12.5)	2.76 ddd (15.6)[e]	Ph6o	Me2A	1/5/27/31/33	31	Ph6$_{ipso}$	137.91 dd (6.0/25.8)
7	To1o	126.31 dd (1.0/3.6)	6.03 pt (7.3)[e]	Me1A/B/Me2o	To2o	3/13/34			
8	To2m	124.65 d (16.3)	6.26 pt (7.4)		To1m	11/15/26/29/34	32	Ph3$_{ipso}$	138.30 dd (6.5/33.4)
9	To1m	124.4 d (6.3)1	6.47 pt (7.4)		To2m	7/12/13/28/34			
10	Ph4m	127.58 d (9.2)	6.86 pt (7.5)		Ph5m	10/14/23/30	33	Ph5$_{ipso}$	138.47 dd (6.5/33.4)
11	To2d	131.63 d (4.6)	6.92 d (7.5)	Me2o		2/8/15/29/34			
12	To1d	130.67 d (8.3)	6.96 dd (7.5)[e]	Me1o		3/9/28/34	34	To2$_{ipso}$	139.52 d (1.7)
13	To1p	127.44 s	7.02 pt (7.3)			7/9/28/34			
14	Ph4p	128.65 s	7.07 d (6.8)		Ph5p	10/23	35	To1$_{ipso}$	140.02 d (13.8)
15	To2p	129.56 s	7.08 d (7.3)			26/29/34			
16	Ph5m	127.78 d (9.5)	~7.17 m (7.6)[f]		Ph4m	16/20/33			
17	Ph6m	128.33 d (8.9)	~7.20 m (7.6)[f]		Ph3m	17/25/31			
18	Ph5p	128.41 bs	~7.23 m[f]		Ph4p	20			
19	Ph6p	128.99 s	~7.31 m[f]			25			
20	Ph5o	130.04 d (12.6)	7.32 m (7.8)[e][f]			18/20			
21	Ph3p	128.76 s	~7.39 m[f]			22/24/32			
22	Ph3m	128.04 d (8.9)	~7.40 m[f]		Ph6m	22/24/32			
23	Ph4o	131.76 d (13.8)	7.40 m (7.7)[f]			14/23			
24	Ph3o	130.51 d (11.5)	7.58 m (7.3)[e][f]	Me2A		21/24			
25	Ph6o	130.58 d (13.5)	7.58 m (7.3)[e][f]	Me3B		19/25			
26	To2o	138.23 d (35.0)	7.64 dd (7.5)[e]	Me2A	To1o	2/15/34			

[a] The numbering scheme refers to Figure 2 with the following addenda: MeX denotes the carbon atom of the methyl group at the backbone of the ligand; Npq refers to the quaternary carbon atom of the neopentane backbone; Meαo$_{ipso}$ refers to the carbon atoms of the *o*-tolyl group α (α = 1−2) bearing the methyl substituent; Toα$_{ipso}$ denotes the corresponding *ipso* carbon atom of the *o*-tolyl groups, while Phβ$_{ipso}$ (β = 3−6) analogously denotes the *ipso* carbons of the phenyl groups. − [b] $^nJ_{CP}$ in Hz is given in brackets. − [c] $^{2/3}J_{HH}$ in Hz is given in brackets. − [d] $^1J_{CH}$ = 126.9 Hz. − [e] $^nJ_{HP}$ = 2.6 Hz (Me3A); 2.2 Hz (Me2A); 12.7 (Me1B); 4.8 Hz (Me1A); 10.7 Hz (Me2B); 11.2 Hz (Me3B); 8.2 Hz (To1o); 4.2 Hz (To1d); 10.4 Hz (Ph5o); 9.7 Hz (Ph3o/Ph6o); 17.7 Hz (To2o). − [f] Signals of individual groups overlap; $^3J_{HH}$ coupling constants were determined by DQF-COSY experiments.

with 37% aq. HCl. The product was extracted with diethyl ether (4 × 50 mL) and the combined organic phases were dried and concentrated in vacuo. The resulting pasty residue was purified by column chromatography on silica gel (20 cm, Ø = 5 cm) using petroleum ether (40/60)/diethyl ether (9:1) as eluent (TLC control, R_f = 0.50) to yield 1.7 g (2.7 mmol, 95%) of ligand **1a** as a colorless oil.

1-[Bis(*o*-tolyl)phosphanyl]-3-(diphenylphosphanyl)-2-(diphenylphosphanylmethyl)-2-methylpropanetricarbonylmolybdenum (1): To a solution of 1.7 g (2.7 mmol) of **1a** in CH_2Cl_2 (50 mL), 815 mg (2.7 mmol) of solid $(MeCN)_3Mo(CO)_3$[29] was added and the mixture was stirred for 2 h at room temperature. During the course of the reaction, the $(MeCN)_3Mo(CO)_3$ slowly dissolved and the color of the solution turned from light-yellow to yellow-brown. The solvent was then removed to leave a brown solid. The crude product was purified by column chromatography on silica gel (10 cm, Ø = 4 cm) using a mixture of petroleum ether (40/60)/CH_2Cl_2 (1:3) as eluent (TLC control: R_f = 0.75) to afford 1.5 g (1.8 mmol, 67%) of **1** as a light-yellow microcrystalline solid. The product was recrystallized from CH_2Cl_2. − IR (CH_2Cl_2): $\tilde{\nu}$ = 1936 (s, CO), 1844 (br. s, CO). − MS(EI); *m/z* (%): 834 (10) [M^+], 806 (12) [M^+ − CO], 778 (40) [M^+ − 2 CO], 750 (30) [M^+ − 3 CO].

1,1,1-Tris[bis(*o*-tolyl)phosphanylmethyl]ethane (3a): 3.87 g (18 mmol) of bis(*o*-tolyl)phosphane[30] was dissolved in DMSO (25 mL) and deprotonated at 0°C by adding 2.02 g (18 mmol) of KO*t*Bu. After warming to room temperature, the deep-red solution was stirred for 1 h. A solution of 0.92 g (5.25 mmol) of 1-chloro-2,2-dichloromethylpropane in DMSO (25 mL) was then slowly added and the resulting mixture was refluxed for 5 h. The mixture was then cooled to room temperature and the DMSO was evaporated in vacuo. The residue was hydrolyzed by adding degassed water (50 mL). After stirring for 16 h, **3a** was extracted with diethyl ether (4 × 50 mL). The combined organic phases were dried over $MgSO_4$ and filtered. Evaporation of the solvent afforded 2.3 g (3.2 mmol, 62%) of **3a** as a white powder; m.p. 176°C. − ^{1}H NMR ($CDCl_3$): δ = 1.1 (s, 3 H, CqCH_3), 2.4 (m, 24 H, ArCH_3, CH_2P), 7.10−7.33 (m, 24 H, arom. H). − ^{13}C NMR ($CDCl_3$): δ = 20.8 (s, Ar*C*H$_3$), 21.3 (s, Ar*C*H$_3$), 42.5 (m, Cq), 125.0−142.2 (m, arom. C). − ^{31}P NMR ($CDCl_3$): δ = −50.9 (s). − MS (FAB); *m/z* (%): 708 (32) [M^+], 617 (100) [M^+ − (*o*-tolyl)], 495 (16) [M^+ − P(*o*-tolyl)$_2$].

1,1,1-Tris[bis(*o*-tolyl)phosphanylmethyl]ethanetricarbonylmolybdenum (3): 708 mg (1 mmol) of the ligand **3a** was dissolved in CH_2Cl_2 (30 mL) and this solution was added to 333 mg (1.1 mmol) of solid $(CH_3CN)_3Mo(CO)_3$[29] at 20°C. The resulting mixture, which immediately turned dark, was stirred for 48 h. Petroleum ether (40/60) (6 mL) was then added and the mixture was filtered through silica gel (2 cm) and Kieselgur (1 cm), resulting in a yellow eluent. Evaporation of the solvent and drying of the residue in vacuo for 48 h afforded 835 mg (0.94 mmol, 94%) of **3** as a pale-yellow powder. A reagent tube filled with a concentrated solution of **3** in CH_2Cl_2 was placed in a Schlenk tube containing a bottom layer of diethyl ether. Vapour diffusion of the diethyl ether at room temperature yielded pale-yellow crystals suitable for X-ray structural analysis within one day.[10] − IR ($CHCl_3$): $\tilde{\nu}$ = 1932 (s, CO), 1835 (br. s, CO). − ^{1}H NMR ($CDCl_3$): δ = 1.65 (m, 3 H, CqCH_3), 1.75−2.0 (m, 18 H, ArCH_3), 2.0−3.0 (br. m, 6 H, CH_2P), 6.5 (m, 6 H, arom. H), 6.8−7.5 (m, 18 H, arom. H). − ^{13}C NMR ($CDCl_3$):

δ = 22.31 (m, Ar*C*H$_3$), 23.22 (m, Ar*C*H$_3$), 38.9 (m, *C*H$_2$P), 42.0 (m, Cq), 125.0−141.3 (m, arom. C), 220 (s, CO). − ^{31}P NMR (CDCl$_3$): δ = 20.0 (s).

Acknowledgments

The financial support by the Deutsche Forschungsgemeinschaft (SFB 247, Normalverfahren HU 151/24-1, /29-1) and the Fonds der Chemischen Industrie is gratefully acknowledged. We are indebted to Mr. T. Jannack for performing mass spectrometric measurements and to the staff of the Microanalytisches Labor of the Organisch-Chemisches Institut, Heidelberg, for providing microanalyses. We wish to acknowledge the early inspiration by the Deutsches Museum, München.

[1] G. Frenking, I. Antes, M. Boehme, S. Dapprich, A. W. Ehlers, V. Jonas, A. Neuhaus, M. Otto, R. Stegmann, A. Veldkamp, S. F. Vyboishchikov, in: *Reviews in Computational Chemistry*, vol. 8 (Eds.: K. B. Lipkowitz, D. B. Boyd), VCH Publishers, Inc., New York, **1996**, chapter 2.
[2] L. J. Bartolotti, K. Flurchick, in: *Reviews in Computational Chemistry*, vol. 7 (Eds.: K. B. Lipkowitz, D. B. Boyd), VCH Publishers, Inc., New York, **1996**, chapter 4.
[3] N. L. Allinger, *J. Am. Chem. Soc.* **1977**, *99*, 8127−8134.
[4] U. Burkert, N. L. Allinger, *Molecular Mechanics*, ACS monograph, Washington DC, **1992**.
[5] P. Comba, T. W. Hambley, *Molecular Modelling of Inorganic Compounds*, VCH, Weinheim, **1995**.
[6] B. J. Hay, *Coord. Chem. Rev.* **1993**, *126*, 177−236.
[7] C. R. Landis, D. M. Root, T. Cleveland, in: *Reviews in Computational Chemistry*, vol. 6 (Eds.: K. B. Lipkowitz, D. B. Boyd), VCH Publishers, Inc., New York, **1995**, chapter 2.
[8] S. Beyreuther, J. Hunger, G. Huttner, S. Mann, L. Zsolnai, *Chem. Ber.* **1996**, *129*, 745−757.
[9] G. Huttner, S. Beyreuther, J. Hunger, in: *Software-Entwicklung in der Chemie 10* (Ed.: J. Gasteiger), GDCH, Frankfurt, **1996**, p. 201−207.
[10] J. Hunger, S. Beyreuther, G. Huttner, K. Allinger, U. Radelof, L. Zsolnai, *Eur. J. Inorg. Chem.* **1998**, 693−702.
[11] J. Hunger, G. Huttner, *J. Comput. Chem.* **1999**, *20*, 455−471.
[12] S. Beyreuther, J. Hunger, S. Cunskis, T. Diercks, A. Frick, E. Planker, G. Huttner, *Eur. J. Inorg. Chem.* **1998,** 1641−1653.
[13] [13a] U. Piantini, O. W. Sørensen, R. R. Ernst, *J. Am Chem. Soc.* **1982**, *104*, 6800−6801. − [13b] M. Rance, O. W. Sørensen, G. Bodenhausen, G. Wagner, R. R. Ernst, K. Wüthrich, *Biochem. Biophys. Res. Commun.* **1983**, *117*, 479−485.
[14] [14a] L. Braunschweiler, R. R. Ernst, *J. Magn. Res.* **1983**, *53*, 521−528. − [14b] A. Bax, D. G. Davis, *J. Magn. Res.* **1985**, *65*, 355−360.
[15] J. Jeener, B. H. Meier, P. Bachmann, R. R. Ernst, *J. Chem. Phys.* **1979**, *71*, 4546−4563.
[16] [16a] G. Bodenhausen, D. J. Ruben, *Chem. Phys. Lett.* **1980**, *69*, 185−188. − [16b] L. E. Kay, P. Keifer, T. Saarinen, *J. Am. Chem. Soc.* **1992**, *114*, 10663−10665. − [16c] A. G. Palmer III, J. Cavanagh, P. E. Wright, M. Rance, *J. Magn. Res.* **1991**, *93*, 151−170. − [16d] J. Schleucher, M. Schwendinger, M. Sattler, P. Schmidt, O. Schedletzky, S. J. Glaser, O. W. Sørensen, C. Griesinger, *J. Biomol. NMR* **1994**, *4*, 301−306.
[17] A. Bax, M. F. Summers. *J. Am Chem. Soc.* **1986**, *108*, 2093−2094.
[18] [18a] G. Binsch, *J. Am. Chem. Soc.* **1969**, *91*, 1304−1309. − [18b] WIN-DYNAMICS 1.0 Release 951220, NMR Dynamic Spectra Simulation and Iteration, Bruker-Franzen Analytik GmbH and K. Il′yasov, O. Nedopekin, Bremen, Germany.
[19] G. Binsch, H. Kessler, *Angew. Chem.* **1980**, *92*, 445−463; *Angew. Chem. Int. Ed. Engl.* **1980**, *19*, 411−429.
[20] J. Sandström, *Dynamic NMR Spectroscopy*, Academic Press, London, **1982**, chapter 7.
[21] C. L. Perrin, T. J. Dwyer, *Chem. Rev.* **1990**, *90*, 935−967.
[22] J. W. Goethe, *Goethe's Werke, Vollständige Ausgabe letzter Hand*, Cottasche Buchhandlung, Stuttgart und Tübingen, **1829**, vol. 22, p. 254, Betrachtungen im Sinne der Wanderer: "Germans, and not only them, are gifted to make science incomprehensible."
[23] For the meaning of the terms "one-ring flip" and "two-ring flip", see ref.[8]
[24] The approach used (*mm2f*, *mm2t*) makes use of the well-scaled force constants of the MM2*[3] force field for the organic part of the molecules. On the other hand, the force constants describing the "inorganic interactions" have been deduced by a minimization procedure based wholly on structural information.[10][11] There is, of course, no direct reference to energetic terms in such a structural database and if the force constants derived from this database are still appropriate on the energy scale, this must result from the indirect constraints imposed on them in the course of their refinement by the dominant force field contribution of the organic part. It was expected that the force constants used for the organic part might automatically force the refinement of the inorganic force field constants to the appropriate scale, as is indeed found.[12]
[25] E. W. Hansen, *Anal. Chem.* **1985**, *57*, 2993−2994.
[26] A. L. Van Geet, *Anal. Chem.* **1970**, *42*, 679−680.
[27] MacroModel 5.0 (MM2*) (see: F. Mohamadi, N. G. J. Richards, W. C. Guida, R. Liskamp, M. Lipton, C. Caufield, G. Chang, T. Hendrickson, W. C. Still, *J. Comput. Chem.* **1990**, *11*, 440−467).
[28] G. Reinhard, R. Soltek, G. Huttner, A. Barth, O. Walter, L. Zsolnai, *Chem. Ber.* **1996**, *129*, 97−108.
[29] [29a] W. S. Tsang, D. W. Meek, A. Wojcicky, *Inorg. Chem.* **1968**, *7*, 1263−1268. − [29b] D. B. Tate, W. R. Knipple, J. M. Augl, *Inorg. Chem.* **1962**, *1*, 433−434.
[30] [30a] F. G. Mann, E. J. Chaplin, *J. Chem. Soc.* **1937**, 527−535. − [30b] G. P. Schiemenz, *Angew. Chem.* **1968**, *80*, 559−560; *Angew. Chem. Int. Ed. Engl.* **1968**, *7*, 544−545. − [30c] Ch. A. Tolman, *J. Am. Chem. Soc.* **1970**, *92*, 2956−2965.

Received July 26, 1999
[I99272]

Sulfur Compounds, 211[‡]

Gas-Phase Acidities of Nine Sulfur Oxoacids of Composition [H_2,S,O_n] (n = 1–4)

André H. Otto[a] and Ralf Steudel*[a]

Keywords: Sulfur oxo acids / Acidity / Ab initio calculations

The gas-phase acidities of the most stable conformations of nine sulfur oxo acids were determined by ab initio MO calculations at the CBS-Q, G2(MP2), and G2 levels of theory. The most accurate G2 results are as follows ($\Delta G°_{298}$ of the deprotonation reaction in kJ mol^{-1}): H–S–O–*H* 1468, *H*–S–O–H 1449, $(HO)_2S$ 1426, *H*–S(=O)OH 1406, H_2S=O 1394, H–S(=O)O*H* 1361, $(HO)_2S$=O 1324, $H_2S(=O)_2$ 1321, H_2O→S 1294, *H*–$S(=O)_2OH$ 1287, H–$S(=O)_2O$*H* 1279, $(HO)_2S(=O)_2$ 1268. These values are in excellent agreement with the few experimental data that can be considered reliable. For molecules of analogous structure, the acidity increases with increasing oxidation number of the sulfur atom. While sulfenic acid, HSO*H*, is as weak an acid as HOCl, sulfurous acid, $(HO)_2SO$, is as strong a proton donor as nitric acid, HNO_3, and sulfonic acid, *H*$S(O)_2OH$, is even stronger than hydrogen iodide, HI, surpassed only by sulfuric acid, H_2SO_4. These results are of relevance to phenomena such as acid rain and aerosol formation in the earth's atmosphere.

Introduction

Sulfur forms a large number of oxo acids, $H_xS_yO_z$, because: (a) the oxidation number(s) of the S atom(s) can vary between –1 and +6 and (b) sulfur–sulfur bonds may occur if $y > 1$.[1–3] Most of these compounds are too unstable to be isolated in pure form. Consequently, the physical and chemical properties of these nevertheless important species are not well-known, and this also holds for their acidities. Only a few experimental and theoretical data are available for the acidities in water and/or in the gas phase.

The most simple ("mononuclear") oxo acids of sulfur are of composition H_2SO_n with n ranging from 1 to 4. However, even in these cases, several isomeric forms are sometimes possible. For example, the oxidation of hydrogen sulfide, H_2S (sulfane), by oxygen atoms (produced by photolysis of ozone) in an argon matrix yields the sulfane oxide H_2S=O as well as the isomeric sulfenic acid H–S–O–H ("oxadisulfane").[4] The latter molecule was shown by ab initio MO calculations to be more stable than the former.[5] The energy barriers for the isomerisations H_2S=O → HSOH and HSOH → H_2S=O were calculated at the HF/6-31G(d) level of theory as 225 and 361 kJ mol^{-1}, respectively.[5f] The acidities of HSOH and H_2S=O, defined as the standard enthalpy change for the deprotonation reactions, were calculated at the MP4/6-311++G(d,p)//MP2(fu)/6-311++G(d,p) level of theory.[5d] At 298 K the following results were obtained (kJ mol^{-1}): 1536 for HSO*H*, 1492 for *H*SOH and 1430 for H_2S=O. The same authors determined the SH acidity of *H*SOH by mass spectrometry as 1481 ± 15 kJ mol^{-1} in very good agreement with the theoretical value.

The energy hypersurface of [H_2,S,O_2] shows stationary points for at least six structures: two conformers of the chain-like sulfur dihydroxide HOSOH, sulfinic acid HS(=O)OH, sulfane dioxide $H_2S(=O)_2$, the chain-like peroxide HSOOH, the branched superoxide H_2S→O=O and the cyclic thiadioxirane H_2S–O^a–O^b(S–O^b).[6a][6b] At the MP4/6-31G(d)//MP2(fu)/6-31G(d) level of theory, the two first-mentioned isomers are considerably more stable than all the others and the chain of C_2 symmetry is the global minimum of what is usually termed as "sulfoxylic acid". The only reliable experimental information on [H_2,S,O_2] is the mass spectrometric observation of the molecule HOSOH, which had been generated by dissociative ionisation of dimethyl sulfate, followed by neutralisation and reionisation.[7] An earlier report on the matrix isolation of sulfinic acid as a photolysis product of an HI–SO_2 mixture in solid argon[8] has been disputed because the reported infrared spectrum of the product mixture does not match the spectra calculated for various [H_2,S,O_2] isomers.[6a] The gas-phase acidities of these isomers were studied at the MP4/6-31G(d)//MP2/3-21G(*) + ZPVE level[6c] and the following $\Delta H°_{298}$ values were obtained: 1444 kJ mol^{-1} for HS(O)O*H* and 1467 kJ mol^{-1} for *H*S(O)OH. Several authors reported the absolute energies both for the acids and the corresponding anions;[6a][6h] this allows the enthalpy change for the deprotonation reaction to be calculated. From the more recent and more reliable data obtained at the MP4/6-31G(d)//MP2(fu)/6-31G(d) level,[6a] the following $\Delta H°_{298}$ values for the deprotonation may be calculated (in kJ mol^{-1}): HOSOH (C_2) 1530, HOSOH (C_s) 1519, *H*S(=O)OH 1477, HS(=O)O*H* 1450, and $H_2S(=O)_2$ 1377.

On the energy hypersurface of [H_2,S,O_3], the well-known molecules of sulfurous acid $(HO)_2S$=O and sulfonic acid

[‡] Part 210: A. Prange, I. Arzberger, C. Engemann, H. Modrow, O. Schumann, H. G. Trüper, R. Steudel, C. Dahl, J. Hormes, *Biochim. Biophys. Acta* **1999**, *1428*, 446–454.

[a] Institut für Anorganische und Analytische Chemie, Technische Universität Berlin, Sekr. C2, D-10623 Berlin, Germany
Fax: (internat.) +49 (0)30/314-26519
E-mail: steudel@schwefel.chem.tu-berlin.de

 © WILEY-VCH Verlag GmbH, D-69451 Weinheim, 2000 1434–1948/00/0404–0617 $ 17.50+.50/0

H–S(=O)$_2$OH were identified as structures of minimal energy but, in addition, a 1:1 adduct of H_2O with SO_2 exists which has also been characterised by infrared and microwave spectroscopy.[9] This adduct will not be discussed further. Here we are mainly interested in the acidities of the two mentioned acids of composition H_2SO_3. Several ab initio MO calculations have shown that gaseous sulfurous acid is more stable than sulfonic acid.[6h][10] At the G2 level of theory, including ZPE correction, the energy difference at 0 K is 41 kJ mol^{-1}.[10c] However, both acids are unstable with respect to the decomposition products H_2O and SO_2. The reaction enthalpies for this decomposition at 298 K are –18 kJ mol^{-1} for (HO)$_2$SO and –53 kJ mol^{-1} for HS(O)$_2$OH at the G2 level[10c] but –45 kJ mol^{-1} were calculated for HS(O)$_2$OH (at 270 K) at the QCISD(T)/6-311++G(d,p)//MP2/6-31G(d) level.[10d] Sulfurous acid was nevertheless observed in the vapour phase by neutralisation–reionisation mass spectrometry.[11] The molecule was generated by ionisation-induced decomposition of diethyl sulfite which loses two molecules of ethene to give (HO)$_2$SO. The fragmentation pattern on collisional activation demonstrated the connectivity of sulfurous acid.

Sulfonic acid has never been observed but its anion H–SO_3^- is well-known from salts such as $CsHSO_3$ and from aqueous solutions. The rational nomenclature for this anion containing an S–H bond is sulfonate ion but it is often termed as hydrogen sulfite or as bisulfite ion, especially in the industrial literature. The name hydrogen sulfite ion should be restricted to the isomer with the connectivity HO–SO_2^-. While solid $CsHSO_3$, according to an X-ray diffraction analysis, contains the sulfonate ion,[12] aqueous solutions of the sodium salt exhibit ^{17}O-NMR signals which can be attributed to both tautomers.[13] From the peak areas, the equilibrium quotient c(HO–SO_2^-)/c(H–SO_3^-) was found to be 4.9 ± 0.1 at 298 K in solutions of ion strength 1.0 M. These results were later confirmed by a Raman spectroscopic investigation of aqueous $NaHSO_3$ solutions.[14] Ab initio MO calculations on the two ions of composition [H,S,O$_3$]$^-$ have been carried out.[6h][15] At the G2 level, the sulfonate ion of C_{3v} symmetry is more stable, by 16 kJ mol^{-1}, than the hydrogen sulfite ion, which surprisingly is of C_1 symmetry.[10c] However, if lower levels of theory are applied, the order of stabilities may be reversed, especially if the symmetry of the hydrogen sulfite ion is restricted to C_s, as has been done in some earlier publications on this subject. Attempts to model the impact of solvation on the stability of the two anions indicated that they are still of very similar energy if dissolved in water.[15c]

The gas-phase acidities of sulfurous and sulfonic acids were studied by various authors.[6h,10b,10c] At the G2 level the deprotonation enthalpies $\Delta H°_{298}$ were calculated as follows (in kJ mol^{-1}): (HO)$_2$SO 1358, *H*S(O)$_2$OH 1323, HS(O)$_2$O*H* 1308.[10c]

Sulfuric acid, H_2SO_4, is the only sulfur oxo acid whose vapour-phase structure was determined experimentally. According to a microwave spectroscopic investigation,[16] the molecule is of C_2 symmetry which was confirmed by a number of ab initio MO calculations.[17] Several conformational (torsional) isomers were theoretically identified at higher energies. In addition, the adduct $SO_3 \cdot H_2O$ was observed by infrared spectroscopy (in matrix isolation experiments),[18] and its gas-phase structure was determined both by microwave spectroscopy[19] and by ab initio MO calculations.[17b,17c] The gas-phase acidity of sulfuric acid was derived from an investigation of the proton transfer in certain ion–molecule reactions as $\Delta G°_{368}$ = 1265 kJ mol^{-1} ($\Delta H°_{368}$ = 1295 kJ mol^{-1}).[20] This value is in excellent agreement with the results of an ab initio MO calculation: At the MP2/6-311++G(d,p)//HF/6-31+G(d) level of theory the deprotonation enthalpy ($\Delta H°$) of H_2SO_4 at 0 K was obtained as 1300 kJ mol^{-1}.[17e]

To obtain accurate gas-phase acidities for the most important of the above-mentioned species *at identical levels of theory*, we calculated the energies of nine acids HA and their corresponding anions A$^-$ at the G2 level of theory, which had formerly been shown to provide reliable acidity data for sulfur compounds, and agree with the best experimental values within ca. 8 kJ mol^{-1}.[21] In addition, the CBS-Q and G2(MP2) methods were applied to all species, since these more economical levels of theory will be used exclusively in two upcoming publications on several larger sulfur oxo acid molecules such as thiosulfuric acid, polythionic acids and polysulfuric acids. In this way a comparison of data for different acids will be possible, as well as a discussion of trends in acidities as a function of molecular structure. Since the gas-phase acidity has been defined in the literature as either $\Delta G°_{298}$ or $\Delta H°_{298}$ of the deprotonation reaction, we also calculated both values for the systems investigated.

Calculations

Ab initio molecular orbital calculations were performed at the CBS-Q,[22] G2(MP2),[23] and G2[24] levels of theory with the GAUSSIAN program system.[25] The G2 method essentially implies an energy calculation at the QCISD(T)/6-311+G(3df,2p) level using geometries optimised at the MP2(full)/6-31G(d) level. Harmonic vibrational wavenumbers were obtained at the HF/6-31G(d) level and were scaled by a factor of 0.8929. All the vibrational eigenvalues of all the molecules investigated were positive. The G2(MP2) method is a modified version of G2 but uses the second-order Møller–Plesset perturbation theory (MP2) for the basis set extension correction rather than the fourth order (MP4). The G2(MP2) method is almost as accurate as the G2 method, but at a substantially reduced computational expense. The excellent performance of these methods and also of CBS-Q in predicting gas-phase acidities of small molecules is well established.[26]

In some cases {[H$_2$,S,O$_3$] and [H$_2$,S,O$_4$]} geometries were calculated with MP2 in combination with the 6-311++G(3df,2p) basis sets. The thermal corrections (no scaling) were obtained using even this level for [H$_2$,S,O$_3$] and less expensive MP2/6-311G++(d,p) calculations for [H$_2$,S,O$_4$]. Then the energies were improved by QCISD(T)/

6-311++G(3df,2p) single point calculations. In addition to the procedures described above, the MP4/6-311++G(d,p) level of theory was applied to the smallest system [H_2,S,O] to optimise the structures.

For details of the quantum chemical methods, see ref.[27] All calculations were carried out on a Cray J90 or on a Linux workstation. To allow for the thermal corrections to the Gibbs free energy of the proton, a value of –0.010654 hartree (–28 kJ mol^{-1}) was used.

Compounds of Composition [H_2,S,O]

To obtain reliable geometries of the three acids H–S–O–H, $H_2S{=}O$, and $H_2O{\rightarrow}S$, as well as of their anions H–O–S$^-$ and H–S–O$^-$, these structures were optimised at the MP4/6-311++G(d,p) level; the results are shown in Table 1. The absolute enthalpies and Gibbs free enthalpies of the species mentioned were calculated by the CBS-Q method based on MP2/6-31G(d′) geometries as well as by the G2(MP2) and G2 methods based on MP2/6-31G(d) geometries. Vibrational wavenumbers and thermal energies were obtained at the HF/6-31G(d′) [CBS-Q] and HF/6-31G(d) [G2(MP2) and G2] levels, respectively. The results are presented in Table 2, and the relative stabilities are shown in Table 3. The stabilities of the acids decrease in the order HSOH > H_2SO > H_2OS. In the case of the anions, HOS$^-$ is more stable than HSO$^-$.

Table 1. Geometries of the acids HSOH, H_2SO, and H_2OS and of their anions HOS$^-$ and HSO$^-$, optimised at the MP4/6-311++G(d,p) level (internuclear distances in pm, bond angles and torsion angles in degrees)

Species	Symmetry	*d*(SH)	*d*(SO)	*d*(HO)	α(OSH)	α(SOH)	τ(HOSH)
HSOH	C_1	134.3	170.1	96.4	97.4	106.7	94.0
H_2SO	C_s	137.9	151.1	–	109.3	–	–
H_2OS	C_s	–	196.6	96.6	–	107.9	–
HOS$^-$	C_s	–	182.4	96.1	–	101.2	–
HSO$^-$	C_s	137.7	162.1	–	105.9	–	–

Table 2. Enthalpies and Gibbs free energies (negative a. u.) of the acids HSOH, H_2SO, and H_2OS and of their anions at 298 K

	Species	CBS-Q	G2(MP2)	G2
H°	HSOH	474.044601	474.027258	474.035959
	H_2SO	474.018747	474.001229	474.008258
	H_2OS	473.983262	473.966092	473.976418
	HOS$^-$	473.483768	473.463909	473.474246
	HSO$^-$	473.475996	473.457653	473.466741
G°	HSOH	474.072204	474.054902	474.063603
	H_2SO	474.045904	474.028399	474.035427
	H_2OS	474.011289	473.994117	474.004443
	HOS$^-$	473.510585	473.490747	473.501084
	HSO$^-$	473.502920	473.484578	473.493666

All geometrical parameters listed in Table 1 have reasonable values. The most stable isomer HSOH is an intermediate between disulfane, HSSH, and hydrogen peroxide, HOOH, and in fact the torsional angle of HSOH (τ = 94°) has a value intermediate between those which have been determined for HSSH (90°)[28] and HOOH (112°).[29] The S–O bond length of 170 pm agrees reasonably well with the experimental value in gaseous CH_3–O–S–S–O–CH_3 (165.3 pm),[30] whose S–O bonds may be considered to be standard single bonds. As expected, the SO bond in the sulfoxide $H_2S{=}O$ (151.1 pm) is much shorter, but, surprisingly, in the "water sulfide" H_2OS (196.6 pm) it is much longer. The latter may therefore be considered to be a donor–acceptor complex of a water molecule and a sulfur atom, symbolised by $H_2O{\rightarrow}S$. Remarkably, the OH bond lengths of $H_2O{\rightarrow}S$ (96.6 pm) and HSOH (96.4 pm) are practically identical, while the SH bond lengths of HSOH (134.3 pm) and $H_2S{=}O$ (137.9 pm) differ substantially. Otherwise, the pyramidal structures of H_2SO and H_2OS are similar, as can be seen from the similar bond angles HSO (109.3°) versus HOS (107.9°). The angles HSH (86.6°) and HOH (105.8°) are similar to those in H_2S (92.1°) and H_2O (104.5°).

Table 3. Relative enthalpies and Gibbs free energies (kJ mol^{-1}) of the acids HSOH, H_2SO, and H_2OS and of their anions HOS$^-$ and HSO$^-$

Species	CBS-Q		G2(MP2)		G2	
	$\Delta H°_{298}$	$\Delta G°_{298}$	$\Delta H°_{298}$	$\Delta G°_{298}$	$\Delta H°_{298}$	$\Delta G°_{298}$
HSOH	0	0	0	0	0	0
H_2SO	68	69	68	70	73	74
H_2OS	161	160	161	160	156	155
HOS$^-$	0	0	0	0	0	0
HSO$^-$	20.4	20.1	16.4	16.2	19.7	19.4

The two isomeric anions differ remarkably in their SO bond strength as indicated by the differing S–O bond lengths of 182.4 pm for the more stable isomer HOS$^-$ and 162.1 pm for HSO$^-$. The latter value suggests that the SO bond has some double-bond character.

Table 4. Gas-phase acidities (kJ mol^{-1}) of HSOH, H_2SO, and H_2OS at 298 K

Species	CBS-Q		G2(MP2)		G2	
	$\Delta H°_{298}$	$\Delta G°_{298}$	$\Delta H°_{298}$	$\Delta G°_{298}$	$\Delta H°_{298}$	$\Delta G°_{298}$
HSO*H*	1499	1467	1502	1469	1501	1468
*H*SOH	1479	1447	1485	1453	1481	1449
H_2SO	1431	1398	1433	1400	1428	1394
H_2OS	1318	1287	1325	1294	1325	1294

The acidities of the three compounds of composition [H_2,S,O] are given in Table 4, both as the reaction enthalpies and the Gibbs free reaction enthalpies of the deprotonation at 298 K. The acidities increase in the order HSO*H* < *H*SOH < H_2SO < H_2OS. The value of $\Delta H°_{298}$ = 1481 kJ mol^{-1}, obtained for *H*SOH at the G2 level, perfectly agrees with the only available experimental value (see Introduction). The fact that *H*SOH is a stronger acid than HSO*H* is due to the stronger OH bond of the latter, but also due to the higher stability of the anion HOS$^-$ which is formed on deprotonation of *H*SOH. On the other hand, H_2OS is a much stronger acid than H_2SO since the rather weak SO bond of H_2OS is turned into the rather strong SO bond in HOS$^-$. In contrast, the strong SO bond of H_2SO

changes on deprotonation to the weaker SO bond in HSO^-. Therefore, H_2SO ($\Delta G°_{298}$ = 1394 kJ mol^{-1}) is as strong a proton donor as nitrous acid HNO_2 ($\Delta G°_{298}$ = 1396 kJ mol^{-1}) while H_2OS ($\Delta G°_{298}$ = 1294 kJ mol^{-1}) is as strong as hydrogen iodide HI ($\Delta G°_{298}$ = 1294 kJ mol^{-1}).[31] The acidities obtained at the CBS-Q and G2(MP2) levels (Table 4) differ by 0.5% or less from the G2 data.

Compounds of Composition [H_2S,O_2]

The geometries of the four most stable acids of composition [H_2,S,O_2], HOSOH (C_2), HOSOH (C_s), HS(O)OH, and $H_2S(O)_2$, are well-known at the MP2(full)/6-31G(d) level[6a] and have not been refined any further in this work. The absolute enthalpies and Gibbs free enthalpies of these species of their anions $HS(O)O^-$ and $HOSO^-$ are given in Table 5; the relative stabilities are presented in Table 6. Compared to the previous work, the order of relative stabilities has not changed. The acidities of the three representative structures are shown in Table 7.

Table 5. Enthalpies and Gibbs free energies (negative a. u.) of the acids HOSOH, $H_2S(O)_2$, and HS(O)OH, and of their anions $HOSO^-$ and HSO_2^-, at 298 K

	Species	Symmetry	CBS-Q	G2(MP2)	G2
	HOSOH	C_2	549.187809	549.161874	549.172641
	HOSOH	C_s	549.185684	549.160021	549.170764
$H°$	$H_2S(O)_2$	C_{2v}	549.168559	549.140765	549.149404
	HS(O)OH	C_1	549.180762	549.154377	549.163664
	$HOSO^-$	C_1	548.632001	548.604945	548.617037
	HSO_2^-	C_1	548.653483	548.625411	548.635399
	HOSOH	C_2	549.217689	549.191849	549.202616
	HOSOH	C_s	549.216266	549.190699	549.201442
$G°$	$H_2S(O)_2$	C_{2v}	549.197793	549.170047	549.178686
	HS(O)OH	C_1	549.210937	549.184628	549.193914
	$HOSO^-$	C_1	548.662513	548.635543	548.647635
	HSO_2^-	C_1	548.682752	548.654719	548.664707

Table 6. Relative enthalpies and Gibbs free energies (kJ mol^{-1}) of the acids HOSOH, $H_2S(O)_2$, and HS(O)OH, and of their anions $HOSO^-$ and HSO_2^- at 298 K

Species	CBS-Q		G2(MP2)		G2	
	$\Delta H°_{298}$	$\Delta G°_{298}$	$\Delta H°_{298}$	$\Delta G°_{298}$	$\Delta H°_{298}$	$\Delta G°_{298}$
HOSOH (C_2)	0	0	0	0	0	0
HOSOH (C_s)	5.6	3.7	4.9	3.0	4.9	3.1
$H_2S(O)_2$	50.5	52.2	55.4	57.2	61.0	62.8
HS(O)OH	18.5	17.7	19.7	19.0	23.6	22.8
HSO_2^-	0	0	0	0	0	0
$HOSO^-$	56.4	53.1	53.7	50.3	48.2	44.8

Table 7. Gas-phase acidities (kJ mol^{-1}) of HOSOH, $H_2S(O)_2$, and HS(O)OH at 298 K

Species	CBS-Q		G2(MP2)		G2	
	$\Delta H°_{298}$	$\Delta G°_{298}$	$\Delta H°_{298}$	$\Delta G°_{298}$	$\Delta H°_{298}$	$\Delta G°_{298}$
HOSOH	1465	1426	1468	1430	1465	1426
$H_2S(O)_2$	1359	1324	1359	1325	1356	1321
HS(O)O*H*	1391	1359	1395	1363	1393	1361
*H*S(O)OH	1447	1412	1449	1414	1442	1406

The most stable isomer HOSOH (C_2 symmetry) is of lowest acidity ($\Delta G°_{298}$ = 1426 kJ mol^{-1}), comparable to hydrogen cyanide, HCN ($\Delta G°_{298}$ = 1420 kJ mol^{-1}). The chain of C_s symmetry is by only 3 kJ mol^{-1} less stable and therefore of practically identical acidity. The asymmetric species HS(O)OH is, by 23 kJ mol^{-1}, less stable than HOSOH (C_2). The OH acidity of this acid ($\Delta G°_{298}$ = 1361 kJ mol^{-1}) is, by 45 kJ mol^{-1}, higher than its SH acidity. This is because the anion $HS(O)O^-$ is more stable than $HOSO^-$. The least stable of the isomers considered here, the tetrahedral molecule $H_2S(=O)_2$ ($\Delta G°_{298}$ = 1321 kJ mol^{-1}) is as strong an acid as trifluoroacetic acid, CF_3COOH ($\Delta G°_{298}$ = 1324 k] mol^{-1}). No experimental acidity data on [H_2,S,O_2] compounds are available for comparison, but it is obvious now that the acidities based on the earlier MP4/6-31G(d)//MP2(fu)/6-31G(d) calculations which were mentioned in the Introduction are too low by 55–90 kJ mol^{-1}.

Sulfurous Acid, $(HO)_2SO$, and Sulfonic Acid, $HS(O)_2OH$

Although sulfurous acid is mentioned in all inorganic chemistry textbooks, its gas-phase geometry has never been studied on a correlated level of theory. The best previous data for $(HO)_2SO$ and $HS(O)_2OH$ are those by Squires,[10b] calculated with the HF/6-31++G(d,p) basis set. The situation for the anions is better: their geometries were determined at the MP2/6-311+G(2df,p) level.[10c] Therefore, we have optimised the structures of the two acids and their anions at the MP2/6-311++G(3df,2p) level. The results are shown in Table 8 The bond lengths of the acids differ by up to 2%, the bond angles by up to 3° and the torsion angles by up to 6° from the best previous data.

The molecule $(HO)_2SO$ can exist as two conformers which both have positive vibrational eigenvalues at all levels of theory investigated. These species are termed as *syn,syn* (**1a**) and *syn,anti* (**1b**) to indicate the orientation of the OH groups (see Figure 1). Their molecular symmetries are C_s and C_1, respectively. The cage-like molecule **1a** represents the global minimum on the energy hypersurface, but **1b** is only slightly less stable (Table 9).

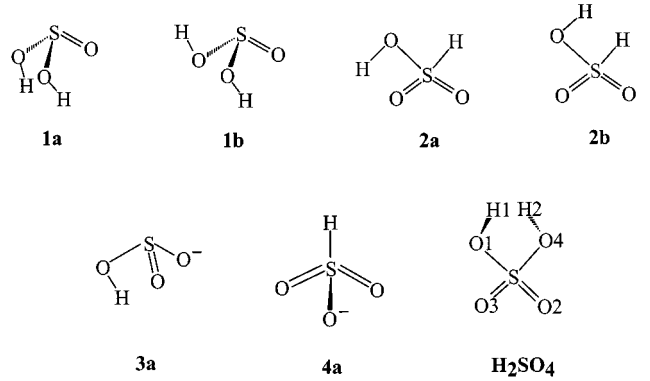


Figure 1. Conformation of the acids of composition [H_2,S,O_3] and of their anions, as well as numbering of atoms in the H_2SO_4 molecule

In a similar fashion, the molecule $HS(O)_2OH$ exists as a *syn* (**2a**) and an *anti* conformer (**2b**) which both are of C_1 symmetry. However, **2b** has one negative eigenvalue of the

Table 8. Geometries of the acids $(HO)_2SO$ and $HS(O)_2OH$, and of their anions $HOSO_2^-$ and HSO_3^-, optimised at the MP2/6-311++G(3df, 2p) level (internuclear distances in pm, bond angles and torsion angles in °)

Species	Symmetry	*d*(H1O1)	*d*(H2O3)	*d*(SH1)	*d*(SO1)	*d*(SO2)	*d*(SO3)	α(SO1H1)	α(SO3H2)	α(O1SO2)	α(O1SO3)	τ(H1O1SO2)	τ(H1O1SO3)	τ(H2O3SO2)
1a, $(HO)_2SO$	C_s (*syn*, *syn*)	97.2	97.2		161.9	145.4	161.9	107.9	107.9	105.8	105.5	20.4	89.6	–89.6
1b, $(HO)_2SO$	C_1 (*syn*, *anti*)	96.8	97.2		163.9	144.2	162.0	108.6	108.3	102.3	98.7	–178.0	71.0	–36.3
2a, $HS(O)_2OH$	C_1 (*syn*)		96.8	133.9	141.9	142.8	158.8		108.3	123.6	108.1			–12.5
3a, $HOSO_2^-$	C_1 (*syn*)	96.8			175.3	147.5	148.9	99.9		102.8	98.7	–107.6	8.6	
4a, HSO_3^-	C_{3v}			135.4	145.8	145.8	145.8			114.6				

Table 9. Enthalpies and Gibbs free energies (negative a. u.) of the acids $(HO)_2SO$ and $HS(O)_2OH$ and of their anions $HOSO_2^-$ and HSO_3^- at 298 K

	Species	Symmetry	CBS-Q	G2(MP2)	G2	QCISD(T)
	1a, $(HO)_2SO$	C_s (*syn*, *syn*)	624.356818	624.321537	624.332814	624.266937
	1b, $(HO)_2SO$	C_1 (*syn*, *anti*)	624.355635	624.320072	624.331614	624.265569
H°	**2a**, $HS(O)_2(OH)$	C_1 (*syn*)	624.345341	624.308397	624.319712	624.254688
	3a, $HOSO_2$	C_1 (*syn*)	623.842567	623.805453	623.818487	623.751103
	4a, HSO_3	C_{3v}	623.851352	623.811820	623.824084	623.757324
	1a, $(HO)_2SO$	C_s (*syn*, *syn*)	624.389897	624.354714	624.365991	624.300412
	1b, $(HO)_2SO$	C_1 (*syn*, *anti*)	624.388558	624.353148	624.364690	624.298709
G°	**2a**, $HS(O)_2(OH)$	C_1 (*syn*)	624.377507	624.340561	624.351876	624.286837
	3a, $HOSO_2^-$	C_1 (*syn*)	623.876716	623.838523	623.851120	623.784615
	4a, HSO_3^-	C_{3v}	623.881168	623.841713	623.853977	623.787285

Table 10. Relative enthalpies and Gibbs free energies (kJ mol^{-1}) of the acids $(OH)_2SO$ and $HS(O)_2OH$ and of their anions $HOSO_2^-$ and HSO_3^-

Species	CBS-Q		G2(MP2)		G2		QCISD(T)	
	$\Delta H°_{298}$	$\Delta G°_{298}$	$\Delta H°_{298}$	$\Delta G°_{298}$	$\Delta H°_{298}$	$\Delta G°_{298}$	$\Delta H°_{298}$	$\Delta G°_{298}$
1a, $(HO)_2SO$	0	0	0	0	0	0	0	0
1b, $(HO)_2SO$	3.1	3.5	3.8	4.1	3.2	3.4	3.6	4.5
2a, $HS(O)_2OH$	30	33	34	37	34	37	32	36
3a, $HOSO_2^-$	21.8	11.7	16.7	8.4	15.8	7.5	16.3	7.0
4a, HSO_3^-	0	0	0	0	0	0	0	0

Hesse matrix if the vibrational data are calculated at the MP2(full)/6-31G(d) level. At the MP2/6-311++G(d,p) level all eigenvalues are positive, but the lowest wavenumber is only 12 cm^{-1}. Furthermore, the MP2/6-311++G(3df,2p) energy of **2b** was found to be higher, by 6 kJ mol^{-1}, than that of **2a** (at 0 K without ZPE correction). Therefore, the species **2b** will not be considered further. The relative enthalpies and Gibbs free enthalpies are listed in Table 10.

Deprotonation of **1a** and **1b** may theoretically result in two conformations of the anion $HOSO_2^-$, but only one (**3a** in Figure 1) has all eigenvalues positive. This species is of C_1 symmetry. Deprotonation of **2a** at the oxygen atom results in the C_{3v} symmetric anion HSO_3^- (**4a**) which is more stable than **3a** (Table 10).

The gas-phase acidities of sulfurous and sulfonic acids were calculated before,[6h][10] but only ΔH values were given. Our data in Table 11 agree with the previous results, but in addition we present $\Delta G°$ values as well as the results obtained at the QCISD(T) level. There is a very good agreement between these different levels of theory. We therefore trust that the theoretical data are reliable; the following data of sulfurous acid **1a** seem to be the best: $\Delta H°_{298} = 1361$, $\Delta G°_{298} = 1326$ kJ mol^{-1}. An experimental deprotonation enthalpy of $\Delta G°_{298} = 1377 \pm 13$ kJ mol^{-1} was reported by Squires.[10b] However, this author already discussed the possibility that the decomposition of sulfurous acid during the mass spectrometric measurement may be responsible for the deviation of the experimental value from his theoretical result ($\Delta H°_{298} = 1380$ kJ mol^{-1}) obtained at the MP4(sdq)/6-31++G(d,p)//HF/6-31++G(d,p) level.

Table 11. Gas-phase acidities (kJ mol^{-1}) of $(HO)_2SO$ and $HS(O)_2OH$ at 298 K

Species	CBS-Q		G2(MP2)		G2		QCISD(T)	
	$\Delta H°_{298}$	$\Delta G°_{298}$	$\Delta H°_{298}$	$\Delta G°_{298}$	$\Delta H°_{298}$	$\Delta G°_{298}$	$\Delta H°_{298}$	$\Delta G°_{298}$
$(HO)_2SO$	1355	1320	1361	1327	1358	1324	1361	1326
$HS(O)_2O\mathit{H}$	1303	1275	1310	1282	1307	1279	1312	1284
$\mathit{H}S(O)_2OH$	1326	1287	1327	1290	1322	1287	1328	1291

As the data in Table 11 show, the acidity of sulfurous acid matches that of trifluoroacetic acid ($\Delta G°_{298} = 1324$ kJ mol^{-1}) and that of nitric acid HNO_3 ($\Delta G°_{298} = 1330$ kJ mol^{-1}), while sulfonic acid is even stronger: the SH acidity is comparable to that of hydrogen iodide, HI, ($\Delta G°_{298} = 1294$ kJ mol^{-1}) and the

OH acidity is close to that of metaphosphoric acid, HPO_3 ($\Delta G°_{298}$ = 1270 kJ mol^{-1}).[31]

Sulfuric Acid, H_2SO_4

The highest level of theory at which the acidity of H_2SO_4 has been studied previously was MP2/6-311++G(d,p)//6-31+G(d).[17e] Structure calculations were carried out at the MP2(full)/6-31+G(d)[17c] and MP2/6-311+G(d,p)[32] levels of theory. In addition, density functional calculations at the B3LYP/6-311++G(2d,2p) level were published.[33] We have recalculated the structure at the MP2/6-311++G(3df,2p) level, and compare the results with the experimental structure in Table 12. There is a remarkably good agreement between the two sets of data. The bond lengths differ by less than 1%, and the bond angles by less than 1.5°. Only the two torsion angles HOSO deviate by ca. 8° from the experimental values. The geometrical parameters of the hydrogen sulfate anion calculated at the same level are also given in Table 12.

Table 12. Calculated geometry of H_2SO_4 (C_2) and of its anion HSO_4^- (C_s, *trans*) optimised at the MP2/6-311++G(3df, 2p) level; comparison with the experimental structure (internuclear distances in pm, bond angles and torsion angles in degrees); for numbering of atoms, see Figure 1

	H_2SO_4 calc.	H_2SO_4 exp.[a]	HSO_4^- calc.
d(H1O1)	96.8	97(1)	96.3
d(SO1)	158.3	157(1)	166.1
d(SO2)	141.9	142(1)	145.4
d(SO3)	141.9	142(1)	145.4
d(SO4)	158.3	157(1)	144.6
α(SO1H1)	108.7	108.5(1.5)	104.3
α(O1SO2)	108.8	108.6(0.5)	104.1
α(O1SO4)	102.1	101(1)	101.3
α(O2SO3)	124.3	123(1)	113.7
α(O2SO4)	105.3	106.4(0.5)	115.6
τ(H1O1SO2)	28.7	21(1)	59.7
τ(H1O1SO4)	–82.3	–91(1)	–59.7

[a] Ref.[16]

The energies of H_2SO_4 and its monoanion were calculated by the standard CBS-Q, G2(MP2), and G2 methods (Table 13). However, it was found that the minimal energy conformation of the anion depends on the basis set. At the MP2(fu)/6-31G(d) [G2] level a conformation of C_1 symmetry was found as the global minimum. At the higher levels MP2/6-31G(d′) [CBS-Q], MP2/6-311++G(d,p), and MP2/6-311++G(3df,2p), the only energy minimum found was that of a structure of C_s symmetry, characterised by a *trans* configuration of the four atoms HOSO located in the plane of symmetry. Therefore, the energies of H_2SO_4 and HSO_4^- were also calculated at these levels. To check whether the calculated acidities can be improved further, we carried out QCISD(T)/6-311++G(3df,2p) energy calculations. However, the results were practically identical with those at the G2 and G2(MP2) levels. These calculated acidities of H_2SO_4 at 298 K perfectly agree with the experimental value measured at 368 K (Table 14).

Table 13. Enthalpies and Gibbs free energies (negative a. u.) of H_2SO_4 and of its anion HSO_4^- at 298 K

	Species	Symmetry	CBS-Q	G2(MP2)	G2	QCISD(T)
H°	H_2SO_4	C_2	699.513641	699.467221	699.481180	699.400683
	HSO_4^-	C_s (*trans*)	699.021094			698.905698
	HSO_4^-	C_1		698.971814	698.986743	
G°	H_2SO_4	C_2	699.547213	699.501036	699.514996	699.434332
	HSO_4^-	C_s (*trans*)	699.055240			698.939772
	HSO_4^-	C_1		699.006334	699.021262	

Table 14. Gas-phase acidities (kJ mol^{-1}) of H_2SO_4 at 298 K

	CBS-Q	G2(MP2)	G2	QCISD(T)	exp.[a]
$\Delta H°_{298}$	1299	1307	1305	1306	1295 ± 11
$\Delta G°_{298}$	1264	1271	1268	1270	1265 ± 10

[a] Ref.[20]

Discussion

In Figure 2, the acidities of the nine investigated oxo acids of sulfur are listed and compared with the acidities of well-known inorganic and simple organic proton donors. The weakest of the

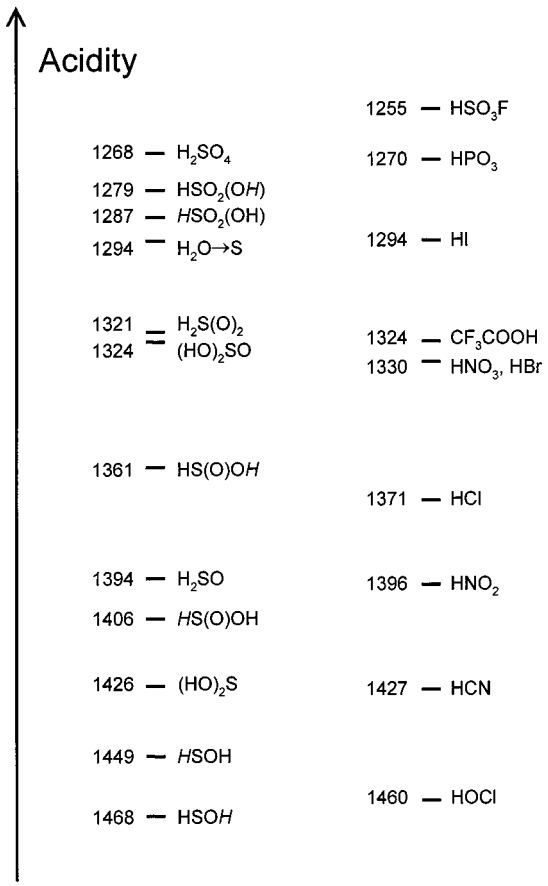


Figure 2. Gas-phase acidities of the sulfur oxo acids [$H_2S_nO_n$] (n = 1–4) relative to the acidities of other inorganic and organic proton donors; the values of $\Delta G°_{298}$ (kJ mol^{-1}) for the deprotonation reaction are given

sulfur acids (sulfenic acid HSO*H*) is as weak a proton donor as HOCl, while sulfuric acid is the strongest of the sulfur oxo acids investigated in this work.

From Figure 2 it can be seen that there is no simple relationship between the oxidation number of the sulfur atom and the OH or SH acidities. The oxidation numbers vary between 0 and +6. However, if only compounds that are structurally related are compared, a clear trend is seen, namely that higher acidities are found with increasing sulfur oxidation number (or number of oxygen atoms). This is demonstrated by the examples shown in Table 15.

Table 15. Influence of the number of oxygen atoms on the gas-phase acidities of sulfur oxo acids

Series (n = 0–2)	Species	$\Delta G°_{298}$ [kJ mol^{-1}]
$H_2S(=O)_n$	H_2S	1443
	$H_2S{=}O$	1394
	$H_2S(=O)_2$	1321
$(HO)_2S(=O)_n$	$(HO)_2S$	1426
	$(HO)_2S{=}O$	1324
	$(HO)_2S(=O)_2$	1268
$HS(=O)_nOH$	*H*SOH	1449
	*H*S(=O)OH	1406
	*H*S(=O)$_2$OH	1287

A surprising result of this study is the rather high acidities of some of the so-called lower oxo acids of sulfur, such as sulfurous acid $(HO)_2SO$ and, in particular, of sulfonic acid, $HS(O)_2OH$, which is almost as strong as sulfuric acid. Even the S*H* acidity of this acid is higher than that of all the hydrogen halides. In the vapour phase these two oxo acids are unstable with respect to H_2O and SO_2, but their formation in the earth′s atmosphere (acid rain) and in certain industrial processes is out of question, since the anions $HOSO_2^-$ and HSO_3^- are stable and these must be in equilibrium with the corresponding acids. If any of the two acids is formed from the corresponding anion, its decomposition into H_2O and SO_2 may be hindered by a substantial energy barrier, as the mass spectrometric observation of $(HO)_2SO$[11] demonstrates.

Several authors have tried to model the behaviour of sulfur oxo acids in water by calculating these molecules inside of or connected to a cluster of water molecules.[33][34] It seems that this is a promising procedure to obtain acidities for aqueous solutions by purely theoretical methods. We will report such calculations on the lower oxo acids of sulfur in a separate publication.

Summary

Nine sulfur oxo acids of composition $[H_2,S,O_n]$ with n = 1–4 were investigated by ab initio MO calculations at the CBS-Q, G2(MP2), and G2 levels of theory, to obtain the enthalpies and Gibbs free energies of the deprotonation reactions in the gas phase at 298 K. As expected, sulfuric acid is the strongest and sulfenic acid HSO*H* is the weakest proton donor. The OH acidity of sulfonic acid, $HS(O)_2OH$, is only slightly lower than that of sulfuric acid, while sulfurous acid, $(HO)_2SO$, is about as strong as nitric acid, $HONO_2$, or hydrogen bromide, HBr. The elusive water → sulfide, $H_2O \rightarrow S$, is also a strong proton donor, comparable to hydrogen iodide, HI. These results are of relevance to the chemistry of sulfur compounds in the earth's atmosphere, where species such as H_2S are oxidised by oxygen atoms, hydrogen peroxide or ozone to give various oxo acids of sulfur. Their acidity then determines the interaction with water molecules which may result in the formation of acid rain and aerosols.[35]

Acknowledgments

This work was supported by the Deutsche Forschungsgemeinschaft, the Verband der Chemischen Industrie and the Konrad-Zuse-Zentrum für Informationstechnologie Berlin.

[1] R. Steudel, *Chemie der Nichtmetalle*, 2nd ed., de Gruyter, Berlin, **1998**.
[2] Greenwood-Earnshaw, *The Chemistry of the Elements*, 2nd ed., Butterworth-Heinemann, Oxford, **1997**.
[3] Holleman-Wiberg, *Lehrbuch der Anorganischen Chemie*, 101st ed., de Gruyter, Berlin, **1995**.
[4] R. R. Smardzewski, M. C. Lin, *J. Chem. Phys.* **1977**, *66*, 3197–3204.
[5] [5a] H. Wallmeier, W. Kutzelnigg, *J. Am. Chem. Soc.* **1979**, *101*, 2804–2814. – [5b] S. Besnainou, J. L. Whitten, *J. Am. Chem. Soc.* **1980**, *102*, 7444–7448. [5c] M. Solà, C. Gonzales, G. Tonachini, H. B. Schlegel, *Theor. Chim. Acta* **1990,** *77*, 281–287. – [5d] R. A. J. O'Hair, C. H. DePuy, V. M. Bierbaum, *J. Phys. Chem.* **1993**, *97*, 7955–7961. – [5e] A. Goumri, J.-D. R. Rocha, D. Laakso, C. E. Smith, P. Marshall, *J. Chem. Phys.* **1994**, *101*, 9405–9411. – [5f] M. Solà, J. Mestres, R. Carbó, M. Duran, *J. Am. Chem. Soc.* **1994**, *116*, 5909–5915.
[6] [6a] T. Steiger, R. Steudel, *J. Mol. Struct. (THEOCHEM)* **1992**, *257*, 313–323. – [6b] F. Jensen, *J. Org. Chem.* **1992**, *57*, 6478–6487. – [6c] D. Laakso, P. Marshall, *J. Phys. Chem.* **1992**, *96*, 2471–2474. – For older studies on certain isomers of H_2SO_2 see: [6d] R. J. Boyd, A. Gupta, R. F. Langler, S. P. Lownie, J. A. Pincock, *Can. J. Chem.* **1980**, *58*, 331–338. – [6e] P. L. M. Plummer, T. S. Chen, K. Y. Law, *Atmospheric Environment* **1984**, *18*, 2769–2774. – [6f] F. Jensen, C. S. Foote, *J. Am. Chem Soc.* **1988**, *110*, 2368–2375. – [6g] Y. Watanabe, N. Kuriki, K. Ishiguro, Y. Sawaki, *J. Am. Chem. Soc.* **1991**, *113*, 2677–2682. – [6h] H. Basch, T. Hoz, in: *The Chemistry of Sulfonic Acids, Esters, and their Derivatives* (Eds.: S. Patai, Z. Rappoport), Wiley, London, **1991**, p. 1–62.
[7] A. J. Frank, M. Sadilek, J. G. Ferrier, F. Turecek, *J. Am. Chem. Soc.* **1997**, *119*, 12343–12353.
[8] M. A. Fender, Y. M. Sayed, F. T. Prochaska, *J. Phys. Chem.* **1991**, *95*, 2811–2814.
[9] [9a] A. Schriver, L. Schriver, J. P. Perchard, *J. Mol. Spectrosc.* **1988**, *127*, 125–142. – [9b] K. Matsamura, F. J. Lovas, R. D. Suenram, *J. Chem. Phys.* **1989**, *91*, 5887–5894.
[10] [10a] N. C. Baird, K. F. Taylor, *J. Comput. Chem.* **1981**, *2*, 225–230. – [10b] R. R. Squires, *Int. J. Mass Spectrom. Ion Proc.* **1992**, *117*, 565–600. – [10c] R. E. Brown, F. Barber, *J. Phys. Chem.* **1995**, *99*, 8071–8075. – [10d] E. Bishenden, D. J. Donaldson, *J. Phys. Chem. A* **1998**, *102*, 4638–4642.
[11] D. Sülzle, M. Verhoeven, J. K. Terlouw, H. Schwarz, *Angew. Chem.* **1988**, *100*, 1591–1592, *Angew. Chem. Int. Ed. Engl.* **1988**, *27*, 1533–1534.
[12] L.-G. Johansson, O. Lindqvist, N.-G. Vannerberg, *Acta Cryst. B* **1980**, *36*, 2523–2526.
[13] D. A. Horner, R. E. Connick, *Inorg. Chem.* **1986**, *25*, 2414–2417.
[14] D. Littlejohn, S. A. Walton, S.-G. Chang, *Applied Spectrosc.* **1992**, *46*, 848–851.
[15] [15a] A. Strömberg, O. Gropen, U. Wahlgren, O. Lindqvist, *Inorg. Chem.* **1983**, *22*, 1129–1133. – [15b] J. A. Noblet, K. A. Schugart, *J. Mol. Struct. (THEOCHEM)* **1994**, *304*, 1–11. – [15c] M. A. Vincent, I. J. Palmer, I. H. Hillier, *J. Mol. Struct. (THEOCHEM)* **1997**, *394*, 1–9.
[16] R. L. Kuczkowski, R. D. Suenram, F. J. Lovas, *J. Am. Chem. Soc.* **1981**, *103*, 2561–2566.
[17] [17a] L. L. Lohr, *J. Mol. Struct.* **1982**, *87*, 221–227. – [17b] T. S. Chen, P. L. M. Plummer, *J. Phys. Chem.* **1985**, *89*, 3689–3693. – [17c] M. Hofmann, P. von Ragué Schleyer, *J. Am. Chem. Soc.* **1994**, *116*,

4947–4952. – [17d] E. M. Evleth, *J. Mol. Struct. (THEOCHEM)* **1994**, *307*, 179–185. – [17e] A. H. Otto, S. Schrader, T. Steiger, M. Schneider, *J. Chem. Soc., Faraday Trans.* **1997**, *93*, 3927–3930.
[18] [18a] B. S. Ault, *Rev. Chem. Intermed.* **1988**, *9*, 233–269. – [18b] L. Schriver, D. Carrere, A. Schriver, K. Jaeger, *Chem. Phys. Lett.* **1991**, *181*, 505–511.
[19] J. A. Philips, M. Canagaratna, H. Goodfriend, K. R. Leopold, *J. Phys. Chem.* **1995**, *99*, 501–504.
[20] A. A. Viggiano, M. J. Henchman, F. Dale, C. A. Deakyne, J. F. Paulson, *J. Am. Chem. Soc.* **1992**, *114*, 4299–4306.
[21] B. J. Smith, L. Radom, *J. Phys. Chem.* **1991**, *95*, 10549–10551.
[22] J. W. Ochterski, G. A. Petersson and J. A. Montgomery, Jr., *J. Chem. Phys.*, 1996, **104**, 2598–2619.
[23] L. A. Curtiss, K. Raghavachari, J. A. Pople, *J. Chem. Phys.* **1993**, *98*, 1293–1298.
[24] L. A. Curtiss, K. Raghavachari, G. W. Trucks, J. A. Pople, *J. Chem. Phys.* **1991**, *94*, 7221–7230.
[25] M. J. Frisch, G. W. Trucks, H. B. Schlegel, P. M. W. Gill, B. G. Johnson, M. A. Robb, J. R. Cheeseman, T. A. Keith, G. A. Petersson, J. A. Montgomery, K. Raghavachari, M. A. Al-Laham, V. G. Zakrzewski, J. V. Ortiz, J. B. Foresman, J. Cioslowski, B. B. Stefanov, A. Nanayakkara, M. Challacombe, C. Y. Peng, P. Y. Ayala, W. Chen, M. W. Wong, J. L. Andres, E. S. Replogle, R. Gomperts, R. L. Martin, D. J. Fox, J. S. Binkley, D. J. Defrees, J. Baker, J. P. Stewart, M. Head-Gordon, C. Gonzalez, J. A. Pople, *GAUSSIAN 94 Revisions D.2* (Cray) and *E.1* (workstation), Gaussian, Inc., Pittsburgh, PA, **1995**.
[26] J. W. Ochterski, G. A. Petersson, K. B. Wiberg, *J. Am. Chem. Soc.* **1995**, *117*, 11299–11308.
[27] J. B. Foresman, A. E. Frisch, *Exploring Chemistry with Electronic Structure Methods*, 2nd ed., Gaussian, Inc., Pittsburgh, PA, **1996**.
[28] J. Hahn, P. Schmidt, K. Reinartz, J. Behrend, G. Winnewisser, K. M. T. Yamada, *Z. Naturforsch. B* **1991**, *46*, 1338–1342.
[29] F.-M. Flaud, C. Camy-Peyret, J. W. C. Johns, B. Carli, *J. Chem. Phys.* **1989**, *91*, 1504–1510.
[30] R. Steudel, H. Schmidt, E. Baumeister, H. Oberhammer, T. Koritsanszky, *J. Phys. Chem.* **1995**, *99*, 8987–8993.
[31] All cited acidities of reference compounds were taken from J. E. Bartmess, "Negative Ion Energetics Data" in *NIST Chemistry WebBook*, NIST Standard Reference Database Number 69, (Eds.: W. G. Mallard, P. J. Linstrom), November **1998**, National Institute of Standards and Technology, Gaithersburg, MD, USA (http://webbook.nist.gov/chemistry).
[32] K. Morokuma, C. Muguruma, *J. Am. Chem. Soc.* **1994**, *116*, 10316–10317.
[33] A. R. Bandy, J. C. Ianni, *J. Phys. Chem. A* **1998**, *102*, 6533–6539.
[34] See for example A. Smith, M. A. Vincent, I. H. Hillier, *J. Phys. Chem. A* **1999**, *103*, 1132–1139; J. A. Tossel, *Chemical Geology* **1997**, *141*, 93–103.
[35] R. Steudel, *Angew. Chem.* **1995**, *107*, 1433–1435, *Angew. Chem. Int. Ed. Engl.* **1995**, *34*, 1313–1315 and references cited therein.

Received September 9, 1999
[I99325]

Sulfonamide-Functionalized Gadolinium DTPA Complexes as Possible Contrast Agents for MRI: A Relaxometric Investigation

Pier Lucio Anelli,[a] Ivano Bertini,*[b] Marco Fragai,[b] Luciano Lattuada,[a] Claudio Luchinat,[c] and Giacomo Parigi[c]

Keywords: NMRD / MRI / Contrast agents / Carbonic anhydrase / Sulfonamides

A novel Gd-DTPA derivative with a built-in sulfonamide (SA) was synthesized as a contrast agent for MRI. The complex was designed to selectively target the enzyme carbonic anhydrase. It is shown that the longitudinal relaxation rates of aqueous solutions of Gd-DTPA-SA in the presence of carbonic anhydrase increase significantly. The binding constant is determined to be 15,000 ± 5,000 M^{-1}. This value ensures substantial formation of the carbonic anhydrase adduct at imaging concentrations of Gd-DTPA-SA. The complex interacts with erythrocytes, presumably due to a high affinity for the carbonic anhydrase present on the outer surface of the latter. This takes place even though the enzyme has a low abundance and is easily saturated by small amounts of Gd-DTPA-SA. The interaction of Gd-DTPA-SA with serum proteins is negligibly small. Therefore, the complex could potentially be tested as a selective contrast agent for compartments outside the blood pool.

Introduction

Contrast agents for MRI are characterized by their large nuclear relaxation capability for the protons of water molecules. In general, a complex of a paramagnetic metal ion, typically gadolinium(III) with seven unpaired electrons, is bound to at least one water molecule, which exchanges rapidly with bulk water. In imaging fields, the gadolinium complex relaxes the protons of the coordinated water at rates ranging from 10^5 s^{-1} for small molecules to 10^6 s^{-1} for macromolecules, whereas the protons of bulk water relax at about 0.4 s^{-1}. If the coordinated water exchanges at a rate of the order of 10^6 s^{-1} or faster, it transfers significant relaxation enhancements to bulk water. This enhancement is what is measured in relaxometry and determines the properties of the contrast agent.[1–3]

Besides low-toxicity requirements, the development of a good contrast agent aims at achieving two major objectives: (i) the increase of the rotational correlation time, τ_r, with respect to the value relative to small complexes, in order to increase the relaxation rates of protons in the perfused tissues, and (ii) the localization of the contrast agent with a larger concentration in some compartments with respect to others nearby. Both requirements can be satisfied by synthesizing a molecule with an efficient targeting system that is able to provide interactions between the agent and specific macromolecular receptors. Such interactions will be regulated by a binding constant, that should be high enough to maximize the effect of the contrast agent even if administered in low doses. Binding constants of the order of 10^4 M^{-1} are large enough to ensure good affinity. The ideal binding constant should also ensure a residence time that is long enough for the MRI acquisition but not so long as to appreciably increase toxicity, as it might happen if the binding constant were much higher.[4]

Organic moieties attached to the complex favor the interaction of the contrast agent with biological molecules or tissues. Three important examples of contrast agents of this class are Gd-BOPTA,[5,6] Gd-EOB-DTPA,[7] and MS-325,[8] which are able to bind noncovalently to serum albumin and can thus highlight the uptake of the gadolinium complex by hepatocytes. Contrast agents have also been proposed to be used as reagents for quantitative in vitro assays, as, for example, Gd-DTPA derivatives containing boronic residues, which should be able to bind to glycated proteins.[9]

Another strategy was used to detect regions in the body or cells where certain enzymes are concentrated. For example, if a gadolinium complex is covalently bound to a galactopyranose residue, so that the access of water to the paramagnetic center is sterically blocked, β-galactosidase, if present, cleaves this bond and thus may expose gadolinium to the solvent.[10] Wherever β-galactosidase is present, the magnetic resonance image is then improved by the contrast agent. If a contrast agent is functionalized with a molecule that is able to specifically react with an enzyme, the contrast agent targets the enzyme and any enzyme-rich tissue. Examples are sulfonamides, which are known to be specific inhibitors of carbonic anhydrase (CA) and have been widely used in medical therapy.[11,12] Carbonic anhydrase is a zinc enzyme present in various tissues in variable amounts.[11] Therefore, different tissues may exhibit different behavior depending on the presence of the enzyme and its accessibility, which could be altered during pathologic processes.[13] Therefore, by synthesizing a Gd-DTPA contrast agent with a sulfonamide (SA) at-

[a] Bracco s.p.a., Milano Research Center,
via Folli 50, 20134 Milano, Italy
[b] Magnetic Resonance Center, Department of Chemistry, University of Florence,
Via Sacconi 6, 50019 Sesto Fiorentino, Italy
E-mail: bertini@cerm.unifi.it
[c] Department of Soil Science and Plant Nutrition, University of Florence,
P.le delle Cascine 28, 50144 Florence, Italy

 © WILEY-VCH Verlag GmbH, D-69451 Weinheim, 2000 1434–1948/00/0404–0625 $ 17.50+.50/0

tached, binding to carbonic anhydrase and relaxation enhancement may be expected.

In this paper, we describe the synthesis of a contrast agent functionalized with the sulfonamide ethylene sulfanilamide (Gd-DTPA-SA). The molecule is shown to bind carbonic anhydrase effectively in vitro with a suitable binding constant and to display a sizable relaxation enhancement. Although not designed as a blood-pool reagent, Gd-DTPA-SA shows a small relaxation enhancement in intact blood with respect to serum, probably as a consequence of its interaction with the small amount of carbonic anhydrase bound to the outside of the erythrocyte membranes.[14]

Results and Discussion

NMRD Characterization of the Gd-DTPA-SA Complex

The paramagnetic relaxivity profile of Gd-DTPA-SA in an aqueous solution at 298 K is shown in Figure 1 (open circles). It is obtained by subtracting the diamagnetic contribution of the solvent relaxation rate in the absence of the paramagnetic compound, R_{1dia}, from the total relaxation rate of the solution, R_1, and normalizing to 1 mM Gd-DTPA-SA.

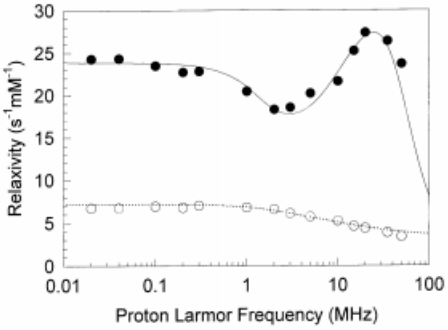


Figure 1. Proton ^{1}H-NMRD profiles of a Gd-DTPA-SA solution at 298 K in the absence (open circles) and in the presence (filled circles) of carbonic anhydrase (1.36 mM); the dotted and the solid lines represent the best fit profiles of the two sets of data

The relaxivity profile of Gd-DTPA-SA appears to be qualitatively and quantitatively very similar to the relaxivity profile of Gd-DTPA.[1] Only one inflection is present, centered at about 10 MHz, corresponding to the ω_s dispersion (where ω_s is the electron Larmor frequency in rad s^{-1}). The data were fitted by taking into account both the outer- and inner-sphere contributions; for comparative purposes, the resulting parameters are reported together with those of Gd-DTPA[1,15,16] (Table 1). The best fit profile is reported as a dotted line in Figure 1. The fit was made by keeping the parameters determining the outer-sphere contribution (the distance of closest approach, d, and the diffusion coefficient, D_{diff}) constant. Two protons were fitted at a distance of about 3 Å, the values of the other parameters being in agreement with those expected from the results of similar complexes,[5,7,15–22] including the increase in the exchange time between bulk and coordinated protons, τ_m, on passing from the binegative Gd-DTPA to the mononegative Gd-DTPA-SA complex.[23]

NMRD Characterization of the Gd-DTPA-SA–Carbonic Anhydrase Complex

Increasing concentrations of CA were added to the Gd-DTPA-SA solution in order to estimate the binding capability of the Gd-DTPA-SA complex. Relaxation measurements of such solutions were performed at 0.02, 0.15, 10, and 15 MHz. Monitoring the field dependence of water proton relaxation allows a better characterization of the parameters responsible for relaxation. Figure 2 shows the water proton longitudinal relaxation rates for solutions with different CA concentrations at 0.02 MHz. A 1:1 binding is assumed as sulfonamides are well known to interact specifically with the catalytic metal ion and the active site of the enzyme in a 1:1 fashion.[13] The data were fitted according to Equations 4–6, and a value for the binding constant of 15,000 ± 5000 M^{-1} was found. The relaxivity of the adduct, R_{add}, was found to be 25.8 s^{-1} mM^{-1} at 0.02 MHz.

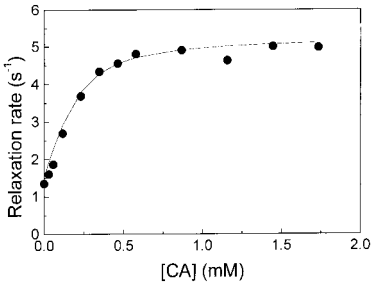


Figure 2. Titration curve of a solution of Gd-DTPA-SA (0.2 mM) with carbonic anhydrase at 0.02 MHz and 298 K

Then, the NMRD profile of a 0.2 mM Gd-DTPA-SA solution with a CA concentration of 1.36 mM (pH 8.1, 298 K) was obtained. This CA concentration ensured that the gadolinium complex was fully bound to CA. The relaxation rate values, after subtraction of the diamagnetic contribu-

Table 1. Best-fit parameters of the ^{1}H-NMRD data on Gd-DTPA and Gd-DTPA-SA in aqueous solution and in a solution containing excess carbonic anhydrase (1.36 mM) at 298 K

Complex	τ_r[a] (10^{-12} s)	τ_v (10^{-12} s)	τ_m (10^{-6} s)	Δ_t cm^{-1}	n_H[b]	r Å	D (ZFS)[c] cm^{-1}	d[b] Å	D (diff. coeff.)[b] (10^{-5} cm^2s^{-1})
[Gd-DTPA][d]	58–73	18–25	0.30	0.034–0.037	2	3.1	0	3.6	2.6
[Gd-DTPA-SA]	64	17	0.50	0.042	2	3.1	0	3.6	2.6
[Gd-DTPA-SA]-CA	12,000	18	0.56	0.017	2	3.0	0.008	3.6	2.6

[a] In the adduct, this value is estimated from the Stokes' equation and kept constant in the fitting procedure. – [b] This value is kept constant in the fitting procedure. – [c] The transient ZFS parameter was introduced to fit the NMRD profile of the adduct only, as it was found not necessary to fit the free complex profile. – [d] From refs. [1, 15, 16]

tion of CA at the same temperature and normalization to 1 mM, are reported in Figure 1 (filled circles). The introduction of CA both increases the relaxivity values and modifies the shape of the profile. The profile now exhibits three inflections: the first (centered at about 1 MHz) can be attributed to the ω_s dispersion, the second (centered at about 10 MHz) is the result of the field-dependent electron relaxation (see below), and the third inflection, for frequencies greater than 30 MHz, is related to the ω_I dispersion (ω_I indicates 2π times the proton Larmor frequency). This behavior is due to a dramatic change in the correlation time for the proton relaxation, given by the shortest time among rotational (τ_r), exchange (τ_m), and electron relaxation (τ_e) time, according to Equation 1.[24]

$$\tau_c^{-1} = \tau_r^{-1} + \tau_m^{-1} + \tau_e^{-1} \quad (1)$$

The rotational correlation time can be estimated from the Stokes-Einstein equation (Equation 2).

$$\tau_r = \frac{4\pi a^3 \eta}{3kT} \quad (2)$$

where a is the radius of the spherical-modeled molecule, η is the viscosity of the solvent, k is the Boltzmann constant and T indicates the temperature. The value of τ_r varies from $\simeq$70 ps for the free complex to $\simeq$12,000 ps for the bound complex (MW $\simeq$30,000). Therefore, τ_r is the dominant correlation time for the nuclear relaxation (according to Equation 1) in the Gd-DTPA-SA solution,[21,25] but it loses its influence when the CA adduct is formed.[21,25] τ_m is likely to be longer, as verified a posteriori (see below). In this case, τ_c is given by the electron relaxation time only and is calculated according to the Bloembergen-Morgan equation (Equation 3).[15,26,27]

$$\tau_e^{-1} = \frac{2\Delta_t^2 (4S(S+1)-3)}{50}\left(\frac{\tau_v}{1+\omega_s^2\tau_v^2} + \frac{4\tau_v}{1+4\omega_s^2\tau_v^2}\right) \quad (3)$$

where ω_s is the electron Larmor frequency, S is the electron spin quantum number, τ_v is the correlation time for electron relaxation and Δ_t^2 is the average quadratic transient zero field splitting.[28] The decay of the electron relaxation rate as a function of the magnetic field is responsible for the peak relaxivity in the 10–50 MHz region of the proton relaxation rate. Therefore, the occurrence of this peak in the high field part of the NMRD profile confirms the presence of binding between Gd-DTPA-SA and CA. The profile was fitted (solid line in Figure 1) and the resulting best-fit parameters are reported in Table 1. With τ_r being fixed at such a large value that it is negligible in the calculation of the correlation time, the fitting procedure provides values of τ_v, τ_m, and Δ_t close to those obtained for other Gd-DTPA derivatives bound to HSA.[7,21,29,30] It should be noted, in particular, that the value of τ_m is almost the same after binding and, in any case, is longer than τ_e. From the fitting, τ_m is the limiting factor for the relaxivity peak between 10–50 MHz. As required for many protein–Gd complex adducts, the effect of a small static zero-field splitting (D) was introduced so that the profile could be reproduced better.[21]

The NMRD measurements show a good binding capability of Gd-DTPA-SA with carbonic anhydrase. The binding constant is 15,000 M^{-1}, compared to 300 M^{-1} for Gd-BOPTA and HSA, 700 M^{-1} for Gd-DTPA-EOB and HSA, or 1,700 for Gd-DOTA-$(BOM)_3$ and HSA.[30] This binding constant ensures that the carbonic anhydrase adduct is largely formed at imaging concentrations. As previous studies have shown,[13] the large value of the binding constant of sulfonamides for CA is accompanied by favorable life times of the gadolinium complex–protein adduct of the order (of a few hours).

The relaxivity of the gadolinium complex at 1 T increases from about 3.5 $mM^{-1}s^{-1}$ when free to about 25 $mM^{-1}s^{-1}$ when bound to the protein. Such an increase is comparable to that of other Gd complexes when they are completely bound to the HSA present in solution.[29] However, such an increase does not occur at the imaging concentration of other Gd complexes (Gd-BOPTA, Gd-EOB-DTPA) because of their relatively small binding constants.[6]

Measurements in Intact Blood

Experiments on human blood were performed to test whether it was possible to detect binding of Gd-DTPA-SA to the small amount of carbonic anhydrase present on the surface of the red cells. Different concentrations of Gd-DTPA-SA were added to human blood samples (and to human serum samples as controls) and relaxation measure-

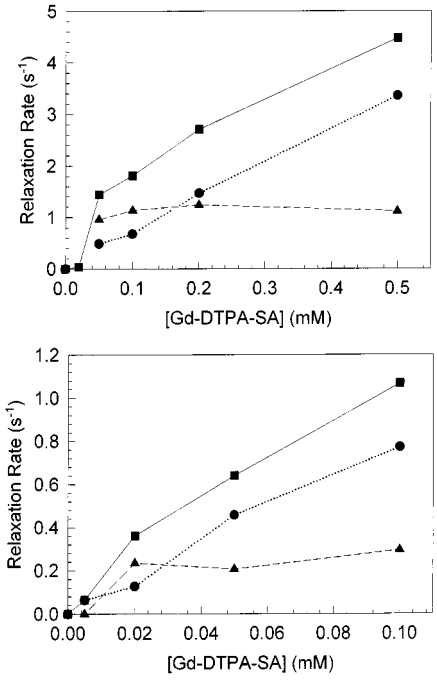


Figure 3. Paramagnetic enhancement in the proton relaxation rate measured in human blood (solid lines) and in serum (dotted lines) as a function of the Gd-DTPA-SA concentration at 0.02 MHz (A) and 50 MHz (B) at 298 K; the differences in relaxation rate between blood and serum are reported as dashed lines

ments at proton Larmor frequencies of 0.02, 0.15, 1.2, 35, and 50 MHz (corresponding to about 0.0005, 0.004, 0.03, 0.8, and 1.2 T) were performed. A small enhancement in proton relaxation was observed. The results obtained at two frequencies (0.02 and 50 MHz), decreased by the diamagnetic contributions, are shown in Figure 3, together with the difference between the paramagnetic enhancements in blood and serum. The low field measurements are more reliable, since the differences detected are much larger with respect to the instrumental precision. The measurements performed at the imaging fields are affected by larger errors, but provide the same indications as the low field experiments. The plots indicate that the Gd complex is bound in the blood sample, while it is free in the serum sample. This is shown by the higher initial increase of relaxation in the blood sample compared to the serum sample. The difference in the two samples levels off to an approximately constant value above Gd concentrations of 0.02–0.04 mM, where the increase in the relaxation rates is linear with the concentration in both blood and serum samples. Presumably, this behavior is a consequence of the saturation of the available carbonic anhydrase on the membranes of the red cells.

Conclusions

We have shown that a Gd-DTPA derivative targeted to bind to carbonic anhydrase in vivo has the desired fundamental properties in terms of binding constant and relaxation enhancements. We have also shown that the compound does not appreciably interact with any soluble macromolecule in serum, and that the amount of carbonic anhydrase present on the outer erythrocyte membranes is too small (although detectable through its enhancement) to block this reagent in the blood pool. Therefore, Gd-DTPA-SA is a potential candidate for in vivo tests for specificity in various tissues outside the blood pool.

Experimental Section

Materials: Carbonic Anhydrase (lyophilized powder from bovine erythrocytes, MW 30000) was purchased from Sigma. *N,N*-Bis(2-{bis[2-(1,1-dimethylethoxy)-2-oxoethyl]amino}ethyl)glycine was supplied by Bracco S.p.A. Human blood and serum were treated with lithium-heparin to prevent coagulation.

Synthesis of Ligands: A schematic summary of the synthesis of Gd-DTPA-SA is reported in Figure 4. *p*-Ethylaminesulfonamide II (236 mg, 1.18 mmol) was added to 20 mL of a DMF solution of *N,N*-bis(2-{bis[2-(1,1-dimethylethoxy)-2-oxoethyl]amino}ethyl)-glycine I (730 mg, 1.18 mmol). Upon the dropwise addition of 0.2 mL of DEPC [$(EtO)_2P(O)CN$] (215 mg, 1.32 mmol), the reaction mixture was maintained at 3 °C using an ice bath. Triethylamine (0.204 mL, 149 mg, 1.48 mmol) was then added slowly to the solution. The reaction was followed by TLC by observing the depletion of the free sulfonamide (R_f = 0.1) and the appearance of the product (R_f = 0.45) with the eluent $CH_2Cl_2/CH_3OH/NH_4OH$ (9:1:0.1). After 10 minutes the amine had fully reacted and the solution was warmed up and allowed to stand at room temperature for 30 minutes. DMF was then removed by vacuum evaporation. The crude product was washed and phase separated in ethyl acetate (33 mL) with a sodium bicarbonate (2 × 25 mL) and saturated sodium chloride solution (2 × 20 mL). Product III (838 mg, yield 89%) was obtained. Its purity was confirmed by using TLC (R_f = 0.45). Its ^{1}H-NMR spectrum was recorded in $CDCl_3$. – ^{1}H NMR: δ = 1.40 (s, 36 H, tBu), 2.4–2.7 (m, 8 H, N–CH_2–CH_2–N), 2.95 (s, 2 H, Ph–CH_2), 3.05 (s, 2 H, N–CH_2–CO), 3.3 (s, 8 H, N–CH_2–COO), 3.5–3.6 (m, 2 H, N–CH_2), 5.6 (s, 2 H, SO_2NH_2), 7.3–7.9 (m, 4 H, Ph), 8.2–8.3 (m, 1 H, NH).

Product III (838 mg, 1.05 mmol) was dissolved in 6 N HCl (8 mL). The mixture was stirred at room temperature for 1 hour and was then washed with CH_2Cl_2 (2 × 10 mL). The aqueous solution was dried and 671 mg (0.98 mmol, yield 93%) of pure compound IV were obtained. An ^{1}H-NMR spectrum was recorded in D_2O. – ^{1}H NMR: δ = 2.8–2.9 (m, 4 H, N–CH_2–CH_2–N), 3.1–3.0 (m, 4 H, N–CH_2–CH_2–N), 3.4–3.3 (m, 2 H, CH_2–Ph), 3.4–3.6 (m, 4 H, N–CH_2–CO–N–CH_2), 4.0 (s, 8 H, N–CH_2–CO), 7.4–7.9 (m, 4 H, Ph).

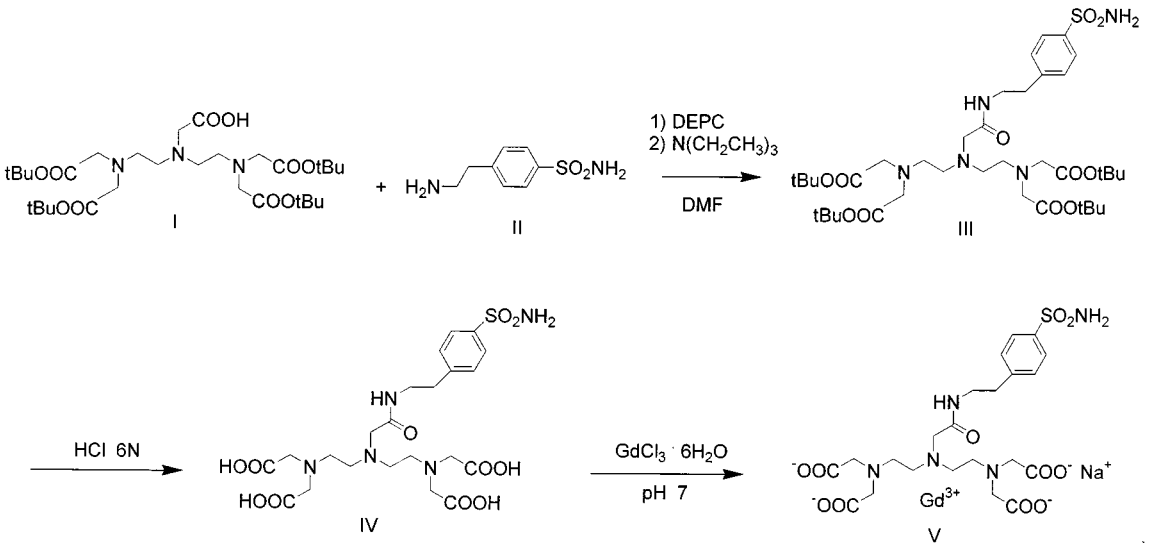


Figure 4. Schematic summary for the synthesis of Gd-DTPA-SA

Complexation and Purification of IV: The complexation and purification procedures follow a protocol already reported.[31] Compound IV (671 mg, 0.98 mmol) was dissolved in 27 mL of distilled water. To this solution 1 N NaOH was added until pH 7 was reached. An aqueous solution (5 mL) of $GdCl_3 \cdot 6H_2O$ (379 mg, 0.98 mmol) was then added slowly, maintaining a pH of 7 by addition of further aliquots of 1 N NaOH. The final crude product V (1.0 g) was obtained by evaporating the solution.

It was dissolved in 10 mL of distilled water and then loaded onto an Amberlite® XAD 1600 resin column (100 mL) and eluted with a CH_3CN/H_2O (9:1) gradient. The fractions containing the complex were evaporated to give 674 mg (0.86 mmol, yield 88%) of the crystalline white product V [negative ion FAB 729 $(M - Na)^-$].

The data collected on a large number of mono and bisamide derivatives of DTPA indicate that these compounds are remarkably stable with respect to dissociation in vivo. Therefore, the same stability is expected for our compound.[4]

Nuclear Magnetic Relaxation Dispersion Experiments: ^1H Nuclear Magnetic Relaxation Dispersion (NMRD) profiles were obtained by plotting the proton relaxation rates, R_1, as a function of the applied magnetic field. The NMRD profiles and all longitudinal water-proton relaxation rate measurements were collected with a Stelar prototype fast field cycling relaxometer or with a Koenig-Brown field cycling relaxometer[25,32] in the 0.01–50 MHz proton Larmor frequency range. Both instruments provide measurements with an error of about ±1%.

NMRD data, with the diamagnetic contribution subtracted, were analyzed according to existing theories, using a program described in ref.[33]

Determination of the Binding Constant: The observed relaxivity R_{obs} is the sum of the contributions from the free GdL complex and the GdL-CA adduct[30,34]

$$R_{obs} = \frac{C_{GdL} - [GdL - CA]}{C_{GdL}} R_{free} + \frac{[GdL - CA]}{C_{GdL}} R_{add} \quad (4)$$

with

$$[GdL\text{-}CA] = \frac{1 + K_A(C_{GdL} + C_{CA}) - \sqrt{(1 + K_A(C_{GdL} + C_{CA}))^2 - 4K_A^2 C_{GdL} C_{CA}}}{2K_A} \quad (5)$$

and

$$K_A = \frac{[GdL\text{-}CA]}{(C_{GdL} - [GdL\text{-}CA])(C_{CA} - [GdL\text{-}CA])} \quad (6)$$

where K_A is the binding constant, C_{GdL} and C_{CA} represent the initial concentrations of both GdL and CA, and R_{free} and R_{add} are the relaxivity of the free complex and the fully bound complex, respectively. Both K_A and R_{add} have been obtained through a two-parameter fitting of the R_{obs} data measured at various CA concentrations. The concentration of the gadolinium complex was 0.2 mM at pH 8.1.

Acknowledgments

For financial support to MF we thank Bracco S.p.A., Italy. For financial support, we also thank MURST ex 40%, Italy, the European Union, TMR-LSF contract ERB FMGE CT950033, and CNR, Progetto Finalizzato Biotecnologie, Italy. We also thank Dr. Claudiu Supuran for discussions and suggestions in the initial stage of this project.

[1] S. H. Koenig, R. D. Brown III, *Progr. NMR Spectrosc.* **1990**, *22*, 487–567.
[2] R. B. Lauffer, *Chem. Rev.* **1987**, *87*, 901–927.
[3] J. A. Peters, J. Huskens, D. J. Raber, *Progr. NMR Spectrosc.* **1996**, *28*, 283–350.
[4] P. Caravan, J. J. Ellison, T. J. McMurry, R. B. Lauffer, *Chem. Rev.* **1999**, *99*, 2293–2351.
[5] F. Uggeri, S. Aime, P. L. Anelli, M. Botta, M. Brocchetta, C. De Haen, G. Ermondi, M. Grandi, P. Paoli, *Inorg. Chem.* **1995**, *34*, 633–642.
[6] F. M. Cavagna, P. Marzola, M. Daprà, F. Maggioni, E. Vicinanza, P. M. Castelli, C. De Haen, C. Luchinat, M. F. Wendland, M. Saeed, C. B. Higgins, *Invest. Radiol. (Suppl. 2)* **1994**, *29*, 50–53.
[7] L. V. Elst, F. Maton, S. Laurent, F. Seghi, F. Chapelle, R. N. Muller, *Magn. Res. Med.* **1997**, *38*, 604–614.
[8] R. B. Lauffer, D. J. Parmelee, S. U. Dunham, H. S. Ouellet, R. P. Dolan, S. Witte, T. J. McMurry, R. C. Walovitch, *Radiology* **1998**, *207*, 529–538.
[9] S. Aime, M. Botta, G. Ermondi, M. Fasano, E. Terreno, *Magn. Res. Imaging* **1992**, *10*, 849–854.
[10] R. A. Moats, S. E. Frazer, T. J. Meade, *Angew. Chem. Int. Ed. Engl.* **1997**, *36*, 726–728.
[11] R. E. Tashian, D. Hewett-Emmett (Eds.), *Biology and Chemistry of the Carbonic Anhydrase,* The New York Academy of Sciences, New York, **1984**.
[12] T. S. Maren, E. O. Couto, *Arch. Biochem. Biophys* **1979**, *196*, 501–510.
[13] T. H. Maren, *Physiol. Rev.* **1967**, *47*, 595–780.
[14] *Carbonic Anhydrase and Modulation of Physiologic and Pathologic Processes in the Organism,* Helicon, Timisoara, **1994**.
[15] D. H. Powell, O. M. N. Dhubhghaill, D. Pubanz, L. Helm, Y. S. Lebedev, W. Schlaepfer, A. E. Merbach, *J. Am. Chem. Soc.* **1996**, *118*, 9333–9346.
[16] S. Aime, M. Fasano, S. Paoletti, E. Terreno, *Gazz. Chim. Ital.* **1995**, *125*, 125–131.
[17] G. Gonzalez, D. H. Powell, V. Tissieres, A. E. Merbach, *J. Phys. Chem.* **1994**, *98*, 53–59.
[18] S. Aime, M. Botta, M. Fasano, S. Paoletti, P. L. Anelli, F. Uggeri, M. Virtuani, *Inorg. Chem.* **1994**, *33*, 4707–4711.
[19] S. Aime, P. L. Anelli, M. Botta, F. Fedeli, M. Grandi, P. Paoli, F. Uggeri, *Inorg. Chem.* **1992**, *31*, 2421–2428.
[20] C. F. G. C. Geraldes, A. M. Urbano, M. C. Alpoim, A. D. Sherry, K.-T. Kuan, R. Rajagopalan, F. Maton, R. N. Muller, *Magn. Res. Imaging* **1995**, *13*, 401–420.
[21] S. W. A. Bligh, A. H. M. S. Chowdhury, D. Kennedy, C. Luchinat, G. Parigi, *Magn. Res. Med.* **1999**, *41*, 767–773.
[22] K. Micskei, L. Helm, E. Brücher, A. E. Merbach, *Inorg. Chem.* **1993**, *32*, 3844–3850.
[23] J. P. Andre, H. R. Maecke, E. Toth, A. E. Merbach, *J. Biol. Inorg. Chem.* **1999**, *4*, 341–347.
[24] I. Solomon, *Phys. Rev.* **1955**, *99*, 559–565.
[25] I. Bertini, C. Luchinat, *NMR of Paramagnetic Molecules in Biological Systems,* Benjamin/Cummings, Menlo Park, CA, **1986**.
[26] Only the field dependence for the longitudinal electron relaxation was used. The field dependence of the transverse electron relaxation may be provided by a different equation; ref. [15,35] but, since the ω_S term in the Solomon equation is already dispersed when the $\omega_S\tau_v$ dispersion occurs, the difference is negligible.
[27] N. Bloembergen, L. O. Morgan, *J. Chem. Phys.* **1961**, *34*, 842–850.
[28] It is possible that some restricted motion of the bound complex characterized by a correlation time shorter than τ_e may contribute another spectral density term (see ref.[36]) However, the satisfactory fitting performed assuming negligible restricted motion (see below) suggests that this effect, if present, is minor.
[29] I. Bertini, C. Luchinat, G. Parigi, G. Quacquarini, P. Marzola, F. M. Cavagna, *Magn. Res. Med.* **1998**, *39*, 124–131.

[30] S. Aime, M. Botta, M. Fasano, S. Geninatti Crich, E. Terreno, *JBIC* **1996**, *1*, 312–319.
[31] D. Parker, K. Pulukkody, F. C. Smith, A. Batsanov, J. A. K. Howard, *J. Chem. Soc. Dalton Trans.* **1994**, 689–693.
[32] S. H. Koenig, R. D. Brown III, in: *NMR Spectroscopy of Cells and Organisms, Vol. II* (Ed.: R. K. Gupta), CRC Press, Boca Raton, **1987**, pp 75–75.
[33] I. Bertini, O. Galas, C. Luchinat, G. Parigi, *J. Magn. Reson. Ser. A* **1995**, *113*, 151–158.
[34] I. Bertini, C. Luchinat, *NMR of paramagnetic substances,* Coord. Chem. Rev. 150, Elsevier, Amsterdam, **1996**.
[35] D. H. Powell, E. Brücher, G. Gonzalez, O. Y. Grinberg, K. Koehler, Y. S. Lebedev, A. E. Merbach, K. Micskei, F. Ottaviani, A. von Zelewsky, *Helv. Chim. Acta* **1993**, *76*, 2129–2146.
[36] G. Lipari, A. Szabo, *J. Am. Chem. Soc.* **1982**, *104*, 4546–4559.
Received September 17, 1999
[I99327]

Second Harmonic Generation and Two-Photon Fluorescence as Nonlinear Optical Properties of Dipolar Mononuclear Sesquifulvalene Complexes

Hans Wong,[a] Timo Meyer-Friedrichsen,[a] Tony Farrell,[a] Christoph Mecker,[a] and Jürgen Heck*[a]

Dedicated to Prof. Dr. Dr. eh. Dr. h.c. H. Sinn on the occasion of his 70th birthday

Keywords: NLO materials / Second harmonic generation / Two-photon fluorescence / Solvatochromism / Electrochemistry / Sesquifulvalene / Sandwich complex

In order to investigate nonlinear optical properties, in particular second harmonic generation (SHG) of organometallic complexes, numerous dipolar monocationic sesquifulvalene complexes of the general form $[Mc-Z-C_7H_6]^+$ have been synthesised (Mc = metallocenyl), wherein the metallocenyl moiety Mc acts as an electron donor, and the tropylium cation $C_7H_6^+$ as an electron acceptor. The mutual electronic influence of the donor and the acceptor groups is warranted by a linking spacer Z, which is a single bond [Mc = $CpFeC_5H_4$ (**4a**); Mc = $CpRuC_5H_4$ (**4b**)], an unsaturated bridge containing olefins [Z = $(E\text{-CH=CH})_n$: n = 1, Mc = $CpFeC_5H_4$ (**25a**); Mc = $CpRuC_5H_4$ (**25b**); n = 2, Mc = $CpFeC_5H_4$ (**26**); n = 3, Mc = $CpFeC_5H_4$ (**27**)], or thiophene units [Z = 2,5-C_4H_2S, Mc = $CpFeC_5H_4$ (**28**); Z = 5,5′-(2,2′-$C_4H_2S)_2$, Mc = $CpFeC_5H_4$ (**29**); Z = 2-(5-*E*-CH=CH)C_4H_2S, Mc = $CpFeC_5H_4$ (**30**)]. For the salts of **4a**·BF_4, **4b**·PF_6 and **25a**·PF_6 X-ray structure determinations have been performed [**4a**·BF_4: orthorhombic, *P*nma, a = 21.75(2), b = 9.900(2), c = 6.881(3) Å, V = 1482.0(15) Å^3, Z = 4; **4b**·PF_6: monoclinic, $P2(1)/c$, a = 8.104(3), b = 18.206(14), c = 11.228(4) Å, β = 107.59(3), V = 1579.1(15) Å^3, Z = 4; **25a**·PF_6: triclinic, $P\bar{1}$, a = 10.067(6), b = 10.496(6), c = 11.418(6) Å, α = 94.07(4), β = 110.96(4), γ = 102.88(5)°, V = 1083.1(11) Å^3, Z = 2]; the solid state structures indicate an almost coplanar arrangement of the organic π-system. Cyclic voltammetry studies reveal an irreversible one-electron reduction and an electrochemically reversible one-electron oxidation step for the ferrocenyl derivatives, whereas the ruthenocenyl derivatives demonstrate an irreversible two-electron oxidation. The redox potentials clearly indicate that the oxidation occurs at the metallocene unit, and the reduction is localised on the tropylium entity. In the electronic absorption spectra two intense bands are observed in the region $400 < \lambda < 900$ nm which undergo strong negative solvatochromic shifts. The origin of the high-energy absorption band is assumed to be an interligand charge-transfer (LL−CT) transition, and the low-energy absorption band is assigned to a donor-acceptor charge-transfer (DA−CT) transition. Whereas the LL−CT is continuously shifted to lower energy with increasing spacer length, the energy of the DA−CT approaches a limiting value. A comparable phenomenon is also observed for the difference between the oxidation and reduction potentials obtained from electrochemical studies. Investigations concerning the nonlinear optical properties of the dipolar cationic sesquifulvalene complexes by means of hyper-Rayleigh scattering (HRS) indicate that the ferrocenyl derivatives fluoresce due to two-photon absorption whereas the ruthenocenyl congeners exhibit second harmonic generation with considerably large first hyperpolarizability which is partly resonance-enhancement based.

Introduction

Materials showing nonlinear optical (NLO) properties have potential applications in photonic devices i.e. for optical data acquisition, storage, transmission and processing. The most prominent NLO features are frequency doubling or even tripling [second and third harmonic generation (SHG and THG)] of incident light, the linear electro-optical effect (Pockels effect) which describes the change of the refractive index of matter with the strength of an applied external electric field, and photorefractivity.[1]

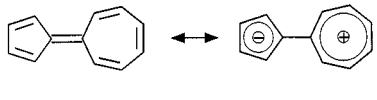
An important class of compounds capable of frequency doubling is composed of an electron donor (D), an acceptor (A) and a π-bridge providing the electronic communication between the donor and acceptor. Such D-π-A compounds are highly polarizable and experimental NLO studies on this kind of organic compounds in a molecular arrangement, incorporated in a polymer, or used as a self-assembled monolayer indeed reveal large SHG effects.[1−3] Our approach to NLO chromophores has been to synthesise organometallic sesquifulvalene-type complexes suitable for SHG, whose NLO properties are characterised by the first hyperpolarizability β. The special features of organometallic complexes have been well documented,[4−6] and include fine-tuning of the molecular polarisation, tailoring of the crystal formation, or fixing additional functional groups as docking spots in supramolecular chemistry.

Very often the change-transfer (CT) states which are very important to achieve high β values (vide infra), can be represented by polar resonance forms[1a] and this also holds for sesquifulvalene (**1**). Although it can be described in terms

[a] Institut für Anorganische und Angewandte Chemie, Universität Hamburg,
Martin-Luther-King-Platz 6, D-20146 Hamburg, Germany,
Fax: (internat.) + 49-4042/838-6348,
E-mail: heck@chemie.uni-hamburg.de

 © WILEY-VCH Verlag GmbH, D-69451 Weinheim, 2000 1434−1948/00/0404−0631 $ 17.50+.50/0

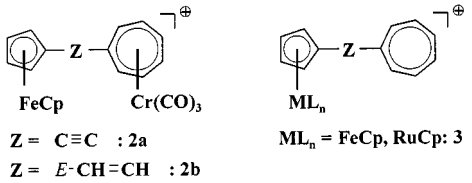
of two resonance forms of different polarities (Scheme 1), sesquifulvalene behaves like a polyene with alternating bond lengths,[7] and its ground state is thus best described by the nonpolar resonance form **A**. Upon excitation charge separation occurs and the resulting structure is likely to be related to the polar resonance form **B**.



1

Scheme 1. Resonance forms of sesquifulvalene (**1**)

Calculation of the first hyperpolarizability β[8][9] of **1** confirms a change in the dipole moment on excitation, but the high reactivity of **1**[10] prevents the experimental determination of its NLO properties. In previous papers we reported the NLO properties of sesquifulvalene-type complexes wherein both aromatic termini of the resonance form **B** are coordinated to metal centres (**2a**, **2b**).[11]

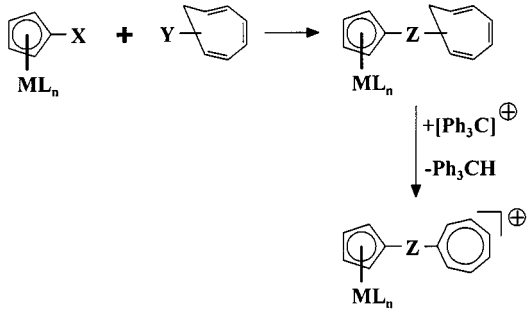


The objective of the present work was to stabilise only the five-membered ring of the aromatic units in **1** by coordination to (η^5-cyclopentadienyl)iron and -ruthenium. Hence, the neutral five-membered ring moiety of the sesquifulvalene complex would act as an electron donor whereas the uncoordinated tropylium cation would behave as an electron accepting group. Such a molecular arrangement creates a dipolar structure in the ground state, which could change upon excitation. Additionally, it was proposed to introduce various bridging functions Z, i.e. olefins and thiophenes, in order to modulate the interaction between the five- and seven-membered ring (**3**). Thiophenes are often used because of their superior thermal stability, and because of their lower resonance stabilisation energy relative to other aromatic spacers. The former HRS studies on the ethenediyl bridged heterodinuclear complex **2b** revealed a large first hyperpolarizability β.[11] It is well-known from dipolar organic NLO chromophores that increasing the number of π-bonds by one between the donor and acceptor increases the experimental β value by a factor of 1.5−2. Therefore the introduction of additional double bonds between the five- and seven-membered ring of the sesquifulvalene complexes appeared to be a very promising endeavour to improve the NLO properties. Just recently, NLO results of related mononuclear sesquifulvalene complexes with a cymantrenyl entity [ML_n = $Mn(CO)_2L$; L = CO, PR_3] instead of MCp as the electron donating group have been published wherein the donor is directly coupled to the tropylium cation or separated by an ethynediyl linker.[12] Thus it would be worthwhile to compare the two families of mononuclear sesquifulvalene complexes concerning their NLO properties.

Results and Discussion

Synthesis

The general strategy to form the desired cationic mononuclear sesquifulvalene complexes was the coupling of functionalised metallocenes with the corresponding cycloheptatriene derivatives to obtain the neutral mononuclear monohydro-sesquifulvalene precursor. The monohydro-sesquifulvalene complexes were converted into the mononuclear cationic sesquifulvalene species by hydride abstraction (Scheme 2).



Scheme 2. General strategy for the synthesis of cationic mononuclear sesquifulvalene complexes

Complexes Without a π-Linker (Z = Single Bond)

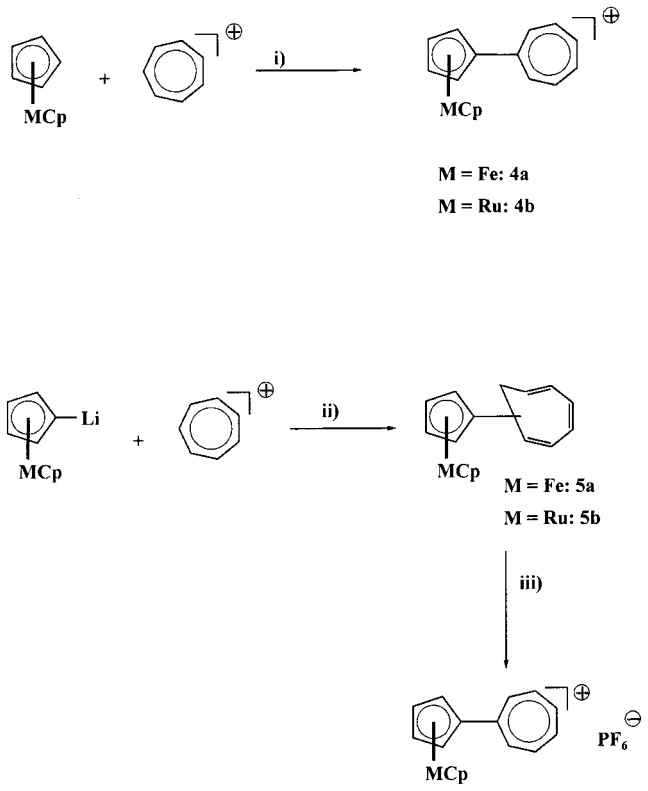
The first published route to the archetypal mononuclear sesquifulvalene complex with the metallocenyl substituent directly linked to the tropylium cation (Z = single bond: **4a**, **4b**) was the electrophilic substitution reaction of ferrocene with the tropylium cation (Scheme 3, i).[13] This method is also applicable to ruthenocene under more vigorous conditions.

However, our experience with the electrophilic substitution reaction revealed difficulties in the purification of the products **4a** and **4b** which were polluted with $[C_7H_7]^+$. Additionally, **4a** was contaminated with paramagnetic impurities which were not easy to remove. Therefore, the nucleophilic addition of monolithiated metallocene[14] to the tropylium cation was preferred yielding the neutral complexes **5a** and **5b** (Scheme 3, ii). The formation of the cationic complexes **4a** and **4b** was subsequently achieved by the reaction of **5a** and **5b** with $[Ph_3C][PF_6]$ (vide infra).

Complexes With Olefinic Linkers [Z = (*E*-CH=CH)$_n$, *n* = 1, 2, 3]

The introduction of one, two or three double bonds between the five- and seven-membered rings was afforded by

Wittig-type reactions of different formyl metallocenes with nucleophiles of the corresponding cycloheptatrienes. Since deprotonated phosphonates are known to react more stereoselectively than phosphoranes in the formation of *E*-olefins,[15] (cycloheptatrienylmethyl)diethylphosphonate (**6**) was prepared in a Michaelis-Arbuzov reaction from 1-chloromethyl-1,3,5-cycloheptatriene.[16] For $n = 1$ the phosphonate **6** underwent a Wittig-Horner-Wadsworth-Emmons (WHWE) reaction in the presence of NaH with the formyl metallocene (M = Fe: **7a**; M = Ru: **7b**[17]) to form the neutral compounds **8a** and **8b** (Scheme 4, i). The elongation of the olefinic bridge (Scheme 4, ii−vii) could be performed by the reaction of the formyl metallocenes **7a** and **7b** with (ethoxycarbonylmethyl)diethylphosphonate in a WHWE reaction. The reduction of the formed ester **9** by $LiAlH_4$ yielded the alcohol **10** which was oxidised with $BaMnO_4$[18] to the vinylogous metallocenyl carbaldehyde **11**. The aldehyde **11** was reacted either with **6**, yielding the cycloheptatrienyl derivative **12**, or was further subjected to the elongation sequence to form the dienyl formyl derivative **13**, which was then linked to the seven-membered ring to give the neutral complex **14**.



Scheme 3. Formation of the monometallic sesquifulvalene complexes **4a** and **4b**: (i) M = Fe, MeCN, reflux; M = Ru, 1,2-$C_2H_4Cl_2$, reflux; (ii) Et_2O, −20°C; (iii) CH_2Cl_2, $[Ph_3C][PF_6]$

Complexes With Thiophene Linkers {Z = 2,5-C_4H_2S or 5,5′-[2,2′-$(C_4H_2S)_2$]}

Another preparatively convenient method to warrant the electronic interaction in dipolar NLO chromophores upon elongation of the dipole is the use of thiophenes as π-linkers.[19−21] These types of complexes have been synthesised starting from 2,5-dibromothiophene[22] (**15**) (Scheme 5). Lithium-bromine exchange and subsequent nucleophilic addition to the tropylium cation led to the formation of 2-bromo-5-cycloheptatrienylthiophene (**16**).[23] Compound **16** was allowed to react with ferrocenyl zinc chloride[24] in a cross-coupling reaction[25] affording a mixture of isomers **A**, **B** and **C** of the monothiophene species **17** (Scheme 5). Thermolysis of the mixture only revealed the isomers **B** and **C** (40:60), which facilitated the final hydride abstraction (vide infra).

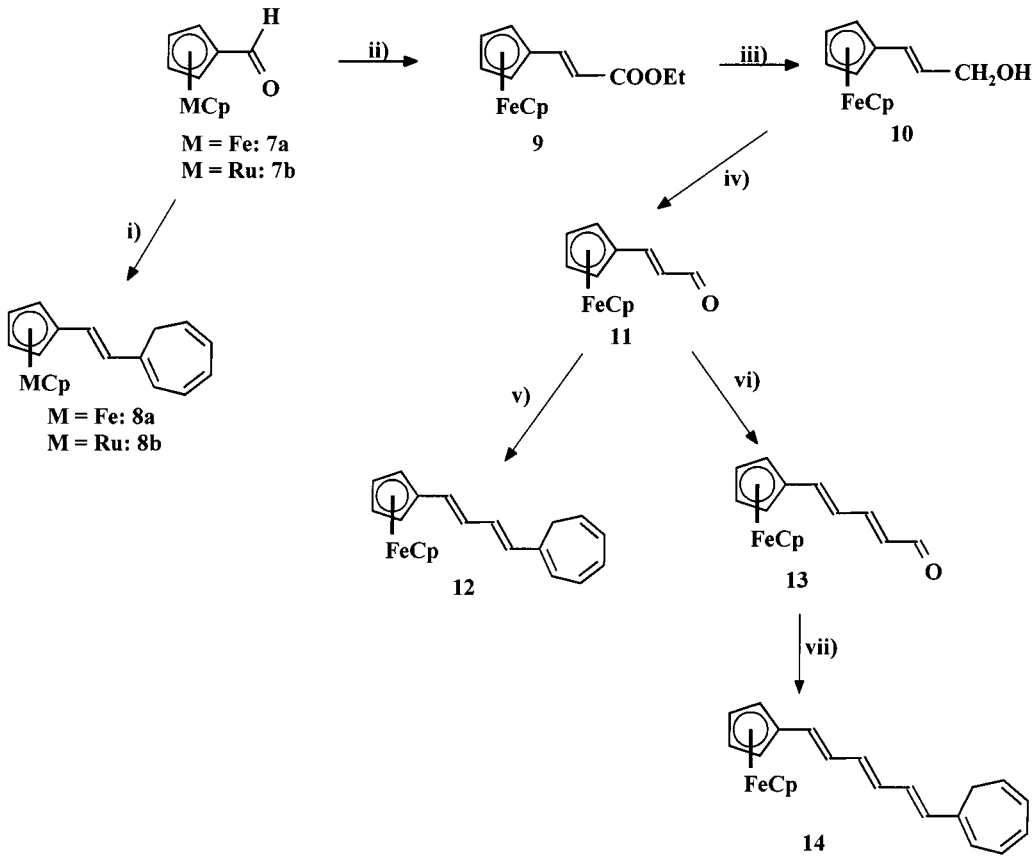
The elongation of the 2,5-thienylene bridge by an additional thiophene unit has been achieved in a Ni-catalysed cross-coupling reaction[26] of the Grignard reagent 2-thienyl magnesium bromide (**18**) with **16** resulting in the formation of the bithiophene derivative **19**[27] (Scheme 6). The bithiophene **19** was lithiated, followed by a zinc-lithium exchange and cross-coupled with iodoferrocene,[14] subsequently yielding the bithiophene bridged monohydro-sesquifulvalene complex **20** as the isomer **A**, which was thermally isomerized to **B**.

Complexes With a Vinylenethienylene Linker [Z = 2-(5-*E*-C_2H_2)C_4H_2S]

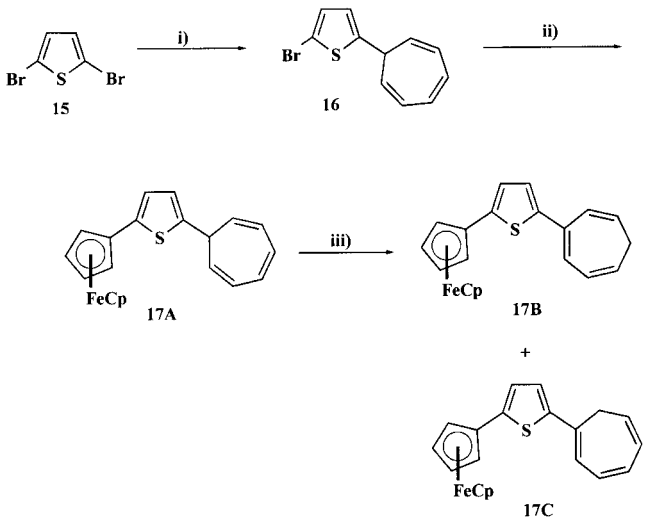
A third way to extend the π-bridge was the combination of an olefinic bond and a thiophene forming a vinylenethienylene bridge.[28] These types of bridges between the donor and an acceptor moiety are easy to synthesise by the formylation[29] of 2-cycloheptatrienylthiophene (**21**),[25] to form compound **22**. Subsequent Wittig reaction of **22** with (ferrocenylmethyl)triphenylphosphorane (**23**)[30][31] afforded the vinylenethienylene-bridged mononuclear monohydro-sesquifulvalene complex **24** (Scheme 7) as a mixture of *E* and *Z* isomers, each of which consisted of two further isomers differing in the position of the sp^3-carbon atom in the seven-membered ring. The isomers were not isolated as, after the hydride abstraction, only one isomer was formed (vide infra).

Formation of the Cationic Sesquifulvalene Complexes

All the sesquifulvalene complexes described above were subjected to hydride abstraction by adding trityl cation to a solution of the neutral complexes (Scheme 8), and was accompanied by a dramatic change in colour from orange-red to deep violet-blue indicating a strong enhancement in the electronic communication between the metallocene and the cationic tropylium entity. All the cations were fully characterised except the cationic sesquifulvalene complex **27** which suffers from a limited stability in solution and in solid state which prevented complete analysis.



Scheme 4. Formation of the olefinic bridged monohydro-sesquifulvalene complexes: (i) THF, −78 °C, $(EtO)_2(O)PCH_2C_7H_7$ (**6**), *n*BuLi; (ii) toluene, 0 °C, $(EtO)_2(O)PCH_2CO_2Et$, *n*BuLi; (iii) Et_2O, $LiAlH_4$, $AlCl_3$; (iv) CH_2Cl_2, $BaMnO_4$; (v) **6**, NaH, DME; (vi) 1. toluene, 0 °C, $(EtO)_2(O)PCH_2CO_2Et$, *n*BuLi, 2. Et_2O, $LiAlH_4$, $AlCl_3$, 3. CH_2Cl_2, $BaMnO_4$; (vii) **6**, NaH, DME



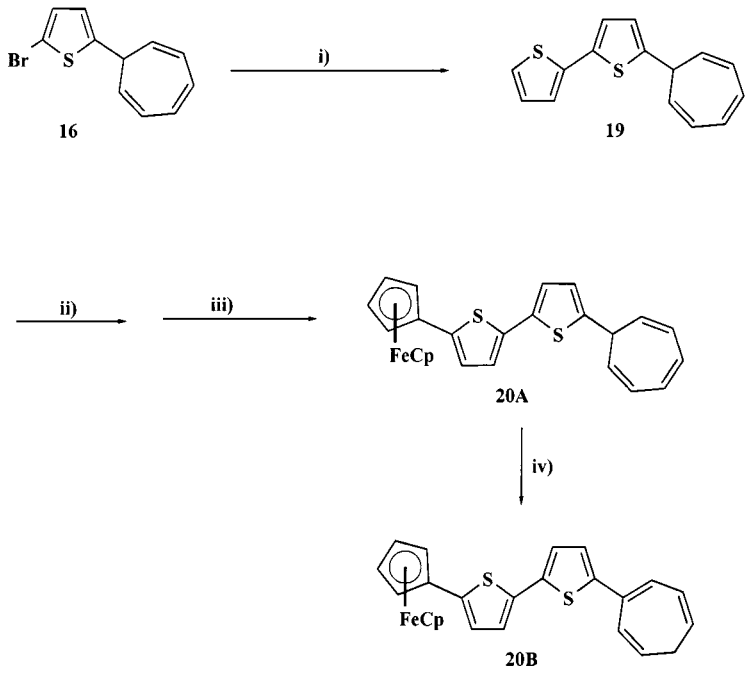
Scheme 5. Formation of the thiophene bridged monohydro-sesquifulvalene complex **17**: (i) 1. THF, −78 °C, *n*BuLi, 2. $[C_7H_7][BF_4]$; (ii) THF, FcZnCl, $Pd(PPh_3)_4$; (iii) toluene, reflux

Structural Results

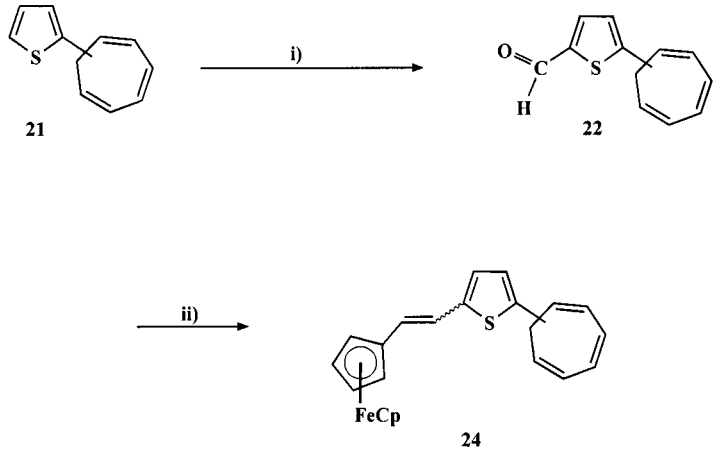
A very important conclusion of the studies on the structural parameters and molecular factors governing the NLO properties, in particular the first hyperpolarizability β, is the correlation between the bond length alternation (BLA) of olefinic bridged D-π-A systems and (i) the dipole change $\Delta\mu_{eg}$ between the ground and the excited CT state, (ii) the electronic transition moment M^2 of the CT transition, and (iii) the energy ΔE of the CT transition.[32][33]

From the sesquifulvalene complexes **4a**, **4b** and **25a** X-ray structure analyses were performed (Figure 1), although for **25a** the accuracy of the structural analysis, which is absolutely necessary for the discussion of a structure-property relationship, suffered from molecular disorder. Two different molecules in the ratio 70:30 lie in almost identical positions and the uncoordinated carbon-carbon double bonds between the five- and seven-membered rings are in a crossed position to each other (Figure 1). The result of an X-ray structure analysis of **4a** has already been published[34] but with less accuracy than obtained in the present work.

The complexes **4a**, **4b** and **25a** all crystallise in centrosymmetric space groups and hence could not be used in the crystalline state for NLO studies to evaluate the SHG. The crystal structures of **4a**, **4b** and **25a** all reveal a virtually coplanar arrangement of the π-termini of the sesquifulvalene ligand (Figure 1, Table 1) as has already been observed in the cymantrenyl congeners.[12][35] The interplanar angle between the five- and seven-membered ring is less than 5°. Within experimental error, the C−C and C−metal dis-



Scheme 6. Formation of the 5,5′-bithienylene bridged monohydro-sesquifulvalene complex **20**: (i) THF, 2-(C_4H_3S)MgBr (**18**), $NiCl_2$dppe; (ii) 1. THF, −78°C, *n*BuLi, 2. $ZnCl_2$; (iii) THF FcI, $Pd(PPh_3)_4$; (iv) toluene, reflux

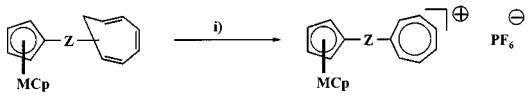


Scheme 7. Synthesis of the vinylenethienylene bridged monohydro-sesquifulvalene complex **24**: (i). 1. THF, −78°C, *n*BuLi, 2. DMF; (ii) THF, *n*BuLi, [$FcCH_2PPh_3$]I

tances in the metallocene moieties are very similar to the corresponding structural data of other metallocene derivatives. The C−C bond lengths of the seven-membered ring in **4a** and **4b** show a small but distinct bond alternation suggesting a slight contribution of the polyene resonance structure **A** (vide supra) to the ground state. Concomitantly the C−C bond linking the five- and seven-membered rings is somewhat shorter than expected for a sp^2-sp^2 carbon-carbon bond. Additionally, it is worth mentioning that the vector of the connecting bond between the two π-termini in **4a** and **4b** is slightly tilted towards the metal centre indicating the electron-withdrawing property of the tropylium part[36] (Table 1).

Redox Properties

The ferrocenyl-containing compounds reveal an electrochemically reversible one-electron oxidation (Figure 2) which is anodically shifted with respect to ferrocene. The amount of the anodic shift depends on the length of the π-linker (Table 2). The reduction of the sesquifulvalene complexes occurs in an irreversible one-electron transfer and at very similar potentials as reported for the unsubstituted tropylium cation.[37] The peak potential E_{pc} also depends on the length of the π-connection. Comparable trends in the redox behaviour are observed for the ruthenocenyl-containing complexes, although the oxidation step is normally



M	Z	
Fe	-	**4a**
Ru	-	**4b**
Fe	*E*-CH=CH	**25a**
Ru	*E*-CH=CH	**25b**
Fe	(*E*-CH=CH)$_2$	**26**
Fe	(*E*-CH=CH)$_3$	**27**
Fe	2,5-C_4H_2S	**28**
Fe	5,5'-[2,2'-(C_4H_2S)]	**29**
Fe	2-(5-*E*-CH=CH)C_4H_2S	**30**

Scheme 8. Synthesis of the cationic mononuclear sesquifulvalene complexes by hydride abstraction: (i) CH_2Cl_2, $[Ph_3C][PF_6]$

Electronic Absorption Spectra

The UV/Vis spectra of the complexes under study are comparable in that the spectra consist of two strong absorption bands in the visible region (Figure 3) with the exception of the ruthenocenyl derivatives in which the high energy absorption bands are shifted towards the near-UV. As can be seen from Table 3 the electronic excitations are governed by a strong blue-shift on increasing the solvent polarity. This strong negative solvatochromism indicates that in the ground state the positive charge is more or less localised on the tropylium moiety of the complexes, whereas upon excitation the positive charge is delocalized or even localised on the opposite part of the complex.

Figure 3 demonstrates the influence of the length of the π-bridge on the electronic absorption spectra: whereas the high energy absorption band is still considerably red shifted, when the π-linker is elongated the longer wavelength absorption band moves to a certain value which may be regarded as the merocyanine limit[39][40] of these mononuclear sesquifulvalene complexes. This behaviour is in accordance with the assignment of the low energy absorption

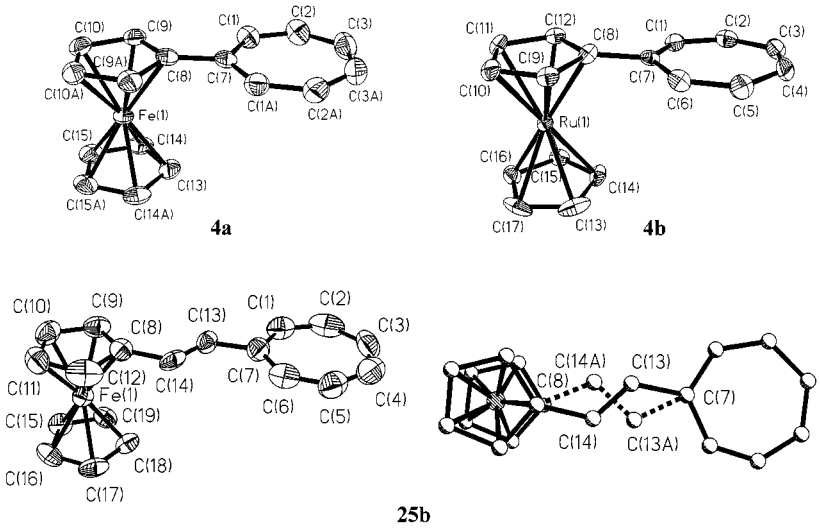


Figure 1. Molecular structures of **4a**, **4b** and **25a** (50% ellipsoids; for **25a** the disordered double bonds are additionally shown (right); the hydrogen atoms, counter ions (BF_4^- and PF_6^-, respectively) and solvent molecules are omitted for clarity)

400−700 mV more anodically shifted (Table 2), and includes an irreversible two-electron transfer.[38] As the π-bridge between the electrophores is extended, the difference of the potentials ΔE between the oxidation and reduction resembles more and more the ΔE value between the oxidation of the free metallocene and the reduction of the unsubstituted tropylium cation.

The electrochemical data make clear that in these sesquifulvalene complexes the nature of the HOMO is still dominated by the neutral donating sandwich units, whereas the character of the LUMO is determined by the cationic tropylium moiety. This combination favours a dipole change upon electronic excitation from the HOMO to the LUMO; ΔE is a relative measure of the energy gap between the HOMO and the LUMO.

band to a donor-acceptor charge transfer (DA−CT) transition. As can be deduced from the electrochemical data the oxidation potential of the ferrocenyl donor continuously approaches the potential of free ferrocene as the π-bridge is extended; similarly, the reduction potential of the acceptor tends towards that of the unsubstituted tropylium cation. Therefore, the energy difference between the donor (HOMO) and the acceptor (LUMO) orbitals has to reach a constant value with increasing π-bridge length, and thus the excitation energy must also reach a limiting value. The close relationship between the electrochemical data and the UV/Vis spectroscopic results is demonstrated by a graphical representation of the ΔE values of the ferrocene-containing complexes as a function of the λ_{max} value of the DA−CT transition (Figure 4).

Table 1. Selected structural data of **4a**, **4b**, and **25a**

Interatomic distances (pm)	**4a**	**4b**	**25a**
C8−C12		145.4(7)	140.6(15)
C8−C9	144.6(3)	144.4(7)	143.9(13)
C9−C10	142.7(4)	141.5(7)	139.5(15)
C10−C11	141.2(6)[a]	143.3(7)	139.4(16)
C11−C12		142.6(7)	141.6(17)
C7−C1	141.5(3)	141.5(7)	137.9(15)
C1−C2	137.7(4)	137.0(7)	140.9(17)
C2−C3	140.0(4)	141.4(8)	145(2)
C3−C4	136.1(7)[b]	136.2(8)	138(2)
C4−C5		140.7(8)	132.9(19)
C5−C6		138.9(7)	131.2(17)
C6−C7		141.0(7)	141.7(14)
M−C8	203.5(3)	215.8(5)	204.2(9)
M−C9	204.8(3)	218.0(5)	202.7(10)
M−C10	206.8(3)	220.5(5)	205.5(11)
M−C11		221.3(5)	205.4(10)
M−C12		216.9(5)	201.3(11)
C7−C8	145.0(5)	147.2(7)	
C8−C13			146.0(19)
C13−C14			131(3)
C7−C14			145(2)
Angles/°			
C8−12[c]/[bridge][d]	175.5°	174.0°	169.8°
[bridge][d]/C1−7[e]	177.0°	177.5°	173.7°
C8−12/C1−7	0°	3.84°	1.69°

[a] Interatomic distance C10−C10a. − [b] Interatomic distance C3−C3a. − [c] C8−12: plane of the five-membered ring. − [d] [bridge]: vector of the C7−C8 bond for **4a** and **4b**, and plane defined by the carbon atoms C7, C8, C13 and C14 for complex **25a**. − [e] C1−7: plane of the seven-membered rings.

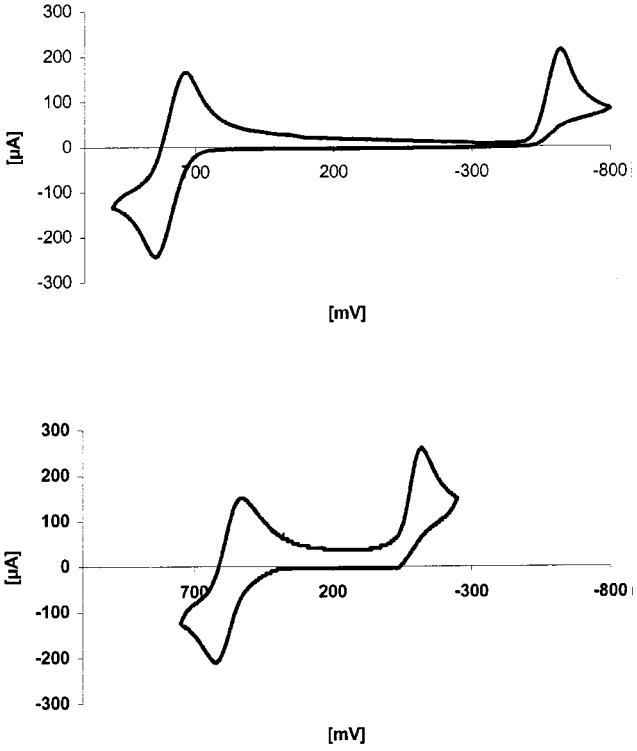


Figure 2. Representative cyclic voltammograms of mononuclear sesquifulvalene complexes: **4a** (top) and **27** (bottom) (E vs. Ag/AgI)

The assignment of the low-energy absorption to the DA−CT transition is also in agreement with the results of

Table 2. Redox potentials[a] of the cationic mononuclear sesquifulvalene complexes of the general form of **3**

ML_n	Z		$E_{1/2}$[a,b]	E_{pc}[a,b,c]	ΔE[b]
FeCp[d]	−	**4a**	0.40	−0.82	1.22
FeCp[d]	*E*-CH=CH	**25a**	0.22	−0.68	0.90
FeCp[d]	$(E\text{-CH=CH})_2$	**26**	0.08	−0.60	0.68
FeCp[d]	$(E\text{-CH=CH})_3$	**27**	0.09	−0.58	0.67
FeCp[d]	$2,5\text{-}C_4H_2S$	**28**	0.20	−0.66	0.82
FeCp[d]	$5,5'\text{-}(2,2'\text{-}C_4H_2S)_2$	**29**	0.10	−0.62	0.72
FeCp[d]	2-(5-*E*-CH=CH)C_4H_2S	**30**	0.10	−0.61	0.71
RuCp[e]	−	**4b**	1.12[f]	−0.85	1.97
RuCp[e]	*E*-CH=CH	**25b**	0.61[f]	−0.68	1.29
			0.61[f,g]	−	−
$[(C_7H_7)]PF_6$[e]	−	−	−	−0.63[h]	

[a] vs. $[FeCp_2]/[FeCp_2]^+$. − [b] in Volts. − [c] Irreversible one-electron reduction, scan rate 100 mV. − [d] In CH_2Cl_2. − [e] In $MeNO_2$. − [f] Irreversible oxidation. − [g] This work, other data ref.[38] − [h] This work, other data ref.[37]

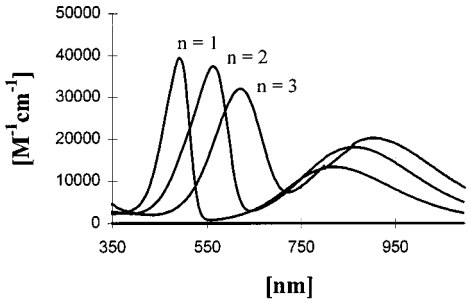


Figure 3. Representative UV/Vis spectra of mononuclear sesquifulvalene complexes $[Fc(E\text{-CH=CH})_nC_7H_6]^+$ demonstrating the effect of different numbers of olefinic spacers between the five- and seven-membered rings on the absorption maxima

the organic dye studies in that unusually long-wavelength absorptions are to be expected when the HOMO and the LUMO are located in different parts of the molecule.[40] Additionally, this assignment is corroborated by the relationship of the positions of the absorption bands on the nature of the donor: the absorption band at higher energy is considerably less influenced than the low lying absorption band upon changing the donating capability as demonstrated for **4a**, **4b** and **25a**, **25b**. It is therefore supposed that the higher-lying absorption band is due to an interligand π-π* transition (LL−CT), which also agrees with the dramatic bathochromic shift of this absorption band when the number of double bonds between the five- and seven-membered ring increases. Several theoretical models[2] have been proposed in an attempt to understand and relate the electronic structure of metallocenyl chromophores to their spectroscopic properties. Our assignment of the absorption bands is in excellent agreement with the latest theoretical treatment[2c] and is based on experimental results.

Non-Linear Optical Studies

The low lying excited states, the facile polarizability and the assignment of the HOMO and LUMO to the donor

Table 3. UV/Vis data of the monometallic sesquifulvalene complexes of the general form of **3**

ML_n	Z		LL−CT λ_{max}[a] (ε)[b]		$\Delta\tilde{\nu}$[c]	DA−CT λ_{max}[a] (ε)[b]		$\Delta\tilde{\nu}$[c]
			CH_2Cl_2	$MeNO_2$		CH_2Cl_2	$MeNO_2$	
FeCp	−	**4a**	400 (14710)	395 (13360)	−316	726 (3570)	700 (3330)	−511
FeCp	*E*-CH=CH	**25a**	490 (39440)	470 (24360)	−868	816 (10460)	765 (9510)	−817
FeCp	(*E*-CH=CH)$_2$	**26**	560 (37380)	520 (24860)	−1373	865 (18090)	780 (12770)	−1260
FeCp	(*E*-CH=CH)$_3$	**27**	621 (32040)	542 (43645)	−2347	903 (20215)	782 (23900)	−1714
FeCp	2,5-C_4H_2S[d]	**28**	530 (42870)	510 (33690)	−740	845 (11210)	760 (9470)	−1324
FeCp	5,5′-[2,2′-$C_4H_2S)_2$][e]	**29**	618 (31130)	560 (27800)	−1676	844 (11210)	700 (9820)	−2437
FeCp	2-(5-*E*-CH=CH)C_4H_2S[f]	**30**	595 20550)	520 (34820)	−2424	885 (8120)	775 (2440)	−1604
RuCp	−	**4b**	410 (14020)	398 (6660)	−740	560 (7360)	536 (18657)	−800
RuCp	*E*-CH=CH	**25b**	477 (16270)	455 (12040)	−1014	642 (22560)	600 (20345)	

[a] In nm. − [b] In $M^{-1}cm^{-1}$. − [c] In cm^{-1}. − [d] 2,5-thienylene bridge. − [e] 5,5′-(2,2′-dithienylene) bridge. − [f] 2-(5-*E*-vinylene)thienylene bridge.

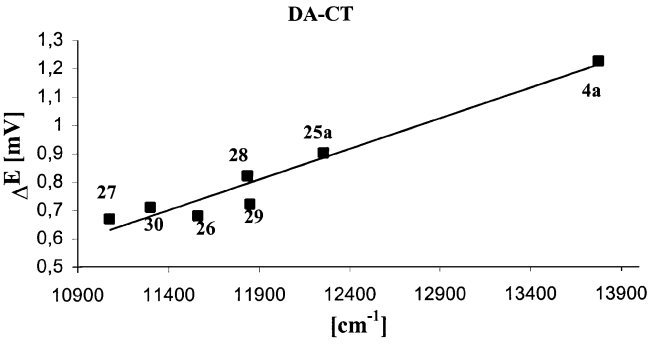


Figure 4. Correlation between the difference of the redox potentials and the λ_{max} values of the DA−CT bands of the ferrocenyl containing sesquifulvalene complexes

and acceptor orbitals, respectively, make sesquifulvalene type complexes most promising NLO candidates. Therefore these complexes were subjected to HRS studies. However, an intrinsic shortcoming of this method may be fluorescence due to two-photon absorption.[41−43]

Using the two-level approximation (Equation 1)[44] to calculate the first hyperpolarizability β indicates that β increases when the energy difference $\Delta E = h\omega_{eg}$ between the ground and the excited states decreases. Nevertheless, in an HRS experiment, the excited state will not be populated although the uptake of two photons of the irradiating frequency ω, and the instantaneous emission of one photon of 2ω will be more probable as the energy $E_{2\omega}$ approaches the energy of the excited state (E_{eg}).[45] When $E_{2\omega}$ equals E_{eg}, the CT state can be populated by the absorption of two photons, whereupon relaxation can occur by means of fluorescence, which may affect considerably the intensity of the measured frequency of the HRS signal (Figure 5).

Since the realisation of the problem of multiphoton absorption-induced fluorescence concerning the determination of first hyperpolarizabilities using the HRS method, several techniques to overcome this problem have been in-

$$\beta\ (-2\omega,\omega,\omega) = \frac{3\Delta\mu g M_{eg}^2}{(\hbar\omega)^2} \cdot \frac{\omega_{eg}^2}{(1-4\omega/\omega_{eg}^2)\cdot(\omega_{eg}^2-\omega^2)} \quad (1)$$

vestigated. These include long wavelength measurement,[47a,47b] time resolved HRS[47c] and the measurement of the two-photon fluorescence spectrum to abstract the fluorescence contribution to the HRS signal.[47d] Recently, Persoons et al.[47e] reported a high frequency demodulating technique to suppress the multiphoton fluorescence contribution to the HRS signal.

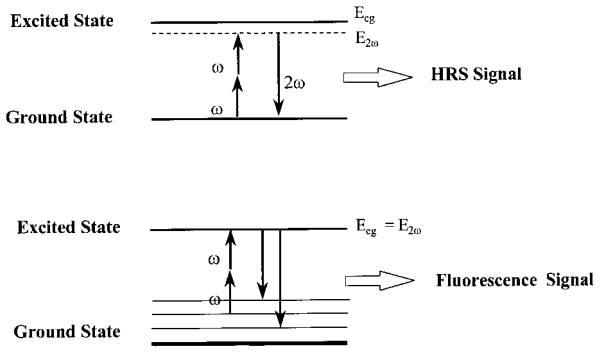


Figure 5. Schematic drawing of the origin of the HRS and the fluorescence signal

In order to check for fluorescence enhancement of the complexes under study we introduced bandpass filters with peak transmittances at different wavelengths in front of the photomultiplier of the HRS set-up.[46] A fluorescence signal should have a very broad line width and a maximum of the emission band which occurs at $\lambda/2$ only by chance.[47d] In sharp contrast to this the line width of the HRS signal is narrow and the maximum has to be fixed. In our investigations we used a Q-switched Nd:YAG laser with λ =

1064 nm, and detected the intensity of the scattered light at $\lambda = 532$ nm to determine the first hyperpolarizability as well as at $\lambda = 400$, 450, 500, 560, 600, 650 and 700 nm to obtain indications of fluorescence.

In Figure 6 the corresponding absorption and emission spectra of the reference *p*-nitroaniline (pNA) are shown corroborating the emission characteristics of the HRS signal of the second harmonic. Comparable HRS signals were recorded for the ruthenocenyl-containing sesquifulvalene complexes **4b** and **25b** as shown in Figure 7, whereas most of the ferrocene derivatives reveal broader emission spectra with a maximum not at $\lambda = 532$ nm (Figure 8), indicating that these ferrocene derivatives exhibit fluorescence. In some cases the solutions of the compounds under study were irradiated at the wavelength of the absorption bands. The failure of any subsequent fluorescence is a strong indication that the fluorescence for the ferrocene derivatives originates from a two-photon absorption.

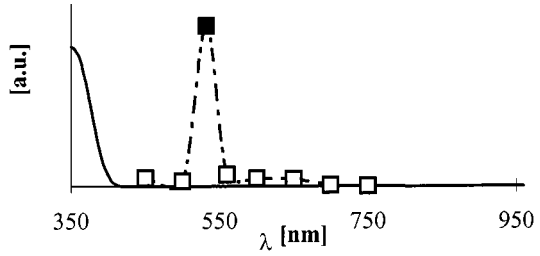


Figure 6. Absorption and emission spectra of the HRS reference *p*-nitroaniline (pNA) (irradiation wavelength $\lambda = 1064$ nm) [squares: λ of measured emission intensities; filled square: position of the HRS signal ($\lambda = 532$ nm)]

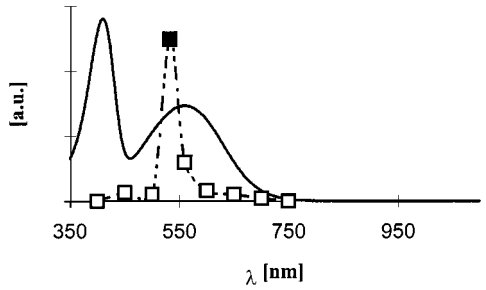


Figure 7. Absorption and emission spectra of the ruthenium sesquifulvalene complex **4b** (irradiation wavelength $\lambda = 1064$ nm; squares: λ of measured emission intensities; filled square: position of the HRS signal ($\lambda = 532$ nm))

In Table 4 the determined β values of the nonfluorescent complexes **4b** and **25b** are shown. Comparing the experimental first hyperpolarizability β and the calculated static hyperpolarizability β_0[50] of **4b** and **25b** it is obvious that the β_0 values are less reliable as the DA−CT maximum approaches the position of the HRS signal. Several features of the estimated β and β_0 values are remarkable:

• As expected from organic NLO chromophores, the first hyperpolarizability increases with increasing chain length (compare **4b** and **25b**). The β and β_0 value of **25b** determined from CH_2Cl_2 and $MeNO_2$ solutions confirm the long wavelength absorption as the DA−CT absorption band and its greater contribution to the first hyperpolarizability. Upon changing the solvent from CH_2Cl_2 to $MeNO_2$ both absorption bands undergo a distinct blue shift, which brings the low energy donor-acceptor absorption band closer to the HRS signal, whereas the LL−CT absorption band is shifted further away; thus, the resonance enhancement is greater for **25b** in $MeNO_2$ than in CH_2Cl_2 solution.

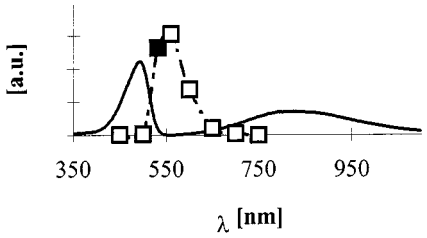


Figure 8. Absorption and emission spectra of the ferrocenyl-containing sesquifulvalene complex **25a** (irradiation wavelength $\lambda = 1064$ nm; squares: λ of measured emission intensities; filled square: position of the HRS signal ($\lambda = 532$ nm))

• These results illustrate that the metallocenes are stronger electron donors than cymantrenyl derivatives.

• Compared to other organometallic mononuclear NLO chromophores with extended π-linkers the results are very promising with regard to the short donor-acceptor distance in the sesquifulvalene-type complexes.

A comparison of the SHG effect between other ferrocenyl complexes[1d,2,36,49] and the corresponding mononuclear sesquifulvalene congeners (**4a**, **25a**, **26**−**30**) is not possible since the latter ferrocene derivatives all show fluorescence. However, our results demonstrate the necessity to check the ferrocenyl-containing D-π-A complexes for fluorescence. Much less work has been performed on NLO chromophores with a ruthenocenyl unit as a donor.[2a, 49] The published data have been obtained from EFISH-measurements at 1.907 μm. In addition to the problem of comparing EFISH and HRS data[41][42] a very recent paper show that first hyperpolarizabilities obtained at different fundamental wavelengths can hardly be compared. However, the β and β_0 values of **25b** listed in Table 4 correspond to values obtained for other sesquifulvalene complexes with ferrocenyl donor units.[11a,51,52]

Conclusions

Various synthetic routes to different dipolar cationic, mononuclear sesquifulvalene complexes, whose application as NLO chromophores appears to be successful, have been reported. Despite the relatively short dipole lengths, strong NLO effects can be obtained which are very promising with respect to longer π-linkers between the neutral donating sandwich and the cationic acceptor group of the seven-membered ring moiety.

Modification of the electronic properties of the donors and acceptors, and of the π-bridge, by chemical means presents the possibility of modulating the NLO properties in-

Table 4. Experimental first hyperpolarizability β[a] and static first hyperpolarizability β_0 (calcd. from Equation 1) of sesquifulvalene complexes tested as nonfluorescent, and examples from the literature for comparison

ML_n		acceptor	Z	λ_{max} [nm]	$\beta \times 10^{30}$ [esu]	$\beta_0 \times 10^{30}$ [esu]	ref.
RuCp[b]	**4b**	$C_7H_6^+$	–	536	378	4	
RuCp	**25b**	$C_7H_6^+$	*E*-CH=CH	600[b]	649	120	
				640[d]	362	105	
$Mn(CO)_3$[c]		$C_7H_6^+$	–	506	38		12
$Mn(CO)_2P(OMe)_3$[c]		$C_7H_6^+$	–	581	53		12
$Mn(CO)_3$[c]		$C_7H_6^+$	C≡C	491	95		12
$Mn(CO)_2P(OMe)_3$[c]		$C_7H_6^+$	C≡C	583	151		12
$Ind(Ph_3P)_2Ru$[b]		Ph–NO_2	C≡C	476	746	119	48a
$Cp(Ph_3P)_2Ru$[e]		*p*-$C_6H_4NO_2$	C≡C–C_6H_4-4-*E*-CH=CH	476	1455	232	48b
FeCp		$Ind(Ph_3P)_2Ru^+$	=C=CH–CH=CH	301[d]	117	73	49a
FeCp		$(\eta^5\text{-}C_4H_3S)Mn(CO)_3^+$	–	514[b]	260	13	49b
FeCp		$(\eta^5\text{-}C_4H_3S)Mn(CO)_3^+$	*E*-CH=CH	536[b]	670	−8	49b
FeCp		$(\eta^5\text{-}C_4H_3S)Mn(CO)_3^+$	$(E\text{-CH=CH})_2$	548[b]	771	34	49b

[a] Determined by hyper-Rayleigh scattering. – [b] Measured in $MeNO_2$, reference: pNA ($\beta = 34.6 \times 10^{-30}$ esu).[46] – [c] Measured in MeCN, reference: pNA ($\beta = 29.2 \times 10^{-30}$ esu). – [d] Measured in CH_2Cl_2, reference: pNA ($\beta = 21.6 \times 10^{-30}$ esu).[46] – [e] Measured in thf, reference: pNA ($\beta = 21.4 \times 10^{-30}$ esu).

volving the results of the first hyperpolarizability β and of the influence on the two-photon absorption. The two-photon fluorescence is observed in particular for mononuclear ferrocenyl derivatives possessing low-lying DA–CT and LL–CT transitions, and is not necessarily a disadvantage because of its potential use in devices for NIR detectors and optical data storage.[53]

Since the chemical modification of metallocenes, particularly ferrocene, is straightforward,[54] the linkage of the sesquifulvalene-type NLO chromophores to polymers or liquid crystalline phases is quite obvious. On the other hand the presented cationic complexes are amphiphilic; hence, they may also have some potential applications for Langmuir–Blodgett films.

Experimental Section

Manipulations were carried out under a N_2 atmosphere and solvents were saturated with N_2. Tetrahydrofuran (THF), diethyl ether (Et_2O), dimethoxyethane (DME), hexane and toluene were freshly distilled from the appropriate alkali metal or metal alloy. Nitromethane ($MeNO_2$), acetonitrile (MeCN) and dichloromethane (CH_2Cl_2) were dried over CaH_2 and distilled under N_2. NMR: Bruker AM 360 and Varian Gemini 200 BB; UV/Vis: Perkin–Elmer Model 554; IR nujol mull, KBr cells, FT-IR 1720X (Perkin–Elmer); EI-MS: 70 eV, Finnigan MAT 311 A; elemental analysis: Heraeus CHN-O-Rapid, Institut für Anorganische und Angewandte Chemie, Universität Hamburg. Formylferrocene, formylruthenocene,[17] chloromethylcycloheptatriene,[16] $BaMnO_4$,[18] 2-bromo-5-cyclohepta-2′,4′,6′-trien-1-ylthiophene (**16**),[22] 2-cycloheptatrienyl-2′,5-bithiophene (**19**)[26] and 2-formyl-5-cycloheptatrienylthiophene (**22**)[30] were synthesised according to literature procedures.

Ferrocenyltropylium Hexafluorophosphate (4a) and Ruthenocenyltropylium Hexafluorophosphate (4b). – Method A

4a: Ferrocene (1.22 g, 6.56 mmol) and tropylium hexafluorophosphate (0.62 g, 2.62 mmol) were stirred in MeCN (30 mL) for 65 h at room temperature. The reaction mixture was filtered and the deep blue-green filtrate was evaporated to dryness. The residue was extracted with toluene to remove the unreacted metallocene, and redissolved in CH_2Cl_2. The product 4a was precipitated by the addition of diethyl ether. Yield: 0.77 g (69.8%). Generally, the product was contaminated by paramagnetic impurities and $[C_7H_7][PF_6]$. Recrystallisation to obtain pure 4a lowers the yield considerably (for spectroscopic data: see below)

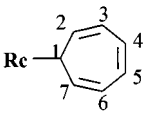
4b: Ruthenocene (0.32 g, 1.4 mmol) and tropylium hexafluorophosphate (0.20 g, 0.85 mmol) were stirred in 1,2-$C_2H_4Cl_2$ (30 mL) at 85°C for 50 h. The workup procedure as described for **4a** yielded 0.25 g (62.8%) of deep blue-violet crystals (for spectroscopic data: see below).

Method B

(Cyclohepta-2,4,6-trien-1-yl)ferrocene (5a): The synthesis of **5a** has been described elsewhere.[11a]

(Cyclohepta-2,4,6-trien-1-yl)ruthenocene (5b): Tropylium hexafluorophosphate (2.60 g, 11 mmol) was added portionwise to a suspension of ruthenocenyl lithium (2.37 g, 10 mmol) in Et_2O (50 mL) at −20 to −30°C. The reaction mixture was allowed to warm slowly to room temperature. After stirring for an additional three hours the solvent was evaporated and the colourless residue extracted with *n*-hexane. The product **5b** was obtained as slightly yellow crystals upon concentration of the hexane extracts. Yield: 2.41 g (75%).

5b: ^1H NMR ($CDCl_3$): δ = 2.28 (t, *J* = 5 Hz, 1 H, H-1), 4.56 (t, 2 H, C_5H_4), 4.57 (s, 5 H, Cp), 4.67 (t, 2 H, C_5H_4), 5.27 (dd, *J* = 3 Hz, *J* = 5 Hz, 2 H, H-2,7), 6.16 (m, 2 H, H-3,6), 6.68 (t, *J* = 3 Hz, 2 H, H-4,5). – ^{13}C NMR ($CDCl_3$): δ = 38.2 (C1), 70.0, 70.6 (C_5H_4, Cp), 94.7 (C_5H_4), 123.6 (C4,5), 127.4 (C2,7), 130.9 (C3,6).



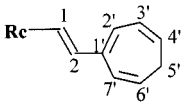
5b

– UV/Vis (CH_2Cl_2): λ_{max}[nm] (ε [M^{-1} cm^{-1}]) 288 (1530), 335 (sh). – EI-MS: *m/z* (%) 322 (80) [M^+ + 1], 321 (100) [M^+]. – $C_{17}H_{16}Ru$ (321.4): calcd. C 63.53, H 5.02; found C 63.45, H 5.13.

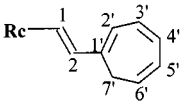
(Cyclohepta-1,3,5-trien-1-ylmethyl)diethylphosphonate (6): 1-Chloromethyl-1,3,5-cycloheptatriene[16](10.0 g, 71 mmol) was stirred in triethylphosphite (13.4 mL, 78 mmol) at 166°C for 8 h. After cooling, the reaction mixture was distilled at 2×10^{-2} mbar. Unreacted 1-chloromethylcyclohepa-1,3,5-triene was recovered at 30°C, and the product **6** obtained at 80°C as a yellow oil. Yield: 13.07 g (76%). – ^{1}H NMR (200 MHz, $CDCl_3$): δ = 1.36 (t, 6 H, CH_2CH_3), 2.48 (d, 2 H, C_7H_7), 2.81 (d, J_{PH} = 23 Hz, 2 H, CH_2P), 4.07 (m, 4 H, CH_2CH_3), 5.38–5.49 (m, 1 H, C_7H_7), 6.12 (m, 2 H, C_7H_7), 6.42–6.62 (m, 2 H, C_7H_7). – EI-MS: *m/z* (%) 242 (12) [M^+], 213 (19) [M^+ – Et], 185 (10) [M^+ – 2Et], 105 (40) [$C_8H_9^+$], 104 (100) [$C_8H_8^+$], 91 (23) [$C_7H_7^+$].

1-(Ferrocenyl)-2-(cycloheptatrienyl)ethene (8a): Complex **7a** was first synthesized by a Wittig reaction of formylferrocene[17] with $Ph_3PCH_2C_7H_7$ to yield a *Z*/*E* mixture of products.[11] Pure *E* isomers could be obtained from the WHWE reaction of formylferrocene with the phosphonate **6** as described for the ruthenocenyl derivative below.

1-Ruthenocenyl-2-(cycloheptatrienyl)ethene (8b): To a solution of the phosphonate **6** (0.57 g, 2.3 mmol) in 2 mL THF at –78°C was added *n*BuLi (1.6 mL of a 1.66 M hexane solution). The reaction mixture was allowed to warm to room temperature, stirred for 1 h and cooled down again to –78° C. Subsequently a solution of formylruthenocene (0.53 g, 2 mmol) in 20 mL of THF was added. The reaction mixture was allowed to warm slowly to room temperature. When the reaction, the course of which was monitored by TLC, had finished, the solvent was evaporated in vacuo, and the residue extracted with hexane. The product **8b** was purified by column chromatography (SiO_2/5% H_2O; hexane/Et_2O 1:1). Yield: 514 mg (75%) of **8b**. As can be deduced from the ^{1}H NMR spectra, the product is a mixture of two isomers which differ in the position of the sp^3-carbon atom in the seven-membered ring. The minor isomer (30%) is 1-ruthenocenyl-2-(cyclohepta-1′,3′,6′-trien-1′-yl)-ethene (isomer A), and the main product is 1-ruthenocenyl-2-(cyclohepta-1′,3′,5′-triene-1′-yl)ethene (isomer B). Both isomers are discernible by the splitting pattern of the high field signal of the sp^3 carbon bound protons between 2 and 3 ppm.



A



B

^{1}H NMR (200 MHz, $CDCl_3$): δ = 2.32 (t, *J* = 6.6 Hz, 2 H, H-5, isomer A), 2.60 (d, *J* = 7.1 Hz, 2 H, H-7′, isomer B), 4.52 (s, 5 H, C_5H_5), 4.58 (m, 2 H, C_5H_4), 4.79 (m. 2 H, C_5H_4), 5.36–5.54 (m, C_7H_7), 6.12–6.56 (m, C_7H_7, H-1, H-2). – EI-MS: *m/z* (%): 260 (67) [M^+], 232 (100) [$C_{10}H_{10}Ru^+$], 167 (56) [$C_5H_5Ru^+$]. – $C_{19}H_{18}Ru$ (347.4): calcd. C 65.69, H 5.22; found C 65.52, H 5.55.

1-Ferrocenyl-2-(ethoxycarbonyl)ethene (9): To a solution of (ethoxycarbonylmethyl)diethylphosphonate (2.78 g, 12 mmol) in toluene (100 mL) at 0°C was added *n*BuLi (7.8 mL of a 1.6 M hexane solution). Stirring was continued for 1 h, and then the reaction mixture was allowed to warm to room temperature. Subsequently it was cooled to 0°C, and a solution of formylferrocene (2.88 g, 14 mmol) in toluene (20 mL) was slowly added. After stirring for 1 h at room temperature the reaction mixture was hydrolysed and extracted with diethyl ether. The organic layer was dried over $MgSO_4$ and the solvent evaporated in vacuo. The residue was purified by column chromatography (Al_2O_3, neutral, 5% H_2O, hexane/diethyl ether 10:1). Yield: 3.15 g (90%). – ^{1}H NMR (200 MHz, C_6D_6): δ = 1.05 (t, *J* = 7.1 Hz, 3 H, CH_3), 3.48 (s, 5 H, C_5H_5), 3.90–4.10 (m, 2 H, C_5H_4), 4.10–4.20 (m, 4 H, CH_2, C_5H_4), 6.24 (d, *J* = 15.8 Hz, 1 H, H-1), 7.81 (d, *J* = 15.8 Hz, 1 H, H-2).

3-Ferrocenyl-2-propenol-1 (10): To a suspension of $LiAlH_4$ (0.4 g, 11 mmol) and $AlCl_3$ (0.40 g, 3 mmol) in diethyl ether (10 mL) at –10°C was added a solution of 1-ferrocenyl-2-(ethoxycarbonyl)ethene (**9**) (2.56 g, 9 mmol) in 8 mL diethyl ether. After stirring at room temperature for 1 h the reaction mixture was hydrolyzed at 0°C and acidified with dilute sulfuric acid. The product **10** was isolated by extraction with diethyl ether. Yield: 2.01 g (99%). – ^{1}H NMR (200 MHz, C_6D_6): δ = 3.9 (m, 2 H, CH_2OH), 3.98 (s, 5 H, C_5H_5), 4.04 (m, 2H. C_5H_4), 4.19 (m, 2 H, C_5H_4), 5.82 (dt, 1 H, H-2), 6.21 (d, 1 H, H-1).

3-Ferrocenylpropenal (11): Barium manganate(VI) (13.9 g, 54 mmol) was added to a solution of 3-ferrocenylpropenol (**10**) (2.01 g, 8.3 mmol) in dichloromethane (50 mL). After 30 min stirring the suspension was filtered and the filtrate evaporated to dryness. The residue was purified by column chromatography (Al_2O_3, neutral, 5% H_2O, hexane/diethyl ether 5:1). Yield: 1.63 g (82%). – ^{1}H NMR (200 MHz, C_6D_6): δ = 4.17 (s, 5 H, C_5H_5), 4.53 (m, 4H. C_5H_4), 6.34 (dd, $J_{1,2}$ = 7.6 Hz, $J_{2,3}$ = 15.4 Hz, 1 H, H-2), 7.42 (d, $J_{2,3}$ = 15.4 Hz, 1 H, H-3), 9.56 (d, $J_{1,2}$ = 7.6 Hz, H-1).

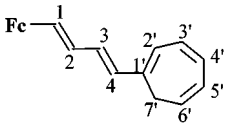
1-Ferrocenyl-4-(ethoxycarbonyl)-1,3-butadiene: The synthesis of 1-ferrocenyl-4-(ethoxycarbonyl)butadiene-1,3 was performed under the same conditions as the synthesis of 1-ferrocenyl-2-(ethoxycarbonyl)ethene (**9**). Quantities used: 1.02 g (4.22 mmol) of (ethoxycarbonylmethyl)diethylphosphonate, 30 mL of toluene, 2.64 mL (4.22 mmol) of *n*BuLi (15% solution in hexane), 1.01 g (4.22 mmol) of 3-ferrocenylpropenal (**11**) in 10 mL of toluene. Yield: 1.10 g (84%). – ^{1}H NMR (200 MHz, C_6D_6): δ = 1.06 (t, *J* = 7.2 Hz, 3 H, CH_3), 3.88 (s, 5 H, C_5H_5), 4.00–4.15 (m, 6 H, CH_2, C_5H_4), 5.99 (d, *J* = 15.2 Hz, 1 H, H-1), 6.32 (m, 2 H, H-2, H-3), 7.55–7.62 (m, 1 H, H-4).

5-Ferrocenyl-2,4-pentadienal (13): To a suspension of $LiAlH_4$ (0.135 g, 3.56 mmol) and $AlCl_3$ (0.158 g, 1.18 mmol) in 5 mL of diethyl ether at 10°C was added a solution of 1-ferrocenyl-4-(ethoxycarbonyl)butadiene (1.0 g, 3.22 mmol) in 4 mL of diethyl ether over 20 minutes. After stirring at room temperature for 1 h, the reaction mixture was hydrolysed with dilute sulfuric acid. Subsequently, the reaction mixture was extracted with diethyl ether. The organic layer was dried over Na_2SO_4 and the solvent was removed in vacuo. The residue of 1-ferrocenyl-1,3-pentadien-1-ol (0.78 g, 2.91 mmol) was dissolved in dichloromethane (20 mL) and oxidised by the addition of $BaMnO_4$ (6.1 g, 24 mmol). After stirring for 30 min the reaction mixture was filtered, the filtrate dried in vacuo and the product purified by column chromatography (Al_2O_3, neutral, 5% H_2O hexane/diethyl ether 5:3). Yield: 0.63 g (81%). – ^{1}H NMR (200 MHz, C_6D_6): δ = 3.89 (s, 5 H, C_5H_5),

4.08 (m, 2 H, C_5H_4), 4.13 (m, 2 H, C_5H_4), 6.00−6.65 (m, 4 H, H-2 − H-5), 9.54 (d, J = 7.8 Hz, 1 H, H-1).

General Procedure for the Synthesis of Mononuclear Monohydrosesquifulvalene Complexes Containing Two or Three Conjugated Double Bonds: A mixture of NaH, phosphonate **6** and the corresponding aldehyde in dimethoxyethane was slowly warmed to 85° C and stirred for 24 h. After cooling to room temperature the reaction mixture was hydrolyzed and extracted with Et_2O. The organic layer was dried with $MgSO_4$ and the product purified by column chromatography.

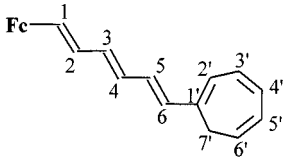
1-Ferrocenyl-4-(cyclohepta-1′,3′,5′-trien-1′-yl)-1,3-butadiene (12): 3-Ferrocenylpropenal (**11**) (1.0 g, 4.42 mmol), phosphonate **6** (1.07 g, 442 mmol), dimethoxyethane (20 mL) and NaH (0.1 g, 4.42 mmol). Column chromatography: Al_2O_3/5% H_2O, hexane/diethyl ether (5:1). Yield: 0.941 g (65%) of **12**.



12

^{1}H NMR (360 MHz, C_6D_6): δ = 2.70 (d, J = 7.2 Hz, 2 H, H-7′), 4.1 (s, 5 H, C_5H_5), 4.11 (m, 2 H, C_5H_4), 4.28 (m, 2 H, C_5H_4), 5.34 (m, 1 H, H-6′), 6.16 (m, 2 H, C_7H_7), 6.28 (m, 1 H, olefinic bridge) 6.43−6.65 (m, 5 H, C_7H_7 and olefinic bridge). − EI-MS: *m*/*z* (%) 328 (100) [M^+], 263 (10) [$M^+ - C_5H_5Fe^+$]. − $C_{21}H_{20}Fe$ (328.2): calcd. C 76.84, H 6.14; found C 75.45, H 6.27.

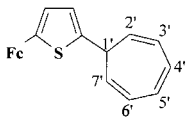
1-Ferrocenyl-6-(cyclohepta-1′,3′,5′-trien-1′-yl)-1,3,5-hexatriene (14): 5-Ferrocenyl-2,4-pentadienal (0.80 g, 3.0 mmol), THF (10 mL), phosphonate **6** (0.73 g, 3 mmol), NaH (0.073 g, 3 mmol). Column chromatography: Al_2O_3/5% H_2O, toluene. Yield: 0.45 g (63%) of **14**.



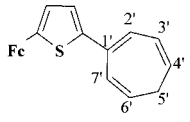
14

^{1}H NMR (360 MHz, C_6D_6): δ = 2.65 (d, J = 7.0 Hz, 2 H, H-7′), 4.00 (s, 5 H, C_5H_4), 4.11 (t, 2 H, C_5H_4), 4.29 (t, 2 H, C_5H_4), 5.31 (m, 1 H, H-6′), 6.13−6.18 (m, 2 H, C_7H_7), 6.29−6.66 (m, 8 H, olefinic bridge, C_7H_7). − EI-MS: *m*/*z* (%): 354 (100) [M^+], 289 (19) [$M^+ - C_5H_5$], 263 (15) [$M^+ - C_7H_7$], 250 (10), 225 (25), 199 (27), 186 (67) [$C_{10}H_{10}Fe^+$], 121 (65) [$C_5H_5Fe^+$]. − $C_{23}H_{22}Fe$ (354.3): calcd. C 77.98, H 6.26; found C 77.04, H 6.34.

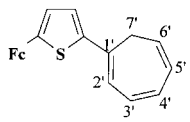
2-Ferrocenyl-5-(cycloheptatrienyl)thiophene (17): A solution of $ZnCl_2(THF)_2$ (3.37 g, 12 mmol) in THF (20 mL) was added to a solution of lithioferrocene[14] at −78°C. After 20 min stirring at −78°C the solution was allowed to warm slowly (40 min) to room temperature and a solution of 2-bromo-5-(cyclohepta-2′,4′,6′-trien-1′-yl)thiophene[22] (2.53 g, 10 mmol) and $Pd(PPh_3)_4$ (0.17 g, 0.1 mmol) in THF (40 mL) was added. After 15 h stirring at room temperature the reaction mixture was quenched with water (2 mL). The solvent was evaporated, the residue extracted with Et_2O (200 mL) in the presence of water (100 mL), and the ether layer was washed two times with 100 mL H_2O. The organic layer was dried over $MgSO_4$ and the product was isolated by column chromatography (Al_2O_3/5% H_2O/diethyl ether). Yield: 1.86 g (52%). The product **17** was a mixture of three isomers in the ratio 73% (**17A**), 14% (**17B**), 12% (**17C**). The composition of this mixture can be changed to 40:60 of isomers **17B** and **17C** by thermolysis in xylene (30 mL) under reflux for 33 h. The isomerisation was monitored by the disappearance of the proton signal H-1′ (2.94) of the isomer **17A**.



17A



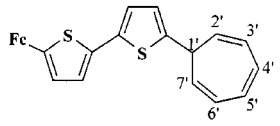
17B



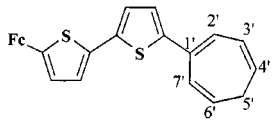
17C

^{1}H NMR (200 MHz, $CDCl_3$): **17A:** δ = 2.94 (t, 1 H, H-1′),), 4.10 (s, 5 H, C_5H_5) 4.26 (m, 2 H, C_5H_4), 4.54 (m, 2 H, C_5H_4), 5.53 (dd, 2 H, H-2′, H-7′), 6.27 (m, 2 H, H-3′, H-6′), 6.74 (m, 2 H, H-4′, H-5′), 6.80 (d, 1 H, C_4H_2S), 6.87 (d, 1 H, C_4H_2S). **17B**, **17C:** δ = 2.39 (t, J = 6.8 Hz, H-5′, **17B**), 2.81 (d, J = 6.8 Hz, H-7′, **17C**), 4.10 (s, C_5H_5), 4.11 (s, C_5H_5), 4.30 (m, C_5H_4), 4.58 (m, C_5H_4), 5.47−5.59 (m, 2 H, C_7H_7), 6.26 (dd, J = 9.4 Hz, J = 6.2 Hz, C_7H_7), 6.48 (d, J = 9.5 Hz, C_7H_7), 6.56−6.64 (m, C_7H_7), 6.86−7.06 (m, C_4H_2S, C_7H_7), 7.14 (d, J = 3.7 Hz, C_4H_2S), 7.20−7.42 (m, C_7H_7), 7.58−7.64 (m, C_4H_2S). − EI-MS: *m*/*z* (%) 358 (100) [M^+], 293 (3) [$M^+ - C_5H_5$], 202 (25) [$M^+ - C_{12}H_{12}$], 121 (21) [$C_5H_5Fe^+$]. − $C_{21}H_{18}FeS$ (358.3): calcd. C 70.40, H 5.06; found C 71.10, H 5.61.

5-Ferrocenyl-5′-(cycloheptatrienyl)-2,2′-bithiophene (20): To a cooled solution (−78°C) of 5-(cycloheptatrienyl)-2,2′-bithiophene (**19**) (1.43 g, 5.6 mmol) in 50 mL of THF was added *n*BuLi (3.5 mL of a 1.6 M hexane solution). The reaction solution was allowed to warm to room temperature, stirred for 40 min and cooled again to −78°C. A $ZnCl_2(THF)_2$ (1.56 g, 5.6 mmol) solution in THF (10 mL) was then added from a syringe. After warming to room temperature and additional stirring for 10 min this reaction mixture was added to a solution of iodoferrocene (1.73 g, 5.6 mmol) and $Pd(PPh_3)_4$ (0.06 g, 0.05 mmol) in THF (20 mL). The red coloured reaction mixture was stirred for 15 h, hydrolyzed with water (1 mL) and dried in vacuo. The solid residue was extracted with Et_2O, the organic layer was washed with water and dried over $MgSO_4$. The pure product was isolated after column chromatography (Al_2O_3/5% H_2O, hexane/ether 8:2). Yield: 1.36 g (55%) of **20** as the isomer A.



20A



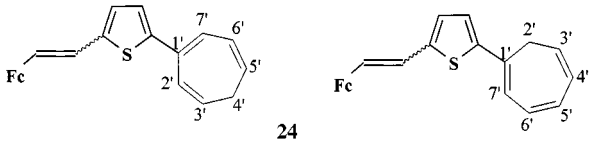
20B

20A: ^{1}H NMR (360 MHz, C_6D_6): δ = 3.09 (dt, J = 5.6 Hz, J = 1.0 Hz, 1 H, H-1′), 3.98 (s, 5 H, C_5H_5), 4.06 (t, 2 H, C_5H_4), 4.46 (t, 2 H, C_5H_4), 5.46 (dd, J = 8.7 Hz, J = 5.7 Hz, 2 H, H-2′, H-7′), 6.06 (m, 2 H, H-3′, H-6′), 6.52 (m, 2 H, H-4′, H-5′), 6.65 (dd, J = 1.0 Hz, J = 3.6 Hz, 1 H, C_4H_2S), 6.75 (d, J = 3.7 Hz, 1 H, C_4H_2S), 6.94 (d, J = 3.6 Hz, 1 H, C_4H_2S), 6.98 (d, J = 3.6 Hz, 1 H, C_4H_2S).

Thermal Rearrangement of the Isomer 20A: A solution of **20A** (0.77 g, 1.75 mmol) dissolved in toluene (8 mL) was refluxed for 24 h. The solution was evaporated to dryness yielding isomer **20B** quantitatively.

20B: ^{1}H NMR (200 MHz, $CDCl_3$): δ = 2.16 (t, *J* = 6.9 Hz, 2 H, H-5′), 3.97 (s, 5 H, C_5H_5), 4.06 (t, 2 H, C_5H_4), 4.46 (t, 2 H, C_5H_4), 5.27 (m, 2 H, H-4′, H-6′), 6.10 (dd, *J* = 9.2 Hz, *J* = 6.1 Hz, 1 H, H-3′), 6.44 (d, *J* = 9.1 Hz, 1 H, H-7′), 6.74 (d, *J* = 3.7 Hz, 1 H, C_4H_2S), 6.85 (d, *J* = 3.7 Hz, 1 H, C_4H_2S), 6.95 (d, *J* = 3.7 Hz, 1 H, C_4H_2S), 6.98 (d, *J* = 3.7 Hz, 1 H, C_4H_2S), 7.00 (d, *J* = 6.1 Hz, 1 H, H-2′). − EI-MS: *m*/*z* (%) 440 (100) [M^+], 121 (21) [$C_5H_5Fe^+$].

1-Ferrocenyl-2-(5′-cycloheptatrienylthien-2′-yl)ethene (24): To a solution of (ferrocenylmethyl)triphenylphosphonium iodide (4.3 g, 7.4 mmol) in THF (70 mL) was added *n*BuLi (4.63 mL of 1.6 M hexane solution). After stirring for 30 min a solution of a 1:2.5 mixture of 2-(cyclohepta-1,3,5-trien-1-yl)-5-formylthiophene and 2-(cyclohepta-1,3,6-trien-1-yl)-5-formylthiophene (**22**) (1.5 g, 7.4 mmol) in THF (10 mL) was added to the Wittig reagent and subsequently stirred for 14 h. The solvent was evaporated in vacuo, and the residue extracted with hexane. The product was purified by column chromatography (Al_2O_3/5% H_2O, hexane). Yield: 1.87 g (66%) of **24**. The product is a mixture of four isomers composed of two pairs of *Z*-and *E*-isomers which differ in the position of the sp^3-carbon atom of the seven-membered ring corresponding to the isomers **22** used as starting material.



24

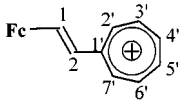
^{1}H NMR (200 MHz, $CDCl_3$): δ = 2.36 and 2.38 (t, *J* = 6.8 Hz, 2 H, H-5′, *E* and *Z* isomer of **24B**), 2.77 and 2.81 (d, *J* = 7.2 Hz, 2 H, H-5, *E* and *Z* isomer of **24A**), 4.13 (s, Cp), 4.26 (m, C_5H_4), 4.44 (m, C_5H_4), 5.51 (m, 2 H, C_7H_7), 6.20−7.10 (C_7H_7 and olefinic bridge). − $C_{23}H_{20}FeS$ (384.3): calcd. C 71.88, H 5.25; found C 71.94, H 5.51.

General Procedure for the Formation of the Cationic Mononuclear Sesquifulvalene Complexes by Hydride Abstraction: To a solution of the corresponding neutral monohydro-sesquifulvalene complex in dichloromethane was added an equimolar amount of trityl hexafluorophosphate dissolved in CH_2Cl_2. The reaction mixture was stirred for 30 min, and the cationic sesquifulvalene complex was precipitated by diluting the dark blue (M = Fe) or dark blue-violet (M = Ru) solution with Et_2O. Recrystallisation was performed by diffusion of Et_2O into a CH_2Cl_2 solution of the sesquifulvalene complexes.

4a·PF_6: Starting material: 0.352 g (1.16 mmol) of **5a** in 20 mL of dichloromethane, and 0.450 g (1.16 mmol) of trityl hexafluorophosphate in 10 mL of dichloromethane. Yield: 0.324 g (63%). ^{1}H NMR (200 MHz, CD_3NO_2): δ = 4.40 (s, 5 H, C_5H_5), 5.45 (t, *J* = 2 Hz, 2 H, C_5H_4), 5.51 (t, *J* = 2 Hz, 2 H, C_5H_4), 8.49−8.78 (m, 6 H, C_7H_6). − ^{13}C NMR (50 MHz, CD_3NO_2): δ = 73.4 (C_5H_4), 75.7 (C_5H_5), 81.8 (C_5H_4), 84.5 (C_q-C_5H_4), 147.9 (C_7H_6), 148.1(C_7H_6), 148.8 (C_7H_6), 175.8 (C_q-C_7H_6). − UV/Vis (CH_2Cl_2): λ_{max} [nm] (ε [$M^{-1}cm^{-1}$]) = 400 (14710), 725 (3570); (CH_3NO_2): λ_{max} [nm] (ε [$M^{-1}cm^{-1}$]) = 395 (13360), 700 (3330). − EI-MS: *m*/*z* (%) 276 (100), [M^+ − PF_6], 186 (25) [M^+ − C_7H_6 − PF_6]. − $C_{17}H_{15}F_6FeP$ (420.1): calcd. C 48.60, H 3.60; found C 48.24, H 3.76.

4b·PF_6: Starting material: 0.643 g (2.00 mmol) of **5b** in 10 mL of dichloromethane, and 0.777 g (2.00 mmol) trityl hexafluorophosphate in 10 mL of dichloromethane. Yield: 62%. − ^{1}H NMR (200 MHz, CD_3NO_2): δ = 4.74 (s, 5 H, C_5H_5), 5.48 (t, *J* = 1 Hz, 2 H, C_5H_4), 5.74 (t, *J* = 1 Hz, 2 H, C_5H_4), 8.44−8.31 (m, 4 H, C_7H_6), 8.67−8.57 (m, 2 H, C_7H_6). − ^{13}C NMR (50 MHz, CD_3NO_2): δ = 73.9 (C_5H_4), 76.8 (C_5H_5), 80.5 (C_5H_4), 88.4 (C_q-C_5H_4), 147.1 (C_7H_6), 149.2 (C_7H_6), 149.4 (C_7H_6), 173.5 (C_q-C_7H_6). − UV/Vis (CH_2Cl_2): λ_{max} [nm] (ε [$M^{-1}cm^{-1}$]) = 410 (14020), 560 (7360); (CH_3NO_2): λ_{max} [nm] (ε [$M^{-1}cm^{-1}$]) = 398 (6655), 536 (3245). − EI-MS: *m*/*z* (%) 322 (10), [M^+ − PF_6], 232 (20) [M^+ − C_7H_6 − PF_6]. − $C_{17}H_{15}F_6PRu$ (465.3): calcd. C 43.88, H 3.25; found C 44.07, H 3.54.

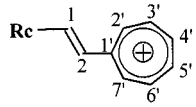
25a·PF_6: Starting material: 0.352 g (1.16 mmol) of **8a** in 20 mL of dichloromethane, and 0.450 g (1.16 mmol) of trityl hexafluorophosphate in 10 mL of dichloromethane. Yield: 0.324 g (63%).



25a

^{1}H NMR (200 MHz, CD_3NO_2): δ = 4.43 (s, 5 H, C_5H_5), 5.03 (t, 2 H, C_5H_4), 5.17 (t, 2 H, C_5H_4) 7.10 (d, *J* = 15.4 Hz, 1 H, H-2), 8.39 (d, *J* = 15.3 Hz, 1 H, H-1), 8.30−8.59 (m, 4 H, H-3′,6′, H-4′,5′) 8.62 (d, *J* = 10.4 Hz, 2 H, H-2′,7′). − ^{13}C NMR (50 MHz, CD_3NO_2): δ = 72.9 (C_5H_4), 73.6 (C_5H_5) 78.6 (C_5H_4), 83.8 (C_q-C_5H_4), 126.7 (C2), 147.9 (C_7H_6), 148.5 (C_7H_6), 148.9 (C_7H_6), 156.0 (C1), 164.7 (C_q-C_7H_6). − UV/Vis (CH_2Cl_2): λ_{max} [nm] (ε [$M^{-1}cm^{-1}$]) = 490 (39440), 816 (10460); (CH_3NO_2): λ_{max} [nm] (ε [$M^{-1}cm^{-1}$]) = 470 (24360), 765 (9510). − $C_{19}H_{17}F_6FeP$ (446.2): calcd: C 51.15, H 3.84; found C 51.17, H 3.93.

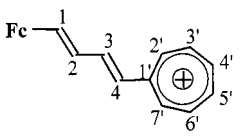
25b·PF_6: Starting material: 0.480 g (1.38 mmol) of **8b** in 20 mL of dichloromethane, and 0.538 g (1.38 mmol) of trityl hexafluorophosphate in 10 mL of dichloromethane. Yield: 0.52 g (77%).



25b

^{1}H NMR (200 MHz, CD_3NO_2): δ = 4.78 (s, 5 H, C_5H_5), 5.20 (t, 2 H, C_5H_4), 5.31 (t, 2 H, C_5H_4) 7.08 (d, *J* = 15.4 Hz, 1 H, H-2), 8.23 (d, *J* = 15.4 Hz, 1 H, H-1), 8.32−8.40 (m, 4 H, H-3′,6′, H-4′,5′) 8.61 (d, *J* = 9.7 Hz, 2 H, H-2′,7′). − ^{13}C NMR (50 MHz, CD_3NO_2): δ = 73.5 (C_5H_4), 74.8 (C_5H_5), 77.7 (C_5H_4), 125.0 (C2), 147.6 (C_7H_6), 148.6 (C_7H_6), 149.3 (C_7H_6), 152.3 (C1). − UV/Vis (CH_2Cl_2): λ_{max} [nm] (ε [$M^{-1}cm^{-1}$]) = 477 (16270), 642 (22560); (CH_3NO_2): λ_{max} [nm] (ε [$M^{-1}cm^{-1}$]) = 455 (12040), 600 (20345). − $C_{19}H_{17}F_6PRu$ (491.4): calcd: C 46.44, H 3.49; found C 45.86, H 3.74.

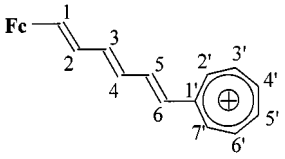
26·PF_6: Starting material: 0.392 g (1.2 mmol) of **12** in 20 mL of dichloromethane, and 0.466 g (1.2 mmol) trityl hexafluorophosphate in 10 mL of dichlorohexane. Yield: 0.429 g (76%).



26

^{1}H NMR (200 MHz, CD_3NO_2): δ = 4.43 (s, 5 H, C_5H_5), 4.85 (s, 2 H, C_5H_4), 4.89 (s, 2 H, C_5H_4), 6.97 (dd, $J_{1,2}$ = 14.7 Hz, $J_{2,3}$ = 3.5 Hz, 1 H, H-2), 6.95 (d, $J_{3,4}$ = 14.7 Hz, 1 H, H-4), 8.06 (dd, $J_{3,4}$ = 14.7 Hz, $J_{2,3}$ = 3.4 Hz, 1 H, H-3), 8.26−8.44 (m, 4 H, H-3′,6′, H-4′,5′), 8.53 (d, $J_{1,2}$ = 14.9 Hz, 1 H, H-1), 8.62 (d, J = 10.1 Hz, 2 H, H-2′,7′). − ^{13}C NMR (50 MHz, CD_3NO_2): δ = 71.9 (C_5H_4), 73.2 (C_5H_5), 76.5 (C_5H_4), 78.6 (C_q-C_5H_4), 128.4 (C2), 130.6 (C4), 148.1 (C_7H_6), 148.9 (C_7H_6), 149.0 (C_7H_6), 152.2 (C1), 155.5 (C3), 166.6 (C_q-C_7H_6). − UV/Vis (CH_2Cl_2): λ_{max} [nm] (ε [$M^{-1}cm^{-1}$]) = 560 (37380), 865 (18090); (CH_3NO_2): λ_{max} [nm] (ε [$M^{-1}cm^{-1}$]) = 520 (24860), 780 (12770). $C_{21}H_{19}F_6FeP$ (472.2): calcd. C 53.42, H 4.06; found C 52.73, H 4.31.

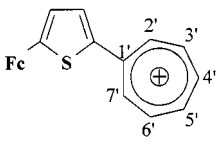
27·PF_6: Starting material: 0.668 g (1.89 mmol) of **14** in 20 mL of dichloromethane, and 0.732 g (1.89 mmol) of trityl hexafluorophosphate in 10 mL of dichloromethane. yield: 0.51 g (54%).



27

^{1}H NMR (360 MHz, CD_2Cl_2): δ = 4.62 (s, 5 H, C_5H_5), 5.18 (m, 4 H, C_5H_4), 6.34 (t, J = 12.7 Hz, 1 H, H-2), 6.47 (t, J = 12.9 Hz, 1 H, H-4), 6.68 (d, J = 14.3 Hz, 1 H, H-6), 7.01 (d, J = 14.5 Hz, 1 H, H-1), 7.27 (t, 1 H, J = 12.7 Hz, H-3), 7.98 (dd, J = 10.0, J = 3.7 Hz, 2 H, C_7H_6), 8.08 (dd, J = 14.6, 11.85 Hz, 1 H, H-5), 8.13 (m, 2 H, C_7H_6), 8.35 (d, J = 10.7 Hz, 2 H, C_7H_6).

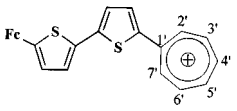
28·PF_6: Starting material: 0.260 g (0.673 mmol) of **17** in 20 mL of dichloromethane, and 0.261 g (0.673 mmol) trityl hexafluorophosphate in 5 mL of dichloromethane. Yield: 0.20 g (60%).



28

^{1}H NMR (200 MHz, CD_3NO_2): δ = 4.25 (s, 5 H, C_5H_5), 4.84 (s, 2 H, C_5H_4), 5.03 (s, 2 H, C_5H_4), 7.45 (d, J = 4.5 Hz, 1 H, C_4H_2S), 8.24 (d, J = 4.4 Hz, 1 H, C_4H_2S), 8.28−8.47 (m, 4 H, H-3′,6′, H-4′,5′), 8.79 (d, J = 10.6 Hz, 2 H, H-2′,7′). − ^{13}C NMR (50 MHz, CD_3NO_2): δ = 70.8 (C_5H_4), 73.5 (C_5H_5), 75.1 (C_5H_4), 78.4 (C_q-C_5H_4), 129.9 (C_4H_2S), 140.6 (C_4H_2S), 141.1 (C_q-C_4H_2S), 146.2 (C_7H_6), 149.4 (C_7H_6), 150.4 (C_7H_6), 160.3 (C_q-C_4H_2S), 168.4 (C_q-C_7H_6). − $C_{21}H_{17}F_6FePS$ (502.2): calcd: C 50.22, H 3.41; found C 50.27, H 3.80.

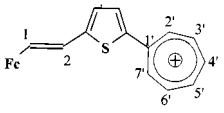
29·PF_6: Starting material: 0.305 g (0.69 mmol) of **20** in 15 mL of dichloromethane, and 0.269 g (0.69 mmol) trityl hexafluorophosphate in 10 mL of dichloromethane. Yield: 0.222 g (55%).



29

^{1}H NMR (200 MHz, CD_3NO_2) δ = 4.37 (s, 5 H, C_5H_5), 5.14 (s, 2 H, C_5H_4), 5.90 (s, 2 H, C_5H_4) 8.13−8.54 (10 H, C_4H_2S and C_7H_6). − ^{13}C NMR (50 MHz, CD_3NO_2): δ = 69.5 (C_5H_4), 72.9 (C_5H_5), 73.1 (C_5H_4), 126.4 (C_4H_2S), 129.4 (C_4H_2S), 131.1 (C_4H_2S), 140.4 (C_4H_2S), 146.4 (C_7H_6), 150.0 (C_7H_6) 150.8 (C_7H_6), (signals of quaternary ^{13}C not observed). − $C_{25}H_{19}F_6FePS$ (552.3): calcd. C 51.39, H 3.28; found C 52.34, H 3.91.

30·PF_6: Starting material: 0.238 g (0.62 mmol) of **24** in 2 mL of dichloromethane, and 0.240 g (0.62 mmol) trityl hexafluorophosphate in 2 mL of dichloromethane. Yield: 0.258 g (79%).



30

^{1}H NMR (200 MHz, CD_2Cl_2) δ = 4.28 (s, 5 H, C_5H_5), 4.70 (m, 4 H, C_5H_4), 6.91 (d, J = 15.6 Hz, 1 H, H-2), 7.34 (d, J = 4.4 Hz, 1 H, C_4H_2S), 7.39 (d, J = 15.4 Hz, 1 H, H-1), 8.17 (d, J = 4.6 Hz, 1 H, C_4H_2S), 8.05 (dd, J = 7.1 Hz, J = 4.1 Hz, 2 H, H-4′,5′), 8.20 (m, 2 H, H-3′,6′), 8.53 (d, J = 10.8 Hz, 2 H, H-2′,7′. − ^{13}C NMR (50 MHz, CD_2Cl_2): δ = 69.7 (C_5H_4), 71.2 (C_5H_5), 73.6 (C_5H_4), 81.8 (C_q-C_5H_4), 117.0 (C2), 130.8 (C_4H_2S), 140.2 (C_4H_2S), 142.1 (C1), 144.3 (C_7H_6), 147.1 (C_7H_6), 148.1 (C_7H_6), 163.4 (C_q-C_7H_6). − $C_{23}H_{19}F_6FePS$ (528.3): calcd. C 52.29, H 3.63; found C 52.28, H 3.95.

X-ray Structure Determination : Crystals suitable for an X-ray structure analysis were obtained by diffusion of Et_2O from the gas phase into CH_2Cl_2 solutions of **4a**, **4b** or **25a**. The data were collected on a four-circle diffractometer Hilger & Watts, Mo-K_α, λ = 0.71073 Å. The structures were solved by direct methods (SHELXS-86).[55] Refinement on F^2 were carried out by full-matrix least-square techniques (SHELXL-93).[56] All non-hydrogen atoms were refined with anisotropic thermal parameters. The hydrogen atoms were refined with a fixed isotropic thermal parameter related by a factor of 1.2 to the value of the equivalent isotropic thermal parameter of their carrier atoms. Weights were optimised in the final refinement cycles (Table 5).

Crystallographic data (excluding structure factors) for the structures reported in this paper have been deposited with the Cambridge Crystallographic Data Centre as supplementary publication no. CCDC-133669 (**4a**), -133670 (**4b**) and -133671 (**25a**). Copies of the data can be obtained free of charge on application to CCDC, 12 Union Road, Cambridge CB2 1EZ, UK [Fax: (internat.) + 44-1223/336-033; E-mail: deposit@ccdc.cam.ac.uk].

Cyclic Voltammetry: An Amel System 5000 was used. The measurements were performed in CH_2Cl_2 and $MeNO_2$ with 0.4 M [N(*n*-Bu)$_4$]ClO_4 as supporting electrolyte, ca. 10^{-3} M solutions of the complexes, a Pt wire as working electrode and a Pt plate (0.6 cm^2) as auxiliary electrode. The given potentials were measured against Ag/Ag^+ and are referenced against $E_{1/2}([FeCp_2]/[FeCp_2]^+)$ = 0 V.

Hyper-Rayleigh Scattering: For experimental set-up see ref.[46]; the measurements were performed at a fundamental wavelength of λ = 1064 nm with a Q-switched Nd:YAG laser; CH_2Cl_2 and $MeNO_2$ solutions were used for the measurements, with concentrations of 10^{-4} to 10^{-6} concerning the complexes under study; *p*-nitroaniline was used as reference [$\beta(CH_2Cl_2) = 21.6 \times 10^{-30}$ esu, $\beta(MeNO_2) = 34.6 \times 10^{-30}$ esu].[46]

Table 5. Crystallographic data of **4a**, **4b** and **25a**

	4a	**4b**	**25a**
Formula	$C_{17}H_{15}BF_4Fe$	$C_{17}H_{15}F_6PRu$	$C_{20}H_{19}Cl_2F_6FeP$
M_r	361.95	465.33	531.07
Crystal system	orthorhombic	monoclinic	triclinic
Space group	*Pnma*	*P*2(1)/*c*	$P\bar{1}$
a/Å	21.75(2)	8.104(3)	10.067(6)
b/Å	9.900(2)	18.206(14)	10.496(6)
c/Å	6.881(3)	11.228(4)	11.418(6)
α/°	–	–	94.07(4)
β/°	–	107.59(3)	110.96(4)
γ/°	–	–	102.88(5)
V/Å^3	1482.0(15)	1579.1(15)	1083.1(11)
Z	4	4	2
ρ_{calcd} /g cm^{-3}	1.622	1.957	1.628
abs. coeff./mm^{-1}	1.055	1.156	1.072
T /K	173(2)	173(2)	293(2)
F(000)	736	920	536
Crystal size/mm^3	0.6 × 0.4 × 0.1	0.4 × 0.3 × 0.1	0.4 × 0.5 × 0.1
θ range /°	2.78 ≤ θ ≤ 30.10	2.64 ≤ θ ≤ 27.57	2.34 ≤ θ ≤ 24.00
Index range	$-1 \le h \le 30$	$-1 \le h \le 10$	$-2 \le h \le 11$
	$-13 \le k \le 1$	$-1 \le k \le 23$	$-12 \le k \le 11$
	$-1 \le l \le 9$	$-14 \le l \le 13$	$-13 \le l \le 12$
Total reflns	3134	4590	4715
Unique reflns	2293	3661	3388
Obs. Reflns [I>2σ(I)]	1773	2640	2147
Parameters/restraints	131/0	227/0	327/0
GooF	1.061	1.000	1.039
R_{int}	0.0175	0.0294	0.0571
R indices [I > 2 σ (I)]	*R*1 = 0.0496	*R*1 = 0.0455	*R*1 = 0.0981
	*wR*2 = 0.1172	*wR*2 = 0.0901	*wR*2 = 0.2490
R indices (all data)	*R*1 = 0.0690	R1 = 0.0778	*R*1 = 0.1468
	*wR*2 = 0.1280	*wR*2 = 0.1012	*wR*2 = 0.2916
Min. max. resd/eÅ^{-3}	−0.647, 0.529	−0.838, 0.775	−0.778, 2.059

Acknowledgments

This work was supported by the Deutsche Forschungsgemeinschaft (DFG, HE 1309/3) and by the European Community (COST D4/0003/94, TMR FMRX-CT98−0166).

[1] [1a] D. J. Williams, *Angew. Chem.* **1984**, *96*, 637−651; *Angew. Chem. Int. Ed. Engl.* **1984**, *23*, 690−703. – [1b] R. W. Boyd, in *Nonlinear Optics*, Academic Press, Inc, **1992**; G. H. Wagnière, in *Linear and Nonlinear Optical Properties of Molecules*, VCH, Weinheim, **1993**. – [1c] P. N. Prasad, D. J. Williams, in *Nonlinear Optical Effects In Molecules & Polymers*, Wiley & Sons, New York, **1991**. – [1d] *Nonlinear Optics of Organic Molecules and Polymers* (Eds.: H. S. Nalwa, S. Miyata), CRC Press, New York, **1997**. – [1e] K. Meerholz, *Angew. Chem.* **1997**, *109*, 981−985; *Angew. Chem. Int. Ed. Engl.* **1997**, *36*, 945−949.

[2] [2a] J. C. Calabrese, L.-T. Cheng, J. C. Green, S. R. Marder, W. Tam, *J. Am. Chem. Soc.* **1991**, *113*, 7227−7232. – [2b] D. R. Canis, M. A. Ratner, T. J. Marks, *J. Am. Chem. Soc.* **1990**, *112*, 8203−8204. – [2c] D. R. Canis, M. A. Ratner, T. J. Marks, *J. Am. Chem. Soc.* **1992**, *114*, 10338−10357. – [2d] D. R. Canis, M. A. Ratner, T. J. Marks, *J. Am. Chem. Soc.* **1994**, *116*, 195−242. – [2e] S. Barlow, H. E. Bunting, C. Ringham, J. C. Green, G. U. Bublitz, S. G. Boxer, I. W. Perry, S. R. Marder, *J. Am. Chem. Soc.* **1999**, *121*, 3715−3723.

[3] T. J. Marks, M. A. Ratner, *Angew. Chem.* **1995**, *107*, 167−187; *Angew. Chem. Int. Ed. Engl.* **1995**, *34*, 155−174.

[4] [4a] N. J. Long, *Angew. Chem.* **1995**, *107*, 37−56; *Angew. Chem. Int. Ed. Engl.* **1995**, *34*, 21−38. –[4b] H. S. Nalwa, *Appl. Organomet. Chem.* **1991**, *5*, 349−377. –[4c] I. R. Whittall, A. M. McDonagh, M. G. Humphrey, M. Samoc, *Adv. Organomet. Chem.* **1998**, *42*, 291−362. –[4d] T. Verbiest, S. Houbrechts, M. Kauranen, K. Clays, A. Persoons, *J. Mater. Chem.* **1997**, *7* (11), 2175−2189.

[5] B. J. Coe, S. Houbrechts, I. Asselberghs, A. Persoons, *Angew. Chem.* **1999**, *111*, 377−380; *Angew. Chem. Int. Ed.* **1999**, *38*, 366−369.

[6] T. Kondo, S. Horiuchi, I. Yagi, S. Ye, K. Uosaki, *J. Am. Chem. Soc.* **1999**, *121*, 391−398.

[7] H. Prinzbach, *Pure Appl. Chem.* **1971**, *28,* 281−329.

[8] J. O. Morley, *J. Am. Chem. Soc.* **1988, 110**, 7660−7663.

[9] G. R. J. Williams, *J. Mol. Struct. (Thermochem)* **1987**, *151*, 215−222.

[10] M. Neuenschwander, W. K. Schenk, *Chimia*. **1972**, *26*, 194−197.

[11] [11a] U. Behrens, H. Bussaard, U. Hagenau, J. Heck, E. Hendrickx, J. Körnich, J. G. M. van der Linden, A. Persoons, A. L. Spek, N. Veldman, B. Voss, H. Wong, *Chem. Eur. J.* **1996**, *2*, 98−103. –[11b] J. Heck, H. C. Brussaard, S. Dabek, T. Meyer-Friedrichsen, H. Wong, *Proc. SPIE, Int. Soc. Opt. Eng.* **1997**, *3*, 53−61.

[12] M. Tamm, A. Grzegorzewski, T. Steiner, T. Jentzsch, W. Werncke, *Organometallics* **1996**, *15*, 4984−4990.

[13] M. Cais, A. Eisenstadt, *J. Am. Chem. Soc.* **1967**, *89*, 5468−5469.

[14] D. Guillaneux, H. B. Kagan, *J. Org. Chem.* **1995**, *60*, 2502−2505.

[15] J. Boutagy, R. Thomas, *Chem.* Rev. **1974**, *74*, 87−99.

[16] L. A. Paquette, H.-J. Kang, C. S. Ra, *J. Am. Chem. Soc.* **1992**, *114*, 7387−7395.

[17] R. Sanders, U. T. Mueller.-Westerhoff, *J. Organomet. Chem.* **1996**, *512*, 219−224.

[18] R. S. Nyholm, P. R. Woolliams, *Inorg. Syn.* **1968**, *11,* 56−61.

[19] F. Effenberger, F. Würthner, *Angew. Chem.* **1993**, *105*, 742−744; *Angew. Chem. Int. Ed. Engl.* **1993**, *32*, 719−721; F. Effenberger, F. Wüthner, F. Steybe, *J. Org. Chem.* **1995**, *60*, 2082−2091.

[20] J. X. Zhang, P. Dubois, R. Jérôme, *J. Chem. Soc., Perkin Trans. 2* **1997**, 1209−1216; S.-S. P. Chou, C.-H. Shen, *Tetrahedron Letters*, **1997**, *36*, 6407−6410; see also ref.[1d], p. 108 ff.

[21] A. Abbotto, S. Bradamante, A. Facchetti, G. A. Pagani, *J. Org.*

Chem. **1997**, *62*, 5755−5765. D. D. Graf, K. R. Mann, *Inorg. Chem.* **1997**, *36*, 141−149.
[22] Y. Golberg, H. Alper, *J. Org. Chem.* **1993, 58**, 3072−3075.
[23] K. Takahashi, T. Sakae, K. Takase, *Chem. Lett.* **1980**, 179.
[24] W.-Y. Wong, W.-T. Wong *J. Chem. Soc., Dalton Trans.* **1996**, 3209−3214.
[25] [25a] T. Nihira, S. Tarutani, K. Takase, K. Takahashi *Heteroycles*, **1995** *41*, 2169−2172. − [25b] E. Negishi, T. Takahashi, A. O. King *Organic Synthesis* **1987**, *66*, 67−72.
[26] R. J. P. Corriu, J. P. Masse, *J. Chem. Soc., Chem. Commun.* **1972**, 141; K. Tamao, K. Sumitani, M. Kumada, *J. Am. Chem. Soc.* **1972**, 94, 4374−4376.
[27] J. M. Tour, R. Wu, *Macromolecules* **1992**, *25*, 1901−1907.
[28] [28a] I.-Y. Wu, J. T. Lin, J. Luo, C.-S. Li, C. Tsai, Y. S. Wen, C.-C. Hsu, F.-F. Yeh, S. Liou, *Organometallics* **1998**, *17*, 2188−2198. − [28b] J. X. Zhang, P. Dubois, R. Jérome, *J. Chem. Soc., Perkin. Trans.* **1997**, *2*, 1209−1216.
[29] M. R. Detty, D. S. Hays, *Heterocycles* **1995**, *40*, 925−937.
[30] P. L. Pauson, W. E. Watts, *J. Chem. Soc*. **1963**, 2990−2996.
[31] H. E. Bunting, M. L. H. Green, S. R. Marder, M. E. Thompson, D. Bloor, V. Kolinsky, R. J. Jones, *Polyhedron* **1992**, *11*, 1489−1499.
[32] C.-T. Chen, S. R. Marder, L.-T. Cheng, *J. Chem. Soc., Chem. Commun.* **1994**, 259−260; S. R. Marder D. N. Beratan, L.-T. Cheng, *Science*, **1991**, *252*, 103−106.
[33] S. R. Marder, B. Kippelen, A. K.-Y. Jen, N. Peyghambarian, *Nature*, **1997**, *388*, 845−851.
[34] S. K. Brownstein, E. J. Gabe, R. C. Hynes, *Can. J. Chem.* **1992**, *70*, 1011−1014.
[35] M. Tamm, A. Grzegorzewski, I. Brüdgam, *J. Organomet. Chem.* **1996**, *519*, 217−220.
[36] U. Hagenau, J. Heck, E. Hendrickx, A. Persoons, T. Schuld, H. Wong, *Inorg. Chem.* **1996**, *35*, 7863−7866.
[37] A. M. Romani, A. Ceccon, A. Venzo, *J. Elektroanal. Chem.* **1981**, *130*, 245−254; A. M. Romani, A. Venzo, A. Ceccon, *J. Elektroanal. Chem.* **1980**, *112*, 147−155.
[38] U. T. Müller-Westerhoff, A. L. Rheingold, G. F. Swiegers, *Angew. Chem.* **1992**, *104*, 1398−1400; *Angew. Chem. Int. Ed. Engl.* **1992**, *31*, 1352−1354; A. F. Diaz, U. T. Müller-Westerhoff, A. Nazzal, M. Tanner, *J. Organomet. Chem.* **1982**, C45−C48.
[39] C. Reichardt, *Solvents and Solvent Effects in Organic Chemistry*, 2nd ed. VCH, Weinheim, **1988**.
[40] M. Klessinger, *Chemie in unserer Zeit* **1978**, *12*, 1−10.
[41] K. Clays, E. Hendrickx, T. Verbiest, A. Persoons, *Adv. Mater.* **1998**, *10*, 643−655.
[42] J. J. Wolff, R. Wortmann, *J. Prakt. Chem.* **1998**, *340*, 99−111.
[43] S. Stadler, G. Bourhill, C. Bräuchle, *J. Phys. Chem.* **1996**, *100*, 6927−6941.
[44] J. L. Oudar, D. S. Chemla, *Chem. Phys.* **1977**, *66*, 2664−2668; E. Hendrickx, K. Clays, A. Persoons, C. Dehu, J. L. Brédas, *J. Am. Chem. Soc.* **1995**, *117*, 3547−3555.
[45] D. L. Andrews, *Adv. Chem. Phys.* **1993**, *85*, 545−606.
[46] K. Clays, A. Persoons, *Rev. Sci. Instrum.* **1992**, *63*, 3285−3289; T. Verbiest, K. Clays, S. Samyn, J. Wolff, B. Reinhartt, A. Persoons, *J. Am. Chem. Soc.* **1994**, *116*, 9320−9323; E. Hendrickx, K. Clays, A. Persoons, *Acc. Chem. Res.* **1988**, *31*, 675−683.
[47] [47a] S. Stadler, R. Dietrich, G. Bourhill, C. Bräuchle, *Optics Letts.* **1996**, *21*, 251−253. − [47b] M. A. Pauley, C. H. Wang, *Rev. Sci. Instrum.* **1999**, *70*, 1277−1284. − [7c] O. F. J. Noordman, N. F. van Hulst, *Chem. Phys. Letts.* **1996**, *253*, 145−150. − [47d] N. W. Song, T.-I. Kang, K. C. Jeoung, S.-J. Jeon, B. R. Cho, D. Kim, *Chem. Phys. Letts.* **1996**, *261*, 307−312; O. K. Song, J. N. Woodford, C. H. Wang, *J. Phys. Chem. A.* **1997**, *101*, 3222−3226. − [47e] G. Olbrechts, R. Strobbe, K. Clays, A. Persoons, *Rev. Sci. Inst.* **1998**, *69*, 2233−2241
[48] [48a] S. Houbrechts, K. Clays, A. Persoons, V. Cadierno, M. P. Gamasa, J. Gimeno, *Organometallics* **1996**, *15*, 5266−5268. − [48b] I. R. Whittall, M. P. Cifuentes, M. G. Humphrey, B. Luther-Davies, M. Samoc, S. Houbrechts, A. Persoons, G. A. Heath, D. Bogsányi, *Organometallics* **1997**, *16*, 2631−2637.
[49] [49a] V. Cadiero, S. Conejero, M. P. Camasa, J. Gimeno, I. Asselberghs, S. Houbrechts, K. Clays, A. Persoons, J. Borge, S. Garcia-Granda, *Organometallics* **1999**, *18*, 582−597. − [49b] I. S. Lee, H. Seo, Y. K. Chung, *Organometallics* **1999**, *18*, 1091−1096. − [49c] O. Briel, K. Sünkel, I. Krossing, H. Nöth, E. Schmälzlin, K. Meerholz, C. Bräuchle, W. Beck, *Eur. J. Inorg. Chem.* **1999**, 483−490. − [49d] I. S. Lee, S. S. Lee, Y. K. Chung, D. Kim, N. W. Song, *Inorg. Chim. Acta* **1998**, *279*, 243−248. − [49e] J. Mata, S. Uriel, E. Peris, R. Llusar, S. Houbrechts, A. Persoons, *J. Organomet. Chem.* **1998**, *562*, 197−202. − [49f] E. Hendrickx, A. Persoons, S. Samson, G. R. Stephenson, *J. Organomet. Chem.* **1997**, *542*, 295−297. − [49g] V. Alain, M. Blanchard-Desce, C.-T. Chen, S. R. Marder, A. Fort, M. Barzoukas, *Synthetic Metals* **1996**, *81*, 133−136. − [49h] K. R. J. Thomas, J. T. Lin, Y. S. Wen, *J. Organomet. Chem.* **1999**, *575*, 301−309. − [49i] R. Herrmann, B. Pedersen, G. Wagner, J.-H. Youn, *J. Organomet. Chem.* **1998**, *571*, 261−266. − [49j] G. G. A. Balavoine, J.-C. Daran, G. Iftime, P. G. Lacroix, E. Manoury, J. A. Delaire, I. Maltey-Fanton, K. Nakatani, S. Di Bella, *Organometallics* **1999**, *18*, 21−29.
[50] β_0 values were calculated using the TLM taking into account only the low lying DA−CT transition. However, it has to be realised that high energy LL−CT absorption may also contribute to the resonance enhancement.
[51] H. Wong, Ph.D. Thesis, University of Hamburg, **1998**.
[52] The SHG effect of the dinuclear complexes published in ref.[11a] and ref.[36] were meanwhile checked for fluorescence due to two photon absorption (TPF). No indication for TPF effects was found: T. Meyer-Friedrichsen, J. Heck, unpublished results.
[53] A. Abota, D. Beljonne, J.-L. Brédas, J. E. Ehrlich, J.-J. Fu, A. A. Heikal, S. E. Hess, T. Kogej, M. D. Levin, S. R. Marder, D. Mc Cord-Maughon, J. W. Perry, H. Röckel, M. Rumi, G. Subraniam, W. W. Webb, X.-L. Wu, C. Xu, *Science* **1998**, *281*, 1653−1656.
[54] *Ferrocenes* (Eds.: A. Togni, T. Hayashi), VCH, **1995**; *Metallocenes* (Eds.: A. Togni, R. L. Halterman), Wiley-VCH, **1998**.
[55] G. M. Sheldrick, SHELXS-86 Program for crystal structure determination, University of Göttingen, Germany, **1986**.
[56] G. M. Sheldrick, SHELXL-93 Program for crystal structure refinement, University of Göttingen, Germany, **1993**.

Received July 5, 1999
[I99243]

Preparation And Structure Of Phosphonium Ions With Intramolecular P ← N Coordination; Novel Diphosphonium Salts And Ionomer Containing Backbone Hypervalent Phosphorus

Francis H. Carré,[a] Claude Chuit,[a] Robert J. P. Corriu,*[a] William E. Douglas,[a] Daniel M. H. Guy,[a] and Catherine Reyé[a]

Keywords: Hypercoordinated phosphorus / Hypervalent phosphorus / Phosphorus / Diphosphonium compounds / Ionomers

Starting from $R'R_2P$ (R′ = 8-dimethylamino-1-naphthyl) containing a donor dimethylamino group, the new phosphonium salts $[R'R_2P(CH_2Ph)]^+Br^-$ [R = Me (**9**) or Ph (**10**)] and $[R'R_2P(p\text{-}CH_2C_6H_4CH_2)PR_2R']^{2+}[2Br]^{2-}$ [R = Ph (**12**)] have been prepared. An interaction between the N and P atoms is evident from the X-ray crystal structure of **10** the N–P distance being less than the sum of the van der Waals radii of the 2 atoms. The geometry of **10** is that of a monocapped tetrahedron whereas the X-ray crystal structure determination shows essentially regular tetrahedral geometry for the analogous compound without the donor amino group, $[(1\text{-}Np)Ph_2P(CH_2Ph)]^+Br^-$ (**11**). Treatment of 1,5-bis(dimethylamino)-2,6-dilithionaphthalene with chlorodiphenylphosphane gave 1,5-bis(dimethylamino)-2,6-bis(diphenylphosphanyl)-naphthalene (**8**) which in the presence of methyl iodide afforded the diphosphonium salt [1,5-bis(dimethylamino)-2,6-bis(diphenylmethylphosphonium)naphthalene]$^{2+}$[2I]$^{2-}$ (**13**). Similarly, treatment of **8** with 1 equivalent of benzyl bromide gave the monophosphonium salt [1,5-bis(dimethylamino)-2-diphenylbenzylphosphonium-6-diphenylphosphanyl-naphthalene]$^+$[Br]$^-$ (**14**) whereas in the presence of 2 equivalents of the same reagent [1,5-bis(dimethylamino)-2,6-bis(diphenylbenzylphosphonium)naphthalene]$^{2+}$[2 Br]$^{2-}$ (**15**) was obtained. The ionomer poly([(1,5-bis{dimethylamino}-2,6-bis{diphenylphosphonium}naphthalene)-(P,P-*p*-xylylene)]$^{2+}$[2 Br]$^{2-}$) (**16**), soluble in liquid SO_2, was prepared by treatment of **8** with α,α′-dibromo-*p*-xylene.

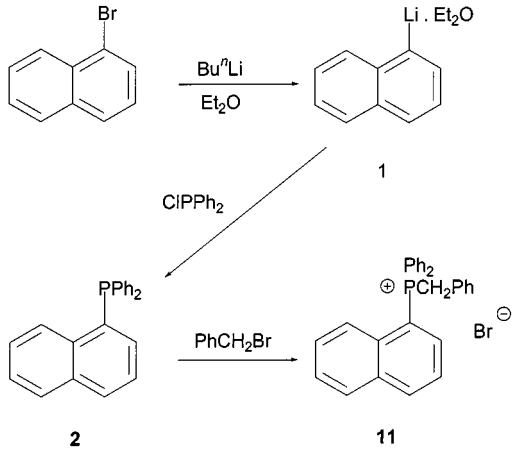
Introduction

Extension of coordination has been widely investigated for phosphoranes[1,2] and silicon compounds[3] but very rarely in the case of phosphanes and phosphonium ions.[4] It has been argued that there is no need to invoke d-orbital participation in the bonding in such hypervalent phosphorus compounds.[5] We have described the preparation, structures and some properties of various phosphanes (and also some phosphonium salts) showing extension of coordination by P←N interactions,[6–8] incorporating in particular the 8-dimethylamino-1-naphthyl ligand first used many years ago for the stabilization of hypercoordinated species[9] and widely applied in silicon chemistry.[3] Here, some new types of such phosphonium salts are reported including those containing two phosphorus atoms, prepared from the 4,8-bis(dimethylamino)-1,5-naphthylidene ligand,[10] in which there are two P←N interactions. The crystal structure of one of the phosphonium salts is compared to that of the corresponding salt without an amine group. We also describe the preparation from this same ligand of a novel ionomer containing hypervalent phosphorus in the backbone.

Results and Discussion

Preparation of Starting Phosphanes

Naphthyllithium (**1**) was prepared by treatment of bromonaphthalene in diethyl ether with *n*-butyllithium[11] (Scheme 1). The presence of one molecule of diethyl ether for each molecule of lithium reagent was shown by the proton NMR spectrum of the hydrolysis product. Naphthyldiphenylphosphane (**2**) was prepared by treatment of **1** with chlorodiphenylphosphane (Scheme 1).

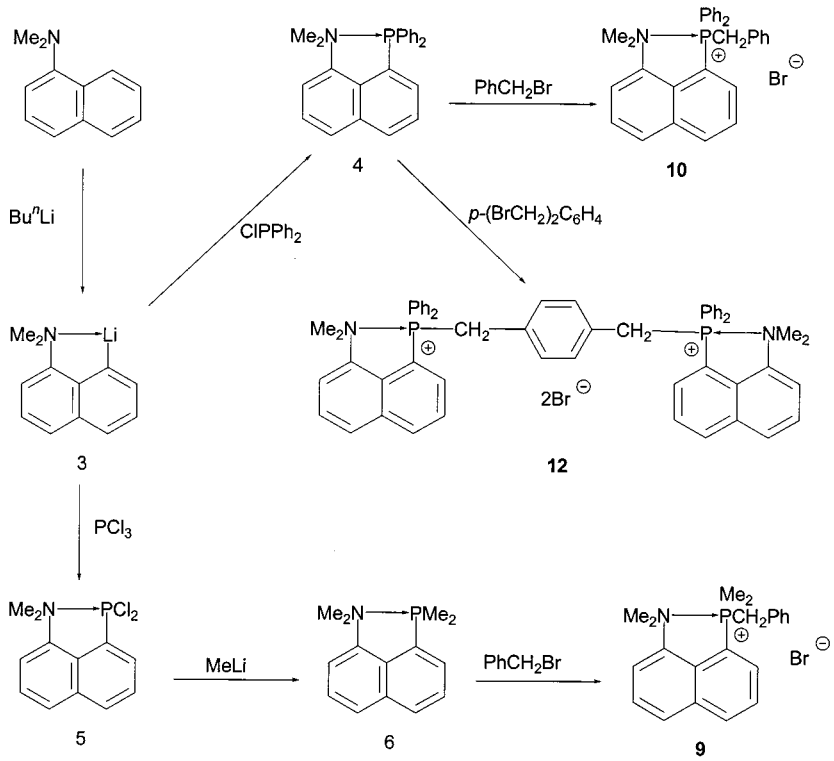


Scheme 1. Preparation of **11**

The hypercoordinate phosphanes were obtained starting from the 8-(dimethylamino)-1-lithionaphthalene (**3**), the latter being prepared quantitatively by treatment of 1-dimethylaminonaphthalene with *n*-butyllithium (Scheme 2).[9] The preparation and the properties of phosphane **4** prepared by treatment of **3** with chlorodiphenylphosphane (Scheme 2) have been previously described;[8,12] a dynamic proton NMR investigation and the X-ray crystal structure determination showed that the geometry of this phosphane

[a] CNRS UMR 5637, Université Montpellier II,
Place E. Bataillon, 34095 Montpellier Cedex 5, France
E-mail: corriu@crit.univ-montp2.fr

 © WILEY-VCH Verlag GmbH, D-69451 Weinheim, 2000 1434–1948/00/0404–0647 $ 17.50+.50/0



Scheme 2. Preparation of hypervalent phosphorus compounds containing the 8-dimethylamino-1-naphthyl ligand

is not symmetric and that the distance between the nitrogen and the phosphorus atoms (2.7 Å) is smaller than the sum of the van der Waals radii of the two atoms (3.4 Å[13]).[8] The geometry of **4** can be described as a monocapped tetrahedron in which the P atom is pseudo-[4+1]-coordinate (taking into account the electron lone pair).[8]

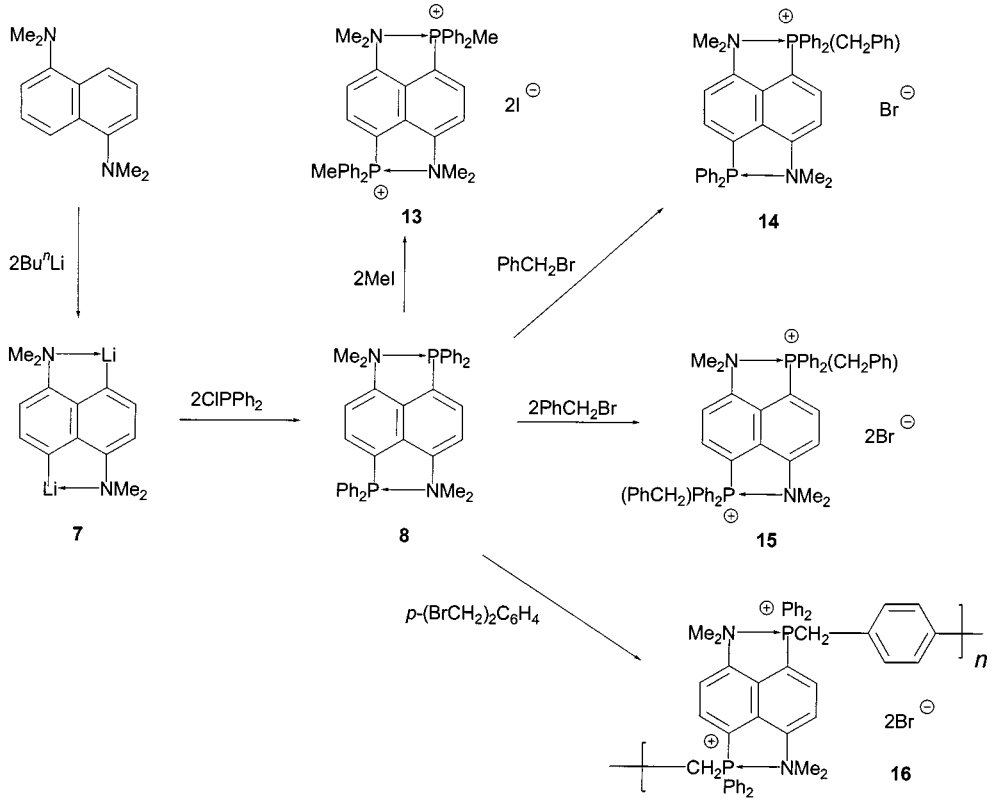
The intermediate dichlorophosphane derivative **5** was obtained by addition of the lithium reagent **3** to a large excess of trichlorophosphane (Scheme 2) at –80 °C. Treatment of **5** with methyllithium gave the dimethylphosphane derivative **6** (Scheme 2). The latter, like **4**, shows a singlet for the amine methyl protons in the proton NMR spectrum at room temperature. However, whereas for **4** this signal is split into two at –95 °C, in the case of **6** at –110 °C (250 MHz) it is merely broadened the permutational isomerization being of lower energy due to the difference in bulk of the phenyl and methyl groups.

Treatment of 1,5-bis(dimethylamino)naphthalene with two equivalents of *n*-butyllithium affords the dilithio reagent **7** (Scheme 3), as we have previously described.[10] Subsequent treatment of **7** with chlorodiphenylphosphane gives the diphosphane **8** containing two hypercoordinate phosphorus atoms (Scheme 3). A dynamic proton NMR study of this compound showed that at –95 °C the singlet corresponding to the amine protons is split into two signals. By use of the Eyring equation the energy of the permutational isomerisation was calculated[14] to be $\Delta G^{\ddagger} = 36.8$ kJ mol^{-1}, a value similar to that previously found for **4**.[8] We have not been able to determine the X-ray crystal structure of **8** but the geometry is most probably similar to that of the corresponding phosphane **4** with a monocapped tetrahedral arrangement of the ligands around each phosphorus.[8]

Preparation of Phosphonium Salts

The very air sensitive hypercoordinate phosphonium salt **9** with methyl groups at P was prepared by treatment of **6** with benzyl bromide (Scheme 2). The analogous stable salt **10** with phenyl groups at P was obtained by reaction of **4** with benzyl bromide. The X-ray crystal structure of **10** (Figure 1) shows a monocapped tetrahedral geometry in which the P atom is [4+1]-coordinate; selected bond lengths and angles are to be found in Table 1 and details of the crystal structure determination in Table 2. The distance between the nitrogen and the phosphorus atoms (2.83 Å) is less than the sum of the van der Waals radii of the 2 atoms (3.4 Å[13]),[8] thus showing that they interact. Indeed, this distance is comparable to the N–N distance (2.79 Å) in 1,8-bis(dimethylamino)naphthalene[15] despite phosphorus being much larger than nitrogen. Moreover, it should be noted that the naphthalene ring in **10** is distorted out of the plane by only *ca.* 17° (dihedral angle between the C9–C1–C2 and C7–C8–C9 planes) whereas for 1,8-bis(dimethylamino)naphthalene[15] the corresponding angle can be evaluated at 28°.

For comparison, the analogous phosphonium salt without the donor nitrogen, $[(1\text{-Np})Ph_2P(CH_2Ph)]^+Br^-$ (**11**), was synthesized by treatment of **2** with benzyl bromide in refluxing toluene (Scheme 1). The X-ray crystal structure analysis of **11** (Figure 2) shows a tetrahedral geometry in



Scheme 3. Preparation of hypervalent phosphorus compounds containing the 4,8-bis(dimethylamino)-1,5-naphthylidene ligand

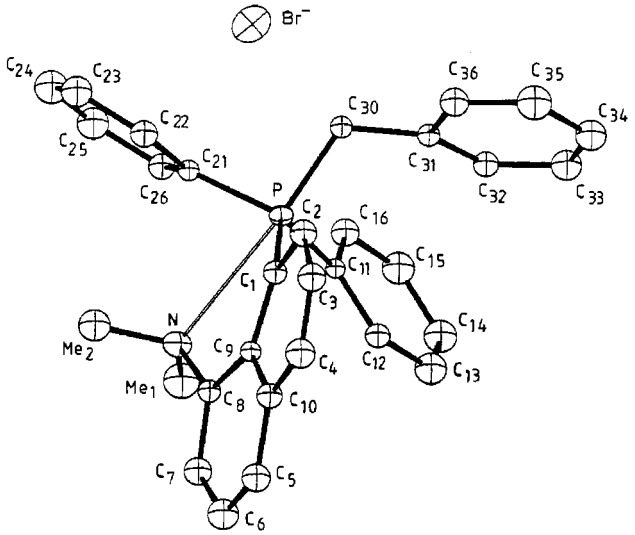


Figure 1. Molecular structure of **10**; hydrogen atoms have been omitted for clarity

which the P atom is 4-coordinate; selected bond lengths and angles are to be found in Table 1 and details of the crystal structure determination in Table 2. Comparison of the angles in **10** and **11** (Table 1) shows that the nitrogen in **10** is opposite to the benzyl group [C(30)] and has little effect on angles C(1)–P–C(30) and C(1)–P–C(11) which remain essentially tetrahedral. However, the presence of the amine group results in a reduction of C(21)–P–C(30) by ca. 9° and C(11)–P–C(30) by ca. 6°, and an enlargement of C(11)–P–C(21) and C(21)–P–C(1) by 5–6°.

Table 1. Selected interatomic distances (Å) and bond angles (°) for **10** and **11**

	10	**11**
P–C(1)	1.820(12)	1.790(5)
P–C(11)	1.787(11)	1.800(5)
P–C(21)	1.796(11)	1.815(5)
P–C(30)	1.844(11)	1.813(5)
P···N	2.826(10)	
N···P–C(30)	175.7(4)	
N···P–C(1)	72.3(4)	
N···P–C(11)	79.1(4)	
N···P–C(21)	75.8(4)	
C(1)–P–C(30)	109.5(5)	108.2(2)
C(11)–P–C(30)	103.6(5)	109.1(2)
C(21)–P–C(30)	99.9(5)	108.9(2)
C(1)–P–C(11)	110.6(5)	110.4(2)
C(11)–P–C(21)	116.4(5)	111.3(2)
C(21)–P–C(1)	115.3(5)	109.0(2)

The ^{1}H NMR resonances for the methylene protons in the hypercoordinate salts **9** (δ_H = 4.4) and **10** (δ_H = 4.7) occur at higher field than in the tetracoordinate salt **11** (δ_H = 5.35). This can be explained by the electron-donating effect of the dimethylamino group coordinated to the phosphorus atom. However, the ^{31}P NMR chemical shift remains essentially unchanged with increase in the coordination number from four (**11**) to five (**9** or **10**) as has previously been observed for hypercoordinated silicon compounds containing the 8-dimethylamino-1-naphthyl ligand.[16]

The analogous compound **12** containing two positively-charged phosphorus atoms was prepared by treating two

Table 2. Summary of crystal data, intensity measurements and refinement for **10** and **11**

	10	**11**
Formula	$C_{31}H_{29}BrNP$	$C_{29}H_{24}BrP$
Cryst. system	triclinic	monoclinic
Space group	*P*–1	$P2_1/c$
a (Å)	9.351(3)	10.123(2)
b (Å)	9.875(3)	20.683(4)
c (Å)	14.664(4)	11.796(3)
α	80.58(2)	
β	74.27(3)	110.29(2)
γ	89.66(3)	
Vol. (Å^3)	1284.8(7)	2316.5(9)
Mol. wt.	526.46	483.4
Z	2	4
$d_{calcd.}$ (gcm^{-3})	1.361	1.386
$d_{measd.}$ (gcm^{-3})	1.32(3)	1.37(2)
Cryst. size (mm)	0.45 × 0.25 × 0.09	0.42 × 0.40 × 0.18
Cryst. colour	colourless	colourless
Recryst. solv.	CH_2Cl_2/heptane, 2:3	ethanol
m.p. (°C)	281.3–282.5	329.5–331.2
Method of data collectn.	ω/φ	ω/φ
Radiation (graphite-monochromated)	Mo-*Kα*	Mo-*Kα*
μ (cm^{-1})	16.6	18.2
2φ limits (°)	4–50	4–50
No of unique reflectns.	3275	3338
No of obsd reflectns.	1548	2106
Final no of variables.	161	180
R	0.0690	0.0396
Rw	0.0705	0.0409
Residual electron density	0.98	0.41

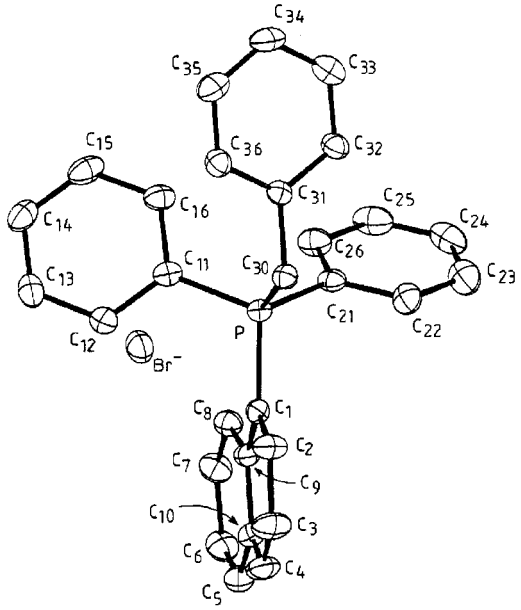


Figure 2. Molecular structure of **11**; hydrogen atoms have been omitted for clarity

equivalents of **4** with one equivalent of α,α'-dibromo-*p*-xylene (Scheme 2). As expected the chemical shifts of the proton and ^{31}P NMR resonances for **12** are very similar to those for **10**, the ^{31}P NMR resonances for these compounds containing phenyl groups occurring at higher field than that for **9** containing methyl groups.

Phosphonium salts containing two hypercoordinate phosphorus atoms were obtained from the diphosphane **8** (Scheme 3). The reactions were followed by ^{31}P NMR, the spectra showing the disappearance of the signal corresponding to the starting phosphane (δ_P = 1.9) and the appearance of the signal corresponding to the phosphonium salt at δ ≈ 23. Salt **13** was prepared by treatment of phosphane **8** with a large excess of methyl iodide in toluene under reflux, the reaction being complete after 4.5 h (Scheme 3).

The compound **14** containing both phosphanyl and phosphonium centres was obtained by treatment of **8** with one equivalent of benzyl bromide the reaction being complete after 60 hours under reflux in toluene (Scheme 3). The ^{31}P NMR spectrum shows a signal at δ 22 characteristic of the phosphonium ion and another at δ = 5 corresponding to the phosphanyl atom, the latter being downfield of that for the starting material **8** (δ_P = 1.9). The proton resonances for the dimethylamino group *peri* to the phosphonium centre (δ_H = 1.7) are shifted upfield compared to those for **8** (δ_H = 2.3) whereas the proton resonances for the dimethylamino group *para* to the phosphonium centre are shifted downfield (δ_H = 2.5).

The analogous salt **15** containing two phosphonium centres was prepared by treatment of **8** with two equivalents of benzyl bromide the reaction being complete in this case after 120 hours under reflux in toluene (Scheme 3). As expected only one ^{31}P NMR signal is observed (δ_P = 24.8) characteristic of the phosphonium ion. The proton NMR spectrum shows all the amine protons to be equivalent (δ_H = 2.08) this signal being upfield of that for **8** (δ_H = 2.3).

The ionomer **16** was prepared by heating **8** with one equivalent of α,α'-dibromo-*p*-xylene in toluene under reflux for 10 d (Scheme 3), the product being insoluble except in

liquid SO_2. The solid state ^{31}P NMR spectrum shows a signal at $\delta = 16$. The conductivity of a compacted disc of the powdered ionomer was found to be 10^{-5} S cm^{-1} (4-point method), and that of a SO_2 solution at –30 °C was 53 S cm^{-1}.

In conclusion, we have shown that an intramolecular donor-acceptor interaction exists in the phosphonium ion **10** and therefore most probably also in the other new phosphonium ions of this type reported here (**9**, **12**, **13–15** and the ionomer **16**). This confirms that the phosphonium ion is able to undergo an extension of coordination. In particular, it should be noted that, as has been previously observed for the analogous silicon compounds,[16] incorporation of the 8-dimethylamino-1-naphthyl ligand to give pentacoordinate phosphane species does not give rise to any substantial change in NMR chemical shift. This independence of NMR chemical shift on coordination number is due to the specific geometry of the ligand and in no way throws doubt[17] on the existence of an N←P (or N←Si) coordinative interaction. On the contrary, a completely coherent picture is found for the structures and chemical behaviour of the totality of penta- and hexacoordinate derivatives formed by intramolecular coordination of either Si or P.

Experimental Section

All reactions were performed using standard Schlenk-tube techniques under an atmosphere of dry argon. Solvents were distilled from appropriate drying agents and degassed before use. ^1H and ^{13}C NMR spectra were obtained using a Bruker DPX-200 spectrometer at 200 MHz and 50.288 MHz, respectively, and ^{31}P NMR spectra on a Bruker 250 AC spectrometer at 101.202 MHz. ^1H and ^{13}C NMR chemical shifts are reported relative to Me_4Si, and ^{31}P chemical shifts relative to H_3PO_4. Infrared spectra were obtained in the region 500–4000 cm^{-1} using a Perkin–Elmer 1600 FT spectrophotometer. Elemental analyses were carried out by the Service Central de Microanalyse du CNRS. Phosphane **4** was prepared from **3** as previously described.[8]

Preparation of 1: Diethyl ether (130 mL) was added at 0 °C to 1.9 M *n*-butyllithium solution in hexane (85 mL, 160 mmol) and the resulting solution was cooled to –20 °C. 1-Bromonaphthalene (20 mL, 140 mmol) was added drop by drop and the mixture was stirred at 0 °C for 1 h and then filtered. The precipitate was washed with pentane and dried under vacuum affording 24.65 g of a white pyrophoric solid ($C_{10}H_7Li \cdot Et_2O$) isolated in 85% yield.

Preparation of 2: Chlorodiphenylphosphane (18 mL, 100 mmol) was added drop by drop to a suspension of **1** (16 g, 76.92 mmol) in diethyl ether (100 mL) at –50 °C. The mixture was then allowed to warm to room temp. and was stirred for 16 h. The resulting white suspension was heated under reflux for 5 h, and was then hydrolysed with 10% NaOH solution (50 mL). The precipitate was washed successively with water, acetone and diethyl ether before being dried under vacuum. The crude product was recrystallized from ethanol to give 13.25 g of the desired product, m.p. 122.3–124.0 °C (yield 55%). – ^1H NMR ($CDCl_3$): δ_H = 7–8.6 (m, aromatic protons). – ^{13}C-{^1H} NMR ($CDCl_3$): δ_C = 126–137 (aromatic carbons). – ^{31}P-{^1H} NMR ($CDCl_3$): δ_P = –13.6 (s). – IR (CCl_4): $\tilde{\nu}$ (cm^{-1}) = 3056 s, 1588 w, 1504 m, 1482 m, 1434 vs, 1386 m, 1329 w, 1094 w, 1027 w. – $C_{22}H_{17}P$ (312.34): calcd. C 84.60, H 5.48, P 9.91; found C 85.01, H 5.48, P 9.78.

Preparation of 3: *n*-Butyllithium in hexane (40 mL, 110 mmol) was added drop by drop to a solution of 1-(dimethylamino)naphthalene (16.54 g, 96.7 mmol) in 250 mL of diethyl ether at room temp. After the mixture had been stirred for 3 d the resulting yellow suspension was filtered and the precipitate was washed thrice with diethyl ether before being dried under vacuum to afford 16.8 g of a yellow pyrophoric fine powder (yield 98%).

Preparation of 5: A suspension of **3** (5.67 g, 32.03 mmol) in 150 mL of diethyl ether was added drop by drop to a solution of trichlorophosphane (12 mL, 137 mmol) in 150 mL of diethyl ether at –80 °C. The mixture was stirred at room temp. overnight. The resulting yellow suspension was filtered and the filtrate was concentrated to give 5.43 g of a yellow solid (yield 62%). – ^1H NMR ($CDCl_3$): δ_H = 2.87 [s, 6 H, $N(CH_3)_2$], 7.5–8.9 (m, 6 H, aromatic protons). – ^{13}C-{^1H} NMR ($CDCl_3$): δ_C = 47.6 (CH_3), 112–148 (aromatic carbons). – ^{31}P-{^1H} NMR ($CDCl_3$): δ_P = 130.85 (s).

Preparation of 6: A 1.25 M solution of methyllithium (28.2 mL, 35.22 mmol) in diethyl ether was added to a suspension of **5** (4.79 g, 17.61 mmol) in 100 mL of diethyl ether. The mixture was stirred at room temperature overnight and then heated under reflux for 3 h. The suspension was hydrolysed by addition of degassed 10% NaOH solution (40 mL). The aqueous layer was extracted with diethyl ether. The combined organic phases were washed with degassed water and dried with $MgSO_4$ before removal of the solvent to give a yellow liquid. Vacuum distillation gave 1.63 g of the desired product (40% yield), b.p. 118–120 °C/0.4 Torr. – ^1H NMR ($CDCl_3$): δ_H = 1.35 [d, $^2J_{1H,31P}$ = 5.7 Hz, 6 H, $P(CH_3)_2$], 2.75 [s, 6 H, $N(CH_3)_2$], 7.3–7.9 (m, 6 H, aromatic protons). – ^{31}P-{^1H} NMR ($CDCl_3$): δ_P = –37.8 (s). – IR (CCl_4): $\tilde{\nu}$ (cm^{-1}) = 3054 m, 2945 s, 2902 s, 2864 s, 2828 vs, 2786 s, 1929 w, 1710 w, 1563 vs, 1500 w, 1477 m, 1453 vs, 1366 vs, 1330 s, 1289 m, 1204 m, 1183 s, 1143 s, 1081 s, 1048 m, 1030 m.

Preparation of 7: *n*-Butyllithium in hexane (110 mL, 310 mmol) was added drop by drop to a solution of 1,5-bis(dimethylamino)naphthalene (30.04 g, 140 mmol) in 500 mL of diethyl ether at room temp.. After the mixture had been stirred for 10 d the resulting yellow suspension was filtered and the precipitate was washed thrice with diethyl ether before being dried under vacuum to afford 30.97 g of a white pyrophoric fine powder (yield 98%).

Preparation of 8: Chlorodiphenylphosphane (10.83 mL, 60 mmol) was added drop by drop to a suspension of **7** (8.52 g, 38 mmol) in 100 mL of diethyl ether at –80 °C. The mixture was then allowed to warm to room temp. and was stirred overnight. The resulting white suspension was heated under reflux for 9 h, and it was then hydrolysed with 10% NaOH solution (100 mL). The precipitate was washed successively with water, acetone and diethyl ether before being dried under vacuum. The crude product was recrystallized from benzene to give 9.6 g of the desired product, m.p. 259.4–263.7 °C (yield 55%). – ^1H NMR ($CDCl_3$): δ_H = 2.3 [s, 12 H, $N(CH_3)_2$], 6.7–7.4 (m, 24 H, aromatic protons). – ^{13}C-{^1H} NMR ($CDCl_3$): δ_C = 46.18 [$N(CH_3)_2$], 118–152 (aromatic carbon atoms). – ^{31}P-{^1H} NMR ($CDCl_3$): δ_P = 1.9 (s). – IR (Nujol): $\tilde{\nu}$ (cm^{-1}) = 3059 m, 2853 vs, 2822 s, 2776 m, 1954 w, 1882 w, 1823 w, 1773 w, 1677 w, 1653 w, 1578 m, 1506 m, 1451 s, 1401 w, 1368 s, 1311 m, 1275 w, 1202 m, 1181 s, 1152 m, 1109 m, 1087 m, 1068 w, 1042 s, 976 vs, 836 m, 826 m, 748 s, 738 vs, 717 m, 697 vs, 668 w, 650 m, 613 s. – $C_{38}H_{36}N_2P_2$ (582.66): C 78.32, H 6.23, N 4.81; found C 78.28, H 6.01, N 4.92.

Preparation of 9: A mixture of **6** (0.33 g, 1.43 mmol) and benzyl bromide (0.17 mL, 1.43 mmol) was heated under reflux in toluene (50 mL) for 3 h. The solvent was removed under vacuum to give 0.53 g of a very air-sensitive white powder (yield 93%). – ^{1}H NMR ($CDCl_3$): δ_H = 2.45 [d, $^2J_{1H,31P}$ = 10 Hz, 6 H, $P(CH_3)_2$], 2.75 [s, 6 H, $N(CH_3)_2$], 4.4 (d, $^2J^1_H{}^{31}_P$ = 15 Hz, 2 H, CH_2), 6.8–8.2 (m, 11 H, aromatic protons). – ^{31}P-{^{1}H} NMR ($CDCl_3$): δ_P = 24.26 (s).

Preparation of 10: A mixture of **4** (2 g, 5.63 mmol) and benzyl bromide (0.67 mL, 5.63 mmol) was heated under reflux in toluene (100 mL) for 9 d. The solvent was then removed under vacuum to give a white solid. The crude product was recrystallized from a mixture of dichloromethane and heptane to give 2.84 g of the desired product, m.p. 281.3–282.5 °C (yield 96%). – ^{1}H NMR ($CDCl_3$): δ_H = 1.5 [s, 6 H, $N(CH_3)_2$], 4.7 (d, $^2J_{1H,31P}$ = 14 Hz, 2 H, CH_2), 6.3–9 (m, 21 H, aromatic protons). – ^{13}C-{^{1}H} NMR ($CDCl_3$): δ_C = 36.14 (d, $^1J_{31P,13C}$ = 48.36 Hz, CH_2), 46.44 (CH_3), 111–151 (aromatic carbons). – ^{31}P-{^{1}H} NMR ($CDCl_3$): δ_P = 22.12 (s). – IR (Nujol): $\tilde{\nu}$ (cm^{-1}) = 3052 w, 2796 w, 1715w, 1694 w, 1570 w, 1497 m, 1438 s, 1412 w, 1376 m, 1338 m, 1286 w, 1209 w, 1195 w, 1152 m, 1114 s, 1105 s, 1081 m, 1036 m, 1023 m, 995 w, 958 w, 929 w, 879 m, 839 s, 831 s, 802 w, 776 vs, 757 s, 727 m, 699 vs, 660.

Preparation of 11: A mixture of naphthyldiphenylphosphane (**2**) (2 g, 6.41 mmol) and benzyl bromide (0.76 g, 6.41 mmol) was heated under reflux in toluene (100 mL) for 6 d. The solvent was removed under vacuum to give a white powder. The crude product was recrystallized from ethanol to give 1.81 g of the desired product, m.p. 329.5–331.2 °C (yield 58%). – ^{1}H NMR ($CDCl_3$): δ_H = 5.35 (d, $^2J_{1H,31P}$ = 15 Hz, 2 H, CH_2), 6.8–8.6 (m, 22 H, aromatic protons). – ^{13}C-{^{1}H} NMR ($CDCl_3$): δ_C = 30.53 (d, $^1J_{13C,31P}$ = 42.78 Hz, CH_2), 112–138 (aromatic carbon atoms). – ^{31}P-{^{1}H} NMR ($CDCl_3$): δ_P = 22.45 (s). – IR (nujol): $\tilde{\nu}$ (cm^{-1}) = 2783 m, 2362 w, 1602 w, 1586 w, 1502 m, 1496 m, 1440 vs, 1377 s, 1338 m, 1318 w, 1262 w, 1214 w, 1166 m, 1110 s, 1074 w, 1033 w, 997 w, 986 w, 921 w, 877 w, 832 m, 800 m, 777 s, 751 s, 717 m, 698 s, 690 s, 664 w, 586 s. – $C_{29}H_{24}BrP$ (483.39): C 72.06, H 5.00; found C 72.06, H 5.09.

Preparation of 12: A mixture of α,α'-dibromo-*p*-xylene (0.74 g, 2.81 mmol) and **4** (2 g, 5.63 mmol) was heated under reflux in toluene (100 mL) for 7 d. The solvent was removed under vacuum to give a white powder. The crude product was recrystallized from a mixture of dichloromethane and pentane to give 1.6 g of the desired product, m.p. 309.9–311.4 °C (yield 58%). – ^{1}H NMR ($CDCl_3$): δ_H = 1.5 [s, 12 H, $N(CH_3)_2$], 4.55 (d, $^2J_{1H,31P}$ = 16 Hz, 4 H, CH_2), 7–9 (m, 36 H, aromatic protons). – ^{13}C-{^{1}H} NMR ($CDCl_3$): δ_C = 38.25 (d, $^1J_{13C,31P}$ = 47.44 Hz, CH_2), 46.4 (CH_3), 110–150 (aromatic carbons). – ^{31}P-{^{1}H} NMR ($CDCl_3$): δ_P = 22.77 (s). – IR (Nujol): $\tilde{\nu}$ (cm^{-1}) = 3053 w, 2854 vs, 2808 w, 1622 w, 1566 w, 1497 w, 1437 s, 1375 s, 1336 m, 1288 w, 1212 w, 1168 m, 1151 w, 1110 s, 1100 m, 1080 w, 1034 w, 1024 w, 995 w, 954 w, 880 w, 826 m, 773 m, 756 s, 724 m, 697 m, 658 w.

Preparation of 13: A mixture of methyl iodide (1.74 g, 28.0 mmol) and **8** (2 g, 3.44 mmol) was heated under reflux in toluene (20 mL) for 4.5 h. The solvent was removed under vacuum to give a white powder. The crude product was recrystallized in a mixture of ethanol and benzene to give 2.48 g of the desired product, m.p. 323.7–324.9 °C (yield 83%). – ^{1}H NMR ($CDCl_3$): δ_H = 2.1 [s, 12 H, $N(CH_3)_2$], 3.1 (d, $^2J_{1H,31P}$ = 13.4 Hz, 6 H, PCH_3), 7.2–7.8 (m, 24 H, aromatic protons). – ^{13}C-{^{1}H} NMR ($CDCl_3$): δ_C = 11.84 (d, $^1J_{13C,31P}$ = 65.17 Hz, PCH_3), 46.67 [$N(CH_3)_2$], 111–157 (aromatic carbon atoms). – ^{31}P-{^{1}H} NMR ($CDCl_3$): δ_P = 23.76 (s). – IR (Nujol): $\tilde{\nu}$ (cm^{-1}) = 1585 w, 1567 m, 1499 s, 1438 vs, 1376 vs, 1318 s, 1211 w, 1155 m, 1121 s, 1101 m, 1038 w, 1012 w, 996 w, 972 m, 914 m, 895 m, 830 w, 785 w, 774 w, 750 s, 715 s, 693 s.

Preparation of 14: A mixture of benzyl bromide (0.61 mL, 5.15 mmol) and **8** (3 g, 5.15 mmol) was heated under reflux in toluene (50 mL) for 60 h. The solvent was removed under vacuum to give a yellow solid, m.p. 275.8–276.5 °C (yield 83%). – ^{1}H NMR ($CDCl_3$): δ_H = 1.7 [s, 6 H, $N(CH_3)_2$ *peri* to P^+], 2.5 [s, 6 H, $N(CH_3)_2$ *para* to P^+], 4.7 (d, $^2J_{1H,31P}$ = 14 Hz, CH_2), 6–7.8 (m, 29 H, aromatic protons). – ^{13}C-{^{1}H} NMR ($CDCl_3$): δ_C = 38.6 (d, $^1J_{13C,31P}$ = 47.23 Hz, CH_2), 45.72 [$N(CH_3)_2$], 46.16 [$N(CH_3)_2$], 119–150 (aromatic carbon atoms). – ^{31}P-{^{1}H} NMR ($CDCl_3$): δ_P = 4.3 (P), 21.91 (P^+). – IR (Nujol): $\tilde{\nu}$ (cm^{-1}) = 3045 w, 1584 w, 1558 w, 1498 m, 1376 vs, 1322 m, 1303 m, 1261 w, 1185 m, 1151 m, 1116 s, 1073 m, 1046 w, 1033 m, 998 m, 971 m, 904 m, 860 m, 837 m, 753 s, 723 m, 697 s.

Preparation of 15: A mixture of benzyl bromide (1.22 mL, 10.30 mmol) and **8** (3 g, 5.15 mmol) was heated under reflux in toluene (50 mL) for 120 h. The solvent was removed under vacuum to give a yellow powder. The crude product was recrystallized from a mixture of ethanol and benzene to give 4.52 g of the desired product, m.p. 294.0–294.6 °C (yield 95%). – ^{1}H NMR ($CDCl_3$): δ_H = 2.08 [s, 12 H, $N(CH_3)_2$], 4.87 (d, $^2J_{1H,31P}$ = 16 Hz, 4 H, CH_2), 6.5–9 (m, 34 H, aromatic protons). – ^{13}C-{^{1}H} NMR ($CDCl_3$): δ_C = 38.8 (d, $^1J_{13C,31P}$ = 47.66 Hz, CH_2), 46.06 (CH_3), 119–150 (aromatic carbons). – ^{31}P-{^{1}H} NMR ($CDCl_3$): δ_P = 24.78 (s). – IR (Nujol): $\tilde{\nu}$ (cm^{-1}) = 2786 w, 1574 w, 1498 s, 1439 vs, 1376 s, 1315 m, 1260 w, 1175 w, 1112 m, 1074 w, 1037 m, 1010 w, 973 w, 904 w, 851 m, 838 m, 786 w, 761 m, 750 s, 726 m, 696 s.

Preparation of 16: A mixture of α,α'-dibromo-*p*-xylene (0.73 g, 2.78 mmol) and **8** (1.62 g, 2.78 mmol) was heated under reflux in toluene (50 mL) for 10 d. The solvent was removed under vacuum to give an orange powder (d 300 °C) which is soluble in liquid SO_2. Solid-state ^{31}P-NMR HPDEC MAS: δ_P = 16. – IR (Nujol): $\tilde{\nu}$ (cm^{-1}) = 2722 w, 1614 w, 1568 m, 1498 s, 1438 vs, 1377 vs, 1315 m, 1261 m, 1211 m, 1157 m, 1110 s, 1033 m, 998 m, 968 m, 899 w, 837 s, 749 m, 720 w, 694 s, 634 w.

X-ray Structure Determinations of 10 and 11: The crystal of **10** used was found to produce only moderate diffraction intensities. The direct methods (SHELXS-86[18]) failed to give the solution of the structure with space groups *P*–1. However, an attempt to solve the structure with the non-centrosymmetric space group *P*1 gave the positions of the bromine anion, the phosphorus atom and four carbon atoms from the naphthyl group. The space group *P*–1 was again assumed to be the correct group and two subsequent Fourier syntheses and a difference Fourier map gave the positions of the remaining atoms. Owing to the small number of observed data, only the bromine, phosphorus and nitrogen atoms were refined anisotropically. The calculated hydrogen atoms[19] were included in the last stages of the refinement. Convergence occurred for the *R* value of 0.0690 (*Rw* = 0.0705). – In the case of **11** the systematic absences revealed the space group $P2_1/c$. Direct methods (SHELXS-86[18]) gave the positions of the bromine anion, the phosphorus atom and the phenyl and some of the naphthyl carbons. Two Fourier maps revealed the remaining carbon atoms. The hydrogen atoms were positioned by calculation[19] and taken into account in the next refinements. After ten cycles of least-squares refinement with anisotropic thermal parameters for all non-hydrogen atoms, the final *R* value was 0.0396 (*Rw* = 0.0409). – The crystal structure data (excluding structure factors) have been deposited with the Cambridge Crystallographic Data Centre as supplementary publication nos. CCDC-114826 (**10**) and -114825 (**11**). Copies

of the data can be obtained free of charge on application to CCDC, 12 Union Road, Cambridge CB2 1EZ, G.B. [Fax: int. code + 44-1223/336-033; E-mail: deposit@ccdc.cam.ac.uk].

[1] R. H. Holmes, *Chem. Rev.* **1996**, *96*, 927.
[2] C. Y. Wong, D. K. Kennepohl, R. G. Cavell, *Chem. Rev.* **1996**, *96*, 1917.
[3] C. Chuit, R. J. P. Corriu, C. Reyé, J. C. Young, *Chem. Rev.* **1993**, *93*, 1371.
[4] C. Chuit, C. Reyé, *Eur. J. Inorg. Chem.* **1998**, 1847.
[5] D. G. Gilheany, *Chem. Rev.* **1994**, *94*, 1339.
[6] C. Chuit, R. J. P. Corriu, P. Monforte, C. Reyé, J. P. Declercq, A. Dubourg, *Angew. Chem. Int. Ed. Engl.* **1993**, *32*, 1430.
[7] M. Chauhan, C. Chuit, R. J. P. Corriu, C. Reyé, J. P. Declercq, A. Dubourg, *J. Organomet. Chem.* **1996**, *510*, 173.
[8] C. Chuit, R. J. P. Corriu, P. Monforte, C. Reyé, J. P. Declercq, A. Dubourg, *J. Organomet. Chem.* **1996**, *511*, 171.
[9] J. T. B. H. Jastrzebski, C. T. Knaap, G. van Koten, *J. Organomet. Chem.* **1983**, *255*, 287.
[10] C. Brelière, R. J. P. Corriu, G. Royo, M. Wong Chi Man, J. Zwecker, *C. R. Acad. Sci. Paris Série II* **1991**, *313*, 1527.
[11] L. Brandsma, H. Verkruijsse, *Preparative Polar Organometallic Chemistry 1*, Springer-Verlag, Berlin, Heidelberg, New York, London, Paris, Tokyo, **1987**.
[12] G. P. Schiemenz, E. Papageorgiou, *Phosphorus and Sulfur* **1982**, *13*, 41.
[13] A. Bondi, *J. Phys. Chem.* **1964**, *68*, 441.
[14] H. Günther, *NMR Spectroscopy*, Wiley, Chichester, **1980**.
[15] H. Einspahr, J. B. Robert, R. E. Marsh, J. D. Roberts, *Acta Cryst.* **1973**, *B29*, 1611.
[16] C. Brelière, R. J. P. Corriu, G. Royo, J. Zwecker, *Organometallics* **1989**, *8*, 1834.
[17] G. P. Schiemenz, B. Schiemenz, S. Petersen, C. Wolff, *Chirality* **1998**, *10*, 180.
[18] G. M. Sheldrick, *SHELXS-86, A Program for Crystal Structure Solution*, Institüt für Anorganische Chemie der Universität: Göttingen, Germany, **1986**.
[19] G. M. Sheldrick, *SHELXS-76, A Program for Crystal Structure Determination*, University of Cambridge: Cambridge, England, **1976**.

Received September 27, 1999
[I99336]

Selective and Environmentally Benign Aerobic Catalytic Oxidation of Alcohols by a Molybdenum-Copper System

Christian Y. Lorber,[a][+] Sebastian P. Smidt,[a] and John A. Osborn*[a]

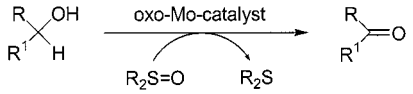
Keywords: Molybdenum / Copper / Oxidation / Alcohols / Catalysis

The oxidation of activated primary and secondary alcohols to the corresponding aldehydes and ketones can be carried out with molecular oxygen, in the presence of the bimetallic molybdenum–copper system $MoO_2(acac)_2$–$Cu(NO_3)_2$ as catalyst.

Introduction

The oxidation of primary and secondary alcohols to aldehydes and ketones, respectively, is a fundamental transformation in organic synthesis, that can be now accomplished by several oxidizing reagents. However, in most cases these reagents are very toxic and must be used in stoichiometric amounts.[1] Considering cost and environmental factors, the development of "green" catalytic processes is an important goal.[2]

During the last few years we have been interested in using high oxidation state oxo complexes of transition metals as catalysts for the oxidation and/or isomerisation of alcohols,[3,4] and we recently discovered the catalytic oxidation of primary and secondary alcohols with *cis*-dioxomolybdenum(VI) complexes with sulfoxides or *N*-oxides as co-oxidants (Scheme 1).[5]

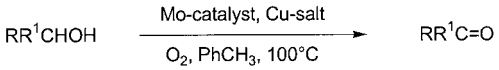


Scheme 1

Although DMSO is a cheap oxidizing agent, DMS would be an unpleasant side-product in large-scale applications. Here we wish to report the selective catalytic oxidation of alcohols by a new heterobimetallic molybdenum-copper system that uses molecular oxygen as the oxidizing source.

Results and Discussion

In our previous catalytic system, $R_2S{=}O$ was used to re-oxidize the molybdenum-dioxo catalyst.[5] Initial investigations showed that substituting $R_2S{=}O$ by dioxygen gave only stoichiometric amount of benzaldehyde for the oxidation of benzylic alcohol. Knowing the capability of copper(I) for the fixation and/or activation of molecular oxygen,[6] we introduced a catalytic amount of copper(I/II) salt in place of the sulfoxide. As we expected, the oxidation of $PhCH_2OH$ was effective with this new heterobimetallic Mo–Cu–O_2 catalytic system in toluene at 100 °C (Scheme 2). Table 1 shows blank experiment results proving that both molybdenum and copper catalysts are essential to oxidize $PhCH_2OH$ to PhCHO under a molecular oxygen atmosphere.



Scheme 2

Table 1. Comparative blank and catalytic experiment results on $PhCH_2OH$ oxidation

Catalyst[a]	t[b] (h)	PhCHO (%)[c]
Mo^{VI}	5	5
Mo^{VI}/O_2	3	6
Cu^{II}	3	0
Cu^{II}/O_2	3	< 2
Fe^{II}/O_2	5	0
Mo^{VI}/Cu^{II}	3	6
$Mo^{VI}/Cu^{II}/O_2$[d]	3	98
$Mo^{VI}/Fe^{II}/O_2$[d]	5	75

[a] Mo^{VI} = 1 equiv. $MoO_2(acac)_2$, Cu^{II} = 1 equiv. $Cu(NO_3)_2$, Fe^{II} = 1 equiv. $FeBr_2$. – [b] 20 equiv. $PhCH_2OH$, 5 equiv. 4-toluic acid, molecular sieves (4 Å), toluene, 100 °C. – [c] GC determination. – [d] Catalytic run.

Typically, a great variety of Mo complexes can be used (e.g. alkoxides, chlorides, dithiocarbamates...), but further studies showed that the nature of the ligands around the molybdenum center is critical to the success of the reaction, with acetylacetonate ($acac^-$) proving the most effective.[7] On the other hand, varying the nature of the copper(II) counterion had little effect on the rate/yield of the reaction, for example $CuSO_4$, $Cu(OAc)_2$, $CuCl_2$, $Cu(NO_3)_2$, $Cu(acac)_2$ and copper(I) salts such as CuCl can also be used. Other transition metals salts known to activate O_2, such as Co^{II}, Fe^{II} and Mn^{II} have also been tested. With $Co(acac)_2$, $MnBr_2$, or $FeBr_2$ instead of a Cu^{II} salt we observed a slower oxidation of $PhCH_2OH$ with selectivities ranging from 75–94%. The Mo–Fe system, although less active, behaved sim-

[a] Laboratoire de Chimie des Métaux de Transition et de Catalyse, UMR 7513 CNRS, Université Louis Pasteur,
4 rue Blaise Pascal, 67000 Strasbourg, France
Fax: (internat.) + 33-3/88416171
E-mail: osborn@chimie.u-strasbg.fr
[+] Present address: Laboratoire de Chimie de Coordination, UPR 8241 CNRS,
205 route de Narbonne, 31077 Toulouse Cedex, France
E-mail: lorber@lcc-toulouse.fr.
Fax: (internat.) + 33-5/615530023

 © WILEY-VCH Verlag GmbH, D-69451 Weinheim, 2000 1434–1948/00/0404–0655 $ 17.50+.50/0

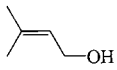
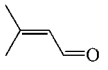
ilarly to the Mo–Cu system, i.e. no oxidation is observed without the Mo catalyst (cf. blank experiments in Table 1); however, we verified that Co^{II} or Mn^{II} alone (i.e. without Mo catalyst) is responsible for some of the alcohol oxidation.[9]

The addition of 5 equivalents of a carboxylic acid (e.g. 4-toluic acid) to the molybdenum-copper system improved the rate and yields of the reaction; stronger acids such as *p*-TsOH have the opposite effect.[10] For similar reasons, we used powdered molecular sieves (4 Å) to trap the water formed during the alcohol oxidation, which improved the catalyst lifetime.[2a,2c,5] Therefore, our typical catalytic system consists of $MoO_2(acac)_2$ (1 equiv.), $Cu(NO_3)_2$ (1 equiv.), 4-toluic acid (5 equiv.), substrate (alcohol, 20 equiv.), powdered activated molecular sieves (4 Å), 1 atm of O_2 in toluene[11] at 100 °C.

The catalytic oxidation of various alcohols takes place under these conditions, and a few results are presented in Table 2. Primary benzylic alcohols are oxidized with nearly total selectivity to aldehydes with no further oxidation to the corresponding acid (Entries 1–5). Secondary benzylic alcohols are oxidized to ketones with good selectivity but at lower rates (Entry 6). Allylic alcohols are oxidized by this method with poor selectivity (Entries 7–8), a common side-reaction being isomerisation[5] to an allylic alcohol or dehydration leading to formation of an ether. Longer periods of reaction are needed for the oxidation of aliphatic alcohols, with only moderate selectivity (Entries 9–12), and in the case of tBuCH$_2$OH further oxidation into tBuCO$_2$H was observed at 120 °C (Entry 11). Attempts to oxidize more than 20 equivalents of substrate lead to lower rates due to deactivation of the catalyst by the water formed. Therefore, the activity of the Mo–Cu system appears to be lower than that of Ru–Cu systems,[2b,2c,4] and is limited to the oxidation of benzylic alcohols.

Studies on the oxidation of a series of *para*-substituted benzylic alcohols (R = Me, H, Cl, CF_3, NO_2) show no correlation with Hammett σ parameters and little variation in rate on the *para* substituent. Hence, benzyl radicals would appear not to be involved in the rate determining step of the oxidation process,[12,13] a conclusion which is further supported by the observation that radical traps such as 2,4,6-tri-*tert*-butylphenol or galvinoxyl have no effect on the rate of the oxidation. The catalytic oxidation of PhCH(D)OH with the Mo–Cu system at 100 °C gives a product ratio of PhCDO/PhCHO = 3.0. In parallel experiments, the overall rate of the catalytic oxidation of PhCH$_2$OH and PhCD$_2$OH at 100 °C gives a value of k_H/k_D = 1.8. Overall, these results support the direct involvement of the benzylic C–H bond in the rate-determining step.

Table 2. Oxidation of various alcohols with the Mo–Cu–O_2 catalytic system

Entry	Substrate[a]	t (h)	Product	Yield %[b]	Conversion %[b]	Selectivity %[b]
1	PhCH$_2$OH	3	PHCHO	98	100	98
2	4-Me-C$_6$H$_4$CH$_2$OH	2.5	4-Me-C$_6$H$_4$CHO	92	100	92
3	4-Cl-C$_6$H$_4$CH$_2$OH	3	4-Cl-C$_6$H$_4$CHO	98	100	98
4	4-NO$_2$-C$_6$H$_4$CH$_2$OH	2	4-NO$_2$-C$_6$H$_4$CHO	97	100	97
5	4-CF$_3$-C$_6$H$_4$CH$_2$OH	5	4-CF$_3$-C$_6$H$_4$CHO	97	100	97
6	PhCH(OH)Et	5	PhC(O)Et	54	60	90
7		1		43[c]	90	48
8	cyclohexen-2-ol	1.5	cyclohexen-2-one	10	83	12[d]
9	cyclohexanol	6	cyclohexanone	37	58	64
10	1-hexanol	10	1-hexanone	16	67	24
11	tBuCH$_2$OH	1	tBuCHO	43[e]	60	72
12	tBuCH$_2$OH	3	tBuCHO / tBuCO$_2$H	13 / 30[e]	66	20[f]

[a] 20 equiv. alcohol, 1 equiv. $MoO_2(acac)_2$, 1 equiv. $Cu(NO_3)_2$, 5 equiv. 4-toluic acid, MS 4 Å, toluene, 100 °C, 1 atm O_2. – [b] GC determination. – [c] Solvent: 1,2-dichlorobenzene, side-reaction: isomerisation into 2-methyl-3-buten-2-ol (32%). – [d] Side-reaction: etherification into ROR (R = cyclohexene) (30%). – [e] At 120 °C. – [f] Selectivity in aldehyde + acid: 66%.

Although the complete mechanism of oxidation with this new catalytic system is not yet fully understood, we propose the catalytic cycle depicted in Figure 1 based on the above observations for the oxidation of PhCH$_2$OH. An initiation would first result in the formation of an alkoxide complex (**a**) by displacement of the acac ligand, as already seen in the oxidation of alcohols with other molybdenum catalysts[5] and by previous experiments carried out in our laboratory, which show that such exchange processes occur

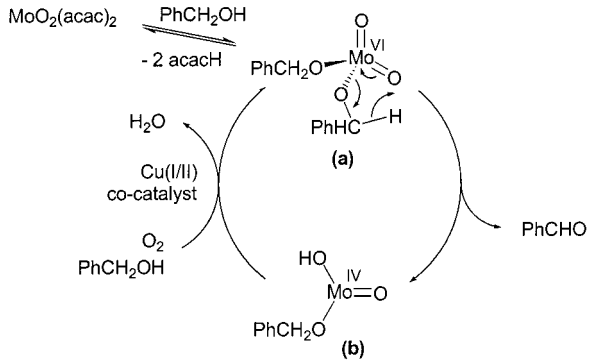


Figure 1. Proposed mechanism for the Mo–Cu–O_2-catalysed oxidation of $PhCH_2OH$; apparently low coordinate species **b** represented in this figure will have additional neutral ligands, such as alcohol, which have been omitted for simplicity

readily at electrophilic Mo^{VI} centers.[3,14] This point is further consistent with the higher rate of oxidation of $PhCH_2OH$ vs. PhCH(Et)OH which may result from the fact that prior coordination of the alcohols to the metal would be disfavored for the latter. A concerted process involving the transfer as a hydride of a β-hydrogen atom of the alkoxo ligand to one of the molybdenum-oxo entities via a five-membered cyclic transition state follows in a rate-determining step, with formation of PhCHO and a Mo^{IV} species (**b**). This transfer would result in the observed moderate primary kinetic isotope effect and is similar to the hydride transfer in other Mo-catalysed systems for the oxidation of alcohols.[5] The reoxidation of (**b**) into (**a**) by the copper salt in the presence of molecular oxygen is unclear. We can exclude a mechanism in which a copper(II) species may serve as the sole oxidant for the molybdenum by a pure redox Wacker-type process,[15] because the oxidation of $PhCH_2OH$ in the absence of molecular oxygen but with a twofold excess of Cu^{II} salt relative to the substrate (i.e. Mo/Cu/substrate = 1:40:20) proceeds with different characteristics (slow rate and very low selectivity in benzaldehyde) than the normal catalytic system under dioxygen atmosphere (Mo/Cu/substrate = 1:1:20).[16] In consequence, the regeneration of the Mo^{VI} active species (**a**) most certainly involves the activation of dioxygen by the copper co-catalyst.[17]

Further studies are needed to clarify the molybdenum reoxidation pathway and the exact function of the copper and carboxylic acid co-catalysts.

Conclusion

In conclusion, we describe a new, ecologically benign, Mo–Cu catalytic system for the aerobic oxidation of alcohols. Although so far limited to the oxidation of benzylic alcohols and with only moderate activities, this catalytic system remains very interesting from a mechanistic point of view and has been extended to the oxidation of alcohols by other oxo-metal complexes with higher activities.[4,21]

Experimental Section

General: All the substrates were purchased from Aldrich or Lancaster and were carefully dried over a suitable drying agent before use, distilled and stored under nitrogen (over molecular sieves 4 Å for liquids) in a glove box. 4-Toluic acid (Aldrich) was dried over P_2O_5 under vacuum. Molecular sieves (4 Å) were activated at 150 °C under vacuum, powdered and stored in a glove box. Toluene was dried over sodium, distilled and stored over molecular sieves in a glove box. $MoO_2(acac)_2$ was purchased from Aldrich or prepared following a literature procedure.[22] $Cu(NO_3)_2$ was obtained by drying $Cu(NO_3)_2{\cdot}2.5H_2O$ under vacuum at 100 °C for 48 hours and stored under nitrogen. $PhCD_2OH$ was prepared by treating ethyl benzoate with $LiAlD_4$ in diethyl ether, followed by hydrolysis with sodium hydroxide (10%), and distillation from CaH_2. PhCH(D)OH was prepared by treating PhCHO with $LiAlD_4$ in THF, followed by hydrolysis with $Na_2SO_4{\cdot}10H_2O$, dried with anhydrous $MgSO_4$, and distilled from CaH_2. The analyses of the catalytic reactions were carried out with a Hewlett–Packard 5890 Series II Gas Chromatograph equipped with a flame ionisation detector (FID) and a Hewlett–Packard HP-1 methyl silicon gum column of length 10 m, diameter 0.53 mm and 2.65 μm film thickness.

General Procedure for the Oxidation of $PhCH_2OH$: In a typical oxidation experiment, under nitrogen (glove box), $PhCH_2OH$ (257 mg, 20 equiv.), $MoO_2(acac)_2$ (39 mg, 1 equiv.), $Cu(NO_3)_2$ (23 mg, 1 equiv.), 4-toluic acid (81 mg, 5 equiv.), powdered molecular sieves (4 Å) (400 mg), and 2 g of toluene were placed in a 5- or 10-mL flask equipped with a stir bar and a reflux condenser. The reaction flask was connected to a molecular oxygen vacuum Schlenk line and heated at 100 °C for 3 h under 1 atm of O_2. Yield of PhCHO: 98% (determined by GC).

Acknowledgments

We would like to thank Dr. B. Meunier, Dr. P. Cassoux, Dr. J. Kress and Dr. J.-P. Le Ny for helpful discussions. We gratefully acknowledge the support of this research by the Centre National de la Recherche Scientifique.

[1] [1a] S. V. Ley, J. Norman, W. P. Griffith, S. P. Marsden, *Synthesis* **1994**, 639–666. – [1b] R. A. Sheldon, J. K. Kochi, in *Metal-Catalyzed Oxidations of Organic Compounds*, Academic Press, New York, **1981**.

[2] For catalytic oxidations see, for example, ref.[1a,4,5] and: [2a] W. P. Griffith, S. V. Ley, G. P. Whitcomb, A. D. White, *J. Chem. Soc., Chem. Commun.* **1987**, 1625–1627. – [2b] R. Lenz, S. V. Ley, *J. Chem. Soc., Perkin Trans. 1* **1997**, 3291–3292. – [2c] I. E. Markó, P. R. Giles, M. Tsukazaki, I. Chellé-Regnaut, C. J. Urch, S. M. Brown, *J. Am. Chem. Soc.* **1997**, *119*, 12661–12662. – [2d] I. E. Markó, P. R. Gilles, M. Tsukazaki, S. M. Brown, C. J. Urch, *Science* **1996**, *274*, 2044–2046. – [2e] A. Dijksman, I. W. C. E. Arends, R. A. Sheldon, *Chem. Commun.* **1999**, 1591–1592. – [2f] S. I. Murahashi, T. Naota, Y. Oda, N. Hirai, *Synlett* **1995**, 733–734.

[3] C. Y. Lorber, J. A. Osborn, *Tetrahedron Lett.* **1996**, *37*, 853–856.

[4] K. S. Coleman, C. Y. Lorber, J. A. Osborn, *Eur. J. Inorg. Chem.* **1998**, 1673–1675.

[5] C. Y. Lorber, I. Pauls, J. A. Osborn, *Bull. Soc. Chim. Fr.* **1996**, *133*, 755–758.

[6] See for example: [6a] N. Kitajima, *Adv. Inorg. Chem.* **1992**, *39*, 1–77. – [6b] N. Kitajima,Y. Moro-oka, *Chem. Rev.* **1994**, *94*, 737–757. – [6c] B. J. Hathaway, in *Comprehensive Coordination Chemistry* (Eds.: G. Wilkinson, R. D. Gillard, J. A. McCleverty), Pergamon Press, **1987**, vol. 5, pp. 534–774. – [6d] K. D. Karlin, Z. Tyeklar, A. D. Zuberbühler, in *Bioinorganic Catalysis* (Ed.: J. Reedijk), Marcel Decker, New York, **1993**, pp. 261–315.

[7] Compare, for example, the oxidation of $PhCH_2OH$ into PhCHO at 100 °C: $MoO_2(acac)_2$ 3 h/98% PhCHO, $MoCl_5$ 5 h/55% PhCHO, $[PPh_4][MoO_2(NCS)_4]$ 6 h/63% PhCHO, $MoO_2(Et_2dtc)_2$ 12 h/82% PhCHO. We have also used with success immobilized Mo catalyst such as PBI·Mo (PBI = polybenz-

imidazol)[8] which is less sensitive to degradation by water (yield of PhCHO after 10 h: 98%).

[8] M. M. Miller, D. C. Sherrington, *J. Chem. Soc., Chem. Commun.* **1994**, 55–56.

[9] H. Mimoun, in *Comprehensive Coordination Chemistry* (Eds.: G. Wilkinson, R. D. Gillard, J. A. McCleverty), Pergamon Press, **1987**, vol. 6, pp.318–410.

[10] Strong acids like *p*-TsOH have a detrimental effect on the catalysis, therefore the beneficial effect observed with a carboxylic acid may not come from its acidic proton character (as previously seen with other alcohols oxidation catalysts[5]) but from the coordinating properties of its carboxylate anion.

[11] 1,2-Dichlorobenzene can also be used, but we observed in some cases unwanted side-products. With donor solvents such as DMF and MeCN, rates are strongly decreasing, probably by inhibition of the copper function.

[12] S. L. Scott, A. Bakac, J. H. Espenson, *J. Am. Chem. Soc.* **1992**, *114*, 4205–4213.

[13] Non linear plots can also be due to other causes such as complications arising from side-reactions, steric effects from large *para* substituents, or cyclic transition states: [13a] H. Maskill, in *The Physical Basis of Organic Chemistry*, Oxford University Press, **1985**, chapter 10, pp. 405–473. – [13b] J. March, in *Advanced Organic Chemistry*, 3rd ed., Wiley Interscience, **1985**, chapter 9, pp. 237–250.

[14] [14a] J. Belgacem, J. Kress, J. A. Osborn, *J. Am. Chem. Soc.* **1992**, *114*, 1501–1502. – [14b] J. Belgacem, J. Kress, J. A. Osborn, *J. Mol. Catal.* **1993**, *86*, 267–285.

[15] S. D. Ittel, G. W. Parshall, in *Homogeneous Catalysis*, 2nd ed., Wiley, New York, **1992**.

[16] In a Wacker-type process, to convert one equivalent of $PhCH_2OH$ to PhCHO, the catalytic system would need two equivalents of Cu catalyst in order to reoxidize the Mo center. To check the possibility of a pure redox Wacker-type process we performed the oxidation of $PhCH_2OH$ (20 equiv.) in the absence of O_2 with 1 equivalent of $MoO_2(acac)_2$ and 40 equiv. of copper(II) salt [$Cu(NO_3)_2$ or $Cu(OAc)_2$], at 100 °C for 3 hours. The reaction was carried out both in the absence of 4-toluic acid and with 5 equivalents of 4-toluic acid. In the reaction performed in the absence of carboxylic acid, we observed only the formation of 2% of PhCHO (instead of 29% with the "normal" Mo–Cu–O_2 system). In the presence of carboxylic acid, we observed the formation of 30% of PhCHO, but with a low selectivity (selectivity was only 60%, instead of 98% for the Mo–Cu–O_2 system). We believe that most of the PhCHO formed in anaerobic conditions in presence of 4-toluic acid results from a Cu-catalysed oxidation of $PhCH_2OH$ because in a blank experiment (40 equivalents Cu^{II}, 5 equivalents 4-toluic acid, but no Mo catalyst) we formed ca. 18% of PhCHO. We also noticed the same behavior with our Mo–Fe system when performing the same kind of experiments with an excess of Fe^{III} salt under argon [$MoO_2(acac)_2$ 1 equivalent, $FeCl_3$ 40 equivalents, 4-toluic acid 5 equivalents, $PhCH_2OH$ 20 equivalents 100 °C, 5 hours] with formation of only 3% PhCHO (with a selectivity in PhCHO of only 4%) which is in contrast to 75% PhCHO (selectivity in PhCHO: 75%) with the Mo–Fe system under O_2 (Mo/Fe 1:1).

[17] Copper(I) and iron(II) complexes are well known to coordinate, activate and transfer molecular oxygen.[6,18–20] We believe the Mo^{IV} complex is first oxidized to Mo^{V} by a redox process induced by the Cu^{II} salt which would generate a Cu^{I} species. The Cu^{I} species is essential for the next step which would involve the activation of O_2 and would result in the oxidation of the Mo^{V} complex with regeneration of the Mo^{VI} catalytic species **a**, possibly through a heterobimetallic μ-peroxo- or μ-oxo-Mo^{VI}–Cu^{II} complex.

[18] See for example: [18a] G. Davies, M. A. El Sayed, R. E. Fasano, *Inorg. Chim. Acta* **1983**, *71*, 95–99. – [18b] S. Mahapatra, J. A. Halfen, E. C. Wilkinson, G. Pan, C. J. Cramer, L. Que, Jr., W. B. Tolman, *J. Am. Chem. Soc.* **1995**, *117*, 8865–8866. – [18c] C. Jallabert, C. Lapinte, H. Rivière, *J. Mol. Catal.* **1980**, *7*, 127–136.

[19] E. Ochiai, *Inorg. Nucl. Chem. Lett.* **1973**, *9*, 987–990.

[20] [20a] A. L. Feig, S. J. Lippard, *Chem. Rev.* **1994**, *94*, 759. – [20b] J. B. Vincent, G. L. Olivier-Lilley, B. Averill, *Chem. Rev.* **1990**, *90*, 1447–1467.

[21] K. S. Coleman, M. Coppe, C. Thomas, J. A. Osborn, *Tetrahedron Lett.* **1999**, *40*, 3723–3726.

[22] M. C. Chakravorti, D. Bandyopadhyay, *Inorg. Synth.* **1992**, *29*, 129–134.

Received October 13, 1999
[I99361]

Structural and Electrical Characterization of the Series $La_{1.33}Na_xMn_xTi_{2-x}O_6$

Ana Isabel Ruiz,[a] María Luisa López,*[a] María Luisa Veiga,[a] and Carlos Pico[a]

Dedicated to Prof. Gaitán on the occasion of his 70th birthday

Keywords: Perovskite phases / Mixed conductors / Materials science / Neutron diffraction / X-ray diffraction

A new series of perovskite-type materials of general formula $La_{1.33}Na_xMn_xTi_{2-x}O_6$ (x = 0.66, 0.55 and 0.44) was obtained and characterized. The common structure is rhombohedral (space group $R\bar{3}c$) although a transition to orthorhombic (space group *Ibmm*) is observed between 400 and 600 K for the x = 0.66 phase. Complex impedance techniques and charge/discharge cycles show a different electrical behavior that varies from a purely electronic conductor (x = 0.66) to a mixed electronic-ionic behavior for the other phases.

Introduction

Complex oxides with a perovskite or perovskite-type structure offer a wide range of interesting electrical properties, e.g. giant magnetoresistance, superconductivity and fast ion conductivity. In this context, complex oxides showing ion-electron conducting properties have received much attention due to their use as electrode materials in solid state batteries.

Perovskite-type oxides based on elements of the first transition series display a wide variety of defect-related phenomena which have their origin in the unfilled 3d electron shell. The relative ease with which electrons can be removed from or added to some metal cations, especially Fe and Mn, means that they often exist in different valence states, depending on the temperature and oxygen partial pressure. This fact also gives rise to a potentially large number of phases, which themselves may deviate from exact stoichiometry in terms of both cation and oxygen contents.[1] On the other hand, defects in perovskite oxides can arise from cation deficiency and the resulting vacancies often form ordered superstructures.

Among the mixed oxides with the perovskite structure, those containing Mn cations have recently attracted a great deal of interest due to their giant negative magnetoresistance effects.[2−4] The parent compound $LaMnO_3$ is an antiferromagnetic insulator in which an orbital ordering is established by means of the cooperative Jahn-Teller effect breaking the degeneracy of the electronic configuration of Mn^{3+} ($t_{2g}^3\ e_g^1$).[5] This order seems to be responsible for an orthorhombic to rhombohedral phase transition at about 873 K which is similar to other structural transitions that take place at elevated temperatures in some related systems.[6,7] It was previously reported[8] that as the orthorhombic (space group *Pbnm*) distortion of the perovskite arrangement decreases, the rare-earth, O1 and O2 atoms approach the ideal positions at (0 0 1/4), (0 1/2 1/4) and (1/4 1/4 0), respectively.

We have recently reported some results on ionic conductors, especially in perovskites of general formula $Ln_{1.33-x}Na_{3x}Ti_2O_6$.[9−10] The partial substitution of titanium by manganese in these compounds could lead to mixed conductors showing high ionic and electronic conductivity. The measurement and control of mixed ionic-electronic conductivities has become recognized as being of technological importance in an increasing number of systems. Therefore, the aim of this paper is to report both the structural and electrical behaviors of $La_{1.33}Na_xMn_xTi_{2-x}O_6$ ($0.66 \geq x \geq 0.44$). A detailed investigation of the phase $La_{1.33}Na_{0.66}Mn_{0.66}Ti_{1.34}O_6$ has been undertaken in order to clarify the parameters controlling the crystal structure of this material. An orthorhombic to rhombohedral transition was found as in $LaMnO_3$. Nevertheless, the orthorhombic space group is different, *Ibmm*, and only a rhombohedral symmetry, $R\bar{3}c$, was found for the remaining compositions. Conductivity measurements were performed and the results are interpreted on the basis of the compositional features.

Results and Discussion

For the series $La_{1.33}Na_xMn_xTi_{2-x}O_6$, pure phases were found in the compositional domain $0.66 \leq x \leq 0.44$. All samples have the characteristic X-ray diffraction patterns of the perovskite structure, in which some reflections are split

Table 1. *R* factors agreement obtained in the refinements by XRD and ND

	XRD refinements (300K)			ND refinements (300K)		
Space group	R_P	R_{WP}	R_B	R_P	R_{WP}	R_B
$R\bar{3}c$	8.73	11.0	9.18	8.56	11.3	7.03
Pbnm	8.29	10.6	9.57	6.30	7.80	5.36
Ibmm	11.6	15.0	9.60	5.79	7.35	4.31

[a] Departamento de Química Inorgánica I,
Facultad de Ciencias Químicas, Universidad Complutense,
28040 Madrid, Spain
Fax: (internat.) + 34-91/394-4352
E-Mail: marisal@eucmax.sim.ucm.es

 © WILEY-VCH Verlag GmbH, D-69451 Weinheim, 2000 1434−1948/00/0404−0659 $ 17.50+.50/0

indicating a noticeable distortion from the ideal cubic symmetry. For $x = 0.66$, the refinement was carried out in the rhombohedral space group $R\bar{3}c$, giving the unit cell parameters $a = 5.488$ Å and $c = 13.451$ Å; the R factors obtained in the refinement are gathered in Table 1.

On the other hand, an orthorhombic symmetry (whose parameters are related to the ideal perovskite ones as follows: $a_o \approx b_o \approx \sqrt{2}\, a_p$ and $c_o \approx 2\, a_p$) could be taken into account if we consider the Goldschmidt[11] factor, $t = [d(A-O)]/[\sqrt{2}\, d(B-O)]$, which is generally used as a tool for studying the perovskite structure. In our case, the value of $t = 0.97$, is compatible with an orthorhombic distortion. The XRD refinements were carried out in the space groups *Pbnm* and *Ibmm,* and the *R* factors obtained are included in Table 1. However these space groups give quite similar values and the results do not allow us to determine which is the more reliable structural model.

Neutron diffraction (ND) data were collected for the phase $La_{1.33}Na_{0.66}Mn_{0.66}Ti_{1.34}O_6$ in order to clarify the space group assignment. The *R* factors obtained by means of ND for the different space groups are also given in Table 1 and these results clearly suggest that the structure is accurately described in the *Ibmm* space group.

Neutron diffraction data were also collected for the same phase ($x = 0.66$) at different temperatures and were refined in an orthorhombic cell (space group *Ibmm*) at temperatures below 400 K that changes to a rhombohedral symmetry (space group $R\bar{3}c$) at higher temperatures (between 600 and 700 K).

The refined atom positions, lattice parameters and *R* factors obtained are listed in Table 2. The agreement between the observed and calculated integrated intensities of both orthorhombic and rhombohedral phases are considered as satisfactory with values of the crystal structure model indicators $R_B \leq 4.35$. The values of R_P and R_{WP} were ≤ 8.21 showing the reliability of the structure analysis.

Table 2. Refined Atomic Positions, Lattice Parameters, and R-factors for $La_{1.33}Na_{0.66}Mn_{0.66}Ti_{1.34}O_6$, obtained by neutron diffraction

		300 K	400 K	600 K	700 K
Space group		*Ibmm*	*Ibmm*	$R\bar{3}c$	$R\bar{3}c$
La/Na	*x*	−0.0042(4)	0.0062(8)	0.0000	0.0000
	y	0.0000	0.0000	0.0000	0.0000
	z	0.2500	0.2500	0.2500	0.2500
Mn/Ti	*x*	0.0000	0.0000	0.0000	0.0000
	y	0.5000	0.5000	0.0000	0.0000
	z	0.0000	0.0000	0.0000	0.0000
O1	*x*	0.0481(6)	0.0477(1)	0.4695(3)	0.4724(5)
	y	0.5000	0.5000	0.0000	0.0000
	z	0.2500	0.2500	0.2500	0.2500
O2	*x*	0.7500	0.7500		
	y	0.2500	0.2500		
	z	0.0214(6)	0.0197(1)		
a (Å)		5.4881(3)	5.4931(4)	5.5055(2)	5.5180(3)
b (Å)		5.4757(2)	5.4821(8)		
c (Å)		7.7407(7)	7.7501(1)	13.4618(1)	13.4844(1)
R_B (%)		4.35	4.21	4.20	4.14
R_P (%)		5.79	6.55	5.73	5.98
R_{WP} (%)		7.36	8.21	7.32	7.67

To illustrate graphically the matches between the complete observed and calculated data, neutron diffraction patterns and difference plots for the orthorhombic (300 K) and the rhombohedral (700 K) forms of $La_{1.33}Na_{0.66}Mn_{0.66}Ti_{1.34}O_6$ are plotted in Figures 1a and 1b, respectively. We will discuss the main characteristic features of both structures separately.

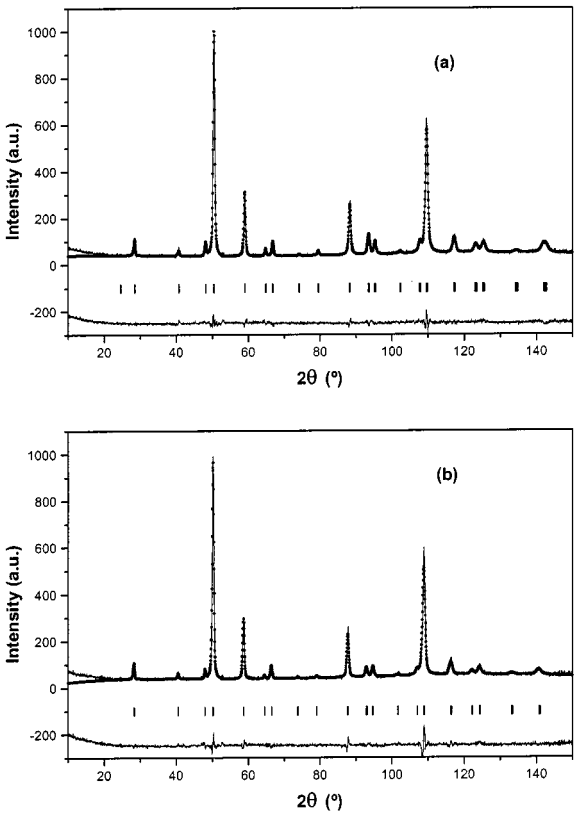


Figure 1. Calculated (full line) and observed (dots) ND patterns and difference spectrum for $La_{1.33}Na_{0.66}Mn_{0.66}Ti_{1.34}O_6$: (a) orthorhombic (300 K) and (b) rhombohedral (700 K)

Orthorhombic $La_{1.33}Na_{0.66}Mn_{0.66}Ti_{1.34}O_6$

The room temperature phase was refined in the orthorhombic space group *Ibmm*. Previous fits of the experimental results in the space group *Pbnm*, that frequently appears in orthorhombic perovskites, give higher *R* factors. In the inner-centered unit cell the Mn and Ti atoms are fixed at the 4b sites, and the La and Na atoms are located at the 4e, the O1 at the 4e and the O2 atoms at the 8g sites. The structure refinement for the title compounds, obtained separately from XRD and ND, are in good agreement and for the remaining compositions only XRD results will be discussed. An examination of the refined atomic coordinates, listed in Table 2, shows that Mn and Ti are placed on the ideal sites and the other atoms are only slightly displaced from their respective ideal positions. A comparison of the atomic coordinates obtained at 300 and 400 K shows that La, Na, O1 and O2 atoms remain nearly unchanged with temperature. Cations in the A-perovskite sites (La/Na) and

Table 3. Interatomic distances (Å) and angles (°) for BO_6 and AO_{12} polyhedra in $La_{1.33}Na_{0.66}Mn_{0.66}Ti_{1.34}O_6$, obtained by neutron diffraction

	300 K	400 K	600 K	700 K
d(Mn/Ti−O1)	1.953(5) (x2)	1.955(3) (x2)	1.951(1) (x2) 1.952(6) (x2)	1.954(8) (x4)
d(Mn/Ti−O2)	1.945(3) (x4)	1.946(1) (x4)	1.954(4) (x2)	1.956(9) (x2)
Mean	1.948	1.949	1.952	1.955
Shannon	2.018	2.018	2.018	2.018
O1−Mn/Ti−O2	89.3(8) (x4) 90.6(1) (x4)	89.0(5) (x4) 91.0(3) (x4)	89.7(8) (x4) 89.8(5) (x2)	89.7(5) (x4) 89.8(7) (x2)
O2−Mn/Ti−O2	89.4(4) (x2) 90.5(2) (x2)	89.5(7) (x2) 90.5(2) (x2)	90.2(3) (x2) 90.3(3) (x4)	90.2(2) (x2) 90.3(6) (x4)
Mn/Ti−O1−Mn/Ti	164.5(4)	164.5(6)		
Mn/Ti−O2−Mn/Ti	170.2(5)	171.0(9)	170.1(2)	171.1(9)
Mean	167.3	167.8	170.1	171.1
La/Na−O1	2.457(6) 2.748(4) (x2) 3.031(2)	2.450(2) 2.750(3) (x2) 3.042(4)	2.581(2) 2.585(1) (x2) 2.754(5) (x4) 2.755(1) (x2)	2.603(1) 2.607(3) (x2) 2.758(2) (x4) 2.759(3) (x2)
La/Na−O2	2.636(1) (x4) 2.847(3) (x4)	2.654(5) (x4) 2.835(6) (x4)	2.755(1) (x2) 2.917(6) 2.921(3) (x2)	2.759(3) (x2) 2.907(2) 2.911(3) (x2)
Mean	2.743	2.746	2.753	2.758
Shannon	2.772	2.772	2.772	2.772

in the B ones (Mn/Ti) will be noted in the following discussion as A and B, respectively.

To study the distortion around the Mn and Ti atoms which are in a BO_6 octahedral coordination, the interatomic distances, O−B−O angles and standard deviations have been calculated and are listed in Table 3. There are two different B−O sets of bond lengths in the octahedra, the average of which scarcely varies (from 1.948 to 1.949 Å) with increasing temperature. The average B−O distances are in good agreement with the sum of the Shannon ionic radii.[12] There are four different O−B−O angles with small deviations from the ideal 90° angle for a cubic perovskite. As can be seen from the interatomic distances and angles, the distortion within the BO_6 octahedron is rather small and the values are closer to ideal ones.

The orthorhombic distortion with respect to a cubic structure can be viewed as the BO_6 octahedra having faces tilted towards or away from each other and therefore the values of the B−O−B angles can be used to study the octahedra tilting. As shown in Table 3, the B−O1−B and B−O2−B angles for the orthorhombic phase $La_{1.33}Na_{0.66}Mn_{0.66}Ti_{1.34}O_6$ are significantly different from 180°, which is the expected value for an ideal cubic perovskite, and the octahedra tilting is ≈12.5°.

Lanthanum and sodium are located in the A sites and inside a twelve-coordinated polyhedron; the respective values of the A−O interatomic distances are gathered in Table 3. In comparison with those of the BO_6 octahedra, the A−O bond lengths vary over a wide range, indicating that these later polyhedra are quite distorted. An inspection of the twelve interatomic distances does not show any discontinuity in the increasing distances, and a division between the eight first-nearest and the four second-nearest oxygen atoms cannot be made, suggesting that it would be a good approximation to assign coordination number 12 to La and Na. The mean A−O distances are of the same order as the Shannon ones.

Rhombohedral $La_{1.33}Na_{0.66}Mn_{0.66}Ti_{1.34}O_6$

The high temperature phase is described as rhombohedral in the space group $R\bar{3}c$. From the hexagonal axes of reference, the A and B atoms are fixed at the 6a and 6b sites, respectively, and the O atoms are located at the 18e ones. The refined atomic coordinates, listed in Table 2, show that only the O atoms are slightly displaced from the ideal positions (1/2 0 1/4) with $\Delta x \approx 0.03$. The refined lattice parameters referring to hexagonal cell coordinates are also given in Table 2 (columns 600 and 700 K), the actual displacement of the O atoms from the ideal positions being about 0.16 Å. The respective values of the rhombohedral unit cell parameters, a_R and α_R, are 5.4990 Å and 60.08° (at 600 K) and 5.5093 Å and 60.10° (at 700 K), respectively.

The refined interatomic distances and angles of the BO_6 octahedron for this high temperature phase are also listed in Table 3, and show that each B atom is surrounded by six almost equidistant O atoms. The O−B−O angles are slightly deviated (± 0.3°) from the ideal value of 90° indicating that the distortion within a BO_6 octahedron is very small. However, the B−O−B angles are significantly different from the ideal angle of 180°, showing that octahedral tiltings remain in the rhombohedral phase. A structural model is depicted in Figure 2, in which the slight nonlinearity of the B−O−B bonds, which are deviated by around 10°, is denoted by the full lines.

The rhombohedral distortion can be viewed as being derived from a rotation of the BO_6 octahedra around the

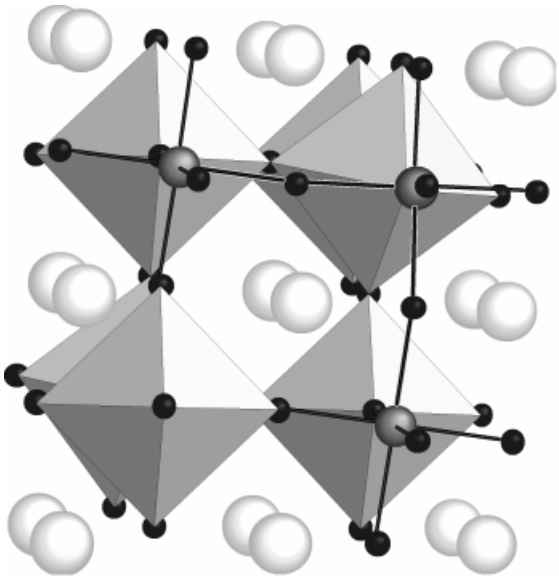


Figure 2. Structural model for compounds with rhombohedral symmetry

three-fold axis by an angle ω from the ideal perovskite position. The angle of rotation ω may be calculated from the oxygen position using $x = (\sqrt{3} - \text{tg}\ \omega)/\sqrt{12}$. The values of ω calculated at 600 and 700 K are 6.03° and 5.46°, respectively. There are different types of A−O distances for the rhombohedral phase of $La_{1.33}Na_{0.66}Mn_{0.66}Ti_{1.34}O_6$. In the absence of a sharp discontinuity in the increasing A−O distances we have assigned a coordination number 12 for the oxygen distorted polyhedra around these A atoms.

As stated above, the phase $LaMnO_3$ shows a cooperative Jahn-Teller effect that seems to be responsible for the orthorhombic to rhombohedral phase transition. Nevertheless, in our material ($x = 0.66$) only a third of the octahedral B-sites are effectively occupied by Mn^{3+}, with Ti^{4+} in the remaining ones, and any cooperative distortion must be excluded. This fact is supported by the similar B−O bond lengths that were encountered. Moreover, in the following phases ($x = 0.55$ and 0.44) only a rhombohedral symmetry appears in the whole range of temperatures studied, and therefore the adoption of such a symmetry in these systems with lower Mn^{3+} content cannot be attributed to a cooperative Jahn-Teller effect.

Rhombohedral $La_{1.33}Na_{0.55}Mn_{0.55}Ti_{1.45}O_6$ and $La_{1.33}Na_{0.44}Mn_{0.44}Ti_{1.56}O_6$

X-ray diffraction data for the phases $x = 0.55$ and 0.44, were tentatively refined on the basis of the space groups *Pbnm* and *Ibmm,* but the best fits were found in a rhombohedral symmetry (space group $R\bar{3}c$). Table 4 gathers the crystal parameters and *R* factors obtained for these compounds and a plot of the final observed, calculated and difference profiles is given in Figure 3 (for the composition $x = 0.44$). The agreements between profiles and *R* factors seem to confirm the validity of the proposed structural model. The basic features of the rhombohedral phases have been confirmed, and the results may be compared with those obtained in our neutron diffraction study.

Table 4. Refined atomic positions, lattice parameters and *R* factors for $La_{1.33}Na_xMn_xTi_{2-x}O_6$ ($x = 0.55$ and 0.44)

		$x = 0.55$	$x = 0.44$
Space group		$R\bar{3}c$	$R\bar{3}c$
La/Na	x	0.000	0.000
	y	0.000	0.000
	z	0.250	0.250
Mn/Ti	x	0.000	0.000
	y	0.000	0.000
	z	0.000	0.000
O1	x	0.462(1)	0.467(8)
	y	0.000	0.000
	z	0.250	0.250
a (Å)		5.493(6)	5.490(1)
c (Å)		13.444(6)	13.434(5)
R_B (%)		7.28	6.74
R_P (%)		7.94	8.57
R_{WP} (%)		10.6	11.2

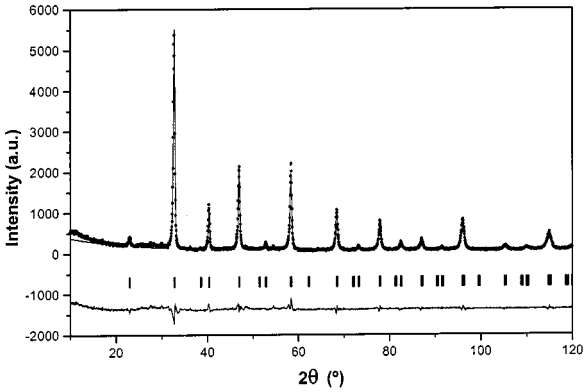


Figure 3. Calculated (full line) and observed (dots) XRD patterns and difference spectrum for $La_{1.33}Na_{0.44}Mn_{0.44}Ti_{1.56}O_6$ (rhombohedral)

On this basis, no differences in B−O bond lengths are encountered (1.952 Å for $x = 0.55$ and 1.948 Å for $x = 0.44$) and all the octahedra are regular. In consequence, the possible presence of a cooperative Jahn-Teller distortion, if it exists at a local level in the MnO_6 octahedra, is undetectable in the structure.

Electrical Properties

Measurements of a.c. impedance spectra have been carried out by alternating current techniques from the complex impedance (Z) plots. Experimental graphs at various temperatures show a semicircle and a spike. An apparent change in the nature of the charge carriers take place from electronic to electronic-ionic mixed conductors when x decreases, and this fact seems to be related to the higher number of cation vacancies in the structure.

Figure 4 shows the Z'' (imaginary part) vs. Z' (real part) plots for $x = 0.66$ at 300 and 326 K; it can be seen that the semicircle is somewhat depressed at this latter temperature.

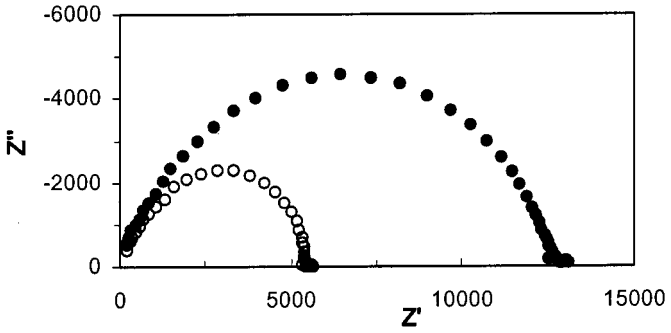


Figure 4. Complex impedance plots at 300 and 326 K for $La_{1.33}Na_{0.66}Mn_{0.66}Ti_{1.34}O_6$

However, for the samples $La_{1.33}Na_{0.55}Mn_{0.55}Ti_{1.45}O_6$ and $La_{1.33}Na_{0.44}Mn_{0.44}Ti_{1.56}O_6$ at temperatures between 298 and 333 K, a semicircle and a spike at low frequencies which is inclined by about 40° with respect to the Z′ axis were observed, and these could be associated with an electrode-electrolyte response (Figure 5, for $x = 0.55$).

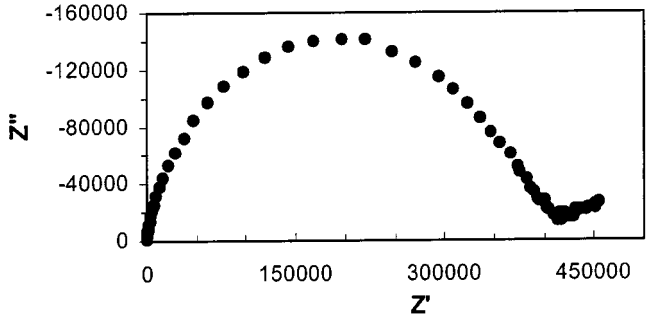


Figure 5. Complex impedance plots at 313 K for $La_{1.33}Na_{0.55}Mn_{0.55}Ti_{1.45}O_6$

Conductivity values for all samples were determined from the complex impedance plots over a wide range of temperatures and they can be fitted to an Arrhenius equation of the form: $\sigma = \sigma_o \times \exp(-Ea/kT)$. Figure 6 shows the linear plots of log σ vs. 1000/T for the three compositions. Conductivity values decrease with decreasing x, this fact being related to the total number of mobile sodium cations in the structure, although the respective activation energies remain almost constant.

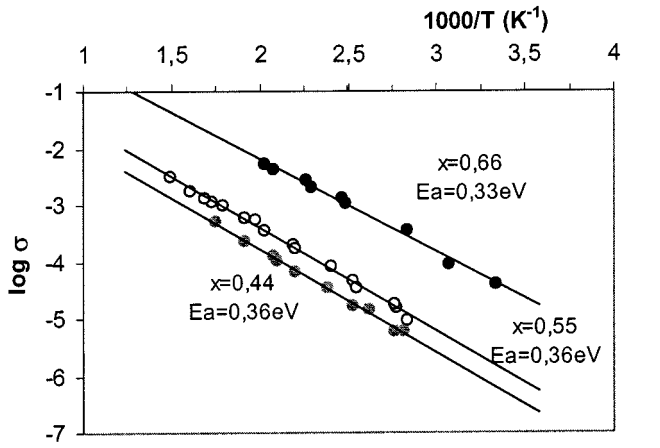


Figure 6. Arrhenius plots for the system $La_{1.33}Na_xMn_xTi_{2-x}O_6$

Charge/discharge experiments on cells consisting of pellets sandwiched between blocking platinum electrodes, showed that significant amounts of current could be passed on the charging cycle but another considerable amount is also detected on subsequently placing the cell in the discharge mode.[13] This phenomenon suggests that the products of charging were stored in the vicinity of the electrodes and were subsequently recovered on discharge, thereby indicating that a certain amount of ionic conduction occurs.

For purely ionic transport, where all the charge passed is stored and released on discharging, the ratio Q_d/Q_c (where Q_d and Q_c are the quantities of charge passed on the discharging and charging mode, respectively) should have the ideal value of unity. In a mixed ionic/electronic conductor, this ratio gives an approximate estimation of the ionic transport number, if one assumes that the reactions occur at the electrode-electrolyte interface during charging. For

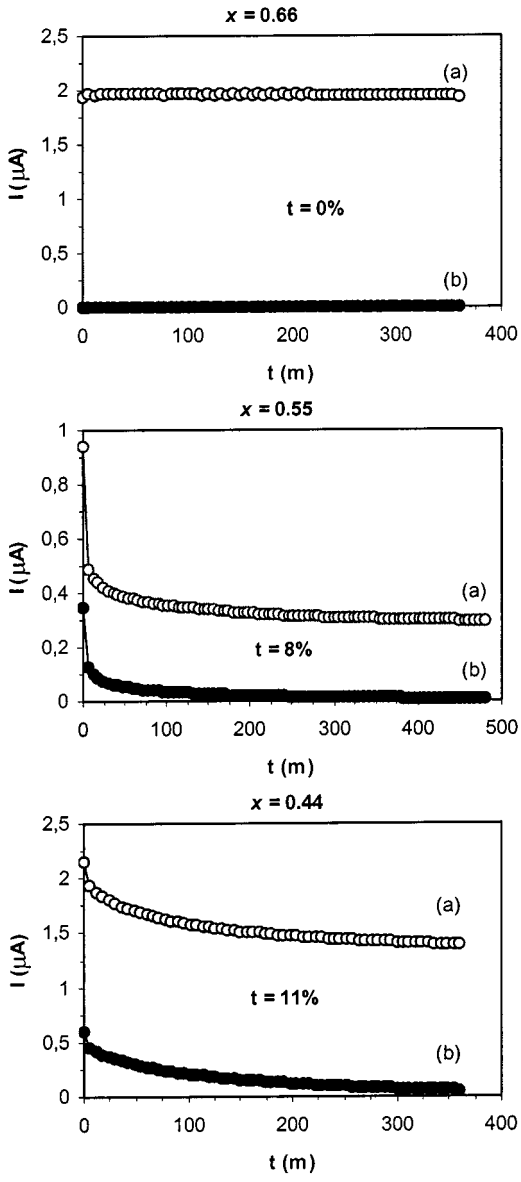


Figure 7. Current vs. time curves for charging/discharging for $x = 0.66$, 0.55 and 0.44 at 313 K (a) charging (b) discharging

purely electronic transport, the discharge current should be zero and the ratio Q_d/Q_c must also be zero. The following results of charging/discharging experiments have been interpreted in terms of these hypotheses.

The experimental results of charge/discharge processes at 313 K for all compositions are summarized in Table 5, and the respective curves are shown in Figure 7. The total charge passed through the system was calculated from the area under the I vs. t curves.

Table 5. Results of charging/discharging experiments at 313 K for $La_{1.33}Na_xMn_xTi_{2-x}O_6$

Composition	Q_c (C)[a]	Q_d (C)[b]	$t \approx Q_d/Q_c$[c]
0.66	7.04×10^{-4}	1.08×10^{-7}	1.53×10^{-4}
0.55	1.61×10^{-4}	1.29×10^{-5}	8.05×10^{-2}
0.44	5.53×10^{-4}	6.04×10^{-5}	1.09×10^{-1}

[a] Amount of charge passed during charging mode. – [b] Amount of charge recovered during discharging mode. – [c] Ionic transport number.

These results seem to confirm the different electric behavior of the materials as a function of their composition. The sample $x = 0.66$ (in which La and Na cations occupy all the A sites in the perovskite structure) behaves as a purely electronic conductor because ionic contribution is hindered. The samples $x = 0.55$ and 0.44 possess a relatively low number of A vacancies to which Na cations can move, and they show a mixed electronic-ionic conduction behavior.

Conclusion

In order to investigate materials with mixed ionic-electronic properties for their use as electrodes in solid-state batteries, some phases of general composition $La_{1.33}Na_x$-$Mn_xTi_{2-x}O_6$ have been obtained. From neutron powder diffraction data a structural transition between the orthorhombic (space group *Ibmm*) and rhombohedral (space group $R\bar{3}c$) symmetries is seen for $x = 0.66$. A similar transition from *Pbnm* to $R\bar{3}c$ symmetry is known for $LaMnO_3$ which is accompanied by an increase in the coordination number of A-cations from 8 to 12. In this respect, the space group *Ibmm* can be considered as a distorted intermediate that maintains the higher coordination number but shows a wide range of A–O bond lengths. The phases $x = 0.55$ and 0.44 adopt the rhombohedral $R\bar{3}c$ symmetry in which the BO_6 octahedra are clearly isolated and do not show any cooperative Jahn-Teller distortion.

All these phases behave as good conductors, on the basis of the relatively low activation energies, and, bearing in mind the absence of vacancies in the A sites when $x = 0.66$, this phase is a pure electronic conductor. The charge/discharge results can be interpreted as a function of the structural features.

Experimental Section

General Remarks: Polycrystalline samples of general composition $La_{1.33}Na_xMn_xTi_{2-x}O_6$ ($x = 0.66$, 0.55 and 0.44) were prepared by a classical ceramic method, from powdered mixtures of La(NO3)3·6H2O, $NaNO_3$, $C_{15}H_{21}MnO_6$ [manganese(III) acetylacetonate] and $C_{10}H_{14}O_5Ti$ (titanyl acetylacetonate), in a stoichiometric ratio, at 973 K for several days.

X-ray diffraction patterns were recorded with a Philips X′Pert-MPD diffractometer and a PW 3050/00 goniometer, using Ni-filtered Cu-K_α radiation and 2θ step size of 0.05°, with a counting time of 12.5 s for each step. The goniometer was connected to a PC controlled by the commercial program PC-APD (Analytical Powder Diffraction Software, 4.0).

The neutron powder diffraction data were recorded at four different temperatures on the D1A high-resolution powder diffractometer ($\lambda = 1.9110$ Å) at the Institut Laue-Langevin (Grenoble, France). The neutron and X-ray diffraction patterns were analyzed through the Rietveld method by the Fullprof program.[14] A pseudo-Voigt function was chosen to generate the line-shape of the diffraction peaks.

Electrical measurements were carried out with a Solartron 1260 Impedance/Gain Phase Analyzer with a frequency range of 0.1 Hz – 10 MHz. Samples were pressed into pellets and then sintered in air at 973 K for 48 h. Blocking electrodes were deposited on two faces of the pellets with platinum paint.

Polarization experiments in dc were carried out at 313 K with a charging voltage of 1 V for the compositions $x = 0.66$, 0.55 and 0.44. These samples and electrodes were the same as those used for conductivity measurements. The equipment includes a standard resistor that was in series with the sample during the charging and discharging cycles.

Acknowledgments

We are indebted to the CICYT (MAT 97–0326-C04–03) for financial support. We acknowledge the ILL for collecting data of ND. One of the authors (A.I.R.) is grateful to the C.A.M. for a grant.

[1] A. Atkinson, *Adv. Ceram.* **1987**, 23, 3.
[2] R. von Helmoth, J. Wecker, B. Holzapfel, L. Schulltz, K. Samwer *Phys. Rev. Lett.* **1993**, 71, 2331.
[3] Y. Tokura, A. Urushibara, Y. Moritomo, T. Arima, A. Asamitsu, G. Kido, N. Furukawa *J. Phys. Soc. Jpn.* **1994**, 63, 3931.
[4] S. Jin, M. McCormack, T. H. Tiefel, R. Ramesh *J. Appl. Phys.* **1994**, 76, 6929.
[5] J. Rodriguez-Carvajal, M. Hennion, F. Moussa, A. H. Moudden *Phys. Rev.* **1998**, B57, R3189.
[6] M. Marezio, J. P. Remeika, P. D. Dernier *Acta Cryst.* **1970**, B26, 2008.
[7] M. Marezio, P. D. Dernier, J. P. Remeika *J. Solid State Chem.* **1972**, 4, 11.
[8] T. C. Huang, W. Parrish, H. Toraya, P. Lacorre, J. B. Torrance *Mat. Res. Bull.* **1990**, 25, 1091.
[9] A. I. Ruiz, M. L. López, M. L. Veiga, C. Pico *Solid St. Ionics* **1998**, 112, 291.
[10] M. A. Arillo, J. Gómez, M. L. López, C. Pico, M. L. Veiga *Solid St. Ionics* **1997**, 95, 241.
[11] V. M. Goldschmidt, *Skr. Nor. Vidensk. Akad.*, Oslo, **1926**, 2.
[12] R. D. Shannon, *Acta Cryst.* **1976**, A32, 751.
[13] H. H. Sumathipala, M. A. K. L. Dissanayake, A. R. West *Solid St. Ionics* **1996**, 86–88, 719.
[14] J. Rodriguez Carvajal, *FULLPROF.* XV Congress of International Union of Crystallography, Toulouse **1990**, p 127, **1994** (Revised version).

Received March 19, 1999
[I99108]

Cathodic Reactions Involved in Corrosion Processes Occurring in Concentrated Nitric Acid at 100 °C

Fanny Balbaud,*[a] Gérard Sanchez,[a] Gérard Santarini,[a] and Gérard Picard[b]

Keywords: Autocatalysis / Cyclic voltammetry / Nitric acid / Nitrogen oxides / Reduction mechanism

In order to explain and analyze the corrosion process of AISI 304 L stainless steel in the presence of nitric acid condensates, the reduction mechanism of nitric acid was studied on a platinum electrode in various nitric acid solutions (4 mol·L^{-1}, 8 mol·L^{-1} and 12 mol·L^{-1}) at 100 °C. Classical electrochemical techniques were used: cyclic voltammetry, chronoamperometry on a stationary electrode as well as on a rotating disk electrode. A reduction mechanism is proposed; this mechanism is autocatalytic and involves a charge-transfer step and a heterogeneous chemical reaction which regenerates the electroactive species at the electrode surface. The electroactive species is assumed to be nitrous acid which is a soluble species. The other compounds involved in the reduction mechanism are NO and NO_2, which are supposed to be adsorbed. The nitric acid concentration influences the major product of the reduction process: NO for concentrations lower than 8 mol·L^{-1} and NO_2 for higher concentrations.

Introduction

Nuclear fuel reprocessing is achieved in France using nitric acid as the dissolution reaction medium. The corrosiveness of nitric acid mixtures leads to the use of corrosion-resistant materials such as austenitic stainless steels or zirconium.

Some potential cases of intergranular corrosion have been identified in experimental devices and studied on non-sensitized stainless steels, for example, in confined and non-renewed nitric acid.[1] However in some specific conditions, uncertainties about the mechanisms involved remain. Corrosion in the presence of nitric acid condensates is one of these cases and can be encountered in any installation handling boiling nitric acid. A specific loop, named ECORCE (Etude de la CORrosion sous Condensat d'Evaporation), designed at the laboratory, revealed a much more severe corrosion of stainless steels by nitric acid condensates than in the liquid bulk under similar conditions of concentration and temperature.[2] In fact, the condensate medium can lead to such highly oxidizing conditions that the corrosion potential of the steel can reach the transpassive domain.

Very few literature data have been found on this phenomenon and no thorough study has been performed. Therefore, in order to understand and analyze the corrosion mechanism of AISI 304 L stainless steel in the presence of nitric acid condensates, a research project was performed in this laboratory. The first step of this study consisted in a thermodynamic analysis of the chemical and electrochemical properties of nitric acid media.[3] This analysis led to a representation of concentrated nitric acid at 100 °C. One of the results of this study concerns the influence of the nitric acid concentration on the reduction species of nitric acid. Major species liable to be found when nitric acid is reduced at potentials close to the equilibrium potential were determined: nitrogen monoxide for nitric acid concentrations lower than 8 mol·L^{-1} and nitrogen dioxide for higher concentrations.[3]

This paper presents the second step of the research project which is the electrochemical investigation of the reduction process of nitric acid at 100 °C occurring on a platinum electrode. The platinum electrode was used as working electrode in order to avoid the oxidation of the electrode material and to focus the research on the reduction process. This electrochemical study appeared necessary as previous corrosion studies performed on AISI 304 L stainless steel in nonrenewed and confined liquid nitric acid[1] revealed the necessity of investigating the cathodic part of the corrosion process by suggesting a major role of the reduction mechanism on the increase in the corrosion rate.

The working temperature in the thermodynamic study[3] and in the electrochemical study was fixed at 100 °C as the metallic wall temperature is close to this value in the condensation zones.

In a last step, it will be necessary to perform a similar electrochemical study on a stainless steel electrode in order to compare the reduction process obtained with the one observed on a platinum electrode and, secondly, to link these results to the results of the corrosion tests performed in the laboratory.[4] The final aim of this research is to ex-

[a] CEA - CEREM, Service de la Corrosion d'Electrochimie et de Chimie des Fluides,
Bâtiment 458, CEA/Saclay, F-91191 Gif sur Yvette Cedex, France
Fax: (internat.) + 33-1/6908-1586
E-mail: fanny.balbaud@cea.fr
[b] Laboratoire d'Electrochimie et de Chimie Analytique (UMR 7575 du C.N.R.S.),
Ecole Nationale Supérieure de Chimie de Paris,
11 rue Pierre et Marie Curie, F-75231 Paris Cedex 05, France
E-mail: picard@ext.jussieu.fr

 © WILEY-VCH Verlag GmbH, D-69451 Weinheim, 2000 1434−1948/00/0404−0665 $ 17.50+.50/0

plain the corrosion mechanism of AISI 304 L stainless steel in the presence of nitric acid condensates.

Literature Data

The Reduction Mechanism of Nitric Acid on a Platinum Electrode

This process has been widely studied over many years.[5–13] All the authors agree on its autocatalytic nature, characterized by the predominant role of the reduction products. It is also generally believed that the nitric acid molecule is not the electroactive species.

In nitric acid solutions of concentrations from 1 to 10 mol·L^{-1}, at 25 °C, containing nitrous acid,[5–12] two different autocatalytic mechanisms have been formulated respectively by Vetter and Schmid.

According to Vetter the mechanism is heterogeneous, as the chemical regeneration of NO_2, assumed to be the electroactive species, occurs at the electrode surface. NO_2 is formed at the interface according to a previous slow heterogeneous chemical reaction. In that case, the stirring of the solution has no influence on the current density.[5–7] This mechanism is described as:

$$(HNO_2)_{ads.} + H^+ = (NO^+)_{ads.} + H_2O$$
$$(NO_3^-)_{ads.} + (NO^+)_{ads.} = (N_2O_4)_{ads.}$$
$$(N_2O_4)_{ads.} = 2(NO_2)_{ads.}$$
$$(NO_2)_{ads.} + e^- = (NO_2^-)_{ads.}$$
$$(NO_2^-)_{ads.} + H^+ = (HNO_2)_{ads.}$$

According to Schmid the mechanism is homogeneous, as the chemical regeneration of NO^+, assumed to be the electroactive species, occurs in the bulk. NO^+ (equivalent to HNO_2) is obtained from the nitrous acid formed in the layer near the electrode. In that case the stirring of the solution provokes a decrease of the current density.[8–12] This mechanism is described as:

$$HNO_2 + H^+ = NO^+ + H_2O$$
$$NO^+ + e^- = NO$$
$$2NO + NO_3^- + H^+ + H_2O = 3HNO_2$$

These two mechanisms, for a long time opposed, have both been validated by Razygraev who worked in a large range of concentrations and temperatures.[13] He supposed that both mechanisms occur on a platinum electrode, but for different potentials, leading to NO_2 (heterogeneous mechanism) or NO (homogeneous mechanism).

The Reduction Mechanism of Nitric Acid on a Stainless Steel Electrode

The same study was performed on stainless steels and alloys by Razygraev.[14] He concluded that an identical sequence of reactions was taking place on the different materials as on the platinum electrode, except that both mechanisms occurred simultaneously on stainless steels.

A recent study on the effect of dissolved chromium species on the corrosion of stainless steel in nitric acid confirmed the autocatalytic characteristic of the reduction of nitric acid on a gold electrode as well as on a stainless steel electrode.[15] This study revealed the lack of influence of Ar, N_2 and N_2O on the corrosion rate of stainless steel and the effect of a continuous bubbling of NO and NO_2, which leads to an increase in the corrosion rate by a catalytic mechanism. However, no reduction mechanism of nitric acid was proposed and the role of the different nitric acid species was not clearly specified.

Conclusions from Literature Data

The knowledge of the corrosion mechanism of AISI 304 L stainless steel in the presence of nitric acid condensates involves the understanding and the analysis of the reduction process of nitric acid.[1]

Literature data on the reduction process of nitric acid occurring on a platinum electrode are very numerous and sometimes contradictory. However, the studies presented in the literature agree on two major points: the reduction mechanism is autocatalytic and the electroactive species is not nitric acid.

The major uncertainties remaining are:

- the identity of the electroactive species at low overvoltages (potential range investigated for the corrosion study): HNO_2, NO^+, NO_2,
- the regeneration site of the electroactive species: electrode surface, solution,
- the influence of the concentration of nitric acid on the reduction process,
- the relationship between the reduction process and the thermodynamic behavior of nitric acid.

In this paper, our aim is to clarify these uncertainties, to identify the major species involved in the reduction process of nitric acid, and to propose a sequence of reactions explaining the experimental facts observed.

Results and Discussion

Various electrochemical techniques have been used: cyclic voltammetry, chronoamperometry with a stationary electrode as well as with a rotating disk electrode.

The values of the Open Circuit Potential (OCP) of the platinum electrode in the nitric acid solutions are given in Table 1. The values of the nitrous acid concentrations are estimated from thermodynamic calculations.[3]

Table 1. Experimental values of the Open Circuit Potential of the platinum electrode in the three nitric acid solutions at 100 °C – corresponding calculated nitrous acid concentration

$[HNO_3]$ [mol·L^{-1}]	OCP [V/SSE][a]	$[HNO_2]$ [mol·L^{-1}]
4	0.550	3.1×10^{-5}
8	0.630	7.5×10^{-6}
12	0.680	7.5×10^{-6}

[a] SSE: $Hg/Hg_2SO_{4(sat.)}$, $K_2SO_{4(sat.)}$.

The electroactivity domain of a solution of nitric acid 4 mol·L^{-1} is presented in Figure 1. The potentials were investigated between 0.400 V/SSE and 1 V/SSE. For higher overvoltages a gaseous evolution occurs.

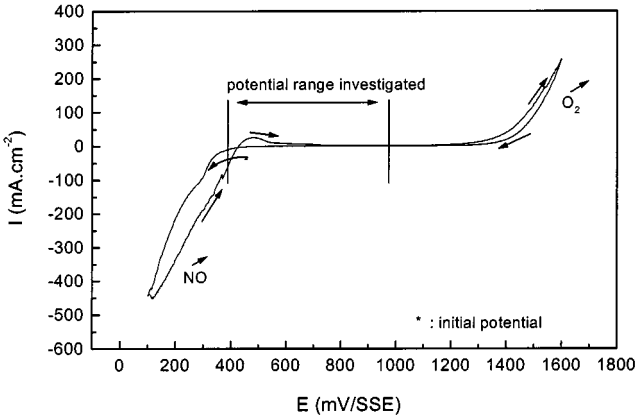


Figure 1. Electroactivity domain of HNO_3 4 mol·L^{-1} at 100 °C at a scan rate of 10 mV·s^{-1}; in reduction, NO evolution; in oxidation, O_2 evolution

Nitric Acid Solutions With No External Additions

Current-Potential Curves at a Low Scan Rate

Figures 2 and 3 show voltammograms obtained on a stationary electrode for nitric acid concentrations of 4 mol·L^{-1}, 8 mol·L^{-1} and 12 mol·L^{-1} at a scan rate of 10 mV·s^{-1}. The curves are presented in a log scale.

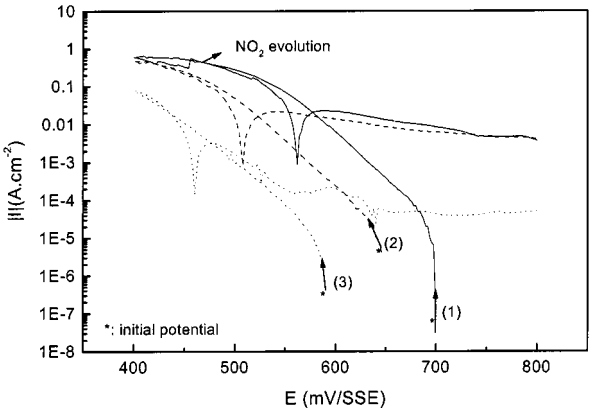


Figure 2. Cyclic voltammograms for HNO_3 solutions of different concentrations at 100 °C at a scan rate of 10 mV·s^{-1}. (1): 12 mol·L^{-1} (2): 8 mol·L^{-1} (3): 4 mol·L^{-1}

For the three solutions, the scans were performed from the OCP to the same potential of 0.400 V/SSE and then reversed (Figure 2). For HNO_3 4 mol·L^{-1}, another curve was placed on the diagram for which the scan was performed down to 0.250 V/SSE (Figure 3).

The oxidation peak is assigned to the oxidation of species formed during the reduction of nitric acid, which is confirmed by the absence of this peak when a scan is performed directly on oxidation.

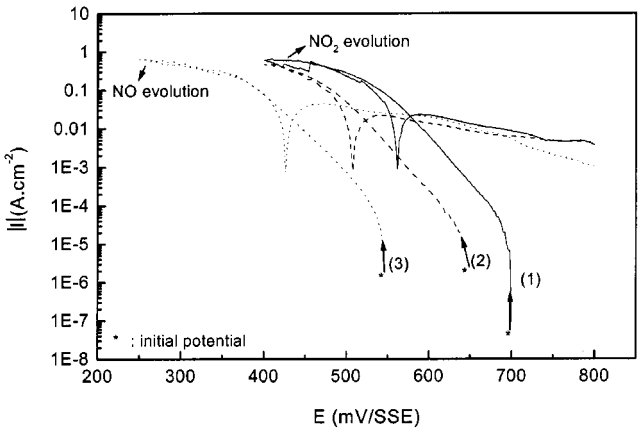


Figure 3. Cyclic voltammograms for HNO_3 solutions of different concentrations at 100 °C at a scan rate of 10 mV·s^{-1}. (1): 12 mol·L^{-1} (2): 8 mol·L^{-1} (3): 4 mol·L^{-1}

The analysis of the experiments and the visual observations show that:

– for the three concentrations, the voltammograms are similar: current densities are almost equal for the same overvoltage (taken from the OCP);
– a red gaseous evolution of NO_2 is observed for HNO_3 12 mol·L^{-1} and 8 mol·L^{-1};
– a colorless gaseous evolution (probably NO) is observed for HNO_3 4 mol·L^{-1} for a potential of 0.250 V whereas no evolution is observed for 0.400 V/SSE.

Figure 4 shows the representation [log$p$(O_2)] versus [–log$p$(HNO_3) and pH] of nitric acid at 100 °C established previously.[3] The curves represent the calculated values of the oxygen pressure for which the partial pressures of NO and NO_2 are equal to 1 bar and the concentration of nitrous acid to 10^{-2} mol·L^{-1}. The links between the oxygen pressure and the experimental potential values are determined by potentiometric measurements for 4 mol·L^{-1}, 8 mol·L^{-1} and 14.4 mol·L^{-1} solutions (determination of the potential for p_{NO2} = 1 bar at the different concentrations) and by considering that $\Delta\log p(O_2) = 1$ for $\Delta E = 2.303RT/4F = 18.5$ mV.[3] For a given potential, the oxygen pressure varies with the nitric acid concentration.

At 100 °C, the electroactivity domain of nitric acid in reduction (nonhatched domain) under a pressure of one bar is divided into two parts. The formation of NO limits the stability domain for concentrations lower than 8 mol·L^{-1} and the formation of NO_2 for higher concentrations. With this diagram, the voltammetric results can be analyzed:

– for HNO_3 12 mol·L^{-1} and 8 mol·L^{-1}, a potential of 0.400 V/SSE applied to the platinum electrode corresponds to oxygen pressures far outside the stability domain of nitric acid and an evolution of NO_2 occurs;
– for HNO_3 4 mol·L^{-1}, the potential of 0.400 V is very near the stability domain of HNO_3. Thus, no gaseous evolution occurs. However, the potential of 0.250 V is located far outside the stability domain and then a gaseous evolution of NO is observed.

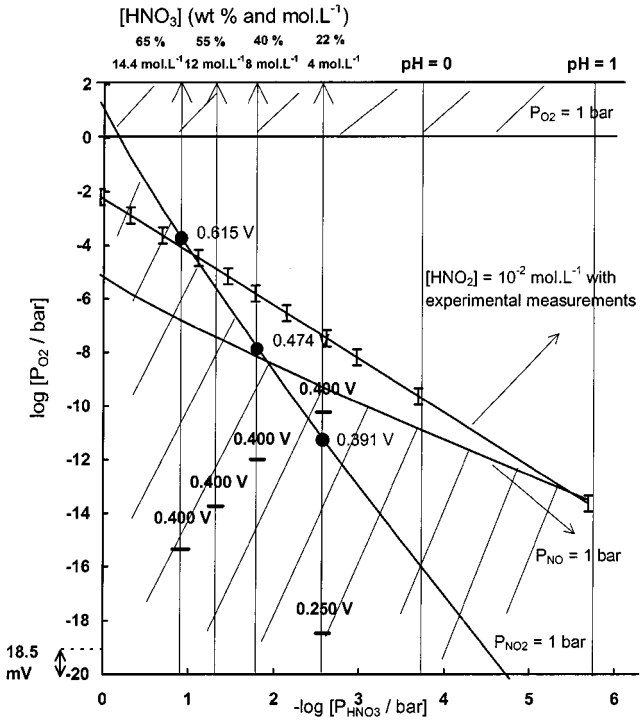


Figure 4. Representation of the chemical and electrochemical properties of concentrated nitric acid at 100 °C. •: Potential values for p_{NO2} = 1 bar (V/SSE at 25 °C); –: potential limits of the electrochemical investigations (V/SSE at 25 °C)

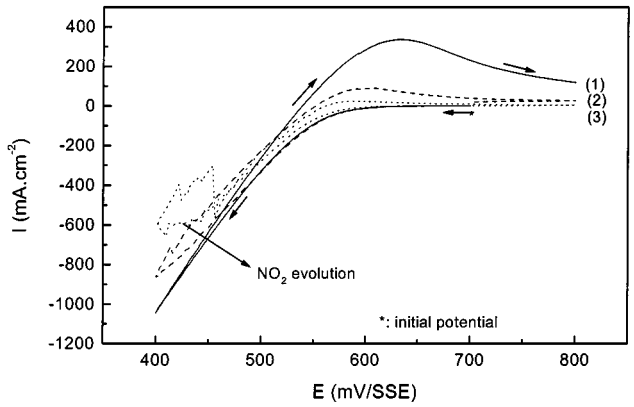


Figure 5. Cyclic voltammograms for HNO_3 12 mol·L^{-1} at 100 °C at different scan rates. (1): 500 mV·s^{-1} (2): 100 mV·s^{-1} (3): 10 mV·s^{-1}

These first results show the dependence of the reduction process on the nitric acid concentration.

Voltammetry

Figure 5, Figure 6 and Figure 7 show, for 12 mol·L^{-1}, 8 mol·L^{-1} and 4 mol·L^{-1} solutions, the voltammograms obtained for scan rates varying from 10 mV·s^{-1} to 500 mV·s^{-1}.

The results obtained are the following:

– for HNO_3 12 mol·L^{-1}, a regular variation of the voltammograms with the scan rate is obtained;

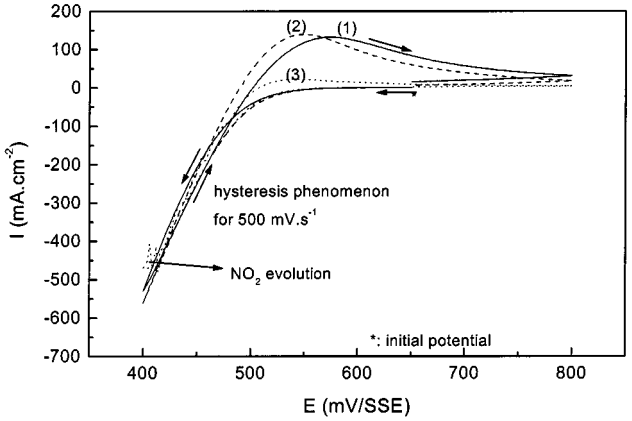


Figure 6. Cyclic voltammograms for HNO_3 8 mol·L^{-1} at 100 °C at different scan rates. (1): 500 mV·s^{-1} (2): 100 mV·s^{-1} (3): 10 mV·s^{-1}

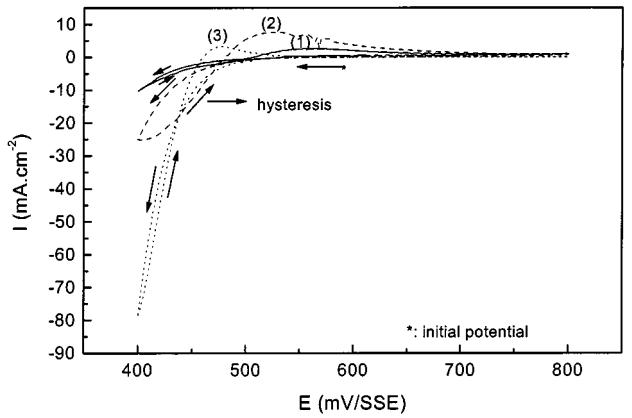


Figure 7. Cyclic voltammograms for HNO_3 4 mol·L^{-1} at 100 °C at different scan rates. (1): 500 mV·s^{-1} (2): 100 mV·s^{-1} (3): 10 mV·s^{-1}

– for HNO_3 8 mol·L^{-1}, a slight hysteresis phenomenon appears for 500 mV·s^{-1};

– for HNO_3 4 mol·L^{-1}, a sharp hysteresis phenomenon appears and the current density in reduction decreases when the scan rate increases;

– for a given scan rate, the current density increases with the nitric acid concentration.

These observations suggest the existence of a relatively slow reaction in the reduction process which is promoted by a high nitric acid concentration.

The analysis of the charges (Table 2) shows that, during the reduction process, some matter is lost: at all concentrations the ratio $|Q_{ox}/Q_{red}|$ is lower than 1 and increases when the scan rate increases. For high nitric acid concentrations, this phenomenon is more marked; the overvoltage applied in reduction is high and the stability domain of nitric acid is exceeded: the small ratio (0.04) obtained at a low scan rate is due to a gaseous evolution (NO_2).

For HNO_3 4 mol·L^{-1}, the overvoltage imposed in reduction is relatively low, the stability domain of nitric acid is not exceeded: no gaseous evolution occurs and the ratio $|Q_{ox}/Q_{red}|$ tends towards 1 for high scan rates.

Chronoamperometry

Experiments on the influence of the nitric acid concentration were performed using chronoamperometry. This tech-

Table 2. Oxidation charge, $Q_{ox.}$ [mC·cm^{-2}], reduction charge, $Q_{red.}$ [mC·cm^{-2}], and ratio $|Q_{ox.}/Q_{red.}|$, as a function of the nitric acid concentration and of the scan rate

$[HNO_3]$ [mol·L^{-1}]	**4**			**8**			**12**		
V [mV·s^{-1}]	$Q_{ox.}$	$Q_{red.}$	$\lvert Q_{ox.}/Q_{red.}\rvert$	$Q_{ox.}$	$Q_{red.}$	$\lvert Q_{ox.}/Q_{red.}\rvert$	$Q_{ox.}$	$Q_{red.}$	$\lvert Q_{ox.}/Q_{red.}\rvert$
500	1.06	−1.5	0.71	51.5	−100.3	0.51	131.1	−297.5	0.44
300	2.05	−3.4	0.60	77.5	−154	0.50	177.2	−490.3	0.36
100	10.4	−20.2	0.51	222.2	−514.6	0.43	144.3	−1305	0.11
30	25.0	−104.0	0.24	592.1	−1958	0.30	182.9	−4430	0.04

nique was used to determine the influence of the stirring of the solution. A reduction potential (near the equilibrium potential) is imposed and when the current is stabilized, the electrode is stirred. The stirring is regulated with a rotating disk electrode (ω = 2000 rpm).

Figure 8 shows the variation of the current density with time for a potential of 0.400 V/SSE and for the different nitric acid concentrations.

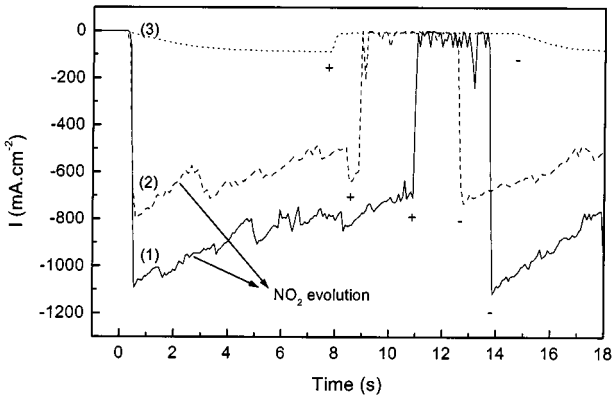


Figure 8. Influence of the stirring on the limiting current density of different nitric acid solutions at 100 °C for a potential of 0.400 V/SSE. ω = 2000 rpm; +: stirring; −: no stirring. (1): 12 mol·L^{-1} (2): 8 mol·L^{-1} (3): 4 mol·L^{-1}

An evolution of nitrogen dioxide is observed for HNO_3 8 mol·L^{-1} and 12 mol·L^{-1}. For all the concentrations the rotation of the electrode leads to a sharp decrease (it becomes nearly equal to zero) of the current density (in magnitude). This inverse dependence of the current density vs. stirring shows that the electroactive species is a soluble species formed at the electrode which diffuses into the solution. When the solution is stirred, the electroactive species is expelled from the electrode. This result is in agreement with Schmid's observations.[8–12] From these first experiments, it is possible to conclude that nitric acid is reduced indirectly through a mechanism involving at least a charge-transfer step and a chemical reaction which regenerates the electroactive species. The electroactive species is a soluble species produced at the electrode by a chemical reaction which is promoted by a high nitric acid concentration.

Influence of the Addition of Nitrous Acid in Solution and of a Flow of Nitrogen Monoxide in the Cell

In order to clarify the species involved, some voltammetric experiments were performed in nitric acid solutions containing reduction products of nitric acid at a significant concentration. The first series was performed with an addition of nitrous acid (nitrites) in solution and the second series with a flow of nitrogen monoxide in the cell.

Current-Potential Curves at a Low Scan Rate

The same experiments (as with nitric acid solutions with no external additions) were performed with an initial nitrite concentration of 10^{-2} mol·L^{-1} in solution. Table 3 gives the OCP of the platinum electrode in the different solutions for a nitrite concentration of 10^{-2} mol·L^{-1}. The values are lower than without nitrites according to the Nernst law:

$$E = E^{0'} - RT/2F \ln[HNO_2]$$

Table 3. Experimental values of the Open Circuit Potential of the platinum electrode in the three nitric acid solutions at 100 °C for a nitrite concentration of 10^{-2} mol·L^{-1}

$[HNO_3]$ [mol·L^{-1}]	OCP [V/SSE]
4	0.457
8	0.514
12	0.564

The experimental values of the apparent standard potentials, for the different nitric acid solutions at 100 °C, have been determined previously.[3]

The influence of the nitric acid concentration was studied for a scan rate of 10 mV·s^{-1} (Figure 9).

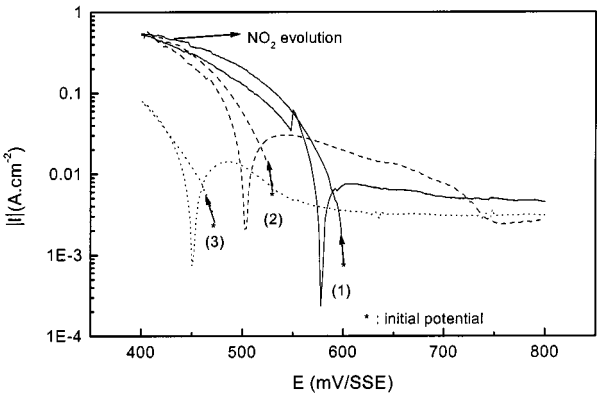


Figure 9. Cyclic voltammograms for HNO_3 solutions of different concentrations at 100 °C containing $[HNO_2] = 10^{-2}$ mol·L^{-1} at a scan rate of 10 mV·s^{-1}. (1): 12 mol·L^{-1} (2): 8 mol·L^{-1} (3): 4 mol·L^{-1}

If the voltammograms are compared with the ones without nitrites, no major differences are observed. The current

densities in reduction are nearly the same with or without nitrites for this scan rate. In oxidation, an increase of the oxidation peak is observed for HNO_3 4 mol·L^{-1} and 8 mol·L^{-1}, which is easily explained as nitrites present in solution undergo oxidation into nitric acid. For HNO_3 12 mol·L^{-1}, a slight decrease of the oxidation current is observed; this phenomenon cannot be readily explained at the moment.

Voltammetry

Figure 10, Figure 11 and Figure 12 show, for 12 mol·L^{-1}, 8 mol·L^{-1} and 4 mol·L^{-1} solutions containing nitrites, respectively, the voltammograms obtained for scan rates varying from 10 mV·s^{-1} to 500 mV·s^{-1}.

The influence of nitrites is more marked for low nitric acid concentrations and high scan rates. The results obtained are:

– for HNO_3 4 mol·L^{-1}, the charge in reduction is multiplied by 1.5 for 50 mV·s^{-1} and by 4 for 500 mV·s^{-1}. Moreover, in the presence of nitrites, the hysteresis disappears even for high scan rates; the evolution of the reoxidation peak current density becomes regular and charges in oxidation are multiplied by 20 for all the scan rates. The chemical regeneration reaction of the active species is slow and limits

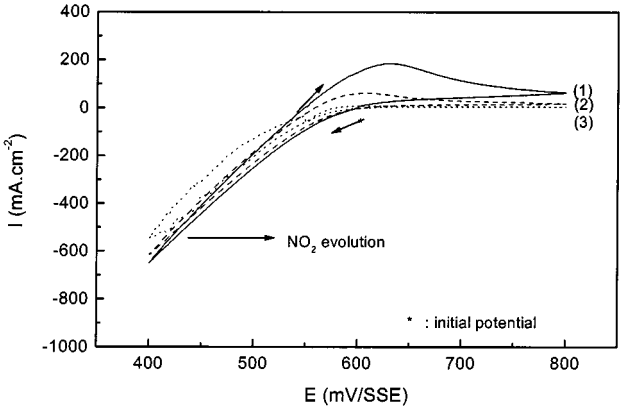


Figure 10. Cyclic voltammograms for HNO_3 12 mol·L^{-1} at 100 °C containing [HNO_2] = 10^{-2} mol·L^{-1} at different scan rates. (1): 500 mV·s^{-1} (2): 100 mV·s^{-1} (3): 10 mV·s^{-1}

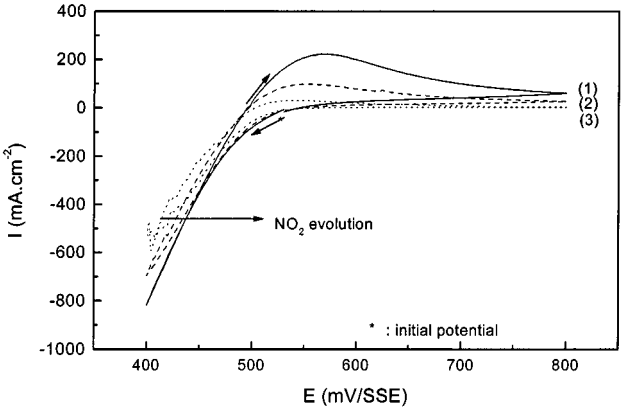


Figure 11. Cyclic voltammograms for HNO_3 8 mol·L^{-1} at 100 °C containing [HNO_2] = 10^{-2} mol·L^{-1} at different scan rates. (1): 500 mV·s^{-1} (2): 100 mV·s^{-1} (3): 10 mV·s^{-1}

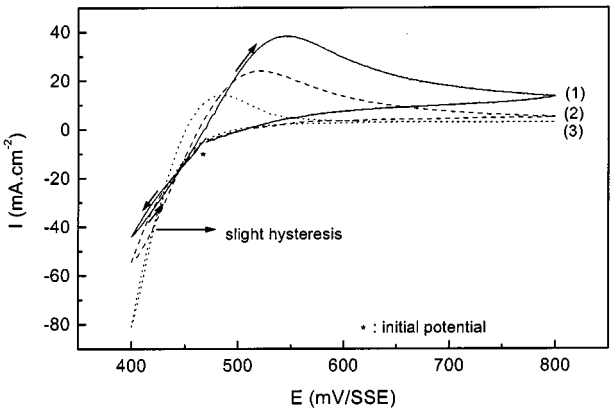


Figure 12. Cyclic voltammograms for HNO_3 4 mol·L^{-1} at 100 °C containing [HNO_2] = 10^{-2} mol·L^{-1} at different scan rates. (1): 500 mV·s^{-1} (2): 100 mV·s^{-1} (3): 10 mV·s^{-1}

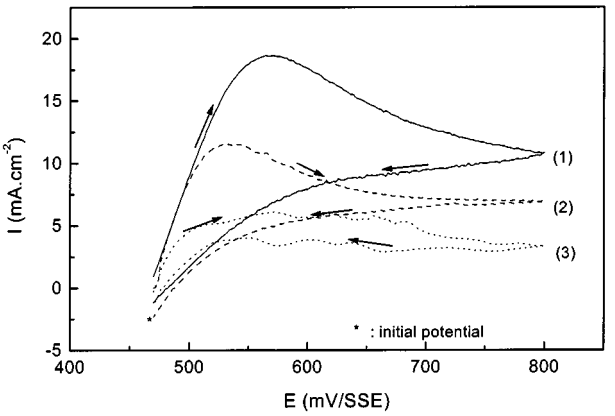


Figure 13. Voltammograms in oxidation for HNO_3 4 mol·L^{-1} containing [HNO_2] = 10^{-2} mol·L^{-1} at 100 °C at different scan rates. (1): 500 mV·s^{-1} (2): 100 mV·s^{-1} (3): 10 mV·s^{-1}

the reduction process. Therefore, the presence of nitrites in solution accelerates the chemical reaction and provokes the disappearance of the hysteresis and the increase in the reduction current densities for high scan rates;

– for HNO_3 8 mol·L^{-1}, the charges in reduction are multiplied by 1.5 for scan rates higher than 30 mV·s^{-1}; in oxidation they are multiplied by 2 for scan rates higher than 300 mV·s^{-1};

– for HNO_3 12 mol·L^{-1}, no major differences are observed with nitrites.

The presence of nitrites promotes the establishment of the steady state in reduction: nitrites in the bulk accelerate the attainment of the concentration in active species near the electrode to reduce nitric acid. For concentrated nitric acid, this concentration is reached rapidly as the chemical regeneration of the active species proceeds easily and therefore a supplementary addition of nitrites does not influence the reduction process.

Direct scans were also performed in oxidation. Figure 13 shows the voltammograms obtained for different scan rates in HNO_3 4 mol·L^{-1}. The same experiments performed in pure nitric acid display a voltammogram without peak which means that the oxidation peak is attributable to the

oxidation of nitrites into nitric acid; this is confirmed by literature data.[16]

If the current density of the oxidation peak is plotted versus the square root of the scan rate for HNO_3 4 mol·L^{-1}, 8 mol·L^{-1} and 12 mol·L^{-1} (Figure 14), a linear variation is obtained in a large range. Thus it is possible to assume that the current is diffusion controlled.

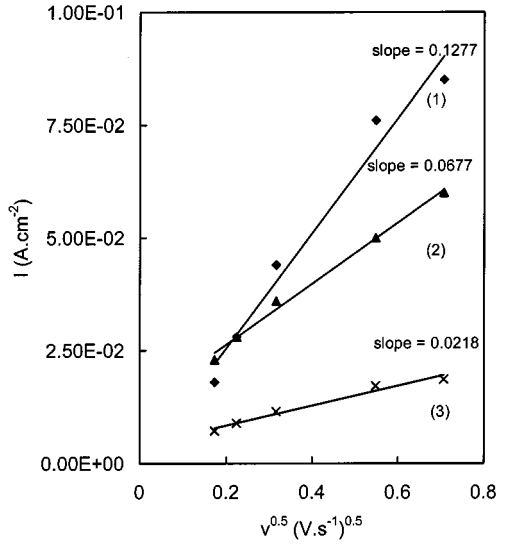


Figure 14. Influence of the scan rate on the variation of the oxidation peak current density for different nitric acid solutions at 100 °C containing approximately [HNO_2] = 10^{-2} mol·L^{-1}. (1): 12 mol·L^{-1} (2): 8 mol·L^{-1} (3): 4 mol·L^{-1}

A diffusion coefficient has been deduced according to:[17a]

$I_p = (2.40 \times 10^5) n^{3/2} D_0^{1/2} v^{1/2} C_0^*$

where

I_p = peak current density [A·cm^{-2}]

n = number of electrons involved in the oxidation charge transfer step

D_0 = diffusion coefficient [cm^2·s^{-1}]

v = scan rate (V·s^{-1})

C_0^* = nitrite concentration [mol·cm^{-3}]

The value of n is $n = 2$, as the oxidation reaction is supposed to be the oxidation of nitrites into nitric acid:

$$HNO_2 + H_2O = HNO_3 + 2H^+ + 2e^-$$

Table 4 shows the diffusion coefficients obtained for a nitrous acid concentration of approximately 10^{-2} mol·L^{-1}, in the different nitric acid solutions.

Table 4. Diffusion coefficient of nitrous acid in nitric acid solutions at 100 °C as a function of nitric acid concentration

[HNO_3] [mol·L^{-1}]	D_0 [cm^2.s^{-1}] and interval of error
4	3×10^{-5} [$8 \times 10^{-6} - 9 \times 10^{-5}$]
8	2×10^{-5} [$5 \times 10^{-6} - 6 \times 10^{-5}$]
12	7×10^{-4} [$2 \times 10^{-4} - 2 \times 10^{-3}$]

The interval of error of the diffusion coefficient is calculated from the error in the value of the concentration of nitrous acid in solution. The concentration of nitrous acid was not directly measured in these experiments. It was calculated from the OCP according to the thermodynamic data obtained previously.[3] The error in the OCP is supposed to be ± 10 mV. The error in the nitrous acid concentration and the error in the diffusion coefficient can then be deduced.

Table 4 shows higher diffusion coefficients for more concentrated HNO_3. This variation may be due to a difference in the chemical form of the diffusing species: for example HNO_2 in less concentrated medium and NO^+ in more concentrated medium. The uncertainty in the measurement minimizes this interpretation and supplementary measurements would be necessary to confirm this result.

Chronoamperometry

Figure 15 shows the variation of the current density with time for a potential of 0.400 V/SSE for the different nitric acid concentrations.

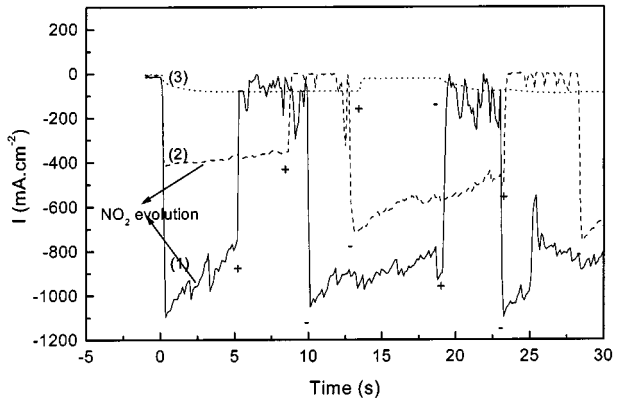


Figure 15. Influence of the stirring on the limiting current density of different nitric acid solutions at 100 °C containing [HNO_2] = 10^{-2} mol·L^{-1} for a potential of 0.400 V/SSE. ω = 2000 rpm; +: stirring; −: no stirring. (1): 12 mol·L^{-1} (2): 8 mol·L^{-1} (3): 4 mol·L^{-1}

The current densities are the same as when there are no nitrites in solution and the stirring of the solution provokes a similar decrease of the current density. Nitrites do not influence the stationary current densities (without stirring) as was already observed with the voltammograms performed at low scan rates.

For HNO_3 4 mol·L^{-1}, the stirring of the electrode provokes a decrease of the stationary current density which stabilizes at a value different from zero: this current is due to the nitrites present in solution.

For HNO_3 8 mol·L^{-1} and 12 mol·L^{-1}, the stirring of the electrode provokes a decrease of the current density similar to when there were no nitrites initially present in solution: the value of the current becomes nearly equal to zero. This result can be explained by the fact that in concentrated nitric acid, nitrites are less stable and an evolution of NO_2 occurs.

Influence of a Flow of Nitrogen Monoxide for HNO_3 4 mol·L^{-1} at 100 °C

The influence of a flow of nitrogen monoxide (flow rate = 1 L·h^{-1}) on the reduction process was studied in

HNO_3 4 mol·L^{-1}. A pressure of p_{NO} = 0.8 bar was imposed by fixing the flow rates of nitrogen monoxide and of an inert gas.

In Figure 16, the voltammograms obtained in the presence of NO and nitrites are compared with the voltammogram obtained without any addition, at a scan rate of 100 mV·s^{-1}. The presence of NO has the same influence as the addition of nitrites: it provokes an increase in the current densities in oxidation and in reduction and the disappearance of the hysteresis. The slight increase in the current densities with NO relative to nitrites is due to the fact that the pressure of NO imposed fixes a concentration in nitrites in solution higher than the concentration added in the other experiments: [HNO_2] = 3.5×10^{-2} mol·L^{-1} (experimental measurement) for p_{NO} = 0.8 bar.

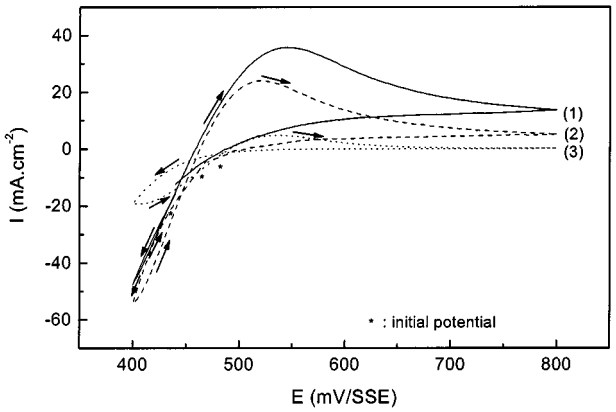


Figure 16. Cyclic voltammograms for HNO_3 4 mol·L^{-1} at 100 °C under different conditions at a scan rate of 100 mV·s^{-1}. (1): p_{NO} = 0.8 bar (2): [HNO_2] = 10^{-2} mol·L^{-1} (3): no addition

Voltammograms were performed at different scan rates in oxidation. Figure 17 presents the results obtained. If the current density of the oxidation peak is plotted versus the square root of the scan rate (Figure 18), a linear variation is obtained similar to the variation obtained in the presence of nitrites.

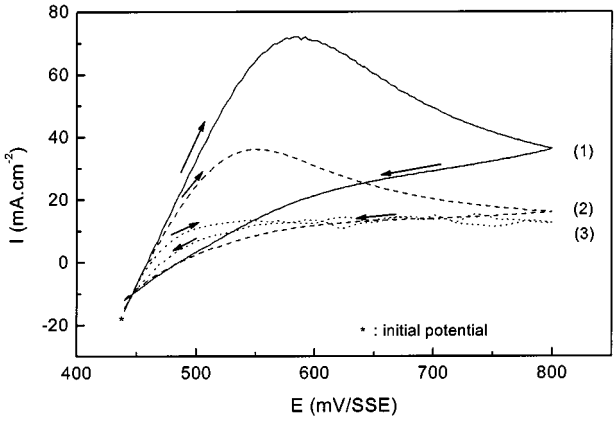


Figure 17. Voltammograms in oxidation for HNO_3 4 mol·L^{-1} under p_{NO} = 0.8 bar at 100 °C at different scan rates. (1): 500 mV·s^{-1} (2): 100 mV·s^{-1} (3): 10 mV·s^{-1}

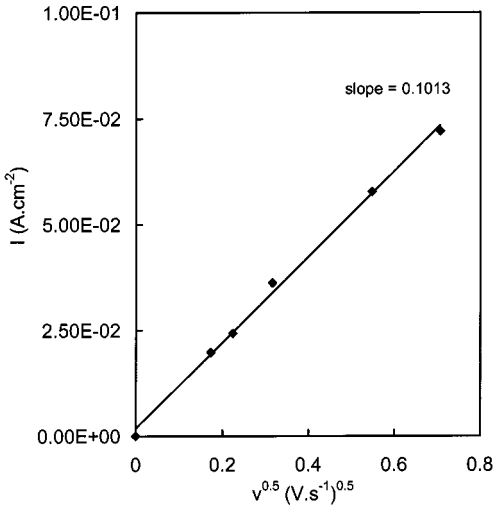


Figure 18. Influence of the scan rate on the variation of the oxidation peak current density for HNO_3 4 mol·L^{-1} at 100 °C under p_{NO} = 0.8 bar

The diffusion coefficient of nitrous acid can be calculated (the interval of error is estimated as in section 'voltammetry'), assuming that the reoxidation peak observed is attributed to the oxidation of nitrites into nitric acid:

$$D_0 = 2 \times 10^{-5}\ \text{cm}^2\cdot\text{s}^{-1}\ [5 \times 10^{-6} - 6 \times 10^{-5}]$$

Chronoamperometric measurements were also performed (Figure 19). The influence of the stirring causes a decrease in the reduction current which stabilizes for a value different from zero. This current is due to the presence of nitrites in solution.

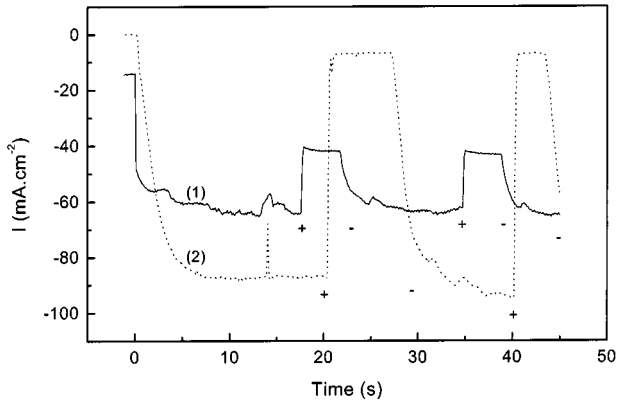


Figure 19. Influence of the stirring on the limiting current density of HNO_3 4 mol·L^{-1} at 100 °C under different conditions for a potential of 0.400 V/SSE. ω = 2000 rpm; +: stirring; −: no stirring. (1): p_{NO} = 0.8 bar (2): no addition

In fact, without stirring, at the steady state, the nitrous acid concentration at the electrode is much higher than in the bulk and this difference is larger for low nitric acid concentrations. When the solution is stirred, the nitrous acid concentration at the electrode is equal to the concentration in solution.

Mechanism of Reduction of Nitric Acid at a Platinum Electrode at 100 °C

It appears from this study that the major parameters for explaining the reduction of nitric acid are firstly the concentration range of nitric acid, and secondly the concentration of nitrous acid. The nitric acid molecule is not directly reduced; it is reduced through an autocatalytic mechanism involving an electrochemical step and a chemical reaction regenerating the active species. The electroactive species is formed at the electrode and diffuses into the solution: this explains the influence of the stirring on the current density. Moreover, it is possible to assume that the electroactive species is a soluble compound. The regeneration reaction is rapid for high HNO_3 concentrations and slow for low concentrations; this provokes the appearance of the hysteresis phenomenon. The electroactive species is believed to be nitrous acid which is the major soluble species present in nitric acid. This is confirmed by the increase in the current densities in reduction in the presence of nitrous acid in solution: this increase is sharp for low nitric acid concentrations and high scan rates and becomes nonexistent for HNO_3 12 mol·L^{-1}. Moreover nitrous acid suppresses the hysteresis phenomenon.

The influence of nitrogen monoxide was shown to be the same as nitrous acid. Therefore it is possible to assume that nitrogen monoxide reacts partly with nitric acid to form nitrous acid. The reduction of nitric acid leads to the formation of NO or NO_2 depending on the potential and the nitric acid concentration.

These conclusions, along with the literature data, allow us to propose a unique reduction mechanism of nitric acid valid for the whole nitric acid concentration range with reaction rates depending on the nitric acid concentration. This mechanism can be divided into two limiting cases, one for the lower concentrations and one for the higher concentrations. In all cases, the charge transfer step is the reduction of nitrous acid into nitrogen monoxide:

$$(HNO_2)_{el.} + H^+ + e^- + s = (NO)_{ads.} + H_2O \quad (1)$$

where 's' represents a free adsorption site.

Then, the chemical regeneration of the active species occurs; this reaction is heterogeneous and produces the electroactive species, HNO_2. It also produces nitrogen dioxide (reduction product for high nitric acid concentrations):[3]

$$HNO_3 + (NO)_{ads.} = (HNO_2)_{el.} + (NO_2)_{ads.} \quad (2)$$

The rate of reaction (2), which is the regeneration reaction, depends on the nitric acid concentration and on the nitrogen monoxide pressure. The rate of the charge transfer step (1) is also influenced, and usually promoted, by a high nitric acid concentration.

A third reaction (3) also occurs:

$$HNO_3 + (HNO_2)_{el.} + 2s = 2(NO_2)_{ads.} + H_2O \quad (3)$$

Reactions(1), (2), (3) are the elementary reactions of the reduction mechanism of nitric acid valid over the whole concentration range. For HNO_3 4 mol·L^{-1}, the regeneration reaction (2) is slow: this causes the hysteresis phenomenon appearing for high scan rates. Therefore, NO formed during the charge transfer step can accumulate and eventually evolve. Reaction (3), in low concentrated medium, promotes the formation of HNO_2, as NO_2 is not stable for concentrations lower than 8 mol·L^{-1}.

Finally, for nitric acid concentrations lower than 8 mol·L^{-1}, the reduction mechanism of nitric acid can be expressed as:

$$(HNO_2)_{el.} + H^+ + e^- + s = (NO)_{ads.} + H_2O \quad (1)$$

$$HNO_3 + 2(NO)_{ads.} + H_2O = 3(HNO_2)_{el.} + 2s \quad (4)$$

where (4) = 2 × (2) – (3)

$$(NO)_{ads.} = (NO)_{g.} + s \quad (5)$$

$$(HNO_2)_{el.} \rightarrow (HNO_2)_{sol.} \quad (6)$$

In the case of HNO_3 12 mol·L^{-1}, the chemical regeneration, reaction (2), promoted by a high nitric acid concentration, is fast and leads to an evolution of NO_2, the stable reduction product for high nitric acid concentrations. The overall reduction mechanism can be described as:

$$(HNO_2)_{el.} + H^+ + e^- + s = (NO)_{ads} + H_2O \quad (1)$$

$$HNO_3 + (NO)_{ads} = (HNO_2)_{el.} + (NO_2)_{ads} \quad (2)$$

$$(NO_2)_{ads} = (NO_2)_{g.} + s \quad (7)$$

$$(HNO_2)_{el.} \rightarrow (HNO_2)_{sol.} \quad (6)$$

Reaction (3) also occurs and is supposed to be at equilibrium. The gaseous species NO and NO_2 are supposed to be adsorbed at the electrode surface, and nitrous acid is a soluble compound formed at the electrode which diffuses into the solution. Therefore, in the reduction mechanism, desorption steps of gaseous species and a diffusion step for nitrous acid have to be added.

Conclusion

The major species involved in the reduction process of nitric acid at low overvoltages have been determined to be HNO_2, NO and NO_2. A mechanism has been proposed, which takes into account the literature data and the experimental results of this paper. It has been shown that: – nitric acid is not the electroactive species; it is reduced indirectly through an autocatalytic process; – nitrous acid is the electroactive species which is reduced into nitrogen monoxide; – nitrous acid is regenerated at the electrode according to a heterogeneous chemical reaction involving nitrogen monox-

ide and nitric acid; – a reduction mechanism for the whole nitric acid concentration range has been proposed depending on the nitric acid concentration: for concentrations higher than 8 mol·L^{-1}, the reduction of nitric acid leads to an evolution of NO_2 and for lower concentrations, it leads to an evolution of NO.

This electrochemical study of the reduction process of nitric acid on a platinum electrode allows us to propose a unique reduction mechanism valid over the whole concentration range. In the next step of our work, similar electrochemical experiments will be performed on a stainless steel electrode to compare the reduction mechanism observed on both materials and then to link the final reduction mechanism with the results of the corrosion tests performed in the laboratory.[4] This last step will be presented in a subsequent paper.

Experimental Section

Reactor Cell: The reactor containing 50 mL of solution was regulated at 100 °C. The working electrode consisted of a platinum disk electrode (area 0.0314 cm^2) polished to a mirror finish. The following circuit was set up for measuring the electrode potential: working electrode/HNO_3, solution 100 °C/HNO_3 solution, 25 °C/saturated KNO_3 solution, 25 °C/saturated K_2SO_4 solution, 25 °C/mercurous sulfate electrode, 25 °C. The reference electrode was a mercurous sulfate electrode (SSE) and is described as: $Hg/Hg_2SO_{4(sat.)}$, $K_2SO_{4(sat.)}$. The potential of this reference electrode versus the standard hydrogen electrode at 25 °C is E_{SSE} = 0.640 V/SHE.[17b]

Electrochemical Apparatus and Procedure: The potential measurements were made with an EGG PAR Model 273 potentiostat. A rotating disk electrode Tacussel EDI 101 T was used to evidence the hydrodynamic effect on the reduction process. Experiments were carried out in 4 mol·L^{-1}, 8 mol·L^{-1}, and 12 mol·L^{-1} nitric acid solutions at 100 °C. The influence of nitrous acid was studied by adding sodium nitrite at a concentration of about 10^{-2} mol·L^{-1} in the solution. The influence of nitrogen monoxide was investigated by imposing a pressure of p_{NO} = 0.8 bar in the cell. The concentration of nitrous acid (nitrite ions) in solution was measured by colorimetry with a Perkin–Elmer UV/Visible spectrometer according to the Griess method.[18]

Acknowledgments

The authors are grateful to COGEMA company for their financial contribution to this work. We also express thanks to SGN company and to M Fauvet from the CEA company for their interest in this work and their scientific support.

[1] J. P. Schosger, F. Dabosi, R. Demay, P. Fauvet, J. P. Moulin, G. Santarini, *Influence of corrosion products on the passivation of AISI 304 L stainless steel in nitric acid media, EUROCORR'96*, session IX, paper 32, Nice, France, **1996**.
[2] P. Fauvet, G. Pinard Legry, *Corrosion aspects in reprocessing technology*, *EUROCORR'92*, Espoo, Finland, **1992**.
[3] F. Balbaud, G. Sanchez, G. Santarini, G. Picard, *Eur. J. Inorg. Chem.* **1999**, *2*, 277–285.
[4] F. Balbaud, G. Sanchez, P. Fauvet, G. Santarini, G. Picard, *Corrosion mechanisms of AISI 304 L stainless steel in the presence of nitric acid condensates*, *EUROCORR'98*, Utrecht, Netherlands, **1998**.
[5] K. Vetter, *Z. Phys. Chem.* **1950**, *194*, 199–206.
[6] K. Vetter, *Z. Phys. Chem.* **1950**, *194*, 284–296.
[7] K. Vetter, *Z. Elektrochem., Ber. Bunsenges. physik. Chem.* **1959**, *63*, 1189–1191.
[8] G. Schmid, *Z. Elektrochem., Ber. Bunsenges. physik. Chem.* **1959**, *63*, 1183–1188.
[9] G. Schmid, J. Delfs, *Z. Elektrochem., Ber. Bunsenges. physik. Chem.* **1959**, *63*, 1192–1197.
[10] G. Schmid, *Z. Elektrochem., Ber. Bunsenges. physik. Chem.* **1961**, *65*, 531–534.
[11] G. Schmid, G. Krichel, *Z. Elektrochem., Ber. Bunsenges. physik. Chem.* **1964**, *68*, 677–688.
[12] G. Schmid, M. A. Lobeck, *Z. Elektrochem., Ber. Bunsenges. physik. Chem.* **1969**, *73*, 89–199.
[13] V. P. Razygraev, M. V. Lebedeva, S. A. Kabakchi, E. Yu. Ponomareva, R. S. Balovneva, L. P. Lobanova, *Zh. Prikl. Khim.* **1988**, *61*, 71–79.
[14] V. P. Razygraev, R. S. Balovneva, E. Yu. Ponomareva, M. V. Lebedeva, *Zashchita Metallov* **1990**, *26*, 54–60.
[15] R. D. Armstrong, G. E. Cleland, G. O. H. Whillock, *J. Appl. Electrochem.* **1998**, *28*, 1205–1211.
[16] D. Dutta, D. Landolt, *J. Electrochem. Soc.* **1972**, *119*, 1320–1325.
[17] [17a] A. J. Bard, L. R. Faulkner, in *Electrochimie: principes et applications*, Masson Cie, Paris, **1983**, p. 245. – [17b] A. J. Bard, L. R. Faulkner, in *Electrochimie: principes et applications*, Masson Cie, Paris, **1983**, p. 785.
[18] G. Charlot, in *Les méthodes de la Chimie Analytique – Analyse quantitative minérale*, Masson Cie, Paris, **1961**, p. 620.

Received May 17, 1999
[I99122]

Reactions Between Dinuclear Cu^{II}–Ni^{II} Complexes and the Nitrito Ligand: A New One-Dimensional Complex $[Cu(oxpn)Ni(\mu\text{-}NO_2)(trimen)]_n(ClO_4)_n$ with Nitrite Acting as a Tridentate Bridging Ligand and Ferro- and Antiferromagnetic Alternation

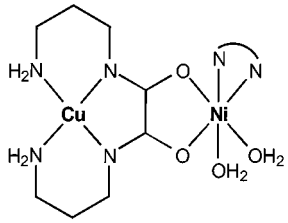
Carmen Diaz,*[a] Joan Ribas,[a] Ramon Costa,[a] Javier Tercero,[a] Mohamed Salah El Fallah[a] Xavier Solans,[b] Mercé Font-Bardía[b]

Keywords: Bridging ligands / Nitrito bridge / Copper / Nickel / Magnetic properties / Supramolecular chemistry

The reaction of $NiX_2 \cdot 6\,H_2O$ (X = NO_3^-, ClO_4^-), bidentate amine, [Cu(oxpn)] [oxpn = *N,N′*-bis(3-aminopropyl)oxamide] and sodium nitrite in ethanolic solution, leads to the formation of new Cu^{2+}–Ni^{2+} complexes of general formula $[Cu(oxpn)Ni(NO_2)(aa)]_n(X)_n$ [**1**, X = ClO_4^-, aa = *N,N,N′*-trimethylethylenediamine (trimen); **2**, X = ClO_4^-, aa = *N,N,N′N′*-tetramethylethylenediamine (tmen); **3**, X = ClO_4^-, aa = *N,N*-dimethyl-*N′*-ethylethylenediamine (dmeten); **4**, X = PF_6^-, aa = trimen; **5**, X = PF_6^-, aa = dmeten]. The structure of complex **1** consists of [Cu(oxpn)Ni(trimen)]$^{2+}$ units linked by a nitrite group acting as a tridentate ligand, giving a one-dimensional system separated by ClO_4^- anions. In contrast, the structure of complex **2** consists of isolated $[Cu(oxpn)Ni(NO_2)(tmen)]^+$ dinuclear units and uncoordinated ClO_4^- anions. The nitrite group acts as a bidentate ligand. Variable-temperature magnetic susceptibility studies were performed on **1–5**. The *J* value through the oxamidato bridge is close to –110 cm^{-1} in all five cases. For complex **1**, considered as a chain, a simulation of the $\chi_M T$ vs *T* was performed with the CLUMAG program. These calculations revealed the influence of the magnetic interactions between the dinuclear entities through the nitrito bridging ligand, on the susceptibility curves at low temperatures.

Introduction

In one-dimensional supramolecular self-assembly processes, we have found that very few complexes starting from polynuclear building blocks have been reported to date. McAuley et al.[1] reported the synthesis of a chloro-bridged polymeric copper(II) complex. Ribas et al., using (S,Se)CN^- bridging ligands, reported a one-dimensional system with Cu_3 entities,[2] and tetranuclear systems starting from Cu^{2+}–Ni^{2+} entities.[3] A one-dimensional structure has been reported from the self-assembly reaction between $[Fe(CN)_6]^{3-}$ and a Mn^{3+} Schiff-base derivative, in which the 1-D architecture is due to hydrogen bonds between trinuclear Mn^{3+}–Fe^{3+}–Mn^{3+} entities.[4] With [Cu(oxpn)], where oxpn is the dianion of *N,N′*-bis(3-aminopropyl)oxamide, the magnetic coupling in Cu–Cu, Cu–Ni or Cu–Mn dinuclear entities is strongly antiferromagnetic, owing to the broad overlap between the magnetic orbitals of the two metal ions through the corresponding molecular orbital of the oxamidato bridge.[5–10] Thus, we started with the dinuclear species $[Cu(oxpn)Ni(H_2O)_2(diamine)]^{2+}$ (Scheme 1) in an attempt to link these molecules ferro- or antiferromagnetically in order to study the spin topology of the final system.



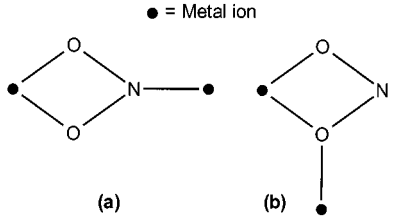
Scheme 1. Structural formula of $[Cu(oxpn)Ni(H_2O)_2(aa)]^{2+}$

The ligand chosen for this was the nitrite group because of the number of different ways in which it can coordinate to a metal centre.[11] The factors influencing the type of nitrite coordination adopted are often delicately balanced. As a monodentate ligand it can bond through either nitrogen or oxygen, while as a bidentate ligand it can chelate or bridge either through nitrogen and oxygen or through oxygen only.[12] Very few examples of tridentate behaviour are known. This coordination mode may be accomplished in two ways. In the first case,[13] the NO_2^- ion is chelated to one metal through the two oxygens and bridged to a second metal ion through the nitrogen atom (Scheme 2a). In the second case,[14] the two metal ions are bridged through a

[a] Departament de Química Inorgànica, Universitat de Barcelona, Martí i Franquès, 1–11, 08028 Barcelona, Spain
Fax: (internat.) +34–93/490-7725
E-mail: cdiaz@kripto.qui.ub.es
[b] Departament de Cristallografia i Mineralogia, Universitat de Barcelona,
Martí i Franquès s/n, 08028 Barcelona, Spain

 © WILEY-VCH Verlag GmbH, D-69451 Weinheim, 2000 1434–1948/00/0404–0675 $ 17.50+.50/0

single oxygen atom while the second oxygen chelates to one of the metal ions (Scheme 2b).



Scheme 2. Trideutate coordination modes for the nitrite ion

Few studies have examined the magnetic exchange mediating properties of the bridging nitrite. Two polymeric Ni^{2+} complexes involving a two atom O,N-bridging mode show a moderate antiferromagnetic interaction ($J \approx -60$ cm^{-1}).[15] A Ni–Mn–Ni trinuclear complex involving the same coordination mode but also with azido bridging ligand has been reported.[12b] An interaction of the same sign and order of magnitude characterises a dinuclear Ni^{2+} complex with a combination of chelation and bridging through a single oxygen atom.[14] A weak ferromagnetic interaction (J = 8 cm^{-1}) is found in a dinuclear Cu^{2+} complex with a single O atom bridging mode[16] and a very weak one (J = 1.33 cm^{-1}) is found in a Mn–Ni bimetallic chain[13b] with nitro coordination at the Ni^{2+} centre and a bidentate nitrito coordination at Mn^{2+}. We report here five compounds of a new family of heterobimetallic polynuclear compounds obtained from Cu(oxpn)–Ni(diamine)–NO_2 with the counteranion ClO_4^- or PF_6^- (diamine = tmen, trimen, dmeten). The crystal structures of $[Cu(oxpn)Ni(\mu\text{-}NO_2)(trimen)]_n(ClO_4)_n$ (**1**), and $[Cu(oxpn)Ni(NO_2)(tmen)]ClO_4$ (**2**) are described. The crystal structure of complex **1** is found to be a chain of dimeric [Cu(oxpn)Ni(trimen)] units linked by the nitrite group acting as a tridentate ligand. The crystal structure of complex **2** is found to be dinuclear with isolated $[Cu(oxpn)Ni(NO_2)(tmen)]^+$ ions. We also report the magnetic properties of the five compounds. The magnetic behaviour of complexes **1** and **2** is markedly different at low temperatures; the other three complexes have an intermediate magnetic behaviour. For all complexes, the magnetic interactions were studied assuming only the strong antiferromagnetic coupling within the dinuclear Cu–Ni entity. Complex **1** was also studied using the ITO method, which reduces the size of the matrices.

Results and Discussion

Crystal Structures

The X-ray crystal structure of **1** consists of dimeric $[Cu(oxpn)Ni(trimen)]^{2+}$ units linked by the nitrite group acting as a tridentate ligand giving a one-dimensional system, separated by ClO_4^- anions. This tridentate nitrite coordination between Cu^{2+} and Ni^{2+}, which has not been reported previously, is a combination of chelation through the two oxygen atoms and bridging through a single oxygen atom (Scheme 2b). Selected bond lengths and angles are listed in Table 1 and the molecular structure and atom labelling is shown in Figure 1. The molecular structure of **2** consists of isolated $[Cu(oxpn)Ni(NO_2)(tmen)]^+$ dinuclear units and uncoordinated ClO_4^- anions. Selected bond lengths and angles are listed in Table 1 and the molecular structure and atom labelling is shown in Figure 2.

Table 1. Selected bond lengths [Å] and angles [deg] for $[Cu(oxpn)Ni(\mu\text{-}NO_2)(trimen)]_n(ClO_4)_n$ (**1**) and $[Cu(oxpn)Ni(NO_2)(tmen)]ClO_4$ (**2**)

Complex **1**			
Ni–O(1)	2.030(7)	Cu–N(3)	1.976(10)
Ni–O(2)	2.050(8)	Cu–N(2)	1.976(10)
Ni–N(6)	2.066(10)	Cu–N(1)	2.016(11)
Ni–O(4)	2.110(11)	Cu–N(4)	2.016(11)
Ni–N(5)	2.119(19)	O(4)–N(7)	1.250(2)
Ni–O(3)	2.152(8)	O(3)–N(7)	1.260(2)
Cu–O(3)	2.609(8)		
O(1)–Ni–O(2)	82.2(3)	N(6)–Ni–O(3)	91.3(4)
O(1)–Ni–N(6)	178.3(4)	O(4)–Ni–O(3)	57.8(4)
O(2)–Ni–N(6)	96.1(4)	N(5)–Ni–O(3)	160.9(4)
O(1)–Ni–O(4)	89.4(3)	N(3)–Cu–N(2)	82.4(4)
O(2)–Ni–O(4)	156.6(4)	N(3)–Cu–N(1)	176.6(5)
N(6)–Ni–O(4)	92.2(4)	N(2)–Cu–N(1)	94.3(4)
O(1)–Ni–N(5)	95.4(3)	N(3)–Cu–N(4)	94.0(5)
O(2)–Ni–N(5)	98.9(4)	N(2)–Cu. –N(4)	175.9(5)
N(6)–Ni–N(5)	84.7(4)	N(1)–Cu–N(4)	89.4(5)
O(4)–Ni–N(5)	103.6(4)	N(7)–O(3)–Ni	94.8(7)
O(1)–Ni–O(3)	89.1(4)	N(7)–O(4)–Ni	97.0(8)
O(2)–Ni–O(3)	100.1(4)	O(3)–N(7)–O(4)	110.4(4)
Cu–O(3)–Ni	58.67(6)		
Complex **2**			
Ni–O(1)	2.124(3)	Cu–N(6)	1.972(4)
Ni–O(2)	2.153(4)	Cu–N(7)	2.020(5)
Ni–O(3)	2.067(3)	Cu–N(8)	2.006(4)
Ni–O(4)	2.008(3)	Cu–N(9)	1.958(4)
Ni–N(1)	2.102(4)	O(1)–N(5)	1.260(6)
Ni–N(2)	2.119(4)	O(2)–N(5)	1.240(6)
O(4)–Ni–O(3)	82.36(11)	N(1)–Ni–O(2)	158.9(2)
O(4)–Ni–N(1)	99.7(2)	N(2)–Ni–O(2)	91.85(14)
O(3)–Ni–N(1)	92.71(14)	O(1)–Ni–O(2)	58.39(14)
O(4)–Ni–N(2)	89.59(12)	N(9)–Cu–N(6)	83.98(14)
O(3)–Ni–N(2)	171.32(12)	N(9)–Cu–N(8)	93.2(2)
N(1)–Ni–N(2)	85.4(2)	N(6)–Cu–N(8)	175.1(2)
O(4)–Ni–O(1)	158.91(14)	N(9)–Cu–N(7)	177.2(2)
O(3)–Ni–O(1)	92.50(12)	N(6)–Cu–N(7)	94.1(2)
N(1)–Ni–O(1)	101.0(2)	N(8)–Cu–N(7)	88.9(2)
N(2)–Ni–O(1)	96.18(13)	N(5)–O(1)–Ni	94.6(3)
O(4)–Ni–O(2)	101.28(14)	N(5)–O(2)–Ni	93.8(3)
O(3)–Ni–O(2)	92.93(14)	O(2)–N(5)–O(1)	113.2(4)

For both complexes, the Ni atoms are in a distorted octahedral environment. The four positions coplanar to the oxamidato bridge are occupied by the two oxygen atoms of this ligand [Ni–O = 2.030, 2.050 Å (**1**) and 2.008, 2.067 Å (**2**)], one nitrogen of the bidentate amine [Ni–N = 2.066 Å (**1**) and 2.119 Å (**2**)] and one oxygen of the nitrite ligand [Ni–O = 2.110 Å (**1**) and 2.124 Å (**2**)]. The other oxygen of the nitrite ligand occupies one of the two remaining positions [Ni–O = 2.152 Å (**1**) and 2.153 Å (**2**)] and the other nitrogen atom of the bidentate amine [Ni–N = 2.119 Å (**1**) and 2.102 Å (**2**)] occupies the other. The coordination polyhedron of Cu^{2+} is different for the two complexes. For complex **1** it can be considered as a square pyramid with apical elongation (4 + 1), the four nitrogen atoms of the oxpn organic ligand are placed in the basal position and the Cu–N

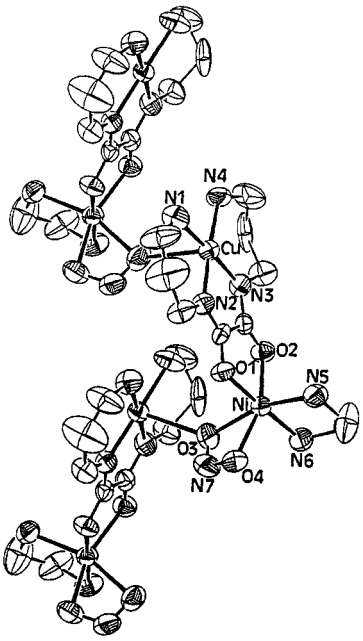


Figure 1. Drawing of the chain part of $[Cu(oxpn)Ni(\mu\text{-}NO_2)(trimen)]_n(ClO_4)_n$ (**1**) with atom labelling scheme; methyl groups have been omitted for clarity

Magnetic Behaviour

Variable temperature (2–300 K) magnetic susceptibility data were collected for microcrystalline samples of compounds **1–5**. From room temperature down to ca. 25 K the $\chi_M T$ vs T plots correspond to the classical behaviour for an isolated Cu–Ni entity coupled antiferromagnetically. From ca. 25 K to 2 K we found two different behaviours: complex **1** shows a clear decrease in $\chi_M T$ from 20 K (0.46 cm^3 mol^{-1} K) to 2 K (0.40 cm^3 mol^{-1} K) and complex **2** shows the typical plateau for a dinuclear Cu–Ni complex, with no decrease in $\chi_M T$ in this zone (Figure 5), while complexes **3**, **4** and **5** show an intermediate behaviour.

The first fit was made from 300 K to ca. 20 K to study only the interaction within each Cu–Ni dinuclear moiety. The spin Hamiltonian that describes the isotropic magnetic exchange interaction in a Cu–Ni dinuclear complex is $H = -JS_{Cu}S_{Ni}$. There are two spin states, $S = 1/2$ and 3/2. Assuming antiferromagnetic coupling, the ground state is $S = 1/2$ ($E = 0$) and the low-lying excited state is $S = 3/2$ ($E = -3J/2$). The g values for each state are related to those of the ions: $g_{3/2} = (1/3g_{Cu} + 2/3g_{Ni})$ and $g_{1/2} = (-1/3g_{Cu} + 4/3g_{Ni})$.[17] By substituting these values in the Van Vleck equation, a typical expression of the molar susceptibility can be deduced. The experimental and theoretical curves of χ_{MT} for complexes **1** and **2** are shown in Figure 5. The J and g values for the five new complexes are listed in Table 2. The J values for the five complexes (close to –110 cm^{-1}) agree with those reported in the literature for the Cu–Ni heterodinuclear complexes with the oxpn bridge.[7]

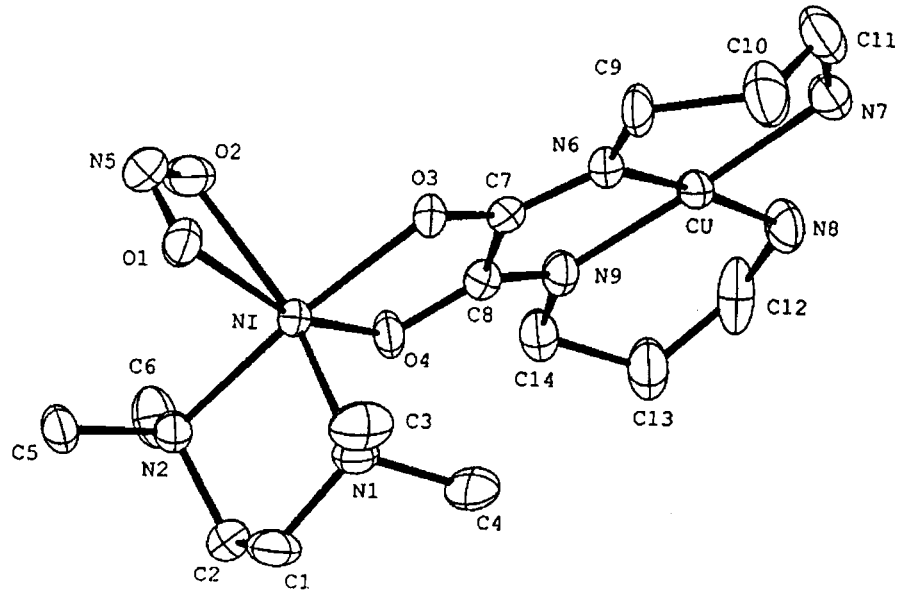


Figure 2. Drawing of the $[Cu(oxpn)Ni(NO_2)(tmen)]ClO_4$ (**2**) with atom labelling scheme; methyl groups have been omitted for clarity

distances are close to 2.0 Å; the coordination is completed by one oxygen of the nitrite bridge (Cu–O = 2.609 Å). For complex **2** the copper atom is coordinated to the four nitrogen atoms of the oxpn organic ligand in a distorted square-planar geometry; the Cu–N distances are close to 2.0 Å. The Cu–Ni distances through the oxamidato bridge are 5.303 Å for complex **1** and 5.293 Å for **2**. The Cu–Ni separation within the dinuclear entities is 4.415 Å for **1** and 6.426 Å for **2**. Schematic representations of the packing for **1** and **2** are given in Figure 3 and Figure 4, respectively.

Study of the Exchange of the Whole Chain for Complex 1

As can be seen from the crystal structure, the chain is formed by dinuclear entities linked by the bridging NO_2^- ligand (Figure 1). Such a ligand can transmit an additional interaction between the Ni–Cu entity causing two different

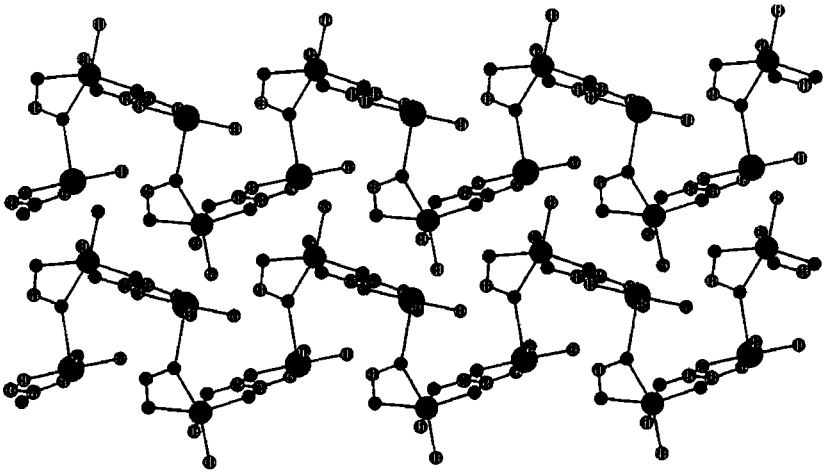


Figure 3. Schematic representation of the packing of $[Cu(oxpn)Ni(\mu\text{-}NO_2)(trimen)]_n(ClO_4)_n$ (**1**)

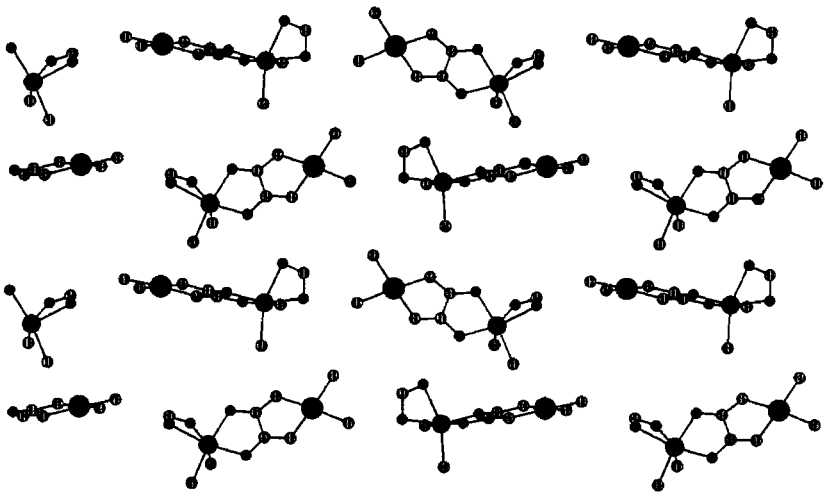


Figure 4. Schematic representation of the packing of $[Cu(oxpn)Ni(NO_2)(tmen)]ClO_4$ (**2**)

forms of the ground state at low temperature. These two forms are shown in Figure 6. If the magnetic interactions between these two entities are weakly ferromagnetic, the resulting total spin value will tend to zero at low temperatures, so the $\chi_M T$ curve would decrease and also tend to zero at these temperatures. In contrast, if the coupling were weakly antiferromagnetic $\chi_M T$ would tend to infinity at low temperatures.

In order to compare the theoretical magnetic behaviour for these extreme cases, a simulation of $\chi_M T$ vs. T for a ring of twelve atoms with alternate $S = 1$ and $S = 1/2$ spins was performed with the CLUMAG program.[18] The J_1 (coupling through the oxamidato bridge) value was fixed at –106 cm^{-1} and g was set at 2.25. The value of J_2 (coupling through the nitrite bridging ligand) was simulated between –20 and 20 cm^{-1}. As expected, with these small J_2 values the variation of $\chi_M T$ vs. T is observed only at low temperatures. The theoretical $\chi_M T$ vs. T curves are shown in Figure 7. When the J_2 coupling is antiferromagnetic $\chi_M T$ increases with decreasing temperature, tending to the six electrons value; when the J_2 coupling is ferromagnetic, $\chi_M T$ decreases with decreasing temperature, tending to zero.

From the magnetic point of view, all these aspects indicate that in this new 1-D complex the antiferromagnetic coupling through the oxamidato bridge is dominant. The coupling through the nitrito bridge is small but positive ($J_2 = 1.1$ cm^{-1} in complex **1** and is lower in the other complexes). A schematic representation of the orthogonality of the magnetic orbitals centred on the metal ions is shown in Figure 8.

The EPR spectra of the five complexes show a single band centred at $g = 2.24$. This band is sharp at low temperature (4 K) and becomes broader at higher temperature (77 and 298 K). This can be assigned to a transition between $|1/2,–1/2\rangle$, $|1/2,1/2\rangle$ of the $S = 1/2$ ground state of the dinuclear entity.

Experimental Section

Syntheses. – Starting Materials: Nickel(II) perchlorate, nickel(II) nitrate, sodium nitrite, ammonium hexafluorophosphate, *N,N,N',N'*-tetramethylethylenediamine (tmen), *N,N,N'*-trimethylethylenediamine (trimen), and *N,N*-dimethyl-*N'*-ethylethylenediam-

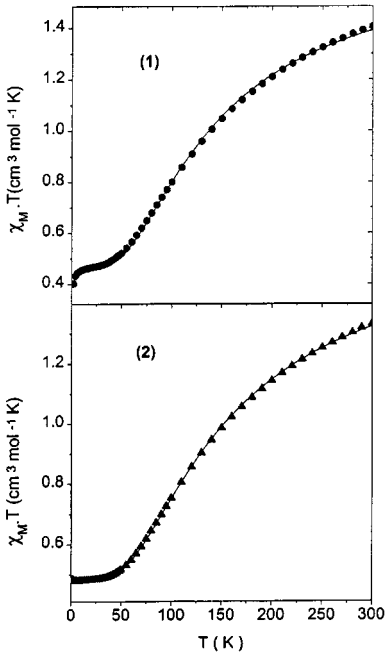


Figure 5. Plot of $\chi_M T$ vs temperature for [Cu(oxpn)Ni(μ-NO_2)(trimen)]$_n$(ClO_4)$_n$ (**1**) and [Cu(oxpn)Ni(NO_2)(tmen)]ClO_4 (**2**); solid lines result from a fit of the data to the appropriate theoretical equation for a [Cu–Ni] complex

Table 2. Best-fit J and g parameters for **1–5** from 300–20 K of the $\chi_M T$ curves

Compound	J (cm^{-1})	g_{Cu}	g_{Ni}	R[a]
1	–106	2.25	2.25	$5\cdot10^{-5}$
2	–113	2.09	2.23	$2\cdot10^{-5}$
3	–108	2.04	2.26	$1\cdot10^{-5}$
4	–113	2.11	2.28	$1\cdot10^{-5}$
5	–111	2.14	2.31	$2\cdot10^{-5}$

[a] $R = \Sigma_i(\chi_{Mcal}T - \chi_{Mobs}T)^2/\Sigma_i(\chi_{Mobs}T)^2$.

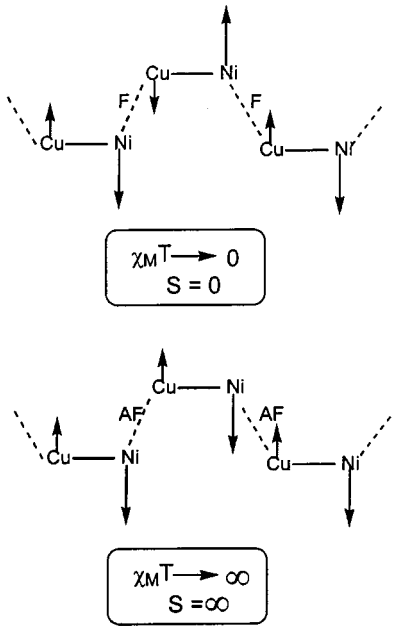


Figure 6. Scheme of the spin topology assuming ferro- or antiferromagnetic coupling between the heterodinuclear [Cu–Ni] entities

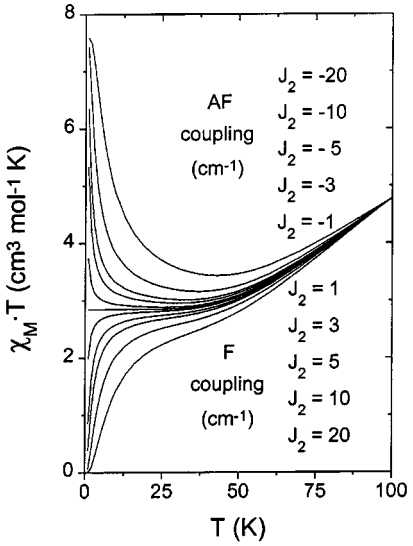


Figure 7. Theoretical curves obtained by the CLUMAG program for different J_2 values; in all cases J_1 and g were maintained constant and equal to the values obtained by fitting the complex **1** as a dinuclear entity: J_1 = –106 cm^{-1} and g = 2.25

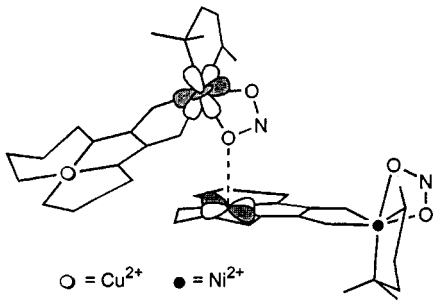


Figure 8. Schematic representation of the orthogonality of the magnetic orbitals centred on the metal ions

ine (dmeten) were purchased from Aldrich and used without further purification. [Cu(oxpn)], where oxpn is the dianion of *N,N'*-bis(3-aminopropyl)oxamide, was synthesised as previously described.[19] Ethanol was distilled before use.

Caution: *Although no incidents were recorded in this study, perchlorate salts containing organic ligands are potentially explosive. They should be prepared in small quantities and handled with extreme care.*

***catena*-[Cu(oxpn)Ni(μ-NO_2)(trimen)]ClO_4 (1):** $NaNO_2$ (2.73 mmol) was added to an ethanolic solution (30 mL) of [Cu(oxpn)Ni(H_2O)$_2$-(trimen)](ClO_4)$_2$ (2.73 mmol), prepared in situ by mixing [Cu(oxpn)] (2.73 mmol), Ni(ClO_4)$_2 \cdot x$ H_2O (2.73 mmol) and trimen (2.73 mmol), with constant stirring. The resulting blue solution was left to evaporate slowly at room temperature. Blue monocrystals suitable for an X-ray determination were collected after one week (yield ca. 70%). – $C_{13}H_{30}ClCuN_7NiO_8$ (570.14): calcd. C 27.38, H 5.30, N 17.20; found C 27.4, H 5.3, N 17.1.

[Cu(oxpn)Ni(NO_2)(tmen)](ClO_4) (2): This complex was prepared in the same way as **1** but with *N,N,N',N'*-tetramethylethylenediamine (tmen) instead of *N,N,N'*-trimethylethylenediamine (trimen). Blue monocrystals suitable for X-ray determination were collected after 10 days (yield ca. 60%). – $C_{14}H_{32}ClCuN_7NiO_8$ (584.15): calcd. C 28.78, H 5.52, N 16.78; Cl, 6.07; found C 28.7, H 5.5, N 16.7; Cl, 6.2.

[Cu(oxpn)Ni(NO_2)(dmeten)](ClO_4) (3): This complex was prepared in the same way as **1** but with *N,N*-dimethyl-*N'*-ethylethylenediamine (dmeten) instead of *N,N,N'*- trimethylethylenediamine (trimen) (yield ca. 65%). – $C_{14}H_{32}ClCuN_7NiO_8$ (584.15): calcd. C 28.78, H 5.52, N 16.78; Cl, 6.07; found C 28.8, H 5.6, N 16.8; Cl, 6.1.

[Cu(oxpn)Ni(NO_2)(trimen)](PF_6) (4): $NaNO_2$ (2.73 mmol) and an ethanolic solution (7 mL) of $(NH_4)PF_6$ (1.36 mmol) were added to an ethanolic solution (30 mL) of [Cu(oxpn)Ni(H_2O)$_2$(trimen)](NO_3)$_2$ (2.73 mmol), prepared in situ by mixing [Cu(oxpn)] (2.73 mmol), Ni(NO_3)$_2$·xH_2O (2.73 mmol) and trimen (2.73 mmol), with constant stirring. The resulting blue solution was left to evaporate slowly at room temperature (yield ca. 70%). – $C_{13}H_{30}CuF_6N_7NiO_4P$ (615.64): calcd. C 25.36, H 4.91, N 15.92; found C 25.2, H 5.1, N 15.8.

[Cu(oxpn)Ni(NO_2)(dmeten)](PF_6) (5): This complex was prepared in the same way as **4** but with *N,N*-dimethyl-*N'*-ethylethylenediamine (dmeten) instead of trimen (yield ca. 60%). – $C_{14}H_{32}CuF_6N_7NiO_4P$ (629.67): calcd. C 26.70, H 5.12, N 15.57; found C 26.8, H 5.2, N 15.4.

Despite all efforts no crystals suitable for X-ray determination were obtained for complexes **3**, **4**, or **5**.

X-ray Crystallography. - [Cu(oxpn)Ni(μ-NO_2)(trimen)]$_n$(ClO_4)$_n$ (1) and [Cu(oxpn)Ni(NO_2)(tmen)]ClO_4 (2): Prismatic crystals (0.1 × 0.2 × 0.2 mm) for **1** and (0.1 × 0.1 × 0.2 mm) for **2** were selected and mounted on an Enraf–Nonius CAD4 four-circle diffractometer. Unit cell parameters were determined from automatic centring of 25 reflections ($12 < \theta < 21°$) and refined by least-squares methods. Intensities were collected with graphite monochromated Mo-K_α radiation, using ω/2θ scan-technique. For **1**, 3522 reflections were measured in the range $2.01 \leq \theta \leq 29.97°$, 3474 of which were nonequivalent by symmetry [R_{int} (on I) = 0.009]; 1763 reflections were assumed as observed applying the condition $I > 2\sigma(I)$. For **2**, 4757 reflections were measured in the range $2.16 \leq \theta \leq 29.94°$, 4710 of which were nonequivalent by symmetry [R_{int} (on I) = 0.017]; 3896 reflections were assumed as observed applying the condition $I > 2\sigma(I)$. Three reflections were measured every 2 h as orientation and intensity controls; significant intensity decay was not observed. Lorentz-polarisation but not absorption corrections were made. The structure was solved by Direct Methods, using SHELXS[20] and refined by full-matrix least-squares method with SHELX93[21] using 3031 reflections for **1** and 4660 reflections for **2** (very negative intensities were not assumed). The function minimised was $\Sigma w \mid F_o \mid^2 - \mid F_c \mid^2 \mid^2$, where $w = [\sigma^2(I) + (0.0795P)^2]^{-1}$ for **1** and $w = [\sigma^2(I) + (0.0842\ P)^2]^{-1}$ for **2**, and $P = (\mid F_o \mid^2 + 2 \mid F_c \mid^2)/3$, f, f' and f'' were taken from ref.[22] The extinction coefficient was 0.0002(2) for **1** and 0.0001(9) for **2**. The chirality of the structure was defined from the Flack coefficient,[23] which is equal to 0.01(3) for **1** for the results given. For complex **1** a carbon atom of the propanediamine moiety and the four O atoms of the perchlorate ion were located in disordered positions; an occupancy factor of 0.5 was assigned according to the height of the Fourier synthesis. 19 H atoms were located from a difference synthesis and refined with overall isotropic temperature factors, using a riding model. The final R (on F) factor was 0.057, wR (on $\mid F_o \mid^2$) = 0.122 and goodness of fit = 1.107 for all observed reflections. The number of parameters refined was 287. Maximum shift/esd = 0.06, mean shift/esd = 0.00. Maximum and minimum peaks in the final difference synthesis were 0.494 and –0.660 eÅ^{-3}, respectively. For complex **2** a carbon atom, C(13), of the oxpn ligand was located in a disordered position. 18 H atoms were located from a difference synthesis and refined with overall isotropic temperature factors and 12 H atoms were computed and refined with an overall isotropic temperature factor, using a riding model. Final R (on F) factor was 0.055, wR (on $\mid F_o \mid^2$) = 0.127 and goodness of fit = 1.115 for all observed reflections. The number of parameters refined was 372. Maximum shift/esd = 0.0, mean shift/esd = 0.00. The maximum and minimum peaks in the final difference synthesis were 0.629 and –0.589 eÅ^{-3}, respectively. Crystallographic data for **1** and **2** are shown in Table 3.

Table 3. Crystallographic data and experimental parameters for [Cu(oxpn)Ni(μ-NO_2)(trimen)]$_n$(ClO_4)$_n$ (**1**) and [Cu(oxpn)Ni(NO_2)(tmen)]ClO_4 (**2**)

	1	**2**
Empirical formula	$C_{13}H_{30}ClCuN_7NiO_8$	$C_{14}H_{32}ClCuN_7NiO_8$
Formula mass	570.14	584.15
Crystal system	monoclinic	orthorhombic
Space group	*Cc*	*Pcab*
T [K]	293(2)	293(2)
λ [Å]	0.71069	0.71069
a [Å]	17.018(2)	14.168(11)
b [Å]	14.706(6)	15.237(2)
c [Å]	11.132(4)	22.321(5)
α [°]	90	90
β [°]	125.06(2)	90
γ [°]	90	90
V [Å^3]	2280.5(13)	4819(4)
Z	4	8
d_{calcd} [g cm^{-3}]	1.661	1.616
μ [mm^{-1}]	1.928	1.827
R [a]	0.0573	0.0552
wR [b]	0.1217	0.1270

[a] R (on F) = $\Sigma \parallel F_o \mid - \mid F_c \parallel / \Sigma \mid F_o \mid$. – [b] wR (on F^2) = $[\Sigma w(F_o^2 - F_c^2)^2 / \Sigma w F_o^4]^{1/2}$.

Atomic positional and thermal parameters, a complete list of bond lengths and angles, and F_o/F_c values are available as supplementary material from one of the authors. Crystallographic data (excluding structure factors) for the structures reported in this paper have been deposited with the Cambridge Crystallographic Data Centre as supplementary publication nos. CCDC-101760 **(1)** and CCDC-118817 **(2)**. Copies of the data can be obtained free of charge on application to CCDC, 12 Union Road, Cambridge CB2 1EZ, UK [Fax: (internat.) +44–1223/336-033; E-mail: deposit@ccdc.cam.ac.uk].

Spectral and Magnetic Measurements: Magnetic measurements were carried out on polycrystalline samples with a Quantum Design MPMS SQUID susceptometer operating at a magnetic field of 0.5 T, between 2 and 300 K. EPR spectra were recorded on powder samples at X-band frequency with a Bruker 300E automatic spectrometer. EPR measurements were carried out in the "Servei de Magnetoquímica" (University of Barcelona).

Acknowledgments

We are very grateful for the financial support given by the Dirección General de Investigación Científica y Técnica (Spain) (Grant PB96/0163). We also thank the group of Dr. D. Gatteschi (Università degli Studi di Firenze) for the providing us with the CLUMAG program and Dra. Núria Clos for recording the EPR measurements.

[1] A. McAuley, S. Subramanian, M. J. Zaworotko, *J. Chem. Soc., Chem. Commun*. **1992**, 1321.
[2] [2a] J. Ribas, C. Diaz, X. Solans, M. Font-Bardía, *Inorg. Chim. Acta* **1995**, *231*, 229. – [2b] J.Ribas, C. Diaz, X. Solans, M. Font-Bardía, *J. Chem. Soc., Dalton Trans.* **1997**, 35.

[3] J. Ribas, C. Diaz, R. Costa, J. Tercero, X. Solans, M. Font-Bardía, H. Stoeckli-Evans, *Inorg. Chem.* **1998**, *37*, 233.
[4] H. Miyasaka, H. Ieda, N. Matsumoto, N. Re, R. Crescenzi, C. Floriani, *Inorg. Chem.* **1998,** *37*, 255.
[5] [5a] Y. Journaux, J. Sletten, O. Kahn, *Inorg. Chem*. **1985**, *24*, 4063. – [5b] F. Lloret, M. Julve, J. Faus, R. Ruiz, I. Castro, M. Mollar, M. Philoche-Levisalles, *Inorg. Chem*. **1992**, *31*, 784. – [5c] J. L. Sanz, B. Cervera, R. Ruiz, C. Boix, J. Faus, F. Lloret, M. Julve, *J. Chem. Soc., Dalton Trans.* **1996**, 1359.
[6] [6a] Z. Zang, D. Liao, Z. Jiang, S. Hao, X. Yao, H. Wang, G. Wang, *Inorg. Chim. Acta* **1990**, *173*, 201. – [6b] . Escuer, R. Vicente, J. Ribas, R. Costa, X. Solans, *Inorg. Chem*. **1992**, *31*, 2627.
[7] [7a] C. Mathoniére, O. Kahn, J. C. Daran, H. Hilbig, F. H. Köhler, *Inorg. Chem*. **1993**, *32*, 4057. – [7b] F. Lloret, Y. Journaux, M. Julve, *Inorg. Chem*. **1990**, *29*, 3967.
[8] O. Kahn, *Adv. Inorg. Chem.* **1996**, *43*, 179.
[9] [9a] M. Verdaguer, M. Julve, A. Michalowicz, O. Kahn, *Inorg. Chem*. **1983**, *22*, 2624. – [9b]Y. Pei, Y. Journaux, O. Kahn, *Inorg. Chem*. **1989**, *28*, 100. – [9c] H. Okawa, M. Koikawa, S. Kida, *J. Chem. Soc., Dalton Trans.* **1990**, 469. – [9d]P. Chaudhuri, M. Winter, B. P. C. Della Védova, E. Bill, S.G. Trautwein, P. Fleischhauer, B. Nuber, J. Weiss, *Inorg. Chem.* **1991**, *30*, 2148.
[10] O. Kahn, *Structure and Bonding*, Springer-Verlag, Berlin, **1987**, *68*, 89.
[11] M. A. Hitchman, C. Rowbotton, *Coord. Chem. Rev.* **1982**, *42*, 55.
[12] [12a] W. B. Tolman *Inorg. Chem*. **1991**, *30*, 4877 and refs. therein. – [12b] T. M. Rajendiran, C. Mathonière, S. Golhen, L. Ouahab, O. Kahn, *Inorg. Chem*. **1998**, *37*, 2651.
[13] [13a] M. Nardelli, G. Pelizzi, *Inorg. Chim. Acta* **1980**, *38*, 15. – [13b] O. Kahn, E. Bakalbassis, C. Mathonière, M. Hagiwara, K. Katsumata, L. Ouahab, *Inorg. Chem*. **1997**, *36*, 1530.
[14] A. Gleizes, A. Meyer, M. A. Hitchman, O. Kahn, *Inorg Chem.* **1982**, *21*, 2257.
[15] A. Meyer, A. Gleizes, J. J. Girerd, M. Verdaguer, O. Kahn, *Inorg. Chem*. **1982**, *21*, 1729.
[16] J. P. Costes, F. Dahan, J. Ruiz, J. P. Laurent, *Inorg. Chim. Acta* **1995**, *239*, 53.
[17] A. Bencini, D. Gatteschi, *EPR of Exchange Coupled Systems*, Springer, Berlin, **1990**, p. 182.
[18] The series of calculations was made using the computer program CLUMAG, which uses the irreducible tensor operator formalism (ITO): D. Gatteschi, L. Pardi, *Gazz Chim. Ital.* **1993**, *123*, 231.
[19] H. Ojima, K. Nonoyama, *Z. Anorg. Allg. Chem*. **1972**, *389*, 75.
[20] G. M. Sheldrick, *Acta Crystallogr.* **1990**, *A46*, 467.
[21] G. M. Sheldrick, SHELXL: *A Computer Program for Crystal Structure Refinement*, Univ. Göttingen, Germany, **1993**.
[22] *International Tables of X-ray Crystallography*, Kynoch Press, Birmingham, **1974**, Vol. 4, pp 99–100 and 149, 1973.
[23] H. D. Flack, *Acta Crystallogr. Sect. A* **1983**, *39*, 876.

Received May 3, 1999
[I99155]

Complexation of Cobalt(II) at the Upper Rim of Two New Calix[4]arene/Bipyridine-Based Podands

Jean-Olivier Dalbavie,[b] Jean-Bernard Regnouf-de-Vains,*[a] Roger Lamartine,[b] Sylvain Lecocq,[c] and Monique Perrin[c]

Keywords: Calix[4]arenes / Bipyridines / Podands / Cobalt complexes

Introduction of one or two 2,2′-bipyridine units at the upper rim of the calix[4]arene platform was performed by means of the Wittig reaction. The resulting alkenes were hydrogenated to give two new bipyridyl-based calixarene podands, which were studied as ligands for Co^{II} cation. The mono-bipyridyldichlorocobalt complex was notably fully characterised by ^{1}H-NMR and X-ray crystal structure analyses, which confirmed the tetrahedral coordination mode involving the bipyridyl subunit and the two chlorine atoms around the cobalt centre.

Introduction

As recently reviewed by Matt et al.,[1] the calixarenes display interesting properties for transition metal chemistry, via their own binding sites (oxygens, aryl rings), or by their ability to act as carriers and spatial organisers of various types of chelating agents, such as esters, phosphanes, or heterocycles. In this domain, our contribution resulted in the synthesis and study of the complexation properties of various podands incorporating 2,2'-bipyridine and 2,2'-bithiazole chelating units at the lower rim of the tetra-*p*-*tert*-butylcalix[4]arene platform.

In order to develop a similar approach at the upper rim, but in a different way than through the potentially coordinating amide links developed by Beer and coll.,[3] we found that the Wittig reaction could be an interesting synthetic tool for building a new family of lipophilic ligands in which the chelating units would be attached by a stable and non-coordinating ethylenic linkage to the calixarene platform.

As a first step, this reaction was applied on the mono[*p*-(formyl)]tris[*p*-(*tert*-butyl)]calix[4]arene model, leading to the conjugated phenol-bipyridyl system **1**.[4] The relative instability of this ligand and its copper(I) complex ([**1**/Cu/**1**]PF_6),[5] especially on chromatographic supports, limited the interest of this family of unsaturated ligand in our field of investigations, and led us to develop the complexation studies of the corresponding saturated podands.

We thus present here the syntheses and some complexation properties towards Cobalt(II) of two new calixarene-based bipyridine ligands, in which the chelating units are bound by an ethylenic linkage to the upper rim of the calixarene platform.

[a] Laboratoire de Chimie Thérapeutique,
UMR 7565 CNRS-UHP, Faculté de Pharmacie,
5, rue Albert Lebrun, F-54001 Nancy Cedex, France
Fax: (internat.) + 333/83178863
E-mail: jean-bernard.regnouf@pharma.u-nancy.fr
[b] Laboratoire de Chimie Industrielle
[c] Laboratoire de Cristallographie, ESA 5078 du CNRS,
Université Claude Bernard Lyon I,
43 Bd du 11 Novembre 1918, F-69622,
Villeurbanne Cedex, France

Results and Discussion

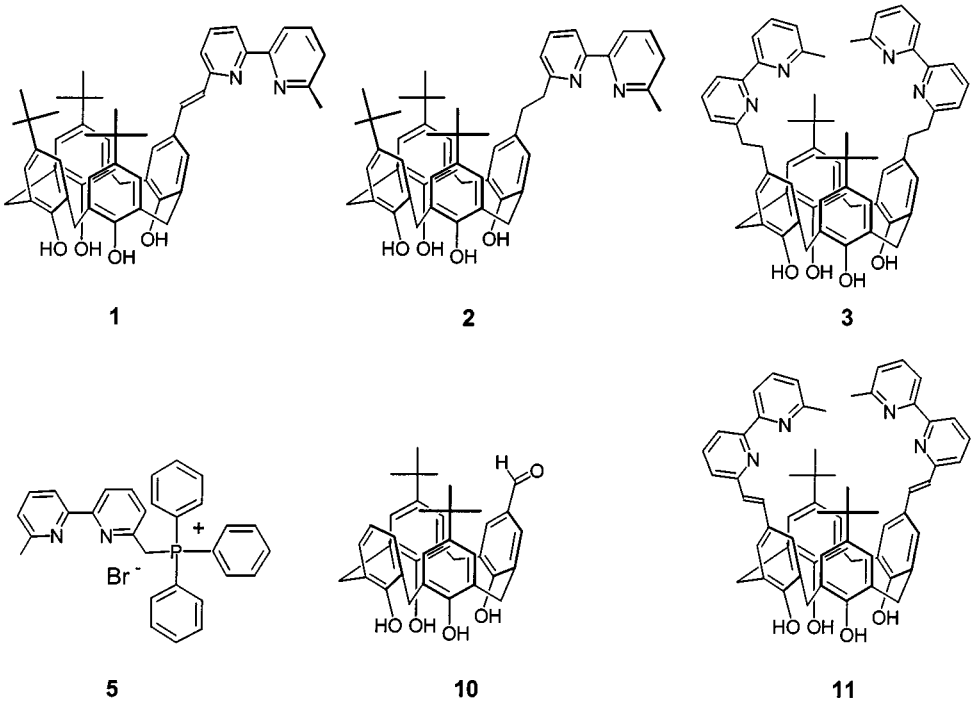
Syntheses of ligands (Scheme 1 *and Scheme* 2*)*. Ligand **2** was obtained quantitatively by catalytic hydrogenation of **1**, but we found it better to reduce the raw Wittig material directly, in order to eliminate the loss of **1** during chromatography. In this way, **2** was obtained in a yield of 40% *vs* the formylcalixarene platform, instead of 27% with isolation of **1**.

The synthetic strategy developed for the disubstituted podand **3** was similar to **1** and **2**, and involved a selective double deterbutylation of the tetra-*p*-*tert*-butylcalix[4]arene **4**, followed by a double Gross formylation[6] applied on the unprotected calixarene platform. The resulting aldehyde was then treated in alcoholic basic conditions with the monophosphonium salt of bipyridine **5** to give the corresponding diene which was directly catalytically hydrogenated into the desired armed calixarene.

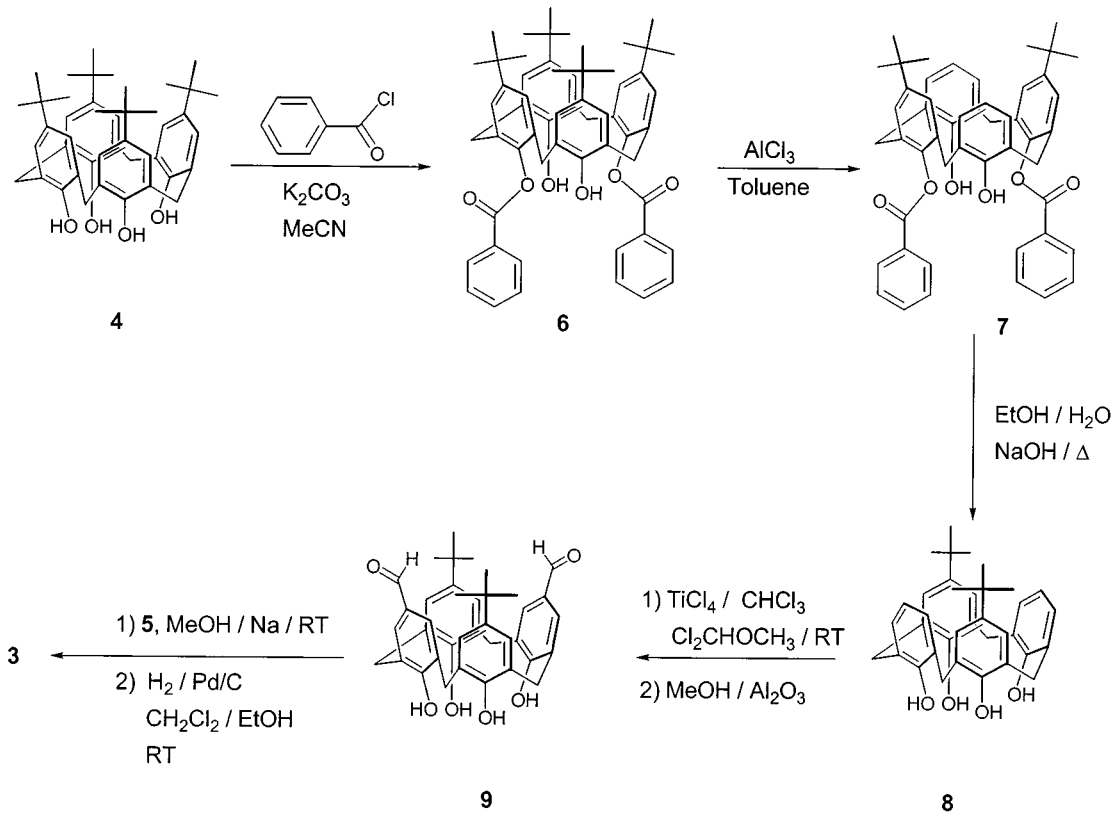
The selective introduction of two chelates at the 5th and 17th positions of the calix[4]arene platform **4** involved a preliminary retro-Friedel and Crafts di-deterbutylation step developed by Gutsche and coll.[7] *via* a selective protective dinitrobenzoylation of two hydroxyl groups in diametrical positions. The resulting diester was obtained in three different acylation media, namely dichlorophenylphosphate/dinitrobenzoic acid/DMF/ pyridine, $AlCl_3$/dinitrobenzoyl chloride/DMF, or dinitrobenzoyl chloride/pyridine systems, with yields of 75, 67, and 95%, respectively. More recently, Huang and coll.[8] described the formation of the dibenzoyl analogue **6** in a benzoyl chloride/$CHCl_3$/NEt_3 medium with a yield of 68%. We found that **6** could easily be synthesised from **4** and benzoyl chloride using MeCN as solvent and K_2CO_3 as base, with a good yield of 91%.

The subsequent retro-Friedel and Crafts deterbutylation step was carried out in toluene using only five equivalents

 © WILEY-VCH Verlag GmbH, D-69451 Weinheim, 2000 1434−1948/00/0404−0683 $ 17.50+.50/0



Scheme 1



Scheme 2

of $AlCl_3$ relative to **6**. The reaction was initiated by a gentle warming and was completed in ca. 1–2 hours, giving **7** with a yield of 80%. Based on the recent work of Magrans and coll., dedicated to the conformational study of 1,3-di-*O*-benzoylated calix[4]arenes,[9] the ^{13}C-NMR analyses of compounds **6** and **7** show that they should not be in a pure cone conformation. The resonance signals of the Ar–CH_2-Ar groups appear at δ = 33.39 and 33.84, respectively, between the standard δ = 31 and 37 values observed for the pure *syn* and *anti* conformations. This suggests that a rapid exchange between the conic and the 1,3-alternate conformations takes

place in solution. Nevertheless, for legibility, **6** and **7** are drawn in the conic conformation in Scheme 2.

The benzoate groups were then removed in alcoholic NaOH at reflux. The 11,23-di-*p*-*tert*-butylcalix[4]arene **8** was thus obtained in an almost quantitative yield.

Introduction of the two formyl groups at the upper rim of **8** failed when the previously described conditions were employed. The use of $TiCl_4$ instead of $SnCl_4$ was successful, affording the bis-aldehyde **9** and some mono-aldehyde **10,** in yields of 65 and 19%, respectively. It is interesting to note that, as previously mentioned,[4] a treatment of the raw electrophilic substitution material over Al_2O_3 was mandatory to liberate the formylated species.

Reaction of **9** with two equivalents of **5**[4] in the presence of an excess of NaOMe in MeOH afforded a mixture of compounds from which only low amounts of pure bis(alkene) **11** were isolated. For this reason, we preferred to hydrogenate the raw Wittig material directly. From the resulting mixture, the bisalkane **3** was isolated after chromatography in a yield of 22%.

Complexation Studies

Cobalt(II) Complex of 2

The reactivity of 6,6'-dimethyl-2,2'-bipyridine (dmbpy) towards Co^{II} cation has notably been studied by Newkome and coll., who prepared, based on UV/Vis spectroscopy and elemental analysis, the neutral tetrahedral $Co(dmbpy)Cl_2$ complex **12**.[10] The same approach applied to an octobipyridylcalix[4]resorcinarene ligand allowed us to prepare, based on UV/Vis spectroscopy, elemental and ES-MS analyses, the corresponding octodichlorocobalt species,[2b] which demonstrated that the presence of a bulky substituent close to the chelating site was not limiting the complexation process.

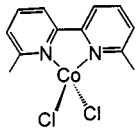
In **2** or **3**, the presence of the ethylenic linkage should give a more pronounced (dimethyl)bipyridine character to the chelating site than in the above-mentioned example, and therefore facilitate the coordination process of Co^{II}.

Thus, reacting **2** with one equivalent of anhydrous $CoCl_2$ in a $MeOH/CH_2Cl_2$ mixture at room temperature gave the light-blue complex **13** (Scheme 3), which was purified by chromatography on Sephadex LH20, and then crystallised as fine needles from a hexane/CH_2Cl_2 mixture. Unfortunately these were unsuitable for X-ray analysis. Elemental analysis was consistent with the presence of 0.2 equivalent of CH_2Cl_2.

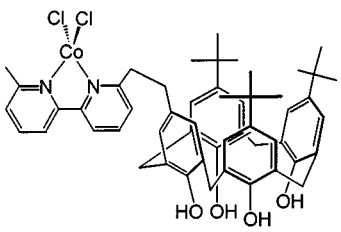
The latter was found in the standard ^{1}H-NMR spectrum of **13**, which also did not display the resonance pattern of the bipyridyl group, thereby confirming the paramagnetic nature of the complex subunit. The remaining part of the molecule, out of the sphere of direct influence of Co^{II}, displayed resonance signals in the expected regions. In $CDCl_3$, at 300 MHz, two singlets assigned to *tert*-butyl groups were found at δ = 1.24 (9 H) and δ = 2.15 (18 H); four broad singlets located at δ = 2.50, 2.95, 3.34, and 3.94 (2 H each) were assigned to the Ar–CH_2-Ar groups, considering that the ethylenic bridge, which supports the effect of the cobalt cation, did not give resonance signals. Changing $CDCl_3$ for CD_2Cl_2 resulted in the transformation of these four singlets into two well-separated broad AB systems, confirming our previous assignment and suggesting a probable rigidification due to a specific interaction between this solvent and the macrocycle.

In the aromatic part, two sharp singlets at δ = 6.92 and 7.06, and a broad one at δ = 7.82, each integrating 2H, were assigned to the aromatic protons of the unsubstituted phenol rings. Finally, a broad singlet located at δ = 9.32 was assigned to the four hydroxyl groups.

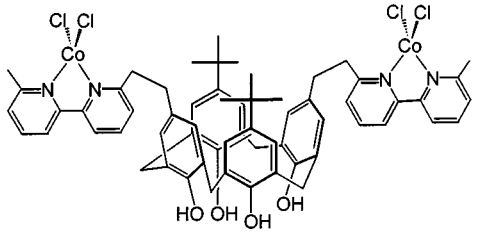
The fact that the resonance signals of protons close to the metallic centre, with regards to the supposed structure of complex **13**, are absent in these classical analytical conditions led us to seek them in a larger frequency domain. Recording data over 65000 Hz (216 ppm at 300 MHz) allowed the exhibition of ten new signals: six relatively sharp singlets ($\Delta\nu_{1/2}$ = 30–38 Hz) integrating for 1 H each, at δ = 70.71, 69.92, 49.10, 46.67, –14.77, and –15.72 that we suspect correspond to the bipyridine protons; a larger singlet



12



13



14

Scheme 3

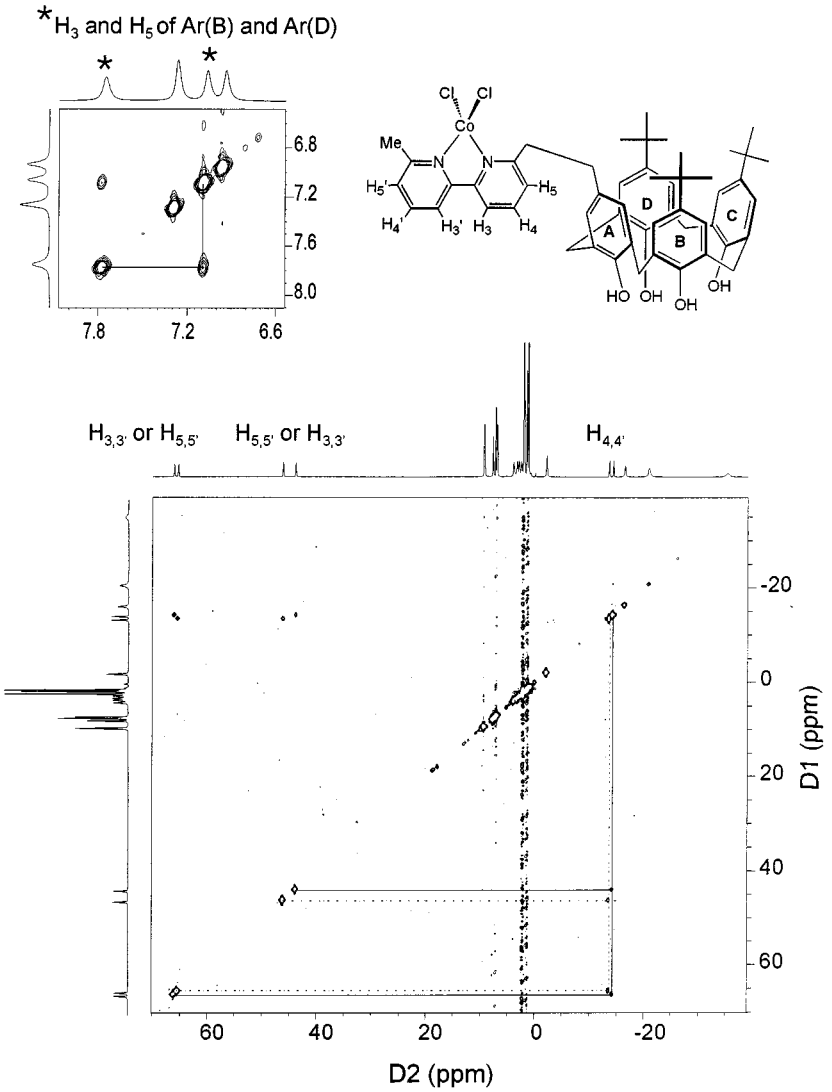


Figure 1. COSY correlations between protons of complex **13** ($CDCl_3$, 500 MHz, 293 K) (main spectrum: bipyridine resonance pattern; offset: aryl resonance pattern)

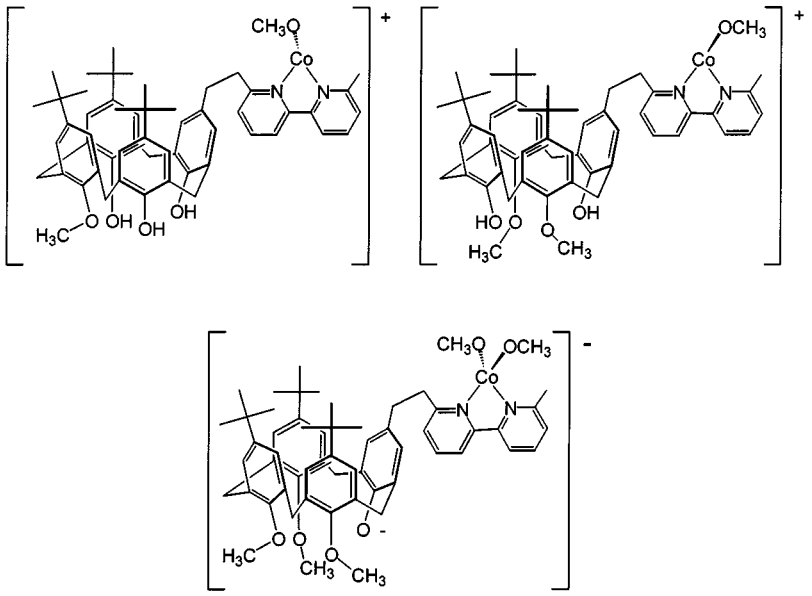
at δ = –2.63 ($\Delta\nu_{1/2}$ = 48 Hz) integrating for 2 H, which was assigned to the substituted phenol ring protons, and three large singlets, one integrating for 2 H ($\Delta\nu_{1/2}$ = 92 Hz) at δ = –17.21, another one integrating for 3 H ($\Delta\nu_{1/2}$ = 169 Hz) at δ = –21.68, and the last singlet integrating for 2 H ($\Delta\nu_{1/2}$ = 300 Hz) at δ = –37.73, which were assigned to the CH_2-phenol, the CH_3-bpy and the CH_2-bpy groups, respectively.

Working at 500 MHz resulted in slight changes in chemical shifts (see Experimental Section). 500-MHz COSY experiment (58000 Hz, 116 ppm) (Figure 1) confirmed the attribution of the bipyridine protons, with two groups of signals at δ = 66.06, 43.87, –14.30, and δ = 65.35, 46.17, –13.52, the negative signals corresponding to the H(4) and H(4') spin systems. Another scalar correlation was found in the calixarene aromatic region between the singlets at δ = 7.75 and δ = 7.07, which were thus assigned to the two lateral phenol rings.

UV/Vis spectroscopy of **13** in CH_2Cl_2 showed a complex ligand-centred absorption pattern associated with a metal-centred transition at 655.5 nm with a molar extinction coefficient of ca. 530 $dm^3.mol^{-1}.cm^{-1}$, identical to the values reported for **12** and corresponding to a tetrahedral coordination mode.[10]

ES-MS analysis confirmed the formation of **13**. The preliminary measurements were performed in CH_2Cl_2 containing some MeOH as proton source. In the positive mode, three peaks corresponding to species containing the native ligand **13** were observed at 846.5, 811.6 and 789.7 a.m.u. and were attributed to the mono-charged cations [**13** – $2Cl^-$ – H^+]$^+$, [**13** – $CoCl_2$ + Na^+]$^+$, and [**13** – $CoCl_2$ + H^+]$^+$, respectively. They were accompanied by compounds of higher molecular weights which were analysed as complex **13** in which one or two phenol groups were *O*-methylated and one chlorine was exchanged with a methoxy anion: 906.6 a.m.u. [$(CH_3O)_2$ **13**–$2Cl^-$ + CH_3O^-]$^+$ and 892.6 a.m.u. [(CH_3O) **13**–$2Cl^-$ + CH_3O^-]$^+$ (Scheme 4).

In the negative mode, which usually gives, in the calixarene family, the mono- or polyphenate anions, the same phenomenon was observed at –50 V, but with a much lower



Scheme 4

intensity, the base peak at 787.6 a.m.u. corresponding to the deprotonated ligand **2**. The molecular peak was observed at 916.6 a.m.u. [**13** – H^+]$^-$, accompanied by the mono- and the bis-dehalogenated species at 880.5 a.m.u. [**13** – Cl^- – $2H^+$]$^-$ and 844.5 a.m.u. [**13** –$2Cl^-$ – $3H^+$]$^-$, respectively. Three peaks at 950.6, 940.6, and 926.6 a.m.u. were attributed to complexes containing one tris-, one bis-, and one monomethylated ligand with a double or single anion metathesis, i.e. [$(CH_3O)_3$**13** –$2Cl^-$ + $2CH_3O^-$ – H^+]$^-$ (Scheme 4), [$(CH_3O)_2$**13** – Cl^- + CH_3O^- – H^+]$^-$, and [(CH_3O) **13** – Cl^- + CH_3O^- – H^+]$^-$. We found in fact, that these methylation reactions and anion metatheses occurred during the analysis: changing the solvent for alcohol-free CH_2Cl_2 (stabilised with 2-methyl-2-butene), gave, in the positive mode (+ 80 V), peaks at 882.5, 846.6, and 789.9 5 a.m.u. which were attributed to [**13** – Cl^-]$^+$, [**13** –$2Cl^-$ – H^+]$^+$, and [**13** – $CoCl_2$ + H^+]$^+$, respectively.

Blue single crystals of complex **13**, suitable for X-ray diffraction analysis, were obtained in a closed tube by liquid diffusion of Et_2O into a solution of **13** in CH_2Cl_2. This study confirmed the presence of the expected dichlorocobalt-bipyridine complex subunit attached by an ethylene link to the upper rim of the tri-*tert*-butylcalix[4]arene platform (Figure 2). The cobalt cation is coordinated in a distorted tetrahedral mode to the two bipyridyl nitrogen atoms and to the two chlorine anions (Table 1), confirming the hypothesis of Newkome et al.[10] The bipyridyl group is parallel to the supporting phenol ring **A**, making with it an angle of only 4.25°.

The cyclic tetramer is in a boat-shaped cone conformation, with the expected usual hydrogen bonds between the hydroxyl groups (2.608–2.731 Ä). The angles between the phenol rings **A**, **B**, **C**, and **D**, and the mean plane defined by the methylene bridges amount to 122.7(2), 118.0(2), 132.7(1), and 117.1(2)°, respectively. Surprisingly, the presence of the bulky complex substituent do not result in the leaning of the supporting phenol ring **A**, while **C**, in the alternate position, is strongly inclined. The *tert*-butyl group of the latter occupies two positions, differing by a rotation of about 60°, with occupancies of 51% and 49%.

Each complex unit is associated with a molecule of Et_2O and one of CH_2Cl_2. The former, which is not shown in Figure 2, is located between the macrocycles, while the latter is trapped into the calixarene cavity, on the level of the *tert*-butyl groups (Figure 3).[11] This molecule of CH_2Cl_2 is found in disordered positions called Cl20–C100–Cl10 (73%) (Figure 2), and Cl30–C200–Cl40 (27%); Cl20 and C200 on one part, Cl40 and C100 on the other part, are positioned on the same sites. The interactions between dichloromethane and calixarene are found between C100 and ring **C** (3.46 Å) and C200 and ring **A** (3.34 Å).

This specific complexation found in the solid state can be correlated with the modifications of the ^{1}H-NMR spectrum of complex **13**, which were previously observed between its $CDCl_3$ and CD_2Cl_2 solutions.

According to the proposal for classification and nomenclature of host-guest type compounds given by Weber and Josel,[12] compound **13** can be defined as a cryptato-tubulato clathrate.

Cobalt(II) Complex of 3

In a similar way, ligand **3** was reacted with two equiv. of $CoCl_2$ to give the dinuclear grey-blue complex **14**. The expected M_2L stoichiometry was verified by UV/Vis spectroscopy in CH_2Cl_2, with an ε value of 1030 dm^3 mol^{-1} cm^{-1} at 656.5 nm, twice the value of **13**, and by C, H, and N elemental analyses. Positive- or negative mode ES-MS analysis of **14** showed methylation reactions and anion metatheses similar to those observed with **13** when methanolic CH_2Cl_2 was used as the solvent (*see Experimental Section*). In the negative mode (–50 V), in alcohol-free CH_2Cl_2, the complex exhibited a single mass of peaks at 1185.5–1189.3

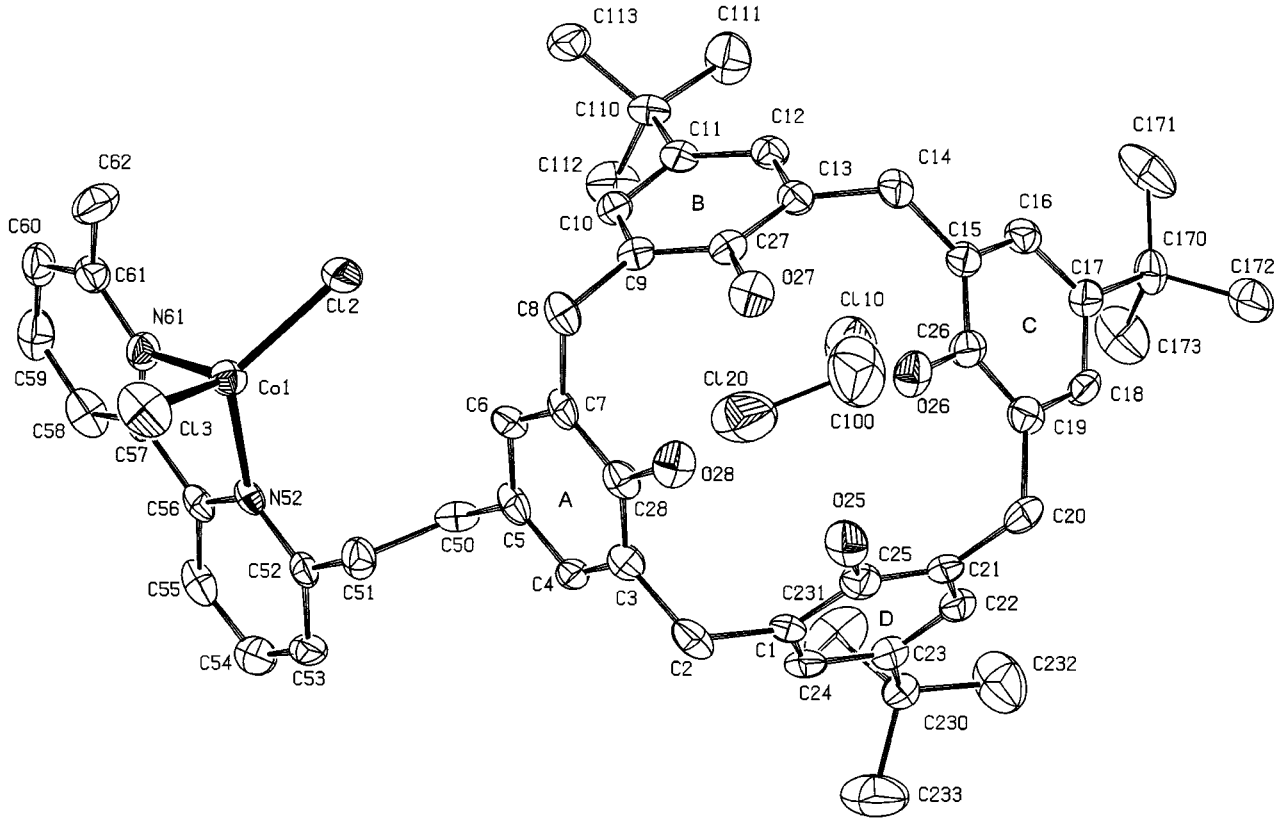


Figure 2. Numbering scheme and ORTEP underside-view of complex **13**

Table 1. Selected geometric parameters around the cobalt centre

Bond lengths [Å]			
Co–N52	2.021(5)	Co–N61	2.027(6)
Co–Cl2	2.213(2)	Co–Cl3	2.222(2)
Bond angles [°]			
Cl2–Co–Cl3	118.4(9)°	N52–Co–N61	82.3(2)
Cl2–Co–N52	119.6(2)°	Cl3–Co–N61	110.1(2)
N52–Co–Cl3	108.7(2)°	N61–Co–Cl2	112.0(2)

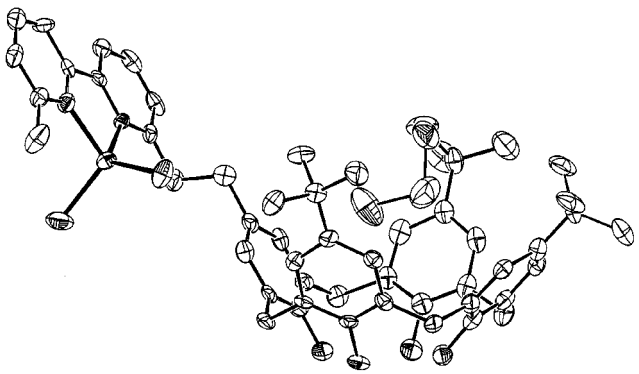


Figure 3. ORTEP side-view of complex **13**

a.m.u. which was attributed to the monophenate species [**14** – H^+]$^-$, confirming the results of UV/Vis and elemental analyses.

Unfortunately, the lack of solubility of **14** did not allow us to verify the ^{1}H-NMR results obtained with **13**.

Conclusion

By a Wittig reaction *plus* hydrogenation process, we have selectively incorporated one and two bipyridine units at the upper rim of *p*-(*tert*-butyl)calix[4]arene platforms. The two new ligands thus obtained displayed coordinating behaviour towards cobalt(II), and the resulting mono- and dinuclear complexes were fully characterised. With the monometallic species, ^{1}H-NMR COSY experiment performed on a large frequency domain allowed us to recover and to assign the bipyridine resonance signals, and X-ray analysis confirmed the tetrahedral coordination of the bipyridine and the two chlorine atoms around the cobalt centre. The complexation studies of other transition metal cations and the building of the tris- and tetra-substituted analogues are now under investigation.

Experimental Section

General: Melting points (°C, uncorrected) were determined on an Electrothermal 9100 in Capillary apparatus. – ^{1}H and ^{13}C NMR spectra were recorded on a Bruker AM 300 or DRX 300 and DRX 500 ($CDCl_3$, TMS as internal standard, chemical shifts in ppm). – Mass spectra (electrospray, ES) were recorded on a Platform Mic-

romass apparatus at the Service Central d'Analyse du CNRS, Solaize. – Infrared spectroscopy was performed on a Mattson 5000 FT apparatus (KBr, $\tilde{\nu}$ in cm^{-1}). – UV spectra were recorded on a Shimadzu UV 2401 PC or a SAFAS UV mc^2 apparatus, λ_{max} in nm, ε in $dm^3\ mol^{-1}\ cm^{-1}$. – Elemental analyses were performed at the Service Central de Microanalyse, Ecole Supérieure de Chimie, Montpellier. – Macherey–Nagel TLC plates were used for chromatography analysis (SiO_2, Polygram SIL G/UV254, ref.805021). All commercially available products were used without further purification unless otherwise specified.

Calix[4]arene-25,26,27,28-tetrol 2. – Indirect Method: To a solution of 0.05 g of **1**[3] ($0.063 \cdot 10^{-3}$ mol) in 5 mL of EtOH/CH_2Cl_2, was added 0.01 g of 5% Pd/C, and H_2 was bubbled through the solution for 1 min. The mixture was stirred at room temp. overnight under H_2 and then filtered over Celite. Evaporation of the filtrate to dryness afforded 0.045 g of pure **2** (90%).

Direct Method: The raw Wittig material obtained from 0.5 g (0.8 mmol) of monoformylcalixarene was neutralised with 1 M HCl and evaporated to dryness. The resulting glassy material was dissolved in 50 mL of CH_2Cl_2, dried over Na_2SO_4 and concentrated to ca. 20 mL. EtOH (30 mL) and 0.2 g of 5% Pd/C were added, and the resulting mixture was stirred under H_2 overnight. The suspension was filtered over Celite and evaporated to dryness. The residue was dissolved in CH_2Cl_2 and addition of MeOH resulted in the precipitation of a raw material which was purified by chromatography (Al_2O_3, CH_2Cl_2/hexane, then CH_2Cl_2/MeOH 99:1) to give 0.25 g of **2** (40%). –UV/Vis (CH_2Cl_2): λ (ε) = 281.0 (23390), 289.0 (24180), 304.0 (10400). – ^{1}H NMR ($CDCl_3$): δ = 1.198 (s, 9 H, *Me*$_3$C); 1.205 (s, 18 H, *Me*$_3$C); 2.62 (s, 3 H, *Me*bpy); 2.80–3.20 (*ABm*, 4 H, C*H*$_2$–C*H*$_2$); 3.45, 4.22 ("q", *AB*, *JAB* = 13 Hz, 4 H, Ar–C*H*$_2$-Ar); 3.45, 4.22 ("q", *AB*, *JAB* = 13 Hz, 4 H, Ar–C*H*$_2$-Ar); 6.93 (s, 2 H, Ar); 7.01–7.07 (m, 7H, 6 H of Ar, 1 H of bpy); 7.02 (d, *J* = 7.6 Hz, 1 H, bpy); 7.64 (t, *J* = 7.6 Hz, 1 H, bpy); 8.19 (*d*, *J* = 7.7 Hz, 1 H, bpy); 8.20 (d, *J* = 7.7 Hz, 1 H, bpy); 10.28 (s, 4H, O*H*). – ^{13}C NMR ($CDCl_3$): δ = 24.67 (*Me*bpy); 31.40, 31.46 (*Me*$_3$C); 32.34, 32.51 (Ar–CH$_2$-Ar); 33.98, 34.03 (Me$_3$*C*); 34.95, 40.07 (*C*H$_2$–CH$_2$); 118.19, 118.53, 122.69, 123.05, 136.97 (C-3, C-4, C-5, C-3', C-4', C-5' of bpy); 125.71, 125.86, 126.03, 129.00 (CH of Ar); 127.41, 127.71, 127.90, 128.31, 135.36, 144.44, 146.37, 146.70, 147.10 (C_o, C_p, C_{ipso} of Ar); 155.90, 155.98, 157.78, 160.67 (C-2, C-2', C-6, C-6', bpy). – ES-MS (neg. mode; –50V); *m*/*z*: 787.7–788.7 [**2** – H$^+$]$^-$. – $C_{53}H_{60}N_2O_4 \cdot 0.25\ CH_2Cl_2$ (810.31): calcd. C 78.93, H 7.53, N 3.46, O 7.90; found C 79.09, H 7.58, N 3.31, O 7.98.

Calix[4]arene-26,28-diol 6: A mixture of finely powdered K_2CO_3 (2.33 g, 17 10^{-3} mol) and 5 g of *p-tert*-butylcalix[4]arene **4** (7.7 10^{-3} mol) in 250 mL of acetonitrile was stirred at 80 °C for 30 min. Benzoyl chloride (1.8 mL, 15.4 10^{-3} mol) was then added by syring, and heating was maintained for 4 h. After cooling, the solvent was evaporated to dryness and the residue dissolved in 100 mL of CH_2Cl_2. The resulting solution was washed with water (3×50 mL), dried over Na_2SO_4, then concentrated to 40 mL on a Rotavapor. The residue was then mixed with 300 mL of EtOH and the resulting cloudy solution was concentrated in vacuo to give 6 g of **6** (91%), white precipitate, m.p. 320–330 °C (dec.). – UV/Vis (CH_2Cl_2): λ (ε) = 278.5 (6100). – IR: $\tilde{\nu}$ = 1735 (C=O). – ^{1}H NMR ($CDCl_3$): δ = 1.01 (s, 18 H, *Me*$_3$C); 1.15 (s, 18 H, *Me*$_3$C); 3.49, 3.97 ("q", *AB*, *JAB* = 14.1 Hz, 8 H, Ar–C*H*$_2$-Ar); 6.91 (s, 4 H, Ar); 7.02 (s, 4 H, Ar); 7.52 (t, *J* = 7.4 Hz, 4 H of C_6H_5); 7.70 (t, *J* = 7.4 Hz, 2 H of C_6H_5); 8.33 (d, *J* = 7.1 Hz, 4 H of C_6H_5). – ^{13}C NMR ($CDCl_3$): δ = 31.53, 31.09 (*Me*$_3$C); 33.39 (Ar–CH$_2$-Ar); 33.86, 34.06 (Me$_3$*C*); 133.71, 130.50, 128.99, 126.12, 125.64 (CH of Ar and C_6H_5); 150.43, 148.87, 143.34, 142.61, 131.92, 127.78, 129.38 (C_o, C_p, C_{ipso} of Ar; C_{ipso} C_6H_5); 165.01 (*C*=O). – ES-MS (neg. mode); *m*/*z*: 855.7 [**6** – H]$^-$; (pos. mode): 857.6 [**6** + H]$^+$. – $C_{58}H_{64}O_6$ (857.15): calcd. C 81.27, H 7.53, O 11.20; found C 81.08, H 7.90, O 11.16.

Calix[4]arene-26,28-diol 7: A mixture of **6** (6 g, $7 \cdot 10^{-3}$ mol) and $AlCl_3$ (4.7 g, 35 10^{-3} mol) in 300 mL of toluene was heated until a red colouration persisted, and then stirred at room temp. for 2 h. H_2O (100 mL) was added, and the resulting emulsion was stirred for 30 min. The toluene phase was washed with water (3×100 mL), the latter extracted with CH_2Cl_2, and the combined organic phases evaporated to dryness. The yellow residue was dissolved in a mixture of CH_2Cl_2 (50 mL) and MeOH (250 mL) and then concentrated in vacuo to ca. 100 mL to give 4.2 g of **7** (80%) as a white precipitate; m.p. 320 °C(dec). – UV/Vis (CH_2Cl_2): λ (ε) = 275.0 (9480), 282.0 (sh, 8330). – IR: $\tilde{\nu}$ = 1735 (C=O). – ^{1}H NMR ($CDCl_3$): δ = 1.08 (s, 18 H, *Me*$_3$C); 3.87, 3.57 ("q", *AB*, *JAB* = 14.1 Hz, 8 H, Ar–C*H*$_2$-Ar); 6.59 (t, *J* = 7.4 Hz, 2 H, Ar); 6.93 (d, *J* = 7.4 Hz, 4 H, Ar); 7.00 (s, 4 H, Ar); 7.52 (t, *J* = 7.7 Hz, 4 H, C_6H_5); 7.72 (t, *J* = 7.4 Hz, 2 H, C_6H_5); 8.22 (d, *J* = 7.0 Hz, 4 H, C_6H_5). – ^{13}C NMR ($CDCl_3$): δ = 31.19 (*Me*$_3$C); 33.84 (Ar–CH$_2$-Ar); 34.15 (Me$_3$*C*); 119.62, 130.70, 129.27, 128.68, 126.31, 133.75 (CH of Ar and C_6H_5); 128.05, 131.95, 144.05, 149.04, 152.91 (C_o, C_p, C_{ipso} of Ar, C_{ipso} of C_6H_5); 164.76 (*C*=O). – ES-MS (neg. mode); *m*/*z*: 535.5 [**7**– H]$^-$. – $C_{50}H_{48}O_6$ (744.94): calcd. C 80.62, H 6.50, O 12.88; found C 80.57, H 6.73, O 12.81.

Calix[4]arene-25,26,27,28-tetrol (8): A mixture of **7** (4.2 g, 5.6 10^{-3} mol) and NaOH (8 g, 200 10^{-3} mol) in a mixture of EtOH (120 mL) and H_2O (40 mL) was heated under reflux for 12 h. After cooling, the solution was acidified to pH 5–6 with HCl to give a white precipitate which was collected by filtration, and then dissolved in CH_2Cl_2. Addition of MeOH resulted in the precipitation of 3 g of **8** (99%), m.p. 300 °C. – UV/Vis (CH_2Cl_2): λ (ε) = 277.5 (10000), 282.5 (sh, 8600). – ^{1}H NMR ($CDCl_3$): δ = 1.25 (s, 18 H, *Me*$_3$C); 4.26, 3.56 ("q", 8 H, Ar–C*H*$_2$-Ar); 6.73 (t, *J* = 7.7 Hz, 2 H, Ar); 7.08 (d, *J* = 7.7 Hz, 4 H, Ar); 7.09 (s, 4 H, Ar); 10.29 (s, 4 H, O*H*). – ^{13}C NMR ($CDCl_3$): δ = 31.52 (*Me*$_3$C); 32.22 (Ar–CH$_2$-Ar); 34.12 (Me$_3$*C*); 129.02, 125.91, 122.37 (CH of Ar); 148.72, 146.77, 144.66, 128.5, 127.56 (C_o, C_p, C_{ipso} of Ar). – ES-MS (neg. mode); *m*/*z*: 535.5 [**8** – H]$^-$. – $C_{36}H_{40}O_4 \cdot 0.9\ CH_2Cl_2$ (613.15): calcd. C 72.28, H 6.87, O 10.44; found C 72.35, H 6.97, O 10.58.

Calix[4]arene-25,26,27,28-tetrol (9) and Calix[4]arene-25,26,27,28-tetrol (10): $TiCl_4$ (1.25 mL, 11.2 10^{-3} mol) was syringed into a soln. of **8** (0.4 g, 0.65 10^{-3} mol) in 10 mL of $CHCl_3$. The resulting red solution was stirred under N_2 during 30 min. Dichloromethylmethyl ether (1 mL, 11.2 10^{-3} mol) was then added dropwise. After 2 h, 25 mL of water was added and stirring was continued for 1 h. After separation, the aqueous phase was washed with CH_2Cl_2 (3×20 mL). The combined organic phases were dried over Na_2SO_4, then concentrated to dryness. The residue was dissolved in 1:1 MeOH/CH_2Cl_2 and 2 g of aluminium oxide were added to give, after ca. 12 h, the raw aldehyde which was purified by chromatography (SiO_2, CH_2Cl_2) to give 0.08 g of the mono aldehyde **10** (19%) and 0.25 g of **9** (64%). – **Compound 9:** m.p. >350 °C. – UV/Vis (CH_2Cl_2): λ (ε) = 281.0 (18300). – IR: $\tilde{\nu}$ = 1680 (C=O). – ^{1}H NMR ($CDCl_3$): δ = 1.24 (s, 18 H, *Me*$_3$C); 4.27,3.69 (br. *AB*, 8 H, Ar–C*H*$_2$-Ar); 7.15 (s, 4 H, Ar); 7.61 (s, 4 H, Ar); 9.74 (s, 2 H, C*H*O); 10.30 (s, 4 H, O*H*). – ^{13}C NMR ($CDCl_3$): δ = 31.50 (*Me*$_3$C), 31.99 (Ar–CH$_2$-Ar); 34.28 (Me$_3$*C*); 126.41, 131.16 (CH of Ar), 126.83, 129.15, 131.30, 145.87, 146.14, 154.70 (C_o, C_p, C_{ipso} of Ar); 190.56 (*C*HO). – ES-MS (pos. mode); *m*/*z*: 615.4 [**9** + Na]$^+$. – $C_{38}H_{40}O_6 \cdot 0.1\ CH_2Cl_2$ (601.23): calcd. C 76.11, H 6.74, O 15.97;

found C 76.20, H 7.18, O 15.58. – **Compound 10:** m.p. > 350 °C. – UV/Vis (CH_2Cl_2): λ (ε) = 280.0 (13500). – IR: ν̃ = 1685 (C=O). – ^{1}H NMR ($CDCl_3$): δ = 1.27 (s, 18 H, *Me*$_3$C); 3.60, 4.29 (br. *AB*, 8 H, Ar–C*H*$_2$-Ar); 6.74 (t, *J* = 7.5 Hz, 1 H, Ar); 7.06 (d, *J* = 7.5 Hz, 2 H, Ar); 7.13 (s, 4 H, Ar); 7.64 (s, 2 H, of Ar); 9.77 (s, 1 H, ArC*H*O); 10.30 (br. s, 4 H, O*H*). – ^{13}C NMR ($CDCl_3$): δ = 31.47 (*Me*$_3$C), 32.06 (Ar–CH_2-Ar); 34.16 (Me$_3$*C*); 122.55, 125.93, 126.29, 129.00, 131.15 (CH of Ar), 125.81, 126.53, 127.82, 128.17, 129.35, 131.12, 145.21, 146.41, 148.53, 154.92 (C$_{o,}$ C$_{p,}$ C$_{ipso}$ of Ar); 190.67 (*C*=O). – ES-MS (pos. mode); *m*/*z*: 587.5 [**10** + Na]$^+$. – $C_{37}H_{40}O_5$·0.8 CH_2Cl_2 (632.67): calcd. C 71.76, H 6.63, O 12.64; found C 71.82, H 6.89, O 12.51.

Calix[4]arene-25,26,27,28-tetrol (3): The bipyridinephosphonium salt **5** (0.585 g, 0.5 10^{-3} mol) was dissolved in a solution of NaOMe in MeOH [10 ml; from 0.097 g of Na (4.05 10^{-3} mol)]. To the resulting yellow solution was added 0.3 g of **9** (0.5 10^{-3} mol). The solution was stirred at room temp. for 6 h and then evaporated to dryness. The raw material was dissolved in CH_2Cl_2 and then washed with 1 M HCl and H_2O. Evaporation of CH_2Cl_2 afforded a glassy material which was dissolved in 10 mL of EtOH and 10 mL of CH_2Cl_2. 30 mg of 5% Pd/C was added and the solution was stirred under a blanket of H_2 overnight. Solid material was filtered over Celite and rinsed with CH_2Cl_2 followed by acetone. The filtrate was evaporated to dryness and the residue was dissolved in 1 mL of CH_2Cl_2. Addition of 10 mL of MeOH resulted in the formation of a white precipitate which was recovered and purified by chromatography (Al_2O_3, CH_2Cl_2/MeOH 97/3) to give 0.105 g of **3** (22%); m.p: 274 °C. – UV/Vis (CH_2Cl_2): λ (ε) = 289.5 (43200). – ^{1}H NMR ($CDCl_3$): δ = 1.21 (s, 18 H, *Me*$_3$C); 2.62 (s, 6 H, *Me*-bpy); 3.06, 2.90 (*ABm*, 8 H, C*H*$_2$C*H*$_2$); 4.24, 3.46 ("q", *AB*, J_{AB} = 13.0 Hz, 8 H, Ar–C*H*$_2$-Ar); 6.91 (s, 4 H, Ar); 7.04 (s, 4 H, Ar); 7.05 (d, *J* = 7.0 Hz, 2 H, bpy); 7.13 (d, *J* = 7.4 Hz, 2 H, bpy); 7.65 (t, *J* = 7.0 Hz, 4 H, bpy); 8.19 (t, *J* = 5.7 Hz, 4 H, bpy); 10.3 (br. s, 4 H, OH). – ^{13}C NMR ($CDCl_3$): δ = 24.68 (*Me*–bpy); 31.47 (*Me*$_3$C); 32.26 (Ar–CH_2–Ar); 34.04 (Me$_3$*C*); 34.95, 40.07 (*C*H$_2$*C*H$_2$); 125.83, 128.98 (CH of Ar); 118.18, 118.49, 122.67, 123.06, 136.98 (CH of bpy); 127.56 128.24, 135.43, 144.48, 146.76 (C$_{o,}$ C$_{p,}$ C$_{ipso}$ of Ar); 155.90, 155.99, 157.80, 160.74 (C(2), C(2'), C(6), C(6') of bpy). – ES-MS (pos. mode); *m*/*z*: 929.5 [**3** + H]$^+$. – $C_{62}H_{64}N_4O_4$·0.1 CH_2Cl_2 (937.72): calcd. C 79.54, H 6.90, N 5.97, O 6.82; found C 79.27, H 6.92, N 5.99, O 6.60.

Calix[4]arene-25,26,27,28-tetrol Cobalt(II) (13): A solution of anhydrous $CoCl_2$ (0.0145 g, 0.111 × 10^{-3} mol) in 3 mL of MeOH was added to a solution of **2** (0.09 g, 0.111 × 10^{-3} mol) in 15 mL of CH_2Cl_2. The resulting blue solution was stirred at room temp. for 3 h and then evaporated to dryness. The blue residue was dissolved in 3 mL of CH_2Cl_2 and purified by chromatography over Sephadex LH20 (CH_2Cl_2). The middle fractions were collected and concentrated; precipitation by hexane gave 0.096 g of **13** (92%), light-blue solid. – UV/Vis (CH_2Cl_2): λ (ε) = 254.5 (12300), 280.0 (16500), 287.5 (14960), 308.0 (10420), 317.0 (11440), 341.0 (6208), 570.5 (284), 655.5 (530). – ^{1}H NMR (500 MHz, $CDCl_3$): δ = –35.24 (br. s, Δν$_{1/2}$ = 300 Hz, 2 H, CH_2–C*H*$_2$-bpy); –20.85 (br. s, Δν$_{1/2}$ = 169 Hz, 3 H, *Me*-bpy); –16.39 (br. s, Δν$_{1/2}$ = 92 Hz, 2 H, C*H*$_2$–CH_2-bpy); –14.30 [s, Δν$_{1/2}$ = 30.50 Hz, 1 H, H(4) or H(4') of bpy]; –13.53 [s, Δν$_{1/2}$ = 30.12 Hz, 1 H, H(4) or H(4') of bpy]; –2.08 [br. s, Δν$_{1/2}$ = 48 Hz, 2 H, Ar(**A**)]; 1.27 (s, Δν$_{1/2}$ = 21.14 Hz, 9 H, *Me*$_3$C); 2.10 (s, Δν$_{1/2}$ = 21.93 Hz, 18 H, *Me*$_3$C); 2.54 (br. s, Δν$_{1/2}$ = 109 Hz, 2 H, Ar–C*H*$_2$–Ar); 3.03 (br. s, Δν$_{1/2}$ = 104.50 Hz, 2H, Ar–C*H*$_2$-Ar); 3.34 (br. s, Δν$_{1/2}$ = 98.70 Hz, 2 H, Ar–C*H*$_2$–Ar); 3.95 (br. s, Δν$_{1/2}$ = 85.25 Hz, 2 H, Ar–C*H*$_2$-Ar); 6.94 [s, Δν$_{1/2}$ = 22.00 Hz, 2 H, Ar(**C**)]; 7.07 [s, Δν$_{1/2}$ = 22.86 Hz, 2 H, H(3) or H(5) of Ar(**B**) and Ar(**D**)]; 7.75 [s, Δν$_{1/2}$ = 26.24 Hz, 2 H, H(5) or H(3) of Ar(**B**) and Ar(**D**)]; 9.33 (s, Δν$_{1/2}$ = 39.60 Hz, 4H, O*H*); 43.87 [s, Δν$_{1/2}$ = 36.50 Hz, 1 H, H(5 or 5') or H(3 or 3') of bpy]; 46.17 [s, Δν$_{1/2}$ = 35.20 Hz, 1 H, H(5' or 5) or H(3' or 3) of bpy]; 65.35 [s, Δν$_{1/2}$ = 36.80 Hz, 1 H, H(3 or 3') or H(5 or 5') of bpy]; 66.06 [s, Δν$_{1/2}$ = 38.62 Hz, 1 H, H(3' or 3) or H(5' or 5) of bpy]. – ES-MS, for $C_{53}H_{60}CoCl_2N_2O_4$ (918.91; 918): *CH_2Cl_2 + amylene, positive mode:* 882.6, 883.6, 884.6, 885.6 [**2** + $CoCl_2$ – Cl$^-$]$^+$; 846.6, 847.7 [**2** + $CoCl_2$ – 2 Cl$^-$ – H$^+$]$^+$; 789.7, 790.7, 791.8 [**2** + H$^+$]$^+$. *CH_2Cl_2 + amylene + MeOH as ionising agent, positive mode*: 906.6, 907.7, 908.8, 909.9 [**2**·(OCH$_3$)$_2$ + $CoCl_2$ – 2 Cl$^-$ + CH_3O^-]$^+$; 892.6, 893.6, 894.6, 895.5 [**2**·(OCH$_3$) + $CoCl_2$ – 2 Cl$^-$ + CH_3O^-]$^+$; 846.5, 847.6, 848.6 [**2** + $CoCl_2$ – 2 Cl$^-$ – H$^+$]$^+$; 811.6, 812.6, 813.6 [**2** + Na$^+$]$^+$; 789.7, 790.7, 791.7 [**2** + H$^+$]$^+$; *negative mode*: major peaks 787.6, 788.6, 789.7 [**2** – H$^+$]$^-$; minor peaks 950.6, 951.6, 952.6 [**2**·(OCH$_3$)$_3$ + $CoCl_2$ – 2 Cl$^-$ + 2 (CH_3O^-) – H$^+$]$^-$; 940.6, 941.6, 942.6 [**2**·(OCH$_3$)$_2$ + $CoCl_2$ – Cl$^-$ + CH_3O^- – H$^+$]$^-$; 926.6, 927.6, 928.6, 929.5 [**2**(OCH$_3$) + $CoCl_2$ – Cl$^-$ + CH_3O^- – H$^+$]$^-$; 916.6, 917.6, 918.6, 919.6 [**2** + $CoCl_2$ – H$^+$]$^-$; 880.5, 881.6, 882.6 [**2** + $CoCl_2$ – Cl$^-$ – 2 H$^+$]$^-$; 844.5, 845.5, 846.6 [**2** + $CoCl_2$ – 2 Cl$^-$ – 3 H$^+$]$^-$. – $C_{53}H_{60}CoCl_2N_2O_4$·0.2 CH_2Cl_2 (935.90): calcd. C 68.27, H 6.50, N 2.99; found C 68.23, H 6.74, N 2.79.

Calix[4]arene-25,26,27,28-tetrol Cobalt(II) (14): A solution of anhydrous $CoCl_2$ (0.018 g, 0.072·10^{-3} mol) in MeOH (6 mL) and CH_2Cl_2 (6 mL) was added to a solution **3** (0.06 g, 0.065·10^{-3} mol) in 30 mL of CH_2Cl_2. The resulting light blue solution was evaporated to dryness; the residue was dissolved in CH_2Cl_2 and then purified by chromatography over Sephadex LH20 (CH_2Cl_2) to give 0.072 g of **14** (92%). Blue-grey powder. – UV/Vis (CH_2Cl_2): λ (ε) = 280.0 (20300); 287.0 (19700), 306.0 (16600); 316.5 (17200); 572.0 (700); 656.5 (1030). – ES-MS: 1) *negative mode, alcohol-free CH_2Cl_2,* –50V: 1185.5, 1187.6, 1188.4, 1189.3 [**3** + 2 $CoCl_2$ – H]$^-$; 2) *positive mode, alcohol-free CH_2Cl_2*, +120V: 851.7, 853.6, 854.7 [**3** + $CoCl_2$ – ($C_{11}H_9N_2$) – Cl]$^+$; 989.5, 990.6, 991.6, 992.6, 994.7 [**3** + $CoCl_2$ –2Cl – H]$^+$; 3) *positive mode, CH_2Cl_2 + MeOH,* +50V: 929.7, 930.6 [**3** + H]$^+$; 951.7, 952.7, 953.7 [**3**·(OCH$_3$) + Na]$^+$; 1032.7, 1033.6, 1034.6 [**3**·(OCH$_3$) + $CoCl_2$ – 2Cl$^-$ + CH_3O^-]$^+$; 1047.6 [**3**·(OCH$_3$)$_2$ + $CoCl_2$ – 2Cl$^-$ + CH_3O^-]$^+$; 4) *negative mode, CH_2Cl_2 + MeOH*, –50V: 731.6, 732.6, 733.5 [**3** – CH_2CH_2bpy]$^-$; 927.7, 928.8, 929.7 [**3** – H]$^-$; 1056.6, 1057.6, 1058.7, 1059.7 [**3** + $CoCl_2$ – H]$^-$; 1065.5, 1067.5, 1068.5 [**3**·(OCH$_3$) + $CoCl_2$ – H]$^-$; 1187.4 [**3** + 2 $CoCl_2$ – H]$^-$. – $C_{62}H_{64}Co_2Cl_4N_4O_4$·$H_2O$ (1206.91): calcd. C 61.70, H 5.51, N 4.64; found C 61.99, H 5.83, N 5.18.

X-ray Crystallographic Study of Complex 13: $C_{53}H_{60}Cl_2Co_1N_2O_4$, CH_2Cl_2, $C_4H_{10}O$, crystal system monoclinic, space group *P*2(1)/*c* with *a* = 24.747(5) Å, *b* = 9.1648(18) Å, *c* = 24.231(5) Å, β = 93.12(3)°, *V* = 5487.5(19) Å^3, $D_{calcd.}$ = 1.305 g/cm^3 and *Z* = 4. The data were collected at 173 K by X-ray diffraction on an Enraf–Nonius Kappa-CCD diffractometer. Full sphere of data was collected by axis rotation with 1°.0 increments over 180°, with 30 s exposures per frame. The crystal to detector distance was 30 mm. Data were analyzed using Kappa-CCD Software.[13] Cell dimensions were refined with HKL Scalepack.[14] The structure was solved with direct methods using the SHELXS programme.[15] Refinement by SHELXL [16] leads to an *R* factor of 0.077 for 3345 F_o > 4 (F_o) and a goodness of fit of 0.947. All nonhydrogen atoms were given anisotropic displacement parameters. All hydrogen atoms were located at their theoretical position and refined as a riding model. EXYZ and EADP instructions were used for the study of the CH_2Cl_2 disorder. The final electron density difference map showed a maximum of 1.23 e.Å^{-3} and a minimum of –0.51 eÅ^{-3}. Molecular graphics were drawn with ORTEP.[17]

Table 2. Crystal data and structure refinement of **13**

Empirical formula	$C_{53}H_{60}Cl_2Co_1N_2O_4{\cdot}CH_2Cl_2{\cdot}C_4H_{10}O$
Mr	1078.23
Crystal system, space group	Monoclinic, *P*2(1)/*c*
Cell dimensions	
a [Å]	24.747(5)
b [Å]	9.1648(18)
c [Å]	24.231(5)
β [°]	93.12(3)
V [Å^3]	5487.5(19)
Z	4
D_x [Mg·m^{-3}]	1.305
D_m	not measured
T [K]	173
Crystal size [mm]	0.36 × 0.18 × 0.04
Color	blue
Enraf–Nonius Kappa-CCD diffractometer	
Wavelength [Å]	0.71073
Absorption correction	none
R_{int}	0
φ limits [°]	2.37 to 27.83
Limiting indices	$-28 \le h \le 28$, $-11 \le k \le 0$, $0 \le l \le 31$
Measured reflections	11633
Independent reflections	10917
Parameters	637
H atoms riding	
S	0.947
R	*R*1 = 0.0767, *wR*2 = 0.1429
Densities (max),(min)[eÅ^{-3}]	1.227 and –0.507

Crystallographic data (excluding structure factors) have been deposited with the Cambridge Crystallographic Data Centre as supplementary publication n° 120557. Copies of the data can be obtained free of charge on application to CCDC, 12 Union Road, Cambridge CB2 1EZ, U.K. [Fax: (internat.) + 44-1223/336033; E-mail: deposit@ccdc.cam.ac.uk]. For other details see Table 2.

Acknowledgments

We are grateful to the MRES for financial support, especially J.-O. D. for a PhD fellowship; to SAFAS (Monaco) and BRUKER S.A. for UV spectroscopy and WINNMR facilities, respectively. We are indebted to Mrs Nicole Marshall for correcting the manuscript.

[1] C. Wieser, D. B. Dieleman, D. Matt, *Coord. Chem. Rev.* **1997**, *165*, 93.
[2] [2a] J.-B. Regnouf-de-Vains, R. Lamartine, *Helv.Chim. Acta* **1994**, *77*, 181. – [2b] J.-B. Regnouf-de-Vains, S. Pellet-Rostaing, R. Lamartine, *Tetrahedron Lett.* **1995**, *36*, 5745. – [2c] J.-B. Regnouf-de-Vains, R. Lamartine, B. Fenet, C. Bavoux, A. Thozet, M. Perrin, *Helv.Chim. Acta* **1995**, *78*, 1607. – [2d] S. Pellet-Rostaing, J.-B. Regnouf-de-Vains, R. Lamartine, *Tetrahedron Lett.* **1996**, *37*,5889. –[2e] S. Pellet-Rostaing, J.-B. Regnouf-de-Vains, R. Lamartine, P. Meallier, S. Guittonneau, B. Fenet, *Helv. Chim. Acta* **1997**, *80*, 1229. – [2f] J.-B. Regnouf-de-Vains, R. Lamartine, B. Fenet, *Helv.Chim. Acta* **1998**, *81*, 661–669.
[3] [3a] P. D. Beer, Z. Chen, A. J. Goulden, A. Grieve, D. Hesek, F. Szemes, T. Wear, *J. Chem. Soc., Chem. Commun.* **1994**, 1269. – [3b] P. D. Beer, *Chem. Commun.* **1996**, 689. – [3c] P. D. Beer, M. G. B. Drew, D. Hezek, M. Shade, F. Szemes, *Chem. Commun.* **1996**, 2161. – [3d] P. D. Beer, J. B. Cooper, *Chem. Commun.* **1998**, 129.
[4] J.-B. Regnouf-de-Vains, R. Lamartine, *Tetrahedron Lett.* **1996**, *37*, 6311.
[5] J.-B. Regnouf-de-Vains, R. Lamartine, poster 33-B, BOSS 6, Gent, Belgium, July 8–12, **1996**.
[6] A. Arduini, G. Manfredi, A. Pochini, A. R. Sicuri, R. Ungaro, *J. Chem. Soc., Chem. Commun.* **1991**, 936.
[7] K. A See, F. R Froncsek, W. H. Watson, R. P. Kashyap, C. D. Gutsche, *J. Org. Chem.* **1991**, *56*, 7256.
[8] Z. T. Huang, G. –Q. Wang, *Synthetic Commun.* **1994**, *24*, 11.
[9] J. O. Magrans, J. de Mendoza, M. Pons, P. Prados, *J. Org. Chem.* **1997**, *62*, 4518.
[10] G. R. Newkome, D. C. Pantaleo, W. E. Puckett, P. L. Ziefle, W. A. Deutsch, *J. Inorg. Nucl. Chem.* **1981**, *43*, 1529.
[11] for an other CH_2Cl_2 complex, see:[11a] J. L. Atwood, S. G. Bott, C. Jones, C. L. Raston, *J. Chem. Soc., Chem. Commun.* **1992**, 1349. – [11b] J. L. Atwood, P. C. Junk, S. M. Lawrence, C. L. Raston, *Supramol. Chem.* **1996**, *7*, 15.
[12] E. Weber, H. P. Josel, *J. Incl. Phenom.* **1983**, *1*, 79.
[13] Enraf–Nonius, *Kappa*-CCD *Software*, **1997**, Enraf–Nonius, Delft, The Nederlands.
[14] Z. Otwinowski, W. Minor, *Methods Enzymol*. **1996**, *276*, 307–326.
[15] G. M. Sheldrick, *SHELXS-97 Program for Crystal Structure Determination* **1997**, University of Gottingen, Germany.
[16] Sheldrick, G.M., *SHELXL-97. Program for the refinement of Crystal Structures.* **1997**, University of Göttingen, Germany.
[17] ORTEP-3 for Windows, L. J. Farrugia, *J. Appl. Cryst.* **1997**, 565.

Received May 31, 1999
[I99192]

Transition Metal Complexes of (Schiff Base)Divalent Group 14 Element Species $[(salen)M]_n{=}M'(CO)_{6-n}$ (n = 1, 2; M = Ge, Sn, Pb; M′ = Cr, W)

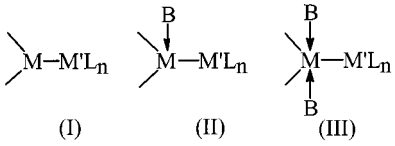
Dominique Agustin,[a] Ghassoub Rima,[a] Heinz Gornitzka,[a] and Jacques Barrau*[a]

Keywords: Germylene / Stannylene / Plumbylene / Schiff base / Transition metal complexes of M_{14} divalent species

The syntheses, characterization, and reactivities of the new stable mono- and *cis*-disubstituted Group 14 metal(II) chromium and tungsten carbonyl complexes (salen)M=M′$(CO)_5$ [salen = 2,2′-*N,N′*-bis(salicylidene)ethylenediamine; M′ = Cr, M = Ge (**4**), Sn (**5**), Pb (**6**); M′ = W, M = Ge (**7**), Sn (**8**), Pb (**9**)] and $[(salen)M]_2$=M′$(CO)_4$ [M′ = W, M = Ge (**10**), Sn (**11**), Pb (**12**); M′ = Cr, M = Sn (**14**), Ge (**15**)] are described. Complexes **4–9** were obtained in high yields by treatment of the M′$(CO)_5 \cdot$ THF intermediates with the stable divalent species (salen)M^{II} [M = Ge (**1**), Sn (**2**), Pb (**3**)]. Direct irradiation of mixtures of (salen)M^{II} and M′$(CO)_6$ resulted in formation of the monosubstituted compounds **4–9** together with the disubstituted species **10–12**, **14**, and **15** in ratios depending on the nature of both M and M′. Pure complexes **10–12** were obtained by two different synthetic approaches starting from the (salen)M^{II} species or the (salen)M=M′$(CO)_5$ complexes. Each of the new complexes has been characterized by ^{1}H- and ^{13}C-NMR, and by ^{119}Sn-NMR in the case of **5**, **8**, **11**, and **14**, as well as by IR spectroscopy in all cases. The molecular structures of **5**, **8**, **11**, and **14**, determined by X-ray structure analyses, reveal a pentacoordinated tin atom. The tin–chromium distances are among the shortest (in particular that in **5**, 2.557 Å) observed for transition metal divalent tin complexes and the tin lies about 0.99 Å above the plane defined by the O_2N_2 atoms of the salen ligand. All these complexes have been found to be unreactive towards water and organic acids. Simple phosphane monosubstitution of carbonyl in **8** using Ph_3P led to the new complex **13**. Reactions with 1,2-bis(diphenylphosphanyl)ethane and 3,5-di-*tert*-butyl-1,2-benzoquinone resulted in displacement of the divalent species from the carbonyl complexes **5** and **8**.

Introduction

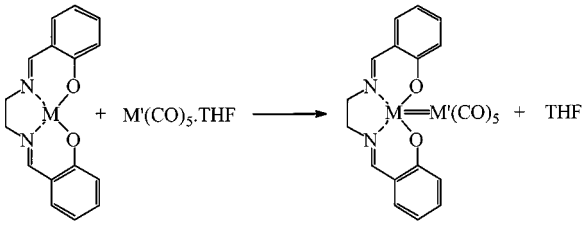
Heavier analogs of carbenes can be used as ligands in transition metal chemistry. They can play an important role in the synthesis of precursors of new materials, and various metallic analogs of carbenic complexes of transition metals have been used or postulated as catalysts in reactions involving the formation or cleavage of M–M bonds. The majority of characterized complexes involve four-coordinate M atoms with type II structures; with bulky or donor substituents, a few structures with a three-coordinate M atom (structure I) have been isolated. Only a few examples of complexes with structures of type III having a five-coordinate M atom have been observed.



(I) (II) (III)

The earlier chemistry of these transition metal complexes with divalent species of Group 14 elements has been summarized in various review articles;[1–5] recent investigations concern mainly tin–Group 6 transition metal complexes.[6–14]

Recently, we reported the synthesis and characterization of new stable divalent germanium, tin, and lead homoleptic species L^2M [L^2 = 2,2′-*N,N′*-bis(salicylidene)ethylenediamine (salen), (*R,R*)-(–)-*N,N′*-bis(3,5-di-*tert*-butylsalicylidene)-1,2-cyclohexanediamine, and *N*-methyl-2,2′-iminobis(8-hydroxyquinoline); M = Ge, Sn, Pb].[15] These compounds are monomeric and feature twofold N···M intramolecular coordination, which lowers the Lewis acidity of the metal atom (characteristic of the free divalent species). Nevertheless, they are efficient σ donors and can be used as monodentate ligands in transition metal chemistry. In this work, we consider the salen compounds (salen)M (M = Ge, Sn, Pb) as precursors of new $L^2M{=}M'(CO)_5$ and $(L^2M)_2{=}M'(CO)_4$ complexes (M = Ge, Sn, Pb; M′ = Cr, W). The syntheses, crystal structures, and some chemical properties of these bimetallic compounds are presented herein.



M = Ge (**1**)
Sn (**2**)
Pb (**3**)

M = Ge ; M'= Cr (**4**), W (**7**)
Sn (**5**) (**8**)
Pb (**6**) (**9**)

Scheme 1

[a] Hétérochimie Fondamentale et Appliquée, UPRES-A 5069 du CNRS, Université Paul-Sabatier,
118 route de Narbonne, F-31062 Toulouse Cedex, France
Fax: (internat.) + 33-5/61 55 82 04
E-mail: barrau@ramses.ups-tlse.fr

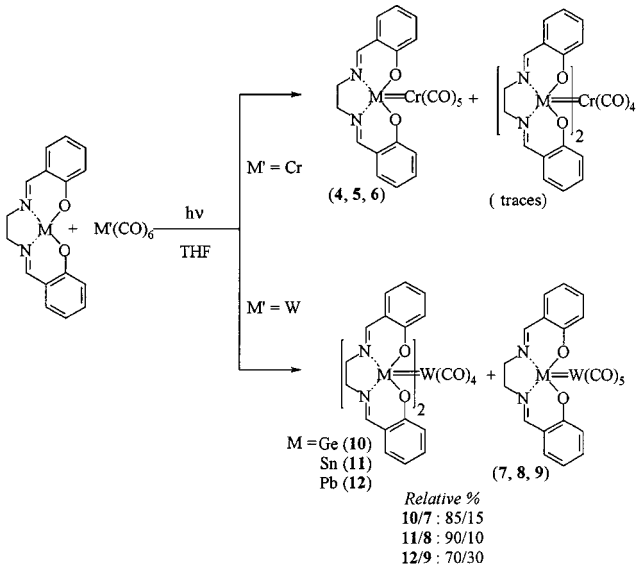
 © WILEY-VCH Verlag GmbH, D-69451 Weinheim, 2000 1434–1948/00/0404–0693 $ 17.50+.50/0

Results and Discussion

Synthesis of Complexes of Divalent Species (salen)M= M′(CO)$_5$ and [(salen)M]$_2$=M′(CO)$_4$ (M = Ge, Sn, Pb; M′ = Cr, W)

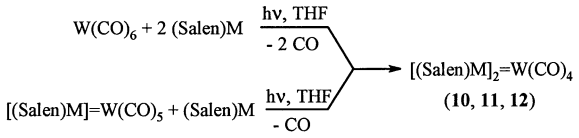
Treatment of the photochemically produced M′(CO)$_5$ · THF intermediates with the (salen)M compounds in THF led to the expected monosubstituted complexes **4–9** in high yields (Scheme 1).

These complexes were obtained as yellow-orange crystalline solids in yields in excess of 80% by recrystallization from $CHCl_3$. They were found to be soluble only in polar and protic solvents (THF, $CHCl_3$, CH_2Cl_2, DMSO, DMF, MeOH). Direct irradiation at room temperature of mixtures of the divalent compounds (salen)M and the hexacarbonyl complexes M′(CO)$_6$ (M′ = Cr, W) also resulted in the formation of the expected monometal(II) complexes in yields depending on the nature of both the Group 14 atom M and the transition metal M′ (Scheme 2). With (salen)germylene and -stannylene, the mono compounds **4** and **5** were produced in high yields when the reactions were carried out using Cr(CO)$_6$. Using W(CO)$_6$ under similar reaction conditions, substitution of more than one carbonyl was observed and the disubstituted compounds **10–12** with the ligands in a *cis* arrangement were formed alongside the monosubstituted species **7–9** (Scheme 2). Extension of this procedure to the reactions of (salen)plumbylene with Cr(CO)$_6$ and W(CO)$_6$ led to complexes **6** in 70% yield and to a mixture of **9** and **12** (30:70, as determined by ^{1}H-NMR), respectively. In contrast, attempts to prepare the (salen)M=M′(CO)$_5$ (M′ = Cr, W) complexes simply by heating mixtures of the starting materials at 80 °C for 24 h proved unsuccessful.



Scheme 2

In view of the particular sensitivity of the tungsten system and the difficulties encountered in separating the mono- and disubstituted tungsten products, we investigated alternative synthetic methods to confirm the structures of **10–12**. Thus, syntheses of pure **10** and **11** were achieved in up to 70% yield by irradiation of a mixture of (salen)M and (salen)M=W(CO)$_5$ or by irradiation of a mixture of two equivalents of (salen)M and one of W(CO)$_6$ (Scheme 3).



Scheme 3

It is interesting to note that under UV irradiation, the *cis*-[(salen)M]$_2$=M′(CO)$_4$ complexes were converted into the *trans* isomers. Such conversions have been particularly well-studied in the case of **11**; irradiation of a solution of *cis*-[(salen)Sn]$_2$=W(CO)$_4$ (**11**) for 6 h resulted in 50% conversion to *trans*-[(salen)Sn]$_2$=W(CO)$_4$ (**11′**). Crystals of **11′** suitable for X-ray structural analysis could not be obtained but its ^{1}H- and ^{13}C-NMR data, a ^{119}Sn-NMR resonance at δ = –374, an IR band at ν_{CO} = 1999 cm^{-1}, and mass spectroscopic data were consistent with the *trans* structure.

Such *cis*/*trans* photochemical isomerizations, as well as thermal reverse conversions, have previously been reported in the case of (carbene)$_2$=W(CO)$_4$.[16] In our case, it has not been possible to unambiguously observe reversion to the thermodynamically favoured *cis* isomer by heating a mixture of **11** and **11′** in the solid state or in solution. When a solid-state 50:50 *cis*/*trans* mixture was maintained at 180 °C for 12 h, the subsequently recorded ^{119}Sn-NMR spectrum featured only resonances due to the *cis* isomer (δ = –348) and due to an unidentified product (δ = –410).

Compounds **4–12** were found to be soluble in polar and protic solvents and insoluble in pentane. All these compounds proved to be stable to moisture.

Physicochemical and Structural Studies of the (salen)M= M′(CO)$_5$ and [(salen)M]$_2$=M′(CO)$_4$ Complexes (M = Ge, Sn, Pb; M′ = Cr, W)

Molecular weight determinations (cryoscopy in benzene) showed **4**, **5**, **7**, and **8** to be monomeric in solution. Compounds **4–12** have been characterized by ^{1}H-, ^{13}C-, and ^{119}Sn-NMR (for the complexes **5**, **8**, and **11**), as well as by IR spectroscopy. ^{1}H- and ^{119}Sn-NMR and IR spectroscopic data are collected in Table 1. The thermal stabilities of these complexes were found to be high; they decompose only on melting, but the germanium and tin complexes proved sufficiently volatile to allow recording of their mass spectra.

The ^{1}H-NMR spectra of complexes **4–12** show different shifts for the signals of the salen ligand relative to those seen for the divalent compounds **1–3**. The most noticeable shifts are seen in the methine proton resonances, which appear at lower field strengths as compared to those of the parent divalent species. For compounds **10–12**, NMR cannot distinguish between the two tin species complexed on the tungsten since the NMR signals of the various protons are similar and therefore non-resolvable. In all cases, as in **1–3**, the chemical shifts and splitting patterns of the CH_2N protons are consistent with the presence of N→M intramolecular coordination in these molecules.

Table 1. Spectroscopic data for compounds **4–12**

		4	**5**	**6**	**7**	**8**	**9**	**10**	**11**	**12**
^{1}H (δ, ppm)	CH_2	3.90	4.01	3.80	3.93	3.99	3.87	3.93	3.81	4.07
	CH=N	8.32	8.42	8.24	8.25	8.73	8.27	8.17	8.43	8.03
^{119}Sn (δ, ppm) ([D$_6$]DMSO)			–137			–328			–348	
IR (Nujol, KBr, cm^{-1})	$\nu_{C=N}$	1630	1638	1620	1620	1641	1630	1620	1638	1625
	$\nu_{C=O}$	1910	1917	1915	1916	1913	1914	1892	1902	1906
		1970	1978	1976	1972	1977	1970	1980	1929	1930
		2047	2047	2048	2067	2063	2060	2009	1954	2015
								2060	2062	2060

The ^{13}C-NMR spectra of **4–12** feature signals with the characteristic chemical shifts of the carbon atoms of the salen ligand, shifted slightly downfield from those in the (salen)M compounds,[15] along with two carbonyl resonances for the monosubstituted complexes **4–9** (relative intensity 1:4) and for the disubstituted complexes **10–12** (relative intensity 1:1).

The ^{119}Sn-NMR spectra of **5**, **8**, and **11** feature singlets at δ = –137, –328, and –348, respectively, which fall within the range of shift values appropriate for pentacoordinate tin compounds; the shift variations between the signal of (salen)Sn and those of the corresponding (salen)Sn=M′(CO)$_5$ complexes reflect the electron-withdrawing effect of the M′(CO)$_5$ groups. The ^1J(^{119}Sn-^{183}W) coupling constants are very similar to those observed in four-coordinate tin(II)–tungsten compounds.[16]

The IR spectra of compounds **4–9** show strong absorptions in the range 1620–1640 cm^{-1} attributable to the $\nu_{C=N}$ stretching frequency under the influence of the N→M intramolecular coordination; these bands are shifted toward higher frequencies by 5–20 cm^{-1} in comparison with the spectra of the free ligands but are not affected to any appreciable extent compared to those observed for the (salen)M compounds. In the metal carbonyl region, three carbonyl bands (A′′$_1$ + A′$_1$ + E) are seen, with an intensity pattern characteristic of C_{4v} local symmetry at chromium or tungsten. Since the unique CO *trans* to the metal M is involved in the A′$_1$ mode, the position of this band [1970 (**4**), 1978 (**5**), 1976 cm^{-1} (**6**)] is indicative[18] of the π-acceptor ability of the (salen)M groups *trans* to the axial carbonyl. IR and ^{13}C-NMR data show that the (salen)M ligands are stronger donors of electron density, but are also π-acceptors. For complexes **10–12**, the appearance of four bands due to the CO groups is compatible with C_{2v} symmetry (*cis* geometry).

The five-coordinate environment about the M atom was confirmed structurally for **5**, **8**, and **11**. Compound **11** represents the first distannylene–tungsten complex [L^{2}Sn]$_2$=W(CO)$_4$ to be structurally characterized. Figure 1, Figure 2, and Figure 3 show solid-state structures of **5**, **8**, and **11**, respectively, together with the numbering scheme adopted. In the case of **11**, the three $CHCl_3$ solvating molecules are omitted for the sake of clarity. Crystal data of **5**, **8**, and **11** are presented in Table 6. Relevant bond lengths and angles in **5**, **8**, and **11** are given in Table 2, Table 3, and Table 4, respectively. In all three compounds, the tin resides in a distorted square-pyramidal geometry with the salen ligand occupying the base plane at Sn–N_2O_2 plane distances of 0.948 Å in **5**, 0.996 Å in **8**, and 1.005 Å and 1.024 Å in **11**. The observed σ Sn–O distances [2.039(3)–2.074(3) Å] are a little longer than classical σ Sn–O bonds (1.94–2.03 Å).[19] The lengths of the Sn←N bonds [2.230(5)–2.288(4) Å] appear to be normal. On going from **5** to **8** and **11**, these Sn–N and Sn–O distances increase as a result of the decreased inductive effect of the transition metal fragment. The tin–chromium or tin–tungsten bonds, which are shorter than typical Sn–M′ (M′ = Cr, W) single bonds,[20] are among the shortest ever observed in transition metal–divalent tin

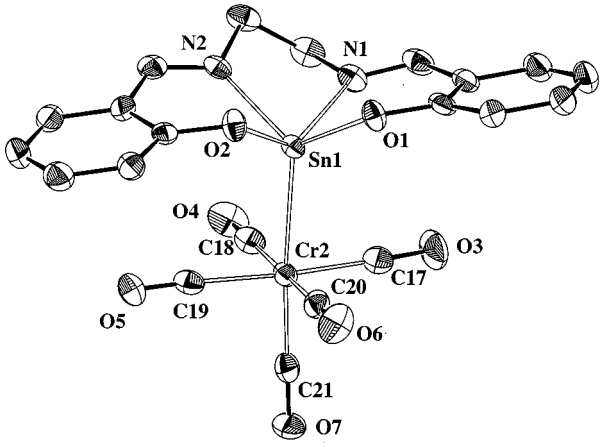


Figure 1. Solid-state structure and atom numbering scheme of (salen)Sn=Cr(CO)$_5$ (**5**)

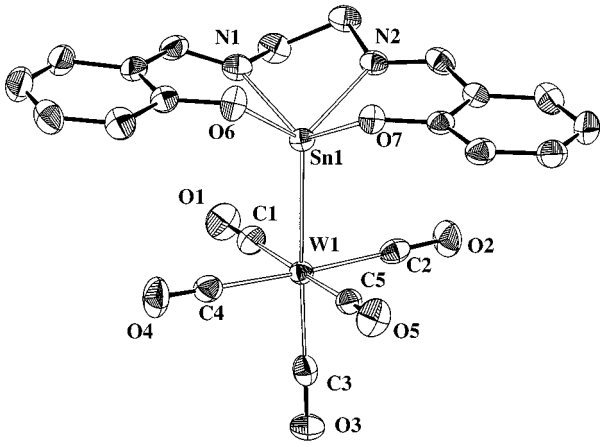


Figure 2. Solid-state structure and atom numbering scheme of (salen)Sn=W(CO)$_5$ (**8**)

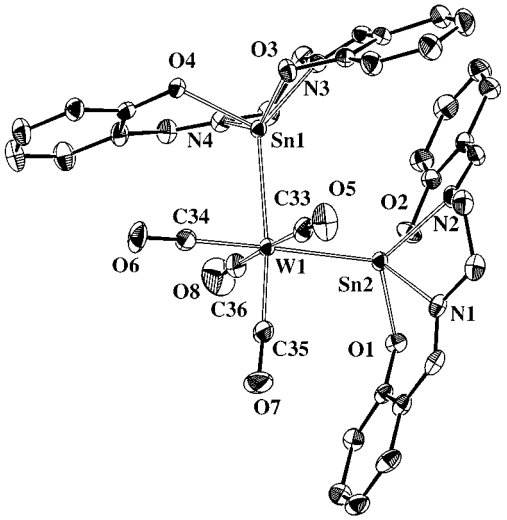


Figure 3. Solid-state structure and atom numbering scheme of $\{[(salen)Sn]_2{=}W(CO)_4\} \cdot 3\,(CHCl_3)$ (**11**); solvent molecules have been omitted for the sake of clarity

Table 2. Selected bond lengths [Å] and angles [deg] in **5**

Distances		Angles	
Sn(1)–Cr(2)	2.578(1)	O(1)–Sn(1)–O(2)	82.27(16)
Sn(1)–O(1)	2.041(4)	O(1)–Sn(1)–N(2)	121.22(16)
Sn(1)–O(2)	2.058(4)	O(2)–Sn(1)–N(2)	80.95(16)
Sn(1)–N(2)	2.230(5)	O(1)–Sn(1)–N(1)	81.41(17)
Sn(1)–N(1)	2.260(5)	O(2)–Sn(1)–N(1)	134.07(18)
Cr(2)–C(21)	1.861(6)	N(2)–Sn(1)–N(1)	71.72(17)
Cr(2)–C(18)	1.873(7)	O(1)–Sn(1)–Cr(2)	120.85(12)
Cr(2)–C(20)	1.886(6)	O(2)–Sn(1)–Cr(2)	115.05(12)
Cr(2)–C(17)	1.894(7)	N(2)–Sn(1)–Cr(2)	117.33(11)
Cr(2)–C(19)	1.915(7)	N(1)–Sn(1)–Cr(2)	110.20(13)

Table 3. Selected bond lengths [Å] and angles [deg] in **8**

Distances		Angles	
W(1)–Sn(1)	2.712(1)	O(6)–Sn(1)–O(7)	81.02(11)
Sn(1)–O(6)	2.039(3)	O(6)–Sn(1)–N(2)	118.87(12)
Sn(1)–O(7)	2.074(3)	O(7)–Sn(1)–N(2)	79.77(11)
Sn(1)–N(2)	2.260(3)	O(6)–Sn(1)–N(1)	80.05(11)
Sn(1)–N(1)	2.261(3)	O(7)–Sn(1)–N(1)	131.39(11)
W(1)–C(3)	1.994(4)	N(2)–Sn(1)–N(1)	71.27(12)
W(1)–C(1)	2.032(4)	O(6)–Sn(1)–W(1)	123.81(9)
W(1)–C(2)	2.039(5)	O(7)–Sn(1)–W(1)	115.95(8)
W(1)–C(4)	2.040(5)	N(2)–Sn(1)–W(1)	116.83(8)
W(1)–C(5)	2.057(4)	N(1)–Sn(1)–W(1)	111.83(9)

complexes, the Sn–Cr distance [2.558(1) Å] in complex **5** being particularly short. These distances reflect a lower electron density at the tin atom in these complexes and may be indicative of double-bond character in the Sn–M′ unit (typical Sn=Cr: 2.60 Å,[7,21,22] Sn=W: 2.74 Å[10,17,23,24]). Thus, it seems that despite its tetradentate capacity the salen ligand does not cancel out the electronic deficiency at the tin atom through N···Sn intramolecular coordination thereby reducing the back-donation by the transition metal. Conversely the solid-state structures suggest that the peculiar arrangement resulting from the structure of the salen ligand maximizes the possibility of [d(M′)-d(p)(Sn)] π overlap.

Table 4. Selected bond lengths [Å] and angles [deg] in **11**

Distances		Angles	
Sn(1)–W(1)	2.711(1)	O(4)–Sn(1)–O(3)	82.57(14)
Sn(1)–O(4)	2.062(3)	O(4)–Sn(1)–N(4)	79.43(14)
Sn(1)–O(3)	2.086(4)	O(3)–Sn(1)–N(4)	137.91(15)
Sn(1)–N(4)	2.265(4)	O(4)–Sn(1)–N(3)	108.90(14)
Sn(1)–N(3)	2.282(4)	O(3)–Sn(1)–N(3)	79.91(14)
Sn(2)–W(1)	2.703(1)	N(4)–Sn(1)–N(3)	70.65(16)
Sn(2)–O(2)	2.066(3)	O(4)–Sn(1)–W(1)	116.76(9)
Sn(2)–O(1)	2.074(3)	O(3)–Sn(1)–W(1)	115.26(11)
Sn(2)–N(2)	2.261(4)	N(4)–Sn(1)–W(1)	106.82(11)
Sn(2)–N(1)	2.288(4)	N(3)–Sn(1)–W(1)	133.06(10)
W(1)–C(35)	1.953(6)	O(2)–Sn(2)–O(1)	79.67(14)
W(1)–C(34)	1.964(6)	O(2)–Sn(2)–N(2)	81.40(16)
W(1)–C(33)	2.013(7)	O(1)–Sn(2)–N(2)	124.75(15)
W(1)–C(36)	2.028(7)	O(2)–Sn(2)–N(1)	125.58(15)
		O(1)–Sn(2)–N(1)	80.00(15)
		N(2)–Sn(2)–N(1)	70.29(17)
		O(2)–Sn(2)–W(1)	125.30(12)
		O(1)–Sn(2)–W(1)	115.03(10)
		N(2)–Sn(2)–W(1)	118.30(11)
		N(1)–Sn(2)–W(1)	109.07(10)
		Sn(2)–W(1)–Sn(1)	96.161(15)

The Sn–W distances in **8** [2.712(1) Å] and **11** [2.711(1) Å and 2.703(1) Å] are very similar, which shows that the strength of the π interaction between the transition metal and the tin atom is not influenced by the number of divalent species on the transition metal. In **5**, **8**, and **11**, the coordination about the Cr or W atom is almost perfectly octahedral. In each compound, the M′–C distances are very similar; the M′–C bonds *trans* to Sn are the shortest, but do not differ significantly from the M′–C equatorial bonds. This suggests that the (salen)Sn ligand is comparable to or slightly poorer than CO as a π acceptor.

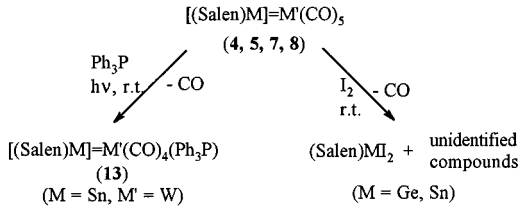
The mass spectra of complexes **4**, **5**, **7**, and **8** exhibit peaks corresponding to molecular ions M^+ [weak (**4** and **7**) or very weak (**5** and **8**) intensity] and to the characteristic fragmentations of such structures (particularly loss of carbonyl groups and of substituents on the Ge and Sn atoms).

Chemical Reactivity of the (salen)M=M′(CO)$_5$ Complexes

Due to their "transition metal–carbene-like" character, the (salen)M=M′(CO)$_5$ complexes would appear to have interesting potential in organometallic chemistry. However, as observed previously, the chemistry of the complexes $L^2M{=}M'(CO)_5$ differs markedly from that of their carbene counterparts despite the many structural similarities.

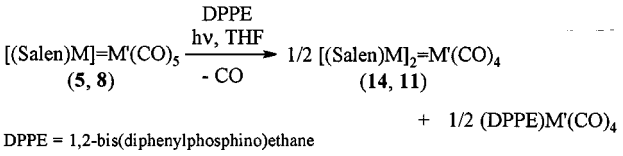
In contrast to their parent compounds (**1–3**) and various $L^2M{=}M'(CO)_5$ complexes, the (salen)M=M′(CO)$_5$ and $[(salen)M]_2{=}M'(CO)_4$ complexes **4–12** were found to be totally unreactive towards water and organic acids (Scheme 3). This lack of reactivity may be attributed to electronic and particularly steric factors, most notably about the tin atom.

With iodine, we observed the expected reactions for compounds with Group 14 metal–transition metal bonds (Scheme 4).



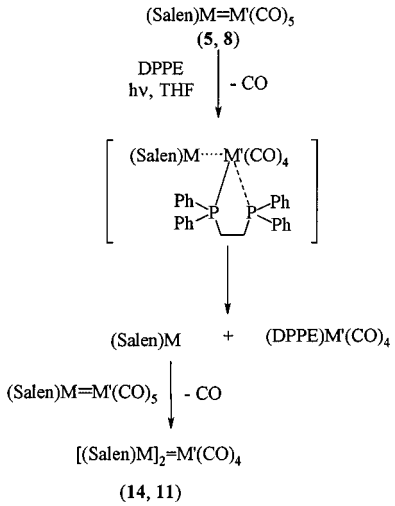
Scheme 4

Since ligands having a lone pair, such as Ph_3P, are able to substitute one or more of the CO groups of metal carbonyls, the monotriphenylphosphane complex of **8** (or **13**, respectively) could easily be prepared by UV irradiation (λ = 254 nm) or by heating (Scheme 4). In contrast, attempted substitution of two CO groups by the chelating ligand 1,2-bis(diphenylphosphanyl)ethane (diphos) were unsuccessful; reactions of this doubly chelating phosphane with **5** and **8** surprisingly led to the distannylene–metal carbonyl complexes **14** and **11**, respectively (Scheme 5).



Scheme 5

Since compounds **5** and **8** are stable towards UV irradiation, it seems that in these cases entry of a second phosphane group into the coordination sphere about M′ causes displacement of the (salen)Sn ligand, which reacts in situ with remaining **5** or **8** to give **14** or **11**, respectively (Scheme 6).



Scheme 6

Complex **14** could be separated from the reaction mixture in the form of orange crystals, by virtue of its low solubility in pentane. The ^{13}C-NMR spectrum and IR data relating to the ν_{CO} region were in agreement with an octahedral coordination sphere about the chromium center and a *cis* geometry. This conclusion was confirmed by an X-ray crystal structure determination (Figure 4, Table 5). The struc-

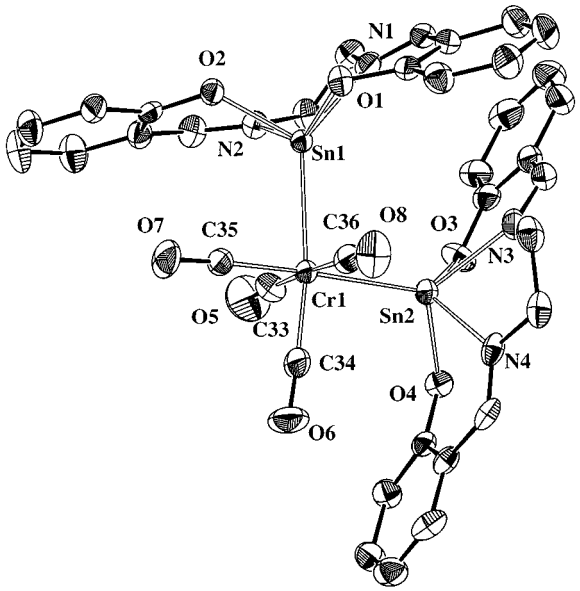
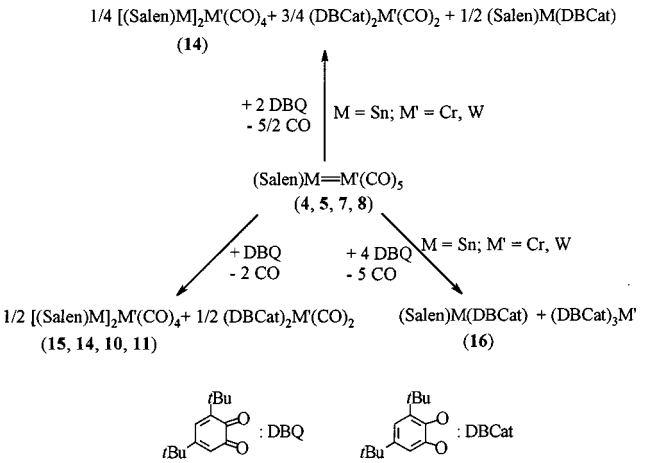


Figure 4. Solid-state structure and atom numbering scheme of $\{[(salen)Sn]_2{=}Cr(CO)_4\} \cdot 3\,(CHCl_3)$ (**14**); solvent molecules have been omitted for the sake of clarity

Table 5. Selected bond lengths [Å] and angles [deg] in **14**

Distances		Angles	
Sn(1)–Cr(1)	2.568(1)	O(1)–Sn(1)–O(2)	82.08(11)
Sn(1)–O(1)	2.085(3)	O(1)–Sn(1)–N(1)	97.34(11)
Sn(1)–O(2)	2.057(3)	O(1)–Sn(1)–N(2)	137.73(13)
Sn(1)–N(2)	2.262(3)	O(2)–Sn(1)–N(1)	107.84(12)
Sn(1)–N(1)	2.288(4)	O(2)–Sn(1)–N(2)	79.49(12)
Sn(2)–Cr(1)	2.555(1)	N(1)–Sn(1)–N(2)	70.68(13)
Sn(2)–O(3)	2.071(3)	O(3)–Sn(2)–O(4)	79.48(12)
Sn(2)–O(4)	2.071(3)	O(3)–Sn(2)–N(3)	81.32(14)
Sn(2)–N(3)	2.255(4)	O(3)–Sn(2)–N(4)	125.70(13)
Sn(2)–N(4)	2.293(4)	O(4)–Sn(2)–N(3)	124.12(13)
Cr(1)–C(33)	1.875(5)	O(4)–Sn(2)–N(4)	79.80(12)
Cr(1)–C(34)	1.833(5)	N(3)–Sn(2)–N(4)	70.34(15)
Cr(1)–C(35)	1.831(5)	Sn(1)–Cr(1)–Sn(2)	96.97(3)
Cr(1)–C(36)	1.875(5)		

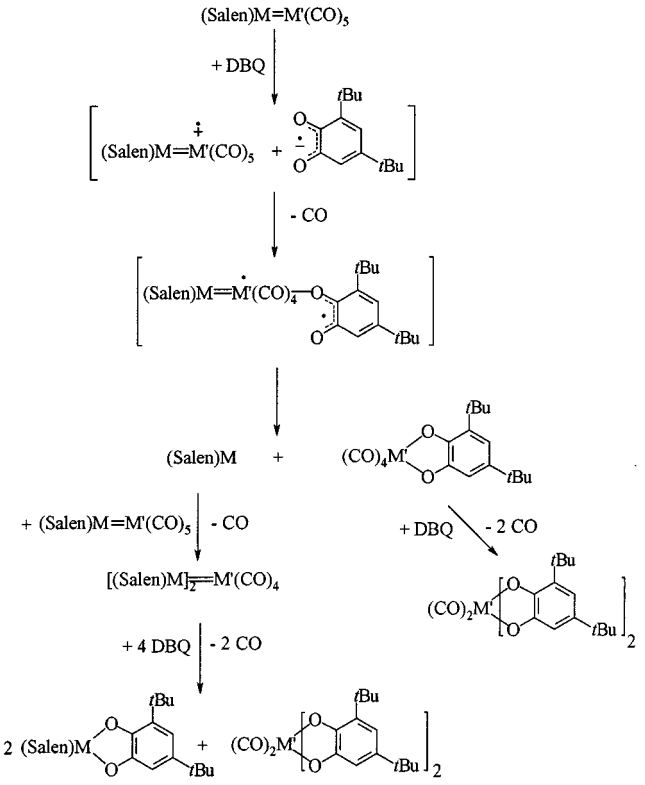


Scheme 7

ture shows similarities to that of **11**; the two *cis*-stannanediyl fragments (salen)Sn, in which the tin atoms show distorted square-pyramidal geometries, are bonded to a $Cr(CO)_4$ fragment with an octahedral environment about the chromium atom. The Cr–Sn distances [2.555(1) and 2.568(1) Å] are indicative of double-bond character in the Cr–Sn unit.

Complexes **4**, **5**, **7**, and **8** were found to react similarly with equimolar amounts of 3,5-di-*tert*-butyl-1,2-benzoquinone (DBQ), leading to **15**, **14**, **10**, and **11**, respectively, along with the $M'(CO)_2(DBCat)_2$ complexes (Scheme 7).

This reaction is consistent with a mechanism involving initial interaction of the quinone with the transition metal atom causing labilization of the M–M′ bond as a result of decreased π-back-bonding (this effect is amplified by chelate ring formation as in the case of the reaction of diphos). The resulting (salen)M ligand then primarily reacts with $(salen)M{=}M'(CO)_5$, leading to the bis-(divalent species)–transition metal complexes $[(salen)M]_2{=}M'(CO)_4$ rather than with the quinone to give the corresponding catecholate **16** (Scheme 8). Supporting evidence for this explanation was obtained by studying the relative reactivities of (salen)Sn towards coordination to the transition metal in $(salen)Sn{=}Cr(CO)_5$ and towards addition to the quinone. Starting with a 1:1:1 mixture of (salen)Sn/DBQ/$(salen)Sn{=}Cr(CO)_5$, the distannylene–chromium complex $[(salen)Sn]_2{=}Cr(CO)_4$ was by far the favored product (ratio 97:3). No evidence of a stable semiquinone intermediate was observed in this reaction. Using two equivalents of 3,5-di-*tert*-butyl-1,2-benzoquinone in addition to the disubstituted complexes, we observed substantial formation of the previously characterized (salen)Sn^{II}-3,5-di-*tert*-butyl-1,2-benzoquinone adduct **16**.[15]



Scheme 8

Conclusion

Several new stable mono- and *cis*-disubstituted Group 14 metal(II)–chromium and tungsten carbonyl complexes have been prepared and their reactivities towards phosphane and 3,5-di-*tert*-butyl-1,2-benzoquinone have been studied. Physicochemical and structural studies have shown that the Group 14 metal resides in a five-coordinate environment.

The Sn–M′ bond lengths observed in the tin complexes are shorter than the typical single-bond lengths and are among the shortest ever observed (in particular the Sn–Cr bond). This indicates that in these complexes, in spite of N→M intramolecular coordination, the divalent species (salen)M behave as σ-donors with π-acceptor properties. These results underline the influence of the stabilizing ligand (bound to the Group 14 element) on the magnitude of the M=M bonding interaction. In short, the (salen)Sn group, with its square-pyramidal geometry, seems to favor the π interaction between the Group 14 element and the chromium or tungsten atom.

Substitution of one CO group has been observed upon reaction with PPh_3. Interestingly, reactions with diphos and 3,5-di-*tert*-butyl-1,2-benzoquinone have been found to lead to the corresponding distannylene metal carbonyl complexes; displacement of the (salen)Sn ligand seems to be the key step in such reactions.

Experimental Section

General: All manipulations were performed under inert atmospheres of nitrogen or argon using standard Schlenk and high-vacuum-line techniques. Dry, oxygen-free solvents were employed throughout. All solvents were distilled from sodium benzophenone or P_2O_5 prior to use. ^{1}H-NMR spectra were recorded on a Bruker AC 80 spectrometer operating at 80 MHz (chemical shifts are reported in ppm relative to internal Me_4Si); ^{13}C-NMR spectra were recorded on an AC 200 spectrometer; the multiplicities of the ^{13}C-NMR signals were determined by the APT technique. ^{1}H-decoupled ^{119}Sn-NMR spectra were recorded on Bruker AC 200 or 400 instruments (chemical shifts are reported in ppm relative to external Me_4Sn). Mass spectra were obtained under electron impact (EI) or chemical ionization (CH_4) conditions at 70 eV and 30 eV, respectively using Hewlett Packard 5989 and Nermag R10-10H spectrometers. IR spectra were recorded on a Perkin–Elmer 1600 FT-IR spectrophotometer. Irradiations were carried out at room temperature using a low-pressure immersion lamp in a quartz glass immersion tube. Molecular weight determinations were carried out with a custom-built apparatus. Melting points (uncorrected) were obtained on a Leitz Biomed hot-plate microscope apparatus. Elemental analyses (C, H, N) were performed at the Microanalysis Laboratory of the Ecole Nationale Supérieure de Chimie de Toulouse.

X-ray Measurements of 5, 8, 11, and 14: Crystal data for all the structures are presented in Table 6. All data were collected at T = 173 K using an oil-coated shock-cooled crystal[25] in each case on

Table 6. Crystallographic data for compounds (salen)Sn=Cr(CO)$_5$ (**5**), (salen)Sn=W(CO)$_5$ (**8**), {[(salen)Sn]$_2$=W(CO)$_4$} · 3 (CHCl$_3$) (**11**), and {[(salen)Sn]$_2$=Cr(CO)$_4$} · 3 (CHCl$_3$) (**14**)

	5	**8**	**11**	**14**
formula	$C_{21}H_{14}CrN_2O_7Sn$	$C_{21}H_{14}N_2O_7SnW$	$C_{39}H_{31}Cl_9N_4O_8Sn_2W$	$C_{39}H_{31}Cl_9N_4O_8Sn_2Cr$
M_T	577.03	708.88	1423.96	1292.11
T [K]	173(2)	173(2)	173(2)	173(2)
crystal system	monoclinic	monoclinic	monoclinic	monoclinic
space group	$P2_1/c$	$P2_1/n$	$C2/c$	$C2/c$
a [Å]	12.213(2)	7.018(1)	22.456(4)	22.437(2)
b [Å]	16.257(3)	14.692(2)	23.240(3)	23.048(3)
c [Å]	11.691(2)	20.821(3)	18.636(3)	18.335(2)
α [°]	90	90	90	90
β [°]	115.24(2)	91.44(2)	96.38(2)	96.08(1)
γ [°]	90	90	90	90
V (Å^3)	2099.6(6)	2146.1(5)	9665(3)	9428.2(18)
Z	4	4	8	8
ρ_{calcd} [Mg/m^3]	1.825	2.194	1.957	1.821
cryst. size [mm]	0.4 × 0.4 × 0.1	0.5 × 0.3 × 0.2	0.6 × 0.5 × 0.5	0.5 × 0.3 × 0.1
μ [mm^{-1}]	1.754	6.566	3.950	1.842
F(000)	1136	1336	5472	5072
$2\varphi_{max}$ [°]	46	48	46	48
refl. collected	15265	16882	38119	38584
indep. refl.	2962	3409	6889	7500
R_{int}	0.0687	0.0426	0.0514	0.0679
absorption correct.	numerical	numerical	numerical	numerical
T_{min}, T_{max}	0.678/0.830	0.219/0.491	0.307/0.603	0.607/0.798
parameters	289	289	640	676
R [$I > 2\sigma(I)$]	0.0468	0.0220	0.0273	0.0294
$wR2$[a] (all data)	0.1086	0.0561	0.0691	0.0618
$(\Delta/\rho)_{min}$ [e.Å^{-3}]	–0.820	–0.702	–0.718	–0.596
$(\Delta/\rho)_{max}$ [e.Å^{-3}]	1.645	0.720	1.238	0.737

[a] $wR2 = \{[\Sigma w(F_c^2 - F_o^2)^2]/[\Sigma w(F_o^2)^2\}^{1/2}$.

a Stoe-IPDS diffractometer employing Mo-K_α (λ = 0.71073 Å) radiation. The structures were solved by direct methods by means of SHELXS-97[26] and refined with all data on F^2 using SHELXL-97.[27] All non-hydrogen atoms were refined anisotropically. Hydrogen atoms were placed in geometrically ideal positions and refined using a riding model. Selected bond lengths and angles in **5**, **8**, **11**, and **14** are presented in tables 2, 3, 4, and 5, respectively. Crystallographic data (excluding structure factors) for the structures reported in this paper have been deposited with the Cambridge Crystallographic Data Centre as supplementary publication nos. CCDC-136101 (**5**), 136102 (**8**), 136103 (**11**), and 136104 (**14**). Copies of the data can be obtained free of charge on application to the CCDC, 12 Union Road, Cambridge CB2 1EZ, U.K. [Fax: (internat.) +44 (0)1223/336033; E-mail: deposit@ccdc.cam.ac.uk].

Synthesis of (salen)Ge=Cr(CO)$_5$ (4). – Procedure 1: A mixture of (salen)Ge[15b] (0.51 g, 1.50 mmol) and Cr(CO)$_6$ (0.33 g, 1.50 mmol) in THF (50 mL) was irradiated for 2 h, during which a red color developed. The solvent was then removed under reduced pressure and the residual solid was treated with pentane. The resulting suspension was filtered and the collected solid was dried in vacuo to afford **4** (0.64 g, 80%) as an orange powder.

Procedure 2: A solution of Cr(CO)$_6$ (0.33 g, 1.50 mmol) in THF (30 mL) was irradiated for 1.5 h. The solution was then purged of CO by passing a stream of nitrogen through it for 15 min., and then a suspension of (salen)Ge (0.51 g, 1.50 mmol) in THF (20 mL) was added. Complex **4** (0.65 g, 83%) was obtained following the same work-up procedure as outlined above; m.p. 280–285 °C (dec.). – ^{1}H NMR (CDCl$_3$): δ = 3.90 (m, 4 H, CH$_2$), 6.50–7.80 (m, 8 H, Ar), 8.32 (s, 2 H, CH=N). – ^{13}C NMR (CDCl$_3$): δ = 59.83 (CH$_2$), 117.03 (CH$_{Ar}$), 118.60 (C$_q$), 118.78 (CH$_{Ar}$), 131.60 (CH$_{Ar}$), 132.49 (CH$_{Ar}$), 161.08 (C$_q$–O), 167.88 (CH=N), 217.08 (C=O *trans*), 218.41 (C=O), 222.47 (C=O), 224.62 (C=O). – IR (Nujol, KBr): $\nu_{C=N}$ 1630; ν_{CO} 1910, 1970, 2047 cm^{-1}. – MS (EI, 70 eV): *m*/*z* = 532 [M$^{+\cdot}$], 504 [M – CO]$^+$, 476 [M – 2 CO]$^+$, 448 [M – 3 CO]$^+$, 420 [M – 4 CO]$^+$, 392 [M – 5 CO]$^+$. – $C_{21}H_{14}CrGeN_2O_7$ (531.94): calcd. C 47.37, H 2.65, N 5.26; found C 47.58, H 2.70, N 5.10.

Synthesis of (salen)Sn=Cr(CO)$_5$ (5). – Procedure 1: A mixture of (salen)Sn[15b] (0.26 g, 0.67 mmol) and Cr(CO)$_6$ (0.15 g, 0.67 mmol) in THF (50 mL) was irradiated for 2 h, during which a red color developed. After removal of the solvent, the crude product was treated with pentane and the resulting suspension was filtered. Crystallization of the collected solid from chloroform afforded **5** (0.31 g, 80%) as red-orange crystals.

Procedure 2: Following a procedure similar to that described for **4**, compound **5** (0.30 g, 83%) was obtained from (salen)Sn (0.24 g, 0.62 mmol) and Cr(CO)$_5$THF (0.17 g, 0.62 mmol); m.p. 270–280 °C (dec.). – ^{1}H NMR ([D$_6$]DMSO): δ = 4.01 (m, 4 H, CH$_2$), 6.50–7.50 (m, 8 H, Ar), 8.42 (s, 2 H, CH=N). – ^{13}C NMR ([D$_6$]DMSO): δ = 52.86 (CH$_2$), 117.77 (CH$_{Ar}$), 118.97 (C$_q$), 122.32 (CH$_{Ar}$), 134.58 (CH$_{Ar}$), 135.90 (CH$_{Ar}$), 165.65 (C$_q$–O), 169.41 (CH=N), 218.54 (C=O), 230 (C=O). – ^{119}Sn{^{1}H} NMR ([D$_6$]DMSO): δ = –149.5. – IR (Nujol, KBr): $\nu_{C=N}$ 1638; ν_{CO} 1917, 1978, 2047 cm^{-1}. – MS (EI, 70 eV): *m*/*z* = 438 [M – 5 CO]$^+$. – $C_{21}H_{14}CrN_2O_7Sn$ (577.92): calcd. C 43.60, H 2.44, N 4.85; found C 43.71, H 2.50, N 4.90.

Synthesis of (salen)Pb=Cr(CO)$_5$ (6): To a suspension of (salen)Pb[15b] (0.15 g, 0.32 mmol) in THF (30 mL) a solution of Cr(CO)$_5$ · THF (0.09 g, 0.32 mmol) in THF (20 mL) was added dropwise. The reaction mixture was stirred at room temperature for 1 h and then the solvent was evaporated under reduced pressure. The residual maroon-orange solid was washed with pentane and dried to afford **6** (0.15 g, 70%); m.p. > 300 °C (dec.). – ^{1}H NMR

([D$_6$]DMSO): δ = 3.80 (m, 4 H, CH$_2$), 6.20–7.40 (m, 8 H, Ar), 8.24 (s, 2 H, CH=N). – IR (Nujol, KBr): $\nu_{C=N}$ 1620; ν_{CO} 1915, 1976, 2048 cm^{-1}. – $C_{21}H_{14}CrN_2O_7Pb$ (665.99): calcd. C 37.84, H 2.12, N 4.21; found C 38.01, H 2.20, N 4.03.

Synthesis of (salen)Ge=W(CO)$_5$ (7): A solution of W(CO)$_5$ · THF (0.15 g, 0.35 mmol) in THF (30 mL) was added dropwise to a suspension of (salen)Ge (0.12 g, 0.35 mmol) in THF (20 mL) and the resulting mixture was stirred at room temperature for 1 h. The solvent was then removed in vacuo and the residual orange solid was washed with pentane. Filtration of the washings and drying of the collected solid gave **7** (0.22 g, 92%) in the form of orange crystals; m.p. 260–270 °C (dec.). – ^{1}H NMR (CDCl$_3$): δ = 3.93 (m, 4 H, CH$_2$), 6.72–7.60 (m, 8 H, Ar), 8.25 (s, 2 H, CH=N). – ^{13}C NMR (CDCl$_3$): δ = 57.25 (CH$_2$), 57.40 (CH$_2$), 118.74 (CH$_{Ar}$), 121.00 (CH$_{Ar}$), 131.87 (CH$_{Ar}$), 133.11 (CH$_{Ar}$), 134.70 (CH$_{Ar}$), 135.22 (CH$_{Ar}$), 138.29 (CH$_{Ar}$), 139.85 (CH$_{Ar}$), 160.92 (C$_q$–O), 167.98 (CH=N), 168.78 (CH=N), 196.37 (C=O), 198.92 (C=O). – IR (Nujol, KBr): $\nu_{C=N}$ 1620; ν_{CO} 1916, 1972, 2067 cm^{-1}. – MS (EI, 70 eV): *m/z* = 662 [M$^{+\cdot}$], 634 [M – CO]$^+$, 608 [M – 2 CO]$^+$, 580 [M – 3 CO]$^+$, 522 [M – 5 CO]$^+$. – $C_{21}H_{14}GeN_2O_7W$ (663.95): calcd. C 37.95, H 2.13, N 4.22; found C 38.20, H 2.29, N 4.10.

Synthesis of (salen)Sn=W(CO)$_5$ (8): A suspension of (salen)Sn (0.11 g, 0.28 mmol) in THF (20 mL) was added dropwise to a solution of W(CO)$_5$ · THF (0.12 g, 0.28 mmol) in the same solvent. The reaction mixture was stirred for a further 30 min, during which an orange color developed. The volatiles were then removed in vacuo and the residual solid product was washed with pentane and purified by crystallization from chloroform to give **8** (0.18 g, 92%) in the form of yellow crystals; m.p. 280–285 °C (dec.). – ^{1}H NMR ([D$_6$]DMSO): δ = 3.99 (m, 4 H, CH$_2$), 6.70–7.00 (m, 8 H, Ar), 8.73 (s, 2 H, CH=N). – ^{13}C NMR ([D$_6$]DMSO): δ = 52.71 (CH$_2$), 117.75 (CH$_{Ar}$), 118.87 (C$_q$), 122.32 (CH$_{Ar}$), 134.55 (CH$_{Ar}$), 135.83 (CH$_{Ar}$), 165.50 (C$_q$–O), 166.99 (CH=N), 197.06 (C=O), 201.16 (C=O). – ^{119}Sn{^{1}H} NMR ([D$_6$]DMSO): δ = –328 ($^2J_{Sn-W}$ = 1458 Hz). – IR (Nujol, KBr): $\nu_{C=N}$ 1641; ν_{CO} 1913, 1977, 2063 cm^{-1}. – MS (EI, 70 eV): *m/z* = 568 [M – 5 CO]$^+$. – $C_{21}H_{14}N_2O_7SnW$ (709.93): calcd. C 35.50, H 1.99, N 3.94; found C 35.70, H 2.12, N 4.00.

Synthesis of (salen)Pb=W(CO)$_5$ (9): In a similar manner, reaction of (salen)Pb (0.15 g, 0.32 mmol) with W(CO)$_5$ · THF (0.13 g, 0.32 mmol) afforded **9** (0.20 g, 79%); m.p. > 300 °C (dec.). – ^{1}H NMR ([D$_6$]DMSO): δ = 3.87 (s, 4 H, CH$_2$), 6.30–7.30 (m, 8 H, Ar), 8.27 (s, 2 H, CH=N). – IR (Nujol, KBr): $\nu_{C=N}$ 1630; ν_{CO} 1914, 1970, 2060 cm^{-1}. – $C_{21}H_{14}N_2O_7PbW$ (798.00): calcd. C 31.58, H 1.77, N 3.51; found C 31.64, H 1.92, N 3.30.

Synthesis of *cis*-[(salen)Ge]$_2$=W(CO)$_4$ (10). – Procedure 1: A mixture of (salen)Ge (0.12 g, 0.36 mmol) and W(CO)$_6$ (0.13 g, 0.36 mmol) in THF (50 mL) was irradiated for 3 h, during which a red-orange color developed. After removal of the solvent, the crude product was washed with pentane and dried to afford a mixture of **10** (85%*) and **7** (15%*) as a red-maroon powder (* relative %).

Procedure 2: A mixture of (salen)Ge (0.25 g, 0.73 mmol) and W(CO)$_6$ (0.13 g, 0.36 mmol) in THF (50 mL) was irradiated for 2.5 h, during which the solution became orange. After removal of the solvent, the crude product was washed with pentane and dried to afford pure **10** (0.65 g, 92%) as an orange powder.

Procedure 3: A mixture of **7** (0.48 g, 0.73 mmol) and (salen)Ge (0.25 g, 0.73 mmol) in THF (50 mL) was irradiated for 4 h. After removal of the solvent, the residue was washed with pentane, the washings were filtered, and the collected solid was dried to give pure **10** (0.62 g, 87%) as orange powder; m.p. 230–240 °C (dec.). – ^{1}H NMR (CDCl$_3$): δ = 3.93 (m, 8 H, CH$_2$), 6.50–7.50 (m, 16 H, Ar), 8.17 (s, 2 H, CH=N). – ^{13}C NMR (CDCl$_3$): δ = 59.79 (CH$_2$), 117.00 (CH$_{Ar}$), 116.43 (C$_q$), 117.10 (CH$_{Ar}$), 131.55 (CH$_{Ar}$), 132.45 (CH$_{Ar}$), 160.91 (C$_q$–O), 166.56 (CH=N), 196.08 (C=O), 196.38 (C=O). – IR (Nujol, KBr): $\nu_{C=N}$ 1620; ν_{CO} 1892, 1980, 2009, 2060 cm^{-1}. – MS (EI, 70 eV): *m/z* = 608 [M – Ge(salen) – 2 CO]$^+$, 522 [M – Ge(salen) – 5 CO]$^+$. – $C_{36}H_{28}Ge_2N_4O_8W$ (975.98): calcd. C 44.26, H 2.89, N 5.74; found C 44.50, H 2.95, N 5.68.

Synthesis of [(salen)Sn]$_2$=W(CO)$_4$ (11). – Procedure 1: A mixture of (salen)Sn (0.27 g, 0.70 mmol) and W(CO)$_6$ (0.25 g, 0.70 mmol) in THF (50 mL) was irradiated for 3 h, during which a red-maroon color developed. The volatiles were then removed in vacuo and the crude product was washed with pentane and dried to afford a mixture of **11** (90%*) and **8** (10%*) as a yellow-orange powder (* relative % as determined by ^{1}H-NMR).

Procedure 2: A mixture of (salen)Sn (0.27 g, 0.70 mmol) and W(CO)$_6$ (0.13 g, 0.35 mmol) in THF (50 mL) was irradiated for 3 h, during which the solution turned pale-orange. After removal of the solvent, the crude product was washed with pentane and dried to afford pure **11** (0.69 g, 92%) as an orange powder.

Procedure 3: A mixture of (salen)Sn (0.55 g, 1.40 mmol) and W(CO)$_6$ (0.26 g, 0.70 mmol) in THF (50 mL) was irradiated for 4 h, during which the solution again turned pale-orange. After removal of the solvent, the crude product was washed with pentane and dried to afford an orange powder consisting of a 30:70 *cis*/*trans* (**11/11′**) mixture, which was characterized by ^{1}H-, ^{13}C-, and ^{119}Sn-NMR and IR spectroscopy.

Procedure 4: As Procedure 2, but after irradiation for 8 h, a 50:50 mixture of **11/11′** was obtained from (salen)Sn (0.55 g, 1.40 mmol) and W(CO)$_6$ (0.26 g, 0.70 mmol).

Procedure 5: According to the previous procedure, pure **11** was obtained from (salen)Sn (0.27 g, 0.70 mmol) and **8** (0.49 g, 0.70 mmol); yield: 0.67 g, 90%. Crystallization from CHCl$_3$ gave **11** · 3 (CHCl$_3$) as orange crystals.

11 (*cis*): m.p. 250–260 °C (dec.). – ^{1}H NMR ([D$_6$]DMSO): δ = 3.78 (s, 4 H, CH$_2$), 6.50–7.50 (m, 16 H, Ar), 8.43 (s, 2 H, CH=N). – ^{13}C NMR ([D$_6$]DMSO): δ = 52.50 (CH$_2$), 116.94 (CH$_{Ar}$), 118.96 (C$_q$), 122.17 (CH$_{Ar}$), 134.37 (CH$_{Ar}$), 135.37 (CH$_{Ar}$), 165.69 (C$_q$–O), 169.32 (CH=N), 202.19 (C=O), 207.30 (C=O). – ^{119}Sn{^{1}H} NMR ([D$_6$]DMSO): δ = –348 ($^2J_{Sn-W}$ = 1456 Hz). – IR (Nujol, KBr): $\nu_{C=N}$ 1638; ν_{CO} 1902, 1929, 1954, 2062 cm^{-1}. – MS (EI, 70 eV): *m/z* = 568 [(salen)SnW$^+$]. – $C_{36}H_{28}N_4O_8Sn_2W$ (1067.94): calcd. C 40.45, H 2.64, N 5.24; found C 40.61, H 2.72, N 5.14.

11′ (*trans*): ^{1}H NMR ([D$_6$]DMSO): δ = 3.82 (s, 4 H, CH$_2$), 6.30–7.50 (m, 16 H, Ar), 8.19 (s, 2 H, CH=N). – ^{13}C NMR ([D$_6$]DMSO): δ = 51.96 (CH$_2$), 115.97 (CH$_{Ar}$), 118.96 (C$_q$), 122.06 (CH$_{Ar}$), 131.56 (CH$_{Ar}$), 132.25 (CH$_{Ar}$), 134.17 (CH$_{Ar}$), 165.82 (C$_q$–O), 167.99 (CH=N), 211.23 (C=O). – ^{119}Sn{^{1}H} NMR ([D$_6$]DMSO): δ = –374. – IR (Nujol, KBr): $\nu_{C=N}$ 1640; ν_{CO} 1999 cm^{-1}.

Synthesis of *cis*-[(salen)Pb]$_2$=W(CO)$_4$ (12). – Procedure 1: A mixture of (salen)Pb (0.15 g, 0.32 mmol) and W(CO)$_6$ (0.11 g, 0.32 mmol) in THF (50 mL) was irradiated for 3 h, during which a maroon color developed. After filtration, the volatiles were removed under reduced pressure. The residue was washed with pentane and dried in vacuo to afford a mixture of **12** (70%*) and **9** (30%*) as a red-brown powder (* relative % as determined by ^{1}H-NMR).

Procedure 2: A mixture of (salen)Pb (0.54 g, 1.14 mmol) and W(CO)$_6$ (0.20 g, 0.57 mmol) in THF (50 mL) was irradiated for 2.5 h, during which the solution turned maroon. After work-up as described in the previous procedure, **12** (0.51 g, 72%) was obtained as an orange powder.

Procedure 3: According to the previous procedure, pure **12** (0.42 g, 60%) was obtained from (salen)Pb (0.27 g, 0.57 mmol) and **9** (0.45 g, 0.57 mmol); m.p. > 300 °C (dec.). – ^{1}H NMR ([D$_6$]DMSO): δ = 4.07 (s, 4 H, CH$_2$), 6.25–7.35 (m, 8 H, Ar), 8.03 (s, 2 H, CH=N). – IR (Nujol, KBr): $\nu_{C=N}$ 1625; ν_{CO} 1906, 1930, 2015, 2060 cm^{-1}. – $C_{36}H_{28}N_4O_8Pb_2W$ (1244.09): calcd. C 34.72, H 2.27, N 4.50; found C 34.90, H 2.40, N 4.32.

Reactions of 4 and 7 with Iodine: To a solution of **4** (0.05 g, 0.10 mmol) or **7** (0.06 g, 0.10 mmol) in DMSO (10 mL) was added iodine (0.03 g, 0.10 mmol). CO was immediately evolved and the solution turned orange. The mixture was stirred at room temperature for 3 h. Subsequent analysis by ^{1}H- and ^{13}C-NMR and by mass spectroscopy revealed that (salen)GeI$_2$ had been produced.[15b]

Reactions of 5 and 8 with Iodine: According to the same procedure as above, reactions of **5** (0.06 g, 0.10 mmol) and **8** (0.07 g, 0.10 mmol) with iodine (0.03 g, 0.10 mmol) afforded (salen)SnI$_2$.[15b]

Synthesis of *cis*-(salen)Sn=W(CO)$_4$(PPh$_3$) (13): A solution of **8** (0.22 g, 0.31 mmol) and triphenylphosphane (0.08 g, 0.31 mmol) in THF (30 mL) was irradiated for 1.5 h. The solvent was then removed in vacuo affording a maroon-orange powder, which was washed with pentane and dried under reduced pressure to give **13** (0.26 g, 90%); m.p. 250–260 °C (dec.). – ^{1}H NMR ([D$_6$]DMSO): δ = 3.77 (s, 4 H, CH$_2$), 6.72–7.60 (m, 23 H, Ar), 8.44 (s, 2 H, CH=N). – ^{13}C NMR ([D$_6$]DMSO): δ = 57.95 (CH$_2$), 122.37 (CH$_{Ar}$), 124.33 (C$_q$), 127.62 (CH$_{Ar}$), 134.18 (CH$_{Ar}$), 134.40 (CH$_{Ar}$), 134.48 (CH$_{Ar}$), 137.41 (CH$_{Ar}$), 137.91 (CH$_{Ar}$), 139.82 (CH$_{Ar}$), 140.80 (CH$_{Ar}$), 171.16 (C$_q$–O), 174.77 (CH=N), 202.34 (C=O), 202.53 (C=O), 207.64 (C=O), 212.74. – ^{119}Sn{^{1}H} NMR ([D$_6$]DMSO): δ = –347.5 (d, $^3J_{Sn-P}$ = 2088 Hz). – ^{31}P{^{1}H} NMR ([D$_6$]DMSO): δ = –16.2 ($^3J_{Sn-P}$= 2088 Hz). – IR (Nujol, KBr): $\nu_{C=N}$ 1639; ν_{CO} 1876, 1977, 2011, 2055 cm^{-1}. – MS (EI, 70 eV): *m*/*z* = 502 [Ph$_3$PW(CO)$_2$]$^+$, 446 [Ph$_3$PW]$^+$, 386 [(salen)Sn]$^{+\cdot}$. – $C_{38}H_{29}N_2O_6PSnW$ (944.03): calcd. C 48.30, H 3.10, N 2.97; found C 48.70, H 3.30, N 2.90.

Reaction of 5 with 1,2-Bis(diphenylphosphanyl)ethane: A solution of **5** (0.22 g, 0.38 mmol) in THF (30 mL) containing 1,2-bis(diphenylphosphanyl)ethane (0.15 g, 0.38 mmol) was irradiated for 2.5 h. The solvent was then removed in vacuo, affording a maroon-orange powder, which was washed with pentane and dried under reduced pressure to give a mixture of **14** and (DPPE)Cr(CO)$_4$. The product was characterized by ^{1}H-, ^{31}P-, and ^{119}Sn-NMR and by IR. Crystallization from CHCl$_3$ gave orange crystals of **14** · 3 (CHCl$_3$). – ^{1}H NMR (CDCl$_3$): δ = 3.99 (m, 4 H, CH$_2$), 6.60–7.50 (m, 10 H, Ar), 8.10 (s, 2 H, CH=N). – ^{13}C NMR (CDCl$_3$): δ = 48.70 (CH$_2$), 118.56 (CH$_{Ar}$), 119.22 (Cq$_{Ar}$), 123.98 (CH$_{Ar}$), 134.37 (CH$_{Ar}$), 136.64 (CH$_{Ar}$), 164.03 (C$_q$–O), 166.66 (C$_q$–O), 170.12 (CH=N), 211.68 (CO *cis*), 218.43 (CO *cis*), 224.99 (CO *trans*). – ^{119}Sn{^{1}H} NMR (CDCl$_3$): δ = –144. – IR (CDCl$_3$, KBr): $\nu_{C=N}$ 1621, ν_{CO} 1931, 1982, 2052 cm^{-1}. – $C_{36}H_{28}CrN_4O_8Sn_2$ (935.93): calcd. C 46.16, H 3.02, N 5.98; found C 46.40, H 3.15, N 5.54.

Reaction of 8 with 1,2-Bis(diphenylphosphanyl)ethane: A solution of **8** (0.22 g, 0.31 mmol) in THF (30 mL) containing 1,2-bis(diphenylphosphanyl)ethane (0.13 g, 0.31 mmol) was irradiated for 2.5 h. The solvent was then removed in vacuo, affording a maroon-orange powder, which was washed with pentane and dried under reduced pressure to give a mixture of **11** and (DPPE)W(CO)$_4$. The product was characterized by ^{1}H-, ^{31}P-, and ^{119}Sn-NMR and by IR.

Reaction of 5 with One Equivalent of DBQ: A mixture of **5** (0.03 g, 0.05 mmol) and DBQ (0.01 g, 0.05 mmol) was dissolved in CHCl$_3$ (5 mL). The color of the solution immediately darkened. The volatiles were subsequently removed under reduced pressure. The crude product was washed with pentane and dried in vacuo to afford **14** (0.02 g, 85%)

Reaction of 7 with One Equivalent of DBQ: A mixture of **7** (0.05 g, 0.10 mmol) and DBQ (0.02 g, 0.10 mmol) was dissolved in CHCl$_3$ (5 mL). The color of the solution immediately darkened and evolution of CO was observed. After stirring for 8 h, the volatiles were removed in vacuo. The crude product was washed with pentane and dried in vacuo to afford **10** (0.04 g, 82%).

Reaction of 8 with One Equivalent of DBQ: A mixture of **8** (0.09 g, 0.12 mmol) and DBQ (0.03 g, 0.12 mmol) was dissolved in CHCl$_3$ (5 mL). The solution immediately turned dark-red. The volatiles were subsequently removed under reduced pressure and the crude product was washed with pentane and dried in vacuo to afford **11** (0.05 g, 78%).

Reaction of 8 with Two Equivalents of DBQ: A mixture of **8** (0.09 g, 0.12 mmol) and DBQ (0.06 g, 0.24 mmol) was dissolved in CHCl$_3$ (5 mL). The solution immediately turned intensely red. The volatiles were subsequently removed under reduced pressure. The crude product was washed with pentane and dried in vacuo to afford a mixture of **11** and **16** (ratio 1:2, as determined by ^{1}H-NMR).

Reaction of 8 with Four Equivalents of DBQ: A mixture of **8** (0.09 g, 0.12 mmol) and DBQ (0.12 g, 0.48 mmol) was dissolved in CHCl$_3$ (10 mL). The solution immediately turned red. The volatiles were subsequently removed in vacuo. The crude product was washed with pentane and dried in vacuo to afford **16** (0.06 g, 83%)

Reaction of 4 with DBQ: A mixture of **4** (0.03 g, 0.05 mmol) and DBQ (0.01 g, 0.05 mmol) was dissolved in CHCl$_3$ (5 mL). The color of the solution immediately darkened and the volatiles were subsequently removed in vacuo. The crude product was washed with pentane and dried in vacuo to afford **15**. – ^{1}H NMR (CDCl$_3$): δ = 4.21 (m, 4 H, CH$_2$), 6.40–7.70 (m, 10 H, Ar), 8.40 (s, 2 H, CH=N). – ^{13}C NMR (CDCl$_3$): δ = 54.50 (CH$_2$), 119.09 (CH$_{Ar}$), 120.89 (Cq$_{Ar}$), 120.13 (CH$_{Ar}$), 134.03 (CH$_{Ar}$), 136.54 (CH$_{Ar}$), 164.20 (C$_q$–O), 161.81 (C$_q$–O), 172.2 (CH=N), 211.70 (CO cis), 217.23 (CO). – $C_{36}H_{28}N_4O_8Ge_2Cr$ (843.97): calcd. C 51.19, H 3.34, N 6.64; found C 51.40, H 3.51, N 6.23.

[1] E. Brooks, H. R. Cros, *J. Organomet. Chem. Rev. A* **1970**, *6*, 227.
[2] M. Veith, O. Recktenwald, *Top. Curr. Chem.* **1982**, *104*, 1.
[3] W. Petz, *Chem. Rev.* **1986**, *86*, 1019.
[4] M. F. Lappert, R. S. Rowe, *Coord. Chem. Rev.* **1990**, *100*, 267.
[5] J. T. B. H. Jastrzebski, G. Van Koten, *Intramolecular Coordination in Organotin Chemistry; Advances in Organometallic Chemistry* **1993**, *35*, 241.
[6] H. Handwerker, C. Leis, R. Probst, P. Bissinger, A. Grohmann, P. Kiprof, E. Herdtweck, J. Blümel, N. Auner, C. Zybill, *Organometallics* **1993**, *12*, 2162.
[7] S. L. Ellis, P. B. Hitchcock, S. A. Holmes, M. F. Lappert, M. J. Slade, *J. Organomet. Chem.* **1993**, *444*, 95.
[8] D. A. Atwood, V. O. Atwood, A. H. Cowley, H. R. Gobran, *Inorg. Chem.* **1993**, *32*, 4671.
[9] N. Tokitoh, K. Manmaru, R. Okazaki, *Organometallics* **1994**, *13*, 167.
[10] M. Weidenbruch, A. Stilter, J. Schlaefke, K. Peters, H. G. von Schnering, *J. Organomet. Chem.* **1995**, *501*, 67.
[11] M. Weidenbruch, A. Stilter, K. Peters, H. G. von Schnering, *Z. Anorg. Allg. Chem.* **1996**, *622*, 534; M. Weidenbruch, A. Stilter, K. Peters, H. G. von Schnering, *Chem. Ber.* **1996**, *129*, 1565.
[12] H. Lang, M. Weinmann, W. Fresch, M. Büchner, B. Schiemenz, *Chem. Commun.* **1996**, 1299.
[13] M. Weidenbruch, A. Stilter, W. Saak, K. Peters, H. G. von Schnering, *J. Organomet. Chem.* **1998**, *560*, 125.
[14] J. Barrau, G. Rima, T. El Amraoui, *J. Organomet. Chem.* **1998**, *570*, 163.

[15] [15a] D. Agustin, G. Rima, J. Barrau, *Main Group Met. Chem.* **1997**, *20*, 791. – [15b] D. Agustin, G. Rima, H. Gornitzka, J. Barrau, *J. Organomet. Chem.* **1999**, *592*, 1.
[16] P. B. Hitchcock, M. F. Lappert, P. Pye, *J. Chem. Soc., Dalton Trans.* **1977**, 2160.
[17] A. L. Balch, E. D. Oram, *Organometallics* **1998**, *7*, 155.
[18] T. J. Marks, *J. Am. Chem. Soc.* **1971**, *93*, 7090.
[19] C. E. Holloway, M. Melnik, *Main Group Met. Chem.* **1998**, *21*, 371.
[20] M. S. Holt, W. L. Wilson, J. H. Nelson, *Chem. Rev.* **1989**, *89*, 11.
[21] K. Jurkschat, A. Tzchach, J. Meunier-Piret, M. Van Meersche, *J. Organomet. Chem.* **1988**, *349*, 143.
[22] J. T. B. H. Jastrzebski, P. A. Van der Schaaf, J. Boersma, G. Van Koten, D. Heijdenrijk, K. Goubitz, D. J. A. de Ridder, *J. Organomet. Chem.* **1989**, *367*, 55.
[23] H. P. Abicht, K. Jurkschat, A. Tzchach, K. Peters, E.-M. Peters, H. G. von Schnering, *J. Organomet. Chem*. **1987**, *326*, 357.
[24] P. Jutzi, B. Hampel, K. Stroppel, C. Krüger, K. Angermund, P. Hofmann, *Chem. Ber.* **1985**, *118*, 2789.
[25] D. Stalke, *Chem. Soc. Rev.* **1998**, *27*, 171.
[26] G. M. Sheldrick, *SHELXS-97*, Program for Crystal Structure Solution, Universität Göttingen, **1997**.
[27] G. M. Sheldrick, *SHELXL-97*, Program for Crystal Structure Refinement, Universität Göttingen, **1997**.

Received July 16, 1999
[I99248]

Synthesis, Spectroscopic and Structural Characterization of New Ru^{II} and Ru^{III} Complexes Containing Triazole- and Thiadiazole-Type Ligands

Marina Biagini Cingi,[a] Maurizio Lanfranchi,*[a] Maria Angela Pellinghelli,[a] and Matteo Tegoni[a]

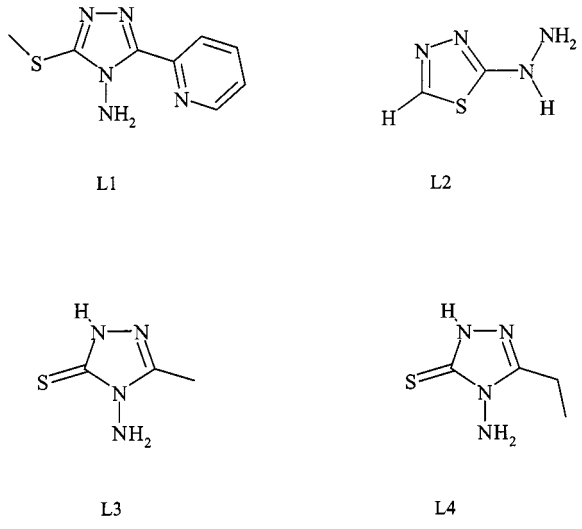
Keywords: Ruthenium / *s*-Triazole / *s*-Triazoline / Oxidations / Crystal structure

The chemical behavior of triazole, thiadiazole, and triazoline derivatives of thiocarbonohydrazide towards *cis*-$[RuCl_2(DMSO)_4]$ (**2**) was studied. Reaction of 4-amino-5-methylthio-3-(2-pyridyl)-1,2,4-triazole (L1) with **2** gave two diastereomeric complexes, *trans,cis*-$[RuCl_2(DMSO)_2(L1)]$ (**3**) and chiral *cis,cis*-$[RuCl_2(DMSO)_2(L1)]$ (**4**). Reaction of **2** with 2-(2-formylhydrazino)-1,3,4-thiadiazole in MeOH gave the complex *trans,cis*-$[RuCl_2(DMSO)_2(L2)]$ (**5**) with concomitant deformylation of the starting ligand. The process was catalyzed by Ru^{II} in very low yield. Synthesis of the Ru complexes of 4-amino-3-methyl-1,2,4-Δ^2-triazoline-5-thione (L3) and 4-amino-3-ethyl-1,2,4-Δ^2-triazoline-5-thione (L4) resulted in an interesting oxidation of the metal promoted by DMSO. Reaction of **2** with these ligands in a 6 N HCl solution led to the isolation of the complexes *mer*-$[RuCl_3(DMSO)(L3)]\cdot 1/2\ H_2O$ (**6**) and *mer*-$[RuCl_3(DMSO)(L4)]\cdot 1/2\ H_2O$ (**7**). The complex *mer*-$[RuCl_3(DMSO)(L4)]\cdot CH_3COOH\cdot H_2O$ (**7'**) was obtained by recrystallization of **7** from ethyl acetate. The complexes **6**, **7**, and **7'** were highly stable in HCl solutions and acetone but not in neutral aqueous solution. To the best of our knowledge this is the first report of Ru^{III} complexes with an N–N–C–S chelating system.

Introduction

Cyclic derivatives of thiocarbonohydrazide and carbonohydrazide are a class of compounds rarely investigated from a structural point of view. They can exhibit analgesic properties[1] and some transition metal complexes have been studied for their pharmacological properties (such as fungicides, acaricides, insecticides, nematicides).[2] The 4-amino-5-thioxo-*s*-triazoline derivatives are known for their capability of complexing a number of soft metal ions.[3] They are also used in fixer compositions for silver halide photographic materials, as corrosion inhibitors, for rapid gravimetric determination of copper, and selective microevaluation of Au^{III}, Tl^{I}, and Ag^{I}.[4] We have previously prepared and structurally characterized complexes of Cu^{II}, Cu^{I}, $Cu^{II/I}$, and Au^{I} with 4-amino-3-methyl-1,2,4-Δ^2-triazoline-5-thione, which may be considered a good stabilizing agent of the low oxidation state.[3,5] This ligand is a weak monoprotic acid which exhibits thione-thiol tautomerism[5] in solution and undergoes an interesting desulfuration reaction promoted by copper(II).[6] In this paper we report our studies on the complexing capability of these ligands towards Ru^{II} and Ru^{III} ions.

Werner-type complexes of ruthenium with cyclic derivatives of thiocarbonohydrazide are a new class of compounds that are of interest for the development of transition metal coordination chemistry. The chloride–dimethyl sulfoxide–ruthenium derivatives containing a nitrogen ligand are of great interest for their potential as non-platinum inorganic antitumor drugs.[7] Moreover the N–N–C–S chelating system is similar to that of thiosemicarbazides and thiosemicarbazones, which constitute an important class of *N,S* donor ligands due to their interesting biological properties.[8] The ligands that we have considered are depicted in Scheme 1. In this report we describe the synthesis and the single-crystal X-ray structures of L1 **1**, L1·HCl **1'**, *trans,cis*-$[RuCl_2(DMSO)_2(L1)]$ (**3**), *cis,cis*-$[RuCl_2(DMSO)_2(L1)]$ (**4**), *trans,cis*-$[RuCl_2(DMSO)_2(L2)]$ (**5**), *mer*-$[RuCl_3(DMSO)(L3)]\cdot 1/2H_2O$ (**6**), *mer*-$[RuCl_3(DMSO)(L4)]\cdot 1/2H_2O$ (**7**) and *mer*-$[RuCl_3(DMSO)(L4)]\cdot CH_3COOH\cdot H_2O$ (**7'**).



Scheme 1. Structures of the ligands

Results and Discussion

Synthesis and Characterization

All complexing reactions were studied using *cis*-$[RuCl_2(DMSO)_4]$ (**2**). The ligands we have considered can

[a] Dipartimento di Chimica Generale ed Inorganica, Chimica Analitica, Chimica Fisica,
Centro di Studio per la Strutturistica Diffrattometrica del CNR, Università degli Studi di Parma
Parco Area delle Scienze 17A, I-43100 Parma, Italy
Fax: (internat.) +39(0)521/905557
E-mail: chimic4@ipruniv.cce.unipr.it

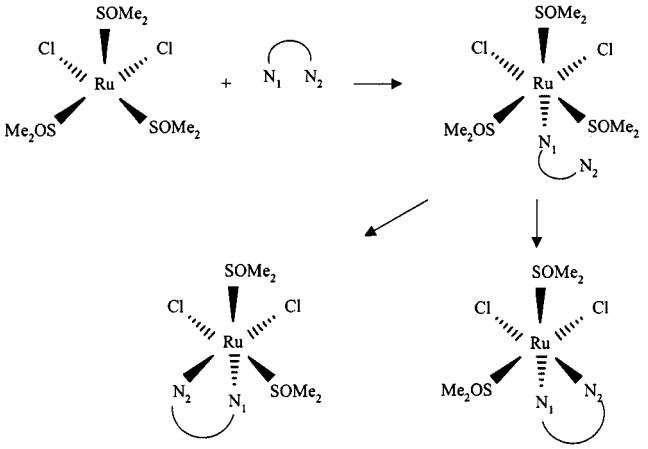
 © WILEY-VCH Verlag GmbH, D-69451 Weinheim, 2000 1434–1948/00/0404–0703 $ 17.50+.50/0

act as monodentate or bidentate *N,N* (L1, L2) or *N,S* (L3, L4) chelating agents; moreover they can interact with the metals through other donating atoms to form polymeric species.[3,5] In L1 the triazole and pyridine fragments are coplanar and can adopt two conformations with the pyridine nitrogen atom on the same side of the exocyclic amine nitrogen atom (**1**) or on the opposite side, as found in **1'**.

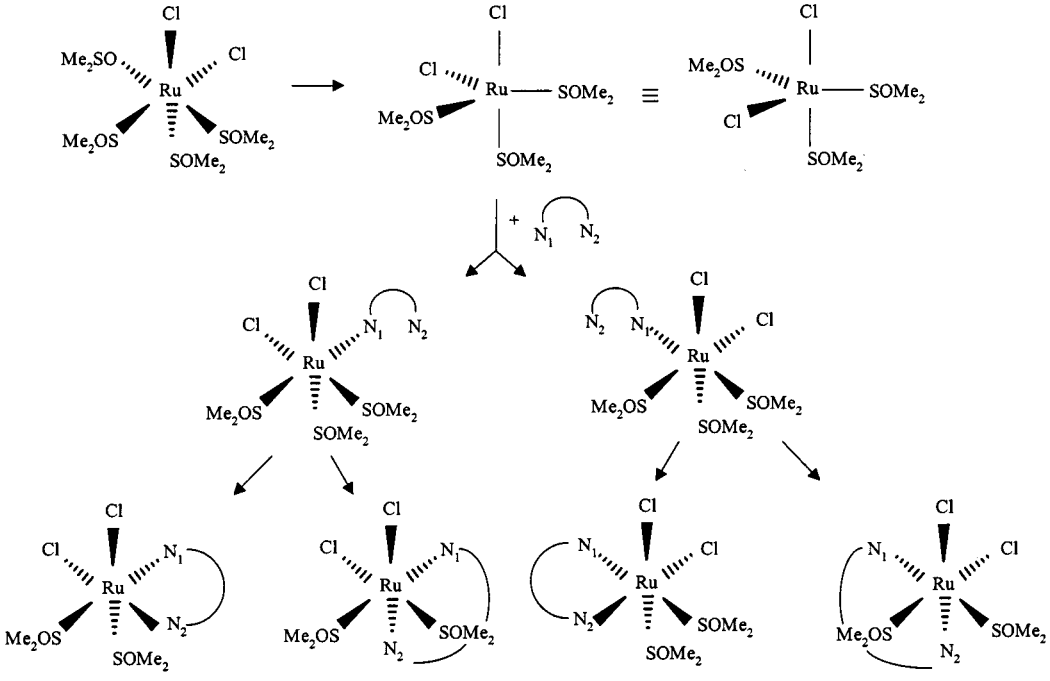
Reaction of **2** with L1 in MeOH produces two diastereomeric complexes, *trans,cis*-[$RuCl_2(DMSO)_2(L1)$] (**3**) and *cis,cis*-[$RuCl_2(DMSO)_2(L1)$] (**4**). The reaction conditions leading to **4** are probably governed by kinetic factors; in fact the complex was obtained only once despite many attempts that led invariably to the formation of **3**. It is well-known that Ru^{II}, a low spin d^6 system, undergoes substitution by a dissociative mechanism.[9] The leaving group in complex **2** is the *O*-coordinated DMSO molecule that lies *trans* to *S*-coordinated DMSO.[10] For steric reasons the trigonal bipyramidal intermediate (TBP) (Scheme 2) will lead to the formation of 100% *cis* isomer **4**, as is also the case of a square pyramid intermediate (SP) (Scheme 3). To explain the formation of **3** we hypothesize a rearrangement of the intermediates TBP or SP to the more stable TBP with three DMSO ligands in equatorial positions, leading to 100% of the *trans*-isomer **3** (Scheme 4). To correctly explain the formation of **4** it is necessary to hypothesize that the first binding of the ligand L1 proceeds through the pyridine nitrogen atom, due to the greater basicity of this atom than that of the triazole [see structure of L1·HCl (**1'**)] even if basicity and nucleophilicity are not equivalent concepts.

Reaction of **2** with 2-(2-formylhydrazino)-1,3,4-thiadiazole in MeOH forms the complex *trans,cis*-[$RuCl_2(DMSO)_2(L2)$] (**5**) in which the ligand is deformylated. This process is catalyzed by Ru^{II} and the yield is very low. A similar deformylation process of [2-(2-formylhydrazino)-1,3,4-thiadiazole] occurs in a 12 M solution of NH_4OH only if Zn^{2+} is added. In an acidic medium rearrangement of the ligand to form 4-amino-1,2,4-Δ^2-triazoline-5-thione was observed. The *trans,cis* isomer may arise through the same mechanism proposed for **3**. In all three complexes **3**, **4**, **5** the *S*-coordinated DMSO molecules are oriented in the same manner with the oxygen atoms lying on an equatorial plane.

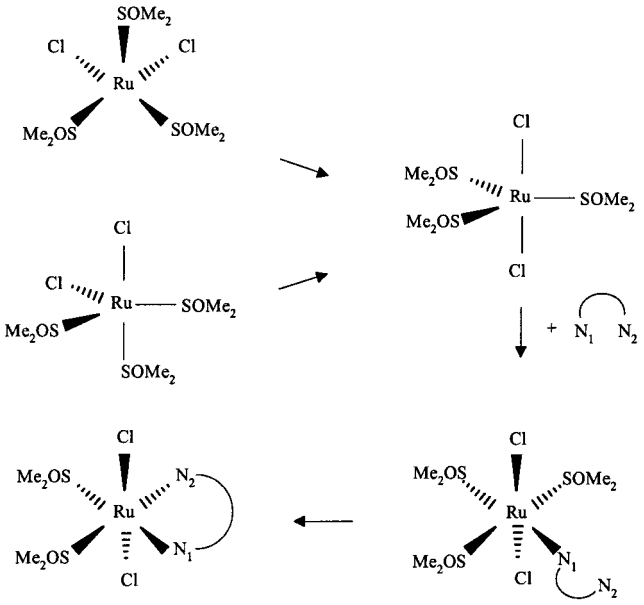
The synthesis of the Ru complexes with L3 and L4 as ligands revealed an interesting oxidative process of the metal. In fact upon treatment of **2** with these ligands in a 6 N HCl solution, Ru^{III} complexes were obtained. This mech-



Scheme 3. Proposed formation pathway of **4** via the SP intermediate



Scheme 2. Proposed formation pathway of **4** via the TBP intermediate



Scheme 4. Proposed formation pathway of **3**

anism does not involve molecular oxygen, as the reaction also proceeds under nitrogen atmosphere. It is well-known that L3 and L4 can act as reducing agents, so the oxidative process has to be due to the presence of DMSO. The oxidizing properties of DMSO in acidic solutions were tested in the presence of Ru^{II}, leading us to hypothesize an equilibrium:

$$2\,Ru^{II} + (CH_3)_2SO + 2\,H^+ \rightleftarrows 2\,Ru^{III} + (CH_3)_2S + H_2O$$

Dimethylsulfide complexes have been synthesized from acidic DMSO solutions,[11] and a similar equilibrium is probably involved in our reaction. In order to detect the dimethylsulfide produced from the reduction of DMSO in our system, the gases evolved during the reaction were allowed to flow through ethylene glycol for 8 h. This solution was analyzed by gas chromatography, showing an appropriate amount of $(CH_3)_2S$. The mechanism we propose involves the formation of a complex having formula $[RuCl_2(DMSO)_2(L)]$ (L = L3 or L4) in which the metal atom undergoes an oxidation process as shown in Scheme 5.

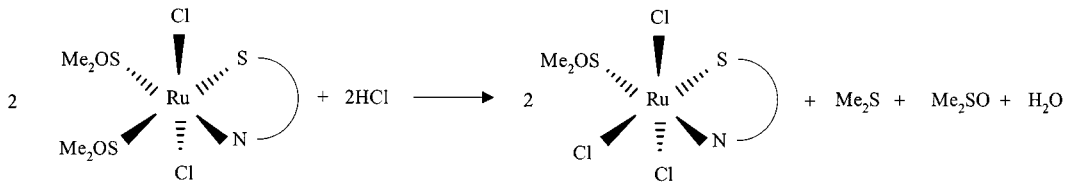
It is probable that during the oxidation, a DMSO molecule coordinated to one ruthenium atom can act as an *S,O* bridging ligand to a second Ru^{II} complex. A simultaneous inner sphere electron transfer mechanism of one electron from each Ru^{II} atom to the bridging DMSO can then occur. The complexes **6**, **7**, and **7'** are not stable in neutral aqueous solutions, whereas they are highly stable in HCl solutions and acetone. Conductivity experiments performed in acetone did not show any increase in molar conductivity, but when a small amount of water was added, the molar conductivity increased dramatically over three hours.

All three complexes synthesized and structurally characterized show a *mer* configuration and to the best of our knowledge this is the first report of Ru^{III} complexes with an N–N–C–S chelating system.

Spectroscopic Investigations

The ^{1}H-NMR spectrum of the complex **3** shows the CH_3 signal of L1 at $\delta = 2.75$, whereas the methyl groups of the two coordinated DMSO ligands give a signal at $\delta = 3.17$. This is in accordance with the assignments for free L1, and of DMSO coordinated to Ru^{II}.[10] The aromatic region shows three multiplets integrating for 1 H in the range $\delta = 7.73$–8.75. The mean shift of these signals with respect to free L1 is about 0.5 ppm, with the exception of the hydrogen atom *ortho* to the pyridine nitrogen atom which gives a signal at $\delta = 10.48$ as compared to $\delta = 8.70$ in free L1. The exocyclic amino group gives signal at $\delta = 6.84$ showing a shift towards higher field of about 0.3 ppm.

Several spectra of the paramagnetic complexes **6** and **7** were collected in different solvents in order to assign the signals and collect data regarding substitution of the DMSO ligand. A spectrum of both complexes in $[D_6]$acetone/$[D_6]$DMSO was collected between $\delta = +50$ and -50 although all the signals were observed between $\delta = +10$ and -12. In some ruthenium(III) complexes,[7] the signal of the methyl groups of the sulfur-coordinated DMSO is observed around $\delta = -14$ as a broad peak. A similar signal near $\delta = -11$ is present in the spectra of **6** and **7**. The signals of the hydrogen atoms of the coordinated amino groups were not located. This is probably due to both the paramagnetic shift and line broadening caused by the presence of the nearby paramagnetic centre. In the complex **6** the signal of the methyl group of L3 was observed as a broad peak at around $\delta = 6.4$. After 14 days this signal became narrower and shifted to $\delta = 5.64$; in the free ligand L3 the methyl group gives a signal at $\delta = 2.23$. In a freshly prepared sample of the analogous complex **7** the signal of the methylene group was observed at $\delta = 5.01$ and neither a shift nor a narrowing of the peak were observed after 16 days, while the signal of the methyl group was observed at $\delta = -0.12$. The signals of these two groups in free L4 are at $\delta = 2.63$ and $\delta = 1.17$, respectively. We have no explanation for the shift of the methyl group signal in the spectrum of **6**, but another important feature arises from these spectra. As the



Scheme 5

distance between the alkyl group and the triazole ring increases, the chemical shifts of the alkyl groups become more similar to those observed in the free ligand. This is probably due to the presence of a non-zero spin density on the triazole ring as a result of back-bonding from the metal to the sulfurous ligand.[12] This may also be the reason why the thioamide hydrogen atom cannot be located between $\delta = +50$ and -50. It should be noted that in the case of the complex **6** the solvent used was a mixture of acetone and DMSO. After 14 days at nearly 300 K no substitution of the coordinated DMSO was observed, strongly suggesting that the ruthenium complex is substitutionally inert. To identify the signal of the acidic thioamide hydrogen atom, a small portion of D_2O was added to the sample of **6** and a spectrum was collected immediately but no change was observed. A week after the addition of D_2O to the sample, the colour of the solution had changed from green to pale yellow. A new spectrum was collected between $\delta = +50$ and -50 but no paramagnetic peaks were observed.

Conductivity Measurements

The complexes **6** and **7** were synthesized in aqueous solution, with the pH maintained around 0 using highly concentrated hydrochloric acid. NMR experiments revealed that when dissolved in anhydrous solvents such as acetone or DMSO, the complex is quite stable for several days. On addition of small portions of water, a dramatic change in the nature of the complex occurs (Figure 1).

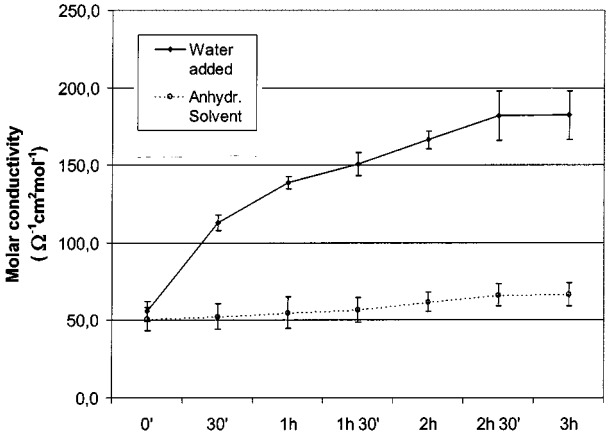


Figure 1. Conductivity measurements of **6**; measurements were made using a $1.016 \cdot 10^{-4}$ M solution of $[RuCl_3(DMSO)(L3)] \cdot 1/2\ H_2O$ in acetone; to follow the reaction, water (0.2 mL) was added to the complex solution (2 mL)

X-ray Structure Analysis

The crystal structures of the ligand L1 (**1**) and of its hydrochloride derivative **1'** are depicted in Figure 2 and Figure 3, respectively. Selected bond lengths and angles are provided in Table 1. The triazole and pyridine rings are essentially coplanar in both compounds {τ[N(1)–C(2)–C(3)–N(5)] = 169.3(2)° for **1** and –0.1(5)° for **1'**} but the molec-

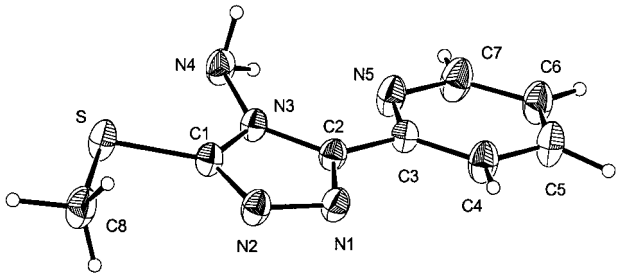


Figure 2. Molecular structure and numbering scheme of compound **1**; thermal ellipsoids are drawn at the 30% probability level

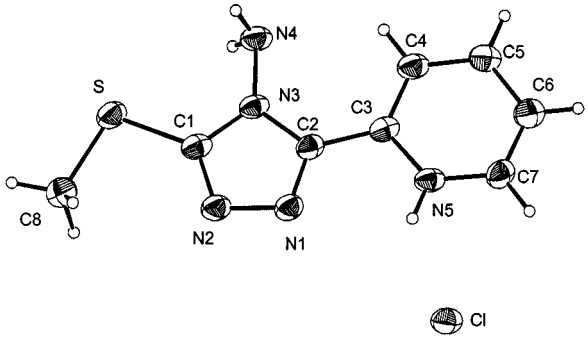


Figure 3. Molecular structure and numbering scheme of compound **1'**; thermal ellipsoids are drawn at the 30% probability level

Table 1. Selected bond lengths [Å] and angles [°] for **1**, **1'**, **3**, and **4**

	1	**1'**	**3**	**4**
Ru–N(1)			2.066(5)	2.032(4)
Ru–N(5)			2.163(6)	2.135(4)
Ru–S(3)			2.257(2)	2.260(1)
Ru–S(2)			2.270(2)	2.243(1)
Ru–Cl(2)			2.390(2)	2.412(1)
Ru–Cl(1)			2.413(2)	2.454(1)
S–C(1)	1.744(3)	1.735(3)	1.726(8)	1.735(5)
S–C(8)	1.798(4)	1.797(3)	1.804(9)	1.756(9)
N(1)–C(2)	1.308(3)	1.312(4)	1.326(8)	1.314(6)
N(1)–N(2)	1.395(3)	1.395(3)	1.400(7)	1.391(6)
N(2)–C(1)	1.310(4)	1.316(4)	1.310(8)	1.310(7)
N(3)–C(1)	1.352(3)	1.367(4)	1.378(8)	1.375(7)
N(3)–C(2)	1.370(3)	1.368(4)	1.372(8)	1.356(6)
N(3)–N(4)	1.411(3)	1.413(4)	1.411(7)	1.412(6)
N(5)–C(7)	1.324(4)	1.326(4)	1.324(8)	1.347(6)
N(5)–C(3)	1.330(5)	1.369(4)	1.360(8)	1.356(6)
N(1)–Ru–N(5)			75.8(2)	76.71(16)
N(1)–Ru–S(3)			92.59(17)	95.60(12)
N(5)–Ru–S(3)			166.50(16)	170.71(11)
N(1)–Ru–S(2)			172.86(16)	92.81(13)
N(5)–Ru–S(2)			99.46(17)	91.08(11)
N(1)–Ru–Cl(2)			93.46(15)	170.74(12)
N(5)–Ru–Cl(2)			84.82(16)	94.07(11)
N(1)–Ru–Cl(1)			85.34(15)	89.49(13)
N(5)–Ru–Cl(1)			89.14(15)	85.60(11)
C(2)–N(1)–N(2)	107.8(2)	107.9(3)	109.7(6)	109.4(4)
C(1)–N(2)–N(1)	106.5(2)	106.5(2)	105.9(6)	105.4(4)
C(1)–N(3)–C(2)	105.5(2)	105.1(3)	106.8(6)	105.6(4)
C(1)–N(3)–N(4)	123.2(2)	128.3(3)	121.3(7)	128.6(4)
C(2)–N(3)–N(4)	131.2(2)	126.6(3)	131.9(7)	125.7(4)
C(3)–N(5)–C(7)	117.7(2)	123.8(3)	116.7(7)	117.8(4)

ules are in different conformations. In both compounds the methyl carbon atoms are synperiplanar with respect to the imine nitrogen atom N(2) (τ[N(2)–C(1)–S–C(8)] = –1.8(2) and –4.2(3)° for **1** and **1'**, respectively). The pyramidal exocyclic amine nitrogen atom N(4) shows the lone pair oriented towards the sulfur atom in **1** and towards the hydrogen atom of the pyridine C(4) atom in **1'**. The most significant differences concerning the bond angles are the C(2)–N(3)–N(4) [131.2(2) and 126.6(3)° for **1** and **1'**, respectively] and the C(2)–C(3)–C(4) [119.1(3)° (**1**), 128.5(3)° (**1'**)] angles, probably due to the different conformations of the amine hydrogen atoms. The larger endocyclic N(5) angle in **1'** is due to the protonation of the pyridine nitrogen atom [123.8(3)° (**1'**), 117.7(2)° (**1**)].

The two Ru^{II} octahedral constitutional isomers *trans*,*cis*-(**3**) and *cis*,*cis*-[$RuCl_2(DMSO)_2$(L1)] (**4**) are shown in Figure 4 and Figure 5, respectively. Selected bond lengths and angles are reported in Table 1. In both complexes the ligand, with N(1) and N(5) synperiplanar, acts as *N*,*N* chelating agent. The torsion angles τ[N(1)–C(2)–C(3)–N(5)] [–8.6(8) and –6.6(8)° for **3** and **4**, respectively] are slightly larger than in **1'**; the S–C_{Me} bond lies on the triazole ring plane in **3** whereas it is out of the plane in **4** due to intramolecular steric hindrance {τ[N(2)–C(1)–S(1)–C(8)] = –2.2(8) and –26.6(7)°}. The conformation of the N(4) amine nitrogen atom in **3** is similar to that found in **1** while in **4** it is similar to that found in **1'**, with the same interaction C(4)–H···N(4) and same trend in the C(2)–N(3)–N(4) bond angles [131.9(7)° (**3**) and 125.7(4)° (**4**)]. In both diastereomeric complexes the DMSO molecules show S=O bonds oriented in the same direction and lying roughly on a coordination plane [N(1)N(5)S(2)S(3)Ru (**3**), N(5)S(2)S(3)-Cl(1)Ru (**4**)] which consequently nearly bisects the C–S–C DMSO bond angles. The *cis*,*cis* isomer is chiral but owing to the centrosymmetric space group both enantiomers are present in the crystal. The OC-6–32-*C* enantiomer is depicted in Figure 5. In both complexes the Ru–N(1) bond lengths involving the imine triazole nitrogen atoms are shorter than the Ru–N(5) ones involving the pyridine N atoms [2.066(5), 2.163(6) Å for **3** and 2.032(4), 2.135(4) Å for **4**, respectively]. The distance Ru–N(1) is longer in **3** than in **4** due to the *trans* influence of the DMSO–*S* ligand.

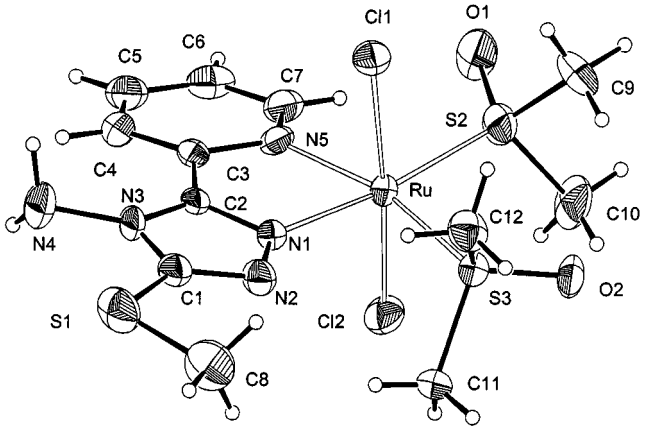


Figure 4. Molecular structure and numbering scheme of complex**3**; thermal ellipsoids are drawn at the 30% probability level

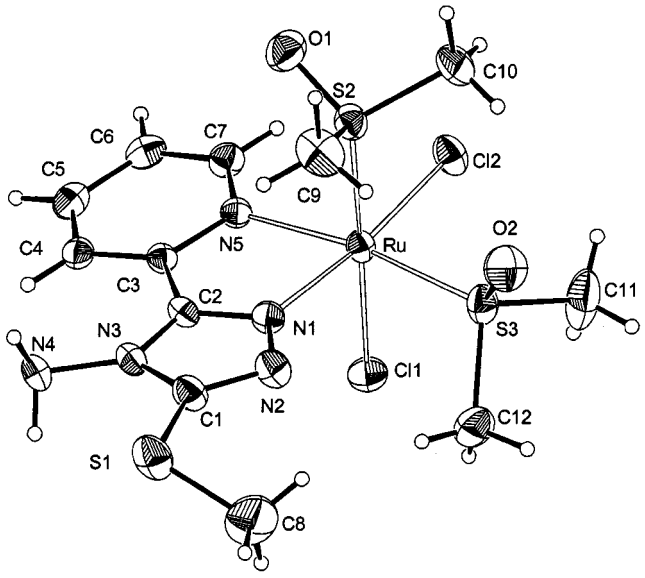


Figure 5. Molecular structure and numbering scheme of complex **4**; thermal ellipsoids are drawn at the 30% probability level

In the octahedral Ru^{II} complex *trans*,*cis*-[$RuCl_2$-$(DMSO)_2$(L2)] (**5**) (Figure 6) the 2-hydrazino-1,3,4-thiadiazole ligand L2 binds via the amine N(4) and the imine N(2) nitrogen atoms. The organic moiety and the ruthenium, sulfur, and oxygen atoms of the two DMSO ligands lie on a crystallographic mirror plane, so that the S=O bonds are oriented in exactly the same direction. The Ru–N(4) bond length involving the amine nitrogen atom is slightly longer than the Ru–N(2) one involving the imine N atom [2.130(6), 2.096(7) Å]. In this case the bite angle [79.3(3)°] is larger than in **3** [75.8(2)°] and **4** [76.7(2)°]. In the coordinated organic ligand the N(3)–C(1) bond length [1.315(12) Å] reveals a high degree of conjugation of the N(3) π orbitals with the heterocyclic ring and consequently a decrease of the double-bond character of the C(1)–N(2) [1.354(11) Å] bond.

In the complexes of Ru^{III} *mer*-[$RuCl_3$(DMSO)-(L3)]·1/2 H_2O (**6**), *mer*-[$RuCl_3$(DMSO)(L4)]·1/2 H_2O (**7**), and *mer*-[$RuCl_3$(DMSO)(L4)]·CH_3COOH·H_2O (**7'**) the 3-substituted 4-amino-Δ^{2-}1,2,4-triazoline-5-thione molecules act as *N*,*S* chelating ligands and the DMSO ligands are *trans* to the amine nitrogen atoms with the S=O bonds in the plane of the chelating ligands and oriented towards the thione S atoms. All complexes show a pseudo-C_s symmetry (Figure 7, Figure 8) except for the C(4) methyl carbon atoms of the ethyl groups in **7** and **7'**. In the three Ru^{III} complexes the Ru–$S(2)_{DMSO}$ bond lengths are ca. 0.05 Å shorter than the Ru–S(1) ones and the Ru–N(4) bond lengths *trans* to S(2) are equivalent (Table 2). The equatorial Ru–Cl(3) bonds are longer than the axial Ru–Cl ones due to the S-*trans* influence of the thione groups. The Ru–S(1) bond length in the three complexes shows some variability but as the bond strength increases a lengthening of the *trans* Ru–Cl(3) bond is observed [Ru–S(1) = 2.326(3) Å (**7**), 2.319(1) Å (**6**), 2.309(1) Å (**7'**), Ru–Cl(3) = 2.375(3) Å (**7**),

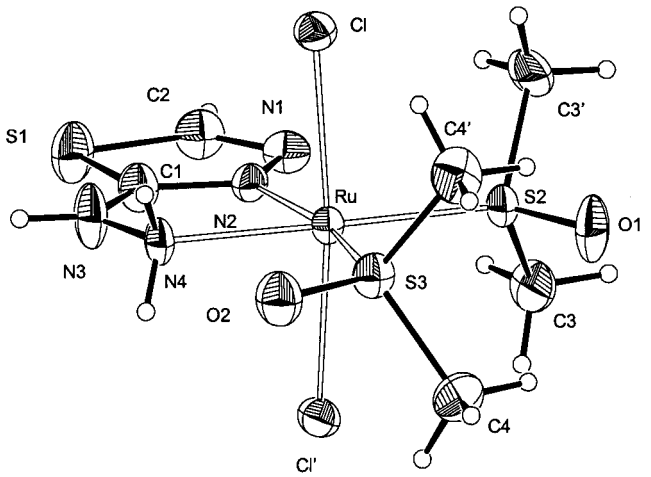


Figure 6. Molecular structure and numbering scheme of complex **5**; thermal ellipsoids are drawn at the 30% probability level; selected bond lengths [Å] and angles [°]: Ru–N(2) 2.096(7), Ru–N(4) 2.130(6), Ru–S(2) 2.242(2), Ru–S(3) 2.253(2), Ru–Cl 2.400(2), S(1)–C(2) 1.702(11), S(1)–C(1) 1.731(11), N(1)–C(2) 1.312(12), N(1)–N(2) 1.355(10), N(2)–C(1) 1.354(11), N(3)–C(1) 1.315(12), N(3)–N(4) 1.413(11); N(2)–Ru–N(4) 79.3(3), N(2)–Ru–S(2) 97.6(2), N(4)–Ru–S(3) 88.3(2), N(2)–Ru–Cl 87.46(4), N(4)–Ru–Cl 87.36(4), C(2)–S(1)–C(1) 86.9(4), C(2)–N(1)–N(2) 109.3(8), C(1)–N(2)–N(1) 114.9(7), C(1)–N(2)–Ru 110.7(6), N(1)–N(2)–Ru 134.4(6), C(1)–N(3)–N(4) 117.1(7), N(3)–N(4)–Ru 110.2(5), N(3)–C(1)–N(2) 122.8(9), N(3)–C(1)–S(1) 125.8(7), N(2)–C(1)–S(1) 111.4(7), N(1)–C(2)–S(1) 117.5(7)

2.386(1) Å (**6**), 2.395(1) Å (**7'**)]. A lengthening of the C(1)–S(1) bonds for the three complexes with respect to the free ligand L3[6] is observed [C(1)–S(1) = 1.705(11), 1.720(6), 1.716(3) and 1.674(6) Å for **7**, **6**, **7'** and L3 respectively]. The coordination alters significantly the double-bond character of the C–S group as is observed to a smaller extent in the copper complexes[3,6] $[CuCl_2(L3)] \cdot H_2O$ [1.693(6), 1.687(6) Å], $[Cu_2Cl_4(L3)]_n \cdot nH_2O$ [1.697(12) Å] and $[Cu_3Cl_5(OH_2)(L3)_2]_n \cdot 2nH_2O$ [1.699(5), 1.694(5) Å].

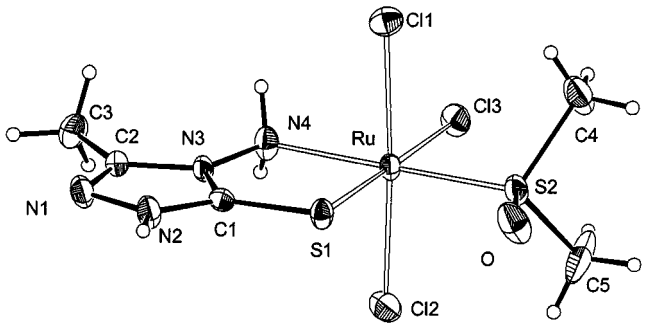


Figure 7. Molecular structure and numbering scheme of complex **6**; the H_2O molecule is omitted for clarity; thermal ellipsoids are drawn at the 30% probability level

To the best of our knowledge the only ruthenium complexes with a neutral ligand and a similar N–N–C–S chelating system are $[(\eta^6\text{-}p\text{-cymene})RuCl(taz)]PF_6$ (taz = 4-amino-2,6-dimethyl-5-oxo-3-thioxo-2,3,4,5-tetrahydro-1,2,4-triazine),[13] $[Ru(HL)(PPh_3)_2Cl]Cl \cdot CH_2Cl_2$ and $[Ru(HL)(PPh_3)(mpi)]Cl_2 \cdot CH_2Cl_2 \cdot 3H_2O$ [HL = methyl 2-pyridyl ketone 4-(4-tolyl)thiosemicarbazone, mpi = methyl(2-pyridyl)methyleneimine],[14] in which the metal has an oxidation state of +2. In the taz complex the C–S distance [1.687(3) Å] supports the double-bond character of the 3-thioxo group[15] and the C–S group is not significantly altered by coordination. In the two HL complexes the C–S bonds, 1.707(6), 1.698(7) Å, are similar to those found in **6**, **7**, and **7'**. In these Ru^{II} cationic complexes the Ru–S bond lengths [2.354(1) Å,[13] 2.386(2), 2.358(2) Å,[14]] are greater than those found in our Ru^{III} complexes, due to the lower oxidation state of the metal.

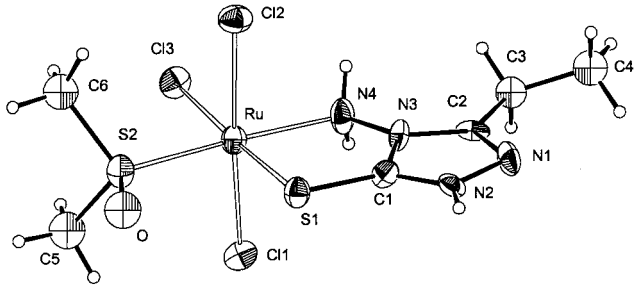


Figure 8. Molecular structure and numbering scheme of complex **7**; the H_2O molecule is omitted for clarity; thermal ellipsoids are drawn at the 30% probability level

Table 2. Selected bond lengths [Å] and angles [°] for **6**, **7**, and **7'**

	6	**7**	**7'**
Ru–N(4)	2.158(5)	2.157(8)	2.162(2)
Ru–S(2)	2.256(1)	2.268(3)	2.267(1)
Ru–S(1)	2.319(1)	2.326(3)	2.309(1)
Ru–Cl(2)	2.353(2)	2.363(3)	2.355(1)
Ru–Cl(1)	2.370(2)	2.368(3)	2.369(1)
Ru–Cl(3)	2.386(1)	2.375(3)	2.395(1)
S(1)–C(1)	1.720(6)	1.705(11)	1.716(3)
N(1)–C(2)	1.287(8)	1.355(11)	1.299(4)
N(1)–N(2)	1.381(7)	1.355(10)	1.381(3)
N(2)–C(1)	1.313(7)	1.313(12)	1.321(4)
N(3)–C(1)	1.334(7)	1.359(12)	1.344(4)
N(3)–C(2)	1.382(10)	1.336(11)	1.392(3)
N(3)–N(4)	1.405(7)	1.411(10)	1.418(3)
N(4)–Ru–S(1)	85.8(1)	86.7(2)	86.96(7)
S(2)–Ru–S(1)	91.09(5)	91.9(1)	90.43(4)
N(4)–Ru–Cl(2)	89.6(2)	89.7(3)	87.14(7)
S(1)–Ru–Cl(2)	90.58(5)	90.4(1)	89.77(3)
N(4)–Ru–Cl(1)	84.9(2)	85.0(3)	88.99(7)
S(1)–Ru–Cl(1)	92.88(5)	91.9(1)	91.04(3)
N(4)–Ru–Cl(3)	92.2(1)	90.5(2)	88.86(7)
C(1)–S(1)–Ru	96.2(2)	96.4(4)	95.8(1)
C(2)–N(1)–N(2)	104.9(5)	103.1(8)	105.3(2)
C(1)–N(2)–N(1)	112.1(5)	114.3(9)	112.2(3)
C(1)–N(3)–C(2)	108.7(5)	109.7(9)	108.7(2)
C(1)–N(3)–N(4)	121.4(5)	123.0(8)	121.6(2)
C(2)–N(3)–N(4)	129.8(5)	126.4(8)	129.6(2)
N(3)–N(4)–Ru	111.9(3)	110.0(5)	110.5(2)

Water molecules of solvation are present in the three Ru^{III} complexes, while in **7'** a free molecule of ethanoic acid cocrystallizes. A broad network of hydrogen bonds is present in every compound structurally characterized.

All Ru complexes display a distorted octahedral coordination and in the *trans*–Cl complexes the axial Cl–Ru–Cl angles [173.95(7)° (**3**), 173.28(9)° (**5**), 173.35(6)° (**6**), 174.13(11)° (**7**), 176.00(3)° (**7'**)] show a significant deviation from linearity forced by the steric hindrance of the DMSO methyl groups. The *trans* Ru–Cl bond lengths in the Ru^{II}

complexes [2.390(2)–2.413(2) Å] compare well with the values found in other *trans*-Cl DMSO Ru^{II} complexes[10,16–21] [2.397(1)–2.432(1) Å]. The lengthening of the Ru–Cl(1) in **4** [2.454(1) Å] reflects the strong *trans* influence of the DMSO ligand, whereas the Ru–Cl(2) bond [2.412(1) Å] *trans* to N(1) agrees with the value found in *cis*,*cis*,*cis*-$[RuCl_2(Me_2SO)_2(py)(Me_3Bzm)]$[22] [2.4148(7) Å] ($Me_3Bzm$ = 1,5,6-trimethylbenzimidazole, py = pyridine). In the Ru^{III} complexes **6**, **7**, **7'**, the *trans* Ru–Cl bond lengths [2.353(2)–2.370(2) Å] are close to the upper limit of the range [2.308(2)–2.366(4) Å] found in other DMSO Ru^{III} complexes.[7,16,23]

Experimental Section

Materials and Instrumentation: Thiocarbonohydrazide, iodomethane, and ruthenium trichloride hydrate were purchased from Aldrich and Fluka. Unless otherwise specified, all reagents and solvents were AR grade and used without further purification. The syntheses of 4-amino-3-methyl-1,2,4-Δ^2-triazoline-5-thione,[24] 4-amino-3-ethyl-1,2,4-Δ^2-triazoline-5-thione,[25] 2-(2-formylhydrazino)-1,3,4-thiadiazole,[25] 4-amino-3-(2-pyridyl)-1,2,4-Δ^2-triazoline-5-thione,[25] and *cis*-dichlorotetrakis(dimethyl sulfoxide)ruthenium(II) [10] (**2**) were performed following reported procedures. – IR spectra were collected on an FT-IR Nicolet 5PC spectrometer using KBr pellets. – ^1H NMR spectra were collected on Bruker WM 300 MHz, AC 300 MHz or AC 100 MHz spectrometers. – Mass spectra were collected on a Finnigan 1020 spectrometer equipped with a MATSSQ 710 quadrupole revealer. – GC analyses were performed with a Carlo Erba MFC 500 equipped with a FID revealer and a CPSIL5CB 100% polysiloxane column (10 m × 0.32 mm, 1.20 μm) (Chrompack, Middleburg, Holland). Helium (purity 99,9%) was used as the carrier gas with a flow rate of 10 mL/min under isothermal conditions (40° C). Elemental analyses were performed using a Carlo Erba Elemental Analyzer EA 1108. – Conductivity measurements were performed using a CRISON microCM 2202 conductimeter equipped with a temperature probe. – Melting points were collected on a Gallenkamp apparatus.

4-Amino-5-methylthio-3-(2-pyridyl)-1,2,4-triazole (1): In a double necked 100 mL round bottomed flask equipped with a condenser NaOH (0.208 g, 5.2 mmol) was dissolved in DMSO (2 mL). A warm solution of 4-amino-3-(2-pyridyl)-1,2,4-Δ^2-triazoline-5-thione (1 g, 5.17 mmol) in DMSO (5 mL) was added dropwise into the flask while stirring. Iodomethane (0.65 mL, 1.48 g, 10.4 mmol) was added dropwise into the flask while stirring and the solution obtained stirred at room temperature for 1.5 h (exothermicity is observed). The solution was added dropwise into water (50 mL) at 0–5 °C. The product was extracted with CH_2Cl_2 (5 × 15 mL), the organic phase washed with water (2 × 15 mL), dried (Na_2SO_4), and concentrated to 1/3 volume under reduced pressure. White crystals of **1** were collected by slow evaporation; the product can also be recrystallized from ethanol. Yield 0.641 g (60%). – m.p. 108–109 °C. – IR (KBr, cm^{-1}): $\tilde{\nu}$ = 3260 (NH_2 asym. str.), 3171 (NH_2 sym. str.), 2923, 1659, 1463, 1420, 1416 (S–CH_3 asym. def.), 1011, 786 (CH_{py} oop def.). – ^1H NMR ([D_6]DMSO): δ = 8.70 (1 H, CH_{py}), 8.07 (1 H, CH_{py}), 8.00 (1 H, CH_{py}), 7.53 (1 H, CH_{py}), 6.55 (2 H, NH_2), 2.65 (3 H, CH_3). – $C_8H_9N_5S$ (207.26): calcd. C 46.36, H 4.38, N 33.79, S 15.47; found C 46.26, H 3.87, N 32.40, S 16.20.

4-Amino-5-methylthio-3-(2-pyridinium)-1,2,4-triazole Chloride (1'): The compound was synthesized by dissolving L1 (0.5 g 2.41 mmol) in a minimum amount of a water:ethanol (1:1) solution. The pH was lowered to ca. 3 by the addition of several drops of ca. 1 N HCl solution. L1' is easily crystallizable as white needles. Yield 0.410 g (70%). – IR (KBr, cm^{-1}): $\tilde{\nu}$ = 3187 (NH_2 str.), 3114 (CH_{py} str.), 1617 (triazole ring def.), 1603, 1541 (NH_2 def.), 1295 (S–CH_3 sym. def.), 1223, 1084, 797 (CH_{py} oop def.), 676 (CH_{py} oop def.), 506. – ^1H NMR ([D_6]DMSO): δ = 8.75 (1 H, CH_{py}), 8.16 (1 H, CH_{py}), 8.03 (1 H, CH_{py}), 7.61 (1 H, CH_{py}), 4.39 (3 H, NH_2 and NH_{py} mediated peak), 2.66 (3 H, CH_3). – $C_8H_{10}ClN_5S$ (297.16): calcd. C 39.42, H 4.16, N 28.73, S 13.15; found C 39.06, H 3.97, N 29.16, S 13.21.

***trans,cis*- (3) and *cis,cis*-Dichlorobis(dimethyl sulfoxide-*S*)(4-amino-5-methylthio-3-(2-pyridyl)-1,2,4-triazole-*N,N'*)ruthenium(II) (4):** The synthesis was performed under nitrogen atmosphere in a three necked 250 mL round bottomed flask equipped with a condenser. **1** (0.064 g, 0.31 mmol) was dissolved in dry methanol (5 mL) and the solution was heated slightly while stirring. A solution of **2** (0.15 g, 0.31 mmol) in dry methanol (10 mL) was added dropwise into the flask and the solution was heated at reflux for 1.5 h. The red-orange solution obtained was poured in a crystallizer and orange crystals of product were collected by slow evaporation. Yield of **3** 0.101 g (60%). – *trans,cis* isomer: IR (KBr, cm^{-1}): $\tilde{\nu}$ = 3273 (NH_2 asym. str.), 3167 (NH_2 sym. str.), 2922 (CH_3 str.), 1620, 1451, 1418 (S–CH_3 asym. def.), 1384, 1092 (S–O DMSO *S*-coord),1069, 1015 (CH_3 DMSO rock),781, 679 (C–S_{DMSO} str.), 426 (Ru–S str.). – ^1H NMR ([D_6]DMSO): δ = 10.48 (1 H, CH_{py}), 8.75 (1 H, CH_{py}), 8.20 (1 H, CH_{py}), 7.73 (1 H, CH_{py}), 6.84 (2 H, NH_2), 3.17 (CH_3 DMSO *S*-coord), 2.75 (3 H, CH_3). – $C_{12}H_{21}Cl_2N_5O_2RuS_3$ (535.49): calcd. C 26.92, H 3.95, N 13.08, S 17.96; found C 27.62, H 4.70, N 12.61, S 17.48. – *cis,cis* isomer: IR (KBr, cm^{-1}): $\tilde{\nu}$ = 3270 (NH_2 asym. str.), 3159 (NH_2 sym. str.), 2919 (CH_3 str.), 1635, 1450, 1411 (S–CH_3 asym. def.), 1096 (S–O DMSO *S*-coord), 1066, 1013 (CH_3 DMSO rock), 780, 678 (C–S_{DMSO} str.), 425 (Ru–S str.). – $C_{12}H_{21}Cl_2N_5O_2RuS_3$ (535.49): calcd. C 26.92, H 3.95, N 13.08, S 17.96; found C 27.37, H 4.24, N 12.76, S 17.63.

***trans,cis*-Dichlorobis(dimethyl sulfoxide-*S*)(2-hydrazino-1,3,4-thiadiazole-*N,N'*)ruthenium(II) (5):** The synthesis was performed under nitrogen atmosphere in a three necked 250 mL round bottomed flask equipped with a condenser. **2** (0.07 g, 0.14 mmol) and 2-(2-formylhydrazino)-1,3,4-thiadiazole (0.041 g, 0.28 mmol) were dissolved in methanol (15 mL) and the solution was heated at reflux while stirring for 1.5 h. The red-orange solution obtained was poured into a crystallizer and red crystals of the product were collected by slow evaporation. Yield 0.012 g (20%). – IR (KBr, cm^{-1}): $\tilde{\nu}$ = 3239 (NH str.), 3180 (NH_2 asym. str.), 3149 (NH_2 sym. str.), 1619 (NH_2 def.), 1216, 1095 (S–O DMSO *S*-coord), 1069, 1013, 687 (C–S_{DMSO} str.), 429 (Ru–S str.). – $C_6H_{16}Cl_2N_4O_2RuS_3$ (444.38): calcd. C 16.21, H 3.62, N 12.60, S 21.64; found C 16.04, H 3.83, N 12.76, S 21.58.

***mer*-Trichloro(dimethyl sulfoxide-*S*)(4-amino-3-methyl-1,2,4-Δ^2-triazoline-5-thione-*N,S*)ruthenium(III) Hemihydrate (6):** In a 100 mL round-bottomed flask, **2** (0.15 g, 0.31 mmol) was added to a suspension of L3 (0.04 g, 0.31 mmol) and HCl (ca. 6 N, 20 mL) while stirring. The mixture was stirred for 0.5 h at room temperature, then the mixture was warmed on a heating plate for 1 h. The green solution obtained was poured into a crystallizer. Dark-green crystals of the product were obtained by slow evaporation. Yield 0.059 g (45%). – IR (KBr, cm^{-1}): $\tilde{\nu}$ = 3449 (OH str.), 3197 (NH str.), 3102 (NH_2 str.), 1610, 1505 (Thioam I), 1124, 1089 (S–O DMSO *S*-coord), 1024, 688 (C–S_{DMSO} str.), 433 (Ru–S str.). – ^1H NMR ([D_6]acetone): δ = 6.4 (br, CH_3), –10.42 (br, CH_3 DMSO *S*-

coord). – $C_5H_{13}Cl_3N_4O_{1.5}RuS_2$ (424.73): calcd. C 14.14, H 3.08, N 13.19, S 15.10; found C 14.32, H 2.83, N 12.83, S 15.30.

***mer*-Trichloro(dimethyl sulfoxide-*S*)(4-amino-3-ethyl-1,2,4-Δ²-triazoline-5-thione-*N,S*)ruthenium(III) Hemihydrate (7):** The procedure was the same as for the synthesis of the previous complex, but using L4 (0.045 g, 0.31 mmol). Green crystals of the product were obtained. Yield 0.061 g (45%). – IR (KBr, cm^{-1}): $\tilde{\nu}$ = 3441 (OH str.), 3194 (NH_2 str.), 1608, 1498 (Thioam I), 1386 (CH_3 rock), 1124 (S–O DMSO *S*-coord), 1029, 684 (C–S_{DMSO} str.), 434 (Ru–S str.) – ^1H NMR ([D_6]acetone): δ = 5.01 (br 2 H, CH_2), –0.12 (3 H, CH_3), –11.15 (br, CH_3 DMSO *S*-coord). – $C_6H_{15}Cl_3N_4O_{1.5}RuS_2$ (438.76): calcd. C 16.43, H 3.45, N 12.77, S 14.61; found C 17.16, H 3.34, N 12.22, S 13.88.

***mer*-Trichloro(dimethyl sulfoxide-*S*)(4-amino-3-methyl-1,2,4-Δ²-triazoline-5-thione-*N,S*)ruthenium(III) Hydrate Acetic Acid Solvate (7'):** In a 100 mL round-bottomed flask **2** (0.15 g, 0.31 mmol) was added to a suspension of L4 (0.045 g, 0.31 mmol) and HCl (ca. 6 N, 20 mL) while stirring. The mixture was stirred for 0.5 h at room temperature, then warmed on a heating plate for 1 h and the green solution obtained was poured in a crystallizer for 24 h. The product was then extracted into ethyl acetate (several portions of 5–10 mL until the organic layer was no longer green). Green crystals of the product

Table 3. Crystallographic data of **1**, **1'**, **3**, and **4** and details of the structure solution and refinement procedures

	1	**1'**	**3**	**4**
Empirical formula	$C_8H_9N_5S$	$C_8H_{10}ClN_5S$	$C_{12}H_{21}Cl_2N_5O_2RuS_3$	$C_{12}H_{21}Cl_2N_5O_2RuS_3$
Formula weight	207.26	243.72	535.49	535.49
Wavelength [Å]	1.54184	0.71073	0.71073	1.54184
Crystal system, space group	Monoclinic, *Cc*	Monoclinic, $P2_1/c$	Monoclinic, $P2_1/c$	Monoclinic, $P2_1/c$
Unit cell dimensions *a* [Å]	8.553(2)	7.754(3)	8.668(3)	11.828(5)
b [Å]	15.830(6)	16.822(7)	12.203(6)	8.314(2)
c [Å]	7.702(2)	8.180(4)	19.632(7)	20.877(9)
β [°]	113.49(2)	91.96(2)	97.27(2)	90.45(2)
Volume [Å³]	956.4(5)	1066.4(8)	2059.9(14)	2052.9(13)
Z, Calculated density [Mg m^{-3}]	4, 1.439	4, 1.518	4, 1.727	4, 1.733
Absorption coefficient [mm^{-1}]	2.744	0.527	1.341	11.584
F(000)	432	504	1080	1080
Crystal size [mm]	0.15 × 0.18 × 0.28	0.22 × 0.31 × 0.40	0.25 × 0.31 × 0.48	0.21 × 0.21 × 0.38
φ range for data collection [°]	5.59 to 69.88	3.48 to 25.01	3.18 to 24.00	3.74 to 69.96
Index ranges	$-8 \le h \le 10$, $-16 \le k \le 19$, $-7 \le l \le 9$	$-9 \le h \le 9$, $0 \le k \le 19$, $0 \le l \le 9$	$-9 \le h \le 9$, $0 \le k \le 13$, $0 \le l \le 22$	$-14 \le h \le 14$, $-5 \le k \le 10$, $-2 \le l \le 25$
Reflections collected/unique, *R*(int)	976/925, 0.0186	2001/1873, 0.1149	3315/3220, 0.0468	3990/3888, 0.0443
Data/restraints/parameters	925/2/158	1873/0/154	3220/0/231	3888/0/238
Goodness-of-fit on F^2[a]	1.103	0.823	0.835	0.970
Final *R* indices [$I > 2\sigma(I)$] (*R*1, *wR*2)	0.0247, 0.0682	0.0376, 0.0623	0.0407, 0.0741	0.0433, 0.1110
R indices (all data) (*R*1, *wR*2)	0.0249, 0.0685	0.1009, 0.0760	0.1095, 0.0903	0.0586, 0.1190
Extinction coefficient	0.0045(6)			
Largest diff. peak and hole [eÅ^{-3}]	0.163 and –0.177	0.290 and –0.248	0.654 and –0.395	0.849 and –1.008

[a] GOOF = $[\Sigma[w(F_o^2 - F_c^2)^2]/(n-p)]^{1/2}$, $R1 = \Sigma \parallel Fo \mid - \mid Fc \parallel / \Sigma \mid Fo \mid$, $wR2 = [\Sigma[w(F_o^2 - F_c^2)^2]/\Sigma[w(F_o^2)^2]]^{1/2}$, $w = 1/[\sigma^2(F_o^2) + (aP)^2 + bP]$, where $P = [\max(F_o^2,0) + 2F_c^2]/3$.

Table 4. Crystallographic data of **5**, **6**, **7**, and **7'** and details of the structure solution and refinement procedures

	5	**6**	**7**	**7'**
Empirical formula	$C_6H_{16}Cl_2N_4O_2RuS_3$	$C_5H_{13}Cl_3N_4O_{1.5}RuS_2$	$C_6H_{15}Cl_3N_4O_{1.5}RuS_2$	$C_8H_{20}Cl_3N_4O_4RuS_2$
Formula weight	444.38	424.73	438.76	507.82
Wavelength [Å]	1.54184	1.54184	0.71073	0.71073
Crystal system, space group	Tetragonal, $P4_2/mbc$	Orthorhombic, *Pcca*	Orthorhombic, *Pccn*	Monoclinic, $P2_1/n$
Unit cell dimensions *a* [Å]	17.597(7)	22.130(7)	23.010(9)	11.029(4)
b [Å]	17.597(7)	10.331(3)	10.542(5)	14.450(6)
c [Å]	9.857(4)	12.290(4)	12.046(6)	12.608(5)
β [°]				110.67(2)
Volume [Å³]	3052(2)	2809.8(15)	2922(2)	1880.0(13)
Z, Calculated density [Mg m^{-3}]	8, 1.934	8, 2.008	4, 1.794	8, 1.995
Absorption coefficient [mm^{-1}]	15.396	17.016	1.901	1.500
F(000)	1776	1680	1744	1020
Crystal size [mm]	0.20 × 0.32 × 0.41	0.21 × 0.21 × 0.45	0.25 × 0.31 × 0.40	0.25 × 0.25 × 0.45
φ range for data collection [°]	5.03 to 69.92	4.28 to 70.02	3.12 to 27.04	3.05 to 30.00
Index ranges	$0 \le h \le 21$, $0 \le k \le 21$, $0 \le l \le 12$	$-13 \le h \le 26$, $-7 \le k \le 12$, $-14 \le l \le 1$	$-29 \le h \le 27$, $-5 \le k \le 13$, $-15 \le l \le 15$	$-15 \le h \le 14$, $0 \le k \le 20$, $0 \le l \le 17$
Reflections collected/unique, *R*(int)	2990/1535, 0.0404	2677/2677, 0.0000	3202/3202, 0.0000	5685/5471, 0.0386
Data/restraints/parameters	1535/0/104	2677/0/158	3202/0/134	5471/0/217
Goodness-of-fit on F^2[a]	1.019	1.024	0.648	0.852
Final *R* indices [$I > 2\sigma(I)$] (*R*1, *wR*2)	0.0483, 0.1230	0.0622, 0.1804	0.0586, 0.1348	0.0304, 0.0589
R indices (all data) (*R*1, *wR*2)	0.0643, 0.1314	0.0679, 0.1882	0.2016, 0.1624	0.0726, 0.0672
Largest diff. peak and hole [eÅ^{-3}]	2.143 and –0.898	1.565 and –2.173	1.638 and –0.740	0.766 and –0.733

[a] GOOF = $\{\Sigma[w(F_o^2 - F_c^2)^2]/(n-p)\}^{1/2}$, $R1 = \Sigma \parallel Fo \mid - \mid Fc \parallel / \Sigma \mid Fo \mid$, $wR2 = \{\Sigma[w(F_o^2 - F_c^2)^2]/\Sigma[w(F_o^2)^2]\}^{1/2}$, $w = 1/[\sigma^2(F_o^2) + (aP)^2 + bP]$, where $P = [\max(F_o^2,0) + 2F_c^2]/3$.

were obtained by slow evaporation. Yield 0.063 g (40%). – IR (KBr, cm^{-1}). $\tilde{\nu}$ = 3470 (OH str.), 3158 (NH_2 asym. str.), 3045 (NH_2 sym. str.), 2925, 1722 (COOH), 1616, 1521 (Thioam I), 1384 (CH_3 rock), 1204, 1081 (S–O DMSO *S*-coord), 1028, 686 (C–S_{DMSO} str.), 605, 432 (Ru–S str.). – $C_8H_{20}Cl_3N_4O_4RuS_2$ (507.82): calcd. C 18.92, H 3.97, N 11.03, S 12.63; found C 18.78, H 4.05, N 10.96, S 12.68.

Experimental Procedure for Conductivity Measurements: Four samples of a solution of **7** in dry acetone ($1.016\ 10^{-4}$ M, 2 mL) were prepared. Distilled water (0.2 mL) was added to two of the four samples, and seven measurements were made (every 30 min), the first immediately after the addition of water. The colour of the samples to which water was added changed from green to pale yellow in 3 h.

X-ray Crystal Structure Determinations: Diffraction data were recorded at 293(2) K with the φ/2φ technique on a Siemens AED (**1**, **5**, **7**), a Philips PW 1100 (**1'**, **3**, **7'**), and an Enraf–Nonius CAD4 diffractometer (**4**, **6**). The individual profiles were analyzed following the method of Lehmann and Larsen.[26] Corrections were made for Lorentz and polarization effects. The structures were solved by direct methods [SIR92][27] and refined by full-matrix least-squares methods based on F^2 using the SHELXL-97[28] program. All the non-hydrogen atoms were refined anisotropically except the ethyl carbon atoms and the oxygen and the methyl carbon atoms of the DMSO ligand in compound **7**. In **1** the hydrogen atoms, taken from a difference Fourier map, were refined freely. In the other compounds, the hydrogen atoms were placed in calculated positions and refined with a riding model, except those of the non-coordinated amine groups, the solvated water hydrogens and the carboxylic hydrogen atoms which were freely refined for the most part. Empirical absorption corrections were applied for compounds **4**, **5**, and **6**.[29] Crystal data and some details of the structure determinations are listed in Table 3 and Table 4. Further details of the crystal structures (excluding structure factors) have been deposited with the Cambridge Crystallographic Data Centre, and can be obtained free of charge on application to The Director, CCDC, 12 Union Road, Cambridge CB2 1EZ, England [Fax: (internat.) +44 (0)1223/336-033; E-mail: deposit@ccdc.cam.ac.uk] on quoting the reference number CCDC-121951–121958, the names of the authors, and the full journal citation. All calculations were carried out on the DIGITAL AlphaStation 255 of the "Centro di Studio per la Strutturistica Diffrattometrica'' del CNR, Parma. The programs PARST[30] and ORTEP[31] were also used.

Acknowledgments

We gratefully acknowledge financial support from the Ministero dell'Università e della Ricerca Scientifica e Tecnologica (MURST) and Consiglio Nazionale delle Ricerche (CNR) (Rome, Italy).

[1] [1a] C. Gors, F. Baert, J. P. Henichart, R. Houssin, *Cryst. Struct. Comm.* **1979**, *8*, 243. – [1b] C. Gors, F. Baert, J. P. Henichart, R. Houssin, *Cryst. Struct. Comm.* **1979**, *8*, 249.

[2] [2a] S. Goel, O. P. Pandey, S. K. Sengupta, *Bull. Soc. Chim. Fr.* **1989**, *6*, 771. – [2b] Q. Bano, N. Tiwari, S. Giri, Nizamuddin, *Indian J. Chem., Sect. B* **1992**, *31B*, 714.

[3] M. Biagini Cingi, F. Bigoli, M. Lanfranchi, M. A. Pellinghelli, A. Vera, E. Buluggiu, *J. Chem. Soc., Dalton Trans.* **1992**, 3145.

[4] [4a] K. R. Habbar, H. V. Sudhakar Nayak, T. Ramachandran, *J. Electrochem. Soc. India* **1983**, *32*, 159. – [4b] R. V. Gadag, M. R. Gajendragad, *J. Indian. Chem. Soc.* **1978**, *55*, 789. – [4c] K. N. Johri, Saxena Shashi, *Microchem. J.* **1978**, *23B*, 453.

[5] M. Biagini Cingi, F. Bigoli, M. Lanfranchi, E. Leporati, M. A. Pellinghelli, C. Foglia, *Inorg. Chim. Acta* **1995**, *235*, 37.

[6] F. Bigoli, M. Lanfranchi, M. A. Pellinghelli, *J. Chem. Res. (S)* **1990**, 214; F. Bigoli, M. Lanfranchi, M. A. Pellinghelli, *J. Chem. Res. (M)* **1990**, 1712.

[7] E. Alessio, G. Balducci, A. Lutman, G. Mestroni, M. Calligaris, W. M. Attia, *Inorg. Chim. Acta* **1993**, *203*, 205, and references therein.

[8] [8a] F. Bregant, S. Pacor, S. Ghosh, S. K. Chattopadhyay, G. Sava, *Anticancer Res.* **1993**, *13*, 1007. – [8b] S. K. Chattopadhyay, S. Ghosh, *Inorg. Chim. Acta* **1987**, *131*, 15. – [8c] S. K. Chattopadhyay, S. Ghosh *Inorg. Chim. Acta* **1989**, *163*, 245.

[9] F. Basolo, R. G. Pearson, *Mechanisms of Inorganic Reactions. A Study of Metal Complexes in Solution*, Wiley, New York, **1958**, pp. 108,163.

[10] E. Alessio, G. Mestroni, G. Nardin, W. M. Attia, M. Calligaris, G. Sava, S. Zorzet, *Inorg. Chem.* **1988**, *27*, 4099.

[11] [11a] M. A. Ledlie, K. G. Allum, I. V. Howell, C. R. Pitkethly, *J. Chem. Soc., Perkin Trans. 1* **1976**, 1734. – [11b] V. Y. Kukushkin, *Coord. Chem. Rev.* **1995**, *139*, 335.

[12] I. Bertini, C. Luchinat, *Coord. Chem. Rev.* **1996**, *150*, 41.

[13] G. García, I. Solano, G. Sánchez, M. D. Santana, G. López, J. Casabó, E. Molins, C. Miravitlles, *J. Organomet. Chem.* **1994**, *467*, 119.

[14] M. Maji, M. Chatterjee, S. Ghosh, S. K. Chattopadhyay, Bo-Mu Wu, T. C. W. Mak, *J. Chem. Soc., Dalton Trans.* **1999**, 135.

[15] E. S. Raper, *Coord. Chem. Rev.* **1985**, *61*, 115.

[16] J. S. Jaswal, S. J. Rettig, B. R. James, *Can. J. Chem.* **1990**, *68*, 1808.

[17] M. Henn, E. Alessio, G. Mestroni, M. Calligaris, W. M. Attia, *Inorg. Chim. Acta* **1991**, *187*, 39.

[18] M. M. Taqui Khan, N. H. Khan, R. I. Kureshy, K. Venkatasubramanian, *Tetrahedron* **1992**, *11*, 431.

[19] C. Anderson, A. L. Beauchamp, *Can. J. Chem.* **1995**, *73*, 471.

[20] C. Price, M. R. J. Elsegood, W. Clegg, N. H. Rees, A. Houlton, *Angew. Chem.* **1997**, *109*, 1823*; Angew. Chem. Int. Ed. Engl.* **1997**, *36*, 1762.

[21] M. Calligaris, O. Carrugo, *Coord. Chem. Rev.* **1996**, *153*, 83.

[22] E. Alessio, M. Calligaris, M. Iwamoto, L. G. Marzilli, *Inorg. Chem.* **1996**, *35*, 2538.

[23] S. Geremia, E. Alessio, F. Todone, *Inorg. Chim. Acta* **1996**, *253*, 87.

[24] M. J. Harrison, R. O. C. Normann, W. A. F. Gladstone, *J. Chem. Soc., C* **1967**, 735.

[25] L. Marchiò, Tesi di Laurea in Chimica, Parma University, Italy, **1997**.

[26] M. S. Lehmann, F. K. Larsen, *Acta Crystallogr., Sect. A* **1974**, *30*, 580.

[27] A. Altomare, G. Cascarano, C. Giacovazzo, A. Gualiardi, M. C. Burla, G. Polidori, M. Camalli, *J. Appl. Crystallogr.* **1994**, *27*, 435.

[28] G. M. Sheldrick, *SHELXL-97 Program for the Refinement of Crystal Structures*, University of Göttingen, Göttingen, Germany, **1997**.

[29] [29a] N. Walker, D. Stuart, *Acta Crystallogr., Sect. A* **1983**, *39*, 158; – [29b] F. Ugozzoli, *Comput. Chem.* **1987**, *11*, 109.

[30] M. Nardelli, *Comput. Chem.* **1983**, *7*, 95.

[31] L. Zsolnai, H. Pritzkow, ZORTEP. ORTEP original program modified for PC. University of Heidelberg, Germany, **1994**.

Received May 27, 1999
[I99205]

Stoichiometric Homo-Aldol Coupling of Acetone, Cyclohexanone, and Acetophenone by the [(η^5-Cp^R)Co] (R = Me_5, 1,2,4-tri-*tert*-butyl) Moiety

Jörg J. Schneider,*[a] Dirk Wolf,[a] Dieter Bläser,[a] and Roland Boese[a]

Keywords: Cobalt / Sandwich complexes / Aldol reactions / Ketones / C_{sp3}−H activation

Acetone, cyclohexanone, and acetophenone react with the toluene-bridged triple-decker complexes [{(η^5-Cp^R)Co}$_2$-μ-(η^4:η^4-toluene)] (R = Me_5 **3**; 1,2,4-tri-*tert*-butyl **4**) by toluene substitution and homo-aldol coupling of two ketone molecules to form the first oxadiene cobalt complexes. These reactions may involve a C_{sp3}–H activation step of the ketones by 14 e$^-$ [(η^5-Cp^R)Co] fragments generated from the triple-decker complexes **3** and **4**. If no acidic protons are present in the position α to the carbonyl carbon position in the ketone, no C_{sp3}–H activation occurs. In agreement with this, benzophenone does not react with complex **3**.

Introduction

During the last decade or so it has been well established, both spectroscopically and crystallographically, that carbonyl compounds are able to coordinate to transition metal fragments and, consequently, metal-mediated reactions, which are stoichiometric or even catalytic in nature, have been studied extensively.[1] The aldol reaction is generally regarded as one of the most powerful carbon–carbon bond forming reactions. The primary metal coordination site is at the C=O group, resulting in three different bonding situations A–C towards the transition metal center (Figure 1).[2] Recent results by Brookhart, who observed selective coordination of phthalaldehyde over acetone with the bis({trimethylsilyl}alkene)(η^5-Me_5C_5)Co complex **1** are striking.[3a] The bis-aldehyde complex **2**, which simultaneously displays coordination modes A and B is formed as the exclusive product from the activation of phthalaldehyde even though acetone was used as the reaction solvent (Scheme 1).[3a] Other examples of similar aldehyde over ketone reactivity are documented for the cobalt complex **1** by the same authors.[3b][3c]

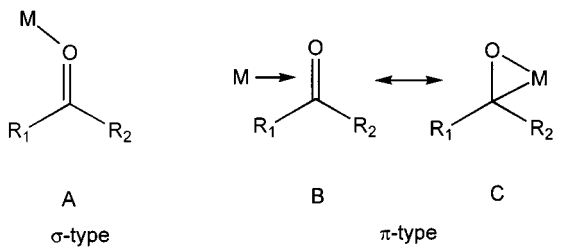
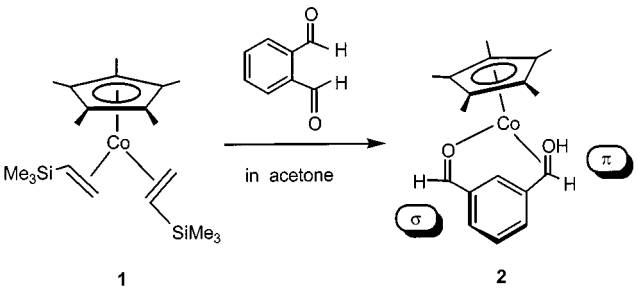


Figure 1. σ- and π-coordination modes of a transition metal fragment M to a ketone; $R_{1,2}$ = H or alkyl



Scheme 1

Herein we report on our studies on the synthesis and structure of cobalt-oxadiene complexes which are formed via a stoichiometric homo-aldol coupling reaction of acetone, cyclohexanone, and acetophenone mediated by 14-e [(η^5-Cp^R)Co] fragments.

Results and Discussion

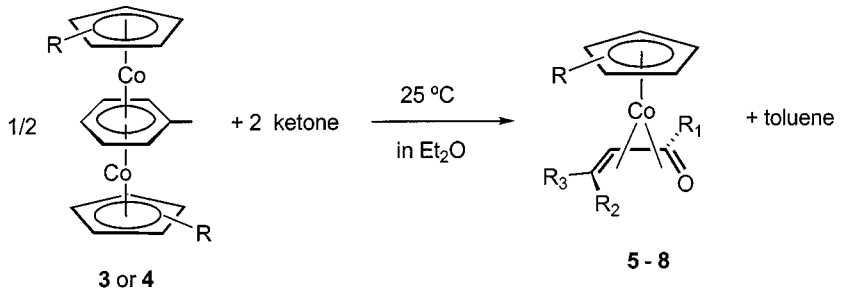
Reaction of [{(η^5-Me_5C_5)Co}$_2$-μ-(η^4:η^4-toluene)] (3) and [{(η^5–1,2,4-tri-*tert*-butyl-C_5H_2)Co}$_2$-μ-(η^4:η^4-toluene)] (4) with Ketones

Reaction of the triple-decker compound [{(η^5-Me_5C_5)Co}$_2$-μ-(η^4:η^4-toluene)] (**3**) either in neat acetone as solvent or with a tenfold excess of acetone in ether results in the formation of the *s-cis*-oxadiene cobalt complex **5** (Scheme 2). No *s-trans* regioisomer was observed. The question of whether the product selectively adopts one of the regioisomers (Figure 2) is of interest since the two arrangements expose different faces of the α, β-unsaturated carbonyl moiety which may lead to different enantioselective additions to this complex.

The reaction of **3** with acetone proceeds stoichiometrically and no free 2-oxo-4-methylpent-3-ene was observed as the organic aldol coupling product resulting from a catalytic reaction sequence. The η^2-keto coordination is characterized by a significant ^{13}C high-field coordination shift of the carbonyl C-atom resonance of $\Delta\delta$ = –72 ppm relative to free acetone.

[a] Institut für Anorganische Chemie der Universität/GH-Essen, Universitätsstrasse 5–7, 45117 Essen
Fax: (internat.) +49 (0)201/1834195
E-mail: joerg.schneider@uni-essen.de

 © WILEY-VCH Verlag GmbH, D-69451 Weinheim, 2000 1434−1948/00/0404−0713 $ 17.50+.50/0



Scheme 2. General reaction scheme for the formation of Co-oxadiene complexes **5–8** via homo-aldol coupling of acetone, cyclohexanone and acetophenone. The characteristic η^4-oxadiene unit of **5–8** is depicted in bold.

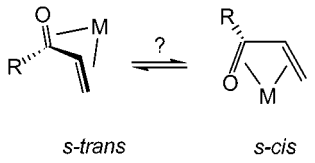
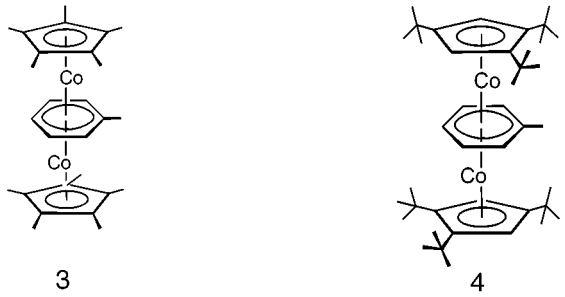


Figure 2. *s-cis* versus *s-trans* arrangement of a metal-oxadiene unit



A tenfold excess of acetophenone in diethyl ether reacts with **3** within 30 minutes to give the oxadiene cobalt complexes [{(η^5-Me_5C_5)Co(η^4-(*E,Z*)-3-methyl-1-oxo-1,3-diphenylbut-2-ene)} **(6)** as a mixture of *cis* and *trans* isomers (ratio 2:3) (Scheme 2). As in the case of **5**, a significant high-field coordination shift of $\Delta\delta$ = –49.2 ppm for the resonance of C1 characterizes the η^2-keto coordination of the [(η^5-Me_5C_5)Co] fragment of **6**. The complete set of ^{13}C-NMR signals for both isomers is not observed probably just due to a low concentration of the sample studied.

When **3** is dissolved in neat cyclohexanone a reaction occurred within two days as judged from the color change from brown red to green black. The oxadiene cobalt complex [(η^5-Me_5C_5)Co(η^4-2-cyclohexylidenecyclohexane-1-one)] **7** is formed in moderate yields. (Scheme 2). ^{1}H- and ^{13}C-NMR spectroscopy shows the formation of only the *s-cis* isomer (assignment via 1D- and 2D-NMR techniques). In the ^{13}C-NMR spectrum the η^2-keto coordination is characterized by a coordination shift of $\Delta\delta$ = –75 ppm for the resonance of C1 relative to free cyclohexanone.

To study the influence of the steric bulk of the [(Cp^R)Co] fragment on the homo-aldol coupling reaction we studied the reaction of acetone with the triple-decker complex **4**. The 1,2,4 tri-*tert*-butyl Cp ligand has already proven its versatility in kinetically stabilizing unusual metal coordination environments.[4,5] When **4** is dissolved together with a tenfold excess of acetone in diethyl ether the reaction proceeds within 12 hours to give the oxadiene complex [{(η^5-$tBu_3C_5H_2$)Co(methyl-2-oxo-pent-3-ene)}] (**8**) whose structure is confirmed by its mass, IR and ^{1}H- and ^{13}C-NMR spectra (see Experimental Section) (Scheme 2). In **8**, as well as in the other oxadiene Co complexes **5–7**, the ν(C=O) stretching frequencies of the complexed η^2-carbonyl moieties are unfortunately obscured by the strong intensity of the stretching frequencies of the Me and 1,2,4-*tert*-butyl residues of the Cp ring ligands.

Molecular Structure of 5

An X-ray crystal structure determination[6] (Figure 3) of **5** reveals the *s-cis*-arrangement of the oxadiene moiety in agreement with the solution NMR results. The C1–O1 distance [1.310(5) Å] of the π-coordinated carbonyl group is in the same range as for the η^2-coordinated C=O group of the dialdehyde complex **1**[3a] as well as for other η^2 bound ketones.[1,7] This suggests a significant amount of π-backbonding from the Co^I d-orbitals into the π^* orbitals of the carbonyl C atom. The Co–O [1.985(3) Å] and the Co1–C2 [1.994(4) Å] distances are in agreement with a symmetrical

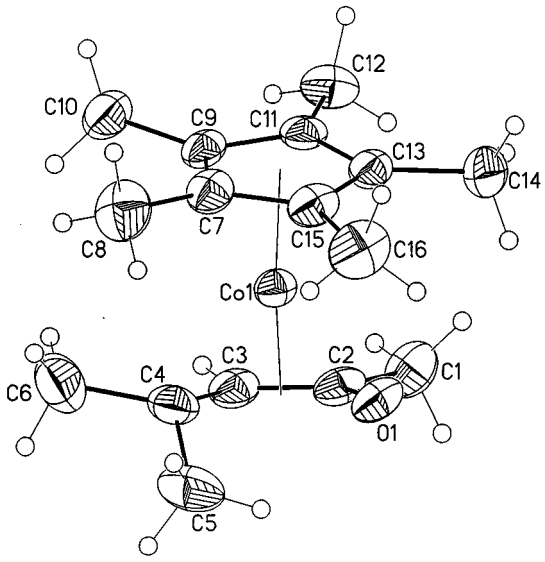


Figure 3, Molecular structure of **5** in the solid state; selected bond length [A] and angles [°]: C(2)–O(1) 1.310(5),C(2)–C(3) 1.396(6), C(3)–C(4) 1.437(6),C(1)–C(2) 1.497(6), C(4)–C(5) 1.503(7), C(4)–C(6) 1529(6), Co(1)–C(2) 1.994(4), Co(1)–O(1) 1.985(3), Co(1)–C(3) 1.985(4), Co(1)–C(4) 2.041(5) O(1)–C(2)–C(3) 116.9(4), C(2)–C(3)–C(4) 119.0(4)

η^2-bonding of the [Co(η^5-C_5Me_5)] fragment to the keto group. The atoms C2, C3, C4, and O1 define an almost ideal plane. The bond length deviation Co–C2 [1.994(4) Å], Co1–C3 [1.985(4) Å], Co1–C4 [2.041(5) Å], and Co1–O [1.985(3) Å] is within experimental error, thus the bonding can be regarded as symmetrical η^4. However, the distance C3–C4 [1.437(6) Å] within the planar oxadiene unit is significantly longer than C2–C3 [1.396(6) Å]. This indicates an intermediate bonding situation between a pure π-coordination mode **A** and a metallacyclic type coordination **B** for **5** in the solid state (Figure 4). **A** and **B** represent the two extremes of coordination for an $M(L)_x$ fragment to a oxadiene ligand system.

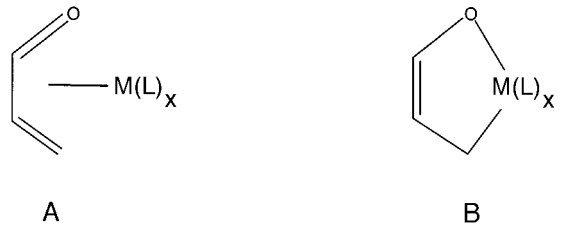
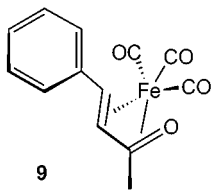


Figure 4. π-Metal coordination **A** versus σ-metallacycle formation **B** in an oxadiene complex

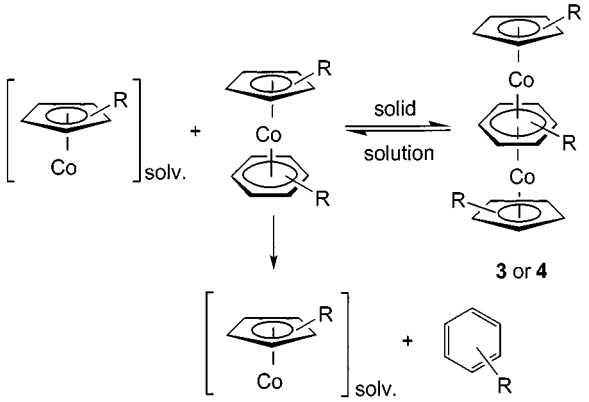
Discussion

Compounds **5–8** belong to a group of organometallic oxadiene complexes of which [(4-phenylbut-3-ene-2-one)-$Fe(CO)_3$] **(9)** represents the first example.[8] This and other enone complexes of a similar bonding type are accessible by standard complexation procedures.[9] In contrast, **5–8** are formed via a Co-mediated aldol-type coupling initiated by reactive 14 e [(η^5-Cp^R)Co] (R = Me_5, 1,2,4-tri-*tert*-butyl) fragments. Their formation from the triple-decker complexes **3** and **4** was verified by detailed mechanistic studies.[5,10] Complexes **3** and **4** are valuable sources of either one or two [(η^5-Cp^R)Co] fragments. The decay of **3** and **4** into [(η^5-Cp^R)Co] (R = Me_5, 1,2,4-tri-*tert*-butyl) fragments (Scheme 3) proceeds in any common donor solvent and is especially fast in the presence of ketones (e.g. acetone).



9

There has been quite intense research on the C–H bond activation by various transition metal complexes especially of the iron group triad which may be followed by functionalization of the activated substrate.[11] A process which combines C–H and C–C coupling reactions is the catalytic

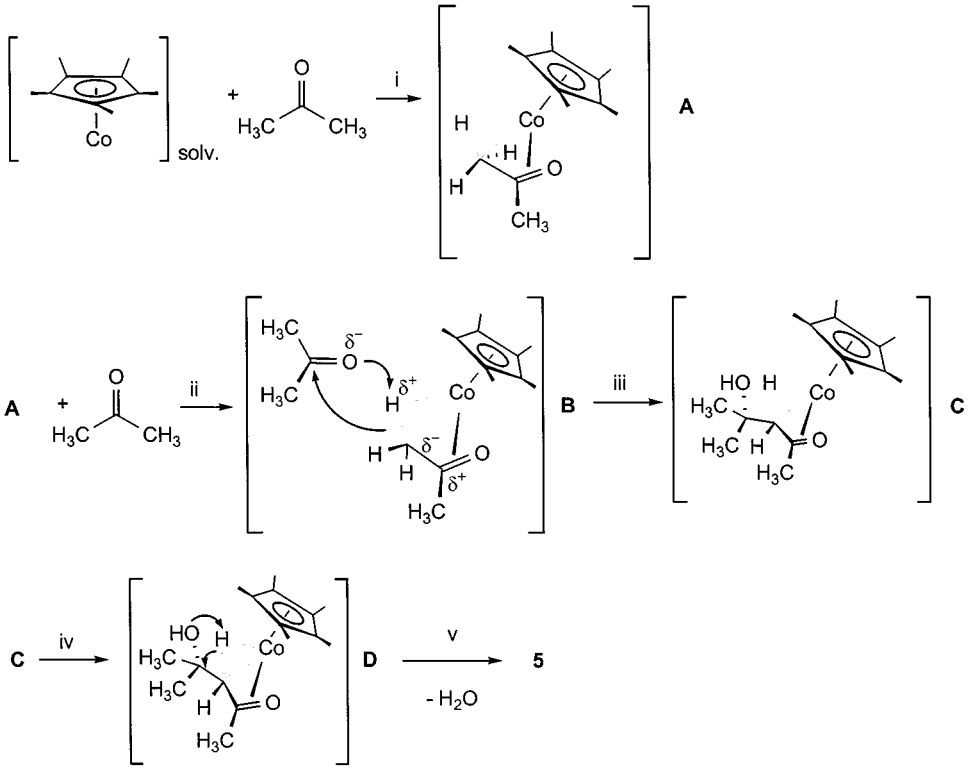


Cp^R = Me_5 or 1,2,4,-tri-*tert*-butyl

Scheme 3. Solid state versus solution equilibrium of the triple-decker complexes **3** and **4**[10]

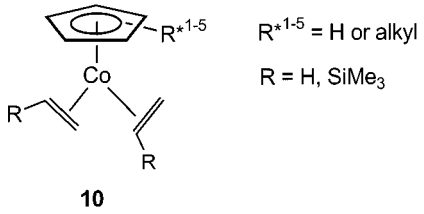
hydroacylation of olefins to form ketones at Rh^I centers studied by Bosnich.[12] However, such reactivity is usually not in the realm of first row transition metal chemistry and only a few cases are reported for organo cobalt complexes but to the best of our knowledge none so far for a C_{sp3}–H bond activation mediated by Co fragments. Extensive studies by Bergman[13], Jones,[14] and Graham[15] have established that 16 e species of the type [(η^5-R_5C_5)ML] (M = Rh, Ir) generated in situ, undergo facile oxidative addition reactions with the C–H bonds of saturated hydrocarbons and arenes. For Co, Brookhart[3a,16] demonstrated facile oxidative addition of aldehydes via the 16 e [(η^5-Me_5C_5)CoL] fragment. However, it is noteworthy with respect to our work that no activation of the less reactive acetone used as solvent is reported by these authors for the [(η^5-Cp^R)CoL] fragment which is derived from **1**. Wadepohl[17] observed facile C_{sp2}–H activation processes of cycloalkenes in the course of the formation of polynuclear [(η^5-Cp^R)Co]-based clusters which are derived from the Jonas complex [(η^5-Cp)Co(ethene)$_2$]. Crucial for the ability of Co centers to participate in C–H-bond activation processes is the generation of reactive sites, especially the formation of either coordinatively unsaturated, electron deficient 16 e [(η^5-Cp^R)Co(L_x)] or even 14 e [(η^5-Cp^R)Co] fragments.[18] C–H activation is assumed to be a significant step in the homo-aldol coupling reaction of the ketones under study herein. This is based on results obtained from the reaction of benzophenone with **3**. Benzophenone contains no acidic protons at the α-carbon position, thus no homo-aldol coupling can be observed with benzophenone which is recovered unchanged from a reaction with **3**. A possible reaction pathway invoking C_{sp3}–H bond activation of acetone, cyclohexanone and acetophenone as crucial reaction step, leading to the oxadiene cobalt complex **5–8** is outlined in Scheme 4 exemplified for the reaction of **3** and acetone.

Reactive 14 e [(η^5-Me_5C_5)Co]$_{solv}$ fragments are generated from **3**. These can first coordinate the keto group of acetone followed by an activation of the hydrogen atoms of the neighboring α-methyl group giving intermediate **A**. Reaction of intermediate **A** with the "acidic" carbonyl carbon



Scheme 4. Proposed reaction scheme for the Co-mediated homo-aldol coupling of acetone

atom of another acetone molecule forms (ii), **B** results in a C–C coupling, leading to intermediate **C** (iii). Finally **C** can eliminate water (v), **D** to yield complex **5**. This elimination of water parallels the classical base catalyzed aldol type coupling reaction.[19]



10

Conclusions

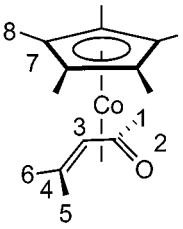
Our findings presented here indicate a pronounced reactivity enhancement of the arene triple-decker type complexes **3** and **4** over half sandwich complexes of type **10**, which in contrast to **3** and **4** do not show similar carbonyl coupling reactions and not even a reactivity towards acetone under similar conditions. This points to the fact that 14 e [(η^5-Cp^R)Co] fragments derived from the triple-deckers **3** and **4** in contrast to 16 e [(η^5-Cp^R)CoL] derived from **10** are able to activate ketones at their C_{sp3}-α-carbon atom under mild conditions. This is to the best of our knowledge the first C_{sp3}–H bond activation of ketones by an organocobalt compound leading to a C–C coupling under neutral and ambient conditions. It remains to be studied if this coupling proceeds regio- and/or stereospecifically with other ketones and if it can be tuned from stoichiometric to catalytic reactivity. Such investigations may open up new synthetic routes with respect to cobalt mediated cycloaddition reactions offering access to complex organic products as in the case of oxadiene complexes of Mo and W.[20]

Experimental Section

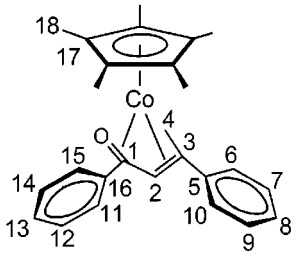
Compounds **3**[21] and **4**[5] were prepared according to published procedures. All ketones were commercial products (purity 99%), they were distilled prior to use and stored under nitrogen in the dark. – The NMR spectra were recorded on a Bruker AC 300 spectrometer (300 MHz for ^{1}H, 75 MHz for ^{13}C) and referenced against the residual protons of the deuterated solvent. – MS spectra were recorded on a MAT 8200 instrument under standard conditions (EI, 70 eV) and the fractional sublimation technique for compound inlet. – T_{vap} gives the individual vaporization temperature of the sublimation process during the MS experiment.

[(η^5-Me_5C_5)Co(η^4-4-methyl-2-oxopent-3-ene)] (5): Complex **3** (0.41 g, 0.85 mmol) was dissolved together with acetone (0.5 g, 8.6 mmol) in 30 mL of diethyl ether. Continued stirring for 24 hours resulted in a color change from red brown to greenish brown. Removal of all volatiles under vacuum gave a semi-solid residue which was dissolved in a minimum amount of pentane. Cooling to –78 °C afforded **5** (0.38 g, 1.31 mmol, 77%) as brown material. The same material resulted when the reaction was performed in acetone only. – MS (EI, 70 eV, T_{vap} 250 °C); *m/z* (%): 292 (100)

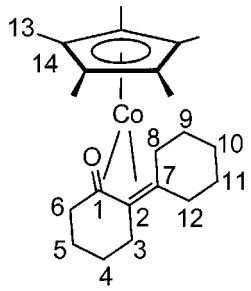
$[M^+]$, 277 (3) $[M^+ - CH_3]$, 249 (20) $[M^+ - CH_3CO]$, 209 (13) $[M^+ - (CH_3)_2C{=}CHCO]$, 192 (70) $[(Me_5C_5)Co]$. – ^1H NMR ($[D_6]$benzene, 300 MHz, 27 °C): δ = 0.95 (s, 3 H), 1.17 (s, 3 H), 1.50 (s, 15 H), 2.13 (s, 3 H), 4.03 (s, 1 H). – $^{13}C\{^1H\}$ NMR ($[D_6]$benzene, 75.1 MHz, 27 °C): δ = 9.4 (C7), 20.9 [C6(5)], 21.8 [C5(6)], 28.2 (C1), 77.9 (C3), 89.1 (C8), 127.2 (C4), 134.9 (C2). – IR (KBr): $\tilde{\nu}$ = 1473, 1448, 1431, 1385, 1351, 1364 (all vs, Me_5C_5), 1236, 1155, 1140, 1065, 1027, 911, 862, 602 (all vs) cm^{-1}. – $C_{16}H_{25}CoO$ (292.29): calcd. C 65.74, H 8.62, Co 20.16; found C 65.85, H 8.69, Co 20.22.



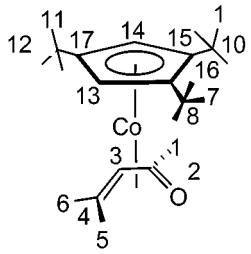
[{(η⁵-Me_5C_5)Co(η⁴-(*E*,*Z*)-3-methyl-1-oxo-1,3-diphenylbut-2-ene)}] (6): Synthetic procedure as described for **5**; crystallization from diethyl ether/pentane (2:1) gives **6** (0.28 g, 0.68 mmol, 63%) as a mixture of its (*E*)- (63%) and (*Z*)-isomers (37%). – MS (EI, 70 eV, T_{vap}: 100 °C); *m*/*z* (%): 416 (100) $[M^+]$, 311 (3) $[M^+ - C_6H_5CO]$, 281 (55) $[M^+ - Me_5C_5]$, 192 10 $[(Me_5C_5)Co]$. – ^1H NMR ($[D_6]$benzene, 300 MHz, 27 °C): δ = 1.23 [s, 15 H, (*Z*)], 1.42 [s, 15 H, (*E*)], 1.54 [s, 3 H, (*E*)], 1.57 [s, 3 H, C4 (*Z*)], 4.99 [s, 1 H, (*E*)], 6.11 [s, 1 H, (*Z*)], 7.17 [m, arenes (*E* + *Z*)], 7.19 [m, arenes (*E* + *Z*)], 7.31 [m, arenes (*E* + *Z*)], 7.39 [m, 3 H, C12–C14 (*E*)], 7.41 [m, 3 H, C12–C14 (*Z*)], 8.16 [m, 2 H, C11, C15 (*E*)], 8.27 [m, 2 H, C11, C15 (*Z*)]. – $^{13}C\{^1H\}$ NMR ($[D_6]$benzene, 75.1 MHz, 27 °C): δ = 8.6 [C17 (*Z*)], 9.0 [C17 (*E*)], 17.1 [C4 (*Z*)], 27.40 [C4 (*E*)], 71.23 [C2 (*Z*)], 71.8 [C2 (*E*)], 89.6 [C18 (*E*)], 89.7 [C18 (*Z*)], 124.5, 124.5, 126.0, 126.7, 127.0, 127.3, 128.6, 129.2, 146.7 (C1). – IR (KBr): $\tilde{\nu}$ = 3055, 3034, 1540, 1488, 762, 695 (all strong, all phenyl), 1488, 1449, 1072, 1022 (all vs, all Me_5C_5) cm^{-1}. – $C_{26}H_{29}CoO$ (416.42): calcd. C 74.99, H 7.02; found C 74.36, H 7.02.



[{(η⁵-Me_5C_5)Co(η⁴-2-cyclohexylidenecyclohexan-1-one)}] (7): Synthetic procedure as described for **5**; crystallization from acetonitrile/ether mixture gives **7** (0.1 g, 0.27 mmol, 22%) as cube-shaped black crystals. – MS (EI, 70 eV, T_{vap} 150 °C); *m*/*z* (%): 372 (100) $[M^+]$, 354 (8) $[M^+ - H_2O]$, 233 (17) $[M^+ - C_9H_{15}]$, 194 (17) $[Me_5Co]$. – ^1H NMR ($[D_6]$benzene, 300 MHz, 27 °C): δ = 1.09 (m, 1 H), 1.52 (m, 2 H), 1.58 (m, 2 H), 1.61 [s, 15 H, C13], 1.77 (m, 2 H), 1.90 (m, 2 H), 1.94 (m, 2 H), 2.0 (m, 1 H), 2.14 (m, 1 H), 2.20 (m, 1 H), 2.32 [t (dd), 1 H], 2.45 (m, 1 H), 2.65 (ddd, 1 H). – $^{13}C\{^1H\}$ NMR ($[D_6]$benzene, 75.1 MHz, 27 °C): δ = 9.4 (C13), 24.2 (sec.), 24.4 (sec.), 26.3 (sec.), 28.1 (sec.), 28.4 (sec.), 28.6 (sec.), 31.0 (sec.), 31.6 (sec.), 32.1 (sec.), 35.7 (sec.), 63.0 (q, C7), 85.5 (q, C2), 88.7 (q, C14), 134.5 (q, C1). – $C_{22}H_{33}CoO$ (372.41): calcd. C 70.95, H 8.93, Co 20.16; found C 71.03, H 9.05.



[{(η⁵-*t*$Bu_3H_2C_5$)Co(4-methyl-2-oxopent-3-ene)}] (8): Synthetic procedure fas described for **5**; crystallization from pentane at –78 °C affords **8** as a brown solid. – MS (EI, 70 eV, T_{vap} = 120 °C); *m*/*z* (%): 390 (32) $[M^+]$, 333 (100) $[M^+ - t\text{Bu}]$, 57 (33) [*t*Bu]. – ^1H NMR ($[D_6]$benzene, 300 MHz, 27 °C): δ = 0.99 [s, 9 H, C11], 1.08 [s, 3 H, C5(6)], 1.18 [s, 3 H, C6(5)], 1.44 [s, 9 H, C7(9)], 1.77 [s, 9 H, C9(7)], 2.29 [s, 3 H, C1], 3.39 [s, 1 H, C13(14)], 4.14 [s, 1 H, C14(13)], 4.69 [s, 1 H, C3], in addition signals due to $[\{(\eta^5\text{-}t\text{Bu}_3H_2C_5)_2Co]$[22] were present in a 1:2 ratio. – $^{13}C\{^1H\}$ NMR ($[D_6]$benzene, 75.1 MHz, 27 °C): δ = 22.2 [C5(6)], 22.7 [C6(5)], 31.3 [C7(9,11)], 31.4 (C1), 32.7 [C9(7,11)], 33.2, 33.4, 35.1 [C11(7,9)], 76.3, 78.1, 79.21, 148.50 (CO). – IR (KBr): $\tilde{\nu}$ = 1486, 1458, 1391, 1242 (all vs, all *t*Bu), 1199, 1163, 1020, 990, 824, 668 (all m) cm^{-1}. – No satisfactory elemental analysis could be obtained due to trace amounts of $[\{(\eta^5\text{-}t\text{Bu}_3C_5)_2Co]$[22] already contained in the starting material **4**.



Reaction of 3 with Benzophenone: Complex **3** (0.31 g, 0.64 mmol) and benzophenone (0.46 g, 2.52 mmol) were dissolved in 30 mL of diethyl ether and stirred for 48 h. Although the color of the solution changed during this time from red-brown to orange-brown, removal of all volatiles gave mainly unchanged benzophenone. However, **3** was no longer present.

Acknowledgments

This work was supported by the DFG (Heisenberg fellowship to J. J. S. and grant SCHN 375/6-1) and the Fonds der Chemischen Industrie. We thank Dr. D. Stöckigt and Dr. K. Seevogel and coworkers (MPI für Kohlenforschung, Mülheim) for recording MS and IR spectra.

[1] [1a] G. Dyker, *Angew. Chem.* **1999**, *111*, 1808–22; *Angew. Chem. Int. Ed.* **1999**, *38*, 1698–1712. – [1b] L. E. Helberg, T. B. Gunnoe, B. C. Brooks, M. Sabat, W. D. Harman, *Organometallics* **1999**, *18*, 573–581, and references cited therein.

[2] For a theoretical discussion of η^2 vs. η^1 bonding see: F. Delbeq, P. Sautet, *J. Am. Chem. Soc.* **1992**, *114*, 2446–2455.

[3] [3a] C. P. Lenges, M. Brookhart, P. S. White, *Angew. Chem.* **1999**, *111*, 535–538; *Angew. Chem. Int. Ed.* **1999**, *38*, 552–555. – [3b] C. P. Lenges, P. S. White, M. Brookhart, *J. Am. Chem. Soc.* **1998**, *120*, 6965–6979. – [3c] C. P. Lenges, M. Brookhart, *J. Am. Chem. Soc.* **1997**, *119*, 3165–3166.

[4] [4a] H. Sitzmann, *Chem. Ber.* **1990**, *123*, 2311–2315. – [4b] J. J.

Schneider, U. Specht, *Z. Naturforsch*. **1995**, *50b*, 684–686. – [4c] J. Okuda, *J. Organomet. Chem*. **1990**, *385*, C39–C42. – [4d] H. Sitzmann, G. Wolmershäuser, *Z. Naturforsch*. **1997**, *52b*, 398–400. – [4e] H. Sitzmann, M. Schär, E. Dorrmann, M. Kelemen, *Z. Anorg. Allg. Chem*. **1997**, *623*, 1609–1613.

[5] J. J. Schneider, D. Wolf, C. Janiak, O. Heinemann, J. Kuhnigk, C. Krüger, *Chem. Eur. J.* **1998**, *4*, 1982–1991.

[6] X-ray crystal structure investigation of **5**: A dark, thin platelike crystal with the approximate dimensions 0.22 × 0.19 × 0.05 mm was investigated at room temperature with a Siemens-Smart System using Mo-K_α radiation. The orthorhombic crystal system has the cell dimensions a = 12.8021(5), b = 14.0394(6), c = 17.1475(6) A, V = 3082.0(2) A^3, Z = 8, ρ = 1.260 g cm^{-3}, μ = 1.101 mm^{-1}, space group *Pbca*. Full-sphere data collection of 21602 reflections (θ_{max} = 25.99°), data reduction (Siemens SAINT Vers. 4.05), empirical absorption correction (Siemens SADABS), max/min transmission 1.00/0.40, 2578 independent reflections [R_{merg} = 0.14 (F^2)], 1359 observed [$F_o > 4\sigma(F)$], structure solution with direct methods and refinement on F^2 of 163 parameters using Siemens SHELXTL Vers. 5.03 resulted in $R1$ = 0.0525 (obs. data) and $wR2$ = 0.1397 (all data), GoF = 0.887, maximum/minium residual electron densities 0.620/−0.286 eA^{-3}. Hydrogen atoms were treated as riding groups with the 1.2 fold (1.5 for methyl groups) isotropic U-values of the equivalent U-values that correspond to the attached C-atoms. Crystallographic data (excluding structure factors) for the structure reported in this paper have been deposited with the Cambridge Crystallographic Data Centre as supplementary publication no. CCDC-130276 **(5)**. Copies of the data can be obtained free of charge on application to The Director, CCDC, 12 Union Road, Cambridge CB2 1EZ, UK [Fax: (internat.) +44–1223/336-033; E-mail: deposit@ccdc.cam.ac.uk].

[7] J. E. Hill, P. E. Fanwick, I. P. Rothwell, *Organometallics* **1992**, *11*, 1771–1773

[8] J. A. S. Howell, B. F. G. Johnson, P. L. Josty, J. Lewis, *J. Organomet. Chem.* **1972**, *39*, 329–333.

[9] [9a] Th. Schmidt, P. Betz, C. Krüger, *J. Organomet. Chem*. **1991**, *402*, 97–104. – [9b] Th. Schmidt, F. Bienewald, R. Goddard, *J. Chem. Soc., Chem. Commun*. **1994**, 1857–1858. – [9c] Th. Schmidt, Habilitation Thesis, University of Cologne **1992**.

[10] J. J. Schneider, D. Wolf, *Z. Naturforsch*. **1998**, *53b*, 1267–1272.

[11] M. Brookhart, M. L. H. Green, *J. Organomet. Chem.* **1983**, *250*, 395–408.

[12] [12a] B. Bosnich, R. W. Barnhart, *Organometallics* **1995**, *14*, 4343–4348. – [12b] B. Bosnich, D. P. Fairlie, *Organometallics* **1988**, *7*, 936–945. – [12c] B. Bosnich, D. P. Fairlie, *Organometallics* **1988**, *7*, 946–954. – [12d] B. Bosnich, J. Whelan, S. H. Bergens, P. Noheda, X. Wang, R. W. Barnhart, *Tetrahedron* **1994**, *50*, 4335–4346. – [12e] B. Bosnich, X. Wang, *Organometallics* **1994**, *13*, 4131–4133. – [12f] B. Bosnich, J. Whelan, S. H. Bergens, P. Noheda, X. Wang, R. W. Barnhart, *J. Am. Chem. Soc*. **1994**, *116*, 1821–1830. – [12g] B. Bosnich, R. W. Barnhart, D. A. Mc. Morran, *Inorg. Chim. Acta* **1997**, *263*, 1–9.

[13] [13a] R. G. Bergman, A. H. Janowicz, *J. Am. Chem. Soc*. **1982**, *104*, 352–354. – [13b] R. G. Bergman, A. H. Janowicz, *J. Am. Chem. Soc*. **1983**, *105*, 3929–3939. – [13c] R. G. Bergman, R. A. Periana, *J. Am. Chem. Soc.* **1986**, *108*, 7346–7355. – [13d] R. G. Bergman, *Science* **1984**, *223*, 902–908.

[14] [14a] W. D. Jones, F. J. Feher, *Organometallics*, **1983**, *2*, 686–687. – [14b] ibid, *J. Am. Chem. Soc.* **1984**, *106*, 1650–1663. – [14c] W. D. Jones, R. Perutz, R. M. Chin, L. Dong, S. B. Duckett, M. G. Partridge, *J. Am. Chem. Soc.* **1993**, *115*, 7685–7695.

[15] [15a] W. A. G. Graham, J. K. Hoyano, *J. Am. Chem. Soc*. **1982**, *104*, 3723–3725. – [15b] W. A. G. Graham, J. K. Hoyano, A. D. Mc Master. *J. Am. Chem. Soc*. **1983**, *105*, 7190–7191.

[16] C. P. Lenges, M. Brookhart, B. E. Grant, *J. Organomet. Chem*. **1997**, *528*, 199–203.

[17] [17a] H. Wadepohl, T. Borchert, H. Büchner, H. Pritzkow, *Chem. Ber*. **1993**, *126*, 1615–1618. – [17b] H. Wadepohl, T. Borchert, H. Pritzkow, *Chem. Commun.* **1995**, 1447–48.

[18] [18a] P. E. Siegbahn, *J. Am. Chem. Soc.* **1996**, *118*, 1487–1496. – [18b] R. G. Bergman, B. C. Moore, A. A. Bengali, *J. Am. Chem. Soc*. **1995**, *117*, 3879–3886.

[19] E. g. Autorenkollektiv, *Organikum,* VEB-Verlag der Wissenschaften, **1977**.

[20] Th. Schmidt, *Chem. Ber./Recueil* **1997**, *130*, 453–461.

[21] J. J. Schneider, U. Denninger, O. Heinemann, C. Krüger, *Angew. Chem*. **1995**, *107*, 631–634; *Angew. Chem. Int. Ed. Engl*. **1995**, *107*, 592–594.

[22] J. J. Schneider, N. Czap, D. Spickermann, C. W. Lehmann, F. Laschi, M. Fontani, P. Zanello, *J. Organomet Chem*. **1999**, *590*, 7–14.

Received July 13, 1999
[I99256]

Syntheses, Structures and Properties of Copper(I) and Copper(II) Complexes of the Ligand *N*,*N*′-Bis[2′-(dimethylamino)ethyl]-*N*,*N*′-dimethylethane-1,2-diamine (Me_6trien)

Michael Becker,[a] Frank W. Heinemann,[a] Falk Knoch,[a] Wolfgang Donaubauer,[a] Günter Liehr,[a] Siegfried Schindler,*[a] Gilad Golub,[b] Haim Cohen,[b] and Dan Meyerstein[b]

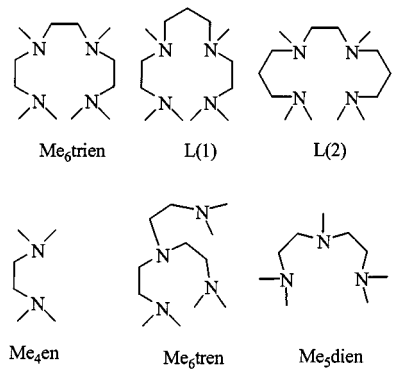
Keywords: Copper / Oxygen / Bioinorganic chemistry / Oxidations / Coordination chemistry

Copper(I) and copper(II) complexes of the ligand *N*,*N*′-bis[2′-(dimethylamino)ethyl]-*N*,*N*′-dimethylethane-1,2-diamine (Me_6trien) were synthesized and structurally characterized. In the solid state the complex cation $[Cu(Me_6trien)]^+$ (**1**) adopts a distorted tetrahedral configuration. Crystallography, EPR measurements, and UV/Vis spectroscopy indicate that the analogous copper(II) complex $[Cu(Me_6trien)Cl]^+$ has a square pyramidal geometry in the solid state as well as in solution. The reaction of **1** with dioxygen was investigated in different solvents. No copper dioxygen intermediates could be detected spectrophotometrically during these reactions.

Introduction

The dioxygen carrier protein hemocyanin (Hc) as well as many other metalloenzymes involved in important biological oxygen transfer reactions contain copper ions in their active sites.[1,2] A fundamental step in metalloenzyme redox reactions is the activation of dioxygen, upon binding at the active site, prior to the reaction with a substrate. Many low molecular weight model complexes for copper proteins have been synthesized and their reactions with dioxygen have been investigated.[1–23] A better understanding of these reactions will assist in the development of new homogeneous catalysts for selective oxidations under mild conditions.[24,25]

In contrast to enzymes, which react in aqueous solutions (although the copper ions are located in a relatively hydrophobic environment) at ambient conditions, the reactions of model complexes with dioxygen usually have to be investigated in organic solvents at low temperatures.[7,10,11,26] Therefore, in order to better model the reactivity of the biological systems, one should ideally study the oxidations of copper(I) complexes by dioxygen in water. This endeavor has been hampered because copper(I) complexes have a great tendency to disproportionate in aqueous solution. However, it is well-known that tertiary amine ligands can stabilize copper(I) in water; for example the copper(I) complex of the macrocyclic ligand 1,4,5,7,7,8,11,12,14,14-decamethyl-1,4,8,11-tetraazacyclo-tetradecane is stable towards oxidation in aqueous solution.[27] Tertiary amines in general have proven to be useful in stabilizing metal complexes in low oxidation states,[28,29] and the thermodynamic properties of a series of Cu^I and Cu^{II} complexes with the tertiary amines Me_6trien, L(1) and L(2) as ligands (Scheme 1) were investigated earlier.[27,29–34] If dioxygen is excluded, dilute solutions of the copper(I) complexes of these amines can easily be synthesized in water by a comproportionation reaction. As an example, the formation of the copper(I) complex of Me_6trien is shown in Equation 1.[31,35]



Scheme 1. Me_6trien = *N*,*N*′-bis[2′-(dimethylamino)ethyl]-*N*,*N*′-dimethylethane-1,2-diamine, L(1) = *N*,*N*′-bis(2′-(dimethylamino)-ethyl)-*N*,*N*′-dimethyl-propane-1,3-diamine, L(2) = *N*,*N*′-bis(2′-(dimethylamino)propyl)-*N*,*N*′-dimethylethane-1,2-diamine, Me_4en = tetramethylethylenediamine, Me_6tren = tris(2-dimethylamino-ethyl)amine), Me_5dien = 1,1,4,7,7-penta methyldiethylethylenetriamine

$$[Cu(II)Me_6trien]^{2+} \xrightarrow{Me_6trien,\ Cu(0)} 2\,[Cu(I)Me_6trien]^{+} \quad (1)$$

[a] Institute for Inorganic Chemistry,
University of Erlangen-Nürnberg,
Egerlandstraße 1, D-91058 Erlangen, Germany
Fax: (internat.) + 49(0)9131/8527387
[b] Chemistry Department, Ben Gurion University of the Negev, Beer-Sheva, Israel
[c] Nuclear Research Centre Negev, Beer-Sheva, Israel
[d] The College of Judea and Samaria, Ariel, Israel

 © WILEY-VCH Verlag GmbH, D-69451 Weinheim, 2000 1434–1948/00/0404–0719 $ 17.50+.50/0

These solutions are stable under inert conditions, but are oxidized immediately to the analogous Cu^{II} complexes by dioxygen.[31,35] As part of our ongoing investigation of the reactions of copper(I) complexes with dioxygen[26,36–42] we therefore investigated these oxidations with the copper(I) complexes of the tertiary amines Me_6trien, L(1) and L(2) in more detail.

Results and Discussion

Synthesis and Crystal Structure of [Cu(Me_6trien)][$CuCl_2$] (1-[$CuCl_2$])

The comproportionation reaction shown in Equation 1 did not allow the synthesis of highly concentrated aqueous solutions of copper(I) complexes. Nevertheless, white crystals were obtained from the reaction of Me_6trien with CuCl in methanol. The molecular structure of the cation of this new complex is shown in Figure 1.

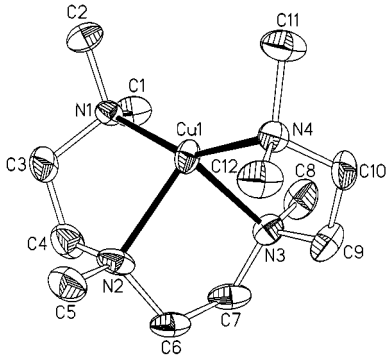


Figure 1. An ORTEP view of **1**; the thermal ellipsoids are at the 30% probability level and the hydrogen atoms are omitted for clarity

Although we had expected to obtain [CuMe_6trien]Cl (**1**-Cl) when mixing the ligand and CuCl in a stoichiometric ratio, it is obvious that the presence of the strong coordinating chloride prevents the reaction with the ligand from completing. Instead, **1**-[$CuCl_2$] is formed. In addition to the complex cation **1**, the asymmetric structural unit contains two halves of dichlorocopper(I) anions. Each of these holds a crystallographically imposed center of symmetry at the copper ion with one independent chloride. The anions are linear with Cu–Cl distances of 2.107(4) and 2.086(2) Å. These are very similar to the values that have been reported in the literature for $[CuCl_2]^-$ complexes.[43–46]

The tertiary amine tetramethylethylenediamine (Me_4en) can be regarded as one half of Me_6trien; the syntheses and structural characterizations of copper(I) complexes with Me_4en in a ratio of 1:2 were reported earlier.[28,45] The complex [Cu(Me_4en)$_2$][$CuCl_2$][45] (**2**-[$CuCl_2$]) is isostructural with **1**-[$CuCl_2$], and both complex cations adopt a distorted tetrahedral configuration. Nevertheless, close inspection of the Cu–N distances in **1** and **2** reveals significant differences. While for **2** the Cu–N bonds are consistent within the 3σ criterion [distances from 2.13(1) to 2.16(1) Å],[45] the two terminal Cu–N bonds in **1** are shorter [2.009(5) and 2.015(5) Å] than the other two Cu–N bonds [2.202(6) and 2.218(6) Å]. This clearly shows that Me_6trien in **1** is under more steric strain than Me_4en in **2**.

It is interesting to compare the molecular structure of **1** to the cation of the copper(I) complex [Cu(Me_6tren)]ClO_4 [**3**-ClO_4, Me_6tren = tris(2-dimethylaminoethyl)amine].[26] Me_6tren is an isomer of Me_6trien. In contrast to the distorted tetrahedral configuration of **1**, the geometry of **3** is best described as trigonal pyramidal (trigonal bipyramidal if the weakly coordinated perchlorate ion in the axial position is included); the copper ion is surrounded by the four amine nitrogen atoms with distances of 2.122(7) Å for the equatorial Cu–N and 2.200(14) Å for the axial Cu–N bonds.

Furthermore, bond lengths and angles in **1** are comparable to those of the complex cation of [Cu(Me_5dien)(CH_3CN)]ClO_4 (Me_5dien = 1,1,4,7,7-pentamethyldiethylethylenetriamine).[47] This compound [bond lengths for Cu–N = 2.04, 2.19, and 2.18 Å, and bond angles for N(1)–Cu–N(2) = 87.2(4) and N(2)–Cu–N(3) = 84.6(4)°] is even more distorted than **1**; its geometry was described as irregular. Me_5dien can be regarded as Me_6trien missing one arm, with the missing arm in the copper(I) complex being substituted by an acetonitrile molecule.

While it is possible to prepare dilute aqueous solutions of **1** by a comproportionation reaction (Equation 1), neither **2**, **3**, or [Cu(Me_5dien)]$^+$ could be obtained under the same conditions. However, we could prepare solutions of **3** in acetonitrile by a comproportionation reaction if Me_6tren was reacted with $CuCl_2 \times 2\ H_2O$ and copper powder under inert conditions. This reaction did not occur if Me_6trien or Me_4en were used as ligands under these conditions.

Reaction of 1 with Dioxygen

Thus far, the reactions of dioxygen with model compounds for copper proteins have been investigated mainly in organic solvents because of the disproportionation of Cu^I to Cu^0 and Cu^{II} in aqueous solutions.[1–4,24,48] For the same reason, knowledge on the kinetics of the oxidation of Cu^I complexes in water is rather limited; usually acetonitrile is chosen as a cosolvent.[39,49–55] Using the tertiary amines Me_6trien, L(1) and L(2) we tried to overcome these difficulties in order to study the formation of copper dioxygen adducts in aqueous solution, which would be similar to the oxidation of deoxy-Hc.

We successfully prepared dilute aqueous solutions of copper(I) complexes according to Equation 1. The kinetic behavior of all three amine complexes was similar; a representative example for the time resolved spectra of the reaction of dioxygen with **1** is shown in Figure 2

During the reaction, only the buildup of the product [Cu(Me_6trien)]$^{2+}$ (**4**) could be observed spectrophotometrically. No intermediate – neither a copper superoxo nor a peroxo complex – was detected. A change in pH from 7.0 to 10.0 did not alter the reaction rates significantly. Also, the rates did not depend on the concentration of dioxygen or the ionic strength. But they increased when the pressure was raised. However, these observations must be treated with caution since a detailed kinetic analysis was not possible. Computational fitting of the absorbance vs. time traces demonstrated that several reaction steps were in-

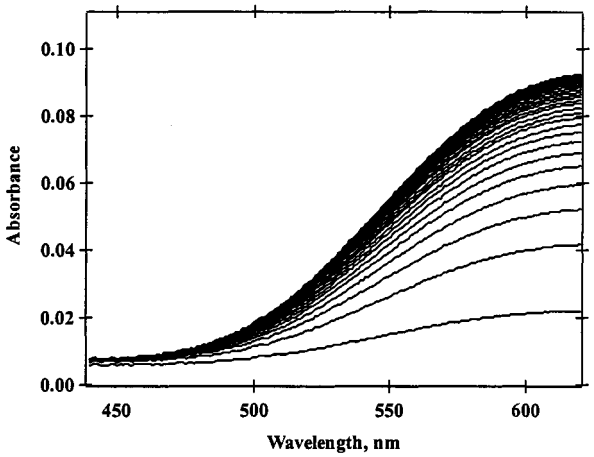


Figure 2. Reaction of **1** with dioxygen at 25 °C in water; the complex was prepared by the comproportionation reaction shown in Equation 1 ([**1**] = 0.5 mM, $[O_2]$ = 0.6225 mM, Δt = 20 s and pH = 8.0)

volved which presumably included higher order terms. To resolve these kinetic traces the spectra of intermediates and broader concentration windows for both reactants would be required.

This behavior was not unexpected because earlier investigations, mainly by Zuberbühler et al., showed that the kinetics of the reactions of copper(I) complexes with dioxygen in water are generally very complicated.[49–53,56–59] Most of these studies were performed in the presence of acetonitrile using the initial-rate treatment for the data analysis. Similar to our measurements, no copper peroxo intermediates were detected spectrophotometrically; often hydrogen peroxide was observed as a product.

To test whether hydrogen peroxide gave rise to additional reaction paths during the oxidation of **1** with dioxygen we investigated the reaction of H_2O_2 with **1** [as well as the copper(I) complexes of L(1) and L(2)]. The oxidation proceeded smoothly, but again complex kinetic behavior was observed and acceptable fitting of the data was not possible.

When small amounts of H_2O_2 were added to an aqueous solution of the copper(II) complexes, changes in the UV/Vis spectrum were not detected. When larger amounts were added (> tenfold excess) bubbles of dioxygen resulting from decomposition of H_2O_2 were observed.

A comparison between the oxidation of **1** and of deoxy-Hc shows clear differences in the reaction behavior. Deoxy-Hc reacts much faster than **1** (ca. 10000 times) with dioxygen (this rate is not dependent on pressure).[60,61] Furthermore, in contrast to the oxidation of **1**, the reaction of the protein is reversible. A major reason for these differences is the fact that the active site of deoxy-Hc is a preorganized dinuclear copper(I) site while **1** is mononuclear. In accordance with this, it has been shown earlier that a preorganized dinuclear copper(I) complex reacted extremely fast with dioxygen in organic solvents.[62] Presently, we are designing new dinuclear copper(I) complexes with tertiary amines in order to develop a system that will react similarly to the protein.

Recently, we found that **3** reacts reversibly with dioxygen in propionitrile or acetone at low temperatures, forming copper superoxo and peroxo complexes.[26][40] This reaction cannot be investigated in aqueous solution because disproportionation of **3** occurs. An investigation in methanol demonstrated that the peroxo complex is not stable in the presence of protons.[26]

The assumption that **1**, an isomer of **3**, would form dioxygen adducts in organic solvents as well, could not be confirmed. The only effect observed when **1** was reacted with dioxygen in methanol, acetone, or propionitrile was a decrease of the overall reaction rate compared to the studies in aqueous solutions. Lowering the temperature to –90 °C also slowed down the oxidation rate. No dioxygen intermediates could be observed spectrophotometrically under these conditions.

For comparison we also investigated the reaction of dioxygen with **2** (prepared in situ from $[Cu(CH_3CN)_4]PF_6$ and Me_4en) in propionitrile or acetone. The kinetic measurements did not provide evidence for the reversible formation of a peroxo intermediate and again an acceptable fitting of the data was not possible. However, it is known (also from kinetic studies) that peroxo and oxo-bridged dinuclear copper species are formed when copper(I) complexes of Me_4en, Et_4en and similar ligands (in a stoichiometric ratio of 1:1) are reacted with dioxygen in organic solvents.[63–70] Recently, a bis μ-oxo-copper complex and a trinuclear cluster with two μ_3-oxide ligands were obtained (and structurally characterized) from the reaction of copper(I) complexes of peralkylated-1,2-cyclohexanediamines with dioxygen.[18,71]

Synthesis and Crystal Structure of $[Cu(Me_6trien)Cl]ClO_4$ (4-Cl–ClO_4)

Copper(II) complexes of Me_6trien were easily prepared. The molecular structure was solved for **4**-Cl–ClO_4; its cation, with a square pyramidal geometry, is shown in Figure 3.

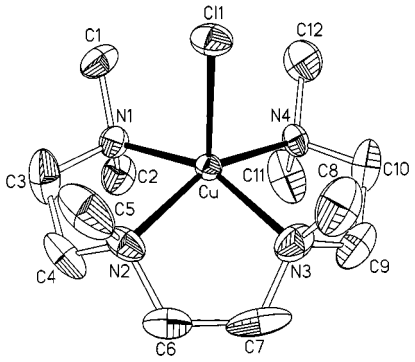


Figure 3. An ORTEP view of the cation of **4**-Cl–ClO_4; the thermal ellipsoids are at the 30% probability level and the hydrogen atoms are omitted for clarity

Structural characterization of copper complexes with Me_6trien or the related amines L(1) and L(2) (Scheme 1) was not available until recently, when the structure of the Cu^{II} complex $[CuL(1)](ClO_4)_2$ [L(1) = *N*,*N*′-bis[2′-(dimethylamino)ethyl]-*N*,*N*′-dimethylpropane-1,3-diamine]

Table 1. Selected bond lengths and bond angles with standard deviations in parentheses for **1**-[$CuCl_2$], **4**-Cl–ClO_4 and **5** × 2 H_2O

Bond lengths (Å) for **1**-[$CuCl_2$]			
Cu(1)–N(1)	2.009(5)	Cu(1)–N(4)	2.015(5)
Cu(1)–N(2)	2.202(6)	Cu(1)–N(3)	2.218(6)
Cu(2)–Cl(1)	2.107(4)	Cu(2)–Cl(1)[a]	2.107(4)
Cu(3)–Cl(2)[b]	2.086(2)	Cu(3)–Cl(2)	2.086(2)
Bond angles (°) for **1**-[$CuCl_2$]			
N(1)–Cu(1)–N(4)	146.8(2)	N(1)–Cu(1)–N(2)	87.3(2)
N(4)–Cu(1)–N(2)	119.3(2)	N(1)–Cu(1)–N(3)	117.7(2)
N(4)–Cu(1)–N(3)	86.4(2)	N(2)–Cu(1)–N(3)	84.5(3)
Cl(1)[a]–Cu(2)–Cl(1)	180.0	Cl(2)[b]–Cu(3)–Cl(2)	180.0
Bond lengths (Å) for **4**-Cl–ClO_4			
Cu–N(2)	2.072(5)	Cu–N(1)	2.158(4)
Cu–N(3)	2.082(5)	Cu–Cl(1)	2.420(2)
Cu–N(4)	2.125(5)		
Bond angles (°) for **4**–Cl–ClO_4			
N(2)–Cu–N(3)	82.4(2)	N(4)–Cu–N(1)	100.0(2)
N(2)–Cu–N(4)	156.0(2)	N(2)–Cu–Cl(1)	103.5(2)
N(3)–Cu–N(4)	85.4(2)	N(3)–Cu–Cl(1)	102.7(2)
N(2)–Cu–N(1)	83.6(2)	N(4)–Cu–Cl(1)	99.2(1)
N(3)–Cu–N(1)	155.9(2)	N(1)–Cu–Cl(1)	99.6(1)
Bond lengths (Å) for **5** × 2 H_2O			
Cu(1)–O(1)	1.911(4)		
Cu(1)–O(1)[c]	1.915(4)		
Cu(1)–N(1)	2.027(4)		
Cu(1)–N(2)	2.040(4)		
Cu(1)–Cu(1)[c]	2.976(1)		
Bond angles (°) for **5** × 2 H_2O			
O(1)–Cu(1)–O(1)[c]	77.9(2)	O(1)[c]–Cu(1)–N(2)	170.7(2)
O(1)–Cu(1)–N(1)	172.7(2)	N(1)–Cu(1)–N(2)	86.7(2)
O(1)[c]–Cu(1)–N(1)	97.4(2)	O(1)–Cu(1)–Cu(1)[c]	39.0(1)
O(1)–Cu(1)–N(2)	97.2(2)	O(1)[c]–Cu(1)–Cu(1)[c]	38.9(1)
N(1)–Cu(1)–Cu(1)[c]	136.0(1)	N(2)–Cu(1)–Cu(1)[c]	135.7(1)

[a] $-x, -y, -z$. – [b] $1-x, -y, -z$. – [c] $-x+1, -y+1, -z+1$.

was reported.[72] L(1) differs from Me_6trien by an additional –CH_2– group. The bond lengths for Cu–N in **4**-Cl–ClO_4 (Table 1) are similar to those generally found for other tertiary amine copper(II) complexes, and differ only slightly from those for [CuL(1)]$(ClO_4)_2$.[72] The main difference between the two structures is that [CuL(1)]$(ClO_4)_2$ has a tetragonally elongated *trans*-CuN_4O_2 coordination sphere with Cu–O distances of 2.562(7) Å while **4**-Cl–ClO_4 is clearly square pyramidal with a Cu–Cl bond length of 2.420(2) Å. No interaction between copper and the perchlorate anion was observed. A direct structural comparison of [CuL(1)]-$(ClO_4)_2$ with **4**-$(ClO_4)_2$ was not possible since the obtained crystals of the latter were not suitable for X-ray crystallography. The Cu–N bond lengths in **4**-Cl–ClO_4 are slightly longer than those in the analogous copper complex [Cu(trien)(SCN)](SCN), with the nonmethylated amine [Cu–N bond length from 2.008(7)–2.030(5) Å].[73] Similarly, the Cu–N bond lengths of [CuL(1)]$(ClO_4)_2$ are longer than in the analogous nonmethylated complex [Cu(2,3,2-tet)]-(ClO_4), (Cu–N bond length from 2.016(6)–2.032(6) Å).[74]

The molecular structure of [Cu(Me_5dien)(H_2O)($OCMe_2$)] was described as distorted square pyramidal [bond lengths Cu–N = 2.036, 2.034, and 2.022 Å, and bond angles for N(1)–Cu–N(3) = 158.8(3) and O(1)–Cu–N(2) = 172.1(4)°] with the acetone molecule in the axial position [bond length Cu–O = 2.222(6) Å].[47] All Cu–ligand bond lengths in this complex are shorter than in **4**-Cl–ClO_4.

The bond lengths for the two isomeric complexes **4**-Cl–ClO_4 and **3**-Cl–ClO_4 [Cu–N_{axial} = 2.040(6) and Cu–$N_{equatorial}$ = 2.186(2) Å] are similar with the exception of the Cu–Cl bond length, which is shorter in **3**-Cl–ClO_4 [2.234(2) Å].[26] Bond angles are different for the two complexes. Complex **4**-Cl–ClO_4 has square pyramidal geometry, while the molecular structure of **3**-Cl–ClO_4 must be described as trigonal bipyramidal.

The different solid state geometries of the two complexes, **4**-Cl–ClO_4 and **3**-Cl–ClO_4, are retained in solution. An absorbance maximum for **4**-Cl–ClO_4 in water at 643 nm (ε = 248 $cm^{-1}M^{-1}$) is typical for a tetragonal distorted copper(II) complex; this coordination is further confirmed by the EPR spectrum [g values: $g(x)$ = 2.042, $g(y)$ = 2.066, $g(z)$ = 2.229; nuclear hyperfine coupling constants: $A(x)$ = 20 G, $A(y)$ = 18 G, $A(z)$ = 168 G]. The same behavior was observed for **4**-$(ClO_4)_2$ [λ_{max} = 643 nm (ε = 248 $cm^{-1}M^{-1}$); g values: $g(x)$ = 2.039, $g(y)$ = 2.064, $g(z)$ = 2.241; nuclear hyperfine coupling constants: $A(x)$ = 19 G, $A(y)$ = 26 G, $A(z)$ = 169 G]. These data are in accord with the results of our earlier measurements with solutions of **4**-SO_4.[29] Furthermore, they are comparable to those reported for [CuL(1)]$(ClO_4)_2$ as discussed above.[72] In contrast, **3**-Cl–ClO_4 represents a

typical trigonal bipyramidal complex with an absorbance maximum at 876 nm (ε = 447 $cm^{-1}M^{-1}$). The trigonal bipyramidal geometry was confirmed by EPR measurements [*g* values: *g*(x) = 2.170, *g*(y) = 2.187, *g*(z) = 2.010; nuclear hyperfine coupling constants: *A*(x) = 88 G, *A*(y) = 96 G, *A*(z) = 81 G]; the spectral parameters are consistent with those measured in the solid state.[75]

Synthesis and Crystal Structure of $[Cu_2(Me_4en)_2(OH)_2](ClO_4)_2 \times 2\ H_2O$ (**5** × 2 H_2O)

Crystalline salts of $[Cu(Me_4en)_2Cl]ClO_4$ could not be synthesized. This was expected since it was previously suggested that the Cu^{II} ion is too small to form a 1:2 complex with Me_4en.[76] When we reacted Me_4en with a mixture of $CuCl_2$ and $Cu(ClO_4)_2$ in the same way as **4**-Cl–ClO_4 was synthesized, we obtained $[Cu_2(Me_4en)_2(OH)_2](ClO_4)_2$ (**5**) instead. The molecular structure of **5** is shown in Figure 4 (bond lengths and angles are given in Table 1).

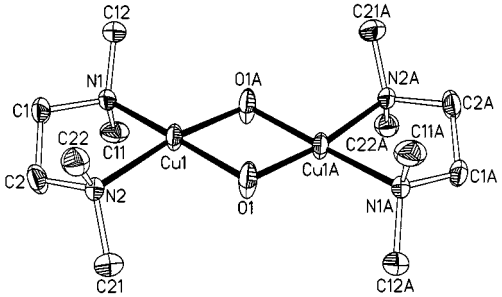


Figure 4. An ORTEP view of the cation of **5** × 2 H_2O; the thermal ellipsoids are at the 30% probability level and the hydrogen atoms are omitted for clarity

A crystal structure of **5** was described earlier by Pavkovik and co-workers.[77] It is not identical with the structure we report here because the latter holds two additional water molecules. This leads to significant differences in the dimensions and the volume of the unit cell. Furthermore, bond lengths and angles in the coordinated Me_4en of the complex described by Pavkovik (bond length C–C 1.377 Å and bond angles of 116.2° and 115.9° around the carbon atoms) do not correspond to the expected C–C bond lengths in this ligand. The authors do not discuss this, but possibly it is due to a disorder in the CH_2–CH_2 group. In contrast to these findings, we obtained a bond length of 1.493(3) Å for the two carbon atoms and bond angles of 109.2(5)° and 109.6(5)°, which are typical for a C–C bond in Me_4en.[78]

Conclusion

The study has shown that copper(I) complexes with related polymethylated aliphatic amines react very differently with dioxygen. Even though it was possible to oxidize **1** [or the copper(I) complexes of L(1) and L(2)] or **2** with dioxygen in different solvents, no dioxygen complexes could be observed as intermediates during these reactions. In contrast, it was shown earlier that the reaction of **3** with dioxygen at low temperatures in nitrile solvents allowed the observation of copper-superoxo and -peroxo complexes as intermediates.[26]

The reason for the different behavior towards dioxygen can be explained by the different geometries of the copper(I)/copper(II) complexes of these ligands. While **3** has a trigonal bipyramidal geometry; in solution a nitrile molecule replaces the weakly coordinated perchlorate,[26] **1** and **2** are best described as pseudo-tetrahedral. The coordination geometry of **3** already closely resembles that of the copper(II) complex, the peroxo product.[26] This is not the case for **1** and **2**. When the pseudo-tetrahedral **1** is oxidized it is turned into the distorted square pyramidal **4**. Evidence for the retention of the coordination geometry in solution is provided by UV/Vis and EPR spectroscopy. Thus, **1** has to undergo a geometrical rearrangement during the reaction with dioxygen; it may even be necessary for one arm of the four dentate ligand to open up before the copper(I) complex can react with dioxygen. Furthermore, the dioxygen ligand in a tetragonal elongated copper complex is kinetically more labile to substitution than in a trigonal bipyramidal geometry. This may be an important reason for the difference in behavior.[79]

It was also found that the nature of the ligand affects the stability of the copper(I) or copper(II) complexes. It was also responsible for the different behavior concerning comproportionation. Furthermore, the study clearly demonstrates that the reactions of copper(I) complexes with dioxygen vary with the solvent used.

The present findings fit well with recent reports on different copper(I) complexes that showed the influence of the ligand and the solvent on the formation of copper complexes with different peroxide binding modes; hereby an equilibrium of a peroxo complex with a bis μ-oxo copper species was discovered.[4,5,7,19–23] While it is still not possible to exactly predict the pathway for the reaction of a copper(I) complex with dioxygen, the findings presented here allow a better understanding of these reactions.

Experimental Section

General Remarks: Reagents and solvents used were of commercially-available reagent-grade quality. Distilled water was used for the preparation of aqueous solutions. The ligand Me_6trien was either synthesized as the free amine,[80] as a hydrochloride salt similar to a published procedure[81] or purchased from Aldrich. $[Cu(CH_3CN)_4]^+$ salts were synthesized and characterized according to literature methods.[82,83] CuCl was either synthesized according to a published procedure[84] or purchased from Aldrich. It was purified in a glove box under an inert atmosphere by washing the light green crystals with methanol until the solid was uniformly white. Preparation and handling of air-sensitive compounds was carried out in a glove box filled with argon (Braun, Garching, Germany; water and dioxygen less than 1 ppm). Air sensitive aqueous solutions were handled by Schlenk techniques or in a glove bag. UV/Vis spectra were measured on a CARY 5G UV/Vis-NIR spectrophotometer. Electron spin resonance measurements at X-band frequency were obtained using a Bruker EMX-113 spectrometer. Samples in methanol/DMF (3:1 mixtures) were measured at 100 K. Time resolved spectra of the reactions of dioxygen with copper(I)

Table 2. The crystal data and structure refinement for **1**-[$CuCl_2$], **4**-Cl–ClO_4 and **5** × 2 H_2O

Complex	**1**-[$CuCl_2$]	**4**-Cl–ClO_4	**5** × 2 H_2O
Empirical formula	$C_{12}H_{30}Cl_2Cu_2N_4$	$C_{12}H_{30}Cl_2CuN_4O_4$	$C_{12}H_{38}Cl_2Cu_2N_4O_{12}$
Formula weight	428.38	428.84	628.44
Temperature (K)	200	293	200
Crystal system	monoclinic	orthorhombic	monoclinic
Space group	$P2_1/n$	$Pna2_1$	$P2_1/c$
a (Å)	14.461(4)	13.075(5)	7.855(1)
b (Å)	14.916(4)	79.721(5)	15.124(2)
c (Å)	8.977(2)	14.861(5)	11.320(2)
β (°)	97.34(2)	90.0	106.77(1)
Volume (Å^3)	1920(1)	1889(1)	1287(1)
Z	4	4	2
Density calcd. (Mg/m^3)	1.482	1.508	1.621
Absorpt. coeffic. (mm^{-1})	2.489	1.461	1.918
F(000)	888	900	652
Crystal size (mm)	0.80 × 0.40 × 0.40	0.53 × 0.45 × 0.34	0.60 × 0.40 × 0.30
Diffractometer used	Siemens P4	Nonius CAD4 MACH3	Siemens P4
scan technique	ω scan	ω-2θ scan	ω scan
θ range for data collect. (°)	2.5 to 27.1	2.5 to 24.05	2.31 to 27.00
Index ranges	$-18 < h < 18$, $-19 < k < 0$, $-11 < l < 3$	$-14 < h < 14$, $-11 < k < 11$, $0 < l < 10$	$-10 < h < 1$, $-1 < k < 19$, $-14 < l < 14$
Reflections collected	5465	14208	3679
Independent refl., R_{int}	4214, 0.0255	2693, 0.1243	2803, 0.0565
Obs. reflect. [$F_o \geq 4\sigma(F)$]	2411	2406	1923
Data/restraints/parameters	4214/0/184	2693/23/ 214	2803/0/230
Goodness of fit on F^2	1.064	1.009	1.057
R_1[a] [$F_o > 4\sigma(F)$]	0.0789	0.0461	0.0560
wR_2[a] (all data)	0.2429	0.1306	0.1467
abs. structure parameter[88]	–	0.03(3)	–
q,r[a]	0.138, 0	0.100, 0	0.0664, 0.8047
Largest diff. peak and hole	3.426, –1.231	0.457, –0.262	0.830, –0.530

[a] $R_1 = \Sigma| F_o| - | F_c || / \Sigma| F_o|$; $wR_2 = \{\Sigma[w(F_o^2 - F_c^2)^2]/\Sigma[w(F_o^2)^2]\}^{1/2}$; $w = 1/[\sigma^2(F_o^2) + (q \times P)^2 + r \times P]$ where $P = (F_o^2 + 2F_c^2)/3$.

complexes were recorded on a modified Hi Tech SF-3 L low temperature stopped-flow unit (Salisbury, UK) equipped with a JM TIDAS 16–500 diode array spectrophotometer (JM, Aalen, Germany). Data fitting was performed using the integrated JM software Kinspec or the program Specfit (Spectrum Software Associates, Chapel Hill, USA). Dioxygen saturated solutions for the kinetic measurements were obtained by passing dioxygen through the solvent for 20 minutes described earlier.[7,10,11,26] Concentration of dioxygen was varied by mixing dioxygen saturated solutions with argon saturated solutions in syringes.

Caution! *Perchlorate salts are potentially explosive and should be handled with great care.*

[Cu(Me_6trien)][$CuCl_2$] (1-[$CuCl_2$]): In a glove box, a solution of Me_6trien (1 g, 4.34 mmol) in 10 mL of methanol was added, with stirring, to a suspension of CuCl (0.42 g, 4.34 mmol) in 10 mL of methanol. The solution turned slightly green and a small amount of red copper metal deposited. After filtration, diethyl ether was added to precipitate the complex. The white solid was filtered off and washed with diethyl ether. Drying in vacuum yielded 0.4 g (43%). – $Cu_2C_{12}H_{30}N_4Cl_2$: calcd. C 33.64, H 7.07, N 13.07; found C 33.89, H 7.14, N 13.13. Colorless crystals of **1**-[$CuCl_2$] were obtained from vapor diffusion of diethyl ether into a methanol solution of CuCl and Me_6trien.

[Cu(Me_6trien)Cl]ClO4 (4-Cl–ClO_4): To a solution of Me_6trien (1.152 g, 5 mmol) in 15 mL of methanol was added a solution of $CuCl_2 \times 2\ H_2O$ (0.42 g, 2.5 mmol) and $Cu(ClO_4)_2 \times 6\ H_2O$ (0.92 g, 2.5 mmol) in 20 mL of water. The solution was stirred for 15 minutes and filtered. After several days turquoise crystals formed suitable for X-ray analysis. Yield 1.4 g (65%). – $CuC_{12}H_{30}N_4Cl_2O_4$: calcd. C 33.61, H 7.05, N 13.06; found C 33.57, H 7.38, N 12.99.

[Cu(Me_6trien])(ClO_4)$_2$ [4-(ClO_4)$_2$]: To a solution of Me_6trien (0.576 g, 2.5 mmol) in 15 mL of methanol was added a solution of $Cu(ClO_4)_2 \times 6\ H_2O$ (0.92 g, 2.5 mmol) in 20 mL of water. Crystals immediately formed and more water was added, while heating the solution on a water bath, until most of the solid material was dissolved. After filtering the solution, deep blue crystals formed on standing for one day. Yield 0.65 g (50%). – $CuC_{12}H_{30}N_4Cl_2O_4 \times 1\ CH_3OH$: calcd. C 29.75, H 6.53, N 10.67; found C 29.67, H 6.52, N 10.93.

[Cu_2(Me_4en)$_2$($OH)_2$](ClO_4)$_2$ (5): To a solution of Me_4en (1.16 g, 10 mmol) in 25 mL of methanol was added a solution of $Cu(ClO_4)_2 \cdot 6H_2O$ (0.92 g, 2.5 mmol) and $CuCl_2 \times 2\ H_2O$ (0.42 g, 2.5 mmol) in 25 mL of water. The solution was stirred for 10 min and filtered. Soon afterwards crystals began to form which were suitable for X-ray analysis. Yield 0.55 g (35%). – $Cu_2C_{12}H_{38}N_4Cl_2O_{12}$: calcd. C 22.93, H 6.09, N 8.92; found C 23.03, H 5.73, N 8.83.

X-ray Crystallographic Study: Crystal data and experimental conditions for **1**-[$CuCl_2$], **4**-Cl–ClO_4 and **5** × 2 H_2O are listed in Table 2. The molecular structures are illustrated in Figures 1, 3, and 4. Selected bond lengths and bond angles with standard deviations in parentheses are presented in Table 1. Intensity data were collected with graphite monochromated Mo-K_α radiation (λ = 0.71073 Å). The collected reflections were corrected for Lorentz and polarization effects (but not for absorption). The structures were solved by direct methods [85,86] and refined by full matrix least squares methods on F^2.[85,87] Hydrogen atoms of **4**-Cl–ClO_4 were calculated for idealized geometries and allowed to ride on their preceding atoms, their isotropic displacement parameters were tied to those of the adjacent atoms by a factor of 1.5. For **1**-[$CuCl_2$] and **5** × 2

H_2O the positions of all hydrogen atoms were localized in a difference Fourier synthesis. The positions and a common isotropic displacement parameter were kept fixed during the refinement of **1**-[$CuCl_2$]. The high residual electron density of **1**-[$CuCl_2$] (3.426 e A^{-3}) is located near the copper atom (0.877 Å), and can be attributed to absorption effects. For **5** × 2 H_2O the positional parameters were refined with a fixed common isotropic displacement parameter. Crystallographic data (excluding structure factors) have been deposited with the Cambridge Crystallographic Data Center as supplementary publication no. CCDC-107373 (**1**-[$CuCl_2$]), –130856 (**4**-Cl–ClO_4), –130857 (**5** × 2 H_2O). Copies of the data can be obtained free of charge from The Director, CCDC, 12 Union Road, Cambridge CB2 1EZ (Fax: int. code + 1223/336-033; E-mail: deposit@ccdc.cam.ac.uk).

Acknowledgments

The authors gratefully acknowledge financial support from the Deutsche Forschungsgemeinschaft (S. S.), the Volkswagen-Stiftung (S. S.) and Deutscher Akademischer Austauschdienst (G. G.). Furthermore they would like to thank Dr. Jens Z. Pedersen (University of Odense, Denmark) for the EPR-measurements, and Prof. Dieter Sellmann and Prof. Rudi van Eldik (University of Erlangen-Nürnberg) for their support of this work.

[1] N. Kitajima, *Adv. Inorg. Chem.* **1992**, *39*, 1–77.
[2] K. D. Karlin, Z. Tyeklár, *Bioinorganic Chemistry of Copper*; Chapman Hall, New York, **1993**.
[3] T. N. Sorrell, *Tetrahedron* **1989**, *45*, 3–68.
[4] N. Kitajima, Y. Moro-oka, *Chem. Rev.* **1994**, *94*, 737–757.
[5] S. Mahapatra, J. A. Halfen, E. C. Wilkinson, L. J. Que, W. B. Tolman, *J. Am. Chem. Soc.* **1994**, *116*, 9785–9786.
[6] S. Mahapatra, J. A. Halfen, E. C. Wilkinson, G. F. Pan, C. J. Cramer, L. Que, W. B. Tolman, *J. Am. Chem. Soc.* **1995**, *117*, 8865–8866.
[7] J. A. Halfen, S. Mahapatra, E. C. Wilkinson, S. Kaderli, V. G. Young, L. Que, A. D. Zuberbühler, W. B. Tolman, *Science* **1996**, *271*, 1397–1400.
[8] L. Casella, M. Gullotti, G. Pallanza, L. Rigoni, *J. Am. Chem. Soc.* **1988**, *110*, 4221–4227.
[9] L. Casella, M. Gullotti, R. Radaelli, P. Di Gennaro, *J. Chem. Soc., Chem. Commun.* **1991**, 1611–1612.
[10] K. D. Karlin, M. S. Nasir, B. I. Cohen, R. W. Cruse, S. Kaderli, A. D. Zuberbühler, *J. Am. Chem. Soc.* **1994**, *116*, 1324–1336.
[11] K. D. Karlin, N. Wei, B. Jung, S. Kaderli, P. Niklaus, A. Zuberbühler, D., *J. Am. Chem. Soc.* **1993**, *115*, 9506–9514.
[12] T. N. Sorrell, D. L. Jameson, *Inorg. Chem.* **1982**, *21*, 1014–1019.
[13] R. Menif, A. E. Martell, P. J. Squattrito, A. Clearfield, *Inorg. Chem.* **1990**, *29*, 4723–4729.
[14] O. J. Gelling, F. van Bolhuis, A. Meetsma, B. L. Feringa, *J. Chem. Soc., Chem. Commun.* **1988**, 552–554.
[15] W. B. Tolman, *Acc. Chem. Res.* **1997**, *30*, 227–237.
[16] D. Ghosh, T. K. Lal, S. Ghosh, R. Mukherjee, *Chem. Comm.* **1996**, 13–14.
[17] N. Kitajima, K. Fujisawa, C. Fujimoto, Y. Moro-oka, S. Hashimoto, T. Kitagawa, K. Toriumi, K. Tatsumi, A. Nakamura, *J. Am. Chem. Soc.* **1992**, *114*, 1277–1291.
[18] A. P. Cole, D. E. Root, P. Mukherjee, E. I. Solomon, T. D. P. Stack, *Science* **1996**, *273*, 1848–1850.
[19] J. Reim, B. Krebs, *Angew. Chem.* **1994**, *106*, 2040–2041, *Angew. Chem. Int. Ed. Engl.* 1969–1971.
[20] T. N. Sorrell, W. E. Allen, P. S. White, *Inorg. Chem.* **1995**, *34*, 952–960.
[21] J. E. Bol, W. L. Driessen, A. Y. N. Ho, B. Maase, L. Que, J. Reedijk, *Angew. Chem.* **1997**, *109*, 1022–1025, Angew. Chem. Int. Ed. Engl. 998–1000.
[22] H. Börzel, P. Comba, C. Katsichis, W. Kiefer, A. Lienke, V. Nagel, H. Pritzkow, *Chem. Eur. J.* **1999**, *5*, 1716–1721.
[23] K. D. Karlin, D.-H. Lee, S. Kaderli, A. D. Zuberbühler, *Chem. Comm.* **1997**, 475–476.
[24] J. Reedijk (Ed.), *Bioinorganic Catalysis*, 2nd ed., Marcel Dekker, New York, **1999**.
[25] R. A. Sheldon, *J. Mol. Catal., A: Chemical*, special ed., **1997**, vol. 117.
[26] M. Becker, F. W. Heinemann, S. Schindler, *Chem. Europ. J.* **1999**, *5*, 3124–3129.
[27] N. Jubran, H. Cohen, Y. Koresh, D. Meyerstein, *J. Chem. Soc., Chem. Commun.* **1984**, 1683–1684.
[28] M. Pasquali, C. Floriani, G. Venturi, A. G. Manfredotti, A. Chiesi-Villa, *J. Am. Chem. Soc.* **1982**, *104*, 4092–4099.
[29] G. Golub, H. Cohen, P. Paoletti, A. Bencini, L. Messori, I. Bertini, D. Meyerstein, *J. Am. Chem. Soc.* **1995**, *117*, 8353–8361.
[30] E. Kimura, T. Koike, M. Kodama, D. Meyerstein, *Inorg. Chem.* **1989**, *28*, 2998–3001.
[31] G. Golub, H. Cohen, D. Meyerstein, *J. Chem. Soc., Chem. Comm.* **1992**, 397–398.
[32] G. Golub, I. Zilbermann, H. Cohen, D. Meyerstein, *Supramolecular Chem.* **1996**, *6*, 275.
[33] G. Golub, A. Lashaz, H. Cohen, P. Paoletti, A. Bencini, B. Valtancoli, D. Meyerstein, *Inorg. Chim. Acta* **1997**, *255*, 111–115.
[34] D. Meyerstein, *Coord. Chem. Rev.* **1999**, *186*, 141–147.
[35] G. Golub, H. Cohen, P. Paoletti, A. Bencini, D. Meyerstein, *J. Chem. Soc., Dalton Trans.* **1996**, 2055–2060.
[36] S. Schindler, D. J. Szalda, C. Creutz, *Inorg. Chem.* **1992**, *31*, 2255–2264.
[37] M. Becker, S. Schindler, R. van Eldik, *Inorg. Chem.* **1994**, *33*, 5370–5371.
[38] S. Ryan, H. Adams, D. E. Fenton, M. Becker, S. Schindler, *Inorg. Chem.* **1998**, *37*, 2134–2140.
[39] S. Goldstein, G. Czapski, R. van Eldik, H. Cohen, D. Meyerstein, *J. Phys. Chem.* **1991**, *95*, 1282–1285.
[40] S. Schindler, C. D. Hubbard, R. van Eldik, *Chem. Soc. Rev.* **1998**, *27*, 387–393.
[41] M. Becker, S. Schindler, K. D. Karlin, T. A. Kaden, S. Kaderli, T. Palanché, A. D. Zuberbühler, *Inorg. Chem.* **1999**, 1989–1995.
[42] N. Navon, H. Cohen, R. van Eldik, D. Meyerstein, *J. Chem. Soc., Dalton Trans.* **1998**, 3663–3666.
[43] S. Andersson, S. Jagner, *Acta Chem. Scand.* **1986**, *A40*, 52–57.
[44] M. Asplund, S. Jagner, M. Nilson, *Acta Chem. Scand.* **1983**, *A37*, 57–62.
[45] L. Engelhardt, M., R. Papsergio, I., A. White, H., *Aust. J. Chem.* **1984**, *37*, 2207–2213.
[46] B. W. Skelton, A. F. Waters, A. White, H., *Aust. J. Chem.* **1991**, *44*, 1207–1215.
[47] M. J. Scott, R. H. Holm, *J. Am. Chem. Soc.* **1994**, *116*, 11357–11367.
[48] E. Spodine, J. Manzur, *Coord. Chem. Rev.* **1992**, *119*, 171–198.
[49] A. D. Zuberbühler in *Metal Ions in Biological Systems* (Ed.: H. Sigel), Marcel Dekker, New York, **1976**, vol. 5, p. 133–189.
[50] H. Gampp, A. Zuberbühler in *Metal Ions in Biological Systems* (Ed.: H. Sigel), Marcel Dekker, New York, **1981**, vol. 12, p. 133–189.
[51] M. Güntensperger, A. Zuberbühler, *Helv. Chim. Acta* **1977**, *60*, 2584–2593.
[52] L. Mi, A. D. Zuberbühler, *Helv. Chim. Acta* **1991**, *75*, 1679–1688.
[53] L. Mi, A. D. Zuberbühler, *Helv. Chim. Acta* **1992**, *75*, 1547–1556.
[54] M. Masarwa, H. Cohen, D. Meyerstein, D. L. Hickman, A. Bakac, J. H. Espenson, *J. Am. Chem. Soc.* **1988**, *110*, 4293–4297.
[55] S. Goldstein, G. Czapski, *Inorg. Chem.* **1985**, *24*, 1087–1092.
[56] K. D. Karlin, J. Zubieta (Eds.), *Copper Coordination Chemistry*, Adenine, New York, **1983**, p. 237–258.
[57] H. Gampp, A. Zuberbühler, *J. Mol. Catal.* **1980**, *7*, 81–88.
[58] H. Gampp, A. D. Zuberbühler, *Chimia* **1978**, *32*, 54–56.
[59] G. Rainoni, A. Zuberbühler, *Chimia* **1974**, *28*, 67–70.
[60] C. R. Andrew, K. P. McKillop, A. G. Sykes, *Biochim. Biophys. Acta* **1993**, *1162*, 105–114.
[61] H. D. Projahn, S. Schindler, R. van Eldik, D. G. Fortier, C. R. Andrew, A. G. Sykes, *Inorg. Chem.* **1995**, *34*, 5935–5941.
[62] R. W. Cruse, S. Kaderli, K. D. Karlin, A. D. Zuberbuehler, *J. Am. Chem. Soc.* **1988**, *110*, 6882–6883.

[63] J. S. Thompson, *J. Am. Chem. Soc.* **1984**, *106*, 8308–8309.
[64] G. Davies, M. A. El-Sayed, *Inorg. Chem.* **1983**, *22*, 1257–1266.
[65] G. Davies, M. A. El Sayed, *Comments Inorg. Chem.* **1985**, *4*, 151–162.
[66] G. Davies, M. A. El-Sayed, M. Henary, *Inorg. Chem.* **1987**, *26*, 3266–3273.
[67] M. A. El-Sayed, El-Toukhy, G. Davies, *Inorg. Chem.* **1985**, *24*, 3387–3390.
[68] M. A. El-Sayed, A. A. Abu-Raqabah, G. Davies, A. El-Toukhy, *Inorg. Chem.* **1989**, *28*, 1909–1914.
[69] M. A. El-Sayed, G. Davies, T. Kasem, S., *Inorg. Chem.* **1990**, *29*, 4730–4735.
[70] J. L. DuBois, P. Mukherjee, A. M. Collier, J. M. Mayer, E. I. Solomon, B. Hedman, T. D. P. Stack, K. O. Hodgson, *J. Am. Chem. Soc.* **1997**, *119*, 8578–8579.
[71] V. Mahadevan, Z. Hou, A. P. Cole, D. E. Root, T. K. Lal, E. I. Solomon, T. D. P. Stack, *J. Am. Chem. Soc.* **1997**, *119*, 11996–11997.
[72] P. V. Bernhardt, *J. Am. Chem. Soc.* **1997**, *119*, 771–774.
[73] G. Marongiu, E. C. Lingafelter, P. Paoletti, *Inorg. Chem.* **1969**, *8*, 2763–2767.
[74] T. G. Fawcett, S. M. Rudich, B. H. Toby, R. A. Lalancette, J. A. Potenza, H. J. Schugar, *Inorg. Chem.* **1980**, *19*, 940–945.
[75] M. Q. Ehsan, Y. Ohba, S. Yamauchi, M. Iwaizumi, *Bull. Chem. Soc. Jpn.* **1996**, *69*, 2201–2209.
[76] D. W. Meek, S. A. Ehrhardt, *Inorg. Chem.* **1965**, *4*, 584–587.
[77] C. Arcus, K. P. Fivizzani, S. F. Pavkovic, *J. Inorg. Nucl. Chem.* **1977**, *39*, 285–287.
[78] E. D. Estes, W. E. Estes, W. E. Hatfield, D. J. Hodgson, *Inorg. Chem.* **1975**, *14*, 106–109.
[79] D. H. Powell, A. E. Merbach, I. Fábián, S. Schindler, R. van Eldik, *Inorg. Chem.* **1994**, *33*, 4468–4473.
[80] R. Barbucci, G. Paoletti, G. Ponticelli, *J. Chem. Soc. A* **1971**, 1637–1640.
[81] R. N. Icke, B. B. Wisegarver, G. A. Alles, H. R. Snyder, *Org. Synth. Coll. Vol.* **1941**, *3*, 723.
[82] M. Ciampolini, N. Nardi, *Inorg. Chem.* **1966**, *5*, 41–44.
[83] G. J. Kubas, B. Monzyk, A. L. Crumbliss, *Inorg. Synth.* **1979**, *19*, 90–92.
[84] R. N. Keller, H. D. Wzcoff, *Inorg. Synth.* **1946**, *2*, 1–4.
[85] *SHELXTL 5.03 for Siemens Crystallographic Research Systems*, Siemens Analytical X-ray Instruments Inc., Madison, WI, USA, **1995**.
[86] A. Altomare, G. Cascarano, C. Giacovazzo, A. Guagliardi, M. C. Burla, G. Polidori, M. Camalli, *J. Appl. Crystallogr.* **1992**, *22*, 389–393.
[87] G. M. Sheldrick, *SHELXL-92*, Univ. of Göttingen, **1992**.
[88] H. D. Flack, *Acta Crystallogr.* **1983**, *A39*, 876.

Received July 20, 1999
[I99266]

Trinuclear Palladium(II) Complexes with 2-Hydroxy-4-methoxyacetophenone N^4-Dimethylthiosemicarbazone: Synthesis, Spectral Studies and Crystal Structure of a Tripalladium Complex

Dimitra Kovala-Demertzi,*[a] Nikolaos Kourkoumelis,[a] Mavroudis A. Demertzis,[a] John R. Miller,[b] Christopher S. Frampton,[c] John K. Swearingen,[d] and Douglas X. West[d]

Keywords: Palladium / S ligands / One-dimensional extended networks / Structure elucidation

The synthesis and spectral characterization of a new *triangular,* trinuclear palladium(II) complex with the dianion of 2-hydroxy-4-methoxyacetophenone N^4-dimethylthiosemicarbazone, 4MeOAp4Me$_2^{2-}$ is reported. The X-ray crystal structure determination of [Pd(4MeOAp4Me$_2$)]$_3$·DMSO shows it to contain a chair-type hexagon of alternating Pd and S atoms which form a molecular bowl. The crystal structure of $H_2$4MeOAp4Me$_2$ shows that it is the *E* isomer with respect to the imine bond of the thiosemicarbazone moiety.

Introduction

Metallic palladium, and its mononuclear and trinuclear palladium(II) compounds, are the catalysts of choice for many reactions.[1] For example, palladium acetate is employed as a homogeneous catalyst in a large number of organic syntheses.[2] Palladium acetate, $Pd_3(\mu\text{-}OAc)_6$, is trinuclear with a triangular arrangement of nonbonded palladium atoms,[3a] and $[Pd_3(\mu\text{-}O_2CMe)_3(\mu\text{-}MeSCHR)_3]$[3b] is a mixed-sphere palladium complex in which the solid state nuclearity and the palladium acetate structure are retained. The structures of both triangular and linear trinuclear palladium(II) complexes have been determined.[3]

Thiosemicarbazones of salicylaldehyde and 2-hydroxyacetophenone have recently attracted considerable attention because of their potential biological properties[4] and catalytic activity.[5] Binuclear copper(II)[6] and nickel(II)[7] complexes of these N^4-substituted thiosemicarbazones have phenoxide bridges. Recently, a trinuclear palladium complex[8] with sulfur bridges, and a trinuclear nickel(II) complex with both Ni–O,O–Ni and Ni–S,O–Ni bridging patterns have been reported.[9] Palladium(II) complexes of 2-formylpyridine, 2-acetylpyridine and 2-benzoylpyridine N^4-substituted thiosemicarbazones have also been studied with regard to their structural and biological properties, and some of them have shown remarkable antitumor activity.[10] Therefore we decided to expand our studies of palladium(II) complexes to include other potentially tridentate thiosemicarbazone ligands and report here the structure of [Pd(4MeOAp4Me$_2$)]$_3$·DMSO (where 4MeOAp4Me$_2$ is the dianion of 2-hydroxy-4-methoxyacetophenone N^4-dimethylthiosemicarbazone), which has Pd–S–Pd bridging. Also included is the crystal structure of the uncomplexed 2-hydroxy-4-methoxyacetophenone N^4-dimethylthiosemicarbazone, $H_2$4MeOAp4Me$_2$.

Results and Discussion

The negative charge distribution on the atoms in a molecule with several donor centers can be used to study the formation of donor-acceptor bonds with a metal. From our

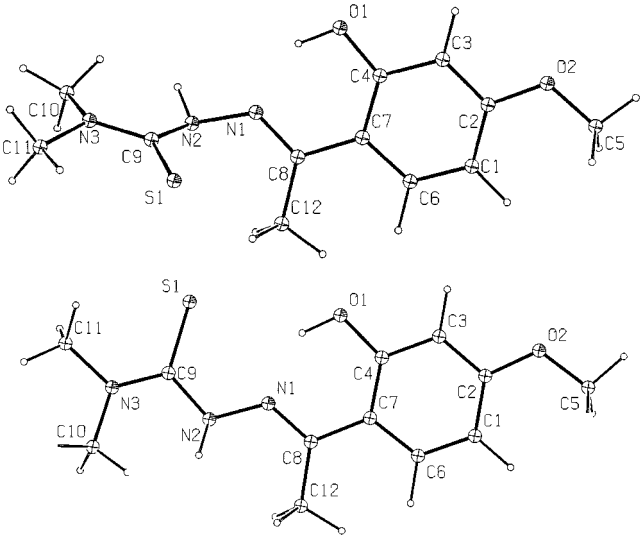


Figure 1. The fully PM3-optimized geometry of the neutral $H_2$4MeOAp4Me$_2$ molecule in the gas phase (a: top) and in methanol (b: bottom); the numbering used in the body of the text is applied

[a] Department of Chemistry, University of Ioannina, 45110 Ioannina, Greece
E-mail: dkovala@cc.uoi.gr
[b] Department of Biological and Chemical Sciences, University of Essex, Wivenhoe Park, Colchester CO4 3SQ, United Kingdom
[c] Roche Discovery Welwyn, Welwyn Garden City, Hertfordshire AL7 3AY, United Kingdom
[d] Department of Chemistry, Illinois State University, Normal, IL 61790-4160, USA

 © WILEY-VCH Verlag GmbH, D-69451 Weinheim, 2000 1434–1948/00/0404–0727 $ 17.50+.50/0

Table 1. The calculated charges, electron densities, ionization potentials, dipole moments and ΔH_f (kcal/mol) for $H_2$4MeOAp4Me$_2$, H_2L, and the dianion 4MeOAp4Me$_2^{2-}$, L^{2-}; atom numbers are in accord with the notation of Figure 1

Atom	Charge[a][b] $H_2$4MeOAp4Me$_2$	Electron densities	Charge[b][c] $H_2$4MeOAp4Me$_2$	Electron densities
O1	–0.258	6.257	–0.333	6.333
O2	–0.184	6.184	–0.231	6.231
N1	–0.261	5.262	–0.238	5.238
N2	0.089	4.911	0.142	4.858
N3	0.075	4.925	0.293	4.707
S	–0.318	6.318	–0.711	6.711
	Charge[a][d] 4MeOAp4Me$_2^{2}$	Electron densities	Charge[c][d] 4MeOAp4Me$_2^{2-}$	Electron densities
O1	–0.563	6.563	–0.755	6.755
O2	–0.229	6.229	–0.244	6.244
N1	–0.066	5.066	–0.209	5.209
N2	–0.244	5.244	–0.203	5.203
N3	–0.029	5.029	–0.028	5.028
S1	–0.699	6.699	–0.918	6.918

[a] In the gas phase. – [b] The dipole moment and the ΔH_f are 4.62 Debye and 1.90 kcal/mol and 15.82 Debye and –24.97 kcal/mol for $H_2$4MeOAp4Me$_2$ in the gas state and in methanol, respectively. – [c] In CH_3OH. – [d] The dipole moment and the ΔH_f are 3.12 Debye and –17.88 kcal/mol and 7.43 Debye) and –223.65 kcal/mol for 4MeOAp4Me$_2^{2-}$ in the gas state and in methanol, respectively.

results the sulfur atom with maximum electron density and negative charge is predicted to be the preferred metal binding site; this agrees with the structural studies. The high effective charge and the high electron density value for the phenolic oxygen O1 and the imine nitrogen N1, also indicate strong electron-donor properties. The effective charges on the nitrogen atoms explain the conjugation of the thiosemicarbazonato moiety. The calculated molecular structures of the neutral $H_2$4MeOAp4Me$_2$ both in the gas phase and methanol are shown in Figure 1. The optimized geometry in methanol is *ZEZ* and is similar to that observed by X-ray diffraction for $H_2$4MeOAp4Me$_2$, the differences being attributable to packing effects. The data in Table 1 show the charge, electron densities for the various atoms, ionization potential, total dipole moment and enthalpy of formation of neutral $H_2$4MeOAp4Me$_2$ and the dianion 4MeOAp4Me$_2^{2-}$, in the gaseous state and in methanol, that have been calculated using MOPAC93.[11] As is evident from these data, the configuration in methanol is the preferred one over the configuration in the gas phase for $H_2$4MeOAp4Me$_2$ and 4MeOAp4Me$_2^{2-}$. The values obtained in methanol solution can be considered as a good approximation of the relative stability of the species in CH_3OH/H_2O. For 4MeOAp4Me$_2^{2-}$ a dramatic difference in stability is seen in methanol and in other polar solvents. The relative stability was computed as 23 and 206 kcal.mol^{-1} for the neutral and dianionic species, respectively.

The interaction of K_2PdCl_4 with $H_2$4MeOAp4Me$_2$ in basic solution (aqueous methanolic ammonia, pH ≈ 9) afforded the trinuclear complexes **1**, **2** and **3** according to the reactions:

$$K_2PdCl_4 \text{ with } H_2\text{4MeOAp4Me}_2 \longrightarrow [Pd(\text{4MeOAp4Me}_2)]_3 \cdot 3\,H_2O\ (\mathbf{1}) + 6\,KCl + 6\,HCl \quad (1)$$

$$\mathbf{1} \longrightarrow [Pd(\text{4MeOAp4Me}_2)]_3\ (\mathbf{2}) + 3\,H_2O \quad (2)$$

$$\mathbf{2} + DMSO \longrightarrow [Pd(\text{4MeOAp4Me}_2)]_3 \cdot DMSO\ (\mathbf{3}) \quad (3)$$

The stoichiometry of the complexes indicates that palladium(II) is coordinated by the doubly charged anion 4MeOAp4Me$_2^{2-}$ formed on the loss of the two protons from the phenolic oxygen and thioamide nitrogen, N2.

Molecular Structures

The structure of the uncomplexed thiosemicarbazone, $H_2$4MeOAp4Me$_2$, with two crystallographically different molecules per unit cell is shown in Figure 2 and the crystallographic data in Table 2, the bond lengths in Table 3 and bond angles in Table 4. The ligand has a *ZEZ* configuration about the bonds C1–C2, N1–C7 and N2–C8. N2H (and N5H) form an intermolecular hydrogen bond to a thione sulfur of an adjacent molecule, and the N2H (and N5H) groups of this molecule form hydrogen bonds to the sulfur atom of the first molecule, resulting in a dimer analogous to the dimer found for a number of heterocyclic thioureas.[12] The crystal packing is stabilized by intermolecular hydrogen bonds of the type C–H···O, O(3a)···H–C(2),[13] and by intramolecular hydrogen bonds. O1H and O3H form bifurcated intramolecular hydrogen bonds with their imine nitrogens, N1 and N3, and sulfur atoms, S1 and S2,

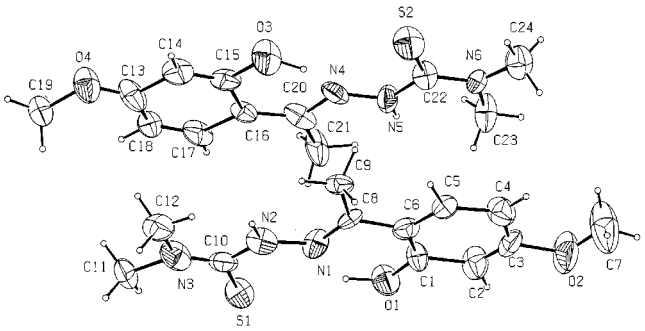


Figure 2. A perspective view of the two crystallographic different molecules of $H_2$4MeOAp4Me$_2$ (atoms at 50% probability)

Table 2. Crystal data and structure refinement for $H_2$4MeOAp4Me$_2$ and [Pd(4MeOAp4Me$_2$)]$_3$·DMSO

Empirical formula	$C_{12}H_{17}N_3O_2S$	$C_{36}H_{45}N_9O_6Pd_3S_3·C_2H_6OS$
Molecular mass	267.3	1193.40
Crystal system	Triclinic	Triclinic
Space group	*P*1 (# 1)	*P*–1 (# 2)
a, Å	8.119(4)	10.2412(1)
b, Å	9.064(2)	12.9971(2)
c, Å	9.629(2)	18.8397(2)
α, °	100.43(2)	92.6569(2)
β, °	101.67(3)	101.0277(7)
γ, °	96.33(3)	109.5790(8)
V, Å^3	674.6(8)	2302.45(5)
Z	2	2
D(calcd.), g cm^{-3}	1.316	1.721
F(000)	284	1200
μ(Mo-K_α), cm^{-1}	2.39	14.0
Crystal size, mm	0.10 × 0.15 × 0.30	0.02 × 0.04 × 0.40
Temperature, K	293(2)	123
λ(Mo-K_α)	0.71073	0.71073
φ min–max, °	1.0–26.38	1.1–26.4
hkl range	0, 10; –11, 11; –12, 12	–12, 12; –16, 16; –23, 23
Total, unique data, *R*(int)	3449, 3317	22641, 9234, 0.035
Observed data	1848 [$I > 3.0\ \sigma(I)$]	7425 [$I > 2.0\ \sigma(I)$]
N(ref), *N*(par)	3317, 330	9244, 564
R, *wR*	0.044, 0.099	0.0387, 0.1051
Goodness-of-fit on F^2	0.628	1.01
Largest diff. peak/hole, eÅ^{-3}	0.52/–0.32	0.81/0.79

Table 3. Selected bond lengths (Å) for $H_2$4MeOAp4Me$_2$ and [Pd(4MeOAp4Me$_2$)]$_3$·DMSO

$H_2$4MeOAp4Me$_2$		[Pd(4MeOAp4Me$_2$)]$_3$·DMSO	
S1–C10	1.65(2)	S1–C10	1.800(6)
N3–C10	1.29(3)	N3–C10	1.358(6)
N2–C10	1.39(2)	N2–C10	1.309(7)
N1–N2	1.39(2)	N1–N2	1.401(5)
N1–C8	1.26(2)	N1–C8	1.316(6)
C1–O1	1.32(2)	C1–O1	1.323(5)
C3–O2	1.48(3)	C3–O2	1.369(6)
S2–C22	1.71(2)	S2–C22	1.821(4)
N6–C22	1.37(2)	N6–C22	1.362(6)
N5–C22	1.36(2)	N5–C22	1.275(6)
N4–N5	1.38(2)	N4–N5	1.406(6)
N4–C20	1.32(2)	N4–C20	1.316(6)
C13–O4	1.25(2)	C13–O3	1.314(5)
C15–O3	1.40(2)	C15–O4	1.373(7)
		S3–C34	1.794(5)
		N9–C34	1.356(5)
		N8–C34	1.306(6)
		N7–N8	1.419(5)
		N7–C32	1.334(6)
		C25–O5	1.322(6)
		C27–O6	1.370(7)
		Pd1–S1	2.2585(12)
		Pd1–S3	2.3347(13)
		Pd2–S1	2.3578(12)
		Pd2–S2	2.2713(12)
		Pd3–S2	2.3579(12)
		Pd3–S3	2.2536(13)
		Pd1–O1	2.000(3)
		Pd1–N1	2.012(4)
		Pd2–O3	1.987(4)
		Pd2–N4	2.004(4)
		Pd3–O5	1.997(3)
		Pd3–N7	2.004(4)

respectively. The various distances and angles for the intramolecular and intermolecular hydrogen bonding of both forms of $H_2$4MeOAp$_4$Me$_2$ are listed in Table 5.

The two crystallographical forms of the $H_2$4MeOAp$_4$Me$_2$ molecules have the greatest differences in the following bond lengths in the thiosemicarbazone moieties: S1–C10, 1.65(2) Å and S2–C22, 1.71(2) Å; N3–C10, 1.29(3) Å and N6–C22, 1.37(2) Å; and N1–C8, 1.27(2) Å and N4–C20, 1.32(2) Å. The bond angles in the thiosemicarbazone moieties having the greatest differences are N3–C10–S1, 126.6(12)° and N6–C22–S2, 122.2(11)°; N1–N2–C10, 121.4(12)° and N4–N5–C22, 116.8(13)° and C8–N1–N2, 121.1(11)° and C20–N4–N5, 115.4(13)°. The phenoxy and methoxy bond lengths and angles are also significantly different suggesting that the differences in the two $H_2$4MeOAp4Me$_2$ molecules are due to packing effects.

The palladium complex **3** crystallizes with a dimethyl sulfoxide solvate molecule. A perspective view of [Pd(4MeOAp4Me$_2$)]$_3$·DMSO with the atomic numbering scheme is shown in Figure 3. The crystallographic data are summarized in Table 2 and selected bond lengths and angles are listed in Table 3 and Table 4, respectively. The core of **3** consists of a six-membered ring of alternating Pd^{II} and S atoms in a chair-like configuration. The remaining two sites of each square planar Pd^{II} center are occupied by the imine nitrogen and the phenoxy oxygen. The dianionic, tridentate ligand has a *ZEZ* configuration about the bonds C1–C6, N1–C8 and N2–C10 for the oxygen, nitrogen and sulfur donor centers. The whole structure forms into a type of bowl with the (3Pd–3S) ring as the base. The bowl almost has a non-crystallographic threefold symmetry except for the disposition of the methoxyphenyl group, C(7)–O(2), on the rim. This type of core has been reported previously for palladium complexes.[14] The dihedral angles between the planes of the two chelate rings (Pd–S–C–N–N) **A** and (Pd–N–C–C–O) **B** are 8.73(13), 0.58(15) and 4.39(17)° for Pd1,

Table 4. Selected bond angles (°) for $H_2$4MeOAp4Me$_2$ and [Pd(4MeOAp4Me$_2$)]$_3$·DMSO

$H_2$4MeOAp4Me$_2$		[Pd(4MeOAp4Me$_2$)]$_3$·DMSO	
N3–C10–S1	126.6(12)	N3–C10–S1	118.4(4)
N2–C10–S1	121.2(12)	N2–C10–S1	122.8(4)
N2–C10–N3	112.1(14)	N2–C10–N3	118.4(4)
N1–N2–C10	121.4(12)	N1–N2–C10	115.9(4)
C8–N1–N2	121.1(11)	C8–N1–N2	114.8(4)
O1–C1–C2	110.6(13)	O1–C1–C2	116.8(4)
N6–C22–S2	122.2(11)	N6–C22–S2	117.1(3)
N5–C22–S2	122.1(11)	N5–C22–S2	122.7(4)
N5–C22–N6	115.6(12)	N5–C22–N6	117.1(3)
N4–N5–C22	116.8(13)	N4–N5–C22	117.0(4)
C20–N4–N5	115.4(13)	C20–N4–N5	114.1(4)
O3–C13–C18	116.0(12)	O3–C13–C18	125.5(5)
		N9–C34–S3	117.6(3)
		N8–C34–S3	123.2(3)
		N8–C34–N9	117.6(3)
		N7–N8–C34	114.3(4)
		C32–N7–N8	114.3(4)
		O5–C25–C30	125.5(5)
Pd_3 Complex		S1–Pd1–S3	89.97(4)
C10–S1–Pd1	95.23(17)	S1–Pd1–O1	178.91(11)
C10–S1–Pd2	104.93(13)	S3–Pd1–O1	91.10(10)
C22–S2–Pd2	95.15(18)	S3–Pd1–N1	172.91(11)
C22–S2–Pd3	103.53(16)	S1–Pd2–S2	92.26(4)
C34–S3–Pd3	96.17(13)	S1–Pd2–O3	89.21(10)
C34–S3–Pd1	101.31(15)	S2–Pd2–O3	176.23(11)
C1–O1–Pd1	122.4(3)	S2–Pd2–N4	85.47(13)
C13–O3–Pd2	125.5(3)	S2–Pd3–S3	90.69(4)
C25–O5–Pd3	123.9(3)	S2–Pd3–O5	90.33(11)
C8–N1–Pd1	125.7(3)	S3–Pd3–O5	178.86(12)
C20–N4–Pd2	119.5(3)	S3–Pd3–N7	85.54(11)
C32–N7–Pd3	125.4(3)	Pd1–S1–Pd2	95.29(4)
N2–N1–Pd1	118.4(3)	S1–Pd1–N1	85.64(11)
N5–N4–Pd2	119.5(3)	Pd2–S2–Pd3	104.18(5)
N8–N7–Pd3	116.1(4)	O1–Pd1–N1	93.27(14)
		Pd1–S3–Pd3	98.43(4)
		S1–Pd2–N4	176.27(12)
		S2–Pd3–N7	175.79(11)
		O3–Pd2–N4	93.24(16)
		O5–Pd3–N7	93.42(15)

Table 5. Distances (Å) and angles (°) for the inter- and intramolecular hydrogen bonding in $H_2$4MeOAp4Me$_2$ and [Pd(4MeOAp4Me$_2$)]$_3$·DMSO

Donor, D	H	Acceptor, A[a]	D···A	H···A	D–H···A
$H_2$4MeOAp4Me$_2$					
O1	H1	N1	2.58(2)	2.00(1)	115.1(8)
O3	H3	N4	2.53(2)	1.68(1)	139.4(7)
O1	H1	S1	3.69(2)	2.71(3)	167.2(7)
O3	H3	S2	3.60(2)	2.76(3)	139.4(7)
N2	H2	S2i	3.65(2)	3.405(3)	98.5(9)
N5	H5	S1i	3.70(2)	3.468(3)	97.7(9)
C(12)	H(12B)	O(3)ii	3.40(2)	2.550(1)	149.2(7)
[Pd(4MeOAp4Me$_2$)]$_2$·DMSO					
C17	H17A	O7i	3.491(7)	2.598(4)	156.7(3)
C19	H19A	O2ii	3.235(7)v	2.546(4)	127.4(3)
C38	H38A	O6iii	3.385(9)	2.488(4)	152.0(4)
C31	H31B	O7a	3.526(8)	2.569(5)	165.5(4)
C36	H36C	S3	3.027(4)	2.5670(11)	102.8(2)
C23	H23C	S2	3.087(6)	2.5816(12)	112.2(3)
C33	H33A	N8	2.649(6)	2.253(4)	102.8(3)
C–H..Cg[b]			H..Cg	X..Cg	C–H..Cg
C5–H5B→ Cg3i			3.020	3.757	135.50
C7–H7B→ Cg6ii			3.225	3.994	126.72
C9–H9A→ Cg1iii			2.698	3.324	122.19
C9–H9B→ Cg1iii			3.196	3.324	88.86
C24–H24A→ Cg9iv			3.277	3.869/P'	120.59
C29–H29A→ Cg9v			2.875	3.752/P'	154.18
C37–H37A→ Cg6iv			2.987	3.691/P'	129.77

[a] Symmetry operations: i: 1 – *x*, 2 – *y*, –*z*; ii: *x*, 1 + *y*, *z*; iii: 1 – *y*, –*z*. – [b] Symmetry operations: i: –1 + *x*, *y*, *z*; ii: –1 + *x*, –1 + *y*, *z*; iii: –*x*, 2 – *y*, 1 – *z*; iv: 1 + *x*, *y*, *z*; v: *x*, –1 + *y*, *z*. Cg1 and Cg3 are referred to the centroids Pd1–S1–C10–N2–N1 and Pd3–S3–C34–N7–N8, respectively, and Cg6 and Cg9 are referred to the centroids Pd2–N4–C20–C18–C13–O3 and C13–C14–C15–C16–C17–C(18), respectively.

Pd2 and Pd3, respectively, indicating that there is some deviation from planarity by the ligands. The plane **A** of Pd1 is tilted by 83.46(14) and 73.58(14)° with respect to the plane **A** of Pd2 and Pd3, respectively.

The distances between the palladium centers [Pd1–Pd2, 3.4118(5) Å; Pd2–Pd3, 3.4746(5) Å; and Pd1–Pd3, 3.6528(5) Å] indicate that there is no direct bond between the palladium atoms. However, a very weak interaction can be postulated in agreement with the reported values for polynuclear palladium complexes [2.549(2)–3.539(1) Å].[3][8][15] The three bond angles involving bridging sulfur atoms are as follows: Pd1–S1–Pd2, 95.29(4)°; Pd2–S2–Pd3, 104.18(5)°; Pd1–S3–Pd3, 98.43(4)°. The Pd–N bond lengths range from 2.004(4) to 2.012(4) Å, the Pd–O distances from 1.987(4) to 2.000(3) Å, and the Pd–S distances from 2.2536(12) to 2.3579(12) Å and are similar to those found in other palladium complexes.[8][10] The greater *trans* influence of the iminic nitrogens can be observed in the lengthening of the *trans* Pd–S distances [2.3579(12)–2.3347(13) Å] with respect to the Pd–S distances *trans* to the phenoxy oxygens [2.2536(12)–2.2713(12) Å]. A comparison of the palladium-donor atom and thiosemicarbazonato moiety bond lengths of **3** and a related palladium complex[8] is shown in Table 6. The negative charge of the dianionic ligand is delocalized over the thiosemicarbazonato moiety and the S–C bond lengths are consistent with increased single bond character, while the imine C–N distances and both thioamide C–N distances indicate considerable double bond character.

The C–S bond length increases from an average of 1.68(2) Å in $H_2$4MeOAp4Me$_2$ to an average of 1.803(5) Å in **3** consistent with this bond's change from a conventional double bond to a single bond. Coordination of the imine nitrogen and phenoxy oxygen causes much smaller changes in the C–N and C–O bond lengths. The thioamide C–N bond (e.g., N2–C10), which formally changes from a single bond to a double bond on coordination, decreases from an average of 1.37(2) Å in $H_2$4MeOAp4Me$_2$ to 1.299(7) Å in **3**. The other thiosemicarbazone bonds' average distances also undergo modest changes on coordination, but the changes are not more than three times the combination of the estimated standard deviations of the bonds in the two compounds. The average bond angles also change on coordination to the palladium centers with most bond angles in the thiosemicarbazone moiety and the phenoxy function increasing or decreasing by at least 5°.

The dimethyl sulfoxide molecule appears to be linked via a three-center hydrogen bond (i.e., bifurcated). This bifurc-

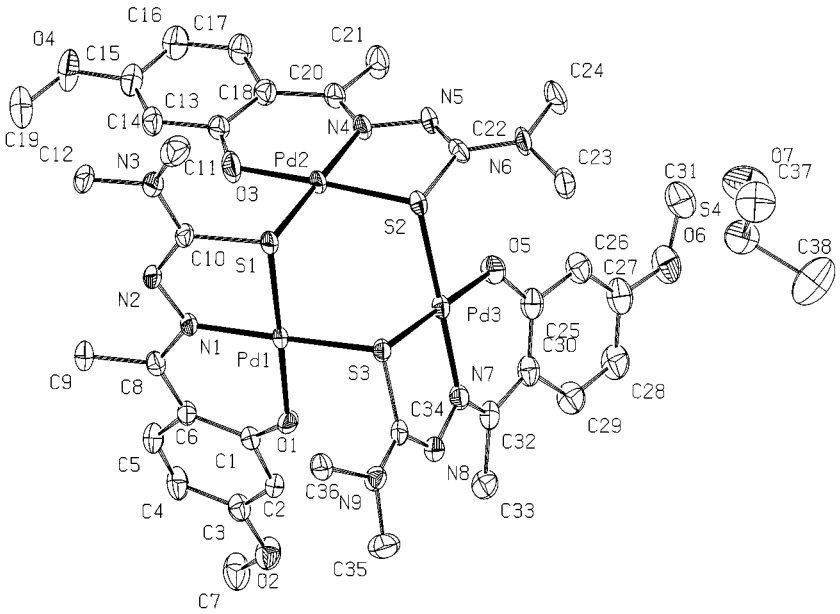


Figure 3. Structural representation of $[Pd(4MeOAp4Me_2)]_3$·DMSO with the labeling scheme; hydrogen atoms are omitted

Table 6. Comparison of bond lengths of trinuclear palladium complexes of 2-hydroxyacetophenone N^4-substituted thiosemicarbazones

Mode	$[Pd(Ap4E)]_3$·DMF[a]	$[Pd(MeOAp4Me_2)]_3$·DMSO[b]
C–S	1.797(7)	1.800(6)
	1.798(8)	1.821(4)
	1.788(6)	1.794(5)
C(S)–NR_2	1.343(9)	1.358(6)
	1.33(1)	1.362(6)
	1.33(1)	1.356(5)
N=C(S)	1.291(9)	1.309(7)
	1.304(8)	1.275(6)
	1.293(9)	1.306(6)
N–N	1.400(8)	1.401(5)
	1.406(8)	1.406(6)
	1.395(8)	1.419(5)
C–O	1.30(1)	1.323(5)
	1.309(9)	1.314(5)
	1.312(9)	1.322(6)
N1=C8	1.314(9)	1.316(6)
	1.306(8)	1.316(6)
	1.296(9)	1.334(6)
Pd–S	2.226(2) 2.332(2)	2.2585(12) 2.3347(13)
	2.250(2) 2.315(2)	2.3578(12) 2.2713(12)
	2.231(2) 2.337(2)	2.3579(12) 2.2536(13)
Pd–O	1.967(5)	2.000(3)
	1.993(5)	1.987(4)
	1.994(6)	1.997(3)
Pd–N	2.005(6)	2.012(4)
	2.002(6)	2.004(4)
	2.020(5)	2.004(4)

[a] Ref.[6], where Ap4E is the dianion of 2-hydroxyacetophenone N^4-ethylthiosemicarbazone. – [b] This work.

ated hydrogen bond involves O7 on dimethyl sulfoxide and the hydrogens on the carbon atom of one trimer, C17···H17A, as well as C31′···H31B′ of an adjacent trimer.[13] Further C–H π interactions[13b] and intramolecular bonds stabilize this structure. Although it is remarkable that there are many contacts, and of different types, the interactions themselves are consistent with the known guidelines for hydrogen bond formation.[13c] For $[Pd(MeOAp4Me_2)]_3$·DMSO, molecular recognition of the hydrogen bonds leads to aggregation and a supramolecular assembly. These interactions are listed in Table 6 and are shown in the packing diagram in Figure 4. The high effective charge on methoxy oxygen atoms and on the sulfoxide oxygen atom help to rationalize the extended network of hydrogen bonding contacts in **3**.

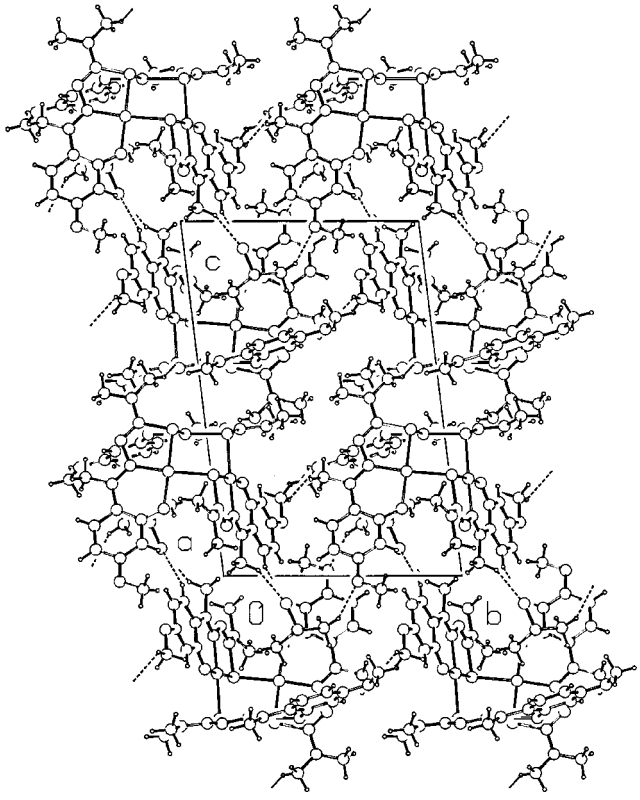


Figure 4. A view of the extended network of the intermolecular hydrogen bonds in $[Pd(4MeOAp4Me_2)]_3$·DMSO along the *a* axis

Spectroscopy

The significant IR bands of $H_2$4MeOAp4Me$_2$ and the three forms of the palladium(II) complex are close in energy to those found in other compounds with tridentate coordination.[9][16] The bands assigned in the spectrum of $H_2$4MeOAp4Me$_2$ shift in the spectrum of the palladium complexes as follows: ν(C=N), from 1556 cm^{-1} to 1541 cm^{-1}; ν(NN), from 1026 cm^{-1} to 1089 cm^{-1}; and ν(CS) (i.e., thioamide IV), from 836 cm^{-1} to 787 cm^{-1}. The palladium-donor atom stretching frequencies are as follows: ν(PdN, imine), 511 cm^{-1}; ν(PdS), 387 cm^{-1}; and ν(PdO), 338 cm^{-1}. Complex **2** exhibits a broad band at 3400 cm^{-1} attributed to the presence of lattice water. The DMSO adduct **3** shows a very strong S–O stretching vibration at 1023 cm^{-1}. This frequency is lower than that for free DMSO (1100–1055 cm^{-1}), suggesting the interaction of DMSO with the trimer complex through oxygen[16] as detailed above.

The main differences between the ^{1}H NMR spectrum of the free $H_2$4MeOAp4Me$_2$ and the trimer complexes are the disappearance of the downfield O1H (and O3H and N2H and N5H) signals. These changes confirm that loss of both hydrogens and metallation occurs, and that the structure of the complex in the solid state persists in $(CD_3)_2SO$ and $CDCl_3$ solutions. The appearance of the OH peak downfield at δ = 13.191 and 12.525 in $(CD_3)_2SO$ and $CDCl_3$, respectively, for $H_2$4MeOAp4Me$_2$ indicates that OH is hydrogen-bonded to $(CD_3)_2SO$ and intramolecularly hydrogen-bonded to the imine nitrogen N1 (and N4) in $CDCl_3$. The position for N2H (and N5H) is downfield at δ = 9.780 and 10.962 in $(CD_3)_2SO$ and $CDCl_3$, respectively, suggesting that this proton is also involved in hydrogen bonding, with more interaction of this proton in $CDCl_3$ solution.[16b] This suggests that a tautomer may exist in solution, similar to that found in 2-acetylpyridine N^4-substituted thiosemicarbazones,[17] and more recently in 2-pyridineformamide N^4-thiosemicarbazones.[18] This would involve N2H (and N5H) shifting to N1 (and N4) to form a bifurcated hydrogen bond with the phenoxy oxygen and thione sulfur.

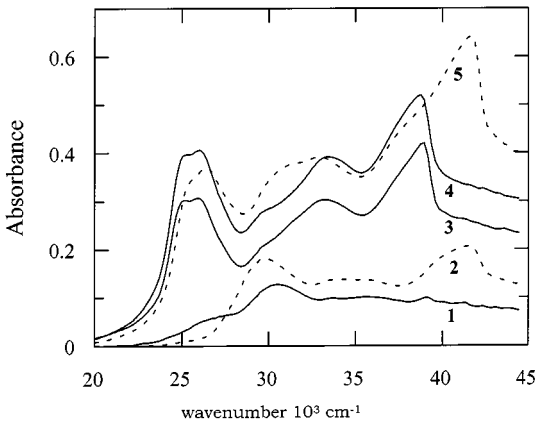


Figure 5. Electronic absorption spectra of $H_2$4MeOAp4Me$_2$; in DMSO (1); in $CHCl_3$ (2); of [Pd(4MeOAp4Me$_2$)]$_3$·3H_2O in DMSO (3); of [Pd(4MeOAp4Me$_2$)]$_3$ in DMSO (4) and of [Pd(4MeOAp4Me$_2$)]$_3$·3H_2O in $CHCl_3$ (5)

The bands of the $H_2$4MeOAp4Me$_2$ at ca. 30000 and 33500 cm^{-1} in the UV/Vis spectrum are due to n → π* transitions of the imine portion of the TSC moiety, and the aromatic ring, respectively.[19] The energies of these two bands are affected by changes in organic solvents due to differences in the mode of hydrogen bonding. The electronic spectrum of the trimer is shown in Figure 5 . Three spin-allowed singlet–singlet d → d transitions are predicted in the visible region of square planar complexes of palladium(II). However, strong charge transfer transitions for [Pd(4MeOAp4Me$_2$)]$_3$ interfere and prevent the observation of all the expected bands. The band at ca. 25000 cm^{-1} is intense and is assigned to a HOMO → LUMO transition.

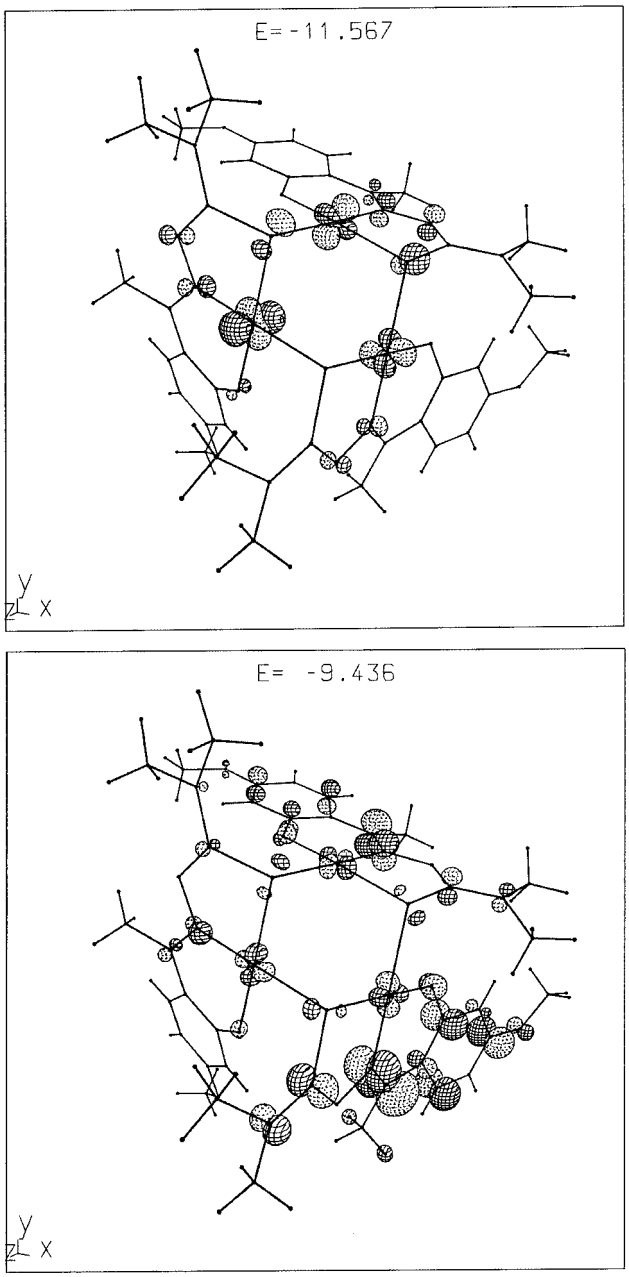


Figure 6. Representation of lowest unoccupied molecular orbital (LUMO: bottom) and highest occupied molecular orbital (HOMO: top) for complex [Pd(4MeOAp4Me$_2$)]$_3$·DMSO

The HOMO and LUMO orbitals are "d"- and π-centered on the metal and on the ligand, respectively. The bands at 25000 and 26000 cm^{-1} are assignable to a combination of d → d and charge transfer transitions.[19] The band at ca. 33000 cm^{-1} is due to the n → π* transition of the thiosemicarbazone moiety (imine, thioamide) and charge transfer involving the TSC moiety (L → M). The maxima at 20000–22000 cm^{-1} and at 26000–28000 cm^{-1} are affected by the nature of the solvent consistent with them having charge-transfer character.

The trinuclear complex was studied by the extended-Hückel method using the CACAO PC Beta-Version 5.0 package.[20] The molecular geometry was established from the crystallographic coordinates of the trinuclear complex. The highest occupied molecular orbital (HOMO; –11.567 eV, Figure 6) is mostly composed of dz2, dxy and dyz and has high percentages of the dz2 (25 %) orbital from Pd1, the dxy (8 %), dyz (10 %) orbitals from Pd2, and dxy (8 %) and dyz (9 %) from Pd3; the lowest unoccupied orbital (LUMO; –9.436 eV, Figure 6) is mostly composed of px orbitals from C32 (–18%), C29 (5%) and N7 (9%). The HOMO's energy is well isolated, strongly suggesting that the assignment of the lowest energy electronic transition can unambiguously be assigned to the computed HOMO–LUMO. This is experimentally addressed. The HOMO–n (n = 1–10) levels are similar in energy, and are more stabilized by ca. 0.5 eV relative to the HOMO. The molecular orbital $HOMO_{-10}$ has components of dxz (20%) from Pd1, dyz (–5%) from Pd2 and p (π) atomic orbitals from N2, N3, N1, C6. This is consistent with a back donation from the metal to π* orbitals from the ligand moieties.[19d]

Experimental Section

General: Solvents were purified and dried according to standard procedures. The palladium(II) complexes were analyzed for C, H and N at the European Environmental Research Institute (Ioannina). Infrared and far-infrared spectra were recorded with a Perkin–Elmer Spectrum GX FT-IR spectrophotometer using KBr (4000–400 cm^{-1}) and polyethylene pellets (400–40 cm^{-1}). Electronic spectra were recorded on a JASCO V-570 spectrophotometer UV/Vis/NIR.

Preparation of the Compounds: 2-Hydroxy-4-methoxyacetophenone N^4-dimethylthiosemicarbazone ($H_2$4MeOAp4Me_2), was prepared by stirring at room temperature a 1:1 ethanol solution (50 mL) of 2-hydroxy-4-methoxyacetophenone (0.05 mol) and N^4-dimethylthiosemicarbazide (0.05 mol) with 3 drops of conc. H_2SO_4 added. N^4-dimethylthiosemicarbazide was prepared following the procedure described by Scovill.[21] The complex Pd(4MeOAp4Me_2)]$_3$·3H_2O (**1**) was prepared directly from the reaction of K_2PdCl_4 (0.392 g, 1.2 mmol) in H_2O (5 mL) and $H_2$4MeOAp4Me_2 (0.267 g, 1 mmol) in CH_3OH (5 mL), with the pH adjusted to ca. 9 with a few drops of a 1.5 M NH_3 solution. After stirring for 24 h at room temperature, the resulting brown powder was filtered off, washed with cold methanol and ether and dried in vacuo over silica gel (yield 70%). – [Pd(MeOAp4Me_2)]$_3$·3H_2O (1169.14): calcd. C 36.98, H 4.39, N 10.78, S 8.23; found C 36.80, H 4.27, N10.95, S 8.40. – Compound **2** was obtained by drying the trihydrate at 40° C initially, and finally at 80° C for 1 h over P_4O_{10} to afford the dehydrated complex [Pd(MeOAp4Me_2)]$_3$. – **2** (1017.07): calcd. C 38.78, H 4.04, N 11.30, S 8.63; found C 38.90, H 4.00, N 11.20, S 8.73. – Slow evaporation of **1** from dimethyl sulfoxide solution yielded dark red crystals of the complex [Pd(MeOAp4Me_2)]$_3$·DMSO (**3**) suitable for X-ray structural analysis. – **3** (1193.40): calcd. C 38.25, H 4.30, N 10.56, S 10.75; found C 38.30, H 4.35, N 10.48, S 10.60.

Crystal Structure Determination of H24MeOAp4Me2 and Complex 3: Crystals of $H_2$4MeOAp4Me_2 were grown by slow concentration of a 1:1 by volume mixture of anhydrous ethanol/acetone and the selected crystal mounted on a glass fiber and used for data collection on a Nonius MACH3 diffractometer. The structure was solved by direct methods[22a] that revealed the positions of all non-hydrogen atoms, and refined on F by a full-matrix least-squares procedures using anisotropic displacement parameters.[22b] The hydrogens attached to nitrogen and oxygen were located by difference Fourier maps and were refined isotropically (U_{iso} = 0.05 Å^2). The remaining hydrogens were located in their calculated positions (C–H 0.96 Å). – A red needle-like crystal, (ca. 0.02 × 0.04 × 0.40 mm) of **3** was mounted on a glass fiber and analyzed with a Bruker SMART 1 K CCD diffractometer equipped with an Oxford Cryosystems Cryostream cooler,[23a] running at 123 K. The data collection nominally covered a sphere of reciprocal space by a combination of five sets of exposures; each exposure set had a different φ angle for the crystal and each exposure covered 0.3° in ω in 30 s. The crystal-to-detector distance was 4.909 cm. Coverage of the unique set was over 98% complete to φ = 26.37° (data truncated at 0.80Å). Data reduction was performed with the program SAINT V4.05.[23b] Crystal decay was monitored by repeating the first 50 frames of data at the end of data collection and analyzing the duplicate reflections. Area detector scaling and absorption corrections were performed by SADABS.[23b] This correction was used to scale the frames of data and to correct for absorption of the primary beam by the crystal support using the method of Blessing.[23c] A correction for absorption of the primary beam by the crystal was not applied. All calculations were performed with SHELXTL.[23d] Crystallographic data for $C_{36}H_{45}N_9O_6Pd_3S_3·C_2H_6OS$ (CCDC-132172) and $C_{12}H_{17}N_3O_2S$ (CCDC-132400) have been deposited with the Cambridge Crystallographic Data Centre. Copies of available material can be obtained, free of charge, on application to CCDC, 12 Union Road, Cambridge CB2 1EZ, UK [Fax: (internat.) + 44-1223/336-033; E-mail: deposit@ccdc.cam.ac.uk].

Calculations: A computational study with a PM3 parameterization scheme[11a] utilizing the eigenvector-following algorithm,[11b] as implemented in the MOPAC93 program,[11c] was used to investigate the prevailing isomer of free $H_2$4MeOAp4Me_2, the monodeprotonated anion, H4MeOAp4Me_2^-, and the diprotonated anion, 4MeOAp4Me_2^{2-}, in the gas phase and simulated solvent bulk (COSMO model[11d]). The complex molecule **3** was studied by the extended-Hückel method using the CACAO PC Beta-Version 5.0 package. The crystallographic coordinates of the complex were used.[20]

[1] Tsuji, *Organic Synthesis with Palladium Compound*, Springer-Verlag, New York, **1980**; R. F. Heck, *Palladium Reagents in Organic Synthesis*, Academic Press, London, **1985**.
[2] [2a] G. W. Parshall, S. D. Ittel, *Homogeneous catalysis*, 2nd ed., Wiley, New York, **1992**. – [2b] F. A. Cotton, S. Han, *Rev. Chim. Miner.* **1983**, 496. – [2c] F. A. Cotton, S. Han, *Rev. Chim. Miner.* **1985**, 277. – [2d] D. H. R. Barton, J. Khamsi, N. Ozbalik, M. Ramesh, J. Sharma, *Tetrahedron* **1989**, *30*, 4661.
[3] [3a] A. C. Skapski, M. Smart, *J. Chem. Soc., Chem. Commun.* **1970**, 658. – [3b] M. Basato, A. Grassi, G. Valle, *Organometallics* **1995**, *14*, 4439. – [3c] A. Deeming, M. N. Meah, P.A. Beates, M.B. Hursthouse, *J. Chem. Soc., Dalton Trans.* **1988**, 2193. – [3d] M. Sommovigo, M. Pasquali, F. Marchetti, P. Leoni, T.

Beringhell, *Inorg. Chem.* **1994**, *33*, 2651. – [3e] M. Parra-Hake, M. F. Retting, R. M. Wing, *Organometallics* **1983**, *2*, 1013. – [3f] P. M. Bailey, A. Kelly, P.M. Maitlis, *J. Chem. Soc., Dalton Trans.* **1978**, 1825. – [3g] M. Basato, C. Bertani, B. Sesto, M. Zecca, A. Grassi, G. Valle, *J. Organometallic Chem.* **1998**, *552*, 277. – [3h] M. Basato, D. Tommasi, M. Zecca, *J. Organometall. Chem.* **1998**, *571*, 115.

[4] D. X. West, S. B. Padhye, P. B. Sonawane, R. C. Chikate, *Asian J. Chem. Rev.* **1990**, *1*, 125.

[5] D. E. Barber, Z. Lu, T. Richardson, R. H. Crabtree, *Inorg. Chem.* **1992**, *31*, 4709.

[6] D. X. West, Y-H. Yang, T. L. Klein, K. I. Goldberg, A. E. Liberta, J. Valdés-Martínez, R. A. Toscano, *Polyhedron* **1995**, *14*, 1681.

[7] D. X. West, Y-H. Yang, T. L. Klein, K. I. Goldberg, A. E. Liberta, J. Valdés-Martínez, S. Hernández-Ortega, *Polyhedron* **1995**, *14*, 3051.

[8] D. Kovala-Demertzi, N. Kourkoumelis, D. X. West, J. Valdés-Martínez, S. Hernández-Ortega, *Eur. J. Inorg. Chem.* **1998**, 861.

[9] A. Berkessel, G. Hermann, O-T. Racuch, M. Buchner, A. Jacobi, G. Huttner, *Chem. Ber.* **1996**, *129*, 1421.

[10] [10a] A. Papageorgiou, Z. Iakovidou, D. Mourelatos, E. Mioglou, L. Boutis, A. Kotsis, D. Kovala-Demertzi, A. Domopoulou, D. X. West, M. A. Demertzis, *Anticancer Res.* **1997**, *17*, 247. – [10b] D. Kovala-Demertzi, A. Domopoulou, M. A. Demertzis, A. Papageorgiou, D. X. West, *Polyhedron* **1997**, *16*, 3625. – [10c] D. Kovala-Demertzi, A. Domopoulou, G. Valle, M. A. Demertzis, A. Papageorgiou, *J. Inorg. Biochem.* **1997**, *68*, 147. – [10d] D. Kovala-Demertzi, M. A. Demertzis, V. Varagi, A. Papageorgiou, D. Mourelatos, E. Mioglou, Z. Iakovidou, A. Kotsis, *Chemotherapy* **1998**, *44*, 421.

[11] [11a] J. J. P. Stewart, *J. Comput. Chem.* **1989**, *10*, 210. – [11b] J. Baker, *J. Comput. Chem.* **1986**, *7*, 385. – [11c] J. J. P. Stewart, *MOPAC93*, Fujitsu Co., **1993**. – [11d] A. Klamt, G. Shurmann, *J. Chem. Soc., Perkin Trans.* **1993**, 799.

[12] J. Valdés-Martínez, S. Hernández-Ortega, D. X. West, L. J. Ackerman, J. K. Swearingen, A. K. Hermetet, *J. Mol. Struct.* **1999**, *478*, 219.

[13] [13a] T. Steiner, B. Lutz, J. van der Maas, A. M. M. Schreurs, J. Kroon, M. Tamm, *Chem. Commun.* **1998**, 171. – [13b] T. Steiner, M. Tamm, A. Grzegorzewski, N. Schulte, N. Veldman, A. M. M. Schreurs, J. Kroon, J. van der Maas, B. Lutz, *J. Chem. Soc., Perkin Trans. 2* **1996**, 2441. – [13c] M. C. Etter, *Acc. Chem. Res.* **1990**, *23*, *120*. – [13d] T. Steiner, *Cryst. Rev.* **1996**, *6*, 1.

[14] [14a] M. Yasui, S. Yoshida, S. Kakuma, S. Shimamato, N. Matsumura, F. Iwasaki, *Bull. Chem. Soc. Jpn.* **1996**, *69*, 2749. – [14b] J. P. Fackler Junior, W. J. Zegarski, *J. Am. Chem. Soc.* **1973,** *95*, 8566. – [14c] Kang-Woo Kim, M.G. Kanatzidis, *J. Am. Chem. Soc*. **1995**, *117*, 5606.

[15] A. G. Quiroga, J. M. Pärez, I. Lopez-Solera, J. R. Masaguer, A. Luque, P. Roman, A. Edwards, C. Alonso, C. Navarro-Ranninger, *J. Med. Chem.* **1998**, *41,* 9, 1399.

[16] [16a] D. X. West, M. M. Salberg, G. A. Bain, A. E. Liberta, *Transition Met. Chem.* **1997**, *22*, 180. – [16b] K. Nakamoto, *Infrared and Raman Spectra of Inorganic and Coordination Compounds*, 5th ed., Wiley, New York, 1997.

[17] D. X. West, G. A. Bain, R. J. Butcher, J. P. Jasinski, R. Y. Pozdniakiv, Y. Li, J. Valdés-Martínez, R. A. Toscano, S. Hernández-Ortega, *Polyhedron* **1996**, *15*, 665.

[18] D. X. West, J. K. Swearingen et al., unpublished results.

[19] [19a] D. Kovala-Demertzi, J. M. Tsangaris, H. O. Desseyn, B. J. Van der Veken, *Bull. Soc. Chim. Belg.* **1987**, *1*, 7. – [19b] A. B. P. Lever, *Inorganic Electronic Spectroscopy*, Elsevier, New York, **1984**. – [19c] G. L. Estiu, A. H. Jubert, J. Costamagna, J. Vargas, *Inorg. Chem.* **1996**, *35*, 263. – [19d] D. Di Leo, F. Berrettini, R. Cini, *J. Chem. Soc., Dalton Trans.* **1998**, 1993.

[20] C. Mealli and D. Proserpio, CACAO PC Beta-Version 5.0, **1998**; C. Mealli, D. Proserpio, *J. Chem. Educ.* **1990**, *11*, 440.

[21] J. P. Scovill, *Phosphorus Sulfur Silicon* **1991**, *60*, 15.

[22] [22a] A. Altomere, G. Cascarano, C. Giacovazzo, A. Guagliardi, M. C. Burla, G. Polidori and M. Camalli, *J. Appl. Crystallogr.* **1994**, *27*, 435. – [22b] S. Mackay, C. Edwards, A. Henderson, C. Gilmore, N. Steward, K. Shankland, A. Donald, University of Glasgow, Scotland, **1997**. – [22c] A. L. Spek, *PLATON: A program for the automated generation of a variety of geometrical entities*, University of Utrecht, The Netherlands, **1997**.

[23] [23a] J. Cosier and A. M. Glazer, *J. Appl. Crystallogr.* **1986**, *19*, 105. – [23b] Bruker AXS Inc., *SMART, SAINT and SADABS Area-detector control and integration software Version 4.*, Bruker AXS Inc., Madison WI 53719, U.S.A., **1998**. – [23c] R. H. Blessing, *Acta Crystallogr., Sect. A* **1995**, *A51*, 33. – [23d] G. M. Sheldrick, *SHELXTL Version 5.10.*, Bruker AXS Inc., Madison, WI 53719, U.S.A, **1998**.

Received August 4, 1999
[I99287]

Adducts of *o*-Silaborane With Water and Methanol

Lars Wesemann,*[a] Michael Trinkaus,[b] Yves Ramjoie,[b] Beate Ganter,[b] Ulli Englert,[b] and Jens Müller*[b]

Keywords: Silaboranes / Cluster compounds / Siloxanes / Silicon / Boranes

The synthesis of alkoxide adducts of *o*-silaborane $[(TMPDAH)_2][(Me_2Si_2B_{10}H_{10})_2O]$ (**3**) and $[TMPDAH][(Me_2Si_2B_{10}H_{10})OMe]$ (**4**) are presented (TMPDA = tetramethylpropylenediamine). For both silaborate clusters **3** and **4** the results of the NMR spectroscopic investigations together with the X-ray single crystal structure determinations are discussed. The geometries of ab initio calculations (HF and B3LYP methods) on the hydroxide adduct $[Si_2B_{10}H_{12}(OH)]^-$ are compared with the structures of **3** and **4**. The dynamic behaviour of the adducts **3** and **4** in solution is discussed with respect to the calculated energy profile for the rotation of the HSi(OH) group.

Introduction

Wade and Williams have developed a classification for borane and heteroborane clusters into groups of different numbers of skeleton electron pairs depending on the number of skeleton atoms.[1,2] On the basis of these rules the structure of a cluster with known composition can often be predicted. A *closo* cluster with n vertices can be transformed into a *nido* cluster by increasing the number of cluster electrons by two. The geometry of this *nido* cluster can be derived from the skeleton of the next higher *closo* cluster ($n + 1$ vertices). Figure 1 shows the thirteen vertex deltahedra and the three primary fragments that result from the removal of a single 4k, a selected 5k, and one of the 6k vertices.

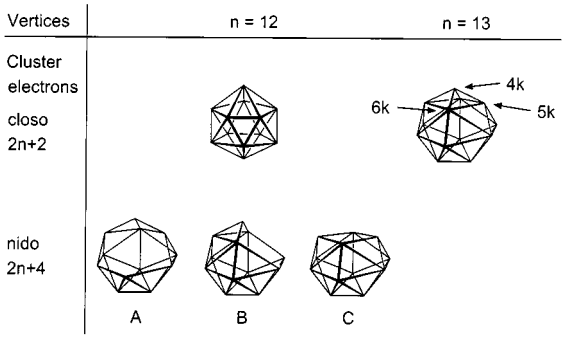
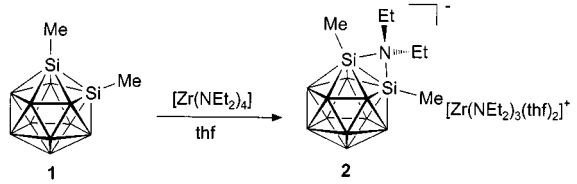


Figure 1. *closo* Clusters with 12 and 13 vertices and *nido* clusters with 12 vertices; in A the 6k vertex, in B the 5k vertex, and in C the 4k vertex is removed

Hawthorne et al. have found a cluster-opening reaction with the reduction of *o*-carborane (geometry A).[3] Examples for geometry B have been published by Paetzold et al. with the adducts of aza-*closo*-dodecaborane(12).[4] So far, 12-vertex *nido* clusters with geometry C, exhibiting a quadrangle as the open cluster face, are unknown.[1] However, *nido* 12-vertex clusters with a geometry other than the primary fragments are known. In the case of the fluxional tetracarbon cluster $R_4C_4B_8H_8$ a variety of cluster geometries has been determined by crystal structure analysis or NMR spectroscopy.[5–7] Depending on the substituents present at the carbon vertices, cluster skeletons exhibiting two neighboring quadrangles or a hexagonal open face have been characterized in the solid state. Adducts of *closo*-heterodicarbaboranes ($MC_2B_9H_{11}$ or $MC_2B_4H_6$) show opened-cluster frameworks, which have been considered as slip distorted geometries with respect to the central heteroatom.[8]

The reaction of the *commo*-cluster $[Si(C_2B_9H_{11})_2]$ with PMe_3 or pyridine results, in both cases, in an opened-cluster geometry.[9] Interestingly, the phosphane removes a boron vertex from the framework and pyridine attacks the silicon resulting in η^1-coordination of the silicon at the cluster.
The first studies on the nucleophilic degradation of 1,2-dimethyl-1,2-disila-*closo*-dodecaborane(12) (*o*-silaborane) (**1**)[10] have resulted in the isolation of a surprising adduct between the *closo*-cluster and dialkylamides.[11] Adducts of this type have been isolated in the case of dimethyl- and diphenyl-*o*-silaborane.[11,12] Regarding the cluster electron count of these adducts, an opened *arachno*-cluster geometry is expected according to the cluster rules. Surprisingly, the adducts show a structure which is closely related to the starting material and is not in agreement with Williams topological systematics (Scheme 1).



Scheme 1

The crystallographically determined structure and the NMR chemical shifts (^{11}B, ^{29}Si) of **1** and **2** have been repro-

[a] Institut für Anorganische Chemie, Universität zu Köln, Greinstraße 6, D-50939 Köln, Germany
[b] Institut für Anorganische Chemie der Technischen Hochschule Aachen, Prof.-Pirlet-Strasse 1, D-52056 Aachen, Germany

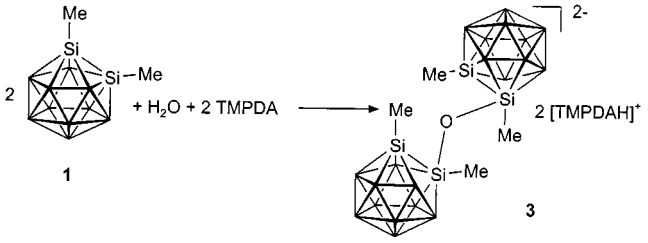
 © WILEY-VCH Verlag GmbH, D-69451 Weinheim, 2000 1434–1948/00/0404–0735 $ 17.50+.50/0

duced by ab initio calculations. The LUMO of the *o*-silaborane should be responsible for the interesting acceptor abilities. This empty orbital is essentially concentrated on the two silicon atoms and shows bonding character with respect to the silicon–silicon distance. In order to get further insight into the acceptor abilities of *o*-silaborane we studied the reaction with other nucleophiles.

Results and Discussion

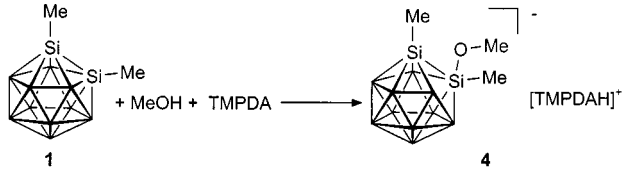
Synthesis, NMR Spectroscopy, and X-ray Diffraction Studies

In this publication we present oxide *o*-silaborane adducts exhibiting a hitherto unknown cluster geometry. By accident we found a reaction of the *closo*-silaborane with water. During our studies on the reactivity of the icosahedral cluster **1** towards tertiary amines, the remaining moisture in the inert gas was found to be the source of water. One equivalent of *o*-silaborane (**1**) reacts with water and one equivalent of tetramethylpropylenediamine (TMPDA) to give the oxide adduct **3** in quantitative yield (Scheme 2).



Scheme 2

The silaborane could be completely recovered after addition of aqueous HCl to a THF solution of the dianion **3**, indicating the reversibility of this acid-base reaction. Exclusion of water from the inert gas enabled us to introduce other less-acidic reagents into this reaction. Thus methanol reacts with TMPDA and one equivalent of *o*-silaborane to give the methoxide adduct **4** (Scheme 3). This adduct formation is also reversible, as is shown by the complete recovery of *o*-silaborane after acidification of a solution of the methoxide adduct **4**.



Scheme 3

Compounds **3** and **4** have been characterized by elemental analysis, multinuclear/multidimensional NMR spectroscopy, and X-ray structure analysis. In both cases crystals suitable for X-ray diffraction were obtained by slow diffusion of hexane into a THF solution of the salts **3** and **4**. Perspective views of the cluster anions of **3** and **4** are depicted in Figure 2 and Figure 3, respectively. Selected interatomic distances are listed in Table 1 and Table 2.

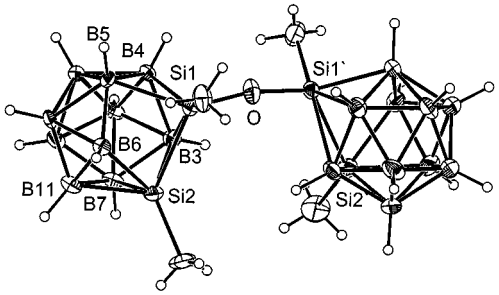


Figure 2. Structure of the anion of **3** in the crystal (PLATON representation,[16] ellipsoids at 30% probability level)

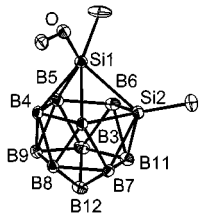


Figure 3. Structure of the anion of **4** in the crystal (PLATON representation,[16] ellipsoids at 30% probability level)

Table 1. Selected interatomic distances in the anion of **3** and **4** [Å]

	Anion of **3**	Anion of **4**
Si–Si	2.391(2), 2.374(2) 2.478(2), 2.364(2)	2.391(2)
Si1–O	1.629(3), 1.647(3) 1.643(4), 1.651(3)	1.674(3)
Si1–B3	2.255(6), 2.281(6) 2.229(6), 2.301(5)	2.254(5)
Si1–B4	2.076(6), 2.092(6) 2.081(5), 2.098(6)	2.081(5)
Si1–B5	2.172(5), 2.141(6) 2.119(6), 2.181(6)	2.126(6)
Si1–B6	2.458(6), 2.408(6) 2.395(6), 2.385(6)	2.400(6)
Si2–B3	2.064(6), 2.075(6) 2.035(6), 2.074(6)	2.082(6)
Si2–B6	2.056(4), 2.048(6) 2.005(5), 2.086(6)	2.040(6)
Si2–B7	2.055(6), 2.048(6) 2.044(6), 2.058(6)	2.051(5)
Si2–B11	2.068(6), 2.053(6) 2.021(6), 2.048(6)	2.060(6)

Table 2. Selected bond angles in the anion of **3** and **4** [°]

	Anion of **3**	Anion of **4**
Si2–Si1–O	120.3(1), 121.0(1) 156.8(1), 123.3(1)	125.0(1)
Si–O–Si	164.2(2), 154.6(2)	–
Si–O–C	–	132.3(3)
Si1–Si2–C2	127.4(3), 127.3(2) 123.4(3), 128.9(1)	126.6(2)
Si2–Si1–C1	114.1(3), 113.7(3) 87.7, 123.3(3)	109.1(3)
O–Si1–B12–B9	84.1(4), 87.2(3), 33.3(4), 98.4(4)	80.9(3)

Two equivalents of the salt $[(TMPDAH)_2][(Me_2Si_2B_{10}H_{10})_2O]$ (**3**) were found to crystallize independently in the asymmetric unit, thus allowing the interatomic parameters of two different Si–O–Si bridged clusters to be discussed. The variations of the Si–O–Si angles [Si1–O1–Si3 164.2(2), Si5–O2–Si7 154.6(2)] and the Si–O bond lengths [Si1–O1 1.629(3), Si3–O1 1.647(3), Si5–O2 1.643(3), Si7–O2 1.651(3)] in the two dianions suggests flexibility of this linkage. This phenomenon has been well-established by several structural and theoretical studies on molecules bear-

ing disiloxane moieties.[17] Thus, an increase in the Si–O–Si angle causes a decrease in the Si–O distance. The presented structural data of the oxide bridged silaboranes are in agreement with this tendency.

The cluster geometries of the oxide and methoxide adducts show a high degree of similarity. In both cases the Si–B distances are in the range of 2.3–2.0 Å. The longest distances between silicon and boron are found in each cluster between Si1, the silicon atom carrying the alkoxide, and B3, the boron atom which is still coordinated to both silicon atoms [2.254(5), 2.255(6), 2.281(6), 2.229(6), 2.301(5) Å]. This adduct formation is also a cluster-opening reaction. The silicon atom attacked by the nucleophile is coordinated to only three boron atoms. Obviously, the bond to the boron atom opposite to the entering nucleophile was broken during adduct formation (see Table 1 Si1–B6). Therefore, the adduct features a quadrangle consisting of two silicon atoms and two boron atoms (Type C in Figure 1). Overall the coordination number of Si1 remains as six. The silicon atom not attached to the oxygen atom is embedded in the cluster framework as in the starting material. The geometry of the oxygen adducts of *o*-silaborane can be derived from the 13-vertex *closo* skeleton by removal of the four-coordinate vertex (4k).

The static geometries of the silaborate derivatives **3** and **4** in the solid state are not compatible with the NMR spectroscopic studies at room temperature. Instead, the number of signals in the ^{1}H-, ^{11}B-, ^{13}C-, and ^{29}Si-NMR spectra equals the number observed for *o*-silaborane, possessing C_{2v} symmetry. A dynamic process involving migration of the oxygen between the neighboring silicon atoms accounts for the smaller number of signals than would be expected for the static compounds. This fluxional process is too rapid on the NMR time scale to be quenched at room temperature.

Ab Initio Calculations

In order to get further insights into the dynamic behavior we studied the oxygen adducts by ab initio calculations.[18] Instead of the anion of compound **4**, we conducted the calculations with the parent compound $[Si_2B_{10}H_{12}(OH)]^-$. Figure 4 shows the relative energies at the HF/6-31G(d) level dependent on the rotation of the SiH(OH) group (see Experimental Section). We chose Si1–B12 as the axis of rotation; i.e., we varied the O–Si1–B12–B9 (Figure 3) torsion angle in steps of 10° and optimized the resulting 19 geometries. We checked that Figure 4 describes an internal reaction path by frequency analyses. This surface scan (Figure 4) clearly shows two minima, **M1** and **M2**, and two transition states, **TS1** and **TS2**. Moreover, we conducted full optimizations for the two equilibrium geometries and the transition state highest in energy (**TS2**), both at the HF/6-31G(d) and the B3LYP/6-31G(d) levels of theory. The calculated structures are depicted in Figure 5 and selected bond lengths and additional data are compiled in Table 3.

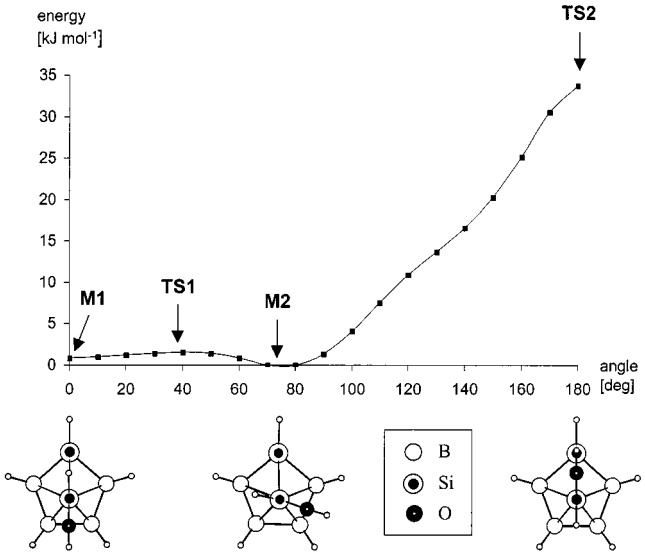


Figure 4. Surface scan for the rotation of the SiH(OH) group in $[Si_2B_{10}H_{12}(OH)]^-$ at the HF/6-31G(d) level

Besides **M1**, **M2**, and **TS2**, Figure 5 shows the two additional geometrical conformers, **M3** and **TS3**. The transition state **TS3** has the OH group symmetrically bound to both Si atoms (C_s point group). This transition state connects two enantiomers of **M3** (C_1 point group) and corresponds to an exchange of the OH group between the two Si atoms. The barrier for this process is only 29.9 kJ mol^{-1} [B3LYP/6-31G(d)].

The major difference between the structures of **M1**, **M2**, **TS1**, and **TS2** on the one side, and **M3** and **TS3** on the other, is the conformation of the OH group. Whereas for **M1**–**TS2** the H atom of the hydroxy group is directed towards the surface of the cluster (torsion angle H–O–Si1–B12 = 180°), for **M3** and **TS3** the H atom is directed in the opposite direction (Figure 5). Obviously, the two reaction coordinates **M1**–**TS1**–**M2**–**TS2** (Figure 4) and **M3**–**TS3** are related by the rotation of the OH group along the Si1–O bond. Therefore, we took several geometries from the surface scan of Figure 4 and rotated the OH group by 180° to give a new set of starting geometries. These optimizations led to two minima at the HF/6-31G(d) level which were similar to **M3**; i.e., 17.4 and 18.8 kJ mol^{-1} higher in energy than **M2**. The barrier for SiH(OH) rotation is just 30.7 kJ mol^{-1} at the B3LYP/6-31G(d) level (Figure 5).

The geometry corresponding to the minimum **M2**, and the structure of the anion of **4**, are very similar. In particular, the calculated and measured torsion angle O–Si1–B12–B9 is 75.3° (75.6°) and 80.9(3)°, respectively. The corresponding torsion angles of the two independent anions of **3** in the solid state are 84.1(4) and 87.2(3)° for one molecular unit, and 33.3(4) and 98.4(4)° for the other molecular unit. These torsion angles are in the flat region of the calculated surface (Figure 4) showing the high degree of flexibility.

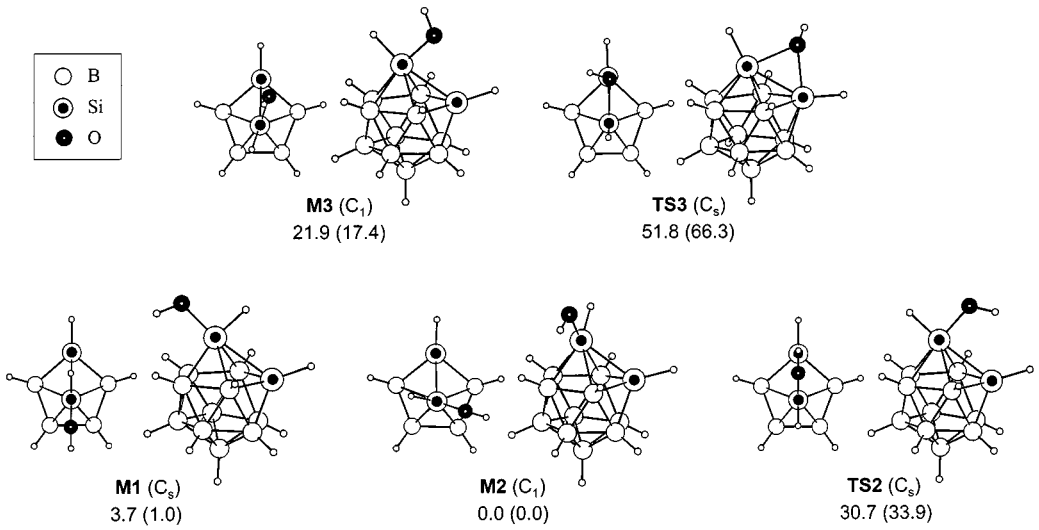


Figure 5. Minimum structures and transition states of $[Si_2B_{10}H_{12}(OH)]^-$; relative energies in kJ mol^{-1} at the B3LYP/6-31G(d) and the HF/6-31G(d) level (in parentheses); two views are depicted for each molecule

Table 3. Bond lengths in Å calculated at the B3LYP/6-31G(d) and the HF/6-31G(d) level (in parentheses)

	M1	M2	M3	TS2	TS3
Si1–Si2	2.492 (2.502)	2.377 (2.377)	2.422 (2.424)	2.461 (2.462)	2.329 (2.315)
Si1–O	1.706 (1.684)	1.708 (1.686)	1.732 (1.708)	1.723 (1.702)	1.996 (1.970)
Si1–B3	2.279 (2.278)	2.288 (2.283)	2.255 (2.257)	2.258 (2.250)	2.103 (2.102)
Si1–B4	2.082 (2.085)	2.112 (2.116)	2.077 (2.083)	2.107 (2.112)	2.066 (2.075)
Si1–B5	2.082 (2.085)	2.116 (2.123)	2.111 (2.116)	2.107 (2.112)	2.071 (2.079)
Si1–B6	2.279 (2.278)	2.391 (2.387)	2.199 (2.197)	2.258 (2.250)	2.111 (2.108)

The geometry corresponding to the transition state **TS3** compares well with the structure of the dimethylamide adduct **2** (Scheme 1).[11]

Experimental Section

General Considerations: All manipulations were carried out under an atmosphere of nitrogen using standard Schlenk techniques. THF was distilled from sodium/benzophenone, and hexane from potassium, and each was stored under nitrogen. – Elemental analyses were performed by the Mikroanalytisches Labor Pascher (Remagen) or the Analytischen Laboratorien (Lindlar). – NMR spectroscopy was performed on a Varian Unity 500 MHz spectrometer (^{1}H: 500 MHz, ^{11}B: 164 MHz, ^{13}C: 125 MHz, ^{29}Si: 100 MHz).

[(TMPDAH)$_2$][(Me$_2$Si$_2$B$_{10}$H$_{10}$)$_2$O] (3): A solution of **1** (264.2 mg, 1.29 mmol) in THF (15 mL) was treated with TMPDA (1.0 g, 7.68 mmol) and H_2O (0.015 mL, 0.94 mmol). The colorless solution was stirred overnight. All volatiles were removed and the remaining colorless solid was characterized by NMR spectroscopy to be almost quantitatively **3**. Crystalline material was obtained by slow diffusion of hexane into a THF solution of **3** (Yield: 426 mg, 0.62 mmol, 96%). – ^{1}H{^{11}B} NMR (500 MHz, TMS, CD_2Cl_2): δ = 0.84 (s, 6 H, SiCH_3), 1.25 (s, 2 H, H9/12), 1.39 (s, 2 H, H4/5/7/11), 1.67 (s, 2 H, H8/10), 1.86 (quin., 2 H, NCH$_2$CH_2CH$_2$N), 1.86 (s, 2 H, H3/6), 2.59 (s, 12 H, NCH_3), 2.98 (t, 4 H, NCH_2CH$_2$CH_2N), 11.19 (s, 1 H, N*H*N). – ^{11}B NMR (160 MHz, $BF_3 \cdot Et_2O$): δ = –11.6 (d, ^1J = 122 Hz, B3/6), –14.5 (d, ^1J = 134 Hz, B8/10), –17.3 (d, ^1J = 122 Hz, B4/5/7/11), –21.1 (d, ^1J = 122 Hz, B9/12). – ^{13}C{^{1}H} NMR (125.6 MHz, TMS): δ = 6.6 (MeSi), 21.7 (s, NCH$_2$*C*H$_2$CH$_2$N), 44.7 [s, N(CH$_3$)$_2$], 60.1 (s, N*C*H$_2$CH$_2$*C*H$_2$N). – ^{29}Si NMR (MHz, TMS): δ = –73.7. – $C_{18}H_{70}B_{20}N_4OSi_4$ (687.35): calcd C 31.46, H 10.27, N 8.15, O 2.33; found C 31.27, H 10.51, N 8.03, O 2.12.

X-ray Crystallographic Analysis of 3: $C_{18}H_{70}B_{20}N_4OSi_4$, ENRAF-Nonius CAD4; Mo-$K_\alpha$ radiation, λ = 0.71073 Å, graphite monochromator; data collection with ω-2θ scan at 203 K, Colorless translucent platelet 0.7 × 0.5 × 0.1 mm, triclinic space group $P\bar{1}$ (no. 2); a = 8.451(2), b = 22.697(3), c = 22.992(3) Å, α = 97.42(1), β = 100.01(1), γ = 100.32(1)°, U = 4214(1) Å^3, Z = 4, ρ_{calcd} = 1.083 gcm^{-3}, μ(Mo-K_α) = 1.60 cm^{-1}, F(000) = 1480; 15805 reflections in the range 2 < θ < 26°, 15226 independent reflections. Structure solution by direct methods[13] and refinement[14] on F^2 for 1366 variables; all nonhydrogen atoms refined isotropically. Convergence at R = 0.074 for 7172 observations with $F_o > 4\sigma F_o$, $wR2$ = 0.154 for all reflections, $w^{-1} = \sigma^2(F_o^2) + \{0.052[\max(F_o^2,0) + 2F_c^2]/3\}^2$, GOF = 0.929.

[TMPDAH][(Me$_2$Si$_2$B$_{10}$H$_{10}$)OMe] (4): A solution of **1** (330.0 mg, 1.61 mmol) in THF (15 mL) was treated with TMPDA (255.3 mg, 1.21 equiv.). After stirring for 30 min CH_3OH (55 mg, 1.07 equiv.) was added. The colorless solution was stirred overnight. All volatiles were removed and the remaining colorless solid was characterized by NMR spectroscopy to be almost quantitatively **4**. Crystalline material was obtained after slow diffusion of hexane into a THF solution of **4** (yield: 572 mg, 1.56 mmol, 97%). – ^{1}H{^{11}B} NMR (500 MHz, TMS, THF): δ = 0.76 (s, 6 H, SiCH_3), 1.22 (s, 2 H, H9/12), 1.37 (s, 4 H, H4/5/7/11), 1.72 (s, 4 H, H3/6/8/10), 1.88 (quin., 2 H, NCH$_2$CH_2CH$_2$N), 2.61 (s, 12 H, NCH_3), 2.97 (t, 4 H, NCH_2CH$_2$CH_2N), 11.04 (s, 1 H, N*H*N). – ^{11}B NMR (160 MHz, $BF_3 \cdot Et_2O$): δ = –13.8 (d, ^1J = 140 Hz, B3/6/8/10), –17.5 (d, ^1J = 128 Hz, B4/5(7/11), –20.5 (d, ^1J = 128 Hz, B9/12). – ^{13}C{^{1}H} NMR (125.6 MHz, TMS): δ = 3.6 (MeSi), 21.2 (NCH$_2$*C*H$_2$CH$_2$N), 44.5 [–N(*C*H$_3$)$_2$], 60.2 (N*C*H$_2$CH$_2$*C*H$_2$N). – ^{29}Si NMR (MHz, TMS): δ = –69.3. – $C_{10}H_{38}B_{10}N_2OSi_2$ (366.71): calcd C 32.75, H 10.45, N 7.64; found C 32.53, H, 10.24, N 7.79.

X-ray Crystallographic Analysis of 4: $C_{10}H_{38}B_{10}N_2OSi_2$, ENRAF-Nonius CAD4; Cu-$K_\alpha$ radiation, $\lambda = 1.54184$ Å, graphite monochromator; data collection with ω-2θ scan at 180 K. Colorless platelet $0.36 \times 0.24 \times 0.08$ mm, monoclinic space group $P2_1/c$ (no. 14); $a = 8.808(1)$, $b = 9.139(1)$, $c = 28.218(7)$ Å, $\beta = 94.24(2)°$, $U = 2265.(1)$ Å^3, $Z = 4$, $\rho_{calcd} = 1.078$ gcm^{-3}, μ(Cu-K_α) = 14.10 cm^{-1}, $F(000) = 792$; 5639 reflections in the scan range $4 < \theta < 70°$, 2599 independent observations with $I > \sigma(I)$ in structure solution with direct methods[13] and refinement[15] on F for 306 variables; all nonhydrogen atoms refined with anisotropic replacement parameters, hydrogen atoms refined isotropically. Convergence at $R = 0.066$, $Rw = 0.063$, $w^{-1} = \sigma^2(F_o)$, $GOF = 1.094$.

Crystallographic data (excluding structure factors) for the structures reported in this paper have been deposited with the Cambridge Crystallographic Data Centre as supplementary publication nos. CCDC-114742 (**3**) and CCDC-114741 (**4**). Copies of the data can be obtained free of charge on application to CCDC, 12 Union Road, Cambridge CB2 1EZ, UK [Fax: (internat.) +44–1223/336-033; E-mail: deposit@ccdc.cam.ac.uk].

Ab Initio Calculations: The Gaussian 94 package,[18] run on a cluster of workstations (*Rechenzentrum der RWTH Aachen*), was applied for all ab initio calculations. The calculations were conducted in redundant internal coordinates. The surface scan of Figure 4 was performed by a step-by-step change of the torsion angle O–Si1–B12–B9 by 10° followed by an optimization of all other geometrical parameters. All full geometry optimizations were conducted without any symmetry restrictions (Figure 5). The total energies E_h (in Hartrees; B3LYP/6-31G(d) and HF/6-31G(d) in parentheses) and ZPVE calculated at HF/6-31G(d) level (in kJ mol^{-1}; in square brackets) are as follows: **M1**: –910.812603 (–907.220984) [483.2], **M2**: –910.814022 (–907.221375) [483.4], **M3**: –910.805689 (–907.214743) [482.1], **TS2**: –910.802310 (–907.208467) [481.8], **TS3**: –910.794274 (–907.196112) [481.4].

Acknowledgments

We are grateful to the Deutsche Forschungsgemeinschaft (DFG-Schwerpunktprogramm "Polyeder") for generous financial support and to the Rechenzentrum der RWTH Aachen for providing generous computer time. Especially, we would like to thank T. Eifert and J. Risch for their support.

[1] K. Wade, *Adv. Inorg. Chem. Radiochem.* **1976**, *18*, 1–66.
[2] R. E. Williams, *Advances in Boron Chemistry* (Ed.: W. Siebert), The Royal Society of Chemistry, Cambridge, **1997**; R. E. Williams, *Adv. Inorg. Chem. Radiochem.* **1976**, *18*, 67–105.
[3] T. D. Getman, C. B. Knobler, M. F. Hawthorne, *Inorg. Chem.* **1990**, *29*, 158–160.
[4] F. Meyer, J. Müller, P. Paetzold, R. Boese, *Angew. Chem*. **1992**, *104*, 1221–1222; *Angew. Chem. Int. Ed.* **1992**, *31*, 1227–1228.
[5] [5a] R. N. Grimes, *Adv. Inorg. Chem. Radiochem.* **1983**, *26*, 55–117; [5b] R. N. Grimes, *Coord. Chem. Rev.* **1995**, *143*, 71–96.
[6] D. P. Freyberg, R. Weiss, E. Sinn, R. N. Grimes, *Inorg. Chem*. **1977**, *16*, 1847–1851.
[7] R. N. Grimes, W. N. Maxwell, R. B. Maynard, E. Sinn, *Inorg. Chem.* **1980**, *19*, 2981–2985.
[8] A. K. Saxena, J. A. Maguire, N. S. Hosmane, *Chem. Rev.* **1997**, *97*, 2421–2461.
[9] D. M. Schubert, W. S. Rees, Jr. C. B. Knobler, M. F. Hawthorne, *Organometallics* **1990**, *9*, 2938–2944.
[10] L. Wesemann, U. Englert, D. Seyferth, *Angew. Chem.* **1995**, *107*, 2435–2436; *Angew. Chem. Int. Ed. Engl.* **1995**, *34*, 2236–2238.
[11] L. Wesemann, Y. Ramjoie, M. Trinkaus, B. Ganter, J. Müller, *Angew. Chem*. **1998**, *110*, 1481–1484; *Angew. Chem. Int. Ed.* **1998**, *37*, 1412–1415.
[12] L. Wesemann, Y. Ramjoie, M. Trinkaus, B. Ganter, *Z. Allg. Anorg. Chem.* **1998**, 624, 1573–1576.
[13] G. M. Sheldrick, *SHELXS86, Program for Structure Solution*, University of Göttingen, Germany, **1986**.
[14] G. M. Sheldrick, *SHELXS93, Program for Structure Refinement*, University of Göttingen, Germany, **1993**.
[15] B. A. Frenz and ENRAF-Nonius, SDP, Version 5.0 (**1989**).
[16] A. L. Spek, *Acta Crystallogr. Sect. A* **1990**, *46*, C34.
[17] F. Cervantes-Lee, H. K. Sharma, K. H. Pannell, A. Derecskei-Kovacs, D. S. Marynick, *Organometallics* **1998**, *17*, 3701–3706; K. M. Baines, A. G. Brooks, P. D. Lickiss, J. F. Sawyer, *Organometallics* **1989**, *8*, 709–716.
[18] All calculations were performed with Gaussian 94, M. J. Frisch, G. W. Trucks, H. B. Schlegel, P. M. W. Gill, B. G. Johnson, M. A. Robb, J. R. Cheeseman, T. Keith, G. A. Petersson, J. A. Montgomery, K. Raghavachari, M. A. Al-Laham, V. G. Zakrzewski, J. V. Ortiz, J. B. Foresman, J. Cioslowski, B. B. Stefanov, A. Nanayakkara, M. Challacombe, C. Y. Peng, P. Y. Ayala, W. Chen, M. W. Wong, J. L. Andres, E. S. Replogle, R. Gomperts, R. L. Martin, D. J. Fox, J. S. Binkley, D. J. Defrees, J. Baker, J. P. Stewart, M. Head-Gordon, C. Gonzalez, J. A. Pople, Gaussian, Inc., Pittsburgh PA, **1995**.

Received August 10, 1999
[I99294]

Bis(terpyridyl)-Ruthenium(II) Units Attached to Polyazacycloalkanes as Sensing Fluorescent Receptors For Transition Metal Ions

Miguel E. Padilla-Tosta,[a] José Manuel Lloris,[a] Ramón Martínez-Máñez,*[a] Angel Benito,[a] Juan Soto,[a] Teresa Pardo,[a] Miguel A. Miranda,[a] and M. Dolores Marcos[b]

Keywords: Terpyridine / Copper sensing / Cyclam / Fluorescence / Solution studies

A synthetic strategy has been devised for the preparation of new compounds in which terpyridyl fragments are linked to 1,4,8,11-tetraazacyclotetradecane (cyclam). Reaction of excess cyclam with 4′-[(4-bromomethyl)phenyl]-2,2′:2″,6′-terpyridine afforded the ligand 1-[4′-*p*-tolyl-(2,2′:6′,2″-terpyridyl)]-1,4,8,11-tetraazacyclotetradecane (L^1) in which the tetraaza macrocycle was covalently attached to one benzyl-terpyridyl fragment. Under similar conditions reaction of cyclam with excess 4′-[(4-bromomethyl)phenyl]-2,2′:2″,6′-terpyridine gave the tetra substituted cyclam derivative 1,4,8,11-[4′-*p*-tolyl-(2,2′:6′,2″-terpyridyl)]-1,4,8,11-tetraazacyclotetradecane (L^2). The multidentate ligand L^2 was crystallographically characterised by single-crystal X-ray diffraction techniques. Reaction of L^1 with $[Ru(mtpy)Cl_3]$ gave the heteroleptic ruthenium(II) complex $[Ru(L^1)(mtpy)][PF_6]_2$ (mtpy = 4′-methyl-2,2′:6′2″-terpyridine). The fluorescent intensity of the metallo-receptor $[Ru(L^1)(mtpy)][PF_6]_2$ was quenched selectively in the presence of copper(II) in an aqueous environment. To gain insight into the nature of this interaction, potentiometric titrations on $[Ru(L^1)(mtpy)]^{2+}$ in the presence of Cu^{2+} were carried out. The quenching of the emission intensity was associated with the presence of the copper $\{Cu[Ru(L^1)(mtpy)]\}^{4+}$ complex in solution. The receptor 1-[4′-methyl-(2,2′:6′,2″-terpyridyl)]-1,4,8,11-tetraazacyclotetradecane (L^3), in which the cyclam fragment is separated from the terpyriyl by a methylene group, has also been synthesised by reaction of 4′-bromomethyl-2,2′:2″,6′-terpyridine and cyclam. With L^3 as starting material, the ruthenium complex $[Ru(L^3)(mtpy)]^{2+}$ was prepared in order to evaluate the effect that the nature of the spacer has on the quenching of the fluorescence upon addition of Cu^{2+}.

Introduction

The assembly of oligopyridyl groups with Ru^{II} or some other transition metals ions to yield polymetallic species has been studied for both practical and fundamental reasons.[1,2] Some examples are: (a) the investigation of energy and electron-transfer processes,[3–8] (b) the exploitation of spectroscopic properties for testing the sensing ability of appended groups towards protons, cations and anions[9,10] and (c) the building up of dendritic species comprising several metal centres for light-harvesting and energy-collection purposes.[11,12] The investigation on these area has mainly been concentrated on building covalently linked metal complexes,[3,5,13] with the building of noncovalent links between components being an alternative pathway.[14] Few examples of these metallo-receptors have demonstrated sensor properties.[15]

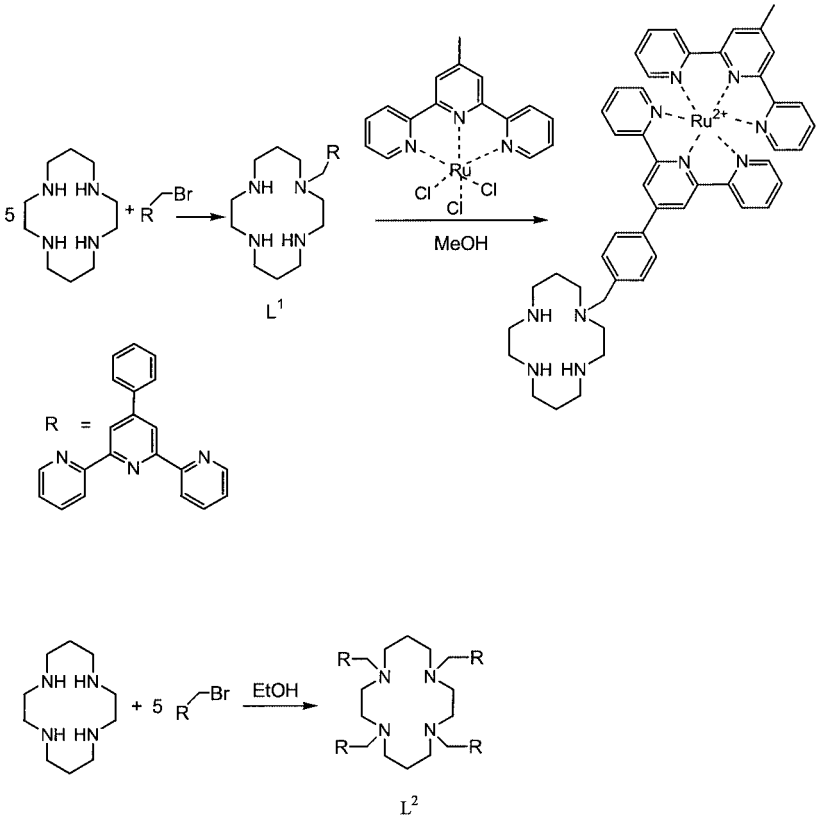
We have synthesised terpyridine-functionalised cyclam ligands and formed complexes with the photoactive Ru^{II} metal ion. The domains of the macrocyclic cavity could allow for the binding of an appropriate guest that might trigger a change in the luminescence of the appended ruthenium metal centre. One of the best known metallo-fluorophores is the tris(2,2'-bipyridyl)-ruthenium(II) core, however the related bis(2,2':6',2''-terpyridine)-ruthenium(II) group has been much less studied as a luminescent signalling subunit.[9,16] We report here that the incorporation of the Cu^{2+} cation into the macrocyclic cavity appended to a bisterpyridyl ruthenium centre changes the emission properties of the $[Ru(tpy)_2]^{2+}$ core, allowing for access to new potential chemosensors based on the fluorophore–spacer–receptor concept.

Results and Discussion

The attachment of polypyridyl fragments to secondary amines in polyazacycloalkanes can be carried out by the use of a polypyridyl fragment containing a CH_2Br substituent. 4'-[(4-Bromomethyl)phenyl]-2,2':6',2''-terpyridine was synthesised following literature procedures.[17] The terpyridine-functionalised cyclam receptor was readily prepared by reaction of the terpyridine derivative with an excessof cyclam in dichloromethane in the presence of NEt_3 at 30° C for 24 hours and further column chromatography in alumina with a mixture of CH_2Cl_2/MeOH (99:1 v/v) as eluent obtaining a ca. 50% yield of L^1 (see Scheme 1). The ^1H NMR spectrum of L^1 shows pyridyl protons in the range of 7.2–8.8 ppm. The proton signals were fully assigned by using $^1H,^1H$ correlation (COSY) spectroscopy. The spectrum is completed by one singlet at 3.7 ppm of the methyl-

[a] Departamento de Química, Universidad Politécnica de Valencia,
Camino de Vera s/n, E-46071 Valencia, Spain
Fax: (internat.)+(34)-96/387-7349
E-mail: rmaez@qim.upv.es
[b] Departamento de Química Inorgánica, Facultad de Química, Universidad de Valencia,
Dr. Moliner 50, E-46100 Burjassot, Valencia, Spain

 © WILEY-VCH Verlag GmbH, D-69451 Weinheim, 2000 1434−1948/00/0404−0741 $ 17.50+.50/0



Scheme 1. Synthesis of L^1 and L^2 and the corresponding ruthenium complex of L^1

enic protons of the tolyl spacer, several overlapped signals in the range 2.40–2.90 of CH_2 groups attached to the nitrogen atoms in the macrocycle and two quintuplets at 1.6–1.8 ppm corresponding to the two nonequivalent central CH_2 groups from the propylene chains in the cyclam macrocycle.

Reaction of cyclam with an excess of 4'-[(4-bromomethyl-)phenyl]-2,2':6',2''-terpyridine in ethanol in the presence of NEt_3 gave L^2 as the unique product (see Scheme 1). The ^1H NMR spectrum of L^2 shows pyridyl protons in the range 7.25–8.70 ppm. The protons of the cyclam moiety appear in the range 1.8–2.8 ppm, whereas the benzylic protons give rise to a singlet at 3.52 ppm.

L^2 has also been characterised by single-crystal X-ray diffraction techniques. Suitable crystals for diffraction purposes were obtained by slow diffusion of diethyl ether into a solution of L^2 in dichloromethane. Some selected bond lengths and angles are listed in Table 1. Figure 1 shows the molecular structure of L^2. The structure consists of a cyclam core substituted with four benzyl-terpyridyl groups, giving a multidentate molecule with a promising geometry containing a central tetraaza and four peripheral terpyridine binding sites. Cyclic tetraamines can exist in several conformations depending on the relative position of the *N*-substituted groups with respect to the N4 plane.[18] Of the five possible conformations for a tetra-substituted cyclam derivative, the crystal structure of L^2 shows that the conformation with two substituents above and two below the mean N4 plane is adopted, the two benzyl-terpyridyl groups above the plane being separated by an ethylene chain. The 2,2':6',2''-terpyridine adopts the usual trans–trans conformation through the C–C interannular bond as has been found in related structures.[19] The terpyridine groups adopt a near-planar conformation with dihedral angles between the planes N(2)–C(10) and N(1)–C(5), N(3)–C(11) and N(2)–C(10), N(5)–C(38) and N(4)–C(45), N(6)–C(40) and N(5)–C(38) of 7.2°, 3.4°, 9.6°, and 13.7°, respectively. The angles between the planes C(16)–C(21) and N(2)–C(11), C(29)–C(34) and N(5)–C(38) are 26.6° and 10.5°, respectively.

Table 1. Selected bond lengths and angles[a]

Length			
N(1)–C(5)	1.307(12)	N(7)–C(22)	1.461(11)
N(1)–C(1)	1.321(13)	N(8)–C(28)	1.464(10)
N(8)–C(26)	1.492(10)	N(7)–C(23)	1.461(10)
N(8)–C(27)	1.480(10)	N(7)–C(24)	1.451(10)
C(1)–C(2)	1.38(2)	C(8)–C(16)	1.508(12)
C(2)–C(3)	1.38((2)	C(19)–C(22)	1.502(13)
C(3)–C(4)	1.371(13)	C(24)–C(25)	1.501(11)
C(4)–C(5)	1.369(12)	C(25)–C(26)	1.519(11)
C(5)–C(6)	1.484(13)		
Angles(°)			
C(9)–C(8)–C(16)	121.2(10)	C(24)–C(25)–C(26)	112.9(8)
C(23)–N(7)–C(22)	110.0(8)	N(8)–C(28)–C(29)	111.0(8)
N(7)–C(22)–C(19)	114.8(9)	N(8)–C(26)–C(25)	110.9(8)

[a] Values in parentheses are standard deviations in the last significant figure.

Reaction of equimolar quantities of L^1 with $Ru(mtpy)Cl_3$ [mtpy = 4'-methyl-2,2':6',2''-terpyridine] in methanol with

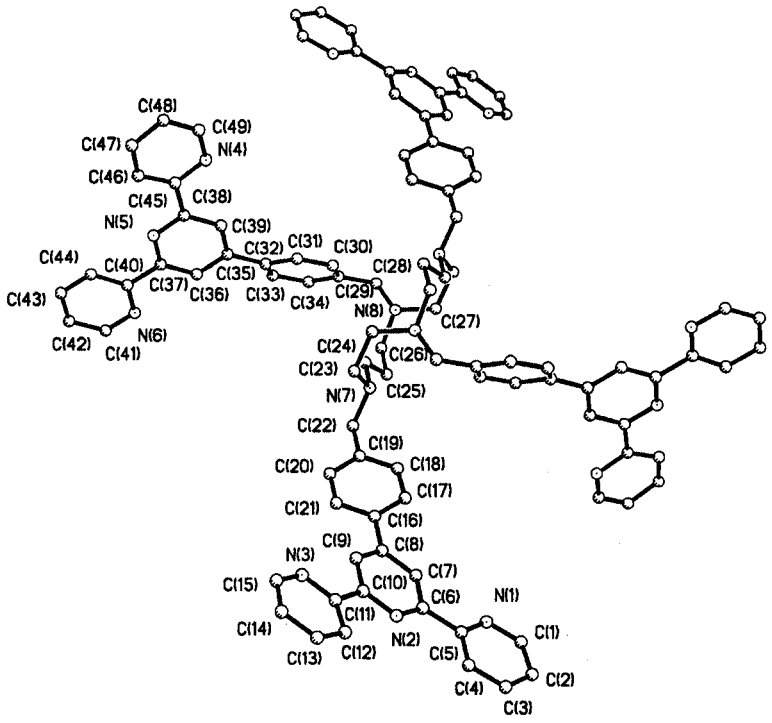


Figure 1. Molecular structure of L^2

the addition of *N*-ethyl-morpholine as mild reductant, afforded the receptor $[Ru(L^1)(mtpy)][PF_6]_2$ after column chromatography in silica using a mixture of acetonitrile/water/saturated aqueous solution of KNO_3 (17:1:2 v/v) as eluent and further precipitation with ammonium hexafluorophosphate (see Scheme 1). The FAB mass spectrum of the bis-terpyridyl ruthenium(II) complex $[Ru(L^1)(mtpy)][PF_6]_2$ showed peaks at m/z = 1161, 1015 and 869 corresponding to $[Ru(L^1)(mtpy)][PF_6]_2$, $[Ru(L^1)(mtpy)][PF_6]^+$ and $Ru(L^1)(mtpy)^{2+}$, respectively. The ^1H NMR spectrum shows the expected signals for the aromatic protons in the range 7.2–9.0 ppm, with two non-equivalent terpyridine groups. The spectrum also contained poorly defined overlapping signals in the 2.8–4 ppm range. The CH_3 of the terminal group appears at 2.93 ppm. Owing to the presence of the acetonitrile signal, the corresponding signal for the central CH_2 groups of the propylene chain in the cyclam cycle were not observed.

The synthesized ruthenium(II) complex contains a polyamine as the "receptor" part of the molecule and a bis(2,2':6',2''-terpyridine)-ruthenium(II) group able to act as signalling subunit. The following study has been carried out mainly to detect the effect that the coordination of the cyclam fragment has on the emission properties of the signalling ruthenium-terpyridine unit. The electronic spectrum of the complexes is as expected for a $[Ru(tpy)_2]^{2+}$ chromophore, with the principal $Ru[d(\pi)] \rightarrow tpy(\pi^*)$ MLCT transition at 484 nm, and the usual intense ligand-centred transitions in the UV region.[20] We have investigated the fluorescence behaviour of acetonitrile/water solutions of the receptor $[Ru(L^1)(mtpy)]^{2+}$ in the presence of transition metal ions M^{2+} (M^{2+} = Ni^{2+}, Cu^{2+}, Zn^{2+}, Cd^{2+}, Hg^{2+} and Pb^{2+}) as a function of the pH (see Figure 2) by luminescence spectroscopy. The continuous protonation of the poly- amine enhanced the emission intensity of the ruthenium core only slightly, indicating that the photoinduced electron transfer mechanism between the lone pair of the amines and the $Ru(tpy)_2^{2+}$ fluorophore is poor. The presence of the transition metals Ni^{2+}, Zn^{2+}, Cd^{2+}, Hg^{2+} and Pb^{2+} does not modify the fluorescence versus pH profile of the free receptor. In contrast, the coordination of Cu^{2+} in the macrocyclic cavity is accompanied by substantial quenching of the luminescence intensity with a minimum centred at pH = 6.9 (see Figures 2 and3).

Figure 2. Relative intensity versus pH for the L and $L-M^{2+}$ systems (L = $[Ru(L^1)(mtpy)][PF_6]_2$; M^{2+} = Cu^{2+}, Ni^{2+}, Zn^{2+}, Cd^{2+}, Pb^{2+}, Hg^{2+}) (λ_{ex} = 484 nm, λ_{em} = 664 nm)

To gain insight into the nature of the interaction of Cu^{2+} with the $Ru(tpy)_2$ fluorophore, two additional studies were carried out: (i) potentiometric titrations on an acetonitrile/water solution of $[Ru(L^1)(mtpy)]^{2+}$ in the presence of Cu^{2+}, and (ii) the synthesis of a parent fluorophore–spacer–receptor multicomponent system where the nature of the spacer was varied.

The protonation and coordination behaviour of L^1 and $[Ru(L^1)(mtpy)]^{2+}$ was studied by potentiometric titrations with KOH of previously acidified solutions in acetonitrile/

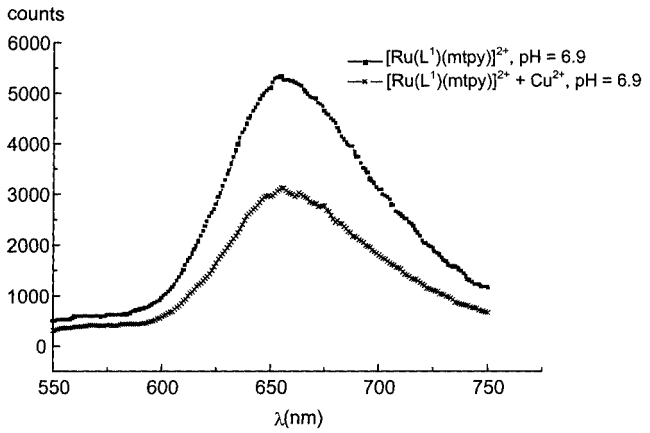


Figure 3. Emission spectra of the $[Ru(L^1)(mtpy)]^{2+}$ cation at pH = 6.9 with and without Cu^{2+}

water (70:30 v/v, 0.1 mol dm^{-3} tetrabutylammonium perchlorate). Additionally the protonation constants of cyclam in acetonitrile/water were also determined. Table 2 shows that $\log K_2 - \log K_3$ for the cyclam is 7.5, but only 3.85 for L^1 and 3.17 for $[Ru(L^1)(mtpy)]^{2+}$. The need to break a hydrogen bond to enable the third proton to become attached has been suggested as an explanation for the large difference between the values of $\log K_2$ and $\log K_3$ in the cyclam. Similar behaviour for cyclam has been observed in water or in THF/water (70:30 v/v).[21] However, this effect disappears in substituted derivatives such as L^1 and $[Ru(L^1)(mtpy)]^{2+}$. Five protonation steps were determined for L^1: the first two protonations probably took place at the macrocyclic moiety; the last three protonations either took place at the terpyridine or at the cyclam. For the $[Ru(L^1)(mtpy)]^{2+}$ complex and cyclam only three protonation constants were observed, the four being too acidic to be determined. Remarkably the $[Ru(L^1)(mtpy)]^{2+}$ complex does not show

Table 2. Stepwise protonation constants (log K) of L^1, $[Ru(L^1)(mtpy)]^{2+}$ and cyclam in acetonitrile/water (70:30 v/v, 0.1 mol dm^{-3} of $[n\text{-}Bu_4N][ClO_4]$

Reaction	L^1	$[Ru(L^1)(mtpy)]$	cyclam
$L + H^+ \rightleftarrows (HL)^+$	10.88(4)[a]	10.33(1)	11.6(2)
$L + 2H^+ \rightleftarrows (H_2L)^{2+}$	19.34(4)	19.08(1)	21.09(1)
$L + 3H^+ \rightleftarrows (H_3L)^{3+}$	23.95(3)	24.66(1)	23.1(2)
$L + 4H^+ \rightleftarrows (H_4L)^{4+}$	26.89(3)		
$L + 5H^+ \rightleftarrows (H_5L)^{5+}$	29.51(2)		
$L + H^+ \rightleftarrows (HL)^+$	10.88	10.33	11.6
$(HL)^+ + H^+ \rightleftarrows (H_2L)^{2+}$	8.46	8.75	9.49
$(H_2L)^{2+} + H^+ \rightleftarrows (H_3L)^{3+}$	4.61	5.58	2.01
$(H_3L)^{3+} + H^+ \rightleftarrows (H_4L)^{4+}$	2.94		
$(H_4L)^{4+} + H^+ \rightleftarrows (H_5L)^{5+}$	2.62		

[a] Values in parentheses are standard deviations in the last significant figure.

substantial basicity difference from L^1 for the first three protonation constants, despite the existence of a positively charged $Ru(tpy)_2^{2+}$ core.

Table 3 shows the stability constants for the formation of Cu^{2+} complexes of $[Ru(L^1)(mtpy)]^{2+}$ in acetonitrile/water (70:30 v/v). The distribution diagram of the $[Ru(L^1)(mtpy)]^{2+}$–H^+–Cu^{2+} is depicted in Figure 4. The receptor $[Ru(L^1)(mtpy)]^{2+}$ forms the complex $\{Cu[Ru(L^1)(mtpy)]\}^{4+}$ existing in the neutral pH range. These species undergo two protonation processes upon lowering of the pH, whereas two additional hydroxo complexes were found to exist at basic pH. The logarithm of the stability constant for the formation of the complex $\{Cu[Ru(L^1)(mtpy)]\}^{4+}$ is 13.30. This value can be compared with that found for the formation of $[Cu(tmfcyclam)]^{2+}$ ($\log K = 19.06$)[22] (where tmfcyclam = 1,4,8,11-tetrakis(ferrocenylmethyl)-tetraazacyclotetradecane), or with that of $[Cu(cyRubipy)]^{10+}$ ($\log K = 6.01$)[23] (where cyRubipy stand for a tetramethyl-$Ru(bipy)_3$-substituted cyclam). In the latter, the Cu^{2+} cation is brought within the range of the electrostatic repulsion from all four of the pendent $[Ru(bipy)_3]^{2+}$ groups while in $Cu[Ru(L^1)(mtpy)]^{4+}$ the Cu^{2+} cation only experiences the electrostatic repulsion of one tolyl-distanced $[Ru(tpy)_2]\}^{2+}$ core. The above could explain the difference in the stability constants of $\{Cu[Ru(L^1)(mtpy)]\}^{4+}$ and $\{Cu[cyRu(bipy)_3]\}^{10+}$ ($\log K$ of $\{Cu[Ru(L^1)(mtpy)]\}^{4+}$ – logK of $\{Cu[cyRu(bipy)_3]\}^{10+}$ = 7.29). Effects of the electrostatic repulsion could also be observed when comparing the stability constants for the formation of the complexes $[Cu(tmfcyclam)]^{2+}$ and

Table 3. Stability constants (log K) for the formation of copper(II) complexes of $[Ru(L^1)(mtpy)]^{2+}$

Reaction	logK
$Cu^{2+} + 2H^+ + L^{2+} \rightleftarrows [Cu(H^2L)]^{6+}$	24.84(5)[a]
$Cu^{2+} + H^+ + L^{2+} \rightleftarrows [Cu(HL)]^{5+}$	19.77(8)
$Cu^{2+} + L^{2+} \rightleftarrows [Cu(L)]^{4+}$	13.30(7)
$Cu^{2+} + L^{2+} + H_2O \rightleftarrows [Cu(L)(OH)]^{3+} + H^+$	4.89(10)
$Cu^{2+} + L^{2+} + 2H_2O \rightleftarrows [Cu(L)(OH)_2]^{2+} + 2H^+$	–4.36(9)

[a] Values in parentheses are standard deviations in the last significant figure.

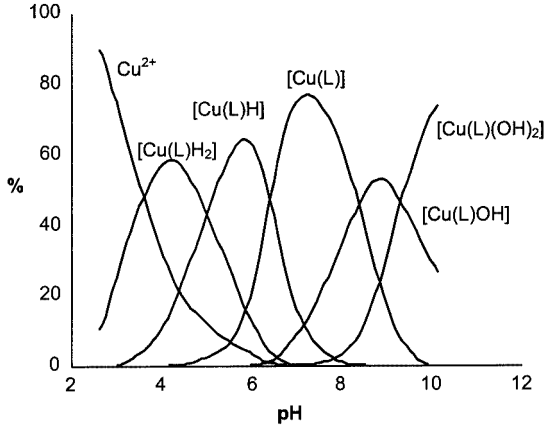


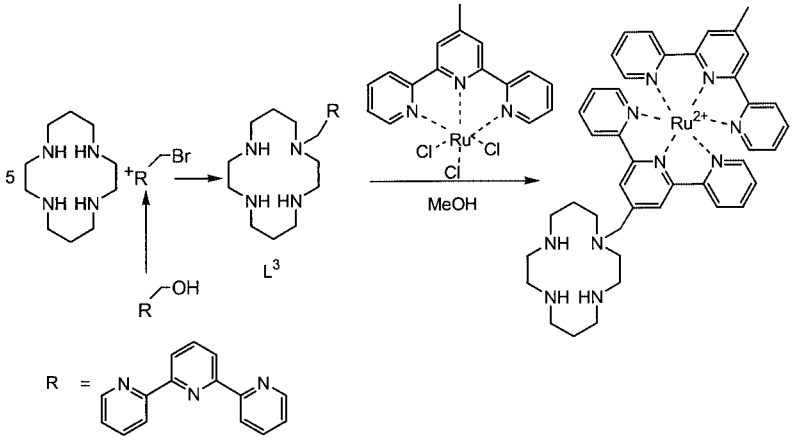
Figure 4. Distribution diagram of the species for the system $[Ru(L^1)(mtpy)]$–Cu^{2+}–H^+

$\{Cu[Ru(L^1)(mtpy)]\}^{4+}$. Despite the existence of the constraints imposed by the tmfcyclam ligand in their interaction with Cu^{2+}, the formation constant for $[Cu(tmfcyclam)]^{2+}$ is larger that that found for $\{Cu[Ru(L^1)(mtpy)]\}^{4+}$ (logK of $[Cu(tmfcyclam)]^{2+}$ – logK of $\{Cu[Ru(L^1)(mtpy)]\}^{4+}$ = 5.76), indicative of the electro-

static repulsion induced by the $[Ru(tpy)_2]^{2+}$ core on the macrocyclic cavity.

Comparison between the distribution diagram in Figure 4 and the I vs. pH curve in Figure 2 provides information about the stoichiometry and the nature of the complexes existing in the pH range where the luminescence is decreased. The quenching of the emission of the $Ru(tpy)_2^{2+}$ fluorophore is related to the presence of the $\{Cu[Ru(L^1)(mtpy)]\}^{4+}$ complex in solution, whereas further coordination of OH^- to the copper metal ion, or protonation of the amine groups in cyclam hinder the quenching.

In order to evaluate the role played by the spacer groups we have also synthesised a parent cyclam terpyridine ligand containing a CH_2 group as spacer instead of a tolyl one as in the case of L^1. For this purpose, the synthesis of the 4'-bromomethyl-2,2':6',2''-terpyridine using the 4'-methyl-2,2':6',2''-terpyridine as starting material was tested using two different routes: (i) by simple bromination of the methyl groups with *N*-bromosuccinimide, or (ii) reaction of CBr_4 with 4'-hydroxymethyl-2,2':6',2''-terpyridine obtained from the methyl derivative. When *N*-bromosuccinimide and catalytic amounts of dibenzoyl peroxide react with 4'-methyl-2,2':6',2''-terpyridine, three products were obtained: monobrominated, dibrominated and starting material. However, the mixture is not amenable to chromatographic separation. In our hands, silica or alumina did not give a very satisfactory separation of the products. The second procedure involves the reaction of 4'-(hydroxymethyl)-2,2':6',2''-terpyridine (OHmtpy) with carbon tetrabromide and triphenylphosphane to give 4'-bromomethyl-2,2':6',2''-terpyridine as the only product in 40% yield (see Scheme 2). 4'-Methyl-2,2':6',2''-terpyridine was reacted with selenium dioxide to give 4'-carbaldehyde-2,2':6',2''-terpyridine which was reduced with $NaBH_4$ to yield the corresponding 4'-(hydroxymethyl)-2,2':6',2''-terpyridine. OHmtpy has been mentioned, but to the best of our knowledge, full experimental information has not been given for its synthesis, so details are included in this paper.



Scheme 2. Synthesis of L^3 and the corresponding ruthenium complex

Reaction of the 4'-bromomethyl-2,2':6',2''-terpyridine with excess cyclam afforded the corresponding L^3 molecule in a 50% yield (see Scheme 2). As expected, the ^1H NMR spectrum of L^3 is very similar to the one of L^1 showing the pyridyl protons in the range 7.2–8.65 ppm. The spectrum is completed by one singlet at 3.62 ppm of the methylenic protons of the spacer, several overlapped signals in the range 2.40–3.10 ppm for the CH_2 groups attached to the nitrogen atoms in the macrocycle and two quintuplets at 1.8–1.95 ppm corresponding to the two nonequivalent central CH_2 groups of the propylenic chains in the cyclam macrocycle. Synthesis of $[Ru(L^3)(mtpy)][PF_6]_2$ ruthenium(II) complex was carried out by a similar method to that used in the synthesis of $[Ru(L^1)(mtpy)][PF_6]_2$ (see Scheme 2). The FAB spectrum of this complex shows peaks at m/z = 1085, 940 and 794, corresponding to $\{[Ru(L^3)(mtpy)]_2[PF_6]\}$, $\{[Ru(L^3)(mtpy)][PF_6]\}^+$ and $\{Ru(L^3)(mtpy)\}^{2+}$, respectively. The ^1H NMR spectrum shows the expected signals for the aromatic protons in the range of 7.2–8.7 ppm with two nonequivalent terpyridine groups. The spectrum also contains poorly defined overlapping signals in the 2.9–3.9 ppm range. The CH_3 of the terminal group appears at 2.93 ppm. As in the spectrum of $[Ru(L^1)(mtpy)]^{2+}$, the presence of the acetonitrile signal hampers the observation of the corresponding signal for the central CH_2 groups of the propylenic chain in the cyclam cycle.

The fluorescence behaviour of acetonitrile/water solutions of the receptor $[Ru(L^3)(mtpy)]^{2+}$ in the presence of transition metal ions M^{2+} (M^{2+} = Ni^{2+}, Cu^{2+}, Zn^{2+}, Cd^{2+}, Hg^{2+} and Pb^{2+}) as a function of the pH has also been studied. The behaviour of the ruthenium complex containing L^3 as ligand is similar to the behaviour observed for the ruthenium complex of L^1. There is a poor enhancement of the emission intensity of the ruthenium core upon protonation of the polyaza macrocycle and whereas the presence of Ni^{2+}, Zn^{2+}, Cd^{2+}, Hg^{2+} and Pb^{2+} does not modify the fluorescence versus pH profile of the free receptor, the coordination of Cu^{2+} quenches the luminescence intensity with a minimum centred at pH = 6.2 (see Figure 5). However, despite the shorter spacer between the cyclam and the $Ru(tpy)_2^{2+}$ core in complex $[Ru(L^3)(mtpy)]^{2+}$ than in $[Ru(L^1)(mtpy)]^{2+}$, a larger quenching is observed for the latter than for the former in the presence of Cu^{2+}.

With regard to the quenching mechanism, preliminary results suggest that the quenching of the fluorescence of the

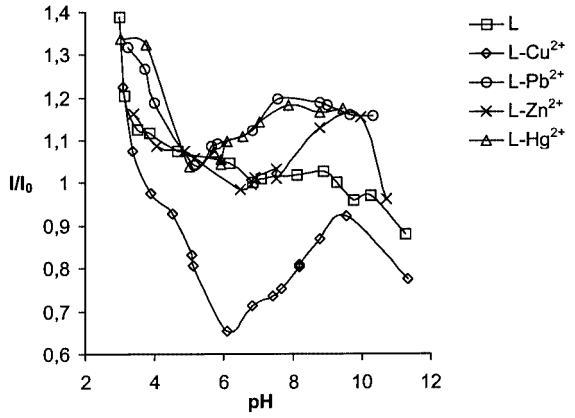


Figure 5. Relative intensity versus pH for the L and L–M^{2+} systems (L = $[Ru(L^3)(mtpy)][PF_6]_2$; M^{2+} = Cu^{2+}, Ni^{2+}, Zn^{2+}, Cd^{2+}, Pb^{2+}, Hg^{2+}) (λ_{ex} = 484 nm, λ_{em} = 625 nm)

$[Ru(L^1)(mtpy)]^{2+}$ and $[Ru(L^3)(mtpy)]^{2+}$ metallo-receptors upon Cu^{2+} binding most likely occurs predominantly by means of an energy transfer, bearing in mind that the electron transfer is unlikely due to the difficulty of oxidation or reduction of $[Cu(cyclam)]^{2+}$.[24] We have calculated the free energy associated with an electron-transfer mechanism by using the emission band intensity, the Ru^{II}/Ru^{III} oxidation potential of the ruthenium bis-terpyridine core ($E_{Ru(III)/Ru(II)}$ = + 1.3 V and the reduction potential for the Cu^{II}/Cu^{I} process ($E_{Cu(II)/Cu(I)}$ = – 1.05 V) in the cyclam environment, and have found a thermodynamically unfavourable ΔG value of +0.45 V for an electron transfer process. Energy-transfer mechanisms would require a close proximity between the fluorophore and the copper metal ion. In this sense, it is remarkable that the quenching is more pronounced in $[Ru(L^1)(mtpy)]^{2+}$ than in $[Ru(L^3)(mtpy)]^{2+}$. In $[Ru(L^1)(mtpy)]^{2+}$, the $Ru(tpy)_2^{2+}$ is separated by a tolyl spacer from the macrocyclic cavity, while in L^3 the spacer is a CH_2 group. The tolyl spacer in L^1 probably favours the movement of the Cu-cyclam core in search of a better overlap between the metal cation in the tetraamine and the $Ru(tpy)_2^{2+}$ fluorophore while in L^3 the CH_2 spacer diminishes this possibility.

Conclusion

We have developed new cyclam receptors functionalised with fluorescent $Ru(tpy)^{2+}$ signalling subunits and have demonstrated that the presence of copper(II) selectively quenches the fluorescence of the ruthenium(II) core more than other common metal ions in an aqueous environment at neutral pH. We have determined that the $\{Cu[Ru(L^1)(mtpy)]\}^{4+}$ complex is responsible for the quenching of the emission of the $[Ru(tpy)_2]^{2+}$ core, whereas further amine protonation or OH^- coordination to the complex hinders the quenching process. Additionally the $[Ru(L^3)(mtpy)]^{2+}$ receptor has also been synthesised and confirmed that Cu^{2+} produces a smaller decrease in fluorescence. An energy-transfer mechanism is suggested. We are currently extending our approach by attaching several macrocyclic structures to ruthenium-terpyridine units and continuing our study on the multireceptor L^2 to obtain dendritic species with several metal centres in order to construct assemblies with tuneable luminescence properties.

Experimental Section

General Remarks: The complexes $[Ru(mtpy)Cl_3]$, 4'-[4-(bromomethyl)phenyl]-2,2':6'.2''-terpyridine (Brmphtpy),[17] 4'-(4-methylphenyl)-2,2':6'.2''-terpyridine (mphtpy) and 2,2':6'.2''-terpyridinyl-4'-carboxaldehyde (CHOtpy), [25] were prepared according to published methods; all other reagents were commercially available and used as received. Photochemical data were obtained with a FS900CDT steady state T-Geometry Fluorometer, Edinburgh Analytical Instruments. All solutions for photophysical studies were rigorously degassed. Concentration of the ligand and metal ion was *ca.* 1.0×10^{-4} mol dm^{-3}. ^1H NMR spectra were recorded with a Varian Gemini spectrometer. Potentiometric titrations were carried out in acetonitrile/water (70:30 v/v, 0.1 mol dm^{-3} tetrabutylammonium perchlorate) using a water-thermostatted reaction vessel at 25.0 ± 0.1 °C under nitrogen. The titrant was added by a Crison microburette 2031. Experimental potentiometric details have been published previously.[26] The concentration of the metals ions was determined using standard methods. The computer program SUPERQUAD[27] was used to calculate the protonation and stability constants. The titration curves for each system (ca. 250 experimental points corresponding to at least three titration curves, pH range investigated 2.5–10.2, concentration of the ligand and metal ion was *ca.* 1.0×10^{-3} mol dm^{-3}) were treated either as a single set or as separate entities without significant variations in the values of the stability constants. Finally the sets of data were merged together and treated simultaneously to give the stability constants.

Synthesis of 4'-(Hydroxymethyl)-2,2':6'.2''-terpyridine (OHmtpy): To a mixture of CHOtpy (1.0 g, 3.8 mmol) in THF (10 mL) was added $NaBH_4$ (200 mg, 5.3 mmol) and the resulting mixture was stirred for 15 min at 0 °C. The reaction mixture was extracted with EtOAc (70 mL), and washed with water (3 × 3 mL) and brine (3 mL). The extract was dried over $MgSO_4$ and evaporated under reduced pressure. The residue was purified by column chromatography on silica gel. Yield 841 mg, 85%.

Synthesis of 4'-(Bromomethyl)-2,2':6'.2''-terpyridine (Brmtpy): To a mixture of OHmtpy (1 mmol) and carbon tetrabromide (2 mmol) in CH_2Cl_2 (5 mL) was added triphenylphosphane (1.1 mmol) at 0 °C in several portions over 15 min. The mixture was stirred for 0.5 h at the same temperature and for 0.5 h at room temperature. In order to remove triphenylphosphane oxide, the mixture was passed through a short silica gel column (10 g) and eluted with CH_2Cl_2. Compound Brmtpy was obtained as a yellow oil that solidified on prolonged drying. Yield 130 mg, 40%. – ^1H NMR (300 MHz, $CDCl_3$): δ = 4.48 (s, 2 H, CH_2Br), 7.29–7.31 [2 H, tpy H(5, 5'')], 7.78–7.81 [2 H, tpy H(4, 4'')], 8.42 [s, 2 H, tpy H(3', 5')], 8.54–8.56 [2 H, tpy H(6, 6'')] and 8.63–8.66 [2 H, tpy H(3, 3'')]. – $C_{16}H_{12}N_3Br.CH_2Cl_2$: calcd. C 49.8, H 3.4, N 10.3; found C 49.6, H 3.1, N 10.3. – FAB-MS: *m/z* (%): 327(30), 325(65), 247(80).

Synthesis of 1-[4'-*p*-Tolyl-(2,2':6',2''-terpyridyl)]-1,4,8,11-tetraazacyclotetradecane (L^1): A mixture of 4'-[4-(bromomethyl)phenyl]-2,2':6'.2''-terpyridine (0.5 mmol) in CH_2Cl_2 (20 mL) was added dropwise to a solution of cyclam (500 mg, 2.5 mmol) in CH_2Cl_2 (20 mL). Et_3N (5 drops) was added, and the solution was heated at 30°C for 24 h. The reaction mixture was washed with water (3

× 3 mL). The organic phase was dried over $MgSO_4$ and evaporated under reduced pressure. The residue was purified by column chromatography on alumina with CH_2Cl_2/CH_3OH (99:1 v/v) as eluent. A pale yellow oil was obtained which solidified on scratching. Yield: 130 mg, 50%. – **L^1**: ^{1}H NMR (300 MHz, $CDCl_3$): δ = 1.60–1.80 (4 H, $CH_2CH_2CH_2$), 2.3–2.9 (16 H, CH_2–N), 3.52 (2 H, Cy–CH_2-tpy), 7.20–7.22 [2 H, tpy H(5, 5'')], 7.34–7.36[2 H, Ph H_m), 7.70–7.72 [2 H, tpy H(4, 4'')], 7.73–7.73 (2 H, Ph H_o), 8.54–8.56 [2 H, tpy H(6, 6'')], 8.57–8.59 [2 H, tpy H(3, 3'')], and 8.62 [s, 2 H, tpy H(3', 5')]. – ^{13}C NMR ($CDCl_3$): δ = 26.17 (CH_2), 28.60 (CH_2), 46–60 (8 CH_2), 71.53 (CH_2), 118.53 (CH, tpy), 121.2 (CH, tpy), 123.64 (CH, tpy), 126.91 (CH, C_6H_4), 129.55 (CH, C_6H_4), 136.82 (CH, tpy), 140.4 (C, tpy), 148.96 (CH, tpy), 149.92 (CH, tpy), 155.8 (C, tpy), 156.14 (C, tpy). – $C_{32}H_{39}N_7.CH_2Cl_2.H_2O$: calcd. C 63.5, H 6.9, N 15.7; found C, 63.0; H, 6.9; N, 15.4. – FAB-MS: *m/z* (%): 522 (100), 323 (40), 212 (50).

Synthesis of 1,4,8,11-[4'-*p*-Tolyl-(2,2':6',2''-terpyridyl)]-1,4,8,11-tetraazacyclotetradecane (L^2): A mixture of Brmphtpy (650 mg, 1.6 mmol) and cyclam (54 mg, 0.27 mmol) in ethanol (50 mL) and in the presence of Et_3N was heated at reflux for 24 h. Yellow crystals were obtained. The residue was purified by column chromatography on alumina using CH_2Cl_2/CH_3OH (97:3 v/v) as eluent. Yield: 70 mg, 20%. **L^2:**. ^{1}H NMR (300 MHz, $CDCl_3$): δ = 1.85 (2 H, $CH_2CH_2CH_2$), 2.62 (8 H, CH_2–N), 2.71 (8 H, CH_2–N), 3.52 (8 H, Cy–CH_2-phtpy),7.25–7.30 [8 H, tpy H(5, 5'')], 7.45–7.50 [8 H, ph), 7.73–7.74 [8 H, ph), 7.75 [8 H, tpy H(4, 4'')], 8.59 [8 H, tpy H(6, 6'')], 8.63–8.66 [8 H, tpy H(3, 3'')] and 8.66 [s, 8 H, tpy H(3', 5')]. – ^{13}C NMR ($CDCl_3$): δ 30.5 (CH_2), 50.5 (4 CH_2), 51.6 (4 CH_2), 59.0 (4 CH_2), 118.8 (CH, tpy), 121.3 (CH, tpy), 123.8 (CH, tpy), 127.0 (CH, C_6H_4), 129.5 (CH, C_6H_4), 136.8 (CH, tpy), 149.0 (CH, tpy), 155.72 (C, tpy), 156.3 (C, tpy). – $C_{98}H_{84}N_{16}{\cdot}2CH_2Cl_2{\cdot}H_2O$: calcd. C 72.5, H 5.3, N 13.5; found C 72.3, H 5.1, N 12.9. – FAB-MS: *m/z* (%): 1487 (100), 1164 (45).

Synthesis of 1-[4'-Methyl-(2,2':6',2''-terpyridyl)]-1,4,8,11-tetraazacyclotetradecane (L^3): L^3 was prepared in the same manner as L^1, by the reaction of cyclam and 4'-(bromomethyl)-2,2':6'.2''-terpyridine. Yield: 110 mg, 50%. **L^3:** ^{1}H NMR (300 MHz, $CDCl_3$): δ = 1.82–1.97 (4 H, $CH_2CH_2CH_2$), 2.4–3.1 (16 H, CH_2–N), 3.62 (2 H, Cy–CH_2-tpy), 7.22–7.24 [2 H, tpy H(5, 5'')], 7.78–7.80 [2 H, tpy H(4, 4'')], 8.40 [s, 2 H, tpy H(3', 5')], 8.53–8.56 [2 H, tpy H(6, 6'')] and 8.60–8.63 [2 H, tpy H(3, 3'')]. – ^{13}C NMR ($CDCl_3$): δ 23.9 (CH_2), 24.2 (CH_2), 45–59 (8 CH_2), 72.38 (CH_2), 121.2 (2 CH, tpy), 123.9 (CH, tpy), 136.9 (CH, tpy), 148.0 (CH, tpy), 150.1 (C, tpy), 155.5 (2 C, tpy). – $C_{26}H_{35}N_7.CH_2Cl_2.H_2O$: calcd. C 59.1, H 7.1, N 17.9; found C 60.0, H 6.9, N 17.4. – FAB-MS: *m/z* (%): 446 (35), 247 (80), 213 (80).

Synthesis of $[Ru(L^1)(mtpy)][PF_6]_2$ and $[Ru(L^3)(mtpy)][PF_6]_2$: These ruthenium complexes were prepared in the same way. A mixture of the appropriate ligand (L^1 105 mg, L^3 89 mg; 0.2 mmol), with $[Ru(mtpy)Cl_3]$ (90 mg, 0.2 mmol) and three drops of *N*-ethylmorpholine as a mild reductor in MeOH (20 mL) was heated at reflux with stirring for 1 h. The resulting deep-red solution was filtered through celite to remove any unchanged $[Ru(mtpy)Cl_3]$ and excess methanolic ammonium hexafluorophosphate was added to the filtrate to precipitate the ligand complexes. Further purification was achieved by chromatography over silica using 17:2:1 acetonitrile/water/saturated aqueous KNO_3 solution. The complexes were isolated as their PF_6^- salts.

$[Ru(L^1)(mtpy)][PF_6]_2$:. Yield: 40 mg, 20%. – ^{1}H NMR (300 MHz, CD_3CN): δ = 2.90 (s, 3 H, CH_3), 3.0–3.5 (16 H, CH_2–N), 3.78–3.82 (2 H, tpy–CH_2–Cy), 7.18–7.20[4 H, tpy H(5,5'')^{1,2}], 7.37–7.39[2 H, tpy H(6,6'')^1], 7.42–7.44[2 H, tpy H(6,6'')^2], 7.74–7.76 (2 H, ph H_m), 7.94–7.96 [4 H, tpy H(4, 4'')^{1,2}], 8.20–8.22 (2 H, ph H_o), 8.48–8.50 [2 H, tpy H(3, 3'')^1], 8.68–8.70 [2 H, tpy H(3, 3'')^2] 8.70 [s, 2 H, tpy H(3', 5')^1] and 9.01 [s, 2 H, tpy H(3', 5')^2].^{1} = mtpy; ^{2} = Cy–spacer–tpy (spacer = tolyl). – $C_{48}H_{52}N_{10}Ru(PF_6)_2.2CH_2Cl_2$: calcd. C 45.1, H 4.2, N 10.5; found C 45.3, H 3.8, N 10.3. – FAB-MS: *m/z* (%): 1161 (8), 1015 (20), 869 (45), 327 (60), 281 (100). – **$[Ru(L^1)(mtpy)][PF_6]_2$:** Yield 30 mg, 15%. – ^{1}H NMR (300 MHz, CD_3CN): δ = 2.97 (s, 3 H, CH_3), 3.0–3.3 (16 H, CH_2–N), 3.7–3.9(2 H, tpy–CH_2–Cy), 7.16–7.18[2 H, tpy H(5,5'')^1], 7.22–7.24 [2 H, tpy H(5, 5'')^2], 7.24–7.26[2 H, tpy H(6,6'')^2], 7.37–7.39[2 H, tpy H(6,6'')^1], 7.92–7.94 [4 H, tpy H(4, 4'')^{1,2}], 8.44–8.46 [2 H, tpy H(3, 3'')^2], 8.50–8.52 [2 H, tpy H(3, 3'')^1] 8.66 [s, 2 H, tpy H(3', 5')^2] and 8.68 [s, 2 H, tpy H(3', 5')^1].^{1} = mtpy; ^{2} = Cy–spacer–tpy (spacer = methylene) – FAB-MS: *m/z* (%): 1085 (20), 939 (26), 793 (45), 595 (60).

X-ray Crystallographic Study: $C_{106}H_{104}N_{16}O_5$, M = 1682.05, triclinic, space group $P\bar{1}$, a = 12.303(4), b = 13.440(5), c = 15.618(6) Å, α = 106.60(3), β = 90.71(3), γ = 101.96(3), Z = 1, U = 2414(2) Å^3, Dc = 1.157 g cm^{-3}, λ(Mo-K_α) = 0.71069 Å, T = 296(2) K, μ(Mo-K_α) = 0.073 mm^{-1}. Measurements were made using a Siemens P4 diffractometer with graphite monochromated Mo-K_α radiation on a yellow crystal of L^2, of dimensions 0.26 × 0.20 × 0.23 mm. A total of 6429 reflections were collected, of which 6090 were unique (R_{int} = 0.0551). Lorentz, polarisation and semi-empirical from psi-scan absorption (Max. and min. transmission 0.4322 and 0.2287) corrections were applied. The structure was solved by direct methods (SHELXTL)[28] and refined by full-matrix least-squared analysis on *F2* (SHELXTL). The refinement converged at R_1 = 0.1077 ($F > 4\sigma(F)$) and wR_2 = 0.3120 (all data). Largest peak and hole in the final difference map +0.44, –0.35 e Å^{-3}. Crystallographic data for the structure reported in this paper have been deposited with the Cambridge Crystallographic Data Centre as supplementary publication no. CCDC-132890. Copies of the data can be obtained free of charge on application to CCDC, 12 Union Road, Cambridge CB2 1EZ, UK [Fax: (internat.)+ 44–1223/336–033; E-mail: deposit@ccdc.cam.ac.uk].

Acknowledgments

We would like to thank the DGICYT (proyecto PB95–1121-C02–02 and 1FD97–0508-C03–01) and Generalitat Valenciana (proyecto GV97-CB-11–62) for support.

[1] L. Fabbrizzi, A. Poggi, *Transitions Metals in Supramolecular Chemistry*, **1994**; J.-M. Lehn, *Supramolecular Chemistry*, VCH, Weinheim.
[2] [2a] A. P. Silva, H. Q. N. Gunaratne, T. Gunnlaugsson, A. J. M. Huxley, C. P. McCoy, J. Rademacher, T. E. Rice, *Chem. Rev.* **1997**, *97*, 1515–1566. – [2b] E. C. Constable, *Chem. Commun*. **1997**, 1073–1080.
[3] [3a] V. Balzani, F. Scandola, *Supramolecular Photochemistry*, Ellis Horwood, Chichester, **1991**. – [3b] V. Balzani, A. Juris, M. Venturi, S. Campagna, S. Serroni, *Chem. Rev.* **1996**, *96*, 759–833.
[4] M. Maestri, N. Armali, V. Balzani, E. C. Constable, A. M. W. Cargill Thompson, *Inorg Chem*. **1995**, *34*, 2759–2767.
[5] F. Barigelletti, L. Flamigni, M. Guardigli, A. Juris, M. Beley, S. Chodorowski-Kimmes, J.-P. Collin. J-P. Sauvage, *Inorg. Chem*. **1996**, *35*, 136–142.
[6] S. L. Larson, C. M. Elliot, D. F. Kelley, *Inorg. Chem*. **1996**, *35*, 2070–2076.
[7] L. Flamigni, F. Barigelletti, N. Armaroli, B. Ventura, J.-P. Collin, J.-P. Sauvage, J. A. Gareth Williams, *Inorg. Chem.* **1999**, *38*, 661–667.
[8] M.T. Indelli, C. A. Bignozzi, F. Scandola, J.-P. Collin, *Inorg Chem*. **1998**, *37*, 6084–6089.

[9] [9a] F. Barigelletti, L. Flamigni, G. Calogero, L. Hammarström, J.-P. Sauvage, J.-P. Collin, *Chem. Commun*. **1998**, 2333–2334. – [9b] M. Padilla-Tosta, J. M. Lloris, R. Martínez-Máñez, T. Pardo, J. Soto, *Inorg. Chim. Acta*. **1999**, *292*, 28–33.
[10] [10a] P. D. Beer, J. Cadman, *N. J. Chem*. **1999**, *23*, 347–349. – [10b] M. C. Grossel, D. G. Hamilton, J. I. Fuller, E. Millan-Barrios, *J. Chem. Soc., Dalton Trans.* **1997**, 3471–3477. – [10c] C. Lopez, J. C. Moutet, E. Saint-Aman, *J. Chem. Soc., Faraday Trans.* **1996**, *92*, 1527–1532.
[11] [11a] V. Balzani, S. Campagna, G. Denti, A. Juris, S. Serroni, M. Venturi, *Acc. Chem. Res.* **1998**, *31*, 26–34. – [11b] F. Vögtle, *Supramolecular Chemistry*, Wiley, Chichester, **1993**.
[12] *Advances in Dendritic Macromolecules* (Ed: G. R. Newkome) J AI Press, Greenwich, **1995**, vol. 2 and references therein.
[13] [13a] A. Harriman, R. Ziessel, *Chem. Commun*. **1996**, 1707–1716. – [13b] F. Barigelletti, L. Flamigni, J-P. Collin, J-P. Sauvage, A. Sour, E. C. Constable, A. M. W. Cargill Thompson, *J. Am. Chem. Soc.* **1994**, *116*, 7692–7699. – [13c] F. Vögtle, M. Frank, M. Nieger, P. Belser, A. Von Zelewsky, V. Balzani, F. Barigelletti, L. De Cola, L. Flamigni, *Angew. Chem. Int. Ed. Engl.* **1993**, 32, 1643–1646.
[14] S. Weidner, Z. Pikramenou, *Chem. Commun*. **1998**, 1473–1474.
[15] [15a] M. A. Mortellaro, D. G. Nocera, *J. Am. Chem. Soc*. **1996**, *118*, 7414. – [15b] Z. Pikramenou, J-a. Yu, A. Ponce, D. G. Nocera, *Coord. Chem. Rev.* **1994**, 132, 181–194. – [15c] F. Szemes, D. Hesek, Z. Chen, S. W. Dent, M. G: B: Drew, A. J. Goulden, A. R. Graydon, A. Grieve, R. J. Mortimer, T. Wear, J. S. Weightman, P. D. Beer, *Inorg. Chem.* **1996**, *35*, 5868–5879.
[16] [16a] V. Wing-Wah Yam, V. Wing-Man Lee, *J. Chem. Soc., Dalton Trans.* 1997, 3005–3010. – [16b] M. Padilla-Tosta, J. M. Lloris, R. Martínez-Máñez, T. Pardo, J. Soto, *Chem. Commun*. submitted.
[17] W. Spahni, G. Calzaferri, *Helv. Chim. Acta* **1984**, *67*, 450–454.
[18] L. F. Lindoy, *The Chemistry of Macrocyclic Ligand Complexes*, Cambridge University Press, Cambridge **1989**.
[19] E. C. Constable A. J. Edwards, R. Martínez-Máñez, P. R. Raithby, A. M. Cargill Thompson, *J. Chem. Soc., Dalton Trans.* **1994**, 645–650.
[20] J. P. Sauvage, J. P. Collin, J. C. Chambron, S. Guillerez, C. Coudret, V. Balzani, F. Barigelletti, L. De Cola, L. Flamigni, *Chem. Rev.* **1994**, *94*, 993–1019.
[21] E. Martell, R.M. Smith, R.M. Motekaitis, *NIST Critical Stability Constants of Metal Complexes Database*, Texas AM University, College Station, **1993**.
[22] J.M. Lloris, R. Martínez-Máñez, T. Pardo, J. Soto, M. E. Padilla-Tosta, *J. Chem. Soc., Dalton Trans.* **1998**, 2635–2641.
[23] A. M. Josceanu, P. Moore, S. C. Rawle, P. Sheldon, S. M. Smith, *Inorg. Chim. Acta.* **1995**, *240*, 159–168.
[24] S. C. Rawle, P. Moore, N. W. Alcock, *J. Chem. Soc., Chem. Commun.* **1992**, 684–687.
[25] K. Potts, D. A. Usifer, A. Guadalupe, H. D. Abruña, *J. Am. Chem. Soc.* **1987**, *109*, 3961–3966.
[26] J. M. Lloris, R. Martínez-Máñez, M. E. Padilla-Tosta, T. Pardo, J. Soto, E. García –España, J. A. Ramírez, M. I. Burguete, S. V. Luis, E. Sinn, *J. Chem. Soc., Dalton Trans.* **1999**, 1779–1784.
[27] P. Gans, A. Sabatini, A. Vacca, *J. Chem. Soc., Dalton Trans.* **1985**, 1195.
[28] *SHELXTL*, Program Version 5.03. Siemens Analytical X-ray Instruments, Madison, WI, **1994**.

Received August 9, 1999
[I99295]

Bis(terpyridyl)-Ruthenium(II) Units Attached to Polyazacycloalkanes as Sensing Fluorescent Receptors For Transition Metal Ions

Miguel E. Padilla-Tosta, José Manuel Lloris, Ramón Martínez-Máñez,* Angel Benito, Juan Soto, Teresa Pardo, Miguel A. Miranda, M. Dolores Marcos

Keywords: Terpyridine / Copper sensing / Cyclam / Fluorescence / Solution studies

Eur. J. Inorg. Chem. **2000**, 741−748

Figure 2 on page 743 of the PDF version is missing; it is provided on this additional page.

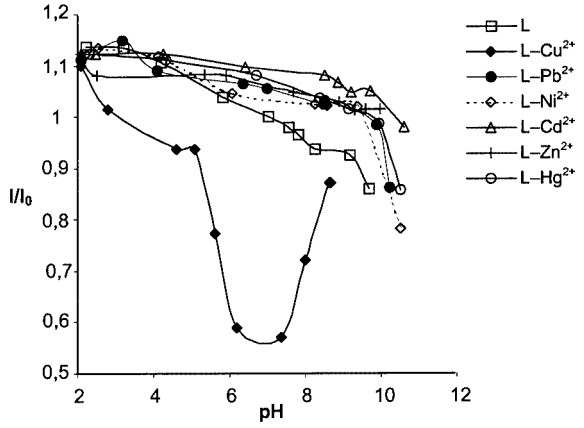


Figure 2. Relative intensity versus pH for the L and $L-M^{2+}$ systems ($L = [Ru(L^1)(mtpy)][PF_6]_2$; $M^{2+} = Cu^{2+}$, Ni^{2+}, Zn^{2+}, Cd^{2+}, Pb^{2+}, Hg^{2+}) (λ_{ex} = 484 nm, λ_{em} = 664 nm)

Non-Luminescent 1,2-Diiminetricarbonylrhenium(I) Chloride Complexes – Synthesis, Electrochemical and Spectroscopic Properties of $Re(DIAN)(CO)_3Cl$ with DIAN = *p*-Substituted Bis(arylimino)acenaphthene

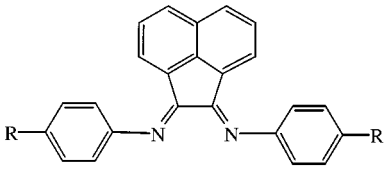
Günther Knör,*[a] Markus Leirer,[a] Tia E. Keyes,[b] Johannes G. Vos,[c] and Arnd Vogler*[a]

Keywords: Rhenium / Diimine ligands / Charge transfer / Solvatochromism / Substituent effects

$Re(1,2\text{-diimine})(CO)_3Cl$ compounds containing the *p*-substituted bis(arylimino)acenaphthene derivatives DIAN-R with R = H, Me, OMe, Br, and Cl were prepared and characterized. The diimine ligands of this series provide unoccupied orbitals at rather low energies and display a pronounced π-accepting strength. This feature determines the electrochemical and spectroscopic properties of the $Re(DIAN\text{-}R)(CO)_3Cl$ complexes. All compounds show rhenium(I) to π*(diimine) metal-to-ligand charge transfer (MLCT) absorptions in the visible spectral region. The maxima of these CT bands systematically shift upon modification of the substituents R and are sensitive to variations of the solvent polarity (negative solvatochromism). $Re(DIAN\text{-}R)(CO)_3Cl$ complexes are non-luminescent both in fluid solution at 298 K and in solvent glass at 77 K.

Introduction

Electronic spectra of complexes of the composition $Re^I(1,2\text{-diimine})(CO)_3(L)$ with L = e.g. halide, CO, phosphane or amine have been studied extensively in recent years.[1,2] These efforts were stimulated by the luminescence behaviour of such compounds, which are characterized by long-lived ^{3}MLCT (triplet metal-to-ligand charge transfer) states. The excited state properties can be utilized for a variety of different purposes such as electron transfer, energy transfer, photochemical CO_2 reduction and the development of optical sensors.[1–4] While mainly polypyridines have been used as 1,2-diimines, ligands with imino groups that are not part of a heterocyclic aromatic system were largely neglected. Since the latter ligands provide π* orbitals at rather low energies,[5–7] the corresponding MLCT absorptions are shifted to much longer wavelengths. Although such complexes may be no longer luminescent owing to the low energy of the MLCT states (energy gap law[8]), they nevertheless could show other useful properties. For example, the charge transfer behaviour might be exploited for nonlinear optical (NLO) devices.[9] For several other applications (e.g. NIR absorbers) photochemical stability is a desireable feature. On the contrary, long-lived excited states tend to participate in bimolecular processes such as the generation of singlet oxygen, which promote photochemical decomposition. It follows that the absence of luminescence from $Re^I(1,2\text{-diimine})(CO)_3(L)$ complexes may present advantages in certain applications. We explored this possibility and selected substituted bis(arylimino)acenaphthenes (DIAN-R)[10] as ligands for the present study (Scheme 1).



Scheme 1. Structural formula of the DIAN-R ligands

These compounds are accessible by standard organic synthesis and can be systematically modified by a variation of the substituents R at the *para* position of their phenyl groups. Owing to the terminal imino groups, the π* energies of these ligands should be rather low. Moreover, since the diimine function is attached to the larger delocalized π-electron system of the acenaphthene moiety, it may be expected to display a high π-accepting strength.

Results and Discussion

The complexes $Re^I(DIAN\text{-}R)(CO)_3Cl$ with R = H, Me, OMe, Br, and Cl have been prepared and characterized by elemental analysis and a variety of spectroscopic techniques. All results are consistent with a pseudooctahedral structure of the compounds and a facial (*fac*) coordination of the carbonyl ligands in agreement with previous studies of other complexes of this type.[1,2]

The absorption spectra of $Re^I(DIAN\text{-}R)(CO)_3Cl$ show various bands below 400 nm and a pronounced absorption in the visible spectral region (Figure l, Table 1). The shorter wavelength bands include certainly intraligand (IL) transitions of the diimines, which absorb as free ligands in the same spectral region. The longer-wavelength band dominating the visible spectrum is assigned to the MLCT transition from rhenium(I) to the π* orbitals of DIAN-R. The charge

[a] Institut für Anorganische Chemie, Universität Regensburg, 93040 Regensburg, Germany
[b] School of Chemistry, Dublin Institute of Technology, Kevin Street, Dublin 8, Ireland
[c] School of Chemical Sciences, Dublin City University, Glasnevin, Dublin 9, Ireland

 © WILEY-VCH Verlag GmbH, D-69451 Weinheim, 2000 1434–1948/00/0404–0749 $ 17.50+.50/0

transfer character of this transition is supported by the fact that the corresponding absorption maxima of all complexes shift to higher energies with increasing solvent polarity (negative solvatochromism). This effect can be evaluated quantitatively by applying different solvent polarity scales such as the empirical E_T parameters[11] or the E^*_{MLCT} values[12] (Figure 2). Generally a linear correlation is observed, although smaller deviations are noticed as previously reported for related complexes.[12] The substituent R of the DIAN-R ligands should also affect the MLCT energy. However, the π* energy of the ligands is only slightly dependent on the nature of R because the phenyl groups at the nitrogen atoms are not coplanar with the diimine moiety.[10] Indeed, a Hammett plot (Figure 3) shows a linear correlation of the σ_p-parameter with the MLCT energies, but the slope (930 cm^{-1}) is rather small. A much stronger dependence on *p*-substituents has been observed for *meso*-tetraphenylporphyrins.[13] In this case the phenyl groups at the *meso* positions are also not coplanar with the porphyrin plane, but the ππ* transitions are more significantly shifted.

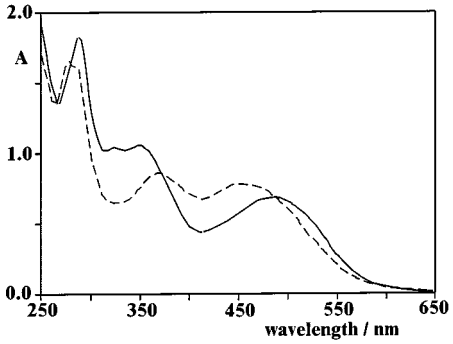


Figure 1. Electronic absorption spectra of Re(DIAN-R)$(CO)_3$Cl with R = OMe (– – –) and R = Cl (—) in acetonitrile solution; $c = 1.3 \cdot 10^{-4}$ M, 1-cm cells

Table 1. UV-VIS spectroscopic data of the Re(DIAN-R)$(CO)_3$Cl complexes in acetonitrile solution at 298 K

R	λ_{max} [nm] (ε [L/(mol·cm)])				
H	474 (5100)	348 (7600)	320 (8000)	286 (13400)	223 (44800)
Me	470 (5700)	355 (8400)	322 (7400)	286 (14200)	219 (57100)
OMe	451 (6600)	370 (7200)	–	285 (13500)	223 (51200)
Br	481 (5600)	350 (8600)	323 (8400)	288 (14800)	223 (65400)
Cl	481 (5100)	349 (7700)	324 (7600)	288 (13300)	224 (54200)

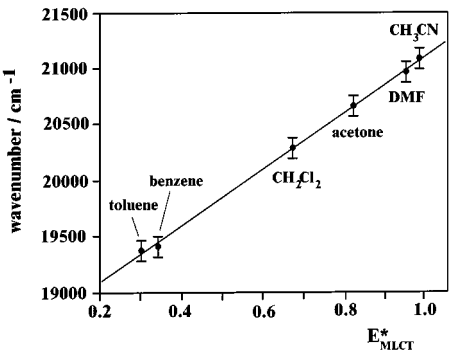


Figure 2. Correlation between the energy of the charge transfer transition of Re(DIAN-H)$(CO)_3$Cl and the solvent parameter E^*_{MLCT} [12]

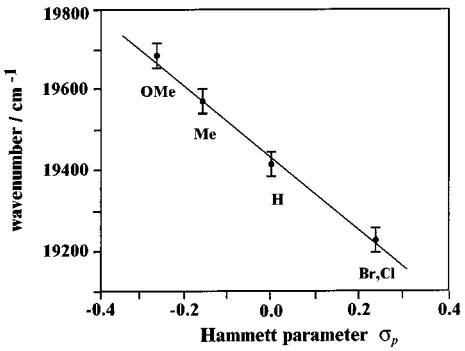


Figure 3. Substituent effects on the MLCT absorption maxima of Re(DIAN-R)$(CO)_3$Cl complexes in benzene at 298 K

To obtain further information about the π-acceptor properties of the bis(arylimino)acenaphthene ligands, electrochemical and spectroelectrochemical experiments were performed with the unsubstituted derivative Re^I(DIAN-H)$(CO)_3$Cl. The first reduction of this compound occurs in cyclic voltammetry as a reversible one-electron step at a redox potential of −0.65 V vs SCE at 298 K in dry DMF containing 0.1 M tetraethylammonium tetrafluoroborate. The reversible spectral changes associated with this process suggest that the first reduction takes place at the DIAN-H ligand. An approximate value of +1.4 V vs SCE can be estimated for the corresponding reaction in the MLCT excited state. These redox potentials reflect the much higher π-acceptor strength of bis(phenylimino)acenaphthene compared to many other frequently used diimine ligands. For example, the compound Re^I(bpy)$(CO)_3$Cl (bpy = 2,2-bipyridyine) displays its first ligand based reduction at the rather negative potential of −1.64 V vs SCE (−1.74 V vs ferrocene/ferrocenium[14]) in the electronic ground state. With exception of the initial reduction wave, the voltammetric response obtained for Re^I(DIAN-H)$(CO)_3$Cl between 1.7 and −2.0 V vs SCE indicates the occurrence of chemical reactions coupled to the heterogeneous electron transfers. Recently, a complex sequence of fragmentation and dimerization steps has been proposed for a related Re^I(1,2-diimine)$(CO)_3$Cl species under similar conditions.[15] A detailed investigation of such processes, however, was not attempted in the present study.

The complexes Re^I(DIAN-R)$(CO)_3$Cl do not show any luminescence at 298 K or 77 K. In general, the emission quantum yields of Re^I(1,2-diimine)$(CO)_3$(L) decrease with decreasing energy of the emitting MLCT state. This behaviour has been attributed to the energy gap law.[1,2,5,8] The same explanation may also apply to the absence of emission from the Re^I(DIAN-R)$(CO)_3$Cl series, since these compounds show their MLCT absorption at distinctly longer wavelength compared to corresponding complexes with polypyridyls as diimine ligands. However, it is surprising that Re^I(DIAN-R)$(CO)_3$Cl complexes do not emit at all, while $[Os(bpy)_3]^{2+}$ and some of its derivatives are luminescent, although their MLCT absorptions appear at similar or longer wavelengths[2] than those of Re^I(DIAN-R)$(CO)_3$Cl. Therefore it cannot be excluded that other effects contribute to the lack of emission from Re^I(DIAN-R)$(CO)_3$Cl.

A decrease of the π* energy of the diimine ligand usually is accompanied by a red-shift of the MLCT absorption. Moreover, a large contribution of the N atomic orbitals to the π* acceptor orbital causes a large overlap stabilization and may lead to an increased mixing of rhenium dπ and ligand Lπ* orbitals.[6] Indeed, the solvatochromism of the Re^{I}(DIAN-R)$(CO)_3Cl$ complexes (average slope = 2860 cm^{-1}) is significantly smaller than that of complexes with polypyridyl ligands[2] [e.g. Re^{I}(bpy)$(CO)_3Cl$, slope = 3120 cm^{-1}], since the "MLCT" transition of the DIAN complexes has less CT character owing to an enhanced delocalization of the participating orbitals. In contrast to polypyridyl complexes, the MLCT transitions of DIAN complexes occur then between strongly bonding dπ and antibonding Lπ* orbitals. The concomittant geometrical changes and the associated skeletal vibrations could facilitate an efficient nonradiative decay.[5,6]

Moreover, a further effect may account for the absence of luminescence from Re^{I}(DIAN-R)$(CO)_3Cl$. The increased back-bonding results in a stabilization of the dπ orbitals, which may drop below the π-orbitals of the chloride ligand.[16] The $Cl^- \rightarrow$ Lπ* diimine LLCT (ligand-to-ligand charge transfer) and MLCT transitions could now be of comparable energies. If the LLCT state is not emissive, its population might provide a new efficient channel for radiationless deactivation.

Experimental Section

Materials and Instrumentation: All starting materials were commercially available and used without further purification. The bis(arylimino)acenaphthene ligands were obtained from acenaphthene quinone and the corresponding *p*-substituted anilines.[10] – Electronic absorption spectra were recorded on a Kontron Uvikon 932 double-beam spectrophotometer and a Shimadzu 3100 UV-VIS/NIR spectrophotometer. – Emission properties were investigated with a Hitachi 850 spectrofluorometer equipped with a Hamamatsu 928 photomultiplier. – The electrochemistry was conducted at a teflon shrouded glassy carbon electrode with SCE reference and platinum mesh auxillary electrode in dry DMF containing 0.1 M tetraethyltetrafluoroborate as electrolyte. – Spectroelectrochemical measurements were carried out with equipment described elsewhere.[17] – IR spectra were measured on a Beckman Acculab 6 spectrometer. – Mass spectra were obtained using Finnigan MAT 95 and Varian MAT 311 instruments. – ^{1}H-NMR data were recorded with a Bruker AC 250 (250 MHz) spectrometer with TMS added as internal standard.

Preparation of the Complexes Re(DIAN-R)$(CO)_3Cl$: A suspension of 181 mg (0.50 mmol) of $Re(CO)_5Cl$ and the equimolar amount of the corresponding bis(arylimino)acenaphthene in 10 mL of toluene was refluxed for 30 min. After cooling the reaction mixture to room temperature and addition of *n*-hexane, the products were obtained as red microcristalline precipitates. The compounds with R = Br and Cl were further purified by chromatography on silica gel using dichloromethane as eluent.

Re(DIAN-H)$(CO)_3Cl$: Yield 289 mg (0.45 mmol, 91%). – IR (KBr): $\tilde{\nu}$ = 3050 cm^{-1} (CH), 2020, 1915, 1890 (CO), 1580 (aromatic rings). – ^{1}H NMR ($CDCl_3$): δ = 8.06 (d, 2 H), 7.00 (d, 2 H), 7.74–7.36 (m, 12 H). – MS (FD^+, $CHCl_3$): *m/z* (%): 638 (100) [M^+]. – $C_{27}H_{16}ClN_2O_3Re$ (638.10): calcd. C 50.82, H 2.53, N 4.39; found: C 50.35, H 2.82, N 4.11.

Re(DIAN-Me)$(CO)_3Cl$: Yield 306 mg (0.46 mmol, 92%). – IR (KBr): $\tilde{\nu}$ = 3030, 2920 cm^{-1} (CH), 2040, 1930, 1890 (CO), 1630, 1600 (aromatic rings). – ^{1}H NMR ($CDCl_3$): δ = 8.09 (d, 2 H), 7.09 (d, 2 H), 7.56–7.28 (m, 10 H), 2.52 (s, 6 H). – MS (FD^+, $CHCl_3$): *m/z* (%): 666.0 (100) [M^+]. – $C_{29}H_{20}ClN_2O_3Re$ (666.15): calcd. C 52.29, H 3.03, N 4.20;. found: C 52.34, H 3.33, N 4.12.

Re(DIAN-OMe)$(CO)_3Cl$: Yield 289 mg (0.45 mmol, 91%). – IR (KBr): $\tilde{\nu}$ = 3070, 3015, 2980, 2850 cm^{-1}(CH), 2040, 1920, 1890 (CO), 1630, 1600 (aromatic rings). – ^{1}H NMR ($CDCl_3$): δ = 8.06 (d, 2 H), 7.17 (d, 2 H), 7.90–7.36 (m, 8 H), 7.19–7.10 (m, 2 H), 3.94 (s, 6H). – MS (FD^+, $CHCl_3$): *m/z* (.%): 698.0 (100) [M^+]. – $C_{29}H_{20}ClN_2O_5Re$ (698.15): calcd. C 49.89, H 2.89, N 4.01; found: C 48.73, H, 2.96, N, 3.81.

Re(DIAN-Br)$(CO)_3Cl$: Yield 111 mg (0.14 mmol, 28%). – IR (KBr): $\tilde{\nu}$ = 2020, 1915, 1885 cm^{-1} (CO). – ^{1}H NMR ($CDCl_3$): δ = 8.11 (dd, 2 H), 7.10 (dd, 2 H), 7.78–7.23 (m, 10 H). – MS (FD^+, $CHCl_3$): *m/z* (%): 796.0 (100) [M^+]. – $C_{27}H_{14}Br_2ClN_2O_3Re$ (795.89): calcd. C 40.75, H 1.77, N 3.52; found: C 40.78, H 2.36, N, 3.20.

Re(DIAN-Cl)$(CO)_3Cl$: Yield 312 mg (0.44 mmol, 88%). – IR (KBr): $\tilde{\nu}$ = 3050, 2960, 2920 cm^{-1} (CH), 2030, 1920, 1890 (CO), 1620, 1595 (aromatic rings). – ^{1}H NMR ($CDCl_3$): δ = 8.06 (dd, 2 H), 7.10 (dd, 2 H), 7.70–7.31 (m, 10 H). – MS (FD^+, $CHCl_3$): *m/z* (%): 706.0 (100) [M^+]. – $C_{27}H_{14}Cl_3N_2O_5Re$ (706.98): calcd. C 45.87, H 2.00, N 3.96; found: C 46.12, H 2.78, N 3.48.

Acknowledgments

Support for this research by the Deutsche Forschungsgemeinschaft is gratefully acknowledged. A. L. Spek is acknowledged for supplementary material on the structures of the DIAN-R ligands.

[1] D. J. Stufkens, A. Vlcek, Jr., *Coord. Chem. Rev.* **1998**, *177*, 127–179.
[2] [2a] D. M. Roundhill, *Photochemistry and Photophysics of Metal Complexes*, Plenum Press, New York, **1994**. – [2b] K. Kalyanasundaram, *Photochemistry of Polypyridine and Porphyrin Complexes*, Academic Press, London, **1992**.
[3] H. Hori, F. P. A. Johnson, K. Koike, O. Ishitani, T. Ibusuki, *J. Photochem. Photobiol. A: Chem.* **1996**, *96*, 171–174.
[4] I. Klimant, P. Belser, O. S. Wolfbeis, *Talanta* **1994**, *41*, 985–991.
[5] A. J. Lees, *Chem. Rev.* **1987**, *87*, 711–743.
[6] D. J. Stufkens, *Coord. Chem. Rev.* **1990**, *104*, 39–112.
[7] J. Reinhold, R. Benedix, P. Birner, H. Hennig, *Inorg. Chim. Acta* **1979**, *33*, 209–213.
[8] J. V. Caspar, T. J. Meyer, *J. Phys. Chem.* **1983**, *87*, 952–957.
[9] [9a] B. J. Coe, S. Houbrechts, I. Asselberghs, A. Persoons, *Angew. Chem.* **1999**, *111*, 377–380; *Angew. Chem. Int. Ed.* **1999**, *38,* 366–369. – [9b] F. W. Vance, J. T. Hupp, *J. Am. Chem. Soc.* **1999**, *121*, 4047–4053.
[10] R. van Asselt, C. J. Elsevier, W. J. J. Smeets, A. L. Spek, R. Benedix, *Recl. Trav. Chim. Pays-Bas* **1994**, *113*, 88–98.
[11] C. Reichardt, *Chem. Rev.* **1994**, *94*, 2319–2358.
[12] D. M. Manuta, A. J. Lees, *Inorg. Chem.* **1983**, *22*, 3825–3828.
[13] A. Ghosh, *J. Molec. Struct. (Theochem)* **1996**, *388*, 359–363.
[14] S. Berger, A. Klein, W. Kaim, J. Fiedler, *Inorg. Chem.* **1998**, *37*, 5664–5671.
[15] G. J. Stor, F. Hartl, J. W. M. van Outersterp, D. J. Stufkens, *Organometallics* **1995**, *14*, 1115–1131.
[16] G. J. Stor, D. J. Stufkens, A. Oskam, *Inorg. Chem.* **1992**, *31*, 1318–1319.
[17] T. E. Keyes, R. J. Forster, M. J. Pradeep, C. G. Coates, J. J. McGarvey, J. G. Vos, *Inorg. Chem.* **1998**, *37*, 5925–5932.

Received August 19, 1999
[I99310]

Rhodium and Iridium β-Diiminate Complexes – Olefin Hydrogenation Step by Step

Peter H. M. Budzelaar,*[a] Nicolle N. P. Moonen,[a] René de Gelder,[a] Jan M. M. Smits,[a] and Anton W. Gal[a]

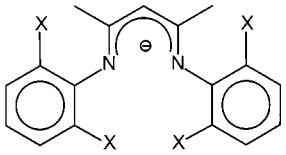
Keywords: Hydrogenation / Isomerization / Rhodium / Iridium / Hydrides

The bulky β-diiminate ligands $[(2,6\text{-}C_6H_3X_2)NC(Me)CHC(Me)N(2,6\text{-}C_6H_3X_2)]^-$ (X = Me, L_{Me}; X = Cl, L_{Cl}) have been found to be effective in stabilizing low coordination numbers (CN) in Rh and Ir complexes. The 14-*e* complex L_{Me}Rh(COE) (COE = cyclooctene) has a three-coordinate T-shaped Rh environment and is nonagostic. Coordinative unsaturation is avoided by incorporation of a small ligand (e.g. N_2, MeCN, olefins), by the intramolecular coordination of a chlorine atom in L_{Cl}Rh(COE), or by an agostic interaction in L_{Me}Rh(norbornene). In solution at room temperature, L_{Me}Rh(COE) undergoes rapid isomerization according to the allyl hydride mechanism; the corresponding 2,3-dimethylbutene complex actually prefers the allyl hydride structure. Rhodium(I) complexes of L_{Me} and L_{Cl} catalyze olefin hydrogenation; hydrogenation of 2,3-dimethylbutene has been shown to be preceded by isomerization. The shielding properties of the bulky β-diiminate ligands allow direct observation of a number of reactive intermediates or their iridium analogues, including an olefin–dihydrogen complex (with Rh) and an olefin dihydride (with Ir). These observations, together with calculations on simple model systems, provide us with snapshots of a plausible hydrogenation cycle. Remarkably, hydrogenation according to this cycle appears to follow a 14-*e*/16-*e* path, in contrast to the more usual 16-*e*/18-*e* paths.

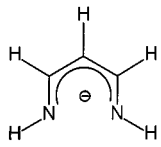
Introduction

Coordinatively unsaturated species are key intermediates in most catalytic cycles. Because of their high reactivity, they can rarely be isolated or even observed directly. Therefore, it is necessary to rely on indirect information (e.g. from trapping experiments or kinetics) to deduce the characteristic properties of such species. Obviously, isolable unsaturated species are of interest because they present an opportunity to study the reactivity of key intermediates *directly*.

We recently found that β-diiminate ligands can be effective in stabilizing low coordination numbers. With early transition metals, this has led to the isolation of stable four-coordinate Ti^{III} and V^{III} dialkyls.[1] In our recent work on late transition metals, we isolated a stable (but still highly reactive) 14-*e* rhodium(I) olefin complex.[2] We now describe the synthesis, characterization, and reactivity of Rh and Ir complexes of two bulky β-diiminate ligands, L_{Me} and L_{Cl}. The Rh complexes have proved to be active in olefin isomerization and hydrogenation. More importantly, we have found that the shielding properties of these ligands allow the direct observation of a number of species that can be envisaged as intermediates in isomerization and hydrogenation cycles, including a rhodium olefin–dihydrogen complex and an iridium olefin–dihydride complex. As an aid to interpretation of the results, B3LYP calculations have been performed on complexes of the model ligand L.



L_{Me} X = Me
L_{Cl} X = Cl



L

Other examples of coordinatively unsaturated species stabilized by bulky ligands have been reported. Some relevant examples are three-coordinate 14-*e* rhodium(I) complexes L_2RhX (L = bulky phosphane)[3] and the remarkable 14-*e* iridium dihydride complex $[P(t\text{Bu})_2Ph]_2IrH_2^+$ described by Caulton.[4] However, we are not aware of any example of a 14-*e* Rh or Ir complex bearing a labile and easily displaceable olefin ligand.

Results and Discussion

Ethene and Cyclooctadiene Complexes

The β-diimine ligand $L_{Me}H$ may easily be prepared by condensation of 2,4-pentanedione and 2,6-dimethylaniline. Reaction with $LiN(i\text{Pr})_2$ in THF produces the lithium salt L_{Me}Li(THF), which is obtained from hexane in the form of off-white crystals. The ligand $L_{Cl}H$ and its lithium salt may be prepared similarly; L_{Cl}Li(THF) forms large yellow crystals from toluene/hexane, which slowly turn reddish on exposure to light.

Reaction of L_RLi(THF) (L_R = L_{Me} or L_{Cl}) with $[Rh(COD)Cl]_2$ (COD = 1,5-cyclooctadiene) produces the

[a] Department of Inorganic Chemistry, University of Nijmegen, Toernooiveld 1, NL-6525 ED Nijmegen, The Netherlands
E-mail: budz@sci.kun.nl

 © WILEY-VCH Verlag GmbH, D-69451 Weinheim, 2000 1434–1948/00/0404–0753 $ 17.50+.50/0

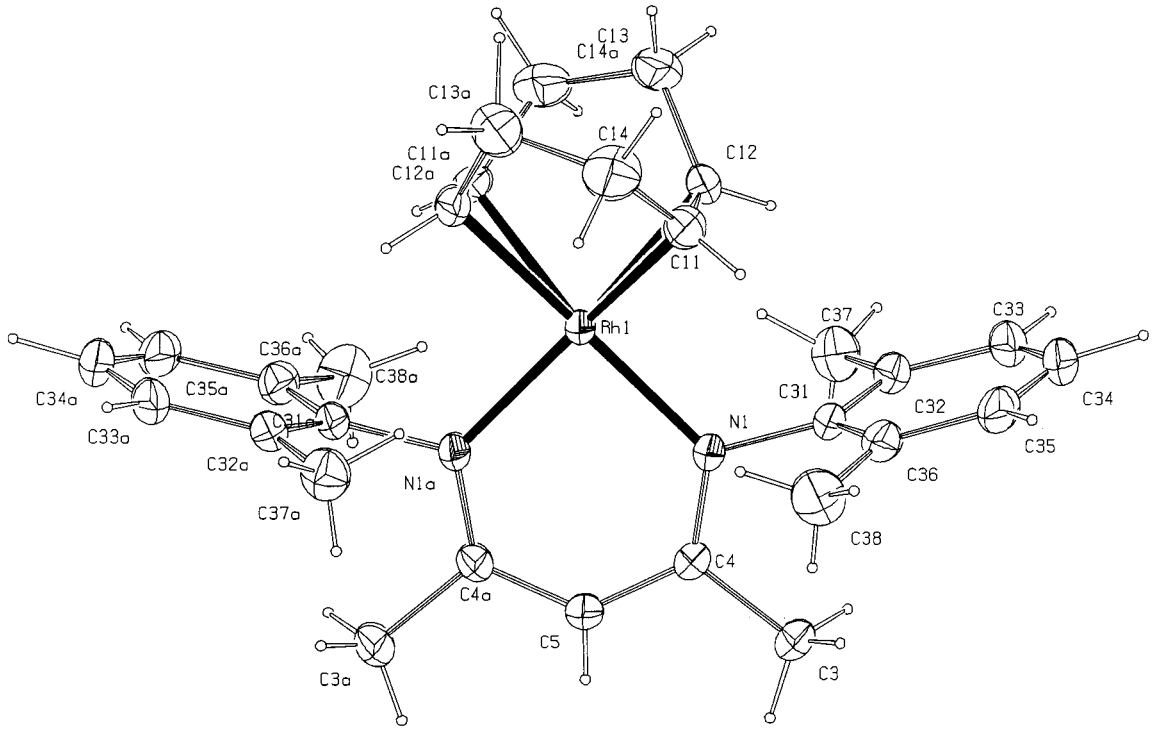


Figure 1. X-ray structure (30% ellipsoids) of $L_{Me}Rh(COD)$; atoms labelled *a* are related to original atoms by a twofold axis through Rh1 and C5; selected bond lengths (Å): Rh1–C11 2.138(2), Rh1–C12 2.169(2), Rh1–N1 2.0953(15)

very stable 16-*e* complexes $L_RRh(COD)$; ethene complexes $L_RRh(C_2H_4)_2$ can be obtained in a similar manner from $[Rh(C_2H_4)_2Cl]_2$. The X-ray structures of $L_{Me}Rh(COD)$ (Figure 1) and $L_{Me}Rh(C_2H_4)_2$ (Figure 2, A) show the expected square-planar coordination geometries. The bis(ethene) complex has perpendicular ethene ligands, which are tilted slightly out of the coordination plane in opposite directions. Distortions of this kind have been observed for *cis*-bis(ethene) complexes containing a chiral ligand; theoretical studies indicate that such structures are relatively easily deformed.[5]

The optimized structure of model complex $LRh(C_2H_4)_2$ shows a regular four-coordinate Rh atom. The calculated Rh–N distance (2.03 Å) is shorter than those observed for $L_{Me}Rh(C_2H_4)_2$ (av. 2.09 Å) and $L_{Me}Rh(COD)$ (av. 2.10 Å), while the Rh–C distances are longer (av. 2.28 Å vs. 2.15 Å). It is possible that the main cause of these discrepancies lies in the choice of model system: the aryl substituents on the L_{Me} ligand will weaken the N–Rh coordination and hence strengthen the Rh–olefin bond relative to the situation in the unsubstituted model ligand L. This means that we can also expect an underestimation of the calculated interaction strength of the LRh fragment with other added ligands.

In the calculated structure of $LRh(C_2H_4)_2$, the centers of the olefin ligands lie exactly in the coordination plane. If, however, the N–Rh–olefin angles are constrained to the value of 94° observed in the X-ray structure of $L_{Me}Rh(C_2H_4)_2$, a nonplanar structure is obtained. This suggests that the nonplanarity in the L_{Me} complex is caused by repulsion between the ethene hydrogens, as a result of the steric demand of the ligand aryl groups. A space-filling model of $L_{Me}Rh(C_2H_4)_2$ indeed shows interlocking of the ethene hydrogens and close contacts between the olefins and the aryl groups (Figure 2, B). Accordingly, the NMR spectra show that ethene rotation is blocked at room temperature. Crowded [bis(oxazolinyl)methanate]Rh(ethene)$_2$ complexes also show hindered rotation,[5] but in relatively open bis(ethene) complexes of β-diketonates and β-ketoiminates ethene rotation is usually fast at room temperature.[6]

Cyclooctene Complexes

The above results suggested that two molecules of a bulkier olefin, e.g. a *cis*-disubstituted olefin, would not fit into the cleft between the aryl groups: the substituents at the double bond of one olefin would interfere either with the arene ring or with the other olefin ligand. Indeed, reaction of $L_{Me}Li(THF)$ with $[Rh(COE)_2Cl]_2$ (COE = cyclooctene) was found to produce the deep-purple *mono*-olefin complex $L_{Me}Rh(COE)$ in moderate yield (70%). This complex proved to be extremely air-sensitive, but otherwise stable at room temperature. The X-ray structure[2] showed the molecule to be disordered over a twofold symmetry axis; this disorder could be refined satisfactorily (Figure 3). The coordination geometry about Rh is roughly T-shaped, but the olefin is shifted somewhat towards the center of the open cleft (N–Rh–olefin = 112°). Remarkably, there are no short agostic interactions.

Unfortunately, the disorder prevents us from obtaining individual distances for the two types of Rh–N bond. In the model compound $LRh(C_2H_4)$, we see a shortening of the Rh–C and Rh–N distances (by 0.07 and 0.04 Å, respectively) relative to those in the bis(ethene) complex. Accord-

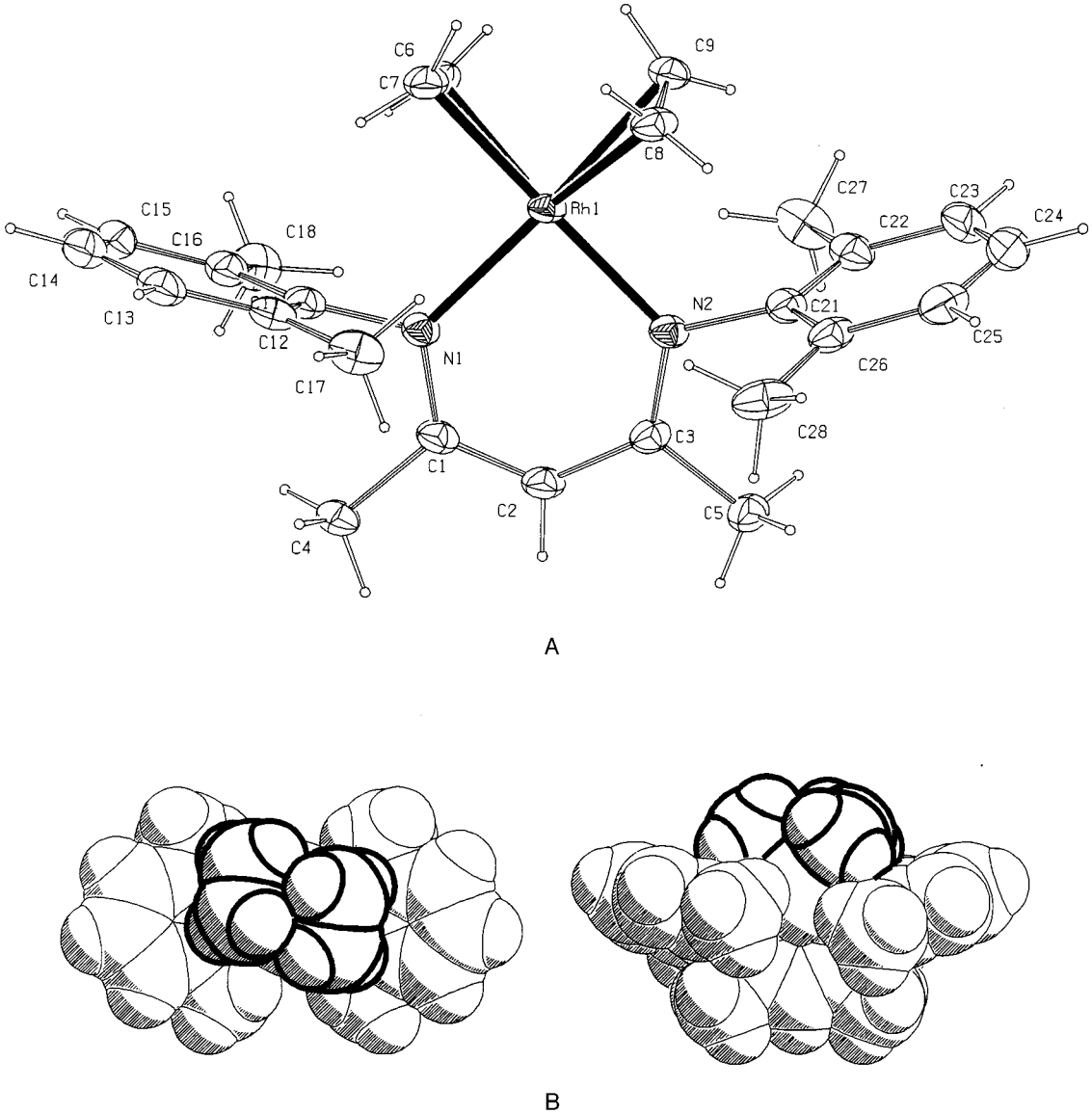


Figure 2. A: X-ray structure (30% ellipsoids) of $L_{Me}Rh(C_2H_4)_2$; B: space-filling model, outline of the ethene ligands emphasized; selected bond lengths (Å) and angles (°): Rh1–C6 2.131(4), Rh1–C7 2.155(4), Rh1–C8 2.133(4), Rh1–C9 2.160(4), Rh1–N1 2.093(3), Rh1–N2 2.086(3), C6–C7 1.390(7), C8–C9 1.367(7); N1–Rh1–N2 89.11(12)

ing to the X-ray data, the Rh–C bonds in $L_{Me}Rh(COE)$ are about 0.08 Å shorter than those in $L_{Me}Rh(C_2H_4)_2$ and $L_{Me}Rh(COD)$, while the Rh–N bonds are about 0.13 Å shorter. However, the X-ray bond lengths obtained for the COE complex must be treated with caution since the two alternative Rh positions, which differ by as much as 0.1 Å, could not be resolved in the structure determination. The N–Rh–olefin angle of 94° calculated for $LRh(C_2H_4)$ is larger than the 88° calculated for $LRh(C_2H_4)_2$, but much smaller than the value of 112° observed in $L_{Me}Rh(COE)$. The calculated barrier associated with ethene transfer between the two vacant sites of $LRh(C_2H_4)$ is only 11 kcal/mol. Thus, we attribute the distortion of $L_{Me}Rh(COE)$ towards a trigonal geometry to the steric demand of the aryl groups, coupled with a low barrier for movement of the olefin.[7]

Solution NMR data at –60 °C[8] are consistent with the solid-state structure, showing discrete resonances for the diiminate halves *cis* and *trans* to the olefin. At room temperature, however, the L_{Me} ligand has effective C_{2v} symmetry, and only two broadened resonances are observed for the cyclooctene ligand in the ^1H spectrum, corresponding to 6 and 8 protons, respectively. We attribute this dynamic behavior to rapid equilibration between olefin and allyl hydride isomers.[9] This scrambles the COE hydrogens in two groups: (i) all *endo* hydrogens (6 H) and (ii) all *exo* hydrogens together with the vinylic hydrogens (8 H). Any intermolecular process would result in complete scrambling of all 14 COE hydrogens.

Owing to the complicated nature of the spectrum, we could not extract the activation energy, but the temperature region in which coalescence is observed (–50 to –20 °C) in-

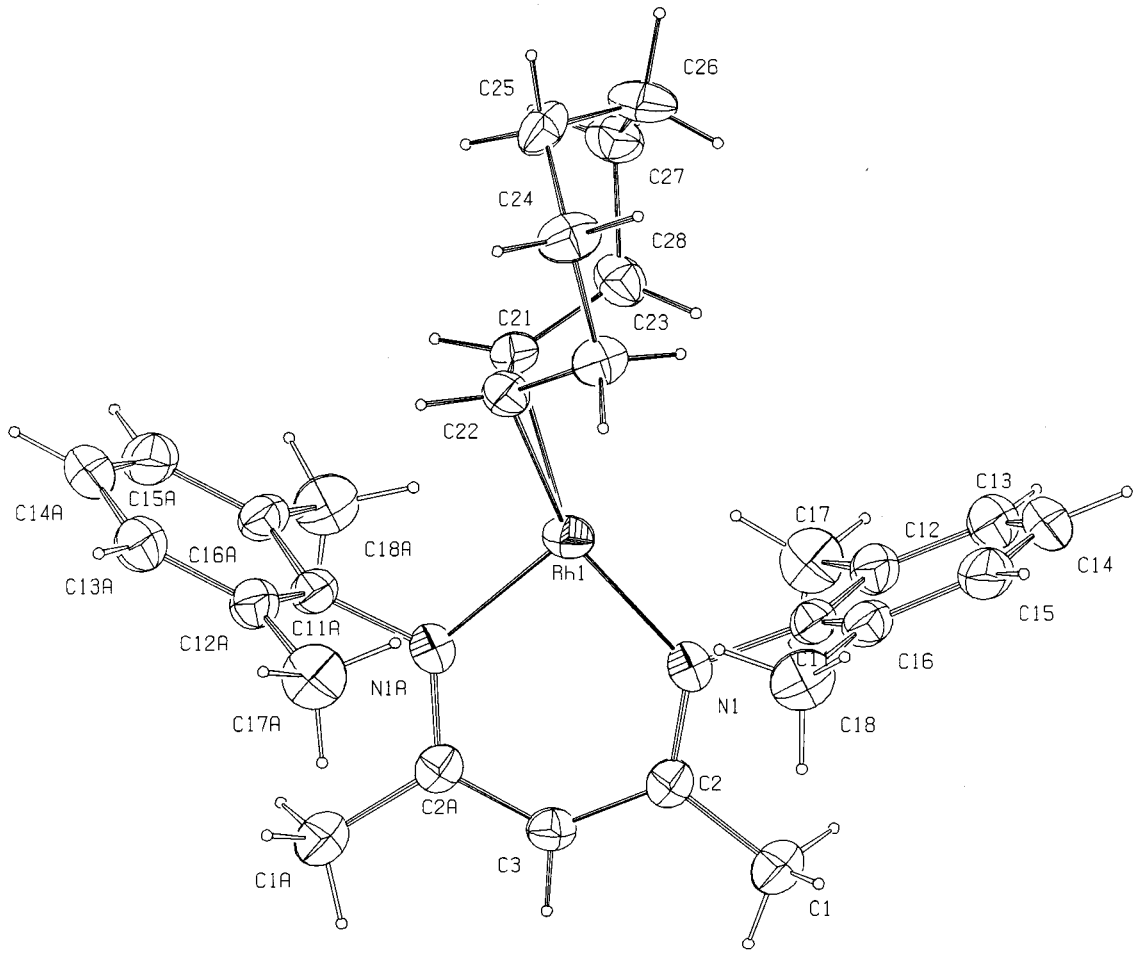


Figure 3. X-ray structure (30% ellipsoids) of $L_{Me}Rh(COE)$ (see ref.[2]); only one of the two cyçlooctene images is shown; atoms labelled *a* are related to original atoms by a twofold axis through Rh1 and C3; selected bond lengths (Å) and angles (°): Rh1–N1 1.955(2), Rh1–C21 2.072(5), Rh1–C22 2.066(6), C21–C22 1.398(7); N1–Rh1–N1a 91.3(1)

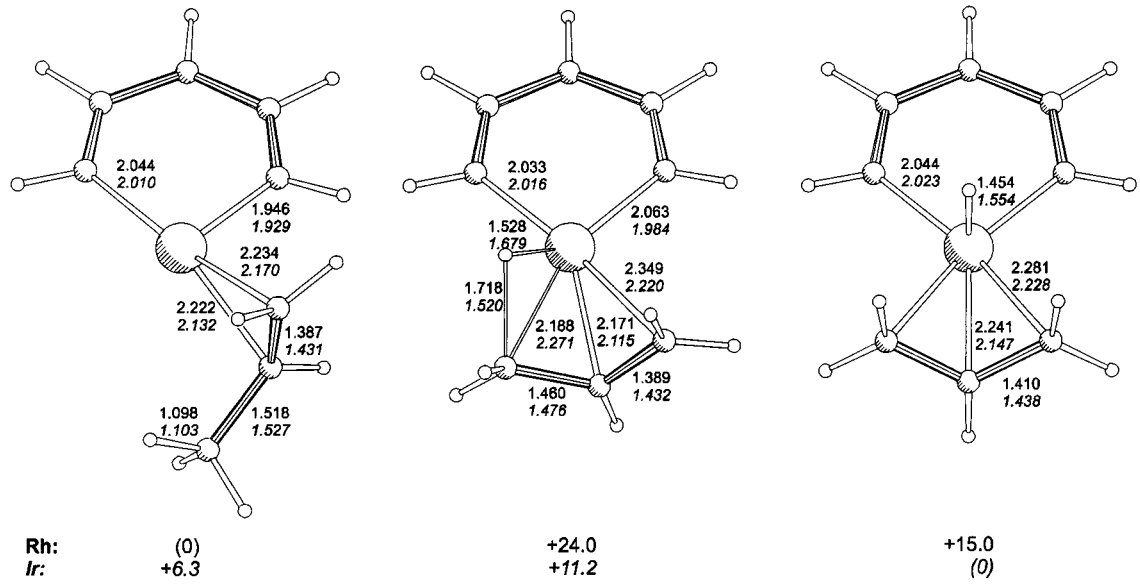


Figure 4. Calculated structures and energies (kcal/mol) for olefin–allyl hydride isomerization of LRh(propene); energies and parameters for the Ir analogs given in italics

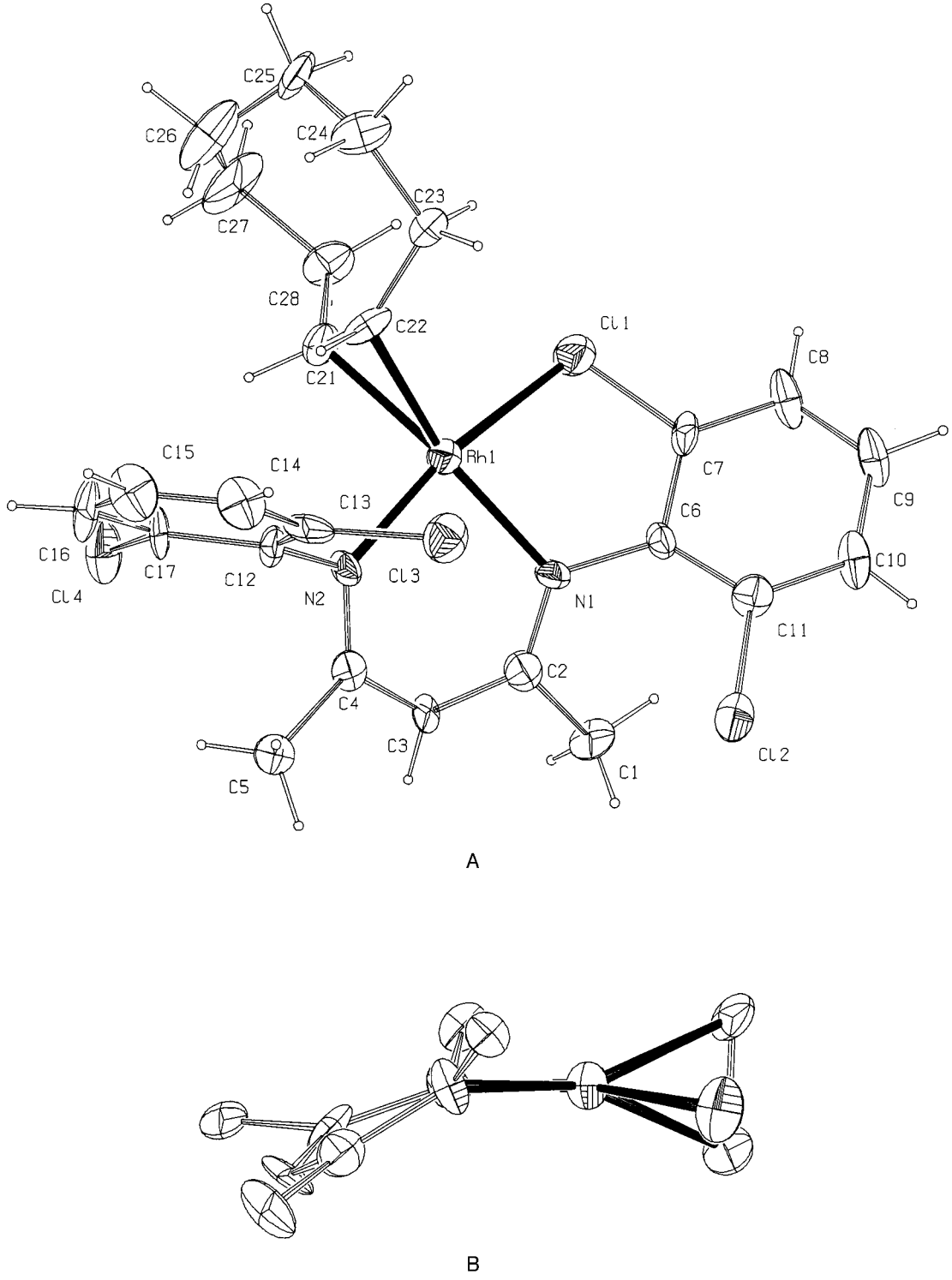


Figure 5. A: X-ray structure (30% ellipsoids) of $L_{Cl}Rh(COE)$; only one of the two independent molecules is shown; B: projection along N1–N2, illustrating the displacement of Rh out of the diiminate plane; selected bond lengths (Å) and angles (°): Rh1–C21 2.088(16), Rh1–C22 2.128(16), Rh1–N1 2.040(12), Rh1–N2 1.996(13), Rh1–Cl1 2.376(5), C21–C22 1.37(2), Rh2–C51 2.155(16), Rh2–C52 2.106(16), Rh2–N31 2.062(14), Rh2–N32 2.048(15), Rh2–Cl31 2.365(5), C51–C52 1.39(2); N1–Rh1–N2 89.2(5), N1–Rh1–Cl1 80.0(4), N31–Rh2–N3 291.2(6), N31–Rh2–Cl31 80.3(4)

dicates a barrier of ca. 12 kcal/mol. B3LYP calculations confirm that the olefin complex LRh(propene) is more stable than the isomeric LRh(allyl)(H),[10] but the calculated energy difference is rather large (15 kcal/mol), and the calculated barrier of 24 kcal/mol is much larger than the experimental value for $L_{Me}Rh(COE)$. The difference of 12 kcal/mol between calculated and observed barriers might be attributable to deficiencies in the theoretical methods used[11] and/or to an absence of steric effects in the model system.[12] Figure 4 shows the calculated structures for the

two isomers and the transition state. The allyl hydride complex has a square-pyramidal structure, with the hydride occupying the apical position and the two outer allyl carbons in equatorial positions.

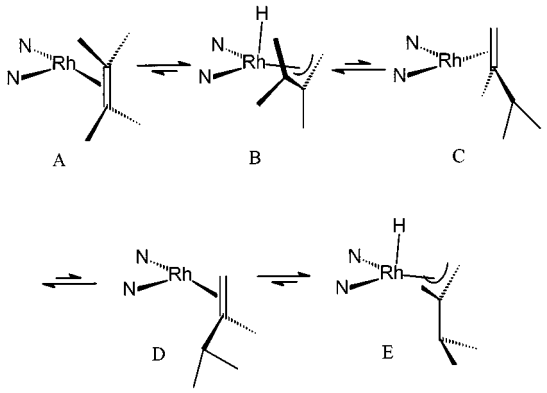
Reaction of $L_{Me}Li(THF)$ with $[Ir(COE)_2Cl]_2$ proceeded more slowly than in the Rh case, and the product was found to be unstable at room temperature (vide infra). Therefore, only a low yield (ca. 10%) of orange "$L_{Me}Ir(COE)$" could be obtained from this reaction. The ^1H- and ^{13}C-NMR spectra of this complex unambiguously establish a static allyl hydride structure $L_{Me}Ir(H)$(cyclooctenyl) ($\delta_H = -46.2$).[13] Repeated attempts to crystallize the product resulted only in poor crystals, which nevertheless allowed the connectivity to be established; this connectivity was consistent with the calculated structure shown in Figure 4. B3LYP calculations indicate that on going from Rh to Ir the relative stabilities of the olefin and allyl hydride isomers are indeed inverted (Figure 4).[14]

In the hope of obtaining a 14-*e* complex with a disorder-free structure, we also prepared red $L_{Cl}Rh(COE)$. The X-ray structure shows coordination of one of the chlorine atoms of the diiminate ligand to the metal (Figure 5). The rhodium atom is displaced out of the diiminate plane to allow close approach to the chlorine. In solution, this complex shows the same allyl hydride dynamic behavior as $L_{Me}Rh(COE)$, although the coalescence temperature is slightly higher. At –60 °C, the allyl hydride exchange is completely frozen out, but exchange of the two chlorine atoms of the chelating dichlorophenyl group remains rapid. The facile dissociation of the Rh–Cl bond in solution, as observed by NMR, does not imply that this is an intrinsically weak interaction. It merely shows that the diiminate ligand deformation needed to achieve Rh–Cl coordination requires nearly as much energy as is gained through formation of the coordination bond.

2,3-Dimethyl-2-butene Complex

When a solution of $L_{Me}Rh(COE)$ in 2,3-dimethyl-2-butene is stirred under hydrogen for a few minutes, all cyclooctene is lost as cyclooctane. After removal of the volatiles, the ^1H-NMR spectrum of the residue in $[D_8]$THF or C_6D_{12} shows strongly broadened signals attributable to a 2,3-dimethylbutene complex.[15] Apparently, *all* olefinic hydrogens in this complex are exchanging on the NMR timescale. Cooling of a $[D_8]$THF solution to –30 °C results in decoalescence of the diiminate 3-H signal into two signals of relative intensity 4:1 and considerable sharpening of the rest of the spectrum. At this temperature, the major component of the mixture (corresponding to the largest 3-H signal) gives rise to fairly sharp isopropyl group resonances (δ = 1.85 and 1.24) and a broad resonance at $\delta = -2.45$, which integrates for approximately 5 protons. Further cooling results in broadening of the resonance at $\delta = -2.45$, but at –60 °C (just above the melting point of THF) the static limit still has not been reached. Because of the multitude of peaks due to the major component and the oxidation product,[15] we cannot assign any peaks due to the minor component in the region δ = 0–2.5. However, below –40 °C, a clear hydride signal is seen at $\delta = -12$ with the appropriate intensity for 1 H of the minor component. In the ^{13}C spectrum, all peaks due to the major component and some peaks due to the minor component can be assigned.

Scheme 1 illustrates the interconversion of the isomers that can be formed from $L_{Me}Rh$(2,3-dimethyl-2-butene). The major component in the low-temperature spectrum must correspond to allyl hydride isomer **E** in equilibrium with olefin complex **D**. The observed average shift of $\delta = -2.45$ for the five protons not belonging to the isopropyl group is compatible with structure **E** but not with **D**. Thus, in contrast to cyclooctene, the equilibrium for this olefin lies on the side of the allyl hydride isomer. The minor component, which gives rise to a hydride resonance below –40 °C, must therefore be allyl hydride isomer **B**. In the olefin complexes **A**, **C**, and **D**, at least one of the substituents at the double bond points towards the diiminate aryl groups. It seems likely that steric repulsion makes the olefin complexes less stable than the allyl hydride isomers **B** and **E**.



Scheme 1. Proposed mechanism for the dynamic behavior of "$L_{Me}Rh$(2,3-dimethyl-2-butene)"

Norbornene Complex

The facile allyl hydride isomerization of cyclooctene and 2,3-dimethylbutene complexes made us wonder whether olefin complexes not containing any available allylic hydrogens would be prone to a similar C–H activation of more remote C–H bonds. Therefore, we tried to prepare a norbornene (NBE) analog of $L_{Me}Rh(COE)$ starting from $[Rh(NBE)_2Cl]_2$. This reaction invariably produced a very dark-colored mixture of complexes. ^1H-NMR showed the presence of a small amount (ca. 10%) of a compound giving signals at $\delta = -10.2$ (dd) and $\delta = -1.2$ (d), but we were not successful in isolating it from the mixture. However, treatment of $L_{Me}Rh(COE)$ with a threefold excess of NBE in hexane resulted in clean formation of the same compound in the form of red-brown crystals. The X-ray structure (Figure 6) shows that it is indeed a close analog of $L_{Me}Rh(COE)$, with a similarly distorted T-shaped coordination geometry. In this case, however, there is a clear agostic interaction with an Rh–H distance of less than 2 Å[16] [RhC = 2.531(4) Å]. This pronounced agostic interac-

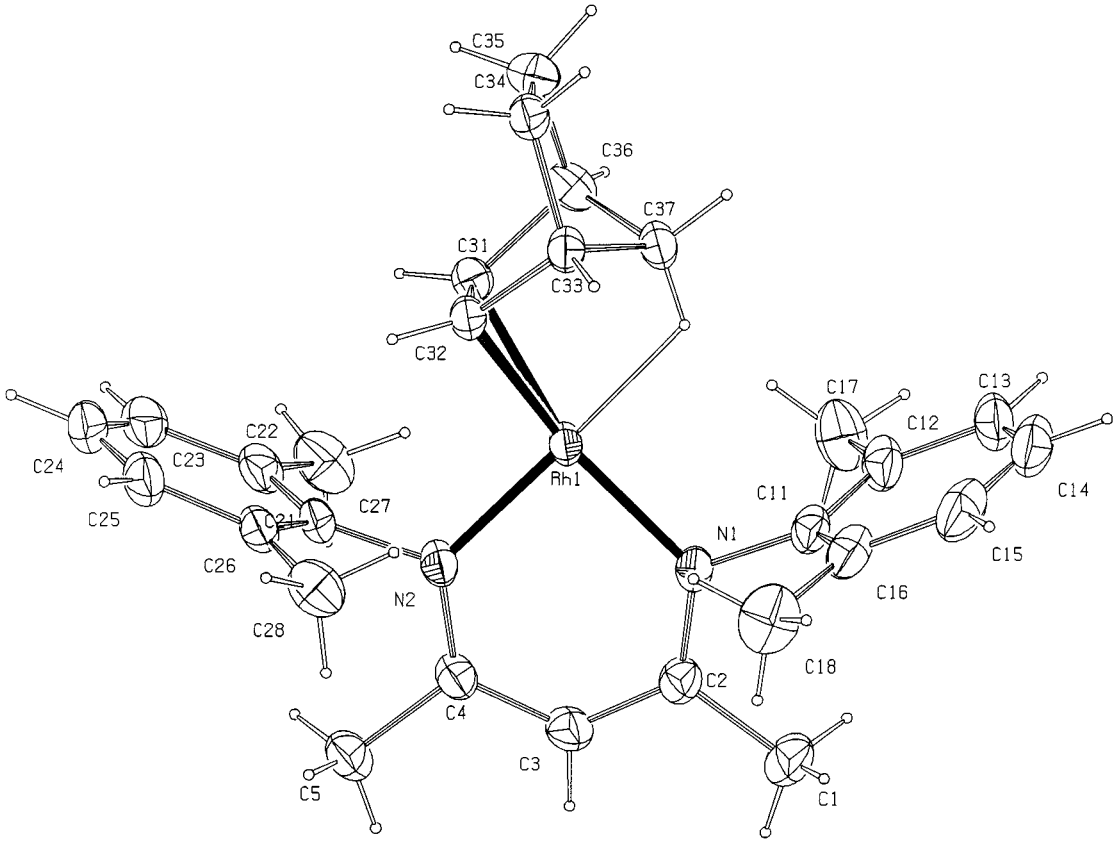


Figure 6. X-ray structure (30% ellipsoids) of $L_{Me}Rh(NBE)$; selected bond lengths (Å) and angles (°): Rh1–C31 2.115(4), Rh1–C32 2.095(4), Rh1–C37 2.531(4), Rh1–N1 2.021(3), Rh1–N2 1.985(3), C31–C32 1.395(6); N1–Rh1–N2 91.12(13)

tion accounts for the unusual high-field shift (δ = –10.2) of the bridge proton, which would more typically be associated with metal-bound hydrides. The alternative formulation as a cyclometallated olefin complex can be ruled out as the RhC distance is much too great for a single bond. Moreover, the methylene carbon is seen to be coupled to both hydrogens (J = 108 and 141 Hz), but shows no measurable coupling to Rh. Close approach of an NBE methylene hydrogen to a metal has also been observed in $(dien)Cu(NBE)^+$ [CuC = 2.78(1) Å, CuH = 2.01(15) Å],[17] but in the three other NBE complexes for which X-ray structures have been reported the distances between the metal and the methylene bridges are much larger: $[(t\text{Bu})_2P(CH_2)_2P(t\text{Bu})_2]Pt(NBE)$ (PtC = 3.18 Å, PtH = 2.75 Å),[18] $Pt(NBE)_3$ (PtC = 3.20/3.13/3.16 Å, PtH = 2.65/2.80/3.01 Å),[19] and a dicopper complex (CuC = 2.96/2.97 Å, CuH = 2.50/2.51 Å).[20]

The observation of a pronounced agostic interaction in $L_{Me}Rh(NBE)$ provides little information concerning the *strength* of this interaction. In fact, the NBE ligand appears to be predisposed towards such an agostic interaction; in the absence of any (repulsive or attractive) Rh–H forces, one would expect a structure very similar to the one observed. One observation that disfavours a strong agostic bond is the fact that such a bond is not observed at all in $L_{Me}Rh(COE)$, despite the fact that only a modest deformation of either the COE or the diiminate ligand would be required to obtain a short Rh–H contact.

In order to clarify this point, we carried out calculations on LRh(NBE). These reproduced most of the features of the X-ray structure of $L_{Me}Rh(NBE)$, although the shortening of Rh-C distances relative to those in the corresponding bis(ethene) complex was overestimated (calcd. 0.09 Å, obsd. 0.04 Å), while that of the Rh-N distances was underestimated (calcd. 0.02 Å, obsd. 0.09 Å). The agostic interaction is somewhat weaker in the calculated structure [RhH = 2.20 Å, RhC = 2.77 Å vs. 2.531(4) Å]; the agostic C–H bond is only slightly elongated (1.108 Å vs. 1.094 Å for the nonagostic bond). The angles about the methylene carbon are normal and there is no significant tilting of the NBE ligand towards the Rh atom. The calculated structure of LRh(NBE) is closer to T-shaped (N−Rh−olefin = 96°) than that observed for $L_{Me}Rh(NBE)$ (N−Rh−olefin = 102°); again, this may probably be attributed to the absence of steric constraints (vide supra) in the model. Fixing the N−Rh−olefin angle at 102° in the calculations costs only 0.7 kcal/mol and results in a slightly longer Rh−olefin bond (2.100 vs. 2.075 Å) and a more pronounced agostic interaction (RhC = 2.72 Å, RhH = 2.13 Å, C−H = 1.110 and 1.095 Å). Nevertheless, there are still no indications that the agostic interaction corresponds to a strong bond.[21]

$L_{Me}Rh(NBE)$ was found to be much less sensitive to air than $L_{Me}Rh(COE)$: a solution in THF had to be shaken in air for several minutes to effect complete oxidation, which was accompanied by liberation of NBE and formation of uncharacterizable rhodium complexes. We assume that the

relative inertness of the NBE complex reflects the inability (for steric reasons) of the NBE ligand to allow access to the fourth coordination site through rotation, and is not related to a large direct agostic bonding energy.

Complexes with Added Ligands

Because of its vacant coordination site, $L_{Me}Rh(COE)$ can be expected to be reactive towards added donor ligands. Indeed, reaction with excess acetonitrile gives yellow $L_{Me}Rh(COE)(MeCN)$, which has the expected square-planar structure (Figure 7). In THF or cyclohexane solution, $L_{Me}Rh(COE)$ reacts with dinitrogen to form brown $L_{Me}Rh(COE)(N_2)$ ($\tilde{\nu}_{NN}$ = 2172 cm^{-1}), from which the N_2 is lost in vacuo. NMR data indicate that the dinitrogen complex also has the expected static square-planar structure. In view of the weakness of the N_2 complexation in $L_{Me}Rh(COE)(N_2)$, it is hardly surprising that agostic $L_{Me}Rh(NBE)$ and 4-coordinate $L_{Cl}Rh(COE)$ do not react with N_2. Reaction of $L_{Me}Rh(COE)$ with excess 1-hexene results in a brown solution, presumably containing $L_{Me}Rh(COE)(hexene)$. On evacuation, this complex loses olefin to give a mixture of $L_{Me}Rh(COE)$ and $L_{Me}Rh(hexene)$ (ca. 4:1 by NMR).

No reaction was observed with TMEDA. NMR spectra of $L_{Me}Rh(COE)$ in cyclohexane, benzene, toluene, and THF are virtually identical, showing the same olefin–allyl hydride dynamic behaviour. Thus, it is evident that THF does not coordinate either.[8] Steric factors may be involved, or it may be that interaction with pure σ-donors such as ethers and amines is weak. Table 1 lists the calculated binding energies for various simple donor molecules at the $LRh(C_2H_4)$ and $LIr(C_2H_4)$ fragments. Bonds to Ir are consistently stronger than those to Rh; for both metals, the order is $H_2 < C_2H_4 \approx$ MeCN $\approx Me_2O \approx N_2 <$ CO. Ligands allowing strong back-donation, such as H_2 and CO, show the largest differences

Table 1. Calculated ligand binding energies of $LRh(C_2H_4)$ and $LIr(C_2H_4)$ fragments [kcal/mol]

Ligand	$LRh(C_2H_4)$	$LIr(C_2H_4)$
CO	40.6	71.2
N_2	30.5	48.2
Me_2O	29.9	35.3
MeCN	28.4	44.7
C_2H_4	24.4	46.3
H_2	11.1	33.2

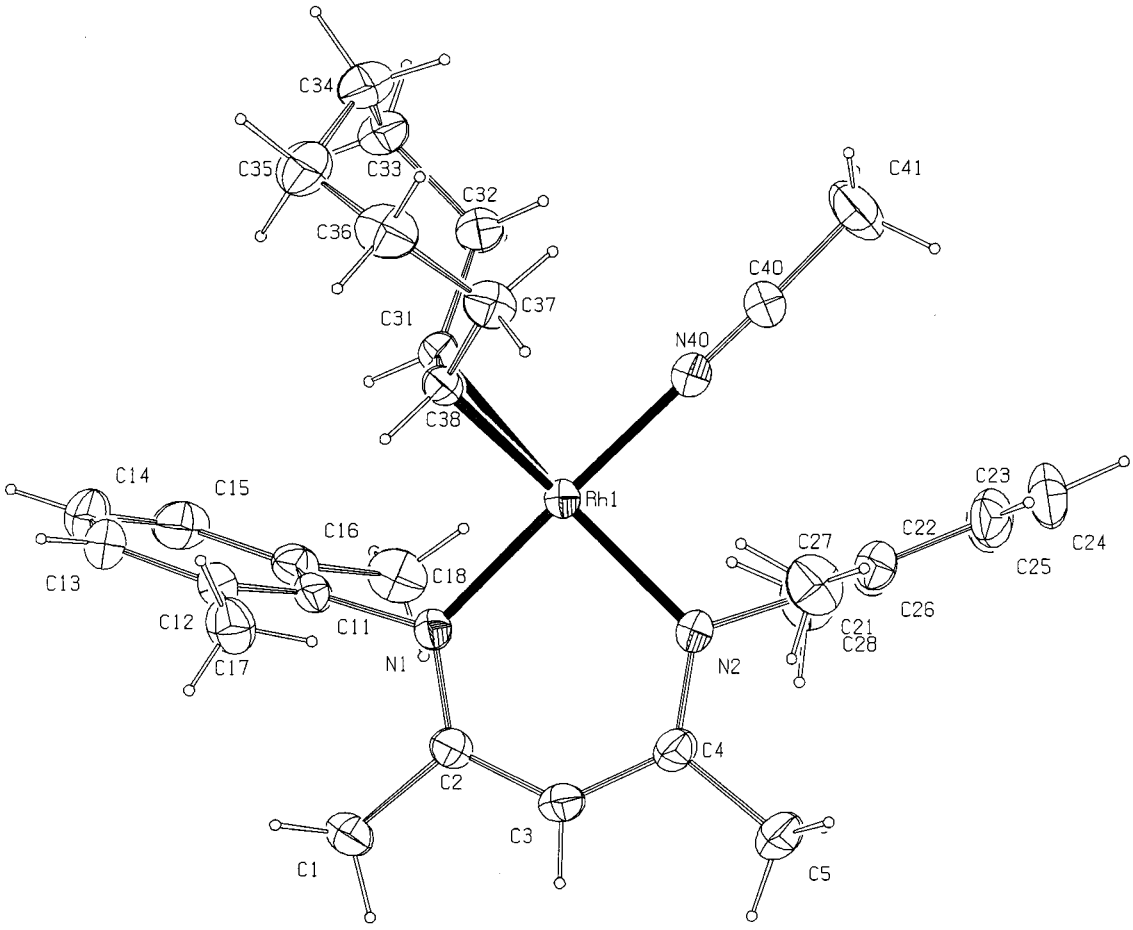


Figure 7. X-ray structure (30% ellipsoids) of $L_{Me}Rh(COE)(MeCN)$; selected bond lengths (Å) and angles (°): Rh1–C31 2.175(2), Rh1–C38 2.115(2), Rh1–N1 2.0598(16), Rh1–N2 2.0821(18), Rh1–N40 1.9899(19), C31–C38 1.399(3), N40–C40 1.136(3); N1–Rh1–N2 89.93(7), N2–Rh1–N40 88.72(7)

between Rh and Ir. The calculated coordination strengths of σ-donors (Me_2O, MeCN) are not much smaller than those of π-acceptors, which suggests that the lack of strong THF coordination is mainly due to steric factors.

Hydrogen Complexes

Reaction of $L_{Me}Rh(COE)$ with hydrogen at –40 °C in [D_8]THF produces $L_{Me}Rh(COE)(H_2)$ (characterized by ^{1}H- and ^{13}C-NMR), the large linewidth of the hydride signal of which is suggestive of a dihydrogen complex (T_1 = 10 ms at –30 °C).[22] If the solution is allowed to warm from –40 °C to 0 °C under a hydrogen atmosphere, kept at 0 °C for a few seconds, and then cooled to –40 °C once more, the dihydrogen complex is no longer present and the dominant species (ca. 50% of the total) is a dinuclear hydride (δ_H = –24.4, J_{RhH} = 25.3 Hz), to which we tentatively assign the composition $(L_{Me}Rh)_2H_4$. This compound decomposes on attempted removal of the solvent at low temperature, and on standing in solution at room temperature, hence it could not be isolated. Deactivation of low-coordinate cationic Ir hydrogenation catalysts has also been shown to involve the formation of hydride cluster complexes.[23]

The iridium complex $L_{Me}Ir(H)$(cyclooctenyl) reacts instantaneously with hydrogen at room temperature to form the stable complex $L_{Me}Ir(COE)H_2$ (δ_H = –22.7), which does not react further with olefins and/or H_2. The X-ray structure of this complex shows a regular T-shaped coordination geometry about Ir (Figure 8). The hydrogens bound to Ir could not be located, but the narrow hydride resonance suggests that in this case we are dealing with a classical dihydride. Surprisingly, $L_{Me}Ir(COE)H_2$ is also one of the decomposition products of $L_{Me}Ir(H)$(cyclooctenyl) in solution at room temperature in the *absence* of H_2. If this decomposition is carried out in a deuterated solvent ([D_8]THF, C_6D_6), a moderate amount of the mono-deuterated complex $L_{Me}Ir(COE)HD$ is formed.[24] The H–D coupling constant of 5.6 Hz is too small for a hydrogen complex, but rather large for a dihydride.[25] The NMR spectra show effective C_{2v} symmetry at room temperature, hence the molecule must be fluxional.

The surprisingly different behaviour of the Rh and Ir complexes towards H_2 is corroborated by the calculated structures of $LRh(C_2H_4)(H_2)$ and $LIr(C_2H_4)H_2$. In both cases, only a single minimum could be located. The Rh

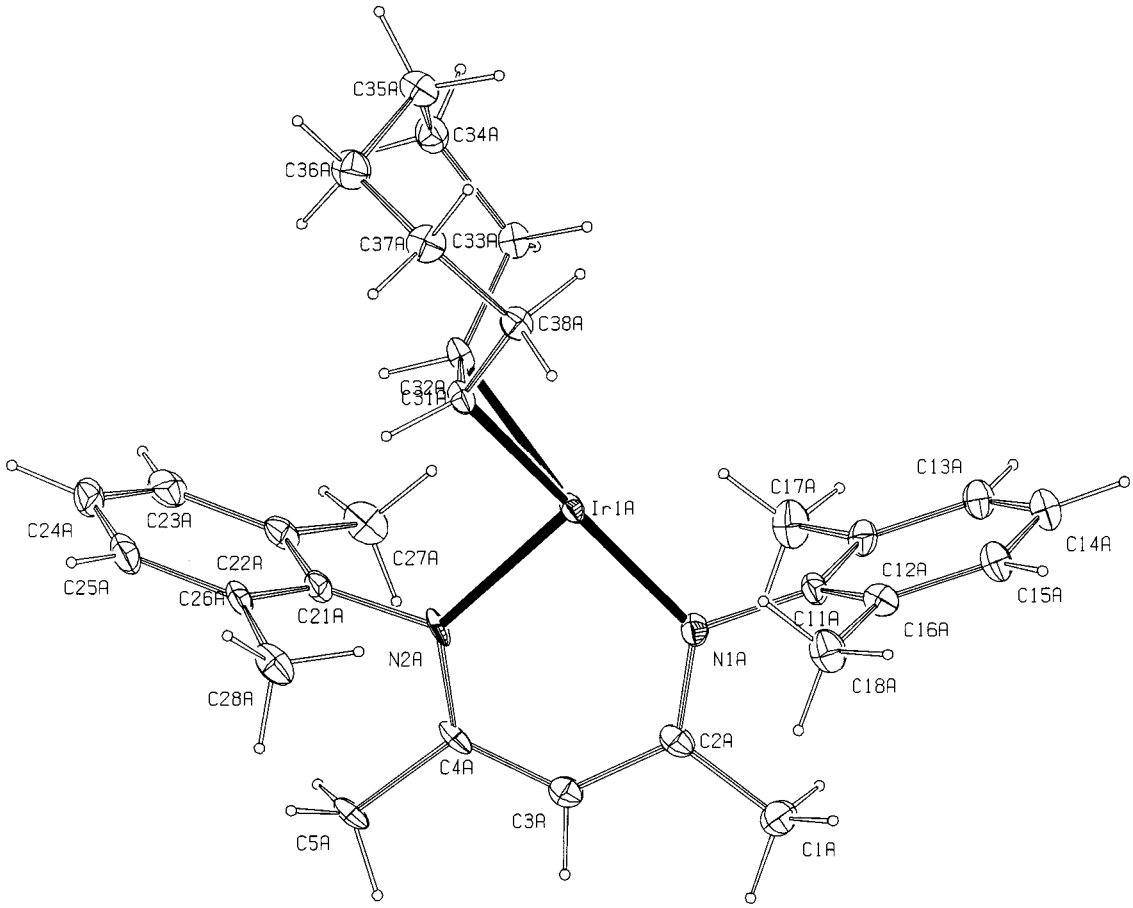


Figure 8. X-ray structure (30% ellipsoids) of $L_{Me}Ir(COE)(H_2)$; only one of the two independent molecules is shown; the hydrides were not located; selected bond lengths (Å) and angles (°): Ir1A–C31A 2.147(4), Ir1A–C32A 2.158(5), Ir1A–N1A 2.036(4), Ir1A–N2A 2.113(4), C31A–C32A 1.411(6), Ir1B–C31B 2.154(6), Ir1B–C32B 2.158(6), Ir1B–N1B 2.036(4), Ir1B–N2B 2.102(4), C31B–C32B 1.421(7); N1A–Ir1A–N2A 89.79(17), N1B–Ir1B–N2B 89.95(17)

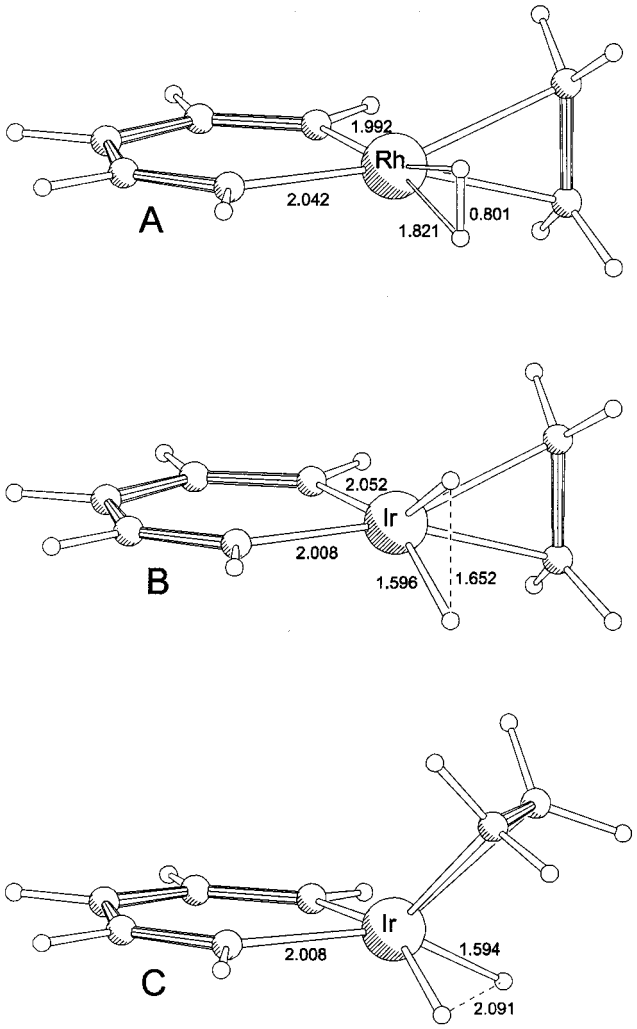


Figure 9. Calculated structures of (A) $LRh(C_2H_4)(H_2)$, (B) $LIr(C_2H_4)H_2$, and (C) the transition state for its left–right isomerization

complex (Figure 9, A) is a loosely bound (11 kcal/mol) square-planar Rh^I dihydrogen complex, in which the H–H bond is only slightly elongated (0.80 Å vs. 0.75 Å in H_2). In contrast, the Ir complex (Figure 9, B) is a strongly bound (33 kcal/mol) trigonal-bipyramidal Ir^{III} dihydride with a nonbonding (but nevertheless rather short) H–H distance of 1.65 Å. The observed fluxionality of $L_{Me}Ir(COE)H_2$ must involve a left–right shift of the olefin. The corresponding calculated transition state for $LIr(C_2H_4)H_2$ (Figure 9, C) has a square-pyramidal structure with an apical olefin ligand and an increased H–H distance of 2.09 Å. The calculated activation energy of 14 kcal/mol is compatible with this rearrangement being fast at room temperature.

Olefin Hydrogenation

$L_{Me}Rh(COE)$ is active as a catalyst in olefin hydrogenation; activity data for a few representative olefins are given in Table 2. Surprisingly, turnovers are comparable for both simple (1-hexene, cyclooctene) and highly substituted (1-methylcyclohexene, 2,3-dimethyl-2-butene) olefins. Bis(cyclohexylidene) is also hydrogenated, albeit with low turnover, but 1-*tert*-butylcyclohexene is not. The catalyst is very sensitive to impurities in the olefin or hydrogen; the turnover numbers in the table are limited by catalyst deactivation. For this reason, we have not tried to obtain kinetic data. The turnovers are not very sensitive to catalyst or olefin concentration, but do show a significant dependence on temperature (COE at 0 °C: 38 turnovers after 2 h, 49 after 4 h) and hydrogen pressure (COE at 20 bar H_2: 170 turnovers after 2 h).

In the case of cyclooctene hydrogenation, the main deactivation product was identified by NMR as $L_{Me}Rh(1,4\text{-COD})$, presumably formed from traces of 1,4-COD in the COE substrate.[26]

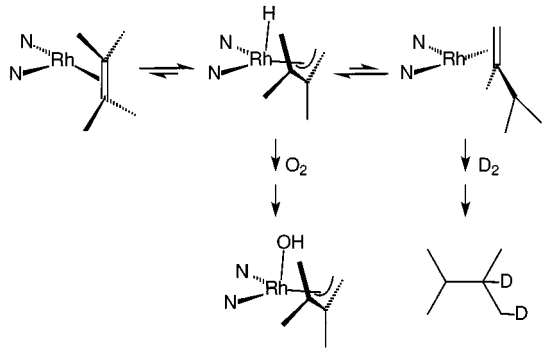
With 2,3-dimethyl-2-butene, the main catalyst deactivation product (ca. 90%) was a deep-green compound, which was identified as $L_{Me}Rh(OH)[\eta^3\text{-}CH_2C(Me)CMe_2]$ by NMR. Its formation can probably be attributed to trapping of an allyl hydride intermediate by traces of oxygen in the hydrogen used. Reduction of 2,3-dimethyl-2-butene with D_2 led to exclusive 1,2-deuteration; no higher deuterated species were detected. This demonstrates that olefin isomerization precedes hydrogenation. Since both cyclooctene and dimethylbutene undergo rapid isomerization according to the olefin–allyl hydride mechanism, it is reasonable to assume that this mechanism is also responsible for the isomerization during catalytic hydrogenation (Scheme 2). Hydrogenation of the trisubstituted olefin 1-methylcyclohexene might also involve an initial isomerization step.

Use of $L_{Me}Rh(COE)$ in hydrogenation is awkward because of its extreme sensitivity. However, less sensitive precursors such as $L_{Me}Rh(C_2H_4)_2$ and $L_{Me}Rh(COE)(MeCN)$ were found to give similar turnovers (see Table 2). Presumably, the active species is the same in all cases. $L_{Me}Rh(COD)$ could not be used as a precursor as it is too stable and does not react with hydrogen even at 100 °C. Catalysts derived from the L_{Cl} ligand give comparable turn-

Table 2. Olefin hydrogenation by β-diiminate Rh complexes

	Total turnover[a]		
Catalyst	cyclooctene	1-methyl-cyclohexene	2,3-dimethyl-2-butene[b]
$L_{Me}Rh(C_2H_4)_2$	77	70	43
$L_{Me}Rh(COE)$	89	44	42
$L_{Me}Rh(COE)(MeCN)$	89	n.d.	42
$L_{Cl}Rh(C_2H_4)_2$	73	42	11

[a] Neat olefin, olefin/catalyst = 125:1, 1 bar H_2, 2 h, room temperature; the catalyst was deactivated at the end of the experiment. – [b] After workup, a small amount of 2,3-epoxy-2,3-dimethylbutane was detected by GC/MS.

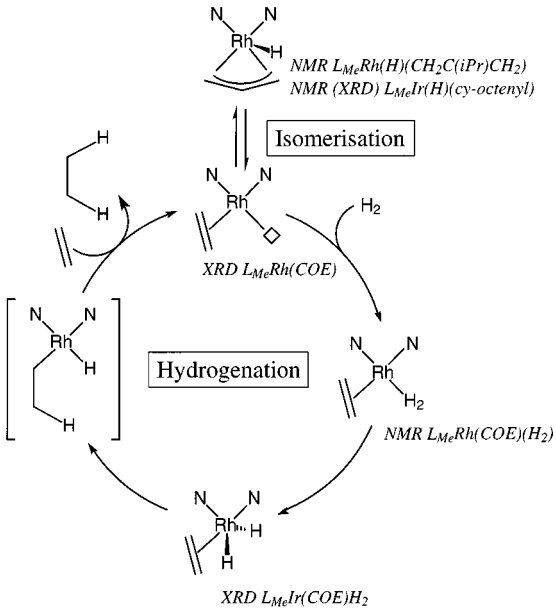


Scheme 2. Hydrogenation of 2,3-dimethyl-2-butene

overs with cyclooctene, but with the more hindered substrates the turnovers are significantly lower. We attribute this to catalyst decomposition through C–Cl oxidative addition,[27] which is able to compete with the coordination of an incoming olefin in the course of hydrogenation.

L_{Me}Ir(H)(cyclooctenyl) does not catalyze olefin hydrogenation, but merely reacts with hydrogen to form the stable dihydride L_{Me}Ir(COE)H_2, as mentioned earlier.

It is tempting to put together a catalytic cycle based on the Rh species (and their Ir analogues) observed in this work. Such a cycle is illustrated in Scheme 3. In the absence of any kinetic data, such a cycle must of course remain speculative.[28] However, it is hard to think of any realistic possibilities for ligand dissociation that would produce alternative active species. Moreover, the marginal stability of the dihydrogen complex L_{Me}Rh(COE)(H_2) is certainly compatible with its involvement in the relatively slow hydrogenation at room temperature. Here, the rate-determining step would probably be the conversion of the dihydrogen complex to a dihydride or its subsequent olefin insertion.



Scheme 3. Proposed cycles for olefin hydrogenation and isomerization based on the species observed; some of the steps of the hydrogenation cycle may be reversible

The cycle in Scheme 3 conforms to the "olefin route", in which the olefin is bound *before* the hydrogen.[29] This certainly happens on initiation, and, in view of the large excess of olefin and the higher calculated olefin binding energy, it most likely happens during propagation as well. However, we cannot exclude that – particularly at high conversions – a hydrogen route might become important. The precise nature of the alkane elimination step (associative or dissociative) also remains unclear.[30]

Most hydrogenation cycles involving Rh or Ir alternate between 16-*e* and 18-*e* species.[28,31] Even in cases where several active species are involved, they all go through intermediates with the same electron count. In our case, the catalysis appears to involve a 14-*e*/16-*e* mechanism, at least for the more hindered olefins, which may be attributed to steric factors.

Conclusions

Bulky β-diiminate ligands (such as L_{Me} and L_{Cl}) are good at stabilizing low coordination numbers, as demonstrated by the present work and by recent reports in the area of early transition metal chemistry. The ligand L_{Me} is particularly useful because its complexes nearly always crystallize well.[32] The ligand L_{Cl} tends to form even better crystallizing complexes, but the reactivity of the C–Cl bonds sometimes introduces complications.

The stabilization of low CN complexes by steric hindrance has allowed us to isolate a number of complexes that would normally be considered as reactive intermediates. Moreover, the use of Ir as a "model" for Rh[33] allows the direct observation of M^{III} species that for Rh would be transient intermediates in conversions between stable M^{I} species. This has allowed us to construct plausible catalytic cycles for hydrogenation and isomerization. Remarkably, the present hydrogenation appears to follow a 14-*e*/16-*e* path instead of the more usual 16-*e*/18-*e* path.

We attribute the observed stabilization of low CN complexes to the shielding of the metal atom by the vertical "walls" of the diiminate aryl groups. A perpendicular orientation of these groups is favoured by the 2,6-disubstitution pattern, which results in a strong repulsive interaction with the backbone methyl groups in a planar conformation. Indeed, work on early transition metal compounds has demonstrated dramatically increased reactivity of a low CN complex on removal of one or both of the substituents on the aryl groups.[1] However, the structure of L_{Cl}Rh(COE) shows that even 2,6-disubstituted aryl groups still have considerable freedom of movement.

One final point of interest is the observation of a pronounced agostic interaction in the L_{Me}Rh(NBE) species but not in L_{Me}Rh(COE). On the basis of both experimental and theoretical evidence, we conclude that in the former system close Rh–H contacts can easily form but do not correspond to strong bonds. Thus, caution should be exercised in equat-

ing small distances with large interaction energies. Such a conclusion is only justified in cases where the ligand undergoes considerable distortion to create the short contact.

Experimental Section

Calculations: All calculations were carried out using the Gaussian program[34] on SGI workstations. The small split-valence 3–21G basis was used for the first-row atoms.[35] For Rh and Ir, relativistic effective core potentials were used for the inner core orbitals and the LanL2DZ basis was used for the valence and outer core electrons;[36] the most diffuse *d* function in this basis was replaced by two components with exponents 1.4142 times higher and lower than the original exponent. Geometries were optimized at the RB3LYP[37] level without any constraints, unless stated otherwise.

Syntheses: All reactions were carried out under Ar. Solvents were distilled from Na/benzophenone prior to use. $[Rh(COD)Cl]_2$,[38] $[Rh(C_2H_4)_2Cl]_2$,[39] $[Rh(COE)_2Cl]_2$, and $[Ir(COE)_2Cl]_2$[40] were prepared according to literature methods.

$L_{Me}H$: A mixture of 2,6-dimethylaniline (30.5 mL, 30 g, 0.25 mol), 2,4-pentanedione (12.7 mL, 12.4 g, 0.12 mol), and *p*-toluenesulfonic acid (21.3 g) in toluene (350 mL) was refluxed for 24 h in a Dean-Stark apparatus. The toluene was then decanted off, and the solid residue was treated with diethyl ether (250 mL), water (200 mL), and $Na_2CO_3 10\ H_2O$ (53 g). After stirring for 25 min, the ether layer was separated, dried with $MgSO_4$, and the solvent was removed in vacuo. The residue was dried in vacuo (10^{-2} bar) at 100 °C for 6 h to remove any remaining free 2,6-dimethylaniline, to give 28.5 g (75%) of $L_{Me}H$. – $C_{21}H_{26}N_2$ (306.45): calcd. C 82.31, H 8.55, N 9.14; found C 81.82, H 8.71, N 8.97. – ^{1}H NMR ($CDCl_3$, 200 MHz): δ = 1.72 (1-H), 4.91 (3-H), 6.96–7.09 (m, *m*- + *p*-H), 2.19 (*o*-CH_3), 12.2 (br., NH). – $^{13}C\{^1H\}$ NMR (75.5 MHz): δ = 20.8 (C-1), 161.2 (C-2), 94.1 (C-3), 144.2 (*i*-C), 132.5 (*o*-C), 128.3 (*m*-C), 124.9 (*p*-C), 18.9 (*o*-CH_3).

$L_{Me}Li(THF)$: To a solution of LH (10 g) in THF (100 mL) was added a solution of $LiN(iPr)_2$ in THF [prepared from 1.6 M *n*-BuLi/hexane (20.5 mL) and diisopropylamine (4.6 mL)]. The solvent was subsequently removed in vacuo and the residue was crystallized from a hot toluene/hexane mixture to give 8.2 g (65%) of LLi(THF). – $C_{25}H_{33}N_2OLi$ (384.49): calcd. C 78.10, H 8.65, N 7.29; found C 78.36, H 8.52, N 7.45. – ^{1}H NMR (C_6D_6, 200 MHz): δ = 1.84 (1-H), 5.00 (3-H), 7.12 (d, *m*-H), 6.96 (t, *p*-H), 2.25 (*o*-CH_3); 2.86, 0.89 (THF). – $^{13}C\{^1H\}$ NMR (50.3 MHz): δ = 22.7 (C-1), 163.2 (C-2), 92.9 (C-3), 152.7 (*i*-C), 130.5 (*o*-C), 128.0 (*m*-C), 121.9 (*p*-C), 18.8 (*o*-CH_3); 67.7, 24.9 (THF).

$L_{Cl}H$: A mixture of 2,6-dichloroaniline (40.5 g, 0.25 mol), 2,4-pentanedione (12.7 mL, 12.4 g, 0.12 mol), and *p*-toluenesulfonic acid (21.3 g) in toluene (350 mL) was refluxed for 24 h in a Dean-Stark apparatus. The toluene was then decanted off, and the solid residue was treated with diethyl ether (250 mL), water (200 mL), and $Na_2CO_3 10\ H_2O$ (53 g). After stirring for 25 min, the ether layer was separated, dried with $MgSO_4$, and the solvent was removed in vacuo. The residue was dried in vacuo (10^{-2} bar) at 100 °C for 6 h to remove any remaining free 2,6-dichloroaniline, and the residue was crystallized from heptane to give 34 g (70%) of $L_{Cl}H$. – $C_{17}H_{14}N_2Cl_4$ (388.12): calcd. C 52.61, H 3.64, N 7.22, Cl 36.54; found C 52.74, H 3.67, N 7.38, Cl 36.43. – ^{1}H NMR ($CDCl_3$, 200 MHz): δ = 1.71 (1-H), 4.94 (3-H), 7.17 (d, *m*-H), 6.86 (t, *p*-H), 12.0 (NH). – $^{13}C\{^1H\}$ NMR (50.3 MHz): δ = 21.4 (C-1), 163.1 (C-2), 95.9 (C-3), 141.1 (*i*-C), 131.7 (*o*-C), 128.6 (*m*-C), 126.2 (*p*-C).

$L_{Cl}Li(THF)$: To a solution of $L_{Cl}H$ (12.6 g) in THF (100 mL) was added a solution of $LiN(iPr)_2$ in THF [prepared from 1.6 M *n*-BuLi/hexane (20.5 mL) and diisopropylamine (4.6 mL)]. The solvent was subsequently removed in vacuo, and the residue was crystallized from a hot toluene/hexane mixture to give 12.2 g (80%) of yellow $L_{Cl}Li(THF)$. – $C_{21}H_{21}N_2OCl_4Li$ (466.16): calcd. C 54.11, H 4.54, N 6.01, Cl 30.42; found C 54.06, H 4.59, N 6.13, Cl 30.54. – ^{1}H NMR (C_6D_6, 200 MHz): δ = 1.82 (1-H), 4.93 (3-H), 7.02 (d, *m*-H), 6.32 (t, *p*-H); 2.96, 0.82 (THF). – $^{13}C\{^1H\}$ NMR (50.3 MHz): δ = 23.5 (C-1), 165.6 (C-2), 95.6 (C-3), 149.5 (*i*-C), 130.7 (*o*-C), 128.7 (*m*-C), 123.0 (*p*-C); 68.2, 25.2 (THF).

$L_{Me}Rh(1,5\text{-}COD)$: A solution of $L_{Me}Li(THF)$ (1.0 g) in THF (10 mL) was added to a suspension of $[Rh(1,5\text{-}COD)Cl]_2$ (0.64 g) in THF (5 mL). The resulting mixture was stirred at room temperature for 2 h, and then the solvent was removed in vacuo. The residue was crystallized from benzene/hexane (2:1) (the hot solution was filtered to remove LiCl) to give yellow crystals of $L_{Me}Rh(1,5\text{-}COD)$ (1.2 g, 88%). – $C_{29}H_{37}N_2Rh$ (516.53): calcd. C 67.43, H 7.22, N 5.42; found C 67.42, H 7.38, N 5.42. – ^{1}H NMR ($CDCl_3$, 200 MHz): δ = 1.55 (1-H), 5.10 (3-H), 6.97–7.11 (m, *m*- + *p*-H), 2.31 (*o*-CH_3), 3.01 (br., CH=CH), 2.12, 1.60 (CH_2). – $^{13}C\{^1H\}$ NMR (50.3 MHz): δ = 25.5 (C-1), 159.3 (C-2), 97.8 (C-3), 150.9 (*i*-C), 132.9 (*o*-C), 128.7 (*m*-C), 124.9 (*p*-C), 19.3 (*o*-CH_3), 79.8 (CH=CH, J_{RhC} = 13 Hz), 31.1 (CH_2).

$L_{Cl}Rh(1,5\text{-}COD)$: A solution of $L_{Cl}Li(THF)$ (0.5 g) in THF (10 mL) was added to a suspension of $[Rh(1,5\text{-}COD)Cl]_2$ (0.26 g) in THF (5 mL). The resulting mixture was stirred at room temperature for 4 h, and then the solvent was removed in vacuo. The residue was crystallized from toluene (70/–20 °C; the hot solution was filtered to remove LiCl) to give yellow crystals of $L_{Cl}Rh(1,5\text{-}COD)$ (0.32 g, 50%). – $C_{25}H_{25}N_2Cl_4Rh$ (598.20): calcd. C 50.20, H 4.21, N 4.68, Cl 23.71; found C 50.14, H 4.12, N 4.69, Cl 23.57. – ^{1}H NMR (C_6D_6, 200 MHz): δ = 1.72 (1-H), 5.28 (3-H), 7.14 (d, *m*-H), 6.45 (t, *p*-H), 3.61 (br., CH=CH), 2.33, 1.56 (m, CH_2). – $^{13}C\{^1H\}$ NMR (50.3 MHz): δ = 25.1 (C-1), 160.9 (C-2), 99.3 (C-3), 147.8 (*i*-C), 132.9 (*o*-C), 128.5 (*m*-C), 125.8 (*p*-C), 78.8 (CH=CH, J_{RhC} = 13 Hz), 30.8 (CH_2).

$L_{Me}Rh(C_2H_4)_2$: A solution of $L_{Me}Li(THF)$ (1.0 g) in THF (10 mL) was added to a suspension of $[Rh(C_2H_4)_2Cl]_2$ (0.51 g) in THF (5 mL). The resulting mixture was stirred at room temperature for 2 h, and then the solvent was removed in vacuo. The residue was crystallized from diethyl ether (30/–20 °C; the warm solution was filtered to remove LiCl) to give very large, dark brown-yellow crystals of $L_{Me}Rh(C_2H_4)_2$ (0.68 g, 50%). Small crystals or powdered material are yellow. – $C_{25}H_{33}N_2Rh$ (464.45): calcd. C 64.54, H 7.16, N 6.03; found C 64.77, H 7.22, N 6.16. – ^{1}H NMR (C_6D_6, 200 MHz): δ = 1.65 (1-H), 5.30 (3-H), 7.04–7.12 (m, *m*- + *p*-H), 2.41 (*o*-CH_3), 2.62, 2.01 (m, C_2H_4). – $^{13}C\{^1H\}$ NMR (50.3 MHz): δ = 25.9 (C-1), 159.5 (C-2), 98.9 (C-3), 150.4 (*i*-C), 133.0 (*o*-C), 129.2 (*m*-C), 125.7 (*p*-C), 19.8 (*o*-CH_3), 63.3 (C_2H_4, J_{RhC} = 11 Hz).

$L_{Cl}Rh(C_2H_4)_2$: A solution of $L_{Cl}Li(THF)$ (0.5 g) in THF (10 mL) was added to a suspension of $[Rh(C_2H_4)_2Cl]_2$ (0.21 g) in THF (5 mL). The resulting mixture was stirred at room temperature for 2 h, and then the solvent was removed in vacuo. The residue was crystallized from diethyl ether (30/–20 °C; the warm solution was filtered to remove LiCl) to give dark-red crystals of $L_{Cl}Rh(C_2H_4)_2$ (0.22 g, 36%). – $C_{21}H_{21}N_2Cl_4Rh$ (546.13): calcd. C 46.19, H 3.88, N 5.13, Cl 25.97; found C 46.21, H 3.89, N 5.25, Cl 25.85. – ^{1}H NMR (C_6D_6, 200 MHz): δ = 1.73 (1-H), 5.29 (3-H), 7.05 (d, *m*-

H), 6.44 (t, *p*-H), 2.88, 2.02 (m, C_2H_4). – $^{13}C\{^1H\}$ NMR (125.76 MHz): δ = 24.2 (C-1), 159.9 (C-2), 98.1 (C-3), 146.1 (*i*-C), 131.8 (*o*-C), 127.4 (*m*-C), 125.0 (*p*-C), 60.8 (C_2H_4, J_{RhC} = 12 Hz).

L_{Me}Rh(COE): A solution of L_{Me}Li(THF) (3.24 g) in THF (10 mL) was added to a suspension of $[Rh(COE)_2Cl]_2$ (3.03 g) in THF (5 mL). The resulting mixture was stirred at room temperature for 1 day, and then the solvent was removed in vacuo. The residue was extracted with two 50 mL portions of warm hexane (60 °C), the combined extracts were concentrated to a volume of 15 mL, and cooled to –20 °C. The next day, a crop of dark-violet crystals had formed. These crystals were recrystallized from fresh hexane to give 3.0 g (66%) of L_{Me}Rh(COE). Crystals suitable for X-ray diffraction analysis were obtained by slow crystallization from cyclohexane. – $C_{29}H_{39}N_2Rh$ (518.55): calcd. C 67.17, H 7.58, N 5.40; found C 67.04, H 7.41, N 5.57. – ^1H NMR (200 MHz, C_6D_{12}, room temp.): δ = 1.72 (1-H), 5.18 (3-H), 7.0–7.1 (m, *m*- + *p*-H), 2.65 (*o*-CH_3), 1.87 (br. s, 8 H), 0.34 (br. s, 6 H) cyclooctene. – ^1H NMR (500 MHz, $[D_8]$THF, –80 °C): δ = 1.55, 1.39 (1-,1′-H), 4.95 (3-H), 7.16, 7.10 (*m*-,*m*′-H), 7.06, 7.05 (*p*-,*p*′-H), 2.70, 2.39 (*o*,*o*′-CH_3), 2.48 (CH=CH), 2.08, 1.5, 1.2, 1.0 (br., CH_2). – $^{13}C\{^1H\}$ NMR (125.7 MHz, $[D_8]$THF, –80 °C): δ = 24.1 (C-1), 26.5 (C-1′, superimposed by solvent signal), 158.6, 156.3, 154.3, 150.9 (C-2, C-2′, *i*-,*i*′-C), 100.4 (C-3, J_{RhC} = 39 Hz), 134.6, 134.5 (*o*-,*o*′-C), 129.9, 129.5 (*m*-,*m*′-C), 126.2, 125.8 (*p*-,*p*′-C), 21.1, 20.4 (*o*,*o*′-CH_3), 64.8 (br., CH=CH), 31.6 (br., CH_2); remaining CH_2 groups not observed.

L_{Me}Ir(cyclooctenyl)(H): A solution of L_{Me}Li(THF) (1.0 g) in diethyl ether (10 mL) was added to a suspension of $[Ir(COE)_2Cl]_2$ (1.16 g) in diethyl ether (5 mL). The resulting mixture was stirred at room temperature for 4 h, and then the solvent was removed in vacuo. The residue was extracted with two 20 mL portions of hexane, the combined extracts were concentrated to a volume of 8 mL, and cooled to –20 °C. After 3 days, orange-red crystals had formed. Concentration of the mother liquor to 3 mL and cooling to –20 °C produced a second crop of crystals. The crystals were dried in vacuo and stored at –20 °C. – $C_{29}H_{39}N_2Ir$ (607.86): calcd. C 57.30, H 6.47, N 4.61; found C 57.08, H 6.56, N 4.74. – ^1H NMR ($[D_8]$THF, –20 °C, 400 MHz): δ = 1.70 (1-H), 5.37 (3-H), 7.20, 7.18 (d, *m*- + *m*′-H), 6.99 (t, *p*-H), 2.16, 2.21 (*o*,*o*′-CH_3), 5.40 (t, 1 H), 2.54 (br. q, 2 H, cyclooctenyl CH), 1.90, 1.27, 1.05, 0.82, 0.25 (br. m, CH_2), –46.19 (IrH). – $^{13}C\{^1H\}$ (100.6 MHz): δ = 23.9 (C-1), 157.6 (C-2), 103.2 (C-3), 157.2 (*i*-C), 132.7, 130.9 (*o*-,*o*′-C), 130.2, 129.8 (*m*-,*m*′-C), 126.0 (*p*-C), 20.3, 20.0 (*o*,*o*′-CH_3), 84.9, 49.6 (cyclooctenyl CH), 32.8, 30.3, 19.9 (CH_2). – IR (KBr): $\tilde{\nu}_{Ir-H}$ = 2122 cm^{-1}.

L_{Cl}Rh(COE): A solution of L_{Cl}Li(THF) (2.0 g) in THF (10 mL) was added to a suspension of $[Rh(COE)_2Cl]_2$ (1.54 g) in THF (10 mL). The resulting mixture was stirred at room temperature for 1 h, and then the solvent was removed in vacuo. The residue was extracted with two 50 mL portions of hexane, the combined extracts were concentrated to dryness in vacuo, and the residue was redissolved in diethyl ether (50 mL). This solution was filtered and then concentrated to a volume of 4 mL and stored overnight at –20 °C. Thereafter, fine red needles had formed, which were filtered off and dried in vacuo to give 0.77 g (30%) of L_{Cl}Rh(COE). – $C_{25}H_{27}N_2Cl_4Rh$ (600.22): calcd. C 50.03, H 4.53, N 4.67, Cl 23.63; found C 49.86, H 4.54, N 4.80, Cl 23.63. – ^1H NMR (200 MHz, C_6D_6, 25 °C): δ = 6.96 (d, 4 H, *m*-H), 6.34 (t, 2 H, *p*-H), 5.36 (s, 1 H, 3-H), 2.2 (v. br., 8 H, COE *exo* ± vinylic), 1.89 (s, 1-H), 1.47 (br., 6 H, COE *endo*). – ^1H NMR (500.13 MHz, $[D_8]$THF, –53 °C[8]): δ = 7.48, 7.39 (m, 2 H each, *m*-,*m*′-H), 7.22, 6.90 (m, 1 H each, *p*-,*p*′-H), 5.30 (s, 1 H, 3-H), 2.20, 1.58 (s, 3 H each, 1-,1′-H), 1.1–2.6 (overlapping multiplets, 14 H, COE). – $^{13}C\{^1H\}$ NMR (125.76 MHz, $[D_8]$THF, –53 °C[8]): δ = 162.5, 162.2 (2-C, 2′-C), 151.7, 146.5 (*i*-,*i*′-C), 133.5, 130.4 (*o*-,*o*′-C), 129.9 (*m*-,*m*′-C), 128.8, 123.7 (*p*-,*p*′-C), 106.6 (C-3), 32.6, 28.2 (COE), 24.6 (C-1); C-1′ and remaining COE resonances not observed.

L_{Me}Rh(C_2Me_4): A suspension of L_{Me}Rh(COE) (0.15 g) in C_2Me_4 (7 mL) was stirred under a hydrogen atmosphere (1 bar) until the solid had completely dissolved (ca. 3 min), giving a dark-brown solution. All volatiles were then removed in vacuo, and the residue was redissolved in $[D_8]$THF for NMR studies (see Results Section). The solution gave rise to small but sharp peaks due to the oxidation product $L_{Me}Rh[\eta^3\text{-}CH_2C(Me)CMe_2](OH)$ (see below); resonances due to the main product were found to be broad at room temperature. At 243 K, all peaks due to the main component $L_{Me}Rh[\eta^3\text{-}CH_2C(iPr)CH_2](H)$ could be assigned: ^1H NMR ($[D_8]$THF, 500 MHz, 243 K): δ = 1.56 (obscured by cyclooctane signal; 1-H), 5.04 (3-H), 7.02, 7.04 (d, *m*-H), 6.90 (t, *p*-H), 2.53, 2.23 (*o*-CH_3), 1.85 (br. sept, H*i*Pr), 1.24 (br. d, CMe_2), –2.45 (br., CH_2 + Rh–H). – $^{13}C\{^1H\}$ NMR (125.7 MHz): δ = 23.4 (C-1), 157.6 (C-2), 99.6 (C-3), 156.8 (*i*-C), 135.0, 131.3 (*o*-C), 129.5 (*m*-C), 126.1 (*p*-C), 19.9, 21.2 (*o*-CH_3), 97.1 (C*i*Pr, J_{RhC} = 11 Hz) (CH_2 obscured by THF), 36.0 (CMe_2), 23.8 (CMe_2). In addition, some peaks due to the minor component $L_{Me}Rh[\eta^3\text{-}CH_2C(Me)CMe_2](H)$ could be tentatively assigned: ^1H NMR (500 MHz, 218 K): δ = 5.03 (3-H), –12.17 (RhH). – $^{13}C\{^1H\}$ NMR (125.7 MHz, 243 K): δ = 158.4 (C-2), 156.4, 155.9 (*i*-,*i*′-C), 133.1 (*o*-C), 130.0, 129.7, 129.3 (*m*-C), 126.4 (*p*-C), 100.0 (C-3), 21.9, 21.1, 20.5 (*o*-CH_3).

L_{Me}Rh(NBE): To a solution of L_{Me}Rh(COE) (0.7 g) in hexane (5 mL) was added NBE (0.5 g). The resulting mixture was stirred at room temperature for 15 min. All volatiles were then removed in vacuo, and the residue was crystallized from hexane (50/–20 °C) to give 0.56 g (83%) of brown-red L_{Me}Rh(NBE). – $C_{28}H_{35}N_2Rh$ (502.50): calcd. C 66.93, H 7.02, N 5.57; found C 66.68, H 6.82, N 5.42. – ^1H NMR (200 MHz, C_6D_{12}): δ = 1.40, 1.60 (1-H), 4.96 (3-H), 6.8–6.9 (m, *m*- + *p*-H), 2.31, 2.61 (*o*-CH_3), 2.55, 2.71 (vinylic and bridgehead H), 0.75 (CH_2CH_2), –0.82 (d, $^2J_{HH}$ = 14.5 Hz, nonagostic HCH), –10.2 (dd, $^2J_{HH}$ = 14.5, J_{RhH} = 11.7 Hz, agostic HCH). – $^{13}C\{^1H\}$ NMR (50.4 MHz, C_6D_{12}): δ = 23.5, 20.9 (C-1), 156.9, 155.7 (C-2), 99.2 (C-3), 158.6, 156.3, 153.3, 150.3 (*i*-C), 133.2 (*o*-C), 128.7, 128.6 (*m*-C), 125.5, 125.2 (*p*-C), 19.9, 19.4 (*o*-CH_3), 65.7 (d, C=C, J_{RhC} = 15 Hz), 47.5 (bridgehead), 29.6 (CH_2CH_2), 16.0 (CH_2). – ^{13}C NMR (125.7 MHz, C_6D_{12}): $^1J_{CH}$ = 108 and 141 Hz for the NBE CH_2. The infrared spectrum (KBr and Nujol mull) did not show any distinct peaks attributable to the agostic C–H bond.

L_{Me}Rh(COE)(N_2): Solutions of L_{Me}Rh(COE)(N_2) were generated by preparing NMR samples of L_{Me}Rh(COE) under nitrogen atmosphere. – ^1H NMR ($[D_8]$THF, 500 MHz): δ = 1.56, 1.75 (1-,1-H′), 5.24 (3-H), 7.16, 7.15 (d, *m*-,*m*′-H), 7.04, 7.09 (t, *p*-,*p*′-H), 2.50, 2.32 (*o*,*o*′-CH_3), 3.04 (CH=CH), 2.14, 1.59, 1.2 (br., CH_2). – $^{13}C\{^1H\}$ NMR (125.7 MHz): δ = 26.6, 23.8 (C-1, C-1′), 160.3, 159.1 (C-2, C-2′), 99.9 (C-3, J_{RhC} = 11 Hz), 156.2, 150.0 (*i*-,*i*′-C), 134.8, 133.3 (*o*-,*o*′-C), 130.1, 29.8 (*m*-,*m*′-C), 127.1, 126.6 (*p*-,*p*′-C), 20.6, 20.1 (*o*,*o*′-CH_3), 76.7 (CH=CH, J_{RhC} = 11 Hz), 32.5, 30.8, 28.1 (CH_2). Essentially pure solid L_{Me}Rh(COE)(N_2) was prepared by dissolving L_{Me}Rh(COE) (0.1 g) in hexane (1 mL) under nitrogen, concentrating the solution to a volume of 0.3 mL in vacuo, and connecting the Schlenk tube to another one containing 6 mL of paraffin oil. After 6 weeks, the hexane had diffused into the paraffin oil and the oily residue had solidified. – IR (Nujol mull): $\tilde{\nu}_{N-N}$ = 2172 cm^{-1}.

$L_{Me}Rh(COE)(MeCN)$: A solution of $L_{Me}Li(THF)$ (0.51 g) in THF (6 mL) was added to a suspension of $[Rh(COE)_2Cl]_2$ (0.48 g) in THF (3 mL) and MeCN (0.75 mL). The resulting mixture was stirred for one day and then the solvents were removed in vacuo. The residue was extracted with two 20 mL portions of cyclohexane. The combined extracts were concentrated to a volume of 10 mL and stored for overnight at 6 °C, which led to the deposition of a yellow powder (0.56 g, 75%). Crystals suitable for X-ray diffraction were obtained by slow crystallization at room temperature. – $C_{31}H_{42}N_3Rh$ (559.60): calcd. C 66.54, H 7.56, N 7.51; found C 66.32, H 7.91, N 7.48. – ^{1}H NMR (C_6D_6, 293 K, 200 MHz): δ = 6.93 (m, *m*-,*p*-H), 5.19 (3-H), 2.80, 2.25, 1.52, 1.27 (m, COE), 2.54, 2.42 (*o*,*o*′-CH_3), 1.69, 1.52 (1-,1′-H), 0.45 (MeCN). – $^{13}C\{^1H\}$ NMR (50.4 MHz): δ = 158.0, 156.0 (C-2, C-2′), 154.3, 149.4 (*i*-,*i*′-C), 133.1, 132.8 (*o*-,*o*′-C), 128 (superimposed by solvent signal, *m*-H), 124.5, 123.2 (*p*-,*p*′-C), 116.1 (CH_3CN), 98.0 (C-3), 66.9 (d, J_{RhC} = 14 Hz, CH=CH), 31.0, 29.7, 26.9 (COE), 25.3, 23.08 (1-,1′-C), 19.5, 19.0 (*o*,*o*′-CH_3), 1.4 (CH_3CN).

$L_{Me}Rh(1,4\text{-}COD)$: $L_{Me}Rh(COE)$ (0.3 g) was dissolved in 1,3-COD (2 mL) and the solution was stirred for 10 min. The solvent was then removed in vacuo, leaving essentially pure $L_{Me}Rh(1,4\text{-}COD)$, which was characterized only by NMR. Heating of the solution in 1,3-COD to 40 °C for 10 min prior to workup resulted in formation of $L_{Me}Rh(1,5\text{-}COD)$. – ^{1}H NMR (C_6H_6, 293 K, 200 MHz): δ = 7.0–7.2 (m, *m*-,*p*-H), 5.25 (3-H), 3.26, 2.7, 2.4, 2.1, 1.7, 1.2 (br. m, 1,4-COD), 2.48, 2.41 (*o*-CH_3), 1.66 (1-H). – $^{13}C\{^1H\}$ NMR (50.3 MHz): δ = 158.3 (C-2), 150.4 (*i*-C), 133.2, 131.8 (*o*-,*o*′-C), 128 (obscured by solvent signal, *m*-,*m*′-C), 124.7 (*p*-C), 98.2 (C-3), 24.9 (C-1), 19.2, 18.9 (*o*,*o*′-CH_3), 72.4 (d, J_{RhC} = 14 Hz), 51.1 (d, J_{RhC} = 8 Hz, C=C), 29.1 (2 C), 28.3, 25.7 (CH_2). The same material remained following hydrogenation of COE with $L_{Me}Rh(COE)$.

$L_{Me}Rh[CH_2C(Me)CMe_2](OH)$: Following hydrogenation experiments with 2,3-dimethyl-2-butene, this compound remained as a deep-green oil. All attempts to crystallize it were unsuccessful. – ^{1}H NMR (C_6H_6, 293 K, 200 MHz): δ = 6.9–7.2 (m, *m*-,*p*-H), 5.26 (3-H), 3.61, 1.84 (br. s, CH_2), 2 × 2.74, 2.57, 2.34 (*o*-CH_3), 1.84, 1.58 (1-H), 1.42, 0.73, 0.50 ($CMeCMe_2$), –1.33 (OH). – $^{13}C\{^1H\}$ NMR (75.5 MHz): δ = 156.9, 153.4 (C-2, C-2′), 153.0, 149.7 (*i*-,*i*′-C), 133.5, 132.9, 132.4, 132.3 (*o*-C), 128 (obscured by solvent signal, *m*-C), 124.4, 124.1 (*p*-,*p*′-C), 98.6 (C-3), 89.9 ($CH_2CMeCMe_2$), 67.7 (d, J_{RhC} = 12 Hz, $CH_2CMeCMe_2$), 50.7 (d, J_{RhC} = 14 Hz, $CH_2CMeCMe_2$), 23.4, 21.4 (C-1, C-1′), 19.4, 19.3, 19.2, 18.8 (*o*-CH_3), 29.0, 26.4, 17.3 ($CH_2CMeCMe_2$).

$L_{Me}Rh(COE)(H_2)$: A solution of $L_{Me}Rh(COE)$ (0.12 g) in $[D_8]$THF (0.7 mL) was cooled to –40 °C and then stirred under hydrogen atmosphere (1 bar) for 3 min. The solution was then cooled to –80 °C and transferred to a cooled NMR tube under Ar. NMR studies showed it to contain $L_{Me}Rh(COE)(H_2)$ as the main Rh complex (ca. 75% of the total; the remainder was $[L_{Me}RhH_2]_2$; see below). – ^{1}H NMR ($[D_8]$THF, 243 K, 500 MHz): δ = 1.51, 1.56 (obscured by cyclooctane signal, 1-,1′-H), 5.12 (3-H), 7.11, 7.02 (d, *m*-,*m*′-H), 7.00, 6.90 (t, *p*-,*p*′-H), 2.39, 2.28 (*o*,*o*′-CH_3), 2.45 (CH=CH), 2.12, 1.59, 1.3 (br., CH_2), –12.8 (br., Rh–H_2; T_1 = 10 ms by inversion-recovery). – $^{13}C\{^1H\}$ NMR (125.7 MHz): δ = 25.8, 22.8 (C-1, C-1′), 160.7, 160.2 (C-2, C-2′), 99.9 (C-3), 158.7, 151.1 (*i*-,*i*′-C), 133.7, 132.1 (*o*-,*o*′-C), 130.1, 129.7 (*m*-,*m*′-C), 126.7, 126.1 (*p*-,*p*′-C), 20.9, 20.2 (*o*,*o*′-CH_3), 76.1 (CH=CH, J_{RhC} = 12 Hz), 35.7, 33.3, 28.0 (CH_2).

$[L_{Me}RhH_2]_2$: The aforementioned solution of (mainly) $L_{Me}Rh(COE)(H_2)$ was transferred back to a Schlenk tube and then warmed (with stirring) to 0 °C under hydrogen atmosphere. After stirring at 0 °C for 10 min, the solution was cooled to –40 °C once more, whereupon NMR spectra were recorded. All the $L_{Me}Rh(COE)(H_2)$ was seen to have been consumed; the solution contained $[L_{Me}RhH_2]_2$ as the main Rh complex (ca. 50% of the total), accompanied by a large number of other compounds in low concentrations. The compound decomposed on standing and on evaporation of the solvent, and all attempts to isolate it were unsuccessful. – ^{1}H NMR ($[D_8]$THF, 243 K, 500 MHz): δ = 1.26 (1-H), 4.94 (3-H), 6.80 (d, *m*-H), 7.02 (t, *p*-H), 1.74 (superimposed by THF signal, *o*-CH_3), –24.23 (t, Rh–H_2, J_{RhHav} = 25 Hz). – $^{13}C\{^1H\}$ NMR (125.7 MHz): δ = 23.6 (C-1), 158.7 (C-2), 100.9 (C-3), 154.3 (*i*-C), 133.8 (*o*-C), 131.2 (*m*-C), 125.3 (*p*-C), 19.8 (*o*-CH_3).

$L_{Me}Ir(COE)H_2$: $L_{Me}Ir(cyclooctenyl)(H)$ (0.2 g) was dissolved in THF (4 mL) and the solution was stirred under hydrogen (1 bar) for 10 min. The volatiles were then removed in vacuo. The reaction was clean and virtually quantitative according to ^{1}H-NMR, but the product was found to be very soluble, even in pentane. X-ray quality crystals were obtained by dissolving the residue in pentane, concentrating the solution to a volume of 0.25 mL, and slowly cooling it to –20 °C. – ^{1}H NMR (C_6D_6, 293 K, 200 MHz): δ = 1.50 (1-H), 5.26 (3-H), 6.96 (d, *m*-H), 6.81 (t, *p*-H), 2.22 (*o*-CH_3), 2.62 (CH=CH), 2.04 (br., =CH–CH_2 *exo*), 0.9–1.3 (br., all other CH_2), –22.6 (IrH_2), –22.74 (IrHD, J_{HD} = 5.6 Hz). – $^{13}C\{^1H\}$ NMR (125.7 MHz): δ = 23.7 (br., C-1), 161 (br., C-2), 102.5 (C-3) (*i*-C not observed), 131.7 (*o*-C), 127.8 (*m*-C), 125.9 (*p*-C), 19.2 (*o*-CH_3), 62.2 (CH=CH), 35.3, 33.2, 26.7 (CH_2). – IR (KBr): $\tilde{\nu}_{Ir-H}$ = 2217 cm^{-1}.

Hydrogenation Experiments

Olefins (COE, 1-methylcyclohexene, 2,3-dimethyl-2-butene, 1-*tert*-butylcyclohexene) were dried over Na and then transferred to a cold trap in vacuo prior to use. The catalyst (ca. 50 mg) was dissolved in neat olefin (1 mL), and the solution was stirred under 1 bar of hydrogen for 2 h. By that time, no more hydrogen was being absorbed. The resulting solution was filtered through alumina to remove Rh and ligand residues, and subsequently analyzed by ^{1}H- and ^{13}C-NMR. Hydrogenation of the solid olefin bis(cyclohexylidene) was carried out in pentane solution [bis(cyclohexylidene) (0.3 g) and $L_{Me}Rh(COE)$ (0.095 g) in pentane (3 mL)]: 5 turnovers (50% conversion) after 2 h (by ^{13}C-NMR).

X-ray Structure Determinations

Crystals were mounted in thin-walled glass capillaries under Ar. Details of all structure determinations are collected in Table 3. Since the glass capillaries prevented an accurate description of the crystal shapes, empirical absorption corrections[41] were applied in most cases (see Table 3). Structures were solved using the PATTY option[42] of the DIRDIF program system.[43] Refinements were carried out with the SHELXL-97 package.[44] All nonhydrogen atoms were refined with anisotropic temperature factors. The hydrogen atoms were placed in calculated positions and refined isotropically in riding mode. All refinements were made by full-matrix least-squares on F^2. Unless otherwise noted, geometrical calculations[45] revealed neither unusual geometric features, nor unusually short intermolecular contacts. Moreover, the calculations revealed no higher symmetry and no solvent accessible areas.

Remarks for Specific Structures. –$L_{Me}Rh(C_2H_4)_2$: The hydrogens of the ethene moieties were freely refined. $L_{Cl}Rh(COE)$: The crystal showed considerable decay (up to 25%) during the measurements, resulting in somewhat higher *R* indices. $L_{Me}Rh(COD)$ and $L_{Me}Rh(COE)(MeCN)$: All hydrogen atoms were freely refined in the final cycles.

Table 3. Details of X-ray structure determinations

Compound	$L_{Me}Rh(COD)$	$L_{Me}Rh(C_2H_4)_2$	$L_{Cl}Rh(COE)$	$L_{Me}Rh(NBE)$	$L_{Me}Rh(COE)(MeCN)$	$L_{Me}Ir(COE)H_2$
Crystal color	transparent brownish	transparent orange-red	transparent orange-brown-red	dark brown-black	transparent yellow-brown	transparent light brown-yellow
Crystal shape	regular fragment	irregular thick platelet	irregular platelet	irregular fragment	irregular fragment	irregular fragment
Crystal size (mm)	0.33 × 0.33 × 0.31	0.51 × 0.45 × 0.16	0.50 × 0.12 × 0.04	0.40 × 0.33 × 0.30	0.50 × 0.22 × 0.22	0.33 × 0.21 × 0.13
Empirical formula	$C_{29}H_{37}N_2Rh$	$C_{25}H_{33}N_2Rh$	$C_{25}H_{27}Cl_4N_2Rh$	$C_{28}H_{35}N_2Rh$	$C_{31}H_{42}N_3Rh$	$C_{29}H_{41}IrN_2$
Formula weight	516.52	464.44	600.20	502.49	559.59	609.84
Temperature [K]	293(2)	208(2)	293(2)	293(2)	150(2)	150(2)
Radiation (graphite mon.)	Mo-K_α	Cu-K_α	Cu-K_α	Cu-K_α	Mo-K_α	Mo-K_α
Wavelength [A]	0.71073	1.54184	1.54184	1.54184	0.71073	0.71073
Crystal system, space group	monoclinic, *C*2/*c*	monoclinic, *P*21/*n*	monoclinic, *P*21/*n*	monoclinic, *P*21/*n*	monoclinic, *P*21/*c*	monoclinic, *P*21/*a*
Unit cell # reflections, θ range [°]	25, 18.506 to 20.343	25, 40.342 to 46.309	25, 12.225 to 19.413	25, 18.704 to 45.402	20212, 1.660 to 26.330	45537, 1.730 to 27.450
a [Å]	14.0042(10)	13.3932(3)	18.705(2)	14.0623(5)	12.7445(2)	17.4950(4)
b [Å]	13.4813(9)	13.4621(3)	7.4768(11)	13.0771(13)	14.6992(4)	14.0151(2)
c [Å]	13.456(4)	13.6582(4)	37.051(6)	14.4341(8)	15.7950(4)	23.0605(6)
α [°]	90	90	90	90	90	90
β [°]	97.187(12)	114.3825(19)	101.939(13)	112.441(4)	106.0702(12)	108.6013(9)
γ [°]	90	90	90	90	90	90
Volume [Å^3]	2520.4(8)	2242.94(10)	5069.7(13)	2453.4(3)	2843.31(11)	5358.9(2)
Z, calcd. density [Mgm^{-3}]	4, 1.361	4, 1.375	8, 1.573	4, 1.360	4, 1.307	8, 1.512
Abs. Coefficient μ [mm^{-1}]	0.696	6.227	9.448	5.737	0.623	5.001
Diffractometer	Enraf–Nonius CAD4	Enraf–Nonius CAD4	Enraf–Nonius CAD4	Enraf–Nonius CAD4	Nonius KappaCCD	Nonius KappaCDD
Scan	θ/2θ	θ/2θ	θ/2θ	θ/2θ	area detector φ and ω	area detector φ and ω
F(000)	1080	968	2432	1048	1176	2448
θ range for data collection[°]	2.71 to 26.31	3.89 to 69.97	2.92 to 62.21	3.73 to 69.91	1.66 to 26.33	1.73 to 27.45
Index ranges	$-12 \le h \le 17$ $-12 \le k \le 16$ $-16 \le l \le 16$	$-16 \le h \le 14$ $0 \le k \le 16$ $0 \le l \le 16$	$-21 \le h \le 0$ $0 \le k \le 8$ $-41 \le l \le 42$	$-17 \le h \le 15$ $0 \le k \le 15$ $0 \le l \le 17$	$-15 \le h \le 15$ $-9 \le k \le 18$ $-19 \le l \le 19$	$-21 \le h \le 22$ $-18 \le k \le 15$ $-29 \le l \le 25$
Refl. collected/unique [R_{int}]	5313/2565 [0.0307]	4439/4256 [0.0944]	8306/8033 [0.1566]	4833/4643 [0.0256]	20212/5776 [0.0576]	45537/12229 [0.0908]
Refl. observed ([$I_0 > 2\sigma(I_0)$])	2458	3935	3022	3905	4563	9290
Semi-emp. ψ-scan abs. corr.	Yes	Yes	Yes	Yes	No	No
Range of rel. transm. factors	1.019 and 0.982	2.390 to 0.713	1.707 to 0.791	1.264 to 0.861		
Data/restraints/parameters	2565/0/201	4256/0/292	8033/0/581	4643/0/286	5776/0/484	12229/0/589
Goodness-of-fit on F^2	1.139	1.044	1.018	1.031	1.037	1.024
SHELXL-97 wt. parameters	0.0321, 1.8277	0.096500, 2.563700	0.0647, 21.5658	0.069900, 2.340900	0.024000, 0.856200	0.080400, 0.000000
Final *R*1, *wR*2 [$I > 2\sigma(I)$]	0.0264, 0.0624	0.0476, 0.1311	0.0930, 0.1639	0.0417, 0.1108	0.0293, 0.0699	0.0460, 0.1182
*R*1, *wR*2 (all data)	0.0277, 0.0629	0.0502, 0.1340	0.2591, 0.2258	0.0506, 0.1171	0.0421, 0.0762	0.0634, 0.1292
Extinction Coefficient		0.0045(3)				
Diff. peak and hole (eÅ^{-3})	0.507 and –0.449	1.396 and –1.478	0.854 and –1.100	1.056 and –0.812	0.335 and –0.526	4.022 and –3.010

$L_{Me}Ir(COE)H_2$: The Ir-bound hydrides were not located. Crystal structure data for $L_{Me}Rh(COD)$, $L_{Me}Rh(C_2H_4)_2$, $L_{Cl}Rh(COE)$, $L_{Me}Rh(NBE)$, $L_{Me}Rh(COE)(MeCN)$, and $L_{Me}Ir(COE)H_2$; calculated total energies and atomic coordinates for the LRh and LIr complexes mentioned in the text. Crystallographic data (excluding structure factors) for the structures reported in this paper have been deposited with the Cambridge Crystallographic Data Centre as supplementary publication nos. CCDC-133849, CCDC-133850, CCDC-133851, CCDC-133852, CCDC-133853, and CCDC-133854. Copies of the data can be obtained free of charge on application to the CCDC, 12 Union Road, Cambridge CB2 1EZ, U.K. [Fax: (internat.) +44 (0)1223 336033; E-mail: deposit@ccdc.cam.ac.uk].

Acknowledgments

We are grateful to P. P. J. Schlebos (KUN) and H. Druijven (University of Groningen) for their able assistance in carrying out some of the NMR measurements. X-ray data for $L_{Me}Ir(COE)H_2$ and $L_{Me}Rh(COE)(MeCN)$ were collected on the CCD diffractometer of the national NWO-CW X-ray facility in Utrecht. Deuteration studies on 2,3-dimethyl-2-butene were carried out by H. van der Heijden and A. B. van Oort at the Shell Research and Technology Centre, Amsterdam. Bis(cyclohexylidene) was kindly provided by R. W. A. Havenith (University of Utrecht). We thank Johnson Matthey for a generous loan of rhodium and iridium chlorides.

[1] P. H. M. Budzelaar, A. B. van Oort, A. G. Orpen, *Eur. J. Inorg. Chem.* **1998**, 1485.

[2] For a preliminary account, see P. H. M. Budzelaar, R. de Gelder, A. W. Gal, *Organometallics* **1998**, *17*, 4122.

[3] Most of these complexes are chloro-bridged dimers in the solid state, but dissociate in solution. See, e.g. [3a] H. L. M. van Gaal, F. G. Moers, J. J. Steggerda, *J. Organomet. Chem.* **1974**, *65*, C43; H. L. M. van Gaal, F. L. A. van den Bekerom, J. P. J. Verlaan, *J. Organomet. Chem.* **1976**, *114*, C35; H. L. M. van Gaal, F. L. A. van den Bekerom, *J. Organomet. Chem.* **1977**, *134*, 237; C. Busetto, A. d'Alfonso, F. Maspero, G. Perego, A. Zazzetta, *J. Chem. Soc., Dalton Trans.* **1977**, 1828; P. R. Hoffman, T. Yoshida, T. Okano, S. Otsuka, J. A. Ibers, *Inorg. Chem.* **1976**, *15*, 2462; T. Yoshida, T. Okano, D. L. Thorn, T. H. Tulip, S. Otsuka, J. A. Ibers, *J. Organomet. Chem.* 1979, *181*, 183; P. Binger, J. Haas, G. Glaser, R. Goddard, C. Krüger, *Chem. Ber.* **1994**, *127*, 1927. – [3b] P. Hofmann, C. Meier, U. Englert, M. U. Schmidt, *Chem. Ber.* **1992**, *125*, 353.

[4] A. C. Cooper, W. E. Streib, O. Eisenstein, K. G. Caulton, *J. Am. Chem. Soc.* **1997**, *119*, 9069; A. C. Cooper, E. Clot, J. C. Huffman, W. E. Streib, F. Maseras, O. Eisenstein, K. G. Caulton, *J. Am. Chem. Soc.* **1999**, *121*, 97.

[5] J. M. Brown, P. J. Guiry, D. W. Price, M. B. Hursthouse, S. Karalulov, *Tetrahedron: Asymmetry* **1994**, *5*, 561.

[6] See, e.g. M. E. Howden, R. D. W. Kemmitt, M. D. Schilling, *J. Chem. Soc., Dalton Trans.* **1980**, 1716.

[7] A distorted T-shape and easy movement of the chlorine atom in three-coordinate bis(phosphane)RhCl complexes has been predicted on the basis of extended-Hückel calculations; see ref. [3b].

[8] The best data were obtained in [D_8]THF. Spectra in [D_8]THF, [D_{12}]cyclohexane (down to 6 °C), and [D_8]toluene (down to

–40 °C) were virtually identical, indicating the absence of significant THF coordination. However, the presence of some arene complexes (to be described in a future paper) in the toluene spectra made interpretation more difficult in these cases.

[9] The allyl hydride mechanism is one of the accepted mechanisms for olefin isomerization. However, only a few examples of rapid equilibration between the two structures have been reported: J. W. Byrne, H. U. Blaser, J. A. Osborn, *J. Am. Chem. Soc.* **1975**, *97*, 3871; H. Bönneman, *Angew. Chem.* **1970**, *82*, 699 (*Int. Ed. Engl.* **1970**, *9*, 736). Decomposition of rhodium(III) allyl hydride complexes to give free olefin has also been demonstrated: J. F. Nixon, B. Wilkins, *J. Organomet. Chem.* **1972**, *44*, C25; **1974**, *80*, 129. For an example of rapid allylic C–H activation at Ir, see R. Dorta, A. Togni, *Organometallics* **1998**, *17*, 5441.

[10] Reductive elimination from palladium(II) and platinum(II) allyl hydrides has been studied computationally: S. Sakaki, H. Satoh, H. Shono, Y. Ujino, *Organometallics* **1996**, *15*, 1713.

[11] The calculated energy difference between the olefin and allyl hydride is very sensitive to the method used. Hartree–Fock gives an even stronger preference for the olefin complex, while pure DFT[2] gives a smaller energy difference and a lower barrier. Apart from correlation treatment, sources of errors could be the basis set (not very large) and the lack of an explicit treatment of direct relativistic effects on the valence electrons.

[12] Steric effects are expected to favor the allyl hydride structure over the olefin complex because of the more "central" position of the allyl group relative to the diiminate aryl groups.

[13] Formation of iridium allyl hydrides from olefin precursors has been reported previously. See, e.g. R. S. Tanke, R. H. Crabtree, *Inorg. Chem.* **1989**, *28*, 3444; Y. Alvarado, O. Boutry, E. Gutiérrez, A. Monge, M. C. Nicasio, M. L. Poveda, P. J. Pérez, C. Ruiz, C. Bianchini, E. Carmona, *Chem. Eur. J.* **1997**, *3*, 860.

[14] The calculated energy difference between the Ir allyl hydride and olefin complexes is rather modest (6 kcal/mol; barrier 11 kcal/mol). If we assume that the 12 kcal/mol error in the case of Rh also applies to Ir, we would expect a preference in the "real" system of 18 kcal/mol and a barrier of 23 kcal/mol, which is compatible with the observed static room temperature spectrum. Unfortunately, L_{Me}Ir(H)(cyclooctenyl) decomposes rapidly on heating in solution, hence we could not verify the onset of dynamic behavior expected at higher temperatures.

[15] In addition to the signals of the dimethylbutene complex, some weak but sharp signals were observed, which could be attributed to the oxidation product L_{Me}Rh(OH)[η^3-$CH_2C(Me)CMe_2$] described in the section on hydrogenation.

[16] The Rh–H distance is calculated as 1.92 Å for a hydrogen placed at a calculated position with a standard C–H bond length of 0.97 Å. The actual C–H distance must be longer, as indicated by the low $^1J_{CH}$. However, the hydrogen atom position could not be refined satisfactorily.

[17] M. Pasquali, C. Floriani, A. Gaetani-Manfredotti, A. Chiesi-Villa, *J. Am. Chem. Soc.* **1978**, *100*, 4918.

[18] N. Carr, B. J. Dunne, L. Mole, A. G. Orpen, J. L. Spencer, *J. Chem. Soc., Dalton Trans.* **1991**, 863.

[19] M. Green, J. A. K. Howard, J. L. Spencer, F. G. A. Stone, *J. Chem. Soc., Dalton Trans.* **1977**, 171.

[20] D. D. LeCloux, S. J. Lippard, *Inorg. Chem.* **1997**, *36*, 4035.

[21] To assess the importance of the pre-organization of NBE, we also optimized the structures of two conformations of LRh(CPE) (CPE = cyclopentene). The CPE complex would be expected to have a weaker agostic interaction since it is less favorably pre-organized. On the other hand, if the interactions were strong, one would certainly expect to see a distortion here, whereas in the NBE complex the pre-organization might be so favorable that the agostic interaction would already be optimal in the undistorted structure. In fact, the energies of the "CH_2 in" and "CH_2 out" conformations of LRh(CPE) differ by less than 3 kcal/mol, and the RhH distance is long even in the "CH_2 in" conformation (2.58 Å; RhC = 2.98 Å; C–H = 1.104 and 1.093 Å). The angle between the $CH_2CH{=}CHCH_2$ plane and the Rh–olefin bond is nearly identical in the two conformations (97° for "CH_2 in", 98° for "CH_2 out"). These observations support our hypothesis that the agostic "bond" is not strong even in the NBE complex. The attractive force is rather weak, but since there is no *repulsive* force and the olefin is pre-organized, a close Rh–H contact still results.

[22] Because of the limited temperature region in which L_{Me}Rh(COE)(H_2) can be observed, T_1(min) studies were not carried out.

[23] See, e.g. R. H. Crabtree, *Acc. Chem. Res.* **1979**, *12*, 331.

[24] For a recent example of H/D exchange catalyzed by an Ir hydride, see E. Gutiérrez-Puebla, A. Monge, M. Paneque, M. L. Poveda, S. Taboada, M. Trujillo, E. Carmona, *J. Am. Chem. Soc.* **1999**, *121*, 346.

[25] See, e.g. B. Moreno, S. Sabo-Etienne, B. Chaudret, A. Rodriguez, F. Jalon, S. Trofimenko, *J. Am. Chem. Soc.* 1995, *117*, 7441; M. T. Bautista, E. P. Cappellani, S. D. Drouin, R. H. Morris, C. T. Schweitzer, A. Sella, J. Zubkowski, *J. Am. Chem. Soc.* **1991**, *113*, 4876 and references cited therein.

[26] The presence of small amounts of a COD isomer (GC/MS) in the COE could be detected by GC. It differed from authentic samples of 1,3-COD and 1,5-COD and so was most likely 1,4-COD. Identification of the deactivation product as a 1,4-COD complex was achieved by comparison with pure L_xRh(1,4-COD) prepared from L_xRh(COE) and 1,3-COD; see details in Experimental Section.

[27] Oxidative addition of aromatic C–halogen bonds will be reported separately.

[28] B. James, *Addition of Hydrogen and Hydrogen Cyanide to Carbon–Carbon Double and Triple Bonds*, in *Comprehensive Organometallic Chemistry* (Ed.: G. Wilkinson), Pergamon, Oxford, **1982**, vol. 8, p 285–369. See also P. A. Chaloner, M. A. Esteruelas, F. Joó, L. A. Oro, *Homogeneous Hydrogenation*, Kluwer, Dordrecht, **1994**.

[29] See, e.g. J. Halpern, D. P. Riley, A. S. C. Chan, J. J. Pluth, *J. Am. Chem. Soc.* **1977**, *99*, 8055; A. S. C. Chan, J. J. Pluth, J. Halpern, *J. Am. Chem. Soc.* **1980**, *102*, 5952; C. R. Landis, J. Halpern, *J. Organomet. Chem.* 1983, *250*, 485; C. R. Landis, J. Halpern, *J. Am. Chem. Soc.* **1987**, *109*, 1746.

[30] In the Wilkinson system, phosphane recoordination is believed to precede alkane elimination (ref.[31]).

[31] See, e.g. J. Halpern, C. S. Wong, *J. Chem. Soc., Chem. Commun.* **1973**, 629; J. Halpern, in *Organotransition Metal Chemistry* (Eds.: Y. Ishii, M. Tsutsui), Plenum, New York, **1975**, p. 109; J. Halpern, T. Okamoto, A. Zakhariev, *J. Mol. Catal.* **1976**, *2*, 65. For theoretical studies, see e.g. A. Dedieu, *Inorg. Chem.* **1980**, *19*, 375; C. Daniel, N. Koga, J. Han, X. Y. Fu, K. Morokuma, *J. Am. Chem. Soc.* **1988**, *110*, 3773.

[32] We have also briefly investigated complexes of related ligands bearing 2,4,6-$Me_3C_6H_2$ and 2,6-(iPr)$_2C_6H_3$ groups at N. The chemistry appears to be similar, but many complexes were obtained as oils and could not be purified.

[33] See, e.g. C. P. Casey, E. L. Paulsen, E. W. Beuttenmueller, B. R. Proft, B. A. Matter, D. R. Powell, *J. Am. Chem. Soc.* **1999**, *121*, 63.

[34] All calculations were carried out with the Gaussian program (*Gaussian 94*, *Revision E.1*, M. J. Frisch, G. W. Trucks, H. B. Schlegel, P. M. W. Gill, B. G. Johnson, M. A. Robb, J. R. Cheeseman, T. Keith, G. A. Petersson, J. A. Montgomery, K. Raghavachari, M. A. Al-Laham, V. G. Zakrzewski, J. V. Ortiz, J. B. Foresman, J. Cioslowski, B. B. Stefanov, A. Nanayakkara, M. Challacombe, C. Y. Peng, P. Y. Ayala, W. Chen, M. W. Wong, J. L. Andres, E. S. Replogle, R. Gomperts, R. L. Martin, D. J. Fox, J. S. Binkley, D. J. Defrees, J. Baker, J. P. Stewart, M. Head-Gordon, C. Gonzalez, J. A. Pople, Gaussian, Inc., Pittsburgh PA, **1995**.

[35] S. Binkley, J. A. Pople, W. J. Hehre, *J. Am. Chem. Soc.* **1980**, *102*, 939.

[36] P. J. Hay, W. R. Wadt, *J. Chem. Phys.* **1985**, *82*, 299.

[37] A. D. Becke, *J. Chem. Phys.* **1993**, *98*, 5648.

[38] G. Giordano, R. H. Crabtree, *Inorg. Synth.* **1990**, *28*, 88.

[39] R. Cramer, *Inorg. Synth.* **1990**, *28*, 86.

[40] A. van der Ent, A. L. Onderdelinden, *Inorg. Synth.* **1990**, *28*, 90.

[41] A. C. T. North, D. C. Philips, F. S. Mathews, *Acta Crystallogr.* **1968**, *A24*, 351.

[42] P. T. Beurskens, G. Beurskens, M. Strumpel, C. E. Nordman, in "Patterson and Pattersons" (Eds.: J. P. Glusker, B. K. Patterson, M. Rossi), Clarendon Press, Oxford, **1987**, p. 356.

[43] P. T. Beurskens, G. Beurskens, W. P. Bosman, R. de Gelder, S. Garcia-Granda, R. O. Gould, R. Israel, J. M. M. Smits, *DIRDIF-96*: A computer program system for crystal structure determination by Patterson methods and direct methods ap-

plied to difference structure factors, Crystallography Laboratory, University of Nijmegen, The Netherlands, **1996**.
[44] G. M. Sheldrick, *SHELXL-97: Program for the refinement of crystal structures*, University of Göttingen, Germany, **1997.**
[45] A. L. Spek, *Acta Crystallogr.* **1990**, *A46*, C34; A. L. Spek, *PLATON-93*: *Program for display and analysis of crystal and molecular structures*, University of Utrecht, The Netherlands, **1995**.

Received September 16, 1999
[I99328]

Cooperative Binding of Nitrile Moieties Within a Bimetallic Pocket: Enforcing Side-On π-Interaction With a High-Spin Nickel(II) Site

Franc Meyer,*[a] Isabella Hyla-Kryspin,[b] Elisabeth Kaifer,[a] and Peter Kircher[a]

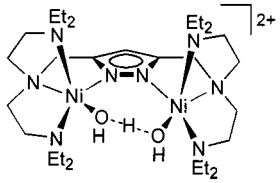
Dedicated to Prof. Dr. Peter Paetzold on the occasion of his 65th birthday

Keywords: Cooperative effects / Coordination modes / Nickel / Bimetallic complexes / π interactions

Different cooperative binding modes of nitriles within the bimetallic pocket of a pyrazolate-based compartmental dinickel(II) site have been studied. The H_3O_2-bridged dinuclear complex **1** reacts with cyanamide to yield **4**, in which a secondary hydrogencyanamido(1–) bridge spans the two metal centers at an unusually short metal–metal distance imposed by the primary ligand matrix. In **5**, a single 2-cyanoguanidine (cnge) molecule is *N*-bound to one nickel(II) ion through its nitrile part and is coordinated to the adjacent metal site through an amido nitrogen. The characteristics of the coordination spheres of the metal centers suggest an additional side-on π-bonding interaction of the nitrile moiety with the second high-spin nickel(II) ion. This unusual interaction is corroborated by comparing the IR bands for the ν(C≡N) stretching vibration of **5** with those of complex **6**, which has two end-on bound cnge molecules, and those of the related mononuclear complex **7**, which lacks a second nickel(II) ion. The nature of the π-bonding interaction in **5** is further analyzed by DFT calculations on relevant model systems. Even though the π-bonding is found to be very weak, it does include some backbonding from occupied 3d MOs at the second high-spin nickel(II) ion to the π* MOs of the nitrile. Such an unconventional π-interaction is suggested to be enforced by the constrained fixation of the nitrile unit within the highly organized coordination pocket of the bimetallic framework. In contrast, the bifunctional 2-hydroxybenzonitrile is accommodated by the distinct binding of the nitrile and phenolate functions to the different metal centers in **8**, which confirms that the simultaneous binding of both an OR-function and an end-on bound nitrile is indeed feasible within the active site pocket. Such a situation is reminiscent of the bimetallic effect that has been assumed to enable the cooperative hydration of nitriles at the dinickel(II) site of **1**. Complexes **4**·$(ClO_4)_2$, **5**·$(ClO_4)_2$, **6**·$(ClO_4)_3$, **7**·$(ClO_4)(BPh_4)$, and **8**·$(ClO_4)_2$ have been characterized structurally by X-ray crystallography.

Introduction

The current interest in multinuclear transition metal complexes is often inspired by the occurrence of multimetallic sites within the active centers of various natural metalloenzymes.[1] The importance of such sites stems not only from their fascinating structural diversity but predominantly from their potential to enable synergetic reactivity of the adjacent metal centers.[2,3] This facilitates the generation of unusual coordination modes of small substrate molecules as well as unique organic transformations at the multimetallic framework which are often otherwise not accessible at monometallic centers. Consequently much effort has been devoted to the search for dinucleating ligand matrices that provide two (or more) coordination compartments in close proximity, in order to favor such sought-after cooperativity within the resulting bimetallic complexes.[4] With this intention in mind we recently investigated a class of pyrazolate-based dinuclear systems whose reactivity patterns can be selectively altered by appropriate changes of the chelating donor side-arms attached to the bridging heterocycle,[5] and which proved to allow novel binding modes and transformations of small molecules within the bimetallic pocket.[6,7] Among these, the dinickel(II) complex **1** (Scheme 1) has turned out to be a valuable system for the modeling of hydrolytic reactions at cooperative dinuclear sites, and, in particular, for investigating functional aspects of the metalloenzyme urease.[7]



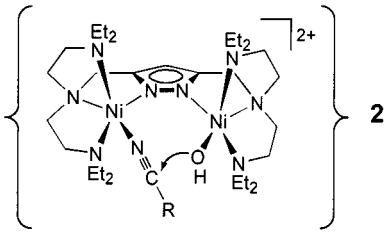
1

Scheme 1. Active dinickel(II) complex **1** (see ref.[7])

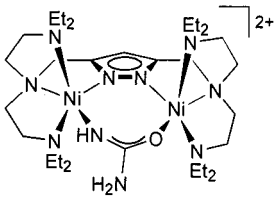
The hydration of nitriles by **1** was assumed to proceed via intermediates such as **2** (Scheme 2), in which the *N*-bound substrate has replaced a water molecule of the former intramolecular H_3O_2 bridge and undergoes subsequent nucleophilic attack by the adjacent hydroxide function to finally form a secondary *N*,*O*-amidato bridge. Alternatively, **1** may exhibit basic rather than nucleophilic behavior, as exemplified by its reaction with urea, which yields an *N*,*O*-bridging

[a] Anorganisch-Chemisches Institut der Universität Heidelberg, Im Neuenheimer Feld 270, 69120 Heidelberg, Germany
Fax: (internat.) + 49-6221/54-5707
E-mail: Franc@sun0.urz.uni-heidelberg.de
[b] Organisch-Chemisches Institut der Universität Heidelberg, Im Neuenheimer Feld 270, D-69120 Heidelberg, Germany

 © WILEY-VCH Verlag GmbH, D-69451 Weinheim, 2000 1434–1948/00/0404–0771 $ 17.50+.50/0

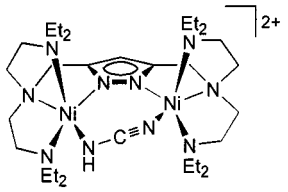


2



3

Scheme 2. Proposed intermediate **2** for reaction of **1** with nitriles (see ref.[7]) and urea-bridged dinickel(II) complex **3** (see ref.[6])



4

Scheme 3. Schematic drawing of **4**

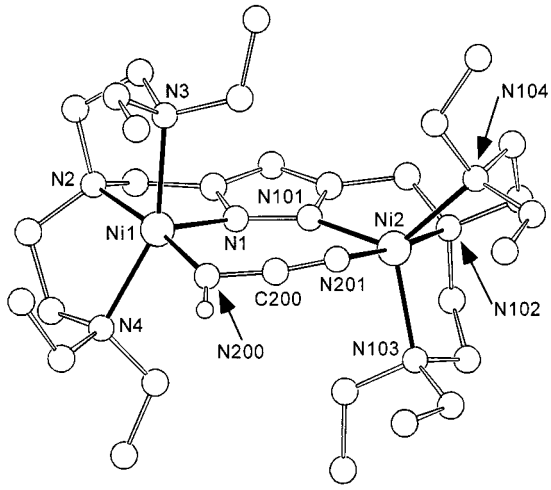


Figure 1. Molecular structure of **4**; in the interests of clarity all hydrogen atoms except H200 have been omitted; selected interatomic distances (Å) and bond angles (°): Ni1–N1 2.012(5), Ni1–N2 2.084(5), Ni1–N3 2.204(5), Ni1–N4 2.163(6), Ni1–N200 1.996(6), Ni2–N101 2.041(5), Ni2–N102 2.091(5), Ni2–N103 2.128(5), Ni2–N104 2.162(5), Ni2–N201 2.016(5), N1–N101 1.386(8), N200–C200 1.286(9), N201–C200 1.176(9), Ni1···Ni2 4.458; N200–C200–N201 172.2(7), Ni1–N200–C200 115.3(5), Ni2–N201–C200 125.9(5)

coordination mode of the deprotonated substrate within the bimetallic pocket (**3**).

In pursuit of studying such transformations mediated by **1**, we now set out to examine whether **3** would also be accessible by hydration of the appropriate nitrile, i.e. cyanamide, according to the situation depicted in **2**. Interest in this study also arose from the fact that cyanamide itself has been recognized as a substrate for both urease (yielding carbon dioxide and ammonia)[8] and Mo-nitrogenase,[9] implying its as-yet-unresolved binding to these multimetallic enzyme active sites. Unexpectedly however, several different binding modes of nitrile moieties at the bimetallic core were found in the course of these investigations, among them an intriguing coordination of cyanoguanidine (the dimeric form of cyanamide) within the clamp of the two metal ions. The present contribution describes the structural and spectroscopic characterization as well as a theoretical study of this novel system. In addition, further structural support for the postulated nitrile hydration intermediate **2** could be obtained.

Results and Discussion

When a solution of **1**·$(ClO_4)_2$ in acetone was treated with cyanamide, a crystalline green product **4**·$(ClO_4)_2$ (Scheme 3) was isolated. This compound has a strong IR absorption of the $\tilde{\nu}$(C≡N) stretch at 2149 cm^{-1} and a single ν(N–H) band at 3282 cm^{-1}. An X-ray diffraction study showed that a hydrogencyanamido(1–) bridging ligand spans the two metal centers and occupies the accessible coordination sites within the pocket of the bimetallic framework (Scheme 3, Figure 1).

The hydrogen atom of this secondary bridge could be located close to N200, which is consistent with the pronounced difference in bond lengths [*d*(C200–N200) = 1.286(9) Å; *d*(C200–N201) = 1.176(9) Å] and confirms N200 as the amido-nitrogen. Furthermore, the μ-NCN(H) proton seems to form a weak hydrogen bond with one of the oxygen atoms of a perchlorate counteranion [*d*(N200···O6) = 3.035 Å].

Obviously the characteristic property of the Ni-bound H_3O_2 unit in **1** to act as a base, which also became apparent in the deprotonation of urea to yield **3**,[6] has caused deprotonation of the cyanamide, with concomitant incorporation of the resulting $HNCN^-$ in a bridging position. The coordination chemistry of the monoanionic cyanamido(1–) ligand has attracted some attention,[10] but only one structurally characterized example of bridging parent $HNCN^-$ has hitherto been reported.[11] In that particular case, a bis(μ-hydrogencyanamido)dicopper(II) core was shown to exhibit a large metal–metal separation of 5.16 Å in conjunction with a slightly shorter C≡N bond length of 1.15(1) Å and larger angles Cu–N≡C of 146.6(8)/144.6(8)°,[11] as compared to *d*(C200–N201) = 1.176(9) Å and Ni2–N201–C200 = 125.9(5)° for **4**. This lends support for the description of the hydrogencyanamido bridge by a significant contribution of limiting form **B** (Scheme 4) at the expense of



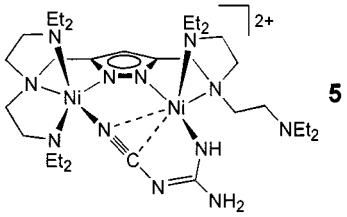
A **B**

Scheme 4. Limiting forms of the hydrogencyanamido(1–) bridge

form **A** in the present case **4**, this apparently being imposed by the rigid pyrazolate-based ligand matrix constraining a relatively short Ni···Ni distance of 4.458 Å. The drastic decrease of $\tilde{\nu}$(C≡N) (2149 cm^{-1} versus 2256 cm^{-1} for free cyanamide) is in accord with this view.

2-Cyanoguanidine within the Bimetallic Pocket

Besides the main product **4**·$(ClO_4)_2$, a few crystals of a different product **5**·$(ClO_4)_2$ were collected from the reaction of **1**·$(ClO_4)_2$ with cyanamide. An IR spectrum indicated the presence of a nitrile unit [major absorption for $\tilde{\nu}$(C≡N) at 2154(s) cm^{-1}] as well as a series of N–H groups (several bands in the range 3200–3450 cm^{-1}) for **5**, and the elemental analysis suggested that two equivalents of the substrate were incorporated in this compound. It thus appeared that the property of the Ni-bound H_3O_2 unit in **1** to act as a base had also induced some dimerization of excess cyanamide to form dicyandiamide (2-cyanoguanidine, cnge), a process that is known to occur readily with cyanamide at pH 8–9.5 in aqueous solution.[12] Accordingly, complex **5**·$(ClO_4)_2$ can be obtained in somewhat better yields by directly treating **1**·$(ClO_4)_2$ with cnge. The overall molecular structure of **5** (Scheme 5) was resolved by X-ray crystallography, the result of which is depicted in Figure 2 and Figure 3.



5

Scheme 5. Schematic drawing of **5**

The 2-cyanoguanidine in its deprotonated form, which is planar within 0.023 Å, is found to be coordinated to the bimetallic site in an unprecedented fashion. Its nitrile function is bound end-on to Ni2 and completes the five-coordination of the latter, which thus displays a ligation sphere intermediate between TB-5 and SPY-5, similar to the metal centers of a variety of previously characterized dinickel(II) complexes with this particular pyrazolate-based ligand framework.[5–7] On the other side the amido nitrogen atom N11 of the deprotonated cnge is coordinated to Ni1. The remaining three *N*-bound hydrogen atoms of the cnge moiety have been located as weak hydrogen bonds to oxygen atoms of the perchlorate counteranions [*d*(N11···O2) = 3.098 Å; *d*(N12···O3) = 2.973 Å; *d*(N12···O8) = 3.030 Å] with one of the latter acting as a twofold hydrogen-bond acceptor towards both N11 and N12. The equivalence of

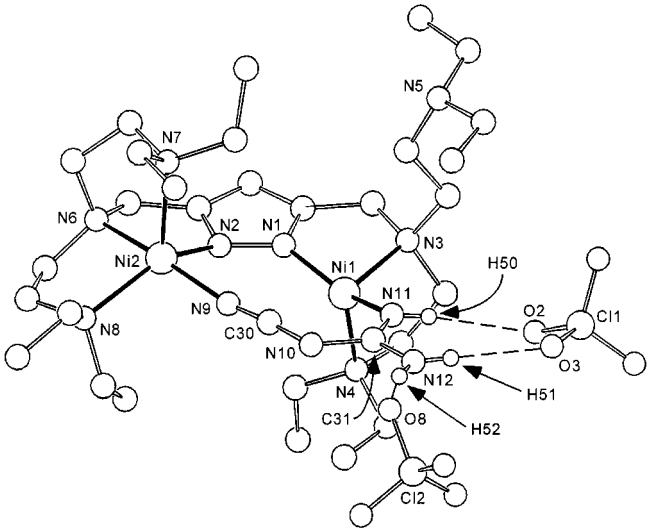


Figure 2. Molecular structure of **5**; in the interests of clarity all hydrogen atoms except those of the cnge moiety have been omitted; selected interatomic distances (Å) and bond angles (°): Ni1–N1 1.918(2), Ni1–N3 2.089(2), Ni1–N4 2.089(2), Ni1–N11 1.952(2), Ni2–N2 1.971(2), Ni2–N6 2.092(2), Ni2–N7 2.154(2), Ni2–N8 2.134(2), N2–N9 2.016(2), N1–N2 1.362(3), N9–C30 1.166(3), C30–N10 1.294(3), N10–C31 1.368(3), C31–N11 1.320(3), C31–N12 1.333(3), Ni1···Ni2 3.985; Ni2–N9–C30 171.2(2), N9–C30–N10 175.1(3), C30–N10–C31 117.8(2)

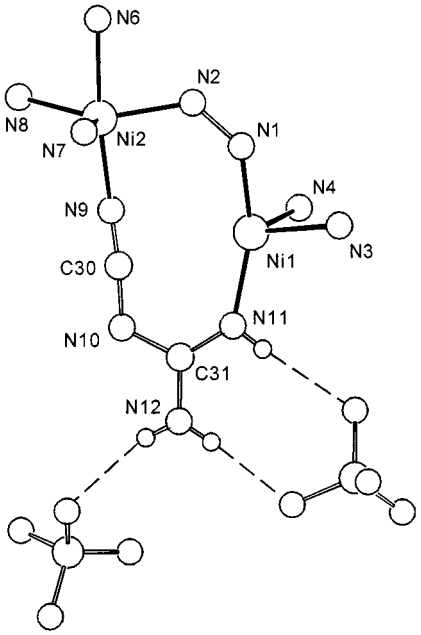
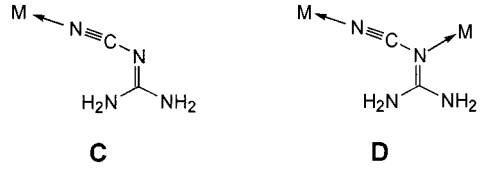


Figure 3. Representation of the central bimetallic core of **5**

the three CN bond lengths of the guanidine moiety (C31–N10/N11/N12), however, suggests the likely presence of other tautomers carrying one of the hydrogen atoms at the central N10 atom.

Unexpectedly the nitrogen donor N5 of one ligand side arm – formerly bound to Ni1 – is now found uncoordinated and dangling in **5**, which leaves the respective nickel(II) ion in a peculiar fourfold coordination environment of *N*-donors [angle N1–Ni1–N11 = 154.19(9)°] with a remaining open coordination space directed towards the inside of the

bimetallic pocket. Closer inspection of the central core of **5** (Figure 3) reveals that the nitrile moiety of the cnge – already bound end-on to Ni(2) – appears to be suitably located within the bimetallic pocket between the two nickel(II) ions to additionally interact with the low-coordinate Ni1 in a side-on fashion, even though the distances *d*(Ni1–N9) = 2.963 Å and *d*(Ni1–C30) = 2.864 Å are rather long. Some nickel complexes featuring side-on coordination of a nitrile unit have previously been structurally characterized, but these generally involve low-valent nickel(0).[13,14] Consistent with the π-backbonding ability of such low-valent nickel(0) species, the CN bonds of the η^2-bound nitriles are significantly lengthened in most of these cases, and their ν(C≡N) stretching frequencies are drastically lowered (to about 1750 cm^{-1}) relative to the free nitriles.[13] The same is also valid for nitriles bound in an η^2- or a μ-η^1,η^2(σ,π)-mode to other transition metals.[15] Cnge itself has repeatedly been used as a ligand towards transition metal ions,[16–20] in particular in copper chemistry,[18–20] and has hitherto been shown to coordinate either in a monodentate form (nitrile *N*-donor, **C**, Scheme 6) or as a bidentate bridging ligand through



Scheme 6. Common binding modes of cnge

both the nitrile and imino-*N* atoms (**D,** Scheme 6), but not through the nitrile-*N* and a terminal amido-*N* as is observed in **5** for the first time.

The IR spectrum of cnge (both free and in coordination compounds) exhibits a characteristic doublet for the ν(C≡N) stretching vibration which has been attributed to the co-existence of different tautomeric forms of the guanidine moiety; the low-frequency component corresponds to the tautomer with conjugated C≡N and C=N bonds[21] (this single tautomer is depicted in all schemes of the present work and is used for the DFT calculations, see below). IR spectroscopic investigations of those cnge complexes of type **C** and **D** studied previously indicated that the ν(C≡N) doublet is generally shifted to slightly higher wavenumbers than free cnge ($\tilde{\nu}$ = 2205 and 2160 cm^{-1}), but that these features can hardly be used to differentiate between different binding modes of cnge.[19] It was furthermore noted that the perturbation of the IR spectra of cnge upon coordination depends more on the strength of its coordination to the metal than on the coordination type, i.e. a strongly bonded cnge showing a M–N–C angle close to 180° is expected to exhibit the most pronounced shift of the ν(C≡N) doublet to higher energy.[19] In the present compound **5** the angle Ni2–N9–C30 amounts to 171.2(2)°, but the main absorption for the ν(C≡N) stretch is found at 2154 cm^{-1} (Table 1). (Two further weak bands occur at somewhat higher energy, i.e. 2180 and 2229 cm^{-1}; it remains speculative whether these bands originate from different tautomers of the cnge fragment.) We tentatively assign the most intense band at lowest energy (2154 cm^{-1}) to the tautomer with conjugated C≡N and C=N bonds. This band exhibits a slight low-frequency shift with respect to free cnge (2160 cm^{-1}), but it is uncertain at this stage whether such a shift is to be attributed to a weak additional side-on interaction of the nitrile moiety with the second Ni1 ion. However, the observed bond length *d*(N9–C30) = 1.166(3) Å in **5** is typical for a CN triple bond and is virtually identical to the value of free cnge [1.1694(3) Å],[22] as is the angle N9–C30–N10 = 175.1(3)° in **5** [vs. 175.1(2)° in free cnge],[22] and hence there is no geometric indication of such an interaction. It should be noted, however, that geometrical changes of the N–C≡N unit upon weak side-on interaction with a high-spin nickel(II) ion should be much less distinct than in the case of a nickel(0) center due to the lower π-backbonding ability of the nickel(II) ion. Furthermore, a short atom distance for the CN triple bond (1.13 Å) has also been observed in the early crystallographic study of a substituted cyanamide π-bonded to a (carbonyl)nickel(0) fragment.[14]

In the case of two copper(I) complexes containing the cation $[Cu_2(cnge)_4]^{2+}$ with three-coordinate metal ions, the dimeric cations were found to stack in the crystal lattice in such a way that the nitrile function of a unidentate cnge molecule is located close to the axial position of a symmetry-related copper atom of a neighboring molecule.[18,19] However, the observed Cu^{I}···nitrile contacts [*d*(Cu···N) = 3.27–3.58 Å and *d*(Cu···C) = 3.50–3.65 Å][19] are much longer than those found for the present complex **5** and, consequently, any side-on binding has been judged unlikely for this copper system.[17]

Magnetic measurements performed on a powdered sample of **5**·$(ClO_4)_2$ confirm the presence of two high-spin nickel(II) ions with μ_{eff} = 3.25 μ_B per nickel ion at 297 K. The temperature dependence of the molar magnetic susceptibility χ and of its inverse 1/χ, as well as of the effective magnetic moment, over the range 297–5.3 K is shown in Figure 4. It reveals the absence of any significant coupling between the two metal ions (the values $|J| < 1$ cm^{-1} and g = 2.27 result from a fit of the experimental data to the

Table 1. IR spectroscopic bands for the ν(C≡N) stretch [cm^{-1}]

	KBr pellet	Acetone
4·$(ClO_4)_2$	2149(vs)	2146
5·$(ClO_4)_2$	2229(w), 2180(w), 2154(s)	2225(m), 2184(s), 2140(sh)
cnge	2205(s), 2160(s)	2184(s), 2144(w)
6·$(ClO_4)_3$	2233(s), 2186(s)	2231(m), 2184(s), 2150(sh)
7·(ClO_4)·(BPh_4)	2227(s), 2183(s)	2228(s), 2184(m)
8·$(ClO_4)_2$	2237(s)	2241

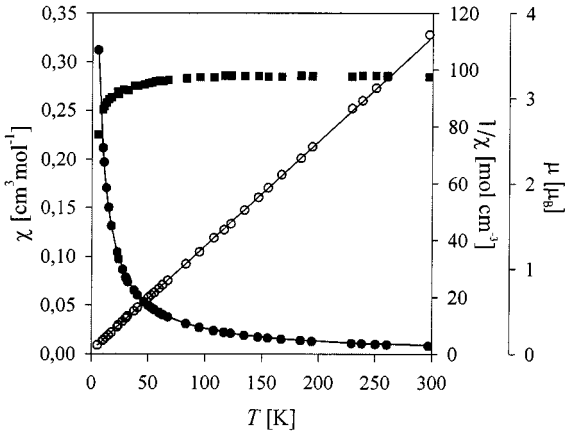
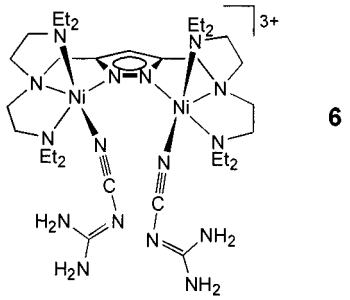


Figure 4. Temperature dependence of the molar magnetic susceptibility χ (filled circles), its inverse 1/χ (open circles), and the magnetic moment per nickel ion (filled squares) for **5**·$(ClO_4)_2$; the solid lines represent the calculated curve fits (Curie-Weiss)

standard expression for the isotropic spin-Hamiltonian $\hat{H} = -2J\hat{S}_1,\hat{S}_2$ with $S_1 = S_2 = 1$;[23] a Curie-Weiss analysis gives $C = 2.71$ and $\varphi = -3.30$).

Analogous Complexes with cnge Purely End-On Bound

In order to shed some more light on a possible contribution of the Ni1 ion to the binding of the C≡N moiety in **5**, two further complexes were investigated for comparison. The first, **6**·$(ClO_4)_3$, was obtained by treating **1**·$(ClO_4)_2$ with a large excess of cnge (Scheme 7). The molecular structure of the cation **6** as elucidated by X-ray crystallography is depicted in Figure 5.



6

Scheme 7. Schematic drawing of **6**

Compound **6** features two neutral cnge ligands within the coordination pocket of the bimetallic framework, each cnge being coordinated to one of the nickel ions in a purely *end-on* fashion (type **C**, Scheme 6). The angles Ni–N–C [171.3(2) and 172.2(2)°] are basically identical to that in **5** [171.2(2)°], and, likewise, all geometric parameters of the cnge ligands in **6** are very similar to those of the cnge fragment in **5**. The cnge-bound hydrogen atoms form several weak hydrogen bonds to perchlorate counteranions or to an acetone solvent molecule included in the crystal lattice (distances N···O in the range 2.9–3.1 Å). Due to the obvious congestion caused by the binding of the two cnge molecules within the bimetallic pocket, the Ni···Ni separation is quite large (4.586 Å) and the metal ions are forced to displace rather drastically out of the plane defined by the pyrazolate heterocycle [+0.784 Å (Ni1) and –0.647 Å (Ni2)]. The exact

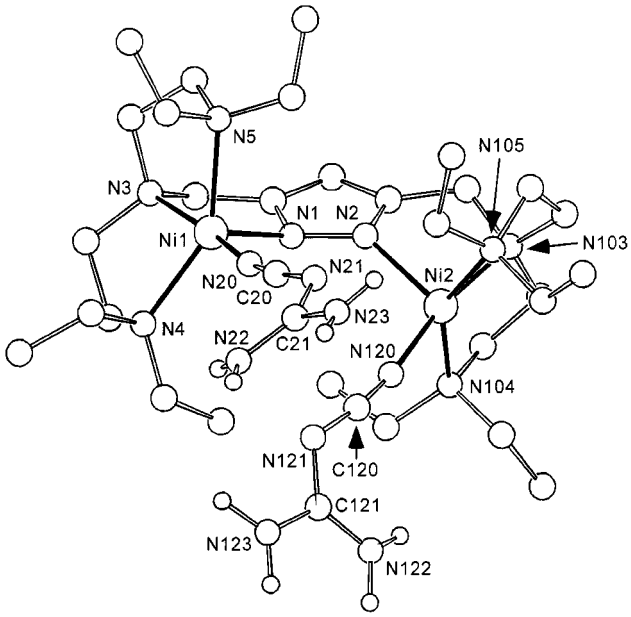
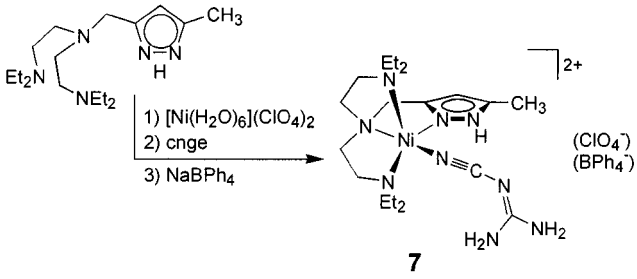


Figure 5. Molecular structure of **6**; selected interatomic distances (Å) and bond angles (°): Ni1–N1 2.035(2), Ni1–N3 2.097(2), Ni1–N4 2.125(2), Ni1–N5 2.158(2), Ni1–N20 1.983(2), Ni2–N2 2.030(2), Ni2–N103 2.097(2), Ni2–N104 2.154(2), Ni2–N105 2.137(2), N2–N120 2.000(2), N1–N2 1.389(3), N20–C20 1.162(3), C20–N21 1.295(3), N21–C21 1.334(3), C21–N22 1.325(3), C21–N23 1.329(3), N120–C120 1.152(3), C120–N121 1.304(3), N121–C121 1.338(3), C121–N122 1.331(3), C121–N123 1.331(3), Ni1···Ni2 4.586; Ni1–N20–C20 171.3(2), N20–C20–N21 170.8(3), Ni2–N120–C120 172.2(2), N120–C120–N121 172.3(3)

process leading to the formation of the tricationic complex **6** from the dicationic precursor **1** remains speculative, as no other products of the reaction could be unambiguously identified.

In order to definitely exclude any effects on the crucial ν(C≡N) vibrational frequencies caused by the distortion of the crowded bimetallic core in **6**, we prepared the corresponding mononuclear complex **7** for comparison



7

Scheme 8. Synthesis of the mononuclear complex **7**·$(ClO_4)(BPh_4)$

(Scheme 8). The compound **7**·$(ClO_4)(BPh_4)$ was obtained in crystalline form by treating the respective mononucleating ligand HL (that provides a single coordination compartment only)[7] with one equivalent each of $[Ni(H_2O)_6](ClO_4)_2$, cnge and $NaBPh_4$. An X-ray crystallographic analysis unequivocally confirmed the constitution of **7** as depicted in Figure 6.

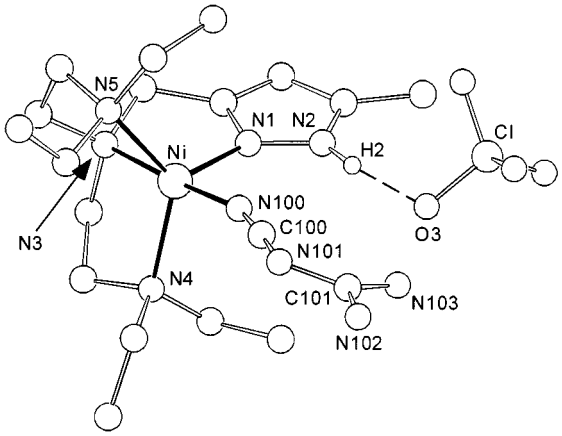


Figure 6. Molecular structure of **7** (only the major position of the disordered cnge moiety is shown); in the interests of clarity all hydrogen atoms except the pyrazole-bound H2 have been omitted; selected interatomic distances (Å) and bond angles (°): Ni–N1 1.991(3), Ni–N3 2.100(3), Ni–N4 2.105(3), Ni–N5 2.153(3), Ni–N100 1.988(4), N100–C100 1.157(7), C100–N101 1.305(7), N101–C101 1.353(7), C101–N102 1.332(7), C101–N103(7), N1–N2 1.362(4); Ni–N100–C100 163.3(4), N100–C100–N101 173.0(6), C100–N101–C101 120.8(5).

The nickel atom is nested in the tran-type coordination compartment [tran = tris(aminoalkyl)amine] and accommodates the end-on bonded cnge ligand in the remaining axial site (type **C**, Scheme 6). As anticipated, the intimate structural details of this situation closely resemble the ones observed for the nickel ions in **6** and for the Ni2 ion in **5**. The pyrazole-bound proton H2 could be located as a hydrogen bond to one of the *O*-atoms of the perchlorate counteranion [*d*(N2···O3) = 2.880 Å], where the perchlorate also forms hydrogen bonds to the terminal amino groups of the cnge [*d*(N103···O2) = 2.926 Å, *d*(N102···O4) = 2.935 Å]. Unfortunately, however, the cnge ligand was found to be disordered over two positions (ratio 85:15), and due to the moderate overall quality of the crystallographic analysis we abstain from any detailed discussion of the pivotal metric parameters of the cnge ligand.

Nevertheless, the isolation of **7** now allowed a more conclusive comparison of the ν(C≡N) stretching frequencies of free cnge with those of cnge *N*-bound to nickel(II) ions either with (**5**) or without (**6**, **7**) an adjacent second nickel(II) center, where the primary nickel(II) ions in all cases are embedded in identical pyrazolate-derived tran-type coordination environments. These values are listed in Table 1.

The complexes **6** and **7**, which feature purely *end-on* bound cnge, display similar IR bands both in acetone solution and in the solid state. As expected, their characteristic doublet for ν(C≡N) is shifted to higher wavenumbers than for free cnge. The overall differences for the low-energy component of the ν(C≡N) stretch (assigned to the tautomer with conjugated C≡N and C=N bonds[21]) are small but nonnegligible, and in the solid state a trend of decreasing frequencies in the order **6** ≈ **7** > free cnge > **5** is found. This experimental result in fact gives evidence for the presence of some (albeit very weak) side-on π-bonding interaction between the nitrile part of the 2-cyanoguanidine ligand and the proximate Ni1 ion in solid **5**. When dissolved in acetone, IR spectra in the region characteristic for ν(C≡N) are quite similar for **5** and **6**, suggesting identical structures in solution that differ from the structure observed for **5** in the solid state.

Theoretical Investigations

With the aim of further substantiating these findings, and in order to describe the electronic structure of complex **5** and to gain deeper insight into the nature of the assumed π-interaction, we have carried out DFT calculations on the simplified complexes **5a**, **7a**, and on the free ligand cnge. In **5a** and **7a** the substituents at the ligand side-arm nitrogen atoms of the parent complexes **5** and **7** have been replaced by hydrogen atoms. We started our investigations with single point calculations for the singlet, triplet, and quintuplet states of **5a** with bond lengths and bond angles taken from the X-ray data of compound **5**. Some selected results are summarized in Table 2.

Table 2. Relative energies (kcal/mol), $<S^2>$ values, atomic spin densities (ρ) and NPA charge (*q*) of the nickel atoms for the singlet, triplet and quintuplet states of **5a**

State	E_{rel}	$<S^2>$	ρNi1	ρNi2	*q*Ni1	*q*Ni2
^{5}**5a**	0.0	6.00	1.733	1.726	+1.454	+1.477
^{3}**5a**	+11.2	2.01	1.733	0.020	+1.455	+1.422
^{1}**5a**	+91.1	0.00	0.000	0.000	+1.252	+1.309

The quintuplet state of **5a** was found to be the ground state, and the states ^{3}**5a** and ^{1}**5a** lie above ^{5}**5a** by 11.2 kcal/mol and 91.1 kcal/mol, respectively. In the case of ^{5}**5a** the calculated atomic spin densities ρ as well as the NPA charges q of the nickel atoms clearly show the high-spin Ni^{II} structures. In the triplet state ^{3}**5a** the Ni2 atom adopts a low-spin configuration (ρNi2 = 0.02), while the spin density at Ni1 (1.733) remains unchanged with respect to ^{5}**5a**. The MO shapes of the metal-centered singly occupied MOs of ^{5}**5a** are shown in Figure 7.

It turns out that the singly occupied MOs of Ni1 have d_{z^2} and d_{xy} character, and consequently its three doubly occupied MOs are of $d_{x^2-y^2}$, d_{yz}, and d_{xz} character. The two latter MOs [d_{yz}, d_{xz}] are well adapted to give side-on backbonding interactions with the in-plane $\pi_\parallel$* and with the out-of plane $\pi_\perp$* MOs of the nitrile π system (Figure 8). At the same time the doubly occupied $3d_{yz}$ and $3d_{xz}$ MOs of Ni2 can give end-on backbonding interactions with the nitrogen p-component of the nitrile π* system (Figure 8). Evidently, the spatial requirements for an effective M→L backbonding in ^{5}**5a** are fulfilled and are similar to those found for Ni(0) moieties complexed to multiple π systems,[24] i.e. an electron density shift from the nickel atoms to the nitrile π* system should indeed be possible.

In order to further explore the nature and the extent of such possible backbonding interactions in complex **5** we have carried out geometry optimizations on ^{5}**5a**, ^{3}**7a**, and on the singlet state of the free cnge ligand. The optimized

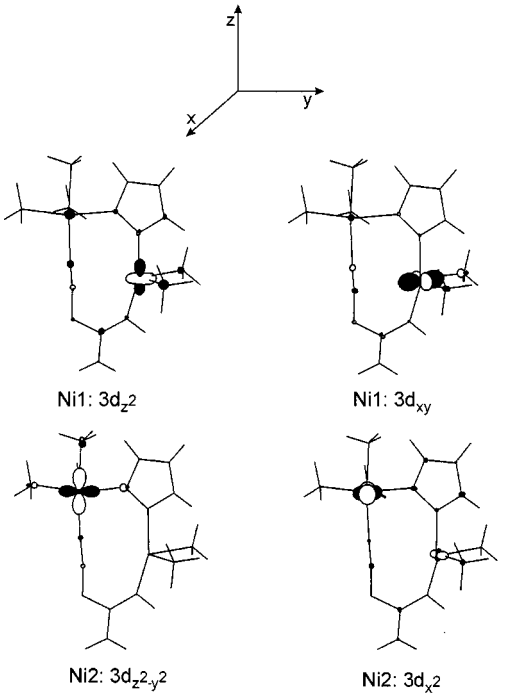


Figure 7. Shapes of the metal-centered singly occupied MOs of ^{5}**5a**

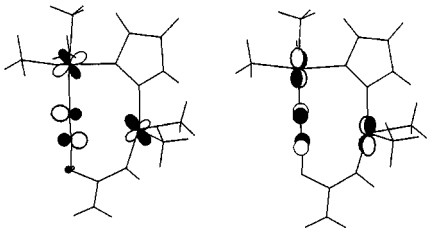


Figure 8. Possible Ni-nitrile backbonding interactions in ^{5}**5a**

structures are shown in Figure 9. According to the vibrational analyses there are no imaginary modes, and consequently these structures represent minima on the potential energy surfaces.

The optimized parameters of the free cnge molecule agree well with the known experimental data.[22] Due to the simplified nature of **5a** and **7a** some of the optimized bond lengths and bond angles differ from those determined by X-ray crystallography for the parent complexes **5** and **7** (Figures 2, 6 and 9). We ascribe these discrepancies to the spatial constraints imposed by the chelate framework of the multidentate ligands in **5** and **7**, which are not effective in the model systems **5a** and **7a**. In the case of **5a** the most striking difference is observed for the optimized Ni2–N≡C bond angle, which is 157.5° (vs. 171.2° in complex **5**). As a result, in **5a** the Ni1 atom and the N and C atoms of the C≡N unit come much closer together [*d*(Ni1–C) = 2.650 Å, *d*(Ni1–N) = 2.448 Å]. We notice, however, that the optimized Ni–N≡C bond angle of **7a** (163.9°) nicely reproduces the experimental value of the mononuclear complex **7** (163.3°). It thus seems that, in **5a**, the nitrile moiety approaches the Ni1 atom in order to enforce the side-on π-bonding interaction, while this is being prevented by the rigid dinucleating ligand matrix in the parent compound **5**.

Upon going from the free cnge ligand to **7a** and **5a**, the optimized C≡N distance increases from 1.163 Å to 1.178 Å and 1.187 Å, respectively. At the same time the calculated stretching frequency, ν(C≡N), decreases from 2209 cm^{-1} (free cnge) to 2189 cm^{-1} (**7a**) and 2143 cm^{-1} (**5a**). The trend of decreasing ν(C≡N) frequencies determined theoretically (free cnge > **7a** > **5a**) differs from that observed experimentally (**7a** > free cnge > **5a**). The calculation (for the gas phase) obviously fails to reproduce the well-known[25] increase in ν(C≡N) that occurs upon end-on binding of the nitrile (in the solid state or in solution), but it suggests that in **7a** the nitrile part of the cnge ligand receives some back-

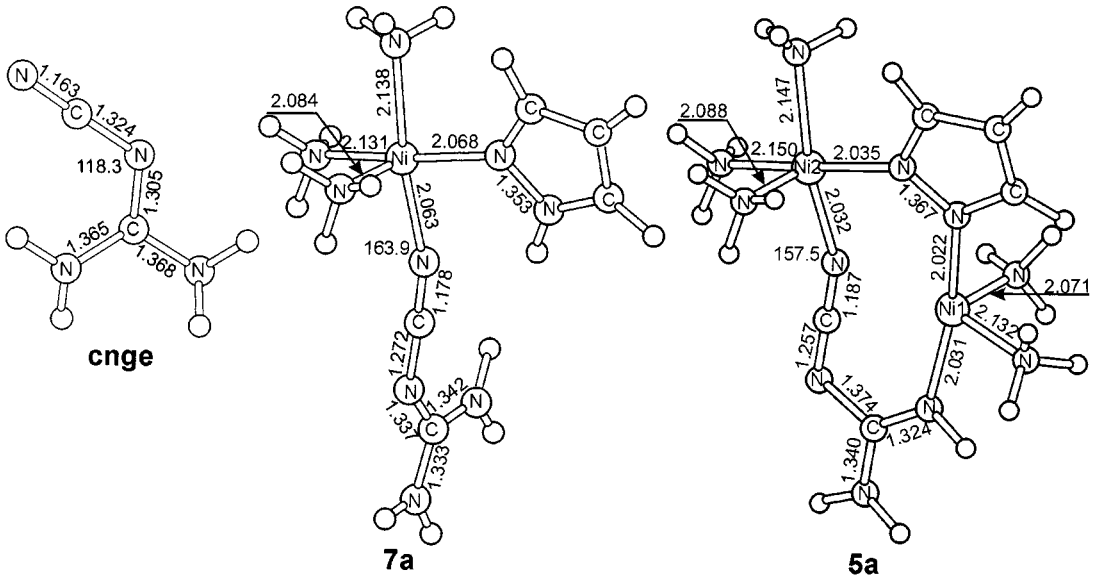


Figure 9. Optimized structures of free cnge, ^{3}**7a** and ^{5}**5a**; bond lengths are given in (Å) and bond angles in (°)

Table 3. Results of NBO and NPA population analyses, optimized C≡N bond lengths and calculated wavenumbers for the ν(C≡N) stretch of cnge, **7a**, and **5a**

	NBO occupation numbers		
	cnge	**7a**	**5a**
σ(C≡N)	1.995	1.990	1.989
π(C≡N)	3.962	3.966	3.935
σ*(C≡N)	0.023	0.029	0.025
π*(C≡N)	0.224	0.456	0.542
	NPA charge		
Ni2		+1.495	+1.477
Ni1			+1.481
–C≡N	–0.023	–0.176	–0.244
d(C≡N) [Å]	1.163	1.178	1.187
$\tilde{\nu}$(C≡N) [cm^{-1}]	2209	2189	2143

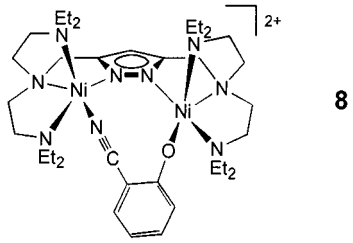
bonding from occupied MOs of the nickel ion (see Figure 8). The calculated NPA charge of the nitrile moiety changes from –0.023 (free cnge) to –0.176 (**7a**), and the population of the nitrile π* MOs increases from 0.224e (free cnge) to 0.456e (**7a**) (Table 3). We suppose that in the experimental complex **7** the end-on Ni–nitrile interactions may have a slightly different character, obviously affecting the observed ν(C≡N) stretching frequencies.

Upon going from **7a** to **5a**, an additional increase of the population of the nitrile π* MOs is discernible (Table 3), while any side-on L→M donation is negligible. With respect to **7a**, the population of the nitrile π* MOs of **5a** is greater by 0.086e. Since in the optimized structure of **5a** the Ni1 atom and the nitrile moiety come closer together than in the parent complex **5**, we also carried out NPA and NBO population analyses using the experimentally determined geometrical parameters of **5**. In this case we observe an increase of the nitrile π* MOs population by 0.049e, suggesting that in **5** the Ni1–nitrile π-bonding has to compete with the structural constraints imposed by the chelate ligands, where these constraints are enforcing a larger nickel–nickel distance and a concomitant weakening of the side-on π-interaction.

In summary, the Ni1–nitrile π-backbonding in **5** can only be characterized as a weak interaction, and this is not surprising when taking into account the large charge of the nickel(II) ion and the contracted character of its 3d shell. The positioning of the nitrile unit within the bimetallic pocket and the resulting weak Ni1–nitrile interaction in ^{5}**5a** apparently block the fifth coordination site of the Ni1 center that otherwise is occupied by an additional donor ligand in all related pyrazolate-based Ni^{II} compounds.[5–7]

Binding of 2-Hydroxybenzonitrile

The question arose as to whether the unusual binding of the C≡N moiety within the bimetallic pocket of **5** is a singular phenomenon and therefore unique to the particular nitrile cnge. We thus reacted **1**·$(ClO_4)_2$ with 2-hydroxybenzonitrile, which in its phenolate form provides a bifunctional ligand of geometric characteristics quite similar to deprotonated cnge. The resulting green complex **8**·$(ClO_4)_2$ (Scheme 9) was obtained in crystalline form, and the molecular structure of the cation as elucidated by X-ray crystallography is depicted in Figure 10.



8

Scheme 9. Schematic drawing of **8**

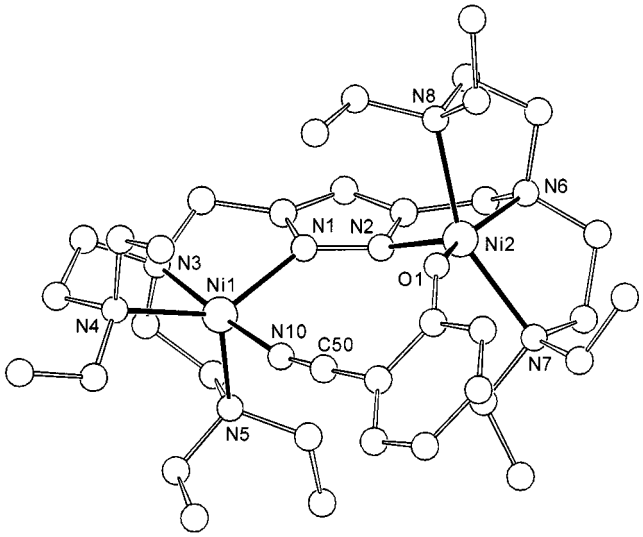


Figure 10. Molecular structure of **8**; selected interatomic distances (Å) and bond angles (°): Ni1–N1 2.050(2), Ni1–N3 2.100(2), Ni1–N4 2.172(2), Ni1–N5 2.111(2), Ni1–N10 1.988(2), Ni2–N2 2.054(2), Ni2–N6 2.087(3), Ni2–N7 2.216(2), Ni2–N8 2.208(2), N2–O1 1.934(2), N1–N2 1.386(3), N10–C50 1.135(4), Ni1···Ni2 4.587; Ni1–N10–C50 167.6(2), N10–C50–C51 176.5(3)

Obviously, the structure of **8** differs fundamentally from those of **5**. Both nickel(II) ions have retained their usual five-coordination with all the ligand side arms of the pyrazolate framework attached to the metal centers; the bifunctional 2-oxybenzonitrile(1–) ligand simply occupies the remaining active coordination sites within the bimetallic pocket. The nitrile unit exhibits plain end-on binding through its *N*-atom [angle N1–N10–C50 = 167.6(2)°] and its ν(C≡N) stretching vibration is found to be unchanged relative to those of free 2-hydroxybenzonitrile [$\tilde{\nu}$ = 2237 cm^{-1}]. These findings emphasize that particular conditions have to prevail in order to favor the weak π-bonding interaction of a nitrile unit with a nearby nickel(II) ion at the expense of the detachment of a ligand *N*-donor from the metal site, as uniquely observed for **5**.

It should finally be noted that the structure of **8** is of interest with respect to the previously proposed cooperative mechanism for the nitrile hydration mediated by **1**, which was assumed to proceed via initial end-on coordination of the nitrile to one of the nickel ions and subsequent nucleo-

philic attack by the adjacent hydroxide as shown for **2** (Scheme 2). Considering the close analogy between a metal-bound hydroxide and the metal-bound phenolate in **8**, the structure found for **8** is reminiscent of this postulated mechanism and at least demonstrates that the simultaneous binding of such an OR-function and a nitrile should, in principle, be feasible within the active site pocket of the dinuclear framework.

Conclusion

Various different binding modes of nitrile moieties at a dinuclear nickel(II) site have been characterized and studied in the present work, where the basic bimetallic framework of **1** once again proved to induce cooperative action of the two proximate metal ions. Cyanamide is incorporated as a hydrogencyanamido(1–) secondary bridge with an unusually short metal–metal separation imposed by the compartmental ligand matrix, representing only the second structurally characterized example of bridging parent $HNCN^-$. The distinct binding of a nitrile and a phenolate function at the adjacent metal centers, as observed in **8**, lends further support for the bimetallic effect that was assumed to enable the cooperative hydration of nitriles at the bimetallic site of **1**: it demonstrates that the simultaneous accommodation of both an OR-function and an end-on-bound nitrile is indeed feasible within the active site pocket of the dinuclear framework.

2-Cyanoguanidine exhibits an unprecedented binding mode within the grip of the two metal ions in **5**: while its nitrile-*N* exhibits the common end-on binding to one nickel atom, and a terminal amido-*N* is coordinated to the other metal site, the structural features suggest an additional side-on interaction of the nitrile unit with the second nickel(II) ion. Combined experimental and theoretical evidence, in particular the trend of decreasing ν(C≡N) stretching frequencies in the series **6** ≈ **7** > free cnge > **5**, as well as the proper spatial arrangement of the crucial molecular orbitals, confirm the presence of a nonnegligible (albeit weak) π-bonding of the nitrile part of the cnge ligand with the adjacent high-spin nickel(II) atom in **5**. This mainly consists of backbonding from the doubly occupied $3d_{yz}$ and $3d_{xz}$ MOs at Ni1 to the π* MOs of the nitrile. We assume that this peculiar π-bonding interaction, which is quite unusual for a high-spin nickel(II) ion nested in a purely *N*-donor environment, and which is expectedly weak, is imposed by the dinuclear pincer effect, i.e. by the seizing of the nitrile within the bimetallic pocket. Apparently, particular geometric conditions have to prevail in order to favor such side-on interaction, and this once again demonstrates the ability of two cooperating metal ions to enable unusual coordination modes by their synergetic action. One could imagine that similar interactions between π-systems and hard metal ions like high-spin nickel(II) might well play a role if enforced within highly organized and constrained substrate binding pockets, e.g. in the protein active site pockets of natural metalloenzymes.

Experimental Section

General Procedures and Methods: All manipulations were carried out under an atmosphere of dry nitrogen with standard Schlenk techniques. Solvents were dried according to established procedures. Compound **1**·$(ClO_4)_2$ and HL were synthesized according to published procedures.[7] – Microanalyses: Mikroanalytische Laboratorien des Organisch-Chemischen Instituts der Universität Heidelberg. – IR spectra: Perkin–Elmer 983G, recorded either as KBr pellets or in acetone solution. – FAB-MS spectra: Finnigan MAT 8230. – Magnetic measurement: Bruker Magnet B-E 15 C8, field-controller B-H 15, variable temperature unit ER4111VT, Sartorius microbalance M 25 D-S. Experimental susceptibility data were corrected for the underlying diamagnetism and temperature-independent paramagnetism [100×10^{-6} cm^3mol^{-1} per nickel(II) ion].[23]

Caution! Although no problems were encountered in this work, transition metal perchlorate complexes are potentially explosive and should be handled with proper precautions.

Complex 4·$(ClO_4)_2$: A solution of **1**·$(ClO_4)_2$ (0.44 g, 0.50 mmol) in EtOH/THF (1:1, 25 mL) was treated with two equivalents of cyanamide and stirred at room temperature for 2 h. All volatile material was then evaporated under reduced pressure, the residue taken up in acetone and the solution layered with light petroleum to gradually yield 0.35 g (0.40 mmol, 80%) green crystals of the product **4**·$(ClO_4)_2$. – IR (KBr): $\tilde{\nu}$ = 3282 (s), 2965 (s), 2933 (s), 2873 (m), 2149 (vs), 1467 (s), 1380 (s), 1089 (vs), 622 (s) cm^{-1}. – MS (FAB, nibeol); *m/z* (%): 779 (100) [**4**·$(ClO_4)^+$], 677/679 (98) [(**4** – 1)/(**4** + 1)$^+$]. – $C_{30}H_{62}Cl_2N_{10}Ni_2O_8$ (879.2): calcd. C 40.99, H 7.11, N 15.93; found C 41.02, H 7.13, N 15.96.

Complex 5·$(ClO_4)_2$: A solution of **1**·$(ClO_4)_2$ (0.78 g, 0.89 mmol) in EtOH/THF (1:1, 25 mL) was treated with 1.2 equivalents of cnge and stirred at room temperature for 2 h. All volatile material was then evaporated under reduced pressure and the oily residue taken up in EtOH/Et_2O (1:4, 25 mL). The green precipitate that formed was separated by filtration and dried under vacuum to afford a light green powder. This was dissolved in acetone and the solution layered with light petroleum to yield 0.16 g (0.17 mmol, 19%) of green crystals of the product **5**·$(ClO_4)_2$. – IR (KBr): $\tilde{\nu}$ = 3432 (m), 3343 (m), 3307 (w), 3232 (w), 2968 (m), 2878 (w), 2229 (w), 2180 (sh), 2154 (s), 1632 (s), 1529 (s), 1478 (s), 1468 (m), 1312 (m), 1096 (vs), 623 (s) cm^{-1}. – $C_{31}H_{64}Cl_2N_{12}Ni_2O_8$ (921.2): calcd. C 40.42, H 7.00, N 18.25; found C 39.95, H 7.07, N 17.40.

Complex 6·$(ClO_4)_2$: A solution of **1**·$(ClO_4)_2$ (0.44 g, 0.50 mmol) in EtOH/THF (1:1, 25 mL) was treated with five equivalents of cnge and stirred at room temperature for 2 h. All volatile material was then evaporated under reduced pressure, the residue taken up in acetone and again treated with three equivalents of cnge. Layering the resulting solution with light petroleum gradually afforded green crystals of the product **6**·$(ClO_4)_3$·acetone (0.11 g, 0.09 mmol, 19%). – IR (KBr): $\tilde{\nu}$ = 3433 (m), 3343 (m), 3238 (m), 2963 (m), 2877 (w), 2233 (s), 2186(s), 1699 (m, acetone), 1641 (s), 1565 (s), 1464 (m), 1259 (m), 1086 (vs), 796 (m), 623 (s) cm^{-1}. – $C_{33}H_{69}Cl_3N_{16}Ni_2O_{12}$·acetone (1163.8): calcd. C 37.15, H 6.50, N 19.26; found C 37.45, H 6.49, N 20.03.

Complex 7·(ClO_4)·(BPh_4): A solution of HL (0.17 g, 0.54 mmol) in EtOH/THF (20 mL, 1:1) was treated with $[Ni(H_2O)_6](ClO_4)_2$ (0.20 g, 0.54 mmol) and cnge (0.05 g, 0.60 mmol) and the reaction mixture stirred for 1 h at room temperature. Then $NaBPh_4$ (0.19 g, 0.56 mmol) was added and the resulting solution layered with light petroleum. Green crystals of **7**·(ClO_4)·(BPh_4)·0.5thf·0.18EtOH

Table 4. Crystal data and refinement details for complexes **4**·$(ClO_4)_2$, **5**·$(ClO_4)_2$, **6**·$(ClO_4)_3$, **7**·(ClO_4)·(BPh_4) and **8**·$(ClO_4)_2$

	4·$(ClO_4)_2$	**5**·$(ClO_4)_2$	**6**·$(ClO_4)_3$	**7**·$(ClO_4)(BPh_4)$	**8**·$(ClO_4)_2$
Formula	$C_{30}H_{62}Cl_2N_{10}Ni_2O_8$	$C_{31}H_{63}Cl_2N_{12}Ni_2O_8$	$C_{33}H_{69}Cl_3N_{16}Ni_2O_{12}$ ·acetone	$C_{36}H_{65}Cl_2N_9Ni_2O_9$· 0.5thf·0.18EtOH	$C_{36}H_{65}Cl_2N_9Ni_2O_9$
M_r	879.2	921.2	1163.9	915.3	956.3
crystal size [mm]	0.03 × 0.15 × 0.30	0.20 × 0.15 × 0.08	0.30 × 0.20 × 0.20	0.08 × 0.30 × 0.30	0.30 × 0.30 × 0.40
crystal system	monoclinic	triclinic	monoclinic	triclinic	monoclinic
space group	*Cc*	$P\bar{1}$	$P2_1/n$	$P\bar{1}$	*C*2/c
a [Å]	8.473(2)	11.474(2)	21.046(4)	10.714(2)	34.338(7)
b [Å]	23.895(5)	12.391(3)	11.178(2)	11.484(2)	9.989(2)
c [Å]	19.412(4)	15.839(3)	24.241(5)	21.713(4)	26.357(5)
α [°]	90	106.40(3)	90	81.06(3)	90
β [°]	90.86(3)	90.77(3)	110.77(3)	89.50(3)	105.40(3)
γ [°]	90	102.27(3)	90	76.35(3)	90
V [Å^3]	3930(1)	2104(1)	5332(1)	2564(1)	8716(3)
$\rho_{calcd.}$ [g·cm^{-3}]	1.486	1.454	1.450	1.184	1.458
Z	4	2	4	2	8
F(000) [e]	1864	976	2456	971	4048
T [K]	200	200	200	200	200
μ (Mo-K_α) [mm^{-1}]	1.154	1.082	0.928	0.479	1.048
hkl range	±10, ±29, ±23	±14, ±15, ±19	–27 to 28, –15 to 14, –34 to 31	±14, ±15, ±29	±42, ±12, ±32
2θ range [°]	3.4−52.2	3.5−52.2	3.6–61.1	3.9−57.4	3.2−52.0
Measured refl.	7791	41676	49853	25867	66921
Unique refl. (*R*int)	7677 (0.084)	8285 (0.069)	14533 (0.089)	13198 (0.079)	8549 (0.088)
Obs. refl. $I > 2\sigma(I)$	6024	5598	7878	6505	6165
refined parameters	505	519	663	664	534
resid. electron dens. [eÅ^{-3}]	0.503/–0.437	0.435/–0.354	0.529/–0.460	0.800/–0.398	1.034/–0.505
R1	0.062	0.039	0.046	0.068	0.042
wR2 (refinement on F^2)	0.142	0.077	0.112	0.230	0.106
Goodness-of-fit	1.029	0.961	0.967	1.016	1.039

gradually formed (0.33 g, 0.36 mmol, 67%). – IR (KBr): $\tilde{\nu}$ = 3421 (s), 3343 (s), 3234 (m), 3046 (m), 2976 (m), 2874 (w), 2227 (s), 2183 (s), 1636 (s), 1550 (s), 1472 (m), 1095 (s), 734 (s), 706 (s) cm^{-1}. – MS (FAB, nibeol); *m*/*z* (%): 466 (44) [$LNi(ClO_4)^+$], 450 (17) [**7**$^+$], 366 (100) [LNi^+]. – $C_{43}H_{59}BClN_9NiO_4$·0.5thf·0.18EtOH (915.3): calcd. C 59.52, H 7.06, N 13.77; found C 58.52, H 7.42, N 13.86.

Complex 8·$(ClO_4)_2$: A solution of **1**·$(ClO_4)_2$ (0.35 g, 0.40 mmol) in EtOH/THF (1:1, 15 mL) was treated with one equivalent of 2-hydroxybenzonitrile (0.048 g, 0.40 mmol) and stirred at room temperature for 1 h. All volatile material was then evaporated under reduced pressure and the residue taken up in acetone and layered with light petroleum. Green crystals of the product **8**·$(ClO_4)_2$ gradually formed (0.31 g, 0.32 mmol, 81%). – IR (KBr): $\tilde{\nu}$ = 2972 (m), 2875 (m), 2237 (s), 1594 (s), 1527 (w), 1476 (s), 1379 (w), 1092 (vs) cm^{-1}. – MS (FAB, nibeol); *m*/*z* (%): 857 (100) [**8**·$(ClO_4)^+$], 755 (90) [**8**$^+$], 378 (65) [**8**$^{2+}$]. – $C_{36}H_{65}Cl_2N_9Ni_2O_9$ (956.3): calcd. C 45.22, H 6.85, N 13.18; found C 44.84, H 6.92, N 12.95.

Calculation Details: The calculations were carried out with the density functional theory method (DFT) known in the literature by its synonym B3LYP.[26] A single extended all-electron basis set was applied in our studies. For Ni we have chosen Wachters (14s,9p,5d) basis set[27] augmented with a 4f polarization function (α_f = 1.29). The contraction scheme of [9s,5p,3d,1f] corresponds to a double- and triple-ζ basis for the core and valence electrons, respectively. The 6–311G basis[28] was used for C, N, and H. The basis set of C and N was augmented by a single 3d polarization function (α_C = 0.626, α_N = 0.913). The geometry optimizations were carried out by using analytical gradient procedures. The presented structures correspond to fully converged geometries with gradients and displacements below the thresholds implemented in Gaussian 98. Vibrational frequencies were obtained from analytic calculations of the Hessian matrices. The calculated frequencies have been scaled by a factor of 0.96. The nature and extent of charge reorganizations was characterized with the help of the natural population analysis (NPA) and natural bond orbital (NBO) methods.[29] The calculations have been carried out with the Gaussian 98 program[30] installed on the IBM RS/6000 workstations of the Universitätsrechenzentrum Heidelberg. For graphical displays we have used the Molek-9000,[31] and GaussView[32] programs.

X-ray Crystallography: The measurements were carried out on a Nonius Kappa CCD diffractometer using graphite-monochromated Mo-K_α radiation. All calculations were performed using the SHELXT PLUS software package. Structures were solved by direct methods with SHELXS-97 and refined with the SHELXL-97 program.[33] The program XPMA[34] was used for graphical handling of the data. Atomic coordinates and thermal parameters of the nonhydrogen atoms were refined in fully or partially anisotropic models by full-matrix least-squares calculation based on F^2. In general the hydrogen atoms were placed at calculated positions and allowed to ride on the atoms they are attached to. The structure of **4**·$(ClO_4)_2$ was treated as a racemic twin. The hydrogen atom H200 of the $HNCN^-$ bridge was located in the difference Fourier synthesis and refined isotropically. In the case of **5**·$(ClO_4)_2$ all hydrogen atoms of the monodeprotonated cnge ligand (H50 – H52) were located and refined. Likewise, for **6**·$(ClO_4)_3$ the protons H22 – H25 and H122 – H125 of the two cnge ligands were located in the difference Fourier map, refined once and then held fixed. One of the terminal ethyl groups (C10 and C14) of **6**·$(ClO_4)_3$ was found to be disordered over two positions (ratio 50:50). In the case of **7**·$(ClO_4)(BPh)_4$ the cnge ligand was found to be partly disordered over two positions (ratio 85:15). The pyrazol-H2 could be found and refined; hydrogen atoms H102, H112, H103, H113 corresponding to the major part of the disordered cnge were located, refined

once and then held fixed. Table 4 compiles the data for the structure determinations. Crystallographic data (excluding structure factors) for the structures reported in this paper have been deposited with the Cambridge Crystallographic Data Centre as supplementary publication no. CCDC 127490 – CCDC-127493 and CCDC-133913. Copies of the data can be obtained free of charge on application to CCDC, 12 Union Road, Cambridge CB2 1EZ, UK [Fax: (internat.) + 44-1223/336-033; E-mail: deposit@ccdc.cam.ac.uk].

Acknowledgments

We sincerely thank Prof. Dr. G. Huttner and Prof. Dr. R. Gleiter for their generous support. Financial support of this work by the Deutsche Forschungsgemeinschaft (SFB 247, Habilitandenstipendium for F. M.) and the Fonds der Chemischen Industrie is gratefully acknowledged.

[1] K. D. Karlin, *Science* **1993**, *261*, 701–708; S. J. Lippard, J. M. Berg, *Principles of Bioinorganic Chemistry*, University Science Books, CF, **1994**; W. Kaim, B. Schwederski, *Bioanorganische Chemie*, Teubner, Stuttgart, **1991**; *Bioinorganic Catalysis* (Ed.: J. Reedijk), Dekker, New York, **1993**; N. Sträter, W. N. Lipscomb, T. Klabunde, B. Krebs, *Angew. Chem.* **1996**, *108*, 2158–2191; *Angew. Chem. Int. Ed. Engl.* **1996**, *35*, 2024–2055.

[2] R. M. Bullock, C. P. Casey, *Acc. Chem. Res.* **1987**, *20*, 167–173; H. Steinhagen, G. Helmchen, *Angew. Chem.* **1996**, *108*, 2489–2492; *Angew. Chem. Int. Ed. Engl.* **1996**, *35*, 2339–2342; D. G. McCollum, B. Bosnich, *Inorg. Chim. Acta* **1998**, *270*, 13–19; E. K. van den Beuken, B. L. Feringa, *Tetrahedron* **1998**, *54*, 12985–13011; R. Than, A. A. Feldmann, B. Krebs, *Coord. Chem. Rev.* **1999**, *182*, 211–241.

[3] M. W. Göbel, *Angew. Chem.* **1994**, *106*, 1201–1203; *Angew. Chem. Int. Ed. Engl.* **1994**, *33*, 1141; M. E. Broussard, B. Juma, S. G. Train, W. J. Peng, S. A. Laneman, G. G. Stanley, *Science* **1993**, *260*, 1784–1788; G. Süss-Fink, *Angew. Chem.* **1994**, *106*, 71–73; *Angew. Chem. Int. Ed. Engl.* **1994**, *33*, 67.

[4] See for example: S. R. Collinson, D. E. Fenton, *Coord. Chem. Rev.* **1996**, *148*, 19–40; D. E. Fenton, H. Okawa, *Chem. Ber./Recueil* **1997**, *130*, 433–442.

[5] F. Meyer, K. Heinze, B. Nuber, L. Zsolnai, *J. Chem. Soc., Dalton Trans.* **1998**, 207–213; F. Meyer, A. Jacobi, B. Nuber, P. Rutsch, L. Zsolnai, *Inorg. Chem.* **1998**, *37*, 1213–1218; M. Konrad, F. Meyer, K. Heinze, L. Zsolnai, *J. Chem. Soc., Dalton Trans.* **1998**, 199–205; F. Meyer, P. Rutsch, *Chem. Commun.* **1998**, 1037–1038.

[6] F. Meyer, H. Pritzkow, *Chem. Commun.* **1998**, 1555–1556.

[7] F. Meyer, E. Kaifer, P. Kircher, K. Heinze, H. Pritzkow, *Chem. Eur. J.* **1999**, *5*, 1617–1630.

[8] L. M. Estermaier, A. H. Sieber, F. Lottspeich, D. H. M. Matern, G. R. Hartmann, *Angew. Chem.* **1992**, *104*, 655–658; *Angew. Chem. Int. Ed. Engl.* **1992**, *31*, 620.

[9] R. W. Miller, R. R. Eady, *Biochim. Biophys. Acta* **1988**, *952*, 290–296.

[10] W. Beck, H. Bock, R. Schlodder, *Z. Naturforsch.* **1974**, *29b*, 75–79.

[11] P. Chauduri, K. Wieghardt, B. Nuber, J. Weiss, *J. Chem. Soc., Chem. Commun.* **1985**, 265–266.

[12] H. Beyer, W. Walter, *Lehrbuch der Organischen Chemie*, S. Hirzel Verlag, Stuttgart, **1988**, p 368.

[13] I. W. Bassi, C. Benedicenti, M. Calcaterra, R. Intrito, G. Rucci, C. Santini, *J. Organomet. Chem.* **1978**, *144*, 225–237; D. Walther, H. Schönberg, E. Dinjus, J. Sieler, *J. Organomet. Chem.* **1987**, *334*, 377–388; J. Sieler, D. Walther, O. Lindquist, L. Andersen, *Z. Anorg. Allg. Chem.* **1988**, *560*, 119–127.

[14] H. Bock, *Angew. Chem.* **1962**, *74*, 695; H. Bock, H. tom Dieck, *Chem. Ber.* **1966**, *99*, 213–226; K. Krogmann, R. Mattes, *Angew. Chem.* **1966**, *78*, 1064; *Angew. Chem. Int. Ed. Engl.* **1966**, *5*, 1046.

[15] M. H. Chisholm, F. A. Cotton, M. W. Extine, L. A. Rankel, *J. Am. Chem. Soc.* **1978**, *100*, 807–811; M. H. Chisholm, J. C. Huffman, N. S. Marchant, *J. Am. Chem. Soc.* **1983**, *105*, 6162–6163; M. H. Chisholm, J. C. Huffman, N. S. Marchant, *Organometallics* **1987**, *6*, 1073–1080; D. M. Hoffman, S. Lee, *Inorg. Chem.* **1992**, *31*, 2675–2676; T. C. Wright, G. Wilkinson, M. Motevalli, M. B. Hursthouse, *J. Chem. Soc., Dalton Trans.* **1986**, 2017–2019; F. J. G. Alonso, M. G. Sanz, V. Riera, A. A. Abril, A. Tiripicchio, F. Ugozzoli, *Organometallics* **1992**, *11*, 801–808; F. A. Cotton, S. C. Haefner, A. P. Sattelberger, *Inorg. Chim. Acta* **1997**, *266*, 55–63.

[16] W. Sacher, U. Nagel, W. Beck, *Chem. Ber.* **1987**, *120*, 895–900; J. Pickardt, B. Kuhn, *Z. Kristallogr.* **1995**, *210*, 901.

[17] M. Fernanda, N. N. Carvalho, A. J. L. Pombeiro, A. Hills, D. L. Hughes, R. L. Richards, *J. Organomet. Chem.* **1993**, *469*, 179–187.

[18] M. J. Begley, P. Hubberstey, P. H. Walton, *J. Chem. Soc., Chem. Commun.* **1989**, 502–503.

[19] M. J. Begley, P. Hubberstey, P. H. Walton, *J. Chem. Soc., Dalton Trans.* **1995**, 957–962.

[20] M. J. Begley, O. Eisenstein, P. Hubberstey, S. Jackson, C. E. Russell, P. H. Walton, *J. Chem. Soc., Dalton Trans.* **1994**, 1935–1942; M. J. Begely, P. Hubberstey, C. E. Russell, P. H. Walton, *J. Chem. Soc., Dalton Trans.* **1994**, 2483–2488; A. J. Blake, P. Hubberstey, W.-S. Li, C. E. Russel, B. J. Smith, L. D. Wraight, *J. Chem. Soc., Dalton Trans.* **1998**, 647–655.

[21] L. A. Sheludyakova, E. V. Sobolev, A. V. Arbuznikow, E. B. Burgina, L. I. Kozhevina, *J. Chem. Soc., Faraday Trans.* **1997**, *93*, 1357–1360.

[22] F. L. Hirshfeld, H. Hope, *Acta Crystallogr.* **1980**, *B36*, 406–415.

[23] C. J. O'Connor, *Progr. Inorg. Chem.* **1982**, *29*, 203–283; O. Kahn, *Molecular Magnetism*, VCH Publishers, New York, **1993**.

[24] I. Hyla-Kryspin, J. Koch, R. Gleiter, T. Klettke, D. Walther, *Organometallics* 1**998**, *17*, 4724–4733.

[25] B. N. Storhoff, H. C. Lewis, Jr., *Coord. Chem. Rev.* **1977**, *23*, 1–29; R. Hoti, Z. Mihalić, H. Vančik, *Croat. Chem. Acta* **1995**, *68*, 359–371.

[26] A. D. Becke, *J. Chem. Phys.* **1992**, *96*, 2155–2160; *J. Chem. Phys.* **1993**, *98*, 5648–5652; S. H. Vosko, L. Wilk, M. Nusair, *Can. J. Phys.* **1980**, *58*, 1200–1211; C. Lee, W. Yang, R. G. Parr, *Phys. Rev. B* **1988**, *37*, 785–789.

[27] A. J. H. Wachters, *J. Chem. Phys.* **1970**, *52*, 1033–1036.

[28] R. Krishnan, J. S. Binkley, R. Seeger, J. A. Pople, *J. Chem. Phys.* **1980**, *72*, 650–654.

[29] J. P. Foster, F. Weinhold, *J. Am. Chem. Soc*. **1980**, *102*, 7211–7218; A. E. Reed, F. Weinhold, *J. Chem. Phys.* **1983**, *78*, 4066–4073; A. E. Reed, R. B. Weinstock, F. Weinhold, *J. Chem. Phys.* **1985**, *83*, 735–746; A. E. Reed, L. A. Curtiss, F. Weinhold, *Chem. Rev.* **1988**, *88*, 899–926.

[30] M. J. Frisch, G. W. Trucks, H. B. Schlegel, G. E. Scuseria, M. A. Robb, J. R. Cheeseman, V. G. Zakrzewski, J. A. Montgomery, Jr., R. E. Stratmann, J. C. Burant, S. Dapprich, J. M. Millam, A. D. Daniels, K. N. Kudin, M. C. Strain, O. Farkas, J. Tomasi, V. Barone, M. Cossi, R. Cammi, B. Mennucci, C. Pomelli, C. Adamo, S. Clifford, J. Ochterski, G. A. Petersson, P. Y. Ayala, Q. Cui, K. Morokuma, D. K. Malick, A. D. Rabuck, K. Raghavachari, J. B. Foresman, J. Cioslowski, J. V. Otitz, B. B. Stefanov, G. Liu, A. Liashenko, P. Piskorz, I. Komaromi, R. Gomperts, R. L. Martin, D. J. Fox, T. Keith, M. A. Al-Laham. C. Y. Peng, A. Nanayakkara, C. Gonzales, M. Challacombe, P. M. W. Gill, B. Johnson, W. Chen, M. W. Wong, J. L. Andres, M. Head-Gordon, E. S. Replogle, and J. A. Pople, *Gaussian 98 Revision A.5*, Gaussian, Inc., Pittsburgh, PA, **1998**.

[31] P. Bischof, *Molek-9000*, Universität Heidelberg, **1998**.

[32] GaussView, Gaussian, Inc., Pittsbourgh, PA, **1998**.

[33] G. M. Sheldrick, *SHELXL-97, Program for Crystal Structure Refinement*, Universität Göttingen, **1997**; *SHELXS-97, Program for Crystal Structure Solution*, Universität Göttingen, **1997**.

[34] L. Zsolnai, G. Huttner, *XPMA*, Universität Heidelberg, **1998**; http://www.rzuser.uni-heidelberg.de/≈v54/xpm.html.

Received September 29, 1999
[I99341]

Reductive Degradation of Tetracobalt Cluster Complexes with a Facial C_8H_8 Ligand – Synthesis of $[Co_3(CO)_3(\mu_3\text{-}CO)_3(\mu_3\text{-}C_8H_8)]^-$ and $[Ru(C_5Me_5)Co_3(CO)_3(\mu_3\text{-}CO)_3(\mu_3\text{-}C_8H_8)]$

Hubert Wadepohl,*[a] Stefan Gebert,[a] Rüdiger Merkel,[a] and Hans Pritzkow[a]

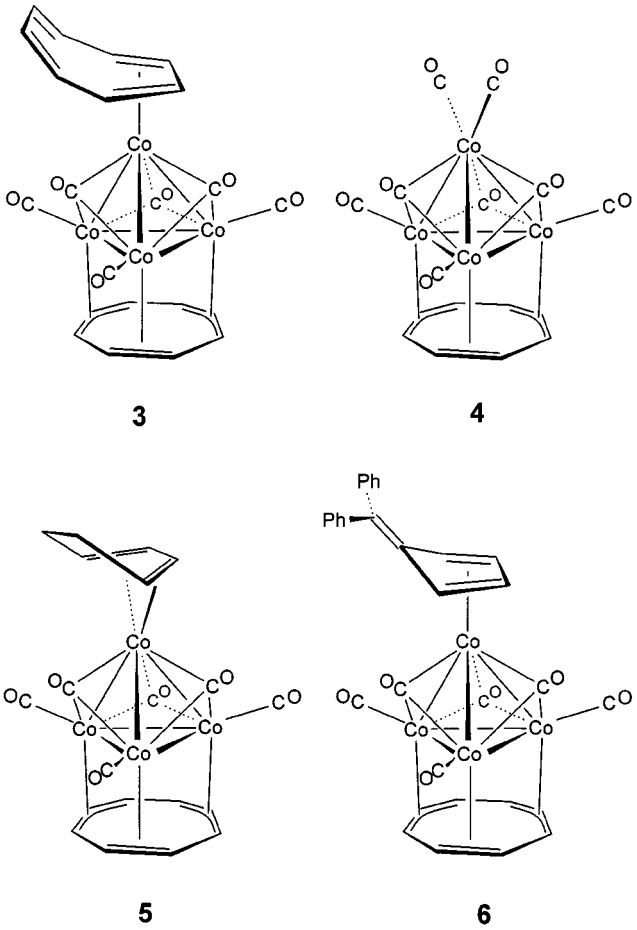
Keywords: Carbocycles / Clusters / Cobalt / Electrochemistry / Facial ligands

Chemical reduction of the cluster complexes $[Co_4(CO)_3(\mu_3\text{-}CO)_3(\mu_3\text{-}C_8H_8)L_2]$ **3** ($L_2 = C_8H_8$), **4** (L = CO), **5** ($L_2 = C_6H_8$) and **6** (L_2 = 6,6-$Ph_2C_6H_4$) gives the trinuclear anion $[Co_3(CO)_3(\mu_2\text{-}CO)_3(\mu_3\text{-}C_8H_8)]^-$ (**7**) in high yield. It is proposed that formation of **7** occurs via degradation of the radical anions $[\mathbf{3}]^-$ – $[\mathbf{6}]^-$, which can be generated reversibly via cyclic voltammetry. The anion **7** is stabilised by the facial C_8H_8 ligand and does not degrade further. Reaction of **7** with $[(C_5Me_5)Ru(NCMe)_3][BF_4]$ results in the formation of $[Ru(C_5Me_5)Co_3(CO)_3(\mu_3\text{-}CO)_3(\mu_3\text{-}C_8H_8)]$ (**8**). The crystal structures of $[NEt_4]^+$-**7**, $[(C_5H_5)_2Co]^+$-**7**, and **8** were determined. In **7** and **8**, the cyclooctatetraene ligand is coordinated to the Co_3 face of the cluster in the facial mode.

Introduction

Transfer of an electron is one of the most basic reactions of molecular metal cluster complexes.[1] Transition metal carbonyl clusters are usually prone to reduction, forming a more or less stable radical anion.[2] Frequently, reduction of the cluster is accompanied or followed by metal–metal bond scission, which may result in a modification of the cluster architecture, a change in nuclearity, or even complete degradation to mononuclear fragments. For example, when reduced electrochemically, $[Co_4(CO)_{12}]$ (**1**) was found to give the unstable monoanion $[Co_4(CO)_{12}]^-$ $[\mathbf{1}]^-$, which in the absence of other reactants decomposes to $[Co(CO)_4]^-$ and cobalt metal.[3] The products of the chemical reduction of **1** are very dependent on the reducing agent and the reaction conditions. With sodium in liquid ammonia, $[Co(CO)_4]^-$ is obtained.[4] The hexanuclear cluster anions $[Co_6(CO)_{15}]^{2-}$ and $[Co_6(CO)_{14}]^{4-}$ are formed with alkali metals or cobaltocene in THF.[5] Finally, the trinuclear $[Co_3(CO)_{10}]^-$ (**2**) can be obtained from **1** and Li[$Co(CO)_4$].[6a]

Recently we described the preparation and structures of a series of tetracobalt cluster complexes $[Co_4(CO)_3(\mu_3\text{-}CO)_3(C_8H_8)L_2]$, e.g. **3** ($L_2 = C_8H_8$), **4** (L = CO), **5** ($L_2 = C_6H_8$), and **6** (L_2 = 6,6-$Ph_2C_6H_4$) with a cyclooctatetraene ligand in the rarely-encountered facial (μ_3-) coordination mode (Scheme 1).[7] In these derivatives of **1**, the facial C_8H_8 ligand was found to resist substitution under a variety of conditions, pointing to a particular stability of the $Co_3(\mu_3\text{-}C_8H_8)$ moiety.[7,8] As described above, degradation of the Co_4 cluster takes place upon reduction of **1**. This disintegration of the metal framework is difficult to control, and frequently leads to a complete breakdown of the cluster. The presence of the facial C_8H_8 ligand might more easily stop this catastrophe at the trinuclear stage.



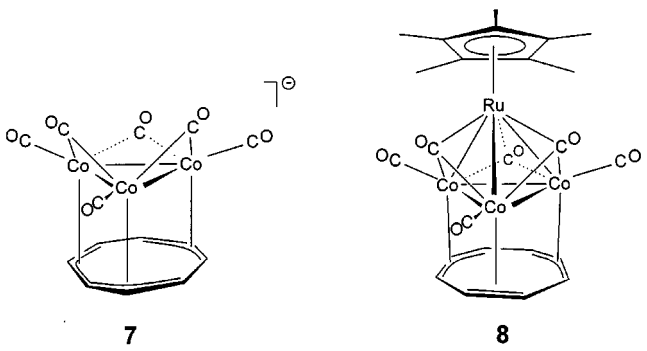
Scheme 1

Here we wish to report the exclusive and quantitative formation of the novel cluster complex anion $[Co_3(CO)_3(\mu_2\text{-}CO)_3(\mu_3\text{-}C_8H_8)]^-$ (**7**) from the reductive degradation of **3**–**6**, and its capping reaction with the $[(C_5Me_5)Ru]^+$ fragment

[a] Anorganisch-chemisches Institut der Ruprecht-Karls-Universität,
Im Neuenheimer Feld 270, D-69120 Heidelberg, Germany
E-mail: bu9@ix.urz.uni-heidelberg.de

 © WILEY-VCH Verlag GmbH, D-69451 Weinheim, 2000 1434−1948/00/0404−0783 $ 17.50+.50/0

to give the heteronuclear cluster complex $[Ru(C_5Me_5)Co_3(CO)_3(\mu_3\text{-}CO)_3(\mu_3\text{-}C_8H_8)]$ (**8**) (Scheme 2).



7 **8**

Scheme 2

Results

Preparative and Spectroscopic Investigations

When treated with an equimolar amount of $Li[HBEt_3]$, the tetranuclear cluster complexes $[Co_4(CO)_3(\mu_3\text{-}CO)_3(C_8H_8)L_2]$ **3–6** are cleanly converted into the trinuclear cluster anion $[Co_3(CO)_3(\mu_2\text{-}CO)_3(\mu_3\text{-}C_8H_8)]^-$ (**7**). Addition of aqueous $[NEt_4]Cl$ results in the precipitation of dark orange $[NEt_4]^+$-**7** in nearly quantitative yield. In contrast, treatment of **6** with $Na_2[Fe(CO)_4]$ in THF only results in a low frequency shift of the bands in the ν(CO) region by about 45 cm^{-1}, without changing the general appearance of the infrared spectrum. Addition of aqueous $[NEt_4]Cl$ in order to crystallise the product as the $[NEt_4]^+$ salt results in the partial reformation of the neutral starting material **6**. Treatment with $[PPh_4]Cl$ in THF causes slow reaction to give the trinuclear anion **7**.

The $[(C_5R_5)_2Co]^+$ (R = H, Me) salts of anion **7** are formed as by-products (10–20% yield) in the reactions of **3** with cyclopentadiene and pentamethylcyclopentadiene, respectively, along with $[Co_4(CO)_3(\mu_3\text{-}CO)_2(\mu_3\text{-}H)(\mu_3\text{-}C_8H_8)(\eta\text{-}C_5R_5)]$ **9a**, **b**[8] (60–70% yield) and $[(C_5R_5)Co(CO)_2]$ (20% yield) (R = H, Me). Reaction of **3** with cobaltocene in THF gives $[(C_5H_5)_2Co]^+$-**7** in nearly quantitative yield. The changes in the IR spectrum after addition of 1.1 equivalents of $Na[C_5H_5]$ to a solution of **3** in THF also indicate the quantitative formation of **7**.

When an equimolar amount of $[(C_5Me_5)Ru(NCMe)_3][BF_4]$ is added to a dichloromethane solution of $[NEt_4]^+$-**7**, a colour change from dark orange to dark red is observed. The heteronuclear cluster complex $[Ru(C_5Me_5)Co_3(CO)_3(\mu_3\text{-}CO)_3(\mu_3\text{-}C_8H_8)]$ (**8**) can be isolated in 45% yield from this mixture after column chromatography. No reaction takes place between $[NEt_4]^+$-**7** and $[Mn(CO)_5Cl]$ or $[(C_5H_5)Fe(CO)_2I]$.

Four bands in the ν(CO) region of the infrared spectrum (1977, 1938, 1782, and 1743 cm^{-1}) are displayed by dichloromethane solutions of **7**. These absorptions do not depend noticeably on the counterion. Complex **8** gives only three ν(CO) bands (2000, 1978, and 1707 cm^{-1}, in CH_2Cl_2). The NMR spectra of **7** and **8**, measured at room temperature, are very simple. The facial C_8H_8 ligand gives only one proton signal [δ = 4.10 (**7**), δ = 3.97 (**8**)] and one carbon NMR resonance [δ = 75.4 (**7**), δ = 70.3 (**8**)]. The ^{13}C NMR resonances for the carbonyl ligands could not be detected, due to the rather low solubility of the complexes. Other resonances in the ^1H and ^{13}C NMR spectra are due to the C_5Me_5 ligand of **8**, and the counterions X^+ ($[NEt_4]^+$ and $[(C_5R_5)_2Co]^+$, respectively) in X^+-**7**.

Electrochemistry

Cyclic voltammograms were recorded in CH_2Cl_2 solution at a scan rate of 100 mV/s. The electrochemical behaviour of the cluster complexes $[Co_4(CO)_6(C_8H_8)L_2]$ **3**, **5**, and **6** is characterised by pseudo-reversible reduction waves. The redox behaviour of the octacarbonyl derivative **4** (L = CO) appears to be more complex. The relevant data are given in Table 1. There are two reduction processes in every case, corresponding to the formation of the monoanions $[Co_4(CO)_6(C_8H_8)L_2]^-$ and dianions $[Co_4(CO)_6(C_8H_8)L_2]^{2-}$, respectively. For complex **4** the first reduction wave is distorted from the ideal shape, indicating a partially irreversible behaviour. The second reduction of **4** is strictly irreversible. Oxidation of the cluster complexes is irreversible, except in the case of complex **6** (L_2 = diphenylfulvene), which shows a pseudo-reversible oxidation wave (Table 1).

Table 1. Electrochemical data ($E_{1/2}$ [V] vs. SCE) for the complexes $[Co_4(CO)_6(C_8H_8)L_2]$ **3–6** (in CH_2Cl_2, supporting electrolyte $[n\text{Bu}_4N][PF_6]$, working electrode glassy carbon, reference electrode SCE, scan rate 100 mV s^{-1})

complex	–2/–1	–1/0	0/+1
3	–1.29	–0.68	
4	–0.99[a]	–0.60[b]	
5	–1.37	–1.02	
6	–1.48	–0.81	0.41

[a] Irreversible. – [b] Partially irreversible.

Crystal and Molecular Structure of $[NEt_4]^+$-7, $[(C_5H_5)_2Co]^+$-7, and 8

Single-crystal X-ray structure determinations were carried out with $[NEt_4]^+$-**7** and with the tetranuclear Co_3Ru cluster complex **8**. Important bond lengths and angles are collected in Table 1 and Table 3. Views of the cluster molecules are presented in Figure 1 and Figure 2. The crystal structure of $[(C_5H_5)]_2Co]^+$-**7** was also determined. Unfortunately, the quality of the diffraction data obtained from this salt did not allow a complete refinement of the structure.

Table 2. Selected bond lengths [Å] and angles [°] for $[Co_3(CO)_6(\mu_3\text{-}C_8H_8)]^-$ (**7**) in $[NEt_4]^+$-**7**.

Co1–Co1A	2.507(2)	Co1–C1	2.516(5)
Co1–Co2	2.530(2)	Co1–C2	2.105(4)
C1–C2	1.402(4)	Co1–C3	2.173(4)
C2–C3	1.409(5)	Co2–C4	2.270(4)
C3–C4	1.426(6)	Co2–C5	2.076(5)
C4–C5	1.408(4)		
Co–C(CO)$_{term.}$	1.742(4), 1.751(5)	Co–C(CO)$_{bridge}$	1.905(4), 1.918(3), 1.899(4)
C2A–C1–C2	137.6(5)	C4–C5–C4A	132.4(5)
C1–C2–C3	132.7(4)	C2–C3–C4	134.0(4)
C3–C4–C5	135.6(4)		

Table 3. Selected bond lengths [Å] and angles [°] for $[Ru(C_5Me_5)Co_3(CO)_6(\mu_3\text{-}C_8H_8)]$ (**8**)

Co1–Co2	2.526(2)	Co2–Co3	2.530(2)
Co1–Co3	2.531(2)	Ru1–Co1	2.589(2)
Ru1–Co2	2.587(2)	Ru1–Co3	2.596(2)
Co1–C44	2.125(10)	Co1–C45	2.098(10)
Co2–C46	2.383(11)	Co2–C47	2.041(10)
Co2–C48	2.226(10)	Co3–C41	2.223(9)
Co3–C42	2.067(9)	Co3–C43	2.354(10)
C41–C42	1.408(14)	C41–C48	1.425(14)
C42–C43	1.394(16)	C43–C44	1.448(16)
C44–C45	1.433(17)	C45–C46	1.425(17)
C46–C47	1.433(18)	C47–C48	1.372(17)
Co–C11, C21, C31	1.769(10)...1.781(11)	Co–C12, C22, C32	1.975(9)...2.019(9)
Ru1–C12, C22, C32	2.092(9)...2.125(9)	Ru–C(C_5Me_5)	2.207(9)...2.240(9)
C48–C41–C42	135(1)	C41–C42–C43	133(1)
C42–C43–C44	136(1)	C43–C44–C45	132(1)
C44–C45–C46	135(1)	C45–C46–C47	133(1)
C46–C47–C48	135(1)	C47–C48–C41	135(1)

The crystal structures of the salts consist of a packing of isolated cations $[NEt_4]^+$ and $[(C_5H_5)_2Co]^+$, respectively, and anions **7**. In both cases, molecular C_s symmetry is imposed on the cluster anions **7** by the space group symmetry. The isosceles triangular array of cobalt atoms is capped by the C_8H_8 ligand in the facial μ_3-η^3:η^3:η^3 coordination mode. Within the experimental errors the anions in the two structures are essentially superimposable. The metal core of complex **8** consists of a distorted Co_3Ru tetrahedron with very nearly C_{3v} symmetry. The facial C_8H_8 ligand binds to the Co_3 face of the cluster in essentially a μ_3-η^2:η^3:η^3 fashion. In both **7** and **8**, the cyclooctatetraene ligands are somewhat puckered and approach a chair-like conformation, with endocyclic torsion angles between 2 and 24°. The pattern of carbon–carbon bond lengths within the μ_3-C_8H_8 rings is rather irregular, spanning the range of 1.402(4)...1.426(6) Å in **7** and 1.372(17)...1.448(16) Å in **8**. In both **7** and **8**, every cobalt atom bears a terminal carbonyl ligand, which is at an angle of about 20° to the Co_3 plane, bent away from the facial C_8H_8 ligand. In **7**, the three remaining carbonyls are bridging the edges of the metal cluster. In complex **8**, the three Co_2Ru faces are fairly symmetrically capped by μ_3-CO ligands.

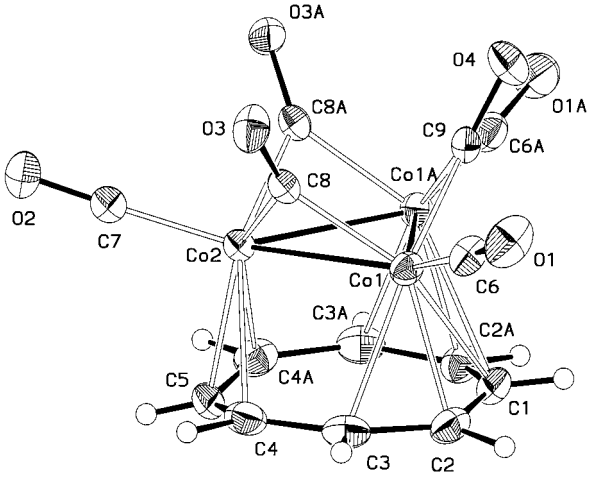


Figure 1. Molecular structure of $[Co_3(CO)_6(\mu_3\text{-}C_8H_8)]^-$ (**7**) in the crystals of $[NEt_4]^+$-**7**

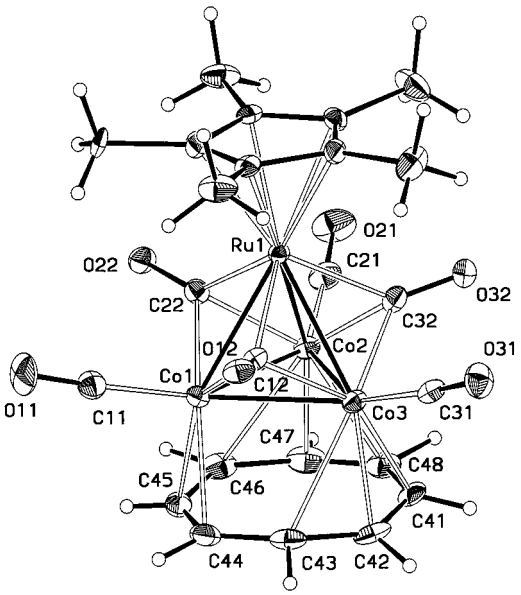


Figure 2. Molecular structure of $[Ru(C_5Me_5)Co_3(CO)_6(\mu_3\text{-}C_8H_8)]$ (**8**)

Discussion

The observed reductive degradation of the μ_3-cyclooctatetraene tetracobalt cluster complexes **3–6** to give the trinuclear **7** has a parallel in the reduction chemistry of the parent binary carbonyl, $[Co_4(CO)_{12}]$ (**1**). However, reduction of **1** is very difficult to stop at the trinuclear stage, $[Co_3(CO)_{10}]^-$ (**2**). This anion is quite unstable and only forms as an ion pair in the presence of a weakly solvated Li^+ counterion.[6] Removal of the stabilising Li^+ from the cluster, e.g. by means of addition of even small percentages of donor ligands such as THF, leads to complete decomposition.[6] As is expected for salts with fairly big organic cations, there is no ion pairing in the crystal structures of $[NEt_4]^+$-**7** and $[(C_5H_5)_2Co]^+$-**7**. These salts can even be heated under reflux in THF for hours without decomposition. Hence, the anion **7** must indeed be greatly stabilised

by the bridging C_8H_8 ligand, compared to the isoelectronic binary carbonyl cluster complex **2**.

We assume that the primary step in the formation of **7** is the transfer of an electron from the reducing agent to the starting clusters **3–6**, to give the tetranuclear radical anions $[\mathbf{3}]^-$ – $[\mathbf{6}]^-$. An alternative nucleophilic attack of **3–6** by hydride from $Li[HBEt_3]$, followed by degradation of the addition product is unlikely. Such a mechanism would not account for the formation of **7** during the reaction of **3** with the cyclopentadienes. We assume that cobaltocene or decamethylcobaltocene, respectively, is formed here from C_5R_5H and $[(C_5R_5)Co(C_8H_8)]$, which is one of the other reaction products. Reduction of the remaining **3** by $[(C_5R_5)_2Co]$ would then lead to the same intermediate as in the reaction with $Li[HBEt_3]$. This view is corroborated by the results of the direct reaction of **3** with cobaltocene that quantitatively generates $[(C_5H_5)_2Co]^+$-**7**.

Spectroscopic evidence for the transient formation of an anionic tetranuclear species comes from the reaction of **6** and $Na_2[Fe(CO)_4]$. The infrared absorptions of the primary product display the pattern characteristic of a $Co_4(CO)_3(\mu_3\text{-}CO)_3$ cluster core; their bathochromic shift relative to those of **6** ($\Delta\tilde{\nu}$ = 40–45 cm^{-1}) is consistent with an anionic tetranuclear cluster, which could be $[\mathbf{6}]^-$ or even $[\mathbf{6}]^{2-}$.

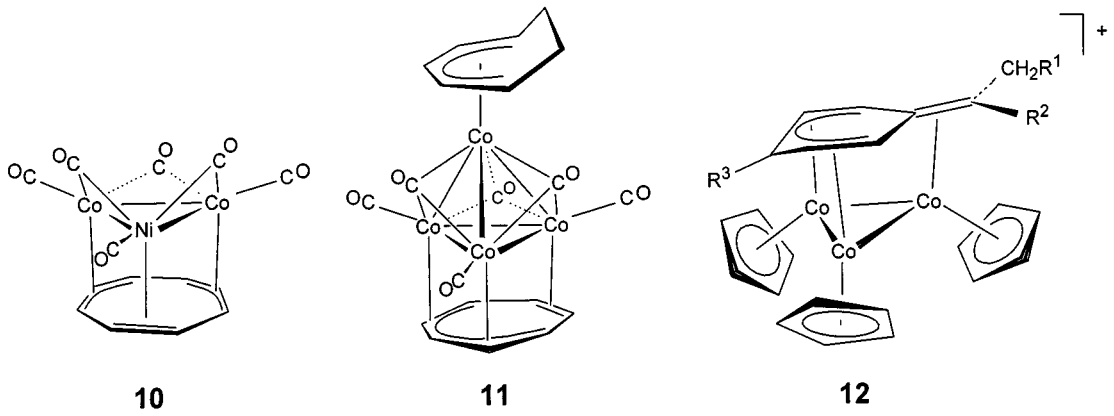
As shown by the cyclic voltammetry experiments, the anions $[\mathbf{3}]^-$, $[\mathbf{5}]^-$ and $[\mathbf{6}]^-$ have a considerable lifetime, at least in the electrochemical double layer. The fragmentation reaction observed after chemical reduction in a preparative scale could be promoted by the different solvent (THF instead of CH_2Cl_2) or else be too slow to have a great effect on the cyclic voltammograms. Complex $[\mathbf{4}]^-$ appears to be more labile in the timescale of our electrochemical experiments. It is however not clear if the observed potential current response is due to the onset of cluster degradation, or to a facile dissociation of carbon monoxide[9] from $[\mathbf{4}]^-$.[10]

The low stability of anionic tetranuclear cluster complexes of cobalt was noted by Chini 30 years ago.[5,11] A stabilisation by the presence of chelating di- and triphosphane ligands was observed.[3] We note here that capping of a Co_3 face in $[Co_4(CO)_{12}]$ (**1**) with the tripodal ligand $HC(PPh_2)_3$ results in a system which does not degrade at all upon reduction,[9,12] in contrast to our C_8H_8-capped cluster **4**.

The structure of the trinuclear anion **7** does not depend on the counterion; it is quite similar to that of its neutral isoelectronic analogue, $[Co_2Ni(CO)_3(\mu_2\text{-}CO)_3(\mu_3\text{-}C_8H_8)]$ (**10**)(Scheme 3).[13] Minor differences are the shorter mean metal–metal distance in **10** (2.514 Å),[13] due to the smaller nickel atom, and the somewhat different coordination mode of the facial C_8H_8 ligand, which is $\mu_3\text{-}\eta^3\text{:}\eta^3\text{:}\eta^3$ in **7** and more like $\mu_3\text{-}\eta^2\text{:}\eta^3\text{:}\eta^3$ in **10**. In the Co_3Ru complex **8**, the C_8H_8 ligand also attains the $\mu_3\text{-}\eta^2\text{:}\eta^3\text{:}\eta^3$ coordination mode, which is the one more commonly found for facially coordinated C_8H_8.[8] In a localised view of the bonding, the π-system of the $\mu_3\text{-}\eta^2\text{:}\eta^3\text{:}\eta^3$-cyclooctatetraene may be grouped into one η^2-coordinated ′ene′ and two η^3-′enyl′ subunits. In the $\mu_3\text{-}\eta^3\text{:}\eta^3\text{:}\eta^3$ ligand, there are three η^3-′enyl′ units, two of which are sharing one carbon atom. This atom (C1 in **7**) is at a very long distance from the nearest Co atoms [Co1 and Co1a, 2.516(5) Å in **7**]. A similar situation was encountered previously involving part of the $\mu_3\text{-}\eta^2\text{:}\eta^3\text{:}\eta^3$-cycloheptatrienyl ligand in the related complex $[Co_4(CO)_3(\mu_3\text{-}CO)_3(\eta^5\text{-}C_7H_9)(\mu_3\text{-}C_7H_7)]$ (**11**) (Scheme 3),[7] and the $\mu\text{-}\eta^3\text{:}\eta^3$-coordinated cyclohexadienyl part of the benzyl ligand in the cations $[\{(C_5H_5)Co\}_3(\mu_3\text{-benzyl})]^+$ (**12**) (Scheme 3).[14]

It should be stressed, however, that we do not wish to attach much significance to the variations in the actual orientation of the facial C_8H_8 ring relative to the bonding M_3 plane, as observed in the crystals. Topologically, there is little difference between these coordination modes; they can be converted into one another by a rather small (less than 8°) rotation of one ring. As indicated by the NMR spectra, rotation of the facial μ_3-cyclooctatetraene ′on top′ of the metal triangle is very easily accomplished in solution. Although the anisotropic displacement parameters of the C_8H_8 ring carbons do not show a large distortion, this dynamic process might be operative in the crystals as well.

The chair-like conformation and the irregular pattern of the carbon–carbon bond lengths of the $\mu_3\text{-}C_8H_8$ rings in **7** and **8** are quite similar to those established earlier for other tri- and tetranuclear cluster complexes with such li-



10 **11** **12**

Scheme 3

gands.[7,8,13] The somewhat greater spread of carbon–carbon bond lengths in the Co_3Ru complex **8** is not significant, due to the larger errors in this structure. The cobalt–cobalt distances in **8** [2.526(2)...2.531(2) Å] are also similar to the corresponding parameters in the Co_4 complexes **3–5** [2.507(2)...2.538(2) Å][7] and in the trinuclear **7** [2.507(2), 2.530(2) Å]. To our knowledge, complex **8** is the first structurally-characterised cobalt containing tetrahedral cluster with a $(C_5R_5)Ru$ vertex. A comparison with data from Co_3Ru clusters with a $Ru(CO)_{3-n}(PR_3)_n$ (n = 0, 1) vertex[15] indicates that Co–Ru bonds are generally slightly longer in these species. This is not unexpected in view of the higher formal oxidation state for Ru in **8**.

In general, the geometry of the $M_3(\mu_3\text{-}C_8H_8)$ subunit does not seem to be influenced much by the nuclearity (three in **7**, four in **3–6** and **8**) and overall charge of the cluster.

Conclusion

In contrast to $[Co_4(CO)_{12}]$ (**1**), reduction of some of its derivatives with a facial C_8H_8 ligand follows a single pathway, and leads to extrusion of a cobalt vertex from the cluster. The product $[Co_3(CO)_6(\mu_3\text{-}C_8H_8)]^-$ (**7**) is appreciably more stable than the corresponding binary carbonyl $[Co_3(CO)_{10}]^-$ (**2**). It is obvious that this is due to an effective stabilisation of the triangular array of cobalt atoms by the bridging cyclopolyene ligand.

Experimental Section

General Procedures: All operations were carried out under an atmosphere of purified nitrogen or argon (BASF R3–11 catalyst) using Schlenk techniques. Solvents were dried by conventional methods. Silica used as a stationary phase for column chromatography was heated to 180–200 °C under vacuum for several days and then stored under nitrogen. The cluster complexes **3–6** were prepared by published methods.[7] – NMR spectra were obtained on Bruker AC 200 and AVANCE DRX200 instruments (200.1 MHz for ^1H, 50.3 MHz for ^{13}C). ^1H and ^{13}C chemical shifts are reported vs. $SiMe_4$ and were determined by reference to internal $SiMe_4$ or residual solvent peaks. – Infrared spectra were recorded in CaF_2 cells with a Bruker IFS-28 Fourier transform spectrometer (optical resolution 0.5 cm^{-1}). – Electrochemical experiments were carried out using a EG & G PARC Model 173 potentiostat and a Model 175 Universal Programmer. Redox potentials are referenced to the standard calomel electrode (SCE). – Elemental analyses were performed locally by the microanalytical laboratory of the Organisch-Chemisches Institut der Universität Heidelberg and by Mikroanalytisches Labor Beller, Göttingen.

$[NEt_4]^+[Co_3(CO)_6(\mu_3\text{-}C_8H_8)]^-$ ($[NEt_4]^+$-7): An equimolar amount of $Li[HBEt_3]$ (1 M solution in THF) is slowly added to 1.63 g (2.7 mmol) of $[Co_4(CO)_6(C_8H_8)_2]$ (**3**) in THF (20 mL). The mixture is stirred for 30 min at room temperature. The solvent is removed under reduced pressure and the residue is redissolved in 5 mL of THF. A solution of 1.0 g (6.0 mmol) of $[NEt_4]Cl$ in 30 mL of water is added dropwise within 30 min. After stirring for 1 h the precipitation of the product is completed by addition of 20 mL of *n*-heptane. The precipitate is collected on a fine glass frit (D4) and

Table 4. Details of the crystal structure determinations of $[NEt_4]^+[Co_3(CO)_6(\mu_3\text{-}C_8H_8)]^-$ ($[NEt_4]^+$-**7**) and $[Ru(C_5Me_5)Co_3(CO)_6(\mu_3\text{-}C_8H_8)]$ (**8**)

	$[NEt_4]^+$-**7**	**8**
empirical formula	$C_{22}H_{28}Co_3NO_6$	$C_{24}H_{23}Co_3O_6Ru$
crystal system	monoclinic	triclinic
space group	$P2_1/m$	$P\text{-}1$
a [Å]	7.922(4)	9.037(4)
b [Å]	16.663(9)	9.692(5)
c [Å]	8.854(5)	13.663(7)
α [°]	90	90.76(4)
β [°]	95.37(5)	93.69(4)
γ [°]	90	106.33(3)
V [Å^3]	1164(1)	1145.4(10)
Z	2	2
M_r	579.25	685.28
d_c [g cm^{-3}]	1.653	1.987
F_{000}	592	680
μ(Mo-K_α) [mm^{-1}]	2.15	2.82
X-radiation, λ [Å]	Mo-K_α, graphite monochromated, 0.71069	
data collect. temperat. [°C]	–70	–70
2 θ range [°]	3–50	3-56
hkl range	±9, 0/19, 0/10	–11/+9, –11/+12, 0/16
reflections measured		
unique reflections	2141	4250
observed [$I \geq 2\sigma(I)$]	1828	2997
parameters refined	217	345
R (obs. reflections only)	0.034	0.055
wR2 (all reflections)	0.088	0.133
($w = 1/[\sigma^2(F) + (A\ P)^2 + B\ P]$,		
A, B	0.0502, 0.59	0.0313, 8.18
P	[max(F_o^2, 0)+2 F_c^2]/3	
GOF	1.058	1.098
Largest diff. peak and hole [eÅ^{-3}]	0.49/–0.44	0.73/–0.85

washed with water, toluene and pentane to give pure dark orange polycrystalline $[NEt_4]^+$-**7** (1.57 g, 100%). – ^{1}H NMR (in CD_2Cl_2): δ = 1.35 (m, 12 H, NCH_2CH_3), 3.24 (m, 8 H, NCH_2CH_3), 4.10 (s, 8 H, C_8H_8). – $^{13}C\{^1H\}$NMR (in C_6D_6): δ = 7.7 (NCH_2CH_3), 53.0 (t, J_{CN} = 3.0 Hz, NCH_2CH_3), 69.1 (C_8H_8). – IR (ν(CO), in CH_2Cl_2): $\tilde{\nu}$ = 1977 (s), 1938 (vs), 1782 (s), 1743 (s) cm^{-1}. – $C_{22}H_{28}Co_3NO_6$ (579.3): C 45.62, H 4.87, N 2.42; found C 45.47, H 4.93, N 2.35.

$[(C_5H_5)_2Co]^+[Co_3(CO)_6(\mu_3\text{-}C_8H_8)]^-$ ($[(C_5H_5)_2Co]^+$-7): A 285 mg (0.46 mmol) sample of **3** and 330 mg (1.7 mmol) of $[(C_5H_5)_2Co]$ are dissolved in 100 mL of toluene at room temperature. A black precipitate is formed immediately, which is collected on a glass frit and washed two times with 10 mL of toluene. The product was recrystallised from THF to give 290 mg (100%) of red $[(C_5H_5)_2Co]^+$-**7**.

$[Ru(C_5Me_5)Co_3(CO)_6(\mu_3\text{-}C_8H_8)]$ (8): A mixture of 720 mg (1.2 mmol) of $[NEt_4]^+$-**7** and 550 mg (1.2 mmol) of $[(C_5Me_5)Ru(NCMe)_3][BF_4]$ in 50 mL of CH_2Cl_2 is stirred at room temperature for 1 h. After filtration of the solution the solvent is removed under reduced pressure and the residue washed with *n*-hexane. The black residue is chromatographed on silica (20·2.5 cm). A broad yellow-brown band is removed first with *n*-hexane/toluene (1:1). The dark red band obtained with CH_2Cl_2 is collected to give black polycrystalline **8** (360 mg, 44%) after removal of solvent in vacuo. ^{1}H NMR (in CD_2Cl_2): δ = 1.84 (s, 15 H, CH_3), 3.97 (s, 8 H, C_8H_8). – $^{13}C\{^1H\}$NMR (in C_6D_6): δ = 9.2 (C_5Me_5), 70.3 (C_8H_8), 105.8 (C_5Me_5). – IR (ν(CO), in THF): $\tilde{\nu}$ = 2000 (sh), 1978 (vs), 1707 (s) cm^{-1}. – $C_{24}H_{23}Co_3O_6Ru$ (685.3): C 42.06, H 3.38; found C 42.24, H 3.41.

Crystal Structure Determinations: Single crystals were grown from a dichloromethane solution at –20 °C ($[NEt_4]^+$-**7**) or by slowly cooling a hot (80 °C) solution in toluene (**8**). Intensity data were collected on a Siemens-Stoe AED2 four circle diffractometer at low temperature and corrected for Lorentz, polarisation and absorption effects (Table 4). A semi-empirical absorption correction was applied (Psi-scans). Crystals of **8** were found to be twinned; the structure was solved and refined using only the nonoverlapping reflections of the individuum which gave the higher intensities. The structures were solved by direct methods, and refined by full matrix least squares based on F^2. All nonhydrogen atoms were given anisotropic displacement parameters. The hydrogen atoms of the cyclooctatetraene rings were located from difference Fourier syntheses and refined with isotropic displacement parameters. All other hydrogens were placed in calculated positions.[16] A limited set of reflection data was also collected from a poorly crystalline specimen of $[(C_5H_5)]_2Co]^+$-**7**. The low quality of this data set allowed the structure to be solved, but was not sufficient for a complete refinement. The calculations were performed using the programs SHELXS-86 and SHELXL-93.[17] Graphical representations were drawn with ORTEP-II[18]

Acknowledgments

This work was supported by the Sonderforschungsbereich 247 der Universität Heidelberg and the Fonds der Chemischen Industrie. H. W. gratefully acknowledges the award of a Heisenberg Fellowship.

[1] H. Vahrenkamp, *Adv. Organomet. Chem.* **1983**, *22*, 169.
[2] W. E. Geiger, *Progr. Inorg. Chem.* **1985**, *33*, 275.
[3] J. Rimmelin, P. Lemoine, M. Gross, D. de Montauzon, *Nouv. J. Chem.* **1983**, *7*, 453.
[4] H. Behrens, R. Weber, *Z. Allg. Anorg. Chem.* **1955**, *281*, 190.
[5] P. Chini, V. Albano, S. Martinengo, *J. Organomet. Chem.* **1969**, *16*, 471.
[6] [6a] G. Fachinetti, *J. Chem. Soc., Chem. Commun.* **1979**, 396. – [6b] H.-N. Adams, G. Fachinetti, J. Strähle, *Angew. Chem.* **1980**, *92*, 411.
[7] H. Wadepohl, S. Gebert, H. Pritzkow, D. Braga, F. Grepioni, *Chem. Eur. J.* **1998,** *4,* 279.
[8] H. Wadepohl, Coord. Chem. Rev. **1999**, *185-186*, 551.
[9] J. Rimmelin, P. Lemoine, M.Gross, A. A. Bahsoun, J. A. Osborn, *Nouv. J. Chem.* **1985**, *9*, 181.
[10] A more detailed study of the electrochemistry of **3**–**6** currently in progress.
[11] P. Chini, B. T. Heaton, *Top. Curr. Chem.* **1977**, *71*, 1.
[12] A. A. Bahsoun, J. A. Osborn, C. Voelker, J. J. Bonnet, G. Lavigne, *Organometallics* **1982**, *1*, 1114.
[13] H. Wadepohl, S. Gebert, R. Merkel, H. Pritzkow, *Chem. Commun.* **1999**, 389.
[14] H. Wadepohl, M. J. Calhorda, M. Herrmann, C. Jost, P. E. M. Lopes, H. Pritzkow, *Organometallics* **1996**, *15*, 5622.
[15] [15a] M. Hidai, M. Orisaku, M. Ue, Y. Koyasu, T. Kodama, Y. Uchida, *Organometallics* **1983**, *2*, 292. – [15b] P. Braunstein, J. Rosé, A. Dedieu, Y. Dusausoy, J.-P. Mangeot, A. Tiripicchio, M. Tiripicchio-Camellini, *J. Chem. Soc., Dalton Trans.* **1986**, 225. – [15c] J. Pursiainen, T. A. Pakkanen, *J. Organomet. Chem.* **1986**, *309*, 187. – [15d] S. Rossi, J. Pursiainen, M. Ahlgren, T. A. Pakkanen, *Organometallics* **1990**, *9*, 475. – [15e] J. Pursiainen, P. Hirva, T. A. Pakkanen, *J. Organomet. Chem.* **1991**, *419*, 193. – [15f] P. Braunstein, Feng Ying Jiao, J. Rosé, P. Granger, F. Balegroune, O. Bars, D. Grandjean, *J. Chem. Soc., Dalton Trans.* **1992**, 2543. – [15g] P. Braunstein, L. Mourey, J. Rosé, P. Granger, T. Richert, F. Balegroune, D. Grandjean, *Organometallics* **1992**, *11*, 2628. – [15h] H. J. Kakkonen, M. Ahlgren, T. A. Pakkanen, J. Pursiainen, *Acta Crystallogr., Sect.C (Cryst. Struct. Comm.)* **1994**, *50*, 528. – [15i] P. Braunstein, J. Rosé, D. Toussaint, S. Jaaskelainen, M. Ahlgren, T. A. Pakkanen, J. Pursiainen, L. Toupet, D. Grandjean, *Organometallics* **1994**, *13*, 2472. – [15j] T. Teppana, S. Jaaskelainen, M. Ahlgren, J. Pursiainen, T. A. Pakkanen, *J. Organomet. Chem.* **1995**, *486*, 217. – [15k] H. J. Kakkonen, M. Ahlgren, J. Pursiainen, T. A. Pakkanen, *J. Organomet. Chem.* **1996**, *507*, 147. – [15l] H. J. Kakkonen, M. Ahlgren, T. A. Pakkanen, J. Pursiainen, *J. Organomet. Chem.* **1996**, *518*, 203.
[16] Crystallographic data (excluding structure factors) for the structures reported in this paper have been deposited with the Cambridge Crystallographic Data Centre as supplementary publication no. CCDC-135215 ($[NEt_4]^+$-**7**) and 135216 (**8**). Copies of the data can be obtained free of charge on application to The Director, CCDC, 12 Union Road, Cambridge CB2 1EZ, UK (Fax: (Internat.) + 44 1223/336 033; E-mail: deposit@ccdc.cam.ac.uk).
[17] *SHELXS-86*: G. M. Sheldrick, *Acta Crystallogr.* **1990**, *A46*, 467; *SHELXL-93*: G. M. Sheldrick, Universität Göttingen **1993**.
[18] *ORTEP-II*: C. K. Johnson, Report ORNL-5138. Oak Ridge National Laboratory, Tennessee, USA.

Received October 4, 1999
[I99345]

Chiral Dilithiomethane Derivatives: Structure Determination and Application in Stereoselective Reactions

Jürgen F. K. Müller[a]

Keywords: Asymmetric synthesis / Chirality / Computer chemistry / Lithium / Dilithiomethane / Sulfoximines

The synthesis and X-ray analysis of chiral dilithiomethane analogues derived from sulfoximines are presented. The structures of the sulfoximine-stabilised mono- and dilithio salts have been compared and allow a rationalization of the second lithiation. Organophosphorus-based dilithiomethane derivatives are also structurally described. The gas-phase structures of *N*,*S*,*S*-trimethylsulfoximine **19** and of its mono- and dilithiated isomers **20–21** were calculated by ab initio methods employing different levels of theory. For an application in asymmetric synthesis, the dilithiation of (*N*-methyl)-*S*-ethyl-*S*-phenylsulfoximine (**11**) afforded a chiral dinucleophile that undergoes highly regio- and stereoselective alkylation reactions with electrophiles. The transmetallation of a chiral dilithiomethane reagent such as **14** with $ClTi(OiPr)_3$ followed by addition of an aldehyde, constitutes a simple one-pot process for the formation of (*E*)-alkenylsulfoximines with excellent diastereoselectivity.

1. Introduction

Since its discovery, dilithiomethane (**2**) has challenged researchers in various fields of chemistry such as synthetic organic chemistry, organometallic chemistry, and computational chemistry. The first landmark was achieved by Ziegler et al. who developed the first synthetic route to dilithiomethane.[1]

$$\underset{\mathbf{1}}{2\,CH_3Li} \xrightarrow{\Delta} \underset{\mathbf{2}}{CH_2Li_2} + CH_4$$

[a] Department of Chemistry, University of Basel
Spitalstrasse 51, 4056 Basel, Switzerland
Fax: (internat.) + 41-61/267-1018
E-Mail: juergen.mueller@unibas.ch

The high reactivity of **2** towards oxygen and moisture, together with its notorious instability and poor solubility in organic solvents, complicated its structural characterisation. After early solid state NMR studies, Stucky et al. suggested an X-ray structure of CD_2Li_2 in 1990 derived from powder diffraction data.[2,3] Computational studies suggested various gas phase structures and even higher aggregates of **2**.[4] For synthetic purposes, however, heteroatom-substituted organolithiums are better qualified than simple alkyllithium compounds. The same is true for heteroatom-substituted geminal dilithiated organic compounds, which have been shown in recent years to possess great synthetic potential.[5] This led to the development of new synthetic strategies, with the aim of synthesising assemblies of complex molecular structures with a minimum of chemical steps more effici-

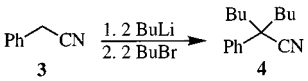


Jürgen Friedrich Karl Müller was born in 1963. He studied chemistry at the University of Freiburg (Germany) from 1983 until 1989 and performed his PhD studies in the group of Prof. Dr. Carsten Bolm at the University of Basel (Switzerland), Department of Organic Chemistry (1990−1993). The topic of the thesis was "Enantioselective catalysis with transition metals". During a postdoctoral stay at the University of Hawaii in the group of Prof. Dr. M. Tius (1994−1995) the author worked in the field of marine natural product synthesis and structure determination. Presently J. F. K. Müller works on his "Habilitation" at the Institute for Inorganic Chemistry of the University of Basel. His general research interests are: structure determination of chiral organo(di)metallics, their application in stereoselective synthesis and computational evaluation. Asymmetric catalysis with chiral sulfur and phosphorus compounds, design and synthesis of enzyme inhibitors.

MICROREVIEWS: This feature introduces the readers to the authors' research through a concise overview of the selected topic. Reference to important work from others in the field is included.

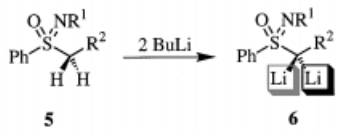
 © WILEY-VCH Verlag GmbH, D-69451 Weinheim, 2000 1434−1948/00/0505−0789 $ 17.50+.50/0

ently. For example, multiple C–C bond formations in a single reaction step have been reported from the reaction of dilithiated nitriles, sulfonamides, sulfones and phosphonates with various electrophiles.[6–9]



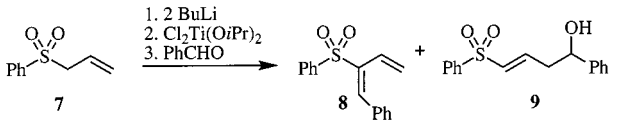
3 4

Unfortunately, a common drawback of all of these reagents is the lack of chirality, which prevents a successful application in asymmetric reactions. If such a dilithiomethane derivative bears a chiral auxiliary adjacent to its geminal dilithiated carbon atom, the two positions of the lithium atoms become nonequivalent because they are in a diastereotopic environment. We have chosen the sulfoximine group, the aza analogue of a sulfone, as a chiral auxiliary, which should allow the twofold abstraction of acidic hydrogen s bound to the adjacent carbon atom in **5**.[10] Phosphorus based chiral auxiliaries, which already have demonstrated a great versatility in asymmetric synthesis, have also to be taken in account.[11]



5 6

One would expect that the reactivity of each geminal bound lithium atom towards electrophiles differs, and might be used for synthetic purposes in asymmetric reactions. Transmetallation with one equivalent of a transition metal compound leads to mixed organodimetallics that are less reactive. This opens the possibility of directing the chemo-, regio-, and stereoselectivity by the appropriate choice of the second metal, which could induce better stereocontrol. Indeed, previous reports on an achiral sulfone **7** demonstrated that such doubly heterometallated lithium-titanium sulfones undergo highly diastereoselective addition to aldehydes forming predominantly (*E*)-alkenes **8** and **9**.[12]



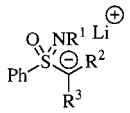
7 8 9

Early investigations into the reactivity of acceptor-substituted organodilithium compounds led finally to the conclusion that, derived from trapping reactions, the intermediates in general have to be geminal dilithio species. This assumption turned out to be erroneous as the first structural investigations of such intermediates have shown. In certain cases NMR and crystallographic studies led to the discovery of the so called "Quasi Dianion Complexes" (QUADAC's), which simulate a second lithiation, but in chemical reality these are complexes between a monolithium compound and a second equivalent of a lithium base as found, for instance, for a "doubly" lithiated nitrile.[13] True dilithiomethane derivatives derived from a sulfone or nitrile are formed only in the presence of a second stabilising group such as trimethylsilyl or vinyl.[14–16] As a consequence, the demand for a structural confirmation of a chiral dilithiomethane derivative has yet to be fulfilled before its synthetic properties can be explored. Recent developments in low temperature diffraction and crystallisation techniques make X-ray crystallography the most powerful instrument for the structure determination of organolithiums.[17] We took advantage of this and started our investigations on the elucidation of the solid-state structures of mono- and dilithiated sulfoximines in combination with quantum chemical calculations, which have been shown to be the method of choice for the determination of the gas phase structures of lithiumorganic compounds.[18]

2. Solid State Structures

2.1 Monolithiated Sulfoximines

Despite their significance in asymmetric synthesis, the structures of monolithiated sulfoximines had not been extensively examined at the time we initiated our studies.



10 a: R^1 = Me, R^2 = R^3 = H
10 b: R^1 = R^2 = $SiMe_3$, R^3 = H
10 c: R^1 = $SiMe_3$, R^2 = H, R^3 = CH=C(Me)$_2$
10 d: R^1 = Me, R^2 = H, R^3 = CH=C(Ph)$_2$
10 e: R^1 = Me, R^2 = H, R^3 = Ph
10 f: R^1 = Me, R^2 = C(Ph)$_2$

Only two crystal structures of lithiated alkyl sulfoximines **10a**, **b** were known and have already been reviewed by Boche in 1989.[19–21] A striking feature in both tetrameric (!) aggregates is the presence of Li–C bonds to the C(α) atom, which are in strong contrast to the typical structures of lithiosulfones, known not to contain any Li–C bonds. It later turned out that in the case of lithiated allylic sulfoximines close similarities to lithiated allylic sulfones are present. A structural study by Gais and co-workers provided evidence for a solvent-separated contact ion pair of **10c**, which is devoid of Li–C contacts.[22] The monomeric species **10c** consists of a [Li(12-crown-4)$_2$] cation and a sulfonimidoyl-substituted allylic anion. The conformation of the lone pair in **10c** suggests a stabilising n_C-$s^*_{S–Ph}$ interaction (negative hyperconjugation) reminiscent of lithiosulfones.[23] Deprotonation induced a planarization of the anionic carbon atom and a pronounced reduction of the S–C(α) bond from 1.794(4) to 1.62(1) Å (Figure 1).

The X-ray structure of a lithiated allylic sulfoximine determined by our group uncovered different structural features.[24] In **10d**, two lithioallylsulfoximine units with opposite chirality are linked by N–Li–O bridges to give an eight-membered ring with the atom sequence (Li–N–S–O)$_2$ (Figure 2). Such a coordination is in good agreement with analogous arrangements in lithiosulfones.[21,25] In dimer **10d** the lithium cations are in a distorted *tetrahedral* environment consisting of the O atoms of two THF molecules and the

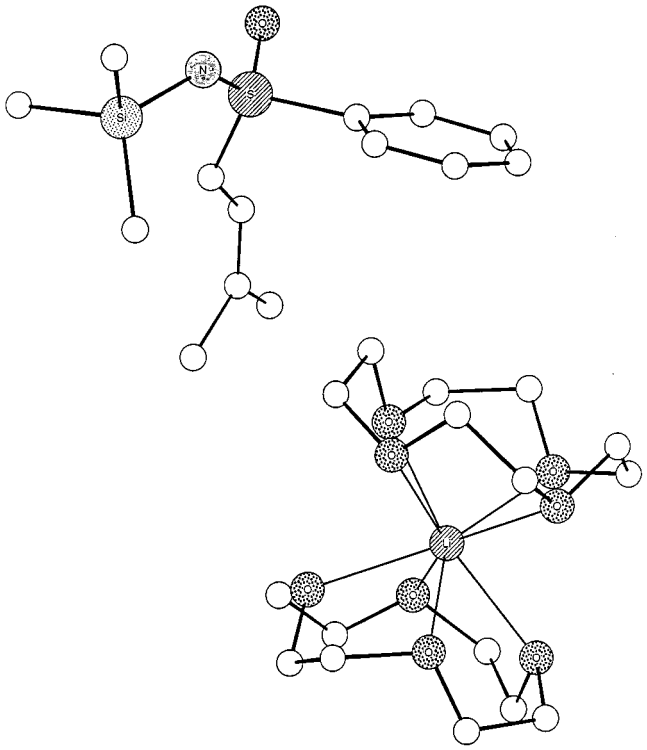


Figure 1. Molecular structure of **10c**; H atoms are omitted for clarity

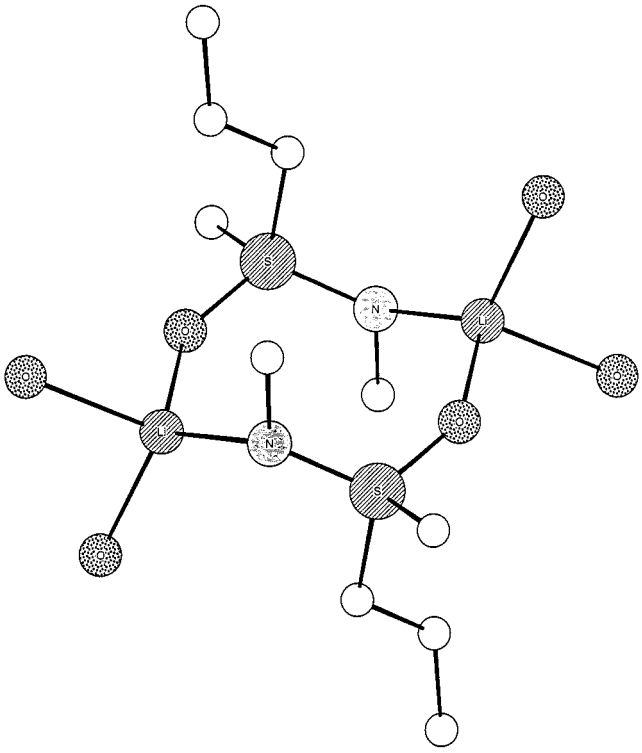


Figure 2. Molecular structure of **10d**; All H atoms, the C atoms of the phenyl groups (except the *ipso*-C's) and of the THF ligands are omitted for clarity

sulfoximine O- and N-atoms. The Li–C bond found in lithioalkylsulfoximines is absent.[19,20] The stabilisation of the negative charge at the C(α) atom by conjugation with the allylic system is more favourable than forming a Li–C bond.

Interestingly, the C(α) atom is pyramidal in spite of the conjugation with the vinyl group and the lone pair at C(α) is orientated in a *gauche* conformation between the O- and N-atoms of the sulfonimidoyl moiety. This allows a stabilisation by negative hyperconjugation.[23] Deprotonation of **10d** is accompanied by a reduction in the S–C(α) bond length of about 0.11 Å, which corresponds to the situation in **10c**. After lithiation only one of the two possible diastereomeric enantiomer pairs has been found in the crystal.

For a benzylic sulfoximine, lithiation leads to dimer **10e** with N–Li–O bridges to give an eight-membered ring with the atom sequence $(Li–N–S–O)_2$ as in **10d**.[26] The lithium cations are in a distorted *tetrahedral* coordination geometry consisting of the N atoms of two TMEDA molecules and the sulfoximine O- and N-atoms. No Li–C bond is found.

The lone pair at C(α) is orientated in a *gauche* conformation between the O and N atoms of the sulfonimidoyl moiety as found for the allylic case. The question as to whether C(α) is pyramidal or not could not be answered with certainty because the benzylic proton has not been located. A significant reduction in the S–C(α) bond length from 1.783(2) Å in the starting material to 1.66(1) Å in **10e** is observed (Figure 3).

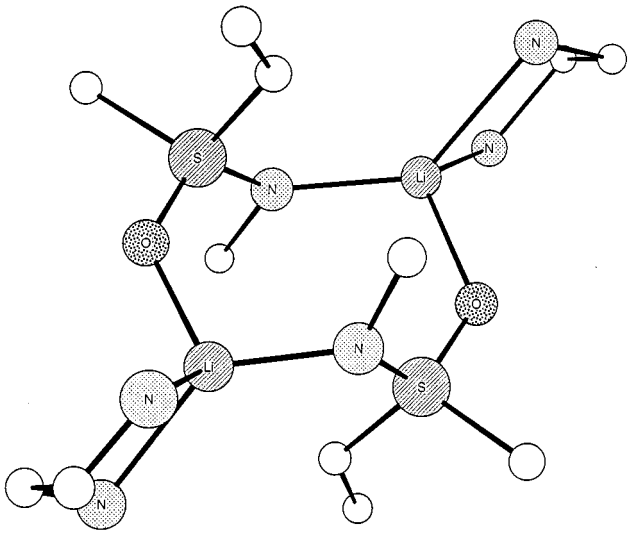


Figure 3. Molecular structure of **10e**; All H atoms, the C atoms of the phenyl groups (except the *ipso*-C's) and of the methyl groups on TMEDA are omitted for clarity

The dinuclear lithium complex **10f** of a lithiated vinylic sulfoximine is bridged through Li-sulfoximine–O bonds, forming two eight-membered rings with the different atomic sequences $(Li–O–S–N)_2$ and $(Li–O–S–C)_2$, respectively.[27] The two halves of the molecule are related by a crystallographic centre of symmetry (Figure 4).

In this complex a Li–C contact with a distance of 2.209(6) Å leads, together with the lithium coordination to the sulfoximine-N-atom, to an Li–N–S–C four-membered ring chelate. In this respect, **10f** differs both from lithiovinylsulfones and lithioallyl(or benzyl)sulfoximines, which do not show Li–C bonds, and from higher associated lithioalkylsulfoximines.[19,20,22,24,28] The *tetrahedral* four-coordination of the lithium cation is completed by coordination

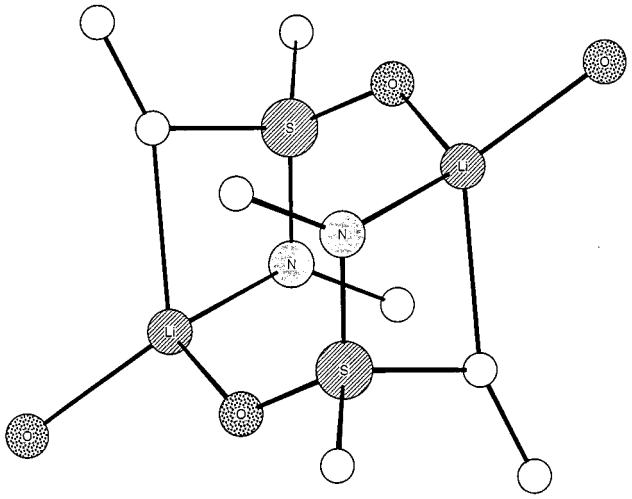


Figure 4. Molecular structure of **10f**; All H atoms, the C atoms of the phenyl groups (except the *ipso*-C's) and of the THF ligands are omitted for clarity

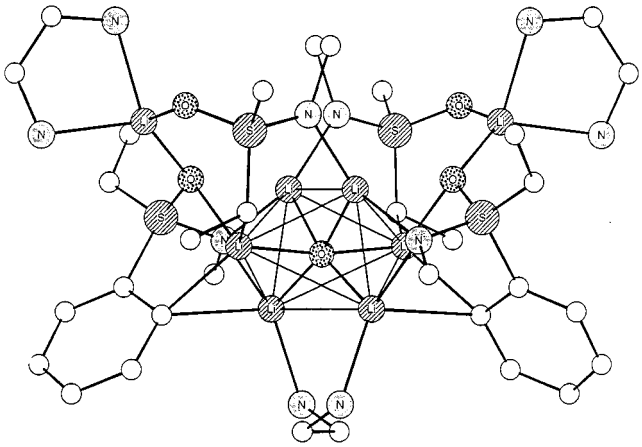
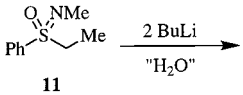


Figure 5. Molecular structure of **12**; all H atoms, the C atoms of the phenyl groups (except the *ipso*-C's) of the monolithiated sulfoximine units and of the methyl groups on TMEDA are omitted for clarity; the thin lines serve to emphasise the geometrical relationship of the Li_6–O core and are not to be considered normal bonds

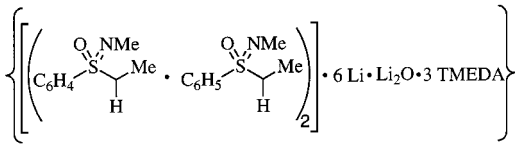
to an O atom of a THF molecule. The S–C(α) bond length is slightly shortened from 1.753(2) Å in the C–H acid to 1.734(3) Å in **10f**. Compared to lithiovinylsulfones this reduction is small and reveals the minor stabilising abilities of the sulfonimidoyl group.[28]

2.2 Dilithiated Sulfoximines

Achiral sulfone- or nitrile-based dilithiomethane compounds have already been investigated in the solid state and have been reviewed previously.[14,15,21] However, an attempt to crystallise a chiral dilithiomethane derivative was first undertaken by our group.[29] Dilithiation of **11** leads to a mixed aggregate containing mono- and dilithiated (*N*-methyl)-*S*-ethyl-*S*-phenyl-sulfoximine units in a 2:2 ratio coordinated by 3 TMEDA ligands. Compound **12** crystallises in the space group *C*2/c and the unit cell contains 4 of the clusters together with 8 disordered TMEDA molecules (Figure 5). The unit cell contains two clusters each composed of two sulfoximine dianions in the (*R*) configuration and two sulfoximine monoanions in the (*S*) configuration. Since the lattice is centrosymmetric, there are two clusters in which these configurations are reversed. This means that an internal chiral resolution has taken place within the clusters. The centre of the aggregate is characterised by a distorted *octahedral* Li_6–O unit due to incorporated Li_2O. In certain cases, Li_2O has been observed in crystalline organolithium compounds where it served as a template for crystallisation.[30] The dianionic subunit in **12** is characterised by two Li–C contacts of the *ortho* C atom to form five-membered ring chelates with the heteroatoms on sulfur and not with a geminal dilithiated structural motif. For Li(2) a coordination to the sulfoximine-O atom, a single O atom derived from Li_2O and a C(α) atom of the neighbouring sulfoximine monoanion is found, whereas Li(4) is coordinated to a sulfoximine N atom, the oxygen of the Li_2O core and an N atom of one TMEDA ligand. For such an *ortho*-directing effect only little data exist for sulfoximines in contrast to sulfones, which are known to be powerful *ortho*-directing groups.[31,32] Despite being deprotonated, a Li–C bond to the C(α) atom is not observed. This is consistent with a substantial S–C multiple bond character, which lowers the basic character of this carbon atom and is supported by a short S–C(α) distance of 1.62 Å (vs. 1.73 Å in protonated sulfoximines).[22,24]



11



12

The anionic C(α) atom has a nearly planar configuration. In the monoanionic sulfoximine moiety, a Li–C(α) contact is observed (2.25 Å) whereas the two heteroatoms are coordinated to two additional Li^+ cations, an arrangement unknown for monolithiated sulfoximines.[19,20,22,24,26,27] In this case, the C(α) atom has a distinct pyramidal configuration. The C(α)–Li bond is arranged in a *gauche* conformation between the N- and O-atoms of the sulfoximine moiety. The coordination sites of the Li atom bonded to the sulfoximine–O are occupied by two nitrogen atoms of the TMEDA ligands and the O atom of the dilithiated sulfoximine, which leads to a bridging of the mono- and dilithio sulfoximine units. A significant shortening of the S–C(α) bond is found (1.66 Å vs. 1.73 Å) in the monoanion, but this is not as pronounced as for the dianionic species where the S–C(α) bond length is 1.62 Å. This additional contraction for the dianion can be explained with the threefold and twofold lithium coordination of the sulfoximine O- and N-atoms, respectively.

The first true heterochiral dilithiomethane derivative was accessible from racemic **13** with 2.5 equivalents of *n*BuLi

and traces of H_2O.[26] A tetrameric heterochiral aggregate **14**, consisting of four dilithiated sulfoximine units and one molecule of Li_2O, which acts as a template for crystallisation, was formed (Figure 6). The core of the aggregate is characterised by a distorted Li_6O-*octahedron*, a structural motif that has been found to be a characteristic feature in **12** and a dilithiated sulfone.[14]

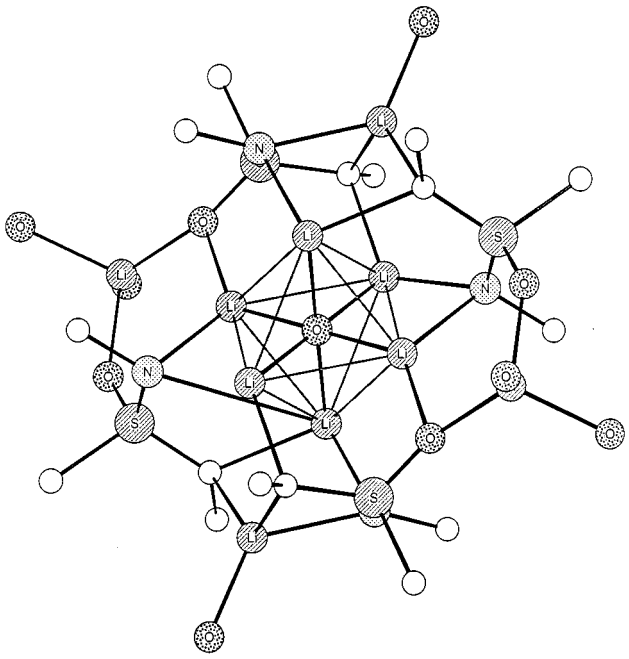
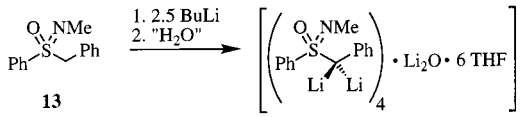


Figure 6. Molecular structure of **14**; all H atoms, the C atoms of the phenyl groups (except the *ipso*-C's) and of the THF ligands are omitted for clarity; the thin lines serve to emphasise the geometrical relationship of the Li_6–O core and are not to be considered normal bonds



Two different dilithiated C atoms are in the asymmetric unit, each connected to two Li^+ ions and therefore distinctly pyramidalized. At C(21) the two Li^+ ions coordinate to a neighbouring sulfoximine nitrogen, forming either Li–C–S–N four-membered ring motifs, as known from monolithiosulfoximines, or C–Li–N–Li–O–S six-membered rings. They also differ in their further coordination sphere: Li(2) shows heteroatom coordination (N,O), whereas Li(5) has one additional C–Li bond, while bridging two different dimetallated C atoms, and a Li–N contact. For C(1), Li(5) is also bound to C(21), leading to a Li–C–Li–C–S–N six-membered ring. The Li^+ in the bridging position complements its fourfold coordination by complexation to a THF oxygen. Li(2) coordinates to the central O atom of the Li_6O core, inducing a six-membered Li–O–Li–O–S–C ring, via the sulfoximine oxygen. The Li–C distances [range 2.19(2)–2.21(2) Å] are similar to that in the monolithiated sulfoximine **10f**. The Li–N distance within the Li–C–S–N chelate [2.23(2) Å] is comparable to that in **10f** and those found in previous investigations. The Li–O bond length to the sulfoximine-O atoms are significantly longer than those within the (Li_6–O) core. A characteristic property is the extremely short S–C(α) bonds [1.61(1), and 1.64(1) Å] compared to **13** [1.783(2) Å] and **10e** [ca. 1.66(1) Å], which is also typical for related sulfones,[14] phosphonates,[33] phosphinimines,[34] and nitriles.[15] The geminal-bound Li atoms adopt a *gauche* conformation between the N- and O-atoms of the sulfoximine moiety and between the sulfoximine-N atom and the *ipso*-C atom, thus confirming sp^3-hybridized C(α) atoms.

In summary, sulfoximines are clearly able to serve as chiral substrates for the creation of well defined chiral dilithio compounds. As a first rule, it seems that those monolithiosulfoximines that do contain C–Li bonds form α,*o*-dilithio salts after the second lithiation. There is no close proximity of the carbon-bound lithium ion to the *ortho* protons of the phenyl group, as one might expect to find for an *ortho* directing effect. We believe that *ortho* attack is favoured because there is less steric hindrance caused by the solvated and C(α)-bound Li^+. For sulfoximines bearing an additional stabilising substituent, such as a phenyl or vinyl group at the C(α) atom, no C–Li bonds but rather N- and O-sulfonimidoyl Li contacts are observed for its monolithiated salts. This induces a closer proximity to the *ortho* protons as in **10d**, **e**. The positioning of the Li ions in the dimeric scaffold in **10d**, **e** prevents the approach of the lithium base to the *ortho* position and directs the second lithiation to the adjacent and freely accessible C(α) atom.

2.3 Dilithiated Phosphonates

Chiral organophosphorus compounds are extraordinarily significant as reagents in asymmetric synthesis.[35] To date, however, phosphorus-stabilised dilithiomethane analogues have been rarely used in synthesis, and the lack of direct evidence led to doubt about the existence of such compounds.[36] The first experimental proof for a geminal dilithiated phosphorus compound is represented by the lithium cluster **16**.[33] The hexameric aggregate consists of six dilithiated phosphonate units and two molecules of dimethylamide. In addition, two Li^+ ions are coordinated by four TMEDA ligands in a distorted *tetrahedral* fashion, balancing the remaining two negative charges. The core of the aggregate is characterised by a Li–O–Li–O four-membered ring and contains the crystallographic inversion centre (Figure 7). Such a structural motif has been found to be an essential feature in these kinds of monolithiated phosphonate, which do not contain C–Li bonds.[37]

There are three different dilithiated C atoms in the asymmetric unit, each connected to two Li^+ ions and distinctly pyramidalized. These geminal bound Li^+ ions coordinate in a similar fashion to a neighbouring phosphonate oxygen, forming C–Li–O–Li four-membered ring motifs. The incorporation of lithium dimethylamide is due to the use of excess *n*BuLi in TMEDA, which leads to the decomposition products *N*,*N*-dimethylvinylamine and lithium dimethylamide at elevated temperatures.[38] However, the excess is essential for the formation of the aggregate because it be-

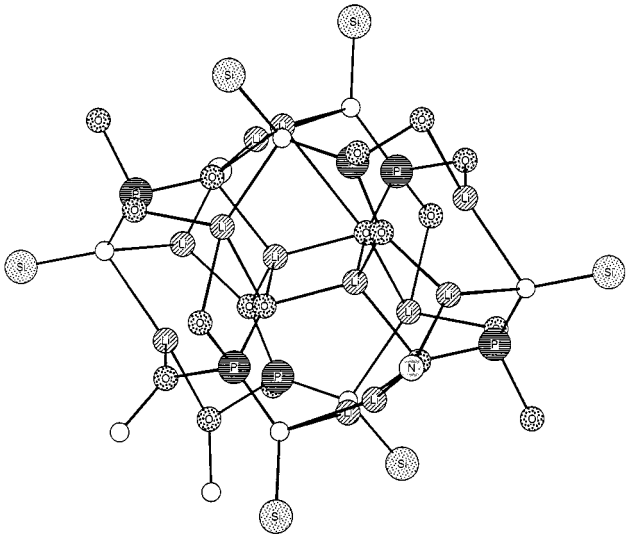
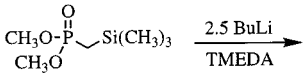
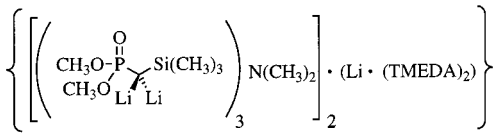


Figure 7. Molecular structure of **16**; all H atoms, the C atoms of the methyl groups on oxygen, nitrogen and silicon are omitted for clarity



15



16

haves as a bridge between the Li atoms. The Li–C distances [range 2.13(1)–2.28(1) Å] can be compared with those in monolithiated phosphonates, which have Li–C distances of 2.21–2.26 Å.[37] The Li–O distances within each C–Li–O–Li chelate [range 1.95(1)–2.85(1) Å] are significantly longer than those within the $(Li–O)_2$ core [1.895(9) and 1.903(9) Å, respectively]. A striking feature is the extremely short P–C bond lengths [1.587(6), 1.604(5) and 1.619(6) Å] compared to neutral (1.80 Å) and monolithiated phosphonates (ca. 1.68 Å). The phosphonate oxygens adopt a *gauche* conformation between the geminal Li^+ cations, clearly indicating a significant degree of pyramidalization. The foundation of this aggregate seems to be the central $(Li–O)_2$ core, which is related to the fundamental structural unit derived from several monolithiophosphonates. We therefore conclude that, after the formation of the typical four-membered rhomboid motif, the incorporation of the second lithium affects only the aggregation sphere outside of the $(Li–O)_2$ core.

2.4 Dilithiated Phosphinimines

Recently, two reports on a remarkable geminal dilithiated phosphinimine were published independently.[34a,34b] The symmetrical bisphosphinime **17** could easily be deprotonated with two equivalents of a strong lithium base to give the dimer **18** (Figure 8).

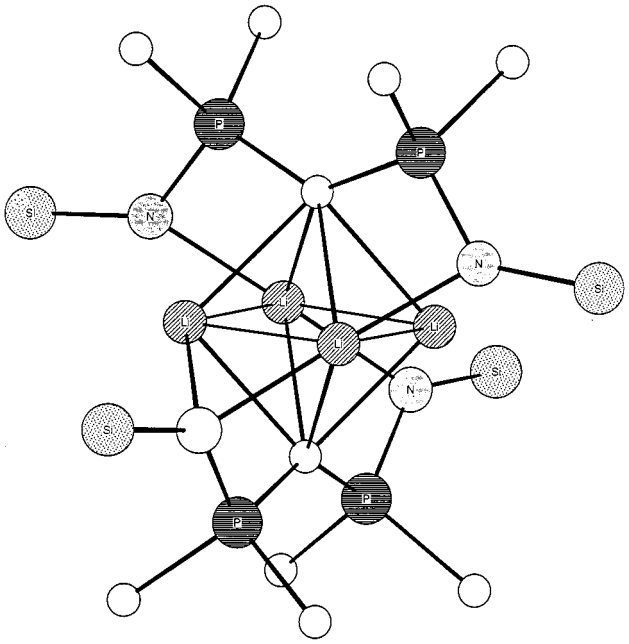


Figure 8. Molecular structure of **18**; all H atoms, the C atoms of the phenyl groups (except the *ipso*-C's) and of the methyl groups on silicon are omitted for clarity; the thin lines serve to emphasise the geometrical relationship of the Li atoms and are not to be considered normal bonds



17 **18**

In this aggregate, two dilithiated phosphinimine units are connected in a "head-to-head" manner, although repulsive interactions should be expected. This is presumably compensated by the chelating properties of the imino N atoms, which bridge two lithium atoms each. The four lithium atoms form a square plane which is capped above and below by the C(α) atoms of the P–C–P ligands, inducing a slightly dissymmetric C_2Li_4 pseudo-*octahedron*. Such a structural motif has already been predicted by computational investigations.[4] The coordination geometry around the dianionic carbon atoms is most remarkable: the N–P–C–P–N units are fairly close to planarity and adopt a perpendicular orientation to each other. In addition, they are also *orthogonal* to the central lithium square. The coordination sphere around each lithium atom is markedly distorted from the ideal *tetrahedral* geometry. The Li–C (ca. 2.38 Å) and the Li–N distances (2.09–2.15 Å) are within the range of related compounds.

3. Computational Investigations

3.1 Mono- and Dilithiated Sulfoximines

Ab initio calculations have been able to determine with considerable success the gas phase structures of achiral and chiral oxygen-, nitrogen-, phosphorus-, and sulfur-stabilized (mono)lithiocarbanions.[39–42] It was our objective to extend these studies from chiral monolithio- to dilithiosulfoximines and to elucidate the possible structures and stabilities of these dilithio intermediates by classical ab initio methods and Density Functional Theory (B3LYP).[24,43] The prochiral model system (*N*-methyl)dimethylsulfoximine **19** was chosen for our computational investigations. Ab initio calculations of the lithiated dimethylsulfoximine **20** yielded 3 different major structural minima **20a–c** (Figure 9).

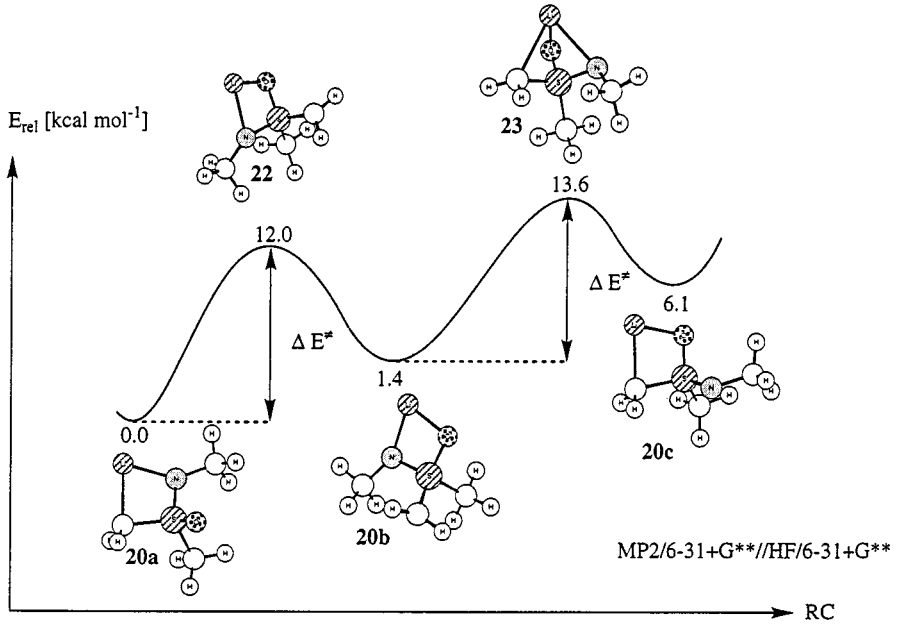
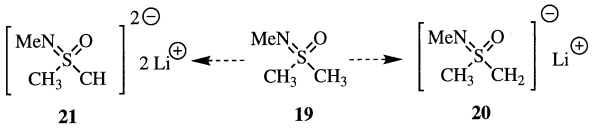


Figure 9. Local energy minima of **20a–c**



21 **19** **20**

Of these, **20a** exhibits a Li–C–S–N four-membered chelate ring; Li–O complexation and a Li–C contact are found in **20c** whereas in **20b** no Li–C contact occurs. In the latter case the sulfoximine O- and N-atoms coordinate to the lithium cation in an orientation reminiscent of typical lithiophenylsulfones and lithioallylsulfoximines.[21,24,25] The Li–N chelate **20a** represents the structure lowest in energy but, surprisingly, the sulfoximine *O*- and *N*-coordinated lithium salt **20b** is only 1.4 kcal/mol higher in energy, whereas the Li–O chelation in **20c** is clearly energetically disfavoured by 6.1 kcal/mol compared to **20a** and **20b**. Lithiation of the dimethylsulfoximine **19** causes a number of distinctive structural changes in **20a–c**: in **20a** a lengthening of the S–N (1.53 vs. 1.58 Å) bond is observed. Similarly the O,C chelation in **20c** lengthens the S–O bond from 1.45 to 1.51 Å while in **20b**, with Li–N, *O*-coordination, both the S–N and S–O bonds are lengthened. The C(α)–Li contact allows only a small shortening of the S–C(α) bond in **20a** (1.72 Å) and **20c** (1.73 Å) whereas in **20b** a significant shortening of the S–C(α) bond is observed (1.63 vs. 1.77 Å in **19**). Structure **22** shows a coordination of the lithium ion to the O and N atoms and can be interpreted as the transition state between the structure minima **20a** and **20b**. The isomers **20b** and **20c** are separated by the transition state **23** by 12.2 kcal/mol. In **23** an unsymmetrical tridentate bonding of the lithium to the O, N, and C(α) atoms is found in contrast to **22** where no Li–C bonding is observed. These characteristics suggest an interconversion mechanism of **20b** to **20c** with **23** as an intermediate. Dilithiation afforded three different local energy minima (Structures **21a–c,** Figure 10).

The isomer **21a** is lowest in energy and exhibits a dilithiospirostructure containing two Li–N–S–C and Li–O–S–C chelates with two different C(α) atoms. A small change in both S–C(α) bond lengths is observed compared to the protonated parent **19** (1.77 Å in **19** vs. 1.73 and 1.75 Å in **21a**). The Li–C distances are 2.09 Å in either case. The lone pairs at the anionic C atoms point away from one another in the direction of each lithium atom, thus minimising the repulsion caused by the two negative charges. Structure **21b** represents a local minimum that is only 2.7 kcal/mol higher in energy. It is characterised by an α,α-dilithiosulfoximine arrangement in which both lithiums are attached to the same C(α) atom. In addition, each lithium is coordinated to one of the two heteroatoms of the sulfonimidoyl moiety, thereby forming (Li–N–S–C) and (Li–O–S–C) four-membered ring chelates, respectively. The S–C(α) bond is signi-

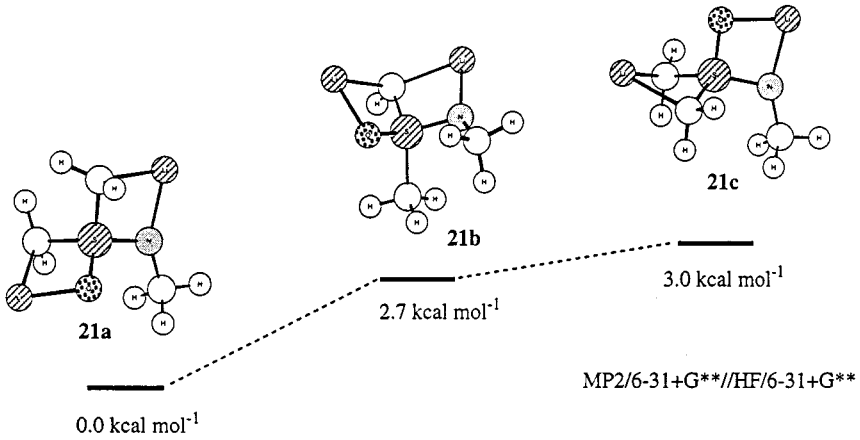


Figure 10. Local energy minima of **21a–c**

ficantly shortened after dimetallation from 1.77 Å to 1.66 Å. The lithium atom coordinating to the sulfoximine oxygen yields the longer Li–C bond with 2.11 Å. In contrast, in the N-chelate the Li–C bond is markedly shorter (2.04 Å). Both planes that are defined by the two four-membered ring chelates form a butterfly-type structure. The lithium atoms are in a diastereotopic environment, which are interesting for synthetic purposes. The local minimum structure **21c** lies 0.3 kcal/mol higher in energy than **21b**. Remarkably, in **21c** one lithium is exclusively coordinated to the heteroatoms of the sulfoximine group whereas the other shows a symmetrical bridging to the C(α) atoms. The twofold carbon coordination of the lithium is unusual, because all other chelation modes of the lithium atoms correspond to structural motifs that have already been calculated for monolithiosulfoximines. The Li–C distances are elongated to 2.23 Å in comparison to the structures **21a** (2.09Å) and **21b** (2.04 and 2.11Å).

A comparison of these major structural minima with the results of MP2(full)/6-31+G** calculations yielded only marginal changes in their geometries and energies. Greater accuracy in the determination of the relative energies may be achieved by applying CBS-Q.[44] These results show a reverse order in the relative stabilities: **21b** becomes slightly energetically favoured over **21c**, but the difference in their energies remains small (see Table 1).

Table 1. Relative energies [in kcal mol^{-1}]

	21a	21b	21c
MP2/6-31+G**//HF/6-31+G**	0.00	2.74	3.01
B3LYP/6-31+G**	0.00	4.87	2.79
CBS-Q (0 K)	0.00	2.23	1.07
CBS-4 (0 K)	0.00	0.72	2.23
MP2 (full)/6-31+G**	0.00	3.02	3.55

The same observation is made for B3LYP/6-31+G**, where **21b** is about 2.1 kcal/mol higher in energy than **21c**.[45] In conclusion, all applied methods show compound **21a** as the global minimum. The isomers **21b** and **21c** are in general 1–5 kcal/mol higher in energy and are fairly close to one another.

3.2 Gas Phase Structures of the Monolithio Sulfoximine Anions and Lithium-Free Dianions

The successive removal of a lithium cation in **21a** resulted in two different monolithiated anions **24a**$^-$ and **24b**$^-$, in which the Li–N–S–C chelate **24a**$^-$ is energetically favoured by ca. 7 kcal/mol over the Li–O–S–C complexation in **24b**$^-$ (see Figure 11 and Table 2).

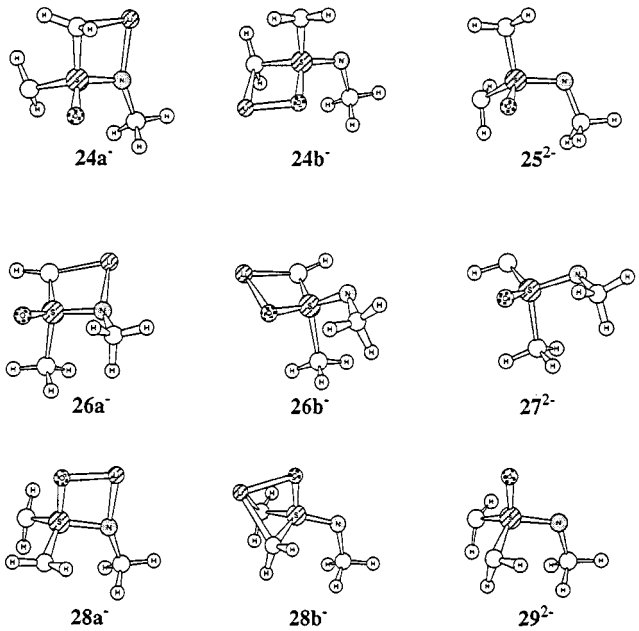


Figure 11. Structure of the monolithio anions **24a,b**$^-$, **26a,b**$^-$, **28a,b**$^-$ and the lithium-free dianions **25**$^{2-}$, **27**$^{2-}$, **29**$^{2-}$

The analogous procedure was also performed with the dilithio salt **21b**. After removal of one lithium the Li–N–S–C complexation is energetically favoured over the Li–O–S–C coordination. The resulting monolithio intermediates **26a**$^-$ and **26b**$^-$ differ distinctly from the structures derived from **21a** even though the complexation energies are similar. The unusual coordination mode of the lithium cations in **21c** leads, after decomplexation of one lithium, either to an exclusively heteroatom-*N*,*O*-coordinated monolithioanion

Table 2. Relative energies of the resulting anions after removal of the lithium cations [in kcal mol^{-1} based on MP2(full)/6-31+G**// HF/6-31+G** calculations]

	Geometries Optimised	Non-optimised	ΔE
24a$^-$	171.6	180.9	9.3
26a$^-$	172.0	181.4	9.4
28a$^-$	169.1	188.3	9.2
24b$^-$	178.4	187.0	8.6
26b$^-$	177.8	192.1	12.3
28b$^-$	170.2	177.1	6.9
25^{2-}	437.6	449.4	11.8
27^{2-}	451.7	465.8	14.1
29^{2-}	439.9	447.6	7.5

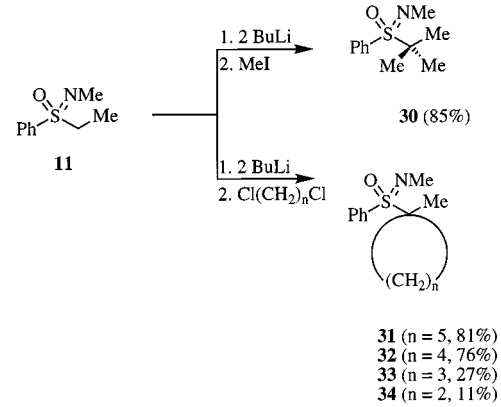
28a$^-$ or to a threefold lithium-coordinated monolithioanion **28b**$^-$. The removal of the second lithium produces a naked 1,3-dianionic species **25**$^{2-}$. The total delithiation requires 437 kcal/mol when starting from the dilithiosulfoximine **21a**. The energy required for the second delithiation amounts to 266 kcal/mol from **24a**$^-$ and 259 kcal/mol from **24b**$^-$. Removal of the second lithium cation affords the α,α-dianion **27**$^{2-}$. The energy required for the twofold delithiation of **21b** amounts to 451 kcal/mol. After removal of the second lithium ion the 1,3-dianion **29**$^{2-}$ is generated (439 kcal/mol), which is closely related to the dianionic species **25**$^{2-}$ with only small differences in their conformations and energies.

4. Applications in Asymmetric Synthesis

4.1 Regio- and Diastereoselective Cyclisations with Biselectrophiles

For the investigation into the use of a chiral dilithiated sulfoximine in asymmetric synthesis, the generated dilithio intermediate **12** has been trapped with various electrophiles.[29] Addition of MeI afforded nearly regioselectively the α,α-dimethylated *S*-*tert*-butyl-*S*-phenylsulfoximine **30** in high yield (85%). Such behaviour was unknown for sulfoximines but is not unusual for sulfones, where an α,*o*-dilithiated species has also been observed that showed a similar reactivity with alkylhalides.[46] NMR-spectroscopic studies by Gais et al. have demonstrated that a temperature dependent transmetallation of an α,*o*- to an α,α-dilithio species is possible.[16] Taking this into account, it becomes reasonable to suggest a transmetallation process as a possible explanation for the observed regioselectivity with dilithiated **11**. This means that, after the first alkylation step in the α-position, a translithiation takes place leading finally to the α,α-dialkylated product. Performing this procedure with a biselectrophile like 1,5-diiodopentane, we expected a similar regioselectivity to the reaction with MeI, which should lead to a ring closure in the α-position.

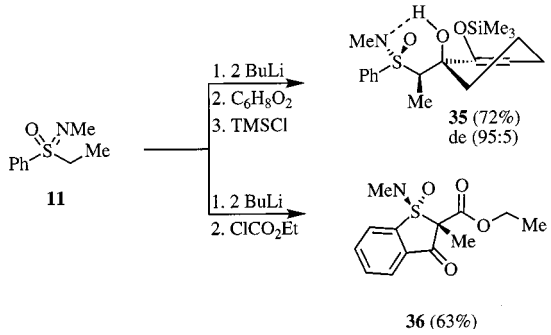
Indeed, a six-membered ring in **31** is formed without any regioisomers and in high yield (81%). With 1,4-diiodobutane a five-membered ring species **32** was obtained in good yield (76%). Cyclisation reactions with shorter bridged bis-



electrophiles showed dramatically lower yields, presumably due to undesired side reactions. The cyclobutane derivative **33** and the cyclopropyl-sulfoximine **34** are therefore only accessible in yields of 27% and 11%.

4.2 Addition to Prochiral Electrophiles

In contrast to the simple biselectrophiles discussed above, cyclohexane-1,2-dione, in the presence of TMSCl, did not undergo ring closure to a cyclopropane derivative. Instead the α,*o*-dilithio species **12** acted as a base and a nucleophile leading, in a synergistic manner in a single reaction-step, to the β-hydroxysulfoximine **35** in high yield (72%) and excellent diastereomeric ratio (95:5). The absolute stereochemistry of the major isomer of **35** has been determined by X-ray structure analysis.

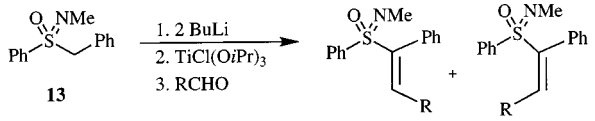


Typical of β-hydroxysulfoximines is the ability to build intramolecular hydrogen bonds to the imino nitrogen to give a six-membered ring with a chair conformation.[47] The methyl group on C(α) and the larger, silyloxy-containing substituent on C(β) are oriented in a pseudo-equatorial fashion. The reaction of the dilithiosulfoximine **12** with ethyl chloroformate afforded, in good yield (63%), the heterocycle **36** as single diastereoisomer. This cyclisation must proceed by a third deprotonation step. NOE experiments confirm that the cis configuration of the C-methyl and *N*-methyl groups is present in the five-membered heterocycle.

4.3 Transmetallation and Alkene Formation

If there are two different metals bound to the same carbon atom of a chiral reagent a new stereocentre might be induced. This principle can be used for the transformation

of chiral information, but has rarely been applied in stereoselective reactions.[12,48] Our approach took advantage of the transmetallation of a geminal dilithiated sulfoximine **14** with $ClTi(OiPr)_3$. Addition of several aldehydes to such a titanated dilithiosulfoximine did not lead to β-hydroxysulfoximines and, instead, only the alkenylsufoximines **37**–**39** were formed. The reactions proceed in a highly diastereoselective fashion leading predominantly to the (*E*)-alkenes.



13

37 R = Ph, 74%, E:Z = 95:5

38 R = *t*Bu, 77%, E:Z = 99:1

39 R = Et, 68%, E:Z = 90:10

5. Conclusion

The first heterochiral dilithiomethane derivative **14** was structurally confirmed by X-ray analysis. A comparison with its monolithiated precursor **10e** revealed a dimer devoid of Li–C contacts. In our opinion, the free accessibility to the anionic C(α) atom in **10e** is responsible for the geminal dilithiation. This is not the case for lithiosulfoximines that form C–Li bonds, as can be seen in lithiated alkyl- or alkenyl-substituted sulfoximines **10a**,**b**,**f**. The second metallation leads to an α,*o*-dilithiosulfoximine. The structures of achiral phosphorus-stabilised geminal dilithio salts have only very recently been confirmed. Since chiral modifications of such compounds are easy to perform, one might expect to use the derived dilithio salts in asymmetric synthesis. The X-ray crystallographic studies on mono- and dilithiated sulfoximines were complemented by quantum chemical calculations on the lithiated (*N*-methyl)dimethylsulfoximine **19**. Three different major energy minima were obtained with the lithium-*N*,*C*-chelate **20a** and the sulfoximine-*N*,*O*-coordinated lithium salt **20b** representing the most stable isomers. In contrast, lithium-*O*,*C*-coordination in **20c** is energetically disfavoured, so that *N*,*C*- and *N*,*O*-coordination should be preferred to *O*,*C*-coordination. Three equilibrium structures for the dilithiated *N*,*S*,*S*-trimethylsulfoximine system were also found, with the dilithiospiro structure **21a** representing the most stable isomer. Only ca. 1–5 kcal/mol higher in energy were the α,α-dilithiosulfoximine **21b** and the isomer **21c**, which have heteroatom contacts to one lithium while the second lithium is associated with both anionic carbon atoms. In conclusion, these results have some important implications for asymmetric synthesis: because reactions with achiral dilithio salts are already meaningful in synthetic sequences one can imagine further synthetic approaches with chiral dilithio compounds derived from the discussed dilithiosulfoximine intermediates **21a** or **21b**. The first multiple stereoselective C–C bond formations with prochiral biselectrophiles have been applied in cyclisation reactions and have led to a new and powerful methodology for the synthesis of new carbo- and heterocycles. The reaction of the dilithiated sulfoximine **11** with cyclohexane-1,2-dione afforded a β-hydroxysulfoximine with high stereocontrol. Transmetallation of **14** with $ClTi(OiPr)_3$ followed by addition of an aldehyde allowed the highly diastereoselective synthesis of (*E*)-alkenylsulfoximines. This new methodology works for the single-step formation of multiple C–C bonds under high regio- and diastereocontrol. Our further studies will focus on this novel concept to create chiral mixed organodimetallics and to apply these compounds in asymmetric synthesis.

[1] K. Ziegler, K. Nagel, M. Patheiger, *Z. Anorg. Allg. Chem.* **1955**, *282*, 345–352.

[2] J. A. Gurak, J. W. Chinn, R. J. Lagow, H. Steinfink, S. C. Yannoni, *Inorg. Chem.* **1984**, *23*, 3717–3720.

[3] G. D. Stucky, M. M. Eddy, W. H. Harrison, R. Lagow, H. Kawa, D. E. Cox, *J. Am. Chem. Soc*. **1990**, *112*, 2425–2427.

[4] [4a] J. B. Collins, J. D. Dill, E. D. Jemmis, Y. Apoloig, P. v. R. Schleyer, R. Seeger, J. A. Pople, *J. Am. Chem. Soc.* **1976**, *98*, 5419–5427. – [4b] E. D. Jemmis, P. v. R. Schleyer, J. A. Pople, *J. Organomet. Chem.* **1978**, *154*, 327–335.

[5] [5a] I. Marek, J.-F. Normant, *Chem. Rev.* **1996**, *96*, 3241–3267. – [5b] C. M. Thomson, in: *Dianion Chemistry in Organic Synthesis*, CRC Press, Boca Raton, Florida, **1994**, pp. 1–250. – [5c] A. Maerker, in: *Lithium Chemistry* (Eds.: A.-M. Sapse, P. v. R. Schleyer), Wiley, New York, **1995**, p. 477–577. – [5d] A. Maerker, M. Theis, *Top. Curr. Chem.* **1987**, *138*, 1–61.

[6] S. Brenner, M. Bovete, *Tetrahedron* **1975**, *31*, 153–158.

[7] [7a] E. M. Kaiser, L. E. Solter, R. A. Schwarz, R. D. Beard, C. R. Hauser, *J. Am. Chem. Soc.* **1971**, *93*, 4237–4242. – [7b] E. M. Kaiser, J. D. Petty, P. L. A. Knutson, *Synthesis* **1977**, 509–550.

[8] [8a] F. Caturia, C. Nájera, *Tetrahedron Lett.* **1996**, *37*, 2833–2836. – [8b] P. Bonete, C. Nájera, *Tetrahedron* **1996**, *52*, 4111–4122.

[9] B. Iorga, F. Eymery, P. Savignac, *Tetrahedron Lett.* **1998**, *39*, 3693–3696.

[10] [10a] C. R. Johnson, *Aldrichim. Acta* **1985**, *18*, 3–11. – [10b] C. Bolm, J. Müller, G. Schlingloff, M. Zehnder, M. Neuburger, *J. Chem. Soc., Chem. Commun.* **1993**, 182–183. – [10c] H.-J. Gais, H. Müller, J. Bund, M. Scommoda, J. Brandt, G. Raabe, *J. Am. Chem. Soc.* **1995**, *117*, 2453–2466. – [10d] M. Reggelin, H. Weinberger, *Angew. Chem. Int. Ed. Engl.* **1994**, *33*, 444–446.

[11] [11a] L. Horner, H. Hoffmann, H. G. Wippel, *Chem. Ber.* **1958**, *91*, 61–63. – [11b] W. S. J. Wadsworth, W. D. Emmons, *J. Am. Chem. Soc.* **1961**, *83*, 1733–1738.

[12] J. Vollhardt, H.-J. Gais, K. L. Lukas, *Angew. Chem. Int. Ed.* **1985**, 24, 608–609.

[13] W. Zarges, M. Marsch, K. Harms, G. Boche, *Angew. Chem. Int. Ed.* **1989**, *28*, 1392–1393.

[14] H.-J. Gais, J. Vollhardt, H. Günther, D. Moskau, H. J. Lindner, S. Braun, *J. Am. Chem. Soc.* **1988**, *110*, 978–980.

[15] W. Zarges, M. Marsch, K. Harms, G. Boche, *Chem. Ber.* **1989**, *122*, 1307–1311.

[16] H.-J. Gais, J. Vollhardt, *Tetrahedron Lett.* **1988**, *29*, 1529–1532.

[17] [17a] T. Kottke, R. J. Lagow, D. Stalke, *J. Appl. Crystallogr.* **1996**, *29*, 465–468.[17b] T. Kottke, D. Stalke, *J. Appl. Crystallogr.* **1993**, *26*, 615–619.

[18] A. Streitwieser, S. M. Bachrach, A. Dorigo, P. v. R. Schleyer, in: *Lithium Chemistry* (Eds.: A.-M. Sapse, P. v. R. Schleyer), Wiley, New York, **1995**, p. 1–43.

[19] H.-J. Gais, I. Erdelmeier, H. J. Lindner, J. Vollhardt, *Angew. Chem. Int. Ed*. **1986**, *25*, 938–939.

[20] H.-J. Gais, U. Dingerdissen, C. Krüger, K. Angermund, *J. Am. Chem. Soc.* **1987**, *109*, 3775–3776.

[21] G. Boche, *Angew. Chem. Int. Ed.* **1989**, *28*, 277–297.

[22] H.-J. Gais, D. Lenz, G. Raabe, *Tetrahedron Lett.* **1995**, *36*, 7437–7440.

[23] [23a] U. Salzner, P. v. R. Schleyer, *J. Am. Chem. Soc*. **1993**, *115*,

10231–10236.[23b] G. Raabe, H.-J. Gais, J. Fleischhauer, *J. Am. Chem. Soc*. **1996**, *118*, 4622–4630.

[24] J. F. K. Müller, R. Batra, B. Spingler, M. Zehnder, *Helv. Chim. Acta* **1996**, *79*, 820–826.

[25] [25a] H.-J. Gais, J. Mueller, J. Vollhardt, *J. Am. Chem. Soc.* **1991**, *113*, 4002–4003. – [25b] H.-J. Gais, G. Hellmann, H. J. Lindner, *Angew. Chem. Int. Ed.* **1990**, *29*, 100–102. – [25c] H.-J. Gais, G. Hellmann, H. Guenther, F. Lopez, H. J. Braun, *Angew. Chem. Int. Ed.* **1989**, *28*, 1025–1027. – [25d] W. Hollstein, M. Marsch, K. Harms, G. Boche, *Angew. Chem. Int. Ed.* **1988**, *27*, 846–847. – [25e] H.-J. Gais, J. Vollhardt, G. Hellmann, H. Paulus, H. J. Lindner, *Tetrahedron Lett.* **1988**, *22*, 1259–1262. – [25f] H.-J. Gais, J. Vollhardt, H. J. Lindner, *Angew. Chem. Int. Ed.* **1986**, *25*, 939–940. – [25g] H.-J. Gais, H. J. Lindner, J. Vollhardt, *Angew. Chem. Int. Ed.* **1985**, *24*, 859–860. – [25h] G. Boche, M. Marsch, K. Harms, G. M. Sheldrick, *Angew. Chem. Int. Ed.* **1985**, *24*, 573–574.

[26] J. F. K. Müller, M. Neuburger, B. Spingler, *Angew. Chem. Int. Ed.* **1999**, *38*, 3549–3552.

[27] J. F. K. Müller, M. Neuburger, M. Zehnder, *Acta Crystallogr., Sect. C* **1997**, *53*, 419–422.

[28] J. F. K. Müller, M. Neuburger, M. Zehnder, *Helv. Chim. Acta* **1995**, *78*, 615–618.

[29] J. F. K. Müller, M. Neuburger, M. Zehnder, *Helv. Chim. Acta* **1997**, *80*, 2182–2190.

[30] [30a] W. Clegg, L. Horsburgh, P. R. Dennison, F. M. Mackenzie, R. E. Mulvey, *Chem. Commun.* **1996**, 1065–1066.[30b] S. C. Ball, I. Cragg-Hine, M. G. Davidson, R. P. Davies, M. I. Lopez-Solera, P. R. Raithby, D. Reed, R. Snaith, E. M. Vogel, *J. Chem. Soc., Chem. Commun.* **1995**, 2147–2148.[30c] C. Lambert, F. Hampel, P. v. R. Schleyer, M. G. Davidson, R. Snaith, *J. Organomet. Chem.* **1995**, *487*, 139–141. – [30d] H. Dietrich, D. Rewicki, *J. Organomet. Chem.* **1981**, *205*, 281–289.

[31] R. F. W. Jackson, A. D. Briggs, P. A. Brown, W. Clegg, M. R. J. Elsegood, C. Frampton, *J. Chem. Soc., Perkin Trans. 1* **1996**, 1673–1682.

[32] For a comprehensive review on *ortho*-metallation reactions see: V. Snieckus, *Chem. Rev.* **1990**, *90*, 879–933.

[33] J. F. K. Müller, M. Neuburger, B. Spingler, *Angew. Chem. Int. Ed.* **1999**, *38*, 92–94.

[34] [34a] C. M. Ong, D. W. Stephan, *J. Am. Chem. Soc*. **1999**, *121*, 2939–2940. – [34b] A. Kasani, R. P. Kamalesh Babu, R. McDonald, R. G. Cavell, *Angew. Chem. Int. Ed.* **1999**, *38*, 1483–1484. – [34c] A. Müller, B. Neumüller, K. Dehnicke, *Chem. Ber.* **1996**, *129*, 253–257.

[35] [35a] J. Clayden, S. Warren, *Angew. Chem. Int. Ed.* **1996**, *35*, 241–270. – [35b] B. E. Maryanoff, A. B. Reitz, *Chem. Rev.* **1989**, *89*, 863–927.

[36] B. Iorga, F. Eymery, P. Savignac, *Tetrahedron Lett.* **1998**, *39*, 4477–4480.

[37] [37a] W. Zarges, M. Marsch, K. Harms, F. Haller, G. Frenking, G. Boche, *Chem. Ber.* **1991**, *124*, 861–866. – [37b] S. E. Denmark, K. A. Swiss, P. C. Miller, S. R. Wilson, *Heteroatom Chem.* **1998**, *9*, 209–218.

[38] G. G. Eberhardt, W. A. Butte, *J. Org. Chem.* **1964**, *29*, 2928–2932.

[39] [39a] G. W. Spitznagel, T. Clark, J. Chandrasekhar, P. v. R. Schleyer, *J. Comput. Chem. 3* **1982**, 363–371. – [39b] F. Bernardi, A. Bottoni, A. Venturini, A. Mangini, *J. Am. Chem. Soc*. **1986**, *108*, 8171–8175.

[40] [40a] T. Clark, P. v. R. Schleyer, K. N. Houk, N. G. Rondan, *J. Chem. Soc., Chem. Commun.* **1981**, 579–581. – [40b] P. v. R. Schleyer, T. Clark, A. J. Kos, G. W. Spitznagel, G. Rohde, D. Arad, K. N. Houk, N. G. Rondan, *J. Am. Chem. Soc*. **1984**, *106*, 6467–6475. – [40c] G. Boche, J. C. W. Lohrenz, A. Opel, in: *Lithium Chemistry* (Eds.: A.-M. Sapse, P. v. R. Schleyer), Wiley, New York, **1995**, 195–226. – [40d] A. M. El-Nahas, P. v. R. Schleyer, *J. Comput. Chem*. **1994**, *15*, 596–625.

[41] [41a] A. Streitwieser Jr., A. Rajca, R. S. McDowell, R. Glaser, *J. Am. Chem. Soc*. **1987**, *109*, 4184–4188. – [41b] S. E. Denmark, C. J. Cramer, *J. Org. Chem*. **1990**, *55*, 1806–1813. – [41c] C. J. Cramer, S. E. Denmark, P. C. Miller, R. L. Dorow, K. A. Swiss, S. R. Wilson, *J. Am. Chem. Soc*. **1994**, *116*, 2437–2447. – [41d] R. Koch, E. Anders, *J. Org. Chem.* **1995**, *60*, 5861–5866. – [41f] M. Kranz, S. E. Denmark, *J. Org. Chem*. **1995**, *60*, 5867–5877. – [41e] M. Kranz, S. E. Denmark, K. A. Swiss, S. R. Wilson, *J. Org. Chem*. **1996**, *61*, 8551–8563.

[42] [42a] S. Wolfe, A. Rauk, I. G. Csizmadia, *J. Am. Chem. Soc*. **1969**, *91*, 1567–1569. – [42b] S. Wolfe, A. Rauk, L. M. Tel, I. G. Csizmadia, *J. Chem. Soc., Chem. Commun*. **1970**, 96–97. – [42c] A. Streitwieser Jr., J. E. Williams, Jr., *J. Am. Chem. Soc*. **1975**, *97*, 191–192. – [42d] S. Wolfe, A. Stolow, L. A. La John, *Tetrahedron Lett.* **1983**, *24*, 4071–4074. – [42e] S. Wolfe, L. A. La John, D. F. Weaver, *Tetrahedron Lett.* **1984**, *25*, 2863–2866. – [42f] T. Clark, in: *Sulfur Centered Reactive Intermediates In Chemistry and Biology* (Eds.: C. Chatgiliaoglu, K.-D. Asmus), NATO ASI Series A, Life Sciences 197, Plenum Press, New York, **1990**, p 13. – [42g] R. Koch, E. Anders, *J. Org. Chem*. **1994**, *59*, 4529–4534.

[43] J. F. K. Müller, R. Batra, *J. Organomet. Chem*. **1999**, *584*, 27–32.

[44] [44a] J. W. Ochterski, G. A. Petersson, K. B. Wiberg, *J. Am. Chem. Soc*. **1995**, *117*, 11299–11308. – [44b] J. W. Ochterski, G. A. Petersson, J. Montgomery, Jr., *J. Chem. Phys.* **1996**, *104*, 2598–2619.

[45] [45a] P. Hohenberg, W. Kohn, *Phys. Rev.* **1964**, *136*, B 864. – [45b] W. Kohn, L. Sham, *J. Phys. Rev.* **1965**, *140*, A 1133. – [45c] J. C. Slater, *International Series in Pure and Applied Physics*, vol. 4 (“The Self-Consistent Field of Molecules and Solids. Quantum Theory”) McGraw-Hill, New York, **1974**. – [45d] A. D. Becke, *Phys. Rev. A* **1988**, *38*, 3098. – [45e] A. D. Becke, *J. Chem. Phys.* **1993**, *98*, 1372–1377. – [45f] J. P. Perdew, Y. Wang, *Phys. Rev. B* **1992**, *45*, 13244. – [45g] R. G. Parr, Y. Wang, *Density-Functional Theory of Atoms and Molecules*, Oxford University Press, Oxford, **1989**.

[46] J. Vollhardt, H.-J. Gais, L. Lukas, *Angew. Chem. Int. Ed*. **1985**, *24*, 608–610.

[47] K.-J. Hwang, E. W. Logusch, L. H. Brannigan, M. R. Thompson, *J. Org. Chem.* **1987**, *52*, 3435–3441.

[48] [48a] J. Vollhardt, H.-J. Gais, K. L. Lukas, *Angew. Chem. Int. Ed.* **1985**, *24*, 696–697. – [48b] H.-J. Gais, J. Vollhardt, H. J. Lindner, H. Paulus, *Angew. Chem. Int. Ed.* **1988**, 27, 1540–1542.

Received August 19, 1999
[I99306]

Microporous Titanosilicates and other Novel Mixed Octahedral-Tetrahedral Framework Oxides

João Rocha*[a] and Michael W. Anderson[b]

Keywords: Zeolites / Microporous zeolites / Titanosilicates / Transition metal

Stable microporous materials, such as zeolites, are extremely important for applications in catalysis, adsorption, ion-exchange, and separation. In this review we describe a new class of stable microporous materials that involves novel mixed octhaedral-tetrahedral framework oxides. The archetypal material is based on titanosilicates, although there is tremendous scope for introducing many other transition metals. These materials not only have potential novel applications in the fields normally associated with zeolites but also possible applications in the areas of optoelectronics, nonlinear optics, batteries, magnetic materials and sensors.

Introduction

Zeolites are crystalline, hydrated aluminosilicates with open three-dimensional structures built of $[SiO_4]^{4-}$ and $[AlO_4]^{5-}$ tetrahedra linked to each other by sharing all the oxygens to form regular intracrystalline cavities and channels of molecular dimensions.[1–3] Silicon-oxygen tetrahedra are electrically neutral when connected together in a three-dimensional network as in quartz (SiO_2). The replacement of Si^{IV} by Al^{III} in such a structure creates an electrical imbalance and, to preserve overall electrical neutrality, each AlO_4 tetrahedron needs a balancing positive charge. This is provided by exchangeable cations held electrostatically within the zeolite. Zeolites possess remarkable physical and

[a] Department of Chemistry, University of Aveiro
3810 Aveiro, Portugal
Fax: (internat.) + 351-234/370-084
E-mail: rocha@dq.ua.pt
[b] UMIST Centre for Microporous Materials, Department of Chemistry,
P. O. Box 88, Manchester M60 1QD, UK
Fax: (internat.) + 44-161/236-7677
E-mail: m.anderson@umist.ac.uk



João Rocha was born in Portugal in 1962. Following his undergraduate studies in Physics and Chemistry at Aveiro University he became assistant in the Department of Chemistry of this University in 1985. In 1987 he joined the group of Jacek Klinowski in Cambridge. His Ph.D. thesis was entitled solid-state NMR studies of kaolinite and related materials and concentrated on the study of the important clay mineral kaolinite and related high-temperature phases.
This was followed by a post-doctoral appointment in Cambridge, still in the group of J. Klinowski, working on solid-state NMR of zeolitic materials. He was appointed Lecturer in Chemistry at University of Aveiro in 1991 and promoted to Professor of Inorganic Chemistry in 1999 and currently heads the Inorganic and Materials Chemistry Centre and the solid-state NMR laboratory. His research interests include: synthesis and characterisation of novel microporous materials; development of new materials for optoelectronics; NMR characterisation of wood and lignocellulosic materials; development of new solid-state NMR techniques for the study of quadrupolar nuclei.



Michael W. Anderson was born in Wimbledon, U.K., in 1960. Following his undergraduate studies in Chemical Physics at Edinburgh University he joined the group of John M. Thomas in Cambridge in 1981. His Ph.D. thesis was entitled Dealuminated Zeolites and concentrated on the removal of aluminium from zeolites using $SiCl_4$. This was followed by three post-doctoral appointments: University of Houston with Larry Kevan working on pulsed EPR measurements of transition metals in zeolites; University of Connecticut with Steve Suib working on catalyst poisoning; University of Cambridge with Jacek Klinowski where he developed in situ NMR methods for monitoring catalytic events in zeolites. He was appointed Lecturer in Chemistry at UMIST in 1990 and promoted to Professor of Materials Chemistry in 1998 and is currently Director of the UMIST Centre for Microporous Materials. His research interests include: experimental and theoretical NMR studies of heterogeneous catalysts; structural studies of mesoporous materials; atomic force microscopy and electron microscopy studies of crystallisation mechanisms; synthesis and applications of novel microporous materials.

MICROREVIEWS: This feature introduces the readers to the authors' research through a concise overview of the selected topic. Reference to important work from others in the field is included.

 © WILEY-VCH Verlag GmbH, D-69451 Weinheim, 2000 1434–1948/00/0505–0801 $ 17.50+.50/0

chemical properties. The most important chemical properties are selective sorption, ion exchange and catalytic activity.

During the 1980s a variety of novel microporous framework structures were synthesised based on an aluminophosphate system.[4] In their pure form the aluminophosphates are termed AlPOs and consist of alternating corner-sharing framework $[AlO_4]^{5-}$ and $[PO_4]^{3-}$ tetrahedral groups. Overall the frameworks have no net charge and, consequently, no cation-exchange properties and little catalytic potential. Framework substitutions are, however, possible and lead to silico-aluminophosphates[5] (SAPOs) and metal-substituted aluminophosphates (MeAPOs).[6] Some of these new materials have the framework topologies of known zeolites while others may have novel structures. In all these materials the framework metal atoms are ostensibly in tetrahedral coordination, although under certain circumstances (for example, various hydration conditions) the coordination might change to five- or six-fold. Porous structures comprised entirely of octahedral sites have also been generated. For example, the manganese oxides known as OMS materials contain only octahedral framework atoms.[7a]

A third, much less explored, compositional possibility for microporous frameworks are structures consisting of interlinked octahedra and tetrahedra. Although clays and related materials, in some way, fall into this category, they only possess two-dimensional co-valent connectivity. Three-dimensional connectivity is required to impart substantial structural stability and we are only concerned with such networks in this review. In 1990 Chapman and Roe were already well aware of the importance of these mixed framework materials.[8] In their words: ''While new structures and compositions of molecular sieves continue to be synthesised, there are indications that attention is turning toward a potentially large class of novel molecular sieve materials composed of interconnected octahedral- and tetrahedral-oxide polyhedra. Such materials will most likely provide examples of new topologies and novel compositions''. In this microreview it is our endeavour to show that some of the most interesting and important developments in the field of zeolites and zeotype materials are taking place in the area of mixed octahedral-tetrahedral oxides. Here, we shall only address the chemistry of silicates and will not be concerned with, in particular, the burgeoning and exciting chemistry of porous phosphates.[7b]

Synthesis

The synthesis of microporous titanosilicates[8–11] and other novel zeotype materials is usually carried out in Teflon-lined autoclaves under hydrothermal conditions with temperatures ranging from ca. 150 to 230 °C and times varying between a few hours and ca. 30 days. In certain cases, the materials have been prepared at relatively high temperatures. For example, single crystals of a titanosilicate analogue of the mineral pharmacosiderite, $Cs_3HTi_4O_4(SiO_4)_3 \cdot 4\,H_2O$, have been obtained hydrothermally in a sealed gold tube at 750 °C for 40 h.[12] The pH of the synthesis gel is normally high, in the range 10–13. Seeding the gel with a small amount of the desired phase (or even with a related solid) is a common practice. The syntheses are in general driven by kinetics, with different metastable phases being formed with time. So far, most research has concentrated on the synthesis of microporous titanosilicates. The experience gathered in this field is guiding the efforts aimed at other systems, most notably zirconosilicates. Hence, here we shall discuss in more detail the synthesis of microporous titanosilicates, particularly ETS-10 (*E*ngelhard *t*itano*s*ilicate material number 10).

The synthesis of ETS-10 was first reported by Kuznicki in 1989.[9] The titanium source used was $TiCl_3$. A slight modification of this method afforded highly crystalline and pure ETS-10 suitable for structural elucidation.[13,14] $TiCl_4$ is another much used (and cheaper) titanium source. For example, using this precursor Das et al.[15] reported a method for the rapid (< 16 h) synthesis of ETS-10. Liu and Thomas[16] have shown that under proper conditions the thermodynamically stable TiO_2 phases of anatase and rutile can be used as suitable titanium sources for the synthesis of porous titanosilicates. A few organotitanium compounds have also been used to prepare microporous titanosilicates. Because they are very sensitive to moisture, these compounds are difficult to handle and require special facilities for their transfer during the gel preparation. For example, Chapman and Roe[8] used $Ti(OC_2H_5)_4$ in the preparation of GTS-1 while Clearfield and co-workers synthesised a novel porous titanosilicate using titanium isopropoxide.[17] Sodium silicate solutions and fumed and colloidal silica are suitable silicon sources. Organosilicon compounds, such as tetraethylorthosilicate have also been used.[17] The synthesis of ETS-10 usually (although not always) requires the presence in the parent gel of both Na^+ and K^+ ions. Other phases, such as some of the AM (*A*veiro/*M*anchester) materials[18] are produced in a pure state only when a single type of cation is present. Potassium fluoride is often used for preparing ETS-10 but its presence is not crucial. A comprehensive study of the hydrothermal synthesis conditions which yield pure and highly crystalline ETS-10 from $TiCl_3$ and anatase has been reported.[19] This work examines the influence on the synthesis of the following parameters: presence of fluoride, sodium, and potassium ions, seeds, H_2O/Si and Si/Ti molar ratios, parent gel pH, temperature, and time. A similar study has been carried out by Das et al., using $TiCl_3$ as the titanium source.[20]

Most porous titanosilicates and other related new materials reported to date can be synthesised without the addition of any organic template molecules. However, several groups have prepared ETS-10 with a range of templates: tetramethylammonium chloride,[21,22] pyrrolidine, tetraethylammonium chloride, tetrapropylammonium bromide,1,2-diaminoethane,[22] choline chloride, and the bromide salt of hexaethyl diquat-5.[23] From the point of view of industrial synthesis scale-up it is very important that many of the new structures can be synthesised in the absence of

costly templating agents. Furthermore, the occluded templates usually need to be removed following synthesis in order to impart microporosity, a procedure that can be both costly and potentially damaging to the framework.

The framework substitution of titanium and silicon by other elements requires a judicious choice of the respective source, which is usually introduced in the parent synthesis gel. The following sources of aluminium, gallium, niobium, and boron for element insertion in the ETS-10 framework have been reported: $NaAlO_2$,[24] $GaCl_3$,[25] $Nb(HC_2O_4)_5$,[26] and $Na_2B_2O_4$[27] (see also refs.[28,29]). In the synthesis of microporous zirconosilicates $ZrCl_4$[30–32] and $Zr(OC_3H_7)_4$[33] have been used as the zirconium sources. The vanadosilicate AM-6, a structural analogue of ETS-10, has been prepared from $VOSO_45H_2O$.[34]

Structure

ETS-10

In 1990 Chapman and Roe published the synthesis and X-ray diffraction pattern of a microporous titanosilicate[8,11] that seemed to have the structure of the mineral zorite by comparison of the diffraction patterns. At about the same time Engelhard Corporation filed a series of patents describing a similar small-pore material, which they named ETS-4 (*E*ngelhard *t*itano*s*ilicate-4) and another wide-pore titanosilicate material named ETS-10.[9,10] Owing to its wide-pore nature and thermal stability ETS-10 is arguably the most important octahedral/tetrahedral framework microporous titanosilicate to be synthesised to date. Consequently, it is important to understand the structure of this material in some detail.

The structure of ETS-10 was solved and reported briefly in 1994 by Anderson et al.[13] and described fully by the same group the following year.[14] Two problems prevented an easy solution to the structure of ETS-10: first, the material could only be synthesised as a powder and, more importantly, the material was inherently disordered. Consequently, conventional diffraction techniques to solve the structure proved inadequate. The following strategy was therefore adopted to elucidate the structure of ETS-10: (i) target the framework ring connectivity and local disorder with high-resolution electron microscopy (HREM); (ii) determine the atomic make-up of the material by chemical analysis; (iii) determine the local silicon environment using ^{29}Si solid-state nuclear magnetic resonance (NMR); (iv) refine a trial structure using a distance-least-squares (DLS) analysis of bond angles and bond lengths; (v) combine the refined structure and known disorder to simulate powder X-ray diffraction data.

The typical crystal morphology of ETS-10 is shown in Figure 1. These scanning electron micrograph images show that (i) the particle has a pseudo-4-fold symmetry along an axis indicated by the large arrow; (ii) traces of faults that are perpendicular to the axis and are indicated by small arrows. This faulted structure is always present in ETS-10 and Figure 1 represents a high quality material.

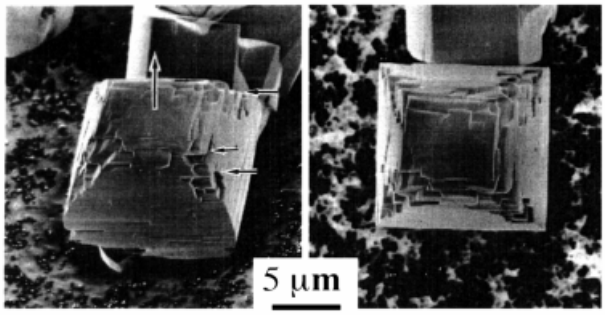


Figure 1. Scanning electron micrograph of a high-quality ETS-10 sample; large arrow depicts pseudo 4-fold axis, small arrows indicate faulting caused be intergrowths

The details of the inherent disorder and the pore structure in ETS-10 are most clearly revealed in the high-resolution electron micrograph (Figure 2). The large 12-ring pores are clearly visible. In order to discern the disorder the reader should note the stacking of these large pores from the bottom of the micrograph to the top. It will be seen that the pores stack randomly to the right or to the left.

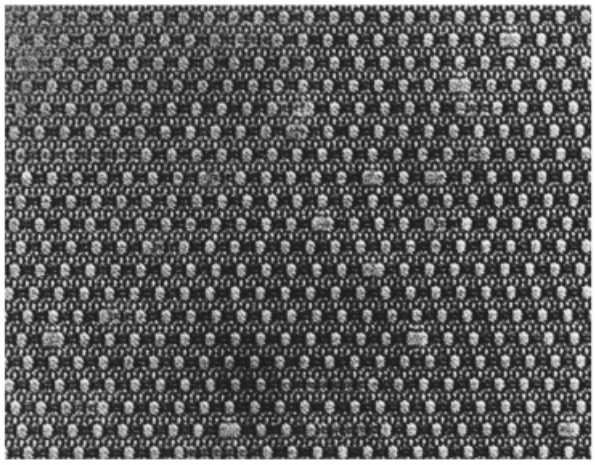


Figure 2. High-resolution electron micrograph of ETS-10

The most interesting aspect of the structure of ETS-10 is that it contains infinite –O–Ti–O–Ti–O– chains (with alternating long/short bonds[35]) that are surrounded by a silicate ring structure. These combine to make up a rod (Figure 33a and 3b) and it is this rod nature that imparts some of the interesting optical properties described in the applications section. Adjacent layers of rods are stacked orthogonal to each other (Figure 3c). These double layers are then stacked with a displacement of 1/4 unit cell in either the [100] direction or the [010] direction to give four possible connections (Figure 3d). If these four possible connections are given equal probability and the stacking is random then the disordered ETS-10 structure is constructed. The pore structure of ETS-10 has 12-rings in all three dimensions; these are straight along [100] and [010] and crooked along the direction of disorder. However, there are only a handful of microporous zeolitic materials with a 3-dimensional 12-ring pore system and in this respect ETS-10 has

excellent diffusion characteristics. It should be noted that the crooked channel is not blocked or the pore volume reduced by the disorder.

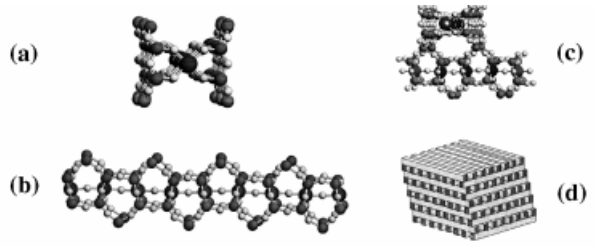


Figure 3. Structural make-up of ETS-10: (a) and (b) show the same rod section of ETS-10 in orthogonal views – large spheres Ti, medium spheres Si and small spheres O; (c) shows how these rods link; (d) shows one possible ordered arrangement of these orthogonol rods

It is interesting to conjecture whether it is possible to construct ordered variants of the ETS-10 structure. The lattice energy difference between different stacking sequences is minimal, however, different sequences result in different pore architecture. A zig-zag stacking of pores results in chiral symmetry and a spiral 12-ring pore in the third dimension. In order to synthesise such a material no doubt a chiral organic templating agent would be required but as yet this has not been achieved.

Mistakes in the stacking sequences (which occur frequently, probably as a result of the crystal growth mechanism) result in line defects in ETS-10 which are in effect double-sized pores. A schematic of the framework connectivity and the incorporation of defects is shown in Figure 4.

The framework formula of this basic unit is $Si_{40}Ti_8O_{104}^{16-}$, which is counterbalanced by 16 monovalent cations. In this original structural work it was impossible to locate the cations in ETS-10. The as-prepared material is 1/4 K^+ and 3/4 Na^+. The most likely location of the cations has been determined by a combination of molecular modelling and, for sodium, ^{23}Na solid-state NMR. Figure 5 shows the final structure of ETS-10 with the cations principally located in sites adjacent to the titanate chains where they balance the charge on the titanium centres.

Very recently a single crystal study on ETS-10 has refined a superposition cell, which essentially regards the structure as a combination of all the ordered variants and confirms in essence all of the previous structural work.[36]

ETS-4

Similar to ETS-10 the nominal structure of ETS-4 suggests that it could have very interesting applications. As noted above, the powder X-ray diffraction pattern of ETS-4 suggests strong similarities with the structure of the natural mineral zorite. In 1973 a naturally occurring alkaline titanosilicate identified as zorite was discovered[37] in trace quantities on the Siberian Tundra. The structure solution of this mineral was published[38] six years later in an article

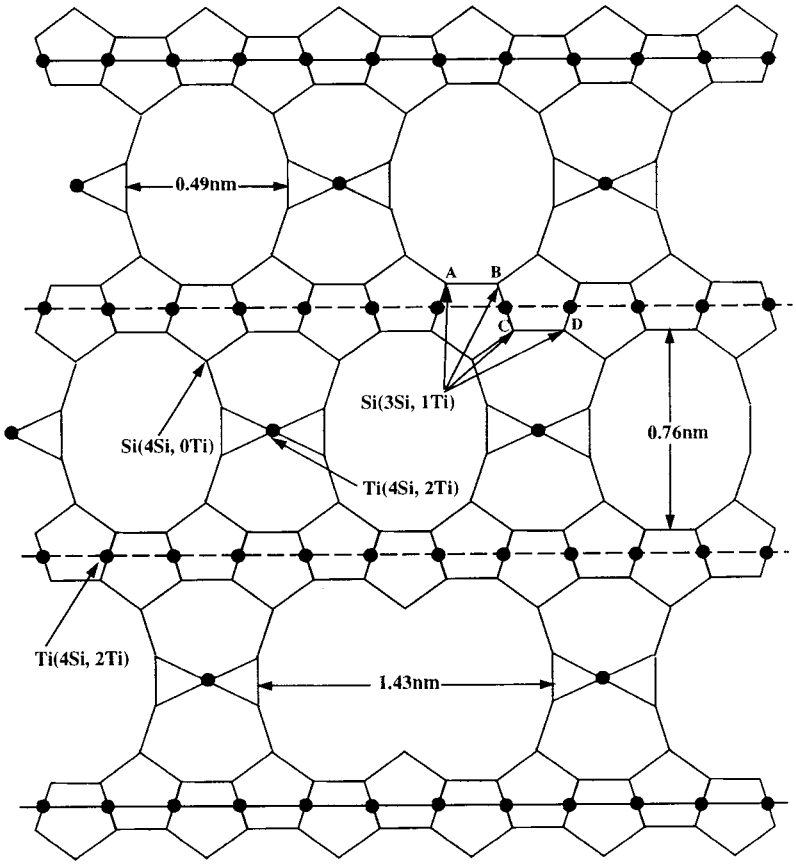


Figure 4. Framework connectivity in ETS-10 showing different chemical and crystallographic environments; also shown is the incorporation of large defects as double pores

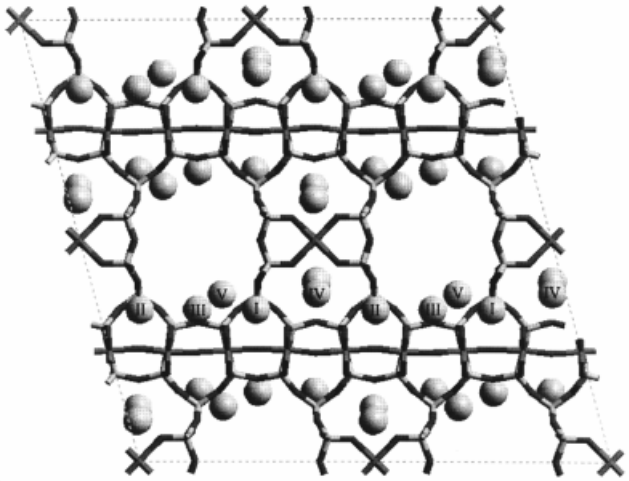


Figure 5. Five cation sites in ETS-10 and their relationship to the framework

entitled "The OD structure of Zorite". According to this contribution,[38] the structure of this mineral is characterised by a highly disordered framework with ostensibly a 2-dimensional channel system. Two orthogonal sets of channels are defined by 12-T/O atom and 8-T atom rings (T = *t*etrahedral silicon; O = *o*ctahedral titanium). In reality, the disorder in zorite results in the larger 12-ring channels becoming partitioned into sections. A molecule diffusing into this 12-T/O ring channel must make detours through the 8-T ring channel system in order to pass freely. Consequently, the adsorption characteristics of zorite are far inferior to that expected for an unfaulted material. Furthermore, zorite lacks thermal stability as internal water acts as part of the structure forming chains through the channel system. When the water is removed the framework structure collapses. Figure 6 shows the framework structure of zorite with possible stacking sequences of ordered end member polymorphs.

In zorite the titanium exists in two different chemical environments, titania rods similar to those in ETS-10, and isolated titania semi-octahedra, which are exposed to the channel system. Consequently, if ETS-4 has the structure of zorite then the accessibility of the titanium centres to the channel system may be a benefit for certain applications, despite the stability issue. The only outstanding problem with the structure of ETS-4 is that the ^{29}Si MAS-NMR spectrum does not agree with the crystal structure. The crystal structure dictates two Si environments Si(2Si,2Ti) and Si(3Si,1Ti) in a ratio of 2:1. The ^{29}Si MAS-NMR spectrum displays two signals, although these are not in the correct ratio. It is still unclear at present how this discrepancy arises but the most reasonable suggestion is that it is due to a large number of defect sites in ETS-4.[39,40]

In terms of stability, the structure of zorite or ETS-4 contains structural water bound in chains along the channel system. At temperatures of 200 °C this water is lost and the structure collapses. At temperatures above 700 °C there is a phase transformation into the dense titanosilicate structure narsarsukite.[41] Because the stoichiometry of ETS-4 and

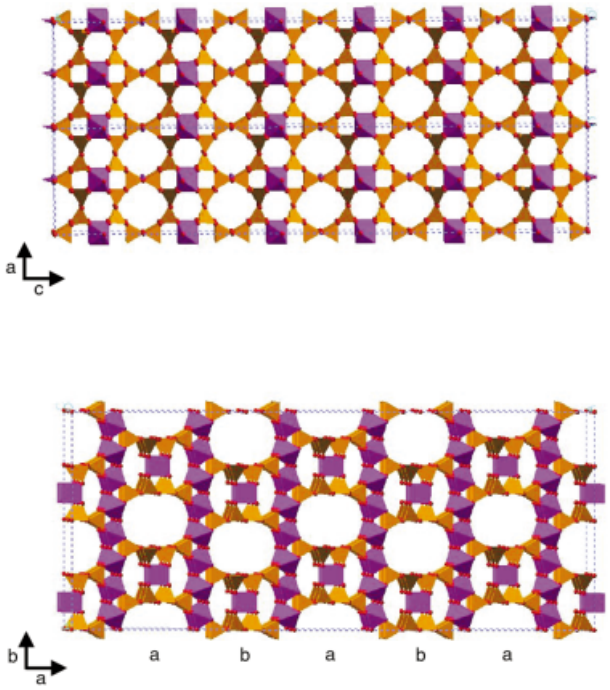


Figure 6. Two orthogonal projections of one possible ordered variant of ETS-4; purple Ti octahedra, brown Si tetrahedra, red spheres oxygens

narsarsukite are different, a quantity of silica must be added to ETS-4 in order to prepare pure narsarsukite at high temperatures.

Other Titanosilicates

In 1994 Clearfield and co-workers reported the synthesis, crystal structure, and ion-exchange properties of a novel porous titanosilicate of ideal composition $Na_2Ti_2O_3SiO_4 \cdot 2\ H_2O$.[17] The structure of this material has been solved from powder X-ray data by ab initio methods. The titanium atoms occur in clusters of four, grouped about the 4_2 axis, and are octahedrally coordinated by oxygen atoms (Figure 7a and 7b). The silicate groups link the titanium clusters into groups of four arranged in a square of about 7.8 Å in length. These squares are linked to similar squares in the *c* direction by sharing corners to form a framework that encloses a tunnel. Half the Na^+ ions are located in the framework, coordinated by silicate oxygen atoms and water molecules. The remaining Na^+ ions reside in the cavity, although some of them are replaced by protons. The Na^+ ions within the tunnels are exchangeable, particularly by Cs^+ ions.

Chapman and Roe[8] have prepared a number of titanosilicate analogues of the mineral pharmacosiderite, a non-aluminosilicate molecular sieve with a framework composition $KFe_4(OH)_4(AsO_4)_3$. Later, Clearfield and co-workers studied by powder X-ray diffraction methods the structure of pharmacosiderite analogues with composition $HM_3Ti_4O_4(SiO_4)_3 \cdot 4\ H_2O$ (M = H^+, K^+, Cs^+).[42] Harrison et al. have been able to grow single crystals of the same cesium phase and solve its structure by single-crystal

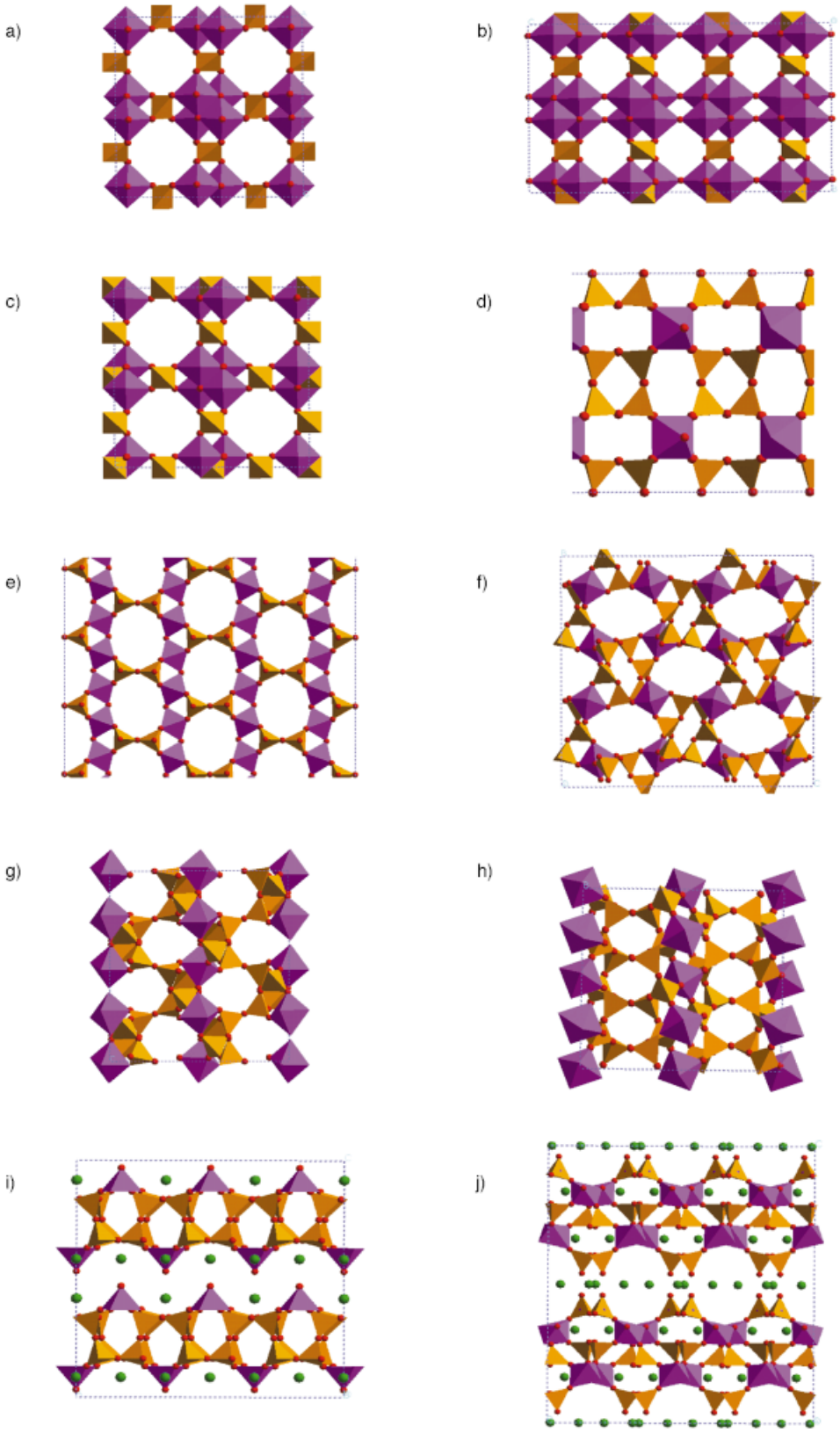


Figure 7. Projection of the structures of: (a) titanosilicate reported by Clearfield et al.[17] along the [001] and (b) [100] directions; (c) pharmacosiderite along [001]; (d) nenadkevichite along [100] and (e) [001]; (f) UND-1 along [100]; (g) penkvilksite 2*O* and AM-3 along [001] and (h) [010]; (i) AM-1 or JDF-L1 along [010]; (j) AM-4 along [100]; purple Ti octahedra, brown Si tetrahedra, green Na cations, red spheres oxygens

methods.[12] These materials possess a most interesting structure built up from TiO_6 octahedra, which share faces to form Ti_4O_4 cubes around the unit-cell corners and have silicate tetrahedra joining the titanium octahedra to form a three-dimensional framework (Figure 7c). Extra-framework Cs^+ species occupy sites slightly displaced from the centres of the intercage eight-ring windows, and also make $CsOH_2$ bonds to the water molecules that reside in the spherical cages.

Nenadkevichite is a rare mineral first found in the Lovozero region (Russia) with the composition $(Na,Ca)(Nb,Ti)Si_2O_7 \cdot H_2O$. The structure of nenadkevichite (from Saint-Hilaire, Quebec, Canada) consists of square rings of silicon tetrahedra Si_4O_{12} in the (100) plane joined together by chains of $(Nb,Ti)O_6$ octahedra in the [100] direction (Figure 7d and 7e).[43] The pores accommodate Na^+ in two partially (0.53 and 0.54) occupied sites and water molecules in two fully occupied sites. Rocha and Anderson and co-workers have been able to prepare a series of synthetic analogues of nenadkevichite with Ti/Nb molar ratios ranging from 0.8 to 17.1 and a purely titaneous sample.[44,45]

Many porous framework titanosilicates contain Ti–O–Ti linkages that often form infinite chains. Interestingly, the materials known as AM-2,[31,32,46–48] UND-1[49] and AM-3[46] do not contain any such linkages. AM-2 is a synthetic potassium titanosilicate analogue of the mineral umbite, a rare zirconosilicate found in the Khibiny alkaline massif (Russia).[50] Although the ideal formula of umbite is $K_2ZrSi_3O_9 \cdot H_2O$, a pronounced substitution of titanium for zirconium occurs. However, the natural occurrence of purely titaneous umbite is unknown. The successful synthesis of umbite materials with different levels of substitution of zirconium by titanium has been reported[31] and indicates the existence of a continuous solid solution that has not been described for any other sodium or potassium zirconosilicate. In the structure of umbite (not shown) the M octahedra, $(Zr,Ti)O_6$, and the T tetrahedra, SiO_4, form a three-dimensional MT-condensed framework.[50] The M octahedron is coordinated to six T tetrahedra. In addition to the M–O–T bonds these tetrahedra also form T–O–T links with each other. The resulting T radical has an identity period of three T tetrahedra and forms an infinite chain. The structures of umbite and the material known as UND-1 ($Na_{2.7}K_{5.3}Ti_4Si_{12}O_{36} \cdot 4\,H_2O$) are very similar.[49] The structure of UND-1 consists (Figure 7f) of six-membered rings of SiO_4 tetrahedra and isolated TiO_6 octahedra. Each TiO_6 octahedron connects, through corner-sharing, to six SiO_4 tetrahedra on the three six-membered rings, thus forming three three-membered rings, while each SiO_4 tetrahedron connects to two isolated TiO_6 octahedra and two other SiO_4 tetrahedra of the same six-membered ring. By such connections, channels running parallel to [100] are formed with eight-membered rings containing alternative –O–Si–O–Ti–O– linkages. The channel wall is covered by seven-membered rings (four SiO_4 tetrahedra and three TiO_6 octahedra) and three-membered rings. There are two cation sites in the structure. One is occupied only by K^+ and is located near the centre of the seven-membered ring of the wall. The other cation site is occupied by 33% K^+ and 67% Na^+ and is located in the large channel near the wall. AM-3 is a sodium titanosilicate analogue of the mineral penkvilksite found in Mont Saint-Hilaire, Québec (Canada), and the Kola Peninsula (Russia) with an ideal formula $Na_4Ti_2Si_8O_{22} \cdot 5\,H_2O$. The mineral occurs in two polytipic modifications, orthorhombic (penkvilksite-2*O*) and monoclinic (penkvilksite-1*M*).[51] These two polytypes have been described according to the OD theory as two of the four possible maximum degree of order polytypes within a family of OD structures formed by two layers.[51] Despite the different space group symmetries the 2*O* (*Pnca*) and 1*M* ($P2_1/c$) polytypes have the same atoms, labeled in the same way, in the asymmetric unit. They differ only in the stacking of the same building blocks. Thus, the following structure description (Figure 7 g and 7h) holds for both polytypes.[51] Penkvilksite contains two independent tetrahedra: The Si1-centred tetrahedra share two corners with other tetrahedra and two corners with TiO_6 octahedra; the Si2-centred tetrahedra share three corners with tetrahedra and one corner with a TiO_6 octahedron. Penkvilksite displays a new kind of connection among SiO_4 tetrahedra. Spirals of corner-sharing tetrahedra develop along [010] and have a periodicity of six tetrahedral units. The Si2-centred tetrahedra are shared between adjacent spirals, which are oriented in an alternate clockwise and counterclockwise fashion. The stacking of the layers along [001] gives rise to tetrahedral layers parallel to (100). The connection of neighbouring layers of tetrahedra is due to Ti^{IV} cations in an octahedral coordination. AM-3 is a synthetic analogue of penkvilksite-2*O*.[46] The synthesis of the 1*M* polytype has been reported recently by Liu et al.[52,53]

The synthesis of a few other microporous framework titanosilicates has also been reported. For example, Chapman and Roe have prepared a synthetic analogue of the mineral vinagradovite[8,54] with a framework composition $Na_8Ti_8Si_{16}O_{52}$. The structure of the mineral is composed of pyroxene chains joined to edge-sharing TiO_6 octahedra, which form brookite columns. These polyhedra define one-dimensional (4 Å) channels containing zeolitic water. A number of other minerals not yet prepared in the laboratory exhibit very interesting frameworks that are connected in a complex way (see the excellent review by J. V. Smith[55]). Verplanckite $[(Mn,Ti,Fe)_6(OH,O)_2(Si_4O_{12})_3]Ba_{12}Cl_9\{(OH,H_2O)_7\}$ has a framework with triple units of (Mn, Ti, Fe) in square-pyramidal coordination and four-rings of silicon tetrahedra.[56] The voids have a free diameter of 7 Å. Muirite, $Ba_{10}(Ca,Mn,Ti)_4Si_8O_{24}(Cl,OH,O)_{12} \cdot 4\,H_2O$, has edge-sharing trigonal prisms and eight-rings of SiO_4.[57]

When attempting to prepare novel microporous framework titanosilicates several groups have obtained layered materials, some of which have very interesting and unusual structures and show potential for being used in a number of applications such as ion exchange. One such material, known as AM-1[14,46] or JDF-L1,[58,59] has the composition $Na_4Ti_2Si_8O_{22} \cdot 4\,H_2O$. This is an unusual non-centrosymmetric tetragonal layered solid that contains five-coordin-

ated Ti^{IV} ions in the form of TiO_5 square pyramids in which each of the vertices of the base is linked to SiO_4 tetrahedra $[TiOO_4(SiO_3)_4]$ to form continuous sheets (Figure 7i).[59] The interlamellar Na^+ ions are exchangeable, for example by protonated alkylamines. AM-4, $Na_3(Na,H)Ti_2O_2[Si_2O_6]_2 \cdot 2\ H_2O$, is yet another example of a layered titanosilicate.[46,60] The crystal structure of AM-4 is built from TiO_6 (M) octahedra and SiO_4 (T) tetrahedra that form layers perpendicular to [001]. Each layer consists of a five-tier sandwich of T–M–T–M–T (Figure 7j). Between the layers are Na^+ cations and water molecules. The former also exist in small cages within the layers. The major features of the structure are zig-zag chains of edge-sharing TiO_6 octahedra running along the [100] direction that are connected together by corner-sharing pyroxene-type SiO_4 tetrahedra. Clearfield et al. reported the synthesis of a layered titanosilicate that seems to be closely related with AM-4.[61] The same group has also carried out a considerable amount of work on the evaluation of synthetic inorganic ion exchangers for cesium and strontium removal from contaminated groudwater and wastewater using (among other materials) several microporous and layered titanosilicates, some of which possess unknown structures (see, for instance, ref.[62] and references therein).

Zirconosilicates

Zirconium silicates occur widely in nature and their formation under hydrothermal conditions (from ca. 300 to 550 °C) has been given considerable attention, though mainly for the solution of general geophysical and mineralogical problems (see ref.[33] and references therein). More than 20 natural and synthetic zirconium silicates are known and for about one-third of them the crystal structures have been solved. Some of the first hydrothermal syntheses of zirconosilicates were carried out by Maurice in 1949.[63] Baussy et al. summarise the early work in this field and report the hydrothermal synthesis of (among others) analogues of the minerals catapleiite ($Na_2ZrSi_3O_9 \cdot 2\ H_2O$) and elpidite ($Na_2ZrSi_6O_{15} \cdot 3\ H_2O$) at 350–500 °C.[64] These materials have also been prepared by others.[65] Jale et al. reported the hydrothermal synthesis of a potassium analogue of elpidite at a relatively low temperature (200 °C).[32] The characteristic feature of the structure of elpidite is the presence of double chains of tetrahedra (epididymite type) connected by zirconium atoms in octahedral coordination (Figure 8a and 8b). The silicate chains form an anionic framework that is saturated by sodium ions. The double chains of tetrahedra are parallel to [100]. Two independent Na^+ cations are present. Na(2) has an octahedral coordination formed by four oxygens of the tetrahedra and two symmetrically equivalent water molecules. Na(1) occurs in a cavity formed by adjacent double chains of tetrahedra and it is bonded to seven oxygens and a water molecule.[66]

Recently, an excellent example of the interesting and promising chemistry of sodium zirconosilicates has been given by Clearfield et al.[33] These workers reported the synthesis, characterisation, and properties of three novel layered materials and five other zirconosilicates. In particular, a synthetic analogue of the mineral gaydonnayite (ideal formula $Na_2ZrSi_3O_9 \cdot 2\ H_2O$) has been prepared. This material has also been synthesised by Rocha and Anderson and co-workers (AV-4)[31] and by Jale et al.[32] The framework of gaydonnayite is composed of sinusoidal single chains of SiO_4 tetrahedra, repeating every six tetrahedra (Figure 8c and 8d).[67] The chains are extend alternately along [011] and [01–1] and are cross-linked by a ZrO_6 octahedron and two distorted NaO_6 octahedra.

Another interesting example of a microporous zirconosilicate is petarasite and its synthetic analogue AV-3.[31,68,69] This rare mineral $[Na_5Zr_2Si_6O_{18}(Cl,OH) \cdot 2\ H_2O]$ possesses a very unusual structure consisting of an open three-dimensional framework built of corner-sharing six-membered rings and ZrO_6 octahedra (Figure 8e and 8f).[68] Elliptical channels (3.5 × 5.5 Å) defined by mixed six-membered rings, consisting of pairs of SiO_4 tetrahedra linked by zirconium octahedra, run parallel to the *b* and *c* axes. Other channels limited by six-membered silicate rings run parallel to the *c* axis. The sodium, chloride and hydroxyl ions and the water molecules reside within the channels. The framework does not collapse until the release of Cl^- at ca. 800 °C.

The preparation of synthetic umbite materials has already been discussed in this microreview. The chemistry of other fascinating microporous framework solids is waiting to be explored. For instance, the mineral lemoynite, $(Na,K)_2CaZr_2Si_{10}O_{26} \cdot 5–6\ H_2O$, possesses a $ZrSi_5O_{13}$ framework with wide open channels where sodium, potassium and calcium cations and water molecules reside.[70] This framework comprises thick (7 Å) layers of hexagons of silicate groups. The sheets are bound together by six-coordinated zirconium atoms. The hexagons are tilted with respect to the layer (001) plane and the architecture of these layers is new.

Niobosilicates

Comparatively few studies are available on microporous framework niobosilicates. In this microreview we have already discussed the work carried out on nenadkevichite analogues containing titanium and niobium.[45,46] Recent work suggests that other niobosilicate materials that show potential as heterogeneous catalysts are yet to be discovered. For example, Rocha and Anderson and co-workers have reported the synthesis of AM-11, a novel microporous sodium niobosilicate.[71] Although its structure is still unknown, this material has a relatively large pore volume and seems to contain NbO_6 octahedra and local silicon environments Si(4Si, 0Nb), Si(3Si, 1Nb) and Si(2Si, 2Nb). A preliminary characterisation of the acid-base properties has shown that AM-11 dehydrates *tert*-butyl alcohol to isobutene with remarkably high activity and selectivity.

Stannosilicates

The hydrothermal synthesis of microporous framework stannosilicates has been pioneered by Corcoran et al. As pointed out by these workers, several minerals containing SnO_6 and SiO_4 polyhedra are known and a few (dense)

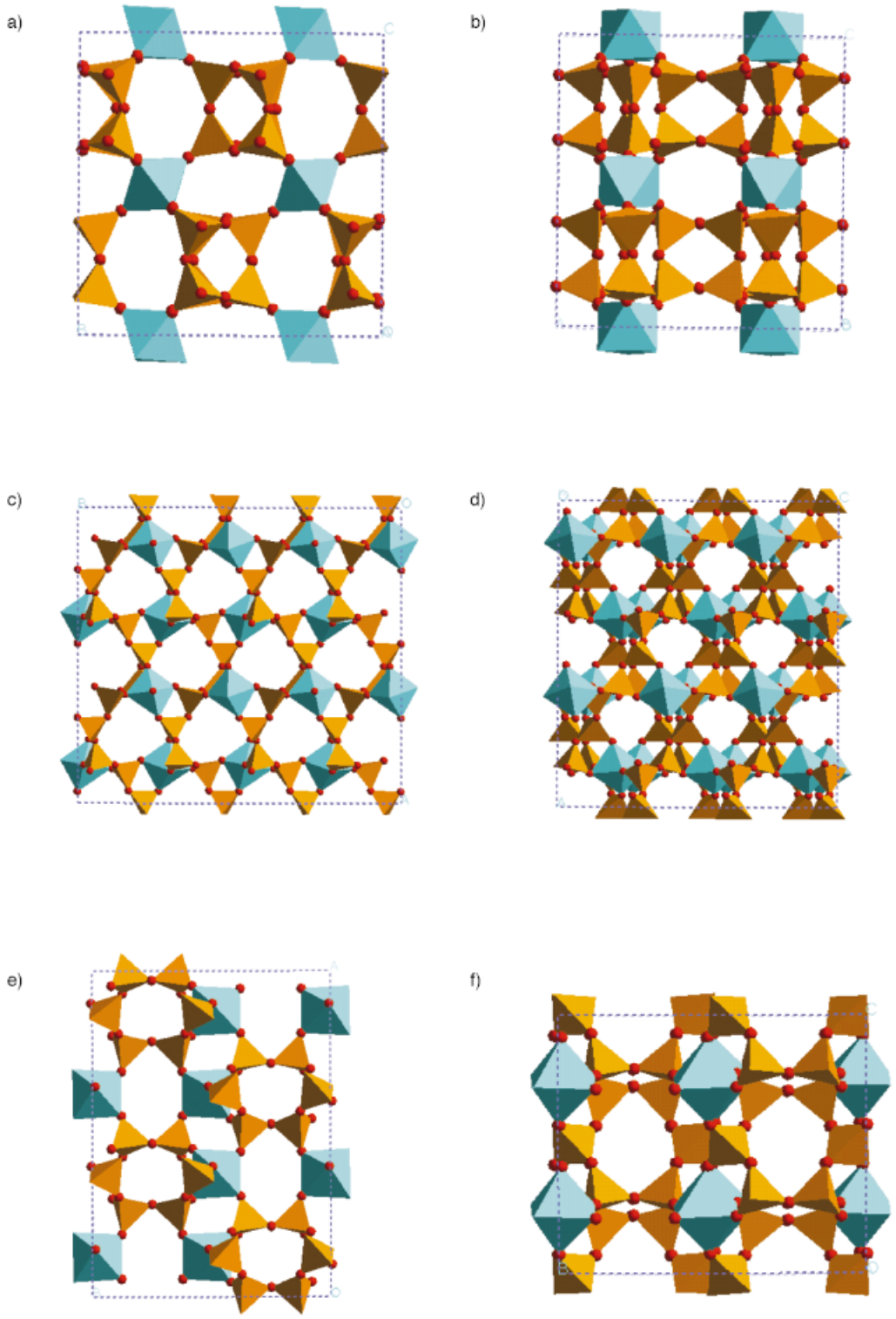


Figure 8. Projections of the structure of: (a) elpidite along the [100] and (b) [010] directions; (c) gaydonnayite and AV-4 along [001] and (d) [010]; (e) petarasite and AV-3 along [001] and (f) [100] directions; blue Zr octahedra, brown Si tetrahedra, red spheres oxygens

stannosilicate phases have been crystallised from high-temperature conditions.[72,73] Two microporous stannosilicates have been reported by Corcoran et al. The orthorhombic phase Sn-A has the composition $Na_8Sn_3Si_{12}O_{34} \cdot n\,H_2O$, while Sn–B has been formulated as $Na_4SnSi_4O_{12} \cdot n\,H_2O$. These materials show reversible water loss and have a significant ion-exchange capacity. A third, layered, stannosilicate ($Na_4SnSi_5O_{14} \cdot n\,H_2O$) has also been reported.[72] Subsequently, Dyer and Jafar reported the synthesis, characterisation and cation-exchange properties of a microporous stannosilicate with a very unusual habit and of composition $Na_{13.5}Sn_{10}Si_{15}O_{36}(OH)_5 \cdot 13.5\,H_2O$.[74] The ion-exchange

behaviour has been shown to be zeolitic in character. The crystal structures of all these solids are, as yet, unknown. Recently, Rocha et al. reported the synthesis and characterisation of two stannosilicates possessing the structures of titanosilicates umbite and UND-1 (Figure 7f).[75]

Vanadosilicates

Although vanadium has already been introduced into the framework of certain zeolites in small amounts, to the best of our knowledge only three microporous framework vanadosilicates are known to contain stoichiometric amounts of vanadium.[34,76,77] Canvasite and pentagonite, dimorphs of the mineral $Ca(VO)(Si_4O_{10}) \cdot 4\,H_2O$, have a framework formed by silicate layers of four- and eight-membered rings of tetrahedra connected vertically by V^{IV} cations that are in a square-pyramidal coordination (Figure 9).[76,77] Replacement of the VO_5 groups by two bridging oxygens would produce a tetrahedral framework topologically identical to that of the zeolite gismondine. The calcium cations and the water molecules reside in the channels formed by the eight-membered rings and between the SiO_2 layers. Canvasite has channels running parallel to the *c* direction with a free diameter of only 3.3 Å in the hydrated state. Hence, both canvasite and pentagonite are likely to behave (at best) as small-pore materials.

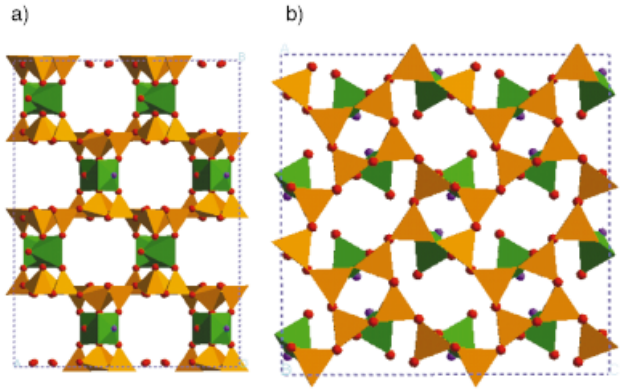


Figure 9. Projection of the structure of canvasite along the (a) [001] and (b) [010] directions; green V square pyramids, brown Si tetrahedra, red spheres oxygens

Recently, the synthesis and structural characterisation of the first large-pore vanadosilicate containing octahedral vanadium and possessing a structure similar to that of titanosilicate ETS-10 has been reported. The presence of stoichiometric amounts of vanadium in the framework of AM-6 gives this material great potential for applications as a catalyst, sorbate or functional material.[34]

Other Silicates

The synthesis of microporous framework silicates of a few other metals have been reported. One such case is AV-1, the synthetic analogue of the rare mineral montregianite (also known as UK-6).[78,79] This is an yttrium silicate, with the formula $Na_4K_2Y_2Si_{16}O_{38} \cdot 10\,H_2O$, that possesses a very unusual structure consisting of two different types of layers alternating along the [010] direction (Figure 10a and 10b):[80] (a) a double silicate sheet, where the single silicate sheet is of the apophyllite type with four- and eight-membered rings, and (b) an open octahedral sheet composed of $[YO_6]$ and three distinct $[NaO_4(H_2O)_2]$ octahedra. The layers are parallel to the (010) plane. The K^+ ions are ten-coordinate and the six water molecules are located within large channels formed by the planar eight-membered silicate rings.

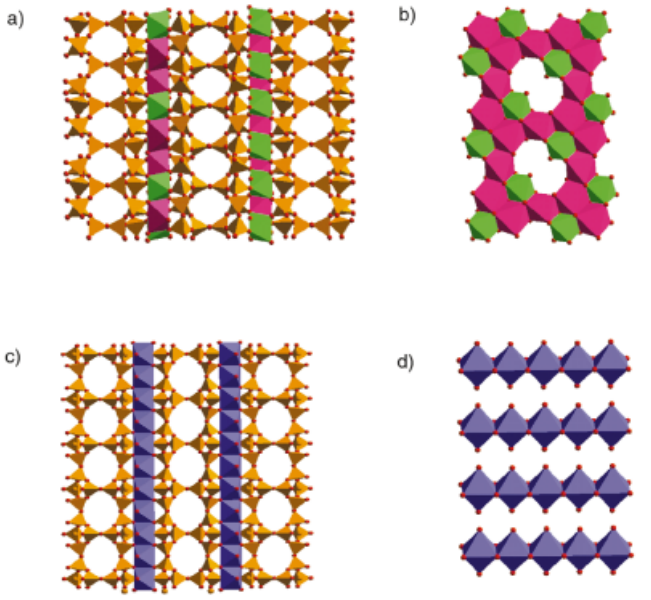


Figure 10. Projection of the structures of: (a) montregianite and AV-1 along the [001] direction; (b) one octahedral layer seen along the [010] direction; (c) rhodesite and AV-2 along [010]; (d) one octahedral layer seen along [100]; green Y octahedra, red Na octahedra, blue Ca octahedra, brown Si tetrahedra, red spheres oxygens

The structure of the alkali calcium silicate mineral rhodesite ($HKCa_2Si_8O_{19} \cdot 6\,H_2O$)[81] and its synthetic analogue AV-2[79] is closely related to that of montregianite. It consists of silicate double layers, chains of edge-sharing $[Ca(O,OH_2)_6]$ octahedra and potassium cations, and additional water molecules within the pores of the silicate double layers (Figure 10c and 10d). Rhodesite and montregianite have double silicate layers of the same topology. In fact, other minerals such as delhayelite, hydrodelhayelite and macdonaldite, all have similar double silicate sheets. In rhodesite these layers possess the maximum topological symmetry (*P*2*mm*) while in montregianite all symmetry has been lost. The structure of rhodesite contains two sets of octahedrally-coordinated calcium ions, which form single chains parallel to [001]. The octahedral chains connect adjacent silicate double layers. While Ca(2) is coordinated to six terminal oxygens that belong to six different SiO_4 tetrahedra, Ca(1) is coordinated to four terminal oxygens from four SiO_4 and two oxygens from water molecules. The extra-framework potassium ions are ten-coordinated to six bridging oxygens and four water molecules.

Characterisation

Disorder

The structures of many microporous materials are disordered and this is the case for the important microporous titanosilicates ETS-10 and ETS-4. It can be assumed that it is likely that a number of the new structures, which will undoubtedly be synthesised in the future, will also be disordered. Disorder should be distinguished from defects. Disorder usually results from the apparent intergrowth of different polymorphs of a structure. In the ideal case this will occur without a disruption in the connectivity of the framework, i.e. internal –OH groups will not be present. Sometimes disorder causes the apparent diffusion pathway through the channel system to be disrupted, as with ETS-4,[39] but sometimes the disorder causes no disruption, as with ETS-10.[13,14] Characterisation of such disordered structures can be complicated, especially if the materials can only be crystallised as microcrystalline powders. The following gives a short description of how a range of characterisation techniques can be powerfully focussed on the problem of characterising disordered materials.

Bulk characterisation techniques generally fall into two categories: those that concern short range effects and those that concern long range effects. This is an important distinction when characterising disordered materials as often, although by no means always, the disorder is manifested beyond the short-length scale. If the disorder occurs on a length scale of tens of Ångstroms, short-range techniques such as high-resolution electron microscopy (HREM), solid-state nuclear magnetic resonance with magic-angle spinning (MAS NMR), infrared spectroscopy (IR), Raman spectroscopy, electronic spectroscopy, and extended X-ray absorption fine structure (EXAFS) will give high quality data. These techniques will behave in the same manner as if there was no disorder. All diffraction techniques, which are inherently long-range techniques, will reflect both the structure and disorder in the material. Consequently, it is often sensible to begin with the short-range techniques and HREM in particular can give information about the possible pore structure and also about how disorder and defects may be incorporated within the material. This is often the cornerstone of any structural analysis. Local chemical environments may be probed in a quantitative fashion using MAS NMR and ^{29}Si is often a useful nucleus in this respect.[82] In favourable circumstances this technique will also yield crystallographic distinctions within a chemical grouping. All these new microporous phases will contain counterbalancing cations and these are often particularly difficult to locate in a disordered material. A common counterbalancing cation is sodium, which is a particularly good NMR nucleus. Because of the quadrupolar nature of ^{23}Na a number of sophisticated modern experiments have been developed known as multiple-quantum NMR spectroscopy. Infrared and Raman spectroscopies can often reveal structural units within a framework. Electronic spectroscopy will show the existence of band gaps, which can be characteristic of certain structures. EXAFS is a useful tool for homing in on a structure towards the end of an analysis. Because of the inability of this technique to distinguish different sites, the data obtained is a composite for the whole sample and is usually of little use in the early stages of structural characterisation. However, EXAFS will reveal very accurate bond lengths in a structure. EXAFS studies on ETS-10 have shown that within the titanate chain the Ti–O bonds are alternately long and short.[35] This will have marked consequences for optical properties.

In the case of ETS-10 this suite of short-range techniques was sufficient to ascertain a framework connectivity for the structure.[13,14] Atomic coordinates can then be refined using simple geometric constraints (bond angles and bond lengths). This is known as a distance-least-squares (or DLS) approach. With suitable interatomic potentials, which exist for titanosilicates[83] but not for some of the more exotic elements, energy minimisation can also be used to refine atomic coordinates. At this stage simulation of HREM images provides one of the best ways to confirm the trial structure.[84]

The diffraction data can be handled in two ways. Usually the diffraction data will consist of sharp and diffuse reflections that are characteristic of the underlying structure and the disorder. By concentrating solely on the sharp reflections it is sometimes possible to define a superposition cell. This is a unit cell that contains structural units in all possible configurations owing to the disorder. Consequently, the unit cell so defined will contain a superposition of framework units with some displacement characteristic of the disorder.

Alternatively the disorder can be incorporated into the calculation of the diffraction data, and a particularly powerful method in this regard is DIFFaX, a technique designed by Treacy, Newsam and Deem in 1991.[85] In this method the structure is built up from structurally perfect layers that are connected according to suitable rules to define the particular disorder observed for the material of interest. In this manner both sharp and diffuse reflections can be simulated. At present it is not possible to use this technique in an iterative fashion, such as Rietveld refinement, and consequently it is best used to confirm structure rather than refine structure.

Isomorphous Framework Substitution

The insertion of heteroatoms into the framework of microporous materials is an important process because it allows the fine-tuning of the their properties. Despite the fact that a considerable amount of work has been carried out on zeolites and other related systems, obtaining unequivocal evidence for framework substitution is not a trivial task and it usually requires the combined use of several techniques. Detailed studies on framework insertion of aluminium, gallium, boron, and niobium on ETS-10 have been reported and we will summarise in the following.

In an attempt to improve the acid characteristics of ETS-10 (and following up the early synthesis work by Kuznicki et al.[28,29]) Rocha and Anderson and co-workers have incorporated aluminium[86,87] and gallium[24,87] into tetrahed-

ral silicon sites, thus generating sites for zeolite-type acidity. These materials are known as ETAS-10 and ETGS-10, respectively. The main evidence for the substitution of silicon by aluminium and gallium in the framework of ETS-10 is provided by solid state NMR. The ^{29}Si MAS-NMR spectra of ETS-10, ETAS-10, and ETGS-10 are shown in Figure 11.

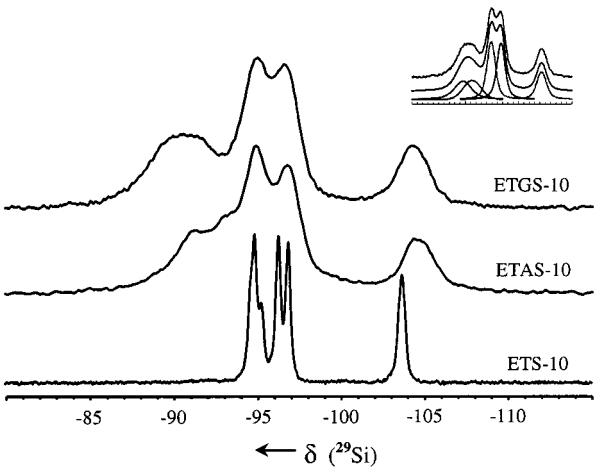


Figure 11. ^{29}Si MAS-NMR spectra of ETS-10, ETAS-10 and ETGS-10; the inset shows a deconvolution of the ETGS-10 spectrum

In ETS-10 there are two types of silicon chemical environments, Si(3Si, 1Ti) and Si(4Si, 0Ti), which give rise to the two groups of resonances at δ = –94 to –97 and ca. –103.7, respectively. The ratio of these environments is 4:1. The spectrum reveals a further crystallographic splitting of the Si(3Si, 1Ti) site. The spectrum of ETAS-10 contains all the ETS-10 resonances plus two other peaks ca. 4 ppm downfield from the Si(3Si, 1Ti) signals. These new peaks become stronger when the framework aluminium concentration increases (Figure 12).

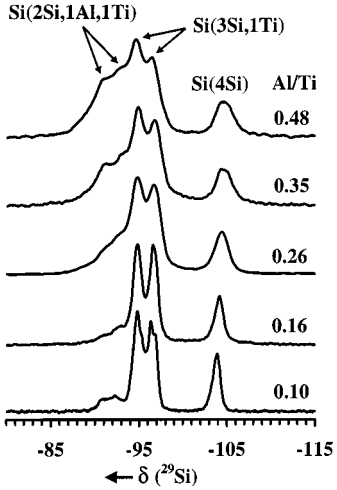
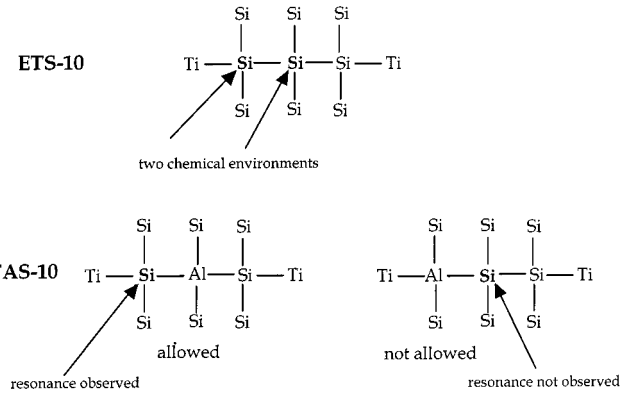


Figure 12. ^{29}Si MAS-NMR spectra of ETAS-10 with the Al/Ti ratios depicted

These signals are ascribed to the framework incorporation of aluminium to produce Si(2Si, 1Al, 1Ti) environments. It is important to note that there is no signal ca. 4 ppm downfield from the Si(4Si, 0Ti) resonance, showing no aluminium substitution neighbouring this silicon site and, hence, providing direct evidence for Al, Ti avoidance.[24,86]



The ^{27}Al MAS-NMR spectrum (not shown) is also indicative of this effect since it contains a single resonance at δ ≈ 60, which is assigned to Al(4Si).

The ^{29}Si MAS-NMR spectrum of gallium-substituted ETS-10 resembles the spectrum of ETAS-10: a broad peak is seen downfield from the Si(3Si, 1Ti) signals. This peak can be deconvoluted into two component signals, each one ca. 1.5 ppm downfield from the Si(2Si, 1Al, 1Ti) resonances, which we assign to Si(2Si, 1Ga, 1Ti) as similar downfield shifts of the ^{29}Si NMR resonances have been reported for gallium-substituted zeolites. No signals are observed in the range δ = –99 to –103.[24,86] On the other hand, the ^{71}Ga MAS-NMR spectrum of fully-hydrated ETGS-10 (not shown) displays a broad peak at δ = 160, which is characteristic of four-coordinated gallium.

Detailed analysis of spectral intensities (I_{Si}) allows framework Si/Al (or Si/Ga) and Si/Ti ratios to be calculated from Equation 1 and Equation 2.

$$\mathrm{Si/Al} = \frac{\sum_{n=0}^{4-m}\sum_{m=0}^{4-n} \mathrm{I}_{\mathrm{Si(nAl,mTi)}}}{0.25\sum_{n=0}^{4-m}\sum_{m=0}^{4-n} \mathrm{nI}_{\mathrm{Si(nAl,mTi)}}} \quad (1)$$

$$\mathrm{Si/Ti} = \frac{\sum_{n=0}^{4-m}\sum_{m=0}^{4-n} \mathrm{I}_{\mathrm{Si(nAl,mTi)}}}{0.25\sum_{n=0}^{4-m}\sum_{m=0}^{4-n} \mathrm{mI}_{\mathrm{Si(nAl,mTi)}}} \quad (2)$$

Increasing the aluminium content in ETAS-10 broadens considerably the ^{29}Si-NMR resonances (Figure 12). In particular, the peak at δ = –104.5 becomes very broad, increasing its Full-Width-at-Half-Maximum (FWHM) from 40 Hz in ETS-10 to 200 Hz in ETAS-10 with Al/Ti = 0.48.[24] In fact, there is an almost perfectly linear correlation between the FWHM of this resonance and the Al/Ti ratio (equivalent to the aluminium content as aluminium replaces silicon and not titanium) of samples. In the case of zeolites the NMR lines are broadened for a number of reasons. Structural disorder, for example, gives rise to a dispersion of chemical shifts. Another important line broadening mech-

anism is the decrease of the spin-spin relaxation times brought about by $^{29}Si/^{27}Al$ dipolar interactions.[88] In order to assess this possibility the spin-spin relaxation times of an ETAS-10 sample with Si/Al = 0.24 has been measured. The two resonances at high frequency have short T_2 times (about 5 ms), confirming their assignment to silicons with aluminium neighbours and, thus, providing further evidence for framework substitution. The peaks attributed to Si(3Si, 1Ti) and Si(4Si) environments have similar, much longer relaxation times (35–49 ms). Therefore, the broadening of the Si(4Si) resonance cannot be explained by the dipolar mechanism discussed above. This effect is most likely caused by the distortion of the lattice upon aluminium incorporation.[86]

It is too early to say whether Al (Ga), Ti avoidance is a general phenomenon in titanoalumino(gallo)silicates. However, it seems logical that, wherever possible, Al (Ga) and Ti will not be neighbours. We have found that at relatively high Al and Ga framework concentrations slight deviations from the Al (Ga), Ti avoidance rule are observed.

The insertion of boron into ETS-10, yielding ETBS-10, has also been reported.[89] As the amount of boron in ETBS-10 increases, a new ^{29}Si MAS-NMR peak, attributed to Si–O–B environments, grows at $\delta \approx -99$ and (as in ETAS-10 and ETGS-10) all the resonances broaden considerably (not shown). On the other hand, the ^{11}B MAS-NMR spectra (not shown) of ETBS-10 samples with different boron contents are similar and contain two groups of very sharp peaks (FWHM ca. 78 Hz) at $\delta \approx -1.4$ and -2.9. This implies that any electric field gradients created by the electronic cloud at the ^{11}B nuclei are very small (quadrupole coupling constant estimated at 40–80 kHz) and shows that boron is in a tetrahedral, rather than a trigonal, coordination and replaces silicon in the framework of ETBS-10. Indeed, it has been reported that hydrated boron-substituted H-ZSM-5 zeolite gives a single sharp ^{11}B-NMR peak at $\delta = -3$.[90] On the other hand, the local environment of any extra-framework boron would, in principle, be more distorted or, at least, a dispersion of boron sites would occur leading to significantly broader ^{11}B MAS-NMR resonances.[89]

The insertion of niobium into the framework of ETS-10, replacing titanium, has been reported to pose particular problems because NMR does not provide strong evidence for it.[91] Indeed, only a relatively small broadening of the ^{29}Si MAS-NMR resonances is observed. In addition, the ^{93}Nb MAS-NMR spectrum recorded with a very fast (32 kHz) spinning rate displays a broad peak at $\delta = 100$ relative to solid Nb_2O_5, suggesting the presence of niobium in a distorted octahedral coordination. However, Raman and FTIR spectroscopies provide strong evidence for this framework substitution. ETS-10 gives a strong and sharp main Raman band at ca. 735 cm^{-1}, assigned to the TiO_6 octahedra (not shown).[91] As the niobium content of the samples increases, this peak shifts slightly and broadens and, simultaneously, a band grows at ca. 664 cm^{-1}. The latter band is typical of NbO_6 octahedra in microporous niobosilicates. The FTIR spectrum of ETS-10 (not shown) displays bands at 446, 550, and 746 cm^{-1}, associated with the TiO_6 octahedra. As the niobium content of the samples increases the intensity of these bands decreases, while a new band at 918 cm^{-1} is seen. This is a further indication that niobium replaces titanium in the ETS-10 framework.

The great (largely overlooked) potential presented by Raman spectroscopy for studying the isomorphous framework substitutions in zeolite-type materials is particularly well illustrated by the synthetic titano-niobosilicate nenadkevichite system.[44,45] The Raman spectra of a sample with Ti/Nb = 0.8 (Figure 13) displays two main bands at 668 and 226 cm^{-1} associated with the NbO_6 octahedra. With increasing titanium content the intensity of these bands decreases (particularly of the former) while simultaneously two other strong bands grow at 764 and 290 cm^{-1}. These bands are attributed to NbO_6 octahedra.

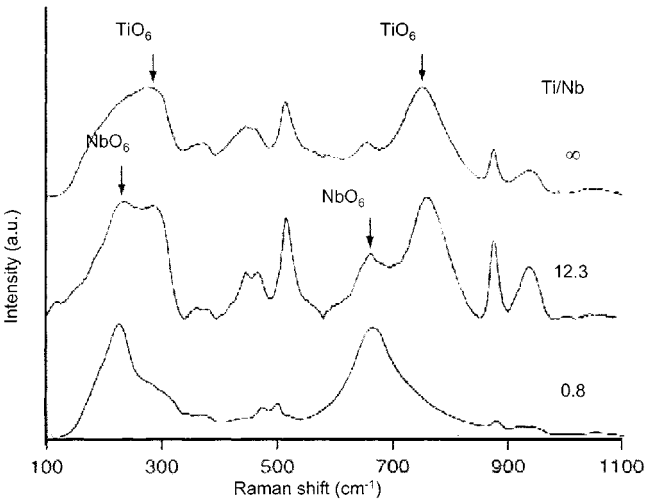


Figure 13. Raman spectra of synthetic nenadkevichite materials; the Ti/Nb ratios are indicated

The titanium for zirconium substitution in synthetic umbite has been studied in detail by powder X-ray diffraction.[31] It has been found that with increasing titanium content the unit cell shrinks in the three directions and its volume decreases systematically from ca. 985 (purely zirconeous sample) to 919 $Å^3$ (titaneous sample). This is not unexpected because Ti^{IV} is smaller than Zr^{IV}. ^{29}Si MAS-NMR spectroscopy provides further evidence for this framework substitution.[31] In the structure of umbite there are three types of Si(2Si, 2Zr) sites with populations 1:1:1.[50] The spectrum of purely zirconeous AM-2 displays a single broad peak at $\delta = -86.5$. In contrast, the spectrum of the purely titaneous sample contains a resonance at $\delta = -87.3$ and two overlapping peaks at about $\delta = -86.2$ and -85.9 in an approximate 1:1:1 intensity ratio, in accord with the crystal structure of umbite. Along the series, it is observed that as the zirconium content of the samples increases, the peak at about $\delta = -86.5$ broadens while the resonance at $\delta = -87.3$ broadens and eventually disappears from the spectrum.

Cation Location (Multiple-Quantum NMR and Computer Modelling)

The framework of these novel microporous materials is anionic and the charge density can be very high. Consider ETS-10, which has a basic formula unit of $Si_{40}Ti_8O_{104}^{16-}$. In other words there are 16 unit charges per 48 metal centres, which would be equivalent to a zeolite with a Si/Al ratio of 2 (which for zeolites is close to the Lowensteinian limit of Si/Al = 1). Moreover, the framework charge centres (at the octahedral Ti^{IV} site) carry an overall two-minus charge. Consequently, the charge distribution is quite different to the monovalent sites in the aluminosilicate zeolites. This will potentially make titanosilicates in this new class particularly attractive for exchanging divalent cations and are indeed particularly selective for some divalent heavy metals such as Pb^{2+} and Cd^{2+}.[9,92] Other materials reported above have an even higher charge density than the theoretical limit for zeolites, e.g. nenadkevichite with a composition $(Na,Ca)(Nb,Ti)Si_2O_7 \cdot H_2O$ is equivalent to a zeolite with Si/Al = 0.5.

It is desirable to characterise the cation site both in terms of crystallographic location and interaction with adsorbed molecules. For quadrupolar cations, such as sodium, the new technique of multiple-quantum MAS NMR is particularly powerful. Historically the NMR study of quadrupolar nuclei has been plagued by the inability to remove the quadrupole interaction, thereby gaining sufficient resolution to observe all possible sites. Two experimentally demanding techniques, dynamic angle spinning (DAS)[93] and double rotation (DOR),[94] were invented to overcome this problem but neither is easily implemented. Recently the technique of multiple-quantum (MQ) MAS NMR has provided a relatively straightforward solution to the problem.

The basic theory behind MQ MAS NMR is now well documented[95–98] and, thus, the following is a brief general overview. Consider the observation of a half-integer ($I > {}^1/_2$) spin nucleus. For a powdered sample, under fast spinning conditions, the frequency for symmetrical (m, $-m$) multiple-quantum transitions involves second- and fourth-rank angular dependent terms. The Legendre polynomials, P_2 and P_4, describing these angular dependencies are (Equation 3 and Equation 4)

$$P_2(\cos\theta) = \left(3\cos^2\theta - 1\right)/2 \quad (3)$$

$$P_4(\cos\theta) = \left(35\cos^4\theta - 30\cos^2\theta + 3\right)/8 \quad (4)$$

where θ is the angle between the spinning axis and the magnetic field B_0. As there is no common root to these polynomials, there is no single spinning axis that can completely remove the second-order quadrupolar broadening.

In the MQ MAS-NMR experiment the sample is spun at the magic angle and the magnetisation evolves sequentially under the triple (or quintuple) quantum Hamiltonian in the first part of time t_1 and under the single-quantum Hamiltonian during the second part. Judicious choice of the length of these evolution periods generates an isotropic echo. The simplest two-dimensional experiment is a two-pulse sequence whereby the pulse phases are cycled in an appropriate manner to select the desired quantum coherence. The projection of the (sheared) MQ MAS NMR spectrum onto axis F1 yields an isotropic, highly resolved spectrum, while the F2 projection is essentially the "conventional" MAS NMR spectrum. The position and profile of a peak in this two-dimensional spectrum immediately yields the isotropic chemical shift for the signal as well as the quadrupole coupling constant, C_Q, and the asymmetry parameter, η. These last two parameters define the quadrupole interaction, which is determined by the local environment of the nucleus. Conversely, if the environment is known then C_Q and η can be determined and compared with the NMR experiment.

Experimentally the technique is straightforward to implement. The hardware required is a conventional MAS NMR probe with smaller coil widths preferred in order to generate large radio-frequency fields. 4 mm rotors or even 2.5 mm rotors are preferable although there is a balance between sensitivity loss and gaining a high radio-frequency field. If the radio-frequency field is insufficient it will not be possible to excite nuclei experiencing a large quadrupolar interaction. These are generally highly coordinated nuclei in a very asymmetric environment.

A combination of MQ MAS NMR and computer modelling has been used to determine the sodium cation siting in ETS-10.[99–101] The ^{23}Na triple-quantum (3Q) MAS NMR spectrum of as-prepared ETS-10 is shown in Figure 14a and comprises two signals. Deconvolution of the isotropic sum projection onto F1 shows them to be in the ratio 2.6:1. The stronger signal comprises two sites, as evidenced by the shoulder in the isotropic F1 projection, with estimated δ_{iso}s and second-order quadrupole effects (SOQEs), $\sqrt{[C_Q^2(1 + (\eta^2/3)]}$ of –7.6 and 1.1 MHz and –7.5 and 1.3 MHz. The weaker signal is equally as broad in F1 and is also likely to comprise more than one site having δ_{iso}s of ca. –1.6 and a SOQEs of ca. 1.7 MHz.

Upon dehydration the weaker of the two signals in the spectrum of the hydrated material has now shifts to a lower F2 frequency (Figure 14b). This is due to an important change in δ_{iso} and SOQE from –1.6 and 1.7 MHz in hydrated ETS-10 to –3.7 and 2.4 MHz, in dehydrated ETS-10. Any sites responsible for this signal are thus strongly affected by dehydration. Although the shape of the stronger signal is slightly altered, it remains unshifted. The two sites largely unaffected by sample dehydration are assigned to sites I and II, which are tucked away on either side of the 12-ring pore (see Figure 5). The change in the position of the weaker signal upon dehydration suggests that any sites that give rise to this signal must be in the vicinity of water molecules and are thus likely to be situated in the pore void. This signal is therefore attributed to sites III and V, which are located at the top of the 12-ring pore near a titanate chain and loosely bound somewhere within the pore, respectively. A number of similar MQ MAS NMR studies have been carried out on a whole range of these novel microporous phases and the results will be published shortly.

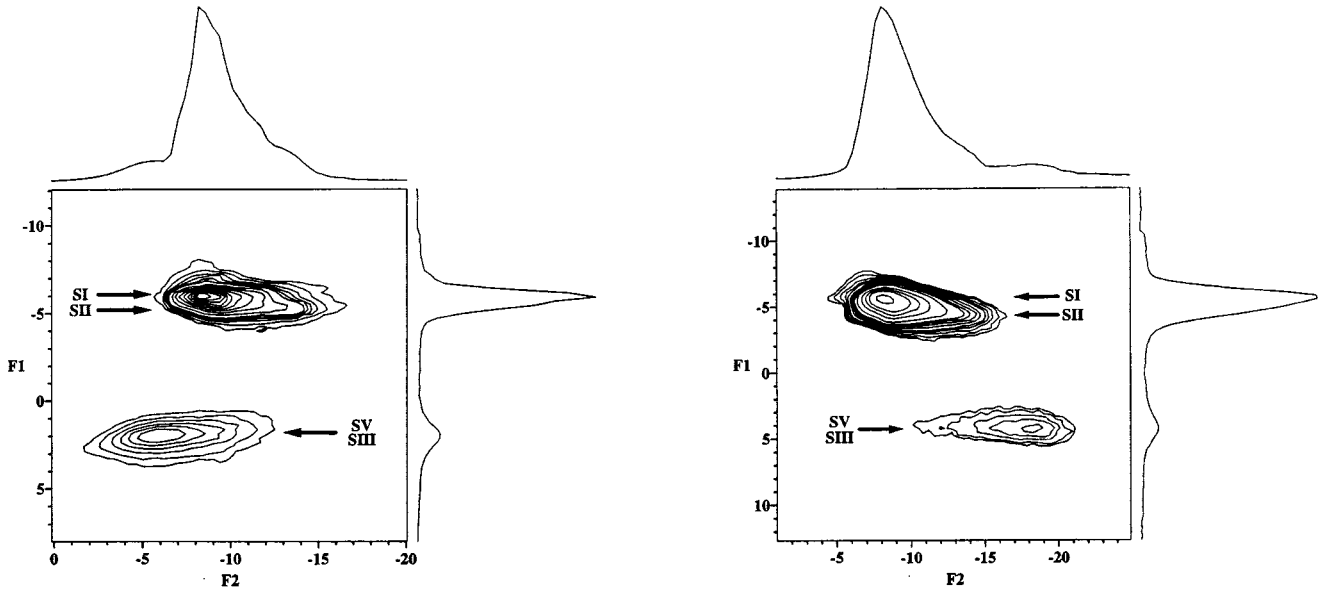


Figure 14. Triple-quantum ^{23}Na MAS-NMR spectra (9.4 T field) of ETS-10 (a) as-prepared and (b) dehydrated sample

Applications

Catalysis

For catalytic applications these novel framework materials present interesting new challenges. Apart from the possibilities for shape-selectivity and high activity through high surface area (similar to zeolites) these new materials possess a number of characteristics that make them particularly interesting as prospective heterogeneous catalysts. To date, only a moderate amount of work has been carried out on catalytic applications of the more stable wide-pore ETS-10 materials. However, this initial work is very encouraging and will no doubt be expanded greatly in the near future. For ETS-10 the catalytic applications have focused on the following attributes: high cation exchange capacity, which leads to many possibilities particularly in base catalysis; facile metal loading for bifuncionality; very low acidity; possible chiral activity; photocatalytic opportunities. It should be pointed out that the titanosilicates with octahedrally-coordinated titanium do not show good properties for oxidation catalysis in comparison to four-coordinate titanium. This is due to the ligand saturation, which prevents further attachment by oxidising agents such as hydrogen peroxide.

A number of papers by Bianchi, Ragaini, and co-workers detail Fischer–Tropsch chemistry over Co and Ru exchanged ETS-10.[102–105] The titanium silicate ETS-10 was found to be a suitable support for metal catalysts, due to its high surface area, high ion-exchange capability and the absence of an acidic function. The importance of alpha-olefin readsorption within the catalyst is discussed and the nature of this readsorption is tailored by effective control of the metal distribution inside the pores of ETS-10. The CO conversion and selectivity obtained also varies depending upon whether the active metal is introduced in the ETS-10 cages by ion-exchange or simply by impregnation.

Two groups, those of Anderson, Rocha, and co-workers[106] and Sivasanker and co-workers,[107–109] have studied the bifunctional reforming reaction of hexane to benzene over Pt-supported basic ETS-10. The basicity of the titanosilicate can be controlled by using samples exchanged with different alkali metals (M = Li, Na, K, Rb, or Cs). A distinct relationship between the intermediate electronegativity (S-int) of the different metal-exchanged ETS-10 samples and the yield of benzene is reported, suggesting the activation of Pt by the basicity of the exchanged metal. Typically ETS-10 samples exhibit greater aromatization activities than related Pt/Al_2O_3 catalysts. The very high basicity of ETS-10 in comparison with, for example zeolite X, is illustrated by Anderson and co-workers in a paper that discusses the relative conversion of 2-propanol to acetone.[110] The same group has also demonstrated how these same properties are effective in aldol chemistry[111] and dehydration of *tert*-butyl alcohol.[112,113] In this latter reaction conversions and selectivities close to 100% are observed at relatively modest temperatures.

One area of possible catalytic activity that has not yet been properly explored is the potential for photo-catalysis. In this respect, the activity of ETS-10 for the photocatalytic degradation of cyclohexanol, cyclododecanol, 2-hexanol, and benzyl alcohol is compared, by Fox and co-workers, with TiO_2 particles included within small and large pore zeolitic supports suspended in acetonitrile.[114] Although the activity was less than that displayed by the titanium-doped silicate TS-1 this work was reported before very much was known about the structure of ETS-10 and how it can be modified. Consequently, this field of research is ripe for exploration, particularly in terms of the optical properties of these novel materials.

Finally, ETS-10 offers the potential for chiral catalysis or asymmetric synthesis if the pure chiral polymorph of ETS-

10 can be synthesised. Along with zeolite β, ETS-10 is currently the only known wide-pore microporous material that possesses a chiral polymorph with a spiral channel. The structures of these as-prepared materials contain an equal proportion of intimately intergrown enantiomorphs and are consequently achiral. The task of synthesising a pure chiral polymorph is, of course, immense. However, with some of the recently developed molecular modelling techniques for designing suitable organic templates to direct the structure, it may well be possible to solve this problem in the next decade.[115]

Optical Properties

Owing to the presence of stoichiometric quantities of transition metals in the framework of these novel microporous materials, they have potential for interesting optical properties.[83,116–119] Most attention to date has again focussed on the microporous material ETS-10. The structure of ETS-10 contains –O–Ti–O–Ti–O– chains, with alternating long and short bonds, which are effectively isolated from each other by a silicate sheath. In effect, therefore, ETS-10 contains monoatomic –O–Ti–O–Ti–O– wires embedded in an insulating SiO_2 environment, a situation that leads to a one-dimensional quantum confinement of electrons or holes within this wire. A blue bandgap shift is associated with this charge carrier confinement within this unprecedented geometrical structure. The effective reduced mass, μ, of electrons and holes within this wire is calculated to be $1.66\ M(e) < \mu < 1.97\ M(e)$, which is consistent with a band gap of 4.03 eV and is quite different to that of bulk TiO_2. This work underlines the possible future role that these microporous materials may play in optoelectronic and nonlinear optical applications. The titanium within the chains can be readily reduced using Na vapour, which effects the following redox couple,[120]

$$Ti^{IV} + Na \rightarrow Ti^{III} + Na^+$$

thereby generating unpaired electrons within the titanate chain and also generating extra cation sites. After such reduction the material is not air stable and is easily reoxidised, generating additional Na_2O within the channels. Such redox couples also give strong indications of possible applications in battery technology.

Recently, Rocha et al. doped ETS-10 with Eu^{3+} and Er^{3+} by ion-exchange techniques and studied the luminescence properties of the resultant materials.[121–122] It has been found that only Eu^{3+}-doped ETS-10 is optically active. Upon calcination at temperatures in excess of 700 °C both materials transform into dense titanosilicate analogues of the mineral narsarsukite [$(Na, K)_2TiSi_4O_{11}$], which is made up of Si_4O_{10} chains that form tubes of rings consisting of four SiO_4 tetrahedra.[123] These tubes are linked by chains of corner-sharing TiO_6 octahedra. The cavities between the Si_4O_{10} tubes and octahedral chains contain Na^+, Eu^{3+} and Er^{3+} cations. Eu^{3+} and Er^{3+}-doped narsarsukite display very interesting luminescence properties. The latter, in particular, exhibits a high and stable room-temperature emission in the visible and in the infrared spectral regions. An efficient energy transfer between the narsarsukite skeleton and the optically active Er^{3+} centres seems to occur.[122]

Adsorption Properties

Dihydrogen, dinitrogen, carbon monoxide, and nitric oxide have all been adsorbed, at nominally liquid nitrogen temperature, on Na^+- and K^+- exchanged ETS-10.[124] IR spectroscopy indicates the formation of $M^+(H_2)$, $M^+(N_2)(n)$, $M^+(CO)(n)$ and $M^+(NO)$ (n = 1, 2, ...; M^+ = Na, K) adducts that prevalently involve alkali-metal cations located in the 12- membered channels. These adducts give main IR absorption bands in the range 4050–4150 cm^{-1} for H_2, 2331–2333 cm^{-1} for N_2, 2148–2176 cm^{-1} for CO, and 1820–1900 cm^{-1} for NO, which are assigned to the fundamental stretching mode of the diatomic molecules polarized by the electric field created by the metal ions. On Na-exchanged samples, the $Na^+(N_2)$ and $Na^+(CO)$ species, formed at the lowest dosage, evolve into $Na^+(N_2)(n)$ and $Na^+(CO)(n)$ (n = 2, 3) species upon increasing the gas phase pressure. This reversible "solvation" process is not observed for K-exchanged samples. There is no comparable precedent for this result for CO adsorbed on zeolites and it is indicative of the unique adsorption characteristics that can be expected with these highly charged, high cation capacity microporous materials.

Cation Exchange

To date there has been very little work on the cation exchange properties of this novel class of material. However, the cation exchange capacity is very high and, in addition, the framework anionic sites are typically divalent, which should be particularly useful for the exchange of divalent cations. Indeed ETS-10 has been shown to be particularly selective for Pb^{2+} [125] and Cd^{2+} [126] ions. Furthermore the penkvilksite structure has been shown to be particularly selective for Li^+ cations,[127] which again may indicate possible applications in battery technology.

Conclusions

In this review it has been shown that a new and exciting field of research into microporous zeotype solids is emerging. These stable silicate materials possess mixed octahedral-tetrahedral frameworks and display entirely new molecular architectures. Although much of the work performed to date has concentrated on titanosilicates, it is clear that the novel porous frameworks may contain many other elements, particularly transition metals such as Zr, Nb, Sn, V, and Y. We anticipate that some of the new materials will find applications in areas usually associated with zeolites. Others, however, may have potential applications in fields such as optoelectronics and nonlinear optics, batteries, magnetic materials and sensors.

Acknowledgments

We thank EC JOULE II (J. R. and M. W. A.), EPSRC (M. W. A.), FCT, PRAXIS XXI, and FEDER (J. R.) for financial support.

We are very grateful to Dr. O. Terasaki for helping to solve the structure of ETS-10 and for the fruitful collaboration between both our groups.

[1] D. W. Breck, *Zeolite Molecular Sieves*, John Wiley & Sons, New York, **1974**.
[2] R. M. Barrer, *Hydrothermal Chemistry of Zeolites*, Academic Press, New York, **1982**.
[3] R. Szostak, *Molecular Sieves*, Van Nostrand Reinhold, New York, **1989**.
[4] S. T. Wilson, S. Oak, B. M. Lok, E. M. Flanigen, W. Plains, US 4 310 440, **1982**.
[5] B. M. Lok, C. A. Messina, R. T. Gajek, T. R. Cannan, E. M. Flanigen, US 4 440 871, **1984**.
[6] S. T. Wilson, S. Oak, E. M. Flanigen, US 4 567 029, **1986**.
[7] [7a] S. L. Suib, *Curr. Opinion Solid State Mater. Sci.* **1998**, *3*, 63. – [7b] R. C. Haushalter, L. A. Mundi, *Chem. Mater.* **1992**, *4*, 31.
[8] D. M. Chapman, A. L. Roe, *Zeolites* **1990**, *10*, 730.
[9] S. M. Kuznicki, US Patent 4 853 202, **1989**.
[10] S. M. Kuznicki, US Patent 4 938 989, **1990**.
[11] D. M. Chapman, US Patent 5 015 453, **1990**.
[12] W. T. A. Harrison, T. E. Gier, G. D. Stucky, *Zeolites* **1995**, *15*, 408.
[13] M. W. Anderson, O. Terasaki, T. Oshuna, A. Philippou, S. P. Mackay, A. Ferreira, J. Rocha, S. Lidin, *Nature* **1994**, *367*, 347.
[14] M. W. Anderson, O. Terasaki, T. Oshuna, P. J. O'Malley, A. Philippou, S. P. Mackay, A. Ferreira, J. Rocha, S. Lidin, *Philos. Mag. B* **1995**, *71*, 813.
[15] T. K. Das, A. J. Chandwadkar, S. Sivasanker, *Chem. Commun.* **1996**, 1105.
[16] X. Liu, J. K. Thomas, *Chem. Commun.* **1996**, 1435.
[17] D. M. Poojary, R. A. Cahill, A. Clearfield, *Chem. Mater.* **1994**, *6*, 2364.
[18] J. Rocha, P. Brandão, Z. Lin, A. P. Esculcas, A. Ferreira, M. W. Anderson, *J. Phys. Chem.* **1996**, *100*, 14978.
[19] J. Rocha, A. Ferreira, Z. Lin, M. W. Anderson, *Microporous Mesoporous Mater.* **1998**, *23*, 1253.
[20] T. K. Das, A. J. Chandwadkar, A. P. Budhkar, A. A. Belhekar, S. Sivasanker, *Microporous Mater.* **1995**, *4*, 195.
[21] V. Valtchev, S. Mintova, *Zeolites* **1994**, *14*, 697.
[22] V. P. Valtchev, *J. Chem. Soc., Chem. Commun.* **1994**, 730.
[23] T. P. Das, A. J. Chandwadkar, A. P. Budhkar, S. Sivasanker, *Microporous Mater.* **1996**, *5*, 401.
[24] M. W. Anderson, A. Philippou, Z. Lin, A. Ferreira, J. Rocha, *Angew. Chem. Int. Ed. Engl.* **1995**, *34*, 1003.
[25] J. Rocha, Z. Lin, A. Ferreira, M. W. Anderson, *J. Chem. Soc., Chem. Commun.* **1995**, 867.
[26] J. Rocha, P. Brandão, J.D. Pedrosa de Jesus, A. Philippou, M. W. Anderson, *Chem. Commun.* **1999**, 471.
[27] J. Rocha, P. Brandão, M. W. Anderson, T. Ohsuna, O. Terasaki, *Chem. Commun.* **1998**, 667.
[28] [28a] S. M. Kuznicki, K. A. Thrush, US 5 244 650, **1993**. – [28b] S. M. Kuznicki, R. J. Madon, G. S. Koermer, K. A. Thrush, EPA 0405978A1, **1991**.
[29] S. M. Kuznicki, A. K. Thrush, WO91/18833, **1991**.
[30] J. Rocha, P. Ferreira, Z. Lin, J. R. Agger, M. W. Anderson, *Chem. Commun.* **1998**, 1268.
[31] Z. Lin, J. Rocha, P. Ferreira, A. Thursfield, J. R. Agger, M. W. Anderson, *J. Phys. Chem. B.* **1999**, *103*, 957.
[32] S. R. Jale, A. Ojo, F. R. Fitch, *Chem. Commun.* **1999**, 411.
[33] A. I. Bortun, L. N. Bortun, A. Clearfield, *Chem. Mater.* **1997**, *9*, 1854.
[34] J. Rocha, P. Brandão, Z. Lin, M. W. Anderson, V. Alfredsson, O. Terasaki, *Angew. Chem. Int. Ed. Engl.* **1997**, *36*, 100.
[35] G. Sankar, R. G. Bell, J. M. Thomas, M. W. Anderson, P. A. Wright, J. Rocha, A. Ferreira, *J. Phys. Chem.* **1996**, *100*, 449.
[36] X. Q. Wang, A. J. Jacobson, *Chem. Commun.* **1999**, 973.
[37] A. N. Mer′kov, I. V. Bussen, E. A. Goiko, E. A. Kul'chitskaya, Y. P. Men′shikov, A. P. Nedorezova, *Zap. Vses. Mineralog. O-va* **1973**, *102*, 54.
[38] P. A. Sandomirskii, N. V. Belov, *Sov. Phys. Crystallogr.* **1979**, *24*, 686.
[39] A. Philippou, M. W. Anderson, *Zeolites* **1996**, *16*, 98.
[40] G. Cruciani, P. DeLuca, A. Nastro, P. Pattison, *Microporous Mesoporous Mater.* **1998**, *21*, 143.
[41] M. Naderi, M. W. Anderson, *Zeolites* **1996**, *17*, 437.
[42] E. A. Behrens, D. M. Poojari, A. Clearfield, *Chem. Mater.* **1996**, *8*, 1236.
[43] P. G. Perrault, C. Boucher, J. Vicat, E. Cannillo, G. Rossi, *Acta Crystallogr., Sect. B* **1973**, *29*, 1432.
[44] J. Rocha, P. Brandão, Z. Lin, A. Kharlamov, M. W. Anderson, *Chem. Commun.* **1996**, 669.
[45] J. Rocha, P. Brandão, Z. Lin, A. P. Esculcas, A. Ferreira, M. W. Anderson, *J. Phys. Chem.* **1996**, *100*, 14978.
[46] Z. Lin, J. Rocha, P. Brandão, A. Ferreira, A. P. Esculcas, J. D. Pedrosa de Jesus, A. Philippou, M. W. Anderson, *J. Phys. Chem.* **1997**, *101*, 7114.
[47] D. M. Poojari, A. I. Bortun, L. N. Bortun, A. Clearfield, *Inorg. Chem.* **1997**, *36*, 3072.
[48] M. S. Dadachov, A. Le Bail, *Eur. J. Solid State Inorg. Chem.* **1997**, *34*, 381.
[49] X. Liu, M. Shang, J. K. Thomas, *Microporous Mater.* **1997**, *10*, 273.
[50] G. D. Ilyushin, *Inorg. Mater.* **1993**, *29*, 853.
[51] S. Merlino, M. Pasero, G. Artioli, A. P. Khomyakov, *Am. Mineral.* **1994**, *79*, 1185.
[52] Y. Liu, H. Du, F. Zhou, W. Pang, *Chem. Commun.* **1997**, 1467.
[53] Y. Liu, H. Du, Y. Xu, H. Ding, W. Pang, Y. Yue, *Microporous Mesoporous Mater.* **1999**, *28*, 511.
[54] R. K. Rastsvetaeve, V. I. Andrianov, *Kristallografiya* **1984**, *29*, 681.
[55] J. V. Smith, *Chem. Rev.* **1988**, *88*, 149.
[56] A. R. Kampf, A. A. Khan, W. H. Baur, *Acta Crystallogr., Sect. B* **1973**, *B29*, 2019.
[57] L. P. Solov'eva, S. V. Borisov, V. V. Bakakin, *Sov. Phys. Crystallogr. (Engl. Transl.)* **1972**, *16*, 1035.
[58] . Du, M. Fang, J. Chen, W. Pang, *J. Mater. Chem.* **1996**, *6*, 1827.
[59] M. A. Roberts, G. Sankar, J. M. Thomas, R. H. Jones, H. Du, M. Fang, J. Chen, W. Pang, R. Xu, *Nature* **1996**, *381*, 401.
[60] M. S. Dadachov, J. Rocha, A. Ferreira, M. W. Anderson, *Chem. Commun.* **1997**, 2371.
[61] A. Clearfield, A. I. Bortun, L. N. Bortun, R. A. Cahill, *Solvent Extr. Ion Exch.* **1997**, *15*, 285.
[62] A. I. Bortun, L. N. Bortun, A. Clearfield, *Solvent Extr. Ion Exch.* **1997**, *15*, 909.
[63] O. D. Maurice, *Econ. Geol.* **1949**, *44*, 721.
[64] G. Baussy, R. Caruba, A. Baumer, G. Turco, *Bull.Soc. fr. Minéral. Crystallogr.* **1974**, *97*, 433.
[65] G. Y. Chao, D. H. Watkinson, *Can. Mineral.* **1974**, *12*, 316.
[66] E. Cannillo, G. Rossi, L. Ungaretti, *Amer. Mineral.* **1973**, *58*, 106.
[67] G. Y. Chao, *Can. Mineral.* **1985**, *23*, 11.
[68] S. Ghose, C. Wan, G. Y. Chao, *Can. Mineral.* **1980**, *18*, 503.
[69] J. Rocha, P. Ferreira, Z. Lin, J. R. Agger, M. W. Anderson, *Chem. Commun.* **1998**, 1269.
[70] Y. Le Page, G. Perrault, *Can. Mineral.* **1976**, *14*, 132.
[71] J. Rocha, P. Brandão, A. Philippou, M. W. Anderson, *Chem. Commun.* **1998**, 2687.
[72] E. W. Corcoran Jr., D. E. W. Vaughan, *Solid State Ionics* **1989**, *32/33*, 423.
[73] E. W. Corcoran Jr., J. M. Newsam, H. E. King Jr., D. E. Waughan, *ACS Symp. Ser.* **1989**, *398*, 603.
[74] [74a] A. Dyer, J. J. Jafar, *J. Chem. Soc., Dalton Trans.* **1990**, 3239. – [74b] A. Dyer, J. J. Jafar, *J. Chem. Soc., Dalton Trans.* **1991**, 2639.
[75] [75a] Z. Lin, J. Rocha, A. Valente, *Chem. Commun.* in press. – [75b] Z. Lin, J. Rocha, A. Ferreira, *J. Mater. Chem.*, submitted.
[76] H. T. Evans Jr., *Amer. Mineral., Sect. B* **1973**, *58*, 412.
[77] R. Rinaldi, J. J. Pluth, J. V. Smith, *Acta Crystallogr., Sect. B* **1975**, *31*, 1598.
[78] J. Rocha, P. Ferreira, Z. Lin, P. Brandão, A. Ferreira, J. D. Pedrosa de Jesus, *Chem. Commun.* **1997**, 2103.
[79] J. Rocha, P. Ferreira, Z. Lin, P. Brandão, A. Ferreira, J. D. Pedrosa de Jesus, *J. Phys. Chem.* **1998**, *102*, 4739.
[80] S. Ghose, P. K. S. Gupta, C. F. Campana, *Am. Mineral.* **1987**, *72*, 365.

[81] K.-F. Hesse, F. Z. Liebau, *Kristallogr.* **1992**, *199*, 25.
[82] A. Labouriau, T. J. Higley, W. L. Earl, *J. Phys. Chem. B* **1998**, *102*, 2897.
[83] A. J. M. deMan, J. Sauer, *J. Phys. Chem.* **1996**, *100*, 5025.
[84] T. Ohsuna, O. Terasaki, D. Watanabe, M. W. Anderson, S. Lidin, *"Zeolites and Related Microporous Materials: State of the Art 1994" Stud. Surf. Sci. Catal.* (Eds.: Weitkamp et al.), **1994**, vol. *84*, p. 413.
[85] M. M. J. Treacy, J. M. Newsam, M. W. Deem, *Proc. Roy. Soc. London A* **1991**, *433*, 499.
[86] M. W. Anderson, J. Rocha, Z. Lin, A. Philippou, I. Orion, A. Ferreira, *Microporous Mater.* **1996**, *6*, 195.
[87] J. Rocha, Z. Lin, A. Ferreira, M. W. Anderson, *J. Chem. Soc., Chem. Commun.* **1995**, 867.
[88] M. W. Anderson, *Magn. Reson. Chem.* **1992**, *30*, 898.
[89] J. Rocha, P. Brandão, M. W. Anderson, T. Ohsuna, O. Terasaki, *Chem. Commun.* **1998**, 667.
[90] K. F. M. G. J. Scholle, W. S. Veeman, *Zeolites* **1985**, *5*, 118.
[91] J. Rocha, P. Brandão, J. D. Pedrosa de Jesus, A. Philippou, M. W. Anderson, *Chem. Commun.* **1999**, 471.
[92] M. W. Anderson, unpublished results.
[93] B. F. Chmelka, K. T. Mueller, A. Pines, J. Stebbins, Y. Wu, J. W. Zwanziger, *Nature* **1989**, *339*, 42.
[94] [94a] A. Samoson, E. Lippmaa, A. Pines, *Mol. Phys.* **1988**, *65*, 1013. – [94b] A. Llor, J. Virlet, *Chem. Phys. Lett.* **1988**, *152*, 248.
[95] L. Frydman, J. S. Harwood, *J. Am. Chem. Soc.* **1995**, *117*, 5367.
[96] J.-P. Amoureux, C. Fernandez, L. Frydman, *Chem. Phys. Lett.* **1996**, *259*, 347.
[97] C. Fernandez, J.-P. Amoureux, *Chem. Phys. Lett.* **1995**, *242*, 449.
[98] A. Medek, J. S. Harwood, L. Frydman, *J. Am. Chem. Soc.* **1995**, *117*, 12779.
[99] M. W. Anderson, J. R. Agger, D. P. Luigi, A. K. Baggaley, J. Rocha, *PCCP* **1999**, *1*, 2287.
[100] J. R. Agger, M. W. Anderson, J. Rocha, D. P. Luigi, M. Naderi, A. K. Baggaley, *Proc. 12th International Zeolite Conf., Baltimore* (Eds.: M. R. S. Treacey et al.), July **1998**, p. 2457.
[101] S. Ganapathy, T. K. Das, R. Vetrivel, S. S. Ray, T. Sen, S. Sivasanker, L. Delevoye, C. Fernandez, J. P. Amoureux, *J. Am. Chem. Soc.* **1998**, *120*, 4752.
[102] C. L. Bianchi, S. Vitali, V. Ragaini, *Stud. Surf. Sci. Catal.* **1998**, *119*, 167.
[103] C. L. Bianchi, S. Ardizzone, V. Ragaini, *Stud. Surf. Sci. Catal.* **1998**, *119*, 173.
[104] C. L. Bianchi, V. Ragaini, *J. Catal.* **1997**, *168*, 70.
[105] C. L. Bianchi, R. Carli, S. Merlotti, V. Ragaini, *Catal. Lett.* **1996**, *41*, 79.
[106] A. Philippou, M. Naderi, N. Pervaiz, J. Rocha, M. W. Anderson, *J. Catal.* **1998**, *178*, 174.
[107] S. B. Waughmode, T. K. Das, R. Vetrivel, S. Sivasanker, *J. Catal.* **1999**, *185*, 265.
[108] T. K. Das, A. J. Chandwadkar, S. Sivasanker, *Stud. Surf. Sci. Catal.* **1998**, *113*, 455.
[109] T. K. Das, A. J. Chandwadkar, H. S. Soni, S. Sivasanker, *Catal. Lett.* **1997**, *44*, 113.
[110] A. Philippou, J. Rocha, M. W. Anderson, *Catal. Lett.* **1999**, *57*, 151.
[111] A. Philippou, M. W. Anderson, *J. Catal.*, in press.
[112] A. Philippou, M. Naderi, J. Rocha, M. W. Anderson, *Catal. Lett.* **1998**, *53*, 221.
[113] T. K. Das, A. J. Chandwadkar, H. S. Soni, S. Sivasanker, *J. Mol. Catal. A – Chemical* **1996**, *107*, 199.
[114] M. A. Fox, K. E. Doan, M. T. Dulay, *Res. Chem. Intermed.* **1994**, *20*, 711.
[115] D. W. Lewis, D. J. Willock, C. R. A. Catlow, J. M. Thomas, G. J. Hutchings, *Nature* **1996**, *382*, 604.
[116] B. Mihailova, V. Valtchev, S. Minatova, L. Konstantinov, *Zeolites* **1996**, *16*, 22.
[117] Y. N. Xu, W. Y. Ching, Z. Q. Gu, *Ferroelectrics* **1997**, *194*, 219.
[118] E. Borello, C. Lamberti, S. Bordiga, A. Zecchina, C.O. Arean, *Appl. Phys. Lett.* **1997**, *71*, 2319.
[119] C. Lamberti, *Microporous Mesoporous Mater.* **1999**, *30*, 155.
[120] A. Zecchina, personal communication.
[121] J. P. Rainho, L. D. Carlos, J. Rocha, *J. Lumin.*, in press.
[122] J. Rocha, L. D. Carlos, J. P. Rainho, Z, Lin, R. M. Almeida, *J. Mater. Chem.*, submitted.
[123] Y. A. Pyatenko, Z. V. Pudvkina, *Kristallografiya* **1960**, *5*, 563.
[124] A. Zecchina, C. O. Arean, G. T. Palomino, F. Geobaldo, C. Lamberti, G. Spoto, S. Bordiga, *PCCP* **1999**, *1*, 1649.
[125] S. M. Kuznicki, K. A. Thrush, US Patent 4 994 191, **1991**.
[126] M. W. Anderson, M. Mohsen, unpublished results.
[127] S. M. Kuznicki, J. S. Curran, X. Yang, US Patent 5 882 624, **1999**.

Received October 12, 1999
[I99360]

An SiO_2-Embedded Nanoscopic Pd/Au Alloy Colloid

Helmut Bönnemann,*[a] Uwe Endruschat,[a] Bernd Tesche,[a] Anna Rufínska,[a] Christian W. Lehmann,[a] Friedrich E. Wagner,[a] George Filoti,[b] Viorica Pârvulescu,[c] and Vasile I. Pârvulescu*[c]

Keywords: Colloids / Sol–gel processes / Immobilization / Heterogeneous catalysts / Hydrogenations

A bimetallic, fully alloyed Pd/Au colloid of 3.0 nm particle size, obtained by the co-reduction of Pd and Au salts with tetraalkylammonium triethylhydroborate, was embedded in a silica matrix employing a modified sol–gel procedure with THF as the solvent. The removal of the protecting tenside led to a mesoporous texture with a comparatively narrow pore distribution. The physical characterisation by a combination of several techniques has shown that the SiO_2-embedded Pd/Au colloid preserves the size and the structural characteristics of the colloidal metal precursor. The new material exhibits catalytic properties in selective hydrogenation.

The incorporation of preformed ligand-stabilized metal clusters and colloids is currently of interest both in basic research[1] and for applications in heterogeneous catalysis.[2a][2b] Bimetallic heterogeneous Pd catalysts have elicited a large interest because of their superior selectivity and their resistance to deactivation which has been observed in several processes of practical importance.[3,4,5] Gold by itself, supported on SiO_2, Al_2O_3 or MgO, shows a rather low catalytic activity,[6] but its addition to Pd was found to lead to an enhanced catalytic activity which has been interpreted in terms of geometric or electronic effects.[7,8]

Most reports on bimetallic Pd catalysts refer to systems prepared via the coimpregnation of the metal salts on solid supports using the incipient wetness technique, followed by calcination.[9,10] However, a vigorous debate is still going on as to whether the resulting Pd–Au particles on the support are fully alloyed.[11] Recent data from a combined XANES and EXAFS study made by Couves and Meeham[12] have emphasized these doubts. Another problem lies in the metal dispersion. There is strong evidence that the addition of Au to Pd salts results in a marked decrease of the dispersion of the bimetallic catalyst systems.[10,13]

Pre-prepared colloidal alloy particles, covered by various protecting shells, offer a different means of access to highly dispersed bimetallic catalyst precursors.[14–19] Following the so called "precursor concept",[20] these pre-prepared nanometals, for which the particle size distribution, composition and structure are rather well defined, may be deposited on various supports to give a new type of heterogeneous bimetallic catalyst.[18–21] Here we report the preparation of a heterogeneous Pd/Au catalyst formed by the embedding of pre-prepared tetraalkylammonium-stabilized Pd/Au alloy particles in a solid SiO_2 matrix following a modified sol–gel process.

The colloidal Pd/Au precursor was prepared in analogy to ref.[18] by the co-reduction of Pd and gold salts with $NOct_4[BEt_3H]$ (= Tetraoctylammonium triethylhydroborate) in dry THF under argon. A solution of palladium acetate (786 mg, 3.5 mmol) and gold chloride (1061 mg, 3.5 mmol) in 300 mL THF was added over the course of 2 h to a vigorously stirred solution of 0.38 M $NOct_4[BET_3H]$ in THF (46.1 mL) at ambient temperature. This process went to completion over the next 16 h and was accompanied by a colour change to black, indicating the formation of colloidal noble metal in solution. The excess of the reducing agent was removed by adding 5 mL acetone to the reaction mixture, which was stirred for another 30 min. The precipitate was removed by filtration and the solvent was evaporated under vacuum (10^{-3} mbar, room temperature, 16 h.). The isolated raw colloidal powder was redispersed in 40 mL diethyl ether and then precipitated by adding 330 mL of an ethanol/methanol mixture, which dissolves any excess protective surfactant. The mixture was allowed to stand for 24 h before the colourless supernatant was removed by decantation. The colloid was precipitated and dried in vacuo. The resulting colloid powder is fully redispersible in THF and has a metal content of 5.28 wt-% Pd and 8.96 wt-% Au (atomic ratio Pd/Au = 53:47). Monometallic Pd and Au colloids were prepared for comparison applying an analogous procedure.[19]

The embedding of the Pd/Au colloid was carried out with tetraethoxysilicate (TEOS) as the precursor for the silica support. However, since the NR_4-stabilized Pd/Au colloids are completely insoluble and even decompose at elevated temperatures in alcoholic solutions, the normal sol–gel procedure has to be modified by using THF as the solvent. The

[a] Max-Planck-Institut für Kohlenforschung, Mülheim an der Ruhr, Abt. Heterogene Katalyse,
Postfach 101353, 45466, Mülheim, Germany
E-mail: Boennemann@mpi-muelheim.mpg.de
[b] Technische Universität München, Physics Department E 15, James Franck Strasse 1, 85747 Garching bei München, Germany
[c] University of Bucharest, Faculty of Chemistry, Department of Catalysis,
B-dul Regina Elisabeta 4–12, Bucharest 70346, Romania
E-mail: v_parvulescu@chim.upb.ro

 © WILEY-VCH Verlag GmbH, D-69451 Weinheim, 2000 1434–1948/00/0505–0819 $ 17.50+.50/0

molar composition of the sol was TEOS/THF/H_2O/HCl = 1:3.5:4:0.05. The colloid was added as a 4.5 wt-% THF solution at room temperature, after refluxing. The sol was stirred vigorously at 70 °C (under reflux) until the gelification was complete (after 2 days). To avoid any decomposition in the presence of air, all steps were carried out under argon. The resulting gel was dried at 110 °C using a ramp of 0.12 °C min^{-1} then calcined in air at 450 °C with a ramp of 0.3 °C min^{-1}. After cooling, the samples were reduced in flowing hydrogen at 450 °C using the same ramp. For comparison, dried samples were subjected directly to reduction without an intermediate calcination. These samples contained 1 wt-% of metal. Thermal activation (450 °C) of such hybrid materials resulted in a porous texture having a rather narrow pore diameter in the region of the mesoporous materials.

The characterisation of the Pd/Au colloids both in the free and in the embedded state was first performed by transmission electron microscopy (TEM), energy dispersive X-ray analysis (EDX), and atomic absorption spectroscopy (AAS). In addition, nitrogen adsorption-desorption curves at 77 K, H_2 chemisorption measurements, solid state ^{29}Si NMR, XRD, SAXS, XPS, and ^{197}Au Mössbauer spectroscopy were applied.

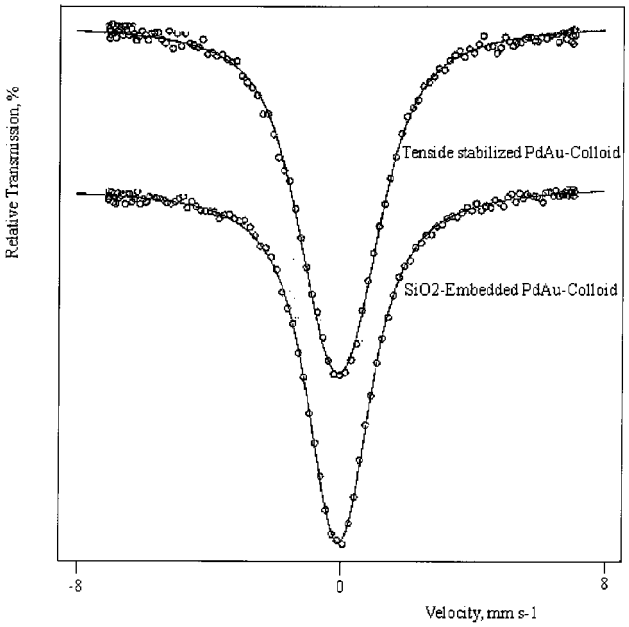


Figure 1. ^{197}Au Mössbauer spectra of tenside-stabilized pure and SiO_2-embedded Pd/Au colloid

Both Mössbauer (see Figure 1) and XRD analyses of the free Pd/Au colloid showed a fully alloyed material consisting of 52% Pd and 48% Au. These values correspond closely to those found by the chemical and EDX analysis. The embedding of the Pd–Au colloids in the sol–gel matrix does not alter the Mössbauer spectrum. There is no difference between the isomer shifts in the free Pd/Au colloid and in the embedded sample, confirming that the colloid structure had not changed during the sol–gel process. The integrity of the incorporated Pd/Au alloy particles remained virtually untouched.

The intensity distributions of XRD patterns of the embedded Au, Pd and Pd/Au colloids correspond to silica and to metallic or bimetallic species. An intense diffraction peak at 22° 2-Θ originates from calcined SiO_2, showing that the support is not totally amorphous. All peaks in the pattern recorded for the bimetallic system containing 1.0 wt-% Pd/Au in SiO_2 correspond to a bimetallic Pd/Au alloy, and no peaks assignable to single Au or Pd species are present. A peak broadening analysis was performed on the basis of FWHM values obtained from peak fitting using a pseudo-Voigt peak shape function. The instrument line broadening was obtained using a standard Si sample. The result indicates a particle size of ca. 3.0 nm both for the Pd/Au and the Au system, whereas the particles in the pure Pd system appear to be larger (ca. 5.6 nm). The composition of the bimetallic Pd/Au alloy was determined from lattice parameter calculations (52 wt-% Au, 48 wt-% Pd; a = 3.976 Å).

Table 1 summarises the textural characteristics of the embedded colloids and the H_2-chemisorption data. The results indicate that in all cases a mesoporous material was present with a rather sharp pore diameter distribution. However, SAXS has shown that the channels are randomly distributed and no tubes (such as those found in MCM materials) are present here. The same information resulted from the TEM analysis. The pore diameter and the mesoporous texture are related to characteristics of the surfactant used. The dispersion of the monometallic Pd colloid in the silica gel matrix was found to be lower than in the case of the bimetallic Pd–Au colloid in the same matrix. For the same metal loading, the Au-containing silica gel matrix exhibited the lowest dispersion. The large differences found between the amounts of physically adsorbed hydrogen and chemisorbed hydrogen, especially for Au, may account for the contribution of the support. TEM measurements (Figure 2) have confirmed a narrow size distribution of the incorporated bimetallic colloid (about 3.0 nm), another proof of the conservation of the characteristics of the colloidal precursor in the incorporated state.

The ^{29}Si CP/MAS NMR spectrum of a Pd/Au SiO_2 sample (1.0 wt-%, preactivated in hydrogen) shows the characteristic structure for Si–O bonds. A ^{29}Si MAS analysis using the "Block decay" procedure indicated that the population of Q^3 species is about 18 %, whereas almost no Q^2 species were found. These data confirm a good polymerisation grade of the silica. The Q^3-to-Q^4 ratio, when compared with published data, was proved to be consistent with the incorporation of the colloids in the silica network.[22] On the basis of the same ^{29}Si MAS analysis it was concluded that the so-called "T surrounding species" are absent.

To test the catalytic properties of the incorporated Pd/Au colloid, we examined the selective semi-hydrogenation of 3-hexyn-1-ol, which gives the corresponding *cis*-hexenol derivative. This is a valuable perfume ingredient.[18] Under standard test conditions, 6.1 mL of 3-hexyn-1-ol were converted without solvent in a stirred 50 mL stainless steel autoclave using 50 mg of catalyst (1 wt-% metal incorporated) at 20 bar hydrogen and 20 °C. The reaction products

Table 1. BET surface area, average pore diameter, hydrogen uptake, metal dispersion, and metallic surface area for the sol–gel-embedded catalysts

Catalyst	BET surface area [$m^2\ g^{-1}$]	Average pore diameter [Å]	Chemisorbed hydrogen			
			H_2 uptake [$cm^3\ g^{-1}$]	Metal dispersion [%]	Metal surface area [$m^2\ g^{-1}_{sample}$]	Metal surface area [$m^2\ g^{-1}_{metal}$]
Pd–SiO_2	319	34	0.30	14.25	0.63	63.2
Au–SiO_2	281	34	0.08	7.38	0.18	17.8
Pd/Au–SiO_2	292	35	0.48	27.60	1.01	101.2

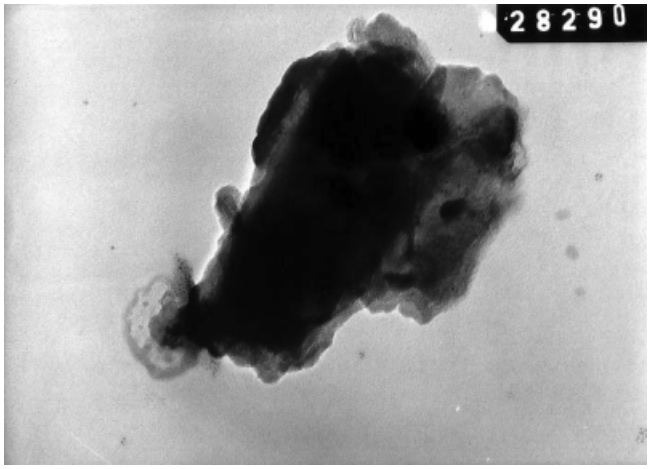


Figure 2. TEM of SiO_2-embedded Pd/Au colloid

were analysed by GC using a Varian 3700–519 chromatograph equipped with a 50 m CW-20M column. The reaction products were identified using the same GC coupled with a Finnigan MAT SSQ7000 mass spectrometer on the basis of pure standards. The results are shown in Figure 3.

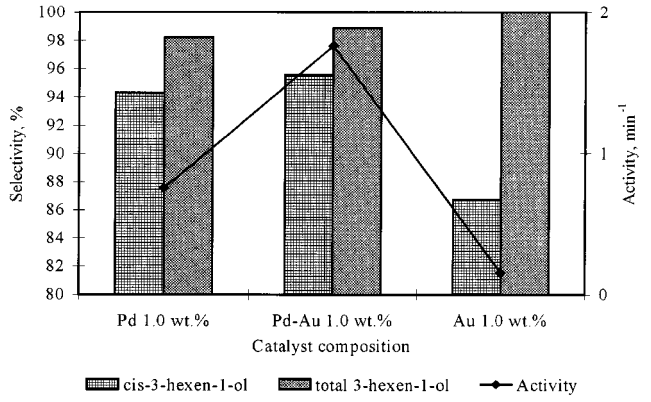


Figure 3. Catalytic activity and selectivity of the embedded colloids in the hydrogenation of 3-hexyn-1-ol

An inspection of Figure 3 shows that the catalytic activity is lowest for the embedded-Au-catalyst sample. As we expected, the catalytic activity of incorporated Pd/Au particles in SiO_2 proved to be superior to monometallic samples. Hexenol and hexanol were the only reaction products. The chemoselectivity towards hexenol reached 100% in the case of embedded Au colloids. Both the other catalysts yielded hexenol and hexanol, the chemoselectivity to hexenol still exceeding 95 %. Both the monometallic Pd and the bimetallic Pd/Au catalysts exhibit a high *cis* selectivity (> 95 %). The performances of the bimetallic Pd/Au catalyst are similar to the highest level reported in the literature.[18] Figure 4 shows the time evolution of the conversion. The selectivity in all the recorded points accounts for the values presented in Figure 3.

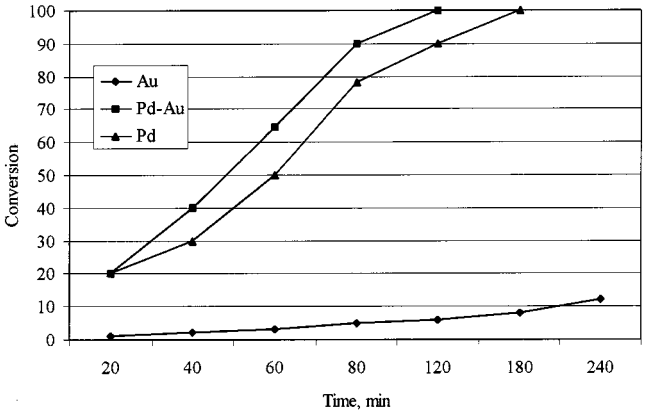


Figure 4. Time evolution of the conversion

Furthermore, we have found that bimetallic Pd–Au colloids incorporated in SiO_2 by sol–gel techniques are active catalysts for selective C,C hydrogenations of unsaturated substrates, e.g. of cinnamaldehyde and styrene. In addition SiO_2-embedded nanoscopic Pd/Au catalysts under these conditions are remarkably resistant to deactivation.

Acknowledgments

V. I. P. thanks the Alexander-von-Humboldt-Stiftung, Bonn, Germany, for the grant of his research fellowship 1997/98 in the Max-Planck-Institut für Kohlenforschung, Mülheim/Ruhr, Germany.

[1] G. Ihlein, B. Junges, U. Jungas, F. Laeri, F. Schüth, U. Vietze, *Appl. Organomet. Chem.* **1998**, *12*, 305–314.
[2] [2a] M. T. Reetz, M. Dugal, *Catal. Lett*. **1999**, *58*, 207–212. – [2b] S. Tao, Z. Zhan, G. Meng, *J. Mater. Sci. Lett*. **1999**, *18*, 707–710.
[3] J. H. Sinfelt, G. H. Via, F. W. Lytle, *Catal. Rev. Sci. Eng.* **1984**, *26*, 81–89.
[4] G. C. Bond, *Chem. Soc. Rev.* **1991**, *20*, 441–458.
[5] R. S. Tanke, Hoechst Celanese *US Pat*. 1 616 015, **1996**.
[6] S. Galvagno, G. Parravano, *J. Catal.* **1978**, *55*, 178–189.
[7] J. W. Sachtler, G. A. Somorjai, *J. Catal.* **1983**, *81*, 77–94.
[8] A. Sachdev, J. Schwank, *J. Catal.* **1989**, *120*, 353–369.

[9] E. L. Kugler, M. Boudart, *J. Catal*. **1979**, *59*, 201–210.

[10] W. Juszczyk, Z. Karpinski, D. Lomot, J. Pielaszek, J. W. Sobtzek, *J. Catal.* **1995**, *151*, 67–76.

[11] J. W. Couves, P. Meeham, *Physica B* **1995**, *208209*, 665–667.

[12] M. Haruta, *Catal. Today* **1997**, *36,* 153–166.

[13] G. Schmid, A. Lehnert, J. -O. Malm, J.-O. Bovin, *Angew. Chem.* **1991**, *103*, 852–854.

[14] M. Harada, K. Asakura, N. Toshima, *J. Phys. Chem.* **1993**, *97*, 5103–5114.

[15] N. Toshima, *Fine Particles Science and Technology* (Ed.: E. Pelizzetti), Kluwer Academic Publishers, **1996**, p. 371–383.

[16] Y. Mizukoshi, K. Okitsu, Y. Maeda, T. A. Yamamoto, R. Oshima, Y. Nagota, *J. Phys. Chem.* **1997**, *101*, 7033–7037.

[17] G. Schmid, H. West, H. Mehles, A. Lehnert, *Inorg. Chem.* **1997**, *36,* 891–895.

[18] H. Bönnemann, W. Brijoux, A. Schulze Tilling, K. Siepen, *Top. Catal*. **1997**, *4*, 217–227.

[19] H. Bönnemann, R. Brinkmann, W. Brijoux, E. Dinjus, Th. Joussen, B. Korall, *Angew. Chem.* **1991**, *103,* 1344–1346.

[20] H. Bönnemann, W. Brijoux, *Advanced Catalysts and Nanostructured Materials* (Ed.: W. R. Moser), Academic Press, San Diego, **1996**, p. 165–196.

[21] J. B. Michel, J. T. Schwartz, *Preparation of Catalysts IV* (Eds.: B. Delmon, P. Grange, P. A. Jacobs, G. Poncelet), vol. 31, Elsevier, Amsterdam, **1987**, p. 669–687.

[22] J. T. Payne, D. A. Reuschle, K. A. Mauritz, *Polym. Prep.* **1997**, *38*, 247–250.

Received November 22, 1999
[I99421]

Linear, Divergent Molecular Receptors – Subtle Effects of Transition Metal Coordination Geometry

Alexander Bilyk,[a] Annegret K. Hall,[a] Jack M. Harrowfield,*[a] Mir Wais Hosseini,[b] Gilles Mislin,[b] Brian W. Skelton,[c] Christopher Taylor,[d] and Allan H. White[c]

Keywords: Thiacalixarene / Trimetallic sandwich / Cobalt / Zinc / Divergent receptors

Reaction between deprotonated *p-tert*-butyltetrathiacalix[4]-arene and Co^{II} or Zn^{II} under strictly defined conditions leads to the formation of sandwich species in which a trimetallic unit is held between two opposed, divergently oriented, staggered *O*- and *S*-bound calixarene ligands in the cone conformation. Despite the isomorphous nature of the crystalline compounds, there is a subtle difference in the coordination of Co^{II} and Zn^{II}, presumably related to the differences in metal radius and electron configuration combined with structural restrictions imposed by the calixarene framework, in that whereas all three Co atoms may be considered six-coordinate (and approximately octahedral), only two of the Zn atoms appear so, the third being five-coordinate and more nearly trigonal bipyramidal in its coordination geometry.

Introduction

The pursuit of the rational design of solid state structure, with the ultimate aim of producing new materials with properties of true utility, can be based upon the exploitation of various chemical forces.[1,2] We have previously demonstrated the feasibility of using (presumably) weak CH_3-π interactions to form one-dimensional "koilates" in which binuclear calix[4]arene metal complexes provide opposed-divergent, double-cavity receptors.[2] A difficulty in this approach arises because of the relatively limited range and possibly the limited stability of appropriate binuclear calix[4]arene derivatives.[2–4] The initial report[5] of the superior transition metal binding properties of *p-tert*-butyltetrathiacalix[4]arene therefore aroused our interest and we have recently characterised[6] an antiferromagnetically coupled dicopper(II) derivative of this calixarene which proved to have a dimeric form in the solid state in which a tetracopper square is sandwiched between opposed, eclipsed calixarene cones, thus justifying our optimism that compounds useful in koilate construction might be obtained. The coordination geometry of the copper atoms in this compound is, however, considerably distorted from any regular form of six-coordination and, in attempting to extend our studies of coordination of the tetrathiacalixarene to the elements adjacent to copper, we have found that this may be an important factor determining the metal/ligand stoichiometry, though not necessarily the opposed double-cavity form of the resultant complex. Thus, we have found that for cobalt(II) and zinc(II), compounds of the stoichiometry $M_3(calH)_2$ (where $calH^{3-}$ is the three-times deprotonated tetrathiacalixarene, $calH_4$) may be isolated. Subsequent structure determinations[7] have shown that the isomorphous cobalt and zinc compounds can indeed be regarded as containing molecular units of this stoichiometry (Figure 1) with, as in the case of the Cu^{II} compound, a small cluster of metal ions sandwiched between two opposed, quasi-staggered calixarene cones. The differences from the copper system may be associated with a stronger tendency to retain a regular octahedral coordination geometry around Co and Zn, with the incompatibility of structural demands being more readily accommodated by the Jahn–Teller accessible Cu^{II} adduct, though this can at best be considered only a partial rationalisation of the detailed differences between these three complexes.

For the preparation of these complexes it is important to adhere closely to a particular procedure to obtain a particular product and to convert it to a crystalline form suitable for X-ray diffraction. With a variety of other metals we have experienced considerable complications due to either polymorphism or alternate stoichiometries. In our initial efforts to obtain the Co and Zn complexes described herein we obtained heterogeneous materials showing only partial solubility in CH_2Cl_2. Interestingly, the ^1H NMR spectrum reported for a Zn^{II} complex[5] isolated from a solvent extraction experiment, is identical to that for the Zn species reported here after recrystallisation. The NMR spectra are consistent with a similar trinuclear species that exists in the solid state (Figure 1) persisting in solution, and where all the protons within each calixarene are chemically inequiva-

[a] Special Research Centre for Advanced Minerals and Materials Processing, University of Western Australia,
Nedlands, WA 6907, Australia
Fax: (internat.) + 61-89/380-1116
E-mail: jmh@chem.uwa.edu.au
[b] Laboratoire de Chimie de Coordination Organique, Institut Le Bel, Université Louis Pasteur de Strasbourg,
4, rue Blaise Pascal, F-67000 Strasbourg, France
[c] Crystallography Centre and Department of Chemistry, University of Western Australia,
Nedlands, WA 6907, Australia
[d] Department of Chemistry, University of Western Australia, Nedlands, WA 6907, Australia

 © WILEY-VCH Verlag GmbH, D-69451 Weinheim, 2000 1434−1948/00/0505−0823 $ 17.50+.50/0

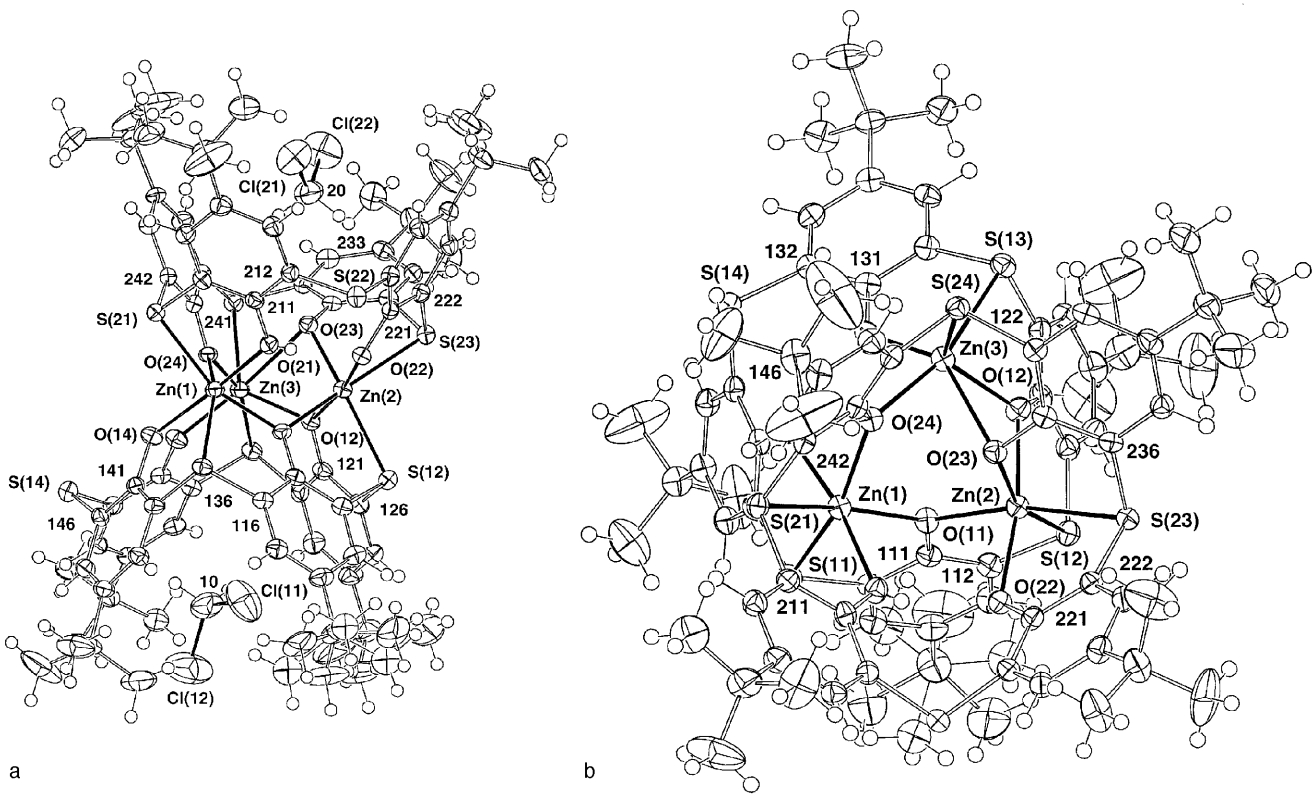


Figure 1. Projections of the zinc complex (a) through and (b) normal to the Zn_3 plane [included CH_2Cl_2 (x2) omitted in the latter]; thermal ellipsoids (50%) are shown for the non-hydrogen atoms, hydrogen atoms having arbitrary radii of 0.1 Å; the chirality of the molecule is most readily appreciated from the relative dispositions of the oxygen pairs O(13,14) and O(21,22) which do not chelate a metal atom, and/or the sulfur atoms S(14,22) which do not bind a metal; note that Zn(2,3) are bridged by a pair of μ-oxo species [O(12,23)] whereas Zn(1,2), (1,3) are bridged by single oxygen atoms O(11), O(24), respectively; note also in (b) that whereas rings 12, 23 are eclipsed at the $M(\mu\text{–}O)_2M$ linkage, the other pairs do not superimpose in this manner. M(1)–M(2,3), M(2)–M(3) are 3.606(1), 3.649(1), 3.144(1) (M = Co) and 3.5092(7), 3.5623(8), 3.2648(7) Å (M = Zn); in (a) H(14) is hidden behind O(14)

lent. We have also found it possible to reproducibly obtain the same $Zn_3(calH)_2$ species by recrystallisation of a solvent extraction product from CH_2Cl_2. However the earlier report of a significantly different Zn complex with the stoichiometry, $Zn_4(cal)(calH_2)_2$,[8] prepared under similar conditions but recrystallised from toluene, highlights the ease with which different forms of the thiacalixarene complexes may be interconverted.

In our isomorphous Co and Zn compounds, the repeating molecular unit in the solid (Figure 1) is a sandwich made up of three metal atoms between two calixarene cones arranged divergently about the metal cluster, each cone containing a dichloromethane molecule. In the case of the Co compound, each metal atom is in an approximately octahedral *cis*-MO_4S_2 environment (Figure 2), though with deviations of up to 20° from the ideal *cis* and *trans* bond angles of 90 and 180°, respectively. This is true for two of the metal atoms in the Zn compound but the third is perhaps better described as having a trigonal bipyramidal coordination environment (Figure 2), a potential sixth (O-donor) ligand atom, which in the Co compound is close enough [2.276(4) Å] to be considered bound, here lying at a distance of 2.652(3) Å. In addition, the Zn–S distances are very disparate for this atom [2.406(1), 2.674(1) Å], perhaps even indicating an approach to 4-coordination, and this disparity in M–S distances is also evident for the corresponding Co atom [Co–S 2.445(1), 2.729(2) Å]. As in the Cu^{II} compound, all donor atoms are derived from the calixarene units, one sulfur atom on each not being involved in coordination and solvent (dichloromethane) molecules only being included within the calixarene cavities and elsewhere within the lattice. The cluster sandwiches are chiral, the only approximate symmetry element being a near two-fold axis passing through one metal atom and bisecting the line joining the other two, true two-fold symmetry seemingly being lost as a result of the coordination sphere irregularities of M(3). The metal atom on the near-C_2 axis has the two phenoxide units bearing residual protons (detected and refined in the structure solution) coordinated to it in a *trans* arrangement [O–M–O 171.0(1)° (Zn), 173.8(1)° (Co)] and interacts with only two phenoxide oxygen atoms

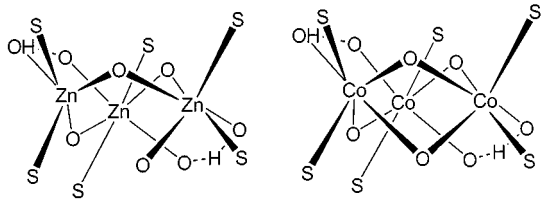


Figure 2. Representation of the coordination environments about the Zn and Co clusters; two of the Zn ions are six-coordinate, the other is five-coordinate, whilst the three Co atoms can be described as six-coordinate

which bridge to the other metal atoms. In the Co compound, each of these has three bridging phenoxide donor atoms, although with Zn, again, only two phenoxide bridging atoms are bound to each. The residual protons on the ligand are probably involved in hydrogen bonding to adjacent phenoxide oxygen atoms [O···O 2.48, 2.49 Å (Zn), 2.44, 2.46 Å (Co)].

Magnetic susceptibility measurements by SQUID magnetometry 4–300 K do not indicate any strong magnetic interactions within the Co compound, with Curie-Weiss behaviour ($\theta = -30°$) being observed, though the room temperature magnetic moment of 8.2 BM is significantly lower than expected for three independent high-spin Co^{II} centres. The possibility exists, however, for the use of connector units in koilate structures which may allow extended interactions within such solids, and we are actively pursuing this hypothesis. The residual phenolic calixarene protons present in the Co and Zn compounds should be removable by base, generating anionic species capable of stronger, electrostatically-assisted association with linker molecules. Many other paramagnetic metal ions may also be readily substituted for Co^{II} in these complexes and we have already isolated rare earth derivatives, for example. It is clear that the strong coordinating properties of tetrathiacalix[4]arene provide a prospect for the far readier development of novel applications in metal ion chemistry than is true of the parent calix[4]arene, though it may be that development of this chemistry will provide insights into further uses of the more extensive class of calixarenes in general.

Experimental Section

General Remarks: All solvents were distilled prior to use except for AR grade DMF which was used as supplied. – ^{1}H NMR spectra were measured in $CDCl_3$ and calibrated to the residual solvent peak on a Bruker ARX500 spectrometer. – FAB mass spectra were recorded on a VG-Analytical ZAB HF spectrometer with 3-nitrobenzyl alcohol as the matrix and the electronic absorption spectra in CH_2Cl_2 solution on a Hewlett–Packard 8452A diode-array spectrometer. – Microanalyses were performed by the Microanalytical Unit at the Australian National University.

$[Zn_3(calH)_2(CH_2Cl_2)_2]\cdot 3CH_2Cl_2$: $CalH_4\cdot CHCl_3$ (200 mg, 240 mmol) was dissolved in DMSO (5 mL) containing NEt_3 (0.1 mL). A solution of $[Zn(DMSO)_6](ClO_4)_2$ (350 mg, 480 mmol) in DMSO (5 mL) was added. The clear solution was left overnight, filtered, and the resulting white powder (90 mg) washed with EtOH (5 mL) and dried in air. The solid was dissolved in CH_2Cl_2, filtered and an equal volume of ethanol carefully added to form a layer above the original solution. After 3 weeks of standing, colourless crystals suitable for structural determination were obtained. The remaining crystals were collected by vacuum filtration, washed with ethanol and dried under reduced pressure to give a white powder (65 mg, 40 μmol). – ^{1}H NMR (500 MHz): δ = 1.22 (s, 36 H, *tert*-butyl), 1.24 (s, 18 H, *tert*-butyl), 1.28(s, 18 H, *tert*-butyl), 7.568 (d, ^1J = 2.5 Hz, 2 H, ArH), 7.569 (d, ^1J = 2.5 Hz, 2 H, ArH), 7.59 (d, ^1J = 2.5 Hz, 2 H, ArH), 7.61 (d, ^1J = 2.5 Hz, 2 H, ArH), 7.65 (d, ^1J = 2.5 Hz, 2 H, ArH), 7.70 (d, ^1J = 2.5 Hz, 2 H, ArH), 7.77 (d, ^1J = 2.5 Hz, 2 H, ArH). – ^{13}C NMR (125.77 MHz): δ = 31.30, 31.36, 31.44, 31.47, 34.06, 34.14, 34.2, 117.8, 118.6, 120.7, 120.76, 120.87, 120.91, 122.2, 122.5, 132.4, 133.4, 134.0, 135.1, 135.26, 135.35, 136.6, 139.1, 140.4, 141.4, 142.5, 156.8, 158.9, 160.0, 161.8. – MS (FAB); *m/z*: 1631 (M^+). – $C_{80}H_{90}O_8S_8Zn_3$ (1632): calcd. C 58.87, H 5.56, S 15.2; found C 58.48, H 5.50, S 15.68. – Electronic spectrum: λ/nm (ε_{max}/M^{-1} cm^{-1}) = 314 (39100).

$[Co_3(calH)_2(CH_2Cl_2)_2]\cdot 3CH_2Cl_2$: $CalH_4\cdot CHCl_3$ (1.0 g, 1.19 mmol) was dissolved in DMF (8 mL) containing NEt_3 (0.5 mL). A solution of $[Co(DMF)_6](ClO_4)_2$ (2.12 g, 3.04 mmol) in DMF (5 mL) was added quickly and a light green precipitate formed immediately. After 2 hours the solid was collected by vacuum filtration, washed with ethanol (5 mL) and dried in air to give a light green powder (0.37 g). This solid was recrystallised by liquid diffusion of EtOH into a CH_2Cl_2 solution to give pale green crystals suitable for structural determination. The remaining crystals were collected by vacuum filtration and dried under reduced pressure to give a light green powder (0.26 g, 150 μmol). – MS (FAB); *m/z*: 1612 (M^+). – $C_{80}H_{90}Co_3O_8S_8$ (1613): calcd. C 55.25, H 5.31, S 14.39; found C 55.67, H 5.30, S 14.30. – Electronic spectrum: λ/nm (ε_{max}/M^{-1} cm^{-1}) = 316 (37400), 380 (sh.; 200), 574 (112), 602 (114).

X-ray Crystallographic Study

Co Compound: $[(CH_2Cl_2)_2(C_{40}H_{45}O_4S_4)_2Co_3]\cdot 3CH_2Cl_2$, $C_{85}H_{100}Cl_{10}Co_3O_8S_8$, M = 2037.6. monoclinic, space group $P2_1/n$, a = 13.294(2), b = 45.401(6), c = 17.510(2) Å, β = 111.034(3)°, V = 9863(4) Å^3, Z = 4, D_c = 1.372 g·cm^{-3}, T = 293(2) K, 109219 ($2\theta_{max}$ = 58° sphere) SAINT/SADABS processed CCD reflections ($T_{min,max}$ = 0.68, 0.89) merged to 24944 unique (R_{int} = 0.048), 11937 with $|F| > 4\sigma|F|$ refining to conventional R, R_w on $|F|$ 0.064, 0.064.

Zn Compound: $[(CH_2Cl_2)_2(C_{40}H_{45}O_4S_4)_2Zn_3]\cdot 2.8CH_2Cl_2$, $C_{84.8}H_{99.6}Cl_{9.6}O_8S_8Zn_3$, M 2040. monoclinic, space group $P2_1/n$, a = 13.085(1), b = 44.800(4), c = 17.503(2) Å, β = 111.934(2)°, V = 9517(3) Å^3, Z = 4, D_c = 1.423 g·cm^{-3}, T 153 K, 106685 ($2\theta_{max}$ = 55° sphere) SAINT/SADABS processed CCD reflections ($T_{min,max}$ = 0.78, 0.96) merged to 21818 unique (R_{int} = 0.048), 17210 with $|F| > 4\sigma|F|$ refining to conventional R, R_w on $|F|$ 0.062, 0.071.

Disorder was more widespread in the cobalt compound, involving *tert*-butyl groups 114, 214, 244 [rotated over two sets of sites, major component occupancies 0.662(7), 0.775(7), 0.743(7), 114 only being disordered in the zinc (0.701(5)], and the lattice dichloromethane molecules 4 (both) and 5 (Zn only). Crystallographic data (excluding structure factors) for the structures reported in this paper have been deposited with the Cambridge Data Centre as supplementary publication no CCDC-137200 (Co compound), CCDC-137201 (Zn compound). Copies of the data can be obtained free of charge on application to CCDC, 12 Union Road, Cambridge CB2 1 EZ, UK [Fax: (internat.) + 44-1223/336-033; E-mail: deposit@ccdc.cam.ac.uk].

Acknowledgments

This work was partly supported by the Australian Research Council.

[1] *Chem. Mater.* **1998**, *10*, Special Issue (Ed.: K. Poeppelmeier) devoted to *Frontiers in Inorganic Solid State Chemistry.*
[2] J. Martz, E. Graf, M. W. Hosseini, A. De Cian, J. Fischer, *J. Mater. Chem.* **1998**, *8*, 2331–2333 and references therein.

[3] D. M. Roundhill, *Progr. Inorg. Chem.* **1995**, *43*, 533.
[4] C. Wieser, C. B. Dieleman, D. Matt, *Coord. Chem. Rev.* **1997**, *165*, 93–162
[5] N. Iki, N. Morohashi, F. Narumi, S. Miyano, *Bull. Chem. Soc. Jpn.* **1998**, *71*, 1597.
[6] G. Mislin, E. Graf, M. W. Hosseini, A. Bilyk, A. K. Hall, J. M. Harrowfield, B. W. Skelton, A. H. White, *Chem. Commun.* **1999**, 373.
[7] *Xtal3.6.1 System* **1999**, (Eds.: S. R. Hall, D. J. du Boulay, R. Olthof-Hazekamp), University of Western Australia.
[8] N. Iki, M. Morohashi, C. Kabuto and S. Miyano, *Chem. Lett.* **1999**, 219.

Received November 29, 1999
[I99433]

Ammonolysis of Trichlorosilanes

Carsten Ackerhans,[a] Bodo Räke,[a] Ralph Krätzner,[a] Peter Müller,[a] Herbert W. Roesky,*[a] and Isabel Usón[a]

Dedicated to Professor Willi Keim on the occasion of his 65th birthday

Keywords: Ammonolysis / Chlorine / Nitrogen / Silicon / Silsesquiazane

The ammonolysis of trichlorosilanes $RSiCl_3$ [R = $CH(SiMe_3)_2$ **(1a)**, Ph **(1b)**, Et **(1c)**] leads to a series of condensed products such as six-membered rings $[(Me_3Si)_2CHSi(OH)NH]_3$ **(2a)** and $[PhSi(NH_2)NH]_3$ **(2b)**, disilazane $[(Me_3Si)_2CHSi(NH_2)_2]_2NH$ **(3)** and the cage compound $(EtSi)_6(NH)_9$ **(4)**. The mixed Si–N–O compound **2a** was obtained when liquid ammonia was not dried over sodium prior to use. The reaction with sodium gives NaCl instead of NH_4Cl as a by-product which is easily removed by filtration.

Introduction

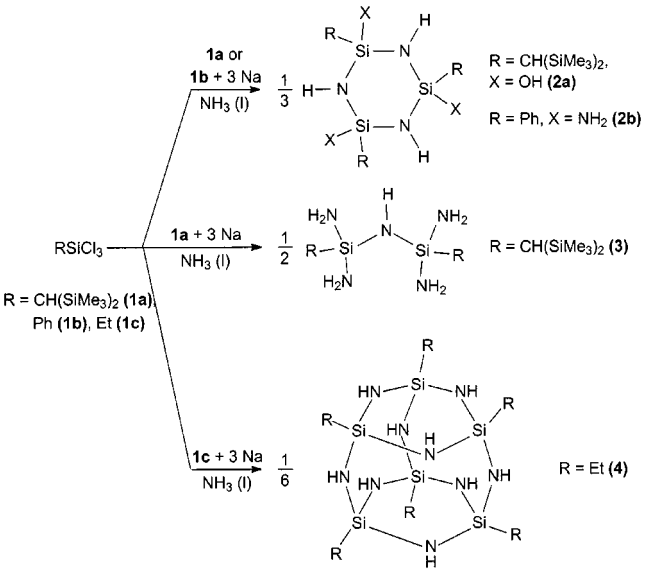
In recent years silicon−nitrogen compounds have gained more and more industrial importance due to the technical use of silicon nitride as a material which is mechanically stable and has a high resistance against heat.[1,2] Moreover, Schnick et al. reported on nitridosilicates, a class of compounds containing a highly polymeric three-dimensional silicon−nitrogen framework with incorporated cations.[3]

In 1993 Power et al. synthesized the first stable product with three NH_2 groups on one silicon atom by ammonolysis of the corresponding trichlorosilane. They used the 2,4,6-$Ph_3C_6H_2$ group as a bulky ligand for this reaction.[4] The chemistry of $RSi(NH_2)_3$ compounds was previously unknown. Consequently we became interested in this class of compounds after studying the isoelectronic compounds $RSi(OH)_3$.[5,6] In these systems R has to be a bulky ligand otherwise the formation of condensation products is observed.[7] Trichlorosilanes with ligands of medium size lead to cyclosilazanes, and trichlorosilanes with small ligands give condensed cage-like products from the reaction with ammonia.[8] Recently we reported the cage-like compound $(MeSi)_6(NH)_9$ using $MeSiCl_3$ in the presence of sodium in liquid ammonia.[9] The advantage of this method is the formation of NaCl instead of NH_4Cl which can be easily removed from the reaction mixture. Our experience has shown that NH_4Cl hinders to some extent the growth of X-ray quality single crystals. In a continuation of our work in liquid ammonia in the presence of sodium we report herein on the reaction using $RSiCl_3$ [R = $CH(SiMe_3)_2$ **(1a)**, Ph **(1b)**, Et **(1c)**] as starting material.

Results and Discussion

Synthesis and Spectra

We investigated the ammonolysis of $RSiCl_3$ compounds with and without sodium following two different routes. In the first approach the trichlorosilane $(Me_3Si)_2CHSiCl_3$ **(1a)** was stirred in liquid ammonia without sodium at −30 °C leading to a six-membered ring system with alternating silicon and nitrogen atoms and a hydroxy group at each ring-silicon atom $[RSi(OH)NH]_3$ [R = $(Me_3Si)_2CH$ **(2a)**] (Scheme 1).



Scheme 1. Reactions of $RSiCl_3$ compounds with ammonia in the presence of sodium

Single crystals suitable for an X-ray crystallographic measurement were isolated from an *n*-hexane solution. In the second route the trichlorosilane $RSiCl_3$ [R = $(Me_3Si)_2CH$ **(1a)**, Ph **(1b)**, Et **(1c)**] was dissolved in toluene

[a] Institut für Anorganische Chemie der Universität Göttingen, Tammannstraße 4, D-37077 Göttingen, Germany
Fax: (internat.) + 49-(0)551/393373
E-mail: hroesky@gwdg.de

 © WILEY-VCH Verlag GmbH, D-69451 Weinheim, 2000 1434−1948/00/0505−0827 $ 17.50+.50/0

and added to a solution of sodium in predried liquid ammonia to give various different types of condensation products (Scheme 1). From the reaction of **1b** we obtained the six-membered Si−N ring **2b**, similar to that of **2a**; however the OH groups at silicon are replaced by the isoelectronic NH_2 groups. In marked contrast is the reaction product using **1a** and liquid ammonia in the presence of sodium. Under these conditions the acyclic disilazane $[(Me_3Si)_2CHSi(NH_2)_2]_2NH$ **(3)** is formed. The reaction of $EtSiCl_3$ **(1c)** in liquid ammonia and sodium resulted in the formation of the cage compound $(EtSi)_6(NH)_9$ **(4)**. We assume that in all of the reactions employing liquid ammonia/sodium, sodium amide is initially formed in situ, and then reacts with the trichlorosilane with formation of sodium chloride. However, probably due to its low solubility, solid $NaNH_2$ in liquid ammonia does not react with the trichlorosilane. All ^1H NMR signals of the NH and NH_2 groups are in the range 0.25−1.80 ppm. The silicon atoms which are bonded to the nitrogen atoms give ^{29}Si NMR signals between −22.0 and −30.8 ppm. In the NMR spectra of product **3** the number of signals for the organic ligands, but not for the two central silicon atoms, are doubled. A possible explanation for this is, that there are two sterically different conformers of the molecule. In the IR spectra we see the typical signals of the NH vibrations between 3350 and 3500 cm^{-1}, and 1535 and 1545 cm^{-1}. The signals of the vibration of the Si−N−Si groups are in the range between 930 and 970 cm^{-1} for the cyclic products **2a**, **2b** and **4**, and at 1162 and 1014 cm^{-1} for the acyclic disilazane (**3**). The mass spectra show the molecular ion peak $[M^+]$ or fragment peaks after elimination of one or two small groups such as Me, NH_2 or OH.

X-ray Structural Analysis

Compound **2a** crystallizes in the trigonal space group $P\bar{3}$ with one third of a molecule in the asymmetric unit. The rest of the molecule is generated by the $\bar{3}$ axis. The core of the structure is a six-membered Si_3N_3 ring showing 41% chair conformation[10] with N and Si atoms occupying alternating sites. To complete the tetrahedral coordination sphere each Si atom in the ring is connected to a hydroxy group and a bis(trimethylsilyl)methyl moiety. All OH groups are oriented in the same direction with respect to the ring plane (Figure 1). The endocyclic N−Si distance is 1.704(2) Å, the angles are 104.6(1)° for N−Si−N and 131.3(1)° for Si−N−Si. The distance between the Si in the ring and the connecting oxygen is 1.673(3) Å; the O−Si−C angle between the hydroxy group and the organic ligand is 106.9(1)°. In the crystal packing two molecules are always bridged by six hydrogen bonds (Figure 2). The distance between the connecting hydroxy groups was calculated to be 1.952 Å between the hydrogen and the accepting oxygen atom. The O−H−O arrangement is nearly linear with an angle of 173.6°.

The single-crystal X-ray structure shows **4** to crystallize in the triclinic space group $P\bar{1}$ with one molecule in the asymmetric unit. The core of **4** consists of two six-membered Si_3N_3 rings in the chair conformation with alternating silicon and nitrogen atoms. The rings are linked by bridging NH groups connected to the Si centers. Thus, a prismatic cage-like structure results (Figure 3). One ethyl group is bonded to each of the silicon atoms. Two groups of nitrogen centers can be differentiated: six are part of the two six-membered rings (av. Si−N distance 1.714 Å) and three are located between the two rings in a bridging posi-

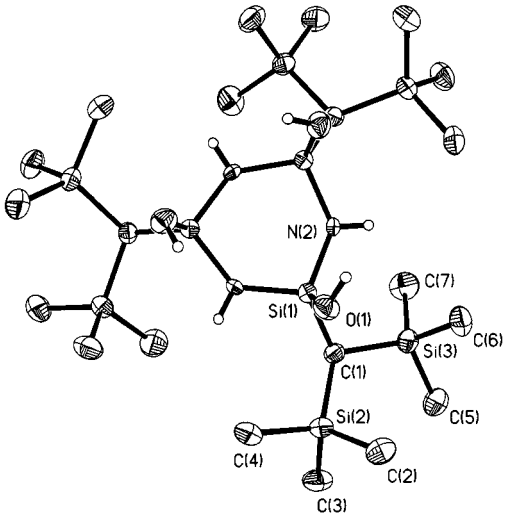


Figure 1. Molecule structure of **2a** in the crystal

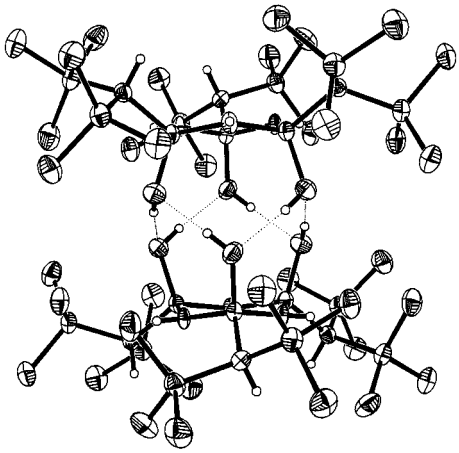


Figure 2. Molecule structure of **2a** with intermolecular hydrogen oxygen bridges

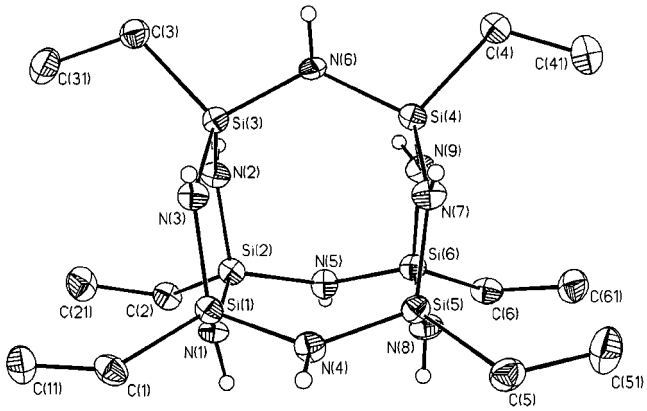


Figure 3. Molecule structure of **4** in the crystal

tion (av. Si−N distance 1.734 Å), which are slightly longer. The silicon centers are all slightly distorted from an ideal tetrahedron. Three groups of angles can be distinguished: the endocyclic N−Si−N angle (av. 131.5°); the somewhat smaller angle between a nitrogen center of one of the rings and a bridging nitrogen center (av. 126.3°); and the C−Si−N angles (av. 109.8°). The nitrogen atoms in the six-membered rings show an almost planar coordination (av. sum of angles 356°). Within the experimental error the bridging N atoms are perfectly planar coordinated (av. sum of angles 360°). The average Si−C bond length of 1.865 Å lies in the range typical for Si−C single bonds.

Conclusion

The grade of condensation and thereby the structure of the aminosilanes is dependent on the size of the ligands. Triaminosilanes with bulky ligands are stable against condensation.[4,7] Small ligands such as methyl and ethyl lead to the formation of a cage.[9] When the ligands are of medium size, then six-membered rings or other low-condensed products are the most favorable configuration. The ammonolysis with sodium in ammonia is superior in handling due to the production of NaCl, rather than NH_4Cl, which can be easily removed from the reaction mixture. It is interesting to note that the ammonolysis of **1a** with ammonia which was not predried with sodium yielded the trihydroxycyclotrisilazane **2a** while the reaction with sodium in predried ammonia gave the acyclic tetraaminodisilazane **3**.

Experimental Section

General: All reactions were performed under dry nitrogen conditions using standard Schlenk and syringe techniques. − The solvents were dried according to literature methods[11] and freshly distilled and saturated with nitrogen prior to use. − Melting points were measured on a Bühler SPA-1 melting point apparatus (uncorrected). − IR spectra were recorded using a BIO-RAD FTS 7 spectrophotometer. − Mass spectra (MS) were obtained with a Finnigan MAT 8200 or a Finnigan MAT 95 spectrometer using the EI technique. − NMR spectra were recorded with a Bruker AM 200 or a Bruker AC 250 spectrometer, δ in ppm relative to external $SiMe_4$. − Elemental analyses were performed at the Analytical Laboratory of the Institute of Inorganic Chemistry at the University of Göttingen.

Trichlorobis(trimethylsilyl)methylsilane (1a): To a suspension of $(SiMe_3)_2CHLi$ (7.4 g, 45 mmol) in toluene (100 mL) was added dropwise tetrachlorosilane (5.7 mL, 8.5 g, 50 mmol). The mixture was refluxed for 3 h, the generated LiCl was removed by filtration and the solvent was removed under vacuum. After distillation at 0.05 mbar, **1a** (10.9 g, 37 mmol, 83%) was obtained as a colorless liquid. − B.p. 45 °C (0.05 mbar). − ^{1}H NMR (C_6D_6): δ = 0.15 [s, $Si(CH_3)_3$]. (The signal from the C*H*-proton was not observed.) − ^{13}C NMR (C_6D_6): δ = 2.45 [$Si(CH_3)_3$], 15.75 ($CSiCl_3$). − ^{29}Si NMR (C_6D_6): δ = 0.37 ($SiMe_3$), 7.95 ($SiCl_3$). − IR (KBr): $\tilde{\nu}$ = 2976, 2955, 2901, 1406, 1269, 1257, 840, 772, 573, 561 cm^{-1}. − MS (EI): *m*/*z* (%) = 279 (100) [M^+ − Me]. − $C_7H_{19}Cl_3Si_3$ (293.8): calcd. C 28.6, H 6.5, Cl 36.2, Si 28.7; found C 28.8, H 6.5, Cl 35.7, Si 28.2.

1,3,5-Tris[bis(trimethylsilyl)methyl]-1,3,5-trihydroxycyclotrisilazane (2a): Ammonia (20 mL) was condensed at −78 °C onto **1a** (5.9 g, 20 mmol) and this mixture was stirred for 2 h under reflux. After warming to room temperature over 3 h, whereby the ammonia vaporized, *n*-hexane (50 mL) was added, the insoluble NH_4Cl was removed by filtration and the filtrate was concentrated in vacuo. A residue of **2a** (2.3 g, 3.5 mmol, 53%) was obtained as a white solid. Slow recrystallization from *n*-hexane (20 mL) resulted in colorless needles of **2a**. − M.p. 110 °C. − ^{1}H NMR (C_6D_6): δ = −0.39 [m, C*H*($SiMe_3$)$_2$, 3 H], 0.29 [m, Si(C*H*$_3$)$_3$, 54 H], 0.50−1.00 (m, N*H*, 3 H), 1.25−1.40 (m, O*H*, 3 H). − ^{29}Si NMR (C_6D_6): δ = −25.1 [*Si*(NH)], −1.5 (*Si*Me_3). − IR (KBr): $\tilde{\nu}$ = 3398, 1541, 1262, 1250, 1204, 1015, 955, 854, 723, 678 cm^{-1}. − MS (EI): *m*/*z* (%) = 624 (100) [M^+ − 2 OH], 607 (81) [M^+ − 3 OH]. − $C_{21}H_{63}N_3O_3Si_9$ (658.6): calcd. C 38.3, H 9.6; found C 36.9, H 9.8.

1,3,5-Triamino-1,3,5-triphenylcyclotrisilazane (2b): To a solution of sodium (3.4 g, 147 mmol) in ammonia (20 mL) was added a solution of $PhSiCl_3$ (10.4 g, 49 mmol) in toluene (100 mL) at −78 °C. After warming to room temperature the mixture was stirred for 1 h. The white precipitate was filtered off and the solvent was removed under vacuum. The residue was washed with *n*-hexane (50 mL) to give **2b** (4.7 g, 11 mmol, 70%) as a white solid. − M.p. 64−68 °C. − ^{1}H NMR (C_6D_6): δ = 0.40−1.80 (m, N*H*, NH_2, 9 H), 7.15 (m, C_6H_5, 10 H), 7.75 (m, C_6H_5, 5 H). − ^{29}Si NMR (C_6D_6): δ = −30.80 [*Si*(NH)] − IR (KBr): $\tilde{\nu}$ = 3468, 3064, 1662, 1620, 1588, 1538, 1427, 1305, 1261, 1198, 1168, 1113, 1028, 936, 918, 892, 845, 727, 699, 611, 478 cm^{-1}. − MS (EI): *m*/*z* (%) = 408 (2) [M^+], 392 (3) [M^+ − NH_2], 376 (4) [M^+ − 2 NH_2]. − $C_{18}H_{24}N_6Si_3$ (408.7): calcd. C 52.9, H 5.92, Si 20.6; found C 52.0, H 5.9, Si 20.6.

1,1,3,3-Tetraamino-1,3-bis[bis(trimethylsilyl)methyl]disilazane (3): Sodium (1.2 g, 52 mmol) was dissolved at −78 °C in liquid ammonia (20 mL). A solution of **1a** (4.6 g, 16 mmol) in toluene (100 mL) was then added dropwise over 30 min. The mixture was stirred for 2 h at −78 °C and, after heating to room temperature within 3 h, whereby the ammonia vaporized, the toluene was removed under vacuum, *n*-hexane (70 mL) was added and the insoluble solid was removed by filtration. After removing the *n*-hexane in vacuo, **3** (3.0 g, 6.6 mmol, 83%) was obtained as a colorless oil. − M.p. 10−15 °C. − ^{1}H NMR (C_6D_6): δ = −0.70 [s, C*H*($SiMe_3$)$_2$, 1 H], −0.62 [s, C*H*($SiMe_3$)$_2$, 1 H], 0.16 [s, Si(C*H*$_3$)$_3$, 18 H], 0.21 [s, Si(C*H*$_3$)$_3$, 18 H], 0.25−1.0 (br. m, N*H*, NH_2, 9 H). − ^{29}Si NMR (C_6D_6): δ = −23.20 [*Si*(NH_2)$_2$], −1.80 (*Si*Me_3), −1.68 (*Si*Me_3). − IR (KBr): $\tilde{\nu}$ = 3482, 3404, 2951, 2891, 1542, 1430, 1401, 1262, 1250, 1162, 1014, 837, 765, 678 cm^{-1}. − MS (EI): *m*/*z* (%) = 437 (40) [M^+ − NH_2], 405 (100) [M^+ − 3 NH_2]. − $C_{14}H_{47}N_5Si_6$ (454.0): calcd. C 37.0, H 10.4; found C 37.0, H 10.4. The osmometric molecular mass determination in toluene gave a molecular weight of 449 Dalton.

Hexaethylsilsesquiazane (4): To a solution of sodium (1.4 g, 60 mmol) in ammonia (20 mL) was added a solution of $EtSiCl_3$ (3.7 g, 20 mmol) in toluene (40 mL) at −78 °C. After warming to room temperature the mixture was stirred for an additional 2 h. The crude product was extracted with *n*-hexane (100 mL). After removing the solvent under vacuum **4** (1.3 g, 78%) was obtained. Recrystallization from diethyl ether (10 mL) gave colorless crystals of **4**. − M.p. 130 °C. − ^{1}H NMR (C_6D_6): δ = 0.58 (m, CH_2, 12 H), 1.05 (m, CH_3, 18 H), 0.58−1.05 (m, N*H*, 9 H). − ^{29}Si NMR (C_6D_6): δ = −22.0 (Me*Si*). − IR (KBr): $\tilde{\nu}$ = 3388, 1304, 1260, 1238, 1196, 1160, 1081, 1011, 964, 935, 841, 794, 769, 722, 685, 640 cm^{-1}. − MS (EI): *m*/*z* (%) = 477 [M^+]. − $C_{12}H_{39}N_9Si_6$ (478.1): calcd. C 30.2, H 8.2; found C 29.6, H 8.2.

Table 1. X-ray structure analysis data of **2a** and **4**

Compound	**2a**	**4**
Formula	$C_{21}H_{63}N_3O_3Si_9$	$C_{12}H_{39}N_9Si_6$
Formula weight	658.55	478.06
Crystal size	0.2 × 0.2 × 0.3	0.2 × 0.2 × 0.1
Crystal system	Trigonal	Triclinic
Space group	$P\bar{3}$	$P\bar{1}$
Unit cell	$a = b = 13.51(1)$ Å $c = 12.64(2)$ Å α = β = 90° γ = 120°	$a = 9.762(2)$ Å $b = 11.515(2)$ Å $c = 11.861(2)$ Å α = 73.79(3)° β = 77.37(3)° γ = 76.69(3)°
Volume	$V = 1997(3)$ Å^3	$V = 1228.7(4)$ Å^3
Z	2	2
Density	1.095 g/cm^3	1.292 g/cm^3
Absorption coefficient	0.323 mm^{-1}	0.358 mm^{-1}
F(000)	720	516
Reflections collected	37064	17087
Independent reflections	1917 (R_{int} = 0.0771)	4810 (R_{int} = 0.0781)
Data/Restr./Param.	1917/1/121	4810/9/277
Data collection range	2.4 ≤ Θ ≤ 23.3°	2.2 ≤ Θ ≤ 26.0°
Final R indices [$I > 2\sigma(I)$][a]	$R1$ = 0.0303 $wR2$ = 0.0730	$R1$ = 0.0462 $wR2$ = 0.1088
Final R indices (all data)	$R1$ = 0.0510 $wR2$ =0.0780	$R1$ = 0.0817 $wR2$ = 0.1192
Goodness-of-fit on F^2[b]	0.972	0.939
Largest diff. peak and hole	0.340 and −0.231 eÅ^{-3}	0.474 and −0.430 eÅ^{-3}

[a] $R1 = \Sigma|F_o - F_c| / \Sigma|F_o|$; $wR2 = [\Sigma w(F_o^2 - F_c^2)^2 / \Sigma wF_o^4]^{1/2}$. – [b] Goodness of fit $S = [\Sigma w(F_o^2 - F_c^2)^2 / \Sigma (n\text{-}p)]^{1/2}$.

X-ray Crystal Structure Analysis:[12] The crystals were mounted on a glass fiber in a rapidly cooled perfluoropolyether.[13] Diffraction data (see Table 1) were collected on a Stoe-Siemens-Huber four-circle diffractometer coupled to a Siemens CCD area detector at 133(2) K, with graphite-monochromated Mo-K_α radiation (λ = 0.71073 Å), performing φ- and ω scans. The structures were solved by direct methods using SHELXS-97[14] and refined against F^2 on all data by full-matrix least-squares with SHELXL-97.[15] All non-hydrogen atoms were refined anisotropically. All hydrogen atoms bonded to carbon were included in the model at geometrically calculated positions and refined using a riding model. The hydrogen atoms bonded to nitrogen were localized in the difference Fourier synthesis and refined with the help of distance restraints and anisotropic displacement parameter restraints. The position of the hydrogen atom bonded to oxygen in **2a** was freely refined.

Acknowledgments

This work was financially supported by the Deutsche Forschungsgemeinschaft.

[1] *Ullmann's Encyclopedia of Industrial Chemistry*, 5. Aufl., VCH, Weinheim **1986**, Vol. A 6, ceramics, 1.
[2] H. Lange, G. Wötting, G. Winter, *Angew. Chem.* **1991**, *103*, 1606−1625; *Angew. Chem. Int. Ed. Engl.* **1991**, *30*, 1579−1591.
[3] H. Huppertz, W. Schnick, *Angew. Chem.* **1997**, *109*, 2765−2767; *Angew. Chem. Int. Ed. Engl.* **1997**, *36*, 2651−2652.
[4] K. Ruhlandt-Senge, R. A. Bartlett, M. M. Olmstead, P. P. Power, *Angew. Chem.* **1993**, *105*, 459−461; *Angew. Chem. Int. Ed. Engl.* **1993**, *32*, 425−427.
[5] R. Murugavel, A. Voigt, M. G. Walawalkar, H. W. Roesky, *Chem. Rev.* **1996**, *96*, 2205−2236.
[6] C. Rennekamp, A. Gouzyr, A. Klemp, H. W. Roesky, C. Brönneke, J. Kärcher, R. Herbst-Irmer, *Angew. Chem.* **1997**, *109*, 413−415; *Angew. Chem. Int. Ed. Engl.* **1997**, *36*, 404−406.
[7] K. Wraage, A. Künzel, M. Noltemeyer, H.-G. Schmidt, H. W. Roesky, *Angew. Chem.* **1995**, *107*, 2954−2956; *Angew. Chem. Int. Ed. Engl.* **1995**, *34*, 2645−2647.
[8] K. A. Adrianov, G. V. Korelev, *J. Organomet. Chem.* **1967**, *7*, 217−225.
[9] B. Räke, H. W. Roesky, I. Usón, P. Müller, *Angew. Chem.* **1998**, *110*, 1508−1510; *Angew. Chem. Int. Ed.* **1998** *37*, 1432−1433.
[10] R. O. Gould, P. Taylor, M. Thorpe, Cremer and Pople Ring Puckering, *Pucker*, Version of 17.3.1995, University of Edinburgh.
[11] Autorenkollektiv, *Organikum*, 19. Aufl., Deutscher Verlag der Wissenschaften, Berlin **1993**.
[12] Crystallographic data (excluding structure factors) for the structures included in this paper have been deposited with the Cambridge Crystallographic Data Centre as supplementary publication nos. CCDC-137377 **(2a)** and -137081 **(4)**. Copies of the data can be obtained free of charge on application to CCDC, 12 Union Road, Cambridge CB2 1EZ, UK [Fax: (internat.) + 44-1223/336-033; Email: deposit@ccdc.cam.ac.uk].
[13] T. Kottke, D. Stalke, *J. Appl. Crystallogr.* **1993**, *26*, 615−619.
[14] G. M. Sheldrick, *Acta Crystallogr., Sect. A* **1990**, *46*, 467−473.
[15] G. M. Sheldrick, *SHELX 97*, Universität Göttingen, **1997**.

Received November 29, 1999
[I99437]

Coordination Chemistry of Calix-Phosphanes: Cooperativity in the Assembly of a Tetragold Calixarene Complex

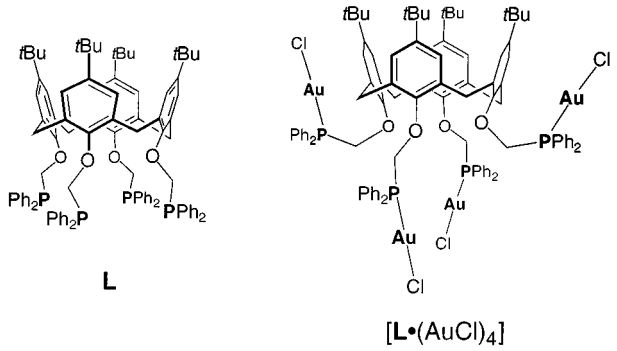
Cedric B. Dieleman,[a] Dominique Matt,*[a] and Anthony Harriman*[b]

Keywords: Metallo-calixarenes / Gold complexes / Tetraphosphane / Stability constants

Assemblage of the tetragold complex [L·(AuCl)$_4$] from *p-tert*-butyl-calix[4]-(OCH$_2$PPh$_2$)$_4$ (L) and [AuCl(tetrahydrothiophene)] was investigated by NMR and UV/Visible spectroscopic titrations. Three steps could be resolved and are assigned, respectively, to addition of one, two and four AuCl units to the macrocyclic ligand. At each stage of metallation, symmetrical species persist on the NMR time scale since the bound AuCl fragments migrate between the different phosphorus centers via both intra- and intermolecular processes. The derived stability constants (logβ_1 = 4.4 ± 0.2, logβ_2 = 7.0 ± 0.7, and logβ_4 = 14.5 ± 2.0) indicate both positive and negative cooperativity during build-up of the tetranuclear species. An X-ray diffraction study made with crystals obtained from an L:Au (1:2) mixture revealed the formation of an unusual binuclear complex whose solid state structure comprises a polymeric chain of [L·AuCl] units linked by pseudo-tetrahedral Au$^+$ ions, each generic unit containing a pendant linear PAuCl fragment. This polymeric species, with its two distinct binding modes, provides a simple rationale by which to explain the role of cooperativity in the overall assembly process.

Introduction

Calixarene-based polytopic ligands are attractive building blocks for the construction of molecules maintaining several *discrete* transition metal centers in close proximity.[1–8] Such intricate architectures provide important opportunities to study metal–metal cooperativity in polynuclear complexes and, inter alia, to extend our understanding of the mechanism of heavy-metal transport in biological systems.[9] As reported recently, the tetra-substituted calix[4]arene **L** possesses the necessary functionality to bind up to four metal centers at the lower rim. This ligand is also known to form bimetallic gold and silver complexes displaying unusual kinetic behavior in solution,[10] although the manner in which such metallo-calixarenes are assembled remains poorly understood. Following a recent study in which we reported the synthesis of the tetranuclear gold complex [**L**·(AuCl)$_4$][10] (Scheme 1) we now describe the stepwise formation of this complex by reaction of **L** with [AuCl(THT)] (THT = tetrahydrothiophene) under conditions that allow the mechanism to be resolved. During this study an unprecedented calixarene polymer could be isolated whose structure is detailed below.



Scheme 1. Drawing of **L** and [**L**·(AuCl)$_4$]

Results and Discussion

As pointed out in a previous study, ^{31}P and ^{1}H NMR spectroscopy suggests that addition of sub-stoichiometric amounts of [AuCl(THT)] to **L** in $CDCl_3$ forms a mono-gold species[11] that co-exists with the free ligand. In fact, careful examination of the NMR spectra shows that excess **L** exchanges with coordinated ligand, since the broad signal due to the mono-gold complex moves upfield with increasing ligand concentration. Furthermore, the NMR spectra show the mono-gold complex to be symmetrical such that, in addition to bimolecular ligand exchange, it appears that the bound AuCl fragment migrates between the four P atoms attached to the calixarene platform. ^{31}P NMR spectra recorded at higher concentrations of [AuCl(THT)] (Au:**L** = 1–4; ligand concentration = 5×10^{-3} M) comprise a singlet whose chemical shift varies over the range 22–33 ppm,[12] while the corresponding ^{1}H NMR spectra confirm the presence of symmetrical species throughout the titration.[13]

X-ray diffraction studies made with crystals isolated from a concentrated **L**:Au (1:2) mixture (CH_2Cl_2, 0.025 M) indicate formation of a binuclear complex whose solid-state structure[14] consists of a polymeric chain of [**L**·AuCl] units linked by trigonal Au$^+$ ions (Figure 1). The basic motif contains a pendant P–Au–Cl fragment while each linking Au cation is bound to three phosphorus atoms, two of which originate from the same calixarene. A chloride anion is ap-

[a] Université Louis Pasteur, UMR 7513 CNRS, Groupe de Chimie Inorganique Moléculaire,
1 rue Blaise Pascal, F-67008 Strasbourg Cedex, France
E-mail: dmatt@chimie.u-strasbg.fr
[b] Department of Chemistry, University of Newcastle,
Newcastle upon Tyne NE1 7RU, UK

 © WILEY-VCH Verlag GmbH, D-69451 Weinheim, 2000 1434–1948/00/0505–0831 $ 17.50+.50/0

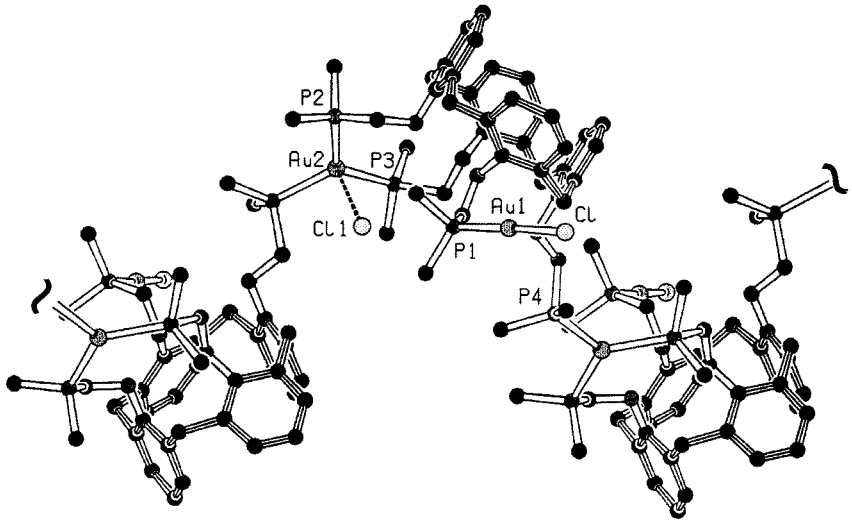


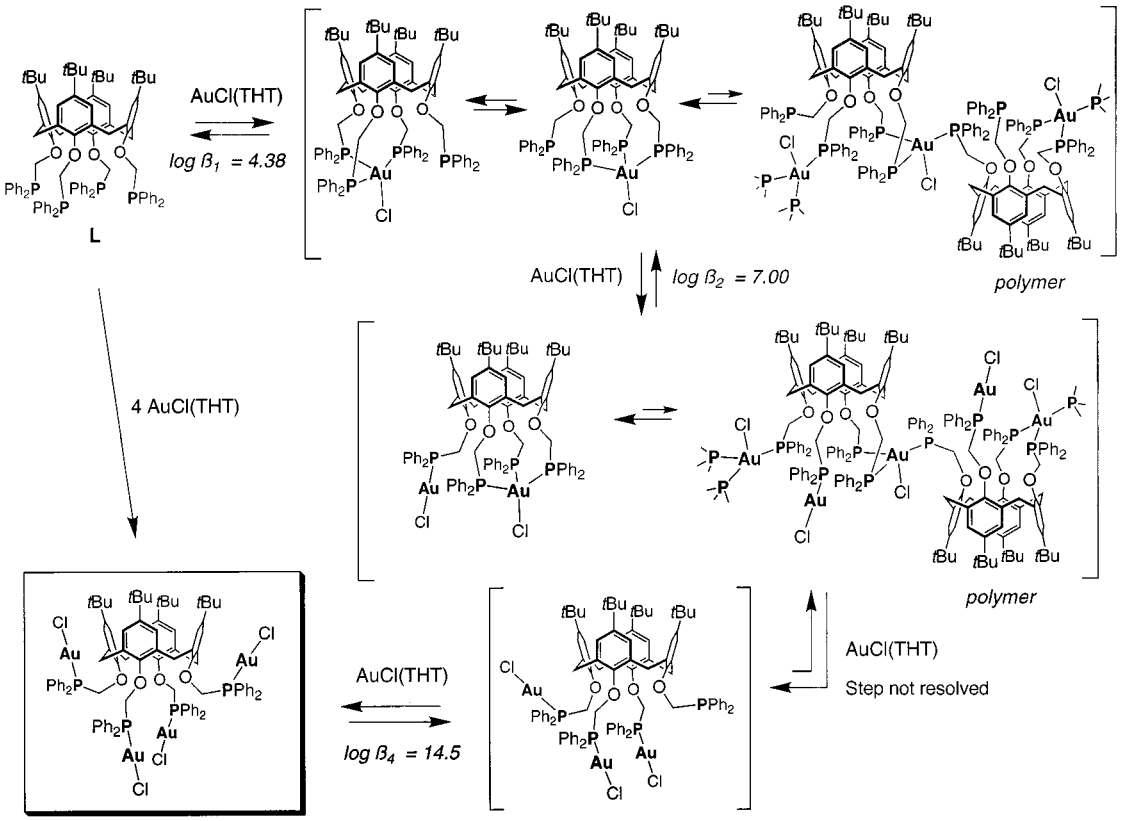
Figure 1. PLATON view of polymeric $[\mathbf{L}\cdot Au_2Cl_2]_\infty$; for clarity the *t*Bu groups have been omitted and only the *ipso* carbon atoms of the PPh_2 aryl rings are shown; selected bond distances (Å) (standard deviations in parentheses): Au(1)–Cl 2.283(7), Au(1)–P(1) 2.254(7), Au(2)–P(2) 2.371(6), Au(2)–P(3) 2.379(6), Au(2)–P′(4) 2.384(6), Au(2)–Cl(1) 3.012(6); dihedral angles between the facing aryl rings of the calixarene matrix: 80.3(7)° and 1.6(7)°

ically sited on each AuP_3 plane, the Au–Cl contact being 3.012(6) Å.[15] This structure differs markedly from known arrangements where AuCl units bound to three P^{III} atoms involve tetrahedral gold atoms.[16–19] It is also noteworthy that this structure contrasts with the numerous gold-linked inorganic polymers for which the gold(I) connector has a coordination number two.[20] The present X-ray structure, which provides a rationale for the bimolecular ligand exchange processes inferred from the NMR studies, is the first indication that gold(I) centers of coordination number two and four co-exist in a single molecule.

The processes leading to formation of $[\mathbf{L}\cdot(AuCl)_4]$ were examined by spectrophotometric titrations with progressive addition of [AuCl(THT)] to **L** (5×10^{-5} M) in acetonitrile at 25 °C. Global analysis of the titration data exposed three discrete steps in the overall assembly. The first step, which corresponds to formation of $[\mathbf{L}\cdot(AuCl)]$, involves a stability constant of $\log\beta_1 = 4.4 \pm 0.2$ while addition of a second AuCl fragment is characterized by $\log\beta_2 = 7.0 \pm 0.7$. Remarkably, addition of further AuCl fragments to $[\mathbf{L}\cdot(AuCl)_2]$ proceeds easily and, in fact, the individual steps leading to attachment of the third and fourth metallic centers could not be resolved. The tetranuclear species $[\mathbf{L}\cdot(AuCl)_4]$, which dominates the equilibrium mixture at high molar ratios of [AuCl(THT)] regardless of total concentration, is formed with $\log\beta_4 = 14.5 \pm 2.0$.

The observed trend in stability constants is best explained by reference to the X-ray structure where two different types of bound AuCl fragments can be seen. Thus, at low molar ratios of Au:**L** the incoming AuCl fragment binds to the calixarene platform with a *pseudo*-tetrahedral geometry by coordinating to three phosphane groups.[21] These phosphanes might be provided by one or two molecules of **L**, according to the total concentration, while the NMR results require that the structure is labile with facile exchange between the various phosphane groups (Scheme 2). This *pseudo*-tetrahedral arrangement is more stable than the corresponding linear P–Au–Cl geometry by ca. 10 kJ mol^{-1}.[22] Attachment of a second AuCl fragment to $[\mathbf{L}\cdot(AuCl)]$ must produce a species having both linear and *pseudo*-tetrahedral P–Au–Cl units, which equilibrate on the NMR timescale, with both monomeric and oligomeric species being possible (Scheme 2).[23] In order to accommodate a third AuCl fragment the more stable *pseudo*-tetrahedral complex must dissociate to allow the formation of two linear P–Au–Cl units. This process involves a small decrease in the Gibbs free energy ($\Delta G° \approx -4$ kJ mol^{-1}) whilst facilitating attachment of the fourth AuCl fragment by providing a vacant phosphane ligand. Therefore, formation of $[\mathbf{L}\cdot(AuCl)_4]$,[10] which is known to possess four linear P–Au–Cl units, proceeds smoothly (Scheme 2).

The present study reveals that formation of $[\mathbf{L}\cdot(AuCl)_4]$ is a stepwise process where both negative and positive cooperativity between the metal centers can take place. The key feature of the overall assembly mechanism involves the interplay between *pseudo*-tetrahedral and linear P–Au–Cl geometries, with the former being more stable but more demanding in the number of phosphane groups. Consequently, the reaction is driven towards the less-stable linear geometry as more metal centers become attached to the platform. This mechanism explains all the known aspects of the reaction, including why $[\mathbf{L}\cdot(AuCl)_2]$ crystallizes and why $[\mathbf{L}\cdot(AuCl)_3]$ is not detected, and is made possible by having X-ray structural data for both $[\mathbf{L}\cdot(AuCl)_2]$ and $[\mathbf{L}\cdot(AuCl)_4]$. Clearly, such switching between different binding geometries within the same molecule is highly unusual and it should be stressed that interconversion is uniquely controlled by the molar ratio. Complexes possessing either of the extreme *pseudo*-tetrahedral or linear geometries can be generated and it will be interesting to determine whether



Scheme 2. Proposed stepwise formation of [**L**·$(AuCl)_4$]; intramolecular migrations of the bound AuCl fragments have not been fully detailed

the exchange processes that occur during the formation of [**L**·$(AuCl)_4$] involve gold–gold interactions.

Experimental Section

Synthesis of Polymeric [L·$(AuCl)_2$]: To a solution of **L** (0.361 g, 0.25 mmol) in CH_2Cl_2 (5 mL) was added a solution of [AuCl(tetrahydrothiophene)] (0.160 g, 0.50 mmol) in CH_2Cl_2 (5 mL). The solution was filtered through Celite. Crystals of $[\mathbf{L}\cdot Au_2Cl_2]_\infty$ were obtained by slow diffusion of hexane into this solution. Yield: 0.290 g, 60%. – ^{31}P NMR (81 MHz, 293 K, CD_2Cl_2): δ = 31.4 (br s). – ^{1}H NMR (200 MHz, 293 K, $CDCl_3$): δ = 7.90–7.28 (40 H, PPh_2), 6.61 (br s, 8 H, *m*-ArH), 4.97 (br s, 8 H, PCH_2O), 4.53 and 2.92 (AB q, ^2J = 12 Hz, 2 × 4 H, $ArCH_2$), 1.04 (s, 36 H, *t*Bu). – $C_{96}H_{100}Au_2Cl_2O_4P_4\cdot 2H_2O$ (1943): calcd. C 59.36, H 5.40; found C 59.30, H 5.20.

Crystal Data for Polymeric [LAu_2Cl_2]·$2H_2O$: $C_{96}H_{100}Au_2Cl_2O_4P_4\cdot 2H_2O$, M = 1943, orthorhombic, space group $P2_12_12_1$, colorless crystals, a = 17.0365(5), b = 23.3634(8), c = 29.038(1) Å, V = 11558(1) Å^3, Z = 4, D_c = 1.12 g·cm^{-3}, μ = 2.670 mm^{-1}, $F(000)$ = 3920. Data were collected on a Nonius KappaCCD diffractometer (graphite Mo-K_α radiation, 0.71073 Å) at –100 °C. 59120 reflections collected ($2.5 \le \varphi \le 26.3°$), 5916 data with $I > 3\sigma(I)$. The structure was solved using the Nonius OpenMoleN[14] package and refined by full-matrix least-squares methods with anisotropic thermal parameters for all non-hydrogen atoms except for one water molecule. The absolute structure was determined by refining Flack's x parameter. Final results: $R(F)$ = 0.058, $wR(F)$ = 0.084, GOF = 1.653, 981 parameters, largest difference peak = 1.084 eÅ^{-3}. Structure graphics were performed with the program PLATON.[24] Crystallographic data (excluding structure factors) for the structure reported in this paper have been deposited with the Cambridge Crystallographic Data Centre as supplementary publication no. CCDC-137702. Copies of the data can be obtained free of charge on application to CCDC, 12 Union Road, Cambridge CB2 1EZ, UK [Fax: (internat) + 44-1223/336-033; E-mail: deposit@ccdc.cam.ac.uk].

Determination of the Binding Constants: The global binding constants log β_n were determined by UV/Visible spectrophotometric titration in acetonitrile (spectroscopic grade). For these measurements, 50 flasks were filled under N_2 atmosphere with a solution of tetraphosphane **L** in acetonitrile (3 mL, 5×10^{-5} M) to which were added variable amounts of [AuCl(THT)] as multiples of 10 μL of a 3×10^{-4} M acetonitrile solution. The Au:L ratios ranged from 0 to 7. The solutions were left for 12 h before measurement. The spectra were recorded between 190 and 310 nm using a quartz cell (1 cm path length) that was thermoregulated at 25 ± 0.5 °C. The absorbance changes monitored were significant enough to be exploited by multiwavelength numerical treatment based on a Benesi–Hildebrandt type equation (program SPECFIT©[25]), which yielded the desired global binding constants log β_n.

[1] P. A. Gale, Z. Chen, M. G. B. Drew, J. A. Heath, P. D. Beer, *Polyhedron* **1998**, *17,* 405–412.
[2] C. Wieser, C. B. Dieleman, D. Matt, *Coord. Chem. Rev.* **1997**, *165,* 93–161.
[3] M. Stolmàr, C. Floriani, A. Chiesi-Villa, C. Rizzoli, *Inorg. Chem.* **1997**, *36,* 1694–1701.
[4] D. M. Roundhill, in *Progress in Inorganic Chemistry,* Vol. 43 (Ed.: K. D. Karlin), Wiley, **1995**, pp 533–593.

[5] S. Pellet-Rostaing, J.-B. Regnouf de Vains, R. Lamartine, *Tetrahedron Lett.* **1995**, *36,* 5745–5748.
[6] C. Dieleman, C. Loeber, D. Matt, A. De Cian, J. Fischer, *J. Chem. Soc., Dalton Trans.* **1995**, 3097–3100.
[7] W. Xu, R. J. Puddephatt, L. Manojlovic-Muir, K. W. Muir, C. S. Frampton, *J. Incl. Phenom.* **1994**, *19,* 277–290.
[8] D. Jacoby, C. Floriani, A. Chiesi-Villa, C. Rizzoli, *J. Chem. Soc., Dalton Trans.* **1993**, 813–814.
[9] R. A. Pufahl, C. P. Singer, K. L. Peariso, S.-J. Lin, P. J. Schmidt, C. J. Fahrni, V. Cizewski Culotta, J. E. Penner-Hahn, T. V. O′Halloran, *Science* **1997**, *278,* 853–856.
[10] C. B. Dieleman, D. Matt, I. Neda, R. Schmutzler, H. Thönessen, P. G. Jones, A. Harriman, *J. Chem. Soc., Dalton Trans.* **1998**, 2115–2121.
[11] For Au:L ≈ 0.5, the ^{31}P NMR spectrum displays a very broad peak at δ ≈ 10 corresponding to the "mono-gold" species and a sharper peak at δ = – 21 due to the free ligand.
[12] The chemical shift of the ^{31}P NMR signal varies with Au:L ratio: δ = 16.6 (1:1 ratio); 31.4 (2:1 ratio); 25.2 (3:1 ratio); 22.7 (4:1 ratio). For the free ligand, δ = –20.4.
[13] All room-temperature ^{31}P NMR spectra display a single peak. On cooling the 2Au:1L solution, the phosphorus signal broadens before splitting into several signals (202 MHz, 183 K). These observations indicate that dynamic processes occur in solution, but the exact nature of the interconverting species could not be inferred from these data. Note, there is no indication of exchange reactions occurring with [L·$(AuCl)_4$] over the temperature range –80 °C/+25 °C.
[14] OpenMoleN, *Interactive Structure Solution,* Nonius B. V., Delft, The Netherlands, **1997**.
[15] Because of the particular position of Cl(1), exactly apically sited above the AuP_3 plane and hence indicative of a bonding interaction, we favor an AuP_3Cl formulation rather than $[AuP_3]^+Cl^-$.
[16] J. Zank, A. Schier, H. Schmidbaur, *J. Chem. Soc., Dalton Trans.* **1999**, 415–420.
[17] M. C. Gimeno, A. Laguna, *Chem. Rev.* **1997**, *97,* 511–522.
[18] S. Attar, W. H. Bearden, N. W. Alcock, E. C. Alyea, J. H. Nelson, *Inorg. Chem.* **1990**, *29,* 425–433.
[19] P. G. Jones, G. M. Sheldrick, J. A. Muir, M. M. Muir, L. B. Pulgar, *J. Chem. Soc., Dalton Trans.* **1982**, 2123–2129.
[20] R. J. Puddephatt, *Chem. Commun.* **1998**, 1055–1062.
[21] P_3-coordination of **L** to a single metal center has been established recently. See: C. B. Dieleman, C. Marsol, D. Matt, A. Harriman, N. Kyritsakas, J.-P. Kintzinger, *J. Chem. Soc., Dalton Trans.* **1999**, 4139–4148. Molecular mechanics computer simulations confirm that intramolecular pseudo-tetrahedral binding is possible.
[22] We assume that β_2 corresponds to formation of the binuclear species possessing both pseudo-tetrahedral and linear AuCl fragments, whereas β_1 refers to formation of the pseudo-tetrahedral geometry. Consequently, ignoring statistical factors, free-energy changes for formation of pseudo-tetrahedral [$\Delta G^\circ = -RT\ln(\beta_1) = -24.5$ kJ mol^{-1}] and linear [$\Delta G^\circ = -RT\ln(\beta_2-\beta_1) = -14.4$ kJ mol^{-1}] sites can be estimated from the titration data. Attaching a third AuCl fragment, assumed to give three linear appendages, corresponds to a crude free-energy change of {$\Delta G^\circ \approx -RT\ln[3(\beta_2-\beta_1)-\beta_2]$} of –4.4 kJ mol^{-1}. Finally, the free energy change for attachment of four linear AuCl fragments {$\Delta G^\circ \approx -RT\ln[4(\beta_2-\beta_1) \approx -58$ kJ mol^{-1}} can be compared to the experimental value ($\Delta G^\circ = -RT\ln(\beta_4) = -80 \pm 12$ kJ mol^{-1}).
[23] Linear P–Au–P coordination occurs in $[LAu_2](PF_6)_2$ but it is most unlikely that such species are formed in the present study. Indeed, $[LAu_2]^{2+}$ does not react with "AuCl" fragments to afford compounds of higher nuclearity.
[24] A. L. Spek, PLATON*, A multipurpose Crystallographic Tool,* Utrecht University, The Netherlands, **1999**.
[25] R. A. Binstead, A. D. Zuberbühler, *SPECFIT* v. 2.1: Spectrum Software Associates: Chapel Hill, NC, **1994**.

Received December 14, 1999
[I99463]

A New Approach to Well-Ordered Quantum Dots

Günter Schmid*[a] and Norbert Beyer[a]

Dedicated to Professor Dr. Heinrich Vahrenkamp on the occasion of his 60th birthday

Keywords: Gold / Clusters / Quantum dots / Monolayers / Amphiphiles

Extended ordered monolayers of ligand stabilized Au_{55} clusters are formed at the phase boundary between water and dichloromethane. The water phase, containing amphiphilic molecules like per-6-deoxy-6-thio-α-cyclodextrin **(1)** or poly(vinylpyrrolidone) **(2)**, is covered by a thin film of a solution of $[Au_{55}(PPh_3)_{12}Cl_6]$ in dichloromethane. The interaction of the cluster molecules with the thiol functions of **1** or the polymer chains of **2** form perfect cluster orders of hexagonal and cubic structure. The monolayers can be transferred onto solid substrates by a simple dipping process. The use of carbon coated copper grids allows the investigation of the monolayers by transmission electron microscopy (TEM). Electron diffraction experiments under a microscope prove the hexagonal and cubic arrangements. The reason for the formation of the one or the other modification is still unknown.

Introduction

Metal particles of the size of Au_{55} clusters (1.4 nm) show quantum size effects (QSE) even at room temperature,[1a−1e] making them promising candidates for future nanoelectronic applications. The first and most important step on this way is to order the clusters in a two-dimensional lattice to become individually addressable. Recently we described the preparation of ordered monolayers of Au_{55} clusters on modified solid surfaces by a simple dip-coating process.[2] In this paper we report the first results on a more generally applicable method to generate highly ordered and extended Au_{55} monolayers at the phase boundary between two liquids.

We believe that two facts are most important for the formation of ordered monolayers. First, an absolutely flat surface is essential. Polymers like PEI as a modifier are believed to form very thin layers that can smooth small roughnesses. Second, the surface should exhibit a large number of sites that are helpful to let the clusters settle down. In the ideal case the interaction between the clusters (or their ligand shell) and the surface should show the same strength everywhere − only a small amount of energy would then be necessary to let the clusters move around to form dense packings. On the other hand, the interaction between the clusters and the anchor groups must be strong enough to adsorb the clusters from solution and to hold them during the preparation process. This very sensitive balance between mobility and fixation determines the success of the self-assembly process.

Keeping these facts in mind we found that a solid surface needs very special conditions to fulfil all these demands. As an alternative we changed from the solid support to the interface between two liquids, exhibiting atomic flatness and isotropic behaviour all over the surface except near the beaker's wall. The long known Langmuir−Blodgett (LB) technique is based on these conditions. However, previous attempts to generate ordered monolayers of clusters by using original LB techniques didn't result in high degrees of order.[1d] Our actual aim was now to find appropriate molecules to provide amphiphilic interfaces between two liquids including useful functions to trap the clusters irreversibly.

Results and Discussion

We selected the CH_2Cl_2 soluble $[Au_{55}(PPh_3)_{12}Cl_6]$ cluster and various water-soluble amphiphilic compounds. Two of them turned out to work best as modifying agents at the phase boundary: per-6-deoxy-6-thio-α-cyclodextrin **(1)** and poly(vinylpyrrolidone) PVP **(2)**. Others like cysteine, cysteamine and poly(1,4-phenylene sulfide) showed similar behaviour; however, the results were not as promising as those with **1** and **2**.

It is to be assumed that the 12 hydroxy groups in **1** function as the hydrophilic part of the basket-like molecule, whereas the six thiol groups are oriented towards the dichloromethane phase to interact with the clusters as shown in Figure 1.

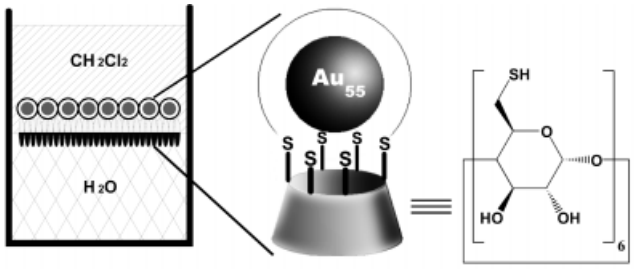


Figure 1. Sketch of the cluster-amphiphile **1** interaction at the phase boundary between water and dichloromethane solution

[a] Institut für Anorganische Chemie der Universität Essen
Universitätsstraße 5−7, D-45117 Essen, Germany
Fax: (internat.) +49-201/183-4195
E-mail: guenter.schmid@uni-essen.de

 © WILEY-VCH Verlag GmbH, D-69451 Weinheim, 2000 1434−1948/00/0505−0835 $ 17.50+.50/0

The function of PVP (**2**) is not as easy to understand as that of **1**. We believe that the polyvinyl backbones form hydrophobic−hydrophobic interactions with the PPh_3 ligands of the clusters.

The experiments were carried out by generating a thin film of a dichloromethane solution of $[Au_{55}(PPh_3)_{12}Cl_6]$ clusters on the aqueous phase containing the amphiphilic compound. Because transmission electron microscopy (TEM) is the most suitable method for examining the success of the experiments, the self-assembled cluster monolayers were transferred onto a carbon-coated copper grid. For good results it is important that the two-phase system does not invert, which may easily happen due to the higher density of the CH_2Cl_2 solution than that of water. This fact presently limits the extension of the monolayers to no more than a few square centimetres. If the CH_2Cl_2 layer becomes too large, it can drop down to the bottom of the flask. If the cluster layer is fished out through the organic phase only a thin, volatile film is covering the surface. If water covers the monolayer it is destroyed during drying.

Following this procedure we were able to generate highly ordered cluster areas in two different structures. A hexagonal and a cubic structure were found beside one another in a sample independent of the surfactant used in the water phase; however, usually the hexagonal structure dominated. The structures were formed in an approximate ratio of 1 to 20 in a number of areas although the cubic arrangements were usually twice as large in extension as the hexagonal ones. Hexagonally structured cluster monolayers, combined with the cyclodextrin **1** and PVP **2**, are shown in Figure 2 and Figure 3, respectively. The insert in Figure 3 shows the electron diffraction pattern, proving the predominately perfect hexagonal architecture.

Figure 4 shows a cut-out of a cubically organized surface, consisting of more than 20,000 clusters. Compound **2** was used as a modifier, as in Figure 3. Here the inserted diffraction pattern was calculated afterwards from the recorded image. The total area is slightly tilted so that the cubic structure is not that easily recognized. This can also be deduced from the diffraction pattern, where the spots show two different distances perpendicular to each other.

It can be assumed that the original areas of ordered clusters at the phase boundary are much larger than those observed under the microscope due to the not yet well developed transfer process from the liquid onto a solid surface. However, we started experiments to improve the procedure by automation.

As reference experiments we tested pure water and, in addition, a water phase containing sodium dodecyl sulfate (SDS). There was absolutely no evidence of cluster assembly in either case. Neither the alkyl chains of the SDS nor the water surface itself showed any attraction for the clusters.

The TEM images of the hexagonal and of the cubic structures showed cluster−cluster distances of 2.3 ± 0.1 nm. This agrees fully with the observed distances in three-dimensional cluster crystals.[3] The value of 2.3 nm seems to be completely independent of the surfactant used. Obviously there is no influence on the clusters if a 40,000 g/mol polymer like **2** or a small molecule like cysteine is used, indicating that the model of the phase boundary as a perfect flat, dense packed support with appropriate anchor groups works pretty well.

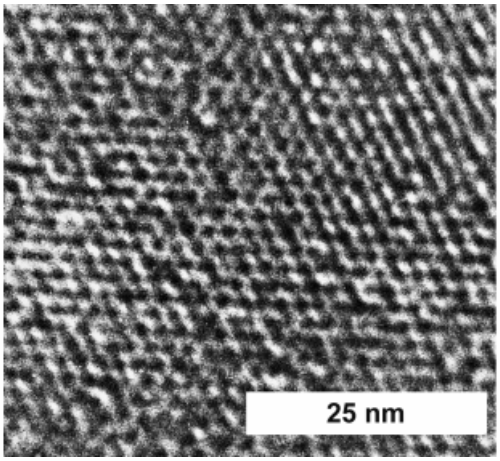


Figure 2. TEM image of a hexagonally ordered area of Au_{55} clusters with a thiol-modified cyclodextrin **1** as amphiphile

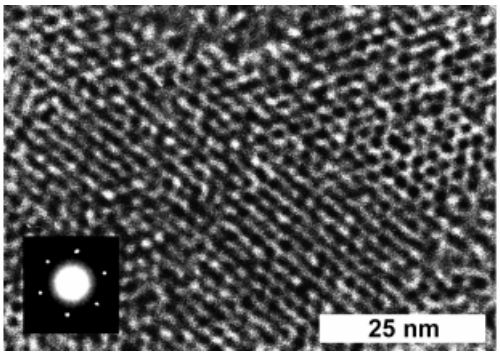


Figure 3. TEM image of a PVP **(2)** supported Au_{55} monolayer; the insert shows the electron diffraction pattern, recorded at a camera length of 4700 mm, proving the hexagonal structure

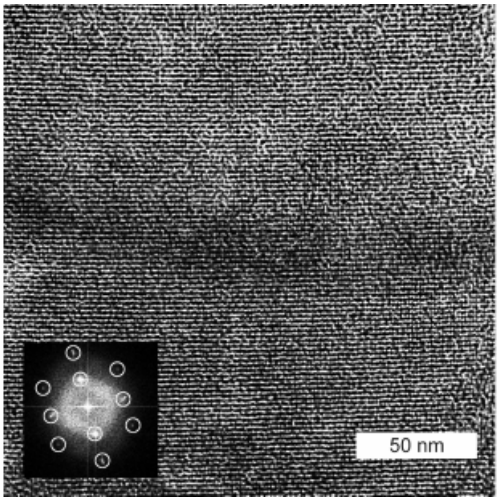


Figure 4. TEM image of a large cubic cluster arrangement; the insert shows the diffraction pattern calculated from the recorded image; the faint spots are marked with circles; the two different distances indicate that the total area was somewhat tilted

Further investigations are still in process. The formation of densely packed cluster layers should have an effect on the surface tension which could be revealed by rheological measurements. There must be strong interactions between the clusters, otherwise these nanometre-thick layers at the phase boundary would not survive under the rough conditions of the sample preparation for the TEM. We also plan to image the interface in situ by means of cryo-TEM. This technique needs very special conditions; however, it will allow snapshots of the formation process itself. Finally we have to use solid supports other than carbon-coated copper grids. First experiments with thin films of silicon carbide gave very promising results which will be reported elsewhere together with further results.

Experimental Section

The synthesis of $[Au_{55}(PPh_3)_{12}Cl_6]$ has been described elsewhere.[4a,4b] Per-6-deoxy-α-cyclodextrin (**1**) was synthezised by G. von Kiedrowski et al., University of Bochum, following published procedures.[5a,5b]. Poly(vinylpyrrolidone) (**2**) K30 (Fluka 81420) was used as received. The ordered $[Au_{55}(PPh_3)_{12}Cl_6]$ monolayers were prepared by adding a small droplet (0.5 mL) of a solution of 0.1 mg/L $[Au_{55}(PPh_3)_{12}Cl_6]$ in CH_2Cl_2 onto the aqueous phase (10 mL) in a tube of 1 cm in diameter, containing 1 mg/L of the amphiphilic compound. This has to be done very carefully to avoid the organic phase falling to the bottom of the tube. After 5−10 minutes the monolayer was formed between the two phases. This film was transferred onto a carbon-coated copper grid (Plano) by dipping it carefully under the surface and then pulling it back slowly, followed by drying in air. The characterization of the samples was carried out by transmission electron microscopy, using a Philips CM 200 FEG at 200 kV.

Acknowledgments

This work was supported by the Deutsche Forschungsgemeinschaft (SFB 452) and the Fonds der Chemischen Industrie. The authors acknowledge financial support by the MSWWF, Nordrhein-Westfalen. We also thank Prof. G. von Kiedrowski and Dipl. Chem. M. Pankau, both Ruhr-Universität Bochum, for providing us with the thiol-modified cyclodextrin.

[1] [1a] U. Simon, G. Schön, G. Schmid, *Angew. Chem.* **1993**, *105*, 264−269; Angew. Chem. Int. Ed. Engl. **1993**, *32*, 250−254. − [1b] G. Schön, U. Simon, Coll. *Polym. Sci.* **1995**, *273*, 101−117. − [1c] G. Schön, U. Simon, Coll. *Polym. Sci.* **1995**, *273*, 202−218. − [1d] L. F. Chi, S. Rakers, M. Hartig, H. Fuchs, G. Schmid, *Thin Solid Films* **1998**, *327−329*, 520−523. − [1e] G. Schmid, L. F. Chi, *Adv. Mater.* **1998**, *10*, 515−526.

[2] G. Schmid, M. Bäumle, N. Beyer. *Angew. Chem*. **2000**, *112*, 187; *Angew. Chem. Int. Ed.* **2000**, *39*, 181−183.

[3] G. Schmid, R. Pugin, Th. Sawitowski, U. Simon, B. Marler, *Chem. Commun.* **1999**, 1303−1304.

[4] [4a] G. Schmid, R. Boese, R. Pfeil, F. Bandermann, S. Meyer, G. H. Calis, J. W. van der Velden, *Chem. Ber.* **1981**, *114*, 3634−3642. − [4b] G. Schmid, *Inorg. Synth.* **1990**, *27*, 214−218.

[5] [5a] M. T. Rojas, R. Königer, J. F. Stoddard, A. E. Kaifer, *J. Am. Chem*. Soc. **1995**, *117*, 336−343. − [5b] G. R. J. Thatcher, *Tetrahedron Lett*. **1196**, *37*, 4647−4650.

Received January 11, 2000
[I00004]

Alkyne[hydrotris(pyrazolyl)borato]tantalum Complexes – An Ethyl Group is a Better α-Agostic Donor Than a Methyl Group

Jean-Cyrille Hierso[a] and Michel Etienne*[a]

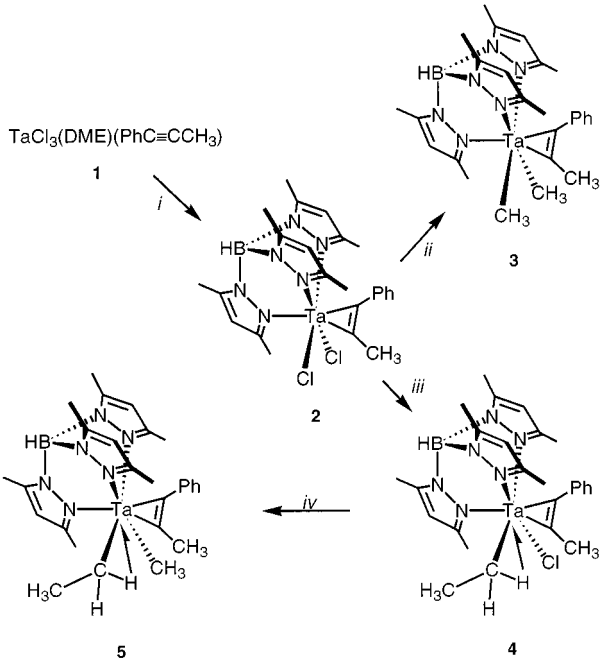
Keywords: Tris(pyrazolyl)borate / Tantalum / Agostic interactions / Alkyne complexes

The synthesis of unprecedented alkyne hydrotris(3,5-dimethylpyrazolyl)borato (Tp^{Me2}) tantalum(III) complexes is reported. The parent dichloro complex $Tp^{Me2}TaCl_2(PhC{\equiv}CCH_3)$ (**2**) is obtained from $TaCl_3(DME)(PhC{\equiv}CCH_3)$ and KTp^{Me2}. **2** reacts with methyllithium to give the dimethyl complex $Tp^{Me2}Ta(CH_3)_2(PhC{\equiv}CCH_3)$ (**3**) and with ethylmagnesium chloride to give the X-ray characterized α-agostic ethyl complex $Tp^{Me2}Ta(Cl)(\mu\text{-}H\text{–}CHCH_3)(PhC{\equiv}CCH_3)$ (**4**). Reaction of **4** with methyllithium generates the mixed methyl ethyl complex $Tp^{Me2}Ta(CH_3)(\mu\text{-}H\text{–}CHCH_3)(PhC{\equiv}CCH_3)$ (**5**) in solution. Spectroscopic data indicate that **5** is α-agostic at the ethyl group only.

Whereas β-agostic interactions in alkyl complexes are electronically favored,[1] steric constraints may induce a preference for an α-agostic interaction even though β-hydrogen atoms are available.[2] Competition between the two effects allowed us to observe the only example of an equilibrium between α- and β-agostic rotamers of an isopropyl group in $Tp^{Me2}Nb(Cl)(i\text{Pr})(PhC{\equiv}CCH_3)$ [Tp^{Me2} = hydrotris(3,5-dimethylpyrazolyl)borate].[3] The steric pressure that causes α-agostic interaction is obviously weaker when the alkyl group is methyl and ascertaining the presence of these interactions then remains a challenge.[4] Together with the synthesis of unprecedented trivalent $Tp^{Me2}Ta$ complexes,[5] we herein provide evidence that the mixed ethyl methyl complex $Tp^{Me2}Ta(CH_3)(\mu\text{-}H\text{–}CHCH_3)(PhC{\equiv}CCH_3)$ is α-agostic at the ethyl group selectively. This unprecedented situation is brought about by the efficient steric control exerted by Tp^{Me2}.

The chemistry we report is summarized in Scheme 1. Addition of one equivalent of KTp^{Me2} to in situ generated[6a][6b] $TaCl_3(DME)(PhC{\equiv}CCH_3)$ (**1**) (DME = 1,2-dimethoxyethane) affords orange crystals of $Tp^{Me2}TaCl_2(PhC{\equiv}CCH_3)$ (**2**) in 40% yield. Just like during the synthesis of $Tp^{Me2}TaCl_2(=N\text{–}t\text{Bu})$,[7] the formation of the by-product $[HB(C_3N_2Me_2H)_3BH][TaCl_6]$ lowers the yield. Addition of KTp^{Me2} to successfully isolated[6c] **1** only improves the yield slightly. $Tp^{Me2}SnCl_3$ does not react with **1**, although this reagent is efficient in the synthesis of tetra- and pentavalent $Tp^{Me2}Ta$ derivatives.[8] **2** has spectroscopic and structural properties akin to those of $Tp^{Me2}NbCl_2(PhC{\equiv}CCH_3)$.[9] Thus, the 4e-alkyne sits in the molecular mirror plane, and two discrete alkyne rotamers, depending on the orientation of the alkyne with respect to Tp^{Me2} are observed up to 373 K (^{1}H NMR, [D$_8$]toluene). The X-ray structure will be described elsewhere.

Both mono- and dialkyl derivatives have been synthesized. Treatment of **1** with two equivalents of methyllithium gives $Tp^{Me2}Ta(CH_3)_2(PhC{\equiv}CCH_3)$ (**3**) in 70% yield. Here the yield is only limited by the high solubility of **3** in alkanes. The equivalent Ta-bound methyl groups of **3** give a singlet at $\delta = 0.76$ in the ^{1}H-NMR spectrum, and a quadruplet centered at $\delta = 59.9$ ($^1J_{CH} = 114$ Hz) in the ^{13}C-NMR spectrum. These data are similar to those for $Tp^{Me2}Nb(CH_3)_2(PhC{\equiv}CCH_3)$[9] and $CpTa(CH_3)_2(ArC{\equiv}CAr)$,[10] and suggest the lack of any significant agostic interaction. The thermally stable $Tp^{Me2}Ta(Cl)(\mu\text{-}H\text{–}CHCH_3)(PhC{\equiv}CCH_3)$ (**4**) is obtained in 80% yield from the reaction between **1** and one equivalent of CH_3CH_2MgCl. A crystal structure analysis (Figure 1) reveals the α-agostic interaction through the distortion of the ethyl group with a very obtuse Ta–Cα–Cβ angle [Ta(1)–C(1)–C(2)= 123.5(3)°]. The Ta–Cα bond [Ta(1)–C(1) =



Scheme 1. (i) KTp^{Me2}, toluene/DME; (ii) 2 $LiCH_3$, diethyl ether; (iii) CH_3CH_2MgCl, diethyl ether; (iv) $LiCH_3$, diethyl ether

[a] Laboratoire de Chimie de Coordination du CNRS, UPR 8241, 205 Route de Narbonne, 31077 Toulouse Cedex 4, France
E-mail: etienne@lcc-toulouse.fr

 © WILEY-VCH Verlag GmbH, D-69451 Weinheim, 2000 1434–1948/00/0505–0839 $ 17.50+.50/0

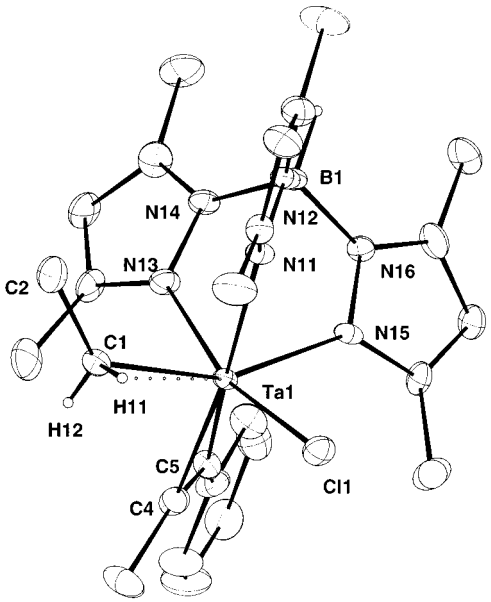


Figure 1. Plot of the molecular structure of $Tp^{Me2}Ta(Cl)(\mu\text{-}H\text{–}CHCH_3)(PhC{\equiv}CCH_3)$ (**4**); selected bond lengths [Å] and angles [°]: Ta(1)–Cl(1) 2.407(1), Ta(1)–C(1) 2.234(5), Ta(1)–C(4) 2.061(5), Ta(1)–C(5) 2.063(5), Ta(1)–H(11) 2.37(6), C(4)–C(5) 1.322(7); Cl(1)–Ta(1)–C(1) 104.4(2), Ta(1)–C(1)–C(2) 123.5(3), Ta(1)–C(1)–H(1) 88.6(43)

2.234(5) Å] remains normal. X-ray data collected at 160 K with an image plate detector combined with absorption corrections allowed the location of the methylene hydrogen atoms. The α-agostic interaction with H(11) is thus further substantiated by the observation of a short Ta···H contact [Ta(1)–H(11) = 2.37(6)°, Ta(1)–C(1)–H(11) = 88.6(43)°]. This interaction is the result of the steric locking of the ethyl group between two adjacent pyrazolyl groups which directs the methylene hydrogen atom in the appropriate location. ^{1}H- and ^{13}C-NMR-spectroscopies also give evidence for the α-agostic interaction in solution. In the room temperature ^{1}H-NMR spectrum, the entire ethyl group yields an AM_3X pattern with one shielded proton [δ = 0.59 (dq, J = 14.6, 6.6 Hz, 1 H, Ta(μ-*H*)CHCH$_3$), 1.40 (dd, J = 7.2, 6.7 Hz, 3 H, TaCH$_2$C*H*$_3$), 3.02 (dq, J = 14.6, 7.5 Hz, 1 H, Ta(μ-H)C*H*CH$_3$]. In the ^{13}C-NMR spectrum, the signal of the Ta-bound carbon atom appears as a doublet of doublets with one low and one high $^1J_{CH}$ [δ = 78.4 (dd, $^1J_{CH}$ = 102, 122 Hz)]. Similar X-ray and spectroscopic data characterize the analogous α-agostic ethyl- and related *n*-alkylniobium derivatives.[2a][2c]

Owing to the increased kinetic stability brought about by tantalum, **4** is thermally stable (373 K, toluene, 24 h) when the niobium analog readily rearranges to $Tp^{Me2}Nb(Cl)(CH_3)(PhC{\equiv}CCH_2CH_3)$ at 343 K (k = 3.0 10^{-5} s^{-1}).[2a] However, this kinetic stability allows the generation of the *unsymmetrical* dialkyl complex $Tp^{Me2}Ta(CH_3)(\mu\text{-}H\text{–}CHCH_3)(PhC{\equiv}CCH_3)$ (**5**) in quantitative yield from **4** and methyllithium in diethyl ether. Although **5** is thermally stable, it slowly decomposes upon attempted isolation. Attempts to synthesize such unsymmetrical niobium complexes lead to alkyl exchange and only dimethyl- and dibenzylniobium complexes have been obtained.[9] ^{1}H- and ^{13}C-NMR data obtained at room temperature on the crude reaction mixture are in favor of a single α-agostic interaction occurring exclusively with the ethyl group. The Ta-bound methyl group of **5** gives a ^{1}H-NMR singlet at δ = 0.68 and a ^{13}C-NMR quadruplet at δ = 55.2 ($^1J_{CH}$ = 116 Hz). In the ^{1}H-NMR spectrum, the diastereotopic methylene protons give a shielded and deshielded doublet of quadruplets at δ = –0.25 (J = 7.4, 15.0 Hz) and 2.46 (J = 7.2, 14.8 Hz). In the ^{13}C-NMR spectrum, the tantalum-bound carbon atom of the ethyl group is characterized by a doublet of doublets centered at δ = 78.0 ($^1J_{CH}$ = 105, 116 Hz). These data, compared to those for the dimethyl complex **3** and for the chloro(ethyl) complex **4**, indicate an α-agostic interaction with the ethyl group selectively. The strength of this interaction cannot be traced from the data: The ^{1}H-NMR chemical shift difference between the signals of the agostic and non-agostic methylene protons is slightly smaller in **4** (2.40 ppm) than in **5** (2.70 ppm) whereas the $^1J_{CH}$ differences are smaller for **5** (10 Hz) than for **4** (20 Hz). The agostic proton is also slightly more shielded in **5**. The ^{1}H-NMR data for **4** do not vary in the temperature range 193–363 K.

Whereas multiple agostic interactions are known, either from a single alkyl group[11a] or from two identical alkyl groups,[11b] it is the first time to our knowledge that two different alkyl groups compete for an agostic bonding. Here, the situation is dominated by the steric demand and directing properties of Tp^{Me2} both of which have little effect, if any, on a methyl group as compared to an ethyl group. The exclusive preference for agostic interaction with the ethyl group is a direct consequence of these properties. This is the main conclusion of this work in addition to the syntheses of the first trivalent $Tp^{Me2}Ta$ complexes.

Experimental Section

All reactions and workup procedures were performed under dry dinitrogen using conventional vacuum-line and Schlenk tube techniques. Toluene, DME, dichloromethane, pentane and *n*-hexane were dried and distilled by refluxing over calcium dihydride under dinitrogen. Diethyl ether was dried and distilled by refluxing over sodium benzophenone under dinitrogen. Tantalum pentachloride, zinc powder, 1-phenyl-1-propyne, methyllithium (1.6 M in diethyl ether) and ethylmagnesium chloride (2.0 M in diethyl ether) were used as received from commercial sources. [D$_6$]Benzene (degassed and stored over molecular sieves under dinitrogen) was used for NMR studies unless stated otherwise. ^{1}H- and ^{13}C-NMR data were acquired with Bruker AC 200, AM 250 or DPX 300. Elemental analyses were performed in the Analytical Service of our laboratory.

$Tp^{Me2}TaCl_2(PhC{\equiv}CCH_3)$ (2): A toluene/DME solution of $TaCl_3(DME)(PhC{\equiv}CCH_3)$, generated from $TaCl_5$ (2.15 g, 6.0 mmol), zinc powder (0.60 g, 9.0 mmol) and $PhC{\equiv}CCH_3$ (0.70 g, 6.0 mmol),[6] was filtered into a suspension of degassed KTp^{Me2} (2.02 g, 6.0 mmol) in DME (10 mL). The slurry was stirred for 5 h and then filtered through Celite to give a bright orange solution. The volatiles were removed under vacuum. The residue was extracted with toluene, filtered and dried under vacuum. This

process was repeated three times to separate the less soluble $[HB(C_3N_2Me_2H)_3BH][TaCl_6]$. $Tp^{Me2}TaCl_2(PhC{\equiv}CCH_3)$ was then obtained as an orange powder (1.60 g, 2.4 mmol, 40% yield). It can be recrystallized from a dichloromethane/hexane (1:1) mixture to give an analytical sample. $C_{24}H_{30}BCl_2N_6Ta$ (665.2): calcd. C 43.4, H 4.4, N 12.7; found C 43.1, H 4.1, N 12.7. – ^{1}H NMR: major isomer: δ = 1.82, 1.96, 2.08, 2.98 (all s, 6, 6, 3, 3 H, $Tp^{Me2}CH_3$), 4.22 (s, 3 H, ≡CCH_3), 5.35, 5.62 (both s, 2, 1 H, Tp^{Me2}CH), 6.83–7.00 (m, 5 H, C_6H_5); minor isomer (some resonances obscured): δ = 1.93, 2.71, 3.00 (all s, 6, 3, 3 H, $Tp^{Me2}CH_3$), 5.44, 5.68 (both s, 2, 1 H, Tp^{Me2}CH), 7.19 (t, J = 7.4 Hz, 1 H, p-C_6H_5), 7.5 (t, J = 7.7 Hz, 2 H, m-C_6H_5), 8.37 (d, J = 7.7 Hz, 2 H, o-C_6H_5); isomer ratio 7:1. – ^{13}C{^{1}H} NMR ($CDCl_3$): major isomer: δ = 12.6, 13.0, 15.3, 15.9 ($Tp^{Me2}CH_3$), 25.7 (≡CCH_3), 108.2, 108.6 ($Tp^{Me2}CH$), 128.6, 128.9, 130.5, 142.4 (C_6H_5), 144.2, 144.5, 153.4, 154.0 ($Tp^{Me2}CCH_3$), 226.8, 269.3 ($CH_3C{\equiv}C$Ph).

$[HB(C_3N_2Me_2H)_3BH][TaCl_6]$: $C_{15}H_{23}B_2Cl_6N_6Ta$ (702.7): calcd. C 25.6, H 3.3, N 11.9; found C 25.6, H 3.8, N 11.3. – ^{1}H NMR (CD_2Cl_2): δ = 2.42 (s, 6 H, CH_3), 6.07 (s, 1 H, CH).

$Tp^{Me2}Ta(CH_3)_2(PhC{\equiv}CCH_3)$ (3): Methyllithium (3.7 mmol, 2.3 mL of a 1.6 M ethereal solution) was added dropwise via syringe at –70 °C to a vigorously stirred suspension of $Tp^{Me2}TaCl_2$-$(PhC{\equiv}CCH_3)$ (1.00 g, 1.4 mmol) in diethyl ether (40 mL). The cooling bath was then removed and the orange suspension slowly turned to pale yellow. The mixture was stirred for 4 h and a white precipitate formed. The solvent was stripped off under vacuum and the residue was extracted three time in a mixture of pentane/diethyl ether (5:1). $Tp^{Me2}Ta(CH_3)_2(PhC{\equiv}CCH_3)$ was obtained as a spectroscopically pure yellow powder after the volatiles were removed. Crystallization from a minimum of pentane gave bright yellow needles (0.66 g, 1.0 mmol, 71% yield). $C_{26}H_{36}BN_6Ta$ (624.4): calcd. C 50.0, H 5.8, N 13.5; found C 50.2, H 5.8, N 13.6. – ^{1}H NMR: major isomer: δ = 0.76 (s, 6 H, TaCH_3), 1.71, 2.05, 2.21, 2.52 (all s, 6, 6, 3, 3 H, $Tp^{Me2}CH_3$), 3.86 (s, 3 H, ≡CCH_3), 5.48, 5.79 (both s, 2, 1 H, Tp^{Me2}CH), 7.05–8.13 (m, 5 H, C_6H_5); minor isomer (some resonances obscured): δ = 0.83 (s, 6 H, TaCH_3), 1.92, 2.04, 2.20, 2.53 (all s, 6, 6, 3, 3 H, $Tp^{Me2}CH_3$), 5.51, 5.78 (both s, 2, 1 H, Tp^{Me2}CH), 7.50 (t, J = 7.7 Hz, 2 H, C_6H_5), 8.10 (d, J = 7.7 Hz, 2 H, C_6H_5); isomer ratio 5:1. – ^{13}C NMR: major isomer: δ = 12.8, 12.7, 15.0, 15.4 ($Tp^{Me2}CH_3$), 25.2 (≡CCH_3), 59.9 (q, J = 114 Hz, TaCH_3), 107.5, 108.6 ($Tp^{Me2}CH$), 143.5, 143.8, 151.7, 151.9 ($Tp^{Me2}CCH_3$), 234.7, 262.3 ($CH_3C{\equiv}C$Ph); minor isomer: δ = 60.7 (TaCH_3).

$Tp^{Me2}Ta(Cl)(CH_2CH_3)(PhC{\equiv}CCH_3)$ (4): An ethereal solution of ethylmagnesium chloride (1.0 mmol, 0.5 mL of a 2.0 M solution) was added via syringe to a vigorously stirred suspension of Tp^{Me2}-$TaCl_2(PhC{\equiv}CCH_3)$ (0.53 g, 0.8 mmol) in diethyl ether (30 mL). The orange suspension slowly turned to a brownish yellow slurry. After filtration, the solution was concentrated to dryness and the residue was extracted with toluene and filtered through a pad of Celite. Concentration of the bright yellow solution to an oil (ca 2 mL) and addition of pentane (10 mL) led to immediate precipitation of golden yellow plates. $Tp^{Me2}Ta(Cl)(CH_2CH_3)(PhC{\equiv}CCH_3)$ (0.26 g, 0.4 mmol, 80% yield) was recovered after filtration and drying under vacuum. – $C_{26}H_{35}BClN_6Ta$ (658.8): calcd. C 47.4, H 5.4, N 12.8; found C 47.4, H, 5.3, N 12.7. – ^{1}H NMR: major isomer: δ = 0.59 [dq, J = 14.6, 6.6 Hz, 1 H, Ta(μ-H)CHCH_3], 1.40 (dd, J= 7.2, 6.7 Hz, 3 H, $TaCH_2CH_3$), 1.62, 1.90, 2.02, 2.03, 2.15, 2.77 (all s, 3 H each, $Tp^{Me2}CH_3$), 3.02 [dq, J = 14.6, 7.5 Hz, 1 H, Ta(μ-H)CHCH_3], 3.91 (s, 3 H, ≡CCH_3), 5.41, 5.52, 5.70 (all s, 1 H each, Tp^{Me2}CH), 6.93–7.09 (m, 5 H, C_6H_5); minor isomer (some resonances obscured): δ = 0.92 [m, 1 H, Ta(μ-H)CHCH_3], 1.81, 1.99, 2.07, 2.13, 2.75, 2.79 (3 H each $Tp^{Me2}CH_3$), 3.15 [m, 1 H, Ta(μ-H)CHCH_3], 5.49, 5.57, 5.69 (all s, 1 H each, Tp^{Me2}CH), 7.17 (t, J= 7.7 Hz, 1 H, p-C_6H_5), 7.49 (t, J= 7.7 Hz, 2 H, m-C_6H_5), 8.24 (dd, J = 8.0, 1.1 Hz, 2 H, o-C_6H_5); isomer ratio 4:1. – ^{13}C NMR: major isomer: δ = 12.7, 12.9, 13.2, 14.8, 15.7, 15.9, 16.0 ($TaCH_2CH_3$, $Tp^{Me2}CH_3$), 25.2 (≡CCH_3), 78.4 (dd, $w_{1/2}$ = 12 Hz, J = 122, 103 Hz, TaCH_2CH_3), 108.0, 108.1, 108.8 ($Tp^{Me2}CH$), 129.1, 130.9, 132.5 (C_6H_5), 144.0, 144.2, 144.3, 151.2, 153.6, 153.9 ($Tp^{Me2}CCH_3$), 227.3, 261.9 ($CH_3C{\equiv}C$Ph); minor isomer: δ = 79.9 ($TaCH_2CH_3$).

$Tp^{Me2}Ta(CH_3)(CH_2CH_3)(PhC{\equiv}CCH_3)$ (5): To an ice/water-cooled (5 °C) suspension of $Tp^{Me2}Ta(Cl)(CH_2CH_3)(PhC{\equiv}CCH_3)$ (0.15 g, 0.23 mmol) in diethyl ether (80 mL) was added via syringe an excess of methyllithium (0.4 mmol, 0.25 mL). The pale yellow mixture turned into a golden yellow solution after ca 15 min. The solution was then stirred for 1 h at room temperature. Various attempts to extract the product using toluene and/or pentane led to rapid decomposition. NMR data were obtained after removing the volatiles under vacuum. – ^{1}H NMR: major isomer: δ = –0.25 [dq, J = 7.2, 14.8 Hz, 1 H, Ta(μ-H)CHCH_3], 0.68 (s, 3 H, TaCH_3) 1.42 (t, J = 7.2 Hz, 3 H, $TaCH_2CH_3$), 1.71, 1.72, 2.04, 2.07, 2.21, 2.51 (all s, 3 H each, $Tp^{Me2}CH_3$), 2.46 [dq, J = 15.0, 7.4 Hz, 1 H, Ta(μ-H)CHCH_3], 3.79 (s, 3 H, ≡CCH_3), 5.47, 5.58, 5.80 (all s, 1 H each, Tp^{Me2}CH), 6.94–7.24 (m, C_6H_5); minor isomer (some resonances obscured): δ = 0.74 (s, 3 H, TaCH_3), 1.91, 1.92, 2.03, 2.06, 2.19, 2.53 (all s, 3 H, $Tp^{Me2}CH_3$), 5.53, 5.62, 5.78 (all s, 1 H, Tp^{Me2}CH), 7.52 (t, J = 7.0 Hz, 2 H, m-C_6H_5), 8.08 (dd, J = 1.5, 8.0 Hz, 2 H, o-C_6H_5); isomer ratio 5:1. – ^{13}C NMR: major isomer: δ = 12.9, 13.0, 13.1, 14.7, 15.2, 15.3, 15.7 ($TaCH_2CH_3$, $Tp^{Me2}CH_3$), 25.0 (≡CCH_3), 55.2 (q, J = 116 Hz, TaCH_3), 78.0 (dd, $w_{1/2}$ = 12 Hz, J = 116, 105 Hz, TaCH_2CH_3), 107.5, 107.6, 108.7 ($Tp^{Me2}CH$), 129.1, 130.9, 132.5 (C_6H_5), 143.9 (*ipso*-C_6H_5), 143.8, 144.0, 144.7, 151.5, 152.1, 152.2 ($Tp^{Me2}CCH_3$), 231.8, 260.2 ($CH_3C{\equiv}$CPh); minor isomer: δ = 55.4 (TaCH_3), 79.3 ($TaCH_2CH_3$).

Crystallographic Study: Single crystals of **4** were obtained from a toluene/pentane solution. Crystal data: $C_{26}H_{35}TaClN_6B$ (571.8), orthorhombic, *Pbca*, a = 15.995(4), b = 19.458(4), c = 17.259(4) Å, V = 5371(1) Å^3, Z = 8, T = 160 K, D = 1.63 Mg m^{-3}, μ = 4.21 mm^{-1}. Data collection was performed with a STOE IPDS diffractometer (Imaging Plate Device) using a graphite- monochromatized Mo-K_α radiation. The structure was solved by direct methods using SIR92.[12] Absorption corrections were applied (min/max trans. 0.5395/0.8161).[13] The refinement was carried out with the CRYSTALS package.[14] 36121 reflections were collected and 5225 found unique (R_{int} = 0.0605). All non-hydrogen atoms were anisotropically refined. Several hydrogen atoms were located from a difference Fourier map but only H(1), H(11) and H(12) were refined with an isotropic thermal parameter [equivalent parameter for H(11) and H(12)]. All the others were included in the calculations in idealized positions (C–H = 0.96 Å) with an isotropic thermal parameter 1.2 times that of the atom to which they were attached. Full-matrix least-square refinements were carried out by minimizing the function $\Sigma w(||F_o| - |F_c||)^2$, where F_o and F_c are the observed and calculated structure factors. A weighting scheme was introduced[15] with $w = w'\{1 - [\Delta F/6\sigma(F)]^2\}^2$. Final $R = \Sigma(||F_o| - |F_c||)/\Sigma|F_o|$, $Rw = [\Sigma w(||F_o| - |F_c||)^2/\Sigma w(|F_o|)^2]^{1/2}$ were 0.0196 and 0.0190, respectively [2820 reflections with $I > 2\sigma(I)$, 328 parameters, *gof* = 1.099, Δρ(min/max) = –0.73/0.54, max ls/esd shift 0.0051]. The plot of the molecular structure was performed with the software CAMERON.[16] Crystallographic data (excluding structure factors) have been deposited with the Cambridge Crystallographic Data Center as supplementary publication number No. CCDC-138605.

Copies of the data can be obtained free of charge on application to CCDC, 12 Union Road, Cambridge CB2 1EZ, UK [Fax: int. code + 44-1223/336-033; E-mail: deposit@ccdc.cam.ac.uk].

Acknowledgments

Thanks are due to Dr. B. Donnadieu for the X-ray data acquisition, and to Drs. J. Jaffart and R. Mathieu for helpful discussions.

[1] M. Brookhart, M. L. H. Green, L.-L. Wong, *Prog. Inorg. Chem.* **1988**, *36*, 1–124. Y. Han, L. Deng, T. Ziegler, *J. Am. Chem. Soc.* **1997**, *119*, 5939–5945. D. G. Musaev, R. D. J. Froese, M. Svensson, K. Morokuma, *J. Am. Chem. Soc.* **1997**, *119*, 367–374. A. Haaland, W. Scherer, K. Ruud, G. S. McGrady, A. J. Downs, O. Swang, *J. Am. Chem. Soc.***1998**, *120*, 3762–3772.

[2] [2a] M. Etienne, R. Mathieu, B. Donnadieu, *J. Am. Chem. Soc.* **1997**, *119*, 3218–3228. – [2b] Z. Guo, D. C. Swenson, R. F. Jordan, *Organometallics* **1994**, *13*, 1424–1432. – [2c] M. Etienne, *Organometallics* **1994**, *13*, 410–412.

[3] J. Jaffart, R. Mathieu, M. Etienne, J. E. McGrady, O. Eisenstein, F. Maseras, *Chem. Commun.* **1998**, 2011–2012.

[4] Z. Dawoodi, M. L. H. Green, V. S. B. Mtetwa, K. Prout, A. J. Schultz, J. M. Williams, T. F. Koetzle, *J. Chem. Soc., Dalton Trans.* **1986**, 1629–1637. M. L. H. Green, A. K. Hugues, N. A. Popham, A. H. H. Stephens, L. L. Wong, *J. Chem. Soc., Dalton Trans.* **1992**, 3077–3082. D. C. Maus, V. Copié, B. Sun, J. M. Griffiths, R. G. Griffin, S. Luo, R. R. Schrock, A. H. Lûu, S. W. Seidel, W. M. Davis, A. Groham, *J. Am. Chem. Soc.* **1996**, *118*, 5665–5671. J. M. Cole, V. C. Gibson, J. A. K. Howard, G. J. McIntyre, G. L. P. Walker, *Chem. Commun.* **1998**, 1829–1830.

[5] General reviews: S. Trofimenko, *Scorpionates – The Coordination Chemistry of Polypyrazolylborate Ligands*, Imperial College Press, London, **1999**. S. Trofimenko, *Chem. Rev.* **1993**, *93*, 943–980. Review on Group-5 metals: M. Etienne, *Coord. Chem. Rev.* **1996**, *156*, 201–236. For *organo*tantalum(V) complexes with Tp′ ligands: D. L. Reger, C. A. Swift, L. Lebioda, *Inorg. Chem.* **1984**, *23*, 349–354. J. M. Boncella, M. L. Cajigal, K. A. Abboud, *Organometallics* **1996**, *15*, 1905–1912. G. Rodriguez, J. P. Graham, W. D. Cotter, C. K. Sperry, G. C. Bazan, B. E. Bursten, *J. Am. Chem. Soc.* **1998**, *120*, 12512–12523.

[6] [6a] K. Takai, Y. Kataoka, K. Utimoto, *J. Org. Chem.* **1990**, *55*, 1707–1708. – [6b] Y. Kataoka, K. Takai, K. Oshima, K. Utimoto, *J. Org. Chem.* **1992**, *57*, 1615–1618. – [6c] (alkyne)(DME)-$TaCl_3$ complexes were not isolated by these authors. We have successfully isolated crystals of $TaCl_3(DME)(PhC{\equiv}CCH_3)$ after addition of *n*-hexane to the crude DME/toluene reaction mixture and cooling to –20 °C (44% yield). – $C_{13}H_{18}Cl_3O_2Ta \cdot 1/4\ C_4H_{10}O_2$ (516.1): calcd. C 32.6, H 4.0; found C 33.0, H 3.5. – ^{1}H NMR ([D$_6$]benzene): δ = 3.01, 3.57, 3.65 (all s, 3 H, $TaOCH_3$ and $\equiv CCH_3$), 3.03 (m, 4 H, CH_2), 3.11 (s, ca. 1.5 H, free CH_2OCH_3), 3.31 (s, 1 H, free CH_2OCH_3), 7.05–7.95 (m, 5 H, $\equiv CC_6H_5$).

[7] J. M. Boncella, M. L. Cajigal, A. S. Gamble, K. A. Abboud, *Polyhedron* **1996**, *15*, 2071–2078.

[8] K. Mashima, T. Oshiki, K. Tani, *Organometallics* **1997**, *16*, 2760–2762.

[9] M. Etienne, F. Biasotto, R. Mathieu, J. L. Templeton, *Organometallics* **1996**, *15*, 1106–1112.

[10] M. D. Curtis, J. Real, W. Hirpo, W. M. Butler, *Organometallics* **1990**, *9*, 66–74.

[11] [11a] J. W. Bruno, G. M. Smith, T. J. Marks, C. K. Fair, A. J. Schultz, J. M. Williams, *J. Am. Chem. Soc.* **1986**, *108*, 40–56. – [11b] A. D. Poole, D. N. Williams, A. M. Kenwright, V. C. Gibson, D. C. R. Hockless, P. A. O'Neil, *Organometallics* **1993**, *12*, 2549–2555.

[12] A. Altomare, G. Cascarano, G. Giacovazzo, A. Guargliardi, M. C. Burla, G. Polidori, M. Camalli, "SIR 92, A program for automatic solution of crystal structures by direct methods", *J. Appl. Crystallogr.* **1994**, *27*, 435.

[13] *X-SHAPE, Crystal Optimisation for Numerical Absorption Correction*, Revision 1.01, STOE and Cie GmbH, Darmstadt, **1996**.

[14] D. J. Watkin, C. K. Prout, R. J. Carruthers, P. Betteridge, *Crystals*, University of Oxford, **1996**, issue 10.

[15] R. J. Carruthers, D. J. Watkin, *Acta Crystallogr.* **1979**, *A35*, 698.

[16] D. J. Watkin, C. K. Prout, L. J. Pearce, *CAMERON*, University of Oxford, Oxford, **1996**.

Received January 12, 2000
[I00005]

Unprecedented Coordination of 4,4′,5,5′-Tetramethyl-2,2′-biphosphinine Doubly Bridging over an Open Triosmium Core

Maarten J. Bakker,[a] Frank W. Vergeer,[a] František Hartl,*[a] Kees Goubitz,[b] Jan Fraanje,[b] Patrick Rosa,[c] and Pascal Le Floch[c]

Keywords: Triosmium cluster / Biphosphinine / Crystal structure / Cyclic voltammetry

The crystal structure of the novel cluster $[Os_3(CO)_{10}$(4,4′,5,5′-tetramethyl-2,2′-biphosphinine)] reveals an unprecedented coordination mode of the biphosphinine ligand that occupies a doubly-bridging position spanning the open osmium triangle. The cluster is photostable, pointing to a localization of the lowest-energy electronic transition largely on the negatively charged biphosphinine ligand.

Introduction

Clusters of the type $[Os_3(CO)_{10}$(α-diimine)] exhibit a very diversified photochemical and redox behaviour which is controlled by the tuneable electronic and steric properties of the α-diimine ligand. Such ligands include 4,4′-di-R-2,2′-bipyridine and pyridine-2-carbaldehyde-*N*′-R-imine (R = alkyl).[1–3] In comparison with σ*N*,σ*N*′-chelated 2,2′-bipyridine, its aromatic phosphorus derivative 4,4′,5,5′-tetramethyl-2,2′-biphosphinine (tmbp) binds as a fairly strong π-acceptor ligand in a variety of mononuclear complexes, and better stabilizes low oxidation states of the metal in the M(σ*P*,σ*P*′-tmbp) chelate ring.[4,5] In addition, it may bind as a cyclophosphahexatriene with localized double bonds, for example in $[Mn_2(CO)_6$(tmbp)] where it chelates to one $Mn(CO)_3$ moiety through the P lone pairs and to the other metal centre through the internal P=C bonds.[6]

The growing interest in biphosphinine complexes prompted us to attempt the synthesis of the cluster $[Os_3(CO)_{10}$(σ*P*,σ*P*′-tmbp)], with the aim of performing a comparative study of its spectroscopic, photochemical and redox properties. Nevertheless, as often encountered in cluster chemistry, our synthetic efforts instead yielded a structural isomer of the intended product, which presents the first example of the biphosphinine coordinated to three transition metal centres as a doubly bridging ligand. Herein we report the synthesis, X-ray crystal structure and brief characterization of this unusual triosmium cluster.

Results and Discussion

The precursor cluster $[Os_3(CO)_{10}(MeCN)_2]$ reacts with tmbp in THF at room temperature to give purple $[Os_3(CO)_{10}(\mu_2P,\mu_2P'$-tmbp)] (**1**, Figure 1). The cluster **1** was isolated and spectroscopically characterized. The X-ray crystal structure is shown in Figure 2. Similarly to the four-electron donor 2,2′-bipyridine in $[Os_3(CO)_{10}$(bpy)], the biphosphinine ligand is chelated at Os(1). In addition, each phosphorus atom forms a bridge between Os(1) and one of the other two osmium centres. The double μ_2-P bridging of tmbp causes cleavage of the Os(1)–Os(2) bond and opening of the osmium triangle [Os(1)–Os(3)–Os(2) = 85.93(2)°]. Secondly, the tmbp ligand becomes strongly distorted and its aromaticity is lifted. In all known mononuclear complexes of tmbp this ligand is perfectly planar, with C–C bond lengths in the rings between 1.38 and 1.41 Å, thus displaying a high degree of aromaticity.[4,5] In contrast, the C–C bond lengths of **1** range from 1.33(2) Å, typical for isolated C=C bonds, to 1.47(2) Å (length of a single C–C bond ≈ 1.53 Å). Importantly, the inter-ring C–C bond length in **1** is rather short [1.41(2) Å] when compared to the characteristic values for the nonreduced uncoordinated ligand (1.49 Å, average of two isomers)[7] and for mononuclear complexes of tmbp (ca. 1.47 Å).[4,5] Also the C–P bonds are rather long [1.77(2)–1.80(2) Å] compared to the C–P bond lengths of "aromatic" tmbp (1.71–1.74 Å).[4,5] These data point to partial reduction of the tmbp ligand by electron transfer from the triosmium core, causing cleavage

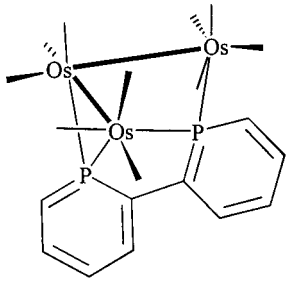


Figure 1. Schematic molecular structure of cluster **1**

[a] Institute of Molecular Chemistry, Universiteit van Amsterdam, Nieuwe Achtergracht 166, 1018 WV Amsterdam, The Netherlands
E-mail: hartl@anorg.chem.uva.nl
[b] Laboratorium voor Kristallografie, Institute of Molecular Chemistry, Universiteit van Amsterdam, Nieuwe Achtergracht 166, 1018 WV Amsterdam, The Netherlands
[c] Laboratoire "Hétéroéléments et Coordination" CNRS UMR 7653, École Polytechnique, 91128 Palaiseau Cedex, France

 © WILEY-VCH Verlag GmbH, D-69451 Weinheim, 2000 1434–1948/00/0505–0843 $ 17.50+.50/0

of the Os–Os bond.[8] Another remarkable feature is the enormous difference between the two Os–P–Os bridge angles: 75.2(1)° [P(2)] spanning the intact Os(1)–Os(3) bond, but 110.0(1)° [P(1)] spanning the nonbonded Os(1) and Os(2) centres.

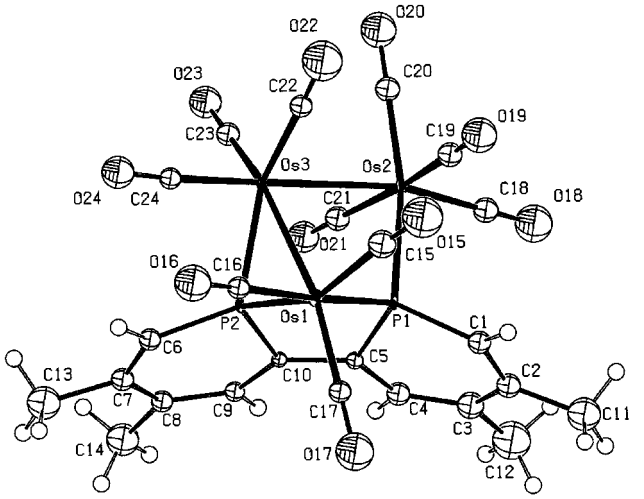


Figure 2. X-ray crystal structure of cluster **1**; selected bond lengths (Å) and angles (°) with standard deviations in parentheses: Os(1)–Os(3) 2.8856(9), Os(2)–Os(3) 2.9567(9), Os(1)–P(1) 2.395(4), Os(2)–P(1) 2.441(4), Os(1)–P(2) 2.351(3), Os(3)–P(2) 2.376(4), P(1)–C(1) 1.77(2), P(1)–C(5) 1.80(2), C(1)–C(2) 1.37(2), C(2)–C(3) 1.46(3), C(3)–C(4) 1.38(2), C(4)–C(5) 1.39(2), P(2)–C(6) 1.78(2), P(2)–C(10) 1.80(1), C(6)–C(7) 1.33(2), C(7)–C(8) 1.47(2), C(8)–C(9) 1.37(2), C(9)–C(10) 1.44(2), C(5)–C(10) 1.41(2); Os(1)–Os(3)–Os(2) 85.93(2), Os(1)–P(1)–Os(2) 110.9(1), Os(1)–P(2)–Os(3) 75.2(1), P(1)–Os(1)–P(2) 75.1(1), C(1)–P(1)–C(5) 100.1(6), C(6)–P(2)–C(10) 101.6(7)

The very different environments of both phosphorus atoms are reflected in their ^{31}P NMR chemical shifts (δ = 26.2 and –146.2). Both values significantly deviate from the strongly positive ^{31}P chemical shifts for "aromatic tmbp" complexes (δ = 178–250).[4,5] The loss of aromaticity is also reflected in the shift of the proton signals to smaller ppm values (ca. 1.5 ppm) compared to those of the noncoordinated tmbp ligand.

Cluster **1** is deep-purple coloured due to a broad absorption band at 540 nm. The corresponding electronic transition exhibits negligible solvatochromism,[9] in contrast to the lowest-energy electronic transition of $[Os_3(CO)_{10}(bpy)]$, which possesses a dominant metal(core)-to-ligand charge transfer character.[1,10] The involved frontier orbitals of **1** probably have a dominant contribution from the tmbp ligand.[8] This may explain the observed inherent photostability of **1**, as no specific metal–ligand or metal–metal bonds are significantly weakened upon visible excitation.[11]

The different electronic structure with regard to that of $[Os_3(CO)_{10}(bpy)]$ is also indicated by the electrochemical behaviour of **1** which, in the first instance, was studied by cyclic voltammetry. At room temperature and at v = 20 mV/s the reduction of **1** is a chemically irreversible two-electron process ($E_{p,c}$ = –1.73 V *vs.* Fc/Fc$^+$), resulting in loss of CO. At v = 100 V/s the reduction becomes a chemically reversible one-electron process ($E_{1/2}$ = –1.74 V *vs.* Fc/Fc$^+$). The reduction potential is more negative than would be expected for a dominantly tmbp-localized reduction of isomeric $[Os_3(CO)_{10}(\sigma P,\sigma P'\text{-tmbp})]$ with a molecular and electronic structure resembling that of $[Os_3(CO)_{10}(\alpha\text{-diimine})]$.[12] On the other hand, the higher stability of the radical anion **1**$^{-\bullet}$ does not correspond to the reduction being localized significantly on the cluster core.[3] We assume that the higher LUMO energy of **1** reflects the partial negative charge on the tmbp ligand, as deduced from the crystallographic data.

A detailed (spectro)electrochemical and quantum chemical investigation of **1** is currently being carried out.[8]

Experimental Section

General: UV/Vis: Varian Cary 4E. – IR: Bio-Rad FTS 60A – NMR: Bruker AMX 300. – MS (FAB): JEOL JMS SX/SX102A four-sector mass spectrometer, coupled to a JEOL MS-MP 7000 data system. – Elemental analyses were performed at H. Kolbe Mikroanalytisches Laboratorium in Mülheim an der Ruhr.

$[Os_3(CO)_{10}(tmbp)]$ (1): $[Os_3(CO)_{10}(MeCN)_2]$[12] (190 mg) and tmbp (45 mg, 0.9 equiv.) were dissolved in freshly distilled THF (50 mL) under an atmosphere of dry N_2. The yellow solution quickly turned red and finally deep purple. After 1.5 h the solvent was evaporated in vacuo, and the crude purple product was purified by column chromatography over silica, eluting with hexane/dichloromethane (20:1). Single crystals suitable for a crystal structure determination were grown from hexane at 293 K.

1: IR (hexane): ν(CO) = 2104 m, 2057 s, 2036 m, 2025 sh, 2022 vs, 2007 w, 1991 m, 1976 m, 1959 w, 1952 w cm^{-1} – ^{1}H NMR (300 MHz, 293 K, $CDCl_3$): δ = 1.90 (s, Me), 2.04 (s, Me), 2.15 (s, Me), 2.20 (s, Me), 6.36 (d, $^2J(P_a–H)$ = 32.1 Hz, 1 H), 6.39 (d, $^2J(P_b–H)$ = 28.5 Hz, 1 H), 6.75 (d, $^3J(P_a–H)$ = 17.4 Hz, 1 H), 6.93 (d, $^3J(P_b–H)$ = 19.2 Hz, 1 H). – ^{31}P{H} NMR (300 MHz, 293 K, $CDCl_3$): δ = –146.2 (d, P_a), 26.2 (d, P_b), $J(P_a–P_b)$ = 108 Hz. – UV/Vis (*n*-hexane): λ = 340 sh, 436 sh, 540 nm. – $C_{24}H_{16}O_{10}Os_3P_2$ (1097): calcd. C 26.28, H 1.47, P 5.65; found C 26.39, H 1.54, P 5.74. – MS (FAB): *m/z* = 1097 [M$^+$].

X-ray Structure of 1: $C_{24}H_{16}O_{10}Os_3P_2$, M = 1097, monoclinic, space group $P2_1/a$, a = 9.8115(8), b = 16.359(1), c = 18.276(1) Å, β = 98.693(6)°, U = 2899.7(3) Å^3, Z = 4, D_x = 2.51 gcm^{-3}, λ(Cu-K_α) = 1.5418 Å, μ(Cu-K_α) = 257.9 cm^{-1}, T = 253 K, F(000) = 1992, 5954 unique reflections measured, final R = 0.060 for 5264 observed reflections. During the measurement the two reference reflections that were measured hourly showed an increase in intensity which could not be explained. This may be the reason why only the heavy atoms (Os and P) could be refined anisotropically. The results of the structure refinement with respect to the geometry of the molecule were, however, satisfactory.

Crystallographic data (excluding structure factors) for the structure reported in this paper have been deposited with the Cambridge Crystallographic Data Centre as supplementary publication no. CCDC-136584. Copies of the data can be obtained free of charge on application to CCDC, 12 Union Road, Cambridge CB2 1EZ, UK [Fax: (internat.) + 44–1223/336–033; E-mail: deposit@ccdc.cam.ac.uk).

Cyclic Voltammetry: Cyclic voltammograms of **1** in freshly distilled THF (with 0.1 M Bu_4NPF_6 as electrolyte) were recorded under argon in a gas-tight single-compartment cell equipped with a Pt-disk

working microelectrode (r = 0.4 mm), a Pt-gauze auxiliary electrode and an Ag-coil pseudoreference electrode. Potential control was achieved with a PAR Model 283 potentiostat.

Photochemistry: Continuous-wave irradiation was performed with a Spectra Physics 2025 argon-ion laser. Nanosecond time-resolved UV/Vis experiments were carried out with 7 ns pulses (fwhm) of a 532 nm line obtained by frequency doubling of the 1064 nm fundamental of a Spectra Physics GCR-3 Nd:YAG laser. Details of the data collection system have been described elsewhere.[2]

Acknowledgments

Mr. T. Mahabiersing is kindly acknowledged for his assistance with the purification of cluster **1**.

[1] J. W. M. van Outersterp, M. T. Garriga Oostenbrink, H. A. Nieuwenhuis, D. J. Stufkens, F. Hartl, *Inorg. Chem.* **1995**, *34*, 6312–6318.
[2] J. Nijhoff, M. J. Bakker, F. Hartl, D. J. Stufkens, W.-F. Fu, R. van Eldik, *Inorg. Chem.* **1998**, *37*, 661–668.
[3] J. Nijhoff, F. Hartl, J. W. M. van Outersterp, D. J. Stufkens, M. J. Calhorda, L. F. Veiros, *J. Organomet. Chem.* **1999**, *573*, 121–133.
[4] F. Mathey, P. Le Floch, *Chem. Ber.* **1996**, *129*, 263–268.
[5] P. Le Floch, F. Mathey, *Coord. Chem. Rev.* **1998**, *179–180*, 771–791.
[6] P. Le Floch, N. Maigrot, L. Ricard, C. Charrier, F. Mathey, *Inorg. Chem.* **1995**, *34*, 5070–5072.
[7] P. Le Floch, D. Carmichael, L. Ricard, F. Mathey, A. Juttand, C. Amatore, *Organometallics* **1992**, *11*, 2475–2479.
[8] M. J. Bakker, F. W. Vergeer, F. Hartl, P. Le Floch, M. J. Calhorda, manuscript in preparation.
[9] UV/Vis absorption maxima of the lowest-energy electronic transition of **1** in different solvents: 540 (hexane), 556 ($\varepsilon = 3.6 \times 10^3$ $M^{-1}cm^{-1}$, THF), 553 (acetonitrile), 559 (pyridine) nm.
[10] M. J. Calhorda, E. Hunstock, L. F. Veiros, F. Hartl, *submitted to J. Phys. Chem. B.*
[11] Cluster **1** is photostable upon continuous irradiation in CCl_4, THF, acetonitrile or pyridine at room temperature (λ_{irr} = 514.5 nm). No UV/Vis transient was observed even on a nanosecond time scale [λ_{irr} = 532 nm, τ(laser pulse) = 7 ns].
[12] The electrode potentials for the one-electron reduction of uncoordinated tmbp and 4,4′-dimethyl-2,2′-bipyridine (dmb) in DMF are $E_{1/2}$ = –1.85 V and –2.16 V *vs.* SCE, respectively.[7] In contrast, for the clusters **1** and $[Os_3(CO)_{10}(\sigma N,\sigma N'\text{-dmb})]$[14] in THF the values are closer, *viz.* $E_{1/2}$ = –1.70 V (208 K) and –1.89 V (213 K) *vs.* $Fc/Fc^{+\cdot}$ respectively.
[13] R. Zoet, J. T. B. H. Jastrzebski, G. van Koten, T. Mahabiersing, K. Vrieze, *Organometallics* **1988**, *7*, 2108–2117.
[14] F. Hartl, unpublished results.

Received November 11, 1999
[I99426]

Temperature-Dependent Photophysical, Photochemical and Redox Properties of Novel Complexes $(CO)_2CpRu–Ru(L_n)–RuCp(CO)_2$ and $(CO)_2CpRu–Ru(L_n)–SnPh_3$ [L_n = $(CO)_2$(*N,N′*-diisopropyl-1,4-diaza-1,3-butadiene)]

Joris van Slageren,[a] František Hartl,*[a] and Derk J. Stufkens[a]

Keywords: Photochemistry / Electrochemistry / Ruthenium compounds / α-Diimine complexes

The photophysical, photochemical and redox properties of the title complexes were investigated. Resonance Raman measurements revealed the lowest-energy electronic transition to possess σ→π* character. At low temperatures, long-lived near-IR emission was observed. Irradiation in solution results in homolytic splitting of a Ru–Ru bond as the primary step, followed by secondary reactions of the radical fragments depending on the experimental conditions. (Spectro)-electrochemical investigations of the title species proved that the axial [$RuCp(CO)_2$] groups exert a stabilising influence on the corresponding radical cations, while destabilising the corresponding radical anions, compared to the redox behaviour of other ruthenium complexes of this type.

Introduction

The photochemical, photophysical and redox properties of the complexes *trans,cis*-[$Ru(L^1)(L^2)(CO)_2$(*i*-Pr–DAB)] (*i*-Pr–DAB = *N,N′*-diisopropyl-1,4-diaza-1,3-butadiene) have been studied extensively in our laboratory.[1–5] In this general formula L^1 and L^2 represent electron donating ligands such as alkyl or metal-containing groups. It was shown that in the lowest excited state of these complexes electron density was transferred from the L^1–Ru–L^2 σ system to the π* orbital of *i*-Pr–DAB, which contrasts with the lowest MLCT state of [$Ru(Cl)(Me)(CO)_2$(*i*-Pr–DAB)] and the XLCT (X = I) state of [$Ru(I)(Me)(CO)_2$(*i*-Pr–DAB)].[6–8] One of the consequences of this σπ* or Sigma-Bond-to-Ligand Charge Transfer (SBLCT) excited state character is a dramatic increase in excited state lifetime.[2] On the other hand, since the L^1–Ru–L^2 σ orbital is high in energy (and hence the corresponding σ* orbital lies relatively low) the dissociative σσ* state is thermally accessible. This imparts all members of the series [$Ru(L^1)(L^2)(CO)_2$(*i*-Pr–DAB)] with a certain degree of photoreactivity.

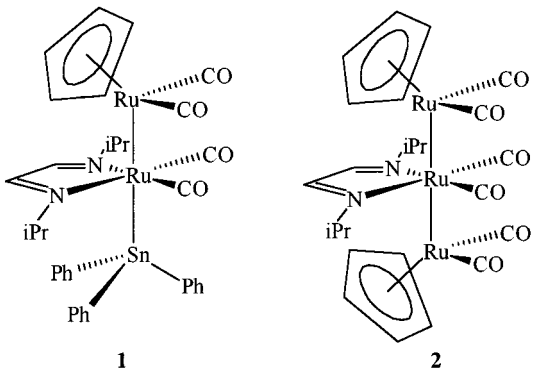
The present study was undertaken to investigate the influence of strongly electron releasing axial ligands on photophysical and photochemical behaviour. Two novel complexes bearing one or two [$RuCp(CO)_2$] groups as axial ligands were therefore synthesized. It was expected that incorporation of these ligands would shift the electronic absorption maximum to lower energy, hence giving rise to near-infrared emission. This is very interesting in view of the challenging application of such compounds as luminescent labels e.g. in biochemical separations, since background luminescence is negligible in the near infrared spectral region. A long luminescence lifetime is also desirable in order to make time-gated detection viable. In order to understand the influence of the electron releasing [$RuCp(CO)_2$] axial ligand(s) on the electronic properties and reactivity of the title complexes in more detail, a (spectro)electrochemical study was also undertaken.

[a] Institute of Molecular Chemistry,
Universiteit van Amsterdam
Nieuwe Achtergracht 166, NL-1018 WV Amsterdam,
The Netherlands
E-mail: hartl@anorg.chem.uva.nl

Results and Discussion

Spectroscopic Properties

The novel title compounds, purple [$Ru(SnPh_3)\{RuCp(CO)_2\}(CO)_2$(*i*-Pr–DAB)] (**1**) and green [$Ru\{RuCp(CO)_2\}_2(CO)_2$(*i*-Pr–DAB)] (**2**) were prepared by addition of $K[RuCp(CO)_2]$ to [$Ru(Cl)(SnPh_3)(CO)_2$(*i*-Pr–DAB)] and [$RuI_2(CO)_2$(*i*-Pr–DAB)], respectively, according to the procedure used for the synthesis of [$Ru\{Re(CO)_5\}_2(CO)_2$(*i*-Pr–DAB)].[9] Both complexes are highly photoreactive in solution, but virtually photostable in the solid state. The ^1H and ^{13}C NMR chemical shifts for the coordinated *i*-Pr–DAB ligand are similar to those found for other *trans,cis*-[$Ru(L^1)(L^2)(CO)_2$(*i*-Pr–DAB)] complexes, pointing to axial positions of the [$RuCp(CO)_2$] groups (See Figure 1). Both **1** and **2** may exist as a mixture of several rotamers in solution.



1 **2**

Figure 1. Schematic molecular structures of the complexes **1** and **2**

 © WILEY-VCH Verlag GmbH, D-69451 Weinheim, 2000 1434–1948/00/0505–0847 $ 17.50+.50/0

Table 1. Spectroscopic data for complexes **1** and **2**

	UV/Vis[a] λ_{max}[b] (ε[c])	Δ[d]	IR[e]	Resonance Raman (cm^{-1})
1	571 (5770), 383, 333, 306	368	1993m, 1960s, 1933s, 1918w	1460s, 1281s, 951s, 829s, 609m, 416w, 242m, 192m
2	605 (7070), 463, 352	82	1991w, 1967s, 1946s, 1926s, 1919sh, 1897w	1459vw, 1281vw, 954m, 833m, 601m, 499w, 320s, 184s, 119s, 104s

[a] In CH_2Cl_2 at room temperature. – [b] nm. – [c] $M^{-1}\cdot cm^{-1}$. – [d] $\Delta = \nu_{max}(MeCN) - \nu_{max}(hexane)$ (in cm^{-1}). – [e] In THF at room temperature.

The electronic absorption data are collected in Table 1. Due to the electron-releasing character of the $[RuCp(CO)_2]$ group, the lowest-energy absorption bands of both **1** and **2** are red-shifted compared to those of other complexes of this series such as $[Ru(SnPh_3)_2(CO)_2(i\text{-Pr–DAB})]$.[9,10] In the case of **1** this absorption band is considerably less solvatochromic than the metal-to-ligand charge transfer (MLCT) band of the structurally related complex $[Ru(Cl)(Me)(CO)_2(i\text{-Pr–DAB})]$,[6] and even less than is found for all presently known non-halide complexes of the $[Ru(L^1)(L^2)(CO)_2(i\text{-Pr–DAB})]$ series.[9,10] For **2** the solvatochromism is negligible. This is indicative of an electronic transition possessing a limited charge transfer character. Upon cooling a 2-MeTHF solution of **1** or **2** to a glassy solid at 80 K, the lowest-energy band shifts to higher energy by ca. 350 cm^{-1}.

In order to characterize the lowest-energy electronic transition, resonance Raman (rR) spectra were recorded for both complexes by irradiation into the corresponding absorption band. This technique relies on the resonance enhancement of Raman intensity for those vibrations which are coupled to the allowed electronic transition, activated by laser excitation. The wavenumbers of the observed Raman bands are collected in Table 1. The rR spectra of **1** and **2** (Figure 2) are significantly different. That of **1** shows resonantly enhanced Raman bands at 1460 cm^{-1} and 1281 cm^{-1}, which belong to ν(CN) and ν(CC) of the coordinated *i*-Pr–DAB ligand, respectively.[2] Their resonance enhancement indicates that the electronic transition involves some degree of charge transfer to the lowest π^*-orbital of the *i*-Pr–DAB ligand. Its occupation gives rise to a lengthening of the C=N bond, a shortening of the central C–C bond, and appearance of the corresponding stretching modes in the rR spectrum. The absence of a resonantly enhanced ν_s(CO) band implies that the π-back-bonding from the central Ru atom to the CO ligands is similar in the ground and excited states, which agrees with a delocalized Ru–Ru(*i*-Pr–DAB)–Sn system and a small charge transfer character of the transition. In contrast, Raman spectra obtained by excitation into predominantly MLCT transitions, for example in the case of $[Ru(Cl)(Me)(CO)_2(i\text{-Pr–DAB})]$, show a pronounced rR effect for ν_s(CO).[6] In the case of **2** the lowest-energy transition has virtually no charge-transfer character since the bands due to the internal stretching vibrations of the *i*-Pr–DAB ligand are absent in the rR spectrum. This observation is in line with the negligible solvatochromism of this absorption band. This effect of the variable charge transfer character on the resonance Raman spectrum is not a particular property of a $\sigma\rightarrow\pi^*$ transition; it has also been found for the ML(CT) transitions of $W(CO)_4(\alpha\text{-diimine})$.[11]

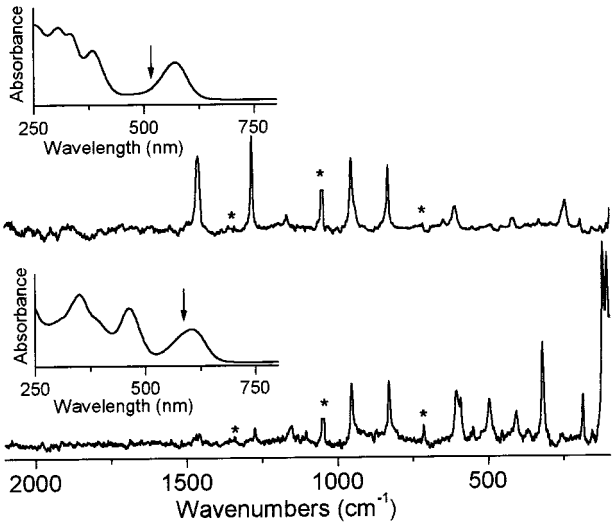


Figure 2. Resonance Raman spectra of **1** (top) and **2** (bottom) recorded by excitation (λ_{exc} = 514.5 and 590 nm, respectively) into the lowest-energy transition of the complexes dispersed in KNO_3 pellets; KNO_3 bands denoted by asterisk; UV/Vis spectra in inserts; λ_{exc} indicated by arrows

Based on the rR data, the lowest-energy absorption band of **1** is assigned to an electronic transition, qualitatively described as σ(Sn–Ru–Ru)$\rightarrow\pi^*$(*i*-Pr–DAB) with some mixing between the σ- and π^*-orbitals. In the case of **2**, this transition occurs between frontier orbitals possessing a strongly mixed σ(Ru–Ru–Ru)–π^*(*i*-Pr–DAB) character. A similar mixing between σ- and π^*-orbitals was revealed by density function calculations on the related model compound $[Ru(SnH_3)_2(CO)_2(H\text{–DAB})]$.[1] These calculations described the HOMO and LUMO as mixed contributions of a Ru p orbital, the sp^3–sp^3 combination of the SnH_3 ligands, and the π^*(H–DAB) orbital. The contribution of the π^*(*i*-Pr–DAB) orbital to the HOMO and LUMO is expected to vary from one complex to another, with a concomitant effect on the charge transfer character and the solvatochromism of the HOMO$\rightarrow$LUMO ($\sigma\rightarrow\pi^*$) transition. Going from **1** to **2**, i.e. replacing the axial $SnPh_3$-ligand by the more electron releasing $[RuCp(CO)_2]$ group, the mixing between the σ and π^* orbitals in both the HOMO and the LUMO increases. As a result the HOMO$\rightarrow$LUMO transition loses most of its charge transfer character, which is reflected in the absence of bands due to the *i*-Pr–DAB stretching vibrations

in the rR spectrum of **2**. In the 1000–100 cm^{-1} region of the rR spectrum of **1**, resonantly enhanced bands can be observed at 951 and 829 cm^{-1} (Ru–*i*-Pr–DAB metallacycle deformations) and at 609, 416, 242, and 192 cm^{-1} (metal–ligand stretching modes). These bands were also observed in the rR spectra of $[Ru(SnPh_3)_2(CO)_2(i\text{-Pr–DAB})]$ and $[Ru(SnPh_3)\{Mn(CO)_5\}(CO)_2(i\text{-Pr–DAB})]$.[2,4] In addition to these vibrations, the rR spectrum of **2** shows extra bands at 499, 320, 119 and 104 cm^{-1}, while the peak at 242 cm^{-1} is missing. The latter two bands are very intense and may belong to a ν(Ru–Ru) or a ν(Ru–Ru–Ru) mode.

Emission Properties

In a 2-MeTHF glass at 80 K, both **1** and **2** show luminescence with a much longer lifetime than that of $[Ru(Cl)(Me)(CO)_2(i\text{-Pr–DAB})]$ (Table 2).[7] This is remarkable, since **1** and **2** emit in the near infrared region, whereas the latter compound emits at much higher energy. At first, this observation seems to be in contradiction with the energy gap law. However, it can be explained by the fact that the lowest excited state has a different character. As mentioned in the introduction, the use of two σ-bound axial donor ligands results in a special type of lowest excited state. In this excited state, some electron density has been transferred from the σ-system, formed by the axial ligands and the central metal atom, to the lowest π* orbital of the α-diimine ligand, hence being called a σπ* state.[1] The long lifetime is a general property of this type of excited state, and can be rationalized as follows: In the σπ* excited state the complexes are less distorted, which is reflected in a smaller Stokes shift

Table 2. Emission properties of compounds **1** and **2** in a 2-MeTHF glass at 80 K (λ_{exc} = 532 nm).

Compound	λ_{abs} (nm)	λ_{em} (nm)	Stokes shift (cm^{-1})	τ (μs)
1	559	830	5841	16
2	593	855	5168	9
$[Ru(Cl)(Me)(CO)_2(i\text{-Pr–DAB})]$[a]	387	650	10455	0.3

[a] From ref.[7].

of their emission (Table 2). This feature originates in the delocalised nature of the electronic system, causing slight distortion of many bonds in the excited state, while the distortion along any normal coordinate is very small. Consequently, the excited state lifetime increases due to the reduction of vibrational overlap between ground and excited state wavefunctions. This situation also applies to related $[Ru(L^1)(L^2)(CO)_2(i\text{-Pr–DAB})]$ complexes, as judged from time-resolved emission and infrared data and from MO calculations.[1,2]

Photochemistry

Complexes **1** and **2** are photoreactive in solution upon irradiation into their lowest (σπ*) absorption band. The photoreactions were monitored with UV/Vis, IR, and EPR spectroscopies. The spectroscopic data of the parent complexes, photoproducts and reference compounds, are collected in Table 3 and the photoreaction pathways are summarized in Scheme 1.

First of all, solutions of **1** and **2** were irradiated in situ in an EPR spectrometer in the presence of a radical trap. The EPR spectrum recorded after irradiation of a THF solution of **1** in the presence of an excess of triphenylphosphane with a high-pressure mercury lamp ($\lambda > 455$ nm) was identical to that of the radical $[Ru(SnPh_3)(PPh_3)(CO)_2(i\text{-Pr–DAB})]^{\bullet}$, obtained by irradiation of $[Ru(SnPh_3)_2(CO)_2(i\text{-Pr–DAB})]$ in the presence of triphenylphosphane.[3] The other radical fragment, $[RuCp(CO)_2]^{\bullet}$, which was also formed by the homolysis of the Ru–Ru bond, was not observed. However, on irriadiation of **1** in toluene containing an excess of nitrosodurene, a different radical species was formed, which was identified as the nitrosodurene-trapped $[RuCp(CO)_2]^{\bullet}$ radical.[12] Exactly the same spectrum was recorded upon irradiation of **2** under the same conditions, proving that in both cases homolytic Ru–Ru bond splitting is the primary photochemical process.

In situ laser irradiation (λ_{exc} = 514.5 nm) of **1** in dichloromethane in an IR spectrometer at room temperature caused the appearance of several new bands in the CO stretching region, while those of the starting compound decreased in intensity. Initially, two bands appeared at 2056 and 2005 cm^{-1}, accompanied by three other bands at 1991, 1965 and 1936 cm^{-1}. The former two bands are assigned to $[RuCp(Cl)(CO)_2]$, in good agreement with the literature values of 2057 and 2009 cm^{-1} in CCl_4.[13] The latter three bands are attributed to $[Ru(SnPh_3)(CO)_2(i\text{-Pr–DAB})]_2$, a product which also results from photolysis of $[Ru(SnPh_3)_2(CO)_2(i\text{-Pr–DAB})]$.[3] In addition, a small peak was detected at 1773 cm^{-1}. It has been assigned to $[RuCp(CO)_2]_2$, its other ν(CO) bands being obscured by the previously mentioned bands.

On prolonged irradiation of the dichloromethane solution of **1**, new bands appeared at 2033 and 1974 cm^{-1} at the expense of the peaks belonging to $[Ru(SnPh_3)(CO)_2(i\text{-Pr–DAB})]_2$. These IR peaks and an absorption band at ca. 440 nm reveal the formation of $[Ru(Cl)(SnPh_3)(CO)_2(i\text{-Pr–DAB})]$, in agreement with literature data for this complex.[3] The dichloromethane solvent apparently does not act as an efficient radical scavenger, allowing the $[Ru(SnPh_3)(CO)_2(i\text{-Pr–DAB})]^{\bullet}$ and $[RuCp(CO)_2]^{\bullet}$ radicals to dimerise before chlorine abstraction from the solvent takes place. This applies particularly to the former radical. The photochemical quantum yield of this reaction was determined, and appeared to be rather high (0.71). These data show that σ→π* excitation of **1** causes homolysis of the Ru–Ru bond, followed by dimerisation or reaction with the solvent (Scheme 1). The Ru–Sn bond remains unaffected.

Irradiation (λ_{exc} = 514.5 nm) of **2** in spin trapping CCl_4 at 263 K gave rise to several new ν(CO) bands belonging to two chlorinated products (Scheme 1). The bands at 2058 and 2009 cm^{-1} belong to $[RuCp(Cl)(CO)_2]$, in agreement with literature data.[13] The second product [ν(CO) at 1974, 1953, 1923 and 1767 cm^{-1}] is assigned to

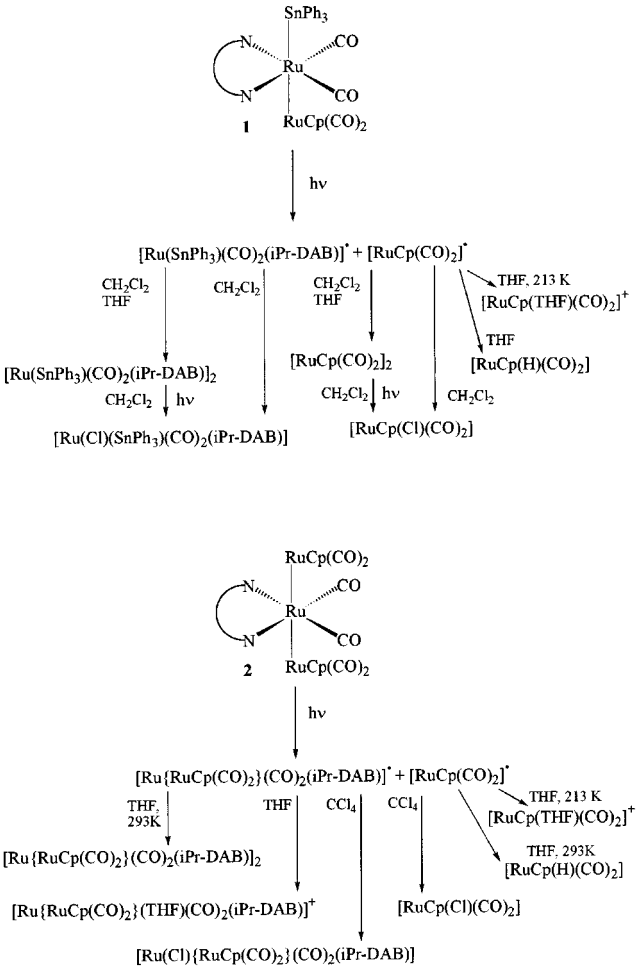
Table 3. Spectroscopic data of complexes **1** and **2** and their photoproducts formed upon 514.5 nm irradiation

Compound	ν(CO) (cm^{-1})	λ_{max} (nm)	solvent; temperature
1	1993m, 1961s, 1933s, 1920sh	308, 334, 384, 571	CH_2Cl_2; 293 K
$[RuCp(Cl)(CO)_2]$	2056, 2005		
$[Ru(Cl)(SnPh_3)(CO)_2(i\text{-Pr–DAB})]$	2032, 1974	≈440	
$[Ru(SnPh_3)(CO)_2(i\text{-Pr–DAB})]_2$	1991w, 1965m, 1936s		
$[RuCp(CO)_2]_2$	1773[a]		
1	1991m, 1958s, 1931s, 1915w		THF; 213 K
$[RuCp(THF)(CO)_2]^+$	2045, 1991		
$[RuCp(H)(CO)_2]$	2026, 1959		
$[Ru(SnPh_3)(CO)_2(i\text{-Pr–DAB})]_2$	1991w, 1959m, 1932s		
$[RuCp(CO)_2]_2$	1991, 1776[a]		
1	1993m, 1960s, 1933s, 1918w	308, 333, 382, 570	THF; 293 K
unassigned	2037, 2010		
$[RuCp(H)(CO)_2]$	2022, 1961		
$[Ru(SnPh_3)(CO)_2(i\text{-Pr–DAB})]_2$	1991w, 1961m, 1935s	385, 690	
$[RuCp(CO)_2]_2$	1991, 1961, 1935, 1783		
2	1996w, 1971s, 1948s, 1929s, 1922sh, 1898w		CCl_4; 263 K
$[RuCp(Cl)(CO)_2]$	2058, 2009		
$[Ru(Cl)\{RuCp(CO)_2\}(CO)_2(i\text{-Pr–DAB})]$	1974s, 1953m, 1923w, 1767w		
2	1990w, 1965s, 1945s, 1924s, 1894w		THF; 213 K
$[RuCp(THF)(CO)_2]^+$	2045, 1990		
$[Ru\{RuCp(CO)_2\}(THF)(CO)_2(i\text{-Pr–DAB})]^+$	1967s, 1943m, 1924w, 1763w		
2	1992w, 1967s, 1946s, 1926s, 1919sh, 1897w	350, 462, 604	THF; 293 K
$[RuCp(H)(CO)_2]$	2023, 1959		
$[Ru\{RuCp(CO)_2\}(THF)(CO)_2(i\text{-Pr–DAB})]^+$	1972s, 1959m, 1925w, 1764w		
$[Ru\{RuCp(CO)_2\}(CO)_2(i\text{-Pr–DAB})]_2$	1988, 1959, 1940	495, 703	
Reference compounds			
$[Ru(SnPh_3)(CO)_2(i\text{-Pr–DAB})]_2$	1988w, 1963m, 1934s	385, 690	THF[b]
$[[Ru(OTf)(SnPh_3)(CO)_2(i\text{-Pr–DAB})]$	2040, 1981		THF[b]
$[RuCp(CO)_2]_2$	2009w, 1997s, 1967m, 1955m, 1936s, 1783s	265, 331	THF
$[RuCp(CO)_2]_2$	1992s, 1965w, 1948w, 1934w, 1778s		THF; 213 K
$[RuCp(CO)_2]_2$	2002s, 1966s, 1936m, 1773s		CH_2Cl_2
$[RuCp(H)(CO)_2]$	2032, 1974		Heptane[c]
$[RuCp(H)(CO)_2]$	2022, 1960		THF
$[RuCp(H)(CO)_2]$	2025, 1953		CH_2Cl_2
$[RuCp(Cl)(CO)_2]$	2057, 2009		CCl_4[d]
$[RuCp(THF)(CO)_2]^+$	2048, 1995		THF[e]
$[Ru(Cl)(SnPh_3)(CO)_2(i\text{-Pr–DAB})]$	2033, 1974		CH_2Cl_2[f]

[a] The other ν(CO) bands are obscured by those of the other photoproducts. – [b] Ref.[3] – [c] Ref.[17] – [d] Ref.[13] – [e] With added NBu_4PF_6 electrolyte. – [f] Ref.[5]

$[Ru(Cl)\{RuCp(CO)_2\}(CO)_2(i\text{-Pr–DAB})]$. The interesting feature of this product is the ν(CO) band due to a bridging carbonyl group (1767 cm^{-1}). We assume that one carbonyl group occupies a Ru–Ru bridging position. The quantum yield of the photochemical reaction of **2** was determined to be 1.16 in CH_2Cl_2. This quantum yield, as well as that for **1** (see above), is much higher than that for $[Ru(SnPh_3)_2(CO)_2(i\text{-Pr–DAB})]$ (0.23), [3] which implies that the Ru–Ru bond is weaker than the Ru–Sn bond. A quantum efficiency higher than 1 may indicate that the radicals formed upon homolytic Ru–Ru bond splitting react with the starting compound in an electron transfer chain reaction. Similar observations were made for several related rhenium, manganese and ruthenium complexes.[14–16]

For comparison, the photochemistry of **1** and **2** was also studied in THF in the absence of radical traps (Scheme 1). In this case the major photoproduct of **1** was clearly $[Ru(SnPh_3)(CO)_2(i\text{-Pr–DAB})]_2$ [ν(CO) = 1991, 1961, 1935 cm^{-1}, λ_{max} = 385, 690 nm]. The other expected dimeric product $[RuCp(CO)_2]_2$ was only formed in a minor amount. In addition, some other bands were observed at 2037, 2022 and 2010 cm^{-1}. These peaks increased in intensity on pro-



Scheme 1. Photochemical pathways of **1** and **2** in various solvents

longed irradiation, at the expense of those belonging to $[RuCp(CO)_2]_2$. The band at 2022 cm^{-1}, together with a band at 1960 cm^{-1} (hidden under the 1961 cm^{-1} band), is assigned to $[RuCp(H)(CO)_2]$, formed by the hydrogen abstraction from the solvent by $[RuCp(CO)_2]^{\bullet}$. The same ν(CO) values were found for $[RuCp(H)(CO)_2]$ synthesized from $Ru_3(CO)_{12}$ and cyclopentadiene.[17] Similar reactions of $[RuCp(CO)_2]^{\bullet}$ were reported recently.[18] The assignment of the 2037 and 2010 cm^{-1} bands is not entirely clear, but they must also belong to a species containing the $[RuCp(CO)_2]$ moiety. On irradiation at 213 K in THF the major products were the same. However, the 2037 and 2010 cm^{-1} bands were absent, whereas a new product was observed with bands at 2045 and 1991 cm^{-1}, fitting nicely with data for the $[RuCp(THF)(CO)_2]^+$ cation (Table 3).

Irradiation of a THF solution of **2** also yielded a mixture of products. Clearly visible are ν(CO) peaks at 2023 and 1960 cm^{-1} due to $[RuCp(H)(CO)_2]$. In addition, there is a series of peaks at 1967, 1943, 1924, and 1766 cm^{-1}, which probably belong to $[Ru\{RuCp(CO)_2\}(THF)(CO)_2(i\text{-Pr–DAB})]^+$, in close correspondence with the ν(CO) values for the chlorinated derivative formed in CCl_4 (vide supra). A third product with ν(CO) bands at 1988, 1960, and 1940 cm^{-1} is proposed to be $[Ru\{RuCp(CO)_2\}(CO)_2(i\text{-Pr–DAB})]_2$. This assignment is not only in agreement with the behaviour of **1**, but is also supported by the investigation of this reaction with UV/Vis spectroscopy. The product spectrum exhibits a low energy absorption band at 703 nm which is characteristic for such a dimer (Figure 3).[3] At low temperatures (213 K) no dimeric products were observed, but only the cationic species $[Ru\{RuCp(CO)_2\}(THF)(CO)_2(i\text{-Pr–DAB})]^+$ and $[RuCp(THF)(CO)_2]^+$. Apparently, the increased viscosity of the solvent at low temperatures hampers the dimerisation of the radical fragments.

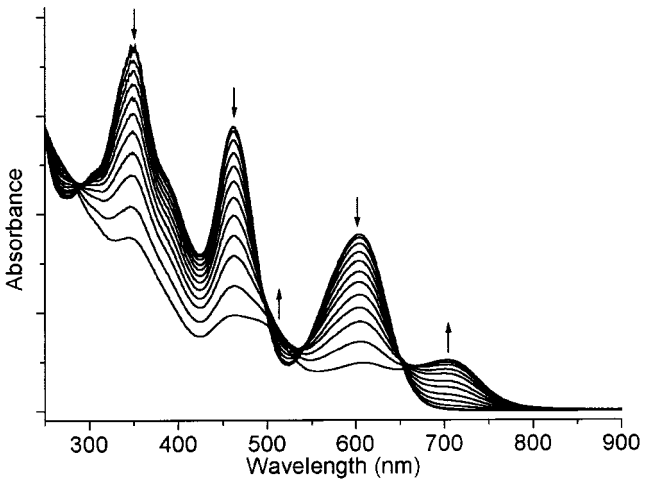


Figure 3. UV/Vis spectral changes accompanying 514.5 nm irradiation of **2** in THF at room temperature

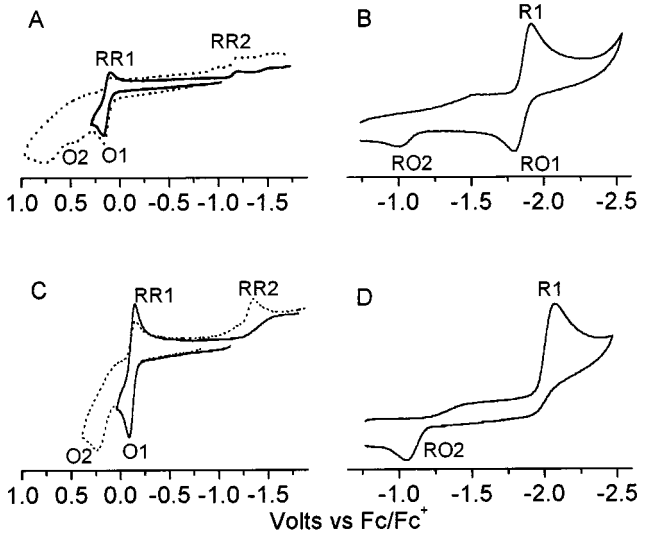


Figure 4. Cyclic voltammograms showing the oxidation of **1** (A) and **2** (C), and the reduction of **1** (B) and **2** (D) in butyronitrile solutions at 213 K

Redox Properties and Reactivity

The complexes **1** and **2** were subjected to a (spectro)electrochemical study. Cyclic voltammograms were recorded at variable temperatures to determine the electrode potentials and to study the reversibility of the corresponding redox processes (Figure 4, Table 4). The nature of the redox products was investigated by IR spectroelectrochemistry. The spectroscopic data are collected in Table 5.

Table 4. Reduction and oxidation potentials (V vs. Fc/Fc^+)

Compound	$E_{p,c}$	$E_{p,a}$	ΔE_p[a]	conditions	reference
1	–1.98	0.16		THF/293 K	this work
1	–1.89[b]	0.17	0.07	*n*-PrCN/213 K	this work
2	–2.04	0.06		THF/293 K	this work
2	–2.11	–0.09	0.06	*n*-PrCN/213 K	this work
$[Ru\{RuCp(CO)_2\}_2(CO)_2(i\text{-Pr–DAB})]^{+\bullet}$		0.24		*n*-PrCN/213 K	this work
$[RuCp(CO)_2]_2$	–2.57	0.37		THF/293 K	this work[c]
$[RuCp(THF)(CO)_2]^+$	–1.47			THF/293 K	this work[c]
$[RuCp(CO)_2]^-$		–1.27		THF/293 K	this work[c]
$[Ru(SnPh_3)_2(CO)_2(i\text{-Pr–DAB})]$	–1.91	0.34			[5]
$[Ru(SnPh_3)(CO)_2(i\text{-Pr–DAB})]^-$		–1.07		THF/293 K	[5]

[a] Anodic process, $\Delta E_p(Fc/Fc^+) = 0.06$ V. – [b] $\Delta E_p = 0.12$ V. – [c] The redox behaviour of the dimer $[RuCp(CO)_2]_2$ in THF was studied independently by cyclic voltammetry and IR spectroelectrochemistry. Literature data in ref.[31,32]

Table 5. IR spectroelectrochemical data for reduction (THF, room temperature) and oxidation (*n*-PrCN, 193 K) products of **1** and **2**

Compound	ν(CO) (cm^{-1})	conditions	reference
1	1992m, 1958s, 1930s, 1913w	*n*-PrCN/193 K	this work
1	1992m, 1969s, 1932s, 1916w	THF/293 K	this work
2	1989w, 1965s, 1946s, 1924s, 1910sh, 1897w	*n*-PrCN/193 K	this work
2	1992w, 1967s, 1946s, 1926s, 1915sh, 1893w	THF/293 K	this work
$[RuCp(n\text{-PrCN})(CO)_2]^+$	2079, 2031	*n*-PrCN/193 K	this work
$[RuCp(MeCN)(CO)_2]^+$	2090, 2044	CH_2Cl_2/293 K	[19]
$[RuCp(CO)_2]^-$	1887, 1801	THF/293 K	this work
$[Ru(SnPh_3)(n\text{-PrCN})(CO)_2(i\text{-Pr–DAB})]^+$	2041, 1987	*n*-PrCN/193 K	this work
$[Ru(SnPh_3)(OTf)(CO)_2(i\text{-Pr–DAB})]$	2040, 1981	THF/293 K	[10]
$[Ru(SnPh_3)(CO)_2(i\text{-Pr–DAB})]^-$	1924, 1856	THF/293 K	[5]
$[Ru\{RuCp(CO)_2\}_2(CO)_2(i\text{-Pr–DAB})]^{+\bullet}$	2021w, 1997s, 1981s, 1962s, 1930w	*n*-PrCN/193 K	this work
$[Ru(n\text{-Pr–CN})_2(CO)_2(i\text{-Pr–DAB})]^{2+\bullet}$	2116, 2060sh	*n*-PrCN/193 K	this work
$[Ru\{RuCp(CO)_2\}(CO)_2(i\text{-Pr–DAB})]^-$	1927, 1847	*n*-PrCN/193 K	this work

At room temperature, the oxidation of **1** is chemically completely irreversible in THF. However, at 213 K in butyronitrile two oxidation waves became apparent, with the first oxidation process (O1) being partly reversible (I_c/I_a = 0.7) on the voltammetric timescale at the scan rate of 100 mV/s (Figure 4, A). The following anodic step (O2) is completely irreversible. The fact that step O1 was found to be more than 150 mV more negatively than that of $[Ru(SnPh_3)_2(CO)_2(i\text{-Pr–DAB})]$[5] indicates that the oxidation of **1** is significantly located on the $[RuCp(CO)_2]$ moiety. Oxidising **1** at O1 led to the appearance of four bands in the IR carbonyl-stretching region. The product formation was independent of the temperature employed. The primary one-electron oxidised product detected at RR1 (Figure 4, A) at 213 K by cyclic voltammetry, is not detectable on the spectroelectrochemical timescale of seconds to minutes. Of the four bands, those at 2079 and 2031 cm^{-1} are attributed to $[RuCp(n\text{-PrCN})(CO)_2]^+$, in accordance with both the literature values of 2090 and 2044 cm^{-1} for $[RuCp(MeCN)(CO)_2]^+$ in CH_2Cl_2[19] and the observation that upon electrochemical oxidation of $[RuCp(CO)_2]_2$ in *n*-PrCN a product with identical ν(CO) wavenumbers was formed (Table 4). The two remaining bands (2042 and 1987 cm^{-1}) must be due to $[Ru(SnPh_3)(n\text{-PrCN})(CO)_2(i\text{-Pr–DAB})]^+$, as their wavenumbers are close to the values found for $[Ru(OTf)(SnPh_3)(CO)_2(i\text{-Pr–DAB})]$ (2041 and 1981 cm^{-1} in THF).[10] Taking these data into account, we propose the following oxidation path for **1**: initially, the unstable radical cation ($\mathbf{1}^{+\bullet}$) is formed, which rapidly splits to give the $[Ru(SnPh_3)(n\text{-PrCN})(CO)_2(i\text{-Pr–DAB})]^+$ cation and the $[RuCp(CO)_2]^\bullet$ radical. The latter species also binds a solvent molecule and converts to the corresponding cation in a second oxidation step. On the reverse scan, small cathodic peaks were observed (RR2, Figure 4, A), but the corresponding processes were not investigated in detail.

The oxidation of **2** is completely irreversible in THF at room temperature. However, at 213 K in butyronitrile at a v = 100 mV/s the first oxidation process (O1) is completely reversible, as indicated by ΔE_p = 61 mV and I_c/I_a = 1 (Figure 4, C). For equimolar solutions of **1** and **2** virtually the same anodic current was observed at E_a(O1) at 213 K. Considering similar values for the diffusion coefficients of **1** and **2,** this reveals that also the oxidation of **2** at low temperatures is a one-electron process. Indeed, the initial oxidation product of **2** observed in the corresponding IR-spectroelectrochemical experiment in *n*-PrCN at 193 K, exhibits a ν(CO) pattern very close to that of the parent compound **2**, but shifted by ca. 35 cm^{-1} to larger wavenumbers [ν(CO) at

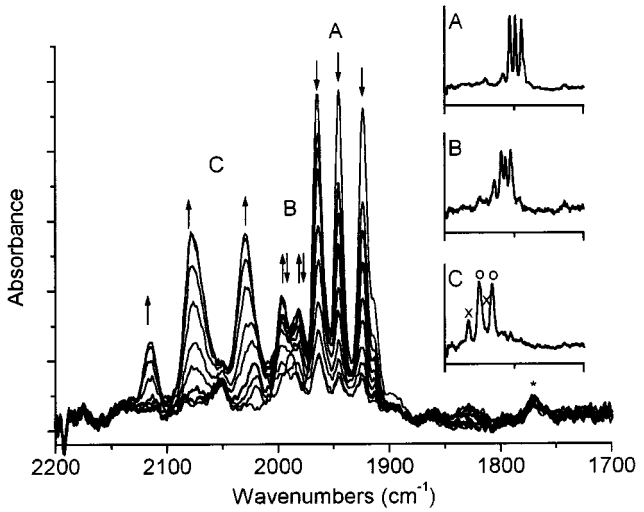


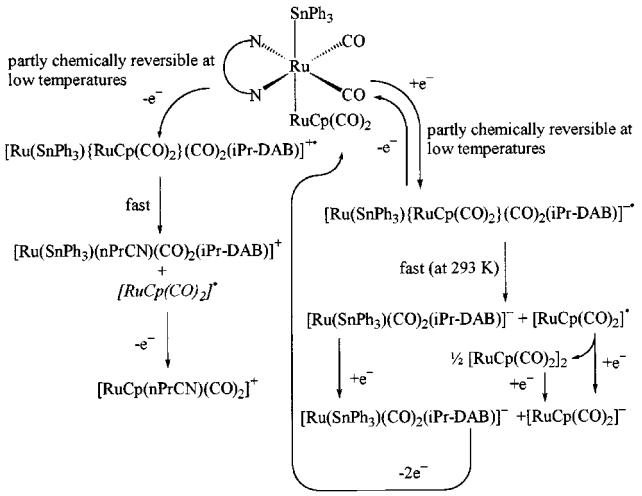
Figure 5. IR spectral changes upon oxidation of **2** in butyronitrile at 193 K. The insets are the parent compound (A), the corresponding radical cation (B), and the secondary oxidation products $[Ru(n\text{-}PrCN)_2(CO)_2(i\text{-}PrDAB)]^{2+}$ and $[RuCp(n\text{-}PrCN)(CO)_2]^+$, indicated by × and o, respectively (C). The asterisk denotes a small $[RuCp(CO)_2]_2$ impurity in the starting compound

2021, 1997, 1981, 1962 and 1930 cm^{-1}, Figure 5]. This points to a similar molecular structure of the one-electron-oxidised product compared to that of neutral **2**. We therefore concluded that at low temperatures the one-electron-oxidised product $[Ru\{RuCp(CO)_2\}_2(CO)_2(i\text{-}Pr\text{–}DAB)]^{+\bullet}$ is stable both on the voltammetric and the spectro-electrochemical time scales. This is the first time that a stable radical cation has been spectroscopically characterised for complexes $[Ru(L^1)(L^2)(CO)_2(\alpha\text{-diimine})]$, albeit at low temperatures.

The second anodic step of **2** (O2) became separated from the reversible O1 step at 213 K, but remained completely irreversible (Figure 4, C). The corresponding oxidation of $\mathbf{2}^{+\bullet}$, followed in situ by IR-spectroscopy at 193 K, produced species with ν(CO) at 2116, 2060 and 2079, 2031 cm^{-1}. The latter two bands are again attributable to $[RuCp(n\text{-}PrCN)(CO)_2]^+$, while the former two bands must be due to a highly positively charged species, e.g. $[Ru(n\text{-}PrCN)_2(CO)_2(i\text{-}Pr\text{–}DAB)]^{2+}$. The secondary oxidation products of $\mathbf{2}^{+\bullet}$ were reduced back at RR2, resulting in a mixture of the parent complex **2** and $[RuCp(CO)_2]_2$.

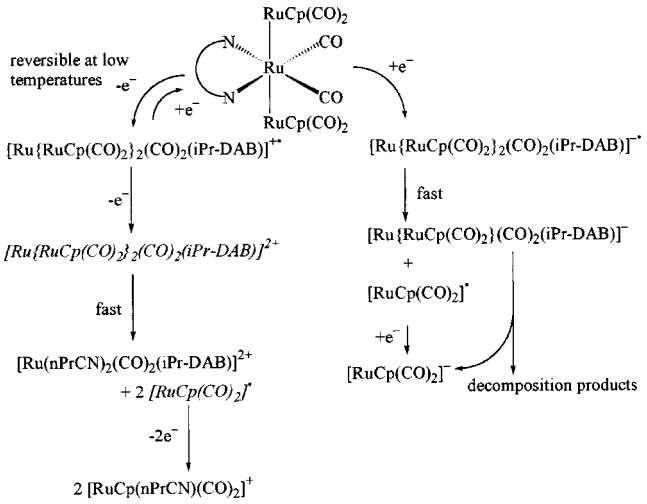
In THF at room temperature, the irreversible reduction of **1** at R1 (see Table 4) produced the IR-detectable anions $[Ru(SnPh_3)(CO)_2(i\text{-}Pr\text{–}DAB)]^-$ [ν(CO) at 1924 and 1855 cm^{-1}][5] and $[RuCp(CO)_2]^-$ [ν(CO) at 1887 and 1801 cm^{-1}, close to the literature data[20]]. In addition to these main bands a smaller ν(CO) peak arose at 1782 cm^{-1}. This peak can be assigned to the dimer $[RuCp(CO)_2]_2$, its remaining peaks being hidden under the other ν(CO) bands (see Table 4). The reduction path of **1** is therefore proposed to involve initially an unstable radical anion, which rapidly falls apart into the stable $[Ru(SnPh_3)(CO)_2(i\text{-}Pr\text{–}DAB]^-$ anion and the $[RuCp(CO)_2]^\bullet$ radical (see Scheme 1). The latter species partly dimerises, but the majority is reduced to the $[RuCp(CO)_2]^-$ anion at the reduction potential of **1**. The fact that the latter reduction potential is similar to that of $[Ru(SnPh_3)_2(CO)_2(i\text{-}Pr\text{–}DAB)]$[5] indicates that reduction takes place primarily on the Ru(*i*-Pr–DAB) moiety.

The radical anion $\mathbf{1}^{-\bullet}$ could only be detected by cyclic voltammetry in butyronitrile at sufficiently low temperatures (Figure 4, B). At 213 K the reduction of **1** is a chemically partly reversible one-electron process with I_a/I_c = 0.78 at v = 100 mV/s (see Figure 4, B). The final reduction products $[Ru(SnPh_3)(CO)_2(i\text{-}Pr\text{–}DAB]^-$ and $[RuCp(CO)_2]^-$ are oxidised at similar electrode potentials (Table 4). Therefore, on the reverse anodic scan the oxidation of the two anions cannot be distinguished and appears as a single anodic peak (RO2) at –1.18 V (THF, room temperature) and –1.00 V vs Fc/Fc^+ (butyronitrile, 213 K, Figure 4, B). IR spectroelectrochemistry revealed that reoxidation of both anions at room temperature at RO2 mainly regenerates the parent complex **1**. In addition, a minor amount of the dimer $[Ru(SnPh_3)(CO)_2(i\text{-}Pr\text{–}DAB]_2$ was produced at the end of the reoxidation. Obviously, $[Ru(SnPh_3)(CO)_2(i\text{-}Pr\text{–}DAB]^-$ was present in a small excess in the thin solution layer after the reduction, and therefore, once all $[RuCp(CO)_2]^-$ had been consumed in the course of the parallel reoxidation, the remaining $[Ru(SnPh_3)(CO)_2(i\text{-}Pr\text{–}DAB]^-$ was oxidised to give the dimer by a previously reported ECEC path.[5]



Scheme 2. Reduction and oxidation pathways of **1** in *n*-PrCN

The reduction of **2** at R1 (Figure 4, D, Table 4) is completely chemically irreversible at moderate voltammetric scan rates, independent of temperatures between 293 and 193 K. Corresponding IR spectroelectrochemical experiments again showed the formation of the $[RuCp(CO)_2]^-$ anion [ν(CO) at 1887 and 1801 cm^{-1}]. Two other ν(CO) bands observed at 1927 and 1847 cm^{-1} are tentatively ascribed to the thermally unstable $[Ru\{RuCp(CO)_2\}(CO)_2(i\text{-}Pr\text{–}DAB]^-$ anion. Attempts to prevent its decomposition by carrying out the reduction of **2** in butyronitrile at 193 K were not successful. Considering the combined voltammetric and spectroelectrochemical results, we conclude that the reduction of **2** initially yields the radical anion $[Ru\{RuCp(CO)_2\}_2(CO)_2(i\text{-}Pr\text{–}DAB)]^{-\bullet}$, which rapidly dissociates into $[Ru\{RuCp(CO)_2\}(CO)_2(i\text{-}Pr\text{–}DAB]^-$ and $[RuCp(CO)_2]^\bullet$. The latter radical further reduces to the cor-



Scheme 3. Reduction and oxidation pathways of **2** in *n*-PrCN

responding anion. No dimerisation of the latter radical was observed in this case, probably due to the more negative reduction potential of **2** (see Table 4). The former anion is thermally unstable and dissociates into another equivalent of $[RuCp(CO)_2]^-$ and unidentified carbonyl products. This decomposition also explains the fact that the reverse oxidation at the anodic peak RO2 at –1.27 V (THF, room temperature) and –1.06 V vs Fc/Fc^+ (butyronitrile, 213 K, Figure 4, D) only concerns the $[RuCp(CO)_2]^-$ anion, yielding mainly the $[RuCp(CO)_2]_2$ dimer instead of recovering the parent complex **2**.

The redox behaviour of the complexes **1** (Scheme 2) and **2** (Scheme 3) differ considerably from that of the complexes $[Ru(L^1)(L^2)(CO)_2(i\text{-Pr–DAB})]$ (L^1, L^2 = $GePh_3$, $SnPh_3$, $PbPh_3$; not all combinations were investigated) previously studied in our laboratory.[5] The latter complexes are reduced reversibly, even at room temperature, producing fairly stable radical anions. In contrast, their oxidation is completely irreversible in the temperature range available. Apparently, coordination of the $SnPh_3$ axial ligands contributes significantly to the stability of the radical anion, mainly due to the strong delocalisation of the SOMO over the $(Ph_3Sn)_2Ru(i\text{-Pr–DAB})$ moiety and also due to the strong Ru–Sn bond.[1] On the other hand, the $[RuCp(CO)_2]$ units exert a stabilising influence on the radical cation, where the π-donor Cp-rings compensate for the reduced electron density on the axial ruthenium atom(s), compared to the neutral precursors. This property of Cp-rings has been recognised e.g. in the complexes $[RuCpX(i\text{-Pr–DAB})]$ (X = Cl, OTf).[21]

Concluding Remarks

The incorporation of one or two strongly donating $[RuCp(CO)_2]$ groups as axial ligands in $[Ru(L^1)(L^2)(CO)_2(i\text{-Pr–DAB})]$ yields complexes with a relatively high-lying $\sigma(L^1\text{–Ru–}L^2)$ HOMO. This is reflected in relatively negative oxidation potentials of **1** and **2** compared to other $[Ru(L^1)(L^2)(CO)_2(i\text{-Pr–DAB})]$ complexes.[1,2] As a further consequence, the emission shifts to the near infrared (NIR) spectral region, with lifetimes in the order of 10 μs at 80 K. This property is very interesting from the viewpoint of the potential use of this type of complexes as NIR emitting labels.[22–25] However, the photochemical reactivity of the studied complexes, which involves homolytic cleavage of a Ru–Ru bond as the primary photoprocess, presents a serious obstacle for such applications. The $[RuCp(CO)_2]$ group(s) also split off upon electrochemical reduction and oxidation of the complexes. The most remarkable difference between the redox behaviour of **1** and **2** and that of the previously studied $[Ru(L^1)(L^2)(CO)_2(i\text{-Pr–DAB})]$ complexes[5], is the stabilising influence of the $[RuCp(CO)_2]$ groups on the one-electron-oxidised products.

Experimental Section

General: $[Ru_3(CO)_{12}]$ (ABCR), I_2 (Merck), $SnClPh_3$ (Aldrich) and $[Ru(CO)_2Cp]_2$ (Strem) were used as received. *N,N′*-diisopropyl-1,4-diaza-1,3-butadiene (*i*-Pr–DAB),[26] $[RuCp(H)(CO)_2]$,[17] $[RuCp(CO)_2]_2$,[17] $[Ru(Cl)(SnPh_3)(CO)_2(i\text{-Pr–DAB})]$,[10] and $[Ru(I)_2(CO)_2(i\text{-Pr–DAB})]$[27] were prepared according to literature procedures. Solvents purchased from Acros (THF, 2-MeTHF, hexanes, dichloromethane) and Merck (heptane) were dried on and distilled from the appropriate drying agent. Silica gel (kieselgel 60, Merck, 70–230 mesh) for column chromatography was dried and activated by heating in vacuo at 160°C overnight. All syntheses and measurements were performed under a nitrogen atmosphere using standard Schlenk techniques. – UV/Vis: Varian Cary 4E and Hewlett-Packard 8453. – IR: Bio-Rad FTS 7 and FTS 60A, the latter equipped with a liquid nitrogen-cooled MCT detector. – NMR: Bruker AMX300 (^1H and ^{13}C) and DRX300 (^{119}Sn). – Resonance Raman: Dilor XY spectrometer, with an SP2040E Ar^+-laser as excitation source and a Wright Instruments CCD-detector. – EPR: Varian E-104A. – FAB-MS: JEOL JMS SX/SX102A four-sector mass spectrometer, coupled to a JEOL MS-MP7000 data system. Elemental analyses were performed at H. Kolbe Mikroanalytisches Laboratorium in Mülheim an der Ruhr.

Time-resolved emission spectra were recorded at 80 K in an Oxford Instruments cryostat. A Spectra Physics GCR-3 Nd:YAG laser, operating at 10 Hz was used as the excitation source. The desired wavelength (532 nm) was obtained by frequency doubling of the 1064 nm fundamental. The setup has been described elsewhere.[16]

Quantum yields of the photoreactions were determined from the disappearance of the parent complexes, following the decay of their lowest-energy absorption band. For this purpose the sample was irradiated within the UV/Vis spectrophotometer with one of the laser lines of an SP2025 Ar^+-ion laser through an optical fiber in a previously described setup.[16]

Cyclic voltammograms (CV) of approximately 10^{-3} M solutions of the parent complexes were recorded with added NBu_4PF_6 (0.1–0.3 M) as supporting electrolyte in a gas-tight, single-compartment, three-electrode cell equipped with platinum disk working (apparent surface area 0.42 mm^2), platinum gauze auxiliary and silver wire pseudoreference electrodes. The cell was connected to a computer-controlled PAR Model 283 potentiostat. Redox potentials are reported relative to $E_{1/2}(Fc/Fc^+)$ ($E_{1/2}$ = 0.575 and 0.43 V vs. SCE in THF and CH_3CN, respectively). Ferrocene was added as internal standard.[28] The scan speed was 100 mV/s. IR-spectroelectrochem-

ical measurements at variable temperatures were performed with ca. 10^{-2} M solutions in previously described optically transparent thin-layer electrochemical (OTTLE) cells.[29,30] The potential was controlled during these measurements by a PA4 (EKOM, Czech Republic) potentiostat.

[Ru(SnPh$_3$)[RuCp(CO)$_2$](CO)$_2$(*i*-Pr–DAB)] (1): [RuCp(CO)$_2$]$_2$ (215.5 mg, 0.48 mmol) was dissolved in 30 mL THF. An excess of 0.6 mL $NaK_{2.8}$ was added through a syringe under stirring. The yellow colour of the reaction mixture changed to brown yellow during the next 45 min, after which IR spectra showed virtually complete conversion into [RuCp(CO)$_2$]$^-$.[20] The resulting solution was added gradually through a syringe to a solution of [Ru(Cl)(SnPh$_3$)(CO)$_2$(*i*-Pr–DAB)] (181.7 mg, 0.24 mmol) in 30 mL THF under the exclusion of light. The reaction mixture turned purple immediately. The solvent was evaporated and the product was purified by column chromatography on activated silica, using a CH_2Cl_2/hexane eluent (1:3 v/v). The product elutes prior to the [RuCp(CO)$_2$]$_2$ main impurity. It was obtained as a purple microcrystalline solid in approximately 50% yield. – ^{1}H NMR ($CDCl_3$): δ = 0.99 {d, 6 H, ^3J = 6.5 Hz, CH(C*H*$_3$)$_2$ pointing toward SnPh$_3$, assignment based on comparison with the ^{1}H NMR spectra of [Ru(SnPh$_3$)$_2$(CO)$_2$(*i*-Pr–DAB)] (δ = 0.97)[1] and **2** (vide infra)}; 1.19 [d, 6 H, ^3J = 6.5 Hz, CH(C*H*$_3$)$_2$ pointing toward RuCp(CO)$_2$], 4.40 [sept, 2 H, ^3J = 6.6 Hz, C*H*(CH$_3$)$_2$], 5.22 (s, 5 H, C_5H_5), 7.27 (m, 9 H, *o*/*p*-SnC_6H_5); 7.38 (m, 6 H, *m*-SnC_6H_5); 7.87 (85% s, 15% d, 2 H, $^4J_{Sn-H}$ = 21 Hz, imine CH). – ^{13}C NMR APT (C_6D_6): δ = 25.1, 24.5 [CH(*C*H$_3$)$_2$], 63.0 [*C*H(CH$_3$)$_2$], 86.4 (C_5H_5), 128.0, 127.7 (s, *m*/*p*-SnC_6H_5), 137.8 (85% s, 15%d, J_{Sn-C} = 34 Hz, *o*-SnC_6H_5), 144.5 (s, *ipso*-SnC_6H_5), 145.4 (s, C=N), 205.7 (s, Ru$_{axial}$–CO), 209.7 (s, Ru$_{central}$–CO). – ^{119}Sn NMR ([D$_6$]acetone): δ = –45.6. – IR (THF): See Table 1. – UV/Vis: See Table 1. – FAB-MS; *m*/*z*: [M$^+$] not detected, 813 [M$^+$ – 2 CO], 764 [M$^+$ – Ph – CO], 649 [M$^+$ – RuCp(CO)$_2$].

[Ru[RuCp(CO)$_2$]$_2$(CO)$_2$(*i*-Pr–DAB)] (2): This compound was synthesized from [Ru(I)$_2$(CO)$_2$(*i*-Pr–DAB)] (103.8 mg, 0.19 mmol) following the same procedure as for **1**. It was obtained as a dark green microcrystalline solid in approximately 50% yield. – ^{1}H NMR ($CDCl_3$): δ = 1.21 [d, 12 H, ^3J = 6.6 Hz, CH(C*H*$_3$)$_2$], 4.36 [sept, 2 H, ^3J = 6.6 Hz, C*H*(CH$_3$)$_2$], 5.24 (s, 10 H, C_5H_5), 7.99 (s, 2 H, imine CH). – ^{13}C NMR APT (C_6D_6): δ = 24.8 [CH(*C*H$_3$)$_2$], 61.6 [*C*H(CH$_3$)$_2$], 86.4 (C_5H_5), 143.7 (C=N), 205.7 (Ru$_{axial}$–CO), 214.6 (Ru$_{central}$–CO). – IR (THF): See Table 1. UV/Vis: See Table 1. – FAB-MS; *m*/*z*: 743 [M$^+$], 521 [M$^+$ – RuCp(CO)$_2$]. – $C_{24}H_{26}N_2O_6Ru_3$ (869.52): calcd. C 38.87, H 3.53, N 3.78; found C 38.69, H 3.36, N 3.70.

[1] M. P. Aarnts, M. P. Wilms, K. Peelen, J. Fraanje, K. Goubitz, F. Hartl, D. J. Stufkens, E. J. Baerends, A. Vlček, Jr., *Inorg. Chem.* **1996,** *35*, 5468–5477.

[2] M. P. Aarnts, D. J. Stufkens, M. P. Wilms, E. J. Baerends, A. Vlček, Jr., I. P. Clark, M. W. George, J. J. Turner, *Chem. Eur. J.* **1996,** *2*, 1556–1565.

[3] M. P. Aarnts, D. J. Stufkens, A. Vlček, Jr., *Inorg. Chim. Acta* **1997,** *266*, 37–46.

[4] M. P. Aarnts, M. P. Wilms, D. J. Stufkens, E. J. Baerends, A. Vlček, Jr, *Organometallics* **1997,** *16*, 2055–2062.

[5] M. P. Aarnts, F. Hartl, K. Peelen, D. J. Stufkens, C. Amatore, J.-N. Verpeaux, *Organometallics* **1997,** *16*, 4686–4695.

[6] H. A. Nieuwenhuis, D. J. Stufkens, A. Oskam, *Inorg. Chem.* **1994,** *33*, 3212–3217.

[7] H. A. Nieuwenhuis, D. J. Stufkens, A. Vlček, Jr., *Inorg. Chem.* **1995,** *34*, 3879–3886.

[8] H. A. Nieuwenhuis, D. J. Stufkens, R. A. McNicholl, A. H. R. Al-Obaidi, C. G. Coates, S. E. J. Bell, J. J. McGarvey, J. Westwell, M. W. George, J. J. Turner, *J. Am. Chem. Soc.* **1995,** *117*, 5579–5585.

[9] M. P. Aarnts, A. Oskam, D. J. Stufkens, J. Fraanje, K. Goubitz, N. Veldman, A. L. Spek, *J. Organomet. Chem.* **1997,** *531*, 191–205.

[10] M. P. Aarnts, D. J. Stufkens, A. Oskam, J. Fraanje, K. Goubitz, *Inorg. Chim. Acta* **1997,** *256*, 93–105.

[11] R. W. Balk, D. J. Stufkens, A. Oskam, *J. Chem. Soc., Dalton Trans.* **1982**, 275–282.

[12] S. Sostero, D. Rehorek, E. Polo, O. Traverso, *Inorg. Chim. Acta* **1993,** *209*, 171–176.

[13] H. B. Abrahamson, M. C. Palazzotto, C. L. Reichel, M. S. Wrighton, *J. Am. Chem. Soc.* **1979,** *101*, 4123–4127.

[14] T. van der Graaf, R. M. J. Hofstra, P. G. M. Schilder, M. Rijkhoff, D. J. Stufkens, J. G. M. van der Linden, *Organometallics* **1991,** *10*, 3668–3679.

[15] H. A. Nieuwenhuis, M. C. E. van de Ven, D. J. Stufkens, A. Oskam, K. Goubitz, *Organometallics* **1995,** *14*, 780–788.

[16] C. J. Kleverlaan, D. J. Stufkens, I. P. Clark, M. W. George, J. J. Turner, D. M. Martino, H. van Willigen, A. Vlček, Jr., *J. Am. Chem. Soc.* **1998,** *120*, 10871–10879.

[17] A. P. Humphries, S. A. R. Knox, *J. Chem. Soc., Dalton Trans.* **1975**, 1710–1714.

[18] W. Macyk, A. Herdegen, A. Karocki, G. Stochel, Z. Stasicka, S. Sostero, O. Traverso, *J. Photochem. Photobiol. A: Chem.* **1997,** *103*, 221–226.

[19] A. Jungbauer, H. Behrens, *Z. Naturforsch. B* **1978,** *33*, 1083–1086.

[20] M. Brookhart, W. B. Studabaker, G. R. Husk, *Organometallics* **1987,** *6*, 1141–1145.

[21] B. de Klerk-Engels, F. Hartl, K. Vrieze, *Inorg. Chim. Acta* **1997,** *254*, 239–250.

[22] S. Akiyama, *Chem. Anal.* **1993,** *77*, 229–251.

[23] I. M. Warner, S. A. Soper, L. B. McGown, *Anal. Chem.* **1996,** *68*, 73R – 91R.

[24] D. C. Williams, *Anal. Chem.* **1995,** *67*, 3427–3432.

[25] G. Patonay, *Adv. Near-Infrared Meas.* **1993,** *1*, 113–138.

[26] H. Bock, H. tom Dieck, *Chem. Ber.* **1967,** *100*, 228–246.

[27] M. J. A. Kraakman, K. Vrieze, H. Kooijman, A. L. Spek, *Organometallics* **1992,** *11*, 3760–3773.

[28] G. Gritzner, J. Kůta, *Pure Appl. Chem.* **1984,** *56*, 461–466.

[29] M. Krejčík, M. Daněk, F. Hartl, *J. Electroanal. Chem. Interfacial Chem.* **1991,** *317*, 179–187.

[30] F. Hartl, H. Luyten, H. A. Nieuwenhuis, G. C. Schoemaker, *Appl. Spectroscopy* **1994,** *48*, 1522–1528.

[31] E. F. Dalton, S. Ching, R. W. Murray, *Inorg. Chem.* **1991,** *12*, 2642–2648.

[32] R. E. Dessy, P. M. Weissman, R. L. Pohl, *J. Am. Chem. Soc.* **1966,** *88*, 5117–5121.

Received September 10, 1999
[I99324]

How to Find Correlations Between Molecular Shape and Packing in a Molecular Crystal: Application of a Novel Strategy to Recognize *n*-Point Polyhedra in Three-Dimensional Space

Stefan Reichling[a] and Gottfried Huttner*[a]

Dedicated to Kurt Mislow, Princeton

Keywords: Crystal packing / Neural networks / Pattern recognition / Organometallic compounds / Close packing

The crystal structures of hundreds of thousands of molecular compounds have now been determined with the quantitative information being stored in large databases. Chemists are generally interested in that specific part of this information which refers to individual molecules. The packing of molecules and their spatial relation to each other is not the focus of interest, even though the material properties of a molecular crystal are determined by both the packing arrangement of the molecules and their specific properties. The lack of interest in packing has at least one obvious reason. It is difficult for the non-expert to find the appropriate packing categories when looking at a principally infinite lattice. A tool performing this search for individual categories of packing in an automatic manner would therefore be of general importance. The development and application of such a tool is described in this paper. Novel strategies to extract a set of n points forming a specific n-point polyhedron from a set of p points ($p > n$) is at its basis. Neural networks and second moment analysis are used as the methods of pattern recognition. In order to correlate packing and shape, second moment analysis of molecular shape is also used. This novel method is applied to three classes of organometallic compounds to determine whether the crystals formed by these compounds belong to any of the three classes *fcc*, *bcc*, or *hcp* in an idealized sense. A strong correlation is found between molecular shape and the membership or nonmembership of these classes. The corresponding program, including appropriate tools for visual representation, is available from the authors.

Introduction

The molecular concept is the basis of chemical reasoning. Even though it is quite complicated to define what a molecule really is, a well-trained chemist will immediately associate a structural representation with this idea and he or she may even take this representation as the idea itself. This kind of reduction has been, and still is, the basis of much of the development of the science of chemistry.

While in earlier days the structures of molecules had generally to be inferred from indirect reasoning, today there is an abundant wealth of structural information available, well-encoded in databases. As this information comes from three-dimensional diffraction analysis, the three-dimensional structures of all the molecules contained in such databases i.e. the coordinates of individual atoms are readily available, as is the mutual arrangement of these molecules within a crystal. While it is evident that such databases add much to the convenience with which a specific structure and even a specific substructure can be found, it is also clear that a collection of very many structures holds a lot of additional information. This additional information is encrypted in the database and one has to ask the proper questions and to apply the proper tools to extract it.

Perhaps the best known example for the validity of this statement is the mapping of a reaction pathway in the early and seminal work of Buergi and Dunitz.[1] The experimental basis for this elegant type of analysis is that the structures of many individual compounds are available within the class of compounds which are relevant to the problem. In another type of application, the conformations adopted by the many individual molecules within one class of compound may be used to find a mechanical model which correctly reproduces and also predicts the conformation of the members of this class.[2] In principle this type of database use builds on the existence or development of intelligent filters that are able to extract the desired information from the wealth of data available. The structure of these filters may be quite different, depending on whether one is looking for reaction pathways[1] or trying to develop a mechanical model.[2] Still, the basic logic is the same: look at the individual structures as snapshots of the geometry of a class of molecules and try to correlate the observed variations with some set of parameters.

It is clear from the above that extracting the hidden information calls for the appropriate tools. As far as molecular structures themselves are concerned, retrieval systems, such as the one built into the most abundant database, the Cambridge Structural Database[3] (hereafter named CSD), are well suited to select classes of compounds, specific kinds of interactions and also specific geometrical arrangements. The situation is much worse if the packing of individual molecules within a crystal is the focus of attention. Although plenty of graphical tools are available to visualize the arrangement of molecules within a three-dimensional

[a] Anorganisch Chemisches Institut der Universität Heidelberg, Im Neuenheimer Feld 270 D-69120 Heidelberg, Germany
Fax: (internat.) + 49-(0)6221/545-707
E-mail: g.huttner@indi.aci.uni-heidelberg.de

 © WILEY-VCH Verlag GmbH, D-69451 Weinheim, 2000 1434−1948/00/0505−0857 $ 17.50+.50/0

lattice, it is very difficult for the non-expert to understand such packing diagrams. "Understanding" in this context means that one would be able to delineate the observed pattern into some archetypal arrangement and thus recognize the basic principles. Projecting this situation onto molecular chemistry: imagine someone who looks at the structure of hexacarbonylchromium and is not able to extract the archetypal octahedron, which is of course apparent to an educated chemist at first glance. The archetypes of arrangements within infinite lattices are more complicated to recognize, one reason being the translational symmetry, and the other being the lack of appropriate training. While solid-state chemists and crystallographers are well trained to reduce a given repetitive architecture to some standard pattern, molecular chemists are generally not so. Looking at any introduction to solid-state chemistry,[4] one will be aware of the power of categorizing compounds by idealizing their geometry such that they may be understood as derivatives of a few basic patterns. Closest packing, hexagonal close packing (*hcp*), cubic close packing (*fcc*) and body-centered packing (*bcc*), are at the basis of the most proliferate idealizations of this type. Referring to the packing of molecules within crystals it has been shown by Kitaigorodskii[5,6] that the idea of closest packing helps to rationalize the individual arrangements.

Definition of the Problem

With the development of what is called supramolecular chemistry,[7–9] i.e. with the increasing awareness of the importance of secondary interactions between molecules, any information about these secondary interactions is more important to the development of chemistry than ever. Structural databases[3] contain an as yet scarcely used and abundant source of information about secondary interactions. It is these secondary interactions which govern the arrangement of molecules within a crystal.

One way to extract part of this information relies upon reconstruction of the observed patterns of packing by making the appropriate choice for the individual terms of the intermolecular potential.[10,11] By doing this for a series of related structures the potential terms may be optimized.[12,13]

Choosing a good starting point for this kind of optimization is guaranteed by yet another method of systematic exploration of aspects of molecular packing: it is found that the centers of gravity of molecules tend to be close to specific compartments of a unit cell.[14] Helpful as this analysis is, it has no direct bearing on the packing of molecules since the position of points in space depends on their coordinates as well as on the metric system to which these coordinates refer. There are – not including translation – an infinite number of three-dimensional possibilities for a set of points if the fractional coordinates are all that is known, since the real position of a point in space is dependent on the lengths of the crystal axes and the angles between them.

Another way would entail the search for specific patterns of packing (c.f. *bcc*, *fcc*, ...) of the molecules as represented by their centers of gravity. Correlation of the appearance of these patterns with parameters describing the shape of the molecules may then be attempted. Basically, this type of approach has been taken by Kitaigorodskii,[6] albeit at a time where computer retrievable databases were not yet common. To make this approach feasible and efficient, tools have to be developed which recognize a specific three-dimensional repetitive pattern automatically. Such tools are still not available, and although it may appear a simple task to use today's pattern recognition techniques to develop such a tool, the problem is quite complicated.

While, given the metric system, the coordinates of n points completely define an n-point pattern, the values of these coordinates depend on translation as well as rotation. A direct search for a specific n-point pattern in three-dimensional space would hence be quite cumbersome. A solution to this problem is to transform the observed patterns into some representation that is independent of rotation and translation, i.e. a representation in internal coordinates. Since the choice of internal reference frame is intentional, this representation of a pattern formed by an ensemble of n points is again not unique and is thus not immediately accessible to analysis by pattern recognition techniques. To make the representations independent of the specific assignment of internal coordinates – i.e. independent of the $n!$ possible choices of labeling n individual points, each by a unique label – instead of analyzing the individual values, which the internal coordinates adopt for a specific arrangement of points, the distribution of these values may be analyzed. Such a distribution may immediately serve as an input to pattern recognition tools. While representing an ensemble of n points in three-dimensional space by a few histographic data does not in general allow reconstruction of the body represented by these points, it is a very efficient way to classify arrangements of n points with respect to symmetry. Different realizations of this type of analysis are described in this paper, i.e. different types of histographic mapping are used as an input to pattern recognition tools. Neural networks[15–18] are trained to differentiate between different types of bodies based on this histographic input.

The problem of analyzing for a specific type of packing within a repetitive pattern, i.e. crystal space, is dealt with in two steps: first the m next neighbors of a given point are determined; this subset of points is then analyzed for the presence of specific polyhedra which are a characteristic consequence of the kind of packing. Thus for instance octahedra are characteristic constituents in a close-packed situation.[19–21] In looking for octahedra, all six-point combinations out of the ensemble of $m + 1$ points (a good value of m being 16 in the search for octahedra in a close packed situation) are formed and automatically analyzed with respect to their potential octahedral arrangement. The few octahedra sorted out from the $\binom{k}{6}$ (read k over six; with $k = m + 1$) point combinations are then further analyzed with respect to their connectivity. From the type of connectivity found, the type of packing (*fcc*, *hcp*, *bcc*) which best approximates the given distribution of points in crystal space is derived.[19–21]

The procedure is applied to a subset of compounds crystallizing in space group *R*3 as well as to a family of tripod–metal complexes $RCH_2C(CH_2X)(CH_2Y)(CH_2Z)ML_n$ (R = H, alkyl, aryl; X, Y, Z = NR_2, OR, SR, PR_2, PRR′) and a selection of $Cr(CO)_5L$ compounds as registered in the CSD[3] (see Experimental Section). Packings which are close to *fcc*, *hcp*, *bcc* drop out automatically by this procedure. Attempts are made to correlate the shape of the molecules with the specific packing observed. It is found that describing the shape in terms of the eigenvalues of the tensor of inertia,[22] i.e. second moment analysis[23] of the molecular shape, produces some insight into the correlation between packing and shape. Second moment analysis is also used as a tool to differentiate different types of arrangements of *n* points in space, i.e. to recognize specific types of polyhedra. It is found to be efficient in this aspect as well and its use combined with neural network analysis produces an efficient filter for sorting out specific *n*-point polyhedra from a given ensemble of *p* points ($p > n$).

Results and Discussion

In this first attempt at automatic pattern recognition in crystal space, the search was limited to the three basic close packing motifs *fcc*, *hcp*, *bcc*. On the other hand, the pattern recognition machinery was designed such that it might also deal with any other type of packing motif.

From the two alternatives of searching in direct or reciprocal space, the first was preferred. If the only goal of analysis of packing motifs was the search for approximate close packed arrangements then search in reciprocal space might be quite effective. Replacing the molecules by atoms at their centers and calculating the diffraction pattern produced by these atoms would map the packing onto reciprocal space. A search for the approximate symmetry of the diffraction pattern and approximate rules of systematic extinction would then reveal the atomic packing pattern in direct space. This kind of analysis, while presumably efficient in the search for close packing motifs, would not easily adapt itself to the search of less specialized packing motifs. Searching for patterns in direct space was therefore preferred.

It might appear that with only three close-packed motifs in mind, a search for characteristic polyhedra such as the cube octahedron (*fcc*) or the anti-cube octahedron (*hcp*) might be the topic of focus. It is however found, as may be understood by imagining these polyhedra,[19–21] that differentiation between these two bodies as a whole is relatively poor. An alternative strategy has therefore been adopted, to search for octahedra and their connectivity from which the packings may be delineated.

Search for Polyhedra

Distance Histogram

An *n*-point polyhedron may be represented by *n*-coordinate triples in three-dimensional space. Since the values of these coordinates are dependent on translation and rotation, a representation in internal coordinates is preferred for pattern recognition purposes. An especially simple representation of this type consists of a vector for the $[n(n-1)/2]$ distances between all pairs of points of the *n*-point ensemble. This vector contains a full description of the polyhedron and may be back-transformed to a corresponding set of coordinates in three-dimensional space which represent the polyhedron. This fact is made use of in distance geometry calculations.[25,26] That the vector holds all the information necessary to reconstruct the body is immediately apparent from the observation that there are $[n(n-1)/2]$ distances and $3n-6$ degrees of freedom for a body with $n > 2$ points. The number of distances will be equal to the degrees of freedom for $n = 3$ and 4, and larger for $n > 4$, meaning that in these cases ($n > 4$) not all of the distances are independent. In each case, the number of independent distances is sufficient to reconstruct the polyhedron. Such a vector containing all $[n(n-1)/2]$ distances is, however, not suited for presentation to a simple pattern recognition algorithm since it may occur in *n*! different forms corresponding to the *n*! permutations of the *n* components in this vector. Only if the labeling scheme to which the vector refers is known, i.e. when the specific connectivity to which it refers to is known, will back-transformation to the coordinates of the *n* points be possible. To create a description of the polyhedron, which is independent of the specific numbering scheme, a histographic representation of

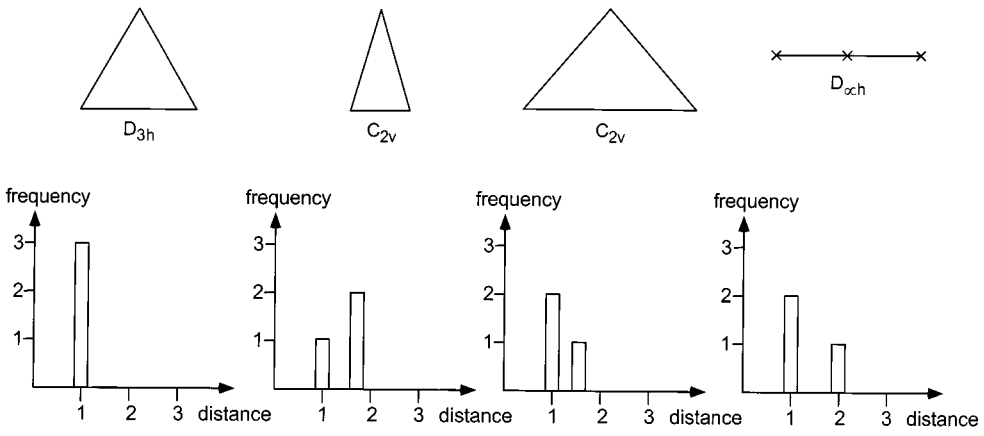


Figure 1. Histographic representation of the effects of symmetry on distance histograms for a set of three points

the vector may be chosen. That is, a histogram showing the frequency with which distances in a specific range occur may be used as input for pattern recognition machinery.

This type of histogram, even though it cannot in general be back-transformed to a three-dimensional representation of the body, is quite characteristic of the individual types of polyhedra. The reason for this is that the symmetry of the polyhedra is encoded in this type of histogram. As an example think of three points in space.

Any pattern formed by three such points is completely characterized by the three distances between these points. While in general these distances may map onto the histogram at any three positions, an arrangement of the points

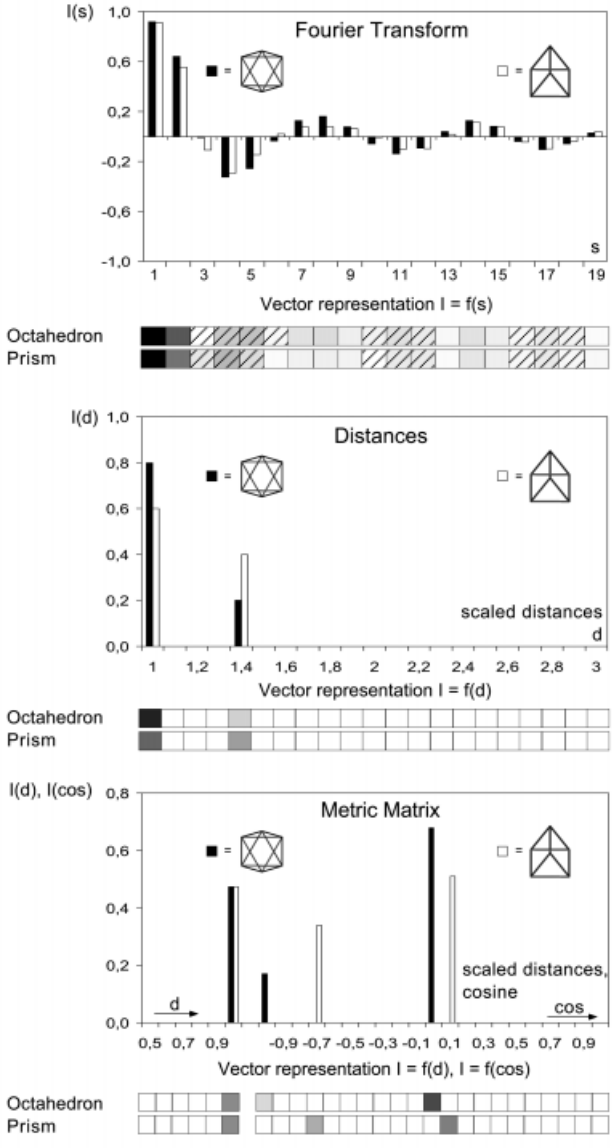


Figure 2. Three methods to represent three-dimensional bodies as a discrete function of just one independent variable. The procedures of obtaining the functions are described in the text. The functions are shown for the examples of a regular octahedron and a regular trigonal prism. The boxes below each function represent the individual components of the vector onto which the functions are mapped. The relative magnitude of the coefficients is indicated by gray shading with black being largest and white being smallest. Negative values of coefficients are indicated by dashed lines.

with any symmetry higher than C_1 will show a specific pattern. If the points conform to an equilateral triangle, the C_3 symmetry of this D_{3h} symmetric body will map itself into the histogram such that the shortest distance is observed three times and there is just one bar in the histogram (Figure 1 left). An isosceles triangle will be represented by two bars, the one corresponding to the two equal distances being twice as high as the one representing the third distance (Figure 1 middle). In the linear arrangement of the $D_{\infty h}$ borderline case of an isosceles triangle, the distance occurring only once will be twice as large as the shortest distance which occurs twice (Figure 1 right). This simple example shows how symmetry mirrors itself in the histographic representation. In this specific case of three points in space, the histographic representation is an unambiguous representation of the body itself. This is because the number of distances is equal to the number of degrees of freedom in this case. The same applies to four points in space, while with $n > 4$ the number of distances exceeds the number of degrees of freedom. In these cases ($n > 4$) the histogram is no longer unambiguous although it still responds in very specific ways to the symmetry of the arrangement of points in space. An example of this type of mapping is represented in Figure 2 (middle) for an octahedron and a trigonal prism.

Histogram for Encoding Distances and Angles: The Metric Matrix Approach

As has already been discussed, a complete set of [$n(n - 1)/2$] distances is a full representation of a body composed of n points in three-dimensional space if the connectivity is also known. It is a representation independent of translation and rotation. Another representation, which is also free of the ambiguities of translation and rotation, consists in the so-called metric matrix of the body (Figure 3 top). To construct this matrix the center of mass of the n points is taken as the origin. The scalar products of all the n vectors radiating from the origin to the n points may then be represented as a symmetric matrix that contains the squares of the distances on the diagonal, and the cosines of the angles sustained by each pair of vectors – each cosine multiplied by the product of the relevant distances – as the off-diagonal terms (Figure 3 top). The appearance of this matrix is also dependent on the scheme used to label the n points and the lines and columns of this matrix may be shuffled around by the $n!$ permutations of the labeling scheme. The matrix itself is thus not immediately suitable for input to a pattern recognition algorithm but the histogram derived from it is. The histogram now consists of two parts, one referring to the distances and the other one to the cosines of the angles (Figure 3 middle). The distances d are mapped onto the interval $0 < d \leq 1$ with the largest distance scaled to 1. Scaling of the cosines is unnecessary since their values are between –1 and +1. The frequencies are scaled such that the values fit in the range $0 \leq$ frequency ≤ 1 (see Experimental Section). The two parts of the histogram (distance, cosine) may be encoded as a vector once the resolution of its two parts (distance, cosine) is defined (Figure 3

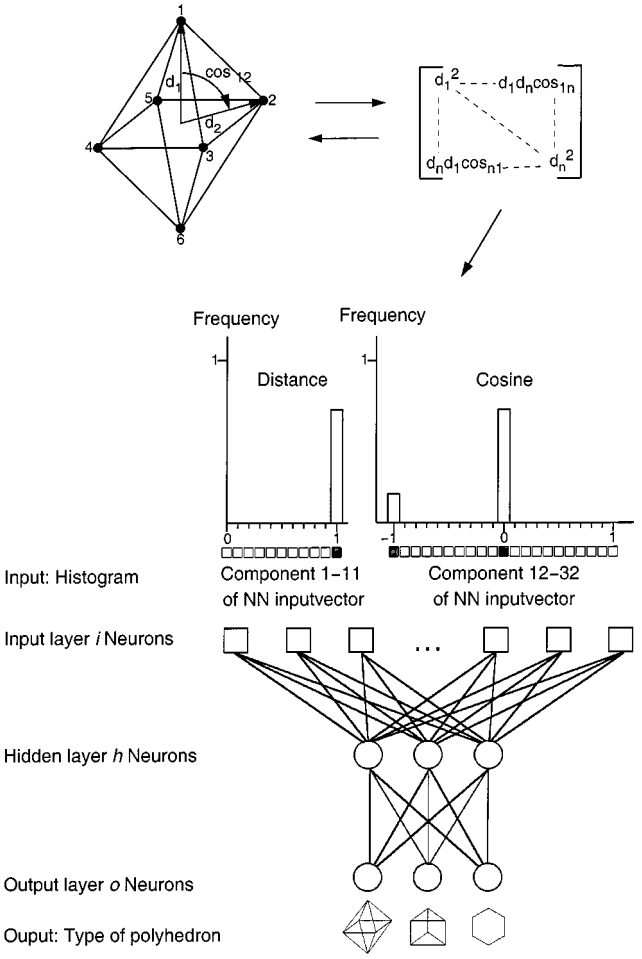


Figure 3. Sorting of *n*-point polyhedra into specific categories by neural networks. The top half of the diagram gives a shorthand illustration of how a vectorial representation of an ensemble of *n* points in space is obtained. An octahedron is deliberately selected as an example. The bottom half illustrates the type of network used. The input layer consists of $i = 32$ neurons to present the vector to the network. A hidden layer of $h = 3$ neurons connects this input layer to the output layer with $o = 3$ neurons. The network is trained to sort the bodies with respect to the class to which they have been assigned to (octahedron, trigonal prism, hexagon).

middle, Figure 2 bottom) and the vector may then be used as the input for a pattern recognition algorithm.

The histograms discussed are a projection of three-dimensional data onto a histographic function with just one independent variable. The advantage of this type of representation is that it is independent of translation and rotation of the body as well as of any permutation of the labeling scheme used to designate the points. Although much information is lost by projecting three-dimensional data this way, the patterns obtained do characterize the symmetry properties of the three-dimensional object (see above).

Fourier Transformation

A different type of projection from three-dimensional space onto a function with just one independent variable consists of a Fourier transformation of the distances spanned by the *n* points of the body. This type of transformation has a long-standing application in electron diffraction[27] and has recently been applied to the condensed description of molecular shape and constitution.[28,29] Application of this procedure is simple as it means to compute the sum

$$I(s) = \sum_{i=1}^{n-1} \sum_{j=i+1}^{n} A_i A_j \frac{\sin sd_{ij}}{sd_{ij}}$$

where *s* refers to the "scattering angle". If the distances *d* are measured in Angstroms its dimension is $Å^{-1}$. Computing this sum for $1 \leq s \leq 50$ produces values of this function at each of these 50 points in *s* space. The function itself is a weighted sum of sine functions of different periodicity. It is found, that for the problems analyzed, as little as the first 19 values of this function are sufficient due to the almost exponential decay of $I(s)$ versus *s*. A vector containing these 19 values of $I(s)$ at $s = 1,2,..,19$ may serve as input to a pattern recognition algorithm (Figure 2 top, $A_i = A_j = 1$ for $i,j = 1...n$).

A comparison of the three methods described, which are able to create specific one-dimensional projections of a set of *n* points in three-dimensional space, is shown in Figure 2. The bodies compared in this example are a regular octahedron and a trigonal prism with all edges of equal length. It can be seen that all three methods are able to differentiate these two types of body. Using the distances only, the discriminative power of the histogram in direct space and its Fourier transform equivalent in reciprocal space do not appear to be very different (Figure 2 top and middle). In fact, it has been found that the simple histographic representation of the distances in direct space is already an efficient tool, so the Fourier transform version of the distance-based code has not been used to a large extent in this work. In addition to the fact that the discriminative power of the Fourier transform representation is not significantly superior to the representation by the distances themselves, it lacks the immediate interpretability of the histogram of distances. In a sense the histogram of distances corresponds to the radial distribution curve to which diffraction data are transformed in order to extract structural information, while the Fourier transform[27] representation corresponds to the diffraction pattern itself. As is seen in Figure 2 a histographic representation of the metric matrix encoding for distances and angles has the highest power of discrimination of the three methods analyzed and is by far preferred.

All the above one-dimensional projections may be seen as kind of spectral representation of the three-dimensional bodies they represent. Specific signatures of these spectra may be interpreted as a kind of fingerprint indicating that some specific body, say an octahedron, trigonal prism, hexagon, tetrahedron, etc. is the origin of this fingerprint. While it is easy to correctly interpret these spectra if the ideal symmetry-defined bodies are at their origin, it is not so simple to extract this type of information by mere inspection if a distorted polyhedron is the origin of the spectra. In fact, if we draw away from the scalar differences for the moment, there is only one octahedron, an ideal body defined by symmetry alone. In the real world, however, there are many arrangements of six points in space which are

close to an octahedral arrangement. Any set of rules defining the extent to which a body may be distorted and still be categorized as belonging to the octahedral class is artificial, and the rules may well change in response to the questions asked. Instead of defining a set of rules in mathematically expressed restrictions of angles and distances, we adopt a different philosophy. It is argued that no arrangement of six points not completely defined by octahedral symmetry is a true octahedron.[30] Nature confronts us with all kinds of six point arrangements but we are still intuitively able to classify these arrangements as say octahedral, trigonal prismatic, and hexagonal by mere inspection of the bodies. Instead of using artificial mathematical rules for the purpose of classification of these bodies we may well rely upon our intuitive interpretation: We look at a body and see it is octahedral. We look at another one and see it is close to a plane hexagon and so on. We then classify the bodies according to what we see. It may be argued that this way of classification lacks any objectivity. However, there is no objectivity in mathematically formulated and artificial classification rules. Adopting the totally subjective view mentioned above introduces the unconventional consideration of personal judgment in science. However, if "truth" is only in the symmetry-defined ideal objects, anything outside this is a matter of taste and purpose. One might like to introduce some kind of objectivity in the manner of social science or psychology: one might present the bodies to be categorized to as many people as time allows and then base classification on a common sense evaluation. Strange as this point of view may appear when uttered in a scientific paper, the thorough logical evaluation of the situation will show that it is completely appropriate to the purpose.[30] The purpose of classification described in this paper is to classify the packing of molecules with respect to categories, which again, not considering scale, are ideals, defined by symmetry alone. Any classification of an observed packing as a distorted version of the ideal is not objective in a scientific sense and is very much biased by our desire to find this relation to one or the other of the ideal patterns.[31]

Neural Network Analysis

Instead of defining a mathematical set of rules to explicitly sort the bodies into different categories, neural networks[15–18] have been trained to choose these categories on the basis of the input vectors of the spectra described above. To train the networks a training set has to be constructed which contains not only the ideal symmetry determined bodies, but also bodies derived from these by random perturbation. To this end, the points defining the ideal body were allowed to occupy positions at random within a perturbation sphere located at the corresponding point of the ideal body. The bodies thus generated where inspected by examining different orientations of their representations on a computer screen and then categorized by inspection. The perturbation spheres were enlarged in a stepwise manner until the chance of finding a perturbed structure showing an apparent relation to the ideal structure was impracticably low e.g. no chance in ten trials. In this way, a training set of 281 polyhedra altogether was produced. The training set comprised the following classes, $n = 4$ square planar, tetrahedral, $n = 5$ pentagon, square pyramidal, trigonal bipyramidal, $n = 6$ hexagon, octahedron, trigonal prism. To analyze the whole set of data with a single network, the vectorial representation of the histograms referring to distance (Figure 2 middle) was augmented by a single coefficient which presented the number of points n underlying the pattern to the network. $1/n$ was used to represent this number. These vectors were then fed into the neural network, which was trained to sort the input into the correct output categories. To validate the trained network function an independent set of 64 distorted polyhedra, comprising all categories to which the network had been trained, was generated as above. It was observed that the categories found by the network were equal to those defined by inspection in 78% of the cases. Some of the "faults" committed by the network are easily explained: A square pyramid may be interpreted as an octahedron due to the fact that neural networks are capable of reconstructing patterns when some of the input data is missing or at error.[17,18] The $1/n$ term (see above) in the input vector did not adequately counter this tendency to pattern reconstitution. Therefore it was decided to use specific pattern recognition machines for every number n of points analyzed and it appeared reasonable to also use the spectral input derived from the metric matrix (Figure 2 bottom). Due to its greater discriminative power, this might not only improve the quality of predictions of the trained network, but it should also abbreviate the time necessary for training the network. The procedure adopted is schematically shown in Figure 3.

For any given arrangement of six points in the data set the metric matrix is calculated. The distances obtained from the diagonal terms of the matrix and the cosines derived from the off-diagonal terms are projected onto histograms, one for the distances and a second for the cosines. A vector representation of these histograms is obtained by discretisation of the distance part (the distances are scaled between zero and one) into 11 intervals and the cosine part into 21 intervals (Figure 3 middle). The vector of these 32 components is used to feed the input layer of a neural network that contains 32 input units. The network consists of this input layer, one hidden layer and one output layer. Whenever an input vector representing a body in the training set is fed into the network, it is simultaneously informed which of the three categories the body belongs to, and how far it is from the ideal. The corresponding qualifier between zero and one (zero no fit, one ideal fit) was obtained by visual inspection (Figure 4) of the body.

Training the network requires feeding the network with the input data and the expected results over and over again until there is no more change between the expected output and the output generated by the network in successive training cycles. At this point of convergence the strength of the connections between the individual neurons (lines in the diagram Figure 3) has been optimized such that the network as a whole automatically sorts the bodies into the cat-

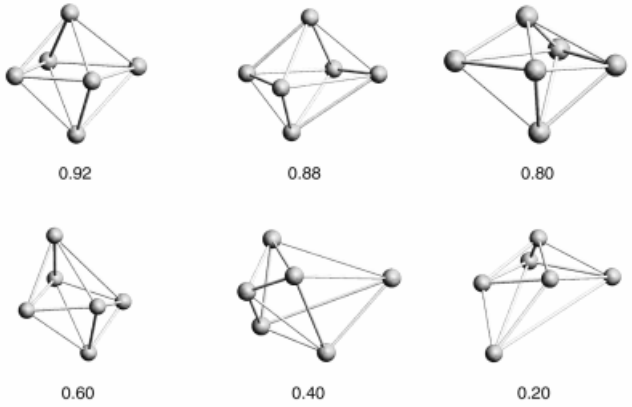


Figure 4. Distorted octahedra and their qualifiers. A few selected examples are shown. The qualifiers q were allotted by visual inspection. For the purpose of training the network only octahedra with qualifiers q greater than or equal to 0.8 were used.

egories in the best way it can. If the network is able to reproduce the artificial categorization of the bodies contained in the training set in an almost quantitative manner, it may be said that the network – with respect to the training bodies – "sees" what a human inspector would see when looking at the bodies themselves. The network is then able to reproduce the categories and qualifiers a human being would allocate by inspection, even for bodies it has never "seen" before. This means the machinery is capable of categorizing bodies in the same manner a human inspection of the bodies would. That is, the time-consuming task of inspecting a three-dimensional body by eye may be transferred to the neural network that produces the same result a human inspector would produce. This protocol was used for the subset of the polyhedra with $n = 6$. Not only was it found to lead to rapid convergence but it also led to a high quality of prediction. Based on a training set of 153 input vectors distributed over the three categories to be identified (octahedron, trigonal prism, hexagon) the square root of the mean standard error (see Experimental Section) after convergence of the training phase was only 0.017. To validate the trained network function, an independent set of 16 distorted polyhedra was generated as above, comprising all categories for which the network had been trained. It was observed that the categories found by the network were equal to those defined by inspection with a deviation between the predetermined and the calculated qualifiers of only 4.5%. Neural networks are thus found to be a sufficient filter to recognize the specific shape of an n-point body from a set of coordinates containing all kinds of n-point arrangements.

Second Moment Analysis

Since it had been found that the manner in which three-dimensional data is reduced to form a vector appropriate for input to the neural network had a large influence on the discriminative power of the trained network, another and a more traditional way of reducing the three-dimensional shape to just a few parameters has been analyzed. If a set of coordinate triples in three-dimensional space is considered to represent the coordinates of n points of equal mass, the tensor of inertia[32] associated with this set reflects the spatial distribution of these points. The lengths of the eigenvectors of this matrix of inertia characterize the shape of the body.[22,32–34] With respect to the bodies analyzed, both an ideal octahedron and an ideal tetrahedron will be characterized by three equal eigenvalues. The rotational symmetry of bodies such as the trigonal prism (C_3), trigonal bipyramid (C_3), and square pyramid (C_4) will produce two eigenvalues of the same size while the third may be different. A planar body such as a hexagon will give rise to one eigenvalue of zero. If the body has rotational symmetry, such as a hexagon with C_6 symmetry, the remaining two eigenvalues will be equal in size. The transformation of a set of points to the coordinate system defined by the eigenvectors of the matrix of inertia is a well established procedure in molecular crystallography, commonly used to define the "best plane" of a set of points.[22] In terms of pattern recognition this method is equivalent to describing the characteristics of a pattern defined by n points in three-dimensional space by its second moments.[23] Thus this method relates to a standard tool in the analysis of distributions which is also a type of pattern recognition technique.

If the masses of the n points of the ensemble analyzed are all taken to be one, the eigenvalues of the matrix of inertia are equal to the sum of the squares of the deviations of the points from the origin (center of mass) along the eigenvector axes. With respect to the bodies analyzed, this means that the eigenvectors will tend to increase with the number of points defining the bodies being analyzed. Thus the number of points is implicitly encoded in the size of the eigenvalues, given that the bodies are scaled such that they fit into a unit sphere and touch the sphere at at least one point. This condition is fulfilled for the training set as described above. In order to retain the information about the number of points n giving rise to a specific set of eigenvalues, and to make results comparable, the eigenvalues have to be scaled in an appropriate way. It has been found through a number of trials that with the conditions met in the training set, the discriminative power of this eigenvector analysis is optimized when each eigenvalue l is replaced by $l' = (1/3.5)\cdot l\cdot n$. To map the results onto a coordinate system defined by the eigenvectors in the interval zero to one, the coordinates are calculated as $l'^2/(l'^2 + 40)$. The results obtained for the training data set using this type of scaling are shown in Figure 5.

It can be seen that the different classes of bodies are, on average, neatly separated in this type of scaled eigenvector diagram. The eigenvalue filter has the advantage of projecting planar bodies onto the YZ plane (X representing the eigenvector axis associated with the smallest eigenvalue and Z corresponding to that with the largest eigenvalue). The only region where there is no clear separation is the one in which octahedra and trigonal prisms are projected (Figure 5). The degree of separation of trigonal bipyramids and square pyramids is also low. Since these bodies are well separated by the neural network technique (see above) it appears that a combination of the eigenvalue filter and the

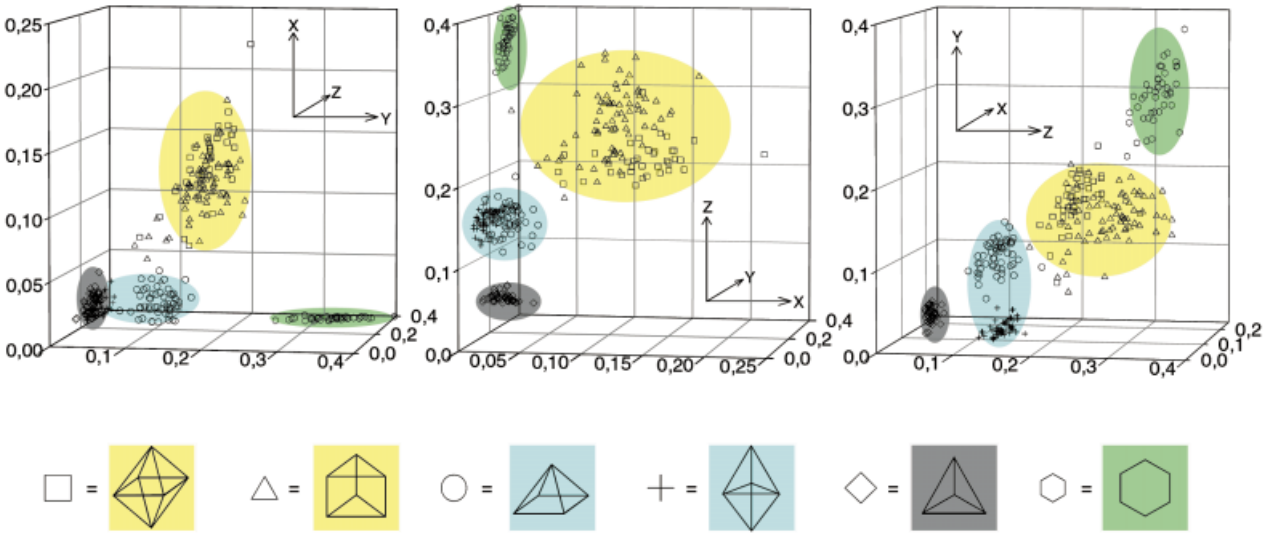


Figure 5. Sorting polyhedra in eigenvector space. The matrix of inertia of a body of n points is calculated with all points given equal weight. The eigenaxes of this matrix define the coordinate system X, Y, Z. The coordinate values are scaled in response to the eigenvalues and to the number of points comprising the body (see text). All three projections onto the eigenvector axes are shown.

neural network filter might be maximally discriminative. This method has therefore been applied as the basis of the work reported below.

Analysis of Packing

In this paper, analysis of the patterns formed by the geometric centers of the molecules within a crystal has been restricted to a search for the three basic types of closest packing. It is clear, however, that the methods developed are applicable to searching for any type of packing pattern.

The analysis has been conducted for the two patterns maximizing density (*fcc*, *hcp*) as well as for the *bcc* pattern, which maximizes the number of closest neighbors.[24] All three of these modes of packing may be described as networks of octahedra.[19–21] In the case of the two dense sphere packings, these octahedra are regular, while in the *bcc* packing mode they are tetragonally compressed. The connectivity of these octahedra, as well as the angles at which they are inclined with respect to each other, are different for the three types of packing (Figure 6; Table 1).

In the *fcc* mode the octahedra are connected via vertices and edges (Figure 6). The angles around the centers of the octahedra at the connecting points are decidedly different for these two types of connections (Table 1). In the *hcp* mode there are three types of connections, vertices, edges, faces (Figure 6) with the associated angles again being

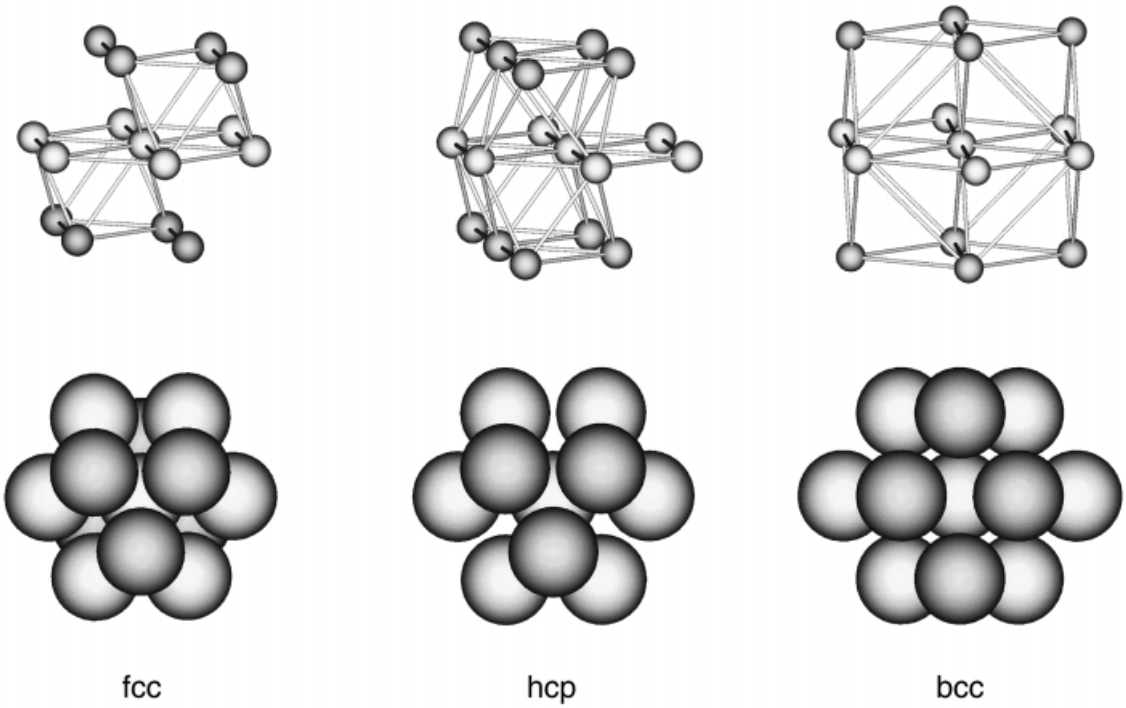


Figure 6. The three types of close packing shown as a network of octahedra (top) and as a stack of layers (bottom)

Table 1. Differentiation of octahedral networks by connection angles. The three basic packing types are described as networks made up of interconnecting octahedra. The octahedra are regular for the *fcc* and *hcp* cases but are tetragonally compressed for the *bcc* case. The values given refer to the angles subtended by the centers of the octahedra and their connecting points in the different modes of connection.

Packing type	Vertex	Edge	Face
fcc	180.0°	90.0°	–
hcp	131.8°	90.0°	70.5°
bcc	180.0°; 135.0°	90.0°	60.0°

within specific ranges (Table 1). The distorted octahedra making up a *bcc* packing also show vertex, edge and face bridging (Figure 6). The angles relevant to these bridging modes are again characteristic for the respective mode (Table 1). A similar type of description may be made with tetrahedra seen as the basic constituents.[19] It was felt that a description based on a network of octahedra[20] might be of higher discriminative power with respect to the problem at hand, since given a random repetitive pattern it is less probable to find six points making up an approximately octahedral shape than it is to find four points conforming to an approximately tetrahedral shape.

Examples

Compounds Crystallizing in Space Group R3

The procedure described above has been applied to a few classes of examples selected either by space group symmetry or by chemical composition. To start, an especially informative example was chosen. When analyzing the packing of a series of compounds which crystallize in the space group *R*3 and which have themselves crystallographic C_3 symmetry, some *bcc* and *fcc* packings should be found within the sample by applying the above methods. In this space group points lying at the C_3 axis will form ideal face-centered and body-centered cubic patterns at specific ratios of the lengths of the a and c axes of their hexagonal cells. A ratio of $a/c = 0.408$ results in an *fcc* packing and a ratio of $a/c = 1.633$ produces a *bcc* pattern.[35] Since the geometric centers of C_3 symmetric molecules necessarily lie on the crystallographic threefold axis, these ratios should also indicate ranges around which the corresponding type of packing will be observed. This means that an a priori assessment of the packing type is possible on the basis of this ratio.

On the other hand, the packing can be analyzed by the pattern recognition techniques described and the relevant packing modes can be delineated from this analysis in each case. If the pattern recognition techniques work well, it is expected that all structures for which the lattice constant ratio predicts a specific type of close packing are independently identified as the same kind of packing. It is in fact found that the predictions by the algorithm are in close agreement with predictions made on the basis of lattice constants (Table 2). This result is highly satisfying since it means that all distorted *fcc* and *bcc* patterns which are a consequence of only the actual axial ratio are found. As shown in Table 2, *bcc* and *fcc* packing modes are also found in ranges which are well outside the exact numbers of $a/c = 0.408$ and 1.633 respectively. The reason for choosing to analyze patterns of packing in space group *R*3 as the first example is also motivated by the idea that perhaps packing and molecular shape are correlated. In space group *R*3, with the centers of gravity of the C_3 symmetric molecules occupying positions at the crystallographic C_3 axis, layers are generated by the very symmetry of the space group. The stacking of these layers, which have the C_3 axis as the normal, is ABC, again solely by virtue of crystallographic symmetry.[35] Whether this kind of stacking of the densely packed layers will approximately correspond to a basic lattice type such as *fcc* depends on the dimensions of the lattice, which are again a consequence of the shape of the molecules.

Table 2. Data set analyzed for compounds crystallizing in space group *R*3. REFCODE refers to the name under which the compound is stored in the CSD. The numbers refer to the numbering scheme used in Figure 7. *a*/*c* gives the corresponding axial ratio with respect to hexagonal setting. The few cases for which a rhombohedral setting is stored in the database have been transformed to the corresponding hexagonal setting (see ref. [35]). Where no value for the *a*/*c* ratio is given the molecules do not occupy positions on a crystallographic C_3 axis. The designators in the columns "packing" refer to the idealized packing type as found by pattern analysis.

REFCODE	No.	*a*/*c*	Packing	REFCODE	No.	*a*/*c*	Packing
CIBKAZ	1	4.87	?	CETJUG	26	1.93	*bcc*
CUKGIY	2	3.00	?	CPPECO10	27	1.64	*bcc*
EFASCO01	3	0.70	?	DAMWET	28	1.92	*bcc*
FEBZIV	4	–	?	DIPYIK	29	1.08	*bcc*
PHPRHO10	5	3.59	?	DODZEB	30	1.80	*bcc*
RERLOP	6	4.60	?	DUSHAA	31	2.11	*bcc*
SUJPUI	7	–	?	FOTGUQ	32	1.19	*bcc*
SUJREU	8	3.58	?	LAMNES	33	1.61	*bcc*
VEKXEO	9	–	?	MSBFEC	34	1.09	*bcc*
VOCXAM	10	–	?	PAFVEX	35	1.54	*bcc*
VUSGIZ	11	2.77	?	PECCUV	36	1.18	*bcc*
VUSGOF	12	2.77	?	PICMET	37	1.74	*bcc*
VUSGUL	13	2.77	?	PPMEIR	38	1.61	*bcc*
YIHTIS	14	–	?	PPMERH	39	1.61	*bcc*
ZEMZIA	15	–	?	RARPEF	40	1.31	*bcc*
ZUDPIX	16	0.79	?	RARVAH	41	1.27	*bcc*
KIFSOH	17	0.87	?	TBZQCR	42	1.18	*bcc*
TEMTOU	18	0.92	?	TFORHI10	43	1.17	*bcc*
VENHIF	19	0.67	?	TICCAJ	44	2.40	*bcc*
TERQIQ	20	2.86	?	TIYLOC	45	2.67	*bcc*
DAJJIH	21	0.30	*fcc*	TONZOL	46	1.35	*bcc*
LIFMUI	22	0.33	*fcc*	VULVAZ	47	1.32	*bcc*
REDBAD	23	0.58	*fcc*	YENHOO	48	3.14	*bcc*
VUGHAG	24	0.67	*fcc*	ZULTOP	49	2.54	*bcc*
VIJGEA	25	1.09	*bcc*				

By using the eigenvalues of the tensor of inertia corresponding to the molecules, we can construct a graph which has the ratio of the length of the eigenaxis of intermediate size, *m*, to the largest one, *l*, (*m*/*l*) on one axis (horizontal axis in Figure 7) and the ratio of the smallest eigenvalue, *s*, to the intermediate one (*s*/*m*) on the other axis (vertical axis in Figure 7). This graph gives an idea of the overall shape of the molecules concerned.

Molecules projected close to the point (1,1) on this diagram are close to spherical in shape. Starting from this point (1,1) along the line $s/m = 1$, the molecular shape is

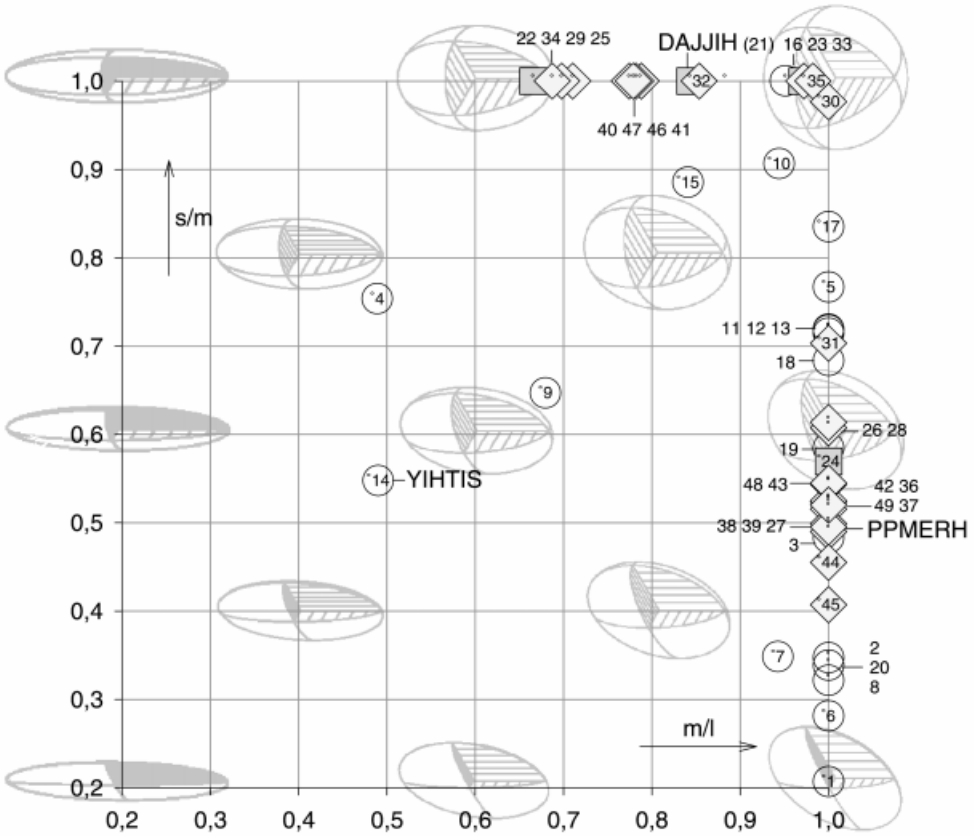


Figure 7. Molecular shape and packing of compounds crystallizing in space group *R*3. The diagram refers to the shape of the ellipsoid of inertia pertaining to each molecule analyzed. The vertical axis gives the ratio of the smallest eigenvalue of this ellipsoid to the intermediate one (*s*/*m*). The horizontal axis refers to the ratio of the intermediate eigenvalue to the largest one (*m*/*l*). The shape of the corresponding ellipsoids is shown in the background of the diagram. The numbers refer to the numbering scheme given in Table 2. In addition, three compounds are named by their REFCODE. The symbols have the following meanings: square *fcc*, diamond *bcc*, circle neither.

increasingly elongated along the C_3 axis. The smaller the value of *m*/*l* the more elongated the ellipsoid. Along the axis *m*/*l* = 1, again starting from the point (1,1), the molecules are increasingly compressed along the C_3 axes the smaller these *s*/*m* values are (Figure 7). Molecules which are not projected onto the axes (*s*/*m* = 1, *m*/*l* = 1) do not have rotational symmetry and all three eigenvalues of the ellipsoids are different. In space group *R*3 this means that these molecules (no 4, 7, 9, 10, 14, 15 see Figure 7, Table 2) are not located at special positions of the unit cell and are not necessarily C_3 symmetric.

The relation of the shape of the ellipsoid of inertia to the true molecular shape is a very reduced one. To present an idea of what this relation looks like Figure 8 shows three selected examples.

Compound no 21 (DAJJIH[36] Figure 7, Figure 8, left) is represented by an elongated ellipsoid. Compound no 39 (PPMERH[36] Figure 7, Figure 8, right) gives rise to a compressed ellipsoid. Both compounds are C_3 symmetric and the ellipsoids therefore show rotational symmetry. The third compound no 14 (YIHTIS[36] Figure 7, Figure 8, middle) gives rise to an ellipsoid with three different axial lengths. Even though the description of the true molecular shapes by their associated ellipsoids of inertia is a very simplified one this method has been used with success to classify the shape of compounds in a general way[33,34] and is also found to be useful in the present context.

When the algorithm described above is applied to the data set, a number of structures are sorted into either one of the two packings *bcc* (diamonds in Figure 7) or *fcc* (squares in Figure 7). Approximate *bcc* packing occurs more often than *fcc* arrangements in the data set analyzed (Figure 7, Table 2). It is to be noted that only structures containing C_3 symmetric molecules fall into these packing categories (*fcc*, *bcc*) and it may be argued that it is the rotational symmetry which allows for the formation of the closely packed layers.

Compounds $Cr(CO)_5L$

To further test the pattern recognition capabilities of the algorithms, a sample of $Cr(CO)_5L$ compounds, showing a wide structural variability and with no space group restrictions were selected for analysis. Among the 99 structures analyzed (Table 3) only 13 were found to fit into either one of the three search patterns *fcc*, *hcp*, *bcc*.

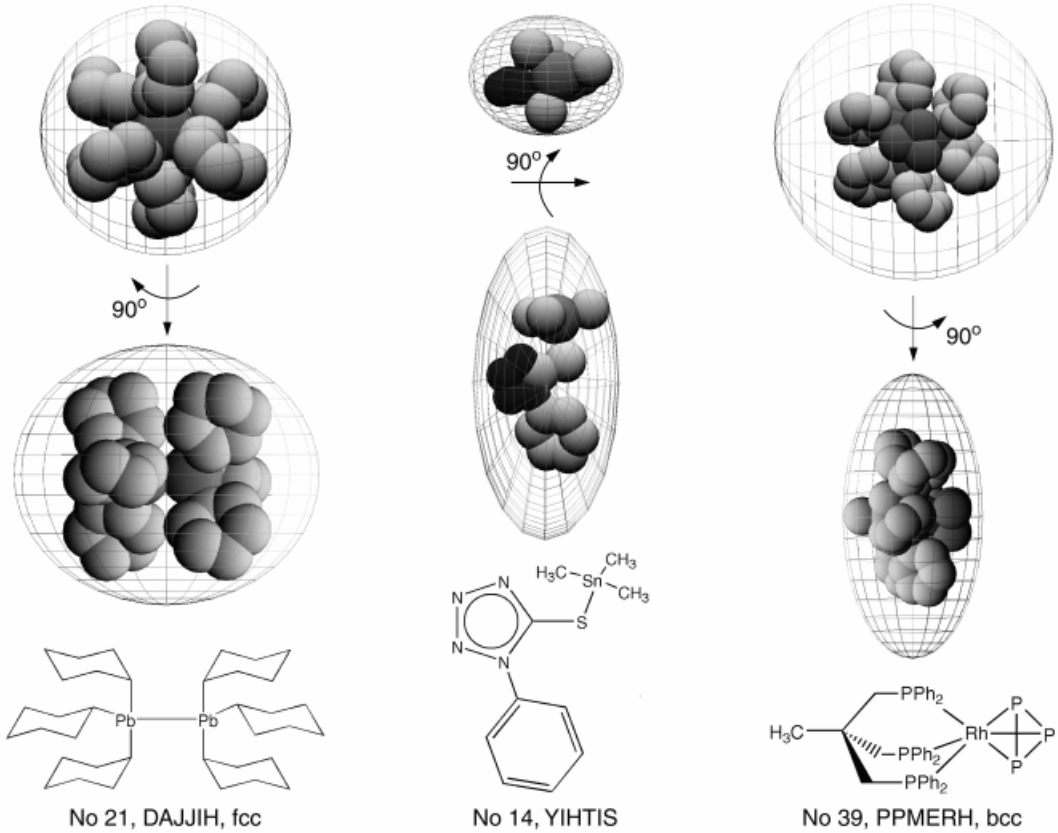


Figure 8. Description of molecular shape by ellipsoids of inertia. The numbers and designators refer to Figure 7 and Table 2. The ellipsoids are scaled such that the molecules fit into their envelope. The labels *fcc* and *bcc* refer to the idealized packing motif of the molecules.

The parent compound $Cr(CO)_6$, being octahedral in shape and thus being represented by a spherical envelope (no 99, coordinates 1,1 in diagram Figure 9) shows almost ideal hexagonal close packing. This has been previously noted by an appropriate visual inspection of the structure[37]. Close to the line $s/m = 1$, i.e. for ellipsoids which have two smaller eigenvalues of equal size, two additional *hcp* patterns are observed (no 90, 95 Figure 9). Close to this line *fcc* and *bcc* patterns are also found (no 83, 85, 89, 92 Figure 9). Out of the 99 structures only 13 are close to one of the idealized packing models, with *fcc* occurring more often than *hcp*, and *bcc* being observed only twice (no 83, 92 Figure 9). It is apparent from Figure 9 that the three basic packing motifs are only found in a range where either s/m or m/l, or both, are greater than 0.8, i.e. in a range where the ellipsoids are not distorted too far from rotational symmetry.

Figure 10 illustrates the relation between molecular shape and ellipsoidal envelope for three selected compounds (no 94, ZUKSED,[36] *fcc*; no 89, YIKSAM,[36] *fcc*; no 92, VOZMUS,[36] *bcc* in Figure 9) which pack in one of the modes analyzed.

Compound 94 gives an impression of how large the deviation from spherical symmetry may be to still allow for an approximate *fcc* type of packing. Compounds 89 and 92 are closer to spherical symmetry (see also diagram Figure 9) and their corresponding ellipsoids are closer to rotational symmetry than the one describing the shape of 94.

Compounds Containing a Tripod-Metal Entity

Due to the interest in the coordination chemistry of tripod metal templates, tripod transition metal compounds were selected as the next class for analysis. All compounds in the set are of the type $RCH_2C(CH_2X)(CH_2Y)(CH_2Z)ML_n$ (R = H, Alkyl, Aryl; X, Y, Z = NR_2, OR, SR, PR_2, PRR′). The constitutional C_3 symmetry of the tripod metal templates, which is exact when X = Y = Z, and may be still approximately so when X and Y and Z are similar, mirrors itself into the diagram Figure 11.

Obviously this constitutional C_3 symmetry is still dominant also in the structure of many of the tripod-ML_n compounds since they project close to the axes $s/m = 1$ and $m/l = 1$. As observed in the two previous examples, structures projecting close to these lines have a high probability of falling into one of the three idealized categories (*fcc*, *hcp*, *bcc*) which define the search pattern of this work. Out of the 44 examples (Table 4) 31 could be categorized this way. Only a few patterns of the *hcp* (no 38, 39, 40 in Figure 11) and *fcc* (no 36, 37 in Figure 11) types are observed. The

Table 3. Data set comprising compounds $Cr(CO)_5L$. REFCODE refers to the name under which the compound is stored in the CSD. The numbers refer to the numbering scheme used in Figure 9. The designators in the columns "packing" refer to the idealized packing type as found by pattern analysis. The designator *hl* assigned to structures 96, 97, and 98 means that the packing of the relevant compounds is characterized by layers of centered hexagons. This side result has been obtained by analyzing the data set on the basis of a filter searching for regular centered hexagons (see text).

REFCODE	No.	Packing	REFCODE	No.	Packing	REFCODE	No.	Packing
BALVIT	1	?	JONMEE	34	?	WAXKUB	67	?
BASTOE10	2	?	JUGWEN	35	?	WETGOR	68	?
BIVTOP	3	?	KAFMUZ	36	?	YESBAZ	69	?
BOVKEC	4	?	KARWEF	37	?	YIPMAL	70	?
CASCUU	5	?	KAXCUH	38	?	YUBTUK	71	?
CATYIF	6	?	KEBMOT	39	?	YUWHAZ	72	?
CHVICR	7	?	KIZWOF	40	?	ZATWAS	73	?
CMPHSC	8	?	KORGED	41	?	ZEPPEP	74	?
CTMTCR	9	?	KUJTOY	42	?	ZIJZOH	75	?
CUFPIC	10	?	LEWYAN	43	?	ZIKCUR	76	?
DAGPUW	11	?	LICBUU	44	?	ZIKDAY	77	?
DARFEH	12	?	LICCAB	45	?	ZITQEY	78	?
DAWXEE	13	?	MEAMCR10	46	?	ZOCCAV	79	?
DEKDUS	14	?	MESTCR	47	?	YETJUC	80	?
DEPTUN	15	?	MTCYCR	48	?	YIZBOY	81	?
DOPKUO	16	?	PCTHFC	49	?	GEWCAM	82	?
EAMNCR10	17	?	PCTXCR	50	?	SUBBIA	83	*bcc*
EMACCR	18	?	PEMSOP	51	?	CNETPA	84	*fcc*
FICZOG	19	?	PEVDAV	52	?	GABYUD	85	*fcc*
FIPCAI	20	?	PMPHCR	53	?	GABZAK	86	*fcc*
FOBPOB	21	?	RARFAR	54	?	LICCEF	87	*fcc*
FOPBIV	22	?	SAKSUS	55	?	YESBED	88	*fcc*
GABZEO	23	?	SASFAT	56	?	YIKSAM	89	*fcc*
GEHBAW	24	?	SEBJEO	57	?	PEZHOR	90	*hcp*
GEVFIW	25	?	TABNEP	58	?	PORGOS	91	*hcp*
GILCUZ	26	?	TACCRC	59	?	VOZMUS	92	*bcc*
HAYXAG	27	?	TAYMOV	60	?	ZIKCOL	93	?
HAYXEK	28	?	TEFXIL	61	?	ZUKSED	94	*fcc*
HEDVOB	29	?	TITHIN	62	?	FONHEV	95	*hcp*
HEPREZ	30	?	TMXTCR10	63	?	WECNIB	96	hl
HEPRID	31	?	VILFUR	64	?	WEDXIM	97	hl
HEZTUB	32	?	VOYJEY	65	?	YUWBIB	98	hl
HIGTUM	33	?	VOYJIC	66	?	FOHCOU	99	*hcp*

greater majority of the patterns correspond to the *bcc* type of packing. By comparing Figure 11 with Figure 7, it appears that *bcc* forms the predominant type of packing in compounds whose inertial tensors give rise to compressed ellipsoids of rotational symmetry with the ratio of eigenvalues *s*/*m* around 0.55.

An illustration of the relation between the molecular shape of tripod metal compounds and the ellipsoids representing them is given in Figure 12.

The two molecules (no 43, NAXHID[36] Figure 12 left; no 42, DUMSUZ[36] Figure 12 middle; see also Figure 11) give rise to ellipsoids with close to rotational symmetry and to a packing which can be classified as idealized *bcc*, while the one showing less apparent symmetry (no 4, LEMFUE[36] Figure 12 right; see also Figure 11) does not fall into one of the three categories with respect to packing.

Correlation Between Packing and Molecular Shape

By comparing the results obtained from trying to correlate the shape of molecules with their mode of packing within a molecular crystal it appears that there is a definitive correlation between the shape and the tendency to pack in one of the three basic packing types, *fcc*, *hcp*, *bcc*. An overlay of Figures 7, 9, 11 is shown in Figure 13.

The results described above for each set of compounds separately are collectively presented in Figure 13. It is apparent that the examples studied map into a range of around $0.3 \leq s/m \leq 1.0$, $0.3 \leq m/l \leq 1.0$. The data tend to accumulate along the lines $s/m = 1$ and especially $m/l = 1$ while the rest of the area $s/m \geq 0.4$, $m/l \geq 0.5$ is almost randomly populated. A total of 193 compounds is represented in Figure 13. The compounds whose packings do not conform to one of the three search patterns are marked by crosses, while the ones that fit are labeled by the appropriate symbols. The area to which the compounds are mapped, and for which assignment to one of the three packing modes is possible, is shaded in yellow in the diagram. Assignment is possible for 73 compounds out of 193. This area is characterized by the symmetry of the ellipsoids describing the shape of the molecules being not too far from rotational. The deviation from rotational symmetry which still allows for one of the three basic packing types may be up to 20% ($s/m = 0.8$, $m/l > 0.8$). When the deviation is larger than this, no *fcc*, *hcp*, or *bcc* packing is found in the sample of 193 compounds (Figure 13). This is a pleasing result as it correlates molecular shape and symmetry with the probability of forming one of the sphere packing modes within a crystal. A possible explanation may be that close packing

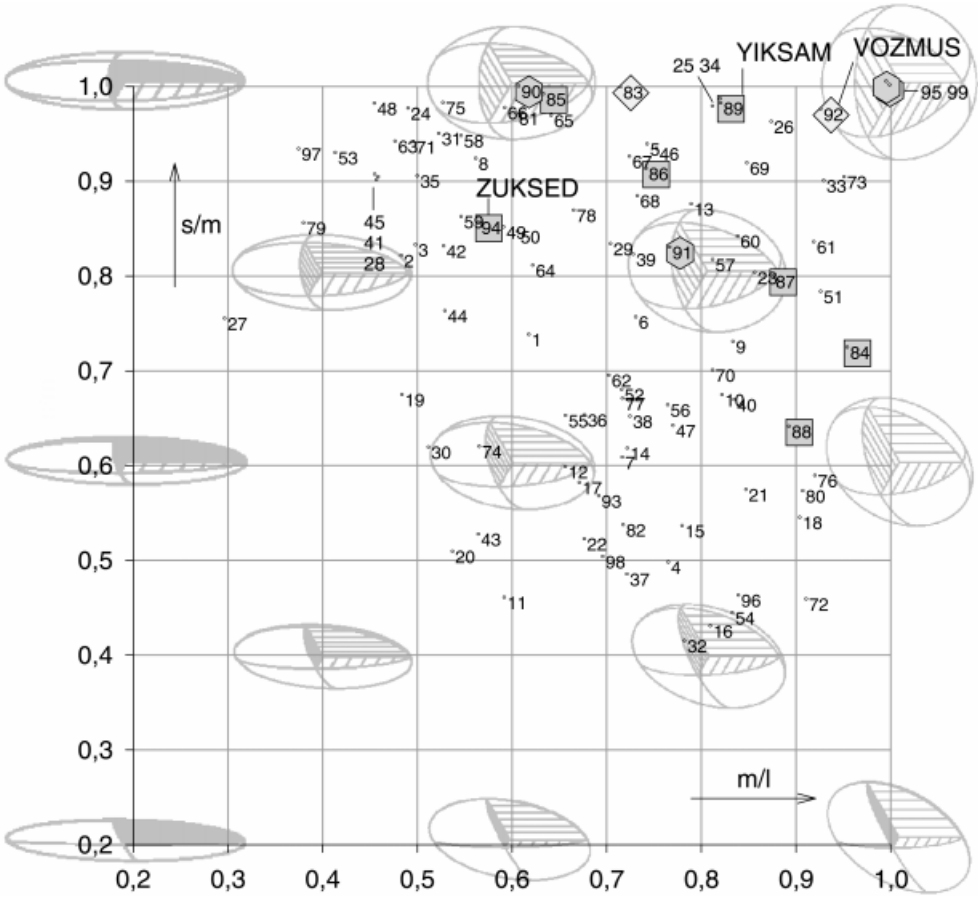


Figure 9. Molecular shape and packing of compounds $Cr(CO)_5L$. The diagram refers to the shape of the ellipsoid of inertia pertaining to each molecule analyzed. The vertical axis gives the ratio of the smallest eigenvalue of this ellipsoid to the intermediate one (*s*/*m*). The horizontal axis refers to the ratio of the intermediate eigenvalue to the largest one (*m*/*l*). The shape of the corresponding ellipsoids is shown in the background of the diagram. The numbers refer to the numbering scheme given in Table 3. In addition, three compounds are named by their REFCODE. The symbols have the following meanings: square *fcc*, diamond *bcc*, hexagon *hcp*.

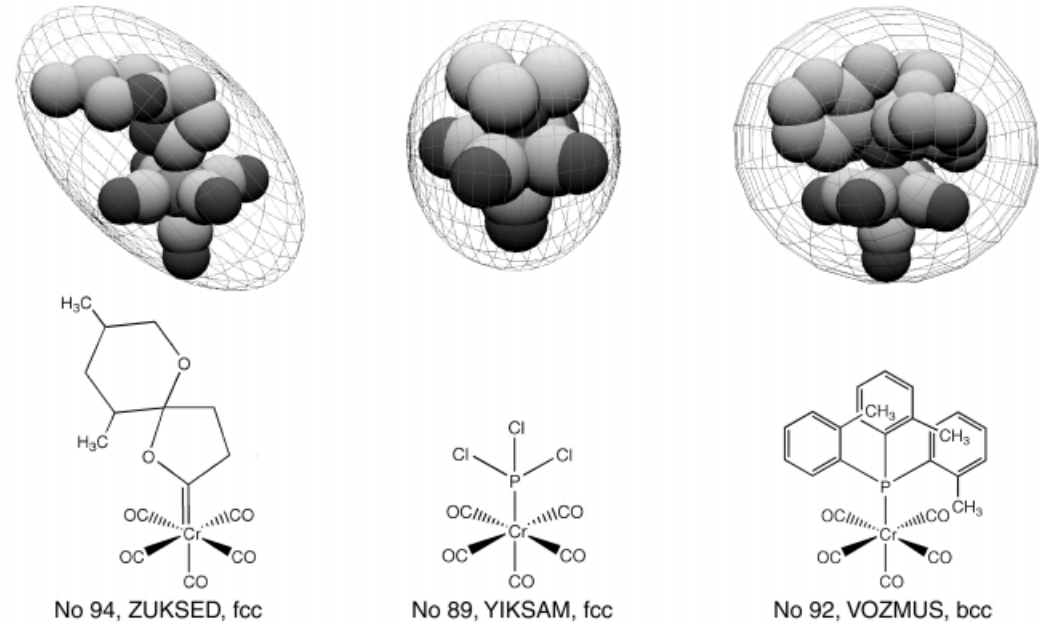


Figure 10. Molecular shape of three selected compounds $Cr(CO)_5L$. The numbers and designators refer to Figure 9 and Table 3. The ellipsoids are scaled such that the molecules fit into their envelope. The labels *fcc* and *bcc* refer to the idealized packing motif of the molecules.

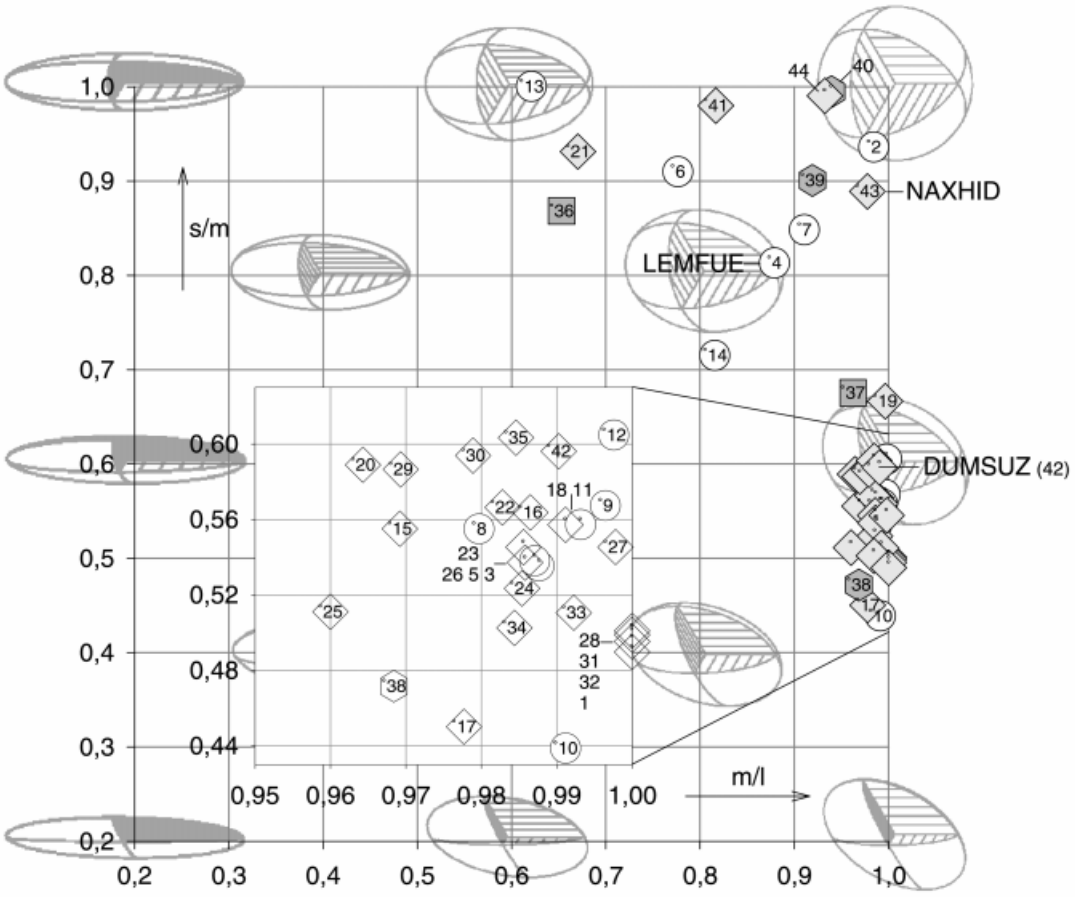


Figure 11. Molecular shape and packing of tripod-metal compounds. The diagram refers to the shape of the ellipsoid of inertia pertaining to each molecule analyzed. The vertical axis gives the ratio of the smallest eigenvalue of this ellipsoid to the intermediate one (s/m). The horizontal axis refers to the ratio of the intermediate eigenvalue to the largest one (m/l). The shape of the corresponding ellipsoids is shown in the background of the diagram. The numbers refer to the numbering scheme given in Table 4. In addition, three compounds are named by their REFCODE. The symbols have the following meanings: square *fcc*, diamond *bcc*, hexagon *hcp*, circle none. – The region around $m/l \approx 1$, $0.4 < s/m < 0.7$ is shown in magnified form in the inset.

Table 4. Data set comprising tripod-metal compounds. REFCODE refers to the name under which the compound is stored in the CSD. The numbers refer to the numbering scheme used in Figure 11. The designators in the columns "packing" refer to the idealized packing type as found by pattern analysis.

REFCODE	No.	Packing	REFCODE	No.	Packing	REFCODE	No.	Packing
CPPECO10	1	*bcc*	BOLJAN	16	*bcc*	PPMEIR	31	*bcc*
COTPMO	2	?	BOMPIC	17	*bcc*	PPMERH	32	*bcc*
LAKYUR	3	?	BURREL10	18	*bcc*	SXPMNI	33	*bcc*
LEMFUE	4	?	CODJIO	19	*bcc*	TPHCOA	34	*bcc*
PAKGOX	5	?	COGWOK	20	*bcc*	TUMYUV	35	*bcc*
RIPFAX	6	?	DOZWUK	21	*bcc*	HAJFED	36	*fcc*
TOTBAF	7	?	DPMENI10	22	*bcc*	HAJFIH	37	*fcc*
ZEPPUF	8	?	FIFBAX	23	*bcc*	DEPNER	38	*hcp*
SUHNAK	9	?	HBPMCO01	24	*bcc*	DUMVIQ	39	*hcp*
VEPSOY	10	?	KEDBIE	25	*bcc*	TOXBEN	40	*hcp*
BELTIV10	11	?	LATNUP	26	*bcc*	CUZTEW	41	*bcc*
ZIWRUS	12	?	PIBYUU	27	*bcc*	DUMSUZ	42	*bcc*
REZYOK	13	?	PICMET	28	*bcc*	NAHXID	43	*bcc*
ROQGUZ	14	?	PMECOS	29	*bcc*	ZIGCOH	44	*bcc*
BISWEF10	15	*bcc*	PMENSE	30	*bcc*			

within layers is optimal when the perimeter of the molecule within the layer is close to circular. The ratios in which the three types of packing *fcc*, *hcp*, *bcc* are observed in the sample shown in Figure 13 is 13:7:53. Even if the sample may be too small to derive any general rule from this finding, one of the reasons which might favor a *bcc* type of

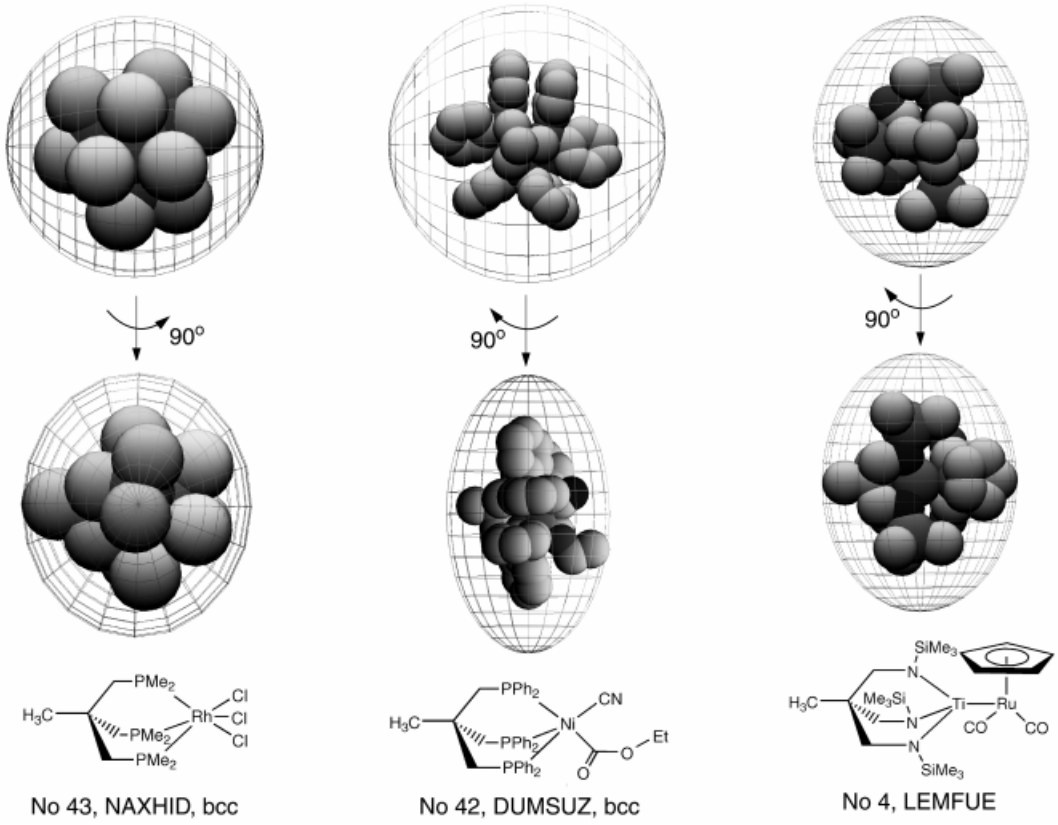


Figure 12. Molecular shape of selected tripod-metal compounds. The numbers and designators refer to Figure 11 and Table 4. The ellipsoids are scaled such that the molecules fit into their envelope. The label *fcc* refers to the idealized packing motif of the molecules.

packing over the other two packing modes is that, with respect to packing spheres, the *fcc* and *hcp* modes are the optimal solutions as far as efficient use of the available space is concerned. Body centered cubic packing, on the other hand, is the optimal solution with respect to maximizing the number of short direct contacts between neighboring spheres.[24] It may well be that maximizing the number of contacts does more to stabilize a molecular crystal than does the optimal use of space.

Conclusion

1. Pattern recognition techniques have been developed which allow for classification of a given set of *n* points in three-dimensional space as being similar to a predefined pattern of the same number of points. The predefined pattern may be any type of chemically interesting polyhedron or may be some other type of pattern that might be of interest. The techniques are such that the quality of fit between a given arrangement of points with one or the other of the predefined categories is quantified as a number between zero and one. Predefinition of patterns relies upon training a neural network to "see" what a human observer would see. Whenever a specific category has to be predefined, a set of training data has to be produced by randomly distorting the ideal pattern. The distorted patterns are inspected and ranked from zero to one according to similarity to and recognizability of the ideal pattern.

2. Several methods to encode three-dimensional structural data into a vector suitable as input to neural networks are reported and it is found that projecting the distance and angle data of the metric matrix of a structure in histographic form onto the vector is a highly efficient strategy.

In addition to this novel pattern recognition technique, the more traditional second moment analysis based upon the matrix of inertia and its eigenvalues is also used.

3. The packing of molecules within a crystal is analyzed with respect to whether the pattern observed might be described as a derivative of one of the three basic types of sphere packing *fcc*, *hcp*, *bcc*. To this end, the molecules are represented by the coordinates of their geometric centers. By symmetry expansion, a minimum number of *m* nearest neighbors within a sphere is generated and all six-point combinations for this set of points are analyzed for octahedral geometry. The octahedral arrangements found are evaluated with respect to their connectivity and to the angles that describe this connectivity. From the type of connectivity found, discrimination between the classes – *fcc*, *hcp*, *bcc*, none of these – is possible.

4. Three sets of compounds – containing a total of 193 organometallic structures – are analyzed with respect to whether the packing modes adopted within the crystals may be described as a variation of one of the three basic types

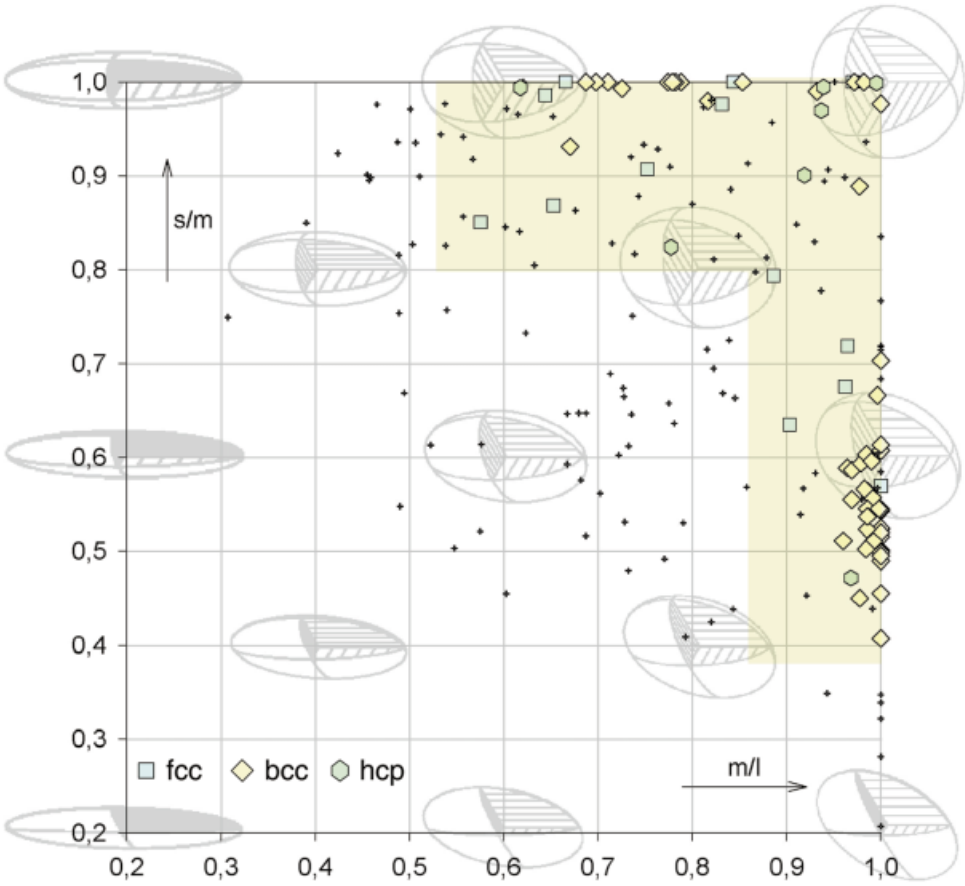


Figure 13. Relation between molecular shape and molecular packing over all data sets analyzed. The diagram refers to the shape of the ellipsoid of inertia pertaining to each molecule analyzed. The vertical axis gives the ratio of the smallest eigenvalue of this ellipsoid to the intermediate one (*s*/*m*). The horizontal axis refers to the ratio of the intermediate eigenvalue to the largest one (*m*/*l*). The shape of the corresponding ellipsoids is shown in the background of the diagram. Only molecules whose shape ellipsoids fall into the area shaded in yellow fall into one of the specified packing categories. Molecules whose shape indicators are shown as a cross do not fall into any of the packing categories analyzed.

of sphere packing. The relevant crystal data are taken from the CSD. One set comprises all organometallic compounds crystallizing in the space group *R*3. The second set contains compounds $Cr(CO)_5L$ and the third one all tripod metal derivatives $RCH_2C(CH_2X)(CH_2Y)(CH_2Z)ML_n$ (R = H, Alkyl, Aryl; X, Y, Z = NR_2, OR, SR, PR_2, PRR′). It is found that the probability of a structure falling into one of the three classes is connected with the shape of the molecules. If the shape is described by the proportions of the eigenvalues of the matrix of inertia corresponding to the molecule, the appropriate diagrams reveal that a packing mode close to one of the three types of sphere packing is most probable when the ellipsoid of inertia has rotational symmetry, i.e. if the compound has approximate C_3 or higher rotational symmetry. Compounds represented by ellipsoids devoid of rotational symmetry may still adopt one of the basic sphere packing types if the relevant eigenvalues do not differ by more than 20% from the mean. At greater ellipticities no match with the search pattern was found.

Experimental Section

Construction of a Data Set Comprising Specified Polyhedra: The data set for training the neural network and calibration of the second moment analysis was generated using a program that allows for the random distortion of ideal polyhedra. From the vertices of an ideal polyhedron, each new vertex of the distorted polyhedron is chosen by randomly selecting a point within a sphere around the vertex of the ideal polyhedron. The degree of distortion can be controlled by the radius of this sphere. As distortion of an ideal polyhedron performed in this way leads rapidly to geometries far from the ideal, a second parameter was introduced to control the distance between the vertices. For each distortion process of a given type of polyhedron, one selects the radius of the distortion sphere (see above), the percentage the distances are allowed to deviate from the ideal polyhedron and the number of distorted polyhedra to be generated. Using this procedure a data set of 381 polyhedra consisting of 37 squares, 43 tetrahedra, 36 pentagons, 55 square pyramids, 54 trigonal bipyramids, 50 hexagons, 73 trigonal prisms, and 38 octahedra including the ideal polyhedra was generated. The degree of distortion was evaluated by visual inspection of each polyhedron. The polyhedron was visualized on a computer screen in any desired orientation. The quality of fit of each polyhedron to the ideal was judged by inspection and a qualifier between $q = 0$ (no fit at all) and $q = 1$ (perfect fit) was allotted. Figure 4 gives an idea of how this subjective assignment of the quality of fit was done. With the specific pattern analysis problem in mind, only those polyhedra for which the qualifier was above 0.8 were incorporated into the training set, giving a total of 381 polyhedra together with the qualifiers (see above). Figure 14 shows six octahedra together with their qualifiers as an example.[38]

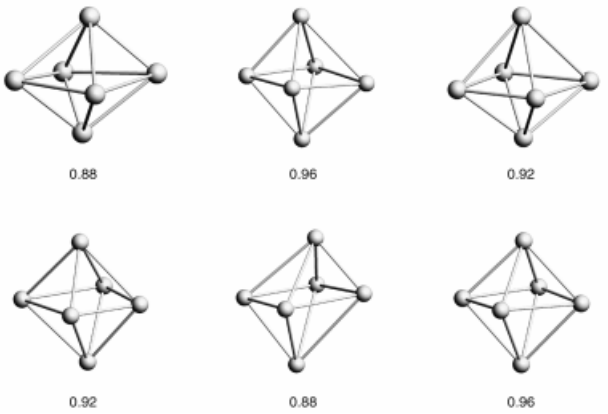


Figure 14. Example of six octahedra with qualifiers above 0.8. The octahedra were generated by randomly distorting an ideal octahedron. The qualifiers indicated by the numbers were allotted by inspection (see text).

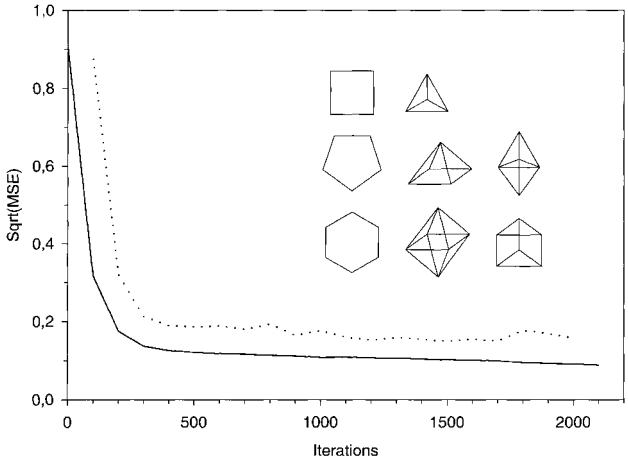


Figure 15. Training of a neural network. The network is designed (see text) to sort the types of polyhedra shown in the inset into their appropriate categories. It was trained on the basis of 281 reference polyhedra. The quality by which the learning pattern is reproduced is represented by the solid line. The quality of prediction for bodies not contained in the training data set is shown by the dashed line.

Sorting of Polyhedra With $4 \leq n \leq 6$ Vertices: The neural network simulator program SNNS,[39] version 4.1 was used. In this work only neural networks of the *feed forward* type were used.[40,41] Such a network consists of an input layer with the number of i input neurons depending on the dimension of the input vector; one or more hidden layers with a number of h hidden neurons and an output layer with the number of o output neurons depending on the dimension of the output vector (see Figure 3). The neurons between each layer are connected and each connection has a specific weight. During the learning process the individual patterns are presented to the network and the weights are adjusted such that the error between the given output vector and the calculated one is minimized.

Figure 15 (solid line) shows the progress of the learning procedure for a network with 27 input neurons, three hidden neurons and nine output neurons, which was trained with a data set containing a total of 281 polyhedra of the types shown in this figure. The shapes of these polyhedra were encoded into a vector based on the method outlined as described in Figure 3 (see above). In contrast to the example shown in Figure 3, the distance part of this vector was limited to only six components, since distances shorter than one half of the maximum distance did not occur in the data set as a consequence of the qualifier being set to q 0.8 (see above). The number of points comprising the individual types of polyhedra was implicitly encoded. Instead of normalizing the ordinate values (''frequency'' in Figure 3) in the histographic representations (for instance by setting the maximal frequency value to one in each case) the frequencies f were mapped onto an ordinate range $0 \leq$ ordinate < 1 by using $f^2/(f^2 + 40)$ as the ordinate value. This means that ordinate values will tend to be larger with larger numbers of points.

As far as convergence of the learning procedure is concerned, the dashed line in Figure 15 shows the root mean square error for a validation data set of 100 patterns containing the same kind of polyhedra as the training set. The root mean square error is defined as the square root of the mean standard error. The mean standard error (MSE) is the sum of the squared deviations between the calculated and the given components of the output vector for all training patterns divided by the number of training patterns. The root mean square error thus indicates the deviation of the output vector as a whole. The deviation of one component of the output vector is calculated as the sum of the squared distances between the calculated and the given output vectors for all training patterns, divided by the number of training patterns and by the number of vector components. The scale of the vertical axis in Figure 15 would then be reduced by a factor of nine (nine output neurons, eight for the bodies shown in Figure 15, a specific one for each body and one extra neuron introduced as a test. This ninth output neuron should only have large numbers $0 \leq q \leq 1$ allotted to it if the body analyzed has no relation to any of the types presented in the training set). The deviation of the individual components is on the order of 0.02 on a scale $0 \leq q \leq 1$. It can be seen that there is no large difference between the straight and the dashed lines. This means that the trained network cannot only recognize the patterns included in the training set but also recognizes patterns which have not been part of the training set.

Sorting of Polyhedra With $n = 6$ Vertices With Respect to Crystal Packing: For the particular problem of pattern recognition with respect to crystal packing, a neural network of the *feed forward* type was trained to filter hexagons, trigonal prisms, and octahedra from ensembles of six points in three-dimensional space. The data set comprised 153 patterns, 43 hexagons, 38 octahedra, and 73 trigonal prisms. This data set was split by random selection into a training set of 137 patterns (35 hexagons, 34 octahedra, 68 prisms) and a validation set of 16 patterns (7 hexagons, 4 octahedra, 5 prisms). The manner in which the data set is separated into different training and validation sets has no great influence on the result. The neural network contained 27 input neurons, six hidden neurons and three output neurons as is schematically shown in Figure 3 where only three hidden neurons are shown. Experiments with different modifications of this type of network suggested that six hidden neurons – as was finally used – is close to the optimum. Each output neuron represents one of the three trained classes (hexagon, octahedron, trigonal prism). The training parameters used with SNNS[39] were as follows:

Learning func: *Backprop Momentum*; Update func: *Topological Order*; Init func: *Randomize Weights*; Learning parameters: *0.6 0.1 0.05 0.05*; Iterations: *500*

Validation of the trained network with the validation data set resulted in a prediction capability of 95.5% with respect to the qualifiers q allocating the polyhedra to their corresponding categories.

The question of practical interest is whether any polyhedron was allocated to an incorrect class. It was found that the classification by the network was 100% correct in this respect, i.e. all polyhedra were correctly assigned to their corresponding class.

Second Moment Analysis: As described above, second moment analysis is another, more traditional method of pattern analysis. The method was used in this case to classify the polyhedra of the data set described at the beginning of the experimental section. For each polyhedron with p vertices one has to calculate the center of mass. The coordinates for each vertex are translated such that the center of mass is at the origin of an orthogonal coordinate system. The new orthogonal coordinates (x_i, y_i, z_i) of the p vertices build up a $3 \times p$ matrix **A**

$$\boldsymbol{A} = \begin{bmatrix} x_1 & x_2 & \cdots & \cdots & x_p \\ y_1 & y_2 & \cdots & \cdots & y_p \\ z_1 & z_2 & \cdots & \cdots & z_p \end{bmatrix}$$

which is multiplied with the transposed matrix $\mathbf{A}^T$ to give a new 3×3 matrix $\mathbf{B} = \mathbf{A}\mathbf{A}^T$. The matrix **B** can be expressed as $\mathbf{B} = \mathbf{X}\Lambda\mathbf{X}^T$, where Λ is the eigenvalue matrix holding the eigenvalues λ_1, λ_2, λ_3 as diagonal elements and **X** is the eigenvector matrix which holds the eigenvectors. The eigenvalues describe the shape of the ellipsoid of inertia which has some relation to the shape of the polyhedron. In order to retain information about the number of points giving rise to a specific set of eigenvalues and at the same time to make results comparable, the eigenvalues have to be scaled in an appropriate way. It has been found through a number of trials that, with the conditions met in the training set, the discriminative power of this eigenvector analysis with respect to separate bodies with n different vertices into individual categories is optimized when each eigenvalue λ_i is replaced by

$$r_i = \lambda_i \cdot \frac{n}{3.5} \quad i = 1,2,3$$

with the scaling function being

$$e_i = \frac{r_i^2}{r_i^2 + 40}$$

The results obtained for the training data set using this type of scaling are shown in Figure 5. The axes X, Y, Z represent the scaled eigenvalues e_i (i = 1, 2, 3). It can be seen that there is a fair separation for some kinds of polyhedra but also that octahedra and trigonal prisms as well as square pyramids and trigonal bipyramids are not well separated. The regions to which the different kinds of polyhedra are mapped to in this diagram are numerically shown in Table 5.

Table 5. Classification of polyhedra by their inertial tensors. The table refers to Figure 5. The coordinates X, Y, Z relate to the eigenvalues of their inertial tensor with a scaling function applied as described in the text. The following abbreviations are used: sq. py square pyramid; trigbpy trigonal bipyramid; oct octahedron; trig pr trigonal prism

Polyhedron	X	Y	Z
Square	0.00–0.0001	0.080–0.130	0.100–0.150
Tetrahedron	0.030–0.055	0.042–0.068	0.054–0.087
Pentagon	0.00–0.0001	0.200–0.242	0.240–0.274
Sq. py/trig bpy	0.031–0.110	0.082–0.183	0.156–0.242
Hexagon	0.00–0.0001	0.370–0.400	0.390–0.430
Oct/trig pr	0.005–0.228	0.156–0.244	0.277–0.510

Packing Analysis: Figure 16 illustrates the general strategy adopted. Given the coordinates of the atoms of the independent molecules within a unit cell and the dimensions and symmetry of the cell, the centers of gravity of all molecules contained in the volume of the unit cell are generated (Figure 16 I→II). The pattern thus obtained is expanded by translational symmetry (Figure 16 II→III). A point in the center of this expanded pattern is selected and its nearest neighbors (16 to start with) are found. Using the pattern recognition tools described above, all octahedra formed by any six of these 16+1 points which are above a certain quality threshold q are found. This qualifier is used to select those six point arrangements which most probably fit together to describe the packing by sharing vertices, edges and faces. In a first attempt, the value of the qualifier $q = 0.9$ is set as the lower limit and from the subgroup of octahedra transgressing this border, pairs of octahedra are selected according to the additional restriction that their qualifiers should be numerically as close together as possible. The connectivity between these pairs of octahedra is then analyzed. The process is repeated with all possible combinations. Based on the entire set of connectivities and their corresponding angles, the packing is classified as belonging to one of the three classes. If no octahedra that fulfill the above conditions are found the thresholds are reduced and the process is repeated. If no fit is found with the qualifiers still having values above $q = 0.8$, the number of points selected in the starting set is increased by one and the procedure is repeated. If no fit is found for up to 24 points in the starting set the packing is considered to not be one of the three types analyzed. In successful cases, this procedure is illustrated as step III→IV in Figure 16. While the thresholds and limits as defined do not have a theoretical foundation, they have been found to be practically sufficient to find any type of packing which has some apparent relation to the three basic packing types analyzed.

Since it is well-known that many patterns of packing involve densely packed layers of molecules, even though these layers are not stacked in such a way as to give rise to one of the three special packing modes discussed above (*fcc*, *hcp*, *bcc*), the search for densely packed layers appears especially worthwhile since the appropriate filters are available (see above). The search may be done by filtering for regular hexagons, independent whether they are centered or not. These hexagons will be filtered out as already described. As an alternative, centered hexagons may be filtered out solely by the application of second moment analysis. This search is done by momentum analysis (see second moment analysis) in order to qualify the seven point arrangements with respect to their planarity (length of the smallest eigenvector). This qualifier *eval* is later used as a parameter in the final filtering function. As a second parameter for this filter-function, the geometric center X of the seven points p_i (i = 1 ... 7) is calculated. The distances d_i from X to all seven points p_i are determined. The smallest of these, d_m, is discarded (the point p_m leading to the smallest distance d_m should be the idealized center of the hexagon). The mean, d_{mean}, of the six distances d_i ($i \neq m$) is calculated. The sum of the differences between the individual distances d_i ($i \neq m$) and their mean value, d_{mean}, is used as the parameter *ldiff*. For a close to regular centered hexagon *ldiff* should be as small as possible. In order to find the hexagons of minimum size the sum of the distances d_i ($i \neq m$) is chosen as the third parameter *lsum*. The filter function *over* is defined as

$$over_i = 1.5 \cdot \left(\frac{eval_i}{eval_{max}}\right) + \left(\frac{ldiff_i}{ldiff_{max}}\right) + \left(\frac{lsum_i}{lsum_{max}}\right)$$

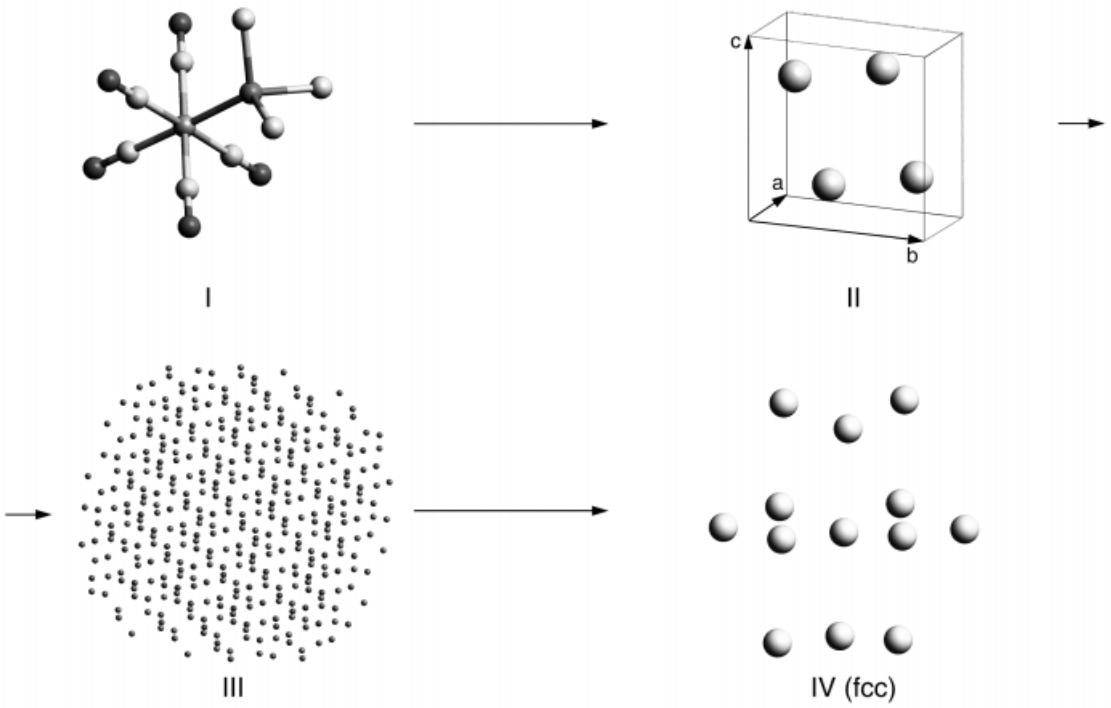


Figure 16. Schematic illustration of the strategy. Molecules within a crystal are replaced by their centers of geometry. The packing of these centers is analyzed by pattern search methods for its similarity to some predefined pattern.

$eval_{max}$ is the largest value of *eval* within the set of seven point arrangements analyzed, comprising a total of 16+1 over 7 individual arrangements. Correspondingly, $ldiff_{max}$ and $lsum_{max}$ are the maximum values found for any seven point combination within the set. Weighting the first term by 1.5 against a weight of 1 for the other terms means that planarity is taken as the most important criterion. The coefficients as well as the type of functions suitable for a filter function have been determined by trial an error. In this manner, any close packed layers are automatically found for any structure analyzed. The centered hexagon with the smallest value *over* is taken as the best plane in the search of an idealized unit cell.

Construction of a Unit Cell: The information about close packed layers obtained by the procedure described above is useful in several aspects. It may be used to project the structure – be it reduced to one central point per molecule or the complete structure – onto this densely packed plane. If the molecules are represented by points, the kind of pattern seen in this projection immediately illustrates the type of packing (see Figure 6). Layer structures with different types of stacking of the individual layers are also immediately identified (see Table 3).

In a second application, the information about layers containing centered hexagons may be used to construct an idealized unit cell. The hexagon is part of a (1,1,1) layer in the *fcc* case (layer stacking ABC) or a (1,1,0) layer in the *bcc* case (layer stacking ABA). In the latter case, even ideal hexagons do not have the full D_{6h} symmetry– which characterizes an *fcc* or *hcp* packing – but are elongated and have maximally D_{2h} symmetry. To find an idealized cube with the appropriate centering with the experimental points as its vertices and centers, the connectivity between the points of such a cube is automatically determined on the basis of the known connectivity of the ideal bodies and of their orientation with respect to the layers.

Figure 17 represents an example of such a body (data from YIKSAM,[36] no. 89 Table 3, Figure 10). In the center of this figure, the body is shown in a projection usually used for illustrating a face-centered cubic cell. At the sides of this figure, projections along the four space diagonals of this body are shown, illustrating that the packing and stacking of close packed planes is very similar in these four directions, as it should be for an *fcc* type packing, where four projections would be identical in the ideal case. The body shown in Figure 17, in addition to not being an exact cube, is not even a parallelepiped and will therefore not be suitable to

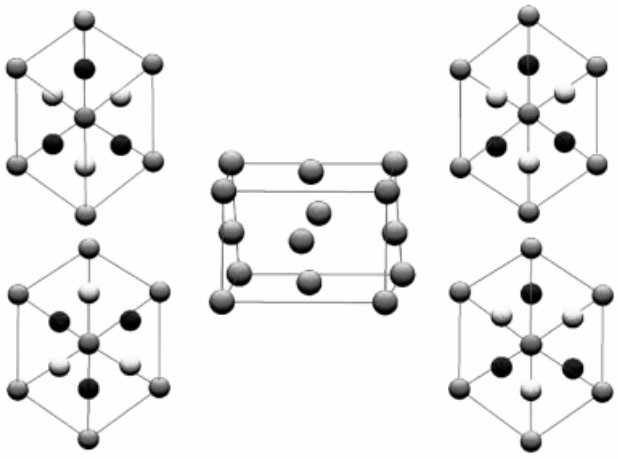


Figure 17. Idealized *fcc* arrangement of one of the specimens analyzed. The figure refers to YIKSAM (Table 3, Figure 10). A projection illustrating the approximate face-centering is shown in the middle. The four independent views of the packing along the four space diagonals of the body shown in the middle are shown at the sides.

describe a crystal, which is an object characterized by translational symmetry. The specific simple example (YIKSAM) is shown in Figure 18 in a two-dimensional projection.

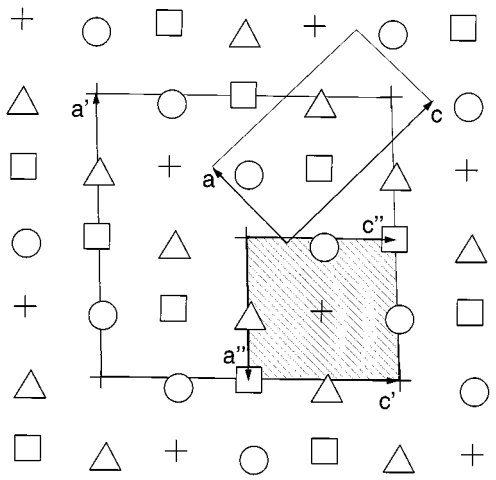


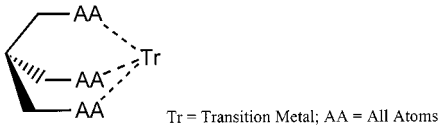
Figure 18. Relation between packing motif and unit cell. The data refer to YIKSAM (Table 3, Figure 10). The packing motif already shown in the middle of Figure 17 is projected onto one of its approximately square faces (shaded area). The axes defining this area are designated a′′, c′′. The axes of the original unit cell are indicated by a and c with the third axis b being perpendicular to a and c. While the shaded area is not yet a repeating unit, a unit cell defined by a′ and c′ is. The length of the axis b has to be doubled.

The crystallographic unit cell is indicated by the vectors a and c. The four points within this unit cell are designated by four different symbols relating to the different coordinates with respect to the third axis b, which is perpendicular to the projection. The idealized face-centered pattern is indicated by an approximately square shaded area. Since the points symbolized by squares and crosses are at approximately the same elevation, they may together form the face of a cube. The points symbolized by circles and triangles again have rather similar coordinates along the b axis but the elevation along this axis is different from that of the points forming the face of the cube. These points (circles, triangles) are the ones centering the faces parallel to the direction of projection. It can be seen that the shaded square is not yet a repetitive unit but that doubling the lengths of its axes a′′, c′′ will give a true repetitive unit, designated by a′ and c′ in the diagram. Once the packing is characterized as belonging to one of the cubic pattern modes, it is possible to construct a body with eight vertices and the respective centering with the experimental points. To find the corresponding repetitive unit the edges of this body, which are close to perpendicular with each other, are used to define a parallelepiped. The axes of this parallelepiped are then expressed in terms of the axes of the original unit cell and based on the restriction that only integer multiples of the original axes are capable of constructing a repetitive pattern, a new unit cell which is a true unit cell and contains the centered bodies as constituents is constructed. This cell may be several times larger than the basic crystallographic unit cell (Figure 18).

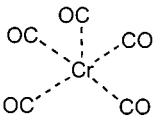
The algebraic details of this transformation are the following: Let a′′, b′′, c′′ be the three vectors which approximately correspond to a description of the body and let a, b, c be the base vectors of the crystallographic unit cell (Figure 18). We then search for a matrix **R**, which transforms the matrix **A** formed by the rows a, b, c into the matrix **B** composed of the rows a′′, b′′, c′′. Since both matrices are nonsingular by definition, the matrix **R** is equal to the product of **B** and the inverse of **A** ($\mathbf{R} = \mathbf{B}\cdot\mathbf{A}^{-1}$; $\mathbf{R}\cdot\mathbf{A} = \mathbf{B}$). The matrix **R** may have non-integer coefficients. Within one row of this matrix, the multipliers that make the coefficients integer, or at least close to integer, are determined and the row is multiplied by the product of these multipliers. Multiplying **A** by this modified matrix results in the best approximation to a cell that is at the same time a true repetitive unit and has the closest relation to the packing type.

Data Sets: All structures were retrieved from the August 1998 version of the CSD.[3] For all searches the parameters NRES = 1 and $Z' \leq 1$ were used. In the case of the structures in the space group *R*3, the parameters SPGN = 146 and atom type Tr were used.

For the molecules with tripodal ligands the search fragment was the following:



For the $Cr(CO)_5L$ structures the search fragment was:



Programs and Equipment: All calculations were carried out on a Silicon Graphics Indigo^2 R4400 workstation, 200 MHz, 128 MB RAM, operating under IRIX 5.3.

The described algorithm was implemented in the new program *crystpack* written in C (≈ 20,000 lines source code) using Motif[42] as graphical user interface and OpenGL[43] for rendering. The program is designed for use under Unix and Linux platforms and is available as source code via www.rzuser.uni-heidelberg.de/~il1/crystpack.html. The program makes use of the SGInfo[44] package. For the purpose of illustration the ZORTEP[45] version of ORTEP[46] and the program package InsightII[47] were used.

Acknowledgments

Fruitful discussions with the late Dr. Laszlo Zsolnai about crystallographic details are gratefully acknowledged, as are the helpful, and at times even enlightening discussions with colleagues Dr. J. Hunger, Dr. S. Beyreuther, and V. Schulz.

[1] H. B. Bürgi, J. D. Dunitz, *Structure Correlation Volume 1 Part II*, VCH, Weinheim, **1994** and references therein.
[2] See for instance: J. Hunger, S. Beyreuther, G. Huttner, K. Allinger, U. Radelof, L. Zsolnai, *Eur. J. Inorg. Chem.* **1998**, 693–702 and references therein.
[3] F. H. Allen, J. E. Davis, J. J. Galloy, O. Johnson, O. Kennard, C. F. Macrae, E. M. Mitchell, G. F. Mitchell, J. M. Smith, D. G. Watson, *J. Chem. Inf. Comput. Sci.* **1991**, 31, 187–204.
[4] See for instance: L. Smart, E. Moore, *Solid State Chemistry: An Introduction*, Chapman Hall, London, **1992**.
[5] A. I. Kitaigorodskii, *J. Phys.* **1945,** 9, 351–352.
[6] A. I. Kitaigorodskii, *Organic Chemical Crystallography*, Consultants Bureau, New York, **1961**.
[7] J. M. Lehn, *Proc. Robert A. Welch Found. Conf. Chem. Res.* **1995**, 11–19.
[8] G. R. Desiraju, C. V. K. Sharma, *Perspect. Supramol. Chem.* **1996**, 31–61.
[9] R. G. Desiraju in: *Compr. Supramol. Chem.* (Eds.: D. D. MacNicol, F. Toda, R. Bishop), Elsevier, Oxford UK, **1996**, Volume 6, p. 1–22.
[10] A. I. Kitaigorodskii, *Molekülkristalle*, Akademie, Berlin, **1979**.

[11] A. I. Kitaigorodskii, *Advan. Struct. Res. Diffr. Methods* **1970**, 3, 173–247.
[12] J. A. Pertsin, A. I. Kitaigorodskii, *The Atom-Atom Potential Method. Applications to Organic Molecular Solids*, Springer Series in Chemical Physics, Vol. 43, Springer, Berlin, **1987**.
[13] A. Gavezzotti, G. Filippini, *Mol. Cryst. Liq. Cryst. Sci. Technol., Sect. A* **1992**, 219, 37–41
[14] W. D. S Motherwell, *Acta Cryst.* **1997**, B53, 726–736.
[15] K. P. Kratzer, *Neuronale Netze – Grundlagen und Anwendungen*, Hanser, Hamburg, **1993**.
[16] H. Ritter, T. Martinez, K. Schulten, *Neuronale Netzwerke – Eine Einführung in die Neuroinformatik selbst-organisierender Netzwerke*, Addison-Wesley, Bonn, **1994**.
[17] A. Zell, *Simulation Neuronaler Netze*, Addison-Wesley, Bonn, **1994**.
[18] J. Zupan, J. Gasteiger, *Neural Networks in Chemistry*, VCH, Weinheim, **1993**.
[19] A. F. Wells, *Structural Inorganic Chemistry*, Fifth Edition, Clarendon Press, Oxford, **1984**.
[20] U. Müller, *Anorganische Strukturchemie*, Teubner, Stuttgart, **1992**.
[21] G. Harsch, R. Schmidt, *Kristallgeometrie – Packungen und Symmetrie in Stereodarstellungen,* Diesterweg, Frankfurt, **1981**.
[22] J. S. Rollett, *Computing Methods in Crystallography*, Pergamon Press, London, **1965**.
[23] G. W. Snedecor, W. G. Cochran, *Statistical Methods*, Iowa State University Press, Ames, **1968**.
[24] F. C. Frank, *Phil. Mag. Letters* **1992**, 66, 81–84.
[25] G. M. Crippen, T. F. Havel, *Distance Geometry and Molecular Conformation,* Research Studies Press Ltd., Sommerset, **1988**.
[26] J. M. Blaney, J. S. Dixon, in: *Reviews in Computational Chemistry Volume 5 Chapter 6* (Ed.: K. B. Lipkowitz, D. B. Boyd), VCH, Weinheim, **1994**.
[27] R. Wierl, *Ann. Phys.* **1931**, 8, 521–564.
[28] J. H. Schuur, P. Selzer, J. Gasteiger, *J. Chem. Inf. Comput. Sci.* **1996**, 36, 334–344.
[29] L. J. Soltzberg, C. L. Wilkins, *J. Am. Chem. Soc.* **1977**, 99, 439–443.
[30] A condensed and easy to read essay on the underlying philosophical problems is to be found in: D. H. Rouvray in: *Fuzzy Logic in Chemistry* (Ed.: D. F. Rouvray), Academic Press, **1997**, chapter 1, p. 1–29; the problem of measuring symmetry has been elegantly treated in: M. Pinsky, D Avnir, *Inorg. Chem.* **1998**, *37*, 5575–5582; D. Avnir, O. Katzenelson, S. Keinan, M. Pinsky, Y. Pinto, Y. Salomon, H. Zabrodsky Hel-Or, *Concepts in Chemistry* (Ed. D. H. Rouvray), Research Studies Press, Somerset, **1997**, chapter 9, p. 283–324.
[31] J. W. Goethe, *Goethes Werke, Vollständige Ausgabe letzter Hand*, Cottasche Buchhandlung, Stuttgart und Tübingen, **1829** Band 22 p. 238, Betrachtungen im Sinne der Wanderer. "Die Theorie an und für sich ist nichts nütze, als insofern sie uns an den Zusammenhang der Erscheinungen glauben macht"; translation: Theory in itself is of no use. It's only purpose is to make us believe in the coherence of phenomena.
[32] H. Goldstein, *Klassische Mechanik*, Akademische Verlagsgesellschaft, Frankfurt, **1963**, V. Kapitel.
[33] D. M. P. Mingos, A. L. Rohl, *J. Chem. Soc., Dalton Trans.* **1991**, 3419–3425.
[34] D. M. P. Mingos, A. L. Rohl, *J. Chem. Soc., Dalton Trans.* **1992**, 3541–3552.
[35] *International Tables for Crystallography*, Volume A 3rd edition, (Ed.: T. Hahn), Kluwer Academic Press, Boston, **1992**, p. 77.
[36] The name is the REFCODE under which the compound is stored in the CSD (see ref. [3]).
[37] D. Braga, F. Grepioni, P. Sabatino, *J. Chem. Soc., Dalton Trans.* **1990**, 3137–3142.
[38] Files containing the coordinates of the polyhedra and the corresponding qualifiers can be accessed over the internet at: www.rzuser.uni-heidelberg.de/il1/crystpack.html.
[39] A. Zell et al., *SNNS User Manual*, Version 4.1, **1995**, http://www.informatik.uni-stuttgart.de/ipvr/bv/projekte/snns/snns.html.
[40] S. Beyreuther, J. Hunger, G. Huttner, S. Mann, L. Zsolnai, *Chem. Ber.* **1996**, *129*, 745–757.
[41] J. Hunger, G. Huttner, *J. Comput. Chem.* **1999**, *20*, 455–471.
[42] M. Brain, *Motif Programming – The Essentials ... and More*, Digital, Newton, **1992**.
[43] M. J. Kilgard, *OpenGL – Programming for the X Window System*, Addison–Wesley, New York, **1996**.
[44] R. W. Grosse-Kunstleve, *Space Group Info's* © **1994–96**, http://www.csb.yale.edu/sginfo
[45] L. Zsolnai, G. Huttner, *University of Heidelberg*, **1994**, http://www.rzuser.uni-heidelberg.de/≈v54/xpm.html.
[46] C. K. Johnson, *ORTEP-II: A FORTRAN Thermal-Ellipsoid Plot Program for Crystal Structure Illustrations*, Oak Ridge National Laboratory Report ORNL-5138, **1976**, http://www.ornl.gov/ortep/ortep.html.
[47] Commercial program package from MSI see: http://www.msi.com.

Received September 9, 1999
[I99320]

Synthesis of the Germanium(I) Compounds $[Ge_2Hal_4]^{2-}$ and Their Reductive Condensation to Octahedral $[Ge_6]^{2-}$ Clusters in an Organometallic Environment

Gerd Renner,[a] Peter Kircher,[a] Gottfried Huttner,*[a] Peter Rutsch,[a] and Katja Heinze[a]

Dedicated to Professor Jürgen Felsche on the occasion of his 60th birthday

Keywords: Germanium(I) / Tetrahalgenodigermanate(2–) / Octahedral $[Ge_6]^{2-}$ clusters / Organometallic derivatives / Carbonyl complexes / Chromium / Tungsten

GeI_2 reacts with $[M_2(CO)_{10}]^{2-}$ (M = Cr, W) leading to reductive coupling of two GeI_2 units to produce the $[Ge_2I_4]^{2-}$ ligands of $[\{(OC)_5M\}I_2Ge–GeI_2\{M(CO)_5\}]^{2-}$ (**1a** and **2a**). The $[Ph_4P]$ salts of these anions have been characterised by X-ray structure analyses as have the $[Ph_4P]$ salts of $[\{(OC)_5M\}Cl_2Ge–GeCl_2\{M(CO)_5\}]^{2-}$ (**1b** and **2b**) obtained from the iodo derivatives **1a** and **2a** by halide metathesis with $[Ph_4P]Cl$. Treatment of GeI_2 with $[W_2(CO)_{10}]^{2-}$ in the presence of 2,2′-bipyridine leads to $[\{(OC)_5W\}I_2Ge–Ge(bipy)\{W(CO)_5\}]$ (**3**). The digermanium ligands in **1**–**3** contain germanium in the unconventional formal oxidation state +I. Reductive condensation of $[\{(OC)_5Cr\}I_2Ge–GeI_2\{Cr(CO)_5\}]^{2-}$ (**1a**) by addition of $[Cr_2(CO)_{10}]^{2-}$ leads to the octahedral cluster $[\{(OC)_5Cr\}_6Ge_6]^{2-}$ (**4**) in a yield of 40%. The sequence of reactions as reported describes the first systematic approach to the synthesis of $[E_6]^{2-}$ clusters.

Introduction

It has recently been shown that mononuclear Sn^{II} or Ge^{II} species may be transformed by group-16 carbonylmetallates to produce the octahedral $[E_6]^{2-}$ clusters (E = Ge, Sn) at the core of the well-characterised compounds $[\{(OC)_5Cr\}_6E_6]^{2-}$.[1] By statistical reasoning, the selective formation of such six-atom aggregates $[E_6]^{2-}$ from six individual constituents – each of which contains only one single element E – is a highly improbable process. Thermodynamic and kinetic control along the reaction pathway must play an important role if, as observed, six mononuclear entities aggregate to form an octahedral species. Because of the high number of oligonuclear intermediates that necessarily line out the pathway of such a process, these thermodynamic and kinetic factors are difficult to control. An extended series of experiments is needed to find the proper conditions for such selective aggregation procedures.

The number of potential steps involved in this type of reaction might be considerably reduced if oligonuclear precursors could be used in the condensation process. With this in mind we have tried to prepare dinuclear precursors that, when appropriately functionalised, would allow better control of the condensation process and a suitable procedure has in fact been developed in the case of germanium.

With germanium as the main-group centre it is known that dinuclear species Ge_2R_6 are intrinsically stable entities.[2] Such organically substituted digermanes do, however, lack the reactive functionalisation necessary to produce dielement E_2 building blocks for the formation of E_6 clusters. Ge_2H_6 might be a potential candidate as it is known that Ge–H bonds may be broken in the presence of organometallic entities,[3] although Ge_2H_6 is not easy to handle and is thus perhaps not the best choice.[4] Moreover, the established procedures for the syntheses of $[\{(OC)_5M\}_6E_6]^{2-}$ clusters all start from mononuclear $EHal_2$ compounds with the anionic pentacarbonylmetal entities $[Cr_2(CO)_{10}]^{2-}$ [5] or $[Cr(CO)_5]^{2-}$ [6] acting as halide abstractors and reducing agents at the same time.[1] The ideal precursors in this respect would therefore be the compounds Ge_2Cl_2 or Ge_2Cl_6; the former compound is still unknown while the latter has been characterised as a rather unstable species.[7] Since these precursors are not available or not suitable as such, one might try to produce them in an organometallically protected form. Since base-stabilised germylene compounds $[(OC)_5M–GeHal_2base]$ (M = Cr, W) are known,[8] a conceptual approach would consist of the reductive coupling of two such entities to give $[\{(OC)_5M\}Hal_2Ge–GeHal_2\{M(CO)_5\}]^{2-}$. This approach receives some additional credit from the observation that $PhPCl_2$ as well as PCl_3 undergo reductive coupling with $[Cr_2(CO)_{10}]^{2-}$ to produce the corresponding diphosphane coordination compounds $[\{(OC)_5Cr\}Cl(R)P–P(R)Cl\{Cr(CO)_5\}]$ (R = Ph,[9] Cl[10]).

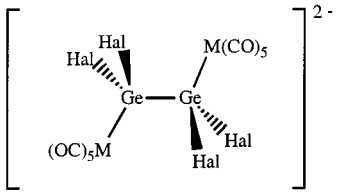
Compounds Containing a $[Ge_2Hal_4]^{2-}$ Ligand

It is shown in this paper that GeI_2 may be reductively coupled by its reaction with $[M_2(CO)_{10}]^{2-}$ (M = Cr, W) to produce $[\{(OC)_5M\}I_2Ge–GeI_2\{M(CO)_5\}]^{2-}$ (**1a** and **2a**, Table 1). Halide exchange by $[Ph_4P]Cl$ leads to the corresponding tetrachlorodigermanate compounds **1b** and **2b** (Table 1).

[a] Anorganisch-Chemisches Institut der Universität Heidelberg
Im Neuenheimer Feld 270, 69120 Heidelberg, Germany
Fax: (internat.) + 49-(0)6221/545707
E-mail: g.huttner@indi.aci.uni-heidelberg.de

 © WILEY-VCH Verlag GmbH, D-69451 Weinheim, 2000 1434–1948/00/0505–0879 $ 17.50+.50/0

Table 1. Complexes of type **1** and **2**



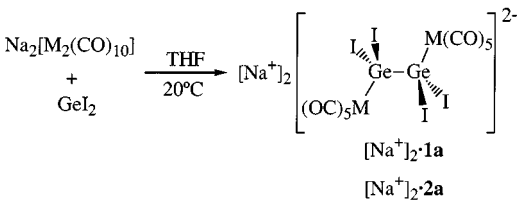
	halide	metal	cation
1a	I	Cr	$[Na^+]$
1a	I	Cr	$[Ph_4P^+]$
1b	Cl	Cr	$[Ph_4P^+]$
2a	I	W	$[Na^+]$
2a	I	W	$[Ph_4P^+]$
2a	I	W	$[nBu_4N^+]$
2b	Cl	W	$[Ph_4P^+]$

These compounds contain the unconventional and hitherto unknown $[Ge_2Hal_4]^{2-}$ ligands with the formal oxidation state of Ge corresponding to +I. In assigning this oxidation state the $Cr(CO)_5$ entities are seen as neutral sixteen-electron Lewis acids with chromium in an oxidation state of zero.

In agreement with the conceptual model, it is further found that $Na_2[\{(OC)_5Cr\}I_2Ge–GeI_2\{Cr(CO)_5\}]$ ($[Na^+]_2$·**1a**) undergoes transformation to the octahedral cluster anion $[\{(OC)_5Cr\}_6Ge_6]^{2-}$ (**4**) by reaction with $[Cr_2(CO)_{10}]^{2-}$ in an overall yield of 40%.

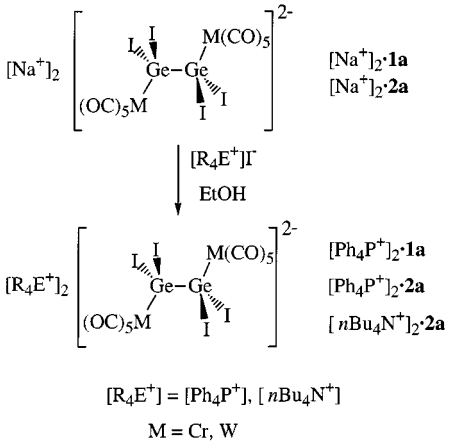
Syntheses and Structures

When a THF solution of $Na_2[Cr_2(CO)_{10}]$ is treated with an equimolar amount of GeI_2, the solution immediately changes colour from orange to red. Chromatography gives $Na_2[\{(OC)_5Cr\}I_2Ge–GeI_2\{Cr(CO)_5\}]$ ($[Na^+]_2$·**1a**) as a red oil (Scheme 1).



Scheme 1. Reaction of $Na_2[M_2(CO)_{10}]$ (M = Cr, W) with GeI_2

The compound $[Ph_4P^+]_2$·**1a** is obtained as a crystalline derivative upon metathesis with $[Ph_4P]I$ in ethanol (Scheme 2).



Scheme 2. Salt metathesis reaction

The anionic constituent of the sodium salt $[Na^+]_2$·**1a** is the same as that of the phosphonium salt $[Ph_4P^+]_2$·**1a**, as evidenced by the $\tilde{\nu}_{CO}$-IR spectra of these compounds (Table 2). The properties of **1a** were therefore fully characterised with $[Ph_4P^+]_2$·**1a** as the example studied (Tables 5 and 6).

Table 2. $\tilde{\nu}_{CO}$-IR spectroscopic data for the compounds **1–2**

	$\tilde{\nu}_{CO}$-IR [cm^{-1}]				
$[Na^+]_2$·**1a** [a]	-	2037s	1970sh	1935vs,br	-
$[Ph_4P^+]_2$·**1a** [b]	-	2034s	1967sh	1933vs	1890s
$[Ph_4P^+]_2$·**1a** [c]	-	2032s	-	1924vs	1892sh
$[Ph_4P^+]_2$·**1b** [b]	-	2030s	1950sh	1930vs	1889vs
$[Ph_4P^+]_2$·**1b** [c]	-	2028s	-	1926vs,br	-
$[Na^+]_2$·**2a** [d]	-	2049s	1967sh	1935vs	1884vs
$[Na^+]_2$·**2a** [a]	-	2052s	-	1934vs,br	1909sh
$[Ph_4P^+]_2$·**2a** [b]	-	2049s	1968sh	1930vs	1885s
$[Ph_4P^+]_2$·**2a** [c]	-	2047s	1963sh	1920vs,br	1889s
$[nBu_4N^+]_2$·**2a** [b]	-	2049s	1967sh	1932vs	1885s
$[nBu_4N^+]_2$·**2a** [d]	2057w	2049s	1967sh	1934vs	1889s
$[nBu_4N^+]_2$·**2a** [c]	-	2049s	1969sh	1929vs	1879s
$[Ph_4P^+]_2$·**2b** [b]	2055w	2046s	1963sh	1929vs	1883vs
3 [d]	2058m	2039s	1958sh	1927vs	-

[a] EtOH. – [b] DMA. – [c] CsI. – [d] THF.

The constitution of **1a**, as given, is in agreement with the spectroscopic data as well as with the microanalytical data. Proof of the constitution of **1a** comes from the X-ray analysis of $[Ph_4P^+]_2$·**1a** (Figure 1, Tables 3 and 7).

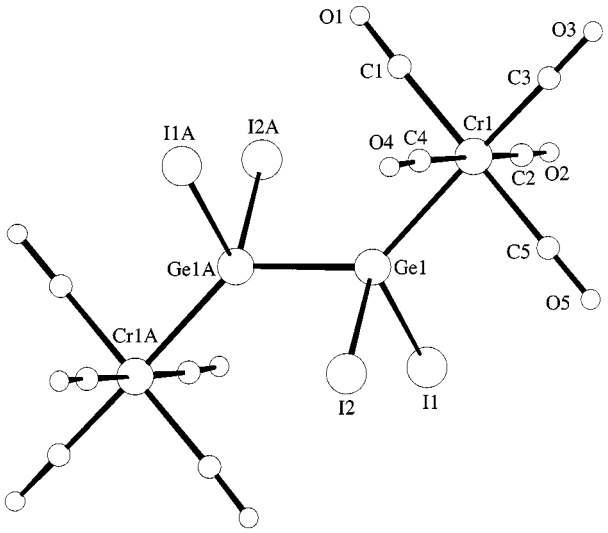


Figure 1. Structure of compound $[Ph_4P^+]_2$·**1a**

The anion has crystallographically imposed inversion symmetry (Table 7). The Ge–Ge bond length is 244.8 pm (Table 3) and is thus well within the range of Ge–Ge distances reported for Ge_2R_6 compounds and their derivatives.[2] The Ge–Cr distances (Table 3) compare favourably with the corresponding distances reported for $[\{(OC)_5Cr\}GeR_2(Donor)]$,[11] as well as with those observed for the mononuclear chelate compounds $[\{(OC)_5Cr\}_2$-Ge(bipy)] and $[\{(OC)_5Cr\}_2$Ge (phen)] (bipy = 2,2′-bipyridine; phen = 1,10-phenanthroline).[12]

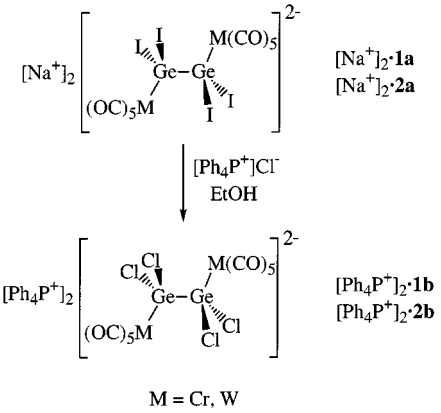
The mean Ge–I bond length of 264.5 pm (Table 3) is similar to that observed for $[\{Cp'(CO)_2Mn\}GeI_3]^-$ (261.6 pm).[13] Corresponding to the inversion symmetry of the molecule, the bonds radiating from the two Ge atoms are in a perfectly staggered arrangement. The pentacarbonylchromium entities are in their conventional idealised octahedral geometry with an overall slight umbrella effect for the equatorial carbonyl groups (Table 3). The CO group C1–O1 – equivalent to C1A–O1A by symmetry – is found to bend in an obverse sense (Table 3). These latter two groups are in close proximity to the GeI_2 entity in the symmetry-related part of the molecule.

The halide functionalities in **1a** are substitutionally labile: treatment of the sodium salt of **1a** (vide supra) with $[Ph_4P]Cl$ results in an exchange of the iodine substituents of **1a** versus chlorine substituents to give **1b** (Scheme 3). Complex **1b** is obtained as a yellow microcrystalline material. The $\tilde{\nu}_{CO}$-IR pattern observed for **1b** is very similar to that shown by **1a** (Table 2). Elemental analysis indicates that halide exchange is not complete under the experimental conditions and the presence of 5 to 10% of unexchanged iodine substituents is inferred from these data (Table 5).

X-ray analysis of $[Ph_4P^+]_2$·**1b** substantiates this hypothesis. Crystals of $[Ph_4P^+]_2$·**1b** are isotypic with those of $[Ph_4P^+]_2$·**1a** (Table 7). The volume of the cell is reduced by about 4% upon substitution of iodine (**1a**) with chlorine (**1b**). The two anions **1a** and **1b** are isostructural in a qualitative sense. The Ge–Ge bond length of 245.5 pm in **1b** (Table 3) is almost equal to that observed for **1a** (244.8 pm,

Table 3. Selected bond lengths [pm], angles [°], and torsion angles [°] for the compounds **1–2**

	$[Ph_4P^+]_2$·**1a** (M = Cr, Hal = I)	$[Ph_4P^+]_2$·**1b** (M = Cr, Hal = Cl)	$[Ph_4P^+]_2$·**2a** (M = W, Hal = I)	$[Ph_4P^+]_2$·**2b** (M = W, Hal = Cl)
Ge1-Ge1A	244.8 (1)	245.5 (1)	245.6 (2)	245.0 (2)
Ge1-M1	246.8 (1)	244.0 (1)	260.6 (1)	258.4 (1)
Ge1-Hal1	264.8 (1)	226.6 (1)	262.8 (1)	225.9 (2)
Ge1-Hal2	264.1 (1)	234.7 (1)	266.2 (1)	238.7 (2)
Hal1-Ge1-Hal2	98.9 (1)	98.3 (1)	97.5 (1)	98.4 (1)
Hal1-Ge1-M1	115.1 (1)	114.9 (1)	115.6 (1)	116.2 (1)
Hal2-Ge1-M1	114.6 (1)	111.7 (1)	110.7 (1)	110.9 (1)
M1-Ge1-Ge1A	132.1 (1)	132.3 (1)	134.8 (1)	130.6 (1)
Hal1-Ge1-Ge1A	95.0 (1)	95.8 (1)	94.4 (1)	96.1 (1)
Hal2-Ge1-Ge1A	94.9 (1)	98.0 (1)	96.8 (1)	99.2 (1)
C1-M1-Ge1	92.8 (2)	90.4 (2)	92.4 (3)	89.4 (3)
C2-M1-Ge1	87.4 (2)	89.2 (2)	89.4 (3)	89.3 (3)
C3-M1-Ge1	178.1 (2)	174.9 (2)	174.4 (3)	174.7 (3)
C4-M1-Ge1	87.9 (2)	87.7 (2)	87.8 (3)	87.0 (3)
C5-M1-Ge1	86.2 (2)	83.5 (2)	86.3 (3)	86.1 (5)
Hal2-Ge1-Ge1A-Hal1A	81	81	81	80
M1A-Ge1A-Ge1-Hal1	49	48	47	47
M1-Ge1-Ge1A-Hal2A	50	51	52	52
C5-M1-Ge1-Hal1	-61	-59	-55	-59
C5-M1-Ge1-Hal2	52	52	54	52



Scheme 3. Salt metathesis reaction combined with an exchange of the iodine versus chlorine substituents

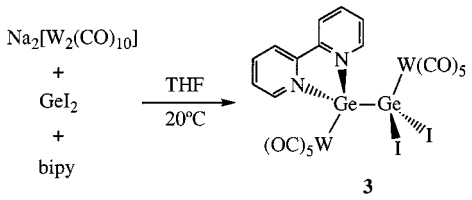
Table 3). The observed discrepancy of the Ge–Cl distances (Table 3), however, as well as the region of residual electron density of 1.6 electrons·10^{-6} pm^{-3} in the neighbourhood of the chlorine substituent Cl2 with the Ge1–Cl2 bond that is apparently too long (Table 3), have to be interpreted in terms of a partial occupancy of the chlorine position by an iodine substituent. Values of individual parameters will therefore be subject to errors and hence do not warrant a detailed discussion. The overall structure of **1b** is nevertheless unequivocally clear from the X-ray analysis.

The mass-spectrometric analyses of $[Ph_4P^+]_2$·**1a** and $[Ph_4P^+]_2$·**1b** show fragmentation patterns which that are in accordance with their assigned constitution (Table 5).

The synthetic strategy leading to the pentacarbonylchromium derivatives **1a** and **1b** works equally well for the pentacarbonyltungsten derivatives **2a** and **2b** (Schemes 1, 2, and 3; Table 1). The anions **2a** and **2b** are isolated as their respective $[Ph_4P^+]$ or $[n Bu_4N^+]$ salts. Single crystals suitable for X-ray analysis could be obtained for their $[Ph_4P^+]$ salts (Tables 3 and 7). As seen from Table 7, the phosphonium salts of **1a**, **1b**, and **2b** form a set of isotypic crystals. The corresponding salt of **2a** also crystallises in a triclinic space group. The cell parameters (Table 7) are, however, numerically quite different from those characterising the above isotypic series. The unit cell observed for $[Ph_4P^+]_2$·**2a** cannot be transformed to a unit cell showing distances and angles that would be in close numerical agreement with those for the isotypic series of the phosphonium salts **1a**, **1b**, and **2b**. Transformation of the cell data of the phosphonium salt of **2a** by {00–1, 100, 0–10} leads to a cell with dimensions (12.76, 12.06, 12.26 [Å]; 69.00, 90.39, 69.09 [°]). On using this transformed unit cell for comparison, the centres of the molecules are seen to have rather similar coordinates in all four salts. In the salt of **2a** the anionic part is, however, at a different rotational position as compared to the orientations of the anions in **1a**, **1b**, and **2b** with respect to the unit cells. By comparing the volumes of the cells (Table 7) it is clear that within the series of phosphonium salts the packing is least efficient in **2a**. This may explain the observation that crystals of $[Ph_4P^+]_2$·**2a** crack when cooled down to 200 K. A phase transition to the more closely packed pattern is in accord with this finding. Nevertheless, the structures of all four compounds (**1a**, **1b**, **2a**, and **2b**) are qualitatively identical with that shown in Figure 1, which illustrates the general arrangement with the structure of **1a** shown as the specific example. In a quantitative respect, the essential difference between the pairs of structures **1a**/**2a** and **1b**/**2b** results from the replacement of the $Cr(CO)_5$ groups in compounds **1** by $W(CO)_5$ groups in compounds **2** (Tables 1, 3, and 7). The torsion angles within the molecules are not affected to a great extent by this replacement and, in particular, the Ge–Ge bond lengths are almost identical in all four compounds within the limits of error, with an average value of 245.2 pm (Table 3). As already observed for **1b**, some of the chlorine positions in **2b** are affected by an incomplete substitution of iodine versus chlorine, with the numerical values of the distances for Ge1–Hal2 in compounds **1b** and **2b** being too large. The remaining distances and angles (Table 3) agree favourably within the set of compounds **1** and **2**. The W–Ge distances observed for **2** are also within the range of W–Ge single bond lengths known to date.[14]

[Hal_2Ge–Ge(bipy)] as a Ligand

It has been observed that formation of the cluster $[\{(OC)_5Cr\}_6Ge_6]^{2-}$ from $Na_2[Cr_2(CO)_{10}]$ and GeI_2 is promoted by the presence of bipy (2,2′-bipyridine)[1a] and so the reactions leading to **1** and **2** were repeated in the presence of bipy. It was hoped that some bipy derivative could be detected that would help to explain the role of the bipy ligand in cluster formation.[1a] However, treatment of $Na_2[Cr_2(CO)_{10}]$ in THF solution with equimolar amounts of GeI_2 and bipy did not produce any new insight into the process. The only products isolated were $[\{(OC)_5Cr\}_2$-Ge(bipy)] and $[\{(OC)_5Cr\}_6Ge_6]^{2-}$, both of which have already been reported.[1a,12] However, the use of $Na_2[W_2(CO)_{10}]$ as the starting material, under otherwise identical conditions, gave the digermanium compound **3** (Scheme 4).



Scheme 4. Reaction of $Na_2[W_2(CO)_{10}]$ with GeI_2 and 2,2′-bipyridine

Compound **3** was purified by column chromatography and the side products $[(OC)_4W(bipy)]$ and $W(CO)_6$ were separated by this procedure.[17] Compound **3** was eluted with THF as a broad red band. Some additional red material was obtained by elution with ethanol and this, by analogy, is thought to contain $[\{(OC)_5W\}_6Ge_6]^{2-}$. Compound **3** was obtained as a red oil by evaporation of the solvent from the combined THF fractions whose $\tilde{\nu}_{CO}$-IR spectra showed only the bands due to **3** (Table 2) with no indication of by-products. Compound **3** could be obtained in a crystal-

line form from its concentrated solutions by a vapour phase diffusion process (see Experimental Section). The red crystals are stable over several days when retained in the mother liquor in the dark. Handling of the crystals is nevertheless problematic since they are found to produce an amorphous material under the conditions of evaporation. It is not yet clear whether this disintegration is due to the reduced pressure – a possibility that is not highly probable since compound **3** is found to crystallise without inclusion of solvent – or whether the material is sensitive to daylight. When the amorphous material that remained after evaporation of the solvent was redissolved, red solutions were obtained and the ^{1}H-NMR spectra of these indicate the presence of a minimum of three different types of coordinated bipy ligands. By comparison with spectra of authentic samples it appears that one of these products is $[(OC)_4W(bipy)]$;[17] the identity of the two other compounds is as yet unknown. The only way to identify the nature of the primary product **3** is therefore by X-ray analysis. Single crystals of **3** were immediately transferred from the mother liquor into perfluorinated oil and then placed onto a diffractometer in as short a period of time as possible while keeping the temperature below –70 °C. This procedure ensured that the crystals survived without disintegration. The structure of **3**, as determined by crystal structure analysis, is depicted in Figure 2 (Table 4).

Crystals of **3** contain discrete molecular entities, the central part of which is the digermanium-derived constituent $[I_2Ge–Ge(bipy)]$ (Figure 2). Each of the germanium centres is coordinated to a $W(CO)_5$ group. One of the germanium centres (Ge1) has two iodine substituents, while the other germanium is coordinated to the bipy ligand (Figure 2). The germanium centres are linked by a Ge–Ge bond, the length of which (248.2 pm) is close to the Ge–Ge bond lengths observed for **1** and **2** (Tables 3 and 4).

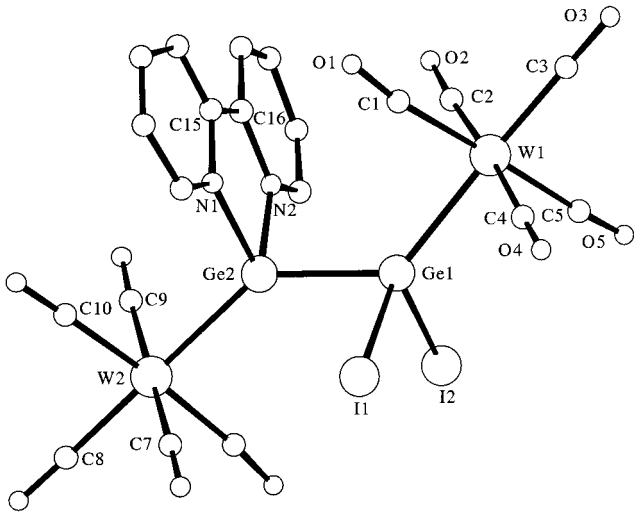


Figure 2. Structure of compound **3**

The Ge–N and Ge–I bond lengths are also within the usual range,[12,13] as are the Ge–W distances[14] (compare Tables 3 and 4). The arrangement of the substituents around the Ge–Ge axis corresponds to that observed for **1** and **2**, with the bonds radiating from the two germanium centres being staggered with respect to one another (Table 4). Even though there is no crystallographically imposed molecular symmetry for **3**, the effective molecular symmetry is close to C_S (for torsion angles, see Table 4). In contrast to the structures of **1** and **2**, the rotation of the $M(CO)_5$ groups around their respective Ge–M axis is close to an eclipsed arrangement in **3** (Table 4, Figure 2); it ap-

Table 4. Selected bond lengths [pm], angles [°], and torsion angles [°] for the compound **3**

Ge1-Ge2	248.2 (3)	N1-Ge2-N2	80.2 (7)
Ge1-W1	259.0 (3)	N1-Ge2-W2	111.8 (5)
Ge1-I1	266.4 (4)	N2-Ge2-W2	111.6 (6)
Ge1-I2	262.0 (3)	C1-W1-Ge1	90.9 (8)
Ge2-W2	259.4 (3)	C2-W1-Ge1	87.3 (6)
Ge2-N1	202.8 (2)	C3-W1-Ge1	177.5 (7)
Ge2-N2	201.4 (2)	C4-W1-Ge1	89.4 (6)
		C5-W1-Ge1	86.8 (6)
W1-Ge1-Ge2-W2	180	I1-Ge1-I2	103.4 (1)
W2-Ge2-Ge1-I2	-48	I1-Ge1-W1	117.8 (1)
W2-Ge2-Ge1-I1	55	I2-Ge1-W1	117.3 (1)
N1-Ge2-Ge1-W1	-40	C6-W2-Ge2	92.4 (7)
N2-Ge2-Ge1-W1	41	C7-W2-Ge2	91.7 (6)
W2-Ge2-N1-C15	-110	C8-W2-Ge2	179.8 (9)
W2-Ge2-N2-C16	107	C9-W2-Ge2	85.7 (7)
C5-W1-Ge1-I1	-13	C10-W2-Ge2	90.8 (6)
C5-W1-Ge1-I2	111	I1-Ge1-Ge2	88.4 (1)
C10-W2-Ge2-N1	-3	I2-Ge1-Ge2	92.8 (1)
C10-W2-Ge2-N2	-91	W1- Ge1-Ge2	130.7 (1)
		W2- Ge2-Ge1	138.7 (1)
		Ge2-N1-C15	115.5 (2)
		Ge2-N2-C16	116.7 (2)

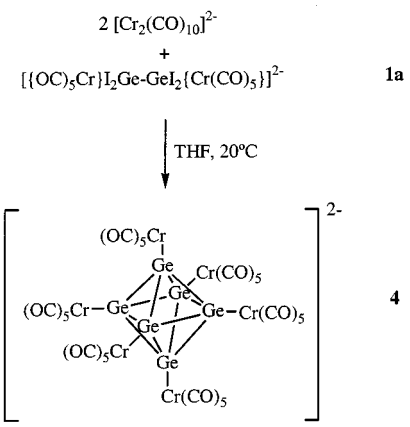
proximates a staggered orientation in the structures **1** and **2** (Table 3, Figure 1).

Compound **3** contains the digermanium species $[I_2Ge–Ge(bipy)]$, which is unknown in the free state and stabilised in **3** by protection with bulky $W(CO)_5$ groups. This digermanium entity may be interpreted in terms of a Lewis base/Lewis acid interaction with the organometallically protected eight electron species $L_nMGe(bipy)$ acting as the base and the equivalently protected six-electron species L_nMGeI_2 as the Lewis acid.[15] This type of interpretation is appealing since the protected six electron species $[(OC)_5M–GeR_2]$[16] are known as such and also in their base-stabilised form.[8] Lewis acid adducts of $[(OC)_5M–Ge(bipy)]$ are equally well known and are well characterised as having $[M(CO)_5]$ as the Lewis acidic group.[12] By whatever electron-counting approach the bonding situation in $[I_2Ge–Ge(bipy)]$ is analysed, it is found that it is in a formal sense isoelectronic to the $[Ge_2Hal_4]^{2–}$ entities of **1** and **2**.

The unsymmetrical substitution of the Ge–Ge entity in **3** might form the basis of its reactivity. To date, however, no attempt to transform **3** into the cluster $[\{(OC)_5W\}_6Ge_6]^{2–}$ has been successful and it may therefore be assumed that compounds of type **3** do not play a key role in the bipy-mediated[1a] synthesis of $[\{(OC)_5W\}_6Ge_6]^{2–}$.

A Straightforward Synthesis of the $[Ge_6]^{2–}$ Core

Even though **3** could not be transformed to produce a $[Ge_6]^{2–}$ cluster, an efficient synthesis of the $[Ge_6]^{2–}$ core has nevertheless been found by following a different strategy (Scheme 5). When THF solutions of $Na_2[\{(OC)_5Cr\}I_2Ge–GeI_2\{Cr(CO)_5\}]$ ($[Na^+]_2$·**1a**) (vide supra) are treated with two equivalents of $Na_2[Cr_2(CO)_{10}]$[5] dissolved in THF, a continuous change of the $\tilde{\nu}_{CO}$-IR spectra of the reaction mixture is observed. While the long-wavelength region is obscured by the bands that are characteristic of $[Cr_2(CO)_{10}]^{2–}$, in the short-wavelength range the bands characteristic of the reaction products are observed to evolve. The band pattern at 2053/2030 cm^{-1} indicates the formation of $[Cr_2(CO)_{10}H]^–$.[5,18] The assignment of this pattern to $[Cr_2(CO)_{10}H]^–$ was corroborated by the independent synthesis of $[Ph_4P][Cr_2(CO)_{10}H]$, which was characterised by single-crystal analysis and comparison with the known structure of this compound,[18] by its proton-NMR signal in CD_2Cl_2 solution at $\delta = –19.4$ and its $\tilde{\nu}_{CO}$-IR spectrum in THF solution.[5,18] A band characteristic of the cluster $[\{(OC)_5Cr\}_6Ge_6]^{2–}$ (**4**) (2043 cm^{-1})[1a] was also found to increase in intensity during the reaction. After complete addition of the two equivalents of $Na_2[Cr_2(CO)_{10}]$ during a period of three hours, the band at 2043 cm^{-1} was found not to increase any further when an additional 0.3 equivalents of $Na_2[Cr_2(CO)_{10}]$ were added. These findings indicate that the formation of the compound that gives rise to the band at 2043 cm^{-1} requires two equivalents of $Na_2[Cr_2(CO)_{10}]$ for completion. The red-brown solution was concentrated, filtered through Kieselgur, and chromatographed on silica gel. $Na_2[\{(OC)_5Cr\}_6Ge_6]$ $\{[Na^+]_2$·**4**$\}$ was obtained as a red ethanolic eluate from which **4** could be precipitated by metathesis with $[Ph_4P]Cl$ in ethanol. The salt $[Ph_4P^+]_2$·**4** was obtained as a microcrystalline red-brown material in fair yields (40%). Crystals were obtained by layering a solution of $[Ph_4P^+]_2$·**4** in DMA (*N*,*N*-dimethylacetamide) with ethanol. The identity of **4** has been inferred by comparison of the unit-cell data obtained for $[Ph_4P^+]_2$·**4** by X-ray analysis with the authentic data.[1a] X-ray analysis of these crystals proved that the sample is identical with authentic $[Ph_4P]_2[\{(OC)_5Cr\}_6Ge_6]$.[1a]



Scheme 5. Reaction of **1a** with $[Cr_2(CO)_{10}]^{2–}$ to produce **4**

Conclusions

In the presence of $M(CO)_5$ moieties (M = Cr, W) germanium(II) halides may be reductively coupled to produce $[Ge_2Hal_4]^{2–}$ ligands. In a formal sense these ligand entities contain germanium in its unconventional +I oxidation state and are formally isoelectronic to P_2R_4 ligands,[9,10] which act as bridging entities in several well-characterised organometallic derivatives. In contrast to P_2R_4, their anionic equivalents $[Ge_2R_4]^{2–}$ are not known but they are found to be stable in their $M(CO)_5$-protected form $[\{(OC)_5M\}I_2Ge–GeI_2\{M(CO)_5\}]^{2–}$ (**1** and **2**).

In the presence of bipy, the organometallically protected ligands of the type $[Hal_2Ge–Ge(bipy)]$ may be obtained under otherwise similar conditions. Here again the formal average oxidation state of germanium is +I and the ligands are not known in the free state but are stable under organometallic protection, as shown for $[\{(OC)_5W\}I_2Ge–Ge(bipy)\{W(CO)_5\}]$ (**3**).

Starting from the digermanium precursor $[\{(OC)_5Cr\}Hal_2Ge–GeHal_2\{Cr(CO)_5\}]^{2–}$ (**1**), a reductive condensation procedure produces $[\{(OC)_5Cr\}_6Ge_6]^{2–}$ (**4**), which has a $[Ge_6]^{2–}$ core. This type of process is the first straightforward approach to the selective synthesis of the $[Ge_6]^{2–}$ core.

Experimental Section

General: All manipulations were carried out under argon by means of standard Schlenk techniques at 20 °C unless mentioned otherwise. All solvents were dried by standard methods and distilled

under argon. The [D6]DMSO and [D6]acetone used for the NMR-spectroscopic measurements were degassed by three successive "freeze-pump-thaw" cycles and dried over 4-Å molecular sieves. Silica gel (Kieselgel z. A. 0.06–0.2 mm, J. T. Baker Chemicals B. V.) used for chromatography and Kieselgur (Kieselgur, gereinigt, geglüht, Erg. B.6, Riedel de Haën AG) used for filtration were degassed at 1 mbar at 130 °C for 12 h and saturated with argon. – NMR: Bruker Avance DPX 200 at 200.13 MHz (^{1}H), 50.323 MHz (^{13}C{^{1}H}), 81.015 MHz (^{31}P{^{1}H}); chemical shifts (δ) in ppm with respect to [D6]DMSO (^{1}H: δ = 2.50; ^{13}C: δ = 39.4) and [D6]acetone (^{1}H: δ = 2.05; ^{13}C: δ = 206.2), respectively, as internal standards and to 85% H_3PO_4 (^{31}P: δ = 0) as external standard. – IR: Bruker FT-IR IFS-66; CaF_2 cells. – UV/Vis/NIR: Perkin–Elmer Lambda 19; cells (0.2 cm; Hellma 110 suprasil). – MS (FAB): Finnigan MAT 8400; Nibeol matrix (4-nitrobenzyl alcohol). – Elemental analysis: Microanalytical Laboratory of the Organisch-Chemisches Institut, Universität Heidelberg. – Melting points: Gallenkamp MFB-595 010; the values are not corrected. – Chemicals: The metallates $Na_2[M_2(CO)_{10}]$[5] (M = Cr, W) and GeI_2[19] were prepared by literature methods. All other chemicals were commercially obtained and used without further purification. – Analytical and spectroscopic data are given in Table 2, Table 5, and Table 6. X-ray data are given in Tables 3, 4, and 7.

$Na_2[\{(OC)_5M\}I_2Ge–GeI_2\{M(CO)_5\}]$ ($[Na^+]_2$·1a, M = Cr; $[Na^+]_2$·2a, M = W): To a stirred orange solution of $Na_2[M_2(CO)_{10}]$ (M = Cr: 430 mg, 1 mmol; M = W: 694 mg, 1 mmol) in THF (50 mL) was added solid GeI_2 (326 mg, 1 mmol) in one portion. The orange solution turned red immediately. After stirring for 1 h, the GeI_2 had completely dissolved and a clear red solution had formed. The reaction mixture was filtered through Kieselgur (3 cm). The resulting red solution was concentrated in vacuo (5 mL) and chromatographed on silica gel (15 cm, Ø = 3 cm; THF). Elution with THF gave one yellow band that contained $[M(CO)_6]$ and $Na[M(CO)_5I]$ (M = Cr, W: identification by IR spectroscopy[20]). A red band remained on the top of the column that was eluted with ethanol. The resulting solution was taken to dryness. $[Na^+]_2$·**1a** and $[Na^+]_2$·**2a**, respectively, were obtained as deep orange oils. The identity of the sodium salts **1a** and **2a** is inferred from metathesis to the corresponding $[Ph_4P]$ salts, which may be fully characterised by various methods, including elemental analysis. The $\tilde{\nu}_{CO}$-IR patterns of the sodium salts and the phosphon-

Table 5. Analytical data for the compounds **1–2**

	m.p. / °C	MS; m/z (%) [fragment]	UV / nm (DMA) λ_{max} (ε [l mol^{-1} cm^{-1}])	mol. formula (mol. Mass)	elemental analysis
$[Ph_4P^+]_2$·**1a**	234-235	980 (7)	296 (25000);	$C_{58}H_{40}O_{10}P_2Cr_2Ge_2I_4$	calcd. C 40.60 H 2.35
	(dec.)	[(M-2PPh$_4$-2CO)]$^-$	366 (3200); 425 (1600)	(1715.67)	found C 40.75 H 2.51
$[Ph_4P^+]_2$·**1b** [a]	247-248	609 (29)	318 (22200);	$C_{58}H_{40}O_{10}P_2Cr_2Ge_2Cl_4$	calcd. C 51.61 H 2.99 [a]
	(dec.)	[(M-2PPh$_4$-CO-Cl)]$^-$	379 (9800)	(1349.92)	found C 50.42 H 2.95
$[Ph_4P^+]_2$·**2a**	201-203	852 (49)	288 (10000);	$C_{58}H_{40}O_{10}P_2W_2Ge_2I_4$	calcd. C 35.19 H 2.04
	(dec.)	[(M-2PPh$_4$-W(CO)$_5$-I]$^-$	311 (7600); 405 (2000)	(1974.40)	found C 34.61 H 2.08
$[n\mathrm{Bu}_4N^+]_2$·**2a**	197-198	1173 (15)	290 (15000);	$C_{42}H_{72}O_{10}N_2W_2Ge_2I_4$	calcd. C 28.25 H 4.06
	(dec.)	[(M-2nBu$_4$N-I)]$^-$	324 (9500); 406 (1500)	(1785.54)	found C 28.21 H 3.88
$[Ph_4P^+]_2$·**2b** [a]	207-208	852 (54)	-	$C_{58}H_{40}O_{10}P_2W_2Ge_2Cl_4$	calcd. C 43.17 H 2.50 [a]
	(dec.)	[(M-2PPh$_4$-3CO)]$^-$	-	(1613.59)	found C 42.18 H 2.46

[a] Partial substitution of Cl by I: calculated formula for $[Ph_4P^+]_2$·**1b**: $C_{58}H_{40}Cl_{3.6}Cr_2Ge_2I_{0.4}O_{10}P_2$; calculated formula for $[Ph_4P^+]_2$·**2b**: $C_{58}H_{40}Cl_{3.6}Cr_2Ge_2I_{0.4}O_{10}P_2$

Table 6. ^{1}H-, ^{31}P{^{1}H}-, and ^{13}C{^{1}H}-NMR spectroscopic data for the compounds **1–2**

	^{1}H					^{31}P{^{1}H}	^{13}C{^{1}H} [i]					
	$H_{arom.}$ [d]	H_α [e]	H_β [f]	H_γ [g]	H_δ [h]		CO_{ax}	CO_{eq}	C_{para}	C_{ortho}	C_{meta}	C_{ipso}
							CO_{ax}	CO_{eq}	C_α	C_β	C_γ	C_δ
$[Ph_4P^+]_2$·**1a** [a]	7.95-7.74	-	-	-	-	23.5	-	219.6	135.2	134.5	130.4	117.6
$[Ph_4P^+]_2$·**1a** [b]	8.00-7.85	-	-	-	-	23.3	-	222.1	136.5	135.8	131.5	119.1
$[Ph_4P^+]_2$·**1b** [a]	7.97-7.69	-	-	-	-	23.3	227.7	220.0	135.2	134.4	130.3	117.6
$[Ph_4P^+]_2$·**2a** [a]	7.96-7.68	-	-	-	-	23.6	-	201.2	135.2	134.4	130.3	117.6
$[Ph_4P^+]_2$·**2a** [c]	7.97-7.60	-	-	-	-	22.8	-	202.6	136.3	135.6	131.3	-
$[n\mathrm{Bu}_4N^+]_2$·**2a** [a]	-	3.17	1.58	1.32	0.94	-	-	201.3	57.4	23.0	19.1	13.3
$[n\mathrm{Bu}_4N^+]_2$·**2a** [b]	-	3.44	1.84	1.42	0.98	-	210.1	202.7	59.4	24.5	20.4	13.9
$[Ph_4P^+]_2$·**2b** [a]	8.02-7.55	-	-	-	-	23.6	205.3	200.0	135.2	134.4	130.3	117.6

[a] [D6]DMSO. – [b] [D6]acetone. – [c] CD_3CN. – [d] Non-resolved multiplets. – [e] t, 2 H. – [f] m, 2 H. – [g] m, 2 H. – [h] t, 3 H. – [i] In case of $[PPh_4]$ salts: C_{para} [d, $^4J(^{31}P,^{13}C)$ = 3 Hz]; C_{ortho} [d, $^4J(^{31}P,^{13}C)$ = 10 Hz]; C_{meta} [d, $^4J(^{31}P,^{13}C)$ = 13 Hz]; C_{ipso} [d, $^4J(^{31}P,^{13}C)$ = 13 Hz]; in case of $[n\mathrm{Bu}_4N]$ salts: C_α, C_β, C_γ, C_δ: carbon atoms of *n*-butyl substituent.

Table 7. Crystal structure data for the compounds **1–3**

compound	$[Ph_4P^+]_2$·**1a**	$[Ph_4P^+]_2$·**1b**	$[Ph_4P^+]_2$·**2a**	$[Ph_4P^+]_2$·**2b**	**3**
formula:	$C_{58}H_{40}O_{10}P_2Cr_2Ge_2I_4$	$C_{58}H_{40}O_{10}P_2Cr_2Ge_2Cl_4$	$C_{58}H_{40}O_{10}P_2W_2Ge_2I_4$	$C_{58}H_{40}O_{10}P_2W_2Ge_2Cl_4$	$C_{20}H_8O_{10}N_2W_2Ge_2I_2$
molecular mass [g]:	1715.67	1349.88	1979.40	1613.59	962.37
crystal dimension [mm]	0.30·0.30·0.30	0.30·0.30·0.30	0.20·0.20·0.20	0.30·0.30·0.30	0.20·0.30·0.20
crystal system:	triclinic	triclinic	triclinic	triclinic	monoclinic
space group (no.):	$P\bar{1}$ (2)	$P\bar{1}$ (2)	$P\bar{1}$ (2)	$P\bar{1}$ (2)	$P2_1/n$ (14)
a [pm]	1196.0 (2)	1117.4 (2)	1204.9 (2)	1122.8 (3)	939.6 (2)
b [pm]	1217.5 (1)	1211.0 (1)	1226.2 (3)	1215.2 (3)	1900.0 (2)
c [pm]	1298.1 (2)	1240.7 (2)	1276.3 (3)	1249.9 (3)	1649.3 (2)
α [°]	70.43 (1)	71.57 (1)	90.39 (3)	70.93 (1)	90.00 (0)
β [°]	88.13 (1)	88.83 (1)	110.91 (3)	88.91 (2)	92.58 (2)
γ [°]	60.65 (1)	68.68 (1)	111.00 (3)	69.02 (2)	90.00 (0)
cell volume [10^6pm^3]:	1532.4 (4)	1475.3 (4)	1624.7 (6)	1497.7 (7)	2941.7 (9)
molecular units / cell:	1	1	1	1	4
density (calculated) [g cm^{-3}]	1.859	1.519	2.023	1.791	2.716
temperature [K]:	200	200	293	200	200
no. reflns. for cell parameter refinement:	30	33		34	37
scan range:	$3.4° \le 2\Theta \le 51.0°$	$3.9° \le 2\Theta \le 48.2°$	$3.5° \le 2\Theta \le 52.2°$	$3.9° \le 2\Theta \le 56.0°$	$3.3° \le 2\Theta \le 49.0°$
scan speed (ω) [° min^{-1}]:	12	12		10	12
integration time [sec/frame]			5		
no. rflns. measured:	5767	5081	19872	8097	5185
no. unique rflns.:	5484	4805	6249	7024	4861
no. rflns. observed ($\ge 2\sigma$):	4839	3886	3294	6229	3111
no. parameters refined:	353	432	353	348	314
residual electron density [·10^{-6} e pm^{-3}]:	0.96 / -1.53	1.61 / -0.56	0.67 / -1.38	3.27 / -4.76	4.36 / -2.08
R_1 / R_w [%] (refinement on F^2)	3.4 / 11.7	4.5 / 13.1	4.5 / 8.8	5.4 / 17.6	6.7 / 17.7

ium salts are similar enough to leave no doubt about the nature of the organometallic anions **1a** and **2a**.

$[Ph_4P]_2[\{(OC)_5M\}I_2Ge–GeI_2\{M(CO)_5\}]$ ($[Ph_4P^+]_2$·1a, M = Cr; $[Ph_4P^+]_2$·2a, M = W): To a stirred orange solution of $[Na^+]_2$·**1a** (541 mg, 0.5 mmol) or $[Na^+]_2$·**2a** (673 mg, 0.5 mmol), respectively, in ethanol (10 mL) was added a suspension of $[Ph_4P]I$ (933 mg, 2 mmol) in ethanol (30 mL). The corresponding yellow $[Ph_4P]$ salts of **1a** or **2a** precipitated immediately. After stirring for 30 min, the solid was separated from the mother liquor by filtration and washed with ethanol (2 × 5 mL), diethyl ether (2 × 5 mL) and dried in vacuo leaving the salts of $[Ph_4P^+]_2$·**1a** and $[Ph_4P^+]_2$·**2a** as yellow powders. Yield: $[Ph_4P^+]_2$·**1a**: 394 mg, 0.23 mmol, 46%; $[Ph_4P^+]_2$·**2a**: 456 mg, 0.23 mmol, 46% (with respect to GeI_2). In order to grow single crystals of $[Ph_4P^+]_2$·**1a** and $[Ph_4P^+]_2$·**2a** the yellow powder was dissolved in DMA (5 mL) and overlayered with ethanol (20 mL). Within 5 d at 20 °C yellow single crystals suitable for X-ray analysis were obtained.

$[Ph_4P]_2[\{(OC)_5M\}Cl_2Ge–GeCl_2\{M(CO)_5\}]$ ($[Ph_4P^+]_2$·1b, M = Cr; $[Ph_4P^+]_2$·2b, M = W): To a stirred orange solution of $[Na^+]_2$·**1a** (541 mg, 0.5 mmol) or $[Na^+]_2$·**2a** (673 mg, 0.5 mmol) in ethanol (30 mL) was added solid $[Ph_4P]Cl$ (750 mg, 2 mmol). The corresponding yellow $[Ph_4P]$ salts of **1b** or **2b** precipitated immediately. Further workup and the growth of single crystals of $[Ph_4P^+]_2$·**1b** or $[Ph_4P^+]_2$·**2b** were achieved following the methods described for $[Ph_4P^+]_2$·**1a**. Yield: $[Ph_4P^+]_2$·**1b**: 310 mg, 0.23 mmol, 46%; $[Ph_4P^+]_2$·**2b**: 370 mg, 0.23 mmol, 46% (with respect to GeI_2). The exchange of iodide versus chloride is almost complete under these conditions, as shown by elemental analysis and X-ray analysis.

$[nBu_4N]_2[\{(OC)_5W\}I_2Ge–GeI_2\{W(CO)_5\}]$ ($[nBu_4N^+]_2$·2a): To a stirred orange solution of $[Na^+]_2$·**2a** (673 mg, 0.5 mmol) in ethanol (30 mL) was added solid $[nBu_4N]I$ (739 mg, 2 mmol). The corresponding yellow $[nBu_4N]$ salt of **2a** precipitated immediately. The subsequent workup followed the method described for $[Ph_4P^+]_2$·**2a**. Yield: $[nBu_4N^+]_2$·**2a**: 482 mg, 0.27 mmol, 54% (with respect to GeI_2).

$[\{(OC)_5W\}I_2Ge–Ge(bipy)\{W(CO)_5\}]$ (3): $Na_2[W_2(CO)_{10}]$ (694 mg, 1 mmol) was dissolved in THF (50 mL) and solid GeI_2 (326 mg, 1 mmol) and solid 2,2′-bipyridine (156 mg, 1 mmol) were added in one portion. The initially clear orange solution turned deep red immediately (GeI_2 dissolved in a period of minutes). After stirring for 1 h, the reaction mixture was filtered through Kieselgur (3 cm). The resulting red solution was concentrated to 5 mL in vacuo and chromatographed on silica gel (15 cm, Ø = 3 cm; diethyl ether). Elution with diethyl ether gave a red band, which was identified by IR spectroscopy to consist of $[W(CO)_6]$ and $[(OC)_4W(bipy)]$.[17,20] Elution with THF gave a second red band containing **3**. This fraction was taken to dryness to leave **3** as a red oil. Single crystals of **3** were obtained by the following procedure: A concentrated THF solution of **3** (348 mg in 5 mL of THF) was shared out between three test tubes (Ø = 1 cm), which were each placed into a Schlenk tube (250 mL). Diethyl ether (30 mL), which was in the Schlenk tube, was allowed to diffuse through the gas phase into the THF solutions (12 h at 20 °C). After this period of time the diethyl ether was replaced by petroleum ether (boiling range 40–60 °C; 50 mL). Vapour diffusion of the petroleum ether for 4 d gave red single crystals of **3** that were suitable for X-ray structure analysis. All operations were carried out in the dark. While the identity of **3** could be determined by X-ray analysis of these crystals at 200 K, dissolving these crystals in CD_2Cl_2 or $[D_6]$acetone at 20 °C resulted in red solutions that contained bipy ligands in three different coordination environments. The ^{1}H-NMR spectra show three sets of

signals that, although not individually resolved, provide evidence that compound **3** disintegrates at least in part under the given experimental conditions. In addition, a satisfactory elemental analysis could not be obtained for **3**.

$[Ph_4P]_2[\{(OC)_5Cr\}_6Ge_6]$ ($[Ph_4P^+]_2$·4): To a stirred orange solution of $[Na^+]_2$·**1a** (541 mg, 0.5 mmol) in THF (30 mL) was added a solution of $Na_2[Cr_2(CO)_{10}]$ (430 mg, 1 mmol) in THF (30 mL) in 10-mL portions during a period of 3 h. During the addition the colour of the solution turned to red-brown. The reaction mixture was filtered through Kieselgur (3 cm), concentrated to 5 mL in vacuo and chromatographed on silica gel (15 cm, Ø = 3 cm; THF). Elution with THF gave a broad yellow band containing $Na[Cr_2(CO)_{10}H]$, which was identified by IR spectroscopy.[5,18] A deep red band remained on top of the column and this was eluted with ethanol. The resulting deep red solution was taken to dryness in vacuo and redissolved in ethanol (10 mL). Addition of solid $[Ph_4P]Cl$ (375 mg, 1 mmol) led to the corresponding red-brown $[Ph_4P]$ salt of **4**, which precipitated immediately. The solid was separated from the mother liquor by filtration, washed with ethanol (2 × 5 mL), diethyl ether (2 × 5 mL) and dried in vacuo. Yield: $[Ph_4P^+]_2$·**4**: 151 mg, 0.07 mmol, 40% (with respect to GeI_2). Single crystals of $[Ph_4P^+]_2$·**4** could be obtained by layering a concentrated DMA solution of $[Ph_4P^+]_2$·**4** (3 mL) with ethanol (20 mL).

X-ray Structure Determinations: The measurements for $[Ph_4P^+]_2$·**1a**, $[Ph_4P^+]_2$·**2b**, and **3** were carried out with a Siemens P4 four-circle diffractometer, data for $[Ph_4P^+]_2$·**2a** were collected with a Nonius Kappa CCD diffractometer, all using Mo-K_α radiation. In the case of the Siemens P4 four-circle diffractometer, measurements of the intensities of three check reflections (measured every 100 reflections) remained constant throughout the data collection, thus indicating crystal and electronic stability. The data collected using a scintillation counter measuring device (Siemens P4) were corrected in the usual way including experimental absorption correction. The data from the CCD device (Nonius Kappa CCD) were processed by the standard Nonius software.[21] All calculations were performed using the SHELXT PLUS software package. Structures were solved by direct methods with the SHELXS-86 program and refined with the SHELXL-93 program.[22] The program XPMA[23] was used for graphical handling of the data. The structures were refined in fully or partially anisotropic models by full-matrix least-squares calculations. Hydrogen atoms were introduced at calculated positions. Table 7 compiles the data for the structure determinations. Crystallographic data for the structures reported in this paper have been deposited with the Cambridge Crystallographic Data Centre as supplementary publication nos. CCDC-135292 ($[Ph_4P^+]_2$·**1a**), -135293 ($[Ph_4P^+]_2$·**1b**), -135291 ($[Ph_4P^+]_2$·**2a**), -135295 ($[Ph_4P^+]_2$·**2b**), -135294 (**3**). Copies of the data can be obtained free of charge on application to CCDC, 12 Union Road, Cambridge CB2 1EZ, UK [Fax: int. code + 44-1223/336-033; E-mail: deposit@ccdc.cam.ac.uk].

[1] [1a] P. Kircher, G. Huttner, K. Heinze, G. Renner, *Angew. Chem.* **1998**, *110*, 1754–1755; *Angew. Chem. Int. Ed.* **1998**, *37*, 1664–1665. – [1b] B. Schiemenz, G. Huttner, *Angew. Chem.* **1993**, *105*, 295–296; *Angew. Chem. Int. Ed. Engl.* **1993**, *32*, 297–298.

[2] [2a] Ph_3Ge–$GePh_3$ (Ge–Ge: 243.7 pm): M. Dräger, L. Ross, *Z. Anorg. Allg. Chem.* **1980**, *490*, 207–216. – [2b] $PhCl_2Ge$–$GeCl_2Ph$ (Ge–Ge: 242.1 pm): K. Häberle, M. Dräger, *Z. Naturforsch.* **1987**, *42b*, 323–329. – [2c] $[\{(Me_3Si)_3Si\}Cl_2Ge$–$GeCl_2\{Si(SiMe_3)_3\}]$ (Ge–Ge = 242.1 pm): S. P. Mallela, R. A. Geanangel, *Inorg. Chem.* **1991**, *30*, 1480–1482. – [2d] $[\{Cp(CO)_2Fe\}R_2Ge$–$GeR_2\{Fe(CO)_2Cp\}]$ (Ge–Ge: 244.8 pm, R_2 = 2,3-dimethylbut-2-ene-1,4-diyl): G. Barsuaskas, D. Lei, M. L. Hampden-Smith, E. N. Duesler, *Polyhedron* **1990**, *9*, 773–779.

[3] [3a] W. Gäde, E. Weiss, *Chem. Ber.* **1981**, *114*, 2399–2404. – [3b] W. Gäde, E. Weiss, *Chem. Ber.* **1984**, *117*, 2464–2468.

[4] L. M. Dennis, R. B. Corey, R. W. Moore, *J. Am. Chem. Soc.* **1924**, *46*, 657–674.

[5] E. Lindner, H. Behrens, S. Birkle, *J. Organomet. Chem.* **1968**, *15*, 165–175.

[6] M. A. Schwindt, T. Lejon, L. S. Hegedus, *Organometallics* **1990**, *9*, 2814–2819.

[7] I. R. Beattie, P. J. Jones, G. Reid, M. Webster, *Inorg. Chem.* **1998**, *37*, 6032–6034.

[8] D. Uhlig, H. Behrens, E. Lindner, *Z. Anorg. Allg. Chem.* **1973**, *401*, 233–242.

[9] G. Huttner, P. Friedrich, H. Willenberg, H.-D. Müller, *Angew. Chem.* **1977**, *89*, 268–269; *Angew. Chem. Int. Ed. Engl.* **1977**, *16*, 260–261.

[10] M. Scheer, K. Schuster, A. Krug, H. Hartnung, *Chem. Ber./Recueil* **1997**, *130*, 1299–1304.

[11] $[\{(OC)_5Cr\}GeCl_2\{ONC_6H_{11}\}]$ (Cr–Ge = 238.8 pm): A. Castel, P. Rivière, J. Satgé, M. Ahbala, J. Jaud, *J. Organomet. Chem.* **1986**, *307*, 205–218.

[12] P. Kircher, G. Huttner, K. Heinze, B. Schiemenz, L. Zsolnai, M. Büchner, A. Driess, *Eur. J. Inorg. Chem.* **1998**, 703–720.

[13] B. Schiemenz, G. Huttner, *Chem. Ber.* **1994**, *127*, 2129–2133.

[14] [14a] G. Huttner, U. Weber, B. Sigwarth, O. Scheidsteger, H. Lang. L. Zsolnai, *J. Organomet. Chem.* **1985**, *282*, 331–348. – [14b] C. Burschka, K. Stroppel, P. Jutzi, *Acta Crystallogr., Sect. B* **1981**, *37*, 1397–1399. – [14c] D. J. Brauer, C. Krüger, *Eur. Cryst. Meeting* **1974**, 435. – [14d] P. Jutzi, B. Hampel, M. B. Hursthouse, A. J. Howes, *J. Organomet. Chem.* **1986**, *299*, 19–27.

[15] H. Schäfer, Diskussionsbemerkung, Münster, **1962**, "Die Verbindungen können sich gegen unsere Beschreibung nicht wehren". Citation in: H. G. von Schnering, *Angew. Chem.* **1981**, *93*, 44–63; *Angew. Chem. Int. Ed. Engl.* **1981**, *20*, 33–52.

[16] [16a] W.-W. du Mont, L. Lange, S. Pohl, W. Saak, *Organometallics* **1990**, *9*, 1395–1399. – [16b] N. Tokitoh, K. Manmaru, R. Okazaki, *Organometallics* **1994**, *13*, 167–171. – [16c] M. F. Lappert, S. J. Miles, P. P. Power, *J. Chem. Soc., Chem. Commun.* **1977**, 458–459. – [16d] P. Jutzi, W. Steiner, E. König, G. Huttner, A. Frank, U. Schubert, *Chem. Ber.* **1978**, *111*, 606–614.

[17] [17a] M. H. B. Stiddard, *J. Chem. Soc.* **1962**, 4712–4715. – [17b] C. S. Kraihanzel, F. A. Cotton, *Inorg. Chem.* **1963**, *2*, 533–540. – [17c] R. J. Angelici, J. R. Graham, *Inorg. Chem.* **1967**, *6*, 988–992.

[18] [18a] R. G. Hayter, *J. Am. Chem. Soc.* **1966**, *88*, 4376–4382. – [18b] L. B. Handy, J. K. Ruff, L. F. Dahl, *J. Am. Chem. Soc.* **1970**, *92*, 7312–7326. – [18c] G. Huttner, P. Kircher, private communication, CCDC-116058.

[19] G. Brauer, *Handbuch der Präparativen Anorganischen Chemie*, 3rd ed., Ferdinand Enke Verlag, Stuttgart, **1981**, vol. 2, p. 727.

[20] F. A. Cotton, C. S. Kraihanzel, *J. Am. Chem. Soc.* **1962**, *84*, 4432–4438.

[21] Collect data collection software, Nonius, **1998**; http://www.nonius.com.

[22] [22a] G. M. Sheldrick, *SHELXS-86 – Program for Crystal Structure Solution*, Universität Göttingen, **1986**; http://www.shelx.uni-ac.gwdg.de/shelx/index.html. – [22b] G. M. Sheldrick, *SHELXL-93 – Program for Crystal Structure Refinement*, Universität Göttingen, **1993**; http://www.shelx.uni-ac.gwdg.de/shelx/index.html. – [22c] *International Tables for X-ray Crystallography*, vol. 4, Kynoch Press, Birmingham, **1974**.

[23] L. Zsolnai, G. Huttner, *XPMA*, Universität Heidelberg, **1998**; http://www.rzuser.uni-heidelberg.de/~v54/xpm.html

Received October 19, 1999
[I99370]

In situ NMR Detection of Dihydrides in the Systems $[RhH(SnCl_3)_5]^{3-}$/Tertiary Phosphanes/Parahydrogen

Claudia Ulrich,[a] Alexei Permin,[b] Valery Petrosyan,[b] and Joachim Bargon*[a]

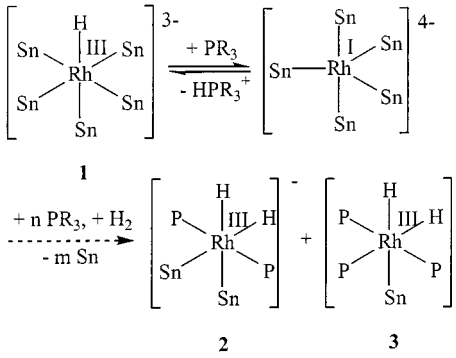
Keywords: Rhodium hydride complexes / Parahydrogen / Tin ligands / Hydrogenations

The oxidative addition of dihydrogen to the $[RhH(SnCl_3)_5]^{3-}$/PR_3 system (PR_3 = PPh_3, $PEtPh_2$, PEt_3) leads to the formation of previously unknown dihydride complexes, the ^{1}H-NMR spectra of which have been studied by means of the ParaHydrogen Induced Polarization (PHIP) method. The composition of the resulting complexes crucially depends on the type of the added phosphane. With PEt_3 as the phosphane and acetonitrile as the solvent, a complex with a $SnCl_2L$ ligand (L = CD_3CN) can be detected. All systems examined catalyze the hydrogenation of phenylacetylene. During these reactions, both the ^{1}H-NMR resonances of the dihydride complexes and those of styrene, the hydrogenation product of phenylacetylene, can be detected simultaneously. In the case of $SnBr_3$ ligands, hydrogen addition in the presence of phosphanes leads to similar dihydride complexes, which were also identified via ^{1}H-NMR spectroscopy. Furthermore, a mixed complex of the structure $[Rh(SnBr_3)_nBr_{6-n}]^{3-}$ has been isolated.

Introduction

The catalytic activity of rhodium complexes containing tin trichloride ligands has been the subject of many studies ever since 1970, when their activity in the dehydrogenation of 2-propanol has first been noted.[1] This reaction and, in particular, the structure of the responsible rhodium-tin complexes have been examined before using ^{119}Sn-NMR spectroscopy.[2] Furthermore, the rhodium(III) monohydride complex **1** has previously been isolated from hydrochloric acid solutions of $RhCl_3$ and $SnCl_2$ and identified with this technique.[3] Reactions of these complexes with tertiary phosphanes have also been studied with ^{31}P- and ^{1}H-NMR spectroscopy, and upon addition of dihydrogen to these systems the formation of two dihydrido complexes **2** and **3** was detected (Scheme 1).[4]

The development of an in situ NMR technique based on ParaHydrogen Induced Polarization (PHIP) allows an extensive study of rhodium dihydride complexes, both stable and transient, via their ^{1}H-NMR spectra, which can be observed during homogeneous catalyzed hydrogenations.[5] Recently, the structure and reactivity of rhodium dihydrides relevant to both Wilkinson- and Schrock-type catalysts as well as their hydrogenation activity were extensively examined by use of PHIP-NMR spectroscopy. This method provides an extraordinary sensitivity for the detection of metal hydrides; therefore, it has been used to observe these typically unstable catalytic intermediates.[5–7] Due to the enhanced resonances, reliable information about the structure of species present in only minor quantities in reaction mixture can thus be obtained. This approach yields valuable insight into both the stereo- and regiochemistry of initial stages of the dihydrogen addition to the substrate.[8]



Scheme 1. Formation of dihydrides from $[HRh(SnCl_3)_5]^{3-}$ in presence of phosphanes and hydrogen, Sn = $SnCl_3$, P = PR_3.

Since reports on tin-containing rhodium dihydrides and the knowledge of their role in homogeneous catalysis are scarce, we have used the PHIP technique to study the reactions of two characteristic prototypes with parahydrogen, namely of the systems $[RhH(SnCl_3)_5]^{3-}$/tertiary phosphane and $RhBr_3$/$SnBr_2$/tertiary phosphane. Recently, platinum(II)-tin hydride complexes were studied in this way,[9] providing a pool of new information about the mechanism of homogeneous, platinum-tin catalyzed hydrogenations of alkynes and alkenes thanks to the identification of previously unknown intermediates. In this study here, we were interested in identifying the consequences, in particular the intermediate products, resulting from the addition of dihydrogen to a variety of tin-containing rhodium complexes. By use of PHIP-NMR spectroscopy we wanted to detect

[a] Institute of Physical and Theoretical Chemistry,
University of Bonn,
Wegelerstrasse 12, D-53115 Bonn, Germany
Fax (internat.) + 49(0)228/739424
E-mail: bargon@uni-bonn.de
[b] Department of Chemistry,
M. V. Lomonosov Moscow State University,
Vorobyevy Gory, 119899 Moscow, Russia,
Fax: (internat.) + 7–095/9395546
E-mail: alp@org.chem.msu.su

 © WILEY-VCH Verlag GmbH, D-69451 Weinheim, 2000 1434–1948/00/0505–0889 $ 17.50+.50/0

previously elusive intermediates occurring during the stepwise tin-for-phosphane substitution as originally described in 1985,[4] in order to obtain more detailed information about the hydrogenation activity of this rhodium-tin system in particular.

Results and Discussion

Of the two rhodium-tin-systems investigated here, the first complex, $[HRh(SnCl_3)_5]^{3-}$, has been obtained and characterized earlier as an isolated rhodium monohydride,[2,3] whereas the second system, $RhBr_3/SnBr_2/HBr$, has not been investigated before.

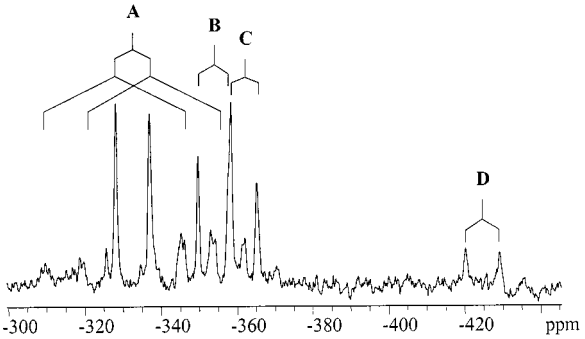


Figure 1. ^{119}Sn-NMR spectrum of the $RhBr_3/SnBr_2/HBr$ system in CD_3CN at –40° C (chemical shifts referenced to external Me_4Sn)

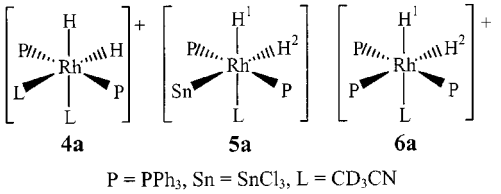
Action of NEt_4^+ onto the latter yields a solid, which was studied by means of NMR spectroscopy. The ^{119}Sn-NMR spectrum (Figure 1) exhibits four main resonances A, B, C, and D, which are due to rhodium-tin-complexes of the type $[Rh(SnBr_3)_nBr_{6-n}]^{3-}$ with typical shifts and coupling values for tin coordinated to rhodium[10] (see Experimental Section). Upon addition of parahydrogen, the ^{1}H-NMR spectrum in acetonitrile reveals no signals of any hydride, by contrast to the chloride analogue. The lack of formation of a monohydride upon addition of tetraethylammonium cations to the $RhBr_3/SnBr_2/HBr$ system seems to be due to the lower reductive ability of tin dibromide in comparison to tin dichloride, which would explain the lack of Rh^I formation and, therefore, the lack of subsequent protonation.

System $[RhH(SnCl_3)_5]^{3-}/PPh_3$

The action of parahydrogen on the $[RhH(SnCl_3)_5]^{3-}$ anion in acetonitrile does not give rise to any detectable dihydrides either. The addition of four equivalents of PPh_3 to the solution causes partial deprotonation of the hydride, since the hydride signal disappears in the ^{1}H-NMR spectrum. Furthermore, the ^{31}P-NMR spectrum reveals the presence of $HPPh_3^+$ at δ = –3 (broad), which undergoes rapid chemical exchange with PPh_3 on the NMR time scale. This behaviour is similar to that of the already described reaction with PBu_3.[4]

$$[HRh(SnCl_3)_5]^{3-} + PBu_3 \rightarrow [Rh(SnCl_3)_5]^{4-} + HPBu_3^+ \quad (1)$$

The subsequent fate of the Rh^I complex is either substitution of the tin ligands by phosphane or back-protonation to **1** as soon as a proton is liberated during the substitution. Addition of parahydrogen at room temperature gives rise to three dihydrides, two of them occurring in polarization (Figure 2).



P = PPh_3, Sn = $SnCl_3$, L = CD_3CN

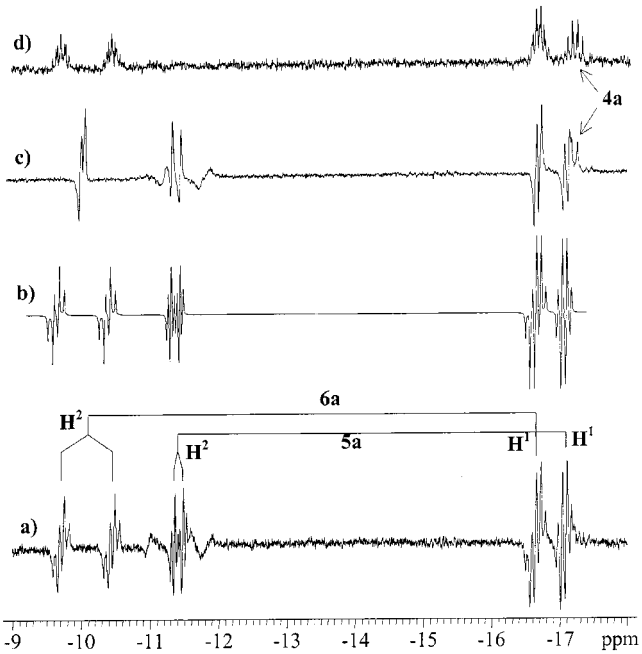


Figure 2. ^{1}H-NMR spectra of the system $[RhH(SnCl_3)_5]^{3-}/PPh_3/H_2$ in CD_3CN; a) PHIP spectrum on heating; b) PHIP++ simulation of **6a** and **5a**; c) PHIP-^{1}H{^{31}P}-NMR spectrum on heating; d) product spectrum after decay of the polarization

The unpolarized hydride resonances at δ = –17.19 are assigned to the chemically equivalent protons of the symmetric complex **4a**. This complex has already been described before.[11] These hydride resonances occur with a multiplicity consisting of doublet of triplets with ^1J(HRh) = –17.5 Hz and ^2J(HP) = 13 Hz (Table 1). The polarized resonances, however, show coupling patterns typical for a bis-phosphane and a tris-phosphane complex, respectively. The bis-phosphane complex **5a** shows one hydride resonance H^2, with a chemical shift value of δ = –11.42, which is typical for a proton in *trans* position to a trichlorostannato ligand. This resonance occurs as a doublet of triplets which are further split into doublets with "antiphase" multiplicity. (In the following the designation "antiphase multiplicity" will be used as an abbreviation universally when referring to multiplets in polarization and a splitting due to ^2J(HH′) coupling between the former two parahydrogen protons). The ^{31}P-decoupled spectrum reveals the rhodium coupling as $^1J(H^2Rh)$ = 25 Hz. The

Table 1. ^{1}H-NMR data of the dihydride complexes

	Formula	^{1}H δ [ppm], J [Hz]
6a	$H_2Rh(PPh_3)_3L$[a]	–16.64 (J_{HH} = –9.5, J_{HRh} = 10, J_{HP} = 13) –10.08 (J_{HRh} = 9.5, J_{HPcis} = 14, $J_{HPtrans}$ = 147)
5a	$H_2Rh(PPh_3)_2(SnCl_3)L$[a]	–17.05 (J_{HH} = –4.5, J_{HRh} = 13, J_{HP} = 13) –11.42 (J_{HRh} = 25, J_{HP} = 9)
4a	$H_2Rh(PPh_3)_2L_2$[a]	–17.19 (J_{HRh} = 17.5, J_{HP} = 13)
3b	$H_2Rh(PEtPh_2)_3(SnCl_3)$	–12.07 (J_{HH} = –6, J_{HRh} = 20, J_{HP} = 10) –10.67 (J_{HRh} = 10, J_{HPcis} = 13, $J_{HPtrans}$ = 130.5, J_{HSn} = 1440)
6b	$H_2Rh(PEtPh_2)_3L$[a]	–17.46 (J_{HH} = –8, J_{HRh} = 13, J_{HP} = 13) –9.82 (J_{HRh} = 13.5, J_{HPcis} = 13.5, $J_{HPtrans}$ = 148)
2c	$H_2Rh(PEt_3)_2(SnCl_3)_2$	–12.52 (J_{HRh} = 25, J_{HP} = 11.5)
3c	$H_2Rh(PEt_3)_3(SnCl_3)$	–12.84 (J_{HH} = –5.5, J_{HRh} = 25, J_{HP} = 12, J_{H119Sn} = 1510, J_{H117Sn} = 1443) –11.48 (J_{HRh} = 11.5, J_{HPcis} = 16, $J_{HPtrans}$ = 131)
8c	$H_2Rh(PEt_3)_3(SnCl_2L)$[a]	–12.40 (J_{HH} = –5, J_{HRh} = 26, J_{HP} = 13, J_{H119Sn} = 1510, J_{H117Sn} = 1443) –10.88 (J_{HRh} = 11, J_{HPcis} = 16, $J_{HPtrans}$ = 158)
7c	$H_2Rh(PEt_3)_2(SnCl_3)_2X$[b]	–18.77 (J_{HH} = –4, J_{HRh} = 16.5, J_{HP} = 15) –12.56 (J_{HRh} = 30, J_{HP} = 11)
9c	$H_2Rh(PEt_3)_3(SnBr_3)$	–13.85 (J_{HH} = –5.5, J_{HRh} = –25, J_{HP} = 12.5) –11.16 (J_{HRh} = 10.5, J_{HPcis} = 15, $J_{HPtrans}$ = 130)
10c	$H_2Rh(PEt_3)_2(SnBr_3)_2$	–13.26 (J_{HRh} = –25, J_{HPcis} = 11.5)
11c	$H_2Rh(PEt_3)_2(SnBr_3)_2X$[b]	–18.77 (J_{HH} = –6, J_{HRh} = –15, J_{HPcis} = 15) –12.56 (J_{HRh} = 31, J_{HPcis} = 12)

[a] L = CD_3CN. – [b] X = Cl, Br, CD_3CN.

other hydride proton, namely H^1 *trans* to acetonitrile, occurs as a high-field pseudo-quadruplet at δ = –17.05 with a rhodium coupling of $^1J(H^1Rh)$ = 13 Hz. The presence of acetonitrile in this complex is confirmed by the fact that the same signals are not detected in the system $RhCl(PPh_3)_3$/$SnCl_2$ (1:5) in [D_6]acetone as the solvent until the addition of minor quantities of acetonitrile.

In the tris-phosphane complex **6a** the large value of $^2J(H^2P)$ = 147 Hz is typical for a *trans*-alignment of the ligands. The ^{31}P-decoupled ^{1}H-NMR spectrum approves this assignment. The high-field shift of H^1 is also due to a *trans* acetonitrile ligand, which is concluded from the observation that the $[Rh(SnBr_3)_nBr_{6-n}]^{3-}$ system gives rise to the same signals upon addition of parahydrogen. Furthermore, these signals can also be detected in the system $RhCl(PPh_3)_3/SnCl_2/PPh_3$ (1:5:7) in CD_3CN.

The complexes **4a** and **6a** are stable and can, therefore, be characterized from their resonances observed in the thermal, i.e., in the regular, "unpolarized" ^{1}H-NMR spectra. Complex **5a,** however, is a transient species which can only be observed in situ, i.e., enhanced by PHIP. The extensive incorporation of acetonitrile into the coordination sphere of the dihydrides can be rationalized by the relatively high π-acceptor properties of triphenylphosphane, which causes its competition with the tin ligands for the filled d-orbitals of rhodium. The tin trihalide ligands have been shown earlier to be relatively strong π-acceptors as well.[12] The instability of complex **5a** could be caused by the high *trans* effect of H^2; therefore, the lability of the tin ligand is enhanced, which causes its dissociation with the formation of **4a**.

System $[RhH(SnCl_3)_5]^{3-}/PEtPh_2$

Upon addition of $PEtPh_2$ to an acetonitrile solution of **1**, deprotonation becomes evident by the appearance of $HPEtPh_2^+$ in the ^{31}P-NMR spectrum at δ = – 8.5 (broad). In addition, several signals in the range of δ = 15 to 45 with typical ^1J(PRh) coupling constants of 90 to 135 Hz

Table 2. ^{31}P-NMR data of the dihydride complexes

Dihydride	Formula	Chemical shifts, δ [ppm], coupling constants J [Hz]
6a	$H_2Rh(PPh_3)_3L$[a]	42.8 (J_{PP} = 19, J_{PRh} = 111) 28.7 (J_{PRh} = 93)
6b	$H_2Rh(PEtPh_2)_3L$[a]	38.8 (J_{PP} = 20, J_{PRh} = 109) 24.3 (J_{PRh} = 96)
3c	$H_2Rh(PEt_3)_3(SnCl_3)$	28.7 (J_{PP} = 22, J_{PRh} = 96) 15.6 (J_{PRh} = 88)

[a] L = CD_3CN

are observed (Table 2). However, the deprotonation of the monohydride does not occur completely, since it can still be detected in the ^{1}H-NMR spectrum.

The admission of parahydrogen gives rise to polarized signals of two dihydrides, **3b** and **6b**, with coupling patterns similar to those of the PPh_3 analogues (Figure 3). The presence of an acetonitrile ligand in **6b** is extrapolated from the observation of the corresponding signals in the PHIP spectra of the bromide system. The signals of **6b** are also detectable in the thermal ^{1}H-NMR spectrum, whereas **3b** is only visible when enhanced by PHIP. The higher stability of **3b** as compared to that of the PPh_3 system, can be explained by the decrease of the π-acceptor properties of $PEtPh_2$ relative to PPh_3; therefore, its competition with the tin ligand is less favourable. It should be mentioned that in this system only tris-phosphane dihydrides are observed.

System $[RhH(SnCl_3)_5]^{3-}/PEt_3$

Upon addition of PEt_3 to an acetonitrile solution of **1**, deprotonation of the monohydride becomes evident by the appearance of $HPEt_3^+$ in the ^{31}P-NMR spectrum at δ = –13.7 (broad). Furthermore, four main signals with ^1J(PRh)

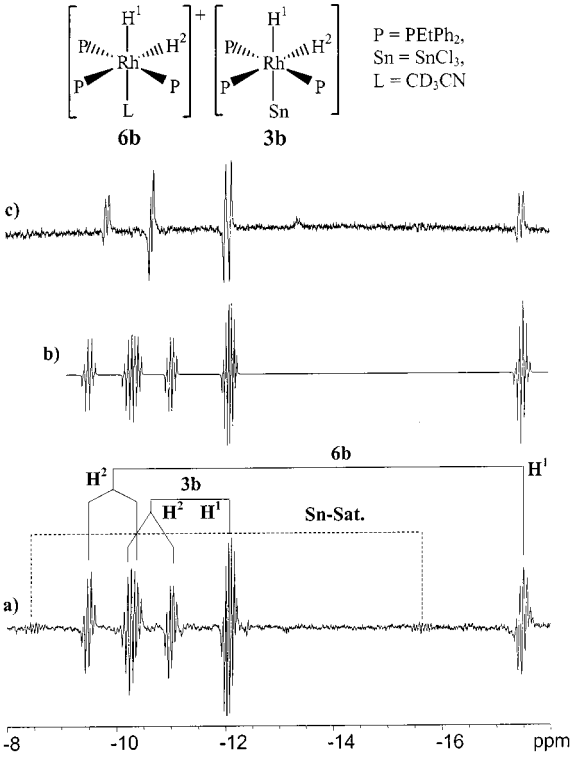
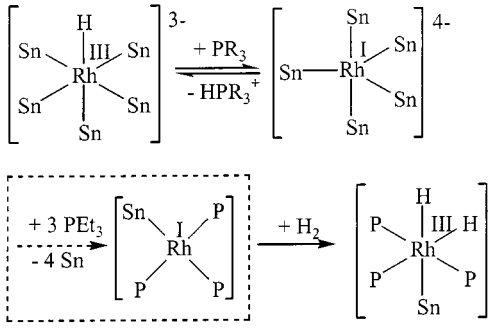


Figure 3. ^{1}H-NMR spectra of the system $[RhH(SnCl_3)_5]^{3-}$/$PEtPh_2$/H_2 in CD_3CN; a) PHIP spectrum on heating; b) PHIP++ simulation of **6b** and **3b**; c) PHIP-^{1}H{^{31}P}-NMR spectrum on heating

couplings of 90, 90, 116, and 137 Hz occur at δ = 7.5, 20.6, 26.4, and 42.2, respectively.

The appearance of polarized dihydrides upon parahydrogen addition depends on the initial P/Rh ratio. When an excess of phosphane (Rh/P = 1:6) is used, the resonances observed correspond to the tris-phosphane *mer*-$H_2Rh(PET_3)_3(SnCl_3)$, **3c**. This complex is also visible in the thermal spectra together with the symmetric complex **2c**, which is formed after prolonged reaction time and upon heating.



Scheme 2. Formation of a tris-phosphane rhodium dihydride at the first stage of the reaction

The dihydride **3c** is apparently the result of an oxidative addition of parahydrogen to $Rh(PET_3)_3(SnCl_3)$ formed at the very beginning of the reaction (Scheme 2). The lack of evidence for the formation of any bis-phosphane dihydrides during the first stage of the reaction can be rationalized to be the consequence of the activating *trans* effect of the first and second PET_3: If three ligands are swiftly replaced by PET_3, only the tris-phosphane is available for the oxidative addition of parahydrogen.

Likewise, at lower PET_3 concentrations (Rh/P = 1:4) the first PHIP spectrum reveals the formation of **3c** only (Figure 4, a). However, upon standing at room temperature, the addition of parahydrogen leads to the emergence of a complicated mixture of PHIP-active dihydrides, as can be concluded from the spectra shown in Figure 4, f.

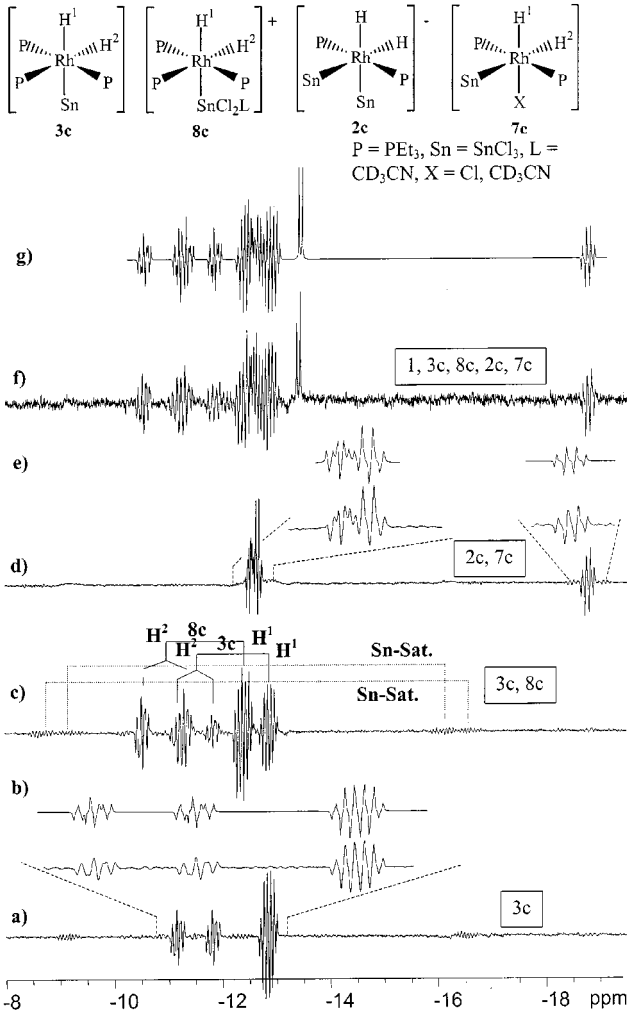
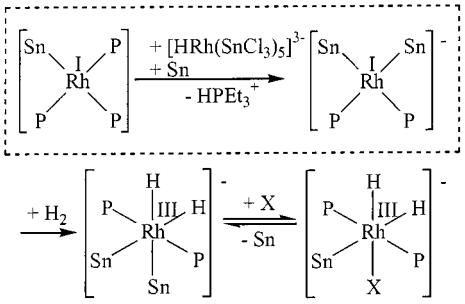


Figure 4. ^{1}H-NMR spectra of the system $[RhH(SnCl_3)_5]^{3-}$/PET_3(1:4)/H_2 in CD_3CN; a) PHIP spectrum immediately after mixing of the reagents; b) PHIP++ simulation of **3c**; c) PHIP spectrum in presence of $AgBF_4$; d) PHIP spectrum on heating; e) PHIP++ simulation of **2c** and **7c**; f) PHIP spectrum after prolonged reaction time; g) PHIP++ simulation of **1**, **2c**, **3c**, **7c**, and **8c**

Heating of the solution changes the patterns (Figure 4, d), apparently because of scrambling of the phosphane throughout the whole system (Scheme 3). Consequently, upon admission of parahydrogen two bis-phosphane dihydrides, **2c** and **7c**, are obtained. The spectral patterns observed correspond to overlapping signals of **2c** (in which the two former parahydrogen protons fail to appear in polarization, possibly due to their maintained symmetry) and the polarized multiplet of **7c**. This assignment has been confirmed by PHIP++ simulation.



Scheme 3. Formation of bis-phosphane rhodium dihydrides after prolonged reaction time

The complicated mixture of resonances observed in the PHIP spectra at room temperature after prolonged reaction times (Figure 4, f) could be analyzed to consist of the overlapping thermal and PHIP signals of **3c**, **2c**, **7c,** and of the starting complex **1,** respectively. This analysis was confirmed via PHIP++ simulation of the expected resonances for the components of this system and a subsequent weighted summation thereof (Figure 4, g).

However, in order to achieve a complete fitting of the observed patterns in the case above, the presence of another tris-phosphane dihydride has to be postulated, namely of **8c**. Its coupling patterns clearly display the *cis*-position alignment of three phosphorus ligands. The chemical shift of the H^1 proton in *cis*-position to phosphorus is characteristic for a *trans*-alignment of the tin-ligand. The difference between the two rather similar dihydrides **3c** and **8c** can only be due to variations in the structure of the tin ligand. As has already been shown before,[13,14] tin(II)chloride possesses additional coordination abilities; therefore, it can coordinate Lewis bases, leading to the formation of $SnCl_2D$ ligands (D = donor). Since this process could be strongly promoted by the abstraction of chloride, we have also recorded the spectra of this system in the presence of added $AgBF_4$ to check out the relevance of this hypothesis. The result shows a strong enhancement of the signals of **8c**, adding support to this suggestion. In addition, tin satellites are clearly visible for the resonance of H^1, exhibiting a value for ^2J(HSn), which is close to that of the related complex **3c**.

By contrast to the PPh_3 and $PEtPh_2$ chloride systems the addition of parahydrogen to the corresponding bromide systems gives rise to relatively stable, tin-containing dihydrides which appear in polarization in the PHIP-NMR spectra. Upon heating, the signals of **9c**, which is the bromide analogue of **3c**, are clearly visible. The complexes **10c** and **11c** can also be detected, which appear to be the tin-tribromide analogues of **2c** and **7c**, respectively. The high-field shift of the hydrogen in *trans*-position to the tin ligand indicates a lower *trans*-effect of $SnBr_3^-$ as compared to that of $SnCl_3^-$. Furthermore, the intensity of the PHIP signals observed in the bromide systems is generally lower than in the corresponding chloride system, apparently because of the lower concentration of Rh^I.

Hydrogenation Experiments

Upon heating, all systems studied hydrogenate added phenylacetylene in a *cis*-manner, as can be concluded from the polarization pattern of the resulting styrene. The hydrogenation activities are rather similar for all these systems.

Characteristically, in all cases investigated, the resonances of the dihydrides are present during the hydrogenation of phenylacetylene to styrene. The apparent lack of formation of any substrate-hydride complexes – similar to those detected in the previously investigated platinum-tin systems[9] – leads us to the conclusion that the observed dihydrides may not be directly included in the catalytic cycle of the hydrogenation, but might just be the precursors for related, catalytically active species. Alternatively, the rates of the individual steps for this catalytic cycle might well be rather different from those of the previously studied platinum-tin system, with the consequence that the rate-determining steps shift with the result that such intermediates, – if they are formed at all -, occur in such minute concentrations that they cannot be detected in spite of the signal enhancement associated with PHIP.

Conclusions

In comparison to PPh_3, the PEt_3 ligand has profound electron donor properties, which causes an extensive incorporation of tin ligands into the resulting dihydrides. Accordingly, when using PPh_3 as the tertiary phosphane, the formation of only one tin-containing dihydride is observed, which is thermally unstable. By contrast, in the system $[RhH(SnCl_3)_5]^{3-}/PEt_3/CD_3CN$/parahydrogen four dihydrides are detectable, which all contain tin ligands. Two of them, namely **3c** and **2c**, are rather stable species. The low stability of the tin-containing complexes with PPh_3 as the ligand is apparently due to the competition of the tin and phosphane ligands. Furthermore, this process is accompanied by more extensive incorporation of acetonitrile into the dihydrides.

In particular, the system $[RhH(SnCl_3)_5]^{3-}/PEtPh_2/CD_3CN$/parahydrogen is remarkable in the sense that it gives rise to tris-phosphane complexes only. This fact can be explained when assuming that there exists a fine balance of σ-donating and π-accepting properties of the phosphane which is apparently optimal for rhodium-phosphorus-binding here.

Experimental Section

General Remarks: All ^1H, ^1H PHIP-, ^{31}P and ^{119}Sn NMR spectra were recorded using a Bruker AC 200 spectrometer; the $^1H\{^{31}P\}$-PHIP NMR spectra were obtained with a Bruker DRX 200 spectrometer. Chemical shifts are referenced to either external TMS (^1H), 85% H_3PO_4 (^{31}P), or $Sn(CH_3)_4$ (^{119}Sn), respectively. For recording the ^{119}Sn spectrum a repetition time of 0.5 s was used, and the accumulation of 28000 scans was necessary to obtain a spectrum with a satisfactory signal-to-noise ratio. In order to obtain the PHIP spectra, excitation pulses corresponding to a flip angle of 45° were used. To record the conventional or "thermal" ^1H NMR spectra, however, the pulse width was set such that it corresponded to the conventional flip angle of 90°. The solvent CD_3CN

was purchased from Aldrich, dried and degassed prior to use, and stored under vacuum. – The simulations of the PHIP-^{1}H NMR spectra were performed using the OS/2-based PHIP++ program, developed by Greve.[15] – The complex $[RhH(SnCl_3)_5][NEt_4]_3$ was prepared as reported in the literature.[3] All starting materials were commercial products (Aldrich) which were used without additional purification.

Typical Preparation of Solutions for Hydrogenation Studies: The Rh^{III} complex, as well as PPh_3, were placed into a screw-capped NMR tube attached to a vacuum line. Then 0.7 mL of dry degassed CD_3CN was condensed into the tube. The weighted amounts of PEt_3 were vacuum-transferred to the sample. After thawing and filling with dry argon, the sample tube was disconnected from the vacuum line and fitted with a septum stopper. The necessary volumes of $PEtPh_2$ were added to the solution of the starting Rh^{III} complex using an Eppendorf micropipette. Parahydrogen was subsequently introduced into the NMR tube through a stainless steel needle through the septum at a pressure of 3 bar. After shaking of the solution in the parahydrogen atmosphere, the tube was inserted into the probe, and the ^{1}H-PHIP spectrum was recorded immediately thereafter.

Tetraethylammonium (Bromo(tribromostannato)rhodium(III) Complexes: 2 g of $SnBr_2$ (7.2 mmol) was added to a stirred solution of 0.3 g $RhBr_3$ (1 mmol) in 10 mL of 3 M HBr under argon. The mixture was heated for 1 h. After the solution had cooled down to room temperature, 0.2 M of NEt_4Br in 3 M HBr was added dropwise. A red precipitate formed which was filtered, washed three times with 3 M HBr, and dried in vacuo. The ^{119}Sn-NMR analysis revealed that the product contained several rhodium-tin complexes of the composition $[Rh(SnBr_3)_nBr_{6-n}][NEt_4]_3$. – ^{119}Sn-NMR ($CD_3CN$): δ = –332 (d, $J_{Rh,Sn}$ = 669 Hz), –354 (d, $J_{Rh,Sn}$ = 603 Hz), –361 (d, $J_{Rh,Sn}$ = 520 Hz), –425 (d, $J_{Rh,Sn}$ = 674 Hz).

Acknowledgments

We thank the Russian Foundation for Basic Research (RFBR), the Deutsche Forschungsgemeinschaft (DFG), and the Fonds der Chemischen Industrie, Frankfurt (Main), Germany, for financial support.

[1] H. B. Charman, *J. Chem. Soc. (B)* **1970**, 584–587.
[2] T. Yamakawa, S. Shinoda, Y. Saito, H. Moriyama, P. S. Pregosin, *Magn. Reson.Chem.* **1985**, *23*, 202–206.
[3] D. P. Krut′ko, A. B. Permin, V. S. Petrosyan, O. A. Reutov, *Izv. Acad. Sci. Ser. Chem.* **1984**, 2787–2790.
[4] D. P. Krut′ko, A. B. Permin, V. S. Petrosyan, O. A. Reutov. *Izv. Acad. Sci. Ser. Chem.* **1985**, 909–914.
[5] [5a] R. Eisenberg, T. C. Eisenschmid, M. S. Chinn, R. U. Kirss, *Adv. Chem. Ser.* **1992**, *230*, 47–74. – [5b] S. B. Duckett, C. J. Sleigh, *Prog. Nucl. Magn. Reson. Spectrosc.* **1999**, *34*, 71–92.
[6] [6a] J. Bargon, J. Kandels, P. Kating, A. Thomas, K. Woelk, *Tetrahedron Lett.* **1990**, *31*, 5721–5724. – [6b] J. Bargon in "*Applied Homogeneous Catalysis with Organometallic Compounds*", (Eds.: B. Cornils, W. A. Herrmann), **1996,** 672–683, VCH–Wiley, Weinheim. – [6c] J. Natterer, J. Bargon, *Prog. Nucl. Magn. Reson. Spectrosc.* **1997**, *31*, 293–315.
[7] S. B. Duckett, C. L. Newell, R. Eisenberg, *J. Am. Chem. Soc.* **1994**, *116*, 10548–10556.
[8] R. Giernoth, P. Hübler, J. Bargon, *Angew. Chem.* **1998**, *110*, 2649–2651.
[9] C. Deibele, A. B. Permin, V. S. Petrosyan, J. Bargon, *Eur. J. Inorg. Chem.* **1998**, 1915–1923.
[10] H. Moriyama, T. Aoki, S. Shinoda, Y. Saito, *J. Chem. Soc., Dalton Trans.* **1981**, 639–644.
[11] J. R. Shapely, R. R. Schrock, J. A. Osborn, *J. Am. Chem. Soc.* **1969**, *91*, 2816–2817.
[12] G. W. Parshall, *J. Am. Chem. Soc.* **1966**, *88*, 704–708.
[13] P. G. Antonov, Y. N. Kukushkin, V. I. Anufriev, *Izv. Vyssh. Uchebn. Zaved. Khim., Khim. Tekhnol.* **1979**, *22*, 128–132.
[14] P. G. Antonov, Y. N. Kukushkin, V. F. Shkredov, V. I. Anufriev, *Izv. Vyssh. Uchebn. Zaved. Khim., Khim. Tekhnol.* **1981**, *24*, 941–948.
[15] [15a] T. Greve, Ph. D. Dissertation, Univ. of Bonn, **1996**. – [15b] J. Natterer, T. Greve, J. Bargon, *Chem. Phys. Lett.* **1998**, *293,* 455–460.

Received November 9, 1999
[I99398]

A Study of the Hydration and Dehydration of Vanadyl Arsenate by X-ray Diffraction Analysis, Infrared and Raman Spectroscopy

Ludvík Beneš,*[a] Klára Melánová,[a] Vítězslav Zima,[a] Miroslava Trchová,[b] Eva Uhlířová,[b] and Pavel Matějka[c]

Keywords: Vanadyl arsenate / Hydrates / Layered compounds / Vibrational spectroscopy / X-ray scattering

The course of the intercalation and deintercalation of water molecules in vanadyl arsenate has been studied by X-ray diffraction analysis and by infrared and Raman spectroscopies. The formation of $VOAsO_4$ hydrates at ambient temperature has been found to depend on relative humidity (r.h.): $VOAsO_4 \cdot 5\,H_2O$ (basal spacing $c = 10.48$ Å) is formed at r.h. above 76%, $VOAsO_4 \cdot 3\,H_2O$ ($c = 8.03$ Å) at 43–76% r.h., $VOAsO_4 \cdot 2\,H_2O$ ($c = 7.33$ Å) at 11–43% r.h.; dehydrated $VOAsO_4$ ($c = 4.18$ Å) exists near 0% r.h. Like the thermal dehydration of $VOPO_4 \cdot 2\,H_2O$, the thermal dehydration of $VOAsO_4 \cdot 3\,H_2O$ proceeds in a stepwise manner so that the dihydrate and monohydrate are formed en route to the anhydrous compound. The arsenate monohydrate is gradually dehydrated over a broad temperature range. The broad diffraction lines observed can be explained in terms of the existence of a disordered phase containing monohydrated and anhydrous forms of vanadyl arsenate. A similar phenomenon has been observed during the dehydration of $VOAsO_4 \cdot 3\,H_2O$ over phosphorus pentoxide at ambient temperature. The hydration of $VOAsO_4$ is different from that of $VOPO_4$. The first step, i.e. the insertion of water that coordinates to the vanadium atoms, is very slow. On the contrary, the uptake of further water molecules with the formation of higher hydrates is fast. It thus seems likely that the filling of one interlayer space with water facilitates the intercalation of further water into neighboring interlayer spaces. Therefore, only higher hydrates together with the original anhydrous phase are observed. Impedance spectral measurements indicate that the conductivity of the trihydrate has a mixed ionic/electronic character.

Introduction

Compounds of the general formula $MOXO_4$ (M = V, Nb, Ta; X = P, As) constitute an isomorphic series. X-ray diffraction studies have established the structures of tetragonal forms of $MOPO_4$[1–3] and $MOAsO_4$,[4,5] which consist of chains of corner-sharing MO_6 octahedra running parallel to the *c* axis. In the *xy* plane, each MO_6 octahedron shares corners with four XO_4 tetrahedra, which link the octahedral chains to produce an $(MOXO_4)_\infty$ layer. These layers are linked along the *c* axis by the *trans*-oxygen vertices of the octahedra to form a three-dimensional lattice.

Hydrates of some of these compounds are known and their formation may be rationalized in terms of cleavage of the long M–O bonds of the respective anhydrous forms and subsequent insertion of a water molecule at the sixth coordination site of the metal in the adjacent layer. Another molecule of water, as in $VOPO_4 \cdot 2\,H_2O$, spans two layers, being simultaneously hydrogen-bonded to each. The crystal structure of this hydrate was studied by neutron powder diffraction techniques on $VOPO_4 \cdot 2\,D_2O$.[6] It confirmed the apical position of the oxygen of the first water molecule in the VO_6 octahedron. The second water molecule was found to lie between two PO_4 tetrahedra of two different $(VOPO_4)_\infty$ layers. Due to the disorder of the second water molecule, its position could not be fully determined. Isostructural hydrates of this kind have been reported for $VOPO_4$,[7,8] $VOAsO_4$,[4] $NbOPO_4$,[9] and $NbOAsO_4$.[5] Molecules other than water can also penetrate between the layers of the anhydrous hosts and can even displace water from $MOXO_4$ hydrates.[10,11]

Vanadyl arsenate forms several hydrates.[4] Vanadyl arsenate trihydrate ($a = 6.39$ Å, $c = 8.08$ Å) can be prepared by refluxing vanadium pentoxide in an excess of arsenic acid (H_3AsO_4). It was found by thermogravimetric analysis that one molecule of water is released at 50 °C forming the dihydrate ($a = 6.37$ Å, $c = 7.39$ Å). The monohydrate is formed at 80 °C and complete dehydration occurs at 105 °C resulting in anhydrous $VOAsO_4$ ($a = 6.33$ Å, $c = 4.18$ Å).

In this paper, we report on a study of these $VOAsO_4$ hydrates. The intercalation and deintercalation of water molecules has been studied by X-ray diffraction analysis and by infrared and Raman spectroscopies. The character of the hydrates has been also studied by alternating current (AC) conductivity.

[a] Joint Laboratory of Solid State Chemistry of the Academy of Sciences of the Czech Republic and the University of Pardubice, Studentská 84, 532 10 Pardubice, Czech Republic
Fax: (internat.) + 420-40/603-6011
E-mail: ludvik.benes@upce.cz
[b] Faculty of Mathematics and Physics, Charles University, V. Holešovičkách 2, 180 00 Prague, Czech Republic
Fax: (internat.) + 420-2/219-12351
E-mail: trchova@mbox.troja.mff.cuni.cz
[c] Department of Analytical Chemistry, Institute of Chemical Technology, Technická 5, 166 28 Prague, Czech Republic

 © WILEY-VCH Verlag GmbH, D-69451 Weinheim, 2000 1434–1948/00/0505–0895 $ 17.50+.50/0

Results and Discussion

In order to study the formation of various hydrates, $VOAsO_4 \cdot 3\ H_2O$ was kept in an atmosphere of controlled relative humidity (r.h.) at ambient temperature. The dependence of basal spacing and water content on relative humidity is illustrated in Figure 1. Vanadyl arsenate trihydrate was found to be stable in the r.h. range from 43% to 76%. At higher r.h., vanadyl arsenate pentahydrate with a basal spacing of 10.48 Å is formed. Vanadyl arsenate dihydrate is observed in the r.h. range from 11% to 43%. In contrast to vanadyl phosphate dihydrate, $VOAsO_4 \cdot 2\ H_2O$ loses its remaining water molecules when the r.h. is close to 0%.

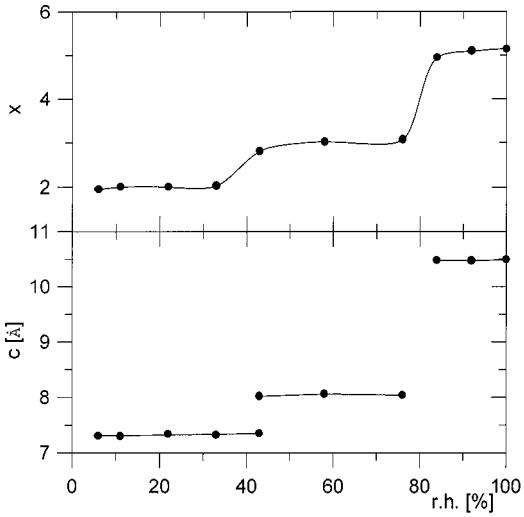


Figure 1. The dependence of the lattice parameter c and water content x of $VOAsO_4 \cdot x\ H_2O$ on relative humidity

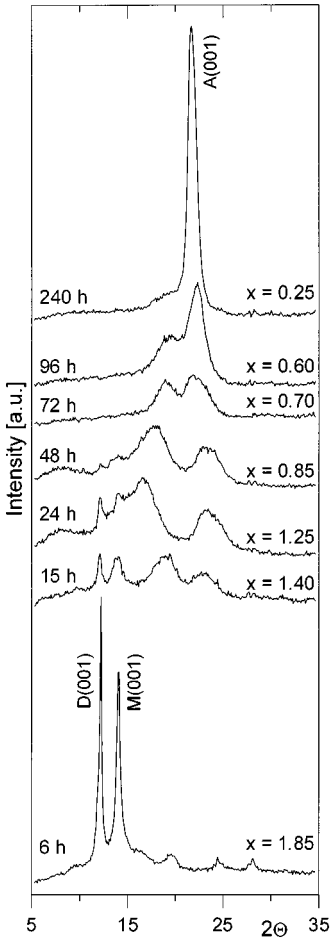


Figure 2. Diffractograms and water content x of $VOAsO_4 \cdot 3\ H_2O$ kept over P_2O_5 as a function of time; the (001) reflections of the dihydrate, monohydrate, and anhydrous compound are denoted as D, M, and A, respectively

The progressive dehydration of $VOAsO_4 \cdot 2\ H_2O$ on storage over phosphorus pentoxide at ambient temperature could be followed by XRD and TG (see Figure 2). After six hours, both the monohydrate and dihydrate were observed. Their (001) diffraction lines were sharp and the water content x became less than two. On continued dehydration, the intensities of these lines decreased, although they remained sharp. In addition, some very broad diffraction lines were seen, the positions and linewidths of which changed during the course of the dehydration. After ten days, the relatively sharp (001) line of anhydrous vanadyl arsenate had appeared. The broadening of the (00l) lines can be explained in terms of a fragmentation of the microcrystals during the dehydration, but the shift in the line positions remains unexplained. The described behavior is similar to that found for a Hendricks–Teller disordered layered lattice,[12] where layers of different types alternate randomly. However, the positions and linewidths calculated from the Hendricks–Teller functions do not correspond to those found experimentally, hence the formation of such a lattice can be excluded. As the diffractogram still shows the line due to the dihydrate after 24 h of dehydration, we presume that there is a random variation of the layers involving dihydrated, monohydrated, and anhydrous $VOAsO_4$.

In situ X-ray diffraction analysis was also employed to follow the dehydration of vanadyl arsenate trihydrate. The sample went through four diffracting phases during heating (see Figure 3). The basal spacings of these phases corresponded to the values found for $VOAsO_4 \cdot 3\ H_2O$ (c = 8.03 Å), $VOAsO_4 \cdot 2\ H_2O$ (c = 7.33 Å), $VOAsO_4 \cdot H_2O$ (c = 6.40 Å), and $VOAsO_4$ (c = 4.18 Å). The transformation of trihydrate to dihydrate was complete at 33 °C. Formation of the monohydrate was found to commence at 51 °C and this species was present up to 57 °C together with the dihydrate. In the temperature range from 63 to 111 °C, only very broad lines were observed. A Hendricks–Teller disordered structure is probably formed in this region. The temperatures of dehydration observed by XRD were lower than those determined by the thermogravimetric method. This difference can be ascribed to the fact that TG measures weight loss caused by evaporation of water released from the interlayer space of the sample.[15]

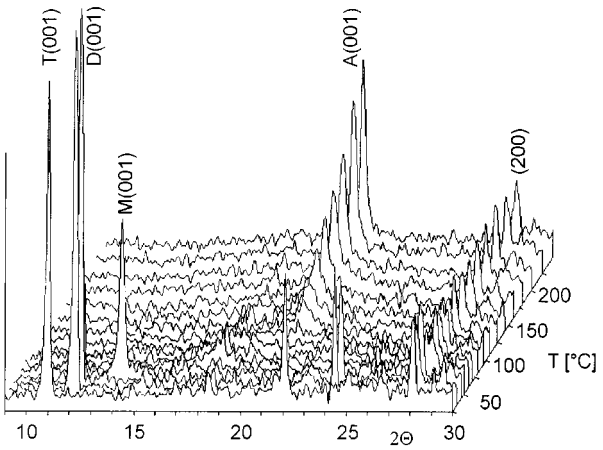


Figure 3. Temperature dependence of the X-ray diffractograms of $VOAsO_4 \cdot 3\ H_2O$

The progressive hydration of anhydrous vanadyl arsenate was studied by XRD at several relative humidities (r.h.). Even at an r.h. as high as 92%, the hydration was found to be very slow in comparison with that of $VOPO_4$.[14,16] After six hours, the intensity of the (001) diffraction line of anhydrous $VOAsO_4$ had decreased to 60% of its original value and the (001) lines of the pentahydrate and dihydrate had appeared. After one day, the intensity of the (001) line of $VOAsO_4$ had decreased to 10% and the prevailing phase was the pentahydrate. After four days, the lines due to anhydrous vanadyl arsenate had disappeared and both the pentahydrate and dihydrate were present. At an r.h. of 76%, the hydration occurred only on the surface of the crystallites of anhydrous $VOAsO_4$. The (001) reflection of the dihydrate appeared at very low intensity after one day and the diffractogram remained the same during a further five days.

Infrared Spectra

The ATR infrared spectrum of anhydrous vanadyl arsenate and the spectra of its dihydrate, trihydrate, and pentahydrate in the range 650 to 2000 cm^{-1} are shown in Figure 4. The observed bands can be fully assigned on the basis of previous studies of the $MOXO_4$ compounds.[17] The spectra have been interpreted in terms of the vibrations of the AsO_4^{3-} tetrahedron by analogy with the fundamental frequencies of the PO_4^{3-} ion in anhydrous $VOPO_4$.[16] The positions of all these bands are shifted to lower wavenumbers due to the mass effect of the As atom compared to P. Table 1 lists the spectra in the terms of the fundamental modes of AsO_4^{3-} ion, the vanadyl V=O vibration, and the O–H stretching and bending modes.

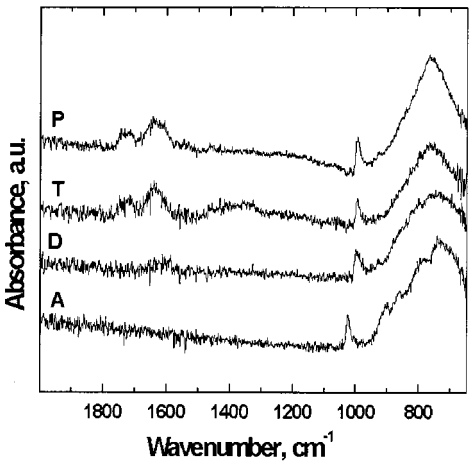


Figure 4. ATR infrared spectra of $VOAsO_4$ (A) and its dihydrate (D), trihydrate (T), and pentahydrate (P)

In the infrared spectrum of anhydrous $VOAsO_4$, the band corresponding to the degenerate antisymmetric $\nu_3(AsO_4^{3-})$ vibration is split into two bands at 905 cm^{-1} and 865 cm^{-1}. The symmetric $\nu_1(AsO_4^{3-})$ vibration at 737 cm^{-1}, which is very strong in the Raman spectrum, also appears in the infrared spectrum provided that the symmetry of the arsenate ion is perturbed from tetrahedral. It is also split in the infrared spectrum, the second band appearing at 793 cm^{-1}. The well-resolved isolated band at 1026 cm^{-1} can reasonably be attributed to the vibration of the vanadyl group V=O.

Vanadyl arsenate trihydrate is stable under ambient conditions. In the infrared spectrum of $VOAsO_4 \cdot 3\ H_2O$, in contrast to that of anhydrous $VOAsO_4$, the two bands due to the degenerate antisymmetric $\nu_3(AsO_4^{3-})$ vibration at 905 and 865 cm^{-1} are not distinguishable. They overlap with the bands of the symmetric $\nu_1(AsO_4^{3-})$ vibration in a broad maximum centred at about 740 cm^{-1}. This can be explained by the fact that there is no longer any internal stress causing

Table 1. Assignments of the observed vibration bands of $VOAsO_4$, $VOAsO_4 \cdot 2\ H_2O$, $VOAsO_4 \cdot 3\ H_2O$, and $VOAsO_4 \cdot 5\ H_2O$

Vibration	V=O	$\nu_3(AsO_4)$ + H_2O vibn.	$\nu_1(AsO_4)$ + H_2O vibn.	$\nu_2(H_2O)$ (C=O)	$\nu_1(H_2O)$	$\nu_3(H_2O)$
$VOAsO_4$	1026 cm^{-1}	905 cm^{-1} 865 cm^{-1}	793 cm^{-1} 737 cm^{-1}	not present	not present	not present
$VOAsO_4 \cdot 2\ H_2O$	1026 cm^{-1} 998 cm^{-1}	n[a]	740 cm^{-1}	1640 cm^{-1}	3500 cm^{-1}	
$VOAsO_4 \cdot 3\ H_2O$	1026 cm^{-1} 998 cm^{-1}	n[a]	740 cm^{-1}	1640 cm^{-1} (1728 cm^{-1})	3400 cm^{-1}	3580 cm^{-1}
$VOAsO_4 \cdot 5\ H_2O$	1026 cm^{-1} 997 cm^{-1}	n[a]	740 cm^{-1}	1635 cm^{-1} (1736 cm^{-1})	3400 cm^{-1}	3600 cm^{-1}

[a] Bands are overlapped or merged with the ν_1 band and cannot be distinguished.

deformation of the AsO_4^{3-} tetrahedron that leads to IR activity of this symmetric vibration. Moreover, these bands also overlap with vibration bands of H_2O molecules, which are usually observed at around 800 cm^{-1}.[16] The vanadyl group vibration band is shifted to 998 cm^{-1} in all hydrates of vanadyl arsenate. As in $VOPO_4$, this effect is caused by the coordination of a water molecule to the vanadium atom, which influences the stretching vibration of the V=O double bond. A band due to the As–O–V lattice vibrations is probably present below 400 cm^{-1}. Besides the position of the vanadyl group absorption, the spectra of all the hydrates differ from that of anhydrous vanadyl arsenate in that H_2O vibration bands are of course present. The deformation vibration of the O–H group is seen at 1640 cm^{-1}. A broad asymmetric band is observed in the region of the valence vibration of the O–H group at 3400 cm^{-1}, together with a maximum at 3580 cm^{-1} (see Table 1). The IR spectrum of the pentahydrate $VOAsO_4 \cdot 5\ H_2O$ is practically identical to that of the trihydrate $VOAsO_4 \cdot 3\ H_2O$. The spectra of these two compounds differ from that of the dihydrate in the presence of a band at about 1728 cm^{-1}, which corresponds to a small degree of contamination by the carbonyl group C=O.

Water molecules penetrated into the sample when pure, completely characterized samples of anhydrous vanadyl arsenate were briefly exposed to atmospheric moisture. The ATR infrared spectra of anhydrous $VOAsO_4$ and its progressive intercalates with water molecules under ambient conditions in the range 650 to 1150 cm^{-1} are presented in Figure 5.

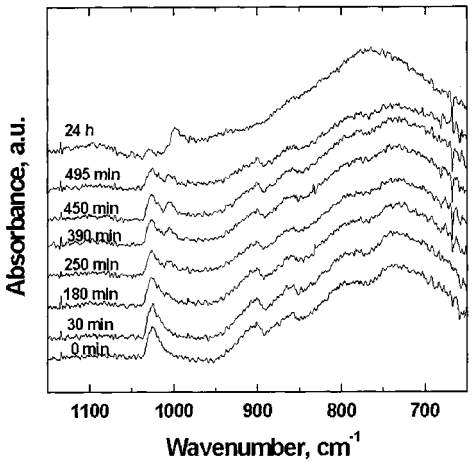


Figure 5. ATR infrared spectrum of anhydrous $VOAsO_4$ and its progressive intercalates with water molecules under ambient conditions

Analysis of these spectra led to the following conclusions:

(i) During the intercalation of water molecules, the intensity of the band at 1026 cm^{-1} due to the vanadyl V=O stretching vibration in the anhydrous form decreases, while a new band appears at 998 cm^{-1}, characteristic of the dihydrate, trihydrate, or pentahydrate.

(ii) Bands due to the symmetric stretching vibration $\nu_1(AsO_4^{3-})$ and the degenerate antisymmetric stretching vibration $\nu_3(AsO_4^{3-})$ change their profile upon hydration and become overlapped with H_2O vibration modes.

(iii) Bands due to deformation and stretching vibrations of water molecules appear at about 1640 cm^{-1} and 3400 cm^{-1} upon hydration.

(iv) The spectrum after 24 hours (Figure 5) is very similar to that of vanadyl arsenate trihydrate (or pentahydrate).

The fact that vanadyl stretching bands are present in both of the aforementioned positions in the initial stages of the intercalation indicates the simultaneous presence of anhydrous and hydrated forms. The changes in the profile of the $\nu_3(AsO_4)$ vibration bands indicate that the system of hydrogen bonds between water molecules and the oxygen of the AsO_4 tetrahedron affects its stretching and bending modes, as was observed for the hydrates of $VOPO_4$.[16]

Raman Spectroscopy

The Raman spectra strongly support the assignments of the bands observed in the infrared spectra of all the studied compounds. Unfortunately, it was not possible to study the kinetics of the hydration process by Raman spectroscopy since the laser irradiation caused a partial escape of water molecules during the measurements. The spectra corresponding to the different hydrated states of the samples between the anhydrous and hydrated forms (spectra 1, 2, and 3 in Figure 6) were obtained by regulation of the incident beam power and of the number of scans.

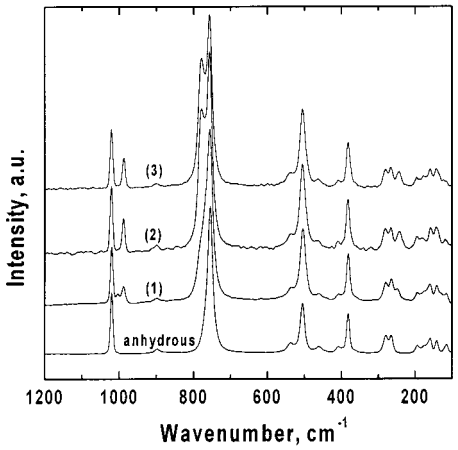


Figure 6. Raman spectra of $VOAsO_4$ and its intermediate hydrate states

The Raman spectrum of anhydrous $VOAsO_4$ (measured in a sealed ampoule) in the range 100 to 1200 cm^{-1} is shown in Figure 6. A strong symmetric $\nu_1(AsO_4^{3-})$ vibration is observed only at 756 cm^{-1}. A very small band due to the degenerate antisymmetric $\nu_3(AsO_4^{3-})$ vibration is observed only at 899 cm^{-1}. The position of the well-resolved isolated band at 1020 cm^{-1} corresponds to the vibration of the vanadyl group V=O in anhydrous vanadyl arsenate. In addition to these features, bands due to symmetric bending vibrations $\nu_4(AsO_4^{3-})$ at 535 cm^{-1} and 506 cm^{-1} and antisymmetric bending vibrations $\nu_2(AsO_4^{3-})$ at 408 and 382 cm^{-1} are also observed in the Raman spectra. The bands at about

270 cm^{-1} can probably be attributed to δ(O–As–O) deformation vibrations.

The effect of water on the spectra of vanadyl arsenate can thus be summarized as follows (see also Figure 6):

(i) In addition to the well-resolved isolated band at 1020 cm^{-1}, attributed to the vibration of the vanadyl group V=O in the anhydrous form of $VOAsO_4$, another peak at 989 cm^{-1} is observed in the Raman spectra of the hydrated forms of $VOAsO_4$.

(ii) A strong symmetric $\nu_1(AsO_4^{3-})$ vibration at 756 cm^{-1} with a strong overlapping shoulder at 780 cm^{-1} is observed.

(iii) A band due to the degenerate antisymmetric $\nu_3(AsO_4^{3-})$ vibration is observed at 899 cm^{-1} and a small shoulder is seen at 920 cm^{-1} in accordance with the infrared results.

AC Conductivity

In order to compare the electrical properties of $VOAsO_4$ with those of the previously studied $VOPO_4$,[20] its AC conductivity was determined by impedance spectroscopy. The impedance data show an arc-shaped dependence of the imaginary versus the real component, which passes through the origin in the complex impedance plot. A resistance connected in parallel with a constant phase element (CPE) was chosen as an equivalent circuit.[18] The dependence of impedance Z (where $Z = Z' - jZ''$) on frequency f for this circuit is given by Equation 1.

$$Z = \frac{R}{1 + \left(j\omega\tau_0\right)^{1-\alpha}} \quad (1)$$

Here, $\omega = 2\pi f$ is the angular frequency, R is the resistance, τ_0 is the relaxation time, and α is a parameter describing a distribution of relaxation times in frequency space. Parameters R, τ_0, and α were estimated from the experimental values by a complex nonlinear least-squares fitting.[19] The conductivity σ_m was then calculated from the estimated resistance R and the dimensions of the sample. The AC impedance curve measured at room temperature and 58% relative humidity was similar to that found for $VOPO_4 2H_2O$[20] indicating similar conductivity behavior. Indeed, the conductivities of $VOPO_4 \cdot 2\,H_2O$ and $VOAsO_4 \cdot 3\,H_2O$ are roughly the same, $\sigma_m = 1.3 \cdot 10^{-5}$ S cm^{-1}. These facts suggest that the electrical properties of $VOXO_4$ materials are not influenced by the atom X. According to these preliminary measurements, the M atom in $MOXO_4$ plays a more important role in the conductivity mechanisms. A more detailed study of the conductivities of these materials is currently underway.

Experimental Section

Materials: Vanadyl arsenate trihydrate was prepared by prolonged boiling of a mixture of vanadium pentoxide and arsenic acid (H_3AsO_4) in water[4] and was stored over a saturated aq. solution of NaBr (r.h. 58%). The samples of $VOAsO_4 \cdot 2\,H_2O$ and $VOAsO_4 \cdot 5\,H_2O$ for IR measurements were obtained by prolonged storage of the trihydrate over saturated solutions of LiCl (r.h. 11%) and KNO_3 (r.h. 92%), respectively. Anhydrous $VOAsO_4$ was prepared by dehydration of the trihydrate at about 300 °C in vacuo for 4 h. The water contents of samples were determined thermogravimetrically. The TG analyses were performed using a Derivatograph C (MOM, Budapest, Hungary). The measurements were performed in air between 20 and 500 °C at a heating rate of 5 K min^{-1}.

X-ray Diffraction: Powder data were obtained with an HZG-4 X-ray diffractometer (Freiberger Präzisionsmechanik, Germany) using Cu-K_α radiation with elimination of Cu-K_β radiation by means of an Ni filter. Diffraction angles were measured in the 2θ range 5–50°. Variable-temperature measurements in the range 20–250 °C were carried out on a thermocouple-controlled heated corundum plate.[21]

Infrared Spectroscopy: IR measurements were made with a Nicolet Impact 400 Fourier transform infrared (FTIR) spectrophotometer in an H_2O-purged environment. An ambient-temperature deuterated triglycine sulfate (DTGS) detector was used for the range from 400 to 4000 cm^{-1}. A Happ–Genzel apodization function was used in all regions and the spectral resolution was 2 cm^{-1}. Approximately 300 scans were accumulated to achieve the signal-to-noise ratio shown. The Baseline Horizontal Attenuated Total Reflection (ATR) accessory with a ZnSe crystal (n = 2.4 at 1000 cm^{-1}) was used in measuring the infrared spectra of the samples. The effective pathlength was approximately a few μm (incident angle 60°, number of reflections 7). The ATR correction was made to eliminate the dependence of the effective pathlength on the wavelength. After some trials, it was found that the best results were obtained when the sample was exposed to the external conditions for a definite time without being removed from the crystal between the subsequent spectral measurements. In this way, the water molecules are deposited on the surface of the ZnSe crystal from the volume and the adsorption of water onto the surface of the sample under investigation is avoided. The vibrational spectrum of each compound was recorded five times using five different samples of the same material. No variation of the studied spectral features was observed between the samples.

Raman Spectroscopy: FT Raman spectra were recorded using an Equinox 55/S Fourier-transform near-infrared (FT-NIR) spectrometer (Bruker) equipped with an FT Raman module FRA 106/S (Bruker). The samples were irradiated with a focused laser beam with a power of 100 mW (Nd-YAG laser, 1064 nm, coherent). The scattered light was collected in a back-scattering geometry. A quartz beamsplitter and a Ge detector (liquid N_2 cooled) were used to obtain interferograms. 128 interferograms were accumulated and subsequently Fourier-transformed using Blackman–Harris 4-term apodization and a zero-filling factor of 8 to obtain final FT Raman spectra in the range 4000–1000 cm^{-1} with 4 cm^{-1} resolution. The FT Raman spectra of pure, well-defined species ($VOAsO_4$, $VOAsO_4 \cdot 3\,H_2O$, $VOAsO_4 \cdot 5\,H_2O$) were recorded from samples in sealed glass ampoules. The ampoules were placed in the sample holder and aligned by the motorized x-y-z sample stage to achieve the optimal optical conditions for sample irradiation and the collection of the scattered light. The FT Raman spectra collected during the intercalation of water were obtained from samples placed in an aluminium cup. The aluminium cup was optically pre-aligned using sulfur as a sample and then the sulfur was replaced by the sample under investigation.

AC Conductivity: Rectangular pellets of dimensions 8 × 3 × 2 mm were prepared by compressing 15 mg of the sample at 2.5 MPa. As

a result of the applied pressure, the layers were preferentially oriented in a plane perpendicular to the direction of the pressure. The opposite sides of the pellets were coated with graphite paste, which served as electrodes, and the AC conductivity was measured along the layers. A Tesla BM 653 impedance meter working in the frequency range 20 Hz to 500 kHz was used for the measurements.

Acknowledgments

This work was supported by the Grant Agency of the Czech Republic, grant no: 203/97/1010 and Grant Agency GAUK, grant no: 37/97/B.

[1] B. Jordan, C. Calvo, *Can. J. Chem*. **1973**, *51*, 2621–2625.
[2] J. M. Longo, P. Kierkegaard, *Acta Chem. Scand*. **1966**, *20*, 72–78.
[3] J. M. Longo, J. W. Pierce, J. A. Kafalas, *Mater. Res. Bull*. **1971**, *6*, 1157–1166.
[4] N. G. Chernorukov, N. P. Egorov, I. A. Korshunov, *Zh. Neorg. Khim*. **1978**, *23*, 2672–2675.
[5] N. G. Chernorukov, N. P. Egorov, I. A. Korshunov, *Izv. Akad. Nauk. SSSR, Neorg. Mater.* **1979**, *15*, 335–338.
[6] M. Tachez, F. Theobald, J. Bernard, A. W. Hewat, *Rev. Chim. Miner.* **1982**, *19*, 291–300.
[7] E. Bordes, P. Courtine, G. Pannetier, *Ann. Chim. (Paris)* **1973**, *8*, 105–113.
[8] G. Ladwig, *Z. Anorg. Allg. Chem*. **1965**, *338*, 266–278.
[9] N. G. Chernorukov, N. P. Egorov, I. R. Mochalova, *Zh. Neorg. Khim*. **1978**, *23*, 2931–2934.
[10] L. Beneš, V. Zima, *Sci. Pap. Univ. Pardubice Ser. A* **1996**, *2*, 121–149; *Chem. Abstr*. **1997**, *126*, 309226m.
[11] J. Kalousová, J. Votinský, L. Beneš, K. Melánová, V. Zima, *Collect. Czech Chem. Commun.* **1998**, *63*, 1–19.
[12] S. Hendricks, E. Teller, *J. Chem. Phys.* **1942**, *10*, 147–167.
[13] D. C. Johnston, S. P. Flysinger, *Phys. Rev. B* **1984**, *30*, 980–984.
[14] L. Beneš, V. Zima, *J. Incl. Phenom*. **1995**, *20*, 381–391.
[15] V. Zima, L. Beneš, J. Málek, M. Vlček, *Mat. Res. Bull*. **1994**, *29*, 687–692.
[16] M. Trchová, P. Čapková, P. Matějka, K. Melánová, L. Beneš, *J. Solid State Chem*. **1999**, *148*, 197–204.
[17] S. D. Ross, *Inorganic Infrared and Raman Spectra*, McGraw-Hill, London, **1972**.
[18] J. R. MacDonald, *Impedance Spectroscopy*, Wiley, New York, **1987**, p. 17.
[19] J. R. MacDonald, *Impedance Spectroscopy*, Wiley, New York, **1987**, p. 180.
[20] V. Zima, M. Vlček, L. Beneš, M. Casciola, L. Massinelli, R. Palombari, *Chem. Mater.* **1996**, *8*, 2505–2509.
[21] L. Beneš, *Sci. Pap. Univ. Pardubice Ser. A* **1996**, *2*, 151–155; *Chem. Abstr*. **1997**, *126*, 310616v.

Received November 12, 1999
[I99405]

Tricarbonyl-η⁶-[(2-thiophenyl)arene]- and -η⁶-[(2-thiophenyl)carbonylarene]-chromium Complexes: Preparation and Conformational Study

Damien Prim,[a] Jean-Philippe Tranchier,[a] Françoise Rose-Munch,[a] Eric Rose,*[a] and Jacqueline Vaissermann[b]

Keywords: Arenetricarbonyl chromium complexes / Palladium / Cross coupling reaction / Thiophenes

The cross coupling reaction of (*p*-chloroanisole)tricarbonylchromium complex (**1**) with thiophene derivatives under palladium-catalyzed conditions leads to the selective formation of tricarbonyl-η⁶-[(2-thiophenyl)arene]- or -η⁶-[(2-thiophenyl)carbonylarene]chromium complexes (**2** or **3**) depending on reaction conditions. The conformation of complexes **2** and **3** in the solid state as well as in solution are reported.

Introduction

Over the last three decades, cross-coupling reactions using Stille, Suzuki, or Negishi methodologies have attracted much attention.[1,2] The unique behaviour of organotin, boron, or zinc reagents with different halogenated aromatics (iodides, bromides, and more recently, chlorides[3]) under palladium catalysis has become one of the most powerful C_{sp2}–C_{sp2} bond formation methods.

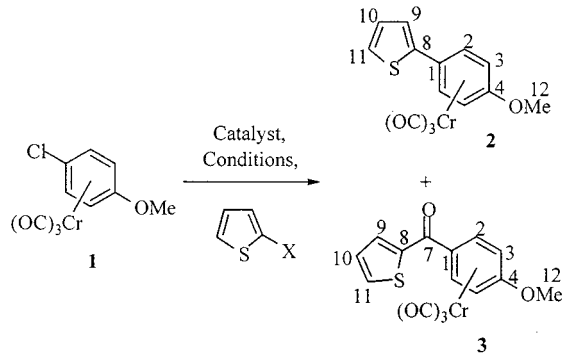
It has been shown that the decrease of the electron density in an aromatic ring due to the presence of the $Cr(CO)_3$ moiety allows an easier oxidative addition of the carbon–halogen bond to the zero-valent palladium active species, which is the initial step of most of the palladium-catalyzed cross coupling processes. This ability allowed for the more frequent inclusion of aryl chloride among the electrophiles, thus enhancing the usefulness of these reactions.[4–6] Since then, palladium-catalyzed processes at π-bond ligands in the presence of $Cr(CO)_3$ groups have been developed.[7]

As part of our current studies on organochromium complexes[8,9] and on cross-coupling reactions,[10,11] we were interested in the preparation of tricarbonyl-η⁶-[(thiophenyl)arene- and -(thiophenyl)carbonylarene]chromium complexes by using a bimetallic activation. This paper describes how the judicious choice of reaction conditions can lead to exceptional selectivities in this class of bond-formation reactions. In particular, in taking advantage of CO insertion under a carbon monoxide atmosphere, exclusive access to carbonylation products can be achieved.

[a] Laboratoire de Synthèse Organique et Organométallique, UMR CNRS 7611, Université Pierre et Marie Curie,
Tour 44–45, 4, Place Jussieu, 75252 Paris Cedex 05, France
Fax: (internat.) +33-1/44275504
E-mail: rose@ccr.jussieu.fr
[b] Laboratoire de Chimie Inorganique et Matériaux Moléculaires, ESA CNRS 7071, Université Pierre et Marie Curie,
Bat F, 4, Place Jussieu, 75252 Paris Cedex 05, France

Results and Discussion

The reaction of *p*-chloroanisole tricarbonylchromium complex (**1**) with thiophene derivatives under palladium-catalyzed conditions (Scheme 1) leads to the formation of two new complexes: the expected thienyl complex **2** but also a second compound due to a carbonyl insertion into the newly formed carbon-carbon bond. We have examined the scope of this reaction with three different thienyl derivatives under several palladium-catalyzed procedures, and the results are presented in Table 1.



Scheme 1

We first tried the classical conditions: $PdCl_2(PPh_3)_2$ in refluxing THF (entry 1), complexes **2** and **3** were obtained in 54% yield in a 3:1 ratio.[12] The two complexes were easily separated by column chromatography, and their spectral data as well as their conformational study in solution and in the solid state will be discussed later (vide infra). If this reaction was performed with (2-thienyl)boronic acid (entry 2) and 2-thienyl zinc chloride[10] (entry 3) (prepared in situ from 2-thienyllithium and anhydrous zinc chloride in THF) complexes **2** and **3** were obtained in a 7:1 ratio (63% yield) and 3.5:1 ratio (19% yield), respectively after silica gel column chromatography. Under milder reaction conditions (room temperature) using Stille-coupling reaction conditions and a modified catalytic system[13] such as $Pd_2(dba)_3$

 © WILEY-VCH Verlag GmbH, D-69451 Weinheim, 2000 1434–1948/00/0505–0901 $ 17.50+.50/0

Table 1. Preparation of complexes **2** and **3**

Entry	X	Catalyst	Conditions	Time [h]	2:3	Yield [%]
1	$SnBu_3$	$PdCl_2(PPh_3)_2$	THF, reflux	18	3:1	54
2	$B(OH)_2$	$Pd(PPh_3)_4$	Acetone, K_2CO_3, reflux	14	7:1	63
3	ZnCl	$Pd(PPh_3)_4$	DMF, 80°	18	3.5:1	19
4	$SnBu_3$	$Pd_2(dba)_3$, 4 $AsPh_3$	DMF, room temp.	20	1:0	82
5	$SnBu_3$	$PdCl_2(PPh_3)_2$	THF, CO, reflux	2	0:1	88

and $AsPPh_3$, where the arsane ligand has been shown to be a more effective dissociative ligand at the transmetallation stage (entry 4), we succeeded in selectively preparing complex **2** in good yield (82%). This selectivity is certainly due to the reaction conditions (room temperature) which inhibit the internal CO migration and therefore the formation of compound **3**. This reaction represents a significant improvement in the synthesis of such complexes. Indeed, the preparation of the [(2-thienyl)-η^6-benzene]tricarbonylchromium complex has already been reported[14] using thermal complexation of the $Cr(CO)_3$ entity to the six-membered ring of 2-phenylthiophene, but with a low yield of 7%. Moreover, if we carried out the coupling reaction under a CO atmosphere as reported in entry 5, we were able to isolate complex **3** as the sole product in high yield (88%).

Conformational Studies in Solution and in the Solid State of Complexes 2 and 3

Solution

The spectral data of complexes **2** and **3** were in good agreement with their respective structures. The IR spectrum of complex **3** showed one band typical for a keto group at 1635 cm^{-1}, besides the bands between 1900 and 1975 cm^{-1} due to CO ligands.

The ^{1}H-NMR data of complexes **2** and **3** are noteworthy to observe the influence by the coordination of the $Cr(CO)_3$ entity and by the conformation of the tripod in solution[15] on the chemical shifts of the protons of the arene. Indeed, protons H-2 and H-3 of complex **2** are privileged spectators vis-à-vis the $Cr(CO)_3$ conformation: they resonate at δ = 5.92 and 5.20 (Table 2, entry 1). Knowing

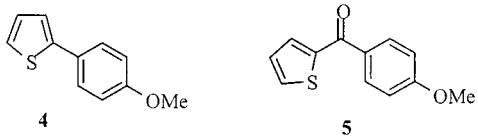


Figure 1. Free arenes

that the protons H-2 and H-3 of the free arene **4** (Figure 1) resonate at δ = 7.60 and 6.96 (Table 2, entry 2), we were able to calculate the shielding of these protons as Δδ = δ(free arene **4**) – δ(complex **2**). In this way we obtained the values of Δδ = 1.68 for H-2 and 1.76 for H-3 in complex **2** (Table 2, entry 3), a small difference of 0.08 ppm! In other words, the coordination of the tricarbonylchromium entity has the same shielding effect on the arene protons. These data are in good agreement with an almost staggered conformation of the $Cr(CO)_3$: indeed the two conformations eclipsing (**2E**, Figure 2) and *anti*-eclipsing the methoxy group (**2AE**, Figure 2), which are in equilibrium, are present in an almost 50:50 ratio.[16]

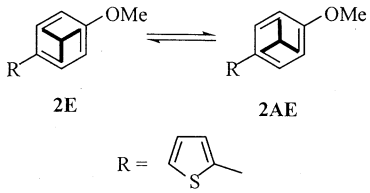


Figure 2. The two conformers of complex **2**

For complex **3**, the shielding of the two protons H-2 and H-3: Δδ = δ(free arene **5**) – δ(complex **3**) are 1.57 and 1.78 ppm, respectively, a difference of 0.21 ppm[17a]

Table 2. ^{1}H- and ^{13}C-NMR data for compounds **2**–**5**

Entry	Compound	H-2	H-3	δ(H-2) – δ(H-3)	Δδ(H-2) – Δδ(H-3)	C-2	C-3
1	2[a]	5.92	5.20	0.72	–	93.3	77.5
2	4[a]	7.60	6.96	0.64	–	127.3	114.1
3	$\Delta\delta^{[a]} = \delta(4) - \delta(2)$	1.68	1.76	–	0.08	34.0	36.6
4	2[b]	5.25	4.37	0.88	–		
5	4[b]	7.43	6.69	0.74	–		
6	$\Delta\delta^{[b]} = \delta(4) - \delta(2)$	2.18	2.32	–	0.14		
7	3[a]	6.32	5.19	1.13	–	95.8	76.6
8	5[a]	7.89	6.97	0.92	–	131.9	144.1
9	$\Delta\delta^{[a]} = \delta(5) - \delta(3)$	1.57	1.78	–	0.21	36.1	37.5
10	3[b]	5.82	4.23	1.59	–		
11	5[b]	7.80	6.59	1.21	–		
12	$\Delta\delta^{[b]} = \delta(5) - \delta(3)$	1.98	2.56	–	0.58		

[a] $CDCl_3$. – [b] C_6D_6.

(Table 2, entry 9). These data are no longer consistent with a mean staggered conformation of the tripod in solution. As the proton H-2 resonates at a lower field (δ = 6.32) with respect to the proton H-3 (δ = 5.19), the population of the conformation eclipsing the methoxy group should be favoured. This can be explained by the synergic effect of the electron-withdrawing keto group which favours an *anti*-eclipsed conformation and of the electron-donating methoxy group which favours the eclipsed conformation.[17b–17f]

Some of the ^{13}C-NMR data of compounds **2–5** are reported in Table 2. First of all, the spectrum of complex **3** displayed, among others, a signal at δ = 230.7 attributed to the carbonyl keto group, whereas carbons of carbonyl ligands appeared as a signal at δ = 232.2. The shielding of the aromatic carbons of the arene ring of complexes **2–5** are, as expected, between 34 and 37 ppm, except the quaternary carbons bearing the methoxy group which are shielded only by 17.1 and 19.8 ppm for complexes **2** and **3**, respectively (Table 2, entries 3 and 9). It is worthy to note that the quaternary carbons C-8 of the thiophene residues of complexes **2** and **3** are also shielded by 17.2 and 22.0 ppm, the other carbons C-9, C-10, C-11 resonating at almost the same field for couples **2**, **4** and **3**, **5**.

Solid State

In order to know more about the conformation of complexes **2** and **3**, they were both subjected to X-ray analysis. The ORTEP views showing the most important bond distances appear in Figure 3 and Figure 4. The conformation of the $Cr(CO)_3$ entities of complexes **2** and **3** are very similar, adopting an almost staggered conformation. The

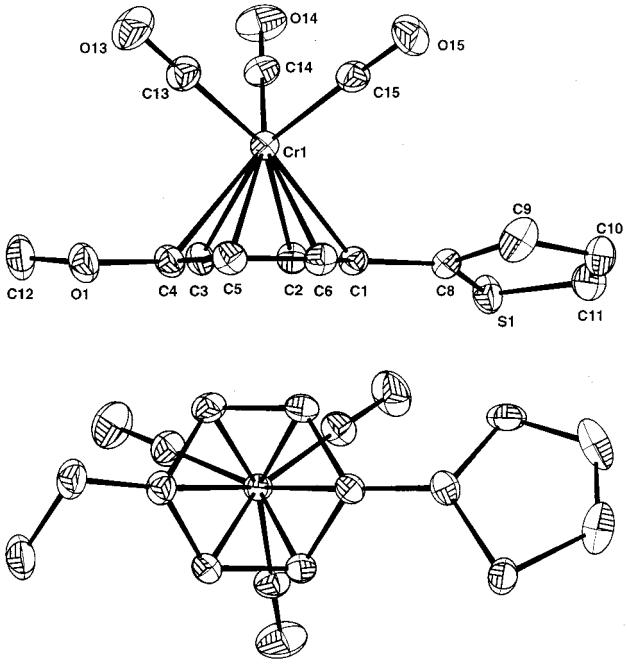


Figure 3. Two views of ORTEP diagram of complex **2**. Selected bond lengths [A]: Cr–C-1 2.233(3), Cr–C-2 2.201(3), Cr–C-3 2.251(3), Cr–C-4 2.289(3), Cr–C-5 2.221(3), Cr–C-6 2.203(3), C-8–C-9 1.46(2), C-10–C-11 1.326(2)

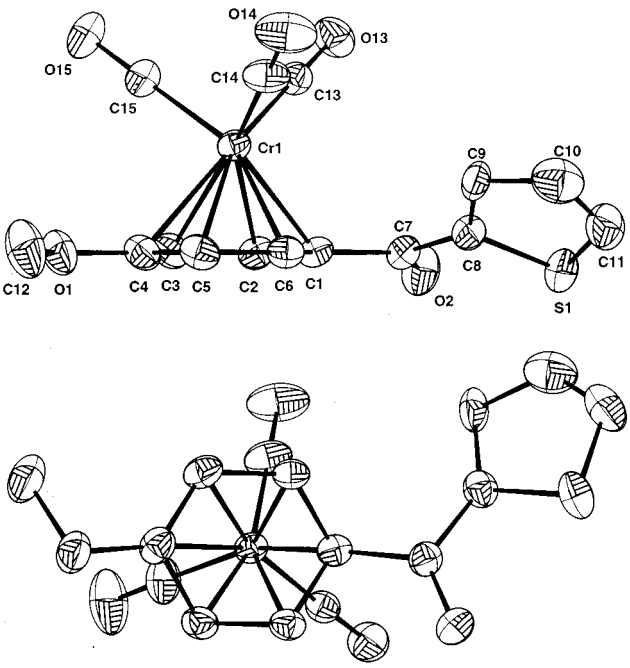


Figure 4. Two views of ORTEP diagram of complex **3**. Selected bond lengths [A]: Cr–C-1 2.181(4), Cr–C-2 2.206(4), Cr–C-3 2.238(4), Cr–C-4 2.282(4), Cr–C-5 2.242(4), Cr–C-6 2.181(4), C-8–C-9 1.52(3), C-10–C-11 1.326(7), C-7–O-2 1.216(5)

values of the torsion angles C-2–C-100–Cr–C-14, C-4–C-100–Cr–C-13, and C-6–C-100–Cr–C-15 for **2** (C-100 being the centre of the six-membered ring) are 22.73°, 22.41°, and 23.12°, respectively. The corresponding values C-2–Cr–C-100–C-13, C-6–Cr–C-100–C-14, and C-4–Cr–C-100–C-15 for **3** are 20.76°, 22.42°, and 21.76°, respectively. These data clearly show that the solid state and solution conformations of the $Cr(CO)_3$ entities are almost the same for complex **2**, but are different for complex **3**. It is interesting to point out that in the case of complex **2**, the thiophene plane is not parallel to the arene plane, the dihedral angle being 19°. In the case of complex **3**, the carbonyl function is not in the plane of the arene ring, the carbonyl pointing out in the direction opposite to the $Cr(CO)_3$ entity with dihedral angles of 14° (with the six-membered arene ring) and of 23° (with the thiophene ring). These features could partially explain why the carbonyl group does not play a complete electron-withdrawing effect in the solid state.

Conclusion

By using the same coupling reaction, we were able to selectively synthesise, in high yield, [(2-thiophenyl)-η⁶-arene]- and [(2-thiophenyl)oxo-η⁶-arene]tricarbonylchromium complexes by slightly modifying the reaction conditions. This methodology addresses the potentiality of this highly versatile bimetallic activation in the preparation of new arenechromiumtricarbonyl complexes.

Experimental Section

General: All experiments were protected at all times from exposure to light and oxygen. Workup procedures were done in air. Tetrahy-

drofuran (THF) used was distilled from sodium benzophenone ketyl under dry nitrogen. – ^{1}H- and ^{13}C-NMR spectra were obtained with Bruker 200 and ARX 400 spectrometers. – Infrared and UV/Vis spectra were recorded with Perkin–Elmer 1420 and Shimadzu 1420 spectrometers, respectively. – Elemental analyses were performed by Le Service de Microanalyses de l'Université Pierre et Marie Curie. – Melting points were measured with a Reichert apparatus. The coupling procedures using 2-thienylzinc chloride and thienylboronic acid had been reported in ref.[10] (4-Anisole)tricarbonylchromium complex was prepared according to ref.[18]

Coupling Reaction with 2-(Tributylstannyl)thiophene. – General Procedure: $Pd_2(dba)_3$ (0.025 g, 0.05 mmol) and $AsPh_3$ (0.06 g, 0.2 mmol) were added successively to complex **1** (0.280 g, 1 mmol) and 20 mL of anhydrous DMF. After 30 min at room temperature, 2-tributylstannylthiophene (0.355 g, 1 mmol) in 5 mL of DMF was added. The mixture was stirred at room temperature for 20 h, poured into 100 mL of ice cold water, and extracted twice with 50 mL of diethyl ether. The combined organic phases were dried on magnesium sulfate and evaporated under reduced pressure. The residue was then purified by flash chromatography on silica gel (petroleum ether/ethyl acetate 75:25) to afford complexes **2** (R_f = 0.36) and **3** (R_f = 0.27) as a yellow and an orange solid, respectively.

Complex 2: M.p. 189–190 °C (Et_2O/petroleum ether 1:1). – IR (CH_2Cl_2): $\tilde{\nu}$ = 1965 cm^{-1} ($Cr(CO)_3$), 1885 cm^{-1} ($Cr(CO)_3$). – UV/Vis (CH_2Cl_2): λ_{max} (ε) = 334 nm (8860), 232 (3400). – ^{1}H NMR ($CDCl_3$): δ = 3.72 (s, 3 H, OCH_3), 5.20 (d, J = 7.1 Hz, 2 H, H-3), 5.92 (d, J = 7.1 Hz, 2 H, H-2), 6.94 (m, 1 H, H-10), 7.18 (d, J = 4.7 Hz, 1 H, H-11), 7.23 (d, J = 3.8 Hz, 1 H, H-9). – ^{1}H NMR (C_6D_6): δ = 2.88 (s, 3 H, OCH_3), 4.37 (d, J = 7.0 Hz, 2 H, H-3), 5.25 (d, J = 7.0 Hz, 2 H, H-2), 6.56 (m, 1 H, H-10), 6.66 (d, J = 4.7 Hz, 1 H, H-11), 6.77 (d, J = 3.4 Hz, 1 H, H-9). – ^{13}C NMR ($CDCl_3$): δ = 56.1 (C-12), 77.5 (C-3), 93.3 (C-2), 96.7 (C-1), 124.6 (C-11), 125.9 (C-9), 127.3 (C-8), 128.0 (C-10), 142.2 (C-4), 232.7 (CO). – MS (70 eV); *m/z* (%): 327 (14) [M^{+1}], 191 (100) [M^{+1} – $Cr(CO)_3$]. – $C_{14}H_{10}CrO_4S$ (326.3): calcd. C 51.33, H 3.09; found C 51.56, H 3.10.

Complex 3: M.p. 160–161 °C (Et_2O/petroleum ether 1:1). – IR (CH_2Cl_2): 1975 cm^{-1} ($Cr(CO)_3$), 1900 cm^{-1} ($Cr(CO)_3$), 1645 (CO). – UV/Vis (CH_2Cl_2): λ_{max} (ε) = 302 nm (39300), 230 (25100). – ^{1}H NMR ($CDCl_3$): δ = 3.78 (s, 3 H, OCH_3), 5.19 (d, J = 7.0 Hz, 2 H, H-3), 6.32 (d, J = 7.1 Hz, 2 H, H-2), 7.17 (m, 1 H, H-10), 7.70 (d, J = 4.9 Hz, 1 H, H-11), 7.84 (d, J = 3.7 Hz, 1 H, H-9). – ^{1}H NMR (C_6D_6): δ = 2.85 (s, 3 H, OCH_3), 4.23 (d, J = 7.1 Hz, 2 H, H-3), 5.82 (d, J = 7.1 Hz, 2 H, H-2), 6.55 (m, 1 H, H-10), 6.81 (d, J = 4.5 Hz, 1 H, H-11), 7.60 (d, J = 3.8 Hz, 1 H, H-9). – ^{13}C NMR ($CDCl_3$): δ = 56.1 (C-12), 76.6 (C-3), 93.3 (C-1), 121.9 (C-8), 128.2 (C-10), 133.2 (C-11), 134.1 (C-9), 144.1 (C-4), 230.7 (C-7), 232.2 (CO). – MS (70 eV); *m/z* (%): 355 (18) [M^{+1}], 219 (40) [M^{+1} – $Cr(CO)_3$]. – $C_{15}H_{10}CrO_5S$ (354.3): calcd. C 50.85, H 2.85; found C 50.67, H 2.70.

Crystal Structure of 2: $[(CO)_3Cr(C_{11}H_{10}OS)]$, M = 326.3, μ = 0.972 mm^{-1}; ρ = 1.59 gcm^{-3} orthorhombic, $P2_12_12_1$, Z = 4, a = 8.111(1), b = 11.196(1), c = 15.027(2) Å, V = 1364.6(3) Å^3, from 25 reflections (34° < 2θ < 34.6°). Cell dimensions and intensities were measured at 295 K on a Nonius CAD4 diffractometer with graphite-monochromated Mo-K_α radiation (λ = 0.71069 Å). ω/20 scans, two standard reflections measured every two hours showed no significant variation 1° < θ < 30° (0 < h 11, 0 < k < 15, 14 < l < 21); 2293 measured reflections, 2268 unique reflections of which 2001 were observed {$[F_o]^2 > 3\sigma([F_o]^2)$}. Data were corrected for Lorentz and polarization effects. The structure was solved by direct methods using SHELXS,[19] all other calculations used CRYSTALS.[20] Atomic scattering factors and anomalous dispersion terms were taken from ref.[21] Full-matrix least-squares refinement based on [F] and a Chebychev weighting scheme gave final values R = 0.0383, wR = 0.0432 and s = 1.04 for 201 variables and 2001 contributing reflections. The maximum shift/esd on the last cycle was 1.71. Non-hydrogen atoms were anisotropically refined. A disorder was observed on the thiophene group between the sulfur atom S(1) and the carbon atom C(9). The best solution was obtained by a model with two positions with an occupancy of approximately 0.63/0.37. Hydrogen atoms were introduced in calculated positions (except on the thiophene group) and only an overall isotropic thermal parameter was refined. The final difference electron density map showed a maximum of 0.27 and a minimum of –0.38 eÅ^{-3}.

Crystal Structure of 3: $[(CO)_3Cr(C_{12}H_{10}O_2S)]$, M = 354.3, μ = 0.892 mm^{-1}; ρ = 1.56 g.cm^{-3} triclinic, P –1, Z = 2, a = 7.355(5), b = 10.520(3), c = 10.665(6) Å, α = 109.56(3), β = 93.65(5), γ = 101.91(4)°, V = 752.9(7) Å^3, from 25 reflections (26° < 2θ < 28°). Cell dimensions and intensities were measured at 295 K on a Nonius CAD4 diffractometer with graphite-monochromated Mo-K_α radiation (λ = 0.71069Å). ω/2θ scans, two standard reflections measured every hour showed no significant variation 1° < θ < 28° (0 < h < 9, –13 < k < 13, 14 < l < 14); 3907 measured reflections, 3628 unique reflections of which 2311 were observed ($[F_o]^2 > 3\sigma([F_o]^2)$); R_{int} = 0.04 for equivalent reflections. Data were corrected for Lorentz and polarization effects. The structure was solved by direct methods using SHELXS,[19] all other calculations used CRYSTALS.[20] Atomic scattering factors and anomalous dispersion terms were taken from ref.[21] Full-matrix least-squares refinement based on [F] and a Chebychev weighting scheme gave final values R = 0.0587, wR = 0.0711 and s = 1.04 for 245 variables and 2311 contributing reflections. The maximum shift/esd on the last cycle was 1.75. Non-hydrogen atoms were anisotropically refined. A disorder was observed on the thiophene group between the sulfur atom S(1) and the carbon atom C(9). The best solution was obtained by a model with two positions with an occupancy of approximately 0.65/0.35. Hydrogen atoms (except on the thiophene group) were located on a difference Fourier map; their coordinates were refined with an overall isotropic thermal parameter. The final difference electron density map showed a maximum of 0.47 and a minimum of –0.58 eÅ^{-3}.

Crystallographic data (excluding structure factors) have been deposited with the Cambridge Crystallographic Data Centre as supplementary publication n° CCDC 132984 and CCDC 132985. Copies of the data can be obtained free of charge on application to CCDC, 12 Union Road, Cambridge CB2 1 EZ, UK (Fax: (internat.) +44-1223/336-033; E-mail: deposit@ccdc.cam.ac.uk).

Acknowledgments

We thank CNRS for financial support.

[1] [1a] E. Negishi, *Acc. Chem. Res.* **1982**, *15*, 340–348. – [1b] E. Erdik, *Tetrahedron* **1992**, *48*, 9577–9648.
[2] [2a] A. Suzuki, *J. Organomet. Chem.* **1999**, *576*, 147–168. – [2b] T. N. Mitchell, *Synthesis* **1992**, 803–815. – [2c] J. K. Stille, *Angew. Chem. Int. Ed. Engl.* **1986**, *25*, 508–524.
[3] [3a] X. Bei, T. Crevier, A. S. Guram, B. Jandeleit, T. S. Powers, H. W. Turner, T. Uno, W. H. Weinberg, *Tetrahedron Lett.* **1999**, *40*, 3855–3858. – [3b] D. W. Old, J. P. Wolfe, S. L. Buchwald, *J. Am. Chem. Soc.* **1998**, *120*, 9722–9723. – [3c] A. F. Littke, G. C. Fu, *Angew. Chem. Int. Ed.* **1998**, *37*, 3387–3388.

[4] [4a] D. Villemin, E. Schigeko, *J. Organomet. Chem*. **1985**, *293*, C10–C12. – [4b] W. Scott, *J. Chem. Soc., Chem. Commun*. **1987**, 1755–1756. – [4c] M. E. Wright, *J. Organomet. Chem.* **1989**, *376*, 353–358.

[5] R. Mutin, C. Lucas, J. Thivolle-Cazat, V. Dufaud, F. Dany, J. M. Basset, *J. Chem. Soc., Chem. Commun*. **1988**, 896–898.

[6] V. Dufaud, J. Thivolle-Cazat, J. M. Basset, R. Mathieu, J. Jaud, J. Vaisserman, *Organometallics* **1991**, *10*, 4005–4015.

[7] [7a] M. Uemura, H. Nishimura, T. Hayashi, *Tetrahedron Lett*. **1993**, *34*, 107–110. – [7b] M. Uemura, H. Nishimura, K. Kamikawa, M. Shiro, *Inorganica Chimica Acta* **1994**, *222*, 63–70. – [7c] M. Uemura, H. Nishimura, K. Kamikawa, K. Nakayama, Y. Hayashi, *Tetrahedron Lett*. **1994**, *35*, 1909–1912. – [7d] M. Uemura, K. Kamikawa, *J. Chem. Soc., Chem. Commun*. **1994**, 2697–2698. – [7e] P. Caldirola, R. Chowdhury, A. M. Johansson, U. Hacksell, *Organometallics* **1995**, *14*, 3897–3900. – [7f] T. Watanabe, K. Kamikawa, M. Uemura, *Tetrahedron Lett*. **1995**, *36*, 6695–6698. – [7g] K. Kamikawa, T. Watanabe, M. Uemura, *Synlett*. **1995**, 1040–1042. – [7h] M. Uemura, A. Daimon, Y. Hayashi, *J. Chem. Soc., Chem. Commun*. **1995**, 1943–1944. – [7i] K. Kamikawa, T. Watanabe, M. Uemura, *J. Org. Chem*. **1996**, *61*, 1375–1384. – [7j] T. Watanabe, M. Uemura, *Chem. Commun.* **1998**, 871–872.

[8] F. Rose-Munch, V. Gagliardini, C. Renard, E. Rose, *Coord. Chem. Rev.* **1998**, *178–180*, 249–268.

[9] F. Rose-Munch, E. Rose, *Current Org. Chem.* **1999**, *3*, 445–467.

[10] D. Prim, G. Kirsch, *J. Chem. Soc., Perkin Trans.1* **1994**, 2603–2606.

[11] Z. F. Plyta, D. Prim, J.P. Tranchier, F. Rose-Munch, E. Rose, *Tetrahedron Lett*. **1999**, *40*, 6769–6771.

[12] To our knowledge, the CO inserted organometallic compound formation was reported in only one example under analogous conditions depending upon the nature of the *ortho*-substituent of the chromium complex (see refs. [7d], [7i]).

[13] [13a] V. Farina, B. Krishnan, *J. Am. Chem. Soc.* **1991**, *113*, 9585–9595. – [13b] V. Farina, B. Krishnan, D. R. Marshall, G. P. Roth, *J. Org. Chem.* **1993**, *58*, 5434–5444.

[14] R. Guilard, J. Tirouflet, P. Fournari, *J. Organomet. Chem*. **1971**, *33*, 195–213.

[15] [15a] J. C. Boutonnet, L. Mordenti, E. Rose, O. Le Martret, G. Precigoux, *J. Organomet. Chem*. **1981**, *221*, 147–156. – [15b] F. Rose-Munch, E. Rose, A. Semra, M. Philoche, *J. Organomet. Chem*. **1989**, *363*, 123–130.

[16] We observed a similar effect during the study of the conformation of the tripod in solution of (2,6-dimethylchlorobenzene)-tricarbonylchromium, where no difference of shielding effect was detected for the aromatic protons (ref. [15b]).

[17] [17a] We also studied the conformation of the $Cr(CO)_3$ tripod in solution in another solvent. In C_6D_6 the H_2 and H_3 proton shielding are $\delta = 2.18$ and 2.32 for complex **2** (Table 2, entry 6). These shielding effects are $\delta = 1.98$ and 2.56 for complex **3**. – [17b] W. R. Jackson, W. B. Jennings, S. C. Renninson, R. Spratt, *J. Chem. Soc. B* **1969**, 1214–1221. – [17c] C. Segard, B. Roques, C. Pommier, G. Guiochon, *Anal. Chem.* **1971**, *43*, 1146–1151. – [17d] F. Van Meurs, J. M. Van der Toorn, H. Van Beckkum, *J. Organomet. Chem*. **1976**, *113*, 341–351. – [17e] A. Solladie-Cavallo, J. Suffert, *Org. Magn. Res.* **1980**, *14*, 426–430. – [17f] J. Brocard, A. Laconi, D. Couturier, *Org. Magn. Res.* **1984**, *22*, 369–371.

[18] C. A. L. Mahaffy, P. L. Pauson, *Inorg. Syntheses* **1990**, *28*, 136–140.

[19] G. M. Sheldrick, *SHELXS-86*, *Program for Crystal Structure Solution*, University of Göttingen, **1986**.

[20] D. J. Watkin, C. K. Prout, J. R. Carruthers, P. W. Betteridge, *Crystals*, issue 10, Chemical Crystallography Laboratory, University of Oxford, U. K. **1996**.

[21] D. T. Cromer, *International Tables for X-ray Crystallography*, vol. IV, Kynoch Press, Birmingham, U. K., **1974**.

Received September 27, 1999
[I99339]

Preparation and Properties of Carbonyliron Complexes of 1-Aza-4-oxa-1,3-butadiene (α-Imino Ketone) – X-ray Crystal Structures of $Fe(CO)_3$[MeN=C(Ph)C(Ph)=O] and $Fe_2(CO)_4$[*t*BuN=C(H)(Me)C(O)(O)C(Me)C(H)=N*t*Bu]

Ron Siebenlist,[a] Hans-Werner Frühauf,*[a] Kees Vrieze,[a] Wilberth J. J. Smeets,[b] and Anthony L. Spek[b]

Keywords: Coordination chemistry / α-Imino ketones / CO complexes / Iron complexes

The reaction of $Fe_2(CO)_9$ at room temperature in THF or toluene with the α-imino ketones $R^1N=C(R^2)–C(R^3)=O$ (L) (R^1 = alkyl, R^2 = H, Me, Ph, R^3 = Me, Ph) (**a–k**), initially results in the formation of the mononuclear chelate $Fe(CO)_3$(α-imino ketone) complexes **6** which can be isolated in moderate (**6h**) to high (**6e–g**) yield. Under these reaction conditions, complexes **6** subsequently react with [$Fe(CO)_4$] fragments or dimerise, to form the dinuclear complexes $Fe_2(CO)_6$(α-imino ketone) (**7a–j**) or $Fe_2(CO)_4$(L–L) (**8a,b,k**), respectively. The complexes **8** contain two α-imino ketone ligands C–C coupled at the ketone carbon atoms. Complexes **8a,b** react with CO at elevated temperatures to quantitatively yield $Fe(CO)_3$(α-imino ketone) (**6a,b**). This reaction can be reversed photochemically. Irradiation of a solution of **6a,b** in the low-energy band results in the reformation of **8a,b** in almost quantitative yield. The extremely air-sensitive complexes **6** and the dinuclear complexes **7** and **8** have been characterised spectroscopically (IR, UV/Vis, ^1H and ^{13}C NMR) and by elemental analysis. The solid state structures of complexes **6g** and **8a** have been determined by single-crystal X-ray diffraction. The molecular structure of **6g** confirms the flat σ-*O*,σ-*N* chelate coordination of the α-imino ketone. The structure of **8a** consists of two metal–metal-bonded $Fe(CO)_2$ units, bridged by a formally 10e-donating dianionic C–C coupled (*t*Bu-ADO) ligand. A mechanism for the formation of complexes **8** is discussed.

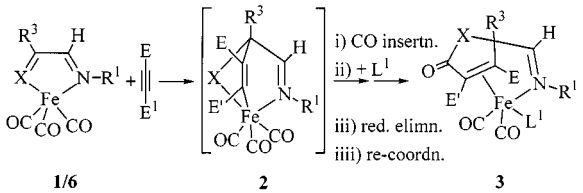
Introduction

The reaction of α-diimine ligands $R^1N=C(H)–C(H)=NR^1$ (R-DAB) (cf. Table 1) and C_5H_4N-2-$C(H)=NR^1$ (R-Pyca) (cf. Table 1) with carbonylmetal compounds of the iron triad leads to the formation of several mono-, di-, and polynuclear complexes.[1–5] The ability to donate the nitrogen lone pairs and the (C=N) imine π-bonds results in a flexible coordination behaviour in which the α-diimine ligand can donate from 2 to 8 electrons to one or more metal centres. An interesting aspect of this versatile coordination behaviour is the activation of the imine bond towards C–C, C–H, C–N, and N–H coupling reactions of R-DAB ligands in the coordination sphere of transition metals with a variety of unsaturated molecules, such as α-diimines[6–10] carbodiimides[11] sulfines,[11] and alkynes.[12–18]

Table 1. Abbreviations used throughout this text

Abbreviation	Explanation
R-DAB	1,4-Diaza-1,3-butadienes of formula $R^1N=C(H)–C(H)=NR^1$
R-Pyca	1,4-Diaza-1,3-dienes of formula C_5H_4N-2-$C(H)=NR^1$
DMAD	Dimethyl acetylenedicarboxylate
MP	Methyl propynoate
*t*Am	2-Methyl-2-butyl
R-ADO	1,6-Di-R-1,6-diazahexa-1,5-diene-3,4-dimethyl-3,4-diolato, $R^1N=C(H)(Me)C(O)HC(O)C(Me)=NR^1$
OPB	2,3-Diolato-2,3-bis(2-pyridyl)butane, [C_5H_4N-2]CMe(O)CMe(O)[2-C_5H_4N]
R-ADA	1,6-Di-R-1,6-diazahexa-1,5-diene-3,4-di-R-aminato, the reductively C–C coupled dimer of R-DAB; $R^1N=C(H)(H)C(NR^1)(H)C(NR^1)C(H)=NR^1$
R-APE	1,2-Di-R-aminato-1,2-bis(2-pyridyl)ethane, the reductively C–C coupled dimer of R-Pyca; [C_5H_4N-2]$CH(NR^1)CH(NR^1)$[2-C_5H_4N]

In a series of previous papers[19–24] we have reported in detail on the C–C coupling reaction of the [(R-DAB)$Fe(CO)_3$] complexes **1** (cf. Scheme 1; X = NR^1, R^3 = H) with the electron-deficient alkynes dimethyl acetylenedicarboxylate (DMAD) (cf. Table 1) and methyl propynoate (MP) (cf. Table 1). The initial step in this reaction can be described as an oxidative 1,3-dipolar [3+2] cycloaddition,



1/6 **2** **3**

X = NR^1, R^3 = H
X = O, R^3 = Ph, Me
E = E^1 = CO_2Me
E = CO_2Me, E^1 = H
L^1 = CO

Scheme 1. Reactions of [$Fe(CO)_3${$R^1N=C(H)–(R^3)C=X$}] (X= NR^1,O) with electron-deficient alkynes

[a] University of Amsterdam, Institute of Molecular Chemistry, Department of Inorganic Chemistry,
Nieuwe Achtergracht 166, 1018 WV Amsterdam, The Netherlands
Fax: (internat.) + 31-20/525-6456
E-mail: hwf@anorg.chem.uva.nl
[b] Utrecht University, Bijvoet Center of Biomolecular Research, Crystal and Structural Chemistry,
Padualaan 8, 3548 CH Utrecht, The Netherlands

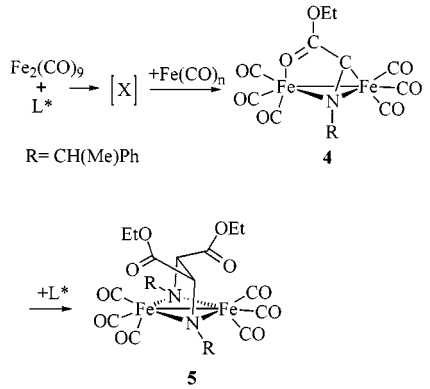
Supporting information for this article is available on the WWW under http://www.wiley-vch.de/home/eurjic or from the author.

 © WILEY-VCH Verlag GmbH, D-69451 Weinheim, 2000 1434–1948/00/0505–0907 $ 17.50+.50/0

in which the electron-deficient alkyne (dipolarophile) adds across the Fe–N=C fragment (1,3-dipole) to give the bicyclo[2.2.1] intermediate **2**. Subsequent insertion of CO and uptake of an additional ligand (L′), followed by reductive elimination and recoordination of the double bond, results in the formation of the [(1,5-dihydropyrrol-2-one)$Fe(CO)_3$] complexes **3**.

In order to broaden the synthetic potential of this reaction we have investigated the closely related [$Fe(CO)_3$(1-aza-4-oxa-1,3-butadiene)] complexes **6** (cf. Scheme 1; X = O, R^3 = Me, Ph), in order to probe their reactivity towards electron-deficient alkynes.[25,26] To this end we studied the coordination behaviour of α-imino ketones towards carbonyliron compounds.

In contrast to the α-diimine chemistry little is known about the coordination behaviour of α-imino ketones towards d^8-metals. α-Imino ketones have been shown to form monodentate *trans*-[$PtCl_2(PR_3)(R^1N{=}C(R^2){-}C(R^3){=}O$][27] and bidentate [$(AlMe_3)_2$(σ,σ-*N,O*–MeN=C(Ph)–C(Ph)=O)] complexes.[28] In these complexes, as well as in the free ligand, the N=C–C=O moiety has a *gauche* conformation with a torsion angle of approximately 90° around the central C–C bond, which is attributed to a minimising of the steric repulsion between the skeleton substituents. The reaction of $Fe_2(CO)_9$ with the closely related α-imino ester PhCH(Me)N=C(H)C(OEt)=O (L*), as described by Weiss et al.,[29] resulted in the formation of two dinuclear products, $Fe_2(CO)_6$(L*) (**4**) and the C–C coupled complex $Fe_2(CO)_6$(L*–L*) (**5**) (cf. Scheme 2).



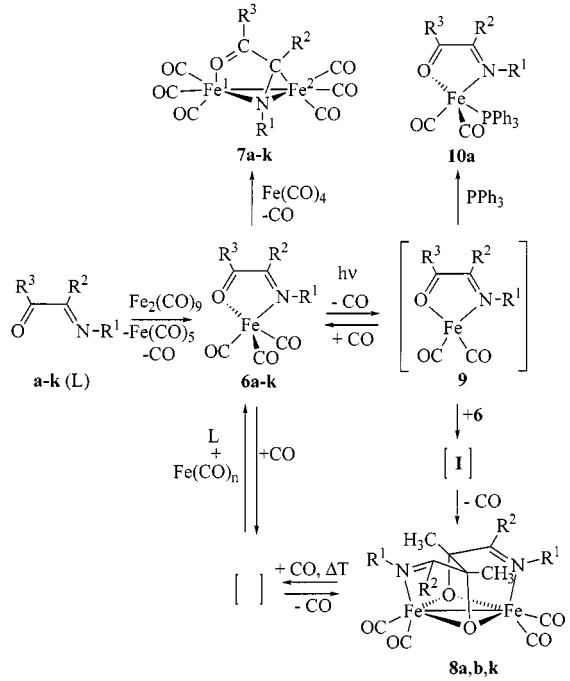
Scheme 2. Reaction of [$Fe_2(CO)_9$] with PhCH(Me)N=C(H)–C(OEt)=O (L*)

In complex **5**, a C–C coupling reaction occurs between the imine C atoms of two α-imino ester ligands. This type of C–C coupling has also been observed in the reaction of R-DAB and R-Pyca with carbonylruthenium compounds,[7] leading to [$Ru_2(CO)_{4,5}$(R-ADA)] (cf. Table 1) and [$Ru_2(CO)_{4,5}$(R-APE)] (cf. Table 1), respectively, but has never been observed for iron.

In this paper we report on the reactions of α-imino ketones (L) with $Fe_2(CO)_9$, which results in the formation of the mononuclear chelate complexes [$Fe(CO)_3$(α-imino ketone)] (**6**) and the dinuclear complexes [$Fe_2(CO)_6$(α-imino ketone)] (**7**) and [$Fe_2(CO)_4$(L–L)] (**8**). Complexes **8** contain two α-imino ketone ligands which are C–C-coupled at the ketone carbon atoms. The influence of the substitution pattern of the α-imino ketone on the formation of the complexes is discussed. The X-ray crystal structures of [$Fe(CO)_3${σ-*N*,σ-*O*-(MeN=C(Ph)–C(Ph)=O)}] (**6g**) and of the newly formed dimeric complex [$Fe_2(CO)_4$(*t*BuN=(H)C(Me)C(O)(O)C(Me)C(H)=N*t*Bu)] (**8a**) are described.

Results and Discussion

The α-imino ketones $R^1N{=}C(R^2){-}C(R^3){=}O$ (L) and the complexes discussed in this investigation are schematically presented in Scheme 3. The type of complex is identified by Arabic numbers. The different α-imino ketones are indicated by the letters **a–k**.



	a	b	c	d	e	f	g	h	i	j	k
R^1	*t*Bu	*t*Am	CH(*i*Pr)$_2$	*p*Tol	*i*Pr	*t*Bu	Me	*p*Tol	*i*Pr	$PhCH_2$	R_1–R_2 =
R^2	H	H	H	H	H	H	Ph	Ph	Ph	Me	-$(CH)_4$-
R^3	Me	Me	Me	Ph	Ph	Ph	Ph	Ph	Ph	Me	Me

Scheme 3. Observed reaction sequence for [$Fe_2(CO)_9$] with the α-imino ketones **a–k**

The reaction of [$Fe_2(CO)_9$] with the α-imino ketones **a–k** at room temperature results in the formation of the mononuclear chelate complexes [$Fe(CO)_3$(α-imino ketone)] (**6e–h**), the new dinuclear complexes [$Fe_2(CO)_6$(α-imino ketone)] (**7a–j**), and the C–C-coupled dimers [$Fe_2(CO)_4$(R-ADO)] (**8a**,**b**) (cf. Table 1) and [$Fe_2(CO)_4$(R-OPB)] (**8k**) (cf. Table 1). Throughout the text [$Fe_2(CO)_4$(L–L)] (**8a,b,k**) is used for these C–C-coupled dimers. The product formation and distribution depends strongly on the substitution pattern of the α-imino ketone and on the solvent.

In all cases the mononuclear chelate complexes [$Fe(CO)_3$(α-imino ketone)] (**6**) are initially formed. However, only when the ligands **e–h** are used are complexes **6** stable enough to be isolated, giving **6h** in moderate yield

and **6e–g** in good to high yields. The complexes **6** react with $[Fe(CO)_4]$ fragments forming $[Fe_2(CO)_6$(α-imino ketone)] (**7a–j**) in moderate to good yield depending on the α-imino ketone used. In complexes **7** the α-imino ketone is σ-*O*,μ_2-*N*,η^2-C=N-coordinated, donating six electrons to the two iron centres. When R^3 = Me, complexes **6** can also react with another equivalent of the α-imino ketone and the carbonyliron compound leading to the new complexes $[Fe_2(CO)_4$(L–L)] in moderate (**8a,b**) or low (**8k**) yield. In complexes **8**, the two α-imino ketones are reductively coupled through the ketone carbon atoms. The resulting bridging ligand is formally dianionic and donates 10 electrons to the two iron centres. Complexes **8a,b** react readily with carbon monoxide (1 atm) at 80 °C to quantitatively regenerate **6a,b**, which under these conditions are stable. Irradiation of a solution of **6a,b** in the low-energy band results in the reformation of complexes **8a–b** in almost quantitative yield. Irradiation of **6a** in the presence of PPh_3 results in the formation of complex **10a** and complex **8a** is not formed. The formed complexes have been characterised by IR, UV/Vis, ^{1}H- and ^{13}C-NMR spectroscopy, elemental analysis, and X-ray crystal structure determinations for complexes **6g** and **8a**. In the following section we will first discuss the structural data and spectroscopic properties of the relevant complexes and subsequently deal with the aspects of their formation, their stability and their reactivity. A mechanism for the formation of complexes **8** is proposed.

Molecular Structure of σ-*N*,σ-*O*-Fe(CO)$_3$[MeN=C(Ph)C(Ph)=O] (6g)

An ORTEP drawing of the molecular structure of **6g** together with the atomic numbering scheme is shown in Figure 1. Selected bond lengths and angles are given in Table 4 (see Supporting Information). The asymmetric unit of the unit cell contains two crystallographically independent molecules. Since these molecules are nearly identical, only one is discussed here.

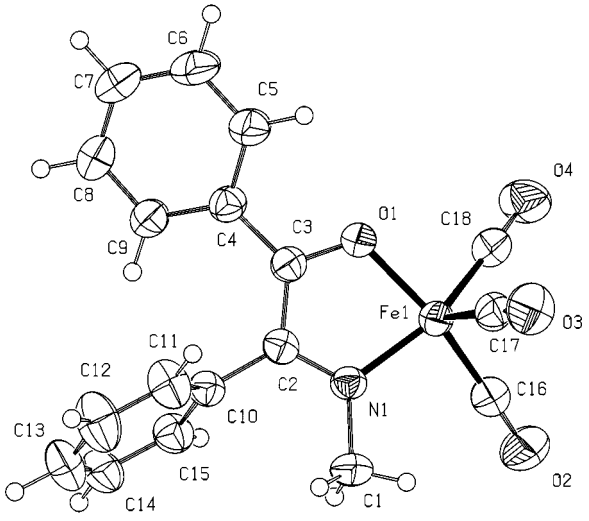


Figure 1. ORTEP drawing (50% probability level) of the molecular structure of **6g**

For a regular five-coordinate d^8 complex, a trigonal-bipyramidal (tbp) or square-pyramidal (sqp) structure might be expected.[40,41] Judging from the angles around the iron atom (cf. Table 4) the coordination around the central iron atom in **6g** more closely resembles a distorted square-pyramidal geometry (89% along the Berry pseudorotation coordinate[42]) with the basal plane defined by N(1), C(16–18), and with Fe(1) 0.353(1) Å above that plane. An ideal tbp or sqp geometry is not possible for these chelate complexes because of the small bite angle of the α-imino ketone (81 ± 1°), a feature also observed in many R-DAB complexes.[40,41,43,44]

The geometries of several five-coordinated [Fe(1,4-dihetero-1,3-butadiene)] complexes, determined by X-ray structures, change from approximately tbp to sqp with increasing π-acceptor properties of the 1,4-dihetero-1,3-butadiene ligand.[44–47] The observed sqp geometry in **6g**, in which the α-imino ketone exhibits good π-acceptor properties, is in agreement with this observation.

The N=C–C=O skeleton is planar within 0.010(3) Å, with the iron atom located 0.03(4) Å above this plane. A similar planar conformation has been found in $[Fe(CO)_2$(*t*-BuNC)(*p*Tol-DAB)],[48] and $[Fe(CO)_3$(MeN=N–N=NMe)].[45] The present example is the first structure showing an intact flat chelate N=C–C=O skeleton, i.e. a conformation with maximum orbital overlap of the C=N and C=O chromophores. From the crystal structure of the free α-imino ketone PhH(Me)CN=C(Ph)–C(Ph)=O, it is known that the N=C–C=O moiety has a torsion angle of 97.7(2)° [46] around the central C–C bond. In monodentate σ-*N*-coordinated *trans*-$[PtCl_2(Et_3)$(*t*BuN=C(H)C(Me)=O)][27] and in the bidentate bridging $[Al(Me_3)_2$-σ,σ′-*N,O*-{MeN=C(Ph)–C(Ph)=O}][28] the torsion angles are 89.0(4)° and 85.9(3)°, respectively (cf. Figure 2). On the basis of these data van Vliet et al.[28] concluded that in the case of α-imino ketones a minimising of the steric repulsion between the ligand substituents is predominant. In $[Fe_2(CO)_6$(PhCH(Me)N=C(H)C(OEt)=O)][29] (**5**) (cf. Scheme 2) an almost flat coordination of the N=C–C=O has been reported; however, in this complex, the N=C imine bond has lost its double-bond character because of the μ_2-*N*,η^2-C=N coordination.

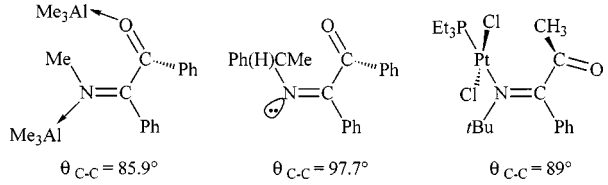


Figure 2. Torsion angles around the central C–C bond of coordinated and free α-imino ketones

The observed planar conformation in **6g** suggests that in the present case the orbital overlap of the imine and ketone moieties, i.e. the formation of a delocalised, low-lying π orbital, prevails over a minimising of the steric interactions between the skeleton substituents. The π*-orbital of the N=C–C=O system, which is antibonding in the C=N and C=O bond and bonding in the central C–C bond, plays an important role for the π-back donation from the electron-rich iron thus allowing the formation of a stable chelate.

Consequently, the coordination of the α-imino ketone to the iron centre in **6g** leads to a significant lengthening of both the imine [C(2)–N(1) = 1.336(3) Å] and the ketone [C(3)–O(1) = 1.295(3) Å] bonds while the central [C(2)–C(3) = 1.410(3) Å] bond is significantly shortened when compared to the C=N, C=O and the central C–C bonds in the free α-imino ketone PhH(Me)CN=C(Ph)C(Ph)=O [1.286(2) Å, 1.209(2) Å and 1.530(2) Å, respectively].[46] The C=O bond is significantly more elongated than the C=N bond (0.086 vs. 0.054 Å), indicating that the chelate coordination exerts a larger effect on the electron density of the C=O than of the C=N bond. This effect is also observed in the ^{13}C-NMR spectra of complexes **8** and might explain the chemoselectivity for C–C coupling at the ketone carbon atom leading to complexes **3** and **8**. Comparable changes in bond lengths, although less pronounced, have been found in [Fe(CO)$_2$(*t*BuNC)(*p*Tol-DAB)][47] and [Fe(CO)$_3$(2,6-*i*Pr$_2$C$_6$H$_3$-DAB)].[40] The Fe–C(16), Fe–C(17) and Fe–C(18) distances of 1.771(3) Å, 1.799(3) Å and 1.802(3) Å, respectively, are within the range of normally observed Fe–CO bond lengths.

Molecular Structure of [Fe$_2$(CO)$_4${*t*BuN=C(H)(Me)C(O)(O)C(Me)(H)C=N*t*Bu}] (8a)

An ORTEP drawing of the molecular structure of [Fe$_2$(CO)$_4$(*t*Bu-ADO)] (**8a**) (cf. Table 1) together with the atomic numbering scheme is shown in Figure 3. Table 5 (see Supporting Information) gives selected bond lengths and bond angles.The molecule consists of two identical Fe(CO)$_2$ units connected by a metal–metal bond and bridged by the newly formed, formally dianionic 10-electron-donating *t*Bu-ADO ligand. The *t*Bu-ADO ligand has been formed by a reductive C–C coupling of two *t*BuN=C(H)–C(Me)=O ligands through the ketone carbon atoms. As a result of this C–C coupling between C(6)–C(8), the former keto groups C(6)–O(1) and C(8)–O(2) have been reduced to anionic olato groups. The molecule exhibits noncrystallographic pseudo C_2 symmetry with the C_2 axis running through the centres of the C(6)–C(8) and the Fe(1)–Fe(2) bonds.

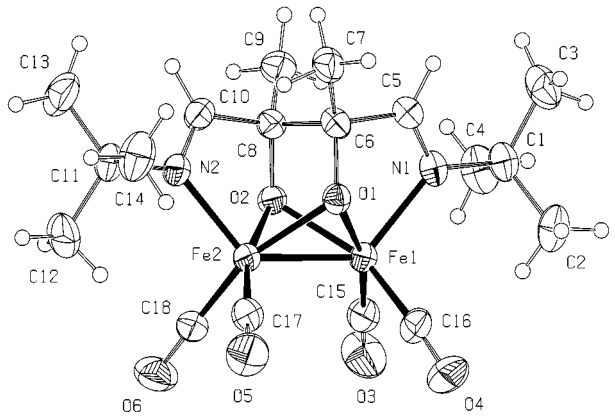


Figure 3. ORTEP drawing (50% probability level) of the molecular structure of **8a**

The Fe(1)–Fe(2) bond length in **8a** is 2.372(2) Å, i.e. a short Fe–Fe bond, since distances in the range of 2.50–2.70 Å are normally observed for single Fe–Fe bonds.[49] The Fe(1)–O(1)–Fe(2) and Fe(1)–O(2)–Fe(2) bond angles are 74.14(14) and 73.78(14)°, respectively, and the Fe–O(carboxylato) bond lengths vary between 1.944(4) and 2.002(4) Å. These bond angles and lengths are comparable to the Fe–X–Fe (X = C, N, O) bond angles and Fe–X (X = C, N, O) bond lengths found in complexes with similar (N,N′), (N,S) and (C,O) bridging ligands.[29,48,50,51] In these complexes comparably short Fe–Fe distances have also been found. The two intact imine moieties are bonded to the iron centre by normal Fe–N=C σ-donor bonds [Fe(1)–N(1) = 2.043(5) Å and Fe(2)–N(2) = 2.030(5) Å]. The angles around the C–C connective bond [C(8)–C(6)–C(5) 107.9(4)° and C(6)–C(8)–C(10) 107.3(4)°] differ only slightly from the optimum value of 109.7° for sp^3-hybridised atoms. In the related complex [Ru$_2$(CO)$_5$(*i*Pr-ADA)], it was concluded from several structural features that the *i*Pr-ADA ligand is forced to coordinate to the ruthenium centres which might explain the facile thermal rupture of the central C–C bond in this complex.[7] From the observed bond angles and lengths in **8a** it appears that the *t*Bu-ADO ligand exhibits no geometrical constraints that could explain the facile fission of the C(6)–C(8) bond under carbon monoxide. The newly formed C–C connective bond C(6)–C(8) in **8a** of 1.587(8) Å is, however, significantly longer than a normal C(sp^3)–C(sp^3) bond. Comparatively long bond lengths have been reported earlier in complexes containing two C–C-coupled R-DAB or α-imino ester ligands[8,29,52–55] and seem to be characteristic for C–C bonds in N–C–C–N moieties in which both nitrogen atoms are covalently coordinated to the metal centres. On dissolution, the dimer [EtZn(*t*Bu-Pyca)]$_2$ [53,54] dissociates to a very small extent into monomers, thus forming an equilibrium mixture showing the weakness of the C–C connective bond. However, [Mo$_2$(CO)$_6$(R-ADA)][55] complexes do not split under carbon monoxide.

In conclusion, we can say that the *t*Bu-ADO ligand in **8a** exhibits no geometrical constraint upon coordination to the iron centres, the newly formed central C(6)–C(8) bond [1.587(8) Å] is longer than normal C–C bonds. Whether or not the facile breaking of the central C(6)–C(8) bond, which is an experimental fact, may be explained by the elongation of C(6)–C(8) remains an open question.

IR, UV/Vis Spectroscopy and Elemental Analysis

The IR, UV/Vis and analytical data of the complexes **6**, **7**, **8** and **10a** are listed in Table 6 (see Supporting Information). The IR spectra of complexes **6** show three strong terminal carbonyl absorptions of equal intensity in the ν(CO) region of 2100–1900 cm^{-1}. The CO absorptions of **6e–g**, and even more so of **6h**, are found at higher frequencies than those of **6a,b** indicating that π-back bonding to the terminal carbonyl ligands decreases on going from **6a** to **6h**. This is a result of the better π-accepting capacity of the α-imino ketones going from ligands **a,b** to **e,f** to **g** and **h**, which bear none, one, two or three electron-withdrawing aromatic groups, respectively.

The six terminal carbonyl ligands of $[Fe_2(CO)_6L]$ (**7a–j**) give rise to six medium to strong absorptions in the ν(CO) region. The pattern of the absorptions is identical to that of $[M_2(CO)_6$(R-DAB/R-Pyca)] (M = Fe, Ru, Os and FeRu).[6,56–59] This strongly suggests that these complexes are isostructural, which is corroborated by the ^{1}H- and ^{13}C-NMR- spectroscopic data. The substituents on the α-imino ketone show only a marginal influence on the frequency of the CO absorption bands of complexes **7**.

The IR spectra of complexes **8** show three terminal carbonyl absorptions, two of high and one of medium intensity. The pattern of the CO absorption bands strongly resembles that of the closely related complex $[Ru_2(CO)_4$(R-ADA)],[6,7] which contains a similarly coupled dimer of R-DAB. The absorption bands are shifted to a higher frequency (approximately 10–20 cm^{-1}) than those of $[Ru_2(CO)_4$(R-ADA)]. Similar shifts to higher frequency are observed for $[M(CO)_3$(R-DAB)] and $[M_2(CO)_6$(R-DAB)] on going from iron to ruthenium.

Electronic Absorption Spectra of Complexes 6 and 8

All complexes **6** show an intense band at about 530 nm. A second band is located at about 410 nm and for complexes **6e–h** a third band is present at approximately 348 nm. The pattern of the bands in the UV/Vis spectra of complexes **6** closely resembles those found for the isostructural complex $[Fe(CO)_3$(R-DAB)],[60] except for the shift of approximately 20 nm to lower energy. The polarity of the solvent has almost no influence on the positions of the absorption bands [λ_{max} **6a**; 524 nm (pentane), 526 nm (toluene), 527 nm (THF)]. This lack of solvatochromic behaviour is also found for $[Fe(CO)_3$(R-DAB)][40,60,61] and $[W(CO)_4$(R-DAB)][61] and is attributed to a strong mixing of the metal d-(HOMO) and α-diimine π*-(LUMO) orbitals. As a result these transitions hardly possess any charge-transfer character, and therefore do not show solvatochromic behaviour. On the basis of these similarities, the band at 530 nm is assigned to several electronic transitions within the metallacycle[40,61] rather than to a charge transfer transition from the metal to the α-imino ketone ligand (MLCT). The band at 410 nm is assigned to a LF transition as for $[Fe(CO)_3$(R-DAB)]. The third band at 348 nm observed in **6e–h** is due to an intra-ligand transition.

Complexes **8a,b** possess a weak band at approximately 640 nm (MLCT) and a strong absorption band at 367 nm. The latter is assigned to the σ–σ* transition of the metal–metal bond. This is corroborated by the increase in intensity of this band upon lowering the temperature, an effect which has been observed before for σ–σ* transitions of metal–metal bonds.[62,63]

Elemental Analyses

Except for **6g**, complexes **6** have not been analysed due to their instability and the fact that they cannot be crystallised. No satisfactory elemental analyses could be obtained for complex **7d** because the isolated oil was not analytically pure and no crystals could be obtained. Complex **8k** has not been analysed because the isolated powder was not analytically pure and the complex decomposes on crystallisation.

NMR Spectroscopy

Tables 6 and 7 with the complete ^{1}H- and ^{13}C-NMR-spectroscopic data of complexes **6**, **7** and **8** are available as Supporting Information.

The ^{1}H- and ^{13}C-NMR spectra of **6a–b** were obtained by splitting **8a–b** under carbon monoxide pressure because, due to the instability of **6a–b**, it was not possible to prepare a suitable NMR sample from the reaction mixture (see Experimental Section). The imine proton resonances (**6a**,**b**,**e**,**f**) are observed between δ = 8.74 and δ = 7.61, whereas in the uncoordinated α-imino ketones the imine proton (**a–f**) resonances are observed between δ = 8.1 and δ = 7.2. The imine and ketone carbon atom resonances are shifted by approximately 12–15 and 20–28 ppm to lower frequency, relative to those of the free ligands, as a result of π-back donation into the low-lying delocalised LUMO of the α-imino ketone. Comparable shifts have been observed for $[Fe(CO)_3$(R-DAB)].[64] The large low-frequency shift of the ketone carbon atom in comparison with the imine carbon atom suggests that the chelate coordination exerts a larger effect on the electron density of the ketone carbon atom. This might be the reason for the observed chemoselectivity in the C–C-coupling reactions, i.e. only coupling at the ketone carbon atom is observed resulting in the formation of complexes **8** and **3** (cf. Scheme 1). Furthermore, it is evident from the X-ray crystal structure of **6g** that the C=O bond is significantly more elongated than the C=N bond, which also suggests a larger effect on the C=O bond upon chelate coordination.

In all complexes **6** the three terminal carbonyl ligands give rise to a single resonance between δ = 212.0 and δ = 214.1, indicating that they rapidly interchange on the NMR time scale at 263 K.

The imine proton and carbon atom resonances of complexes **7** are observed between δ = 4.78–3.77 and δ = 65–90, respectively. These large shifts to lower frequency of approximately 4 ppm and 80 ppm are typical for a μ^2-*N*,η^2-C=N coordination of the C=N moiety of the α-imino ketone and have also been observed in $[M_2(CO)_6$(R-DAB)] (M = Fe, Ru, Os and FeRu) complexes.[6,57–59] The resonances of the ketone carbon atoms are only marginally shifted relative to those of the free ligand.

Because of the asymmetric coordination of the α-imino ketone ligand, the six terminal carbonyl ligands in complexes **7** are inequivalent. In a rigid carbonylmetal skeleton this should result in six independent resonances for the carbonyl groups. However, at 263 K complexes **7** show four resonances with relative intensities of 1:3:1:1 going from high to low frequency. This indicates a local scrambling of the carbonyl groups on one metal centre, which has also been observed in $[Fe_2(CO)_6$(R-DAB)] complexes.[65] This exchange process has been demonstrated for complex **7f** in CD_2Cl_2. At 183 K the six carbonyl ligands give rise to six separate signals, showing that at this temperature the ter-

minal carbonyl ligands on both metal centres are at the limit of slow exchange. The individual assignment of the CO resonances to either one of the two $Fe(CO)_3$ moieties is not clear from this dynamic behaviour but can reasonably be deduced from the ^{13}CO-NMR-spectroscopic data of $[FeRu(CO)_6$(R-Pyca)] complexes. From the crystal structure of $[FeRu(CO)_6$(*i*Pr-Pyca)],[59] it is known that the μ_2-*N*,η^2-C=N coordination of the C=N moiety is directed towards the iron centre. In the ^{13}CO-NMR spectra of these complexes recorded at 263 K the Fe–CO signals appeared as one sharp resonance and the Ru–CO signals as three separate resonances. Consequently, in our case, the three signals of equal intensity (263 K) correspond to the μ_2-*N*,σ-*O*-coordinated $Fe^1(CO)_3$ moiety and the broad resonance corresponds to the three carbonyl groups of the $Fe^2(CO)_3$ moiety, which is μ_2-*N*,η^2-C=N-coordinated through the C=N bond of the α-imino ketone (cf. Scheme 3).

In complexes **8a**,**b** the imine-proton and carbon-atom resonances are observed between δ = 7.55–7.80 and δ = 169.5–174.0, respectively, indicating that the imine moiety is σ-*N*-coordinated to the iron centre. The signals of the reductively coupled ketone carbon atoms in **8** accordingly show a pronounced coordination shift (ca. 120 ppm) to lower frequency and are observed around δ = 80. The four terminal carbonyl ligands give rise to two resonances between δ = 217 and δ = 218, indicating pairwise exchange at each iron centre.

Reactions of α-Imino Ketones with Carbonyliron

Complex Formation

The formation, stability and yield of complexes **6**, **7** and **8** strongly depends on the R^1, R^2, and R^3 substituents attached to the imine nitrogen atom, the imine carbon, and the ketone carbon atom, respectively. In the following sections we will first discuss the formation of complexes **6** and **7** and the factors that influence their stability. Subsequently, the formation of complex **8** is discussed and a mechanism is proposed.

Formation and Reactivity of $[Fe(CO)_3$(α-imino ketone)] (6)

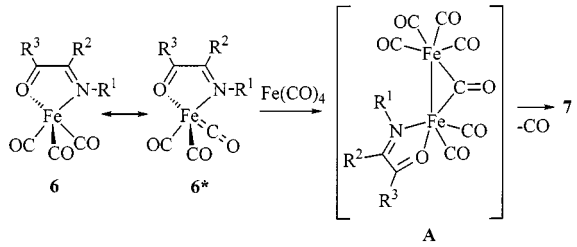
The reaction of $[Fe_2(CO)_9]$ with the α-imino ketones **a–k** at room temperature in THF or toluene results in the initial formation of the deep purple chelate $[Fe(CO)_3$(α-imino ketone)] complexes **6**, probably via a monodenate *N*-coordinated $[Fe(CO)_4$(α-imino ketone)] intermediate, as a result of the better σ-coordinating properties of the C=N moiety than the C=O moiety,[27,66] according to Equation 1.

$$[Fe_2(CO)_9] + \text{α-imino ketone} \rightarrow [Fe(CO)_3(\text{α-imino ketone})]\ (\mathbf{6}) + [Fe(CO)_5] + CO \quad (1)$$

In THF no formation of **6i** was observed. In toluene, however, low concentrations of **6i** were formed which, under the reaction conditions, rapidly reacts further to **7i**. Analogous to $[Fe(CO)_3$(R-DAB)], complexes **6** are intensely coloured, highly air-sensitive and could not be isolated pure in the solid state except for **6g**. Complexes **6** are soluble and stable in common solvents as hexane, Et_2O, toluene and THF, but decompose in chlorinated solvents like $CHCl_3$, as is the case for $[M(CO)_3$(R-DAB)] (M = Fe, Ru).[7] Complexes **6a,b** react photochemically to form the corresponding complexes **8a,b**. Irradiation of **6e–g**, however, does not lead to the corresponding C–C coupled complexes **8** but results in slow decomposition of **6e–g**.

Formation and Reactivity of $[Fe_2(CO)_6$(α-Imino Ketone)] (7)

The $[Fe_2(CO)_6$(α-imino ketone)] complexes **7** are formed in THF and toluene by reaction of $[Fe(CO)_3$(α-imino ketone)] (**6**) with $Fe(CO)_4$ (cf. Scheme 4). Complexes **7** are probably formed via the CO-bridged intermediate **A**, similar to the proposed intermediate for the formation of $[Fe_2(CO)_6$(R-DAB)].[67] The formation of **A** can be described as an isolobal analogue[68,69] of the addition of an olefin to a carbene giving a cyclopropane ring system. In the present case, $Fe(CO)_4$ is isolobal with a carbene and the Fe–C bond of a terminal CO ligand in **6** is, in its resonance structure (**6***), isolobal with an olefin. Addition results in the formation of intermediate **A**, and subsequent coordination of the C=N π-bond with concomitant loss of CO completes the structure of complex **7**.



Scheme 4. Proposed reaction mechanism for the formation of **7**

Complexes **7** are isolated as red-brown crystalline solids, except for **7d**, and are air-stable in crystalline form. The stoichiometry of complexes **7** has been established by elemental analyses. The α-imino ketone in complexes **7** is σ-*O*,μ_2-*N*,η^2-C=N-coordinated to the two iron centres and donates six electrons, as can be concluded from the IR, ^{1}H-NMR, and ^{13}C-NMR spectra. An analogous coordination has been found for the closely related α-imino ester complex $[Fe_2(CO)_6\{PhCH(Me)N{=}C(H)C(OEt){=}O\}]$[29] (**5**) (cf. Scheme 2). No formation of the alternative possible six-electron coordination mode, i.e. σ-*N*,μ_2-*O*,η^2-C=O, has been observed. In the α-imino ketone 2-acetylpyridine (**k**), the C=N π-bond is not available for η^2 coordination because it is part of an aromatic pyridine system. Therefore, σ-*N*,μ_2-*O*,η^2-C=O is the only accessible six-electron coordination mode. However, with ketone **k** only complex **8k** is formed and the formation of a complex with a σ-*N*,μ_2-*O*,η^2-C=O coordination mode is not observed. With the closely related α-imino ketones 2-benzoylpyridine and pyridine-2-carboxaldehyde (i.e. bearing a phenyl group and a proton on the ketone carbon atom, respectively) no isolable complexes are formed. Since initially the mononuclear chelate $[Fe(CO)_3\{C_5H_4N$-2-$C(R^3){=}NR^1\}]$ complexes are formed, indicated by the deep blue colour of the reaction mixture,

this means that either complexes with a σ-*N*,μ_2-*O*,η^2-C=O coordination of the α-imino ketone are not formed, or they decompose under the reaction conditions.

The yields of complexes **7** depend strongly on the ligand used. Generally the yields are higher for the ligands with a phenyl substituent on the ketone carbon atom than for those bearing a methyl group. In the latter case the lowest yields are found for ligands **a** and **b** (ca. 17%). With these ligands, however, complexes **8a,b** are formed in ca. 25% yield leading to a total yield of binuclear complexes of 40 to 45%. Furthermore, it is apparent that when R^1 (the imine nitrogen substituent) is an aryl group the yield is much lower than for R^1 = alkyl. This observation can be accounted for in terms of the lower basicity of the imine donor site for aryl vs. alkyl; if R^1 is aryl, this will lead to a less-efficient μ_2-*N*,η^2-C=N interaction. As a consequence, under these conditions complexes **7d**,**h** react with $Fe(CO)_n$ fragments to give unknown products, which lowers the yields. This has also been found in $[Fe_2(CO)_6$(Aryl-Pyca)] complexes.[70]

Reaction With Free Ligand

Complexes **7** do not react thermally or photochemically with an excess of free ligand. Consequently, **7** is not an intermediate in the formation of **8**.

Reaction With CO

Treatment of $[Fe_2(CO)_6$(R-DAB)] with carbon monoxide (40–50 bar) at elevated temperatures yielded the monomeric complexes $[Fe(CO)_3$(R-DAB)] and $[Fe(CO)_5]$.[43,70] This route should also be convenient for the formation of the monomeric $[Fe(CO)_3$(α-imino ketone)] complexes **6**. However, reaction of $[Fe_2(CO)_6$(α-imino ketone)] (**7**) with CO leads only to decomposition, and the monomeric complexes **6** are not detected. The η^2-C=N coordination is probably stronger than the σ-*O* coordination and, consequently, the coordinated keto oxygen atom is substituted by CO, which triggers the decomposition of **7**.

Factors that Influence the Formation and Stability of Complexes 6 and 7

It has been mentioned before that the N=C–C=O skeleton has a conformational preference for a near orthogonality of the N=C and C=O groups (cf. Figure 2), caused by steric interactions of the ligand substituents, especially on the 1,3-and 2,4-positions.[27,28,46]

The crystal structure of **6g** confirms that the α-imino ketone is σ-*N*,σ-*O* chelating in a flat planar *cis* conformation. This planar coordination of an intact N=C–C=O moiety shown in **6g** has never been observed before. So, the primary factor that influences the formation and stability of complexes **6** is whether the α-imino ketone can sterically easily adopt a planar or near planar *cis* conformation. Furthermore, the stability of complexes **6** depends on the σ-donor and π-accepting properties of the α-imino ketone ligand upon coordination. Because the energy of the n-electrons at the oxygen is much lower than at the nitrogen atom, α-imino ketones are weaker donors than diazabutadienes. The unoccupied orbitals of the iron centre are at still higher energy than the n-electrons at the nitrogen atom.[66,71] Consequently, reinforcement of the dative bond by significant π-back donation is required for the formation of stable chelate complexes **6**.[66] The extent of π-back donation depends on the energy level of the π*-LUMO, which in turn can be tuned with the ligand substituents, especially the substituent on the ketone carbon atom. As a consequence, electron-donating groups (like methyl) disfavour chelate coordination, while electron-withdrawing groups (like phenyl) will lead to more stable complexes. It should be noted that when the level of the π*-LUMO is lowered too far in energy this can lead to a redox reaction in which the metal centre is oxidised, leading to decomposition of the formed complexes.[66]

Thirdly, the stability of complexes **6** depends on the propensity of η^2-C=N coordination to a second metal fragment, giving rise to the formation of complexes **7**. The propensity of the analogous R-DAB towards η^2-C=N coordination has been studied by Staal et al.[17] and decreases on going from RCH_2 to R_2CH to R_3C for the imine nitrogen substituent on R-DAB. The propensity towards η^2-C=N coordination will also depend on the substituent on the imine carbon atom and decreases in the order H > Me >> Ph, as has been found in the reactivity of complexes $[\{C_5H_4N$-2-$C(R^3)=NR^1\}Fe(CO)_3]$ (R^3= H, Me, Ph) towards $Fe(CO)_4$ fragments.[70]

Considering these factors it is understandable that for the α-imino ketones **e–g**, and less so for **h**, the stable complexes **6e–h** are formed. All three have an electron-withdrawing phenyl substituent on the ketone carbon atom which favours the formation of a stable chelate. The α-imino ketones **g** and **h** have relatively small substituents on the imine nitrogen atom and a bulky phenyl substituent on the imine carbon atom, while the α-imino ketones **e,f** have relatively bulky *i*Pr and *t*Bu groups on the nitrogen but only a proton on the imine carbon atom. This means that these α-imino ketones can easily adopt a planar *cis* conformation and subsequently form the stable complexes **6e–h**. The reaction of **6e** → **7e** is more favourable than the reaction **6f** → **7f** because of the greater propensity for η^2-C=N coordination (R_2CH vs. R_3C) of ligand **e**, which is corroborated by the higher yields of **7e**. For the α-imino ketone **h**, the steric influence of the *p*Tol group is similar to that of a cyclohexyl, but electronic influences also play an important role as can be seen from the instability of **7d**,**h** (see above). Complex **6h** slowly decomposes in solution, which could be due to the inferior σ-donating capacity of the nitrogen or to an internal redox reaction because of the low-lying π*-LUMO.

When relatively bulky substituents are attached to both the imine nitrogen and carbon atoms (**c**,**i**) it is difficult for these ligands to adopt the planar *cis* conformation. This is confirmed by the observation that only very low concentrations of **6c**,**i** are formed during the reaction, i.e. no intensive colouring of the reaction mixture is observed. The reaction of α-imino ketone **i** in THF resulted only in the formation of $[Fe(CO)_4$(THF)] and free ligand. Performing the same

reaction in toluene, a less coordinating solvent, resulted in the formation of **7i** in good yield by a fast reaction of **6i** with $Fe(CO)_4$. This demonstrates particularly well the poor chelating properties of α-imino ketones when they cannot easily adopt a planar *cis* geometry.

The ligands **a–c** have a methyl substituent on the ketone carbon, a proton on the imine carbon, and a big aliphatic substituent on the imine nitrogen atom. In principle this set of substituents appears sterically suitable for the formation of complexes **6**. However, complexes **6a–c** cannot be isolated in high yield. With ligand **c**, complex **6c** is formed in very low concentrations, i.e. no intense colouring of the reaction mixture is observed. Apparently, the 2,4-dimethyl-3-pentyl substituent on the imine nitrogen atom in ligand **c** is so bulky that the planar *cis* conformation is strongly disfavoured, i.e **6c** is formed in low concentrations and quickly reacts further to form complex **7c** in 38% yield. The reduced yields of **7a**,**b** (ca. 17%) have to be ascribed to the formation of **8a,b** and the sterically disfavoured η^2-C=N coordination due to the tertiary (CR_3) substituent on the imine nitrogen in **a**,**b** as opposed to the secondary substituent (CHR_2) in **c**. The methyl substituent on the ketone carbon atom also contributes to the overall low yields because it restricts the coordination of the oxygen atom through reduced π-back donation. Under the reaction conditions this probably leads to a slow chelate formation and consequently decomposition of the initially formed $[Fe(CO)_4\{R^1N{=}C(R^2){-}C(R^3){=}O\}]$ complexes which are known to be very labile.[68,69]

Formation and Reactivity of $Fe_2(CO)_4$(L-L) (8a,b,k)

Complexes **8a**,**b**,**k** are synthesised in moderate (**8a,b**) or low (**8k**) yield by reaction of the ligands **a,b,k** with $[Fe_2(CO)_9]$, according to Equation 2.

$$2\,[Fe_2(CO)_9] + 2\,\alpha\text{-imino ketone} \rightarrow [Fe_2(CO)_4(L{-}L)]\,(\mathbf{8}) + 2\,[Fe(CO)_5] + 4\,CO \quad (2)$$

They are isolated as dark green powders and are air-stable (**8a,b**) in their crystalline form. They are readily soluble in toluene, acetone, CH_2Cl_2 and THF. In solution **8a,b** are slightly light-sensitive whereas **8k** is very light-sensitive, especially in chlorinated solvents. Irradiation of the isostructural $[Mo_2(CO)_6(t\text{Bu-ADA})]$ at the Mo–Mo-σ,σ* transition results in the formation of $[Mo_2(CO)_6(t\text{Bu-DAB})_2]$,[63] i.e. fission of the C–C bond. Irradiation of **8a,b** at the high-energy slope (λ = 350 nm) of the metal–metal bond σ,σ* transition (**8a**; λ_{max} = 362 nm), however, leads to a fast (CH_2Cl_2) or slow (THF) decomposition of the starting complexes, and formation of $[Fe_2(CO)_4(\alpha\text{-imino ketone})_2]$ is not observed.

Heating a solution of **8a,b** (0.21 mmol, 50 mL) in toluene under CO at 80 °C for ca. 40 min causes fission of the central C–C bond between the two α-imino ketone ligands and of the metal–metal bond giving the mononuclear complexes **6a,b** in quantitative yield, according to Equation 3.

$$[Fe_2(CO)_4(L{-}L)] + 2\,CO \rightarrow 2\,[Fe(CO)_3(\alpha\text{-imino ketone})] \quad (3)$$

Irradiation of a toluene or THF solution of **6a,b** at the low-energy band (**6a**; λ_{max} = 526 nm) with the 514.5-nm line of an argon ion laser at room temperature leads to reformation of **8a,b** in high yield (cf. Figure 4).

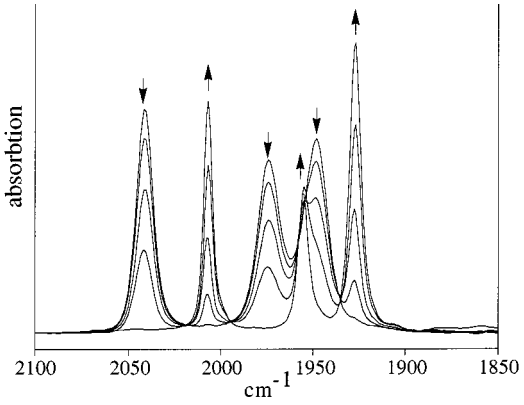
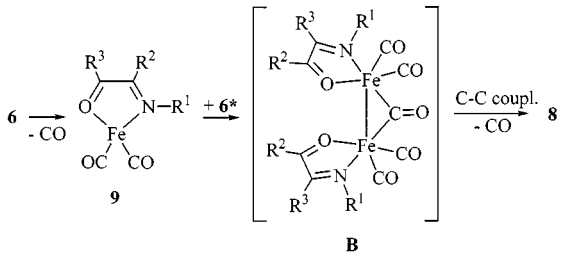


Figure 4. IR-spectral changes in the terminal carbonyl region during the irradiation of $[Fe(CO)_3\{t\text{BuN}{=}C(H){-}C(Me){=}O\}]$ (**6a**) in toluene at 293 K (514.5 nm); formation of **8a**

The irradiation times in THF are longer than those in toluene. The reaction time can be shortened in both cases by purging the solution with nitrogen gas, or degassing the solution under vacuum during irradiation. This observation can be explained by assuming the occurrence of an intermediate (**I** in Scheme 3) with the composition $[Fe_2(CO)_5(\alpha\text{-imino ketone})_2]$, which is formed by the loss of CO from **6a** and subsequent reaction of the highly reactive $[Fe(CO)_2(\alpha\text{-imino ketone})]$ (**9**) with the parent complex **6a**. For intermediate **I**, a metal–metal-bonded structure **B**, containing a bridging CO and two chelating α-imino ketone ligands, can be envisaged. A similar intermediate has been proposed for the formation of $[Ru_2(CO)_{4,5}(\text{R-IAE})]$.[7] The formation of **B**, like the formation of **A**, can be seen as an isolobal analogue to the reaction between a carbene and an olefin (cf. Scheme 5). In the present case, $[Fe(CO)_2(\alpha\text{-imino ketone})]$ (**9**) is a d^8-ML_4 fragment, like $Fe(CO)_4$, and is thus isolobal with a carbene. Subsequent addition to the Fe=C bond in **6*** (isolobal with an olefin, Scheme 4) leads to the formation of **B** which contains, as opposed to intermediate **A**, two chelating α-imino ketones. Reductive C–C coupling of the ketone carbon atoms with concomitant extrusion of CO results in the formation of **8a,b,k**. Further support for structure **B** stems from the formation of the isostructural complexes $[Fe_2(CO)_5(c\text{Hex-DAB})_2]$[60] and $[Ru_2(CO)_5\{CH(i\text{Pr})_2\text{-DAB}\}_2]$[72] upon irradiation of $[Fe(CO)_3(c\text{Hex-DAB})]$ and $[Ru(CO)_3\{CH(i\text{Pr})_2\text{-DAB}\}]$ in hexane at 150 K. However, in these cases no C–C bond formation was observed even upon warming the solution.

In order to obtain spectroscopic proof for the proposed mechanism, low-temperature IR and UV/Vis experiments were carried out. Irradiation of **6a** in 2-MeTHF at –120 °C leads initially to the formation of a single photoproduct and upon longer irradiation in the formation of **8a**. The new photoproduct has two CO stretching frequencies at 1962 and 1881 cm^{-1}, a shift of approximately 75 cm^{-1} to lower frequency with respect to those of **6a**, which points to the



Scheme 5. Proposed reaction mechanism for the formation of **8**

formation of $[Fe(CO)_2(2\text{-MeTHF})\{t\text{BuN}{=}C(H)\text{–}C(Me){=}O\}]$ (**9a**·2-MeTHF), i.e. loss of CO. The low-frequency shift is due to the good σ-donor capacity of 2-MeTHF at low temperature. In the UV/Vis spectrum, a new intense band is observed at 496 nm, which means that the ML band is shifted somewhat to higher energy on substitution of CO for 2-MeTHF. Irradiation in the presence of PPh_3 results, under the same conditions (–120 °C) or at room temperature, in the formation of the stable complex $[Fe(CO)_2(PPh_3)\{t\text{BuN}{=}C(H)\text{–}C(Me){=}O\}]$ (**10a**) [IR: 1967, 1903 cm^{-1}; UV: 560 nm (cf. Scheme 3)], and complex **8a** is not observed. Thermally (–120 °C), **9a** reacts back to form the parent complex **6a** (95%) and, to a small extent, to **8a** (5%). Irradiation of **6a** in toluene at –80 °C leads, as at room temperature, to the formation of **8a** accompanied by some decomposition; no intermediates are observed. These observations firmly support the proposal that the first step in the photochemical reaction is loss of CO. Depending on the stabilising effect of the σ-donor ligand present in solution, the initially formed labile 16e-$[Fe(CO)_2\{t\text{BuN}{=}C(H)\text{–}C(Me){=}O\}]$ intermediate (**9a**) can be trapped and isolated (PPh_3), stabilised at low temperature (2-MeTHF) or allowed to react further to form **8a** (toluene).

Irradiation of **6a** in hexane at –100 °C leads predominantly to **8a** together with a new photoproduct in approximately 10% yield. Due to the limited solubility of **8a** in hexane at –100 °C, and probably also of the new photoproduct, they both precipitate from the solution, thus giving rise to rather weak and broad absorptions. However, it can still be seen that the new photoproduct has a bridging CO ligand (1780 cm^{-1}) and three or four absorptions in the terminal region. This supports the formation of the CO-bridged structure **B**, which is furthermore corroborated by the absorption band at 797 nm in the UV/Vis spectrum. Similarly, $[Fe_2(CO)_5(c\text{Hex-DAB})_2]$ has an absorption band at 740 nm. It must be emphasised, however, that the conclusion that **B** is the only intermediate in the C–C-coupling reaction is not justified, since it was only observed at low concentrations. Extended photochemical studies are needed to obtain more detailed information about the reaction pathway **6** → **8**.

The question as to whether or not structure **B** is also an intermediate in the thermal C–C-coupling (**6** → **8**) or -decoupling (**8** → **6**) reaction is difficult to answer. It was mentioned earlier that complexes **6a,b** are stable in the pure form, i.e. they do not react back to their corresponding complexes **8**. As a consequence, under the reaction conditions, complexes other than **6** must play a role in the reaction pathway **6** → **8**. The decoupling reaction of **8a,b** → **6a,b** has been followed by means of high-pressure ^{1}H-NMR spectroscopy (see Experimental Section). However, an intermediate has not been observed during the conversion from **6** → **8**. It seems likely, however, that an intermediate like structure **B** should also be present in the thermal reaction.

As shown earlier, the C–C-coupled complexes **8** are only formed with ligands **a,b** and **k** which all bear a methyl substituent on the ketone carbon atom, whereas for the corresponding phenyl-substituted ligands **e** and **f** C–C coupling is not observed. Apparently, the methyl substituent is of decisive importance for the formation of **8**. This effect is most probably due to electronic factors (see below), although steric reasons cannot be excluded. The exclusive coupling at the ketone carbon atom is in line with the 1,3-dipolar reactivity, i.e. exclusive addition at the Fe–O=C fragment is observed (cf. Scheme 1). From this it might be concluded that the factors which determine the reactivity for 1,3-dipolar cycloadditions and the C–C coupling reactions discussed here are possibly similar. It has been shown that the 1,3-dipolar reactivity[26,73–75] decreases upon exchange of an electron-donating substituent for an electron-withdrawing substituent (Me → Ph). So analogously, the reactivity for C–C coupling to form **8** might decrease in this order. With ligand **j** the corresponding C–C-coupling product **8j** is not observed which is probably due to steric interactions of the methyl groups on both the ketone and the imine carbon atoms.

The yields of **8a,b** in the thermal reaction are almost identical in THF and toluene. On first sight, lower yields are expected in THF due to its better σ-donor capacity, thus stabilising $[Fe(CO)_2(\alpha\text{-imino ketone})]$, i.e. less-effective formation of intermediate **B** and accordingly **8**. However, in THF higher concentrations of $[Fe(CO)_3(\alpha\text{-imino ketone})]$ are present which results in a more effective formation of intermediate **B**. This is in agreement with the observation that $[Fe_2(CO)_5(c\text{Hex-DAB})_2]$ is only formed at rather high concentrations of $[Fe(CO)_3(c\text{Hex-DAB})]$. Furthermore, this is in line with the observation that **8c** is not formed as **6c** is present in very low concentration. Interestingly, the reaction of ligand **k** with $[Fe_2(CO)_9]$ in THF does not lead to **8k**, while in toluene it is formed in low yield. Obviously, in this case, THF inhibits the formation of **8k**.

Experimental Section

General Remarks: ^{1}H- and ^{13}C-NMR spectra were recorded with a Bruker AMX-300 spectrometer. Chemical shifts are reported relative to TMS (δ = 0) in the deuterated solvents indicated. – The IR spectra were recorded with a BioRad FTS-7 FTIR spectrophotometer or with a Perkin–Elmer 283 IR spectrophotometer. – Electronic absorption spectra were measured with a Perkin–Elmer Lambda 5 UV/Vis spectrophotometer or with a Varian Cary 4E spectrophotometer. – For low-temperature IR and UV/Vis measurements an Oxford Instruments DN 1704/54 liquid-nitrogen cryostat was used. The irradiations were carried out using the 514.5-nm line of an SP 2025 argon ion laser or a Philips HPK 125-W

high pressure mercury lamp equipped with the appropriate interference (λ = 500 nm) filter. – Elemental analyses were carried out by Dornis und Kolbe, Microanalytisches Laboratorium, Mülheim a. d. Ruhr, Germany. All solvents were carefully dried and distilled under nitrogen before use. All preparations were carried out under dry nitrogen by conventional Schlenk techniques. – Silica gel for column chromatography (Kieselgel 60, 70–230 mesh, E. Merck, Darmstadt, Germany) was dried and activated prior to use by heating to 180 °C under vacuum for 16 h. $Fe_2(CO)_9$[30] and the α-imino ketones **a**,**b**,**d–j**[31,33] were prepared according to published procedures. $Fe(CO)_5$ (Strem Chemicals) and 2-acetylpyridine (**k**) (Janssen) were used as commercially obtained.

The new α-imino ketone **c**, having R^1 = 2,4-dimethyl-3-pentyl [$CH(iPr)_2$] (cf. Table 1), R^2 = H, R^3 = Me, was synthesised according to the literature procedure for ligands **a**,**b**.[33] Yield 65%. – IR (pentane, cm^{-1}): $\tilde{\nu}$ = 1708 (vs) ν(C=O), 1650 (m) ν(C=N). – ^1H NMR ($CDCl_3$, room temp.): δ = 7.46 (s, 1 H, N=C*H*), 2.51 (t, *J* = 6.0 Hz, 1 H, N–C*H*), 2.39 (s, 3 H, CH_3), 2.06 (dsept, *J* = 6.0 Hz, 6.9 Hz, 1 H, C*H*), 0.83, 0.82 [d, *J* = 6.9 Hz, 2 × 6 H, $CH(CH_3)_2$]. – ^{13}C NMR ($CDCl_3$, room temp.): δ = 199.1 (*C*=O), 159.5 (*C*=N), 83.2 (N–CH), 29.6 (C–CH), 25.03 (CH_3), 20.5, 18.4 [$CH(CH_3)_2$].

The explanations for the acronyms used in this paper are given in Table 1.

The general procedures for the preparation of complexes **6e–h**, **7a–j** and **8a,b,k** are given below, details are listed in Table 2.

Synthesis of [Fe(CO)$_3$(α-imino ketone)] (6e–h): To a stirred suspension of [$Fe_2(CO)_9$] in 40 mL of THF was added 0.5 g of the respective α-imino ketone (cf. Table 2), whereupon the solution immediately turned dark purple. After all the free ligand had been consumed [monitored by the decrease of the ν(C=O) band of the ligand], the solution was filtered to remove the unchanged [$Fe_2(CO)_9$]. The solution was concentrated to dryness and the residue was redissolved in 60 mL of pentane (**6e–g**) or 30 mL of pentane/5 mL Et_2O (**6h**) and filtered again. For **6e,f** the solution was concentrated to dryness, yielding **6e,f** as deep purple oils in 80% (**6e**) or 90% (**6f**) yield. Due to their instability these complexes are best used directly after preparation or stored in pentane solution at –30 °C. Cooling a pentane solution of **6g** to –20 °C resulted in dark purple lustrous crystals in about 35% yield, which were suitable for X-ray diffraction. Subsequent crystallisation from a concentrated mother liquor at –30 °C led to a second batch of crystals of **6g** (35%), giving a total yield of 70%. The second batch of crystals often contained small amounts of [$Fe_2(CO)_6$(L)] (**7g**, < 5%), also formed under these reaction conditions. Cooling the pentane/Et_2O solution of **6h** to –30 °C resulted in a red voluminous precipitate, and **6h** was isolated as a pink-red powder in about 30% yield containing small amounts of [$Fe_2(CO)_6$(L)] (**9h,** <5%). Complex **6h** decomposes within 1 d at room temperature and should be stored at temperatures below –20 °C. Due to the instability of **6e,f,h**, and the fact that they cannot be crystallised, no elemental analyses could be obtained.

Synthesis of [Fe(CO)$_3${*t*AmN=C(H)–C(Me)=O}] (6b): Solutions of **6b** to be used in situ for further reactions were synthesised according to the literature procedure for **6a** (cf. Table 1).[25,26]

Synthesis of [Fe$_2$(CO)$_6$(L)] (7a–j) and [Fe$_2$(CO)$_4$(L–L)] (8a,b,k): To a stirred suspension of [$Fe_2(CO)_9$] in 40 mL of THF or toluene was added 0.5 g of the respective α-imino ketone (cf. Table 2), whereupon the solution turned dark purple (**a,b**) or blue (**k**). The reaction mixture was stirred for 3 h (THF) or 16 h (toluene) during which time the colour of the reaction mixture changed from dark purple/blue to red-brown. After evaporation of the solvent, the residue was redissolved in a minimum of CH_2Cl_2 and the products were purified by column chromatography on silica gel (column 1 × 15 cm). Elution with pentane afforded a green fraction, containing [$Fe_3(CO)_{12}$]. Further elution with pentane/Et_2O (ratio cf. Table 2) afforded a red-brown fraction which, after evaporation of the solvent, gave [$Fe_2(CO)_6$(L)] (**7a–j**) as a red-brown oil or powder. Crystallisation from pentane at –60 °C resulted in most cases in red-brown crystalline products, the yields varied between 15 and 75% (isolated product) depending on the ligand. Subsequent elution with Et_2O/CH_2Cl_2 (ratio cf. Table 2) afforded a dark green fraction which, after evaporation of the solvent, yielded [$Fe_2(CO)_4$(L–L)]

Table 2. Syntheses of complexes **6e–h**, **7a–j** and **8a**,**b**,**k**

	Ligand substituents			Ligand (mmol)[a]	$Fe_2(CO)_9$ [g, (mmol)]	Solvent (reaction time)[b]	Elution ratio[c]	Yield (%)[d]
Compd.	R^1	R^2	R^3					
6e	*i*Pr	H	Ph	2.65	1.3 (3.60)	THF (1)		75
6f	*t*Bu	H	Ph	2.64	1.2 (3.30)	THF (1)		90
6g	Me	Ph	Ph	2.24	2.5 (6.96)	THF (2)		70
6h	*p*Tol	Ph	Ph	1.67	1.3 (3.60)	THF (0.5)		30
7a	*t*Bu	H	Me	3.73	3.1 (6.52)	THF (3)	7:1	16
7b	*t*Am	H	Me	3.74	3.0 (6.24)	THF (3)	7:1	16
7c	$CHiPr_2$	H	Me	2.75	2.6 (7.14)	THF (3)	7:1	36
7d[e]	*p*Tol	H	Ph	2.24	2.0 (5.50)	THF (2)	7:1	17
7e	*i*Pr	H	Ph	2.65	2.1 (5.70)	THF (3)	7:1	63
7f	*t*Bu	H	Ph	2.64	3.0 (6.24)	THF (3)	7:1	57
7g[f]	Me	Ph	Ph	2.24	2.5 (6.67)	Tol (14)	6:2	75
7h[e]	*p*Tol	Ph	Ph	1.67	1.6 (4.37)	Tol (14)	7:1	25
7i[e]	*i*Pr	Ph	Ph	1.77	2.2 (6.00)	Tol (14)	6:2	64
7j	Benzyl	Me	Me	2.65	2.6 (7.70)	THF (3)	6:4	44
8a	*t*Bu	H	Me	3.73	3.1 (6.52)	THF (3)	2:3	25
8b	*t*Am	H	Me	3.54	3.0 (6.24)	THF (3)	2:3	27
8k[g]	2-Pyridine		Me	4.13	3.0 (6.24)	Tol (14)	3:2	4

[a] Based on 0.5 g of the respective α-imino ketone. – [b] Solvent used, THF (tetrahydrofuran) or Tol (toluene) and the reaction time in hours. – [c] Ratio of pentane/Et_2O for elution of **7a–i** and the ratio of Et_2O/CH_2Cl_2 for elution of **8a**,**b**,**k**. – [d] Yield based on α-imino ketone consumed. – [e] After the reaction was stopped air was bubbled through the solution for 5 min to destroy the mononuclear [Fe(CO)$_3$(α-imino ketone)] complex present. – [f] Green-brown fraction, crystallisation from pentane/Et_2O (5:1) yields a green brown micro crystalline precipitate. – [g] Reaction mixture turned intensively blue.

Table 3. Crystallographic data for **6g** and **8a**

Compound	**6g**	**8a**
Empirical formula	$C_{18}H_{13}FeNO_4$	$C_{18}H_{26}Fe_2N_2O_6$
Molecular mass	363.15	478.11
Space group	$P\bar{1}$ (no. 2)	$P\bar{1}$ (no. 2)
Crystal system	triclinic	triclinic
a [Å]	10.6110(14),	7.974(2)
b [Å]	12.1544(13),	11.377(14)
c [Å]	14.5221(11)	13.525(10)
α [°]	88.96(1)	74.24(9)
β [°]	75.20(1)	78.95(4)
γ [°]	67.75(1)	69.98(7)
V [Å^3]	1669.6(4)	1104(2)
Z	4	2
$D_{calcd.}$ [g cm^{-3}]	1.445(3)	1.439(2)
F(000)	744.0	496.0
μ [cm^{-1}]	9.2	13.5
Crystal size [mm]	0.52 × 0.63 × 0.20	0.10 × 0.20 × 0.75
Data collection		
Temperature [K]	295	295
θmin/θmax [°]	1.5, 27.50	1.57, 27.50
Radiation (monochromated)	Mo-K_α (graphite), 0.71073 Å	Mo-K_α (graphite), 0.71073 Å
Δω [°]	0.83 + 0.35tanθ	0.53 + 0.35tanθ
Horizontal and vertical aperture [mm]	2.95, 4.0	3.0, 4.0
X-ray exposure time [h]	51	35
Linear decay (%)	1.0	1.0
Reference reflections	–2 3 0, 4 2 5, 5 3 2	2 2 3, 3 2 –2, –2 4 2
Index ranges	*h*: –13 – 13 *k*: –15 – 15 *l*: –18 – 18	*h*: 0 – 10 *k*: –13 – 14 *l*: –17 – 17
Total data	8495	5445
Unique data	7610	5077
Observed data	6062 [$I > 2.5\sigma(I)$]	3706 [$I > 2.5\sigma(I)$]
Refinement		
No. of refl. and params.	6062, 441	3706, 278
Weighting scheme	$w = 1.0/[\sigma^2(F)]$	$w = 1.0/[\sigma^2(F) + 0.000699\ F^2]$
Final *R*, w*R*, *S*	0.0380, 0.0418, 0.80	0.0546, 0.0791, 1.10
Isotr. therm. par. H atoms [Å^2]	0.075(2)/0.095(5) for CH/CH$_3$	0.081(4)
$(\Delta/\sigma)_{av}$ in final cycle	0.0222	0.0142
min./max. resd. density [e/Å^3]	–0.45, 0.45	–0.83, 0.95

(**8a,b,k**) as a green powder. Crystallisation from pentane/CH_2Cl_2 (2:3) resulted in dark green needles of **8a,b**, in 25 and 27% yield, respectively. Crystals of **8a** were suitable for X-ray diffraction. Complex **8k** was formed in only 4% yield and decomposed on crystallisation.

Preparation of Solutions of 6b for ^{1}H- and ^{13}C-NMR Spectroscopy: A solution of ca. 80 mg **8b** in 2.5 mL of [D$_6$]acetone was placed in a high-pressure NMR tube and kept at 313 K for 5 h under 35 bar carbon monoxide. This resulted in a complete conversion into **6b**.

Reaction of [Fe$_2$(CO)$_4$(L–L)] (8a,b) with Carbon Monoxide. – Formation of 6a,b: Compound **8a** (0.100 g, 0.21 mmol) or **8b** (0.106 g, 0.21 mmol) was dissolved in 50 mL of toluene and stirred under carbon monoxide for 40 min at 80 °C. During this time the colour of the solution turned from green to intense purple. The reaction was followed by IR spectroscopy and showed that **8a,b** had been quantitatively converted into **6a–b**.

Photochemical conversion of [Fe(CO)$_3$(L)] (6a,b) in [Fe$_2$(CO)$_4$(L–L)] (8a,b): A toluene solution containing **6a,b** (0.21 mmol, 50 mL) was irradiated into the high-energy slope of the low-energy band (λ_{max} = 526 nm) with the 514.5-nm line of an argon ion laser at room temperature. The reaction was followed by IR spectroscopy. Complete conversion of **6** to **8** took approximately 1 h, during which time the colour of the solution gradually changed from intense purple to green/brown. Due to some decomposition of **6a,b**, the formed products **8a,b** had to be purified by column chromatography. Elution with CH_2Cl_2 afforded a dark green fraction which, after evaporation of the solvent, yielded [Fe$_2$(CO)$_4$(L–L)] (**8a,b**) as a green powder in 90% yield.

X-ray Crystal Structure Determination of 6g and 8a: Dark opaque crystals were mounted under nitrogen in a Lindemann glass capillary (**6g**) or glued on a glass fibre (**8a**) and transferred to an Enraf–Nonius CAD-4T rotating-anode diffractometer for data collection. Unit-cell parameters were determined from least-squares treatment of the SET4 setting angles of 25 reflections and were checked for the presence of higher lattice symmetry.[34] The crystals of **6g** and **8a** show broad reflection profiles. All data were collected with ω/2θ scan mode, and were corrected for Lp and for the observed linear decay of the intensity control reflections; redundant data were merged into a unique data set. An empirical absorption correction was applied for both compounds with the DIFABS[34] method (correction range 0.646–1.440 for **6g** and 0.614–1.180 for **8a**). The structures were solved with either standard Patterson methods (**8a**) or direct methods (**6g**) (SHELXS86)[35] and subsequent difference Fourier syntheses. Refinement on *F* was carried out by full-matrix least-squares techniques. A small cavity at 0,0,1/2 of 49 Å^3 was found in the unit cell of **8a**. However, no significant residual density could be detected in that area (PLATON).[36] Hydrogen atoms were introduced at calculated positions [C–H = 0.98 Å] and included in the refinement riding on their carrier atoms. All non-H atoms were refined with anisotropic thermal parameters, H atoms were refined with common isotropic thermal parameters. Weights were introduced in the final refinement cycles. Neutral atom scattering factors were taken from[37] and corrected for anom-

alous dispersion.[38] All calculations were performed with SHELX76[39] and the PLATON package[36] (geometrical calculations and illustrations) on a DEC-5000 cluster. Crystal data and numerical details of the structure determinations are given in Table 3.

Supporting information for this article (Tables 4 and 5 with selected bond lengths and angles for **6g** and **8a**, Table 6 with IR, UV/Vis, and analytical data, and Tables 7 and 8 with ^{1}H- and ^{13}C-NMR-spectroscopic data for compounds **6**, **7**, and **8**) is available on the WWW under http://www.wiley-vch.de/home/eurjic or from the author. Crystallographic data (excluding structure factors) for the structures of **6g** and **8a** have been deposited with the Cambridge Crystallographic Data Centre as supplementary publication nos. CCDC-137484 (**8a**), and -137485 (**6g**). Copies of the data can be obtained free of charge on application to CCDC, 12 Union Road, Cambridge CB2 1EZ, UK [Fax: (internat.) + 44-1223/336-033; E-mail: deposit@ccdc.cam.ac.uk].

Acknowledgments

This investigation was in part supported (W. J. J. S., A. L. S.) by the Netherlands Foundation for Chemical Research (SON) with financial aid from the Netherlands Organisation for Scientific Research (NWO). We are indebted to J.-M. Ernsting for practical assistance with recording NMR data and to B. D. Rossenaar for practical assistance with recording LT-IR and UV/Vis data.

[1] G. van Koten, K. Vrieze, *Adv. Organomet. Chem.* **1982**, *21*, 151–239.
[2] K. Vrieze, G. van Koten, *Inorg. Chim. Acta* **1985**, *100*, 79–96.
[3] K. Vrieze, *J. Organomet. Chem.* **1986**, *300*, 307–326.
[4] R. Zoet, G. van Koten, C. H. Stam, D. J. Stufkens, K. Vrieze, *Organometallics* **1988**, *7*, 2118–2123.
[5] R. Zoet, J. T. B. H. Jastrzebski, G. van Koten, T. Mahabiersing, K. Vrieze, C. H. Stam, D. Heijdenrijk, *Organometallics* **1988**, *7*, 2108–2117.
[6] L. H. Staal, L. Polm, R. W. Balk, G. van Koten, K. Vrieze, A. M. F. Brouwer, *Inorg. Chem.* **1980**, *19*, 3343–3351.
[7] W. P. Mul, C. J. Elsevier, H.-W. Frühauf, K. Vrieze, I. Pein, M. C. Zoutberg, C. H. Stam, *Inorg. Chem.* **1990**, *29*, 2336–2345.
[8] J. Keijsper, G. van Koten, K. Vrieze, M. C. Zoutberg, C. H. Stam, *Organometallics* **1985**, *4*, 1306–1308.
[9] J. Keijsper, L. H. Polm, G. van Koten, K. Vrieze, G. Abbel, C. H. Stam, *Inorg. Chem.* **1984**, *23*, 2142–2148.
[10] L. H. Polm, C. J. Elsevier, G. van Koten, J. M. Ernsting, D. J. Stufkens, K. Vrieze, R. R. Andréa, C. H. Stam, *Organometallics* **1987**, *6*, 1096–1104.
[11] J. Keijsper, L. H. Polm, G. van Koten, K. Vrieze, C. H. Stam, J. D. Schagen, *Inorg. Chim. Acta* **1985**, *103*, 137–149.
[12] F. Muller, G. van Koten, K. Vrieze, D. Heijdenrijk, B. B. Krijnen, C. H. Stam, *Organometallics* **1989**, *8*, 41–48.
[13] F. Muller, G. van Koten, M. J. A. Kraakman, K. Vrieze, R. Zoet, K. A. A. Duineveld, D. Heijdenrijk, C. H. Stam, M. C. Zoutberg, *Organometallics* **1989**, *8*, 982–991.
[14] F. Muller, G. van Koten, K. Vrieze, D. Heijdenrijk, *Organometallics* **1989**, *8*, 33–40.
[15] F. Muller, G. van Koten, K. Vrieze, K. A. A. Duineveld, D. Heijdenrijk, A. N. S. Mak, C. H. Stam, *Organometallics* **1989**, *8*, 1324–1330.
[16] F. Muller, G. van Koten, K. Vrieze, D. Heijdenrijk, *Inorg. Chim. Acta* **1989**, *158*, 69–79.
[17] L. H. Staal, L. Polm, K. Vrieze, F. Ploeger, C. H. Stam, *Inorg. Chem.* **1981**, *20*, 3590–3597.
[18] L. H. Staal, G. van Koten, K. Vrieze, B. van Santen, C. H. Stam, *Inorg. Chem.* **1981**, *20*, 3598–3606.
[19] H.-W. Frühauf, F. Seils, R. J. Goddard, M. J. Romão, *Angew. Chem. Int. Ed. Engl.* **1983**, *22*, 992–993; *Angew. Chem.* **1983**, *95*, 1014–1415; *Angew. Chem. Suppl*. **1983**, 1435–1450.
[20] H.-W. Frühauf, F. Seils, R. J. Goddard, M. J. Romão, *Organometallics* **1985**, *4*, 948–949.
[21] H.-W. Frühauf, F. Seils, *J. Organomet. Chem.* **1986**, *302*, 59–64.
[22] H.-W. Frühauf, F. Seils, *J. Organomet. Chem.* **1987**, *323*, 67–76.
[23] H.-W. Frühauf, F. Seils, C. H. Stam, *Organometallics* **1989**, *8*, 2338–2343.
[24] P. P. M. de Lange, H.-W. Frühauf, M. van Wijnkoop, M. J. A. Kraakman, M. Kranenburg, A. H. J. P. Groot, J. Fraanje, Y. Wang, M. Numan, *Organometallics* **1993**, *12*, 417–427.
[25] M. van Wijnkoop, R. Siebenlist, P. P. M. de Lange, H.-W. Frühauf, K. Vrieze, W. J. J. Smeets, A. L. Spek, *Organometallics* **1993**, *12*, 4172–4181.
[26] M. van Wijnkoop, R. Siebenlist, J. M. Ernsting, P. P. M. de Lange, H.-W. Frühauf, E. Horn, A. L. Spek, *J. Organomet. Chem.* **1993**, *482*, 99–109; and references cited therein.
[27] M. R. P. van Vliet, G. van Koten, J. A. M. van Beek, K. Vrieze, F. Muller, C. H. Stam, *Inorg. Chim. Acta* **1986**, *112*, 77–85.
[28] M. R. P. van Vliet, G. van Koten, M. A. Rotteveel, M. Scharp, K. Vrieze, B. Kojic-Prodic, A. L. Spek, A. J. M. Duisenberg, *Organometallics* **1986**, *5*, 1389–1394.
[29] A. de Cian, R. E. Weiss, Y. Chauvin, D. Commereuc, D. Hugo, *J. Chem. Soc., Chem. Commun.* **1976**, 249–250.
[30] $[Fe_2(CO)_9]$ was prepared by a slightly modified literature procedure (E. H. Braye, W. Hübel, *Inorg. Synth.* **1966**, *8*, 178) using a quartz Schlenk tube and starting with 25 mL of $Fe(CO)_5$, 150 mL of glacial acetic acid and 10 mL of acetic anhydride (the latter was added to prevent the mixture containing too much water). A rayonet RS photochemical reactor (λ_{max} = 2500 Å) was used for irradiation and a continuous stream of air was used to cool the reaction mixture. Filtration, washing with water, ethanol, ether, and subsequently drying in vacuo gave $[Fe_2(CO)_9]$ usually in more than 90% yield.
[31] B. Alcaide, G. Escobar, R. Pérez-Ossario, J. Plumet, D. Sanz, *J. Chem. Research (M)* **1984**, 1466–1488; *J. Chem. Research (S)* **1984**, 144–145.
[32] W. B. Wheatley, W. E. Fitzgibbon, L. C. Cheney, *J. Org. Chem.* **1953**, *18*, 1564–1571.
[33] H. van der Poel, G. van Koten, *Synth. Commun.* **1978**, *8*, 305–313.
[34] N. Walker, D. Stuart, *Acta Crystallogr., Sect. A* **1983**, *A39*, 158–166.
[35] G. M. Sheldrick, *SHELXS86, Program for crystal structure determination*, Univ. of Göttingen, Germany, **1986**.
[36] A. L. Spek, *Acta Crystallogr., Sect. A* **1990**, *A46*, C34.
[37] D. T. Cromer, J. B. Mann, *Acta Crystallogr., Sect. A* **1968**, *A24*, 321–324.
[38] D. T. Cromer, D. Liberman, *J. Chem. Phys.* **1970**, *53*, 1891–1898.
[39] G. M. Sheldrick, *SHELX76, Crystal structure analysis package*, Univ. of Cambridge: Cambridge, England, **1976**.
[40] M. Kokkes, D. J. Stufkens, A. Oskam, *J. Chem. Soc., Dalton Trans.* **1983**, 439–445.
[41] H.-W. Frühauf, I. Pein, F. Seils, *Organometallics* **1987**, *6*, 1613–1620.
[42] R. R. Holmes, in *Progress in Inorganic Chemistry* (Ed.: S. J. Lippard), Wiley, Cambridge, Massachusetts, **1984**, vol. 32, pp. 119–236.
[43] H.-W. Frühauf, G. Wolmershäuser, *Chem. Ber.* **1982**, *115*, 1070–1082.
[44] M. A. De Paoli, H.-W. Frühauf, F.-W. Grevels, E. A. Koerner von Gustorf, W. Riemer, C. J. Krüger, *J. Organomet. Chem.* **1977**, *136*, 219–233.
[45] R. J. Doedens, *J. Chem. Soc., Chem. Commun.* **1968**, 1271–1272.
[46] I. Fonseca, S. Martinez-Carrera, S. Garcia-Blanco, *Acta Crystallogr., Sect. B* **1979**, *B35*, 2643–2646.
[47] P. P. M. de Lange, M. J. A. Kraakman, M. van Wijnkoop, H.-W. Frühauf, K. Vrieze, W. J. J. Smeets, A. L. Spek, *Inorg. Chim. Acta* **1992**, *196*, 151–160.
[48] S. Aime, L. Milone, E. Sappa, A. Tirpicchio, M. Tirpicchio Camellini, *J. Chem. Soc., Dalton Trans.* **1979**, 1155–1159.
[49] J. Meunier-Piret, P. Piret, M. van Meersche, *Acta Crystallogr.* **1965**, *19*, 85–91.
[50] H. Kisch, P. Reiser, F. Knoch, *Chem. Ber.* **1991**, *124*, 1143–1148.
[51] P. G. Le Borgne, D. Grandjean, *Acta Crystallogr., Sect. B* **1973**, *B29*, 1040–1046.

[52] A. L. Spek, J. T. B. H. Jastrzebski, K. Vrieze, *Acta Crystallogr., Sect. C* **1987**, *43*, 2006–2007.
[53] E. Wissing, S. van der Linden, E. Rijnberg, J. Boersma, W. J. J. Smeets, A. L. Spek, G. van Koten, *Organometallics* **1994**, *13*, 2602–2608.
[54] G. van Koten, J. B. T. H. Jastrzebski, K. Vrieze, *J. Organomet. Chem.* **1983**, *250*, 49–61.
[55] L. H. Staal, A. Oskam, K. Vrieze, E. Roosendaal, H. Schenk, *Inorg. Chem.* **1979**, *6*, 1634–1640.
[56] H.-W. Frühauf, A. Landers, R. J. Goddard, C. Krüger, *Angew. Chem.* **1978**, *90*, 56–57; *Angew. Chem. Int. Ed. Engl.* **1978**, *17*, 64–65.
[57] L. H. Staal, G. van Koten, K. Vrieze, *J. Organomet. Chem.* **1981**, *206*, 99–108.
[58] R. Zoet, G. van Koten, G. Muller, K. Vrieze, M. van Wijnkoop, K. Goubitz, C. J. G. van Halen, C. H. Stam, *Inorg. Chim. Acta* **1988**, *149*, 193–208.
[59] M. J. Kraakman, C. J. Elsevier, J.-M. Ernsting, K. Vrieze, K. Goubitz, *Inorg. Chim. Acta* **1993**, *203*, 129–143.
[60] H. K. van Dijk, D. J. Stufkens, A. Oskam, *J. Am. Chem. Soc.* **1989**, *111*, 541–547.
[61] D. J. Stufkens, *Coord. Chem. Rev.* **1990**, *104*, 39–112; and refs. cited therein.
[62] H. B. Abrahamson, C. C. Frazier, D. S. Ginley, H. B. Gray, J. Lilienthal, D. R. Tyler, M. S. Wrighton, *Inorg. Chem.* **1977**, *16*, 1554–1556.
[63] R. R. Andréa, H. E. de Jager, D. J. Stufkens, A. Oskam, *J. Organomet. Chem.* **1986**, *316*, C24–C28.
[64] D. Leibfritz, H. tom Dieck, *J. Organomet. Chem.* **1976**, *105*, 255–261.
[65] L. H. Staal, J. Keijsper, L. Polm, K. Vrieze, *J. Organomet. Chem.* **1981**, *204*, 101–113.
[66] H. Friedel, I. W. Renk, H. tom Dieck, *J. Organomet. Chem.* **1971**, *26*, 247–259.
[67] H.-W. Frühauf, J. Breuer, *J. Organomet. Chem.* **1984**, *277*, C13–C17.
[68] R. Rosenthal, I. Wender, in *Organic Syntheses via Metal Carbonyls* (Eds.: I. Wender, P. Pino), Interscience Publishers, New York, **1968**, vol. 1; pp. 405–466.
[69] M. Kilner, in *Advances in Organometallic Chemistry* (Eds.: F. G. A. Stone, R. West), Academic Press, Inc., New York, **1972**, vol. 10, pp. 115–198.
[70] H.-W. Frühauf, F.-W. Grevels, A. Landers, *J. Organomet. Chem.* **1979**, *178*, 349–360.
[71] I. W. Renk, H. tom Dieck, *Chem. Ber.* **1972**, *105*, 1403–1418.
[72] H. K. van Dijk, J. J. Kok, D. J. Stufkens, A. Oskam, *J. Organomet. Chem.* **1989**, *362*, 163–177.
[73] K. N. Houk, J. Sims, R. E. Duke, R. W. Strozier, J. K. George, *J. Am. Chem. Soc.* **1973**, *95*, 7287–7301.
[74] K. N. Houk, J. Sims, C. R. Watts, L. J. Luskus, *J. Am. Chem. Soc.* **1973**, *95*, 7301–7315.
[75] K. N. Houk, *Acc. Chem. Res.* **1975**, *8*, 361–369.

Received October 6, 1999
[I99351]

Sulfur Compounds, 212[‡]

Preparation of Organic Polysulfanes R_2S_n (n = 5, 7, 8, 9) from Sulfenyl Chlorides, RSCl, and Transition Metal Polysulfido Complexes

Ralf Steudel,*[a] Karin Hassenberg,[a] Vera Münchow,[a] Oliver Schumann,[a] and Joachim Pickardt[a]

Keywords: Sulfur / Titanium / Zinc / Polysulfido complexes / Sulfur heterocycles / Polysulfides / Polysulfanes / Sulfenyl chlorides

The preparation of seven novel organic polysulfanes is reported. Bis(n-octyl)heptasulfane R_2S_7 **1** is formed upon reaction of RSCl with $[Cp_2TiS_5]$, while the corresponding nonasulfane R_2S_9 **2** is obtained by reaction of RSSCl with $[Cp_2TiS_5]$. The bis(n-octyl)pentasulfane R_2S_5 **3** is obtained from RSCl and $[(Cp'_2TiCl)_2S_3]$ by transfer of the S_3 ligand at 20 °C. The new alkyl polysulfanes **1**–**3** have been obtained in quantitative yields. They are liquids at 20 °C, having freezing points below –50 °C, but do not form mesogenic phases. Reactions of $[Cp_2TiS_5]$ with 2-naphthyl- and 4-chlorophenyl sulfenyl chloride furnish the corresponding heptasulfanes **4** and **5**, respectively, which are solids at 20 °C. 1,2-Benzodisulfenyl chloride $C_6H_4(SCl)_2$ reacts with $[(Cp'_2TiCl)_2S_3]$ to give the known 1,2,3,4,5-benzopentathiepin $C_6H_4S_5$ **6**, with $[Cp_2TiS_5]$ to give the novel 1,2,3,4,5,6,7-benzoheptathionin $C_6H_4S_7$ **7**, and with $[(TMEDA)ZnS_6]$ to give the novel 1,2,3,4,5,6,7,8-benzooctathiecin $C_6H_4S_8$ **8**. The cyclic polysulfanes **6**–**8** are solids at 20 °C and have been recovered in yields of 60–83%. The orthorhombic structure of 1,2-$C_6H_4S_7$ has been investigated by single-crystal X-ray diffraction analysis. The molecules are found to be located at sites of C_s symmetry and the motif of the C_2S_7 heterocycle is +–+–+–+–, with the torsion angle of zero at the carbon–carbon bond. The three internuclear SS distances measure 205.0(1), 203.7(1), and 205.7(1) pm.

Introduction

Sulfur-rich organic polysulfanes R_2S_n ($n > 2$) may be synthesized by a variety of methods starting from either thiols, sulfenyl chlorides, elemental sulfur, sulfanes (H_2S_n), chlorosulfanes (S_nCl_2), ionic polysulfides (e.g. Na_2S_n), or other sulfur compounds.[1] In most cases, mixtures of polysulfanes of varying chain length n are obtained, which have to be separated by repeated crystallization or by chromatography. Such separations have to be conducted under mild conditions owing to the thermal and thermodynamic instability of the longer-chain polysulfanes, which tend to equilibrate with species of other chain lengths or to split off S_8, S_7, or S_6 (Equation 1 and 2):[2]

$$2\ R_2S_n \rightarrow R_2S_{n+x} + R_2S_{n-x} \quad (1)$$

$$R_2S_n \rightarrow R_2S_{n-8} + S_8\ (n > 8) \quad (2)$$

In recent years, the enormous potential of titanocene polysulfide complexes for the synthesis of novel homocyclic and heterocyclic organic and inorganic sulfur compounds has been demonstrated.[3,4,5,6] Using these reagents, a large number of interesting sulfur-rich species have been prepared, for which no synthetic route had hitherto been available. When organic sulfenyl chlorides or related SCl compounds are allowed to react with titanocene pentasulfide, chain-like polysulfanes with up to nine sulfur atoms may be generated (Equation 3 and 4; Cp = η^5-C_5H_5):[7,8]

$$2\ CCl_3SCl + [Cp_2TiS_5] \rightarrow (CCl_3)_2S_7 + [Cp_2TiCl_2] \quad (3)$$

$$2\ i\text{PrOSSCl} + [Cp_2TiS_5] \rightarrow (i\text{PrO})_2S_9 + [Cp_2TiCl_2] \quad (4)$$

In a similar fashion, bifunctional organic sulfenyl chlorides and chlorodisulfanes have been treated with titanocene pentasulfide or similar complexes, thereby generating cyclic sulfur-rich polysulfanes with up to 11 sulfur atoms (Equation 5 and 6):[9,10,11]

$$1,2\text{-}C_2H_4(SCl)_2 + [Cp_2TiS_5] \rightarrow C_2H_4S_7 + [Cp_2TiCl_2] \quad (5)$$

$$1,2\text{-}C_7H_{10}(SCl)(SSCl) + [Cp_2TiS_5] \rightarrow C_7H_{10}S_8 + [Cp_2TiCl_2] \quad (6)$$

A relatively new titanocene polysulfide complex is $[Cp'_2Ti(Cl)–S_3–(Cl)TiCp'_2]$,[12] which reacts with sulfenyl chlorides as an S_3 group transfer reagent (Equation 7 and 8; Cp′ = $CH_3C_5H_4$):[13]

$$C_{10}H_{12}(SCl)_2 + [(Cp'_2TiCl)_2S_3] \rightarrow C_{10}H_{12}S_5 + 2\ [Cp'_2TiCl_2] \quad (7)$$

$$C_{10}H_{12}(SCl)(SSCl) + [(Cp'_2TiCl)_2S_3] \rightarrow C_{10}H_{12}S_6 + 2\ [Cp'_2TiCl_2] \quad (8)$$

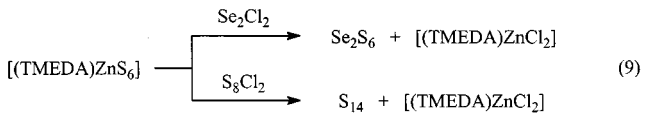
In this work, we report the synthesis of five chain-like and three cyclic organic polysulfanes with between 5 and 9 sulfur atoms. In the case of the chain-like species, we used alkyl as well as aryl substituents. The n-octyl substituent was employed in the hope that the rather long chains of (n-

[‡] Part 211: A. H. Otto, R. Steudel, *Eur. J. Inorg. Chem.*, in print.

[a] Institut für Anorganische und Analytische Chemie, Sekr. C2, Technische Universität Berlin, D-10623 Berlin, Germany
Fax: (internat.) + 49-(0)30/314-26529
E-mail: steudel@schwefel.chem.tu-berlin.de

 © WILEY-VCH Verlag GmbH, D-69451 Weinheim, 2000 1434–1948/00/0505–0921 $ 17.50+.50/0

octyl)$_2S_n$ would result in a high degree of anisotropy and consequently in mesogenic properties. The aryl groups 4-chlorophenyl and 2-naphthyl were used in the expectation that readily crystallizable products suitable for X-ray crystallographic analysis would be obtained. In the case of the cyclic species, 1,2-substituted benzene was used for the same reason. A further aim of this work was to study the utility of the zinc polysulfide chelate complex [(TMEDA)ZnS_6] in the preparation of sulfur-rich organic heterocycles. This compound has previously been used to prepare inorganic rings such as 1,2-Se_2S_6 [14] and S_{14} (Equation 9).[15]



(9)

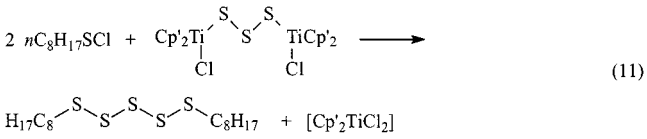
Results and Discussion

Aliphatic Polysulfanes[16]

Octylsulfenyl chloride was prepared by chlorination of *n*-octanethiol. Titanocene pentasulfide was found to react with this sulfenyl chloride at temperatures below 0 °C in carbon disulfide to quantitatively afford bis(*n*-octyl)heptasulfane **1** (Equation 10; $x = 1$). This compound is a viscous red liquid at ambient temperature and has a freezing point of –60 °C.

$$2\ n C_8H_{17}S_xCl + [Cp_2TiS_5] \rightarrow (nC_8H_{17})_2S_{5+2x} + [Cp_2TiCl_2] \quad (10)$$

Reaction of *n*-octanethiol with dichlorosulfane gives *n*-octylchlorodisulfane, which reacts with titanocene pentasulfide under the same experimental conditions as above to yield the orange bis(*n*-octyl)nonasulfane **2** (Equation 10; $x = 2$). This product freezes to a glass at –52 °C. Bis(*n*-octyl)pentasulfane **3**, a yellow liquid with freezing point –67 °C, was prepared by the reaction of *n*-octylsulfenyl chloride with bis[bis(methylcyclopentadienyl)chlorotitanium]trisulfide [(Cp′$_2$TiCl)$_2S_3$] in carbon disulfide at low temperatures (Equation 11; Cp′ = $CH_3C_5H_4$).



(11)

Analyses by ^{1}H-NMR and HPLC showed that the unusual red color of the heptasulfane 1 is not due to traces of titanocene pentasulfide or titanocene dichloride as might be suspected. Bis(*n*-octyl)nonasulfane **2** is the most sulfur-rich of all selectively available diorganylpolysulfanes that is *liquid* at ambient temperature.

The lengths of the sulfur chains in these novel compounds have been assessed not only by microanalysis, but also by reversed-phase HPLC. A linear relationship exists between the number of sulfur atoms in the chain (n_S) and the natural logarithm of the capacity factor (ln k'), which is calculated from the retention time. This has previously been demonstrated for other polysulfanes bearing alkyl and aryl substituents.[10,11,13,17] On heating of the nonasulfane **2** at 80 °C for 30 min., decomposition occurred resulting in a mixture of polysulfanes with up to 15 sulfur atoms. A plot of ln k' versus the number of sulfur atoms n_S for the bis(*n*-octyl)polysulfanes formed in this reaction is shown in Figure 1.

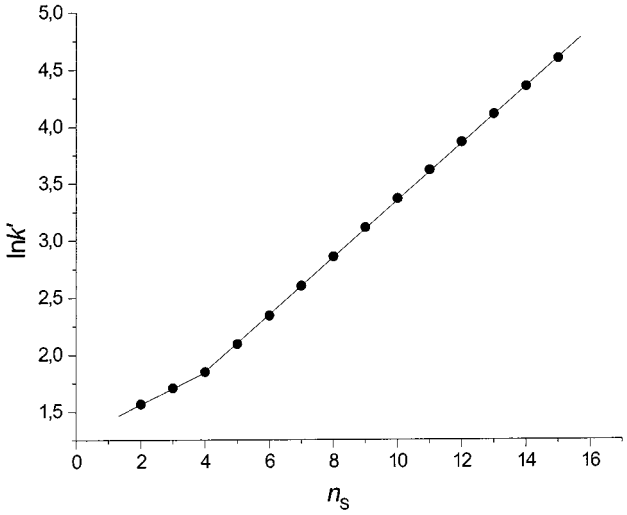


Figure 1. Dependence of the chromatographic retention times of the bis(*n*-octyl)polysulfanes $(C_8H_{17})_2S_n$ (n = 2–15) on the number of sulfur atoms n_S; here, ln k' is plotted against n_S [$k' = (t_r - t_0)/t_0$; t_0 = dead time, t_r = retention time]

Table 1. Retention data (retention times t_R, capacity factors k', and retention index values *RS*) of the homologous series $(C_8H_{17})_2S_n$ (n = 2–15)

n_S	t_R [min]	ln k'	*RS*	n_S	t_R [min]	ln k'	*RS*
2	8.10	1.565	941	9	32.83	3.111	1384
3	9.11	1.706	982	10	41.92	3.365	1457
4	10.28	1.847	1022	11	53.41	3.615	1529
5	12.47	2.092	1092	12	67.93	3.861	1599
6	15.96	2.342	1164	13	86.19	4.104	1669
7	20.23	2.600	1238	14	109.89	4.350	1740
8	25.69	2.854	1311	15	139.91	4.595	1810

The chromatographic data and the retention indices *RS* [18] derived therefrom are given in Table 1. The retention indices are independent of the chromatographic system used and can therefore be used for the identification of these species in a similar manner as spectroscopic data.

The chromatograms of the pure products **1**–**3** showed neither traces of other polysulfanes nor of sulfur homocycles, the other products of the disproportionation of polysulfanes according to Equations 1 and 2. The three liquid bis(*n*-octyl)polysulfanes can be stored at –25 °C for several months without decomposition. After storage at ambient temperatures for three days, HPLC analysis showed that about 10% of the products had undergone disproportionation. The ^{1}H- and ^{13}C-NMR spectra of **1**–**3** did not reveal any unusual features. The proton signals exhibit a very slight downfield shift with increasing number of sulfur

atoms, reflecting the increase in acidity of the sulfanes H_2S_n with increasing chain length n.[19]

The infrared spectra of **1**–**3**, recorded at ambient temperatures, are almost identical. They show mainly the absorptions of the *n*-octyl substituents, i.e. strong signals due to the CH stretching modes in the range 2850–2960 cm^{-1} and the CH_2 bending modes between 1200 and 1470 cm^{-1}. More interesting are the SS stretching modes, which can best be detected by Raman spectroscopy. The low-temperature (–135 °C) Raman spectra exhibit, besides weak to strong lines in the ranges 2700–3000 cm^{-1} and 1300–1500 cm^{-1} attributable to the *n*-octyl substituents, several lines between 420 and 510 cm^{-1}, which are characteristic of catenated sulfur. In this region, the spectrum of $(nC_8H_{17})_2S_5$ is characterized by three peaks at 435, 459, and 493 cm^{-1}, and a shoulder at 505 cm^{-1}. The heptasulfane spectrum features four lines at 429, 445, 470, and 495 cm^{-1}, and a shoulder at 463 cm^{-1}. The Raman spectrum of $(nC_8H_{17})_2S_9$ features medium to strong lines at 423, 437, 463, and 494 cm^{-1}, with shoulders at 452 and 472 cm^{-1}. All these lines must stem from SS stretching modes as the Raman spectrum of *n*-octanethiol does not feature any lines in this region (see Figure 2). The number of lines in the region 400–510 cm^{-1} is smaller than the expected number of SS stretching modes of **1**–**3**, indicating that there must be some coincidental degeneracies.

In view of the low freezing points of these liquid polysulfanes, no mesogenic properties were to be expected near room temperature. All three compounds solidify as glasses on rapid cooling to –70 °C.

Aromatic Polysulfanes

Chain-Like Heptasulfanes[20]

The 2-naphthyl and 4-chlorophenyl groups have previously been used in the preparation of relatively stable sulfur-rich derivatives, from which it can be concluded that these residues stabilize either sterically or electronically the thermodynamically unstable sulfur compounds. Since the corresponding sulfenyl chlorides are readily available,[21] we have prepared bis(2-naphthyl)heptasulfane **4** and bis(4-chlorophenyl)heptasulfane **5** by reaction with titanocene pentasulfide (Equation 12).

$$2\ RSCl + [Cp_2TiS_5] \rightarrow R_2S_7 + [Cp_2TiCl_2] \quad (12)$$

These reactions were carried out at 20 °C in carbon disulfide solution; **4** was obtained as a pale-yellow powder in 51% yield, while **5** formed lemon-yellow microcrystals (44% yield). Despite the bulky substituents, these compounds are characterized by relatively low melting points of 55 °C (**4**) and 40 °C (**5**). Reversed-phase HPLC analyses of the rapidly quenched melts did not reveal the presence of any decomposition products. However, when the heptasulfanes were heated to twice the melting temperatures (110 °C and 80 °C, respectively) for 5 min., the naphthyl derivative decomposed to give a mixture of polysulfanes R_2S_n with up to 11 sulfur atoms, while the chlorophenyl derivative produced a similar series of homologous sulfanes with 3–12 sulfur atoms. As mentioned above, such homologous series can be analysed by the systematic increase of the retention

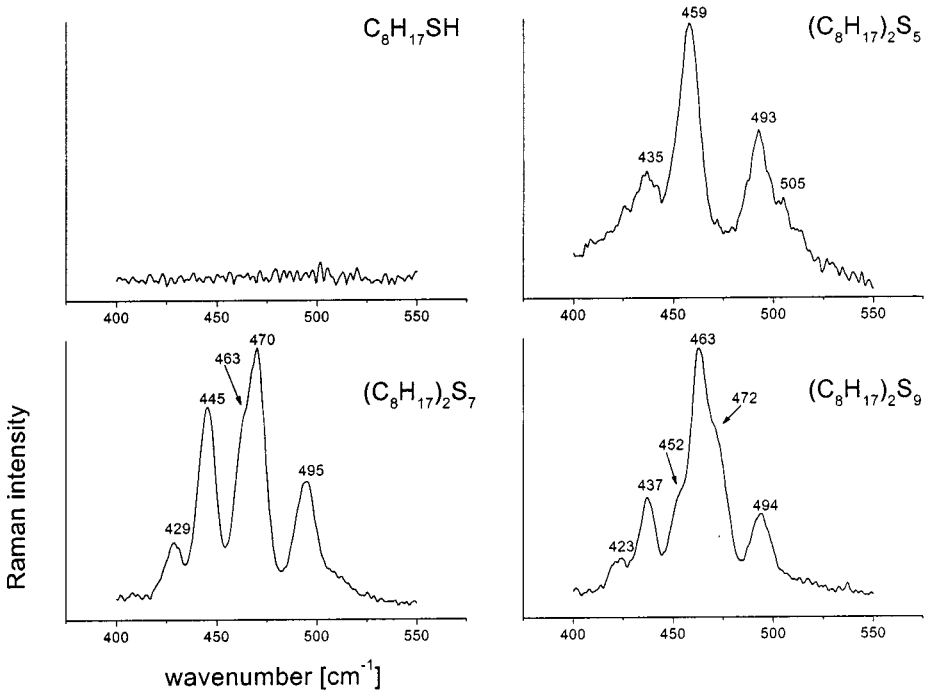


Figure 2. Raman spectra of *n*-octanethiol and of the bis(*n*-octyl)polysulfanes $(nC_8H_{17})_2S_n$ (n = 5, 7, 9) in the range 400–550 cm^{-1}

time with increasing number n_S of sulfur atoms. The retention index *RS* is a linear function of n_S and the following data were determined using methanol as an eluent:

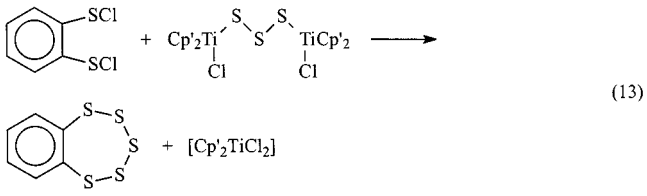
$RS = a + bn_S$
4: n_S = 2–11, a = 517, b = 69
5: n_S = 2–12, a = 382, b = 67

The linear correlation coefficients were better than 0.999.

Both heptasulfanes were found to be well-soluble in carbon disulfide and in chlorinated aliphatic hydrocarbons. They may be stored for long periods at 4 °C without decomposition, but slow decomposition occurs at 20 °C. HPLC analysis, mass spectrometry, as well as infrared, Raman, ^{1}H- and ^{13}C-NMR spectroscopic data confirmed the identities and purities of **4** and **5**. Their low melting points can be explained as follows. The torsion angle at SS bonds is usually about 90°, but may be positive or negative (enantiomeric forms). A chain with six SS bonds can therefore theoretically exist as $2^6 = 64$ conformational isomers. It has previously been shown that many of these conformers will be of almost identical energy.[22] However, in crystals of polysulfanes usually only one conformer is found.[1] It therefore seems reasonable to assume that only a single conformation of the CSSSSSSSC chain is present in solid **4** and **5**, while several conformations will be present in their melts, thus resulting in a strong increase in entropy. The melting temperature T_m and the melting entropy ΔS_m are inversely related to each other, with the melting enthalpy as an additional factor: $T_m = \Delta H_m/\Delta S_m$. Therefore, long chain-like polysulfanes are either liquid at 20 °C or have melting points only slightly above ambient temperature.

Cyclic Polysulfanes

The titanocene complex $[(Cp'_2TiCl)_2S_3]$ reacts with 1,2-benzenebis(sulfenyl chloride), prepared by chlorination of 1,2-benzenedithiol, at low temperatures in carbon disulfide solution to yield the known yellow 1,2,3,4,5-benzopentathiepin **6** (Equation 13).



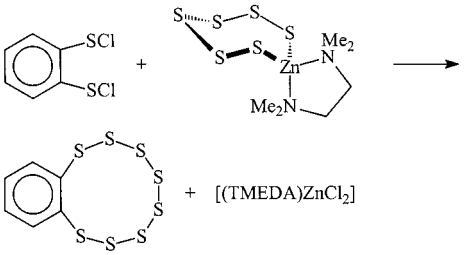
(13)

Compound **6** was first synthesized by Fehér and Langer[23] by condensation of 1,2-benzenedithiol $C_6H_4(SH)_2$ with dichlorotrisulfane S_3Cl_2. It was obtained in a yield of just 50% and was seemingly not very pure since the reported melting point of 65–66 °C differs substantially from our measurements. Our product was analytically, chromatographically, and spectroscopically pure and was found to melt at 58 °C. It was recovered in 73% yield. In 1979, Fehér and Engelen determined the molecular and crystal structure of **6**,[24] and in 1984 Chenard and Miller reported a new synthesis of **6** from 1,2-benzothiadiazole and elemental sulfur in the presence of DABCO at 160–185 °C (yield 54%).[25] The melting point of **6** measured by these authors was 58–60 °C, which agrees well with our findings.

Under similar conditions as those used to generate **6**, 1,2-benzenebis(sulfenyl chloride) was found to react with titanocene pentasulfide to yield the novel 1,2,3,4,5,6,7-benzoheptathionin **7**, which was obtained in 83% yield as a yellow solid with m.p. 107 °C (Equation 14).

$$1,2\text{-}C_6H_4(SCl)_2 + [Cp_2TiS_5] \rightarrow 1,2\text{-}C_6H_4S_7 + [Cp_2TiCl_2] \qquad (14)$$

The new octasulfane 1,2,3,4,5,6,7,8-benzooctathiecin **8**, a yellow solid with m.p. 73 °C, was obtained in 60% yield following reaction of the zinc hexasulfido chelate complex $[(TMEDA)ZnS_6]$ [26] with 1,2-benzenebis(sulfenyl chloride) in carbon disulfide at ambient temperature (Equation 15; TMEDA = tetramethylethylenediamine).



(15)

The number of sulfur atoms in these cyclic polysulfides can again be assessed by reversed-phase HPLC, since there is a linear relationship between the number of sulfur atoms in the ring and the logarithm of the capacity factor (not shown). The ^{1}H-NMR spectra of **6**–**8** each feature an AA′BB′ system, which is centered at δ = 7.61 for the C_2S_5 ring, at δ = 7.63 for the C_2S_7 ring, and at δ = 7.59 for the C_2S_8 ring. The ^{13}C-NMR spectra feature only three signals in the expected region. The infrared spectra are all very similar, in line with expectation. They are dominated by a very strong absorption near 750 cm^{-1}, which is typical for 1,2-substituted benzene rings. More interesting are the Raman spectra, which show the SS stretching modes between 400 and 520 cm^{-1} (see Figure 3). The three heterocycles each exhibit a distinct pattern of SS stretching modes. In the relevant region, the spectrum of the benzopentathiepin features four lines at 418, 429, 467, and 490 cm^{-1}, that of the benzoheptathionine features five lines at 436, 451, 471, 495, and 518 cm^{-1} and a shoulder at 480 cm^{-1}, while that of the benzooctathiocene is characterized by six lines at 416, 428, 438, 460, 467, and 512 cm^{-1} with shoulders at 476 and 515 cm^{-1}.

The crystal structure of $C_6H_4S_7$ was determined by single-crystal X-ray diffraction analysis. The crystals were found to be orthorhombic with four molecules in the unit cell and a density of 1.765 g cm^{-3} at 20 °C. The molecules have C_s symmetry (Figure 4). The crystallographic mirror plane passes through the center of the C3–C3′ bond and contains S4.

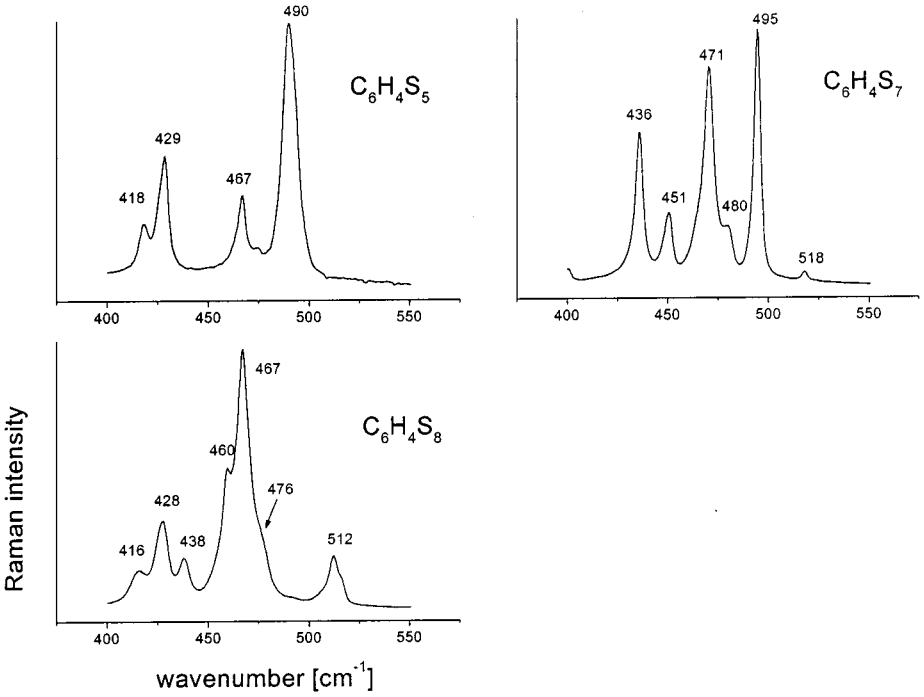


Figure 3. Raman spectra of the solid 1,2-benzenepolysulfanes $C_6H_4S_n$ (n = 5, 7, and 8) at 20 °C in the range 400–550 cm^{-1}

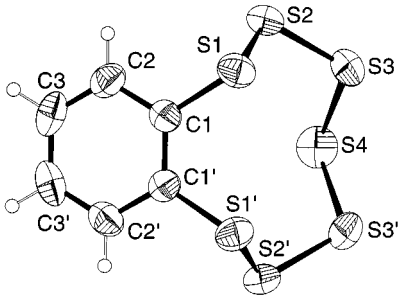


Figure 4. Structure of the 1,2-$C_6H_4S_7$ molecule in the crystal (PLATON plot)

Table 2. Selected bond lengths [pm], valence angles [°], and torsion angles [°] for $C_6H_4S_7$ (symmetry transformations used to generate equivalent atoms: $' = x, -y + 1/2, z$)

S(1)−S(2)	205.02(14)	S(1)–S(2)–S(3)	108.20(6)
S(2)−S(3)	203.73(13)	S(2)–S(3)–S(4)	109.66(6)
S(3)−S(4)	205.73(13)	S(3)–S(4)–S(3′)	103.76(8)
		C(1)–S(1)–S(2)	101.04(11)
S(1)−C(1)	177.0(3)	C(1′)–C(1)–S(1)	121.67(10)
C(1)−C(1′)	138.3(6)	C(1′)–C(1)–C(2)	119.4(2)
C(1)−C(2)	139.2(5)	C(2)–C(1)–S(1)	118.9(2)
C(2)−C(3)	136.9(5)	C(1)–C(2)–C(3)	120.6(3)
C(3)−C(3′)	138.2(8)	C(2)–C(3)–C(3′)	120.0(2)
C(1)–S(1)–S(2)–S(3)	103.60(12)	S(2)–S(1)–C(1)–C(2)	66.5(3)
S(1)–S(2)–S(3)–S(4)	–84.73(7)	C(1′)–C(1)–C(2)–C(3)	2.0(4)
S(2)–S(3)–S(4)–S(3′)	110.18(7)	S(1)–C(1)–C(2)–C(3)	180.0(3)
S(2)–S(1)–C(1)–C(1′)	–115.57(7)	C(1)–C(2)–C(3)–C(3′)	–2.0(4)

Selected internuclear distances, bond angles, and torsion angles are listed in Table 2.

The geometrical parameters show the expected values with an arithmetic mean of 138.1 pm for the CC bonds and an average of 204.8 pm for the SS bonds. The latter value is identical to the average bond length in S_8. There is a slight alternation in the SS bond lengths in **7**: d(S1−S2) = 205.0(1), d(S2−S3) = 203.7(1), and d(S3−S4) = 205.7(1) pm. The conformations of sulfur homocycles and sulfur-rich heterocycles can best be characterized by the *motif*, which describes the order of the signs of the torsion angles around the ring. The motif for the C_2S_7 heterocycle is +-+-0+-+-, with a value of zero at the carbon–carbon bond. Such a motif has not previously been observed for any nine-membered heterocycle of the type C_xS_y. The absolute values of the torsion angles at the SS bonds lie between 85° and 110° (see Table 2).

Conclusions

We have shown that sulfur-rich organic polysulfanes can be prepared in good yield not only from titanocene polysulfido complexes, but also from the relatively new zinc hexasulfido complex, despite the presence of the amine TMEDA. Normally, amines catalyze the decomposition of thermodynamically unstable polysulfur compounds. The novel bis(*n*-octyl)polysulfanes described here, which consist of chains of more than 20 non-hydrogen atoms, do not form mesogenic phases at ambient temperature since their freezing temperatures are quite low. These chains most probably have a random coil conformation rather than a straight chain structure in the liquid phase and therefore the materials solidify as glasses. The chain-like polysulfanes bearing aromatic substituents are solids at 20 °C, even when the sulfur chain is quite long. Most probably, they exist as *a single* conformer in the solid state, but as many rotational isomers in the liquid state, leading to a high melting entropy and hence to a depression of the melting temperature. Once

again, we have observed that the homologous members of the series R_2S_n with n = 2–12 exhibit a systematic increase in their reversed-phase HPLC retention times with increasing number of sulfur atoms.

Experimental Section

General: The reactions were carried out under exclusion of moisture using carefully dried solvents. The chromatographic system used has been described previously.[11] Octadecylsilane (C18) was used as a stationary phase throughout. The following spectrometers were used: Nicolet Magna 750 FT-IR spectrometer (using KBr or CsCl sample discs); Bruker RFS 100 FT Raman spectrometer, equipped with an Nd-YAG laser (1064 nm); Bruker ARX 200 and ARX 400 NMR spectrometers.

Synthesis of Bis(*n*-octyl)pentasulfane (1): *n*-Octylsulfenyl chloride was first prepared by chlorination of the corresponding thiol with one equivalent of sulfuryl chloride in dichloromethane at 0 °C according to standard procedures. At –70 °C, a solution of the sulfenyl chloride (0.181 g, 1 mmol) in CS_2 (25 mL) was added dropwise over a period of 1 h to a solution of $[(Cp'_2TiCl)_2S_3]$ (0.290 g, 0.5 mmol) in CS_2 (25 mL), which resulted in a color change from dark-green to light-red. The reaction mixture was allowed to warm to 20 °C, the volume was reduced to one-half of the original, and then the concentrated solution was cooled to –50 °C for several hours. The precipitated $[Cp'_2TiCl_2]$ was filtered off. This procedure (partial evaporation of the solvent and subsequent cooling) was repeated until no more titanocene dichloride was precipitated. The remaining solvent was then completely removed under reduced pressure yielding the liquid product. Yield: 0.193 g (quantitative); freezing temp. –66 to –68 °C. – $C_{16}H_{34}S_5$ (386.8): calcd. C 49.7, H 8.9, S 41.5; found C 50.8, H 8.2, S 40.4. – UV/Vis (methanol): λ_{max} (%) = 216 nm (100), 292 (sh). – MS (120 °C): *m*/*z* (%) = 386 (23) [M^+], 322 (100). – ^{1}H NMR (200 MHz, $CDCl_3$): δ = 2.99 (t, 4 H), 1.78 (tt, 4 H), 1.45–1.29 (br. s, 20 H), 0.89 (t, 6 H). – $^{13}C\{^1H\}$ NMR (50 MHz, $CDCl_3$): δ = 39.9, 31.8, 29.1, 29.1, 28.8, 28.4, 22.6, 14.1. – Raman (80 mW, 20 °C): $\tilde{\nu}$ = 505 cm^{-1} (SS), 493 (SS), 459 (SS), 435 (SS).

Synthesis of Bis(*n*-octyl)heptasulfane (2) and -nonasulfane (3): To a stirred solution of $[Cp_2TiS_5]$ (0.846 g, 2.5 mmol) in CS_2 (30 mL) at –20 °C (**2**) or at –70 °C (**3**), a solution of *n*-octylsulfenyl chloride (0.904 g, 5 mmol) or *n*-octylchlorodisulfane (1.064 g, 5 mmol) in CS_2 (40 mL) was added dropwise. [The chlorodisulfane, a yellow viscous liquid, had been prepared from the thiol (10 mmol) and SCl_2 (12 mmol) in CH_3OtBu at –70 to +20 °C]. The color turned from dark-red to light-red. The precipitated $[Cp_2TiCl_2]$ was removed by filtration at 20 °C in the case of **2** and at –20 °C in the case of **3** and the filtrate was concentrated to one-half of its original volume. After cooling to –50 °C for several hours, the precipitated $[Cp_2TiCl_2]$ was filtered off. On complete removal of the solvent under reduced pressure, the liquid polysulfane was obtained. Yield: 1.127 g of the heptasulfane or 1.290 g of the nonasulfane (both quantitative). – **2:** freezing temp. –61 °C. – $C_{16}H_{34}S_7$ (450.9): calcd. C 42.6, H 7.6, S 49.8; found C 43.3, H 7.8, S 48.0. – UV/Vis (methanol): λ_{max} (%) = 226 nm (100), 300 (sh). – MS (160 °C): *m*/*z* (%) = 450 (1) [M^+], 418 (7) [M^+ – S], 386 (10) [M^+ – 2S], 322 (100) [M^+ – 4S]. – ^{1}H NMR (200 MHz, $CDCl_3$): δ = 3.00 (t, 4 H), 179 (tt, 4 H), 1.46–1.29 (br. s, 20 H), 0.90 (t, 6 H). – ^{13}C NMR (50 MHz, $CDCl_3$): δ = 39.8, 31.8, 29.1, 29.1, 28.9, 28.4, 22.6, 14.1. – Raman (40 mW, –135 °C): $\tilde{\nu}$ = 429 cm^{-1} (SS), 445 (SS), 463 (SS), 470 (SS), 495 (SS). – **3:** freezing temp. –53 °C. – $C_{16}H_{34}S_9$ (515.1): calcd. C 37.3, H 6.7, S 56.0; found C 37.7, H 6.4, S 56.3. – UV/Vis (methanol): λ_{max} (%) = 228 nm (100), 284 (sh). – MS (160 °C): *m*/*z* (%) = 450 (0.2) [M^+ – 2S], 418 (2) [M^+ – 3S], 386 (4) [M^+ – 4S], 145 (100) [$C_8H_{17}S$]. – ^{1}H NMR (200 MHz, $CDCl_3$): δ = 3.01 (t, 4 H), 1.79 (tt, 4 H), 1.47–1.29 (br. s, 20 H), 0.90 (t, 6 H). – ^{13}C NMR (50 MHz, $CDCl_3$): δ = 39.8, 31.8, 29.1, 28.9, 28.4, 22.6, 14.1. – Raman (40 mW, –135 °C): $\tilde{\nu}$ = 423 cm^{-1} (SS), 437 (SS), 452 (SS), 463 (SS), 472 (SS), 494 (SS).

Synthesis of Bis(2-naphthyl)heptasulfane (4): To a stirred solution of $C_{10}H_7SCl$ (0.29 g, 1.49 mmol) in CS_2 (40 mL), $[Cp_2TiS_5]$ (0.25 g, 0.74 mmol) was added at 20 °C under an N_2 atmosphere. After the color had changed to orange-red, the precipitated $[Cp_2TiCl_2]$ was filtered off and the filtrate was stirred with a few mg of silica gel to bind residual titanocene dichloride. After filtration, the solvent was evaporated to leave a yellow oil, which was dissolved in a small volume of CH_2Cl_2. A little *n*-hexane was added and the mixture was concentrated until some turbidity appeared. It was then cooled to –50 °C, which led to the deposition of crystals of **4**. The collected crystals were washed with *n*-hexane and dried to give **4** as a yellow powder, m.p. 55–58 °C; yield 0.18 g (51%). – $C_{20}H_{14}S_7$ (478.8): calcd. C 50.2, H 3.0, S 46.9; found C 50.1, H 3.1, S 45.3. – UV/Vis (methanol): λ_{max} (%) = 222 nm (92), 233 (97), 236 (100), 240 (98), 281 (34), 334 (14). – MS (210 °C): *m*/*z* (%) = 446 (0.3) [M^+ – S], 115 (100) [C_9H_7]. – ^{1}H NMR (200 MHz, CD_2Cl_2): δ = 8.09 (d), 7.83 (m), 7.68 (dd), 7.53 (m). – ^{13}C NMR (50 MHz, CD_2Cl_2): δ = 127.0, 127.5, 127.8, 127.8, 129.3, 129.9, 133.0, 133.1, 133.4. – Raman (40 mW; 20 °C): $\tilde{\nu}$ = 394 cm^{-1} (m), 417 (sh), 430 (vs), 441 (s), 473 (vs), 505 (sh), 511 (s), 521 (m).

Synthesis of Bis(4-chlorophenyl)heptasulfane (5): To a stirred solution of $[Cp_2TiS_5]$ (1.00 g, 2.96 mmol) in CS_2 (70 mL), ClC_6H_4SCl (1.06 g, 5.91 mmol) was added at 20 °C. After 5 min., the color had changed to orange and the precipitated $[Cp_2TiCl_2]$ was filtered off. A few mg of silica gel was added to the filtrate to bind residual titanocene dichloride. After stirring for a few min., the solution was filtered, the filtrate was concentrated to a volume of 5 mL, and then *n*-pentane (10 mL), MTB ether (15 mL), and ethanol (15 mL) were added. The solvents were then evaporated until the solution became turbid. Cooling of the solution to –78 °C led to the deposition of crystals of **5** (m.p. 40 °C), which were filtered off, washed with *n*-pentane, and dried in air; yield 0.58 g (44%). – $C_{12}H_8Cl_2S_7$ (447.6): calcd. C 32.2, H 1.8, S 50.2; found C 32.3, H 1.7, S 50.2. – UV/Vis (methanol): λ_{max} (%) = 211 nm (93), 240 (100), 292 (30), 327 (23). – MS (160 °C): *m*/*z* (%) = 418 (0.2), 414 (0.4) [M^+ – S], 382 (2) [M^+ – 2S], 175 (100) [$C_6H_4ClS_2$]. – ^{1}H NMR (200 MHz, CD_2Cl_2): δ = 7.57 (dm, 4 H), 7.36 (dm, 4 H). – ^{13}C NMR (50 MHz, CD_2Cl_2): δ = 129.5, 132.0, 134.4, 135.0. – Raman (40 mW; 20 °C): $\tilde{\nu}$ = 376 cm^{-1} (m), 419 (w), 435 (vs), 456 (vw), 473 (vs), 509 (m), 541 (m).

Synthesis of 1,2,3,4,5-Benzopentathiepin (6): To a stirred solution of $[(Cp'_2TiCl)_2S_3]$ (0.150 g, 0.259 mmol) in CS_2 (40 mL) at –78 °C, a solution of 1,2-benzenebis(sulfenyl chloride) (0.055 g, 0.259 mmol) in CS_2 (40 mL) was added dropwise over a period of 20 min. [The bis(sulfenyl chloride) had been prepared by chlorination of the corresponding dithiol using elemental chlorine in CCl_4 at 0 °C]. On warming the reaction mixture to ambient temperature, the color changed from dark-green to light-red. After filtering off the precipitated $[Cp'_2TiCl_2]$, the filtrate was concentrated to one-quarter of its original volume and the mixture was cooled to –55 °C for several hours. After another filtration, the solvent was completely removed under reduced pressure. The yellow crude product was recrystallized from a mixture of CS_2 and CH_3OtBu (1:1). Yield: 0.045 g (73%); m.p. 58 °C. – $C_6H_4S_5$ (236.4): calcd. C

30.4, H 1.7, S 67.7; found C 30.3, H 1.4, S 66.1. – UV/Vis (methanol): λ_{max} (%) = 223 nm (100), 272 (sh), 314 (sh). – MS (88 °C): *m/z* (%) = 236 (16) [M^+], 172 (100) [$M^+ - S_2$]. – ^{1}H NMR (200 MHz, CD_2Cl_2): δ = 7.85 (m, 2 H), 7.36 (m, 2 H). – ^{13}C NMR (50 MHz, $CDCl_3$): δ = 143.8, 135.8, 129.6. – Raman (150 mW, 20 °C): $\tilde{\nu}$ = 418 cm^{-1} (SS), 428 (SS), 467 (SS), 490 (SS).

Synthesis of 1,2,3,4,5,6,7-Benzoheptathionin (7): The synthesis was carried out in analogy to the preparation of **4** starting from [Cp_2TiS_5] (0.8 g, 2.37 mmol) in CS_2 (150 mL) and 1,2-benzenebis(sulfenyl chloride) (0.5 g, 2.37 mmol) in CS_2 (50 mL). Yield: 0.59 g (83%); m.p. 107 °C. – $C_6H_4S_7$ (300.6): calcd. C 24.0, H 1.3; found C 24.2, H 1.1. – UV/Vis (methanol): λ_{max} (%) = 218 nm (100), 295 (sh). – MS (149 °C): *m/z* (%) = 300 (2) [M^+], 172 (100) [$C_6H_4S_3$]. – ^{1}H NMR (200 MHz, CD_2Cl_2): δ = 7.77 (m, 2 H), 7.48 (m, 2 H). – ^{13}C NMR (50 MHz, $CDCl_3$): δ = 137.9, 135.2, 131.3. – Raman (150 mW, 20 °C): $\tilde{\nu}$ = 436 cm^{-1} (SS), 451 (SS), 471 (SS), 495 (SS), 518 (SS).

Synthesis of 1,2,3,4,5,6,7,8-Benzooctathiecin (8): To a stirred solution of [(TMEDA)ZnS_6] (0.326 g, 0.94 mmol) in CS_2 (30 mL), a solution of 1,2-benzenebis(sulfenyl chloride) (0.2 g, 0.94 mmol) in CS_2 (20 mL) was added dropwise over a period of 30 min. After stirring for 1 h, the precipitated [(TMEDA)$ZnCl_2$] was filtered off and the solvent was removed completely from the filtrate. The crude yellow oil was crystallized from a mixture of CS_2 and MTB ether (1:1). Yield: 0.19 g (60%); m.p. 73 °C. – $C_6H_4S_8$ (332.6): calcd. C 21.7, H 1.2; found C 21.2, H 0.9. – UV/Vis (methanol): λ_{max} (%) = 213 nm (100), 235 (sh), 318 (sh). – MS (120 °C): *m/z* (%) = 332 (1) [M^+], 172 (100) [$C_6H_4S_3$]. – ^{1}H NMR (200 MHz, CD_2Cl_2): δ = 7.74 (m, 2 H), 7.43 (m, 2 H). – ^{13}C NMR (50 MHz, $CDCl_3$): δ = 139.4, 133.9, 129.8. – Raman (150 mW, 20°C): $\tilde{\nu}$ = 416 cm^{-1} (SS), 428 (SS), 438 (SS), 460 (SS), 467 (SS), 512 (SS).

Table 3. Crystal data and structure refinement for $C_6H_4S_7$

Empirical formula	$C_6H_4S_7$
Formula weight	300.51
Temperature [K]	293(2)
Wavelength [Å]	0.71073
Crystal system	orthorhombic
Space group	*Pnma*
Z	4
a [Å]	17.7990(7)
b [Å]	13.2422(6)
c [Å]	4.7990(2)
V [Å^3]	1131.11(8)
D (calcd.) [g cm^{-3}]	1.765
μ [mm^{-1}]	1.342
Crystal size [mm]	0.3 × 0.08 × 0.08
2θ range [°]	4.58–55.00
Index ranges	*h* ±22, *k* +17, *l* ±6
Collected reflections	7947
Independent reflections	1358 (R_{int} = 0.0625)
Obsd. with $I > 2\sigma(I)$	916
Data/restraints/parameters	1358/0/61
Goodness-of-fit on F^2	1.119
R_1 [$I > 2\sigma(I)$]	0.0507
R_1 (all data)	0.0889
Largest diff. peak/hole [eÅ^{-3}]	0.425/–0.229

Crystallography: Crystals were obtained by dissolving **7** in carbon disulfide and adding *n*-hexane until the mixture became turbid. On cooling this mixture to 4 °C, crystals separated. Diffraction measurements were made at room temperature using a Siemens SMART CCD diffractometer (Mo-K_α radiation, 10 s per frame, 0.3° ω-scan increments, specimen–detector distance 3 cm). Preliminary lattice constants were obtained from 45 orientation frames and final unit cell dimensions by refinement of the reflections obtained from all frames. The compound crystallizes in the space group *Pnma* (no. 62). An empirical absorption correction (SADABS[27]) was performed. Structure solution and refinement were performed using SHELXTL.[28] H atom positions were calculated assuming trigonal-planar coordination of C atoms with C–H distances of 93 pm and were refined as riding on the C atoms with isotropic temperature factors 1.2$U_{equiv.}$ of the corresponding C atoms. A summary of data collection and refinement is given in Table 3. Crystallographic data (excluding structure factors) have been deposited with the Cambridge Crystallographic Data Centre as supplementary publication no. CCDC-136074. Copies of the data can be obtained free of charge on application to the CCDC, 12 Union Road, Cambridge CB2 1EZ, U.K. [Fax.: (internat.) +44 (0)1223 336033; E-mail: deposit@ccdc.cam.ac.uk].

Acknowledgments

This work was supported by the Deutsche Forschungsgemeinschaft and the Verband der Chemischen Industrie.

[1] Review: R. Steudel, M. Kustos, *Encyclopedia of Inorganic Chemistry* (Ed.: B. King), Vol. 7, J. Wiley, Chichester, **1994**, pp. 4009–4038.
[2] R. Steudel, *Top. Curr. Chem.* **1982**, *102*, 149–176.
[3] R. Steudel, in *The Chemistry of Inorganic Ring Systems* (Ed.: R. Steudel), Chapt. 13, Elsevier Science Publ., Amsterdam, **1992**, pp. 233–253.
[4] R. Steudel, M. Kustos, M. Pridöhl, U. Westphal, *Phosphorus, Sulfur, Silicon* **1994**, *93/94*, 61–72.
[5] R. Steudel, M. Kustos, V. Münchow, U. Westphal, *Chem. Ber.* **1997**, *130*, 757–764.
[6] H. W. Roesky, H. Zamankhan, J. W. Bats, H. Fuess, *Angew. Chem.* **1980**, *92*, 122; *Angew. Chem. Int. Ed. Engl.* **1980**, *19*, 125.
[7] R. Steudel, M. Pridöhl, J. Buschmann, P. Luger, *Chem. Ber.* **1995**, *128*, 725–728.
[8] H. Schmidt, R. Steudel, *Z. Naturforsch. Part B* **1990**, *45*, 557–558.
[9] M. Kustos, J. Pickardt, J. Albertsen, R. Steudel, *Z. Naturforsch. Part B* **1993**, *48*, 928–934.
[10] R. Steudel, M. Kustos, *Phosphorus, Sulfur, Silicon* **1991**, *62*, 127–137.
[11] R. Steudel, V. Münchow, J. Pickardt, *Z. Anorg. Allg. Chem.* **1996**, *622*, 1594–1600.
[12] R. Steudel, M. Kustos, A. Prenzel, *Z. Naturforsch. Part B* **1997**, *52*, 79–82.
[13] M. Kustos, R. Steudel, *J. Org. Chem.* **1995**, *60*, 8056–8061.
[14] A. K. Verma, T. B. Rauchfuss, *Inorg. Chem.* **1995**, *34*, 6199.
[15] R. Steudel, O. Schumann, J. Buschmann, P. Luger, *Angew. Chem.* **1998**, *110*, 2502–2504; *Angew. Chem. Int. Ed.* **1998**, *37*, 2377–2378.
[16] For more details, see O. Schumann, Doctoral Dissertation, Techn. Univ. Berlin, **1999**.
[17] R. Steudel, S. Förster, J. Albertsen, *Chem. Ber.* **1991**, *124*, 2357–2359.
[18] R. Steudel, E.-M. Strauss, D. Jensen, *Z. Naturforsch. Part B* **1990**, *45*, 1282–1290.
[19] A. H. Otto, R. Steudel, *Eur. J. Inorg. Chem.* **1999**, 2057–2061.
[20] For more details, see V. Münchow, Doctoral Dissertation, Techn. Univ. Berlin, **1996**.
[21] T. Zincke, K. Eismayer, *Ber. Dtsch. Chem. Ges.* **1918**, *51*, 751. E. Gebauer-Fülnegg, *J. Am. Chem. Soc.* **1927**, *49*, 2270.
[22] Y. Drozdova, K. Miaskiewicz, R. Steudel, *Z. Naturforsch. Part B* **1995**, *50*, 889–893.
[23] F. Fehér, M. Langer, *Tetrahedron Lett.* **1971**, *24*, 2125.
[24] F. Fehér, B. Engelen, *Z. Anorg. Allg. Chem.* **1979**, *452*, 37.
[25] B. L. Chenard, T. J. Miller, *J. Org. Chem.* **1984**, *49*, 1221.

[26] A. K. Verma, T. B. Rauchfuss, S. R. Wilson, *Inorg. Chem.* **1995**, *34*, 3072.
[27] G. M. Sheldrick, *SADABS*, University of Göttingen, Germany, **1996**.
[28] G. M. Sheldrick, *SHELXTL Software Reference Manual*, version 5.1, Bruker AXS Inc., Madison, Wisconsin, USA, **1997**.
Received October 19, 1999
[I99372]

Cationic *ansa*-(η^5-Cyclopentadienyl)(η^6-arene) Complexes of Titanium[+]

Patrick J. W. Deckers,[a] Arjan J. van der Linden,[b] Auke Meetsma,[a] and Bart Hessen*[a]

Keywords: Titanium / Cyclopentadienes / Arene complexes / Cations / Bridging ligands

The half-sandwich titanium trimethyl complex (η^5-$C_5H_4CMe_2Ar$)$TiMe_3$ (Ar = 3,5-$Me_2C_6H_3$) reacts with the Lewis acid $B(C_6F_5)_3$ to give the ionic Ti^{IV} *ansa*-cyclopentadienyl-arene complex [(η^5,η^6-$C_5H_4CMe_2Ar$)$TiMe_2$]-[$MeB(C_6F_5)_3$]. In bromobenzene solvent, addition of more $B(C_6F_5)_3$ leads to C_6F_5/Me exchange and, subsequently, to formation of an unusual dimeric Ti^{III} dicationic species, {[(η^5,η^6-$C_5H_4CMe_2Ar$)Ti(μ-Br)]$_2$}[$B(C_6F_5)_4$]$_2$, which was structurally characterized. Its formation involves reduction of the transition-metal center, solvent C–Br cleavage and perfluoroaryl-group scrambling.

Introduction

Cationic titanium half-sandwich (mono-cyclopentadienyl) species show interesting catalytic activity, especially in the syndiotactic polymerization of styrene[1] and the polymerization of propene to high molecular weight atactic polypropene.[2] There has been some debate in the literature about the nature of the actual active species in these systems, e.g. whether Ti^{IV} or Ti^{III} species are involved, or both.[3] As the cationic species [(η^5-C_5R_5)$TiMe_2$]$^+$ are highly electron-deficient we sought ways of stabilizing these, without resorting to strong heteroatom-based Lewis basic moieties, in order to study their reactive properties. Baird et al. found that [(η^5-C_5Me_5)MMe_2]$^+$ cations (M = Ti, Zr, Hf) can bind arenes reversibly,[4] and that this interaction is significantly stronger for Zr and Hf (for which a related crystal structure has been reported[5]) than for Ti. We thus set out to prepare half-sandwich titanium complexes with benzyl-substituted Cp-ligands to use these interactions in an intramolecular fashion. The feasibility of this was suggested by observations of Chien, Rausch et al. on the [η^5-$C_5Me_4(CH_2CH_2Ph)$]$TiMe_3$ + [Ph_3C][$B(C_6F_5)_4$] system, where NMR evidence was obtained for η^6-coordination of the arene moiety in the thermally labile cationic dimethyl species.[6] In this contribution we describe the synthesis of neutral and cationic titanium complexes with the benzyl-substituted cyclopentadienyl ligand [$C_5H_4CMe_2Ar$]$^-$ (Ar = 3,5-dimethylphenyl).

The cationic *ansa*-cyclopentadienyl-arene complex [(η^5,η^6-$C_5H_4CMe_2Ar$)$TiMe_2$][$MeB(C_6F_5)_3$] was found to be quite stable in bromobenzene solution at ambient temperature, but it reacts with the Lewis acid $B(C_6F_5)_3$ via Me/C_6F_5 scrambling. This species subsequently undergoes a highly unusual transformation, resulting in a dicationic dimeric Ti^{III} complex. The crystal structure of this product represents the first structural characterization of an *ansa*-cyclopentadienyl-arene early transition-metal compound.

Results and Discussion

The synthesis of the benzyl-cyclopentadienyl salt Li[$C_5H_4CMe_2Ar$] (Ar = 3,5-dimethylphenyl) is straightforward, proceeding through addition of ArLi (obtained from ArBr and *n*BuLi) to 6,6-dimethylfulvene, analogous to the preparation of Li[$C_5H_4CMe_2Ph$].[7] The 3,5-(dimethyl)-phenyl group was chosen initially to provide a stronger donor interaction (in [Cp*MMe_2(arene)]$^+$ toluene is more strongly bound than benzene[4]) and to make arene cyclometallation[8] less favorable. Reaction of this Li salt with $TiCl_4$ in dichloromethane afforded ($C_5H_4CMe_2Ar$)$TiCl_3$, which was methylated in benzene solvent using Me_2Mg(dioxane) to give the trimethyl derivative ($C_5H_4CMe_2Ar$)$TiMe_3$ (**1**).

In [D_2]-1,1,2,2-tetrachloroethane or [D_5]bromobenzene solvent, **1** reacts with 1 equiv. of the Lewis acid $B(C_6F_5)_3$ to give deep red solutions of a species that was identified by 1D and 2D NMR techniques as the ionic *ansa*-cyclopentadienyl-arene complex [(η^5,η^6-$C_5H_4CMe_2Ar$)$TiMe_2$][$MeB(C_6F_5)_3$] (**2**, Scheme 1).

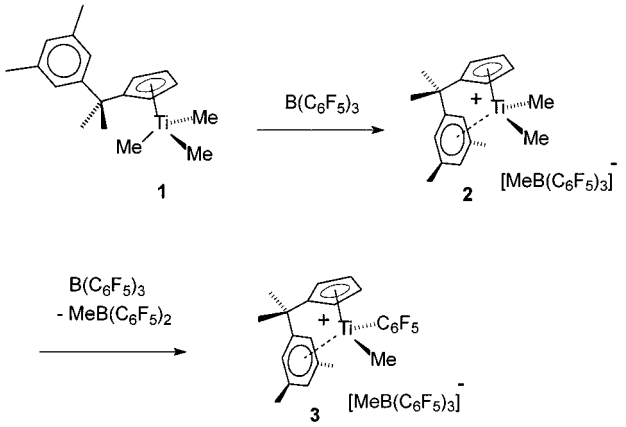
The resonances for the [$MeB(C_6F_5)_3$]$^-$ anion are consistent with those for a noncoordinated anion,[9] and the resonances for the arene moiety show substantial coordination chemical shifts (downfield for *o*-C and *p*-C, upfield for *m*-C; the *o*-H proton resonances are found upfield shifted at δ = 5.91). The chemical shift difference between the two sets of Cp protons also increases strongly ($\Delta\delta$ = 1.59 in **2** and 0.14 in **1**). Compound **2** is a 16-electron complex and does not readily react with propene or styrene at ambient temperature (as seen from NMR-tube-scale experiments). This suggests that the arene moiety is fairly strongly bound. Addition of a drop of [D_8]THF to a C_6D_5Br solution of **2** shows a shift of the Cp and aryl proton resonances back to

[+] Netherlands Institute for Catalysis Research (NIOK) publication no. RUG-99-4-04

[a] Center for Catalytic Olefin Polymerization, Department of Chemistry, University of Groningen,
Nijenborgh 4, NL-9747 AG Groningen, The Netherlands
E-mail: hessen@chem.rug.nl
[b] Shell Research and Technology Centre Amsterdam,
P. O. Box 38000, NL-1030 BN Amsterdam, The Netherlands

Supporting information for this article is available on the WWW under http://www.wiley-vch.de/home/eurjic or from the author.

 © WILEY-VCH Verlag GmbH, D-69451 Weinheim, 2000 1434–1948/00/0505–0929 $ 17.50+.50/0



Scheme 1. Generation of the cationic species **2** and **3**

"normal" chemical shift ranges, indicating release of the arene moiety in the presence of a hard Lewis base to give a $[(\eta^5\text{-}C_5H_4CMe_2Ar)TiMe_2(THF)_x][MeB(C_6F_5)_3]$ species. Compound **2** is reasonably stable in $C_2D_2Cl_4$ or $[D_5]$bromobenzene and only very gradually decomposes at ambient temperature. Solutions of **2**, prepared in situ in $[D_5]$bromobenzene, produced a few deep brown-green crystals upon standing at ambient temperatures for several days (vide infra).

The presence of one equivalent of excess $B(C_6F_5)_3$ in bromobenzene solutions of **2** resulted in a reaction (complete in about 20–24 h at ambient temperature) forming $MeB(C_6F_5)_2$[10] and an organometallic species that, based on NMR spectroscopy, was identified as the mixed methyl/perfluoroaryl species $[(\eta^5,\eta^6\text{-}C_5H_4CMe_2Ar)Ti(C_6F_5)Me][MeB(C_6F_5)_3]$ (**3**, Scheme 1). The ^{19}F NMR spectrum shows a C_6F_5 group with a downfield shifted *o*-F resonance, and the ^{13}C NMR spectrum a triplet with $^3J_{CF} = 7.3$ Hz at $\delta = 102.7$ for the Ti–Me group. These features are consistent with a $Ti(Me)(C_6F_5)$ species.[11] The ^1H NMR resonances of **3** are broad at ambient temperature, but at –30 °C they reveal an asymmetric structure, and the retention of the η^5,η^6-coordination mode of the ancillary ligand. Thus the addition of an extra equivalent of the Lewis acid induces a scrambling of Ti-bound and B-bound hydrocarbyl groups. Upon standing at ambient temperature the solution produces brown-green crystals that (based on lattice parameters) are identical to those that are (more slowly) formed in solutions of **2**.

An X-ray structure determination showed that these crystals are of the salt $\{[(\eta^5,\eta^6\text{-}C_5H_4CMe_2Ar)Ti(\mu\text{-}Br)]_2\}[B(C_6F_5)_4]_2$ (**4**, Figure 1).

In this compound a dicationic dimeric Ti^{III} *ansa*-cyclopentadienyl-arene bromide complex is complemented by two tetrakis(pentafluorophenyl)borate anions. The dication is centrosymmetric, with nearly equivalent Ti–Br bond lengths in the $Ti(\mu\text{-}Br)_2Ti$ bridge. The Ti–Br distances are, on average, 0.085 Å shorter than in the isoelectronic neutral $[(C_5H_4Me)_2Ti(\mu\text{-}Br)]_2$ complex[12] and this, combined with the wider Br–Ti–Br' angle, results in a Ti···Ti distance of 3.7858(9) Å in **4** that is 0.34 Å shorter than in the latter compound. The bend angle of the Cp-arene ligand backbone, C(5)–C(6)–C(7), is quite acute at 95.8(3)°, and the Cp(centroid)–Ti–Ar(centroid) angle is 125.0°. The arene ring does not deviate significantly from planarity, but the bonding to the Ti atom is highly asymmetric, with Ti–C(7), Ti–C(8) and Ti–C(12) being much shorter than the Ti–C(9), –C(10) and –C(11) distances. This results in a slight lengthening of the C(7)–C(8) and C(7)–C(12) bonds relative to the other arene C–C bonds.

The formation of compound **4** is remarkable for at least two reasons: a) the reaction of a Ti^{IV} cation with a Lewis acid in a halogenated solvent yields a Ti^{III} halide species, and b) starting from a cation with the $[MeB(C_6F_5)_3]^-$ counterion, a product is formed with $[B(C_6F_5)_4]^-$ counterions. This indicates that the reaction involves a reduction of the

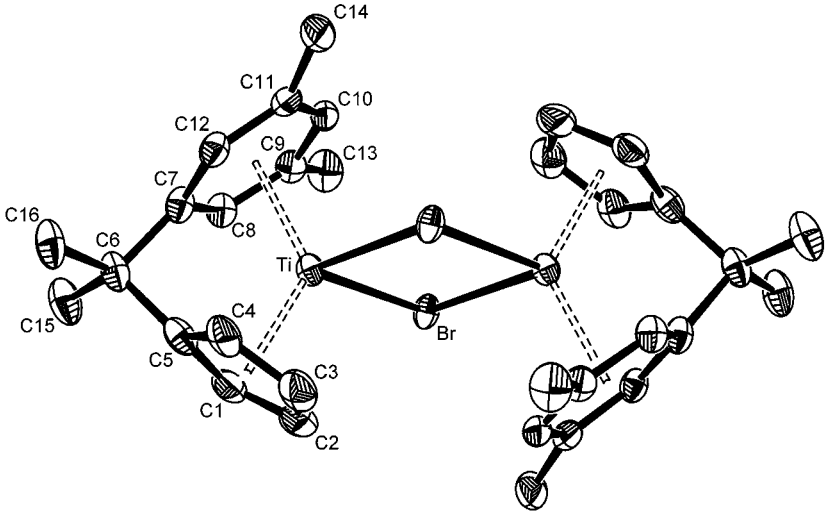


Figure 1. ORTEP diagram of the molecular structure of the cationic part of **4**; hydrogen atoms are omitted for clarity; selected interatomic distances [Å] and angles [°]: Ti–Br 2.6250(7), Ti–Br' 2.6334(7), Ti–C(1) 2.341(4), Ti–C(2) 2.410(5), Ti–C(3) 2.383(5), Ti–C(4) 2.313(4), Ti–C(5) 2.323(3), Ti–C(7) 2.379(3), Ti–C(8) 2.473(4), Ti–C(9) 2.674(4), Ti–C(10) 2.725(3), Ti–C(11) 2.713(4), Ti–C(12) 2.470(4), C(7)–C(8) 1.419(6), C(8)–C(9) 1.393(5), C(9)–C(10) 1.393(6), C(10)–C(11) 1.394(6), C(11)–C(12) 1.395(5), C(7)–C(12) 1.410(6); Br–Ti–Br' 87.90(2), Ti–Br–Ti' 92.10(2), C(5)–C(6)–C(7) 95.8(3), C(15)–C(6)–C(16) 107.6(3)

metal center, cleavage of the solvent C–Br bond, and a scrambling of the substituents on the borane/borate species. In C_6D_5Br solvent, formation of $CH_3C_6D_5$ is seen (GC/MS). The isolated yield of **4** is rather low (18%) and precise reactive pathways in this transformation are, as yet, unclear, but the observations made so far are of interest. For instance, they may shed some light on the way in which Ti^{III} centers can be generated by the reaction of Ti^{IV} alkyls with an excess of Lewis acid activator (note that Grassi et al. use chlorobenzene as solvent for their ESR experiments with Cp^*TiMe_3 and Lewis acids[3b]). It also demonstrates the dynamic nature of perfluoroarylborate "weakly coordinating" anions, in which tetraarylborates may be formed from alkyltriarylborates (an interesting contrast to the aryl abstraction from the $[B(C_6F_5)_4]^-$ anion, recently reported by Bochmann et al.[13]).

In conclusion, we have observed the formation of a cationic *ansa*-Cp-arene titanium dimethyl species, hydrocarbyl ligand scrambling on this species induced by the presence of excess Lewis acid, and a highly unusual degradation of a cationic Ti^{IV} species in bromobenzene to produce a Ti^{III} complex, the first structurally characterized *ansa*-Cp-arene early transition-metal derivative. These observations provide an interesting insight into the possible activation and degradation processes in titanium-based half-sandwich olefin polymerization catalysts, and we are presently studying related hemilabile monocyclopentadienyl Ti^{IV} species to increase our understanding of this chemistry.

Experimental Section

General: All experiments were performed under a nitrogen atmosphere with standard Schlenk and glove-box techniques. Deuterated solvents (Aldrich, Acros) were either degassed and dried over molecular sieves ($C_2D_2Cl_4$, C_6D_5Br, CD_2Cl_2) or dried over Na/K alloy and vacuum transferred before use. Dichloromethane was distilled from P_2O_5, C_6H_5Br from Ca chips, other solvents were distilled from Na/K alloy or Na (toluene) before use. – NMR spectra were recorded on Varian Gemini 200/300, Inova 400 and Unity 500 spectrometers. The ^{1}H-NMR spectra were referenced to resonances of residual protons in the deuterated solvents. Chemical shifts (δ) are given relative to tetramethylsilane (downfield shifts are positive). Li[$C_5H_4CMe_2Ar$] (Ar = 3,5-dimethylphenyl) was prepared analogously to the derivative with Ar = Ph[7] using 3,5-dimethylphenyllithium prepared in hexane from the corresponding aryl bromide and *n*BuLi. 6,6-Dimethylfulvene and 5-bromo-3-methyltoluene (Aldrich) were used as purchased.

Preparation of (η^5-$C_5H_4CMe_2Ar$)$TiCl_3$: To a stirred solution of $TiCl_4$ (1.0 g, 5.3 mmol) in 20 mL of dichloromethane, cooled at –40 °C, was added solid Li[$C_5H_4CMe_2Ar$] (1.16 g, 5.3 mmol). The red suspension was warmed to room temperature and stirred for 16 h. The salts were separated by centrifugation and subsequent decanting. The solvent was removed in vacuo from the supernatant, and the resulting red-brown oil was extracted with pentane. Cooling the extract to –40 °C yielded orange crystals of the title compound. Yield: 1.28 g (3.50 mmol, 66%). – ^{1}H NMR ([D_6]benzene): δ = 6.69 (s, 2 H, *o-H*), 6.66 (s, 1 H, *p-H*), 6.37 (ps. t, 2 H, Cp), 6.03 (ps. t, 2 H, Cp), 2.10 (s, 6 H, Ar–CH_3), 1.63 [s, 6 H, C(CH_3)$_2$]. – ^{13}C{^{1}H} NMR (CD_2Cl_2): δ = 158.0 (Ar C_{ipso}), 149.8 (Cp C_{ipso}), 140.2 (Ar *m-C*), 130.3 (Ar *p-C*H), 126.5 (Cp *C*H), 126.0 (Ar *o-C*H), 124.5 (Cp *C*H), 43.1 (*C*Me$_2$), 30.8 [C(*C*H$_3$)$_2$], 23.4 (Ar–CH$_3$). – $C_{16}H_{19}Cl_3Ti$ (365.6): calcd. C 52.57, H 5.24, Cl 29.09, Ti 13.10; found C 52.42, H 5.32, Cl 28.91, Ti 12.85.

Preparation of (η^5-$C_5H_4CMe_2Ar$)$TiMe_3$ (1): To a solution of ($C_5H_4CMe_2Ar$)$TiCl_3$ (0.95 g, 2.6 mmol) in 15 mL of benzene was added $Me_2Mg(dioxane)_{0.5}$ (1.86 g, 4.0 mmol). The suspension was stirred at ambient temperature while the color changed gradually from red to yellow. The mixture was centrifuged and the salts were separated by decantation. The solvent was removed in vacuo, and the residue extracted with pentane. Evaporation of the solvent yielded **1** as a yellow oil that solidified on standing. The compound is very soluble in pentane, but may be crystallized from this solvent at low temperature to yield analytically pure material. – ^{1}H NMR ([D_6]benzene): δ = 6.94 (s, 2 H, *o-H*), 6.69 (s, 1 H, *p-H*), 5.95 (ps. t, 2 H, Cp), 5.81 (ps. t, 2 H, Cp), 2.15 (s, 6 H, Ar–CH_3), 1.45 [s, 6 H, C(CH_3)$_2$], 1.31 (s, 9 H, Ti–CH_3) . – ^{13}C NMR ([D_6]benzene): δ = 150.3 (s, Ar C_{ipso}), 144.7 (s, Cp C_{ipso}), 137.4 (s, Ar *m-C*), 129 (Ar *p-C*H, part. overlapped by solvent), 124.3 (d, J_{CH} = 149 Hz, Ar *o-C*H), 114.0 (d, J_{CH} = 167 Hz, Cp *C*H), 109.5 (d, J_{CH} = 171 Hz, Cp *C*H), 63.0 (q, J_{CH} = 120 Hz, Ti-*C*H$_3$), 39.7 (s, *C*Me$_2$), 29.6 [q, J_{CH} = 132 Hz, C(*C*H$_3$)$_2$], 21.6 (q, J_{CH} = 121 Hz, Ar–CH$_3$). – $C_{19}H_{28}Ti$ (304.3): calcd. C 74.99, H 9.27, Ti 15.73; found C 74.80, H 9.29, Ti 15.50.

Generation of [(η^5,η^6-$C_5H_4CMe_2Ar$)$TiMe_2$][$MeB(C_6F_5)_3$] (2): A solution of **1** (13.5 mg, 44.3 μmol) in 0.25 mL of $C_2D_2Cl_4$ was added to a solution of $B(C_6F_5)_3$ (22.7 mg, 44.3 μmol) in 0.25 mL of $C_2D_2Cl_4$ to give a deep red solution of **2**. The reaction proceeds in a similar fashion in C_6D_5Br solvent. – ^{1}H NMR (C_6D_5Br): δ = 7.02 (s, 1 H, *p-H*), 6.74 (ps. t, 2 H, Cp), 5.91 (s, 2 H, *o-H*), 5.15 (ps. t, 2 H, Cp), 2.10 (s, 6 H, Ar–CH_3), 1.07 [6 H, C(CH_3)$_2$, + 3 H B–CH_3], 0.34 (s, 6 H, Ti–CH_3). – ^{13}C NMR ($C_2D_2Cl_4$, –40 °C): δ = 155.2 (s, Ar C_{ipso}), 151.2 (d, J_{CF} = 236 Hz, *o-C*F), 140.3 (d, J_{CF} = 236 Hz, *p-C*F), 139.2 (d, J_{CF} = 236 Hz, *m-C*F), 138.0 (s, Cp C_{ipso}), 135.3 (d, J_{CH} = 166 Hz, Ar *p-C*H), 131.4 (br, C_6F_5 C_{ipso}), 128.2 (d, J_{CH} = 186 Hz, Ar *o-C*H), 125.3 (d, J_{CH} = 166 Hz, Cp *C*H), 123.4 (s, Ar *m-C*), 115.9 (d, J_{CH} = 172 Hz, Cp *C*H), 74.4 (q, J_{CH} = 126 Hz, Ti–CH$_3$), 43.9 (s, *C*Me$_2$), 25.8 [q, J_{CH} = 130 Hz, C(*C*H$_3$)$_2$], 21.6 (q, J_{CH} = 126 Hz, Ar–CH$_3$), 13.5 (br, B–CH$_3$). – ^{19}F NMR ($C_2D_2Cl_4$): δ = –132.8 (*o-F*), –164.1 (*p-F*), –166.7 (*m-F*).

Reaction of 2 with [D_8]THF: To a deep red solution of **2** in C_6D_5Br, prepared as described above, was added a drop of [D_8]THF, resulting in a red solution of [(η^5-$C_5H_4CMe_2Ar$)Ti-Me_2(THF)$_n$][$MeB(C_6F_5)_3$]. – ^{1}H NMR (C_6D_5Br/[D_8]THF): δ = 6.72 (s, 2 H, *o-H*), 6.66 (s, 1 H, *p-H*), 6.14 (ps. t, 2 H, Cp), 6.04 (ps. t, 2 H, Cp), 2.14 (s, 6 H, Ar–CH_3), 1.37 [6 H, C(CH_3)$_2$ + 6 H, Ti–CH_3], 1.04 (br, 3 H, B–CH_3).

Reaction of 2 with $B(C_6F_5)_3$: In an NMR tube with a Teflon (Young) valve, a solution of **2** was prepared as described above, but using two equivalents of $B(C_6F_5)_3$ per Ti. The tube was allowed to stand at ambient temperature, and was monitored at regular intervals by ^{1}H and ^{19}F NMR. After 24 h all of **2** had disappeared, giving **3** and $MeB(C_6F_5)_2$.

3: ^{1}H NMR (C_6D_5Br, –30 °C): δ = 6.85 and 6.80 (br, 1 H each, Cp), 6.71 (s, 1 H, *p*-H), 5.96 and 5.74 (s, 1 H each, *o-H*), 5.66 and 5.53 (br, 1 H each, Cp), 2.11 and 1.38 (s, 3 H each, Ar–CH_3), 1.13–1.09 [total 9 H, C(CH_3)$_2$ + Ti–CH_3]. – ^{13}C{^{1}H} NMR (C_6D_5Br, –30 °C): δ = 102.7 (t, $^3J_{CF}$ = 7.3 Hz, Ti–CH$_3$), 40.5 [*C*(CH$_3$)$_2$], 22.2 [C(*C*H$_3$)$_2$], 20.2, 21.0 (Ar–CH$_3$), aromatic resonances poorly resolved. – ^{19}F NMR (C_6D_5Br, –30 °C): δ = –114.3 (*o*-F, Ti–Ar), –

132.9 (*o*-F, B–Ar), –149.9 (*p*-F, Ti–Ar), –159.5 (*m*-F, Ti–Ar), –164.7 (*p*-F, B–Ar), –167.3 (*m*-F, B–Ar).

$MeB(C_6F_5)_2$: ^{1}H NMR (C_6D_5Br, 20 °C): δ = 1.52 (quint., $^5J_{HF}$ = 2 Hz, B–Me). – ^{19}F NMR (C_6D_5Br, –30 °C): δ = –129.9 (*o*-F), –147.5 (*p*-F), –161.5 (*m*-F).

Formation of $\{[(\eta^5,\eta^6\text{-}C_5H_4CMe_2Ar)Ti(\mu\text{-}Br)]_2\}[B(C_6F_5)_4]_2$ (4): A solution of **1** (0.120 g, 0.39 mmol) in 5 mL of bromobenzene was added to $B(C_6F_5)_3$ (0.40 g, 0.78 mmol). Over a period of 3 weeks at ambient temperature green-brown crystals separated from the solution. The supernatant was decanted and the crystals rinsed twice with 10 mL of pentane. Yield: 0.070 g (34 μmol, 18%) of analytically pure **4**. – $C_{80}H_{38}B_2Br_2F_{40}Ti_2$ (2036.3): calcd. C 47.19, H 1.88, Ti 4.70; found C 47.03, H 2.22, Ti 4.58.

Crystal Structure Analysis of 4: Enraf–Nonius CAD4-F diffractometer, Mo-K_α radiation (λ = 0.71073 Å), T = 130 K; monoclinic, $P2_1/n$, a = 13.616(2), b = 16.014(1), c = 17.702(2) Å, β = 109.01(1), V = 3649.4(7) Å^3, Z = 2, D_x = 1.853 g cm^{-3}, μ = 14.7 cm^{-1}. The structure was solved by direct methods. A final refinement on F^2 converged at $wR(F^2)$ = 0.1143 for 7118 reflections with $F_o^2 \geq 0$ and $R(F)$ = 0.0415 for 5390 reflections with $F_o \geq 4\sigma(F_o)$ and 644 parameters.

Crystallographic data (excluding structure factors) for the structure reported in this paper have been deposited with the Cambridge Crystallographic Data Centre as supplementary publication no. CCDC-135683. Copies of the data can be obtained free of charge on application to CCDC, 12 Union Road, Cambridge CB2 1EZ, UK [Fax: (internat.) + 44-1223/336-033; E-mail: deposit@ccdc.cam.ac.uk].

Note Added in Proof (February 28, 2000): During the processing of this contribution a paper was published describing the generation and NMR-spectroscopic characterization (in CD_2Cl_2 solvent at –60 °C) of the cation $[\eta^5,\eta^6\text{-}C_5H_4CMe_2Ph)TiMe_2]^+$.[14]

Acknowledgments

This investigation was supported by a grant from Shell International Chemicals B.V. and the Dutch Polymer Institute (DPI).

[1] [1a] T. Ishihara, T. Seimiga, M. Kuramoto, M. Uoi, *Macromolecules* **1986**, *19*, 2464–2465. – [1b] T. Ishihara, M. Kuramoto, M. Uoi, *Macromolecules* **1988**, *21*, 3356–3360. – [1c] For more recent work in this area, see: P. Foster, J. C. W. Chien, M. D. Rausch, *Organometallics* **1996**, *15*, 2404–2409 and references cited therein.

[2] J. Sassmanshausen, M. Bochmann, J. Rosch, D. Lilge, *J. Organomet. Chem.* **1998**, *548*, 23–28.

[3] [3a] T. E. Ready, R. Gurge, J. C. W. Chien, M. D. Rausch, *Organometallics* **1998**, *17*, 5236–5239. – [3b] A. Grassi, S. Saccheo, A. Zambelli, F. Laschi, *Macromolecules* **1998**, *31*, 5588–5591. – [3c] A. Grassi, A. Zambelli, F. Laschi, *Organometallics* **1996**, *15*, 480–482. – [3d] Q. Wang, R. Quyoum, D. J. Gillis, M.-J. Tudoret, D. Jeremic, B. K. Hunter, M. C. Baird, *Organometallics* **1996**, *15*, 693–703.

[4] D. J. Gillis, M.-J. Tudoret, M. C. Baird, *J. Am. Chem. Soc.* **1993**, *115*, 2543–2545.

[5] S. J. Lancaster, O. B. Robinson, M. Bochmann, S. J. Coles, M. B. Hursthouse, *Organometallics* **1995**, *14*, 2456–2462.

[6] J. C. Flores, J. S. Wood, J. C. W. Chien, M. D. Rausch, *Organometallics* **1996**, *15*, 4944–4950.

[7] [7a] G. Tainturier, B. Gautheron, P. Renaut, P. Etievant, *C. R. Acad. Sci. Paris, Sér. C* **1975**, *281*, 951–954. – [7b] P. Renaut, G. Tainturier, B. Gautheron, *J. Organomet. Chem.* **1978**, *148*, 35–42.

[8] G. Erker, T. Mühlenbernd, *J. Organomet. Chem.* **1987**, *319*, 201–211.

[9] A. D. Horton, J. de With, A. J. van der Linden, H. van de Weg, *Organometallics* **1996**, *15*, 2672–2674.

[10] [10a] B. Qian, D. L. Ward, M. R. Smith III, *Organometallics* **1998**, *17*, 3070–3076. – [10b] P. Biagini, G. Lugli, F. Garbassi, P. Andreussi, *Eur. Pat. Appl.* EP 667 357, **1995**.

[11] M. J. Sarsfield, S. W. Ewart, T. L. Tremblay, A. W. Roszak, M. C. Baird, *J. Chem. Soc., Dalton Trans.* **1997**, 3097–3104.

[12] R. Jungst, D. Sekutowski, J. Davis, M. Luly, G. Stucky, *Inorg. Chem.* **1977**, *16*, 1645–1655.

[13] M. Bochmann, M. J. Sarsfield, *Organometallics* **1998**, *17*, 5908–5912.

[14] J. Sassmannshausen, A. K. Powell, C. E. Anson, S. Wocadlo, M. Bochmann, *J. Organomet. Chem.* **1999**, *592*, 84–94.

Received October 29, 1999
[I99383]

Reaction of the Tetrachalcogenides [ME_4(dppe)] (M = Pd, E = S; M = Pt, E = S, Se) with Activated Alkynes to Form Dithiolenes and Diselenolenes

Susan Ford,[a] Mark R. Lewtas,[a] Christopher P. Morley,*[a] and Massimo Di Vaira[b]

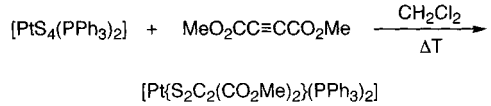
Keywords: Palladium / Platinum / Dithiolenes / Diselenolenes / Sulfur / Selenium

The tetrachalcogenides [ME_4(dppe)] (M = Pd, E = S; M = Pt, E = S, Se) react with the activated alkynes $RO_2CC{\equiv}CCO_2R$ (R = Me, Et) to form the dithiolenes and diselenolenes [M{$E_2C_2(CO_2R)_2$}(dppe)]; the structures of the compounds with E = S, R = Et have been determined by X-ray crystallography; [PdS_4(dppe)] also reacts with the carbene complex [$W(CO)_5${C(OEt)C≡CPh}] to yield the bimetallic dithiolene [Pd{S_2C_2[C(OEt)$W(CO)_5$]Ph}(dppe)].

Introduction

For many years, the potentially useful electrochemical and optical properties of transition metal dithiolenes have attracted the attention of chemists, physicists, and materials scientists.[1] Possible areas of application include molecular electronics, infrared dyes, liquid crystals, and catalysis.[2–4] By contrast, the selenium analogues of dithiolenes (diselenolenes) have been little studied,[5–10] largely because of the lack of generally applicable preparative methods. These complexes are, however, attractive synthetic targets since the incorporation of selenium should lead to a smaller HOMO–LUMO gap and an increase in the strength of intermolecular interactions in the solid state.

We are interested in the potential reactivity of metal polychalcogenides towards activated alkynes to yield dithiolenes and diselenolenes. Treatment of [$PtS_4(PPh_3)_2$][11] with dimethyl acetylenedicarboxylate (DMAD) has already been shown to lead to the dithiolene [Pt{$S_2C_2(CO_2Me)_2$}-$(PPh_3)_2$] (Scheme 1).[12]



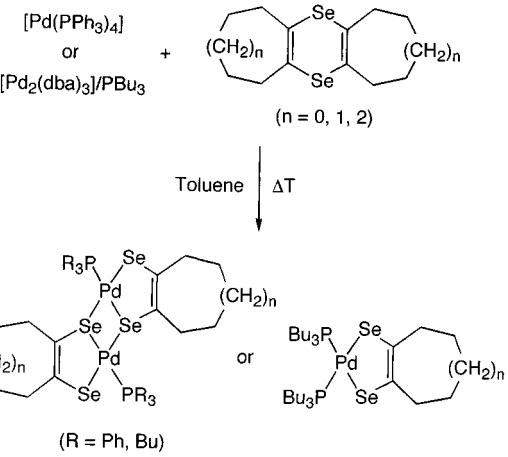
Scheme 1

In a parallel study, we have recently prepared palladium diselenolenes bearing hydrocarbon substituents from Pd^0 complexes and 1,4-diselenines (Scheme 2).[13,14]

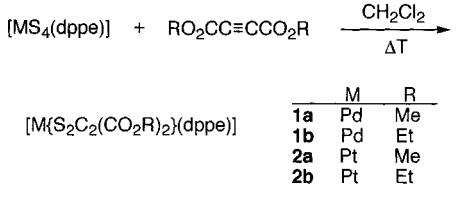
We now report the preparation of a number of dithiolenes and diselenolenes starting from the tetrachalcogenides [PdS_4(dppe)], [PtS_4(dppe)], and [$PtSe_4$(dppe)][15] [dppe = 1,2-bis(diphenylphosphanyl)ethane].

Results and Discussion

The polychalcogenides [PdS_4(dppe)], [PtS_4(dppe)], and [$PtSe_4$(dppe)] are readily prepared from appropriate M^0 precursors and the elemental chalcogen. In an extension of the work of Dudis et al.[12] stirring [MS_4(dppe)] (M = Pd, Pt) with an activated alkyne (dimethyl or diethyl acetylenedicarboxylate) in dichloromethane at reflux leads to formation of the dithiolenes **1a**,**b** (M = Pd) and **2a**,**b** (M = Pt) (Scheme 3).

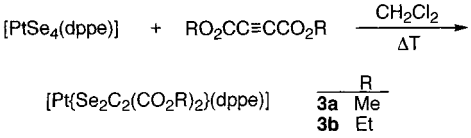


Scheme 2



Scheme 3

The tetraselenide [$PtSe_4$(dppe)] reacts in an analogous fashion to yield the diselenolenes **3a**,**b** (Scheme 4). A similar reaction of the MSe_4 fragment has previously been observed for the anionic tungsten complex $[WSe(Se_4)_2]^{2-}$.[16]



Scheme 4

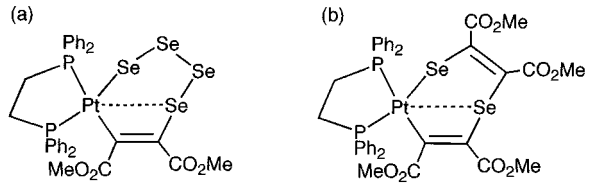
[a] Department of Chemistry, University of Wales Swansea, Singleton Park, Swansea SA2 8PP, UK
[b] Dipartimento di Chimica, Università degli Studi di Firenze, Via Maragliano 75/77, 50144 Firenze, Italy

 © WILEY-VCH Verlag GmbH, D-69451 Weinheim, 2000 1434–1948/00/0505–0933 $ 17.50+.50/0

The reactivity within this system of the three tetrachalcogenides is noticeably different, with [PdS_4(dppe)] being the most reactive, followed by [$PtSe_4$(dppe)] and then [PtS_4(dppe)].

The reaction of [$PtSe_4$(dppe)] with a large excess of DMAD was monitored by ^{31}P-NMR spectroscopy. An intermediate is formed in the early stages of the reaction that has inequivalent phosphorus nuclei [**4a**: P_A, δ = 49.5, $J(^{195}Pt\text{-}^{31}P)$ = 1906 Hz; P_B, δ = 48.5, $J(^{195}Pt\text{-}^{31}P)$ = 3166 Hz; $J(^{31}P_A\text{-}^{31}P_B)$ = 10.8 Hz]. This intermediate is not present once the starting material has been consumed. The final phosphorus-containing product is predominantly the diselenolene **3a**, but there is also a second species present in low concentration [**5a**: P_A, δ = 45.6, $J(^{195}Pt\text{-}^{31}P)$ = 3223 Hz; P_B, δ = 43.9, $J(^{195}Pt\text{-}^{31}P)$ = 2054 Hz; $J(^{31}P_A\text{-}^{31}P_B)$ = 7.4 Hz]. The coupling constants in the ^{31}P-NMR spectra of **4a** and **5a** are comparable with those in the selenaketocarbene complex [$Pt(SeC_8H_{12})(PPh_3)_2$],[17] which has one phosphorus atom *trans* to selenium and one *trans* to carbon.

The reaction of [$Ti(\eta^5\text{-}C_5H_5)_2Se_5$] with DMAD to yield [$Ti(\eta^5\text{-}C_5H_5)_2\{Se_2C_2(CO_2Me)_2\}$] has been studied by Bollinger and Rauchfuss.[8] They showed that the mechanism involves binding of the alkyne to the chalcogenide chelate ring in the rate-determining step. The structure of an adduct between DMAD and the dithiolene [$Rh(\eta^5\text{-}C_5H_5)\{S_2C_2(CO_2Me)_2\}$] has been reported.[18] In this compound a new metal–carbon bond has been generated by insertion of the alkyne into the metal–chalcogen bond. We therefore tentatively assign the structures shown in Figure 1 to **4a** and **5a**.



4a **5a**

Figure 1. Proposed structures of **4a** and **5a**

Compounds **1a**, **2a**, and **3a** could not be obtained in a pure state due to the formation of polymeric material derived from DMAD, although the NMR-spectroscopic and mass-spectrometric data confirm their formulation as [$M\{E_2C_2(CO_2Me)_2\}$(dppe)] (**1a**: M = Pd, E = S; **2a**: M = Pt, E = S; **3a**: M = Pt, E = Se). No such problems were, however, encountered with the ethyl derivatives **1b**, **2b**, and **3b**, which were characterised by standard analytical and spectroscopic methods. It seems likely that the greater size of the ethyl substituents in DEAD inhibits the formation of a species analogous to **5a**, which might function as an intermediate in the polymerisation process.

The crystal structures of the isomorphous compounds **1b** and **2b** were determined by X-ray diffraction (Figure 2, Table 1). There are only very small differences between them, with the bonding in the dithiolene unit being slightly asymmetric in each case: One M–S bond is ca. 0.02 Å longer than the other, and one P–M–S angle is significantly expanded [**1b**: 96.51(5)° vs. 89.83(4)°; **2b**: 96.16(5)° vs. 90.26(5)°]. This feature does not appear to have been observed before in the structures of palladium and platinum dithiolenes, and is probably to be attributed to packing effects.

The structures of relatively few palladium mono-dithiolenes have been reported. The Pd–S distances in **1b** (2.284, 2.310 Å) are in the range of those previously observed (2.274–2.324 Å),[19] and are comparable with those in [Pd{$S_2C_2(CH_2CH_2\text{-}N\text{-}$2-pyridinium)}(dppe)][$BPh_4$] (2.297, 2.303 Å).[20] Platinum mono-dithiolenes are more numerous, in part because of interest in their luminescent properties. The Pt–P distances in **2b** (2.268, 2.265 Å) may be compared with those in [Pt{$S_2C_2S_2CS$}(dppe)] (2.258, 2.250 Å)[21] and [Pt{$S_2C_2(CN)_2$}(dppe)] (2.262, 2.252 Å).[22] Comparable Pt–S distances to those in **2b** (2.297, 2.318 Å) are found in [Pt{$S_2C_2(CO_2Me)_2$}{$P(OMe)_3$}$_2$] (2.300, 2.302 Å)[23] and [Pt{$S_2C_2(CO_2Me)_2$}(PPh_3)$_2$] (2.304 Å).[12]

Crystals of **3b** suitable for study by X-ray diffraction could not be obtained. The spectroscopic data are, however, entirely in accord with a structure for **3b** analogous to those of **1b** and **2b**. The NMR data for all three compounds are strikingly similar. There are small, but significant differences between the palladium and platinum derivatives [particularly in the value of $\delta(^{31}P)$], which we have observed in other dppe complexes of these metals. Replacement of the sulfur in **2b** by selenium (**3b**) leads to a slight upfield shift in $\delta(^{13}C)$ for the dichalcogenolene carbons. This is accompanied by a slight downfield shift in $\delta(^{31}P)$ and an increase in the platinum-phosphorus coupling constant [$J(^{31}P\text{-}^{195}Pt)$]. These changes may imply that the diselenolene ring in **3b** has a marginally greater electron density than the dithiolene ring in **2b**. A similar increase in $J(^{31}P\text{-}^{195}Pt)$ was observed by Rauchfuss et al. for the analogous triphenylphosphane derivatives [Pt{$E_2C_2(CO_2Me)_2$}(PPh_3)$_2$] (E = S, Se).[8]

The ^{77}Se-NMR spectrum of **3b** is shown in Figure 3, together with the satellite structure of the ^{31}P resonance. Analysis of the data allows evaluation of the three coupling constants in this system: $J(^{31}P_{trans}\text{-}^{77}Se)$ = 64.3 Hz; $J(^{31}P_{cis}\text{-}^{77}Se)$ = 31.8 Hz; $J(^{31}P\text{-}^{31}P)$ = 13.9 Hz. The values of $J(^{31}P\text{-}^{77}Se)$ are significantly higher than those previously determined in platinum selenolate complexes,[24] but are comparable with that reported for the diselenolene [Pt{Se_2C_2-$(CO_2Me)_2$}(PPh_3)$_2$] (52 Hz, presumably an average value).[8]

In the IR spectra of **1b**, **2b**, and **3b** four bands corresponding to C=O stretching are observed and these are at lower frequencies (by ca. 10–100 cm^{-1}) than $\nu_{C=O}$ in DEAD (1724 cm^{-1}). There is an accompanying small decrease (by ca. 20 cm^{-1}) of the C–O stretching frequency from its value in DEAD, which is 1255 cm^{-1}. These changes are reflected in a substantial increase (by ca. 16 ppm) in the ^{13}C-NMR chemical shift of the carbonyl carbon atoms [in DEAD $\delta(CO)$ = 151.7]. All the compounds give intense molecular ions in their FAB mass spectra. Ions corresponding to the expected fragmentation patterns are also observed, of which

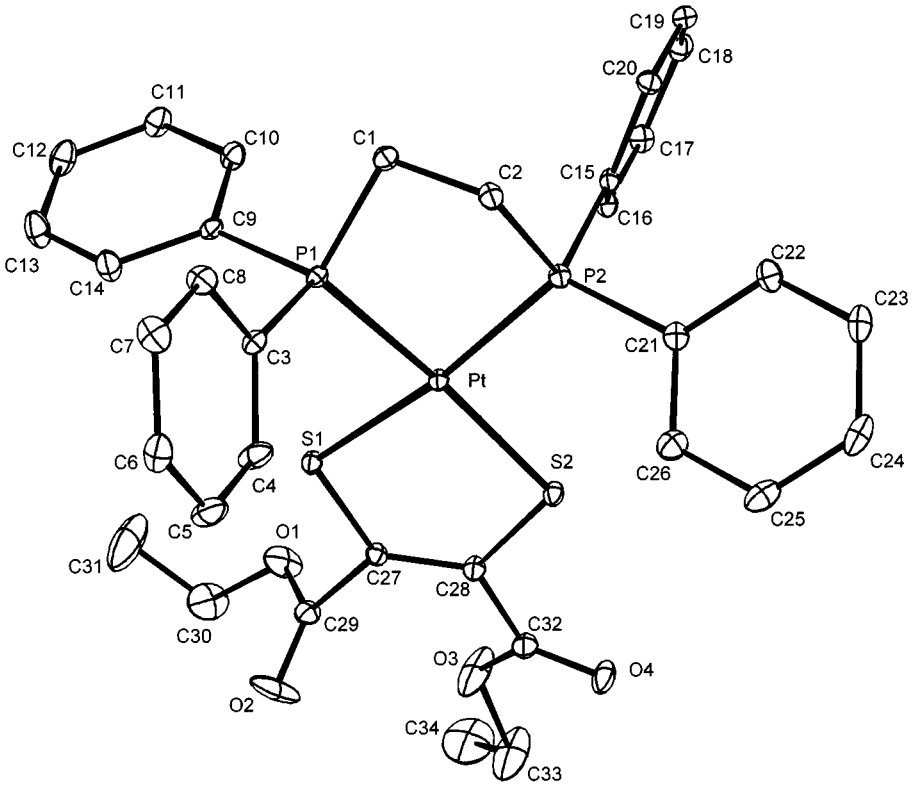


Figure 2. Molecular stuctures of [M{$S_2C_2(CO_2R)_2$}(dppe)] [M = Pd, **1b**; M = Pt, **2b** (shown)]

Table 1. Selected bond lengths [Å] and angles [°] for [M{S_2C_2-$(CO_2R)_2$}(dppe)] (M = Pd, **1b**; M = Pt, **2b**)

	1b (M = Pd)	**2b** (M = Pt)
M–P(1)	2.2775(13)	2.268(2)
M–P(2)	2.2766(14)	2.265(2)
M–S(1)	2.2837(14)	2.297(2)
M–S(2)	2.3096(14)	2.318(2)
S(1)–C(27)	1.726(5)	1.730(6)
S(2)–C(28)	1.760(5)	1.767(6)
C(27)–C(28)	1.354(7)	1.341(8)
P(1)–M–P(2)	84.72(4)	85.05(5)
P(2)–M–S(2)	96.51(5)	96.16(5)
S(2)–M–S(1)	89.41(4)	89.02(5)
S(1)–M–P(1)	89.83(4)	90.26(5)
S(1)–C(27)–C(28)	123.3(4)	123.8(5)
C(27)–C(28)–S(2)	121.8(4)	121.8(4)
M–S(1)–C(27)	103.2(2)	103.1(2)
M–S(2)–C(28)	102.2(2)	102.3(2)

those arising from loss of DEAD {i.e. $[ME_2(dppe)]^+$} are particularly prominent.

No products could be isolated from the reactions of $[ME_4(dppe)]$ (M = Pd, E = S; M = Pt, E = S, Se) with less activated alkynes, such as PhC≡CH, PhC≡CPh, HC≡CCO_2Et, or PhC≡CCO_2Et. In the case of the most reactive of the tetrachalcogenides ($[PdS_4(dppe)]$), treatment with PhC≡CCO_2Et did lead to the observation of a new AB pattern in the ^{31}P-NMR spectrum, analysis of which yielded δ = 50.5, 50.2, J = 41.0 Hz. This is presumed to arise from the unsymmetrical dithiolene [Pd{S_2C_2-

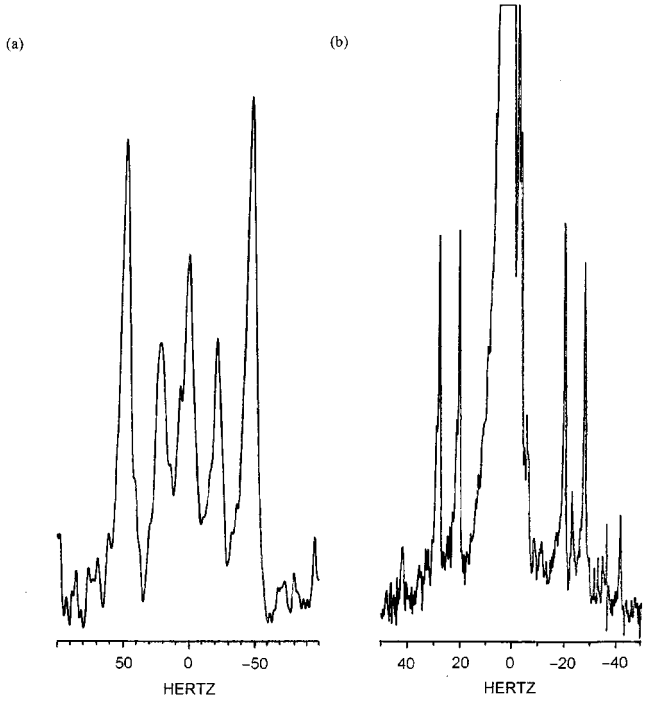
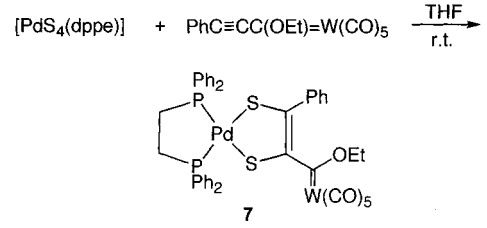


Figure 3. NMR spectra of **3b**: (a) structure of ^{77}Se resonance, (b) satellite structure of ^{31}P resonance; analysis of the data gives J(^{31}P-^{77}Se) = 64.3 Hz, 31.8 Hz; J(^{31}P-^{31}P) = 13.9 Hz

$(CO_2Et)Ph$}(dppe)] (**6**), as the molecular ion for this species was observed in the mass spectrum of the reaction mixture. The NMR data are also strikingly similar to those for

[Pd{S_2C_2[C(OEt)$W(CO)_5$]Ph}(dppe)] (**7**) (vide infra). The extent of conversion into product was, however, very low, and separation of compound **6** was not achieved.

The carbene complex [$W(CO)_5${C(OEt)C≡CPh}][25] is an alkyne bearing a highly electron-withdrawing substituent. It reacts with [PdS_4(dppe)] {but not with the platinum tetrachalcogenides [PtE_4(dppe)] (E = S, Se)} at room temperature in tetrahydrofuran solution to yield the unsymmetrical dithiolene [Pd{S_2C_2[C(OEt)$W(CO)_5$]Ph}(dppe)] (**7**) in moderate yield (Scheme 5). The reaction could not be performed in dichloromethane, as decomposition occurs in this solvent. Some starting material remains unchanged and must be separated from the product by column chromatography. There are also a number of unidentified by-products. Compound **7** could not be obtained as a crystalline solid, but its composition is assured on the basis of NMR, UV/Vis, and IR spectroscopy and mass spectrometry.



Scheme 5

The ^{31}P-NMR spectrum of **7** contains the expected AB pattern for the inequivalent phosphorus atoms. Analysis of the data gives δ(^{31}P) = 50.0, 49.1; ^2J(^{31}P-^{31}P) = 40.9 Hz. The chemical shifts are similar to those observed for the symmetrical palladium dithiolenes **1a,b**. The coupling constant is comparable with that for the palladium diselenolene [Pd{$Se_2C_7H_{10}$}(PBu_3)$_2$] (44 Hz),[14] and is significantly greater than that for the platinum analogue **3b** (13.9 Hz).

The ^{13}C-NMR spectrum of **7** has many similarities to that of **1b**. Each of the carbon atoms in the phenyl rings and the CH_2 group of dppe forms the X part of an AA′X system, and should therefore give rise to five lines in the spectrum. The outermost lines are often weak and were not observed in **1b**. In **7** the phenyl rings bound to the two inequivalent phosphorus atoms are themselves inequivalent, so we expect to see a doubling of the number of lines. This is essentially what is observed, although overlapping occurs in some cases. The greatest discrimination occurs for the carbon atoms in the dithiolene. These have chemical shifts of δ = 145.0 and δ = 138.5 in **7**. Although the equivalent single resonance was too weak to be observed in **1b**, in **2b** and **3b** it is at δ = 139.5 and 137.3, respectively. We assign the resonance at δ = 145.0 to the carbon bearing the highly electron-withdrawing carbene substituent.

Bands corresponding to C≡O stretching are not observed in the IR spectrum of **7**. This is surprising, given their prominence in the spectrum of the carbene starting material. Convincing evidence for the presence of the carbonyl ligands is, however, provided by the FAB mass spectrum. In addition to an intense molecular ion centred on *m/z* = 1051, there are clusters of peaks around *m/z* = 967 (M^+ – 3 CO) and *m/z* = 911 (M^+ – 5 CO), as well as several other fragments resulting from carbonyl loss.

Overall, it can be seen that the reactions of palladium and platinum tetrachalcogenides with activated alkynes provide an effective route to dithiolenes and diselenolenes bearing highly electron-withdrawing groups. This preparative method is thus complementary to the use of 1,2,3-selenadiazoles or 1,4-diselenines, which enables the synthesis of hydrocarbyl-substituted derivatives. We are now proceeding to examine in more detail the photophysical and electrochemical properties of this class of compound.

Experimental Section

General: All reactions were performed using standard Schlenk techniques and pre-dried solvents under dinitrogen. – ^{1}H- and ^{13}C-NMR spectra: Bruker AC400; tetramethylsilane as internal standard. ^{31}P-, ^{77}Se-, and ^{195}Pt-NMR spectra: Bruker WM250; 85% phosphoric acid, dimethyl selenide, or sodium hexachloroplatinate as external standard. – IR spectra: Perkin–Elmer 1725X. – UV/Vis spectra: Perkin–Elmer Lambda 9. – Mass spectra were recorded by the EPSRC Mass Spectrometry Centre, using Fast Atom Bombardment (FAB). Values of *m/z* quoted are for isotopomers containing ^{80}Se, ^{106}Pd, or ^{195}Pt as appropriate; expected isotope distribution patterns were observed. – Elemental analyses were performed by the analytical service of the University of Wales, Cardiff.

Bis(diphenylphosphanyl)ethane(tetrasulfido-*S*,*S*)palladium and -platinum,[12] bis(diphenylphosphanyl)ethane(tetraselenido-*Se*,*Se*)-platinum[14], and pentacarbonyl[phenylethynyl(ethoxy)carbene]-tungsten[25] were prepared by literature procedures.

Palladium Dithiolenes (1a,b), Platinum Dithiolenes (2a,b) and Platinum Diselenolenes (3a,b): The same general procedure was used for all three types of compound. A mixture of [ME_4(dppe)] [0.063 g (M = Pd, E = S), 0.072 g (M = Pt, E = S) or 0.091 g (M = Pt, E = Se), 0.1 mmol] and dimethyl or diethyl acetylenedicarboxylate (0.43 g or 0.48 g, 3.0 mmol) in dichloromethane (50 mL) was heated under reflux for a prolonged period (**1a**,**b**: 18 h; **2a**,**b**: 6 d; **3a**,**b**: 4 d). After this time, a brown or red solid had precipitated. The mixture was filtered, and the solvent removed from the filtrate by evaporation under reduced pressure to leave an oily yellow to orange solid. This was purified by recrystallisation from a mixture of dichloromethane and petroleum ether (b.p. 30–40 °C). The products of the reaction with DMAD (**1a**, **2a**, **3a**) could not be obtained free of a polymeric impurity. Compounds **1b**, **2b**, **3b** are air-stable crystalline solids (**1b**, pale orange; **2b**, cream; **3b**, yellow) that are soluble in a wide range of organic solvents.

1a: ^{31}P NMR: δ = 52.0. – MS; *m/z*: 710 [M^+].

1b: Yield: 0.052 g, 70%. – M.p. 248 °C (dec.). – $C_{34}H_{34}O_4P_2PdS_2$: calcd. C 55.3, H 4.63; found C 55.3, H 4.76. – ^{1}H NMR: δ = 7.82 (m, 8 H), 7.48 (m, 12 H), 4.18 (q, *J* = 7 Hz, 4 H), 2.49 (m, 4 H), 1.25 (t, *J* = 7 Hz, 6 H). – ^{13}C NMR: (*C*=O, *C*=*C* not observed), δ = 133.5 [average J(^{13}C-^{31}P) = 6 Hz], 131.6, 129.5 [PC_{Ar}, average J(^{13}C-^{31}P) = 19 Hz], 129.0 [average J(^{13}C-^{31}P) = 5 Hz], 61.0 [OCH_2], 27.9 [PCH_2, average J(^{13}C-^{31}P) = 24 Hz], 14.1 [CH_3]. – ^{31}P NMR: δ = 52.0. – IR (KBr disk): $\tilde{\nu}$ = 3053 m, 2962 s, 2918 s, 2850 m, 1713 m, 1693 m, 1638 m, 1619 m, 1527 m, 1436 s, 1234 vs, 1102 vs, 1030 s, 804 m, 748 m, 716 m, 705 m, 692 s, 530 s, 484 w cm^{-1}. – UV/Vis (CH_2Cl_2), λ_{max} (ε [dm^3 cm^{-1} mol^{-1}]) = 230

Table 2. Crystallographic data for [M{$S_2C_2(CO_2R)_2$}(dppe)] (M = Pd, **1b**; M = Pt, **2b**)

Compound	**1b**	**2b**
Formula	$C_{34}H_{34}O_4P_2PdS_2$	$C_{34}H_{34}O_4P_2PtS_2$
M_r	739.07	827.76
Crystal system	Monoclinic	Monoclinic
Space group	$P2_1/c$ (No. 14)	$P2_1/c$ (No. 14)
a [Å]	14.229(4)	14.279(2)
b [Å]	16.124(4)	16.165(3)
c [Å]	14.881(3)	14.907(2)
β [°]	90.14(2)	90.11(1)
V [Å^3]	3414(2)	3441(1)
Z	4	4
D_c [Mg m^{-3}]	1.438	1.598
Crystal size [mm]	0.15 × 0.50 × 0.50	0.15 × 0.25 × 0.55
μ [mm^{-1}]	0.795	9.927
Radiation	Mo-K_α (λ = 0.71069 Å)	Cu-K_α (λ = 1.54184 Å)
Data collected	±h, +k, +l	2.6 redundancy
Scan type	ω-2θ	CCD ω scans
2θ range for data [°]	5–50	6–115
Reflections collected	6295	11425
Unique reflections	5999 (R_{int} = 0.020)	4332 (R_{int} = 0.042)
Unique observed reflections with $I > 2\sigma(I)$	4446	3556
No. of parameters	390	390
$R1$ (observed reflections)	0.043	0.033
$R1$ (all unique reflections)	0.071	0.039
$wR2$	0.113	0.079
Goodness of fit	1.018	0.952
Largest features (max., min.) in final ΔF map [e Å^{-3}]	0.73, –0.58	0.93, –1.06

(30000), 280 (31000), 490 (150), 570 (1200) nm. – MS; *m*/*z*: 738 [M$^+$].

2a: ^{31}P NMR, δ = 44.9 [J(^{195}Pt-^{31}P) 2769 Hz]. – MS; *m*/*z*: 799 [M$^+$].

2b: Yield: 0.050 g, 60%. – M.p. 145 °C (dec.). – $C_{34}H_{34}O_4P_2PtS_2$: calcd. C 49.3, H 4.14; found C 46.9, H 4.33. – ^{1}H NMR: δ = 7.79 (m, 8 H), 7.45 (m, 12 H), 4.20 (q, J = 7 Hz, 4 H), 2.47 (m, 4 H), 1.25 (t, J = 7 Hz, 6 H). – ^{13}C NMR: δ = 167.1 [*C*=O], 139.5 [*C*=*C*, J(^{13}C-^{31}P) not resolved], 133.6 [average J(^{13}C-^{31}P) = 6 Hz], 131.6, 129.6 [P*C*$_{Ar}$, average J(^{13}C-^{31}P) = 30 Hz], 128.8 [average J(^{13}C-^{31}P) = 5 Hz], 61.1 [O*C*H$_2$], 28.6 [P*C*H$_2$, J(^{13}C-^{31}P) not resolved], 14.1 [*C*H$_3$]. – ^{31}P NMR: δ = 44.9 [J(^{195}Pt-^{31}P) = 2767 Hz]. – IR (KBr): $\tilde{\nu}$ = 3001 m, 2963 s, 2925 vs, 2858 m, 1717 s, 1695 s, 1638 vs, 1619 vs, 1526 s, 1436 m, 1385 m, 1236 s, 1103 s, 1040 m, 750 w, 717 m, 692 m, 617 s, 533 vs, 485 vs cm^{-1}. – UV/Vis (CH_2Cl_2), λ_{max} (ε [dm^3 cm^{-1} mol^{-1}]) = 230 (45000), 260 (35000), 320 (5800), 370 (770) nm. – MS; *m*/*z*: 827 [M$^+$].

3a: ^{31}P NMR: δ = 45.8 [J(^{195}Pt-^{31}P) = 2794 Hz]. – MS; *m*/*z*: 895 [M$^+$].

3b: Yield: 0.060 g, 65%. – M.p. 195 °C (dec.). – $C_{34}H_{34}O_4P_2PtSe_2$: calcd. C 44.3, H 3.72; found C 42.9, H 3.66. – ^{1}H NMR: δ = 7.75 (m, 8 H), 7.47 (m, 12 H), 4.18 (q, J = 7 Hz, 4 H), 2.43 (m, 4 H), 1.24 (t, J = 7 Hz, 6 H). – ^{13}C NMR: δ = 168.2 [*C*=O], 137.3 [*C*=*C*, average J(^{13}C-^{31}P) = 7 Hz], 133.5 [average J(^{13}C-^{31}P) = 5 Hz], 131.6, 129.5 [P*C*$_{Ar}$, average J(^{13}C-^{31}P) = 29 Hz], 128.8 [average J(^{13}C-^{31}P) = 5 Hz], 61.2 [O*C*H$_2$], 28.8 [P*C*H$_2$, average J(^{13}C-^{31}P) = 25 Hz], 14.1 [*C*H$_3$]. – ^{31}P NMR: δ = 45.8 [J(^{195}Pt-^{31}P) = 2790 Hz]. – ^{77}Se NMR: δ = 483 [J(^{77}Se-^{31}P) = 64.3, 31.8 Hz; J(^{31}P-^{31}P) = 13.9 Hz]. – ^{195}Pt NMR: δ = –2921 [J(^{195}Pt-^{31}P) = 2790 Hz]. – IR (KBr): $\tilde{\nu}$ = 2919 s, 2850 m, 1720 m, 1688 m, 1639 m, 1619 m, 1532 m, 1437 m, 1385 w, 1230 vs, 1105 m, 1034 m, 999 m, 751 w, 717 m, 704 m, 692 m, 618 w, 535 s, 487 m cm^{-1}. – UV/Vis (CH_2Cl_2), λ_{max} (ε [dm^3 cm^{-1} mol^{-1}]) = 230 (12000), 290 (9500), 310 (3700), 320 (3500), 330 (2600), 350 (1900), 370 (580) nm. – MS; *m*/*z*: 923 [M$^+$].

Palladium Complex 7: A mixture of [PdS_4(dppe)] (0.063 g, 0.1 mmol) and [$W(CO)_5${=C(OEt)C≡CPh}] (0.048 g, 0.1 mmol) in THF (100 mL) was stirred at room temperature for 4 h. During this time the solution became cloudy and some of the [PdS_4(dppe)] remained undissolved. The solvent was removed from the mixture by evaporation under reduced pressure to give a dark red oily solid, which was chromatographed on a short column of silica, using toluene as eluent. A band was collected that was yellow on the column. On changing the eluent to dichloromethane, four bands were collected that were light brown, yellow, orange and pink in order of elution. The third of these contained the product, which was isolated as a dark red-brown oily solid after removal of the solvent. The others yielded dppe disulfide, [PdS_4(dppe)], and small amounts of unidentified compounds.

7: Yield: 0.036 g, 34%. – ^{1}H NMR: δ = 7.80 (m, 7 H), 7.42 (m, 15 H), 7.16 (m, 3 H), 4.18 (q, J = 7 Hz, 2 H), 2.48 (m, 4 H), 0.66 (t, J = 7 Hz, 3 H). – ^{13}C NMR: (*C*=O, *C*=W not observed), δ = 145.0 [*C*=C, J(^{13}C-^{31}P) not resolved], 138.5 [C=*C*, J(^{13}C-^{31}P) not resolved], 133.5 [four peaks], 131.4, 129.9 [P*C*$_{Ar}$, average J(^{13}C-^{31}P) = 22 Hz], 129.0 [four peaks], 128.4, 127.3, 126.2, C*C*$_{Ar}$ not observed, 67.4 [O*C*H$_2$], 27.9 [*C*H$_2$P, seven peaks], 12.7 [*C*H$_3$]. – ^{31}P NMR: δ = 50.0, 49.1 [AB: J(^{31}P-^{31}P) = 40.9 Hz]. – IR (KBr): $\tilde{\nu}$ = 2920 vs, 2850 s, 1635 m, 1465 w, 1435 m, 1384 w, 1234 m, 1102 s, 801 w, 745 w, 692 m, 529 m, 480 w cm^{-1}. – UV/Vis (CH_2Cl_2), λ_{max} (ε [dm^3 cm^{-1} mol^{-1}]) = 230 (90000), 270 (73000), 420 (16000), 480 (7300) nm. – MS; *m*/*z*: 1051 [M$^+$].

X-ray Crystallography: Details of the crystal structure determinations are given in Table 2. Measurements were carried out at room temperature with an Enraf–Nonius CAD4 diffractometer for **1b**, using graphite-monochromated Mo-K_α radiation, and with a Bruker-AXS CCD platform mounted on a rotating anode generator equipped with Göbel mirrors for **2b**, using Cu-K_α radiation. No crystal decay was observed during data collections, although **2b** was found to decompose if Mo-K_α radiation was used. Empirical corrections for absorption were applied, based on ψ scans (**1b**) or SADABS[26] (**2b**) [min., max. transmission factors: 0.93, 0.98 (**1b**);

0.412, 1.000 (**2b**)]. Structure solution was by direct methods, with SIR97,[27] and Fourier cycles with SHELXL-93,[28] which was also used for structure refinements. The final refinement cycles were performed against F^2 with all nonhydrogen atoms anisotropic and hydrogen atoms in calculated positions. Crystallographic data (excluding structure factors) for the structures reported in this paper have been deposited with the Cambridge Crystallographic Data Centre as supplementary publications CCDC-136286 (**1b**) and -136287 (**2b**). Copies of the data can be obtained free of charge on application to CCDC, 12 Union Road, Cambridge CB2 1EZ, UK [Fax: (internat.) + 44-1223/336-033; E-mail: deposit@ccdc.cam.ac.uk].

Acknowledgments

We thank EPSRC for the provision of research studentships to S. F. and M. R. L., Johnson Matthey plc for the loan of palladium and platinum salts, and the Ministero dell' Università e della Ricerca Scientifica e Tecnologica for financial support to M. d. V.

[1] U. T. Müller-Westerhoff, B. Vance, in *Comprehensive Coordination Chemistry* (Ed.: G. Wilkinson), Pergamon, Oxford, **1988**, vol. 2, ch. 16.5, pp. 595–631.
[2] P. Cassoux, L. Valade, H. Kobayashi, R. A. Clark, A. E. Underhill, *Coord. Chem. Rev.* **1991**, *110*, 115–160.
[3] T. Bjørnholm, T. Geisler, J. C. Petersen, D. R. Grieve, N. C. Schiødt, *Non-Linear Optics* **1995**, *10*, 129–137.
[4] A. T. Coomber, D. Beljonne, R. H. Friend, J. L. Brédas, A. Charlton, N. Robertson, A. E. Underhill, M. Kurmoo, P. Day, *Nature* **1996**, *380*, 144–146.
[5] D. J. Sandman, J. C. Stark, G. W. Allen, L. A. Acampora, S. Jansen, M. T. Jones, G. J. Ashwell, B. M. Foxman, *Inorg. Chem.* **1987**, *26*, 1664–1669; B. Gautheron, G. Tainturier, S. Pouly, F. Theobald, H. Vivier, A. Laarif, *Organometallics* **1984**, *3*, 1495–1499; T. M. Klapötke, *Phosphorus Sulfur Silicon* **1989**, *41*, 105–111.
[6] G. C. Papavassiliou, *Mol. Cryst. Liq. Cryst.* **1982**, *86*, 159–162; G. Matsubayashi, A. Yokazawa, *J. Chem. Soc., Dalton Trans.* **1990**, 3535–3539; C. Faulmann, J.-P. Legros, P. Cassoux, J. Cornelissen, L. Brossard, M. Inokuchi, H. Tajima, M. Tokumoto, *J. Chem. Soc., Dalton Trans.* **1994**, 249–254; S. Zeltner, R. M. Olk, M. Pink, S. Jelonek, P. Jorchel, T. Gelbrich, J. Sieler, R. Kirmse, *Z. Anorg. Allg. Chem.* **1996**, *622*, 1979–1986.
[7] W. B. Heuer, P. J. Squattrito, B. M. Hoffman, J. A. Ibers, *J. Am. Chem. Soc.* **1988**, *110*, 792–803; F. Wudl, E. T. Zellers, S. D. Cox, *Inorg. Chem.* **1985**, *24*, 2864–2866.
[8] C. M. Bollinger, T. B. Rauchfuss, *Inorg. Chem.* **1982**, *21*, 3947–3954.
[9] Y. Okano, H. Sawa, S. Aonuma, R. Kato, *Chem. Lett.* **1993**, 1851–1854; R. D. McCullough, J. A. Belot, J. Seth, A. L. Rheingold, G. P. A. Yap, D. O. Cowan, *J. Mater. Chem.* **1995**, *5*, 1581–1587.
[10] M. Kajitani, R. Ochiai, K. Dohki, N. Kobayashi, T. Akiyama, A. Sugimori, *Bull. Chem. Soc. Jpn.* **1989**, *62*, 3266–3271; E. J. Miller, S. J. Landon, T. B. Brill, *Organometallics* **1985**, *4*, 533–538.
[11] J. Chatt, D. M. P. Mingos, *J. Chem. Soc. A* **1970**, 1243–1245; R. R. Gukathasan, R. H. Morris, A. Walker, *Can. J. Chem.* **1983**, *61*, 2490–2492.
[12] D. S. Dudis, C. King, J. P. Fackler Jr., *Inorg. Chim. Acta* **1991**, *181*, 99–102.
[13] S. Ford, P. K. Khanna, C. P. Morley, M. DiVaira, *J. Chem. Soc., Dalton Trans.* **1999**, 791–794.
[14] S. Ford, C. P. Morley, M. DiVaira, *New J. Chem.* **1999**, *23*, 811–813.
[15] M. R. Lewtas, C. P. Morley, M. DiVaira, *Polyhedron*, accepted for publication.
[16] M. A. Ansari, C. H. Mahler, J. A. Ibers, *Inorg. Chem.* **1989**, *28*, 2669–2674.
[17] P. W. Khanna, C. P. Morley, *J. Chem. Res. (S)* **1995**, 64–65.
[18] M. Kajitani, T. Suetsugu, R. Wakabayashi, A. Igarashi, T. Akiyama, A. Sugimori, *J. Organomet. Chem.* **1985**, *293*, C15-C18; M. Kajitani, T. Suetsugu, T. Takagi, S. Sugimori, K. Aoki, H. Yamazaki, *J. Organomet. Chem.* **1995**, *487*, C8–C14.
[19] C. Kraffert, D. Walther, K. Peters, O. Lindqvist, V. Langer, J. Sieler, J. Reinhold, E. Hoyer, *Z. Anorg. Allg. Chem.* **1990**, *588*, 167–180; N. G. Connelly, J. G. Crossley, A. G. Orpen, *J. Chem. Soc., Chem. Commun.* **1992**, 1568–1571; M. Ebihara, M. Tsuchiya, T. Kawamura, *Acta Cryst., Sect. C* **1994**, *50*, 1880–1802.
[20] K. A. van Houten, D. C. Heath, C. A. Barringer, A. L. Rheingold, R. S. Pilato, *Inorg. Chem.* **1998**, *37*, 4647–4653.
[21] R. Vicente, J. Ribas, X. Solans, M. Font-Attaba, A. Mari, P. de Loth, P. Cassoux, *Inorg. Chim. Acta* **1987**, *132*, 229–236.
[22] J. M. Bevilacqua, J. A. Zuleta, R. Eisenberg, *Inorg. Chem.* **1994**, *33*, 258–266.
[23] J. M. Bevilacqua, R. Eisenberg, *Inorg. Chem.* **1994**, *33*, 2913–2923.
[24] P. K. Khanna, C. P. Morley, M. B. Hursthouse, K. M. A. Malik, O. W. Howarth, *Heteroatom Chem.* **1995**, *6*, 519–524.
[25] E. O. Fischer, F. R. Kreissl, *J. Organomet. Chem.* **1972**, *35*, C47–C51.
[26] G. M. Sheldrick, *SADABS, Program for CCD data absorption correction*, University of Göttingen.
[27] A. Altomare, M. C. Burla, M. Camalli, G. L. Cascarano, C. Giacovazzo, A. Guagliardi, A. G. G. Moliterni, G. Polidori, R. Spagna, *J. Appl. Crystallogr.* **1999**, *32*, 115–119.
[28] G. M. Sheldrick, *SHELXL-93, Program for Crystal Structure Refinement*, University of Göttingen, **1993**.

Received November 2, 1999
[I99388]

On the Hydrolysis of tBu$_2$Ge(OEt)$_2$: Supramolecular Self Assembly in the Solid State of 2 tBu$_2$Ge(OH)$_2$, (tBu$_2$GeOH)$_2$O, and H$_2$O

Jens Beckmann,[a][+] Klaus Jurkschat,*[a] and Markus Schürmann[a]

Dedicated to Professor Stanislaw Pasynkiewicz on the occasion of his 70th birthday

Keywords: Germanium / Germanol / Hydrogen bonds / X-ray structure

The hydrolysis of tBu$_2$Ge(OEt)$_2$ is described. Depending on the amount of water used either tBu$_2$Ge(OH)$_2$ (**1**) or a mixture of the latter and (tBu$_2$GeOH)$_2$O (**2**) were obtained. A cocrystallate consisting of 2tBu$_2$Ge(OH)$_2$, (tBu$_2$GeOH)$_2$O and water was the subject of a single crystal X-ray diffraction study. In the solid state the individual molecules are connected by hydrogen bonds giving rise to the formation of a polymeric double chain ribbon.

Introduction

Organosilanols represent a well established class of compounds. In the solid state they are connected through hydrogen bonds and adopt various secondary structural motifs.[1] Organosilanols find applications as building blocks for the synthesis of molecular metallasiloxanes and related materials.[2] In contrast, only a very few examples of organogermanols are known, presumably because of their higher sensitivity toward self-condensation than organosilanols. For organogermanols, hydrogen bonding is also observed in the solid state.[3] As part of our ongoing studies on metallastannoxanes we prepared tBu$_2$Ge(OH)$_2$ by hydrolysis of tBu$_2$Ge(OEt)$_2$, and used this product for further investigations. Despite the mild reaction conditions applied, in one case a mixture of tBu$_2$Ge(OH)$_2$ and (tBu$_2$GeOH)$_2$O was obtained. Attempts to separate this mixture by fractional crystallization afforded a cocrystallate of 2tBu$_2$Ge(OH)$_2$, (tBu$_2$GeOH)$_2$O, and water, the structure of which is reported in this paper.

Results and Discussion

The hydrolysis of tBu$_2$Ge(OEt)$_2$ with a slight excess of water provided a mixture of the germanols tBu$_2$Ge(OH)$_2$ (**1**) and (tBu$_2$GeOH)$_2$O (**2**) whereas the use of a large excess of water exclusively gave tBu$_2$Ge(OH)$_2$ (**1**) (Equation 1).

$$3\,t\mathrm{Bu_2Ge(OEt)_2} \xrightarrow[-\ \mathrm{EtOH}]{\mathrm{H_2O}} \underset{\mathbf{1}}{t\mathrm{Bu_2Ge(OH)_2}} + \underset{\mathbf{2}}{(t\mathrm{Bu_2GeOH})_2\mathrm{O}} \qquad (1)$$

Compound **2** is the first example of a 1,1,3,3-tetraorganogermanoxane-1,3-diol. Recently, Puff et al. reported the low-yield synthesis of tBu$_2$Ge(OH)$_2$ (**1**) by the hydrolysis of tBu$_2$GeCl$_2$.[3a,4] Moreover, the authors used tBu$_2$Ge(OH)$_2$ (**1**) for the preparation of the diorganogermanium oxide *cyclo*-(tBu$_2$GeO)$_3$ which was obtained in moderate yield.[3a,4] However, no information was given on the identity of by-products such as **2**, or higher oligomers, from these reactions.

After the first crop of **1** had been isolated attempts to separate the above-mentioned mixture of **1** and **2** by fractional crystallisation failed. Instead, we obtained a single crystalline material which, according to ^{1}H NMR spectroscopy, consisted of a mixture of **1** and **2** in the ratio of 2:1. In this context it is worth mentioning that Weidenbruch et al., by the same method, succeeded in the separation of the silicon analogues tBu$_2$Si(OH)$_2$ and (tBu$_2$SiOH)$_2$O.[5]

The molecular structure of the cocrystallate is shown in Figure 1. Crystallographic data are given in Table 1 and selected bond lengths and angles are listed in Table 2.

The asymmetric unit indeed contains two molecules of **1**, a molecule of **2** and, in addition, a molecule of water; these three components are connected by a framework of hydrogen bonds (Figure 1). The mean Ge–O and Ge–C bond lengths amount to 1.77 and 1.96 Å, respectively, and are comparable with those of other organogermanols.[3] The germanium atoms of **1** and **2** show distorted tetrahedral configurations with the greatest deviations of 121.8(2) and 119.6(2)°, respectively, found for the C–Ge–C bond angles, due to the steric demand of the bulky *tert*-butyl groups. The Ge–O–Ge bond angle in **2** amounts to 143.9(2)° which is by 10.9 and 8.7° greater than the corresponding angles in (tBu$_2$GeO)$_3$[3a] and (Ph$_3$Ge)$_2$O,[6] respectively. Bearing in mind the variety of different hydrogen bonding frameworks in solid organosilanols, it is quite remarkable that the secondary structural motifs within this cocrystallate, and individual tBu$_2$Ge(OH)$_2$ (**1**)[3a] and tBu$_2$Si(OH)$_2$,[7] are virtually the same and adopt polymeric double chain ribbons (Figure 2). Selected hydrogen bond lengths and angles are listed

[a] Lehrstuhl für Anorganische Chemie II der Universität Dortmund,
44221 Dortmund, Germany
Fax: (internat.) + 49-231/755-5048
E-mail: kjur@platon.chemie.uni-dortmund.de

[+] This work contains part of the Ph. D. Thesis of J. B., Dortmund University, **1999**.

 © WILEY-VCH Verlag GmbH, D-69451 Weinheim, 2000 1434–1948/00/0505–0939 $ 17.50+.50/0

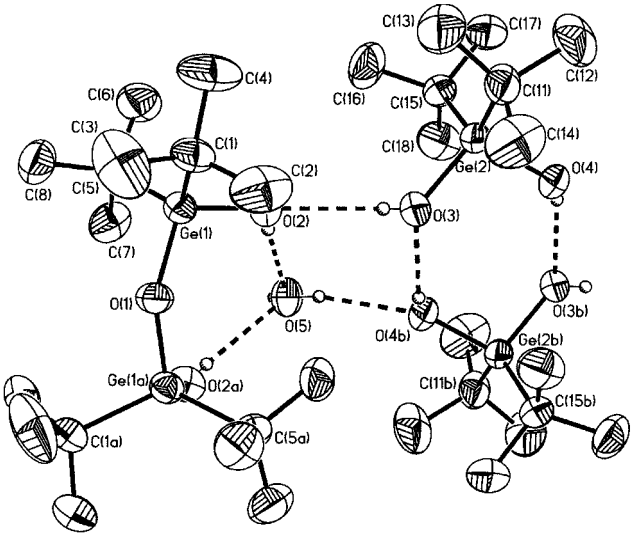


Figure 1. General view (SHELXTL-PLUS) of the cocrystallate showing 30% probability displacement ellipsoids and the atom numbering scheme

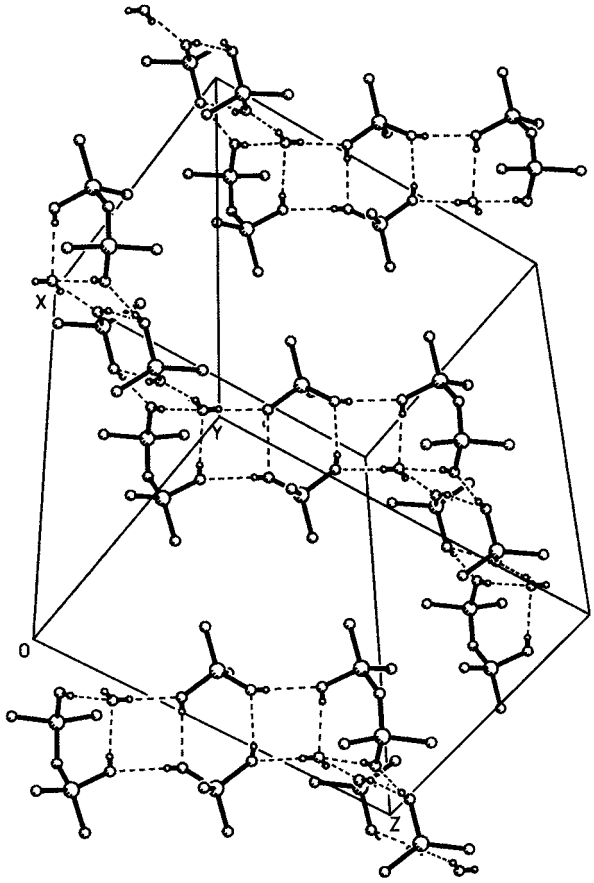


Figure 2. Perspective view (SHELXTL-PLUS) of the hydrogen bonding in the crystal lattice

in Table 3. The observed O···O distances in the cocrystallate are within the range of related compounds, e.g. organosilanols, and show no particularities.[1]

With the view that the crystals can be regarded as supramolecular entities, a comprehensive knowledge of the parameters which control the solid state structures is very welcome.[8] In this context it is obvious that the bulky *tert*-butyl groups dominate the structures of the above-mentioned compounds. This assumption is further supported by the isotypic di-*tert*-butyl element oxides (tBu$_2$MO)$_3$ (M = Si, Ge, Sn)[3a,9a,9b] and di-*tert*-butyl element imides (tBu$_2$MNH)$_3$ (M = Si, Sn).[10a,10b]

Table 1. Crystal data and structure refinement for 2tBu$_2$Ge(OH)$_2$·(tBu$_2$GeOH)$_2$O·H$_2$O

Formula	$C_{16}H_{38}Ge_2O_3 \cdot 2C_8H_{20}GeO_2 \cdot H_2O$
Form. wt.	883.3
Cryst. syst.	monoclinic
Cryst. size, mm	0.20 × 0.20 × 0.18
Space group	*C2/c*
a, Å	21.875(1)
b, Å	13.109(1)
c, Å	16.519(1)
β, deg	94.268(1)
V, Å^3	4723.8(5)
Z	4
ρ_{calcd}, Mg/m^3	1.242
ρ_{measd}, Mg/m^3	1.248(3)
μ, mm^{-1}	2.557
F(000)	1856
θ range, °	3.51 to 22.43
Index ranges	$-23 \le h \le 23$ $-14 \le k \le 14$ $-17 \le l \le 17$
No. of reflns.	23045
Completeness to θ_{max}	95.6
No. of indep. reflns./R_{int}	3071/0.0590
No. of reflns obsd with [$I > 2\sigma(I)$]	1965
No. refined params	229
GooF (F^2)	0.948
*R*1 (*F*) [$I > 2\sigma(I)$]	0.0321
*wR*2 (*F*2) (all data)	0.0691
$(\Delta/\sigma)_{max}$	<0.001
Largest diff peak/hole, e/Å^3	0.217/–0.283

Experimental Section

General Remarks: tBu$_2$Ge(OEt)$_2$ was synthesized by the reaction of tBuLi with Ge(OEt)$_4$.[11] – NMR spectra were recorded on a Bruker DRX 400 spectrometer operating at 400.13 MHz (^{1}H) and 100.62 MHz (^{13}C). Chemical shifts (δ) are given in ppm relative to SiMe$_4$. – Mass spectra were obtained on a Finnigan MAT 8230 spectrometer. – IR spectra were recorded on a Bruker FTIR IFS 113v spectrometer. – The elemental analyses were performed on an instrument from Carlo Erba Strumentazione (Modell 1106). – The density of single crystals was determined using a Micromeritics Accu Pyc 1330.

Synthesis of Di-*tert*-butylgermane Diol (1) and 1,1,3,3-Tetra-*tert*-butyldigermanoxane-1,3-diol (2): A solution of tBu$_2$Ge(OEt)$_2$ (5.54 g, 20.0 mmol) in ethanol (50 mL) was treated with water (900 mg, 50.0 mmol) and heated for 15 h at 40 °C. The solvent was then removed in vacuo. The residue was recrystallized several times from chloroform at –10 °C affording colorless crystals of **1** as the first fraction (1.4 g, 6.3 mmol, 32%, m.p. 146 °C). – ^{1}H NMR (400.13 MHz, $CDCl_3$): δ = 1.49 (s, 2 H, GeO*H*) 1.70 (s, 18 H, GeC*Me$_3$*). – ^{13}C{^{1}H} NMR (100.62 MHz, $CDCl_3$): δ = 29.1 (Ge*C*Me$_3$) 27.4 (GeC*Me$_3$*). – IR (KBr): ν_{OH} = 3248 (bs) cm^{-1}. – $C_8H_{20}GeO_2$ (220.9): C 43.50, H 9.13; found C 44.00, H 9.43. – From the residue a second crystalline fraction was obtained (2.8 g)

Table 2. Selected bond lengths [Å] and angles [°] for $2\,tBu_2Ge(OH)_2{\cdot}(tBu_2GeOH)_2O{\cdot}H_2O$

Ge(1)–O(1)	1.7599(12)	Ge(1)–O(2)	1.779(4)
Ge(1)–C(1)	1.962(4)	Ge(1)–C(5)	1.957(4)
Ge(2)–O(3)	1.783(3)	Ge(2)–O(4)	1.772(4)
Ge(2)–C(11)	1.963(5)	Ge(2)–C(15)	1.953(4)
O(1)–Ge(1)–O(2)	109.12(18)	O(1)–Ge(1)–C(1)	105.49(17)
O(1)–Ge(1)–C(5)	109.14(13)	O(2)–Ge(1)–C(1)	105.8(2)
O(2)–Ge(1)–C(5)	107.3(2)	C(1)–Ge(1)–C(5)	119.6(2)
O(3)–Ge(2)–O(4)	103.04(18)	O(3)–Ge(2)–C(11)	108.7(2)
O(3)–Ge(2)–C(15)	108.62(17)	O(4)–Ge(2)–C(11)	103.7(2)
O(4)–Ge(2)–C(15)	109.4(2)	C(11)–Ge(2)–C(15)	121.8(2)
Ge(1)–O(1)–Ge(1a)[a]	143.9(2)		
O(2)–Ge(1)–O(1)–Ge(1a)	–28.09(17)	C(1)–Ge(1)–O(1)–Ge(1a)	–141.40(16)
C(5)–Ge(1)–O(1)–Ge(1a)	88.88(15)		

[a] Symmetry transformations used to generate equivalent atoms: $a = -x + 1, y, -z + 0.5$.

Table 3. Hydrogen bond lengths [Å] and angles [°] for $2tBu_2Ge(OH)_2{\cdot}(tBu_2GeOH)_2O{\cdot}H_2O$

D–H···A	d (D–H)	d (H···A)	d (D···A)	(D–H–A)
O(2)–H(2')···O(5)	0.58(5)	2.27(5)	2.840(7)	173(8)
O(3)–H(3')···O(2b)[a]	0.61(4)	2.24(4)	2.849(5)	175(7)
O(4)–H(4')···O(3c)[b]	0.60(5)	2.20(5)	2.775(6)	162(8)
O(5)–H(5")···O(4)	0.65(6)	2.21(6)	2.829(4)	162(8)

[a] Symmetry transformations used to generate equivalent atoms: $b = x, -y + 1, z + 0.5$. – [b]Symmetry transformations used to generate equivalent atoms: $c = -x + 1, -y + 1, -z + 1$.

which, according to ^{1}H NMR spectroscopy, still contained a mixture of **1** and **2** in a ratio of about 2:1. From the second fraction a single crystal was taken for the X-ray diffraction studies. From the remainder, compound **2** (850 mg, 2.0 mmol, 20%, m.p. 87 °C) was isolated by size-exclusion chromatography (Sephadex-G20, CH_2Cl_2). – ^{1}H NMR (400.13 MHz, $CDCl_3$): δ = 1.85 (s, 2 H, GeOH) 1.11 (s, 36 H, GeC*Me*$_3$). – ^{13}C{^{1}H} NMR (100.62 MHz, $CDCl_3$): δ = 29.8 (GeC*Me*$_3$), 27.9 (GeC*Me*$_3$). – IR (KBr) ν_{OH}: 3314 (bm) cm^{-1}. – MS; *m/z* (%): 367 (50) [$M^+ - C_4H_9$], 349 (28) [$M^+ - C_4H_{11}O$], 293 (72) [$M^+ - C_8H_{19}O$], 277 (22) [$M^+ - C_8H_{19}O_2$]. – $C_{16}H_{38}Ge_2O_3$ (423.7): C 45.35, H 9.04; found C 45.83, H 9.90. – Using the same procedure with a large excess of water (25 mL), the diorganogermane diol **1** was formed almost quantitatively.

X-ray Crystallography: Intensity data for the colorless crystals grown from chloroform were collected on a Nonius Kappa CCD diffractometer with graphite-monochromated Mo-K_α (0.71069 Å) radiation at 291 K. The data collection covered almost the whole sphere of reciprocal space with 360 frames via ω-rotation (Δ/ω = 1°) at two times 20s per frame. The crystal-to-detector distance was 3.0 cm. Crystal decay was monitored by repeating the initial frames at the end of data collection. Analyzing the duplicate reflections there was no indication for any decay. The data were not corrected for absorption effects. The structure was solved by direct methods SHELXS97[12a] and successive difference-Fourier syntheses. Refinement applied full-matrix least-squares methods SHELXL97.[12b] – The H atoms of the hydroxy groups and the water molecule were located in the difference Fourier map and refined isotropically. The other H atoms were placed in geometrically calculated positions using a riding model (including free rotation about C–C) and refined with a common isotropic temperature factor [C–$H_{prim.}$ 0.96 Å; U_{iso} 0.160(4) Å^2]. – Atomic scattering factors for neutral atoms and real and imaginary dispersion terms were taken from the International Tables for X-ray Crystallography.[12c] The figures were created by SHELXTL-Plus.[12d] Crystallographic data are given in Table 1, selected bond distances and angles in Table 2, and hydrogen bond distances and angles in Table 3. – Crystallographic data for the structures reported in this paper have been deposited with the Cambridge Crystallographic Data Centre as supplementary publication no. CCDC-136796. Copies of the data can be obtained free of charge on application to CCDC, 12 Union Road, Cambridge CB2 1EZ, UK [Fax: (internat.) + 44-1223/336-033; E-mail: deposit@ccdc.cam.ac.uk].

Acknowledgments

We thank the Deutsche Forschungsgemeinschaft and the Fonds der Chemischen Industrie for financial support.

[1] P. D. Lickiss, *Adv. Inorg. Chem*. **1995**, *42*, 147–262.
[2] R. Murugavel, A. Voigt, M. G. Walawalker, H. W. Roesky, *Chem. Rev.* **1996**, *96*, 2205–2236.
[3] [3a] H. Puff, S. Franken, W. Schuh, W. Schwab, *J. Organomet. Chem*. **1983**, *254*, 33–41. – [3b] G. Ferguson, J. F. Gallagher, D. Murphy, T. R. Spalding, C. Glidewell, H. D. Holden, *Acta Cryst*. **1992**, *C48*, 1228–1231. – [3c] C. Glidewell, M. B. Hursthouse, D. Lloyd, K. W. Lumbard, R. L. Short, *J. Chem. Res.* **1996**, *400*, 3319–3323. – [3d] A. Kawachi, Y. Tanaka, K. Tamao, *Organometallics* **1997**, *16*, 5102–5107.
[4] H. Puff, S. Franken, W. Schuh, W. Schwab, *J. Organomet. Chem*. **1983**, *244*, C41–C42.
[5] M. Weidenbruch, H. Pesel, D. V. Hieu, *Z. Naturforsch*. **1980**, *35b*, 31–34.
[6] C. Glidewell, D. C. Liles, *Acta Cryst*. **1978**, *B34*, 119–124.
[7] N.H. Buttrus, C. Eaborn, P.B. Hitchcock, A.K. Saxena, *J. Organomet. Chem*. **1985**, *284*, 291–297.
[8] [8a] G. R. Desiraju, *Angew. Chem. Int. Ed. Engl*. **1995**, *34*, 2328–2361. – [8b] G. R. Desiraju, *Chem. Commun*. **1997**, 1475–1482. – [8c] D. Braga, F. Grepioni, G. R. Desiraju, *J. Organomet. Chem*. **1997**, *548*, 33–43. –
[9] [9a] W. Clegg, *Acta Cryst*. **1982**, *B38*, 1648–1649. – [9b] H. Puff, W. Schuh, R. Sievers, W. Wald, R. Zimmer, *J. Organomet. Chem*. **1984**, *260*, 271–280.
[10] [10a] W. Clegg, G. M. Sheldrick, D. Stalke, *Acta Cryst*. **1984**, *C40*, 433–434. – [10b] H. Puff, D. Hänssgen, N. Beckermann, A. Roloff, W. Schuh, *J. Organomet. Chem*. **1989**, *373*, 37–47.
[11] M. Weidenbruch, A. Ritschl, K. Peters, H. G. von Schnering, *J. Organomet. Chem*. **1992**, *438*, 39–44.
[12] [12a] G. M. Sheldrick, *Acta Cryst*. **1990**, *A46*, 467–473. – [12b] G. M. Sheldrick, University of Göttingen, **1997**. – [12c] *International Tables for Crystallography*, Kluwer Academic Publishers, Dordrecht, **1992**, Vol. C. – [12d] G. M. Sheldrick, SHELXTL-PLUS. Release 4.1 Siemens Analytical X-ray Instruments Inc., **1991**.

Received November 18, 1999
[I99413]

New Di- and Trinuclear Complexes with Pyrazolato Bridges. Crystal Structures of $[\{(C_6F_5)_2Pd(\mu\text{-}pz)(\mu\text{-}Cl)\}_2Pd]^{2-}$ and $[(C_6F_5)_2Pd(\mu\text{-}pz)_2Pd(\eta^3\text{-}C_4H_7)]$ (pz = pyrazolate)

José Ruiz,*[a] Félix Florenciano,[a] Miguel A. Sánchez,[a] Gregorio López,[a] M. Carmen Ramírez de Arellano,[b] and José Pérez[a]

Keywords: Pyrazolate complexes / Palladium / Platinum / N ligands / Bridging ligands

Trinuclear complexes containing pyrazolate bridging ligands of the type $[NBu_4]_2[\{(C_6F_5)_2\ M(\mu\text{-}pz)(\mu\text{-}X)\}_2M']$ (M, M′= Pd or Pt; X= Cl, OH, or pz) (Hpz = pyrazole) have been prepared using $[NBu_4][M(C_6F_5)_2(acac)]$ (acac = acetylacetonate) or $[NBu_4]_2[M_2(C_6F_5)_4(\mu\text{-}OH)_2]$ and $[M'Cl_2(Hpz)_2]$ or $[M'(Hpz)_4]^{2+}$ as starting materials. Asymmetric homo- and heterobimetallic complexes of the types $[NBu_4][R_2M(\mu\text{-}pz)_2Pd(\eta^3\text{-allyl})]$ and $[R_2M(\mu\text{-}pz)_2M'L_2]$ (allyl = C_3H_5 or C_4H_7; L_2 = 2 PEt_3 or bipy; R = C_6F_5 or C_6Cl_5; M, M′ = Pd or Pt) have been obtained starting from $[NBu_4][MR_2(pzHpz)]$ and $[Pd(\eta^3\text{-allyl})(acac)]$ or $[M'L_2Cl_2]$, respectively. The identity of the new complexes has been established by NMR (^1H, ^{19}F and ^{31}P) spectroscopy. The crystal structure of $[\{(C_6F_5)_2Pd(\mu\text{-}pz)(\mu\text{-}Cl)\}_2Pd]^{2-}$ has an inversion centre, with a bent appearance of the $Pd_3(\mu\text{-}pz)_2(\mu\text{-}Cl)_2$ moiety. The crystal structure of $[(C_6F_5)_2Pd(\mu\text{-}pz)_2Pd(\eta^3\text{-}C_4H_7)]$ has also been determined by single-crystal X-ray diffraction, where a boat conformation of the central "Pd_2N_4" six-membered rings is observed.

Introduction

Metal pyrazolate (pz) complexes have attracted considerable interest in recent years due to their versatile coordination chemistry,[1–10] and to a number of potential properties of these compounds such as catalytic activity [11] and bioactivity.[12] Pyrazolate exobidentate ligands can firmly hold two metal atoms in close proximity, thereby allowing extensive electron delocalization between the two centres. Homobimetallic pyrazolate-bridged nickel,[7,13] palladium,[14] and platinum[15] complexes $[\{M(C_6F_5)_2(\mu\text{-}pz)\}_2]^{2-}$ have previously been prepared in our laboratory by reaction between the basic $[\{M(C_6F_5)_2(\mu\text{-}OH)\}_2]^{2-}$ and the acidic pyrazole. We have also recently described[16] the preparation and characterization of mononuclear pyrazole-pyrazolate complexes of palladium(II) and platinum(II) $[NBu_4][R_2M(pzHpz)]$ (M = Pd, Pt; R = C_6F_5, C_6Cl_5; Hpz = pyrazole), which contain an acidic pyrazole ligand and which could act as metalloligands towards a variety of metallic fragments showing η^2 coordination mode, a synthetic strategy widely and successfully applied by Oro et al. to rhodium, ruthenium and iridium chemistry.[4–6,17,18] Studies of the reactivity of some palladium and platinum pyrazolate complexes towards Lewis acid metal complexes have been very recently reported.[9,10]

Oligomeric compounds of the type $[\{R_nM(\mu\text{-}pz)(\mu\text{-}X)\}_2M']^{m-}$ (M, M′ = Pd or Pt) are rare and only $[\{RM(\mu\text{-}pz)(\mu\text{-}X)\}_2M']$ (R = η^3-C_3H_5, η^3-C_4H_7) have been described.[19] In this paper we report the synthesis and characterization of trinuclear complexes of the type $[\{(C_6F_5)_2M(\mu\text{-}pz)(\mu\text{-}X)\}_2M']^{2-}$ (M, M′ = Pd or Pt; X = Cl, OH, or pz) as well as the preparation of asymmetric homo- and heterobimetallic complexes MM′ (M = Pd, Pt; M′ = Pd or Pt) with pyrazolato bridging ligands by using $[R_2M(pzHpz)]^-$ as a building block. The X-ray crystal structures of $[\{(C_6F_5)_2Pd(\mu\text{-}pz)(\mu\text{-}Cl)\}_2Pd]^{2-}$ (which is so far the first complex of this kind to be structurally characterized) and $[(C_6F_5)_2Pd(\mu\text{-}pz)_2Pd(\eta^3\text{-}C_4H_7)]$ are also reported.

The complexes $[NBu_4][M(C_6F_5)_2(acac)]$, $[NBu_4]_2[M_2(C_6F_5)_4(\mu\text{-}OH)_2]$, $[NBu_4][MR_2(pzHpz)]$ (M = Pd, Pt) and $[Pd(\eta^3\text{-allyl})(acac)]$ have shown to be useful precursors for the synthesis of the polynuclear compounds reported herein.

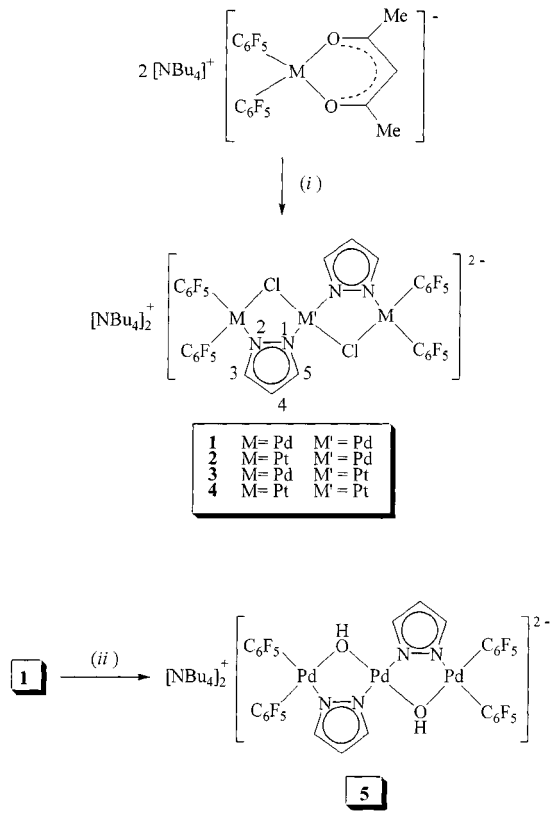
Results and Discussion

The reaction (2:1) between the mononuclear complex $[NBu_4][M(C_6F_5)_2(acac)]$ (M′ Pd or Pt) and *trans*-$[M'(pzH)_2Cl_2]$ (M′ Pd or Pt) in acetone or methanol leads to the corresponding trinuclear complex $[NBu_4]_2[\{(C_6F_5)_2M(\mu\text{-}pz)(\mu\text{-}Cl)\}_2M']$ (M, M′ = Pd or Pt) (Scheme 1) with the concomitant release of Hacac.

Elemental analyses of these complexes are satisfactory and the complexes have been characterized by IR, ^1H and $^{19}F\{^1H\}$ NMR spectroscopy. Measurements of the molar conductivity in acetone indicate that they behave as 2:1 electrolytes.[20] The IR spectra of complexes **1–4** show the characteristic absorptions of the C_6F_5 group[21] at 1630, 1490, 1450, 1050, 950 cm^{-1} and a split band at ca. 800 cm^{-1}, derived from the so-called X-sensitive mode in C_6F_5-halogen

[a] Departamento de Química Inorgánica, Universidad de Murcia, E-30071 Murcia, Spain
E-mail: jruiz@fcu.um.es
[b] Departamento de Química Orgánica, Facultad de Farmacia, Universidad de Valencia, 46100 Valencia, Spain
E-mail: mcra@uv.es

 © WILEY-VCH Verlag GmbH, D-69451 Weinheim, 2000 1434–1948/00/0505–0943 $ 17.50+.50/0

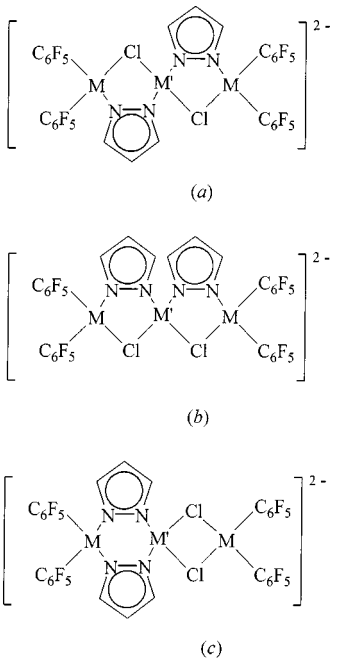


Scheme 1. (i) $M'Cl_2(pzH)_2$; (ii) 2 NBu_4OH

molecules, which is characteristic of the *cis*-$Pd(C_6F_5)_2$ fragment [16,22] and behaves like a ν(M–C) band.[23] The ^1H NMR spectra exhibit a set of three resonances for the pyrazolate rings which indicates that only one of the three possible geometrical isomers (Scheme 2) is present in solution. Taking into account the *trans* geometry of the complexes $[M'(pzH)_2Cl_2]$, (M′ = Pd[19] or Pt[24]) an *anti* arrangement (Scheme 2a) should be the most probable structure for these trinuclear complexes, and this is confirmed by an X-ray diffraction study of complex **1** (vide infra).

In all cases the resonance at δ = 5.8 or 5.9 is assigned to the 4-H. The resonance at δ = 6.84 or 6.87 in complexes **2** or **4**, respectively, appears flanked by ^{195}Pt satellites which suggests that it should be assigned to 3-H (with the numbering given in Scheme 1). The observed values for $J(^{195}Pt-^1H)$ (ca. 15 Hz) agree with the values found in the literature.[9,16,25] The ^{19}F NMR spectroscopy patterns are consistent with the presence of two nonequivalent C_6F_5 groups, one trans to Cl and one trans to pz. As expected, the *ortho* F signals of complexes **2** and **4** are flanked by the satellites due to coupling to ^{195}Pt.

The structure of **1** is shown in Figure 1 and selected bond lengths and angles in Table 1. Insofar as we know this is the first tripalladium species of this kind to be structurally characterized. Since Pd(2) lies on an inversion centre, the "central" PdN_2Cl_2 unit is square planar. The geometry around the Pd(1) is essentially square-planar as well, the deviation of Pd(1) from the best plane through the atoms defining the coordination plane is 0.005(1) Å. The Pd_2(μ-pz)(μ-Cl) unit has an envelope conformation at Cl. The "central" PdN_2Cl_2 unit makes dihedral angles of 124.70(7)° to the "terminal" PdNCl planes, giving a bent appearance to the $Pd_3(\mu\text{-pz})_2(\mu\text{-Cl})_2$ moiety. The bridging chlorine to Pd(2) distances are significantly shorter than those to Pd(1). The Pd(2)Cl distance, 2.313(1) Å, is in the range found for chlorine trans to chlorine on Pd^{II}.[26] In a similar way the Pd(2)N distances are shorter than those of Pd(1)N. The distances between the central Pd(2) and the two Pd(1) atoms are 3.484 Å and show no significant metal–metal interactions. The pyrazolato rings are planar with the atoms defining the plane all being coplanar within 0.002(2) Å. The two pentafluorophenyl rings bonded to Pd(1) are planar and rotated 81.9(1)° with respect to each other. The rings present distortions as indicated by the values of the C–C–C angles which range from 113.7 to 124.3 °. This type of distortion has already been observed in other fluorophenyl rings.[27]



Scheme 2. Geometrical isomers of complexes **1**–**4**

The addition of [NBu_4]OH (aq) to a dichloromethane solution of **1** gives rise to the yellow hydroxo- homotrinuclear $[NBu_4]_2[\{(C_6F_5)_2Pd(\mu\text{-pz})(\mu\text{-OH})\}_2Pd]$ (**5**). The presence of the hydroxo- ligand is manifested by the observation of the characteristic IR absorption in the vicinity of 3600 cm^{-1} and of a high-field proton resonance at δ –1.82.[14] The X-ray crystal structure of the related binuclear hydroxo pyrazolate platinum complex $[NBu_4]_2[\{(C_6F_5)_2Pt\}_2(\mu\text{-pz})(\mu\text{-OH})]$ has previously been reported.[15]

The reaction (1:2:1) between $[NBu_4]_2[M_2(C_6F_5)_4(\mu\text{-OH})_2]$ (M′ = Pd or Pt), [NBu_4]OH (aq) and $[M'(pzH)_4]Cl_2$ (M = Pd or Pt) leads to the formation of the white trimeric complexes $[NBu_4]_2[\{(C_6F_5)_2M(\mu\text{-pz})_2)\}_2M']$ (M, M′ = Pd or Pt) **6–8** (Scheme 3) containing four pyrazolate anions as bridging ligands. The ^1H NMR spectra exhibit a unique set of three resonances with relative intensities of 4:4:4 for the pyrazolato rings. The ^{19}F NMR spectra of compounds **6–8**

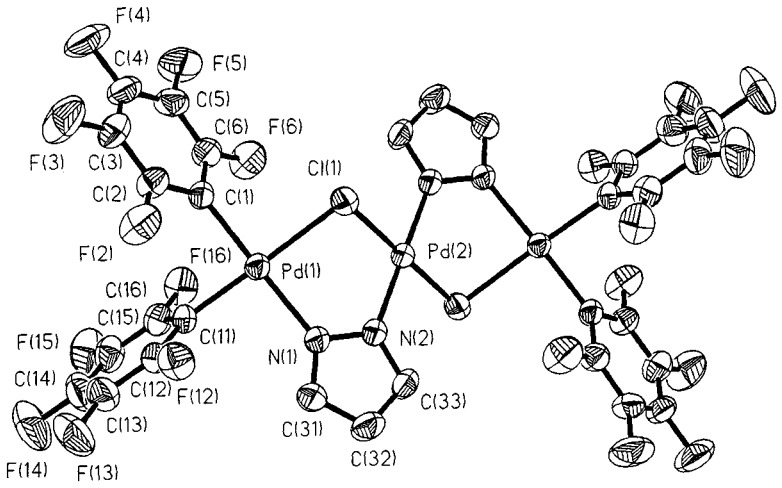
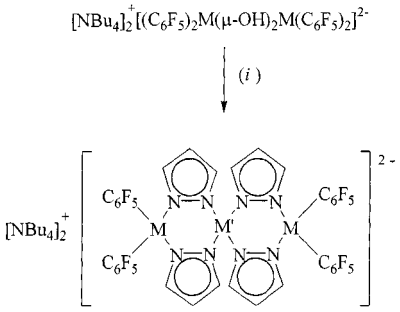


Figure 1. Structure of **1** showing the atom numbering scheme; hydrogen atoms have been omitted for clarity

Table 1. Selected distances (Å) and bond angles (deg) for complex **1**

Bond Distances		Bond Angles	
Pd(1)–C(1)	1.995(3)	C(1)–Pd(1)–C(11)	86.57(14)
Pd(1)–N(1)	2.076(3)	C(11)–Pd(1)–N(1)	95.26(13)
Pd(2)–N(2)[a]	2.001(3)	C(11)–Pd(1)–Cl(1)	178.03(10)
Pd(2)–Cl(1)[a]	2.013(3)	N(2)[a]–Pd(2)–N(2)	180.0
Pd(1)–C(11)	1.999(4)	N(2)–Pd(2)–Cl(1)[a]	91.67(9)
Pd(1)–Cl(1)	2.4025(11)	N(2)–Pd(2)–Cl(1)	88.33(9)
Pd(2)–N(2)	2.001(3)	C(1)–Pd(1)–N(1)	177.28(12)
Pd(2)–Cl(1)	2.3125(10)	C(1)–Pd(1)–Cl(1)	92.01(11)
		N(1)–Pd(1)–Cl(1)	86.20(10)
		N(2)[a]–Pd(2)–Cl(1)[a]	88.33(9)
		N(2)[a]–Pd(2)–Cl(1)	91.67(9)
		Cl(1)[a]–Pd(2)–Cl(1)	180.0

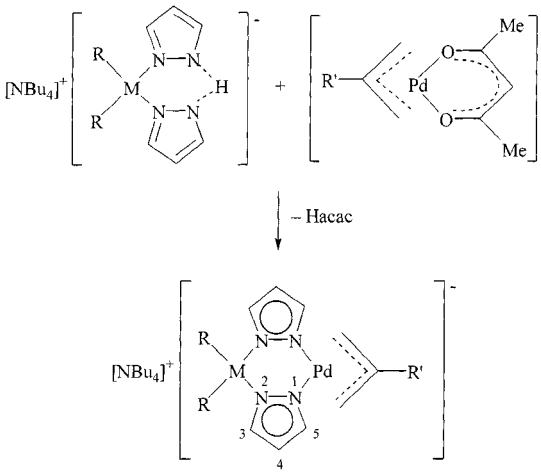
[a] Symmetry transformations used to generate equivalent atoms: $-x + 1, -y + 1, -z + 1$.



6	M = Pd	M' = Pd
7	M = Pd	M' = Pt
8	M = Pt	M' = Pt

Scheme 3. (i) $M'(pzH)_4Cl_2/2\ NBu_4OH$

at room temperature show the presence of two resonances for the *ortho* F atoms together with a resonance for the *para* F atom which suggests that rotation around the Pd–C bond is hindered. A boat conformation of the central $MM'N_4$ six-membered rings should be expected.[10,23]



9	M = Pd,	R = C_6F_5,	R' = Me
10	M = Pd,	R = C_6F_5,	R' = H
11	M = Pd,	R = C_6Cl_5,	R' = Me
12	M = Pd,	R = C_6Cl_5,	R' = H
13	M = Pt,	R = C_6F_5,	R' = Me
14	M = Pt,	R = C_6F_5,	R' = H

Scheme 4. Synthesis of allyl complexes **9**–**14**

The mononuclear palladium or platinum complexes *cis*-$[MR_2(pzHpz)]^-$ (R = C_6F_5 or C_6Cl_5) react with [Pd(acac)(η^3-allyl)] (allyl = C_3H_5 or C_4H_7) to give [$R_2M(\mu$-$pz)_2Pd(\eta^3$-allyl)] complexes (Scheme 4) with the concomitant release of Hacac. The related metal complexes [Ir(η^5-C_5Me_5)$(pz)_2$(Hpz)] or [Ru(η^6-*p*-cymene)$(pz)_2$(Hpz)] give similar reactions.[5,6,17,18]

The new complexes **9–14** have been characterized on the basis of partial elemental analysis and spectroscopic data. The IR spectra show the bands assigned to the C_6F_5 (1630, 1490, 1460, 1050 and 950 cm^{-1})[20] or the C_6Cl_5 (1315, 1285, 1220 and 670 cm^{-1})[28] groups. Morever, a split absorption located at ca. 800 cm^{-1} in the spectra of the bis(pentahalophenyl) derivatives [22,29] is observed. Complexes **9–14** be-

have in acetone as 1:1 electrolytes,[19] in accordance with the formulae given.

The two signals observed in the *ortho*-F region of the ^{19}F NMR spectra of compounds **13** and **14** indicate that rotation of the C_6F_5 groups around the carbon–metal bond is hindered.

The ^1H NMR spectra consist of three resonances with relative intensities of 2:2:2 for the heterocyclic rings. The resonance at $\delta = 5.9–5.4$ in the spectra of complexes **9–14** are unambiguously assigned to the 4-H atom (the numbering given in Scheme 4). The high-field pyrazolyl resonance at ca. $\delta = 7.3–7.1$ should be assigned to 3-H because this signal is flanked by ^{195}Pt satellites in the spectra of compounds **13** and **14**.

The ^1H NMR spectra of complexes **10, 12** and **14** also show three resonances with an intensity ratio of 1: 2: 2 in the allylic group region, whereas the spectra of complexes **9**, **11** and **13** show three singlets for the methylallyl group with the expected intensity ratio of 2:2:3.

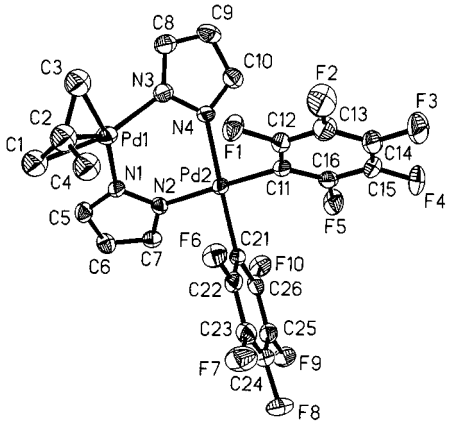


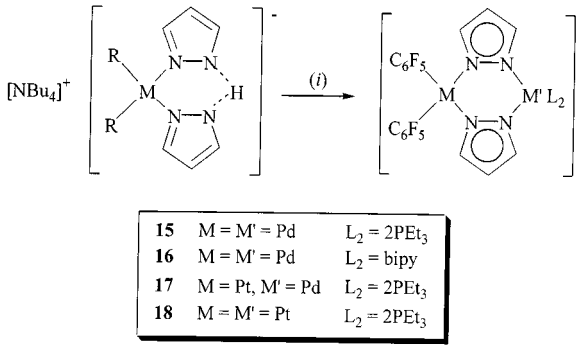
Figure 2. Structure of the anion of **9** showing the atom numbering scheme; hydrogen atoms have been omitted for clarity

The crystal structure of the anion of complex **9** is shown in Figure 2 and selected bond lengths and angles in Table 2. The structure shows an asymmetric dinuclear complex in which the Pd(η^3-allyl) and the Pd(C_6F_5)$_2$ units are bridged by two pyrazolate ligands. The Pd(1)–Pd(2) vector is coplanar with both pyrazolate ligands (mean deviations 0.035 and 0.048 Å). The Pd(1)–N(1)–N(2)–Pd(2)–N(4)–N(3) ring exhibits a typical boat conformation with a dihedral angle Pd(1)–Pd(2)–N(1)–N(2) and Pd(1)–Pd(2)–N(3)–N(4) of 65.3°. The allyl ligand is bonded to the Pd(1) atom in an asymmetric η^3-mode [Pd(1)–C(1) 2.172(9) and Pd(1)–C(3) 2.110(9) Å]. The vector joining the centre of the C(1)–C(2)–C(3) fragment and the Pd(1) atom makes an angle of 65.2° with the allyl plane. The Pd(2) centre shows a square planar geometry.

Although the hydrogen of the (pyrazole)(pyrazolato) complexes [MR_2(pz)(Hpz)]$^-$ (M = Pd or Pt) cannot be abstracted by reaction with an additional mol of NBu_4OH, in the presence of chloro complexes of the type [$M'Cl_2L_2$] (M' = Pd or Pt; L_2 = 2 PEt_3 or bipy), both metal complexes allow the preparation, in acetone, of the new heterodinuclear complexes [$(C_6F_5)_2M(\mu\text{-pz})_2M'L_2$] (**15–18**; Scheme 5), which were recrystallized from dichloromethane/hexane.

Table 2. Selected distances (Å) and bond angles (deg) for complex **9**

Bond Distances		Bond Angles	
Pd(1)–C(1)	2.172(9)	N(3)–Pd(1)–N(1)	93.40(14)
Pd(1)–C(2)	2.149(8)	N(3)–Pd(1)–C(3)	99.2(2)
Pd(1)–C(3)	2.110(9)	N(1)–Pd(1)–C(1)	97.3(2)
Pd(1)–N(1)	2.071(3)	N(1)–Pd(1)–C(3)	116.3(3)
Pd(1)–N(3)	2.066(4)	N(3)–Pd(1)–C(1)	165.5(2)
Pd(2)–C(11)	2.012(5)	N(3)–Pd(1)–C(2)	134.7(2)
Pd(2)–C(21)	2.012(4)	N(1)–Pd(1)–C(2)	129.4(2)
Pd(2)–N(2)	2.066(4)	C(1)–C(2)–C(3)	111.5(8)
Pd(2)–N(4)	2.057(3)	C(11)–Pd(2)–C(21)	86.7(2)
		C(11)–Pd(2)–N(4)	90.5(2)
		C(11)–Pd(2)–N(2)	176.4(2)
		C(21)–Pd(2)–N(2)	91.8(2)
		C(21)–Pd(2)–N(4)	177.2(2)
		N(4)–Pd(2)–N(2)	90.98(14)



15	M = M' = Pd	$L_2 = 2PEt_3$
16	M = M' = Pd	L_2 = bipy
17	M = Pt, M' = Pd	$L_2 = 2PEt_3$
18	M = M' = Pt	$L_2 = 2PEt_3$

Scheme 5. (i) $NBu_4OH/[M'Cl_2L_2]$

All complexes give satisfactory analytical data. The ^1H NMR spectrum of complex **17** exhibits a resonance at $\delta = 7.41$, flanked by ^{195}Pt satellites. The ^{19}F NMR spectra of complexes **15, 17** and **18** show a broad resonance for the *ortho* F atoms, but a unique resonance for the *para* F atom, indicating partial restriction in the rotation around the M–C bond. Two multiplets for the methylene and methyl groups of the PEt_3 ligands are observed in the ^1H NMR spectra, in agreement with previous results.[30,31]

The presence of two resonances in the ^{19}F NMR spectrum of **16** for the *ortho* F atoms together with a resonance for the *para* F atom suggest again that rotation around the Pd–C bond is restricted even at room temperature.

The ^{31}P NMR spectra of **15** and **17** show a unique resonance whereas complex **18** exhibits a singlet with ^{195}Pt satellites (J_{Pt-P} = 3060 Hz). Several heteropolymetallic systems involving platinum(II) and palladium(II) of general formula [(L–L)M(μ-az)$_2$M'X$_2$] (where L–L is a chelating ligand, M = Pt or Pd, M' = Zn, Cd or Ni) have recently been reported.[9,25]

Experimental Section

General Methods: C, H and N analyses were performed with a Carlo Erba model EA 1108 microanalyzer. – Decomposition temperatures were determined with a Mettler TG-50 thermobalance

with a heating rate of 10°C min^{-1}. – Molar conductivities were measured in an acetone solution ($c \approx 5 \times 10^{-4}$ mol dm^{-3}) with a Crison 525 conductimeter. – The NMR spectra were recorded on a Bruker AC 200E (^{1}H) or Varian Unity 300 (^{19}F, ^{31}P) spectrometer. – Infrared spectra were recorded on a Perkin–Elmer 16F PC FT-IR spectrophotometer using nujol mulls between polyethylene sheets. – The starting complexes $[NBu_4]_2[M_2(C_6F_5)_4(\mu\text{-}OH)_2]$ (M = Pd[14] or Pt[32]), [Pd(acac)(allyl)] (allyl = C_3H_5 or C_4H_7),[23] $[NBu_4][MR_2(pzHpz)]$ (M = Pd or Pt, R = C_6F_5 or C_6Cl_5),[16] $[NBu_4][M(C_6F_5)_2(acac)]$ (M = Pd or Pt),[14,32] $[ML_2Cl_2]$ (L_2 = PEt_3, M = Pd,[33] Pt;[34] L_2 = bipy, M′ Pd;[35] L = Hpz, M = Pd,[23] Pt[24]) and $[M(pzH)_4]Cl_2$ (M = Pd or Pt)[24] were prepared as described in the literature.

$[NBu_4]_2[\{(C_6F_5)_2Pd(\mu\text{-}pz)(\mu\text{-}Cl)\}_2M]$ M = Pd (1) or Pt (3): *trans*-$M(pzH)_2Cl_2$ (M = Pd, Pt) (0.064 mmol) was added to a solution of $[NBu_4][Pd(C_6F_5)_2(acac)]$ (100 mg, 0.13 mmol) in acetone (15 cm^3), the solution was stirred at room temperature for 30 min and the solvent was then partially evaporated under reduced pressure. On addition of ether and hexane the yellow complexes **1** and **3** precipitated and were filtered off and air-dried.

1: Yield 85%. – $C_{62}H_{78}Cl_2F_{20}N_6Pd_3$ (1677): calcd. C 44.4, H 4.7, N 5.0; found C 44.1, H 4.5, N 4.9. – M.p. 219 °C (dec.). – Λ_M = 171 S cm^2 mol^{-1}. – IR (nujol): $\tilde{\nu}$ = 796, 782 cm^{-1} (Pd-C_6F_5). – ^{1}H NMR ([D$_6$]acetone, TMS): δ = 7.47 (d, $J_{4,5}$ = 2.1 Hz, 2 H, H^5), 6.64 (d, $J_{3,4}$ = 1.7 Hz, 2 H, H^3), 5.83 (pseudo-t, 2 H, H^4). – ^{19}F NMR ([D$_6$]acetone, $CFCl_3$): δ = –112.9 (d, $J_{o,m}$ = 28.7 Hz, 4 F_o), –113.5 (d, $J_{o,m}$ = 27.6 Hz, 4 F_o), –163.7 (t, $J_{m,p}$ = 20.3 Hz, 2 F_p), –164.2 (t, $J_{m,p}$ = 19.1 Hz, 2 F_p), –165.2 (m, 4 F_m), –165.9 (m, 4 F_m).

3: Yield 74%. – $C_{62}H_{78}Cl_2F_{20}N_6Pd_2Pt$ (1766): calcd. C 42.2, H 4.5, N 4.8; found C 42.4, H 4.5, N 4.9. – M.p. = 211 °C (dec.). – Λ_M = 165 S cm^2 mol^{-1}. – IR (nujol): $\tilde{\nu}$ = 796, 784 cm^{-1} (Pd-C_6F_5). – ^{1}H NMR ([D$_6$]acetone, TMS): δ = 7.58 (d, $J_{4,5}$ = 1.9 Hz, 2 H, H^5), 6.84 (br, 2 H, H^3), 5.88 (pseudo-t, 2 H, H^4). – ^{19}F NMR ([D$_6$]acetone, $CFCl_3$): δ = –112.8 (d, $J_{o,m}$ = 25.6 Hz, 4 F_o), –113.4 (d, $J_{o,m}$ = 26.2 Hz, 4 F_o), –163.6 (t, $J_{m,p}$ = 19.5 Hz, 2 F_p), –164.1 (t, $J_{m,p}$ = 19.2 Hz, 2 F_p), –165.3 (m, 4 F_m), –165.8 (m, 4 F_m).

$[NBu_4]_2[\{(C_6F_5)_2Pt(\mu\text{-}pz)(\mu\text{-}Cl)\}_2M]$ M = Pd (2) or Pt (4): *trans*-$M(pzH)_2Cl_2$ (M= Pd, Pt) (0.046 mmol) was added to a solution of $[NBu_4][(C_6F_5)_2Pt(acac)]$ (80.0 mg, 0.1 mmol) in methanol (15 cm^3), the solution was stirred at room temperature for 6 h and the solvent was then partially evaporated under reduced pressure. The precipitate was collected by filtration and air-dried. Both compounds were recrystallized from dichloromethane/hexane.

2: Yield 75%. – $C_{62}H_{78}Cl_2F_{20}N_6PdPt_2$ (1855): calcd. C 40.2, H 4.2, N 4.5; found C 40.1, H 4.2, N 4.4. – M.p. = 225 °C (dec.). – Λ_M = 165 S cm^2 mol^{-1}. – IR (nujol): $\tilde{\nu}$ = 796, 782 cm^{-1} (Pt-C_6F_5). – ^{1}H NMR ([D$_6$]acetone, TMS): δ = 7.47 (br, 2 H, H^5), 6.84 (br, J_{HPt} = 15 Hz, 2 H, H^3), 5.87 (br pseudo-t, 2 H, H^4). – ^{19}F NMR ([D$_6$]acetone, $CFCl_3$): δ = –117.5 (d, $J_{o,m}$ = 23.1, J_{PtFo} = 446.6, J_{PtFo} = 550.2 Hz, 8F_o), –166.4 (t, $J_{m,p}$ = 19.7 Hz, 2 F_p), –166.7 (t, $J_{m,p}$ = 19.7 Hz, 2 F_p), –167.4 (m, 4 F_m), –167.8 (m, 4 F_m).

4: Yield 70%. – $C_{62}H_{78}Cl_2F_{20}N_6Pt_3$ (1943): calcd. C 38.1, H 4.1, N 4.3; found C 38.3, H 4.1, N 4.4. – M.p. = 246 °C (dec.). – Λ_M = 169 S cm^2 mol^{-1}. – IR (nujol): $\tilde{\nu}$ = 808, 798 cm^{-1} (Pt-C_6F_5). – ^{1}H NMR ([D$_6$]acetone, TMS): δ = 7.62 (d, $J_{4,5}$ = 1.7 Hz, 2 H, H^5), 6.87 (d, $J_{3,4}$ = 1.8, J_{HPt}= 15.1 Hz, 2 H, H^3), 5.94 (pseudo-t, 2 H, H^4). – ^{19}F NMR ([D$_6$]acetone, $CFCl_3$): δ = –117.6 (d, $J_{o,m}$ = 29.0, J_{PtFo} = 442.2, J_{PtFo} = 556.7 Hz, 8F_o), –166.2 (t, $J_{m,p}$ = 19.7 Hz, 2 F_p), –166.4 (t, $J_{m,p}$ = 20.0 Hz, 2 F_p), –167.3 (m, 4 F_m), –167.7 (m, 4 F_m).

$[NBu_4]_2[\{(C_6F_5)_2Pd(\mu\text{-}pz)(\mu\text{-}OH)\}_2Pd]$ (5): A 20% solution of $[NBu_4]OH$ (0.055 cm^3, 0.072 mmol) was added to a solution of **1** (60.0 mg, 0.036 mmol) in dichloromethane (10 cm^3). The solution was stirred at room temperature for 30 min and then concentrated to dryness. Addition of methanol and water followed by vigorous stirring rendered a yellow suspension, from which a yellow solid was filtered off and air-dried. – Yield 70%. – $C_{62}H_{80}F_{20}N_6O_2Pd_3$ (1641): calcd. C 45.4, H 4.9, N 5.1; found C 45.2, H 4.7, N 5.0. – M.p. = 185 °C (dec.). – Λ_M = 193 S cm^2 mol^{-1}. – IR (nujol): $\tilde{\nu}$ = 3606 cm^{-1} (OH str), 794, 780 cm^{-1} (Pd-C_6F_5). – ^{1}H NMR ([D$_6$]acetone, TMS): δ = 7.0 (d, $J_{4,5}$ = 1.7 Hz, 2 H, H^5), 6.56 (br, 2 H, H^3), 5.82 (pseudo-t, 2 H, H^4), –1.82 (s, 2 H, OH). – ^{19}F NMR ([D$_6$]acetone, $CFCl_3$): δ = –112.9 (d, $J_{o,m}$ = 27.1 Hz, 4 F_o), –113.6 (d, $J_{o,m}$ = 25.6 Hz, 4 F_o), –164.9 (t, $J_{m,p}$ = 19.7 Hz, 2 F_p), –165.0 (t, $J_{m,p}$ = 20.0 Hz, 2 F_p), –166.1 (m, 8 F_m).

$[NBu_4]_2[\{(C_6F_5)_2Pd(\mu\text{-}pz)_2)\}_2M]$ M = Pd (6) or Pt (7): A 20% solution of $[NBu_4]OH$ (0.18 cm^3, 0.142 mmol), followed by $M(pzH)_4Cl_2$ (M′Pd, Pt) (0.071 mmol) were added to a solution of $[NBu_4]_2[(C_6F_5)_2Pd(\mu\text{-}OH)_2Pd(C_6F_5)_2]$ (100 mg, 0.071 mmol) in *N,N*-dimethylformamide (5 cm^3). The solution was stirred at room temperature for 1 h and on addition of water complexes **6** and **7** precipitated as white solids which were collected by filtration, washed with diethyl ether and air-dried.

6: Yield 85%. – $C_{68}H_{84}F_{20}N_{10}Pd_3$ (1747): calcd. C 46.9, H 4.9, N 8.0; found C 46.9, H 4.9, N 7.7. – M.p. = 272 °C (dec.). – Λ_M = 176 S cm^2 mol^{-1}. – IR (nujol): $\tilde{\nu}$ = 792, 778 cm^{-1} (Pd-C_6F_5). – ^{1}H NMR ([D$_6$]acetone, TMS): δ = 7.08 (d, $J_{4,5}$ = 1.6 Hz, 4 H, H^5), 6.89 (d, $J_{3,4}$ = 1.7 Hz, 4 H, H^3), 5.80 (pseudo-t, 4 H, H^4). – ^{19}F NMR ([D$_6$]acetone, $CFCl_3$): δ = –113.0 (d, $J_{o,m}$ = 30.7 Hz, 4 F_o), –114.9 (d, $J_{o,m}$ = 20.7 Hz, 4 F_o), –165.9 (t, J = 19.7 Hz, 4 F_p), –166.8 (br, 8 F_m).

7: Yield 82%. – $C_{68}H_{84}F_{20}N_{10}Pd_2Pt$ (1829): calcd. C 44.7, H 4.6, N 7.7; found C 44.4, H 4.3, N 7.5. – M.p. = 304 °C (dec.). – Λ_M = 199 S cm^2 mol^{-1}. – IR (nujol): $\tilde{\nu}$ = 792, 778 cm^{-1} (Pd-C_6F_5). – ^{1}H NMR ([D$_6$]acetone, TMS): δ = 7.08 (d, $J_{4,5}$ = 2.1 Hz, 4 H, H^5), 6.93 (d, $J_{3,4}$ = 1.8 Hz, 4 H, H^3), 5.83 (pseudo-t, 4 H, H^4). – ^{19}F NMR ([D$_6$]acetone, $CFCl_3$): δ = –113.1 (d, $J_{o,m}$ = 28.9 Hz, 4 F_o), –114.7 (d, $J_{o,m}$ = 27.5 Hz, 4 F_o), –166.0 (t, $J_{m,p}$ 19.1 Hz, 4 F_p), –166.8 (br, 8F_m).

$[NBu_4]_2[\{(C_6F_5)_2Pt(\mu\text{-}pz)_2)\}_2Pt]$ (8): A 20% solution of $[NBu_4]OH$ (0.13 cm^3, 0.10 mmol), followed by $Pt(pzH)_4Cl_2$ (26.32 mg, 0.10 mmol) were added to a solution of $[[NBu_4]_2[(C_6F_5)_2Pt(\mu\text{-}OH)_2Pt(C_6F_5)_2]$ (80.0 mg, 0.05 mmol) in methanol (10 cm^3). The solution was stirred at room temperature for 4 h and the solvent was then partially evaporated under reduced pressure. On addition of water the white complex **8** precipitated and was filtered off and air-dried. – Yield 72%. – $C_{68}H_{84}F_{20}N_{10}PdPt_2$ (1918): calcd. C 42.6, H 4.4, N 7.3; found C 42.7, H 4.2, N 7.1. – M.p. = 295 °C (dec.). – Λ_M = 180 S cm^2 mol^{-1}. – IR (nujol): $\tilde{\nu}$ = 804, 792 cm^{-1} (Pt-C_6F_5). – ^{1}H NMR ([D$_6$]acetone, TMS): δ = 7.17 (d, $J_{3,4}$ = 1.7 Hz, J_{HPt} = 15.6 Hz, 4 H, H^3), 6.97 (d, $J_{4,5}$ = 1.7 Hz, 4 H, H^5), 5.87 (pt, J = 2.0 Hz, 4 H, H^4). – ^{19}F NMR ([D$_6$]acetone, $CFCl_3$): δ = –116.2 (br, J_{PtFo} = 465 Hz, 4 F_o), –117.3 (br, J_{PtFo} = 506 Hz, 4 F_o), –166.7 (m, 4 F_p+ 8 F_m).

$[NBu_4][R_2M(\mu\text{-}pz)_2Pd(\eta^3\text{-}allyl)]$ (9–14): [Pd (allyl)(acac)] (allyl = C_3H_5 or C_4H_7) (0.122 mmol) was added to a solution of $[NBu_4][R_2M(pzHpz)]$ (M = Pd or Pt, R = C_6F_5 or C_6Cl_5) (0.122 mmol) in dichloromethane (8 cm^3). The solution was stirred at room temperature for 30 min and the solvent was then partially evaporated under reduced pressure. On addition of hexane the

white complexes **9–14** precipitated and were filtered off and air-dried (see Scheme 4).

9: Yield 70%. – $C_{38}H_{43}F_{10}N_5Pd_2$ (972.6): calcd. C 46.9, H 4.5, N 7.2; found C 46.6, H 4.8, N 7.2. – M.p. = 247 °C (dec.). – Λ_M = 102 S cm^2 mol^{-1}. – IR (nujol): $\tilde{\nu}$ = 785, 775 cm^{-1} (Pd-C_6F_5). – ^{1}H NMR ([D$_6$]acetone, TMS): δ = 7.30 (d, $J_{4,5}$ = 1.8 Hz, 2 H, H^5), 7.10 (d, $J_{3,4}$ = 1.8 Hz, 2 H, H^3), 5.88 (pt, 2 H, H^4), 3.49 (s, 2 H, H_{syn}), 2.86 (s, 2 H, H_{anti}), 2.30 (s, 3 H, CH_3). – ^{19}F NMR ([D$_6$]acetone, $CFCl_3$): δ = –113.4 (d, $J_{o,m}$ = 32.2 Hz, 2 F_o), –114.2 (d, $J_{o,m}$ = 32.2 Hz, 2 F_o), –166.1 (t, $J_{m,p}$ 19.8 Hz, 2 F_P), –166.7 (m, 4 F_m).

10: Yield 75%. – $C_{37}H_{41}F_{10}N_5Pd_2$ (958.6): calcd. C 46.4, H 4.3, N 7.3; found C 46.1, H 4.6, N 7.2. – M.p. = 284 °C (dec.). – Λ_M = 91 S cm^2 mol^{-1}. – IR (nujol): $\tilde{\nu}$ = 785, 775 cm^{-1} (Pd-C_6F_5). – ^{1}H NMR ([D$_6$]acetone, TMS): δ = 7.30 (d, $J_{4,5}$ = 1.9 Hz, 2 H, H^5), 7.13 (d, $J_{3,4}$ = 1.9 Hz, 2 H, H^3), 5.91 (pt, 2 H, H^4), 5.74 (m, 1 H, H^2), 3.75 (d, J = 6.9 Hz, 2 H, H_{syn}), 3.05 (d, J = 12.3 Hz, 2 H, H_{anti}). – ^{19}F NMR ([D$_6$]acetone, $CFCl_3$): δ = –113.9 (d, $J_{o,m}$ = 31.6 Hz Hz, 4 F_o), –166.0 (t, $J_{m,p}$ = 20.0 Hz, 2 F_p), –166.7 (m, 4 F_m).

11: Yield 75%. – $C_{38}H_{43}Cl_{10}N_5Pd_2$ (1137): calcd. C 40.1, H 3.8, N 6.2; found C 39.9, H 4.0, N 5.9. – M.p. = 234 °C (dec.). – Λ_M = 100 S cm^2 mol^{-1}. – IR (nujol): $\tilde{\nu}$ = 830, 825 cm^{-1} (Pd-C_6Cl_5). – ^{1}H NMR ([D$_6$]acetone, TMS): δ = 7.33 (d, $J_{4,5}$ = 1.7 Hz, 2 H, H^5), 7.29 (d, $J_{3,4}$ = 1.7 Hz, 2 H, H^3), 5.84 (pt, 2 H, H^4), 3.48 (s, 2 H, H_{syn}), 2.87 (s, 2 H, H_{anti}), 2.23 (s, 3 H, CH_3).

12: Yield 70%. – $C_{37}H_{41}Cl_{10}N_5Pd_2$ (1123): calcd. C 39.6, H 3.7, N 6.2; found C 39.6, H 3.9, N 6.2. – M.p. = 230 °C (dec.). – Λ_M = 101 S cm^2 mol^{-1}. – IR (nujol): $\tilde{\nu}$ = 835, 825 cm^{-1} (Pd-C_6Cl_5). – ^{1}H NMR ([D$_6$]acetone, TMS): δ = 7.32 (d, $J_{4,5}$ = 1.9 Hz, 2 H, H^5), 7.30 (d, $J_{3,4}$ = 1.9 Hz 2 H, H^3), 5.84 (pt, 2 H, H^4), 5.69 (m, 1 H, H^2), 3.69 (d, J = 6.9 Hz, 2 H, H_{syn}), 3.00 (d, J = 12.4 Hz, 2 H, H_{anti}).

13: Yield 84%. – $C_{38}H_{43}F_{10}N_5PdPt$ (1061): calcd. C 43.0, H 4.1, N 6.6; found C 43.1, H 4.0, N 6.3. – M.p. = 324 °C (dec.). – Λ_M = 97 S cm^2 mol^{-1}. – IR (nujol): $\tilde{\nu}$ = 800, 790 cm^{-1} (Pt-C_6F_5). – ^{1}H NMR ([D$_6$]acetone, TMS): δ = 7.30 (d, $J_{4,5}$ = 1.8 Hz, 2 H, H^5), 7.20 (d, $J_{3,4}$ = 1.8, J_{HPt} = 14.5 Hz, 2 H, H^3), 5.92 (pt, 2 H, H^4), 3.50 (s, 2 H, H_{syn}), 2.80 (s, 2 H, H_{anti}), 2.28 (s, 3 H, CH_3). – ^{19}F NMR ([D$_6$]acetone, $CFCl_3$): δ = –117.2 (br, J_{PtFo} = 507.6 Hz, 2 F_o), –117.7 (br, J_{PtFo} = 505.8 Hz, 2 F_o), –168.0 (m, 2 F_p + 4 F_m).

14: Yield 90%. – $C_{37}H_{41}F_{10}N_5PdPt$ (1047): calcd. C 42.4, H 4.0, N 6.7; found C 42.3, H 4.3, N 6.6. – M.p. = 328 °C (dec.). – Λ_M = 99 S cm^2 mol^{-1}. – IR (nujol): $\tilde{\nu}$ = 800, 790 cm^{-1} (Pt-C_6F_5). – ^{1}H NMR ([D$_6$]acetone, TMS): δ = 7.28 (d, $J_{4,5}$ = 1.8 Hz, 2 H, H^5), 7.24 (d, J = 1.8, J_{HPt} = 13.5 Hz, 2 H, H^3), 5.93 (pt, 2 H, H^4), 5.70 (m, 1 H, H^2), 3.75 (d, J = 6.9 Hz, 2 H, H_{syn}), 3.04 (d, J = 12.3 Hz, 2 H, H_{anti}). – ^{19}F NMR ([D$_6$]acetone, $CFCl_3$): δ = –117.5 (br, J_{PtFo} = 507.9 Hz, 4 F_o), –167.8 (m, 2 F_p + 4 F_m).

[$R_2M(\mu\text{-pz})_2M'L_2$] (15–18): A 20% solution of [NBu$_4$]OH (0.122 mmol) was added to a solution of [NBu$_4$]-[M(C_6F_5)$_2$(pz)(Hpz)] (M = Pd or Pt) (0.122 mmol) in acetone (5 cm^3). After stirring for 5 min, [M′L_2Cl_2] (M′ = Pd, Pt; L_2 = 2 PEt_3, bipy) (0.122 mmol) was added to initially yield a suspension, that slowly changed to a solution that was stirred for 2 h (5 h for **18**) and then partially evaporated under reduced pressure. On addition of methanol/water the white complexes **15–18** precipitated. They were filtered off, washed with water and air-dried. Complexes **15–18** were recrystallized from dichloromethane/hexane (see Scheme 5).

15: Yield 53%. – $C_{30}H_{36}F_{10}N_4P_2Pd_2$ (917.4): calcd. C 39.3, H 4.0, N 6.1; found C 39.3, H 4.0, N 5.8. – M.p. = 289 °C (dec.). – IR (nujol): $\tilde{\nu}$ = 790, 780 cm^{-1} (Pd-C_6F_5). – ^{1}H NMR ([D$_6$]acetone, TMS): δ = 7.34 (br, 4 H), 6.01 (br, 2 H, H^4), 1.91 (m, 12 H, CH_2), 1.20 (dt, J_{HH} = 7.2 Hz, J_{PH} = 17.8, 18 H, CH_3). – ^{19}F NMR ([D$_6$]acetone, $CFCl_3$): δ = –113.1 (br, 4 F_o), –164.6 (t, 2 F_p, $J_{m,p}$ 19.7 Hz), –166.1 (m, 4 F_m). – ^{31}P NMR ([D$_6$]acetone, H_3PO_4): δ = 25.0 (s).

16: Yield 55%. – $C_{28}H_{14}F_{10}N_6Pd_2$ (837.3): calcd. C 40.2, H 1.7, N 10.0; found C 40.1, H 2.0, N 9.9. – M.p. = 318 °C (dec.). – IR (nujol): $\tilde{\nu}$ = 790, 780 cm^{-1} (Pd-C_6F_5). – ^{1}H NMR ([D$_6$]acetone, TMS): δ = 8.74 (d, J = 8.2 Hz, 2 H, H$^{3,3'}$ of bipy), 8.50 (m, 2 H, H$^{4,4'}$ of bipy), 7.85 (d, J = 1.4 Hz, 2 H, H$^{6,6'}$ of bipy), 7.82 (m, 2 H, H$^{5,5'}$ of bipy), 7.59 (d, J = 2.0 Hz, 2 H of pz), 7.31 (d, J = 2.0 Hz, 2 H of pz), 6.19 (pt, 2 H, H^4 of pz). – ^{19}F NMR ([D$_6$]acetone, $CFCl_3$): δ = –114.3 (br, 2 F_o), –115.3 (br, 2 F_o), –164.8 (t, $J_{m,p}$ = 18.3 Hz, 2 F_o), –166.3 (br, 4 F_m).

17: Yield 60%. – $C_{30}H_{36}F_{10}N_4P_2PdPt$ (1006): calcd. C 35.8, H 3.6, N 5.6; found C 36.0, H 3.7, N 5.3. – M.p. = 294 °C (dec.). – IR (nujol): $\tilde{\nu}$ = 800, 790 cm^{-1} (Pt-C_6F_5). – ^{1}H NMR ([D$_6$]acetone, TMS): δ = 7.41 (d, $J_{3,4}$ = 1.9, J_{HPt} = 14 Hz, 2 H, H^3), 7.35 (d, $J_{4,5}$ = 1.9 Hz, 2 H, H^5), 6.06 (pseudo-t, 2 H, H^4), 1.93 (m, 12 H, CH_2), 1.22 (dt, J_{HH} = 7.4, J_{PH} = 17.1 Hz, 18 H, CH_3). – ^{19}F NMR ([D$_6$]acetone, $CFCl_3$): δ = –116.2 (br, J_{Fo-Pt} = 514 Hz, 4 F_o), –167.3 (t, $J_{m,p}$ 19.7 Hz, 2 F_p), –167.4 (m, 4 F_m). – ^{31}P NMR ([D$_6$]-acetone, H_3PO_4): δ = 24.8 (s).

18: Yield 50%. – $C_{30}H_{36}F_{10}N_4P_2Pt_2$ (1094.72): calcd. C 32.9, H 3.3, N 5.1; found C 32.7, H 3.5, N 5.2. – M.p. = 298 °C (dec.). – IR (nujol): $\tilde{\nu}$ = 800, 790 cm^{-1} (Pt-C_6F_5). – ^{1}H NMR ([D$_6$]acetone, TMS): δ = 7.43 (br, 2 H), 7.39 (d, J = 2.1 Hz, 2 H), 6.11 (pt, 2 H, H^4), 1.95 (m, 12 H, CH_2), 1.17 (dt, J_{HH} = 7.5, J_{PH} = 16.9 Hz, 18 H, CH_3). – ^{19}F NMR ([D$_6$]acetone, $CFCl_3$): δ = –116.3 (br, J_{FoPt} = 457 Hz, 4 F_o), –166.3 (t, $J_{m,p}$ = 19.7 Hz, 2 F_p), –167.3 (m, 4 F_m). – ^{31}P NMR ([D$_6$]acetone, H_3PO_4): δ = –0.3 (s, J_{Pt-P} = 3060 Hz).

Determination of the X-ray Crystal Structure of 1 and 9: Crystals of **1** and **9** suitable for X-ray diffraction studies were grown from dichloromethane/hexane liquid diffusion, mounted on glass fibres

Table 3. Crystallographic data for compounds **1** and **9**

	1	**9**
Molecular formula	$C_{62}H_{78}Cl_2F_{20}N_6Pd_3$	$C_{38}H_{49}F_{10}N_5Pd_2$
M	1677	978.6
Crystal system	Monoclinic	Monoclinic
a (Å)	16.322(3)	12.7632(7)
b (Å)	10.486(2)	16.4972(10)
c (Å)	20.866(4)	20.3623(12)
β (°)	102.76(10)	100.989(4)
V (Å^3)	3483.1(12)	2208.8(4)
T (K)	291(2)	173(2)
Space group	$P2_1/c$	$P2_1/n$
Z	2	4
D_{calc} (g cm^{-3})	1.599	1.544
μ(Mo-K_α)/mm^{-1}	0.939	0.931
Reflections measured	11659	10069
Independent reflections	9532	7390
R_{int}	0.0519	0.0423
$R1$ [$I > 2\sigma(I)$][a]	0.0480	0.0343
$wR2$ (all data)[b]	0.1191	0.1027
Maximum shift/σ	0.001	0.001
Maximum Δρ (eÅ^{-3})	0.493	0.899

[a] $R1 = \Sigma||F_o| - |F_c||/\Sigma|F_o|$, $wR2 = \{\Sigma[w(F_o^2 - F_c^2)^2]/\Sigma\, w(F_o^2)^2\}^{0.5}$. – [b] $w = 1/[\sigma^2(F_o^2) + (aP)^2 + bP]$, where $P = (2F_c^2 + F_o^2)/3$ and a and b are constants set by the program.

and transferred to the diffractometer (Siemens P4) as summarised in Table 3.

Cell constants were refined from 31 (compound **1**) or 62 (compound **9**) reflections in the 2θ range 10–25°. Crystal data were corrected for absorption using ψ-scans. The structures were solved by the heavy atom method and refined anisotropically on F^2 (program SHELXL-93).[36] Hydrogen atoms were included using a riding model. For compound **9** the allyl ligand is disordered over two sites (68 and 32% refined occupancy).

Crystallographic data (excluding structure factors) for the structures reported in this paper have been deposited with the Cambridge Crystallographic Data Centre as supplementary publication no. CCDC-137011 (for complex **9**) and CCDC-137012 (for complex **1**). Copies of the data can be obtained free of charge on application to CCDC, 12 Union Road, Cambridge CB2 1EZ, UK [Fax: (internat.) + 44-1223/336-033; E-mail: deposit@ccdc.cam.ac.uk].

Acknowledgments

Financial support from the DGES (project PB97–1036), Spain, is gratefully acknowledged. F. F. and J. P. thank the University of Murcia and the Ministerio de Educación y Ciencia (Spain), respectively, for research grants.

[1] S. Trofimenko, *Prog. Inorg. Chem.* **1986**, *34*, 115.
[2] A. P. Sadimenko, S. S. Basson, *Coord. Chem. Rev.* **1996**, *147*, 247.
[3] G. La Monica, G. A. Ardizzoia, *Prog. Inorg. Chem.* **1997**, *46*, 151.
[4] C. Tejel, J. M. Villoro, M. A. Ciriano, J. A. López, E. Eguizábal, F. J. Lahoz, V. I. Bakhmutov, L. A. Oro, *Organometallics* **1996**, *15*, 2967.
[5] D. Carmona, F. J. Lahoz, R. Atencio, A. J. Edwards, L. A. Oro, M. P. Lamata, M. Esteban, S. Trofimenko, *Inorg. Chem.* **1996**, *35*, 2549.
[6] D. Carmona, J. Ferrer, R. Atencio, F. J. Lahoz, L. A. Oro, M. P. Lamata, *Organometallics* **1995**, *14*, 2057.
[7] G. López, G. García, J. Ruiz, G. Sánchez, J. García, C. Vicente, *J. Chem. Soc., Chem. Commun.* **1988**, 2429.
[8] N. Masciocchi, M. Moret, A. Sironi, G. Ardizzoia, S. Cenini, G. La Monica, *J. Chem. Soc., Chem. Commun.* **1995**, 1955.
[9] C. Pettinari, F. Marchetti, A. Cingolani, S. I. Troyanov, A. Drozdov, *J. Chem. Soc., Dalton Trans.* **1998**, 3335.
[10] L. Falvello, J. Forniés, A. Martín, R. Navarro, V. Sicilia, P. Villarroya., *Chem. Commun.* **1998**, 2429.
[11] F. Maury, *J. Phys. IV* **1995**, *5*, C5–449.
[12] R. Abul, M. B. Cleaver, J. S. Taylor, *Inorg. Chem.* **1992**, *31*, 3636.
[13] G. López, G. García, G. Sánchez, J. García, J. Ruiz, J. A. Hermoso, A. Vegas, M. Martínez-Ripoll, *Inorg. Chem.* **1992**, *31*, 1518.
[14] G. López, J. Ruiz, G. García, C. Vicente, J. Casabó, E. Molins, C. Miravitlles, *Inorg. Chem.* **1991**, *30*, 2605.
[15] G. López, J. Ruiz, G. García, C. Vicente, V. Rodríguez, G. Sánchez, J. A. Hermoso, M. Martínez-Ripoll, *J. Chem. Soc., Dalton Trans.* **1992**, 1681.
[16] G. López, J. Ruiz, C. Vicente, J. M. Martí, G. García, P. A. Chaloner, P. B. Hitchcock, R. M. Harrison, *Organometallics* **1992**, *11*, 4090.
[17] D. Carmona, F. J. Lahoz, L. A. Oro, M. P. Lamata, S. Buzarra, *Organometallics* **1991**, *10*, 3123.
[18] D. Carmona, J. Ferrer, F. J. Lahoz, L. A. Oro, J. Reyes, M. Esteban, *J. Chem. Soc., Dalton Trans.* **1991**, 2811; and references therein.
[19] M. T. Pinillos, C. Tejel, L. A. Oro, M. C. Apreda, C. Foces-Foces, F. H. Cano, *J. Chem. Soc., Dalton Trans.* **1989**, 1133.
[20] W. J. Geary, *Coord. Chem. Rev.* **1971**, *7*, 81.
[21] D. A. Long, D. Steel, *Spectrochim. Acta* **1963**, *19*, 1955.
[22] E. Alonso, J. Forniés, C. Fortuño, M. Tomás, *J. Chem. Soc., Dalton Trans.* **1995**, 3777.
[23] E. Maslowski,*Vibrational Spectra of Organometallic Compounds*, Wiley: New York, **1977**; p 437.
[24] C. G. van Kralingen, J. K. de Ridder, J. Reedijk, *Transition Met. Chem*. **1980**, *5*, 73.
[25] A. L. Bandini, G. Banditelli, M. A. Cinellu, G. Sanna, G. Minghetti, F. Demartin, M. Manassero, *Inorg. Chem.* **1989**, *28*, 404.
[26] M. Parra-Hake, M. F. Rettig, R. M. Wing, *Organometallics* **1983**, *2*, 8.
[27] P. G. Jones, *J. Organomet. Chem.* **1988**, *345*, 405.
[28] J. Casabó, J. M. Coronas, J. Sales, *Inorg. Chim. Acta* **1974**, *11*, 5.
[29] R. Usón, J. Forniés, F. Martínez, M. Tomás, J. Reoyo, *Organometallics* **1983**, *2*, 1386.
[30] F. J. Hopton, A. J. Rest, D. T. Rosevear, F. G. A. Stone, *J. Chem. Soc.* **1966**, 1326.
[31] G. López, J. Ruiz, G. García, J. M. Martí, G. Sánchez, J. García, *J. Organomet. Chem.* **1991**, *412*, 435.
[32] G. López, J. Ruiz, G. García, C. Vicente, J. M. Martí, J. A. Hermoso, A. Vegas and M. Martínez-Ripoll, *J. Chem. Soc., Dalton Trans.* **1992**, 53.
[33] R. Usón, J. Forniés, F. Martínez, *J. Organomet. Chem.* **1977**, *132*, 429.
[34] G. W. Parshall, *Inorg. Synth.* **1970**, *12*, 27.
[35] F. L. Wimmer, S. Wimmer, P. Castan, *Inorg. Synth*. **1992**, *29*,185.
[36] G. M. Sheldrick, SHELXL-93; University of Göttingen, **1993**, Göttingen, Germany).

Received November 23, 1999
[I99418]

Rational Design of Homo and Hetero Hexanuclear Coordination Compounds: Syntheses and Magnetic Properties of $[Cu_2^{II}M_4^{II}]$ (M = Cu, Ni) Species and the Crystal Structure of $\{[Cu(tmen)(H_2O)]_2[Cu(tmen)]_2[Cu_2L](H_2O)\}(ClO_4)_4 \cdot 2\,H_2O$

Ally Aukauloo,*[a] Xavier Ottenwaelder,[a] Rafael Ruiz,[a][+] Yves Journaux,*[a] Yu Pei,[a] Eric Rivière[a] and M. Carmen Muñoz[b]

Keywords: Copper / Nickel / Amides / Polynuclear complexes / Magnetic properties

New homo- and heterometallic hexanuclear complexes of formula $\{[Cu(tmen)(H_2O)]_2[Cu(tmen)]_2[Cu_2L](H_2O)\}(ClO_4)_4 \cdot 2\,H_2O$ **[Cu_6-tmen]** $\{[Cu(pmdien)]_4[Cu_2L]\}(ClO_4)_4 \cdot 4\,H_2O$ **[Cu_6-pmdien]** and $\{[Ni(cyclam)]_4[Cu_2L]\}(ClO_4)_4 \cdot 4\,H_2O$ **[Cu_2Ni_4-cyclam]** [H_8L = tetrakis(aminomethylene)methanetetrakis(oxamic acid), tmen = *N,N,N′,N′*-tetramethylethylenediamine, pmdien = *N,N,N′,N′,N″*-pentamethyldiethylenetriamine, and cyclam = 1,4,8,11-tetraazacyclotetradecane] have been synthesized. The crystal structure of **[Cu_6-tmen]** has been determined by single-crystal X-ray diffraction. The structure consists of cationic $\{[Cu(tmen)(H_2O)]_2[Cu(tmen)]_2[Cu_2L](H_2O)\}^{4+}$ hexanuclear units. The hexanuclear cation is made up of two symmetry-related oxamato-bridged trinuclear units connected through the central carbon atom C(6) of the L^{8-} ligand. Variable-temperature magnetic susceptibility measurements (1.8–300 K) have been performed for these series of complexes including the dinuclear precursors of formula $Na_4[Cu_2L] \cdot 10.5\,H_2O$ **[Cu_2-Na]**, $(NMe_4)_4[Cu_2L] \cdot 4\,H_2O$ **[Cu_2-NMe_4]** and $(PPh_4)_4[Cu_2L] \cdot 6\,H_2O$ **[Cu_2-PPh_4]**. The magnetic data have been interpreted. Evidence of a weak intramolecular ferromagnetic interaction between the two Cu^{II} ions in $[Cu_2L]^{4-}$ has been observed. For the hexanuclear species, the interaction through the oxamato bridge was found to be equal to –6790, –2650, and –1643 yJ (–342, –133, and –82 cm^{-1}) for **[Cu_6-tmen]**, **[Cu_6-pmdien]**, and **[Cu_2Ni_4-cyclam]**, respectively. In these complexes, the weak intramolecular ferromagnetic coupling between the two Cu^{II} ions within the dinuclear synthon was masked by intermolecular interactions or local anisotropy.

Introduction

One of the current challenges for inorganic chemists is the design and synthesis of high nuclearity complexes of the first row transition metal ions in a controlled fashion.[1–2] The pathways used to obtain these intriguing species are based, essentially, on the following synthetic schemes: i) the self-assembly method,[3–10] ii) the use of polynucleating ligands,[11–12] or iii) the use of complexes as ligands.[13–18] In the former case, the nature of the final products cannot be determined a priori. In contrast, the latter two methods proceed step by step. Hence they provide an alternative route to gain control of both the nuclearity and the dimensionality of the polymetallic edifice and, furthermore, allow the preparation of species containing metal ions of different natures, i.e. heterometallic complexes.

In a previous paper,[19] we described the synthesis of a new dinuclear copper(II) complex $[Cu_2L]^{4-}$ (Figure 1), where L^{8-} is the bis-tetradentate chelating ligand *N,N′,N″,N‴*-tetramethylenemethanetetrakis(oxamato). This dinuclear complex can be used as a building block for the synthesis of high nuclearity complexes or extended networks, following the strategy of "complexes as ligands". The design of this molecular synthon fulfils several important criteria. Firstly, $[Cu_2L]^{4-}$ is potentially a tetrakis-bidentate ligand that can coordinate to four other metal ions through the external oxygen atoms. The use of ancillary ligands on these metal ions avoids polymerisation, and leads to polynuclear species instead of extended networks. Also, the chelating nature of the oxamate groups ensures high values for the stability constants of the polynuclear complexes. Secondly, from a topological point of view, the connectivity number of four of this ligand is favourable for the construction of high-spin dendrimer-like molecules, and also for the synthesis of molecular-based magnets, since the critical temperature T_C is related to the number of neighbours of each magnetic centre.[20] Furthermore, the geometry of the ligand with non-coplanarity between the two planes containing the copper ions, as shown in Figure 1, has been designed with the aim of inducing a ferromagnetic coupling between the two Cu^{II} ions.[21] Such a coupling should, therefore, lead to a molecular synthon with an $S = 1$ ground state. Polynuclear complexes or extended networks built with this dinuclear complex are expected to have attractive magnetic properties.

This "complexes as ligands" strategy has been successfully applied in the preparation of the homometallic hexanuclear complexes $\{[Cu(tmen)(H_2O)]_2[Cu(tmen)]_2[Cu_2L]\}$-

[a] Laboratoire de Chimie Inorganique, UMR 8613 CNRS, Bat 420 Université de Paris-Sud, F-91405 Orsay, France
Fax: (internat.) + 33-1/69154754
E-mail: jour@icmo.u-psud.fr
[b] Departamento de Física Aplicada, Universidad Politécnica de València, E-46071 València, Spain
[+] Present address: Departament de Quimica Inorganica Universitat de València E-46100 Burjassot (València) Spain

 © WILEY-VCH Verlag GmbH, D-69451 Weinheim, 2000 1434–1948/00/0505–0951 $ 17.50+.50/0

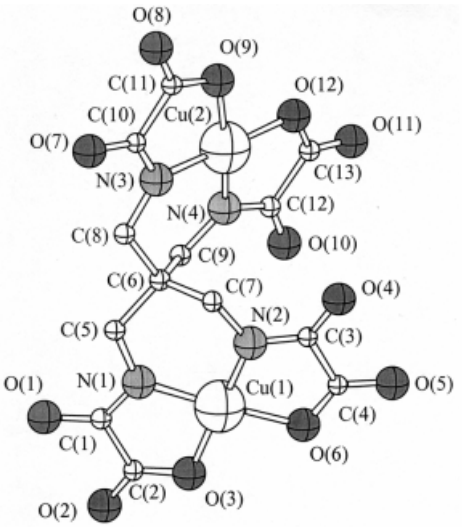


Figure 1. Perspective view of the anionic dinuclear unit $[Cu_2L]^{4-}$ of **[Cu_2–Na]** (hydrogen atoms have been omitted for clarity); crystallographic data of this compound are reported in reference[19]

$(H_2O)\}(ClO_4)_4 \cdot 2\,H_2O$ **[Cu_6-tmen]** (tmen = *N,N,N′,N′*-tetramethylethylenediamine) and $\{[Cu(pmdien)]_4[Cu_2L]\}(ClO_4)_4 \cdot 4\,H_2O$ **[Cu_6-pmdien]** (pmdien = *N,N,N′,N′,N″*-pentamethyldiethylenetriamine), and a heterometallic hexanuclear complex $\{[Ni(cyclam)]_4[Cu_2L]\}(ClO_4)_4 \cdot 4\,H_2O$ **[Cu_2Ni_4-cyclam]**. We report herein their synthesis and magnetic characterisations as well as the magnetic properties of their dinuclear precursors $Na_4[Cu_2L] \cdot 10.5\,H_2O$ **[Cu_2-Na]**, $(NMe_4)_4[Cu_2L] \cdot 4\,H_2O$ **[Cu_2-NMe_4]** and $(PPh_4)_4[Cu_2L] \cdot 6\,H_2O$ **[Cu_2-PPh_4]**, and the X-ray structural determination of **[Cu_6-tmen]**.

Results and Discussion

Synthesis of the Complexes

The dinuclear precursors were obtained by reaction of the tetraethyl ester derivative of the ligand (Et_4H_4L) with NaOH or NMe_4OH, for **[Cu_2-Na]** and **[Cu_2-NMe_4]** respectively, followed by addition of Cu^{2+}. The tetraphenylphosphonium derivative **[Cu_2-PPh_4]** was then obtained by successive metatheses with Ag^+ and PPh_4^+. The hexanuclear compounds were synthesised by adding four equivalents of an external complex to the dinuclear **[Cu_2-Na]** precursor and isolated as microcrystalline powders after slow evaporation of the solvent. External complexes were Ni(cyclam)$(ClO_4)_2(H_2O)_2$, or in situ generated Cu(tmen)$(ClO_4)_2$ or Cu(pmdien)$(ClO_4)_2$.

Crystal Structure Analysis

The structure of **[Cu_6-tmen]** consists of hexameric copper(II) complex cations, $\{[Cu(tmen)(H_2O)]_2[Cu(tmen)]_2[Cu_2L](H_2O)\}^{4+}$ (Figure 2), perchlorate anions and crystallisation water molecules. The hexanuclear cation is made up of two symmetry-related oxamato-bridged trinuclear units (I = 1 – *x*, *y*, –*z*) connected through the central carbon atom C(6) which lies on a crystallographic twofold axis, in accordance with the C_2 space group.

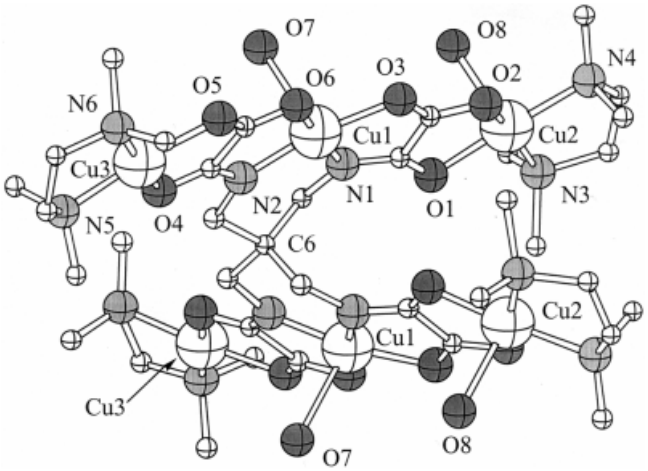


Figure 2. Perspective view of the cationic hexanuclear unit $\{[Cu(tmen)(H_2O)]_2[Cu(tmen)]_2Cu_2L(H_2O)\}^{4+}$ of **[Cu_6-tmen]** with the atom-numbering scheme (hydrogen atoms have been omitted for clarity); selected bond lengths [pm] and angles [°] with standard deviations in parentheses: Cu(1)–N(1) 192.6(5), Cu(1)–N(2) 191.7(5), Cu(1)–O(3) 196.1(4), Cu(1)–O(6) 196.3(4), Cu(2)–N(3) 192.9(5), Cu(2)–N(4) 191.9(5), Cu(2)–O(9) 196.6(4), Cu(2)–O(12) 198.2(4); N(2)–Cu(1)–N(1) 96.7(2), O(3)–Cu(1)–N(1) 84.3(2), O(6)–Cu(1)–N(1) 173.4(2), N(2)–Cu(1)–O(3) 176.8(2), N(2)–Cu(1)–O(6) 84.2(2), O(6)–Cu(1)–O(3) 95.1(2), N(3)–Cu(2)–N(4) 95.2(2), O(9)–Cu(2)–N(3) 84.4(2), O(12)–Cu(2)–N(3) 179.0(2), N(4)–Cu(2)–O(9) 172.4(2), N(4)–Cu(2)–O(12) 83.9(2), O(12)–Cu(2)–O(9) 96.4(2)

Within each trinuclear fragment, the terminal Cu(2) and Cu(3) atoms are (4 + 1) and (4 + 2) coordinated, respectively. Their basal planes are formed by two amino nitrogen atoms from the tmen ligand and two oxygen atoms from the oxamato bridge. The apical positions are filled by the oxygen atom O(8) from the water molecule (234 pm) in the former, and the O(10) and O(13) atoms from two weakly bound perchlorate anions (272 pm) in the latter. The central Cu(1) atom has a (4 + 1) coordination environment, with an equatorial plane occupied by two deprotonated amido nitrogen atoms and two carboxylate oxygen atoms from the oxamato groups. The fifth axial position is occupied by the water oxygen atom O(7) (250 pm). The metal atoms Cu(1) and Cu(2) are displaced from the least-square basal plane toward the apical water molecule by 15 and 20 pm, respectively, while the Cu(3) atom shows no deviation from the mean plane. The basal planes of the three copper(II) ions in the trinuclear unit are almost coplanar [dihedral angles of 7(2), 6(2), and 5(2)° for Cu(1)–Cu(2), Cu(1)–Cu(3), and Cu(2)–Cu(3), respectively], in contrast to those of the central copper(II) ions from the $[Cu_2L]$ fragment [43.2(8)° for $Cu(1)–Cu^{I}(1)$].

In the crystal, two neighbouring hexanuclear entities (II = 1 – *x*, *y*, 1 – *z*) are linked through the oxygen atom O(7) from apical water which acts as a bridge between the central copper(II) ions, thus leading to a chain along the *c* axis (Figure 3). The $Cu(1)–O(7)–Cu^{II}(1)$ angle is 124(2)°. The intramolecular metal–metal separations Cu(1)···Cu(2), Cu(1)···Cu(3), Cu(2)···Cu(3), and $Cu(1)\cdots Cu^{I}(1)$ are 514,

513, 1024, and 591 pm, respectively, whereas the intermolecular one Cu(1)···Cu^{II}(1) is 442 pm.

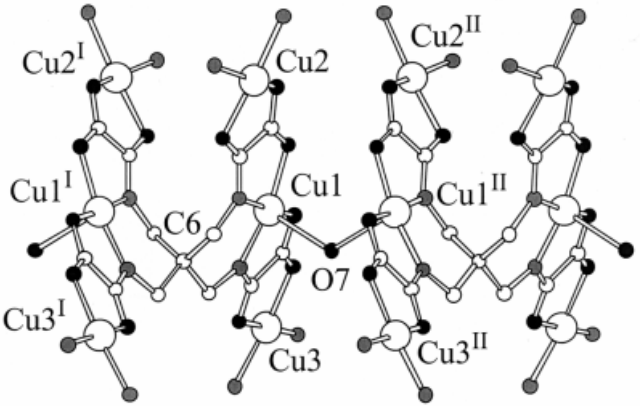


Figure 3. View of two symmetry-related hexanuclear complexes (II: $1-x$, y, $1-z$) belonging to the chain which runs along the c axis; the carbon atoms of the tmen ligands and the oxygen atoms of coordinated water and perchlorate molecules have been omitted for clarity

Magnetic Properties of Dinuclear Precursors

The magnetic properties of **[Cu$_2$-Na]**, **[Cu$_2$-NMe$_4$]** and **[Cu$_2$-PPh$_4$]** (SQUID, 1.8–300 K) are depicted in Figure 4. The magnetic properties of the dinuclear copper(II) complexes strongly depend on the nature of the counter-cation. As can be seen for **[Cu$_2$-Na]**, the $\chi_M T$ curve smoothly decreases upon cooling below 5 K, showing that the dominant interaction between Cu^{II} ions is antiferromagnetic. On the contrary, upon cooling **[Cu$_2$-NMe$_4$]** and **[Cu$_2$-PPh$_4$]**, the increase of the $\chi_M T$ product indicates that the coupling between the Cu^{II} ions is ferromagnetic. The best fits are obtained using the following parameters J = –4.6 yJ (–0.23 cm^{-1}), g = 2.10, 5.4 yJ (0.27 cm^{-1}), g = 2.05 and 23.8 yJ (1.2 cm^{-1}), g = 2.02 for **[Cu$_2$-Na]**, **[Cu$_2$-NMe$_4$]** and **[Cu$_2$-PPh$_4$]**, respectively ($H = -JS_1 \cdot S_2$).[22] The agreement factors R defined as $\Sigma(\chi_M T_{exp}-\chi_M T_{theo})^2/\Sigma(\chi_M T_{exp})^2$ are then equal to $4.6\cdot10^{-5}$, $7\cdot10^{-6}$, and $4\cdot10^{-5}$ for **[Cu$_2$-Na]**, **[Cu$_2$-NMe$_4$]**, and **[Cu$_2$-PPh$_4$]**, respectively.

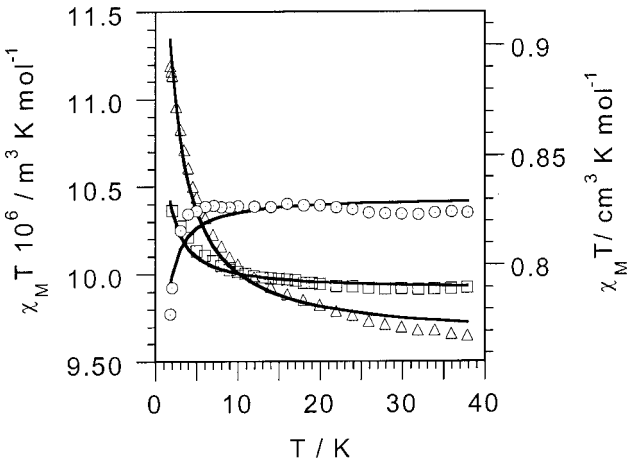


Figure 4. Thermal variation of the magnetic susceptibility of **[Cu$_2$Na]** (⊙), **[Cu$_2$NMe$_4$]** (□) and **[Cu$_2$PPh$_4$]** (Δ) in the form of $\chi_M T$ versus T plot; the lines are the calculated curves

The antiferromagnetic interaction obtained for [Cu$_2$Na] can be explained in light of its crystal structure. The dinuclear units are not isolated within the crystal, as the oxygen atoms of oxamato groups of [Cu$_2$L]$^{4-}$ are coordinated to the Na^{I} ions leading to an extended 3D network.[19] The antiferromagnetic coupling between the Cu^{II} ions is probably due to the interaction through the Na^{I} ions and not from the interaction through the carbon atoms linking the two Cu^{II} ions. This analysis is reinforced by the magnetic behaviour of **[Cu$_2$-NMe$_4$]** and **[Cu$_2$-PPh$_4$]**. For these two compounds, where organic cations are present and cannot be coordinated to the external oxygen atoms of the oxamato group, the coupling is, as expected, ferromagnetic. Moreover, the magnitude of the coupling seems to be related to the size of the counter-cation, i.e. the bulkier the counter-cation, the more pronounced the coupling. Even though no crystallographic structures of these compounds are yet available, the stronger ferromagnetic interaction is observed for the PPh_4^+ salt where the intermolecular interactions are expected to be the smallest.

Magnetic Properties of Hexanuclear Species

The magnetic properties of the hexanuclear complexes **[Cu$_6$-tmen]** and **[Cu$_6$-pmdien]** are shown in Figure 5. At room temperature, $\chi_M T$ is equal to 14.9 μm^3 K mol^{-1} (1.19 cm^3 K mol^{-1}) and 24.6 μm^3 K mol^{-1} (1.96 cm^3 K mol^{-1}) for **[Cu$_6$-tmen]** and **[Cu$_6$-pmdien]**, respectively. These values are lower than expected for six noninteracting copper(II) ions (31.2 μm^3 K mol^{-1}). For both compounds, $\chi_M T$ decreases upon cooling to reach a constant value of 10.0 μm^3 K mol^{-1} (0.798 cm^3 K mol^{-1}) around 100 K for **[Cu$_6$-tmen]** and 10.2 μm^3 K mol^{-1} (0.811 cm^3 K mol^{-1}) around 20 K for **[Cu$_6$-pmdien]**. Upon further cooling, $\chi_M T$ decreases abruptly below 20 K for **[Cu$_6$-tmen]** and 8 K for **[Cu$_6$-pmdien]**. At 1.8 K, $\chi_M T$ values are equal to 6.36 μm^3 K mol^{-1} (0.506 cm^3 K mol^{-1}) and 9.31 μm^3 K mol^{-1} (0.741 cm^3 K mol^{-1}) for **[Cu$_6$-tmen]** and **[Cu$_6$-pmdien]**, respectively. In the high temperature region, these observed trends are typical of strongly coupled trinuclear Cu^{II} complexes and the plateaux correspond to temperature ranges where the $S = {}^1/_2$ ground states of the trinuclear units are the only populated states.

The rapid decrease in the $\chi_M T$ products at low temperature is interpreted as arising from a weak interaction between the trinuclear units. To take this into account, the effective spin Hamiltonian shown in Equation 1 has been used where $S_A = S_B = {}^1/_2$ correspond to the two ground-state doublets of the Cu$_3^{II}$ trimeric units, defined as A and B in this perturbational treatment.[23]

$$H = -J(S_{A1}S_{A2} + S_{A1}S_{A3} + S_{B1}S_{B2} + S_{B1}S_{B3}) - j_{eff}S_AS_B + g\beta(S_{A1} + S_{A2} + S_{A3} + S_{B1} + S_{B2} + S_{B3})\cdot B \quad (1)$$

Over the whole temperature range, the theoretical curves derived from the above Hamiltonian closely follow the experimental data for both compounds. The best fits are obtained using the following parameters J = –6790 yJ (–342 cm^{-1}), j_{eff} = –31.8 yJ (–1.6 cm^{-1}), g = 2.07 and J = –2650 yJ (–133 cm^{-1}), j_{eff} = –10.7 yJ (–0.54 cm^{-1}), g =

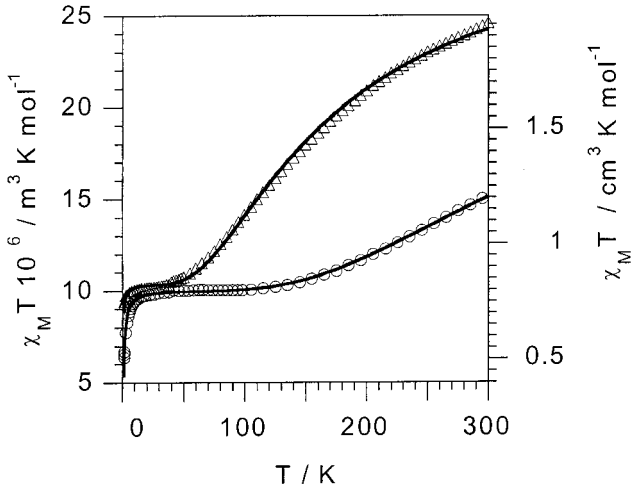


Figure 5. Thermal variation of the magnetic susceptibility of **[Cu$_6$-tmen]** (Δ) and **[Cu$_6$-pmdien]** (O) in the form of $\chi_M T$ versus T plot; the lines are the calculated curves

2.10 for **[Cu$_6$-tmen]** and **[Cu$_6$-pmdien]**, respectively (solid lines in Figure 5). The agreement factors R are then equal to $1.91 \cdot 10^{-4}$ and $7.4 \cdot 10^{-5}$, respectively. In **[Cu$_6$-tmen]**, the exchange interaction parameter J between Cu(1) and Cu(2) or equivalently, Cu(1) and Cu(3) ($J = J_{12} = J_{13}$) through the oxamato bridge is in excellent agreement with that of the related trinuclear complex {[Cu(tmen)]$_2$Cu(pba)}-(ClO$_4$)$_2$,[24] where J is equal to –7530 yJ (–379 cm^{-1}). As for the effective interaction parameter j_{eff} between the two trinuclear units, it may be related to the exchange parameter J_{Cu-Cu} between the two central Cu^{II} ions by the expression $j_{eff} = 1/9 \cdot J_{Cu-Cu}$, i.e. J_{Cu-Cu} = –278 yJ (–14 cm^{-1}).[25] This value may be associated with two different pathways for the interaction between the trinuclear units. The first is an intramolecular coupling between the two trinuclear units of the same molecule, through the N–C–C–C–N σ-bond moiety. The other takes place between units of two different molecules, due to the Cu(1) ions which are connected by the apical O(7) oxygen (Figure 3). The latter pathway takes preference as coupling occurs through only one atom. This preference is also supported by a comparison between the value of –278 yJ for this interaction and those of the dinuclear units **[Cu$_2$-NMe$_4$]** and **[Cu$_2$-PPh$_4$]** (+5.4 and +23.8 yJ). It is noteworthy that there is no improvement in the quality of the fit for the low temperature data by using an alternating $S = {}^1/_2$ chain model. In other words, it is not possible to determine from the magnetic data the respective contribution of the intra- and intermolecular interactions.

The lack of crystallographic structure renders the thorough analysis of the magnetic behaviour of **[Cu$_6$-pmdien]** difficult. Nevertheless, the J value through the oxamato bridge (–2650 yJ) is also in very good agreement with that of the related trinuclear complex {[Cu(pmdien)]$_2$Cu(pba)}-(PPh$_4$)$_2$,[24] where J is equal to –3020 yJ (–152 cm^{-1}). In **[Cu$_6$-pmdien]**, the j_{eff} value of –10.7 yJ is likewise associated to intermolecular interaction. The weaker interaction through the oxamato bridge for **[Cu$_6$-pmdien]** than for **[Cu$_6$-tmen]** stems from the relative orientation of the magnetic orbitals in these complexes. In the latter compound, all magnetic orbitals lie almost in the same plane, ensuring a maximum overlap between them. On the contrary, in **[Cu$_6$-pmdien]** the magnetic orbitals of the Cu^{II} ions are not coplanar, and hence leads to a decrease in the orbital overlapping.[24][26][27]

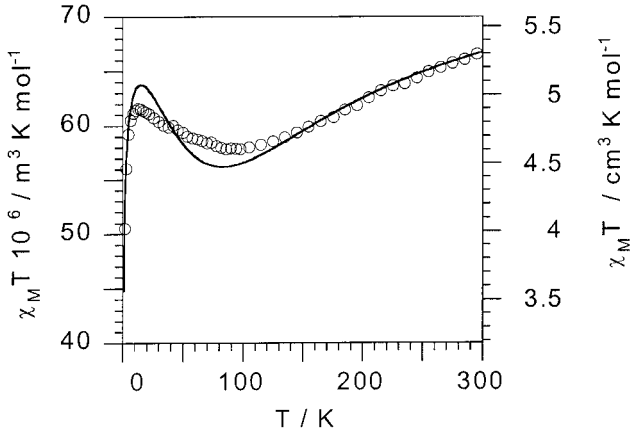


Figure 6. Thermal variation of the magnetic susceptibility **[Cu$_2$Ni$_4$-cyclam]** in the form of $\chi_M T$ versus T plot: (O) experimental data, calculated curve (line)

The magnetic properties of **[Cu$_2$Ni$_4$-cyclam]** are depicted in Figure 6. At room temperature $\chi_M T$ is equal to 66.6 μm^3 K mol^{-1} (5.3 cm^3 K mol^{-1}) which is close to 71.3 μm^3 K mol^{-1}, the expected value for noninteracting ions (for g_{Cu} = 2.1 and g_{Ni} = 2.2). The $\chi_M T$ product first decreases upon cooling, reaches a minimum around 80 K, then increases to a maximum at about 15 K with $\chi_M T$ equal to 66.6 μm^3 K mol^{-1}, and finally decreases again upon cooling to 2 K.

The expected behaviour of **[Cu$_2$Ni$_4$-cyclam]** is that of [NiCuNi] heterotrinuclear species, with a weak interaction between the trinuclear units in the low temperature region. In fact, the experimental curve can be fitted using the theoretical law of a trinuclear [NiCuNi] complex.[13][28] In this model, the decrease of $\chi_M T$ at low temperature is attributed to the zero field splitting in the $S = {}^3/_2$ ground state of the [NiCuNi] trinuclear unit. The best fit of the experimental data is obtained using the following parameters J = –1704 yJ (–85 cm^{-1}), D = –69.6 yJ (–3.5 cm^{-1}), g_{Ni} = 2.30 and g_{Cu} = 2.15. The agreement factor R is then equal to $5.2 \cdot 10^{-4}$. On the other hand, the experimental data can also be fitted to a hexanuclear model using the effective spin Hamiltonian (1) with $S_A = S_B = {}^3/_2$ being the two quadruplets ground states of the [NiCuNi] trimeric units, defined as A and B. For this model, the best fit of the data is obtained with the following parameters J = –1643 yJ (–82 cm^{-1}), j_{eff} = –1.4 yJ (–0.068 cm^{-1}), g_{Ni} = 2.30 and g_{Cu} = 2.15. The agreement factor R is then equal to $4.5 \cdot 10^{-4}$. The effective interaction parameter j_{eff} between the two trinuclear units may be related to the exchange parameter J_{Cu-Cu} between the two central Cu^{II} ions by the expression $j_{eff} = 1/25 \cdot J_{Cu-Cu}$

i.e. J_{Cu-Cu} = –34 yJ (–1.7 cm^{-1}). For both models, the interaction through the oxamato bridge is smaller than that of the related [NiCuNi] trinuclear complexes. Recently, the role of peripheral ligand on the coupling constant has been studied in oxalato-bridged nickel(II) complexes.[29] With four nitrogens as donor atoms, the peripheral cyclam ligand is expected to induce a coupling close to that of the cth ligand (cth = 2,4,4,9,9,11-hexamathyl-1,5,8,12-tetraazacyclotetradacane), that is –2470 yJ (–124.5 cm^{-1}).[13] This is not observed experimentally, but in the absence of an X-ray analysis of the compound, it is not possible to give a satisfactory explanation to this relatively small value of the exchange interaction through the oxamato bridge.

It should be noted that the theoretical curves for the two alternative models are almost indistinguishable, showing that the D and j_{eff} parameters are strongly correlated. This renders impossible an unambiguous determination of D and j_{eff} by a fit of the magnetic data with a theoretical model including the two parameters. Nevertheless, **[Cu_2Ni_4-cyclam]** is EPR silent indicating that both effects are not negligible. First, the weak interaction j_{eff} between two trinuclear subunits leads to integer spin values for the hexanuclear species. Second, the large value for the Ni^{II} single ions zero field splitting makes the low lying integer spin states EPR silent. Unfortunately, neither the magnetic data nor the EPR spectra are able to give the relative values of D and j_{eff}. Hence, we cannot rule out the possibility of the weak ferromagnetic coupling between the trinuclear subunits associated with large values of the zero field splitting in the low lying states in **[Cu_2Ni_4-cyclam]**.

Conclusion

We have obtained three new hexanuclear species with a new dinuclear Cu^{II} molecular synthon. The non-coplanarity of the Cu^{II}'s coordination environment favours a ferromagnetic coupling between the two ions as shown by the magnetic properties of **[Cu_2-NMe_4]** and **[Cu_2-PPh_4]**. However, the ferromagnetic coupling between the two Cu^{II} ions within the dinuclear synthon is weak and often masked by intermolecular interactions, as in **[Cu_2-Na]** and **[Cu_6-tmen]**, or local anisotropy as in **[Cu_2Ni_4-cyclam]**. To overcome this problem, we are presently working on new polynuclear synthons with different spacers that should induce larger ferromagnetic couplings. To the best of our knowledge, only ligands allowing the synthesis of homo-hexanuclear[12] or hetero-tetranuclear species have been described in the literature.[30][31] The tetrakis-bidentate molecular synthon $[Cu_2L]^{4-}$ reported here, is a unique example of a building block allowing the synthesis of homo- and heterometallic hexanuclear complexes in a rational fashion. Taking advantage of the design of $[Cu_2L]^{4-}$, high-spin (S = 9) heterometallic hexanuclear species with Mn^{II} or Fe^{III} ions are in the process of being synthesised. We are also using this tetrakis-bidentate complex as a ligand to obtain extended networks. The non-coplanar connectivity of four should lead to both a graphite-like hexagonal 2D array and a diamond like 3D network, and possibly to high-temperature molecular-based magnets.

Experimental Section

General: All reagents were obtained from commercial sources and used as received. The tetraethyl ester derivative Et_4H_4L of the ligand was synthesed following a literature procedure.[19] – Elemental analyses were performed by the Microanalytical Service of ICNS (CNRS). – IR spectra were carried out on a Spectrum 1000 FT-IR spectrophotometer (Perkin–Elmer). – Magnetic measurements in the 1.8–300 K temperature range were carried out with a MPMS5 SQUID susceptometer (Quantum Design Inc). – EPR measurements were performed at 100 K on a Bruker ER 200 E at X-band on solid samples.

Syntheses and General Physical Properties of the Dinuclear Complex: The dicopper(II) complex was obtained by reaction of the tetraethyl ester derivative of the ligand (Et_4H_4L) with Cu^{2+} in basic aqueous media and isolated as its sodium, tetramethylammonium, and tetraphenylphosphonium salts.

[Cu_2-Na]: The synthesis and characterisation of the sodium salt $Na_4[Cu_2L] \cdot 10.5\ H_2O$ have previously been described.[19]

[Cu_2-NMe_4]: The tetramethylammonium derivative $(NMe_4)_4[Cu_2L] \cdot 4\ H_2O$ was synthesised and isolated in a similar manner to that of **[Cu_2-Na]**: To a suspension of the tetraethyl ester derivative Et_4H_4L (1.33 g, 2.5 mmol) in water (50 mL) was added NMe_4OH (8.9 mL of a 25% methanolic solution, 22 mmol). After stirring for 5 min at room temperature, an aqueous solution (25 mL) of $Cu(NO_3)_2 \cdot 3\ H_2O$ (1.20 g, 5 mmol) was added dropwise. The deep-blue solution was then filtered and the solvent volume was reduced to 10 mL on a rotary evaporator. Slow addition of absolute ethanol to the mother liquor gave a hygroscopic purple solid which was collected by filtration, washed with ethanol and ether, and dried under vacuum (74%). – $C_{13}H_8Cu_2N_4O_{12}[N(C_4H_{12})_4]_4 \cdot 4\ H_2O$ (1629.7): calcd. C 38.36, H 7.10, Cu 13.9, N 12.34; found C 37.88, H 6.79, Cu 13.6, N 12.26. – IR (KBr): $\tilde{\nu}$ = 1635 and 1602 cm^{-1} (C=O).

[Cu_2-PPh_4]: The tetraphenylphosphonium derivative $(PPh_4)_4[Cu_2L] \cdot 6\ H_2O$ was synthesised from **[Cu_2-Na]** by successive metatheses with Ag^+ and PPh_4^+: To a solution of **[Cu_2-Na]** (140 mg, 0.17 mmol) in water (10 mL) was added solid silver nitrate (31 mg, 0.18 mmol). After stirring for 5 min, the purple precipitate that formed in a quantitative yield was collected by filtration, washed successively with water, ethanol and ether, and then dried under vacuum. To a suspension of this solid (152 mg, 0.16 mmol) in water (5 mL) was added an aqueous solution (10 mL) of tetraphenylphosphonium chloride (235 mg, 0.63 mmol). Silver chloride appeared as a white solid. After stirring for 15 min, the purple blue solution was filtered and evaporated to dryness. The solid residue was dissolved in the minimum amount of acetonitrile and 5 mL of acetone was added. Addition of ether allowed the isolation of a hygroscopic purple precipitate which was collected by filtration, washed with ether and kept in a dessicator (94%). – $C_{13}H_8Cu_2N_4O_{12}[P(C_6H_5)_4]_4 \cdot 6\ H_2O$ (2005): calcd. C 65.30, H 5.03, Cu 6.34, N 2.79; found C 65.54, H 5.04, Cu 6.26, N 2.87. – IR (KBr): $\tilde{\nu}$ = 1634 and 1603 cm^{-1} (C=O).

Syntheses and General Physical Properties of the Hexanuclear Complexes: These compounds were synthesised in a straightforward

manner from the dinuclear copper(II) complex **[Cu_2-Na]** and the appropriate external complex.

[Cu_6-tmen]: The hexacopper complex $\{[Cu(tmen)(H_2O)]_2[Cu(tmen)]_2[Cu_2L](H_2O)\}(ClO_4)_4 \cdot 2\,H_2O$ was synthesed in the following way with $[Cu(tmen)]^{2+}$ prepared in situ from a 1:1 mixture of Cu^{2+} and the corresponding diamine: To a solution of copper(II) perchlorate (0.74 g, 2.0 mmol) and *N,N,N′,N′*-tetramethylethylenediamine (302 μL, 2 mmol) in water (20 mL) was added under stirring an aqueous solution (10 mL) of **[Cu_2-Na]** (0.39 g, 0.5 mmol). Slow evaporation at room temperature of the deep-blue filtered solution gave, after a few days, a microcrystalline deep-blue powder which was filtered off and air-dried. – $C_{37}H_{82}Cl_4Cu_6N_{12}O_{33}$ (1746.2): calcd. C 25.45, H 4.73, N 9.63; found C 25.72, H 4.83, N 9.58. – IR (KBr): $\tilde{\nu}$ = 1634 and 1600 cm^{-1} (C=O), 1120 and 1086 cm^{-1} (Cl–O; ClO_4^-). A single crystal of **[Cu_6-tmen]** of low quality but good enough for a complete structure determination was selected. Up to now, attempts to obtain single crystals of higher quality by recrystallization from various solvents (water, methanol, acetonitrile) have been unsuccessful.

[Cu_6-pmdien]: The other hexacopper complex $\{[Cu(pmdien)]_4[Cu_2L]\}(ClO_4)_4 \cdot 4\,H_2O$ was formed by the same procedure with *N,N,N′,N′,N″*-pentamethyldiethylenetriamine (418 μL, 2 mmol) in place of *N,N,N′,N′*-tetramethylethylenediamine. After slow evaporation, a deep-blue microcrystalline powder formed, but no well-shaped crystals of a sufficient quality for X-ray analysis were obtained. – $C_{49}H_{100}Cl_4Cu_6N_{16}O_{28} \cdot 4\,H_2O$ (1956.6): calcd. C 30.08, H 5.56, Cl 7.25, N 11.45; found C 29.92, H 5.58, Cl 7.33, N 11.41. – IR (KBr): $\tilde{\nu}$ = 1620 cm^{-1} (C=O), 1121 and 1089 cm^{-1} (Cl–O; ClO_4^-).

[Cu_2Ni_4-cyclam]: The polymetallic complex $\{[Ni(cyclam)]_4[Cu_2L]\}(ClO_4)_4 \cdot 4\,H_2O$ was obtained as follows: To a solution of Ni(cyclam)$(H_2O)_2(ClO_4)_2$ (198 mg, 0.4 mmol) in 1:1 water/acetonitrile (6 mL) was added solid **[Cu_2-Na]** (82 mg, 0.1 mmol). After stirring for 30 min at 40 °C all the solid had dissolved to give a purple-red solution. Slow evaporation at room temperature afforded crystalline material of very low quality for X-ray analysis. All attempts at isolating crystals of good quality by recrystallisation were unsuccessful. – $C_{53}H_{104}Cl_4Cu_2N_{20}Ni_4O_{28} \cdot 4\,H_2O$ (2045.3): calcd. C 31.12, H 5.52, Cl 6.93, N 13.70; found C 30.98, H 5.51, Cl 7.06, N 13.73. – IR (KBr): $\tilde{\nu}$ = 1614 cm^{-1} (C=O), 1114 and 1086 (Cl–O; ClO_4^-), 2925 and 2869 (N–H; cyclam).

X-ray Crystallographic Study: Crystal structure analysis of the selected crystal of **[Cu_6-tmen]**: Enraf–Nonius CAD-4 diffractometer, Mo-K_α radiation, λ = 71.069 pm, graphite monochromator, 293 K. Data collection solution and refinement: *w*-2θ, Lorentz and polarisation effects and absorption correction, standard Patterson methods with subsequent full-matrix least-squares method refinement SHELX86, SHELX93.[32,33] $C_{37}H_{82}Cl_4Cu_6N_{12}O_{33}$, monoclinic, space group C_2, a = 2807.1(10), b = 1430.4(6), c = 872.1(7) pm, β = 95.28(2)°, V = 3.487(3) nm^3, Z = 4, r_{calcd} = 1.65 g cm^{-3}, m = 2.04 mm^{-1}, $1 \le \theta \le 25°$, crystal size 0.10 × 0.10 × 0.10 mm. 2395 Unique reflections, and 2344 assumed as observed with $I > 2\sigma(I)$. The hydrogen atoms were not found or calculated. Refinement of 363 variables with anisotropic thermal parameters for all atoms except for the O(5) atom which was refined with an overall isotropic thermal parameter gave R = 0.105 and R_w = 0.251 with Σ = 1.09. The crystal drawings were carried out with the CRYSTAL MAKER[34] program. Crystallographic data (excluding structure factors) for the structure reported in this paper have been deposited with the Cambridge Crystallographic Data Centre as supplementary publication no. CCDC-101561. Copies of the data can be obtained free of charge on application to CCDC, 12 Union Road, Cambridge CB21EZ, UK [fax: (internat.) + 44-1223/336-033; E-mail: deposit@ccdc.cam.ac.uk].

Acknowledgments

This work was supported by the CNRS (France) and the DGICYT, Ministerio de Educación y Ciencia (Spain), through project PB94–1002 for post-doctoral grants.

[1] O. Kahn in: *Magnetism of heteropolymetallic systems* (Ed.: O. Kahn), Springer-Verlag, Berlin, Heidelberg, **1987**, p. 89–167.
[2] O. Kahn, *Adv. Inorg. Chem.* **1995**, *43*, 179–259.
[3] G. Christou, *Acc. Chem. Res.* **1989**, *22*, 328.
[4] E. K. Brechin, S. G. Harris, A. Harrison, S. Parsons, A. G. Whittaker, R. E. P. Winpenny, *Chem. Commun.* **1997**, 653–654.
[5] A. K. Powell, S. L. Heath, D. Gatteschi, L. Pardi, R. Sessoli, F. Del Giallo, F. Pieralli, *J. Am. Chem. Soc.* **1995**, *117*, 2491–2502.
[6] D. Gatteschi, A. Caneschi, R. Sessoli, A. Cornia, *Chem. Soc. Rev.* **1996**, 101–109.
[7] D. Gatteschi, A. Caneschi, L. Pardi, *Science* **1994**, *265*, 1054–1058.
[8] J. A. Real, G. De Munno, R. Chiappetta, F. Lloret, Y. Journaux, J.-C. Colin, G. Blondin, *Angew. Chem.* **1994**, *106*, 1223; *Angew. Chem. Int. Ed.* **1994**, *33*, 1184–1186.
[9] S. P. Watton, P. Fuhrmann, L. E. Pence, A. Caneschi, A. Cornia, G. L. Abbati, S. J. Lippard, *Angew. Chem.* **1997**, *109*, 2917–2919; *Angew. Chem. Int. Ed.* **1997**, *36*, 2774–2776.
[10] J. L. Heinrich, P. A. Berseth, J. R. Long, *Chem. Commun.* **1998**, 1231–1232.
[11] C. N. Verani, T. Weyhermüller, E. Rentschler, E. Bill, P. Chaudhuri, *Chem. Commun.* **1998**, 2475–2476.
[12] S. Tandon, L. K. Thompson, J. N. Bridson, C. Benelli, *Inorg. Chem.* **1995**, *34*, 5507–5515.
[13] P. Yu, Y. Journaux, O. Kahn, *Inorg. Chem.* **1988**, *27*, 399–404.
[14] F. Lloret, Y. Journaux, M. Julve, *Inorg. Chem.* **1990**, *29*, 3967–3972.
[15] T. Mallah, C. Auberger, M. Verdaguer, P. Veillet, *Chem. Commun.* **1995**, 61–62.
[16] S. W. Gordon-Wylie, E. Bominaar, T. J. Collins, J. M. Workman, B. J. Claus, R. E. Patterson, S. E. Williams, B. J. Conklin, G. T. Yee, S. T. Weintraub, *Chem. Eur. J.* **1995**, *1*, 528–537.
[17] P. Yu, Y. Journaux, O. Kahn, *Inorg. Chem.* **1989**, *28*, 100–103.
[18] M. Mitsumi, H. Okawa, H. Sakiyma, M. Ohba, N. Matsumoto, T. Kurisaki, H. Wakita, *J. Chem. Soc., Dalton Trans.* **1993**, 2991–2994.
[19] A. Aukauloo, X. Ottenwaelder, R. Ruiz, Y. Journaux, P. Yu, E. Rivière, B. Cervera, C. Muñoz, *Eur. J. Inorg. Chem.* **1999**, *2*, 209–212.
[20] R. Ruiz, C. Surville-Barland, Y. Journaux, J.-C. Colin, I. Castro, B. Cervera, M. Julve, F. Lloret, F. Sapiña, *Chem. Mater.* **1997**, *9*, 201–209.
[21] H. Oshio, T. Watanabe, A. Ohto, T. Ito, T. Ikoma, S. Tero-Kubota, *Inorg. Chem.* **1997**, *36*, 3014–3021.
[22] This paper uses the SI units. The molar magnetic susceptibility χ_M is expressed in $m^3\ mol^{-1}$. The conversion factor to the irrational emu quantity $\chi_M^{(ir)}$ is $10^6/4\pi$. The energies are expressed in 10^{-24} Joule. The submultiple prefix for 10^{-24} is yocto, its symbol is y. Therefore 1 yJ means 10^{-24} Joule. The conversion factor to cm^{-1} is 5.034 10^{-2} (1 $cm^{-1} \approx$ 20 yJ).
[23] Y. Journaux, J. Sletten, O. Kahn, *Inorg. Chem.* **1986**, *25*, 439–447.
[24] R. Costa, A. Garcia, J. Ribas, T. Mallah, Y. Journaux, J. Sletten, X. Solans, *Inorg. Chem.* **1993**, *32*, 3733–3742.
[25] The effective intertrinuclear interaction parameter j_{eff} can be related to the local interaction parameter J_{ij} between metal centres from each trinuclear unit through the relation

$$j_{eff} = J_{ij}\,\frac{S(S+1) + S_i(S_i+1) - S^*(S^*+1)}{2S(S+1)} \cdot \frac{S(S+1) + S_j(S_j+1) - S^{\#}(S^{\#}+1)}{2S(S+1)}$$

where J_{ij} is the interaction between the ions i and j belonging to the two different trinuclear units, S^* and $S^{\#}$ are the intermediate spin values in the trinuclear unit in the chosen coupling scheme.

[26] M. Julve, M. Verdaguer, A. Gleizes, M. Philoche-Levisalles, O. Kahn, *Inorg. Chem.* **1984**, *23*, 3808–3818.

[27] Y. Journaux, J. Sletten, O. Kahn, *Inorg. Chem.* **1985**, *24*, 4063–4069.

[28] J. Ribas, C. Diaz, R. Costa, Y. Journaux, C. Mathonière, O. Kahn, A. Gleizes, *Inorg. Chem.* **1990**, *29*, 2042.

[29] P. Román, C. Guzmán-Miralles, A. Luque, J. Beitia, J. Cano, M. Julve, F. Lloret, S. Alvarez, *Inorg. Chem.* **1996**, *35*, 3741–3751.

[30] C. Krebs, M. Winter, T. Weyhermüller, E. Bill, K. Wieghardt, P. Chaudhuri, *Chem. Commun.* **1995**, 1913–1915.

[31] Y. Journaux, R. Ruiz, A. Aukauloo, P. Yu, *Mol. Cryst. Liq. Cryst.* **1997**, *305*, 193–202.

[32] G. M. Sheldrick, *SHELX-86 A Program for Crystal Structure Determination*, Göttingen, **1986**.

[33] G. M. Sheldrick, *SHELXL-93 Program for the Refinement of Crystal Structures*, Göttingen, **1993**.

[34] D. Palmer, *CrystalMaker*, Bicester, **1993**.

Received July 13, 1999
[I99257]

Preparation, Properties, and Reactions of Metal-Containing Heterocycles, 101[‡]

Inclusion of Copper(I) into a Novel Bipyridine-Containing Tetraphosphadiplatinacyclophane

Ekkehard Lindner,*[a] Robert Veigel,[a] Kirstin Ortner,[a] Christiane Nachtigal,[a] and Manfred Steimann[a]

Dedicated to Professor Heinrich Vahrenkamp on the occasion of his 60th birthday

Keywords: Bipyridyldiphosphane ligands / Macrocycles / Metallacyclophanes / Platinum / Supramolecular chemistry

The 5,5′-bis(hydroxyalkyl)-2,2′-bipyridines **4a–c** (Scheme 1) were prepared either in one step (**4b**, **4c**) or in four steps (**4a**) starting with 5,5′-dimethyl-2,2′-bipyridine in each case. Reaction of **4a–c** with mesyl chloride afforded the bis(mesylates) $[–C_5H_3N–(CH_2)_n–CH_2–OSO_2Me]_2$ **5a–c** [n = 1 (**a**), 2 (**b**), 3 (**c**)], which could easily be transformed into the diphosphanes **6a–c** by reaction with $LiPPh_2$. Treatment of **6c**, **6b** with $Cl_2Pt(NCPh)_2$ and $(RC_6H_4)_2Pt(COD)$ according to the high-dilution method resulted in the formation of the tetraphosphadiplatinacyclophanes $[–C_5H_3N–(CH_2)_4–PPh_2PtCl_2PPh_2–(CH_2)_4–C_5H_3N–]_2$ (**7c**) and $[–C_5H_3N–(CH_2)_3–PPh_2Pt(C_6H_4R)_2–PPh_2–(CH_2)_3–C_5H_3N–]_2$ (**8b**, **9b**) (**8b**: R = H, **9b**: R = *t*Bu), respectively (Scheme 2). The molecular structures of **8b** and **9b** were elucidated by X-ray structural analyses. The noncoordinated bipyridine moieties in **8b** were employed to encapsulate copper(I) to give the host/guest complex **10b** (Scheme 3), which was investigated by FAB-MS, NMR spectroscopy, and cyclovoltammetry. **10b** exhibited a quasi-reversible oxidation at $E_{1/2}$ = –0.31 V and an electrodeposition-redissolution redox system at $E_{1/2}$ = –0.79 V, owing to the formation of copper at the surface of the working electrode.

Introduction

Since the systematic investigations of metal-containing macrocycles by Fujita et al.,[1] great interest emerged in the synthesis and design of such systems.[2] A couple of years later, the first synthesis of typical metallacyclophanes was published in the literature.[3] This kind of macrocycle presents the classically bridged cyclophane structure with aromatic units at the bottom and the top of the molecule, whereas the metals are located in the center of the aliphatic chain.[4] The introduction of transition metal fragments leads to a remarkable influence on the structure of the cyclophane framework.[3,5] Furthermore, a new potential reactive center is obtained, which can, for example, be used for the insertion of carbon monoxide into M–C σ bonds[3,5] or for catalysis.[6] Meanwhile several methods for the incorporation of transition metals into the cyclophane framework are known.[5,7,8] Most of these metallacyclophanes were obtained by reaction of metal-containing precursors with tertiary phosphanes or aliphatic and aromatic amines, in particular bipyridine.[9] Surprisingly, little attention has been paid to hybrid bipyridylphosphane ligands,[10] which combine the coordination chemistry of a remarkable chelator with that of a tertiary phosphane. Recently, Ziessel et al. described the generation of such a ligand and its employment in the formation of an interesting ruthenium(II)- and copper(I)-containing macrocycle.[10c,10d] In this case, the bipyridine core was provided with only one phosphane. Therefore, both donor types were needed to accomplish cyclization.

The present work deals with the construction of bipyridyldiphosphane ligands, which allows for the formation of metallacyclophanes by using only the P donors. Consequently, the resulting metallacyclophanes should have the capability to encapsulate metal ions by the formation of metal–nitrogen bonds, thus representing an important step in the design of organometallic analogues of the tris(bipyridine) cages published by Vögtle et al.[11] In this context, it was necessary to provide the macrocycle with sufficient flexibility. To achieve this goal, three novel PNNP ligands with methylene spacer units of different length between the phosphane and the bipyridine were made accessible. To prevent the formation of mononuclear species, less common 5,5′-substituted bipyridines were introduced.

Results and Discussion

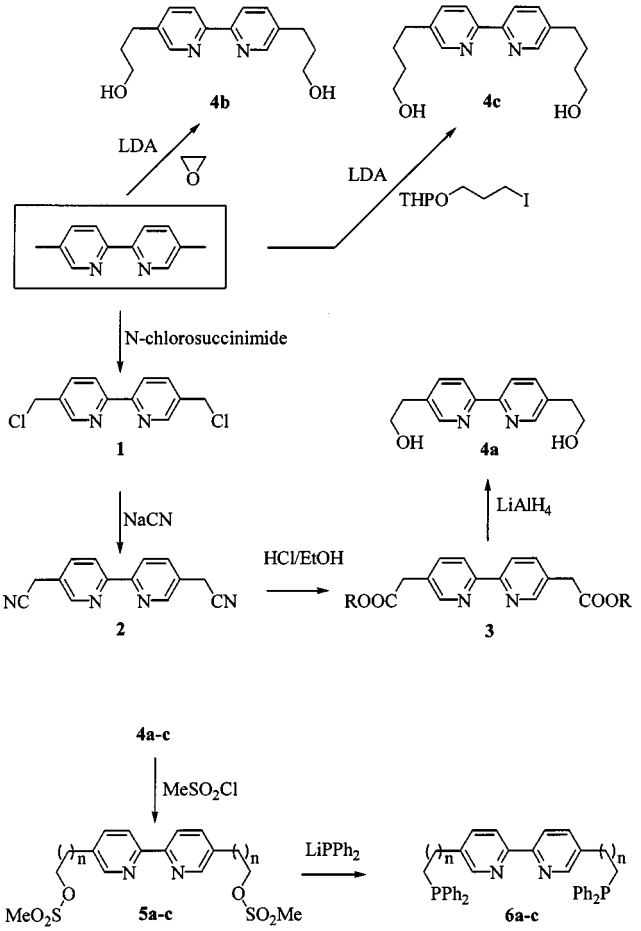
Synthesis of Ligands

For the diols **4a–c** which are important intermediates in the synthesis of the bipyridyldiphosphane ligands **6a–c** (Scheme 1), three different approaches had to be investigated. The diol **4a** was obtained in a conventional four-step process, starting with 5,5′-dimethyl-2,2′-bipyridine.[11a] Chlorination with *N*-chlorosuccinimide afforded compound **1** in which both chlorides were subsequently exchanged by

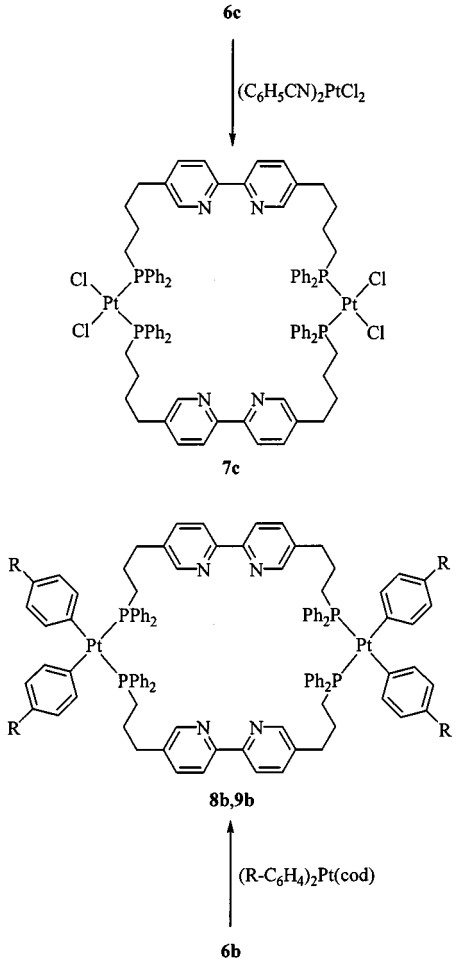
[‡] Part 100: E. Lindner, M. Mohr, C. Nachtigal, R. Fawzi, G. Henkel, *J. Organomet. Chem.*, in press.

[a] Institut für Anorganische Chemie der Universität Tübingen, Auf der Morgenstelle 18, 72076 Tübingen, Germany
Fax: (internat.) + 49-7071/29-5306
E-mail: ekkehard.lindner@uni-tuebingen.de

 © WILEY-VCH Verlag GmbH, D-69451 Weinheim, 2000 1434–1948/00/0505–0959 $ 17.50+.50/0



Scheme 1. Synthesis of the diols **4a–c** and their conversion into the bipyridyldiphosphanes **6a–c** [*n* = 1 (**a**), 2 (**b**), 3 (**c**); LDA = lithium diisopropylamide; THP = tetrahydropyran]



Scheme 2. Tetraphosphadiplatinacyclophanes **7c**, **8b**, and **9b** [R = H (**8b**), *t*Bu (**9b**)]

cyanides to achieve chain propagation. Acid catalyzed ethanolysis of **2** led to the bifunctionalized ester **3**, which was finally reduced with $LiAlH_4$ to form the target molecule **4a**. In contrast, the diols **4b**[12] and **4c** were made accessible in a one pot reaction. In both cases, 5,5′-dimethyl-2,2′-bipyridine was consecutively deprotonated with lithium diisopropylamide and reacted with oxirane and 1-tetrahydropyranyloxy-3-iodopropane,[13] respectively.

Treatment of the diols **4a–c** with mesyl chloride resulted in the formation of the corresponding dimesylates **5a–c**. This excellent leaving group was then replaced for phosphanes by the reaction of **5a–c** with $LiPPh_2$ to give the bipyridyldiphosphanes **6a–c**. The compounds **6a–c** were obtained as colorless, slightly air-sensitive solids, which were soluble in all common organic solvents with the exception of hydrocarbons and alcohols. Their molecular composition was corroborated by FAB mass spectra displaying in each case the expected molecular peak. Both phosphorus donors in **6a–c** are chemically equivalent, giving rise to a singlet each between δ = –15.1 and –15.5 in the $^{31}P\{^1H\}$-NMR spectra ($CDCl_3$).

Platinacyclophanes

Under high-dilution conditions, the bipyridyldiphosphane ligand **6c** reacted with bis(benzonitrile)dichloroplatinum(II)[14] in CH_2Cl_2 to give the 38-membered macrocycle **7c** in remarkably good yields (Scheme 2). An ES mass spectrum confirmed the dinuclear assembly of this molecule. Owing to the 5,5′-substitution pattern in **6c**, the formation of the undesired mononuclear cyclophane was successfully prevented. From a dichloromethane solution **7c** precipitated as a colorless, thermally stable solid when this solvent was removed in vacuo. It is only slightly soluble in dichloromethane and hot chloroform.

The $^{31}P\{^1H\}$-NMR spectrum of **7c** (in CD_2Cl_2) displayed a singlet at δ = 8.4 which was assigned to the four chemically equivalent phosphorus atoms, and a doublet for the ^{195}Pt satellites. The coupling constant of 3646 Hz is typical for a *cis*-$PtCl_2$ arrangement.[15] In the downfield part of the $^{13}C\{^1H\}$-NMR spectrum of **7c** (in CD_2Cl_2), six singlets and three complex multiplets resulting from AXX′ spin systems were assigned to the five bipyridine- and *para*-substituted carbon atoms of the $P(C_6H_5)_2$ units and to the *ipso*-, *ortho*-, and *meta*-carbon atoms of the phosphorus-bound phenyl groups, respectively.[15] Two further AXX′ patterns at δ = 30.0 and 25.4 were ascribed to the α- and β-carbon atoms of the alkyl chain adjacent to the phosphorus atom.[15] Finally, a multiplet at δ = 32.5 consisted of overlapping peaks of the aliphatic γ- and δ-carbon atoms.

Analogous reactions of the bipyridyldiphosphanes **6a**,**b** with bis(benzonitrile) dichloroplatinum(II) afforded poorly soluble products of either polymers or platinacyclophanes, and hence no distinction or separation was possible. Since the solubility of platinacyclophanes of the above-mentioned type is strongly dependent on the kind of the ligands attached to platinum, for further reactions cyclooctadienediphenylplatinum(II)[16] was employed as a starting material. When (COD)Pt(C_6H_5)$_2$ was allowed to react with the ligands **6a**–**c** under high-dilution conditions, soluble products could be obtained. However, only the tetraphosphadiplatinacyclophane **8b** was isolated in acceptable yields (Scheme 2). In the case of **8a**,**c** not only were the yields very low, but several by-products were also formed. The reasons for this behavior can be summarized as follows: (i) owing to the chelate effect of cyclooctadiene and the strengthening of the metal–carbon π back bond caused by the *trans*-positioned phenyl ligands which are strong σ donors, cyclooctadienediphenylplatinum(II) does not react as fast as bis(benzonitrile)dichloroplatinum(II).[16] This decrease in reaction rate exerts a negative impact on the effectiveness of the high dilution method.[17] (ii) In the case of the employment of cyclooctadienediphenylplatinum, the coordination of the bipyridine moiety in the ligands **6a**–**c** to platinum occurs as a side reaction. Although the ratio of coordinated bipyridine to phosphane is very low, this phenomenon upsets the exact stoichiometry of the starting compounds and favours an undesired polymerization. Nevertheless, the tetraphosphadiplatinacyclophane **8b** was obtained in more than 20% yield, while the isolation of the corresponding tetraphosphadiplatinacyclophanes **8a** and **8c** with shorter and longer alkyl chains failed. This suggested that the size of the 34-membered macrocycle **8b** represents an entropic maximum or enthalpic minimum with regard to the cyclization.[18]

By slow evaporation of the solvent, **8b** crystallized from a mixture of dichloromethane and methanol in the form of pale yellow plates, which were temperature-sensitive and dissolved readily in halogenated hydrocarbons and hot benzene. An FAB mass spectrum of **8b** displayed the expected molecular peak at *m*/*z* = 1915. The $^{31}P\{^1H\}$-NMR spectrum (in CD_2Cl_2) consisted of a singlet at δ = 8.8 along with a doublet for the ^{195}Pt satellites with a coupling constant of 1773 Hz, typical for the *cis*-diphenyldiphosphaneplatinum(II) fragment.[19] The downfield part of the $^{13}C\{^1H\}$-NMR spectrum of **8b** revealed six singlets and three AXX′ spin systems[20] which could be assigned in the same way as in the corresponding spectrum of **7b**. Additionally, three singlets and one AXX′ pattern with platinum satellites were ascribed to the carbon atoms of the Pt(C_6H_5)$_2$ unit.[19] In the upfield part of the spectrum, three AXX′ patterns were found, which were assigned to the three methylene groups of the alkyl chain.

The introduction of diareneplatinum(II) in the synthesis of metallacyclophanes creates a new possibility for tuning the properties of such compounds by varying the aromatic core. In the last years, a plethora of diareneplatinum(II) compounds with different properties with regard to crystallization, solubility, reactivity, and steric demand of the organometallic fragment was reported.[21] To investigate the practicability of these variations a bulky *tert*-butyl group was introduced in the *para*-position of the phenyl ligand. To achieve this goal, bis(*tert*-butylphenyl)cyclooctadieneplatinum(II)[19] was treated with the bipyridyldiphosphane **6b** under high-dilution conditions in CH_2Cl_2. The resulting macrocycle **9b** was obtained in a comparable yield to **8b**, but crystallized even better, which simplified the isolation of the compound. The $^{31}P\{^1H\}$- and $^{13}C\{^1H\}$-NMR spectra of **9b** were similar to those of **8b**, but revealed two additional singlets, related to the *tert*-butyl group in the former case. The FAB mass spectrum displayed the expected molecular peak at *m*/*z* = 2138.

X-ray Crystal Structures of 8b and 9b

Crystals of the tetraphosphadiplatinacyclophanes **8b** and **9b**, suitable for X-ray crystallography were obtained by slow concentration of a solution of **8b**, **9b** in dichloromethane/methanol. ORTEP diagrams of the molecular structures of **8b**, **9b** with atomic labeling are depicted in Figure 1 and Figure 2, respectively. Because of disordered solvent molecules, the diffraction data are of somewhat restricted quality which, however, is not unusual for macrocycles of the size presented in this investigation.[8,9,10b,22] Surprisingly, both structures are rather similar, despite the steric congestion of the bulky *tert*-butyl groups in **9b**. In both cases, the cavity has the shape of a parallelogram, with edges of lengths of 10.00(2)/11.83(2) Å and 9.92(4)/11.77(3) Å (C16–C3A/C16–C3) for **8b** and **9b**, respectively. The vertices of these parallelograms are occupied by the atoms C3, C3A and C16, C16A with distances of 15.84(3)/15.14(3) Å (**8b**) and 14.58(3)/16.18(6) Å (**9b**). The Pt1–Pt1A distances are 9.782(2) Å (**8b**) and 9.645(3) Å (**9b**). Owing to the center of inversion, the opposite pyridyl units are arranged face to face. The normals of the adjacent pyridyl rings form angles of 15.6(9)° (**8b**) and 14.8(9)° (**9b**). Also very similar are the distances of the bridging atoms of the opposite bipyridine groups (C7–C10A) with 12.08(2) Å (**8b**) and 12.07(3) Å (**9b**). In **8b** and **9b**, one P–phenyl and both Pt–phenyl substituents point to the interior of the macrocycle and exert a shielding effect on the access to the cavity. Nevertheless, a water molecule is encapsulated in **8b** which is not the case in **9b** containing additional bulky and hydrophobic *tert*-butyl groups. Remarkably, the water molecules in **8b** are located in the center of the macrocycle and simultaneously at the vertices of the triclinic unit cell (Figure 3). The two platinum atoms of each macrocycle and the encapsulated water molecule are arranged on an axis, which is indicated by dotted lines. Figure 3 demonstrates the appearance of tubes formed by the macrocycles along the *b* axis.

Encapsulation of Copper(I)

The tetraphosphadimetallacyclophanes **7c**, **8b**, and **9b** are provided with bipyridine units, which are available to coordinate transition metals which prefer a tetrahedral envir-

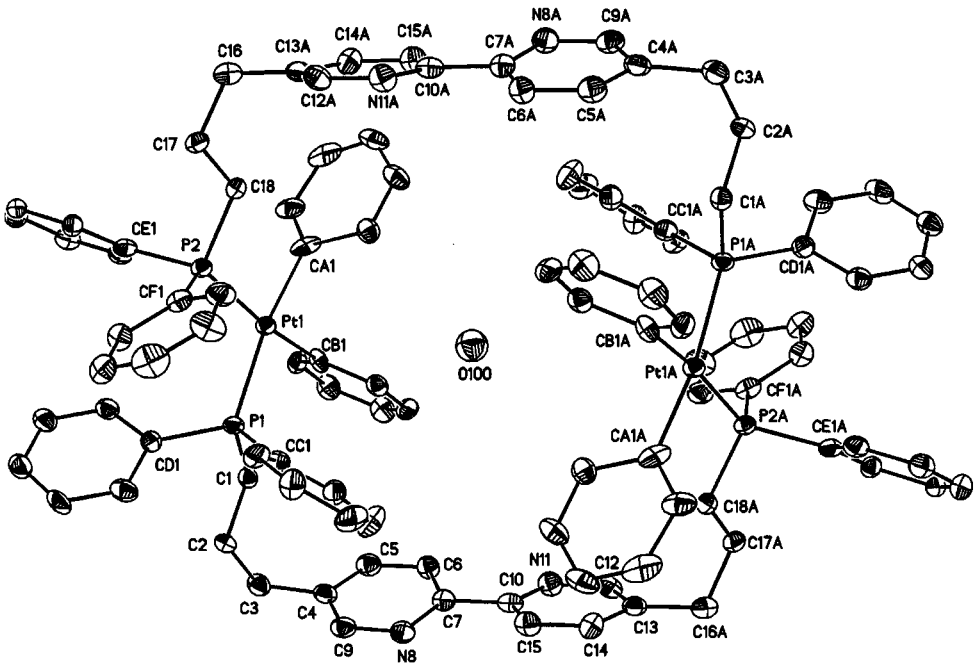


Figure 1. Molecular structure of **8b** · 3 H_2O · 2 CH_2Cl_2 in the crystal; ORTEP plot with thermal ellipsoids at 20% probability; hydrogen atoms are omitted for clarity; selected distances [A]: Pt1–CA1 = Pt1A–CA1A = 2.01(2), Pt1–CB1 = Pt1A–CB1A = 2.02(1), Pt1–P1 = Pt1A–P1A = 2.313(3), Pt1–P2 = Pt1A–P2A = 2.330(3)

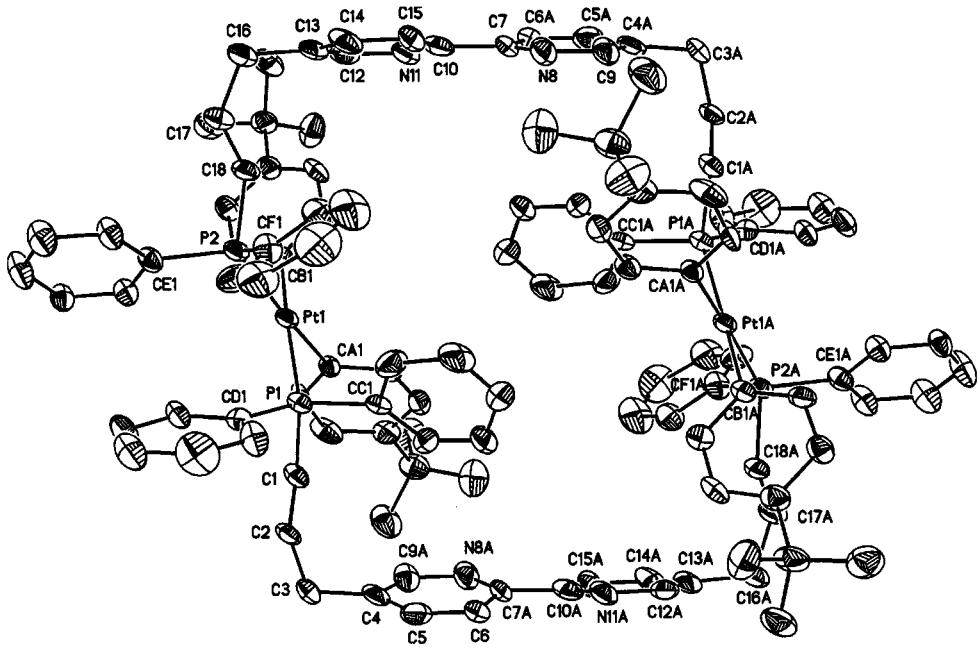


Figure 2. Molecular structure of **9b** · 2 CH_2Cl_2 in the crystal; ORTEP plot with thermal ellipsoids at 20% probability; hydrogen atoms are omitted for clarity; selected distances [A]: Pt1–CA1 = Pt1A–CA1A = 2.03(2), Pt1–CB1 = Pt1A–CB1A = 2.08(2), Pt1–P1 = Pt1A–P1A = 2.310(6), Pt1–P2 = Pt1A–P2A = 2.315(5)

onment. The incorporation of the bipyridine ligands into a macrocyclic framework should enhance the stability of such a complex. This phenomenon is known as the macrocyclic effect.[23] Owing to its better solubility, the macrocycle **8b** was chosen for encapsulation studies. Upon treatment of a solution of **8b** in dichloromethane with $[Cu(NCMe)_4][BF_4]$,[24] its color immediately turned from pale yellow to deep red, indicating the formation of a bis(bipyridine)copper(I) complex. Indeed, after purification the host/guest compound **10b** (Scheme 3) was obtained as a red–brown solid, which was air- and temperature-sensitive. An FAB mass spectrum confirmed the composition of **10b**. The $^{31}P\{^1H\}$-NMR spectrum of **10b** was still characterized by a singlet (δ = 9.8) along with two platinum satellites ($^1J_{PtP}$ = 1778 Hz). Only the ^{13}C-NMR signals of the bipyridine framework show a difference in chemical shifts of up to

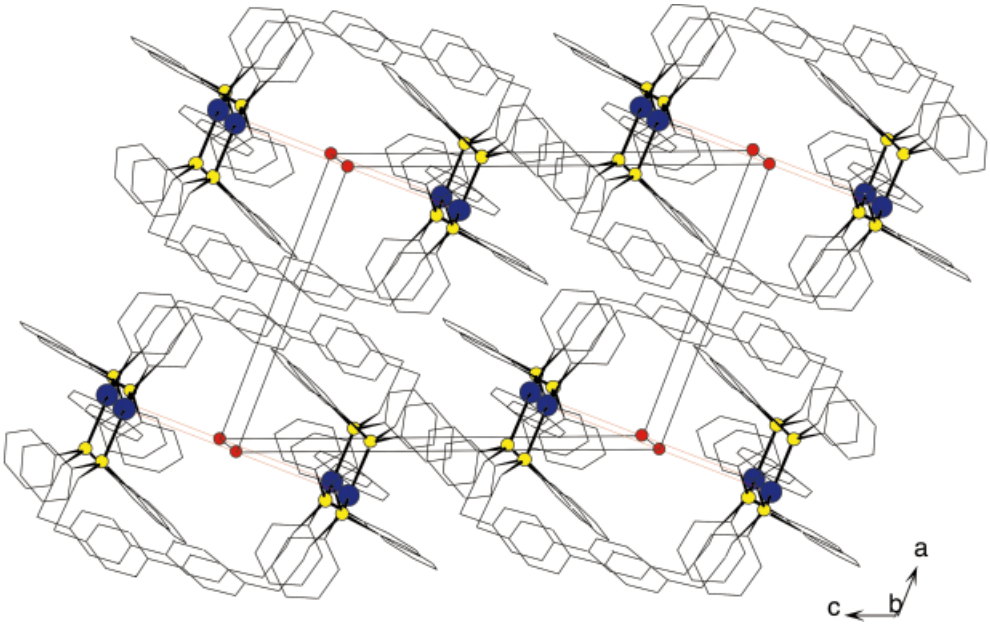
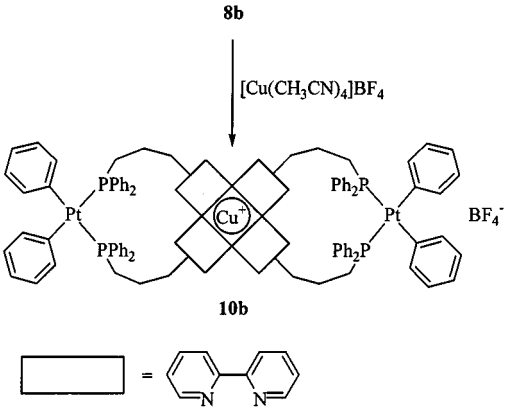


Figure 3. A view of the tubes formed by the macrocycle **8b** along the *b* axis of the crystal



Scheme 3. Encapsulation of copper(I) into the macrocycle **8b**

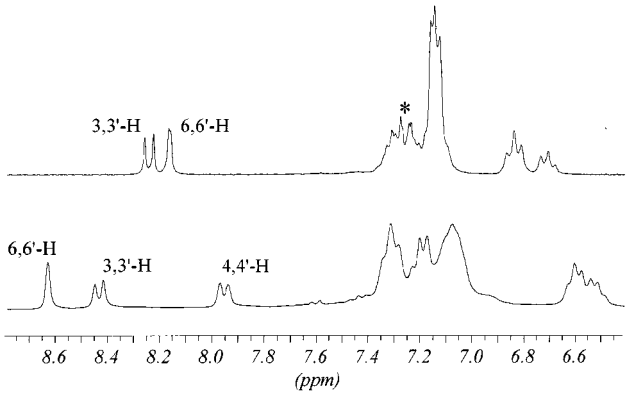


Figure 4. Comparison of the aromatic part of the ^{1}H-NMR spectra of **8b** (top) and **10b** (bottom); resonances of protons of the bipyridine units are labeled; the asterisk marks the position of the 4,4′-H resonances of the bipyridine units in **8b** as determined by a 2D COSY NMR experiment

4.5 ppm, which was traced back to the coordination of copper(I); all other ^{13}C resonances were similar to those of **8b**. A comparison of the downfield part of the ^{1}H-NMR spectra of **10b** and **8b** showed that the resonances of the bipyridine protons also underwent remarkable shifts (Figure 4). The tetrahedral coordination of copper(I)[25] is responsible for a lowering of the symmetry causing a prochirality of the protons of the alkyl chain in **10b**.[26] Because of this prochirality, their ^{1}H-NMR signals are broadened, which is rationalized by an ABCDEFXX′ spin system. In particular, the ^{1}H-NMR signals of the γ-methylene groups adjacent to the bipyridine backbone were examined by a comparison of the HMQC spectra of **10b** and **8b**. As a result, the change of the splitting pattern from a triplet (**8b**) to *two* multiplets (**10b**) is observed, which is explained by the magnetic nonequivalence of the two protons, caused by their prochirality. Apart from a slight broadening of the ^{1}H and ^{13}C resonances, no chemical exchange effects[27] were observed, which is in agreement with the use of the non-coordinating counterion[27b,28] and solvent,[29] the chelate effect of the macrocyclic ligand,[23,30] the shielding of the copper center by the bulky organometallic units, and the rigidity of the host/guest complex **10b**. In the ^{19}F-NMR spectrum of **10b**, the presence of the counterion BF_4^- is confirmed by a singlet at $\delta = -153.0$. An intensive absorption at 1056 cm^{-1} in the IR spectrum is assigned to the triply degenerate BF_3 vibration.

The electrochemical behavior of the host/guest complex **10b** was investigated by cyclic voltammetry. A quasi-reversible wave at $E_{1/2} = -0.31$ V vs. fc/fc$^+$ in CH_2Cl_2/CH_3CN was attributed to the Cu^I/Cu^{II} redox system. The $E_{1/2}$ value was similar to that of $[Cu(bipy)_2]^+$ [31] and its derivatives which are not substituted at the 6-position.[32] Typical of the low $E_{1/2}$ value was the easy and fast oxidation of copper(I) to copper(II) when a solution of **10b** was exposed to air. This was accompanied by a change in color from deep red to green.[33] Obviously, the above-mentioned stabilization of the bis(bipyridine)copper(I) complex does not include inertness toward oxygen, which can only be achieved by the introduction of substituents at the 6-position.[34,35]

On the other hand, such air-sensitive bis(bipyridine)copper(I) systems have applications in the field of redox catalysis.[36,37]

A electrodeposition–redissolution peak system at $E_{1/2}$ = –0.79 V is traced back to the formation of copper(0) at the surface of the working electrode.[31] Finally, an irreversible peak was found at 0.92 V caused by the oxidation of the diphenyldiphosphaneplatinum(II) fragment.

Conclusion

The incorporation of transition metals into the framework of cyclophanes has opened new perspectives in the field of macrocyclic chemistry.[5–9] Most of these systems were constructed using phosphorus or nitrogen donor functions and in particular they were provided with diphenylphosphane or bipyridine units.[9] However, surprisingly little attention has been paid to systems which combine both types of these ligand systems.[10] In the present investigation, the synthesis of new hybrid bipyridylphosphane ligands was introduced, enabling the formation of metallacyclophanes by the employment of P donors only. Major problems that had to be overcome to achieve the desired binuclear macrocycles were the formation of polymers, the premature complexation of bipyridine as a side reaction, and the poor solubility of the products. These drawbacks could largely be eliminated by variation of both the organometallic fragment and the length of the alkyl chain between the bipyridine and the phosphane units. As a result of these examinations, the tetraphosphadiplatinacyclophanes **8b** and **9b** were obtained, which exhibit satisfactory solubility and crystallization properties. At least two methylene groups between bipyridine and the phosphane were a prerequisite for sufficient flexibility to include tetrahedrally coordinated transition metals. The occurrence of undesirable mononuclear products was successfully prevented by the 5,5′-substitution pattern at the bipyridine cores. Owing to the presence of bipyridines which were still uncoordinated and the solubility of the macrocycle **8b** in solvents of medium polarity, it was possible to encapsulate copper(I) in **8b**. The resulting host/guest complex **10b** has three metal atoms with different coordination environments. The macrocycles described in this publication also represent an important step in the design of organometallic analogues of the tris(bipyridine) cages published by Vögtle et al.[11]

Experimental Section

General: All reactions were carried out under dry argon. Solvents were dried with appropriate reagents and stored under dry argon. – Column chromatography was performed using activated silica gel, 0.063–0.200 mm (Merck); column dimensions are reported in the specific sections describing the synthesis of the respective compounds. – Elemental analyses were carried out with a Carlo Erba 1106 and an Elementar Vario EL analyzer. Cl and S analyses were carried out according to Schöniger.[38] Chlorine and sulphur were determined as described by Dirscherl and Erne[39] according to Brunisholz and Michot,[40] and Wagner,[41] respectively. Copper and platinum were quantitatively analyzed with a Varian AA20 spectrometer. – Mass spectra: EI-MS Finnigan TSQ 70 (200 °C). FD- and FAB-MS: Finnigan 711A (8 kV), modified by AMD. ESI spectra were recorded with a triple-quadrupole mass spectrometer API III (Sciex, Thornhill, Canada) equipped with a nebulizer-assisted electrospray source. – FT-IR: Bruker IFS 48. – ^{1}H, ^{13}C{^{1}H}, ^{31}P{^{1}H}, and ^{19}F{^{1}H} NMR: Bruker DRX 250 spectrometer operating at 250.13, 62.90, 101.26, and 235.33 MHz, respectively. ^{1}H chemical shifts were referenced to the residual proton peaks of the solvent and are quoted in ppm downfield from TMS. ^{13}C chemical shifts were calibrated against the deuterated solvent multiplets and referenced to TMS. ^{31}P chemical shifts were measured relative to external 85% H_3PO_4 with downfield values being taken as positive. ^{19}F chemical shifts were measured relative to external 0.05% 1,3,5-trifluorotoluene. The assignment of the signals has been supported by DEPT-135 (Distortionless Enhancement by Polarization Transfer), homonuclear, and heteronuclear correlation spectra, when necessary. – The electrochemical experiments were performed with a Bioanalytical Systems (BAS, West Lafayette, IN) CV-50 W electrochemical workstation controlled by a standard 80486 personal computer (control program version 2.0). For electroanalytical experiments a Metrohm Pt electrode tip (Filderstadt, Germany) was used as working electrode. The counter electrode was a Pt wire of 1 mm diameter. A single-unit Habber–Luggin double reference-electrode[42] was used. The resulting potential values refer to Ag/Ag^+ (0.01 M in CH_3CN/0.1 M NBu_4PF_6). Ferrocene was used as an external standard. Its potential was determined by separate cyclic voltammetric experiments in the respective solvent, and all potentials were rescaled to $E°$(fc/fc^+) (0.145 V in CH_2Cl_2/CH_3CN vs Ag/Ag^+). All potentials in the present paper are reported relative to the fc/fc^+ standard.[43] For cyclic voltammetry, a gas-tight full-glass three-electrode cell was used: its assembly for the experiments has been described.[44] The cell was purged with argon before it was filled with the electrolyte. Background curves were recorded before adding the substrate to the solution. These were later subtracted from the experimental data with substrate. The automatic BAS CV-50 W *iR*-drop compensation facility was used for all experiments. – *N*-Chlorosuccinimide, lithium aluminum hydride, oxirane, ferrocene, and methanesulfonyl chloride were of commercial grade and used without further purification; the latter was stored under argon. 5,5′-Dimethyl-2,2′-bipyridine,[11] 1-tetrahydropyranyloxy-3-iodopropane,[13] lithium diphenylphosphide,[45] bis(benzonitrile)-dichloroplatinum(II),[14] cyclooctadienediphenylplatinum(II),[16] and bis(*tert*-butylphenyl)cyclooctadieneplatinum(II)[19] were synthesized according to literature methods.

5,5′-Bis(chloromethyl)-2,2′-bipyridine (1): 5,5′-Dimethyl-2,2′-bipyridine (30.0 g, 163.0 mmol), *N*-chlorosuccinimide (52.2 g, 391.2 mmol), and benzoyl peroxide (500 mg, 1.74 mmol) were suspended in CCl_4 (1300 mL). The suspension was heated at reflux for 48 h, and filtered hot (P3). The filtrate was concentrated to 200 mL under reduced pressure and the precipitated product was collected on a filter (P3). The crude product was purified by recrystallization from benzene. Yield 20.9 g (50.6%), colorless solid, m.p. 165 °C. – ^{1}H NMR ($CDCl_3$): δ = 8.67 (d, $^4J_{HH}$ = 2.0 Hz, 2 H, 6,6′-H, bipy), 8.40 (d, $^3J_{HH}$ = 8.2 Hz, 2 H, 3,3′-H, bipy), 7.86 (dd, $^3J_{HH}$ = 8.2 Hz, $^4J_{HH}$ = 2.0 Hz, 2 H, 4,4′-H, bipy), 4.64 (s, 4 H, CH_2Cl). – ^{13}C{^{1}H} NMR ($CDCl_3$): δ = 155.7 (s, C, bipy), 149.2 (s, CH, bipy), 137.4 (s, CH, bipy), 133.6 (s, C, bipy), 121.3 (s, CH, bipy), 43.2 (s, CH_2Cl). – MS (EI); *m/z*: 252.0 [M^+]. – $C_{12}H_{10}Cl_2N_2$ (253.1): calcd. C 56.94, H 3.98, Cl 28.01, N 11.07; found C 57.10, H 3.83, Cl 27.91, N 10.95.

5,5′-Bis(cyanomethyl)-2,2′-bipyridine (2): Compound **1** (15.0 g, 59.3 mmol) was dissolved in a mixture of ethanol (400 mL) and concentrated hydrochloric acid (7 mL). This solution was added dropwise over a period of 30 min to a refluxing solution of sodium cyanide (23.6 g, 480.6 mmol) in 500 mL of water and 500 mL of ethanol (***Caution: Generation of hydrogen cyanide!***). The solution was then heated at reflux for further 2 h and concentrated to a volume of 200 mL under reduced pressure. The remaining solution was diluted with 800 mL of water and the solution was stirred for 30 min. The precipitated product was filtered (P3) and washed with water (2 × 100 mL). The residue was dissolved in 300 mL of acetone and filtered (P3). The solvent of the filtrate was evaporated to dryness to give the crude product, which was used without further purification. Yield 8.3 g (59.3%), brown solid. For analytical data **2** was purified by sublimation and a colorless solid was obtained, m.p. 197 °C. – IR (KBr): $\tilde{\nu}$ = 2256 cm^{-1} (CN). – ^1H NMR ([D$_6$]acetone): δ = 8.72 (d, $^4J_{HH}$ = 1.9 Hz, 2 H, 6,6′-H, bipy), 8.51 (d, $^3J_{HH}$ = 8.2 Hz, 2 H, 3,3′-H, bipy), 7.99 (dd, $^3J_{HH}$ = 8.2 Hz, $^4J_{HH}$ = 1.9 Hz, 2 H, 4,4′-H, bipy), 4.14 (s, 4 H, CH_2CN). – $^{13}C\{^1H\}$ NMR ([D$_6$]acetone): δ = 155.9 (s, C, bipy), 149.8 (s, CH, bipy), 137.7 (s, CH, bipy), 129.0 (s, C, bipy), 121.6 (s, CH, bipy), 118.6 (s, CH_2CN), 21.0 (s, CH_2CN). – MS (EI); *m*/*z*: 234.0 [M$^+$]. – $C_{14}H_{10}N_4$ (234.3): calcd. C 71.78, H 4.30, N 23.92; found C 71.80, H 4.14, N 23.37.

Diester 3: To a suspension of **2** (7.7 g, 32.9 mmol) in 500 mL of ethanol, at 0 °C dry hydrogen chloride was added until saturation was achieved. The solution was heated at reflux for 18 h and concentrated to dryness under reduced pressure. The residue was suspended in 200 mL of water, neutralized with $NaHCO_3$, and extracted with ethyl acetate (2 × 300 mL). The combined organic layers were dried with Na_2SO_4, filtered (P3), and the solution was concentrated to dryness under reduced pressure. The product was purified by column chromatography (ethyl acetate, diameter/length of column 7/50 cm). Yield 5.3 g (48.8%), colorless solid. – M.p. 76 °C. – IR (KBr): $\tilde{\nu}$ = 1736 cm^{-1} (CO). – ^1H NMR ($CDCl_3$): δ = 8.52 (d, $^4J_{HH}$ = 2.0 Hz, 2 H, 6,6′-H, bipy), 8.30 (d, $^3J_{HH}$ = 8.1 Hz, 2 H, 3,3′-H, bipy), 7.69 (dd, $^3J_{HH}$ = 8.1 Hz, $^4J_{HH}$ = 2.0 Hz, 2 H, 4,4′-H, bipy), 4.10 (q, $^3J_{HH}$ = 7.1 Hz, 4 H, $COOCH_2CH_3$), 3.61 (s, 4 H, $CH_2COOC_2H_5$), 1.18 (t, $^3J_{HH}$ = 7.1 Hz, 6 H, $COOCH_2CH_3$). – $^{13}C\{^1H\}$ NMR ($CDCl_3$): δ = 154.6 (s, C, bipy), 149.6 (s, CH, bipy), 137.6 (s, CH, bipy), 129.8 (s, C, bipy), 120.5 (s, CH, bipy) 61.0 (s, $COOCH_2CH_3$), 38.2 (s, $CH_2COOC_2H_5$), 14.0 (s, $COOCH_2CH_3$). – MS (EI); *m*/*z*: 328.1 [M$^+$]. – $C_{18}H_{20}N_2O_4$ (328.4): calcd. C 65.84, H 6.14, N 8.53; found C 65.52, H 6.14, N 8.56.

Diol 4a: Lithium aluminum hydride (1.18 g, 31.03 mmol) was suspended in 100 mL of THF and the suspension was added dropwise to an ice-cold solution of **3** (5.09 g, 15.50 mmol) in 200 mL of THF. The resulting suspension was stirred for 4 h at room temperature, then cautiously quenched with water and concentrated to dryness. The residue was dissolved in 120 mL of water and extracted continuously with diethyl ether for 48 h. The organic layer was dried with Na_2SO_4, filtered (P3), and concentrated. The crude product was purified using column chromatography (dichloromethane/methanol, 7:1, diameter/length of column 7/50). Yield 2.15 g (56.8%), colorless solid, m.p 146 °C. – ^1H NMR (CD_3OD): δ = 8.49 (d, $^4J_{HH}$ = 2.0 Hz, 2 H, 6,6′-H, bipy), 8.14 (d, $^3J_{HH}$ = 8.2 Hz, 2 H, 3,3′-H, bipy), 7.79 (dd, $^3J_{HH}$ = 8.2 Hz, $^4J_{HH}$ = 2.0 Hz, 2 H, 4,4′-H, bipy), 3.82 (t, $^3J_{HH}$ = 6.7 Hz, 4 H, CH_2CH_2OH), 2.90 (t, $^3J_{HH}$ = 6.7 Hz, 4 H, CH_2CH_2OH). – $^{13}C\{^1H\}$ NMR (CD_3OD): δ = 154.7 (s, C, bipy), 150.3 (s, CH, bipy), 139.1 (s, CH, bipy), 136.4 (s, C, bipy), 122.1 (s, CH, bipy), 63.1 (s, CH_2CH_2OH), 36.7 (s, CH_2CH_2OH). – MS (EI); *m*/*z*: 244.1 [M$^+$]. – $C_{14}H_{16}N_2O_2$ (244.3): calcd. C 68.83, H 6.60, N 11.47; found C 68.31, H 6.11, N 11.27.

Diol 4b: A freshly prepared solution of 100.0 mmol of lithium diisopropylamide in 375 mL of a 1:2 mixture of *n*-hexane and THF was added dropwise to a solution of 5,5′-dimethyl-2,2′-bipyridine (18.4 g, 100.0 mmol) in 700 mL of THF at –50 °C. The solution was then allowed to warm to room temperature and stirred for 1 h. Then it was cooled to –50 °C and oxirane (4.9 g, 111.4 mmol) was added. Subsequently the solution was heated to 40 °C for 4 h, while the condenser was kept at –30 °C. The complete procedure had to be repeated. The solution was then quenched with a saturated aqueous NH_4Cl solution until pH = 7 was achieved. THF was removed under reduced pressure and the resulting suspension was extracted seven times with a 2:1 mixture of dichloromethane and ethyl acetate. The combined organic layers were dried with Na_2SO_4, filtered (P3), and concentrated. The crude product was purified by column chromatography (dichloromethane/methanol, 10:1, diameter/length of column 7/50). Yield 6.32 g (23.2%), colorless solid, m.p. 119 °C. – ^1H NMR (CD_3OD): δ = 8.47 (d, $^4J_{HH}$ = 2.0 Hz, 2 H, 6,6′-H, bipy), 8.14 (d, $^3J_{HH}$ = 8.2 Hz, 2 H, 3,3′-H, bipy), 7.75 (dd, $^3J_{HH}$ = 8.2 Hz, $^4J_{HH}$ = 2.0 Hz, 2 H, 4,4′-H, bipy), 3.59 (t, $^3J_{HH}$ = 6.3 Hz, 4 H, $CH_2CH_2CH_2OH$), 2.76 (t, $^3J_{HH}$ = 7.8 Hz, 4 H, $CH_2CH_2CH_2OH$) 1.86 (m, 4 H, $CH_2CH_2CH_2OH$). – $^{13}C\{^1H\}$ NMR (CD_3OD): δ = 155.0 (s, C, bipy), 150.3 (s, CH, bipy), 139.5 (s, CH, bipy), 138.7 (s, C, bipy), 122.3 (s, CH, bipy), 61.9 (s, $CH_2CH_2CH_2OH$), 35.0 (s, $CH_2CH_2CH_2OH$), 30.0 (s, $CH_2CH_2CH_2OH$). – MS (EI); *m*/*z*: 272.1 [M$^+$]. – $C_{16}H_{20}N_2O_2$ (272.3): calcd. C 70.56, H 7.40, N 10.29; found C 70.40, H 7.35, N 10.34.

Diol 4c: A freshly prepared solution of 100.0 mmol of lithium diisopropylamide in 375 mL of a 1:2 mixture of *n*-hexane and THF was added dropwise to a solution of 5,5′-dimethyl-2,2′-bipyridine (18.4 g, 100.0 mmol) in 700 mL of THF at –50 °C. The solution was allowed to warm to room temperature and stirred for 1 h. Then it was cooled to –78 °C and 1-iodo-3-(tetrahydropyranyloxy)propane (28.4 g, 105.2 mmol) was added dropwise. The solution was allowed to warm to room temperature and stirred for 30 min. The complete procedure was repeated. The solution was then quenched with 1 M hydrochloric acid until pH = 0 was achieved, stirred for an additional hour and neutralized with $NaHCO_3$. THF was removed under reduced pressure and the resulting suspension was extracted seven times with a 2:1 mixture of dichloromethane and ethyl acetate. The combined organic layers were dried with Na_2SO_4, filtered (P3), and concentrated. The crude product was purified by column chromatography (dichloromethane/methanol, 10:1, diameter/length of column 7/50). Yield 6.11 g (20.4%), colorless solid, m.p. 109 °C. – ^1H NMR (CD_3OD): δ = 8.48 (d, $^4J_{HH}$ = 2.1 Hz, 2 H, 6,6′-H, bipy), 8.17 (d, $^3J_{HH}$ = 8.1 Hz, 2 H, 3,3′-H, bipy), 7.80 (dd, $^3J_{HH}$ = 8.1 Hz, $^4J_{HH}$ = 2.1 Hz, 2 H, 4,4′-H, bipy), 3.57 (t, $^3J_{HH}$ = 6.3 Hz, 4 H, $CH_2CH_2CH_2CH_2OH$), 2.73 (t, $^3J_{HH}$ = 7.5 Hz, 4 H, $CH_2CH_2CH_2CH_2OH$) 1.74 (m, 4 H, CH_2), 1.59 (m, 4 H, CH_2). – $^{13}C\{^1H\}$ NMR (CD_3OD): δ = 155.1 (s, C, bipy), 150.4 (s, CH, bipy), 140.0 (s, CH, bipy), 138.8 (s, C, bipy), 122.4 (s, CH, bipy), 62.8 (s, $CH_2CH_2CH_2CH_2OH$), 33.6 (s, CH_2), 33.3 (s, CH_2), 28.8 (s, CH_2). – MS (EI); *m*/*z*: 300.1 [M$^+$]. – $C_{18}H_{24}N_2O_2$ (300.4): calcd. C 71.96, H 8.06, N 9.32; found C 72.33, H 8.01, N 9.48.

General Procedure for the Preparation of the Dimesylates 5a–c: Methanesulfonyl chloride (2.50 g, 22.0 mmol) in 20 mL of dichloromethane was added dropwise to a suspension of **5a–c** (10.0 mmol) and triethylamine (2.22 g, 22.0 mmol) in 200 mL of dichloromethane at 0 °C. The reaction mixture was allowed to

warm to room temperature, stirred for 1 h, and washed with 100 mL of a diluted aqueous $NaHCO_3$ solution. The aqueous layer was reextracted with 100 mL of dichloromethane and the combined organic layers were dried with Na_2SO_4, filtered (P3), and concentrated to dryness. The products were washed with 20 mL of cold methanol (0 °C) and dried in vacuo.

Dimesylate 5a: Yield 3.61 g (90.3%), colorless solid, m.p. >130 °C (dec.). – ^{1}H NMR ($CDCl_3$): δ = 8.56 (d, $^4J_{HH}$ = 1.9 Hz, 2 H, 6,6′-H, bipy), 8.35 (d, $^3J_{HH}$ = 8.2 Hz, 2 H, 3,3′-H, bipy), 7.72 (dd, $^3J_{HH}$ = 8.2 Hz, $^4J_{HH}$ = 1.9 Hz, 2 H, 4,4′-H, bipy), 3.13 (t, $^3J_{HH}$ = 6.6 Hz, 4 H, $CH_2CH_2OSO_2CH_3$), 3.13 (t, $^3J_{HH}$ = 6.6 Hz, 4 H, $CH_2CH_2OSO_2CH_3$), 2.93 (s, 6 H, $CH_2CH_2OSO_2CH_3$). – ^{13}C{^{1}H} NMR ($CDCl_3$): δ = 154.8 (s, C, bipy), 149.7 (s, CH, bipy), 137.7 (s, CH, bipy), 132.4 (s, C, bipy), 121.1 (s, CH, bipy), 69.3 (s, $CH_2CH_2OSO_2CH_3$), 37.7 (s, $CH_2CH_2OSO_2CH_3$), 32.9 (s, $CH_2CH_2OSO_2CH_3$). – MS (FD, 30 °C); *m/z*: 400.1 [M$^+$]. – $C_{16}H_{20}N_2O_6S_2$ (400.6): calcd. C 47.99, H 5.03, N 7.00, S 16.01; found C 47.98, H 5.08, N 6.93, S 15.73.

Dimesylate 5b: Yield 3.60 g (84.2%), colorless solid, m.p. >130 °C (dec.). – ^{1}H NMR ($CDCl_3$): δ = 8.54 (d, $^4J_{HH}$ = 2.0 Hz, 2 H, 6,6′-H, bipy), 8.32 (d, $^3J_{HH}$ = 8.1 Hz, 2 H, 3,3′-H, bipy), 7.67 (dd, $^3J_{HH}$ = 8.1 Hz, $^4J_{HH}$ = 2.0 Hz, 2 H, 4,4′-H, bipy), 4.27 (t, $^3J_{HH}$ = 6.2 Hz, 4 H, $CH_2CH_2CH_2OSO_2CH_3$), 3.00 (s, 6 H, $CH_2CH_2CH_2OSO_2CH_3$), 2.84 (t, $^3J_{HH}$ = 7.6 Hz, 4 H, $CH_2CH_2CH_2OSO_2CH_3$), 2.13 (m, 4 H, $CH_2CH_2CH_2OSO_2CH_3$). – ^{13}C{^{1}H} NMR ($CDCl_3$): δ = 154.1 (s, C, bipy), 149.2 (s, CH, bipy), 137.4 (s, CH, bipy), 136.1 (s, C, bipy), 121.1 (s, CH, bipy), 68.8 (s, $CH_2CH_2CH_2OSO_2CH_3$), 37.6 (s, $CH_2CH_2CH_2OSO_2CH_3$), 30.5 (s, $CH_2CH_2CH_2OSO_2CH_3$), 28.8 (s, $CH_2CH_2CH_2OSO_2CH_3$). – MS (FD, 30 °C); *m/z*: 428.0 [M$^+$]. – $C_{18}H_{24}N_2O_6S_2$ (428.6): calcd. C 50.45, H 5.64, N 6.54, S 14.97; found C 49.96, H 5.73, N 6.41, S 14.82.

Dimesylate 5c: Yield 3.71 g (81.4%), colorless solid, m.p. >130 °C (dec.). – ^{1}H NMR ($CDCl_3$): δ = 8.45 (d, $^4J_{HH}$ = 2.1 Hz, 2 H, 6,6′-H, bipy), 8.24 (d, $^3J_{HH}$ = 8.1 Hz, 2 H, 3,3′-H, bipy), 7.59 (dd, $^3J_{HH}$ = 8.1 Hz, $^4J_{HH}$ = 2.1 Hz, 2 H, 4,4′-H, bipy), 4.21 (t, $^3J_{HH}$ = 6.0 Hz, 4 H, $CH_2CH_2CH_2CH_2OSO_2CH_3$), 2.96 (s, 6 H, $CH_2CH_2CH_2CH_2OSO_2CH_3$), 2.68 (t, $^3J_{HH}$ = 6.8 Hz, 4 H, $CH_2CH_2CH_2CH_2OSO_2CH_3$), 1.65–1.85 (m, 8 H, $CH_2CH_2CH_2CH_2OSO_2CH_3$). – ^{13}C{^{1}H} NMR ($CDCl_3$): δ = 154.1 (s, C, bipy), 149.1 (s, CH, bipy), 137.0 (s, CH, bipy), 136.9 (s, C, bipy), 120.7 (s, CH, bipy), 69.7 (s, $CH_2CH_2CH_2CH_2OSO_2CH_3$), 37.6 (s, $CH_2CH_2CH_2CH_2OSO_2CH_3$), 30.5 (s, $CH_2CH_2CH_2CH_2OSO_2CH_3$), 28.7 (s, CH_2), 27.0 (s, CH_2). – MS (FD, 30 °C); *m/z*: 456.0 [M$^+$]. – $C_{20}H_{28}N_2O_6S_2$ (456.6): calcd. C 52.61, H 6.18, N 6.13, S 14.04; found C 52.50, H 6.32, N 6.14, S 14.04.

General Procedure for the Preparation of the Diphosphanes 6a–c: A freshly prepared solution of lithium diphenylphosphide (1.69 g, 8.8 mmol) in 50 mL of THF was added dropwise to a solution of 8.0 mmol of **6a–c** in 200 mL of THF at –78 °C. The solution was allowed to warm to room temperature, stirred for 30 min and quenched with degassed water. The solvent was completly removed under reduced pressure and the residue was washed two times with 10 mL of cold methanol (0 °C). The remainder was dissolved in 50 mL of dichloromethane, and the solution was filtered (P4), and then concentrated in vacuo.

Diphosphane 6a: Yield 4.23 g (91.1%), colorless, slightly air-sensitive solid, m.p. 156 °C. – ^{1}H NMR ($CDCl_3$): δ = 8.45 (d, $^4J_{HH}$ = 1.9 Hz, 2 H, 6,6′-H, bipy), 8.26 (d, $^3J_{HH}$ = 8.2 Hz, 2 H, 3,3′-H, bipy), 7.59 (dd, $^3J_{HH}$ = 8.2 Hz, $^4J_{HH}$ = 1.9 Hz, 2 H, 4,4′-H, bipy), 7.47–7.27 (m, 20 H, Ph), 2.75 (m, 4 H, $CH_2CH_2PPh_2$), 2.36 (m, 4 H, $CH_2CH_2PPh_2$). – ^{13}C{^{1}H} NMR ($CDCl_3$): δ = 153.8 (s, C, bipy), 149.0 (s, CH, bipy), 138.3–138.0 (m, *ipso*-Ph and C, bipy), 136.9 (s, CH, bipy), 132.8 (d, $^2J_{PC}$ = 18.6 Hz, *ortho*-Ph), 128.9 (s, *para*-Ph), 128.7 (d, $^3J_{PC}$ = 6.4 Hz, *meta*-Ph), 121.1 (s, CH, bipy), 29.9 (d, CH_2), 29.3 (d, CH_2). – ^{31}P{^{1}H} NMR ($CDCl_3$): δ = –15.1 (s). – MS (FAB, 30 °C); *m/z*: 581.3 [M$^+$ + H]. – $C_{38}H_{34}N_2P_2$ (580.6): calcd. C 78.61, H 5.90, N 4.82; found C 78.29, H 5.51, N 4.69.

Diphosphane 6b: Yield 4.30 g (88.4%), colorless, slightly air sensitive solid, m.p. 163 °C. – ^{1}H NMR ($CDCl_3$): δ = 8.45 (d, $^4J_{HH}$ = 2.0 Hz, 2 H, 6,6′-H, bipy), 8.23 (d, $^3J_{HH}$ = 8.1 Hz, 2 H, 3,3′-H, bipy), 7.55 (dd, $^3J_{HH}$ = 8.1 Hz, $^4J_{HH}$ = 2.0 Hz, 2 H, 4,4′-H, bipy), 7.42–7.28 (m, 20 H, Ph) 2.78 (t, $^3J_{HH}$ = 7.2 Hz, 4 H, $CH_2CH_2CH_2PPh_2$), 2.06 (m, 4 H, $CH_2CH_2CH_2PPh_2$), 1.73 (m, 4 H, $CH_2CH_2CH_2PPh_2$). – ^{13}C{^{1}H} NMR ($CDCl_3$): δ = 154.3 (s, C, bipy), 149.6 (s, CH, bipy), 138.6 (d, $^1J_{PC}$ = 12.8 Hz, *ipso*-Ph), 137.1 (s, C, bipy), 137.0 (s, CH, bipy), 132.8 (d, $^2J_{PC}$ = 18.5 Hz, *ortho*-Ph), 128.8–128.5 (m, *meta*- and *para*-Ph), 120.6 (s, CH, bipy), 34.1 (d, $^3J_{PC}$ = 13.8 Hz, $CH_2CH_2CH_2PPh_2$), 27.7–27.3 (m, 8 H, $CH_2CH_2CH_2PPh_2$). – ^{31}P{^{1}H} NMR ($CDCl_3$): δ = –15.5 (s). – MS (FAB, 50 °C); *m/z*: 609.0 [M$^+$ + H]. – $C_{40}H_{38}N_2P_2$ (608.7): calcd. C 78.93, H 6.29, N 4.60; found C 79.06, H 6.44, N 4.45.

Diphosphane 6c: Yield 4.51 g (88.6%), colorless, slightly air sensitive solid, m.p. 132 °C. – ^{1}H NMR ($CDCl_3$): δ = 8.41 (d, $^4J_{HH}$ = 2.0 Hz, 2 H, 6,6′-H, bipy), 8.20 (d, $^3J_{HH}$ = 8.2 Hz, 2 H, 3,3′-H, bipy), 7.50 (dd, $^3J_{HH}$ = 8.2 Hz, $^4J_{HH}$ = 2.0 Hz, 2 H, 4,4′-H, bipy), 7.43–7.25 (m, 20 H, PPh_2), 2.60 (t, $^3J_{HH}$ = 7.6 Hz, 4 H, $CH_2CH_2CH_2CH_2PPh_2$), 2.06 (m, 4 H, $CH_2CH_2CH_2CH_2PPh_2$), 1.87–1.68 (m, 8 H, $CH_2CH_2CH_2CH_2PPh_2$). – ^{13}C{^{1}H} NMR ($CDCl_3$): δ = 154.1 (s, C, bipy), 149.3 (s, CH, bipy), 138.8 (d, $^1J_{PC}$ = 13.0 Hz, *ipso*-Ph), 137.5 (s, C, bipy), 136.7 (s, CH, bipy), 132.8 (d, $^2J_{PC}$ = 18.5 Hz, *ortho*-Ph), 128.6 (s, *para*-Ph), 128.5 (d, $^3J_{PC}$ = 6.5 Hz, *meta*-Ph), 120.5 (s, CH, bipy), 32.5–32.2 (m, $CH_2CH_2CH_2CH_2PPh_2$ and $CH_2CH_2CH_2CH_2PPh_2$) 28.0 (d, $^1J_{PC}$ = 11.5 Hz, $CH_2CH_2CH_2CH_2PPh_2$), 25.7 (d, $^2J_{PC}$ = 16.2 Hz, $CH_2CH_2CH_2CH_2PPh_2$). – ^{31}P{^{1}H} NMR ($CDCl_3$): δ = –15.3 (s). – MS (FAB, 30 °C); *m/z*: 637.3 [M$^+$ + H]. – $C_{42}H_{42}N_2P_2$ (636.8): calcd. C 79.22, H 6.65, N 4.40; found C 78.83, H 6.70, N 4.21.

Tetrachlorodiplatinacyclophane 7c: Solutions of bis(benzonitrile)-dichloroplatinum(II) (1.35 g, 2.858 mmol) and of **6c** (1.82 g, 2.860 mmol) in 200 mL of dichloromethane each were simultaneously added dropwise within 2 h into 200 mL of dichloromethane. After the solution was stirred for 30 min and concentrated to 10 mL in vacuo, polymeric fractions precipitated. These were removed by filtration (P4) and the filtrate was concentrated to dryness. The residue was washed intensively with *n*-pentane, dissolved in 100 mL of hot chloroform, and the resulting solution was cooled to room temperature, filtered (P4), and concentrated to dryness. Yield: 1.52 g (58.9%), colorless solid, m.p. >290 °C (dec.). – ^{1}H NMR (CD_2Cl_2): δ = 8.35 (d, 4 H, 6,6′-H, bipy), 8.24 (d, $^3J_{HH}$ = 8.1 Hz, 4 H, 3,3′-H, bipy), 7.53–7.18 (m, 44 H, PPh_2 and 4,4′-H, bipy), 2.54 (t, $^3J_{HH}$ = 7.6 Hz, 8 H, $CH_2CH_2CH_2CH_2PPh_2$), 2.12 (m, 8 H, $CH_2CH_2CH_2CH_2PPh_2$), 1.75–1.48 (m, 16 H, $CH_2CH_2CH_2CH_2PPh_2$). – ^{13}C{^{1}H} NMR (CD_2Cl_2): δ = 154.6 (s, C, bipy), 149.8 (s, CH, bipy), 137.9 (s, C, bipy), 137.1 (s, CH, bipy), 134.0 (m,[46] *N* = 9.5 Hz, *ortho*-Ph), 131.7 (s, *para*-Ph), 130.1 (m,[46] *N* = 58.8 Hz, *ipso*-Ph), 129.0 (m,[46] *N* = 10.2 Hz, *meta*-Ph), 120.8 (s, CH, bipy), 32.9–32.1 (m, $CH_2CH_2CH_2CH_2PPh_2$), 30.0 (m,[46] *N* = 39.5 Hz, $CH_2CH_2CH_2CH_2PPh_2$), 25.4 (s br,[14,46] $CH_2CH_2CH_2CH_2PPh_2$). – ^{31}P{^{1}H} NMR (CD_2Cl_2): δ = 8.4 (s, d, $^1J_{PtP}$ = 3646 Hz). – MS (ES); *m/z*: 1769.4 [M$^+$ – Cl]. –

$C_{84}H_{84}Cl_4N_4P_4Pt_2$ (1805.5): calcd. C 55.88, H 4.69, Cl 7.85, N 3.10, Pt 21.61; found C 55.65, H 4.73, Cl 7.70, N 3.41, Pt 20.96.

General Procedure for the Tetraaryldiplatinacyclophanes 8b and 9b: Solutions of cyclooctadienediphenylplatinum(II) or bis(*tert*-butylphenyl)cyclooctadieneplatinum(II) (3.38 mmol) and of **6b** (2.06 g, 3.39 mmol) in 400 mL of dichloromethane each were simultaneously added dropwise during 5 h into 500 mL of dichloromethane. The solution was stirred overnight and concentrated. The residue was purified by column chromatography (dichloromethane/methanol, 50:1, diameter/length of column 7/50) and recrystallized twice from dichloromethane/methanol.

Tetraphenyldiplatinacyclophane 8b: Yield: 670 mg (20.7%), pale yellow plates, m.p. >150 °C (dec.). – ^{1}H NMR (CD_2Cl_2): δ = 8.26 (d, $^3J_{HH}$ = 8.2 Hz, 4 H, 3,3′-H, bipy), 8.18 (d, $^4J_{HH}$ = 2.0 Hz, 4 H, 6,6′-H, bipy), 7.37–7.10 (m, 52 H, Ph_2P, Ph_2Pt and 4,4′-H, bipy), 6.92–6.67 (m, 12 H, Ph_2Pt), 2.19 (t, $^3J_{HH}$ = 6.3 Hz, 8 H, $CH_2CH_2CH_2PPh_2$), 1.65–1.25 (m, 16 H, $CH_2CH_2CH_2PPh_2$). – ^{13}C{^{1}H} NMR (CD_2Cl_2): δ = 161.5 (m,[46] $^1J_{PtC}$ = 840.8 Hz, *ipso*-Ph_2Pt), 154.5 (s, C, bipy), 149.8 (s, CH, bipy), 137.7–136.8 (m, C, bipy, CH, bipy, *ortho*-Ph_2Pt), 133.5 (m,[46] *N* = 10.0 Hz, *ortho*-Ph_2P), 132.9 (m,[46] *N* = 41.3 Hz, *ipso*-Ph_2P), 130.1 (s, *para*-Ph_2P), 128.4 (m,[46] *N* = 8.5 Hz, *meta*-Ph_2P), 127.5 (s, d, $^3J_{PtC}$ = 65.5 Hz, *meta*-Ph_2Pt), 121.6 (s, *para*-Ph_2Pt), 120.4 (s, CH, bipy), 34.2 (m,[46] *N* = 13.5 Hz, $CH_2CH_2CH_2PPh_2$), 27.8 (m,[46] *N* = 33.4 Hz, $CH_2CH_2CH_2PPh_2$), 26.6 (s, br,[14,46] $CH_2CH_2CH_2PPh_2$). – ^{31}P{^{1}H} NMR (CD_2Cl_2): δ = 8.8 (s, d, $^1J_{PtP}$ = 1773 Hz). – MS (FAB, 30 °C); *m/z*: 1915.6 [M^+], 1761.0 [M^+– 2 Ph], 1684.4 [M^+– 3 Ph], 1607.3 [M^+– 4 Ph]. – $C_{104}H_{96}N_4P_4Pt_2$ (1916.0): calcd. C 65.20, H 5.05, N 2.92, Pt 20.36; found C 65.16, H 5.28, N 2.97, Pt 19.95.

Tetrakis(*tert*-butylphenyl)diplatinacyclophane 9b: Yield: 840 mg (23.2%), pale yellow plates, m.p. >145 °C (dec.). – ^{1}H NMR (CD_2Cl_2): δ = 8.25 (d, $^3J_{HH}$ = 8.2 Hz, 4 H, 3,3′-H, bipy), 8.15 (d, $^4J_{HH}$ = 2.0 Hz, 4 H, 6,6′-H, bipy), 7.36–7.12 (m, 52 H, Ph_2P, Ph_2Pt and 4,4′-H, bipy), 6.98–6.89 (m, 8 H, $PtPh_2$), 2.14 (t, $^3J_{HH}$ = 6.3 Hz, 8 H, $CH_2CH_2CH_2PPh_2$), 1.58–1.22 [m, 52 H, $CH_2CH_2CH_2PPh_2$, and $C(CH_3)_3$]. – ^{13}C{^{1}H} NMR (CD_2Cl_2): δ = 157.4 [m,[46] *ipso*-(*tert*-butylPh)$_2$Pt], 154.5 (s, C, bipy), 149.8 (s, CH, bipy), 144.0 [s, *para*-(*tert*-butylPh)$_2$Pt], 137.2 (s, C, bipy) 137.1 (s, CH, bipy), 136.6 [s, d, $^2J_{PtC}$ = 34.8 Hz, *ortho*-(*tert*-butylPh)$_2$Pt], 133.5 (m,[46] *N* = 10.7 Hz, *ortho*-Ph_2P), 133.0 (m,[46] *N* = 41.3 Hz, *ipso*-Ph_2P), 130.0 (s, *para*-Ph_2P), 128.4 (m,[46] *N* = 9.3 Hz, *meta*–Ph_2P), 124.4 [s, d, $^3J_{PtC}$ = 64.0 Hz, *meta*-(*tert*-butylPh)$_2$Pt], 120.6 (s, CH, bipy), 34.3–34.0 [m, $CH_2CH_2CH_2PPh_2$ and $C(CH_3)_3$],

Table 1. Crystal data, data collection and structure refinement for compounds **8b** and **9b**

	8b	**9b**
Crystal data		
Empirical formula	$C_{106}H_{106}Cl_4N_4O_3P_4Pt_2$	$C_{122}H_{132}Cl_4N_4P_4Pt_2$
Formula weight	2139.81	2310.18
Crystal system	Triclinic	Orthorhombic
Space group	$P\bar{1}$	*Pbcn*
Z	1	4
$d_{calcd.}$[g/cm^3]	1.444	1.307
a [Å]	12.422(2)	19.769(6)
b [Å]	12.970(1)	23.409(5)
c [Å]	16.723(2)	25.374(8)
α [°]	90.11(1)	90
β [°]	110.29(1)	90
γ [°]	102.26(1)	90
V [Å^3]	2461(1)	11742(6)
μ [mm^{-1}]	7.252	2.572
F(000)	1078	4704
Data Collection		
Radiation	Cu-K_α	Mo-K_α
Monochromator	graphite	graphite
Crystal size [mm]	0.25 × 0.25 × 0.15	0.20 × 0.30 × 0.40
Temperature [K]	213	173
Scan mode	ω	ω
$\theta_{min/max}$ [°]	2.77/32.52	2.06/27.60
hkl range	*h* –1/14	*h* –1/25
	k –15/14	*k* –30/1
	l –19/18	*l* –33/1
Measured reflections	9619	15388
Unique reflections	8352	13356
Absorption correction	Ψ scans	none
T_{max}/T_{min}	0.9715/0.6456	
Refinement		
Refinement method	Full-matrix least-squares on F^2	Full-matrix least-squares on F^2
Data/restraints/parameters	8352/2/573	13356/0/598
Hydrogen treatment	Calculated except solvent molecules	calculated
Final *R* Values [$I > 2\sigma(I)$]		
*R*1[a]	0.0891	0.1154
*wR*2[b]	0.2333	0.3174
$\rho_{residual}$(max/min) [eÅ^{-3}]	3.465/–5.865	4.393/–2.292

[a] $R1 = \Sigma||F_o| - |Fc||/\Sigma|F_o|$. – [b] $wR2 = \{\Sigma[w(F_o^2 - F_c^2)^2]/[\Sigma[w(F_o^2)]\}^{1/2}$; $w = 1/[\delta^2(F_o^2) + (ap)^2 + bp]$; $p = (F_o^2 + 2F_c^2)/3$; $a = 0.0946$; $b = 8.58$. – $S = \{\Sigma[w(F_o^2 - F_c^2)^2]/(n - p)\}^{1/2}$.

31.9 [s, C(CH_3)$_3$], 27.7 (m,[46] N = 32.7 Hz, $CH_2CH_2CH_2PPh_2$), 26.5 (s, br,[14,46] $CH_2CH_2CH_2PPh_2$). – $^{31}P\{^1H\}$ NMR (CD_2Cl_2): δ = 9.1 (s, d, $^1J_{PtP}$ = 1763 Hz). – MS (FAB, 30 °C); *m/z*: 2138.8 [M^+ – H], 1873.5 [M^+ – 2 *tert*-butylPh], 1740.2 [M^+ – 3 *tert*-butylPh], 1607.2 [M^+ – 4 *tert*-butylPh]. – $C_{120}H_{128}N_4P_4Pt_2$ (2140.4): calcd. C 67.34, H 6.03, N 2.62, Pt 18.23; found C 67.11, H 6.06, N 2.44, Pt 17.88.

Copper Complex 10b: $[Cu(CH_3CN)_4][BF_4]$ (47.2 mg, 0.15 mmol) in 4 mL of acetonitrile was added to a solution of **8b** (287.4 mg, 0.15 mmol) in 10 mL of dichloromethane. The solution was stirred for 15 min and concentrated. The residue was dissolved in 10 mL of dichloromethane, precipitated with 40 mL of *n*-pentane, filtered (P4), and washed with benzene/dichlormethane (1:1). Yield: 257.6 mg (83.1%), red-brown, air-sensitive solid. – IR (KBr): $\tilde{\nu}$ = 1056 cm^{-1} (BF_4). – UV/Vis (CD_2Cl_2): χ_{max} = 300.9, 314.2, 433.0 nm. – ^1H NMR (CD_2Cl_2): δ = 8.64 (s, 4 H, 6,6′-H, bipy), 8.44 (d, $^3J_{HH}$ = 8.1 Hz, 4 H, 3,3′-H, bipy), 7.96 (d, $^3J_{HH}$ = 8.1 Hz, 4 H, 4,4′-H, bipy), 7.39–6.98 (m, 48 H, Ph_2P and Ph_2Pt), 6.66–6.47 (m, 12 H, Ph_2Pt), 3.02–1.08 (m, 24 H, $CH_2CH_2CH_2PPh_2$). – $^{13}C\{^1H\}$ NMR (CD_2Cl_2): δ = 161.0 (m,[46] *ipso*-Ph_2Pt), 151.0 (s, C, bipy), 148.4 (s, CH, bipy), 141.7 (s, C, bipy), 139.1 (s, CH, bipy), 137.0 (s, d, $^2J_{PtC}$ = 29.9 Hz, *ortho*-Ph_2Pt), 134.2–132.3 (m, *ipso*- and *ortho*-Ph_2P), 130.0 (s, *para*-Ph_2P), 128.5 (m,[46] N = 8.8 Hz, *meta*-Ph_2P), 127.3 (s, d, $^3J_{PtC}$ = 64.0 Hz, *meta*-Ph_2Pt), 122.3 (s, CH, bipy), 121.5 (s, *para*-Ph_2Pt), 35.0 (m,[46] N = 16.8 Hz, $CH_2CH_2CH_2PPh_2$), 28.6 (s, br,[14,46] $CH_2CH_2CH_2PPh_2$), 26.3 (m,[46] N = 34.9 Hz $CH_2CH_2CH_2PPh_2$). – $^{31}P\{^1H\}$ NMR (CD_2Cl_2): δ = 9.8 (s, d, $^1J_{PtP}$ = 1778 Hz). – $^{19}F\{^1H\}$ NMR (CD_2Cl_2): δ = –153.0 (s, br). – MS (FAB, 30 °C); *m/z*: 1979.4 [M^+ – BF_4], 1670.4 [M^+ – BF_4 – 4 Ph]. – $C_{104}H_{96}BCuF_4N_4P_4Pt_2 \cdot 2\ CH_2Cl_2$ (2236.2): calcd. C 56.93, H 4.51, Cu 2.84, N 2.51, Pt 17.45; found C 56.59, H 4.32, Cu 2.32, N 2.44, Pt 16.67.

X-ray Structural Determination of the Diplatinacyclophanes 8b · 3 H_2O · 2 CH_2Cl_2 and 9b · 2 CH_2Cl_2: Crystallographic data for both compounds are summarized in Table 1. Single crystals of **8b** and **9b** were obtained from a dichloromethane/methanol solution. Each crystal was mounted on a goniometer head and transferred to a Siemens P4 diffractometer (Mo-K_α radiation, graphite monochromator) and to an Enraf Nonius CAD4 diffractometer (Cu-K_α, graphite monochromator), respectively. Accurate unit cell parameters and orientation matrices were determined by least-squares refinement of setting angles of a set of well-centered reflections. Reduced cell calculations did not indicate higher lattice symmetry for **8b** than $P\bar{1}$, while **9b** crystallizes in the orthorhombic space group *Pbcn*. Data were corrected for LP effects and for observed linear decay. An empirical absorption correction via Ψ-scan was applied for **8b**. The structures were solved by direct methods (SHELXS)[47] and refined by least-squares methods based on F^2 using SHELXL 97.[48] All non-hydrogen atoms except the solvent molecules were refined anisotropically. All hydrogen atoms were located in calculated positions, with the exception of those of the solvent molecules in **8b**. Crystallographic data for both structures reported in this paper have been deposited with the Cambridge Crystallographic Data Centre as supplementary publication nos. CCDC-131421 for **8b** and CCDC-131420 for **9b**. Copies of the data can be obtained free of charge on application to CCDC, 12 Union Road, Cambridge CB2 1EZ, UK [Fax: (int. code) + 44-1223/336-033; E-mail: deposit@ccdc.cam.ac.uk].

Acknowledgments

R. V. wishes to thank the Land Baden-Württemberg for the award of a Ph.D. fellowship (Landesgraduiertenförderungsgesetz). Support of this research by the Deutsche Forschungsgemeinschaft and the Fonds der Chemischen Industrie is gratefully acknowledged. Degussa AG is thanked for supplying starting materials. We are also indebted to Priv.-Doz. Dr. H. A. Mayer, Institut für Anorganische Chemie, University of Tübingen and Prof. Dr. B. Speiser, Institut für Organische Chemie, University of Tübingen, for helpful discussions regarding the interpretation of the NMR spectra and CV measurements, respectively.

[1] M. Fujita, J. Yakaki, K. Ogura, *J. Am. Chem. Soc.* **1990**, *112*, 5645–5646.

[2] [2a] H. Plenio, *Angew. Chem.* **1997**, *109*, 358–360; *Angew. Chem. Int. Ed. Engl.* **1997**, *36*, 348–351. – [2b] B. Olenyuk, J. A. Whiteford, P. J. Stang, *J. Am. Chem. Soc.* **1996**, *118*, 8221–8230. – [2c] J. Manna, J. A. Whiteford, P. J. Stang, D. C. Muddiman, R. D. Smith, *J. Am. Chem. Soc.* **1996**, *118*, 8731–8732. – [2d] J. Manna, C. J. Kuehl, J. A. Whiteford, P. J. Stang, D. C. Muddiman, S. A. Hofstadler, R. D. Smith, *J. Am. Chem. Soc.* **1997**, *119*, 11611–11619. – [2e] R. W. Saalfrank, A. Dresel, V. Seitz, S. Trummer, F. Hampel, M. Teichert, D. Stalke, C. Stadler, J. Daub, V. Schünemann, A. X. Trautwein, *Chem. Eur. J.* **1997**, *3*, 2058–2062. – [2f] R. W. Saalfrank, V. Seitz, D. L. Caulder, K. N. Raymond, M. Teichert, D. Stalke, *Eur. J. Inorg. Chem.* **1998**, 1313–1317. – [2g] C. M. Drain, J. –M. Lehn, *J. Chem. Soc., Chem. Commun.* **1994**, 2313–2315. – [2h] M. –C. Lagunas, R. A. Cossage, W. J. J. Smeets, A. L. Spek, G. van Koten, *Eur. J. Inorg. Chem.* **1998**, 163–168. – [2i] J. E. Kingston, L. Ashford, P. D. Beer, M. G. B. Drew, *J. Chem. Soc., Dalton Trans.* **1999**, 251–257. – [2j] G. M. Gray, C. H. Duffey, *Organometallics* **1995**, *14*, 238–244. – [2k] G. M. Gray, A. Varshney, C. H. Duffey, *Organometallics* **1995**, *14*, 245–250. – [2l] F. M. Romero, R. Ziessel, A. Dupont-Gervais, A. van Dorsselaer, *J. Chem. Soc., Chem. Commun.* **1996**, 551–553. – [2m] S. M. AlQaisi, K. J. Galat, M. Chai, D.G. Ray III, P. L. Rinaldi, C. A. Tessier, W. J. Youngs, *J. Am. Chem. Soc.* **1998**, *120*, 12149–12150. – [2n] W. Uhl, T. Spies, W. Saak, *Eur. J. Inorg. Chem.* **1998,** 1661–1665.

[3] E. Lindner, W. Wassing, R. Fawzi, M. Steimann, *Angew. Chem.* **1994**, *106*, 363–365; *Angew. Chem. Int. Ed. Engl.* **1994**, *33*, 321–323.

[4] F. Vögtle in: *Cyclophan-Chemie* (Eds.: C. Elschenbroich, F. Hensel, H. Hopf), Teubner, Stuttgart, **1990**.

[5] [5a] E. Lindner, M. W. Pitsch, R. Fawzi, M. Steimann, *Chem. Ber.* **1996**, *129*, 639–645. – [5b] E. Lindner, W. Wassing, M. W. Pitsch, R. Fawzi, M. Steimann, *Inorg. Chim. Acta* **1994**, *220*, 107–113.

[6] I. A. Bagatin, D. Matt, *Inorg. Chem*. **1999**, *38*, 1585–1591.

[7] P. J. Dyson, A. G. Hulkes, P. Suman, *J. Chem. Soc., Chem. Commun.* **1996**, 2223–2224.

[8] J. Nitschke, T. D. Tilley, *J. Org. Chem.* **1998**, *63*, 3673–3676.

[9] [9a] E. Lindner, C. Hermann, G. Baum, D. Fenske, *Eur. J. Inorg. Chem.* **1999**, 679–685. – [9b] G. C. Dol, S. Gaemers, M. Hietikko, P. C. J. Kamer, P. W. N. M. van Leeuwen, R. J. M. Nolte, *Eur. J. Inorg. Chem.* **1998**, 1975–1985. – [9c] C. M. Hartshorn, P. J. Steel, *Inorg. Chem.* **1996**, *35*, 6902–6903. – [9d] J. R. Farrell, C. A. Mirkin, I. A. Guzei, L. M. Liable–Sands, A. L. Rheingold, *Angew. Chem*. **1998**, *110*, 484–486; *Angew. Chem. Int. Ed.* **1998**, *37*, 465–467. – [9e] J. R. Farrell, C. A. Mirkin, *J. Am. Chem. Soc.* **1998**, *120*, 11834–11835. – [9f] M. E. van der Boom, M. Gozin, Y. Ben–David, L. J. W. Shimon, F. Frolow, H. –B. Kraatz, D. Milstein, *Inorg. Chem.* **1996**, *35*, 7068–7073. – [9g] M. A. Houghton, A. Bilyk, M. M. Harding, P. Turner, T. W. Hambley, *J. Chem. Soc., Dalton Trans.* **1997**, 2725–2733.

[10] [10a] A. A. Bahsoun, R. Ziessel, *Nouv. J. Chim.* **1985**, *9*, 225–229. – [10b] R. Ziessel, *Tetrahedron Lett.* **1989**, *30*, 463–465. – [10c] R. Ziessel, D. Matt, L. Toupet, *J. Chem. Soc., Chem. Commun.* **1995**, 2033–2034. – [10d] R. Ziessel, L. Toupet, S. Chardon–Noblat, A. Deronzier, D. Matt, *J. Chem. Soc., Dalton Trans.* **1997**, 3777–3784.

[11] [11a] F. Ebmeyer, F. Vögtle, *Chem. Ber.* **1989**, *122*, 1725–1727. – [11b] F. Ebmeyer, F. Vögtle, *Angew. Chem.* **1989**, *101*, 95–96; *Angew. Chem. Int. Ed. Engl*. **1989**, *28*, 79–80. – [11c] S. Grammenudi, F. Vögtle, *Angew. Chem.* **1986**, *98*, 1119–1121; *Angew. Chem. Int. Ed. Engl*. **1986**, *98*, 1119–1121. – [11d] F. Barigelletti, L. de Cola, V. Balzani, P. Belser, A. v. Zelewsky, F.

Vögtle, F. Ebmeyer, S. Grammenudi, *J. Am. Chem. Soc.* **1989**, *111*, 4662.
[12] A. D. Hamilton, H. –D. Rubin, A. B. Bocarsly, *J. Am. Chem. Soc.* **1984,** *106*, 7255–7257.
[13] G. L. Hodgson, D. F. MacSweeney, T. Money, *J. Chem. Soc., Perkin Trans.* **1973**, 2113–2130.
[14] T. Uchiyama, Y. Toshiyasu, Y. Nakamura, T. Miwa, S. Kawaguchi, *Bull. Chem. Soc. Jpn.* **1981**, *54*, 181–185.
[15] A. Varshney, M. L. Webster, G. M. Gray, *Inorg. Chem.* **1992**, *31*, 2580–2587.
[16] H. C. Clark, L. E. Manzer, *J. Organomet. Chem.* **1973**, *59*, 411–428.
[17] [17a] L. Rossa, F. Vögtle, in: *Synthesis of Medio- and Macrocyclic Compounds by High Dilution Principle Techniques: Topics in Current Chemistry* (Ed.: F. Vögtle), Springer, Heidelberg, **1983**, vol. 113, *Cyclophanes I*, p 1. – [17b] P. Knops, N. Sendhoff, H.-B. Mekelburger, F. Vögtle, in: *High Dilution Reactions – New Synthetic Applications: Topics in Current Chemistry* (Ed.: E. Weber, F. Vögtle) Springer, Heidelberg **1992**, vol. 161, *Macrocycles*, p. 1.
[18] E. Lindner, T. Leibfritz, R. Fawzi, M. Steimann, *Chem. Ber./Receuil* **1997**, *130*, 347–356.
[19] U. Bayer, H. A. Brune, *Z. Naturforsch.* **1983**, *38b*, 226–236.
[20] Partially overlapped with the peaks of the *ortho*-carbon atom of the $Pt(C_6H_5)_2$ unit.
[21] [21a] G. K. Anderson in: *Comprehensive Organometallic Chemistry II* (Eds.: E. W. Abel, F. G. A. Stone, G. Wilkinson) **1995**, vol. 9, p. 431–532. – [21b] H. A. Brune, J. Unsin, H. G. Alt, G. Schmidtberg, K. H. Spohn, *Chem. Ber.* **1984**, *117*, 1606–1619.
[22] [22a] M. Fujita, O. Sasaki, T. Mitsuhashi, T. Fujita, J. Yazaki, K. Yamaguchi, K. Ogura, *J. Chem. Soc., Chem. Commun.* **1996**, 1535–1536. – [22b] S. L. James, D. M. P. Mingos, A. J. P. White, D. J. Williams, *J. Chem. Soc., Chem. Commun.* **1998**, 2323–2324. – [22c] P. N. W. Baxter, J. –M. Lehn, B. O. Kneisel, G. Baum, D. Fenske, *Chem. Eur. J.* **1999**, *5*, 113–120. – [22d] J. E. Kingston, L. Ashford, P. D. Beer, M. G. B. Drew, *J. Chem. Soc., Dalton Trans.* **1999**, 251–257.
[23] J.-M. Lehn, Supramolecular Chemistry, VCH, Weinheim **1995**, p. 18 and references cited therein.
[24] G. J. Kubas, *Inorg. Synth.* **1979**, *19*, 90–92.
[25] [25a] B. W. Skelton, A. F. Waters, A. H. White, *Aust. J. Chem.* **1991**, *44*, 1207–1215. – [25b] M. Munakata, S. Kitagawa, A. Asahara, H. Masuda, *Bull. Chem. Soc. Jpn.* **1987**, *60*, 1927–1929.
[26] N. Sachsinger, C. D. Hall, *J. Organomet. Chem.* **1997**, *531*, 61–65.
[27] [27a] S. Kitagawa, M. Munakata, N. Miyaji, *Inorg. Chem.* **1982**, *21*, 3842–3843. – [27b] D. R. McMillin, J. R. Kirchhoff, K. V. Goodwin, *Coord. Chem. Rev.* **1985**, *64*, 83–92.
[28] S. Kitagawa, M. Munakata, *Inorg. Chem.* **1981**, *20*, 2261–2267.
[29] R. Ziessel, M.-T. Youinou, *Angew. Chem*. **1993**, *105*, 929–932; *Angew. Chem. Int. Ed. Engl*. **1993**, *32*, 877–880.
[30] Sauvage et al. observed a surprisingly strong stabilization of a bis(α,α′-diimine)copper(I) complex by the incorporation of the two α,α′-diimine ligands into a macrocyclic framework: J.-C. Chambron, J.-P. Sauvage, *Tetrahedron Lett.* **1986**, *27*, 865–868.
[31] J.-C. Chambron, J.-P. Sauvage, *New J. Chem.* **1990**, *14*, 883–889.
[32] R. James, R. J. P. Williams, *J. Chem. Soc.* **1961**, 2007–2019.
[33] M. Schmittel, C. Michel, A. Ganz, M. Herderich, *J. Prakt. Chem.* **1999**, *341*, 228–236.
[34] M.-T. Youinou, R. Ziessel, J.-M. Lehn, *Inorg. Chem.* **1991**, *30*, 2144–2148.
[35] Recent examples for bis(bipyridine)copper(I) complexes, which are substituted in 4- or 5-positions are: [35a] P. Ghosh, D. Shabat, S. Kumar, S. C. Sinha, F. Grynszpan, J. Li, L. Noodleman, E. Keinan, *Nature* **1996**, *382*, 339–341. – [35b] P. R. Ashton, V. Balzani, A. Credi, O. Kocian, D. Pasini, L. Prodi, N. Spencer, J. F. Stoddart, M. S. Tolley, M. Venturi, A. J. P. White, D. J. Williams, *Chem. Eur. J.* **1998**, *4*, 590–607. – [35c] B. König, O. Möller, H. Zieg, *J. Prakt. Chem*. **1996**, *338*, 549–552. – [35d] G. Nuding, K. Nakashima, R. Iguchi, T. Ishii, S. Shinkai, *Tetrahedron Lett.* **1998**, *39*, 9473–9476. – [35e] M.-H. Shu, W.-Y. Sun, C.-Y. Duan, Y.-J. Fu, W.-J. Zhang, W.-X. Tang, *J. Chem. Soc., Dalton Trans.* **1999**, 729–734.
[36] [36a] A. Sobkowiak, A. Qui, X. Liu, A. Llobet, D. T. Sawyer, *J. Am. Chem. Soc.* **1993**, *115*, 609–614. – [36b] M. Munakata, S. Nishibayashi, H. Sakamoto, *J. Chem. Soc., Chem. Commun.* **1980**, 219.
[37] The incorporation of reactive metal centers is gaining increasing interest in supramolecular chemistry. Recent Examples are: [37a] Ref.[6]. – [37b] P. Molenveld, J. F. J. Engbersen, H. Kooijman, A. L. Spek, D. N. Reinhoudt, *J. Am. Chem. Soc.* **1998**, *120*, 6729–6737. – [37c] H. K. A. C. Coolen, J. A. M. Meeuwis, P. W. N. M. van Leeuwen, R. J. M. Nolte, *J. Am. Chem. Soc.* **1995**, *117*, 11906–11913.
[38] [38a] W. Schöniger, *Microchim. Acta* **1955**, 123–129. – [38b] W. Schöniger, *Michrochim. Acta* **1956**, 869–876.
[39] A. Dirscherl, F. Erne, *Microchim. Acta* **1961**, 866–873.
[40] G. Brunisholz, J. Michot, *Helv. Chim. Acta.* **1954**, *37*, 598–602.
[41] H. Wagner, *Michrochim. Acta* **1957**, 19–23.
[42] B. Gollas, B. Krauss, B. Speiser, H. Stahl, *Curr. Sep.* **1994**, *13*, 42–44.
[43] G. Gritzner, J. Kuta, *J. Pure Appl. Chem.* **1984**, *56*, 462.
[44] S. Dümmling, E. Eichhorn, S. Schneider, B. Speiser, M. Würde, *Curr. Sep.* **1996**, *15*, 53–56.
[45] S. Meyer, Ph. D. Thesis, University of Tübingen **1987**.
[46] m: AXX′ pattern.
[47] G. M. Sheldrick, *Acta Crystallogr. Sect. A* **1995**, *51*, 33–38 ("SHELXS V5.03 program for crystal structure solution", University of Göttingen, Germany).
[48] G. M. Sheldrick, *SHELXTL V5.03 program for crystal structure refinement*, University of Göttingen, Germany, **1995**.

Received July 19, 1999
[I99264]

Experimental Evidence for a Second Coordination Sphere Water Molecule in the Hydration Structure of YbDTPA – Insights for a Re-Assessment of the Relaxivity Data of GdDTPA

Kenneth Irvin Hardcastle,*[a] Mauro Botta,*[b] Mauro Fasano,[c] and Giuseppe Digilio[d]

Keywords: Lanthanides / Ytterbium / MRI contrast agents / Solid-state structures / Hydration

The low temperature (–100 °C) X-ray structure of the complex $K_2[Yb(DTPA)(H_2O)]$ has been determined. The metal ion is at the center of a tricapped trigonal prism and is nine-coordinate, binding to the three nitrogens and five oxygens of the ligand and one water molecule. From the structure obtained, three well-defined hydration shells can be observed consisting of: i) one coordinated water molecule; ii) several water molecules in the outer coordination sphere of the Yb^{III} ion and iii) one water molecule surprisingly close to the metal center and hydrogen-bonded to proximate carboxylate groups. A variable-field and temperature NMRD study of the corresponding Gd complex has been performed and the data interpreted by taking into account the presence of second-sphere water molecule(s). The results of the analysis are in excellent agreement with the X-ray structural data.

Introduction

The use of paramagnetic metal complexes to alter the nuclear magnetic relaxation times of water protons in tissues is a well established procedure in clinical diagnosis for enhancing the contrast between healthy and diseased regions in MRI (**M**agnetic **R**esonance **I**maging) images.[1] Currently, about 35% of the MRI examinations are performed with the use of contrast enhancing agents (CA). The most common class of these compounds are neutral or negatively charged polyaminocarboxylate complexes of Gd^{III}, both linear and macrocyclic, which are extracellular, nonspecific CA which rapidly diffuse throughout the body after injection and are excreted via the renal route.[2–4] The first of these complexes to be considered as a CA and to be tested on humans was $[Gd(DTPA)(H_2O)]^{2-}$ ($DTPA^{5-}$ = diethylenetriamine-*N*,*N*′,*N*′′-pentaacetate).[5] Much is known about this compound; the ligand is octadentate and fully exploits its chelating ability towards lanthanide(III) ions to form thermodynamically stable tricapped trigonal structures where one of the capping positions is occupied by a water molecule. In solution the complexes are stereochemically non-rigid and the fluxional process involves conformational inversion of the ethylenediamine rings and rotation of the acetate arms which corresponds to the interconversion between two enantiomeric forms;[6,7] isostructurality across the lanthanide series has been suggested by the analysis of NMR data.[8] The coordination sphere of the Gd^{III} complex is completed by a water molecule that has a mean residence lifetime of about 300 ns at 298 K, as assessed by Merbach et al. by ^{17}O NMR.[9] It is common practice to evaluate the efficacy of a given Gd complex as a CA in terms of the relaxivity parameter, r_{1p} ($mM^{-1}\ s^{-1}$), the net increment in the water proton longitudinal relaxation rate per millimolar concentration of the paramagnetic compound.[1,2] The relaxivity reflects the efficiency of the nuclear-electron dipolar coupling between the nuclear magnetic moment of the water protons and the electronic magnetic moment of the metal ion and is traditionally described on the basis of a model that considers two distinct contributions: *inner sphere*, related to the exchange of the bound water molecule(s) from the coordination site to the bulk, and *outer sphere*, which involves the water molecules diffusing near the paramagnetic center during their translational diffusion.[10] The relaxivity has a strong dependence upon the applied magnetic field strength and from the analysis of this dependence (NMRD, **N**uclear **M**agnetic **R**elaxation **D**ispersion profiles) several important structural and dynamic parameters may be obtained.[11] However, the polar nature of these complexes, featuring negative charges localized on the carboxylate groups, has recently suggested the presence of structured, hydrogen-bonded water molecules in the second coordination sphere of Gd^{III} and thus a possible inadequacy in the physical model used for the interpretation of the relaxation data and the analysis of the NMRD profiles.[1,12–14] The contribution

[a] Department of Chemistry, California State University Northridge,
18111 Nordhoff Street, Northridge, CA 91330–8262 (USA)
Fax: (internat.) +1–818–677–2912
E-mail: ken.hardcastle@csun.edu
[b] Dipartimento di Scienze e Tecnologie Avanzate, Universita' del Piemonte Orientale "Amedeo Avogadro'', Corso Borsalino 54, 15400 Alessandria (Italy)
Fax: (internat.) +39–011–670–7524
E-mail: botta@ch.unito.it
[c] Dipartimento di Chimica I.F.M., Universita' di Torino, Via P. Giuria 7, 10125 Torino (Italy)
[d] Bioindustry Park del Canavese, Via Ribes 5, Colleretto Giacosa (TO)

 © WILEY-VCH Verlag GmbH, D-69451 Weinheim, 2000 1434–1948/00/0505–0971 $ 17.50+.50/0

of second sphere water molecules to r_{1p} has been suggested in a few special cases over the last few years by some indirect evidence, but the possibility of its more general role and its influence on the correct evaluation of the relaxation parameters has not yet been discussed.[15] Here we report on a low temperature single crystal X-ray structural determination of K_2[Yb(DTPA)(H_2O)] where the hydration structure of the complex is clearly detectable and provides firm evidence of a water molecule adjacent to the carboxylate oxygens at a distance sufficiently close to the metal ion to be able to influence significantly the relaxivity of the corresponding Gd^{III} complex. On the basis of these findings, the NMRD data are reinterpreted and the new set of relaxation parameters are found to be in a better agreement with the available structural data.

Results and Discussion

Solid State Structural Characterization

Table 1 lists some selected interatomic distances for K_2[Yb(DTPA)(H_2O)]; the molecular geometry of the anion, [Yb(DTPA)(H_2O)]$^{2-}$, along with associated water molecules is shown in Figure 1. The Yb^{III} ion is surrounded by nine coordinating atoms: three nitrogen atoms, N1, N2, N3, five carboxylato oxygen atoms, O1, O3, O5, O7 and O9 and a bound water molecule, O1 W, which form a tri-capped trigonal prism (TTP) geometry around the central ytterbium ion. The capping atoms are the bound water, O1 W, and N1 and N3 (crystallographic data see Table 2).

Table 1. Selected interatomic distances [Å] for K_2[Yb(DTPA)-(H_2O)]

Yb(1)–N(1)	2.553(5)	Yb(1)–O(5)	2.291(4)
Yb(1)–N(2)	2.553(5)	Yb(1)–O(7)	2.320(4)
Yb(1)–N(3)	2.742(5)	Yb(1)–O(9)	2.303(4)
Yb(1)–O(1)	2.295(4)	Yb(1)–O(1 W)	2.423(4)
Yb(1)–O(3)	2.324(4)	Yb(1)–O(7 W)	4.178(4)
Yb(1)–H(7WA)	3.280(7)	Yb(1)–H(7WB)	4.539(7)

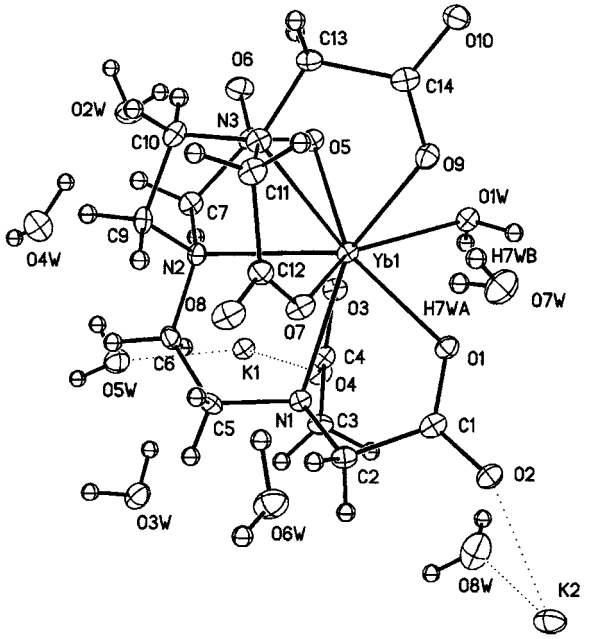


Figure 1. Solid state structure of K_2[Yb(DTPA)(H_2O)]

The geometry of the ligand can also be described as a monocapped square antiprism (CSAP); however, the distortions from a regular geometry are much greater in this configuration than in the trigonal prism geometry. For example, in the trigonal prismatic geometry, only the Yb–N2 distance is significantly longer, 2.553(5) Å, than the Yb–O1, O3, O6, O7, O10 distances, 2.307(4) Å (ave); whereas with the square antiprism geometry, the N1, N2, N3, O7 atom deviations from a regular plane are +0.24, –0.21, +0.25 and –0.28 Å, respectively. The geometry of the anion, [Yb(DTPA)(H_2O)]$^{2-}$ is very similar to that of other lanthanide DTPA complexes of gadolinium[16,17] and neodymium.[18] The bound water molecule to ytterbium ion distance, Yb–O1 W, is 2.423(4) Å, which is significantly shorter than the corresponding distance in the analogous Gd^{III} complex of 2.490 Å. Interestingly, unlike the few structures of lanthanide complexes with DTPA previously reported, in this low temperature X-ray diffraction study we were able to observe the hydration structure of the complex. The structure of K_2[Yb(DTPA)(H_2O)] has eight associated water molecules, one bound water, O1 W, and six water molecules in the outer coordination sphere surrounding the anionic ytterbium complex, at an average distance of 5.8 Å from the Yb to the oxygen atoms of the water molecules. One additional water molecule, O7 W, was located 4.18 Å from the ytterbium atom and strongly hydrogen-bonded to the carboxylate oxygen atoms O1, O7 and O9 at distances of 2.38–2.54 Å, respectively, which are significantly shorter than the van der Waals distance and within the accepted range for hydrogen bonds .

Relaxometry

The water proton longitudinal relaxation rate is strongly enhanced in a solution containing a paramagnetic Gd^{III} complex and the measured value, R_1^{obs} (s^{-1}), is normally resolved into three contributions:

$$R_1^{obs} = R_{1p}^{is} + R_{1p}^{os} + R_1^{w} \quad (1)$$

where R_1^w is the background diamagnetic term, corresponding to the water relaxation rate in a solution of a related diamagnetic derivative, R_{1p}^{is} the represents the contribution arising from exchange ($k_{ex} = 1/\tau_M$) of the metal-bound water molecule(s) from the coordination site to the bulk solvent and R_{1p}^{os} is the contribution associated with the solvent molecules diffusing near the paramagnetic center in the outer coordination sphere. The inner sphere relaxation rate arises from the modulation of the dipolar electron-nucleus interaction by chemical exchange (τ_M), electron spin relaxation (τ_S) and reorientation of the Gd–O_w vector (τ_R) and is described in terms of the following set of Equations:[2,10]

Table 2. Crystal data and structure refinement for $K_2[Yb(DTPA)(H_2O)]$

Identification code	$K_2[YbDTPA(H_2O)]$	
Empirical formula	$C_{14}H_{34}K_2N_3O_{18}Yb$	
Formula weight	783.68	
Temperature	173(2) K	
Wavelength	0.71073 Å	
Crystal system	Triclinic	
Space group	$P\bar{1}$	
Unit cell dimensions	a = 9.558(3) Å	α = 76.92(5)°.
	b = 11.277(9) Å	β = 87.02(3)°.
	c = 13.412(7) Å	γ = 69.04(5)°.
Volume	1314.3(13) Å^3	
Z	2	
Density (calculated)	1.980 Mg/m^3	
Absorption coefficient	3.961 mm^{-1}	
F(000)	782	
Crystal size	0.40 × 0.32 × 0.25 mm^3	
Theta range for data collection	1.56 to 27.47°.	
Index ranges	$-12 \le h \le 12$, $-14 \le k \le 14$, $-17 \le l \le 17$	
Reflections collected	7824	
Independent reflections	6016 [R_{int} = 0.0288]	
Absorption correction	Psi scans	
Max. and min. transmission	0.4792 and 0.3211	
Refinement method	Full-matrix least-squares on F^2	
Data/restraints/parameters	6016/16/351	
Goodness-of-fit on F^2	1.404	
Final R indices [$I > 2\sigma(I)$]	$R1$ = 0.0406, $wR2$ = 0.1142	
R indices (all data)	$R1$ = 0.0418, $wR2$ = 0.1150	
Largest diff. peak and hole	2.250 and –1.404 e.Å^{-3}	

$$R_{1p}^{is} = \frac{[M]\times q}{55.6} \times \frac{1}{T_{1M} + \tau_M} \quad (2)$$

$$\frac{1}{T_{1M}} = \frac{2}{15}\left(\frac{\mu_0}{4\pi}\right)^2 \frac{\hbar^2\gamma_S^2\gamma_I^2}{r_{GdH}^6} S(S+1)\left[\frac{3\tau_{c1}}{1+\omega_I^2\tau_{c1}^2} + \frac{7\tau_{c2}}{1+\omega_S^2\tau_{c2}^2}\right] \quad (3)$$

$$\frac{1}{\tau_{ci}} = \frac{1}{\tau_M} + \frac{1}{\tau_R} + \frac{1}{\tau_{Si}} \qquad i = 1, 2 \quad (4)$$

$$\left(\frac{1}{\tau_{S1}}\right)^{ZFS} = \Delta^2\tau_v\left(\frac{2.4}{1+\omega_S^2\tau_v^2} + \frac{9.6}{1+4\omega_S^2\tau_v^2}\right) \quad (5)$$

$$\left(\frac{1}{\tau_{S2}}\right)^{ZFS} = \Delta^2\tau_v\left[\frac{5.26}{1+0.372\omega_S^2\tau_v^2} + \frac{7.18}{1+1.24\omega_S\tau_v}\right] \quad (6)$$

In Equations 2–6 [M] is the molar concentration of the paramagnetic complex; q is the number of water molecules coordinated to the metal ion; τ_M is their mean residence lifetime; T_{1M} is their longitudinal relaxation time; S is the electron spin quantum number; γ_H is the proton nuclear magnetogyric ratio; g and β are the electronic g factor and Bohr magneton, respectively; r_{Gd-H} is the distance between the metal ion and the protons of the coordinated water molecules; ω_H and ω_S are the proton and electron Larmor frequencies, respectively; τ_R is the reorientational correlation time; and τ_{S1} and τ_{S2} are the longitudinal and transverse electron spin relaxation times. These latter terms, in analogy with the nuclear magnetic relaxation times, have a frequency dependence which is normally represented by Equations 5 and 6 where τ_v is the correlation time associated with the modulation of the electron-lattice interaction and Δ is the square root of the average quadratic (transient) zero-field splitting tensor. This latter term is often expressed in terms of τ_{S0}, the limiting value of the electronic relaxation time at zero magnetic field, according to the expression:

$$\Delta^2 = \frac{1}{12\tau_{S0}\tau_v} \quad (7)$$

The outer-sphere relaxivity has a dependence on the electronic relaxation times, τ_{S1} and τ_{S2} of the metal ion, on the distance of closest approach of solute and solvent (d), on the sum of solvent and solute diffusion constants (D) and on the magnetic field strength. This term is well described by the Freed equation modified in a form suitable for small paramagnetic metal chelates:

$$R_{1p}^{os} = C^{os}\left(\frac{1}{aD}\right)\left[7J(\omega_S) + 3J(\omega_H)\right] \quad (8)$$

where C^{os} is a constant ($5.8\cdot10^{-13}$ s^{-2}M^{-1}) and the dependence on the electronic relaxation times is expressed in the non-Lorentzian spectral density functions $J(\omega_i)$.[19] Thus the paramagnetic contribution to the water protons' relaxation rate implicitly contains very useful information for a series of important structural and dynamic parameters which would allow for a complete characterization of the solute and its interaction with the solvent. In order to obtain reliable values for these parameters the magnetic field dependence of r_{1p} through Equations 3–6 is exploited by measuring the paramagnetic relaxation rate as a function of the applied magnetic field strength. This is best done by

using specialized instrumentation, the field-cycling relaxometer, which switches magnetic field strength very rapidly over the desired range (typically corresponding to proton Larmor frequencies of 0.01 to 50 MHz), thus allowing a complete and accurate dataset to be recorded in about 0.5 h. The $1/T_1$ dataset, otherwise known as a NMRD profile, represents the sum of the spectral density functions of the active relaxation mechanisms and can be fitted to the inner- and outer-sphere equations to yield the values of the relaxation parameters.[11]

For small, rapidly tumbling Gd^{III} chelates the NMRD profile near room temperature is flat, ie. r_{1p} assumes a constant value for frequency values up to about 1–2 MHz, then it decreases because of the dispersion of the $\omega_S\ \tau_{c2}$ term in Equation 3 and tends to level off in the high field region. For polyaminocarboxylate complexes with $q = 1$, inner- and outer sphere terms at the imaging fields (10–60 MHz) make a similar contribution to the relaxivity, the contribution being determined primarily by the terms τ_R/r^6_{Gd-H} (r^{is}_{1p}) and d^2/D (r^{os}_{1p}).[2,11] For this reason, complexes of similar size and molecular weight are expected to have similar relaxivity at these magnetic fields. Normally, the NMRD profiles are not sensitive to the value of τ_M, which at 25 °C is of the order of a few hundred nanoseconds for enneacoordinate Gd^{III} chelates and thus makes a negligible contribution to τ_{ci} (Equation 4). In the low field region r_{1p} is affected by the value of the electronic relaxation time which varies from one complex to another as a result of their different symmetries, rigidities and donor atoms.[20,21] In Figure 2, the experimental NMRD data of $[Gd(DTPA)(H_2O)]^{2-}$ are reported as measured at 25 °C and pH = 7.2. Because of the particularly important role played by this complex in the field of MRI contrast agents, where it has been considered as a reference in the development of new compounds, its profile is well-known and has been analyzed and discussed in considerable detail, primarily by S. H. Koenig and R. D. Brown III.[11]

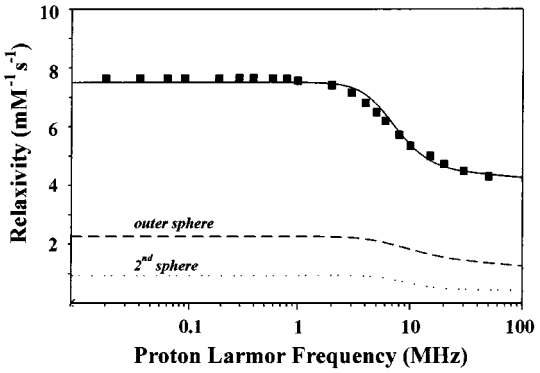


Figure 2. NMRD profile at 25 °C and pH = 7.2 of $Na_2[Gd(DTPA)(H_2O)]$. The curve through the data points has been calculated with the parameters of Table 3, obtained through a best-fitting procedure to equations for paramagnetic relaxation, as described in the text. The lower dashed and dotted curves represent the outer- and 2nd sphere contributions, respectively.

An excellent fit of the data to both inner and outer sphere theory was obtained by considering as adjustable parameters τ_{S0} (85 ps), τ_v (20 ps), τ_R (80 ps) and r_{Gd-H} (3.05 Å), whereas reasonable assumptions were made with regard to d (3.6 Å), D (the diffusion constant of the complex is assumed to be about 25% that of water), q (= 1) and τ_M (1 ns). This interpretation, based on resolution of the data into inner and outer sphere contributions, has proven to be very useful for comparing the data of different complexes, understanding the relaxometric behavior as a function of viscosity, temperature and pH and provides a good basis for rational design of new CA.

However, when one compares the parameters of the fitting procedure with the available structural data on a series of related Gd^{III} complexes several discrepancies are found. The solid state X-ray structures of numerous Gd^{III} chelates reveal that the $Gd–O_w$ distance does not show significant variation from a value of about 2.45 Å, which corresponds to a r_{Gd-H} value of about 2.9 Å.[16,17,22] When compared to the fitted value of 3.05 Å, this represents a significant difference, considering that the relaxivity has a dependence on the inverse of the 6th power of this parameter. On the other hand, the value of 3.6 Å for the closest distance of approach of the outer sphere water molecules to the paramagnetic center is far too short, even shorter than metal-ligand proton distances found in Ln^{III} complexes with DTPA. The X-ray structural determination presented here clearly indicates for this parameter an average value of 4.5 Å, which implies a contribution of the outer sphere relaxivity which is markedly lower than normally calculated. The reorientational correlation time, τ_R = 80 ps, is sensibly longer than the value, about 70 ps, calculated from ^{13}C NMR data on diamagnetic derivatives (La^{III}, Y^{III} or Lu^{III} complexes), probably a consequence of its strong correlation with the value of r_{Gd-H} . On the other hand, when we try to fit the NMRD profile by fixing the parameters r_{Gd-H}, d, D and τ_R to more realistic values (and by using $q = 1$ and τ_M = 360 ns, as calculated by Merbach et al.),[9] a very poor result is obtained. The much larger value of d reduces by almost 50% the contribution of r^{os}_{1p} and is not compensated by the shorter value of the distance r_{Gd-H} . We tried to account for the remaining contribution to the relaxivity by including into the fitting model a term which considers the dipolar interaction of second sphere water molecules with the paramagnetic Gd^{III} ion (r^{2s}_{1p}). Over the last 15 years this contribution has seldom been taken into account for the interpretation of relaxometric data and, in the case of MRI contrast agents, only in studies involving small Gd^{III} chelates with $q = 0$.[12,15] The X-ray crystal structure of $[Yb(DTPA)(H_2O)]^{2-}$ provides clear evidence of the presence of a water molecule hydrogen-bonded to oxygen atoms of adjacent carboxylate groups and at a distance significantly closer than that of the outer sphere solvent molecules. In fact, the orientation of this water molecule, directed towards the metal ion, is such that a hydrogen atom is located only 3.28 Å from Gd^{III}. A contribution to relaxivity is thus expected provided that the mean residence lifetime of the molecule is longer than the diffusional correlation time, i.e. the time necessary for the solvent and the metal complex to diffuse apart from each other (proportional to d^2/D, about 50 ps). Under this condition,

Table 3. Best fitting parameters derived from the variable temperature NMRD data of $Na_2[Gd(DTPA)(H_2O)]$

Parameter	4 °C	10 °C	18 °C	25 °C	32 °C	39 °C
τ_{SO} (ps)	85	82	74	72	73	65
τ_V (ps)	35	31	27	22	19	17
τ_M (ns)	1270	864	531	363	241	166
τ_R (ps)	126	106	86	65	61	52
D (10^5 cm^2s^{-1})	1.62	1.92	2.38	2.84	3.38	3.99
τ_{M_1} (ps)	156	129	101	94	67	56

the second sphere water molecule experiences rotation of the complex and its effect to the measured solvent relaxation rate can be evaluated by using the inner sphere approach. We then fitted the experimental NMRD data at 25 °C with a model that includes the second sphere term and thus 3 more parameters: the number of the second sphere water molecules, q_{2S}, their distance from Gd^{III}, r_{2S} and their mean residence lifetime τ_{M2S}. The total number of relaxation parameters is 11, but several of them can be fixed by using structural data or can be estimated by using values obtained with other techniques. An accurate value of τ_M has been obtained by Merbach and co-workers by ^{17}O NMR ($\tau_M \cong 360$ ns at 25 °C); τ_R has been calculated by ^{13}C NMR relaxation data to be about 70 ps; r_{Gd-H} is allowed to vary slightly about the value of 2.93 Å estimated from X-ray data; the D value has been previously assessed by the analysis of NMRD profiles for complexes whose relaxivity is exclusively controlled by the outer sphere term ($q = 0$); to d we may assign the value of 4.50 Å as estimated before. The adjustable parameters are then the electronic relaxation time (τ_{S0} and τ_v), τ_{M2S} and q_{2S}/r_{2S}, whereas τ_R and τ_M were allowed to vary a little from the initial estimates in order to optimize the fitting. The results of the fitting procedure of the data measured at 4, 10, 18, 25, 32 and 39 °C to this model are reported in Table 3. In Figure 2 the experimental and calculated profiles at 25 °C, along with the calculated contributions of the outer- and second sphere components are shown. The experimental data for all temperatures are fit nicely with a set of structural parameters that match the crystallographic data, reproduce very well previous estimates on the electronic relaxation times and water exchange lifetime and account for a second sphere water contribution of about 13% of the observed relaxivity at low fields. The calculated (20 MHz; 25 °C) temperature dependence of the second sphere contribution is reported in Figure 3 and shows an exponential decrease with increasing temperature, in accord with the fitting results, indicating that the residence lifetime of the hydrogen-bonded water molecules represents the dominant correlation time of the dipolar interaction. This behavior is in agreement with the expectation that at high temperatures the lifetime of the hydrogen-bonding interaction becomes so short as to approach the diffusion limit, where this contribution vanishes.

The best fit value of q_{2S}/r_{2S} is $1.5 \cdot 10^7$ cm^{-1} which could be assigned to a water molecule with a proton at 3.28 Å from the Gd^{III} ion by analogy with the crystal structure of the Yb complex. Clearly, this is only an approximation, as

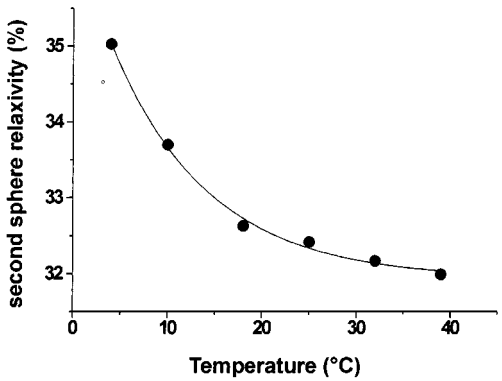


Figure 3. Temperature dependence of the second sphere contribution (%) to the overall relaxivity of $[Gd(DTPA)(H_2O)]^{2-}$ at 20 MHz and 25 °C.

the number of water molecules hydrogen-bonded to the carboxylate groups is surely higher than one. On the other hand, it must be stressed that the technique is only capable of detecting the effects associated with those solvent molecules whose mean residence lifetime is sufficiently long. Thus, it cannot be excluded that the second sphere contribution evidenced in this work is attributable to a single water molecule located in a well-defined position, as revealed by the X-ray crystal structure. The estimated residence lifetime of this water is 94 ps at 25 °C, in good agreement with previous estimates on related systems.

It is generally assumed that the temperature dependence of the correlation time τ_v (and of Δ^2) follows

$$\frac{1}{\tau_v} = \frac{RT}{Nh} exp\left(\Delta S^{\#} / R - \Delta H^{\#} / RT\right) \quad (9)$$

an Eyring behavior (Equation 9) and the plot of data versus temperature, reported in a linear form in Figure 4, represents a good check of the reliability and accuracy of the fitting procedure. The two straight lines in Figure 4 have R factors > 0.99 indicating that the assumptions made for deriving the parameters listed in Table 3 are reasonable and provide correct estimates of the electronic relaxation times of Gd^{III}.

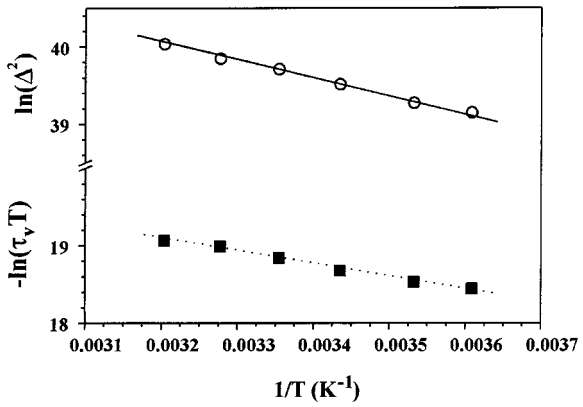


Figure 4. Temperature dependence of the relaxation parameters Δ^2 and $\tau_V T$, calculated from the best-fitting procedure of the NMRD profiles measured at 4, 10, 18, 25, 32 and 39 °C.

Conclusion

The X-ray crystal structure of K_2[Yb(DTPA)(H_2O)] shows that the coordination polyhedron around the metal ion is very similar to that previously found for the Gd^{III} complex, with a nine-coordinate ligand environment composed of the three amine nitrogens, five carboxylate oxygens and one water molecule. The coordination geometry is best described as a tricapped trigonal prism. Additional water molecules have been localized and described as belonging to the outer- and second hydration spheres of the metal ion. In particular, the second sphere water molecule is involved in an hydrogen bond network with the bound water and the uncoordinated carboxylate oxygens and is located very close to the metal ion. From the X-ray results we have reconsidered the NMRD relaxivity profiles of the MRI contrast agent [Gd(DTPA)(H_2O)]$^{2-}$, based on a model comprising contributions from the water molecules in the three different environments: inner-, outer- and second sphere. An excellent fit of the experimental data to this model has been obtained with a set of the relaxation parameters which is in much better agreement with the available structural data. The contribution of the second sphere term is about 10% of the total relaxivity but is very important for a correct and more realistic interpretation of the experimental data. Furthermore, its contribution could be optimized and the relaxivity enhanced through suitable ligand design.[23]

Experimental Section

General Remarks: $GdCl_3 \cdot 6H_2O$, $YbCl_3 \cdot 6H_2O$ and H_5DTPA were purchased from Aldrich. The metal complexes were prepared by mixing stoichiometric amounts of the ligand and of the metal chloride and by adjusting the pH to 7 with KOH. The solutions were kept at room temperature under vigorous stirring for one hour until the pH stabilized. The compounds were then purified by precipitation by addition of acetone. In the case of K_2[Gd(DTPA)(H_2O)], the absence of free metal ion was assessed by the constant value of the water proton relaxation rate, measured at 298 K and 20 MHz, after successive additions of a small excess of the free ligand. The paramagnetic solutions of the Gd^{III} complex for the ^{1}H low resolution NMR study were prepared by weight of the solid compound and their concentrations (1–2 mM) measured by relaxometry from the known value of the relaxivity at 312 K. A 0.15 M solution of the Yb^{III} complex was prepared in D_2O and the purity of the compound was ascertained by recording the ^{1}H NMR spectrum. Crystals suitable for the X-ray diffraction study were obtained after very slow evaporation at room temperature of a concentrated aqueous solution of the complex.

^{1}H NMR Measurements: Water proton relaxation measurements (20 MHz, 25 °C) were carried out with a Stelar Spinmaster Spectrometer (Mede, Pv, Italy) on 0.5–2 mM solutions of K_2[Gd(DTPA)(H_2O)] at pH = 7.2, I = 0.1. Spin-lattice relaxation times T_1 were measured by the standard inversion recovery method with typical 90° pulse width of 3.5 ms, 16 experiments of 4 scans. The reproducibility of the data is ±1%. The $1/T_1$ nuclear magnetic relaxation dispersion profiles of water protons were measured at 4, 10, 18, 25 and 39 °C using 1.5 mM solutions of the complex on the field-cycling Koenig–Brown relaxometer of the University of Torino (Italy). The temperature was controlled by circulating a freon from an external bath and measured by a thermometer inserted into the freon close to the sample. The reproducibilities of the measured T_1 values were estimated to be ±2%.

X-ray Crystallographic Study

A suitable crystal of K_2[Yb(DTPA)(H_2O)] was coated with Paratone oil, placed on the end of a silica fiber and mounted in a goniometer head on the Nonius CAD4 diffractometer in a stream of cold nitrogen gas. The crystal was centered optically and unit cell parameters and an orientation matrix for data collection were obtained at –100 °C by using the centering program in the CAD4 system. Details of the crystal data are given in Table 2 The actual scan range was calculated by scan width = scan range + 0.35 tanθ and backgrounds were measured by using the moving-crystal – moving-counter technique at the beginning and end of each scan. Two representative reflections were monitored every 2 h as a check on instrument and crystal stability. Lorentz, polarization, and decay corrections were applied to the data as well as an absorption correction based on a series of ψ scans. The weighting scheme used during refinement was $1/\sigma^2$, based on counting statistics.

The structure was solved by Direct Methods using SHELXTL/PC V5.03[24] which revealed the positions of most of the non-hydrogen atoms. All other non-hydrogen atoms were found by successive difference Fourier syntheses including the ytterbium-bound water, O(1 W), the second sphere water molecule, O(7 W) and the outer sphere water molecules, O(2,3,4,5,6,8 W). Hydrogen atoms were placed their expected chemical positions using the HFIX command for all ligand hydrogens, but hydrogens attached to oxygen-water molecules were identified from a difference Fourier; all hydrogens were included in the final cycles of least squares with isotropic U_{ij} 's related to the atoms on which they rode. All other non-hydrogen atoms were refined anisotropically.

Neutral atom scattering factors and values of $\Delta f'$ and $\Delta f''$ were taken from Volume C of the *International Tables for X-ray Crystallography.*[25] Structure refinement and preparation of figures and tables for publication were carried out on PCs by using SHELXTL/PC V5.03.[24] Crystallographic data (excluding structure factors) for the structure reported in this paper have been deposited with the Cambridge Crystallographic Data Centre as supplementary publication no. CCDC- 133337. Copies of the data can be obtained free of charge on application to CCDC, 12 Union Road, Cambridge CB2 1EZ, UK [Fax: (internat.) + 44–1223/336–033; E-mail: deposit@ccdc.cam.ac.uk].

Acknowledgments

We gratefully thank the NATO Science Program for a travel grant (M.B. and K.H.) and MURST and C.N.R. Legge 95/95 for financial support.

[1] R. B. Lauffer, *Chem. Rev.* **1987**, *87*, 901–927.
[2] [2a] S. Aime, M. Botta, M. Fasano, E. Terreno, *Chem. Soc. Rev.* **1998**, *27*, 19–29. – [2b] S. Aime, M. Botta, M. Fasano, S. Geninatti Crich, E. Terreno, *Coord. Chem Rev.* **1999**, *185–186*, 321–333.
[3] M. F. Tweedle, in *Lanthanide Probes in Life, Chemical and Earth Sciences* (Eds: J.-C. Bunzli, G. R. Choppin), Elsevier, Amsterdam, **1989**, chapter 5.
[4] J. A. Peters, J. Huskens, D. J. Raber, *Prog. NMR Spectrosc.* **1996**, *28*, 283–350.
[5] G. M. Bydder, in *Magnetic Resonance Imaging* (Eds: D. D. Stark, W. G. Bradley, Jr.), The C. V. Mosby Company, St. Louis, **1988**, chapter 10.

[6] J. A. Peters, *Inorg. Chem.* **1988**, *27*, 4686–4691.
[7] S. Aime, M. Botta, *Inorg. Chim. Acta* **1990**, *177*, 101–105.
[8] B. J. Jenkins, R. B. Lauffer, *Inorg. Chem.* **1988**, *27*, 4730–4738.
[9] K. Micksei, L. Helm, E. Brücher, A. E. Merbach, *Inorg. Chem.* **1993**, *32*, 3844–3850.
[10] L. Banci, I. Bertini, C. Luchinat, *Nuclear and Electron Relaxation*, VCH, Weinheim, **1991**.
[11] S. H. Koenig, R. D. Brown III, *Prog. NMR Spectrosc.* **1990**, *22*, 487–567.
[12] S. Aime, M. Botta, D. Parker, J. A. G. Williams, *J. Chem. Soc., Dalton Trans.* **1996**, 17–23.
[13] J. W. Chen, F. P. Auteri, D. E. Budil, R. L. Belford, R. B. Clarkson *J. Phys. Chem.* **1994**, *98*, 13452–13459.
[14] J. W. Chen, R. L. Belford, R. B. Clarkson *J. Phys. Chem.* **1998**, *102*, 2117–2130.
[15] M. Botta, presented at the COST D1 European Workshop, Coimbra, August 18–19, 1995.
[16] H. Gries, H. Miklautz, *Physiol. Chem. Phys. Med. NMR* **1984**, *16*, 105–112.
[17] M. B. Inoue, M. Inoue, Q. Fernando *Inorg. Chim. Acta* **1995**, *232*, 203–206.
[18] J. J. Stezowski, J. L. Hoard, *Isr. J. Chem*. **1984**, *24*, 323–334.
[19] J. H. Freed, *J. Chem. Phys.* **1978**, *68*, 4034–4039.
[20] S. Aime, M. Botta, G. Ermondi, F. Fedeli, F. Uggeri, *Inorg. Chem.* **1992**, *31*, 1100–1103
[21] S. Aime, P. L. Anelli, M. Botta, F. Fedeli, M. Grandi, P. Paoli, F. Uggeri, *Inorg. Chem.* **1994**, *33*, 2422–2428.
[22] C. A. Chang, L. C. Francesconi, M. F. Malley, K. Kumar, J. Z. Gougoutas, M. F. Tweedle, D. W. Lee, L. J. Wilson, *Inorg. Chem.* **1993**, *32*, 3501–3508.
[23] M. Botta, *Eur. J. Inorg. Chem*., **2000**, 399–407.
[24] SHELXTL/PC V5.03, Bruker AXS, Madison, WI, U. S. A.
[25] A. J. C. Wilson (ed), *International Tables for X-ray Crystallography, Volume C.* Kluwer Academic Publishers, Dordrecht, **1992**, Tables 6.1.1.4 (pp. 500–502) and 4.2.6.8 (pp. 219–222).

Received August 19, 1999
[I99308]

Borabenzene Derivatives, 31[‡]

Enantiomerically Pure Complexes of Manganese, Iron, and Zirconium with Pinene-Fused Boratabenzene Ligands – Structures of *exo*-FeCp*($C_{13}H_{17}BNMe_2$) and *exo*,*exo*-$ZrCl_2(C_{13}H_{17}BNMe_2)_2$

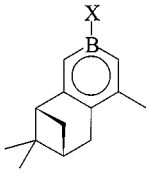
Gerhard E. Herberich,*[a] Ulli Englert,[a] Beate Ganter,[a] and Mario Pons[a]

Keywords: Boron / Transition metals / Sandwich complexes / Boratabenzene / Pinene

Complexes of pinene-fused boratabenzene ligands [(1*R*,9*R*)-6,10,10-trimethyl-4-boratatricyclo[7.1.1.$0^{2,7}$]undeca-2,4,6-trienes] $C_{13}H_{17}BX$ (with **a**: X = NMe_2; **b**: X = OMe; **c**: X = Me) are described. The lithium salt Li($C_{13}H_{17}BNMe_2$) [Li(**1a**)] reacts with [Cp*Fe(NCMe)$_3$]PF_6 and with $Mn(CO)_3Br(py)_2$ to give diastereomeric mixtures FeCp*($C_{13}H_{17}BNMe_2$) (**4a**) and $Mn(CO)_3(C_{13}H_{17}BNMe_2)$ (**7**). The mixture **4a** undergoes solvolysis in methanol to produce methoxy compounds **4b**, which in turn react with LiMe in Et_2O to give methyl derivatives **4c**. The lithium salts Li($C_{13}H_{17}BX$) [Li(**1a**–**c**)] react with $ZrCl_4$ in toluene or Et_2O to give *exo*,*exo*-$ZrCl_2(C_{13}H_{17}BX)_2$ complexes (**8a**–**c**). The dimethyl derivative *exo*,*exo*-$ZrMe_2(C_{13}H_{17}BNMe_2)_2$ (**9**) can also be prepared from **8a**/LiMe in Et_2O. NOE difference spectra have been analyzed to determine the configurations of the diastereomers and to establish a chemical shift criterion for assessing the configuration of the metal–ligand coordination. An independent confirmation of the product stereochemistries has been obtained by single-crystal X-ray structure determinations of *exo*-**4a** and **8a**.

Introduction

In previous work, we developed a synthetic route to enantiomerically pure, pinene-fused lithium boratabenzenes Li(**1a**–**c**).[1] In this paper, we describe the first transition metal complexes of the ligands **1a**–**c**.

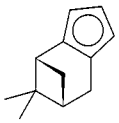


1

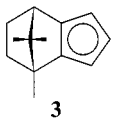
a: X = NMe_2
b: X = OMe
c: X = Me

The motivation for this research stems from analogous cyclopentadienyl chemistry. Chiral metallocenes[2] have been employed as catalyst precursors in stereoregular olefin polymerization,[3] in enantioselective synthesis,[4] and as auxiliary ligands in asymmetric catalysis.[5,6]

The chirality of a metallocene may have different origins.[7] Annulated chiral cyclopentadienyl ligands derived from the chiral pool are of particular interest. They promise well-defined asymmetry and stereocontrol. Using enantiomerically pure starting materials, enantiomerically pure complexes are obtained. Early and important examples are the camphor-derived CamCp ligand (**2**)[8] and the pinene-derived PinCp (**3**).[9] Finally, it should be noted that the ligands **2** and **3** as well as **1a**–**c** possess diastereotopic faces, the more crowded *endo* face with the dimethylmethylene bridge, and the less crowded *exo* face with an ethylene bridge in the case of **2** and a methylene bridge in the case of **1** and **3**. As a consequence, complex formation with these ligands will usually produce mixtures of *exo* and *endo* diastereomers.



2



3

Results and Discussion

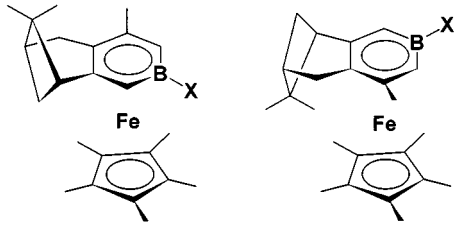
(Pentamethylcyclopentadienyl)iron Complexes

First we describe complexes of the ligands **1a**–**c** with the FeCp* fragment. The simpler 1-methylboratabenzene derivative Fe(C_5H_5BMe)Cp*[10] has previously been synthesized in near quantitative yield from [Cp*Fe(NCMe)$_3$]PF_6[11] and Li(C_5H_5BMe).[12] Using the same general method,[13] [Cp*Fe(NCMe)$_3$]PF_6 was treated with the 4-dimethylamino compound Li(**1a**) in the form of its TMEDA adduct[1b] to give a mixture of the two diastereomers *exo*-FeCp*(**1a**) [≡ *exo*-**4a**] and *endo*-FeCp*(**1a**) [≡ *endo*-**4a**] as a deep-red crystalline solid in near quantitative yield (97%). The *exo* isomer was invariably formed preferentially, along with 10–25% of the *endo* isomer. Pure *exo* isomer *exo*-**4a** could be obtained by fractional crystallization from hexane in acceptable yield (50%). In methanol solution, the diastereomeric mixture **4a** slowly underwent solvolysis (60 °C, 24 h) to give, after workup, a corresponding mixture of the methoxy compounds **4b** as a red oil (100%). Treatment of **4b** with

[‡] Part 30: G. E. Herberich, X. Zheng, J. Rosenplänter, U. Englert, *Organometallics* **1999**, *18*, 4747-4752.

[a] Institut für Anorganische Chemie, Technische Hochschule Aachen,
D-52056 Aachen, Germany
Fax: (internat.) +49-241/8888-288
E-mail: gerhard.herberich@ac.rwth-aachen.de

 © WILEY-VCH Verlag GmbH, D-69451 Weinheim, 2000 1434–1948/00/0505–0979 $ 17.50+.50/0



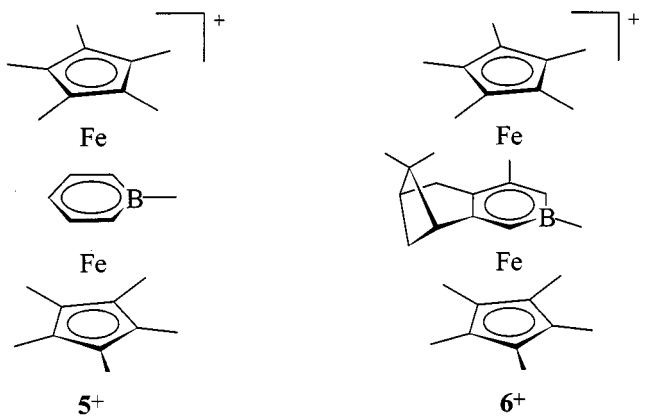
exo - 4 endo - 4

a: X = NMe_2, b: X = OMe, c: X = Me

LiMe in Et_2O led to a smooth substitution to afford a mixture of the methyl compounds **4c** as a slowly solidifying deep-red oil (97%).

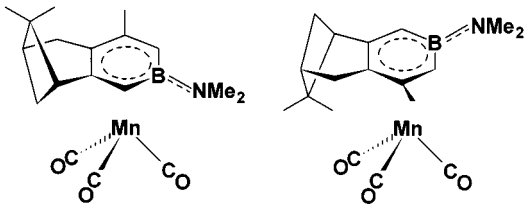
Careful analysis of the NMR spectra in combination with NOE difference spectra led to the conclusion that the major isomer in these mixtures **4a**–**c** was the *exo* diastereomer. This assignment was later confirmed by an X-ray structure determination of *exo*-**4a** (see below).

A fully satisfying preparative-scale separation of the diastereomers could not be achieved in any of the three cases. However, in the case of **4c**, which has an unreactive substituent at boron, a catalyzed isomerization could be observed. In an NMR tube, the diastereomeric mixture **4c** was dissolved in [D_6]acetone and treated with a catalytic amount of [Cp*Fe(NCMe)$_3$]PF_6 at ambient temperature; within a few hours complete isomerization to the clearly more stable *exo*-**4c** isomer had occurred. This observation can readily be explained. The sterically less crowded Fe(C_5H_5BMe)Cp* reacts with [Cp*Fe(NCMe)$_3$]PF_6 in dichloromethane with reversible formation of the triple-decker complex [Cp*Fe(μ-C_5H_5BMe)FeCp*]PF_6 [≡ (**5**)PF_6].[10] With the bulkier pinene-fused boratabenzene ligand **1c**, the corresponding triple-decker species $\mathbf{6}^+$ should be highly destabilized. The equilibrium of the triple-decker formation will be shifted to the left and the concentration of the triple-decker cation will be too low for its detection by NMR. On the other hand, we may assume that $\mathbf{6}^+$ is still energetically accessible, thus providing a low-energy isomerization pathway. This type of equilibration of diastereomers was first established by ourselves in the case of the diastereomeric isodicyclopentadienyl (Idcp) complexes *endo*- and *exo*-Ru(Icdp)Cp*.[14]



A Tricarbonylmanganese Complex

The tricarbonylmanganese complex Mn(CO)$_3$(**1a**) [≡ **7**] was chosen as a further example of a late transition metal complex. In reactions with *C*-unsubstituted lithium 1-aminoboratabenzenes, the complex [Mn(CO)$_3$(NCMe)$_3$]PF_6[15] has been successfully used as a source of the Mn(CO)$_3$ fragment.[16] However, treatment of the presumably much more basic[17] Li(TMEDA)(**1a**) with [Mn(CO)$_3$(NCMe)$_3$]PF_6 in THF led to protonation of $\mathbf{1a}^-$ and the pinene-fused dihydroborinine H(**1a**) (with the proton added at C-5)[1b] was isolated in near quantitative yield. We then used MnBr(CO)$_3$(py)$_2$[18] (see Experimental Section for an improved preparation); reaction with Li(**1a**) gave mixtures of the two diastereomers *exo*-**7** and *endo*-**7** as orange, light-sensitive oils.



exo - 7 endo - 7

A systematic variation of the reaction conditions[19] showed that nonpolar solvents favor the formation of *exo*-**7** (in hexane, 65 °C, 72 h; diastereomeric ratio *exo*/*endo* = 76:24), whereas in THF *endo*-**7** is obtained preferentially (65 °C, 2 h; *exo*/*endo* = 36:64). Pure *exo*-**7** could readily be obtained from mixtures **7** with high *exo*/*endo* ratios as a yellow, light-sensitive solid by two fractional crystallizations from hexane. In contrast, pure isomer *endo*-**7** could not be isolated.

Zirconium Complexes

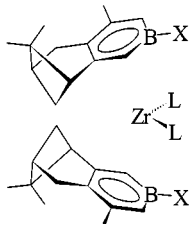
The synthesis of enantiomerically pure bis(ligand) complexes of zirconium seemed to be a particularly interesting goal. A number of simple achiral bis(boratabenzene)dichlorozirconium complexes,[20,21,22a] achiral *ansa*-,[22a] as well as some chiral *ansa*-compounds[22b] have been described. In combination with MAO, these complexes are active catalysts for olefin polymerization.[21,22]

The reaction of freshly sublimed $ZrCl_4$ with the lithium boratabenzene Li(**1a**) in toluene or diethyl ether produces the bis(ligand) complex **8a** as a blue to purple solid in a crude yield of 55%. The main by-product (20–30%) results from protonation of $\mathbf{1a}^-$ and is in fact the pinene-fused dihydroborinine H(**1a**) mentioned above. In THF, the protonation of $\mathbf{1a}^-$ becomes almost entirely predominant.

For a bis(ligand) complex, three diastereomers with *exo*,*exo*, *exo*,*endo*, and *endo*,*endo* coordination may be expected, but only the *exo*,*exo* diastereomer is found experimentally. This result is in accord with similar findings made for the analogous reaction with Paquette's pinene-fused lithium cyclopentadienide.[23]

The methoxy compound Li(**1b**) and the methyl compound Li(**1c**) also give bis(ligand) complexes, i.e. the orange compounds **8b** and **8c**, both of which also have the *exo*,*exo* configuration according to their spectral data. Loss of starting material by protonation is less significant in these cases [ca. 10% of Li(**1b**), negligible in the synthesis of **8c**], presumably because of the lower basicities of the corresponding anions.

The bis(boratabenzene)zirconium complex $ZrCl_2(C_5H_5BNiPr_2)_2$ can readily be methylated with LiMe in Et_2O to give the corresponding dimethyl derivative $ZrMe_2(C_5H_5BNiPr_2)_2$.[21a] Analogously, a solution of **8a** can be titrated with LiMe in Et_2O. The end of the titration is indicated by a color change from purple to deep-red; the dimethyl derivative **9** thus obtained can be crystallized from toluene to give small red crystals.



8: L = Cl; **a**: X = NMe_2, **b**: X = OMe, **c**: X = Me
9: L = Me, X = NMe_2

NMR Spectroscopic Distinction of Diastereomers

In the preceding paper on pinene-fused boratabenzenes, we discussed the characteristic spectroscopic features of these compounds and the assignment techniques used.[1a] In the present work, the only additional point of interest with regard to the NMR characterization is the distinction of the diastereomers and the assignment of *exo* and *endo* configurations, respectively. Selected ^{1}H-NMR data are presented in Table 1. In the case of the diastereomeric FeCp* complexes *exo*-**4a**–**c** and *endo*-**4a**–**c**, NOE difference spectra for the proton signals of the Cp* ligand and for the protons 10-Me_{endo}, and 11-H_{endo} (and to a lesser extent also 8-H_{endo} and 8-H_{exo}), respectively, can be used to assign these signals and to determine the configuration of the complex in question.

For the pairs of diastereomers of **4a**–**c**, chemical shift patterns emerge that show an unambiguous correlation with the configuration of the metal–ligand bond. The pair of manganese complexes *exo*-**7** and *endo*-**7** (for which the NOE assignment technique is not applicable) also conform to this pattern. In the case of the zirconium complexes **8a**–**c** and **9**, where only one diastereomer is found, the data (especially for the pair of methyl groups 10-Me_{exo}/10-Me_{endo} and the relatively high chemical shift values for 11-H_{endo}) indicate an *exo* configuration of the metal–ligand bond, and hence an *exo*,*exo* configuration of the complexes. These conclusions are in agreement with the results of the structure determinations described below.

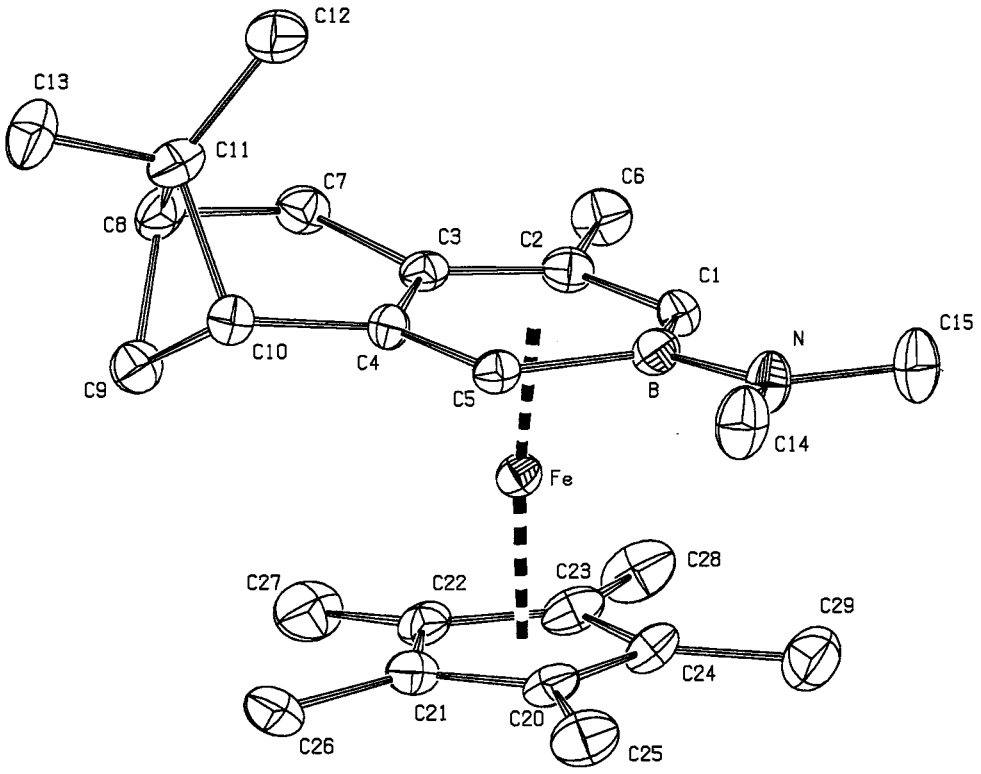
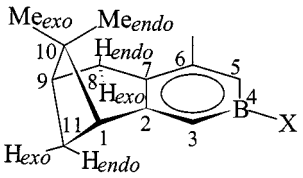


Figure 1. Molecular structure (PLATON plot, see ref.[25], at a 30% probability level) of *exo*-**4a** in the crystal; selected bond lengths [Å] for *exo*-**4a**: Fe–C1 2.121(5), Fe–C2 2.088(4), Fe–C3 2.114(4), Fe–C5 2.134(4), Fe–B 2.352(6), Fe–C(Cp*) 2.072 (av.), B–N 1.438(7), C1–B 1.519(7), C1–C2 1.409(6), C2–C3 1.413(6), C3–C4 1.435(5), C4–C5 1.397(6), C5–B 1.525(7), Fe–Cp* 1.6815(6), Fe–(C_5B) 1.5931(6)



1

Table 1. Selected ^{1}H-NMR chemical shift data

Compound[a]	10-Me$_{exo}$	10-Me$_{endo}$	11-H$_{exo}$	11-H$_{endo}$	8-H$_{exo}$	8-H$_{endo}$
exo-**4a**	1.32	0.60	2.58	2.10	2.63	2.25
exo-**4b**	1.29	0.56	2.56	2.04	2.59	2.20
exo-**4c**	1.28	0.51	2.56	2.04	2.62	2.20
endo-**4a**	1.30	1.66	2.39	0.75	2.24[b]	2.57[b]
endo-**4b**	1.28	1.60	2.37	0.71	2.12[b]	2.51[b]
endo-**4c**	1.28	1.60	2.35	0.66	–[c]	2.53
exo-**7**[b]	1.11	0.56	2.39	1.84	2.48	2.24
endo-**7**[b]	1.09	1.35	2.32	0.88	2.20	2.51
8a	1.33	0.56	2.37	1.83	3.30	2.65
8b	1.35	0.55	2.49	1.73	3.26	2.69
8c	1.35	0.48	2.49	1.69	3.25	2.68
9	1.35	0.67	2.33	1.22	2.97	2.79

[a] Measured in C_6D_6 for the Fe and Mn complexes and in CD_2Cl_2 for the Zr compounds. – [b] Assignments are not confirmed by NOE difference spectra. – [c] Signal obscured.

Structure of the Iron Complex *exo*-4a

A sample of pure *exo*-**4a** was recrystallized from hexane at –30 °C to give deep-red crystals of good quality. Complex *exo*-**4a** crystallizes in the chiral orthorhombic space group $P2_12_12_1$. The structure determination confirmed the *exo* configuration of *exo*-**4a** (Figure 1).

The molecule shows a typical sandwich structure. The atoms C1C5 are essentially coplanar [maximum vertical displacement of 0.021(4) Å for C3], but the aminoboranediyl group is bent away from the metal and the boron atom resides 0.191(5) Å above the C1C5 plane. There are several indications of transannular repulsive interactions. The ring–ring conformation places the methylene group between two methyl groups of the Cp* ligand and the same is true for the B–NMe_2 group. There is a marked bending of the sandwich, which results in an increased distance between the Cp* ligand and the *endo*-methylene bridge; the angle between the best Cp* plane and the best C_5B plane amounts to 5.0(1)°. The slip distortion[25] of the boratabenzene ring amounts to 0.11 Å and is smaller than that in Fe(C_5H_5BMe)Cp* (0.15 Å).[10] This detail may seem surprising, but an increase in the slip distortion would be counteracted by an increase in the transannular repulsion of the *endo*-methylene bridge. Finally, we note the relatively long Fe–B distance of 2.352(6) Å and the relatively short B–N distance of 1.438(7) Å. These features demonstrate the often documented π-interaction between the boron p_z orbital and the nitrogen lone pair.

Structure of the Bis(ligand) Zirconium Complex 8a

Crystals suitable for X-ray crystallographic analysis were obtained by crystallization of **8a** from toluene at –30 °C. Complex **8a** crystallizes in the chiral orthorhombic space group $P2_12_12_1$ and displays a bent-sandwich structure with a bending angle of 131.65(14)° (Figure 2 and 3). The front view illustrates the approximate C_2-symmetry of this complex.

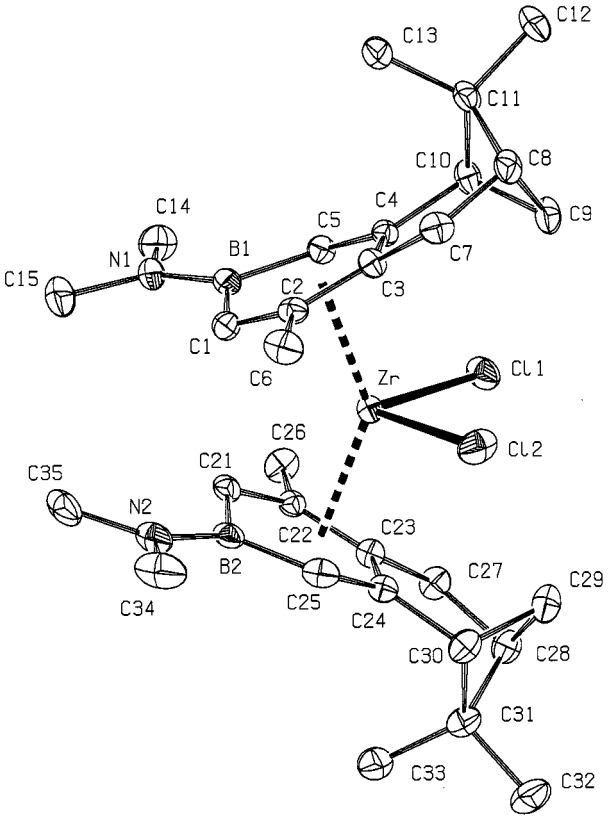


Figure 2. Side view of the molecular structure (PLATON plot, see ref.[25]) of **8a** in the crystal; selected bond lengths [A] and angles [°] for **8a**: Zr–Cl1 2.437(1), Zr–Cl2 2.428(1), Zr–C1 2.642(3), Zr–C2 2.615(3), Zr–C3 2.628(3), Zr–C4 2.627(3), Zr–C5 2.622(3), Zr–B1 2.901(4), Zr–C21 2.593(3), Zr–C22 2.599(3), Zr–C23 2.641(3), Zr–C24 2.685(3), Zr–C25 2.656(3), Zr–B2 2.860(4); Cl1–Zr–Cl2 94.85(3)

The planes C1C5 and C21C25 of the boratabenzene ligands are good planes [with a maximum vertical displacement of 0.017(3) Å]; the aminoboranediyl groups are bent away from the metal with vertical displacements of 0.271(4) Å for B1 and 0.229(4) Å for B2. The average Zr–B distance of 2.88 Å is comparable with the corresponding distances in $ZrCl_2(C_5H_5BMe)_2$ (2.81 Å),[20] $ZrCl_2$(4-Bu*t*$C_5H_4BPh)_2$ (2.80 Å),[21a] $ZrCl_2(C_5H_5BOEt)_2$ (2.83 Å),[21c] and $ZrCl_2(C_5H_5BNiPr_2)_2$ [2.98 Å; B–N 1.396(6) Å].[21a] The average B–N bond length amounts to 1.419 Å and indicates considerable π-interaction between the boron and the exocyclic substituent. This weakens the Zr–B interaction and as a consequence markedly lengthened Zr–B distances are found. A more subtle question is why this situation results in a shorter Zr–B distance and a longer B–N bond length in **8a** as compared to the values in $ZrCl_2(C_5H_5BNiPr_2)_2$.[21a] We suggest that this difference is due to steric effects. The

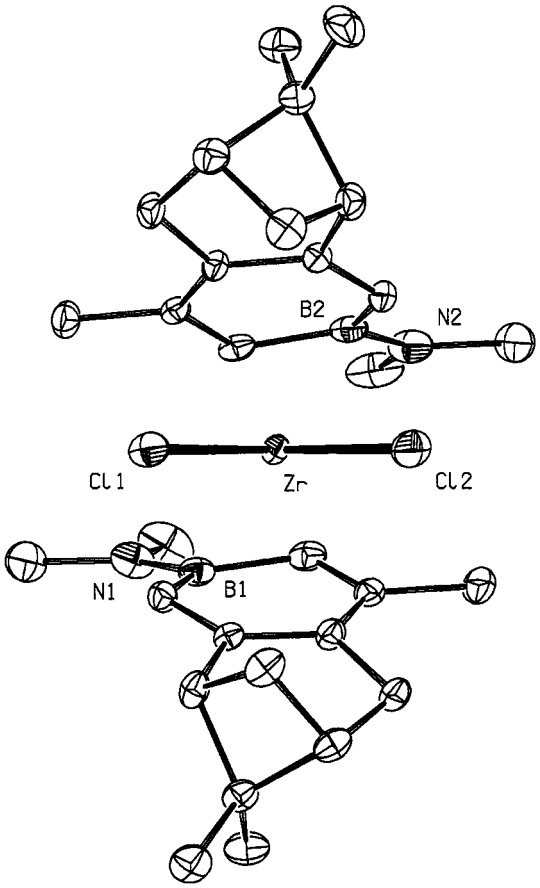


Figure 3. Front view of the molecular structure (PLATON plot, see ref.[25]) of **8a** in the crystal

bulky pinene part of the ligand in **8a** shifts the Zr atom towards the boron (as explained above in the case of *exo*-**4a**) and this results in shorter Zr–B distances and remarkably small slip distortions of just 0.12 and 0.15 Å for the two ligands. The bulky N*i*Pr$_2$ group in ZrCl$_2$(C$_5$H$_5$BN*i*Pr$_2$)$_2$ can be expected to have the opposite effect, resulting in particularly long Zr–B distances and particularly short B–N bond lengths.

Concluding Remarks

In this paper we have described the first transition metal complexes of pinene-fused boratabenzene ligands. With complex fragments incorporating late d-metals, complex formation gives diastereomeric mixtures in most cases, with a marked preference for the the sterically less congested *exo* diastereomers. In contrast, the bis(ligand)zirconium complexes are formed exclusively as *exo*,*exo* isomeric products. Parallels with earlier work by Paquette's group on complexes of the pinene-fused cyclopentadienyl ligand are evident. The pinene-fused Cp also shows a pronounced preference for coordination of the metal at the less hindered *exo* face.[9] Considering the data presented here, this preference seems to be less strong for the pinene-fused boratabenzenes.

Experimental Section

General Remarks: Reactions were carried out under an atmosphere of dinitrogen by employing conventional Schlenk techniques. Hexane was distilled from potassium, toluene from sodium, THF and Et$_2$O from sodium benzophenone ketyl, and CH$_2$Cl$_2$ from CaH$_2$. Electron-impact mass spectra were recorded on a Finnigan MAT-95 spectrometer with a nominal electron energy of 70 eV. Elemental analyses were performed by the Analytische Laboratorien Prof. Dr. H. Malissa und G. Reuter GmbH, D-51789 Lindlar. Melting points were determined in sealed capillaries on a Büchi 510 melting point apparatus and are uncorrected. NMR spectra were recorded on a Varian Unity 500 (^{1}H, 500 MHz; ^{13}C{^{1}H}, 125.7 MHz; ^{11}B{^{1}H}, 160.4 MHz), a Varian VXR 300 (^{1}H, 300 MHz; ^{13}C{^{1}H}, 75.4 MHz), or a Rototec/Picinotti Mini-FID spectrometer (^{11}B{^{1}H}, 29 MHz). Chemical shifts, measured at ambient temperature, are quoted relative to internal TMS for ^{1}H and ^{13}C, and relative to external BF$_3$·Et$_2$O for ^{11}B.

FeCp*(C$_{13}$H$_{17}$BNMe$_2$) (4a): A solution of Li(TMEDA)(**1a**) (1.23 g, 3.50 mmol) in THF (20 mL) was added to [Cp*Fe(NCMe)$_3$]PF$_6$ (1.56 g, 3.40 mmol) in acetonitrile (20 mL). The mixture immediately turned red and was left at ambient temperature for 12 h. After careful removal of the volatiles, the resulting residue was triturated with hexane. Filtration through a frit covered with kieselguhr and concentration of the filtrate in vacuo left a red oil, which was purified by chromatography on alumina (deactivated with 5% H$_2$O, 5 cm layer) using pentane containing 1% triethylamine as eluent. Removal of the solvents gave **4a** (1.38 g, 97%) as a red oil; the diastereomeric ratio *exo*/*endo* was found to vary between 3:1 and 9:1. Pure *exo* isomer *exo*-**4a** could be obtained from hexane at –30 °C as deep-red crystals in 50% yield; barely air-sensitive, soluble in hexane, benzene, THF, and CH$_2$Cl$_2$; m.p. 116 °C.

***exo*-4a**: ^{1}H NMR (500 MHz, C$_6$D$_6$): δ = 3.10 (d, *J* = 2.1 Hz, 5-H), 2.98 (d, *J* = 2.1 Hz, 3-H), 2.98 (br. s, NMe), 2.96 (br. s, NMe), 2.63 (dd, *J* = 15.7, 2.4 Hz, 8-H$_{exo}$), 2.58 (dddd, *J* = 9.2, 5.8, 5.8, 1.5 Hz, 11-H$_{exo}$), 2.25 (ddd, *J* = 15.7, 2.5, 1.5 Hz, 8-H$_{endo}$), 2.18 (dd, *J* = 5.8, 5.5 Hz, 1-H), 2.17 (dddd, *J* = 5.8, 5.5, 2.5, 2.4 Hz, 9-H), 2.10 (d, *J* = 9.2 Hz, 11-H$_{endo}$), 1.81 (s, 6-Me), 1.59 (s, Cp*), 1.32 (s, 10-Me$_{exo}$), 0.60 (s, 10-Me$_{endo}$). – ^{13}C{^{1}H} NMR (126 MHz, C$_6$D$_6$): δ = 113.7 (C-2), 98.3 (C-6), 80.8 (*C*$_5$Me$_5$), 79.5 (C-7), 66.3 (br., C-5), 64.8 (br., C-3), 48.4 (C-1), 41.3 (C-9), 39.9 (br., NMe$_2$), 39.4 (C-10), 33.7 (C-11), 29.4 (C-8), 26.8 (10-Me$_{exo}$), 21.3 (10-Me$_{endo}$), 20.9 (6-Me), 10.5 (C$_5$*Me*$_5$). – ^{11}B{^{1}H} NMR (160 MHz, C$_6$D$_6$): δ = 20. – MS: *m*/*z* (%) = 419 (100) [M$^+$], 364 (13) [M$^+$ – NMe$_2$]. – C$_{25}$H$_{38}$BFeN (419.3): calcd. C 71.62, H 9.14, N 3.34; found C 71.41, H 9.25, N 3.38.

***endo*-4a**: ^{1}H NMR (300 MHz, C$_6$D$_6$): δ = 3.08 (d, *J* = 2.0 Hz, 5-H), 2.96 (br. s, NMe$_2$), 2.84 (d, *J* = 2.0 Hz, 3-H), 2.57 and 2.24 (dm, *J* = 16.8 Hz, 1 H each, 8-H$_{exo}$, 8-H$_{endo}$), 2.39 (ddd, *J* = 9.1, 5.4, 5.4 Hz, 11-H$_{exo}$), 2.30 (dd, *J* = 5.7, 5.4 Hz, 1-H), 2.10 (m, 9-H), 1.87 (s, 6-Me), 1.66 (s, 10-Me$_{endo}$), 1.59 (s, Cp*), 1.30 (s, 10-Me$_{exo}$), 0.75 (d, *J* = 9.1 Hz, 11-H$_{endo}$). – ^{13}C{^{1}H} NMR (75 MHz, C$_6$D$_6$): δ = 118.0 (C-2), 97.9 (C-6), 80.4 (*C*$_5$Me$_5$), 79.8 (C-7), 67–64 (br., C-3 and C-5), 49.5 (C-1), 41.1 (C-9), 40.1 (br., NMe$_2$), 38.8 (C-10), 35.1 (C-11), 28.9 (C-8), 27.4 (10-Me$_{exo}$), 23.8 (10-Me$_{endo}$), 21.4 (6-Me), 10.9 (C$_5$*Me*$_5$). – ^{11}B{^{1}H} NMR (29 MHz, C$_6$D$_6$): δ = 20.

FeCp*(C$_{13}$H$_{17}$BOMe) (4b): A solution of **4a** (356 mg, 0.85 mmol) in methanol (10 mL) was kept at 60 °C for 24 h. Removal of the solvent in vacuo left **4b** (344 mg, 100%) as a red oil; isomer distri-

bution unchanged; barely air-sensitive, readily soluble in hexane, benzene, diethyl ether, and methanol. – MS: *m*/*z* (%) = 406 (3) [M^+], 56 (100). – $C_{24}H_{35}BFeO$ (406.2): calcd. C 70.97, H 8.69; found C 69.86, H 8.84.

***exo*-4b**: ^{1}H NMR (500 MHz, C_6D_6): δ = 3.84 (s, OMe), 3.46 (d, *J* = 2.1 Hz, 5-H), 3.34 (d, *J* = 2.1 Hz, 3-H), 2.59 (dd, *J* = 15.9, 2.7 Hz, 8-H$_{exo}$), 2.56 (dddd, *J* = 9.2, 6.1, 5.8, 1.2 Hz, 11-H$_{exo}$), 2.20 (ddd, *J* = 15.9, 2.4, 1.2 Hz, 8-H$_{endo}$), 2.16 (dd, *J* = 5.8, 5.5 Hz, 1-H), 2.13 (dddd, *J* = 6.1, 5.5, 2.7, 2.4 Hz, 9-H), 2.04 (d, *J* = 9.2 Hz, 11-H$_{endo}$), 1.76 (s, 6-Me), 1.60 (s, Cp*), 1.29 (s, 10-Me$_{exo}$), 0.56 (s, 10-Me$_{endo}$). – ^{13}C{^{1}H} NMR (126 MHz, C_6D_6): δ = 114.7 (C-2), 99.6 (C-6), 80.8 (C_5Me_5), 80.4 (C-7), 71.2 (br., C-5), 69.5 (br., C-3), 53.6 (OMe), 48.2 (C-1), 41.2 (C-9), 39.2 (C-10), 33.6 (C-11), 29.4 (C-8), 26.7 (10-Me$_{exo}$), 21.2 (10-Me$_{endo}$), 20.5 (6-Me), 10.3 (C_5Me_5). – ^{11}B{^{1}H} NMR (29 MHz, C_6D_6): δ = 25.

***endo*-4b**: ^{1}H NMR (500 MHz, C_6D_6): δ = 3.86 (s, OMe), 3.49 (d, *J* = 1.8 Hz, 5-H), 3.26 (d, *J* = 1.8 Hz, 3-H), 2.51 (dd, *J* = 16.2, 2.4 Hz, 8-H$_{endo}$), 2.37 (ddd, *J* = 9.2, 6.1, 5.8 Hz, 11-H$_{exo}$), 2.31 (dd, *J* = 5.8, 5.5 Hz, 1-H), 2.13 (dddd, *J* = 6.1, 5.5, 2.7, 2.4 Hz, 9-H), 2.12 (m, 8-H$_{exo}$), 1.82 (s, 6-Me), 1.61 (s, Cp*), 1.60 (s, 10-Me$_{endo}$), 1.28 (s, 10-Me$_{exo}$), 0.71 (d, *J* = 9.2 Hz, 11-H$_{endo}$). – ^{13}C{^{1}H} NMR (126 MHz, C_6D_6): δ = 119.3 (C-2), 99.3 (C-6), 81.0 (C-7), 80.4 (C_5Me_5), 71.4 (br., C-5), 64.4 (br., C-3), 53.6 (OMe), 49.4 (C-1), 40.9 (C-9), 38.6 (C-10), 34.9 (C-11), 28.8 (C-8), 27.2 (10-Me$_{exo}$), 23.6 (10-Me$_{endo}$), 21.0 (6-Me), 10.6 (C_5Me_5). – ^{11}B{^{1}H} NMR (29 MHz, C_6D_6): δ = 25.

FeCp*($C_{13}H_{17}$BMe) (4c): A solution of **4b** (215 mg, 0.53 mmol) in diethyl ether (4 mL) was cooled to –50 °C. LiMe (0.4 mL, 1.6 M in diethyl ether, 0.64 mmol) was added and the mixture was allowed to warm to room temperature overnight. After the addition of a small amount of alumina at –50 °C, the solution was filtered through alumina (deactivated with 5% H_2O, 5 cm layer) using pentane as eluent. Removal of the volatiles in vacuo left **4c** (206 mg, 100%) as a red, slowly solidifying oil; isomer distribution unchanged; barely air-sensitive, readily soluble in hexane, benzene, diethyl ether, and acetone. – MS: *m*/*z* (%) = 390 (100) [M^+]. – $C_{24}H_{35}BFe$ (390.2): calcd. C 73.88, H 9.04; found C 73.68, H 9.25.

***exo*-4c**: ^{1}H NMR (500 MHz, C_6D_6): δ = 3.80 (d, *J* = 1.2 Hz, 5-H), 3.70 (d, *J* = 1.2 Hz, 3-H), 2.62 (dd, *J* = 15.9, 2.8 Hz, 8-H$_{exo}$), 2.56 (m, 11-H$_{exo}$), 2.20 (m, 8-H$_{endo}$), 2.19 (dd, *J* = 5.8, 5.5 Hz, 1-H), 2.13 (m, 9-H), 2.04 (d, *J* = 9.2 Hz, 11-H$_{endo}$), 1.77 (s, 6-Me), 1.53 (s, Cp*), 1.28 (s, 10-Me$_{exo}$), 1.14 (s, BMe), 0.51 (s, 10-Me$_{endo}$). – ^{13}C{^{1}H} NMR (126 MHz, C_6D_6): δ = 114.1 (C-2), 98.8 (C-6), 82.9 (C-7), 80.4 (C_5Me_5), 84.9 and 83.5 (br., C-3 and C-5), 48.1 (C-1), 41.1 (C-9), 39.2 (C-10), 33.3 (C-11), 29.4 (C-8), 26.6 (10-Me$_{exo}$), 21.1 (10-Me$_{endo}$), 20.4 (6-Me), 10.1 (C_5Me_5), 1.3 (BMe). – ^{11}B{^{1}H} NMR (160 MHz, C_6D_6): δ = 20.

***endo*-4c**: ^{1}H NMR (500 MHz, C_6D_6): δ = 3.80 (d, *J* = 1.2 Hz, 5-H), 3.68 (d, *J* = 1.2 Hz, 3-H), 2.53 (m, 8-H$_{endo}$), 2.35 (m, 2 H, 1-H and 11-H$_{exo}$), 2.01 (m, 9-H), 1.84 (s, 6-Me), 1.60 (s, 10-Me$_{endo}$), 1.54 (s, Cp*), 1.26 (s, 10-Me$_{exo}$), 1.20 (s, BMe), 0.66 (d, *J* = 8.2 Hz, 11-H$_{endo}$). – ^{13}C{^{1}H} NMR (126 MHz, C_6D_6): δ = 79.9 (C_5Me_5), 49.5 (C-1), 40.9 (C-9), 38.4 (C-10), 34.8 (C-11), 28.9 (C-8), 27.2 (10-Me$_{exo}$), 23.8 (10-Me$_{endo}$), 20.9 (6-Me), 10.6 (C_5Me_5). – ^{11}B{^{1}H} NMR (160 MHz, C_6D_6): δ = 20. – Signals due to 8-H$_{exo}$, C-2, C-3, BMe, C-5, C-6, and C-7 could not be located; note that many signals are almost superimposed by those of the *exo* isomer.

MnBr(CO)$_3$(py)$_2$: Pyridine (20 mL) was added with stirring to MnBr(CO)$_5$,[18b] which resulted in rapid gas evolution (CO). As far as possible, light was excluded during the subsequent steps. When the gas evolution had subsided, the mixture was warmed to 80 °C for 1 h, then slowly allowed to cool to ambient temperature. Hexane (60 mL) was added and the deposited orange solid was collected on a frit. It was then washed through the frit by dissolving it in CH_2Cl_2. Removal of the solvent in vacuo left the orange-red crystalline product (9.65 g, 98%); light-sensitive, insoluble in hexane and toluene, soluble in pyridine, THF, and CH_2Cl_2. – ^{1}H NMR (250 MHz, CD_2Cl_2): δ = 8.74 (m, 2-/6-H), 7.61 (m, 4-H), 7.31 (m, 3-/5-H). – IR (CD_2Cl_2): $\tilde{\nu}$ = 2030 (s), 1944 (s), 1910 cm^{-1} (m).

Mn(CO)$_3$($C_{13}H_{17}$BNMe$_2$) (7): A solution of Li(**1a**) (873 mg, containing a known amount of THF, 3.10 mmol) in hexane (20 mL) was added to a suspension of MnBr(CO)$_3$(C_5H_5N)$_2$ (1.13 g, 3.00 mmol) in hexane (75 mL) at 65 °C by means of a cannula. The mixture was kept at 65 °C for 72 h and then filtered through a frit covered with kieselguhr. Removal of the volatiles left **7** (1.00 g, 91%) as an orange oil; the diastereomeric ratio *exo*/*endo* was found to be 3:1. The pure *exo* isomer was isolated as a yellow-orange shiny solid by fractional crystallization from hexane at –30 °C; m.p. 87 °C; soluble in hexane, benzene, THF, and diethyl ether; light-sensitive. When the same reaction was carried out in THF for 2 h at 65 °C, an orange oil with a diastereomeric ratio *exo*/*endo* of 1:2 in favour of the *endo* isomer was obtained.

***exo*-7**: ^{1}H NMR (500 MHz, C_6D_6): δ = 3.54 (d, *J* = 2.5 Hz, 5-H), 3.32 (d, *J* = 2.5 Hz, 3-H), 2.69 (br. s, NMe), 2.62 (br. s, NMe), 2.48 (dd, *J* = 16.3, 3.1 Hz, 8-H$_{exo}$), 2.39 (dddd, *J* = 9.8, 6.1, 5.5, 1.5 Hz, 11-H$_{exo}$), 2.24 (ddd, *J* = 16.3, 2.8, 1.5 Hz, 8-H$_{endo}$), 2.08 (dd, *J* = 5.5, 5.5 Hz, 1-H), 1.87 (dddd, *J* = 6.1, 5.5, 3.1, 2.8 Hz, 9-H), 1.84 (d, *J* = 9.8 Hz, 11-H$_{endo}$), 1.74 (s, 6-Me), 1.11 (s, 10-Me$_{exo}$), 0.56 (s, 10-Me$_{endo}$). – ^{13}C{^{1}H} NMR (126 MHz, C_6D_6): δ = 223.2 (CO), 134.7 (C-2), 120.0 (C-6), 91.0 (C-7), 78.6 (br., C-5), 72.4 (br., C-3), 49.6 (C-1), 40.9 (C-9), 38.8 (C-10), 38.5 (NMe$_2$), 33.2 (C-11), 30.1 (C-8), 26.3 (10-Me$_{exo}$), 21.3 (6-Me), 21.1 (10-Me$_{endo}$). – ^{11}B{^{1}H} NMR (160 MHz, C_6D_6): δ = 23. – MS: *m*/*z* (%) = 367 (14) [M^+], 311 (9) [M^+ – 2 CO], 283 (100) [M^+ – 3 CO], 228 (2) [M^+ – Mn(CO)$_3$], 55 (5) [Mn^+]. – $C_{18}H_{23}BMnNO_3$ (367.1): calcd. C 58.89, H 6.31, N 3.82; found C 60.08, H 6.04, N 3.82.

***endo*-7**: ^{1}H NMR (500 MHz, C_6D_6): δ = 3.64 (d, *J* = 2.5 Hz, 5-H), 3.09 (d, *J* = 2.5 Hz, 3-H), 2.75 (br. s, NMe), 2.62 (br. s, NMe), 2.51 (dd, *J* = 16.6, 2.4 Hz, 8-H$_{endo}$), 2.32 (ddd, *J* = 9.5, 5.8, 5.5 Hz, 11-H$_{exo}$), 2.20 (dd, *J* = 16.6, 3.6 Hz, 8-H$_{exo}$), 2.13 (dd, *J* = 5.5, 5.5 Hz, 1-H), 1.87 (dddd, *J* = 5.8, 5.5, 3.6, 2.4 Hz, 9-H), 1.70 (s, 6-Me), 1.35 (s, 10-Me$_{endo}$), 1.09 (s, 10-Me$_{exo}$), 0.88 (d, *J* = 9.5 Hz, 11-H$_{endo}$). – ^{13}C{^{1}H} NMR (126 MHz, C_6D_6): δ = 223.2 (CO), 134.2 (C-2), 119.9 (C-6), 93.0 (C-7), 79.6 (br., C-5), 65.9 (br., C-3), 49.6 (C-1), 41.1 (C-9), 39.9 (C-10), 38.5 (NMe$_2$), 34.4 (C-11), 29.8 (C-8), 27.2 (10-Me$_{exo}$), 23.5 (10-Me$_{endo}$), 21.3 (6-Me). – ^{11}B{^{1}H} NMR (160 MHz, C_6D_6): δ = 23.

***exo*,*exo*-ZrCl$_2$($C_{13}H_{17}$BNMe$_2$)$_2$ (8a):** A suspension of $ZrCl_4$ (743 mg, 3.19 mmol) in diethyl ether (20 mL) was cooled to –50 °C. Li(**1a**) (1.60 g, containing a known amount of THF, 6.32 mmol) in diethyl ether (30 mL) was then added dropwise through a cannula. The mixture was allowed to warm to room temperature and then stirred for 50 h. After removal of the volatiles, the residue was triturated with hexane (30 mL) and the resulting deep-purple suspension was cooled to –78 °C. The blue-purple solid was collected on a G4-frit at this temperature, washed with cold hexane (2 × 5 mL), and finally extracted from the frit with dichloromethane. Removal of the solvent left **8a** (1.08 g, 55%) as a fine microcrystalline powder. The product could be crystallized by dissolving it in hot toluene and cooling the solution to –30 °C (yield 50%); m.p. (dec.) 150 °C; slightly soluble in hexane and diethyl ether, soluble in benzene,

very soluble in CH_2Cl_2. – ^{1}H NMR (500 MHz, CD_2Cl_2): δ = 5.67 (d, *J* = 3.4 Hz, 5-H), 4.79 (d, *J* = 3.4 Hz, 3-H), 3.30 (dd, *J* = 16.5, 3.1 Hz, 8-H$_{exo}$), 3.01 (s, NMe), 2.74 (s, NMe), 2.65 (ddd, *J* = 16.5, 3.1, 1.2 Hz, 8-H$_{endo}$), 2.47 (dd, *J* = 5.8, 5.5 Hz, 1-H), 2.37 (dddd, *J* = 9.8, 6.1, 5.5, 1.2 Hz, 11-H$_{exo}$), 2.21 (dddd, *J* = 6.1, 5.8, 3.1, 3.1 Hz, 9-H), 1.83 (d, *J* = 9.8 Hz, 11-H$_{endo}$), 1.81 (s, 6-Me), 1.33 (s, 10-Me$_{exo}$), 0.56 (s, 10-Me$_{endo}$). – ^{13}C{^{1}H} NMR (126 MHz, CD_2Cl_2): δ = 163.0 (C-2), 148.3 (C-6), 121.9 (C-7), 116.8 (br., C-5), 108.0 (br., C-3), 53.2 (C-1), 40.6 (C-9), 39.3 (C-10), 39.3 (NMe), 38.4 (NMe), 31.7 (C-8), 31.1 (C-11), 26.2 (10-Me$_{exo}$), 24.2 (6-Me), 21.2 (10-Me$_{endo}$). – ^{11}B{^{1}H} NMR (160 MHz, CD_2Cl_2): δ = 34. – MS: *m*/*z* (%) = 618 (6) [M^+], 574 (4) [M^+ – NMe_2], 390 (100) [M^+ – $C_{13}H_{17}BNMe_2$], 229 (57) [$C_{13}H_{18}BNMe_2^+$]. – $C_{30}H_{46}B_2Cl_2N_2Zr$ (618.5): calcd. C 58.26, H 7.50, N 4.53; found C 58.32, H 7.47, N 4.67.

***exo*,*exo*-ZrCl$_2$(C$_{13}$H$_{17}$BOMe)$_2$ (8b):** A suspension of $ZrCl_4$ (116 mg, 0.50 mmol) in diethyl ether (3 mL) was cooled to –50 °C. Li(**1b**) (255 mg, containing a known amount of THF, 0.98 mmol) in diethyl ether (3 mL) was then added dropwise through a cannula. The mixture was allowed to warm to room temperature and stirring was continued for 72 h. Filtration of the red-orange suspension through a frit covered with kieselguhr and concentration of the filtrate in vacuo left an orange solid. Trituration with hot toluene and filtration gave a clear solution, from which **8b** (60 mg, 20%) could be obtained at –30 °C as an impure orange powder; soluble in benzene, diethyl ether, and CH_2Cl_2. – ^{1}H NMR (500 MHz, CD_2Cl_2): δ = 5.80 (d, *J* = 3.4 Hz, 5-H), 4.77 (d, *J* = 3.4 Hz, 3-H), 3.77 (s, OMe), 3.26 (dd, *J* = 16.5, 2.8 Hz, 8-H$_{exo}$), 2.69 (ddd, *J* = 16.5, 2.8, 1.2 Hz, 8-H$_{endo}$), 2.55 (dd, *J* = 5.5, 5.5 Hz, 1-H), 2.49 (dddd, *J* = 10.1, 6.1, 5.5, 1.2 Hz, 11-H$_{exo}$), 2.23 (dddd, *J* = 6.1, 5.8, 3.1, 2.8 Hz, 9-H), 1.97 (s, 6-Me), 1.75 (d, *J* = 10.1 Hz, 11-H$_{endo}$), 1.35 (s, 10-Me$_{exo}$), 0.55 (s, 10-Me$_{endo}$). – ^{13}C{^{1}H} NMR (126 MHz, CD_2Cl_2): δ = 167.7 (C-2), 153.7 (C-6), 125.9 (C-7), 119.9 (br., C-5), 107.1 (br., C-3), 53.4 (C-1), 52.8 (OMe), 40.2 (C-9), 39.0 (C-10), 32.4 (C-8), 32.0 (C-11), 26.1 (10-Me$_{exo}$), 24.6 (6-Me), 21.2 (10-Me$_{endo}$). – ^{11}B{^{1}H} NMR (160 MHz, CD_2Cl_2): δ = 38. – $C_{28}H_{40}B_2Cl_2O_2Zr$ (592.4): calcd. C 56.77, H 6.81; found C 56.69, H 6.73.

***exo*,*exo*-ZrCl$_2$(C$_{13}$H$_{17}$BMe)$_2$ (8c):** A suspension of $ZrCl_4$ (232 mg, 1.00 mmol) in diethyl ether (3 mL) was cooled to –60 °C. Li(**1c**) (416 mg, 2.02 mmol) in diethyl ether (6 mL) was then added dropwise through a cannula. The mixture was allowed to warm to room temperature and stirring was continued for one week. Filtration of the red-orange suspension through a frit covered with kieselguhr and concentration of the filtrate in vacuo left **8c** (560 mg, 100%) as an impure orange powder; moderately soluble in hexane, soluble in benzene, diethyl ether, THF, and CH_2Cl_2. – ^{1}H NMR (500 MHz, CD_2Cl_2): δ = 6.42 (d, *J* = 2.7 Hz, 5-H), 5.47 (d, *J* = 2.7 Hz, 3-H), 3.25 (dd, *J* = 17.1, 3.1 Hz, 8-H$_{exo}$), 2.68 (ddd, *J* = 17.1, 2.8, 1.2 Hz, 8-H$_{endo}$), 2.58 (dd, *J* = 5.8, 5.5 Hz, 1-H), 2.49 (dddd, *J* = 10.1, 6.1, 5.5, 1.2 Hz, 11-H$_{exo}$), 2.24 (dddd, *J* = 6.1, 5.8, 3.1, 2.8 Hz, 9-H), 1.93 (s, 6-Me), 1.69 (d, *J* = 10.1 Hz, 11-H$_{endo}$), 1.35 (s, 10-Me$_{exo}$), 0.92 (s, BMe), 0.48 (s, 10-Me$_{endo}$). – ^{13}C{^{1}H} NMR (126 MHz, CD_2Cl_2): δ = 165.2 (C-2), 150.8 (C-6), 133.2 (br., C-5), 131.3 (C-7), 124.9 (br., C-3), 53.0 (C-1), 40.2 (C-9), 39.0 (C-10), 32.8 (C-8), 31.6 (C-11), 26.1 (10-Me$_{exo}$), 23.6 (6-Me), 21.1 (10-Me$_{endo}$), 6.9 (br., BMe). – ^{11}B{^{1}H} NMR (160 MHz, CD_2Cl_2): δ = 43. – MS: *m*/*z* (%): 560 (5) [M^+], 361 (70) [M^+ – $C_{13}H_{17}BMe$].

***exo*,*exo*-ZrMe$_2$(C$_{13}$H$_{17}$BNMe$_2$)$_2$ (9):** A solution of LiMe (0.80 mL, 1.6 M in diethyl ether, 1.28 mmol) was added to **8a** (380 mg, 0.61 mmol) in diethyl ether (20 mL). After the addition of 2 equivalents, the mixture had turned red. Stirring was continued for 5 min. Filtration and removal of the solvent in vacuo gave **9** (331 mg, 93%) as a red oil. Crystallization from THF at –30 °C gave small red crystals (60%); m.p. (dec.) 160 °C; slightly soluble in hexane, soluble in benzene, diethyl ether, and THF, very soluble in CH_2Cl_2. – ^{1}H NMR (500 MHz, CD_2Cl_2): δ = 5.20 (d, *J* = 3.4 Hz, 5-H), 4.74 (d, *J* = 3.4 Hz, 3-H), 2.97 (dd, *J* = 15.9, 3.1 Hz, 8-H$_{exo}$), 2.79 (ddd, *J* = 15.9, 2.7, 1.2 Hz, 8-H$_{endo}$), 2.67 (br. s, NMe_2), 2.41 (dd, *J* = 5.8, 5.5 Hz, 1-H), 2.33 (dddd, *J* = 9.8, 6.1, 5.5, 1.2 Hz, 11-H$_{exo}$), 2.23 (dddd, *J* = 6.1, 5.8, 3.1, 2.7 Hz, 9-H), 1.96 (s, 6-Me), 1.35 (s, 10-Me$_{exo}$), 1.22 (d, *J* = 9.8 Hz, 11-H$_{endo}$), 0.67 (s, 10-Me$_{endo}$), –0.42 (s, ZrMe). – ^{13}C{^{1}H} NMR (126 MHz, CD_2Cl_2): δ = 156.3 (C-2), 146.0 (C-6), 116.3 (br., C-5), 111.9 (C-7), 107.9 (br., C-3), 52.8 (C-1), 42.9 (ZrMe), 40.7 (C-9), 39.9 (C-10), 38.7 (NMe), 38.7 (NMe), 31.3 (C-8), 30.3 (C-11), 26.3 (10-Me$_{exo}$), 23.9 (6-Me), 21.0 (10-Me$_{endo}$). – ^{11}B{^{1}H} NMR (160 MHz, CD_2Cl_2): δ = 32. – MS: *m*/*z* (%) = 348 (1) [M^+ – $C_{13}H_{17}BNMe_2$], 333 (1) [348$^+$ – Me]. – $C_{32}H_{52}B_2N_2Zr$ (577.6): calcd. C 66.54, H 9.07, N 4.85; found C 66.77, H 9.30, N 4.81.

X-ray Structure Determination of *exo*-4a: $C_{25}H_{38}BFeN$; formula mass 419.25 g·mol^{-1}, orthorhombic space group $P2_12_12_1$ (no. 19); *a* = 7.974(4), *b* = 16.783(4), *c* = 17.128(7) Å, *V* = 2292(3) Å^3, *Z* = 4, $d_{calcd.}$ = 1.21 g·cm^{-3}, μ_{lin} = 0.67 mm^{-1}. Enraf–Nonius CAD4 diffractometer; Mo-K_α radiation (λ = 0.71073 Å); graphite monochromator. Data collection at 223 K on a red crystal of dimensions ca. 0.50 × 0.40 × 0.35 mm^3 using ω/2θ scans in the diffraction range 3 < θ < 26° yielded 4798 reflections, which were corrected for Lorentz and polarization effects; no absorption correction was applied. After merging symmetry-equivalent data, 4478 unique reflections remained for structure solution by direct methods[26] and subsequent Fourier difference syntheses. Least-squares refinement on structure factors[27] was performed with anisotropic displacement parameters for all non-hydrogen atoms and with isotropic displacement parameters for all hydrogen atoms. Convergence was obtained for 405 variables, 3811 unique observations with $I > 1.0\ \sigma(I)$ at $R = 0.058$, $R_w = 0.050$, GoF = 1.079. A final difference Fourier map showed fluctuations of less than 0.50 e·Å^{-3}.[28]

X-ray Structure Determination of 8a: $C_{30}H_{46}B_2Cl_2N_2Zr$; formula mass 618.46 g·mol^{-1}, orthorhombic space group $P2_12_12_1$ (no. 19); *a* = 9.162(3), *b* = 17.777(3), *c* = 18.841(5) Å, *V* = 3069(1) Å^3, *Z* = 4, $d_{calcd.}$ = 1.34 g·cm^{-3}, μ_{lin} = 0.55 mm^{-1}. Enraf–Nonius CAD4 diffractometer; Mo-K_α radiation (λ = 0.71073 Å); graphite monochromator. Data collection at 203 K on a blue translucent platelet of dimensions ca. 0.50 × 0.50 × 0.20 mm^3 using ω/2θ scans in the diffraction range 2 < θ < 28° yielded 9358 reflections. The data were corrected for Lorentz and polarization effects, and an empirical absorption correction based on azimuthal scans[29] (min. rel. trans. 0.861, max. rel. trans. 1.000) was applied. After merging symmetry-equivalent data, 6869 unique reflections remained for structure solution by direct methods[26] and subsequent Fourier difference syntheses. Least-squares refinement on structure factors[27] was performed with anisotropic displacement parameters for all non-hydrogen atoms and with hydrogen atoms in calculated positions [C–H = 0.98 Å, U_{iso}(H) = 1.3 U_{eq}(C)]. Convergence was obtained for 334 variables, 6228 unique observations with $I > 1.0\ \sigma(I)$ at $R = 0.040$, $R_w = 0.041$, GoF = 1.095. A final difference Fourier map showed fluctuations of less than 0.62 eÅ^{-3}.[28]

Acknowledgments

This work was generously supported by the Deutsche Forschungsgemeinschaft and the Fonds der Chemischen Industrie.

[1] [1a] G. E. Herberich, U. Englert, B. Ganter, M. Pons, R. Wang, *Organometallics* **1999**, *18*, 3406–3413. – [1b] G. E. Herberich, B. Ganter, M. Pons, *Organometallics* **1998**, *17*, 1254–1256.
[2] R. L. Halterman in *Metallocenes*, vols. 1 and 2 (Eds.: A. Togni, R. L. Halterman), Wiley-VCH, Weinheim, Germany, **1998**, 456–544.
[3] [3a] C. Janiak in *Metallocenes*, vol. 2 (Eds.: A. Togni, R. L. Halterman), Wiley-VCH, Weinheim, Germany, **1998**, 547–623. – [3b] *Ziegler Catalysts* (Eds.: G. Fink, R. Mülhaupt, H.-H. Brintzinger), Springer-Verlag, Berlin, **1995**. – [3c] Y. Okamoto, T. Nakano, *Chem. Rev.* **1994**, *94*, 349–372.
[4] [4a] A. H. Hoveyda, J. P. Morken in *Metallocenes*, vol. 2 (Eds.: A. Togni, R. L. Halterman), Wiley-VCH, Weinheim, Germany, **1998**, 625–683. – [4b] A. H. Hoveyda, J. P. Morken, *Angew. Chem.* **1996**, *108*, 1378–1401; *Angew. Chem. Int. Ed. Engl.* **1996**, *35*, 1262–1284.
[5] [5a] *Catalytic Asymmetric Synthesis* (Ed.: I. Ojima), VCH, Weinheim, Germany, **1993**. – [5b] *Handbook of Enantioselective Catalysis with Transition Metal Compounds* (Eds.: H. Brunner, W. Zettlmeier), VCH, Weinheim, Germany, **1993**.
[6] [6a] A. Togni in *Metallocenes*, vol. 2 (Eds.: A. Togni, R. L. Halterman), Wiley-VCH, Weinheim, Germany, **1998**, 685–721. – [6b] A. Togni, *Angew. Chem.* **1996**, *108*, 1581–1583; *Angew. Chem. Int. Ed. Engl.* **1996**, *35*, 1475–1477. – [6c] *Ferrocenes* (Eds.: A. Togni, T. Hayashi), VCH, Weinheim, Germany, **1995**.
[7] R. L. Halterman, *Chem. Rev.* **1992**, *92*, 965–994.
[8] [8a] L. A. Paquette, K. J. Moriarty, J. A. McKinney, R. D. Rogers, *Organometallics* **1989**, *8*, 1707–1713. – [8b] R. L. Halterman, K. P. C. Vollhardt, *Tetrahedron Lett.* **1986**, *27*, 1461–1462.
[9] L. A. Paquette, M. Gugelchuk, M. L. McLaughlin, *J. Org. Chem.* **1987**, *52*, 4732–4740.
[10] G. E. Herberich, U. Englert, B. Ganter, C. Lamertz, *Organometallics* **1996**, *15*, 5236–5241.
[11] D. Catheline, D. Astruc, *Organometallics* **1984**, *3*, 1094–1100.
[12] G. E. Herberich, B. Schmidt, U. Englert, *Organometallics* **1995**, *14*, 471–480.
[13] G. E. Herberich, A. Gaffke, H. J. Eckenrath, *Organometallics* **1998**, *17*, 5931–5932.
[14] G. E. Herberich, U. J. Jansen, *Organometallics* **1995**, *14*, 834–841.
[15] R. H. Reimann, E. Singleton, *J. Chem. Soc.* **1975**, 808–813.
[16] A. J. Ashe III, J. W. Kampf, C. Müller, M. Schneider, *Organometallics* **1996**, *15*, 387–393.
[17] For the 1,2-dihydroborinine $C_5H_6BNiPr_2$, pK_a(DMSO) = 17.7; for the 1,4-isomer pK_a(DMSO) = 17.8, see ref.[16] Methyl groups attached to sp^2 carbon atoms in cyclopentadienes increase the pK_a(DMSO) by ca. 2.0 units: F. G. Bordwell, M. J. Bausch, *J. Am. Chem. Soc.* **1983**, *105*, 6188–6189.
[18] [18a] E. W. Abel, G. Wilkinson, *J. Chem. Soc.* **1959**, 1501–1505. – [18b] M. H. Quick, R. J. Angelici, *Inorg. Synth.* **1990**, *28*, 156.
[19] M. Pons, Dissertation, Technische Hochschule Aachen, Aachen, Germany, **1999**, p. 34.
[20] G. E. Herberich, U. Englert, A. Schmitz, *Organometallics* **1997**, *16*, 3751–3757.
[21] [21a] G. C. Bazan, G. Rodriguez, A. J. Ashe III, S. Al-Ahmad, C. Müller, *J. Am. Chem. Soc.* **1996**, *118*, 2291–2292. – [21b] G. C. Bazan, G. Rodriguez, A. J. Ashe III, S. Al-Ahmad, J. W. Kampf, *Organometallics* **1997**, *16*, 2492–2494. – [21c] J. S. Rogers, G. C. Bazan, C. K. Sperry, *J. Am. Chem. Soc.* **1997**, *119*, 9305–9306. – [21d] R. W. Barnhart, G. C. Bazan, T. Mourey, *J. Am. Chem. Soc.* **1998**, *120*, 1082–1083.
[22] [22a] A. J. Ashe III, S. Al-Ahmad, X. Fang, J. W. Kampf, *J. Am. Chem. Soc.* **1998**, *120*, 3883–3888.[22b] J. S. Rogers, R. J. Lachicotte, G. C. Bazan, *J. Am. Chem. Soc.* **1999**, *121*, 1288.
[23] L. A. Paquette, K. J. Moriarty, R. D. Rogers, *Organometallics* **1989**, *8*, 1506–1511.
[24] A. L. Spek, *Acta Crystallogr.* **1990**, *A46*, C34.
[25] The slip distortion is defined as the distance between the geometric center of the C_5B ring and the projection of the metal atom onto the ring plane.
[26] G. M. Sheldrick, *SHELXS-86*, *Program for Crystal Structure Solution*, University of Göttingen, Göttingen, Germany, **1986**.
[27] B. A. Frenz, Enraf–Nonius SDP Version 5.0, Delft, The Netherlands, **1989**, and local programs.
[28] Crystallographic data (excluding structure factors) for the structures reported in this paper have been deposited with the Cambridge Crystallographic Data Centre as supplementary publication nos. CCDC-134091 (*exo*-**4a**) and CCDC-134092 (**8a**). Copies of the data can be obtained free of charge on application to the CCDC, 12 Union Road, Cambridge CB2 1EZ, U.K. [Fax: (internat.) +44 (0)1223 336033; E-mail: deposit@ccdc.cam.ac.uk].
[29] A. C. T. North, D. C. Phillips, F. S. Mathews, *Acta Crystallogr.* **1968**, *A24,* 351–359.

Received September 6, 1999
[I99317]

Standard Molar Enthalpies of Formation of Mg and Ca Alkoxides

Teresa Barreira[a] and João Paulo Leal*[a]

Keywords: Thermochemistry / Alkaline-Earth Alkoxides / Enthalpy of Formation / Calcium / Magnesium

The enthalpies of formation of some alkaline-earth alkoxides were determined by reaction-solution calorimetry (Δ_fH^o[Mg(OMe)$_2$] = –792.6±1.2 kJ/mol; Δ_fH^o[Mg(OEt)$_2$] = –847.9±2.7 kJ/mol; Δ_fH^o[Ca(OMe)$_2$] = –890.8±6.4 kJ/mol; Δ_fH^o[Ca(OEt)$_2$] = –924.5±2.6 kJ/mol; Δ_fH^o[Ca(OBu)$_2$] = –989.8±5.4 kJ/mol) and allowed us to extend a previously developed model for predicting the enthalpies of formation of Be, Sr and Ba alkoxides.

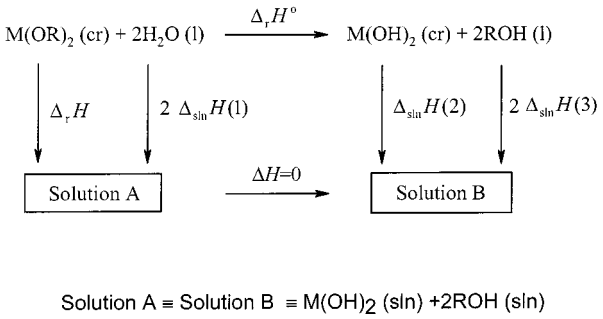
Introduction

Alkaline and alkaline-earth metal alkoxide compounds are of major importance in synthetic chemistry.[1] However, thermochemical data for these substances is rather scarce. Previous results obtained for sodium and lithium alkoxides[2,3] show that there exists a linear relation between the enthalpies of formation of the alkoxides and those of the corresponding alcohols for short-chain unbranched alkoxides. A model based on the alkoxide energy calculations and a simple electrostatic model was also developed, which enabled us to predict unknown alkali metal alkoxide enthalpies of formation.

In this paper we extend the previously developed model to alkaline-earth alkoxides and use it for the prediction of some unmeasured Be, Sr and Ba alkoxides.

Results and Discussion

The enthalpies of formation of magnesium and calcium alkoxides were calculated according to Scheme 1 (reaction with water, used for all the compounds studied in this paper) or Scheme 2 [reaction with 0.1 M HCl, used for Ca(OEt)$_2$]. In these schemes, Δ_rH^o represents the reaction enthalpy with all the compounds in their standard state, Δ_rH the experimentally measured reaction enthalpy, $\Delta_{sln}H(2)$ the dissolution enthalpy for stoichiometric amounts of M(OH)$_2$ in H_2O, $\Delta_{sln}H(3)$ the dissolution enthalpy of the alcohol in H_2O + M(OH)$_2$, $\Delta_{sln}H(5)$ the dissolution of $CaCl_2$ in 0.1 M HCl, $\Delta_{sln}H(6)$ the dissolution of ethanol in a 0.1 M HCl + $CaCl_2$ solution, and $\Delta_{sln}H(7)$ the dissolution of water in 0.1 M HCl solution. $\Delta_{sln}H(1)$ (dissolution of water in water) and $\Delta_{sln}H(4)$ (dissolution of 0.1 M HCl in 0.1 M HCl) are obviously zero.



Scheme 1. Reaction with water

As the concentrations of M(OH)$_2$ in solution were always very small [about 1 mol M(OH)$_2$ in 4 × 10^5 mol water] an infinite dilution can be assumed and $\Delta_{sln}H(2)$ can be calculated as –2.30 kJ/mol for magnesium hydroxide and –16.73 kJ/mol for the calcium analogue using the data in Table 1.[4,5] In the cases of ethanol and methanol, $\Delta_{sln}H(3)$ values were calculated from the differences between the enthalpies of formation of the pure alcohols and the respective enthalpies of formation at infinite dilution in water (Table 2 and Equation 1 and 2). $\Delta_{sln}H(3)$ for butanol was taken as −7.39 ± 0.59 kJ/mol.[3]

$$\Delta_{sln}H(3)\ (MeOH) = \Delta_fH^o\ (CH_3OH,\infty\ H_2O) - \Delta_fH^o\ (CH_3OH,l) = -7.3 \pm 0.4\ kJ/mol \quad (1)$$

$$\Delta_{sln}H(3)\ (EtOH) = \Delta_fH^o\ (C_2H_5OH,\infty\ H_2O) - \Delta_fH^o\ (C_2H_5OH,\ l) = -10.7 \pm 0.6\ kJ/mol \quad (2)$$

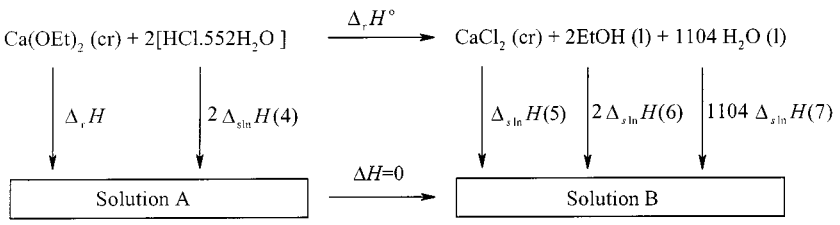
The fact that the above $\Delta_{sln}H(3)$ values were obtained in water and not in H_2O + M(OH)$_2$ solutions should not be relevant due to the low concentrations of M(OH)$_2$ in solution. This is in keeping with the values in a previous publication[3] where the dissolution of butanol in water, H_2O + LiOH and H_2O + NaOH was measured, and showed no difference within experimental error.

The enthalpies of formation of aqueous 0.1 M HCl and crystalline calcium chloride are known (Table 1). The dissolution of calcium chloride in 0.1 M HCl and of ethanol in $CaCl_2$ + 0.1 M HCl solution was measured (Table 2). The dissolution of water in the solvent is negligible (smaller than the detection limit of the apparatus) and even when multiplied by 1104 yields a minor contribution to the final Δ_rH^o value (smaller than the experimental error). Therefore, $\Delta_{sln}H(7)$ was neglected.

Schemes 1 and 2 lead to Equations 3 and 4, that allow the calculation of the enthalpies of formation of the metal alkoxides shown in Table 3.

[a] Departamento de Química, Instituto Tecnológico e Nuclear, 2686–953 Sacavém, Portugal
Fax: (internat.) + 351-1/994-1455
E-mail: jpleal@itn1.itn.pt

 © WILEY-VCH Verlag GmbH, D-69451 Weinheim, 2000 1434−1948/00/0505−0987 $ 17.50+.50/0



Solution A ≡ Solution B ≡ $CaCl_2$ (sln) +2EtOH (sln) + n ($HCl \cdot 552H_2O$)

Scheme 2. Reaction with 0.1 M HCl

Table 1. Auxiliary data (T = 298.15 K)

Compound	$\Delta_f H^o$ (kJ/mol)	Ref.
H_2O, l	–285.830	4
CH_3OH, l	–239.1±0.3	5
$CH_3OH \cdot \infty H_2O$	–246.4±0.3	5
C_2H_5OH, l	–277.5±0.4	5
$C_2H_5OH \cdot \infty H_2O$	–288.2±0.4	5
C_4H_9OH, l	–327.3±0.4	5
$Mg(OH)_2$, cr	–924.54	4
$Mg(OH)_2$, ai	–926.84	4
Mg, g	147.70	4
$Ca(OH)_2$, cr	–986.09	4
$Ca(OH)_2$, ai	–1002.82	4
Ca, g	178.2	4
$CaCl_2$, cr	–795.8	4
$HCl \cdot 552\ H_2O$	–166.596	4

Table 2. Dissolution enthalpies (T = 298.15 K)

Compound	$\Delta_{sln}H(3)$ (kJ/mol)[a]	$\Delta_{sln}H(6)$ (kJ/mol)[b]	$\Delta_{sln}H(5)$ (kJ/mol)[c]
CH_3OH	–7.3±0.4[d]	–	–
C_2H_5OH	–10.7±0.6[d]	–9.4±1.6	–
C_4H_9OH	–7.39±0.59[e]	–	–
$CaCl_2$	–	–	–81.8±1.1

[a] Dissolution in water. – [b] Dissolution in 0.1 M HCl + $CaCl_2$. – [c] Dissolution in 0.1 M HCl. – [d] Calculated from data in Table 1. – [e] Measured in ref.[3]

Table 3. Reaction enthalpies, and standard enthalpies of formation of magnesium and calcium alkoxides (T = 298.15 K).

Alkoxide	$\Delta_r H$[a] (kJ/mol)	$\Delta_f H^o$[$M(OR)_2$,cr] (kJ/mol)	$\Delta_r H^o$[a] (kJ/mol)
$Mg(OMe)_2$	–55.4±0.7	–792.6±1.2	–38.5±1.1
$Mg(OEt)_2$	–83.7±2.3	–847.9±2.7	–60.0±2.6
$Ca(OMe)_2$	–33.2±6.3	–890.8±6.4	–1.9±6.4
$Ca(OEt)_2$	–83.1±2.2	–924.5±2.6	–45.0±2.5
–	–192.1±9.1[b]	–926.1±9.7	–
$Ca(OBu)_2$	–110.7±5.2	–989.8±5.4	–79.2±5.3

[a] Reaction with water unless stated otherwise. – [b] Reaction with 0.1 M HCl.

$$\Delta_f H^o [M(OR)_2] = \Delta_f H^o [M(OH)_2,cr] + 2\Delta_f H^o [ROH, l] - 2\Delta_f H^o [H_2O, l] - \Delta_r H + \Delta_{sln} H(2) + 2\Delta_{sln} H(3) \quad (3)$$

$$\Delta_f H^o [Ca(OEt)_2, cr] = \Delta_f H^o [CaCl_2,cr] + 2\Delta_f H^o [EtOH, 1] - 2\Delta_f H^o [HCl \cdot 552H_2O] - \Delta_r H + \Delta_{sln} H(5) + 2\Delta_{sln} H(6) + 1104\ \Delta_{sln} H(7) \quad (4)$$

As a first comment we note the good agreement between the values for the enthalpy of formation of $Ca(OEt)_2$ obtained by the two different methods referred to above. Since the reaction with HCl was studied mainly to test the consistency of the results, in all subsequent calculations the values derived from the reactions with water will be used.

A plot of the enthalpies of formation of the crystalline alkoxides against the enthalpies of formation of the corresponding alcohols in their standard reference states is shown in Figure 1. This type of plot has been used before for many compound families,[6] including sodium[2] and lithium alkoxides,[3] and it is useful to assess the reliability of the data. For calcium alkoxides, and using the three points for R = Me, Et and Bu, a fairly linear correlation (r = 0.9922; uncertainty intervals are standard deviations) (Equation 5) is obtained. The slope defined by the two points for Mg alkoxides (R = Me and Et) is 1.44.

$$\Delta_f H^o (Ca(OR)_2) = (1.13 \pm 0.14)\ \Delta_f H^o (ROH, l) - (617 \pm 39) \quad (5)$$

To understand the plot of Figure 1 (or Equation 5) we can use Equation 6, where $\Delta_r H^o$ is simply defined in terms of the standard enthalpies of formation of reactants and products. If a linear correlation between $\Delta_f H^o$ [$M(OR)_2$,cr] and $\Delta_f H^o$ (ROH,l) is observed, this means that $\Delta_r H^o$ is constant for several R. On the other hand, as evidenced by Equation 6, the slope of the line should be close to 2 (the number of alkoxide ligands bound to M). However, this is not observed either for Mg or Ca compounds, nor is $\Delta_r H^o$ constant (Table 3) in Equation 5. Similar behaviour had been noticed for some K, Rb and Cs alkoxides.[7] This type of plot should work well only if the crystal structure has little effect on the energetics. Since none of the crystal structures are known, and since changing the anions and/or the cations is very likely to change the crystal structure, Figure 1 should be used mainly as a visual aid to find trends in the values.

$$\Delta_f H^o [M(OR)_2, cr] = 2\Delta_f H^o [ROH, l] + \Delta_f H^o [M(OH)_2, cr] - 2\Delta_f H^o [H_2O, l] - \Delta_r H^o \quad (6)$$

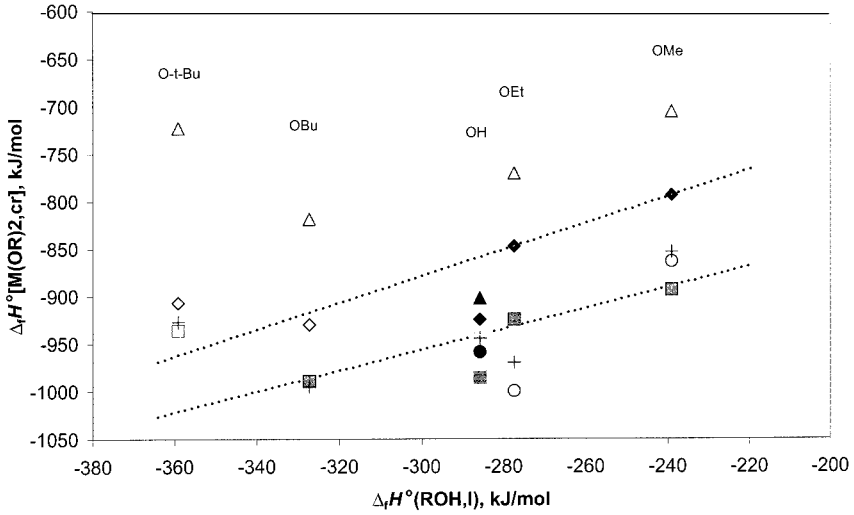
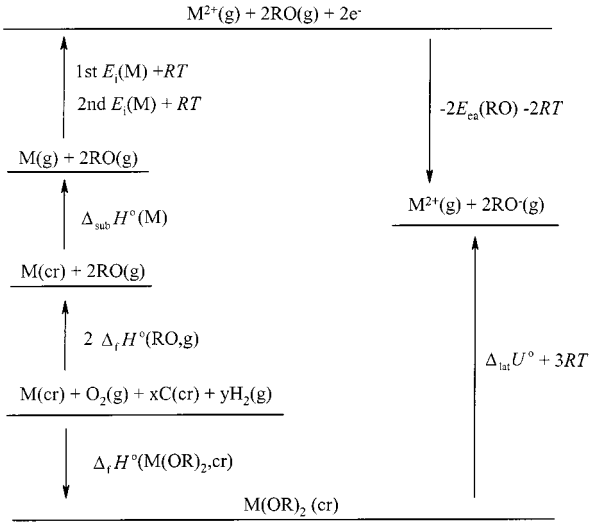


Figure 1. Enthalpies of formation of alkaline-earth metal alkoxides versus the enthalpies of formation of the corresponding alcohols (experimental data: filled symbols; estimated data: empty symbols; Be: triangle; Mg: diamond; Ca: square; Sr: circle; Ba: cross); the lower line is a linear regression using the three experimental values for Ca, and the upper line is simply a line passing through the two experimental Mg values, which are included mainly as a visual guide

Table 4. Lattice energies of magnesium and calcium alkoxides

Alkoxide $M(OR)_2$[a]	$\Delta_f H°(RO_2,g)$ (kJ/mol)[c]	EA(OR) (kJ/mol)[d]	$\Delta_{lat}U°[M(OR)_2]$ (kJ/mol)
$Mg(OH)_2$[b]	39±4	176.4±1.0	2990.8±8.2
$Mg(OMe)_2$	18±4	151.4±2.1	2866.9±9.1
$Mg(OEt)_2$	–17±4	166.5±3.2	2822±10
$Ca(OH)_2$[b]	39±4	176.4±1.0	2629.8±8.2
$Ca(OMe)_2$	18±4	151.4±2.1	2542±11
$Ca(OEt)_2$	–17±4	166.5±3.2	2476±10
$Ca(OBu)_2$	–63±4	171±14	2440±30

[a] $\Delta_{sub}H°(Mg)$ = 147.70 kJ/mol,[4] $\Delta_{sub}H°(Ca)$ = 178.2 kJ/mol,[4] 1st E_i (Mg) = 743.935,[4] 2nd E_i (Mg) = 1456.869,[4] 1st E_i (Ca) = 596.05,[4] 2nd E_i (Ca) = 1151.65.[4] – [b] $\Delta_f H°[M(OH)_2]$ taken from Table 1. – [c] Taken from D. F. McMillen, D. M. Golden, *Ann. Rev. Phys. Chem.* **1982**, *33*, 493. – [d] Taken from S. G. Lias, J. E. Bartmess, J. F. Liebman, J. L. Holmes, R. D. Levin, W. G. Mallard, *J. Phys. Chem.*, **1988**, *17*, Suppl. no. 1.



Scheme 3

Another way of discussing the data in Table 4 involves the calculation of lattice energies ($\Delta_{lat}U°$) of magnesium and calcium alkoxides.

These values, displayed in Table 4, were obtained from the standard enthalpies of formation of the alkoxides and from literature data, according to Scheme 3. The high ionic character of the alkoxides is indicated by their lattice energies, which are under 200 kJ/mol lower than the lattice energies of the corresponding hydroxides.

Let us assume a simple ionic model and the Kapustinskii approximation represented by Equation 7.[8] In this expression, v represents the number of ions in the molecule, Z_+ and Z_- the charges of the cation and anion and r_+ and r_- the respective radii in pm. As the ionic radii of Mg^{2+} and Ca^{2+} are known,[9] the ionic radii of the alkoxide anions can be derived from the data in Table 4. The results are shown in Table 5, which also includes early data for alkaline-earth and alkali metal alkoxides [2,3,7] and estimates of the radii of the alkoxide ions in some alkaline-earth metal alkoxides not studied in this work.

$$\Delta_{lat}U° = \frac{1.079\times10^5 . v . Z_+ Z_-}{r_+ + r_-} \quad (7)$$

The radii calculated by the above procedure are called "thermochemical radii" and have no special physical meaning, apart from reproducing lattice energies when introduced in Equation 7. It is to be noted that the values of the *n*-butoxy anion always have a greater error than the others. This is mainly due to the huge error in the electroaffinity of the butoxy ion.

Using these estimated radii and Scheme 3, it is possible to calculate the enthalpies of formation for some unknown alkaline-earth metal alkoxides (Table 6). The error bars are

Table 5. Thermochemical radii[a] calculated or estimated[b] for the alkoxide ions in alkali and alkaline-earth metal alkoxides[c]

RO^-	$Be(OR)_2$	LiOR[e]	$Mg(OR)_2$	NaOR[f]	$Ca(OR)_2$	KOR[g]	$Sr(OR)_2$	RbOR[g]	$Ba(OR)_2$	CsOR[g]
HO^-	120.2±1.1[d]	119.8±1.3	130.5±1.2	127.4±1.5	132.2±1.3	121±3	130.4±1.3[d]	118±3	129.7±1.4[d]	116±3
MeO^-	(130±2)	130.1±1.5	**139.8±1.2**	141.8±1.9	**140.6±1.5**	138±4	(140±6)	131±4	(140±6)	131±4
EtO^-	(132±2)	132.4±1.6	**143.4±1.3**	145.2±2.0	**147.5±1.5**	134±4	(136±6)	127±3	(138±6)	129±4
nBuO$^-$	(135±4)	135.0±3.6	(145±5)	144.9±4.8	**151.3±3.4**	144±10			(148±12)	139±10
tBuO$^-$	(146±3)	146.1±2.1	(154±3)	154.2±3.0	(167±8)	160±6			(170±8)	160±6

[a] Thermochemical radii studied in the present paper are in bold. – [b] Estimated thermochemical radii in parentheses[c] $r_+(Li^+)$ = 90 ±1 pm, $r_+(Na^+)$ = 116 ±1 pm, $r_+(K^+)$ = 152 ±1 pm, $r_+(Rb^+)$ = 166 ±1 pm, $r_+(Cs^+)$ = 181 ±1 pm, $r_+(Be^{2+})$ = 59 ±1 pm, $r_+(Mg^{2+})$ = 86 ±1 pm, $r_+(Ca^{2+})$ = 114 ±1 pm, $r_+(Sr^{2+})$ = 132±1 pm, $r_+(Ba^{2+})$ = 149±1 pm.[9] – [d] Δ_fH^o[Be(OH)$_2$,cr] = –902.5 kJ/mol, Δ_fH^o[Sr(OH)$_2$,cr] = –959.0 kJ/mol, Δ_fH^o[Ba(OH)$_2$,cr] = –944.7 kJ/mol, $\Delta_fH^o(Be^{2+},g)$ = 2993.23 kJ/mol, $\Delta_fH^o(Sr^{2+},g)$ = 1790.54 kJ/mol, $\Delta_fH^o(Ba^{2+},g)$ = 1660.38 kJ/mol.[4] – [e] Calculated from data in ref.[3] – [f] Calculated from data in ref.[2] – [g] From ref.[7]

large (50 kJ/mol excluding the butoxides and 90 kJ/mol for the butoxides) when compared with those for the alkoxides measured on this paper (2–6 kJ/mol). The main reason is that a small error in the radii will be amplified in the lattice energy values (since $\Delta_{lat}U^o$ is a big value) and therefore in the values of the enthalpy of formation.

Table 6. Lattice energies and enthalpies of formation of alkaline–earth alkoxides; estimated values in parentheses

Alkoxide	$\Delta_{lat}U^o$ kJ/mol	Δ_fH^o[M(OR)$_2$] kJ/mol
$Be(OMe)_2$	(3425±40)	(–706±41)
$Be(OEt)_2$	(3390±40)	(–771±41)
$Be(OBu)_2$	(3337±71)	(–819±77)
$Be(Ot Bu)_2$[a]	(3158±49)	(–723±51)
$Mg(OMe)_2$	2866.9±9.1	–792.6±1.2
$Mg(OEt)_2$	2822±10	–847.9±2.7
$Mg(OBu)_2$	(2803±62)	(–930±68)
$Mg(Ot Bu)_2$[a]	(2698±36)	(–907±39)
$Ca(OMe)_2$	2542±11	–890.8±6.4
$Ca(OEt)_2$	2476±10	–924.5±2.6
$Ca(OBu)_2$	2440±30	–989.8±5.4
$Ca(Ot Bu)_2$[a]	(2304±66)	(–936±68)
$Sr(OMe)_2$	(2380±53)	(–864±54)
$Sr(OEt)_2$	(2416±55)	(–1000±56)
$Sr(OBu)_2$	–	–
$Sr(Ot Bu)_2$[a]	–	–
$Ba(OMe)_2$	(2240±47)	(–854±48)
$Ba(OEt)_2$	(2256±48)	(–970±49)
$Ba(OBu)_2$	(2180±88)	(–995±93)
$Ba(Ot Bu)_2$[a]	(2029±51)	(–927±53)

[a] $\Delta_fH^o(Ot Bu)$ = –91±5 kJ/mol from D. F. McMillen, D. M. Golden, *Ann. Rev. Phys. Chem.* **1982**, *33*, 493; $E_{ea}(Ot Bu)$ = 184.4±5.2 from S. G. Lias, J. E. Bartmess, J. F. Liebman, J. L. Holmes, R. D. Levin, W. G. Mallard, *J. Phys. Chem.* **1988**, *17*, Suppl. no. 1.

Nevertheless, if no other values exist, those can be quite useful. In the future we intend to extend this study to other alkaline-earth metal alkoxides to achieve better data for these compounds.

Knowing the structures would give deep insight into in these kinds of compounds. Despite all efforts, it has not yet been possible to obtain single crystals, and powder studies have yet to be undertaken.

Experimental Section

Materials: Methanol (Merck, 99.8%) and ethanol (Merck, 99.8%) were pre-dried over calcium sulfate, refluxed over activated magnesium and iodine, and finally distilled. Butanol (Sigma, 99.0%) was dried over calcium hydride and distilled. Magnesium (turnings, Sigma) and calcium (granules, Sigma) were used as supplied and stored in an oxygen- and water-free glovebox. Iodine was sublimed twice before use. Pentane was distilled over P_2O_5 and stored in the glovebox over 4 Å molecular sieves.

Physical Measurements: Infrared spectra were determined using a Perkin–Elmer 577 spectrophotometer with samples mounted as Nujol mulls between KBr plates. Elemental analyses were performed on a Perkin–Elmer 240 C (C, H) automatic analyzer or by gravimetric analyses (Mg as magnesium oxide,[10] Ca as calcium oxalate[11]). Iodine was qualitatively analyzed by an energy-dispersive X-ray spectrometer with a primary photon beam produced by a high power rhodium anode X-ray tube (Kevex Delta XRF Analyst System).

Alkoxide Syntheses: The studied alkoxides are moisture sensitive. Therefore, all syntheses were performed inside an oxygen- and water-free (<5 ppm) glovebox. Alcohols were degassed before use. Magnesium alkoxides were prepared by addition of the metal to an excess of alcohol (methanol or ethanol) containing a small amount of sublimed iodine (acting as a catalyst) and stirred for several days inside the glovebox at room temperature. The solution was taken to dryness, washed twice with pentane and dried under high vacuum (10^{-4}–10^{-5} Torr). The calcium alkoxides (methoxy, ethoxy and butoxy) were synthesized in a similar way without adding the catalyst. One of the problems that may occur is the formation of metal hydroxides due to the presence of water, and which are virtually impossible to separate from the alkoxides. Another problem is ensuring that the alkoxides are completely dry, i.e. all the excess alcohol must be removed. IR spectra showed that all the alkoxides used in

Table 7. Elemental analysis of magnesium and calcium alkoxides

Alkoxide	Found %C	%H	%M	Theoretical %C	%H	%M
$Mg(OMe)_2$	27.95	6.77	–	27.90	7.03	–
$Mg(OEt)_2$	39.83	8.51	21.1	41.99	8.81	21.24
$Ca(OMe)_2$	23.21	5.97	–	23.52	5.92	–
$Ca(OEt)_2$	38.23	7.82	31.0	36.90	7.74	30.78
$Ca(OBu)_2$	51.03	9.65	–	51.57	9.74	–

this work were alcohol- and hydroxide-free. Elemental analysis of the alkoxides (C, H, metal) was also performed (metal analysis on only some of them) to assess the purity (Table 7). For the magnesium compounds energy-dispersive X-ray spectrometry was conducted to check if any iodine was incorporated, the result always being negative.

Reaction-Solution Calorimetry: The calorimeter used was specially built for the study of oxygen- and water-sensitive compounds, and the experimental procedure was described in a previous paper.[2] All measurements were made near 298.15 K, and the results are averages of at least four runs. The errors presented are twice the standard deviation of the mean in each case. To determine the enthalpies of formation of the alkoxides, their reactions with water were studied in the calorimeter. As a test for consistency, the reaction of $Ca(OEt)_2$ with a 0.1 M aqueous solution of HCl was also studied.

Acknowledgments

The authors thank Dr. Fátima Araújo (ITN) for energy-dispersive X-ray spectrometry analysis. Financial support from FCT (PRAXIS/2/2.1/QUI/51/94) is gratefully acknowledged.

[1] E.g. A. Streitwieser Jr., C. H. Heathcock, *Introduction to Organic Chemistry* (3rd ed.), Macmillan, New York, **1985**.
[2] J. P. Leal, A. Pires de Matos and J. A. Martinho Simões, *J. Organomet. Chem.*, **1991**, *403*, 1.
[3] J. P. Leal and J. A. Martinho Simões, *J. Organomet. Chem.*, **1993**, *460*, 131.
[4] D. D. Wagman, W. H. Evans, V. B. Parker, R. H. Schumm, I. Halow, S. M. Bailey, *K*. L. Churney and R. L. Nutall, *The NBS Tables of Chemical Thermodynamics Properties, J. Phys. Chem.*, **1982**, *11*, 2.
[5] J. B. Pedley, R. D. Naylor and S. P. Kirby, *Thermochemical Data of Organic Compounds* (2nd ed.), Chapman and Hall, New York, **1986**.
[6] J. A. Martinho Simões, in *Energetics of Organometallic Species* (Ed.: J. A. Martinho Simões), NATO-ASI Series, Kluwer, Dordrecht, **1992** and references cited therein.
[7] [7a] P. Nunes, PhD. thesis, IST, **1999**. – [7b] J. P. Leal, M. E. Minas da Piedade, P. Nunes, private communication.
[8] Kapustinskii noticed that, in the formula for the lattice energy in an ionic model, dividing the Madelung constants by the number of ions in the molecule gives a new constant, which is almost independent of the structure of the lattice. He also assumed the repulsive part of the energy to be 1/9 the attractive part and split the internuclear equilibrium distance in a sum of two radii (r+ and r-). This equation is a simplification of the Born-Lande equation and thus works on the assumption of spherical particles, but if the thermochemical radii is not given a physical meaning but used as a parameter for calculation, as we have done here, the equation can be used for non-spherical particles (e.g. *n*-butoxy). For a detailed discussion see e.g. D. A. Johnson, *Some Thermodynamic Aspects of Inorganic Chemistry*, 2nd ed., Cambridge University Press, Cambridge, **1982**.
[9] R. D. Shannon, *Acta Cryst.* **1976**, *A32*, 751.
[10] W. W. Scott, *Scott's Standard Methods of Chemical Analysis*, 5th ed., Vol. 1, (Ed.: N. H. Furman), D. Van Nostrand Company Inc., **1939** p. 211.
[11] *Applied Inorganic Analysis* (Eds.: W. F. Hillehrand, G. E. F. Lundell, H. A. Bright and J. I. Hoffman), 2nd ed., John Wiley and Sons, Inc., New York, **1955**, pp. 642–643.

Received September 13, 1999
[I99326]

Protonation of [tpmRu(PPh$_3$)$_2$H]BF$_4$ [tpm = Tris(pyrazolyl)methane] – Formation of Unusual Hydrogen-Bonded Species

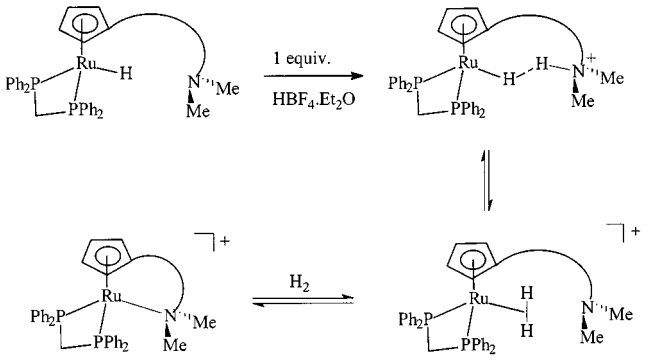
Hei Shing Chu,[a] Zhitao Xu,[b] Siu Man Ng,[a] Chak Po Lau,*[a] and Zhenyang Lin*[b]

Keywords: Ruthenium / Dihydrogen complexes / Dihydrogen bonding / Hydride protonation

Protonation of [tpmRu(PPh$_3$)$_2$H](BF$_4$) with excess HBF$_4$Et$_2$O in CD$_2$Cl$_2$ yielded, in a straightforward manner, the dicationic η^2-dihydrogen complex [tpmRu(PPh$_3$)$_2$(H$_2$)](BF$_4$)$_2$, which, as expected, is more acidic than its monocationic Tp [Tp = hydrotris(pyrazolyl)borate] analog [TpRu(PPh$_3$)$_2$(H$_2$)]BF$_4$ (pK_a: 2.8 vs. 7.6). The complex [tpmRu(PPh$_3$)$_2$(H$_2$)](BF$_4$)$_2$ is unstable towards H$_2$ loss at ambient temperature. However, acidification of [tpmRu(PPh$_3$)$_2$H]BF$_4$ with excess aqueous HBF$_4$ or aqueous triflic acid in [D$_8$]THF gave very interesting results. Variable-temperature ^{1}H- and ^{31}P-NMR studies revealed that the aqueous acid did not fully protonate the metal hydride to form the dihydrogen complex, but a hydrogen-bonded species was obtained. The feature of this species is that the strength of its Ru–H···H–(H$_2$O)$_m$ interaction decreases with temperature; this phenomenon is unusual because other complexes containing dihydrogen bonds show enhanced M–H···H–X interaction as the temperature is lowered. Decrease of the dihydrogen-bond strength with temperature in the present case can be attributed to the decline of acidity that results from the formation of larger H$^+$(H$_2$O)$_n$ ($n > m$) clusters at lower temperatures; steric hindrance of these large clusters also contribute to the weakening of the dihydrogen bonding interactions. At higher temperatures, facile H/H exchange occurs in Ru–H···H–(H$_2$O)$_m$ via the intermediacy of a "hydrogen-bonded dihydrogen complex" Ru–(H$_2$)···(H$_2$O)$_m$. To investigate the effect of the H$^+$(H$_2$O)$_m$ cluster size on the strength of the dihydrogen bonding in [tpmRu(PPh$_3$)$_2$H]$^+$, molecular orbital calculations at the B3LYP level have been performed on model systems, [tpmRu(PH$_3$)$_2$H]$^+$ + H$^+$(H$_2$O) and [tpmRu(PH$_3$)$_2$H]$^+$ + H$^+$(H$_2$O)$_2$. The results provide further support to the notion that the formation of larger H$^+$(H$_2$O)$_n$ clusters weakens the Ru–H····H(H$_2$O)$_n$ dihydrogen bonding interaction.

Introduction

The recent discovery of intramolecular[1] and intermolecular[2] M–H···H–A dihydrogen bonding between a transition-metal hydride and a hydrogen-bond donor containing an O–H or an N–H group has attracted much attention. It has been shown that such hydride–proton interactions may significantly contribute to the stabilization of organometallic structures in mononuclear complexes[3] and cluster hydride derivatives.[1h,4] They may also be very important in the elucidation of reaction pathways occurring on the surface of transition-metal clusters bearing hydride ligands.[1h,4] Furthermore, complexes containing dihydrogen bonding have been proposed as intermediates for the formation of η^2-dihydrogen complexes or heterolytic cleavage of η^2-H$_2$ ligand.[5] This proposal has been vividly demonstrated by our recent work on intramolecularly hydrogen-bonded ruthenium complexes containing [2-(dimethylamino)ethyl]cyclopentadienyl and [3-(dimethylamino)propyl]cyclopentadienyl ligands (Scheme 1). The intramolecularly hydrogen-bonded complexes were unequivocally characterized by relaxation time T_1 measurements and spin saturation transfer study; the dihydrogen complexes in Scheme 1 were unstable toward H$_2$ loss.[6]



Scheme 1

Chaudret et al.[7] have recently reported the first direct observation of an intermolecular dynamic proton transfer equilibrium: *trans*-(dppm)$_2$HRuH···HOPh ⇌ *trans*-[(dppm)$_2$HRu(H$_2$)]$^+$(OPh)$^-$, when excess PhOH was added to a C$_6$D$_6$ or C$_7$D$_8$ solution of (dppm)$_2$RuH$_2$. The use of 10 equiv. of the more acidic alcohol, hexafluoroisopropyl alcohol (HFP) in place of PhOH resulted in complete proton transfer to give the η^2-dihydrogen complex *trans*-[(dppm)$_2$HRu(H$_2$)]$^+$[OCH(CF$_3$)$_2$]$^-$ immediately. Therefore, it seems that isolation of the hydrogen-bonded complex

[a] Department of Applied Biology Chemical Technology, The Hong Kong Polytechnic University, Hung Hom, Kowloon, Hong Kong, China
Fax: (internat.) + 852-2364-9932
E-mail: bccplau@polyu.edu.hk
[b] Department of Chemistry, The Hong Kong University of Science and Technology, Clear Water Bay, Kowloon, Hong Kong, China
Fax: (internat.) + 852-2358-1594
E-mail: chzlin@ust.hk

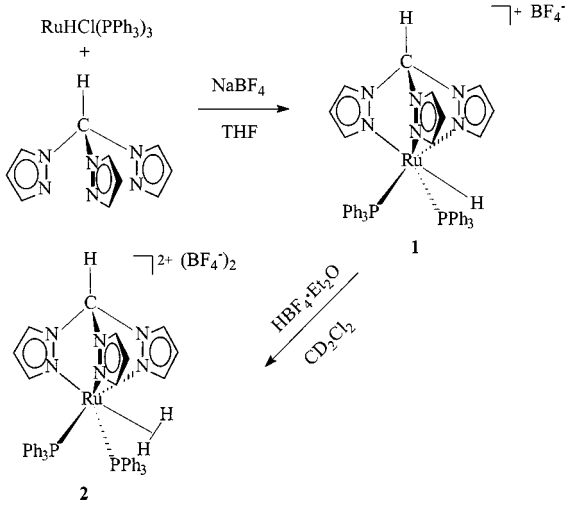
 © WILEY-VCH Verlag GmbH, D-69451 Weinheim, 2000 1434–1948/00/0505–0993 $ 17.50+.50/0

L_nM–H···HA is very dependent on the acid strength of HA. We report here that protonation of the monocationic ruthenium hydride complex $[tpmRu(PPh_3)_2H]^+$ [tpm = tris(pyrazolyl)methane] with $HBF_4{\cdot}Et_2O$ in CD_2Cl_2 readily yields the dicationic η^2-dihydrogen complex $[tpmRu(PPh_3)_2(H_2)]^{2+}$, while on the other hand, acidification of the hydride precursor with aqueous HBF_4 or aqueous CF_3SO_3H in [D$_8$]THF generates a hydrogen-bonded species $[tpmRu(PPh_3)_2H{\cdots}H(H_2O)_m]^{2+}$, which displays some unusual and interesting behaviors in variable temperature ^{1}H- and ^{31}P-NMR spectroscopy.

Results and Discussion

Synthesis, Characterization, and Acidity Measurement of $[tpmRu(PPh_3)_2(H_2)](BF_4)_2$ (2)

The dihydrogen complex $[tpmRu(PPh_3)_2(H_2)](BF_4)_2$ (**2**) was synthesized according to the sequence shown in Scheme 2. Reaction of $RuHCl(PPh_3)_3$ with tpm and $NaBF_4$ in THF gave $[tpmRu(PPh_3)_2H]BF_4$ (**1**); adoption of the synthetic route of the analogous Tp complex $TpRu(PPh_3)_2H$ [Tp = hydrotris(pyrazolyl)borate][8] to **1** was not successful. The Tp hydride complex was prepared by sodium borohydride reduction of the chloro precursor $TpRu(PPh_3)_2Cl$, which in turn was synthesized by reaction of $RuCl_2(PPh_3)_3$ with KTp.[9] An analogous reaction of $RuCl_2(PPh_3)_3$ with tpm in the presence of $NaBF_4$ did not, however, yield $[tpmRu(PPh_3)_2Cl]BF_4$ in a pure form, instead it was contaminated with some reddish brown solids. We have learned that the reaction of the neutral facial ligand 1,4,7-trimethyl-1,4,7-triazacyclononane (^{Me}Cn) with $RuCl_2(PPh_3)_3$ and $NaBF_4$ is always plagued by impurities too.[10]



Scheme 2

The ^{1}H-NMR spectrum of **1** shows the hydride signal as a triplet at $\delta = -13.98$ ($J_{HP} = 27.6$ Hz). The coupling constant is similar to those reported for analogous complexes with three-legged piano-stool structures. For example, J = 34.0 Hz for $CpRu(PPh_3)_2H$,[11] and 26.4 Hz for $TpRu(PPh_3)_2H$.[8] The presence of the hydride ligand is also confirmed by IR spectroscopy, which shows the ν(Ru–H) at 2054 cm^{-1} (KBr). That the net positive charge in **1** improves the Ru–H binding is evidenced by comparison of its ν(Ru–H) with that of $TpRu(PPh_3)_2H$ [ν(Ru–H) = 2008 cm^{-1}, KBr].[8] The ^{31}P{^{1}H}-NMR spectrum of **1** shows one resonance at $\delta = 68.3$, indicative of the chemical equivalence of the phosphorous atoms. The molecular dihydrogen complex **2** was prepared in situ by protonation of **1** with $HBF_4{\cdot}Et_2O$ in [D$_2$]dichloromethane at –50 °C.

The presence of the η^2-H_2 moiety in **2** was confirmed by variable-temperature relaxation time T_1 measurements and the observation of a large $^1J_{HD}$ value for the corresponding isotopomer $[tpmRu(PPh_3)_2(HD)](BF_4)_2$. The ^{1}H-NMR spectrum of **2** showed a broad signal at $\delta = -8.04$, integrating for two hydrogen atoms. A minimum T_1 value of 24 ms was recorded at 241 K and 400 MHz. Acidification of **1** with excess DBF_4 gave the η^2-HD isotopomer, which showed a 1:1:1 triplet ($^1J_{HD}$ = 31.1 Hz) of a 1:2:1 triplet ($^2J_{HP}$ = 5.7 Hz) centered at $\delta = -8.06$ in the ^{1}H-NMR spectrum.

The pseudo aqueous pK_a of **2** was estimated by studying the equilibrium shown in Equation 1 with ^{1}H NMR in CD_2Cl_2, using the hydride complex $[^{Me}CnRu(dppe)H]^+$ (^{Me}Cn = 1,4,7-trimethyl-1,4,7-triazacyclononane) as the base.

$$[tpmRu(PPh_3)_2(H_2)]^{2+} + [^{Me}CnRu(dppe)H]^+ \rightleftharpoons [tpmRu(PPh_3)_2H]^+ + [^{Me}CnRu(dppe)(H_2)]^{2+} \quad (1)$$

The pseudo aqueous pK_a value of $[^{Me}CnRu(dppe)(H_2)]^{2+}$ has been determined previously in CD_2Cl_2 using a similar method.[12a] The equilibrium mixture could be conveniently obtained by protonating a mixture of $[tpmRu(PPh_3)_2H]^+$ and $[^{Me}CnRu(dppe)H]^+$ with a limited amount of $HBF_4{\cdot}Et_2O$. The equilibrium was obtained at –60 °C because the η^2-dihydrogen complex **2** is unstable towards H_2 loss at higher temperatures. The relative concentrations of the dihydrogen complexes and metal hydrides in the equilibrium were estimated from integration of the upfield hydride signals in the ^{1}H-NMR spectrum. The pK_a of **2** was estimated to be 3 according to Equation 2. K_{eq} in Equation 2 is the equilibrium constant of Equation 1.

$$pK_a(\mathbf{2}) = pK_{eq} + pK_a([^{Me}CnRu(dppe)(H_2)]^{2+}) \quad (2)$$

The dihydrogen complex **2** is a new entry into the relatively small family of dicationic η^2-dihydrogen complexes.[12] In contrast to the abundance of monocationic dihydrogen complexes, the number of well-characterized dicationic dihydrogen complexes is still limited. The double positive charge of the metal center in these complexes lowers the effectiveness of $d\sigma(M)\rightarrow\sigma^*(H_2)$ back bonding, and increases the $\sigma(H_2)\rightarrow d\sigma(M)$ interaction. It is therefore expected that depletion of electron density in the η^2-H_2 ligand renders the dicationic dihydrogen complexes very

acidic. Dicationic dihydrogen complexes, which demonstrate high reactivity toward heterolysis of η^2-H_2 ($pK_a < -2$) and high room-temperature stability with respect to loss of H_2, both in solid state and in solution, have recently been reported, including $[Os(bpy)(PR_3)_2(CO)(H_2)]^{2+}$ (PR_3 = PPh_3, $PMePh_2$; bpy = 2,2′-bipyridine),[12b][12c] $[Os(phen)(PPh_3)_2(CO)(H_2)]^{2+}$ (phen = 1,10-phenanthroline),[12c] $[Os(dppp)_2(CO)(H_2)]^{2+}$,[12d] *trans*-$[Os(dppe)_2(CH_3CN)(H_2)]^{2+}$,[12e] and *trans*-$[Fe(dppe)_2(L)(H_2)]^{2+}$ (L = CO, CNH).[12f] A strong $\sigma(H_2)\rightarrow d\sigma(M)$ interaction is believed to be dominant in these complexes.

Less stable (H_2 loss at room temperature), but acidic dicationic dihydrogen complexes are exemplified by $[Os(P\mathit{i}Pr_3)_2(CH_3CN)_3(H_2)]^{2+}$,[12g] $[Ru(bpy)(PPh_3)_2(CO)(H_2)]^{2+}$,[12c] and $[Ru(dppp)_2(CO)(H_2)]^{2+}$.[12d] We have recently reported the synthesis and acidity of some dicationic dihydrogen complexes containing the facial triazacyclononane ligands $[^{R}CnRu(L)(L')(H_2)]^{2+}$ [^{H}Cn = 1,4,7-triazacyclononane, ^{Me}Cn = 1,4,7-trimethyl-1,4,7-triazacyclononane; L,L′ = $(PPh_3)_2$, dppe, and CO, PPh_3]; the acidity of the complexes $[^{H}CnRu(PPh_3)_2(H_2)]^{2+}$ (pK_a = 4.5) and $[^{Me}CnRu(dppe)(H_2)]^{2+}$ (pK_a = 3.8), although low in comparison to those of the aforementioned dicationic dihydrogen complexes, are nevertheless significantly higher than those of their monocationic hydrotris(pyrazolyl)borato (Tp) and Cp analogoues (by 3–4 pK_a units). The carbonyl-containing complexes $[^{H}CnRu(PPh_3)(CO)(H_2)]^{2+}$ (pK_a = –1.3) and $[^{Me}CnRu(PPh_3)(CO)(H_2)]^{2+}$ (pK_a = –2.6) are also more acidic than their monocationic Tp counterpart $[TpRu(PPh_3)(CO)(H_2)]^{+}$ (pK_a = –0.6), but to a smaller extent. The non-carbonyl-containing ^{R}Cn dihydrogen complexes are stable in the solid state at room temperature, but in solution the η^2-H_2 ligand is displaced by strongly coordinating solvent such as acetonitrile.[12a] It should be mentioned that dicationic dihydrogen complexes are not necessarily acidic, for example, $[Os(NH_3)_4(L)(H_2)]^{2+}$ [12h,12i] and $[Os(en)_2(L)(H_2)]^{2+}$,[12j] reported by Taube and co-workers, which tightly bind H_2, are not acidic, probably due to the strong electron-donating effect of the NH_3 and en ligands.

The fact that complex **2** is more acidic than the analogous dicationic ^{R}Cn dihydrogen complexes $[^{H}CnRu(PPh_3)_2(H_2)]^{2+}$ [12a] and $[^{Me}CnRu(PPh_3)_2(H_2)]^{2+}$ [12a] seems to indicate that the tpm ligand is less electron donating than ^{R}Cn. As expected, **2** is significantly more acidic than the analogous monocationic Tp and Cp complexes. On the other hand, the stability of **2** is lower than that of the ^{R}Cn, Tp, and Cp counterparts. The η^2-H_2 of **2** is labile at –15 °C. In fact, addition of $HBF_4{\cdot}Et_2O$ to **1** in CD_2Cl_2 at room temperature resulted in immediate evolution of H_2, which gave a signal at δ = 4.62 in the ^{1}H-NMR spectrum. The major product of the reaction was the aquo complex $[tpmRu(PPh_3)_2(H_2O)](BF_4)_2$ (**3**),[13] which was formed by displacement of η^2-H_2 by residual H_2O in the solvent, only a trace amount of **2** was detected (vide infra). It is noteworthy that the T_1(min) of **2** is larger than that of the monocationic analog $[TpRu(PPh_3)_2(H_2)]BF_4$,[8] and its $^1J_{HD}$ value is smaller than that of the latter. The weaker H–H interaction of the η^2-H_2 ligand in **2** relative to that of the η^2-H_2 in $[TpRu(PPh_3)_2(H_2)]BF_4$ may be due the fact that the tpm ruthenium fragment $[tpmRu(PPh_3)_2]^{2+}$ is a stronger σ-acceptor than the Tp counterpart. Morris has pointed out that the lower H–H bond strength of the η^2-H_2 in $[Os(pys)(PPh_3)_2(CO)(H_2)]BF_4$ (pys = 2-pyridinethiolate) is a result of the strong $\sigma(H_2)\rightarrow d\sigma(M)$ interaction.[14]

Acidification of [tpmRu(PPh$_3$)$_2$H](BF$_4$) (1) with Aqueous HBF$_4$ or Aqueous CF$_3$SO$_3$H

While protonation of **1** with excess $HBF_4{\cdot}Et_2O$ in CD_2Cl_2 generated **2** in a straightforward manner, acidification of **1** in [D$_8$]THF with excess aqueous HBF_4 or aqueous CF_3SO_3H gave quite different results. No dihydrogen gas evolution was detected, even when the acidification was carried out at room temperature; and no signal seemed to be observable in the upfield region of the ^{1}H-NMR spectrum (Figure 1, left). However, a very broad signal became detectable at –15°C; and it gradually evolved into a broad triplet as the temperature was lowered to –45°C; the broad triplet sharpened when the temperature was further decreased to –60°C . The spectral change with temperature was found to be reversible, i.e. the triplet gradually broadened into the baseline again with increasing temperature. Concurrent off-resonance decoupled ^{31}P-NMR spectra are also shown in Figure 1 (right). It can be seen that as the triplet hydride peak starts broadening out at –45 °C, H–P coupling in the ^{31}P-NMR spectrum disappears. The phosphorus peak also sharpens as the hydride signal broadens into the baseline. Like the VT ^{1}H-NMR study, the spectral changes with temperature in the ^{31}P-NMR measurements are also reversible. In fact, if the protonation reaction was carried out at –60°C, and the temperature gradually raised to 20°C, the sets of ^{1}H- and ^{31}P-NMR spectra collected at various temperatures were identical to those depicted in Figure 1. It is interesting to note that throughout the whole variable-temperature NMR study, signals pertaining to η^2-H_2 ligand and free H_2 were not observed.

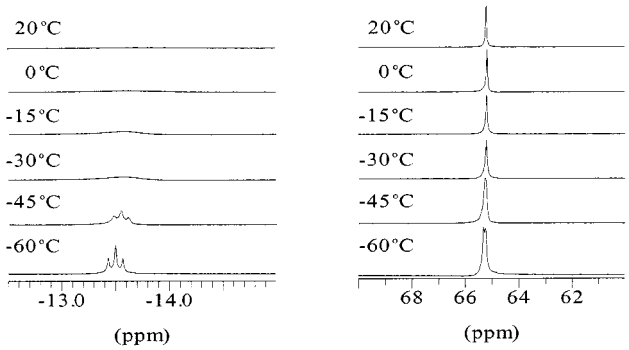
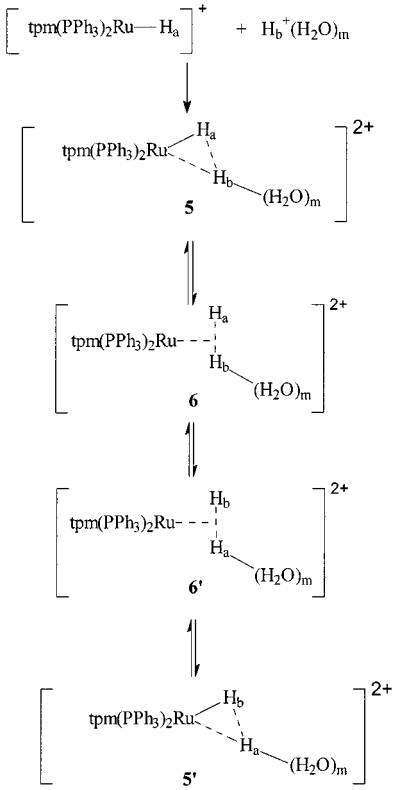


Figure 1. Variable-temperature (left) ^{1}H-NMR spectra (upfield region) and (right) ^{31}P-NMR spectra of $[tpmRu(PPh_3)_2H]^+$ + aq HBF_4 in [D$_8$]THF

The fact that acidification of **1** with aqueous HBF_4 or aqueous CF_3SO_3H in [D$_8$]THF gave identical result, as revealed by VT ^{1}H- and ^{31}P-NMR studies, seemed to indicate that the two acids were leveled to the same species in the

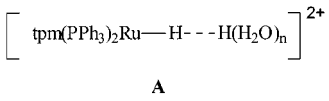
two systems. We assume that the acids were both leveled to $H^+(H_2O)_m$, and have to admit that the precise state of solvation of H^+ was unknown.[15] It seems, however, that the pK_a value (–1.74)[16] commonly assigned to H_3O^+ does not reflect the actual acidity of the aqueous HBF_4 or aqueous CF_3SO_3H in our case. Failure to generate the dihydrogen complex **2** with aqueous HBF_4 or aqueous CF_3SO_3H implies that acidity of either acid might only be close to or even lower than that of $[tpmRu(PPh_3)_2(H_2)]^{2+}$, and therefore is not able to effect complete proton transfer to **1**. In our recent work, we have attributed deprotonation of the η^2-H_2 ligands in $[TpRu(L_2)(H_2)]^+$ [L_2 = $(PPh_3)_2$, dppe][8][12a] and $[^RCnRu(L_2)(H_2)]^{2+}$ [^RCn = 1,4,7-triazacyclononane, 1,4,7-trimethyl-1,4,7-triazacyclononane; L_2 = $(PPh_3)_2$, dppe][12a] by H_2O in THF/H_2O or organic/aqueous mixed solvents to strong solvation of H^+ by H_2O; all these complexes have pK_a values higher than 3.



Scheme 3

Spectral changes of the hydride signal in the VT ^{1}H-NMR study of the acidification reaction of **1** with aqueous acid are contrary to the behaviors of the hydride signals of complexes containing dihydrogen bonding. The hydride signals of these complexes usually broaden as the temperature goes down, due to strengthening of the M–H···H–X interaction, and they sharpen as the temperature is increased because of weakening of the dihydrogen bonding. The unusual spectral behavior displayed by the hydride ligand of **1** in the acidification process can be reconciled by the sequence depicted in Scheme 3. Acidification of **1** with aqueous acid generates the hydrogen-bonded species **5**; at higher temperature, rapid H/H exchange between Ru–H and $H^+(H_2O)_m$ (**5** ⇌ **5′**) via the intermediacies of a pair of transient η^2-dihydrogen complexes (**6** and **6′**) leads to broadening-out of the hydride signal. The feature of this pair (**6** and **6′**) is that the η^2-H_2 ligand, which is hydrogen-bonded to the $(H_2O)_m$, does not dissociate readily from the metal center, and that might be the reason for not observing free H_2 in the course of the VT ^{1}H-NMR study. Analogously, Crabtree et al. have very recently reported that hydrogen-bonding provided by a pendant amine group is the key factor that allows stabilization of an Ir–(HF) complex.[17] Species similar to **5** (or **5′**) and **6** (or **6′**) have been proposed as intermediates in the protonation of *cis*-$[FeH_2\{PCH_2CH_2PPh_2)_3\}]$ to form the η^2-dihydrogen complex.[18]

At low temperature (–60° C), acidity decreases due to higher degree of solvation of H^+, i.e. formation of larger cluster $H^+(H_2O)_n$; Ru–H···H$(H_2O)_n$, dihydrogen bonding in **A** weakens and therefore results in sharpening of the hydride signal.



A

Weakening of the dihydrogen bonding in **A** at low temperature can also be rationalized in terms of steric effect of the large cluster $H^+(H_2O)_n$.

Another possible scenario for the protonation of **1** with aqueous acid is the occurrence of a rapid proton transfer between **1** and H_2O (Equation 3); lowering the temperature would slow down this proton exchange and the low temperature spectrum closely resembles that of complex **1**. But the equilibrium depicted in Equation 3 does not seem to be in congruence with the VT NMR spectra shown Figure 1.

$$[tpmRu(PPh_3)_2H]^+ + H_3O^+ \rightleftharpoons [tpmRu(PPh_3)_2(H_2)]^{2+} + H_2O \quad (3)$$

1 **2**

If such a rapid proton transfer occurs, it is most likely that a weighted average of hydride signals of **1** and **2** is observed, and the phosphorus signal is also an average of those of **1** and **2**. However, careful examination of the VT ^{1}H- and ^{31}P-NMR spectra does not reveal the existence of these average signals. It is also noteworthy that no H_2 loss was observed when the system was allowed to stand at room temperature. Had the equilibrium depicted in Equation 3 existed, the equilibrating **2** should have evolved H_2 while standing at room temperature. We have learned that **2** is unstable with respect to H_2 loss at –15 °C.

Dihydrogen bonding between the protonated water cluster $H(H_2O)_m^+$ and the hydride in **5** (or **5′**) was characterized by IR spectroscopy in THF at room temperature. A THF solution of **2** showed the ν(RuH) band at 2040 cm^{-1}, upon addition of 10 equiv. of aqueous HBF_4, this band was shifted to a lower wavenumber at 1967 cm^{-1}. Berke, Epstein, and co-workers have characterized intermolecular hydrogen bonding of acidic alcohols to the hydride ligand of $WH(CO)_2(NO)L_2$ by IR spectroscopy in hexane at 200 K. The IR spectrum of the tungsten hydride complex showed

a low-wavenumber shoulder in the ν(WH) band, in the presence of 3 equiv. of hexafluoro-2-propanol (HFIP).[2e] Unfortunately, it is not possible to characterize the dihydrogen bonding between **2** and protonated water cluster by measurement of T_1(min) because the strength of the Ru–H···H(H$_2$O)$_{m\ or\ n}$ dihydrogen bond in the system varies with temperature. Furthermore, it is not possible to measure T_1 at –30 °C or above since the hydride signal broadens into the baseline at these temperatures. Acidification of **1** with HBF$_4$·Et$_2$O in CD$_3$OD/[D$_8$]THF gave practically identical results as the protonation of **1** with aqueous HBF$_4$ in [D$_8$]THF. This is not surprising since it is expected that methanol behaves very similarly to H$_2$O in this process. Quantum chemical calculations described in the following section also seem to support our proposal of Scheme 3.

At this point, we would like to comment on the formation of aquo complex [tpmRu(PPh$_3$)$_2$(H$_2$O)](BF$_4$)$_2$ (**3**) in the room-temperature protonation reaction of **1** with HBF$_4$·Et$_2$O in CD$_2$Cl$_2$. The predominant form of acid in this system is Et$_2$OH$^+$, which is strong enough to fully protonate **1** to form **2**. The trace amount of water present in the system does not form the hydrogen-bonded species **5** (or **5′**) with **2** because it is protonated by Et$_2$OH$^+$ (Equation 4), which is a stronger acid than **2**. At –15°C or above, the η^2-H$_2$ ligand in **2** becomes labile, and the coordinatively unsaturated species generated upon dissociation of H$_2$ from **2** abstracts H$_2$O from the equilibrium (Equation 4) to form the thermodynamically stable aquo complex **3**.

$$Et_2OH^+ + H_2O \rightleftharpoons Et_2O + H_3O^+ \quad (4)$$

The H/H exchange proposed in Scheme 3 was further supported by H/D exchange, which occurred in the acidification of a [D$_8$]THF solution of **1** with CF$_3$SO$_3$D/D$_2$O. It was found that addition of CF$_3$SO$_3$D/D$_2$O (v/v, 1:1) to a [D$_8$]THF solution of **1** at room temperature led to immediate broadening of the hydride signal into the baseline. The upfield triplet signal, which re-appeared as the temperature was lowered to –60 °C, diminished considerably due to H/D exchange.

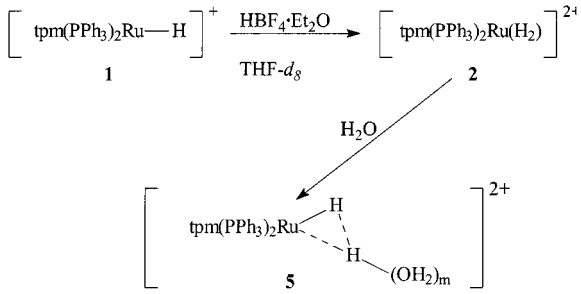
Structure **5** (or **5′**) can be viewed as an intermediate on the reaction path that leads to transient **6** (or **6′**), and then to the product of complete proton transfer from an acid to the metal hydride precursor. Gusev and Reinhart have very recently proposed that reactions of anionic ruthenium and rhenium hydrides with phenylacetylene first generate the hydrogen-bonded species [L$_n$M–H···H–C≡CPh]$^-$, which equilibrates with the transient [L$_n$M(μ-H$_2$)(CCPh)]$^-$ (Equation 5). The latter, which is analogous to **6** (or **6′**), then undergoes hydride transfer to the C$_\alpha$ atom of phenylacetylene to form the [L$_n$M–C(Ph)=CH$_2$]$^-$ vinyl intermediate.[19]



(5)

Generation of the Hydrogen-Bonded Complex from 2

We have been able to generate the hydrogen-bonded complex **5** from the η^2-dihydrogen complex **2**, and have monitored this transformation by using ^{1}H-NMR spectroscopy. Complex **2** was first formed in a 5-mm NMR tube by acidification of a [D$_8$]THF solution of **1** (0.4 mL) with 1 equiv. of HBF$_4$·Et$_2$O at –30 °C, subsequent addition of 50 μL of H$_2$O to the solution led to the disappearance of the η^2-H$_2$ signal of **2** and concomitant appearance of the very broad peak of the hydrogen-bonded hydride of **5** (Scheme 4).



Scheme 4

Quantum Chemical Study

The broadening/sharpening changes of the hydride signal for the dihydrogen-bonded species **5** observed in the variable-temperature NMR experiments show unusual behavior when compared to other dihydrogen bonded systems.[2e,7] In order to provide an insight into the understanding of the unusual behavior, quantum mechanical calculations at the density-functional B3LYP level of theory have been undertaken to investigate the structural details for the following model systems: [tpmRu(PH$_3$)$_2$H]$^+$, [tpmRu(PH$_3$)$_2$(H$_2$)]$^{2+}$, [tpmRu(PH$_3$)$_2$H]$^+$ + H$^+$(H$_2$O), and [tpmRu(PH$_3$)$_2$H]$^+$ + H$^+$(H$_2$O)$_2$. The [tpmRu(PH$_3$)$_2$(H$_2$)]$^{2+}$ system represents the complete proton transfer product in organic solvent. The latter two model systems represent the corresponding situation in aqueous/THF solution, and the relevant calculations allow us to study the effect of water aggregation on the dihydrogen bonding. They can also provide information on the structural details of protonated products under different acidity because one can consider that HBF$_4$·Et$_2$O is more acidic than H$^+$(H$_2$O), which in turn, is more acidic than H$^+$(H$_2$O)$_2$. It should be noted that the model systems cannot be directly related to the experimental systems because the actual degree of water aggregation in each experimental system cannot be well-defined. Therefore, the calculated H···H distances for different numbers of water molecules in the model systems are only useful in considering the trend, which qualitatively accounts for the effect of water aggregation on the dihydrogen bonding.

The optimized structures for the four model systems are shown in Figure 2. Consistent with the experimental finding that the direct protonation of [tmpRu(PPh$_3$)$_2$H]$^+$ with HBF$_4$·Et$_2$O in an organic solvent gives a non-classical dihydrogen complex, [tpmRu(PH$_3$)$_2$(H$_2$)]$^{2+}$. The H–H distance in this dihydrogen complex is calculated to be 0.81 Å with a symmetrical coordination of the η^2-H$_2$ unit (Ru–H: 1.82 Å).[20]

The calculations for the [tpmRu(PH$_3$)$_2$H]$^+$ + H$^+$(H$_2$O) system give a similar result. The system can be described as [tpmRu(PH$_3$)$_2$(H$_2$)···OH$_2$]$^{2+}$, again a non-classical dihydro-

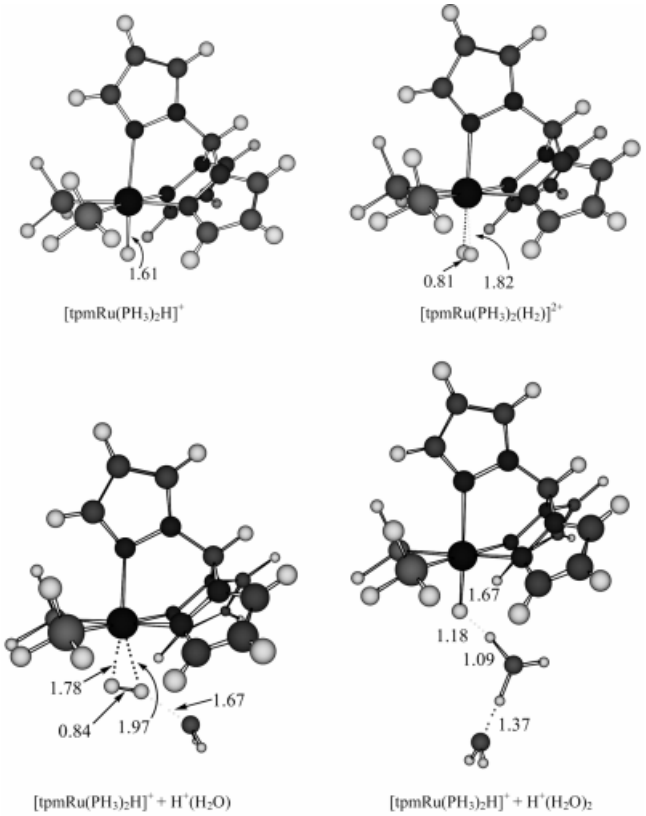


Figure 2. Optimized structures for model systems: $[tpmRu(PH_3)_2H]^+$, $[tpmRu(PH_3)_2(\eta^2\text{-}H_2)]^{2+}$, $[tpmRu(PH_3)_2H]^+ + H^+(H_2O)$, and $[tpmRu(PH_3)_2H]^+ + H^+(H_2O)_2$

gen complex, a weak hydrogen bond exists between one of the two hydrogen atoms and the oxygen atom of H_2O (H···O: 1.67 Å). The H–H distance (0.84 Å) in the η^2-H_2 unit lengthens only slightly, although the coordination of the η^2-H_2 ligand becomes unsymmetrical. The Ru–H distance on the side of the O···H hydrogen bonding is lengthened (1.97 Å) while the other is shortened (1.78 Å). The results of these calculations for the mono-water system suggest that $H^+(H_2O)$ is still very acidic, resulting in the formation of non-classical structure upon protonation.

Surprisingly, further association with one more water molecule, which gives the $[tpmRu(PH_3)_2H]^+ + H^+(H_2O)_2$ system, leads to a species that is close to a classical hydride. The metal-hydride distance, calculated to be 1.67 Å, is within the range of classical M–H distance[20g,21] {1.61 Å in $[tpmRu(PH_3)_2H]^+$}. In this system, the hydride ligand was also found to have a significant interaction with the proton from the $H^+(H_2O)_2$ unit. The H···H distance was calculated to be 1.18 Å. The typical H···H distance in other M–H···H–X systems is around 1.8 Å.[5] Apparently, in the current system, the hydride acceptor [H^+ in $H^+(H_2O)_2$] is very protonic when compared to other systems studied previously.[2e,7] In the structure of $[tpmRu(PH_3)_2H]^+ \cdots H^+(H_2O)_2$, one can clearly see the aggregate of $H^+(H_2O)_2$, which can be formulated as $H^+(H_2O)\cdots OH_2$. The additional H_2O is only weakly bounded through normal hydrogen bonding.

These calculations indicate that the mono-water system prefers a dihydrogen non-classical structure, while the di-water system adopts a structure close to a classical hydride. Though weakly bound, the presence of an additional water molecule surprisingly switches the non-classical structure to a classical one with M–H···H–X dihydrogen bonding. This result suggests that a fast exchange can occur between classical and non-classical structures, as proposed in Scheme 3, when temperature increases. The association and dissociation of the weakly bound water molecule can be strongly influenced by temperature.

The current work deals with the effect of water aggregation on the H···H dihydrogen bonding. The stability of these dicationic hydrogen-bonded systems is another important topic that requires further attention. Theoretically, the evaluation of the H···H bonding strengths in the studied systems involves the charge-separation processes. Therefore, much higher levels of theory are necessary in order to produce some meaningful results. Clearly, the stability of these systems should be further studied both theoretically and experimentally.

Conclusion

We have shown in this study, the species that are proposed as intermediates along the reaction pathway of protonation of metal hydrides to form η^2-dihydrogen complexes. One of these species is a hydrogen-bonded metal hydride, $[tpmRu(PPh_3)_2H\cdots H(H_2O)_n]^{2+}$ (**A**), which is formed by acidification of $[tpmRu(PPh_3)_2H]^+$ with aqueous HBF_4 in [D_8]THF at –60 °C. The comparatively weak Ru–H···$H(H_2O)_n$ dihydrogen interaction is attributable to lower acidity and larger steric hindrance of the bulky $H^+(H_2O)_n$ clusters, which are the major forms of acid at low temperature. At higher temperatures, the degree of aquation of H^+ decreases and the smaller clusters $H^+(H_2O)_m$ ($m < n$) exhibit relatively higher acidity, therefore the species **5** (or **5′**) with stronger dihydrogen bonding become the major species in solution. Finally, a full-fledged η^2-dihydrogen complex $[tpmRu(PPh_3)_2(H_2)]^{2+}$ is generated when $tpmRu(PPh_3)_2H$ is protonated with $HBF_4{\cdot}Et_2O$ in CD_2Cl_2. The results of our quantum chemical calculations at B3LYP level on model systems, $[tpmRu(PH_3)_2H]^+ + H^+(H_2O)$ and $[tpmRu(PH_3)_2H]^+ + H^+(H_2O)_2$, indeed suggest that the Ru–H···$H(H_2O)_m$ dihydrogen bonding interaction greatly depends on the size of the water cluster. For the mono-water model system, a non-classical dihydrogen complex is preferred. The di-water system, however, gives a Ru–H···$H(H_2O)_2$ dihydrogen bonded species.

The acidification of metal hydrides normally leads to either non-classical η^2-H_2 dihydrogen complexes or formation of species with the M–H···H–X interaction (dihydrogen bonding). Strongly acidic conditions give non-classical complexes, while weakly acidic conditions result in dihydrogen bonding. Here, we demonstrate that the strength of hydride-proton interaction can be tuned through the association of water molecules to H^+.

Experimental Section

All reactions were performed under dry nitrogen using standard Schlenk techniques. Solvents were distilled under nitrogen from appropriate drying agents[22] (solvent/drying agent): methanol/Mg/I$_2$, ethanol/Mg/I$_2$, acetonitrile/CaH$_2$, dichloromethane/CaH$_2$, tetrahydrofuran/Na/benzophenone, diethyl ether/Na, *n*-hexane/Na. Ruthenium trichloride, RuCl$_3$·3H$_2$O, pyrazole, sodium tetrafluoroborate, and [D$_1$]trifluoromethanesulfonic acid were purchased from Aldrich. Tetrafluoroboric acid in ethereal solution and aqueous solution were obtained from Fluka. Triphenylphosphane was obtained from Merck and was recrystallized from ethanol before use. The complexes RuHCl(PPh$_3$)$_3$ [23] and [^{Me}CnRu(dppe)H]BF$_4$ (^{Me}Cn = 1,4,7-trimethyl-1,4,7-triazacyclononane)[12a] were synthesized according to literature methods. – Infrared spectra were obtained from a Nicolet Magna 750 Ft-IR spectrophotometer. ^{1}H-NMR spectra were recorded with a Bruker DPX-400 spectrometer; chemical shifts were reported relative to residual protons of the deuterated solvents. ^{31}P-NMR spectrum were measured at 161.7 MHz with a Bruker DPX-400 spectrometer; chemical shifts of these spectra were externally referenced to 85% H$_3$PO$_4$ in D$_2$O (δ = 0). Relaxation-time T_1 measurements were carried out at 400 MHz by the inversion-recovery method using the standard 180°–τ–90° pulse sequences. Elemental analyses were performed by M–H–W laboratories, Phoenix, AZ.

Trispyrazolylmethane (tpm): The ligand tpm was prepared by following a literature method,[24] with some modifications. A solution of pyrazole (10.00 g, 0.15 mmol) in 30 mL of THF was added to a vigorously stirred suspension of potassium (1.9 g, 50 mmol) in 200 mL of THF. After the potassium had completely reacted, chloroform (6.0 mL, 6.5 mmol) was slowly added over a period of 2 h, and the colloidal mixture was stirred under reflux for 36 h. The mixture was filtered at room temperature to remove the KCl, and the solvent of the filtrate was removed by using a rotary evaporator to yield a dark brown sludge. Pure trispyrazolylmethane was obtained by sublimation of the dark brown sludge. Yield: 3.1 g (9.5% based on pyrazole used).

[tpmRu(PPh$_3$)$_2$H]BF$_4$ (1): Samples of RuHCl(PPh$_3$)$_3$ (0.60 g, 0.60 mmol), tpm (0.15 g, 0.70 mmol), and NaBF$_4$ (0.072 g 0.66 mmol) were dissolved is 20 mL of THF and the solution was stirred at room temperature for 1 h. The solution was then concentrated to dryness under vacuum, and the residue was washed with methanol. Pure product was obtained by recrystallization of the residue with dichloromethane/hexane. Yield: 0.48 g (87%). – C$_{46}$H$_{41}$BF$_4$N$_6$P$_2$Ru: calcd. C 59.55, H 4.45, N 9.06; found C 59.48, H 4.48, N 8.94. – IR (KBr, cm^{-1}): ν(Ru–H) = 2054 (m). – ^{1}H NMR ([D$_6$]acetone, 400 MHz, 25 °C): δ = –13.82 (t, 1 H, $^3J_{HP}$ = 27.8 Hz), 5.99 (t, 2 H, pz, $^3J_{HH}$ = 2.36 Hz), 6.31 (t, 1 H, pz, $^3J_{HH}$ = 2.35 Hz), 6.83 (d, 1 H, pz, $^3J_{HH}$ = 1.70 Hz), 6.88 (d, 2 H, pz, $^3J_{HH}$ = 1.82 Hz), 7.13–7.37 (m, 30 H of PPh$_3$), 8.21 (d, 2 H, pz, $^3J_{HH}$ = 2.59 Hz), 8.48 (d, 1 H, pz, $^3J_{HH}$ = 2.57 Hz), 9.33 (s, 1 H, pz$_3$C*H*). – ^{31}P{^{1}H} NMR (CD$_2$Cl$_2$, 161.70 MHz, 25 °C): δ = 70.6 (s).

In Situ Preparation of [tpmRu(PPh$_3$)$_2$(H$_2$)](BF$_4$)$_2$ (2): A sample of **1** (10 mg, 11 μmol) was dissolved in 0.4 mL of [D$_2$]dichloromethane, the solution was cooled to –50 °C inside the NMR probe, 1.3 μL of HBF$_4$ (13 μmol, 54% solution in diethyl ether) was then added. A period of 15 min was allowed for completion of the reaction before NMR spectra were recorded. – ^{1}H NMR (CD$_2$Cl$_2$, 400 MHz, –50 °C): δ = –8.04 [br. s, 2 H, Ru–(H$_2$)], 5.34 (s, 1 H, pz), 5.76 (s, 1 H, pz), 5.93 (s, 2 H, pz), 6.32 (s, 2 H, pz), 6.98–7.50 (m, 30 H of PPh$_3$), 7.98 (s, 2 H, pz), 8.41 (s, 1 H, pz), 9.33 (s, 1 H, pz$_3$C*H*). – ^{31}P{^{1}H} NMR (CD$_2$CL$_2$, 161.70 MHz, –50 °C): δ = 48.2 (s). Variable- temperature T_1 measurements on the H$_2$ signal were carried out by the inversion-recovery method using standard 180°–τ–90° pulse sequence. – T_1 (400 MHz, ms): 41.3 (203 K), 32.9 (213 K), 28.2 (223 K), 25.2 (233 K), 23.9 (243 K), 28.7 (253 K). T_1(min) (400 MHz, 241 K): 24.0 ms.

In Situ Preparation of [tpmRu(PPh$_3$)$_2$(HD)](BF$_4$)$_2$ ([D$_1$]-2): A sample of **1** (18 mg, 20 μmol) was dissolved in 0.4 mL of [D$_2$]dichloromethane. After cooling the solution to –50 °C, 2.1 μL of DBF$_4$ solution was added. – ^{1}H NMR (CD$_2$Cl$_2$, 400 MHz, –50 °C): δ = –8.06 (tt, J_{HD} = 31.1 Hz, J_{HP} = 5.8 Hz).

[tpmRu(PPh$_3$)$_2$(H$_2$O)](BF$_4$)$_2$ (3): A sample of **1** (300 mg, 0.3 mmol) was dissolved in 20 mL of CH$_2$Cl$_2$, excess HBF$_4$·Et$_2$O (100 μL, 54% solution in diethyl ether) was added, followed by addition of 5 μL of H$_2$O. The solution was stirred at room temperature for 30 min, and was then concentrated to dryness under vacuum to yield a pale yellow solid, which was washed with 20 mL of diethyl ether. Yield: 270 mg (88%). – C$_{46}$H$_{42}$B$_2$F$_8$N$_6$OP$_2$Ru: calcd. C 53.55, H 4.10, N 8.15; found C 53.36, H 3.93, N 8.07. – ^{1}H NMR (CD$_2$Cl$_2$, 400 MHz, 20 °C): δ = 9.91 (s, 1 H, pz$_3$C*H*), 8.79 (d, 1 H, pz, $^3J_{HH}$ = 2.90 Hz), 8.55 (d, 2 H, pz, $^3J_{HH}$ = 2.78 Hz), 7.60–7.34 (m, 30H of PPh$_3$), 6.90 (d, 1 H, pz, $^3J_{HH}$ = 1.98 Hz), 6.43 (t, 2 H, pz, $^3J_{HH}$ = 2.48 Hz), 5.86 (t, 1 H, pz, $^3J_{HH}$ = 2.68 Hz), 5.52 (d, 1 H, pz, $^3J_{HH}$ = 2.31 Hz), 3.71 (s, 2 H, *H*$_2$O). – ^{31}P{^{1}H} NMR (CD$_2$Cl$_2$, 162 MHz, 20 °C): δ = 44.1 (s).

Acidity Measurement: The pK_a value of [tpmRu(PPh$_3$)$_2$(H$_2$)](BF$_4$)$_2$ was estimated by studying the equilibrium shown in Equation 1. In the experiment, appropriate amounts of [tpmRu(PPh$_3$)$_2$H]BF$_4$ and [^{Me}CnRu(dppe)H]BF$_4$ were dissolved in CD$_2$Cl$_2$ in an NMR tube, and a limited amount of HBF$_4$·Et$_2$O was then added. The ^{1}H-NMR spectrum was immediately taken at –60 °C. Relative molar concentrations of the equilibrated species were derived from the ^{1}H-NMR integrations of the hydride signals.

Protonation of [tpmRu(PPh$_3$)$_2$H]BF$_4$ (1) with Aqueous HBF$_4$: A sample of [tpmRu(PPh$_3$)$_2$H]BF$_4$ (**1**) (10 mg, 0.011 mmol) was dissolved in 0.4 mL of [D$_8$]THF in a 5-mm NMR tube, and 10 μL of aqueous HBF$_4$ (8 M) was added. The VT ^{1}H-NMR spectra were immediately taken.

Computational Details: The quantum mechanical calculations at the density-functional B3LYP level of theory used the effective core potentials of Wadt and Hay with double-ζ valence functions[25] for the Ru and P atoms. The standard 3–21G basis sets were applied to the first-row elements H, C, and N, with those hydrogens directly involved in hydrogen bonding (and dihydrogen bonding) augmented by single-ζ polarization functions (i.e. 3–21 g**).[26] The use of the 3–21G basis set in the calculations allows us to keep the computational expense reasonable due to the large size of the tmp ligand. All structures were fully optimized with the Gaussian98 package.[27]

Acknowledgments

This work was supported by the Hong Kong Research Grants Council (Project No. PolyU5178/99P), the Hong Kong Polytechnic University, and the Hong Kong University of Science and Technology.

[1] [1a] W. Yao, R. H. Crabtree, *Inorg. Chem.* **1996**, *35*, 3007–3011. – [1b] E. Peris, J. C. Lee, Jr., J. R. Rambo, O. Eisenstein, R. H. Crabtree, *J. Am. Chem. Soc.* **1995**, *117*, 3485–3491. – [1c] J. C. Lee, Jr., A. L. Rheingold, B. Muller, P. S. Pregosin, R. H.

Crabtree, *J. Chem. Soc., Chem. Commun.* **1994**, 1021–1022. – [1d] W. Xu, A. J. Lough, R. H. Morris, *Inorg. Chem.* **1996**, *35*, 1549–1555. – [1e] S. Park, A. J. Lough, R. H. Morris, *Inorg. Chem.* **1996**, *35*, 3001–3006. – [1f] A. J. Lough, S. Park, R. Ramachandran, R. H. Morris, *J. Am. Chem. Soc.* **1994**, *116*, 8356–8357. – [1g] S. Park, R. Ramachandran, A. J. Lough, R. H. Morris, *J. Chem. Soc., Chem. Commun.* **1994**, 2001–2002. – [1h] S. Aime, R. Gobetto, E. Valls, *Organometallics* **1997**, *16*, 5140–5141. – [1i] R. C. Stevens, R. Bau, D. Milstein, O. Blum, T. F. Koetzle, *J. Chem. Soc., Dalton Trans.* **1990**, 1429–1432.

[2] [2a] K. Abdur-Rashid, D. G. Gusev, S. E. Landau, A. J. Lough,, R. H. Morris, *J. Am. Chem. Soc.* **1998**, *120*, 11826–11827. – [2b] B. P. Patel, J. Wessel, W. Yao, J. C. Lee, Jr., E. Peris, T. F. Koetzle, G. P. A. Yap, J. B. Fortin, J. S. Ricci, G. Sini, A. Albinati, O. Eisenstein, A. L. Rheingold, R. H. Crabtree, *New J. Chem.* **1997**, *21*, 413–421. – [2c] J. A. Ayllon, S. Sabo-Etienne, B. Chaudret, S. Ulrich, H.-H. Limbach, *Inorg. Chim. Acta* **1997**, *259*, 1–4. – [2d] N. V. Belkova, E. S. Shubina, A. V. Ionidis, L. M. Epstein, H. Jacobsen, A. Messmer, H. Berke, *Inorg. Chem.* **1997**, *36*, 1522–1525. – [2e] E. S. Shubina, N. V. Belkova, A. N. Krylov, E. V. Vorontsov, L. M.Epstein, D. G. Gusev, M. Niedermann, H. Berke, *J. Am. Chem. Soc.* **1996**, *118*, 1105–1112. – [2f] B. P. Patel, W. Yao, G. P. A. Yap, A. L. Rheingold, R. H Crabtree, *Chem. Commun.* **1996**, 991–992. – [2g] E. Peris, J. Wessel, B. P. Patel, *J. Chem. Soc., Chem. Commun.* **1995**, 2175–2176. – [2h] J. Wessel, J. C. Lee, Jr., E. Peris, G. P. A. Yap, J. B. Fortin, J. S. Ricci, G. Sini, A. Albinati, T. F. Koetzle, O. Eisenstein, A. L. Rheingold, R. H. Crabtree, *Angew. Chem. Int. Ed. Engl.* **1995**, *34*, 2507–2509.

[3] R. H. Crabtree, P. E. M. Siegbahn, O. Eisenstein, A. L. Rheingold, T. Koetzle, *Acc. Chem. Res.* **1996**, *29*, 348–354.

[4] S. Aime, M. Férriz, R. Gobetto, E. Valls, *Organometallics* **1999**, *18*, 2030–2032.

[5] [5a] R. H. Crabtree, *Science* **1998**, *282*, 2000–2001. – [5b] R. H. Crabtree, *J. Organomet. Chem.* **1998**, *557*, 111–115.

[6] H. S. Chu, C. P. Lau, K. Y. Wong, W. T. Wong, *Organometallics* **1998**, *17*, 2768–2777.

[7] J. A. Ayllón, C. Gervaux, S. Sabo-Etienne, B. Chaudret, *Organometallics* **1997**, *16*, 2000–2002.

[8] W. C. Chan, C. P. Lau, Y. Z. Chen, Y. Q. Fang, S. M. Ng, G. Jia, *Organometallics* **1997**, *16*, 34–44.

[9] N. W. Alcock, I. D. Burns, A. F. Hill, K. S. Claire, *Inorg. Chem.* **1992**, *31*, 2906–2908.

[10] S. M. Ng, M. Phil. Thesis, The Hong Kong Polytechnic University, **1998**.

[11] M. I. Bruce, M. G. Humphrey, G. A. Swincer, R. C. Wallis, *Aust. J. Chem.* **1984**, *37*, 1747–1755.

[12] Some recent examples of dicationic η^2-dihydrogen complexes: [12a] S. M. Ng, Y. Q. Fang, C. P. Lau, W. T. Wong, G. Jia, *Organometallics* **1998**, *17*, 2052–2059. – [12b] D. M. Heinekey, T. A. Luther, *Inorg. Chem.* **1996**, *35*, 4396–4399. – [12c] T. A. Luther, D. M. Heinekey, *Inorg. Chem.* **1998**, *37*, 127–132. – [12d] E. Rocchini, A. Mezzetti, H. Rüegger, U. Burckhardt, V. Gramlich, A. Del Zotto, P. Martinuzzi, P. Rigo, *Inorg. Chem.* **1997**, *36*, 711–720. – [12e] M. Schlaf, A. J. Lough, P. A. Maltby, R. H. Morris, *Organometallics* **1996**, *15*, 2270–2278. – [12f] C. E. Forde, S. E. Landau, R. H. Morris, *J. Chem. Soc., Dalton Trans.* **1997**, 1663–1664. – [12g] K.-T. Smith, M. Tilset, R. Kuhlman, K. G. Caulton, *J. Am. Chem. Soc.* **1995**, *117*, 9473–9480. – [12h] W. D. Harman, H. Taube, *J. Am. Chem. Soc.* **1990**, *112*, 2261–2263. – [12i] Z.-W. Li, H. Taube, *J. Am. Chem. Soc.* **1991**, *113*, 8946–8947. – [12j] Z.-W. Li, H. Taube, *J. Am. Chem. Soc.* **1994**, *116*, 9506–9513.

[13] See experimental section for independent synthesis and characterization of **3**.

[14] M. Schlaf,, R. H. Morris, *J. Chem. Soc., Chem. Commun.* **1995**, 625–626.

[15] T. H. Lowry, K. S. Richardson, *Mechanism and Theory in Organic Chemistry*, 3rd ed., Harper Collins: New York, **1987**, chapter 3.

[16] C. D. Ritchie, *Physical Organic Chemistry, The Fundamental Concept*, Marcel Dekker: New York, **1990**, p 238.

[17] D.-H. Lee, H. J. Kwon, B. P. Patel, L. M. Liable-Sands, A. L. Rheingold, R. H. Crabtree, *Organometallics* **1999**, *18*, 1615–1621.

[18] M. G. Basallote, J. Durán, M. J. Fernández-Trujillo, M. A. Máñez, J. Rodríguez de la Torre, *J. Chem. Soc., Dalton Trans.* **1998**, 745–750.

[19] B. Reinhart, D. G. Gusev, *New J. Chem.* **1999**, 1–3.

[20] For theoretical calculations on hydride and dihydrogen complexes see for example: [20a] J. S. Craw, G. B. Bacskay, N. S. Hush, *J. Am. Chem. Soc.* **1994**, *116*, 5937–5948. – [20b] S. Dapprich, G. Frenking, *Organometallics* **1996**, *15*, 4547–4551. – [20c] I. Bytheway, G. B. Backsay, N. S. Hush, *J. Phys. Chem.* **1996**, *100*, 6023–6031. – [20d] Z. Lin, M. B. Hall, *Coord. Chem. Rev.* **1994**, *135*, 845–819 and references therein. [20e] J. Li, T. Ziegler, *Organometallics*, **1996**, *15*, 3844–3849. – [20f] Z. Xu, I. Bytheway, G. Jia, Z. Lin, *Organometallics* **1999**, *18*, 1761–1766. – [20g] R. Gelabert, M. Moreno, J. M. Lluch, Lledós, A. *J. Am. Chem. Soc.* **1997**, *119*, 9840–9847. – [20h] R. Gelabert, M. Moreno, J. M. Lluch, A. Lledós, *J. Am. Chem. Soc.* **1998**, *120*, 8168–8176.

[21] For experimental Ru–H bond lengths of Ru hydrides, see for instances: [21a] B. Chin, A. J. Lough, R. H. Morris, C. T. Schweitzer, C. D'Agostino, *Inorg. Chem.* **1994,** *33*, 6278–6288. – [21b] E. P. Cappellani, S. D. Drouin, G. Jia, P. A. Maltby, R. H. Morris, C. T. Schweitzer, *J. Am. Chem. Soc.* **1994**, *116*, 3375–3388. – [21c] P. A. Maltby, M. Schlaf, M. Steinbeck, A. J. Lough, R. H. Morris, W. T. Klooster, *J. Am. Chem. Soc*. **1996**, *118*, 5396–5407.

[22] D. R. Perrin, W. L. Armanego, *Purification of Laboratory Chemicals*, 2nd ed., Pergmon, Oxford, U.K., **1980**.

[23] P. S. Hallman, T. A. Stephenson, G. Wilkinson, *Inorg. Synth.* **1970**, *12*, 237–240.

[24] B. Huckel, *Chem. Ber.* **1937**, 2024–5026.

[25] P. J. Hay, W. R. Wadt, *J. Chem. Phys.* **1985**, *82*, 299–310.

[26] S. Huzinaga, *Gaussian basis sets for molecular calculations*, Amsterdam, Elsevier Science Pub. Co., **1984**.

[27] M. J. Frisch, G. W. Trucks, H. B. Schlegel, G. E. Scuseria, M. A. Robb, J. R. Cheeseman, V. G. Zakrzewski, J. A. Montgomery, Jr., R. E. Stratmann, J. C. Burant, S. Dapprich, J. M. Millam, A. D. Daniels, K. N. Kudin, M. C. Strain, O. Farkas, J. Tomasi, V. Barone, M. Cossi, R. Cammi, B. Mennucci, C. Pomelli, C. Adamo, S. Clifford, J. Ochterski, G. A. Petersson, P. Y. Ayala, Q. Cui, K. Morokuma, D. K. Malick, A. D. Rabuck, K. Raghavachari, J. B. Foresman, J. Cioslowski, J. V. Ortiz, B. B. Stefanov, G. Liu, A. Liashenko, P. Piskorz, I. Komaromi, R. Gomperts, R. L. Martin, D. J. Fox, T. Keith, M. A. Al-Laham, C. Y. Peng, A. Nanayakkara, C. Gonzalez, M. Challacombe, P. M. W. Gill, B. Johnson, W. Chen, M. W. Wong, J. L. Andres, C. Gonzalez, M. Head-Gordon, E. S. Replogle, J. A. Pople, *Gaussian 98, Revision A.5*, Gaussian, Inc., Pittsburgh PA, **1998**.

Received September 22, 1999
[I99335]

Spectroscopic Study of the Hydration Equilibria and Water Exchange Dynamics of Lanthanide(III) Complexes of 1,7-Bis(carboxymethyl)-1,4,7,10-tetraazacyclododecane (DO2A)

Fabrice Yerly,[a] Frank A. Dunand,[a] Éva Tóth,[a] Artur Figueirinha,[b] Zoltán Kovács,[c] A. Dean Sherry,[d] Carlos F. G. C. Geraldes,*[b] and André E. Merbach*[a]

Keywords: Imaging agents / Lanthanides / NMR spectroscopy / DNA cleavage

The hydration state of a series of $[Ln(DO2A)(H_2O)_n]^+$ complexes in aqueous solution at pH = 6.4–7.0 was studied by measuring the lanthanide-induced ^{17}O shifts (LIS) of water [Ln includes elements from Ce to Yb; DO2A = 1,7-bis(carboxymethyl)-1,4,7,10-tetraazacyclododecane]. Their contact contribution, obtained from Reilley plots, indicated a decrease in the inner-sphere water coordination number of the $[Ln(DO2A)(H_2O)_n]^+$ complexes from $n = 3$ (Ce–Eu), to $n = 2$ (Tb–Yb). A temperature-dependent UV/Vis absorption study of the 578–582 nm $^7F_0 \rightarrow {}^5D_0$ transition band of $[Eu(DO2A)(H_2O)_n]^+$ in aqueous solution showed that this complex is present in an equilibrium between eight- and nine-coordinate species with $n = 2$ and $n = 3$, respectively. The hydration equilibrium parameters ($2 \rightleftarrows 3$), $K_{2-3}^{298} = 4.0 \pm 0.2$, $\Delta H_{2-3}^0 = -12.1 \pm 1$ kJ mol^{-1} and $\Delta S_{2-3}^0 = -28.9 \pm 3$ J mol^{-1} K^{-1},correspond to an average hydration number of 2.65–2.85 in the temperature range 273–363 K. A variable temperature, multiple field ^{17}O NMR study combined with direct EPR measurements of the transverse electronic relaxation rates has been used to obtain the parameters characterizing water exchange, rotation and electronic relaxation, all influencing the proton relaxivity of $[Gd(DO2A)(H_2O)_{2-3}]^+$. The small increase in the water exchange rate of $[Gd(DO2A)(H_2O)_{2-3}]^+$ ($k_{ex}^{298} = (10 \pm 5) \times 10^6 s^{-1}$) relative to that of$[Gd(DOTA)(H_2O)]^-$ (4.8×10^6 s^{-1}) is a consequence of an unfavorable interplay of charge and hydration equilibria. The value of $\tau_R^{298} = 40 \pm 1$ ps is short, and the electronic relaxation rate ($1/T_{2e} \approx 1.2 \times 10^{10}$ s^{-1}) is fast relative to $[Gd(DOTA)(H_2O)]^-$ ($1.3–2.4 \times 10^9$ s^{-1} for $B = 0.34$ T). These parameters negate to some extent the expected increase in proton relaxivity of the $[Gd(DO2A)(H_2O)_{2-3}]^+$ complex.

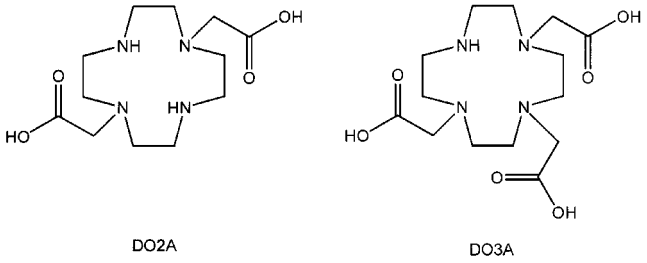
Introduction

There is a continued strong interest in the synthesis and characterization of trivalent lanthanide complexes, largely driven by biological and medical applications in magnetic resonance imaging (MRI),[1] NMR shift reagents,[2] luminescence probes[3] and DNA/RNA cleavage agents.[4] Macrocyclic ligands are often targeted because they form thermodynamically and kinetically stable complexes with Ln^{3+} ions, thereby making them particularly attractive for these types of biomedical applications. A classic example is the $[Gd(DOTA)(H_2O)]^-$ complex, a widely used MRI contrast agent [DOTA = 1,4,7,10-tetrakis(carboxymethyl)-1,4,7,10-tetraazacyclododecane]. One feature of $[Gd(DOTA)(H_2O)]^-$ that is common to most other commercially available contrast agents is its lack of tissue specificity. One approach to obtain tissue-specific MRI contrast agents has been the synthesis of positively charged Gd^{III} complexes which target bone tissue.[5] It has been proposed that the mechanism of bone uptake is related to the ability of positively charged complexes to mimic biological cations (Ca^{2+}, K^+, etc.) in their interactions with anionic bone surfaces.[5b] Cationic complexes also serve as candidates for DNA/RNA ribonuclease mimics, provided they have free coordination sites (inner-sphere waters) available to coordinate with nucleotides.[6] Removal of one or two carboxylates from the ligand DOTA results in a decrease in complex stability and an increase in the number of inner-sphere water molecules [see structures of DO3A = 1,4,7-tris(carboxymethyl)-1,4,7,10-tetraazacyclododecane and DO2A = 1,7-bis(carboxymethyl)-1,4,7,10-tetraazacyclododecane in Scheme 1].

A recent UV/Vis study of $[Eu(DO3A)(H_2O)_n]$ has shown that in aqueous solution this complex is present in an equilibrium between eight- and nine-coordinate species having one and two inner-sphere water molecules, respectively.[7] Among other parameters, including the rate of molecular tumbling and electronic relaxation, the exchange rate of these coordinated water molecules is an important factor in

[a] Institute of Inorganic and Analytical Chemistry, University of Lausanne, BCH, CH-1015 Lausanne, Switzerland
[b] Department of Biochemistry, Faculty of Science and Technology, and Center of Neurosciences, University of Coimbra, Apartado 3126, 3000 Coimbra, Portugal
[c] Department of Chemistry, The University of Texas at Dallas, P. O. Box 830688, Richardson, TX 75083–0688, U.S.A.
[d] See address [c] and The Mary Nell and Ralph B. Rogers Magnetic Resonance Center, Department of Radiology, University of Texas Southwestern Medical Center, 5801 Forest Park Rd., Dallas, TX 75235–9085, U.S.A.
Supporting information for this article is available on the WWW under http://www.wiley-vch.de/home/eurjic or from the author.

 © WILEY-VCH Verlag GmbH, D-69451 Weinheim, 2000 1434–1948/00/0505–1001 $ 17.50+.50/0



Scheme 1. Structure of the ligands DO2A and DO3A

determining the proton relaxivity, hence the efficiency of the Gd^{III} complex as an MRI contrast agent.

The objective of this work was to study the hydration state of several $[Ln(DO2A)(H_2O)_n]^+$ complexes and to evaluate the factors that influence the proton relaxivity of $[Gd(DO2A)(H_2O)_n]^+$. Although the low stability constant recently reported for $[Gd(DO2A)(H_2O)_n]^+$,[8] much lower than the value reported previously,[5c] indicates that this complex may not be suitable for biomedical applications, it serves as a useful model of a complex having more than a single inner-sphere water molecule, and the influence of this on water relaxivity. To get information on structural similarities or changes along the Ln^{III} series, lanthanide induced ^{17}O shifts (LIS) of water have been measured for the whole series of lanthanide(III) DO2A complexes and analyzed in terms of Reilley plots.[9] The UV/Vis spectra of $[Eu(DO2A)(H_2O)_n]^+$ gave unambiguous evidence for the existence of a hydration equilibrium for this complex. A variable temperature, multiple field ^{17}O NMR study combined with direct measurements of the transverse electronic relaxation rates has been used to determine the water exchange rate of $[Gd(DO2A)(H_2O)_n]^+$.

Results and Discussion

Lanthanide Induced ^{17}O NMR Shift Measurements

To obtain the number of inner-sphere water molecules, n, in the $[Ln(DO2A)(H_2O)_n]^+$ complexes, ^{17}O NMR chemical shifts were measured on 0.020 M solutions of those complexes in 2% ^{17}O-enriched water (Ln = La, Ce, Pr, Nd, Eu, Dy, Ho, Er, Yb and Lu), at pH 7–8, 346 K and 9.4 T. To ensure that the complexes are fully formed (for 0.020 M solutions, at pH > 7.8 for the La^{III} complex, at pH > 6.8 for the Gd^{III} complex, and at pH > 6.5 for the Lu^{III} complex),[8] complexation was verified by ^1H NMR spectroscopy. As there are two conflicting reports on the thermodynamic stability constant for $[Gd(DO2A)(H_2O)_n]^+$,[5c,8] the lower stability constant value was assumed when preparing the complexes so as to ensure that all metal was complexed. Although some complexes may have one partially hydrolyzed, inner-sphere water molecule under the conditions used here (the value of the hydrolysis constant obtained for the $[Eu(DO2A)(H_2O)_n]^+$ complex has been reported to be $pK_a^{Eu} = 8.1 \pm 0.3$),[8] such ionization would not affect the measured ^{17}O shift values of bulk water.[1b]

The ^{17}O shift (Δ) of water in the presence of a paramagnetic complex has diamagnetic (Δ_d), contact (Δ_c) and pseudocontact contributions (Δ_p).[1b] The value of Δ_d was taken as the average shift observed in the La^{3+} and Lu^{3+} complexes. The remaining sum, $\Delta_c + \Delta_p$, can be expressed as a product of terms, one characteristic of the Ln^{3+} ion but independent of the structure of the complex ($<S_z>$ and C^D, respectively) and another characteristic of the complex but independent of the Ln^{3+} ion (F and G, respectively). Thus, the paramagnetic shift induced by the lanthanide (LIS) Δ' is given by Equation 1:[1b,10,11]

$$\Delta' = \Delta - \Delta_d = \Delta_c + \Delta_p = <S_z> F + C^D G \quad (1)$$

Values of $<S_z>$ and C^D were taken from the literature[10,11] and Equation 1 was rearranged into a linear form to give Equation 2:[9,12]

$$\Delta'/C^D = <S_z> F/C^D + G \quad (2)$$

For an isostructural series of Ln^{3+} complexes, a plot of Δ'/C^D vs. $<S_z>/C^D$ should be linear. Deviations from linearity have been taken as evidence for a change in structure along the Ln^{III} series.[1b,9,12]

The observed ^{17}O LIS values of water at 346 K were extrapolated to $\rho_W = [Ln]/[H_2O] = 1$. Since water exchange between the bulk and the inner coordination sphere of the $[Ln(DO2A)(H_2O)_n]^+$ complexes is fast,[5c] the extrapolated ^{17}O shift values correspond to nΔ.[13] A plot of ^{17}O shifts according to Equation 2 does not follow a single linear correlation but rather divides into two groups (Ce–Eu and Dy–Yb) with a "break" near the middle of the lanthanide series (see Figure 1).

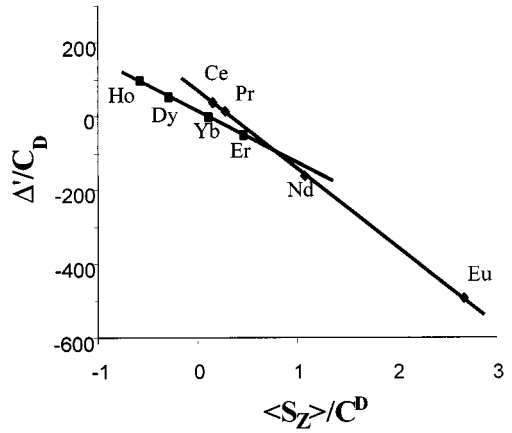


Figure 1. Plot of Δ'/C^D versus $<S_z>/C^D$ for the ^{17}O resonance of the $[Ln(DO2A)(H_2O)_n]$ complexes at 346 K

Such a break could reflect a change in the water coordination number of the complexes along the lanthanide series. A linear regression analysis[9] of the two sets of data gives nF = –211 ± 1 and nG = 72.5 ± 2.1 for Ln = Ce–Eu, and nF = –140 ± 4 and nG = 12.2 ± 1.7 for Ln = Dy–Yb. The ^{17}O LIS of the coordinated water molecules is dominated by the contact contribution[1b] as shown by the large F values. The values of F for Ln^{3+}-bound ^{17}O nuclei are known to be rather constant at –70 ± 11 at 346 K.[1b,13] Using this constant and the values of nF obtained from the plot, values of $n = 3 \pm 0.3$ and $n = 2 \pm 0.3$ were estimated

for the Ce–Eu and Dy–Yb series, respectively. The value of $n = 2$ for the heavier Ln ion complexes agrees with the previously published value for $[Dy(DO2A)(H_2O)_n]^+$ derived from a ^{17}O shift titration.[5c] The calculated values of nG and n also led us to values of $G = 21.2 \pm 0.7$ for Ce–Eu and $G = 6.1 \pm 0.8$ for Dy–Yb. This decrease in the average geometric term G for the ^{17}O nuclei of the coordinated water molecules from the first to the second half of the Ln series is also in agreement with the proposed decrease in the water coordination number. In fact, the change of $n = 3$, with a possible monocapped square antiprismatic coordination geometry of the Ln ion in $[Ln(DO2A)(H_2O)_3]^+$, to $n = 2$, with a possible square antiprismatic coordination geometry of the Ln ion in $[Ln(DO2A)(H_2O)_2]^+$, would correspond to a loss of the water molecule in the capping position. This coordination position makes the largest contribution to the G value.

UV/Vis Measurements

The ^{17}O LIS measurements indicated that a structural change occurs in the middle of the Ln^{III} series near Eu^{III}. Eu^{III} has a transition band in the visible spectrum at 578–582 nm ($^7F_0 \rightarrow {}^5D_0$) which is very sensitive to changes in the coordination environment and has been previously used to characterize coordination equilibria for Eu^{III} complexes.[7,14,15] In accordance with the ^{17}O LIS measurements, the UV/Vis spectrum of a $[Eu(DO2A)(H_2O)_n]^+$ solution clearly shows the presence of two coordination species (a representative spectrum is given in Figure 2).

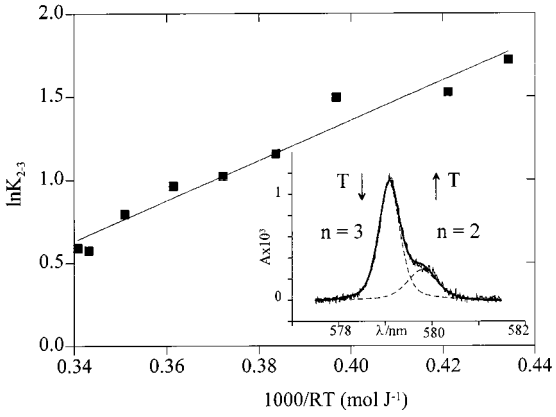


Figure 2. Ratio of the integrals of the two transition bands ($n = 2$ and $n = 3$) in the UV/Vis spectrum of $[Eu(DO2A)(H_2O)_n]^+$ as a function of the inverse temperature; the line represents a linear least-squares fit to the data points; the resulting parameters are $\Delta H^0 = -12.1 \pm 1$ kJ mol^{-1}, $\Delta S^0 = -28.9 \pm 3$ J mol^{-1} K^{-1}; the inserted figure shows a typical UV/Vis spectrum of the Eu^{3+} $^7F_0 \rightarrow {}^5D_0$ transition in a $[Eu(DO2A)(H_2O)_n]^+$ solution ($T = 323.0$ K; $c_{Eu} = 0.01$ M); the dashed lines represent the fitted contributions of the two peaks to the overall spectrum, itself given by the solid line

Chang et al. recently published a pH-dependent luminescence study of $[Eu(DO2A)(H_2O)_n]^+$ in the pH range 5.2–9.6 (ambient temperature).[8] The luminescence spectra present two bands of varying intensity as a function of pH, assigned to the $[Eu(DO2A)(H_2O)_3]^+$ and $[Eu(DO2A)(H_2O)_2(OH)]$ species. Based on the relative peak intensities, they estimated a hydrolysis constant of 8.1 ± 0.3 (pK_a). Since the pH of our $[Eu(DO2A)(H_2O)_n]^+$ sample was 6.4, the amount of any deprotonated complex would be negligible and hence this cannot explain the second absorption band in the spectrum. Moreover, the intensity of one band increases while that of the other decreases with increasing temperature, a feature characteristic of hydration equilibria. Since $DO2A^{2-}$ has 6 donor atoms and coordination numbers of 8 or 9 are generally observed for Eu^{III} complexes, the equilibrium can be depicted as shown in Equation 3:

$$[Eu(DO2A)(H_2O)_2]^+ + H_2O \rightleftarrows [Eu(DO2A)(H_2O)_3]^+ \quad (3)$$

A comparison of the position of the two transition bands with those of previously studied 8- and 9-coordinate Eu^{III} poly(aminocarboxylate) complexes[7,15] is consistent with this assignment. The band at $\lambda_{max} \approx 579.8$ nm, which gains intensity with increasing temperature, is assigned to the complex of lower coordination number, $[Eu(DO2A)(H_2O)_2]^+$, while the band at $\lambda_{max} \approx 579.0$ nm can be assigned to $[Eu(DO2A)(H_2O)_3]^+$.

The hydration equilibrium constant is defined by Equation 4:

$$K_{2-3} = \frac{[Eu(DO2A)(H_2O)_3]^+}{[Eu(DO2A)(H_2O)_2]^+} \quad (4)$$

The reaction enthalpy, $\Delta H_{2-3}°$, and the reaction entropy, $\Delta S_{2-3}°$, for the equilibrium can be obtained from the temperature dependence of K_{2-3} (Equation 5):

$$\ln K_{2-3} = \frac{\Delta S^0_{2-3}}{R} - \frac{\Delta H^0_{2-3}}{RT} \quad (5)$$

The spectra were analyzed with a program developed in our laboratory,[15] which relates the ratio of the integrals of the two bands to the equilibrium constant. The temperature dependence of the ratio of the band integrals is presented in Figure 2. A fitting of the data to Equation 5 gave values for $\Delta H^0_{2-3} = -12.1 \pm 1$ kJ mol^{-1}, $\Delta S^0_{2-3} = -28.9 \pm 3$ J mol^{-1} K^{-1} and $K^{298}_{2-3} = 4.0 \pm 0.2$. This corresponds to an average hydration number of 2.65–2.85 for $[Eu(DO2A)(H_2O)_{2-3}]^+$ in the temperature range 273–363 K.

It should also be noted that in the spectra reported by Chang et al., a small shoulder on one of the bands was present. Though not interpreted by the authors, it could represent differently hydrated species. In their study, the number of inner-sphere water molecules as determined by differences in excited-state lifetimes in H_2O and D_2O[16] was found to be $n = 3.0$ for the fully protonated species. However, it does not preclude the existence of a hydration equilibrium since the usual error in the value of n determined by this method is approximately ± 0.2.

^{17}O NMR and EPR Measurements

Transverse and longitudinal ^{17}O relaxation rates and chemical shifts were measured for $[Gd(DO2A)(H_2O)_n]^+$ at

1.41, 9.4 and 14.1 T as a function of temperature. The UV/Vis measurements performed on the corresponding $[Eu(DO2A)(H_2O)_n]^+$ complex indicated that this complex is present in two hydrated forms. There is no direct method to study hydration equilibrium for a Gd^{III} complex, so one can only rely on the results obtained for the nearest neighbor, Eu^{III}. In the case of $[Ln(DO3A)(H_2O)_n]$, a luminescence study of the Tb^{III} complex and the UV/Vis measurements on the corresponding Eu^{III} chelate both resulted in similar values for the water coordination number (n = 1.8 and 1.9, respectively), indicating that it is reasonable to assume the same hydration equilibria for the Gd^{III} and Eu^{III} complexes. This means that in a solution of $[Gd(DO2A)(H_2O)_n]^+$ there are two species (the bis- and tris-hydrated complex) both of which can, in principle, exchange with bulk water. Consequently, any analysis of the transverse relaxation rates in this system should be treated as a three-site exchange problem.

We recently compared the analyses of ^{17}O NMR data of $[Gd(DO3A)(H_2O)_n]$ (n = 1 and 2) performed with the rigorous three-site exchange approach using Kubo–Sack matrices versus the more typical Swift–Connick treatment by assuming a temperature-dependent value for the mole fraction of bound water.[7] The two approaches gave the same results for parameters derived from the ^{17}O NMR data. This led us to conclude that, in such cases, where the equilibrium between the two differently hydrated species is strongly shifted towards one complex (for both $[Gd(DO2A)(H_2O)_n]^+$ and $[Gd(DO3A)(H_2O)_n]$ it was the nine-coordinate complex), the simpler Swift–Connick treatment provides sufficiently precise results, and application of the more complicated Kubo–Sack formalism is not necessary. Therefore the present ^{17}O NMR data for $[Gd(DO2A)(H_2O)_n]^+$ have been analyzed by means of the Swift–Connick equations, according to the method previously described.[7,17,18] For the mole fraction of bound water (P_m), we used a temperature-dependent value calculated on the basis of ΔH^0_{2-3} and ΔS^0_{2-3} obtained for $[Eu(DO2A)(H_2O)_{2-3}]^+$ in the UV/Vis study. In the calculations, the electronic relaxation rates measured by EPR at 0.34 T (X-band) have been fitted simultaneously with the ^{17}O NMR data. The transverse electronic relaxation rate ($1.2 \pm 0.1 \times 10^{10}$ s^{-1}) measured at 0.34 T was independent of temperature over the range T = 274 – 356 K. The transverse ^{17}O relaxation rates and chemical shifts as well as the fitted curves are presented in Figure 3.

The fit resulted in the following parameters: $k_{ex}^{298} = 10 \pm 5 \times 10^6$ s^{-1}, $\Delta H^{\neq} = 21.3 \pm 4$ kJ/mol, $\Delta S^{\neq} = -39 \pm 11$ kJ/mol $\tau_R^{298} = 40 \pm 1$ ps, $E_R = 16.4 \pm 0.7$ kJ/mol, $\tau_v^{298} = 16 \pm 1$ ps, $E_v = 1.0$ kJ/mol, $\Delta^2 = 1.06 \pm 0.02 \times 10^{20}$ s^{-2} and $A/\hbar = -3.4 \pm 0.2 \times 10^6$ rad s^{-1}.

Previous ^{17}O NMR studies on numerous Gd^{III} complexes have shown that the rate and mechanism of water exchange is strongly related to the inner-sphere structure of the chelate. These findings suggested that, for complexes with a hydration equilibrium, less energy is needed to pass from the reactant to the transition state since both are already present in solution. Thus, one might expect an increased

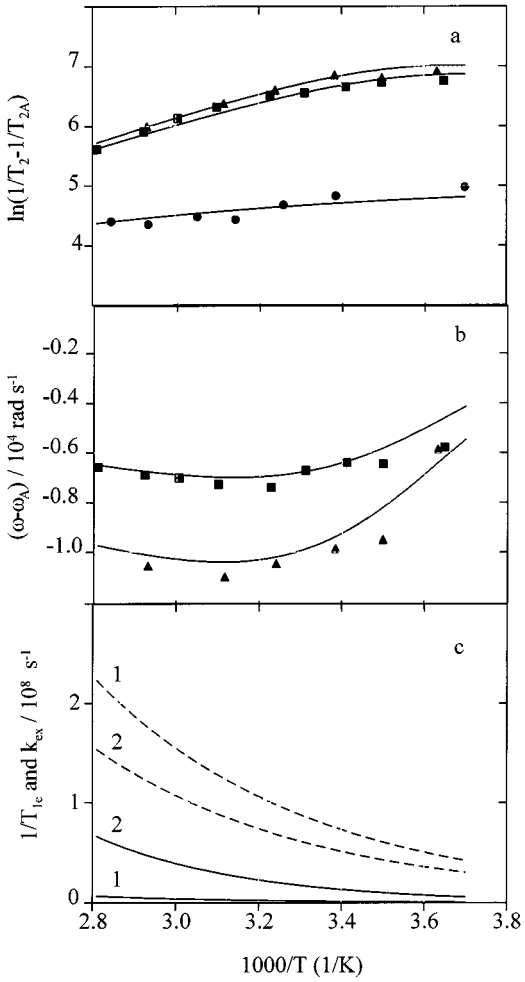


Figure 3. Temperature dependence of the transverse ^{17}O relaxation enhancements (a) and chemical shifts (b) at B = 14.1 T (σ), 9.4 T (n) and 1.41 T (l); the solid lines correspond to the simultaneous least-squares fit to all data points according to the Swift and Connick equations using a temperature dependent P_m value; the lower part of the figure (c) represents k_{ex} (solid lines) and $1/T_{1e}$ (dashed lines), the two contributions to the overall correlation time that governs the transverse ^{17}O relaxation, as computed for the two limiting cases of $k_{ex}^{298} = 5 \times 10^6$ (1) and 15×10^6 s^{-1} (2) (see text)

water exchange rate for $[Gd(DO2A)(H_2O)_{2-3}]^+$ than for a system like $[Gd(DOTA)(H_2O)]^-$ having a single hydrated species. Contrary to expectations for both $[Gd(DO2A)(H_2O)_{2-3}]^+$ and $[Gd(DO3A)(H_2O)_{1-2}]$, only a limited gain in the water exchange rate was observed {about two-fold compared with $[Gd(DOTA)(H_2O)]^-$ ($k_{ex}^{298} = 10 \times 10^6$ s^{-1} and 11×10^6 s^{-1} for the DO2A and DO3A complexes, respectively, versus 4.8×10^6 s^{-1} for the DOTA complex)}.[7] However, a second confounding factor that one must consider in these complexes is the increase in overall positive charge on the DO3A and DO2A complexes. A previous study on the Gd^{III} complex of the pentacarboxylate $DOTASA^{5-}$ has clearly shown that a higher negative charge favors fast water exchange, as k_{ex}^{298} of $[Gd(DOTASA)(H_2O)]^{2-}$ was about 50% higher than that of $[Gd(DOTA)(H_2O)]^-$ ($H_5DOTASA$ = 1,4,7,10-tetraazacyclododecane-1-succinic acid-4,7,10-triacetic acid).[19] A similar effect was observed upon substitution of one carboxylate of

$DOTA^{4-}$ or $DTPA^{5-}$ by noncharged amide groups. In both systems, the water exchange rate diminished by a factor of 3–4. Thus, the limited increase in the water exchange rate of $[Gd(DO2A)(H_2O)_{2-3}]^+$ or $[Gd(DO3A)(H_2O)_{1-2}]$ relative to that of $[Gd(DOTA)(H_2O)]^-$ must reflect two opposing effects: the favorable hydration equilibrium effect partially cancelled by the unfavorable charge effects.

The k_{ex} values as cited above correspond to the exchange of one water molecule, hence the overall water exchange rate is about twice the k_{ex} of $[Gd(DO3A)(H_2O)_{1-2}]$ (the average hydration number close to 2) and three times the k_{ex} of $[Gd(DO2A)(H_2O)_{2-3}]^+$ (the average hydration number close to 3). Consequently, the overall water-exchange rates of $[Gd(DO3A)(H_2O)_{1-2}]$ and $[Gd(DO2A)(H_2O)_{2-3}]^+$ relative to that of $[Gd(DOTA)(H_2O)]^-$ were greater by a factor 4 and 6, respectively.

It should be noted that the error in k_{ex}^{298} determined in this study is exceptionally high. The reason lies in the unfavorable interplay of water exchange and electronic relaxation for this system. For $[Gd(DO2A)(H_2O)_{2-3}]^+$, a slow exchange region, where the $1/T_2$ values are directly proportional to the water exchange rate, does not exist over the temperature range examined (the transverse relaxation rate enhancement never increases with temperature; see Figure 3). In the fast and intermediate exchange regions, the relaxation rate of the Gd^{III} electron spin also contributes to the measured $1/T_2$ values. Thus, one needs information on the electronic relaxation rate to extract an accurate value for k_{ex}. We have performed further measurements of the transverse electronic relaxation rates by EPR (unfortunately the magnetic field is quite different from that used in the ^{17}O study) and ^{17}O transverse relaxation rates at three different magnetic fields, in order to achieve this goal. The latter information usually allows better definition of the electronic relaxation contribution, which is the field-dependent term in $1/T_2$. Despite these efforts, the uncertainty in the water exchange rate remained unusually high. Figure 3(c) summarizes the contribution of k_{ex} and the longitudinal electronic relaxation rate, $1/T_{1e}$, to the overall correlation time that governs the ^{17}O transverse relaxation ($1/\tau_{s1,2} = k_{ex} + 1/T_{1e}$). The plots clearly show that, at all temperatures, the contribution of $1/T_{1e}$ is larger than that of k_{ex}. The relatively fast electronic relaxation is directly evidenced by the $1/T_{2e}$ values measured by EPR (ca. 1.2×10^{10} s^{-1}) and independent of temperature for $[Gd(DO2A)(H_2O)_{2-3}]^+$, but in the range $1.3–2.4\times10^9$ s^{-1} for $[Gd(DOTA)(H_2O)]^-$ ($B = 0.34$ T). Interestingly, the electronic-relaxation times obtained from NMRD profiles for positively charged pyridine containing DO2A-like Gd^{III} complexes have also been reported to be shorter than for $[Gd(DOTA)(H_2O)]^-$.[5b]

Implications for Water Proton Relaxivity

The relaxivity of $[Gd(DO2A)(H_2O)_n]^+$ in the pH region where the complex is fully formed is proportional to its hydration state (n).[20] However, deprotonation of one of the inner-sphere water molecules in the $[Gd(DO2A)(H_2O)_n]^+$ complexes, leading to the $[Gd(DO2A)(H_2O)_{n-1}(OH)]$ species could modify the relaxivity at high pH. It has been reported in several systems that at high pH values, OH^- catalyzed proton exchange becomes important and the proton-exchange rate determining the proton relaxivity cannot be simply given by the water-exchange rate. The hydration and hydrolysis equilibria have been studied for the Eu^{III} complex,[8] where the tris-aqua form predominates, $K_{2-3}^{298} = 4.0 \pm 0.2$. Therefore the value of the hydrolysis constant, $pK_a^{Eu} = 8.1 \pm 0.3$,[8] which is an average of the hydrolysis constants for the two species with $n = 2$ and 3 weighted by their concentrations, corresponds almost exclusively to the deprotonation of the trihydrated complex, $[Eu(DO2A)(H_2O)_3]^+$. Assuming that the hydration and hydrolysis equilibria of the Gd^{III} and Eu^{III} complexes are similar, their ionization pK_a values should also be similar and no changes in relaxivity of $[Gd(DO2A)(H_2O)_n]^+$ due to hydrolysis are expected below pH $\approx$ 7.1.

A relaxivity of 6.49 $mM^{-1}s^{-1}$ has been reported previously[5b] for $[Gd(DO2A)(H_2O)_n]^+$ at pH 7.0, 298 K and 40 MHz. A simulation using an average n of 2.8 and the parameters obtained from the ^{17}O NMR and EPR study estimated a relaxivity of 6.18 $mM^{-1}s^{-1}$ at the same frequency and temperature, consistent with the measured value.

As discussed in the introduction, the Gd^{III} complexes with hydration equilibrium were expected to have higher water-exchange rates than chelates with a single hydration state. Such accelerated water exchange could result in a significant increase in proton relaxivity for macromolecular derivatives of such systems where the relaxivity is limited by slow water exchange. For $[Gd(DO2A)(H_2O)_{2-3}]^+$ itself, water exchange has no observable effect on the proton relaxivity since it is exclusively limited by fast rotation (and perhaps by fast electronic relaxation). However, in a macromolecular agent the substitution of $DOTA^{4-}$ with $DO2A^{2-}$ could result in a significant increase in proton relaxivity, since the water exchange rate would be increased by a factor of 6.

Conclusion

The hydration equilibrium and dynamics of a series of $[Ln(DO2A)(H_2O)_n]^+$ complexes in aqueous solution at pH = 6.4 – 7.0 was studied by several spectroscopic techniques. An analysis of the lanthanide induced ^{17}O shifts (LIS) of bulk water provided evidence for a decrease in the number of inner-sphere coordinated water molecules in the $[Ln(DO2A)(H_2O)_n]^+$ complexes, changing from $n = 3$ to $n = 2$ near Eu^{III}. A temperature-dependent UV/Vis study of $[Eu(DO2A)(H_2O)_n]^+$ in aqueous solution provided further evidence for an equilibrium between eight- and nine-coordinate species (n = 2,3), with the nine-coordinate $[Eu(DO2A)(H_2O)_3]^+$ species predominating.

A variable temperature, multiple field ^{17}O NMR study combined with direct EPR measurements has been used to calculate the parameters characterizing water exchange, rotation and electronic relaxation, all of which influence the proton relaxivity of $[Gd(DO2A)(H_2O)_{2-3}]^+$. The limited in-

crease in water exchange rate, $k_{ex}^{298} = 10 \pm 5 \times 10^6$ s^{-1}, compared with $[Gd(DOTA)(H_2O)]^-$ (4.8×10^6 s^{-1}) is a consequence of the opposite influence of the charge and of the hydration equilibrium. However, as there are 2.8 times as many water molecules on average in the $[Gd(DO2A)(H_2O)_{2-3}]^+$ complex compared with $[Gd(DOTA)(H_2O)]^-$ (298 K), the overall gain in water exchange is significant. The proton relaxivity of $[Gd(DO2A)(H_2O)_{2-3}]^+$ is lower than expected, despite the favorable water coordination number of this complex. This reflects a combination of favorable and unfavorable parameters that contribute to its relaxivity, in particular a relatively slow water exchange rate, a short τ_R, and a fast electronic relaxation rate.

Experimental Section

Sample Preparation: The $DO2A^{2-}$ ligand was synthesized by a previously published method.[21] The $[Ln(DO2A)(H_2O)_n]$ complexes were prepared by mixing equimolar quantities of the ligand and metal solutions, followed by heating (353 K) for two hours. The pH was regularly adjusted to 6 – 7. The ^{17}O NMR shift measurements for the series of Ln^{III} complexes (different from Gd^{III}) were performed on 0.020 mM $[Ln(DO2A)(H_2O)_n]^+$ solutions (pH = 7.0). The ^{17}O NMR measurements for the Gd^{III} complex were performed on a 0.0119 mol/kg $[Gd(DO2A)(H_2O)_n]^+$ solution (pH = 6.53); a $[Y(DO2A)(H_2O)_n]^+$ solution of the same pH and concentration was used as an external reference. To improve sensitivity, ^{17}O-enriched water (10% $H_2^{17}O$, Yeda R&D Co.) was added to the solutions resulting in a 2% ^{17}O enrichment. The absence of free Ln^{III} ion was verified with xylenol orange indicator.[22]

UV/Visible Spectrophotometry: UV/Visible spectra of a $[Eu(DO2A)(H_2O)_n]^+$ solution (c_{Eu} = 0.01 M; pH = 6.5) were recorded in the temperature range 277–350 K on a Perkin–Elmer Lambda 19 spectrometer, using thermostated cells with a 10 cm optical length (λ = 577.5 – 581.5 nm).

^{17}O NMR Measurements: The ^{17}O NMR shift study of the $[Ln(DO2A)(H_2O)_n]^+$ series of complexes was performed using a Bruker AM-400 spectrometer (9.4 T; 54.2 MHz) at 346 K. The samples were introduced in spherical glass bulbs inside 10 mm NMR tubes, with a drop of nitromethane as an internal shift reference. The spectra were run unlocked. Downfield-induced shifts were taken as positive. A variable temperature ^{17}O NMR study of $[Gd(DO2A)(H_2O)_n]^+$ was performed at 3 different magnetic fields using Bruker spectrometers: AMX2–600 (14.1 T, 81.4 MHz), AM-400 (9.4 T; 54.2 MHz) and a 1.41 T, 8.14 MHz electromagnet were connected to an AC-200 console. Bruker VT-1000 temperature control units were used to stabilize the temperature, which was measured by a substitution technique.[23] Bulk water longitudinal relaxation rates, $1/T_1$, were obtained by the inversion recovery method,[24] and transverse relaxation rates, $1/T_2$, by the Carr–Purcell–Meiboom–Gill spin echo technique.[25]

Data Analysis: The least-squares fitting was performed by the program Scientist® for Windows® by Micromath®, version 2.0 The reported errors correspond to one standard deviation obtained by the statistical analysis.

Acknowledgments

We thank Dr. Lothar Helm for helpful discussions. We are grateful to the Swiss National Science Foundation, the Office for Education and Science (OFES), Nycomed Amersham Imaging, the Portuguese Foundation of Science and Technology (grant Praxis 2/2.2/SAU/1194/95), and to the Robert A. Welch Foundation (AT-584) for financial support. This research was carried out in the frame of the EC COST D8 action and the EU-BIOMED program (MACE project).

[1] [1a] R. B. Lauffer, *Chem. Rev.* **1987**, *87*, 901. – [1b] J. A. Peters, J. Huskens, D. J. Raber, *Prog. Nucl. Magn. Reson. Spectr.* **1996**, *28*, 283.
[2] A. D. Sherry, C. F. G. C. Geraldes, in *Lanthanide Probes in Life, Chemical and Earth Sciences, Theory and Practice* (Eds.: J.-C. G. Bünzli, G. R. Choppin), Elsevier, Amsterdam, **1986**, Chapter 4.
[3] [3a] J. M. Lehn, C. O. Roth, *Helv. Chim. Acta* **1991**, *74*, 572. – [3b] F. S. Richardson, *Chem. Rev.* **1982**, *82*, 541.
[4] J. R. Morrow, L. A. Buttrey, V. M. Shelton, K. A. Berback, *J. Am. Chem. Soc.* **1992**, *114*, 1903.
[5] [5a] W. D. Kim, D. C. Hrncir, G. E. Kiefer, A. D. Sherry, *Inorg. Chem.* **1995**, *34*, 2225. – [5b] W. D. Kim, G. E. Kiefer, G. E. Maton, K. McMillan, R. N. Muller, A. D. Sherry, *Inorg. Chem.* **1995**, *34*, 2233. – [5c] J. Huskens, D. A. Torres, Z. Kovacs, J. P. André, C. F. G. C. Geraldes, A. D. Sherry, *Inorg. Chem.* **1997**, *36*, 1495. – [5d] S. Aime, M. Botta, S. G. Crich, G. B. Giovenzanna, G. Jommi, R. Pagliarin, M. Sisti, *Inorg. Chem.* **1997**, *36*, 2992.
[6] S. Amin, H. R. Morrow, C. H. Lake, M. R. Churchill, *Angew. Chem. Int. Ed. Engl.* **1994**, *33*, 773.
[7] É. Tóth, O. M. Ni Dhubhghaill, G. Besson, L. Helm, A. E. Merbach, *Magn. Res. Chem.* **1999**, *37*, 701.
[8] C. A. Chang, Y.-H. Chen, H.-Y. Chen, F.-K. Shieh, *J. Chem. Soc., Dalton Trans.* **1998**, 3243.
[9] C. N. Reilley, B. W. Good, R. D. Allendoerfer, *Anal. Chem.* **1976**, *48*, 1446.
[10] [10a] R. M. Golding, M. P. Halton, *Aust. J. Chem.* **1972**, *25*, 2577. – [10b] A. A. Pinkerton, M. Rossier, S. Stavros, *J. Magn. Reson.* **1985,** *64,* 420.
[11] B. Bleaney, *J. Magn. Reson.* **1972,** *8,* 91.
[12] J. Reuben, *J. Magn. Reson.* **1982,** *50*, 233.
[13] C. F. G. C. Geraldes, A. M. Urbano, M. A. Hoefnagel, J. A. Peters, *J. Chem. Soc., Dalton. Trans*, **1992**, 463, and references therein.
[14] G. Geier, C. K. Jorgensen, *Chem. Phys. Lett.*, **1971**, 263.
[15] N. Graeppi, D. H. Powell, G. Laurenzcy, L. Zékány, A. E. Merbach, *Inorg. Chim. Acta*, **1994**, *235*, 311.
[16] [16a] W. D. Horrocks, Jr., D. R. Sudnick, *J. Am. Chem. Soc.* **1979**, *101*, 334. – [16b] W. D. Horrocks, Jr., M. Albin, *Prog. In Org. Chem.* **1984**, *31*, 1.
[17] K. Micskei, L. Helm, E. Brücher, A. E. Merbach, *Inorg. Chem.* **1993**, *32*, 3844.
[18] G. Gonzalez, D. H. Powell, V. Tissières, A. E. Merbach, *J. Phys. Chem.*, **1994**, *98*, 53.
[19] J. P. André, H. Maecke, É. Tóth, A. E. Merbach, *J. Biol. Inorg. Chem.* **1999**, *4,* 341.
[20] X. Zang, C. A. Chang, H. G. Brittain, J. M. Garrison, J. Telser, M. Tweedle, *Inorg. Chem.* **1992**, *31*, 5597.
[21] Z. Kovacs, A. D. Sherry, *J. Chem. Soc., Chem. Commun.* **1995**, 185.
[22] G. Brunisholz, M. Randin, *Helv. Chim. Acta* **1959**, *42*, 1927.
[23] C. Amman, P. Meier, A. E. Merbach, *J. Magn. Reson.* **1982**, *46*, 319.
[24] R. V. Vold, J. S. Waugh, M. P. Klein, D. E. Phelps, *J. Chem. Phys.* **1968**, *48*, 3831.
[25] S. Meiboom, D. Gill, *Rev. Sci. Instrum.* **1958**, *29*, 688.

Received December 21, 1999
[I99338]

Linkage Isomerization in Pt^{II}–9-Methyladenine Complexes

Jorma Arpalahti,*[a] Karel D. Klika,[a] and Satu Molander[a]

Keywords: Linkage isomerization / NMR spectroscopy / Nucleobases / Platinum / Structure elucidation

Bis(9-methyladenine) complexes of *cis*-$Pt^{II}(NH_3)_2$ undergo slow linkage isomerization from the N7 to the N1 site in aqueous solution at elevated temperatures. The ratio of the isomeric complexes during the isomerization process indicates that whilst Pt^{II} prefers the N(7) site in the adenine moiety kinetically, it is the N(1) coordination mode which is thermodynamically more stable. The crystal structures of the isomers do not reveal any unusual features; the few apparently structurally significant differences in the bond angles in the N(1)-bound bis(complex) merely reflect the poor quality of the crystal and/or crystal packing effects rather than a direct result emanating from the coordination mode of the ligand.

Introduction

Of the naturally occurring nucleobases, the adenine moiety exhibits the most flexible binding-site behavior with metal ions. In 9-substituted adenine derivatives, the ring nitrogens N(1) and N(7) are the predominant binding sites;[1] in aqueous solution the distribution of the metal ion between these sites depends on the pH, the metal, and the other ligands coordinated to the metal.[2] When coordination to both of these sites is blocked binding may then occur at N(3).[3] In exceptional cases, various metal ions may also bind to the exocyclic amino group with a concomitant loss of a proton.[4–6]

The site distribution of the metal ion is pH-dependent due to the different basicities of the adenine nitrogen atoms and in this respect, the N(1),N(7) dichotomy of 9-substituted adenines has received considerable attention. Whilst hard 3d transition metal ions slightly favor the N(7) site over the N(1) site,[7] softer metal species such as Pd^{II} appear to prefer the N(1) site.[1a] With inert cations like Pt^{II}, however, care must be taken to distinguish the kinetically preferred binding site from the thermodynamically more stable one. Recently, we have shown that monofunctional, aquated Pt^{II}(dien) kinetically favors the N(7) site in adenosine, although it is the N(1) binding mode which is thermodynamically more stable.[8] (The slow isomerization process takes several days at 65 °C in aqueous solution.) With bifunctional Pt^{II} compounds, such as the biologically important Pt^{II} diamines, the majority of studies reveal only N(7) coordination,[2,9] with only rare instances of the Pt^{II} binding to other sites in the adenine moiety such as N(1),[10–12] or N(6)[6b]. Although the Pt^{II}–N bond is generally considered inert, the relatively easy bond rearrangement found in platinated oligonucleotides[11b,13] have led to this dogma being questioned.[12] Together with the novel S→N migration of coordinated Pt in sulfur containing biomolecules,[14] this has led to tremendous interest in the linkage isomerization in Pt-nucleobase complexes.[6,12] In this work we report the isomerization of bis(9-methyladenine) complexes of *cis*-$Pt^{II}(NH_3)_2$ in aqueous solution. The isomeric complexes exhibiting the N(1),N(1); N(1),N(7); and N(7),N(7) binding modes of Pt^{II} in the adenine moiety have been structurally characterized by X-ray crystallography and by ^{1}H-, ^{13}C-, and ^{195}Pt-NMR spectroscopy. To our knowledge, the former two complexes represent the first examples of mononuclear Pt^{II} bis(complexes) in which the adenine moiety displays the N(1) binding mode.

Results and Discussion

The isomerization of the bis(complexes) of 9-methyladenine (9-made), *cis*-$[Pt(NH_3)_2$(9-made-*N*7)$_2]^{2+}$ (**1**), *cis*-$[Pt(NH_3)_2$(9-made–*N*1)(9-made-*N*7)$]^{2+}$ (**2**) *cis*-$[Pt(NH_3)_2$(9-made-*N*1)$_2]^{2+}$ (**3**), can be conveniently followed by HPLC (see Figure 1).

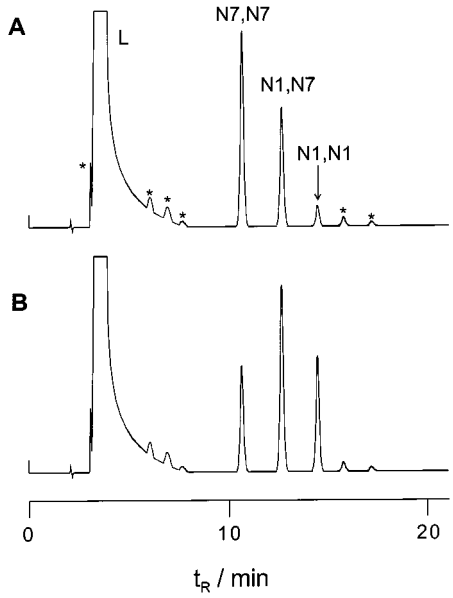


Figure 1. HPLC profiles of the isomerization mixture after 1 h (A) and 15 d (B). Notation: L is free 9-methyladenine, while the isomeric complexes are denoted as Pt binding sites; * denote unknown species

[a] Department of Chemistry, University of Turku,
FIN-20014, Turku, Finland
Fax: (internat.) + 358-2-333 6700
E-mail: jorma.arpalahti@utu.fi

 © WILEY-VCH Verlag GmbH, D-69451 Weinheim, 2000 1434−1948/00/0505−1007 $ 17.50+.50/0

When compared to free nucleobase, the bis(complexes) have longer retention times and the complexes follow an elution order of **1** < **2** < **3**. In a solution containing a slight excess of the ligand ($[Pt]_T/[L]_T$ = 1:2.5), the N(7) coordination mode predominates at the beginning of complexation

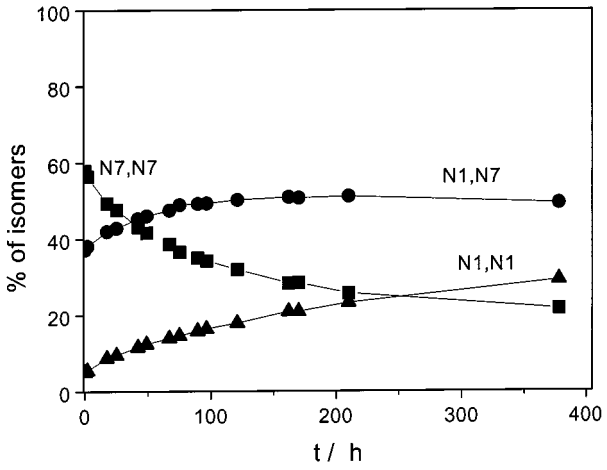


Figure 2. The relative percentage of different complexes (based on peak areas at 260 nm) during the isomerization process in aqueous solution at 80–85 °C

(Figure 2). However, when kept at ca. 85 °C for several days a slow N(7)→N(1) isomerization takes place, as shown by the diminution of the N(7),N(7)-bound species and an increase in the N(1),N(7)- and the N(1),N(1)-bound species. The time-dependent concentrations of the different complexes indicate that it is the N(7) binding mode which is kinetically preferred, whereas it is the N(1) site which forms the thermodynamically more stable complexes; this is in line with findings for monofunctional Pt^{II}.[8] Interestingly, the amount of the bis(complex) with the mixed N(1),N(7) coordination mode first increases and then only very slowly decreases indicating stepwise N(7)→N(1) isomerization. The slowness of the reaction, as compared to intramolecular bond rearrangements,[6] suggests that in this case the isomerization results from the breaking and reformation of Pt-nucleobase bonds. Unfortunately, the data do not allow definitive conclusion about the reaction path, i.e. solvent path and/or direct nucleophilic attack of the free nucleobase on the complex for both are expected to be very slow.[1b]

The kinetic preference of Pt^{II} for the adenine N(7) site may be attributed to steric hindrance by the exocyclic amino group that limits the platination of the N(1) site[7,10] despite its stronger basicity.[15] Because the N(7)→N(1) isomerization is slow even at elevated temperatures, reflecting the high thermodynamic stability of the Pt–N bond,[15] it is not surprising therefore that the formation of bis(complexes) exhibiting only the N(1) binding mode has been previously overlooked.[11a]

The ^1H, ^{13}C, and ^{195}Pt spectral data for the dications **1**, **2**, and **3** are listed in Table 1. All three complexes in aqueous solutions show evidence of dynamic processes, as indicated by the splitting and/or broadening of the ^1H, ^{13}C, and ^{195}Pt signals. In all likelihood, the dynamic process in effect is the restricted rotation of the nucleobase(s) about the Pt–N bond resulting from the close spatial proximity of the Pt^{II} atom and the exocyclic amino group of the adenine moiety. This spatial proximity is particularly close for the N(1)-bound species[6a,8] and consistent with this, **3** displays the strongest effects. Nevertheless, the observed ^1H chemical shifts corroborate the assignment of the Pt binding modes showing significant downfield shifts by those signals near the proposed coordination site. The δ_{Pt} values of all three isomeric complexes are close to –2500 ppm, typical for a PtN_4 coordination sphere.[16]

Crystal Stuctures

The crystal structure analyses confirmed the Pt^{II} binding modes of the isomeric complexes and the thermal ellipsoids of the dications of **1a – 3a** are shown in Figures 3, 4, and 5, respectively; selected interatomic distances and angles are listed in Table 2.

The crystallographic data, experimental details and results of structure refinements are listed in Table 3. In all complexes, the Pt^{II} coordination sphere is nearly square-planar with normal and very similar Pt–N bond lengths and angles, except in **1**, where the Pt–N(7a) distance of 2.021(6) Å seems to be significantly shorter (3.8σ[17]) than the Pt–N(11) distance of 2.056(7) Å. Otherwise the cation of **1a** is very similar to the corresponding one of the nitrate salt.[9] The complexed nucleobases are orientated in a head-to-tail fashion in **1** and **2**, whereas in **3** their orientation is head-to-head. The latter is of particular interest, as it brings the exocyclic C(6)–NH_2 groups onto the same side of the PtN_4 plane. The N(6)···Pt distance of 3.21(1) Å in **3** is close to that found in **2** for the N(1)-bound 9-made, viz. 3.149(8) Å, and comparable to those reported earlier for other N(1) platinated adenine derivatives.[6a,8] With the N(1) binding mode, the exocyclic amino group is significantly closer to the Pt^{II} atom than it is in N(7)-bound species; the N(6)···Pt distance is 3.446(8) Å in the N(7)-bound 9-made of **2,** and 3.430(7) Å (unit A) and 3.515(7) Å (unit B) in **1**. The close proximity of the Pt^{II} and N(6) atoms may indicate a hydrogen bond type of interaction between these two atoms. The calculated values for the N(6)H···Pt distances and the N(6)–H(6)···Pt angles of 2.76 Å and 114° [H(6B)] in **3**, 2.67 Å and 116° [H(6A1)], and 2.75 Å and 139° [H(6B2)] in **2**, 2.73 Å and 139° [H(6A2)], and 2.82 Å and 139° [H(6B2)] in **1** are, at least for the N(7)-bound species, close to the values given in the literature for this type of interaction, viz. 2.2–3.5 Å and >120°, respectively.[18] Irrespective of this interaction being present, the Pt^{II} atom lies virtually in the plane defined by the four coordinating nitrogen atoms and deviates by less than 0.02 Å from this plane in all three complexes.

The corresponding bond lengths and angles of the base moieties in **1** and **2** are very similar and they do not significantly deviate from the values given for uncomplexed 9-methyladenine.[19] The same holds true also for the bond lengths in **3**, where the several seemingly large differences become insignificant when the large e.s.d.s are taken into account, e.g. the C(4)–C(5) bond. However, some of the ring angles in **3** display significant changes when compared

Table 1. ^{1}H, ^{13}C, and ^{195}Pt chemical shifts in ppm for **1**, **2**, and **3**

Chem. shifts[a]		δ_{Pt}	δ_H			δ_C					
Compounds			H2	H8	CH_3	C2	C4	C5	C6	C8	CH_3
1[b]		–2476	8.292 {8.33} (8.240)[c]	8.628 {8.63} (8.764)[c]	3.799 {3.81}	156.41	151.75	118.23	156.45	147.03	33.56
2[d]	N(1)[e]	–2527	8.639 (8.826)	8.010 (8.040)	3.702 (3.759)	155.59 (155.25)	150.36 [f]	121.42 (121.31)[c]	157.90 (157.84)	147.30 [g]	32.63 [g]
	N(7)[e]		8.260 (8.224)	8.695 (8.844)	3.819 (3.836)	156.33 [g]	151.71 [f]	118.20 (118.34)[c]	156.37 [g]	147.16 (146.81)	33.57 [g]
3[h]		–2565 (–2583)	8.797 (8.883)	8.153 (8.158)	3.812 (3.829)	156.31 (155.28)	150.39 (150.46)	121.2 (121.0)	157.79[i] (157.96) [i]	147.09 (147.18)	32.82 (32.86)

[a] Spectra recorded in D_2O (^{1}H) or in H_2O/D_2O (^{13}C and ^{195}Pt). – [b] Possibly two sets of signals in a ratio of 9:1, the values for the minor species in parenthesis; data from ref. [9] in braces – [c] Questionable. – [d] Two sets of signals for each nucleobase in a ratio of ca. 8:2, data for the minor species in parenthesis. – [e] Binding mode of 9-made and associated ^{1}H and ^{13}C chemical shifts. – [f] Not observed. – [g] Known to be hidden beneath other signals from the 2-D spectra. – [h] Two signals in a ratio of ca. 2:1 were detected for all nuclei. The values in parenthesis refer to the minor signal. – [i] Signal shows a shoulder 0.06 ppm upfield.

Table 2. Selected interatomic distances and angles for isomeric complexes **1**, **2**, and **3**

	1		**2**		**3**
Pt–N(10)	2.037(7)		2.044(7)		2.046(8)
Pt–N(11)	2.056(7)		2.033(8)		
Pt–N(1)			2.046(7)		2.038(11)
Pt–N(7)	2.031(7)[a]	2.021(6)[b]	2.022(7)		
N(1)–C(2)	1.334(12)	1.330(12)	1.389(11)[c]	1.330(13)[d]	1.29(3)
N(1)–C(6)	1.365(12)	1.343(11)	1.366(11)	1.358(11)	1.42(3)
N(3)–C(2)	1.340(12)	1.338(12)	1.306(12)	1.315(13)	1.40(3)
N(3)–C(4)	1.355(11)	1.347(11)	1.348(11)	1.351(11)	1.45(5)
N(6)–C(6)	1.331(11)	1.326(10)	1.324(11)	1.338(12)	1.28(2)
N(7)–C(5)	1.405(10)	1.389(10)	1.394(11)	1.412(11)	1.41(3)
N(7)–C(8)	1.314(10)	1.320(10)	1.323(12)	1.316(12)	1.33(2)
N(9)–C(4)	1.375(11)	1.370(11)	1.368(11)	1.372(12)	1.40(2)
N(9)–C(8)	1.358(11)	1.350(11)	1.365(12)	1.357(11)	1.42(4)
N(9)–C(9)	1.460(10)	1.474(10)	1.456(11)	1.465(13)	1.44(3)
C(4)–C(5)	1.375(11)	1.377(11)	1.380(12)	1.379(12)	1.24(6)
C(5)–C(6)	1.394(11)	1.429(11)	1.394(12)	1.377(13)	1.34(4)
N(10)–Pt–N(11)	89.1(3)		89.8(3)		
N(7)–Pt–N(7)	90.9(3)				
N(1)–Pt–N(7)			90.7(3)		
N(1)–Pt–N(1)#[e]					88.9(5)
N(1)–Pt–N(10)			179.2(3)		179.1(15)
N(1)–Pt–N(10)#[f]					90.7(4)
N(1)–Pt–N(11)			90.8(3)		
N(7)–Pt–N(10)	177.7(3)[a]	90.9(3)[b]	88.7(3)		
N(7)–Pt–N(11)	89.2(3)	179.7(3)	178.1(3)		
C(2)–N(1)–C(6)	119.0(8)	119.8(8)	119.0(7)[c]	118.3(9)[d]	119.6(11)
C(2)–N(3)–C(4)	110.4(7)	110.6(7)	112.1(8)	110.6(8)	107(2)
C(5)–N(7)–C(8)	106.4(7)	105.5(7)	103.5(8)	106.6(8)	109(2)
C(4)–N(9)–C(8)	106.0(6)	107.1(7)	106.4(7)	106.5(8)	91(3)
C(4)–N(9)–C(9)	126.9(8)	127.0(8)	127.9(8)	127.6(8)	143(3)
C(8)–N(9)–C(9)	127.0(8)	126.0(8)	125.3(8)	125.7(8)	125.4(17)
N(1)–C(2)–N(3)	129.3(9)	128.8(9)	127.7(8)	129.9(9)	127(2)
C(5)–C(4)–N(9)	108.1(7)	106.5(7)	106.0(8)	108.3(8)	127(4)
C(5)–C(4)–N(3)	126.0(8)	127.3(7)	125.9(8)	125.4(9)	130.2(17)
N(3)–C(4)–N(9)	125.9(7)	126.2(7)	128.1(8)	126.3(8)	103(4)
C(4)–C(5)–C(6)	118.8(8)	116.4(7)	119.3(8)	118.6(8)	119(3)
C(4)–C(5)–N(7)	107.2(7)	108.9(7)	110.6(8)	106.7(8)	98(3)
C(6)–C(5)–N(7)	133.9(7)	134.7(7)	130.1(8)	134.7(9)	142(4)
C(5)–C(6)–N(6)	125.3(8)	124.5(8)	123.5(8)	124.8(8)	117(3)
C(5)–C(6)–N(1)	116.5(8)	117.1(7)	115.9(8)	117.1(9)	118(3)
N(1)–C(6)–N(6)	118.2(8)	118.4(8)	120.6(8)	118.1(8)	125(2)
N(7)–C(8)–N(9)	112.2(7)	112.1(7)	113.5(8)	111.9(8)	114.1(14)

[a] Unit A. – [b] Unit B. – [c] For N(1)-bound 9-made (unit A). – [d] For N(7)-bound 9-made (unit B). – [e] N(1)# generated by symmetry transformation: $-x + 3/2, y, z$. – [f] N(10)# generated by symmetry transformation: $-x+3/2, y, z$.

Table 3. Crystal data and structure refinement for the isomeric complexes *cis*-$[Pt(NH_3)_2(9\text{-made-}N7)_2](ClO_4)_2 \cdot 2\,H_2O$ (**1a**), *cis*-$[Pt(NH_3)_2(9\text{-made-}N1)(9\text{-made-}N7)](ClO_4)_2$ (**2a**), and *cis*-$[Pt(NH_3)_2(9\text{-made-}N1)_2](PF_6)_2 \cdot 3\,H_2O$ (**3a**)

	1	**2**	**3**
Empirical formula	$C_{12}H_{24}Cl_2N_{12}O_{10}Pt$	$C_{12}H_{20}Cl_2N_{12}O_8Pt$	$C_{12}H_{26}F_{12}N_{12}O_3P_2Pt$
Molecular mass	762.42	726.39	871.48
Crystal system	triclinic	triclinic	orthorhombic
Spące group	*P*–1	*P*–1	*Ama*2
a [Å]	9.564(3)	10.2393(10)	20.875(3)
b [Å]	16.117(5)	15.455(3)	15.524(4)
c [Å]	7.9983(14)	7.4399(10)	8.742(6)
α [°]	91.995(19)	98.614(12)	90
β [°]	90.69(3)	91.663(9)	90
χ [°]	104.68(3)	89.441(10)	90
V [Å^3]	1191.7(6)	1163.6(3)	2833(2)
Z	2	2	4
D(calcd.) [g cm^{-3}]	2.125	2.073	2.043
μ [mm^{-1}]	6.188	6.326	5.185
F(000)	744	704	1688
Crystal size [mm]	0.12 × 0.34 × 0.36	0.12 × 0.14 × 0.18	0.20 × 0.20 × 0.16
θ range [°]	1.31–25.05	1.99–25.16	1.95–27.49
Index ranges	+11, ±19, ±10	+12, ±18, ±9	+27, –20, +11
Reflections collected	4206	4343	1785
independent (R_{int})	4206 (0.0000)	4096 (0.0364)	1785 (0.0000)
observed [$I > 2\sigma I$]	3665	3359	1170
Absorption correction	ψ scan		
Transmission	1.000–0.661	1.000–0.667	1.000–0.696
Refinement method	Full-matrix least-squares on F^2		
Data/restraints/parameters	4026/10/334	4096/42/311	1785/13/199
Goodness-of-fit on F^2	1.065	1.078	1.038
R indices[a] [$I > 2\sigma I$]	$R_1 = 0.0401$	$R_1 = 0.0387$	$R_1 = 0.0422$
	$wR2 = 0.0991$	$wR2 = 0.0890$	$wR2 = 0.0785$
R indices (all data)	$R_1 = 0.0532$	$R_1 = 0.0654$	$R_1 = 0.1021$
	$wR2 = 0.1047$	$wR2 = 0.1004$	$wR2 = 0.0926$
Largest diff. peak and hole [eÅ^{-3}]	2.125 and –2.240	1.569 and –1.247	1.372 and –0.926

[a] $R_1 = \Sigma||F_o| - |F_c||/\Sigma|F_o|$, $wR_2 = \{\Sigma\,[w(F_o^2 - F_c^2)^2]/\Sigma\,[\,w(F_o^2)^2]\}^{1/2}$ and $w = 1/[\sigma^2(F_o^2) + (aP)^2 + bP)]$, where $P = (2\,F_c^2 + F_o^2)/3$.

to isomers **1** and **2** and to the uncomplexed ligand. The most significant difference can be seen in the N(3)–C(4)–N(9) angle of 103(4)°, which differs by 6.2σ[17] from that in the N(1)-bound 9-made of **2**, viz.128.1(8)°. Other significant differences include the angles C(4)–N(9)–C(8) (5.2σ from that in **1**, unit B), C(4)–N(9)–C(9) (5.2σ from that in **1**, unit A), C(5)–C(4)–N(9) (5.1σ) and C(4)–C(5)–N(7) (4.1σ) from that in **2** [N(1)-bound 9-made]. It seems to us that these differences merely reflect the poor quality of the crystal and/or crystal packing effects rather than a direct result emanating from the coordination mode of the ligand,[20] since the majority of the significant differences are seen relative to the N(1)-bound ligand in **2**.

The packing of the isomeric complexes is predominantly stabilized by hydrogen bonding involving primarily the am(m)ine hydrogens and anions and/or lattice water (Table 4). Additional H-bonds may be formed between the exocyclic amino groups and endocyclic nitrogens in **2a**, and between water molecules in **1a** and **3a**. By contrast, stacking of the base moieties seems to be relative unimportant in stabilizing the crystal lattice. In **1a**, the neighboring bases are orientated in a head-to-tail fashion with a distance of 3.64 Å between the centers of the 5- and 6-membered rings, which may indicate a weak stacking interaction. With **2a** and **3a**, the distances between the neighboring heteroaromatic rings are > 4 Å.

Conclusions

The isomerization of the bis(9-methyladenine) complexes of *cis*-$Pt^{II}(NH_3)_2$ in aqueous solution is a very slow process. The ratio of the isomeric complexes as a function of time indicates that Pt^{II} kinetically prefers the N(7) site in the adenine moiety, whilst it is the N(1) coordination mode which is thermodynamically more stable. The slowness of the reaction, as compared to the intramolecular Pt^{II}–N bond rearrangement,[6b] suggests that the isomerization of the bis(complexes) results from the breaking and reformation of Pt-nucleobase bonds, although no definitive conclusion about the reaction path can be made. In this respect, the relative easy bond rearrangements in platinated oligonucleotides (single stranded or double stranded)[11b,13] are strongly suggestive for an intramolecular migration mechanism. The crystal structures of the isomers do not reveal any unusual features, except for those few apparently significant differences in the bond angles in the N(1)-bound bis(complex), which merely reflect the poor quality of the crystal and/or crystal packing effects rather than a direct result emanating from the coordination mode of the ligand. The packing of the isomeric complexes is predominantly stabilized by hydrogen bonding, whilst stacking of the base moieties seems to be relative unimportant in stabilizing the crystal lattice.

Table 4. Possible hydrogen bonds (D–H···A) for **1a – 3a**

D–H···A[a]	*d*(D···A) [Å]; <(DHA) [°]	Symmetry transformation
Compound **1a**		
N(6A)–H(6A1)···N(1A)	3.05(1); 156.4	$-x, -y + 1, -z + 2$
N(6B)–H(6B1)···N(1B)	3.02(1); 171.1	$-x + 1, -y, -z + 2$
N(10)–H(10A)···O(6)	3.00(1); 168.5	$x - 1, y, z$
N(10)–H(10C)···O(1)	3.09(1); 163.6	
N(11)–H(11C)···N(3A)	3.01(1); 170.1	$-x + 1, -y + 1, -z + 2$
N(11)–H(11A)···O(7)	3.02(1); 167.3	$x - 1, y, z$
N(11)–H(11B)···O(2)	3.05(1); 167.0	
O(9)···O(10)	2.80(1)	$x, y, z - 1$
O(9)···O(3)	2.98(2)	
O(9)···O(8)	2.86(2)	
O(10)···O(5)	2.71(3)	
Compound **2a**		
N(6A)–H(6A1)···O(2A)	2.78(2); 135.8	$x, y, z + 1$
N(6A)–H(6A2)···N(7A)	2.94(1): 157.8	$-x + 1, -y + 2, -z + 2$
N(6B)–H(6B1)···N(1B)	3.00(1); 168.2	$-x + 2, -y + 1, -z + 1$
N(10)–H(12B)···O(6A)	2.73(2); 131.6	
N(10)–H(12C)···O(4A)	3.02(2); 152.8	$x, y, z + 1$
N(11)–H(11B)···O(7A)	2.94(2); 165.7	$-x + 1, -y + 1, -z + 2$
N(11)–H(11A)···O(6B)	3.03(2); 163.6	
Compound **3a**		
N(6)–H(6A)···O(1A)	2.78(7); 166.8	
N(6)–H(6B)···F(2)	2.83(5); 128.7	$x, y + {}^1/_2, z + {}^1/_2$
N(10)–H(10B)···O(2B)	2.94(7); 144.7	$x, y + {}^1/_2, z - {}^1/_2$
N(10)–H(10B)···O(2A)	2.96(3); 166.7	$x, y + {}^1/_2, z - {}^1/_2$
O(1B)···O(2A)	2.55(3)	
O(1B)···O(2B)	2.86(9)	

[a] The water hydrogens could not be located from the electron density maps.

Experimental Section

General Remarks: The NMR measurements were carried out in D_2O (^1H) or in H_2O/D_2O (^{13}C and ^{195}Pt) at ambient temperature. Spectra were acquired on a JEOL Alpha 500 spectrometer equipped with a 5 mm tunable probe operating at 500.16 MHz for ^1H, 125.78 MHz for ^{13}C, and 107.21 MHz for ^{195}Pt.[8] The ^1H and ^{13}C spectra were referenced internally to sodium 4,4-dimethyl-4-silapentanesulfonate (DSS), assigned as $\delta = 0.015$ ppm for proton and 0 ppm for carbon; the ^{195}Pt spectra were referenced externally to $[PtCl_4]^{2-}$ (δ_{Pt} –1625 ppm from $[PtCl_6]^{2-}$). The assignments of the ^1H and ^{13}C resonances were based on HMQC, DEPT, and HMBC spectra and by comparison to the assignments of the Pt^{II}(dien) complexes of adenosine.[8] – The HPLC measurements were carried out on a Merck-Hitachi chromatograph using an end-capped RP-18 column (5 μm, E. Merck AG) and a water/methanol (85:15) mixture (0.05 M $NaClO_4$, pH 3) as eluent. – Adenine was purchased from Sigma, $NaClO_4 \cdot H_2O$ and DMF from E. Merck AG, and $NaPF_6$ (98%) from Ventron; all were used as received.

Isomerization Procedure: Treatment of *cis*-$[PtI_2(NH_3)_2]$[21] (970 mg, 2.0 mmol) with two equivalents of $AgNO_3$ in 10 mL of water for two hours at 60 °C gave a clear solution of the diaqua species upon removing the AgI precipitate by filtration. After the addition of 9-methyladenine[22] (9-made, 550 mg, 3.7 mmol) into 7.4 mL of the Pt^{II} solution, the mixture was stirred at 80–85 °C and the progress of the isomerization was intermittantly followed by HPLC. After 15 days, the reaction was stopped (the mixture began to turn yellow together with the formation of some black solid), the mixture was filtered, and the filtrate was left to evaporate to dryness at ambient temperature. The solid residue was treated with 30 mL of boiling methanol to remove most of the unchanged 9-made. According to HPLC analysis the remaining solid residue (620 mg) contained ca. 20% of 9-made and ca. 75% of the desired isomers. The isomeric complexes were isolated and purified by fractional crystallization with different anions, as described below.

***cis*-[Pt(NH$_3$)$_2$(9-made-*N*7)$_2$](ClO$_4$)$_2$ · 2 H$_2$O (1a):** The crude product obtained above was dissolved in 2 mL of water with gentle warming. Slow cooling to +4 °C afforded a crystalline product with a composition of [**2**] ≈ [**1**] > [**3**] as deduced by HPLC analysis. Repeated recrystallizations from a minimal amount of water finally gave ca. 50 mg of chromatographically pure crystals of **1** with NO_3^- as the counter ion. Alternatively, and more conveniently, **1** was prepared by dissolving 9-made (120 mg, 0.8 mmol) in 2 mL of 1 M HNO_3 [to prevent N(1) platination], followed by the addition of 0.38 equiv. of *cis*-$[Pt(NH_3)_2(H_2O)_2]^{2+}$ in 5 mL of water. After stirring for 48 h at ca. 35 °C, the filtered solution was neutralized with 1 M NaOH, which afforded 125 mg of pale yellow crystals (50% from Pt) upon cooling to +4 °C. The isomeric purity of the product (>99%) was ascertained by HPLC analysis. Finally, **1** was crystallized as a perchlorate (**1a**) by dissolving the dinitrate in 1 M $NaClO_4$. – $C_{12}H_{24}Cl_2N_{12}O_{10}Pt$ (762.42): calcd. C 18.90, H 3.17, N 22.05; found C 18.80, H 3.02, N 21.82.

***cis*-[Pt(NH$_3$)$_2$(9-made-*N*1)(9-made-*N*7)](ClO$_4$)$_2$ (2a):** All of the solutions obtained from the above fractional crystallizations were pooled, which gave a mixture with a relative composition of [**2**] > [**3**] > [**1**]. This solution was concentrated to ca. 1 mL; after the addition of 1 mL of 1 M $NaClO_4$ to the mixture, crystals (ca. 320 mg) were obtained at +4 °C. The filtered crystalline product was then dissolved in 1.5 mL of DMF.[23] Crude **2a**, obtained at –20 °C after the addition of 0.2 mL of water and 6 mL of ethanol to the solution, was filtered off and washed with cold water. Recrystallization from a minimal amount water gave 120 mg of chromatographically pure **2a**. – $C_{12}H_{20}Cl_2N_{12}O_8Pt$ (726.39): calcd. C 19.84, H 2.78, N 23.14; found C 19.91, H 2.91, N 22.72.

***cis*-[Pt(NH$_3$)$_2$(9-made-*N*1)$_2$](PF$_6$)$_2$ · 3 H$_2$O (3a):** The DMF solution and washings of **2a** were evaporated to dryness at ambient temperature. The solid residue was washed with cold 0.1 M $HClO_4$ to remove most of the remaining **2a**. Dissolving the residue in 1 mL of water yielded 50 mg of chromatographically pure **3a** at +4 °C after the addition of 1 mL of 1 M $NaPF_6$ (pH 5, adjusted with 1 M NaOH) to the solution. – $C_{12}H_{26}F_{12}N_{12}O_3P_2Pt$ (871.48): calcd. C 16.54, H 3.01, N 19.29; found C 16.41, H 2.81, N 18.98.

X-ray Diffraction Studies: All X-ray data were collected on a Rigaku AFC5S diffractometer at ambient temperature with Mo-K_α radiation (λ = 0.71069 Å). Unit cell parameters were obtained from a least-squares fit of 25 reflections [41.60 < 2θ < 45.48° (**1a**), 40.82 < 2θ < 46.60° (**2a**), and 20.95 < 2θ < 31.61° (**3a**)]. Intensity data were collected by the ω/2θ scan technique to a maximum 2θ value of 50° (55° for **3a**). The intensities of three standard reflections were measured every 150 data points in all cases, and they showed no intensity decay. The intensities of the reflections were corrected for Lorenz, polarisation and absorption (empirical) effects.[24] The structures were solved by standard Patterson and difference Fourier methods and refined by full-matrix least-squares calculations employing SHELXL-97.[25] All atoms except hydrogen were refined with anisotropic temperature factors. In all complexes the hydrogen atoms are at the calculated positions. The final cycle of refinement gave for the structure **1a**, R_1 = 0.0401 and $wR2$ = 0.0991 for the observed data [$I > 2\sigma(I)$] and 334 parameters and R_1 = 0.0532 and $wR2$ = 0.1047 for all data. For **2a**, refinement converged at R_1 = 0.0387 and $wR2$ = 0.0890 for the observed data and 311 parameters and R_1 = 0.0654 and $wR2$ = 0.1004 for all data. For **3a** the final refinement cycle gave R_1 = 0.0422 and $wR2$ = 0.0785 for the observed data and 200 parameters and R_1 = 0.1021 and $wR2$ = 0.0926 for all data. Crystallographic data and experimental details are given in Table 2, selected bond lengths and angles are given in Table 3, and possible hydrogen bonds in Table 4. Data reduction and subsequent calculations were performed with *teXsan for Windows*.[26] Figures were drawn with *Ortep-3 for Windows*.[27] Crystallographic data (excluding structure factors) for the structures reported in this paper have been deposited with the Cambridge Crystallographic Data Centre as supplementary publication no. CCDC-135162 (**1a**), CCDC-135163 (**2a**), and CCDC-135164 (**3a**). Copies of the data can be obtained free of charge on application to CCDC, 12 Union Road Cambridge, CB2 1EZ, UK [Fax: +44 (0)1223/336-033; E-mail: deposit@ccdc.cam.ac.uk].

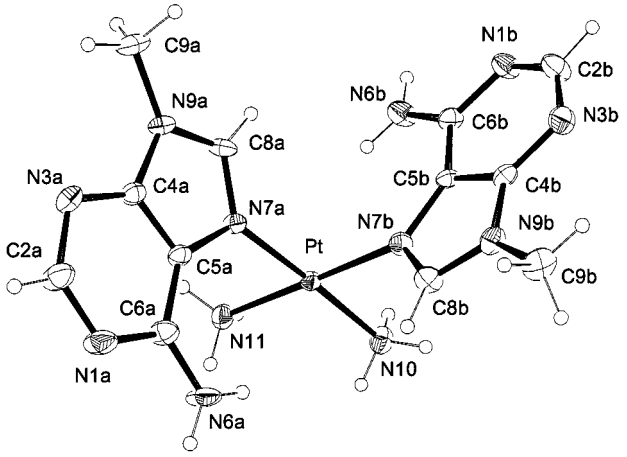


Figure 3. ORTEP plot of the cation of *cis*-[Pt(NH$_3$)$_2$(9-made-*N*7)$_2$](ClO$_4$)$_2$ · 2 H$_2$O (**1a**) showing 30% probability ellipsoids

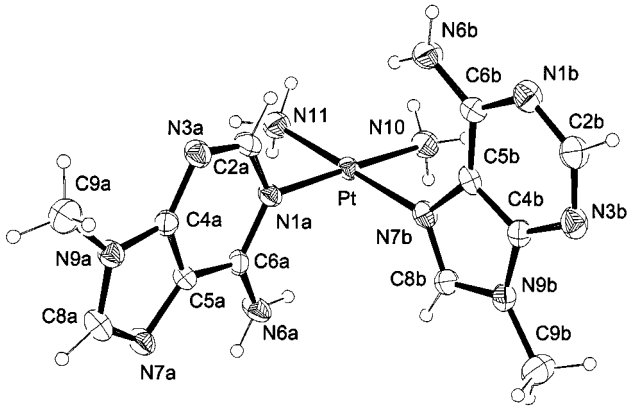


Figure 4. ORTEP plot of the cation of *cis*-[Pt(NH$_3$)$_2$(9-made-*N*1)(9-made-*N*7)](ClO$_4$)$_2$ (**2a**) showing 30% probability ellipsoids

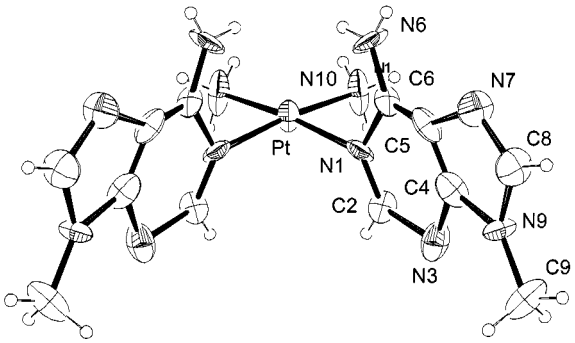


Figure 5. ORTEP plot of the cation of *cis*-[Pt(NH$_3$)$_2$(9-made-*N*1)$_2$](PF$_6$)$_2$ · 3 H$_2$O (**3a**) showing 30% probability ellipsoids

Acknowledgments

We thank Dr. Reijo Sillanpää for helpfull discussions concerning the X-ray crystal structure analysis. This work is a part of the COST Action D8/004/97 (Chemistry of Metals in Medicine).

[1] [1a] R. B. Martin, in: *Cisplatin – Chemistry and Biochemistry of a Leading Anticancer Drug* (Ed.: B. Lippert). Verlag Helvetica Chimica Acta, Zürich, **1999**, 183–205. – [1b] J. Arpalahti, in: *Cisplatin – Chemistry and Biochemistry of a Leading Anticancer Drug* (Ed.: B. Lippert). Verlag Helvetica Chimica Acta, Zürich, **1999**, 207–222.
[2] B. Lippert, in: *Progress in Inorganic Chemistry, Vol. 37* (Ed.: S. J. Lippard). Wiley, New York, **1989**, 1–97.
[3] C. Meiser, B. Song, E. Freisinger, M. Peilert, H. Sigel, B. Lippert, *Chem. Eur. J.* **1997**, *3*, 388–398.
[4] [4a] L. Y. Kuo, M. G. Kanatzidis, M. Sabat, A. L. Tipton, T. J. Marks, *J. Am. Chem. Soc.* **1991**, *113*, 9027–9045. – [4b] F. Zamora, M. Kunsman, M. Sabat, B. Lippert, *Inorg. Chem.* **1997**, *36*, 1583–1587.
[5] [5a] M. J. Clarke, *J. Am Chem. Soc.*, **1978**, *100*, 5068–5075. – [5b] G. Lowe, T. Vilaivan, *Perkin Trans. 1*, **1996**, 1499–1503.
[6] [6a] J. Arpalahti, K. D. Klika, *Eur. J. Inorg. Chem.* **1999**, 1199–1201. – [6b] J. Viljanen, K. D. Klika, R. Sillanpää, J. Arpalahti, *Inorg. Chem* **1999**, *38*, 4924–4925.
[7] J. Arpalahti, E. Ottoila, *Inorg. Chim. Acta* **1985**, *107*, 105–110.
[8] J. Arpalahti, K. D. Klika, R. Sillanpää, R. Kivekäs, *Dalton Trans.* **1998**, 1397–1402.
[9] A. Iakovidis, N. Hadjiliadis, F. Dahan, J.-P. Laussac, B. Lippert, *Inorg. Chim. Acta*, **1990**, *175*, 57–63.

[10] J. Arpalahti, P. Lehikoinen, *Inorg. Chim. Acta* **1989**, *159*, 115–120.
[11] [11a] A. Eastman, *Biochemistry* **1982**, *21*, 6732–6736. – [11b] K. Inagaki, M. Alink, A. Nagai, Y. Kidani, J. Reedijk, *Inorg. Chem*. **1990**, *29*, 2183–2185.
[12] B. Lippert, *Coord. Chem. Rev.* **1999**, *182*, 263–295.
[13] [13a] S. L. Bruhn, J. H. Toney, S. J. Lippard, in: *Progress in Inorganic Chemistry, Vol. 38* (Ed.: S. J. Lippard). Wiley, New York, **1990**, 477–516. – [13b] M. Boudvillain, R. Dalbiès, M. Leng, in: *Metal Ions in Biological Systems, Vol. 33* (Eds.: A. Sigel, H. Sigel). Marcel Dekker, New York, **1996**, 87–103. – [13c] D. Yang, S. S. G. E. van Boom, J. Reedijk, J. H. van Boom, A. H.-J. Wang, *Biochemistry*, **1995**, *34*, 12912–12920.
[14] J. Reedijk, J. M. Teuben, in: *Metal Ions in Biological Systems, Vol. 32* (Eds.: A. Sigel, H. Sigel). Marcel Dekker, New York, **1996**, 339–362.
[15] M. Mikola, K. D. Klika, A. Hakala, J. Arpalahti, *Inorg. Chem*. **1999**, *38*, 571–578.
[16] T. G. Appleton, J. R. Hall, S. F. Ralph, *Inorg. Chem*. **1985**, *24*, 4685–4693.
[17] σ defined as $\sigma = (\sigma_1^2+\sigma_2^2)^{1/2}$ with σ_1 and σ_2 being the errors in angles that are compared (see ref. [4b]).
[18] [18a] W. Yao, O. Eisenstein, R. H. Crabtree, *Inorg. Chim. Acta* **1997**, *254*, 105–111. – [18b] D. Braga, F. Grepioni, E. Tedesco, K. Biradha, G. R. Desiraju, *Organometallics* **1997**, *16*, 1846–1856.
[19] [19a] T. J. Kistenmacher, M. Rossi, *Acta Crystallogr*. **1977**, *B33*, 253–257. – [19b] R. K. McMullan, P. Benci, B. M. Craven, *Acta Crystallogr*. **1980**, *B36*, 1424–1430.
[20] The employment of NO_3^- or ClO_4^- as the counter ion gave crystals of very poor quality.
[21] S.C. Dhara, *Indian J. Chem*. **1970**, *8*, 194–194.
[22] H. Lönnberg, J. Ylikoski, J. Arpalahti, E. Ottoila, A. Vesala, *Acta Chem. Scand.* **1985**, *A39*, 171–180.
[23] According to HPLC analysis the crystalline product contained **2** (80%) and **3** (20%); this ratio could not be changed by repeated recrystallizations from water.
[24] A. C. T. North, D. C. Phillips, F. S. Mathews, *Acta Crystallogr*. **1968**, *A24* 351–359.
[25] G. M. Sheldrick, *SHELXL 97*, *Program for the Refinement of Crystal Structures*, University of Göttingen, **1997**.
[26] *teXsan for Windows. Structure Analysis Software,* Molecular Structure Corporation, Texas 77381, USA (1997).
[27] L. J. Farrugia, *J. App. Cryst.,* **1997**, *30*, 565.

Received October 4, 1999
[I99344]

Synthesis and Characterization of Some Metal Complexes with New Nitrogen–Oxygen Donor Macrocyclic Ligands – X-ray Crystal Structures of a 26-Membered Reduced Monoprotonated Macrocycle and a 20-Membered Pendant-Arm Schiff-Base Macrocyclic Cadmium(II) Complex

Manuel Vicente,[a] Carlos Lodeiro,[a] Harry Adams,[b] Rufina Bastida,*[a] Andrés de Blas,[c] David E. Fenton,[b] Alejandro Macías,[a] Adolfo Rodríguez,[a] and Teresa Rodríguez-Blas[c]

Keywords: Metal complexes / Template synthesis / Schiff bases / Oxaazamacrocycles

New series of macrocyclic Schiff-base lanthanide(III), yttrium(III), and cadmium(II) complexes, $[M(\mathbf{1})]X_n$ (X = NO_3^-, M = Y, Ln = La–Yb except Pm and Dy; X = ClO_4^-, M = Cd, La, Ce, Pr, Sm, Gd, or Er) and $[M(\mathbf{3})]X_n$ (X = NO_3^-, M = Dy; X = ClO_4^-, M = Er and Cd), have been prepared by cyclocondensation of O^1,O^7-bis(2-formylphenyl)-1,4,7-trioxaheptane with O^1,O^7-bis(2-aninyl)-1,4,7-trioxaheptane (**1**) or tris(2-aminoethyl)amine (**3**) in the presence of the appropriate metal salt as a template agent. The Schiff-base macrocycles **1** and **3** are also formed in the absence of a metal ion. Treatment of **1** with $NaBH_4$ in methanol gives the diamine macrocycle **2**. The reactions of Ln^{III}, Cd^{II}, and Y^{III} ions with **2** have also been investigated. The crystal structures of the monoprotonated ligand **2** and of the complex $[Cd(\mathbf{3})](ClO_4)_2$ have been determined by X-ray diffraction analysis.

Introduction

Enormous progress in macrocyclic chemistry has been made in the past decade.[1–4] The number of new macrocyclic ligand molecules designed and synthesized has increased significantly and their structures have become much more complex. One reason for the interest in this field is that it offers exciting possibilities for creative minds to construct novel supramolecular assemblies that are capable of performing highly specific molecular functions. The precise molecular recognition between macrocyclic ligands and their guests provides a good opportunity for studying key aspects of supramolecular chemistry, which are also significant in a variety of disciplines including chemistry, biology, physics, medicine, and related science and technology.

In the course of our research programme on the synthesis and characterization of new coordination complexes of lanthanides, we have reported the synthesis of lanthanide(III) complexes with several N_xO_y-donor macrocyclic ligands containing aromatic, head, and lateral units.[5–10] The compound O^1,O^7-bis(2-formylphenyl)-1,4,7-trioxaheptane has been used as a dicarbonyl precursor in the design of macrocyclic ligands incorporating mixed donor atoms. Most efforts to date have focused on its use in the synthesis of oxaazapolyamine macrocycles as complexing agents for transition metal or heavy metal ions.[11–14] In contrast, little has been reported on its use in the synthesis of Schiff-base macrocycles and their metal complexes.[15–17]

An important aspect of the present work has been the synthesis of two novel dibenzo-substituted Schiff-base macrocycles derived from O^1,O^7-bis(2-formylphenyl)-1,4,7-trioxaheptane, specifically the 26-membered N_2O_6-donor macrocycle **1** and the 20-membered N_4O_3-donor pendant-arm macrocycle **3** (Scheme 1).

The coordination abilities of **1** and **3** towards lanthanide(III) ions have been investigated and, as an extension of these studies, a comparative investigation of the interactions of Y^{III} and Cd^{II} with these ligands has also been carried out. In macrocycle **3**, the role of the amine moiety as an axial coordinating pendant arm has been confirmed by X-ray structural analysis of the complex $[Cd(\mathbf{3})](ClO_4)_2$. The Schiff-base ligand **1** has been reduced to the corresponding saturated macrocycle **2** in order to increase its flexibility and the complexation behaviour of **2** towards the aforementioned metal ions has also been investigated. We also report the X-ray crystal structure of the monoprotonated macrocycle **2**.

Results and Discussion

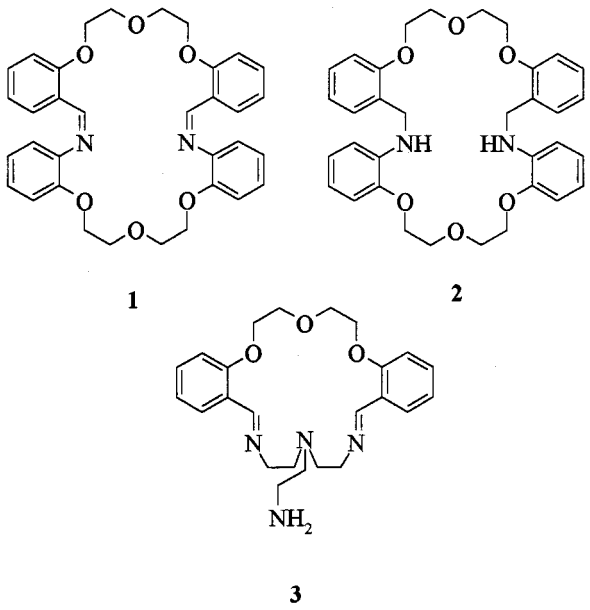
Macrocycle 1 and Its Metal Complexes

The non-template reaction of O^1,O^7-bis(2-formylphenyl)-1,4,7-trioxaheptane and O^1,O^7-bis(2-aninyl)-1,4,7-trioxa-

[a] Departamento de Química Inorgánica, Universidad de Santiago de Compostela,
Avenida de las Ciencias s/n, E-15706 Santiago de Compostela, Spain
Fax: (internat.) +34 981 597525
E-mail: qibastid@usc.es
[b] Department of Chemistry, Dainton Building, The University of Sheffield,
Sheffield S3 7HF, U.K.
Fax: (internat.) +44 (0)114 2738673
E-mail: d.fenton@sheffield.ac.uk
[c] Departamento de Química Fundamental e Industrial, Universidade de A Coruña,
Campus da Zapateira s/n, E-15701 A Coruña, Spain
Fax: (internat.) +34 981 167065
E-mail: mayter@udc.es

Supporting information for this article is available on the WWW under http://www.wiley-vch.de/home/eurjic or from the author.

 © WILEY-VCH Verlag GmbH, D-69451 Weinheim, 2000 1434–1948/00/0505–1015 $ 17.50+.50/0



Scheme 1. Macrocycle **1**: 12,13,15,16,29,30,32,33-octahydrotetrabenzo[*h*,*l*,*u*,*y*][1,4,7,14,17,20,10,24]hexaoxadiazacyclohexacosine; macrocycle **2**: 5,6,12,13,15,16,22,23,29,30,32,33-dodecahydrotetrabenzo[*h*,*l*,*u*,*y*][1,4,7,14,17,20,10,24]hexaoxadiazacyclohexacosine, macrocycle **3**: 2-(8,9,10,11,19,20,22,23-octahydro-7*H*-dibenzo[*h*,*s*][1,4,7,11,14, 17]trioxatriazacycloicosin-9-yl)-1-ethylamine

heptane in methanol yields the Schiff-base macrocycle **1**. It was not found necessary to carry out this ring-closure under high-dilution conditions. The product was isolated as an air-stable orange-yellow solid in 75% yield and was characterized by elemental analysis, FAB MS, IR, and ^{1}H-NMR spectroscopy. The FAB mass spectrum shows the parent-ion peak at m/z = 567, confirming the [1+1] cyclic nature of the Schiff-base ligand. The IR spectrum features a strong band at 1620 cm^{-1} attributable to the azomethine group. The ^{1}H-NMR spectrum in CD_3CN solution is complicated and shows more than the expected number of signals; a signal at δ = 8.91 can be attributed to the CH=N- proton. The complexity may be due to hydration and hydrolysis of imine bonds leading to carbinolamine formation and reversal of the Schiff base reaction.[18]

Cyclocondensation reactions carried out in the presence of metal salts (M = Y, Ln, Cd) yielded solids, which were characterized as the metal complexes $[M(\mathbf{1})]X_n \cdot x\,H_2O$ (X = NO_3^-, M = Y, La–Yb except Pm and Dy; X = ClO_4^-, M = Cd, La, Ce, Pr, Sm, Gd, or Er). Their analytical and conductivity data are presented in Table 1. The molar conductivities of the nitrate complexes in acetonitrile fall within the range reported for 2:1 electrolytes in this solvent.[19] This implies that one anion must be coordinated, at least in MeCN solution, and most probably in the solid state as well. The perchlorate complexes of La, Ce, Pr, Sm, and Er have conductivities between those for 2:1 and 3:1 electrolytes and the Gd and Cd complexes have values corresponding to 2:1 electrolytes, reflecting the weak coordination ability of the perchlorate anion. The FAB mass spectral results confirm the monomeric [1+1] (dicarbonyl + diamine) nature of the complexes, the most intense peak corresponding to $[\mathbf{1} + H]^+$. The spectra of the complexes frequently show peaks due to $[Ln(\mathbf{1})X_2]^+$ and for the cadmium complex peaks corresponding to $[Cd(\mathbf{1})(ClO_4)]^+$ at m/z = 779 and $[Cd(\mathbf{1})]^+$ at m/z = 680 are seen.

The complexes have similar IR spectra and the data are again consistent with the presence of imine bonds, each complex exhibiting the ν(C=N) mode at ca. 1644 cm^{-1},[20] while no bands attributable to C=O or NH_2 groups are detected. The shift of the imine band to higher wavenumbers upon complexation suggests coordination through the imine nitrogen atoms.[21,22] In the complexes derived from La^{III} nitrate and Cd^{II} and Sm^{III} perchlorates, a ν(C=N) band at ca. 1624 cm^{-1} is also seen, suggesting that in these cases only one imine N atom may be bound to the metal. The water present in the majority of the complexes (giving broad absorption bands at ca. 3450 cm^{-1}) is probably lattice and/or coordinated water.[23] All nitrate complexes exhibit absorption bands characteristic of both coordinated [ca. 1450 (ν_5), 1300 (ν_1), and 1030 (ν_2) cm^{-1}] and ionic (ca. 1380 cm^{-1}) nitrate.[24–26] The magnitude of the separation of the nitrate stretching vibrations ($\nu_5 - \nu_1$) of ca. 160 cm^{-1} is indicative of bidentate coordination.[27]

The IR spectra of the perchlorate complexes feature split bands attributable to the asymmetric Cl–O stretching mode at ca. 1080 cm^{-1} (ν_3) and the asymmetric Cl–O bending mode (ν_4) at ca. 620 cm^{-1}, suggesting that both bound and free anions are present.[28,29] The highest-energy band comprises three well-resolved maxima at ca. 1140, 1120, and 1080 cm^{-1}. However, as ν_{as}(C–O–C) for the polyether chains of the ligand also falls in this region it is not possible to precisely define the coordination mode.

The UV/visible spectra of macrocycle **1** and the corresponding metal complexes were recorded using 10^{-3}–10^{-6} M solutions in acetonitrile. For the complexes, the spectra were recorded immediately after preparation of the solutions and again after these solution had been set aside for periods of one day and one week. The spectra were found to be reproducible and no loss of the metal ion in solution could be detected. The positions of the absorption maxima, the extinction coefficients, and the linear correlation coefficients are available as Supporting Information. The free macrocycle exhibits two strong, broad absorption bands at ca. 251 and 320 nm, corresponding to the π-π* transitions of benzene rings and azomethine groups.[30] In the spectra of the metal complexes, the π-π* absorption bands are red-shifted with respect to their positions in the spectrum of **1**. The perchlorate complexes of La^{III} and Ce^{III} exhibit three strong absorptions at around 274, 317, and 391 nm; the spectra of the other complexes are similar, featuring four absorptions around 246, 291, 315, and 391 nm; the band around 246 nm may arise from charge-transfer transitions.[31,32]

Room temperature emission spectra were recorded using 10^{-6} M acetonitrile solutions of the free ligand **1** and of the $[Ln(\mathbf{1})]X_3$ (Ln = La, Nd, Eu, Gd, Tb, Lu; X = NO_3^-) and $[Cd(\mathbf{1})](ClO_4)_2$ complexes. The spectrum of the free ligand was recorded following excitation at 265 nm, which resulted

Table 1. Analytical, yield and molar conductance (in MeCN) data for the complexes $[M(\mathbf{1})]X_n \cdot x\,H_2O$ (calculated values are given in parentheses)

M	x	Analysis (%)			Yield (%)	Λ_M (Ω^{-1} cm^2mol^{-1})	Colour
		C	N	H			
$X = NO_3^-$							
Y[a]	3	47.85 (48.35)	6.70 (6.70)	5.25 (5.80)	31	225	pale brown
La	7	40.30 (40.15)	6.85 (6.90)	4.55 (4.75)	41	289	yellow/orange
Ce	3	43.60 (43.15)	7.05 (7.40)	4.85 (4.25)	51	278	orange
Pr[b]	–	47.00 (47.20)	7.30 (7.25)	4.70 (4.60)	34	220	orange
Nd	8	38.80 (39.25)	7.25 (6.80)	4.65 (4.85)	55	296	yellow/orange
Sm	2	43.10 (43.50)	7.40 (7.45)	3.95 (4.10)	44	246	yellow/green
Eu	4	42.30 (41.80)	7.00 (7.15)	4.40 (4.30)	27	237	orange
Gd	3	41.65 (42.35)	7.75 (7.30)	3.95 (4.20)	52	270	orange
Tb	5	40.25 (40.75)	7.20 (7.00)	3.90 (4.45)	18	229	dark orange
Ho	2	42.00 (42.80)	7.65 (7.35)	4.05 (4.00)	78	284	brown
Er	3	42.10 (41.95)	6.70 (7.20)	4.10 (4.15)	46	291	pale orange
Tm	7	38.90 (39.00)	6.45 (6.70)	4.10 (4.60)	50	279	orange
Yb	8	37.95 (38.20)	6.40 (6.55)	4.40 (4.70)	58	244	orange
$X = ClO_4^-$							
Cd	8	39.40 (39.90)	2.80 (2.75)	4.75 (4.90)	64	291	yellow
La	5	37.40 (37.40)	2.60 (2.55)	4.10 (4.05)	87	369	orange
Ce	5	37.25 (37.35)	2.75 (2.55)	3.75 (4.05)	51	409	dark orange
Pr	2	39.05 (39.20)	2.50 (2.70)	3.90 (3.70)	30	433	dark green
Sm	11	33.75 (33.65)	2.20 (2.30)	5.10 (4.65)	68	386	red-orange
Gd	1	39.90 (39.30)	2.40 (2.70)	4.55 (3.50)	62	277	orange
Er	6	35.55 (35.85)	2.55 (2.45)	3.85 (4.05)	64	386	orange

[a] $[M(\mathbf{1})]X_n \cdot x\,H_2O \cdot 2\,Et_2O$. – [b] $[M(\mathbf{1})]X_n \cdot Et_2O$.

in a low fluorescent emission. It was not possible to observe an antenna effect[33] and the luminescent quantum yield could not be calculated because of the low residual intensity of the emission.

Macrocycle 2 and Its Metal Complexes

It has previously been reported that diamine-containing oxaazamacrocyclic ligands derived from O^1,O^7-bis(2-formylphenyl)-1,4,7-trioxaheptane can be prepared by a non-template cyclocondensation of the precursor dialdehyde and the appropriate diamine, followed by in situ reduction with sodium borohydride.[12] We have found that a similar procedure may successfully be employed for the preparation of the reduced macrocycle **2**. The FAB mass spectrum shows a highest molecular weight peak at m/z = 571, corresponding to $[\mathbf{2} + H]^+$, while the IR spectrum features a secondary amine N–H stretching band at ca. 3410 cm^{-1} and no imine band at ca. 1620 cm^{-1}. Comparison of the ^{1}H-NMR spectra of macrocycles **1** and **2** reveals the disappearance of the signal at δ = ca. 8.91 due to the imine proton and the appearance of a new broad singlet signal at δ = 3.65 corresponding to the N*H*CH_2 amine protons.

Complexation reactions of macrocycle **2** with hydrated metal salts ($X = NO_3^-$, M = Y, La, Ce, Pr, Sm, Gd, Er, or Lu; $X = ClO_4^-$, M = Cd, La, Pr, Gd, or Er) were carried out in order to investigate the coordination capability of this more flexible and hydrolytically stable ligand towards the Ln^{III}, Y^{III}, and Cd^{II} ions. In most cases, the microana-

Table 2. Analytical, yield and molar conductance (in MeCN) data for the complexes $[M_m(\mathbf{2})]X_n \cdot x\,H_2O$ (calculated values are given in parentheses)

M	m	x	Analysis (%)			Yield (%)	Λ_M (Ω^{-1} cm^2mol^{-1})	Colour
			C	N	H			
$X = NO_3^-$								
Y[a]	1	–	41.50 (41.60)	7.20 (6.85)	4.15 (3.95)	93	283	yellow
La[b]	1	–	38.50 (38.10)	6.30 (6.20)	3.40 (3.55)	84	251	pale yellow
Ce[c]	1	–	35.70 (35.40)	5.65 (5.60)	3.55 (3.30)	85	274	yellow
Pr	1	9	38.05 (38.55)	6.70 (6.60)	5.60 (5.35)	63	219	pale yellow
Sm	1	9	38.80 (38.20)	6.40 (6.55)	5.70 (5.30)	51	290	pale yellow
Gd[d]	2	–	32.90 (32.85)	8.25 (8.30)	3.75 (3.70)	77	375	pale yellow
Er[e]	2	–	32.30 (32.10)	8.60 (8.55)	3.25 (3.25)	31	295	yellow
Lu	2	7	29.80 (29.10)	7.85 (8.00)	3.95 (3.75)	19	315	pale yellow
$X = ClO_4^-$								
Cd	1	2	44.55 (44.50)	3.05 (3.05)	4.60 (4.60)	14	220	yellow
La	1	3	38.90 (38.45)	2.90 (2.65)	4.35 (4.20)	20	225	pale yellow
Pr	1	2	38.50 (39.05)	3.00 (2.70)	4.05 (4.05)	41	388	yellow
Gd	2	9	24.95 (24.85)	1.80 (1.70)	4.00 (3.45)	79	395	orange
Er	2	2	26.65 (26.55)	1.70 (1.80)	2.55 (2.75)	50	339	orange

[a] $[M_m(\mathbf{2})]X_n \cdot 1.5\,CHCl_3$. – [b] $[M_m(\mathbf{2})]X_n \cdot 2\,CHCl_3$. – [c] $[M_m(\mathbf{2})]X_n \cdot 3\,CHCl_3$. – [d] $[M_m(\mathbf{2})]X_n \cdot 3\,CH_3OH$. – [e] $[M_m(\mathbf{2})]X_n \cdot CH_3OH$.

lytical data (Table 2) were in accord with the formation of mononuclear complexes of the type $[M(\mathbf{2})]X_n \cdot x\,H_2O$ (X = NO_3^-, M = Y, La, Ce, Pr, Sm; X = ClO_4^-, M = Cd, La, Pr). However, in contrast to the complexes of macrocycle **1**, elemental analyses of complexes of the heavier lanthanides Gd, Er (NO_3^-, ClO_4^-), and Lu (NO_3^-) were indicative of dinuclear complexes of the general formula $[Ln_2(\mathbf{2})]X_6$. These may arise from the increased flexibility of the reduced macrocycle, allowing the accommodation of the smaller cations; attempts to obtain the corresponding mononuclear complexes were unsuccessful. The molar conductivities of the complexes $[M(\mathbf{2})]X_n \cdot x\,H_2O$ in acetonitrile were found to fall in the range reported for 2:1 electrolytes in this solvent.[19]

The FAB mass spectra of the complexes invariably show the peak corresponding to the free macrocycle. The spectra of the yttrium, cerium, and cadmium complexes also show peaks corresponding to $[Y(\mathbf{2})(NO_3)]^+$ (m/z = 721), $[Ce(\mathbf{2})(NO_3)_2]^+$ (m/z = 834) and $[Cd(\mathbf{2})(ClO_4)]^+$ (m/z = 783).

The IR spectra of the nitrate complexes feature several bands in the region associated with nitrate vibrations, from which it is evident that these species contain both coordinated and ionic nitrate groups.[24,25] The two most intense nitrate absorptions, associated with $\nu(N{=}O)$ and $\nu_a(NO_2)$, appear at ca. 1450 and 1300 cm^{-1}. The $\Delta\nu$ separations between the two highest frequency bands fall in the range 154–213 cm^{-1}, suggesting bidentate coordination of the nitrate anions.[27] In the spectra of the perchlorate complexes, the higher-energy band (ν_3) consists of three maxima at ca. 1137, 1120, and 1080 cm^{-1}. The ν_4 band also shows splitting with maxima at ca. 636 and 624 cm^{-1}. The splitting of these bands is indicative of coordination of at least one of the perchlorate anions to the metal,[28,29] but as with the complexes of macrocycle **1** a full assignment is hindered by the presence of ligand bands.

The UV/visible spectra of macrocycle **2** and the corresponding metal complexes were recorded using 10^{-3}–10^{-6} M acetonitrile solutions. The free macrocycle exhibits three broad absorption bands at ca. 250, 277, and 293 nm, corresponding to the π-π* transitions of benzene rings and azomethine groups.[30] In the spectra of the metal complexes, the π-π* absorption bands are red-shifted with respect to their positions in the spectrum of macrocycle **2**. Emission spectra of the free ligand **2** and some of its metal complexes were recorded using 10^{-6} M acetonitrile solutions. Low fluorescent emissions were observed, similar to those seen with macrocycle **1** and its metal complexes.

Crystal Structure of $[(\mathbf{2})H](ClO_4) \cdot CHCl_3$

Single crystals of $[(\mathbf{2})H](ClO_4) \cdot CHCl_3$ suitable for X-ray analysis were obtained by slow crystallization from a solution of the complex $[Cd(\mathbf{2})](ClO_4)_2 \cdot 2\,H_2O$ in diethyl ether/chloroform open to the atmosphere. The crystal structure of the cation is shown in Figure 1. There are two $[(\mathbf{2})H](ClO_4) \cdot CHCl_3$ groups in the asymmetric unit. Only one of the two amine nitrogen atoms in the ligand is protonated and the flexibility of the macrocycle allows it to adopt a folded conformation. This is reinforced by intramolecular hydrogen-bond interactions. The perchlorate ions and the solvent molecules are not involved in hydrogen-bond interactions with macrocycle **2**. The bond lengths and angles fall within the expected ranges.

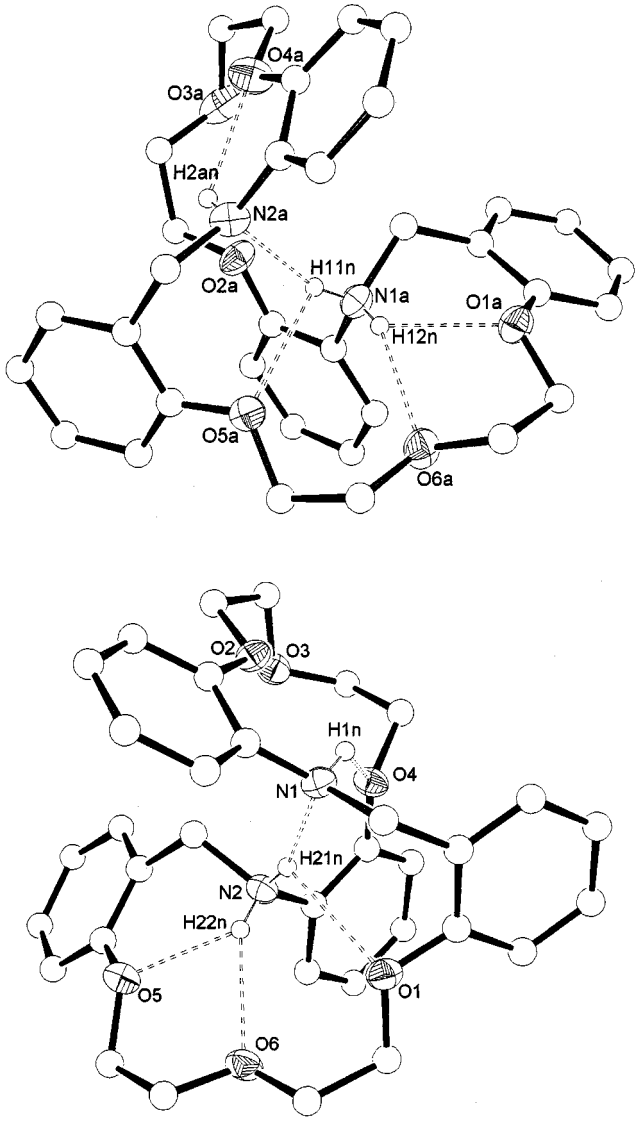


Figure 1. Molecules 1 and 2 of the protonated macrocycle **2** in the asymmetric unit of $[(\mathbf{2})H](ClO_4) \cdot CHCl_3$

Macrocycle 3 and Its Metal Complexes

Reactions of heterocyclic dialdehydes with tris(2-aminoethyl)amine give cryptands,[34–36] while the reaction of 2,6-diacetylpyridine with tris(2-aminoethyl)amine in the presence of metal templates gives a [2+2] pendant-armed Schiff-base macrocycle resulting from the condensation of two molecules of each precursor.[37] It was therefore extremely interesting to find that the non-template reaction of O^1,O^7-bis(2-formylphenyl)-1,4,7-trioxaheptane and tris(2-aminoethyl)amine in acetonitrile produced a rare example of an amino pendant-armed [1+1] Schiff-base macrocycle, i.e. **3**.

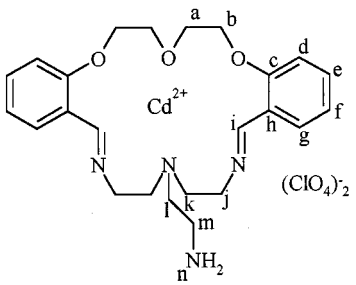
The compound was isolated as a yellow solid, and was found to be stable in air and moderately soluble in most common organic solvents. The IR spectrum features a strong peak at 1636 cm^{-1} due to C=N while no bands attributable to C=O groups are detectable. The primary amine stretching modes of the *pendant-arm* NH_2 group cannot be assigned owing to the presence of an intense broad band centred at ca. 3400 cm^{-1}. The latter is consistent with the presence of water, as is also suggested by the microanalytical data. The FAB mass spectrum shows the parent peak at m/z = 425, confirming the [1+1] cyclic nature of the Schiff base. The ^{1}H-NMR spectrum recorded in $CDCl_3$ solution features two imine proton singlets at δ = 8.79 and δ = 8.77, suggesting the possible presence of conformers in solution. The C_6H_4 protons give rise to a multiplet at δ = 7.96–6.84, while the CH_2CH_2 chains give rise to four multiplets in the aliphatic region. The complex nature of these signals could stem from the presence of related conformers in solution or from the magnetic inequivalence of the geminal hydrogen pairs caused by restricted rotation about the C–C bond.[38,39] In the pendant arm, this restriction could possibly be due to hydrogen-bonding effects. The broad singlet at δ = 1.84–1.95 may be assigned to the NH_2 group, as was confirmed by deuterium exchange when D_2O was added to the $CDCl_3$ solution. No change in the spectrum of the macrocycle was observed after 24 h, demonstrating a greater stability of this ligand compared with macrocycle **1**.

Metal-template reactions between equimolar amounts of O^1,O^7-bis(2-formylphenyl)-1,4,7-trioxaheptane and tris(2-aminoethyl)amine in the presence of hydrated lanthanide nitrates or perchlorates gave analytically pure products formulated as $[Ln(\mathbf{3})]X_3 \cdot x\,H_2O$ only for Er (X = ClO_4^-) and Dy (X = NO_3^-). Attempts to obtain other Ln^{III} complexes by changing the experimental conditions were unsuccessful and it was possible to identify complexes derived from the precursor amine as the major components of the products. The complexes cannot be prepared by a two-step procedure involving preparation of the free macrocycle followed by a complexation reaction with the requisite lanthanide salt.

The IR spectra of $[Er(\mathbf{3})](ClO_4)_3 \cdot 2\,H_2O$ and $[Dy(\mathbf{3})](NO_3)_3 \cdot H_2O$ show the imine band at ca. 1638 cm^{-1}. This band is slightly shifted in comparison to its position in the spectrum of the free ligand. The ν(NH_2) band is masked by a broad band at ca. 3400 cm^{-1} due to the water present in the complexes. Bands attributable to the perchlorate groups are present in the spectrum of the Er complex at ca. 1120, 1109, and 1088 cm^{-1} (ν_3) and at 627 and 637 cm^{-1} (ν_4), suggesting the presence of coordinated perchlorate groups. The spectrum of the Dy complex features bands at ca. 1458 (ν_5), 1298 (ν_1), and 1030 (ν_2) cm^{-1}, indicative of bidentate nitrate groups, as well as a band at 1383 cm^{-1} due to ionic nitrate. The molar conductance of the Dy complex in dimethylformamide (71 $\Omega^{-1}cm^2mol^{-1}$) is in the range reported for 1:1 electrolytes in this solvent,[19] indicating strong coordination of the nitrate ions. The very limited solubility of the Er complex in various solvents prohibited the measurement of conductivity. The FAB mass spectra of the complexes feature a peak corresponding to the free macrocycle **3** at m/z = 425; in neither case was the molecular ion observed.

When the template reaction was carried out in the presence of hydrated cadmium perchlorate, $[Cd(\mathbf{3})](ClO_4)_2$ was isolated as a white solid. It was found that direct reaction of macrocycle **3** with the metal salt could also be exploited for the synthesis of the complex. The molar conductivity in acetonitrile (307 $\Omega^{-1}cm^2mol^{-1}$) indicates that the complex is

Table 3. ^{1}H- and ^{13}C-NMR data (250 MHz) for $[Cd(\mathbf{3})](ClO_4)_2$ in CD_3CN



Assignment	Shift (δ value)	Integration	*J*/Hz	Assignment	Shift (δ value)
H_i	8.37 (s)	2 H	^3J (^{1}H,^{111,113}Cd) 43	C_a	66.7
H_f	7.50 (t)	1 H	^3J (H_e,H_f) 7.5	C_b	67.2
H_d	7.19 (t)	1 H	^4J (H_d,H_f) 1.8	C_c	156.1
H_e	7.36 (dd)	1 H	^3J (H_e,H_d) 7.9	C_d	113.9
H_g	6.86 (d)	1 H	^3J (H_g,H_f) 8.3	C_e	134.7
H_a, H_b, H_j, H_k, H_l, H_m	4.59–4.49 (m)	2 H		C_f	121.1
	4.21–3.99 (m)	6 H		C_g	133.8
	3.93–3.81 (m)	2 H		C_h	122.5
	3.64–3.53 (m)	2 H		C_i	169.9
	3.03–2.96 (m)	8 H		C_j	57.2
H_n	3.39–3.22 (br. s)	2 H		C_k	55.0
				C_l	54.2
				C_m	37.5

a 2:1 electrolyte, hence the ClO_4^- anion is not coordinated in solution. In the IR spectrum of the complex, the strong absorption at 1642 cm^{-1} corresponds to the expected C=N vibration of the Schiff base; this band is shifted to higher wavenumber than in the free ligand. Two strong peaks at 3354 and 3274 cm^{-1} can be attributed to the vibration of the primary amine, and the spectrum also features single bands attributable to ionic ClO_4^- anions at 1080 cm^{-1} (ν_3) and 620 cm^{-1} (ν_4). The FAB mass spectrum shows peaks attributable to $[Cd(\mathbf{3})ClO_4]^+$ at m/z = 637 and $[Cd(\mathbf{3})]^+$ at m/z = 537. The ^{1}H-NMR spectrum (Table 3), recorded immediately after dissolution in CD_3CN, features only a single imine proton peak at δ = 8.37, along with two cadmium satellites [$^3J(^1H,^{111,113}Cd) \approx 43$ Hz]. A broad signal is observed at δ = ca. 3.39, corresponding to the pendant-amine protons. A spectrum recorded after 24 h showed no significant changes, demonstrating the stability of the cadmium perchlorate complex in solution. Recrystallization of the complex from acetonitrile resulted in the formation of crystals suitable for an X-ray crystallographic study.

Description of the Structure of $[Cd(3)](ClO_4)_2$

The X-ray crystal structure of complex $[Cd(\mathbf{3})](ClO_4)_2$ is shown in Figure 2, together with selected bond lengths and angles at the metal, and confirms that a single cadmium cation is coordinated by macrocycle **3**. The perchlorate anions do not interact with the metal. The flexibility of the macrocycle allows it to adopt a folded cleft-like conformation that encapsulates the metal, giving an irregular 7-coordinated N_4O_3 complex in which the Cd ion interacts with all heteroatoms of the ligand. Similar 7-coordination of Cd^{II} has been observed in other macrocyclic complexes.[40,41] The cadmium–nitrogen bond lengths range from 2.254(4) Å [Cd–pendant amine nitrogen N(4)] to 2.492(4) Å [Cd–tertiary amine nitrogen N(2)], with the distances between the metal and the two imino nitrogens and the pendant amino nitrogen N(4) being shorter than the standard Cd–N bond length of 2.33 ± 0.005 Å,[42] thus indicating strong coordinative bonds between these N atoms and the metal. The three Cd–ether oxygen bonds appear to be somewhat elongated, although they fall within the range of 2.36–2.84 Å reported for similar bonds in other cadmium(II) complexes.[43–45] The distances and angles in the ligand are normal. The folding of the macrocycle to achieve the hepta-coordination results in an almost coplanar arrangement of the two phenyl rings [interplanar angle 19.9(2)°].

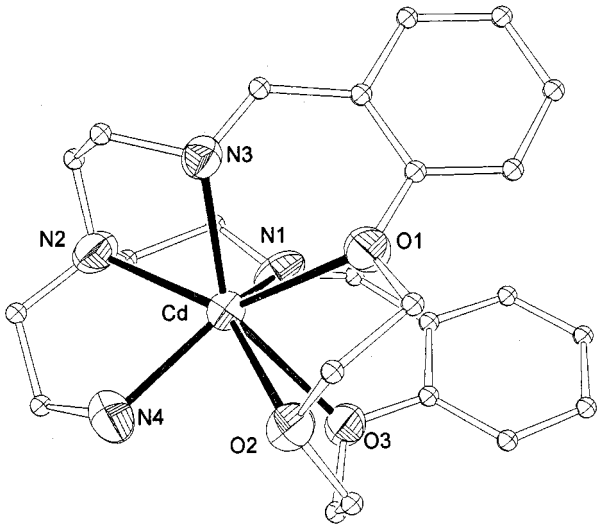


Figure 2. Crystal structure of the cation in $[Cd(\mathbf{3})](ClO_4)_2$: selected bond lengths (Å) and angles (°) at the metal: Cd–N4, 2.254(4), Cd–N1 2.268(4), Cd–N3 2.309(3), Cd–N2 2.492(4), Cd–O1 2.558(3), Cd–O3 2.581(3), Cd–O2 2.605(3); N4–Cd–N1 123.73(18), N4–Cd–N3 119.48(17), N1–Cd–N3 93.73(12), N4–Cd–N2 74.42(16), N1–Cd–N2 75.57(14), N3–Cd–N2 71.56(12), N4–Cd–O1 135.57(15), N1–Cd–O1 96.73(13), N3–Cd–O1 69.55(11), N2–Cd–O1 139.71(11), N4–Cd–O3 95.23(16), N1–Cd–O3 70.56(118), N3–Cd–O3 144.46(10), N2–Cd–O3 130.12(11), O1–Cd–O3 80.58(10), N4–Cd–O2 75.00(15), N1–Cd–O2 132.22(11), N3–Cd–O2 115.41(10), N2–Cd–O2 147.45(12), O1–Cd–O2 63.44(9), O3–Cd–O2 63.76(9)

Conclusions

The cyclocondensation of O^1,O^7-bis(2-formylphenyl)-1,4,7-trioxaheptane with O^1,O^7-bis(2-aninyl)-1,4,7-trioxaheptane gives the oxa-aza Schiff-base macrocycle **1**, which, on reaction with $NaBH_4$, is readily reduced to macrocycle **2**. Mononuclear lanthanide complexes have been prepared from both macrocycles, with dinuclear complexes being formed only by the more flexible ligand **2** and the smaller lanthanide ions. Most interestingly, the reaction of O^1,O^7-bis(2-formylphenyl)-1,4,7-trioxaheptane with tris(2-aminoethyl)amine has been found to give a rare example of an amino pendant-armed [1+1] Schiff-base macrocycle **3** rather than a cryptand or a [2+2] macrocycle. The integrity of the macrocycle **3** has been confirmed by a crystal structure determination of the complex $[Cd(\mathbf{3})](ClO_4)_2$. This type of functionalized macrocycle should provide opportunities for the synthesis of a wide range of derivatives suitable as precursors for polynuclear complexation.

Experimental Section

Measurements: Elemental analyses were carried out by the University of Santiago de Compostela Microanalytical Service on Carlo Erba 1108 and Leco CNHS-932 microanalysers. – Infrared spectra were recorded with samples between KBr discs using a Mattson Cygnus 100 spectrophotometer. – Proton NMR spectra were recorded on a Bruker WM-300 spectrometer. – Positive-ion FAB mass spectra were recorded on a Kratos MS50TC spectrometer using a 3-nitrobenzyl alcohol (*m*NBA) matrix. Conductivity measurements were carried out on 10^{-3} mol dm^{-3} acetonitrile solutions at 20 °C using a WTW LF-3 conductivimeter. The electronic absorption spectra of the complexes (10^{-3}–10^{-6} M acetonitrile solutions) were measured in the range 300–900 nm using Hitachi U-3200 and Perkin–Elmer Lambda 6 spectrophotometers. Emission spectra were recorded on a SPEX F111 Fluorolog spectrofluorimeter.

Chemicals and Starting Materials: O^1,O^7-Bis(2-formylphenyl)-1,4,7-trioxaheptane was prepared according to a literature method;[17] O^1,O^7-bis(2-aninyl)-1,4,7-trioxaheptane was prepared by reduction of the corresponding dinitro precursor using a proced-

ure similar to that described previously.[46–49] Tris(2-aminoethyl)-amine and the metal salts were commercial products (from Alfa and Aldrich) and were used without further purification. Solvents were of reagent grade and were purified by the usual methods. ***Caution:*** Perchlorate salts are potentially explosive! Only small amounts of material should be prepared and handled with great care; particular caution must be exercised when they are heated in vacuo.

Condensation of O^1,O^7-Bis(2-formylphenyl)-1,4,7-trioxaheptane with O^1,O^7-Bis(2-aninyl)-1,4,7-trioxaheptane in the Absence of Metal Ions: A solution of O^1,O^7-bis(2-aninyl)-1,4,7-trioxaheptane (0.28 g, 1 mmol) in hot methanol (50 mL) was added dropwise to a refluxing solution of O^1,O^7-bis(2-formylphenyl)-1,4,7-trioxaheptane (0.31 g, 1 mmol) in hot methanol (50 mL). The resulting solution was gently refluxed with magnetic stirring for ca. 5 h. The colour changed to yellow and an orange-brown powder precipitated, which was filtered off. The solution was then concentrated using a rotary evaporator; on leaving the concentrated filtrate to stand, an orange-yellow powder precipitated, which was filtered off, washed with diethyl ether, and dried in vacuo. This product was characterized as the macrocyclic ligand. Yield 75%; m.p. 160 °C. – IR (KBr): $\tilde{\nu}$ = 1620 cm^{-1} $(C{=}N)_{imi}$, 1590 (C=C). – MS (FAB; *m*NBA): *m*/z = 567 [**1** + H]$^+$.– HR MS: *m*/*z* = 566 (100%) $C_{34}H_{34}N_2O_6$. – ^{1}H NMR (CD_3CN): δ = 8.9 (s, 2 H, $HC{=}N_{imi}$). – $C_{34}H_{34}N_2O_6 \cdot 0.5\,H_2O$: calcd. C 70.95, H 6.15, N 4.90; found C 70.80, H 6.10, N 5.25.

Reaction of O^1,O^7-Bis(2-formylphenyl)-1,4,7-trioxaheptane and O^1,O^7-Bis(2-aninyl)-1,4,7-trioxaheptane in the Presence of Metal Ions: General Procedure for [M(1)][X]$_n$: To a refluxing solution of O^1,O^7-bis(2-formylphenyl)-1,4,7-trioxaheptane (1 mmol) in hot methanol (25 mL) was added a solution of the hydrated metal salt (1 mmol) (M = Y, Cd, Ln = La–Yb except Pm and Dy) in methanol (15 mL). The resulting solution was magnetically stirred and heated while a methanolic solution of O^1,O^7-bis(2-aninyl)-1,4,7-trioxaheptane (1 mmol) was slowly added. Following the addition, refluxing was continued for ca. 4–5 h. The solution was then concentrated in a rotary evaporator to a volume of ca. 10–15 mL. An equal volume of acetonitrile/diethyl ether was slowly infused into the solution, which led to the deposition of a powdery precipitate. The product was filtered off, washed with absolute ethanol, and dried in vacuo. Microanalytical data are given in Table 1. The compounds were found to be air-stable, soluble in methanol, dimethylformamide, dimethyl sulfoxide, acetonitrile, pyridine, dichloromethane, nitrobenzene, and nitromethane, moderately soluble in absolute ethanol, and insoluble in diethyl ether, water, chloroform, and cyclohexane.

Synthesis of Macrocycle 2: The reduction was carried out according to a modification of a literature method.[49,50] O^1,O^7-Bis(2-aninyl)-1,4,7-trioxaheptane (4.0 mmol) in warm methanol (150 mL) was slowly added to a solution of O^1,O^7-bis(2-formylphenyl)-1,4,7-trioxaheptane (4.0 mmol) in warm methanol (300 mL). The resulting mixture was refluxed for 1 h, cooled, and then solid $NaBH_4$ (65 mmol) was carefully added portionwise with stirring. When effervescence had ceased, a white precipitate was observed, which was collected by filtration. This product was washed with water and characterized as the macrocycle. The filtrate was concentrated to dryness in a rotary evaporator and the residue was taken up in dichloromethane (150 mL). The resulting solution was stirred for ca. 72 h. A grey precipitate was removed by filtration and the solution was dried over anhydrous sodium sulfate. It was then concentrated to a volume of ca. 10–15 mL in a rotary evaporator whereupon diethyl ether was added, which led to the deposition of a white product. This was filtered off, washed with absolute ethanol, and dried in vacuo to give a second crop of the macrocyclic product. The compound was found to be air-stable, soluble in warm chloroform/benzene (1:1); moderately soluble in hot methanol and chloroform, and insoluble in acetonitrile, absolute ethanol, diethyl ether, dimethylformamide, dimethyl sulfoxide, pyridine, and water. Yield 40%; m.p. 179–181 °C. – IR (KBr): $\tilde{\nu}$ = 3364 cm^{-1} (NH), 1601 (C=C). – MS (FAB; *m*NBA): *m*/*z* = 571 [**2** + H]$^+$. – HR MS: *m*/*z* = 570 (100%) $C_{34}H_{38}N_2O_6$.– ^{1}H NMR ($CDCl_3$): δ = 7.42–6.67 (m, 16 H, C_6H_4), 4.75 (s, 4 H, CH_2NH), 4.23–3.87 (m, 16 H, OCH_2CH_2), 3.65 (br. s, 2 H, NH). – $C_{34}H_{38}N_2O_6 \cdot H_2O$: calcd. C 69.40, H 6.50, N 8.10; found C 69.50, H 6.75, N 7.95.

Crystal Structure of [(2)H](ClO$_4$) · CHCl$_3$: A yellow plate-like crystal of $[C_{34}H_{39}N_2O_6](ClO_4) \cdot CHCl_3$ (790.48), dimensions 0.5 × 0.5 × 0.2 mm, crystallized from diethyl ether/chloroform, was used for the structure determination. The chosen crystal was mounted on a glass fibre using an epoxy resin. Data were collected by means of a Bruker Smart CCD area detector with an Oxford Cryosystems low-temperature system held at 150 K. Cell parameters were refined from the setting angles of 140 reflections (θ range 1.35–28.48). Reflections were measured from a hemisphere of data composed of frames each covering 0.3° in ω. Of the 24613 reflections measured, all of which were corrected for Lorentz and polarization effects and for absorption (maximum and minimum transmission coefficients of 0.893 and 0.223), 9824 independent reflections exceeded the significance level $F/\sigma(F) > 4.0$. The structure was solved by direct methods and refined by full-matrix least-squares methods on F^2. Hydrogen atoms were placed in geometrically idealized positions and refined with a riding model (including torsional freedom for methyl groups) with U_{iso} restrained as 1.2 (or 1.5 for methyl groups) times U_{eq} of the carrier atom. Refinement converged at a final $R = 0.0745$ ($wR2 = 0.2321$ for all 16888 unique data, 943 parameters, mean and maximum Δ/σ 0.000, 0.0001) with allowance for the thermal anisotropy of all non-hydrogen atoms. Minimum and maximum final electron density –0.816 and 0.987 eÅ^{-3}. A weighting scheme $w = 1/[\sigma^2(F_o^2) + (0.1408P)^2 + 0.0000P]$, where $P = (F_o^2 + 2F_c^2)/3$, was used in the latter stages of refinement. Complex scattering factors were taken from the SHELXTL program package[51] as implemented on a Viglen Pentium computer, while molecular graphics were derived from ORTEP-3.[52] A summary of the experimental and structure solution procedure is given in Table 4.

Metal Complexes of Macrocycle 2. – General Procedure: The appropriate metal salt (0.15 mmol) was dissolved in methanol (10 mL) and added to a stirred solution of the ligand **2** (0.15 mmol) in chloroform/benzene (20 mL + 20 mL). An immediate colour change was usually observed and a precipitate began to deposit. The mixture was then stirred for 3 days at room temperature. The product was subsequently filtered off and dried in vacuo. The filtrate was concentrated in a rotary evaporator to leave an oil. On treatment with diethyl ether, a solid was obtained, which was filtered off and dried in vacuo. This reaction was attempted with $Cd(ClO_4)_2 \cdot x\,H_2O$ and $Y(NO_3)_3 \cdot x\,H_2O$, the nitrates of La, Ce, Pr, Sm, Gd, Er, and Lu, and the perchlorates of La, Pr, Gd, and Er. Microanalytical data of the relevant products are given in Table 2. The complexes were found to be air-stable, soluble in acetonitrile, chloroform, dimethylformamide, and dimethyl sulfoxide, moderately soluble in methanol and dichloromethane, and insoluble in absolute ethanol, cyclohexane, diethyl ether, and water.

Reaction of O^1,O^7-Bis(2-formylphenyl)-1,4,7-trioxaheptane and Tris(2-aminoethyl)amine in the Absence of Metal Ions: A solution of O^1,O^7-bis(2-formylphenyl)-1,4,7-trioxaheptane (0.31 g, 1 mmol)

Table 4. Crystal data and structure refinement for $[C_{34}H_{39}N_2O_6](ClO_4) \cdot CHCl_3$

Empirical formula	$C_{35}H_{40}Cl_4N_2O_{10}$
Formula weight	790.48
Temperature [K]	423(2)
Wavelength [Å]	0.71073
Crystal system, space group	triclinic, *P*-1
Unit cell dimensions:	
a [Å]	10.4438(11)
b [Å]	11.9470(12)
c [Å]	30.724(3) Å
α [°]	90.619(2)
β [°]	99.485(2)
γ [°]	102.441(2)
Volume [Å^3]	3688.1(7)
Z	4
Calculated density [Mg/m^3]	1.328
Absorption coefficient [mm^{-1}]	0.243
F(000)	1528
Crystal size [mm]	0.5 × 0.5 × 0.2
θ range for data collection [°]	1.35 to 28.48
Index ranges	$-13 \le h \le 9$ $-14 \le k \le 15$ $-40 \le l \le 40$
Reflections collected/unique	24613/16888 [*R*(int) = 0.0464]
Completeness to 2θ	28.48°; 90.7%
Absorption correction	None
Refinement method	Full-matrix least-squares on F^2
Data/restraints/parameters	16888/0/943
Goodness-of-fit on F^2	0.990
Final *R* indices [$I > 2\sigma(I)$]	*R*1 = 0.0745, *wR*2 = 0.1982
R indices (all data)	*R*1 = 0.1200, *wR*2 = 0.2321
Largest diff. peak and hole	0.987 and –0.816 e · Å^{-3}

in hot acetonitrile (100 mL) was added dropwise to a refluxing solution of tris(2-aminoethyl)amine (0.15 mL, 1 mmol) in hot acetonitrile (300 mL). The resulting solution was gently refluxed with magnetic stirring for ca. 3 h. The colour of the reaction mixture changed to yellow and first an unidentified precipitate was deposited, which was removed by filtration. The filtrate was then concentrated to a volume of ca. 10 mL and a yellow product was obtained. This was collected by filtration, washed with diethyl ether, and dried in vacuo to give macrocycle **3** in 25% yield; m.p. 115 °C (dec.) – IR (KBr): $\tilde{\nu}$ = 1636 cm^{-1} (C=N)$_{imi}$. – ^{1}H NMR ($CDCl_3$): δ = 8.79–8.77 (s, 2 H, HC=N$_{imi}$), 7.96–6.84 (m, 8 H, C_6H_4), 4.24–4.14 (m, 4 H, CH_2O), 4.00–3.84 (m, 4 H, CH_2O-aryl), 3.71–3.62 (m, 4 H, C*H*$_2$N=CH), 2.92–2.60 (m, 8 H, CH_2-N$_{ternary}$), 1.94–1.85 (br. s, 2 H, NH_2). – MS (FAB; *m*NBA): *m*/*z* = 425 [**3** + H]$^+$. – MS(EI): P$^+$ = 394 [**3** – CH_2NH_2]$^+$. – $C_{24}H_{32}N_4O_3 \cdot 1.5\ H_2O$: calcd. C 63.85, H 7.75, N 12.45; found C 64.40, H 7.50, N 12.40.

Reaction of *O*^{1},*O*^{7}-Bis(2-formylphenyl)-1,4,7-trioxaheptane and Tris(2-aminoethyl)amine in the Presence of Metal Ions: General Procedure for [M(3)][X]$_n$: To a refluxing solution of tris(2-aminoethyl)-amine (1 mmol) in either hot methanol, acetonitrile, or absolute ethanol (50 mL) was added a solution of the hydrated lanthanide salt (1 mmol) (X = ClO_4^-, Ln = La, Ce, Gd, Er or Ho; X = NO_3^-, Ln = La, Pr, Sm, Eu, Gd, Tb, Dy, Ho, Er, Tm, Yb, or Lu) in the same solvent (50 mL). The resulting mixture was magnetically stirred and heated for 1 h, during which a methanolic or ethanolic solution (50 mL) of *O*^{1},*O*^{7}-bis(2-formylphenyl)-1,4,7-trioxaheptane (1 mmol) was slowly added. Refluxing was continued for ca. 3–4 h. The solution was then concentrated in a rotary evaporator to a volume of ca. 10–15 mL. An equal volume of diethyl ether was slowly infused into the concentrated solution, which led to the deposition of a yellow powdery precipitate. The product was filtered off and dried in vacuo. The products thus obtained gave unsatisfactory analytical results. When the methanol/diethyl ether or ethanol/diethyl ether solution was concentrated to dryness once more and further diethyl ether was added, a second product was isolated by filtration and identified as the metal complex only in the cases of the reactions with erbium perchlorate and dysprosium nitrate. In the reactions with the other Ln^{III} nitrates or perchlorates, no analytically pure products could be isolated. The compounds were found to be air-sensitive. When the same reaction was carried out with Cd^{II} perchlorate in absolute ethanol, the product isolated was characterized as the [Cd(**3**)]$(ClO_4)_2$ complex; recrystallization from acetonitrile resulted in the formation of crystals suitable for X-ray crystallographic analysis.

[Er(3)](ClO$_4$)$_3$ · 2 H$_2$O: Solvent: Methanol. Yield: 16%. – IR (KBr): $\tilde{\nu}$ = 1637 cm^{-1} (C=N)$_{imi}$, 1600 (C=C), 1120, 1109, 1088, 627, and 636 (ClO_4^-). – MS (FAB; *m*NBA): *m*/*z* = 425 [**3** + H]$^+$. – $C_{24}H_{36}N_4O_{17}Cl_3Er$: calcd. C 31.10, H 3.90, N 6.05; found C 30.60, H 3.75, N 6.80. The yellow complex was found to be moderately soluble in acetonitrile, dimethylformamide, and acetone, but insoluble in methanol, chloroform, absolute ethanol, dimethyl sulfoxide, diethyl ether, and water.

[Dy(3)](NO$_3$)$_3$ · H$_2$O: Solvent: Acetonitrile. Yield: 63%. – IR (KBr): $\tilde{\nu}$ = 1638 cm^{-1} (C=N)$_{imi}$, 1600 (C=C), 1458, 1383, 1298, 1046, and 1030 (NO_3^-). – MS (FAB; *m*NBA): *m*/*z* = 425 [**3** + H]$^+$. – Λ_M (DMF): 71 Ω^{-1}cm^{2}mol^{-1}. – $C_{24}H_{34}N_7O_{13}Dy$: calcd. C 37.55, H 4.50, N 12.75; found C 37.50, H 4.80, N 12.55. The yellow complex was found to be soluble in dimethylformamide and dimethyl sulfoxide, moderately soluble in acetonitrile, methanol, chloroform, absolute ethanol, and acetone, and insoluble in diethyl ether and water.

[Cd(3)](ClO$_4$)$_2$: Solvent: Absolute ethanol; the order of addition of tris(2-aminoethyl)amine and *O*^{1},*O*^{7}-bis(2-formylphenyl)-1,4,7-trioxaheptane was reversed. The white precipitate obtained directly from the reaction mixture was filtered off and dried in vacuo. Yield: 36%. – IR (KBr): 1642 cm^{-1} (C=N)$_{imi}$, 1116, 1083, 1039, and 620 (ClO_4^-). – ^{1}H- and ^{13}C-NMR spectra; see Table 3. – MS (FAB; *m*NBA): *m*/*z* = 637 [Cd(**3**)(ClO_4)]$^+$, 537 [Cd(**3**)]$^+$. – $C_{24}H_{32}N_4O_{11}Cl_2Cd$: calcd. C 39.20, H 4.40, N 7.60; found C 39.35,

Table 5. Crystal data and structure refinement of [Cd(**3**)]$(ClO_4)_2$

Empirical formula	$C_{24}H_{32}CdCl_2N_4O_{11}$
Formula weight	735.84
Temperature [K]	293(2)
Wavelength [Å]	0.71073
Crystal system	monoclinic
Space group	*P*21/*n*
Unit cell dimensions:	
a [Å]	11.7207(2)
b [Å]	18.2691(2)
c [Å]	13.5708(2)
β [°]	100.3439(3)
Volume [Å^3]	2858.64(7)
Z	4
Calculated density [Mg/m^3]	1.710
Absorption coefficient [mm^{-1}]	1.017
F(000)	1496
Crystal size [mm]	0.55 × 0.30 × 0.05
θ range for data collection [°]	1.89 to 28.29
Index ranges	$-14 \le h \le 15$ $-24 \le k \le 12$ $-18 \le l \le 16$
Reflections collected/unique	20796/7078 [*R*(int) = 0.0360]
Refinement method	Full-matrix least-squares on F^2
Data/restraints/parameters	7078/0/387
Goodness-of-fit on F^2	1.022
Final *R* indices [$I > 2\sigma(I)$]	R_1 = 0.0472, wR_2 = 0.1179
R indices (all data)	R_1 = 0.0722, wR_2 = 0.1335
Largest diff. peak and hole	1.151 and -0.749 eÅ^{-3}

H 4.40, N 7.30. The complex was found to be air-stable, soluble in acetonitrile, dimethylformamide, and dimethyl sulfoxide, but insoluble in methanol, chloroform, absolute ethanol, acetone, diethyl ether, and water. Recrystallization from acetonitrile resulted in the formation of crystals suitable for an X-ray crystallographic study.

Crystal Structure of [Cd(3)](ClO$_4$)$_2$: A colorless, plate-like crystal of $[Cd(C_{24}H_{32}N_4O_3)](ClO_4)_2$ (735.84), crystallized from acetonitrile solution, with dimensions 0.55 × 0.30 × 0.05 mm, was used for the structure determination. The chosen crystal was mounted on a glass fibre using an epoxy resin. Data were collected using a Siemens SMART CCD area detector single-crystal diffractometer with graphite-monochromated Mo-K_α radiation (λ = 0.71073 Å). Preliminary unit cell constants were determined from a set of 45 narrow-frame scans (0.3 in ω). A total of 1420 frames of intensity data were collected with a width of 0.3° per frame and a counting time of 20 s/frame at a crystal-to-detector distance of 4.5 cm. The collected frames were integrated using an orientation matrix determined from the narrow-frame scans and refined using Siemens SAINT[53] software on all observed reflections. Absorption corrections were applied by means of the SADABS[54] program (maximum and minimum transmission coefficients, 1.0000 and 0.7650). The integration process yielded 20796 reflections, of which 7078 were independent. The structure was solved using SHELX-97[55] by the heavy atom method (Cd atom) and subsequent Fourier difference synthesis, and refined by full-matrix least-squares methods on F^2. The amine hydrogen atoms were located on a Fourier map. All other hydrogen atoms were included in calculated positions and refined in riding mode with U(H) equal to 1.2 times U_{eq} of the parent atom. Molecular graphics were generated using ORTEP-3.[52] A summary of the experimental and structure solution procedure is given in Table 5.

Crystallographic data (excluding structure factors) for the structures reported in this paper have been deposited with the Cambridge Crystallographic Data Centre as supplementary publication nos. CCDC-135465 for [(2)H](ClO$_4$) · CHCl$_3$ and CCDC-135464 for [Cd(**3**)](ClO$_4$)$_2$. Copies of the data can be obtained free of charge on application to the CCDC, 12 Union Road, Cambridge CB2 1EZ, U.K. [Fax: (internat.) +44 (0)1223 336033; E-mail: deposit@ccdc.cam.ac.uk].

Acknowledgments

We thank A Xunta de Galicia (XUGA 20903B96 and PGIDT99PXI20902B) for financial support.

[1] B. Dietrich, P. Viout, J.-M. Lehn, *Macrocyclic Chemistry*, VCH, Weinheim, **1993**.
[2] V. Alexander, *Chem. Rev.* **1995**, *95*, 273–342.
[3] L. F. Lindoy, *Pure Appl. Chem.* **1997**, 2179–2186.
[4] H. Okawa, H. Furutachi, D. E. Fenton, *Coord. Chem. Rev.* **1998**, *174*, 51–75.
[5] R. Bandín, R. Bastida, A. de Blas, P. Castro, D. E. Fenton, A. Macías, A. Rodríguez, T. Rodríguez-Blas, *J. Chem. Soc., Dalton Trans.* **1994**, 1185–1188.
[6] R. Bastida, A. de Blas, P. Castro, D. E. Fenton, A. Macías, R. Rial, A. Rodríguez, T. Rodríguez-Blas, *J. Chem. Soc., Dalton Trans.* **1996**, 1493–1497.
[7] H. Adams, R. Bastida, A. de Blas, M. Carnota, D. E. Fenton, A. Macías, A. Rodríguez, T. Rodríguez-Blas, *Polyhedron* **1997**, *16*, 567–572.
[8] C. Lodeiro, R. Bastida, A. de Blas, D. E. Fenton, A. Macías, A. Rodríguez, T. Rodríguez-Blas, *Inorg. Chim. Acta* **1998**, *267*, 55–62.
[9] L. Valencia, R. Bastida, A. de Blas, D. E. Fenton, A. Macías, A. Rodríguez, T. Rodríguez- Blas, *Inorg. Chim. Acta* **1998**, *282*, 42–49.
[10] E. Bértolo, R. Bastida, A. de Blas, D. E. Fenton, A. Macías, A. Rodríguez, T. Rodríguez-Blas, A. Villar, *Z. Naturforsch.* **1998**, *53b*, 1445–1454.
[11] K. R. Adam,. A. J. Leong, L. F. Lindoy, H. C. Lip, B. W. Skelton, A. H. White, *J. Am. Chem. Soc.* **1983**, *105*, 4645–4651.
[12] C. A. Davis, P. A. Duckworth, L. F. Lindoy, W. E. Moody, *Aust. J. Chem.* **1995**, *48*, 1819–1825.
[13] C. A. Davis, A. J. Leong, L. F. Lindoy, J. Kim, S. Lee, *Aust. J. Chem.* **1998**, *51*, 189–193.
[14] C. A. Davis, P. A. Duckworth, A. J. Leong, L. F. Lindoy, A. Bashall, M. McPartlin, *Inorg. Chim. Acta* **1998**, *273*, 372–378.
[15] T. Hökelek, Z. Kiliç, S. Bilge, *Acta Crystallogr.* **1999**, *C55*, 248–250.
[16] T. Hökelek, Z. Kiliç, S. Bilge, *Acta Crystallogr.* **1999**, *C55*, 381–383.
[17] L. P. Battaglia, A. C. Bonamartini, A. Mangia, *Inorg. Chim. Acta* **1980**, *42*, 191–196.
[18] K. K. Abid, D. E. Fenton, *Inorg. Chim. Acta* **1984**, *95*, 119–125.
[19] W. J. Geary, *Coord. Chem. Rev.* **1971**, *7*, 81–122.
[20] V. A. J. Aruma, V. Alexander, *Inorg. Chim. Acta* **1996**, *249*, 93–100.
[21] S. M. Peng, G. C. Gordon, V. L. Goedken, *Inorg. Chem.* **1978**, *17*, 119–126.
[22] N. S. Gill, R. H. Nuttall, D. E. Scaife, *J. Inorg. Nucl. Chem.* **1961**, *18*, 79–87.
[23] K. Nakamoto, *Infrared and Raman Spectra of Inorganic and Coordination Compounds*, Wiley-Interscience, New York, 3rd ed., **1978**.
[24] S. Aime, M. Botta, U. Casellato, S. Tamburini, P. A. Vigato, *Inorg. Chem.* **1995**, *34*, 5825–5831.
[25] N. F. Curtis, Y. M. Curtis, *Inorg. Chem.* **1965**, *4*, 804–813.
[26] A. B. P. Lever, E. Mantovani, B. S. Ramaswamy, *Can. J. Chem.* **1971**, *49*, 1957–1964.
[27] R. J. Ferrano, *J. Inorg. Nucl. Chem.* **1959**, *10*, 319–322.
[28] S. F. Pavkovic, D. W. Meek, *Inorg. Chem.* **1965**, *4*, 1091–1098.
[29] M. R. Rosenthall, *J. Chem. Educ.* **1973**, *50*, 331–335.
[30] E. Pretsch, T. Clerc, J. Seibl, W. Simon, *Tables of Spectral Data for Structure Determination of Organic Compounds*, 2nd. ed., Springer-Verlag, **1989**.
[31] D. S. Kumar, V. Alexander, *Inorg. Chim. Acta* **1995**, *238*, 63–71.
[32] L. J. Charbonnnière, C. Balsiger, K. J. Schenk, J. G. Bünzli, *J. Chem. Soc., Dalton Trans.* **1998**, 505–510.
[33] N. Sabbatini, S. Perathoner, V. Balzani, B. Alpha, J.-M. Lehn, *Supramolecular Photochemistry* (Eds.: V. Balzani, D. Reidel), Reidel Publishing Company, **1987**, 187–206.
[34] M. G. B. Drew, D. MacDowell , J. Nelson, *Polyhedron* **1988**, *7*, 2229–2232.
[35] D. MacDowell, J. Nelson, *Tetrahedron Lett.* **1988**, 385–386.
[36] D. MacDowell, J. Nelson, V. McKee, *Polyhedron* **1989**, *8*, 1143–1145.
[37] S. R. Collinson, D. E. Fenton, *Coord. Chem. Rev.* **1996**, *148*, 19–40.
[38] N. A. Bailey, C. O. Rodríguez de Barbarín, D. E. Fenton, P. C. Hellier, P. D. Hempstead, M. Kanesato, P. B.Leeson, *J. Chem. Soc., Dalton Trans.* **1995**, 765–770.
[39] H. Adams, N. A. Bailey, M. J. S. Dwyer, D. E. Fenton, P. C. Hellier, P. D. Hempstead, J. M. Latour, *J. Chem. Soc., Dalton Trans.* **1993**, 1207–1216.
[40] K. R. Adam, K. P. Dancey, A. J. Leong, L. F. Lindoy, B. J. McCool, M. McPartlin, P. A. Tasker, *J. Am. Chem. Soc.* **1988**, *110*, 8471–8477.
[41] K. R. Adam, S. P. H. Arshad, D. S. Baldwin, P. A. Duckworth, A. J. Leong, L. F. Lindoy, B. J. McCool, M. McPartlin, B. A. Tailor, P. A. Tasker, *Inorg. Chem.* **1994**, *33*, 1194–1200.
[42] C. J. Harding, Q. Lu, J. F. Malone, D. J. Marrs, N. Martin, V. McKee, J. Nelson, *J. Chem. Soc., Dalton Trans.* **1995**, 1739–1747.
[43] R. Iwamoto, H. Wakano, *J. Am. Chem. Soc.* **1976**, *98*, 3764–3768.
[44] C. E. Boman, *Acta Crystallogr., Sect. B.* **1977**, *33*, 1529–1533.
[45] L. Malmsten, *Acta Crystallogr., Sect. B.* **1979**, *35*, 1702–1704.
[46] R. D. Canon, B. Chiswell, L. M. Venanzi, *J. Chem. Soc., Sec. A.* **1967**, 1277–1281.
[47] A. Bashall, D. E. Fenton, A. J. Leong, L. F. Lindoy, M.

McPartlin, B. P. Murphy, P. A. Tasker, *J. Chem. Soc., Dalton Trans.* **1987**, 2543–2553.
[48] A. Horbarzewski, J. F. Biernat, *Inorg. Chim. Acta* **1983**, *74*, 131–134.
[49] N. A. Bailey, D. E. Fenton, S. J. Kitchen, T. H. Lilley, M. G. Williams, P. A. Tasker, A. J. Leong, L. F. Lindoy, *J. Chem. Soc., Dalton Trans.* **1991**, 627–637.
[50] P. G. Grimsley, L. F. Lindoy, H. C. Lip, R. J. Smith, J. T. Baker, *Aust. J. Chem*. **1977**, *30*, 2095–2098.
[51] SHELXL, *An Integrated System for Solving and Refining Crystal Structures from Diffraction Data [Revision 5.1]*, Bruker AXS Ltd.
[52] L. J. Farrugia, *J. Appl. Cryst*. **1997**, *30*, 565.
[53] saint *Software Reference Manual*, *Siemens Analytical X-ray Instruments Inc*., Madison, Wisconsin, USA, **1995**.
[54] G. M. Sheldrick, Sadabs, *Program for Empirical Absorption Correction of Area Detector Data*, University of Göttingen, Germany, **1996**.
[55] G. M. Sheldrick, SHELX-97, *An Integrated System for Solving and Refining Crystal Structures from Diffraction Data*, University of Göttingen, Germany, **1997**.

Received October 6, 1999
[I99352]

Novel Nitrido- and Oxo(phthalocyaninato) Complexes of Molybdenum, Tungsten and Rhenium

Karsten Frick,[a] Sanjiv Verma,[a] Jörg Sundermeyer,[b] and Michael Hanack*[a]

Keywords: Phthalocyanines / Nitrides / Oxo complexes / Rhenium / Molybdenum / Tungsten

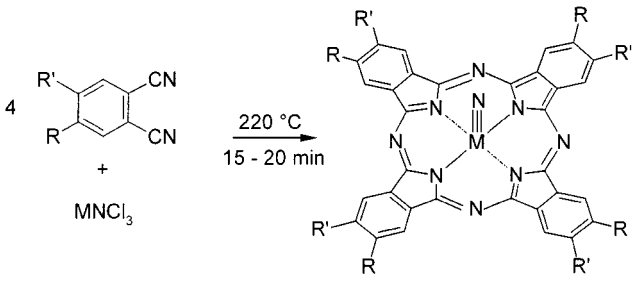
The synthesis of new nitrido(phthalocyaninato)molybdenum (**1**–**4**) and -tungsten complexes (**5**–**7**) starting from the corresponding phthalonitriles and $MNCl_3$ (M = Mo, W) is reported. In addition, the reaction of (tBu$_4$Pc)WN (**6**) with PPh_3 leading, after several steps, to the diamagnetic compound (tBu$_4$Pc)WO (**7**) is described. The reaction of (tBu$_4$Pc)ReN (**9**) with PPh_3 leads to [(tBu$_4$Pc)ReO]$_2$ (**12**), and of [(C$_5$H$_{11}$)$_8$Pc]ReN (**10**) with PPh_3 leads, under different conditions, to {[(C$_5$H$_{11}$)$_8$Pc]ReO}$_2$O (**11**).

Introduction

Continuing with our work on nitrido(phthalocyaninato)-metal compounds[1] we report here on the synthesis and properties of novel nitrido(phthalocyaninato)metal complexes of molybdenum and tungsten, as well as two other oxo(phthalocyaninato)rhenium dimers. The aim of our work on the paramagnetic PcMN complexes (M = Mo, W) is to reduce them to the anionic phthalocyaninato complexes PcMN$^-$ and to investigate their subsequent reaction with electrophiles to obtain new nitrido-bridged phthalocyaninato complexes. These complexes should be more reactive in their nitrido functionality than the nitrido-bridged rhenium phthalocyanines which we have reported recently.[1]

Until now, the few publications concerning molybdenum phthalocyanines mostly concentrate on oxophthalocyaninatomolybdenum(IV), PcMoO.[2] Some porphyrinato complexes of molybdenum are known.[3] The most interesting are (TMP)MoN (TMP = tetramesitylporphyrinato), (TTP)MoN (TTP = tetratolylporphyrinato) and (TPP)MoN (TPP = tetraphenylporphyrinato) because the molybdenum is in the +5 oxidation state and in a planar arrangement with the porphyrinato ligand.[4]

The preparation of unsubstituted[5] and substituted PcMoN is successful starting from the appropriate phthalonitriles and $MoNCl_3$[6,7], by melting them at 220 °C for 15 to 20 minutes (Scheme 1). The dark green PcMoN (**1**) can be separated from its impurities by Soxhlet extraction with acetone and toluene. The substituted complexes (R$_8$Pc)MoN [R = C$_3$H$_7$ (**2**), C$_4$H$_9$ (**3**), C$_5$H$_{11}$ (**4**)] are purified by column chromatography on Al_2O_3 with toluene and by washing with methanol. The yield is 65% in the case of **1**. The yields are higher for the substituted PcMoN complexes [**2** (11%), **3** (8%), **4** (10%)] than for the corresponding nitrido(phthalocyaninato)rhenium complexes.[1] We assume that either the excess dinitrile is responsible for the Cl radical abstraction from $MNCl_3$, or that Cl$^-$ is oxidized to Cl_2 with reduction of the metal center.



	1	2	3	4	5	6	7
M	Mo	Mo	Mo	Mo	W	W	W
R	H	C$_3$H$_7$	C$_4$H$_9$	C$_5$H$_{11}$	H	H	C$_5$H$_{11}$
R'	H	C$_3$H$_7$	C$_4$H$_9$	C$_5$H$_{11}$	H	*t*Bu	C$_5$H$_{11}$

Scheme 1. Synthesis and structure of nitrido(phthalocyaninato)metal complexes

The M$^+$ peak for PcMoN (**1**) in the FAB-MS is observed at m/z = 623.1 (calcd. 622.5). The complexes (R$_8$Pc)MoN [R = C$_3$H$_7$ (**2**), C$_4$H$_9$ (**3**), C$_5$H$_{11}$ (**4**)] show their M$^+$ peak in the FD-MS with the expected isotopic pattern. The infrared spectra of **1**–**4** are difficult to interpret. Usually the Mo≡N stretching vibration[6] is observed higher than 1000 cm^{-1} and the Mo=O vibration in phthalocyanines appears at $\tilde{\nu}$ =

[a] Institut für Organische Chemie, Lehrstuhl II,
Universität Tübingen,
Auf der Morgenstelle 18, D-72076 Tübingen, Germany
Fax: (internat.) + 49-7071/295-244
E-mail: hanack@uni-tuebingen.de
http://www.uni-tuebingen.de/hanack/index.html
[b] Fachbereich Chemie, Universität Marburg,
Hans Meerwein Straße, D-35032 Marburg, Germany
Fax: (internat.) + 49-6421/282-8917
E-mail: jsu@chemie.uni-marburg.de

 © WILEY-VCH Verlag GmbH, D-69451 Weinheim, 2000 1434–1948/00/0505–1025 $ 17.50+.50/0

Table 1. EPR, IR and UV data of the new phthalocyanines

	EPR g	IR [cm^{-1}] $\nu_{M\equiv N}$	UV [nm] λ (Q)
PcMoN (**1**)	1.97	953	703.5 (ClN)[a]
[$(C_3H_7)_8$Pc]MoN (**2**)	1.97	974	709.0 (toluene)
[$(C_4H_9)_8$Pc]MoN (**3**)	1.97	962	711.5 (toluene)
[$(C_5H_{11})_8$Pc]MoN (**4**)	1.97	974	716.0 (toluene)
PcWN (**5**)	1.88	953	751.0 (ClN)[a]
(tBu$_4$Pc)WN (**6**)	1.89	959	745.0 (toluene)
[$(C_5H_{11})_8$Pc]WN (**7**)	1.89	957	770.5 (toluene)
PcWO (**8**)	–	$\nu_{W=O}$ = 1047[b]	674.5 (toluene)
[(tBu$_4$Pc)Re(O)]$_2$ (**12**)	–	$\nu_{Re=O}$ = 960[b]	652.5 (chloroform)
{[$(C_5H_{11})_8$Pc]Re(O)}$_2$O (**11**)	–	–	701.5 (chloroform)

[a] ClN = 1-chloronaphthalene. – [b] Tentative assignment.

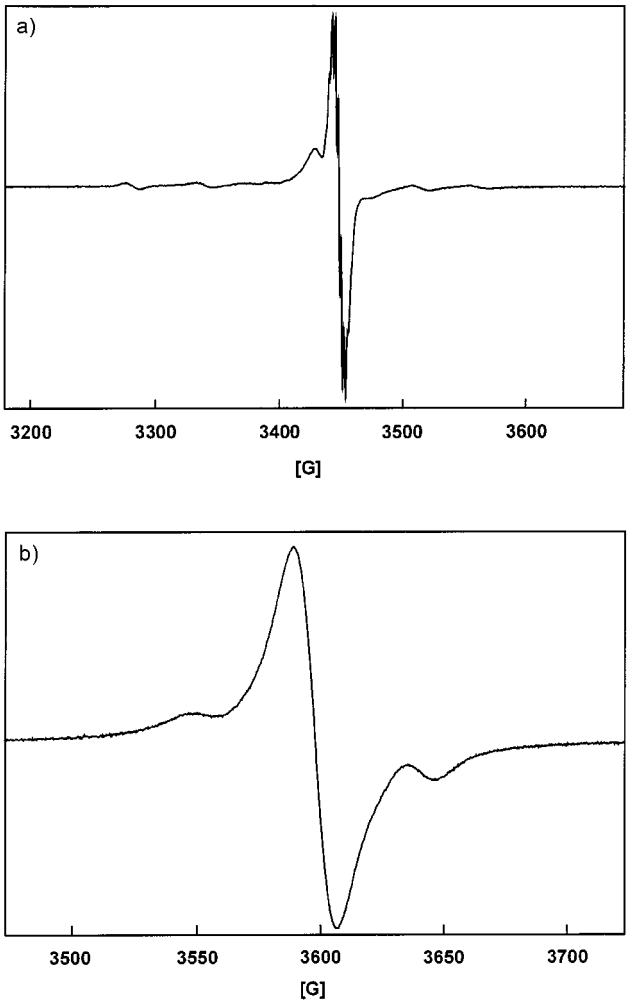


Figure 1. EPR spectra of a) PcMoN (**1**) and b) $(C_5H_{11})_8$PcWN (**7**)

950–980 cm^{-1}.[2a] For PcMoN (**1**) and (R_8Pc)MoN **2**–**4** the Mo≡N stretching vibration is observed below 1000 cm^{-1} (Table 1). The lowered value of the stretching vibration can be explained by interaction of the nitrogen lone pair with the following Lewis acidic Mo center within the same stack, which reduces the bond order of MoN. In PcReN the Re≡N stretching vibration is located at $\tilde{\nu}$ = 978 cm^{-1} due to the same effect.[1b,1c] This lowering is not unusual, e.g. in $MoNF_4^-$ the band for MoN is located at $\tilde{\nu}$ = 969 cm^{-1}.[8] The UV/Vis spectrum of **1** in solution and as a KBr pellet indicates the presence of dimers: the maximum of the Q-band in solution (chloroform) is seen at λ = 703.5 nm (satellites are located at λ = 639.5 and 602.5 nm) and a shoulder is seen at λ = 777.0 nm in the solution spectrum and at λ = 791.5 nm in the solid state. Under the assumption of a Davidov–Kasha exciton interaction,[9] the shoulders at λ = 649.5 and 791.5 nm are due to dimers with an interaction of ΔE = 2750 cm^{-1}. In contrast to **1** the UV/Vis spectra of **2**–**4** show the usual Q- and B-bands of monomeric phthalocyanines. As an element of group six, molybdenum in the oxidation state +5 has a d^1 configuration with one unpaired electron. An EPR spectrum of PcMoN (**1**) in 1-chloronaphthalene shows intense central lines (g = 1.97) due to the coupling of the electron with the five nitrogens. Six weaker lines seen symmetrically on both the right and the left side of the central signal are due to the electron–Mo^{95}/Mo^{97} coupling (Figure 1a). The simulated spectrum corresponds to the measured spectrum. The spectra of the more soluble compounds **2**–**4** show the same patterns (Table 1). The g factor for the complexes **1**–**4** is 1.97.

Some phthalocyaninato complexes of tungsten have been synthesized,[10] but only in $PcWCl_3$[10a] and (ClPc)W(O)OH[11] is the metal in the +5 oxidation state. These examples indicate that nitrido(phthalocyaninato)-tungsten complexes should also exist. With the same synthetic strategy as for the PcMoN compounds, unsubstituted, tetra- and octasubstituted nitrido(phthalocyaninato)-tungsten complexes **5**–**7** are obtained (Scheme 1). Their stability against moisture is greater than that observed for the molybdenum phthalocyanines **1**–**4**. PcWN (**5**) is separated from its impurities by Soxhlet extraction with ethanol, acetone and toluene and isolated as a dark green powder in high yield (70%). The M^+ peak of **5** in the FAB-MS appears at m/z = 709.9 (calcd. 710.1). Purification of (tBu$_4$Pc)WN (**6**) and [$(C_5H_{11})_8$Pc]WN (**7**) is not possible by column chromatography. The excess of phthalonitrile in the substituted complexes **6** and **7** is separated by Soxhlet extraction (hexane), further impurities are precipitated with dichloromethane/hexane. The synthesis of $(C_5H_{11})_8$PcWN (**7**) can be carried out in a higher yield using $W(NTos)_2Cl_2$[12] instead of $WNCl_3$. Impurities are separated by washing the crude product with methanol and precipitated with dichloromethane/hexane. The molecular ions of compounds **6** and **7** can be seen in the FD-MS with the expected isotopic pattern. The IR spectrum of **5** is quite similar to that of PcReN[1b,1c] and almost the same as that of PcMoN (**1**). All phthalocyanine vibrations are in the usual regions. The W≡N vibration is expected between 1000 and 950 cm^{-1}. A band of medium intensity at $\tilde{\nu}$ = 953 cm^{-1} is assigned to this vibration (Figure 2). The W=O vibration in (ClPc)W(O)OH[11] is also found around $\tilde{\nu}$ = 953 cm^{-1}. This indicates that the W≡N vibration appears at lower wavelength due to the interaction with the next metal center within a stack as explained for PcMoN

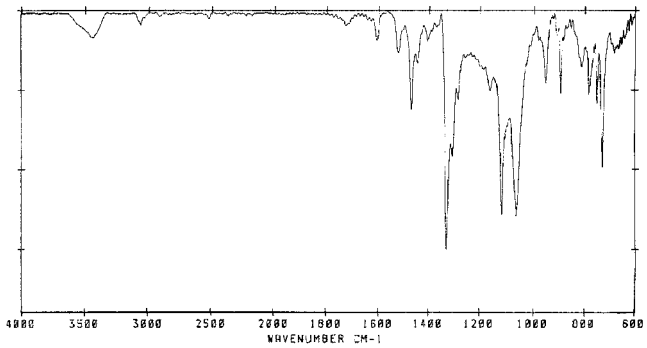


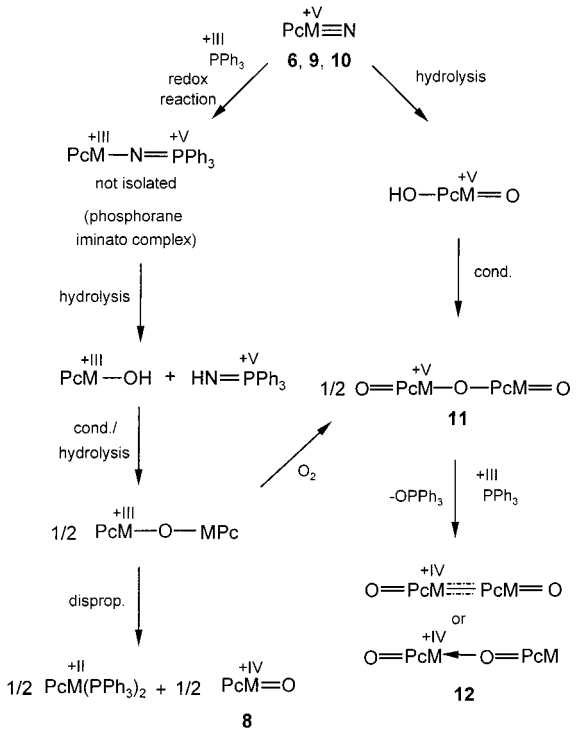
Figure 2. IR spectrum of PcWN (**5**)

(**1**). The W≡N vibration in the soluble complexes **6** and **7** is observed at $\tilde{\nu}$ = 959 (**6**) and 957 cm^{-1} (**7**) (Table 1).

In (ClPc)W(O)OH the maximum of the Q-band is at λ = 730 nm.[11] PcWN (**5**) shows a red shift in the Q-band maximum at λ = 751.0 nm (Table 1); the Q-band is broadened and shows two shoulders at λ = 699.5 and 673.5 nm. A shoulder at higher wavelength cannot be found, which indicates that only monomeric units of **5** are present in solution. (tBu$_4$Pc)WN (**6**) and [$(C_5H_{11})_8$Pc]WN (**7**) show broadened Q-bands at λ = 745.0 (**6**) and 770.5 nm (**7**). The d^1-electron configuration of tungsten in PcWN (**5**), (tBu$_4$Pc)WN (**6**) and [$(C_5H_{11})_8$Pc]WN (**7**) allows the recording of their EPR spectra. Compound **6** exhibits a broad intense signal at g = 1.88 without hyperfine structure due to the electron–nitrogen or electron–tungsten coupling (Table 1). This is quite normal for powder spectra even at 77 K.[11] However, **6** and **7** show an electron–W^{183} coupling in toluene solution (Figure 1b). Two signals, besides the main resonance, with an intensity of about 7% appear [g = 1.89 (**6**, **7**)] (Table 1).

Reactions of PcReN[13] and PcMoO[2f] complexes with phosphanes have been the focus of recent studies. To date, the exact mechanism of the reaction of the PcMN complexes **6**, (tBu$_4$Pc)ReN (**9**), [$(C_5H_{11})_8$Pc]ReN (**10**) with PPh_3 is unknown but we suggest two pathways (Scheme 2). The first possible mechanism involves nucleophilic attack of the phosphane at the LUMO of the nitrido complex having mainly the character of an MN–π*-orbital.[6] This redox reaction would lead to a phosphorane iminato complex that could undergo hydrolysis to finally yield PcWO (**8**) as described in Scheme 2. The second pathway begins with hydrolysis of **6**, **9** and **10**. After condensation **11** is obtained which can be reduced with PPh_3 to the phthalocyaninatometal complex **12**.

As a first attempt the reaction of (tBu$_4$Pc)WN (**6**) with PPh_3 was investigated. After column chromatography only (tBu$_4$Pc)WO (**8**) was isolated in 50% yield. The FD-MS spectrum of **8** shows the expected molecular peak at m/z = 936.5 (calcd. 936.3) in accordance with the calculated isotopic pattern. An interesting result is indicated in the IR spectrum of **8** in which the W≡N stretching vibration disappears. All other vibrations show very little or no difference in intensity or wave number. The assignment of the W=O vibration is difficult, however a shoulder at $\tilde{\nu}$ = 1047 cm^{-1} could correspond to this vibration (Table 1). In the UV/Vis spectrum of **8** the Q-band shows a heavy blue shift relative to (tBu$_4$Pc)WN (**6**), with a maximum at λ = 674.5 nm and shoulders at λ = 725.0 and 611.0 nm (Table 1). In the same way the B-band is shifted to lower wavelength. The ^{1}H NMR spectrum of diamagnetic (tBu$_4$Pc)WO (**8**) shows the signals of the tBu groups between δ = 1.60–2.26 due to the structural isomers present in tetrasubstituted phthalocyanines. The signals of the aromatic protons are found between δ = 7.5–8.6.



Scheme 2. Mechanism leading to PcWO (**8**), [tBu$_4$PcRe(O)]$_2$ (**12**) and [$(C_5H_{11})_8$PcRe(O)]$_2$O (**11**)

The reaction of PcMN with PPh_3 is studied further with the nitridophthalocyaninatorhenium complexes (tBu$_4$Pc)ReN (**9**) and [$(C_5H_{11})_8$Pc]ReN (**10**). Recently the reaction of Re_2O_7 and phthalonitrile with PPh_3 leading to the formation of $(PcRe)_2$ was reported.[14] In the first step of this reaction $(PPh_3)_2$PcRe was formed, after heating to 350 °C $(PcRe)_2$ was obtained. $(PPh_3)_2$PcRe was also successfully prepared starting from "PcReO" and PPh_3.[13] The reaction of **9** and **10** with PPh_3 at different reaction temperatures gives different products (Scheme 2). At lower temperatures μ-oxo[oxoocta(n-pentyl)phthalocyaninato]rhenium {[$(C_5H_{11})_8$Pc]Re(O)}$_2$O (**11**) is obtained, while at higher temperatures (350 °C) rhenium is reduced to the +4 oxidation state. After column chromatography on Al_2O_3 with toluene and dichloromethane as eluents, [(tBu$_4$Pc)Re(O)]$_2$ (**12**) is isolated. There are two possible structures for **12**: first, the stacking of a second molecule in trans-position to form a μ-oxo bridged dimer, and second a dimer with a rhenium-rhenium bond. From the UV/Vis spectra we assume that the dimeric complex [(tBu$_4$Pc)Re(O)]$_2$ (**12**) with a rhenium–rhenium bond is obtained. In the FD-MS the

molecular peak for **12** is found at *m/z* = 1876.6 (calcd. 1876.4) and the signal of the monomeric fragment (tBu$_4$Pc)Re(O)$^+$ appears at *m/z* = 938.2. The IR spectrum of **12** shows differences from that of the starting material (tBu$_4$Pc)ReN (**9**). The Re≡N vibration disappears; however, the Re=O vibration is not seen due to strong new ligand vibrations in that region. In the UV/Vis spectrum of **12** in chloroform the dimerization is proved by the blue shift of the Q-band to λ = 652.5 nm relative to (tBu$_4$Pc)ReN (**9**) [λ_{max} (Q) = 698 nm (CH_2Cl_2)] and the appearance of the forbidden Q$^-$-band at λ = 801.5 nm (Figure 3a, Table 1). The exciton interaction is calculated to be ΔE = 2850 cm^{-1}, while for (PcRe)$_2$ the calculated value is lower than 2400 cm^{-1}.[14] The interaction caused by the distance of the macrocycles is dependent on the radius of the metal ions. In (PcRe)$_2$ the oxidation state of rhenium is +2, but in **12** it is +4. The effect of the sterically demanding tBu groups on the distance of the macrocycles is low.[15] With the UV/Vis spectrum as KBr pellet the exciton interaction in the solid state is ascertained to be ΔE = 2000 cm^{-1}. A higher distance of the macrocycles is concluded from these results and may be explained by an eclipsed conformation in the solid state. In solution, **12** rotates to the staggered conformation. A change of conformation was also established for (PcRe)$_2$.[14] In the presence of light, a chloroform solution of **12** decomposes as seen by the appearance of a greater absorbance of the monomer band at λ = 692.0 nm.

In the ^{1}H NMR spectrum of [(tBu$_4$Pc)Re(O)]$_2$ (**12**) a broadening of the signals due to the interaction of two macrocycles and the structural isomers is seen. The signals of the aromatic protons are between δ = 9.58–9.49 and δ = 8.50–8.39, while the tBu groups are shifted to lower field (δ = 2.15–1.81) than for (tBu$_4$Pc)ReN (**9**).

The reaction of [(C$_5$H$_{11}$)$_8$Pc]ReN (**10**) with PPh$_3$ at 250 °C for 30 minutes leads to the μ-oxo dimer [{(C$_5$H$_{11}$)$_8$Pc}Re(O)]$_2$O (**11**) as a product of hydrolysis (Scheme 2). Compound **11** is separated from its impurities by column chromatography on Al$_2$O$_3$. Unchanged **10** is first obtained with toluene and **11** is then eluted with dichloromethane in 18% yield. The shorter reaction time at lower temperature does not reduce the rhenium. The mechanism of the reaction is still unknown but a suggested mechanism can be seen in Scheme 2. The calculated and observed isotopic pattern of the molecular peak at *m/z* = 2568.2 in the FD-MS are in agreement.

In the IR spectrum **11** shows two new intense bands at $\tilde{\nu}$ = 685 and 658 cm^{-1}. The Re≡N vibration disappears with the formation of a new band at $\tilde{\nu}$ = 802 cm^{-1}. There are different possibilities of a $M_2O_3^{4+}$ unit, e.g. (TTP)Nb$_2$O$_3$ has three μ-oxo-bridges.[16] This is not the case for **11** because in (tBu$_4$Pc)Re(O)OEt the Re=O vibration is assigned to $\tilde{\nu}$ = 949 cm^{-1}.[15] The O=PcRe–O–PcRe=O units in phthalocyanines are in a linear arrangement due to steric reasons. In linear complexes the Re–O–Re vibration is located between 650–700 cm^{-1}. In [(OEP)ReO]$_2$O (OEP = octaethylporphyrinato) this vibration is observed at $\tilde{\nu}$ = 675 cm^{-1}.[17] Consequently the new band at 802 cm^{-1} is assigned to a ligand vibration. The Re=O vibration is not found in the expected region due to strong bands at $\tilde{\nu}$ = 685 and 658 cm^{-1}. Another possible explanation for the new bands is that in a linear arrangement of O=PcRe–O–PcRe=O, vibrational coupling of the $\nu_{Re=O}$ and ν_{Re-O} modes may occur shifting $\nu_{Re=O}$ to lower (802 cm^{-1}) and ν_{Re-O} to higher frequencies (685/658 cm^{-1}). Dimerization is again confirmed by the UV/Vis spectrum of **11** in chloroform (Figure 3c). A red shift in the Q-band to λ = 701.5 nm is seen and the forbidden Q$^-$-band is located at λ = 778.5 nm (Table 1). From these data the exciton interaction is estimated to be ΔE = 1410 cm^{-1}, in the solid state it is calculated to be ΔE = 1450 cm^{-1}. The appearance of the Q$^-$-band may be explained by a lowering of symmetry. These results indicate that the conformation of **11** has not changed. In the ^{1}H NMR and the ^{13}C-DEPT-135 NMR spectra all expected signals are observed. The 16 equivalent aromatic protons show a singlet at δ = 8.80. The signals of the different methylene groups appear separate and are easily assigned. The methyl group shows its resonance as a triplet at δ = 1.20. In the ^{13}C-DEPT-135 spectrum all CH-signals occur in the expected region.

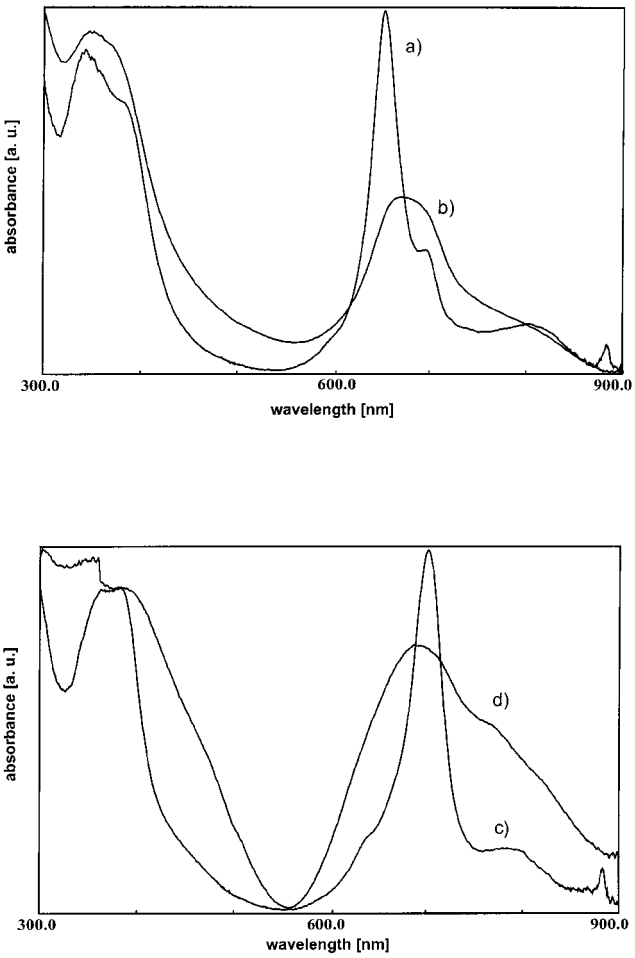


Figure 3. UV/Vis spectra of a) **12** in chloroform b) **12** as a KBr pellet c) **11** in chloroform d) **11** as KBr pellet

Experimental Section

$W(NTos)_2Cl_2$,[12] $MoNCl_3$,[7] $WNCl_3$,[7] 4-*tert*-butylphthalonitrile,[18] 4,5-di-*n*-alkylphthalonitriles[19] (alkyl = propyl, butyl, pentyl), nitrido(tetra-*tert*-butyl-phthalocyaninato)rhenium[1,15] and nitrido[octa(*n*-pentyl)phthalocyaninato)rhenium[1] were prepared according to known procedures.

FT-IR: Bruker IFS 48. – UV/Vis: Shimadzu UV−365. – MS: Varian Mat 711 (EI, FD). – ^1H, ^{13}C, ^{11}B NMR: Bruker AC 250 (^1H: 250.133, ^{13}C: 62.902, ^{11}B: 80.251 MHz). – Elemental Analyses: Carlo Erba Elemental Analyser 1104, 1106. – EPR: Bruker ESP 300 (X-band).

Nitrido(phthalocyaninato)molybdenum (1): Phthalonitrile (393 mg, 3.08 mmol) was heated with $MoNCl_3$ (147.9 mg, 0.68 mmol) at 220 °C. The temperature was held constant for 20 minutes. After cooling the reaction to room temperature the solid was crushed in a mortar and Soxhlet extracted with acetone and toluene to remove impurities. Yield: PcMoN (**1**) (275 mg, 65%) as a dark green powder. – IR (KBr): $\tilde{\nu}$ = 1605 cm^{-1}, 1549, 1470, 1414, 1331, 1304, 1163, 1119, 1090, 1066, 953 (Mo≡N), 906, 895, 804, 781, 750, 729. – UV/Vis (1-chloronaphthalene): λ = 396.5 nm, 602.5, 639.5, 664.5, 703.5, 777.0. – UV/Vis (KBr): λ = 365.0 nm, 509.5, 609.5, 649.5, 732.0, 791.5. – MS (FAB): *m*/*z* = 623.1 (M^+), 514.7 (M^+ – MoN). – EPR (1-chloronaphthalene, room temp.): *g* = 1.97.

Nitrido[octa(*n*-alkyl)phthalocyaninato]molybdenum [alkyl = propyl (2), butyl (3), pentyl (4)]: The appropriate 4,5-di-*n*-alkylphthalonitrile (2.08 mmol) was melted with $MoNCl_3$ (100 mg, 0.46 mmol) at 220 °C for 15 minutes. Most of the impurities were removed by column chromatography in the dark on Al_2O_3 with toluene (two or three times). The solid was then washed several times with methanol. Yield: $[(C_3H_7)_8Pc]MoN$ (**2**) (58 mg, 11%), $[(C_4H_9)_8Pc]MoN$ (**3**) (33 mg, 8%) and $[(C_5H_{11})_8Pc]MoN$ (**4**) (48 mg, 10%) as green powders.

2: IR (KBr): $\tilde{\nu}$ = 2959 cm^{-1}, 2932, 1618, 1501, 1454, 1402, 1377, 1325, 1261, 1105, 1013, 974 (Mo≡N), 905, 802, 756, 702. – UV/Vis (toluene): λ = 348.5 nm, 647.5, 672.5, 709.0. – MS (FD) (toluene): *m*/*z* = 959.8 (M^+). – EPR (toluene, room temp.): *g* = 1.97.

3: IR (KBr): $\tilde{\nu}$ = 3423 cm^{-1}, 3290, 3036, 2957, 2870, 1715, 1643, 1620, 1460, 1377, 1337, 1321, 1211, 1173, 1103, 1013, 962 (Mo≡N), 901, 754, 704. – UV/Vis (toluene): λ = 351.5 nm, 614.5, 647.5, 673.0, 711.5. – MS (FD) (toluene): *m*/*z* = 1072.3 (M^+), 962.4 (M^+ – MoN). – EPR (toluene, room temp.): *g* = 1.97.

4: IR (KBr): $\tilde{\nu}$ = 2957 cm^{-1}, 2928, 1684, 1645, 1618, 1566, 1520, 1456, 1377, 1330, 1261, 1103, 1015, 974 (Mo≡N), 899, 802, 754, 733. – UV/Vis (toluene): λ = 353.5 nm, 649.5, 679.0, 716.0. – MS (FD) (toluene): *m*/*z* = 1184.8 (M^+). – EPR (toluene, room temp.): *g* = 1.97.

Nitrido(phthalocyaninato)tungsten (5): Phthalonitrile (260 mg, 2.04 mmol) was mixed with $WNCl_3$ (138 mg, 0.45 mmol) and melted at 220 °C for 20 minutes. The crude product was then extracted with EtOH, acetone and toluene. Yield: PcWN (**5**) (230 mg, 72%) as a dark green solid. – IR (KBr): $\tilde{\nu}$ = 1604 cm^{-1}, 1470, 1445, 1331, 1308, 1159, 1119, 1064, 953 (W≡N), 895, 812, 783, 750, 729. – UV/Vis (1-chloronaphthalene): λ = 359.5 nm, 673.5, 699.5, 751.0. – UV/Vis (KBr): λ = 355.0 nm, 622.5, 674.5, 704.0, 753.0. – MS (FAB): *m*/*z* = 709.9 (M^+). – EPR (solid state, 77 K): *g* = 1.88.

Nitrido[tetra(*tert*-butyl)phthalocyaninato]tungsten (6): A mixture of 4-*tert*-butylphthalonitrile (700 mg, 3.8 mmol) and $WNCl_3$ (255 mg, 0.84 mmol) was heated to 220 °C for 15 minutes. The solid was crushed in a mortar and Soxhlet extracted with hexane to remove the unreacted phthalonitrile. Further impurities were precipitated with CH_2Cl_2/hexane. The solvent was then removed to give (tBu$_4$Pc)WN (**6**) (110 mg, 14%) as a green solid. – IR (KBr): $\tilde{\nu}$ = 3443 cm^{-1}, 3069, 2963, 2905, 1612, 1516, 1483, 1394, 1366, 1323, 1258, 1200, 1150, 1072, 959 (W≡N), 930, 833, 762, 748. – UV/Vis (toluene): λ = 365.0 nm, 677.0, 745.0. – MS (IS) (MeOH): *m*/*z* = 934.5 (M^+). – MS (FAB): *m*/*z* = 934.3 (M^+). – EPR (toluene, room temp.): *g* = 1.89.

Nitrido[octa(*n*-pentyl)phthalocyaninato]tungsten (7). Method a): 4,5-Di-*n*-pentylphthalonitrile (500 mg, 1.87 mmol) was melted with $WNCl_3$ (114 mg, 0.37 mmol) at 220 °C for 15 minutes. After extraction of the excess of phthalonitrile with hexane, further impurities were precipitated three times with CH_2Cl_2/hexane. Removal of the solvent under vacuum gave $[(C_5H_{11})_8Pc]WN$ (**7**) (43 mg, 9%) as a green solid. **Method b):** 4,5-Di-*n*-pentylphthalonitrile (800 mg, 3.0 mmol) was reacted with $W(NTos)_2Cl_2$ (413 mg, 0.66 mmol) at 220 °C for 10 min. The crude product was first washed with three times methanol and further impurities were then precipitated from CH_2Cl_2/hexane (5×). The solution was separated from solid impurities and the solvent was removed yielding **7** (107 mg, 13%). – IR (KBr): $\tilde{\nu}$ = 3437 cm^{-1}, 3024, 2957, 2928, 2870, 1614, 1483, 1454, 1396, 1325, 1157, 1076, 1011, 957 (W≡N), 893, 814, 746, 733, 685. – UV/Vis (toluene): λ = 376.0 nm, 695.5, 770.5. – MS (FD) (toluene): *m*/*z* = 1270.7 (M^+). – EPR (toluene, room temp.): *g* = 1.89.

Oxo[tetra(*tert*-butyl)phthalocyaninato]tungsten (8): (tBu$_4$Pc)WN (31 mg, 0.033 mmol) (**6**) was slowly heated with PPh_3 (31 mg, 0.33 mmol) to 250 °C. The temperature was held for 1 h. After cooling to room temperature the solid was chromatographed on Al_2O_3 (10% H_2O) with chloroform as the eluent. The product was then eluted with THF. Finally, further impurities were extracted with hexane to give 15 mg (49%) (tBu$_4$Pc)WO (**8**). – IR (KBr): $\tilde{\nu}$ = 3165 cm^{-1}, 3076, 2963, 2907, 1734, 1722, 1614, 1483, 1464, 1394, 1366, 1327, 1281, 1255, 1200, 1146, 1080, 928, 893, 831, 748, 685, 665. – UV/Vis (toluene): λ = 356.5 nm, 611.0, 674.5, 725.0. – MS (FD) (CH_2Cl_2): *m*/*z* = 936.5 (M^+). – ^1H NMR ($CDCl_3$): δ = 1.60–2.26 (36 H, *t*Bu). – ^{13}C NMR ($CDCl_3$): δ = 31.0 (CCH_3), 32.1 (CCH_3).

μ-Oxo[oxo{octa(*n*-pentyl)}phthalocyaninato]rhenium (11): (tBu$_4$Pc)-ReN (22.0 mg, 0.0235 mmol) was slowly heated with PPh_3 (61.7 mg, 0.235 mmol) to 220 °C at 6 × 10^{-2} mbar. The temperature was held for 30 minutes. The crude product was then chromatographed on Al_2O_3 with toluene to remove the impurities. Compound **11** was eluted with CH_2Cl_2. Yield: $[\{(C_5H_{11})_8Pc\}Re(O)]_2O$ (**11**) (11 mg, 18%). – IR (KBr): $\tilde{\nu}$ = 2957 cm^{-1}, 2928, 1620, 1485, 1456, 1398, 1377, 1340, 1261, 1138, 1116, 1032, 891, 802, 723, 685, 658. – UV/Vis ($CHCl_3$): λ = 363.5 nm, 380.5, 637.0, 701.5, 778.5. – UV/Vis (KBr): λ = 383.0 nm, 691.0, 768.0, 818.5. – MS (FD) (toluene): *m*/*z* = 2568.2 (M^+). – ^1H NMR ($CDCl_3$): δ = 1.17–1.23 (t, 24 H, CH_3), 1.72–1.80 (m, 16 H, CH_3CH_2), 1.91–1.99 (m, 16 H, $CH_3CH_2CH_2$), 2.24–2.30 (m, 16 H, $ArCH_2CH_2$), 3.41–3.48 (m, 16 H, $ArCH_2$), 8.80 (8 H, H-b). – ^{13}C NMR ($CDCl_3$): δ = 14.5 (CH_3), 23.1 (CH_3CH_2), 32.4 ($CH_3CH_2CH_2$), 32.7 ($ArCH_2CH_2$), 34.8 ($ArCH_2$), 123.9 (C-b), 135.8 (C-c), 143.4 (C-a), 145.4 (C-d). – ^{13}C NMR (DEPT 135, $CDCl_3$): δ = 14.5 (CH_3), 23.1 (CH_3CH_2), 32.4 ($CH_3CH_2CH_2$), 32.7 ($ArCH_2CH_2$), 34.8 ($ArCH_2$), 123.9 (C-b). – $C_{144}H_{192}N_{16}O_3Re$ (2567.6): calcd. C 67.36, H 7.54, N 8.73; found C 65.55, H 7.29, N 8.15.

Bis[oxo{tetra(tert-butyl)}phthalocyaninato]rhenium (12): For the synthesis see **11** above. Temperature: 250 °C; reaction time: 45 mi-

nutes. Yield: $[(t\mathrm{Bu}_4\mathrm{Pc})\mathrm{Re(O)}]_2$ (**12**) (5 mg, 11%). – IR (KBr): $\tilde{\nu}$ = 2959 cm^{-1}, 2924, 1614, 1485, 1393, 1366, 1335, 1281, 1258, 1198, 1151, 1111, 1092, 1051, 933, 833, 831, 754, 733, 714, 694, 673. – UV/Vis ($CHCl_3$): λ = 343.0 nm, 380.5, 652.5, 695.0, 801.5. – UV/Vis (KBr): λ = 346.0 nm, 669.5, 774.5. – MS (FD) (toluene): *m*/*z* = 940.2 (M^+/2), 1876.0 (M^+ – O). – ^{1}H NMR ($CDCl_3$): δ = 1.70–2.20 (m, 36 H, *t*Bu), 7.70–9.70 (m, 12 H, H-Ar). – $C_{96}H_{96}N_{16}O_3Re_2$ (1894.3): calcd. C 61.32, H 5.15, N 11.93; found C 58.65, H 4.97, N 11.10.

Acknowledgments

We wish to thank the Deutsche Forschungsgemeinschaft (Schwerpunktprogramm "Nitridobrücken", II C10–3221008) for financial support of this work.

[1] [1a] K. Frick, U. Ziener and M. Hanack, *Eur. J. Inorg. Chem.* **1999**, 1309–1313. – [1b] U. Ziener, K. Dürr, M. Hanack, *Synth. Met* **1995**, *71*, 2285–2286. – [1c] U. Ziener, M. Hanack, *Chem. Ber.* **1994**, *127*, 1681–1685.

[2] [2a] V. Börschel, J. Strähle, *Z. Naturforsch.* **1984**, *39b*, 1664–1667. – [2b] H. A. O. Hill, M. M. Norgett, *J. Chem. Soc., (A) Inorg. Phys. Theor.* **1966**, 1476–1478. – [2c] S. J. Edmondson, P. C. H. Mitchell, *Polyhedron* **1986**, *5*, 315–317. – [2d] G. Ferraudi, T. Nyokong, M. Feliz, M. Perkovic, D. P. Rilemma, *Inorg. Chim. Acta* **1994**, *215*, 27–32. – [2e] T. Nyokong, *Polyhedron* **1994**, *13*, 215–220. – [2f] M. Gorsch, H. Homborg, *Z. Anorg. Allg. Chem.* **1998**, *624*, 634–641.

[3] [3a] T. S. Srivastava, E. B. Fleischer, *J. Am. Chem. Soc.* **1970**, *92*, 5518–5519. – [3b] T. Diebold, B. Chevrier, R. Weiss, *Inorg. Chem.* **1979**, *18*, 1193–1200.

[4] J. C. Kim, W. S. Rees, V. L. Goedken, *Inorg. Chem.* **1994**, *33*, 3191–3194.

[5] T. Mayer-Uhma, H. Homborg, unpublished.

[6] [6a] K. Dehnicke, J. Strähle, *Angew. Chem. Int. Ed. Engl.* **1981**, *93*, 451–464. – [6b] K. Dehnicke, J. Strähle, *Angew. Chem. Int. Ed. Engl.* **1992**, *104*, 978–1000.

[7] K. Dehnicke, U. Weiher, J. Strähle, *Z. Naturforsch.* **1977**, *B32*, 1484–1486.

[8] D. Fenske, W. Liebelt, K. Dehnicke, *Z. Anorg. Allg. Chem.* **1980**, *467*, 83–88.

[9] M. Kasha, in *Spectroscopy of the Excited State* (Eds.: B. DiBartolo, D. Pacheco, V. Goldberg), Plenum Press, New York **1976**, 337.

[10] [10a] V. G. Shishkin, M. I. Al′yanov, F. P. Snegireva, *Khim. Khim. Tekhnol.* **1976**, *19*, 1348–1351; CA 86:37094. – [10b] M. I. Al′yanov, F. P. Snegireva, V. G. Shishkin, V. F. Borodkin, *Otkrytiya, Izobret., Prom. Obraztsy, Tovarnye Znaki* **1975**, *52*, 56; CA 83:115362.

[11] J. Padilla, M. I. Litter, A. Campero, *Anal. de Quim.* **1993**, *89*, 177–180.

[12] K. Korn, A. Schorm, J. Sundermeyer, *Z. Anorg. Allg. Chem.*, in press.

[13] M. Göldner, A. Kienast, H. Homborg, *Z. Anorg. Allg. Chem.* **1998**, *624*, 141–146.

[14] M. Göldner, H. Hückstädt, K. S. Murray, B. Moubaraki, H. Homborg, *Z. Anorg. Allg. Chem.* **1998**, *624*, 288–294.

[15] U. Ziener, *Dissertation*, Universität Tübingen, **1995**.

[16] J. F. Johnson, W. R. Scheidt, *J. Am. Chem. Soc.* **1977**, *99*, 294–295.

[17] J. W. Buchler, S. B. Kruppa, *Z. Naturforsch.* **1990**, *45b*, 518–530.

[18] [18a] S. A. Mikhalenko, S.V. Barkanova, O. C. Lebedev, E. A. Luk′yanets, *Zh. Obshch. Khim.* **1971**, *41*, 2725; *J. Gen. Chem. USSR* **1971**, *41*, 2770–2773. – [18b] B. W. Werner, A. T. Peters, *J. Chem. Soc.* **1952**, 680–686. – [18c] M. Hanack, R. Fay, *Recl. Trav. Chim. Pays-Bas* **1986,** *105*, 427–433.

[19] M. Hanack, P. Haisch, H. Lehmann, L. R. Subramanian, *Synthesis* **1993**, 387–390.

Received October 6, 1999
[I99353]

Structure and Dynamic Behavior of (η^3-Allyl)bromodicarbonylmolybdenum(II) Complexes Containing Polydentate 2-Pyridylphosphanes or Their Oxides as Chelating Ligands: Occurrence of Three Fluxional Processes

Pablo Espinet,*[a] Rosa Hernando,[a] Gonzalo Iturbe,[a] Fernando Villafañe,[a] A. Guy Orpen,[b] and Isabel Pascual[b]

Keywords: Molybdenum / Fluxionality / Pyridylphosphanes / Phosphane oxides / Polydentate ligands

The pseudo-octahedral complexes [Mo(η^3-allyl)Br(CO)$_2$(P-Py$_n$Ph$_{3-n}$-*P,N*)] (Py = 2-pyridyl; n = 2, 3) and [Mo(η^3-allyl)Br(CO)$_2$(OPPy$_m$Ph$_{3-m}$-*O,N*)] (m = 1, 2, 3) undergo three different dynamic processes in solution, depending on the chelating ligand. The complexes containing PPhPy$_2$ and PPy$_3$ as chelating *P,N*-donors undergo a novel "pivoted double switch" mechanism which scrambles two *equatorial* coordination sites with racemization, while maintaining the identity of the phosphorus atom *trans* to the allyl ligand. The complexes containing 2-pyridylphosphane oxides as chelating *O,N*-donors undergo a nondissociative intramolecular trigonal-twist (or turnstile) rearrangement which maintains the identity of the phosphane oxide oxygen atom coordinated in an *equatorial* position. All the complexes containing uncoordinated pyridyls undergo a slow dissociative exchange of pyridyls without coordination site scrambling. The structure of the complex [Mo(η^3-allyl)Br(CO)$_2$(OPPy$_3$-*O,N*)] has been determined by X-ray diffraction.

Introduction

The coordination of 2-pyridylphosphanes or their P-substituted derivatives has allowed the elucidation of many dynamic processes in solution. Our group is currently carrying out a study of their behavior with different metals, such as palladium, platinum[1] and molybdenum.[2] In the course of these studies, we decided to explore the behavior of 2-pyridylphosphanes[3] or their oxides towards (η^3-allyl)bromodicarbonylmolybdenum(II), with the aim of understanding how the ligands coordinate to this metal moiety (there are very few reports on hybrid chelating or tripodal ligands coordinated to this system), and examine possible dynamic processes in solution.

The complexes [Mo(η^3-allyl)X(CO)$_2$(L^1)(L^2)] (X = anionic ligand; L^1, L^2 = two monodentate neutral ligands, or one bidentate neutral ligand), show two possible solid state structures, as depicted in Figure 1 (**A** and **B**). Both are pseudo-octahedral complexes if the η^3-allyl ligand is considered as occupying one coordination site with its terminal atoms oriented over the carbonyl groups, which has been demonstrated to be the most energetically favorable arrangement.[4] In structure **A** the anionic ligand occupies the *axial* position, *trans* to the allyl group, giving rise to C_s symmetry with a σ plane which bisects the allyl group and contains the metal atom, whereas in structure **B** the anionic ligand X occupies one of the *equatorial* positions leading to a C_1 geometry. The adoption of one of these two possible arrangements in the solid state does not seem to follow clear rules. Structure A is usually observed when X is a halogen or a pseudohalogen and L–L is a bidentate nitrogen donor ligand, such as bipy.[5] However, structure B has been found for trifluoroacetate as the anionic ligand and 1,10-phenanthroline as the chelate,[6] or when the neutral ligands are two pyrazols and bromide is the anionic ligand.[7]

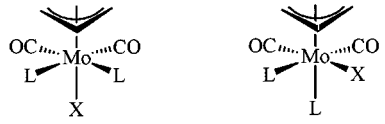


Figure 1. Two possible structures, **A** and **B**, for [Mo(η^3-allyl)X(CO)$_2$(L^1)(L^2)]

Several solution dynamic processes have been detected for this type of complex: the nondissociative trigonal-twist rearrangement[8] or turnstile mechanism,[1c,9] in which there is an intramolecular rotation of the "XL$_2$" face, was first established for L$_2$ = diphosphane and X = halogen. This process has since then been observed for a variety of "XL$_2$" systems, including cationic complexes with XL$_2$ = neutral tridentate nitrogen donor ligand.[10] Other solution processes detected for these complexes are the substitution of the neutral ligands (usually nitrogen donors) by solvents such as MeCN or water,[10b,11] and the η^3–η^1–η^3 rearrangement of the allyl ligand, which has been proposed for tridentate nitrogen donor ligands such as trispyrazolylborate or bispyrazolylaminomethane.[12]

[a] Departamento de Química Inorgánica, Facultad de Ciencias, Universidad de Valladolid, 47005 Valladolid, Spain
E-mail: espinet@qi.uva.es
[b] School of Chemistry, University of Bristol, Bristol BS8 1TS, U.K.
E-mail: Guy.Orpen@bris.ac.uk
Supporting Information for this article is available on the WWW under http://www.wiley-vch.de/home/eurjic or from the author.

 © WILEY-VCH Verlag GmbH, D-69451 Weinheim, 2000 1434–1948/00/0505–1031 $ 17.50+.50/0

Results and Discussion

[Mo(η³-allyl)Br(CO)$_2$(PPy$_n$Ph$_{3-n}$-*P,N*)] (*n* = 2, 3)

The complexes [Mo(η³-allyl)Br(CO)$_2$(PPy$_n$Ph$_{3-n}$-*P,N*)] [*n* = 2 (**1**), 3 (**2**)] were obtained by displacement of the nitrile ligands in [Mo(η³-allyl)Br(CO)$_2$(MeCN)$_2$] with PPy$_2$Ph or PPy$_3$.[13] All attempts to obtain a similar complex with PPyPh$_2$ were unsuccessful. This may be due to electronic factors since PPyPh$_2$ is a weaker donor than the other pyridylphosphanes.[14] The IR spectra of **1** and **2** in the C–O stretching region show two bands, as expected for *cis* dicarbonyl complexes. Their low electrical conductivity in solution indicates that the complexes are neutral, supporting coordination of the bromo ligand to the molybdenum atom.

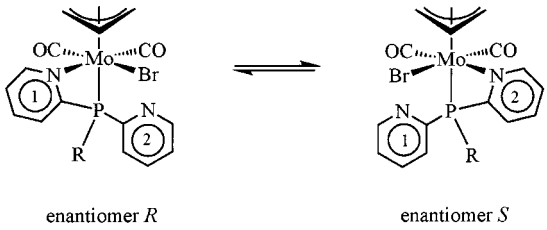
Characterization of [Mo(η³-allyl)Br(CO)$_2$(PPy$_2$Ph-*P,N*)] (1)

The low temperature ^{1}H NMR spectrum (–60 °C) corresponds to an asymmetric complex, the signals of the allyl group displaying the expected ABCDX pattern. Two doublets are observed for the H^6 protons of the pyridyls: one at very low field (9.60 ppm) typical of a pyridyl ligand coordinated *cis* to a halogen ligand, as has been clearly established for square planar geometries;[15] and the second (9.12 ppm) in the typical range of H^6 for uncoordinated pyridyls. Thus, for complex **1** at low temperature, these data support the *P,N*-coordination of the PPy$_2$Ph ligand.

However, a symmetrically averaged spectrum (revealing a racemization process) is observed at high temperature (+55 °C): the allyl group displays an A$_2$M$_2$X pattern where both H^{anti} are equivalent, as well as both H^{syn}, and only one doublet (9.46 ppm) is detected for both pyridyl H^6 atoms. Therefore, the dynamic process detected results in simultaneous equivalence of the two pyridyl groups and both ends of the allyl group. The phosphorus atom of PPy$_2$Ph is not directly involved in the dynamic process, and its chemical shift remains practically unchanged from –60 °C to +55 °C (–8.7 ppm in the ^{31}P{^{1}H} NMR spectra). This implies it coordinates in the *axial* position *trans* to the allyl group in a structure of type B (Figure 1).

The only process consistent with this NMR behavior is the racemization shown in Scheme 1 (R = Ph for **1**). In this exchange process, the pyridyl groups always occupy the same position when coordinated, and the Br ligand switches between two *equatorial* positions. We will refer to this process as a "pivoted double switch" mechanism.

Both the geometry of the molecule and the dynamic process in complex **1** were confirmed by a phase sensitive 2-D ^{1}H NOESY spectrum recorded at –50 °C, shown in Figure 2. At this temperature, the significant signals have split and the interchange process is slow. In Figure 2 a (positive peaks), cross-peaks due to chemical exchange of magnetization are detected between both H^{syn}, and also between both H^{anti} of the allyl group (the latter are difficult to observe because their signals almost overlap); whereas for the aromatic protons, cross-peaks relate the H^6 protons of the coordinated and uncoordinated pyridyls at this temperature. Figure 2b shows negative cross peaks due to NOEs between both H^6–H^{central}, H^{syn}–H^{anti}, and H^6–other aromatic protons. The latter two are expected NOEs, and do not provide structural information, but the first correlation indicates a close spatial proximity of the H^{central} of the allyl ligand and both H^6 atoms. A similar NOE has been reported for a complex containing a phenanthroline coordinated in the



Scheme 1. "Pivoted double switch" mechanism in complexes **1** (R = Ph) and **2** (R = Py)

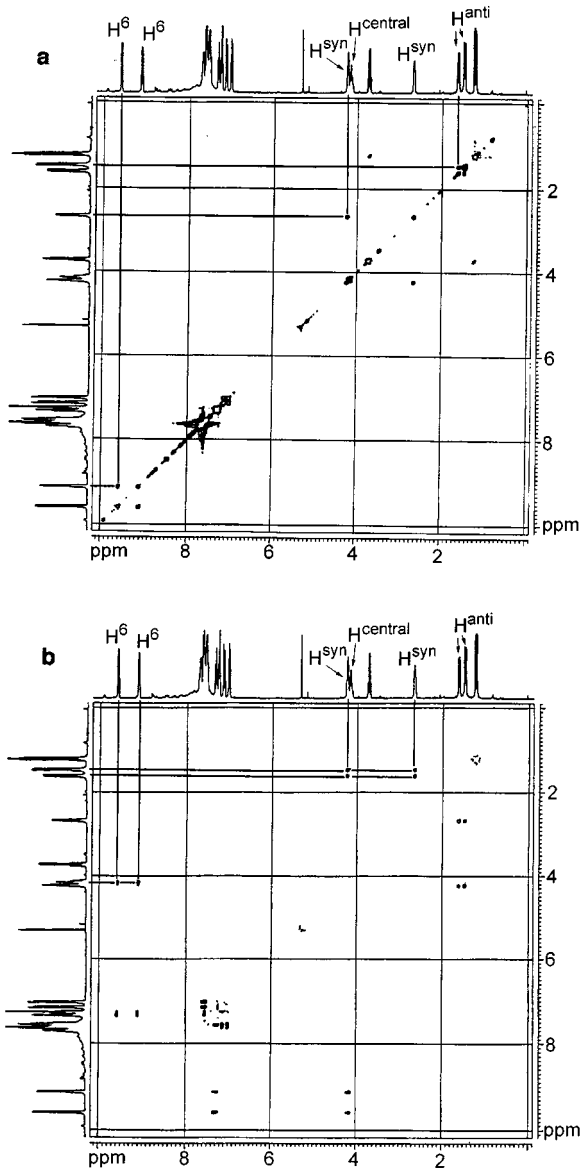


Figure 2. Phase sensitive 2-D NOESY experiment carried out for **1** at –50 °C. (a) Positive peaks due to chemical exchange of magnetization. (b) Negative peaks due to NOEs

same position as the pyridyl in our system.[6] The observation of two intense cross-peaks between $H^{central}$ and the two H^6 at lower field in complex **1** must presumably be related to the dynamic process shown in Scheme 1.

Characterization of [Mo(η^3-allyl)Br(CO)$_2$(PPy$_3$-*P,N*)] (2)

All the main features observed for **1** are also detected for **2**. The $^{31}P\{^1H\}$ NMR spectra at different temperatures (from +55 °C to –60 °C) show only one invariant singlet at –10.0 ppm. The ^1H NMR spectrum at –60 °C supports the existence of only one asymmetric complex in solution (which is a racemic mixture, as before), where three doublets are observed for the H^6 protons of the three pyridyls present: one at very low field (9.56 ppm) for the pyridyl coordinated *cis* to the bromo ligand,[15] and two more for the H^6 of the uncoordinated pyridyls (9.11 and 8.98 ppm). The ^1H NMR spectra at room temperature and above correspond to a symmetric averaged species where the allyl group displays the expected A_2M_2X pattern, and the signals of two H^6 (one coordinated and one uncoordinated) have coalesced to one broad signal, whereas the H^6 of the third pyridyl (that at higher field) remains nonequivalent. This indicates that the exchange process depicted in Scheme 1 (with R = Py in **2**) affects only one of the two uncoordinated pyridyls, the one which is able to coordinate by virtue of its geometry.

The ^1H NMR spectrum at 55 °C shows a slight broadening of all the signals, which is not observed in the spectrum of **1** at this temperature, suggesting that the third pyridyl begins to become involved in a second, and slower, exchange process. This second process interchanging the third pyridyl with the other two is too slow to be detected by variable temperature NMR (decomposition of the sample is observed upon further heating), but could be confirmed by a phase sensitive 2-D ^1H NOESY experiment. Chemical exchange is detected between both H^{syn}, between both H^{anti}, and between two H^6 (as for **1**), but in addition less intense cross peaks relating these two H^6 with the third H^6 (8.98 ppm) are also observed, supporting the involvement of the third pyridyl (R in Scheme 1) in a slower exchange equilibrium.

Discussion of the Dynamic Process of Complexes 1 and 2

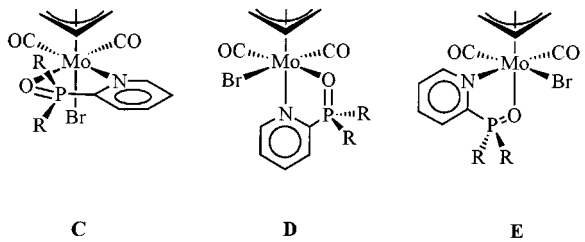
The dynamic process shown in Scheme 1 for complexes **1** and **2** seems not to have precedent in the literature for the (η^3-allyl)bromodicarbonylmolybdenum(II) system, so the mechanism of interconversion deserves further discussion. All dissociative mechanisms can be discarded. An η^3–η^1–η^3 rearrangement of the allyl ligand would render H^{anti} and H^{syn} equivalent giving an A_4X pattern for the allyl group in the ^1H NMR spectra, which is not observed. A mechanism involving dissociation of the coordinated pyridyl ligand with concomitant rotation about the Mo–P may also be discounted, as the second slow process detected for **2**, which exchanges the three pyridyls, in fact requires decoordination of the pyridyl to allow for rotation around the Mo–P bond and hence coordination of the third pyridyl (Scheme 1). Hence, if decoordination of the coordinated pyridyl was occurring for the process in Scheme 1, the exchange of the third pyridyl should take place at the same rate (assuming rotation about the Mo–P bond is rapid), which is not observed. Dissociation of the bromo ligand may also be discounted since addition of excess bromide [5:1 as NBu_4Br in $(CD_3)_2CO$ solution of **2**][16] did not reduce the exchange rate.

To ascertain whether the dynamic process was associative, $\Delta S^{\ddagger}$ was determined by line shape analysis using the DNMR6 program for complex **2** (data taken from –40 to +40 °C). The value obtained, -2 ± 4 J mol^{-1} K^{-1}, is too low to unequivocally support an associative mechanism for this process, although values close to zero have been found for processes which have been finally identified as associative.[1b] Therefore, either an associative or a concerted mechanism may be proposed for this dynamic process, as the dissociative path can be definitely discarded.

[Mo(η^3-allyl)Br(CO)$_2$(OPPy$_n$Ph$_{3-n}$-*O,N*)] (*n* = 1, 2, 3)

The complexes [Mo(η^3-allyl)Br(CO)$_2$(OPPy$_n$Ph$_{3-n}$-*O,N*)] [*n* = 1 (**3**), 2 (**4**), 3 (**5**)] were obtained by displacement of the nitrile ligands in [Mo(η^3-allyl)Br(CO)$_2$(MeCN)$_2$] with the ligands $OPPyPh_2$, $OPPy_2Ph$, and $OPPy_3$ to obtain **3**, **4**, and **5**, respectively. Complex **4** could also be obtained by oxidative addition of allyl bromide to [Mo(CO)$_3$(OPPy$_2$Ph-*O,N*$_2$)].

The three complexes show two C–O stretching bands in the solid state, as expected for *cis* dicarbonyl complexes. Complexes **3** and **5** also display two C–O stretching bands in solution, whereas **4** shows four. According to the isomer equilibria discussed below, four bands should be expected (at least when all the isomers are noticeably abundant). However, the bands for each pair of isomers **C** and **D** are almost coincident (Figure 3). In fact careful examination of the IR C–O bands reveals that they are asymmetric and show shoulders, but the presence of **C** and **D** isomers only becomes clear in the NMR spectra. The IR spectra of the solid complexes **3–5** do not show bands in the 1300–1200 cm^{-1} region, where the P–O stretching absorptions of the free ligands are found. This implies coordination of the ligands as oxygen donors, although the assignment of the band due to P–O stretching is very difficult, due to the pres-



C **D** **E**

Figure 3. Three possible isomers C, D, and E, for complexes **3–5**

ence of other absorptions in the expected range for O-bonded phosphane oxides.[17]

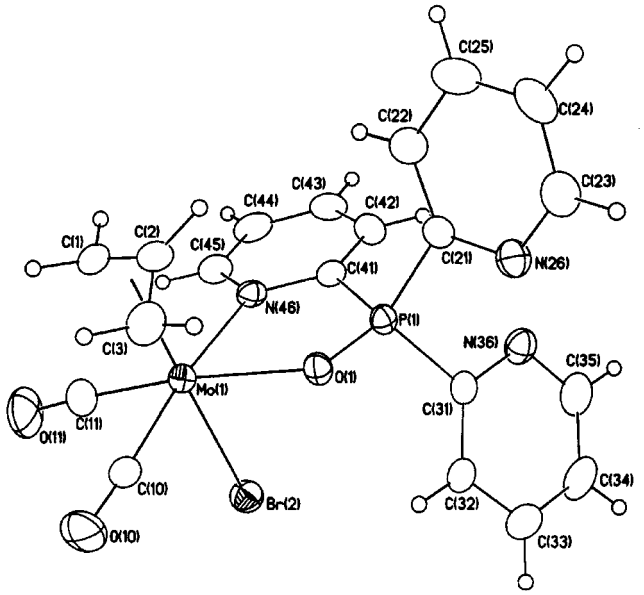


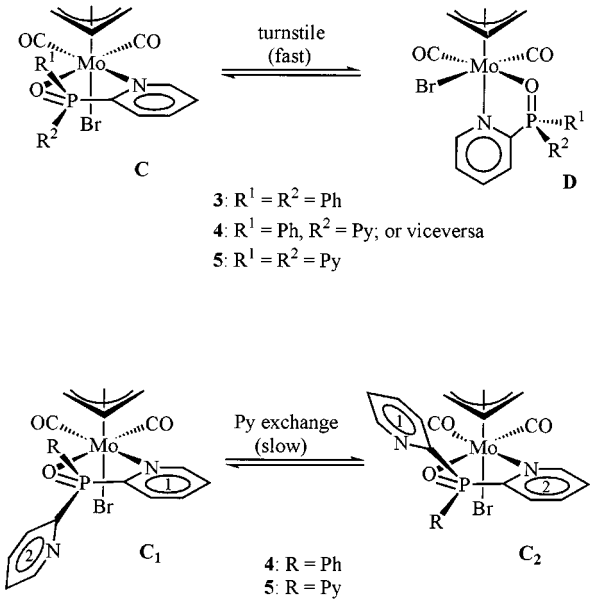
Figure 4. Displacement ellipsoid drawing of **5** showing the atom numbering scheme;tThe ellipsoids are drawn at 30% probability level

Table 1. Selected bond (Å) and angles (deg) for **5**

Mo(1)–C(10)	1.934(7)	Mo(1)–C(11)	1.934(8)
Mo(1)–C(1)	2.314(6)	Mo(1)–C(3)	2.301(7)
Mo(1)–C(2)	2.196(6)	Mo(1)–Br(2)	2.6429(8)
Mo(1)–O(1)	2.256(4)	Mo(1)–N(46)	2.323(5)
C(1)–C(2)	1.380(9)	C(2)–C(3)	1.415(9)
P(1)–O(1)	1.501(4)	P(1)–C(41)	1.817(6)
C(10)–O(10)	1.149(8)	C(11)–O(11)	1.130(8)
C(10)–Mo(1)–C(11)	78.7(3)	O(1)–Mo(1)–N(46)	76.8(2)
C(11)–Mo(1)–N(46)	99.5(3)	C(10)–Mo(1)–O(1)	103.5(2)
C(10)–Mo(1)–N(46)	171.0(2)	C(11)–Mo(1)–O(1)	170.0(2)
C(10)–Mo(1)–Br(2)	89.2(2)	C(11)–Mo(1)–Br(2)	85.5(2)
O(1)–Mo(1)–Br(2)	84.76(10)	N(46)–Mo(1)–Br(2)	81.87(11)
Mo(1)–N(46)–C(41)	120.8(4)	N(46)–C(41)–P(1)	113.4(4)
C(41)–P(1)–O(1)	108.8(3)	P(1)–O(1)–Mo(1)	120.1(2)
Mo(1)–C(1)–C(2)	67.7(3)	Mo(1)–C(3)–C(2)	67.7(4)
C(1)–C(2)–Mo(1)	76.9(4)	C(3)–C(2)–Mo(1)	75.7(4)
C(1)–C(2)–C(3)	115.1(6)		

The low electrical conductivities in solution indicate that the complexes **3–5** are neutral, with the bromo ligand coordinated to the molybdenum atom. Only the three isomers **C**, **D**, and **E**, shown in Figure 3, can be proposed in accordance with the IR and conductivity data. The molecules are chiral, and Figure 3 shows the *R* enantiomers only.

The $^{31}P\{^{1}H\}$ NMR spectra of complexes **3** and **5** show two singlets of different intensity at low temperature, which coalesce on heating. This implies that a dynamic process interchanging two of the three possible isomers in Figure 3 is occurring. Twice as many signals are observed in the $^{31}P\{^{1}H\}$ NMR spectra of **4**, that is, four singlets at –60 °C which coalesce to two singlets of different intensity at 50 °C. In this complex the R groups are different (Ph and Py), thus the isomers, which are enantiomers in **3** and **5** (and which therefore have indistinguishable NMR spectra) become diastereoisomers for **4**, doubling the number of signals; but again only two of the three structures **C**, **D**, or **E** are involved. The exchange process observed corresponds exactly to the trigonal-twist mechanism described in the literature for the complex [Mo(η³-allyl)I(CO)$_2$(arphos)],[8] and needs no further discussion except for identification of the two isomers involved. This was achieved as described below.



Scheme 2. Dynamic processes in complexes **3**, **4**, and **5**: fast nondissociative intramolecular trigonal-twist (or turnstile) rearrangement in complexes **3**, **4**, and **5** and slow pyridyl-exchange equilibria in complexes **4** and **5**

Structure of [Mo(η³-allyl)Br(CO)$_2$(OPPy$_3$-*O,N*)] (5)

An X-ray structural determination was carried out for [Mo(η³-allyl)Br(CO)$_2$(OPPy$_3$-*O,N*)] (**5**). The structure is shown in Figure 4, and Table 1 lists relevant distances and angles. The molybdenum atom is *pseudo*-octahedrally coordinated, assuming that the allyl group occupies one site. The two carbonyls and the allyl are mutually *cis*, with the terminal carbon atoms of the allyl moiety oriented over the carbonyls, as usually found for this class of complex.[4] The observed structure is of the form labeled **C** in Figure 3. The P–O distance is slightly elongated compared to those found in palladium(II) complexes containing the OPPy$_2$Ph ligand, where the oxygen atom is not coordinated to the metal: P–O = 1.480(2) and 1.482(2) Å in [Pd(C$_6$F$_5$)X(OPPy$_2$Ph-*N$_2$*)] (X = Br and C$_6$F$_5$, respectively)[1b] *cf.* 1.501(4) Å in **5**. The donor atoms of the OPPy$_3$ ligand coordinated in the *equatorial* positions have different donor properties, but this seems to induce very little asymmetry in the *trans* carbonyl groups: the Mo–C distances are equal [1.934(7) and 1.934(8) Å] and the C–O distances show insignificant differences [1.149(8) and 1.130(8) Å]. The allyl group is also essentially symmetrical [C–C = 1.380(9) and 1.415(9) Å; Mo–C^{terminal} = 2.314(6) and 2.301(7) Å]. This indicates that the different donor properties of the atoms in the *equatorial* sites do not induce observable asymmetry in the allyl ligand, as has been previously reported.[10a] The distances

and angles of the allyl group found in **5** are very similar to those reported for [Mo(η^3-allyl)(acac)(CO)$_2$(py)],[18] which also contains an oxygen donor ligand and a nitrogen donor ligand in the *equatorial* positions.

Discussion of the Dynamic Process of Complexes 3–5

When an NMR sample of **5** in $CDCl_3$ was prepared in a liquid nitrogen bath, and then allowed to melt and simultaneously dissolve at –60 °C in the NMR probe, only one isomer was found, which is logically assigned to structure **C**. The solution was then warmed to room temperature to establish the equilibrium between the isomers, and a phase sensitive 2-D ^{1}H NOESY spectrum was recorded at –50 °C. Negative peaks associated to NOE are not observed, which disfavors structure **E** for which an NOE between the coordinated pyridyl and some of the allyl protons would be expected (H^6–$H^{central}$ correlations were observed for **1** and **2**). Consequently, we assign structure **D** to the second isomer. Positive peaks were observed between $H^{central}$, and each H^{syn} and H^{anti} of the two isomers **C** and **D**, but not between the two H^{syn} or between the two H^{anti} atoms of each isomer. In other words, there was no racemization of the molecule and the two halves of the allyl group remained inequivalent during the fluxional processes. Finally, there were also weak cross peaks showing exchange of the coordinated and the free pyridyl groups.

Thus two types of exchange are operative in these systems, which are depicted in the general Scheme 2. The faster movement is a nondissociative intramolecular trigonal-twist (or turnstile) rearrangement, converting diastereoisomers **C** and **D**. This is the only mechanism operating for $R^1 = R^2 =$ Ph (in **3**). The second and slower movement (it is barely observed in the one dimensional spectrum of **5** at 55 °C as a broadening of the signals) is an exchange of pyridyls without racemization. In this respect, it is very different from the "pivoted double switch" as seen in **1** and **2**. The conservation of the asymmetry allows decoordination of the oxygen to give a *N,N*-bonded intermediate to be discounted, as this would create a symmetry plane. In fact, in conjunction with the observation of pyridyl exchange of **1** and **2**, a dissociative mechanism is more plausible, with the incoming pyridyl group taking the site left vacant by dissociation. This, as shown in Scheme 2, converts $\mathbf{C_1}$ to $\mathbf{C_2}$, these being identical for **5**, but diastereoisomers for **4**. The slowness of this mechanism is also consistent with a dissociative process.

Conclusion

The systems studied here reveal the existence of three mechanisms, depending on the chelating ligand. The slowest mechanism is common to both ligands that have uncoordinated pyridyls, which is a dissociative exchange of pyridyls without scrambling of coordination sites. The second, shown by the pyridylphosphane oxides, is the well-known nondissociative intramolecular trigonal-twist (or turnstile) mechanism, which produces scrambling of the coordination sites but retaining the elements of chirality (i.e. without racemization). Finally, for bis- or trispyridylphosphane, the pendant pyridyl triggers a novel "pivoted double switch" mechanism scrambling two coordination sites with racemization. A different but somewhat related case has been discussed in detail elsewhere.[19]

Experimental Section

General Remarks: All reactions were carried out under an atmosphere of pre-purified dinitrogen. Solvents were purified according to standard procedures.[20] [Mo(η^3-allyl)Br(CO)$_2$(MeCN)$_2$],[21] [Mo(CO)$_3$(OPPy$_2$Ph-*O,N*$_2$)],[2b] and 2-pyridylphosphanes were prepared as previously described,[22] and their oxides were synthesized by standard methods.[23] The synthesis of [Mo(η^3-allyl)Br(CO)$_2$(PPy$_2$Ph-*P,N*)] has been previously reported.[2a]

The progress of the reactions involving carbonyl complexes was monitored by solution IR spectra in the 2100–1700 cm^{-1} region. Filtrations were carried out on dry Celite without exclusion of air. The products are air-stable solids which were recrystallized at –20 °C.

Infrared spectra were recorded on Perkin–Elmer 883 or 1720X apparatus in NaCl cells for solutions, and as Nujol mulls or KBr pellets for solids. NMR spectra were recorded on Bruker AC-300 or ARX-300 instruments in $CDCl_3$. NMR spectra were referred to TMS or 85% aqueous H_3PO_4. Elemental analyses were performed on a Perkin–Elmer 2400B microanalyzer. The electrical conductivity measurements were carried out at room temperature with a Crison 522 conductivity meter using $5\cdot10^{-4}$ M solutions; the range of molar conductivity for 1:1 electrolytes is 75–95 S·cm^2·mol^{-1} in nitromethane solutions.[24]

General Method for the Preparation of the Complexes: A 100 mL Schlenk flask was successively charged with equimolar amounts (0.2–0.5 mmol) of [Mo(η^3-allyl)Br(CO)$_2$(MeCN)$_2$], the respective ligand, and CH_2Cl_2 (10–25 mL). The solution was stirred at room temperature for 15 min., and then EtOH or hexane was added (5–15 mL). Concentration of the solution in vacuo and cooling to –20 °C gave microcrystalline solids, which were filtered, washed with Et_2O (3 × 3 mL approximately), and dried in vacuo. The yields, color, and spectroscopic data of the products obtained are given below.

[Mo(η^3-allyl)Br(CO)$_2$(PPy$_2$Ph-*P,N*)] (1):[2a] $^{31}P\{^1H\}$ NMR (room temp.): δ = –8.7 (s). – ^{1}H NMR (55 °C): δ = 9.46 (d, *J* = 5 Hz, 2 H^6 of coordinated + uncoordinated Py), 7.76 (m, 3 H), 7.63 (m, 2 H), 7.52 (m, 2 H), 7.27 (m, 2 H), 7.07 (d, *J* = 8 Hz, 2 H), 4.15 (m, 1 H^c), 3.40 (br, 2 H^s), 1.54 (d, *J* = 9.5 Hz, 2 H^a). – ^{1}H NMR (room temp.): δ = 9.43 (br, 2 H^6 of coordinated + uncoordinated Py), 7.72 (m, 3 H), 7.63 (m, 2 H), 7.53 (m, 2 H), 7.28 (m, 2 H), 7.08 (d, *J* = 8 Hz, 2 H), 4.15 (m, 1 H^c), 1.54 (d, *J* = 9.5 Hz, 2 H^a). – ^{1}H NMR (–60 °C): δ = 9.60 (d, *J* = 5.5 Hz, 1 H^6 of coordinated Py), 9.12 (d, *J* = 5.5 Hz, 1 H^6 of uncoordinated Py), 7.63 (m, 7 H), 7.34 (t, *J* = 6 Hz, 1 H), 7.27 (t, *J* = 6 Hz, 1 H), 7.16 (d, *J* = 8 Hz, 1 H), 7.03 (d, *J* = 8 Hz, 1 H), 4.24 (br, 1 H^s), 4.17 (m, 1 H^c), 2.67 (br, 1 H^s), 1.63 (d, *J* = 10 Hz, 1 H^a), 1.48 (d, *J* = 10 Hz, 1 H^a). Other spectroscopic and analytical data have been reported previously.[2a]

[Mo(η^3-allyl)Br(CO)$_2$(PPy$_3$-*P,N*)] (2): 46%, yellow. – $^{31}P\{^1H\}$ NMR (room temp.): δ = –10.0 (s). – ^{1}H NMR (55 °C): δ = 9.50

(br, 2 H^6 of coordinated + uncoordinated Py), 9.00 (br, 1 H^6 of uncoordinated Py), 8.20 (br, 1 H), 8.0 (br, 1 H), 7.50 (br, 3 H), 7.20 (br, 2 H), 7.00 (br, 2 H), 4.10 (brm, 1 H^c), 3.50 (br, 2 H^s), 1.56 (d, J = 9.5 Hz, 2 H^a). – ^{1}H NMR (room temp.): δ = 9.50 (br, 2 H^6), 9.08 (d, J = 4.5 Hz, 1 H^6 of uncoordinated Py), 8.22 (t, J = 7 Hz, 1 H), 8.00 (m, 1 H), 7.58 (m, 1 H), 7.52 (m, 2 H), 7.25 (m, 2 H), 6.94 (d, J = 8 Hz, 2 H), 4.14 (m, 1 H^c), 1.56 (d, J = 9.5 Hz, 2 H^a). – ^{1}H NMR (–60 °C): δ = 9.56 (d, J = 5.5 Hz, 1 H^6 of coordinated Py), 9.11 (d, J = 5.5 Hz, 1 H^6 of uncoordinated Py), 8.98 (d, J = 4 Hz, 1 H^6 of uncoordinated Py), 8.29 (t, J = 8 Hz, 1 H), 8.07 (t, J = 7.5 Hz, 1 H), 7.66 (t, J = 6 Hz, 1 H), 7.57 (q, J = 7 Hz, 2 H), 7.32 (m, 2 H), 7.02 (d, J = 8 Hz, 1 H), 6.85 (d, J = 8 Hz, 1 H), 4.3 (br, 1 H^s), 4.16 (m, 1 H^c), 2.7 (br, 1 H^s), 1.65 (d, J = 9.5 Hz, 1 H^a), 1.50 (d, J = 9.5 Hz, 1 H^a). – IR (CH_2Cl_2): $\tilde{\nu}$ = 1948 vs, 1851s cm^{-1}. – IR (Nujol): $\tilde{\nu}$ = 1940 vs, 1828 vs, 1652 w, 1587 w, 1571 w, 1456 s, 1424 m, 1275 w, 1066 w, 1045 w, 987 w, 807 w, 769 m, 752 w, 737 w cm^{-1}. – $C_{20}H_{17}BrMoN_3O_2P$ (538.19): calcd. C 44.63, H 3.18, N 7.81; found C 44.29, H 3.50, N 7.49. – Conduct. Λ_M ($MeNO_2$): 9 $S{\cdot}cm^2{\cdot}mol^{-1}$.

[Mo(η³-allyl)Br(CO)$_2$(OPPyPh$_2$-*O,N*)] (3): 59%, red. – $^{31}P\{^1H\}$ NMR (room temp.): δ = 48.6 (br). – $^{31}P\{^1H\}$ NMR (–60 °C): δ = 51.4 (s, isomer D), 49.5 (s, isomer C). – ^{1}H NMR (room temp.): δ = 9.70 (br, 1 H^6, Py), 7.92 (m, 1 H, Py), 7.73 (m, 9 H, Py + Ph), 7.48 (m, 3 H, Py + Ph), 4.20 (br, 1 H^s), 4.10 (br, 1 H^c), 3.31 (br, 1 H^s), 1.54 (d, J = 9.5 Hz, 1 H^a), 1.31 (d, J = 9.5 Hz, 1 H^a). – ^{1}H NMR (–60 °C): δ = 9.76 (d, J = 5 Hz, 1 H^6, Py, isomer C), 8.98 (d, J = 5 Hz, 1 H^6, Py, isomer D), 7.97 (m, 1 H^6, Py, isomers C + D), 7.76 (m, 9 H, Py + Ph, isomers C + D), 7.48 (m, 3 H, Py + Ph, isomers C + D), 4.35 (br, 1 H^s, isomer C), 4.24 (m, 1 H^c, isomer C), 3.45 (br, 1 H^s, isomer C), 3.38 (br, 1 H^s, isomer D), 3.22 (m, 1 H^c, isomer D), 3.06 (br, 1 H^s, isomer D), 1.55 (d, J = 9.5 Hz, 1 H^a, isomer C), 1.43 (d partially overlapped with the next signal, 1 H^a, isomer D), 1.41 (d, J = 9.5 Hz, 1 H^a, isomer C), 1.27 (d, J = 9.5 Hz, 1 H^a, isomer D); ratio isomer C/isomer D = 1:0.2. – IR (CH_2Cl_2): $\tilde{\nu}$ = 1937 vs, 1838 s cm^{-1}. – IR (KBr pellet): $\tilde{\nu}$ = 3058 w, 1924 vs, 1830 vs, 1588 w, 1485 w, 1459 w, 1439 m, 1314 w, 1285 w, 1167 w, 1152 s, 1141 s, 1123 m, 1086 w, 1073 w, 1055 w, 1027 w, 1012 w, 998 w, 925 w, 766 w, 740 m, 726 m, 695 m, 634 w, 609 w, 560 s, 537 s, 507 w, 481 w, 448 w cm^{-1}. – $C_{22}H_{19}BrMoNO_3P$ (552.22): calcd. C 47.85, H 3.47, N 2.54; found C 47.60, H 3.57, N 2.73. – Conduct. Λ_M ($MeNO_2$): 10 $S{\cdot}cm^2{\cdot}mol^{-1}$.

[Mo(η³-allyl)Br(CO)$_2$(OPPy$_2$Ph-*O,N*)] (4): 72%, orange. Complex **4** was also obtained by an alternative method: A 100 mL Schlenk flask was successively charged with [Mo(CO)$_3$(OPPy$_2$Ph-*O,N*$_2$)] (0.092 g, 0.2 mmol), $CHCl_3$ (20 mL), and allyl bromide (1 mL, 11.5 mmol). An immediate color change from dark purple to orange was observed. After 5 min stirring at room temp., the volatiles were removed in vacuo and the orange residue was recrystallized from CH_2Cl_2/hexane giving 0.052 g (47%) of **4**. – $^{31}P\{^1H\}$ NMR (room temp.): δ = 39.4 (br, m), 35.4 (s, M). – $^{31}P\{^1H\}$ NMR (–60 °C): δ = 42.7 (s, isomer D of m), 40.7 (s, isomer C of m), 36.4 (s, isomer D of M), 35.2 (s, isomer C of M). – ^{1}H NMR (room temp.): δ = 9.60 (br, 1 H^6 of coordinated Py, M + m), 8.86 (d, J = 4.5 Hz, 1 H^6 of uncoordinated Py, m), 8.75 (d, J = 4.5 Hz, 1 H^6 of uncoordinated Py, M), 8.39 (t, J = 7 Hz, 1 H, M), 8.24 (m, 1 H, M + m), 7.91 (m, 4H of M + 5 H of m), 7.56 (m, 5 H of M + 5 H of m), 4.20 [br, 1 H^s of (M + m)+ 1 H^c of (M + m)], 3.44 (br, 1H^s of M + m), 1.58 (d, J = 9.5 Hz, 1 H^a of M), 1.56 (d, J = 9.5 Hz, 1 H^a of m), 1.41 (d, J = 9.5 Hz, 1 H^a of m), 1.39 (d, J = 9.5 Hz, 1 H^a of M). – ^{1}H NMR (–60 °C): δ = 9.72 (d, J = 5.5 Hz, 1 H^6 of coordinated Py, isomer C of M), 9.68 (d, J = 5.5 Hz, 1 H^6 of coordinated Py, isomer C of m), 8.90 (brm, 1 H^6 of uncoordinated Py, isomer C + D of m), 8.78 (d, J = 4.5 Hz, 1 H^6 of uncoordinated Py, isomer C of M), 8.72 (d, J = 4.5 Hz, 1 H^6 of uncoordinated Py, isomer D of M), 8.33 (m), 7.96 (m), 7.62 (m), 4.39 (br, 1 H^s, isomer C of M + m), 4.30 (m, 1 H^c, isomer C of M + m), 3.61 (br, 1 H^s, isomer C of m), 3.52 [br, 1 H^s of isomer C of m and 1 H^c of isomer D (M or m)], 3.25 [m, 1 H^c of isomer D (M or m)], 3.18 (br, 1 H^s, isomer D of M), 3.16 (br, 1 H^s, isomer D of m), 1.61 (d, J = 9.5 Hz, 1 H^a, isomer C of M), 1.58 (d, J = 9.5 Hz, 1 H^a, isomer C of m), 1.50 (d, J = 9.5 Hz, 1 H^a, isomer C of m), 1.43 (d, J = 9.5 Hz, 1 H^a, isomer C of M), 1.35 (m, H^a, isomer D of M + m); M = major equilibrium; m = minor equilibrium; ratio M/m = 1:0.8; Ratio isomer C/isomer D for each equilibrium = 1:0.2. –

Table 2. Crystal data and structure refinement for **5**

Empirical formula	$C_{20}H_{17}BrMoN_3O_3P$
Formula weight	554.17
Temperature	293(2) K
Wavelength	0.71073 Å
Crystal system	Monoclinic
Space group	C2/c
Unit cell dimensions	a = 20.5279(14) Å, α = 90°
	b = 12.0329(8) Å, β = 96.146(10)°
	c = 17.1172(11) Å, γ = 90°
Volume	4203.8(5) Å^3
z	8
Density (calculated)	1.751 Mg/m^3
Absorption coefficient	2.627 mm^{-1}
F(000)	2192
Crystal size	0.2 × 0.2 × 0.15 mm
Theta range for data collection	2.24 to 25.02°
Index ranges	–17 h 24, –14 k 14, –19 l 20
Reflections collected	9749
Independent reflections	3685 [R(int) = 0.0534]
Refinement method	Full-matrix least-squares on F^2
Data/restraints/parameters	3679/0/262
Goodness-of-fit on F^2	1.154
Final R indices [$I > 2\sigma(I)$]	$R1$ = 0.0485, $wR2$ = 0.0897
R indices (all data)	$R1$ = 0.0830, $wR2$ = 0.1078
Weighting scheme calc.	$1/[\sigma^2(F_o^2) + (0.0297\ P)^2 + 16.4861\ P]$, where $P = (F_o^2 + 2\ F_c^2)/3$
Largest diff. peak and hole	0.0384 and –0.494 e/Å^3

IR (CH_2Cl_2): $\tilde{\nu}$ = 1950 s(sh), 1937vs, 1858 m(sh), 1839 s cm^{-1}. – IR (KBr pellet): $\tilde{\nu}$ = 3060 w, 1923 vs, 1828 vs, 1587 w, 1574 w, 1440 m, 1285 w, 1169 m, 1154 m, 1134 s, 1096 m, 1011 w, 988 w, 807 w, 774 w, 748 s, 694 w, 560 s, 540 s, 508 w, 449 w cm^{-1}. – $C_{21}H_{18}BrMoN_2O_3P$ (553.21): calcd. C 45.59, H 3.28, N 5.06; found C 45.36, H 3.01, N 5.06. – Conduct. Λ_M ($MeNO_2$): 18 $S{\cdot}cm^2{\cdot}mol^{-1}$.

[Mo(η^3-allyl)Br(CO)$_2$(OPPy$_3$-*O*,*N*)] (5): 47%, red. – $^{31}P\{^1H\}$ NMR (room temp.): δ = 34.0 (br). – $^{31}P\{^1H\}$ NMR (–60 °C): δ = 36.4 (s, isomer C), 32.1 (s, isomer D). – ^1H NMR (room temp.): δ = 9.50 (br, 1 H^6 of coordinated Py), 8.82 (d, J = 4.5 Hz, 1 H^6 of uncoordinated Py), 8.70 (d, J = 4.5 Hz, 1 H^6 of uncoordinated Py), 8.37 (m, 2 H), 7.90 (m, 4 H), 7.69 (br, 1 H), 7.51 (m, 1 H), 7.44 (m, 1 H), 4.10 (br, 1 H^s + 1 H^c), 3.40 (br, 1 H^s), 1.54 (d, J = 9.5 Hz, 1 H^a), 1.36 (d, J = 9.5 Hz, 1 H^a). – ^1H NMR (–60 °C): δ = 9.76 (d, J = 5 Hz, 1 H^6 of coordinated Py, isomer C), 8.94 (d, J = 5 Hz, 1 H^6 of coordinated Py, isomer D), 8.88 (d, J = 4.5 Hz, 1 H^6 of uncoordinated Py, isomer C), 8.84 (d, J = 4.5 Hz, 1 H^6 of uncoordinated Py, isomer D), 8.76 (d, J = 4.5 Hz, 1 H^6 of uncoordinated Py, isomer C), 8.72 (d, J = 4.5 Hz, 1 H^6 of uncoordinated Py, isomer D), 8.50 (t, J = 7 Hz, 1 H, isomer D), 8.43 (t, J = 6.5 Hz, 1 H, isomer C), 8.27 (t, J = 7 Hz, 1 H, isomer C), 8.22 (t, J = 6.5 Hz, 1 H, isomer D), 7.90 (m, 5 H, isomers C + D), 7.60 (m, 1 H, isomers C + D), 7.50 (d, J = 5 Hz, 1 H, isomers C + D), 4.37 (br, 1 H^s, isomer C), 4.27 (m, 1 H^c, isomer C), 3.82 (m, 1 H^c, isomer D), 3.55 (br, 1 H^s, isomer C), 3.33 (br, 1 H^s, isomer D), 3.26 (br, 1 H^s, isomer D), 1.59 (d, J = 9.5 Hz, 1 H^a, isomer C), 1.47 (d, J = 9.5 Hz, 1 H^a, isomer D), 1.41 (d, J = 9.5 Hz, 1 H^a, isomer C), 1.38 (d, J = 9.5 Hz, 1 H^a, isomer D); ratio isomer C/isomer D = 1:0.9. – IR (CH_2Cl_2): $\tilde{\nu}$ = 1950 vs, 1854 s cm^{-1}. – IR (Nujol): $\tilde{\nu}$ = 1936 vs, 1838 vs, 1589 w, 1577 m, 1430 m, 1285 w, 1220 w, 1177 m, 1163 m, 1148 m, 1104 m, 1085 m, 1057 w, 1010 w, 988 w, 771 w, 748 m cm^{-1}. – $C_{20}H_{17}BrMoN_3O_3P$ (554.19): calcd. C 43.35, H 3.09, N 7.58; found C 43.27, H 3.17, N 7.69. – Conduct. Λ_M ($MeNO_2$): 20 $S{\cdot}cm^2{\cdot}mol^{-1}$.

X-ray Crystallographic Analysis of 5: Crystal data and other details of the structure analysis are presented in Table 2. Red crystals of **5** were recrystallized from dichloromethane/diethyl ether and showed a block-like habit. One of these crystals was mounted on a glass fiber with epoxy resin. All diffraction measurements were made at room temperature with a Siemens SMART[25] diffractometer using graphite monochromated Mo-K_α radiation. A full hemisphere of reciprocal space was scanned by 0.3° ω steps with the area detector center held at 2θ = –27°. A total of 1321 data frames were collected for 10 seconds exposure per frame. The reflections were integrated using the SAINT program.[26] No crystal decay over the period of data collection was observed. A total of 10001 diffracted intensities were measured, 3685 unique observations remained after averaging of duplicate and equivalent measurements (R_{int} = 0.0579) and deletion of the systematic absences. Of these 2587 had $I > 2\sigma(I)$. An empirical absorption and detector correction was applied, effective transmission coefficients were in the range 0.878 to 0.634. Lorentz and polarization corrections were applied. The structure was solved by direct and Fourier methods, and refined using full-matrix least-squares refinement on F^2.[27] All non-hydrogen atoms were assigned anisotropic displacement parameters and refined without positional constraints. All hydrogen atoms were constrained to idealized geometries and assigned isotropic displacement parameters 1.2 times the U_{iso} value of their attached carbon for aromatic hydrogens. Final residuals and other details are given in Table 1.[28] Weights, w, were set to minimize the variation in S as a function of $|F_o|$. Final difference electron density maps showed no significant features. Complex neutral-atom scattering factors were taken from ref.[29].

Crystallographic data (excluding structure factors) for the structure reported in this paper have been deposited with the Cambridge Crystallographic Data Centre as supplementary publication no. CCDC-134122. Copies of the data can be obtained free of charge on application to CCDC, 12 Union Road, Cambridge CB2 1EZ, UK [Fax: (internat.) + 44-1223/336-033; E-mail: deposit@ccdc.cam.ac.uk].

Acknowledgments

The authors in Valladolid thank the D.G.I.C.Y.T. of Spain for financial support (Project PB96–0363), and the Bristol authors the UK EPSRC for financial support.

[1] [1a] J. A. Casares, S. Coco, P. Espinet, Y.-S. Lin, *Organometallics* **1995**, *14*, 3058–3067. – [1b] J. A. Casares, P. Espinet, J. M. Martínez-Ilarduya, Y.-S. Lin, *Organometallics* **1997**, *16*, 770–779. – [1c] J. A. Casares, P. Espinet, *Inorg. Chem.* **1997**, *36*, 5428–5431.

[2] [2a] P. Espinet, P. Gómez-Elipe, F. Villafañe, *J. Organomet. Chem.* **1993**, *450*, 145–150. – [2b] J. A. Casares, P. Espinet, R. Hernando, G. Iturbe, F. Villafañe, D. D. Ellis, A. G. Orpen, *Inorg. Chem.* **1997**, *36*, 44–49.

[3] G. R. Newkome, *Chem. Rev.* **1993**, *93*, 2067–2089.

[4] M. D. Curtis, O. Eisenstein, *Organometallics* **1984**, 3, 887–895.

[5] [5a] R. Davis, L. A. P. Kane-Maguire, in *Comprehensive Organometallic Chemistry* (Eds.: G. Wilkinson, F. G. A. Stone, E. W. Abel), Pergamon, Oxford, UK, **1982**, Volume 8, 1156–1159. – [5b] M. W. Whiteley, in *Comprehensive Organometallic Chemistry II* (Eds.: G. Wilkinson, F. G. A. Stone, E. W. Abel), Pergamon, Oxford, UK, 1995. Volume 12, J. A. Labinger, M. J. Winter, eds.; 337–338.

[6] M. P. T. Sjögren, H. Frisell, B. Åkermark, P.-O. Norrby, L. Eriksson, A. Vitagliano, *Organometallics* **1997**, *16*, 942–950.

[7] F. A. Cotton, R. L. Luck, *Acta Crystallogr., Sect. C* **1990**, *46*, 138–140.

[8] J. W. Faller, D. A. Haitko, R. D. Adams, D. F. Chodosh, *J. Am. Chem. Soc.* **1979**, *101*, 865–876.

[9] I. Ugi, D. Marquarding, H. Klusacek, P. Gillespie, *Acc. Chem. Res.* **1971**, *4*, 288–296.

[10] [10a] B. J. Brisdon, M. Cartwright, A. G. W. Hodson, M. F. Mahon, K. C. Molloy, *J. Organomet. Chem.* **1992**, *435*, 319–335. – [10b] B. J. Brisdon, M. Cartwright, A. G. W. Hodson, *J. Organomet. Chem.* **1984**, *277*, 85–90. – [10c] K.-B. Shiu, K.-S. Liou, C. P. Cheng, B.-R. Fang, Y. Wang, G.-H. Lee, W.-J. Vong, *Organometallics* **1989**, *8*, 1219–1224.

[11] K.-B. Shiu, C.-J. Chang, S.-L. Wang, F.-L. Liao, *J. Organomet. Chem.* **1991**, *407*, 225235.

[12] [12a] S. K. Chowdhury, M. Nandi, V. S. Joshi, A. Sarker, *Organometallics* **1997**, *16*, 1806–1809. – [12b] D. S. Frohnapfel, P. S. White, J. L. Templeton, H. Rüegger, P. S. Pregosin, *Ibid* **1997**, *16*, 3737–3750. – [12c] K.-B. Shiu, C.-J. Chang, Y. Wang, M.-C. Cheng, *J. Organomet. Chem.* **1991**, *406*, 363–369.

[13] The preparation of **1** was described previously in ref.[2a], but the structure was assigned mistakenly from the 80 MHz NMR data. The new data now available from a 300 MHz apparatus allows us to correct that mistake here.

[14] R. P. Schutte, S. J. Rettig, A. M. Joshi, B. R. James, *Inorg. Chem.* **1997**, *36*, 5809–5817.

[15] [15a] P. K. Byers, A. J. Canty, *Organometallics*, **1990**, *9*, 210–220. – [15b] R. E. Rülke, J. M. Ernsting, A. L. Spek, C. J. Elsevier, P. W. N. M. Leeuwen, K. Vrieze, *Inorg. Chem.* **1993**, *32*, 5769–5778.

[16] $(CD_3)_2CO$ solution has to be used in order to avoid ion pairs detected in $CDCl_3$ solutions (ref.[1a]).

[17] K. Nakamoto, *Infrared and Raman Spectra of Inorganic and Coordination Compounds*, 3rd ed., Wiley, New York, **1978**, p. 209.

[18] B. J. Brisdon, A. A. Woolf, *J. Chem. Soc., Dalton Trans.* **1978**, 291–295.

[19] M. A. Alonso, J. A. Casares, P. Espinet, K. Soulantica, *Angew. Chem. Int. Ed. Eng.* **1999**, *38*, 533–535.

[20] D. D. Perrin, W. L. F. Armarego, *Purification of Laboratory Chemicals*, 3rd ed., Pergamon Press, Oxford, **1988**.

[21] H. tom Dieck, H. Friedel, *J. Organomet. Chem.* **1968**, *4*, 375–385.
[22] [22a] F. R. Keene, M. R. Snow, P. J. Stephenson, E. R. T. Tiekink, *Inorg. Chem.* **1988**, *27*, 2040–2045. – [22b] K. Kurtev, D. Ribola, R. A. Jones, D. J. Cole-Hamilton, G. Wilkinson, *J. Chem. Soc., Dalton Trans.* **1980**, 55–58. – [22c] H. Schmidbaur, Y. Inoguchi, *Z. Naturforsch, Teil B.* **1980**, *35*, 1329–1334.
[23] [23a] F. G. Mann, J. Watson, *J. Org. Chem.* **1948**, *13*, 502–531. – [23b] G. R. Newkome, D. C. Hager, *J. Org. Chem.* **1978**, *43*, 947–949.
[24] W. Geary, *Coord. Chem. Rev.* **1971**, *7*, 81–122.
[25] SMART Siemens Molecular Analysis Research Tool V4.014 copyright **1989–94**, Siemens Analytical X-ray, Madison, WI, USA.
[26] SAINT (Siemens Area detector INTegration) program, Siemens Analytical X-ray, Madison, WI, USA.
[27] SHELXTL Rev. 5.0, Siemens Analytical X-ray, 1994.
[28] $R1 = \Sigma||F_o| - |F_c||/\Sigma|F_o|$; $wR2 = [\Sigma w(F_o^2 - F_c^2)^2/\Sigma w(F_o^2)^2]^{1/2}$; $S = [\Sigma w(F_o^2 - F_c^2)^2/(N - NV)]^{1/2}$; ($N$ = data + restraints; NV = parameters).
[29] *International Tables for Crystallography*, Vol. C, **1992**, Kluwer, Dordrecht.

Received October 14, 1999
[I99363]

Metal-Containing Amphiphiles: Orthometallated Iridium(III) Complexes with Substituted 6′-Phenyl-2,2′-bipyridines

Francesco Neve*[a] and Alessandra Crispini[a]

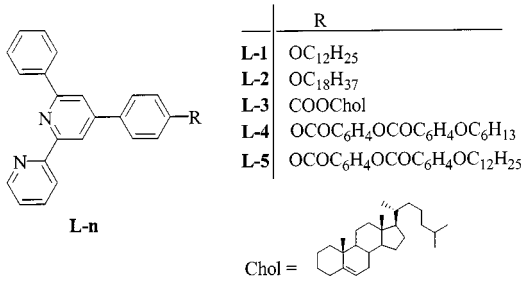
Keywords: Iridium / Amphiphiles / N ligands / Structure elucidation

The reaction of 4′-functionalized 6′-phenyl-2,2′-bipyridine ligands (**L-*n***) with the dimer $[(ppy)_2IrCl]_2$ (ppy = 2-phenylpyridine anion) and subsequent counterion exchange affords a new series of cationic orthometallated iridium(III) complexes, $[(ppy)_2Ir(L\text{-}n)][PF_6]$ (**1**–**5**), which have been characterized by spectroscopic methods. These complexes have a large shape anisotropy and significant amphiphilic character. The crystal structure of **4** has been determined by X-ray diffraction.

Introduction

The coexistence of distinct hydrophobic and hydrophilic moieties in the same structure is the key factor inducing segregation of dissimilar parts thus generating supramolecular anisotropic assemblies. In this light amphiphilic molecules, either neutral or ionic, are known to self-organise into a great variety of supramolecular structures both in solution and in the solid state.[1,2] On the other hand, since the incorporation of a transition metal ion into the polar part may impart additional features to the resulting amphiphile, metal coordination has been considered a simple way of preparing novel classes of amphiphiles. Recently, redox-active,[3,4] photo-active[3] or simply surface-active[5] amphiphilic complexes have been prepared. In addition, liquid-crystal behaviour has also been described for both thermotropic (temperature-active)[6,7] and lyotropic (concentration-active)[8] metal-containing amphiphiles.

We recently reported the synthesis of new 6′-phenyl-2,2′-bipyridines bearing promesogenic substituents in the 4′-position.[9] Our investigation showed that strongly anisometric, photoactive complexes with square-planar geometry could be obtained with these ligands,[9,10] which eventually exhibited liquid-crystalline properties.[11] In order to prepare new amphiphilic complexes, we have focused our attention on 6′-phenyl-2,2′-bipyridine ligands that bear highly hydrophobic substituents (**L-*n*** in Scheme 1) and which, at the same time, may afford species with a high aspect ratio (i.e. width-to-length ratio). Here we report on the synthesis and structural characterization of the series of Ir^{III} cationic complexes $[(ppy)_2Ir(\mathbf{L}\text{-}n)][PF_6]$ (**1**–**5**) which are based on the ligands **L-*n*** (n = 1–5) and which also contain the orthometallated $\{(ppy)_2Ir\}$ fragment (ppy = orthometallated 2-phenylpyridine). The synthesis of ligands **L-2** and **L-3** is also reported here for the first time.



Scheme 1

Anisometric Ligands

The functionalized **L-*n*** ligands present either alkoxy (–OR) or ester (–COOR or –OCOR) functions in the periphery of the *N*,*N*-chelating site (Scheme 1). Such an arrangement leads to the formation of ligands with a large anisometry (i.e. shape anisotropy) provided a terminal group ensures the right content of aliphatic carbon atoms.

Derivatization of the 6′-phenyl-2,2′-bipyridine moiety can be accomplished following two different synthetic strategies. The build-up of the 2,2′-bipyridine skeleton through a Kröhnke-type[12] synthesis may follow (see the preparation of **L-2**) or precede the introduction of the peripheral substituent usually through condensation reactions (as for **L-3**). The latter strategy seems to be more valuable since it potentially allows a wide variety of derivatives to be prepared.[11]

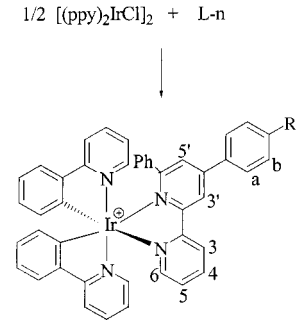
Orthometallated Iridium(III) Complexes

Bridge-splitting reactions of $[(ppy)_2IrCl]_2$ with *N*,*N*-chelating ligands are commonplace when the incorporation of the orthometallated $\{(ppy)_2Ir\}$ fragment into a mononuclear[13] or multinuclear[14] species is desired. Likewise, the cationic complexes **1**–**5** were obtained in good yield upon reaction of the dimer $[(ppy)_2IrCl]_2$ with the **L-*n*** ligands under reflux conditions in a dichloromethane/methanol mixture (Scheme 2). Metathesis of the chloride counterion with excess NH_4PF_6 gave the final products $[(ppy)_2Ir(L\text{-}n)][PF_6]$.

The ^1H NMR spectroscopic characterization of **1**–**5** showed that only a single isomer resulted from the reaction. From the NMR evidence it follows that both the pyridine

[a] Dipartimento di Chimica, Università della Calabria
I-87030 Arcavacata di Rende (CS), Italy
Fax: (internat.) + 39-0984/492-044
E-mail: f.neve@unical.it

 © WILEY-VCH Verlag GmbH, D-69451 Weinheim, 2000 1434−1948/00/0505−1039 $ 17.50+.50/0



1 – 5

	R
1	$OC_{12}H_{25}$
2	$OC_{18}H_{37}$
3	COOChol
4	$OCOC_6H_4OCOC_6H_4OC_6H_{13}$
5	$OCOC_6H_4OCOC_6H_4OC_{12}H_{25}$

Scheme 2

rings of **L** are involved in the coordination and no metallation has occurred. Although no attempt was made to assign all the resonances of the spectra (e.g. the proton spectrum of **3** shows some 19 distinct signals or groups of signals in the aromatic region), it is apparent that all the complexes belong to an isostructural series, where the two metallated ppy ligands for each complex experience through-space shielding effects different from each other.

Complexes **1**–**5** are insoluble in water, but reasonably soluble in dichloromethane or chloroform (with **1** and **2** showing the best solubility) affording air-stable solutions. All complexes are also very soluble in acetonitrile and solutions of **1**–**5** in this solvent were used to measure the electronic absorption spectra. The absorption spectra of all the complexes are dominated by a broad band peaking in the UV region and extending to the visible. The maximum of this band is around 270 nm, and receives its main contribution from ligand-centred LC transitions involving the metallated phenylpyridine ligands.[15] The absorptions which appear as shoulders of the main band probably arise from spin-allowed MLCT transitions. In particular spin-allowed Ir→(**L-*n***) CT transitions probably dominate the lowest energy portion of the spectra.[13,16,17] Finally, the very weak features reaching into the visible region may correspond to formally spin-forbidden MLCT transitions. A more detailed assignment of the electronic absorption spectra of **1**–**5** is, however, beyond the scope of the present work.

Crystal Structure of 4

Despite the poor tendency to crystallize of the remaining members of the series **1**–**5**, single crystals of **4** were easily obtained at ambient temperature by slow diffusion of methanol into chloroform solutions of the complex. An X-ray analysis showed the presence in the unit cell of two crystallographically independent molecules with similar metric parameters and the same configuration at the metal (Table 1). Figure 1 shows a perspective drawing of one of the cations (cation **1**).

Table 1. Selected bond lengths [Å] and angles [°] for complex **4**

Cation **1**		Cation **2**	
Ir(1)–N(1)	2.06(1)	Ir(2)–N(5)	2.05(1)
Ir(1)–N(2)	1.98(1)	Ir(2)–N(6)	2.07(1)
Ir(1)–N(3)	2.14(1)	Ir(2)–N(7)	2.16(1)
Ir(1)–N(4)	2.21(1)	Ir(2)–N(8)	2.24(1)
Ir(1)–C(6)	2.03(1)	Ir(2)–C(70)	2.02(1)
Ir(1)–C(17)	2.00(1)	Ir(2)–C(81)	2.05(1)
N(1)–Ir(1)–N(4)	96.6(4)	N(5)–Ir(2)–N(8)	93.7(4)
N(1)–Ir(1)–C(6)	82.8(6)	N(5)–Ir(2)–C(70)	80.7(4)
N(1)–Ir(1)–N(3)	87.9(4)	N(5)–Ir(2)–N(7)	93.3(4)
N(2)–Ir(1)–N(1)	171.9(4)	N(6)–Ir(2)–N(5)	169.7(4)
N(2)–Ir(1)–N(3)	99.4(4)	N(6)–Ir(2)–N(7)	96.0(4)
N(2)–Ir(1)–N(4)	88.7(4)	N(6)–Ir(2)–N(8)	92.7(4)
N(2)–Ir(1)–C(6)	93.1(6)	N(6)–Ir(2)–C(70)	94.4(3)
N(3)–Ir(1)–N(4)	75.9(4)	N(7)–Ir(2)–N(8)	75.6(4)
C(6)–Ir(1)–N(3)	94.0(5)	C(70)–Ir(2)–N(7)	93.8(3)
C(6)–Ir(1)–N(4)	169.9(5)	C(70)–Ir(2)–N(8)	167.7(3)
C(17)–Ir(1)–N(1)	92.5(5)	C(81)–Ir(2)–N(5)	89.7(5)
C(17)–Ir(1)–N(2)	79.9(5)	C(81)–Ir(2)–N(6)	80.7(5)
C(17)–Ir(1)–N(3)	175.3(4)	C(81)–Ir(2)–N(7)	174.4(4)
C(17)–Ir(1)–N(4)	108.7(4)	C(81)–Ir(2)–N(8)	109.0(4)
C(17)–Ir(1)–C(6)	81.4(5)	C(81)–Ir(2)–C(70)	82.1(4)

Although the study revealed several causes of disorder which affected the general accuracy, the molecular and crystal features are well established. The metal centre displays a slightly distorted octahedral geometry with *trans* angles at the Ir^{III} centre spanning the range 167–176°. The C-donor atoms of the metallated ppy ligands adopt a *cis* configuration as in the parent dimer,[18] showing a remarkable *trans*-influence which is in good agreement with similar observations on related complexes[13b,17,19,20]. The pyridine rings of the **L-4** ligand are almost coplanar (dihedral angle between the two mean planes of 10°), whereas the rotationally free 6′-phenyl ring is found to be nearly orthogonal to the mean plane of the coordinated **L-4** ligand (tilt angle of 82°). The hexyloxy chain of cation **1** deviates from a fully *trans*-planar conformation with the C(59)–C(60) and C(62)–C(63) bonds in a *gauche* conformation (66 and 69°, respectively). The corresponding chain of cation **2** shows a slightly different sequence of conformations (i.e. *tttgg*).

The mutual orientation between the two molecules in the asymmetric unit is such that the central pyridine ring of the **L-4** ligand of one cation faces the 4′-phenyl ring of the second cation thus resulting in a slipped *head*-to-*tail* arrangement. The packing diagram shows a layered structure with layers stacking along the *b* axis (Figure 2). In particular, the alternating tilt of the hydrocarbon chain axes along *b* generates a herringbone motif.

Thermal Behaviour of Complexes 1–5

Since some of the free **L-*n*** ligands are thermotropic liquid crystals,[11] we tried to ascertain whether complexes **1**–**5** displayed a thermotropic phase behaviour using thermal polarizing optical microscopy and differential scanning calorimetry (DSC) techniques. Although some notable differ-

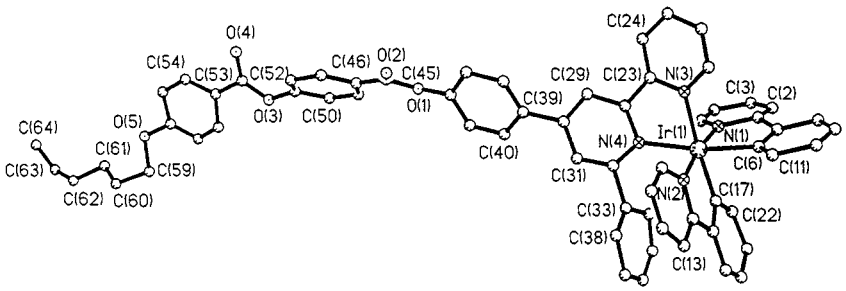


Figure 1. A perspective view and numbering scheme of cation **1** of complex **4**; all atoms are shown as arbitrarily sized circles; H atoms omitted for clarity

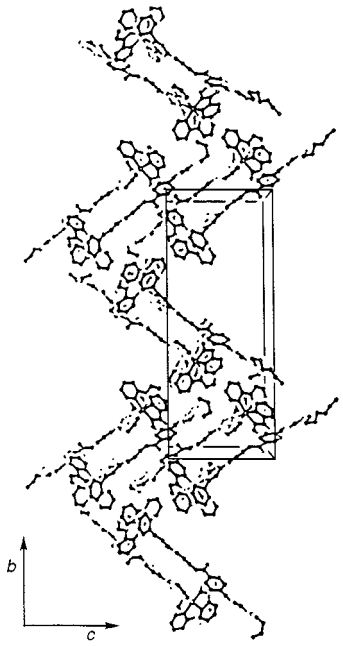


Figure 2. Packing diagram of **4** viewed down the *a* axis

ences were observed, both techniques confirmed the absence of liquid-crystalline behaviour along the whole series of complexes. Thus, while **1** and **4** clearly melt to an isotropic liquid, compounds **2** and **5** very smoothly become plastic solids on heating (above 140 and 170 °C, respectively) with fading birefringence. No clearing (or decomposition) is then observed till ca. 300°C, and cooling affords only glassy solids. The behaviour of **3** is even less clear, roughly matching that of **2**.

The above observations show that, whereas the cations $[(ppy)_2Ir(L\text{-}n)]^+$ possess a suitable polar/apolar ratio of their molecular parts which may guarantee phase separation, the bulkiness of the six-coordinate head-group in **1**–**5** somewhat reduces the structural anisotropy of the **L-*n*** ligands and no compensation for such a reduction is available from dipolar and/or dispersive interactions in the melt. In conclusion, we have prepared ionic metal-containing amphiphiles which failed to display mesogenic properties as pure species. Other properties are more predictable (e.g. photoluminescence) although unexplored. Attempts are in progress to design materials with improved properties.

Experimental Section

Materials and Methods: Ammonium acetate (Lancaster), 1-[2-oxo-2-(phenyl)ethyl]pyridinium bromide [hereafter *N*-(phenacyl)pyridinium bromide] (Lancaster), cholesterol (Lancaster), 1,3-dicyclohexylcarbodiimide (Aldrich) and 4-(pyrrolidino)pyridine (Aldrich) were used as received. The complex $[(ppy)_2IrCl]_2$ was prepared as described in the literature.[16a] The diester ligands 4′-{4-[4-(hexyloxybenzoyloxy)benzoyloxy]phenyl}-6′-phenyl-2,2′-bipyridine (**L-4**) and 4′-{4-[4-(dodecyloxybenzoyloxy)benzoyloxy]-phenyl}-6′-phenyl-2,2′-bipyridine (**L-5**) were obtained according to a method recently devised in our laboratory.[11] The synthesis of 4′-(4′′-carboxyphenyl)-6′-phenyl-2,2′-bipyridine to be used as starting material in the preparation of the ligand **L-3** has been reported elsewhere.[20] All reactions and manipulations of the complexes were performed in air. – ^{1}H NMR spectra were recorded at room temperature on a 300-MHz Bruker AC300 spectrometer. Chemical shifts are reported relative to internal TMS. – IR spectra were obtained as nujol mulls or KBr pellets on a Perkin–Elmer System-2000 FT-IR spectrophotometer. – Optical observations were carried out with a Zeiss Axioskop polarizing microscope equipped with a Linkam CO 600 heating stage and a temperature control unit. – Melting temperatures were measured by differential scanning calorimetry (DSC) with a Perkin–Elmer DSC-7. – Elemental analyses of the new complexes were performed by the Microanalytical Service of our department.

4′-(4′′-Octadecyloxyphenyl)-6′-phenyl-2,2′-bipyridine (L-2): The ligand **L-2** was prepared in a way similar to that for the previously reported **L-1**.[10] A solution of *N*-(phenacyl)pyridinium bromide (0.52 g, 1.88 mmol), 1-(2-pyridyl)-3-[4-(octadecyloxy)phenyl]propen-1-one (0.90 g, 1.88 mmol), and ammonium acetate (1.45 g, 18.8 mmol) in methanol (25 mL) was heated to reflux for 8 h. A brown precipitate was obtained after cooling the reaction mixture to 0 °C. Purification of the crude solid by column chromatography on SiO_2 (CH_2Cl_2 and diethyl ether as consecutive eluents) yielded the product after workup as a pinkish-brown flaky solid in low yield (18%). M.p. 92 °C. – ^{1}H NMR (300 MHz, $CDCl_3$): δ = 8.72 (br d, 1 H), 8.69 (d, J = 8.1 Hz, 1 H), 8.62 (d, J = 1.4 Hz, 1 H), 8.20 (m, 2 H), 7.96 (d, J = 1.4 Hz, 1 H), 7.86 (t d, J = 7.6 Hz, J = 5.0 Hz, J = 1.7 Hz, 1 H), 7.79 (d, J = 8.6 Hz, 2 H), 7.52 (m, 3 H), 7.34 (m, 1 H), 4.03 (t, 2 H, OCH_2), 1.80 (m, 2 H, OCH_2CH_2), 1.49–1.20 [m, 30 H, $(CH_2)_{15}$], 0.88 (t, 3 H, CH_3).

4′-[(Cholesteryloxycarbonyl)phenyl]-6′-phenyl-2,2′-bipyridine (L-3): Cholesterol (0.08 g, 0.2 mmol), 4′-(4′′-carboxyphenyl)-6′-phenyl-2,2′-bipyridine (0.07 g, 0.2 mmol), 1,3-dicyclohexylcarbodiimide (0.04 g, 0.2 mmol) and 4-(pyrrolidino)pyridine (0.004 g, 0.03 mmol) were suspended in degassed CH_2Cl_2 (30 mL) and stirred under a dry nitrogen atmosphere for 24 h. A white precipitate was removed

by filtration, and the colourless filtrate was consecutively washed with 5% acetic acid (20 mL) and water (2 × 20 mL). The organic phase was dried over sodium sulfate and rotary-evaporated to dryness. The desired product was obtained as a white solid after purification of the solid residue by column chromatography (SiO_2, CH_2Cl_2/3% MeOH). Yield: 31%. – IR (KBr): $\tilde{\nu}$ = 1716 cm^{-1} (CO). – ^1H NMR (300 MHz, $CDCl_3$): δ = 8.74–8.69 (m, 2 H), 8.66 (br s, 1 H), 8.23–8.17 (m, 4 H), 8.00 (br s, 1 H), 7.90–7.86 (m, 3 H), 7.57–7.45 (m, 3 H), 7.36 (m, 1 H), 5.44 (br d, 1 H, chol.), 4.92 (m, 1 H, chol.), 2.53–0.68 (m, 43 H, chol.).

General Procedure for the Synthesis of the Complexes 1–5: A stirred suspension of the appropriate ligand (0.06 mmol) and $[(ppy)_2IrCl]_2$ (0.03 mmol) in CH_2Cl_2/MeOH (10 ml; 6:4) was heated to reflux. Clear orange or brown solutions were observed within 10 min. After 2 h, the solution was allowed to cool to ambient temperature. Then, a saturated solution of a five-fold excess (based on the ligand) of NH_4PF_6 in MeOH was added and stirring was continued for a further 30 min. The products were isolated after partial evaporation of the solvents under reduced pressure, washed with methanol and diethyl ether, and dried in vacuo.

[(ppy)$_2$Ir(L-1)][PF$_6$] (1): Yield: 65%, brown powder. – M.p. (DSC) 187 °C. – IR (KBr): $\tilde{\nu}$ = 842 cm^{-1} (PF) cm^{-1}. – UV/Vis (acetonitrile): λ_{max} (log ε) = 271 nm (4.64), 315sh (4.52), 383sh (4.02). – ^1H NMR (300 MHz, CD_3CN): δ = 8.88 (d, *J* = 8.2 Hz, 1 H, 3-H), 8.83 (br s, 1 H, 3′-H), 8.19 (br t, 1 H, 4-H), 7.92 (d, *J* = 8.6 Hz, 2 H, a-H), 7.81–7.69 (m, 6 H), 7.54 (br s, 1 H, 5′-H), 7.48 (d, *J* = 7.5 Hz, 1 H), 7.31 (br m, 1 H, 5-H), 7.20 (d, *J* = 7.6 Hz, 1 H), 7.10–7.05 (m, 3 H), 6.95–6.88 (m, 2 H), 6.81–6.70 (m, 3 H), 6.59–6.54 (m, 2 H), 6.36 (br t, 1 H), 5.93 (d, *J* = 7.5 Hz, 1 H), 5.57 (d, *J* = 7.5 Hz, 1 H), 4.03 (t, 2 H, OCH_2), 1.80 (m, 2 H, OCH_2CH_2), 1.46–1.27 (m, 18 H, $(CH_2)_9$), 0.88 (t, 3 H, CH_3). – $C_{56}H_{56}F_6IrN_4OP$ (1138): calcd. C 59.09, H 4.92, N 4.92; found C 58.72, H 5.23, N 5.10.

[(ppy)$_2$Ir(L-2)][PF$_6$] (2): Yield (after chromatography on silica gel with CH_2Cl_2/5% MeOH as eluent): 24%, orange-brown powder. – IR (KBr): $\tilde{\nu}$ = 843 cm^{-1} (PF). – UV/Vis (acetonitrile): λ_{max} (log ε) = 272 nm (4.63), 314sh (4.49), 377sh (4.01). – ^1H NMR ($CDCl_3$): δ = 8.86 (d, *J* = 7.9 Hz, 1 H, 3-H), 8.81 (d, *J* = 2.0 Hz, 1 H, 3′-H), 8.17 (br t, 1 H, 4-H), 7.91 (d, *J* = 8.8 Hz, 2 H, a-H), 7.85–7.67 (m, 6 H), 7.54 (br s, 1 H, 5′-H), 7.47 (d, *J* = 7.0 Hz, 1 H), 7.30 (br m, 1 H, 5-H), 7.19 (d, *J* = 7.0 Hz, 1 H), 7.07–7.04 (m, 3 H), 6.94–6.87 (m, 2 H), 6.80–6.70 (m, 3 H), 6.58–6.53 (m, 2 H), 6.35 (br t, 1 H), 5.92 (d, *J* = 7.9 Hz, 1 H), 5.57 (d, *J* = 7.9 Hz, 1 H), 4.01 (t, 2 H, OCH_2), 1.79 (m, 2 H, OCH_2CH_2), 1.45–1.25 [m, 30 H, $(CH_2)_{15}$], 0.87 (t, 3 H, CH_3). – $C_{62}H_{68}F_6IrN_4OP$ (1222): calcd. C 60.92, H 5.61, N 4.58; found C 61.08, H 5.78, N 4.34.

[(ppy)$_2$Ir(L-3)][PF$_6$] (3): Yield: 81%, orange powder. – IR (KBr): $\tilde{\nu}$ = 1716 cm^{-1} (CO), 842 (PF). – UV/Vis (acetonitrile): λ_{max} (log ε) = 270 nm (4.44), 317sh (4.08), 386sh (3.57). – ^1H NMR (300 MHz, CD_3CN): δ = 8.82 (d, *J* = 2.0 Hz, 1 H, 3′-H), 8.74 (d, *J* = 7.8 Hz, 1 H, 3-H), 8.20 (d, *J* = 8.9 Hz, 2 H, b-H), 8.16 (t, *J* = 7.8 Hz, 1 H, 4-H), 8.08 (d, *J* = 8.9 Hz, 2 H, a-H), 7.96–7.89 (m, 4 H), 7.84 (d, *J* = 6.0 Hz, 2 H), 7.79 (d, *J* = 2.0 Hz, 1 H, 5′-H), 7.69 (d, *J* = 5.9 Hz, 1 H), 7.61 (d, *J* = 7.8 Hz, 1 H), 7.13–7.07 (m, 2 H), 6.98–6.92 (m, 2 H), 6.82 (t, *J* = 7.0 Hz, 1 H), 6.77 (t, *J* = 7.8 Hz, 2 H), 6.65 (br s, 2 H), 6.57 (t, *J* = 7.0 Hz, 1 H), 6.37 (d, *J* = 7.4 Hz, 1 H), 5.96 (d, *J* = 7.0 Hz, 1 H), 5.57 (d, *J* = 7.0 Hz, 1 H), 5.45 (d, *J* = 4.9 Hz, 1 H, chol.), 4.81 (m, 1 H, chol.), 2.5–0.7 (m, 43 H, chol.). – $C_{72}H_{76}F_6IrN_4O_2P$ (1366): calcd. C 63.28, H 5.61, N 4.10; found C 63.02, H 5.62, N 4.12.

[(ppy)$_2$Ir(L-4)][PF$_6$] (4): Yield: 80%, bright yellow powder. – M.p. (DSC) 288 °C. – IR (KBr): $\tilde{\nu}$ = 1740, 1733 cm^{-1} (CO), 840 (PF). – UV/Vis (acetonitrile): λ_{max} (log ε) = 270 nm (4.61), 320sh (4.14), 380sh (3.60). – ^1H NMR (300 MHz, CD_3CN): δ = 8.83 (br s, 1 H, 3′-H), 8.74 (d, *J* = 8.2 Hz, 1 H, 3-H), 8.31 (d, *J* = 8.5 Hz, 2 H), 8.22–8.02 (m, 5 H), 7.98–7.83 (m, 6 H), 7.80 (br s, 1 H, 5-H), 7.68 (d, *J* = 5.7 Hz, 1 H), 7.61 (d, *J* = 7.6 Hz, 1 H), 7.54–7.44 (m, 5 H), 7.31 (d, *J* = 7.8 Hz, 1 H), 7.17–7.06 (m, 4 H), 6.95 (m, 2 H), 6.83 (br t, 1 H), 6.77 (t, *J* = 7.8 Hz, 2 H), 6.66 (v br s, 2 H), 6.58 (t, *J* = 7.4 Hz, 1 H), 6.38 (t, *J* = 7.4 Hz, 1 H), 5.97 (d, *J* = 7.7 Hz, 1 H), 5.58 (d, *J* = 7.7 Hz, 1 H), 4.12 (t, 2 H, OCH_2), 1.80 (m, 2 H, OCH_2CH_2), 1.41–1.36 [m, 6 H, $(CH_2)_3$], 0.94 (t, 3 H, CH_3). – $C_{64}H_{52}F_6IrN_4O_5P$ (1294): calcd. C 59.39, H 4.05, N 4.33; found C 59.30, H 4.17, N 4.21.

[(ppy)$_2$Ir(L-5)][PF$_6$] (5): Yield: 75%, brownish orange powder. – IR (KBr): $\tilde{\nu}$ = 1736 cm^{-1} (CO), 842 (PF). – UV/Vis (acetonitrile): λ_{max} (log ε) = 270 nm (4.71), 321sh (4.27), 381sh (3.72). – ^1H NMR (300 MHz, CD_3CN): δ = 8.83 (br s, 1 H, 3′-H), 8.74 (d, *J* = 8.2 Hz, 1 H, 3-H), 8.31 (d, *J* = 8.5 Hz, 2 H), 8.18–8.02 (m, 5 H), 7.98–7.83 (m, 6 H), 7.80 (d, *J* = 1.8 Hz, 1 H, 5′-H), 7.66 (d, *J* = 5.8 Hz, 1 H), 7.63 (d, *J* = 8.0 Hz, 1 H), 7.53–7.43 (m, 5 H), 7.30 (d, *J* = 8.0 Hz, 1 H), 7.17–7.06 (m, 4 H), 6.95 (m, 2 H), 6.83 (t, *J* = 7.7 Hz, 1 H), 6.76 (t, *J* = 7.8 Hz, 2 H), 6.65 (v br s, 2 H), 6.57 (t, *J* = 7.6 Hz, 1 H), 6.37 (t, *J* = 7.4 Hz, 1 H), 5.96 (d, *J* = 7.7 Hz, 1 H), 5.58 (d, *J* = 7.5 Hz, 1 H), 4.07 (t, 2 H, OCH_2), 1.81 (m, 2 H, OCH_2CH_2), 1.45–1.28 [m, 18 H, $(CH_2)_9$], 0.89 (t, 3 H, CH_3). – $C_{70}H_{64}F_6IrN_4O_5P$ (1378): calcd. C 60.99, H 4.68, N 4.06; found C 60.56, H 4.57, N 4.27.

Crystal Structure Determination: Diffraction data for complex **4** were collected on a Siemens (Bruker) SMART area detector diffractometer by using graphite-monochromated Mo-K_α radiation (λ = 0.71073 Å) with the ω-2θ method (*T* = 163 K). Data were corrected for absorption (SADABS)[21] and Lorentz-polarization effects. The structure was solved by direct methods using SHELXS-97[22] and refined by full-matrix least-squares on F^2 (SHELXL-97).[22] Crystal data and structure refinements parameters are given in Table 2. All nonhydrogen atoms were refined anisotropically. Hydrogen atoms were placed in calculated positions with fixed contri-

Table 2. Crystal data, data collection parameters, solution and refinement for complex **4**

Empirical formula	$C_{64}H_{52}F_6IrN_4O_5P$
Formula weight	1294
Crystal system	monoclinic
Space group	$P2_1/c$
a [Å]	22.037(11)
b [Å]	34.821(22)
c [Å]	13.987(6)
α [°]	90
β [°]	90.38(4)
γ [°]	90
V [Å^3]	10733(10)
Z	8
$d_{calcd.}$ [g cm^{-3}]	1.602
Crystal size [mm]	0.19 × 0.15 × 0.08
μ [mm^{-1}]	2.596
Transmission (min/max)	0.701/0.928
2θ range [°]	3.0–50
Index range (*h*, *k*, *l*)	–26 26, –41 41, –16 16
Reflections collected	93561
Independent reflections	18890
Observed reflections [$I > 2\sigma(I)$]	11149
Parameters	1368
Final *R* indices	*R*1 = 0.0903, *wR*2 = 0.1631
R indices (all data)	*R*1 = 0.1569, *wR*2 = 0.1760
Goodness-of-fit on F^2	1.562

butions (U = 0.08 Å^2). The two sets of C atoms [C(33) through C(38)] and [C(97) through C(102)] have been refined as rigid regular hexagons with default C–C bond lengths of 1.39 Å.

Crystallographic data (excluding structure factors) for the structure included in this paper have been deposited with the Cambridge Crystallographic Data Centre as supplementary publication no. CCDC-112438. Copies of the data can be obtained free of charge on application to CCDC, 12 Union Road, Cambridge CB2 1EZ, UK [Fax: (internat.) + 44-1223/336-033; Email: deposit@ccdc.cam.ac.uk].

Acknowledgments

Financial support from the Italian Ministero dell′Università e della Ricerca Scientifica e Tecnologica (MURST) and Consiglio Nazionale delle Ricerche (CNR) is gratefully acknowledged. The authors are also grateful to Jonathan Charmant and Professor G. A. Orpen (University of Bristol) and to Professor P. Dapporto (University of Florence) for X-ray data collection and helpful comments.

[1] F. Vögtle, *Supramolecular Chemistry*, Wiley, Chichester, UK, **1991**; J. M. Lehn, *Supramolecular Chemistry: Concepts and Perspectives*, VCH, Weinheim, **1995**.

[2] J.-H. Fuhrhop, J. Köning, *Membranes and Molecular Assemblies: the Synkinetic Approach*, The Royal Society of Chemistry, Cambridge, **1994**.

[3] V. W.-W. Yam, V. C.-Y. Lau, K.-Z. Wang, K.-K. Cheung, *J. Mater. Chem.* **1998**, *8*, 89–97.

[4] H. Masui, R. W. Murray, *Inorg. Chem.* **1997**, *36*, 5118–5126.

[5] I. A. Fallis, P. C. Griffiths, D. E. Hibbs, M. B. Hursthouse, A. L. Winnington, *Chem. Commun.* **1998**, 665–666.

[6] F. Neve, M. Ghedini, G. De Munno, A.-M. Levelut, *Chem. Mater.* **1995**, *7*, 688–693.

[7] F. Neve, *Adv. Mater.* **1996**, *8*, 277–289.

[8] J. D. Holbrey, G. J. T. Tiddy, D. W. Bruce, *J. Chem. Soc., Dalton Trans.* **1995**, 1769–1774.

[9] F. Neve, M. Ghedini, A. Crispini, *Chem. Commun*. **1996**, 2463–2464.

[10] F. Neve, A. Crispini, S. Campagna, *Inorg. Chem*. **1997**, *36*, 6150–6156.

[11] F. Neve, M. Ghedini, O. Francescangeli, S. Campagna, *Liq. Cryst.* **1998**, *24*, 673–680.

[12] F. Kröhnke, *Synthesis* **1976**, 1–24.

[13] [13a] Y. Ohsawa, S. Sprouse, K. A. King, M. K. De Armond, K. W. Hanck, R. J. Watts, *J. Phys. Chem.* **1987**, *91,* 1047–1054. – [13b] J. H. van Diemen, J. G. Haasnoot, R. Hage, E. Müller, J. Reedijk, *Inorg. Chim. Acta* **1991**, *181*, 245–251. – [13c] P. Didier, L. Ortmans, A. Kirsch-De Mesmaeker, R. J. Watts, *Inorg. Chem.* **1993**, *32,* 5239–5245. – [13d] G. Calogero, G. Giuffrida, S. Serroni, V. Ricevuto, S. Campagna, *Inorg. Chem.* **1995**, *34*, 541–545.

[14] J. H. van Diemen, R. Hage, H. E. B. Lempers, J. Reedijk, J. G. Vos, L. De Cola, F. Barigelletti, V. Balzani, *Inorg. Chem.* **1992**, *31*, 3518–3522. – S. Serroni, A. Juris, S. Campagna, M. Venturi, G. Denti, V. Balzani, *J. Am. Chem. Soc.* **1994**, *116*, 9086–9091.

[15] M. Maestri, V. Balzani, C. Deuschel-Cornioley, A. von Zelewsky, *Adv. Photochem.* **1992**, *17,* 1–68.

[16] [16a] S. Sprouse, K. A. King, P. J. Spellane, R. J. Watts, *J. Am. Chem. Soc*. **1984**, *106*, 6647–6653. – [16b] K. A. King, R. J. Watts, *J. Am. Chem. Soc*. **1987**, *109*, 1589–1590. – [16c] F. O. Garces, K. A. King, R. J. Watts, *Inorg. Chem*. **1988**, *27*, 3464–3471. – [16d] B. Schmid, F. O. Garces, R. J. Watts, *Inorg. Chem.* **1994**, *33,* 9–14.

[17] M. G. Colombo, T. C. Brunold, T. Riedner, H. U. Güdel, M. Förtsch, H.-B. Bürgi, *Inorg. Chem.* **1994**, *33*, 545–550.

[18] F. O. Garces, K. Dedeian, N. L. Keder, R. J. Watts, *Acta Crystallogr.* **1993**, *C49*, 1117–1120.

[19] R. Urban, R. Kramer, S. Mihan, K. Polborn, B. Wagner, W. Beck, *J. Organomet. Chem.* **1996**, *517*, 191–200.

[20] F. Neve, A. Crispini, S. Campagna, S. Serroni, *Inorg. Chem*. **1999**, *38*, 2250–2258.

[21] G. M. Sheldrick, *SADABS, Program for Empirical Absorption Correction*, Universität Göttingen, **1997**.

[22] G. M. Sheldrick, *SHELXL-97*, *Program for Crystal Structure Refinement*, Universität Göttingen, **1997**; *SHELXS-97*, *Program for Crystal Structure Solution*, Universität Göttingen, **1997**.

Received October 15, 1999
[I99364]

Synthesis and Chemistry of Dithiadiazole Free Radicals [4-(4′-C_5H_4N)CN_2S_2] and [4-(3′-C_5H_4N)CN_2S_2]; X-ray Crystal Structures of [Pd_3{μ-SNC(Ar′)NS–*S*,*S*′}$_2$(PPh_3)$_4$] (Ar′ = 4′-C_5H_4N, 4′-$C_5H_4NBEt_3$ and 3′-$C_5H_4NBEt_3$)

Wai-Kwok Wong,*[a] Chaode Sun,[a] Wai-Yeung Wong,[a] Daniel W. J. Kwong,[a] and Wing-Tak Wong[b]

Keywords: Palladium / Dithiadiazole / Radicals

Two new 1,2,3,5-dithiadiazoles, [4-(4′-C_5H_4N)CN_2S_2] (**L¹**) and [4-(3′-C_5H_4N)CN_2S_2] (**L²**), with different pyridyl groups at the 4-position were prepared. As Lewis bases, the dithiadiazoles reacted with Lewis acids via their pyridyl groups to form acid-base adducts with retention of the five-membered dithiadiazole ring. Ligands **L¹** and **L²** reacted with excess triethylborane to give **L¹**BEt_3 and **L²**BEt_3 (**1a** and **1b**) and with $Mn(CO)_5Br$ to give the *fac*-$Mn(CO)_3Br(L^1)_2$ (**2a**) and *fac*-$Mn(CO)_3Br(L^2)_2$ (**2b**) complexes. When reacted with Pd^0 complexes, namely, $Pd(PPh_3)_4$ and a mixture of $[Pd_2(dba)_3]$ and dppf, the dithiadiazoles underwent ring-opening reaction by reductive cleavage of the S–S bond of the dithiadiazole ring. The resulting formation of Pd–S bonds gave the corresponding trinuclear complexes [Pd_3{μ-SNC(4′-C_5H_4N)NS-*S*,*S*′}$_2$(PPh_3)$_4$] (**3a**), [Pd_3{μ-SNC(3′-C_5H_4N)NS-*S*,*S*′}$_2$(PPh_3)$_4$] (**3b**), and [Pd_3{μ-SNC(4′-C_5H_4N)NS-*S*,*S*′}$_2$(dppf)$_2$] (**4**) [dba = dibenzylideneacetone, dppf = 1,1′-bis(diphenylphosphanyl)-ferrocene]. Complexes **3a** and **3b** reacted with excess triethylborane to give the corresponding acid-base adducts [Pd_3{μ-SNC(4′-$C_5H_4NBEt_3$)NS-*S*,*S*′}$_2$(PPh_3)$_4$] (**5a**) and [Pd_3{μ-SNC(3′-$C_5H_4NBEt_3$)NS-*S*,*S*′}$_2$(PPh_3)$_4$] (**5b**.) Complex **3a** reacted with $Mn(CO)_5Br$ to give {[Pd_3{μ-SNC(4′-C_5H_4N)NS-*S*,*S*′}$_2$(PPh_3)$_4$][$MnBr(CO)_3$]}$_n$ (**6**). The structures of **3a**, **5a**, and **5b** were established by X-ray crystallography.

Introduction

1,2,3,5-Dithiadiazoles belong to a remarkable and new class of stable free radicals which exist as a monomer–dimer equilibrium in the solid state and in solution.[1–10] These radicals have attracted special attention because they can act as molecular building blocks in the preparation of both conducting materials and "organic" magnets. Another interesting property is their ability to act as chelating or bridging ligands for transition metals. When reacted with low-valent transition metal complexes, the radical species underwent reductive cleavage of the S–S bond of the dithiadiazolyl ring with the formation of metal–sulfur bonds. However, so far only the reactivity of the phenyl derivative $(PhCNSSN)_2$ toward low-valent transition metal complexes has been studied.[11–15]

In this paper, we report the syntheses of two new 1,2,3,5-dithiadiazoles with different pyridyl groups at the 4-position and their reactivities toward low-valent transition metal complexes. These ligands have two different reactive sites, namely, the pyridyl group and the dithiadiazolyl ring. When reacted via the pyridyl group, these ligands simply act as Lewis bases with ring-retention. When reacted via the dithiadiazolyl group, these ligands undergo ring-opening reaction with the cleavage of the S–S bond and the formation of metal–sulfur bonds.

[a] Department of Chemistry, Hong Kong Baptist University, Waterloo Road, Kowloon Tong, Hong Kong
Fax: (internat.) + 852/2339-7348
E-mail: wkwong@hkbu.edu.hk
[b] Department of Chemistry, The University of Hong Kong, Pokfulam Road, Hong Kong

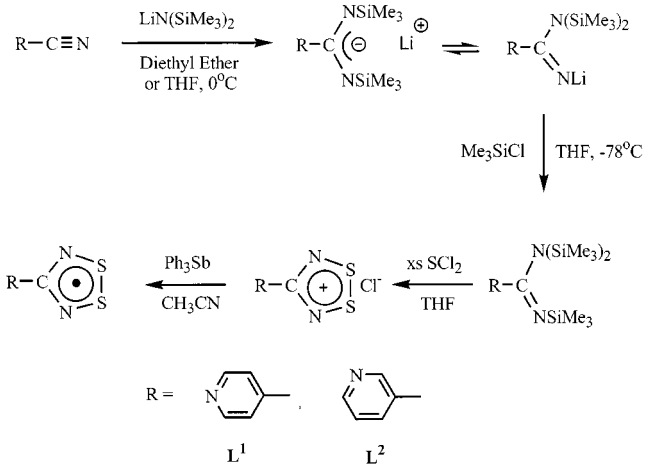
Results and Discussion

Preparation of L^1 and L^2

The compounds [4-(4′-NC_5H_4)CN_2S_2] (**L¹**) and [4-(3′-NC_5H_4)CN_2S_2] (**L²**) were prepared according to the synthetic routes shown in Scheme 1, in low to moderate yields (33% for **L¹**; 50% for **L²**) as black solids after sublimation. Both compounds are only slightly soluble in common organic solvents and are sensitive to air and moisture. The IR spectra (KBr) of ligands **L¹** and **L²** showed the characteristic absorption peaks for substituted dithiadiazole ring at 1140 (m), 810 (s), 656 (s), 510 (m), and 1146 (m), 809 (s), 667 (s), 511 (m) cm^{-1}, respectively.[1] The low-resolution mass spectra (LRMS) of **L¹** and **L²** operated in EI mode exhibited the highest mass peak at *m*/*z* 364 with the most abundant peak at *m*/*z* 182 corresponding to the dimer $[(NC_5H_4)CN_2S_2]_2$ and the monomer $[(NC_5H_4)CN_2S_2]$, respectively. The solid-state EPR spectra of **L¹** and **L²** both displayed a broad peak compared with the diphenyl picrylhydrazyl (DPPH) standard. The *g*-value was determined to be 2.014 which is characteristic of a single unpaired electron. It is likely that dissociation of $(RCN_2S_2)_2$ (R = 4-pyridyl and 3-pyridyl) to the monomer, similar to that observed in $(PhCN_2S_2)_2$[16] and $[S_6N_4]^{2+}$ salts,[17,18] takes place in the solid state.

Both **L¹** and **L²** exhibited concentration- and temperature-dependent solution EPR spectra. At their saturated concentration in toluene, the room temperature solution EPR spectra of both **L¹** and **L²** showed a broad peak at $g = 2.014$. However, when the solution was diluted ten-fold, the EPR spectra exhibited a simple 1:2:3:2:1 quintuplet pattern. These observations are indicative of the occurrence of

 © WILEY-VCH Verlag GmbH, D-69451 Weinheim, 2000 1434–1948/00/0505–1045 $ 17.50+.50/0



Scheme 1

an electron spin exchange process, commonly observed in free radical systems in solution, where two radicals collide and exchange electrons. At saturated concentration, the rate of this bi-molecular process is very high, resulting in a severe broadening of the EPR resonances. With a ten-fold dilution, the rate of this bi-molecular exchange became sufficiently slow that the intrinsic EPR resonances of the free radicals were not significantly affected and the hyperfine splitting pattern became observable. The 1:2:3:2:1 hyperfine splitting pattern of **L¹** and **L²** suggested that the unpaired electron was delocalized over the five-membered ring and coupled to the two equivalent ^{14}N nuclei. The observation of a *g*-factor of 2.014 together with a hyperfine coupling constant *A* of ca. 0.50 mT indicates that the pyridyl group does not exert any significant effect on the single unpaired electron on the dithiadiazole ring. The solution became EPR-silent when cooled down to liquid-nitrogen temperature (i.e., –196°C), suggesting that **L¹** and **L²** no longer exist as monomers at this temperature. Since an eclipsed dimeric structure has been found for the analogous 4-phenyl-1,2-dithia-3,5-diazole in its crystalline state,[19] the formation of such a dimeric structure for both **L¹** and **L²** at –196°C, which will allow for an antiferromagnetic coupling between the two unpaired electrons on the two 5-membered rings, could well explain the quenching of the EPR signals observed at this temperature.

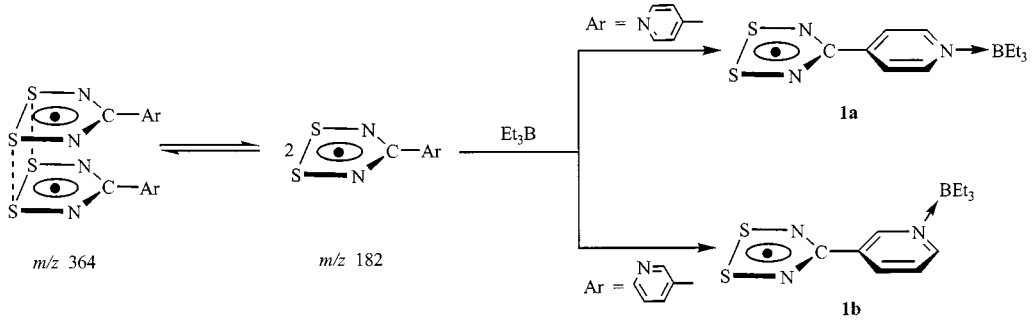
Reaction with Triethylborane

When a suspension of **L¹** or **L²** was allowed to react with excess triethylborane in dichloromethane or toluene at ambient temperature, a dark-red clear solution was immediately obtained. The EPR behaviour of the resultant solution was very similar to that of **L¹** or **L²**. The EPR spectra exhibited a single peak at $g = 2.014$ and after dilution with a relevant solvent, a quintet signal with an intensity pattern of 1:2:3:2:1 and a *g* value of 2.014 ($A = 0.50$ mT). Attempts to isolate the products in pure crystalline form only led to the isolation of an air-sensitive dark-red viscous oil. The EPR data showed that the products retained the characteristics of the dithiadiazolyl ring. This suggested that the products were probably the acid-base adducts **L¹** · BEt_3 (**1a**) and **L²** · BEt_3 (**1b**), which were formed by the interaction of the pyridyl group of **L¹** and **L²** with triethylborane as shown in Scheme 2. However, this could not preclude the possibility that triethylborane also formed acid-base adducts with the dimers of **L¹** and **L²**.

Reaction with $Mn(CO)_5Br$

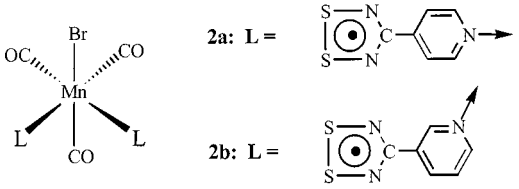
When ligand **L¹** was allowed to react with an excess of $Mn(CO)_5Br$ in tetrahydrofuran at 55 °C for 4 h, workup gave the stoichiometric product $C_{15}H_8BrMnN_6O_3S_4 \cdot 2.5\ H_2O$ (**2a** · 2.5 H_2O), as reddish-brown tiny crystals, in moderate yield (56%). In the carbonyl region of its IR spectrum (KBr), **2a** exhibited three very strong absorptions at 2030, 1942, and 1909 cm^{-1}, characteristic of a *fac*-$Mn(CO)_3$ configuration. Complex **2a** exhibited a broad peak and a quintuplet with a relative intensity pattern of 1:2:3:2:1 in its solid state and tetrahydrofuran solution EPR spectra, respectively. The measured *g* value of 2.014 indicates the presence of a single electron and the five-line pattern ($A = 0.50$ mT) observed was due to the coupling of the single electron with two equivalent ^{14}N nuclei in the dithiadiazolyl ring. The EPR spectra of **2a** were similar to those of **L¹**, indicating retention of the dithiadiazolyl ring. LRMS (EI mode) of **2a** exhibited a peak at *m/z* 182 for **L¹** while the parent peak of **2a** was not observed. Based on the above spectroscopic and analytical data, compound **2a** could be formulated as *fac*-$Mn(CO)_3Br(\mathbf{L^1})_2$.

Similarly, when **L²** was allowed to react with $Mn(CO)_5Br$, work up gave the reddish-brown stoichiometric solid $C_{15}H_8BrMnN_6O_3S_4 \cdot H_2O$ (**2b** · H_2O) in good yield (75%).



Scheme 2

The spectroscopic data of **2b** were very similar to those of **2a**. In the carbonyl region of its IR spectrum (KBr), **2b** showed three very strong absorptions at 2028, 1947, and 1912 cm^{-1}, characteristic of a *fac*-$Mn(CO)_3$ configuration. Compound **2b** also exhibited a broad peak and a quintet with an intensity pattern of 1:2:3:2:1 in its solid state and tetrahydrofuran solution EPR spectra, respectively. The measured *g*-value was 2.014 with the hyperfine coupling constant $A = 0.51$ mT. Compound **2b** was also formulated as *fac*-$Mn(CO)_3Br(\mathbf{L^2})_2$.

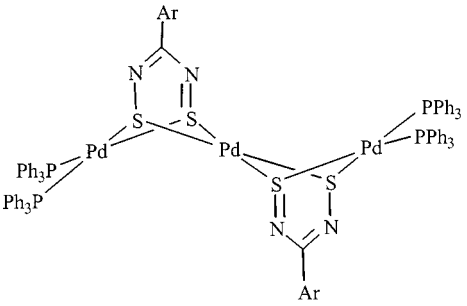


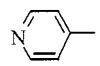
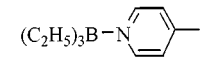
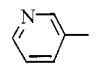
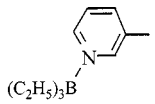
Preparation of $[Pd_3\{\mu\text{-SNC(Ar}')\text{NS–}S,S'\}_2(PPh_3)_4]$

Ar′ = 4′-C_5H_4N

When $\mathbf{L^1}$ was allowed to react with 4 equivalents of $Pd(PPh_3)_4$ in toluene for 4 h at ambient temperature, workup gave red crystals of $(Ph_3P)_4Pd_3(C_{12}H_8N_6S_4) \cdot 0.25\,CH_2Cl_2$, **3a** · $0.25\,CH_2Cl_2$, in good yield (70%) after recrystallization from a dichloromethane solution. In the IR spectrum of **3a**, absorption corresponding to $\mathbf{L^1}$ (characterized by strong absorptions at 1140, 810, 656, and 510 cm^{-1}) were not observed. Instead three strong absorptions at 1434, 691, and 527 cm^{-1} were detected. This IR spectrum was indicative of a ring opening reaction between the two sulfur-sulfur atoms. In addition to the pyridyl and phenyl carbons, the $^{13}C\text{-}\{^1H\}$ NMR spectrum of **3a** gave a singlet at $\delta = 174.0$ for the C=N carbon of the amidine group. The ^1H-NMR spectrum of **3a** showed resonances at $\delta = 8.52$ (dd, 4 H, $J = 4.6$, 1.6 Hz) and 8.11 (dd, 4 H, $J = 4.6$, 1.6 Hz) for the pyridyl α- and β-protons, respectively, and at $\delta = 7.12$ (t, 12 H, $J = 7.3$ Hz), 6.97 (t, 24 H, $J = 7.3$ Hz), and 6.83 (m, 24 H) for the phenyl protons. The $^{31}P\text{-}\{^1H\}$ NMR spectrum of **3a** in $CDCl_3$ exhibited only a singlet at $\delta = 27.5$ for the PPh_3 groups, indicating that all the triphenylphosphane groups were equivalent. LRMS (positive FAB) of **3a** exhibited a parent peak at *m/z* 1731 [(M + 1) for ^{106}Pd]. Based on the above spectroscopic data, compound **3a** could be formulated as $[Pd_3\{\mu\text{-SNC(4}'\text{-}C_5H_4N)\text{NS-}S,S'\}_2(PPh_3)_4]$ with a structure similar to that of $[Pd_3\{\mu\text{-SNC(Ph)NS-}S,S'\}_2(PPh_3)_4]$ as shown below.[15] This was confirmed by an X-ray crystallographic study.

Crystals of **3a** · 2 $(C_2H_5)_2O$ suitable for X-ray diffraction study were grown from a dichloromethane/diethyl ether mixture. A perspective drawing of **3a** is shown in Figure 1 and selected bond lengths and angles are given in Table 1. The solid state structure of **3a** is consistent with its spectroscopic data. The structure of **3a** is composed of a linear Pd_3 chain bridged by two SNC(4-C_5H_4N)NS ligands in which the terminal Pd atoms are related through a crystallographic inversion center at Pd(2). Both Pd(1) and Pd(2)



3a: Ar = 
5a: Ar = 
3b: Ar = 
5b: Ar = 

atoms possess a square planar geometry. The terminal Pd atoms have a PdP_2S_2 environment whereas the central Pd is bound only to the dithiadiazolyl S atoms, thus producing a PdS_4 coordination geometry. This structure is analogous to those of $[Pt_3\{\mu\text{-SNC(Ph)NS-}S,S'\}_2(PPh_3)_4]$ and $[Pd_3\{\mu\text{-SNC(Ph)NS-}S,S'\}_2(PPh_3)_4]$ reported previously.[15] In **3a**, the dithiadiazolyl ligands take up a bridging mode between Pd(1) and Pd(2) with a Pd···Pd distance of 2.852(1) Å. Such metal–metal distance is slightly longer than the sum of the metallic radii (2.76 Å for Pd), suggesting that no metal-metal bond exists.

As a bridging ligand, the S–S bond in the dithiadiazolyl ring has been broken. The S(1)–N(1) and S(2)–N(2) distances are 1.64(1) and 1.65(1) Å, respectively. The N(1)–C(1) and N(2)–C(1) distances of 1.34(1) and 1.331(1) Å, respectively, are also intermediate between those expected for carbon-nitrogen single (1.46 Å) and double (1.26 Å) bonds. All these indicate some degree of electron delocalization about the SNCNS framework. This delocalization is also reflected in the S(1)–N(1)–C(1) and S(2)–N(2)–C(1) bond angles of 125.6(9) and 124.2(9)°, respectively, which deviate significantly from that expected for a tetrahedral sp^3 nitrogen atom and are closer to a sp^2 nitrogen atom.

Ar′ = 3′-C_5H_4N

When two equivalents of $\mathbf{L^2}$ were allowed to react with 3 equivalents of $Pd(PPh_3)_4$ in toluene for 4 h at ambient temperature, workup gave a stoichiometric red solid, $(Ph_3P)_4Pd_3(C_{12}H_8N_6S_4)1.7CH_2Cl_2$ (**3b** · $1.7\,CH_2Cl_2$) in good yield (60%) after recrystallization from dichloromethane. The spectroscopic data of **3b** were very similar to those of **3a**. Compound **3b** exhibited a similar IR spectrum to that of **3a** with three strong absorptions at 1433, 692, and 526 cm^{-1}. In addition to the pyridyl and phenyl carbons, the $^{13}C\text{-}\{^1H\}$ NMR spectrum of **3a** exhibited a singlet at $\delta = 173.9$ for the C=N carbon of the amidine group. The $^{31}P\text{-}\{^1H\}$ NMR spectrum of **3b** in $CDCl_3$ gave only a singlet at $\delta = 27.5$ for the PPh_3 groups. The ^1H-NMR spectrum of **3b** exhibited resonances at $\delta = 9.46$ (d, 2 H, $J = 1.6$ Hz), 8.50 (dd, 4 H, $J = 4.6$, 1.6 Hz), and 8.39 (dt, 2 H, $J = 8.4$, 1.6 Hz) for the pyridyl protons, and at $\delta = 7.25$–6.82 (60

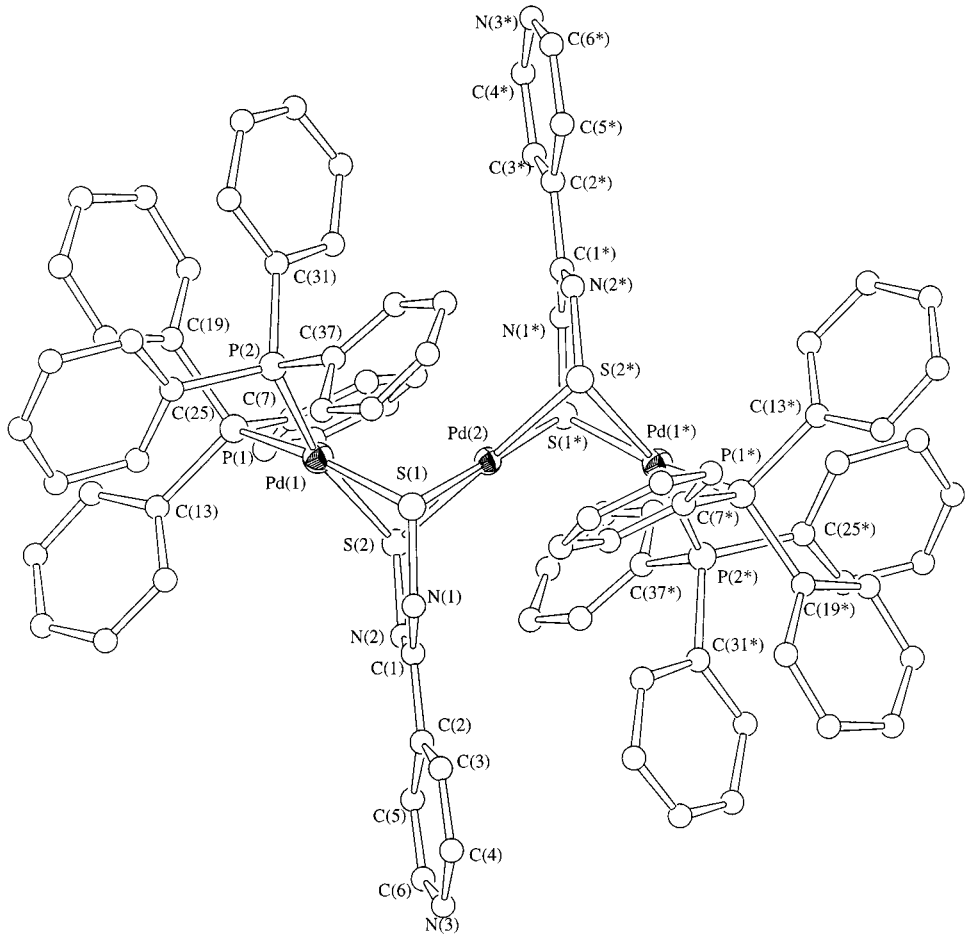
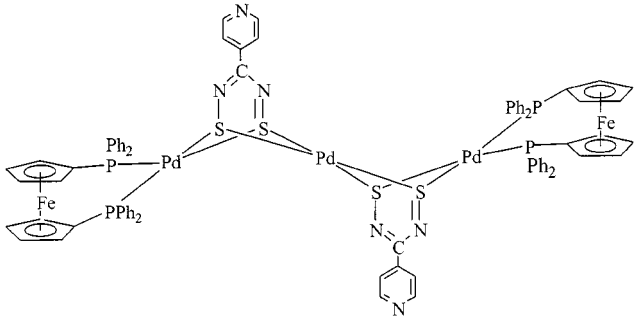


Figure 1. A perspective drawing of the molecular structure of **3a**

H, m) for the phenyl protons. LRMS (positive FAB) of **3b** exhibited a parent peak at *m/z* 1731 [(M + 1) for ^{106}Pd]. Based on the above spectroscopic and analytical data, a centrosymmetric trinuclear complex with a structure similar to that of **3a** was proposed for **3b**.

Preparation of [Pd_3{μ-SNC(4′-NC_5H_4)NS–*S,S′*}$_2$(dppf)$_2$] (4)

When one equivalent of $\mathbf{L^1}$ was allowed to react with a mixture of two equivalents of 1,1′-bis(diphenylphosphanyl)ferrocene (dppf) and one equivalent of tris(dibenzylideneacetone)dipalladium [$Pd_2(dba)_3$] in toluene for one day at room temperature, workup gave a stoichiometric red solid of $(dppf)_2Pd_3(C_{12}H_8N_6S_4) \cdot 0.5\,CH_2Cl_2$ (**4** · 0.25 CH_2Cl_2) in a moderate yield (50%). In addition to the pyridyl and phenyl carbon signals, the ^{13}C-{^1H} NMR spectrum of **4** exhibited three broad singlets at δ = 73.3, 72.3, and 72.0 for the cyclopentadienyl carbon atoms. The ^{31}P-{^1H} NMR spectrum of **4** in $CDCl_3$ exhibited only a singlet at δ = 25.5 for the phosphanyl groups. The ^1H-NMR spectrum of **4** exhibited two doublets at δ = 8.56 (d, 4 H, *J* = 6.2 Hz) and 8.22 (d, 4 H, *J* = 6.2 Hz) for the pyridyl protons, a complex multiplet at δ = 7.52–7.08 (m, 48 H) for the phenyl protons, and four singlets at δ = 3.92 (s, 4 H), 3.68 (s, 4 H), 3.65 (s, 4 H), and 3.61 (s, 4 H) for the cyclopentadienyl protons. LRMS (positive FAB) of **4** exhibited a parent ion peak at *m/z* 1791 [(M + 1) for ^{106}Pd]. Based on the spectroscopic and analytical data, compound **4** could be formulated as [Pd_3{μ-SNC(4′-NC_5H_4)NS-*S,S′*}$_2$(dppf)$_2$] with the structure as shown below.



4

Reaction of Triethylborane with 3a and 3b

When an excess amount of triethylborane was allowed to react with **3a** and **3b** in CH_2Cl_2/hexane mixture for one day at ambient temperature, workup gave red crystals of **5a** and **5b** of the same stoichiometry $(Ph_3P)_4Pd_3(C_{12}H_8N_6S_4)$-$(BEt_3)_2$ in 74 and 71% yield, respectively. Compound **5a** exhibited a spectroscopic pattern similar to that of **3a**. In

Table 1. Selected bond lengths [Å] and angles [°] for compounds **3a**, **5a**, and **5b**

Compound **3a**					
Pd(1)···Pd(2)	2.852(1)	Pd(1)–P(1)	2.357(3)	S(1)–N(1)	1.64(1)
Pd(1)–S(1)	2.360(3)	Pd(1)–P(2)	2.341(4)	S(2)–N(2)	1.65(1)
Pd(1)–S(2)	2.388(3)	Pd(2)–S(1)	2.337(3)	N(1)–C(1)	1.34(1)
N(2)–C(1)	1.33(1)	Pd(2)–S(2)	2.357(3)		
Pd(1)–Pd(2)–Pd(1*)	180.0	S(1)–Pd(1)–P(2)	89.2(1)	S(1)–Pd(2)–S(2)	81.0(1)
S(1)–Pd(1)–P(1)	169.0(1)	S(2)–Pd(1)–P(2)	165.7(1)	Pd(1)–S(1)–Pd(2)	74.8(1)
S(2)–Pd(1)–P(1)	89.3(1)	S(1)–Pd(1)–S(2)	79.9(1)	Pd(1)–S(2)–Pd(2)	73.89(9)
S(1)–N(1)–C(1)	125.6(9)	N(1)–C(1)–N(2)	131(1)	Pd(2)–Pd(1)–S(2)	52.56(8)
S(2)–N(2)–C(1)	124.2(9)	Pd(2)–Pd(1)–S(1)	52.24(8)	P(1)–Pd(1)–P(2)	101.8(1)
Compound **5a**					
Pd(1)···Pd(2)	2.8638(5)	Pd(1)–P(1)	2.338(2)	S(1)–N(1)	1.641(5)
Pd(1)–S(1)	2.387(2)	Pd(1)–P(2)	2.338(2)	S(2)–N(2)	1.663(5)
Pd(1)–S(2)	2.368(2)	Pd(2)–S(1)	2.351(1)	N(1)–C(37)	1.333(8)
Pd(2)–S(2)	2.344(2)	N(2)–C(37)	1.326(7)	B(1)–N(3)	1.69(1)
Pd(1)–Pd(2)–Pd(1*)	180.0	P(1)–Pd(1)–P(2)	102.47(6)	S(1)–Pd(2)–S(2)	98.30(5)
S(1)–Pd(1)–P(1)	86.77(5)	S(2)–Pd(1)–P(2)	90.99(6)	Pd(1)–S(1)–Pd(2)	74.37(4)
S(2)–Pd(1)–P(1)	166.42(6)	S(1)–Pd(1)–S(2)	84.46(5)	Pd(1)–S(2)–Pd(2)	74.87(5)
S(1)–N(1)–C(37)	124.6(4)	N(1)–C(37)–N(2)	132.3(6)	Pd(2)–Pd(1)–S(2)	52.19(4)
S(2)–N(2)–C(37)	125.2(4)	Pd(2)–Pd(1)–S(1)	52.24(4)	C(40)–N(3)–B(1)	119.9(8)
Compound **5b**					
Pd(1)···Pd(2)	2.884(1)	Pd(2)–P(1)	2.348(2)	S(1)–N(1)	1.662(6)
Pd(1)–S(1)	2.342(2)	Pd(2)–P(2)	2.326(3)	S(2)–N(2)	1.663(6)
Pd(1)–S(2)	2.349(2)	Pd(2)–S(1)	2.378(3)	N(1)–C(1)	1.33(1)
N(2)–C(1)	1.33(1)	B(1)–N(3)	1.66(1)	Pd(2)–S(2)	2.371(2)
Pd(2)–Pd(1)–Pd(2*)	180.0	P(1)–Pd(2)–P(2)	101.06(7)	S(1)–Pd(2)–S(2)	80.04(7)
S(1)–Pd(2)–P(1)	88.95(7)	S(2)–Pd(2)–P(1)	167.11(8)	Pd(1)–S(1)–Pd(2)	75.31(7)
S(2)–Pd(2)–P(2)	90.90(7)	S(1)–Pd(1)–S(2)	81.26(7)	Pd(1)–S(2)–Pd(2)	75.32(7)
S(1)–N(1)–C(1)	123.7(5)	N(1)–C(1)–N(2)	132.7(7)	Pd(1)–Pd(2)–S(2)	51.98(5)
S(2)–N(2)–C(1)	125.0(5)	Pd(1)–Pd(2)–S(1)	51.77(5)	C(3)–N(3)–B(1)	120.1(8)

the IR spectrum (KBr), other than the three strong absorptions at 1435, 692, and 520 cm^{-1}, the observation of *v*(Py, CN) at 1619 cm^{-1}, a shift of ca. 34 cm^{-1} from that of **3a** (1585 cm^{-1}), indicated B–N bond formation. In addition to the ethyl resonance, the ^{1}H-NMR spectrum of **5a** also exhibited two resonances at δ = 8.47 (d, 4 H, *J* = 6.6 Hz) and 8.35 (d, 4 H, *J* = 6.6 Hz) for the α-H and β-H of the pyridyl group, respectively. The slight upfield shift of ca. 0.05 ppm for the α-H signal from that of **3a** (δ = 8.52) and downfield shift of ca. 0.24 ppm for the β-H signal from that of **3a** (δ = 8.11) were also characteristic of the formation of B–N dative bond. The ^{31}P-{^{1}H} NMR spectrum of **5a** in $CDCl_3$ exhibited a singlet at δ = 27.5 for the PPh_3 groups. LRMS (positive FAB) of **5a** exhibited an ion peak at *m*/*z* 1731 [(M – 2 BEt_3 + 1) for ^{106}Pd]. Based on the above spectroscopic data, compound **5a** could be envisaged as an acid-base adduct of the triethylborane and the pyridyl groups of **3a**, and formulated as [Pd_3{μ-SNC(4′-$C_5H_4NBEt_3$)NS-*S,S′*}$_2$(PPh_3)$_4$].

Other than the phenyl protons, the ^{1}H-NMR spectrum of **5b** showed resonances of the triethylborane protons at δ = 0.60 (m, 18 H) and 0.51 (m, 12 H), and the pyridyl protons at δ = 9.47 (2 H, br s), 8.47 (m, 4 H), and 7.85 (s, 2 H). The ^{31}P-{^{1}H} NMR spectrum of **5b** in $CDCl_3$ exhibited only a singlet at δ = 26.9 for the PPh_3 groups. LRMS (positive FAB) of **5b** exhibited an ion peak at *m*/*z* 1731 [(M – 2 BEt_3 + 1) for ^{106}Pd]. Thus, compound **5b** could also be formulated as [Pd_3{μ-SNC(3′-$C_5H_4N \cdot BEt_3$)NS-*S,S′*}$_2$(PPh_3)$_4$]. The structures of both compounds **5a** and **5b** were ascertained by X-ray crystallography.

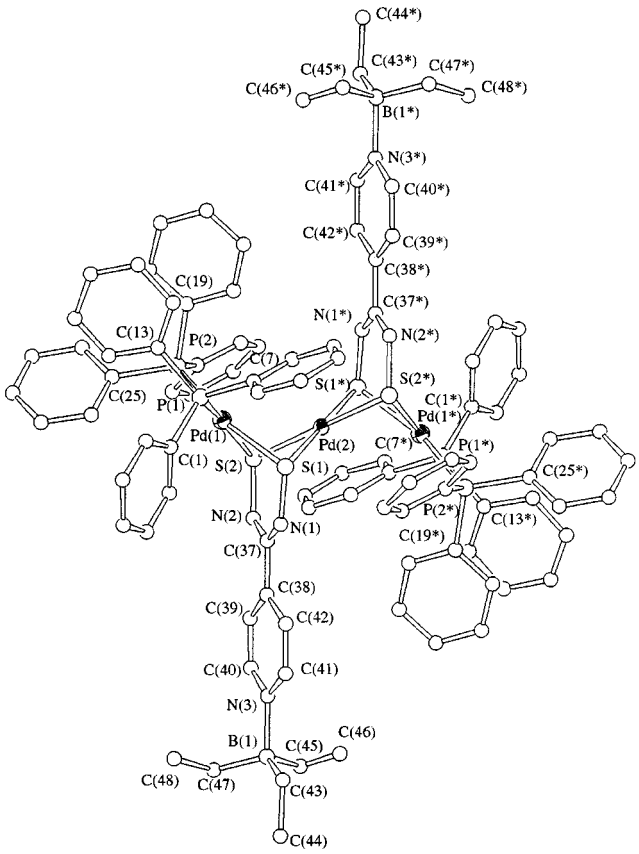


Figure 2. A perspective drawing of the molecular structure of **5a**

Crystals of **5a** · 4 CH_2Cl_2 and **5b** · 4 CH_2Cl_2 suitable for X-ray diffraction studies were grown from a solution of the respective compound in a dichloromethane/hexane mixture. Perspective drawings of the compounds are shown in Figure 2 and Figure 3, respectively. Selected bond lengths and angles are given in Table 1. The solid state structures of **5a** and **5b** are consistent with their spectroscopic data. Crystal structure analyses revealed that the triethylborane groups interact with the pyridyl groups of **3a** and **3b** forming acid-base adducts with a B–N distance of 1.69(1) and 1.66(1) Å, respectively. Other than the presence of triethylborane groups at the pyridyl groups, the structures of **5a** and **5b** are very similar to that of **3a** and **3b**.

Preparation of {[Pd_3{μ-SNC(4′-C_5H_4N)NS–*S,S′*}$_2$-(PPh_3)$_4$][$Mn(CO)_3Br$]}$_n$ (6)

When **3a** was allowed to react with 2 equivalents of $Mn(CO)_5Br$ in dichloromethane for one day at ambient tem-

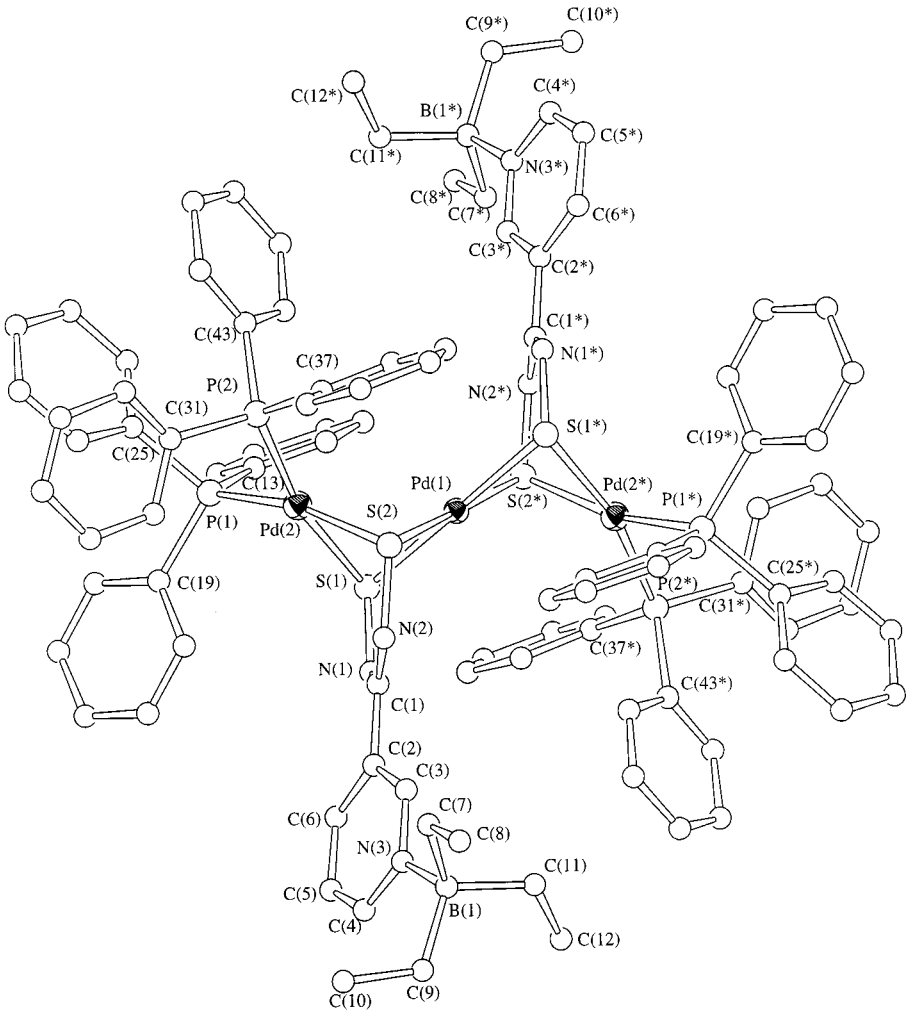
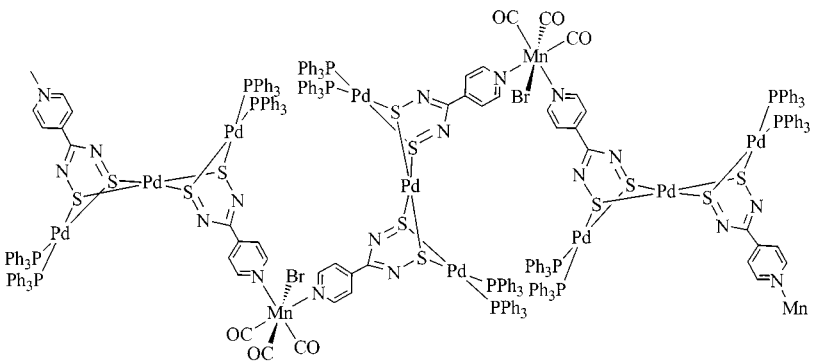


Figure 3. A perspective drawing of the molecular structure of **5b**



6

perature, workup gave a stoichiometric red solid of $(Ph_3P)_4Pd_3(C_{12}H_8N_6S_4)[Mn(CO)_3Br] \cdot 1.5\ CH_2Cl_2$ (**6** · 1.5 CH_2Cl_2) in a moderate yield of 55%. In the IR spectrum (KBr), compound **6** exhibited three very strong absorptions in the terminal carbonyl region at 2024, 1935, and 1905 cm^{-1}, which were indicative of a *fac*-$Mn(CO)_3$ configuration; and ν(Py, CN) at 1606 cm^{-1}, a shift of ca. 21 cm^{-1} from that of **3a** (1585 cm^{-1}), indicating the formation of Mn–N bonds. The Mn–N bond formation was also reflected in the chemical shifts of the pyridyl protons in the ^{1}H-NMR spectrum ($CDCl_3$), in which the α-H and β-H signals were shifted downfield from δ = 8.52 and 8.11 for **3a** to δ = 8.71 and 8.14 for **6**. The ^{1}H-NMR spectrum of **6** exhibited two resonances of relative intensity 4:30 for the pyridyl and phenyl protons, respectively. The ^{31}P-{^{1}H} NMR spectrum of **6** in $CDCl_3$ gave only a singlet at δ = 27.4 for the PPh_3 groups. LRMS (positive FAB) of **6** exhibited an ion peak at *m*/*z* 1730 {[M – $MnBr(CO)_3$] for ^{106}Pd}. Based on the spectroscopic and analytical data, compound **6** could be formulated as $\{[Pd_3\{\mu\text{-}SNC(4'\text{-}C_5H_4N)NS\text{-}S,S'\}_2(PPh_3)_4][Mn(CO)_3Br]\}_n$ with a possible structure shown below. In **6**, complex **3a** and $Mn(CO)_3Br$ were linked alternately together in a linear manner, in which the central metal Mn possesses an octahedral geometry with the three carbonyl ligands in a *fac* configuration, while the two nitrogen atoms adopt a *cis* configuration. The two nitrogen atoms coordinated to the same metal Mn came from two different molecules of **3a**. Thus, **6** could also be described as two $Mn(CO)_3Br$ and one bridging **3a** ligand alternately linking together in a linear geometry.

Experimental Section

General Procedures: Unless otherwise stated, manipulations were performed under oxygen-free nitrogen using standard techniques in a glovebox. Solvents were dried by standard procedures, distilled and de-aerated prior to use. All chemicals used were of reagent grade, obtained from the Aldrich Chemical Company and, where appropriate, degassed before use. The compounds $Pd(PPh_3)_4$,[20] dppf,[21] and $Pd_2(dba)_3$[22] were prepared according to literature methods. – Microanalyses were performed by the Shanghai Institute of Organic Chemistry, Chinese Academy of Sciences, China. – The melting points were obtained in glass capillaries and were uncorrected. – Infrared spectra were recorded with a Nicolet Nagna-IR 550 spectrometer and NMR spectra with a JEOL EX270 spectrometer. Chemical shifts of ^{1}H and ^{13}C-{^{1}H} NMR spectra were referenced to internal deuteriated solvents and then recalculated to $SiMe_4$ (δ = 0.00), those of ^{31}P-{^{1}H} NMR spectra were referenced to external 85% H_3PO_4 (δ = 0.00). The EPR spectra were obtained with an X-band JEOL JES TE-100 spectrometer at room temperature, low-resolution mass spectra with a Finnigan MAT SSQ-710 or MAT 95 spectrometer either in EI or FAB (positive ion) mode.

[4-(4′-NC_5H_4)CN_2S_2] L^1: A solution of $Li[N(SiMe_3)_2]$, generated in situ by treating $(Me_3Si)_2NH$ (32.94 g, 200 mmol) in diethyl ether (100 mL) with *n*BuLi (122 mL of 1.6 M, 200 mmol) in hexane, was slowly added to a solution of 4-cyanopyridine (20.8 g, 200 mmol) in tetrahydrofuran (70 mL) at 0 °C. The resulting dark-red solution was warmed to room temperature and allowed to react overnight. The solvent was removed in vacuo to give a dark red residue that was then suspended in toluene (400 mL). A solution of Me_3SiCl (22.4 g, 200 mmol) in toluene (100 mL) was then slowly added to the suspension at room temperature. Upon complete addition, the solution mixture was stirred under reflux for 7 h, then at room temperature overnight. The resultant reaction mixture was then filtered to afford a red filtrate, which was pumped dry before acetonitrile (200 mL) was added. A solution of sulfur dichloride (42 g, 400 mmol) in acetonitrile (50 mL) was then slowly added. The mixture was stirred at room temperature for 24 h and then filtered to afford crude 4-(4′-pyridyl)dithiadiazolylium chloride as a yellow solid, which was washed once with a 1:1 mixture of acetonitrile/toluene (200 mL) and then suspended in acetonitrile (200 mL). A solution of triphenylantimony (72 g, 200 mmol) in acetonitrile (100 mL) was slowly added to the suspension at room temperature to give a dark purple precipitate. The reaction mixture was allowed to stir at room temperature for 2 h before the solvent was removed in vacuo to give a dark purple residue. Sublimation of the residual solid at 110°C/0.05 Torr afforded a dark red solid of [4-(4′-NC_5H_4)CN_2S_2]. Yield: 12.1 g, 33.3%; m. p. 252–254°C (dec.). – $C_6H_4N_3S_2 \cdot H_2O$ (200.25): calcd. C 36.0, H 3.0, N 21.0, S 32.0; found C 36.0, H 2.9, N 20.8, S 31.0. – IR (cm^{-1}, in KBr): $\tilde{\nu}$ = 3388 vs, 3332 s, 3266 s, 3120 m, 3028 m, 1945 w, 1693 m, 1649 m, 1599 s, 1560 w, 1417 vs, 1377 s, 1230 m, 1140 m, 1062 m, 1018 m, 1000 m, 913 w, 828 s, 810 s, 785 vs, 747 w, 736 w, 667 m, 656 vs, 618 w, 510 m, 464 w. – LRMS (EI mode); *m*/*z*: 364 [M_2 for ^{32}S] and 182 [M for ^{32}S]. – EPR (in toluene): g = 2.014, A = 0.52 mT (five lines with relative intensity 1:2:3:2:1).

[4-(3′-NC_5H_4)CN_2S_2] L^2: The compound was prepared as described for L^1. $LiN(SiMe_3)_2$ (2.7 g, 164 mmol), 3-cyanopyridine (17.4 g, 164 mmol), $SiMe_3Cl$ (17.8 g, 164 mmol), sulfur dichloride (51.7 g, 492 mmol), and triphenylantimony (29.2 g, 82 mmol) were used. A dark red powder was obtained after sublimation (100°C/0.03 Torr). Yield: 14.9 g, 50%; m. p. 215–217°C (dec.). – $C_6H_4N_3S_2 \cdot 0.25\ H_2O$ (186.74): calcd. C 38.6, H 2.4, N 22.5, S 34.3; found C 38.4, H 2.4, N 21.9, S 33.7. – IR (cm^{-1}, KBr): $\tilde{\nu}$ = 3608 w, 3423 m, 3067 m, 3038 m, 2964 w, 1686 m, 1589 m, 1480 w, 1429 m, 1375 vs, 1325 m, 1244 m, 1189 m, 1146 m, 1116 w, 1091 w, 1040 m, 1026 s, 905 w, 834 m, 809 vs, 782 vs, 698 vs, 667 s, 627 m, 511 m, 459 m. – LRMS (EI mode); *m*/*z*: 364 [M_2 for ^{32}S] and 182 [M for ^{32}S]. – EPR (in toluene): g = 2.013, A = 0.51 mT (five lines with relative intensity 1:2:3:2:1).

***fac*-$MnBr(CO)_3(L^1)_2$ (2a):** $Mn(CO)_5Br$ (0.58 g, 2.1 mmol) and L^1 (0.19 g, 1.04 mmol) were stirred in tetrahydrofuran (20 mL) at 55°C for 4 h to yield a reddish-brown solution and a small amount of yellow precipitate. After cooling to room temperature, the solution was filtered. The red-brown filtrate was cooled to –5°C to give tiny reddish-brown needle crystals, which were filtered and dried in vacuo. Yield: 0.18 g, 56%; m. p. 167–169°C (dec.). – $C_{15}H_8BrMnN_6O_3S_4 \cdot 2.5\ H_2O$ (628.37): calcd. C 28.7, H 2.1, N 13.4, S 20.4; found C 28.6, H 1.9, N 13.5, S 19.3. – IR (cm^{-1}, in KBr): $\tilde{\nu}$ = 3410 m, 3103 m, 2975 m, 2927 m, 2866 w, 2030 vs, 1942 vs, 1909 vs, 1686 m, 1612 m, 1421 m, 1375 m, 1222 m, 1098 m, 1059 m, 1019 m, 842 m, 778 m, 681w, 648 w, 630 m, 517 m. – EPR (in THF): g = 2.014, A = 0.50 mT, quintuplet with relative intensity: 1:2:3:2:1. (in solid): g = 2.011.

***fac*-$MnBr(CO)_3(L^2)_2$ (2b):** A solution of $Mn(CO)_5Br$ (0.04 g, 0.15 mmol) and L^2 (0.05 g, 0.27 mmol) in tetrahydrofuran (10 mL) was stirred under reflux for 4 h to yield a reddish-brown precipitate. The precipitate was filtered off, washed with tetrahydrofuran (3 × 4 mL) and dried in vacuo. Yield: 0.06 g, 74%; m. p. 155–157°C (dec.). – $C_{15}H_8BrMnN_6O_3S_4 \cdot H_2O$ (601.33): calcd. C 30.0, H 1.7,

N 14.0, S 21.3; found C 29.8, H 1.6, N 13.5, S 20.8. – IR (cm^{-1}, in KBr): $\tilde{\nu}$ = 3379 m, 3201 m, 3058 m, 2854 w, 2028 vs, 1947 vs, 1912 vs, 1610 m, 1573 w, 1463 m, 1435 s, 1415 m, 1331 w, 1258 w, 1193 w, 1102 m, 1027 w, 999 w, 830 w, 806 w, 744 m, 708 m, 694 s, 673 m, 635 m, 524 s, 492 w. – EPR (in THF): g = 2.014, A = 0.51 mT, quintuplet with relative intensity 1:2:3:2:1; (in solid): g = 2.014.

[Pd_3{μ-SNC(4′-NC_5H_4)NS-*S,S′*}$_2$(PPh_3)$_4$] (3a): Solid **L^1** (0.07 g, 0.38 mmol) was added to a stirred suspension of $Pd(PPh_3)_4$ (0.84 g, 0.73 mmol) in toluene (14 mL) at ambient temperature. The reaction mixture was then stirred for 4 h to give a red precipitate. The red precipitate was filtered off, washed with toluene (2 × 6 mL) and dried in vacuo. The red precipitate was then re-dissolved in hot dichloromethane (20 mL) to give a deep red solution, which was filtered and cooled to –30°C to give red block crystals. The crystals were filtered and dried in vacuo. Yield: 0.22 g, 66%; m. p. 250–252°C (dec.). – $C_{84}H_{68}N_6P_4Pd_3S_4 \cdot 0.25\ CH_2Cl_2$ (1753.97): calcd. C 57.7, H 3.9, N 4.8, S 7.3; found C 58.0, H 3.9, N 4.7, S 7.3. – IR (cm^{-1}, in KBr): $\tilde{\nu}$ = 3049 w, 2940 w, 2853 w, 1585 m, 1478 m, 1434 s, 1418 m, 1309 m, 1264 w, 1181 w, 1155 w, 1094 m, 1057 w, 1026 w, 998 w, 840 w, 821 w, 746 m, 737 m, 715 vs, 691 vs, 671 s, 618 w, 527 s, 519 vs, 506 s, 492 s, 459 w, 445 w, 424 w. – NMR ($CDCl_3$): ^{31}P-{^{1}H}, PPh_3, δ = 27.5 (s); ^{13}C-{^{1}H}, C=N carbon atom, 174.0 (br, s); pyridyl carbon atoms, 150.1, 149.4, and 121.7; phenyl carbon atoms, 133.9 (t, J = 6.1 Hz), 129.9, 128.2 (t, J = 4.9 Hz); ^{1}H, pyridyl protons, δ = 8.52 (dd, 4 H, J = 4.6, 1.6 Hz), 8.11 (dd, 4 H, J = 4.6, 1.6 Hz); phenyl protons, 7.12 (t, 12 H, J = 7.3 Hz), 6.97 (t, 24 H, J = 7.3 Hz), 6.83 (m, 24 H); dichloromethane protons, 5.23 (s). – LRMS (FAB: +ve mode) *m*/*z*: 1731 [(M + 1) for ^{106}Pd].

[Pd_3{μ-SNC(3′-NC_5H_4)NS-*S,S′*}$_2$(PPh_3)$_4$] (3b): The compound was prepared as described for **3a**. $Pd(PPh_3)_4$ (4.0 g, 3.46 mmol) and **L^2** (0.42 g, 2.31 mmol) were used. Yield: 1.19 g, 55%; m. p. 254–256°C (dec.). – $C_{84}H_{68}N_6P_4Pd_3S_4 \cdot 1.7\ CH_2Cl_2$ (1877.11): calcd. C 54.8, H 3.8, N 4.5, S 6.8; found C 54.8, H 3.6, N 4.5, S 7.1. – IR (cm^{-1}, in KBr): $\tilde{\nu}$ = 3050 w, 2963 w, 1640 m (br), 1583 m, 1476 m, 1433 s, 1384 m, 1310 m, 1261 m, 1196 w, 1153 m, 1093 s, 1023 m, 997 m, 907 w, 801 s (br), 741 s (br), 719 m, 691 vs, 670 s, 618 w, 543 w, 526 s, 519 vs, 493 s, 431 w, 422 w, 406 w. – NMR ($CDCl_3$): ^{31}P-{^{1}H}, PPh_3, δ = 27.5 (s); ^{13}C-{^{1}H}, C=N carbon atom, 173.9 (s); pyridyl carbon atoms, 149.1, 148.7, 138.4 134.6 and 122.7; phenyl carbon atoms, 134.0 (t, J = 6.1 Hz), 131.0 (dd, J = 20.8, 19.5 Hz), 129.8, 128.2 (t, J = 4.9 Hz); ^{1}H, pyridyl protons: δ = 9.46 (d, 2 H, J = 1.6 Hz), 8.50 (dd, 4 H, J = 4.6, 1.6 Hz) and 8.39 (dt, 2 H, J = 8.4, 1.6 Hz); phenyl protons, 7.25–6.82 (m, 60 H); dichloromethane protons, 5.23 (s). – LRMS (FAB: +ve mode) *m*/*z*: 1731 [(M + 1) for ^{106}Pd].

[Pd_3{μ-SNC(4′-NC_5H_4)NS-*S,S′*}$_2$(dppf)$_2$] (4): Solid [4-(4′-NC_5H_4)-CN_2S_2]$_2$ (**L^1**) (0.20 g, 0.55 mmol) was added to a stirred solution of $Pd_2(dba)_3$ (0.50 g, 0.55 mmol) and dppf (0.61 g, 1.10 mmol) in toluene (18 mL) at ambient temperature. The reaction mixture was then stirred for one day to give a red precipitate, which was filtered, washed with toluene (6 mL), and dried in vacuo. Further washing the red precipitate with hot dichloromethane (20 mL) gave a red residue, which was dried in vacuo. The red residue was then recrystallized from hot chloroform to give tiny red crystals. Yield: 0.49 g, 49%; m. p. 256–258°C (dec.). – $C_{80}H_{64}Fe_2N_6P_4Pd_3S_4 \cdot 0.25\ CHCl_3$ (1822.62): calcd. C 52.9, H 3.5, N 4.6, S 7.0; found C 52.7, H 3.7, N 5.0, S 7.2. – IR (cm^{-1}, in KBr): $\tilde{\nu}$ = 3112 s, 2964 m, 2924 m, 2853 w, 1589 s, 1480 m, 1435 vs, 1420 s, 1402 m, 1310 s, 1261 w, 1164 m, 1098 m, 1027 m, 998 w, 524 m, 519 m, 487 vs, 464 m, 439 m. – NMR ($CDCl_3$): ^{31}P-{^{1}H}, phosphanyl groups, δ = 25.5 (s); ^{13}C-{^{1}H}, phenyl and pyridyl carbon atoms, 149.2, 135.6, 132.2, 131.1, 128.1, 125.1, 123.0 and 121.5; cyclopentadienyl carbon atoms, 73.3 (br, s), 72.3 (br, s) and 72.0 (br, s); ^{1}H, pyridyl protons, 8.56 (d, 4 H, J = 6.2 Hz), 8.22 (d, 4 H, J = 6.2 Hz); phenyl protons, 7.52–7.08 (m, 48 H); cyclopentadienyl protons, 3.92 (s, 4 H), 3.68 (s, 4 H), 3.65 (s, 4 H) and 3.61 (s, 4 H). – LRMS (FAB: +ve mode) *m*/*z*: 1791 [(M + 1) for ^{106}Pd].

[Pd_3{μ-SNC(4′-C_5H_4NBEt_3)NS-*S,S′*}$_2$(PPh_3)$_4$] (5a): A solution of triethylborane (0.2 mL of 1M, 0.2 mmol) in hexane was carefully layered over a solution of **3a** (0.17 g, 0.10 mmol) in dichloromethane (10 mL). The resultant solution was left undisturbed at ambi-

Table 2. Summary of crystal data for compounds **3a**, **5a**, and **5b**

	3a	**5a**	**5b**
Empirical formula	$C_{92}H_{88}N_6O_2P_4Pd_3S_4$	$C_{100}H_{106}B_2Cl_8N_6P_4Pd_3S_4$	$C_{100}H_{106}B_2Cl_8N_6P_4Pd_3S_4$
Molecular mass	1881.08	2268.56	2268.56
Crystal system	Triclinic	Monoclinic	Triclinic
Space group	*P*–1 (no. 2)	$P2_1/n$ (no. 14)	$P\bar{1}$ (no. 2)
a [Å]	13.901(4)	15.671(1)	15.101(8)
b [Å]	13.925(2)	21.800(1)	15.91(1)
c [Å]	10.999(2)	17.187(1)	12.095(6)
α [°]	93.38(1)	90	101.41(5)
β [°]	98.69(2)	116.98(1)	104.28(5)
γ [°]	80.81(2)	90	107.59(5)
U [$Å^3$]	2076.4(7)	5232.5(7)	2565(3)
Z	1	2	1
μ(Mo-K_α) [cm^{-1}]	8.74	7.99	9.21
Temperature [K]	298	298	298
Reflections collected	5685	44557	6980
Independent reflections (R_{int})	5415 (0.030)	9555 (0.070)	6670 (0.033)
Observed reflections	3744 [$I > 1.50\sigma(I)$]	6347 [$I > 1.50\sigma(I)$]	4484 ($I > 3.00\sigma(I)$]
R	0.068	0.058	0.070
R_w [a]	0.084	0.054	0.082

[a] Weighting scheme $w = 4F_o^2/[\sigma^2(F_o^2) + pF_o^2]^2$.

ent temperature for 24 h to give red crystals, which were filtered and dried in vacuo. Yield: 0.16 g, 73%; m. p. 213–215°C (dec.). – $C_{96}H_{98}B_2N_6P_4Pd_3S_4 \cdot 3\ CH_2Cl_2$ (2183.50): calcd. C 54.5, H 4.8, N 3.9; found C 54.4, H 4.7, N 3.8. – IR (cm^{-1}, in KBr): $\tilde{\nu}$ = 3053 m, 2900 m, 2859 s, 1619 s, 1587 m, 1480 m, 1435 vs, 1309 m, 1268 m, 1160 m, 1094 m, 1040 m, 998 m, 892 w, 852 m, 823 w, 798 m, 738 s, 723 vs, 692 vs, 662 s, 618 w, 527 s, 520 vs, 507 s, 492 m, 447 w, 430 w, 411 w. – NMR ($CDCl_3$): ^{31}P-{^1H}, PPh_3, δ = 27.5 (s); ^1H, pyridyl protons, 8.47 (d, 4 H, *J* = 6.6 Hz), 8.35 (d, 4 H, *J* = 6.6, Hz); phenyl protons, 7.19 (t, 24 H, *J* = 7.3 Hz), 7.02 (t, 24 H, *J* = 7.3 Hz), 6.89 (m, 24 H); dichloromethane protons, 5.28 (s); ethyl protons, 0.66 (t, 18 H, *J* = 7.6 Hz) and 0.49 (q, 12 H, *J* = 7.6 Hz). – LRMS (FAB: +ve mode) *m/z*: 1731 [(M –2BEt_3 + 1) for ^{106}Pd].

[Pd_3{μ-SNC(3′-NC_5H_4)$NBEt_3$)NS-*S,S*′}$_2(PPh_3)_4$] (5b): Compound **5b** was prepared as described for **5a**. Triethylborane (excess) and **3b** (0.14 g, 0.08 mmol) were used. Yield: 0.13 g, 71%; m. p. 208–210°C (dec.). – $C_{96}H_{98}B_2N_6P_4Pd_3S_4 \cdot 4\ CH_2Cl_2$ (2268.42): calcd. C 53.0, H 4.7, N 3.7; found C 53.2, H 4.7, N 3.8. – IR (cm^{-1}, in KBr): $\tilde{\nu}$ = 3054 w, 2936 w, 2898 w, 2856 m, 2814 w, 1614 w, 1575 m, 1478 m, 1434 s, 1309 m, 1185 w, 1162 m, 1094 m, 1051 w, 1026 w, 996 w, 891 w, 874 w, 799 w, 742 s, 692 vs, 624 w, 521 s, 506 s, 436 m. – NMR ($CDCl_3$): ^{31}P-{^1H}, PPh_3, δ = 26.9 (s); ^1H, pyridyl protons, 9.47 (br. s, 2 H), 8.47 (m, 4 H), 7.85 (s, 2 H); phenyl protons, 7.12 (t, 12 H, *J* = 6.7 Hz), 6.97 (t, 24 H, *J* = 6.7 Hz), 6.85 (m, 24 H); dichloromethane protons, 5.24 (s); ethyl protons, 0.60 (m, 18 H) and 0.51 (m, 12 H). – LRMS (FAB: +ve mode) *m/z*: 1731 [(M – 2 BEt_3 + 1) for ^{106}Pd].

{[Pd_3{μ-SNC(4′-NC_5H_4)NS-*S,S*′}$_2(PPh_3)_4$][$BrMn(CO)_3$]}$_n$ (6): A solution of $Mn(CO)_5Br$ (0.045 g, 0.16 mmol) in dichloromethane (6 mL) was added to a solution of **3a** (0.14 g, 0.08 mmol) in dichloromethane (6 mL) at ambient temperature to give a deep-red solution. The resultant solution was stirred overnight at ambient temperature and then filtered. The solvent of the filtrate was removed in vacuo and the residue was washed with diethyl ether (3 × 5 mL) and dried in vacuo to afford a reddish-brown solid. Yield 0.09 g, 54%. m. p. 196–198°C (dec.). – $C_{87}H_{68}BrMnN_6P_4Pd_3S_4O_3 \cdot 1.5\ CH_2Cl_2$ (2079.00): calcd. C 51.1, H 3.4, Br 3.9, N 4.0, S 6.2; found C 51.0, H 3.4, Br 4.1, N 4.1, S 6.3. – IR (cm^{-1}, in KBr): $\tilde{\nu}$ = 3053 m, 2024 vs, 1935 vs, 1905 vs, 1641 m, 1606 m, 1480 m, 1434 s, 1384 m, 1311 m, 1184 w, 1174 m, 1095 m, 1079 m, 1026 m, 998 m, 849 w, 494 m, 440 m (br). – NMR ($CDCl_3$): ^{31}P-{^1H}, PPh_3, δ = 27.4 (s); ^1H, pyridyl protons, 8.71 (4 H_α, br, s), 8.14 (4 H_β, br, s); phenyl protons, 7.15–6.84 (m). – LRMS (FAB: +ve mode) *m/z* 1730 {[M – $MnBr(CO)_3$] for ^{106}Pd}.

X-ray Crystallography: Suitable crystals of **3a**, **5a**, and **5b** were mounted and sealed in Lindemann capillaries. All pertinent crystallographic data and other experimental details are summarised in Table 2. Intensity data of **3a** and **5b** were collected with a Rigaku AFC7R diffractometer, and that for **5a** with an MAR research image plate scanner using graphite-monochromated Mo-K_α radiation (λ = 0.71073 Å) at room temperature. All intensity data were corrected for Lorentz polarisation effects. Empirical absorption corrections based on the ψ-scan method were employed for **3a** and **5b**, whereas an approximation of absorption corrections by inter-image scaling was applied for **5a**. For **5a**, 60 3° frames with an exposure time of 5 min per frame were used. The structures were solved by a combination of direct methods (SIR 92) [23] and Fourier difference techniques, and refined by full-matrix least-squares analysis on *F* until convergence was reached. However, in compound **3a**, attempts to refine all non-hydrogen atoms anisotropically gave unreasonably high displacement parameters for the atoms. Therefore, only the heavy atoms (Pd, S, and P) were included in subsequent refinement cycles. The atoms of the ether solvent molecule in **3a** were fixed throughout in the refinement processes. Hydrogen atoms on the organic moieties were generated at their ideal positions (C–H 0.95 Å) and allowed to ride on their respective parent carbon atoms. All calculations were performed with a Silicon-Graphics computer using the program package TEXSAN.[24] Crystallographic data (excluding structure factors) for the structure(s) reported in this paper have been deposited with the Cambridge Crystallographic Data Centre as supplementary publication no. CCDC-135684 to -135686. Copies of the data can be obtained free of charge on application to CCDC, 12 Union Road, Cambridge CB2 1EZ, UK [Fax: int. code + 44-1223/336-033; E-mail: deposit@ccdc.cam.ac.uk].

Acknowledgments

W.-K. Wong thanks the Hong Kong Baptist University and the Hong Kong Research Grants Council for financial support. W.-T. Wong thanks the Hong Kong Research Grants Council and the University of Hong Kong for financial support.

[1] A. J. Banister, N. R. M. Smith, R. G. Hey, *J. Chem. Soc., Perkin Trans. 1* **1983**, 1181–1186.
[2] P. D. B. Belluz, A. W. Cordes, E. M. Kristof, P. V. Kristof, S. W. Liblong, R T. Oakley, *J. Am. Chem. Soc.* **1989**, *111*, 9276–9278.
[3] A. W. Cordes, R. C. Haddon, R. T. Oakley, L. F. Schneemeyer, J. V. Waszczak, K. M. Young, N. M. Zimmerman, *J. Am. Chem. Soc.* **1991**, *113*, 582–588.
[4] A. W. Cordes, R. C. Haddon, R. G. Hicks, R. T. Oakley, T. T. M. Palstra, L. F. Schneemeyer, J. V. Waszczak, *J. Am. Chem. Soc.* **1992**, *114*, 5000–5004.
[5] A. W. Cordes, R. C. Haddon, R. G. Hicks, R. T. Oakley, T. T. M. Palstra, *Inorg. Chem.* **1992**, *31*, 1802–1808.
[6] A. W. Cordes, C. M. Chamchoumis, R. G. Hicks, R. T. Oakley, K. M. Young, R. C. Haddon, *Can. J. Chem.* **1992**, *70*, 919–925.
[7] C. Aherne, A, J. Banister, A. W. Luke, J. M. Rawson, R. J. Whitehead, *J. Chem. Soc., Dalton Trans.* **1992**, 1277–1282.
[8] A. J. Banister, Ian Lavender, J. M. Rawson, W. Clegg, B. K. Tanner, R. J. Whitehead, *J. Chem. Soc., Dalton Trans.* **1993**, 1421–1429.
[9] A. W. Cordes, N. A. George, R. C. Haddon, D. K. Kennepohl, R. T. Oakley, T. T. M. Palstra, R. W. Reed, *Chem. Mater.* **1996**, *8*, 2774–2778.
[10] A. J. Banister, A. S. Batsanow, O. G. Dawe, P. L. Herbertson, J. A. K. Howard, S. Lynn, I. May, J. N. B. Smith, J. M. Rawson, T. E. Rogers, B. K. Tanner, G. Antorrena, F. Palacio, *J. Chem. Soc., Dalton Trans.* **1997**, 2539–2541.
[11] A. J. Banister, I. B. Gorrell, W. Clegg, K. A. Jørgensen, *J. Chem. Soc., Dalton Trans.* **1991**, 1105–1109.
[12] A. J. Banister, I. B. Gorrell, S. E. Lawrence, C. W. Lehmann, I. May, G. Tate, A. J. Blake, J. M. Rawson, *J. Chem. Soc., Chem. Commun.* **1994**, 1779–1780.
[13] A. J. Banister, I. May, *Phosphorus, Sulfur, Silicon Relat. Elem.* **1994**, *93*, 447–448.
[14] A. J. Banister, I. B. Gorrell, A. J. K. Howard, S. E. Lawrence, C. W. Lehmann, I. May, J. M. Rawson, B. K. Tanner, C. I. Gregory, A. J. Blake, S. P. Fricker, *J. Chem. Soc., Dalton Trans.* **1997**, 377–384.
[15] A. J. Banister, A. J. K. Howard, I. May, J. M. Rawson, *Chem. Commun.* **1997**, 1763–1764.
[16] G. G. Alange, A. J. Banister, B. Bell, P. W. Millen, *J. Chem. Soc., Perkin Trans. 1* **1979**, 1192–1194.
[17] H. W. Roesky, M. Witt, J. Schimokowiak, M. Schmidt, M. Noltemeyer, G. M. Sheldrick, *Angew. Chem. Int. Ed. Engl.* **1982**, *21*, 538–539.
[18] K. W. H. Small, A. J. Banister, Z. V. Hanptman, *J. Chem. Soc., Dalton Trans.* **1984**, 1377–1381.

[19] A. Vegas, A. Perez-Salazar, A. J. Banister, R. G. Hey, *J. Chem. Soc., Dalton Trans.* **1980**, 1812–1815.
[20] R. J. Angelici, *Reagents for Transition Metal Complexes and Organometallic Syntheses, Inorganic Syntheses*, vol. 28 (Ed.: D. R. Coulson), Wiley, , USA, **1990**, p.107
[21] J. J. Bishop, A. Davison, M. L. Katcher, D. W. Lichtenberg, R. E. Merrill, J. C. Smart, *J. Organomet. Chem*. **1971**, *27*, 241–249.
[22] T. Ukai, H. Kawazura, Y. Ishii, *J. Organomet. Chem*. **1974**, *65*, 253–266.
[23] SIR92: A. Altomare, M. Cascarano, C. Giacovazzo, A. Guagliardi, *J. Appl. Crystallogr.* **1992**, *25*, 310.
[24] *TEXSAN*, Crystal Structure Analysis Package, Molecular Structure Corporation, Houston, TX, **1985** and **1992**.
Received October 18, 1999
[I99365]

Fixation of Carbon Dioxide by Oxalic Amidinato Magnesium Complexes: Structures and Reactions of Trimetallic Magnesium Carbamato and Related Complexes

Mario Ruben,[c] Dirk Walther,*[a] René Knake,[a] Helmar Görls,[a] and Rainer Beckert[b]

Dedicated to Professor Heinrich Vahrenkamp on the occasion of his 60th birthday

Keywords: Carbon dioxide fixation / Magnesium / N ligands / C–C coupling

The reaction of oxalic amidines R^1–N=C(NHR^2)–C(NHR^2)=N–R^1 with CH_3MgX followed by uptake of CO_2 results in the formation of the trimeric carbamato complexes [R^1–N=C(NR^2–COO)–C(NR^{2}COO)=N–R^1]$_3$Mg$_3$(THF)$_6$ (**2a**: R^1 = R^2 = Ph; **2b**: R^1 = R^2 = *p*-tolyl) as the thermodynamically stable final products of the reaction. Their X-ray crystal structures show that the three metal centres are in a linear arrangement. The central magnesium ion is octahedrally surrounded by six O-donor atoms of the μ_2-carbamato bridges, while both peripheral magnesium ions are facially coordinated by three O-donor atoms of the carbamato groups and three THF molecules. This coordination sphere can be considered as a structural model for the active centre in the ribulose-1,5-bisphosphate carboxylase/oxygenase enzyme. Compound **2a** reacts with $ZnCl_2$ or $CoBr_2$, with CO_2 elimination, to form dimeric complexes of the type [X$_2$M(oxalamidinato)MX$_2$][Mg(DMF)$_6$] (M = Zn, Co; X = Cl, Br). X-ray crystal structure analyses show that the d-metals are tetrahedrally coordinated. The magnesium-bromide-containing intermediates in the formation of **2a** and **2b** are able to transfer CO_2 to acetophenone, thus simulating the CO_2 activation step in enzymatic biotin-dependent carboxylation reactions.

Introduction

Biological transformation reactions of carbon dioxide into organic material by C–C linkage are either activated by biotin-depending enzymes (Acetyl CoA carboxylase) in the fatty acids synthesis, or catalysed by Rubisco in the dark reaction of natural photosynthesis. In both enzymes carbamato magnesium complexes seems to play an essential role. In biotin-containing systems the carbamato magnesium complexes are carriers of "active CO_2" which can be transferred to C–H bonds to form the C–COOH group. However, neither the structure of the carbamato complex nor the mechanism of the CO_2 activation reaction have yet been established.[1–8]

In contrast, in Rubisco the carbamato group does not act as a CO_2 source, but is proposed to serve as proton relay which abstracts the C3 proton from ribulose-1,5-bisphosphate. The resulting enol reacts with carbon dioxide in the coordination sphere of the magnesium centre to form a new C–C bond (for reviews see refs.[9–11]). The structure of various forms of Rubisco have been elucidated by X-ray crystallography.[9] In the substrate-free complex the Mg^{II} centre is octahedrally surrounded by a monodentate carbamato group, two carboxylato ligands and three water molecules.[12]

It is noteworthy that, so far, the chemistry of abiotic carbamato magnesium complexes is poorly developed, especially with respect to the understanding of their reactivity as CO_2-transfer reagents.[13–19] Furthermore, structurally elucidated complexes which might act as structural or functional models for the above-mentioned enzymes are very rare. Only one organometallic mixed Al–Mg alkyl compound has been structurally characterised.[20a] Recently the X-ray structure of an oligomer consisting of six diethylcarbamato–Mg units has also been reported.[20b]

We describe here the synthesis, structure, and reactivity of a variety of new magnesium carbamato complexes which may act as models for the above-mentioned CO_2-transforming systems. The complexes were synthesised from magnesium oxalic amidinates or from the di(isopropyl)amido magnesium complex and carbon dioxide.

Results and Discussion

Synthesis and Structure of Carbamato Mg Complexes

The reaction of tetraphenyloxalic amidine **H_2A** (2.56 mmol, Figure 1) with two equivalents of CH_3MgBr in 50 mL of THF resulted in the deprotonation of the ligand and formation of methane. Subsequent reaction with CO_2 at –20 °C afforded a white precipitate (**1a**, 60%). According to the elemental analyses it was contaminated with ca. 10% of complex **2a** which was formed by elimination of $MgBr_2$

[a] Institut für Anorganische und Analytische Chemie der Universität Jena,
August-Bebel-Straße 2, 07743 Jena, Germany
[b] Institut für Organische Chemie und Makromolekulare Chemie der Universität Jena,
Humboldtstraße, 07743 Jena, Germany
[c] Institut für Anorganische und Analytische Chemie der Universität Jena,
August-Bebel-Straße 2, 07743 Jena, Germany;
On leave from the Laboratoire de Chimie Supramoléculaire, ISIS/ULP Strasbourg, 4 rue Blaise Pascal, 67000 Strasbourg, France

 © WILEY-VCH Verlag GmbH, D-69451 Weinheim, 2000 1434–1948/00/0505–1055 $ 17.50+.50/0

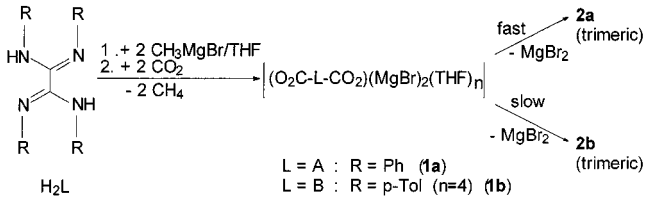


Figure 1. Pathway of the formation of **2a** and **2b**

from **1a**. Colourless crystals of pure **2a** could be obtained from the filtrate in 30% yield.

When the synthesis was carried out in dilute solution (90 mL of THF) only pure **2a** was isolated in 80% yield. In contrast, the product of the analogous reaction with tetra-*p*-tolyloxalic amidine was analytically pure **1b** (Figure 1).

The IR spectrum of **2a** exhibits two bands in the region of the C=O and C=N valence frequencies at 1630 (less intense) and 1656 cm^{-1} (more intense). This suggests that both C=N and carbamato groups are present in the molecule.

Elemental analysis of **2a** showed that there was no bromide in the CO_2 insertion product and pointed to the analytical composition of $[Mg(CO_2)_2(\mathbf{A})(THF)_2]_n$. A spectroscopically identical product was obtained by using dried air for the CO_2 insertion.

Single crystals of **2a** were grown from a dilute THF solution. The X-ray crystal structure revealed a trimeric structure of the product in which three magnesium centres are connected by six μ_2-carbamato bridges according to the above-mentioned analytical composition $[Mg(CO_2)_2(\mathbf{A})(THF)_2]_3$. Figure 2 shows the molecular structure of the

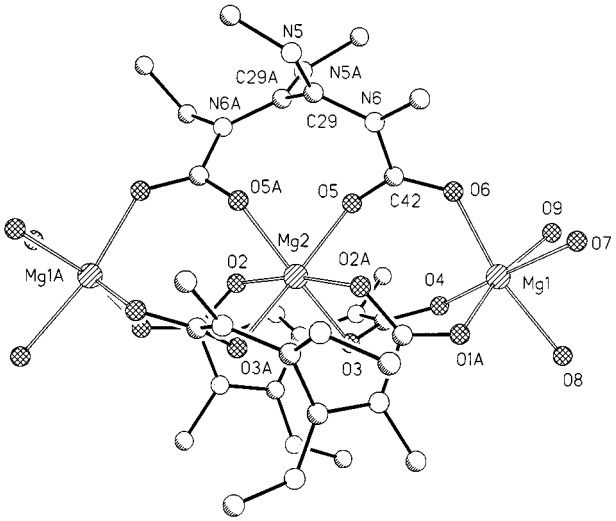


Figure 2. View of the inner sphere of complex **2a** with selected bond lengths [Å] and bond angles [°]: Mg1–O1A 2.021(6), Mg1–O4 2.026(5), Mg1–O6 2.016(6), Mg1–O7 2.169(6), Mg1–O8 2.144(6), Mg1–O9 2.110(7), Mg2–O2 2.075(4), Mg2–O3 2.089(6), Mg2–O5 2.076(6), C42–O5 1.239(8), C42–O6 1.263(9), N6–C29 1.377(10), N6–C42 1.420(10), N5–C29 1.271(10), C29–C29A 1.54(2); O1A–Mg1–O4 97.0(2), O1A–Mg1–O6 98.7(3), O1A–Mg1–O7 89.5(2), O1A–Mg1–O8 85.7(3), O1A–Mg1–O9 168.4(3), O2–Mg2–O2A 170.6(3), O2–Mg2–O3 84.9(2), O2–Mg2–O3A 88.8(2), O2–Mg2–O5 96.3(2), O2–Mg2–O5A 90.6(2), O5–C42–O6 127.6(7), N5–C29–N6 120.3(7); symmetry transformation used to generate equivalent atoms A: $-x - 1, -y, z$

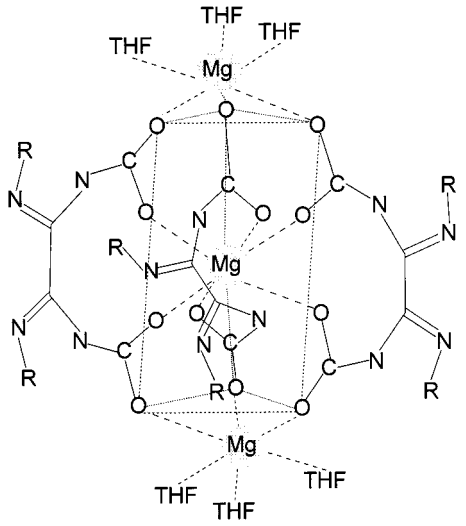


Figure 3. Coordination of the three carbamato strains in **2a** around the Mg centres

molecule and Figure 3 the inner part of **2a**. Relevant bond lengths and angles are also summarised in Figure 2.

The shape of the molecule resembles a straight prism (h = 6.4 Å) with two eclipsed (by 17°) triangles (3 × 3 × 3 Å) (Figure 3). The three magnesium atoms are exactly linear (the Mg–Mg–Mg angle is 180°) and lie within a distance of d_{Mg} = 4.211(6) Å. The central magnesium ion is surrounded by six O-donor atoms of the μ_2-carbamato bridges in an octahedral fashion, while the two peripheral magnesium ions are facially coordinated by three O-donor atoms of the carbamato groups and three THF molecules. The six negatively charged carbamato groups in **2a** have almost identical C–O distances [1.25(1) Å] and O–C–O angles [127.0(4) –127.6(4)°]. Three strongly twisted oxalamidine groups are located above the edges of the prism, with the 1,2-diimine units directed outwards, with a torsion angle for the N=C–C=N groups of 122.3°.

Thus, the molecule exhibits three soft Lewis base centres (the uncoordinated 1,2-diimine units) above the edges of the prism and two (potentially hard) Lewis centres (the peripheral magnesium atoms) above the basic triangles of the same prism. Because of the energetically unfavourable "hard-soft" combination the Lewis acid and base centres do not proceed to polymers. However, the free 1,2-diimine units can react with further metal centres (vide infra).

The ^{13}C-NMR spectrum of **2a** in [D$_6$]DMSO has only twelve resonances which correspond to the carboxylated oxalic amidinato ligands. The very strong carbamate signal appears at δ = 159.5 and the signals for THF at δ = 67.9 and 26.3. This simple pattern clearly shows that the highly symmetrical trimeric structure found by X-ray diffraction remains intact in solution.

The coordination of the peripheral magnesium atoms resembles the coordination of the magnesium ion in the substrate-free Rubisco enzyme[4] in which the magnesium centre also has an octahedral environment formed by three facially coordinated COO groups (one from a carbamato ligand and two from carboxylato groups) and three coord-

inated solvent molecules (water). However, the Mg–O(carbamato) distances in **2a** [d_{Mg-O} = 2.016(6)–2.169(6) Å] are significantly shorter than in the enzyme crystal (d_{Mg-O} = 2.31 Å).

In contrast to the above-described reaction with tetraphenyloxalic amidine, the reaction of tetra-*p*-tolyloxalic amidine **H_2B** with CH_3MgBr, followed by treatment with carbon dioxide, resulted in the pure bromo magnesium complex **1b** with the analytical composition $[(MgBr)_2(CO_2)_2$-(**B**)$(THF)_4]_n$ which was isolated as a microcrystalline solid. In this reaction the subsequent elimination of $MgBr_2$ proceeded very slowly (Figure 1). Nevertheless, some crystals of bromide-free carbamato complex **2b** could be obtained from the reaction mixture after some weeks. Compound **2b** was found to be isostructural with **2a** by an X-ray structural analysis.

The ^{13}C-NMR investigations of **1b** pointed to a molecule with only low symmetry; the signal of the carbamato group was found at δ = 161.7. The IR spectrum showed a strong band at 1639 cm^{-1} which may be assigned to the carbonyl group of the carbamato ligand. Since single crystals of **1b** could not be isolated, the structure of this compound remains unknown.

To gain further insight into the coordination sphere in MgBr-containing carbamato complexes, we have also synthesised complex **3** by deprotonation of $(isopropyl)_2NH$ with one equivalent MeMgBr and subsequent reaction with CO_2 to form a white, crystalline product with the analytical composition $[(iPr)_2–N–CO_2–MgBr(THF)_2]_2$ in high yield (95%) (Equation 1).

$$\begin{aligned} &2\,(i\mathrm{Pr})_2\mathrm{NH} + 2\,\mathrm{CH_3MgBr} + n\,\mathrm{THF} \rightarrow \\ &2\,(i\mathrm{Pr})_2\mathrm{N–MgBr(THF)_n} + 2\,\mathrm{CH_4} \\ &2\,(i\mathrm{Pr})_2\mathrm{N–MgBr(THF)}_n + 2\,\mathrm{CO_2} \rightarrow \\ &[(i\mathrm{Pr})_2\mathrm{N–CO_2)(MgBr(THF)_2]_2} + n - 2\,\mathrm{THF} \end{aligned} \quad (1)$$

The ^{1}H-NMR spectrum of **3** ([D_6]DMSO, 20 °C) shows only the resonances for the protons of the isopropyl group (δ = 1.17, 1.20, and 3.28) and the protons of THF (δ = 1.73, 3.57). However, no signal for the N–H proton was found. Furthermore, the ^{13}C-NMR spectrum exhibits only one, weak carbamate signal at δ = 166.39 in [D_7]DMF. In addition, the IR spectrum showed no band for the N–H stretching frequency in the 3300 cm^{-1} region. An X-ray crystal structure determination showed the dimeric structure of **3**, which is shown in Figure 4 along with relevant bond lengths and angles. The coordination sphere around the magnesium ions consists of three oxygen donor atoms of the bridging carbamato groups, two axially coordinated THF molecules and one monodentate bromide anion, and can be described as a distorted octahedron. Two of the carbamato oxygens are bonded at a distance of 1.963(2) Å, while the third one is more weakly bound with a bond length of 2.358(2) Å. Both carbamato groups act as tridentate bridging ligands and form, together with the two Mg ions, a planar eight-membered ring with a Mg–Mg distance of 3.277(2) Å.

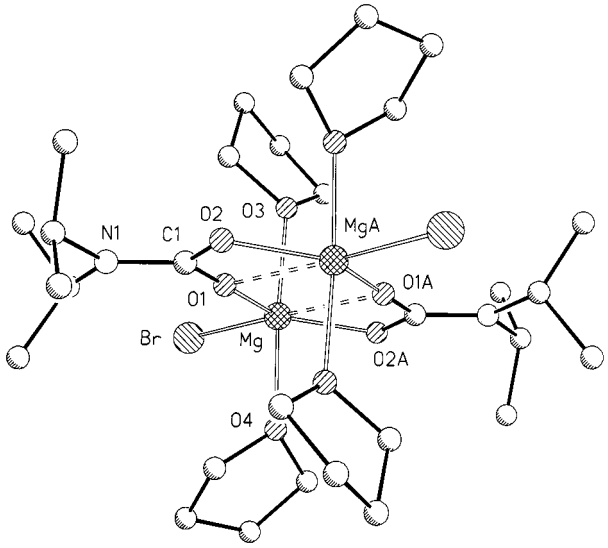
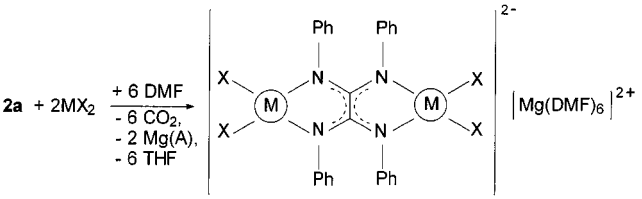


Figure 4. Molecular structure of the dimeric complex **3** with selected bond lengths [Å] and bond angles [°]: Mg–Br 2.572(1), Mg–O1 1.963(2), Mg–O2A 2.042(2), Mg–O1A 2.358(2), Mg–O3 2.117(2), Mg–O4 2.119(2), C1–O1 1.286(3), C1–O2 1.262(4), C1–N1 1.348(4); Br–Mg–O1 108.88(7), Br–Mg–O1A 168.95(7), Br–Mg–O2A 110.06(7), Br–Mg–O3 89.92(7), Br–Mg–O4 91.49(7), O1–C1–O2 118.8(3), N1–C1–O1 120.5(3), N1–C1–O2 120.7(3); symmetry transformation used to generate equivalent atoms A: $-x + 2, -y + 2, -z + 2$

Reactions of the Carbamato Complexes With Metal Halides

The reaction of **2a** with $ZnCl_2$ in DMF gave the yellow, sparingly soluble complex $[Cl_2Zn(A)ZnCl_2][Mg(DMF)_6]$ (**4**) in 80% yield (with respect to $ZnCl_2$) even when the starting materials were reacted in the molar ratio 1:1. Using an excess of $ZnCl_2$ (6:1) resulted in higher yields of **4** (Figure 5)



4 : M = Zn, X = Cl
5 : M = Co, X = Br

Figure 5. Formation reaction of the dimeric complexes **4** and **5**

An X-ray crystal structure determination (Figure 6) and FAB-MS showed a complex anion with two tetrahedrally coordinated zinc ions bridged by the deprotonated oxalamidine ligand. The electrostatic charge is counterbalanced by a magnesium ion which is surrounded by six DMF molecules. No CO_2 is present in the complex. This structure seems to indicate that coordination of metal fragments at the peripheral 1,2-diimine units of the trimeric complex **2a** causes steric strain in the inner part of the trimer leading to a complete rearrangement of the molecule with elimination of CO_2 and formation of the dimer **4**.

The same reaction was observed when $CoBr_2$ was treated with **2a** (Figure 5). Single crystals of the resulting green Co complex **5** were obtained from THF. According to the X-

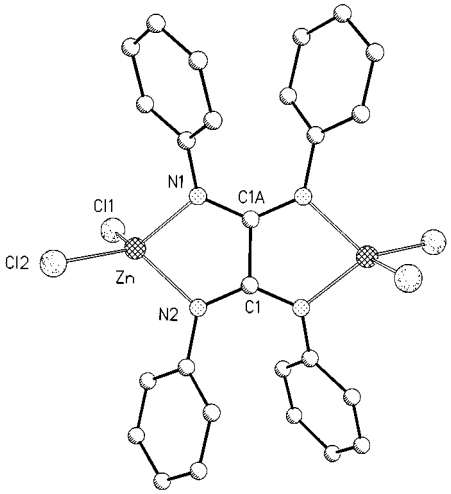


Figure 6. Molecular structure of **4** with selected bond lengths [Å] and bond angles [°] (the cation $[Mg(DMF)_6]^{2+}$ is omitted for clarity): Zn–Cl1 2.296(1), Zn–Cl2 2.278(1), Zn–N1 2.016(5), Zn–N2 2.020(5), N1–C1A 1.338(7), N2–C1 1.320(7), C1–C1A 1.565(11); Cl1–Zn–Cl2 113.10(7), Cl1–Zn–N1 114.7(1), Cl1–Zn–N2 111.1(1), N1–C1A–N2A 131.9(5), N2–C1–C1A 114.4(6); symmetry transformation used to generate equivalent atoms A: $-x + 2$, $-y + 2$, $-z + 1$

ray structural analysis, compound **5** exhibits the same dimeric structure as found for the Zn complex **4**. The bond lengths and angles in the bridging oxalic amidinate, and between the tetrahedral Co^{II} centres and the nitrogen donor atoms, are also similar (Figure 7).

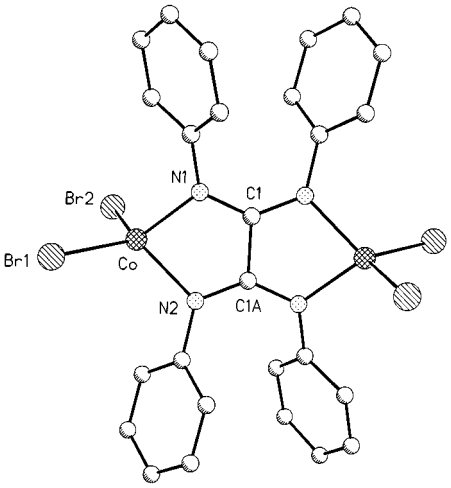


Figure 7. Molecular structure of **5** with selected bond lengths [Å] and bond angles [°] (the cation $[Mg(DMF)_6]^{2+}$ is omitted for clarity): Co–Br1 2.375(1), Co–Br2 2.375(1), Co–N1 1.986(6), Co–N2 1.999(6), N1–C1 1.340(9), N2–C1A 1.328(9), C1–C1A 1.555(13); Br1–Co–Br2 112.30(6), Br1–Co–N1 115.6(1), Br1–Co–N2 115.0(1), N1–C1–N2A 132.7(6), N1–C1–C1A 113.2(8); symmetry transformation used to generate equivalent atoms A: $-x + 1$, $-y + 1$, $-z + 2$

Carboxylation of Acetophenone

Acetophenone was used as the substrate for CO_2 transfer reactions because it contains the CH_3CO–R group which is carboxylated in biotion-dependent reactions as well. The reaction of acetophenone with the carbamato complexes **1b** or **1a** (contaminated with ca. 10% of the inactive trimer **2a**) either in THF at 70 °C or in DMF at room temperature, followed by hydrolysis, resulted in the formation of the carboxylation product benzoylic acid. The free carboxylic acid could either be determined by NMR spectroscopy or by HPLC determination. Although the yields of this C–C-linkage reaction were low (10%), the reaction may be considered as a model step for the CO_2 transfer reaction of carboxybiotin in biological reactions which proceed with acetylCoA to form the carboxylated product HOOC–CH_2–CO–CoA. In contrast, **2a**, **2b**, and **3** do not contain "activated" CO_2. This suggests that the coordination environment of the metal centre essentially influences the reactivity of the carbamato–Mg group.

Conclusions

In the present paper we have shown that carbamato magnesium complexes can be synthesised by treating oxalic amidines or di(isopropyl)amine with CH_3MgBr, followed by uptake of CO_2. The complexes **2a**, **2b**, and **3** represent structurally elucidated carbamato magnesium complexes which are of interest with respect to the magnesium containing active centres of biotin-dependent enzymes and Rubisco. The reaction of $ZnCl_2$ or $CoBr_2$ with the free diimine groups of **2a** results in the complete elimination of CO_2 and a rearrangement of the system to form the dinuclear complexes **4** and **5**.

Whereas **2a**, **2b**, and **3** are not able to transfer CO_2 to compounds with C–H-acidic bonds, both the carbamato complexes **1b** and **1a** (containing ca. 10% of the inactive trimer **2a**) react with acetophenone to form benzoylic acid upon hydrolysis, simulating the C–C linking step in biotin-dependent CO_2 transfer reactions.

Experimental Section

General: The oxalic amidine ligands were prepared according to literature procedures.[21] CH_3MgBr and CH_3MgCl (3 M in diethyl ether), purchased from Aldrich, and pure CO_2 (4.8) from Linde AG, were used without additional purification.

All reactions were carried out under argon with standard Schlenk techniques and all solvents dried and distilled before use.

^{1}H-NMR spectra were obtained with a Bruker AC 200 MHz spectrometer and all spectra were referenced to TMS or deuterated solvent as an internal standard. FAB mass spectra were obtained with a Finnigan MAT SSQ 710 spectrometer (2,4-dimethoxybenzyl alcohol as matrix). IR measurements were carried out with a Perkin–Elmer System 2000 FT-IR. Analytical HPLC experiments were carried out using a water HPLC system, consisting of a Knauer HPLC pump 64, a Rheodyne 7125 5 μL injector loop, a Merck Li Chrophor RP 18 (5μm) column and a Knauer variable wavelength detector at $\lambda = 295$ nm. The system was controlled by Knauer HPLC 2.21a software. The mobile phase used was 50:50 CH_3CN/H_2O containing 0.01 M KH_2PO_4 and adjusted to pH = 2. Elemental analyses were carried out at the Microanalytical Laboratory of the Friedrich Schiller University, Jena. Metals were determined by complexometric titration of an aqueous solution, obtained by reaction of the complex with dilute H_2SO_4, followed by extraction

of the organic products with diethyl ether and subsequent addition of ammonia. Halogen was determined by titration with silver nitrate.

$[Mg(CO_2)_2(A)(THF)_2]_3$ (2a): One equivalent (per N–H group) of CH_3MgBr (3 M in diethyl ether) was added slowly to a stirred solution of ligand H_2A (1 g, 2.56 mmol) in 50 mL of anhydrous THF until the gas evolution was finished. Then the yellowish solution was cooled to –20 °C and CO_2 was bubbled through the solution for some minutes. The resulting solution was shaken at room temperature for 1 h. After 24 h, a white precipitate of product **1a** (containing ca. 10% **2a** as calculated from the elemental analysis) was isolated by filtration, washed three times with diethyl ether and subsequently dried in vacuo. Yield: 60%. Additionally, pure complex **2a** crystallised from the mother liquor after standing overnight. Yield: 30% of pure **2a**.

When the reaction was carried out in 90 mL of THF as solvent and a CH_3MgBr solution in toluene was used, only pure crystalline **2a** was isolated in 80% yield.

Single crystals of **2a** were obtained by reducing the remaining THF solution to half volume and allowing to crystallise at room temperature, or by recrystallisation of the isolated crude product **1a** from THF. Longer reaction times and higher temperatures resulted in the formation of **2a** in higher yields by accomplished $MgBr_2$ extrusion.

2a: $C_{108}H_{108}Mg_3N_{12}O_{18}$ (1935.03): calcd. C 67.0, H 5.6, Mg 3.8, N 8.7; found C 66.3, H 5.8, Mg 3.7, N 8.7. – ^{1}H NMR ([D$_6$]DMSO, 20 °C): δ = 6.63–7.28 (m, arom.). – ^{13}C NMR ([D$_6$]DMSO, 20 °C): δ = 25.2, 67.1 (THF), 120.4, 121.6, 122.0, 124.4, 127.2, 128.2, (arom., phenyl), 143.3 (*ipso*-C-amine), 149.3 (N=C–N), 150.4 (*ipso*-C-imine), 159.5 (carbamate). – IR (nujol): $\tilde{\nu}$ = 1592 (C=C_{arom}), 1630, 1656, (N–COO, C=N) cm^{-1}.

Mixture 1a/2a: (90:10) {**1a**: $[Mg_2Br_2(CO_2)_2(A)(THF)_4]_n$}: calcd. C 56.6, H 4.9, Br 13.4 Mg 5.0, N 6.3; found C 55.4, H 5.3, Br 13.4, Mg 5.0, N 5.8.

$[Mg_2Br_2(CO_2)_2(B)(THF)_4]_n$ (1b): The reaction was carried out as described above for **2a**. The main product in this reaction was **1b**. Yield 92%. – $C_{48}H_{60}Br_2Mg_2N_4O_8$ (1029.5): calcd. C 56.0, H 5.9, Br 15.4, Mg 4,7, N 5.4; found C 55.0, H 6.1, Br 14.1, Mg 4.5, N 5.3. – ^{1}H NMR ([D$_6$]DMSO, 20 °C): δ = 1.73 (dd, 16 H, CH_2), 2.13, 2.26 (2 × s, 12 H, CH_3), 3.57 (dd, 16 H, CH_2), 7.27–6.62 (m, 20 H, arom.). – ^{13}C NMR ([D$_6$]DMSO, 20 °C): δ = 20.8, 20.9, (CH_3), 25.2, 67.0 (CH_2, THF), 120.0, 121.7, 122.3, 128.8, 129.2, 130.8, 131.7, 134.9 (arom. tolyl), 141.6 (*ipso*-C-amine), 148.1 (N=C–N), 151.0 (*ipso*-C-imine), 161.7 (carbamate). – IR (Nujol): $\tilde{\nu}$ = 1592 (C=C_{arom}), 1630, 1639 (N–COO, C=N) cm^{-1}.

Single crystals of **2b** were isolated from the mother liquor after storage at –20 °C for some weeks. Yield: 5%. Characterization by X-ray analysis.

$[(iPr)_2NCO_2MgBr(THF)_2]_2$ (3): The reaction was analogously carried out as described for **2a.** Yield 95%. – $C_{30}H_{60}Br_2Mg_2N_2O_8$ (785.2): calcd. C 45.9, H 7.7, Br 20.4, N 3.6; found: C 44.6, H 8.2, Br 24.1, N 3.6. – ^{1}H NMR ([D$_6$]DMSO, 20 °C): δ = 1.17 (s, 6 H, CH_3), 1.20 (s, 6 H, CH_3), 1.73 (dd, 8 H, CH_2, THF), 3.28 (m, 2 H, CH), 3.57 (dd, 8 H, O–CH_2, THF). – ^{13}C NMR ([D$_6$]DMSO, 20 °C): δ = 19.9 (CH_3), 28.8 (CH_2, THF), 34.2 (C–H), 67.8 (O–CH_2, THF), 166.3 (carbamate). – IR (Nujol): $\tilde{\nu}$ = 1578 cm^{-1} (carbamate).

$[Mg(DMF)_6][Zn_2(A)Cl_4]$ (4): Compound **2a** (100 mg, 5.2·10^{-5} mol) was dissolved in 1 mL of anhydrous DMF and $ZnCl_2$ (42 mg, 31.2·10^{-5} mol), dissolved in 1 mL of DMF, was added. After a few minutes of stirring, a yellow solid precipitated. The solid was filtered off, washed with THF and dried in vacuo. Single crystals were grown from the mother liquor at room temperature. Yield: 152 mg (87%). – $C_{44}H_{62}Cl_2MgN_{10}O_6Zn_2$ (1123.9): calcd. C 47.0, H 5.5, Cl 12.6, N 12.5; found C 42.7, H 5.1, Cl 12.6, N 11.2. – ^{1}H NMR ([D$_6$]DMSO, 20 °C) δ = 2.72 (s, CH_3, 18 H, DMF), 2.88 (s, CH_3, 18 H, DMF), 6.55–6.82 (m, 20 H, arom.), 7.94 (s, 6 H, CH, DMF). – IR (nujol): $\tilde{\nu}$ = 1591 (C=C_{arom}), 1659 (C=O, DMF) cm^{-1}. – FAB-MS [DMBA]: *m*/*z* = 945 [M$^+$ – 2 DMF – Cl + 2 H], 622 [M$^+$ – 6 DMF – Mg – Cl + 2 H].

$[Mg(DMF)_6][Co_2(A)Br_4]$ (5): This compound was prepared in a similar manner to **4**. Single crystals of the green compound were grown from a solution of the redissolved product in DMF at –20 °C. IR (nujol): $\tilde{\nu}$ = 1659 (C=O, DMF), 1591 (C=C_{arom}) cm^{-1}. – FAB-MS [DMBA]: *m*/*z* = 1288 [M$^+$], 838 [M$^+$ – 2 DMF – Cl + 2 H – 2 DMF + 2 H$^+$], 602 [**A**CoBr(DMF) + 2 H$^+$], 528 [**A**CoBr + 2 H$^+$].

Carboxylation of Acetophenone: Compound **1b** (1.35 mol), dissolved in 70 mL, of anhydrous DMF was treated with 1.2 mL of acetophenone and the resulting solution was stirred for 12 h at room temperature. The resulting benzoyl acetic acid was determined either by aqueous work up or by HPLC.

By Wet Workup: After removal of the DMF in vacuo, the remaining residue was hydrolysed with 50 mL of 25% HCl and the water phase extracted three times with diethyl ether. The organic phase was washed with a 10% solution of Na_2CO_3 and the separated water phase was acidified carefully until pH = 5 and subsequently extracted with diethyl ether. The diethyl ether phase was dried with solid Na_2SO_4 and the solvent removed in vacuo to give benzoyl acetic acid as a white solid. Yield 5–10%. – ^{1}H NMR ([D$_6$]acetone, 20 °C): δ = 4.02 (–CH_2–).

By HPLC: Benzoyl acetic acid was determined by comparison with an authentic sample of benzoylic acid. Yield: 6–10%.

The reaction product **1a/2a** (90:10) reacts analogously to form 6–10% benzoylic acid.

Crystal Structure Determinations: The intensity data for the compounds **2a** and **3** were collected with a Nonius CAD4 diffractometer and for the other compounds with a Nonius Kappa CCD diffractometer, using graphite-monochromated Mo-K_α radiation. Data were corrected for Lorentz and polarization effects. Only the compounds **3** and **5** were corrected for absorption effects.[22,23]

The structures were solved by direct methods (SHELXS[24]) and refined by full-matrix least-squares techniques against F_o^2 (SHELXL-97[25]). For compound **4** the hydrogen atoms were located by difference Fourier synthesis and refined isotropically; the hydrogen atoms of the other compounds were included at calculated positions with fixed thermal parameters. All non-hydrogen atoms were refined anisotropically.[25] XP (SIEMENS Analytical X-ray Instruments, Inc.) was used for structure representations.

Crystal Data for 2a:[26] $C_{108}H_{108}Mg_3N_{12}O_{18} \cdot 1.5\,C_4H_8O$, M_r = 2043.15 gmol^{-1}, colourless prism, size 0.40 × 0.38 × 0.36 mm, orthorhombic, space group *Aba*2, crystal is a racemic twin, *a* = 17.978(2), *b* = 23.753(3), *c* = 28.248(3) Å, *V* = 12063 (1) Å^3, *T* = –90 °C, *Z* = 4, $\rho_{calcd.}$ = 1.125 gcm^{-3}, μ (Mo-K_α) = 0.91 cm^{-1}, *F*(000) = 4320, 6269 reflections in *h*(0/22), *k*(0/29), *l*(0/35), measured in the range 2.27° ≤ Θ ≤ 26.33°, 6269 independent reflections, 3659 reflections with $F_o > 4\,\sigma(F_o)$, 620 parameters, 1 restraint, $R1_{obs}$ = 0.086, $wR2_{obs}$ = 0.218, $R1_{all}$ = 0.177, $wR2_{all}$ = 0.274,

GOOF = 1.765, largest difference peak and hole: 0.862/–0.332 e Å^{-3}.

Crystal Data for 2b: $C_{146}H_{180}Mg_3N_{12}O_{24}$, M_r = 2559.95 gmol^{-1}, colourless prism, size 0.40 × 0.35 × 0.30 mm, monoclinic, space group $P2_1/c$, a = 24.085(2), b = 18.1640(10), c = 30.297(3) Å, β = 91.274(4) °, V = 13251.1(19) Å^3, T = –90 °C, Z = 4, $\rho_{calcd.}$ = 1.283 gcm^{-3}, μ (Mo-K_α) = 1 cm^{-1}, F(000) = 5472, 30541 reflections in h(–25/25), k(0/20), l(–30/32), measured in the range 2.44° ≤ Θ ≤ 23.28°, completeness Θ_{max} = 97.2%, 17884 independent reflections, R_{int} = 0.099, 10749 reflections with $F_o > 4\,\sigma(F_o)$, 1438 parameters, 0 restraints, $R1_{obs}$ = 0.225, wR^2_{obs} = 0.542, $R1_{all}$ = 0.281, wR^2_{all} = 0.580, GOOF = 1.255, largest difference peak and hole: 1.063/–0.694 e Å^{-3}.

Crystal Data for 3:[26] $C_{30}H_{60}Br_2Mg_2N_2O_8$, M_r = 785.24 gmol^{-1}, colourless prism, size 0.40 × 0.35 × 0.35 mm, monoclinic, space group $P2_1/n$, a = 11.062(3), b = 11.743(2), c = 15.184(3) Å, β = 101.38(2)°, V = 1933.6(7) Å^3, T = –90 °C, Z = 2, $\rho_{calcd.}$ = 1.349 gcm^{-3}, μ (Mo-K_α) = 21.73 cm^{-1}, ψ scan, $trans_{min.}$: 0.117, $trans_{max.}$: 0.279, F(000) = 824, 3762 reflections in h(0/13), k(–14/0), l(–18/17), measured in the range 2.21° ≤ Θ ≤ 26.30°, 3579 independent reflections, R_{int} = 0.028, 2440 reflections with $F_o > 4\,\sigma(F_o)$, 319 parameters, 0 restraints, $R1_{obs}$ = 0.035, wR^2_{obs} = 0.075, $R1_{all}$ = 0.084, wR^2_{all} = 0.091, GOOF = 1.080, largest difference peak and hole: 0.305/–0.504 e Å^{-3}.

Crystal Data for 4:[26] $[C_{18}H_{42}MgN_6O_6]^+[C_{26}H_{20}Cl_4N_4Zn_2]^-$, M_r = 1123.9 gmol^{-1}, colourless prism, size 0.32 × 0.30 × 0.28 mm, triclinic, space group P–1, a = 9.6879(4), b = 10.9384(4), c = 13.9082(4) Å, α = 78.401(2), β = 71.791(2), γ = 78.934(2) °, V = 1358.19(8) Å^3, T = –90 °C, Z = 1, $\rho_{calcd.}$ = 1.367 gcm^{-3}, μ (Mo-K_α) = 11.43 cm^{-1}, F(000) = 578, 12317 reflections in h(0/12), k(–13/13), l(–16/17), measured in the range 3.12° ≤ Θ ≤ 26.35°, completeness Θ_{max} = 99.2%, 5496 independent reflections, R_{int} = 0.036, 4374 reflections with $F_o > 4\sigma(F_o)$, 304 parameters, 0 restraints, $R1_{obs}$ = 0.083, wR^2_{obs} = 0.210, $R1_{all}$ = 0.104, wR^2_{all} = 0.228, GOOF = 1.004, largest difference peak and hole: 1.419/–1.350 e Å^{-3}.

Crystal Data for 5:[26] $[C_{18}H_{42}MgN_6O_6]^+[C_{26}H_{20}Co_2Br_4N_4]^-$, M_r = 1282.80 gmol^{-1}, colourless prism, size 0.28 × 0.22 × 0.11 mm, triclinic, space group P–1, a = 9.8104(6), b = 11.0742(5), c = 14.0020(9) Å, α = 76.997(3), β = 71.602(2), γ = 78.400(3) °, V = 1392.46(14) Å^3, T = –90 °C, Z = 1, $\rho_{calcd.}$ = 1.530 gcm^{-3}, μ (Mo-K_α) = 35.27 cm^{-1}, semi-empirical, $trans_{min.}$: 0.432, $trans_{max.}$: 0.776, F(000) = 644, 9237 reflections in h(0/12), k(–13/13), l(–16/17), measured in the range 3.04° ≤ Θ ≤ 26.49°, completeness Θ_{max} = 98.5%, 5693 independent reflections, R_{int} = 0.085, 3271 reflections with $F_o > 4\sigma(F_o)$, 304 parameters, 0 restraints, $R1_{obs}$ = 0.078, wR^2_{obs} = 0.178, $R1_{all}$ = 0.1527, wR^2_{all} = 0.2164, GOOF = 0.986, largest difference peak and hole: 0.706/–1.020 e Å^{-3}.

Acknowledgments

Financial support for this work from the Deutsche Forschungsgemeinschaft (SFB 436), the VW-Stiftung and the Fonds der Chemischen Industrie is gratefully acknowledged. M. R. wishes to thank the Studienstiftung des Deutschen Volkes for a grant.

[1] S. D. Taylor, R. Kluger, *J. Am. Chem. Soc*. **1993**, *115*, 867–871.
[2] D. J. Kuo, I. A. Rose, *J. Am. Chem. Soc*. **1993**, *115*, 387–390.
[3] H. Martini, J. Retey, *Angew. Chem*. **1993**, *105*, 287–289; *Angew. Chem. Int. Ed. Engl*. **1993**, *32,* 278–280.
[4] F. Lynen, J. Knappe, E. Lorch, G. Jütting, E. Ringelmann, *Angew. Chem.***1959**, *71*, 481–486.
[5] F. Lynen, J. Knappe, E. Lorch, G. Jütting, E. Ringelmann, J. P. Lachance, *Biochem. Z*. **1961**, *335*, 123–167.
[6] S. Berger, A. Braune, W. Buckel, U. Härtel, M.-L. Lee, *Angew. Chem*. **1996**, *108*, 2259–2261; *Angew. Chem. Int. Ed. Engl*. **1996**, *35*, 2132–2133.
[7] Y. Musashi, T. Hamada, S. Sakaki, *J. Am. Chem. Soc*. **1995**, *117*, 11320–11326.
[8] T. J. Andrews, G. H. Lorimer, N. E. Tolbert, *Biochem*. **1973**, *12*, 11–17.
[9] W. W. Cleland, T. J. Andrews, S. Gutteridge, F. C. Hartman, G. H. Lorimer, *Chem. Rev*. **1998**, *98*, 549–561.
[10] W. A. King, J. E. Gready, T. J. Andrews, *Biochem*. **1998**, *37*, 15414–15422.
[11] I. Anderson, S. Knight, Y. Lindqvist, T. Lundqvist, C.-I. Bränden, G. H. Lorimer, *Nature* **1989**, *337*, 229–234.
[12] T. C. Taylor, I. Anderson, *Nat. Struct. Biol*. **1996**, *3*, 95–101.
[13] A. S. Mildvan, D. C. Fry, E. H. Serpersu, in: *Enzymatic and Model Carboxylation and Reduction Reactions for Carbon Dioxide Utilization* (Eds.: M. Aresta, J. V. Schloss), Kluwer Academic Publishers, Dordrecht, The Netherlands, **1990**, p. 321–345.
[14] D. Walther, U. Ritter, R. Kempe, J. Sieler, B. Undeutsch, *Chem. Ber*. **1992**, *125*, 1529–1536.
[15] R. E. Tirpak, R. S. Olsen, M. W. Rathke, *J. Org. Chem*. **1985**, *50*, 4877–4879.
[16] N. Matsamura, N. Asai, S. Yoneda, *J. Chem. Soc., Chem. Commun*. **1983**, 1487–1488.
[17] N. Matsamura, T. Ohba, S. Yoneda, *Chem. Lett*. **1983**, 317–318.
[18] N. Matsamura, T. Ohba, H. Inoue, *Bull. Chem. Soc*. **1982,** *55*, 3949–3950.
[19] D. Walther, M. Ruben, S. Rau, *Coord. Chem. Rev*. **1999**, *182*, 68–100.
[20] [20a] C. C. Chang, B. Srinivas, M. L. Wu, W. H. Chiang, M. Y. Chiang, C. S. Hsiung, *Organometallics* **1995,** *14*, 5150–5159. – [20b] C. C. Chang, M. S. Ameerunisha, *Coord. Chem. Rev*. **1999**, *189*, 199–278 and references therein.
[21] A. Bauer, *Ber. Dtsch. Chem. Ges.* **1907**, *40*, 2650–2662.
[22] *MOLEN, An Interactive Structure Solution Procedure*, Enraf–Nonius, Delft, The Netherlands, **1990.**
[23] Z. Otwinowski, W. Minor, "Processing of X-ray Diffraction Data Collected in Oscillation Mode", in: *Methods in Enzymology*, vol. 276, "Macromolecular Crystallography", Part A (Eds.: C.W. Carter, R.M. Sweet), Academic Press, **1997**, pp. 307–326.
[24] G. M. Sheldrick, *Acta Crystallogr. Sect. A* **1990**, *46*, 467–473.
[25] G. M. Sheldrick, *SHELXL-97*, University of Göttingen, Germany, **1993**.
[26] Crystallographic data (excluding structure factors) for the structures included in this paper have been deposited with the Cambridge Crystallographic Data Centre as supplementary publication no. CCDC-407983 (**2a**), -135156 (**2b**), -135157 (**3**), -135158 (**4**), -135159 (**5**). Copies of the data can be obtained free of charge on application to CCDC, 12 Union Road, Cambridge CB2 1EZ, UK [Fax: (internat.) + 44-1223/336-033; E-mail: deposit@ccdc.cam.ac.uk].

Received July 13, 1999
[I99373]

Organolanthanoids, 24[‡] Organoamido- and Aryloxo-Lanthanoids, 21[‡]

Syntheses and Structures of Bis(aryloxo)fluoroytterbium(III) Complexes, $[Yb(OAr)_2F(THF)]_2$ (OAr = OC_6H_2-2,6-*t*Bu_2-4-R; R = H, Me, *t*Bu), and Bis(cyclopentadienyl)fluoroytterbium(III) Complexes, $[YbCp_2F]_3$, $[Yb(MeCp)_2F]_4$, $[YbCp_2F(OPPh_3)]_2$, and $[Yb(MeCp)_2F(THF)]_2$

Glen B. Deacon,*[a] Gerd Meyer,[b] and Dirk Stellfeldt[b]

Dedicated to Prof. Dr. Othmar Stelzer on the occasion of his 60th birthday

Keywords: Lanthanide(III) / Ytterbium / Aryloxides / Fluorine / C–F Activation

Reaction of $[Yb(OAr)_2(THF)_3]$ (OAr = OC_6H_2-2,6-*t*Bu_2-4-R; R = H, Me, *t*Bu) with perfluorodecalin in THF at room temperature results in C–F activation and formation of the first heteroleptic aryloxofluorolanthanoid complexes, $[Yb(OAr)_2F(THF)]_2$. Oxidation of bis(cyclopentadienyl)ytterbium(II) with perfluoro(methylcyclohexane) or perfluorodecalin in DME surprisingly gives unsolvated $[YbCp_2F]_3$. The analogous reaction of bis(methylcyclopentadienyl)ytterbium(II) yields unsolvated $[Yb(MeCp)_2F]_4$, whilst in THF, the oxidation provides $[Yb(MeCp)_2F(THF)]_2$. Treatment of $[YbCp_2F(THF)]_2$ with triphenylphosphane oxide gives $[YbCp_2F(OPPh_3)]_2$. X-ray structure determinations revealed $[Yb(OAr)_2F(THF)]_2$ (R = H or *t*Bu) to be centrosymmetric fluoride-bridged dimers with five-coordination for ytterbium. Examination of the structures of the cyclopentadienyl complexes showed that $[YbCp_2F]_3$ is trimeric with formal eight-coordination for ytterbium and a planar $(YbF)_3$ ring, whereas $[Yb(MeCp)_2F]_4$ is an eight-coordinate tetramer having a puckered $(YbF)_4$ ring with F–Yb–F angles of ca. 90° and Yb–F–Yb angles close to 180° [178.9(4), 168.4(3)°]. Both $[Yb(MeCp)_2F(THF)]_2$ and $[YbCp_2F(OPPh_3)]_2$ are nine-coordinate fluoride-bridged dimers.

Introduction

Heteroleptic lanthanoid fluorides $[LnF_nL_{3-n}]$ [L = cyclopentadienyl (Cp), OAr, OR, NR_2 etc.] provide a synthetic challenge since the high stability of lanthanoid fluorides[3] may favour rearrangement into LnF_3 and LnL_3. {A tendency in this direction is shown by the isolation of the fluoride-rich, multiple-fluoride-bridged cage $[Yb_5(C_5Me_5)_6F_9]$ from the reaction of $[Yb(C_5Me_5)_2(OEt_2)]$ with C_9F_{18} in toluene.[3]} They are also of interest as potential olefin polymerisation catalysts, especially in view of the success of cyclopentadienylzirconium fluorides[4] in this role.[5] Complexes of this type are extremely rare,[6–14] there being no reported aryloxofluorolanthanoid complexes[9–12] and few examples of cyclopentadienylfluorolanthanoids.[3,6–8,12–21] We now report the syntheses and structures of the first aryloxofluorolanthanoid complexes, $[Yb(OAr)_2F(THF)]_2$ (OAr = OC_6H_2-2,6-*t*Bu_2-4-R; R = H, Me, *t*Bu), and some new bis(cyclopentadienyl)fluorolanthanoid(III) complexes, $[YbCp_2F]_3$, $[Yb(MeCp)_2F]_4$, and $[YbCp_2F(OPPh_3)]_2$, as well as a new synthesis and the structure of the previously reported,[3] but structurally uncharacterized, $[Yb(MeCp)_2F(THF)]_2$.

Results and Discussion

Syntheses

Reaction of the ytterbium(II) aryloxides $[Yb(OAr)_2(THF)_3]$ (OAr = OC_6H_2-2,6-*t*Bu_2-4-R; R = H, Me, *t*Bu) with perfluorodecalin gives the corresponding heteroleptic bis(aryloxo)fluorolanthanoid(III) complexes, shown (below) to be the dimers $[Yb(OAr)_2F(THF)]_2$.

$$2\,[Yb(OAr)_2(THF)_3] + C_{10}F_{18} \rightarrow [Yb(OAr)_2F(THF)]_2 + \text{unsaturated fluorocarbons} \quad (1)$$

Pefluorodecalin was recently introduced as an oxidant in lanthanoid chemistry in the synthesis of $[YbCp_2F(THF)]_2$.[21] This provided the first example of C–F activation of a saturated fluorocarbon by a lanthanoid complex. The compound has also been used to give Group 4 organometallic fluorides.[22]

The versatility of perfluorocycloalkanes in the preparation of heteroleptic lanthanoid fluorides is also illustrated

[‡] Part 23: Ref.[1] Part 20: Ref.[2]

[a] Chemistry Department, Monash University, Victoria 3800, Australia, Fax: (internat.) + 61-3/9905-4597, E-mail: Glen.Deacon@sci.monash.edu.au
[b] Institut für Anorganische Chemie, Universität zu Köln, Greinstraße 6, 50939 Köln, Fax: (internat.) + 49-221/470-5083, E-mail: Gerd.Meyer@uni-koeln.de

 © WILEY-VCH Verlag GmbH, D-69451 Weinheim, 2000 1434–1948/00/0505–1061 $ 17.50+.50/0

by syntheses of new bis(cyclopentadienyl)fluoroytterbium(III) complexes. Thus, reaction of $[YbCp_2(DME)]$ with perfluorodecalin or perfluoro(methylcyclohexane) in 1,2-dimethoxyethane surprisingly yields *unsolvated* bis(cyclopentadienyl)fluoroytterbium(III), shown to be trimeric (Equation 2).

$$3\ [YbCp_2(DME)] + C_{10}F_{18}\ (C_7F_{14}) \rightarrow [YbCp_2F]_3 + \text{unsaturated fluorocarbons} \quad (2)$$

This contrasts isolation of the solvated complex $[YbCp_2F(THF)]_2$ from the synthesis in tetrahydrofuran.[21] A similar reaction of $[Yb(MeCp)_2(THF)]$ with perfluorodecalin in DME also gives an *unsolvated* complex, revealed to be the novel and unexpected tetramer, $[Yb(MeCp)_2F]_4$, by X-ray crystallography.

$$4\ [Yb(MeCp)_2(THF)] + C_{10}F_{18} \rightarrow [Yb(MeCp)_2F]_4 + \text{unsaturated fluorocarbons} \quad (3)$$

The use of THF as a solvent for this reaction provides $Yb(MeCp)_2F(THF)$, which has been previously prepared by C–F activation of the more reactive perfluoro-2,3-dimethylpent-2-ene in THF.[3] These syntheses (1)–(3) establish oxidation of ytterbium(II) compounds by perfluorodecalin to be a general route to heteroleptic ytterbium(III) fluorides. However, perfluoro(methylcyclohexane) was an unsatisfactory oxidant for $[Yb(MeCp)_2(THF)]$ in THF [cf. $YbCp_2(DME)$[21]] and hence is a less widely applicable reagent. The low-moderate yields are probably due to incomplete deposition of the products, which have appreciable solubility in the reaction media, rather than competing reactions. Any LnF_3 formed by rearrangement (see Introduction) would have coprecipitated with the heteroleptic fluoro complexes, precluding the observed satisfactory analyses (below). In the present syntheses, the reduction products were not examined, but it has been shown that the oxidation of $[YbCp_2(DME)]$ by perfluoro(methylcyclohexane) yields perfluorotoluene and *p*-, *m*-, and *o*-$HC_6F_4CF_3$,[21] and that reduction of perfluorodecalin by low oxidation state group 4 metallocenes gives perfluoronaphthalene and specific hydropolyfluoronaphthalenes.[23]

The first complex of a bis(cyclopentadienyl)fluorolanthanoid with a ligand other than an ether has been obtained by displacement of coordinated THF by triphenylphosphane oxide.

$$[YbCp_2F(THF)]_2 + 2\ Ph_3PO \rightarrow [YbCp_2F(OPPh_3)]_2 + 2\ THF \quad (4)$$

It is of interest that this could be achieved without incurring rearrangement into the strongly-bonded phosphane oxide complex $[YbCp_3(OPPh_3)]$[1] and the highly stable[3] YbF_3.

Characterization

The composition of the complexes was established by lanthanoid metal and fluorine analyses. The latter were very valuable, particularly for the highly hydrolytically labile $[Yb(OAr)_2F(THF)]_2$ complexes, in view of the similarity in molecular weights between the fluoro and the corresponding hydroxo complexes. Further, the presence of fluorine in single crystals of $[Yb(OC_6H_2\text{-}2,4,6\text{-}t\text{Bu}_3)_2F(THF)]_2 \cdot 3\ THF$ was established by EDAX-measurements. The THF of solvation was lost on drying under vacuum in isolation of the bulk product. By contrast, for OAr = $OC_6H_3\text{-}2,6\text{-}t\text{Bu}_2$, both bulk product and single crystals have the same composition. The extreme sensitivity of $[Yb(OAr)_2F(THF)]_2$ compounds to hydrolysis was illustrated by the invariable observation of weak bands at ca. 3600 cm^{-1} in their infrared spectra, near to reported ν(OH) absorptions [3685, 3651m(sp)] of $[Yb(OC_6H_2\text{-}2,4,6\text{-}t\text{Bu}_3)_2(OH)(THF)]_2$,[24] and these bands intensified rapidly on brief deliberate exposure of the mulls/disk to the atmosphere. (The plate protected Nujol mulls or the KBr disks were briefly in air on transfer to the chamber of the IR spectrometer). Extreme sensitivity is not observed for the cyclopentadienylfluoroytterbium(III) complexes, which showed no analogous absorption in similarly recorded spectra. When solutions of the complexes were stored for several days to grow single crystals (see Experimental Section), there was no evidence of decomposition into LnF_3.

For the tetrahydrofuran complexes, absorption bands at 1050–1020 cm^{-1} and 880–860 cm^{-1} can be attributed to ring stretching modes of coordinated THF, shifted from the free ligand values (1070, 912 cm^{-1}) as expected on coordination[25] {e.g. compare $[Yb(MeCp)_2F(THF)]_2$ and $[Yb(MeCp)_2F]_4$; Experimental Section}, though phenolate absorption also occurs in the latter region.[26] By contrast the spectra of $[YbCp_2F]_3$ and $[Yb(MeCp)_2F]_4$, isolated from DME, do not show any absorption at 900–840 cm^{-1} corresponding to the intense absorption of free DME at 858 cm^{-1},[27] expected at higher energy on coordination.[28] In the spectrum of $[YbCp_2F(OPPh_3)]_2$, ν(PO) is observed at 1179 cm^{-1}, lowered from the free ligand value (1195 cm^{-1}) as expected on coordination.[29] The relatively small shift is consistent with observations for other $Ln(OPPh_3)$ complexes, which show a decrease in the shift of ν(PO) from La to Lu.[1,30]

Comparison of the far infrared spectra of $[Yb(OAr)_2F(THF)]_2$ and $[Yb(OAr)_2(THF)_3]$ complexes (Experimental section) suggests an intense ν(YbF) absorption is located at 390–375 cm^{-1} (Table 1) with the possibility of a second absorption (expected for a halogen-bridged dimeric structure[31]) near 300 cm^{-1} at least for OAr = $OC_6H_2\text{-}2,6\text{-}t\text{Bu}_2\text{-}4\text{-R}$, R = Me, or *t*Bu. The former are at higher frequencies than reported ν(YbF) values (330–298 cm^{-1})[3,21] for formally eight and nine-coordinate bis(cyclopentadienyl)fluorolanthanoid(III) complexes (Table 1), consistent with the lower coordination number, and are expectedly lower than ν(YbF) (569, 546 cm^{-1}) of matrix isolated, three-coordinate YbF_3.[32] No infrared absorption band was observed for $[YbCp_2F]_3$ at 350–275 cm^{-1}, where ν(YbF) is expected, but the Raman spectrum showed a ν(YbF) line at 336 cm^{-1}. Thus, ν(YbF) for the highly symmetrical structure (see below), is infrared inactive. For the less symmet-

rical $[Yb(MeCp)_2F]_4$, ν(YbF) was observed in the infrared spectrum, and the assignment for $[Yb(MeCp)_2F(THF)]_2$ is in agreement with that reported[3] (Table 1). There is some uncertainty over ν(YbF) of $[YbCp_2F(OPPh_3)]_2$ as Ph_3PO has weak absorption in the relevant region,[33] but the higher frequency band of two near 300 cm^{-1} seems the more likely. Overall, it is not possible to distinguish between eight- and nine-coordinate bis(cyclopentadienyl)fluorolanthanoid(III) complexes on the basis of ν(YbF) frequencies (Table 1).

Table 1. ν(Yb–F) frequencies of heteroleptic fluorolanthanoid(III) complexes

Compound	ν(Yb–F) [cm^{-1}][a]
$[Yb(OC_6H_3\text{-}2,6\text{-}t\text{Bu}_2)_2F(THF)]_2$[b]	387, 304 (?)
$[Yb(OC_6H_2\text{-}2,6\text{-}t\text{Bu}_2\text{-}4\text{-}Me)_2F(THF)]_2$[b]	381, 302
$[Yb(OC_6H_2\text{-}2,4,6\text{-}t\text{Bu}_3)_2F(THF)]_2$[b]	375, 304
$[YbCp_2F]_3$[b]	336 (Raman)
$[Yb(MeCp)_2F]_4$[b]	328
$[YbCp_2F(OPPh_3)]_2$[b]	306 (?)
$[Yb(MeCp)_2F(THF)]_2$[b]	332 (326[3])
$[YbCp_2F(THF)]_2$[21]	298
$[Eu(Me_5C_5)_2F(OEt_2)]$[3]	311
$[Sm(Me_5C_5)_2F(OEt_2)]$[3]	304
$[Yb(Me_5C_5)_2F(OEt_2)]$[3]	303

[a] From far infrared spectra, except where indicated otherwise. – [b] This work.

No metal containing ions were observed in the mass spectra of $[Yb(OAr)_2F(THF)]_2$ complexes, but trinuclear and dinuclear ions were observed for $[YbCp_2F]_3$, $[Yb(MeCp)_2F]_4$, $[YbCp_2F(OPPh_3)]_2$ and $[Yb(MeCp)_2F(THF)]_2$. In each case the highest observed ion was $[Yb_3L_5F_3]^+$ (L = Cp or MeCp) or this ion ±H. (For the methylcyclopentadienyl complexes, this ion was close to the instrument limit, hence the possibility of formation of tetranuclear ions cannot be ruled out.) An analogous ion was the highest observed in the spectra of $[YbCp_2F(THF)]_2$,[21] $[ScCp_2F]_3$,[15] and $[Sm(t\text{BuCp})_2F]_3$.[20] Formation of trinuclear ions for the dimeric complexes $[YbCp_2F(OPPh_3)]_2$ and $[Yb(MeCp)_2F(THF)]_2$ evidently involves thermally induced dissociation of the neutral ligand and further association, as observed for $[YbCp_2F(THF)]_2$.[21] Because of such reactions, the mass spectra are an uncertain guide as to solid state structures. In general the fragmentation patterns of the Cp complexes were similar to those of $[YbCp_2F(THF)]_2$ [21] and $[ScCp_2F]_3$,[15] whilst those of the MeCp complexes showed features (loss of $MeCp^•$, $Me^•$, and, for the THF complex, $H^•$) similar to those of $[Ln(MeCp)_3]$.[34] However there was no evidence of the electron impact-induced ring expansions shown by $[Ln(MeCp)_3]$.[34] For the phosphane oxide complex, no ions with coordinated Ph_3PO were observed, although such ions, notably $LnCp_2(OPPh_3)^+$, have been observed with low intensity in the mass spectra of some $[LnCp_3(OPR_3)]$ complexes.[1]

X-ray Crystal Structures

1. $[Yb(OC_6H_2\text{-}2,6\text{-}t\text{Bu}_2\text{-}4\text{-}X)_2F(THF)]_2$ (X = H or *t*Bu): X-ray crystallography has shown that the complexes $[Yb(OC_6H_2\text{-}2,6\text{-}t\text{Bu}_2\text{-}4\text{-}X)_2F(THF)]_2$ (X = H or *t*Bu) are dimeric with bridging fluorides and five-coordinate ytterbium. In each case the fluoride bridging is somewhat unsymmetrical (0.04–0.07 Å), the differences being significant on consideration of the errors in bond lengths. Selected bond lengths and angles for the X = H complex and for the two crystallographically independent X = *t*Bu molecules are listed in Table 2, whilst the structure of $[Yb(OC_6H_3\text{-}2,6\text{-}t\text{Bu}_2)_2F(THF)]_2$ is displayed in Figure 1, and that of molecule 1 of $[Yb(OC_6H_2\text{-}2,4,6\text{-}t\text{Bu}_3)_2F(THF)]_2$ in Figure 2. The stereochemistry is very irregular, but can be regarded as distorted trigonal bipyramidal with an aryloxide oxygen and a fluorine apical (ArO–Yb–F 150–153°), and the other aryloxide oxygen, O(THF), and the other fluorine equatorial. A similar arrangement is observed in $[Yb(OC_6H_2\text{-}2,4,6\text{-}t\text{Bu}_3)_2OH(THF)]_2$ [24] where the apical ArO–Yb–OH angle is somewhat larger [156.2(3)°] than the ArO–Yb–F angles (Table 2). A similar arrangement of Cp ring centres, THF oxygen, and bridging fluorides is observed in $[YbCp_2F(THF)]_2$,[21] $[Yb(MeCp)_2F(THF)]_2$, and $[YbCp_2F(OPPh_3)]_2$, (below), but the largest (transoid) angle, O(THF)–Yb–F, is only ca. 140°. Moreover, $[Yb(OAr)_2F(THF)]_2$ complexes have one of the bulky ligands in an apical position, whereas neither of the larger groups (Cp/MeCp) is apical in the cyclopentadienyl complexes. At first sight, the Yb–(μ-F) distances (Table 2) are surprisingly long for a five-coordinate complex, since they are comparable with those of the nine-coordinate dimers, $[YbCp_2F(THF)]_2$,[21] $[Yb(MeCp)_2F(THF)]_2$, and $[YbCp_2F(OPPh_3)]_2$ (see below), as well as those [2.206(5), 2.196(5) Å] of the two sets of Yb–(μ–F) bonds in eight-coordinate $[Yb_5(C_5Me_5)_6(\mu_4\text{-}F)(\mu_3\text{-}F)_2(\mu\text{-}F)_6]$.[3] On the basis of the data for the cyclopentadienyl compounds[3,21] and the variation of ionic radius with coordination number,[35] a Yb–(μ-F) distance of ca. 2.0 Å might be expected in $[Yb(OAr)_2F(THF)]_2$ complexes. This would be near terminal Yb–F distances [2.015(4), 2.026(2) Å] in monomeric eight-coordinate $[Yb(C_5Me_5)_2F(L)]$ (L = THF or Et_2O) complexes.[3] However there is actually quite wide variation in the limited range of bridging Yb–F distances reported[3,16,17,21]. Thus, Yb–(μ_3-F) distances for eight-coordinate Yb^{III} in $[Yb_5(C_5Me_5)_6(\mu_4\text{-}F)(\mu_3\text{-}F)_2(\mu\text{-}F)_6]$ are much longer [2.319(6)–2.468(6) Å] than Yb–(μ-F) above, and Yb–(μ_4-F) lenghts cover a narrower range (2.365–2.387 Å).[3] By contrast, Yb^{III}–(μ-F) distances for fluoride ions bridging Yb^{III} and Yb^{II} in seven-coordinate $[Yb_2(C_5Me_5)_4(\mu\text{-}F)]$[17] and eight-coordinate (for Yb^{III}) $[Yb_4(C_5Me_5)_6(\mu\text{-}F)_4]$[16] are very short at 2.084(2) and 2.129 ± 0.002 Å respectively. Even Sm–(μ-F) of eight-coordinate $[Sm(C_5H_4\text{-}t\text{Bu})_2F]_3$ [20] and $[Sm\{C_5H_3\text{–}1,3\text{-}(SiMe_3)_2\}_2F]_2$ [19] differ by ca. 0.06 Å. In the present complexes, the relatively long (for coordination number 5) Yb–(μ-F) distances are attributed to steric crowding around ytterbium. The sum of the steric coordination numbers[36] of the ligands for the $[Yb(OAr)_2F(THF)]_2$ complexes is 8.0, whereas the values for the topologically related $[YbCp_2F(THF)]_2$ [21] and $[Yb(MeCp)_2F(THF)]_2$ are 7.3–7.5, indicative of less steric hindrance. Thus long Yb–(μ-F) bonds in the $[Yb(OAr)_2F(THF)]_2$ complexes are reasonable because of

Table 2. Selected bond lengths (Å) and angles (°) for $[Yb(OC_6H_3\text{-}2,6\text{-}tBu_2)_2F(THF)]_2$ and $[Yb(OC_6H_2\text{-}2,4,6\text{-}tBu_3)_2F(THF)]_2 \cdot 3\ THF$

	$[Yb(OC_6H_3\text{-}2,6\text{-}tBu_2)_2F(THF)]_2$	$[Yb(OC_6H_2\text{–}2,4,6\text{-}tBu_3)_2F(THF)]_2 \cdot 3\ THF$ molecule 1	molecule 2	
Yb(1)–F(1)	2.172(4)	2.170(4)	2.169(5)	Yb(2)–F(2)
Yb(1)–F(1a)	2.213(3)	2.239(4)	2.225(5)	Yb(2)–F(2a)
Yb(1)–O(1)	2.043(3)	2.061(6)	2.053(6)	Yb(2)–O(4)
Yb(1)–O(2)	2.062(4)	2.053(6)	2.073(5)	Yb(2)–O(5)
Yb(1)–O(3)	2.301(4)	2.315(6)	2.332(6)	Yb(2)–O(6)
Yb(1)–F(1)–Yb(1a)	111.3(1)	110.7(2)	111.1(2)	Yb(2)–F(2)–Yb(2a)
F(1)–Yb(1)–F(1a)	68.7(1)	69.3(2)	68.9(2)	F(2)–Yb(2)–F(2a)
O(1)–Yb(1)–F(1)	107.6(1)	102.8(2)	109.3(2)	O(4)–Yb(2)–F(2)
O(1)–Yb(1)–F(1a)	100.2(1)	152.7(2)	100.7(2)	O(4)–Yb(2)–F(2a)
O(1)–Yb(1)–O(2)	108.0(1)	109.1(2)	108.6(2)	O(4)–Yb(2)–O(5)
O(1)–Yb(1)–O(3)	112.9(1)	89.3(2)	113.7(2)	O(4)–Yb(2)–O(6)
O(2)–Yb(1)–F(1)	104.6(1)	109.7(2)	103.0(2)	O(5)–Yb(2)–F(2)
O(2)–Yb(1)–F(1a)	151.7(2)	98.1(2)	150.5(2)	O(5)–Yb(2)–F(2a)
O(2)–Yb(1)–O(3)	88.9(1)	113.1(2)	88.1(2)	O(5)–Yb(2)–O(6)
O(3)–Yb(1)–F(1)	130.6(2)	128.4(2)	129.1(2)	O(6)–Yb(2)–F(2)
O(3)–Yb(1)–F(1a)	77.3(1)	77.3(2)	77.4(2)	O(6)–Yb(2)–F(2a)

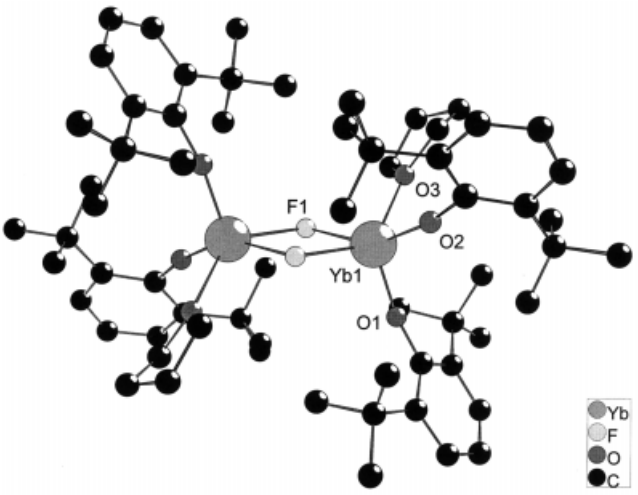


Figure 1. The molecular structure of $[Yb(OC_6H_3\text{-}2,6\text{-}tBu_2)_2F(THF)]_2$

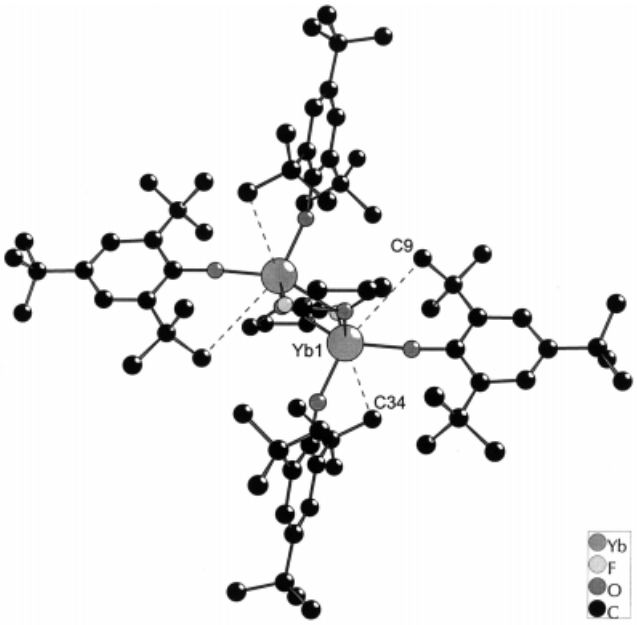


Figure 2. The molecular structure of molecule 1 of $[Yb(OC_6H_2\text{-}2,4,6\text{-}tBu_3)_2F(THF)]_2$ showing the close Yb···C(Me) contacts

crowding, and there are also relatively long Yb–O(THF) bonds (see below).

The average Yb–O(THF) distance (2.32 Å) is somewhat shorter than that [2.363(8) Å] of five-coordinate $[Yb(OC_6H_2\text{-}2,6\text{-}tBu)_2OH(THF)]_2$.[24] Subtraction of an extrapolated radius (from the data of Shannon[35]) for five-coordinate Yb^{3+} from Yb–O(THF) gives 1.51 Å, typical of values (1.48–1.59 Å) derived from Ln–O(THF) of low coordinate complexes with bulky aryloxides.[24,26,37] This is larger than subtraction values of 1.34 ± 0.05 Å derived from Ln–O(THF) of cyclopentadienyllanthanoid complexes[38] and specifically 1.37 Å from Yb–O(THF) of $[YbCp_2F(THF)]_2$ [21] and reflects bond lenghtening induced by steric crowding as noted for Yb–(μ-F) above. The Yb–OAr distances are comparable with those of both five-coordinate $[Yb(OC_6H_2\text{–}2,4,6\text{-}tBu_3)_2OH(THF)]_2$ [24] and $[Yb(OC_6H_3\text{-}2,6\text{-}Ph_2)_3(THF)_2]$,[37a] and subtraction of the 5-coordinate Yb^{3+} radius from <Yb–OAr> gives 1.25 Å, quite typical of values derived from data for low coordinate Yb^{II} and Yb^{III} aryloxides.[24,26,37]

Further evidence of considerable steric crowding in the $[Yb(OAr)_2F(THF)]_2$ complexes is provided by the existence of short Yb···C(Me) and C(Me)···C(Me) separations (Table 3) and the former are displayed for molecule 1 of $[Yb(OC_6H_2\text{-}2,4,6\text{-}tBu_3)_2F(THF)]_2$ in Figure 2. The listed Yb···C(Me) distances are less than the sum (3.94 Å) of the metallic radius of ytterbium[39] (which can be viewed as a pseudo van der Waals radius) and the van der Waals radius of a methyl group.[40] However these contacts are significantly longer than can be attributed to agostic Yb···C(alkyl) contacts (ca. 2.9–3.2 Å)[16,41] and are thus approaches induced by ligand congestion. The close C(Me)···C(Me) contacts that also reflect congestion are between methyls of *different tert*-butyl groups on the same or different Yb atoms. Their separations are less than two methyl van der Waals

Table 3. Non bonding close Yb···C and C(Me)···C(Me) contacts (Å) in $[Yb(OC_6H_2\text{-}2,6\text{-}t\text{Bu-}4\text{-}X]_2$ complexes

Compound	X = H		X = *t*Bu molecule 1		X = *t*Bu molecule 2	
Yb···C(Me)	Yb(1)···C(28)	3.578(6)	Yb(1)···C(9)	3.65(4)	Yb(2)···C(67)	3.67(4)
	Yb(1)···C(8)	3.747(6)	Yb(1)···C(34)	3.65(2)	Yb(2)···C(48)	3.73(2)
C(Me)···C(Me)	C(14)···C(23)[a]	3.52(1)	C(17)···C(34)[a]	3.81(3)	C(57)···C(76)[a]	3.56(2)
	C(8)···C(22)[a]	3.77(1)	C(17)···C(27)[a]	3.86(3)	C(57)···C(75)[a]	3.96(3)
	C(9)···C(28)[b]	3.565(7)	C(8)···C(26)[b]	3.93(3)	C(48)···C(75)[a]	3.73(4)
	C(12)···C(27)[b]	3.790(9)	C(9)···C(35)[b]	3.81(3)	C(49)···C(67)[b]	3.65(3)
	C(12)···C(28)[b]	3.954(9)			C(66)···C(58)[b]	3.86(6)

[a] Both Me groups are on one Yb atom. – [b] Me groups on different Yb atoms.

radii. In addition to these contacts there are also a number just above the sum of the van der Waals radii.

2. $[YbCp_2F]_3$: Unsolvated bis(cyclopentadienyl)fluoroytterbium(III) crystallizes as a trimer with eight-coordinate ytterbium ions, and is the first *unsolvated unsubstituted* cyclopentadienyllanthanoid fluoride to be structurally characterized, though similar trimers have been observed for $[ScCp_2F]_3$,[15] $[Sm(C_5H_4\text{-}t\text{Bu})_2F]_3$,[20] and $[Sm(C_5Me_5)_2Cl]_3$.[42] Selected bond lengths and angles are given in Table 4 and the structure is shown in Figure 3. The structure features a planar Yb_3F_3 ring with near equal Yb–F bond lengths, but with one Yb–F–Yb and one F–Yb–F angle slightly different from the other two. However, these slight variations are of little consequence and the structure is sufficiently symmetrical for ν(Yb–F) to be infrared inactive and observed only in the Raman spectrum (Table 1). There is little variation in <Ln–C> bond lengths between $[YbCp_2F]_3$ (Figure 3) and $[ScCp_2F]_3$,[15] $[Sm(C_5H_4\text{-}t\text{Bu})_2F]_3$ [20] and $[Sm(C_5Me_5)Cl]_3$ [42] and in <Ln–F> between the three fluorides, when allowance is made for variation in Ln^{3+} radii. Thus subtraction of the ionic radius for eight-coordinate Ln^{3+} from <Ln–C> gives 1.61, 1.60, 1.63, and 1.65 Å for the respective compounds. These values are in the normal range[43] and compare with 1.60 Å similarly derived from <Yb–C> of $[YbCp_2F(THF)]_2$.[21] A similar subtraction from <Ln–F> of the first three compounds gives 1.17, 1.18, and 1.17 Å, respectively. Values from <Ln–F> of $[YbCp_2F(THF)]_2$ [21] (1.15 Å) and $[Sm\{C_5H_3\text{-}1,3\text{-}(SiMe_3)_2\}_2F]_2$ [19] (1.22 Å) lie either side of the values for the trimers, and all are well below similarly derived values (1.36 and 1.41 Å) for the two different Yb–F bonds of the bulky $[Yb(OAr)_2F(THF)]_2$ complexes (above). Of the four trimeric bis(cyclopentadienyl)lanthanoid(III) halide structures (Figure 3 and refs.[15,20,42]), the present complex has the largest X–Ln–X (X = Cl or F) angle and the smallest Ln–X–Ln angle, a result that is unexpected since the group contains the complex of the much smaller Sc^{3+}. Although the cen–Yb–cen (cen = centroid of a Cp ring) angle is in

Table 4. Selected bond lengths and angles for $[YbCp_2F]_3$ and $[Yb(MeCp)_2F]_4$

Distance (Å)		Angle (°)	
$[YbCp_2F]_3$			
Yb(1)–F(1)	2.147(9)	Yb(1)–F(1)–Yb(2)	154.1(4)
Yb(1)–F(3)	2.16(1)	Yb(1)–F(3)–Yb(3)	148.9(4)
Yb(2)–F(1)	2.146(9)	Yb(2)–F(2)–Yb(3)	154.6(4)
Yb(2)–F(2)	2.157(9)	F(1)–Yb(2)–F(2)	85.5(3)
Yb(3)–F(2)	2.143(9)	F(1)–Yb(1)–F(3)	88.7(3)
Yb(3)–F(3)	2.18(1)	F(2)–Yb(3)–F(3)	88.1(3)
<Yb–C>	2.59	Cen(1)–Yb(1)–F(1)	106.4
Yb(1)–Cen(1)	2.33	Cen(1)–Yb(1)–F(3)	107.2
Yb(1)–Cen(2)	2.33	Cen(2)–Yb(1)–F(1)	107.7
Yb(2)–Cen(3)	2.31	Cen(2)–Yb(1)–F(3)	109.7
Yb(2)–Cen(4)	2.31	Cen(1)–Yb(1)–Cen(2)	129.5
Yb(3)–Cen(5)	2.32	Cen(3)–Yb(2)–F(1)	107.6
Yb(3)–Cen(6)	2.32	Cen(3)–Yb(2)–F(2)	107.9
		Cen(4)–Yb(2)–F(1)	108.8
		Cen(4)–Yb(2)–F(2)	108.9
		Cen(3)–Yb(2)–Cen(4)	129.4
		Cen(5)–Yb(3)–F(2)	106.8
		Cen(5)–Yb(3)–F(3)	107.9
		Cen(6)–Yb(3)–F(2)	109.4
		Cen(6)–Yb(3)–F(3)	107.4
		Cen(5)–Yb(3)–Cen(6)	129.4
$[Yb(MeCp)_2F]_4$			
Yb(1)–F(1)	2.163(6)	F(1)–Yb(1)–F(2)	91.4(3)
Yb(1)–F(2)	2.173(6)	Yb(2)–F(1)–Yb(1)	178.9(4)
Yb(2)–F(1)	2.136(6)	F(1)–Yb(2)–F(2)	92.2(3)
Yb(2)–F(2)	2.145(6)	Yb(2)–F(2)–Yb(1)	168.4(3)
<Yb–C>	2.59	Cen(1)–Yb(1)–F(1)	107.6
Yb(1)–Cen(1)	2.31	Cen(1)–Yb(1)–F(2)	110.4
Yb(1)–Cen(2)	2.29	Cen(2)–Yb(1)–F(1)	107.1
Yb(2)–Cen(3)	2.31	Cen(2)–Yb(1)–F(2)	107.1
Yb(2)–Cen(4)	2.31	Cen(1)–Yb(1)–Cen(2)	127.2
		Cen(3)–Yb(2)–F(1)	106.5
		Cen(3)–Yb(2)–F(2)	108.0
		Cen(4)–Yb(2)–F(1)	107.9
		Cen(4)–Yb(2)–F(2)	108.0
		Cen(3)–Yb(2)–Cen(4)	128.2

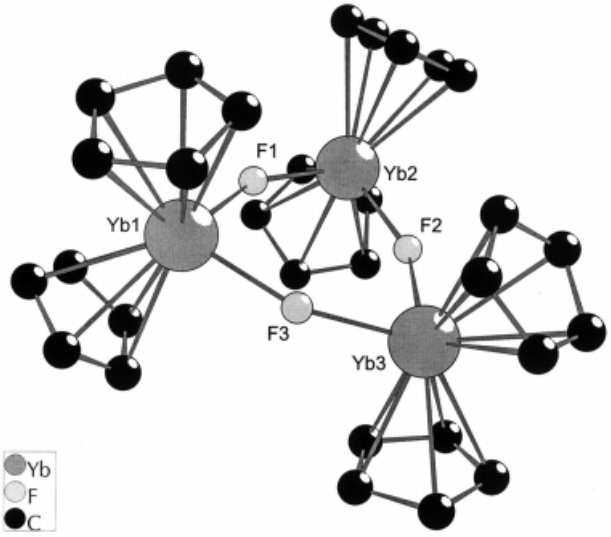


Figure 3. The molecular structure of $[YbCp_2F]_3$

the range (127–140°) for 8-coordinate complexes, it is close to the overlap with the range (113–129°) for 9-coordinate complexes (see literature cited in ref.[21]). The sum of the steric coordination numbers of the ligands[36] is quite low at 6.1, especially compared with 7.3 for $[YbCp_2F(THF)]_2$, and highlights the surprising failure to obtain a solvate from DME. A dimer with chelating DME and 10-coordinate ytterbium would have a sum of steric coordination numbers of 7.9. Whilst comparable with the value 8.0 for $[Yb(OAr)_2F(THF)]_2$ complexes, it may be too large when other alternatives are available. A monomer with chelating DME would have a reasonable value of 6.85, but the molecule would have only one stable Yb–F bond per Yb compared with two in dimers and trimers. However, a dimer with unidentate DME (known refs.[28,44] in lanthanoid chemistry) would allow two Yb–F bonds/Yb and a reasonable steric coordination number sum of 7.0. Despite this, the sterically unsaturated $[YbCp_2F]_3$ is preferred. With this structure, the non bonding Yb(n)···Yb(m) separations [(1)/(2) 4.186; (1)/(3) 4.185; (2)/(3) 4.196 Å] and F(n)···F(m) separations [(1)/(2) 2.885; (1)/(3) 2.975; (2)/(3) 2.981 Å] exceed those for the solvated dimer $[Yb(MeCp)_2F(THF)]_2$ (Yb···Yb 3.666 Å; F···F 2.465 Å). From the structural data for $[Sm(C_5H_3\text{-}1,3\text{-}(SiMe_3)_2)_2F]_2$,[19] a Yb···Yb separation of ca. 3.60 Å in the unsolvated dimer "$[YbCp_2F]_2$" can be estimated. This reinforces the lack of crowding revealed by steric coordination numbers.

3. $[Yb(MeCp)_2F]_4$: Crystallization of this heteroleptic fluoride from DME as a tetramer with eight-coordinate Yb^{III} is particularly surprising. Not only is the complex not solvated, but it is the first tetrameric bis(cyclopentadienyl)lanthanoid(III) fluoride. Previously only an unsolvated dimer,[19] trimers,[15,20] and a solvated dimer[21] have been isolated. The nearest similar structure is the mixed oxidation state ($Yb^{II,III}$) $[Yb_4(C_5Me_5)_6(\mu\text{-}F)_4]$,[16] which has eight-coordinate Yb^{III} and five-coordinate Yb^{II}. Selected bond lengths and angles for $[Yb(MeCp)_2F]_4$ are given in Table 4.

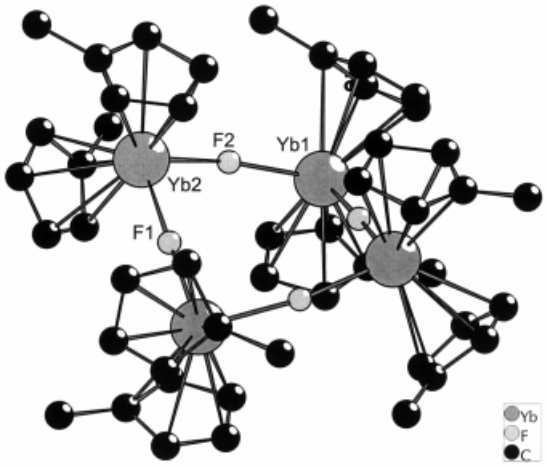


Figure 4. The molecular structure of $[Yb(MeCp)_2F]_4$

The structure is displayed in Figure 4. The eight-membered Yb_4F_4 ring is puckered with Yb–F–Yb angles near linear and F–Yb–F angles near 90° (Table 4). Similar F–Yb–F angles are observed in $[Yb_4(C_5Me_5)_6(\mu\text{-}F)_4]$,[16] but the Yb–F–Yb angles [160.0(2), 157.3(2)°] show much greater deviation from linearity than in $[Yb(MeCp)_2F]_4$. The four fluorine atoms are near coplanar (max. deviation 0.007 Å) with the plane parallel to the [101] plane, but the two different ytterbium atoms are very substantially displaced [Yb(1) +0.605 Å; Yb(2) −0.575 Å] from the F_4 plane. In $[Yb_4(C_5Me_5)_6(\mu\text{-}F)_4]$ the Yb^{III} atoms are similarly displaced from the F_4 plane, but the Yb^{II} atoms are only slightly displaced.[16] The average Yb–C and Yb–F distances are virtually identical with those of $[YbCp_2F]_3$, and subtraction of the ionic radius[35] for eight-coordinate Yb^{3+} gives 1.60 and 1.17 Å respectively. Although the methylcyclopentadienyl ligand is somewhat bulkier than Cp, the cen–Yb–cen angles are marginally smaller for the MeCp complex and are approaching the limit for eight-coordinate complexes (see literature cited in ref.[21]). As with $[YbCp_2F]_3$, the sum of the steric coordination numbers for the ligands[36] is small at 6.3, and contrasts 7.5 for the solvated dimer $[Yb(MeCp)_2F(THF)]_2$ (below). Again, a solvated monomer "$[Yb(MeCp)_2F(DME)]$" with chelating DME or a dimer solvated with unidentate DME are sterically viable. Formation of a tetramer leads to even longer Yb···Yb and F···F separations (4.296/4.299 and 3.088/3.106 Å, respectively) than in the trimer with the *less bulky* ligand. Whilst this should minimise non-bonding interactions, several molecules with closer Ln···Ln and F···F separations are isolable. In particular, the highly crowded $[Yb(OAr)_2F(THF)]_2$ dimers have average Yb···Yb separations of 3.635 Å and average F···F separations of 2.49 Å.

4. $[YbCp_2F(OPPh_3)]_2$ and $[Yb(MeCp)_2F(THF)]_2$: Both complexes were established as fluoride-bridged dimers with nine-coordinate ytterbium. The structures are displayed in Figure 5 and Figure 6, and bond length and angle data are compared with those of $[YbCp_2F(THF)]_2$ in Table 5. Two independent molecules are observed for the phosphane oxide complex, but data are listed for only one owing to the low precision of the determination. A structure was needed for the previously reported[3] $[Yb(MeCp)_2F(THF)]$, since both monomeric $[Yb(C_5Me_5)_2F(THF)]$[3] and dimeric $[YbCp_2F(THF)]_2$[21] structural analogues exist.

The arrangement of centroids of the cyclopentadienyl rings, the fluorines, and the oxygen donor atom can be viewed as distorted trigonal bipyramidal with oxygen and one bridging fluoride in the apical positions. For the phosphane oxide complex, within the error limits, the Yb–C, Yb–F, and Yb–O distances show no unexpected features. The bond lengths of $[Yb(MeCp)_2F(THF)]_2$ show interesting trends, when compared with those of $[YbCp_2F(THF)]_2$.[21] From <Yb–C> and <Yb–F> values, there is a hint of bond lengthening in the methylcyclopentadienyl compound, but the size of the estimated standard deviations in the earlier determination[21] makes the comparison uncertain. However Yb–O(THF) is clearly larger for $[Yb(MeCp)_2F(THF)]_2$. Subtraction of the ionic radius for nine-coordinate Yb^{3+} gives 1.45 Å, which is higher than usual (1.34 ± 0.05 Å)[38] for THF complexes of

Table 5. Selected bond lengths and angles of $[Yb(MeCp)_2F(THF)]_2$, $[YbCp_2F(THF)]_2$,[21] and $[YbCp_2F(OPPh_3)]_2$

	$[Yb(MeCp)_2F(THF)]_2$	$[YbCp_2F(THF)]_2$ [a]	$[YbCp_2F(OPPh_3)]_2$ molecule 2
Distance (Å)			
Yb(1)–F(1)	2.186(3)	2.161(9)	2.18(2)
Yb(1)–F(1a)	2.231(3)	2.215(9)	2.20(2)
Yb(1)–O(1)	2.490(4)	2.41(1)	2.19(2)
<Yb–C>	2.67	2.64	2.65
<Yb–Cen>	2.39	2.37	2.37
Yb···Yb	3.666	3.651	3.686
Angle (°)			
F(1)–Yb(1)–F(1a)	67.8(1)	66.9(4)	65.1(9)
Yb(1)–F(1)–Yb(1a)	112.2(1)	113.1(4)	114.9(9)
O(1)–Yb(1)–F(1)	73.5(1)	72.9(3)	76.2(8)
O(1)–Yb(1)–F(1a)	141.2	139.8(3)	141.3(8)
O(1)–Yb(1)–Cen(1)	97.0	98.9	100
O(1)–Yb(1)–Cen(2)	98.5	98.5	97
Cen(1)–Yb(1)–Cen(2)	125.2	123.9	124
Cen(1)–Yb(1)–F(1)	114.0	116.4	120
Cen(1)–Yb(1)–F(1a)	100.9	99.7	98
Cen(2)–Yb(1)–F(1)	120.8	119.6	116
Cen(2)–Yb(1)–F(1a)	98.7	100.1	100

[a] Numbering of F(1) and F(1a) inverted from that reported (ref.[21]) to correspond to that used [Yb(1)–F(1) shortest] in the present molecules.

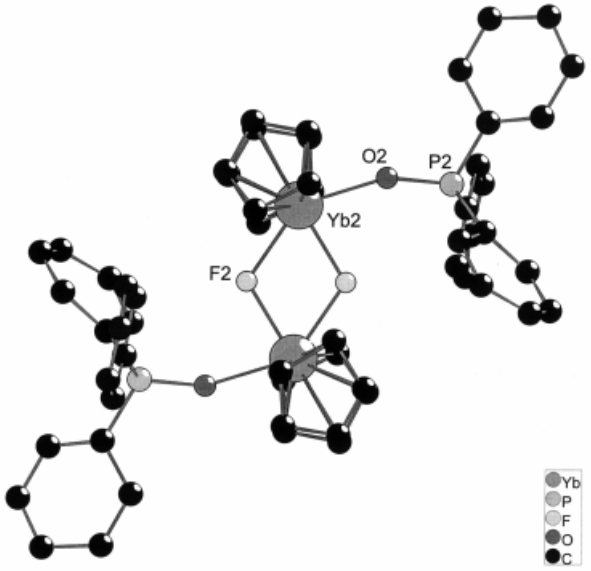


Figure 5. The molecular structure of molecule 2 of $[YbCp_2F(OPPh_3)]_2$

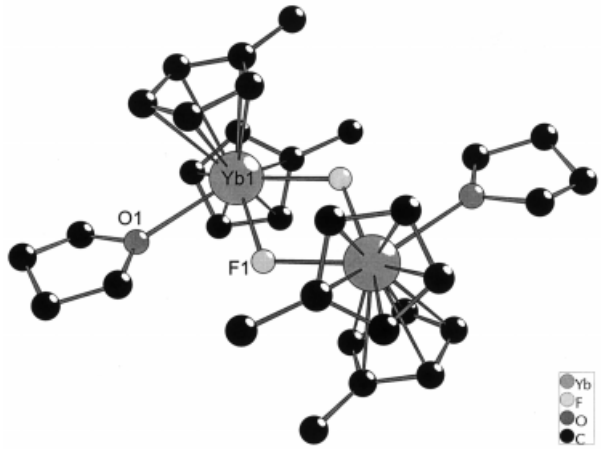


Figure 6. The molecular structure of $[Yb(MeCp)_2F(THF)]_2$

cyclopentadienyllanthanoids, e.g. 1.37 Å for $[YbCp_2F(THF)]_2$ [21] and 1.34 Å for monomeric $[Yb(C_5Me_5)_2F(THF)]$, and approaching values (1.49–1.59 Å)[24,26,37] derived from Yb-O(THF) of THF complexes of bulky lanthanoid aryloxides (see e.g. $[Yb(OAr)_2F(THF)]_2$ above). Thus the small increase in cyclopentadienyl ligand bulkiness from $[YbCp_2F(THF)]_2$ to $[Yb(MeCp)_2F(THF)]_2$ (sum of ligand steric coordination numbers 7.3 and 7.5 respectively) is sufficient to weaken the Yb–O bond significantly. It also becomes apparent why $[Yb(C_5Me_5)_2F(THF)]$[3] is monomeric, not dimeric. The dimer would have a ligand steric coordination number sum of 8.2, higher even than for $[Yb(OAr)_2F(THF)]_2$ (8.0), and THF would plausibily be dissociated, whereas the steric coordination number sum for the monomer is 7.2, comparable with $[YbCp_2F(THF)]_2$, permitting an uncrowded Yb–O bond.

From the packing diagrams, it is evident that the molecules of the above dimers, trimer, and tetramer are well separated and non interacting. In $[YbCp_2F]_3$, the trimeric molecules are parallel to one another in alternating layers, whilst in $[Yb(MeCp)_2F]_4$ the planes of the four fluorines of the tetramers align parallel to the [101] plane. The two independent molecules of $[Yb(OC_6H_2\text{-}2,4,6\text{-}t\text{Bu}_3)_2F(THF)]_2$ are perpendicular to each other.

Conclusions

The present study establishes that a range of heteroleptic lanthanoid fluorides can be prepared, including aryloxides, and that considerable structural variety is exhibited. A heteroleptic aryloxide chloride analogous to the

$[Yb(OAr)_2F(THF)]_2$ complexes is known, viz. $[Sm(OC_6H_2$-2,6-tBu_2-4-Me$)_2Cl(THF)]_2$,[45] but the larger iodide gives a slightly more crowded monomer $[Ln(OAr)_2I(THF)_2]$ (Ln = Sm[45] or Yb[46]). There are both chloride and hydride analogues of $[Ln(Cp$ or MeCp$)_2FL]_2$ where L = THF (see ref.[21] and literature cited therein), but not for L = Ph_3PO, and $[Sm(C_5Me_5)_2Cl]_3$ [42] is related to $[YbCp_2F]_3$. However there is no homocyclic chloride tetramer structurally similar to $[Yb(MeCp)_2F]_4$.[12–14] Although the tetramer $[GdCp_2Cl]_4$ is known, the structure is a dimer of dimers with a ladder arrangement[13]. Isolation of $[YbCp_2F]_3$ and $[Yb($-$MeCp)_2F]_4$ unsolvated from DME is striking, and contrasts the formation of $[Yb(Cp$ or MeCp$)_2F(THF)]_2$. The corresponding DME complexes would have the more unusual[28,44] unidentate DME and appear unable to compete with the very uncrowded unsolvated trimer and tetramer.

Experimental Section

General: The lanthanoid(II) reactants and lanthanoid(III) products are extremely air- and moisture-sensitive, hence all operations were carried out under purified Ar or N_2. Unless indicated otherwise, handling methods and solvent purification were as described previously.[47] – Infrared spectra (4000–600 cm^{-1}) were obtained for Nujol mulls between NaCl plates with a Nicolet 5PC-FTIR-spectrometer or as KBr disks with a Bruker 66V/S instrument. Far infrared spectra (600–50 cm^{-1}) were recorded for polyethylene disks with a Bruker IFS 66V/S spectrometer. – The Raman spectrum was obtained for a solid sample in a sealed capillary with a Bruker FRA 106/S instrument. – Mass spectra were recorded with a Varian MAT CH5-DF mass spectrometer. The aryloxofluoroytterbium(III) complexes showed only ligand ions and the data are not listed. For the cyclopentadienylfluoroytterbium(III) compounds, clusters with the correct isotope pattern for the assignments given were observed. – The Energy Dispersive Analysis through X-ray (EDAX) measurement was carried out with an ECON IV PV 9900–26 instrument, II. Physikalische Institut, Universität zu Köln. – Metal analysis were effected as described previously.[47] Fluorine analyses for samples sealed under Ar in gelatin capsules were carried out by the method of Campbell.[48] Perfluorodecalin and perfluoro(methylcyclohexane), from Avocado Chemicals, were dried over molecular sieves (4 Å), degassed, and vacuum transferred to storage vessels. Ytterbium(II) aryloxides were prepared as described previously[26] and had IR spectra in agreement with those reported. Far IR spectra – for comparison with trivalent complexes (below): $[Yb(OC_6H_3$-2,6-$tBu_2)_2(THF)_3]$: $\tilde{\nu}$ = 590 w cm^{-1}, 534 m (br), 490 w, 459 w, 441 m, 383 w, 333 s, 309 m, 270 w, 184 w, 143 w (br). $[Yb(OC_6H_2$-2,6-tBu_2-4-Me$)_2(THF)_3]$: $\tilde{\nu}$ = 577 m cm^{-1}, 564 w, 527 s (br), 501 s, 353 s, 302 s, 223 w, 180 w, 149 w, 116 w. $[Yb(OC_6H_2$-2,4,6-$tBu_3)_2(THF)_3]$: $\tilde{\nu}$ = 578 vw cm^{-1}, 537 m, 519 s, 491 vw, 447 m, 358 s (br), 263 w (br), 170 w, 144 m, 87 w. The divalent ytterbocenes $[YbCp_2(DME)]$ and $[Yb(MeCp)_2(THF)]$ were also prepared by reported methods.[49]

Bis(aryloxo)fluorolanthanoid(III) Complexes $[Yb(OAr)_2F(THF)]_2$: The appropriate $[Yb(OC_6H_2$-2,6-tBu_2-4-R$)_2(THF)_3]$ (R = H, Me, *t*Bu) complex (ca. 0.30–0.40 mmol) and perfluorodecalin (mol ratio 4:1) were stirred in THF (2.5 mL) at room temperature for 48 h. The resulting suspension was heated to 50 °C and then cooled to room temperature, when the deposited solid was filtered off and washed twice with THF (0.5 mL) and dried for at least 3 h under vacuum. The products were obtained as bright orange microcrystalline powders in 25–30% yield.

Di{bis(2,6-di-*tert*-butylphenolato)(μ-fluoro)(tetrahydrofuran)ytterbium(III)}: IR (Nujol): $\tilde{\nu}$ = 3077 w cm^{-1}, 3063 w, 1584 w, 1410 s, 1358 m, 1316 w, 1260 s, 1246 s, 1200 m, 1130 w, 1105 m, 1036 w, 1003 m, 953 w, 924 w, 914 w, 870 s, 821 w, 750 s, 662 m. – Far-IR: $\tilde{\nu}$ = 589 w cm^{-1}, 573 w, 562 w, 547 s, 526 w, 494 m, 451 m, 387 s (br), 338 vs, 304 m, 279 m, 207 s, 140 w, 125 w. – $C_{64}H_{100}F_2O_6Yb_2$ (1349.52): calcd. F 2.82, Yb 25.64; found F 2.59, Yb 25.41. Single crystals were obtained by storage of a THF solution in a dry box for 4 weeks.

Di{bis(2,6-di-*tert*-butyl-4-methylphenolato)(μ-fluoro)(tetrahydrofuran)ytterbium(III)}: IR (KBr disk): $\tilde{\nu}$ = 3059 w cm^{-1}, 2955 s, 2913 s, 2869 m, 1459 m, 1419 s, 1386 m, 1356 w, 1260 s (br), 1219 m, 1202 w, 1149 w, 1122 w, 1067 w, 1020 m, 915 w, 887 w, 861 m, 830 m, 807 w, 780 w. – Far-IR: $\tilde{\nu}$ = 577 w cm^{-1}, 563 w, 537 vs, 401 w (sh), 381 s (br), 356 m, 325 w (sh), 314 m, 302 m, 219 w, 190w. – $C_{68}H_{108}F_2O_6Yb_2$ (1408.70): calcd. F 2.70, Yb 24.62; found F 2.50, Yb 24.53.

Di{(μ-fluoro)(tetrahydrofuran)bis(2,4,6-tri-*tert*-butylphenolato)ytterbium(III)}: IR (Nujol): $\tilde{\nu}$ = 3067 w cm^{-1}, 1584 w, 1408 s, 1360 m (sh), 1260 s, 1246 s, 1200 w, 1130 w, 1105 w, 1036 w, 1003 w, 953 w, 914 w, 870 m, 822 w, 797 w, 750 s, 662 w. – Far-IR: $\tilde{\nu}$ = 539 s cm^{-1}, 475 w (sh), 461 m, 375 s (br), 359 s (sh), 304 m, 273 w, 206 m, 183 w. – $C_{80}H_{132}F_2O_6Yb_2$ (1574.00): calcd. F 2.41, Yb 21.99; found F 2.42, Yb 22.18. Single crystals of the complex as a tris(tetrahydrofuran) solvate were obtained by storage of a saturated THF solution at –20 °C for 2 d, and were shown to contain fluorine by EDAX measurements.

Bis(cyclopentadienyl)fluoroytterbium(III) Complexes. – Tri{bis(cyclopentadienyl)(μ-fluoro)ytterbium(III)}: To a solution of $[YbCp_2(DME)]$ (1.0 g, 2.5 mmol) in DME (10 mL), perfluoro(methylcyclohexane) (0.23 g, 0.51 mmol) was added. The biphasic system was stirred for 48 h at room temperature. The resulting yellow precipitate was filtered off and washed twice with DME (3 mL). The product was dried for 3 h under vacuum (yield 45%). – IR (Nujol): $\tilde{\nu}$ = 3077 w cm^{-1}, 2708 w, 1653 w, 1576 w, 1152 w, 1067 w, 1011 s, 774 vs, 667 w, 621 w. – Far IR: $\tilde{\nu}$ = 480 s (br) cm^{-1}, 265 m, 230 w, 194 m, 114 w. – Raman Spectrum: $\tilde{\nu}$ = 938 w cm^{-1}, 629 s, 336 m, 119 m. – MS (20 eV, 260 °C), *m/z* (%): 901 (100) $[Yb_3Cp_5F_3]^+$, 836 (2.5) $[Yb_3Cp_4F_3]^+$, 644 (10) $[Yb_2Cp_4F_3]^+$, 625 (5.4) $[Yb_2Cp_4F_2]^+$, 579 (38) $[Yb_2Cp_3F_2]^+$, 533 (2.6) $[Yb_2Cp_2F_2]^+$, 369 (18) $[YbCp_3]^+$, 304 (76) $[YbCp_2]^+$, 239 (31) $[YbCp]^+$, 173 (1.6) $[Yb]^+$, 66 (41) $[CpH]^+$, 65 (27) $[Cp]^+$, 39 (24) $[HF_2]^+$, 19 (57) $[F]^+$. – $C_{30}H_{30}F_3Yb_3$ (966.69): calcd. F 5.90, Yb 53.70; found F 5.66 Yb 53.36. – A saturated DME solution was stored for 3 weeks at –20 °C giving yellow crystals of the title compound suitable for X-ray crystallography. An analogous preparation using perfluorodecalin gave the compound in 49% yield.

Tetra{(μ-fluoro)bis(methylcyclopentadienyl)ytterbium(III)}: To $[Yb($-$MeCp)_2(THF)]$ (1.06 g, 2.6 mmol) and perfluorodecalin (0.30 g, 0.66 mmol), DME (2.5 mL) was added. The solution became emerald green and the biphasic system was stirred for 24 h at room temperature. An orange solid was precipitated after 2 h. This was filtered off and washed twice with DME (0.5 mL) and dried for 3 h under vacuum (yield 25%). – IR (KBr): $\tilde{\nu}$ = 3083 w cm^{-1}, 2927 m, 2864 m, 1703 w, 1634 w, 1534 w, 1486 w, 1454 m, 1381 w, 1350 w, 1237 w, 1038 s, 933 m, 830 s, 768 vs, 623 w. – Far IR: $\tilde{\nu}$ = 470 vs (br) cm^{-1}, 328 s, 260 s, 230 m, 197 m, 164 w, 144 w. – MS (20 eV, 205 °C), *m/z* (%): 971 (44) $[Yb_3(MeCp)_5F_3]^+$, 957 (29)

Table 6. Crystallographic data for $[Yb(OC_6H_3\text{-}2,6\text{-}t\text{Bu}_2)_2F(THF)]_2$ and $[Yb(OC_6H_2\text{-}2,4,6\text{-}t\text{Bu}_3)_2F(THF)]_2 \cdot 3$ THF

	$[Yb(OC_6H_3\text{-}2,6\text{-}t\text{Bu}_2)_2F(THF)]_2$	$[Yb(OC_6H_2\text{-}2,4,6\text{-}t\text{Bu}_3)_2F(THF)]_2 \cdot 3$ THF
Empirical formula	$C_{64}H_{100}F_2O_6Yb_2$	$C_{92}H_{156}F_2O_9Yb_2$
Formula weight [g/mol]	1349.52	1790.25
Temperature [K]	293(2)	123(2)
Radiation Mo-K_α [pm]	71.073	71.073
Crystal system	orthorhombic	triclinic
Space group	*Pbca* (Nr. 61)	$P\bar{1}$ (No. 2)
Cell dimensions [Å, °]	a = 19.628(2) b = 15.567(2) c = 20.728(2)	a = 15.871(3) b = 16.098(3) c = 19.346(3) α = 92.96(2) β = 106.24(2) γ = 101.41(2)
Volume/10^6 [pm^3]	6333(1)	4622(1)
Z	4	2
Density [g/cm^3] calcd.	1.415	1.286
Absorption coefficient [mm^{-1}]	2.844	1.961
F(000)	2759	1876
2θ range	3.88° < 2θ < 45°	4.0° < 2θ < 42°
Diffractometer	STOE-IPDS	STOE-IPDS
Number of reflections collected	40376	25790
Data/restraints/parameters	4138/0/334	9493/0/901
Goodness of Fit	0.905	1.000
R indices [$I > 2\sigma(I)$]	$R1$ = 0.0291, $wR2$ = 0.0364	$R1$ = 0.0504, $wR2$ = 0.1257
R indices (all data)	$R1$ = 0.0613, $wR2$ = 0.0388	$R1$ = 0.0636, $wR2$ = 0.1365

Table 7. Crystallographic data for $[YbCp_2F]_3$, $[Yb(MeCp)_2F]_4$, $[Yb(MeCp)_2F(THF)]_2$, and $[YbCp_2F(OPPh_3)]_2$

	$[YbCp_2F]_3$	$[Yb(MeCp)_2F]_4$	$[Yb(MeCp)_2F(THF)]_2$	$[YbCp_2F(OPPh_3)]_2$
Empirical formula	$C_{30}H_{30}F_3Yb_3$	$C_{48}H_{56}F_4Yb_4$	$C_{32}H_{44}F_2O_2Yb_2$	$C_{56}H_{50}F_2O_2P_2Yb_2$
Formula weight [g/mol]	966.69	1401.09	844.75	1200.98
Temperature [K]	293(2)	293(2)	293(2)	293(2)
Radiation Mo-K_α [pm]	71.073	71.073	71.073	71.073
Crystal system	monoclinic	monoclinic	monoclinic	triclinic
Space group	*Cc* (Nr. 9)	*Ia* (Nr. 9)	$P2_1/c$ (Nr. 14)	$P\bar{1}$(No. 2)
Cell dimensions [Å, °]	a = 17.331(3) b = 15.544(2) c = 10.691(2) β = 91.59(2)	a = 11.820(2) b = 8.5812(9) c = 22.470(4) β = 92.98(4)	a = 8.575(1) b = 19.444(2) c = 9.313(1) β = 98.05(2)	a = 10.525(5) b = 12.481(7) c = 22.35(2) α = 97.2(1) β = 92.63(1) γ = 106.0(6)
Volume/10^6 [pm^3]	2878.9(7)	2276.1(6)	1537.4(3)	2789(4)
Z	4	2	2	2
Density [g/cm^3] calcd.	2.230	2.044	1.825	1.430
Absorption coefficient [mm^{-1}]	9.290	7.839	5.817	3.432
F(000)	1787	1320	820	1180
2θ range	5.14° < 2θ < 50.50°	5.86° < 2θ < 50.00°	4.88° < 2θ < 56.20°	4.92° < 2θ < 37.50°
Diffractometer	STOE-IPDS	STOE-IPDS	STOE-IPDS	STOE-IPDS
Number of reflections collected	10357	7833	14262	10478
Data/restraints/parameters	4994/2/277	3648/1/262	3454/0/172	4163/9/297
Goodness of Fit	1.000	0.985	0.941	0.703
R-indices [$I > 2\sigma(I)$]	$R1$ = 0.0420, $wR2$ = 0.0737	$R1$ = 0.0282, $wR2$ = 0.0604	$R1$ = 0.0315, $wR2$ = 0.0575	$R1$ = 0.0719, $wR2$ = 0.1566
R-indices (all data)	$R1$ = 0.0639, $wR2$ = 0.0769	$R1$ = 0.0344, $wR2$ = 0.0622	$R1$ = 0.0615, $wR2$ = 0.0637	$R1$ = 0.1701, $wR2$ = 0.1876

$[Yb_3(MeCp)_4(Cp)F_3]^+$, 942 (7.2) $[Yb_3(MeCp)_3(Cp)(C_5H_4)F_3]^+$, 700 (18) $[Yb_2(MeCp)_4F_2]^+$, 686 (5.4) $[Yb_2(MeCp)_3(Cp)F_2]^+$, 621 (82) $[Yb_2(MeCp)_3F_2]^+$, 607 (21) $[Yb_2(MeCp)_2(Cp)F_2]^+$, 594 (1.1) $[Yb_2(MeCp)(Cp)(C_5H_6)F_2]^+$, 542 (10) $[Yb_2(MeCp)_2F_2]^+$, 528 (1.4) $[Yb_2(MeCp)_2(Cp)F_2]^+$, 463 (3.3) $[Yb_2(MeCp)F_2]^+$, 411 (16) $[Yb_3(MeCp)_3]^+$, 397 (4.1) $[Yb(MeCp)_2(Cp)]^+$, 332 (100) $[Yb(MeCp)_2]^+$, 318 (14) $[Yb(MeCp)(Cp)]^+$, 253 (39) $[Yb(MeCp)]^+$, 239 (3.6) $[Yb(Cp)]^+$, 174 (2.2) $[Yb]^+$, 79 (57) $[MeCp]^+$, 67 (10.3) $[CpH]^+$. – $C_{48}H_{56}F_4Yb_4$ (1401.09): calcd. F 5.42, Yb 49.40; found F 5.27, Yb 49.61. Single crystals for X-ray analysis were obtained by isothermal evaporation of DME in a U-tube, with the solution in one arm at room temperature, and the other arm cooled in liquid nitrogen.

Di{bis(cyclopentadienyl)(μ-fluoro)(triphenylphosphane oxide)-ytterbium(III)}: $[YbCp_2(DME)]$ (0.59 g, 1.5 mmol) and perfluorodecalin (0.17 g, 3.8 mmol) were stirred in THF (4 mL) at room temperature for 24 h. The colour of the solution changed to dark brown and a yellow solid precipitated. To this mixture, THF (4 mL) and $OPPh_3$ (0.42 g, 1.5 mmol) were added. After stirring for 24 h at room temperature and 3 d at 50 °C, the resulting yellow precipitate was filtered off. The pale yellow solid was washed twice with

THF (2 mL) and dried for 3 h under vacuum (yield 34%). – IR (KBr): $\tilde{\nu}$ = 3084 m cm^{-1}, 3059 m, 1650 w, 1591 w, 1486 w, 1438 s, 1179 s (br), 1124 s, 1098 m, 1071 w, 1012 s, 926 w, 873 w, 846 w, 779 s (br), 747 s, 726 s, 692 s. – Far IR: $\tilde{\nu}$ = 540 s cm^{-1}, 514 w, 476 s, 458 s (br), 421 w, 389 w, 306 m, 292 m, 254 m, 225 w, 203 m (sh), 195 s, 141 w, 117 w. – MS (20 eV, 280 °C), *m/z* (%): 902 (1.7) $[Yb_3Cp_5F_3H]^+$, 643 (0.7) $[Yb_2Cp_3F_2(C_5H_4)]^+$, 578 (1.4) $[Yb_2Cp_2F_2(C_5H_4)]^+$, 513 (0.3) $[Yb_2CpF_2(C_5H_4)]^+$, 369 (8.8) $[YbCp_3]^+$, 304 (18) $[YbCp_2]^+$, 278 (57) $[OPPh_3]^+$, 277 (100) $[OPPh_2(C_6H_4)]^+$, 239 (15) $[CpYb]^+$, 201 (17) $[OPPh_2]^+$, 185 (8.6) $[PPh_2]^+$, 154 (3.6) $[Ph_2]^+$, 77 (4.3) $[Ph]^+$, 65 (2.9) $[Cp]^+$, 39 (3.5) $[HF_2]^+$. – $C_{56}H_{50}F_2O_2P_2Yb_2$ (1200.98): calcd. F 3.16; found F 3.22. Slow evaporation of the THF filtrate in a U-tube yielded yellow needles of $[YbCp_2F(OPPh_3)]_2$ suitable for X-ray crystallography.

Di{(μ-fluoro)bis(methylcyclopentadienyl)(tetrahydrofuran)ytterbium-(III)}: $[Yb(MeCp)_2(THF)]$ (0.76 g, 1.8 mmol) and perfluorodecalin (0.21 g, 4.5 mmol) were stirred for 48 h in THF (2.5 mL) at room temperature. The mixture was warmed up to 50 °C for 2 h and then slowly cooled. The microcrystalline precipitate was filtered off and washed twice with 0.5 mL of THF (yield 24%). – IR (Nujol): $\tilde{\nu}$ = 3079 w cm^{-1}, 1239 w, 1067 w, 1049 m, 1034 m, 932 m, 835 s, 766 vs, 616 w. – Far IR: $\tilde{\nu}$ = 468 vs (br) cm^{-1}, 331 s, 268 s, 229 m, 197 m, 116 w. – MS (20 eV, 215 °C), *m/z* (%): 970 (47) $[Yb_3(MeCp)_4(CpCH_2)F_3]^+$, 956 (29) $[Yb_3(MeCp)_4(C_5H_4)F_3]^+$, 943 (7.7) $[Yb_3(MeCp)_3(Cp)_2F_3]^+$, 700 (12) $[Yb_2(MeCp)_4F_2]^+$, 684 (3.4) $[Yb_2(MeCp)_3(Cp)F_2]^+$, 621 (38) $[Yb_2(MeCp)_3F_2]^+$, 609 (8.6) $[Yb_2(MeCp)_2(C_5H_7)F_2]^+$, 542 (4.9) $[Yb_2(MeCp)_2F_2]^+$, 528 (1.1) $[Yb_2(MeCp)(Cp)F_2]^+$, 411 (29) $[Yb(MeCp)_3]^+$, 397 (7.3) $[Yb(MeCp)_2(Cp)]^+$, 332 (100) $[Yb(MeCp)_2]^+$, 318 (17) $[Yb(MeCp)(Cp)]^+$, 253 (51) $[Yb(MeCp)]^+$, 239 (6.6) $[Yb(Cp)]^+$, 174 (2.2) $[Yb]^+$, 79 (66) $[MeCp]^+$, 39 (12) $[HF_2]^+$. – $C_{32}H_{44}F_2O_2Yb_2$ (844.75): calcd. F 4.50, Yb 41.00; found F 4.29, Yb 41.38. – Single crystals were obtained by isothermal evaporation of the filtrate in a U-tube. An attempt to effect a similar synthesis with perfluoro(methylcyclohexane) at room temperature for 7 d showed the reaction to be very slow.

X-ray Structure Determination: Crystals were mounted in 0.2/0.3 mm diameter glass capillaries under dry argon in a glove box. Data sets were measured with an IPDS diffractometer (imaging plate system STOE) using Mo-K_α radiation and a graphite monochromator (Table 6 and Table 7). Structure determinations were carried out with the programs SHELX-96 and SHELX-97.[50] Numerical absorption corrections for $[YbCp_2F]_3$, $[Yb(MeCp)_2F]_4$, $[Yb(MeCp)_2F(THF)]_2$, and $[Yb(OC_6H_2\text{-}2,6\text{-}tBu_2\text{-}4\text{-}X)_2F(THF)]_2$ were run after crystal face optimisation (X-Shape[51] and X-RED[52]). Neutral atom scattering factors were from International Tables, vol. C.[53] Complete lists of atomic coordinates, bond lengths and angles, thermal parameters, and hydrogen atom coordinates are available from the Cambridge Crystallographic Data Centre as supplementary publication nos. CCDC-136401–136406. Copies of the data can be obtained free of charge on application to CCDC, 12 Union Road, Cambridge CB121EZ (UK) [Fax: (int. code) + 44-1223/336-033; E-mail: deposit@ccdc.cam.ac.uk].

Acknowledgments

We are especially grateful to the Fonds der Chemischen Chemie, Frankfurt am Main, for a Kekulé stipend for D. S., and to the Australian Research Council for support.

[1] G. B. Deacon, G. D. Fallon, C.M. Forsyth, B. M. Gatehouse, P. C. Junk, A. Philosof, P. A. White, *J. Organomet. Chem.* **1998**, *565*, 201–210.
[2] G. B. Deacon, C. M. Forsyth, P. C. Junk, B. W. Skelton, A. H. White, *Chem. Eur. J.* **1999**, *5*, 1452–1459.
[3] P. L. Watson, T. H. Tulip, I. Williams, *Organometallics* **1990**, *9*, 1999–2009.
[4] A. Herzog, F.-Q. Liu, H. W. Roesky, A. Demsar, K. Keller, M. Noltemeyer, F. Pauer, *Organometallics* **1994**, *13*, 1251–1256.
[5] W. Kaminsky, S. Lenk, V. Scholz, H. W. Roesky, A. Herzog, *Macromolecules* **1997**, *30*, 7647–7650.
[6] J. L. Kiplinger, T. G. Richmond, C. E. Osterberg, *Chem. Rev.* **1994**, *94*, 373–421.
[7] H. Dorn, E. F. Murphy, S. A. A. Shah, H. W. Roesky, *J. Fluorine Chem.* **1997**, *86*, 121- 125.
[8] J. Burdenine, B. Jedlicka, R. H. Crabtree, *Chem. Ber./Recueil* **1997**, *130*, 145–154.
[9] R. C. Mehrotra, A. Singh, U. M. Tripathi, *Chem. Rev.* **1991**, *91*, 1287–1303.
[10] W. J. Evans, *New. J. Chem.* **1995**, *19*, 727–750.
[11] L. G. Hubert-Pfalzgraf, *New. J. Chem.* **1995**, *19*, 525–533.
[12] M. N. Bochkarev, L. N. Zakharov, G. S. Kalinina (Eds.), *Organoderivatives of the Rare Earth Elements*, Kluwer, Dordrecht, **1995**.
[13] H. Schumann, J. A. Meese-Marktscheffel, L. Esser, *Chem. Rev.* **1995**, *95*, 865–986.
[14] F. T. Edelmann, in E. W. Abel, F. G. A. Stone, G. Wilkinson (Eds.), *Comprehensive Organometallic Chemistry II*, vol. 4, Pergamon, Oxford, **1995**, chapter 2.
[15] F. Bottomley, D. E. Paez, P. S. White, *J. Organomet. Chem.* **1985**, *291*, 35–41.
[16] C. J. Burns, D. J. Berg, R. A. Andersen, *J. Chem. Soc., Chem. Commun.* **1987**, 272–273.
[17] C. J. Burns, R. A. Andersen, *J. Chem. Soc., Chem. Commun.* **1989**, 136–137.
[18] E. Lork, R. Mews, J. Petersen, P. G. Watson, *XVIIth International Conference on Organometallic Chemistry*, Brisbane, Australia, July **1996**.
[19] Z. Xie, Z. Liu, F. Xue, T. C. W. Mak, *J. Organomet. Chem.* **1997**, *539*, 127–130.
[20] H. Schumann, M. R. Keitsch, J. Winterfeldt, J. Demtschuk, *J. Organomet. Chem.* **1996**, *525*, 279–281.
[21] G. B. Deacon, S. C. Harris, G. Meyer, D. Stellfeldt, D. L. Wilkinson, G. Zelesny, *J. Organomet. Chem.* **1998**, *552*, 165–170.
[22] J. L. Kiplinger, T. G. Richmond, *J. Am. Chem. Soc.* **1996**, *118*, 1805–1806.
[23] J. L. Kiplinger, T. G. Richmond, *J. Chem. Soc., Chem. Commun.* **1996**, 1115–1116.
[24] G. B. Deacon, T. Feng, S. Nickel, M. I. Ogden, A. H. White, *Aust. J. Chem.* **1992**, *45*, 671–683.
[25] [25a] J. Lewis, J. R. Miller, R. L. Richards, A. Thompson, *J. Chem. Soc.* **1965**, 5850–5860. – [25b] R. J. H. Clark, J. Lewis, D. J. Machin, R. S. Nyholm, *J. Chem. Soc.* **1963**, 379–387.
[26] G. B. Deacon, T. Feng, P. MacKinnon, R. H. Newnham, S. Nickel, B. W. Skelton, A. H. White, *Aust. J. Chem.* **1993**, *46*, 387–399.
[27] *Documentation of Molecular Spectroscopy*, Spectrum No 16116, Verlag-Chemie, Weinheim, **1970**.
[28] See, e.g.: J. E. Cosgriff, G. B. Deacon, G. D. Fallon, B. M. Gatehouse, H. Schumann, R. Weimann, *Chem. Ber.* **1996**, *129*, 953–958.
[29] F. A. Cotton, R. D. Barnes, E. Bannister, *J. Chem. Soc.* **1960**, 2199–2203.
[30] [30a] D. R. Cousins, F. A. Hart, *J. Inorg. Nucl. Chem.* **1967**, *29*, 1745–1757. – [30b] J. E. Cosgriff, G. B. Deacon, B. M. Gatehouse, *Aust. J. Chem.* **1993**, *46*, 1881–1896.
[31] G. B. Deacon, S. C. Harris, G. Meyer, D. Stellfeldt, D. L. Wilkinson, G. Zelesny, *J. Organomet. Chem.* **1996**, *525*, 247–254.
[32] R. H. Hauge, J. W. Hastie, J. L. Margrave, *J. Less Common Met.* **1971**, *23*, 359–365.
[33] G. B. Deacon, J. H. S. Green, *Spectrochim. Acta* **1969**, *25A*, 355–364.
[34] G. Paolucci, R. D. Fischer, H. Breitbach, B. Pelli, P. Traldi, *Organometallics* **1988**, *7*, 1918–1923.

[35] R. D. Shannon, *Acta Crystallogr., Sect. A* **1976**, *32*, 751–767.
[36] J. Marçalo, A. P. de Matos, *Polyhedron* **1989**, *8*, 2431–2437.
[37] [37a] G. B. Deacon, T. Feng, B. W. Skelton, A. H. White, *Aust. J. Chem.* **1995**, *48*, 741–756; [37b] G. B. Deacon, T. Feng, P. C. Junk, B. W. Skelton, A. H. White, *Chem. Ber./Recueil* **1997**, *130*, 851–857. – [37c] G. B. Deacon, S. Nickel, P. MacKinnon, E. R. T. Tiekink, *Aust. J. Chem.* **1990**, *43*, 1245–1257.
[38] G. B. Deacon, P. I. MacKinnon, T. W. Hambley, J. C. Taylor, *J. Organomet. Chem.* **1983**, *259*, 91–97.
[39] A. F. Wells, *Structural Inorganic Chemistry*, 4th ed., Clarendon, Oxford, **1975**.
[40] L. Pauling, *The Nature of the Chemical Bond*, 3rd ed., Cornell University Press, Ithaca, New York. **1960**.
[41] See, e.g.: [41a] J. M. Boncella, R. A. Andersen, *Organometallics* **1985**, *4*, 205–206. – [41b] H. Heijden, C. J. Shaverien, A. G. Orpen, *Organometallics* **1989**, *8*, 255–258. – [41c] T. D. Tilley, R. A. Andersen, A. Zalkin, *Inorg. Chem.* **1984**, *23*, 2271–2276.
[42] W. J. Evans, D. E. Drummond, J. W. Grate, H. Zhang, J. L. Atwood, *J. Am. Chem. Soc.* **1987**, *109*, 3928–3936.
[43] K. N. Raymond, C. W. Eigenbrot, *Acc. Chem. Res.* **1980**, *13*, 276–283.
[44] M. N. Bochkarev, I. L. Fedushkin, A. A. Fagin, T. V. Petrovskaya, J. W. Ziller, R. N. R. Broomhall-Dillard, W. J. Evans, *Angew. Chem.* **1997**, *109*, 123–124.
[45] Z. Hou, A. Fujita, T. Yoshimura, A. Jesorka, Y. Zhang, H. Yamazaki, Y. Wakatsuki, *Inorg. Chem.* **1996**, *35*, 7190–7195.
[46] G. Zelesny, Doctoral Thesis, University of Cologne, **1998**.
[47] G. B. Deacon, C. M. Forsyth, B. M. Gatehouse, A. Philosof, B. W. Skelton, A. H. White, P. A. White, *Aust. J. Chem.* **1997**, *50*, 959–970.
[48] A. D. Campbell, P. A. Dawson, *Mikrochim. Acta* **1983**, *1*, 489–494.
[49] [49a] G. B. Deacon, A. J. Koplick, T. D. Tuong, *Aust. J. Chem.* **1984**, *37*, 517–525. – [49b] G. B. Deacon, G. N. Pain, T. D. Tuong, *Inorg. Synth.* **1990**, *28*, 291–297. – [49c] G. B. Deacon, G. N. Pain, T. D. Tuong in *Herrmann-Brauer, Synthetic Methods of Organometallic and Inorganic Chemistry*, 3rd ed. (Ed. W.A. Herrmann), G. Thieme, Stuttgart, **1997**, vol. 6, pp. 54–55.
[50] [50a] G. M. Sheldrick, *SHELXS-96 (-97), Program for the Solution of Crystal Structures,* Göttingen **1996 (1997)**. – [50b] G. M. Sheldrick, *SHELXL-96 (-97), Program for the Refinement of Crystal Structures from Diffraction Data*, Göttingen **1996 (1997)**.
[51] STOE Cie GmbH, X-Shape: *Crystal optimisation for numerical absorption correction*, Darmstadt, **1996**.
[52] STOE Cie GmbH, X-Red: *Data reduction for STADI4 and IPDS*, Darmstadt, **1996**.
[53] R. J. C. Wilson (Ed.), *International Tables of Crystallography*, vol. C, Kluwer Academic Publishers, Dordrecht, **1992**.

Received October 28, 1999
[I99382]

Density Functional Study of Possible Intermediates in the Mechanism of Olefin Cyclopropanation Catalyzed by Metal Carboxylates

Cristóbal Rodríguez-García,[a] Òscar González-Blanco,[a] Antonio Oliva,[a] Rosa M. Ortuño,[a] and Vicenç Branchadell*[a]

Keywords: Carbene complexes / Carboxylato complexes / Density functional calculations / Palladium / Rhodium

The structures of several complexes arising from the interaction between methylene and palladium and rhodium diformates were optimized through density functional calculations. For palladium, mono-, di-, and trimeric complexes were considered. The results obtained show that in all cases the most stable structures correspond to complexes in which methylene has inserted in one of the M–O bonds, while metal–carbene complexes are energy minima only for monomeric palladium diformate and for rhodium diformate. Trimeric palladium formate is thermodynamically stable upon fragmentation. However, when it reacts with methylene, fragmentation becomes favorable. The role of the resulting monomeric complex in the olefin cyclopropanation mechanism catalyzed by palladium dicarboxylates is discussed.

Introduction

The reaction of olefins with diazomethane catalyzed by transition metal complexes is one of the methods for obtaining cyclopropane derivatives.[1–2] The generally accepted mechanism for this reaction involves the formation of a metal–carbene complex as intermediate. Pfeiffer and Dötz[3] have recently reported the first direct spectroscopic observation of such an intermediate for cyclopropanation reactions of enol ethers catalyzed by Cr^0 complexes.

Rhodium and palladium diacetates are among the most efficient catalysts for the cyclopropanation of olefins by diazo compounds. Because their ability to coordinate olefins differs, different mechanisms for these two catalysts have been postulated.[4] For rhodium, the first step would be the formation of the metal–carbene complex that would then react with the olefin, whereas for palladium a metal–olefin complex would be formed before the attack at diazomethane.

Ortuño et al.[5] have reported that in the reaction between diazomethane and chiral cyclohexenones catalyzed by palladium diacetate, the methylenation can take place both at the C–C double bond and at the carbonyl group, the site-selectivity of the process depending on the nature of the substituents in cyclohexenone. The knowledge of the structure of the intermediate arising from the interaction between diazomethane and palladium diacetate seems crucial for understanding the origin of this selectivity.

Metal–carbene complexes have also been studied from a theoretical point of view.[6–13] Vyboishchikov and Frenking[13] have recently studied a series of tungsten–carbene complexes and have analyzed the nature of the bonding. For low-valent complexes, such as $(CO)_5WCH_2$, the bonding can be analyzed in terms of an electron donation from the HOMO of singlet methylene to the corresponding empty d orbital of the metal and a back-donation from one of the doubly occupied dπ orbitals of the metal to the virtual $1b_1$ orbital of singlet methylene. On the other hand, for high-valent complexes, such as Cl_4WCH_2, the bonding is better described as a covalent double bond arising from the interaction between metal and methylene open-shell fragments. In this case, the metal–carbene bond is stronger (larger bond dissociation energy and shorter bond length).

In this paper we present a theoretical study of complexes arising from the reaction between diazomethane and palladium dicarboxylates, which can be relevant in the olefin cyclopropanation mechanism. The alkyl groups have been modeled by hydrogen atoms to simplify the calculations.

Computational Details

Molecular geometries were fully optimized at the generalized gradient approximation (GGA) level of calculation with Becke's[14] exchange potential and the correlation potential of Perdew and Wang[15] (BPW91) implemented in the ADF program.[16–18] The inner electrons of the metal (up to the 3d shell), C, and O were treated within the frozen-core approximation.[17] For the valence space, a basis set of uncontracted Slater-type orbitals was used.[19] The basis set for the metal is triple-ξ. The valence basis set for C, O, and H is of the double-ξ type, supplemented with a set of 3d (C and O) and 2p (H) polarization functions. At this level of calculation the computed bonding energy of $PdCH_2$ is 49.4 kcal mol^{-1}, in excellent agreement with the value obtained by Siegbahn,[20] using the MCPF method (51.0 kcal mol^{-1}).

Relativistic effects were considered in all atoms through the so-called quasi-relativistic method,[21] in which the first-order scalar relativistic Pauli Hamiltonian is diagonalized in the space of the nonrelativistic solutions. These effects were included in the geometry optimization.

[a] Departament de Química,
Universitat Autònoma de Barcelona, Edifici Cn,
08193 Bellaterra, Spain
Fax: (internat.) +34-935812920
E-mail: vicenc@klingon.uab.es

 © WILEY-VCH Verlag GmbH, D-69451 Weinheim, 2000 1434–1948/00/0505–1073 $ 17.50+.50/0

Molecular geometries were also optimized at the local density approximation[22] (LDA) level of calculation with the Gaussian-98 program.[23] These geometries were used to calculate harmonic vibrational frequencies. In these calculations we used the effective core potentials of Hay and Wadt[24] for the metal atoms. For the remaining atoms we used the D95 basis set[25] supplemented with a set of 3d polarization functions for C and O.

Results and Discussion

Palladium diacetate has a trimeric structure in the solid state.[26] We optimized the geometry of trimeric palladium diformate as well as those corresponding to the dimer and the monomer. For comparison, we also studied dimeric rhodium diformate.[27] The optimized geometries of these complexes are shown in Figure 1 and selected geometry parameters are presented in Table 1.

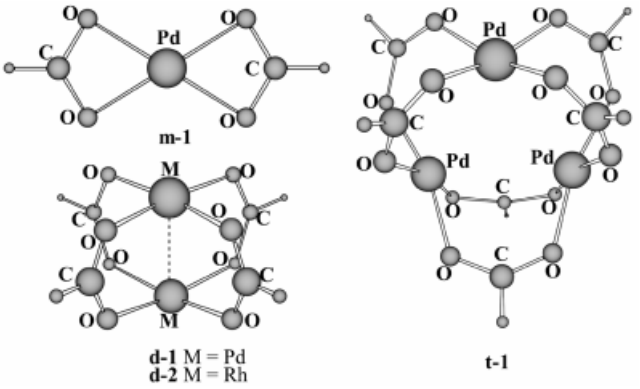


Figure 1. Structures of palladium and rhodium diformates

Table 1. Selected geometry parameters obtained for palladium and rhodium diformate

Structure[a]	M–O[b]	O–C	M–O–C	O–C–O	O–M–O	M–M
m-1	2.082	1.278	89.2	118.2	63.5	
d-1	2.07	1.271	118.1	131.1	89.8	2.581
d-2	2.059	1.270	116.8	128.9	90.0	2.380
t-1[c]	2.049	1.262	127.5	131.5	92.5	3.242
	(1.989)	(1.237)	(130.9)	(125.6)		(3.131)

[a] See Figure 1. – [b] Distances in Å, angles in degrees. – [c] Experimental values corresponding to the crystal structure of palladium diacetate are given in parentheses (ref.[26a]).

Monomeric palladium diformate, **m-1**, has D_{2h} symmetry with the two formate ligands in a bidentate coordination mode, in such a way that Pd is in a square-planar environment, as expected for d^8 ML_4 complexes.

Dimeric palladium diformate, **d-1**, and rhodium diformate, **d-2**, have D_{4h} symmetry. Both metal atoms are linked to each other through four bridging formate ligands, so that each metal atom is also in a square-planar environment. In this environment, Rh^{II} has a d^7 electron configuration. The d orbital pointing to the four oxygen atoms of the coordination plane is empty, while the d_{z^2} orbital, which is perpendicular to the coordination plane, is singly occupied. The interaction between the d_{z^2} orbitals of both Rh atoms leads to a single Rh–Rh bond in **d-2**. The geometry parameters obtained for this complex are very similar to those reported by Cotton and Feng.[28] On the other hand, for the palladium dimeric complex, **d-1**, there is no metal–metal bond, since the dz^2 orbitals of both Pd atoms are doubly occupied. The relatively short value of the Pd–Pd distance is due to the bridging ligands and it is similar to values observed for other Pd^{II} dinuclear complexes.[28]

The trimeric palladium diformate, **t-1**, has D_{3h} symmetry, with the three Pd atoms forming an equilateral triangle (see Figure 1). Two formate bridges link each pair of Pd atoms, leading to a square-planar environment for all metal centers. The optimized geometry parameters obtained for **t-1** (see Table 1) are in very good agreement with the crystal structure determined for palladium diacetate.[26]

Even though palladium diacetate has a trimeric structure in the solid state, in solution it could also exist as a monomer or a dimer. Fragmentation of **t-1** could take place according to the following steps:

t-1 → **d-1** + **m-1** (1)

d-1 → **m-1** + **m-1** (2)

Table 2. Variation of energy and of thermodynamic functions; computed for palladium diformate fragmentation

Step	ΔE[a]	$\Delta H°_{298}$ [a]	$\Delta S°_{298}$[b]	$\Delta G°_{298}$[a]
1	30.9	29.3	43.3	16.4
2	28.1	26.2	48.9	11.6

[a] In kcal mol^{-1}. – [b] In cal K^{-1} mol^{-1}.

Table 2 presents the computed values for energies and thermodynamic functions associated with these steps. Fragmentation of **t-1** is energetically and thermodynamically unfavorable in the gas phase. However, we cannot exclude the possibility that the solvent effect or the coordination of an additional ligand make this process feasible. For this reason, we will consider the formation of carbene complexes from the three forms of palladium diformate.

For comparison, we also considered the fragmentation of **d-2**, which would lead to planar monomeric rhodium diformate in a ^2A_g state. This process is energetically more unfavorable than the fragmentation of **d-1**, the computed fragmentation energy being 80.3 kcal mol^{-1}, since it would involve the cleavage of a Rh–Rh bond, whereas for the palladium complex the metal–metal interaction is repulsive.

For the interaction of methylene with **m-1**, we obtained two different structures (see Figure 2): a Pd–CH_2 complex with C_2 symmetry (**m-3**) and a structure in which methylene has inserted into one of the Pd–O bonds (**m-4**). Both structures are energy minima, since all their vibrational frequencies are real. The **m-3** structure can be considered as a distorted trigonal bipyramid in which O1 and O2 are in the axial positions. The inserted structure **m-4** is 35.3 kcal mol^{-1} more stable than **m-3** and the coordination is square planar.

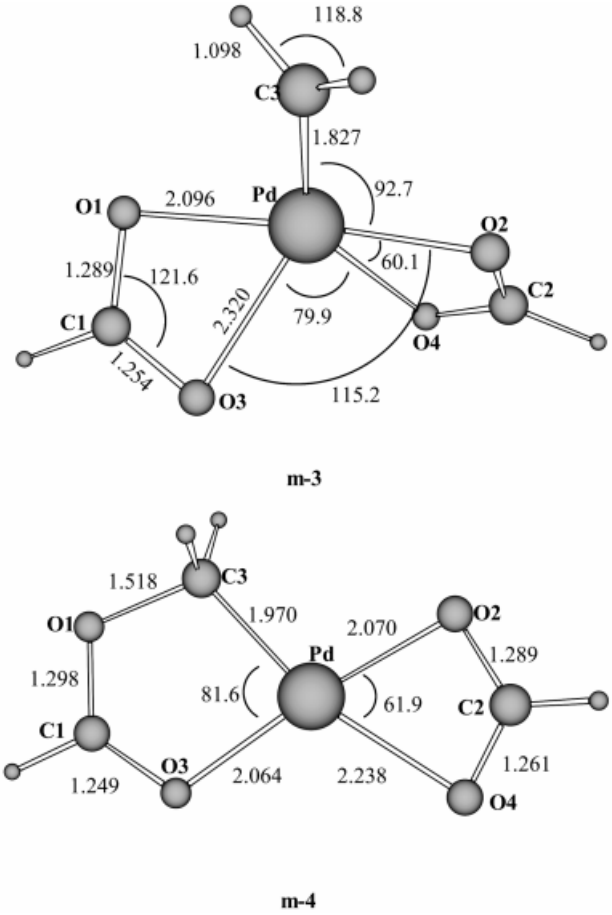


Figure 2. Structures of complexes arising from the interaction between methylene and monomeric palladium diformate; distances are in Å and angles in degrees

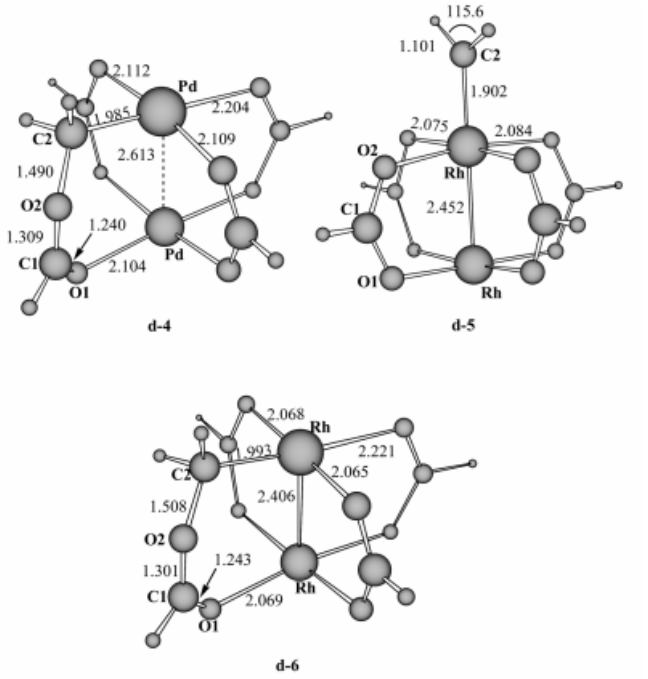


Figure 3. Structures of complexes arising from the interaction between methylene and dimeric rhodium and palladium diformates; distances are in Å and angles in degrees

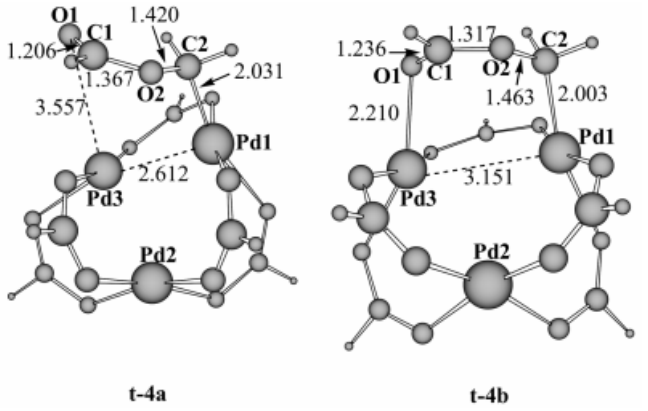


Figure 4. Structures of complexes arising from the interaction between methylene and trimeric palladium diformate; distances are in Å and angles in degrees

Figure 3 represents the structures obtained for the interaction of methylene with dimeric complexes **d-1** and **d-2**. For rhodium diformate, we obtained a metal–carbene complex with C_{2v} symmetry (**d-5**). A similar structure was optimized for palladium diformate, but it has three imaginary frequencies, of symmetries a_2, b_1, and b_2. By lowering the symmetry to C_2, a structure with one imaginary frequency of b symmetry is obtained. Relaxation of all symmetry constraints leads to a structure in which the CH_2 group has inserted into one of the Pd–O bonds (**d-4**). This structure is 35.4 kcal mol^{-1} lower in energy than the C_{2v} Pd–CH_2 structure. A similar CH_2-inserted structure was also obtained for Rh (**d-6**), this structure being 16.6 kcal mol^{-1} lower in energy than **d-5**.

For the interaction between **t-1** and methylene, we obtained a Pd–CH_2 structure with C_2 symmetry. However, this structure is not an energy minimum, since it has an imaginary frequency of b symmetry. When symmetry restrictions are removed, this structure evolves to the CH_2-inserted complex **t-4a** represented in Figure 4. This structure is 32.3 kcal mol^{-1} lower in energy than the C_2 one. Figure 4 shows that in **t-4a** one of the Pd atoms is surrounded by only three oxygen atoms, and that the C1–O1 carbonyl group is not interacting with any of the Pd atoms. We also optimized the geometry of a CH_2-inserted structure in which all Pd atoms are linked through bidentate ligands, as in dimeric complexes **d-4** and **d-6**. The obtained structure, **t-4b**, which is also shown in Figure 4, is 6.0 kcal higher in energy than **t-4a**.

The value of the Pd1–Pd3 distance in **t-4a** (see Figure 4) and the fact that Pd3 is only coordinated to three oxygen atoms seem to indicate that some kind of bonding interaction exists between Pd1 and Pd3. This interaction could be viewed as the electron donation from an occupied dz^2-type orbital perpendicular to the Pd1 coordination plane to an empty d orbital of Pd3. In this way, Pd3 would be in a square-planar tetracoordinated environment, while Pd1 would be in a square-pyramidal pentacoordinated environment.

Structure **t-4b** would be more similar to the CH_2-inserted structures obtained for the monomer and the dimer. However, it is destabilized with respect to **t-4a**. The reason is that the Pd1–Pd3 distance is too large for a bridging ligand such as CH_2OCHO. In the monomeric complex **m-4**, all the C and O atoms of the CH_2OCHO bidentate ligand are in the same plane as Pd, so that the C1–O1–C3–Pd dihedral angle is 0°. In the dimeric complexes, the CH_2OCHO bridging ligand is not coplanar with the metal atoms and the C1–O2–C2–M dihedral angle is –59.4° for **d-4** (M = Pd) and –57.8° for **d-6** (M = Rh). Finally, in **t-4b**, the C1–O2–C2–Pd1 dihedral angle is –80.1°. This large deviation from planarity makes **t-4b** unstable with respect to **t-4a**.

These results suggest that a metal–carbene complex does not exist for dimeric and trimeric palladium dicarboxylates. This kind of structure would exist for monomeric palladium dicarboxylates and for dimeric rhodium dicarboxylates, but, in both cases, the metal–carbene complex would be unstable with respect to methylene insertion in one of the M–O bonds. To rationalize these results, we will analyze the metal–carbene bond in complexes **m-3** and **d-5**.

For comparison, we also optimized the geometries of $(CO)_5WCH_2$ and Cl_4WCH_2 as representative examples of different kinds of metal–carbene complexes. The results obtained, which are summarized in Table 3, are very similar to those reported by Vyboishchikov and Frenking.[13] If we compare the values of the M–CH_2 bond length and of the internal geometry parameters of the methylene group corresponding to **m-3** (Figure 2) and **d-5** (Figure 3) with those

Table 3. Selected geometry parameters of $(CO)_5WCH_2$ and Cl_4WCH_2

Complex	Geometry parameter[a]	
$(CO)_5WCH_2$	W–C[b]	2.070
	C–H	1.101
	H–C–H	108.9
Cl_4WCH_2	W–C	1.881
	C–H	1.097
	H–C–H	115.6

[a] Bond lengths in Å and bond angles in degrees. – [b] Methylene C atom.

presented in Table 3, we observe that Pd and Rh complexes are more similar to Cl_4WCH_2 than to $(CO)_5WCH_2$. So, **m-3** and **d-5** complexes would be better viewed as arising from the interaction of the $^3B_1$ ground state of methylene with the corresponding metal fragment also in a triplet state, as shown in Figure 5.

According to the extended transition state method,[30] the M–CH_2 bonding energy (*BE*) can be formally partitioned into the following terms

$$BE = -(\Delta E_{prep} + \Delta E_{st} + \Delta E_{orb})$$

The preparation energy term, ΔE_{prep}, is the energy difference between the ground state equilibrium geometry of each fragment and the geometry and electronic state they have in the complex. ΔE_{st}, is the steric energy term and represents the interaction energy between both prepared fragments with the geometries corresponding to the final complex, but with the densities that each fragment would have if the other fragment was absent. Finally, the orbital interaction term, ΔE_{orb}, takes into account the stabilization produced when the densities of both fragments are allowed to relax.

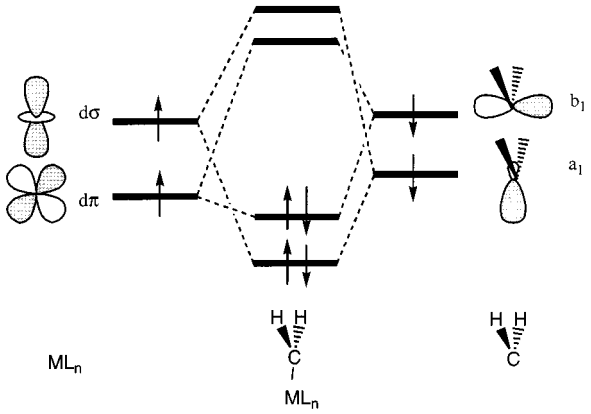


Figure 5. Schematic orbital interaction diagram for triplet methylene and a metal fragment

The formation of the M–CH_2 bond requires monooccupied dσ and dπ orbitals in the metal. These orbitals are doubly occupied in the ground state structure of **m-1**, where the only vacant metal d orbital is the one pointing to the four oxygen atoms (d_{xy}). In the prepared fragment, this orbital is doubly occupied, so that the interaction with the formate ligands becomes repulsive. Geometry distortion relieves this repulsion, leading to the structure shown in Figure 3.

For the metal fragment of **d-5**, the dσ orbital is the unoccupied antibonding combination of the Rh dz^2 orbitals, while dπ is the doubly occupied antibonding combination of the corresponding Rh d orbitals. The preparation of the metal fragment involves a promotion from dπ to dσ. Since dσ is a Rh–Rh antibonding orbital, the Rh–Rh bond becomes weaker upon complex formation (see Table 1 and Figure 3).

We separated the orbital interaction term into two contributions:

$$\Delta E_{orb} = \Delta E_{\sigma+\pi} + \Delta E_{pol}$$

The first term arises from a calculation in which all virtual orbitals of both fragments were removed, so that the energy stabilization is due only to the metal–carbene double bond formation. σ and π contributions can be separated, since the corresponding orbitals belong to different symmetry species, both in **m-3** (*a* and *b*) and in **d-5** (a_1 and b_1). The second term (ΔE_{pol}) is the additional stabilization produced when all virtual orbitals are included in the calculation and can be attributed to the polarization of the densities of both fragments.

Table 4 shows that the M–CH_2 bonds in **m-3** and **d-5** are weaker than in Cl_4WCH_2. The energy partition analysis shows that the dominant factor is the strength of σ and π interactions. The M–CH_2 bond is polarized towards

methylene. The Mulliken population analysis shows that the charge in the CH_2 fragment is –0.33 for **m-3** and –0.39 for **d-5**. The value obtained for Cl_4WCH_2 is –0.45, so that the donor ability of the metal fragments in **m-3** and **d-5** is lower than that of WCl_4.

Table 4. Components of the M–CH_2 bonding energy of metal–carbene complexes. See text for definitions; energies in kcal mol^{-1}

	Cl_4WCH_2	m-3	d-5
ΔE_{prep}	36.3	30.8	23.2
ΔE_{Pauli}	261.1	215.6	190.8
ΔE_{elstat}	–186.5	–150.2	–126.8
ΔE_{st}	74.6	65.4	64.0
ΔE_{σ}	–113.3	–95.0	–91.7
ΔE_{π}	–48.7	–34.0	–22.3
$\Delta E_{\sigma+\pi}$	–160.0	–129.0	–114.0
ΔE_{pol}	–36.6	–22.9	–26.5
BE	85.7	55.7	53.3

Since the M–CH_2 bond in **m-3** and **d-5** is not strong enough, these complexes are unstable with respect to methylene insertion in one of the M–O bonds. This process, which restores the square-planar coordination arrangement around the metal, involves the cleavage of a M–O bond and the formation of a σ M–C bond. For dimeric and trimeric palladium diformate, metal–carbene complexes are much more destabilized and do not correspond to stable structures. In these cases, the preparation energy of the metal fragment would be notably larger than for **m-3** and **d-5** and the rigidity of the structures does not allow a similar geometry relaxation as the one observed for the monomer.

We have seen that trimeric palladium diformate is thermodynamically stable with respect to fragmentation. Let us now consider the fragmentation of the methylene-inserted structure **t-4a**. This fragmentation can take place through the following steps:

t-4a → **d-1** + **m-4** (3)

t-4a → **d-4** + **m-1** (4)

d-4 → **m-4** + **m-1** (5)

Table 5. Variation of energy and thermodynamic functions for the fragmentation of **t-4a**

Step	ΔE[a]	$\Delta H°_{298}$[a]	$\Delta S°_{298}$[b]	$\Delta G°_{298}$[a]
3	4.3	2.6	39.2	–9.1
4	17.9	17.0	42.3	4.4
5	14.5	12.8	45.8	–0.9

[a] In kcal mol^{-1}. – [b] In cal K^{-1} mol^{-1}.

Table 5 contains the energies and variation of thermodynamic functions associated with these processes. Fragmentation is energetically unfavorable, but the inclusion of the entropy contribution makes step 3 thermodynamically favorable. These results can be compared with those corresponding to the fragmentation of **t-1** (Table 2), which was unfavorable even when the entropy contribution was considered.

Thus, **t-4a** is unstable with respect to fragmentation even in the gas phase and the monomeric **m-4** complex, which would be the product of such a process, could be envisaged as an intermediate in the cyclopropanation mechanism. A possible mechanistic scheme for the reaction between diazomethane and ethylene catalyzed by palladium dicarboxylates is presented in Figure 6. In the first step, the reaction between diazomethane and **t-1** leads to the formation of **t-4a**. Then, the fragmentation of this complex leads to **m-4**. Reaction between this complex and ethylene would lead to the formation of the corresponding cyclopropane derivative and **m-1**, which could also react with diazomethane to regenerate **m-4**. The reaction between **m-4** and the olefin is expected to involve several steps, such as the coordination of the olefin to Pd and the formation of a metalacyclobutane intermediate. The detailed study of this process, including the location of transition states, is currently in progress. The computed Gibbs energies presented in Figure 6 show that the overall mechanism is thermodynamically feasible for the cyclopropanation of ethylene.

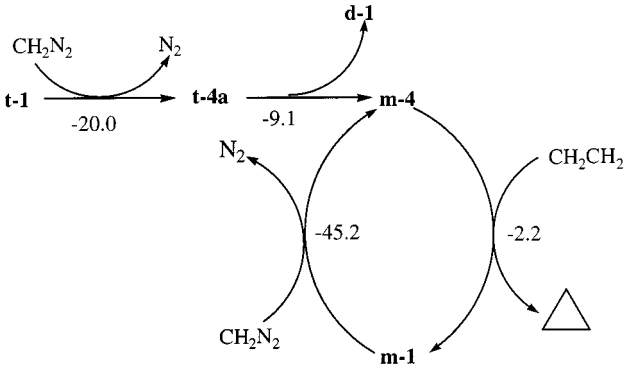


Figure 6. Possible mechanism for cyclopropanation of ethylene by diazomethane catalyzed by palladium diformate; values of reaction Gibbs energies are given in kcal mol^{-1}

As we mentioned in the introduction, other mechanisms involving the prior coordination of the olefin to palladium diacetate had also been postulated.[4] Our results showed that the coordination of an additional ligand in a tetracoordinated Pd^{II} complex requires an important rearrangement of the ligands to minimize metal–ligand repulsion. We saw that this rearrangement is not possible for the coordination of methylene in dimeric and trimeric palladium complexes. Similar behavior is expected for other ligands such as ethylene. So, a palladium–ethylene complex would only be formed from the monomeric structure **m-1**. We optimized the geometry of this complex and the obtained structure is shown in Figure 7. This structure can be consid-

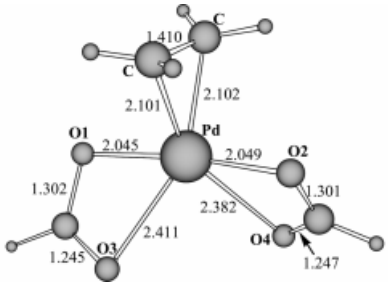


Figure 7. Structure of complexes arising from the interaction between ethylene and monomeric palladium diformate; distances are in Å

ered to be trigonal bipyramidal with ethylene in one of the equatorial positions. Compared to **m-4** (Figure 2), the Pd–O3 and Pd–O4 distances are notably larger in the ethylene complex, while Pd–O1 and Pd–O2 distances are slightly shorter. The computed Pd–ethylene bond dissociation energy is 16.8 kcal mol^{-1}. We also optimized the geometry of a complex in which ethylene inserts in one of the Pd–O bonds, but it is 2.7 kcal mol^{-1} higher in energy than the ethylene-coordinated complex.

The reaction between **m-1** and diazomethane to yield **m-4** and N_2 has a reaction energy of –47.2 kcal mol^{-1}, so that it is energetically much more favorable than the formation of the ethylene-coordinated complex. Cui et al.[31] studied the reaction between Cu and diazomethane to form $CuCH_2$ and N_2 theoretically, and observed that the reaction proceeds without an energy barrier and with a reaction energy of –34.9 kcal mol^{-1}. The formation of **m-4** from **m-1** and diazomethane involves an important rearrangement of the formate ligands, so that an energy barrier is expected for this process. Since this rearrangement is also necessary for ethylene coordination, the corresponding energy barriers are expected to be similar.

These results suggest that the mechanism for the cyclopropanation of olefins by diazomethane catalyzed by palladium dicarboxylates does not involve the prior formation of a metal–olefin complex. On the other hand, metal–carbene complexes are unstable with respect to methylene insertion in one of the Pd–O bonds, so that these CH_2-inserted species could be intermediates in the cyclopropanation mechanism.

Concluding Remarks

We optimized the geometries of several complexes arising from the interaction between methylene and palladium and rhodium diformates. In all cases, the most stable structures correspond to complexes in which methylene has inserted into one of the M–O bonds, while metal–carbene complexes correspond to energy minima only for monomeric palladium diformate and for dimeric rhodium diformate. In these cases, the analysis of the metal–carbene bonding shows that the bond is weaker than for other complexes, such as Cl_4WCH_2, due to a lower σ and π donor ability of the metal fragment.

Trimeric palladium formate (**t-1**) is thermodynamically stable upon fragmentation. However, when it forms a complex with methylene (**t-4a)**, fragmentation becomes favorable. The resulting monomeric complex **m-4** can be envisaged as an intermediate in the olefin cyclopropanation mechanism catalyzed by palladium dicarboxylates.

Acknowledgments

This work has been financially supported by DGESIC (PB97–0214). Computer time from Centre de Supercomputació de Catalunya (CESCA) and a doctoral fellowship from the Universitat Autònoma de Barcelona to C. R. are gratefully acknowledged. Finally, the authors thank Dr. Gabriel Aullón for helpful discussions on dimeric Pd^{II} complexes.

[1] M. P. Doyle, *Chem. Rev.* **1986**, *86*, 919.
[2] M. P. Doyle in: *Comprehensive Organometallic Chemistry 2, Vol 12* (Eds.: E. W. Abel, F. G. A. Stone, G. Wilkinson), Pergamon, New York, **1995**, p. 387.
[3] J. Pfeiffer, K. H. Dötz, *Angew. Chem. Int. Ed. Engl.* **1997**, *36*, 2828.
[4] A. J. Anciaux, A. J. Hubert, A. F. Noels, N. Petiniot, P. Teyssié, *J. Org. Chem.* **1980**, *45*, 695.
[5] R. M. Ortuño, J. Ibarzo, A. Alvarez-Larena, J. F. Piniella, *Tetrahedron Lett.* **1996**, *37*, 4059.
[6] D. Spangler, J. J. Wendolowski, M. Dupuis, M. M. L. Chen, H. F. Schaeffer III, *J. Am. Chem. Soc.* **1981**, *103*, 3985.
[7] [7a] H. Nakatsuji, J. Ushio, S. Han, T. Yonezawa, *J. Am. Chem. Soc.* **1983**, *105*, 426. – [7b] J. Ushio, H. Nakatsuji, T. Yonezawa, *J. Am. Chem. Soc.* **1984**, *106*, 5892.
[8] T. E. Taylor, M. B. Hall, *J. Am. Chem. Soc.* **1984**, *106*, 1576.
[9] M. Sodupe, J. M. Lluch, A. Oliva, J. Bertrán, *Organometallics* **1989**, *8*, 1837.
[10] T. R. Cundari, M. S. Gordon, *J. Am. Chem. Soc.* **1991**, *113*, 5231.
[11] A. Márquez, J. Fernandez Sanz, *J. Am. Chem. Soc.* **1992**, *114*, 2903.
[12] [12a] H. Jacobsen, G. Schreckenbach, T. Ziegler, *J. Phys. Chem.* **1994**, *98*, 11406. – [12b] H. Jacobsen, T. Ziegler, *Inorg. Chem.* **1996**, *35*, 775.
[13] S. Vyboishchikov, G. Frenking, *Chem. Eur. J.* **1998**, *4*, 1428.
[14] A. D. Becke, *Phys. Rev. A* **1988**, *38*, 3098.
[15] [15a] Y. Wang,. J. P. Perdew, *Phys. Rev. B* **1991**, *44*, 13298. – [15b] J. P. Perdew, J. A. Chevary, S. H. Vosko, K. A. Jackson, M. R. Pederson, D. J. Singh, C. Fiolhais, *Phys. Rev. B* **1992**, *46*, 6671.
[16] ADF 2.3, Theoretical Chemistry, Vrije Universiteit, Amsterdam.
[17] E .J. Baerends, D. E. Ellis, P. Ros, *Chem. Phys.* **1973**, *2*, 41.
[18] G. te Velde, E. J. Baerends, *J. Comp. Phys.* **1992**, *99*, 84.
[19] P. Vernooijs, G. J. Snijders, E. J. Baerends, *Slater Type Basis Functions for the Whole Periodic System*; Internal Report: Vrije Universiteit Amsterdam, The Netherlands, 1981.
[20] P. E. M. Siegbahn, *Chem. Phys. Lett.* **1993**, *201*, 15.
[21] T. Ziegler, V. Tschinke, E. J. Baerends, J. Snijders, W. Ravenek, *J. Phys. Chem.* **1989**, *93*, 3050.
[22] [22a] O. Gunnarsson, I. Lundquist, *Phys. Rev.* **1974**, *B10*, 1319. – [22b] S. H. Vosko, L. Wilk, M. Nusair, *Can. J. Phys.* **1980**, *58*, 1200.
[23] M. J. Frisch, G. W. Trucks, H. B. Schlegel, G. E. Scuseria, M. A. Robb, J. R. Cheeseman, V. G. Zakrzewski, J. A. Montgomery, Jr., R. E. Stratmann, J. C. Burant, S. Dapprich, J. M. Millam, A. D. Daniels, K. N. Kudin, M. C. Strain, O. Farkas, J. Tomasi, V. Barone, M. Cossi, R. Cammi, B. Mennucci, C. Pomelli, C. Adamo, S. Clifford, J. Ochterski, G. A. Petersson, P. Y. Ayala, Q. Cui, K. Morokuma, D. K. Malick, A. D. Rabuck, K. Raghavachari, J. B. Foresman, J. Cioslowski, J. V. Ortiz, B. B. Stefanov, G. Liu, A. Liashenko, P. Piskorz, I. Komaromi, R. Gomperts, R. L. Martin, D. J. Fox, T. Keith, M. A. Al-Laham, C. Y. Peng, A. Nanayakkara, C. Gonzalez, M. Challacombe, P. M. W. Gill, B. Johnson, W. Chen, M. W. Wong, J. L. Andres, C. Gonzalez, M. Head-Gordon, E. S. Replogle, J. A. Pople, *Gaussian 98*, Revision A.5; Gaussian, Inc.: Pittsburgh PA, **1998**.
[24] P. J. Hay, W. R. Wadt, *J. Chem. Phys.* **1985**, *82*, 299.
[25] T. H. Dunning Jr., P. J. Hay in: *Modern Theoretical Chemistry*, *Vol 3* (Ed.: H. F. Schaeffer III), Plenum, New York, **1976**, p. 1.
[26] [26a] F. A. Cotton, S. Han, *Rev. Chim. Minerale.* **1983**, *20*, 496. – [26b] D. H. R. Barton, J. Khamsi, N. Ozbalik, M. Ramesh, J. C. Sarma, *Tetrahedron Lett.* **1989**, *30*, 4661.
[27] F. A. Cotton, B. G. DeBoer, M. D. LaPrade, J. R. Pipal, D. A. Ucko, *Acta Crystalogr.* **1971**, *B27*, 1664.
[28] F. A. Cotton, X. Feng, *J. Am. Chem. Soc.* **1998**, *120*, 3387.
[29] G. Aullón, P. Alemany, S. Alvarez, *Inorg. Chem.* **1996**, *35*, 5061, and references therein.
[30] T. Ziegler, A. Rauk,. *Theoret. Chim. Acta* **1977**, *46*, 1.
[31] Q. Cui, D. G. Musaev, M. Svensson, K. Morokuma, *J. Phys. Chem.* **1996**, *100*, 10936.

Received November 9, 1999
[I99397]

Transition Metal Complexes with Sulfur Ligands, 143[‡]

Coordination of CO, NO, N_2H_2, and Other Nitrogenase Relevant Small Molecules to Sulfur-Rich Ruthenium Complexes with the New Ligand 'tpS_4'$^{2-}$ = 1,2-Bis(2-mercaptophenylthio)phenylene(2–)

Dieter Sellmann,*[a] Klaus Engl,[a] Frank W. Heinemann,[a] and Joachim Sieler[b]

Dedicated to Professor Heinrich Vahrenkamp on the occasion of his 60th birthday

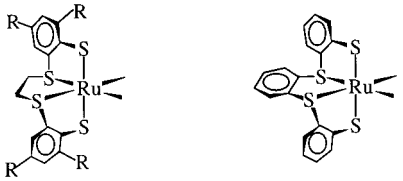
Keywords: Ruthenium / S ligands / Hydrazine / Diazene

In the search for ruthenium complexes with sulfur-dominated coordination spheres that bind, activate, or stabilize nitrogenase relevant molecules, complexes containing the new and robust tetradentate ligand 'tpS_4'–H_2 were synthesized. Treatment of $[RuCl_2(PPh_3)_3]$ with 'tpS_4'$^{2-}$ gives $[Ru(PPh_3)_2('tpS_4')]$ (**1**), which contains two labile PPh_3 ligands. The reaction of **1** with PEt_3 or DMSO led to substitution of both PPh_3 ligands, yielding $[Ru(PEt_3)_2('tpS_4')]$ (**2**) and $[Ru(DMSO)_2('tpS_4')]$ (**3**), respectively. When treated with nitrogenous ligands, complex **1** lost only one PPh_3 ligand to yield $[Ru(L)(PPh_3)('tpS_4')]$ complexes where L = py (**7**), NH_3 (**8**), N_2H_4 (**9**), NH_2NHMe (**10**), and CH_3CN (**12**), all of which are labile. The labile acetonitrile complex $[Ru(CH_3CN)(PPh_3)('tpS_4')]$ (**12**) proved to be particularly suited as a precursor for the syntheses of other $[Ru(L)(PPh_3)('tpS_4')]$ complexes. The 18 and 19 valence electron NO complexes $[Ru(NO)(PPh_3)('tpS_4')]BF_4$ (**13**) and $[Ru(NO)(PPh_3)('tpS_4')]$ (**14**), $(NEt_4)[Ru(N_3)(PPh_3)('tpS_4')]$ (**15**), $[Ru(I)(PPh_3)('tpS_4')]$ (**16**), and $[Ru(N_3)(PPh_3)('tpS_4')]$ (**17**) were obtained starting from complex **12**. The labile mononuclear hydrazine complex $[Ru(N_2H_4)(PPh_3)('tpS_4')]$ (**9**) gave the dinuclear complex $[\mu\text{-}N_2H_4\{Ru(PPh_3)('tpS_4')\}_2]$ (**18**) by dissociation of hydrazine. The dinuclear diazene complex $[\mu\text{-}N_2H_2\{Ru(PPh_3)('tpS_4')\}_2]$ (**19**) was obtained by oxidation of **9** and more readily from $[Ru(CH_3CN)(PPh_3)('tpS_4')]$ (**12**) and N_2H_2, which was generated in situ from $K_2N_2(CO_2)_2$ and acetic acid. The molecular structures of **7**, **13**, **16**, **18**, and **19** were determined by X-ray structure analyses. The complexes **18** and **19** represent the first complexes containing the hydrazine/diazene couple, which enables us to compare both the bonding features and the formation of N–H···S bridges when hydrazine and diazene bind to transition metal sulfur sites.

Introduction

The stabilization, or coordination and activation of small molecules such as CO, N_2, H_2, NO, N_3^-, N_2H_2, N_2H_4, and NH_3 by transition metal sulfur complexes is of pivotal interest for understanding the molecular mechanisms of nitrogenases.[1] It can be assumed that these molecules interact with the FeMo, FeV, or FeFe cofactors that are the active sites of nitrogenases. The FeMo cofactors of FeMo nitrogenase in the resting state have been shown by X-ray crystallography to contain $[Fe_7MoS_9]$ clusters.[2] Similar structures are assumed for the FeV or FeFe cofactors of the alternative FeV and FeFe nitrogenases.[3] However, the functioning of these clusters has remained unexplained, not least because a compound that models basic structural *and* functional principles of the cofactors has yet to be found. In particular, these principles are metal sulfur sites *and* the mild catalytic reduction of N_2 with biologically compatible redox potentials.[4]

In our search for such compounds we have found that both the [Ru('S_4')] fragments and their tertiary butyl derivatives [Ru('$^{bu}S_4$')] coordinate the complete series of above mentioned molecules, with the exception of N_2 (Scheme 1).[5]



Scheme 1. [Ru('$^{R}S_4$')] and [Ru('tpS_4')]

Another shortcoming of the [Ru('$^{R}S_4$')] complexes are ligand C–S cleavage reactions. In most cases, the [Ru('$^{R}S_4$')] fragments prove to be robust and the '$^{R}S_4$'$^{2-}$ ligands stay intact, behaving as spectator ligands. However, under strongly reducing or photolytic conditions, in reactions with

[‡] Part 142: D. Sellmann, K. Engl, F. W. Heinemann, *Eur. J. Inorg. Chem.*, in press.

[a] Institut für Anorganische Chemie der Universität Erlangen-Nürnberg,
Egerlandstraße 1, 91058 Erlangen, Germany
Fax: (internat.) + 49-9131/852-7367
E-mail: sellmann@anorganik.chemie.uni-erlangen.de
[b] Institut für Anorganische Chemie der Universität Leipzig,
Linnéstraße 3, 04103 Leipzig, Germany

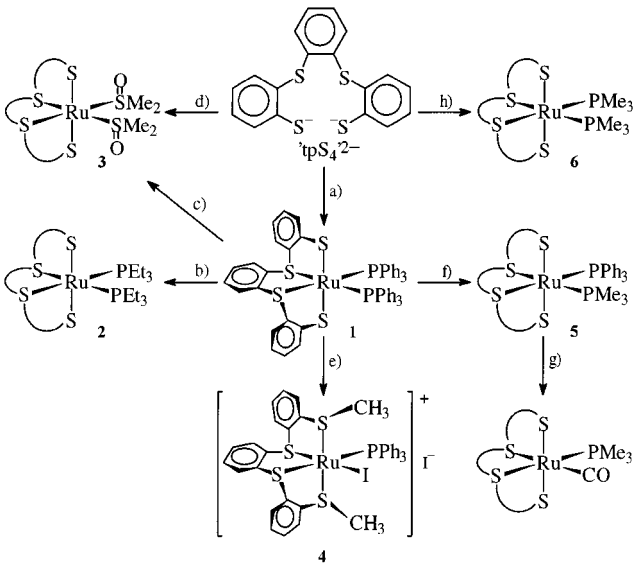
 © WILEY-VCH Verlag GmbH, D-69451 Weinheim, 2000 1434–1948/00/0505–1079 $ 17.50+.50/0

electron-rich metal complexes, and in reactions involving 19 valence electron complexes, C(alkyl)–S cleavage reactions take place yielding, among other products, 1,2-benzenedithiolate, or vinylthio(2-mercapto)benzene(1–) ligands and ethylene.[6] Since aromatic C–S bonds are more stable towards cleavage than C(alkyl)–S bonds, we synthesized the new dithioether–dithiolate ligand 'tpS_4'$^{2-}$ = 1,2-bis(2-mercaptophenylthio)phenylene(2–), which contains exclusively aromatic C–S bonds. In a previous paper we described the syntheses of 'tpS_4'$^{2-}$ and a few Ru, Os, and Ni complexes containing [M('tpS_4')] fragments, demonstrating that the 'tpS_4'$^{2-}$ ligand coordinates metals in the same helical manner as the '$^{R}S_4$'$^{2-}$ ligands and is indeed stable toward C–S cleavage.[7] Preliminary tests also indicated that analogous [Ru('$^{R}S_4$')] and [Ru('tpS_4')] complexes can have quite different substitution reactivity. This prompted us to systematically investigate the synthesis and reactivity of [Ru('tpS_4')] complexes, focusing on hydrazine, nitrosyl, and azido derivatives as potential N_2 complex precursors,[8] because subtle differences in the [Ru('$^{R}S_4$')] and [Ru('tpS_4')] fragments may be decisive in the binding or nonbinding of N_2.[9]

Results

Syntheses of [Ru('tpS_4')] Complexes with DMSO, Phosphanes, and Nitrogenous Coligands

In the search for labile [Ru(L)(L')('tpS_4')] complexes we probed the exchange of PPh_3 in the readily accessible [Ru(PPh_3)$_2$('tpS_4')] (**1**) (Scheme 2).[7]



Scheme 2. Phosphane and DMSO exchange reactions of [Ru(PPh_3)$_2$('tpS_4')]: a) + [$RuCl_2(PPh_3)_3$], THF, 4 h, room temperature (room temp.); b) + exc. PEt_3, THF, 3 min, reflux; c) DMSO, 5 min, reflux; d) + [$RuCl_2(DMSO)_4$], THF, 2.5 d, room temp.; e) + CH_3I, 2 h, room temp.; f) + exc. PMe_3, THF, 3 h, room temp.; g) + CO (1bar), THF, 4 d, room temp.; h) + [$RuCl_2(PMe_3)_4$], MeOH, 4 h, reflux

When **1** was treated with PEt_3, [Ru(PEt_3)$_2$('tpS_4')] (**2**) formed. Formation of the mixed phosphane complex [Ru(PEt_3)(PPh_3)('tpS_4')] was not observed. Brief heating of **1** in DMSO yielded [Ru(DMSO)$_2$('tpS_4')] (**3**) which could be readily obtained directly from [$RuCl_2(DMSO)_4$] and 'tpS_4'$^{2-}$. With regard to the PEt_3 and DMSO reactions, the reactivity of **1** is in contrast to that of the parent complex [Ru(PPh_3)$_2$('S_4')] which exchanges only one or none of its PPh_3 ligands under comparable conditions. An analogous behavior of **1** and the parent complex [Ru(PPh_3)$_2$('S_4')] was found in the reactions with MeI and PMe_3. Treatment of **1** in CH_2Cl_2 with excess MeI afforded the doubly methylated derivative [Ru(I)(PPh_3)('tpS_4–Me_2')]I (**4**) in isomerically pure form. PMe_3 was able to substitute only one PPh_3 ligand in **1** to give [Ru(PMe_3)(PPh_3)('tpS_4')] (**5**), even when an excess of PMe_3 was applied and the temperature was raised. The bis(PMe_3) complex [Ru(PMe_3)$_2$('tpS_4')] (**6**) formed from [$RuCl_2(PMe_3)_4$] and Li_2–'tpS_4' in boiling MeOH.

In order to probe the lability of PMe_3 versus that of PPh_3 in [Ru(PMe_3)(PPh_3)('tpS_4')] (**5**), complex **5** was treated with CO under standard conditions. Monitoring the reaction by IR and NMR spectroscopy as well as mass spectrometry showed the formation of [Ru(CO)(PMe_3)('tpS_4')], indicating that in **5** the large PPh_3 is more labile than the small PMe_3 ligand.

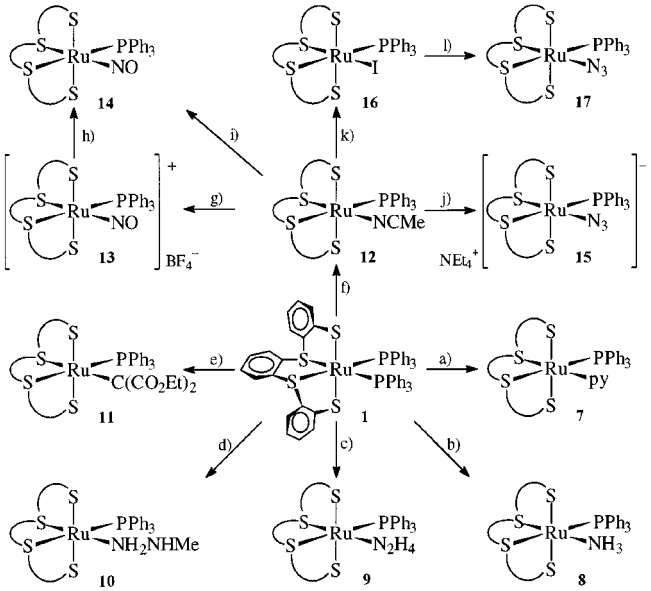
The complexes **2**–**6** proved to be less labile than the PPh_3 complex **1** and were not suited for exchange reactions with nitrogenous ligands. Attempts to exchange directly one PPh_3 in **1** for such ligands succeeded with pyridine, hydrazine(s), ammonia, and even diazomalonic ethyl ester, but failed for NO, NO^+, or N_3^-. In order to achieve their coordination it was necessary to proceed via the acetonitrile complex [Ru(MeCN)(PPh_3)('tpS_4')] (**12**). Scheme 3 summarizes these reactions and complexes.

Brief heating of **1** in pyridine gave [Ru(py)(PPh_3)('tpS_4')] (**7**). Treatment of **1** in THF with an excess of NH_3 gas, N_2H_4, or N_2H_3Me likewise afforded [Ru(NH_3)(PPh_3)('tpS_4')] (**8**), [Ru(N_2H_4)(PPh_3)('tpS_4')] (**9**), and [Ru(N_2H_3Me)(PPh_3)('tpS_4')] (**10**). In order to drive the reactions to completion, the solutions were usually heated to boiling for a short time. The conversion of **9** into a dinuclear hydrazine complex is described below.

A reaction was also observed between **1** and diethyl diazomalonate [$N_2C(CO_2Et)_2$)] in boiling THF. Monitoring the reaction by ^1H NMR spectroscopy showed that the primary product is presumably [Ru{$N_2C(CO_2Et)_2$}(PPh_3)('tpS_4')], which rapidly transforms into the carbene complex [Ru{$C(CO_2Et)_2$}(PPh_3)('tpS_4')] (**11**).

These results indicate that nitrogenous ligands are able to selectively substitute one PPh_3 in [Ru(PPh_3)$_2$('tpS_4')] (**1**). In the quest for labile solvent complex derivatives of **1**, which had so far remained inaccessible, we now tried to obtain the acetonitrile complex [Ru(MeCN)(PPh_3)('tpS_4')] (**12**). The yellow complex **12** formed from boiling acetonitrile solutions of **1**, could be isolated in solid state, completely characterized, and proved an excellent starting material for further complexes.

The reaction of **12** with CO at ambient conditions established the lability of the MeCN ligand. The CO complex



Scheme 3. Coordination of nitrogenous ligands to the [Ru(PPh$_3$)('tpS$_4$')] fragment: a) pyridine, 10 min, reflux; b) + NH$_3$ (gaseous), THF, 5 min, reflux; c) + exc. N$_2$H$_4$, THF, 10 min, reflux; d) + exc. NH$_2$NHMe, THF, 45 min, reflux; e) +exc. N$_2$C(CO$_2$Et)$_2$, THF, 4 h, reflux; f) MeCN, 3 h, reflux; g) + NOBF$_4$, CH$_2$Cl$_2$, 3 h, room temp.; h) + LiBEt$_3$ H, THF, 30 min, room temp.; i) NO (gaseous), CH$_2$Cl$_2$, 20 h, room temp.; j) + NEt$_4$N$_3$, acetone, 3 h, room temp.; k) + 0.5 I$_2$, THF 12 h, room temp.; l) + exc. NEt$_4$N$_3$, acetone, 3 d, room temp.

[Ru(CO)(PPh$_3$)('tpS$_4$')] [ν(CO) = 1964 cm^{-1}] formed nearly instantly. [Ru(CO)(PPh$_3$)('tpS$_4$')] also formed directly from **1** and CO. However, this reaction needed ca. 12 h to go to completion.[7]

Treatment of **12** with one equivalent of NOBF$_4$ yielded [Ru(NO)(PPh$_3$)('tpS$_4$')]BF$_4$ (**13**). Complex **13** is the first 18 valence electron nitrosyl complex with an [RuPS$_4$] core characterized by X-ray structure determination. It was of particular interest as a test complex for probing the stability of the 'tpS$_4$'$^{2-}$ ligand towards reduction.

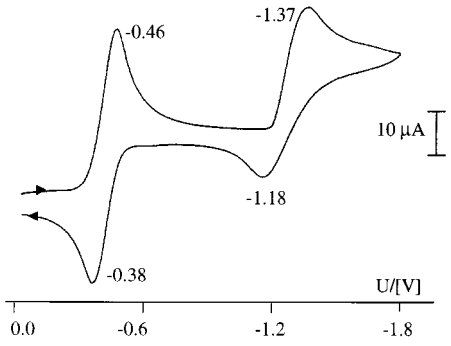


Figure 1. Cyclic voltammogram of [Ru(NO)(PPh$_3$)('tpS$_4$')]BF$_4$ (**13**) in CH$_2$Cl$_2$ (10^{-3} M, 10^{-1} M NBu$_4$PF$_6$, v = 0.05Vs^{-1})

The cyclic voltammogram (CV) of **13** in CH$_2$Cl$_2$ (Figure 1) exhibited two redox waves in the cathodic region. The redox wave at $E_{1/2}$ = –0.42 V could be assigned to the reversible reduction [Ru(NO)(PPh$_3$)('tpS$_4$')]$^+$/[Ru(NO)(PPh$_3$)('tpS$_4$')]^0 and indicated the viability of the neutral 19 valence electron nitrosyl complex [Ru(NO)(PPh$_3$)('tpS$_4$')] (**14**).

This result was corroborated by chemical reduction of **13** and the reaction of the acetonitrile complex **12** with NO gas. Monitoring the reaction of **13** with LiBEt$_3$H in THF by IR spectroscopy showed that the ν(NO) band of **13** at 1850 cm^{-1} was replaced by a new band at 1602 cm^{-1}. No gas was evolved, and the intensity and frequency of the 1602 cm^{-1} band was found to be compatible with the formation of **14**.[10] Treating **12** with NO gas in CH$_2$Cl$_2$ led to a strong ν(NO) band appearing in the same region at 1605 cm^{-1}. Complex **14** could be precipitated from this solution as red-brown solid by the addition of *n*-hexane. Complex **14** is highly reactive and almost instantly oxidized by traces of air to give the [Ru(NO)(PPh$_3$)('tpS$_4$')]$^+$ cation, as indicated by the ν(NO) band at 1842 cm^{-1} (KBr). Complex **14** is paramagnetic and was only characterized by elemental analyses, IR spectroscopy, and mass spectrometry, which confirmed that the 'tpS$_4$'$^{2-}$ ligand remained intact.

Attempts to convert the nitrosyl ligands of either cationic **13** or neutral **14** into dinitrogen ligands by reactions with azide or ammonia have so far been unsuccessful. For the alternate route, in which the ligating azide is converted into N$_2$ by attack with NO$^+$, azido complexes were needed. Treatment of **12** in acetone with one equivalent of NEt$_4$N$_3$ yielded the azido complex (NEt$_4$)[Ru(N$_3$)(PPh$_3$)('tpS$_4$')] (**15**) whose formation could be established by IR and ^{1}H NMR spectroscopy. However, **15** proved to be too labile to obtain ^{13}C and ^{31}P NMR spectra and rapidly decomposed, even in the solid state, to give a brown mixture of intractable products. Repeated attempts to purify **15** by recrystallization were unsuccessful. For these reasons, we tried to obtain a potentially more stable Ru^{III} azide complex via the Ru^{III} iodide complex [Ru(I)(PPh$_3$)('tpS$_4$')] (**16**). Complex **16** formed from the reaction of the acetonitrile complex **12** with half an equivalent of iodine, and could be characterized by X-ray crystallography. The subsequent reaction of **16** with NEt$_4$N$_3$ yielded [Ru(N$_3$)(PPh$_3$)('tpS$_4$')] (**17**) which was isolated in pure state and characterized by IR spectroscopy and mass spectrometry. As expected, and confirmed from the ^{1}H NMR spectra showing broad and unresolved peaks, **16** and **17** are both paramagnetic. Complex **17** was further characterized by its cyclic voltammogram (Figure 2).

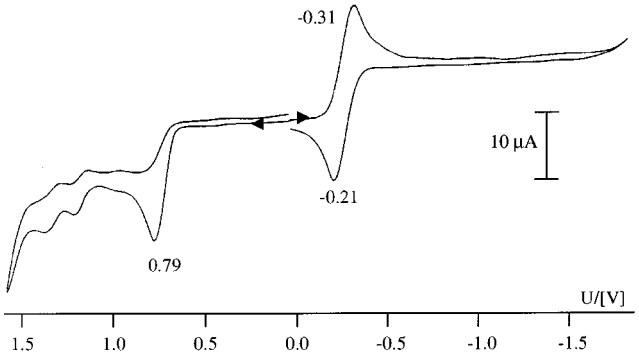


Figure 2. Cyclic voltammogram of [Ru(N$_3$)(PPh$_3$)('tpS$_4$')]BF$_4$ (**17**) in CH$_2$Cl$_2$ (10^{-3} M, 10^{-1} M NBu$_4$PF$_6$, v = 0.02Vs^{-1})

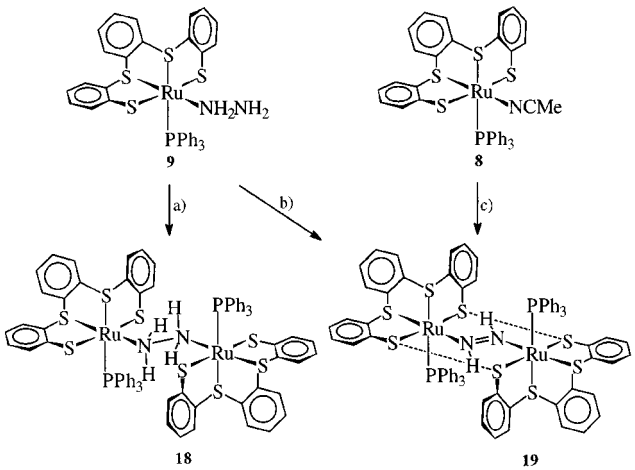
In the cathodic region, **17** showed a reversible redox wave at $E_{1/2}$ = –0.26 V. It is compatible with the reversible reduc-

tion of **17** to give the anion of the Ru^{II} complex **15**. Attempts to convert **17** photolytically, thermally, or by treatment with HBF_4 in CH_2Cl_2 into a dinitrogen complex remained unsuccessful.

Dinuclear Hydrazine and Diazene Complexes with [Ru(PPh$_3$)('tpS$_4$')] Fragments

The unsuccessful attempts to obtain a [Ru(PPh_3)('tpS_4')] dinitrogen complex via nitrosyl or azide precursors prompted us to return to the hydrazine complex [Ru(N_2H_4)(PPh_3)('tpS_4')] (**9**). As mentioned above, the N_2H_4 ligand is labile. In this respect **9** resembles the other [Ru(L)(PPh_3)('tpS_4')] complexes in which L is a σ-N donor ligand.

The complex [Ru(N_2H_4)(PPh_3)('tpS_4')] (**9**) did not yield a dinitrogen complex either. However, further investigation led to the characterization of [μ-N_2H_4{Ru(PPh_3)('tpS_4')}$_2$] (**18**) and [μ-N_2H_2{Ru(PPh_3)('tpS_4')}$_2$] (**19**) which represent the first hydrazine and diazene couple characterized by X-ray structure determination (Scheme 4).



Scheme 4. Formation of dinuclear hydrazine and diazene complexes with [Ru(PPh_3)('tpS_4')] fragments: a) CH_2Cl_2, 7 d, room temp.; b) + O_2, CH_2Cl_2, 36 h, room temp.; c) + exc. $K_2N_2(CO_2)_2$, + exc. CH_3CO_2H, THF, 3 h, room temp.

Attempts to recrystallize **9** from CH_2Cl_2/MeOH mixtures afforded yellow microcrystals that proved so sparingly soluble that no NMR spectra could be recorded. The elemental analyses and IR spectra indicated that two molecules of mononuclear **9** had formed the dinuclear hydrazine complex **18** by dissociation of hydrazine. Carrying out the same experiment in THF/Et_2O mixtures afforded single crystals of **18**·4THF, which could be structurally characterized. When the CH_2Cl_2 solutions of the hydrazine complex **9** were treated with atmospheric oxygen, their color turned from yellow to dark green and green crystals precipitated. They were also sparingly soluble, but we were able to record a ^1H NMR spectrum which exhibited a signal at δ = 14.59, indicative of an N_2H_2 ligand in a centrosymmetric dinuclear diazene complex of the type [μ-N_2H_2{Ru(PPh_3)('tpS_4')}$_2$] (**19**). Intense absorptions at 307 and 463 nm in the UV/Vis spectrum also suggested the formation of **19**, which was finally and unambiguously characterized by an X-ray crystal structure determination of **19**·4CH_2Cl_2.

The aerial oxidation of **9** afforded **19** in yields of 25%. A potential reason for the low yield is that the dinuclear hydrazine complex **18** must form before subsequent oxidation occurs to give **19**. Therefore we sought a better synthesis of **19** and found that much higher yields (> 80%) were obtained from the reaction of the labile acetonitrile complex **12** with N_2H_2, which was generated in situ by acidolysis of $K_2N_2(CO_2)_2$ with dilute acetic acid in THF. This trapping of the unstable diazene in solution is possible with particular metal sulfur complex fragments and was first discovered with the synthesis of [μ-N_2H_2{Fe(PPr_3)('S_4')}$_2$].[11]

General Properties and Spectroscopic Characterization of [Ru(L)(L')('tpS$_4$')] Complexes

As far as possible, all [Ru(L)(L')('tpS_4')] complexes have been characterized by the common spectroscopic methods and elemental analyses. The molecular structures of **7**, **13**, **16**, **18**, and **19** have been determined by X-ray structure analysis. All Ru^{II} complexes are diamagnetic, while the two Ru^{III} complexes are paramagnetic as indicated by their ^1H NMR spectra. The colors of the complexes range from yellow or orange (**1**–**12**), to green (**17**, **19**) and brown (**13**, **14**, **16**). All complexes, except the dinuclear species **18** and **19**, show moderate to good solubilities in CH_2Cl_2. The IR spectra of all complexes in KBr exhibit the typical absorptions of the [Ru('tpS_4')] fragment. A strong ν(CO) absorption at 1968 cm^{-1} and a strong δ(PCH) at 953 cm^{-1} characterize [Ru(CO)(PMe_3)('tpS_4')]. A ν(SO) band at 1015 cm^{-1} indicates sulfur coordination of DMSO in [Ru$(DMSO)_2$('tpS_4')] (**3**). Weak ν(NH) (3334, 3292, 3245, 3164 cm^{-1}) and ν(CN) (2271 cm^{-1}) bands readily identify [Ru(N_2H_4)(PPh_3)('tpS_4')] (**9**) and [Ru(MeCN)(PPh_3)('tpS_4')] (**12**) respectively. Strong ν(NO) bands at 1852 and 1598 cm^{-1} characterize the nitrosyl complexes **13** and **14**. The azide complexes **15** and **17** show characteristic ν(N_3) absorptions at 2029 and 2036 cm^{-1}. The ^1H NMR spectra of C_2-symmetric [Ru$(L)_2$('tpS_4')] complexes exhibit a typical set of six multiplets for the aromatic 'tpS_4' protons. This multiplet changes when the symmetry is lowered to C_1 in [Ru(L)(L')('tpS_4')] complexes. In all [Ru(L)(PPh_3)('tpS_4')] complexes, the 'tpS_4' multiplets are superimposed on the PPh_3 multiplets. Thus, the [Ru(L)(PPh_3)('tpS_4')] complexes usually are more readily identified by their ^{13}C and ^{31}P NMR spectra.

However, the ^1H NMR spectrum of [Ru(I)(PPh_3)('tpS_4–Me_2')]I (**4**) showed two singlets for the methyl groups, establishing that only one of several possible isomers had formed. The ^1H NMR spectra of **8** and **12** exhibited characteristic singlets at δ = 1.70 and 1.75, indicating the coordination of ammonia and acetonitrile. The hydrazine complex **9** gave rise to two multiplets at δ = 4.2 and 4.1 which are attributed to the Ru-bound NH_2 group, and a broad singlet at δ = 3.4 which is assigned to the terminal NH_2 group. The N_2H_2 singlet at δ = 14.59 is characteristic of the diazene complex [μ-N_2H_2{Ru(PPh_3)('tpS_4')}$_2$] (**19**). Complex **19** was further characterized by its UV/Vis spectrum, showing a strong absorption at 463 nm (ε = 8162 L

mol^{-1} cm^{-1}) which is characteristic of the 4c-6 e^- π bond system of [M=NH=NH=M] fragments (Figure 3).[12]

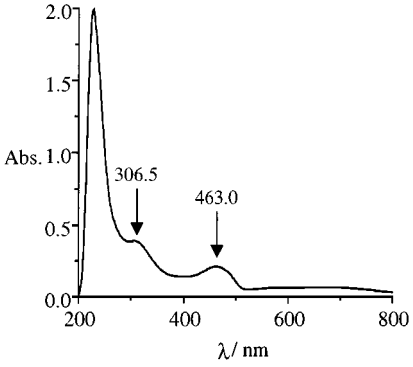


Figure 3. UV/Vis spectrum of $[\mu\text{–}N_2H_2\{Ru(PPh_3)(\text{'}tpS_4\text{'})\}_2]$ in CH_2Cl_2

X-ray Structure Analysis

The molecular structures of [Ru(py)(PPh_3)('tpS_4')] (**7**), [Ru(NO)(PPh_3)('tpS_4')]BF_4·CH_2Cl_2 (**13**·CH_2Cl_2), [Ru(I)(PPh_3)('tpS_4')]·CH_2Cl_2 (**16**·CH_2Cl_2), [μ-N_2H_4\{Ru(PPh_3)('tpS_4')\}$_2$]·4THF (**18**·4THF), and [μ-N_2H_2\{Ru(PPh_3)('tpS_4')\}$_2$]·4CH_2Cl_2 (**19**·4CH_2Cl_2) were determined by X-ray crystallography and are shown in Figure 4. Table 1 lists selected distances and angles.

In all cases the crystal lattices contain discrete molecules or ions. All compounds exhibit six-coordinate Ru centers, helical coordination of the 'tpS_4'$^{2-}$ ligands with *trans*-thiolate and *cis*-thioether S donors, and *cis* coordination of the ligands PPh_3 and L = py, NO, I, N_2H_4, N_2H_2.

Distances and angles lie in the range observed for related [Ru('S_4')] complexes. For example, in both the [Ru('tpS_4')] and [Ru('S_4')] complexes, the average Ru–S distances are found to be in the narrow range of 233–238 pm. This is worthy of note, in light of the different properties of the coligands which coordinate to the [RuS_4] cores, such as the σ-π ligands CO, NO^+ or N_2H_2, or the σ ligands N_2H_4 and pyridine. Even in the Ru^{III} complex [Ru(I)(PPh_3)('tpS_4')]·CH_2Cl_2 (**16**·CH_2Cl_2), the average Ru–S distance (234 pm) does not significantly differ from that of Ru^{II} complexes. This invariance of averaged M–S distances in low-spin complexes having no electrons in antibonding orbitals has been previously discussed and can be traced back to the bonding properties of sulfur ligands, which can function as σ-donor, σ-donor–π-acceptor, and σ-donor–π-donor ligands.[13–15]

The diazene and hydrazine complexes **19**·4CH_2Cl_2 and **18**·4THF deserve special consideration. They represent the first structurally characterized complexes containing the N_2H_2/N_2H_4 couple, and enable comparison of both the differing bonding situations and the formation of N–H···S bridges when hydrazine or diazene bind to transition metal

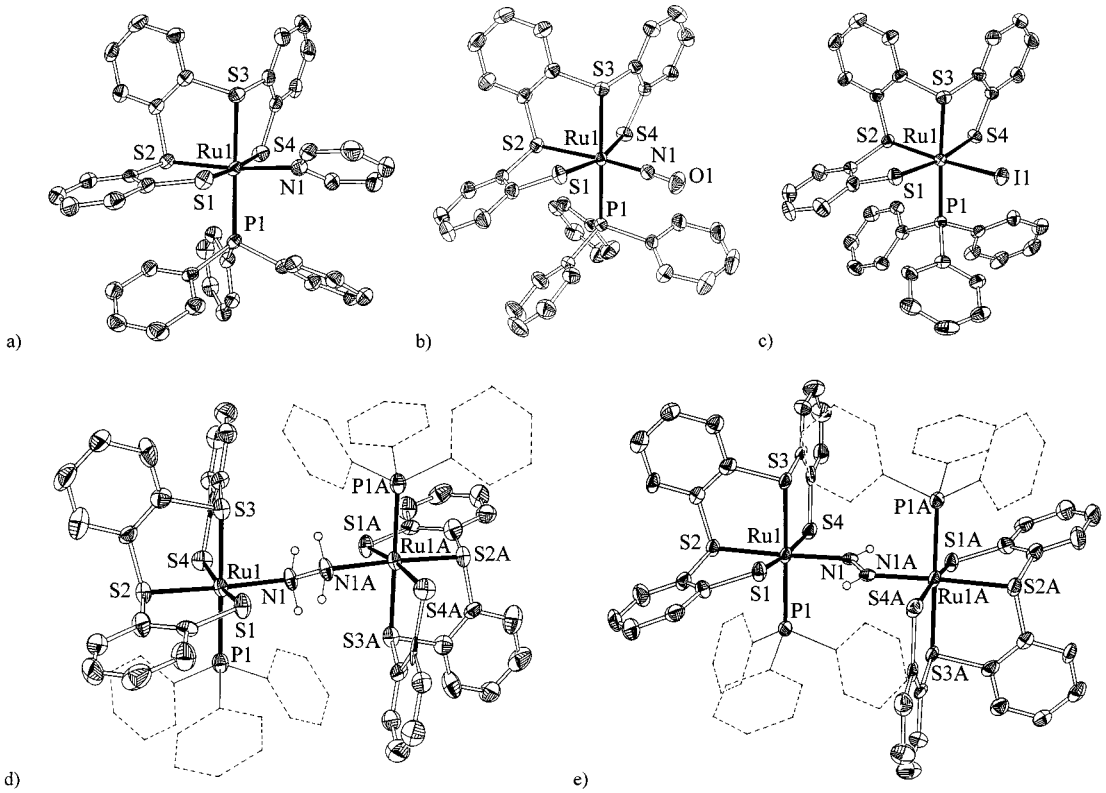


Figure 4. Molecular structures of a) [Ru(py)(PPh_3)('tpS_4')] (**7**), b) [Ru(NO)(PPh_3)('tpS_4')]BF_4·CH_2Cl_2 (**13**·CH_2Cl_2), c) [Ru(I)(PPh_3)('tpS_4')]·CH_2Cl_2 (**16**·CH_2Cl_2), d) [μ-N_2H_4\{Ru(PPh_3)('tpS_4')\}$_2$]·4THF (**18**·4THF), and e) [μ-N_2H_2\{Ru(PPh_3)('tpS_4')\}$_2$]·4CH_2Cl_2 (**19**·4CH_2Cl_2) (50% probability ellipsoids; C-bonded H atoms, solvent molecules, and BF_4^- anions omitted)

Table 1. Selected distances [pm] and angles [°] of [Ru(py)(PPh_3)('tpS_4')] (**7**), [Ru(NO)(PPh_3)('tpS_4')]BF_4·CH_2Cl_2 (**13**·CH_2Cl_2), [Ru(I)(PPh_3)('tpS_4')]·CH_2Cl_2 (**16**·CH_2Cl_2), [μ-N_2H_4{Ru(PPh_3)('tpS_4')$}_2$]·4THF (**18**·4THF), and [μ-N_2H_2{Ru(PPh_3)('tpS_4')$}_2$]·4CH_2Cl_2 (**19**·4CH_2Cl_2)

Complex (L)	**7** (py)	**13**·CH_2Cl_2 (NO^+)	**16**·CH_2Cl_2 (I)	**18**·4THF (N_2H_4)	**19**·4CH_2Cl_2 (N_2H_2)
Ru1–S1	238.5(1)	242.1(1)	236.0(2)	239.1(4)	239.8(2)
Ru1–S2	227.7(1)	239.1(1)	233.1(1)	227.5(4)	232.9(2)
Ru1–S3	234.1(1)	238.4(1)	234.2(1)	234.5(4)	234.5(2)
Ru1–S4	240.3(1)	236.2(1)	231.3(2)	239.4(4)	239.4(2)
Ru1–P1	234.5(1)	242.4(1)	237.7(2)	232.1(4)	235.8(2)
Ru1–L	215.5(3)	175.6(3)	271.18(6)	214.4(9)	203.0(7)
N1–N1A	–	–	–	149(2)	129(1)
N1–H1	–	–	–	102	88
S4–H1	–	–	–	298	289
S1A–H1	–	–	–	258	258
S3A–H2	–	–	–	288	–
S1–Ru1–S4	176.00(4)	165.45(4)	170.13(6)	171.9(1)	172.25(9)
S2–Ru1–S3	88.21(4)	86.49(3)	88.49(5)	88.6(1)	87.50(8)
S3–Ru1–P1	177.93(4)	174.88(3)	175.13(5)	179.8(2)	178.12(9)
S2–Ru1–P1	93.56(4)	91.91(3)	96.15(5)	91.6(1)	92.49(8)
S2–Ru1–L	172.42(10)	172.88(10)	169.19(4)	175.8(3)	175.8(2)
Ru1–N1–N1A	–	–	–	117.1(9)	127.4(7)
Ru1–N1–H1	–	–	–	112.3	121.7
N1–N1A–H1	–	–	–	97.2	110.9

sulfur sites. Both complexes possess a crystallographically imposed inversion symmetry. The N_2H_2 and N_2H_4 ligands bridge two enantiomeric [Ru(PPh_3)('tpS_4')] fragments, and the centers of the N–N bonds represent the inversion centers. The average Ru–S distances in the hydrazine complex **18**·4THF (235.1 pm) and the diazene complex **19**·4CH_2Cl_2 (236.6 pm) are also similar. The difference of 1.5 pm is a result of different Ru–S2 distances *trans* to the N_2H_4 and N_2H_2 ligands, which are 227.5(4) pm (**18**·4THF) vs. 232.9(2) pm (**19**·4CH_2Cl_2). All other Ru–S distances are identical within the 3σ criterion in both **18**·4THF and **19**·4CH_2Cl_2.

The Ru–S2 distance of **19**·4CH_2Cl_2 [232.9(2) pm] indicates the *trans* bond lengthening influence of the σ-π ligand N_2H_2, since the corresponding Ru–S2 distances of the σ ligand N_2H_4 and pyridine complexes **18**·4THF [227.5(4) pm] and **7** [227.7(1) pm] are shorter. The Ru–S distances *trans* to N_2H_2 in the closely related complexes [μ-N_2H_2{Ru(PPh_3)('S_4')$}_2$] [228.2(2) pm] and [μ-N_2H_2{Ru(PPh_3)('$^{bu}S_4$')$}_2$] [230.7(3) pm][12] are slightly shorter than in **19**·4CH_2Cl_2. Nonetheless, as in **19**·4CH_2Cl_2, the Ru–S bonds *trans* to the N_2H_2 ligand always represent the shortest Ru–S bonds in [μ-N_2H_2{RuS_4}$_2$] complexes so far characterized.

The different bonding properties of N_2H_2 and N_2H_4 are also illustrated by the Ru–N distances of **18**·4THF [214.4(9) pm] and **19**·4CH_2Cl_2 [203.0(7) pm], indicating Ru–N single and partial Ru–N double bonds. The Ru–N distance in **18**·4THF is comparable with that of the pyridine complex **7** [215.5(3) pm], while the Ru–N distance in **19**·4CH_2Cl_2 is rationalized by the [M=NH=NH=M] 4c-6e$^-$ π bonding system, which is characteristic of this type of [μ-N_2H_2{M}$_2$] complex.[12] The N–N distances in **18**·4THF [149(2) pm] and in **19**·4CH_2Cl_2 [129(1) pm] correspond with N–N single and slightly elongated N–N double bonds.

In both **18**·4THF and **19**·4CH_2Cl_2, the Ru centers and the thiolate donors form approximated planes. When least-squares planes are calculated through the six atoms Ru1, S1, S4, Ru1A, S1A, and S4A, the largest deviations from these planes are observed for the Ru centers, being 11.0(2) pm (**18**·4THF) and 10.8(1) pm (**19**·4CH_2Cl_2), respectively. In the diazene complex **19**·4CH_2Cl_2, the diazene N atoms are also coplanar, deviating by only 5.5(6) pm. In the hydrazine complex **18**·4THF, the hydrazine N atoms show a large deviation of 25.9(9) pm from the respective plane. This deviation gives rise to a step-like arrangement of the two enantiomeric [Ru(NH_2)(PPh_3)('tpS_4')] halves of **18**·4THF. The step height, calculated as distance between the two least-squares planes [Ru1, S1, S2, S4, N1] and [Ru1A, S1A, S2A, S4A, N1A], is 52.8 pm. The step-like arrangement of the two [$RuNPS_4$] cores in **18**·4THF is also reflected by the [S4–Ru1–N1–N1A] torsion angle of –151.9(1)°. [In the diazene complex, in which the Ru, the thiolate S and diazene N atoms form a nearly perfect plane, the corresponding angle is 173.9(9)°, close to the ideal of 180°.]

The arrangement of Ru, thiolate S, diazene N, or hydrazine N atoms enables the formation of stabilizing N–H···S hydrogen bonds in both **18**·4THF and **19**·4CH_2Cl_2. The N–H···S bonds are indicated by both the N–H···S vectors and the distances, which are shorter than the sum of the corresponding van der Waals radii (r_H = 120 pm, r_S = 185 pm) (Figure 5).

In the diazene complex **19**·4CH_2Cl_2, two bifurcated and nearly planar N–H···S_2 (thiolate) bridges exist [*d*(H1···S1A) = 258 pm, *d*(H1···S4) = 289 pm]. In the hydrazine complex **18**·4THF, two similar but nonplanar bifurcated hydrogen bonds are indicated by the H1···S1A (258 pm) and H1···S4 (298 pm) distances. It is significant that in the hydrazine complex the H2···S3A and the corresponding H2A···S3 distances of 288 pm indicate two additional hydrogen bonds between the thioether S atoms S3 and S3A and the NH_2 group atoms H2, and H2A. (Assuming sp^3 hybridization of the thioether S donors, the lone pairs at S3 and S3A indeed point directly at the positions of H2 and H2A respectively.)

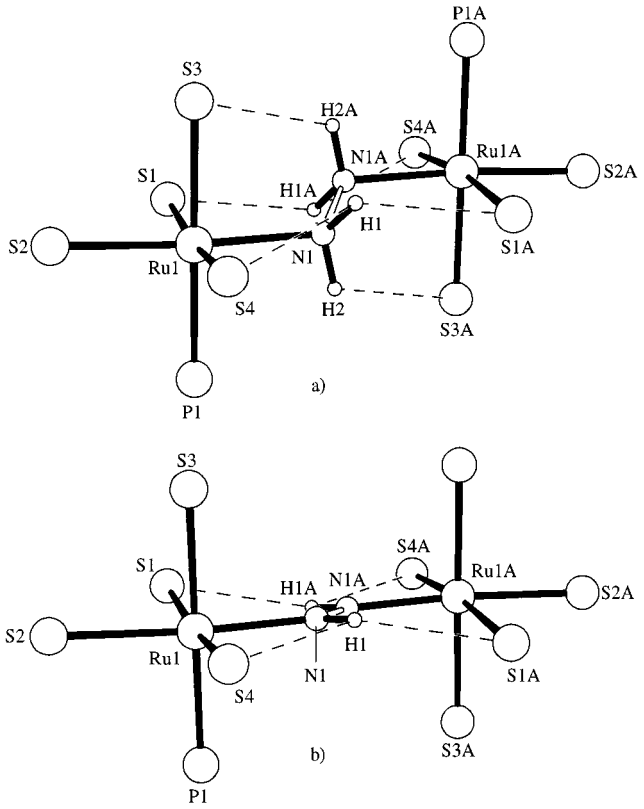


Figure 5. The [μ-N_2H_x{$RuPS_4$}$_2$] cores of a) **18**·4THF (x = 4) and b) **19**·4CH_2Cl_2 (x = 2) illustrating the [μ-N_2H_x{RuS_2(thiolate)}$_2$] planes and NH···S bridges

Due to the inversion center, the two NH_2 groups in **18**·4THF assume a staggered conformation, in contrast to the conformation in free hydrazine which exhibits a dihedral angle of about 95°.[16]

Discussion and Conclusion

The [Ru('tpS_4')] fragment exhibits a similarly versatile coordination chemistry as the [Ru('$^RS_4$')] fragments and binds a large number of coligands ranging from CO, NO, CR_2, PR_3 to N_3^-, N_2H_2, N_2H_4, and NH_3. In addition, [Ru('tpS_4')] complexes undergo reactions and yield species not yet observed with [Ru('$^RS_4$')] fragments. For example, [Ru(PPh_3)$_2$('tpS_4')] (**1**) exchanges both of its PPh_3 ligands with DMSO or PEt_3. When the [Ru(NO)(PPh_3)('tpS_4')]$^+$ (**13**) cation is reduced to give the neutral 19 valence electron species [Ru(NO)(PPh_3)('tpS_4')] (**14**), the 'tpS_4'$^{2-}$ ligand stays intact, in contrast to the '$^RS_4$'$^{2-}$ ligands, which undergo C–S cleavage reactions.[6]

In the search for labile [Ru('tpS_4')] precursor complexes, [Ru(PPh_3)$_2$('tpS_4')] (**1**) was found to exclusively exchange one PPh_3 for nitrogenous ligands. This enabled the synthesis of N_2H_4 and NH_3 complexes and, in particular, of the acetonitrile complex [Ru(MeCN)(PPh_3)('tpS_4')] (**12**). Complex **12** made feasible the synthesis of the azido, iodo, and nitrosyl complexes. All attempts to obtain dinitrogen complexes have so far remained unsuccessful also with the [Ru('tpS_4')] fragment. However, structurally characterized transition metal sulfur complexes containing the hydrazine and diazene couple could be obtained for the first time. The complexes [μ-N_2H_4{Ru(PPh_3)('tpS_4')}$_2$] (**18**) and [μ-N_2H_2{Ru(PPh_3)('tpS_4')}$_2$] (**19**) permitted a detailed analysis of the structural and bonding properties of hydrazine versus diazene complexes. The structural parameters indicate bifurcated N–H···S_2(thiolate) hydrogen bonds in both **18** and **19** and additional N–H···S(thioether) bridges in the hydrazine complex **18**. The increased number of N–H···S hydrogen bonds formed when going from the diazene to hydrazine complexes is significant with regard to the "open-side" model of the FeMoco function in nitrogenases.[4a], [13a] According to this model, N_2 is activated through binding to two low-spin Fe^{II} centers in [S, N, O] coordination spheres. Over the course of three subsequent [2 H^+, 2 e^-] reduction steps yielding NH_3 via N_2H_2 and N_2H_4 intermediates, an increased number of N–H···S(O) hydrogen bonds is instrumental in keeping the redox potential in the range –280 mV to ca. –500 mV, which are the both the thermodynamic limiting and biologically compatible values of enzymatic N_2 reduction.

Experimental Section

General Methods: Unless otherwise noted, all reactions and operations were carried out at room temperature under nitrogen using standard Schlenk techniques. Solvents were dried and distilled before use. As far as possible, reactions were monitored by IR or NMR spectroscopy. – Spectra were recorded with the following instruments: IR (KBr disks or CaF_2 cuvettes, solvent bands were compensated): Perkin–Elmer 983, 1620 FT IR, and 16PC FT-IR. – NMR: Jeol FT-JNM-GX 270, EX 270, and Lambda LA 400 with the protio solvent signals used as a reference. Chemical shifts are quoted on the δ scale (downfield shifts are positive) relative to tetramethylsilane (^{1}H, ^{13}C{^{1}H} NMR) or 85% H_3PO_4 (^{31}P{^{1}H} NMR). Spectra were recorded at 25 °C. – Mass spectra: Jeol MSTATION 700 spectrometer. – UV/Vis: Shimadzu UV-3101 – Elemental analysis: Carlo Erba EA 1106 or 1108 analyzer. – Cyclic voltammetry was performed with a PAR 264A potentiostat using a three-electrode cell with glassy carbon ROTEL A working, Pt reference and Pt counter electrodes. Solutions were 10^{-3} M in complex. TBA[PF_6] (10^{-1} M) was used as conducting electrolyte. Potentials were referenced to the normal hydrogen electrode via Fc/Fc$^+$ as internal standard (E_{Fc/Fc^+} = +0.4 V versus normal hydrogen electrode).[17] – $N_2C(CO_2Et_2)_2$,[18] $K_2C_2N_2O_4$,[19] [$RuCl_2$-$(DMSO)_4$],[20] [$RuCl_2(PMe_3)_4$],[21] NEt_4N_3,[22] [Ru(PPh_3)$_2$-('tpS_4')] (**1**),[7] and 'tpS_4'–H_2,[7] were prepared as described in the literature, LiOMe, MeI, $NOBF_4$, $LiBEt_3H$, NH_2NHMe, and N_2H_4 were purchased from Aldrich.

[Ru(PEt_3)$_2$('tpS_4')] (2): PEt_3 (0.5 mL, 3.4 mmol) was added to a yellow-orange suspension of [Ru(PPh_3)$_2$('tpS_4')] (**1**) (190 mg, 0.19 mmol) in THF (10 mL) and heated at reflux for 3 min. The resultant yellow solution was cooled to room temperature, and concentrated to dryness. The yellow residue was dissolved in THF (5 mL), the resulting solution was filtered, layered with *n*-hexane (50 mL) and cooled to –30 °C. Yellow microcrystals precipitated, which were separated after 1 d, washed with *n*-hexane (40 mL) and dried in vacuo. Yield: 70 mg of **2**·0.5THF (50%). – $C_{32}H_{46}O_{0.5}P_2RuS_4$ (**2**·0.5THF) (730.0): calcd. C 52.65, H 6.35, S

17.57; found C 52.90, H 6.56, S 17.21. – MS (FD, CH_2Cl_2, ^{102}Ru); *m/z*: 694 [Ru(PEt_3)$_2$('tpS_4')]$^+$. – ^1H NMR (CD_2Cl_2, 269.6 MHz): δ = 7.95–7.85 (m, 2 H, C_6H_4), 7.75 (d, 2 H, C_6H_4), 7.35 (d, 2 H, C_6H_4), 7.25–7.18 (m, 2 H, C_6H_4), 6.90–6.75 (m, 4 H, C_6H_4), 1.95–1.75 (m, 12 H, P–CH_2CH$_3$), 1.10–0.97 (m, 15 H, P–CH$_2$CH_3). – $^{13}C\{^1H\}$ NMR (100.40 MHz, CD_2Cl_2): δ = 158.9, 138.6, 136.8, 132.0, 131.5, 130.2, 129.7, 128.8, 121.1 [*C*(aryl)], 19.2 (t, P–*C*H$_2$CH$_3$), 8.5 (P–CH$_2$*C*H$_3$). – $^{31}P\{^1H\}$ NMR (109.38 MHz, CD_2Cl_2): δ = 18.0 (s).

[Ru(DMSO)$_2$('tpS$_4$')] (3): A yellow-orange suspension of [Ru(PPh_3)$_2$('tpS_4')] (**1**) (196 mg, 0.20 mmol) in DMSO (15 mL) was heated at reflux for 5 min, yielding a yellow-green solution. The solution was cooled to room temperature, combined with MeOH (75 mL), and stirred for 12 h. A yellow solid precipitated, which was separated, washed with MeOH (30 mL), Et_2O (20 mL), and dried in vacuo. Despite several recrystallizations from CH_2Cl_2/MeOH, satisfactory elemental analyses could not be obtained. However, the NMR spectra of the yellow solid showed the absence of any PPh_3 resulting from the precursor complex **1**. Yield: 50 mg of **3** (41%). – $C_{22}H_{24}O_2RuS_6$ (**3**) (613.9): calcd. C 43.05, H 3.94; found C 44.42, H 4.13. – IR (KBr): $\tilde{\nu}$ = 1015 cm^{-1}, s, ν(SO). – MS (FD, CH_2Cl_2, ^{102}Ru); *m/z*: 614 [Ru(DMSO)$_2$('tpS_4')]$^+$. – ^1H NMR (269.6 MHz, CD_2Cl_2): δ = 7.85–7.80 (m, 2 H, C_6H_4), 7.65 (d, 2 H, C_6H_4), 7.50 (d, 2 H, C_6H_4), 7.33–7.28 (m, 2 H, C_6H_4), 7.00 (t, 2 H, C_6H_4), 6.87 (t, 2 H, C_6H_4), 3.25 (s, 3 H, S–CH_3), 3.05 (s, 3 H, S–CH_3). – $^{13}C\{^1H\}$ NMR (100.40 MHz, CD_2Cl_2): δ = 153.9, 137.1, 136.9, 132.5, 131.8, 130.7, 130.6, 130.0, 122.8, (C_6H_4), 46.3, 44.9 (S–*C*H$_3$).

[Ru(I)(PPh$_3$)('tpS$_4$–Me$_2$')]I (4): MeI (0.5 mL, 8.0 mmol) was added while stirring to a yellow-orange solution of [Ru(PPh_3)$_2$('tpS_4')] (**1**) (140 mg, 0.14 mmol) in CH_2Cl_2 (30 mL) which changed its color to yellow over the course of 2 h. After addition of *n*-hexane (40 mL), a yellow solid precipitated, which was separated, washed with MeOH (10 mL), *n*-hexane (20 mL), and dried in vacuo. Recrystallization from CH_2Cl_2/Et_2O (20 mL/ 40 mL) yielded yellow crystals, which were separated, washed with Et_2O (20 mL), and dried in vacuo. Yield: 100 mg of **4** (71%). – $C_{38}H_{33}I_2PRuS_4$ (**4**) (1004): calcd. C 45.47, H 3.31, S 12.78; found C 45.25, H 3.50, S 12.59. – ^1H NMR (CD_2Cl_2, 269.6 MHz): δ = 8.30 (t, 2 H, C_6H_4), 8.00 (d, 1 H, C_6H_4), 7.90–7.80 (m, 1 H, C_6H_4), 7.75–7.60 [m, 8 H, C_6H_4 and P(C_6H_5)$_3$], 7.60–7.30 [m, 15 H, C_6H_4 and P(C_6H_5)$_3$], 2.85 (s, 3 H, S–CH_3), 2.05 (s, 3 H, S–CH_3). – $^{31}P\{^1H\}$ NMR (109.38 MHz, CD_2Cl_2): δ = 23.5 (s).

[Ru(PMe$_3$)(PPh$_3$)('tpS$_4$')] (5): PMe_3 (0.8 mL, 7.70 mmol) was added to a yellow suspension of [Ru(PPh_3)$_2$('tpS_4')] (**1**) (400 mg, 0.41 mmol) in THF (15 mL). The suspension was stirred for 3 h, during the course of which a yellow solution resulted, which was filtered and concentrated to dryness to give a yellow residue. The residue was digested with *n*-hexane (40 mL) for 1 h, separated, washed with *n*-hexane (40 mL), and dried in vacuo. Yield 180 mg of **5** (55%). – $C_{39}H_{36}P_2RuS_4$ (**5**) (796.0): calcd. C 58.85, H 4.56, S 16.11; found C 59.10, H 4.57, S 15.52. – IR (KBr): $\tilde{\nu}$ = 953 cm^{-1}, δ(PCH). – MS (FD, CH_2Cl_2, ^{102} Ru); *m/z*: 796 [Ru(PMe_3)(PPh_3)('tpS_4')]$^+$. – ^1H NMR (269.6 MHz, CD_2Cl_2): δ = 7.86–7.74 (m, 3 H, C_6H_4), 7.59–7.46 [m, 7 H, C_6H_4 and P(C_6H_5)$_3$], 7.26–7.23 [m, 11 H, C_6H_4 and P(C_6H_5)$_3$], 7.09 (d, 1 H, C_6H_4), 6.96–6.94 (m, 2 H, C_6H_4), 6.85 (t, 1 H, C_6H_4), 6.65 (t, 1 H, C_6H_4), 6.56 (t, 1 H, C_6H_4), 1.16 [d, *J* = 4.32 Hz, 9 H, P(CH_3)]. – $^{13}C\{^1H\}$ NMR (67.8 MHz, CD_2Cl_2): δ = 159.0 (d, J_{PC} = 5.96 Hz), 156.2 (d, J_{PC} = 7.95 Hz), 138.9, 138.7, 138.2, 138.0, 136.6, 136.1, 135.9, 135.3, 134.6 (d, J_{PC} = 9.93 Hz), 132.2, 131.4, 130.5, 129.8 (d, J_{PC} = 3.48 Hz), 129.7, 129.5, 129.2, 128.5, 127.4 (d, J_{PC} = 8.94 Hz), 121.2, 121.1 [*C*(aryl)], 18.3 [d, J_{PC} = 9.94 Hz, (P(*C*H$_3$)], 17.9 [d, J_{PC} = 9.94, (P(*C*H$_3$)]. – $^{31}P\{^1H\}$ NMR (109.38 MHz, CD_2Cl_2): δ = –6.5 (d, *P*Me$_3$), +37 (d, *P*Ph$_3$).

[Ru(PMe$_3$)$_2$('tpS$_4$')] (6): Solid Li_2–'tpS_4' (159 mg, 0.43 mmol) was added to a stirred suspension of [RuCl_2(PMe_3)$_4$] (205 mg, 0.43 mmol) in MeOH (10 mL), which was heated at reflux for 4 h, yielding a yellow solution from which yellow microcrystals started precipitating. Cooling to room temperature completed the precipitation. The resulting yellow microcrystals were separated, washed with MeOH (15 mL) and *n*-hexane (20 mL), and dried in vacuo. Yield: 120 mg of **6** (46%). – $C_{24}H_{30}P_2RuS_4$ (**6**) (609.8): calcd. C 47.27, H 4.96, S 21.03; found C 47.20, H 4.88, S 21.11. – IR (KBr, cm^{-1}): $\tilde{\nu}$ = 958, 943 vs, δ(PCH). – MS (FD, CH_2Cl_2, ^{102}Ru); *m/z*: 610 [Ru(PMe_3)$_2$('tpS_4')]$^+$. – ^1H NMR ([D$_8$]THF, 399.65 MHz): δ = 7.97–7.93 (m, 2 H, C_6H_4), 7.77 (d, 2 H, C_6H_4), 7.29 (d, 2 H, C_6H_4), 7.20–7.16 (m, 2 H, C_6H_4), 6.80–6.76 (m, 2 H, C_6H_4), 6.72–6.68 (m, 2 H, C_6H_4), 1.41 (d, *J* = 4.28 Hz, 18 H, P–CH_3). – $^{13}C\{^1H\}$ NMR (100.40 MHz, [D$_8$]THF): δ = 159.8 (t), 139.7 (t), 137.3, 132.7–132.5 (m), 132.5, 130.9, 130.0, 128.8, 121.0 [*C*(aryl)], 18.9–18.0 (m, P–*C*H$_3$). – $^{31}P\{^1H\}$ NMR (161.70 MHz, [D$_8$]THF): δ = 7.7 (s).

[Ru(py)(PPh$_3$)('tpS$_4$')] (7): A yellow-orange suspension of [Ru(PPh_3)$_2$('tpS_4')] (**1**) (235 mg, 0.24 mmol) in pyridine (7 mL) was heated at reflux for 10 min to give an orange-red solution. The solution was cooled to room temperature, combined with MeOH (70 mL), and stirred for 1 h. A yellow solid precipitated, which was separated, washed with MeOH (40 mL) and Et_2O (40 mL), and dried in vacuo. Yield 125 mg of **7** (65%). – $C_{41}H_{32}NPRuS_4$ (**7**) (799.0): calcd. C 61.63, H 4.04, N 1.75, S 16.05; found C 61.41, H 3.89, N 1.99, S 16.15. – MS (FD,CH_2Cl_2, ^{102}Ru); *m/z*: 799 [Ru(py)(PPh_3)('tpS_4')]$^+$. – ^1H NMR (269.6 MHz, CD_2Cl_2): δ = 8.50 [d, 2 H, *o*-*H*(py)], 7.95 (d, 1 H, C_6H_4), 7.70 (d, 1 H, C_6H_4), 7.65–7.60 (m, 1 H, C_6H_4), 7.53–7.48 (m, 1 H, C_6H_4), 7.40–7.30 [m, 6 H, C_6H_4 and P(C_6H_5)$_3$], 7.25–7.10 [m, 12 H, C_6H_4, P(C_6H_5)$_3$ and py], 7.05–6.90 (m, 3 H, C_6H_4), 6.80–6.75 (m, 3 H, C_6H_4), 6.65 (t, 1 H, C_6H_4), 6.55 (t, 1 H, C_6H_4). – $^{31}P\{^1H\}$ NMR (109.38 MHz, CD_2Cl_2): δ = 41.50 (s).

[Ru(NH$_3$)(PPh$_3$)('tpS$_4$')] (8): NH_3 gas was bubbled through a refluxing yellow-orange suspension of [Ru(PPh_3)$_2$('tpS_4')] (**1**) (200 mg, 0.20 mmol) in THF (25 mL) for 5 min. A yellow-orange solution resulted which was cooled to room temperature, combined with *n*-hexane (100 mL), and stirred for 2 h. A yellow solid precipitated, which was separated, washed with *n*-hexane (40 mL), and dried in vacuo. Yield 100 mg of **8**·THF (65%). – $C_{38}H_{34}NO_{0.5}PRuS_4$ (**8**·0.5THF) (773.0): calcd. C 59.04, H 4.43, N 1.81, S 16.59; found C 59.03, H 4.21, N 1.67, S 16.33. – IR (KBr, cm^{-1}): $\tilde{\nu}$ = 3348, 3245, ν(NH). – ^1H NMR (399.65 MHz, CD_2Cl_2) δ = 7.95 (d, 1 H, C_6H_4), 7.86 (d, 2 H, C_6H_4), 7.69–7.64 [m, 6 H, C_6H_4 and P(C_6H_5)$_3$], 7.46 (d, 1 H, C_6H_4), 7.36–7.26 [m, 12 H, C_6H_4 and P(C_6H_5)$_3$], 6.97 (t, 1 H, C_6H_4), 6.90–6.86 (m, 2 H, C_6H_4), 6.57–6.52 (m, 2 H, C_6H_4), 1.70 (s, 3 H, NH_3). – $^{31}P\{^1H\}$ NMR (109.38 MHz, CD_2Cl_2): δ = 47.5 (s).

[Ru(N$_2$H$_4$)(PPh$_3$)('tpS$_4$')] (9): N_2H_4 (0.25 mL, 8.00 mmol) was added to a stirred yellow-orange suspension of [Ru(PPh_3)$_2$('tpS_4')] (**1**) (250 mg, 0.25 mmol) in THF (20 mL), which was heated at reflux for 10 min to give a yellow-orange solution. The solution was cooled to room temperature, filtered, combined with *n*-hexane (80 mL), and stirred for 1 h. A yellow solid precipitated, which was separated, washed with MeOH (10 mL) and *n*-hexane (40 mL), and dried in vacuo. Yield: 100 mg of **9** (53%). – $C_{36}H_{31}N_2PRuS_4$ (**9**) (752.0): calcd. C 57.50, H 4.16, N 3.73, S 17.06; found C 56.74, H 4.37, N 3.64, S 16.86. – IR (KBr, cm^{-1}): $\tilde{\nu}$ = 3334, 3292, 3245, 3164

ν(NH). – MS (FD, CH_2Cl_2, ^{102}Ru); *m/z*: 749 [Ru(N$_2$H)(PPh_3)('tpS_4')]$^+$. – ^{1}H NMR (269.6 MHz, CD_2Cl_2): δ = 7.95 (d, 1 H, C_6H_4), 7.85–7.77 (m, 2 H, C_6H_4), 7.65–7.59 [m, 6 H, C_6H_4 and P(C_6H_5)$_3$], 7.47 (d, 1 H, C_6H_4), 7.27–7.22 [m, 12 H, C_6H_4 and P(C_6H_5)$_3$], 7.98–6.82 (m, 3 H, C_6H_4), 6.53–6.50 (m, 2 H, C_6H_4), 4.20 (m, 1 H, NH_2), 4.09 (m, 2 H, NH_2), 3.36 (s, 1 H, NH_2). – ^{31}P{^{1}H} NMR (109.38 MHz, CD_2Cl_2): δ = 44.0 (s).

[Ru(N_2H_3Me)(PPh_3)('tpS_4')] (10): N_2H_3Me (0.52 mL, 10.0 mmol) was added to a yellow-orange suspension of [Ru(PPh_3)$_2$('tpS_4')] (**1**) (200 mg, 0.20 mmol) in THF (10 mL). The suspension was heated at reflux for 45 min, during the course of which a yellow-orange solution resulted. The solution was cooled to room temperature, filtered, and combined with *n*-hexane (80 mL). A yellow solid precipitated, which was separated, washed with MeOH (10 mL), *n*-hexane (20 mL), and dried in vacuo. Yield: 105 mg of **10** (69%). – $C_{37}H_{33}N_2PRuS_4$ (**10**) (766.0): calcd. C 58.02, H 4.34, N 3.66, S 16.74; found C 57.06, H 4.43, N 3.67, S 16.38. – ^{1}H NMR (269.6 MHz, CD_2Cl_2): δ = 7.95 (d, 1 H, C_6H_4), 7.84 (d, 1 H, C_6H_4), 7.79–7.75 (m, 1 H, C_6H_4), 7.67–7.61 [m, 6 H, C_6H_4 and P(C_6H_5)$_3$], 7.45 (d, 1 H, C_6H_4), 7.28–7.20 [m, 12 H, C_6H_4 and P(C_6H_5)$_3$], 6.95–6.80 (m, 3 H, C_6H_4), 6.54–6.48 (m, 2 H, C_6H_4), 3.97 (t, *J* = 4.16 Hz, 1 H, NH_2), 3.84–3.81 (m, 1 H, NH_2), 3.38–3.29 (m, 1 H, NH_2), 2.09 (d, *J* = 6.88 Hz, 3 H, CH_3). – ^{13}C{^{1}H} NMR (67.8 MHz, CD_2Cl_2): δ = 156.7 (d, J_{PC} = 6.22 Hz), 153.1, 142.3, 142.2, 139.0, 135.9, 135.8, 134.1 (d, J_{PC} = 9.84 Hz), 133.5, 132.9, 132.3, 131.7 (d, J_{PC} = 5.17 Hz), 131.2, 130.7, 130.2, 129.8, 129.6, 129.3, 128.4, 128.0 (d, J_{PC} = 9.32 Hz), 121.8, 120.9 [*C*(aryl)], 42.8 (*C*H$_3$). – ^{31}P{^{1}H} NMR (109.38 MHz, CD_2Cl_2): δ = 47.0 (s).

[Ru{$C(CO_2Et)_2$}(PPh_3)('tpS_4')] (11): $N_2C(CO_2Et)_2$ (0.5 mL, 3.10 mmol) was added to a yellow-orange suspension of [Ru(PPh_3)$_2$('tpS_4')] (**1**) (200 mg, 0.20 mmol) in THF (15 mL). The suspension was heated at reflux for 4 h, over the course of which a yellow-orange solution resulted. The solution was cooled to room temperature, filtered, and combined with *n*-hexane (40 mL). A yellow solid precipitated, which was separated, washed with *n*-hexane (20 mL), and dried in vacuo. Yield: 100 mg of **11** (57%). – $C_{43}H_{37}O_4PRuS_4$ (**11**) (878.1): calcd. C 58.82, H 4.25, N 0.00, S 14.61; found C 58.76, H 4.21, N 0.41, S 13.90. – IR (KBr, cm^{-1}): $\tilde{\nu}$ = 1674, 1640 ν(CO). – MS (FD, CH_2Cl_2, ^{102}Ru); *m/z*: 878 [Ru{$C(CO_2Et)_2$}('tpS_4')]$^+$. – ^{1}H NMR (269.6 MHz, CD_2Cl_2): δ = 8.06–8.03 (m 1 H, C_6H_4), 7.94 (d, 2 H, C_6H_4), 7.71–7.65 [m, 5 H, C_6H_4 and P(C_6H_5)$_3$], 7.58 (d, 1 H, C_6H_4), 7.49 (t, 1 H, C_6H_4), 7.33–7.16 [m, 14 H, C_6H_4 and P(C_6H_5)$_3$], 6.86 (d, 1 H, C_6H_4), 6.67 (t, 1 H, C_6H_4), 6.40 (t, 1 H, C_6H_4), 4.30–4.14 (m, 1 H, COOCH_2CH$_3$), 4.03–3.83 (m, 2 H, COOCH_2CH$_3$), 3.76–3.64 (m, 1 H, COOCH_2CH$_3$), 1.16 (t, *J* = 3.58 Hz, 3 H, $COOCH_2CH_3$), 1.06 (t, *J* = 3.47 Hz, 3 H, $COOCH_2CH_3$). – ^{31}P{^{1}H} NMR (109.38 MHz, CD_2Cl_2): δ = 31.0 (s).

[Ru(MeCN)(PPh_3)('tpS_4')] (12): A yellow-orange suspension of [Ru(PPh_3)$_2$('tpS_4')] (275 mg, 0.28 mmol) in acetonitrile (35 mL) was heated at reflux for 3 h, yielding a yellow-orange solution. The solution was cooled to room temperature, filtered, concentrated in volume to 20 mL, combined with MeOH (50 mL), and stirred for 1 h. A yellow solid precipitated, which was separated, washed with MeOH (20 mL), Et_2O (40 mL), and dried in vacuo. Yield 150 mg of **12** (70%). – $C_{38}H_{30}NPRuS_4$ (**12**) (761.0): calcd. C 59.98, H 3.97, N 1.84, S 16.85; found C 59.87, H 4.09, N 2.01, S 16.69. – IR (KBr, cm^{-1}): $\tilde{\nu}$ = 2271 ν(CN). – MS (FD, CH_2Cl_2, ^{102}Ru); *m/z*: 720 [Ru(PPh_3)('tpS_4')]$^+$. – ^{1}H NMR (CD_2Cl_2, 269.6 MHz): δ = 7.95 (d, 1 H, C_6H_4), 7.80 (d, 1 H, C_6H_4), 7.70–7.60 [m, 7 H, C_6H_4 and P(C_6H_5)$_3$], 7.45–7.40 (m, 1 H, C_6H_4), 7.30–7.20 [m, 10 H, C_6H_4 and P(C_6H_5)$_3$], 7.15–7.05 (m, 2 H, C_6H_4), 6.95–6.80 (m, 3 H, C_6H_4), 6.55–6.45(m, 2 H, C_6H_4), 1.75 (s, 3 H, CH_3). – ^{31}P{^{1}H} NMR (109.38 MHz, CD_2Cl_2): δ = 42.5 (s).

[Ru(NO)(PPh_3)('tpS_4')]BF_4 (13): Solid $NOBF_4$ (29 mg, 0.25 mmol) was added to a stirred solution of [Ru(MeCN)(PPh_3)('tpS_4')] (**12**) (190 mg, 0.25 mmol) in CH_2Cl_2 (15 mL), whose color changed from yellow to red over the course of 3 h. Undissolved material was removed by filtration, and Et_2O (80 mL) was added dropwise to the filtrate. A red-brown solid precipitated, which was separated, washed with Et_2O (20 mL), and dried in vacuo. Yield: 85 mg of **13**·0.25CH_2Cl_2 (40%). – $C_{36.25}H_{27.5}BCl_{0.5}F_4NOPRuS_4$ (**13**·0.25CH_2Cl_2) (858.0): calcd. C 50.75, H 3.23, N 1.63, S 14.95; found C 50.74, H 3.41, N 1.62, S 14.80. – IR (KBr, cm^{-1}): $\tilde{\nu}$ = 1852 ν(NO). – MS (FD, CH_2Cl_2, ^{102}Ru); *m/z*: 750 [Ru(NO)(PPh_3)$_2$('tpS_4')]$^+$. – ^{1}H NMR (CD_2Cl_2, 269.6 MHz): δ = 8.13 (d, 1 H, C_6H_4), 7.90 (d, 1 H, C_6H_4), 7.67–7.47 [m, 18 H, C_6H_4 and P(C_6H_5)$_3$], 7.43–7.40 (m, 1 H, C_6H_4), 7.31–7.11 (m, 3 H, C_6H_4), 7.00–6.96 (m, 2 H, C_6H_4), 6.88–6.81 (m, 1 H, C_6H_4). – ^{13}C{^{1}H} NMR (100.40 MHz, CD_2Cl_2): δ = 151.3 (d), 150.2, 134.5, 134.3, 133.7, 133.3, 133.3, 133.2, 133.0, 132.9, 132.0, 131.7, 131.5, 131.2, 129.9, 129.6, 129.5, 129.2, 126.7, 126.3, 125.7, 125.5 [*C*(aryl)]. – ^{31}P{^{1}H} NMR (109.38 MHz, CD_2Cl_2): δ = 25.0 (s).

[Ru(NO)(PPh_3)('tpS_4')] (14): NO gas was bubbled through a yellow solution of [Ru(MeCN)(PPh_3)('tpS_4')] (**12**) (210 mg, 0.28 mmol) in CH_2Cl_2 (20 mL) for 1 min. A deep-red solution resulted, which was stirred for 20 h. After addition of *n*-hexane (30 mL) a red-brown solid precipated, which was separated, washed with *n*-hexane (20 mL), and dried in vacuo. Yield 70 mg of **14** (34%). – $C_{36}H_{27}NOPRuS_4$ (**14**) (749.9): calcd. C 57.66, H 3.63, N 1.87, S 17.10; found C 55.03, H 3.67, N 2.04, S 17.18. – IR (KBr, cm^{-1}): $\tilde{\nu}$ = 1598 ν(NO). – MS (FD, CH_2Cl_2, ^{102}Ru); *m/z*: 750 [Ru(NO)(PPh_3)$_2$('tpS_4')]$^+$.

(NEt_4)[Ru(N_3)(PPh_3)('tpS_4')] (15): NEt_4N_3 (50 mg, 0.29 mmol) was added to a yellow suspension of [Ru(MeCN)(PPh_3)('tpS_4')] (**12**) (220 mg, 0.29 mmol) in acetone (20 mL). Under exclusion of light, the mixture was stirred for 3 h during which time an orange solution resulted. Addition of Et_2O (80 mL) to the solution yielded an orange solid, which was separated after 1 h, washed with Et_2O (40 mL) and dried in vacuo. Yield: 146 mg of **15** (56%). – $C_{44}H_{47}N_4PRuS_4$ (**15**) (892.2): calcd. 59.24, H 5.31, N 6.28, S 14.37; found C 58.07, H 5.47, N 5.81, S 15.10. – IR (KBr, cm^{-1}): $\tilde{\nu}$ = 2029 ν(N_3). – ^{1}H NMR ([D$_6$]acetone, 269.6 MHz): δ = 8.87 (d, 1 H, C_6H_4), 8.73–8.68 (m, 1 H, C_6H_4), 8.58–8.53 [m, 6 H, C_6H_4 and P(C_6H_5)$_3$], 8.43 (d, 1 H, C_6H_4), 8.00–7.90 [m, 13 H, C_6H_4 and P(C_6H_5)$_3$], 7.79 (d, 1 H, C_6H_4), 7.68–7.58 (m, 2 H, C_6H_4), 7.33–7.27 (m, 1 H, C_6H_4), 7.15–7.10 (m, 1 H, C_6H_4), 4.15 (q, *J* = 3.71 Hz, 8 H, N–CH_2), 2.10–2.05 (m, 12 H, N–CH_2–CH_3).

[Ru(I)(PPh_3)('tpS_4')] (16): Elemental iodine (40 mg, 0.16 mmol) was added to a stirred suspension of [Ru(MeCN)(PPh_3)('tpS_4')] (**12**) (240 mg, 0.31 mmol) in THF (15 mL). Over the course of 5 min a clear red solution resulted from which dark red microcrystals crystallized. The crystals were separated after 12 h, washed with THF (20 mL), Et_2O (20 mL), and dried in vacuo. Yield: 200 mg of **16**·THF (70%). – $C_{40}H_{35}IOPRuS_4$ (**16**·THF) (918.9): calcd. C 52.28, H 3.84, S 13.96; found C 52.43, H 3.92, S 13.80. – MS (FD, CH_2Cl_2, ^{102}Ru); *m/z*: 847 [Ru(I)(PPh_3)$_2$('tpS_4')]$^+$.

[Ru(N_3)(PPh_3)('tpS_4')] (17): NEt_4N_3 (67 mg, 0.39 mmol) was added to a stirred suspension of [Ru(I)(PPh_3)('tpS_4')]·THF (**16**) (165 mg, 0.18 mmol) in acetone (15 mL). Under exclusion of light, the suspension was stirred for 2.5 d during which time its color changed to yellow-green. The yellow-green solid was separated, washed with MeOH (40 mL), acetone (40 mL) and Et_2O (20 mL), and dried in

Table 2. Selected crystallographic data of [Ru(py)(PPh$_3$)('tpS$_4$')] (**7**), [Ru(NO)(PPh$_3$)('tpS$_4$')]BF$_4$·CH$_2$Cl$_2$ (**13**·CH$_2$Cl$_2$), [Ru(I)(PPh$_3$)-('tpS$_4$')]·CH$_2$Cl$_2$ (**16**·CH$_2$Cl$_2$), [μ-N$_2$H$_4${Ru(PPh$_3$)('tpS$_4$')}$_2$]·4THF (**18**·4THF), and [μ-N$_2$H$_2${Ru(PPh$_3$)('tpS$_4$')}$_2$]·4CH$_2$Cl$_2$ (**19**·4CH$_2$Cl$_2$)

Compound	**7**	**13**·CH$_2$Cl$_2$	**16**·CH$_2$Cl$_2$	**18**·4THF	**19**·4CH$_2$Cl$_2$
Empirical formula	$C_{41}H_{32}NPRuS_4$	$C_{37}H_{29}BCl_2F_4NOPRuS_4$	$C_{37}H_{29}Cl_2IPRuS_4$	$C_{88}H_{90}N_2O_4P_2Ru_2S_8$	$C_{76}H_{64}Cl_8N_2P_2Ru_2S_8$
M_r [g/mol]	799.0	921.6	931.7	1760	1809
Crystal size [mm]	0.44 × 0.30 × 0.16	0.42 × 0.35 × 0.12	0.30 × 0.30 × 0.20	0.30 × 0.30 × 0.10	0.20 × 0.15 × 0.01
F(000)	816	928	1844	910	916
Crystal system	triclinic	triclinic	monoclinic	triclinic	triclinic
Space group	$P\bar{1}$	$P\bar{1}$	$P2_1/c$	$P\bar{1}$	$P\bar{1}$
a [pm]	984.0(2)	1037.6(1)	1094.0(1)	1034.8(4)	1102.96(4)
b [pm]	1007.9(1)	1205.9(1)	2452.8(3)	1451.7(4)	1334.71(5)
c [pm]	1794.4(3)	1676.2(2)	1369.0(1)	1479.3(6)	1545.90(5)
α [°]	88.76(1)	105.46(1)	90	115.90(2)	65.840(1)
β [°]	82.48(2)	96.00(1)	96.48(1)	91.90(2)	82.152(1)
γ [°]	77.12(1)	105.78(1)	90	93.68(3)	68.199(1)
V [nm^3]	1.7199(5)	1.9095(3)	3.6501(6)	1.990(1)	1.9276(1)
Z	2	2	4	1	1
$d_{calcd.}$ [g/cm^3]	1.543	1.603	1.695	1.469	1.559
μ [mm^{-1}]	0.778	0.863	1.721	0.683	0.972
Diffractometer	Siemens P4	Siemens P4	Siemens P4	Siemens P4	CCD (Bruker AXS)
Radiation [pm]	Mo-K_α (λ = 71.073)	Mo-K_α (λ = 71.073)	Mo-K_α (λ = 71.073)	Mo-K_α (λ = 71.073)	Mo-K_α (λ = 71.073)
Temperature [K]	200(2)	200(2)	200(2)	200(2)	210(2)
Scan technique	ω scan	ω scan	ω scan	ω scan	ω scan
2Θ range [°]	4.0–54.0	3.6–54.0	3.7–54.0	4.8–50.0	3.5–54.5
Scan speed [°/min]	4.0–40.0	4.0–40.0	5.0–50.0	8.0	–
Meas. reflections	8884	9579	9649	7698	10881
Indep. reflections	7497	8178	7956	6526	6557
R_{int} [%]	3.98	5.42	4.30	9.46	7.50
Obsd. reflections	5550	6189	6163	2795	3697
σ criterion	$F_o \geq 4\sigma(F)$	$F_o \geq 4\sigma(F)$	$F_o \geq 4\sigma(F)$	$F_o \geq 4\sigma(F)$	$F_o \geq 4\sigma(F)$
$R1$; $wR2$ [%]	4.33; 10.35	4.72; 10.79	4.22; 11.68	8.61; 16.49	7.26; 21.07
Ref. parameters	561	605	506	478	461

vacuo. Yield: 85 mg of **17**·0.5Me$_2$CO. – $C_{37.5}H_{30}N_3O_{0.5}PRuS_4$ (**17**·0.5Me$_2$CO) (791.0): calcd. C 56.94, H 3.82, N 5.31, S 16.22; found C 56.58, H 3.82, N 5.10, S 16.02. – IR (KBr, cm^{-1}): $\tilde{\nu}$ = 2036 ν (N_3). – MS (FD, CH_2Cl_2, ^{102}Ru); *m*/*z*: 762 [Ru(N_3)-(PPh$_3$)$_2$('tpS$_4$')]$^+$.

[μ-N$_2$H$_4${Ru(PPh$_3$)('tpS$_4$')}$_2$] (18): [Ru(N_2H_4)(PPh$_3$)('tpS$_4$')] (**9**) (120 mg, 0.16 mmol) was dissolved in CH_2Cl_2 (7 mL) and the solution was stirred for 7 d. After addition of MeOH (10 mL), yellow microcrystals precipitated, which were separated, washed with MeOH (10 mL), Et_2O (15 mL), and dried in vacuo. Yield: 20 mg of **17**·0.75CH_2Cl_2 (16%). – $C_{72.75}H_{59.5}Cl_{1.5}N_2P_2Ru_2S_8$ (**18**·0.75CH_2Cl_2) (1536): calcd. C 56.90, H 3.91, N 1.82, S 16.71; found C 56.72, H 4.03, N 2.01, S 16.30

[μ-N$_2$H$_2${Ru(PPh$_3$)('tpS$_4$')}$_2$] (19). – a) From [Ru(N_2H_4)-(PPh$_3$)('tpS$_4$')] (9) and O$_2$: [Ru(N_2H_4)(PPh$_3$)('tpS$_4$')] (**9**) (145 mg, 0.19 mmol) was dissolved in CH_2Cl_2 (20 mL) in a Schlenk tube that was closed by a septum. Air (20 mL, 0.19 mmol O_2) was injected into the solution by means of a syringe. Over the course of 36 h, the solution changed color from yellow to green, and green microcrystals precipitated. They were separated, washed with CH_2Cl_2 (5 mL), MeOH (15 mL), H_2O (10 mL) and Et_2O (20 mL), and dried in vacuo. Yield: 35 mg of **19**·CH_2Cl_2 (24%). – $C_{73}H_{58}Cl_2N_2P_2Ru_2S_8$ (**19**·CH_2Cl_2) (1555): calcd. C 56.40, H 3.76, N 1.80, S 16.50; found C 56.27, H 3.73, N 1.99, S 16.55. – UV/Vis (CH_2Cl_2): λ_{max} (nm) = 306.5 (ε = 15159 L mol^{-1} cm^{-1}), 463 (ε = 8162 L mol^{-1} cm^{-1}). – **b) From [Ru(MeCN)(PPh$_3$)('tpS$_4$')] (12), K$_2$N$_2$(CO$_2$)$_2$ and HAc:** 0.2 M acetic acid (3.45 mL, 0.69 mmol) was added dropwise to a stirred suspension of [Ru(-MeCN)(PPh$_3$)('tpS$_4$')] (**12**) (175 mg, 0.23 mmol) and $K_2N_2(CO_2)_2$ (134 mg, 0.69 mmol)in THF (25 mL). A dark green solution resulted with evolution of gas. Over the course of 5 min a green solid precipitated, which was separated after 3 h, washed with H_2O (15 mL), THF (25 mL), Et_2O (25 mL), and dried in vacuo. Yield: 153 mg of **19**·2H_2O (88%). – $C_{72}H_{60}N_2O_2P_2Ru_2S_8$ (**19**·2H_2O) (1506): calcd. C 57.43, H 4.02, N 1.86, S 17.03; found C 57.26, H 3.95, N 1.77, S 16.67.

X-ray Structure Analyses of [Ru(py)(PPh$_3$)('tpS$_4$')] (7), [Ru(NO)(PPh$_3$)('tpS$_4$')]BF$_4$·CH$_2$Cl$_2$ (13·CH$_2$Cl$_2$), [Ru(I)(PPh$_3$)-('tpS$_4$')]·CH$_2$Cl$_2$ (16·CH$_2$Cl$_2$), [μ-N$_2$H$_4${Ru(PPh$_3$)('tpS$_4$')}$_2$]·4THF (18·4THF), and [μ-N$_2$H$_2${Ru(PPh$_3$)('tpS$_4$')}$_2$]·4CH$_2$Cl$_2$ (19·4CH$_2$Cl$_2$): Orange crystals of **7** were grown by layering a hot pyridine solution of **7** with MeOH. Dark-brown platelets of **13**·CH_2Cl_2 formed when a saturated CH_2Cl_2 solution of **13** was layered with *n*-hexane. Black rhombohedra of [Ru(I)(PPh$_3$)('tpS$_4$')]·CH_2Cl_2 (**16**·CH_2Cl_2) were obtained when a saturated CH_2Cl_2 solution of **16** was layered with MeOH. Yellow platelets of [μ-N_2H_4{Ru(PPh$_3$)('tpS$_4$')}$_2$]·4THF (**18**·4THF) crystallized from a THF solution of **18** layered with Et_2O. Green platelets of **19**·4CH_2Cl_2 formed when air was injected into a yellow solution of [Ru(N_2H_4)(PPh$_3$)('tpS$_4$')] (**9**) in CH_2Cl_2. – Suitable single crystals were mounted by using the oil-drop mounting technique.[23] For all data sets Lorentz and polarization corrections were applied. For **18**·4THF absorption effects have been neglected. A ψ-scan absorption correction has been applied for **7** (T_{min} = 0.4357, T_{max} = 0.4699), **13**·CH_2Cl_2 (T_{min} = 0.4254, T_{max} = 0.4680), and **16**·CH_2Cl_2 (T_{min} = 0.2677, T_{max} = 0.3412). An empirical correction was used for **19**·4CH_2Cl_2 (SADABS, T_{min} = 0.8294, T_{max} = 0.9923).[24] All structures were solved by direct methods and were refined using full-matrix least-squares procedures on F^2 (SHELXTL 5.03).[25] – All non-hydrogen atoms were refined anisotropically. The positions of the hydrogen atoms were taken from a difference Fourier map and were either refined isotropically (**7**), refined with a common isotropic displacement parameter (**13**·CH_2Cl_2 and **16**·CH_2Cl_2) or were kept fixed with a common isotropic displacement parameter

(**18**·4THF, **19**·4CH_2Cl_2). The BF_4 anion in the structure of **13**·CH_2Cl_2 is disordered around the B1-F11 vector, where two possible sites have been refined such that they are both equally occupied (50%). Furthermore, the solvate CH_2Cl_2 molecule is disordered with two different sites having occupancies of 74(4)% and 26(4)% respectively. In **16**·CH_2Cl_2, one Cl atom of the solvate molecule is disordered. Two possible sites have been refined with occupancies of 61(5)% and 39(5)%. In **19**·4CH_2Cl_2 two of the solvate molecules are disordered with site occupancies of the two possible sites being refined to 77(1)% and 29(1)%. The hydrogen atoms of the solvate molecules in all structures are geometrically positioned. Selected crystallographic data are summarized in Table 2.[26]

Acknowledgments

Financial support of this work by the Deutsche Forschungsgemeinschaft and the Fonds der Chemischen Industrie is gratefully acknowledged.

[1] B. K. Burgess, D. J. Lowe, *Chem. Rev.* **1996**, *96*, 2983–3011.
[2] J. B. Howard, D. C. Rees, *Chem . Rev.* **1996**, *96*, 2965–2982.
[3] R. R. Eady, *Chem. Rev.* **1996**, *96*, 3013–3030.
[4] [4a] D. Sellmann, J. Utz, N. Blum, F. W. Heinemann, *Coord. Chem. Rev.* **1999**, *190–192*, 607–627. – [4b] R. N. F. Thorneley, D. J. Lowe, J. Biolog. *Inorg. Chem.* **1996**, *1*, 576–580. – [4c] I. Dance, *J. Biolog. Inorg. Chem.* **1996**, *1*, 581–586. – [4d] D. Sellmann, J. Sutter, *J. Biolog. Inorg. Chem.* **1996**, *1*, 587–593. – [4e] D. Coucouvanis, *J. Biolog. Inorg. Chem.* **1996**, *1*, 594–600. – [4f] C. J. Rickett, *J. Biolog. Inorg. Chem.* **1996**, *1*, 601–606. – [4g] G. J. Leigh, *Eur. J. Biochem.* **1995**, *229*, 14–20.
[5] D. Sellmann, T. Gottschalk-Gaudig, F. W. Heinemann, *Inorg. Chem.* **1998**, *37*, 3982–3988 and literature cited therein.
[6] D. Sellmann, I. Barth, F. Knoch, M. Moll, *Inorg. Chem.* **1990**, *29*, 1822–1826.
[7] D. Sellmann, K. Engl, T. Gottschalk-Gaudig, F. W. Heinemann, *Eur. J. Inorg Chem.* **1999**, 333–339.
[8] F. Bottomley, in *A Treatise on Dinitrogen Fixation* (Eds.: R. W. F. Hardy, F. Bottomley, R. C. Burns), Wiley, New York, **1979**, p. 109–167.
[9] J. Chatt, D. P. Meloille, R. L. Richards, *J. Chem. Soc.* **1969**, 2841–2844.
[10] D. Sellmann, H. Kunstmann, F. Knoch, M. Moll, *Inorg. Chim. Acta* **1988**, *154*, 157–167.
[11] D. Sellmann, A. Hennige, *Angew. Chem.* **1997**, *108*, 270–271; *Angew. Chem. Int. Ed. Engl.* **1997**, *36*, 276–278.
[12] [12a] D. Sellmann, E. Böhlen, M. Waeber, G. Huttner, L. Zsolnai, *Angew. Chem.* **1985**, *97*, 984–985; *Angew. Chem. Int. Ed. Engl.* **1985**, *24*, 981–982. – [12b] D. Sellmann, J. Käppler, F. Knoch, M. Moll, *Inorg. Chem.* **1993**, *32*, 960–964.
[13] [13a] D. Sellmann, J. Sutter, *Acc. Chem. Res.* **1997**, *30*, 460–469. – [13b] D. Sellmann, J. Sutter, in "Transition Metal Sulfur Chemistry: Biological and Industrial Significance" (Eds.: E. I. Stiefel, K. Matsumoto), *ACS Symp. Ser.* **1996**, *653*, 101–116. – [13c] D. Sellmann, T. Becker, F. Knoch, *Chem. Eur. J.* **1996**, *2*, 1092–1098.
[14] T. Gottschalk-Gaudig, Dissertation, University Erlangen-Nürnberg, **1997**, p. 94–96.
[15] D. Sellmann, T. Gottschalk-Gaudig, F. W. Heinemann, *Inorg. Chim. Acta* **1998**, *269*, 63–72.
[16] N. N. Greenwood, A. Earnshaw, *Chemie der Elemente*, VCH Weinheim, **1988**, p. 546.
[17] M. Koepp, H. Wendt, H. Strehlow, *Z. Elektrochem.* **1960**, *64*, 483–491.
[18] M. Regitz, *Chem. Ber.* **1966**, *99*, 3128–3147.
[19] J. Thiele, *Justus Liebigs Ann. Chem.* **1892**, *271*, 127.
[20] I. P. Evans, A. Spencer, G. Wilkinson, *J. Chem. Soc., Dalton Trans.* **1973**, 204–209.
[21] H. Schmidbaur, G. Blaschke, *Z. Naturforsch.* **1980**, *35b*, 584–587.
[22] D. Sellmann, W. Weber, *J. Organomet. Chem.* **1986**, *304*, 195–205.
[23] H. Hope, in *Experimental Organometallic Chemistry* (Eds.: Al L. Wayda, M. Y. Darensbourg), *ACS Symp. Ser.* **1987**, *357*, 257–262.
[24] R. H. Blessing, *Acta Crystallogr.* **1995**, *A51*, 33–37.
[25] *SHELXTL 5.03 for Siemens Crystallographic Research Systems*, Siemens Analytical X-ray Instruments Inc., Madison, WI, USA, **1995**.
[26] Crystallographic data (excluding structure factors) for the structures reported in this paper have been deposited with the Cambridge Crystallographic Data Centre as CCDC-133763 (**7**), -133764 (**13**·CH_2Cl_2), -133765 (**16**·CH_2Cl_2), -133766 (**18**·4THF), -133767 (**19**·4CH_2Cl_2). Copies of the data can be obtained free of charge on application to The Director, CCDC, 12 Union Road, Cambridge CB2 1EZ, UK [Fax: (internat.) + 44-1223/336-033, E-mail: deposit@ccdc.cam.ac.uk].

Received November 9, 1999
[I99400]

The Syntheses and Molecular Structure of a Branched Oligosilyl Anion with a Record of Nine Silicon Atoms and of the First Branched Oligosilyl Dianion

Yitzhak Apeloig,*[a] Gady Korogodsky,[a] Dmitry Bravo-Zhivotovskii,*[a] Dieter Bläser,[b] and Roland Boese[b]

Keywords: Silicon / Silyl anions / Lithium / Silanes / Polysilyl dianions / α,ω-Dilithiooligosilanes

$(Me_3Si)_3Si(Me_2Si)_2(Me_3Si)_2SiLi$ (**1**) and $LiSi(Me_3Si)_2(Me_2Si)_2Si(Me_3Si)_2Li$ (**2**) were synthesized by the reaction of $(Me_3Si)_3Si(Me_2Si)_2Si(Me_3Si)_3$ in THF with one or two mol-equivalents, respectively, of MeLi. Both **1** and **2** were characterized spectroscopically and by trapping reactions, and **1** also by X-ray crystallography.

Introduction

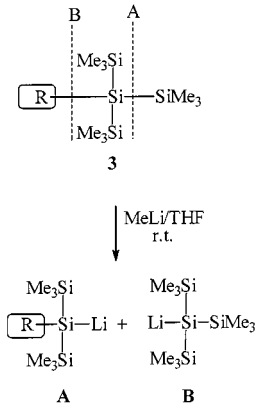
Silyl anions are potentially important reagents in synthesis[1] and they are probably involved in the formation and degradation of polysilanes.[2] However, the number and variety of synthetically useful silyl anions and the information on their structures is very limited,[1] especially in comparison to carbanions; e.g., $CH_3(CH_2)_nCH_2Li$ reagents are widely used in synthesis, while the analogous $Me_3Si(SiMe_2)_nSiMe_2Li$ are unknown, except for $Me_3SiSiMe_2Li$.[3] Of contemporary interest is the branched "hypersilyl" anion, $(Me_3Si)_3Si^-$, first prepared in situ[4] and later isolated as stable THF[5a,5b] or DME[5c] complexes of the lithium salt, e.g., $(Me_3Si)_3SiLi{\cdot}3THF$. The large steric requirements,[6] the interesting electronic properties[7] and the solubility of its derivatives in organic solvents has made the $(Me_3Si)_3Si$ group a popular ligand in main-group[8] and in transition-metal chemistry.[9] Recently, several new branched polysilyl anions have been synthesized by us[10a] (and were used to prepare novel stable silenes[10b]), as well as by other groups.[11] However, these anions have a relatively small number of silicon atoms, and in anions which were structurally characterized the maximum number of silicon atoms is only four.[10a,11a]

We report here[12] the synthesis and the full structural characterization of a new branched polysilyl anion $(Me_3Si)_3SiMe_2SiMe_2Si(Me_3Si)_2SiLi{\cdot}3THF$ (**1**) holding two records for silyl anions: (a) It has nine silicon atoms – the highest known; and (b) it has a chain of 5 silicon atoms (including the anionic center) – the longest known. We also report on the synthesis of the first known branched oligosilyl dianion, the corresponding nTHF·$LiSi(Me_3Si)_2Me_2SiMe_2Si(Me_3Si)_2SiLi{\cdot}n$THF (**2**).

[a] Department of Chemistry and the Lise Meitner-Minerva Center for Computational Quantum Chemistry, Technion-Israel Institute of Technology
Haifa 32000, Israel
Fax: (internat.) + 972-4/823-3735
E-mail: chrapel@tx.technion.ac.il
[b] Institut für Anorganische Chemie der Universität-GH Essen
Universitätstrasse 3–5, 45117 Essen, Germany
Fax: (internat.) + 49-201/183-2535
E-mail: boese@structchem.uni-essen.de

Results and Discussion

Recently we found[10a] that the products obtained from the reaction of branched polysilanes **3** with methyllithium (Scheme 1) depend on the substituent R as follows: when R has one or two silicon atoms (series 1) CH_3Li attacks preferentially at the sterically less-hindered Si atom, yielding the silyllithium **A** (bond A is cleaved). However, when R is a branched polysilane fragment (series 2) only $(Me_3Si)_3SiLi$ (**B**) was obtained (bond B is cleaved).



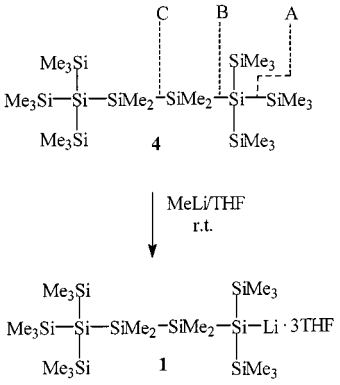
Series 1: R = $SiMe_2tBu$, $SiMe_2SiMe_3$; $SiMe_2SiMe_2tBu$.
Series 2: R = $SiMe(SiMe_3)_2$; $Si(SiMe_3)_3$; $SiMe_2Si(SiMe_3)_3$; $SiMeHSi(SiMe_3)_3$.

Scheme 1

To gain a better understanding of the reaction in Scheme 1 we also studied the cleavage of the doubly branched polysilane **4**.[13] Reaction of **4** with one equivalent of MeLi leads to cleavage of bond A [i.e., **4** behaves as a member of series 1, even though it possesses a $(Me_3Si)_3Si$ fragment], producing the novel branched polysilyl anion **1** (Scheme 2). The structure of **1** was first assigned by isolating the expected trapping products $(Me_3Si)_3SiMe_2SiMe_2Si(Me_3Si)_2SiR$ (R = tBuMe$_2$Si, PhMe$_2$Si, CH_3OCH_2) when treated with tBuMe$_2$SiCl, PhMe$_2$SiCl and CH_3OCH_2Cl, respectively (see Experimental Section). These compounds were characterized by their ^1H, ^{13}C and ^{29}Si NMR spectra

 © WILEY-VCH Verlag GmbH, D-69451 Weinheim, 2000 1434–1948/00/0505–1091 $ 17.50+.50/0

and finally by X-ray crystallography. To the best of our knowledge, **1** is *the isolated silyl anion with the highest number of silicon atoms* (i.e., nine) *and with the longest polysilicon chain* (5 silicon atoms), of any other known silyl anion.



Scheme 2

Our results contrast with those of Pannell et al.[13] who reported that the reaction of **4** with CH_3Li followed by reaction with CH_3I yields $(Me_3Si)_4Si$, implying the presence of $(Me_3Si)_3SiMe_2SiLi$ and thus cleavage of bond C in **4**. Preliminary experiments aimed at the resolving this discrepancy, which we have carried out, suggest that Pannell's observation may result from the presence of impurities in the precursor which was used. Thus, when **4** was purified by crystallization (according to Pannell's procedure[13]) reaction with CH_3Li followed by addition of water led exclusively to $(Me_3Si)_4Si$ (as observed by Pannell et al.[13] who, however, used CH_3I). No traces of $(Me_3Si)_3SiSiMe_2H$ (expected if bond C in **4** is cleaved) were detected. On the other hand, **4** (which was carefully purified by liquid chromatography) produced only **1**.[14] HPLC chromatography of **4** purified by crystallization, showed 10% of two additional compounds, yet unidentified. We therefore speculate that these impurities catalyze the production of $(Me_3Si)_4Si$ which was observed by Pannell et al.[13]

The structure of **1**·3THF, as determined by X-ray crystallography, is shown in Figure 1. Except for $(Me_3Si)_3SiLi$[5] and the closely related *t*$BuMe_2Si(Me_3Si)_2SiLi$·3THF[10a] this is the only other reported X-ray structure of a solvated[15] branched silyllithium compound.

Table 1 summarizes the most important structural parameters of the four known solvated[15] branched silyl lithium compounds: **1**·3THF, $(Me_3Si)_3SiLi$·3THF (**5**·3THF), *t*$BuMe_2Si(Me_3Si)_2SiLi$·3THF (**6**·3THF)[10a] and $(Me_3SiMe_2Si)_3SiLi$·3THF (**7**·3THF) – recently synthesized by our group.[16] In general the four structures are quite similar, but some differences can be noted;[17] *r*(Si–Li) in **1**·3THF (2.657 Å) is similar to that in **5**·3THF (2.644 Å),[5a] and in **6**·3THF (2.684 Å)[10a] but it is 0.11 Å shorter than in **7**·3THF (2.767 Å). We refrain from interpreting these differences because quantum-mechanical calculations show that the force-constant for the Si–Li bond stretching is very small,[16] so that even small effects (including crystal packing forces), can cause significant changes in *r*(Si–Li). The

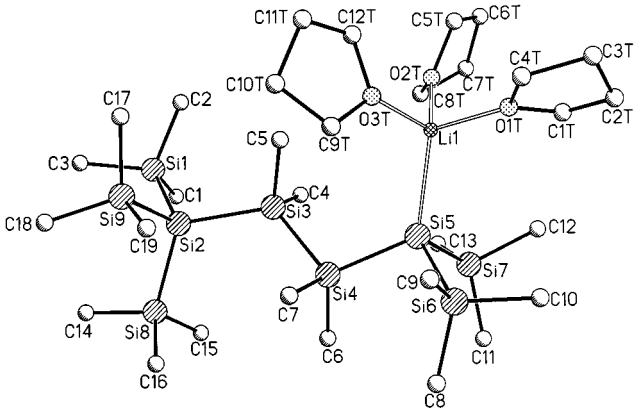


Figure 1. Molecular structure of **1**; hydrogen atoms have been omitted for clarity; selected bond lengths (Å) and bond angles (°): Si(1)–Si(2) 2.361(1), Si(2)–Si(9) 2.355(2), Si(2)–Si(8) 2.348(1), Si(2)–Si(3) 2.378(1), Si(3)–Si(4) 2.355(1), Si(4)–Si(5) 2.363(1), Si(7)–Si(5) 2.352(1), Si(6)–Si(5) 2.348(1), Si(5)–Li, 2.657(6); Si(1)–Si(2)–Si(9) 105.9(1), Si(1)–Si(2)–Si(8) 107.3(1), Si(2)–Si(3)–Si(4) 118.2(1), Si(3)–Si(4)–Si(5) 109.9(1), Si(4)–Si(5)–Si(6) 101.0(1), Si(4)–Si(5)–Si(7) 104.2(1), Si(6)–Si(5)–Si(7) 100.2(1)

Table 1. Selected bond lengths [Å] and bond angles [°] for solvated branched silyllithium compounds and silanes

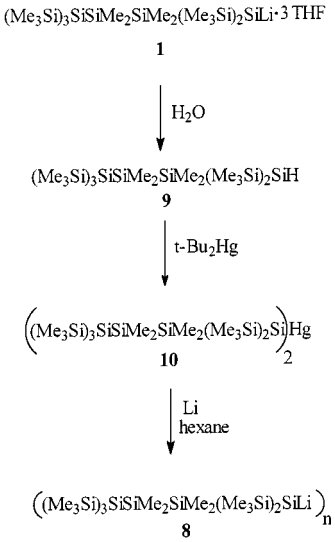
Compound	*r*(Si–Li)	*r*(Si–Si)[a]		α(Si–Si–Si)[b]	
		individual	average	individual	average
1·3THF	2.657(6)	2.352, 2.348, 2.363	2.355	100.2, 101.0, 104.2	101.7
5·3THF[5a]	2.644(12)	2.330[c]	2.330	102.4[c]	102.4
5·3THF[5b]	2.669(13)	2.330, 2.328, 2.336	2.331	103.1, 101.7, 103.1	102.6
5·1.5DME[5c]	2.630(5)	2.338, 2.347, 2.340	2.342	104.7, 104.0, 103.1	103.9
6·3THF[10a]	2.684(9)	2.353, 2.346, 2.341	2.347	105.4, 99.4, 100.0	101.6
7·3THF[16]	2.767(11)	2.361[c]	2.361	100.1[c]	100.1
$(Me_3Si)_4Si$[5a]		2.346[c]	2.346[c]	109.5[c]	109.5[c]
4[13]		2.361, 2.355, 2.345, 2.375	2.359	107.0, 109.0, 115.3	110.3

[a] Between the central silicon atom (the anionic center) and an α-silicon atom. – [b] Around the central silicon atom (the anionic center). – [c] All values are identical by symmetry.

Si–Si bonds around the anionic center [Si(5)] are slightly longer in **1**·3THF, **6**·3THF and **7**·3THF than in **5**·3THF, (average bond lengths: 2.355 Å, 2.347 Å, 2.361 Å and 2.334 Å, respectively), probably reflecting repulsions between the bulky branched silicon chains. The average Si–Si–Si angles around Si(5) are similar in all compounds. Comparison with the neutral silane **4**[13] reveals distortions in the polysilicon backbone of **1**·3THF; the Si(2)–Si(3) and Si(4)–Si(5) bonds in **1**·3THF are slightly elongated, while *r*[Si(3)–Si(4)] is slightly shortened relative to **4**. The Si(3)–Si(4)–Si(5) angle in **1**·3THF is contracted to 109.9° (117.1° in **4**), while the Si(2)–Si(3)–Si(4) angles in **1**·3THF and **4** are similar.

The ^{29}Si NMR chemical shift of the anionic center Si(5) in **1** is at δ = –181.5, strongly shielded, as expected, compared to the corresponding silane **4** (δ = –119.6). This shift is similar to that observed on going from $(Me_3Si)_4Si$ (δ = –135.5) to $(Me_3Si)_3SiLi$·3THF (δ = –189.0). A comparison

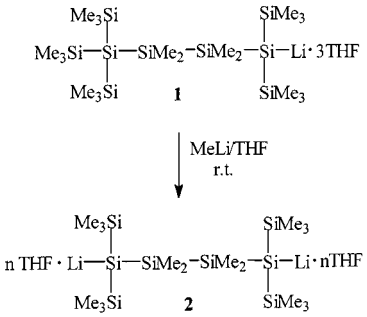
with other silyl anions shows that the ^{29}Si chemical shift of the anionic center in **1** is shifted slightly downfield compared to that in $(Me_3Si)_3SiLi{\cdot}3THF$ (δ = –189.0) and slightly upfield compared with that in **7**·3THF (δ = –176.8). These changes probably reflect a combination of steric and electronic effects. Interestingly, in **1** the chemical shifts of Si(4) (δ = –22.2) and of the more remote Si(3) (δ = –33.5) are shifted in opposite directions (by 7 ppm downfield and by 4 ppm upfield, respectively) relative to their positions in **4** (δ = –29.5). The chemical shift of Si(2) in **1** (δ = –129.9) is shifted upfield by 10.3 ppm relative to **4** (δ = –119.6).



Scheme 3

We have also prepared, according to Scheme 3, the unsolvated analogue of **1**, i.e. **8**. Compound **1** was first hydrolyzed to the corresponding oligosilane **9** which was then reacted with tBu$_2$Hg to give the corresponding disilylmercury compound **10**. Compound **10** was then reacted with Li in hexane to give unsolvated **8**. Compound **8** was characterized by ^1H, ^{13}C, and ^{29}Si NMR spectroscopy and by its reaction products with tBuMe$_2$SiCl, HMe$_2$SiCl and CH_3OCH_2Cl (see Experimental Section), but we have not yet been able to obtain suitable crystals of **8** for an X-ray analysis. In analogy with other similar silyl lithium compounds[1,2] we assume that **8** is a dimer (i.e. n = 2).

Compound **1** reacts (in THF) with an additional equivalent of CH_3Li to give the corresponding dianion **2** (Scheme 4) which has a total of 8 silicon atoms and a chain



Scheme 4

of 4 silicon atoms. The proposed structure of **2** is supported by ^1H, ^{13}C and ^{29}Si NMR spectroscopy and by the isolation of the expected trapping products: R(Me$_3$Si)$_2$SiMe$_2$SiMe$_2$-SiSi(SiMe$_3$)$_2$R (R = SiMe$_2$$t$Bu, SiMe$_2H, CH_2OCH_3$) in the reactions with tBuMe$_2$SiCl, ClSiMe$_2$H and ClCH$_2$OCH$_3$, respectively (see Experimental Section). Recently we have also isolated the unsolvated **2**.[16] Attempts to crystallize **2** in order to determine its molecular structure by X-ray crystallography are in progress. Several linear α,ω-dilithium oligosilanes were reported previously.[11b,18] However, **2** is the first isolated and spectroscopically characterized branched silyldilithium compound.

Conclusion

We have synthesized, isolated and determined using X-ray crystallography the molecular structure of a new branched polysilyllithium compound $(Me_3Si)_3SiMe_2$-$SiMe_2Si(Me_3Si)_2SiLi{\cdot}3THF$ (**1**) holding two records for silyl anions: (a) it has nine silicon atoms – the highest known; and (b) it has a chain of 5 silicon atoms (including the anionic center) – the longest known. We have also synthesized the first branched oligosilyldilithium compound, the corresponding nTHF·LiSi(Me$_3$Si)$_2$Me$_2$SiMe$_2$Si(Me$_3$Si)$_2$SiLi·nTHF (**2**). Compounds **1** and **2** are expected to have a variety of synthetic applications; e.g., most recently Lambert et al. have applied **1** (prepared according to our procedure[12]) for synthesizing a nanometer-scale dendritic polysilane.

We are continuing our efforts to synthesize even longer branched polysilyl anions and to study their properties and their potential applications.

Experimental Section

General Remarks: Standard Schlenk techniques were used for all syntheses and all sample manipulations. – NMR spectra were recorded at room temperature in C_6D_6 solution using a Bruker EM-200 or Bruker-400 instruments. – Mass spectroscopy (MS) data were obtained with a Finnigan MAT TSQ 45 triplestage quadrupole mass spectrometer.

(Me$_3$Si)$_3$SiMe$_2$SiMe$_2$Si(Me$_3$Si)$_2$SiLi·3THF (1): Compound **4**[13] (7.0 g, 11.3 mmol) in dry THF (30 mL) was placed in a Schlenk flask under vacuum, and 9 mL of a 1.4 M solution of CH_3Li in diethyl ether was added in 10 portions over 72 h (conversion was followed by NMR spectroscopy). The THF solvent was removed and **1** was crystallized from hexane to give 6.5 g of colorless crystals of **1**·3THF (75% yield), suitable for X-ray analysis. – ^1H NMR (C_6D_6): δ = 0.42 [s, 27 H, Si(SiMe$_3$)$_3$], 0.55 [s, 18 H, SiLi(SiMe$_3$)$_2$], 0.60 (s, 6 H, SiMe$_2$), 0.73 (s, 6 H, SiMe$_2$), 1.37 (m, 12 H, CH$_2$ of THF), 3.50 (m, 12 H, OCH$_2$ of THF). – ^{13}C NMR (C_6D_6): δ = 3.7 [Si(SiMe$_3$)$_3$], 1.6 (SiMe$_2$), 6.9 (SiMe$_2$), 7.5 [SiLi(SiMe$_3$)$_2$], 25.3 (CH$_2$ of THF), 68.5 (OCH$_2$ of THF). – ^{29}Si NMR (C_6D_6): δ = –181.5 [*Si*Li(SiMe$_3$)$_2$], –129.9 [*Si*(SiMe$_3$)$_3$], –33.5 (SiMe$_2$), –22.2 (SiMe$_2$), –9.4 [Si(*Si*Me$_3$)$_3$], –5.0 [SiLi(*Si*Me$_3$)$_2$].

***n*THF·LiSi(Me$_3$Si)$_2$Me$_2$SiMe$_2$Si(Me$_3$Si)$_2$SiLi·*n*THF (2):** Compound **1** (6.5 g, 8.5 mmol) in dry THF (30 mL) was placed in a Schlenk flask under vacuum, and 9 mL of a 1.4 M solution of CH_3Li in ether was added in 10 portions over 72 h (conversion was

followed by NMR spectroscopy). Removal of the solvent gave 4.7 g of **2**·*n*THF (60% yield). – ^{1}H NMR (C_6D_6): δ = 0.49 [s, 36 H, $SiLi(SiMe_3)_2$], 0.64 (s, 12 H, $SiMe_2$), 1.37 (m, 12 H, CH_2 of THF), 3.50 (m, 12 H, OCH_2 of THF). – ^{29}Si NMR (C_6D_6): δ = –187.6 [*Si*$Li(SiMe_3)_2$], –25.6 ($SiMe_2$), –4.3 [$SiLi(SiMe_3)_2$].

Trapping Reactions. – General Procedure: The trapping reagent (15 mmol) in 50 mL of toluene was added to a solution of **1** (10 mmol) or **2** (5 mmol) in 40 mL of toluene cooled to –78 °C. All operations were carried out under vacuum using Schlenk techniques. The reaction mixture was stirred at room temperature for 10 h. The pure products were isolated after filtration of the reaction mixture and evaporation of the solvent, in yields which generally exceeded 90%.

Reaction of 1 with $PhMe_2SiCl$. – $(Me_3Si)_3SiMe_2SiMe_2Si(Me_3Si)_2SiSiMe_2Ph$: ^{1}H NMR ($C_6D_6$): δ = 0.31 [s, 27 H, $Si(SiMe_3)_3$], 0.33 [s, 18 H, $Si(Si\mathit{Me}_3)_2SiMe_2Ph$], 0.40 [s, 6 H, $Si(SiMe_3)_2Si\mathit{Me}_2Ph$], 0.50 (s, 6 H, $SiMe_2$), 0.59 (s, 6 H, $SiMe_2$), 7.19 [m, 3 H, $Si(SiMe_3)_2SiMe_2\mathit{Ph}$], 7.56 [m, 2 H, $Si(SiMe_3)_2SiMe_2\mathit{Ph}$]. – ^{13}C NMR ($C_6D_6$): δ = 1.4 ($SiMe_2$), 1.7 ($SiMe_2$), 2.4 [$Si(SiMe_3)_2Si\mathit{Me}_2Ph$], 3.8 [$Si(SiMe_3)_3$], 3.9 [$Si(Si\mathit{Me}_3)_2SiMe_2Ph$], 127.9, 129.6, 133.3, 134.7 [$Si(SiMe_3)_2SiMe_2\mathit{Ph}$]. – ^{29}Si NMR ($C_6D_6$): δ = –127.3 [*Si*$(SiMe_3)_3$], –125.8 [*Si*$(SiMe_3)_2SiMe_2Ph$], –29.0 ($SiMe_2$), –28.8 ($SiMe_2$), –9.4 [$Si(\mathit{Si}Me_3)_3$], –9.0 [$Si(\mathit{Si}Me_3)_2SiMe_2Ph$], –2.1 [$Si(SiMe_3)_2\mathit{Si}Me_2Ph$]. – MS (CI); *m*/*z*: 674 [M^+ + 2], 657 [M^+ – Me], 595 [M^+ – Ph].

Reaction of 1 with tBuMe$_2$SiCl. – $(Me_3Si)_3SiMe_2SiMe_2Si(Me_3Si)_2SiSiMe_2tBu$: ^{1}H NMR ($C_6D_6$): δ = 0.28 [s, 6 H, $Si(SiMe_3)_2Si\mathit{Me}_2t$Bu], 0.34 [s,27 H, $Si(SiMe_3)_3$], 0.37 [s, 18 H, $Si(Si\mathit{Me}_3)_2SiMe_2t$Bu], 0.57 (s, 6 H, $SiMe_2$), 0.60 (s, 6 H, $SiMe_2$), 1.02 [m, 3 H, $Si(SiMe_3)_2SiMe_2t$Bu]. – ^{13}C NMR (C_6D_6): δ = 0.2 [$Si(SiMe_3)_2Si\mathit{Me}_2t$Bu], 2.0 ($SiMe_2$), 2.7 ($SiMe_2$), 3.9 [$Si(SiMe_3)_3$], 5.0 [$Si(Si\mathit{Me}_3)_2SiMe_2t$Bu], 19.1 [$Si(SiMe_3)_2SiMe_2C\mathit{CH}_3$], 28.6 [$Si(SiMe_3)_2SiMe_2\mathbf{C}CH_3$]. – ^{29}Si NMR ($C_6D_6$): δ = –127.7 [*Si*$(SiMe_3)_3$], –126.6 [*Si*$(SiMe_3)_2SiMe_2t$Bu], –29.3 ($SiMe_2$), –27.0 ($SiMe_2$), –9.4 [$Si(\mathit{Si}Me_3)_3$], –9.0 [$Si(\mathit{Si}Me_3)_2SiMe_2t$Bu], 5.7 [$Si(SiMe_3)_2\mathit{Si}Me_2t$Bu]. – MS (CI); *m*/*z*: 652 [M^+ + 2], 637 [M^+ + 2 – Me], 595 [M^+ + 2 – tBu].

Reaction of 1 with H_2O. – $(Me_3Si)_3SiMe_2SiMe_2Si(Me_3Si)_2SiH$ (9): ^{1}H NMR (C_6D_6): δ = 0.28 [s, 18 H, $Si(Si\mathit{Me}_3)_2H$], 0.32 [s, 27 H, $Si(SiMe_3)_3$], 0.45 (s, 6 H, $SiMe_2$), 0.46 (s, 6 H, $SiMe_2$), 2.7 [s, 1 H, $Si(SiMe_3)_2\mathit{H}$]. – MS (EI); *m*/*z*: 449 [M^+ – $HSi(SiMe_3)$], 375 [M^+ – $HSi(SiMe_3)_2$].

Reaction of 1 with $ClCH_2OCH_3$. – $(Me_3Si)_3SiMe_2SiMe_2Si(Me_3Si)_2SiCH_2OCH_3$: ^{1}H NMR ($C_6D_6$): δ = 0.32 [s, 18 H, $Si(Si\mathit{Me}_3)_2CH_2OCH_3$], 0.33 [s, 27 H, $Si(SiMe_3)_3$], 0.51 (s, 6 H, $SiMe_2$), 0.54 (s, 6 H, $SiMe_2$), 3.13 [s, 3 H, $Si(SiMe_3)_2CH_2O\mathit{CH}_3$], 3.48 [s, 2 H, $Si(SiMe_3)_2\mathit{CH}_2OCH_3$]. – ^{13}C NMR ($C_6D_6$): δ = –0.4 ($SiMe_2$), 0.9 ($SiMe_2$), 1.8 [$Si(Si\mathit{Me}_3)_2CH_2OCH_3$], 3.6 [$Si(SiMe_3)_3$], 62.9 [$Si(SiMe_3)_2\mathit{CH}_2OCH_3$], 63.1 [$Si(SiMe_3)_2CH_2O\mathit{CH}_3$]. – ^{29}Si NMR ($C_6D_6$): δ = –128.3 [*Si*$(SiMe_3)_3$], –76.2 [*Si*$(SiMe_3)_2CH_2OCH_3$], –32.8 ($SiMe_2$), –31.0 ($SiMe_2$), –11.7 [$Si(\mathit{Si}Me_3)_2CH_2OCH_3$], –9.5 [$Si(\mathit{Si}Me_3)_3$]. – MS (EI); *m*/*z*: 567 [M^+ – Me], 637 [M^+ – Si $SiMe_3)_3$].

Reaction of 2 with $PhMe_2SiCl$. – $PhMe_2SiSi(Me_3Si)_2Me_2SiMe_2Si(Me_3Si)_2SiSiMe_2Ph$: ^{1}H NMR ($C_6D_6$): δ = 0.29 [s, 36 H, $Si(Si\mathit{Me}_3)_2SiMe_2Ph$], 0.38 [s, 12 H, $Si(SiMe_3)_2Si\mathit{Me}_2Ph$)], 0.57 (s, 12 H, $SiMe_2$), 7.57 [m, 5 H, $Si(SiMe_3)_2SiMe_2\mathit{Ph}$]. – ^{13}C NMR ($C_6D_6$): δ = 1.5 ($SiMe_2$), 2.5 [$Si(SiMe_3)_2Si\mathit{Me}_2Ph$], 4.0 [$Si(Si\mathit{Me}_3)_2SiMe_2Ph$], 129.6, 134.7, 141.5 [$Si(SiMe_3)_2SiMe_2\mathit{Ph}$]. – ^{29}Si NMR ($C_6D_6$): δ = –126.2 [*Si*$(SiMe_3)_2SiMe_2Ph$], –28.6 ($SiMe_2$), –12.1 [$Si(SiMe_3)_2\mathit{Si}Me_2Ph$], –9.0 [$Si(\mathit{Si}Me_3)_2SiMe_2Ph$]. – MS (CI); *m*/*z*: 703 [M^+ – 2Me], 657 [M^+ – Ph].

Reaction of 2 with tBuMe$_2$SiCl. – $tBuMe_2SiSi(Me_3Si)_2Me_2SiMe_2Si(Me_3Si)_2SiSiMe_2tBu$: ^{1}H NMR ($C_6D_6$): δ = 0.27 [s, 12 H, $Si(SiMe_3)_2Si\mathit{Me}_2t$Bu], 0.31 [s, 36 H, $Si(SiMe_3)_2$], 0.63 (s, 12 H, $SiMe_2$), 1.03 [s, 18 H, $Si(SiMe_3)_2SiMe_2t$Bu].

Reaction of 2 with H_2O. – $HSi(Me_3Si)_2Me_2SiMe_2Si(Me_3Si)_2SiH$: ^{1}H NMR ($C_6D_6$): δ = 0.28 [s, 36 H, $Si(SiMe_3)_2$], 0.44 (s, 12 H, $SiMe_2$), 2.70 [s, 1 H, $Si(SiMe_3)_2H$].

Synthesis of 8. – 1. Synthesis of the Precursor $[(Me_3Si)_3SiMe_2Si-Me_2Si(Me_3Si)_2Si]_2Hg$ (10): (tBu)$_2$Hg (0.99 g, 3.15 mmol) and **9** (6.5 mmol) (see above) were heated under argon to 120 °C. The reaction mixture was stirred for 4 h, during which time 5.25 mmol of 2-methylpropane was formed. Evaporation of the volatile compounds and crystallization of the reaction mixture from pentane gave **10** (3.40 g, 85% yield). – ^{1}H NMR (C_6D_6): δ = 0.44 [s, 18 H, $Si(SiMe_3)_2$], 0.54 [s, 27 H, $Si(SiMe_3)_3$], 0.63 (s, 6 H, $SiMe_2$), 0.64 (s, 6 H, $SiMe_2$). – ^{13}C NMR (C_6D_6): δ = 3.6 [$Si(SiMe_3)_3$], 5.5 [$Si(SiMe_3)_2$], 25.8 ($SiMe_2$), 67.8 ($SiMe_2$). – ^{29}Si NMR (C_6D_6): δ = –128.9 [*Si*$(SiMe_3)_3$], –53.1 [*Si*$(SiMe_3)_2$], –33.0 ($SiMe_2$), –19.2 ($SiMe_2$), –9.4 [$Si(\mathit{Si}Me_3)_3$], –2.7 [$Si(\mathit{Si}Me_3)_2$].

2. Synthesis of $(Me_3Si)_3SiMe_2SiMe_2Si(Me_3Si)_2SiLi$ (8): A hexane solution of **10** (3.4 g, 2.67 mmol) was sonicated with an excess of Li. After Hg precipitation the solvent was separated from the metallic residue. Evaporation of hexane gave **8** (2.5 g, 85% yield). – ^{1}H NMR (C_6D_6): δ = 0.42 [s, 27 H, $Si(SiMe_3)_3$], 0.55 [s, 18 H, $SiLi(SiMe_3)_2$], 0.60 (s, 6 H, $SiMe_2$), 0.73 (s, 6 H, $SiMe_2$). – ^{13}C NMR (C_6D_6): δ = 1.4 ($SiMe_2$), 3.8 [$Si(SiMe_3)_3$], 6.5 ($SiMe_2$), 7.6 [$SiLi(SiMe_3)_2$]. – ^{29}Si NMR (C_6D_6): δ = –181.5 [*Si*$Li(SiMe_3)_2$], –129.9 [*Si*$(SiMe_3)_3$], –33.0 ($SiMe_2$), –22.6 ($SiMe_2$), –9.4 [$Si(\mathit{Si}Me_3)_3$], –5.0 [$SiLi(\mathit{Si}Me_3)_2$].

X-ray Crystallographic Study: Crystal data of **1**·3THF: $C_{19}H_{57}LiSi_9{\cdot}3C_4H_8O$, crystal dimensions 0.37 × 0.29 × 0.24 mm, measured on a Nicolet R3 diffractometer with Mo-K_α radiation at T = 128 K. Cell dimensions: a = 19.071(3), b = 15.113(2), c = 17.379(3) Å, V = 5009(1) Å^3, orthorhombic crystal system, Z = 4, $d_{calcd.}$ = 1.010 g·cm^{-3}, μ = 0.263 mm^{-1}, space group $Pca2_1$, data collection of 10872 intensities ($2\Theta_{max}$ = 50°), 8347 independent (R_{merg} = 0.0190), 7531 observed [$F_o > 4\sigma(F)$], structure solution with direct methods (Siemens-SHELXS) and refinement on F^2 (Siemens-SHELXTL 5.03) (397 parameters). The hydrogen atom positions were calculated and refined as rigid groups with the 1.2-fold (1.5 for methyl groups) U_{iso} values of the corresponding C atoms. The absolute structure was confirmed by refinement of the x parameter resulting in –0.27(13). $R1$ = 0.0460, $wR2$ (all data) = 0.1255, $w^{-1} = \sigma^2(F_o^2) + (0.0839\ P)^2 + 2.0556\ P$, where $P = [(\max F_o^2) + (2F_c^2)]/3$, GoF ($F^2$) = 1.04, maximum residual electron density 0.780 eÅ^{-3}. Crystallographic data (excluding structure factors) for the structure reported in this paper have been deposited with the Cambridge Crystallographic Data Centre as supplementary publication no. CCDC-1994140. Copies of the data can be obtained free of charge on application to CCDC, 12 Union Road, Cambridge CB2 1EZ, UK [Fax: (internat.) + 44-1223/336-033; E-mail: deposit@ccdc.cam.ac.uk].

Acknowledgments

This research was supported by the German-Israel Binational Foundation (GIF), by the Minerva Foundation and by the Fund for the Promotion of Research at the Technion. Y. Apeloig is grate-

ful to the Humboldt Foundation for a senior Research Award and to Professor H. Schwarz (TU Berlin) for his warm hospitality during his Humboldt tenure.

[1] [1a] J. Belzner, U. Dehner, in *The Chemistry of Organic Silicon Compounds*, part 2 (Ed.: Z. Rappoport, Y. Apeloig,), Wiley, New York **1998**, p. 779. – [1b] P. Lickiss, C. Smith, *Coord. Chem. Rev.* **1995**, *145*, 75. – [1c] K. Tomao, A. Kawachi, *Adv. Organomet. Chem*. **1995**, *38*, 1. – [1d] A. Sekiguchi, *Coord. Chem. Rev.*, in press.

[2] K. Sakamoto, K. Obata, H. Hirata, M. Nakajiama, H. Sakurai, *J. Am. Chem. Soc*. **1989**, *111,* 7641.

[3] A. Sekiguchi, M. Nanjo, C. Kabuto, H. Sakurai, *Organometallics* **1995**, *14*, 2630.

[4] H. Gilman,. C. L. Smith, *J. Organomet. Chem*. **1967**, *8*, 245.

[5] [5a] A. Heine, R. Herbest-Irmer, G. Sheldrick, D. Stalke, *Inorg. Chem*. **1993**, *32*, 2694. – [5b] H. Dias, M. Olmstead, K. Ruhlandt-Senge, P. Power, *J. Organomet. Chem.* **1993**, *462*, 1. – [5c] G. Becker, H. Hartmann, A. Münch, H. *Z.* Riffel, *Z. Anorg. Allg. Chem*. **1985**, *530*, 29.

[6] J. Frey, E. Schottland, Z. Rappoport, D. Bravo-Zhivotovskii, M. Nakash, M. Botoshansky, M. Kaftory, Y. Apeloig, *J. Chem. Soc., Perkin Trans. 2* **1994**, 2555.

[7] [7a] H. Bock, J. Meuret, K. Ruppert, *J. Organomet. Chem.* **1993**, *446*, 113. – [7b] H. Bock, J. Meuret, K. Ruppert, *Angew. Chem. Int. Ed. Engl.* **1993**, *32*, 414.

[8] A. Heine, D. Stalke, *Angew. Chem. Int. Ed. Engl.* **1993**, *32*, 121.

[9] [9a] M. Eisen, in *The Chemistry of Organic Silicon Compounds*, part 2 (Eds.: Z. Rappoport, Y. Apeloig), Wiley, New York, **1998**, p. 2037. – [9b] T. D. Tilley, in *The Chemistry of Organic Silicon Compounds* (Eds.: S. Patai, Z. Rappoport), Wiley, New York, **1989**, p. 1415.

[10] [10a] Y. Apeloig, M. Yuzefovich, M. Bendikov, D. Bravo-Zhivotovskii, *Organometallics* **1997**, *16*, 1265. – [10b] Y. Apeloig, M. Bendikov, M. Yuzefovich, M. Nakash, D. Bravo-Zhivotovskii, D. Blaser, R. Boese, *J. Am. Chem. Soc.* **1996**, *118*, 12228.

[11] [11a] A. Sekiguchi, M. Nanjo, C. Kabuto, H. Sakurai, *Angew. Chem. Int. Ed. Engl.* **1997**, *36*, 113. – [11b] C. Marshner, C. Mechtler, *Tetrahedron Lett.* **1999**, *40*, 7777.

[12] Reported in part in the *11th Int. Sym. on Organosilicon Chemistry* (Montpellier, France), **1996**, PA 55.

[13] S. Whittaker, M. Brun, F. Cervantes-Lee, K. Pannell, *J. Organomet. Chem.* **1995**, *499*, 247.

[14] [14a] Lambert et. al.[14b] have recently reported results identical to ours. – [14b] J. B. Lambert, H. Wu, *Organometallics* **1998**, *17*, 4904.

[15] The structures of the unsolvated dimeric $[Me(PhMe_2Si)_2SiLi]_2$ and $[Ph(Me_3Si)_2SiLi]_2$ were reported recently,[11a] but these compounds, being nonsolvated, have different structural characteristics from the solvated silyl lithium compounds and therefore they are not discussed here.

[16] D. Bravo-Zhivotovskii, Y. Apeloig et al., to be published.

[17] In the structural discussion we use the structure of **5**·3THF reported by Sheldrick et al.,[5a] who reported the structures of both pure **5**·3THF and of **5**·3THF cocrystallized with $Si(SiMe_3)_4$. The structural data of Power et al.[5b] is very similar to that reported by Sheldrick for **5**·3THF cocrystalized with $Si(SiMe_3)_4$ [5a] but the presence or absence of $Si(SiMe_3)_4$ was not mentioned.[5b] We therefore assumed that the most reliable data for pure **5**·3THF is that reported in ref.[5a]

[18] [18a] J. Belzner, U. Dehnert, D. Stalke, *Angew. Chem. Int. Ed. Engl*. **1994**, *33*, 2450. – [18b] W. Ando, T. Wakahara, T. Akasaka, S. Nagase, *Organometallics* **1994**, *13*, 4683. – [18c] G. Becker, H. Hartmann, E. Hengge, Z. Schrank, *Z. Anorg. Allg. Chem*. **1989**, *572*, 63. – [18d] H. Gilman, G. L. Schwebke, *J. Am. Chem. Soc*. **1963**, *85*, 1016. – [18e] H. Gilman, D. J. Peterson., A. W. Jarvie, H. S. Winkler, *J. Am. Chem. Soc*. **1956**, *82*, 2076.

Received November 18, 1999
[I99414]

(β-Octafluoro-*meso*-tetraarylporphyrin)manganese Complexes: Synthesis, Characterization and Catalytic Behaviour in Monooxygenation Reactions

Emmanuel Porhiel,[a] Arnaud Bondon,*[a] and Jacques Leroy[b]

Keywords: Fluorinated porphyrins / Electrochemistry / Manganese / Oxidation catalysis

The synthesis and characterization of manganese complexes of β-octafluoro-*meso*-tetraarylporphyrins are reported. The presence of the electron-withdrawing β-fluorine atoms induces a very large shift of the redox potential for the oxidation of the manganese(II) derivatives. With the *meso*-aryl group bearing two *ortho*-chlorine atoms (2,6-dichlorophenyl) or five fluorine atoms (pentafluorophenyl), metal complexation leads to the isolation of pure manganese(II) compounds. The stability and catalytic activity of these new derivatives have been studied using hydrogen peroxide and iodosylbenzene as oxidants, and standard substrates for epoxidation and hydroxylation reactions. The results are compared to those obtained with the β-hydrogenated analogs under the same conditions. In the case of hydrogen peroxide, the high level of porphyrin degradation prevents efficient catalytic activity. With iodosylbenzene as oxidant, both stability and epoxidation are similar to those of the β-hydrogenated porphyrins, however, a substantial improvement in the efficiency of the hydroxylation of cyclohexane is observed with up to 33 turnovers with (perfluorotetraphenylporphyrin)manganese(II).

Introduction

Metalloporphyrins have long been known to catalyze the oxidation of various substrates. These catalytic reactions can be performed with a large variety of oxygen donors such as iodosylbenzene (PhIO), peroxides (hydrogen or alkyl), hypochlorites, potassium peroxysulfate, *N*-oxides or molecular oxygen.[1–4] Although various metalloporphyrins have been shown to be catalytically efficient,[5] the most studied ones are those containing iron and manganese. Despite substantial progress towards the use of metalloporphyrins as catalysts to perform cytochrome-P450-like oxidative reactions, especially in the hydroxylation of alkanes, synthesis of new porphyrins with electron-withdrawing substituents is still a challenge. The objective is to prepare porphyrins characterized by very high redox potentials which should resist oxidative decomposition and exhibit a very high efficiency in oxidation catalysis. Three generations of metalloporphyrins have been successively studied: i) the unsubstituted core-planar tetraphenylporphyrin (TPP),[6–9] ii) the porphyrins bearing substituents on the *meso*-aryl groups[10–13] and iii) the porphyrins β-octahalogenated or β-substituted with other electron-withdrawing groups.[14–18] In the latter group, the chloro and the bromo derivatives have been extensively studied whereas the fluorinated compounds have only recently been reported.[19,20]

In a misleading paper published in 1989, the ferric "Teflon" porphyrin [2,3,7,8,12,13,17,18-octafluoro-5,10,15,20-tetrakis(pentafluorophenyl)porphyrin] was reported to be very stable and very efficient for epoxidation and hydroxylation with hydrogen peroxide.[21] Not only was the characterization of the β-fluorinated porphyrins shown to be erroneous,[19,20] but the purported catalytic activities have been invalidated.[22] With the exception of the hydroxylation of aromatic compounds involving the use of a large excess of the substrate anisole[23] or toluene,[24] β-octahalogenation of metalloporphyrins leads to catalysts relatively unstable towards hydrogen peroxide[22,25,26] or hypochlorites.[27] Nevertheless, a great improvement in catalytic activity occurs through β-octahalogenation of *meso*-tetrakis(2,6-dichlorophenyl)porphyrin when using $KHSO_5$,[15] PhIO[22,28] or molecular oxygen[17] as oxidants. Surprisingly, the β-octahalogenation of the *meso*-tetrakis(pentafluorophenyl)porphyrin does not improve the efficiency of the epoxidation or hydroxylation with PhIO,[22,28] but does so for the hydroxylation of alkanes with molecular oxygen.[17]

The origin of the increased activity associated with the presence of electron-withdrawing substituents at the β-pyrrolic position is mainly related to a large anodic shift in the first oxidation potential[20,29–39] and to distortion of the macrocycle.[33,40–42]

Our previous work has shown that the β-fluorination of porphyriniron complexes leads to an increased catalytic activity with regard to the hydroxylation of alkanes.[22] However, with H_2O_2, the expected higher stability of the porphyriniron derivatives was not observed.[22] In the present study, we have prepared and characterized the manganese complexes of 2,3,7,8,12,13,17,18-octafluoro-5,10,15,20-tetraphenylporphyrin (β-F_8TPP), 2,3,7,8,12,13,17,18-octafluoro-5,10,15,20-tetrakis(2,6-dichlorophenyl)porphyrin (β-F_8TDCPP) and 2,3,7,8,12,13,17,18-octafluoro-5,10,15,20-tetrakis(pentafluorophenyl)porphyrin (β-F_8TPFPP,

[a] Laboratoire de Chimie Organométallique et Biologique, UMR CNRS 6509, Université de Rennes 1, 35042 Rennes cedex, France
Fax: (internat.) + 33-2/99281646
E-mail: Arnaud.Bondon@univ-rennes1.fr
[b] Ecole Normale Supérieure, Département de Chimie, UMR CNRS 8640, 24 rue Lhomond, 75231 Paris cedex 05, France

 © WILEY-VCH Verlag GmbH, D-69451 Weinheim, 2000 1434–1948/00/0505–1097 $ 17.50+.50/0

also called perfluorotetraphenylporphyrin). Their stability in the presence of PhIO and H_2O_2 has been measured, as well as their catalytic behaviour in the epoxidation of cyclooctene and the hydroxylation of cyclohexane.

Results

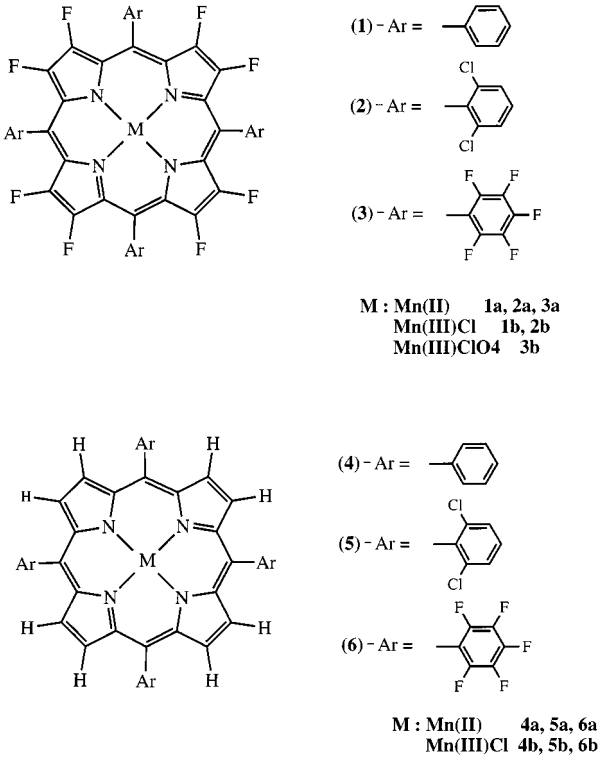
Synthesis of Metalloporphyrins

Preparation of the (β-octafluoro-*meso*-tetraarylporphyrin)manganese complexes (Scheme 1) was carried out under standard conditions,[43] from free-base porphyrins using a ten-fold excess of $Mn(OAc)_2{\cdot}4H_2O$ in DMF under an inert gas. Metallation was achieved after refluxing for a few minutes. Pure Mn^{II}(β-F_8TPP) complex (**1a**) could be obtained if the reaction was performed under anaerobic conditions, whereas pure manganese(II) complexes were always isolated, even after refluxing for several hours, under aerobic conditions, with the β-F_8TDCPP and β-F_8TPFPP porphyrins. These complexes, (β-F_8TDCPP)Mn^{II} (**2a**) and (β-F_8TPFPP)Mn^{II} (**3a**), obtained in high yield (>90%) after purification by column chromatography, are perfectly stable in air. In contrast, the complex (β-F_8TPP)Mn^{II} (**1a**) must be stored as an acetonitrile solution because slow oxidation occurs in air even in the solid state. A second step to prepare the manganese(III) derivatives is necessary, the protocol depending on the nature of the aryl groups. The complex (β-F_8TPP)Mn^{III}Cl (**1b**) was obtained from **1a** by autooxidation during column chromatography on silica gel. The compound (β-F_8TDCPP)Mn^{III}Cl (**2b**) can be prepared from **2a** by oxidation with iron perchlorate or ferricinium salt in dichloromethane solution. Attempts to isolate pure (β-F_8TPFPP)Mn^{III}Cl were unsuccessful because the manganese(III) complex is readily reduced to the Mn^{II} complex **3a**, but the perchloratomanganese(III) complex **3b** could be obtained in dichloromethane by addition of solid iron perchlorate.

Characterization of Metalloporphyrins

UV/Visible Spectroscopy

The electronic absorption spectra of the β-fluorinated manganese complexes in $CHCl_3$ are summarized in Table 1. The manganese(II) complexes display a hypsochromic shift of 13–16 nm compared to the β-hydrogenated analogs. The Soret bands of both (β-F_8TPP)Mn (**1a**) or (β-F_8TPFPP)Mn (**3a**) are found at 419 nm and that of the complex (β-F_8TDCPP)Mn (**2a**) at 422 nm. As for the β-hydrogenated analogs, two Q bands (551 and 588 nm) are observed for complex **1a** and only one near 550 nm for complexes **2a** and **3a**. The corresponding manganese(III) derivatives exhibit a Soret absorption at 474 nm for **1b** and **2b**, with a blue shift of only 3–4 nm as compared to **4b** and **5b**, respectively. However, the (perfluorotetraphenyl)porphyrin complex **3b** displays a shift of 14 nm (Soret band at 458 nm) relative to the hydrogenated complex **6b**.



Scheme 1. Structure and labels of porphyrinmanganese compounds

Table 1. UV/Vis data of various β-fluoroporphyrinmanganese complexes and other analogs [λ_{max} (nm)]

Compound	Soret band		Q bands			
(β-F_8TPP)Mn^{II} (**1a**)			419	549	586	
(β-F_8TDCPP)Mn^{II} (**2a**)			422	551	585	
(β-F_8TPFPP)Mn^{II} (**3a**)			546			
(TPP)Mn^{II} (**4a**)[a]			435	564	601	
(TDCPP)Mn^{II} (**5a**)[b]			435	567		
(TPFPP)Mn^{II} (**6a**)			432	561		
(β-F_8TPP)Mn^{III}Cl (**1b**)	365		474	519	572	607
(β-F_8TDCPP)Mn^{III}Cl (**2b**)	363		474		571	605
(β-F_8TPFPP)$Mn^{III}ClO_4$ (**3b**)	367		458		550	
(TPP)Mn^{III}Cl (**4b**)	375	401[c]	478	526	581	617
(TDCPP)Mn^{III}Cl (**5b**)	371	391[c]	477		579	606
(TPFPP)Mn^{III}Cl (**6b**)	365	395[c]	477		576	605

[a] From ref.[67]. – [b] From ref.[45]. – [c] Shoulder.

Electrochemistry

The redox potential data for the manganese compounds were obtained by cyclic voltammetry in dichloromethane containing 0.1 M Bu_4NPF_6 as supporting electrolyte. Results are referenced to the SCE and summarized in Table 2. All complexes undergo a reversible Mn^{II}/Mn^{III} process with $E^{1/2}$ ranging from –0.34 V for **4** to 0.70 V for **3**. Similar values have already been reported for the hydrogenated complexes **4**–**6**.[24,44,45] The potentials of the β-fluorinated porphyrinmanganese complexes are significantly higher than those of their hydrogenated analogs. The most important anodic shift is +0.82 V for (β-F_8TPFPP)Mn (**3**), compared to (TPFPP)Mn (**6**). Smaller shifts are observed be-

Table 2. Electrochemical data for porphyrinmanganese complexes (V vs. SCE)

Porphyrin complexes[a]	Ring oxidation		Mn^{II}/Mn^{III}	Ring reduction	
(β-F_8TPP)Mn (**1**)	n. o.[b]	1.51	0.16	–1.28	–1.53[c]
(β-F_8TDCPP)Mn (**2**)	n. o.	n. o.	0.30	–1.14	–1.40
(β-F_8TPFPP)Mn (**3**)	n. o.	n. o.	0.70	–0.64	–1.08
(TPP)Mn (**4**)[d]	1.53	1.09	–0.34	–1.58	n. o.
(TDCPP)Mn (**5**)[d]	n. o.	1.43	–0.28	–1.34	–1.50[c]
(TPFPP)Mn (**6**)[d]	n. o.	1.41[c]	–0.12	–1.26	–1.55

[a] Cyclic voltammetry conditions: in CH_2Cl_2 containing 1 mM porphyrinmanganese complexes and 0.1 M Bu_4NPF_6; scan rate, 50 $mV \cdot s^{-1}$. – [b] Not observed. – [c] Irreversible process, E^{ox}_p or E^{red}_p. – [d] These metalloporphyrins have been previously studied with different solvents: **4**,[44] **5**[45] and **6**.[24]

tween **2** and **5** (+0.58 V) and between **1** and **4** (+0.5 V). Furthermore, the amplitude of the redox potential values, which follows the order **1** < **2** < **3**, is larger than that of the hydrogenated complexes, which follows the order **4** < **5** < **6**. With the exception of the complex **1**, which shows a second oxidation wave at 1.51 V, there are no accessible oxidation waves, up to 1.8 V, for the complexes **2** and **3**. Two reversible reductions are often observed with manganese complexes.[46] The presence of the eight fluorine atoms induces small shifts at lower potentials for the complexes **1** and **2**, whereas a much larger influence is observed in the case of **3** with differences of 0.62 V and 0.47 V for the first and the second reduction waves, respectively.

Nuclear Magnetic Resonance

The fluorine chemical shifts of the new β-fluorinated porphyrinmanganese complexes are reported in the Experimental Section. To the best of our knowledge, only one report has been dedicated to fluorine-NMR study of (pentafluorophenyl)porphyrin derivatives complexed by zinc, iron or ruthenium.[47] With the paramagnetic manganese complexes, the resonances of the β-fluorine atoms are broadened beyond detection in the case of manganese(II) derivatives, whereas for the manganese(III) complexes broad signals are detected at δ = –4.9, –4.2 and –2.8 for complexes **1b**, **2b** and **3b**, respectively. The chemical shifts seem to correlate with the redox potential for the reduction of the manganese complexes [δ (ppm) = –5.44 + 3.8 $E^{1/2}$ (V); correlation coefficient: 0.993], but additional compounds would be needed to confirm this relationship.

Oxidation with Iodosylbenzene

Stability in the Absence of Substrate

The robustness of porphyrinmanganese complexes towards PhIO as oxidant has been studied at room temperature under aerobic conditions, both in the absence and presence of a co-catalyst such as 1-methylimidazole or ammonium acetate, and in the absence of substrate. The ratio catalyst/oxidant/co-catalyst employed was 1:100:10. An excess of cyclooctene was added to the cuvette prior to measurement to convert high-valent manganese species into Mn^{III} derivatives, allowing us to estimate the decrease of the Soret band of the Mn^{III} complexes (Table 3). Addition of cyclooctene was necessary since manganese complexes react with iodosylbenzene to generate, in the absence of substrate, (porphyrin)Mn^{IV} complexes.[48,49] A dimeric complex [(PhIO)TPPMn^{IV}Cl]$_2$O has been characterized by a broad Soret band at 421 nm in chlorobenzene.[48] Under similar conditions, but in dichloromethane, a Soret band was observed at 426 nm for the new complexes obtained from **4b** and **5b**, and at 417 nm from **6b**. With the β-fluorinated porphyrinmanganese complexes, the addition of PhIO to **1**(**a** or **b**), **2**(**a** or **b**) and **3a** produces new intermediates, characterized by Soret bands at 412, 410 and 404 nm, respectively, irrespective of the oxidation state of the starting complexes Mn^{II} or Mn^{III} (Table 4). Once again, β-fluorination leads to a blue-shift of 13–16 nm when compared with the β-hydrogenated analogs.

The results obtained show that with 1-methylimidazole or without co-catalyst, the β-fluorinated porphyrinmanganese(II) or -manganese(III) complexes show a similar robustness comparable with the β-hydrogenated analogs. It must be emphasized that the sterically protected porphyrins **2a**, **2b** and **5b** are very stable (loss <5%) even under the drastic conditions employed. On the other hand, the decomposition of complexes **3a** and **6b** is around 50%. In the absence of co-catalyst, complexes **1a**, **1b** and **4b** are quite stable, exhibiting only a 15 to 19% decrease in the intensity of Soret band. With a co-catalyst this decrease is ca. 55%. The stability depends on the nature of the aryl groups and increases in the order $C_6H_5 < C_6F_5 < C_6H_3Cl_2$, which applies both for the β-hydrogenated and the β-fluorinated porphyrins. With ammonium acetate as co-catalyst the stabilities of the catalysts were close to those observed with imidazole. However, with this co-catalyst, the reaction of PhIO with **2a**,**b** and **3a** leads to new complexes characterized by Soret peaks at 407 and 401 nm, respectively. These species still remain after addition of cyclooctene and have not been further characterized.

Epoxidation

The catalytic activity of the porphyrinmanganese complexes in cyclooctene epoxidation has been evaluated using unusually drastic catalytic conditions with a cyclooctene/PhIO/co-catalyst/catalyst ratio of 100:100:10:1 (Table 5). Thus, the epoxide yields, calculated relative to the substrate and the oxidant, which are in equal amounts, correspond directly to the turnover numbers.

Table 3. Stability of various porphyrinmanganese complexes towards PhIO

Catalyst	Decrease in Soret absorbance (%)[a]		Catalyst
(β-F_8TPP)Mn (**1a** or **1b**)[b]	55 (15)[c]	56 (19)[c]	(TPP)Mn^{III}Cl (**4b**)
(β-F_8TDCPP)Mn (**2a** or **2b**)[b]	5 (0)[c]	3 (0)[c]	(TDCPP)Mn^{III}Cl (**5b**)
(β-F_8TPFPP)Mn^{II} (**3a**)	48 (47)[c]	53 (51)[c]	(TPFPP)Mn^{III}Cl (**6b**)

[a] Porphyrin complexes were dissolved in dichloromethane (2 mM) with 1-methylimidazole (10 equiv.) and PhIO (100 equiv.) was added at 25 °C. After 15 min, 20 μL of cyclooctene was added in the cuvette and UV/Vis measurement was performed. – [b] Reduced and oxidized manganese complexes give identical values. – [c] In parentheses, same experiment without co-catalyst.

Table 4. UV/Vis data of the porphyrinmanganese complexes obtained after addition of iodosylbenzene [λ_{max} (nm), at 25 °C in CH_2Cl_2]

Intermediate	From	Soret band		Intermediate	From
"(β-F_8TPP)Mn^{IV}"	**1a** or **1b**	412	426 (421)[a]	"(TPP)Mn^{IV}"	**4b**
"(β-F_8TDCPP)Mn^{IV}"	**2a** or **2b**	410	426	"(TDCPP)Mn^{IV}"	**5b**
"(β-F_8TPFPP)Mn^{IV}"	**3a**	404	417	"(TPFPP)Mn^{IV}"	**6b**

[a] From ref.[48] in chlorobenzene.

Table 5. Cyclooctene epoxidation by PhIO catalyzed by porphyrinmanganese complexes

Catalyst	Epoxide yield (%)[a] Cyclooctene/PhIO		Catalyst
(β-F_8TPP)Mn (**1a** or **1b**)[b]	43 (42)[c]	42 (43)[c]	(TPP)Mn^{III}Cl (**4b**)
(β-F_8TDCPP)Mn (**2a** or **2b**)[b]	73 (71)[c]	73 (74)[c]	(TDCPP)Mn^{III}Cl (**5b**)
(β-F_8TPFPP)Mn^{II} (**3a**)	63 (60)[c]	59 (60)[c]	(TPFPP)Mn^{III}Cl (**6b**)

[a] Cyclooctene/PhIO/1-MeIm/catalyst = 100:100:10:1 in CH_2Cl_2 (catalyst at 2 mM), at room temperature. Yields were determined by GC after 1 h and based on starting cyclooctene. – [b] Reduced and oxidized manganese complexes give identical values. – [c] In parentheses, $CH_3CO_2NH_4$ used as co-catalyst with same ratio.

With 1-methylimidazole or ammonium acetate as co-catalyst, the activities of β-fluorinated (porphyrin)Mn^{II} or -Mn^{III} catalysts are very similar. Surprisingly, the results are also comparable to those obtained with the β-hydrogenated analogs. The epoxide yield was found to be about 43% for catalysts **1a**,**b** or **4b** and 60% for **3a** or **6b**. The best yields, of ca. 73%, were observed with the protected manganese complexes **2a**,**b** and **5b**. Therefore the activity is dependant on the nature of the aryl groups and increases in the order $C_6H_5 < C_6F_5 < C_6H_3Cl_2$.

Hydroxylation

The hydroxylation of cyclohexane was chosen to evaluate the catalytic activity of the porphyrinmanganese complexes. We used the same ratio as for epoxidation, namely a cyclohexane/PhIO/co-catalyst/catalyst ratio equal to 100:100:10:1, and the results are reported in Table 6. Again, we noticed similar activities for both β-fluorinated Mn^{II} and Mn^{III} catalysts. However, in this case, the presence of β-fluorine atoms improves the cyclohexane hydroxylation. In particular, with 1-methylimidazole, a two-fold increase in yield was observed with the catalyst **2**, as compared with **5b**. The best hydroxylation yield is obtained with the (perfluorotetraphenyl)porphyrin complex **3a**, with a 33% yield of cyclohexanol in the presence of 1-methylimidazole as co-catalyst. The activity depends also on the nature of the aryl groups, increasing in the order: $C_6H_5 < C_6H_3Cl_2 < C_6F_5$, in contrast to that observed for epoxidation. Finally, the co-catalyst clearly has an effect on the yields, 1-methylimidazole being more effective than ammonium acetate.

Oxidation with Hydrogen Peroxide

Stability in the Absence of Substrate

The stability of the manganese porphyrins was studied with a H_2O_2/co-catalyst/porphyrin ratio of 100:10:1, under aerobic conditions at room temperature (Table 7). Usually, acetonitrile is used for diluting hydrogen peroxide, but in this solvent complexes **2a** and **3a** remain in the reduced state, even in the presence of H_2O_2. Coordination of acetonitrile prevents reaction with H_2O_2. Moreover, the addition of acetonitrile to a dichloromethane solution of complex **2b** induces its reduction to the Mn^{II} complex **2a**. Therefore, we used methanol as co-solvent to assess the stability and catalytic activities of complexes **2a** and **2b**. However, the most electron-deficient catalyst **3a** was found to be unreactive towards H_2O_2 in methanol.

The effect of the co-solvent on the reactivity of the porphyrin complexes **2a** and **2b** was shown to be crucial, but the nature of the co-solvent is also important when measuring the stability of the β-hydrogenated complexes **4–6**. The complex **6b** is stable with acetonitrile as co-solvent and partially decomposed in the presence of methanol, whereas complex **5b** shows the opposite behaviour. The introduction of fluorine at the β-position of (TPP)Mn seems to stabilize the complex in acetonitrile but not in methanol. Degrada-

Table 6. Cyclohexane hydroxylation by PhIO, catalyzed by porphyrinmanganese complexes

Catalyst	Cyclohexane/PhIO with $CH_3CO_2NH_4$	Product yield (%)[a] Cyclohexanol + -one	Cyclohexane/PhIO with 1-MeIm
(β-F_8TPP)Mn (**1a** or **1b**)[b]	–		8
(β-F_8TDCPP)Mn (**2a** or **2b**)[b]	8		20
(β-F_8TPFPP)Mn^{II} (**3a**)	12		33
(TPP)Mn^{III}Cl (**4b**)	–		4
(TDCPP)Mn^{III}Cl (**5b**)	5		9
(TPFPP)Mn^{III}Cl (**6b**)	9		26

[a] Cyclohexane/PhIO/co-catalyst/catalyst = 100:100:10:1 in CH_2Cl_2 (catalyst at 2 mM), at room temp. Yields were determinated by GC after 1 h and based on starting cyclohexane. – [b] Reduced and oxidized manganese complexes give identical values.

Table 7. Stability of various porphyrinmanganese complexes towards H_2O_2

Catalyst	Decrease in Soret absorbance (%)[a]				Catalyst
	CH_2Cl_2/CH_3CN	CH_2Cl_2/CH_3OH	CH_2Cl_2/CH_3CN	CH_2Cl_2/CH_3OH	
(β-F_8TPP)Mn^{II} (**1a**)	100	100			
(β-F_8TPP)Mn^{III}Cl (**1b**)	36	79	65	61	(TPP)Mn^{III}Cl (**4b**)
(β-F_8TDCPP)Mn^{II} (**2a**)	< 5[b]	52			
(β-F_8TDCPP)Mn^{III}Cl (**2b**)	< 5[c]	54	27	9	(TDCPP)Mn^{III}Cl (**5b**)
(β-F_8TPFPP)Mn^{II} (**3a**)	< 5[b]	< 5[b]			
			3	37	(TPFPP)Mn^{III}Cl (**6b**)

[a] H_2O_2 was added at once (100 equiv., 3% in CH_3CN or CH_3OH) to the porphyrinmanganese complex (2 mM) in CH_2Cl_2/CH_3CN (1:1) or CH_2Cl_2/CH_3OH (1:1) and the decrease was measured after 15 min at 25 °C. – [b] The complex remains as Mn^{II}. – [c] The complex is reduced to Mn^{II}.

tion of ca. 53% was measured for both Mn^{II} and Mn^{III} complexes **2a**, **2b**, much more important than that observed for the hydrogenated analog. Finally, the oxidized and reduced complexes **2a**, **2b** show the same decrease in intensity of the Soret band whereas the stability of complex **1** depends on the oxidation state. Bleaching of the reduced form **1a** is very rapid with both co-solvents even though the oxidized form **1b** decays more slowly and is sensitive to the nature of the co-solvent.9

Epoxidation and Hydroxylation

The olefin epoxidation activity of the porphyrinmanganese complexes was investigated by epoxidation of cyclooctene, with a cyclooctene/H_2O_2/$CH_3CO_2NH_4$/catalyst ratio of 100:200:10:1, in CH_2Cl_2/CH_3CN and CH_2Cl_2/CH_3OH mixtures (Table 8). As suggested by the stability test, the complex **3a** is inactive in these solvent mixtures. Both oxidation states of (β-F_8TDCPP)manganese complexes **2a** and **2b** are also inactive in acetonitrile. However, in methanol, a similar efficiency was observed for the two complexes. With a 15% yield of cyclooctene epoxide, these

Table 9. Oxidation in acetone by H_2O_2, catalyzed by (β-F_8TPFPP)Mn^{II} and (TPFPP)Mn^{III}Cl

Catalyst	Product yield (%)[a] Cyclooctene + H_2O_2 8 equiv. Epoxide	Cyclohexane + H_2O_2 8 equiv. ol + -one
(β-F_8TPFPP)Mn^{II} (**3a**)	32	9
(TPFPP)Mn^{III}Cl (**6b**)	44	4

[a] Substrate/H_2O_2/$CH_3CO_2NH_4$/catalyst = 100:800:10:1 (catalyst at 2 mM), at room temperature. H_2O_2 35% was added (2 molar equivalent relative to substrate) at 0, 10, 20 and 30 min. Mn(P), substrate and co-catalyst were dissolved in CH_2Cl_2/CH_3COCH_3 (80:20).

Table 8. Cyclooctene epoxidation by H_2O_2, catalyzed by porphyrinmanganese complexes

Catalyst	Epoxide yield (%)[a]				Catalyst
	CH_2Cl_2/CH_3CN	CH_2Cl_2/CH_3OH	CH_2Cl_2/CH_3CN	CH_2Cl_2/CH_3OH	
(β-F_8TPP)Mn^{II} (**1a**)	1	–			
(β-F_8TPP)Mn^{III}Cl (**1b**)	1	1	4	5	(TPP)Mn^{III}Cl (**4b**)
(β-F_8TDCPP)Mn^{II} (**2a**)	n. d.[b]	16			
(β-F_8TDCPP)Mn^{III}Cl (**2b**)	n. d.[b]	14	> 98	48	(TDCPP)Mn^{III}Cl (**5b**)
(β-F_8TPFPP)Mn^{II} (**3a**)	n. d.[b]	n. d.[b]	69	41	(TPFPP)Mn^{III}Cl (**6b**)

[a] Cyclooctene/H_2O_2/$CH_3CO_2NH_4$/catalyst = 100:200:10:1 (catalyst at 2 mM), at room temperature. Yields were determined by GC after 1 h and based on starting cyclooctene. Mn(P), substrate and co-catalyst were dissolved in CH_2Cl_2/CH_3CN or CH_3OH (1:1); concentrated aqueous H_2O_2 diluted to 3% in the indicated solvent, was added by 2 additions of 1 molar equivalent relative to cyclooctene, at 0 and 20 min. – [b] Not detected.

β-fluorinated porphyrinmanganese complexes were less efficient than the analog (TDCPP)MnCl (**5b**). The same applies for the complexes of β-F_8TPP, **1a** and **1b**, which exhibit poor activities that are even inferior to the hydrogen equivalent **4b**.

In order to gain some insight into the catalytic activities of (perfluorotetraphenylporphyrin)manganese, a co-solvent which permits oxidations with H_2O_2 was required. With acetone as co-solvent instead of acetonitrile or methanol, we found that the perfluorotetraphenylporphyrin complex **3a** reacts with hydrogen peroxide.[50] A decrease in the Soret absorption of the (β-F_8TPFPP)Mn band was observed by UV/Vis spectroscopy, but without appearance of the Mn^{III} band, presumably due to a rapid return to the reduced form. In this system, even in the presence of the substrate, part of the hydrogen peroxide was consumed and reduced to water by the continual oxidation of Mn^{II} to Mn^{III}, to the detriment of substrate oxidation. Consequently, the use of a larger amount of H_2O_2 (8 equivalents relative to the substrate) led to a yield of epoxide of 32% (Table 9).

Hydroxylation reactions were only performed with the perfluorotetraphenylporphyrin complex **3a** and its β-hydrogenated analog **6b** (Table 9) based on their reasonable yields obtained for epoxidation. The yields of hydroxylation with these two porphyrinmanganese complexes are low although a slight increase is observed through β-fluorination.

Discussion

In some cases, β-octachlorinated or β-octabrominated porphyrins display higher activities, especially in hydroxylation catalysis. However, due to the strong electron-withdrawing character of the fluorine atoms, recent calculations have predicted that β-octafluorination should exert an electronic effect significantly larger than that of β-octachlorination or β-octabromination.[51] Furthermore, the effect on the energy level of the HOMO should be even more pronounced because the core distortion induced by steric hindrance between the aryl groups and the β-chlorine or -bromine is absent with the smaller fluorine atoms. This saddle distortion is responsible for some destabilization of the HOMO, resulting in a decrease in the first oxidation potential.[33,39,52] In a sense, the erroneous paper by Tsuchiya and Seno[21] corresponded to the expected improvement in stability and efficiency in hydroxylation catalysis. We recently unambiguously demonstrated the erroneous character of these results using authentic iron complexes of β-octafluorinated porphyrins. On the other hand, an increase in the efficiency of the catalyst for alkane hydroxylation is associated with β-octafluorination.[22]

Synthesis and Characterization

Manganese complexation results in the formation of stable Mn^{II} derivatives. Oxidation of manganese is not observed for complexes **2** and **3**, even during prolonged reflux in air, in contrast with β-octachlorinated or β-octabrominated porphyrins,[15] but in agreement with electrochemical data. The presence of the β-fluorine atoms induces a blue-shift in the Mn^{II} and Mn^{III} UV/Vis spectra as compared to the hydrogenated compounds. The amplitude of these blue-shifts varies in the range 5–20 nm depending on the oxidation state of the metal and the aryl substituents. This range is very close to the observed variation for the free-base porphyrins[19,20] or iron complexes.[53] This result, consistent with the planar structure of the β-octafluorinated porphyrins,[20,54] contrasts with the strong red-shifts observed for other β-octahalogenated derivatives which are associated with a large macrocycle distortion. However, the crystallographic structure of the pentacoordinated (H_2O)β-F_8TPPZn complex shows a pronounced saddle shape,[19] which is more likely attributable to crystal packing. Also surprising, but possibly related to the same variations between the solution and the solid state, is the near-planar structure of the hexacoordinated zinc complex of the β-heptanitrotetraphenylporphyrin,[18] whereas strong red-shifts of the Soret band are observed for the β-(nitro)$_{1-7}$porphyrins.[18,28,30,38]

The data for one-electron redox potentials are also in agreement with the strong electron-withdrawing character of the fluorine atoms. β-Octafluorinated porphyrinmanganese(III) complexes are more easily reduced to manganese(II) complexes than the hydrogenated analogs. Redox potentials of 0.16 V and 0.30 V are found for the derivatives **1** and **2**, respectively, whereas complex **3** exhibits a value of 0.70 V which corresponds to the highest redox potential for a halogenated porphyrin. Only the (β-heptanitrotetraphenylporphyrin)manganese complex was reported to have a higher potential (0.94 V).[38] Similarly, positive shifts of the potentials are observed, but to a lesser extent, for the first and the second ring reduction. These data explain why the complexes are isolated as reduced manganese derivatives as well as their extreme stability of the reduced state. For example, the complexes **2** and **3** remain as Mn^{II} under reflux in air, whereas the (β-octabromotetramesitylporphyrin)Mn^{II} is converted into the Mn^{III} complex.[15]

Oxidation Reactions

Over the last few years, the main objective in the search for new metalloporphyrins as oxidation catalysts has been the preparation of very stable and efficient molecules. In accordance with this aim, we have performed all tests of stability and catalytic activity under severe conditions, with equimolar proportions of oxidant and substrate. The catalyst was used at 1% relative to the oxidant, even for the measures of stability. These conditions allowed us to obtain directly the turnover number without any protection by excess substrate. Consequently, most of our results correspond to relatively modest yields. Furthermore, analysis of the influence of the β-octafluorination required us to carry out the experiments on the nonfluorinated porphyrinmanganese complexes under the same conditions.

Iodosylbenzene

This oxidant is not a good one in terms of the environment, but has been extensively used in order to assess the

catalytic properties of metalloporphyrins. It has been used as oxygen donor with porphyrinmanganese complexes for some time.[8,9] Beside porphyrin modifications, an improvement is associated with the use of imidazole as co-catalyst, corresponding to an enhancement of the reaction rate.[55] In this study, we used 1-methylimidazole or ammonium acetate as co-catalysts, the latter known to be a good co-catalyst in oxidation reactions with hydrogen peroxide.[56]

The study of the stability of the new β-octafluorinated porphyrinmanganese derivatives towards iodosylbenzene, in the absence of substrate, gave unexpected results. The decrease in the intensity of the Soret band is the same for both the β-octafluorinated complexes **1–3** and the β-octahydrogenated analogs **4–6**. The amount of decomposition is also independent of the manganese oxidation state in the starting compounds, the reduced state being available in the complexes **1–3**. The addition of 1-methylimidazole as co-catalyst induces a difference in the case of the tetraphenyl derivatives **1** and **4** only, with a larger (or at least faster) decomposition of these catalysts. The extent of the decrease in intensity of the Soret band was measured after addition of cyclooctene because an intermediate was formed during the reaction of the manganese complexes with iodosylbenzene. These intermediates are converted into Mn^{III} by adding the substrate with concomitant formation of epoxide, characteristic of a higher oxidation state of manganese. Mn^{IV} complexes have been extensively studied,[1,48,49,57–60] and the formation of a dimeric (μ-oxo)porphyrinmanganese complex that contains one iodosylbenzene per manganese has been reported.[48] This product was characterized by a Soret band at 421 nm. Compared to the non-β-halogenated derivatives **4–6**, a blue-shift of the Soret bands of 13–16 nm is also observed for the β-fluorinated complexes **1–3**. This analogous result suggests the formation of Mn^{IV} derivatives.

As far as the epoxidation catalysis is concerned, the absence of any significant difference in the yields of epoxidation between the β-fluorinated and the β-hydrogenated complexes is surprising. The best systems contain *meso*-2,6-dichlorophenyl as the aryl group, independent of the substitution at the β-positions. According to the results of the stability study, the use of catalysts with reduced or oxidized manganese leads to a very similar outcome suggesting the same reactive intermediates. Finally, the use of co-catalysts increases the rate of the reactions as previously observed,[55] without any difference in the turnover numbers obtained with 1-methylimidazole or ammonium acetate.

In contrast to epoxidation, large variations in the yields of hydroxylation of cyclohexane are observed, depending on: i) the presence of β-fluorine atoms, ii) the absence or the nature of co-catalyst and iii) the nature of the aryl group of the tetraarylporphyrins. 1-Methylimidazole has been shown to be an efficient co-catalyst favoring a high-valent (oxo)Mn intermediate.[61] With this co-catalyst, conversion of cyclohexane lies in the range 5–25% for the β-hydrogenated complexes **4–6** and 8–33% for the β-fluorinated porphyrinmanganese complexes **1–3**. The increase in the turnover number is close to 100% for Ar = phenyl (**1** and **4**) and dichlorophenyl (**2** and **5**) and 30% for Ar = pentafluorophenyl (**3** and **6**), with up to 33 turnovers for the perfluorotetraphenylporphyrin catalyst. It should also be emphasized that, in contrast with the epoxidation reaction, the best yields are obtained with Ar = pentafluorophenyl (**3** and **6**) rather than Ar = dichlorophenyl (**2** and **5**). Similarly, the efficiency for the hydroxylation of linear alkane by PhIO by tetraarylporphyriniron complexes is larger for Ar = pentafluorophenyl than for Ar = dichlorophenyl.[62]

Hydrogen Peroxide

The conditions employed correspond to two bulk additions of equimolar hydrogen peroxide (relative to the substrate) rather than dropwise addition. We used ammonium acetate as co-catalyst which has been shown to be more efficient than imidazole and carboxylic acids.[56] However, the studies have been complicated by the high metal oxidation potentials of the β-fluoroporphyrin complexes, corresponding to a very easy reduction of the manganese. Acetonitrile, the most common solvent for homogeneous reaction with H_2O_2, binds and stabilizes Mn^{II} complexes. Even methanol is able to prevent the reaction of hydrogen peroxide with (perfluorotetraphenylporphyrin)manganese. For this last porphyrin derivative, we have found a way to perform catalytic studies using acetone as solvent.

Under the conditions employed, the main finding is the instability of the β-fluoroporphyrinmanganese complexes towards hydrogen peroxide. Similar results have already been reported for β-chloro- or β-bromoporphyrinmanganese complexes.[25,26] However, good yields of hydroxylation have been reported, but in the presence of very large excess of substrate and very small oxidant/catalyst ratios.[23,24] The large amount of decomposition of the β-fluoroporphyrins, previously encountered with the iron complexes, has been associated with the high reactivity of the β-fluorinated positions towards homolytic cleavage, or nucleophilic attack of H_2O_2.[22] We have observed that β-fluoroporphyrinzinc complexes exhibit good stability towards H_2O_2, while extensive protection of β-halogenated porphyrins can be achieved with the use of radical scavengers.[26] Overall, these data are more in favor of the homolytic cleavage of hydrogen peroxide.

Conclusion

Many factors are involved in the catalytic activity of metalloporphyrins. Among these are the reactivity of the oxometal intermediate, the steric protection due to the substituents on the aryl groups, the distortion of the macrocycle, the resistance towards oxidation of the porphyrin and also the nature of the co-catalyst, the oxidant and the effect of solvent. It is still difficult to rationalize why the *meso*-tetraarylmetalloporphyrins are so efficient when the aryl groups are 2,6-dichlorophenyl or pentafluorophenyl. However, the olefin requires a less reactive oxometal intermediate for epoxidation than alkane hydroxylation. In the for-

mer reaction, steric protection due to the chlorine atoms of the dichlorophenyl group could be considered an important factor in efficient epoxidation. With alkane hydroxylation, more electron-deficient metalloporphyrins are responsible for an increase in the reactivity of the oxometal species, which favors a higher yield in hydroxylation. This view is consistent with the very small differences in the results obtained with iodosylbenzene, associated with the β-fluorination of the porphyrin in epoxidation, whereas larger effects are observed in the hydroxylation of cyclohexane. With hydrogen peroxide, the high level of decomposition prevents any improvement in epoxidation from being detected, as was previously observed with iron β-chloro- or -bromoporphyrins[26] and β-fluoroporphyrins.[22] However, a small increase in hydroxylation is observed with the (perfluorotetraphenylporphyrin)manganese as compared to the β-hydrogenated analog.

In conclusion, these results, as well as those obtained with β-fluoroporphyriniron complexes,[22] show an improvement in the reactivity of the oxometal intermediate leading to better yields in reactions of hydroxylation.

Experimental Section

General: All solvents were distilled prior to use. Chemical reagents were obtained from commercial sources. PhIO was prepared according to a literature procedure.[63] – UV/Vis spectra were recorded with a Uvikon 941 spectrometer. – NMR spectra were recorded with a Bruker 200 DPX spectrometer in $CDCl_3$ (^1H: 200 MHz, ^{19}F: 188 MHz). – Cyclic voltammograms were measured with a PAR M 263, the $E^{1/2}$ values (V) are reported versus SCE. – FAB mass spectrometry was performed, at the CRMPO, with a ZabSepc TOF Micromass. – Gas chromatography analyses were performed with a GC 121 DFL Delsi instrument. – Analytical thin layer chromatography was performed on commercial aluminium sheets coated with silica gel 60 F_{254} (Merck).

General Complexation Procedure for β-Octafluoroporphyrins: The porphyrins were prepared as previously reported using the Lindsey procedure[64] by condensation of the desired aldehyde and 3,4-difluoropyrrole.[19,65,66] To a suspension of the porphyrin (10 mmol) in DMF (5 mL), under argon, $Mn(OAc)_2{\cdot}4H_2O$ (10 equiv.) was added, and then the mixture was heated to reflux.[43] The complexation was completed within 5 min and after cooling the solvent was removed under vacuum. The complexes **2a** and **3a** were dissolved in dichloromethane and the solutions were filtered through a short silica gel column and concentrated. The complex **1a** was dissolved in dichloromethane/*n*-hexane (1:1 in volume) and the solution filtered and concentrated. **1a** was stored in acetonitrile to prevent oxidation.

Oxidation of Mn^{II} Complexes to $Mn^{III}Cl$: The complex **1a** obtained after evaporation of DMF, was chromatographed on a silica gel column (CH_2Cl_2/CH_3OH, 90:10). The solvents were removed and the residue was dissolved in CH_2Cl_2, washed with 3 M HCl, dried with NaCl and concentrated to give the complex **1b**. An excess of solid $FeClO_4$ was added to the complex **2a** in dichloromethane, and the oxidation monitored by UV/Vis spectroscopy. After filtration, the solution was washed with 3 M HCl, dried with NaCl and concentrated to give the complex **2b**.

The complex **3b** was prepared in situ by addition of a small excess of iron perchlorate to **3a** in dichloromethane.

[2,3,7,8,12,13,17,18-Octafluoro-5,10,15,20-tetraphenylporphyrin]-manganese(II) (1a): MS (FAB HRMS); *m/z* (%): 811.0923 (100) [M^+]; calcd. for $C_{44}H_{20}F_8MnN_4$: 811.0941. – UV/Vis (CH_2Cl_2): λ_{max} (log ε) = 419 (5.08), 549 (3.95), 586 nm (3.87). – CV (CH_2Cl_2/Bu_4NPF_6): E = 1.51 V, 0.16 V, –1.28 V, –1.53 V.

[5,10,15,20-Tetrakis(2,6-dichlorophenyl)-2,3,7,8,12,13,17,18-octafluoroporphyrin]manganese(II) (2a): R_f: 0.78 (silica gel, dichloromethane, room temperature) – MS (FAB HRMS); *m/z* (%): 1082.7796 (100) [M^+]; calcd. for $C_{44}H_{12}{}^{35}Cl_8F_8MnN_4$: 1082.7823. – UV/Vis ($CHCl_3$): λ_{max} nm (log ε) = 422 (5.13), 551 (4.11), 585 (3.79). – CV (CH_2Cl_2/Bu_4NPF_6): E = 0.30 V, –1.14 V, –1.40 V.

[2,3,7,8,12,13,17,18-Octafluoro-5,10,15,20-tetrakis(pentafluorophenyl)porphyrin]manganese(II) (3a): R_f: 0.61 (silica gel, dichloromethane, room temperature). – MS (FAB HRMS); *m/z* (%): 1170.9057 (100) [M^+]; calcd. for $C_{44}F_{28}MnN_4$: 1170.9056. – UV/Vis ($CHCl_3$): λ_{max} (log ε) = 419 (5.24), 546 nm (4.28). – ^{19}F NMR ($CDCl_3/CD_3OD$, 80:20; δ in ppm referenced to $CFCl_3$): δ = –131.93 (br., 8 F, *o*-F), –148.38 (s, 4 F, *p*-F), –157.57 (s, 8 F, *m*-F). – CV (CH_2Cl_2/Bu_4NPF_6): E = 0.70 V, –0.64 V, –1.08 V.

[2,3,7,8,12,13,17,18-Octafluoro-5,10,15,20-tetraphenylporphyrin]-manganese(III) Chloride (1b): R_f: 0.25 (silica gel, dichloromethane/methanol 95:5, room temperature). – UV/Vis ($CHCl_3$): λ_{max} (log ε) = 365 (4.73), 474 (4.62), 572 (3.89), 607 nm (3.95). – ^{19}F NMR ($CDCl_3$): δ = –4.9 (br., 8 F, β-F).

[5,10,15,20-Tetrakis(2,6-dichlorophenyl)-2,3,7,8,12,13,17,18-octafluoroporphyrin]manganese(III) Chloride (2b): UV/Vis (CH_2Cl_2): λ_{max} (log ε) = 363 (4.89), 474 (4.72), 571 (4.03), 605 nm (3.89). – ^{19}F NMR ($CDCl_3$): δ = –4.2 (br., 8 F, β-F).

[2,3,7,8,12,13,17,18-Octafluoro-5,10,15,20-tetrakis(pentafluorophenyl)porphyrin]manganese(III) Perchlorate (3b): UV/Vis (CH_2Cl_2): λ_{max} (log ε) = 367 (4.83), 458 (4.82), 547 nm (4.05). – ^{19}F NMR ($CDCl_3/CD_3OD$, 80:20): δ = 2.8 (br., 8 F, β-F), –141.60 (br., 8 F, *o*-F), –149.73 (s, 4 F, *p*-F), –160.57 (s, 8 F, *m*-F).

Oxidation Procedure: All reactions were carried out, in duplicate, at room temperature, under aerobic conditions in a tube stirred by a Vortex.

Oxidation with Iodosylbenzene: To the desired porphyrinmanganese complex (0.4 μmol), substrate (cyclooctene or cyclohexane, 40 μmol), and co-catalyst (4 μmol when present), in 200 μL of CH_2Cl_2, PhIO (40 μmol, 8.8 mg) was added in a single aliquot. The reaction mixtures were analyzed by gas chromatography and UV/Vis at 20 min and 60 min by taking 10-μL aliquots.

Oxidation with Hydrogen Peroxide: To the desired porphyrinmanganese complex (0.4 μmol), substrate (cyclooctene or cyclohexane, 40 μmol), and $AcONH_4$ as co-catalyst (4 μmol) in 200 μL of CH_2Cl_2/CH_3OH or CH_2Cl_2/CH_3CN (1:1 in volume), two additions of 50 μL (one molar equivalent, relative to the substrate) of H_2O_2, diluted to 3% in CH_3OH or CH_3CN, were performed at 0 min and 20 min. The reaction mixtures were analyzed by gas chromatography at 20 min and 60 min by taking 10-μL aliquots.

Oxidation in Acetone with Hydrogen Peroxide: To the desired manganese porphyrin (0.4 μmol), substrate (cyclooctene or cyclohexane, 40 μmol), and $AcONH_4$ as co-catalyst (4 μmol) in 200 μL of CH_2Cl_2/CH_3COCH_3 (80:20), concentrated (35%) aqueous solution of H_2O_2 (5 μL, two equivalents relative to the substrate) was added

at 0, 10, 20 and 30 min. The reaction mixtures were analyzed by gas chromatography at 20 min and 60 min by taking 10-μL aliquots.

Acknowledgments

We thank Dr. B. Meunier for fruitful comments and Dr. P. de Oliveira for a careful reading of the manuscript and gratefully acknowledge the financial support of the Brittany Region as a grant to E. P.

[1] *Metalloporphyrins in Catalytic Oxidations* (Ed. R. A. Sheldon), Marcel Dekker, New York, **1994**.
[2] D. Mansuy, *Coord. Chem. Rev.* **1993**, *125*, 129–141.
[3] B. Meunier, *Chem. Rev.* **1992**, *92*, 1411–1456.
[4] M. J. Gunter, P. Turner, *Coord. Chem. Rev.* **1991**, *108*, 115–161.
[5] D. Mansuy, J. F. Bartoli, J. C. Chottard, M. Lange, *Angew. Chem. Int. Ed. Engl.* **1980**, *19*, 909–910.
[6] J. T. Groves, T. E. Nemo, R. S. Myers, *J. Am. Chem. Soc.* **1979**, *101*, 1032–1033.
[7] C. K. Chang, M. S. Kuo, *J. Am. Chem. Soc.* **1979**, *101*, 3413–3415.
[8] C. L. Hill, B. C. Schardt, *J. Am. Chem. Soc.* **1980**, *102*, 6374–6375.
[9] J. T. Groves, W. J. Kruper, R. C. Haushalter, *J. Am. Chem. Soc.* **1980**, *102*, 6375–6377.
[10] C. K. Chang, F. Ebina, *J. Chem. Soc., Chem. Commun.* **1981**, 778–779.
[11] J. T. Groves, R. C. Haushalter, M. Nakamura, T. E. Nemo, B. J. Evans, *J. Am. Chem. Soc.* **1981**, *103*, 2884–2886.
[12] P. S. Traylor, D. Dolphin, T. G. Traylor, *J. Chem. Soc., Chem. Commun.* **1984**, 279–280.
[13] B. R. Cook, T. J. Reinert, K. S. Suslick, *J. Am. Chem. Soc.* **1986**, *108*, 7281–7286.
[14] T. G. Traylor, S. Tsuchiya, *Inorg. Chem.* **1987**, *26*, 1338–1339.
[15] P. Hoffman, A. Robert, B. Meunier, *Bull. Soc. Chim. Fr.* **1992**, *129*, 85–97.
[16] T. Wijesekera, A. Matsumoto, D. Dolphin, D. Lexa, *Angew. Chem. Int. Ed. Engl.* **1990**, *29*, 1028–1030.
[17] J. E. Lyons, P. E. Ellis, H. K. Myers, *J. Catal.* **1995**, *155*, 59–73.
[18] K. Ozette, P. Leduc, M. Palacio, J. F. Bartoli, K. M. Barkigia, J. Fajer, P. Battioni, D. Mansuy, *J. Am. Chem. Soc.* **1997**, *119*, 6442–6443.
[19] J. Leroy, A. Bondon, L. Toupet, C. Rolando, *Chem. Eur. J.* **1997**, *3*, 1890–1893.
[20] E. K. Woller, S. G. DiMagno, *J. Org. Chem.* **1997**, *62*, 1588–1593.
[21] S. Tsuchiya, M. Seno, *Chem. Lett.* **1989**, 263–264.
[22] E. Porhiel, A. Bondon, J. Leroy, *Tetrahedron Lett.* **1998**, *39*, 4829–4830.
[23] M. N. Carrier, C. Scheer, P. Gouvine, J. F. Bartoli, P. Battioni, D. Mansuy, *Tetrahedron Lett.* **1990**, *31*, 6645–6648.
[24] K. Iida, M. Nango, K. Okada, S. Matsumoto, M. Matsuura, K. Yamashita, K. Tsuda, Y. Kurono, Y. Kimura, *Chem. Lett.* **1994**, 1307–1310.
[25] P. Hoffman, G. Labat, A. Robert, B. Meunier, *Tetrahedron Lett.* **1990**, *31*, 1991–1994.
[26] A. M. d. A. Rocha Gonsalves, R. A. W. Johnstone, M. M. Pereira, J. Shaw, A. J. F. Sobral, *Tetrahedron Lett.* **1991**, *32*, 1355–1358.
[27] A. M. d. A. Rocha Gonsalves, M. M. Pereira, A. C. Serra, R. A. W. Johnstone, M. L. P. G. Nunes, *J. Chem. Soc., Perkin Trans. 1* **1994**, 2053–2057.
[28] J. F. Bartoli, P. Battioni, W. R. De Foor, D. Mansuy, *J. Chem. Soc., Chem. Commun.* **1994**, 23–24.
[29] A. Giraudeau, H. J. Callot, M. Gross, *Inorg. Chem.* **1979**, *18*, 201–206.
[30] A. Giraudeau, H. J. Callot, J. Jordan, I. Ezhar, M. Gross, *J. Am. Chem. Soc.* **1979**, *101*, 3857–3862.
[31] P. Bhyrappa, V. Krishnan, *Inorg. Chem.* **1991**, *30*, 239–245.
[32] K. M. Kadish, F. D'Souza, A. Villard, M. Autret, E. Van Caemelbecke, P. Bianco, A. Antonini, P. Tagliatesta, *Inorg. Chem.* **1994**, *33*, 5169–5170.
[33] P. Ochsenbein, K. Ayougou, D. Mandon, J. Fischer, R. Weiss, R. N. Austin, K. Jayaraj, A. Gold, J. Terner, J. Fajer, *Angew. Chem. Int. Ed. Engl.* **1994**, *33*, 348–350.
[34] J. A. Hodge, M. G. Hill, H. B. Gray, *Inorg. Chem.* **1995**, *34*, 809–812.
[35] P. Tagliatesta, J. Li, M. Autret, E. Van Caemelbecke, A. Villard, F. D'Souza, K. M. Kadish, *Inorg. Chem.* **1996**, *35*, 5570–5576.
[36] M. Autret, Z. Ou, A. Antonini, T. Boschi, P. Tagliatesta, K. M. Kadish, *J. Chem. Soc., Dalton Trans.* **1996**, 2793–2797.
[37] G. Hariprasad, S. Dahal, B. G. Maiya, *J. Chem. Soc., Dalton Trans.* **1996**, 3429–3436.
[38] K. Ozette, P. Battioni, P. Leduc, J. F. Bartoli, D. Mansuy, *Inorg. Chim. Acta* **1998**, *272*, 4–6.
[39] F. D'Souza, M. E. Zandler, P. Tagliatesta, Z. Ou, J. Shao, E. Van Caemelbecke, K. M. Kadish, *Inorg. Chem.* **1998**, *37*, 4567–4572.
[40] D. Mandon, P. Ochsenbein, J. Fischer, R. Weiss, K. Jayaraj, R. N. Austin, A. Gold, P. S. White, O. Brigaud, P. Battioni, D. Mansuy, *Inorg. Chem.* **1992**, *31*, 2044–2049.
[41] L. M. Henling, W. P. Schaefer, J. A. Hodge, M. E. Hughes, H. B. Gray, J. E. Lyons, P. E. Ellis, *Acta Crystallogr.* **1993**, *C49*, 1743–1747.
[42] W. P. Schaefer, J. A. Hodge, M. E. Hughes, H. B. Gray, J. E. Lyons, P. E. Ellis, R. W. Wagner, *Acta Crystallogr.* **1993**, *C49*, 1342–1345.
[43] A. D. Adler, F. R. Longo, F. Kampas, J. Kim, *J. Inorg. Nucl. Chem.* **1970**, *32*, 2443–2445.
[44] S. L. Kelly, K. M. Kadish, *Inorg. Chem.* **1982**, *21*, 3631–3639.
[45] S. Jeon, H. K. Lee, Y. K. Choi, *Bull. Korean Chem. Soc.* **1996**, *17*, 929.
[46] L. J. Boucher, *Coord. Chem. Rev.* **1972**, *7*, 289–329.
[47] E. R. Birnbaum, J. A. Hodge, M. W. Grinstaff, W. P. Schaefer, L. Henling, J. A. Labinger, J. E. Bercaw, H. B. Gray, *Inorg. Chem.* **1995**, *34*, 3625–3632.
[48] J. A. Smegal, B. C. Schardt, C. L. Hill, *J. Am. Chem. Soc.* **1983**, *105*, 3510–3515.
[49] J. A. Smegal, C. L. Hill, *J. Am. Chem. Soc.* **1983**, *105*, 2920–2922.
[50] Preliminary study has shown that *t*BuOOH reacts with the perfluorotetraphenylporphyrin, even in the presence of acetonitrile. This result may suggest the reaction of acetone with hydrogen peroxide giving a transient alkyl hydroperoxide which is able to react with **3a**, in contrast with hydrogen peroxide.
[51] A. Ghosh, *J. Am. Chem. Soc.* **1995**, *117*, 4691–4699.
[52] K. M. Barkigia, L. Chantranupong, K. M. Smith, J. Fajer, *J. Am. Chem. Soc.* **1988**, *110*, 7566–7567.
[53] E. Porhiel, A. Bondon, J. Leroy, unpublished results.
[54] J. Leroy, A. Bondon, L. Toupet, *Acta Crystallogr.* **1999**, *C55*, 464–466.
[55] E. Guilmet, B. Meunier, *Nouv. J. Chim.* **1982**, *6*, 511–513.
[56] A. Thellend, P. Battioni, D. Mansuy, *J. Chem. Soc., Chem. Commun.* **1994**, 1035–1036.
[57] J. A. Smegal, C. L. Hill, *J. Am. Chem. Soc.* **1983**, *105*, 3515–3521.
[58] J. T. Groves, M. K. Stern, *J. Am. Chem. Soc.* **1987**, *109*, 3812–3814.
[59] J. T. Groves, M. K. Stern, *J. Am. Chem. Soc.* **1988**, *110*, 8628–8638.
[60] R. D. Arasasingham, G. X. He, T. C. Bruice, *J. Am. Chem. Soc.* **1993**, *115*, 7985–7991.
[61] P. Battioni, J. P. Renaud, J. F. Bartoli, M. Reina-Ariles, M. Fort, D. Mansuy, *J. Am. Chem. Soc.* **1988**, *110*, 8462–8470.
[62] J. F. Bartoli, O. Brigaud, P. Battioni, D. Mansuy, *J. Chem. Soc., Chem. Commun.* **1991**, 440–442.
[63] H. Saltzman, J. G. Sharefkin, *Org. Synth.* **1973**, *3*, 658–659.
[64] J. S. Lindsey, R. W. Wagner, *J. Org. Chem.* **1989**, *54*, 828–836.
[65] J. Leroy, C. Wakselman, *Tetrahedron Lett.* **1994**, *35*, 8605–8608.
[66] E. K. Woller, V. V. Smirnov, S. G. DiMagno, *J. Org. Chem.* **1998**, *63*, 5706–5707.
[67] R. D. Jones, D. A. Summerville, F. Basolo, *J. Am. Chem. Soc.* **1978**, *100*, 4416–4424.

Received November 12, 1999
[I99417]

Metal-Catalyzed Oxidations, 10[‡]

New Insights into the Mechanism of Hydroperoxide Activation by Investigation of Dynamic Processes in the Coordination Sphere of Seven-Coordinated Molybdenum Peroxo Complexes

Angelika Hroch,[a] Gerd Gemmecker,[a] and Werner R. Thiel*[b]

Dedicated to Prof. O. Nuyken on the occasion of his 60th birthday

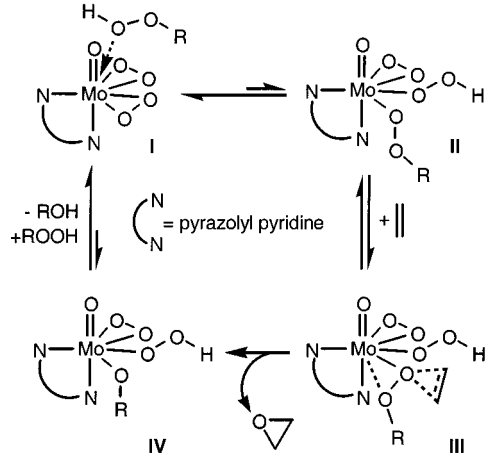
Keywords: Catalysis / Densitiy functional theory / Epoxidation / Reaction mechanisms

Seven-coordinated molybdenum oxobisperoxo complexes with chelate nitrogen donors like pyrazolylpyridines are catalysts for the epoxidation of olefins. An NMR spectroscopic and quantumchemical study on the fluxionality of the chelate ligand proves that during this process partial ligand dissociation takes place. This gave rise to a detailed theoretical study on the activation of CH_3OOH at the model complex $(NH_3)_2MoO(O_2)_2$ including dissociation of one of the ammonia ligands and proton transfer from the hydroperoxide to one of the peroxo ligands.

Introduction

During the last decades, a series of mechanistic studies on the olefin epoxidation with hydroperoxides catalyzed by high-valent transition metal complexes was carried out to get a deeper insight into the elementary steps of the activation of the oxidising agent,[2–5] but also to understand the transfer of chirality in the synthetically important enantio- and diastereoselective epoxidation of allylic alcohols.[6] As a result of these investigations, it is more and more accepted that the activation of alkyl hydroperoxides (ROOH) is performed by an intermediate η^2-coordination of the peroxidic agent to the Lewis acidic metal centre.[7–12] This is considered to be an "umpolung" of the electron rich alkyl peroxide allowing an electrophilic attack to the olefin. The intermediate alkyl peroxo complexes are usually generated by ligand exchange from suitable precursor complexes, but some transition metal alkyl peroxo complexes have been isolated[13–21] and a few exhibiting η^2-coordination of ROOH have been structurally characterised.[9,10,22] An analogous sequence may be postulated when hydrogen peroxide is used as the oxidising agent, but the final prove of a M–OOH structural motive is still lacking.

We investigated the mechanism of the olefin epoxidation with seven-coordinated molybdenum peroxo complexes of the type $MoO(O_2)_2(L–L)$ (L–L = pyrazolylpyridine ligand) during the last years[23–28] and were able to show that these complexes do not transfer oxygen from one of the η^2-O_2 ligands to the olefin, neither via a spirocyclic transition state nor by precoordination of the olefin to molybdenum as it was postulated in the literature. Instead, they act as activators of the oxidising agent ROOH as it is known from other high valent transition metal complexes. Based upon these results, a new mechanism for the olefin epoxidation with molybdenum peroxo complexes could be proposed (Scheme 1), wherein the oxidising agent coordinates to the Mo^{VI} centre (**I**), undergoes a proton transfer to one of the peroxo ligands (**II**) and is activated for oxygen transfer by η^2-coordination (**III**). This mechanistic idea was supported by a series of experiments especially concerning the proton transfer and kinetic aspects.[25,26]



Scheme 1

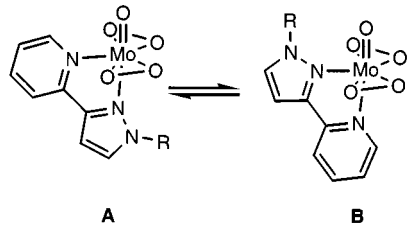
[‡] Part 9: Ref.[1]

[a] Institut für Organische Chemie und Biochemie II, Technische Universität München, Lichtenbergstrasse 4, 85747 Garching, E-mail: angelika.hroch@ch.tum.de; gerd.gemmecker@ch.tum.de
[b] Institut für Anorganische Chemie, Technische Universität München, Lichtenbergstrasse 4, 85747 Garching, E-mail: werner.thiel@ch.tum.de

Supporting information for this article is available on the WWW under http://www.wiley-vch.de/home/eurjic or from the author.

 © WILEY-VCH Verlag GmbH, D-69451 Weinheim, 2000 1434–1948/00/0505–1107 $ 17.50+.50/0

Owing to the asymmetric nature of the ligand bearing two different nitrogen donor centres, these peroxo complexes exist in two isomeric forms **A** and **B**, which differ in the orientation of the aromatic rings relative to the axial oxo ligand and which are in equilibrium in solution (Scheme 2, R = alkyl, $-CH_2COOEt$). This special feature gave us insight into the role of the Lewis acidity of the metal centre which can be tuned by the donor properties of the chelate ligands and allowed for the first time to establish a quantitative relationship between the structure of an epoxidation catalyst and its activity.[27]



Scheme 2

In the present paper, we report on the NMR spectroscopic investigation of the isomerisation process (**A** $\rightleftarrows$ **B**). In addition to the kinetic and thermodynamic data obtained herein, this investigation opens up the door to the activation of ROOH at peroxo complexes, which we elucidated by means of computational methods.

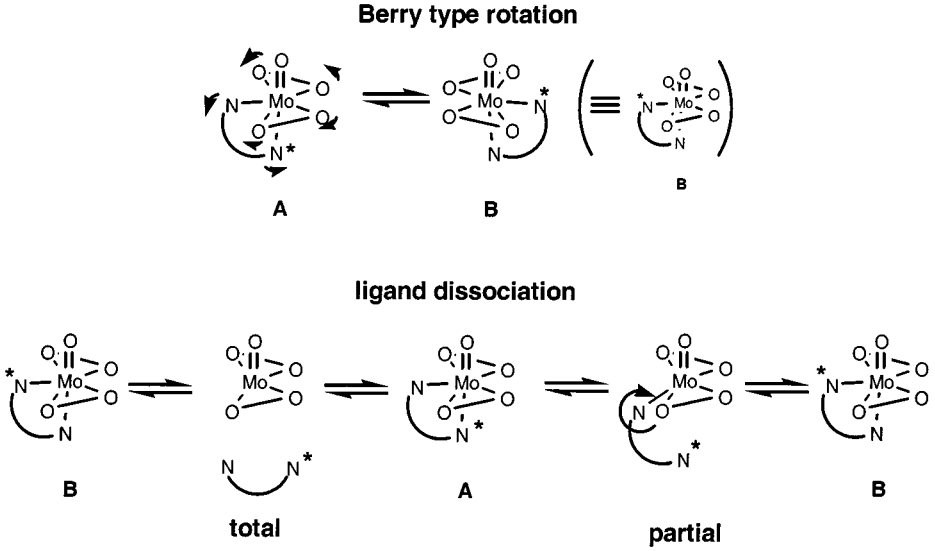
Results and Discussion

For long, the existence of the two isomers **A** and **B** was discussed as a more or less static phenomenon, since simple temperature dependent NMR experiments did not show any significant change in the spectra of the pyrazolylpyridine complexes up to a temperature of 100 °C. This simple image had to be improved when the fluxionality of these systems was preliminarily examined[29] by one dimensional spin transfer experiments, which allow the determination of slow dynamic processes.[30,31]

From a formal point of view, the isomer equilibration (**A** $\rightleftarrows$ **B**) can be achieved either by a Berry-type process of ligand fluxionality (Scheme 3, top) or by ligand dissociation (either complete or partial dissociation; Scheme 3, bottom).

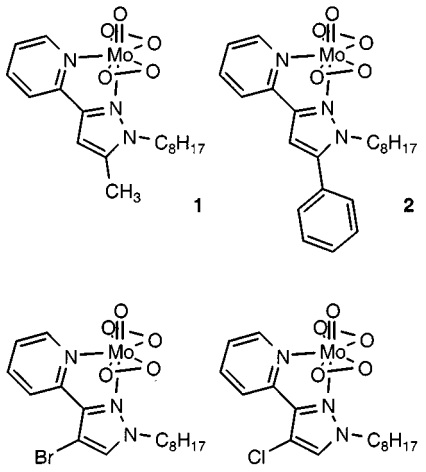
While a Berry-type rotation may be considered unfavourable due to the chelating ligands (pyrazolylpyridine, η^2-O_2-), ligand dissociation from the high valent transition metal centre Mo^{VI} will also be an endothermic process. For a more accurate and extended determination of these processes and the related kinetic and thermodynamic data, the oxobisperoxo molybdenum complexes **1–4**, bearing pyrazolylpyridine ligands with different substituents at the pyrazole moiety, were investigated by temperature-dependent two dimensional NOESY[32] experiments. A common feature of the peroxo complexes investigated are positive entropies of activation (ca. 42–76 $JK^{-1}mol^{-1}$), which prove a dissociation to take place in the rate determining step of the equilibration and therefore rule out a Berry-type rotation. The energies of activation derived from the kinetic data are found in a range of ca. 89–110 $kJmol^{-1}$ (Table 1).

Since these NMR experiments do not allow to distinguish between a partial and a complete ligand dissociation, we investigated the dissociation process by quantum chemical calculations on the model complex $MoO(\eta^2\text{-}O_2)_2(NH_3)_2$ using density functional theory (B3LYP-method[33–35] with LanL2DZ* basis set[36–39]) . The complex geometries resulting from these calculations are in good agreement with the bond parameters obtained from X-ray structure analysis of analogous molybdenum peroxo complexes.[23,24,28,40–42] Figure 1 shows a comparison between the calculated structural parameters and those of oxodiperoxo[3-(2-pyridyl)-1-pyrazolylacetic acid ethyl ester]molybdenum(VI).[23] All calculated bond lengths are found slightly too long, which is due to the applied method.[43] Only the distance between the apical NH_3 ligand and the



Scheme 3

Table 1. Activation parameters (from NOESY data) for the isomer equilibration of some molybdenum peroxo complexes



	1	2	3	4
E_A	111.0	108.1	97.1	89.1
$\Delta H^{\ddagger}$	108.4	105.6	94.6	86.6
$\Delta S^{\ddagger}$	76.2	77.0	71.0	42.7

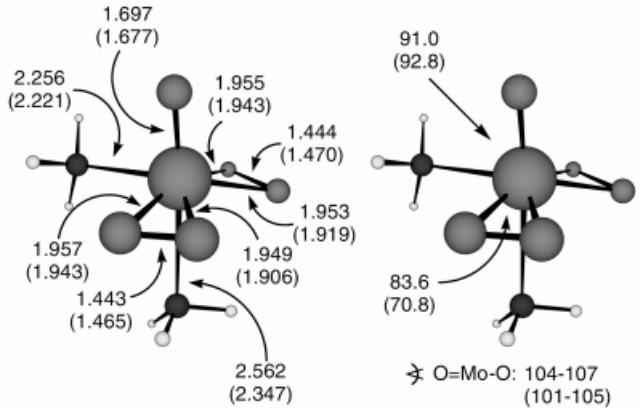


Figure 1. Calculated (DFT) bond lengths (left side) and bond angles (right side) of $MoO(\eta^2\text{-}O_2)_2(NH_3)_2$ compared with values obtained by X-ray structure analysis (in parentheses)[23]

molybdenum centre is calculated much too long, implicating a flat PES (potential energy surface). The same feature has already been described for the ligated water molecule in the rhenium peroxo complex $ReO(\eta^2\text{-}O_2)_2(CH_3)(H_2O)$ by Rösch et al.[44]

Ligand dissociation obviously is an endothermic process: we calculated 56.2 kJmol^{-1} for the dissociation of the axial NH_3 ligand, about 165 kJmol^{-1} for the dissociation of the equatorial NH_3 ligand, and 241.9 kJmol^{-1} for the dissociation of both NH_3 ligands (Figure 2, Table 2). While calculation of $MoO(\eta^2\text{-}O_2)_2(ax\text{-}NH_3)(eq\text{-}NH_3)$ (**a**), $MoO(\eta^2\text{-}O_2)_2(eq\text{-}NH_3)$ (**c**), and $MoO(\eta^2\text{-}O_2)_2$ (**d**), resulted in stable geometries, geometry optimisation of the axially-coordinated isomer **b** lead to **c**. Therefore, the dissociation energy

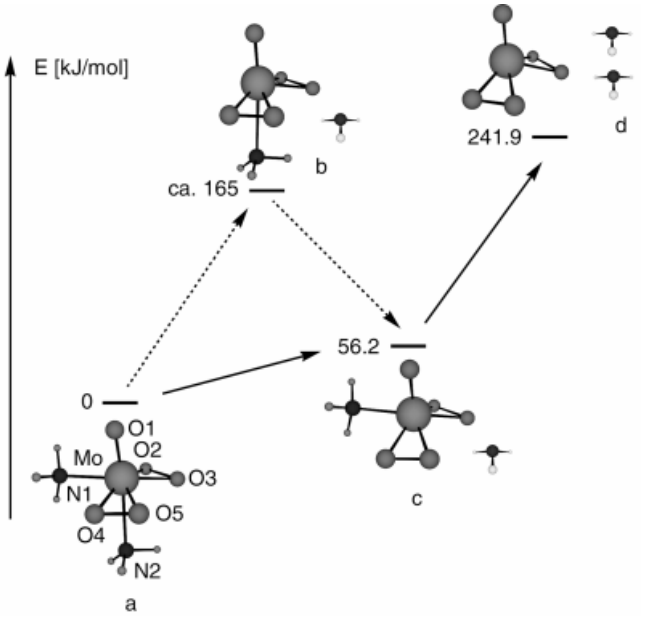


Figure 2. Energy profile (DFT) of the subsequent dissociation of NH_3 ligands from of $MoO(\eta^2\text{-}O_2)_2(NH_3)_2$

Table 2. Dissociation energies and structural features (DFT) of the complexes shown in Figure 2

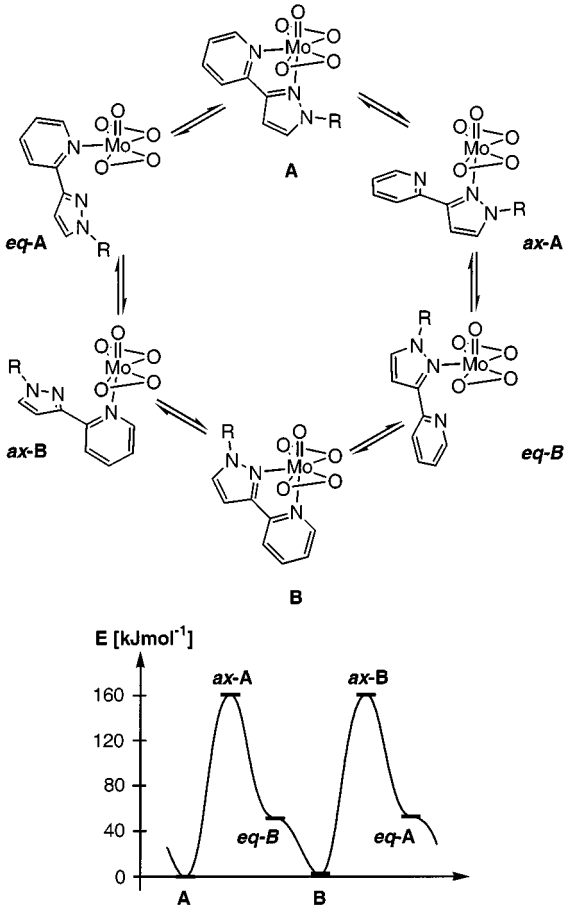
	a	**b**[a]	**c**	**d**
		Energy [kJmol^{-1}]		
	0[b]	ca. 165	56.2	241.9
		Bond lengths [Å]		
Mo–N1	2.256	–	2.242	–
Mo–N2	2.562	2.563	–	–
Mo–O1	1.697	1.697	1.692	1.683
Mo–O2	1.955	1.955	1.926	1.910
Mo–O3	1.953	1.953	1.950	1.944
Mo–O4	1.957	1.957	1.926	1.910
Mo–O5	1.949	1.949	1.949	1.944
O2–O3	1.444	1.444	1.446	1.431
O4–O5	1.443	1.443	1.446	1.431

[a] The dissociation energy to complex **b** was obtained by a single point calculation, the bond parameters were taken from compound **a**. – [b] By definition.

related to isomer **b** could just be obtained by a single point calculation.

As the geometry of the $MoO(\eta^2\text{-}O_2)_2$ centre does not change dramatically by addition of one or two NH_3 ligands (Table 2), the energies of activation obtained from the NMR experiments should be somehow related to one of the calculated dissociation energies. Since 242 kJmol^{-1} for the complete ligand dissociation is far from the experimentally found value of about 100 kJmol^{-1}, we propose a partial ligand dissociation as the key step in the isomerisation process. This agrees with the observation that peroxo complexes of this type undergo a relatively slow decomposition in the presence of excess trifluoroacetic acid (after 15 min about 10–15% of decomp.) in $CHCl_3$ solution.[45] A complete dissociation of the chelate ligand would give rise to a rapid protonation of the liberated ligand and precipitation of a polymeric molybdenum peroxide. Additionally the

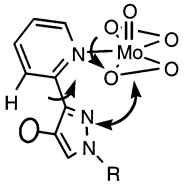
catalytic activity of the complexes strongly depends on the substituent pattern of the donor ligand, which also makes a complete ligand dissociation unfavourable. Based on the quantum chemical calculations, spectroscopic investigations and reactivity studies, the isomerisation process depicted in Scheme 4 is proposed.



Scheme 4

Since we could not find a stable axially coordinated intermediate $MoO(\eta^2\text{-}O_2)_2(ax\text{-}NH_3)$ in our calculations, the compounds ***ax*-A** and ***ax*-B** may be discussed as transition states in the isomerisation sequence. The species ***eq*-A** and ***eq*-B** represent flat minima or saddle points of the PES, which correlates with the dissociative nature of the rate determining step.

While the activation energies obtained from the NOESY kinetics qualitatively reflect the strengths of the Mo–N bonds to be broken and therefore the donor potencies of the appropriate chelate ligands, the entropies of activation give an idea about the increase of ligand fluxionality after partial dissociation. They should depend on the substitution pattern of the pyrazolyl fragment: bulky substituents in 4-position (Br) as well as substituents forming H interactions with the proton in the 3-position of the pyridine ring (Cl) will hinder the free rotation around the pyrazole–pyridine bond (Scheme 5) and decrease the entropy of activation (Table 1).



Scheme 5

Beside the clarification of the equilibration process, these investigations may open up a new insight into mechanistic details of the olefin epoxidation with seven-coordinated molybdenum peroxo catalysts. The intermediate $16e^-$ complex **II** of the postulated epoxidation mechanism (Scheme 1) still may undergo a η^2-coordination of the alkyl hydroperoxide to give the activated species **III** ($18e^-$). However, its Lewis acidity should be rather moderate and the derived eight-coordinated species **III** can be considered as sterically overcrowded, which makes the activation process unfavourable. In contrast, partial ligand dissociation would open a coordination site at the molybdenum centre for coordination/activation of the alkyl hydroperoxide, and additionally enhance its Lewis acidity. For that reason, we investigated by quantum chemical calculations the interaction of methyl hydroperoxide (CH_3OOH) with both, the seven-coordinated model system $MoO(\eta^2\text{-}O_2)_2(NH_3)_2$ (**a**) and its six-coordinated congener $MoO(\eta^2\text{-}O_2)_2(eq\text{-}NH_3)$ (**c**), which has been calculated to be just about 56 $kJmol^{-1}$ higher in energy.

A first interaction of a hydroperoxide with a seven-coordinated peroxo species of the type **I** (Scheme 1) may result either from a hydrogen bond between one or both of the peroxo ligands, an attack of one of the Lewis basic oxygen atoms of the hydroperoxide at the molybdenum center, or by a combination of both. For the first mode as a series of stable geometries were found by computational calculations ($\mathbf{e_1}$, $\mathbf{e_2}$, $\mathbf{e_3}$). Despite the well-known fact that density functional theory is not the best method for the calculation of weak interactions like hydrogen bonds,[46] we believe that the geometries and energies we found may give an impression about the first approach of a hydroperoxide to the peroxo complex. The hydrogen bonded system is stabilised by 46.6 to 67.7 $kJmol^{-1}$ compared to free $MoO(\eta^2\text{-}O_2)_2(NH_3)_2/CH_3OOH$ (Figure 3, Table 3). Taking into account that one of the ammonia ligands also forms hydrogen bonds to the hydroperoxide in all the calculated structures and that the calculations do not include any solvent effect, the calculated energies reflect quite well the energy of an intermolecular hydrogen bond in complex **5** (Scheme 6, S = solvent), which was estimated to 8–20 $kJmol^{-1}$ by NMR spectroscopic investigations.[28] **5** forms intramolecular H-bonds to an $\eta^2\text{-}O_2$ ligand in nonpolar solvents like chloroform, intermolecular H-bonds to the solvent in polar solvents like acetone and intermolecular H-bonds to an $\eta^2\text{-}O_2$ ligand of another peroxo complex in the solid state structure.[28]

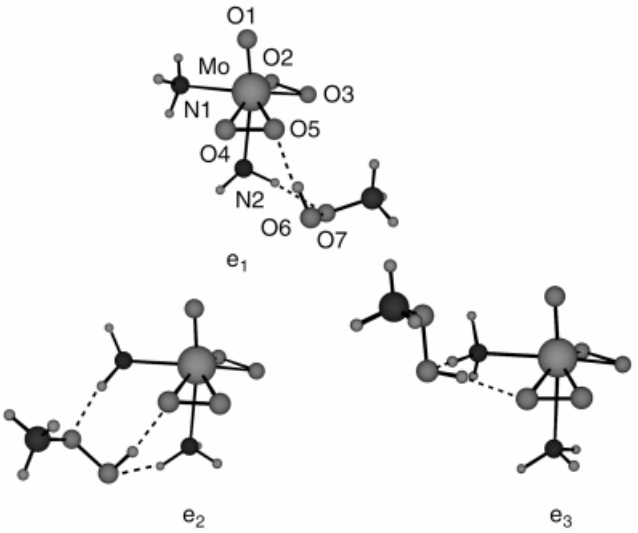


Figure 3. Different modes of H bonding between CH_3OOH and $MoO(\eta^2\text{-}O_2)_2(NH_3)_2$

Table 3. Energetic and structural features (DFT) of the complexes shown in Figure 3

	$\mathbf{e_1}$	$\mathbf{e_2}$	$\mathbf{e_3}$
		Energy[a] [kJmol^{-1}]	
	–46.6	–67.7	–53.1
		Bond lengths [Å]	
Mo–N1	2.261	2.249	2.244
Mo–N2	2.505	2.512	2.538
Mo–O1	1.698	1.696	1.695
Mo–O2	1.959	1.956	1.953
Mo–O3	1.943	1.943	1.947
Mo–O4	1.963	1.985	1.971
Mo–O5	1.966	1.957	1.964
O4···HO	–	1.761	1.893
O5···HO	1.847	–	–
O6···HN	–	2.232	1.984
O7···HN	1.954	1.947	–

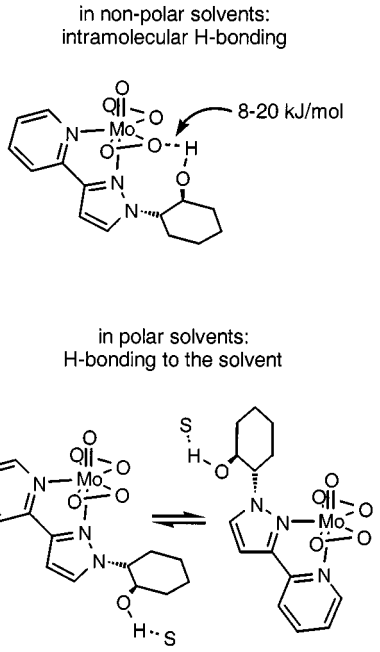
[a] Compared to free $MoO(\eta^2\text{-}O_2)_2(NH_3)_2$ + CH_3OOH.

Up to now it was not possible to find a local minimum on the PES representing a Lewis acid/base interaction between $MoO(\eta^2\text{-}O_2)_2(NH_3)_2$ (**a**) and CH_3OOH or a combination of the latter feature with hydrogen bonding.

Proton transfer from the hydroperoxide to either the rear or the front oxygen atom of one of the peroxo ligands results in the formation isomeric species of the type **II** $MoO(\eta^2\text{-}O_2)(OOH)(OOCH_3)(NH_3)_2$ ($\mathbf{f_1}$, $\mathbf{f_2}$, $\mathbf{f_3}$), all lower in energy than the starting materials (Figure 4, Table 4).

They are stabilised by intramolecular hydrogen bonding ($\mathbf{f_1}$, $\mathbf{f_2}$) between the proton of the hydroperoxo ligand and the α-oxygen atom of the alkyl peroxo ligand, forming a five-membered ring system and hydrogen bonds to one or both of the ammonia ligands. Along with these theoretical studies we investigated the behaviour of oxobisperoxo(pyrazolylpyridine)molybdenum complexes in the presence of excess *t*BuOOH by NMR. NMR spectroscopy did not prove any interaction between the hydroperoxide and the molybdenum complex, which may either be explained by the different steric demand of *t*BuOOH and CH_3OOH or by a certain error related to the computational method due to the simplification of the donor ligand by NH_3 and by neglect of solvent effects. However, it is indisputable that the energies assigned to the proton transfer and the opening of one $\eta^2\text{-}O_2$ ligand to form a $Mo(OOH)(OOCH_3)$ fragment are low, which makes the existence of species of the type **II** (Scheme 1) in equilibrium with **I** feasible.

Parallel to the seven-coordinated system $MoO(\eta^2\text{-}O_2)_2(NH_3)_2$ (**a**) the interaction of CH_3OOH with the six-coordinated complex $MoO(\eta^2\text{-}O_2)_2(eq\text{-}NH_3)$ (**c**) was investigated. As shown before, dissociation of the axial donor was found to be low in energy. Although unproductive in the



Scheme 6

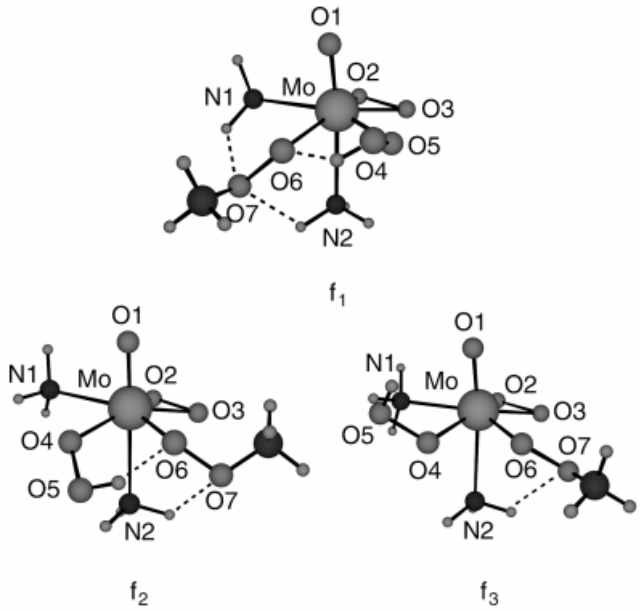


Figure 4. Isomeric species of the type $MoO(\eta^2\text{-}O_2)(OOH)(OOCH_3)(NH_3)_2$

Table 4. Energetic and structural features (DFT) of the complexes shown in Figure 4

	$\mathbf{f_1}$	$\mathbf{f_2}$	$\mathbf{f_3}$
		Energy[a] [kJmol^{-1}]	
	–20.7	–37.1	–20.6
		Bond lengths [Å]	
Mo–N1	2.307	2.305	2.274
Mo–N2	2.458	2.479	2.457
Mo–O1	1.698	1.704	1.705
Mo–O2	1.943	1.958	1.957
Mo–O3	1.970	1.966	1.965
Mo–O4	2.838	1.995	2.044
Mo–O5	1.974	2.989	2.963
Mo–O6	2.074	2.012	1.978
O6···HO	1.853	1.821	–
O7···HN	2.249/2.020	2.374	2.241

[a] Compared to free $MoO(\eta^2\text{-}O_2)_2(NH_3)_2 + CH_3OOH$.

Table 5. Energetic and structural features (DFT) of the complexes shown in Figure 5

	$\mathbf{g_1}$	$\mathbf{g_2}$	$\mathbf{g_3}$
		Energy[a] [kJmol^{-1}]	
	+7.0	+16.4	–1.5
		Bond lengths [Å]	
Mo–N1	2.232	2.230	2.226
Mo–O1	1.689	1.689	1.687
Mo–O2	1.938	1.936	1.944
Mo–O3	1.949	1.943	1.948
Mo–O4	1.952	1.950	1.943
Mo–O5	1.951	1.962	1.967
Mo–O6	2.798	2.798	2.749
Mo–O7	3.997	3.714	3.541
O4···HO	2.341	2.347	2.272
O5···HO	2.732	2.234	2.022
O6···HN	2.169	2.371	2.316

[a] Related to the reaction: **a** + $CH_3OOH \rightarrow$ **g** + NH_3.

isomerisation process of the pyrazolylpyridine complexes (Scheme 4), it may be considered as the key step in the activation of the alkyl hydroperoxide.

We therefore investigated structures of the type $MoO(\eta^2\text{-}O_2)_2(eq\text{-}NH_3)(ax\text{-}CH_3OOH)$ (**g**) by means of computational methods and found three minima on the PES (there may even be more). The energies of these compounds (Table 5), wherein the hydroperoxide can be bound to the molybdenum centre by either the protonated ($\mathbf{g_1}$, $\mathbf{g_2}$) or the alkylated ($\mathbf{g_3}$) oxygen atom, are related to the reaction $MoO(\eta^2\text{-}O_2)_2(NH_3)_2 + CH_3OOH \rightarrow MoO(\eta^2\text{-}O_2)_2(eq\text{-}NH_3)(ax\text{-}CH_3OOH) + NH_3$. The data prove that methyl hydroperoxide is able to stabilise the molybdenum centre in the same manner as ammonia does it. This is promoted by interactions between the proton of the hydroperoxide and one or two of the oxygen atoms of an η^2-peroxo ligand and one of the NH_3 protons with the coordinating oxygen atom of the hydroperoxide, reflecting the basicity of CH_3OOH (Figure 5, Table 5).

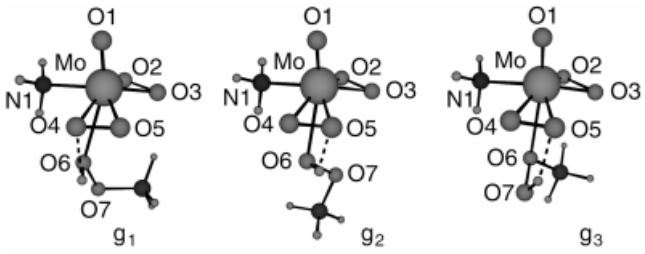


Figure 5. Structures of CH_3OOH adducts to $MoO(\eta^2\text{-}O_2)_2(eq\text{-}NH_3)$

The weak hydrogen bond between OOH and (η^2-O_2) can again be considered as the first step of a proton transfer from the hydroperoxide to the peroxo ligand as discussed before. Proton transfer leads to a series of isomeric molybdenum complexes of the type $MoO(\eta^2\text{-}O_2)(eq\text{-}NH_3)(OOH)(OOCH_3)$ (**h**) showing different ligand conformations (Figure 6 shows three examples, there may be more). The energies given in Table 6 are related to the reaction $MoO(\eta^2\text{-}O_2)_2(NH_3)_2 + CH_3OOH \rightarrow MoO(\eta^2\text{-}O_2)(\eta^1\text{-}O_2H)(eq\text{-}NH_3)(\eta^1\text{-}OOCH_3) + NH_3$.

The intramolecular proton transfer should be a rapid process with a low barrier of activation, it is only slightly endothermic. In all cases we observed, the complexes are stabilised by hydrogen bonds and by η^2-coordination of the methyl hydroperoxo and/or the hydroperoxo ligand, a feature which was not found in the complexes $MoO(\eta^2\text{-}O_2)(OOH)(OOCH_3)(NH_3)_2$ ($\mathbf{f_1}$–$\mathbf{f_3}$, Figure 4). This shows that previous partial dissociation of one donor ligand from a seven-coordinated peroxo complex is energetically feasible and that the activation of the hydroperoxide for oxygen transfer may start with such a dissociative process.

The calculated Mo–O–O angles lie between the data of complexes bearing η^1-coordinated (112–118°[13–21]) and η^2-coordinated alkyl peroxo ligands (59–65°[9,10,20]).

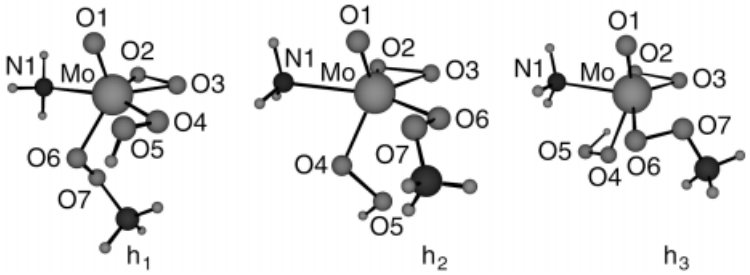
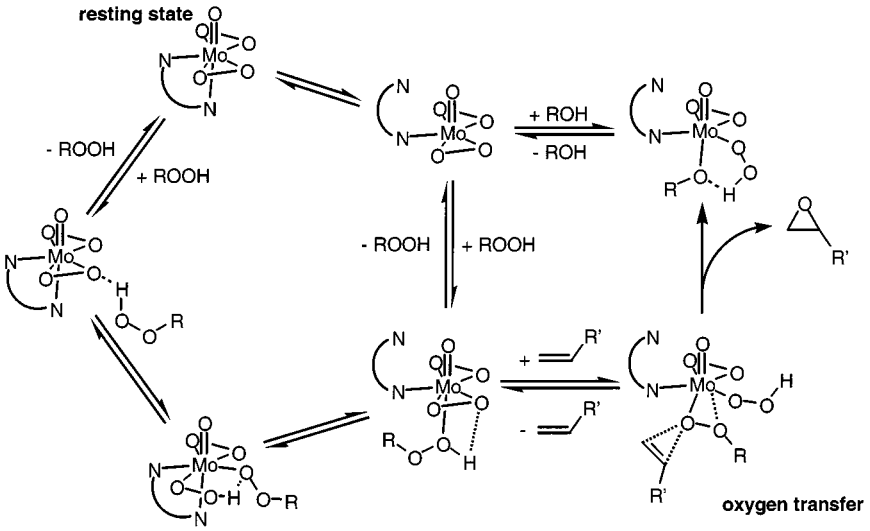


Figure 6. Calculated geometries of molybdenum complexes of the type $MoO(\eta^2\text{-}O_2)(eq\text{-}NH_3)(OOH)(OOCH_3)$

Table 6. Energetic and structural features (DFT) of the complexes shown in Figure 6

	$\mathbf{h_1}$	$\mathbf{h_2}$	$\mathbf{h_3}$
		Energy[a] [kJmol^{-1}]	
	25.8	44.0	79.0
		Bond lengths [Å]	
Mo–N1	2.326	2.368	2.253
Mo–O1	1.692	1.699	1.712
Mo–O2	1.929	1.921	1.996
Mo–O3	1.952	1.954	1.923
Mo–O4	1.974	1.976	2.071
Mo–O5	2.640	2.742	3.108
Mo–O6	2.106	1.957	2.105
Mo–O7	2.492	2.597	2.150
O2···HO	–	–	2.033
O6···HO	2.193	–	–
O7···HN	2.468	–	–
		Bond angles [°]	
Mo–O4–O5	100.0	105.1	117.3
Mo–O6–O7	90.1	98.3	76.4

[a]Related to the reaction: **a** + CH_3OOH → **h** + NH_3.



Scheme 7

The overall mechanistic idea resulting from the NMR investigations and the computational calculations is shown in Scheme 7, wherein the seven-coordinated oxobisperoxo complex represents a kind of resting state in the catalytic cycle.

Thus, seven-coordinated molybdenum peroxo complexes bearing chelate pyrazolylpyridine ligands do not undergo a direct oxygen transfer from an η^2-coordinated peroxo ligand to an olefin but activate a potential oxidising agent for oxygen transfer, similar to other high valent and highly Lewis acidic transition metal centres. This includes the requirement of basic ligands to undergo a proton transfer reaction prior to the activation of the hydroperoxide. η^2-Coordinated peroxo ligands are ideal for this purpose since they are weak π donors, which preserves the Lewis acidity of the metal centre. They remain ligated to the metal in a η^1-coordination mode allowing rapid intramolecular proton transfer after the oxygen transfer to regenerate the catalyst.

Conclusion

As shown by NMR spectroscopy and quantum chemical calculations, ligand fluxionality may play an important role in the activation of the hydroperoxide. We were able to show, that the energies related with a partial ligand dissociation and intra- and intermolecular proton transfer reactions are low and that η^2-coordination of an alkylperoxo ligand stabilises six-coordinated molybdenum species.

Experimental Section

NMR spectra were recorded with a Bruker DMX 600 spectrometer and processed by Silicon Graphics workstations with the X-WIN-NMR software package. The 1D spectra and the 2D NOESY spectra were measured at different temperatures/mixing times: **1** (297.3 K/2s, 306.8 K/2 s, 316.3 K/2 s, 325.8 K/2 s), **2** (297.3 K/1 s, 306.8 K/1 s, 316.3 K/1 s), **3** (287.9 K/1 s, 297.3 K/0.5 s, 306.8 K/0.3 s, 316.3 K/0.2 s), **4** (290.0 K/1 s, 300.0 K/0.5 s, 310.0 K/0.2 s, 320 K/0.1 s). – Quantum chemical calculations were performed with the program Gaussian98W using the B3LYP gradient-corrected exchange-correlation functional[33–35] in combination with the Los Alamos effective core potentials on molybdenum atoms together with a gaussian valence basis set of double zeta quality (LanL2DZ).[36–39] The orbital basis sets of carbon, nitrogen and oxygen atoms were augmented by a single set of polarisation functions.[47] Full geometry optimisations were carried out in C_1 symmetry using analytical gradient techniques and the resulting structures were confirmed to be true minima by diagonalisation of the analytical Hessian Matrix.

Acknowledgments

We wish to thank the Deutsche Forschungsgemeinschaft (Schwerpunktprogramm "Peroxidchemie"), the Fonds der Chemischen Industrie for financial support and Prof. W. A. Herrmann and Prof. H. Kessler for logistic support of this work.

[1] H. Glas, E. Herdtweck, G. R. J. Artus, W. R. Thiel, *Inorg. Chem.* **1998**, *37*, 3644.

[2] F. Di Furia, G. Modena, *Pure Appl. Chem.* **1982**, *54*, 1853.
[3] K. A. Jorgensen, *Chem. Rev.* **1989**, *89*, 431.
[4] K. A. Jørgensen, R. Hoffman, *Acta Chem. Scand., Ser. B* **1986**, *40*, 411.
[5] M. J. Filatov, K. V. Shalyaev, E. P. Talsi, *J. Mol. Catal.* **1994**, *87*, L5.
[6] D. J. Berrisford, C. Bolm, K. B. Sharpless, *Angew. Chem.* **1995**, *107*, 1159; *Angew. Chem. Int. Ed. Engl.* 1995, *34*, 1059.
[7] G. Boche, F. Bosold, J. C. W. Lohrenz, *Angew. Chem.* **1994**, *106*, 1228; *Angew. Chem. Int. Ed. Engl.* **1994**, *33*, 1161.
[8] R. D. Bach, M.-D. Su, J. L. Andrés, H. B. Schlegel, *J. Am. Chem. Soc.* **1993**, *115*, 8763.
[9] G. Boche, K. Möbus, K. Harms, J. C. W. Lohrenz, M. Marsch, *Chem. Eur. J.* **1996**, *2*, 604.
[10] G. Boche, K. Möbus, K. Harms, M. Marsch, *J. Am. Chem. Soc.* **1996**, *118*, 2770.
[11] Y.-D. Wu, D. K. W. Lai, *J. Am. Chem. Soc.* **1995**, *117*, 11327.
[12] Y.-D. Wu, D. K. W. Lai, *J. Org. Chem.* **1995**, *60*, 673.
[13] G. Ferguson, M. Parvez, P. K. Monaghan, R. J. Puddephat, *J. Chem. Soc., Chem. Commun.* **1983**, 267.
[14] G. Ferguson, M. Parvez, P. K. Monaghan, R. J. Puddephat, *Organometallics* **1984**, *4*, 1669.
[15] H. Mimoun, R. Charpentier, A. Mitschler, J. Fischer, R. Weiss, *J. Am. Chem. Soc.* **1989**, *102*, 1047.
[16] G. Strukul, R. A. Michelin, J. D. Orbell, L. Randaccio, *Inorg. Chem.* **1983**, *22*, 3706.
[17] C. Giannotti, C. Fontaine, A. Chiaroni, C. Riche, *J. Organomet. Chem.* **1976**, *113*, 57.
[18] L. Saussine, E. Brazi, A. Robine, H. Mimoun, J. Fischer, R. Weiss, *J. Am. Chem. Soc.* **1985**, *107*, 3534.
[19] A. van Asselt, B. D. Santasiero, J. E. Bercaw, *J. Am. Chem. Soc.* **1986**, *108*, 8291.
[20] N. Katajima, T. Katayama, K. Fujisawa, Y. Iwata, Y. Moro-oka, *J. Am. Chem. Soc.* **1993**, *115*, 7872.
[21] M. Akita, T. Miyaji, S. Hikichi, Y. Moro-oka, *Chem. Commun.* **1998**, 1005.
[22] H. Mimoun, P. Chaumette, M. Mignard, L. Saussine, J. Fischer, R. Weiss, *New J. Chem.* **1983**, *7*, 467.
[23] W. R. Thiel, M. Angstl, T. Priermeier, *Chem. Ber.* **1994**, *127*, 2373.
[24] W. R. Thiel, T. Priermeier, *Angew. Chem.* **1995**, *107*, 1870; *Angew. Chem. Int. Ed. Engl.* **1995**, *34*, 1737.
[25] W. R. Thiel, *Chem. Ber.* **1996**, *129*, 575.
[26] W. R. Thiel, *J. Mol. Catal. A: Chemical*, **1997**, *117*, 449.
[27] W. R. Thiel, J. Eppinger, *Chemistry Eur. J.*, **1997**, *3*, 696.
[28] H. Glas, M. Spiegler, W. R. Thiel, *Eur. J. Inorg. Chem.* **1988**, *1*, 275.
[29] W. R. Thiel, M. Mattner, unpublished results.
[30] S. Forsén, R. A. Hoffman, *Acta Chem. Scand.* **1963**, *17*, 1787.
[31] S. Braun, H.-O. Kalinowski, S. Berger, *100 and More Basic NMR Experiments*, VCH, **1996**.
[32] J. Evans, *Biomolecular NMR Spectroscopy*, Oxford University Press, **1995**.
[33] C. Lee, W. Yang, R. G. Parr, *Phys. Rev.* **1988**, *B37*, 785.
[34] A. D. Becke, *Phys. Rev.* **1988**, *A38*, 3098.
[35] B. Miehlich, A. Savin, H. Stoll, H. Preuss, *Chem. Phys. Lett.* **1989**, *157*, 200.
[36] J. B. Foresman, T. A. Keith, K. B. Wiberg, J. Snoonian, M. J. Frisch, *J. Phys. Chem.* **1996**, *100*, 16098.
[37] W. J. Stevens, H. Basch, J. Krauss, *J. Chem. Phys.* **1984**, *81*, 6026.
[38] W. J. Stevens, M. Krauss, H. Basch, P. G. Jasien, *Can. J. Chem.* **1992**, *70*, 612.
[39] T. R. Cundari, W. J. Stevens, *J. Chem. Phys.* **1993**, *98*, 5555.
[40] E. O. Schlemper, G. N. Schrautzer, L. A. Hughes, *Polyhedron* **1984**, *3*, 377.
[41] W. A. Herrmann, W. R. Thiel, J. G. Kuchler, *Chem. Ber.* **1990**, *123*, 1953.
[42] W. A. Herrmann, W. R. Thiel, J. G. Kuchler, J. Behm, E. Herdtweck, *Chem. Ber.* **1990**, *123*, 1963.
[43] T. Ziegler, *Can. J. Chem.* **1995**, *73*, 743.
[44] P. Gisdakis, S. Antonczak, S. Köstlmeier, W. A. Herrmann, N. Rösch, *Angew. Chem.* **1998**, *110*, 2333; *Angew. Chem. Int. Ed.* **1998**, *37*, 2211.
[45] In a spectroscopic study[25] on the interaction of Brønsted and Lewis acids on oxobisperoxo(pyrazolylpyridine)molybdenum complexes, we were able to show a selective attack of protons at the peroxo ligands of the molecule.
[46] E. Ruiz, D. R. Salahub, A. Vela, *J. Chem. Phys.* **1996**, *100*, 12265.
[47] P. C. Hariharan, J. A. Pople, *Theor. Chim. Acta* **1973**, *28*, 213.

Received November 25, 1999
[I99429]

Reaction of Organolithium Compounds with Alkali Metal Alkoxides – A Route to Superbases

Lubomír Lochmann[a]

Keywords: Alkali metals / Organolithium compounds / Alkali metal alkoxides / Metal exchange / Metallation

Organolithium compounds and lithium alkoxides form adducts, the reactivities of which are similar to those of the parent organolithium compounds. On the other hand, with heavy alkali metal alkoxides a metal interchange takes place, which gives rise to heavy alkali metal organic compounds. This is accompanied by a dramatic increase in the reactivity of the system, hence the name "Superbase" (SB) may be applied. This metal interchange is a general reaction and proceeds not only with organolithium compounds but also with lithium amides and lithium enolates of ketones and esters. SBs readily react with organic substrates to give heavy alkali metal derivatives of the substrate. Such reactions, followed by conversion with an electrophile, find wide application in organic synthesis. The properties of SBs may be further enhanced by using a greater than equimolar amount of a highly-branched heavy alkali metal alkoxide (R^2OM). In this review, the mechanism of SB reactions with substrates is discussed and the stoichiometric participation rather than catalytic effect of R^2OM is documented. Although various routes for the reaction of SBs with substrates may be envisaged, a heavy alkali metal organic compound is involved in all cases.

Introduction

Organolithium compounds react with alkali metal alkoxides in different ways depending on the metal of the alkoxide. Lithium alkoxides and organolithium compounds form adducts, the reactivities of which approach those of the parent organolithium compounds. On the other hand, heavy alkali metal alkoxides undergo a metal interchange with organolithium species, giving rise to heavy alkali metal organic compounds and lithium alkoxides. The reactivities of these systems are dramatically enhanced and this phenomenon warrants the name Superbase (SB). SBs are extremely strong bases; they readily react with many organic compounds and thus represent useful tools in organic synthesis.

The very first reference to the system prepared from butyllithium and sodium or potassium *tert*-butoxide can be found in a U.S. patent[1] [applied for on Nov. 14, 1963 by Wofford (Phillips Petroleum Co.)], where its use as a polymerization catalyst is described. A paper on this topic appeared much later.[2] The next account of this system appeared in a Czech patent[3] (applied for on Dec. 30, 1964, by Lochmann et al.), which was followed by a lecture[4] and a paper by the same authors[5] (submitted on Nov. 24, 1965). These communications and the following papers[6,7] described the metal interchange leading to the generation of heavy alkali metal organic compounds, as well as the formation of the latter through reaction of SBs with organic

[a] Institute of Macromolecular Chemistry, Academy of Sciences of the Czech Republic,
Heyrovský Sq. 2, 162 06 Prague 6, Czech Republic
Fax: (internat.) + 420-2/367981
E-mail: lochmann@imc.cas.cz



Lubomír Lochmann was born in Prague, Czech Republic, in 1926. He studied chemistry at the Faculty of Chemical Technology, Czech Technical University, Prague, and obtained his M.Sc. degree in 1949. Between 1955 and 1960 he worked in industry and was engaged in the synthesis of fine organic chemicals. He joined the Institute of Macromolecular Chemistry, Academy of Sciences of the Czech Republic, Prague, in 1961 and has been active there up to the present time as a leading scientist. He obtained his Ph.D. degree in 1968 and D.Sc. degree in 1998 from the same Institute. In 1992 and 1993 he was a Visiting Scientist at Cornell University, Ithaca, N.Y., USA, with Prof. J. M. J. Fréchet. His main scientific interests are organic compounds of alkali metals (alkali metal carbanions, amides, and alkoxides; their interactions, formation, and reactions of Superbases) and anionic polymerization, in particular that of (meth)acrylate esters (mechanism, growth centre properties, block copolymers). He is an author of 80 scientific papers, 25 patents, and 3 reviews. For the discovery of the lithium–heavy alkali metal interchange and of Superbases, he received an Award of the Czechoslovak Bureau of Patents and Discoveries (1991).

MICROREVIEWS: This feature introduces the readers to the authors' research through a concise overview of the selected topic. Reference to important work from others in the field is included.

 © WILEY-VCH Verlag GmbH, D-69451 Weinheim, 2000 1434–1948/00/0606–1115 $ 17.50+.50/0

substrates. Subsequently, the general nature of this metal interchange was established and more effective SBs were discovered.[7–11] Eventually, Schlosser submitted a paper (on Aug. 4, 1966) describing an increased reactivity of butyllithium (BuLi) in the presence of potassium *tert*-butoxide and explained this phenomenon in terms of solvation of the BuLi by the oxygen atom of the alkoxide, akin to the solvation of organometallics by ethers. Metallations of several substrates and their subsequent conversions into derivatives through in situ reactions with electrophiles were also described in this paper.[12] This author went on to investigate reactions of SBs with many organic substrates and contributed substantially to the use of SBs in organic synthesis; the relevant results have been summarized in two reviews.[13,14] The properties of SBs have also been investigated in other laboratories. Some salient accounts can be found in refs.[15–23]

The bulk of this review is focussed on the formation and properties of SBs based on results obtained by the author. As SBs find such widespread application in synthetic chemistry, a complete listing of their uses is beyond the scope of this survey (see other reports[13,14,24,25]). Some reactions with specific substrates are described here in greater detail merely in the context of elucidating the reaction mechanism. Throughout this paper, the term "organolithium compounds" is used to denote compounds having a carbon–lithium, a nitrogen–lithium, or an enolate group–lithium bond.

Interaction of Organolithium Compounds with Lithium Alkoxides

Preparation and Properties of $[R^1Li{\cdot}R^2OLi]_x$ Adducts

In mixtures of organolithium compounds and lithium alkoxides, adducts are formed according to Scheme 1.[26–29] This interaction is complex in nature, which stems from the ability of these compounds to form supermolecular aggregates.[30–32] The degree and strength of alkali metal alkoxide aggregation is controlled by the steric requirement of the alkoxy group and the properties of the metal.

$$1/x\,[R^1Li]_x + n\;1/y\,[R^2OLi]_y \rightleftharpoons 1/z\,[R^1Li \cdot n\,R^2OLi]_z$$

Scheme 1

In terms of increasing adduct stability, such systems may be ordered as shown in Scheme 2. Bulky organolithium compounds form adducts less readily than simple ones, whereas the opposite is true for the alkoxides. This is probably due to the fact that the stability of supermolecular aggregates of alkoxides decreases with increased branching, and that this no longer disfavours adduct formation. In accordance with these conclusions, the adduct composed of butyllithium (BuLi) and lithium *tert*-butoxide (*t*BuOLi) is easily formed, whereas lithium methoxide is unable to form such adducts.

Increasing bulkiness of RLi ↓	C_4H_9Li	+	$(CH_3)_3COLi$	↑ Increasing bulkiness of the alkoxide	**Increasing adduct stability**
	$(CH_3)_2CHLi$	+	$(CH_3)_3COLi$		
	$(CH_3)_3CLi$	+	$(CH_3)_3COLi$		
	C_4H_9Li	+	C_4H_9OLi		
	C_4H_9Li	+	CH_3OLi		

Scheme 2

Structure of the $[C_4H_9Li{\cdot}(CH_3)_3COLi]_x$ Adduct

The structure of this adduct, which is isolable in crystalline form, was investigated by Boche et al. by means of X-ray diffraction analysis.[33] It was found to consist of tetrameric aggregates containing two kinds of Li atoms, some being bound to two C atoms and one O atom, the others to one C atom and two O atoms. The degree of aggregation of this adduct in benzene solution is also equal to four,[28,34] hence a solution structure similar to that in the crystalline state may be anticipated.

Reactivity of $[R^1Li{\cdot}R^2OLi]_x$ Adducts

The interaction of organolithium compounds with lithium alkoxides is also manifested in a change in the reactivity of the former,[35–38] although the effect is not so pronounced in this case. The addition of BuLi to 1,1-diphenylethene was chosen for a systematic investigation of the effect of lithium alkoxides on the reaction rate.[35] The ratios of the respective rate constants obtained in the absence and presence of various Li alkoxides at two different concentrations are given in Table 1. The effects of the lithium alkoxides on the rate of addition of BuLi are seen to be negligible, apart from in the case of lithium (–)-(1*R*)-menthoxide. At the lower concentration used, even this effect became very slight.

Table 1. Rate constants for the addition of butyllithium (BuLi) to 1,1-diphenylethene (DPE) in the presence of lithium alkoxides (ROLi)

R	ROLi[a] [10^{-2} mol/L]	BuLi [10^{-2} mol/L]	DPE [10^{-2} mol/L]	k_m/k[b]
(–)-(1*R*)-Menthyl	15.0	15.0	0.1010	4.65
(–)-(1*R*)-Menthyl	1.5	1.5	0.0101	1.20
tert-Butyl	15.0	15.0	0.1010	1.70
tert-Butyl	1.5	1.5	0.0101	0.93
Butyl	12.3[c]	15.0	0.1010	1.43
Butyl	1.1[c]	1.5	0.0101	0.82

[a] In benzene at 29 °C. [b] k_m and k are the rate constants for the addition of butyllithium to DPE in the presence and absence of ROLi, respectively. [c] Saturated solution of lithium butoxide in the corresponding butyllithium solution.

Thus, in summary, it can be stated that lithium alkoxides influence the reactivity of BuLi only to a small extent.

Reaction of Organolithium Compounds with Heavy Alkali Metal Alkoxides – Formation of Superbases

Exchange of Li by Na, K, Rb, Cs

In continuation of the above investigation, it was found that heavy alkali metal alkoxides, in contrast to lithium alkoxides, increase the reactivity of organolithium compounds to a great extent, by a factor of more than 10^6. This is due to another reaction, which occurs in such systems after formation of an initial adduct (similar to the adducts with lithium alkoxides), namely a lithium–heavy alkali metal interchange as generalized in Scheme 3.[3–7,39–43] This interchange gives rise to organic compounds of heavy alkali metals and lithium alkoxides. It was first observed with organolithium compounds containing a C–Li bond, as that in BuLi.[3–6] Subsequently, it was also verified for compounds with an N–Li bond, as that in lithium diisopropylamide,[40] and finally it was found to occur with lithium enolates of esters[42] or ketones, such as lithiated pinacoline.[43] The structure of the starting heavy alkali metal alkoxide may also be varied, tertiary alkoxides being most suited for practical applications, while methoxides are unsuitable. Hence, the validity of this metal interchange scheme is quite general. The systems ($R^1Li + R^2OM$) are often called Superbases due to their increased reactivities.

$$R^1Li + R^2OM \rightarrow R^1M + R^2OLi \qquad (M = Na, K, Rb, Cs)$$

R^1Li represents compounds with C–Li, or N–Li, as well as enolate group $-Li\left(\left[>C{=}C(Y){-}O\right]-Li\right.$, where Y = OR or R) bonds. R^2OM is a tertiary, secondary or primary alkoxide (methoxides excluded).

Scheme 3

Thus, the reactions according to Scheme 4 may proceed.

$$C_4H_9Li + (CH_3)_2(C_2H_5)CONa \text{ (or K)} \rightarrow C_4H_9Na \text{ (or K)} + (CH_3)_2(C_2H_5)COLi$$

$$(iso\text{-}C_3H_7)_2NLi + (CH_3)_3CONa \text{ (or K)} \rightarrow (iso\text{-}C_3H_7)_2NNa \text{ (or K)} + (CH_3)_3COLi$$

$$(CH_3)_2CLiCOOC_2H_5 + (CH_3)_3CONa \text{ (or K)} \rightarrow (CH_3)_2CNa(\text{or K})COOC_2H_5 + (CH_3)_3COLi$$

Scheme 4

This metal interchange takes place not only in hydrocarbon media, from which the reaction product is precipitated, but also in media in which the product remains in solution, as has been verified either by EPR[16] or NMR[15,44] spectroscopy. These results indicate that separation of the reaction product is not the only driving force for the metal interchange.

An SB based on 2-ethylhexyllithium has recently been developed, which exhibits good solubility even in aliphatic hydrocarbons in the absence of any additive[41] (2-ethylhexylsodium is known to be soluble in hexane[45]). This modification is very convenient for reactions of SBs with organic substrates, particularly with those that are insoluble in hydrocarbons. Alternative solvent systems (e.g. with electron-donating solvents at low temperatures) are not compatible with all compounds.

Synthesis of Heavy Alkali Metal Organic Compounds Through Metal Interchange

Organic compounds of heavy alkali metals formed by metal interchange (Scheme 3) can in some cases be isolated in high yield and in a high state of purity,[5–7,39–43] making this a method of choice for their preparation. The procedure is extremely simple: hydrocarbon solutions of the organolithium compound and the heavy alkali metal alkoxide (both ca. 1 M) are mixed under stirring at room temperature; the insoluble product typically separates within a few minutes and can be collected by filtration. It should be noted that the purities of the starting compounds and solvents are of critical importance with regard to the quality of the product. Heavy alkali metal alkoxides soluble in hydrocarbons, such as potassium 2-methyl-2-butoxide (*tert*-pentoxide) (*t*PeOK) or menthoxide (rather than *t*BuOK) are best suited for the metal interchange and give rise to pure organopotassium compounds.

A number of pure heavy alkali metal organic compounds have been prepared through such metal interchange: compounds with a C–heavy alkali metal bond may be obtained from *n*-alkyl or aryllithium compounds in good yields (see Table 2). Their heavy alkali metal contents are close to the calculated values and the Li contents are generally less than 0.5%. For further details concerning this reaction, see refs.[47–53] Some organolithium compounds are barely soluble in aliphatic hydrocarbons, such as methyl- or phenyllithium. In these cases, the use of diethyl ether as a solvent or cosolvent has been proposed by Weiss.[54]

Several heavy alkali metal substituted amides have been prepared in benzene solution according to Scheme 3 (Table 3). Metal interchange with lithium amides that are well-soluble in benzene, e.g. lithium diisopropylamide, gives rise to heavy alkali metal amides of high purity in appreciable yields.[40]

Heavy alkali metal enolates of esters and ketones may also be prepared from the corresponding lithium enolates according to Scheme 3 (cf. Table 3 in ref.[7]). However, these compounds are more conveniently prepared by direct metallation of the parent carbonyl compounds with sodium or potassium hexamethyldisilazanes.[42,43]

Interaction of Organopotassium Compounds with Alkali Metal Alkoxides

The behaviour of organopotassium compounds towards alkali metal alkoxides seems to be very variable. Simple alkylpotassium compounds do not form adducts with potassium *tert*-pentoxide (*t*PeOK) or menthoxide, even in an excess of the alkoxide[55] (Scheme 5, Table 2), but do so with a three molar amount of lithium *tert*-pentoxide (*t*PeOLi), as is illustrated in the case of butylpotassium (formed by metal interchange)[56] (Scheme 6).

Table 2. Preparation of alkyl(aryl)sodium and potassium compounds by metal interchange

Reactants[a]			Isolated products				
R^1Li	R^2OM	$[R^2OM]/[R^1Li]$	R^1M	Yield %	Metal content[b] [%] M found	M calcd.	Li
C_4H_9Li	$(CH_3)_3CONa$	1.3	C_4H_9Na	83	28.02	28.70	0.10
$C_8H_{17}Li$	$(CH_3)_2(C_2H_5)CONa$	1.0	$C_8H_{17}Na$[c]	83	16.46	16.88	0.08
$C_{12}H_{25}Li$	$(CH_3)_3CONa$	1.0	$C_{12}H_{25}Na$	59	12.42	11.95	0.29
C_6H_5Li[d]	$(CH_3)_3CONa$	1.5	C_6H_5Na	80	21.5	23.0	0.50
C_4H_9Li	$(CH_3)_2(C_2H_5)COK$	1.0	C_4H_9K[c]	76	40.36	40.65	0.50
C_4H_9Li	$(CH_3)_2(C_2H_5)COK$	3	C_4H_9K[c]	92	41.02	40.65	0.12
$C_8H_{17}Li$	$(CH_3)_2(C_2H_5)COK$	1	$C_8H_{17}K$	88	25.15	25.67	0.26
$C_{12}H_{25}Li$	(–)-(1*R*)-menthoxide K	1.0	$C_{12}H_{25}K$	58	18.7	18.78	0.15

[a] In heptane or cyclohexane at 25 °C. – [b] Atomic absorption spectrometry. – [c] Impurities < 1%. [d] In the presence of diethyl ether (ref. [54]).

Table 3. Preparation of substituted sodium or potassium amides by metal interchange

R^1R^2NM	Yield[a] [%]	Metal content[b] [%] M found	M calcd.	Li	N content[c] [%] found	calcd.
$(iso\text{-}C_3H_7)_2NNa$	68	18.80	18.66	0.15	11.26	11.37
$(iso\text{-}C_3H_7)(C_6H_{11})NNa$	78	14.78	17.08	0.07	8.21	8.58
$(C_6H_{11})_2NNa$	91	11.59	11.31	0.11	6.73	6.89
$(iso\text{-}C_3H_7)(C_6H_{11})NK$	59	22.26	21.80	0.25	7.76	7.81
$(C_6H_{11})_2NK$	74	17.01	17.82	0.17	6.21	6.38

[a] In benzene at 25 °C; $[R^2OM]/[LiNR^1R^3]$ = 1.0–1.3. – [b] Determined by atomic absorption spectrometry. – [c] According to Kjeldahl analysis.

BuLi + (1–3) *t*PeOK → *t*PeOLi + (0–2) *t*PeOK + BuK
(no adducts formation)

Scheme 5

BuLi + *t*PeOK + 2 *t*PeOLi → (Bu, *t*PeO)(Li, K) (mixed adduct)

Scheme 6

This mixed aggregate was isolated and was found to have an Li/K molar ratio of ca. 1.4 and a Bu/*t*PeO group ratio of ca. 1.2.

Benzyl- and phenylpotassium (formed by arene metallation by SB) behave in just the opposite manner: they do not react with *t*PeOLi (even in excess), but do form adducts with excess *t*PeOK[41,57] (Scheme 7).

BuLi + *t*PeOK + $PhCH_3$ → BuH + *t*PeOLi + $PhCH_2K$

but: BuLi + 3 *t*PeOK + $PhCH_3$ →
BuH + *t*PeOLi + [$PhCH_2K \cdot n$ *t*PeOK]

PhK + *t*PeOK → [PhK · *n* *t*PeOK]

Scheme 7

The mixed benzylpotassium + *t*PeOK adduct was isolated as a microcrystalline solid; after hydrolysis a $PhCH_3$/*t*PeOH ratio of ca. 1.6 and an Li content of 0.4% were found.

Reaction of Superbases with Substrates

General Aspects and Synthesis of Heavy Alkali Metal Derivatives of the Substrates

It is well-known that heavy alkali metal organic compounds are much more reactive than the corresponding lithium derivatives. The formation of such a compound in the system organolithium compound + heavy alkali metal alkoxide is the predominant reason for the high reactivity of SBs towards organic substrates.[5,44,56]

These reactions may be very different in nature (Scheme 8). Some examples, not covering all the potential applications, are hydrogen–metal exchange (metallation), addition to multiple C=C or other bonds, Wurtz-type coupling with organic halides (even with non-activated halides such as BuBr), and the initiation of anionic polymerization.

$R^1Li + R^2OM + R^3H \rightarrow R^1H + R^2OLi + R^3M$ [$pK(R^1H) > pK(R^3H)$]

$R^1Li + R^2OM + (C_6H_4)_2C{=}CH_2 \rightarrow (C_6H_4)_2CM{-}CH_2{-}R^1 + R^2OLi$

$R^1Li + R^2OM + R^3X \rightarrow R^1{-}R^3 + MX + R^2OLi$ + side-products (X = Br, I)

$R^1Li + R^2OM + n\ CH_2{=}C(CH_3)COOCH_3 \rightarrow R^1{-}[{-}CH_2{-}(CH_3)COOCH_3){-}]_{n-1}{-}CH_2{-}(CH_3)COOCH_3)M + R^2OLi$ (M = Na, K, Rb, Cs)

Scheme 8

A common feature of all the reactions shown in Scheme 8 is that the resulting derivative of the substrate contains predominantly the heavy alkali metal.[5–7,41] This was confirmed by determining the individual alkali metals in the organometallic products isolated prior to protolysis. Hence, metal interchange must also be involved in reactions of SBs with organic substrates. These reactions can thus be used for the preparation of heavy alkali metal derivatives of the substrates. Some examples are shown in Table 4, where the isolated yields of the organometallic products are good, their heavy alkali metal contents are in good agreement with the calculated values, and the Li contents are below

Table 4. Reaction of organic compounds of lithium (R^1Li), heavy alkali metal alkoxides (R^2OM), and organic substrates

Reactants			Product	Yield	Metal content[a] [%]		
R^1Li	R^2OM	Organic substrate		[%]	M found	M calculated	Li
C_4H_9Li	$(CH_3)_3COK$	$C_6H_5CH_3$	$C_6H_5CH_2K$	93	28.35	30.02	0.40
C_4H_9Li	(-)(1*R*)-menthoxide K	C_6H_6	C_6H_5K	89	31.20	33.65	0.37
C_4H_9Li	(-)(1*R*)-menthoxide K	$C_6H_5CH(CH_3)_2$	$C_6H_5CK(CH_3)_2$[b]	92	22.30	24.70	0.44
C_4H_9Li	$(CH_3)_2(C_2H_5)ONa$	$Ph_2C{=}CH_2$	$Ph_2CNaC_5H_{11}$	86	7.90	8.83	0.08
$C_4H_9CH(C_2H_5)CH_2Li$	$CH_2(C_2H_5)COK$	$C_6H_5CH_3$	$C_6H_5CH_2K$	99	28.27	30.02	0.19
$(iso\text{-}C_3H_7)_2NLi$	$(CH_3)_3COK$	$C_6H_5CH_3$	$C_6H_5CH_2K$[c]	89	29.85	30.02	0.37
$(CH_3)_2(C{=}C(OCH_3){-}O)Li$	$(CH_3)_3COK$	$CH_2{=}C(CH_3){-}COOCH_3$	PMMA[d]				

[a] By atomic absorption spectrometry in the isolated organometallic product. – [b] Mixture of regioisomers. – [c] Nitrogen content 1.26%, i.e. contaminated with a small amount of potassium diisopropylamide. – [d] Poly(methyl methacrylate) obtained in a higher limiting conversion than in the absence of the alkoxide and with a microstructure corresponding to organopotassium initiators.

0.5%. For other examples of the preparation of heavy alkali metal organic compounds, see refs.[58,59] Conversely, there are also cases where the product composition does not match the calculated values and depends rather strongly on the reaction conditions, as will be shown below.

The substrate metallated with the SB may alternatively be reacted with an electrophile without isolation, and this is the way in which SBs are most often used in organic synthesis (see refs.[13,14,24,25]).

In principle, reactions of SBs with substrates can be carried out in one of two different ways. In Method A, the organolithium compound and heavy alkali metal alkoxide are mixed in an appropriate solvent prior to addition of the substrate. In Method B, one component of the SB is mixed with the substrate first, and only then is the other component of the SB added. In the latter case, the SB acts in statu nascendi[56,60] and shows slightly higher reaction rates; however, the conditions in the course of the reaction are neither constant nor well defined.

Typical procedures for the reaction of substrates with SBs are as follows: the substrate (in excess relative to R^1Li, if possible) is mixed with the SB components (according to Method A or B), the ratio R^2OM/R^1Li being 1.1–1.3 (for synthesis of the organometallic compound) or 2–3 (for use in organic synthesis; see below), in an appropriate solvent (typically an aliphatic hydrocarbon) at room temperature and the resulting mixture is stirred for 0.5–3 h under an inert gas. Potassium *tert*-pentoxide is preferred to *t*BuOK. Prolonged stirring and/or an increase in the temperature do not generally increase the yield but lead only to more side reactions. Ethereal solvents may be used at lower reaction temperatures and with substrates having a higher C–H acidity. Generally speaking, better yields of the desired metallated compounds are obtained with substrates having less sterically hindered and more acidic reaction sites and under conditions that favour the metallation (e.g. with an excess of the substrate in cases, where only monometalation is attempted).

Reactions of Superbases with Aromatic Hydrocarbons

The metallation of aromatic hydrocarbons has been studied in detail in order to elucidate the mechanism of SB reactions. This investigation involved the isolation of metallated substrates prior to their hydrolysis and analysis.

Metallation of toluene with the SB derived from 2-ethylhexyllithium (EtHexLi) and *t*PeOK was investigated first.[41] Table 5 highlights the key finding that under all conditions used for these experiments, relatively pure benzylpotassium with a low Li content was formed. The quality of the benzylpotassium was not affected even at ratios of *t*PeOK/EtHexLi below unity, e.g. at a ratio of 0.3. In this case, however, the yield of benzylpotassium was lower and corresponded exactly to the amount of potassium alkoxide present. This shows that potassium alkoxide actually participates in the metallation in a stoichiometric amount and is not merely a catalyst. As soon as all the potassium alkoxide is consumed, no further metallation takes place in spite of the presence of some remaining organolithium compound. Thus, metal interchange is substantial for reactions of SBs with organic substrates.

The reduced concentration of potassium alkoxide in an SB is also reflected in an extraordinarily decreased rate of metallation. Using equimolar amounts of the alkoxide and EtHexLi, the metallation of toluene is complete within ca. 10 min. However, with an SB containing only 0.3 equivalents of the alkoxide, the limiting yield of benzylpotassium was only obtained after more than 20 h.

The product of toluene metallation using an SB containing an excess of *t*PeOK was analyzed in a similar manner. With a small excess of this alkoxide, e.g. 1.3 molar, the quality of benzylpotassium formed remained virtually unchanged. On the other hand, with a large excess, e.g. 3

Table 5. Metallation of toluene with 2-ethylhexyllithium (EtHexLi) and potassium *tert*-pentoxide (*t*PeOK)

Reaction conditions[a]			Reaction product[b]					
[*t*PeOK]/ [EtHexLi]	[PhCH]$_3$/ [*t*PeOK]	Time [h]	Yield of solid[c] [%]	Metal content[d] [%]		[K]/[Li]	Content[e] [mol-%]	
				K	Li		$PhCH_3$	*t*PeOH
0.3	5	1	20	27.1	0.6	8.0	98	2.0
0.3	5	23	29	27.2	0.5	9.7	87	0.5
0.6	5	1	60	27.6	0.5	9.8	97	2.0
1.0	5	1	100	28.3	0.2	25.0	95	2.8
1.0	1	1	100	28.8	0.2	25.5	84	4.8
3.0	5	1	138[f]	28.6	0.4	12.7	70[f]	42[f]

[a] In heptane at 20 °C. – [b] Isolated as a solid before hydrolysis. – [c] Calculated as $PhCH_2K$, relative to EtHexLi. – [d] By atomic absorption spectrometry. – [e] By GLC after hydrolysis of the isolated product. – [f] Adduct of $PhCH_2K$ with *t*PeOK.

molar, an adduct of benzylpotassium with the excess of potassium alkoxide was isolated following toluene metallation. This excess of *t*PeOK in the SB causes an approximately 10-fold increase in the rate of toluene metallation in comparison with the SB composed of equimolar amounts of the components.

Further, the effect of lithium alkoxide concentration on the rate of toluene metallation with the SB prepared from BuLi and *t*PeOK was investigated.[56] The molar ratio of lithium *tert*-pentoxide (*t*PeOLi) to butylpotassium in the SB was varied in the range 7:1 to 0:1, either through the addition of an excess of the lithium alkoxide or by removing the lithium alkoxide from the SB reaction mixture by repeated washing prior to toluene addition. It would appear (Table 6) that the toluene metallation rate is influenced only slightly by the lithium alkoxide, and that the metallation rate in the presence of excess of the lithium alkoxide is decreased rather than increased. It should be stressed that the reactivity of neat butylpotassium, as obtained by complete removal of the *t*PeOLi after the metal interchange by washing, is of the same order of magnitude as that of the equimolar butylpotassium + *t*PeOLi mixture formed according to Scheme 3. Thus, in contrast to the potassium alkoxide, lithium alkoxide does not play a substantial role for the high reactivity of the SB.

Metallations of other aromatic hydrocarbons were investigated by employing the same procedure. Table 7 shows that the metallation of benzene is much more dependent on the reaction conditions than that of toluene.[57,61] In the case of benzene, the concentration of the substrate plays a most important role. Phenylpotassium was obtained in good yield and in a highly pure state at the highest benzene concentrations, e.g. if benzene was used as a solvent. With decreasing benzene concentration, the amounts of lithium and alkoxides in the product increased. These parameters could be somewhat improved by using a higher concentration of the potassium alkoxide; however, other conditions did not affect the product quality to any significant extent. Metallations of other aromatic hydrocarbons, such as cumene[62] or naphthalene,[55] with SBs were found to be even less straightforward (Table 8). Thus, optimal conditions for the metallation of aromatic hydrocarbons have to be assessed in each individual case.

Table 6. Metallation of toluene with Superbases prepared from butyllithium and alkali metal alkoxides followed by reaction with methyl iodide

Starting base system	molar ratio	Actual base system[a]	molar ratio	Method/ base form[b]	Conversion[c] [%]	$t_{1/2}$ [h]	Rate factor[d]	Product yield[e] [mol-%]		
								PhEt	xylenes	others[f]
BuLi		BuLi		A/sol.	0	$>>10^4$	$<<10^{-6}$	0	0	0
BuLi + *t*PeOLi	1:3	BuLi + *t*PeOLi	1:3	A/sol.	0	$>>10^4$	$<<10^{-6}$	0	0	0
BuLi + *t*PeOLi + *t*PeOK	1:6:1	BuK + *t*PeOLi	1:7	A/sol.	67	0.13	0.3	44	21	2
BuLi + *t*PeOLi + *t*PeOK	1:3:1	BuK + *t*PeOLi	1:4	A/sol.	67	0.072	0.5	46	21	0
BuLi + *t*PeOK	1:1	BuK + *t*PeOLi	1:1	A/insol.	73	0.036	1.0	43	18	12
BuLi + *t*PeOK	1:1	BuK[g]		A/insol.	71	0.042	0.9	54	8	9
BuLi + *t*PeOK	1:3	BuK + *t*PeOK + *t*PeOLi	1:2:1	A/insol.	96	0.005	7.2	86	2	8
BuLi + *t*PeOK	1:1	–		B/sol.	76	0.017	2.1	39	17	20
BuLi + *t* BuOLi + *t*PeOK	1:3:1	–		B/sol.	77	0.10	0.4	32	13	32

[a] After reaction according to Scheme 3. – [b] Method A: [BuLi + *t*PeOK] + toluene; Method B: [BuLi + toluene] + *t*PeOK; solution or insoluble; both in heptane at 20 °C. – [c] Toluene conversion after 30 min. – [d] $F = t_{1/2}$ (standard)/$t_{1/2}$. – [e] Reaction mixture quenched with methyl iodide 30 min. after toluene addition. – [f] 100 – (unchanged toluene + ethylbenzene + xylenes). – [g] *t*PeOLi removed before toluene addition by washing with heptane under strictly inert conditions.

A marked improvement in the product quality was observed when a small amount of diethyl ether was present during the metallation (Table 8).[55,57] In this way, the amounts of Li and other impurities present in the product could be halved or reduced even further.

The described dependence of the product composition on the substrate structure and reaction conditions may be re-

Table 7. Metallation of benzene with 2-ethylhexyllithium (EtHexLi) and potassium *tert*-pentoxide (*t*PeOK)

Reaction conditions[a]		Reaction product[b]			
[PhH]/ [EtHexLi]	[*t*PeOK]/ [EtHexLi]	Yield of solid[c] [mol-%]	[K]/[Li]	Content[d] [mol-%] PhH	*t*PeOH
31	1	97	12.3	93	3.4
5	1	98	5.9	86	5.5
1	1	90	2.4	82	11.3
1	1.3	91	6.6	77	10.4

[a] In heptane at 20 °C, 1 h. – [b] Isolated as a solid before hydrolysis. – [c] Calculated as PhK, relative to EtHexLi. – [d] After hydrolysis of the isolated product, determined by GLC.

Table 8. Metallation of aromatic hydrocarbons (ArH) with alkyllithium compounds (RLi) and potassium *tert*-pentoxide (*t*PeOK) and the influence of diethyl ether (Et_2O)

Reaction conditions[a]				Reaction product[b]	
ArH	RLi	[*t*PeOK]/ [RLi]	[Et_2O]/ [RLi]	Yield[c] [mol-%]	[K]/[Li]
Benzene	EtHexLi	1	0	90	2.4
Benzene	EtHexLi	1	6	70	8.3
Benzene	EtHexLi	1.3	0	91	6.6
Benzene	EtHexLi	1.3	6	82	16.3
Cumene	BuLi	1.1	0	75	4.1
Cumene	BuLi	1.1	6	43	30.5
Naphthalene	BuLi	1.1	0	71	1.9
Naphthalene	BuLi	1.1	6	75	3.0
Naphthalene	BuLi	1.1	15	85	3.1

[a] In heptane at 20 °C, [ArH]/[RLi] = 1. – [b] Isolated as a solid before hydrolysis. – [c] Calculated as ArK, related to RLi.

lated to the ability of organometallic compounds to form supermolecular aggregates. The course of metallation is controlled predominantly by kinetic effects. In those cases where the substrate is metallated slowly, either due to its structure or a low concentration, the concentration of the resulting organometallic product is also low. In this situation, other alkali metal compounds, such as alkoxides or Li compounds, are co-aggregated or co-precipitated with the product to a significant extent, yielding a low-purity product. Solvation of the organic alkali metal compounds with electron-donor solvents such as diethyl ether stabilizes the organometallics at lower degrees of aggregation and increases the metallation rate, which leads to higher product concentrations. Accordingly, the presence of diethyl ether during the metallation of aromatic hydrocarbons has been shown to have a favourable effect on the product purity.

Reactions of Superbases with Olefins

SBs can react with olefins in two different ways: by substitution of an olefinic hydrogen by the alkali metal (see for instance[21,22,25]) or by the addition of SB across the olefinic double bond.

Olefins with polarized double bonds add organometallics across this double bond, giving rise to new organometallic compounds. In some cases, addition of the new organometallic to the olefin may be repeated many times, ultimately leading to polymers (anionic polymerization).

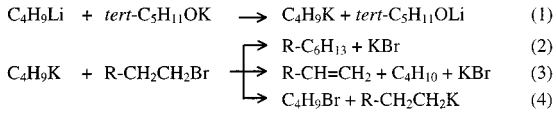
Following reactions of 1,1-diphenylethene (1,1-DPE, anionic polymerization of which is difficult) with SBs prepared from BuLi and *t*PeOK or *t*PeONa, the organometallic products were isolated and analyzed.[55] The results indicated that addition of SB across the double bond was the major reaction rather than hydrogen–metal exchange. The reactivity of the 1,1-diphenylhexylpotassium formed in this reaction was so high that addition to another 1,1-DPE molecule was possible. Thus, reaction of a three-fold molar amount of 1,1-DPE relative to the SB resulted in the predominant formation of 1,1,3,3-tetraphenyloctylpotassium. The lithium content in all isolated products was < 0.4%.

Another example of SB addition across an activated C=C double bond is seen in the anionic polymerization of methyl methacrylate, which is readily initiated by the SBs generated from a lithium ester enolate and sodium or potassium *tert*-butoxides.[7,63,64] The microstructure of the obtained poly(methyl methacrylate) revealed that metal interchange occurred even in this system and that the heavy alkali metal enolate was the active species in this polymerization.

Thus, lithium–potassium (sodium) interchange according to Scheme 3 takes place even in the case of additions of SBs to the C=C double bonds.

Reaction of Superbases with Organic Halides

Non-activated organic halides, such as butyl or octyl bromides, react with BuLi in hydrocarbons only to a negligible extent. If, however, a heavy alkali metal alkoxide is added to such a mixture, a fast or even vigorous reaction commences, in which products of C–C coupling are formed



Scheme 9

(e.g. reaction 2 in Scheme 9), or β-elimination of hydrogen halide (e.g. reaction 3 in Scheme 9) and halogen–metal exchange (e.g. reaction 4 in Scheme 9) take place.[65] Besides these main products, only lithium alkoxide and heavy alkali metal halide are detected in the mixtures prior to hydrolysis. Obviously, at some stage of the reaction the lithium–heavy alkali metal exchange must have occurred (e.g. reaction 1 in Scheme 9).

Under favourable conditions, i.e. with primary or aromatic bromides or iodides, the reaction can be conducted in such a way that a high yield of the C–C coupling product is obtained, e.g. over 80%. Hence, the reaction between SBs and organic halides may be regarded as an improvement of the Wurtz hydrocarbon synthesis.

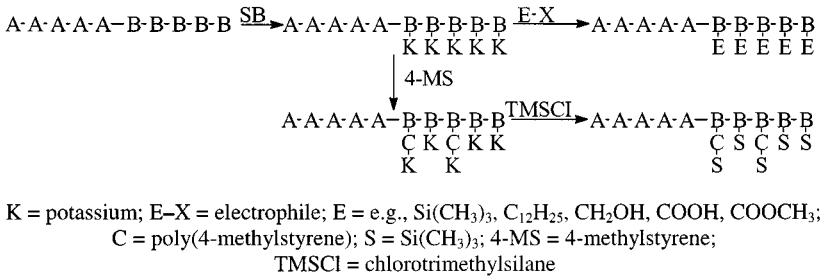
Use of Superbases in Polymer Chemistry

It emerged that SBs are also useful in polymer chemistry as initiators of anionic polymerization.[1,66–68] Another, even more promising use of SBs in polymer chemistry lies in the chemical modification of some polymers.

A suitable reagent for the metallation of some non-polar polymers was found about two decades ago, namely a mixture of BuLi and *N,N,N,N*-tetramethylethylenediamine (TMEDA).[69–71] SBs prepared from organolithium compounds and potassium alkoxides, however, seem to be superior to the TMEDA reagent because of higher reactivity, efficiency,[23,55] and regioselectivity.[72]

The procedure for multi-site functionalization of polymers using SBs involves two steps: (i) metallation of the polymer with the SB, which results in a multi-site potassium-metallated polymer, and (ii) in situ reaction of the metallated intermediate with an electrophile, giving rise to the multi-site functionalized polymer.[62] A similar procedure was suggested independently by Nemes.[73] Due to the high reactivity of the carbon–potassium bond in the metallated intermediate, the choice of electrophiles for step (ii) is wide and polymers with diverse functional groups are easily accessible. The procedure has been applied to various polymers, such as polystyrene,[62] polybutadiene,[74] poly(4-methylstyrene),[55] and polyether dendrimers.[75,76] In this way, polymers randomly substituted to various degrees with diverse functional groups are obtained in a simple one-pot process.

Non-polar copolymers, both random and block (e.g. A–B), can likewise be multi-site-functionalized employing a method similar to that described for homopolymers. If the difference in C–H acidities of various units (blocks) is sufficiently high ($pK_A - pK_B > 2$), it is possible to selectively metallate the more acidic units in the copolymer by appropriate choice of the SB.[72] For instance, the methyl groups in the block copolymer polystyrene-*block*-poly(4-methylstyrene) are selectively substituted, as illustrated in Scheme 10.



K = potassium; E–X = electrophile; E = e.g., $Si(CH_3)_3$, $C_{12}H_{25}$, CH_2OH, COOH, $COOCH_3$;
C = poly(4-methylstyrene); S = $Si(CH_3)_3$; 4-MS = 4-methylstyrene;
TMSCl = chlorotrimethylsilane

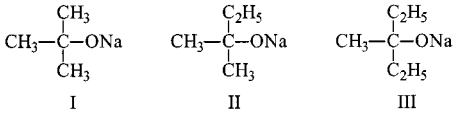
Scheme 10

The metallated (co)polymer intermediate is also effective as a multifunctional initiator of anionic polymerization, giving rise to grafted (co)polymers. In Scheme 10, this is shown for the case of grafting a block copolymer.[77]

By virtue of the great flexibility of the method, an appreciable number of novel random or block copolymers or diverse structures made up of selectively grafted (co)polymers can be prepared.

More Effective Modifications of Superbases (Second-Generation SBs)

The reactivity of an SB not only depends on the structure of the parent organolithium compound, it is also influenced by the alkoxide component. The effect of the structure and concentration of the heavy alkali metal alkoxide on SB properties has been investigated[8–11,56] using sodium alkoxides of structures I, II, and III (Scheme 11).



Scheme 11

In order to assess the SB reactivity, the time–conversion dependence in the reaction of modified SBs with organic halides was monitored. Some results are shown in Figure 1,

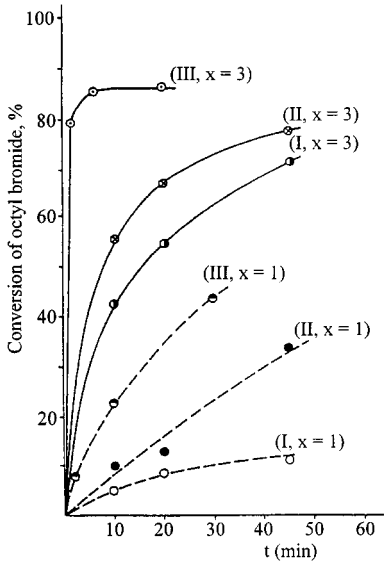


Figure 1. Conversion of octyl bromide in the reaction with various Superbases [C_4H_9Li + *x* RONa] in heptane at –30 °C (by Br ion determination); R = *tert*-butyl (I), *tert*-pentyl (II), 3-methylpentan-3-yl (III) (see Scheme 11); *x* = 1 or 3

in which the time–conversion curves for the reaction of octyl bromide with SBs of various compositions are plotted. It can clearly be seen that the reaction rate increases with the alkoxide concentration in the SB and with the degree of branching of the alkoxide.[9] The corresponding acceleration factors are summarized in Table 9. Rate accelerations caused by a similar modification of the SB could also be observed in metallations of aromatic hydrocarbons.

The effect of the alkoxide structure on SB properties is evidently associated with the degree of substitution on the alkoxide in the vicinity of the OM group. It was mentioned above that the strength of the alkoxide aggregation decreases with increasing substitution. The alkoxide autoaggregation competes with its other interactions and, there-

Table 9. Rates of reaction of octyl bromide with various Superbases [C_4H_9Li + *x* RONa] and yields of dodecane (coupling product) in heptane at –30 °C

RONa R	[RONa]/ [C_4H_9Li] [*x*]	Reaction half-time [min]	Total acceleration factor	Yield of dodecane [%]
tert-butyl	1	> 1000	1	35
tert-pentyl	1	74	> 13	47
3-methylpentan-3-yl	1	40	> 25	55
tert-butyl	3	16	> 60	75
tert-pentyl	3	8	> 125	81
3-methylpentan-3-yl	3	0.8	> 1250	53[a]

[a] An appreciable amount of another reaction product was formed.

fore, these interactions can be expected to be favoured with more substituted alkoxides. The effects and structures of alkoxides I, II, and III (Scheme 11) are in accord with this statement. From a practical point of view, SBs prepared from *tert*-pentoxides appear to be much more suited for metallations than those prepared from *tert*-butoxides.

The structure and concentration of the heavy alkali metal alkoxide also affect the regioselectivity in reactions of SBs with substrates. For instance, in the reaction of an SB with octyl bromide, the yield of dodecane (the expected product of the C–C coupling) increased from 47 to 81% when the alkoxide to BuLi ratio was increased from 1 to 3 (Table 9).[9] Another striking example is the metallation of ethylbenzene (Figure 2).[11] Metallation of this substrate with various SBs followed by quenching with methyl iodide should give rise to cumene. In the reaction using the standard SB derived from BuLi and one equivalent of *t*BuOK, only 30% of cumene was obtained and the limiting conversion of ethylbenzene reached just 65% (curves 1a and 2a). On the other hand, use of a modified SB prepared from BuLi and three equivalents of potassium 3-methyl-3-pentoxide (a more branched alkoxide, akin to structure III in Scheme 11) (*t*MePeOK) under the same conditions resulted in 88% of cumene and a 100% conversion of ethylbenzene (curves 1b and 2b). Moreover, the metallation rate was about 10 times higher using the modified SB compared to that with the standard one.

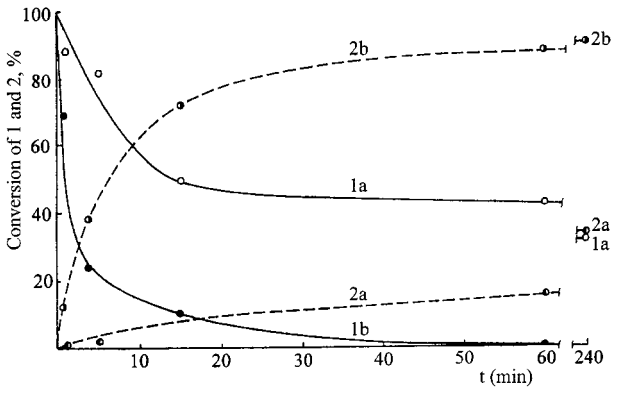


Figure 2. Metallation of ethylbenzene with various Superbases; $[BuLi]_0$ = 0.27 mol/L, heptane, 20 °C, metallation quenched with methyl iodide; curves: 1 (a,b) = ethylbenzene, 2 (a,b) = cumene; curves a: [ethylbenzene]/[BuLi]/[*t*BuOK] = 1:1:1; curves b: [ethylbenzene]/[BuLi]/[potassium 3-methyl-3-pentoxide] = 1:1:3

Consequently, the properties of the first-generation Superbases, prepared using one equivalent of heavy alkali metal *tert*-butoxide, have been considerably improved by using larger amounts of a more branched alkoxide of the same metal. Therefore, the latter can be designated as second-generation Superbases. They are more advantageous in organic and polymer chemistry in that they give higher yields of the desired products in a more straightforward process.

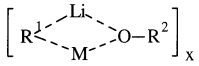
The origins of the novel properties of second-generation Superbases are probably complex. The described effect of heavy alkali metal alkoxides may be due to the formation of new SB supermolecular aggregate species possessing increased reactivities. More probably, however, the reasons may merely be physicochemical in origin, such as a change in the metal interchange equilibrium and/or rate, or a change in the solubilities or degrees of aggregation of the reaction components.

Reaction Mechanism

Mechanism of the Metal Interchange in the System R^1Li + R^2OM

Only limited information is available on the mechanism of the reaction between organolithium compounds and heavy alkali metal alkoxides. The situation is complicated by the autoaggregation of these compounds.

When organolithium compounds interact with heavy alkali metal alkoxides, an intermediate adduct is formed first, which is similar to the adducts of lithium alkoxides (see above) with the simplified structural units shown in Scheme 12. The adduct formation is obviously a dynamic equilibrium reaction.[28] An ab initio computational study of the model system R^1Li + R^2OM (M = Na to Cs) showed that an adduct of the type depicted in Scheme 12 is the most stable in the system.[78] Further transformation of this adduct was not predicted in this study, obviously due to the simplified model structures and conditions (gas phase). Another computational study dealt with the system CH_3Li–CH_3OK, from which it was concluded that an intermediate 1:3 adduct was the most reactive.[79] The X-ray structure of a compound with intramolecular bridging similar to that in Scheme 12 has also been described.[80]



Scheme 12

In the next step, transformation of the [$R^1Li{\cdot}R^2OM$] intermediate according to Scheme 3 takes place. With the assumption that this intermediate has a structure similar to that of the BuLi + *t*BuOLi adduct,[33] the metal atoms bound to two oxygen atoms and one carbon atom could be lithium, while those bound to two carbon atoms and one oxygen atom could be the heavy alkali metal. If this were the case, splitting of the intermediate adduct to an organic heavy alkali metal compound and lithium alkoxide in the following reaction step may easily be envisaged.

The lithium–heavy alkali metal interchange proceeds in the direction opposite to the assumed one because it leads to a product containing a more electropositive heavy alkali metal bound to a less electronegative atom than the oxygen of the alkoxide, i.e. to a carbon or nitrogen atom, or to an enolate group. Therefore, the question of the driving force for this interchange is of great importance. The exchange process is certainly supported by a shift in the reaction equilibria due to the precipitation of the least soluble component in hydrocarbon solvents, which is most often the heavy alkali metal organic compound. However, the metal interchange also takes place in solution[15,16,44] and, therefore, some other effects must also be operative. The formation of an oxygen–lithium bond in the lithium alkoxide could be one of these effects. According to the HSAB principle, this alkoxide would seem to be thermodynamically more stable than the heavy alkali metal alkoxides. Moreover, lithium alkoxides appear as products in all kinds of metal interchange reactions, such as those reported above (Scheme 3). Another factor could be the different stabilities of supermolecular aggregates of various alkali metal alkoxides. The greater stability of lithium alkoxides compared with the corresponding heavy alkali metal alkoxides is reflected in the fact that various aprotic donor solvents have a less pronounced effect on the degree of aggregation of the former.[32]

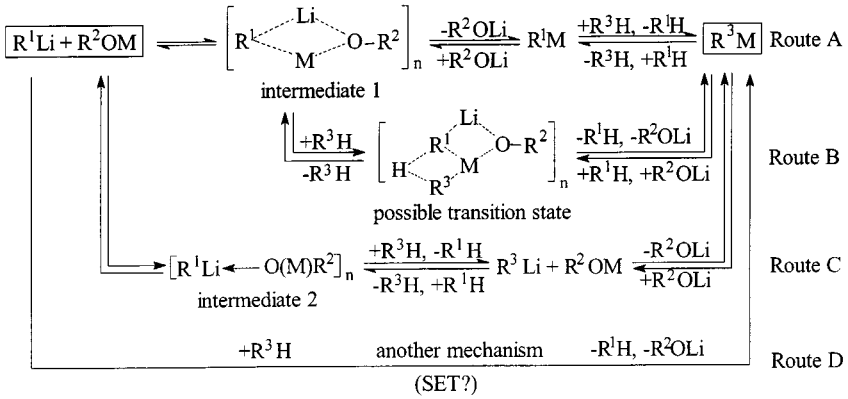
Mechanism of Reactions of Superbases with Organic Substrates

As mentioned above, two procedures can be used for the reaction of an organic substrate with an SB prepared from R^1Li and R^2OM. In Method A, the SB components are mixed first and only then is the substrate added. In this case, the heavy alkali metal organic compound is precipitated following metal interchange prior to addition of the substrate. There are then two possible modes of reaction of the substrate: (i) either the substrate is adsorbed onto the surface of the precipitate and the reaction takes place there, or (ii) the substrate reacts in solution with a very low concentration of the precipitated compound. In neither case can participation of alkali metal alkoxides present in the system be completely ruled out as, for instance, they may change the solubility or adsorption. Indeed, it follows from Table 6 that to some extent these alkoxides influence the behaviour of the organopotassium precipitate in the reaction with toluene: the reaction rate is increased in the presence of an excess of potassium alkoxide and decreased when the lithium alkoxide is in excess. Moreover, a change in the product distribution as a result of the presence of the alkoxides has also been observed,[56] in agreement with an earlier finding.[60] Nevertheless, in all these cases, the organopotassium compound in any form should remain the principal reagent (cf. below).

In the second commonly used procedure, Method B, the organic substrate is mixed with one component of the SB first and only then is the other SB component added. In this case, various routes can be suggested for the transition from the initial to the final stages, the structures of both of which are well established.

In the case of metallation of hydrocarbon R^3H, some of these pathways can be defined as shown in Scheme 13. According to Route A, the intermediate adduct 1 is first decomposed to the lithium alkoxide and the heavy alkali metal compound, which in a further step metallates the hydrocarbon R^3H to give a heavy alkali metal derivative. On the other hand, the intermediate adduct of type 1 (precursor of the C–heavy alkali metal compound) may also react directly with the substrate, yielding the heavy alkali metal derivative of the substrate through a transition state with a structure as that depicted in Scheme 13. This pathway is designated as Route B.

In the intermediate type 2, proposed in ref.,[12] activation of the organolithium compound is assumed to occur through solvation of the heavy alkali metal alkoxide, akin to that by electron-donor solvents (Route C). In this case, metallation should produce a lithium derivative of the substrate. In order to obtain the heavy alkali metal substituted substrate (as is isolated), an additional lithium–heavy alkali metal interchange must be assumed. The reason for this interchange is not clear within this hypothesis. Moreover, this idea does not explain why *t*BuOK increases the reactivity of BuLi through "solvation" to such an enormous extent ($>> 10^6$ times, ref.[56]), whereas *t*BuOLi is almost inactive in this respect (see above). It is questionable as to whether the difference in polarities of the O–Li and O–M bonds (M = Na, K, Rb, Cs) could cause such a change in the



Scheme 13

BuLi behaviour. Consequently, the mechanism of Route C is difficult to rationalize.

Finally, other mechanisms, e.g. those involving single-electron transfer (SET mechanism) cannot be ruled out either and are summarized in Route D.

The isolation of the heavy alkali metal derivative as the final product as well as the stoichiometric participation of the heavy alkali metal alkoxide in the reactions of SBs with organic substrates (see above) would seem to favour Routes A and B.

Structure of the "Active" Species in Reactions of Superbases

Let us summarize principal information on the R^1Li + R^2OM system: (i) After mixing of these components of the SB, metal interchange gives rise to the heavy alkali metal organic compound R^1M, which may be isolated in a pure state by washing. (ii) The organometallic products obtained from reactions of SBs with substrates isolated prior to hydrolysis contain predominantly the heavy alkali metal and only traces of lithium. This is found in reactions of SBs with substrates of different types, i.e. in metallations, in additions to double bonds, and in reactions with organic halides or polymers. (iii) Potassium alkoxide participates in reactions of SBs with substrates in a stoichiometric amount and does not merely act as a catalyst or as an activator of R^1Li. SBs having an R^2OM/R^1Li ratio below unity no longer metallate the substrate once all the R^2OM has been consumed, in spite of some unchanged R^1Li still being present. (iv) The reactivity of R^1Li + R^2OM mixtures is only slightly influenced by the concentration of the lithium alkoxide formed in the metal interchange. For instance, after complete removal of *t*PeOLi, BuK shows approximately the same reactivity as an equimolar mixture of the SB components. Mixtures of BuK with excess *t*PeOLi exhibit a decreased reactivity and, therefore, the formation of such an adduct cannot be responsible for the high SB reactivity. (v) The reactivities of SBs prepared from R^1Li and various R^2OM species increase with increasing concentration and bulkiness of R^2OM. (vi) A detailed NMR investigation of the system generated from triphenylmethyllithium and caesium 3-ethylhept-3-oxide in THF solution has shown that triphenylmethylcaesium and lithium 3-ethyl-3-heptoxide are formed through metal interchange and that they exist as separate species rather than as an adduct.[44]

Considering the points (i) to (vi), it can be concluded that in the reaction of a substrate with the R^1Li + R^2OM system, the metal interchange is the essential step and that the "active" species should be the heavy alkali metal organic compound or a derivative thereof.

When trying to decide which of the possible mechanisms proposed for the reactions of SBs with substrates is in fact correct, it should be borne in mind that the system involves a number of partial reactions, including coordination and aggregation equilibria. This makes the system very flexible. The rate and equilibrium constants may specifically depend on the properties of a given system, i.e. the structures of the reactants, the reaction conditions, and the reaction type. For instance, the extent of participation of Routes A and B in a reaction of an SB with a particular substrate depends primarily on the ratio of the rate constants for cleavage of the intermediate 1 according to Route A and those for direct metallation of the substrate by this intermediate. This ratio may be different in specific cases; thus, a substrate that is metallated more slowly would prefer Route A, while a more readily metallated substrate would be subject to a greater contribution from Route B.

Hence, it is questionable as to whether the reactions of SBs with substrates invariably proceed in exactly the same way. It could also be the case that one mechanism may predominate under certain conditions while another may become more important under other circumstances. Thus, any search for a "single universal active species" in SB reactions is irrelevant. Nevertheless, regardless of the actual path taken by the SB reactions with substrates, the metal interchange must take place at some stage in all cases and is an integral part of the reaction.

Acknowledgments

Financial funding for preparation of this article provided by the Grant Agency of the Czech Republic (Grant No. 203/97/0538) is much appreciated.

[1] C. F. Wofford (to Phillips Petroleum Co.), *US Patent* 3,294.768; appl. November 14, **1963**.
[2] H. L. Hsieh, C. F. Wofford, *J. Polym. Sci., Part A-1* **1969**, *7*, 449.
[3] L. Lochmann, J. Pospíšil, D. Lím, *Czech. Pat.* 132.254; appl. December 30, **1964**; *Chem. Abstr.* **1970**, *73*, 25642f.
[4] J. Báča, L. Lochmann, K. Jůzl, J, Čoupek, D. Lím, Symposium on Macromolecules, Prague, 1965, Preprint No. P 508, submitted June 6, 1965; *J. Polym. Sci., Part C* **1968**, *16*, 3865.
[5] L. Lochmann, J. Pospíšil, D. Lím, *Tetrahedron Lett.* **1966**, 257.
[6] L. Lochmann, D. Lím, *J. Organomet. Chem.* **1971**, *28*, 153.
[7] L. Lochmann, J. Trekoval, *Collect. Czech. Chem. Commun.* **1988**, *53*, 76.
[8] L. Lochmann, *J. Organomet. Chem.* **1989**, *364*, 281.
[9] L. Lochmann, *J. Organomet. Chem.* **1989**, *376*, 1.
[10] H. Andringa, H. D. Verkruijsse, L. Brandsma, L. Lochmann, *J. Organomet. Chem.* **1990**, *393*, 307.
[11] L. Lochmann, J. Petránek, *Tetrahedron Lett.* **1991**, *32*, 1483.
[12] M. Schlosser, *J. Organomet. Chem.* **1967**, *8*, 9.
[13] M. Schlosser, *Pure Appl. Chem.* **1988**, *60*, 1627.
[14] M. Schlosser, *Mod. Synth. Methods* **1992**, *6*, 227.
[15] G. Boche, H. Etzrodt, *Tetrahedron Lett.* **1983**, *24*, 5477.
[16] D. Wilhelm, T. Clark, P. v. R. Schleyer, J. Courtneige, A. G. Davies, *J. Organomet. Chem.* **1984**, *273*, C1.
[17] D. Wilhelm, T. Clark, P. v. R. Schleyer, *J. Chem. Soc., Chem. Commun.* **1983**, 211.
[18] C. Schade, W. Bauer, P. v. R. Schleyer, *J. Organomet. Chem.* **1985**, *295*, C25.
[19] R. Pi, W. Bauer, B. Brix, C. Schade, P. v. R. Schleyer, *J. Organomet. Chem.* **1986**, *306*, C1.
[20] L. Brandsma, H. D. Verkruijsse, C. Schade, P. v. R. Schleyer, *J. Chem. Soc., Chem. Commun.* **1986**, 260.
[21] B. Gordon III, M. Blumenthal, *Polym. Bull. (Berlin)* **1985**, *14*, 69.
[22] J. J. Bahl, R. B. Bates, B. Gordon III, *J. Org. Chem.* **1979**, *44*, 2290.
[23] N. S. Mills, A. R. Rusinko III, *J. Org. Chem.* **1986**, *51*, 2567.
[24] L. Brandsma, H. D. Verkruijsse, *Preparative Polar Organometallic Chemistry*, vol. 1, Springer, Berlin, **1987**.
[25] L. Brandsma, *Preparative Polar Organometallic Chemistry*, vol. 2, Springer, Berlin, **1990**.

[26] T. L. Brown, J. A. Ladd, G. M. Newman, *J. Organomet. Chem.* **1965**, *3*, 1.
[27] M. Y. Darensbourg, B. Y. Kimura, G. E. Hartwell, T. L. Brown, *J. Am. Chem. Soc.* **1970**, *92*, 1236.
[28] J. F. McGarrity, C. A. Ogle, *J. Am. Chem. Soc.* **1985**, *107*, 1805.
[29] L. Lochmann, J. Pospíšil, J. Vodňanský, J. Trekoval, D. Lím, *Collect. Czech. Chem. Commun.* **1965**, *30*, 2187.
[30] G. E. Coates, K. Wade, *Organometallic Compounds*, vol. I, Methuen, London, **1967**.
[31] W. N. Setzer, P. v. R. Schleyer, *Adv. Organomet. Chem.* **1985**, *24*, 353; cf. also: C. Schade, P. v. R. Schleyer, *Adv. Organomet. Chem.* **1987**, *27*, 169.
[32] V. Halaška, L. Lochmann, D. Lím, *Collect. Czech. Chem. Commun.* **1968**, *33*, 3245.
[33] M. Marsch, K. Harms, L. Lochmann, G. Boche, *Angew. Chem.* **1990**, *102*, 334; *Angew. Chem. Int. Ed. Engl.* **1990**, *29*.
[34] V. Halaška, L. Lochmann, *Collect. Czech. Chem. Commun.* **1973**, *38*, 1780.
[35] L. Lochmann, R. Lukáš, *Collect. Czech. Chem. Commun.* **1972**, *37*, 569.
[36] J. F. McGarrity, C. A. Ogle, Z. Brich, H.-R. Loosli, *J. Am. Chem. Soc.* **1985**, *107*, 1810.
[37] H. L. Hsieh, *J. Polym. Sci. A-1* **1970**, *8*, 533.
[38] P. Caubére, *Chem. Rev.* **1993**, *93*, 2317.
[39] L. Lochmann, J. Trekoval, Czechoslovak Discovery No. 60, Czechoslovak Bureau of Patents and Discoveries, Prague, **1991**.
[40] L. Lochmann, J. Trekoval, *J. Organomet. Chem.* **1979**, *179*, 123.
[41] L. Lochmann, J. Trekoval, *J. Organomet. Chem.* **1987**, *326*, 1.
[42] L. Lochmann, J. Trekoval, *J. Organomet. Chem.* **1975**, *99*, 329.
[43] L. Lochmann, R. L. De, J. Trekoval, *J. Organomet. Chem.* **1978**, *156*, 307.
[44] W. Bauer, L. Lochmann, *J. Am. Chem. Soc.* **1992**, *114*, 7482.
[45] Eur. Patent Appl. 41306; *Chem. Abstr.* **1981**, *96*, 123007. Preparation of a heptane solution of 2-ethylhexylsodium was checked in the author's laboratory. Protolysis of this solution gave almost the expected amount of 3-methylheptane.
[46] L. Lochmann, J. Čoupek, D. Lím, *Collect. Czech. Chem. Commun.* **1970**, *35*, 733.
[47] H. F. Ebel, *Methoden Org. Chem. (Houben-Weyl)*, **1970**, vol. XIII/1, p. 388.
[48] W. H. Glaze, D. P. Duncan, *J. Organomet. Chem.* **1975**, *99*, 11.
[49] S. H. Bertz, Ch. P. Gibson, G. Dabbagh, *Organometallics* **1988**, *7*, 227.
[50] E. Weiss, G. Sauermann, *Chem Ber.* **1970**, *103*, 265.
[51] E. Weiss, G. Sauermann, *J. Organomet. Chem.* **1970**, *21*, 1.
[52] E. Weiss, H. Koester, *Chem. Ber.* **1977**, *110*, 717.
[53] E. Weiss, G. Sauermann, G. Thirase, *Chem. Ber.* **1983**, *116*, 741.
[54] G. Thirase, E. Weiss, *J. Organomet. Chem.* **1974**, *81*, C1.
[55] L. Lochmann, unpublished results.
[56] L. Lochmann, H. Jakubův, L. Brandsma, *Collect. Czech. Chem. Commun.* **1993**, *58*, 1445.
[57] L. Lochmann, *Collect. Czech. Chem. Commun.* **1987**, *52*, 2710.
[58] D. Hoffmann, W. Bauer, F. Hampel, N. J. R. van Eikema Hommes, P. v. R. Schleyer, P. Otto, U. Pieper, D. Stalke, D. S. Wright, R. Snaith, *J. Am. Chem. Soc.* **1994**, *116*, 528.
[59] D. Bucca, B. Gordon III, *Macromolecules* **1994**, *27*, 862.
[60] M. Schlosser, S. Strunk, *Tetrahedron Lett.* **1984**, *25*, 741.
[61] L. Lochmann, M. Fossatelli, L. Brandsma, *Recl. Trav. Chim. Pays-Bas* **1990**, *109*, 529.
[62] L. Lochmann, J. M. J. Fréchet, *Macromolecules* **1996**, *29*, 1767.
[63] L. Lochmann, M. Rodová, J. Trekoval, *J. Polym. Sci., Polym. Chem. Ed.* **1974**, *12*, 2091.
[64] L. Lochmann, D. Doskočilová, J. Trekoval, *Collect. Czech. Chem. Commun.* **1977**, *42*, 1355.
[65] L. Lochmann, J. Trekoval, *Collect. Czech. Chem. Commun.* **1986**, *51*, 1439.
[66] B. Gordon III, J. E. Loftus, D. Bucca, *Polym. Prepr.* **1988**, *29(2)*, 21.
[67] I. Yu. Kirchevskaya, A. R. Samotsvetov, N. P. Seredina, N. I. Urazov, V. P. Shatalov, *Vysokomol. Soedin., Ser. A* **1976**, *18*, 1844; *Chem. Abstr.* **1976**, *85*, 178051o.
[68] T. C. Cheng, A. F. Halasa, *J. Polym. Sci., Polym. Chem. Ed.* **1976**, *14*, 573.
[69] M. J. Farral, J. M. J. Fréchet, *J. Org. Chem.* **1976**, *41*, 3877.
[70] G. Clouet, J. Brossas, *Makromol. Chem.* **1979**, *180*, 867.
[71] G. J. Beinert, J. G. Zilliox, J. E. Herz, *Makromol. Chem.* **1993**, *194*, 3184.
[72] L. Lochmann, M. Janata, P. Holler, Z. Tuzar, P. Kratochvíl, *Macromolecules* **1996**, *29*, 8092.
[73] S. Nemes, J. Borbély, J. Borda, T. Kelen, *Polym. Bull. (Berlin)* **1991**, *27*, 123.
[74] A. F. Halasa, G. B. Mitchell, M. Stayer, D. P. Tate, A. E. Oberster, R. W. Koch, *J. Polym. Sci., Polym. Chem. Ed.* **1976**, *14*, 497.
[75] L. Lochmann, K. L. Wooley, P. T. Ivanova, J. M. J. Fréchet, *J. Am. Chem. Soc.* **1993**, *115*, 7043.
[76] J. M. J. Fréchet, L. Lochmann, V. Šmigol, F. Švec, *J. Chromatogr. A* **1994**, *667*, 284.
[77] M. Janata, L. Lochmann, J. Brus, P. Holler, Z. Tuzar, P. Kratochvíl, B. Schmitt, W. Radke, A. H. E. Müller, *Macromolecules* **1997**, *30*, 7370.
[78] T. Kremer, S. Harder, M. Junge, P. v. R. Schleyer, *Organometallics* **1996**, *15*, 585.
[79] G. Ghio, G. Tonachini, P. Venturello, *Tetrahedron* **1996**, *52*, 7053.
[80] S. Harder, A. Streitwieser, *Angew. Chem. Int. Ed. Engl.* **1993**, *32*, 1066.

Received September 30, 1999
[I99340]

The Formation of a Solid from the Reaction $SiCl_4(g) + O_2(g) \rightarrow SiO_2(s) + 2Cl_2(g)$

Michael Binnewies*[a] and Karl Jug[b]

Dedicated to Prof. Dr. Heinrich Vahrenkamp on the occasion of his 60th birthday

Keywords: Growth pattern / Chemical vapor deposition / Silicon / Chlorine / Oxygen / Thermochemistry

The formation of a solid by the reaction of small gaseous molecules during a CVD or CVT experiment is a highly complicated process. In the case of the combustion of silicon(IV) chloride in oxygen, which leads to solid silicon dioxide, hundreds of intermediate chlorosiloxanes have been detected. On the basis of their compositions, structures, and stabilities, growth mechanisms of Si–O networks can be derived. The stepwise formation of solid SiO_2 can be described in terms of three basic reactions: (i) formation of highly reactive $O{=}SiCl_2$, (ii) insertion of $O{=}SiCl_2$ into an Si–Cl bond, and (iii) thermally induced elimination of $SiCl_4$ from the resulting chlorosiloxanes.

1. Introduction

Although solid-state chemistry has been largely concerned with the structures, physical and chemical properties, and broad applications of solids, over the past 30 years solid-state chemists have become increasingly interested in their formation and in the intermediates involved during the formation process. Nowadays, cluster compounds are considered and discussed as connecting links between molecules and solids. Whereas these were considered as rare exceptions in the 1960s,[1] more and more examples have been found, in particular as a result of the impressive development in the area of X-ray analysis, of substances that can be classified as cluster compounds. The principle of condensed clusters[2] accounts for their role as links between molecules and solids. Colloids, as examples of giant clusters with 10^3 to 10^9 atoms, are also included in the discussion.[3] In general, clusters represent small fragments of the structures of solids. From the present viewpoint, it can be stated that the traditional separation between molecules and solids is nei-

[a] Institut für Anorganische Chemie, Universität Hannover, Callinstraße 9, D-30167 Hannover, Germany
Fax: (internat.) +49-511/762-19032
E-mail: binn@mbox.aca.uni-hannover.de
[b] Theoretische Chemie, Universität Hannover, Am Kleinen Felde 30, D-30167 Hannover, Germany
Fax: (internat.) +49-511/762-5939



Michael Binnewies studied chemistry in Münster/Westfalen, where he received his Diploma in 1971 and his Dr. rer. nat. in 1973. He worked on solid-gas equilibria in metal halide systems under the direction of Harald Schäfer. Further work involved the mass spectrometric characterization of highly reactive molecules containing main group elements. In 1988, he took up a professorship in Freiburg/Br. Since 1992, he has been Professor of Inorganic Chemistry at the University of Hannover. His current research interests lie in the fields of chemical vapour transport reactions and main group chemistry.



Karl Jug studied physics in Frankfurt/Main, where he received his Diploma in physics in 1964 and his Dr. phil. nat. in physical chemistry in 1965. His research work, under the direction of Hermann Hartmann, was on quantum chemical modelling of the spectra of inorganic and organic compounds. From 1965 to 1967, he was head of staff of Theoretica Chimica Acta in Frankfurt/M., before he moved to the IIT in Chicago to work with Peter Lykos. He was Assistant Professor in 1969 and Associate Professor in 1971 at St. Louis University. He returned to Germany in 1975 to take up a position as Professor of Theoretical Chemistry at the University of Hannover. His research interests have focussed on semiempirical methods and the theoretical basis of chemical concepts (charge, bonding, diradicals, aromaticity). In applied work, he has been concerned with thermal and photochemical reactions of organic compounds, the structures and reactivities of organic and inorganic compounds and clusters, the cluster simulation of solid-state surfaces, and heterogeneous catalysis.

MICROREVIEWS: This feature introduces the readers to the authors' research through a concise overview of the selected topic. Reference to important work from others in the field is included.

 © WILEY-VCH Verlag GmbH, D-69451 Weinheim, 2000 1434–1948/00/0606–1127 $ 17.50+.50/0

ther up to date nor scientifically substantiated. While the structural borderline between molecules and solids has become largely indistinct, the physical properties of compounds in this transition range are becoming increasingly interesting. Typical co-operative phenomena, such as electrical conductivity, do not appear abruptly, but change continuously over a certain range.

Whereas solid compounds have generally been characterized after their formation, in the transition range between molecules and solids the relevant formation pathways and mechanisms have not been so well investigated. In the case of the title reaction, i.e. the formation of solid SiO_2 from $SiCl_4$ and oxygen, this chemically – from the viewpoint of substance change – interesting question has now been investigated and is largely understood. This subject is reviewed here.

2. Thermodynamic Aspects

Reactions of chlorides of elements with oxygen to give the corresponding oxides and chlorine are found to be exothermic for almost all elements. The Gibbs energy ΔG^0_R is almost always negative. The reaction equilibrium generally lies on the side of the oxide, as is the case with silicon. At 298 K, a reaction enthalpy of –248.2 kJ/mol and a reaction entropy of 48.3 J/(Kmol)[4,5] are calculated for the title reaction and consequently ΔG^0_R (298) = –233 kJ/mol. The equilibrium at 298 K therefore lies close to the product SiO_2. This also holds true for temperatures of 1000 or 2000 K, although the equilibrium constant decreases with increasing temperature. In spite of this extreme equilibrium situation, if an oxygen flow containing $SiCl_4$ is passed through a heated tube about 30 cm in length, noticeable reaction only occurs at temperatures above 700–800 °C. In the temperature range 800–1000 °C, the resulting product is, however, not the SiO_2 that would be expected from a thermodynamic point of view. Instead, a multitude of chlorosiloxanes $Si_xO_yCl_z$ are formed. In these compounds, the chlorine atoms of the starting $SiCl_4$ are only partially replaced by oxygen atoms. The compounds are considered as intermediates that are formed in the course of the reaction. Their investigation allows an insight into the mode of formation of the solid silicon dioxide and the individual steps involved. If the reaction temperature is increased to above 1000 °C, the reaction rate becomes considerably enhanced. The title reaction proceeds very quickly without noticeable by-product formation to give the final products SiO_2 and Cl_2. Under these conditions, the experimental possibility of trapping the intermediates in order to learn more about the reaction process is lost. For a better understanding of the reaction process, the temperature range between 700 and 1000 °C, in which the chlorosiloxanes are formed, is therefore of special interest.

3. Chlorosiloxanes

3.1 Literature Survey

3.1.1 Experimental Facts

In the following, a tabular survey of the literature on perchlorosiloxanes[6–34] with up to 10 silicon atoms per molecule and their mode of formation is given (Table 1).

Beyond the listed compounds, the title reaction leads to the formation of numerous other higher chlorosiloxanes with molar weights up to 7000 D. These contain between 11 and about 70 silicon atoms per molecule, and have quite different oxygen and chlorine contents. The formulae of about 250 other chlorosiloxanes with molar weights up to 5000 D have been reported following mass spectrometric investigations, which are listed below. Details can be found in the literature.[34]

$Si_{11}O_{12}Cl_{20}$, $Si_{11}O_{13}Cl_{18}$, $Si_{11}O_{14}Cl_{16}$, $Si_{11}O_{15}Cl_{14}$, $Si_{12}O_{13}Cl_{22}$, $Si_{12}O_{14}Cl_{20}$, $Si_{12}O_{15}Cl_{18}$, $Si_{12}O_{16}Cl_{16}$, $Si_{12}O_{17}Cl_{14}$, $Si_{13}O_{14}Cl_{24}$, $Si_{13}O_{15}Cl_{22}$, $Si_{13}O_{16}Cl_{20}$, $Si_{13}O_{17}Cl_{18}$, $Si_{13}O_{18}Cl_{16}$, $Si_{13}O_{19}Cl_{14}$, $Si_{13}O_{20}Cl_{12}$, $Si_{14}O_{16}Cl_{24}$, $Si_{14}O_{17}Cl_{22}$, $Si_{14}O_{18}Cl_{20}$, $Si_{14}O_{19}Cl_{18}$, $Si_{14}O_{20}Cl_{16}$, $Si_{15}O_{17}Cl_{26}$, $Si_{15}O_{18}Cl_{24}$, $Si_{15}O_{19}Cl_{22}$, $Si_{15}O_{20}Cl_{20}$, $Si_{15}O_{21}Cl_{18}$, $Si_{15}O_{22}Cl_{16}$, $Si_{16}O_{19}Cl_{26}$, $Si_{16}O_{20}Cl_{24}$, $Si_{16}O_{21}Cl_{22}$, $Si_{16}O_{22}Cl_{20}$, $Si_{16}O_{23}Cl_{18}$, $Si_{16}O_{24}Cl_{16}$, $Si_{17}O_{20}Cl_{28}$, $Si_{17}O_{21}Cl_{26}$, $Si_{17}O_{22}Cl_{24}$, $Si_{17}O_{23}Cl_{22}$, $Si_{17}O_{24}Cl_{20}$, $Si_{17}O_{25}Cl_{18}$, $Si_{18}O_{21}Cl_{30}$, $Si_{18}O_{22}Cl_{28}$, $Si_{18}O_{23}Cl_{26}$, $Si_{18}O_{24}Cl_{24}$, $Si_{18}O_{25}Cl_{22}$, $Si_{18}O_{26}Cl_{20}$, $Si_{18}O_{27}Cl_{18}$, $Si_{18}O_{28}Cl_{16}$, $Si_{19}O_{22}Cl_{32}$, $Si_{19}O_{23}Cl_{30}$, $Si_{19}O_{24}Cl_{28}$, $Si_{19}O_{25}Cl_{26}$, $Si_{19}O_{26}Cl_{24}$, $Si_{19}O_{27}Cl_{22}$, $Si_{19}O_{28}Cl_{20}$, $Si_{20}O_{23}Cl_{34}$, $Si_{20}O_{24}Cl_{32}$, $Si_{20}O_{25}Cl_{30}$, $Si_{20}O_{26}Cl_{28}$, $Si_{20}O_{30}Cl_{20}$, $Si_{21}O_{25}Cl_{34}$, $Si_{21}O_{26}Cl_{32}$, $Si_{21}O_{27}Cl_{30}$, $Si_{21}O_{28}Cl_{28}$, $Si_{21}O_{29}Cl_{26}$, $Si_{22}O_{26}Cl_{36}$, $Si_{22}O_{27}Cl_{34}$, $Si_{22}O_{28}Cl_{32}$, $Si_{22}O_{29}Cl_{30}$, $Si_{22}O_{30}Cl_{28}$, $Si_{22}O_{31}Cl_{26}$, $Si_{22}O_{32}Cl_{24}$, $Si_{23}O_{27}Cl_{38}$, $Si_{23}O_{28}Cl_{36}$, $Si_{23}O_{29}Cl_{34}$, $Si_{23}O_{30}Cl_{32}$, $Si_{23}O_{31}Cl_{30}$, $Si_{23}O_{32}Cl_{28}$, $Si_{23}O_{33}Cl_{26}$, $Si_{23}O_{34}Cl_{24}$, $Si_{24}O_{28}Cl_{40}$, $Si_{24}O_{29}Cl_{38}$, $Si_{24}O_{30}Cl_{36}$, $Si_{24}O_{31}Cl_{34}$, $Si_{24}O_{32}Cl_{32}$, $Si_{24}O_{33}Cl_{30}$, $Si_{24}O_{34}Cl_{28}$, $Si_{24}O_{35}Cl_{26}$, $Si_{24}O_{36}Cl_{24}$, $Si_{25}O_{29}Cl_{42}$, $Si_{25}O_{30}Cl_{40}$, $Si_{25}O_{31}Cl_{38}$, $Si_{25}O_{32}Cl_{36}$, $Si_{25}O_{33}Cl_{34}$, $Si_{25}O_{34}Cl_{32}$, $Si_{25}O_{35}Cl_{30}$, $Si_{25}O_{36}Cl_{28}$, $Si_{25}O_{37}Cl_{26}$, $Si_{26}O_{31}Cl_{42}$, $Si_{26}O_{32}Cl_{40}$, $Si_{26}O_{33}Cl_{38}$, $Si_{26}O_{34}Cl_{36}$, $Si_{26}O_{35}Cl_{34}$, $Si_{26}O_{37}Cl_{30}$, $Si_{26}O_{38}Cl_{28}$, $Si_{26}O_{39}Cl_{26}$, $Si_{27}O_{32}Cl_{44}$, $Si_{27}O_{33}Cl_{42}$, $Si_{27}O_{34}Cl_{40}$, $Si_{27}O_{35}Cl_{38}$, $Si_{27}O_{36}Cl_{36}$, $Si_{28}O_{33}Cl_{46}$, $Si_{28}O_{34}Cl_{44}$, $Si_{28}O_{35}Cl_{42}$, $Si_{28}O_{36}Cl_{40}$, $Si_{28}O_{37}Cl_{38}$, $Si_{28}O_{43}Cl_{26}$, $Si_{29}O_{35}Cl_{46}$, $Si_{29}O_{36}Cl_{44}$, $Si_{29}O_{37}Cl_{42}$, $Si_{29}O_{38}Cl_{40}$, $Si_{29}O_{39}Cl_{38}$, $Si_{29}O_{40}Cl_{36}$, $Si_{29}O_{41}Cl_{34}$, $Si_{30}O_{36}Cl_{48}$, $Si_{30}O_{37}Cl_{46}$, $Si_{30}O_{38}Cl_{44}$, $Si_{30}O_{39}Cl_{42}$, $Si_{30}O_{40}Cl_{40}$, $Si_{30}O_{41}Cl_{38}$, $Si_{30}O_{42}Cl_{36}$, $Si_{30}O_{43}Cl_{34}$, $Si_{30}O_{44}Cl_{32}$, $Si_{31}O_{37}Cl_{50}$, $Si_{31}O_{38}Cl_{48}$, $Si_{31}O_{39}Cl_{46}$, $Si_{31}O_{40}Cl_{44}$, $Si_{31}O_{41}Cl_{42}$, $Si_{31}O_{42}Cl_{40}$, $Si_{31}O_{43}Cl_{38}$, $Si_{31}O_{44}Cl_{36}$, $Si_{31}O_{45}Cl_{34}$, $Si_{31}O_{47}Cl_{30}$, $Si_{32}O_{39}Cl_{50}$, $Si_{32}O_{40}Cl_{48}$, $Si_{32}O_{41}Cl_{46}$, $Si_{32}O_{42}Cl_{44}$, $Si_{32}O_{43}Cl_{42}$, $Si_{32}O_{44}Cl_{40}$, $Si_{32}O_{45}Cl_{38}$, $Si_{32}O_{46}Cl_{36}$, $Si_{32}O_{47}Cl_{34}$, $Si_{32}O_{48}Cl_{32}$, $Si_{32}O_{49}Cl_{30}$, $Si_{33}O_{39}Cl_{54}$, $Si_{33}O_{40}Cl_{52}$, $Si_{33}O_{41}Cl_{50}$, $Si_{33}O_{42}Cl_{48}$, $Si_{33}O_{43}Cl_{46}$, $Si_{33}O_{44}Cl_{44}$, $Si_{33}O_{45}Cl_{42}$, $Si_{33}O_{46}Cl_{40}$, $Si_{33}O_{47}Cl_{38}$, $Si_{33}O_{48}Cl_{36}$, $Si_{33}O_{49}Cl_{34}$, $Si_{33}O_{50}Cl_{32}$, $Si_{34}O_{41}Cl_{54}$, $Si_{34}O_{42}Cl_{52}$, $Si_{34}O_{43}Cl_{50}$, $Si_{34}O_{44}Cl_{48}$, $Si_{34}O_{45}Cl_{46}$, $Si_{34}O_{46}Cl_{44}$, $Si_{34}O_{47}Cl_{42}$, $Si_{34}O_{49}Cl_{38}$, $Si_{34}O_{50}Cl_{36}$, $Si_{34}O_{51}Cl_{34}$, $Si_{34}O_{52}Cl_{32}$, $Si_{35}O_{42}Cl_{56}$, $Si_{35}O_{43}Cl_{54}$, $Si_{35}O_{44}Cl_{52}$, $Si_{35}O_{45}Cl_{50}$, $Si_{35}O_{46}Cl_{48}$, $Si_{35}O_{47}Cl_{46}$, $Si_{35}O_{48}Cl_{44}$, $Si_{35}O_{50}Cl_{40}$, $Si_{35}O_{51}Cl_{38}$, $Si_{35}O_{52}Cl_{36}$, $Si_{35}O_{53}Cl_{34}$, $Si_{35}O_{54}Cl_{32}$, $Si_{36}O_{43}Cl_{58}$, $Si_{36}O_{44}Cl_{56}$, $Si_{36}O_{45}Cl_{54}$, $Si_{36}O_{46}Cl_{52}$, $Si_{36}O_{47}Cl_{50}$, $Si_{36}O_{48}Cl_{48}$, $Si_{36}O_{49}Cl_{46}$, $Si_{36}O_{52}Cl_{40}$, $Si_{36}O_{54}Cl_{36}$, $Si_{36}O_{55}Cl_{34}$, $Si_{36}O_{56}Cl_{32}$, $Si_{37}O_{44}Cl_{60}$, $Si_{37}O_{45}Cl_{58}$, $Si_{37}O_{46}Cl_{56}$, $Si_{37}O_{47}Cl_{54}$, $Si_{37}O_{48}Cl_{52}$, $Si_{37}O_{49}Cl_{50}$, $Si_{37}O_{52}Cl_{44}$, $Si_{37}O_{53}Cl_{42}$, $Si_{37}O_{54}Cl_{40}$, $Si_{37}O_{56}Cl_{36}$, $Si_{37}O_{57}Cl_{34}$,

Table 1. Survey of chlorosiloxanes with up to 10 Si atoms with mode of formation, characterization, and references

Chlorosiloxane	Formation[‡]	Characterization method	References
$SiOCl_2$	9	[c][g]	[6][40][42]
Si_2OCl_6	1–8	[a][b][c][d][e][g][h]	[6–29][42]
$Si_2O_2Cl_4$	4	[g][h]	[17][42]
Si_3OCl_8	3, 4, 7	[h]	[7][18]
$Si_3O_2Cl_8$	1–4, 7, 8	[a][b][c][d][h]	[7][11–17][20–22][27][30–32][42]
$Si_3O_3Cl_6$	1–4, 8	[a][b][c][d][e][g][h]	[7][12–15][17][27][31–33][42]
Si_4OCl_{10}	4	[h]	[7]
$Si_4O_2Cl_{10}$	4	[h]	[7]
$Si_4O_3Cl_{10}$	1–4, 7, 2a	[a][b][c][d][g][h]	[7][10–14][16][17][20][22][27][30–32][42]
$Si_4O_4Cl_8$	1–4, 6, 7	[a][b][c][d][e][g][h]	[7][9–14][27][29][31–34][43]
$Si_4O_5Cl_6$	1, 3, 4	[g][h]	[7][17][31][34][42]
$Si_5O_3Cl_{12}$	4	[h]	[7]
$Si_5O_4Cl_{12}$	1–4, 7	[a][b][h]	[7][11][13][17][20][22][27][30][32][43]
$Si_5O_5Cl_{10}$	1, 3, 4	[a][b][g][h]	[7][12][14][17][27][31][32][42]
$Si_5O_6Cl_8$	1, 3, 4	[b][g][h]	[7][14][17][31][32][34][43]
$Si_5O_7Cl_6$	1	[h]	[31][34][43]
$Si_6O_5Cl_{14}$	1, 2, 2a, 4, 7	[a][b][h]	[7][11][13][17][22][27][29][32]
$Si_6O_6Cl_{12}$	1, 3, 4	[h]	[7][17][31][32][43]
$Si_6O_7Cl_{10}$	1, 3, 4	[a][b][h]	[7][17][27][31][32][34][43]
$Si_6O_8Cl_8$	1	[a][b][h]	[7][17][27][31][32][34][43]
$Si_6O_9Cl_6$	1	[h]	[31][34]
$Si_7O_6Cl_{16}$	1, 2, 4, 7	[a][b][h]	[7][11][13][22][32]
$Si_7O_7Cl_{14}$	1, 4	[h]	[7][32][34]
$Si_7O_8Cl_{12}$	1, 3	[a][b][h]	[7][31][32][43]
$Si_7O_9Cl_{10}$	1, 3	[h]	[7][31][32][43]
$Si_7O_{10}Cl_8$	1	[h]	[31][34]
$Si_8O_7Cl_{18}$	1	[h]	[32]
$Si_8O_8Cl_{16}$	1	[h]	[28][32][34]
$Si_8O_9Cl_{14}$	1	[h]	[28][32][34]
$Si_8O_{10}Cl_{12}$	1	[a][h]	[10][31][34][43]
$Si_8O_{11}Cl_{10}$	1	[a][b][g][h]	[31][34][42]
$Si_8O_{12}Cl_8$	1	[a][d][h]	[10][31][34–36][43]
$Si_8O_{14}Cl_4$	1	[a][h]	[10]
$Si_9O_8Cl_{20}$	1	[h]	[32]
$Si_9O_9Cl_{18}$	1	[h]	[32][34]
$Si_9O_{10}Cl_{16}$	1	[h]	[32][34]
$Si_9O_{11}Cl_{14}$	1	[h]	[32][34]
$Si_9O_{12}Cl_{12}$	1	[h]	[34]
$Si_9O_{13}Cl_{10}$	1	[h]	[34]
$Si_{10}O_9Cl_{22}$	1	[h]	[32]
$Si_{10}O_{10}Cl_{20}$	1	[h]	[32]
$Si_{10}O_{11}Cl_{18}$	1	[h]	[32][34]
$Si_{10}O_{12}Cl_{16}$	1	[h]	[34][43]
$Si_{10}O_{13}Cl_{14}$	1	[h]	[34][43]
$Si_{10}O_{14}Cl_{12}$	1	[h]	[34]
$Si_{10}O_{15}Cl_{10}$		[g]	[43]

[‡] Methods of formation and conditions: 1: $SiCl_4 + O_2$, ΔT; 2: $SiCl_4 + H_2O$; 2a: $Si_2OCl_6 + H_2O$; 2b: $Si_4O_4Cl_8 + H_2O$; 3: Si_2OCl_6, ΔT; 4: Si_2OCl_6, plasma; 5: $SiCl_4 + SO_3$, ΔT; 6: $SiCl_4 + NO_x$, ΔT; 7: $Si + O_2 + Cl_2$, ΔT; 7a: $SiC + O_2 + Cl_2$, ΔT; 8: $SiCl_3OBz$ (Bz = Benzyl), ΔT. 9: $SiO + Cl_2$, h·ν. – [a] Analytical determination of the composition. – [b] ^{29}Si NMR spectroscopy. – [c] Infrared spectroscopy. – [d] Raman spectroscopy. – [e] Electron diffraction. – [f] X-ray diffraction. – [g] Quantum chemical calculations. – [h] Mass spectrometry.

$Si_{38}O_{46}Cl_{60}$, $Si_{38}O_{47}Cl_{58}$, $Si_{38}O_{48}Cl_{56}$, $Si_{38}O_{49}Cl_{54}$, $Si_{38}O_{50}Cl_{52}$, $Si_{38}O_{51}Cl_{50}$, $Si_{38}O_{55}Cl_{42}$, $Si_{38}O_{57}Cl_{38}$, $Si_{38}O_{58}Cl_{36}$, $Si_{39}O_{47}Cl_{62}$, $Si_{39}O_{48}Cl_{60}$, $Si_{39}O_{49}Cl_{58}$, $Si_{39}O_{50}Cl_{56}$, $Si_{39}O_{51}Cl_{54}$, $Si_{39}O_{58}Cl_{40}$, $Si_{39}O_{59}Cl_{38}$, $Si_{39}O_{61}Cl_{34}$, $Si_{39}O_{62}Cl_{32}$, $Si_{40}O_{47}Cl_{66}$, $Si_{40}O_{48}Cl_{64}$, $Si_{40}O_{50}Cl_{60}$, $Si_{40}O_{51}Cl_{58}$, $Si_{40}O_{52}Cl_{56}$, $Si_{40}O_{53}Cl_{54}$, $Si_{41}O_{49}Cl_{66}$, $Si_{41}O_{50}Cl_{64}$, $Si_{41}O_{51}Cl_{62}$, $Si_{41}O_{52}Cl_{60}$, $Si_{41}O_{53}Cl_{58}$, $Si_{41}O_{54}Cl_{56}$, $Si_{41}O_{64}Cl_{36}$, $Si_{42}O_{50}Cl_{68}$, $Si_{42}O_{51}Cl_{66}$, $Si_{42}O_{52}Cl_{64}$, $Si_{42}O_{53}Cl_{62}$, $Si_{42}O_{54}Cl_{60}$, $Si_{43}O_{53}Cl_{66}$, $Si_{43}O_{54}Cl_{64}$, $Si_{43}O_{55}Cl_{62}$, $Si_{43}O_{56}Cl_{60}$, $Si_{43}O_{57}Cl_{58}$, $Si_{44}O_{56}Cl_{64}$, $Si_{44}O_{57}Cl_{62}$, $Si_{44}O_{58}Cl_{60}$, $Si_{44}O_{59}Cl_{58}$, $Si_{45}O_{59}Cl_{62}$, $Si_{45}O_{60}Cl_{60}$.

To give a complete survey of chlorosiloxanes, we have also listed in Table 1 such compounds that are not formed by the title reaction. In the following, however, only the thermally formed chlorosiloxanes are discussed. The present compounds can be classified as belonging to a homologous series of the general formula $Si_nO_{n+x}Cl_{2(n-x)}$ ($x = -1$ to 24). We observe that particularly oxygen-rich chlorosiloxanes (large x) are favoured in the case of large molecules (large n). This is to be expected, because x cannot exceed n. For $x = n$, the limit of Si_nO_{2n}, i.e. SiO_2 is obtained. The composition of a chlorosiloxane closely corresponds to its structure. This will be demonstrated in Section 3.2.

As can be seen, the reaction of $SiCl_4$ with oxygen results in the formation of an unusual multitude of chlorosiloxanes. The number of Si atoms ranges from 1 up to about 70 per molecule. With just a few exceptions, all of the aforementioned chlorosiloxanes can be prepared in significant amounts, although often not in pure form. In particular, the higher molecular weight siloxanes [$n(Si) > 10$] can only be characterized in mixtures owing to separation difficult-

ies. Whereas the lower homologues can be separated by distillation[13] and the medium weight homologues by gas chromatography,[32] separation of the high molecular weight compounds has proved insurmountable. The sensitivity of chlorosiloxanes to hydrolysis makes separation even more difficult, although it should also be noted that this is reduced with increasing oxygen content. However, with increasing oxygen content the molar weight increases accordingly. Adjacent compounds become more and more similar with respect to their physical and chemical properties and hence separation becomes more difficult.

3.1.2 Theoretical Methods

A difficulty in evaluating the experimental results is the structural characterization of the chlorosiloxanes described by the general molecular formula $Si_nO_{n+x}Cl_{2(n-x)}$. Whereas for a few Si atoms it is possible to obtain an appropriate structure by application of simple valence rules, this is no longer the case for larger systems due to the sharp increase in the number of possible isomers. Moreover, structural data such as bond lengths and bond angles, as well as the relative stabilities of the isomers, cannot be experimentally determined in a simple way. Here, quantum chemical methods can offer additional information to complement that obtained in the experimental investigations. So-called ab initio methods are mainly based on the Hartree–Fock method in the self-consistent field (SCF) approximation. Here, the electrons are described by one-electron functions, the molecular orbitals (MOs), where each MO for an electron is calculated in the field of the nuclei and the average field of all the other electrons. This one-electron approximation can be improved by the inclusion of the correlation between the electrons. This is achieved by applying configuration interaction (CI) or perturbation theory (MP2). Since ab initio calculations are very demanding in terms of computer time due to the increased basis sets and the inclusion of correlation, their application is restricted to systems with a few dozen atoms.

For comparative studies, which are necessary in the case of siloxanes because of the multitude of compounds, semiempirical methods are more appropriate. Here, one also starts from the SCF method and tries to considerably reduce the computer time by applying approximations. In this way, the differential overlaps of the atomic orbitals are neglected (ZDO approximation) and the remaining integrals are in part empirically adjusted. The first procedure can be justified by the orthogonalization of the atomic orbitals. The second leads to an implicit inclusion of correlation and therefore often to substantial improvements in the prediction of structures and stabilities. As a result of the continuous improvements of semiempirical methods, large systems with more than a hundred atoms can now be reliably calculated, once smaller systems have been tested by making comparisons with experimental data or highly accurate ab initio calculations. Semiempirical methods suitable for the calculation of larger molecules with first and second row atoms are AM1,[35] PM3,[36] MNDO/d,[37] and SINDO1[38] or its improved version MSINDO.[39]

Siloxanes were at first studied only sporadically.[40] Here, the basic system $SiOCl_2$ played a special role. As a single molecule it is undoubtedly stable, but is extremely reactive. It is possible that it is formed from Si_2OCl_6, which is easily accessible experimentally. Relevant calculations were performed ab initio with large basis sets and correlation.[41] SINDO1 calculations were first performed for small systems with up to eight Si atoms. The emphasis was on structure and stability with the aim of deriving rules for predicting the preferred formation of isomers.[42] These selected systems were $Si_nO_{n-1}Cl_{2(n+1)}$ (n = 2–4), $Si_nO_nCl_{2n}$ (n = 2–5), $Si_nO_{n+1}Cl_{2(n-1)}$ (n = 4, 5), and $Si_nO_{n+3}Cl_{2(n-3)}$ (n = 8). In order to gain insight into the growth mechanism, the palette of these small systems was extended to $Si_nO_{n-1}Cl_{2(n+1)}$ (n = 5), $Si_nO_nCl_{2n}$ (n = 6), $Si_nO_{n+1}Cl_{2(n-1)}$ (n = 6, 7), $Si_nO_{n+2}Cl_{2(n-2)}$ (n = 5–8, 10), and $Si_nO_{n+3}Cl_{2(n-3)}$ (n = 10, 12).[43] In order to understand the growth mechanism, additional calculations were needed, which introduced interesting new aspects, in particular with regard to the silsesquioxanes $Si_{2n}O_{3n}Cl_{2n}$ (n = 2–8, 10, 12, 18, 24, 30) and polycycles $Si_{2n}O_{3n-3}Cl_{2(n+3)}$ (n = 9, 15).

3.2 Structures of Chlorosiloxanes

Mainly on the basis of ^{29}Si NMR studies, but also by crystal structure analyses, the structures of a substantial number of chlorosiloxanes have been determined.[13,14,27,28,31,44–46] For the characterization of such species, the chlorosiloxanes have first been prepared and then derivatized (esterified) with retention of the Si–O backbone, and the derivatives have been structurally characterized. In the following, only the siloxanes formed by the title reaction will be discussed. A compilation of the experimentally determined connection patterns is presented in Table 2 in the form of structure diagrams. For completeness, the atomic connections of chlorosiloxanes prepared in a different way are additionally listed in Table 3.

From the survey, the relationship between the structures of the molecules and their compositions can be seen. The chlorosiloxanes $Si_nO_{n+x}Cl_{2(n-x)}$ with $x = -1$ form chains and both unbranched and branched catenated structures are found.[13] For $x = 0$, Si–O monocyclic rings are observed, which often bear side groups[31] of the same composition. It should be mentioned that among the prepared chlorosiloxanes there are no four-membered rings of the Si_2O_2 type. This is in agreement with the structural chemistry of silicon dioxide and silicates, as well as with the results of quantum chemical calculations.[42] Three-dimensional polycyclic Si–O structures are formed when $x \geq 1$. Increasing oxygen content leads to an increase in the three-dimensional character of the Si–O framework. The largest chlorosilsesquioxane with an experimentally determined structure is $Si_8O_{12}Cl_8$,[46] which has a cubane-like cage structure. The compound $Si_8O_{12}(OCH_3)_8$ has in fact been studied previously.[47] However, this structure was obtained in a different way and will not be discussed here.

Table 2. Survey of structures of thermally formed chlorosiloxanes; M: silicon atom bonded to one oxygen atom; D: silicon atom bonded to two oxygen atoms; T: silicon atom bonded to three oxygen atoms; Q: silicon atom bonded to four oxygen atoms

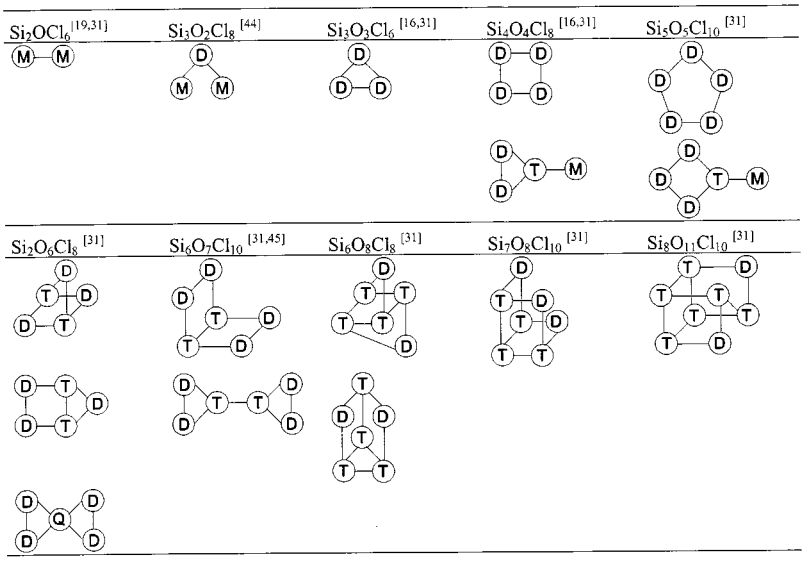
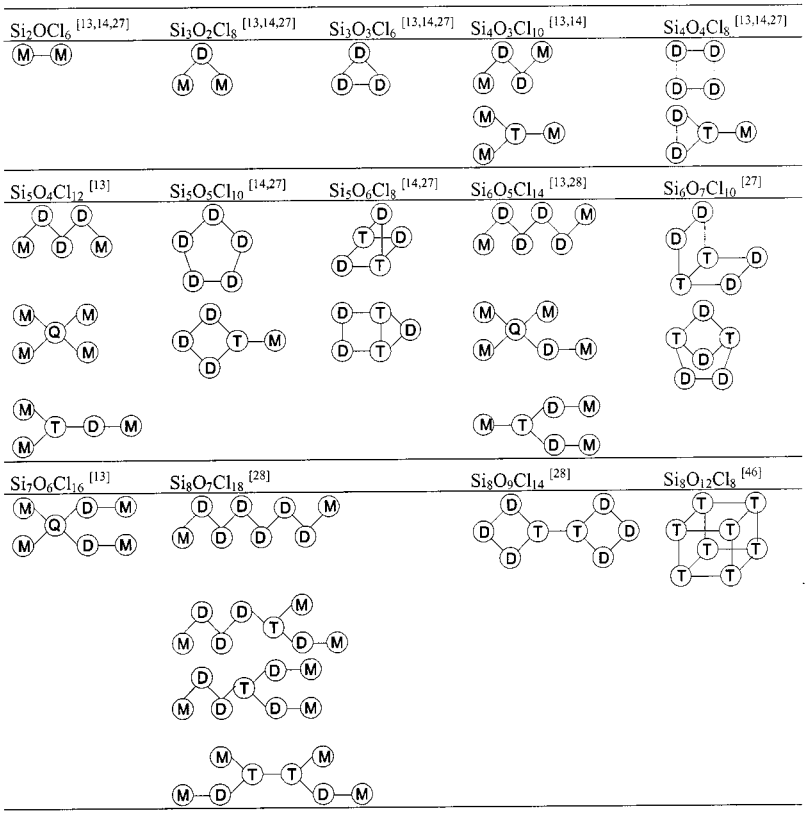
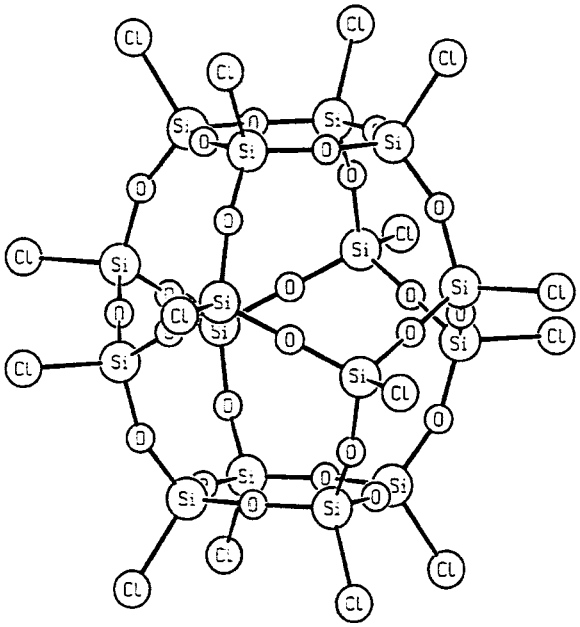


Table 3. Survey of structures of other chlorosiloxanes not thermally formed

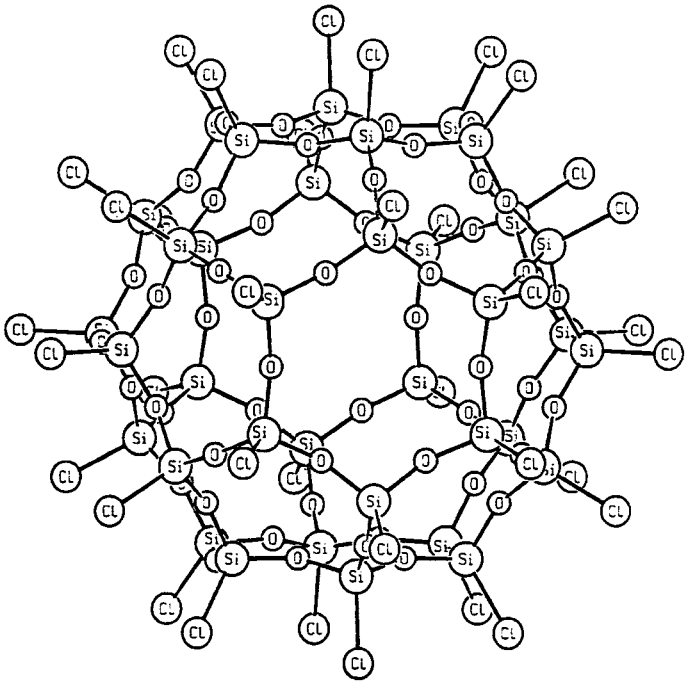


Larger molecules have to date eluded experimental structure determination for the aforementioned reasons, but the results of quantum chemical calculations are available, on the basis of which cage-like structures can be expected for siloxanes with up to 40 Si atoms.[43,48] Particularly comprehensive information is available for hydridosilsesquioxanes $Si_{2n}O_{3n}H_{2n}$,[48] which are built up analogously to the chlorosilsesquioxanes $Si_{2n}O_{3n}Cl_{2n}$. In Figure 1, the expected structures of a few representative compounds are presented.

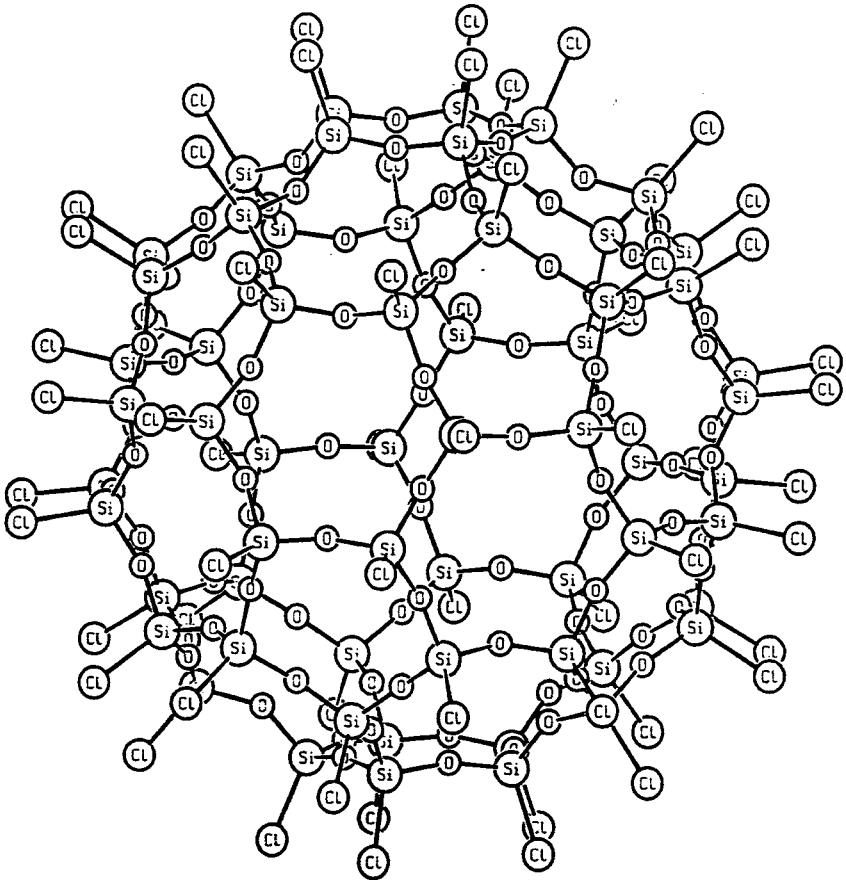
A common feature of all the structures, determined both experimentally and theoretically, is that they contain differently connected six-, eight-, ten-, and twelve-membered rings. The preferred ring size can be established from stabilization curves and the growth patterns.[43,48] The findings



$Si_{16}O_{24}Cl_{16}$ (D_{4d})



$Si_{36}O_{54}Cl_{36}$ (D_{6h})



$Si_{60}O_{90}Cl_{60}$ (I_h)

Figure 1. Quantum chemically calculated structures of some silsesquioxanes

are in agreement with studies on the stabilities of monocyclic chlorosiloxanes, which led us to expect very similar stabilities for rings of different sizes,[43] although with larger rings being somewhat more stabilized. However, with a further increase in ring size, the energy decreases once more so that a saturation is reached for twelve-membered rings. A balanced combination of rings (ten- and twelve-membered) is more stable than a combination of small (six- and eight-membered) and large (twelve- and higher-membered) rings.

3.3 Stability of Chlorosiloxanes

For none of the chlorosiloxanes discussed here have heats of formation or entropies been experimentally determined, hence a discussion of their thermodynamic stabilities has to rely on quantum chemical calculations, estimates, and practical experience.

The fact that these compounds are formed at temperatures slightly less than 1000 °C seems to suggest that they are thermodynamically stable. However, there are also literature reports pertaining to their thermal decomposition at similar temperatures.[7,30] Considering the rather complicated decomposition reaction of a chlorosiloxane, it is apparent that silicon tetrachloride and a variety of oxygen-rich chlorosiloxanes will invariably be formed. In the resultant product(s) of the thermolysis, the number of silicon atoms can be either smaller (a), equally large (b), or both larger and smaller (c). Let us now consider these three possible decomposition reactions and formulate for each case one of the many possible reaction equations in a general form. In the following, we choose one example of each case and discuss its likelihood.

(a) Decomposition of a gaseous chlorosiloxane under cleavage of $SiCl_4$: [30]

$$Si_nO_{n+x}Cl_{2(n-x)} \rightarrow SiCl_4 + Si_{n-1}O_{n+x}Cl_{2(n-x-2)} \quad (1)$$

$$Si_4O_3Cl_{10} \rightarrow SiCl_4 + Si_3O_3Cl_6 \; (n = 4, x = -1) \quad (2)$$

(b) Decomposition of a chlorosiloxane with n Si atoms with formation of an oxygen-richer and an oxygen-poorer chlorosiloxane with n Si atoms in each:

$$2Si_nO_{n+x}Cl_{2(n-x)} \rightarrow Si_nO_{n+x+1}Cl_{2(n-x-1)} + Si_nO_{n+x-1}Cl_{2(n-x+1)} \quad (3)$$

$$2Si_4O_4Cl_8 \rightarrow Si_4O_5Cl_6 + Si_4O_3Cl_{10} \quad (4)$$

(c) Decomposition of a chlorosiloxane with n Si atoms with formation of a larger (n + 1 Si atoms) and a smaller (n – 1 Si atoms) siloxane:

$$2Si_nO_{n+x}Cl_{2(n-x)} \rightarrow Si_{n+1}O_{n+x+1}Cl_{2(n-x+1)} + Si_{n-1}O_{n+x-1}Cl_{2(n-x-1)} \quad (5)$$

$$2Si_4O_4Cl_8 \rightarrow Si_5O_5Cl_{10} + Si_3O_3Cl_6 \quad (6)$$

In all such cases, the total number of Si–O and Si–Cl bonds remains unchanged in the course of the reaction. Since one can assume that the bond energies in such chemically similar systems will have similar values, heats of reaction close to 0 kJ/mol are to be expected. The entropies of the reactions of types (a)–(c) are, however, more significant, at least in case (a). If a chlorosiloxane decomposes into several smaller molecules [reaction type (a)], the increase in the number of molecules means that such a process will invariably proceed under entropy gain (considering the homogeneous gas-phase reaction). This reaction entropy can be expected to be of the order of 120–160 J/(Kmol) for a change in the number of molecules (Δv) of +1. If a chlorosiloxane decomposes into two comparatively equal siloxanes, distinguished only by their oxygen content [reaction type (b)], such a reaction occurs without a change in the number of molecules and hence its associated entropy will be close to 0 J/(Kmol). The same holds for a reaction of type (c). Of course, mixed forms of reactions (a)–(c) are conceivable. For case (a), a temperature-independent ($\Delta H = 0$) equilibrium constant of $e^{120/R}$ to $e^{160/R} \approx 10^6$ to 10^8 is obtained from the above considerations. Almost complete decomposition is thus to be expected from a thermodynamic point of view. For cases (b) and (c), equilibrium constants of about $e^0 = 1$ are to be expected. The decomposition products should thus be present in similar concentrations as the reactant. For each of the resulting decomposition products (other than $SiCl_4$), analogous considerations can be made. In summary, we can state from a thermodynamic point of view that each chlorosiloxane should undergo decomposition. The most favoured decomposition reaction is the cleavage of $SiCl_4$, which should eventually lead to SiO_2 and $SiCl_4$. Consideration of the discussed decomposition reactions from a molecular point of view (kinetic aspect) also leads to a clear preference for decomposition reaction (a). To bring about reaction (a), only the necessary activation energy from a collision with an energy-rich molecule or the (hot) wall of the reaction vessel has to be supplied. For reactions (b) and (c), however, a collision of two molecules of equal composition is necessary. This is rather improbable in the complex reaction mixture. Unimolecular reactions leading to the products of reactions (b) and (c) are inconceivable.

The results of these considerations clearly show that from both thermodynamic and kinetic points of view, all chlorosiloxanes must be unstable. They decompose to give $SiCl_4$ along with oxygen-richer siloxanes. This is consistent with all the experimental evidence.[7,30,49,50]

4. Build-Up and Decomposition Reactions: Growth of Si–O Frameworks

In Section 3.1, it was shown that an impressive number of descendants, i.e. chlorosiloxanes of quite different composition with molar weights up to 7000 D, can be generated. We suspect that further chlorosiloxanes with even higher molar weights are formed, which remain undetected.[50] The formation of such a wealth of reaction products in this seemingly simple reaction leads to the conjecture that a highly reactive intermediate is involved, which reacts with numerous reaction partners in a non-specific manner, thereby generating the broad spectrum of products. Recent matrix-spectroscopic studies have shown that in both the

reaction of $SiCl_4$ with O_2 and the thermolysis of Si_2OCl_6, the initial step at about 1000 °C leads to the formation of $O{=}SiCl_2$.[51] Although silaphosgene has long been known as a molecule that can be isolated in a matrix,[6] its presence in high-temperature vapours has now been demonstrated for the first time. Thermodynamic calculations [without consideration of SiO_2(s) and subsequent reactions of $O{=}SiCl_2$] lead us to expect that $O{=}SiCl_2$ should appear in the temperature range from about 1100 K to 1700 K, in concentrations peaking at 1400 K.[51] The performed experiments support this expectation. The temperature at which $O{=}SiCl_2$ first appears in appreciable concentrations (about 1100 K) is identical to that at which the reaction of $SiCl_4$ with O_2 commences and chlorosiloxanes are formed. This can be taken as strong evidence that $O{=}SiCl_2$ is involved in the formation of chlorosiloxanes. The initial step in the thermolysis of Si_2OCl_6 also leads to silaphosgene,[51] as well as to a build-up of higher chlorosiloxanes.[7,30,49] Here, the key role of silaphosgene in the build-up of catena-siloxanes has been demonstrated.[49] The chemical properties of $O{=}SiCl_2$ are not known. In view of the unusual coordination number of three at silicon and the presence of an Si–O double bond, it can be expected to be a highly reactive molecule. Although the value of its standard heat of formation is highly negative at –702.1 kJ/mol,[40] decomposition into solid SiO_2 and $SiCl_4$ can be expected on the basis of literature data concerning the stabilities of other silicon compounds.[4] In the case of the reaction of $SiCl_4$ with O_2, a great excess of $SiCl_4$ is available as a potential reaction partner. Silaphosgene could react with it by inserting into an Si–Cl bond with the formation of Si_2OCl_6:

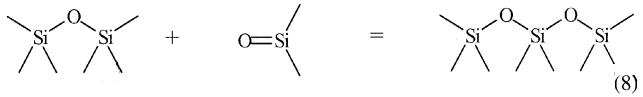


(7)

In fact, Si_2OCl_6 is also the main product when $SiCl_4$ and O_2 are reacted in the temperature range 700–950 °C. If Si_2OCl_6 is indeed formed, it is also available as a reaction partner for silaphosgene.

For catena-siloxanes with 4 or more silicon atoms, several isomers are formed, which can be separated, to some extent, by gas chromatography.[50] This growth of unbranched and branched chains is terminated for chain lengths of about 10 Si atoms.[32] Larger catena-siloxanes have not hitherto been observed.

This mechanism allows some understanding of the growth of the chains. However, it does not provide an explanation for the formation of mono- and oligocyclic siloxanes (see Table 1). In a growth reaction, $O{=}SiCl_2$ will invariably introduce Si and O atoms into the newly formed



(8)

siloxanes in a 1:1 ratio. In this way, no chlorosiloxanes with more oxygen than silicon atoms can be formed. Since these are, however, undoubtedly formed, the insertion of $O{=}SiCl_2$ cannot be the only reaction responsible for the build-up of the Si–O frameworks of oxygen-rich siloxanes and eventually therefore of solid SiO_2. In Section 3.2, it was explained that all chlorosiloxanes must decompose for entropy reasons, preferably according to the following decomposition reaction:

$$Si_nO_{n+x}Cl_{2(n-x)} \rightarrow SiCl_4 + Si_{n-1}O_{n+x}Cl_{2(n-x-2)} \quad (9)$$

For each such decomposition step, the stepwise built-up chlorosiloxane is decomposed once more, but in a stoichiometrically different way than for the build-up. Whereas in a growth reaction, the Si and O atoms are invariably introduced in equal numbers, only Si and Cl are cleaved in the decomposition process (eq. 9). All oxygen atoms are retained by the decomposing molecule. In this way, the molecules becomes smaller after each decomposition step, but concurrently oxygen-richer. Step by step, siloxanes with three-dimensional, cage-like Si–O frameworks are generated.

In Figure 2, we attempt to represent graphically the interplay between growth and decomposition. For chlorosiloxanes $Si_nO_{n+x}Cl_{2(n-x)}$, the ratio $(n+x)/n$ of the number of mol of oxygen and silicon is plotted against the number n of Si atoms per molecule for a series of x values.

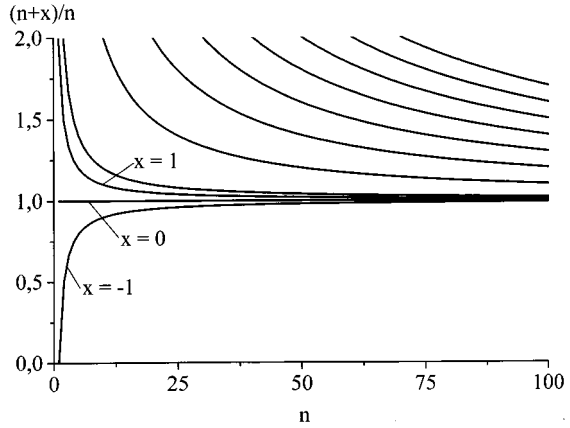


Figure 2. Dependence of the composition of homologous chlorosiloxanes on the number of silicon atoms

The generated sequences of points can be connected with hyperbola-like curves. Each of these curves corresponds to a homologous series of chlorosiloxanes; the lowest to the catena-siloxanes ($x = -1$), the next to the cyclosiloxanes ($x = 0$), etc. If growth and decomposition steps are introduced (in the form of arrows) into this diagram, Figure 3 is obtained.

Starting from $SiCl_4$, first Si_2OCl_6 is formed, then a further increase in the chain length occurs, for example up to $Si_5O_4Cl_{12}$. If this decomposes with formation of $SiCl_4$, $Si_4O_4Cl_8$ is formed, which can grow for example up to $Si_7O_7Cl_{14}$, before this in turn decomposes into the bicyclic

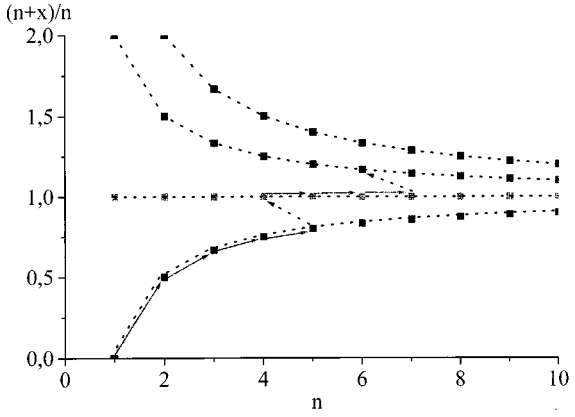


Figure 3. Growth pathways of chlorosiloxanes

$Si_6O_7Cl_7$. In this way, the stepwise transformation of $SiCl_4$ to SiO_2 can be followed almost continuously.

For thermolysis of Si_2OCl_6 in a closed vessel, it has been shown[49] that the rate of the growth reaction [v(growth)] is greater than that of the decomposition reaction [v(decomposition)]. Therefore, at a constant temperature, more and more chlorosiloxanes are formed. In studies of the influence of temperature on the formation of chlorosiloxanes it is found that the relative amount of increasingly oxygen-rich siloxanes increases.[30,49] This means that the rate of decomposition reaction, which leads to the formation of oxygen-rich compounds, has a higher temperature coefficient than that of the growth reaction. The following inequalities hold:

$$v(\text{growth}) > v(\text{decomposition}),$$
$$dv(\text{growth})/dT < dv(\text{decomposition})/dT$$

This means that with increasing temperature a point must be reached where the overall decomposition reaction proceeds more rapidly than the overall growth reaction. The two curves intersect at a temperature T_s. This is schematically represented in Figure 4.

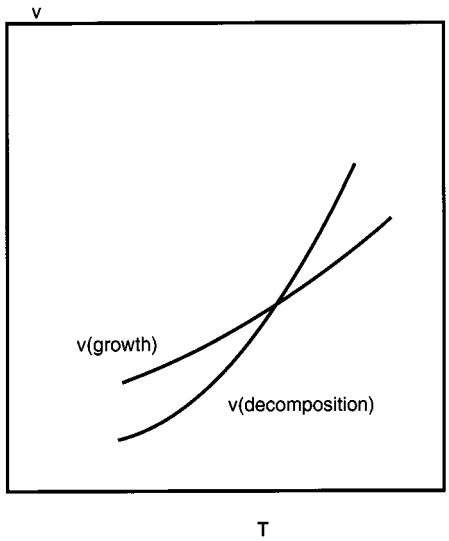


Figure 4. Temperature-dependence of the growth and decomposition rates of chlorosiloxanes

This temperature is at first unknown. Also unknown is to what (average) molar weight the molecules have grown at this point. It is certain that the reaction process discussed on the basis of the experimental results takes place below T_s.

In summary, we can say that $O{=}SiCl_2$ is formed in a first step of the reaction between $SiCl_4$ and O_2. This is a highly reactive molecule, which reacts with all reaction partners possessing an Si–Cl bond with formation of an Si–O–Si group. This is a typical growth reaction and leads to a variety of catena-siloxanes starting from $SiCl_4$. However, siloxanes with a ratio n(O)/n(Si) greater than one cannot originate in this way. They are formed from chlorosiloxanes by entropy-driven cleavage of $SiCl_4$. In this way, the molecules become smaller once more, but oxygen-richer. Their compositions approach that of the final product SiO_2. Species with up to about 70 Si atoms and molar weights of 7000 D could be followed experimentally. As regards the further reaction, we can only speculate. However, it is unlikely that there will be any change in the fundamental reaction pattern, which is governed by the decomposition of chlorosiloxanes. If we extrapolate on the basis of the described findings, two alternative possibilities arise depending on the reaction conditions.

(a) The reaction temperature is always below T_s: As long as the formed siloxanes are at the reaction temperature and $O{=}SiCl_2$ is available as a reaction partner, the molecules will keep growing and become increasingly oxygen-rich. This growth cannot proceed indefinitely as the volatility of the siloxanes decreases with increasing molar weight. Eventually, condensed phases must arise. In particular, this will occur if the residence period of the siloxanes in the reaction zone, and consequently the time for molecular growth, is long. As an alternative to the condensation of high molecular weight chlorosiloxanes, the formation of aerosols, small suspended particles with diameters of 10^{-7} to 10^{-3} cm, appears likely. The formation of such an aerosol, which shows no tendency to undergo condensation, is not unusual. Indeed, in the technological processing of light-wave conductors, such aerosols present an exhaust air problem. Here, an oxygen flow loaded with $SiCl_4$, $GeCl_4$, BCl_3, $POCl_3$ and other compounds is passed through a heated tube of very pure quartz glass so that the oxides of the aforementioned elements are deposited on the interior of the quartz tube. From this so-called "preform", light-wave guides for optical data transfer are manufactured. This reaction, which is very similar to the one discussed, does not proceed to completion either. A portion of the introduced halogen compounds leaves the reaction tube as smoke, which is difficult to condense or filter. Whether such a suspended particle follows the same growth and decomposition mechanisms as a large siloxane molecule is not clear, but is nevertheless conceivable.

(b) The reaction temperature exceeds T_s: The decomposition reactions (in particular $SiCl_4$ cleavage) proceed more rapidly than the formation reactions. However, such molecules cannot completely decompose in this way. If $SiCl_4$ is cleaved, Si and Cl atoms are lost in a ratio of 1:4. If, in

the limiting situation, all Cl atoms are eliminated, we can formulate the following equation:

$$Si_nO_{n+x}Cl_{2(n-x)} = 0.5(n-x)SiCl_4 + Si_{(n+x)/2}O_{(n+x)} \quad (10)$$

An $(SiO_2)_{(n+x)/2}$ "molecule" would have to be formed, an oligomer of the monomer SiO_2,[6] i.e. an SiO_2 cluster with a molar weight not much lower than that of the chlorosiloxane from which it originated.

Since a fundamental change of the whole Si–O framework is unlikely in this process, a structural relationship between the formed SiO_2 and the high molecular weight chlorosiloxanes can be expected. Quantum chemical calculations on the structures and stabilities of SiO_2 clusters seem quite interesting this context.

It is found experimentally that the reaction of $SiCl_4$ with oxygen leads to larger and larger amounts of increasingly oxygen-rich chlorosiloxanes with increasing temperature. Depending on the experimental conditions, a point just below 1000 °C is reached at which the reaction behaviour changes abruptly within a temperature interval of just a few degrees.[50] This sudden change in the reaction behaviour could be connected with the marked intersection point T_s. No more chlorosiloxanes with typically molecular properties (relatively high fugacity, solubility in non-polar organic solvents) are formed, but rather a white, X-ray-amorphous solid, which mainly consists of "SiO_2" with variable but low chlorine content (< 5%). The globular particles have diameters of about 0.1 μm and are reminiscent of the industrial product "Aerosil" (Degussa–Hüls). This is formed in a similar way, under similar conditions. Thus, gaseous $SiCl_4$ is blown into an oxyhydrogen flame at temperatures of about 1000 °C. Depending on the reaction conditions, SiO_2 particles with diameters between 7 and 50 nm are formed. The reactions occurring in the flame are unknown. In principle, three reaction partners are initially available for the $SiCl_4$: H_2, O_2, and H_2O. If H_2 and O_2 are introduced in the ratio 2:1, they should react primarily as in the oxyhydrogen reaction and water will be the primary reaction partner for $SiCl_4$. In a first step, trichlorosilanol $SiCl_3OH$ will thus be generated with elimination of HCl.[17] This can then react in a similar manner as $O{=}SiCl_2$ with $SiCl_4$ or chlorosiloxanes with formation of Si–O–Si bonds.[52] The interplay between growth and decomposition should be analogous to the situation discussed above. If a globular Aerosil particle with a diameter of 7 nm and densely packed oxygen atoms is considered, we can estimate that such a particle contains 10^5 O atoms. This corresponds to a formula of $Si_{50000}O_{100000}$ in molecular language. Such a giant molecule is thus separated from the chlorosiloxane with about 50 Si atoms by three orders of magnitude. Nevertheless, a continuous transition from the high molecular weight chlorosiloxanes to these solid-state particles is not unlikely. The properties and uses of Aerosil and related products are described in company reports.[53–55]

Finally, two questions will be addressed:

(a) Why is X-ray amorphous SiO_2 formed?

(b) Does the situation described for the system Si/O/Cl apply to elements other than silicon?

Let us start with (a): It is obvious that SiO_2 formed in fractions of a second in an oxyhydrogen flame cannot be well-ordered and crystalline. An equally amorphous product is formed if an oxygen stream loaded with $SiCl_4$ is passed through a heating section of about 40 cm[50] at a relatively low flow velocity. The thermolysis of Si_2OCl_6 in a closed system for an extended time of several weeks also leads to amorphous products.[50] This latter observation would suggest that the reaction time is of lesser importance. Although as a typical glass-forming substance, SiO_2 is a material that is normally solidified from a melt, it can be obtained in crystalline form from media of low viscosity, such as supercritical water (hydrothermolysis of α-quartz). An intrinsic property of SiO_2 is therefore probably not the reason. Thus, this phenomenon is seemingly related to the discussed reaction course. In the discussion of the structures of the initially formed chlorosiloxanes, it was pointed out that rings of different sizes arise in the monocyclic and oligocyclic siloxanes. In the course of the reaction, these rings become linked to form increasingly complicated three-dimensional structures. For the silsesquioxanes in particular, quantum chemical calculations were performed to gain insight into the stabilities of isomeric siloxanes. These showed that beyond molecular sizes of about 48 silicon atoms, structures with skeletons akin to that in crystalline SiO_2 become favoured.[43,56] In the example shown in Figure 5, two isomers of $Si_{48}O_{72}Cl_{48}$ are depicted; the upper one is an Si–O framework corresponding to the so-called α-cage, while the lower one corresponds to the structure of β-tridymite.

The latter isomer is more stable according to new MSINDO calculations.[56] The stability of such a bulk-like structure is also greater than that of a fullerene-like cage structure with 12 ten-membered and 14 twelve-membered rings.[48] The growth of fullerene-like structures can occur in two steps in the presence of water and is accompanied by the elimination of HCl. The insertion mechanism has been described previously.[48] In cases where the intermediately formed chlorosiloxanes show bulk-like structures even at the beginning of their growth, we would, of course, expect crystalline SiO_2. However, this is not the case, as was made clear in Section 3.2. If the growth of Si–O frameworks starts in a different way than the formation and condensation of Si–O twelve-membered rings (as in crystalline SiO_2) and molecules of the type depicted in the upper portion of Figure 5 are initially formed, it is difficult to conceive that a rearrangement to a bulk-like, albeit more stable structure (Figure 5, below), would occur. It seems, therefore, that the initial growth of chlorosiloxane molecules with a few dozen Si atoms is responsible for the non-occurrence of bulk-like crystalline SiO_2.

(b) The question arises as to whether the discussed mechanisms are also applicable to other material systems, and whether intermediates analogous to those of the present reaction are also observable for other elements. There are relatively few examples in the literature of elements that

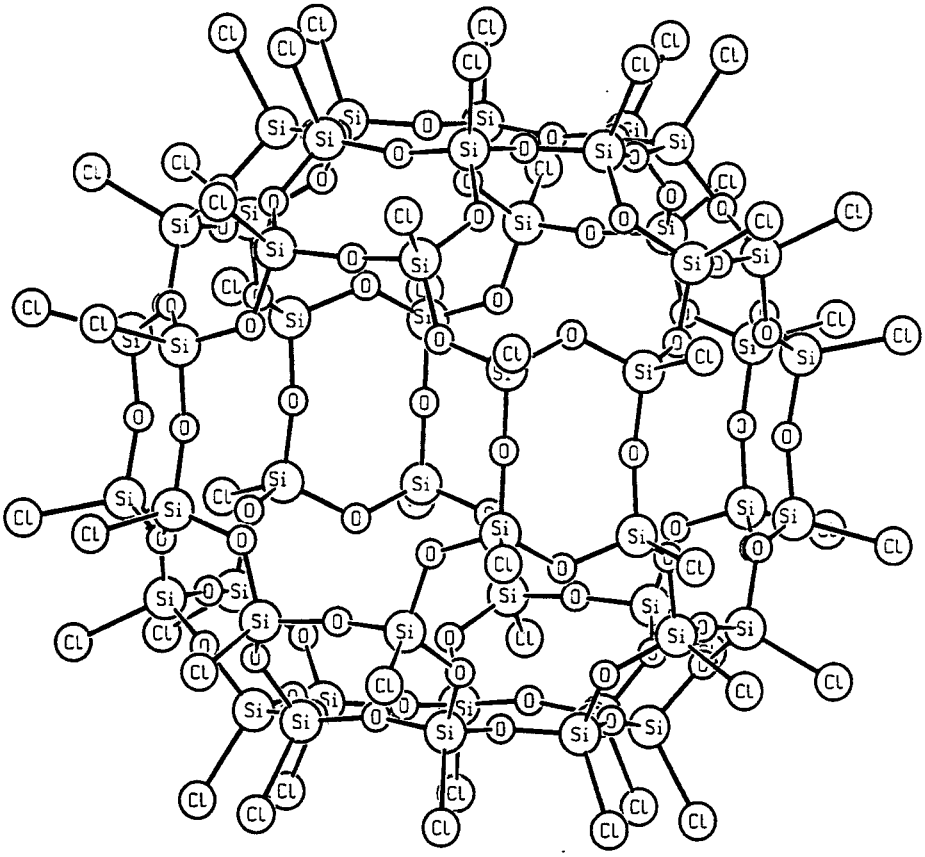


Figure 5. Quantum chemically calculated structures of two isomeric silsesquioxanes (Si_{48}); top: α-cage; bottom: tridymite structure

form molecular oxyhalides that can be discussed as intermediates of the reactions of halides with oxygen. These are mainly the metalloids and non-metals, as well as a few transition elements (fifth, sixth, and seventh subgroups). Oxyhalides of germanium, which correspond to those of silicon, but are thermally more labile, are known in somewhat larger numbers.[57] No other element shows the variety of molecular oxyhalides as silicon. In the group of one of the authors (M.B.), analogous experiments on other systems have been attempted, most notably on the reaction of $TiCl_4$ with oxygen. Despite extensive efforts, the search for corresponding intermediates was in this and many other cases fruitless. Clearly, silicon represents a special situation. If we consider the similarities and differences of the material systems Si/O/Cl and Ti/O/Cl, we can say the structural chemistry of silicon is characterized by the coordination number 4 and tetrahedral coordination, whereas for titanium oxides the coordination number 6 dominates. In contrast to titanium, for silicon the transition from chloride to oxide proceeds without a change in the coordination number or geometry. Therefore, a stepwise substitution of Cl by O atoms is possible for silicon, without destruction of the short-range order. This is not possible for the transition of molecular chloride to oxide in the case of titanium. The reaction of $TiCl_4$ with oxygen also leads also to the oxide and may conceivably pass through similar intermediates. However, even if these are indeed formed, they are so unstable and have such a short lifetime that they cannot be isolated or observed experimentally. This argument holds true not only for titanium, but also for almost all metals.

Acknowledgments

We thank the following co-workers for their contributions to this work: Dr. M. Jerzembek, Dr. A. Kornick, Dr. H. Quellhorst, Dr. D. Wichmann, and Dr. A. Wilkening. We thank the Deutsche Forschungsgemeinschaft for financial support as part of the program "Specific phenomena in silicon chemistry".

[1] H. Schäfer, H. G. v. Schnering, *Angew. Chem*. **1964**, *76*, 833.
[2] A. Simon, *Angew. Chem*. **1981**, *93*, 23; *Angew. Chem. Int. Ed. Engl*. **1981**, *20*, 1.
[3] G. Schmid, *Clusters and Colloids*, VCH, Weinheim, **1994**.
[4] M. Binnewies, E. Milke, *Thermochemical Data of Elements and Compounds*, Wiley-VCH, Weinheim, **1999**.
[5] JANAF Thermochemical Tables 3rd. Ed., ACS, NBSB, New York, **1985**.
[6] H. Schnöckel, *Z. Anorg. Allg. Chem.* **1980**, *460*, 37.
[7] A. Kornick, M. Binnewies, *Z. Anorg. Allg. Chem.* **1990**, *587*, 167.
[8] F. C. Friedel, A. Ladenburg, *J. Liebigs Ann. Chem.* **1868**, 355.
[9] H. Rheinboldt, W. Wisfeld, *J. Liebigs Ann. Chem.* **1935**, *517*, 197.
[10] L. Troost, P. Hautefeuille, *Bull. Soc. Chim. Fr.* **1871**, *16*, 240.
[11] W. C. Schumb, D. F. Holloway, *J. Am. Chem. Soc.* **1941**, *63*, 2753.
[12] D. W. S. Chambers, C. J. Wilkins, *J. Chem. Soc., Chem. Commun.* **1960**, 5088.
[13] H. C. Marsmann, E. Meyer, M. Vongehr, E. F. Weber, *Makromol. Chem.* **1983**, *184*, 1817.
[14] E. Bertling, H. C. Marsmann, *Phys. Chem. Minerals* **1988**, *16*, 295.
[15] E. A. Chernyshev, N. A. Mudrova, T. L. Krasnova, Yu. M. Ushakov, A. B. Petrunin, M. G. Kuznetsova, *J. Gen. Chem. USSR* **1992**, *62*, 1076.
[16] U. Wannagat, D. Burgdorf, H. Bürger, G. Pawelke, *Z. Naturforsch*. B **1991**, *46b*, 1039.
[17] A. Kornick, M. Binnewies, *Z. Anorg. Allg. Chem.* **1990**, *587*, 157.
[18] J. E. Marra, E. R. Kreidler, N. S. Jacobson, D. S. Fox, *J. Electrochem. Soc*. **1988**, *135*, 1571.
[19] W. Airey, C. Glidewell, D. W. Ranking, A. G. Ranking, *J. Mol. Struct.* **1971**, *8*, 413.
[20] J. Goubeau, R. Warncke, *Z. Anorg. Allg. Chem.* **1949**, *259*, 109.
[21] W. C. Schumb, A. J. Stevens, *J. Am. Chem. Soc.* **1947**, *69*, 726.
[22] W. C. Schumb, A. J. Stevens, *J. Am. Chem. Soc.* **1950**, *72*, 3178.
[23] J. R. Durig, J. Flanagan, V. F. Kalinsky, *J. Mol. Struct*. **1975**, *27*, 241.
[24] J. R. Durig. E. L. Varetti, W. J. Natter, A. Müller, *J. Mol. Struct.* **1978**, *49*, 43.
[25] H. Aleman, J. Lielmezs, *Thermochim. Acta* **1992**, *194*, 87.
[26] B. S. Suresh, D. K. Padma, *Polyhedron* **1986**, *5*, 1579.
[27] E. Bertling, H. C. Marsmann, *Z. Anorg. Allg. Chem.* **1989**, *578*, 166.
[28] H. C. Marsmann, E. Meyer, *Makromol. Chem.* **1987**, *188*, 887.
[29] R. M. Atkins, V. A. Hoban, *J. Mater. Res.* **1989**, *4*, 641.
[30] Yu. Borisova, G. S. Gol'din, L. S. Baturina, V. P. Voloshenko, S. V. Sin'ko, *Russ. J. Gen. Chem*. **1993**, *63*, 269.
[31] H. C. Marsmann, E. Meyer, *Z. Anorg. Allg. Chem.* **1987**, *548,* 193.
[32] H. Quellhorst, A. Wilkening, M. Binnewies, *Z. Anorg. Allg. Chem.* **1997**, *623*, 1871.
[33] U. Wannagat, G. Bogedain, A. Scherwan, H. C. Marsmann, D. J. Brauer, H. Bürger, F. Dörrenbach, G. Pawelke, *Z. Naturforsch.* B **1991**, *46b*, 931.
[34] M. Binnewies, M. Jerzembeck, A. Wilkening, *Z. Anorg. Allg. Chem.* **1997**, *623*, 1875.
[35] M. J. S. Dewar, E. G. Zoebisch, E. F. Healey, J. J. P. Stewart, *J. Am. Chem. Soc*. **1987**, *107*, 3902.
[36] J. J. P. Stewart, *J. Comput. Chem*. **1989**, *10*, 209–221.
[37] W. Thiel, A. A. Voityuk, *Theor. Chim. Acta* **1992**, *81*, 391.
[38] D. N. Nanda, K. Jug, *Theor. Chim. Acta* **1980**, *57*, 95; K. Jug, R. Iffert, J. Schulz, *Int. J. Quantum Chem*. **1987**, *32,* 265.
[39] B. Ahlswede, K. Jug, *J. Comput. Chem*. **1999**, 20, 563–572.
[40] J. J. P. Stewart, M. S. Gordon, *Phosphorus, Sulfur, and Silicon* **1990**, *47*, 105.
[41] D. Wichmann, K. Jug, *Chem. Phys.* **1998**, *236*, 87.
[42] K. Jug, D. Wichmann, *J. Mol. Struct. (Theochem.)* **1994**, *313*, 155.
[43] K. Jug, D. Wichmann, *J. Mol. Struct. (Theochem.)* **1997**, *398–399*, 365.
[44] H. Borrmann, M. Binnewies, *Z. Krist*., in press.
[45] J. Magull, M. Binnewies, *Z. Krist*., in press.
[46] K. W. Törnroos, G. Calzaferri, R. Imhof, *Acta Cryst. C* **1995**, *51*, 1732.
[47] V. W. Day, W. G. Klemperer, V. V. Mainz, D. M. Müller, *J. Am. Chem. Soc.* **1985**, *107,* 8262.
[48] D. Wichmann, K. Jug, *J. Phys. Chem. B.* **1999**, *103*, 10087.
[49] A. Wilkening, M. Binnewies, *Z. Naturforsch. B,* in press.
[50] A. Wilkening, Ph. D, thesis, University of Hannover, 1998.
[51] M. Junker, A. Wilkening, M. Binnewies, Hg. Schnöckel, *Eur. J. Inorg. Chem.* **1999**, 1531.
[52] H. Quellhorst, A. Wilkening, N. Söger, M. Binnewies, *Z. Naturforsch*. **1999**, *54b*, 577.
[53] DEGUSSA, Schriftenreihe Pigmente, Nr. 11.
[54] DEGUSSA, Schriftenreihe Pigmente, Nr. 56.
[55] DEGUSSA, Aerosil – Pyrogene Kieselsäuren.
[56] K. Jug, D. Wichmann, unpublished results.
[57] S. Lieke, M. Binnewies, *Z. Anorg. Allg. Chem*. **1997**, *623*, 1705.

Received November 10, 1999
[I99409]

Selective C−H Bond Activation with Na_2PtCl_4 in Inverted Micelles

S. Gaemers,[a] K. Keune,[a] A. M. Kluwer,[a] and C. J. Elsevier*[a]

Keywords: Platinum / Micelles / C−H activation / NMR spectroscopy / Inverted micelles

The selective C–H activation of *n*-heptane and methylcyclohexane with Na_2PtCl_4 under mild conditions in water in inverted micelles is described.

Introduction

The selective activation and functionalisation of aliphatic hydrocarbons is of great interest.[1,2] In particular, the transformation of aliphatic hydrocarbons under mild reaction conditions to, for example, alcohols and aldehydes presents a problem. The activation of C−H bonds is thermodynamically not a difficult process, but the selective activation of C−H bonds of specific sp^3 carbon atoms is troublesome.[3,4] The use of appropriate transition metal catalysts may alleviate this problem.[5] To date several (catalytic) reactions are known for the conversion of hydrocarbons to functionalised hydrocarbons.[1,4−7] The activation of C−H bonds has been achieved by using $[PtCl_4]^{2-}$ as the catalyst with various substrates.[8,9] Such reactions are often performed under highly acidic conditions in aqueous solutions containing CF_3COOH or H_2SO_4.[2,6,8,9] For the selective C−H activation of hydrocarbons with platinum(II), we decided to introduce a water-soluble platinum salt in an aliphatic reaction medium by means of inverted micelles. The reaction rates in water[10−13] and in biphasic systems[14] (water in oil micro-emulsions) can be increased by using inverted micelles as this increases the surface contact area between catalyst and substrate. We decided to use inverted micelles of AOT[15] as this surfactant has been well studied and is commercially available.

The incubation of inverted micelles of AOT containing a 0.20 M solution of Na_2PtCl_4 in D_2O during several hours at 353 K resulted in the selective C−H activation of the CH_3 moieties of *n*-heptane and methylcyclohexane, as witnessed by the observed H-D exchange. The use of D_2O enables a stable ^2H lock during ^{195}Pt NMR experiments and allows for the observation of the exchange of protons for deuterons in the Pt^{II}-mediated C−H activation, see below.

Water and Platinum Loading

The size and shape of inverted micelles is determined (apart from the type of surfactant, solvent, concentration) by the amount of water present in inverted micelles. The water/AOT ratio is expressed as W_0 (W_0 = [H_2O]/[AOT]). Variations of W_0 cause changes in the size and structure of the inverted micelles,[16] the volume of the micro-droplets, the rotational correlation time (τ_c) of the inverted micelles[17] and the water-structure in the inverted micelles.[18] Therefore, it is of vital importance to control the W_0 parameter. When performing catalysis or spectroscopy in inverted micelles, the concentration of the compound(s) of interest (catalyst and/or substrates) is an important parameter as well; it is closely related to W_0 and may influence the size and shape of inverted micelles in a similar manner. The concentration of Na_2PtCl_4 in inverted micelles may influence the maximum water loading of the inverted micelles. Therefore, the maximum platinum concentration that can be reached in a solution of inverted AOT micelles in *n*-heptane has been determined by titration,[19,20] the results of which are shown in Figure 1.

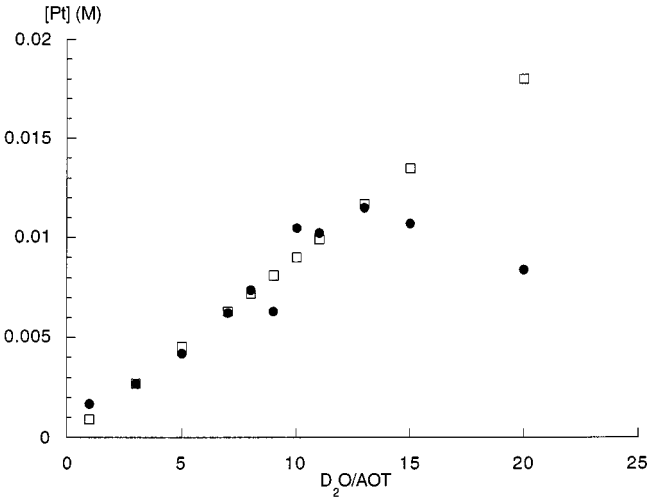


Figure 1. Titration of a solution of 0.25 M AOT in *n*-heptane with a 0.2 M solution of Na_2PtCl_4 in D_2O; filled circles are the measured platinum concentrations, open squares are the calculated concentrations

At the W_0 value where the measured concentration starts to deviate from the calculated concentration, the maximum platinum loading for the inverted micelles is reached.[21] Up to W_0 = 13 the concentration of platinum *in* the inverted micelle is 0.2 M. No precipitation of the platinum salt or exclusion of water was observed below this value. The ex-

[a] Institute of Molecular Chemistry, Universiteit van Amsterdam, Nieuwe Achtergracht 166, 1018 WV Amsterdam, The Netherlands Fax: (internat.) +31-20/525-6456 E-mail: else4@anorg.chem.uva.nl

 © WILEY-VCH Verlag GmbH, D-69451 Weinheim, 2000 1434−1948/00/0606−1139 $ 17.50+.50/0

periments in micellar solutions have been performed at $W_0 = 10$. The orange/brown colour of the micellar solutions clearly indicates that the platinum salt is indeed dissolved in the inverted micelles. No coloration of the aliphatic solvents occurs in the absence of AOT.

^{195}Pt NMR Spectroscopy

In order to assess putative interactions between the surface of the inverted micelles and the Na_2PtCl_4, we performed a ^{195}Pt NMR study (see Table 1). As the ^{195}Pt chemical shift is very sensitive to small changes in the chemical environment of the salt, interactions between the inverted micelle and Na_2PtCl_4 are expected to appear as variations in the ^{195}Pt chemical shift. Note that a decrease of the ^{195}Pt chemical shift by 11 ppm is observed when varying the Na_2PtCl_4 concentration from 0.05 M to 0.2 M in D_2O. As we did not observe any changes of the ^{195}Pt chemical shift in inverted micelles of AOT (where the concentration is 0.2 M) relative to the chemical shift in a 0.2 M D_2O solution of Na_2PtCl_4, it can be concluded that the environment of the platinum(II) species in inverted micelles is comparable to that in D_2O solution.

Table 1. ^{195}Pt chemical shift data of Na_2PtCl_4 in inverted micelles in various solvents, $[Na_2PtCl_4] = 0.2$ M

	Solvent	[AOT][a]	$\delta(^{195}Pt)$[b]
1	D_2O[c]	–	−1614
2	D_2O	–	−1625
3	heptane	0.25	−1626
4	hexane	0.25	−1626
5	pentane	0.25	−1624

[a] AOT concentration in mols/L. – [b] $\delta(^{195}Pt)$ in ppm. – [c] 0.05 M solution.

H-D Exchange

We observe that H-D exchange of the methyl protons of *n*-heptane with deuterons from D_2O readily proceeds at 353 K in inverted micelles of AOT, as indicated by ^{2}H NMR spectroscopy and GC-MS. Stacked plots of the ^{2}H NMR spectra of 0.25 M AOT in *n*-heptane or methylcyclohexane containing 0.2 M Na_2PtCl_4 in D_2O are shown in Figure 2. Monitoring the ^{2}H NMR intensity of *n*-heptane of a micellar solution of AOT containing Na_2PtCl_4 at 353 K as a function of time, showed an increase of the integral of the methyl resonance by a factor of 2.5. Similarly, an increase of the deuterium content was observed for the methyl group of methylcyclohexane. GC-MS spectra of methylcyclohexane after H-D exchange showed a deuteration level in the isotope pattern three times higher than the natural abundance. No concomitant increase of the integral of the ^{2}H NMR resonance of the methylene protons was observed in either case. This observation is proof of the selective enrichment of the methyl groups with ^{2}H due to exchange of protons with deuterons from D_2O. Comparison with a blank experiment showed that no enrichment in deuterium of the terminal methyl groups takes place in the absence of the platinum salt. Hence, this enrichment must

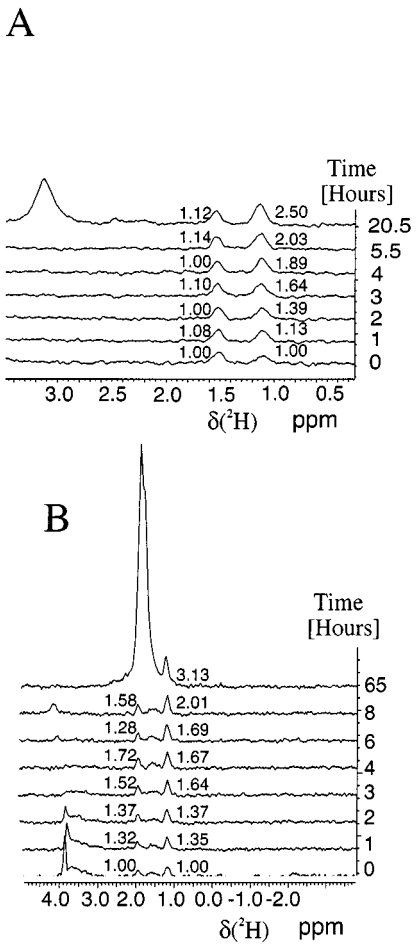


Figure 2. Stacked plots of ^{2}H NMR spectra recorded at 353 K of a micellar solution of AOT containing a 0.2 M D_2O solution of Na_2PtCl_4, demonstrating the H-D exchange in the methyl groups of *n*-heptane (A) and methylcyclohexane (B); an increase of the ^{2}H intensity of the *methyl* resonances is observed exclusively; the intensities at t = 0 have been arbitrarily calibrated at 1.00

stem from selective C−H activation by platinum(II) followed by exchange of the proton by a deuteron from D_2O.

This finding exemplifies the selective activation of the terminal methyl groups of aliphatic hydrocarbons in inverted micelles. Based on the total amount of platinum present in solution, we calculated that a sub-stoichiometric conversion (minimum value 10%) has been obtained so far.

After the H-D exchange had ceased, a colourless two phase system containing metallic platinum was obtained. The reason for the formation of metallic platinum is presently unknown. The signal observed at 1.5 ppm in Figure 2b might be the result of the hydrolysis of AOT, resulting in 2-ethyl-1-hexanol.

Conclusions and Outlook

The use of inverted micelles of AOT in a biphasic system of water-solubilised platinum salts in aliphatic solvents offers a very mild and selective route for the C−H bond activation of CH_3 groups in hydrocarbons. This may have in-

teresting implications for new routes towards terminally substituted (linear) alkane derivatives.

We now aim at employing a more stable surfactant, which may increase the lifetime of the micro-emulsion. The intrinsic features of inverted micelles in biphasic systems, such as a high contact area and ease of separation of the catalyst from products, deserve further attention in connection with the activation of C−element bonds.

Experimental Section

The surfactant sodium bis(2-ethylhexyl)sulfosuccinate (AOT) was dried by azeotropically distilling the salt three times with benzene followed by drying overnight in vacuo. Solutions of inverted micelles containing Na_2PtCl_4 were prepared by the addition of 135 μL of a 0.2 M stock solution of the appropriate platinum salt in D_2O to a 0.25 M AOT stock solution in *n*-heptane or methylcyclohexane. Stirring for at least two hours resulted in yellow or brown optically transparent solutions, which are stable for several days at room temperature. The solutions of inverted micelles containing Na_2PtCl_4 (0.2 M) thus obtained were heated to 353 K in a closed NMR tube, preferably a 10 mm od, 8 mm id sapphire HP NMR tube to prevent evaporation of the solvent. The HP NMR tube has been described in detail elsewhere.[22,23] For every ^2H NMR spectrum 512 scans were acquired at 353 K using the broad band channel of a 10 mm broad band 10 MHz-121 MHz-{^1H} probe (^1H at 300 MHz). The pulse duration was 5 μs (≈30° pulse), a 1.0 s preaquisition delay was used, during which the HOD resonance was saturated by CW irradiation.

[1] [1a]R. G. Bergman, *Science* **1984**, *223*, 902. − [1b]R. H. Crabtree, *Chem. Rev.* **1995**, *95*, 987.

[2] M. Lin, T. Hogan, A. Sen, *J. Am. Chem. Soc.* **1997**, *119*, 6048.

[3] H. E. Bryndza, L. K. Fong, R. A. Paciello, W. Tam, J. E. Bercaw, *J. Am. Chem. Soc.* **1987**, *109*, 1444.

[4] [4a]A. Sen, *Acc. Chem. Res.* **1998**, *31*, 550. − [4b]B. Rybtchinsky, D. Milstein, *Angew. Chem. Int. Ed.* **1999**, *38*, 870.

[5] D. D. Wick, K. I. Goldberg, *J. Am. Chem. Soc.* **1997**, *119*, 10235.

[6] R. A. Periana, D. J. Taube, S. Gamble, H. Taube, T. Satoh, H. Fujii, *Science* **1998**, *280*, 560.

[7] M. Lin, T. E. Hogan, A. Sen, *J. Am. Chem. Soc.* **1996**, *118*, 4574.

[8] [8a]J. A. Labinger, A. M. Herring, D. K. Lyon, G. A. Luinstra, J. E. Bercaw, I. T. Horváth, K. Eller, *Organometallics* **1993**, *12*, 895. − [8b]G. A. Luinstra, L. Wang, S. S. Stahl, J. A. Labinger, J. E. Bercaw, *J. Organomet. Chem.* **1995**, *504*, 75.

[9] A. E. Shilov, G. B. Shul′pin, *Chem. Rev.* **1997**, *97*, 2879.

[10] Y. Zhang, P. Sun, *Tetrahedron: Asymmetry* **1996**, *7*, 3055.

[11] S. Otto, J. B. F. N. Engberts, J. C. T. Kwak, *J. Am. Chem. Soc.* **1998**, *120*, 9517.

[12] Y. Ikushima, Z. Shervani, N. Saito, N. Hatakeda, O. Sato, T. Aizawa, M. Arai, *Chem. Eng. Sci.* **1999**, *54*, 2859.

[13] F. Van Vyve , A. Renken, *Catal. Today* **1999**, *48*, 237

[14] C. Larpent, F. Brisse-Le Menn, H. Patin, *J. Mol. Catal.* **1991**, *65*, L35.

[15] Aerosol-OT; bis(2-ethylhexyl)sulfosuccinate sodium salt.

[16] C. H. Cho, M. Chung, J. Lee, T. Nguyen, S. Singh, M. Vedamuthu, S. Yao, J.-B. Zhu , G. W. Robinson, *J. Phys. Chem.* **1995**, *99*, 7806.

[17] H. Hauser, G. Haering, A. Pande, P. L. Luisi, *J. Phys. Chem.* **1989**, *93*, 7869.

[18] G. Onori, A. Santucci, *J. Phys. Chem.* **1993**, *97*, 5430.

[19] A solution of 0.25 M AOT in *n*-heptane was titrated with a stock solution of 0.2 M Na_2PtCl_4 in D_2O. The concentration of the AOT solution used (0.25 M) is well above the critical micelle concentration of AOT, which is 0.4 mM in aliphatic solvents.[20] The platinum concentration of the solutions of inverted micelles were determined by UV/Vis absorption spectrometry at 375 nm for a number of W_0 values. A blank solution of 0.25 M AOT devoid of platinum showed no absorption at 375 nm. The extinction coefficient of the micellar solutions was calculated from the known concentration where $W_0 = 3$ and was 132 M^{-1} cm^{-1} for Na_2PtCl_4.

[20] [20a] M. Ueno, H. Kishimoto , Y. Kyogoku, *Chem. Lett.* **1977**, 599. − [20b] F. Heatly, *J. Chem. Soc., Faraday Trans.* **1987**, *83*, 517.

[21] The concentration as determined by UV/Vis deviates from the calculated concentration Na_2PtCl_4 for $W_0 > 13$. Above this value, the micelles either only take up water and exclude platinum, or exclude both water and platinum from the interior of the inverted micelles.

[22] D. C. Roe, *J. Magn. Reson.* **1985**, *63*, 388.

[23] C. J. Elsevier, *J. Mol. Catal.* **1994**, *92*, 285.

Received December 29, 1999
[I99475]

New Silyl-Substituted Tin-Nitrogen Heterocubanes: Fourfold Metal-Coordinated Nitrogen and Exceptional Chemical and NMR Properties

Michael Veith,*[a] Michael Opsölder,[a] Michael Zimmer,[a] and Volker Huch[a]

Dedicated to Prof. Schmutzler on the occasion of his 65th birthday

Keywords: Tin / Nitrogen / Cage compounds / Cluster compounds / Fourfold metal-coordinated nitrogen

The synthesis of new silyl-substituted tin-nitrogen heterocubanes and the structural analysis of $[Me_3SiNSn]_4$ is described. A sharp signal in the ^{14}N NMR spectrum and a septet in the ^{119}Sn NMR spectrum are among the interesting properties of this new type of compound with nitrogen surrounded by four (hemi)metals.

Introduction

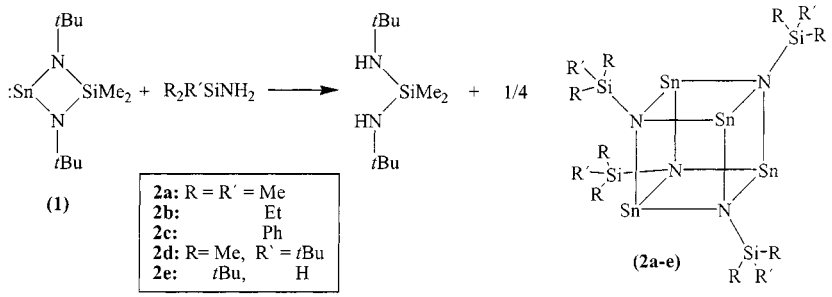
Iminostannylenes of the type $[SnNR]_4$ have been known for about twenty years and were prepared and examined with varying substituents (e.g. R = *t*Bu,[1] *i*Pr, NMe_2,[2] 2,6-$iPr_2C_6H_3$, $BMes_2$,[3] C_6H_{11}, 2-$CH_2C_5H_4N$,[4] Ph[5]).[6] The main structural feature of these compounds is a Sn_4N_4 cage which represents a distorted heterocubane or two interpenetrating tetrahedrons (Sn_4 or N_4), with the R ligands at the nitrogen atoms.

Results and Discussion

From the reaction of the cyclic diazastannylene **1** with primary silylamines (Scheme 1) it was possible to extend the spectrum of substituents to give a new class with silicon, which is the most electropositive element bonded to the nitrogen atom up to now. In addition, the nitrogen carries four electropositive ligands (three metals, one hemimetal) which is unusual for this element. To the best of our knowledge, only three compounds have been characterized by crystal structure analysis where nitrogen is surrounded by four tin(IV) atoms[7] or two silicon and two germanium(II) atoms.[8]

Because of the high condensation tendency of trimethylsilylamine,[9] it had to be synthesised and reacted in situ with **1** to obtain directly **2a**. With other silylamines, we obtained a seconorcubane-like cage $Sn_3H_2(NSiRR'_2)_4$ as an intermediate in the synthesis of **2b–e**, which is analogous to the reaction observed with *tert*-butylamine.[1a] At high temperatures and with reduced pressure (240 °C, 0.01 Torr) it can be transformed to the corresponding cubane-like cage.

The X-ray structure analysis of **2a** reveals, to a good approximation, a $\bar{4}3m$ (T_d) molecular symmetry, but the molecule has only one crystallographic mirror plane passing through Sn(1)−Sn(2)−N(1)−N(2). At the four corners of the distorted Sn_4N_4 cube the Me_3Si groups are located in a staggered form towards the divalent tin atoms (Figure 1). Compound **2a** is the first compound known to us where a nitrogen atom is surrounded by three tin atoms and one silicon atom. The Sn−N bonds in **2a** are slightly shorter than those in the *tert*-butyl-derivative $[tBuNSn]_4$, whereas the Si−N bonds are exceptionally short. The average distance is only about 173 pm whereas 179−183 pm is expected for quaternary nitrogen; only a few exceptions are known.[10]



Scheme 1. General synthesis for $[R'R_2Si–NSu]_4$ (**2a**–**2e**)

Because of this special coordination environment the nitrogen shows unusual NMR properties which are not usually found for (metal)organic compounds. The four electropositive elements surround the ^{14}N nucleus so symmetric-

[a] Institut für Anorganische Chemie, Universität des Saarlandes, Postfach 151150, D-66701 Saarbrücken, Germany
Fax: (internat.) + 49-681/302-3995
E-mail: veith@rz.uni-sb.de

 © WILEY-VCH Verlag GmbH, D-69451 Weinheim, 2000 1434−1948/00/0606−1143 $ 17.50+.50/0

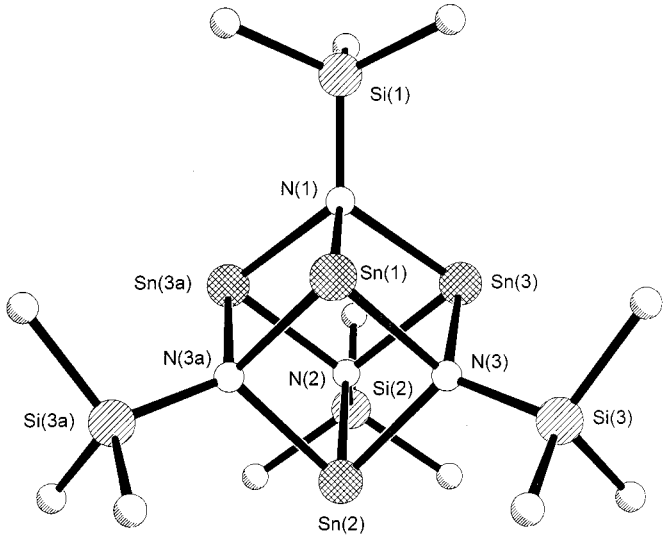


Figure 1. X-ray structure of **2a**; carbon atoms are not labelled; selected distances (average) [pm] and angles [°]: Sn−N 219.6(4), Sn−Sn 329.5(1), Si−N 172.7(4); N−Sn−N 82.3(2), Sn−N−Sn 97.2(2)

ally that its quadrupole moment does not affect the measurability of a ^{14}N NMR spectrum in a negative way. It is possible to get good ^{14}N signals with a half-height width of 8 Hz for the compounds **2a−e**; these signals are accompanied by Sn satellites (integration: approximately 35% of the signal, as expected[11] for three Sn atoms).[12] In addition to that the three ^{14}N nuclei ($I = 1$) around each ^{119}Sn atom split the tin resonance into a septet with an intensity ratio of 1:3:6:7:6:3:1 (Figure 2). The small satellite signals marked with stars are ^{117}Sn satellites with $^2J(^{117}Sn,^{119}Sn) = 57$ Hz, as proved by simulation[13] of the spectrum.

The tests on the reactivity of **2b** showed a remarkable stability of the Sn−N and Si−N bonds. No reaction could be observed with $AlCl_3$, $SnCl_4$, $ZnCl_2$, CuCl, Me_3SnCl, Ph_3SnCl, Me_3SiN_3, LiOMe, NaO*t*Bu, *t*BuOH, LiOH or NH_3, even under drastic conditions with some of them. This is probably due to the special bonding situation of the nitrogen with the neighbouring atoms.

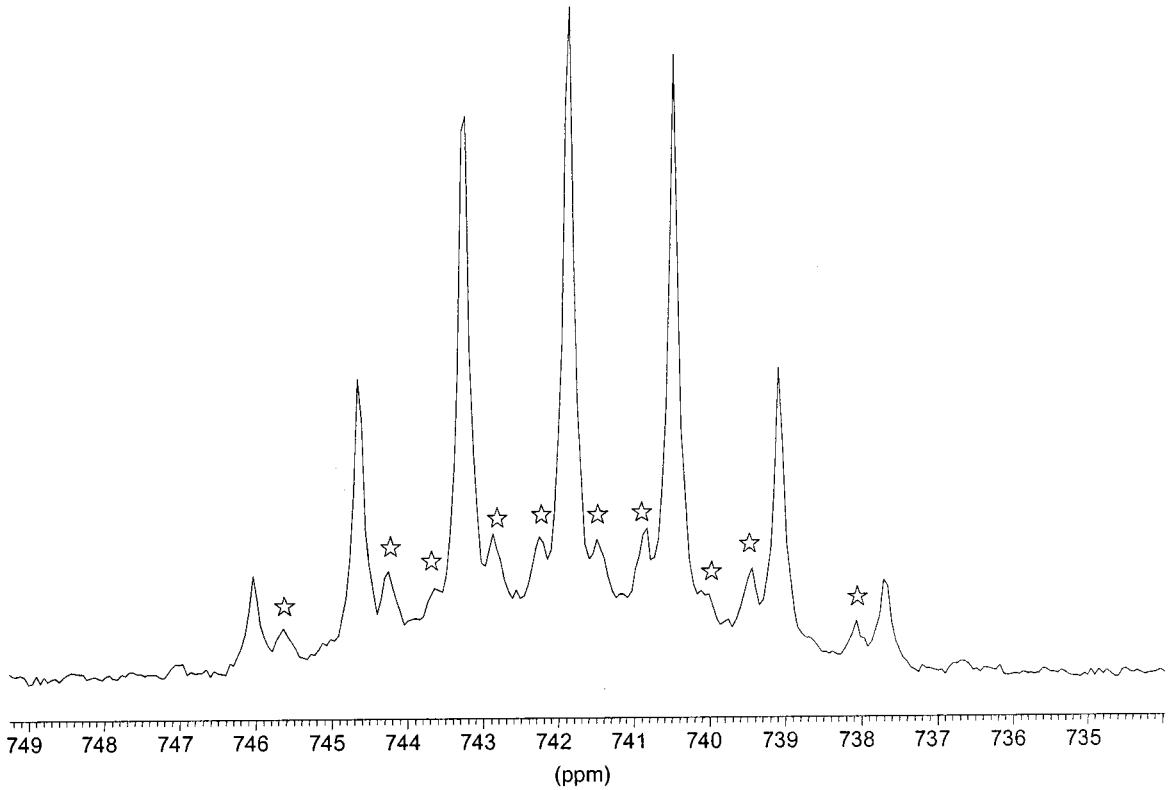


Figure 2. ^{119}Sn NMR spectrum of **2d**; couplings to three ^{14}N nuclei ($I = 1$) are responsible for the extraordinary splitting of the ^{119}Sn signal into a septet with a coupling constant of $^1J(^{14}N,^{119}Sn) = 103.8$ Hz, the signal intensities are in the ratio 1:3:6:7:6:3:1; the peaks marked with stars are ^{117}Sn satellite signals with $^2J(^{117}Sn, ^{119}Sn) = 57$ Hz

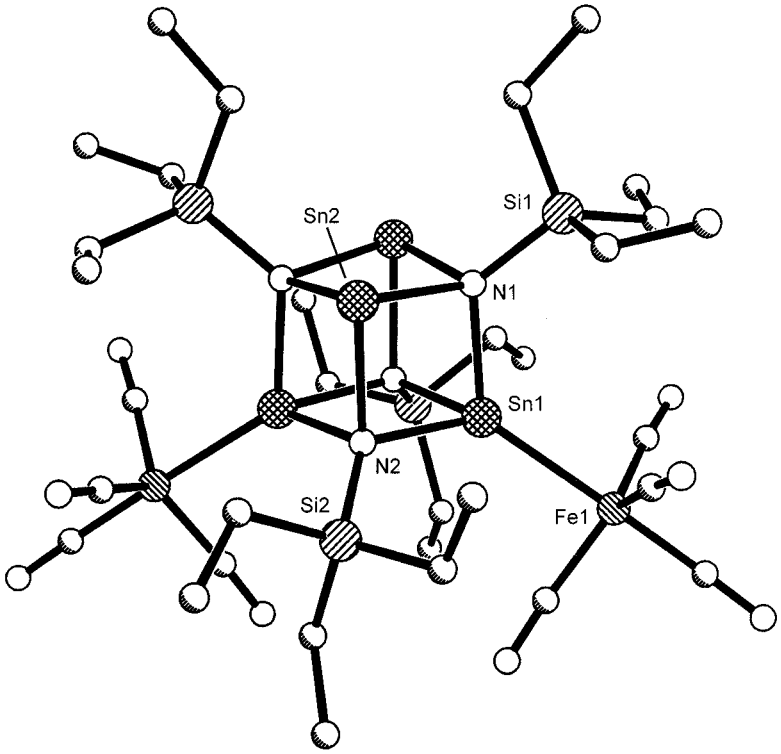


Figure 3. X-ray structure of **3**; carbon and oxygen atoms are not labelled; selected distances [pm] and angles [°]: Sn(1)−N (av.) 215.2(3), Sn(2)−N 224.4(3), Sn(1)−Sn(1a) 321.5(1), Sn(1/1a)−Sn(2/2a) (av.) 327.4(1), Sn(2)−Sn(2a) 332.6(1), Sn(1)−Fe(1) 248.4(1); N−Sn(1)−N (av.) 85.2(1), N−Sn(2)−N (av.) 81.5(1), Sn−N(1)−Sn (av.) 97.1(1), Sn−N(2)−Sn (av.) 95.4(1)

However, it was possible to make use of the Lewis base properties of two of the tin atoms. The reaction of $Fe_2(CO)_9$ with **2b** gave the molecule $[Et_3SiNSn]_4[Fe(CO)_4]_2$ **(3)**. A similar molecule, $[t\text{BuNSn}]_4[Cr(CO)_5]_2$,[14] is known. The structure of **3** (Figure 3) shows a crystallographic twofold axis (C_2) orthogonal to the cube faces Sn(1)−N(2)−Sn(1a)−N(2a) and Sn(2)−N(1)−Sn(2a)−N(1a). The Sn_4N_4 core is close to a C_{2v} (mm2) symmetry. The Sn(1)−N and Sn(1)−Sn(1a) contacts are considerably shorter than in **2a**. The reason for this is the shift of electron density from tin to iron and with that the Et_3Si groups make way for the iron carbonyls, as shown by the larger angles at Sn(1) and the different Si−N−Sn angles.

Experimental Section

General: All substances were handled under an atmosphere of dry nitrogen and solvents were dried and stored over sodium.

$[Me_3SiNSn]_4$ (2a): Me_3SiCl (11 g, 0.1 mol) in 50 mL hexane was added dropwise at −50 °C to liquid ammonia (50 mL). The ammonia was then removed in vacuo at the same temperature. The cold solution was decanted from the NH_4Cl precipitate, added to a solution of **1**[15] (3.2 g, 10 mmol) in hexane (10 mL) and was then allowed to warm to room temperature. After removing all volatile substances the crude product was purified by sublimation (0.01 Torr, 200 °C). m.p. 238 °C, 72% yield. − ^{1}H NMR (200.13 MHz, C_6D_6): δ = 0.26 (s).

$[R_2R'SiNSn]$ (2b−e): A solution of **1** (2.4 g, 7.5 mmol) was added dropwise to a solution of the silylamine (10 mmol; **b**: Et_3SiNH_2, **c**: Ph_3SiNH_2, **d**: $Me_2t\text{BuNH}_2$,[17] **e**: $t\text{Bu}_2\text{HSiNH}_2$[16]) in 10 mL toluene. After stirring for two hours it was refluxed for one hour. The volatile substances were removed in vacuum and the seconorcubane-like intermediate was pyrolysed in vacuo at 0.01 Torr and 250 °C. The formed silylamine was cold trapped and the product sublimed. − ^{1}H NMR (200.13 MHz, C_6D_6/C_7D_8) **2b**: δ = 0.86 (q), 1.15 (t); **2c**: δ = 7.05−7.25 (m), 7.58−7.63 (m); **2d**: δ = 0.26 (s), 1.10 (s); **2e**: δ = 1.24 (s), 4.30 [s, $^3J(^1H, ^{117/119}Sn)$ = 18 Hz].

$[Et_3SiNSn]_4[Fe(CO)_4]_2$ (3): $Fe_2(CO)_9$ (0.76 g, 2.1 mmol) and **2b** (0.40 g, 0.40 mmol) were heated to 65 °C in toluene (10 mL) for 2 hours (the colour changed from orange to green) and then to 100 °C for 6 hours. Toluene and $Fe(CO)_5$ were then removed in vacuum. The mixture of crude product and $Fe_3(CO)_{12}$ was diluted with hexane, filtered and concentrated to obtain crystals of the product (82% yield) which were recrystallized from toluene. − ^{1}H NMR (200.13 MHz, C_6D_6): δ = 1.09/1.86 (broad signals).

All compounds gave correct elemental analyses. A molecular weight determination of **2b** in benzene (cryoscopy) gave a mass of 997.8 g·mol^{-1} (calcd. 992.0 g·mol^{-1}).

X-ray Crystallography

2a: Stoe AED2 diffractometer, Mo-K_α radiation (λ = 71.073 pm), 298 K, crystal size 1.0 × 0.7 × 0.5 mm, monoclinic, space group *C2/m* with a = 2646.8(5) pm, b = 1216.0(2) pm, c = 1097.8(2) pm, β = 110.79(3)°, V = 3303106 pm^3, Z = 4; ρ = 1.841 Mg m^{-3}; μ = 3.15 mm^{-1}, 1.65° ≤ θ ≤ 27.51°, −12 ≤ h ≤ 34, −14 ≤ k ≤ 15, −14 ≤ l ≤ 13, 7583 reflections measured, 3980 independent, empirical absorption correction (min. 0.537, max. 0.998), *R1* = 0.0388, *wR2* = 0.1094, GOF 1.354, no restraints, 133 parameters, remaining electron density max. 1.042 × 10^{-6}, min. −0.796 × 10^{-6} e·pm^{-3}.

3: Stoe IPDS diffractometer, Mo-K_α radiation (λ = 71.073 pm), 220 K, crystal size 0.8 × 0.5 × 0.3 mm, monoclinic, space group

*C*2/*c* with $a = 1775.0(4)$ pm, $b = 1998.7(4)$ pm, $c = 1792.9(4)$ pm, $\beta = 100.00(3)°$, $V = 6264106$ pm^3, $Z = 4$; $\rho = 1.603$ Mg·m^{-3}; $\mu = 2.14$ mm^{-1}, $2.34° \leq \theta \leq 23.95°$, $-20 \leq h \leq 20$, $-22 \leq k \leq 22$, $-20 \leq l \leq 20$, 19455 measured reflections, 4731 independent, *R1* = 0.0323, *wR2* = 0.0909, GOF 1.111, no restraints, 291 parameters, remaining electron density max. 0.907×10^{-6}, min. -0.485×10^{-6} e pm^{-3}.

The structures described in this paper were solved with the heavy-atom method and refined towards F^2 for all observed reflections (solution and refinement with SHELXS97, hydrogen atoms were calculated in ideal tetrahedral geometry and optimised).

Crystallographic data (excluding structure factors) for the structure(s) reported in this paper have been deposited with the Cambridge Crystallographic Data Centre as supplementary publication nos. CCDC-142230 (**2a**) and -142231 (**3**). Copies of the data can be obtained free of charge on application to CCDC, 12 Union Road, Cambridge CB2 1EZ, UK [Fax: (internat.) + 44-1223/336-033; E-mail: deposit@ccdc.cam.ac.uk].

Acknowledgments

This work was supported by the Deutsche Forschungsgemeinschaft within the scope of the Schwerpunkt Halbleiter und Metallcluster and the Fond der Chemischen Industrie. We also thank Mrs. Maria Jarczyk for her assistance.

[1] [1a]M. Veith, M.-L. Sommer, D. Jäger, *Chem. Ber.* **1979**, *112*, 2581−2587; − [1b]M. Veith, O. Recktenwald, *Z. Naturforsch., Teil B* **1983**, *38*, 1054−1061.
[2] M. Veith, G. Schlemmer, *Chem. Ber.* **1982**, *115*, 2141−2152.
[3] H. Chen, R. A. Bartlett, H. V. R. Dias, M. M. Olmstead, P. P. Power, *Inorg. Chem.* **1991**, *30*, 3390−3394.
[4] R. E. Allan, M. A. Beswick, A. J. Edwards, M. A. Paver, M.-A. Rennie, P. R. Raithby, D. S. Wright, *J. Chem. Soc., Dalton Trans.* **1995**, 1991−1994.
[5] W. J. Grigsby, T. Hascall, J. J. Ellison, M. M. Olmstead, P. P. Power, *Inorg. Chem.* **1996**, *35*, 3254−3261.
[6] M. Veith, *Chem. Rev.* **1990**, *90*, 3−16.
[7] [7a]C. Kober, H. Nöth, W. Storch, *Chem. Ber.* **1997**, *130*, 765−769; − [7b]R. Bettenhausen, W. Milius, W. Schnick, *Chem. Eur. J.* **1997**, *3*, 1337−1341.
[8] M. Veith, M. Zimmer, *Z. Anorg. Allg. Chem.* **1996**, *622*, 1471−1477.
[9] N. Wiberg, W. Uhlenbrock, *Chem. Ber.* **1971**, *104*, 2643−2645.
[10] M. Veith, M. Grosser, O. Recktenwald, *J. Organomet. Chem.* **1981**, *216*, 27−38.
[11] M. S. Holt, W. L. Wilson, J. H. Nelson, *Chem. Rev.* **1989**, *89*, 11−49.
[12] ^{14}N NMR (14.462 MHz) **2a**: δ = −329; **2b**: δ = −324; **2c**: δ = −322; **2d**: δ = −327. − ^{119}Sn NMR [74.631 MHz, $^1J(^{14}N,^{119}Sn)$ in Hz] **2a**: δ = 782/100.6; **2b**: δ = 753/102.2; **2c**: δ = 565/103.5; **2d**: δ = 741/103.8; **2e**: δ = 594/106.9; **3**: δ = 489, 520. − ^{29}Si NMR [39.761 MHz, $^2J(^{29}Si,^{117/119}Sn)$ in Hz] **2a**: δ = 4.17/29.4; **2b**: δ = 7.50/16.4; **2c**: δ = −15.1/17.7; **2d**: δ = 8.22/17.6; **2e**: δ = 11.9/15.5.
[13] WIN-DAISY, Bruker-Franzen Analytik GmbH, Bremen, Germany.
[14] M. Veith, magazin forschung **1992**(1), 33−40, Universität des Saarlandes; Saarbrücken, Germany.
[15] M. Veith, *Angew. Chem.* **1975**, *87*, 287−288; *Angew. Chem. Int. Ed. Engl.* **1975**, *14*, 263−264
[16] D. M. Choquette, M. J. Timm, J. L. Hobbs, M. M. Rahim, K. J. Ahmed, R. P. Planalp, *Organometallics* **1992**, *11*, 529−534.
[17] J. R. Bowser, R. H. Neilson, R. L. Wells, *Inorg. Chem.* **1978**, *17*, 1882−1886.

Received March 2, 2000
[I00081]

The First Ru^{II} Bipyridyl-Capped Cyclodextrin: Evidence of Electron-Transfer Through the Cavity

Dominique Armspach,*[a] Dominique Matt,*[a] and Anthony Harriman[b]

Keywords: Cyclodextrins / Ruthenium / N ligands / Electron transfer / Inclusion compounds

The narrow rim of an α-cyclodextrin has been AD-capped with a photoactive ruthenium(II) tris(2,2′-bipyridyl) fragment giving a diastereomeric mixture of complexes that bind 1,4-benzoquinone in water. Steady-state and time-resolved emission studies have been used to probe electron-transfer processes occurring inside and outside the cavity.

Introduction

Supramolecular assemblies displaying *vectorial* photoinduced electron-transfer (ET) reactions have attracted much attention in recent years from the view point of designing efficient artificial photosynthetic systems and light-driven molecular machines.[1−5] In order to gain a better understanding of through-space ET processes, it is necessary to closely position the reactants in a *rigid* manner but to avoid either direct orbital contact or a connecting organic framework. Here, we describe the synthesis and photophysical properties of a water-soluble α-cyclodextrin (α-CD) host for which a photoactive ruthenium(II) centre is held, for the first time, at a *fixed* distance above the receptor. Our approach involves capping the α-CD with a difunctionalized 2,2′-pyridyl ligand before subsequent metallation. The resulting complex is expected to behave as a metallo-receptor which, upon illumination, will transfer an electron between the excited metal centre and a redox-active substrate trapped in the cavity. Photoactive Ru^{II}(bipy) centres appended to cyclodextrin receptors have been reported previously, but these systems contain *flexible* Ru−CD connectors, thus preventing full geometrical control of the ET process.[6]

Results and Discussion

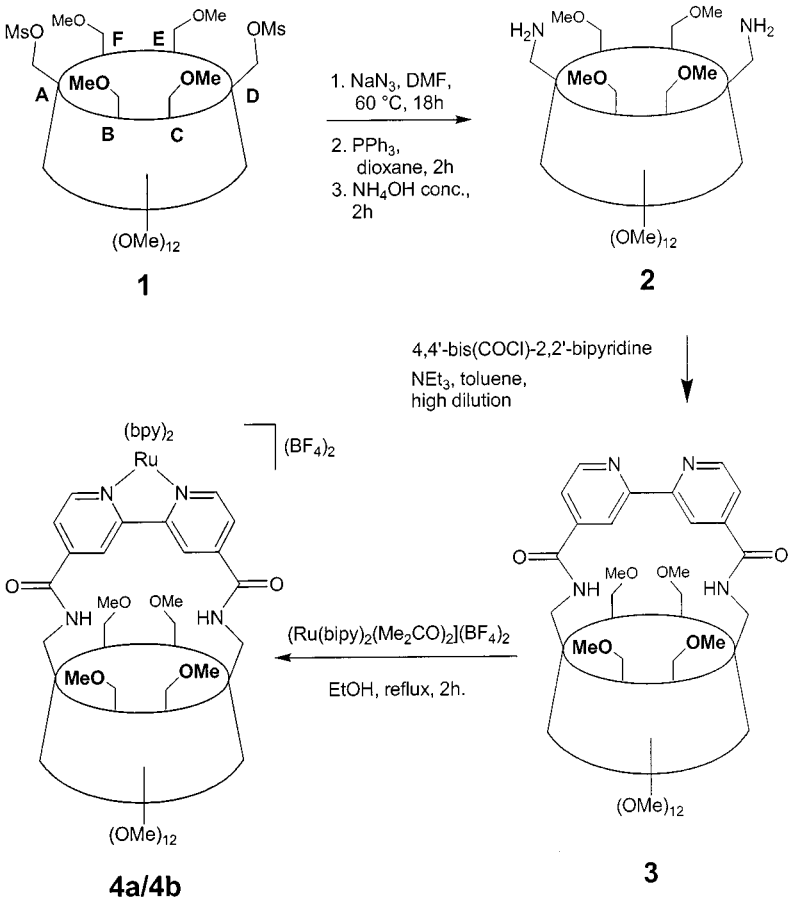
The key precursor for our study is 6A,6D-diamino-6A,6D-dideoxy-hexadeca-*O*-methyl-α-CD (**2**) which allows effective capping with diacid chlorides and good solubility in organic solvents. Compound **2** was synthesised in two steps from the dimesylate **1**[7] according to Scheme 1. Macrocyclisation of **2** under high dilution with 4,4′-bis(chlorocarbonyl)-2,2′-bipyridine in the presence of triethylamine afforded the "exo"-bipy ligand **3** in ca. 50% yield which, on treatment with the solvent complex $[Ru(bipy)_2(Me_2CO)_2][BF_4]_2$, gave an equimolar mixture of the diastereomeric complexes **4a/4b**[8] which was not resolved (see Experimental Section). Unlike ligand **3**, these complexes are soluble in water as well as in organic solvents.

Both ^1H NMR and ^{13}C NMR spectroscopy revealed the diastereomeric nature of the ruthenium complexes **4a/4b**. Each individual compound retains the C_2 symmetry of the ligand. Complexes **4a/4b** undergo chemical shift changes in D_2O upon addition of varying amounts of 1,4-benzoquinone (BQ) indicative of bimolecular association (Figure 1). A titration procedure involving the measurement of chemicals shifts for aqueous solutions containing excess BQ confirmed the 1:1 stoichiometry of the resultant supramolecular assembly and indicated an association constant (K_a) of $9 \pm 3\ M^{-1}$.[9] The CIS[10] (complexation-induced shift on 100% complexation) values obtained from these ^1H NMR spectra are listed in Table 1 for nonoverlapping probes and provide clear indication for the inclusion of BQ into the CD cavity. Amongst the most significant changes are those experienced by the H-3,3′ protons ($\Delta\delta_{max} = +0.22$, vs. +0.05 for H-5,5′ and +0.03 ppm for H-6,6′) of the 4,4′-dicarbonyl-2,2′-bipyridyl fragment, the only 2,2′-bipyridyl (bipy) protons that point towards the cavity interior. Interestingly, some of the CD MeO-3 protons[10] which also point towards the interior of the cavity are strongly upfield shifted ($\Delta\delta_{max} = -0.20$ and −0.23) whereas others are slightly downfield shifted or remain unchanged ($\Delta\delta_{max} = +0.05$ and −0.01) (Figure 1), suggesting that a particular guest orientation within the CD cavity is favoured, perhaps because of some structural distortion imposed by the bipy cap. Furthermore, the chemical shift change found for the H_{CD}-5 protons[11] ($\Delta\delta_{max} = +0.13$) is consistent with medium immersion of BQ.[10]

Luminescence from the metal complex in **4** is quenched upon addition of BQ but Stern-Volmer plots show *pronounced* positive deviations from linearity without reaching a plateau at high quinone concentrations (Figure 2). This situation arises from a combination of both diffusional and static emission quenching processes, as confirmed by time-

[a] Groupe de Chimie Inorganique Moléculaire, Université Louis Pasteur,
UMR 7513 CNRS, 1 rue Blaise Pascal, F-67008 Strasbourg Cedex, France
E-mail: armyou@chimie.u-strasbg.fr
dmatt@chimie.u-strasbg.fr
[b] Department of Chemistry, University of Newcastle, Newcastle upon Tyne NE1 7RU, U.K.

 © WILEY-VCH Verlag GmbH, D-69451 Weinheim, 2000 1434−1948/00/0606−1147 $ 17.50+.50/0



Scheme 1. Synthesis of the diastereomeric mixture **4a/4b**

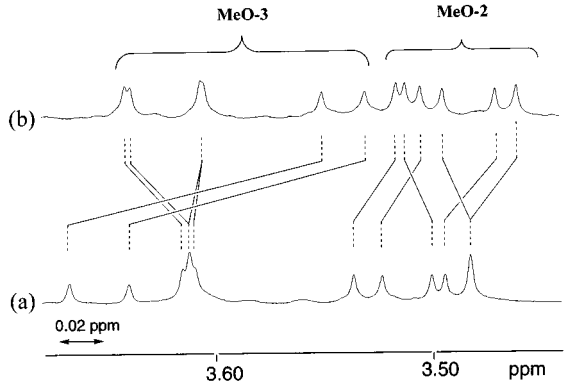


Figure 1. ^{1}H NMR (500 MHz) spectra in the MeO-2 and MeO-3 regions: (a) spectrum of **4a/4b** in the absence of 1,4-benzoquinone; (b) spectrum of **4a/4b** in the presence of 40 equiv. of 1,4-benzoquinone

resolved luminescence studies. Fitting the titration data collected over a wide variation in BQ concentration, however, requires a second diffusional process which becomes important only at high BQ concentrations. These results are readily accommodated within a model for which BQ quenches emission from **4** via a diffusional process having a bimolecular rate constant of 3×10^9 M^{-1} s^{-1} and that competes with inclusion of BQ into the cavity. The second diffusional step, which also occurs with a bimolecular rate constant of 3×10^9 M^{-1} s^{-1}, can now be assigned to quenching of residual emission from the BQ·**4** complex. The best fit to the luminescence data gives $K_a = 45$ M^{-1} and indicates that the encapsulated quinone quenches the excited state of the metal complex with a first-order rate constant of 3.0×10^7 s^{-1}. Insisting on $K_a = 10$ M^{-1}, as indicated by the NMR studies, raises this latter rate constant to 4.7×10^7 s^{-1}. Each quenching step is attributed to ET from the triplet excited metal complex to BQ, although the radical ion products could not be detected by transient absorption spectroscopy.

The NMR studies indicate that the BQ guest is located at an edge-to-edge separation distance (R) of ca. 7 Å[12] from the bipy capping unit. Since the rate of electron transfer usually decreases exponentially with increasing R according to $k = A \exp(-\beta R)$, where the pre-exponential factor A has a value of ca. 10^{13} s^{-1}, we can approximate the attenuation factor β as being ca. 1.8 Å^{-1}. This means that the cavity exerts a serious damping effect on the rate of ET, being comparable to that of a solvent molecule. In the present study, the preferential 3D orientation of an electron-accepting guest takes place within an AD-capped α-CD and, for the first time, photoinduced ET within a Ru(bipy)−cyclodextrin receptor that guests a benzoquinone is shown to occur. Although the rigidified metalloreceptor **4** facilitates study of through-space, light-induced electron transfer in which a variety of redox-active substrates could

Table 1. ^1H NMR chemical shifts data ($\Delta\delta$ values)[a] for the **4a/4b** mixture; BQ in D_2O at 25 °C

Ligand of **4**	Probe[a][b] H-3,3′	H-4,4′	H-5,5′	H-6,6′	H_{CD}-1	H_{CD}-2	H_{CD}-5	MeO-2	MeO-3	MeO-6
2,2′-bipyridine	< 0.01	< 0.01	< 0.01	+0.03 < 0.01	–	–	–	–	–	–
3	+0.22 +0.21	–	+0.05	+0.03	+0.05 −0.02 < 0.01	+0.04 −0.07 −0.04	+0.13 +0.07 +0.04	+0.02 −0.04 −0.04	−0.20 −0.23 +0.05 < 0.01	– −0.05 +0.04

[a] The $\Delta\delta$ values relate to the chemical shift changes experienced by nonoverlapping probe protons in the host on 100% 1:1 complexation (CIS values). They were obtained after treatment of the binding data by an iterative nonlinear curve fitting program. All measurements were carried out using external $Me_4Si/CDCl_3$ as reference. The H_{CD}-3, H_{CD}-4, and H_{CD}-6 protons could not be identified. – [b] H-n,n′ stands for bipy protons while H_{CD}-n corresponds to cyclodextrin signals. For some probes two distinct signals were observed either because of diastereomer distinction, or because of the presence of two nonequivalent H atoms belonging to the same diastereomer.

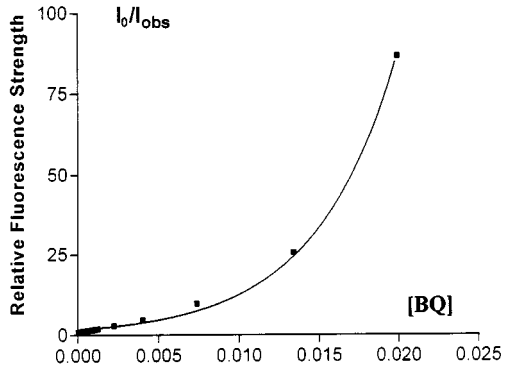


Figure 2. Stern-Volmer plot for the Ru-quinone system derived from **4a/4b**; [Ru] = 1.94×10^{-5} M in H_2O, at 25 °C; [Q] in mol/L

be used, it is necessary to optimise the binding process. This is most easily accomplished by enlarging the cavity and such studies are now underway.

Experimental Section

General: All manipulations were performed under dry nitrogen using purified solvents. A COSY experiment on complexes **4a/4b** allowed precise assignment of the bipy protons. The luminescence experiments were performed using a Perkin−Elmer LS 50B spectrofluorometer at room temperature. Full details for the synthesis of compounds **2** and **3** will be described elsewhere. For the atom numbering of α-cyclodextrin, see ref.[13].

Compound 2: yield 88% (starting from **1**). M.p. 184−186 °C. − ^1H NMR (200.13 MHz, $CDCl_3$): δ = 1.40 (br s, 4 H, NH_2), 3.38 (s, 6 H, CH_3O-6), 3.39 (s, 6 H, CH_3O-6), 3.49 (s, 18 H, CH_3O), 3.63 (s, 6 H, CH_3O), 3.64 (s, 6 H, CH_3O), 3.65 (s, 6 H, CH_3O), 2.99−3.94 (m, 36 H, H_{CD}-2, H_{CD}-3, H_{CD}-4, H_{CD}-5 and H_{CD}-6), 5.02 (d, ^3J = 3 Hz, 2 H, H_{CD}-1), 5.06 (d, ^3J = 3.5 Hz, 4 H, H_{CD}-1). − $^{13}C\{^1H\}$ NMR (50.32 MHz, $CDCl_3$): δ = 42.7 (CH_2N), 57.8 (×2) and 58.0 (CH_3O), 59.0 and 59.1 (CH_3O-6), 61.7 and 61.8 (×2) (CH_3O), 71.1, 71.2, and 72.4 (C_{CD}-5), 71.1 (×2) (C_{CD}-$6^{B,C,E,F}$), 81.3 (×3), 82.2 (×4), 82.5, 83.2 (C_{CD}-2, C_{CD}-3, and C_{CD}-4), 99.8, 100.0, and 100.3 (C_{CD}-1). − $C_{52}H_{94}N_2O_{28}$ (1195): calcd. C 52.25, H 7.93, N 2.34; found C 52.19, H 8.00, N 2.22.

Ligand 3: yield 50%. M.p. 195−197 °C. − IR (KBr): $\tilde{\nu}$ = 1655 (CO) cm^{-1}. − ^1H NMR (200.13 MHz, $CDCl_3$): δ = 3.02 (s, 6 H, CH_3O-6), 3.12 (s, 6 H, CH_3O-6), 3.45 (s, 6 H, CH_3O), 3.47 (s, 12 H, CH_3O), 3.60 (s, 6 H, CH_3O), 3.63 (s, 6 H, CH_3O), 3.65 (s, 6 H, CH_3O), 3.13−4.14 (m, 36 H, H_{CD}-2, H_{CD}-3, H_{CD}-4, H_{CD}-5 and H_{CD}-6), 4.94 (d, ^3J = 3 Hz, 2 H, H_{CD}-1), 5.00 (d, ^3J = 3.5 Hz, 2 H, H_{CD}-1), 5.03 (d, ^3J = 3.1 Hz, 2 H, H_{CD}-1), 7.57 (br. t, 2 H, CONH), 7.89 (d, ^3J = 5 Hz, 2 H, H_{pyr}-5,5′), 8.28 (s, 2 H, H_{pyr}-3,3′), 8.96 (d, ^3J = 5 Hz, 2 H, H_{pyr}-6,6′). − $^{13}C\{^1H\}$ NMR (50.32 MHz, $CDCl_3$): δ = 43.2 (CH_2NH), 57.8 and 58.1 (×2) (CH_3O), 58.8 and 59.1 (CH_3O-6), 61.6 and 61.7 (×2) (CH_3O), 70.7, 71.4, and 72.9 (C_{CD}-5), 70.9 and 72.3 (C_{CD}-$6^{B,C,E,F}$), 80.6, 81.3, 81.4, 81.8 (×3), 82.1 (×2), 82.3, and 85.8 (C_{CD}-2, C_{CD}-3, and C_{CD}-4), 99.5, 99.6, and 100.1 (C_{CD}-1), 118.7 (C_{pyr}-5,5′), 121.7(C_{pyr}-3,3′), 142.3 (C_{pyr}-4,4′), 151.8 (C_{pyr}-6,6′), 157.1 (C_{pyr}-2,2′), 164.5 (CONH). − $C_{64}H_{98}N_4O_{30}$ (1404): calcd. C 54.77, H 7.04, N 3.99; found C 54.70, H 7.09, N 3.84.

Complexes 4a + 4b (mixture): A mixture of *cis*-$RuCl_2(bipy)_2$ (0.074 g, 0.14 mmol) and $AgBF_4$ (0.064 g, 0.32 mmol) in acetone (20 mL) was refluxed for 2 h. After cooling, the filtered solution was added to a solution of **3** (0.200 g, 0.14 mmol) in ethanol (10 mL). Acetone was removed under reduced pressure and the ethanolic solution was stirred under reflux for 2 h. A solution of $NaBF_4$ in water (1 M, ca. 20 mL) was then added to the mixture. Extraction with CH_2Cl_2 (3 × 50 mL) and drying over $MgSO_4$ afforded **4** as a mixture of two diastereomers.[8] Yield: 0.270 g, 95%. − IR (KBr): $\tilde{\nu}$ = 1655 (CO) cm^{-1} − UV/Vis (H_2O): λ_{max} (ε) = 485 (11000), 421 (10400). − ^1H NMR (500.14 MHz, D_2O, ext. ref.: $SiMe_4$ in $CDCl_3$): δ = 2.60 (s, 6 H, CH_3O-6), 2.92 (s, 6 H, CH_3O-6), 3.05 (s, 6 H, CH_3O-6), 3.21 (s, 6 H, CH_3O-6), 3.23−3.37 (6dd, ^3J = 2.8 and 9.7 Hz, 12 H, H_{CD}-2), 3.48 (s, 12 H, CH_3O-2), 3.49 (s, 6 H, CH_3O-2), 3.50 (s, 6 H, CH_3O-2), 3.52 (s, 6 H, CH_3O-2), 3.54 (s, 6 H, CH_3O-2), 3.55−4.22 (m, 48 H, H_{CD}-3, H_{CD}-4, and H_{CD}-6), 3.96−4.20 (m, 6 H, H_{CD}-5), 5.11 (d, ^3J = 3.7 Hz, 2 H, H_{CD}-1), 5.12 (d, ^3J = 3.7 Hz, 2 H, H_{CD}-1), 5.16 (d, ^3J = 2.8 Hz, 2 H, H_{CD}-1), 5.20 (d, ^3J = 2.8 Hz, 2 H, H_{CD}-1), 5.27 (d, ^3J = 3.4 Hz, 2 H, H_{CD}-1), 5.29 (d, ^3J = 3.4 Hz, 2 H, H_{CD}-1), 7.35−7.43 (m, 8 H, H_{pyr}-5,5′), 7.68 (d, ^3J = 5.4 Hz, 2 H, H_{pyr}-6,6′), 7.72 (d, ^3J = 5.4 Hz, 2 H, H_{pyr}-6,6′), 7.80 (dd, ^3J = 5.5 Hz and ^4J = 1.8 Hz, 4 H, H_{pyr}-5,5′ connected to CD), 7.82 (d, ^3J = 5.4 Hz, 2 H, H_{pyr}-6,6′), 7.86 (d, ^3J = 5.4 Hz, 2 H, H_{pyr}-6,6′), 8.04−8.13 (m, 12 H, H_{pyr}-4.4′ of bipy and H_{pyr}-6,6′ connected to CD), 8.57−8.59 (m, 8 H, H_{pyr}-3,3′), 9.07 (d, ^4J = 1.8 Hz, 2 H, H_{pyr}-3,3′ connected to CD), 9.12 (d, ^4J = 1.8 Hz, 2 H, H_{pyr}-3,3′ connected to CD). − $^{13}C\{^1H\}$ NMR (50.32 MHz, $CDCl_3$): δ = 44.3 (×2) (CH_2NH), 57.4 (×2), 57.7 (×2) and 57.6 (×2) (CH_3O), 58.5 (×2), 58.7 and 58.9 (CH_3O-6), 61.5 (×2), 61.7 (×2) and 62.0 (×2) (CH_3O), 70.1(×2), 70.4 (×2), and 70.5 (×2) (C_{CD}-5), 70.7 (×2) and 71.3 (×2) (C_{CD}-$6^{B,C,E,F}$), 80.3 (×2), 81.9 (×4), 82.1 (×2), 82.3 (×4), 82.4 (×2), 82.6 (×2), and 84.2 (×2) (C_{CD}-2, C_{CD}-3, and C_{CD}-4), 99.9 (×2), 100.2 (×2), and 100.4 (×2) (C_{CD}-1), 120.1 (×2), 124.6

(×4) (C_{pyr}-3,3′), 127.7 (×2), 127.9 (×2), and 128.5 (×2) (C_{pyr}-5,5′), 138.4 (×2), 138.6 (×2), 143.3 and 143.4 (C_{pyr}-4,4′), 150.5 (×2), 151.2 (×2), 152.1 (×2) (C_{pyr}-6,6′), 156.0 (×2), 156.7 (×2), 157.3 (×2) (C_{pyr}-2,2′), 162.2 (×2) (CONH). − FAB-MS: *m/z* (%) = 1903 (15) $(M - BF_4)^+$, 1816 (100) $(M - 2BF_4)^+$. − $C_{84}H_{114}B_2F_8N_8O_{30}Ru$ (1991): calcd. C 50.69, H 5.77, N 5.63; found C 50.62, H 5.90, N 5.41.

The determination of the association constants is based on the chemical shift variation of certain nonoverlapping H-signals upon addition of an excess (3−40 equiv.) of BQ to a 2.7×10^{-3} M solution of **4** in D_2O. The data were treated by a nonlinear regression analysis program in order to extract K_a and CIS values. A similar procedure was used to evaluate the K_a value ($K_a = 8 \pm 3\ M^{-1}$) for the complex formed between [hexakis(2,3,6-tri-*O*-methyl-α-cyclodextrin] (TM-α-CD) and BQ. Comparison of the two K_a values suggests that the [$Ru(bipy)_2$(4,4′-biscarbonylbipy)] cap has little influence on the complexation process.

Emission spectra (room temperature, $\lambda_{exc} = 460$ nm) in air-saturated water were obtained for a concentration of complex **4** that was maintained constant throughout the titration (1.94×10^{-5} M). The quinone concentration ranges from 1.94×10^{-5} M to 2.00×10^{-2} M.

[1] I. Willner, E. Kaganer, E. Joselevich, H. Dürr, E. David, M. J. Günter, M. R. Johnston, *Coord. Chem. Rev.* **1998**, *171,* 261−285.

[2] R. Breslow, S. D. Dong, *Chem. Rev.* **1998**, *98,* 1997−2011.

[3] J.-C. Chambron, J.-P. Collin, J.-P. Dalbavie, C. Dietrich-Buchecker, V. Heitz, F. Odobel, N. Solladié, J.-P. Sauvage, *Coord. Chem. Rev.* **1998**, *180,* 1299−1312.

[4] P. R. Ashton, R. Ballardini, V. Balzani, E. C. Constable, A. Credi, O. Kocian, S. J. Langford, J. A. Preece, L. Prodi, E. R. Schofield, N. Spencer, J. F. Stoddart, S. Wenger, *Chem. Eur. J.* **1998**, *4,* 2413−2422.

[5] P. Piotrowak, *Chem. Soc. Rev.* **1999**, *28,* 143−150.

[6] R. Deschenaux, T. Ruch, P.-F. Deschenaux, A. Juris, R. Ziessel, *Helvetica Chim. Acta* **1995**, *78,* 619−628.

[7] D. Armspach, D. Matt, *Chem. Commun.* **1999**, 1073−1074.

[8] Molecule **4** combines an enantiomerically pure cyclodextrin fragment with the dissymetric ruthenium centre. This combination results in the formation of two diastereomers.

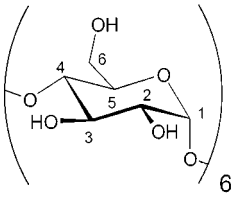
[9] Both diastereomers **4a/4b** were found to undergo similar chemical shift changes upon complexation with BQ and therefore identical K_a values for the 1:1 complexes were obtained. Probes giving the maximum chemical shift changes were used to evaluate the K_a values, namely H-3,3′ protons of the 4,4′-dicarbonyl-2,2′-bipyridyl moiety and one of the CD MeO-3 signals.

[10] H.-J. Schneider, F. Hacket, V. Rüdiger, H. Ikeda, *Chem. Rev.* **1998**, *98,* 1755−1785.

[11] Unfortunately, the H_{CD}-3 signals which are usually strongly upfield-shifted, even for a shallow complexation process, could not be identified as a result of signal overlap. However, the H_{CD}-3 signal of the (TM-α-CD)·BQ complex could be clearly seen and undergoes a significant upfield-shift on complexation (CIS = −0.42 ppm on 100% complexation). Based on this probe, an association constant of $8 \pm 3\ M^{-1}$ was determined; this value is in agreement with that obtained for BQ complexation with **4a/4b** ($9 \pm 3\ M^{-1}$).

[12] This value was estimated on the basis of the NMR CIS values found for protons located in the CD cavity together with molecular models. Clearly, the large chemical shift changes on BQ-complexation experienced by some of the MeO-3 protons indicate a shallow guest inclusion of the guest at the cavity entrance. For steric reasons the *OO*-axis of included BQ was assumed to be oriented along the CD C_2 axis. The estimated edge-to-edge separation stands for the distance between an N atom of the substituted bipy and the nearest BQ-oxygen atom.

[13] Numbering in α-CD:



6

Received December 13, 1999
[I99455]

Preparation, Characterization and Crystal Structure of the Dinuclear Chromium Complex $\{(C_5H_5)Cr[\mu\text{-}CH_2SiMe_2{-}N(SiMe_3)]\}_2$

Rino Messere,[a] Marie-Rose Spirlet,[b] Dominique Jan,[c] Albert Demonceau,[c] and Alfred F. Noels*[c]

Keywords: Chromium / Cyclopentadienes / Si ligands / Metallacycles

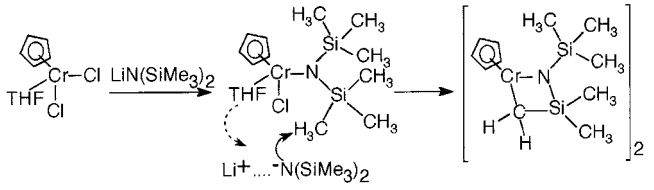
The complex $\{(C_5H_5)Cr[\mu\text{-}CH_2SiMe_2{-}N(SiMe_3)]\}_2$ (**1**) was obtained by reacting lithium bis(trimethylsilyl)amide (**2**) with $CpCrCl_2{\cdot}THF$. A single crystal X-ray diffraction study revealed that the complex is dimeric with two [μ-CH_2SiMe_2–$N(SiMe_3)$] bridging units and a *cis* configuration of the two cyclopentadienyl ligands. Bond distances and angles are compared with those observed in $[(C_5Me_5)Cr^{I}Me]_2$ and $[(C_5H_5)Cr^{III}Me_2]_2$.

Introduction

Chromium-based heterogeneous catalysts have a long-standing use in the commercial polymerization of small olefins. The search for soluble analogues has led Theopold et al. to synthesize a variety of low valent chromium complexes.[1] In this context, different permethylated cyclopentadienyl complexes of Cr^{II} and Cr^{III} have been fully identified as monomeric and/or dimeric species,[2] revealing new structures and reactivities towards olefins.[3]

We now report the first example of a cyclopentadienyl complex of chromium(III) containing a bidentate alkyl-amido ligand. Although amido derivatives of Si, Ti, V, Fe and Cr have been reported,[4] amide complexes of chromium are rare and, to date, never simultaneously ligated to a Cp ligand.

The new complex was readily obtained from $CpCrCl_2{\cdot}THF$ (or $[CpCrCl_2]_n$) and $LiN(SiMe_3)_2$, (**2**). Reaction of $CpCrCl_2{\cdot}THF$ with three equivalents of $LiN(SiMe_3)_2$ in THF produced a dark violet solution from which, instead of the expected complex $[(C_5H_5)Cr(NSiMe_3)_2]$, an unprecedented dimeric complex $\{(C_5H_5)Cr[\mu\text{-}CH_2SiMe_2{-}N(SiMe_3)]\}_2$ **(1)** (Scheme 1) was isolated as a crystalline material in 55% yield after purification.



Scheme 1. Synthesis of di-Cr^{III} complex **1**

At this preliminary stage, complex **1** appears to result from a C–H σ bond metathesis similar to that described by Berno et al. for a similar vanadium complex,[5] the deprotonation being performed by $LiN(SiMe_3)_2$ which acts as a base rather than as a nucleophile.

The ^1H NMR spectrum of paramagnetic **1** displays broadened, intense absorptions which are characteristic of the CH_3 groups [δ = 0.62 (*C20, C21* and *C22*, 9 H); δ = 2.28 (s, 3 H), −1.79 (s, 3 H), *C 19, C 18*; δ = 27.2 (μ-CH_2)]. The ^{13}C NMR spectrum displays three broad absorptions at 46.3, 35.1 and 2.7 ppm and a doublet at 89 ppm. The FTIR spectrum shows the characteristic absorptions of the Si–N and Si–CH_3 stretching at 850 and 1250 cm^{-1}.

The molecular structure of **1** has been unambiguously established by an X-ray structure analysis.

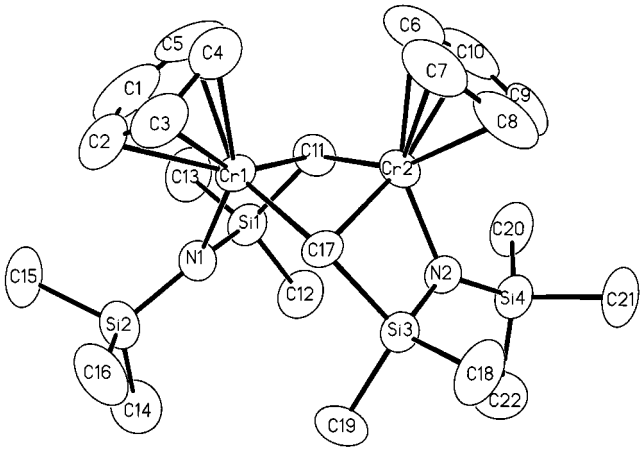


Figure 1. X-ray structure of **1** with atom labelling scheme

Figure 1 shows the geometry and the atom labelling scheme for the molecule. It appears indeed that **1** is a dimer consisting of two $[(C_5H_5)Cr]$ moieties bridged by two [μ-$CH_2SiMe_2{-}N(SiMe_3)$] units. The two Cp ligands are unexpectedly in a *cis* arrangement. Selected bond lengths and

[a] Glaceries de Saint-Roch-Saint-Gobain; Direction R&D, Centre Développement Bâtiment (CDB),
Rue des Glaces Nationales, 169 B-5060 Sambreville, Belgium
[b] Physique expérimentale, B5, University of Liège,
4000 Sart-Tilman, Belgium
[c] Center for Education and Research on Macromolecules, B6a, University of Liège,
B-4000 Sart-Tilman, Belgium
Fax: (internat.) + 32-4/366-3497
E-mail: AF.Noels@ulg.ac.be

 © WILEY-VCH Verlag GmbH, D-69451 Weinheim, 2000 1434–1948/00/0606–1151 $ 17.50+.50/0

angles are reported hereafter. The two bridging units form two almost p1anar (within 0.10 Å) four-membered metallaazasilacyclobutane rings (an example where a cyclobutane ring is made up of four different elements!), and form the dimeric unit by sharing the CH_2 groups with the two Cr atoms. The two bridging carbon atoms are almost symmetrically placed between the two Cr atoms [Cr1−C11 = 2.163(5), Cr1−C17 = 2.221(5), Cr2−C11 = 2.217(5), Cr2−C17 = 2.172(5) Å] but are significantly longer than typical Cr^{III}−C alkyl σ-bonds (2.09 Å).[6] The coordination about each chromium has approximate C_{3v} symmetry with the center of the Cp ring at the apex and the bridging methyl carbons and the nitrogen at the base of a distorted tetrahedron. The two tetrahedrons are joined by sharing a C−C edge. The Cr−C bond lengths of C_5H_5Cr are in the range expected for η^5-coordinated cyclopentadienyl rings. The distortion of the coordination polyhedrons is reflected by the angles subtended at the chromium atoms. While the C−Cr−C and N−Cr−C angles are less than 109°, the Cp−Cr−C and Cp−Cr−N angles are nearly identical but greater than 109°. The Cr−C (bridging) mean distance of 2.193(5) Å is in agreement with the mean value of 2.186 Å observed in $[(C_5Me_5)Cr^{II}Me]]_2$ [1b] and 2.188 Å observed in $[(C_5H_5)(CH_3)Cr^{III}Me]_2$.[2b] The chromium−chromium distance of 2.662(2) Å is fairly short and close to the value (2.606 Å) reported for the dimeric complex $\{(C_5H_5)(CH_3)Cr^{III}Me\}_2$.[2b] In light of the theoretical MO-analysis of metal−metal bonding in related paramagnetic chromium(III) complexes by Janiak et al.,[6] such short distances are consistent with metal−metal interactions, although we do not care to speculate about the exact bond order or bond strength of this interaction. This Cr−Cr bond remains, however, considerably longer than that of a Cr^{III} bis(μ-alkylidene) complex (2.262 Å) recently described by Theopold et al., the shortest metal−metal distance found so far in Cr^{III} alkyls.[7]

Complex **1** alone is inactive in the polymerization of ethylene and addition of an alkylaluminium is required to initiate ethylene polymerization. Polymerization results will be reported in due course.

Experimental Section

All reactions were carried out under an atmosphere of purified nitrogen. Solvents were distilled, dried and kept under nitrogen before use.

$(C_5H_5)CrCl_2\cdot THF$: Finely divided $CrCl_3\cdot THF_3$ (10 g) was poured into 200 mL of dry deoxygenated THF. A solution of CpNa in THF (1 M, 20 mL) at 0° C was added to this suspension and the resulting green solution stirred for 1 hour at 0 °C. The solution was then warmed to 20 °C and kept for one hour at that temperature. The green solution turned blue. The solution was then taken to dryness under low pressure to yield a blue product. This dark solid was washed with pentane (100 mL) at 20 °C to yield a blue, hygroscopic powder after drying under vacuum at 30 °C. Yield 95%.

$\{(C_5H_5)Cr[\mu\text{-}CH_2SiMe_2\text{−}N(SiMe_3)]\}_2$ (1): $(C_5H_5)CrCl_2\cdot THF$ (0.1 g) was dissolved in 50 mL of purified THF under an inert atmosphere. To this solution was added a solution of $LiN(SiMe_3)_2$ (1 M, 2.7 mL) in THF at 10 °C. The reaction mixture was then stirred at 20° C for 4 hours after which the solution was taken to dryness under low pressure, yielding a black solid. This dark product was extracted with pentane (20 mL) and then with toluene (2 × 30 mL). The combined toluene filtrate was kept at −20 °C for 2 days to yield a dark-violet solid. Yield 55%.

X-ray Crystallographic Study:[8] Crystal data for $C_{22}Cr_2N_2Si_4$ (M_r = 508.6): monoclinic system with cell dimensions at 20 °C of a = 14.847(3)Å, b = 11.172(2) Å, c = 17.889(3) Å, β = 93.43(3)°; V = 2962(1) Å^3; μ(Mo-K_α) = 0.904 mm^{-1}; F(000) = 1000; space group $P2_1/c$ with Z = 4 and $D_{calcd.}$ = 1.141 g/cm^3. A selected specimen (0.45 × 0.35 × 0.35 mm.) was sealed in a thin-walled glass capillary under argon. The X-ray diffraction data were obtained with a Siemens R3m/V four-circle computer-controlled X-ray diffractometer (graphite-monochromated Mo-K_α radiation: λ = 0.71073 Å) at 293 K. The unit cell parameters and standard deviations were calculated for the setting angles of 25 reflections with 10° < 2θ < 35°. The space group $P2_1/c$ was unequivocally established from systematic absences. The intensities of 7519 reflections corresponding to 3823 independent reflections ($R_{int.}$ = 0.038) were measured by the ω scan technique in the range 3.5° < 2θ < 45.0° (h: −15 → 15, k: −12 → 12, l: −19 → 19). Three standard reflections were monitored every 97 reflections to check crystal stability. No decrease of intensity during data collection was observed. Data were corrected for Lorentz polarization and absorption effects, the latter with a semi-empirical method. The transmission factors range from 0.765 to 0.967. The structure was solved by direct methods and Fourier techniques. Full-matrix least-squares refinement was carried out against F^2. The thermal behavior of the nonhydrogen atoms was treated anisotropically. Riding H atoms, with C−H bond lengths of 0.95 Å and a fixed isotropic U of 0.08 Å were included in the refinement. The final agreement factors were 0.056 for 2914 reflections with $F_o^2 > 2\sigma(F_o^2)$ and 271 parameters. The maximum shift/e.s.d. in the final cycle was less than 0.001. The highest peak in the final difference Fourier map was 0.703 eÅ^{-3}. Calculations were performed with Siemens SHELXTL PLUS package programs.[9]

Acknowledgments

We are grateful to the Interuniversity Institute for Nuclear Sciences and to the National Fund for Scientific Research (Brussels) for financial support to the laboratory of Analytical Chemistry and Radiochemistry of the University of Liege. We also thank the "National Fund for Scientific Research" (F.N.R.S.), Belgium, for the purchase of major instrumentation.

[1] [1a] K. H. Theopold, *Acc. Chem. Res.* **1990**, *23*, 263−270. − [1b] R. A. Heintz, R. L. Ostrander, A. L. Rheingold, K. H. Theopold, *J. Am. Chem. Soc.* **1994**, *116*, 11387−11396. − [1c] K. H. Theopold, *Eur. J. Inorg. Chem.* **1998**, 15−24.

[2] [2a] S. K. Noh, S. C. Sendlinger, C. Janiak, K. H. Theopold, *J. Am. Chem. Soc.* **1989**, *111*, 9127−9129. − [2b] D. S. Richeson, J. F. Mitchell, K. H. Theopold, *Organometallics.* **1989**, *8*, 2570−2577.

[3] [3a] K. H. Theopold, R. A. Heintz, S. K. Noh, B. J. Thomas, in *Advance in Chemistry Series* (Eds.: W. R. Moser, D. W. Slocum), ACS, Washington, DC, **1992**, *230*, 591−602. − [3b] G. Bhandari, Y. Y. Kim, J. M. McFarland, A. L. Rheingold, K. H. Theopold, *Organometallics* **1995**, *14*, 738−745. − [3c] G. Bhandari, A. L. Rheingold, K. H. Theopold, *Chem. Eur. J.* **1995**, *1*, 199−203. − [3d] P. A. White, J. Calabrese, K. H. Theopold, *Organometallics* **1996**, *15*, 5473−5475.

[4] [4a] B. Horvath, J. Strutz, E. Z. Horvath, *Z. Anorg. Allg. Chem.* **1979**, *457*, 38−50. − [4b] D. Reardon, I. Kovacs, K. B. P.

Ruppa, K. Feghali, S. Gambarotta, J. Petersen, *Chem. Eur. J.* **1997**, *3*, 1482−1488.
[5] P. Berno, R. Minhas, S. K. Hao, S. Gambarotta, *Organometallics* **1994**, *13*, 1052−1054.
[6] C. Janiak, J. Silvestre, K. H. Theopold, *Chem. Ber.* **1993**, *126*, 631−643.
[7] R. A. Heintz, S. Leelasubcharoen, L. M. Liable-Sands, A. L. Rheingold, K. H. Theopold, *Organometallics* **1998**, *17*, 5477−5485.
[8] Crystallographic data (excluding structure factors) for the structure reported in this paper have been deposited with the Cambridge Crystallographic Data Centre as supplementary publication no CCDC-117153. Copies of the data can be obtained free of charge on application to CCDC, 12 Union Road, Cambridge CB2 1EZ, UK [Fax: (internat.) + 44-1223/336-033; E-mail: deposit@ccdc.cam.ac.uk].
[9] *SHELXTL-Plus.* G. M. Sheldrick (**1991**). Release 4. 1. Siemens Analytical Instrument Inc., Madison, Wisconsin, USA.

Received June 7, 1999
[I99207]

Synthesis and Structure of Cyclotrigermenium Salts of Tetrakis{3,5-bis(trifluoromethyl)phenyl}borate, Tetrakis(pentafluorophenyl)borate and Tetrakis{4-[*tert*-butyl(dimethyl)silyl]-2,3,5,6-tetrafluorophenyl}borate: A Stable Free Germyl Cation in the Condensed Phase

Akira Sekiguchi,*[a] Norihisa Fukaya,[a] Masaaki Ichinohe,[a] and Yutaka Ishida[a]

Keywords: Cations / Electron transfer / Germanium / Small ring systems

The reaction of tetrakis(tri-*tert*-butylsilyl)cyclotrigermene (**1a**) with $Ph_3C^+[3,5\text{-}(CF_3)_2C_6H_3]_4B^-$ ($TFPB^-$), $Ph_3C^+(C_6F_5)_4B^-$ ($TPFPB^-$), and $Ph_3C^+[4\text{-}(t\text{BuMe}_2\text{Si})C_6F_4]_4B^-$ ($TSFPB^-$) in benzene produced the stable free tris(tri-*tert*-butylsilyl)cyclotrigermenium ion ($\mathbf{2a}^+$) with the corresponding tetraarylborate as the counterion. The crystal structures of $\mathbf{2a}^+TFPB^-$ and $\mathbf{2a}^+TSFPB^-$ reveal a free germyl cation with a two π-electron system. The three-membered ring of germanium atoms constitutes an almost equilateral triangle. The cyclotrigermenium tetraarylborates, $\mathbf{2a}^+TFPB^-$, $\mathbf{2a}^+TPFPB^-$, and $\mathbf{2a}^+TSFPB^-$, are stable in solution. The spectroscopic data show that $\mathbf{2a}^+$ is a free germyl cation, does not coordinate to either the solvent molecules (dichloromethane, chloroform, toluene, or diethyl ether) or the counter anions ($TFPB^-$, $TPFPB^-$, or $TSFPB^-$). The tris(tri-*tert*-butylgermyl)cyclotrigermenium ion ($\mathbf{2b}^+$) was also characterized.

Introduction

The chemistry of tricoordinated germyl and silyl cations in the condensed phase has developed rapidly in recent years.[1] Their study is, however, at an early stage compared to that of the carbocations.[2] Over the years, many efforts have been directed towards the synthesis and characterization of free germyl and silyl cations in the condensed phase.[3] In 1997, Lambert and Zhao successfully synthesized the trimesitylsilyl cation, which was a long-sought free silyl cation.[4] Although they did not perform an X-ray study, convincing evidence of its existence was given by its ^{29}Si NMR chemical shift in aromatic solvents.[4,5] The presence of the free silyl cation has been strongly supported by ab initio calculations, demonstrating good agreement between the calculated and experimental ^{29}Si NMR chemical shifts.[6]

In contrast to the silyl cations, very little experimental work has been reported on the germyl cation in the condensed phase.[5,7] Recently, we isolated and characterized $[(t\text{Bu}_3\text{SiGe})_3^+BPh_4^-]$ ($\mathbf{2a}^+TPB^-$, TPB^- = tetraphenylborate) by the reaction of tetrakis(tri-*tert*-butylsilyl)cyclotrigermene with $Ph_3C^+TPB^-$, which was the first example of a free germyl cation with a two π-electron system.[8,9] However, a problem of the TPB anion is its chemical instability.[10] $\mathbf{2a}^+TPB^-$ can survive in a solution of dichloromethane only at temperatures below −78 °C.

$[3,5\text{-}(CF_3)_2C_6H_3]_4B^-$ ($TFPB^-$, tetrakis{3,5-bis(trifluoromethyl)phenyl}borate),[11] $(C_6F_5)_4B^-$ ($TPFPB^-$, tetrakis(pentafluorophenyl)borate),[12] and $[4\text{-}(t\text{BuMe}_2\text{Si})C_6F_4]_4B^-$ ($TSFPB^-$, tetrakis{4-[*tert*-butyl(dimethyl)silyl]-2,3,5,6-tetrafluorophenyl}borate)[13] are known to be stable borate anions. These counter anions should increase the stability of the resulting cyclotrigermenium ion. This prompted us to examine the reaction of $t\text{Bu}_3\text{E}$- substituted cyclotrigermenes **1a** (E = Si)[14] and **1b** (E = Ge)[14] with $Ph_3C^+TFPB^-$, $Ph_3C^+TPFPB^-$, and $Ph_3C^+TSFPB^-$, producing $[(t\text{Bu}_3\text{EGe})_3^+TFPB^-]$, $[(t\text{Bu}_3\text{EGe})_3^+TPFPB^-]$, and $[(t\text{Bu}_3\text{EGe})_3^+TSFPB^-]$ (E = Si, Ge). These germyl cations can survive for extensive periods without decomposition both in solution and the solid state. We report here spectroscopic and structural evidence that $\mathbf{2}^+TFPB^-$, $\mathbf{2}^+TPFPB^-$, and $\mathbf{2}^+TSFPB^-$ incorporate free germyl cations, which do not coordinate to either the solvent molecules dichloromethane, chloroform, toluene or diethyl ether, or the counter anions $TFPB^-$, $TPFPB^-$, or $TSFPB^-$.

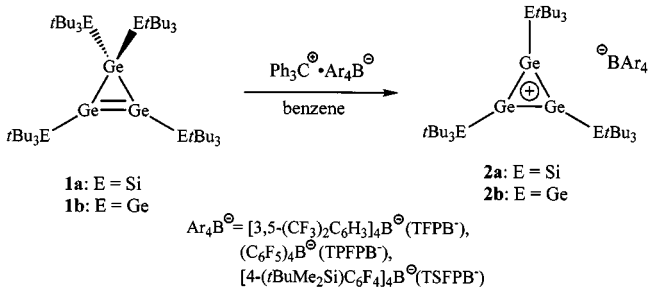
Results and Discussion

Synthesis of $\mathbf{2}^+TFPB^-$, $\mathbf{2}^+TPFPB^-$, and $\mathbf{2}^+TSFPB^-$

Synthesis was carried out under an inert atmosphere by standard Schlenk and high-vacuum line techniques. Dry oxygen-free benzene was introduced by vacuum transfer to a mixture of $(t\text{Bu}_3\text{Si})_4Ge_3$ (**1a**) and $Ph_3C^+TFPB^-$, and the mixture was stirred at room temperature. The solution immediately changed from the dark red color of **1a** to yellow, and a brown powder formed. The solvent was removed under vacuum and the resulting solid was washed with hexane in a glove box to afford $\mathbf{2a}^+TFPB^-$ as a yellow powder in 81% yield (Scheme 1). Despite the large steric congestion, the reaction is very rapid and is complete within 5 min. The reaction is possibly initiated by electron transfer from **1a** to the trityl cation followed by elimination of a $t\text{Bu}_3\text{Si}$ radical through cleavage of the weak exocyclic Si-Ge bond to produce $\mathbf{2a}^+TFPB^-$.[15] The reaction of **1b** with $Ph_3C^+TFPB^-$

[a] Department of Chemistry, University of Tsukuba, Tsukuba, Ibaraki 305-8571, Japan
Fax: (internat.) + 81-298/53-4314
E-mail: sekiguch@staff.chem.tsukuba.ac.jp

 © WILEY-VCH Verlag GmbH, D-69451 Weinheim, 2000 1434−1948/00/0606−1155 $ 17.50+.50/0



Scheme 1

in benzene also proceeded to give **2b**$^+$TFPB$^-$ in 76% yield. Both **2a**$^+$TFPB$^-$ and **2b**$^+$TFPB$^-$ are soluble in dichloromethane, but only slightly soluble in toluene. Similarly to the reaction with Ph_3C^+TFPB$^-$, the reaction of **1a** and **1b** with Ph_3C^+TPFPB$^-$ in benzene produced **2a**$^+$TPFPB$^-$ (80%) and **2b**$^+$TPFPB$^-$ (80%), respectively. However, several attempts to obtain crystals of these complexes failed. The reaction of **1a** with Ph_3C^+TSFPB$^-$ in benzene produced **2a**$^+$TSFPB$^-$ as orange crystals in 88% yield. The tetraarylborate derivatives of the cyclotrigermenium ion are extremely air- and moisture-sensitive, and the yellow color disappeared immediately when solutions were exposed to the air.

Crystal Structures of 2a$^+$TFPB$^-$ and 2a$^+$TSFPB$^-$

Recrystallization of **2a**$^+$TFPB$^-$ from toluene yielded yellow-orange crystals suitable for X-ray crystallography; its molecular structure is shown in Figure 1. The three-membered ring consisting of germanium atoms forms an almost equilateral triangle, as determined by the internal bond angles of 59.79(3) to 60.28(3) °. The Ge−Ge distances of the three-membered ring are almost equal, ranging from 2.3284(8) to 2.3398(8) Å (av. 2.3333(8) Å). The Ge−Ge bond lengths observed for **2a**$^+$TFPB$^-$ (Figure 1) are intermediate between the Ge=Ge double bond (2.239(4) Å) and

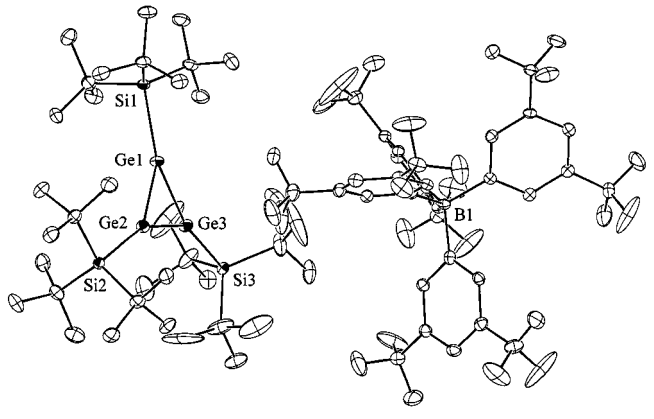


Figure 1. Perspective view of **2a**$^+$TFPB$^-$ in the crystal at the 30% probability level (hydrogen atoms are omitted for the clarity). Selected bond lengths (Å): Ge1−Ge2, 2.3316(9); Ge1−Ge3, 2.3284(8); Ge2−Ge3, 2.3398(8); Ge1−Si1, 2.425(1); Ge2−Si2, 2.442(1); Ge3−Si3, 2.444(1). Selected bond angles (deg): Ge2−Ge1−Ge3, 60.28(3); Ge2−Ge1−Si1, 150.58(5); Ge3−Ge1−Si1, 148.55(5); Ge1−Ge2−Ge3, 59.79(3); Ge1−Ge2−Si2, 145.94(5); Ge3−Ge2−Si2, 152.75(5); Ge1−Ge3−Ge2, 59.93(3); Ge1−Ge3−Si3, 152.36(5); Ge2−Ge3−Si3, 146.70(5).

the Ge−Ge single bond (2.522(4) Å) of the precursor **1a**.[14] The three silicon atoms are nearly coplanar with the central three-membered ring. The bond lengths of the Ge−Si bonds (Ge1−Si1, 2.425(1) Å; Ge2−Si2, 2.442(1) Å; Ge3−Si3, 2.444(1) Å) of **2a**$^+$TFPB$^-$ are shorter than those of **1a**[14] (2.629(7) Å for the Ge−Si bond length of sp^3 Ge atom and 2.448(7) Å for the Ge−Si bond length of sp^2 Ge atoms).

The perspective view appears to show a weak electrostatic interaction between the germanium and fluorine atoms. The three closest distances range from 3.823 to 5.097 Å, as depicted in Figure 2. However, these distances are longer than the sum (3.57 Å) of the van der Waals radii for germanium and fluorine atoms.[16] Undoubtedly, CF_3 groups of the counter anion are sufficiently remote from the germanium center to preclude any covalent interaction.

We have also obtained X-ray diffraction data for **2a**$^+$TSFPB$^-$, which was obtained by recrystallization from toluene. Due to the steric bulkiness of the *t*BuMe$_2$Si group attached to the *para* positions of the phenyl rings of borate anion, no interaction between the cation moiety and the counter anion can be found (Figure 3). As a consequence, the skeleton of the three-membered framework forms an equilateral triangle; the Ge−Ge bond lengths are 2.3310(8) Å for Ge1−Ge2, 2.3315(7) Å for Ge1−Ge3, and 2.3349(8) Å for Ge2−Ge3, and the Ge−Ge−Ge bond angles are 60.10(2)° for Ge2−Ge1−Ge3, 59.96(2)° for Ge1−Ge2−Ge3, 59.94(2)° for Ge1−Ge3−Ge2. In addition, the silicon atoms of the *t*Bu$_3$Si groups attached to the germanium atoms are in approximately the same plane as the three-membered ring, as determined by the sum of the respective bond angles around the germanium atoms (e.g. 359.99(4)° for Ge1, 359.96(4)° for Ge2, and 359.86(5)° for Ge3).

These structural features for **2a**$^+$TFPB$^-$ and **2a**$^+$TSFPB$^-$ are practically the same as those of **2a**$^+$TPB$^-$,[8a] i.e. the counter anion does not affect the framework of the cyclotrigermenium ion. Thus, the crystal structure of the cyclotrigermenium ion reveals a free germyl cation with a two π-electron system. The three germanium atoms form an equilateral triangle similar to its carbon analog, the cyclopropenium ion.[17]

The structures of **2a**$^+$TFPB$^-$ and **2a**$^+$TSFPB$^-$ presented here are very close to those predicted by a calculation on the corresponding D_{3h} $(HGe)_3^+$ isomer.[7d] The observed average Ge−Ge distances for **2a**$^+$TFPB$^-$ and **2a**$^+$TSFPB$^-$ are 2.3333(8) Å and 2.3325(8) Å, compared with the calculated value of 2.361 Å for a $(HGe)_3^+$ ion with D_{3h} symmetry. The theoretical calculations also predict a hydrogen-bridged nonplanar structure with C_{3v} symmetry that has a lower energy than that of a planar one with D_{3h} symmetry.[7d] However, the more stable hydrogen-bridged $(HGe)_3^+$ isomer cannot be expected when the hydrogens are replaced by other groups. Due to the steric hindrance and electronic properties of the *t*Bu$_3$Si group,[18] the cyclotrigermenium ion favors a planar structure similar to that of the cyclopropenium ion. A cyclotrigallane dianion, Na_2[(2,6-$Mes_2C_6H_3$)Ga]$_3$ (Mes = 2,4,6-trimethylphenyl), has been

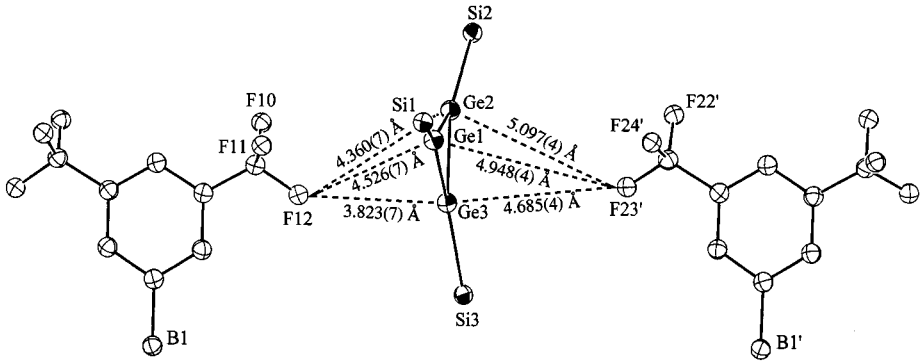


Figure 2. Section from the structure of $\mathbf{2a}^{+}$TFPB^{-} with the closest atomic distances between Ge and F.

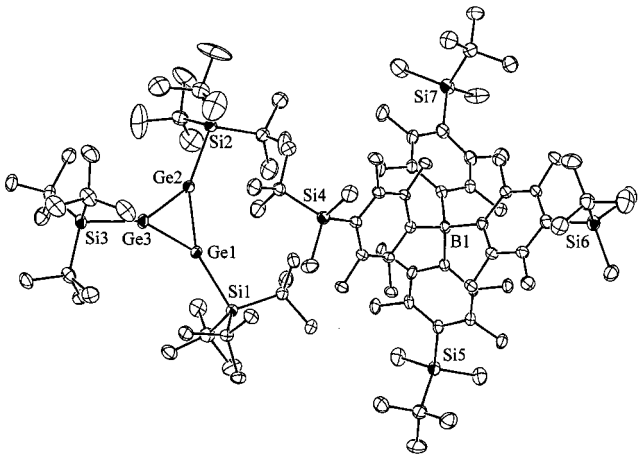


Figure 3. Perspective view of $\mathbf{2a}^{+}$TSFPB^{-} in the crystal at the 30% probability level (hydrogen atoms are omitted for the clarity). Selected bond lengths (Å): Ge1−Ge2, 2.3310(8); Ge1−Ge3, 2.3315(7); Ge2−Ge3, 2.3349(8); Ge1−Si1, 2.420(1); Ge2−Si2, 2.460 (1); Ge3−Si3, 2.434(1). Selected bond angles (deg): Ge2−Ge1−Ge3, 60.10(2); Ge2−Ge1−Si1, 151.17(4); Ge3−Ge1−Si1, 148.72 (4); Ge1−Ge2−Ge3, 59.96(2); Ge1−Ge2−Si2, 150.86(4); Ge3−Ge2−Si2, 149.14(4); Ge1−Ge3−Ge2, 59.94(2); Ge1−Ge3−Si3, 151.94(5); Ge2−Ge3−Si3, 147.98(5).

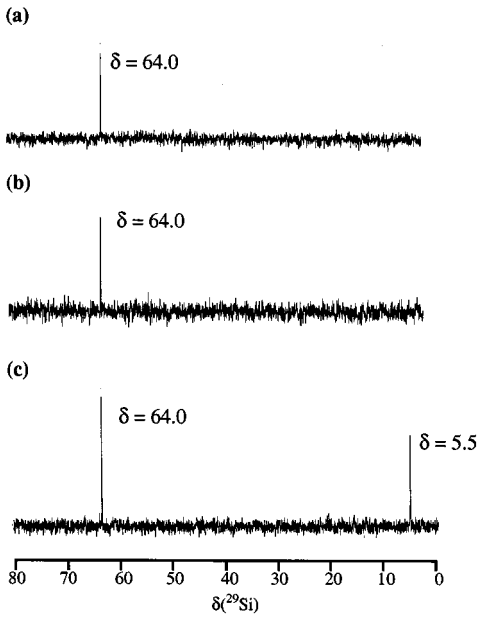


Figure 4. ^{29}Si NMR spectra of $\mathbf{2a}^{+}$TFPB^{-} (a), $\mathbf{2a}^{+}$TPFPB^{-} (b), $\mathbf{2a}^{+}$TSFPB^{-} (c) in CD_2Cl_2 at 298 K.

synthesized as a metallic ring system possessing aromatic character.[19]

Free Cyclotrigermenium Ion in Solution

The evidence for the free cyclotrigermenium ion is supported by the NMR spectroscopic data. The ^{1}H, ^{13}C, and ^{29}Si NMR chemical shifts for the cyclotrigermenium moiety of $\mathbf{2a}^{+}$TFPB^{-}, $\mathbf{2a}^{+}$TPFPB^{-}, and $\mathbf{2a}^{+}$TSFPB^{-} in CD_2Cl_2 are practically the same (see the Experimental Section). For example, ^{29}Si NMR chemical shifts of $\mathbf{2a}^{+}$TFPB^{-}, $\mathbf{2a}^{+}$TPFPB^{-}, and $\mathbf{2a}^{+}$TSFPB^{-}, as shown in Figure 4, are independent of the counter anion. The ^{29}Si NMR chemical shift of $\mathbf{2a}^{+}$TFPB^{-} is also essentially the same in the different solvents, appearing at $\delta = 64.0$ in CD_2Cl_2, $\delta = 64.2$ in $CDCl_3$, $\delta = 64.4$ in [D$_8$]toluene, and $\delta = 64.5$ in Et_2O. This independence from the both counter anion and solvent clearly indicates that $\mathbf{2a}^{+}$ is a free germyl cation in solution.

The large downfield shift of the ^{29}Si NMR resonance of $\mathbf{2a}^{+}$, relative to that of **1** ($\delta = 37.2$ for tBu$_3$Si attached to the saturated Ge atom and 50.1 for tBu$_3$Si attached to the Ge=Ge double bond), is due to the positive charge on the cyclotrigermenium ion. The positive charge is not localized on the germanium atoms, but is significantly transferred to the silicon centers. According to the Mulliken charges, most of the positive charge is distributed on the silicon atoms of the substituents rather than on the ring germanium atoms. It has been reported that the positive charge on the ring carbon atoms of cyclopropenium cations $(RC)_3^{+}$ decreases with decreasing electronegativity of the substituent: +0.200 (R = CH$_3$), +0.026 (R = H), −0.243 (R = SiH$_3$).[20] The atomic (Mulliken) charges on $(H_3SiGe)_3^{+}$, according to the HF/6−31G* level calculations, indicate a similar delocalization of the positive charge: −0.07 for the ring germanium

atoms, +0.64 for the silicon atoms of the SiH_3 substituents.[21]

Conclusion

Treatment of tetrakis(tri-*tert*-butylsilyl)cyclotrigermene (**1a**) with the trityl cation in benzene produces the stable free tris(tri-*tert*-butylsilyl)cyclotrigermenium ion (**2a**$^+$) with three different counter anions. The crystal structures and the spectroscopic data show that **2a**$^+$ is a free germyl cation, which does not coordinate to either the counter anions or the solvent molecules.

Experimental Section

All manipulations were carried out under an inert atmosphere in a MBRAUN MB 150B-G gas-replacement type glove box or by standard Schlenk and high-vacuum line techniques. − ^{1}H NMR spectra were recorded at 300.1 MHz on a Bruker AC-300 FT NMR spectrometer. ^{13}C and ^{29}Si NMR spectra were collected on a Bruker AC-300 at 75.5, 59.6 MHz, respectively. − All solvents were dried and degassed over potassium mirror in vacuo prior to use in the preparation of cyclotrigermenium ion. The cyclotrigermenes **1a**,[14] **1b**,[14] and trityl cations Ph_3C^+ $[3,5\text{-}(CF_3)_2C_6H_3]_4B^-$ (TFPB$^-$),[11] $Ph_3C^+(C_6F_5)_4B^-$ (TPFPB$^-$),[12] and Ph_3C^+[4-(*t*Bu-Me_2Si) $C_6F_4]_4B^-$ (TSFPB$^-$)[13] were prepared according to literature procedures. On account of the inclusion of solvent molecules, no satisfactory elemental analyses data for the cyclotrigermenium salts could be obtained.

Tris(tri-*tert*-butylsilyl)cyclotrigermenium Tetrakis[3,5-bis(trifluoromethyl)phenyl]borate (2a$^+$TFPB$^-$): Dry oxygen-free benzene was introduced by vacuum transfer to a mixture of **1a** (60 mg, 0.06 mmol) and Ph_3C^+TFPB$^-$ (65 mg, 0.06 mmol), and the mixture was stirred at room temperature for 10 min. The dark red solution of **1a** became yellow, and brown powder was formed. The solvent was removed under vacuum and the resulting solid was washed with hexane in a glove box to afford a yellow powder of **2a**$^+$TFPB$^-$ (80 mg, 81%). M.p. 132−134 °C (dec). − ^{1}H NMR (CD_2Cl_2): δ = 1.40 (s, 81 H), 7.56 (s, 4 H), 7.73 (s, 8 H). − ^{13}C{^{1}H} NMR (CD_2Cl_2): δ = 27.2, 31.8, 117.8, 125.0 [q, $^1J(^{13}C\text{-}^{19}F)$ = 270 Hz], 129.1−129.9 (m), 135.2, 162.2 [q, $^1J(^{13}C\text{-}^{11}B)$ = 50 Hz]. − ^{29}Si{^{1}H} NMR (CD_2Cl_2): δ = 64.0.

Tris(tri-*tert*-butylsilyl)cyclotrigermenium Tetrakis(pentafluorophenyl)borate (2a$^+$TPFPB$^-$): By the procedure described above, the reaction of **1a** (60 mg, 0.06 mmol) and Ph_3C^+TPFPB$^-$ (55 mg, 0.06 mmol) provided **2a**$^+$TPFPB$^-$ (ca. 80%) as a yellow waxy solid. − ^{1}H NMR (CD_2Cl_2): δ = 1.40 (s, 81 H). − ^{13}C{^{1}H} NMR (CD_2Cl_2): δ = 27.2, 31.8, 124.0−125.5 (m), 136.7 [d, $^1J(^{13}C\text{-}^{19}F)$ = 240 Hz], 138.6 [d, $^1J(^{13}C\text{-}^{19}F)$ = 240 Hz], 148.5 [d, $^1J(^{13}C\text{-}^{19}F)$ = 240 Hz]. − ^{29}Si{^{1}H} NMR (CD_2Cl_2): δ = 64.0.

Tris(tri-*tert*-butylgermyl)cyclotrigermenium Tetrakis[3,5-bis(trifluoromethyl)phenyl]borate (2b$^+$TFPB$^-$): By the procedure described above, the reaction of **2b** (30 mg, 0.03 mmol) and Ph_3C^+TFPB$^-$ (30 mg, 0.03 mmol) provided **2b**$^+$TPFPB$^-$ (34 mg, 76%) as yellow crystals. M.p. 112−114 °C (dec). − ^{1}H NMR (CD_2Cl_2): δ = 1.48 (s, 81 H), 7.56 (s, 4 H), 7.73 (s, 8 H). − ^{13}C{^{1}H} NMR (CD_2Cl_2): δ = 32.4, 37.1, 117.8, 125.0 [q, $^1J(^{13}C\text{-}^{19}F)$ = 270 Hz], 129.1−129.9 (m), 135.2, 162.2 [q, $^1J(^{13}C\text{-}^{11}B)$ = 50 Hz].

Tris(tri-*tert*-butylgermyl)cyclotrigermenium Tetrakis(pentafluorophenyl)borate (2b$^+$TPFPB$^-$): By the procedure described above, the reaction of **2b** (30 mg, 0.03 mmol) and Ph_3C^+TPFPB$^-$ (25 mg, 0.03 mmol) provided **2b**$^+$TPFPB$^-$ (ca. 80%) as a yellow waxy solid. − ^{1}H NMR (CD_2Cl_2): δ = 1.48 (s, 81 H). − ^{13}C{^{1}H} NMR (CD_2Cl_2): δ = 32.4, 37.1, 124.0−125.5 (m), 136.7 [d, $^1J(^{13}C\text{-}^{19}F)$ = 240 Hz], 138.6 [d, $^1J(^{13}C\text{-}^{19}F)$ = 240 Hz], 148.5 [d, $^1J(^{13}C\text{-}^{19}F)$ = 240 Hz].

Tris(tri-*tert*-butylsilyl)cyclotrigermenium Tetrakis{4-[*tert*-butyl(dimethyl)silyl]-2,3,5,6-tetrafluorophenyl}borate) (2a$^+$TSFPB$^-$): By the procedure described above, the reaction of **2a** (200 mg, 0.20 mmol) and Ph_3C^+TSFPB$^-$ (258 mg, 0.20 mmol) provided **2a**$^+$TSFPB$^-$ (326 mg, 88%) as orange crystals. M.p. 154−156 °C (dec). − ^{1}H NMR (CD_2Cl_2): δ = 0.33 (s, 24 H), 0.90 (s, 36 H), 1.41 (s, 81 H). − ^{13}C{^{1}H} NMR (CD_2Cl_2): δ = −3.2, 18.3, 27.0, 27.7, 32.3, 108.8 [t, $^2J(^{13}C\text{-}^{19}F)$ = 33 Hz], 134.3−135.8 (m), 149.2 [d, $^1J(^{13}C\text{-}^{19}F)$ = 262 Hz]. − ^{29}Si{^{1}H} NMR (CD_2Cl_2): δ = 5.47, 64.0.

X-ray Crystal Structure Determination of 2a$^+$TFPB$^-$ and 2a$^+$TSFPB$^-$: Single crystals of **2a**$^+$TFPB$^-$ and **2a**$^+$TSFPB$^-$ suitable for X-ray diffraction were grown from toluene solutions. The X-ray crystallographic experiments were performed on a MacScience DIP2020 or DIP2030 image plate diffractometer equipped with graphite-monochromatized Mo-K_α radiation (λ = 0.71073). Crystal data for **2a**$^+$TFPB$^-$ at 120 K: $M_F = C_{68}H_{93}BF_{24}Ge_3Si_3$, Mr = 1679.27, monoclinic, a = 16.912(1) Å, b = 20.919(1) Å, c = 23.399(1) Å, β = 108.147(4)°, V = 7866.4(7) Å^3, space group = $P2_1/n$, Z = 4, $D_{calcd.}$ = 1.418 g/cm^3, R = 0.0849 (R_w = 0.2153 for all data). Crystal data for **2a**$^+$TSFPB$^-$(C_7H_8)$_2$ at 120 K: $M_F = C_{98}H_{157}BF_{16}Ge_3Si_7$, Mr = 2064.54, orthorhombic, a = 13.3320(5) Å, b = 20.5110(3) Å, c = 40.638(1) Å, V = 11112.6(5)Å ^{3}, space group = $Pc2_1n$, Z = 4, $D_{calcd.}$ = 1.234 g/cm^3, R = 0.0523 (R_w = 0.1512 for all data). Crystallographic data (excluding structure factors) for the structures reported in this paper have been deposited with the Cambridge Crystallographic Data Centre as supplementary publication nos. CCDC-137540 and 137541. Copies of the data can be obtained free of charge on application to CCDC, 12 Union Road, Cambridge CB2 1EZ, UK [Fax: (internat.) +44(1223)336−033; E-mail:deposit@ccdc.cam.ac.uk].

Computational Details: Calculations at the Hartree−Fock (HF) level were performed by using the Gaussian 94 computer program.[21] The 6−31G* basis set was used for all geometry optimizations.

Acknowledgments

This work was supported by a Grant-in-Aid for Scientific Research (Nos. 09239101, 10304051, 1113321, 11166209) from the Ministry of Education, Science and Culture of Japan, and TARA (Tsukuba Advanced Research Alliance) fund.

[1] For reviews, see: [1a] R. J. P. Corriu, M. Henner, *J. Organomet. Chem.* **1974**, *74*, 1. – [1b] J. B. Lambert, L. Kania, S. Zhang, *Chem. Rev.* **1995**, *95*, 1191. – [1c] C. Maerker, J. Kapp, P. v. R. Schleyer, *Organosilicon Chemistry: from Molecules to Materials,* (Eds.: N. Auner, J. Weis), VCH, Weinheim, Vol. II, **1996**. – [1d] P. v. R. Schleyer, *Science* **1997**, *275*, 39. – [1e] J. Belzner, *Angew. Chem. Int. Ed. Engl.* **1997**, *36*, 1277.

[2] G. A. Olah, *Angew. Chem. Int. Ed. Engl.* **1995**, *34*, 1393.

[3] [3a] G. A. Olah, G. Rasul, L. Heiliger, J. Bausch, G. K. S. Prakash, *J. Am. Chem. Soc.* **1992**, *114*, 7737. – [3b] M. Kira, T. Hino, H. Sakurai, *J. Am. Chem. Soc.* **1992**, *14*, 6697. – [3c] S. R. Bahr, P. Boudjouk, *J. Am. Chem. Soc.* **1993**, *115*, 4514. – [3d] L. Olsson, D. Cremer, *Chem. Phys. Lett.* **1993**, *215*, 433. –

[3e] P. v. R. Schleyer, P. Buzek, T. Müller, Y.Apeloig, H.-U. Siehl, *Angew. Chem. Int. Ed. Engl.* **1993**, *32*, 1471. – [3f] J. B. Lambert, S. Zhang, C. L. Stern, J. C. Huffman, *Science* **1993**, *260*, 1917. – [3g] C. A. Reed, Z. Xie, R. Bau, A. Benesi, *Science* **1993**, *262*, 402. – [3h] L. Pauling, *Science* **1994**, *263*, 983. – [3i] G. A. Olah, G. Rasul, X.-Y. Li, H. A. Buchholz, G. Sandford, G. K. S. Prakash, *Science* **1994**, *263*, 983. – [3j] J. B. Lambert, S. Zhang, *Science* **1994**, *263*, 984. – [3k] C. A. Reed, Z. Xie, *Science* **1994**, *263*, 985. – [3l] Z. Xie, R. Bau, C. A. Reed, *J. Chem. Soc., Chem. Commun.* **1994**, 2519. – [3m] L. Olsson, C.-H. Ottosson, D. Cremer, *J. Am. Chem. Soc*. **1995**, *117*, 7460. – [3n] G. A. Olah, X.-Y. Li, Q. Wang, G. Rasul, G. K. S. Prakash, *J. Am. Chem. Soc*. **1995**, *117*, 8962. – [3o] Z. Xie, R. Bau, A. Benesi, C. A. Reed, *Organometallics* **1995**, *14*, 3933. – [3p] G. A. Olah, G. Rasul, H. A. Buchholz, X.-Y. Li, G. K. S. Prakash, *Bull. Soc. Chim. Fr.* **1995**, *132*, 569. – [3q] Z. Xie, J. Manning, R. W. Reed, R. Mathur, P. D. W. Boyd, A. Benesi, C. A. Reed, *J. Am. Chem. Soc.* **1996**, *118*, 2922. – [3r] M. Arshadi, D. Johnels, U. Edlund, C.-H. Ottosson, D. Cremer, *J. Am. Chem. Soc*. **1996**, *118*, 5120. – [3s] H.-U. Steinberger, T. Müller, N. Auner, C. Maerker, P. v. R. Schleyer, *Angew. Chem. Int. Ed. Engl.* **1997**, *36*, 626.

[4] J. B. Lambert, Y. Zhao, *Angew. Chem. Int. Ed. Engl.* **1997**, *36*, 400.

[5] J. B. Lambert, Y. Zhao, H. Wu, W. C. Tse, B. Kuhlmann, *J. Am. Chem. Soc.* **1999**, *121*, 5001.

[6] T. Müller, Y. Zhao, J. B. Lambert, *Organometallics* **1998**, *17*, 278.

[7] [7a] P. Jutzi, *Adv. Organomet. Chem.* **1986**, *26*, 217. – [7b] J. B. Lambert, S. M. Ciro, C. L. Stern, *J. Organomet. Chem.* **1995**, *499*, 49. – [7c] H. V. R. Dias, Z. Wang, *J. Am. Chem. Soc.* **1997**, *119*, 4650. – [7d] For the theoretical calculation of $A_3H_3^+$ cations (A = C, Si, Ge, Sn), see: E. D. Jemmis, G. N. Srinivas, J. Leszczynski, J. Kapp, A. A. Korkin, P. v. R. Schleyer, *J. Am. Chem. Soc.* **1995**, *117*, 11361.

[8] [8a] A. Sekiguchi, M. Tsukamoto, M. Ichinohe, *Science* **1997**, *275*, 60. – [8b] M. Ichinohe, N. Fukaya, A. Sekiguchi, *Chem. Lett.* **1998**, 1045.

[9] For the cyclotrigermenyl radical, see: M. Olmstead, L. Pu, R. S. Simons, P. P. Power, *Chem. Commun.* **1997**, 1595.

[10] S. H. Strauss, *Chem. Rev.* **1993**, *93*, 927.

[11] S. R. Bahr, P. Boudjouk, *J. Org. Chem.* **1992**, *57*, 5545.

[12] J. C. W. Chien, W.-M. Tsai, M. D. Raush, *J. Am. Chem. Soc.* **1991**, *113*, 8570.

[13] [13a] L. Jia, X. Yang, A. Ishihara, T. J. Marks, *Organometallics* **1995**, *14*, 3135. – [13b] L. Jia, X. Yang, C. L. Stern, T. J. Marks, *Organometallics* **1997**, *16*, 842.

[14] A. Sekiguchi, H. Yamazaki, C. Kabuto, H. Sakurai, S. Nagase, *J. Am. Chem. Soc.* **1995**, *117*, 8025.

[15] The fates of tBu$_3$Si and Ph$_3$C radicals are not clear, although we have observed the presence of tBu$_3$SiF, Ph$_3$CH, and an unidentified unstable product, which may be formed by the attack of tBu$_3$Si radical on the *para* position of Ph$_3$C radical.

[16] A. Bondi, *J. Phys. Chem.* **1964**, *68*, 443.

[17] [17a] R. Breslow, *J. Am. Chem. Soc.* **1957**, *79*, 5318. – [17b] R. Breslow, C. Yuan, *J. Am. Chem. Soc.* **1958**, *80*, 5991. – [17c] M. Sundaralingam, L. H. Lensen, *J. Am. Chem. Soc.* **1966**, *88*, 198. – [17d] R. Breslow, *Pure Appl. Chem.* **1971**, *28*, 111. – [17e] A. T. Ku, M. Sundaralingam, *J. Am. Chem. Soc.* **1972**, *94*, 1688. – [17f] F. H. Allen, *Tetrahedron* **1982**, *38*, 645. – [17g] M. W. Wong, L. Radom, *J. Am. Chem. Soc.* **1989**, *111*, 6976. – [17h] W.-K. Li, N. V. Riggs, *J. Mol. Struct.* **1992**, *89*, 189.

[18] Electropositive substituents such as the silyl group prefers planar Ge=Ge double bonds to *trans*-bent structures. In addition, remarkable relief of the strain of three-membered rings comprising of the Group 14 elements by the electropositive substituent is predicted by theoretical calculations, see: [18a] S. Nagase, *Pure Appl. Chem.* **1993**, *65*, 675. – [18b] A. Sekiguchi, S. Nagase, in *The Chemistry of Organic Silicon Compounds*, Vol. 2, Part 1, (Eds.: Z. Rappoport, Y. Apeloig), John Wiley & Sons Ltd. **1998**, Chapter 3.

[19] $Na_2[(2,6\text{-}Mes_2C_6H_3)Ga]_3$ and $K_2[(2,6\text{-}Mes_2C_6H_3)Ga]_3$ (Mes = 2,4,6- trimethylphenyl), which are isoelectronic with cyclotrigermenium ion, have been synthesized, see: [19a] X.-W. Li, W. T. Pennington, G. H. Robinson, *J. Am. Chem. Soc.* **1995**, *117*, 7578. – [19b] X.-W. Li, Y. Xie, P. R. Schreiner, K. D. Gripper, R. C. Crittendon, C. F. Campana, H. F. Schaefer, G. H. Robinson, *Organometallics* **1996**, *15*, 3798.

[20] A. de Meijere, D. Faber, M. Noltemeyer, R. Boese, T. Haumann, T. Müller, M. Bendikov, E. Matzner, Y. Apeloig, *J. Org. Chem.* **1996**, *61*, 8564.

[21] M. J. Frisch, G. W. Trucks, H. B. Schlegel, P. M. W. Gill, B. G. Johnson, M. A. Robb, J. R. Cheeseman, T. Keith, G. A. Petersson, J. A. Montgomery, K. Raghavachari, M. A. Al Laham, V. G. Zakrzewski, J. V. Ortiz, J. B. Foresman, J. Cioslowski, B. B. Stefanov, A. Nanayakkara, M. Challacombe, C. Y. Peng, P. Y. Ayala, W. Chen, M. W. Wong, J. L. Andres, E. S. Replogle, R. Gomperts, R. L. Martin, D. J. Fox, J. S. Binkley, D. J. Defrees, J. Baker, J. P. Stewart, M. Head-Gordon, C. Gonzalez, J. A. Pople, *Gaussian 94*, Revision E.2; Gaussian, Inc.: Pittsburgh, PA, **1995**.

Received December 10, 1999
[I99449]

First Hyperpolarizabilities of Manganese(I)−Chromium(0) Sesquifulvalene Complexes

Matthias Tamm,*[a] Thomas Bannenberg,[a] Kim Baum,[a] Roland Fröhlich,[b] Thomas Steiner,[c] Timo Meyer-Friedrichsen,[d] and Jürgen Heck[d]

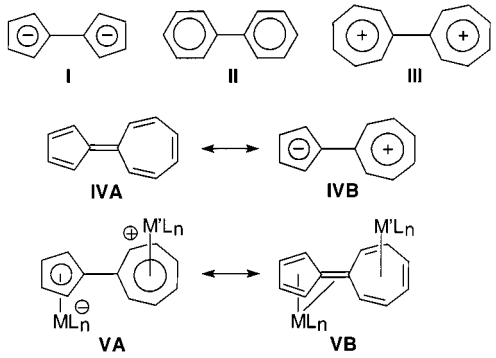
Dedicated to Hedda Meyer on the occasion of her 60th birthday

Keywords: Sesquifulvalene / Manganese / Chromium / Heterobimetallic complexes / Nonlinear optics

The synthesis of monometallic manganese and bimetallic manganese–chromium complexes incorporating the sesquifulvalene derivatives 2-(2,4,6-cycloheptatrien-1-ylidene)indene (**VI**) and [(2,4,6-cycloheptatrien-1-ylidene)ethenylidene]cyclopentadiene (**VII**) is reported. Charge separation is observed upon complexation and stabilization of **VI** and **VII** by metal centers, and the spectroscopic and structural properties of [(**VI**)$Mn(CO)_3$]BF_4 (**6**), [$(OC)_3$Mn(μ-**VI**)$Cr(CO)_3$]BF_4 (**8**), [(**VII**)$Mn(CO)_3$]BF_4 (**13**), and [$(OC)_3$Mn(μ-**VII**)$Mn(CO)_3$]BF_4 (**15**) are clearly indicative of sesquifulvalene ligands coordinated in a dipolar η^5 or μ-η^5:η^7 fashion, respectively. The coplanar cyclopentadienyl and cycloheptatrienyl fragments act as strongly coupled electron-donating and -accepting groups and strong negative solvatochromism is observed for complexes **6**, **8**, **13**, and **15**. Accordingly, exceptionally large first molecular hyperpolarizabilities β have been determined by means of hyper Raleigh scattering for the bimetallic species **8** and **15**, as well as for some related compounds. The X-ray crystal structures of *anti*-[$(OC)_3$Mn(μ-η^5:η^7-**VI**)$Cr(CO)_3$] (**8**) and *syn*-[$(OC)_3$Mn(μ-η^5:η^7-**VII**)$Cr(CO)_3$] (**15**) are reported.

Introduction

In recent years, considerable effort has been devoted to exploring the organometallic chemistry of η-cycloheptatrienyl ligands and significant progress has been made in the development of new synthetic routes to their metal complexes.[1] However, η-cycloheptatrienyl transition metal complexes, M(η-C_7H_7), still remain poorly explored in comparison with the analogous η-cyclopentadienyl, M(η-C_5H_5), and benzene systems, M(η-C_6H_6). This also holds true in the area of bimetallic complexes with conjugated hydrocarbon-bridged transition metal fragments, which is dominated by ligands containing five- and six-membered rings,[2] e.g. bicyclopentadienyl (**I**)[3,4] and biphenyl (**II**)[5] (Scheme 1). On the other hand, related complexes with the iso-π-electronic hydrocarbon bicycloheptatrienyl (**III**) have been reported only recently by Whiteley and co-workers.[6] Direct linkage of an anionic cyclopentadienyl unit and a cationic cycloheptatrienylium unit gives the cross-conjugated hydrocarbon sesquifulvalene (**IV**), which constitutes a dipolar structural isomer of biphenyl (**II**). Despite the fact that **IV** can be described by resonance structure **IVB** containing two aromatic subunits, it is quite unstable and behaves like a polyene with alternating bond lengths;[7] its ground state electronic structure is best represented by the apolar canonical form **IVA**.



Scheme 1

In contrast, charge separation is observed upon complexation and stabilization of **I** and its derivatives by transition metal fragments,[8−10] and heterobimetallic iron−chromium[9] and manganese−chromium[10] complexes of type **V** have been obtained. The spectroscopic and structural properties of the latter are clearly indicative of sesquifulvalene ligands coordinated in a dipolar μ-η^5:η^7 fashion (resonance structure **VA**, Scheme 1). In these complexes, the cyclopentadienyl and cycloheptatrienyl frag-

[a] Anorganisch-Chemisches Institut,
Westfälische Wilhelms-Universität,
Wilhelm-Klemm-Straße 8, D-48149 Münster, Germany
Fax (internat.): +49(0)251/8333108
E-mail: mtamm@uni-muenster.de
[b] Organisch-Chemisches Institut,
Westfälische Wilhelms-Universität,
Corrensstraße 40, D-48149 Münster, Germany
[c] Institut für Kristallographie, Freie Universität Berlin,
Takustraße 6, D-14195 Berlin, Germany
[d] Institut für Anorganische und Angewandte Chemie,
Universität Hamburg,
Martin-Luther-King-Platz 6, D-20146 Hamburg, Germany

 © WILEY-VCH Verlag GmbH, D-69451 Weinheim, 2000 1434−1948/00/0606−1161 $ 17.50+.50/0

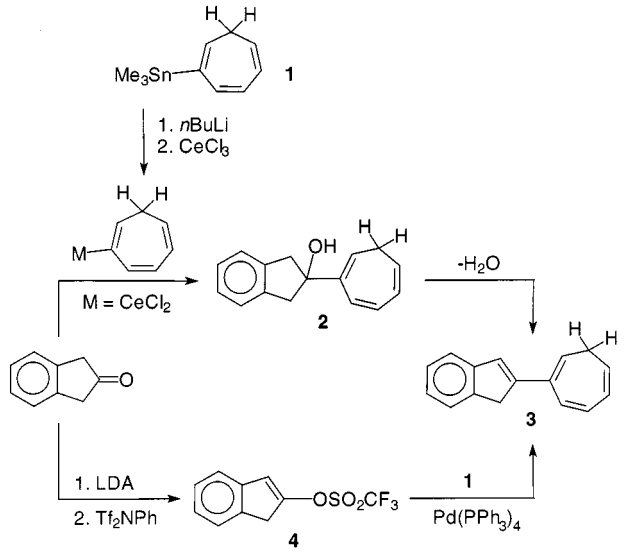
ments act as strongly coupled electron-donating and -accepting groups, respectively, and thus together meet the requirements for the classical construction of compounds with large SHG (second harmonic generation) efficiencies.[11] Accordingly, it has been observed that sesquifulvalene complexes exhibit unusually pronounced nonlinear optical (NLO) properties, and their first molecular hyperpolarizabilities β are among the highest ever measured for organometallic NLO chromophores.[12]

In continuation of our work on transition metal complexes with dipolar cycloheptatrienyl ligands,[8−10,13] we report herein on the syntheses and properties of mono- and bimetallic complexes incorporating either the benzanellated sesquifulvalene derivative 2-(2,4,6-cycloheptatrien-1-ylidene)indene (**VI**) (complexes **6**, **8**) or the "cumulogous" sesquifulvalene [(2,4,6-cycloheptatrien-1-ylidene)ethenylidene]-cyclopentadiene (**VII**) (complexes **13**, **15**). Furthermore, an investigation of the first molecular hyperpolarizabilities of various manganese sesquifulvalene complexes using the hyper Raleigh scattering technique is presented.

Results and Discussion

Synthesis of Complexes 6 and 8

The preparation of sesquifulvalene complexes has hitherto been accomplished by template syntheses, which usually involve a C−C coupling reaction between a cyclopentadienyl complex and a cycloheptatrienyl derivative, followed by complexation of the cycloheptatrienyl unit and/or hydride abstraction.[8]−[10] This synthetic procedure is limited to cyclopentadienyl complexes that can readily be functionalized at the five-membered ring, e.g. by metallation and halogenation reactions.[14] In order to develop methods more widely applicable to the preparation of sesquifulvalene complexes, we became interested in employing dihydrosesquifulvalenes such as **3** (Scheme 2), which can be deprotonated and transferred to metal centers in the same way as ordinary cyclopentadiene derivatives.[15] In principle, dihydrosesquifulvalenes can be prepared by addition of a nucleophilic cyclopentadienyl anion to an electrophilic tropylium cation yielding 1,3,5-cycloheptatrienes bearing the Cp residue in the allylic 7-position.[16] These hydrocarbons are of limited use, however, as complexation of the seven-membered ring can lead to two different stereoisomers with *exo* and *endo* configurations, and this may hamper the ensuing hydride abstraction.[10,17] Therefore, as a suitable starting material we chose 2-trimethylstannyl-1,3,5-cycloheptatriene (**1**), which is functionalized in a vinylic rather than the allylic position, and which can be obtained directly from cycloheptatriene by metallation and subsequent reaction with Me_3SnCl.[10,18] The 1,3,5-cycloheptatrien-2-yl anion can easily be generated and used as a nucleophile by transmetallation of **1** with *n*BuLi.[13b,13c] Hence, its addition to cyclopentenones and subsequent dehydration of the resulting adducts by acidic workup should lead to appropriately substituted dihydrosesquifulvalenes.[15,19]

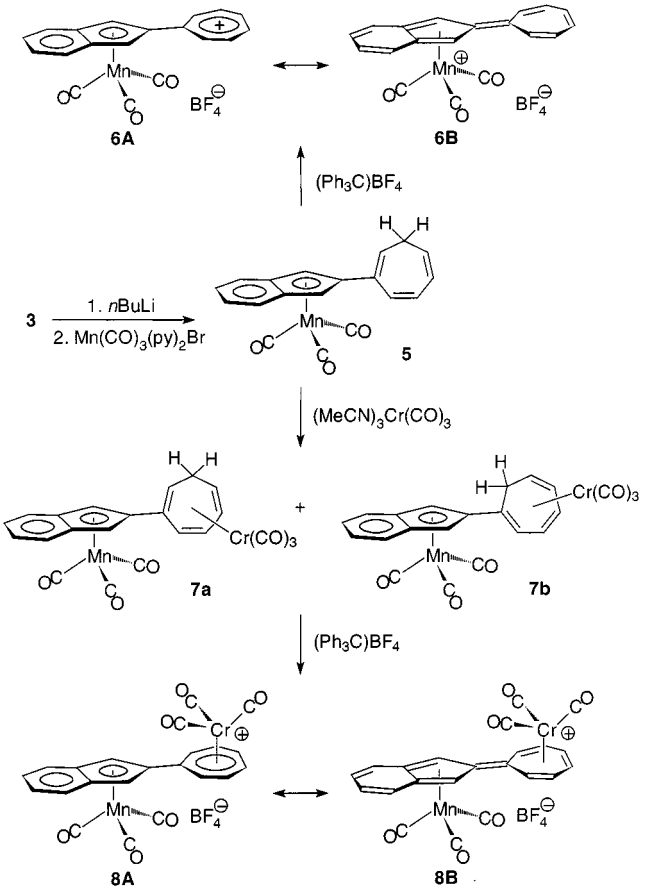


Scheme 2

To test the strategy outlined above, we started with 2-indanone, since the dihydrosesquifulvalene **3** was expected to be stable and isolable in isomerically pure form as a result of benzanellation in the 4,5-positions (Scheme 2). The alcohol **2**, however, could only be isolated in 26% yield from the reaction of 2-indanone with RLi (R = 1,3,5-cycloheptatrienyl-2-yl). Evidently, the lithium complex not only acts as a nucleophile towards the ketone, but the desired addition to the carbonyl group is accompanied by significant simple deprotonation.[20] As organocerium compounds generally exhibit higher nucleophilicity and reduced basicity compared to organolithium compounds,[21] the undesired formation of the enolate anion could be suppressed to some extent by employing $RCeCl_2$ (R = 1,3,5-cycloheptatrienyl-2-yl), although the yield still remained quite low (40%). Dehydration of **2** was then achieved by refluxing in benzene in the presence of a catalytic amount of *p*-toluenesulfonic acid using a water trap; subsequent chromatographic separation afforded **3** as a crystalline white solid.[22]

To improve the poor overall yield of **3** (10−20% based on 2-indanone), an alternative route involving a Stille coupling reaction[23] between the triflate **4** and the stannane **1** was used (Scheme 2).[24] Triflate **4** was prepared by deprotonation of 2-indanone with lithium diisopropylamide (LDA) and subsequent reaction of the intermediate enolate with bis(trifluoromethanesulfonato)phenylamine (Tf_2NPh).[25] Stille coupling with a catalytic amount of $Pd(PPh_3)_4$ afforded **3** in at least moderate yield (60% based on **1**, 45% based on 2-indanone). The dihydrosesquifulvalene **3** proved to be indefinitely stable at 0 °C under argon, but was found to slowly decompose in solution over a period of several hours with the deposition of a precipitate. All resonances in the ^1H and ^{13}C NMR spectra could unambiguously be assigned by means of correlated two-dimensional NMR spectroscopy ($^1H,^1H$ and $^1H,^{13}C$ COSY).

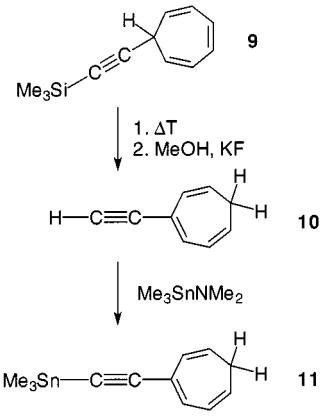
Compound **3** could then be used for the preparation of cycloheptatrienyl-substituted indenyl complexes. In order to assess the influence of benzanellation on the electronic and



Scheme 3

optical properties of sesquifulvalene complexes derived from **3**, complexes **6** and **8** were prepared and compared with the known parent compounds **16** and **17** (Figure 3, vide infra). Treatment of **3** with *n*BuLi followed by $Mn(CO)_3(pyridine)_2Br$[19b,26] produced the cymantrene derivative **5** (Scheme 3). Hydride abstraction at this stage using triphenylcarbenium tetrafluoroborate, $(Ph_3C)BF_4$, led to the monometallic benzosesquifulvalene complex **6**, which could be quantitatively isolated in the form of red-brown crystals. Alternatively, reaction of **5** with $(MeCN)_3Cr(CO)_3$ in refluxing THF gave a mixture of the two bimetallic isomers **7a** and **7b** (**7a**:**7b** ≈ 60:40, Scheme 3). Comparison with the spectroscopic data of related complexes[10] revealed that in **7a** the $Cr(CO)_3$ group is coordinated to a 1,3,5-cycloheptatrien-2-yl ring as expected, whereas **7b** contains a 1,3,5-cycloheptatrien-1-yl ring. The formation of **7b** must have resulted from thermal rearrangement of the coordinated cycloheptatrienyl ring in **7a** through a 1,5-sigmatropic hydrogen migration.[17,27] As both complexes are racemic mixtures of two enantiomers, six resonances are observed for the diastereotopic indenyl protons of each isomer.

Nevertheless, **7a** and **7b** are equally useful for the synthesis of the bimetallic sesquifulvalene complex **8** as the *exo* hydrogen atom in both isomers is easily accessible for hydride abstraction. Indeed, **8** was formed quantitatively upon treatment with $(Ph_3C)BF_4$ and could be isolated in the form of orange-brown crystals.



Scheme 4

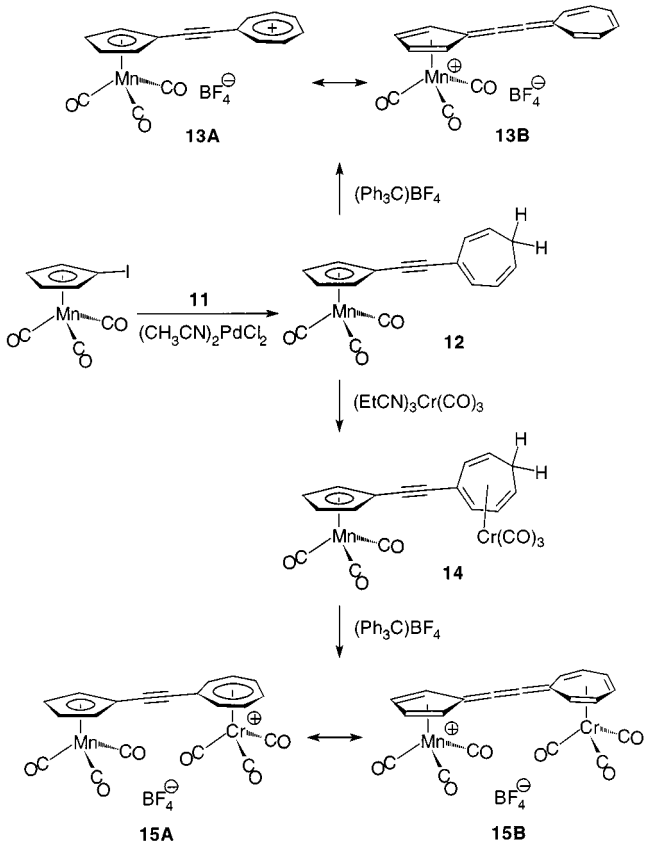
Synthesis of Complexes 13 and 15

The monometallic complex **13** has previously been obtained from the reaction of $[\eta^5\text{-}(LiC{\equiv}CC_5H_4)Mn(CO)_3]$ with tropylium salts, followed by hydride abstraction.[8a] However, the complexation of the intermediate 1,3,5-cycloheptatrien-7-yl derivative could again lead to an isomeric mixture of *exo* and *endo* isomers, which would hamper the required reaction with the trityl cation (vide supra). In order to obtain suitably functionalized ethynylcycloheptatriene derivatives that would allow a high-yielding synthesis of **15**, we followed a route involving the stannane **11** (Scheme 4). 7-Trimethylsilylethynyl-1,3,5-cycloheptatriene (**9**) was found to undergo thermal rearrangement in DMF at 135 °C.[28] Desilylation in methanol in the presence of a catalytic amount of KF[29] followed by distillation yielded a mixture of isomeric hydrocarbons composed almost entirely of 3-ethynyl-1,3,5-cycloheptatriene (**10**) formed by just one 1,5-hydrogen shift. Further hydrogen migrations led to the formation of cycloheptatrienes substituted in the 1- and 2-positions. Treatment of **10** with Me_3SnNMe_2 gave **11**, which could then be used in Stille coupling reactions.

Thus, the Pd-catalyzed reaction of **11** with iodocymantrene, $[\eta^5\text{-}(C_5H_4I)Mn(CO)_3]$,[14a,14b] in DMF afforded a yellow oil, which crystallized on standing at 4 °C for a couple of days (Scheme 5). At this stage, the 1,3,5-cycloheptatrien-3-yl derivative **12** was the only isomer detectable by NMR spectroscopy. As expected, hydride abstraction gave the known monometallic sesquifulvalene complex **13**,[8b] whereas reaction with $(EtCN)_3Cr(CO)_3$ at room temperature produced bimetallic **14**. As the two sides of the seven-membered ring in **13** are enantiotopic, **14** forms a racemic mixture of two enantiomers and its ^{13}C NMR spectrum features five cyclopentadienyl resonances due to the diastereotopic carbon atoms. The allylic *exo* hydrogen atom in **14** is again easily accessible to the trityl cation and **15** can be isolated in quantitative yield as yellow-orange crystals following treatment with $(Ph_3C)BF_4$.

Structural Characterization of Sesquifulvalene Complexes 8 and 15

The molecular structure of the cation in **8** is depicted in Figure 1. The five- and seven-membered rings are almost



Scheme 5

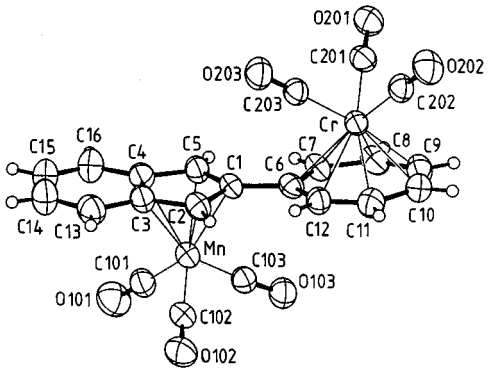


Figure 1. ORTEP drawing of the cation in **8**; selected bond lengths [Å] and angles [°]: Mn−C1 2.110(8), Mn−C2 2.125(11), Mn−C3 2.207(11), Mn−C4 2.236(10), Mn−C5 2.151(10), C1−C2 1.433(12), C2−C3 1.440(14), C3−C4 1.41(2), C4−C5 1.436(13), C5−C1 1.432(12), C1−C6 1.489(12), C6−C7 1.391(12), C7−C8 1.422(14), C8−C9 1.38(2), C9−C10 1.40(2), C10−C11 1.45(2), C11−C12 1.321(14), C12−C6 1.440(13), Cr−C6 2.277(9), Cr−C7 2.222(9), Cr−C8 2.210(10), Cr−C9 2.224(11), Cr−C10 2.206(11), Cr−C11 2.219(11), Cr−C12 2.215(10); (C1−5)(C6−12) 4.6(6)°

perfectly coplanar [dihedral angle of 4.6(6)°]. The ligand coordinates to the $Mn(CO)_3$ and $Cr(CO)_3$ fragments in η^5 and η^7 modes, respectively, and the fragments adopt an *anti*-facial arrangement. Unfortunately, due to the high absorption coefficient (see Experimental Section), the structure could only be refined with reduced accuracy, thus preventing a very detailed discussion of the bonding geometry. Nevertheless, the inter-ring bond length in **8** [C1−C6 = 1.489(12) Å] clearly corresponds to a $C(sp^2)-C(sp^2)$ single

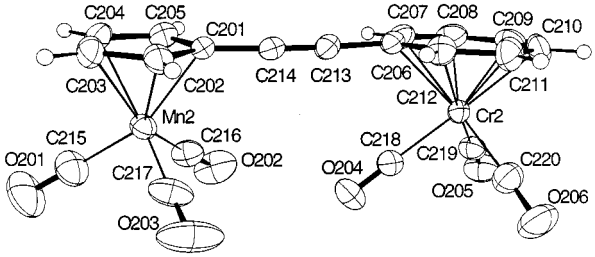


Figure 2. ORTEP drawing of one cation in **15**·CH_2Cl_2; the asymmetric unit contains two independent molecules of **15**; selected bond lengths [Å] and angles [°]: molecule 2 [molecule 1] Mn2−C201 2.122(3) [2.132(3)], Mn2−C202 2.124(3) [2.134(3)], Mn2−C203 2.139(3) [2.148(3)], Mn2−C204 2.150(3) [2.144(3)], Mn2−C205 2.134(3) [2.135(3)], C201−C202 1.422(5) [1.421(4)], C202−C203 1.400(5) [1.403(4)], C203−C204 1.403(6) [1.407(5)], C204−C205 1.403(5) [1.405(4)], C201−C214 1.424(4) [1.424(4)], C214−C213 1.186(4) [1.189(4)], C213−C206 1.434(4) [1.435(4)], C206−C207 1.416(4) [1.407(4)], C207−C208 1.382(4) [1.394(4)], C208−C209 1.400(5) [1.404(5)], C209−C210 1.377(6) [1.382(5)], C210−C211 1.416(6) [1.411(5)], C211−C212 1.395(5) [1.386(4)], C212−C206 1.411(4) [1.425(4)], Cr2−C206 2.261(3) [2.266(3)], Cr2−C207 2.234(3) [2.249(3)], Cr2−C208 2.223(3) [2.210(3)], Cr2−C209 2.221(3) [2.235(3)], Cr2−C210 2.222(3) [2.231(3)], Cr2−C211 2.213(4) [2.222(3)], Cr2−C212 2.251(3) [2.234(3)]; C201−C214−C213 177.8(3) [178.2(3)], C214−C213−C206 176.1(3) [177.5(3)]; (C201−205)(C206−212) 5.4(0)° [17.2(0)°]

bond, and hence the solid-state structure of **8** is evidently that of an indenyl-cycloheptatrienyl complex and is best described by canonical form **8A** in Scheme 4. However, a minor contribution from resonance form **8B** could be deduced from the observation that the bonding between the seven-membered ring and the $Cr(CO)_3$ moiety is slightly distorted towards a fulvene-type coordination geometry, the Cr−C6 bond length [2.277(9) Å] being significantly longer than the remaining Cr−C distances [average 2.216(10) Å].

In **15**, the asymmetric unit contains two independent molecules with both cations adopting a *syn*-facial conformation. The molecular structure of one cation is shown in Figure 2. The two cations differ slightly in the relative orientations of their *cyclo*-C_5 and *cyclo*-C_7 units, the relevant dihedral angles being 5.4(4)° and 17.2(4)°. Within experimental error, the bond lengths and angles in the two molecules are almost identical and correspond to a solid-state structure best described by canonical form **15A** in Scheme 5. For instance, the C(sp)−C(sp) bonds are clearly triple bonds [C113−C114 = 1.189(4) Å and C213−C214 = 1.186(4) Å]. Furthermore, the intra-ring bond lengths do not alternate significantly, as befits aromatic cyclopentadienyl and cycloheptatrienyl units.

Spectroscopic Properties of Sesquifulvalene Derivatives

The NMR spectroscopic data of the mono- and bimetallic complexes **6**, **8**, **13**, and **15** confirm that complexation of the sesquifulvalene derivatives leads to charge separation within the ligands and to dipolar coordination of the respective hydrocarbon. Accordingly, low-field resonances at $\delta \approx 9$ are observed for the cycloheptatrienyl protons in monometallic **6** and **13**, which fall in the expected range for tropylium cations of the type $(C_7H_6R)^+$.[30] As a result of coordination of the seven-membered rings to the $Cr(CO)_3$ moieties, these resonances are shifted to significantly higher

Table 1. UV/Vis data for complexes **6**, **8**, **13**, and **15**

Compound	λ_{max} [nm] CH_2Cl_2	CH_3CN	$\Delta\tilde{\nu}$ [cm^{-1}]
6	501	471	−1270
8	486	468	−790
13	537	491	−1740
15	449	429	−1040

field in bimetallic **8** and **15** (δ = 6.25−6.50) and are wholly consistent with the values expected for cycloheptatrienyl complexes of the type [η^7-(C_7H_6R)$Cr(CO)_3$].[17,31]

As mentioned above, the four sesquifulvalene derivatives are intensely colored compounds. They show strong solvatochromic behaviour and their UV/Vis spectra are markedly solvent-dependent, which is usually a good indication of possible NLO activity.[32] The lowest-energy band λ_{max} (Table 1) is most strongly shifted upon changing the solvent from dichloromethane to acetonitrile ($\Delta\tilde{\nu}$ ranging from −790 cm^{-1} in **8** to −1740 cm^{-1} in **13**). On the basis of these hypsochromic shifts (negative solvatochromic behaviour), the lowest-energy transition in these systems can be assigned to a π to π^* CT transition,[33] which is APPROXIMATELY (!) represented by the canonical forms **A** (ground state) and **B** (excited state) shown in Scheme 3 for **6** and **8** and in Scheme 5 for **13** and **15**.

The bimetallic derivatives **8** and **15** absorb at higher energy than the corresponding monometallic complexes **6** and **13**, and λ_{max} is hypsochromically shifted upon complexation of the seven-membered ring. This observation implies that interaction of the $Cr(CO)_3$ group with the cycloheptatrienyl unit increases the HOMO/LUMO energy gap of the relevant π to π^* CT excitation. In other words, the [(C_7H_6R)$Cr(CO)_3$] moiety has a stronger ability to effectively stabilize a positive charge than the "naked" tropylium system, which leads to an increase in the energy difference between the two limiting resonance structures **A** and **B** (Schemes 3 and 5).

Nonlinear Optical Properties of Sesquifulvalene Derivatives

It has been demonstrated that sesquifulvalene complexes are among the most promising organometallic candidates for nonlinear optical applications.[9] Consequently, we have measured the first molecular hyperpolarizabilities β of selected monometallic manganese and bimetallic manganese−chromium sesquifulvalene complexes (Figure 3) using the hyper Raleigh scattering technique (HRS), which allows determination of β in solution even for ionic compounds.[34] Here, HRS experiments were performed with an Nd:YAG laser (λ = 1064 nm). The intensity of the frequency-doubled scattered light ($\lambda/2$ = 532 nm) was measured as a function of the concentration of the NLO chromophore. The results are shown in Table 2.

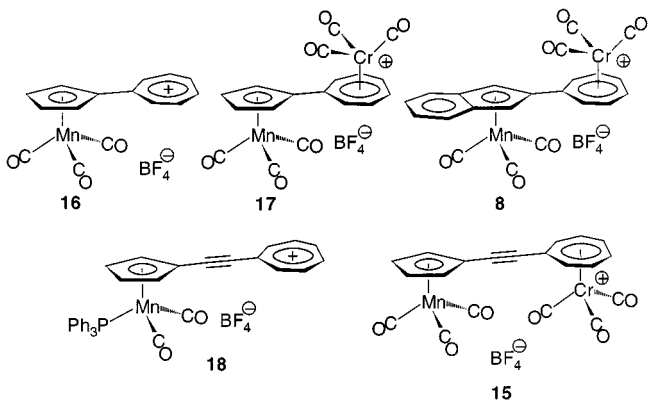


Figure 3. Sesquifulvalene complexes studied by hyper Raleigh scattering

Table 2. UV/Vis and NLO data for selected sesquifulvalene complexes

Compound	Solvent[a]	λ_{max}, nm	β, 10^{-30} esu[b]	β_0, 10^{-30} esu[b][c]
8	CH_3NO_2	435	112	31
15	CH_2Cl_2	449	244	58
16	CH_3NO_2	510	240	15
17	CH_3NO_2	445	77	19
18	CH_2Cl_2	751	226	113

[a] Solutions of *p*-nitroaniline as external reference [$\beta(CH_2Cl_2)$ = 21.6 × 10^{-30} esu, $\beta(CH_3NO_2)$ = 34.6 × 10^{-30} esu]. − [b] β-values in electrostatic units (esu) of the CGS systems (Gaussian system); [β_{CGS}] = cm^4/statV = esu; [β_{SI}] = Cm^3/V^2 = C^3m^3/J^2; β_{SI} = $(1/3)^3$ × 10^{-19} β_{CGS} (see ref.[12a]). − [c] β_0 = β [(1 − $4\lambda_{max}^2/\lambda^2$) (1 − $\lambda_{max}^2/\lambda^2$)] with λ = 1064 nm (Nd:YAG laser) (see refs.[34a,35]).

The β values in Table 2 are unusually large owing to resonance enhancement, which occurs when the frequency of the charge-transfer excitation is close to the frequency of the stimulating laser or close to the doubled frequency. Therefore, extrapolation of the dynamic hyperpolarizabilities β to their static counterparts β_0 was accomplished by means of the two-level model (Table 2).[34a,35] The first molecular hyperpolarizabilities presented here are very high compared to those of organic[11,36] or organometallic[12] compounds with chromophores of similar lengths. Comparison of the nonlinear optical efficiency of bimetallic **15** with that of the related ferrocene derivative [(C_5H_5)Fe(μ-η^5:η^7-C_5H_4−C≡C−C_7H_6)$Cr(CO)_3$]BF_4 (β_0 = 105 × 10^{-30} esu)[9] shows that the ferrocene moiety is superior to the cymantrene unit, (C_5H_4R)$Mn(CO)_3$, probably due to its stronger electron-donating ability. However, the electronic and optical properties of these manganese complexes can be easily and efficiently tuned by ligand substitution reactions,[8b] and the introduction of a phosphane ligand to give monometallic **18** results in extraordinary frequency-doubling characteristics. Furthermore, this protocol could be extended to the introduction of readily available chiral phosphanes leading to optically active compounds that can be expected to crystallize in noncentrosymmetric space groups, thereby fulfilling a crucial requirement for the observation of macroscopic NLO effects.[11,12]

Conclusion

In summary, we have presented new methods for the syntheses of sesquifulvalene complexes that can be considered

as widely applicable for the preparation of various other bimetallic complexes. In particular, use of the appropriately substituted cycloheptatrienyl derivatives **3** and **11** circumvents the *exo*/*endo* problem encountered with the 1,3,5-cycloheptatrien-7-yl derivatives and facilitates high-yielding syntheses. Finally, the first hyperpolarizabilities determined for various manganese sesquifulvalene complexes confirm the suitability of such complexes for nonlinear optical applications.

Experimental Section

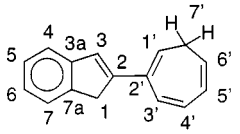
General: All operations were performed under an atmosphere of dry argon by using Schlenk and vacuum techniques. Solvents were dried by standard methods and distilled prior to use. The following compounds were prepared as described in the literature: $Mn(CO)_3(pyridine)_2Br$,[26] $(C_5H_4I)Mn(CO)_3$,[14a] $(CH_3CN)_3Cr(CO)_3$,[37] $(CH_3CH_2CN)_3Cr(CO)_3$,[38] 2-trimethylstannyl-1,3,5-cycloheptatriene (**1**).[10] The synthesis of **13** has been published previously.[8a] Complete assignment of all resonances in **3** and **10** was achieved with the aid of two-dimensional NMR spectroscopy ($^1H,^1H$ and $^1H,^{13}C$ COSY experiments).

2-(1,3,5-Cycloheptatrien-2-yl)indan-2-ol (2). − Method A: A solution of **1** (1.59 g, 6.24 mmol) in THF (30 mL) was treated with *n*-butyllithium (2.5 mL of a 2.5 M solution in hexane, 6.3 mmol) at −78 °C. After stirring for 45 min, a solution of 2-indanone (0.79 g, 5.98 mmol) in THF (15 mL) was added. The reaction mixture was then allowed to warm to room temperature and stirring was continued for 12 h. Quenching with aqueous HCl (24%, 2 mL) and ice (6 g) resulted in the formation of **2**. After 30 min, the reaction mixture was made alkaline with aqueous ammonia solution (3.5%) and then diluted with brine (20 mL). It was then extracted with diethyl ether (3 × 20 mL) and the combined extracts were dried over Na_2SO_4 and concentrated. Chromatography of the residue on alumina (4% H_2O) eluting with dichloromethane gave **2** as a white solid. Yield: 0.35 g (26%).

Method B: At −78 °C, a suspension of $CeCl_3$ (2.88 g, 11.68 mmol) in THF (35 mL) was added to a solution containing the 1,3,5-cycloheptatrien-2-yl anion, which had been generated from a solution of **1** (2.54 g, 9.96 mmol) in THF (50 mL) and *n*-butyllithium (4.0 mL of a 2.5 M solution in hexane, 10.0 mmol) as described above (Method A). After stirring for 30 min, a solution of 2-indanone (1.19 g, 9.00 mmol) in THF (9 mL) was added dropwise and stirring was continued for 15 h at −74 °C. The reaction mixture was then allowed to warm to room temperature, whereupon TMEDA (ca. 2.6 mL) was added. After 30 min, the reaction mixture was quenched with aqueous $NaHCO_3$ and diluted with brine. Extraction with dichloromethane (3 × 100 mL), drying of the combined extracts with Na_2SO_4, and evaporation of the solvent afforded **2**, which could be purified chromatographically as described above. Yield: 0.81 g (40%). − ^1H NMR ($CDCl_3$, 400 MHz): δ = 7.32−7.22 (m, 4 H, C_6H_4), 6.83 (d, 1 H, C_7 ring: CH), 6.65 (dd, 1 H, C_7 ring: CH), 6.15 (dd, 1 H, C_7 ring: CH), 5.63 (t, 1 H, C_7 ring: CH), 5.54 (dt, 1 H, C_7 ring: CH), 3.36 (d, 2 H, C_5 ring: CH_2), 3.06 (d, 2 H, C_5 ring: CH_2), 2.26 (t, 2 H, C_7 ring: CH_2); no OH resonance could be observed.

2-(1,3,5-Cycloheptatrien-2-yl)indene (3). − Method A: A solution of **2** (1.75 g, 7.80 mmol) in benzene (30 mL) was treated with a catalytic amount of *p*-toluenesulfonic acid and refluxed for 12 h in an apparatus fitted with a water trap. After removal of the solvent in vacuo, the crude product was purified by chromatography on silica (4% H_2O) using petroleum ether/dichloromethane (3:1) as eluent to afford **3** as a white crystalline solid. Yield: 0.60 g (37%).

Method B: At room temperature, a suspension of lithium chloride (2.41 g, 56.85 mmol) and $Pd(PPh_3)_4$ (0.18 g, 0.16 mmol) in THF (20 mL) was treated with a solution of **4** (2.05 g, 7.76 mmol) in THF (20 mL). After stirring for 15 min, a solution of stannane **1** (1.97 g, 7.73 mmol) in THF (20 mL) was added and the resulting mixture was refluxed for 16 h. The dark-green solution thus obtained was then diluted with pentane (200 mL) and treated with aqueous ammonia solution (10%, 3 × 75 mL). The organic layer was separated, dried with Na_2SO_4, and the solvent was removed in vacuo. Crude **3** (Figure 4) could be purified chromatographically as described above. Yield: 0.98 g (61%); m.p. 92 °C. − ^1H NMR ($CDCl_3$, 400 MHz): δ = 7.37 (d, *J* = 6 Hz, 1 H, 7-H), 7.29 (d, *J* = 6 Hz, 1 H, 4-H), 7.22 (dd, *J* = 6 Hz, 6 Hz, 1 H, 6-H), 7.13 (dd, *J* = 6 Hz, 6 Hz, 1 H, 5-H), 7.07 (d, *J* = 9 Hz, 1 H, 3′-H), 6.78 (s, 1 H, 3-H), 6.69 (dd, *J* = 9 Hz, 5 Hz, 1 H, 4′-H), 6.18 (dd, *J* = 6 Hz, 5 Hz, 1 H, 5′-H), 5.74 (t, *J* = 8 Hz, 1 H, 1′-H), 5.60 (td, *J* = 8 Hz, 6 Hz, 1 H, 6′-H), 3.56 (s, 2 H, 1-H), 2.35 (t, *J* = 8 Hz, 2 H, 7′-H). − ^{13}C NMR ($CDCl_3$, 100.4 MHz): δ = 146.6 (C-7a), 145.5 (C-3a), 142.7 (C-2), 134.4 (C-2′), 131.5 (C-4′), 130.1 (C-3′), 127.0 (C-3), 126.9 (C-5′), 126.4 (C-6), 124.5 (C-5), 123.7 (C-6′), 123.4 (C-7), 120.7 (C-4), 119.7 (C-1′), 39.1 (C-1), 27.7 (C-7′). − MS (EI); *m*/*z* (%): 206 (100) [M^+], 191 (43) [$M - CH_3]^+$, 115 (26) [$M - C_7H_7]^+$, 91 (76) [$M - C_9H_7]^+$, 65 (5) [$M - C_9H_7 - C_2H_2]^+$. − $C_{16}H_{14}$ (206.3): calcd. C 93.16, H 6.84; found C 92.01, H 6.81



3

Figure 4. Numbering scheme for **3**

1*H*-Inden-2-yl Trifluoromethanesulfonate (4): A solution of diisopropylamine (2.1 mL, 15.0 mmol) in THF (15 mL) was treated with *n*-butyllithium (5.3 mL of a 2.5 M solution in hexane, 13.3 mmol) at −78 °C and the resulting mixture was allowed to warm to room temperature. The LDA solution thus obtained was then cooled to −78 °C once more, whereupon a solution of 2-indanone (1.39 g, 10.52 mmol) in THF (11 mL) was added. After 15 min at −78 °C, stirring was continued for 2 h at ambient temperature. The enolate solution was then treated with a solution of *N*,*N*-bis(trifluoromethanesulfonyl)aniline (4.20 g, 11.76 mmol) in THF (25 mL) at −78 °C and the resulting mixture was stirred at room temperature for 10 h. It was then diluted with aqueous NH_4Cl solution (20 mL) and extracted with diethyl ether (3 × 40 mL). After removal of the solvent from the combined extracts, the oily residue was purified by column chromatography on silica (4% H_2O) using petroleum ether/dichloromethane (5:1) as eluent to afford the sulfonate **4** as a yellow oil, which was dried in vacuo. Yield: 2.05 g (74%). − ^1H NMR ($CDCl_3$, 250 MHz): δ = 7.42−7.24 (m, 4 H, C_6H_4), 6.70 (s, 1 H, 1-H), 3.68 (s, 2 H, 3-H).

Manganese Complex 5: At −50 °C, a solution of **3** (0.98 g, 4.75 mmol) in THF (40 mL) was treated with *n*-butyllithium (2.0 mL of a 2.5 M solution in hexane, 5.0 mmol). After stirring for 60 min, a solution of $Mn(pyridine)_2(CO)_3Br$ (2.10 g, 5.57 mmol) in THF (60 mL) was added dropwise and the resulting mixture was refluxed for 3 h. Removal of the solvent in vacuo and purification of the residue by column chromatography on alumina (4% H_2O)

eluting with petroleum ether/dichloromethane (5:1) afforded **5** as a yellow crystalline solid. Yield: 1.04 g (64%); m.p. 41 °C. − ^{1}H NMR ($CDCl_3$, 400 MHz): δ = 7.44 (d, 2 H, C_6 ring: CH), 7.09−7.07 (m, 3 H, C_6 ring: CH + C_7 ring: CH), 6.74 (s, 2 H, C_5 ring: CH), 6.23−6.19 (m, 2 H, C_7 ring: CH), 5.73 (t, 1 H, C_7 ring: CH), 5.54 (dt, 1 H, C_7 ring: CH), 2.40 (t, 2 H, CH_2). − ^{13}C NMR ($CDCl_3$, 100.4 MHz): δ = 224.9 (Mn−CO), 132.7 (C_7 ring: CH), 130.5 (C_7 ring: C-2), 129.3, 127.0 (C_7 ring: CH), 126.4, 125.2 (C_6 ring: CH), 122.9, 119.1 (C_7 ring: CH), 108.9 (C_5 ring: C-1), 103.1 ($C_{5/6}$ ring: C), 69.9 (C_5 ring: CH), 27.5 (CH_2). − MS (EI); *m*/*z* (%): 344 (11) [M^+], 316 (4) [M − CO]$^+$, 288 (5) [M − 2CO]$^+$, 260 (64) [M − 3CO]$^+$, 205 (100) [M − 3CO − Mn]$^+$, 191 (28) [M − 3CO − Mn − CH_2]$^+$, 178 (7) [M − 3CO − Mn − H − C_2H_2]$^+$. − IR (KBr): ν (CO) = 2010, 1935, 1914 cm^{-1}. − $C_{19}H_{13}MnO_3$ (344.3): calcd. C 66.29, H 3.81; found C 65.89, H 4.19.

Manganese Benzosesquifulvalene Complex 6: At −78 °C, a solution of **5** (130 mg, 0.38 mmol) in dichloromethane (5 mL) was treated with a solution of $(Ph_3C)BF_4$ (90 mg, 0.27 mmol) in dichloromethane (5 mL). The reaction mixture was allowed to warm to room temperature and stirring was continued for 1 h. On addition of diethyl ether (80 mL), **6** precipitated as a red-brown crystalline solid and was collected by filtration. Yield: (70 mg, 60%). − ^{1}H NMR (CD_3CN, 250 MHz): δ = 9.16 (m, 2 H, C_7 ring: CH), 8.87 (m, 4 H, C_7 ring: CH), 7.78 (m, 2 H, C_6 ring: CH), 7.30 (m, 2 H, C_6 ring: CH), 6.44 (s, 2 H, C_5 ring: CH). − ^{13}C NMR (CH_3CN, 100.4 MHz): δ = 224.9 (Mn−CO), 166.7 (C_7 ring: C-1), 154.1 (C_7 ring: CH), 153.5 (C_7 ring: CH), 150.8 (C_7 ring: CH), 129.8 (C_6 ring: CH), 126.0 (C_6 ring: CH), 106.6 ($C_{5/6}$ ring: C), 98.7 (C_5 ring: C-1), 77.3 (C_5 ring: CH). − MS (FAB POS); *m*/*z* (%): 343 (100) [M^+], 287 (8) [M − 2CO]$^+$, 259 (65) [M − 3CO]$^+$, 204 (67) [M − 3CO − Mn]$^+$, 178 (10) [M − 3CO − Mn − C_2H_2]$^+$. − IR (KBr): ν (CO) = 2017, 1953, 1928 cm^{-1}. − UV/Vis (CH_2Cl_2): λ (lg ε) = 297 (4.17), 501 (4.45) nm. − UV/Vis (CH_3CN): λ (lg ε) = 296 (4.05), 354 (4.09), 471 (4.25) nm. − $C_{19}H_{12}BF_4MnO_3$ (430.0): calcd. C 53.07, H 2.81; found C 53.42, H 3.68.

Mixture of Manganese−Chromium Complexes 7a, 7b: A mixture of $(MeCN)_3Cr(CO)_3$ (0.83 g, 3.20 mmol) and **5** (0.85 g, 2.47 mmol) was dissolved in THF (50 mL) and the resulting solution was refluxed for 60 min The solvent was then removed in vacuo and the residue was extracted with dichloromethane. Purification by column chromatography on alumina (4% H_2O) eluting with petroleum ether/dichloromethane (4:1) afforded the mixture **7a/7b** as a red-brown solid. Yield: 0.74 g (62%). − MS (EI); *m*/*z* (%): 480 (21) [M^+], 424 (8) [M − 2CO]$^+$, 396 (46) [M − 3CO]$^+$, 368 (10) [M − 4CO]$^+$, 340 (69) [M − 5CO]$^+$, 312 (100) [M − 6CO]$^+$, 257 (87) [M − 6CO − Mn]$^+$, 205 (24) [M − 6CO − Mn − Cr]$^+$. − IR (KBr): ν (CO) = 2060, 2018, 1938 cm^{-1}. − $C_{22}H_{13}CrMnO_6$ (480.3): calcd. C 55.02, H 2.73; found C 55.60, H 3.08

Manganese−Chromium Benzosesquifulvalene Complex 8: At −78 °C, a solution of **7** (0.74 g, 1.54 mmol) in dichloromethane (10 mL) was treated with a solution of $(Ph_3C)BF_4$ (0.41 g, 1.24 mmol) in dichloromethane (5 mL). The reaction mixture was allowed to warm to room temperature, whereupon stirring was continued for a further 90 min. On addition of diethyl ether (90 mL), **8** was precipitated as orange-brown crystals and was collected by filtration. Yield: 0.55 g (79%). − ^{1}H NMR (CD_3CN, 250 MHz): δ = 7.64 (m, 2 H, C_6 ring: CH), 7.28 (m, 2 H, C_6 ring: CH), 6.74−6.50 (m, 6 H, C_7 ring: CH), 6.16 (s, 2 H, C_5 ring: CH). − ^{13}C NMR (CD_3CN, 100.4 MHz): δ = 225.40 (Cr−CO), 221.46 (Mn−CO), 129.21 (C_6 ring: CH), 125.99 (C_6 ring: CH), 119.45 (C_7 ring: C-1), 105.77 (C_7 ring: CH), 105.31 ($C_{5/6}$ ring: C), 104.85 (C_7 ring: CH), 102.07 (C_5 ring: C-1), 101.91 (C_7 ring: CH), 74.17 (C_5 ring: CH). − MS (FAB POS); *m*/*z* (%): 479 (66) [M^+], 423 (34) [M − 2CO]$^+$, 395 (85) [M − 3CO]$^+$, 259 (42), [M − 6CO − Cr]$^+$, 204 (63), [M − 6CO − Cr − Mn]$^+$. − IR (KBr): ν (CO) = 2012, 1923, 1873 cm^{-1}. − UV/Vis (CH_2Cl_2): λ (lg ε) = 321 (2.77), 486 (2.44) nm. − UV/Vis (CH_3CN): λ (lg ε) = 299 (3.38), 468 (2.86) nm. − $C_{22}H_{12}BCrF_4MnO_6$ (566.1): calcd. C 46.68, H 2.14; found C 45.32, H 2.65

X-ray Crystal Structure Analysis of 8:[39] $C_{22}H_{12}BCrF_4MnO_6$, M_r = 566.1, dark brown crystal, dimensions 0.65 × 0.25 × 0.20 mm, *a* = 16.486(3) Å, *b* = 7.992(1) Å, *c* = 17.548(5) Å, β = 102.60(2)°, *V* = 2256.4(8) Å^3, $\rho_{calcd.}$ = 1.666 g cm^{-3}, *F*(000) = 1128 e, μ = 9.173 mm^{-1}, no absorption correction applied, *Z* = 4, monoclinic, space group $P2_1/a$ (No. 14), λ = 1.54176 Å, *T* = 293 K, ω scans, 2850 reflections collected in the θ range between 2.58 and 59.94° (−18 ≤ *h* ≤ 17, 0 ≤ *k* ≤ 8, 0 ≤ *l* ≤ 19), 2834 observed reflections [$I \geq 2\sigma(I)$], 320 refined parameters, R = 0.0962, wR^2 = 0.2516, max. residual electron density 0.926 (−0.463) e Å^{-3}. Data were collected with an Enraf−Nonius Turbo-CAD4 diffractometer equipped with a rotating anode generator. Structure solution with SHELXS-86, structure refinement with SHELXL-93, graphics with ORTEP.

7-(Trimethylsilylethynyl)-1,3,5-cycloheptatriene (9): A solution of trimethylsilylacetylene (3.04 g, 30.0 mmol) in THF (10 mL) was treated with *n*-butyllithium (12.4 mL, 2.5 M solution in hexane, 31.0 mmol) at −40 °C. After stirring for 30 min at ambient temperature, the acetylide solution was added to a suspension of $(C_7H_7)BF_4$ (5.0 g, 28.1 mmol) in THF (100 mL) at −40 °C. The reaction mixture was stirred for 1 h at this temperature and then allowed to warm to room temperature, whereupon saturated NH_4Cl solution (100 mL) was added. The resulting mixture was extracted with diethyl ether (3 × 50 mL) and the combined extracts were dried over $MgSO_4$. Evaporation of the solvent and distillation of the residue at 0.07 mbar and 50−52 °C afforded **9** as a clear, yellowish oil. Yield: 4.36 g (82%). − ^{1}H NMR ($CDCl_3$, 200 MHz): δ = 6.63 (m, 2 H, 3,4-H), 6.18 (m, 2 H, 2,5-H), 5.33 (dd, 2 H, 1,6-H), 2.50 (tt, 1 H, 7-H), 0.20 (s, 9 H, $SiCH_3$). − ^{13}C NMR ($CDCl_3$, 50.3 MHz): δ = 130.9 (C-3,4), 124.6 (C-2,5), 123.0 (C-1,6), 108.0 (*C*≡C−$SiMe_3$), 84.5 (C≡*C*−$SiMe_3$), 32.6 (C-7), 0.1 ($SiCH_3$).

3-Ethynyl-1,3,5-cycloheptatriene (10): A solution of **9** (4.0 g, 21.2 mmol) in DMF (40 mL) was heated to 150 °C for 3 h. After evaporation of the solvent, the dark-brown concentrated reaction mixture was taken up in methanol and treated with a catalytic amount of KF (50 mg). The resulting mixture was stirred for 3 days at room temperature, then cooled to 0 °C, whereupon the product was separated by adding saturated NH_4Cl solution (60 mL). Extraction with diethyl ether (3 × 10 mL), drying of the combined extracts over $MgSO_4$, and careful removal of the solvent in vacuo afforded crude **10**, which could be obtained as a colorless liquid by distillation at 15 mbar. Yield: 1.52 g (62%). − ^{1}H NMR ($CDCl_3$, 400 MHz): δ = 6.95 (d, *J* = 6 Hz, 1 H, 4-H), 6.19 (d, *J* = 9 Hz, 1 H, 2-H), 6.17 (dd, *J* = 9 Hz, 6 Hz, 1 H, 5-H), 5.51 (dt, *J* = 9 Hz, 7 Hz, 1 H, 6-H), 5.39 (dt, *J* = 9 Hz, 7 Hz, 1 H, 1-H), 3.02 (s, 1 H, C≡CH), 2.28 (dd, *J* = 7 Hz, 7 Hz, 2 H, CH_2). − ^{13}C NMR ($CDCl_3$, 100.4 MHz): δ = 137.1 (C-4), 128.2 (C-2), 126.3 (C-5), 124.4 (C-3), 124.0 (C-6), 121.8 (C-1), 85.4 (*C*≡CH), 77.1 (C≡*C*H), 27.6 (C-7). − MS (EI); *m*/*z* (%): 116 (41) [M^+], 115 (100) [M − H]$^+$.

3-(Trimethylstannylethynyl)-1,3,5-cycloheptatriene (11): Me_3SnNMe_2 (1.8 g, 8.6 mmol) was added to **10** (1.0 g, 8.6 mmol) and the reaction mixture was stirred without a solvent for 5 min at ambient temperature. After evaporation of the Me_2NH formed, **11** was isolated in quantitative yield as a yellow-orange oil, which was suffi-

ciently pure for use in further reactions. – ^{1}H NMR ($CDCl_3$, 200 MHz): δ = 6.91 (d, 1 H, CH), 6.16 (d + dd, 2 H, CH), 5.44 (m, 2 H, CH), 2.28 (t, 2 H, CH_2), 0.31 ($SnCH_3$). – ^{13}C NMR ($CDCl_3$, 50.3 MHz): δ = 136.3, 128.5, 126.4 (CH), 125.7 (Sn−C≡C−*C*), 123.6, 121.8 (CH), 110.6, 93.3 (C≡C), 27.6 (CH_2), −7.7 ($SnCH_3$).

Manganese Complex 12: $(C_5H_4I)Mn(CO)_3$ (2.44 g, 7.39 mmol) and **11** (1.80 g, 6.45 mmol) were dissolved in DMF (50 mL) and $Pd(CH_3CN)_2Cl_2$ (60 mg) was added. The solution turned brown and stirring was continued for 12 h at room temperature. After the addition of diethyl ether (50 mL) followed by a solution of KF (750 mg) in water (25 mL), the mixture was stirred for 1 h while argon was bubbled through it. The organic phase was then separated and washed with water (3 × 100 mL). The combined aqueous phases were extracted with diethyl ether (2 × 50 mL) and the ethereal extracts were dried over $MgSO_4$. After removal of the solvent in vacuo, the crude product was purified by chromatography on silica (4% H_2O) eluting with petroleum ether/CH_2Cl_2 (10:1). Evaporation of the solvent from the appropriate fraction afforded **12** as a yellow oil, which solidified on storage in a refrigerator at 4 °C. Yield: 2.05 g (87%). – ^{1}H NMR ($CDCl_3$, 200 MHz): δ = 6.91 (d, 1 H, C_7 ring: CH), 6.18 (m, 2 H, C_7 ring: CH), 5.46 (m, 2 H, C_7 ring: CH), 5.00 (br. s, 2 H, C_5 ring: CH), 4.69 (br. s, 2 H, C_5 ring: CH), 2.31 (t, 2 H, CH_2). – ^{13}C NMR ($CDCl_3$, 50.3 MHz): δ = 224.3 (Mn−CO), 136.7, 127.8, 126.3 (C_7 ring: CH), 124.5 (C_7 ring: C-3), 124.1, 122.0 (C_7 ring: CH), 90.5 (C_5 ring: C-1), 86.0 (C_5 ring: CH), 83.1 (C≡C), 82.0 (C_5 ring: CH), 81.4 (C≡C), 27.6 (CH_2). – MS (EI); *m*/*z* (%): 318 (84) [M^+], 262 (71) [M − 2CO]$^+$, 234 (100) [M − 3CO]$^+$, 179 (62) [M − 3CO − Mn]$^+$. – IR(KBr): $\tilde{\nu}$ = 2222 (C≡C), 2021, 1932 (CO) cm^{-1}. – $C_{17}H_{11}MnO_3$ (318.2): calcd. C 64.17, H 3.48; found C 64.10, H 3.77.

Manganese−Chromium Complex 14: To a solution of **12** (1.0 g, 3.1 mmol) in THF (20 mL) was added $(CH_3CH_2CN)_3Cr(CO)_3$ (1.1 g, 3.8 mmol) as a solid. The mixture was stirred at ambient temperature for 3 days. After removal of the solvent in vacuo, the crude product was purified by chromatography on silica (4% H_2O) eluting with petroleum ether/CH_2Cl_2 (3:1). Evaporation of the solvent afforded **14** as an orange-red crystalline solid. Yield: 770 mg (55%). – ^{1}H NMR ($CDCl_3$, 200 MHz): δ = 6.29 (d, 1 H, C_7 ring: CH), 5.09 (s, 2 H, C_5 ring: CH), 5.00 (d, 1 H, C_7 ring: CH), 4.83 (t, 1 H, C_7 ring: CH), 4.74 (s, 2 H, C_5 ring: CH), 3.39 (m, 2 H, C_7 ring: CH), 2.95 (m, 1 H, 7-*endo*-H), 1.83 (dm, 1 H, 7-*exo*-H). – ^{13}C NMR ($CDCl_3$, 50.3 MHz): δ = 231.2 (Cr−CO), 224.1 (Mn−CO), 103.9, 100.7, 99.2 (C_7 ring: CH), 94.9 (C_7 ring: C-3), 89.5 (C_5 ring: C-1), 86.8, 86.6, 82.3, 82.2 (C_5 ring: diastereotopic CH), 81.1, 78.4 (C≡C), 57.5, 56.7 (C_7 ring: CH), 23.9 (CH_2). – MS (EI): *m*/*z* (%) = 454 (3) [M^+], 398 (3) [M − 2CO]$^+$, 370 (8) [M − 3CO]$^+$, 314 (6) [M − 5CO]$^+$, 286 (19) [M − 6CO]$^+$, 234 (27) [M − 6CO − Cr]$^+$, 179 (35) [M − 6CO − Mn − Cr]$^+$, 52 (100) Cr^+. – IR (KBr): ν (CO) = 2023, 1955, 1925, 1890 cm^{-1}. – $C_{20}H_{11}CrMnO_6$ (454.2): calcd. C 52.88, H 2.44; found C 52.06, H 2.65.

Manganese−Chromium Complex 15: A solution of **14** (0.50 g, 1.10 mmol) in dichloromethane (15 mL) was added dropwise to a stirred solution of $(Ph_3C)BF_4$ (0.33 g, 1.00 mmol) in dichloromethane (5 mL) at 0 °C. The resulting mixture was allowed to warm to room temperature and stirring was continued for 2 h. The reaction mixture was then poured into rapidly stirred diethyl ether (100 mL), which led to the precipitation of **15** as a dark-yellow, crystalline solid. Crystallization from dichloromethane afforded **15**·CH_2Cl_2 as red crystals. Yield: 535 mg (90%). – ^{1}H NMR (CD_2Cl_2, 200 MHz): δ = 6.76 (m, 2 H, C_7 ring: CH), 6.64 (m, 2 H, C_7 ring: CH), 6.49 (d, 2 H, C_7 ring: CH), 5.31 (m, 2 H, C_5 ring: CH), 4.88 (m, 2 H, C_5 ring: CH). – ^{13}C NMR (CD_2Cl_2, 50.3 MHz): δ = 224.2 (Cr−CO), 219.7 (Mn−CO), 107.1 (C_7 ring: C-1), 105.2 (C_7 ring: CH), 104.8 (C_7 ring: CH), 104.2 (C_7 ring: CH), 91.8 (C_5 ring: C-1), 89.6 (C_5 ring: CH), 85.4 (C≡C), 83.8 (C_5 ring: CH), 75.6 (C≡C). – MS (ESI): *m*/*z* (%) = 453 (100) [M^+], 369 (88) [M − 3CO]$^+$, 313 (100) [M − 5CO]$^+$, 285 (24) [M − 6CO]$^+$. – IR (KBr): $\tilde{\nu}$ = 2227 (C≡C), 2061, 2022, 1935 (CO) cm^{-1}. – UV/Vis (CH_2Cl_2): λ (lg ε) = 266 (4.24), 309 (4.18), 449 (3.74) nm. – UV/Vis (CH_3CN): λ (lg ε) = 300 (4.24), 334 (4.12), 429 (3.75) nm. – $C_{20}H_{10}BCrF_4MnO_6{\cdot}CH_2Cl_2$ (625.0): calcd. C 40.36, H 1.94; found C 39.83, H 1.82.

X-ray Crystal Structure Analysis of 15·CH_2Cl_2:[39] $C_{20}H_{10}BCrF_4MnO_6{\cdot}CH_2Cl_2$, M_r = 625.0, dark-red crystal, dimensions 0.30 × 0.15 × 0.05 mm, *a* = 20.387(1) Å, *b* = 7.354(1) Å, *c* = 32.882(1) Å, β = 96.12(1)°, *V* = 4901.8(7) Å^3, $\rho_{calcd.}$ = 1.694 g cm^{-3}, *F*(000) = 2480 e, μ = 12.42 cm^{-1}, absorption correction (0.707 ≤ *T* ≤ 0.941), *Z* = 8, monoclinic, space group $P2_1/n$ (No. 14), λ = 0.71073 Å, *T* = 198 K, ω and φ scans, 30148 reflections collected (±*h*, ±*k*, ±*l*), [(sinθ)/λ] = 0.65 Å^{-1}, 11195 independent (R_{int} = 0.041) and 8158 observed reflections [$I \geq 2\sigma(I)$], 649 refined parameters, *R* = 0.052, wR^2 = 0.127, max. residual electron density 1.17 (−1.08) e Å^{-3}, hydrogens calculated and refined as riding atoms, two chemically identical molecules with different conformations in the asymmetric unit. Data were collected with a Nonius KappaCCD diffractometer equipped with a rotating anode generator. Programs used: data acquisition COLLECT, data reduction DENZO-SMN, absorption correction SORTAV, structure solution SHELXS-86, structure refinement SHELXL-97, graphics DIAMOND.

Hyper Raleigh Scattering: For the experimental set-up, see ref.[34c] As the incident light source a Nd:YAG laser with a wavelength of 1064 nm was used. All measurements were made in dry CH_2Cl_2 or CH_3NO_2 with concentrations in the range 10^{-6} to 10^{-4} M and *p*-nitroaniline (*p*-NA) as a reference [$\beta_{p\text{-NA}}(CH_2Cl_2) = 21.6 \times 10^{-30}$ esu; $\beta_{p\text{-NA}}(CH_3NO_2) = 34.6 \times 10^{-30}$ esu]. The solutions were kept in darkness to prevent decomposition by daylight and were checked by recording UV/Vis spectra. An estimate of β absorption corrections was calculated as suggested in ref.[40] All compounds were checked for nonfluorescence by using interference filters of varying peak transmittance.[41]

Acknowledgments

This work was financially supported by the Deutsche Forschungsgemeinschaft (Ta 189/1-4,5) and the Fonds der Chemischen Industrie. M. T., T. B., and K. B. are grateful to Prof. Dr. F. E. Hahn for his generous support. The excellent technical assistance of D. Beck is also gratefully acknowledged.

[1] M. L. H. Green, D. K. P. Ng, *Chem. Rev.* **1995**, *95*, 439.
[2] [2a] W. Beck, B. Niemer, M. Wieser, *Angew. Chem.* **1993**, *105*, 969; *Angew. Chem. Int. Ed. Engl.* **1993**, *32*, 923. – [2b] S. Barlow, D. O'Hare, *Chem. Rev.* **1997**, *97*, 637. – [2c] D. Astruc, *Acc. Chem. Res.* **1997**, *30*, 383.
[3] For recent work, see: [3a] R. Boese, J. K. Cammack, A. J. Matzger, K. Pflug, W. B. Tolman, K. P. C. Vollhardt, T. W. Weidman, *J. Am. Chem. Soc.* **1997**, *119*, 6757. – [3b] P. A. McGovern, K. P. C. Vollhardt, *Chem. Commun.* **1996**, 1593. – [3c] I. Kovács, M. C. Baird, *Organometallics* **1996**, *15*, 3588. – [3d] D. S. Brown, M. H. Delville, K. P. C. Vollhardt, D. Astruc, *Organometallics* **1996**, *15*, 2360. – [3e] I. Kovács, M. C. Baird, *Organometallics* **1995**, *14*, 5469. – [3f] R. C. Kerber, B. Waldbaum, *Organometallics* **1995**, *14*, 4742. – [3g] I. Kovács, M. C. Baird, *Organometallics* **1995**, *14*, 4084. – [3h] I. Kovács, M. C. Baird, *Organometallics* **1995**, *14*, 4074. – [3i] T. T. Chin, W. E.

Geiger, *Organometallics* **1995**, *14*, 1316. – [3j] M. Tilset, K. P. C. Vollhardt, R. Boese, *Organometallics* **1994**, *13*, 3146. – [3k] D. S. Brown, M.-H. Delville-Desbois, R. Boese, K. P. C. Vollhardt, D. Astruc, *Angew. Chem.* **1994**, *106*, 715; *Angew. Chem. Int. Ed. Engl.* **1994**, *33*, 661. – [3l] A. P. Kahn, R. Boese, J. Blümel, K. P. C. Vollhardt, *J. Organomet. Chem.* **1994**, *472*, 149. – [3m] C. G. Kreiter, W. Conrad, R. Exner, *Z. Naturforsch.* **1993**, *48b*, 1635. – [3n] H. El Amouri, J. Vaissermann, Y. Besace, K. P. C. Vollhardt, G. E. Ball, *Organometallics* **1993**, *12*, 605. – [3o] R. Boese, M. A. Huffman, K. P. C. Vollhardt, *Angew. Chem.* **1991**, *103*, 1542; *Angew. Chem. Int. Ed. Engl.* **1991**, *30*, 1463.

[4] For earlier work, see: P. A. McGovern, K. P. C. Vollhardt, *Synlett* **1990**, 493.

[5] [5a] S. S. Lee, T.-Y. Lee, J. E. Lee, I. S. Lee, Y. K. Chung, M. S. Lah, *Organometallics* **1996**, *15*, 3664. – [5b] D. T. Pierce, W. E. Geiger, *Inorg. Chem.* **1994**, *33*, 373. – [5c] W. E. Geiger, N. Van Order, Jr., D. T. Pierce, T. E. Bitterwolf, A. L. Rheingold, N. D. Chasteen, *Organometallics* **1991**, *10*, 2403. – [5d] T. E. Bitterwolf, K. S. Raghuveer, *Inorg. Chim. Acta* **1990**, *172*, 59. – [5e] K.-D. Plitzko, G. Wehrle, B. Gollas, B. Rapko, J. Dannheim, V. Boekelheide, *J. Am. Chem. Soc.* **1990**, *112*, 6556. – [5f] C. Elschenbroich, J. Heck, W. Massa, M. Birkhahn, *Chem. Ber.* **1990**, *123*, 2321. – [5g] N. Van Order, Jr., W. E. Geiger, T. E. Bitterwolf, A. L. Rheingold, *J. Am. Chem. Soc.* **1987**, *109*, 5680. – [5h] T. E. Bitterwolf, *J. Organomet. Chem.* **1980**, *252*, 305. – [5i] C. Elschenbroich, J. Heck, *J. Am. Chem. Soc.* **1979**, *101*, 6773.

[6] R. L. Beddoes, E. S. Davies, M. W. Whiteley, *J. Chem. Soc., Dalton Trans.* **1995**, 3231.

[7] W. K. Schenk, R. Kyburz, M. Neuenschwander, *Helv. Chim. Acta* **1975**, *58*, 117.

[8] [8a] M. Tamm, A. Grzegorzewski, I. Brüdgam, *J. Organomet. Chem.* **1996**, *519*, 217. – [8b] M. Tamm, A. Grzegorzewski, T. Steiner, T. Jentzsch, W. Werncke, *Organometallics* **1996**, *15*, 4984.

[9] U. Behrens, H. Brussard, U. Hagenau, J. Heck, E. Hendrickx, J. Körnich, J. G. M. van der Linden, A. Persoons, A. L. Spek, N. Veldman, B. Voss, H. Wong, *Chem. Eur. J.* **1996**, *2*, 98.

[10] M. Tamm, A. Grzegorzewski, T. Steiner, *Chem. Ber./Recueil* **1997**, *130*, 225.

[11] [11a] W. Nie, *Adv. Mater.* **1993**, *5*, 520. – [11b] S. R. Marder, J. W. Perry, *Adv. Mater.* **1993**, *5*, 804. – [11c] D. R. Kanis, M. A. Ratner, T. J. Marks, *Chem. Rev.* **1994**, *94*, 195. – [11d] T. J. Marks, M. A. Ratner, *Angew. Chem.* **1995**, *107*, 167; *Angew. Chem. Int. Ed. Engl.* **1995**, *34*, 155.

[12] [12a] N. J. Long, *Angew. Chem.* **1995**, *107*, 37; *Angew. Chem. Int. Ed. Engl.* **1995**, *34*, 6. – [12b] I. R. Whittal, A. M. McDonagh, M. G. Humphrey, M. Samoc, *Adv. Organomet. Chem.* **1998**, *42*, 291. – [12c] I. R. Whittal, A. M. McDonagh, M. G. Humphrey, M. Samoc, *Adv. Organomet. Chem.* **1998**, *43*, 349.

[13] [13a] M. Tamm, T. Jentzsch, W. Werncke, *Organometallics* **1997**, *16*, 1418. – [13b] M. Tamm, A. Grzegorzewski, I. Brüdgam, H. Hartl, *Chem. Commun.* **1997**, 2227. – [13c] M. Tamm, A. Grzegorzewski, I. Brüdgam, H. Hartl, *J. Chem. Soc., Dalton Trans.* **1998**, 3523−3528.

[14] [14a] C. Lo Sterzo, M. M. Miller, J. K. Stille, *Organometallics* **1989**, *8*, 2331. – [14b] C. Lo Sterzo, J. K. Stille, *Organometallics* **1990**, *9*, 687. – [14c] D. Guillaneux, H. B. Kagan, *J. Org. Chem.* **1995**, *60*, 2502.

[15] C. Janiak, H. Schumann, *Adv. Organomet. Chem.* **1991**, *33*, 331.

[16] [16a] J. D. White, T. Furuta, M. McCamish, *Synth. Commun.* **1973**, *3*, 425. – [16b] H. Prinzbach, D. Seip, G. Englert, *Liebigs Ann. Chem.* **1966**, *698*, 57. – [16c] H. Prinzbach, D. Seip, L. Knothe, W. Faisst, *Liebigs Ann. Chem.* **1966**, *698*, 34. – [16d] H. Prinzbach, *Pure Appl. Chem.* **1971**, *28*, 281. – [16e] H. Prinzbach, H. Knöfel, *Angew. Chem.* **1969**, *81*, 900; *Angew. Chem. Int. Ed. Engl.* **1969**, *8*, 881.

[17] A. Roberts, M. W. Whiteley, *J. Organomet. Chem.* **1993**, *458*, 131.

[18] M. Stähle, R. Lehmann, J. Kramar, M. Schlosser, *Chimia* **1985**, *39*, 229.

[19] [19a] M. Enders, R. Rudolph, H. Pritzkow, *Chem. Ber.* **1996**, *129*, 459. – [19b] H. Plenio, D. Burth, *Organometallics* **1996**, *15*, 1151.

[20] F. A. Carey, R. J. Sundberg, *Organische Chemie* (Eds.: H. J. Schäfer, D. Hoppe, G. Erker), VCH, Weinheim, **1995**, p. 1134.

[21] [21a] T. Imamoto, T. Kusumoto, Y. Tawarayama, Y. Sugiura, T. Mita, Y. Hatanaka, M. Yokohama, *J. Org. Chem.* **1984**, *49*, 3904. – [21b] C. R. Johnson, B. D. Tait, *J. Org. Chem.* **1987**, *52*, 281.

[22] T. E. Ready, J. C. Chien, M. D. Rausch, *J. Organomet. Chem.* **1996**, *519*, 21.

[23] J. K. Stille, *Angew. Chem.* **1986**, *98*, 504; *Angew. Chem. Int. Ed. Engl.* **1986**, *25*, 508.

[24] W. J. Scott, G. T. Crisp, J. K. Stille, *J. Am. Chem. Soc.* **1984**, *106*, 4630.

[25] [25a] J. L. Mascareñas, L. A. Sarandeses, L. Castedo, A. Mouriño, *Tetrahedron* **1991**, *47*, 3485. – [25b] J. McMurry, W. J. Scott, *Tetrahedron Lett.* **1983**, *24*, 979. – [25c] P. J. Stang, M. Hanack, L. R. Subramanian, *Synthesis* **1982**, 85.

[26] E. W. Abel, G. Wilkinson, *J. Chem. Soc.* **1959**, 1501.

[27] H. Wadepohl, W. Galm, H. Pritzkow, *Organometallics* **1996**, *15*, 570 and references cited therein.

[28] [28a] P. Bönzil, M. Neuenschwander, P. Engel, *Helv. Chim. Acta* **1990**, *73*, 1685. – [28b] G. Cavicchio, G. Gaudiano, P. P. Ponti, *Tetrahedron Lett.* **1980**, *21*, 2333.

[29] L. Guo, J. D. Bradshaw, C. A. Tessier, W. J. Youngs, *J. Chem. Soc., Chem. Commun.* **1994**, 243.

[30] T. Asao, M. Oda in *Methoden der Organischen Chemie (Houben-Weyl)*, vol. V/2c (Ed.: H. Kropf), Georg Thieme Verlag, Stuttgart, **1985**, p. 49, and references cited therein.

[31] The ^{1}H NMR spectrum (CD_3CN) of $[(C_7H_7)Cr(CO)_3]BF_4$ features one resonance at $\delta = 6.52$.

[32] M. S. Paley, J. M. Harris, H. Looser, J. C. Baumert, G. C. Bjorklund, D. Jundt, R. J. Twieg, *J. Org. Chem.* **1989**, *54*, 3774.

[33] [33a] C. Reichardt, *Chem. Rev.* **1994**, *94*, 2319. – [33b] C. Reichardt, *Solvents and Solvent Effects in Organic Chemistry*, VCH, Weinheim, **1988**. – [33c] H. G. O. Becker, *Einführung in die Photochemie*, Deutscher Verlag der Wissenschaften, Berlin, **1991**.

[34] [34a] E. Hendrickx, K. Clays, A. Persoons, C. Dehu, J. L. Brédas, *J. Am. Chem. Soc.* **1995**, *117*, 3547. – [34b] K. Clays, A. Persoons, *Phys. Rev. Lett.* **1991**, *66*, 2980. – [34c] K. Clays, A. Persoons, *Rev. Sci. Instrum.* **1992**, *63*, 3285.

[35] J. L. Oudar, D. S. Chemla, *J. Chem Phys.* **1977**, *66*, 2664.

[36] [36a] P. Nguyen, G. Lesley, T. B. Marder, I. Ledoux, J. Zyss, *Chem. Mater.* **1997**, *9*, 406. – [36b] L.-T. Cheng, W. Tam, S. H. Stevenson, G. R. Meredith, G. Rikken, S. R. Marder, *J. Phys. Chem.* **1991**, *95*, 10631. – [36c] L.-T. Cheng, W. Tam, S. R. Marder, A. E. Stiegman, G. Rikken, C. W. Spangler, *J. Phys. Chem.* **1991**, *95*, 10643.

[37] W. P. Fehlhammer, W. A. Herrmann, K. Öfele in *Handbuch der Präparativen Anorganischen Chemie* (Ed.: G. Brauer), Ferdinand Enke Verlag, Stuttgart, **1981**, vol. 3, p. 1866 and p. 2020.

[38] G. J. Kubas, L. S. van der Sluys, *Inorg. Synth.* **1990**, *28*, 29.

[39] Crystallographic data (excluding structure factors) for the structures reported in this paper have been deposited with the Cambridge Crystallographic Data Centre as supplementary publication nos. CCDC-133372 (**15**·CH_2Cl_2) and CCDC-133373 (**8**). Copies of the data can be obtained free of charge on application to The Director, CCDC, 12 Union Road, Cambridge CB2 1EZ, UK [Fax: (internat.) +44-1223/336033, E-mail: deposit@ccdc.cam.ac.uk].

[40] W. M. Laidlaw, R. G. Denning, T. Verbiest, E. Chauchard, A. Persoons, *Nature* **1993**, *363*, 58.

[41] J. Heck, S. Dabek, T. Meyer-Friedrichsen, H. Wong, *Coord. Chem. Rev.* **1999**, *190−192*, 1217.

Received September 6, 1999
[I99319]

Dissociation Patterns of Small $Fe_mO_n^+$ (m = 1–4, $n \leq 6$) Cluster Cations Formed Upon Chemical Ionization of $Fe(CO)_5/O_2$ Mixtures

Detlef Schröder,[a] Phillip Jackson,[a] and Helmut Schwarz*[a]

Keywords: Clusters / Iron oxides / Mass spectrometry / Metal peroxides / Oxidation

The collisional activation mass spectra of cationic iron oxide clusters $Fe_mO_n^+$ (m = 1–4, $n \leq 6$) prepared by chemical ionization of $Fe(CO)_5/O_2$ mixtures show remarkable trends in the fragmentation behaviors, which can be attributed to the formal oxidation states of iron. (i) The preferential fragmentation pathways of $Fe_mO_n^+$ clusters with $m/n \geq 1$ correspond to losses of atomic oxygen as well as FeO units. (ii) For $Fe_mO_n^+$ clusters with $1 > m/n > 2/3$, losses of neutral FeO_2 begin to compete with those of O and FeO. (iii) For FeO_2^+ and the oxygen-rich clusters $Fe_2O_3^+$ and $Fe_4O_6^+$ (m/n = 2/3), losses of molecular oxygen predominate, while this channel is more or less irrelevant for the other $Fe_mO_n^+$ cations. These observations are interpreted using peroxide structures for the oxygen-rich $Fe_mO_n^+$ ions, thereby preventing the need for formal high-valent iron(IV) in these clusters.

Introduction

Ionic iron oxide clusters $Fe_mO_n^{+/-}$ can be generated by sputtering neutral iron oxide,[1,2] by seeding Smalley-type expansion sources for iron clusters with oxygen,[3–5] or by reacting cationic Fe_m^+ clusters with suitable oxidants.[6–10] As far as cations are concerned, most of these methods are restricted to metal-rich clusters with $m/n \geq 1$, i.e. clusters containing iron in formal oxidation states up to Fe^{III}. High-valent metal-oxo species that are potentially attractive as oxidants (e.g. the dinuclear Fe^{IV} oxide core of methane monooxygenase)[11,12] are usually not formed.

A viable approach for synthesizing oxygen-rich Fe/O clusters in the gas phase is by means of redox reactions, which we refer to hereafter as the chemical route to metal-oxide clusters.[6,13] Upon chemical ionization of a mixture of $Fe(CO)_5$ with an excess of oxygen, a complex sequence of reactions occurs that ultimately leads to the formation of oxygen-rich $Fe_mO_n^+$ clusters [see Equations (1) – (5)].

Ionization

$$O_2 + e \rightarrow O_2^+ + 2e \quad (1)$$

Charge transfer

$$Fe(CO)_5 + O_2^+ \rightarrow Fe(CO)_n^+ + nCO + O_2 \quad (2)$$

Clustering

$$Fe(CO)_n^+ + Fe(CO)_5 \rightarrow Fe_2(CO)_m^+ + (5 + n - m)CO \quad (3)$$

Oxidation

$$Fe_2(CO)_m^+ + O_2 \rightarrow Fe_2O(CO)_p^+ + CO_2 + (m - p - 1)CO \quad (4)$$

$$Fe_2O(CO)_p^+ + O_2 \rightarrow Fe_2O_2^+ + CO_2 + (p - 1)CO \quad (5)$$

[a] Institut für Organische Chemie der Technischen Universität Berlin,
Straße des 17. Juni 135, D-10623 Berlin
Fax: (internat.) + 49-30/314 21102
E-mail: df@www.chem.tu-berlin.de

Let us illustrate this manifold by describing a plausible route for the formation of $Fe_2O_2^+$ as an example. The sequence starts with electron ionization of O_2 as the major component of the neutral mixture [Equation (1)], followed by (dissociative) charge transfer to yield iron-carbonyl cations [Equation (2)]. These ions then undergo clustering with neutral $Fe(CO)_5$ to afford dinuclear iron-carbonyl clusters [Equation (3)],[6,14,15] followed by stepwise oxidation of the clusters by dioxygen [Equations (4) and (5)].[6,16] Side reactions lead to $Fe_2O_3^+$ and trace amounts of Fe_2O^+ (see below). Similarly, higher $Fe_mO_n^+$ clusters are accessible through this scheme, and their abundances very much depend on the $Fe(CO)_5/O_2$ mixing ratios and other ionization parameters such as overall pressure, repeller voltage etc. Under typical CI conditions, reasonably intense signals can be achieved for (i) FeO^+ and FeO_2^+, (ii) $Fe_2O_2^+$ and $Fe_2O_3^+$, (iii) $Fe_3O_3^+$ and $Fe_3O_4^+$, as well as (iv) $Fe_4O_4^+$, $Fe_4O_5^+$, and $Fe_4O_6^+$ (Table 1). More abundant Fe_2O^+ fluxes than those obtained by chemical ionization of $Fe(CO)_5/O_2$ can be achieved by electron ionization of dicyclopentadienyldinitrosyldiiron $[Cp_2Fe_2(NO)_2]$.[17]

Results and Discussion

The $Fe_mO_n^+$ cations were probed by their collisional activation (CA) mass spectra (Table 1); the results for the mononuclear species FeO^+ and FeO_2^+ are presented for comparative purposes only and are not discussed.[18] While the fragmentation patterns of the $Fe_mO_n^+$ clusters appear rather complex at the first inspection, some insightful aspects are revealed if the formal oxidation state of iron is considered as an additional parameter. In this formalism, we assume that oxygen acts as a strict two-electron acceptor, i.e. O^{2-}, count the positive charge as additional valence, and avoid split valencies of the atoms. For example, we assign Fe_2O^+ as containing one Fe^I and one Fe^{II}; it is thus denoted as Fe^I/Fe^{II}. Accordingly, $Fe_2O_2^+$ is Fe^{II}/Fe^{III},

 © WILEY-VCH Verlag GmbH, D-69451 Weinheim, 2000 1434–1948/00/0606–1171 $ 17.50+.50/0

Table 1. Representative neutral losses and mass differences (in amu) observed in the CA mass spectra of $Fe_mO_n^+$ clusters formed by CI of $Fe(CO)_5/O_2$ mixtures.

[a][b]	averaged valence[c]	O –16	O_2 –32	Fe –56	FeO –72	FeO_2 –88	FeO_3 –104	Fe_2O_2 –144	Fe_2O_3 –160	Fe_2O_4 –176	Fe_3O_3 –216	Fe_3O_4 –232
FeO^+	3.0	100										
FeO_2^+	5.0[d]	50	100		1							
Fe_2O^+[e]	1.5	60		25	100							
$Fe_2O_2^+$	2.5	100	10	2	8	40						
$Fe_2O_3^+$	3.5	40	100		1	3	5					
$Fe_3O_3^+$	2.33	60	3		100	45	5					
$Fe_3O_4^+$	3.0	100	12		2	20	8			1		
$Fe_4O_4^+$	2.25	5	1		100	5		25	15	5	4	10
$Fe_4O_5^+$	2.75	65	8		2	100	5	8	1			
$Fe_4O_6^+$	3.25	8	100		1	2	15			5		

[a] Formal assignments of the elemental compositions. For example, loss of FeO_3 could also correspond to FeO + O_2, FeO_2 + O, FeO + 2 O etc. – [b] Intensities given relative to the base peaks = 100%. For the sake of clarity, some minor fragments below 5% are omitted. – [c] See text for the formalism. – [d] For discussions of the structural dichotomy of $[Fe,O_2]^{0/+}$, see refs.[18,27]. – [e] Fe_2O^+ is formed in only minor amounts upon CI of $Fe(CO)_5/O_2$ mixtures; $Cp_2Fe_2(NO)_2$ was instead used as precursor.[17]

$Fe_2O_3^+$ is Fe^{III}/Fe^{IV}, $Fe_3O_3^+$ is 2 Fe^{II}/Fe^{III}, etc. The corresponding net oxidation states of the iron atoms in the clusters are 1.5 in Fe_2O^+, 2.5 in $Fe_2O_2^+$, 3.5 in $Fe_2O_3^+$, and 2.3 in $Fe_3O_3^+$.

Using this formalism, the fragmentation patterns can be categorized as follows. (i) For low-valent $Fe_mO_n^+$ clusters ($m/n \geq 1$), losses of FeO prevail, (ii) for $Fe_mO_n^+$ species with $1 > m/n > 2/3$, loss of FeO_2 begins to compete, and (iii) for $Fe_mO_n^+$ ions with $m/n = 2/3$, i.e. $Fe_2O_3^+$ and $Fe_4O_6^+$, loss of molecular oxygen is the dominant pathway. While these patterns can be deduced from Table 1, a more obvious representation is provided by Figure 1, in which only the fractional losses of FeO, FeO_2, and O_2 are considered. Loss of atomic oxygen is not regarded as structurally characteristic and, moreover, it is likely to be overestimated in collisional activation employing kilo electron-volt energies because momentum transfer in high-energy collisions and collection efficiencies favor observation of fragments due to losses of light neutrals.

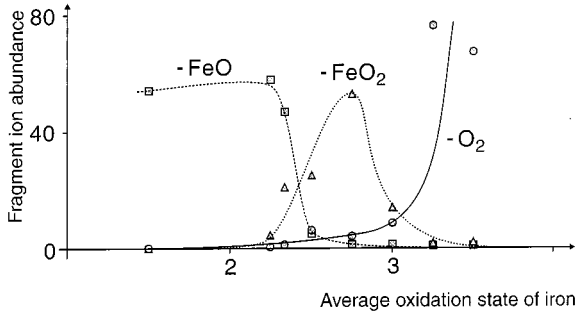


Figure 1. Normalized intensities of FeO (■), FeO_2 (▲), and O_2 (•) losses from $Fe_mO_n^+$ clusters as a function of the averaged oxidation state of the iron atoms; the lines serve just as a guide. Normalization is made to the sum of all fragments observed and the oxidation states are calculated as outlined in the text; for example, a formal oxidation state of 2.5 is attributed to $Fe_2O_2^+$, i.e. Fe^{II}/Fe^{III} that is one Fe^{II} and one Fe^{III}.

Unlike the iron-rich $Fe_mO_n^+$ clusters with $m > n$ studied by Armentrout and co-workers,[7,9] expulsion of neutral iron atoms (or Fe_n aggregates) is rarely observed for the ions under study. Expulsion of FeO units from the low-valent species is formally associated with preservation of the oxidation states of the remaining metal atoms while increasing the average, e.g. loss of the iron(II) compound FeO from $Fe_4O_4^+$ to afford $Fe_3O_3^+$ leads from $3Fe^{II}/Fe^{III}$ to $2Fe^{II}/Fe^{III}$. If we assign neutral FeO_2 to formal iron(IV),[19,20] loss of this neutral corresponds to a disproportionation of the oxidation states between ions and neutrals. In this formalism, losses of molecular oxygen correspond to four-electron reductions of the clusters.

Energetics

The fragmentations observed in the CA spectra cannot directly be related to the associated thermochemical thresholds of the respective channels because collisions occurring in the kilo electronvolt regime do not sample equilibrium. Nevertheless, some correlations can be seen for those clusters for which additional thermochemical information is available.[21]

For example, the predominance of FeO loss from Fe_2O^+ over those of O and Fe, respectively, is consistent with the thermochemistry of the fragments; expressed as sums of heats of formations these are $\Sigma\Delta_fH(Fe^+ + FeO) = 338$ kcal/mol, $\Sigma\Delta_fH(Fe_2^+ + O) = 375$ kcal/mol, and $\Sigma\Delta_fH(FeO^+ + Fe) = 360$ kcal/mol.[21] Similarly, the prevalence of FeO_2 over FeO losses from $Fe_2O_2^+$ is in keeping with the thermochemical thresholds of these channels, i.e. $\Sigma\Delta_fH(FeO^+ + FeO) = 318$ kcal/mol versus $\Sigma\Delta_fH(Fe^+ + FeO_2) = 297$ kcal/mol; note that the base peak due to loss of an O atom has an energy demand of $\Sigma\Delta_fH(Fe_2O^+ + O) = 314$ kcal/mol. Likewise, the competition of FeO and FeO_2 losses for $Fe_3O_3^+$ [Equations (6) and (7)] is consistent with the thermochemical information available. Thus, $D(OFe_2^+–O) \approx D(Fe_2^+–O)$[8] and $D(Fe_2^+–O) = 119 \pm 3$ kcal/mol[7,9] in conjunction with $\Delta_fH(FeO) = 57 \pm 3$ kcal/mol and two nicely consistent values of $\Delta_fH(FeO_2) = 18 \pm 5$ kcal/mol[22] and 15 ± 3 kcal/mol,[3,23,24] respectively, imply $\Sigma\Delta_fH(Fe_2O_2^+ + FeO) = 253$ kcal/mol and $\Sigma\Delta_fH(Fe_2O^+ + FeO_2) = 272$ kcal/mol. Even though the energetics for $Fe_3O_3^+$ are undetermined, these values suggest a difference of about 20 kcal/mol in favor of Equation (6), which is in

accord with the observed preference for this channel in the CA spectrum of $Fe_3O_3^+$.

$$Fe_3O_3^+ \rightarrow Fe_2O_2^+ + FeO \quad (6)$$

$$Fe_3O_3^+ \rightarrow Fe_2O^+ + FeO_2 \quad (7)$$

$$Fe_3O_3^+ \rightarrow Fe_3O^+ + O_2 \quad (8)$$

Interestingly, while loss of dioxygen from $Fe_3O_3^+$ according to Equation (8) has a comparable energy demand, $\Sigma\Delta_f H(Fe_3O^+ + O_2) = 269$ kcal/mol, this channel is hardly observed experimentally (Table 1). Hence, the absence (or occurrence) of O_2 loss is subject to kinetic rather than thermodynamic restrictions. Thereby, it could reflect structural motifs of the ionic species being probed. We note in passing that, although conceivable, loss of two O atoms instead of molecular oxygen in Equation (8) is much more energy demanding [$\Sigma\Delta_f H(Fe_3O^+ + 2O) = 387$ kcal/mol]. Thus, sequential oxygen-atom loss is not considered to play a major role in the experimentally observed fragmentation pattern.

Structures

Unambiguous conclusions about the geometric structures of the $Fe_mO_n^+$ clusters cannot be derived from the fragmentation patterns; for example, already eight different isomers need to be considered for the four-atomic, neutral Fe_2O_2 cluster.[25] However, it is precisely the loss of molecular oxygen that at least provides intuitive guides to the possible cluster structures generated. Specifically, intense dioxygen losses observed for oxygen-rich $Fe_2O_3^+$ and $Fe_4O_6^+$ species imply the presence of peroxide units in these clusters while this motif is less likely in the other clusters. Here, the term "peroxide unit" only refers to the presence of O–O bonds in the cluster; whether these are best described as μ^2 peroxo ligands or η^1/η^2 dioxygen complexes is a matter of spin coupling,[18,20,26] which is presently unknown for the cationic $Fe_mO_n^+$ clusters studied here.

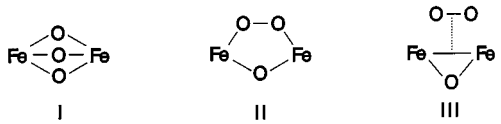
Another, indirect indication of peroxidic structures for $Fe_2O_3^+$ and $Fe_4O_6^+$ is the complete absence of $Fe_3O_5^+$ upon chemical ionization of $Fe(CO)_5/O_2$ mixtures; putative $Fe_3O_5^+$ (250 amu) turns out to be exclusively [$Fe_3O_5H_2^+$] (252 amu) containing one ^{54}Fe isotope; most probably $Fe_3O_4^+ \cdot H_2O$. A possible rationale for these observations is that, among the ions formed in the CI plasma, $Fe_2O(CO)^+$ and $Fe_4O_4(CO)^+$, but not $Fe_3O_3(CO)^+$, are observed. These iron oxide carbonyl clusters are in turn likely to serve as precursors for the formation of $Fe_2O_3^+$ and $Fe_4O_6^+$, respectively, by exchange of the CO ligand by dioxygen; a reaction that also occurs for the mononuclear species, i.e. $Fe(CO)^+ + O_2 \rightarrow FeO_2^+ + CO$.[18] Absence of $Fe_3O_3(CO)^+$ as a precursor can account for the failure to generate $Fe_3O_5^+$ in the $Fe(CO)_5/O_2$ plasma. In turn, the presence of O−O bonds in $Fe_2O_3^+$ and $Fe_4O_6^+$ is implied. Thus, we suggest that $Fe_2O_3^+$ is, for example, formed in Equation (9) from an intermediate carbonyl cluster, i.e. the ligand replacement in Equation (9) competes with the oxidation of the cluster according to Equation (5).

$$Fe_2O(CO)^+ + O_2 \rightarrow Fe_2O_3^+ + CO \quad (9)$$

Oxidation States and Fragmentation Routes

In the series of oxygen-deficient $Fe_mO_n^+$ clusters studied as transients by Armentrout and co-workers,[7,9,10] losses of Fe and Fe_2 units prevailed. In terms of the net oxidation state, these evaporations of neutral Fe units increase the formal cluster valencies, e.g. $Fe_5O_2^+ \rightarrow Fe_3O_2^+ + Fe_2$ leads from an averaged oxidation state of 1.0 in the reactant to 1.67 in the product Fe/O cluster. For the $Fe_mO_n^+$ clusters with $m = n$, our results show preferential losses of the iron(II) compound FeO, e.g. $Fe_3O_3^+ \rightarrow Fe_2O_2^+ + FeO$ corresponds to an increase of the formal valence state from 2.33 in the reactant to 2.5 in the Fe/O cluster formed while the oxidation states of the atoms remain unchanged in reactants and products, i.e. both $2Fe^{II}/Fe^{III}$.

Loss of neutral FeO_2 from the clusters with $m < n$ corresponds to a formal disproportionation of valencies, e.g. from 2.5 in $Fe_2O_2^+$ to 1.0 in the ionic product Fe^+ and 4.0 in neutral FeO_2. Consideration of formal oxidation states also provides a rationale for the switch from FeO to FeO_2 loss upon increasing oxygen content. For example, loss of FeO from $Fe_3O_4^+$ would lead to $Fe_2O_3^+$, which has a high-valent iron(IV) or bearing a peroxidic O−O bond, both features that are considered energetically demanding. Instead, disproportionation with concomitant loss of neutral FeO_2 leads to $Fe_2O_2^+$, an Fe/O cluster with reasonably strong Fe−O bonds.[7–9]

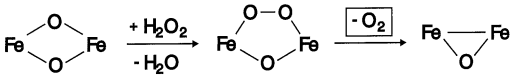


Scheme 1

The oxygen-rich $Fe_mO_n^+$ clusters with $m/n = 2/3$ show preferential losses of molecular oxygen. If these clusters were indeed oxide and not peroxide clusters, high-valent iron(IV) would be present, e.g. Fe^{III}/Fe^{IV} for structure **I** of $Fe_2O_3^+$ (Scheme 1). Involvement of peroxidic structures enables iron to adopt lower oxidation states. For example, the formal valencies in the bridged peroxide **II** are Fe^{II}/Fe^{III} and only Fe^{I}/Fe^{II} in the corresponding dioxygen complex **III**. The avoidance of high valencies is consistent with the mode of generation as well as the fragmentation behavior observed in the experiments. Hence, we suggest that oxygen-rich Fe/O clusters trade-off high oxidation states and prefer the formation of peroxo units instead.

From a conceptual point of view, the formation of peroxo units in the oxygen-rich Fe/O clusters and the associated ability to release molecular oxygen suggest a catalase activity of polynuclear Fe/O clusters. That is, instead of forming

high-valent iron-oxo species with hydrogen peroxide, Fe/O clusters can mediate the disproportionation of H_2O_2 into H_2O and 1/2 O_2 via peroxidic metal clusters as intermediates (Scheme 2). In particular, the near degeneracy of low-lying electronic states of different multiplicities in transition metal oxide clusters may counter the spin problem associated with the release of O_2 in its triplet ground state.[27,28] We will continue to address these points in the context of studies of the catalytic activation of peroxides by transition metals in the gas phase.[29,30]



Scheme 2

As demonstrated in this study, collisional activation of cationic Fe/O clusters can provide qualitative insights into structural features, i.e. the presence of O−O bonds, but definitely not more than that. In particular, no precise information about the bonding schemes, e.g. symmetric versus antisymmetric clusters, presence of Fe−Fe bonds, nature of the bridging ligands etc., not to mention spin states, can be discerned. Nevertheless, these kinds of phenomenological studies of transition metal oxide clusters will continue to be important for the time being due to inadequacies of otherwise powerful theoretical methods. While recent applications of density functional theory have proven rather promising for mononuclear iron compounds,[31] there are grave difficulties for these methods in the treatment of coordinatively unsaturated transition metal oxide clusters.[11,12,25]

Experimental Section

The experiments were performed with a modified VG ZAB/HF/AMD 604 four-sector mass spectrometer of BEBE configuration, which has been described elsewhere.[32] The $Fe_mO_n^+$ cations were generated as described above by chemical ionization (CI) of mixtures of $Fe(CO)_5$ and oxygen in ratios varying from ca. 1:5 to 1:50. We note in passing that chemical ionization of mixtures containing high concentrations of oxygen drastically reduces the lifetimes of the tungsten filaments used in the ion source from months (or even years) to a few hours. Better yields of Fe_2O^+ were obtained by electron ionization of $Cp_2Fe_2(NO)_2$.[17] After acceleration to a kinetic energy of 8 keV, the ions of interest were mass-selected using B(1) and E(1) at mass resolutions $m/\Delta m$ between 3000 and 5000. Collisional activation (CA) in the field-free region between E(1) and B(2) was affected using oxygen at 80% transmittance of the incident ion beam. The fragmentation products were scanned using B(2), detected, on-line processed, and accumulated using the AMD/Intectra data system.

An inherent interference for $Fe_mO_n^+$ cations formed upon CI of $Fe(CO)_5/O_2$ mixtures are the carbonyl clusters of the type $Fe_{m-1}(CO)_2O_n^+$, because Fe and 2CO have the same nominal mass (both 56 amu). These interferences are readily apparent as characteristic losses of carbon monoxide (28 amu) in the CA mass spectra, and such losses are not observed for pure $Fe_mO_n^+$ clusters. In practise, these interferences were minimized by appropriate adjustment of the mass resolution whilst maintaining an excess of O_2 in the mixtures, thereby favoring oxidation of all iron-containing ions to the corresponding oxide clusters. Another possible interference is due to clusters in which one ^{56}FeO unit is replaced by an ion-dipole complex with residual water containing the lighter ^{54}Fe isotope (both 72 amu); this interference is readily identified by characteristic loss of water (18 amu) in the CA spectrum of these ions. With the notable exception of formal $Fe_3O_5^+$ (see above), these hydrated iron oxide cluster ions were of negligible abundance.

Acknowledgments

Financial support by the Deutsche Forschungsgemeinschaft, the Volkswagen Stiftung, and the Fonds der Chemischen Industrie is gratefully acknowledged. We thank Prof. J. Müller for providing us with a sample of $Cp_2Fe_2(NO)_2$.

[1] B. Maunit, A. Hachimi, P. Manuelli, P. J. Calba, J. F. Muller, *Int. J. Mass Spectrom. Ion Processes* **1996**, *156*, 173.
[2] M. C. Oliveira, J. Marcalo, M. C. Vieira, M. A. Almoster Ferreira, *Int. J. Mass Spectrom. Ion Processes* **1999**, *185/186/187*, 825.
[3] H. Wu, S. R. Desai, L.-S. Wang, *J. Am. Chem. Soc.* **1996**, *118*, 5296.
[4] S. J. Riley, E. K. Parks, G. C. Nieman, L. G. Polo, S. Wexler, *J. Chem. Phys.* **1984**, *80*, 1360.
[5] R. L. Whetten, D. M. Cox, D. J. Trevor, A. Kaldor, *J. Phys. Chem.* **1985**, *89*, 566.
[6] D. B. Jacobon, B. S. Freiser, *J. Am. Chem. Soc.* **1986**, *108*, 27.
[7] S. K. Loh, L. Lian, P. B. Armentrout, *J. Chem. Phys.* **1989**, *91*, 6148.
[8] O. Gehret, M. P. Irion, *Chem. Eur. J.* **1996**, *2*, 598.
[9] J. B. Griffin, P. B. Armentrout, *J. Chem. Phys.* **1997**, *106*, 4448.
[10] J. B. Griffin, P. B. Armentrout, *J. Chem. Phys.* **1997**, *107*, 5345.
[11] P. E. M. Siegbahn, R. H. Crabtree, *J. Am. Chem. Soc.* **1997**, *119*, 3103.
[12] K. Yoshizawa, T. Ohta, T. Yamabe, *Bull. Chem. Soc. Jpn.* **1998**, *71*, 1899.
[13] J. N. Harvey, D. Schröder, H. Schwarz, *Inorg. Chim. Acta* **1998**, *273*, 111.
[14] M. S. Foster, J. L. Beauchamp, *J. Am. Chem. Soc.* **1975**, *97*, 4808.
[15] E. L. Kerley, D. H. Russell, *J. Am. Chem. Soc.* **1990**, *112*, 5959.
[16] S. W. Buckner, B. S. Freiser, *J. Phys. Chem.* **1989**, *93*, 3667, and references cited therein.
[17] D. Schröder, J. Müller, H. Schwarz, *Organometallics* **1993**, *12*, 1972.
[18] D. Schröder, A. Fiedler, J. Schwarz, H. Schwarz, *Inorg. Chem.* **1994**, *33*, 5094.
[19] Z. Cao, M. Duran, M. Solà, *Chem. Phys. Lett.* **1997**, *274*, 411.
[20] L. Andrews, G. V. Chertihin, A. Ricca, C. W. Bauschlicher, *J. Am. Chem. Soc.* **1996**, *118*, 467.
[21] P. B. Armentrout, B. L. Kickel, in *Organometallic Ion Chemistry* (Ed. B. S. Freiser), Kluwer, Dordrecht, **1996**, p 1.
[22] D. L. Hildenbrand, *Chem. Phys. Lett.* **1975**, *34*, 252.
[23] E. A. Kaibicheva, E. B. Rudnyi, L. N. Sidorov, *Russ. J. Phys. Chem.* **1992**, *66*, 1679.
[24] J. Fan, L.-S. Wang, *J. Chem. Phys.* **1995**, *102*, 8714.
[25] Z. Cao, M. Duran, M. Solà, *J. Chem. Soc., Faraday Trans.* **1998**, *94*, 2877.
[26] A. Fiedler, I. Kretzschmar, D. Schröder, H. Schwarz *J. Am. Chem. Soc.* **1996**, *118*, 9941.
[27] D. Schröder, A. Fiedler, W. A. Herrmann, H. Schwarz, *Angew.*

Chem. **1995**, 107, 2714; *Angew. Chem. Int. Ed. Engl.* **1995**, *34*, 2517.
[28] D. Schröder, C. A. Schalley, H. Schwarz, in *Peroxide Chemistry* (Ed. W. Adam), Wiley-VCH, Weinheim, in press.
[29] R. Wesendrup, C. A. Schalley, D. Schröder, H. Schwarz, *Chem. Eur. J.* **1995**, *1*, 608.
[30] C. A. Schalley, R. Wesendrup, D. Schröder, H. Schwarz, *Organometallics* **1996**, *15*, 678.
[31] M. N. Glukhovtsev, R. D. Bach, C. J. Nagel, *J. Phys. Chem. A* **1997**, *101*, 316.
[32] C. A. Schalley, D. Schröder, H. Schwarz, *Int. J. Mass Spectrom. Ion Processes* **1996**, *153*, 173.

Received November 4, 1999
[I99395]

Syntheses, Structures, and Reactivity of Hexaborylbenzene Derivatives

Christian Ester,[a] Andreas Maderna,[a] Hans Pritzkow,[a] and Walter Siebert*[a]

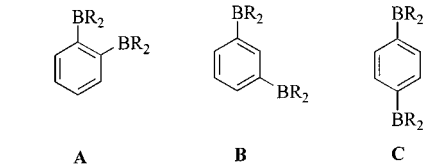
Dedicated to Prof. Heinrich Vahrenkamp on the occasion of his 60th birthday

Keywords: Hexaborylbenzenes / Bis(boryl)acetylenes / Cyclooligomerization / Catalysts / Boranes / Boron

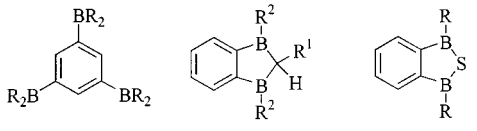
The hexaborylbenzene derivatives **2a** and **2b** have been obtained by transition metal catalyzed {[$CpCo(CO)_2$], [$Co_2(CO)_8$], [Ni(cod)$_2$]} cyclotrimerization of bis(1,3,2-benzodioxaborol-2-yl)acetylene (**1a**) and bis[1,3,2-(2,3-naphtho)-dioxaborol-2-yl]acetylene (**1b**). Reaction of [$Co_2(CO)_8$] with **1a** yielded the bis(1,3,2-dioxaborol-2-yl)dicobaltatetrahedrane derivative **3a**, which has been subjected to X-ray structure analysis. Reaction of stoichiometric amounts of **3a** and diphenylacetylene was found to give the bis(boryl)tetraphenylbenzene derivative **4**, while **3a** and mono(1,3,2-benzodioxaborol-2-yl)acetylene (**5**) reacted to yield the tetraborylbenzene derivative **6**. $AlMe_3$ and $AlEt_3$ were found to react with **2a**,**b** to furnish $C_6(BMe_2)_6$ (**7a**) and $C_6(BEt_2)_6$ (**7b**), respectively. With pyridine, the hexafunctional Lewis acid **7a** formed the crystalline bis(pyridine) adduct $C_6(BMe_2)_6{\cdot}(NC_5H_5)_2$ (**8a**). Thermolysis of $C_6(BEt_2)_6$ (**7b**) resulted in the intramolecular elimination of ethane to give the 1,2,3,4-bis(2′,3′-dihydro-1′,3′-diborole)-5,6-bis(diethylboryl)benzene compound **9b**. The molecular structure of the hexaborylbenzene pyridine adduct **8a** has been determined by X-ray structure analysis.

Introduction

Over the past two decades, borylbenzene compounds have become an area of particular interest in relation to the syntheses of boraheterocycles[1] and of polymeric graphite-like boron−carbon frameworks.[2] Several derivatives of the bis(boryl)benzene isomers **A**, **B**, and **C** are known. Kaufmann[3] obtained 1,2-bis(dichloroboryl)benzene **A** (R = Cl) by silicon−boron exchange with BCl_3, while Eisch et al.[4] synthesized the bis(diethylboryl)benzene derivatives of **A**, **B**, and **C** (R = Et) through tin−boron exchange by reacting the corresponding bis(trimethylstannyl)benzenes with Et_2BX (X = Cl, Br).

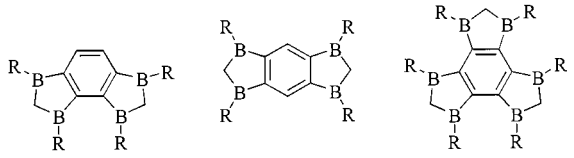


A **B** **C**



D **E** **F**

The formation and electrochemical properties of bis(boryl)benzene derivatives **C** (R = Ph, Mes) have been studied by Kaim and Schulz.[5] The synthesis of a 1,3,5-tris(boryl)-benzene derivative of **D** (R = Br, OH) was achieved by Stern and Washburn[6] by means of a Friedel−Crafts reaction. Okada, Oda, et al.[7] obtained the mesityl derivatives of **B** and **D** by treating dimesitylfluoroborane with Grignard solutions prepared from 1,3-dibromo- and 1,3,5-tribromobenzene.



G **H** **I**

The benzo-1,3-diborole heterocycle **E** (R^1 = H, Me; R^2 = Cl, Me, NMe_2) has been synthesized by tin−boron exchange of 1,2-bis(trimethylstannyl)benzene with bis(dichloroboryl)methane derivatives, and its ligand properties have been studied in the context of complex formation.[8] The redox reaction between 1,2-diiodobenzene, BI_3, and $(IBS)_3$ led to the formation of the benzo-2,5-diiodo-1,2,5-thiadiborole derivative **F** (R = I), in which the iodine could easily be substituted, thereby allowing access to a variety of derivatives.[9] Its dimethyl derivative (**F**, R = Me) formed the first stable tricarbonylironthiaborane complex.[10] Bis- and tris(2,3-dihydro-1,3-diborole)benzene compounds **G**−**I** are of interest with regard to the synthesis of doubly- and triply-stacked complexes with bridging 1,3-diborolyl ligands. Tetra- and hexaborylbenzenes are potential precursors for the preparation of boron-containing polymers. A graphite-like web $(C_3B)_n$, in which each boron atom is connected to three carbon atoms, should be feasible by polycondensation of $C_6(BR_2)_6$ with elimination of BR_3. We report herein on the synthesis of hexaborylbenzene derivatives by transition metal catalyzed cyclotrimerization of

[a] Anorganisch-Chemisches Institut der Universität,
Im Neuenheimer Feld 270, D-69120 Heidelberg, Germany
Fax: (internat.) +49(0)6221/54−5609
E-mail: ci5@ix.urz.uni-heidelberg.de

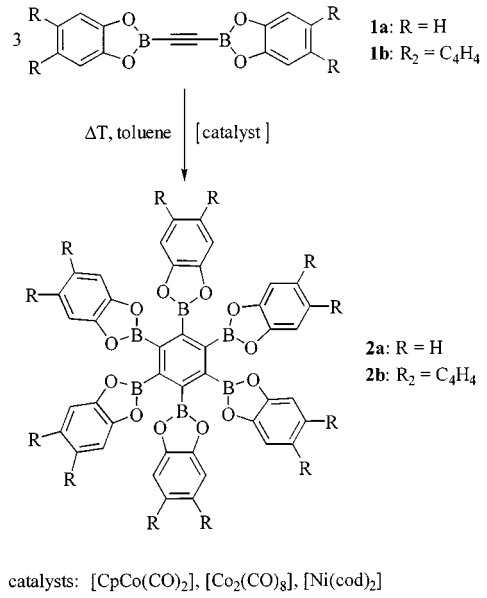
 © WILEY-VCH Verlag GmbH, D-69451 Weinheim, 2000 1434−1948/00/0606−1177 $ 17.50+.50/0

bis(boryl)acetylene derivatives and on the reactivities of these compounds. A preliminary account of our work has been reported previously.[11]

Results and Discussion

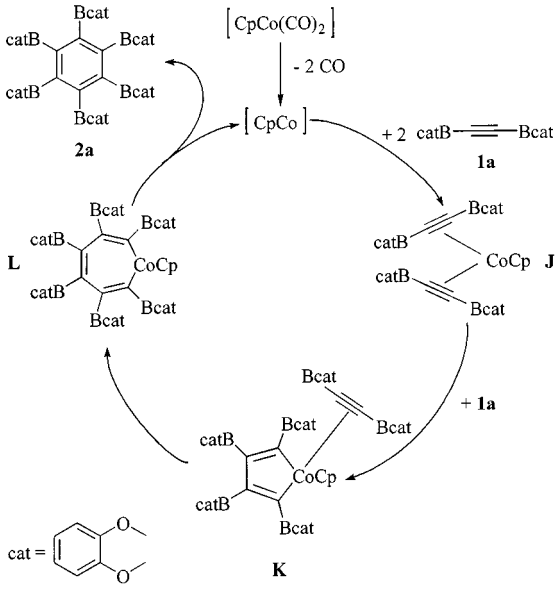
Hexakis(1,3,2-benzodioxaborolyl)benzene (2a) and Hexakis{1,3,2-naphtho[2,3-*d*]dioxaborolyl}benzene (2b)

Since the early report of thermal trimerization of acetylene to benzene by Berthelot,[12] and the first transition metal catalyzed version of this reaction by Reppe,[13] the [2+2+2] cyclotrimerization of acetylenes has been extensively studied. A large number of transition metal complexes as well as Ziegler-type catalysts[14] are known to catalyze this reaction.[15] The formation of substituted arenes by cobalt-catalyzed [2+2+2] cyclotrimerization of alkynes is well-known and has found widespread application in organic synthesis.[16] In an analogous manner, the diborylacetylene **1a**[17] (R = H) has been cyclotrimerized in the presence of (η^5-cyclopentadienyl)dicarbonyl-cobalt in refluxing toluene to give the hexaborylbenzene derivative **2a** (R = H) in 75% yield (Scheme 1).[11]



Scheme 1

Compound **2a** is only slightly soluble in most organic solvents; in methanol, a slow reaction leading to the formation of $H_4C_6O_2BOMe$ takes place. Purification of **2a** can be accomplished by repeated washing with toluene. The ^{11}B NMR spectrum in [D_4]MeOH shows a broad signal at δ = 29 due to **2a** and a sharp one at δ = 19.0 attributable to the methanolysis product $H_4C_6O_2BOCD_3$. A characteristic feature of borylbenzenes is the broad ^{13}C NMR resonance signal of the *ipso* carbon atom(s) of the central C_6 ring (δ = 130−150).[18] **2a** exhibits a resonance at δ = 143 due to the *ipso* carbon atoms, which is shifted by 50 ppm to lower field as compared to that of the bis(boryl)acetylene **1a**. This reflects the change of the hybridization of the carbon atoms from sp to sp^2. The ^{13}C NMR signals of the aromatic carbons of the catecholyl substituents appear at δ = 116.3, 120.8, and 146.2. The ^1H NMR spectrum features one multiplet at δ = 6.61−6.77 due to the aromatic protons. EI-MS data confirm the identity of **2a** through the appearance of ion peaks at *m*/*z* = 785 [M^+] and 667 [$M^+ - H_4C_6O_2B$].



Scheme 2

Similarly, the bis(boryl)acetylene **1b** ($R_2 = C_4H_4$) could be trimerized in the presence of a catalytic amount of $CpCo(CO)_2$ to give hexakis{1,3,2-naphtho[2,3-*d*]dioxaborolyl}benzene (**2b**, $R_2 = C_4H_4$) in good yield (Scheme 1). Compound **2b** was characterized by ^1H, ^{13}C, and ^{11}B NMR spectroscopy, elemental analysis, and mass spectrometry. The ^1H NMR spectrum shows the expected multiplet at δ = 7.14−7.59 due to the aromatic protons. In the ^{13}C NMR spectrum, the signals due to the naphthol substituent are seen at δ = 110.8, 124.4−131.0, and 147.8, while that due to the carbons of the benzene ring appears at δ = 144. The ^{11}B NMR shift of δ = 28.3 is comparable with that seen for **2a** (R = H). In the EI mass spectrum of **2b**, the molecular ion appears at *m*/*z* = 1085 and shows the expected isotopic pattern.

Catalytic Cycles with [CpCo(CO)$_2$], [Co$_2$(CO)$_8$], and [Ni(cod)$_2$]

The postulated mechanism of [$CpCo(CO)_2$]-catalyzed cyclotrimerization[16] of acetylene is illustrated for diborylacetylenes in Scheme 2. It is likely that under thermal conditions two alkyne moieties displace the two CO ligands at the metal to form the diborylacetylene complex **J**. Subsequent reductive coupling of the alkynes would then give a coordinatively unsaturated cobaltacyclopentadiene complex. Complexation of a third molecule of **1a** could then lead to **K**, which would be followed by alkyne insertion to form the cobaltacycloheptatriene **L**. Finally, reductive elimination of the CpCo complex fragment would account for the formation of the observed hexaborylbenzene **2a**. Recently, Vollhardt et al.[19] succeeded in synthesizing a cobaltacyclopentadiene−alkyne complex of type **K**, thus

seemingly proving this mechanism, although no direct evidence for the intermediacy of the postulated cobaltacycloheptatriene was obtained. Indeed, theoretical investigations of the mechanism at ab initio and density functional (DFT) levels[20] indicate that a cobaltacycloheptatriene (in Scheme 2) is in fact very unlikely to occur.

Analogously, the catalytic trimerization of **1a** with octacarbonyldicobalt leads to the hexaborylbenzene derivative **2a** in 70% yield. The proposed mechanism of this catalytic cyclotrimerization is outlined in Scheme 3. In the first step of the catalytic cycle, the elimination of two CO ligands leads to the unsaturated species $[Co_2(CO)_6]$, which then reacts with **1a** to give the bis(boryl)dicobaltatetrahedrane **M** (**3a**) (Scheme 3). Insertion of one molecule of bis(boryl)acetylene **1a** leads to complex **N**, which reacts with a third acetylene molecule to give **O**. Subsequent reductive elimination yields the hexaborylbenzene **2a**. An intermediate of the type **O** obtained from the reaction of acetylene, *tert*-butylacetylene, and octacarbonyldicobalt has been characterized by X-ray structure analysis.[21]

In the past, numerous compounds incorporating benzene or cyclooctatetraene derivatives have been synthesized in the presence of nickel catalysts.[22a][22b] It was found that the [2+2+2] cycloaddition of **1a** to give the hexaborylbenzene derivative **2a** was also catalyzed by $[Ni(cod)_2]$ in 80% yield. The proposed mechanism of the catalytic cyclotrimerization with $[Ni(cod)_2]$ is similar to that with $[CpCo(CO)_2]$ (Scheme 2).

Synthesis and Properties of Bis(borolyl)dicobaltatetrahedrane (3a)

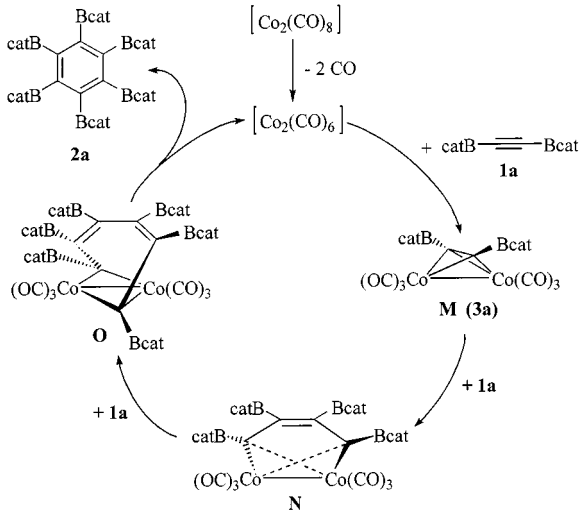
In 1956, it was found that acetylene and substituted acetylenes are capable of displacing two carbonyl groups from $[Co_2(CO)_8]$ to yield dicobaltatetrahedranes.[23] To investigate the mechanism of the cyclotrimerization with $[Co_2(CO)_8]$ as catalyst, the first intermediate **M** of the catalytic cycle was synthesized. Thus, the bis(borolyl)dicobaltatetrahedrane **3a** was prepared in 45% yield by treating the bis(boryl)ethyne **1a** with one equivalent of $[Co_2(CO)_8]$ in dichloromethane at room temperature (Scheme 4). **3a** was isolated by column chromatography on Florisil® and characterized by ^1H, ^{13}C, and ^{11}B NMR, IR, mass spectrometry, as well as an X-ray structure analysis.

The ^1H NMR spectrum shows the signal due to the aromatic protons at $\delta = 6.85-7.29$. In the ^{13}C NMR spectrum, the arene carbon atoms give rise to signals at $\delta = 111.5$, 122.0, and 147.4. The signals of the carbon atoms bonded to boron are observed at $\delta = 96$, while those of the carbonyl ligands appear at $\delta = 197.4$. The ^{11}B NMR signal, seen at $\delta = 33.1$, is shifted to low field ($\Delta\delta = 10$ ppm) as compared to that of the bis(boryl)acetylene **1a**. The IR spectrum of **3a** features three absorption bands at $\tilde{\nu} = 2102$, 2066, and 2038 cm^{-1} attributable to the CO ligands. In the mass spectrum (EI) of **3a**, the molecular ion peak appears at $m/z = 548$ and shows the expected isotopic distribution as well as the appropriate fragmentation pattern arising from the stepwise loss of the six CO ligands.

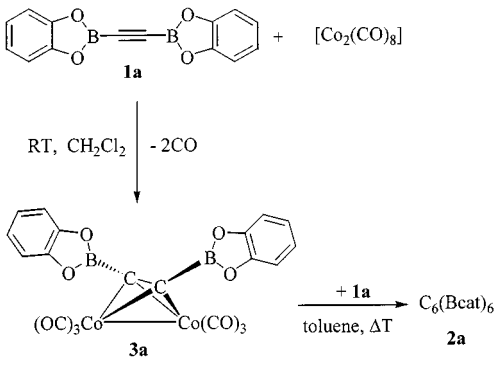
The bis(1,3,2-benzodioxaborolyl)dicobaltatetrahedrane (**3a**) was shown to catalyze the trimerization of **1a**, thus verifying the catalytic cycle with $[Co_2(CO)_8]$. Catalytic amounts of **3a** and the diborylacetylene **1a** were allowed to react in refluxing toluene for 24 h. The resulting product was the expected hexakis(1,3,2-benzodioxaborolyl)benzene (**2a**, Scheme 4).

Bis(1,3,2-benzodioxaborolyl)tetraphenylbenzene and Tetrakis(1,3,2-benzodioxaborolyl)benzene

Since the syntheses of the first dicobaltatetrahedranes,[23] numerous cobalt complexes have been reported.[24] However, the use of C_2Co_2 clusters for the preparation of substituted arenes has not been studied in detail. We have explored this route and have found that heating of diphenylacetylene and a stoichiometric amount of **3a** in toluene results in the formation of bis(1,3,2-benzodioxaborolyl)tetraphenylbenzene (**4**) in good yield (Scheme 5). Compound **4** was characterized by ^1H, ^{13}C, and ^{11}B NMR spectroscopy, and by mass spectrometry. The ^1H NMR spectrum shows the expected multiplet due to the aromatic protons at $\delta = 6.60-7.30$. In the ^{13}C NMR spectrum, the signals attributable to the benzodioxaborolyl substituent appear at $\delta = 112.6$, 122.5, and 148.5, while those of the phenyl substituents are seen at $\delta = 125.8$, 127.3, 131.4, and 141.7. The ^{11}B NMR spectrum features one signal at $\delta = 32.3$. In the HR-

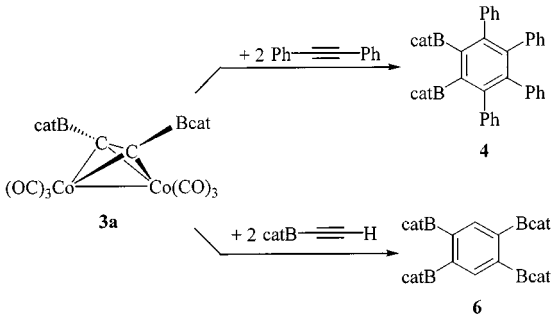


Scheme 3



Scheme 4

EI mass spectrum, the molecular ion peak of **4** is seen at m/z = 618 and shows the expected isotopic pattern.



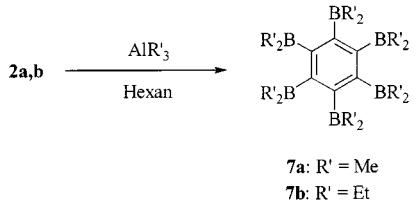
Scheme 5

Analogously, the bis(borolyl)dicobaltatetrahedrane (**3a**) reacts with the monoborylacetylene **5** to give the tetrakis(1,3,2-benzodioxaborolyl)benzene (**6**) (Scheme 5). To the best of our knowledge, this represents the first example of the synthesis of a tetraborylbenzene derivative through a stoichiometric reaction of a transition metal cluster and an acetylene.

Tetrakis(1,3,2-benzodioxaborolyl)benzene (**6**) is − in contrast to the hexaboryl derivatives **2a**,**b**, which are only slightly soluble in most organic solvents − highly soluble in toluene and chlorinated solvents. The molecular ion peak of **6** is detected in the HR-EI mass spectrum at m/z = 550. In the ^{11}B NMR spectrum, one signal is seen at δ = 22.2, while the ^{1}H NMR spectrum shows a signal at δ = 6.83−7.20 due to the protons of the catecholyl ligand. The signals of the two aromatic protons of the central benzene ring are not detected. In the ^{13}C NMR spectrum, the carbon atoms of the catecholyl ligand give rise to signals at δ = 111.6, 121.8, and 146.5. It would seem that **6** consists not only of the 1,2,4,5-isomer, but is rather a mixture of the 1,2,4,5-, 1,2,3,4-, and 1,2,3,5-isomers.

Substitution of the Catechol Groups in 2a,b

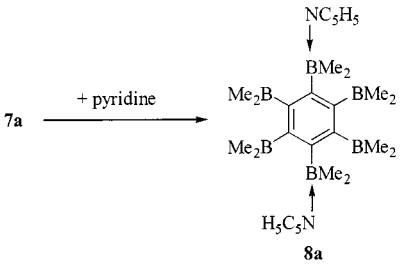
In analogy to the cleavage of the B−O bonds in 2-alkyl-1,3,2-benzodioxaborole derivatives with Grignard reagents,[25] treatment of a suspension of **2a**,**b** in hexane with trimethylaluminum furnishes hexakis(dimethylboryl)benzene (**7a**) (Scheme 6). Purification of the crude product could only be achieved by column chromatography on Florisil®, which allowed pure **7a** to be isolated in 24% yield. Compound **7a** is a low melting, colorless solid, which, in contrast to **2a**,**b**, is extremely sensitive to air and moisture. It was characterized by ^{1}H-, ^{13}C-, and ^{11}B NMR spectroscopy, and by mass spectrometry. The ^{1}H NMR spectrum shows only one signal at δ = 0.95, attributable to the B−CH_3 groups. In the ^{13}C NMR spectrum, the *ipso* carbon atoms of the benzene ring give rise to signals at δ = 149.1, while the B−CH_3 groups resonate at δ = 18.6. The ^{11}B NMR spectrum features one broad signal at δ = 85.1, which is in the range typical for alkylated boron compounds.[26] In the HR-EI mass spectrum of **8a**, the molecular ion peak is seen at m/z = 317 and shows the expected isotopic distribution.



Scheme 6

On treating **2a**,**b** with triethylaluminum, the hexakis(diethylboryl)benzene (**7b**) is formed. As in the case of the methyl analogue, purification could only be achieved by chromatography on a column of Florisil®. Compound **7b** was found to be soluble in hexane and also proved to be sensitive to air and moisture. In the ^{1}H NMR spectrum, a triplet (J = 7.1 Hz) is seen at δ = 1.07 due to the methyl groups, along with a quadruplet at δ = 1.34 due to the methylene units. The ^{13}C NMR spectrum of **7b** features two signals at δ = 9.9 and 23.9 attributable to the ethyl substituents, while the resonances of the benzene carbon atoms are seen at δ = 146.8. The ^{11}B NMR shift of δ = 83.7 is comparable with the shift of **7a** quoted above. In the HR-EI mass spectrum, the molecular ion peak appears at m/z = 485.5.

The hexaborylbenzene derivatives **7a**,**b** possess six electron-poor boryl groups and may be regarded as hexafunctional Lewis acids. Therefore, pyridine was added to a solution of **7a** in hexane (Scheme 7). At −15 °C, a white precipitate was obtained, which was found to consist of two crystalline products, a microcrystalline compound and colorless needles.



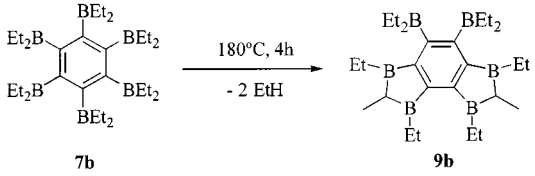
Scheme 7

NMR and mass spectral data showed this precipitate to be composed of $C_6(BMe)_6$ and pyridine. The ^{11}B NMR spectrum in [D_8]THF shows signals at δ = 55.4, 3.1, and 48.8, the latter being attributable to the protolysis product Me_2BOH. The signal at δ = 55.4 can be assigned to [$C_6(BMe_2)_6 \cdot (NC_5H_5)_2$] (**8a**), in which only two pyridines are coordinated, while the broad peak centered at δ = 3.1 corresponds to a compound in which all the boron atoms are tetracoordinated. It is likely that the boron atoms in **7a** are completely coordinated by pyridine, although we are unable to prove this. Evidently, the two pyridine ligands in **8a** are not fixed, but undergo rapid exchange with the neighboring boryl groups so that only an averaged signal

(δ = 55.4) is seen in the ^{11}B NMR spectrum. In the mass spectrum (EI) of **8a**, the molecular ion peak of **2a** (*m*/*z* = 317), without the two pyridine molecules, is observed.

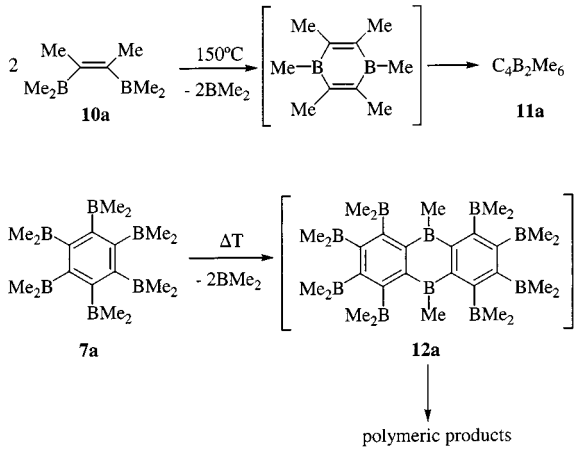
Thermolysis of Hexakis(diethylboryl)benzene (7b)

In 1968, Binger reported the first synthesis of the derivative 1,3,4,5-tetraethyl-2,3-dihydro-2-methyl-1,3-diborole, which involved thermolysis of *cis*-3,4-diethyl-3,4-bis(diethylboryl)hexene[27] at 160 °C. Similarly, a sample of **7b** was heated to 180 °C for 4 h in an argon stream. The reaction was accompanied by the evolution of ethane and the color changed from white to yellow. NMR and mass spectral data indicated that 1,2,3,4-bis(1′,3′-diborole-2′,3′-dihydro)-5,6-bis(boryl)benzene (**9b**) had been formed (Scheme 8). This represents the first example of a benzo derivative with two attached 1,3-diborole rings. In the ^{11}B NMR spectrum, one broad signal is seen at δ = 77.0, which is shifted upfield by 8 ppm compared to that of $C_6(BEt_2)_6$ (**7b**). The ^{13}C NMR spectrum of **9b** features three signals at δ = 7.8, 9.8, and 10.9 due to the three different methyl groups. The resonances of the methylene carbon atoms are found at δ = 24.2 and 25.6, while the bridging methylene carbon atoms give a signal at δ = 67.8. The signal due to the arene carbon atoms is seen at δ = 154.0. In the mass spectrum (EI) of **9b**, the molecular ion peak is seen at *m*/*z* = 425 and shows the expected isotopic distribution.



Scheme 8

Binger also reported the thermolysis of the *cis*-2,3-dimethyl-2,3-bis(dimethylboryl)hexene[27] at 150 °C to give, via the 1,4-hexamethyldiboracyclohexadiene, the *nido*-tetracarbahexaborane(6) (**11a**) (Scheme 9). Analogously, methyl derivative **7a** was heated to 150 °C in the hope of isolating the condensation product **12a** (Scheme 9). However, no low molecular weight species such as **12a** could be detected; only insoluble brown products were obtained, which may have web-like structures.



Scheme 9

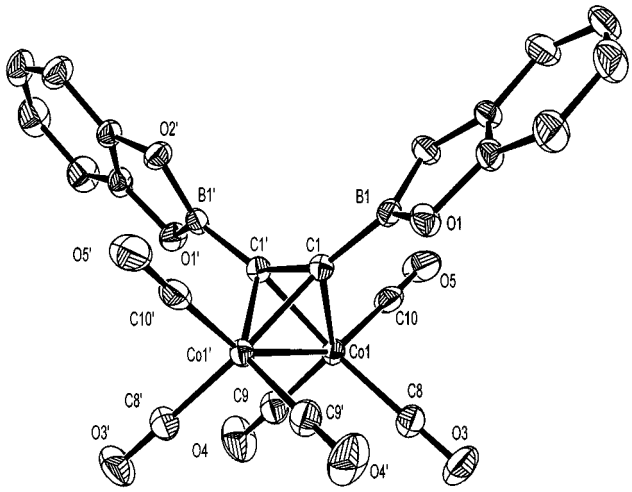


Figure 1. Structure of **3a** in the crystal; selected bond lengths [Å] and angles [°]: Co1–Co1′ 2.472(2), C1–C1′ 1.345(7), Co1–C1 1.983(4), Co1–C1′ 1.953(4), B1–C1 1.518(5), B1–O1 1.379(5), B1–O2 1.387(5); Co1–C1–Co1′ 77.8(1), Co1–C1–C1′ 68.8(2), Co1′–C1–C1′ 71.2(2), B1–C1–C1′ 145.2(2), O1–B1–O2 111.8(3), B1–C1–Co1 127.8(3), B1–C1–Co1′ 137.0(3)

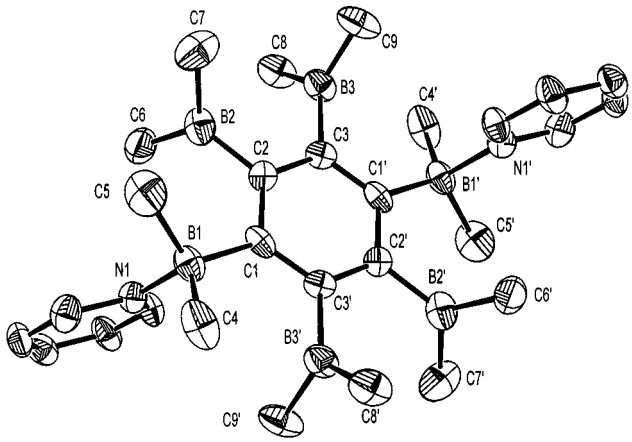


Figure 2. Structure of **8a** in the crystal; selected bond lengths [Å]: B1–C1 1.668(11), B1–N1 1.667(10), B2–C2 1.585(12), B3–C3 1.561(11), C1–C2 1.437(9), C2–C3 1.391(9), C3–C1′ 1.422(9)

Crystal Structures

The structure of **3a** was characterized by performing a single-crystal X-ray analysis (crystal data and structure refinement parameters for **3a** and **8a** are presented in Table 1). The dark-red crystals of **3a**, grown at 4 °C from a solution in toluene, belong to the monoclinic system, space group *C*2/*c* and have four formula units in the unit cell.

The molecular structure (Figure 1) shows the Co_2C_2 framework; each cobalt atom is surrounded by three CO ligands and each carbon atom bears a terminal $BO_2C_6H_4$ group. The C1–C14 distance of 1.345 Å is similar to that in other Co_2C_2 tetrahedrane compounds.[28a,28b] The

Tabelle 1. Crystal data and structure refinement for **3a** and **8a**

	3a	**8a**
Empirical formula	$C_{20}H_8B_2Co_2O_{10}\cdot C_7H_8$	$C_{28}H_{46}B_6N_2$
Formula mass	639.9	475.6
Crystal system	monoclinic	trigonal
Space group	*C*2/*c*	$R\bar{3}$
Unit cell		
a [Å]	16.290(12)	31.25(2)
b [Å]	14.573(10)	31.25(2)
c [Å]	14.148(11)	9.942(7)
α [deg]	90	90
β [deg]	124.31	90
γ [deg]	90	120
Volume [Å^3]	2774(4)	8408(10)
Z	4	9
Calcd. density [g/cm^3]	1.532	1.306
Absorp. coeff. [mm^{-1}]	1.251	0.05
F(000)	1288	2322
Crystal size [mm]	0.3 × 0.4 × 0.6	0.2 × 0.2 × 0.3
Θ-range [deg]	25	22.5
Index ranges	−19/+16, 0/+17, 0/+16	−26/+28, 0/+33, 0/+9
No. of reflections		
unique	2439	1926
observed [$I > 2\sigma(I)$]	2067	731
Transmission	0.631−0.787	−
Parameters	171	171
Final *R* indices		
*R*1 [$I > 2\sigma(I)$]	0.047	0.086
*wR*2	0.133	0.242
T [°C]	−65	−70
Largest diff. peak/hole [e/Å]	1.08/−0.45	0.17/−0.17

Co1−Co1 distance (2.472 Å) falls within the normal range.[28a][28b]

To elucidate the structure of **8a**, an X-ray diffraction study was carried out. A single crystal was grown from a solution in hexane at −15 °C. The determined structure is shown in Figure 2. **8a** crystallizes in the trigonal space group $R\bar{3}$ with nine formula units in the unit cell.

The crystal structure analysis reveals that in the donor−acceptor compound **8a**, two pyridines are coordinated to *para*-BMe_2 groups in *anterti* positions (Figure 2). The boron atoms of the remaining four boryl groups are coordinated in a planar fashion, the BC_2 planes being perpendicular to the central benzene plane. The distances C1−C2 (1.438 Å), C2−C3 (1.391 Å), and C3−C1 (1.422 Å) in the aromatic ring are somewhat elongated.

Experimental Section

General: All manipulations of compounds were performed with rigorous exclusion of air and moisture under an argon atmosphere using standard Schlenk techniques. Solvents were dried with the appropriate drying agents and distilled under a nitrogen atmosphere. − Column chromatography: Florisil® (Fluka), 100−200 mesh. − Elemental analyses were carried out at the Microanalytical Laboratory, Universität Heidelberg. − Melting points (uncorrected) were obtained on a Büchi apparatus using samples sealed in capillaries under argon. − ^{1}H, ^{13}C, and ^{11}B NMR: Bruker AC 200 spectrometer; ^{1}H and ^{13}C spectra were referenced to $(CH_3)_4Si$; ^{11}B spectra to $BF_3\cdot Et_2O$. − IR spectra were recorded on a Bruker IFS 28 FT spectrometer. − Mass spectra were obtained on Finnigan MAT 8230 and Jeol MStation IMS-700 spectrometers operating in EI and FD modes. − Bis(1,3,2-benzodioxaborol-2-yl)acetylene (**1a**),[17] $(Me_3Sn)_2C_2$,[29] $[Ni(cod)_2]$,[30] and $[CpCo(C_2H_4)_2]$[31] were prepared according to literature procedures. $[CpCo(CO)_2]$, $[Co_2(CO)_8]$, and 2,3-dihydroxynaphthalene were purchased from Aldrich®.

2-Chloro-[1,3,2-(2,3-naphtho)dioxaborole]: To a solution of BCl_3 (39.0 g, 0.33 mol) in CH_2Cl_2 (500 mL), 2,3-dihydroxynaphthalene (50.0 g, 0.31 mol) was added at −78 °C. The mixture was allowed to warm to room temperature and stirred for a further 12 h. It was then concentrated and the resulting crystalline precipitate was collected by filtration. Yield: 61.3 g (96%), colorless needles; m.p. 152 °C. − ^{1}H NMR (200.1 MHz, $CDCl_3$): δ = 7.84−7.44 (m, 6 H, arene H). − ^{13}C NMR (50.3 MHz, $CDCl_3$): δ = 108.8, 125.3, 127.8, 130.4, 147.3 ($C_{10}H_6$). − ^{11}B NMR (64.2 MHz, $CDCl_3$): δ = 29.9. − MS (70 eV, EI): *m*/*z* (%) = 204 (100) [M^+].

Bis[1,3,2-(2,3-naphtho)dioxaborol-2-yl]acetylene (1b): To a solution of $(Me_3Sn)_2C_2$ (4.00 g, 11.4 mmol) in toluene (50 mL), $C_{10}H_6O_2BCl$ (4.65 g, 22.8 mmol) in toluene (150 mL) was added at −78 °C. The mixture was allowed to warm to room temperature and stirred for a further 24 h. It was then concentrated and the resulting precipitate was collected by filtration. Yield: 3.73 g (91%) of **1b** as a colorless, crystalline, air-stable solid; m.p. 255 °C. − ^{1}H NMR (200.1 MHz, [D$_4$]MeOH): δ = 7.54−7.10 (m, 12 H, arene H). − ^{13}C NMR (50.3 MHz, [D$_4$]MeOH): δ = 110.2, 124.1, 126.4, 131.5, 148.3 ($C_{10}H_6$), 98 (BCCB). − ^{11}B NMR (64.2 MHz, [D$_4$]MeOH): δ = 22.1. − MS (70 eV, EI): *m*/*z* (%) = 362 (100) [M^+].

Hexakis(1,3,2-benzodioxaborolyl)benzene (2a). − Catalyst [CpCo(CO)$_2$]: To a suspension of **1a** (2.28 g, 8.7 mmol) in toluene (30 mL), (η^5-cyclopentadienyl)dicarbonylcobalt (0.09 g, 0.5 mmol) was added at room temperature. The mixture was then heated under reflux for 48 h. After cooling, the resulting precipitate was collected by filtration, washed several times with toluene, and dried in vacuo. Yield: 1.71 g (75%) of **2a** as a white, air-stable powder; m.p. > 310 °C. − ^{1}H NMR (200.1 MHz, [D$_4$]MeOH): δ = 6.61−6.77

(m, 24 H, arene H). − ^{13}C NMR (50.3 MHz, [D$_4$]MeOH): δ = 116.3, 120.8, 146.2 (C_6H_4), 143 (br., C_{ar}−B). − ^{11}B NMR (64.2 MHz, [D$_4$]MeOH): δ = 29.3. − MS (70 eV, HR-EI): *m/z* (%) = 785.1879 (100) [M$^+$; calcd. $^{12}C_{42}{}^{1}H_{24}{}^{10}B_1{}^{11}B_5{}^{16}O_{12}$: 785.1862]. − $C_{42}H_{24}B_6O_{12}$ (785.51): calcd. C 64.22, H 3.08; found C 64.06, H 3.26.

Catalyst [$Co_2(CO)_8$]: A suspension of **1a** (1.02 g, 3.9 mmol) and octacarbonyldicobalt (0.13 g, 0.4 mL) in toluene (30 mL) was heated for 24 h under reflux. Workup was carried out as above. Yield: 0.69 g (68%) of **2a**.

Catalyst [Ni(cod)$_2$]: A suspension of **1a** (1.38 g, 5.3 mmol) and [Ni(C_8H_8)$_2$] (0.08 g, 0.3 mmol) in toluene (40 mL) was heated for 20 h under reflux. Workup was carried out as above. Yield: 1.07 g (77%) of **2a**.

Catalyst 3a: A suspension of **1a** (1.12 g, 4.3 mmol) and bis(1,3,2-benzodioxaborolyl)dicobalttetrahedrane (**3a**) (0.11 g, 0.2 mmol) in toluene (30 mL) was heated for 24 h under reflux. Workup was carried out as above. Yield: 0.63 g (56%) of **2a**.

Hexakis{1,3,2-naphtho[2,3-*d*]dioxaborolyl}benzene (2b): A suspension of **1b** (2.03 g, 5.6 mmol) and (η^5-cyclopentadienyl)dicarbonylcobalt (0.08 g, 0.4 mmol) in toluene (30 mL) was heated for 48 h under reflux. Workup was carried out as for **2a**. Yield: 1.28 g (63%) of **2b** as a white, air-stable powder; m.p. > 310 °C. − ^{1}H NMR (200.1 MHz, [D$_4$]MeOH): δ = 7.14−7.59 (m, 36 H, arene H). − ^{13}C NMR (50.3 MHz, [D$_4$]MeOH): δ = 110.8, 124.4, 127.0, 131.0, 147.8 ($C_{10}H_6$), 144 (br., C_{ar}−B). − ^{11}B NMR (64.2 MHz, [D$_4$]MeOH): δ = 28.3. − MS (70 eV, EI): *m/z* (%) = 1085 (7) [M$^+$], 917 (4) [M$^+$ − $C_{10}H_6O_2B$], 749 (3) [M$^+$ − 2 $C_{10}H_6O_2B$]. − $C_{66}H_{36}B_6O_{12}$ (1086): calcd. C 73.00, H 3.34; found C 71.40, H 3.39.

Bis(borolyl)dicobaltatetrahedrane (3a): To a solution of bis(1,3,2-benzodioxaborole-2-yl)acetylene (**1a**; 1.22 g, 4.7 mmol) in CH_2Cl_2 (40 mL), a solution of octacarbonyldicobalt (1.61 g, 4.7 mmol) in CH_2Cl_2 (20 mL) was added dropwise at room temperature. An immediate reaction ensued, as indicated by the evolution of carbon monoxide. The mixture was stirred for 20 h at room temperature and thereafter for 2 h at reflux temperature. To the red-brown solution was then added Florisil® (10 g) and the solvent was removed in vacuo. The residue was separated by column chromatography (Florisil®/hexane) to give two fractions. Using hexane as eluent, [$Co_2(CO)_8$] was obtained first. The second fraction (hexane/toluene, 1:1) was found to contain **3a**. Yield: 1.17 g (45%) of **3a** as a red, air-sensitive solid; m.p. 102 °C. − ^{1}H NMR (200.1 MHz, C_6D_6): δ = 6.85−7.29 (m, 8 H, C_{ar}H). − ^{13}C NMR (50.3 MHz, C_6D_6): δ = 111.5, 122.0, and 147.4 (C_{ar}), 96 (br., C−B), 197.4 (CO). − ^{11}B NMR (64.2 MHz, C_6D_6): δ = 33.1. − IR (hexane): $\tilde{\nu}$ [cm^{-1}] = 2102 (s), 2066 (vs), 2038 (vs). − MS (70 eV, EI): *m/z* (%) = 548 (2) [M$^+$], 520 (7) [M$^+$ − CO], 492 (9) [M$^+$ − 2 CO], 464 (6) [M$^+$ − 3 CO], 436 (9) [M$^+$ − 4 CO], 408 (23) [M$^+$ − 5 CO], 380 (13) [M$^+$ − 6 CO], 321 (8) [M$^+$ − 6 CO − Co], 262 (100) [M$^+$ − 6 CO − 2 Co].

Bis(1,3,2-benzodioxaborolyl)tetraphenylbenzene (4): To a solution of **3a** (1.14 g, 2.1 mmol) in toluene (30 mL), diphenylacetylene (0.75 g, 4.2 mmol) was added at room temperature. The resulting mixture was stirred for 24 h under reflux. After cooling, the brown solution thus obtained was filtered and the filtrate was concentrated to dryness in vacuo. The residue was washed several times with hexane and dried in vacuo. Yield: 1.01 g (76%) of **4** as a white, air-stable powder. − ^{1}H NMR (200.1 MHz, $CDCl_3$): δ = 6.60−7.30 (m, 28 H, arene H). − ^{13}C NMR (50.3 MHz, $CDCl_3$): δ = 112.6, 122.5, 148.5 (C_6H_4), 125.8, 127.3, 131.4, 141.7 (C_6H_5), 145 (br., C_{ar}−B). − ^{11}B NMR (64.2 MHz, $CDCl_3$): δ = 32.3. − MS (70 eV, HR-EI): *m/z* (%) = 618.21839 (45) [M$^+$; calcd. $^{12}C_{42}{}^{1}H_{28}{}^{11}B_2{}^{16}O_4$: 618.21869].

Tetrakis(1,3,2-benzodioxaborolyl)benzene (6): To a solution of **3a** (1.06 g, 1.9 mmol) in toluene (25 mL), monoborylacetylene[32] **5** (0.56 g, 3.9 mmol) was added at room temperature. The resulting mixture was stirred for 24 h under reflux. After cooling, the brown solution thus obtained was filtered and the filtrate was concentrated to dryness in vacuo. The residue was washed several times with hexane and dried in vacuo. Yield: 0.83 g (79%) of **6** as a white, air-stable powder. − ^{1}H NMR (200.1 MHz, $CDCl_3$): δ = 6.83−7.20 (m, 16 H, arene H, catecholyl); C_{ar}−H not observed . − ^{13}C NMR (50.3 MHz, $CDCl_3$): δ = 111.6, 121.8, 146.5 (C_6H_4); C_{ar}−B and C_{ar}−H not observed. − ^{11}B NMR (64.2 MHz, $CDCl_3$): δ = 22.2. − MS (70 eV, HR-EI): *m/z* (%) = 550.1371 (83) [M$^+$; calcd. $^{12}C_{30}{}^{1}H_{18}{}^{11}B_4{}^{16}O_8$: 550.1365]; Δmmu = 0.6.

Hexakis(dimethylboryl)benzene (7a): To a suspension of **2a** (1.51 g, 1.9 mmol) [or **2b** (1.67 g, 1.5 mmol)] in hexane (40 mL), trimethylaluminum (0.56 g, 7.8 mmol) [0.45 g, 6.2 mmol] was added dropwise at −20 °C. The reaction mixture was allowed to warm to room temperature, stirred for 24 h, and then heated under reflux for 2 h. The brown-yellow solution thus obtained was filtered and the filtrate was concentrated to dryness in vacuo. The oily residue was redissolved in hexane (10 mL) and separated by column chromatography (Florisil®/hexane). Yield: 0.14 g (24%) [0.10 g (20%)] of **7a** as a colorless, air-sensitive solid; m.p. 34 °C. − ^{1}H NMR (200.1 MHz, C_6D_6): δ = 0.96 (s, 36 H, BCH_3). − ^{13}C NMR (50.3 MHz, C_6D_6): δ = 18.6 (BCH_3), 149.1 [C_{ar}−B(CH_3)$_2$]. − ^{11}B NMR (64.2 MHz, C_6D_6): δ = 85.1. − MS (70 eV, EI): *m/z* (%) = 317 (27) [M$^+$], 302 (7) [M$^+$ − CH_3], 246 (13) [M$^+$ − B(CH_3)$_2$ − 2 CH_3]; HR-EI: *m/z* (%) = 317.34155 (29) [M$^+$; calcd. $^{12}C_{18}{}^{1}H_{36}{}^{10}B_1{}^{11}B_5$: 317.34116]; Δ mmu = 0.39.

Hexakis(diethylboryl)benzene (7b): To a suspension of **2a** (1.32 g, 1.7 mmol) [or **2b** (1.53 g, 1.4 mmol)] in hexane (35 mL), triethylaluminum (0.77 g, 6.7 mmol) [0.64 g, 5.6 mmol] was added dropwise at −20 °C. Workup was carried out as for **7a**. Yield: 0.33 g (40%) [0.19 g (28%)] of **7b** as a colorless, air-sensitive solid; m.p. 48 °C. − ^{1}H NMR (200.1 MHz, C_6D_6): δ = 1.07 (t, *J* = 7.1 Hz, 36 H, CH_2CH_3), 1.34 (q, *J* = 7.3 Hz, 24 H, CH_2CH_3). − ^{13}C NMR (50.3 MHz, C_6D_6): δ = 9.9 (CH_2CH_3), 23.9 (CH_2CH_3), 146.8 [C_{ar}−B(CH_2CH_3)$_2$]. − ^{11}B NMR (64.2 MHz, C_6D_6): δ = 83.7. − MS (70 eV, EI): *m/z* (%) = 485.5 (54) [M$^+$], 456 (9) [M$^+$ − C_2H_5], 428 (5) [M$^+$ − 2 C_2H_5], 348 (22) [M$^+$ − 2 B(C_2H_5)$_2$]; HR-EI: *m/z* (%) = 485.5330 (5) [M$^+$; calcd. $^{12}C_{30}{}^{1}H_{60}{}^{10}B_1{}^{11}B_5$: 485.5290]; Δ mmu = 4.0.

Hexakis(dimethylboryl)benzene−Bipyridine Adduct (8a): Hexakis(-dimethylboryl)benzene **7a**, obtained from **2a** (1.21 g, 1.5 mmol) and trimethylaluminum (0.44 g, 6.0 mmol), was dissolved in hexane (12 mL) and then pyridine (2 mL) was added. The reaction mixture was cooled to −15 °C, whereupon a white precipitate was deposited. Yield: 0.22 g (30%) of **8a** as colorless, air-sensitive needles; m.p. 110 °C. − ^{1}H NMR (200.1 MHz, [D$_8$]THF): δ = 0.90 (s, BCH_3), 1.28 [s, B(CH_3)$_2$−NC_5H_5], 6.96 (m, C_5H_5N), 7.71 (m, C_5H_5N), 8.49 (m, C_5H_5N). − ^{13}C NMR (50.3 MHz, [D$_8$]THF): δ = 1.5 [B(CH_3)$_2$−NC_5H_5], 19.3 (BCH_3), 128.5, 134.3, 146.2 (C_5H_5N), 144.7 [$CB(CH_3)_2$]. − ^{11}B NMR (64.2 MHz, [D$_8$]THF): δ = 55.4. − MS (70 eV, EI): *m/z* (%) = 317 (35) [M$^+$ − 2 C_5H_5N], 302 (7) [M$^+$ − 2 C_5H_5N − CH_3], 246 (11) [M$^+$ − 2 C_5H_5N − B(CH_3)$_2$ − 2 CH_3], 79 (100) [C_5H_5N].

1,2,3,4-Bis(1,3-diborole)-5,6-bis(boryl)benzene (9b): Under argon, hexakis(diethylboryl)benzene (**7b**; 0.21 g, 0.4 mmol) was slowly

heated without a solvent to 180 °C and maintained at this temperature for 4 h. Yield: 0.14 g (77%) of a yellow, air-sensitive oily residue. – ^{1}H NMR (200.1 MHz, C_6D_6): δ = 1.04 (m, CH_2CH_3), 1.52 (m, CH_2CH_3), 3.5 ($CHCH_3$). – ^{13}C NMR (50.3 MHz, C_6D_6): δ = 7.8 ($CHCH_3$), 9.8 [$B(CH_2CH_3)_2$], 10.9 [$B(CH_2CH_3)$], 24.2 [$B(CH_2CH_3)_2$], 25.6 [$B(CH_2CH_3)$], 67.8 ($CHCH_3$), 154 [$C-B(CH_2CH_3)_2$]. – ^{11}B NMR (64.2 MHz, C_6D_6): δ = 77. – MS (70 eV, EI): *m/z* (%) = 425 (42) [M^+], 396 (71) [$M^+ - C_2H_5$], 327 (21) [$M^+ - C_2H_5 - B(C_2H_5)_2$], 298 (13) [$M^+ - 2\ C_2H_5 - B(C_2H_5)_2$].

Crystal Structure Determinations of 3a and 8a: Crystal data and details of the structure determinations are listed in Table 1. Unique sets of intensity data were collected at −65 °C and −70 °C on a Siemens−Stoe AED four-circle diffractometer (Mo-K_α radiation, λ = 0.7107 Å, graphite monochromator, ω-scans). Empirical absorption corrections (ψ-scans) were applied. The structures were solved by direct methods (SHELXS-86)[33] and refined by least-squares methods based on F^2 with all measured reflections (SHELXL-97).[34] All nonhydrogen atoms were refined anisotropically. Hydrogen atoms were included in calculated positions or as part of rigid groups (CH_3).

Crystallographic data (excluding structure factors) for the structures reported in this paper have been deposited with the Cambridge Crystallographic Data Centre as supplementary publication nos. CCDC-137769 (**3a**) and CCDC-137770 (**8a**). Copies of the data can be obtained free of charge on application to the CCDC, 12 Union Road, Cambridge CB2 1EZ, U.K. [Fax: (internat.) +44 (0)1223/336033; E-mail: deposit@ccdc.cam.ac.uk]

[1] J. H. Morris in *Comprehensive Organometallic Chemistry* (Eds.: G. Wilkinson, F. G. A. Stone, E. Abel), Vol. 1, Pergamon Press, Oxford, **1982**, p. 311−380.

[2] M. Müller, V. S. Iyer, C. Kübel, V. Enkelmann, K. Müllen, *Angew. Chem.* **1997**, *109*, 1679−1682; *Angew. Chem. Int. Ed. Engl.* **1997**, *36*, 1607−1610.

[3] [3a]D. E. Kaufmann, *Chem. Ber.* **1987**, *120*, 901. – [3b]D. E. Kaufmann, W. Schacht, *Chem. Ber.* **1987**, *120*, 1331−1338.

[4] J. J. Eisch, B. W. Kotowicz, *Eur. J. Inorg. Chem.* **1998**, 761−769.

[5] [5a]W. Kaim, A. Schulz, *Angew. Chem.* **1984**, *46*, 611; *Angew. Chem. Int. Ed. Engl.* **1984**, *23*, 615. – [5b]W. Kaim, A. Schulz, *Chem. Ber.* **1989**, *122*, 1863.

[6] D. R. Stern, R. M. Washburn, U.S. Pat. 3092652, *C. A.* **1963**, 11556.

[7] K. Okada, T. Sugawa, M. Oda, *J. Chem. Soc., Chem. Commun.* **1992**, 74−75.

[8] H. Schulz, T. Deforth, W. Siebert, *Z. Naturforsch.* **1993**, *48b*, 68−71.

[9] B. Asgarouladi, R. Full, K.-J. Schaper, W. Siebert, *Chem. Ber.* **1974**, *107*, 34.

[10] W. Siebert, G. Augustin, R. Full, C. Krüger, I.-H. Tsay, *Angew. Chem.* **1975**, *87*, 286.

[11] A. Maderna, H. Pritzkow, W. Siebert, *Angew. Chem.* **1996**, *108*, 1664; *Angew. Chem. Int. Ed. Engl.* **1996**, *35*, 1501.

[12] M. C. R. Berthelot, *Acad. Sci.* **1866**, *62*, 905.

[13] W. Reppe, O. Schlichting, K. Klager, T. Toepel, *Justus Liebigs Ann. Chem.* **1948**, *560*, 1.

[14] [14a] L. S. Meriwether, E. C. Clothup, G. W. Kennerly, R. N. Reusch, *J. Org. Chem.* **1961**, *26*, 5155. – [14b] V. O. Reikhstel'd, K. L. Makovetskii, *Russ. Chem. Rev.* **1966**, *35*, 510.

[15] [15a] N. E. Shore, *Chem. Rev.* **1988**, *88*, 1081−1119. – [15b] B. M. Trost, *Science* **1991**, *254*, 1472−1477. – [15c] M. Lautens, W. Klute, W. Tam, *Chem. Rev.* **1996**, *96*, 49−92.

[16] K. P. C. Vollhardt, *Angew. Chem.* **1984**, *96*, 525−542; *Angew. Chem. Int. Ed. Engl.* **1984**, *23*, 539.

[17] H. Schulz, G. Gabbert, H. Pritzkow, W. Siebert, *Chem. Ber.* **1993**, *126*, 1593−1595.

[18] D. E. Kaufmann, R. Boese, A. Scheer, *Chem. Ber.* **1994**, *127*, 2349.

[19] R. Diercks, B. E. Eaton, S. Gürtzgen, S. Jalisatgi, A. J. Matzger, R. H. Radde, K. P. C. Vollhardt, *J. Am. Chem. Soc.* **1998**, *120*, 8247−8248.

[20] J. H. Hardesty, J. B. Koerner, T. A. Albright, G.-Y. Lee, *J. Am. Chem. Soc.* **1999**, *121*, 6055−6067.

[21] O. S. Mills, G. Robinson, *Proc. Chem. Soc.* **1964**, 187.

[22] [22a] G. Wilke, *Pure Appl. Chem.* **1978**, *50*, 677−690. – [22b] J. J. Eisch, A. M. Piotrowski, A. A. Aradi, C. Krüger, M. J. Rom, *Z. Naturforsch.* **1985**, *40b*, 624.

[23] H. Greenfield, H. W. Sterberg, R. A. Friedel, J. H. Wotiz, R. Markby, I. Wender, *J. Am. Chem. Soc.* **1956**, *78*, 120.

[24] E. Sappa, A. Tiripicchio, P. Braunstein, *Chem. Rev.* **1983**, *83*, 203−239.

[25] S. Cabiddu, A. Maccioni, M. Secci, *Gazz. Chim. Ital.* **1972**, *102*, 555.

[26] H. Nöth, B. Wrackmeyer, *Nuclear Magnetic Resonance Spectroscopy of Boron Compounds*, Springer Verlag, Berlin, Heidelberg, New York, **1978**.

[27] P. Binger, *Angew. Chem.* **1968**, *80*, 288.

[28] [28a] W. G. Sly, J. Am. Chem. Soc. ***1959***, 81, *18*. – [28b] *F. A. Cotton, J. D. Jamerson, B. R. Stults,* J. Am. Chem. Soc. ***1976***, 98, *1774*.

[29] B. Wrackmeyer, H. Nöth, *J. Organomet. Chem.* **1976**, *108*, C21−C25.

[30] B. Heyn, B. Hipler, G. Kreisel, H. Schreer, D. Walter, in "*Anorganische Synthesechemie*", Springer Verlag, **1986**.

[31] K. Jonas, C. Krüger, *Angew. Chem. Int. Ed. Engl.* **1980**, *19*, 520.

[32] Y. Gu, *Diploma Thesis*, Universität Heidelberg, **1996**.

[33] G. M. Sheldrick, *SHELXS-86*, Universität Göttingen, **1986**.

[34] G. M. Sheldrick, *SHELXL-97*, Universität Göttingen, **1997**.

Received December 13, 1999
[I99454]

Transition-Metal Substituted Phosphaalkenes, 41[‡]

Syntheses and Structures of *C*-Monoamino-*P*-ferriophosphaalkenes $[(\eta^5\text{-}C_5Me_5)(CO)_2FeP{=}CR^1(NR^2_2)]$ (R^1 = Ph, *t*Bu, 3,4,5-$(MeO)_3C_6H_2$; NR^2_2 = NMe_2, Piperidino)

Lothar Weber,*[a] Stefan Kleinebekel,[a] Annette Rühlicke,[a] Hans-Georg Stammler,[a] and Beate Neumann[a]

Dedicated to Professor Gerd Becker on the occasion of his 60th birthday

Keywords: Phosphaalkenes / Iron / Condensation reactions

Reaction of equimolar amounts of the carbenium iodides $[Me_2N(R)CSMe]I$ [**1a**: R = Ph; **1b**: *t*Bu; **1c**: 3,4,5-$(MeO)_3C_6H_2$], [pip(Ph)CSMe]I (**1d**) (pip = piperidino), and $LiP(SiMe_3)_2 \cdot$ DME afforded phosphaalkenes $Me_2N(R)C{=}PSiMe_3$ (**2a–c**) and pip(Ph)C=$PSiMe_3$ (**2d**). Combination of **2a–d** with $[(\eta^5\text{-}C_5Me_5)(CO)_2FeCl]$ led to the formation of $[(\eta^5\text{-}C_5Me_5)(CO)_2\text{-}FeP{=}C(R)NMe_2]$ [**3a**: R = Ph; **3b**: *t*Bu; **3c**: 3,4,5-$(MeO)_3C_6H_2$] and $[(\eta^5\text{-}C_5Me_5)(CO)_2FeP{=}C(Ph)pip]$ (**3d**). Compounds **2a–d** and **3a–d** were characterized by means of spectroscopy (IR, ^1H, $^{13}C\{^1H\}$, $^{31}P\{^1H\}$ NMR). The molecular structures of **3a** and **3b** were determined by X-ray diffraction analysis. The results of an X-ray study on $[(\eta^5\text{-}C_5Me_5)(CO)_2Fe{-}P{=}C(Ph)SiMe_3]$ (**3g**) for comparison are also included. All experimental observations are rationalized by the assumption that complexes **3a**, **3c**, and **3d** are phosphaalkenes with an inverse π-electron distribution ($P^{\delta-}\,C^{\delta+}$) and are comparable to $[(\eta^5\text{-}C_5Me_5)(CO)_2FeP{=}C(NMe_2)_2]$ (**3e**), whereas **3b** is better regarded as phosphaalkene with a normal polarization ($P^{\delta+}\,C^{\delta-}$) of the P=C bond, similar to that given in **3g**.

Introduction

Within the last 15 years metallophosphaalkenes have emerged from being laboratory curiosities to become versatile synthons in organoelement and coordination chemistry.[1] P-metallophosphaalkenes are now accessible by a variety of different synthetic pathways (Scheme 1).

In methods (a)[2] and (b),[3] the P=C double bond was built up during a sequence of condensation and rearrangement steps, whereas in routes (c),[4] (d),[5] and (e),[6] reactants with preformed P=C bonds were involved. The organophosphorus precursor of route (f) is a phosphaalkyne, the bond order of which was reduced from 3 to 2 by hydroruthenation.[7] To date it is obvious that all the synthetic principles depicted in Scheme 1 suffer from limited generality. Thus, route (e) was limited to Fe and Ru derivatives. The ferriophosphaalkene **3e** is interesting because its P=C bond displays an inverse π-electron distribution. This leads to a highly nucleophilic phosphorus center, and consistently, to a rich and versatile chemistry with inorganic, organometallic, and organic electrophiles.[1,8]

We were now interested in experimentally determining the borderline between "classically polarized" metallophosphaalkenes such as $(\eta^5\text{-}C_5Me_5)(CO)_2FeP{=}C(SiMe_3)R$, (R = $SiMe_3$, Ph)[4] and $(\eta^5\text{-}C_5Me_5)(CO)_2FeP{=}C(O\text{-}SiMe_3)(R)$ (R = Ph, *t*Bu, Mes)[2] on the one hand, and "inversely polarized" phosphaalkenes on the other hand.

One possible experimental approach to this target was based on the replacement of one amino substituent in **3e** by an organic group that cannot participate in π-conjugation with the P=C bond.

Results and Discussion

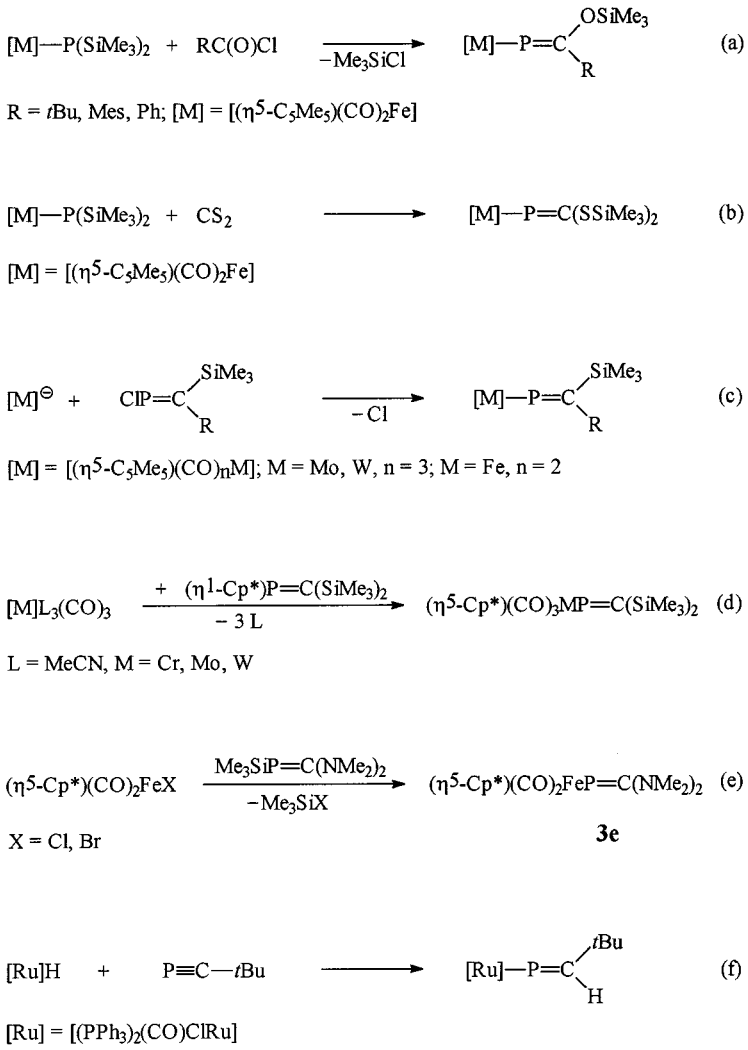
For the preparation of ferriophosphaalkenes with only one amino group at the methylene carbon atom, a synthetic route according to reaction (e) (Scheme 1) seemed promising. The required P-silylated phosphaalkenes were formed by the reaction of equimolar amounts of the (methylthiomethylene)immonium iodides **1a–d** and $LiP(SiMe_3)_2 \cdot$ DME[9] in a mixture of *n*-pentane and 1,2-dimethoxyethane (DME, −75 °C → room temperature). Within 24 h the reaction mixtures slowly turned orange.

Orange $Me_3SiP{=}CR^1(NR^2_2)$ (**2a–d**) were isolated as oils in moderate yields (38–62%) after filtration and removal of solvents. Phosphaalkenes **2a** and **2b** were purified by vacuum distillation to afford light yellow oils. The distillates were still contaminated with some $P(SiMe_3)_3$, which was invariably formed as a by-product. Due to its inherent thermolability, the attempted distillation of **2c** and **2d** was thwarted by decomposition. This approach parallels our

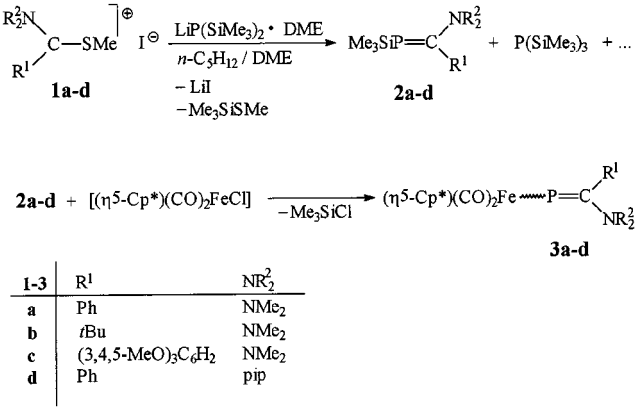
[‡] Part 40: L. Weber, M. H. Scheffer, H.-G. Stammler, A. Stammler, *Eur. J. Inorg. Chem.* **1999**, 1607–1611.

[a] Fakultät für Chemie der Universität Bielefeld, Universitätsstrasse 25, D-33615 Bielefeld, Germany
Fax: (internat.) + 49-(0)521/106-6146
E-mail: lothar.weber@uni-bielefeld.de

 © WILEY-VCH Verlag GmbH, D-69451 Weinheim, 2000 1434–1948/00/0606–1185 $ 17.50+.50/0



Scheme 1. Synthetic routes to P-metallophosphaalkenes



1-3	R^1	NR^2_2
a	Ph	NMe_2
b	*t*Bu	NMe_2
c	(3,4,5-MeO)$_3$C$_6$H$_2$	NMe_2
d	Ph	pip

Scheme 2. Synthesis of phosphaalkenes **2a−d** and **3a−d**; pip = NC_5H_{10}

previous synthesis of $Me_3SiP{=}C(NMe_2)_2$ (**2e**) from LiP(SiMe$_3$)$_2$ · DME and [(Me$_2$N)$_2$CSMe]I,[10] and constitutes a generalization of the reaction principle. The novel phosphaalkenes **2a−d** are sensitive to oxygen and moisture. Upon combination of **2a−d** with one equivalent of (η^5-C_5Me_5)(CO)$_2$FeCl[11] in a mixture of *n*-pentane and DME, a reaction occurred in the temperature range −75 to 20 °C to give the red microcrystalline ferriophosphaalkenes **3a−d** in 34 to 67% yield.

The replacement of one dimethylamino group in $Me_3SiP{=}C(NMe_2)_2$ (**2e**) ($\delta^{31}P$ = 46.5)[10] by an aryl ring resulted in slight downfield shifts to δ = 50.3 (**2c**), 54.3 (**2a**), and 59.5 (**2d**). The introduction of one *tert*-butyl group, however, was accompanied by a more pronounced deshielding in **2b** (δ = 68.7).

In the $^{13}C\{^1H\}$ NMR spectra of **2a**, **2c**, and **2d**, the doublets of the methylene carbon atoms of the P=C bond are insignificantly shifted δ ^{13}C = 204.7−205.1 when compared with **2e** (δ = 204.0). Also, the coupling constants $^1J_{P,C}$ decrease from 85.0 Hz in **2e** to 64.4−65.4 Hz. Interestingly, in the *tert*-butyl derivative **2b** the carbon atom of the P=C bonds was observed at much lower field (δ = 219.7) with an increased coupling constant ($^1J_{P,C}$ = 94.1 Hz). Two discrete singlet resonances for the methyl groups of the dimethylamino function in **2a** and **2c** are paralleled by two broad singlets, each accounting for 3-H atoms in the ^{1}H-NMR spec-

tra, and point to a hindered rotation of the amino group about the N-C_{sp^2} bond at room temperature. In **2b** only one resonance for the NMe_2 group in the $^{13}C\{^1H\}$ as well as the ^1H-NMR spectra was measured. The replacement of the trimethylsilyl group in **2a–d** by the [(η^5-C_5Me_5)-$(CO)_2Fe$] fragment caused strong downfield shifts in the $^{31}P\{^1H\}$-NMR spectra. Ferriophosphaalkenes **3a** (δ = 232.0), **3c** (δ = 225.4), and **3d** (δ = 225.4) also display more deshielded $^{31}P\{^1H\}$-NMR resonances in comparison to (η^5-C_5Me_5)$(CO)_2FeP{=}C(NMe_2)_2$ (**3e**) (δ = 135.5).[6] This observation indicates that the inverse polarity in the novel products is considerably reduced with respect to **3e**. This effect is much more evident with the *tert*-butyl-substituted ferriophosphaalkene **3b**, where a singlet at $\delta^{31}P$ = 409.0 was registered. At this point it is helpful to compare our data with the ^{31}P-NMR-resonances of the "classically" polarized ferriophosphaalkenes (η^5-C_5Me_5)$(CO)_2FeP{=}C(SiMe_3)_2$ (δ = 641.5)[4] and (η^5-C_5Me_5)$(CO)_2FeP{=}C(Ph)(SiMe_3)$ (δ = 520.7).[4] On the ground of ^{31}P-NMR spectroscopy, compound **3b** should not be considered as an inversely polarized phosphaalkene. The ^{13}C nuclei of the P=C bond in **3a–d** experience small high fields ($\Delta\delta^{13}C$ = 2.4–5.0 ppm) relative to precursors **2a–d**. The $^1J_{P,C}$ coupling constants of **2a**, **2c**, and **2d** were increased by ca. 20 Hz. An opposite trend, however, was observed with **2b** and **3b**, where the metallation was accompanied by a decrease of the coupling constant $^1J_{P,C}$ by 18.8 Hz. Again, a bonding situation in **3b** different from that in **3a**, **c**, and **d** might be anticipated. In the ^{13}C-NMR spectra of **3a–d** the carbonyl ligands give rise to singlets in the narrow range of δ = 218.0 to 218.5. The high-field shift in comparison to (η^5-C_5Me_5)$(CO)_2$-$FeP{=}C(NMe_2)_2$ (**3e**) agrees with a smaller degree of charge transfer from the organophosphorus ligand via the iron atom onto the carbonyls in **3a–d**. This is also reflected in the IR spectra of **3a–d**, where two intense ν(CO) bands at 1987–1989 cm^{-1} and 1940–1941 cm^{-1} are hypsochromically shifted when compared with **3e** (1973 and 1925 cm^{-1}). In the classically polarized phosphaalkenes (η^5-C_5Me_5)-$(CO)_2FeP{=}C(SiMe_3)_2$ (**3f**) and (η^5-C_5Me_5)$(CO)_2FeP{=}$ $C(Ph)(SiMe_3)$ (**3g**) the ^{13}C(CO) NMR signals were observed at δ = 217.6 and 216.1, respectively, and the ν(CO) bands in the IR spectra occurred at $\tilde{\nu}$ = 1988 and 1942 or 1993 and 1940 cm^{-1}, respectively.[4]

This spectroscopic evidence may be interpreted as with **3b**, as if the borderline between the inversely polarized ferriophosphaalkene **3e** and the more classically polarized compounds **3f** and **3g** has been trespassed.

To further substantiate this idea, X-ray structural analyses of **3a** and **3b** were necessary.

X-ray Structural Analysis of 3a

Single crystals of **3a** were grown from toluene at −30 °C. The molecular structure of **3a** is related to that of the metallophosphaalkene **3e**.[6] The molecule displays a distorted "piano stool" geometry [P(1)–Fe(1)–C(11) 91.8(1)°, P(1)–Fe(1)–C(12) 93.3(1)°, C(11)–Fe(1)–C(12) 96.5(2)°] (Figure 1).

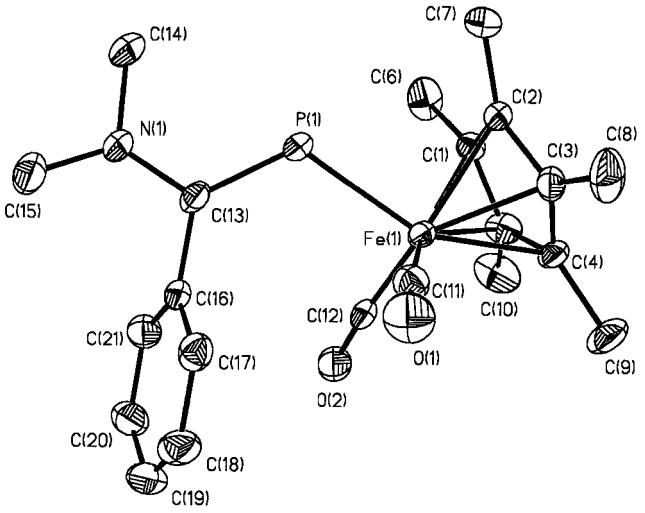


Figure 1. Molecular structure of **3a** in the crystal; selected bond lengths [Å] and angles [°]: Fe(1)–P(1) 2.316(1), Fe(1)–C(11) 1.764(4), Fe(1)–C(12) 1.766(4), P(1)–C(13) 1.717(4), N(1)–C(13) 1.399(4), N(1)–C(14) 1.452(5), N(1)–C(15) 1.449(5), C(13)–C(16) 1.495(5), O(1)–C(11) 1.138(5), O(2)–C(12) 1.137(4); P(1)–Fe(1)–C(11) 91.8(1), P(1)–Fe(1)–C(12) 93.3(1), C(11)–Fe(1)–C(12) 96.5(2), Fe(1)–C(11)–O(1) 176.2(4), Fe(1)–C(12)–O(2) 174.1(3), Fe(1)–P(1)–C(13) 118.9(1), P(1)–C(13)–N(1) 120.0(3), P(1)–C(13)–C(16) 126.1(2), N(1)–C(13)–C(16) 113.7(3), C(13)–N(1)–C(14) 118.5(3), C(13)–N(1)–C(15) 120.8(3), C(14)–N(1)–C(15) 113.3(3)

Two of the legs are represented by nearly linear terminal carbonyl ligands. The organophosphorus ligand is connected with the $(C_5Me_5)(CO)_2Fe$ fragment by a Fe–P single bond of 2.316(1) Å, which compares well with that in **3e** [2.325(2) Å]. The same holds true for the P=C bond lengths in both molecules [**3a**: 1.717(4) Å; **3e**: 1.709(5) Å], which fall in the typical region of 1.70–1.76 Å usually determined for amino-substituted phosphaalkenes.[12] The P=C bond is in an (*E*) configuration, with the iron atom and the phenyl group on the same side of the molecule. Presumably due to steric congestion, the angles Fe(1)–P(1)–C(13) [118.9(1)°] and P(1)–C(13)–C(16) [126.1(2)°] are markedly different. The phenyl ring is twisted out of the plane defined by the atoms Fe(1), P(1), and C(13) by 70.7°. The angle at the P atom in **3e** was found to be 117.9(2)°. The carbon atom C(13) in **3a** is in a trigonal-planar configuration (sum of angles = 359.8°), featuring a bond length of 1.399(4) Å to the slightly pyramidal nitrogen atom (sum of angles = 352.6°). The plane defined by the atom C(13), C(14), and C(15) encloses an angle of 16.6° with the plane through the atoms Fe(1), P(1), and C(13). This allows for effective π-conjugation of the lone-pair at the nitrogen atom with the P=C bond. In line with this, bond N(1)–C(13) is markedly shorter than the calculated value for a $C_{(sp^2)}$–$N_{(sp^2)}$ single bond (1.45 Å).[12] In **3e**, the pyramidal geometry was only observed for the N atom of the *trans*-oriented dimethylamino group [sum of angles = 350.5°, *d*(CN) = 1.410(7) Å]. The NMe_2 unit in a *cis*-disposition to the iron atom of **3e** was planar [sum of angles = 360.0°, *d*(CN) = 1.372(8) Å].

X-ray Structural Analysis of 3b

Single crystals of **3b** were grown from toluene at −30 °C. Again the molecule possesses a distorted piano stool configuration at the $(\eta^5\text{-}C_5Me_5)(CO)_2Fe$ unit (Figure 2).

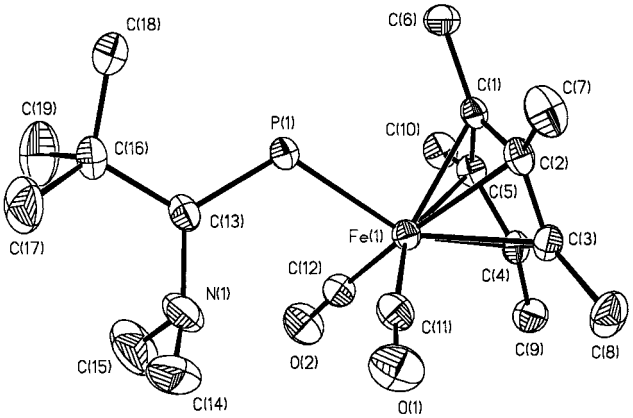


Figure 2. Molecular structure of **3b** in the crystal; selected bond lengths [Å] and angles [°]: Fe(1)−P(1) 2.276(1), Fe(1)−C(11) 1.756(3), Fe(1)−C(12) 1.756(3), P(1)−C(13) 1.697(3), N(1)−C(13) 1.448(4), N(1)−C(14) 1.447(5), N(1)−C(15) 1.449(5), C(13)−C(16) 1.551(4); P(1)−Fe(1)−C(11) 89.7(1), P(1)−Fe(1)−C(12) 90.0(1), C(11)−Fe(1)−C(12) 97.1(1), Fe(1)−C(11)−O(1) 173.8(3), Fe(1)−C(12)−O(2) 174.6(3), Fe(1)−P(1)−C(13) 117.0(1), P(1)−C(13)−N(1) 120.8(2), P(1)−C(13)−C(16) 118.8(2), N(1)−C(13)−C(16) 120.4(2), C(13)−N(1)−C(14) 118.1(3), C(13)−N(1)−C(15) 118.0(3), C(14)−N(1)−C(15) 112.1(3)

The Fe−P bond of 2.276(1) Å, however, is much shorter than in **3a**. Interestingly, the dimethylamino group at the P=C double bond [P(1)−C(13) = 1.697(3) Å] is oriented nearly perpendicular to the plane defined by the atoms Fe(1), P(1), and C(13) (= 86.7°) thus preventing any notable π-conjugation. In keeping with this, the atomic distance N(1)−C(13) of 1.448(4) Å is much longer than in **3a** and compares well with the remaining bond lengths N(1)−C(14) [1.447(5) Å], and N(1)−C(15) [1.449(5) Å]. The nitrogen atom is slightly pyramidal [sum of angles = 348.2°] with its lone pair directed towards the carbonyl ligands. The atom C(13) is trigonal-planarly ligated with a *tert*-butyl group in *trans*-disposition to the bulky $(\eta^5\text{-}C_5Me_5)(CO)_2Fe$ unit. The valence angle at the P atom [117.0(1)°] compares well with those in **2a** and **2e** (vide supra). The peculiarities in the spectroscopic data of **2b** in relation to those of **2a** and **2e** can be rationalized by a non-existent N(lone pair)−P=C π conjugation, which is the prerequisite for excess electron density to the P atom. The lack of electronic repulsion between an electron abundant phosphorus atom and the (also) electron-rich iron-complex fragment in **3b** allows for a much shorter Fe−P distance. To further support these arguments, the X-ray structural analysis of the "classically" polarized ferriophosphaalkene $[(\eta^5\text{-}C_5Me_5)(CO)_2FeP{=}C(Ph)(SiMe_3)]$ (**3g**)[4,13] is included in this paper.

X-ray Structural Analysis of 3g

Single crystals of **3g** were grown from *n*-pentane at −4 °C. The analysis shows that the molecule is bisected by a mirror plane defined by the atoms Si(1), C(10), P(1), and Fe(1) (Figure 3).

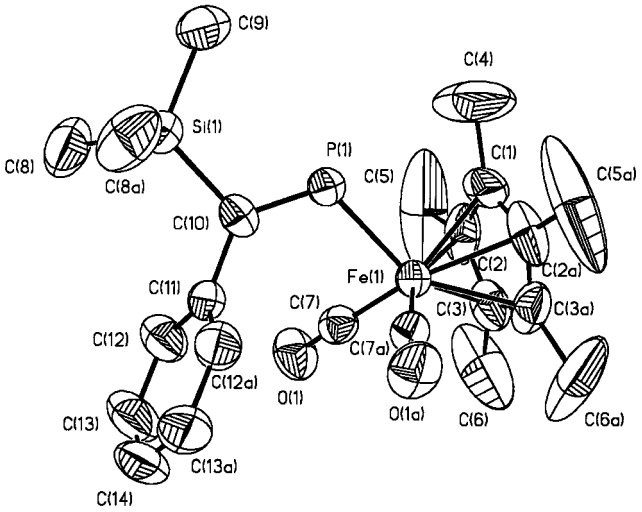


Figure 3. Molecular structure of **3g** in the crystal; selected bond lengths [Å] and angles [°]: Fe(1)−P(1) 2.269(2), Fe(1)−C(7) 1.749(5), P(1)−C(10) 1.665(6), C(10)−Si(1) 1.887(7), C(10)−C(11) 1.484(8), O(1)−C(7) 1.148(5); P(1)−Fe(1)−C(7) 90.2(2), C(7)−Fe(1)−C(7a) 99.0(3), Fe(1)−P(1)−C(10) 119.3(2), P(1)−C(10)−Si(1) 117.6(5), P(1)−C(10)−C(11) 129.4(5), Si(1)−C(10)−C(11) 112.9(4), Fe(1)−C(7)−O(1) 174.5(4)

The pentamethylcyclopentadienyl ring is disordered. The organophosphorus ligand in the "piano stool"-configured complex fragment is of primary interest for our discussion. As is observed for **3a**, an (*E*) configuration at the P=C double bond with an orthogonally directed phenyl ring in the vicinity of the $Fe(CO)_2$ unit is observed. However, in marked contrast to **3a** the bond Fe(1)−P(1) [2.269(2) Å] is shorter and compares more favorably with the bond encountered in **3b**. The P=C double bond of **3g** [1.665(6) Å] is shorter than in the inversely polarized phosphaalkenes **3a** and **3e**, and more typical for "classically polarized" phosphaalkenes without π-donating atoms at the methylene carbon atom. The valence angle Fe(1)−P(1)−C(10) of 119.3(2)° compares well with the corresponding data in **3a**, **3b**, and **3e**. The angle P(1)−C(10)−C(11) [129.5(4)°] at the trigonal planar carbon atom C(10) [sum of angles = 360.0°] is markedly more obtuse than the angle P(1)−C(10)−Si(1) [117.6(5) Å] at the side opposite to the bulky iron-complex fragment.

Conclusions

In a series of ferriophosphaalkenes of the type $[(\eta^5\text{-}C_5Me_5)(CO)_2FeP{=}CR^1(NR^2_2)]$ (R^1 = Ph, *t*Bu, 3,4,5-$(MeO)_3C_6H_2$; NR^2_2 = NMe_2, pip) it was demonstrated that the phenomenon of an inverse electron density distribution $P^{\delta-}\ C^{\delta+}$ is only realized whenever an allylic-like π-conjuga-

tion of the lone pair at the N atom with the P=C π-bond is possible. In such molecules, where the lone pair at the nitrogen atom is oriented perpendicular to the PC-π-system, a classical behavior concerning the polarity of the P=C bond ($P^{\delta+}$ $C^{\delta-}$) is observed. In an earlier paper Appel already pointed to a correlation between ^{31}P-NMR shifts of amino-substituted phosphaalkenes and the dihedral angle between the plane that includes the atoms P, C, N, and the NR_2 plane.[14]

Experimental Section

All manipulations were performed under dry nitrogen. Solvents were rigorously dried with an appropriate drying agent and freshly distilled before use. − The following compounds were prepared according to literature procedures: Thioamides $PhC(S)NMe_2$, tBuC(S)NMe_2, and {3,4,5-$(MeO)_3C_6H_2$}C(S)NMe_2 were obtained from the corresponding amides and P_4S_{10}.[15] PhC(S)pip was synthesized from benzaldehyde, piperidine, and sulfur.[16] The carbenium salts [PhC(SMe)NMe_2)I (**1a**)[17] and [PhC(SMe)pip]I (**1d**)[18] resulted from the corresponding thioamides and methyl iodide. [η^5-$Cp^*(CO)_2FeCl$],[11] $LiP(SiMe_3)_2 \cdot DME$[9] − IR spectra: Bruker FT-IR VECTOR 22. − ^{1}H-, ^{13}C-, ^{29}Si-, and ^{31}P-NMR spectra at room temp.; Bruker AC 100 (^{1}H, 100.13 MHz; ^{31}P, 40.53 MHz), Bruker Avance DRX 500 (^{1}H, 500.13 MHz; ^{13}C, 125.75 MHz; ^{29}Si, 99.53 MHz; ^{31}P, 202.46 MHz) references: $SiMe_4$ (^{1}H, ^{13}C, ^{29}Si), 85% D_3PO_4 (^{31}P).

[Me_2N(tBu)CSMe]I (1b): A solution of iodomethane (9.38 g, 66.1 mmol) in diethyl ether (60 mL) was added dropwise at ambient temp. to an ethereal solution (250 mL) of tBuC(S)NMe_2 (9.38 g, 66.1 mmol). Stirring was continued for 24 h. The precipitate was filtered, washed with diethyl ether (2 × 30 mL) and dried in vacuo to give 10.52 g (56%) of **1b** as a white powder. − ^{1}H NMR ($CDCl_3$): δ = 1.44 (s, 9 H, tBu), 2.94 (s, 3 H, SCH_3), 3.76 (s, 6 H, NCH_3). − ^{13}C{^{1}H} NMR ($CDCl_3$): δ = 23.3 (s, SCH_3), 28.7 [s, C(CH_3)$_3$], 44.3 [s, $C(CH_3)_3$], 49.4 (s, NCH_3), 53.5 (s, NCH_3), 203.7 (s, CH_3SC). − $C_8H_{18}INS$ (287.2): calcd. C 33.46, H 6.32, N 4.88; found C 33.41, H 6.05, N 4.90.

[{3,4,5-$(MeO)_3C_6H_2$}C(NMe_2)SMe]I (1c): A solution of {3,4,5-$(MeO)_3C_6H_2$}C(S)NMe_2 (9.1 g, 35.6 mmol) in diethyl ether (500 mL) was slowly combined with iodomethane (5.06 g, 35.6 mmol). After 24 h of stirring at room temp. it was filtered to afford 6.28 g (44%) of **1c** as a colorless powder. − ^{1}H NMR ($CDCl_3$): δ = 2.29 (s, 3 H, SCH_3), 3.53 (s, 3 H, NCH_3), 3.81 (s, 3 H, p-OCH_3), 3.86 (s, 6 H, m-OCH_3), 6.99 (s, 2 H, H-phenyl). − ^{13}C{^{1}H} NMR ($CDCl_3$): δ = 18.7 (s, SCH_3), 45.8 (s, NCH_3), 49.0 (s, NCH_3), 57.2 (s, m-OCH_3), 60.8 (s, p-OCH_3), 104.1 (s, C-o-phenyl), 124.2 (s, C-i-phenyl), 140.1 (s, C-p-phenyl), 154.3 (s, C-m-phenyl), 190.7 (s, $CSCH_3$). − $C_{13}H_{20}INO_3S$ (397.4): calcd. C 39.30, H 5.07, N 3.53; found C 39.02, H 5.10, N 3.53.

Me_3SiP=C(Ph)NMe_2 (2a): To a slurry of [Me_2N(Ph)CSMe]I (**1a**) (27.60 g, 89.8 mmol) in a mixture of n-pentane (100 mL) and 1,2-dimethoxyethane (DME) (100 mL) at 0 °C was slowly added a solution of $LiP(SiMe_3)_2 \cdot DME$ (24.70 g, 89.8 mmol) in a mixture of n-pentane (70 mL) and DME (70 mL). The dark yellow slurry was warmed to room temp. and stirred for another 16 h. It was filtered, and the filter cake was washed with 30 mL of DME and then with two portions of 30 mL of n-pentane. Solvents and volatile components were removed in vacuo to afford a deep orange residue. The crude product was purified by vacuum distillation (bp = 55−75 °C, 5Pa) to give 11.50 g (54%) of **2a** as a light yellow oil, which contained small amounts of $P(SiMe_3)_3$ as an impurity. − ^{1}H NMR (C_6D_6): δ = 0.10 (d, $^3J_{P,H}$ = 4.7 Hz, 9 H, $SiCH_3$), 2.20 (s, br, 3 H, NCH_3), 3.07 (s, br, 3 H, NCH_3), 6.96−7.03 (m, 5 H, Ph). − ^{13}C{^{1}H} NMR (C_6D_6): δ = 2.5 (d, $^2J_{P,C}$ = 16.6 Hz, $SiCH_3$), 42.1 (s, NCH_3), 42.3 (s, NCH_3), 127.1−128.3 (C-o-, m-, p-phenyl), 143.5 (d, $^2J_{P,C}$ = 9.0 Hz, C-i-phenyl), 204.7 (d, $^1J_{P,C}$ = 65.2 Hz, P=C). − ^{29}Si{^{1}H} NMR (C_6D_6): δ = −4.1 (d, $^1J_{P,Si}$ = 56.1 Hz). − ^{31}P{^{1}H} NMR (C_6D_6): δ = 54.3 s. Analytically samples of **2a** could not be obtained due to partial decomposition to $P(SiMe_3)_3$.

Me_3SiP=C(tBu)NMe_2 (2b): A slurry of **1b** (7.97 g, 28.0 mmol) in a mixture of 60 mL of n-pentane and 30 mL of DME was treated at −30 °C with a solution of $LiP(SiMe_3)_2 \cdot DME$ in 60 mL of a 1:1 mixture of n-pentane and DME. Stirring at room temp. was stopped after 3 h, and the slurry was filtered. From the dark yellow filtrate 2.31 g (38%) of yellow **2b** was isolated by distillation (bp: 55−60 °C, 10 Pa). − ^{1}H NMR (C_6D_6): δ = 0.31 (d, $^3J_{P,H}$ = 13.9 Hz, 9 H, $SiCH_3$), 1.35 (d, $^3J_{P,H}$ = 1.2 Hz, 9 H, tBu), 2.76 (s, 6 H, NCH_3). − ^{13}C{^{1}H} NMR (C_6D_6): δ = 2.7 (d, $^2J_{P,C}$ = 13.0 Hz, $SiCH_3$), 31.6 [s, C(CH_3)$_3$], 43.7 [d, $^2J_{P,C}$ = 25.0 Hz, $C(CH_3)_3$], 47.80 (s, NCH_3), 219.7 (d, $^1J_{P,C}$ = 94.1 Hz, P=C). − ^{29}Si{^{1}H} NMR (C_6D_6): δ = −3.1 (d, $^1J_{P,Si}$ = 74.5 Hz). − ^{31}P{^{1}H} NMR (C_6D_6: δ = 68.7 s. − Analytically pure samples of **2b** could not be obtained. Major impurity is $P(SiMe_3)_3$.

Me_3SiP=C[3,4,5-$(MeO)_3C_6H_2$]NMe_2 (2c): A slurry of **1c** (17.80 g, 45.0 mmol) in a mixture of 50 mL of n-pentane and 50 mL of DME was cooled to −70 °C, and a solution of $LiP(SiMe_3)_2 \cdot DME$ (12.40 g, 45.0 mmol) was added dropwise. It was warmed to room temp. and stirred for 4 h. Filtration and removal of volatile components in vacuo led to 8.20 g of crude orange **2c** (56%). The thermolabile oil was contaminated with $P(SiMe_3)_3$ and decomposed completely upon distillation. − ^{1}H NMR (C_6D_6): δ = 0.17 (d, $^3J_{P,H}$ = 4.5 Hz, 9 H, $SiCH_3$), 2.34 (s, br, 3 H, NCH_3), 3.15 (s, br, 3H. NCH_3), 3.38 (s, 6 H, m-OCH_3), 3.81 (s, 3 H, p-OCH_3), 6.27 (s, 2 H, Ph). − ^{13}C{^{1}H} NMR (C_6D_6): δ = 2.6 (d, $^2J_{P,C}$ = 12.6 Hz, $SiCH_3$), 42.0 (s, NCH_3), 42.2 (s, NCH_3), 55.7 (s, m-OCH_3), 60.7 (s, p-OCH_3), 105.5 (d, $^3J_{P,C}$ = 14.6 Hz, C-o-phenyl), 138.6 (d, $^2J_{P,C}$ = 9.3 Hz, C-i-phenyl), 138.8 (s, C-p-phenyl), 153.7 (s, C-m-phenyl), 204.8 (d, $^1J_{P,C}$ = 65.4 Hz, P=C). −^{29}Si{^{1}H} NMR (C_6D_6): δ = −4.1 (d, $^1J_{P,Si}$ = 56.1 Hz). − ^{31}P{^{1}H} NMR (C_6D_6): δ = 50.3 s. Analytically pure samples of **2c** could not be obtained. Major impurity is $P(SiMe_3)_3$.

Me_3SiP=C(Ph)pip (2d): Similarly, crude thermolabile **2d** (2.27 g, 62%) was obtained as an orange oil from **1d** (4.80 g, 13.2 mmol) and $LiP(SiMe_3)_2$ DME (3.79 g, 13.8 mmol) in a mixture of n-pentane and DME at −50 °C. Stirring of the resulting yellow slurry at room temp. was maintained for 16 h. − ^{1}H NMR (C_6D_6): δ = 0.11 (d, $^3J_{P,H}$ = 4.6 Hz, 9 H, $SiCH_3$), 1.17 (s, br, 6 H, CH_2), 2.70 (s, br, 2 H, NCH_2), 3.90 (s, br, 2 H, NCH_2), 6.98−7.09 (m, 5 H, Ph). − ^{13}C{^{1}H} NMR (C_6D_6): δ = 2.5 (d, $^2J_{P,C}$ = 14.3 Hz, $SiCH_3$), 24.5 (s, br, CH_2), 26.8 (s, br, CH_2), 50.9 (s, NCH_2), 127.5−128.8 (C-o-, m-, p- phenyl), 146.6 (d, $^2J_{P,C}$ = 8.6 Hz, C-i-phenyl), 205.1 (d, $^1J_{P,C}$ = 64.8 Hz, P=C). − ^{29}Si{^{1}H} NMR (C_6D_6): δ = 3.5 (d, $^1J_{P,Si}$ = 57.5 Hz). − ^{31}P{^{1}H} NMR (C_6D_6): δ = 59.5 s. Analytically pure samples of **2d** could not be obtained. Major impurity is $P(SiMe_3)_3$.

[(η^5-C_5Me_5)$(CO)_2$FeP=C(Ph)NMe_2] (3a): A solution of **2a** (4.60 g, 19.5 mmol) in DME (30 mL) was added to a slurry of [(η^5-C_5Me_5)-$(CO)_2$FeCl] (5.50 g, 19.5 mmol) in cold n-pentane (40 mL, −30 °C).

Table 1. Crystal data and data collection parameters

Compound	**3a**	**3b**	**3g**
formula	$C_{21}H_{26}FeNO_2P$	$C_{19}H_{30}FeNO_2P$	$C_{22}H_{29}FeO_2PSi$
M_r	411.25	391.26	440.36
crystal dimensions [mm]	0.6 × 0.45 × 0.3	0.5 × 0.4 × 0.15	0.25 × 0.15 × 0.15
crystal system	orthorhombic	monoclinic	monoclinic
space group	$Pca2_1$	$P2_1/n$	$P2_1/m$
a [Å]	13.689(5)	10.613(4)	8.820(4)
b [Å]	8.536(2)	12.821(6)	12.567(9)
c [Å]	17.590(4)	15.351(6)	10.804(4)
β [°]	90	104.67(3)	102.93(3)
V [Å^3]	2055.4(10)	2020.7(14)	1167.2(11)
Z	4	4	2
$\rho_{calcd.}$ [Mg m^{-3}]	1.329	1.286	1.253
μ [mm^{-1}]	0.826	0.836	0.779
F(000)	864	832	464
T [K]	173	173	293
2 θ [°]	4.8−60.0	4.2−60.0	3.9−60.0
no refl. collected	6180	6168	7530
no. refl. unique	5691	5883	3562
no. refl. $I > 2\sigma(I)$	4406	4201	1252
R(int)	0.0463	0.0426	0.1527
refined parameters	242	240	142
GOF	1.025	1.033	0.990
R_F [$I > 2\sigma(I)$]	0.0510	0.0543	0.0737
wR_F^2 [$I > 2\sigma(I)$]	0.1064	0.1291	0.1060
Δρ max/min [e Å^{-3}]	0.384/−0.630	0.915/−0.696	0.4/−0.4

After warming up to ambient temp. the solution was stirred for 16 h. Solvents and volatile components were removed in vacuo to give a dark brown solid residue. This material was triturated with diethyl ether, filtered, and the filter-cake was washed with diethyl ether (2 × 20 mL). The filtrate was concentrated until the appearance of the first crystals and than stored at −28 °C. Product **3a** (5.41 g, 67 mmol) was isolated as dark-red needles. − IR (Nujol, cm^{-1}): $\tilde{\nu}$ = 1989 vs, (CO), 1941 vs (CO). − ^{1}H NMR (C_6D_6): δ = 1.46 [s, 15 H, $C_5(CH_3)_5$], 2.91 (s, 3 H, NCH_3), 2.92 (s, 3 H, NCH_3), 7.05−7.53 (m, 5 H, Ph). − ^{13}C{^{1}H} NMR (C_6D_6): δ = 9.0 [s, $C_5(CH_3)_5$], 43.7 (s, NCH_3), 95.7 [s, $C_5(CH_3)_5$], 126.9−129.8 (s, C-*o*-, *m*-, *p*-phenyl), 146.1 (d, $^2J_{P,C}$ = 7.7 Hz, C-*i*-phenyl), 199.8 (d, $^1J_{P,C}$ = 84.3 Hz, P=C), 218.1 (s, CO). − ^{31}P{^{1}H} NMR (C_6D_6): δ = 232.0 s. − $C_{21}H_{26}FeNO_2P$ (411.3) calcd. C 61.33, H 6.37, N 3.41; found C 61.18, H 6.28, N 3.40.

[(η^5-C_5Me_5)(CO)$_2$FeP=C(*t*Bu)NMe$_2$] (3b): A slurry of [(η^5-C_5Me_5)-(CO)$_2$FeCl] (1.11 g, 4.0 mmol) in *n*-pentane (20 mL) was combined with the solution of **2b** (0.85 g, 4.0 mmol) in 20 mL of DME. Analogous work-up furnished compound **3b** (0.80 g, 51%) as red needles. − IR (Nujol, cm^{-1}): $\tilde{\nu}$ = 1987 vs (CO), 1940 vs (CO). − ^{1}H NMR (C_6D_6): δ = 1.48 [s, 15 H, $C_5(CH_3)_5$], 1.56 [s, 9 H, $C(CH_3)_3$], 2.93 (s, 6 H, NCH_3). − ^{13}C{^{1}H} NMR (C_6D_6): δ = 9.1 [s, $C_5(CH_3)_5$], 34.0 [d, $^3J_{P,C}$ = 14.6 Hz, $C(CH_3)_3$], 46.4 (s, NCH_3), 48.4 [d, $^2J_{P,C}$ = 28.4 Hz, $C(CH_3)_3$], 96.1 [s, $C(CH_3)_5$], 217.3 (d, $^1J_{P,C}$ = 75.3 Hz, P=C), 218.3 (s, CO). − ^{31}P{^{1}H} NMR (C_6D_6): δ = 409.0 s. − $C_{19}H_{30}FeNO_2P$ (391.3): calcd. C 58.32, H 7.73, N 3.58; found C 58.28, H 7.73, N 3.26.

[(η^5-C_5Me_5)(CO)$_2$FeP=C[3,4,5-(MeO)$_3$C$_6$H$_2$]NMe$_2$] (3c): Analogously, dark-red crystals (0.55 g, 34%) of **3c** were synthesized from [(η^5-C_5Me_5)(CO)$_2$FeCl] (0.91 g, 3.2 mmol) and **2c** (1.06 g, 3.2 mmol) in a 1:1 mixture of DME and *n*-pentane at −50 °C. Stirring at room temp. was maintained for 16 h. − IR (Nujol, cm^{-1}): $\tilde{\nu}$ = 1971 vs (CO), 1935 vs (CO). − ^{1}H NMR (C_6D_6): δ = 1.45 [s, 15 H, $C_5(CH_3)_5$], 2.99 (s, 3 H, NCH_3), 3.00 (s, 3 H, NCH_3), 3.54 (s, 6 H, *m*-OCH_3), 3.89 (s, 3 H, *p*-OCH_3), 6.75 (s, 2 H, Ph). − ^{13}C{^{1}H} NMR (C_6D_6): δ = 9.0 [s, $C_5(CH_3)_5$], 4.35 (NCH_3), 42.6 (s, NCH_3), 55.6 (s, *m*-OCH_3), 55.9 (s, *m*-OCH_3), 60.6 (s, *p*-OCH_3), 95.8 [s, $C_5(CH_3)_5$], 107.4 (s, C-*o*-phenyl), 138.6 (s, C-*p*-phenyl), 141.3 (d, $^2J_{P,C}$ = 7.7 Hz, C-*i*-phenyl), 153.5 (s, C-*m*-phenyl). 199.8 (d, $^1J_{P,C}$ = 84.8 Hz, P=C), 218.5 (s, CO). − ^{31}P{^{1}H} NMR (C_6D_6): δ = 225.4 s. − $C_{24}H_{32}FeNO_5P$ (501.3): calcd. C 57.50, H 6.43, N 2.79; found C 57.23, H 6.56, N 2.71.

[(η^5-C_5Me_5)(CO)$_2$FeP=C(Ph)pip] (3d): Compound **3d** (0.79 g, 38%) resulted as red-brown needles from the reaction of [(η^5-C_5Me_5)-(CO)$_2$FeCl] (1.31 g, 4.6 mmol) and 1.28 g (4.6 mmol) of **2d** in an *n*-pentane/DME mixture at −78 °C. − IR (Nujol, cm^{-1}): $\tilde{\nu}$ = 1990 vs (CO), 1941 vs (CO). − ^{1}H NMR (C_6D_6): δ = 1.30−1.51 (m, 6 H, CH_2), 1.45 [s, 15 H, $C_5(CH_3)_5$], 3.44 (t, $^3J_{HH}$ = 5.4 Hz, NCH_2), 7.08−7.62 (m, 5 H, Ph). − ^{13}C{^{1}H} NMR (C_6D_6): δ = 9.0 [s, $C_5(CH_3)_5$], 24.9 (s, CH_2), 26.2 (s, CH_2), 52.7 (d, $^3J_{P,C}$ = 18.4 Hz, NCH_2), 95.8 [s, $C_5(CH_3)_5$], 127.0−130.0 (C-*o*-, *m*-, *p*-phenyl), 146.5 (d, $^2J_{P,C}$ = 7.2 Hz, C-*i*-phenyl), 201.3 (d, $^1J_{P,C}$ = 82.9 Hz, P=C), 218.0 (s, CO). − ^{31}P{^{1}H} NMR (C_6D_6): δ = 256.4 s. − $C_{24}H_{30}FeNO_2P$ (451.3): calcd. C 63.87, H 6.70, N 3.10; found C 63.77, H 6.50, N 3.07.

X-ray Crystallography: Crystallographic data were collected with a Siemens $P2_1$ four circle diffractometer with Mo-K_α (graphite monochromator, λ = 0.71073 Å). Crystallographic programs used for the structure solution and refinement were from SHELXTL PLUS and SHELXL-97. The structures were solved by Direct Methods and were refined by using full-matrix least squares on F^2 of all unique reflections with anisotropic thermal parameters for all non-hydrogen atoms. Hydrogen atoms were included at calculated positions with U(H) = 1.2 U_{eq} for groups, U(H) = 1.5 U_{eq} for CH_3 groups. Crystal data of the compounds are listed in Table 1.[19]

Acknowledgments

This work was generously supported by the Deutsche Forschungsgemeinschaft (Bonn, Germany) and the Fonds der Chemischen In-

dustrie (Frankfurt, Main, Germany) which are gratefully acknowledged.

[1] L. Weber, *Angew. Chem.* **1996**, *108*, 292−310; *Angew. Chem. Int. Ed.* **1996**, *35*, 271−288.

[2] [2a]L. Weber, K. Reizig, M. Frebel, R. Boese, M. Polk, *J. Organomet. Chem.* **1986**, *306*, 105−114. − [2b]L. Weber, K. Reizig, M. Frebel, *Chem. Ber.* **1986**, *119*, 1857−1867.

[3] L. Weber, S. Uthmann, H. Bögge, A. Müller, H.-G. Stammler, B. Neumann, *Organometallics* **1998**, *17*, 3593−3598.

[4] E. Niecke, H.-J. Metternich, M. Nieger, D. Gudat, P. Wenderoth, W. Malisch, C. Hahner, W. Reich, *Chem. Ber.* **1993**, *126*, 1299−1309.

[5] D. Gudat, E. Niecke, B. Krebs, M. Dartmann, *Chimia* **1985**, *39*, 277−279.

[6] L. Weber, O. Kaminski, H.-G. Stammler, B. Neumann, V. D. Romanenko, *Z. Naturforsch. B* **1993**, *48*, 1748−1794.

[7] [7a]R. B. Bedford, A. F. Hill, C. Jones, *Angew. Chem.* **1996**, *108*, 587−589; *Angew. Chem. Int. Ed. Engl.* **1996**, *35*, 347. − [7b]R. B. Bedford, A. F. Hill, C. Jones, A. J. P. White, D. J. Williams, J. D. E. T. Wilton-Ely, *Organometallics* **1998**, *17*, 4744−4753.

[8] L. Weber, M. H. Scheffer, H.-G. Stammler, B. Neumann, W. W. Schoeller, A. Sundermann, K. K. Laali, *Organometallics* **1999**, *18*, 4216−4221.

[9] G. Fritz, W. Hölderich, *Z. Anorg. Allg. Chem.* **1976**, *422*, 104−114.

[10] L. Weber, O. Kaminski, *Synthesis* **1995**, 158.

[11] R. B. King, M. B. Bisnette, *J. Organomet. Chem.* **1967**, *8*, 287−297.

[12] A. N. Chernega, A. V. Ruban, V. D. Romanenko, L. N. Markovskii, A. A. Korkin, M. Y. Antipin, Y. T. Struchkov, *Heteroatom. Chem.* **1991**, *2*, 229−241.

[13] A. Rühlicke, PhD Thesis, University of Bielefeld, **1994**.

[14] R. Appel, F. Knoll, I. Ruppert, *Angew. Chem.* **1981**, *93*, 771−784; *Angew. Chem. Int. Ed. Engl.* **1981**, *20*, 731.

[15] S. Raucher, P. Klein, *J. Org. Chem.* **1981**, *46*, 3558−3559.

[16] [16a] M. F. Aly, R. Grigg, *Tetrahedron* **1988**, *44*, 7271−7282. − [16b] F. Cornea, C. Cervasov, M. Ciureanu, *Spectrochim. Acta.* **1980**, *36a*, 775−782.

[17] F. Stansfield, *J. Chem. Soc. Perkin, Trans I* **1984**, 2933−2935.

[18] D. A. Field, F. Stansfield, *J. Chem. Soc.* **1952**, 4067−4075.

[19] Further details of the crystal structure investigations are available on request from the Cambridge Crystallographic Data Centre, CCDC, 12 Union Road, Cambridge CB 21EZ, UK, [Fax: int. code +44−1223/336-0335, E-mail: deposit@ccdc.cam.nc.uk], on quoting the depository numbers CCDC-137935 (**3a**), CCDC-137936 (**3b**), and CCDC-137937 (**3g**), together with the names of the authors, and the journal citation.

Received December 14, 1999
[I99458]

Molecular Architecture with 2,2′-Bipyrazine and Metal Ions: Infinite Loop and Molecular Square

Ralf-Dieter Schnebeck,[a] Eva Freisinger,[a] and Bernhard Lippert*[a]

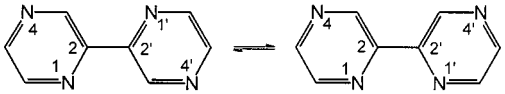
Dedicated to Professor Heinrich Vahrenkamp on the occasion of his 60th birthday

Keywords: N ligands / Palladium / Platinum / Silver / Molecular architecture / Structure elucidation

The potential of $[L_2Pd(2,2'\text{-bpz-}N^1,N^{1'})]^{2+}$ [L_2 = en (**1**), L = H_2O (**4a**), 2,2′-bpz = 2,2′-bipyrazine] for use as an angular element in the generation of self-organized systems of variable molecular architecture has been studied. Ag^+ forms an infinite loop **3** with **1**, in which the metal ions function as cross-linking agents between the organic entities 2,2′-bpz. Complex **4a**, on the other hand, self-assembles as a bis(μ-OH) dinuclear species **4b**, and in the presence of 4,4′-bipyridine (4,4′-bpy) as a molecular square **6** with the heteroaromatic 4,4′-bpy ligands representing the cross-linking entities.

Introduction

The generation of regularly shaped molecules ("molecular architecture") from organic ligands and metal entities is an area of great current interest.[1] Our own activities in this field have centered on combinations of linear (*trans*-a_2Pt^{II} with a = NH_3 or CH_3NH_2; Hg^{2+}) or *cis*-square planar (*cis*-a_2Pt^{II}, $enPt^{II}$, $enPd^{II}$) metal fragments and nucleobases or other heterocyclic ligands.[2] Among others, we have been able to isolate and characterize molecular rectangles,[3] hexagons,[4] open boxes,[4,5] triangles,[6] and barrels.[7] The use of 2,2′-bipyrazine (2,2′-bpz) proved to be particularly fortunate since it provided a large number of different metal-binding patterns due to the availability of four ring N donor atoms and its structural flexibility about the central C2−C2′ bond (Scheme 1).



Scheme 1

Interestingly, $enPd^{II}$ forms a mononuclear chelate with 2,2′-bpz, $[enPd(2,2'\text{-bpz-}N^1,N^{1'})]^{2+}$ (**1**),[6a] whereas under comparable conditions $enPt^{II}$ forms a cyclic trinuclear structure, $[\{enPt(2,2'\text{-bpz-}N^4,N^{4'})\}_3]^{6+}$,[7] which is to be considered the kinetic product of this reaction. It can be converted into the analogous chelate with $N(1),N(1')$−metal binding on prolonged heating.[7] The triangle can exist as different conformers, depending on the mutual orientation of the two pyrazine moieties of the 2,2′-bpz ligand.[7] Both the mononuclear Pd complex[6] and the Pt triangle[6a,7] can be applied as building blocks for larger aggregates by combining them with suitable metal fragments. For example, three $[enPd(2,2'\text{-bpz-}N^1,N^{1'})]^{2+}$ cations and three *trans*-$(NH_3)_2Pt^{II}$ units form a flat triangle **2** with Pd^{II} at the corners and Pt^{II} in the middle of the sides of the triangle,[6c] whereas combination of the Pt triangle $[\{enPt(2,2'\text{-bpz-}N^4,N^{4'})\}_3]^{6+}$ with three $enPd^{II}$ yields a hexanuclear molecular vase[6b] or with three Ag^+, a container compound.[7] Anion inclusion is a general phenomenon of all these compounds.

In continuation of this work we report herein the product obtained by cocrystallizing **1** with $AgClO_4$, as well as our efforts to prepare *cis*-$[(H_2O)_2M(2,2'\text{-bpz-}N^1,N^{1'})]^{2+}$ (M = Pd^{II}, Pt^{II}) instead of coordinatively saturated $[enPd(bpz\text{-}N^1,N^{1'})]^{2+}$ species and to probe their use as building blocks for regularly shaped macrocyclic compounds.

Results and Discussion

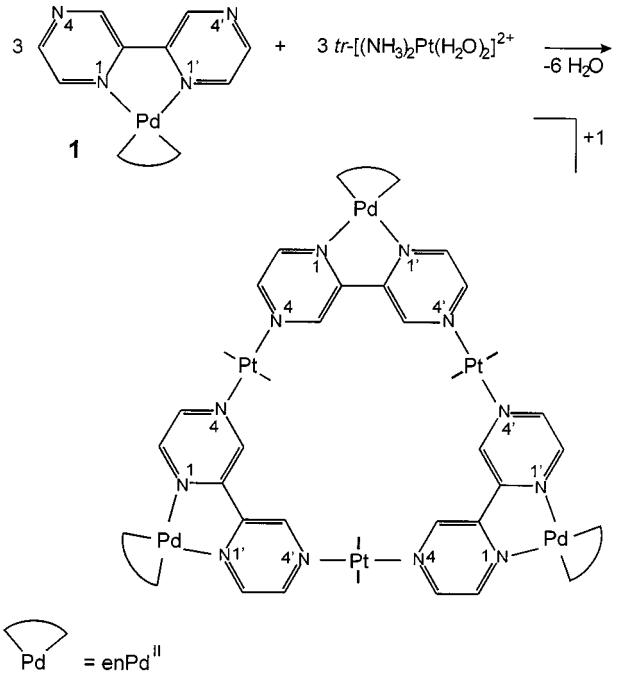
Infinite Loop Structure

As mentioned in the introduction, $[enPd(2,2'\text{-bpz-}N^1,N^{1'})]^{2+}$ (**1**) forms a triangle **2** with *trans*-$[(NH_3)_2Pt(H_2O)_2]^{2+}$, with the bpz ligands essentially coplanar with the six metal ions (Scheme 2).[6c] Although **2** forms an arrangement in the solid state that gives rise to a channel with a string of ClO_4^- anions in its center, the presence of the NH_3 ligands at Pt^{II} and their orientation essentially perpendicular to the plane of the triangle precludes any direct stacking of the cations. Rather, counter anions and water molecules are assisting formation of the channel. An obvious idea was to apply linearly coordinated metal ions such as Ag^+ instead of *trans*-$(NH_3)_2Pt^{II}$ in order to achieve neat stacking of the 2,2′-bpz entities. At the same time the use of Ag^+ instead of Pt^{2+} would somewhat reduce the high positive charge of the hexanuclear cation. However, the experiment carried out with $AgClO_4$ did not yield the anticipated closed triangular structure and neither did it generate a helical nor a polymeric open zigzag chain. Rather, as revealed by X-ray crystallography, an infinite loop is formed.

Figure 1 provides different views of the polymeric structure of $\{[enPd(2,2'\text{-bpz})Ag](ClO_4)_3\}_\infty$ (**3**). Selected bond

[a] Fachbereich Chemie, Universität Dortmund,
44221 Dortmund, Germany
Fax: (internat.) + 49-(0)231/755-3797

 © WILEY-VCH Verlag GmbH, D-69451 Weinheim, 2000 1434−1948/00/0606−1193 $ 17.50+.50/0



Scheme 2

lengths and angles of **3** are listed in Table 1. The geometry of the enPd(2,2′-bpz) moiety is normal.[6a] Ag(1) cross-links two [enPd(2,2′-bpz-N^1,$N^{1'}$)]$^{2+}$ fragments via two N(4) positions in a linear fashion, whereas there is a 160.4(3)° angle about Ag(2). It appears 1that deviation from linearity about the second silver ion is caused by the asymmetry of weak Ag(2)···$OClO_3^-$ interactions (Figure 2). The two enPd(2,2′-bpz) units bound to Ag(1) are coplanar, but those bound to Ag(2) form a dihedral angle of 30.5(2)°. As a consequence, Pd−Pd distances across Ag(1) are longer [13.930(2) Å] than those across Ag(2) [13.542(3) Å], and likewise distances between the Ag centers differ [Ag(1)···Ag(1′), 6.780(2) Å; Ag(2)···Ag(2′), 13.559(3) Å]. As evident from Figure 1, the respective metal cations are arranged in a collinear fashion along the *x* axis.

Table 1. Selected bond lengths [Å] and angles [°] of **3**

Pd(1)−N(1)	2.020(5)	N(1)−Pd(1)−N(12)	177.3(2)
Pd(1)−N(12)	2.025(5)	N(1)−Pd(1)−N(11)	98.2(2)
Pd(1)−N(11)	2.027(5)	N(12)−Pd(1)−N(11)	82.7(2)
Pd(1)−N(1′)	2.035(4)	N(1)−Pd(1)−N(1′)	80.3(2)
Ag(1)−N(4)	2.202(5)	N(12)−Pd(1)−N(1′)	98.8(2)
Ag(2)−N(4′)	2.200(4)	N(11)−Pd(1)−N(1′)	178.4(2)
		N(4)[a]−Ag(1)−N(4)	180
		N(4′)[b]−Ag(2)−N(4′)	160.4(3)

Symmetry operation: [a] $-x+1, -y, -z$. − [b] $-x+1, y, -z-1/2$.

Triangle vs. Alternatives

Reaction of **1** with Ag^+ can, in principle, lead to a triangle, an infinite helix, an infinite zigzag chain, or an infinite loop (Scheme 3). Formation of monomeric species with PdAg or $PdAg_2$ stoichiometry is not considered here. With $AgClO_4$ the loop structure is exclusively formed. Inspection of the solid state structure reveals why **3**, unlike the structurally related Pd_3Pt_3 compound **2**, does not from a triangle. At the same time it provides clues regarding the re-

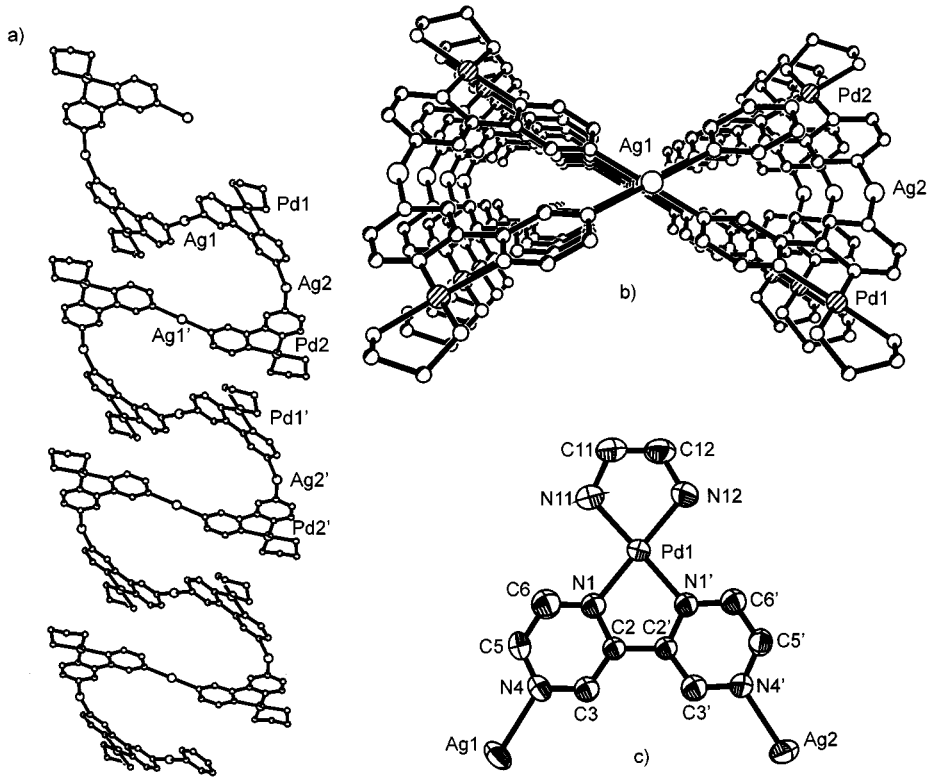


Figure 1. Side view (a), view along the *x* axis (b), and view of a section of [enPd(2,2′-bpz)Ag](ClO$_4$)$_3$ (**3**) (c); central Ag(1) ions are 6.780(2) Å apart, outer Ag(2) as well as Pd(1) ions are 13.559(3) Å apart, which correspond to the length of the crystallographic *c* axis

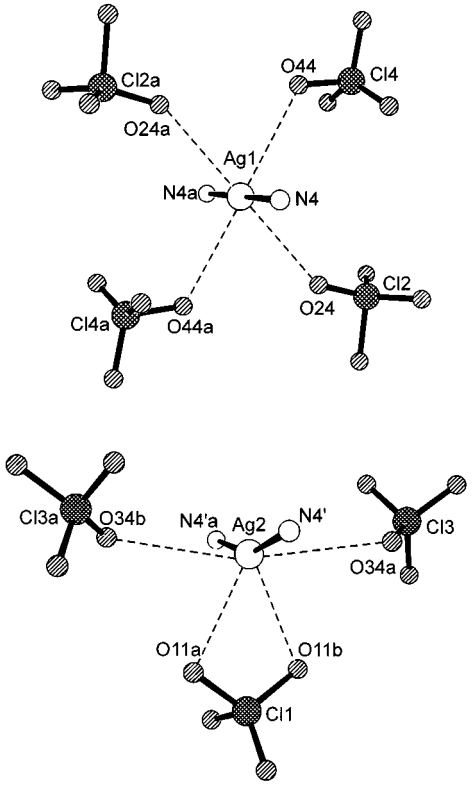


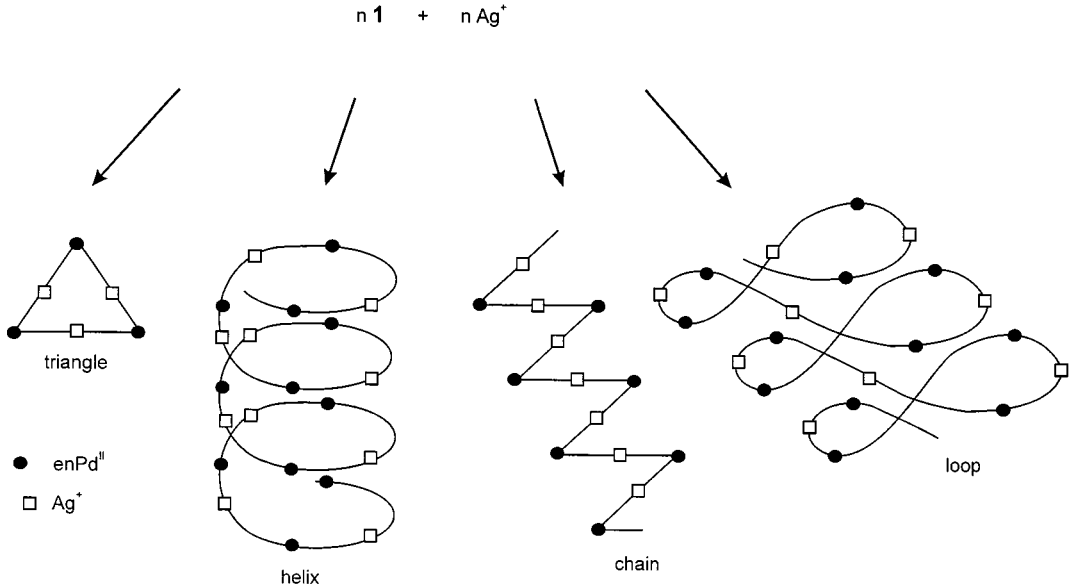
Figure 2. Different environments of Ag(1) and Ag(2) ions; Ag···O contacts are as follows: Ag(1)···O(44), 2.770(7) Å; Ag(2)···O(34a), 2.96(2) Å; Ag(2)···O(11a), 2.71(2) Å; Ag(1)···O(24), 2.71(2) Å

quirements for formation of all four feasible arrangements. There are two geometrical features that prevent closure of a Pd_3Ag_3 combination to form a triangle: First, the loss of coplanarity of the enPd(2,2′-bpz) entities cross-linked by Ag(2). Second, the *head-tail* orientation of the two enPd(2,2′-bpz) entities cross-linked by Ag(1). For formation of a closed triangle, mutual *head-head* orientation of all three enPd(2,2′-bpz) units is absolutely essential. It appears that the loss of collinearity about Ag(2) is of less importance, even though it might facilitate the propeller twist, hence loss of coplanarity of the two bpz ligands bound to Ag(2). The two geometrical parameters mentioned above therefore determine which of the three possible alternatives to the triangle is formed (Table 2).

Table 2. Relationship between possible structures derived from [enPd(2,2′-bpz- N^1,$N^{1'}$)]$^{2+}$ and linear metal entities from geometrical parameters

Structure	Angles [°] between three adjacent bpz ligands	Mutual orientation of adjacent bpz ligands
Triangle	ca. 0	all *head-head*
1D helix	at least 1 angle ≠ 0	all *head-head*
Loop	at least 1 angle ≠ 0	1 *head-tail*
Zigzag chain	0 or ≠ 0	all *head-tail*

We suspect that in addition to concentration effects, which should favor formation of a triangle in more dilute solution and of polymeric structures in concentrated solution, the role of the anions may be crucial in determining the solid-state structure. Although we have varied the Ag salts ($AgNO_3$, $AgPF_6$), we were unable to obtain crystals of sufficient quality for X-ray analysis with NO_3^- and PF_6^- anions. According to ^{1}H-NMR spectroscopy, **3** is labile in aqueous solution and dissociates into **1**, Ag^+, and ClO_4^-. Crystallization thus necessarily occurs from a concentrated solution, thereby favoring a polymeric structure. We note that polymeric helical structures are quite common in systems comprised of heterocyclic N-donor ligands, Ag^+ ions and poorly coordinating anions.[8] There is also an interesting parallel in the literature between our previously described Pd_3Pt_3 triangle[6c] and the polymeric PdAg structure of **3**: Kim et al.[9] have described a molecular triangle comprised of $enPt^{II}$ corners and sides that consist of pseudorotaxanes [cucurbituril entity treaded by the bifunctional

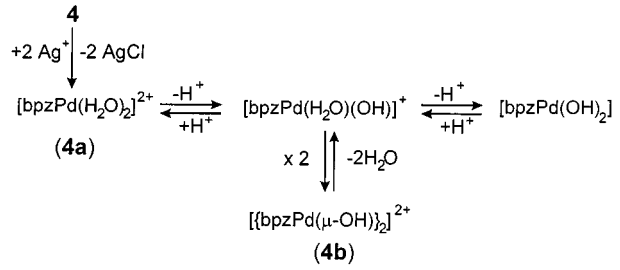


Scheme 3

N,*N*′-bis(3-pyridylmethyl)-1,4-diaminopentane], yet find formation of a 1D helix when enPt^{II} is replaced by Ag^+.[10]

Utility of *cis*-[$(H_2O)_2$M(2,2′-bpz-N^1,$N^{1'}$)]$^{2+}$ as Building Block

Our previous efforts to use 2,2′-bpz compounds had focused on coordinatively saturated enM^{II} (M = Pd or Pt) complexes with this ligand. In order to generate a molecular architecture with **1** (triangle,[6a] loop, vase[7]) bridging metal ions had to be applied. Their function was to cross-link N(4) positions. By replacing the en ligand by two Cl^- ligands, building blocks which have the potential of additional substitution of the Cl^- ligands are feasible, and hence permit an extension in two directions: Metal cross-linking through the available N(4) sites as in the case of **1** (above) and/or coordination of bridging ligands by substitution of the chloro ligands. In order to further pursue this option, we have prepared [Cl_2Pd(2,2′-bpz-N^1,$N^{1'}$)] (**4**) by reaction of K_2PdCl_4 with 2,2′-bpz and subsequently abstracted the Cl^- ligands by $AgNO_3$ to produce [$(H_2O)_2$Pd(2,2′-bpz-N^1,$N^{1'}$)]$(NO_3)_2$ (**4a**) (Scheme 4). pD-dependent ^{1}H-NMR spectra of **4a** (Figure 3) reveal formation of at least one kinetically inert (NMR time scale!) intermediate between [$(H_2O)_2$Pd(2,2′-bpz)]$^{2+}$ at low pH and the high-pH species [$(OH)_2$Pd(2,2′-bpz)]. Isolation on a preparative scale proved that this species is the dinuclear, μ-OH bridged complex [(2,2′-bpz)Pd$(OH)_2$Pd(2,2′-bpz)]$(NO_3)_2$ (**4b**). Spectra in the pD = 6−7 range indicate the presence of yet another, unidentified species. In analogy to the behavior of *cis*-[$(NH_3)_2$Pt$(H_2O)_2$]$^{2+}$,[11] [enPt$(H_2O)_2$]$^{2+}$,[12] and [enPd$(H_2O)_2$]$^{2+}$,[13] which form both μ-OH dimers, μ-OH trimers and even μ-OH tetramers,[12a] these resonances might be due to one of these higher oligomers. There is no indication of any (measurable) oligomerization of **4a** via the available N(4) sites of the 2,2′-bpz ligand.



Scheme 4

The cation of [(2,2′-bpz-N^1,$N^{1'}$)Pd$(OH)_2$Pd(2,2′-bpz-N^1,$N^{1'}$)]$(NO_3)_2$·4 H_2O (**4b**) is depicted in Figure 4. Selected interatomic distances and angles are given in Table 3.

The geometry of the central PdO_2Pd core compares very well with that of the μ-OH Pt^{II} dimer mentioned above,[11a] except that the Pd···Pd separation is somewhat shorter than that of Pt···Pt. Features of the (bpz-N^1,$N^{1'}$)Pd^{II} entity are similar to those observed in related complexes.[6,7] Dinuclear cations of **4b** are arranged like the tiles of a roof in stacks with parallel 2,2′-bpz ligands approximately 3.1 Å apart. NO_3^- anions and water molecules run in channels between individual stacks and interconnect these by hydrogen-bond formation and weak axial Pd···ONO_2 contacts. For example, NO_3^- is hydrogen-bonded to a μ-OH group [2.805(4) Å], has a contact with Pd [3.370(4) Å], and forms another hydrogen bond with a water molecule [2.807(5) Å] which in turn shows a weak contact [3.38(4) Å] with C(5)H of 2,2′-bpz in a neighboring stack.

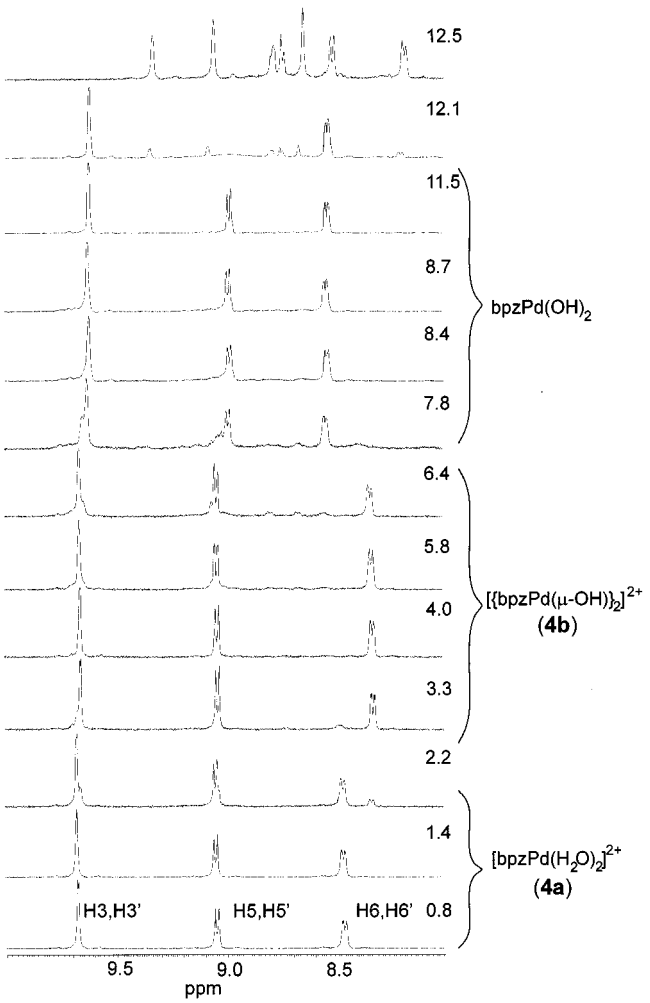


Figure 3. pD-dependent ^{1}H-NMR spectra of [(2,2′-bpz)Pd$(H_2O)_2$]$^{2+}$ in D_2O; above pD = 12 complex decomposition or rearrangement reactions take place

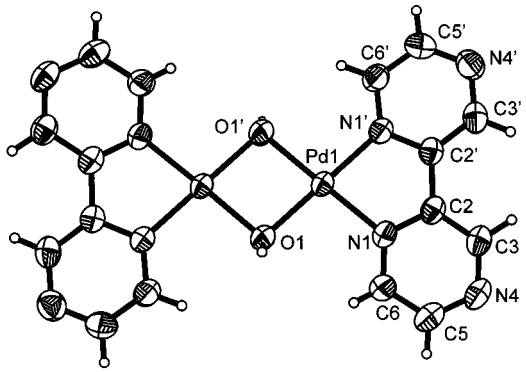


Figure 4. Molecular cation of [(2,2′-bpz-N^1,$N^{1'}$)Pd$(OH)_2$Pd(2,2′-bpz-N^1,$N^{1'}$)] $(NO_3)_2$·4 H_2O (**4b**) with atom numbering scheme; the Pt analogue **5b** is isostructural and not shown

Table 3. Selected bond lengths [Å] and angles [°] of **4b**

Pd(1)−N(1′)	1.981(3)	N(1′)−Pd(1)−N(1)	81.5(1)
Pd(1)−N(1)	1.994(2)	N(1′)−Pd(1)−O(1)[a]	178.5(1)
Pd(1)−O(1)[a]	2.005(2)	N(1)−Pd(1)−O(1)[a]	98.8(1)
Pd(1)−O(1)	2.005(2)	N(1′)−Pd(1)−O(1)	97.4(1)
Pd(1)−Pd(1)[a]	3.0185(6)	N(1)−Pd(1)−O(1)	178.6(1)
		O(1)[a]−Pd(1)−O(1)	82.3(1)
		Pd(1)[a]−O(1)−Pd(1)	97.7(1)

[a] Symmetry operation: $-x, -y, -z + 1$.

Table 4. Selected bond lengths [Å] and angles [°] of the Pt analogue of **4b**, compound **5b**

Pt(1)−N(1′)	1.960(8)	N(1′)−Pt(1)−N(1)	81.6(3)
Pt(1)−N(1)	1.975(7)	N(1′)−Pt(1)−O(1)	178.7(3)
Pt(1)−O(1)	2.009(7)	N(1)−Pt(1)−O(1)	99.6(3)
Pt(1)−O(1)[a]	2.036(7)	N(1′)−Pt(1)−O(1)[a]	98.7(3)
Pt(1)−Pt(1)[a]	3.0972(8)	N(1)−Pt(1)−O(1)[a]	179.5(3)
		O(1)−Pt(1)−O(1)[a]	80.0(3)
		Pt(1)−O(1)−Pt(1)[a]	100.0(3)

[a] Symmetry operation: $-x, -y + 2, -z + 1$.

Similarly to **4**, the corresponding Pt complex **5** was prepared, although it was not isolated in analytically pure form. Treatment of **5** with $AgNO_3$ and crystallization at pH ≈ 3 gave the isostructural Pt analogue of **4b** [(2,2′-bpz-N^1,$N^{1'}$)Pt(OH)$_2$Pt(2,2′-bpz-N^1,$N^{1'}$)](NO$_3$)$_2$·4 H$_2$O (**5b**) in crystalline form, yet low yield. The compound is not shown, but selected structural details are listed in Table 4. The purity of **5b** was also established by ^{195}Pt- as well as ^{1}H-NMR spectroscopy in D_2O [δ = 9.64 (s, H3, H3′), 9.02 (d, J = 4 Hz, H5, H5′), 8.88 (d, H6, H6′)]. The position of the ^{195}Pt-NMR singlet at δ = −1442 agrees well with that of the μ-OH dimer derived from (*trans*-1,2-diaminocyclohexane)Pt^{II},[14] but differs from that of *cis*-[(NH$_3$)$_2$Pt(OH)$_2$Pt(NH$_3$)$_2$]$^{2+}$ (δ = −1156).[15] Addition of DNO_3 (pD = 1) converts **5b** into monomeric [(D$_2$O)$_2$Pt(2,2′-bpz)]$^{2+}$ (^{1}H-NMR resonances at δ = 9.69, 9.04, 8.84), while addition of NaOD (pD = 7) in a slow reaction gives [(OH)$_2$Pt(2,2′-bpz)] (^{1}H-NMR resonances at δ = 9.49, 9.04, 8.88).

Open Molecular Box ("Square")

Conversion of **4b** to [(H$_2$O)$_2$Pd(2,2′-bpz-N^1,$N^{1'}$)]$^{2+}$ (**4a**) and subsequent reaction with 4,4′-bipyridine (4,4′-bpy) yielded the cyclic compound [{(bpz-N^1,$N^{1'}$)Pd(4,4′-bpy)}$_4$](NO$_3$)$_8$·14.4 H$_2$O (**6**) in high yield. Figure 5 gives a view of the tetranuclear cation.

Table 5. Selected bond lengths [Å] and angles [°] of **6**

Pd(1)−N(11a)	2.010(8)	N(11a)−Pd(1)−N(11b)	80.6(3)
Pd(1)−N(11b)	2.008(8)	N(11a)−Pd(1)−N(11c)	173.5(3)
Pd(1)−N(11c)	2.001(8)	N(11a)−Pd(1)−N(21d)	95.9(3)
Pd(1)−N(21d)	2.009(8)	N(11b)−Pd(1)−N(11c)	94.7(3)
		N(11b)−Pd(1)−N(21d)	175.9(4)
		N(11c)−Pd(1)−N(21d)	88.9(3)
Pd(2)−N(21a)	2.035(8)	N(21a)−Pd(2)−N(21b)	80.3(3)
Pd(2)−N(21b)	2.009(8)	N(21a)−Pd(2)−N(21c)	175.0(3)
Pd(2)−N(21c)	2.003(8)	N(21a)−Pd(2)−N(11d)[a]	96.1(3)
Pd(2)−N(11d)[a]	2.034(8)	N(21b)−Pd(2)−N(21c)	95.4(3)
		N(21b)−Pd(2)−N(11d)[a]	174.6(3)
		N(21c)−Pd(2)−N(11d)[a]	88.4(3)

[a] Symmetry operation: $-x + 1, -y, -z + 2$.

Salient structural features are listed in Table 5. The cation bears a close resemblance to related molecular squares[16] built of 4,4′-bpy sides and segments of two-dimensional networks containing the 4,4′-bpy square motif, respect-

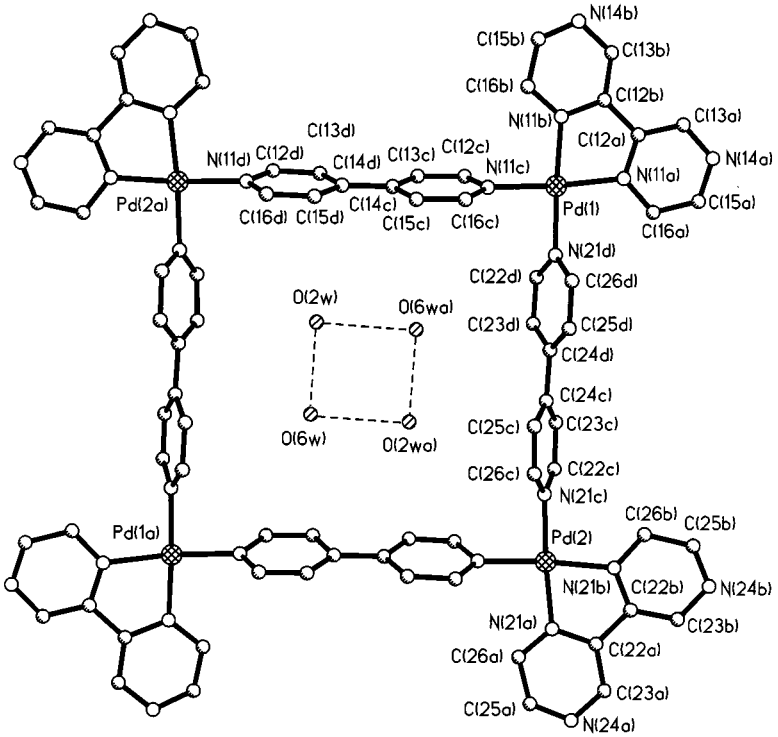


Figure 5. View of tetranuclear cation of **6** with four water molecules inserted

ively.[17] The four heavy-metal ions are exactly coplanar (as opposed to a strongly puckered, hence nonplanar arrangement as seen with bulky phosphane groups at the metal entities[16]), forming a square with edge-to-edge distances of ca. 11.057(3) Å and diagonal Pd···Pd distances of 15.703(4) Å [Pd(1)···Pd(1)] and 15.603(4) Å [Pd(2)···Pd(2)]. Of the 4,4′-bpy units in **6**, two are markedly twisted [41.6(3)°] about the central C−C bond, while the two others are hardly twisted [1.5(7)°]. Nevertheless, the four 4,4′-bpy ligands are approximately perpendicular to the Pd_4 square, thus making **6** in essence an "open box".[18] The coordination geometries of the Pd corner units deviate markedly from the ideal square-plane as far as angles are concerned. Four water molecules, interacting through H bonds [O(2w)···O(6w), 2.97(2) Å] and almost coplanar with the Pd_4 plane [deviations 0.26(2) Å for O(2w); 0.25(2) Å for O(6w)], reside in the center of the square. Tetranuclear cations of **6** stack, at a distance of 6.302(1) Å between Pd centers, in such a way as to produce long channels (Figure 6), which run along the *y* axis. Individual segments of the channel (Pd_4 squares) are interrupted by four NO_3^- anions, which are oriented parallel to the Pd_4 plane and sandwiched between individual squares. Pd···O distances are 3.02(1) Å [Pd(1)···O(22)] and 3.09(1) Å [Pd(2)···O(12)]. The remaining anions are distributed as follows: Pairs of NO_3^- anions (50% occupancy) are oriented perpendicular to the Pd_4 planes in the space between layers of Pd_4 squares. They show multiple hydrogen bonding interactions with additional water molecules. The remaining NO_3^- anions (three per tetranuclear cation) reside at the outside of the square, hence between individual channels.

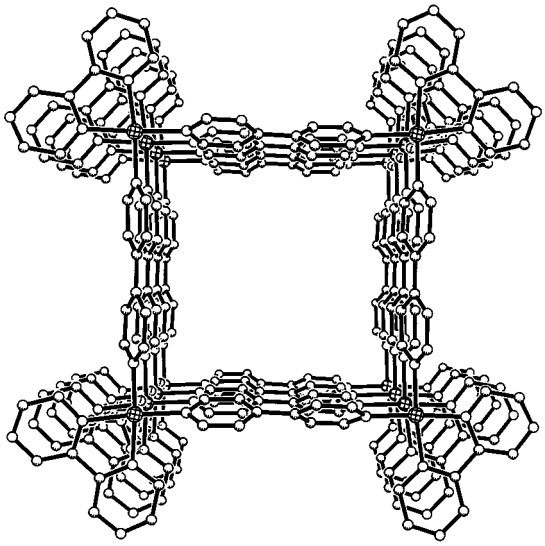
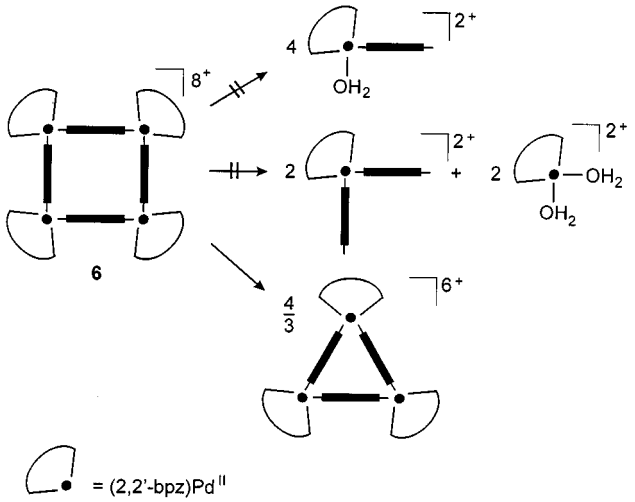


Figure 6. Packing diagram with channel formed by cations of **6**; the view is along the *y* axis; nearest intercationic Pd···Pd distances are 6.302(1) Å; water molecules and NO_3^- anions are omitted

Formation of similar channels has been reported before,[16,17,19] occasionally with inclusion of strongly hydrophobic guests such as *o*-halobenzene[17] or naphthalene.[19]

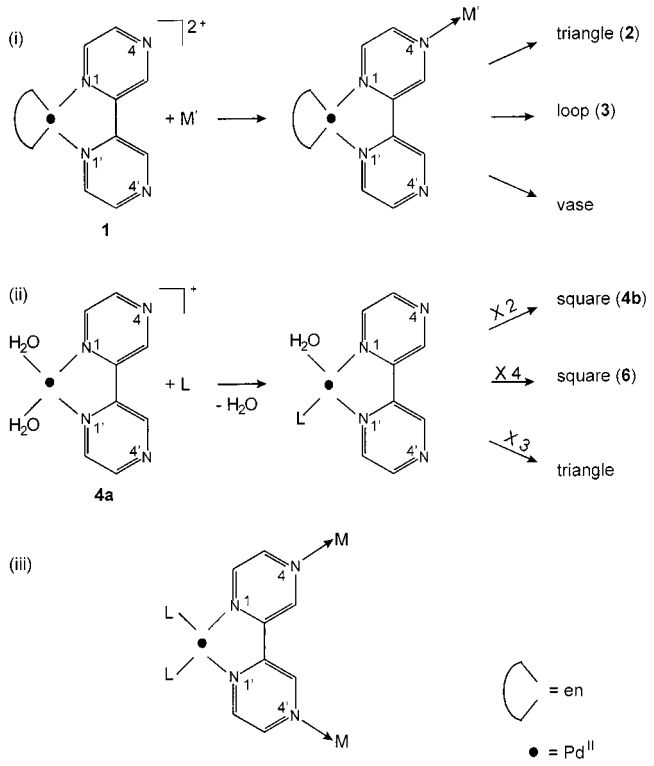
In aqueous solution (pD = 2) **6** coexists with a second species. In addition to the five ^{1}H-NMR resonances due to the 2,2′-bpz ligands (H3, H3′; H5, H5′; H6, H6′) and the two protons H_α and H_β of 4,4′-bpy, a second set of resonances (ca. 30−35% of the former at a concentration of 0.016 M of dissolved tetramer **6**) is observed. The assignment of the individual resonances is straightforward on the basis of differences in H,H coupling constants and 2D-NMR experiments, respectively. The simplicity of the signal patterns of 2,2′-bpz and 4,4′-bpy resonances of both species present in solution are neither consistent with dissociation of tetranuclear **6** into monomeric $[(2,2'\text{-bpz})Pd(4,4'\text{-bpy-}N^1)(D_2O)]^{2+}$ (expected doubling of bpz and bpy resonances due to nonequivalence of two halves of these molecules) nor dissociation into $[(2,2'\text{-bpz})Pd(4,4'\text{-bpy-}N^1)_2]^{2+}$ and free $[(2,2'\text{-bpz})Pd(D_2O)_2]^{2+}$ (expected doubling of bpy resonances; two sets of bpz resonances). We tentatively favor a proposal made by Fujita et al.,[19] according to which the molecular square assembled from $(2,2'\text{-bpy})Pd^{II}$ (2,2′-bpy = 2,2′-bipyridine) and 4,4′-bpy equilibrates in solution with a cyclic trinuclear species[19] (Scheme 5). An interesting detail of the ^{1}H-NMR spectrum of dissolved **6** (c.f. Experimental Section) supporting this view refers to the chemical shift of the protons H6, H6′ of the 2,2′-bpz ligands in the two species: In the major species, which is assigned to the square, this resonance (d, $^3J_{5,6}$ = 3 Hz) occurs at δ = 7.98 while in the minor one, tentatively assigned to the cyclic trimer, this doublet is found at δ = 8.38. From model building it becomes clear that H6, H6′ of 2,2′-bpz is experiencing the ring current of the pyridine ring of the 4,4′-bpy ligands to a larger extent than is to be anticipated for a triangular structure. Therefore it is to be expected that H6, H6′ of 2,2′-bpz resonates upfield from that of the molecular triangle in the case of a molecular square.



Scheme 5

Conclusions

As outlined in Scheme 6, $[L_2Pd(2,2'\text{-bpz-}N^1,N^{1'})]^{2+}$ cations [L_2 = en (**1**), L = H_2O (**4a**)] represent useful angular units for the generation of larger cationic aggregates. There are two principal ways by which this can be achieved. (i) When additional metal ions M′ bind to the available N(4) positions of the chelating 2,2′-bpz ligand in **1** and cross-



Scheme 6

link to other cations **1**, depending on the geometry of M′, flat triangles [M′ = *trans*-$(NH_3)_2Pt^{II}$ **2**[6c]], loop structures ($M' = Ag^+$ in **3**) or hexanuclear vases (M′ = $enPd^{II}$ [7]) can form. (ii) Compound **4a** can likewise act as an angular unit upon substitution of the aqua ligands by other bridging ligands L. These may be small (OH^- in **4b**) or large (4,4′-bpy in **6**) and may themselves be angular (OH^-) or linear units (4,4′-bpy). Of course, variations of these motifs are possible, e.g. upon use of M′−L−M′ fragments in (i) or L−M′−L linear units in (ii). Finally there is, in principle, also the possibility of combining (i) and (ii) in such a way as to use **4a** as a cross element in molecular architecture [option (iii) in Scheme 6].

Experimental Section

2,2′-Bpz[20] and [enPd(2,2′-bpz-$N^1,N^{1'}$)]$(ClO_4)_2$ (**1**)[6a] were prepared as reported. 4,4′-Bipyridine was obtained commercially.

[enPd(2,2′-bpz-$N^1,N^{1'}$)Ag]$_n(ClO_4)_{3n}$ (3): [enPd(2,2′-bpz-$N^1,N^{1'}$)]$(ClO_4)_2$ (**1**) (100.00 mg, 0.191 mmol) was dissolved in water (10 mL) and stirred with $AgClO_4$ (43.00 mg, 0.191 mmol) for 1 d at room temperature. The yellow solution was then filtered, concentrated to 3 mL by rotary evaporation, and then kept at 4 °C. Yellow **3** was obtained in 79% yield (110.28 mg) within 4 d. $C_{10}H_{14}AgCl_3N_6O_{12}Pd$ (730.89): calcd. C 16.4, H 1.9, N 11.4; found C 16.2, H 1.9, N 11.3. ***Caution!*** Perchlorate salts are potentially explosive and should be used in small quantities only.

[Cl_2Pd(2,2′-bpz-$N^1,N^{1'}$)] (4): 2,2′-bpz (100.00 mg, 0.63 mmol) and K_2PdCl_4 (206.00 mg, 0.63 mmol) were suspended in water (20 mL) and stirred for 1 d at room temperature. The yellow solid was then filtered off and washed with $CHCl_3$ (10 mL) (95% yield, 200.78 mg). $C_8H_6Cl_2N_4Pd$ (335.48): calcd. C 28.6, H 1.8, N 16.7; found C 28.3, H 1.9, N 16.5.

[$(H_2O)_2$Pd(2,2′-bpz-$N^1,N^{1'}$)]$(NO_3)_2$ (4a): The complex was prepared in situ by treating **4** with 2 equiv. of $AgNO_3$ in H_2O or alternatively by acidification (HNO_3, pH < 3) of an aqueous solution of **4b**. − ^{1}H NMR (200 MHz, D_2O, TSP, pD < 3): δ = 8.47 (dd, $^3J_{5,6}$ = 3 Hz, 2 H, arom., $^5J_{3,6}$ = 1.1 Hz, 2 H, arom.), 9.05 (d, $^3J_{5,6}$ = 3 Hz, 2 H, arom.), 9.68 (d, $^5J_{3,6}$ = 1 Hz, 2 H, arom.).

[(2,2′-bpz-$N^1,N^{1'}$)Pd$(OH)_2$Pd(2,2′-bpz-$N^1,N^{1'}$)]$(NO_3)_2$·4 H_2O (4b): **4** (300.00 mg, 0.994 mmol) was suspended in water (15 mL) and stirred for 24 h at room temperature with $AgNO_3$ (338.00 mg, 1.988 mmol). After removal of AgCl by filtration, the pH value was adjusted to 3, then the reaction mixture was heated to 60 °C and filtered again. Yellow-orange crystals of **4b** were isolated in 62% yield (222.85 mg) within 1 d at 4 °C. $C_{16}H_{18}N_{10}Pd_2O_{10}$ (723.21 for dihydrate): calcd. C 26.6, H 2.5, N 19.4; found C 26.7, H 2.4, N 19.3. − ^{1}H NMR (200 MHz, D_2O, TSP, pD = 5.5): δ = 8.34 (dd, $^3J_{5,6}$ = 3 Hz, 2 H, arom., $^5J_{3,6}$ = 1.1 Hz, 2 H, arom.), 9.05 (d, $^3J_{5,6}$ = 3 Hz, 2 H, arom.), 9.66 (d, $^5J_{3,6}$ = 1 Hz, 2 H, arom.).

[Cl_2Pt(2,2′-bpz-$N^1,N^{1'}$)] (5): 2,2′-bpz (100.00 mg, 0.63 mmol) and K_2PtCl_4 (262.00 mg, 0.63 mmol) were suspended in water (15 mL) and stirred for 4 d at 80 °C. The yellow solid was then filtered off, washed with $CHCl_3$ (10 mL) and dried. **5** could not be isolated in pure form and possibly contained a compound with (2,2′-bpz-$N^4,N^{4'}$)Pt^{II} species.

[(2,2′-bpz-$N^1,N^{1'}$)Pt$(OH)_2$Pt(2,2′-bpz-$N^1,N^{1'}$)]$(NO_3)_2$·4 H_2O (5b): Crude **5** (369.00 mg, 0.87 mmol) was suspended in water (15 mL) and stirred for 24 h at 80 °C with $AgNO_3$ (338.00 mg, 1.988 mmol). After removal of AgCl by filtration, the pH value was adjusted to 3, the reaction mixture heated to 60 °C and filtered again. Yellow-orange crystals of **5b** were isolated in less than 5% yield (22.00 mg)

Table 6. X-ray data for **3**, **4b**, **5b**, and **6**

	3	**4b**	**5b**	**6**
Empirical formula	$C_{10}H_{14}AgCl_3N_6O_{12}Pd$	$C_8H_{11}N_5O_6Pd$	$C_8H_{11}N_5O_6Pt$	$C_{36}H_{42.4}N_{16}O_{19.2}Pd_2$
Molecular mass	730.89	379.62	468.31	1219.26
Space group	*Pbcn*	$P2_1/n$	$P2_1/n$	$P2_1/n$
a [Å]	17.946(4)	7.0430(10)	7.0440(10)	27.231(5)
b [Å]	17.616(4)	23.222(5)	23.100(5)	6.3020(10)
c [Å]	13.559(3)	7.893(2)	7.985(2)	27.273(5)
β [°]		106.22(3)	106.68(3)	91.02(3)
V [Å^3]	4286.5(17)	1239.5(4)	1244.6(4)	4679.6(14)
Z	8	4	4	4
T [K]	293(2)	293(2)	293(2)	293(2)
μ [mm^{-1}]	2.200	1.533	11.310	0.863
R_1 (obs. data)[a]	0.0361	0.0276	0.0374	0.0661
wR_2 (obs. data)[b]	0.0904	0.0634	0.0913	0.1416

[a] $R_1 = \Sigma \, ||F| - |F_c|| / \Sigma \, |F|$. − [b] $wR_2 = [\Sigma w(F^2 - F_c^2)^2 / \Sigma w(F^2)^2]^{1/2}$.

within 1 d at 4 °C. − ^{1}H NMR (200 MHz, D_2O, TSP, pD = 4.2): δ = 8.71 (d, $^3J_{5,6}$ = 4 Hz, 2 H, arom.), 9.02 (d, $^3J_{5,6}$ = 4 Hz, 2 H, arom.), 9.62 (s, 2 H, arom.).

[{(2,2′-bpz-N^1,$N^{1'}$)Pd(4,4′-bpy)}$_4$](NO$_3$)$_8$·14.4 H$_2$O (6): 4b (88.00 mg, 0.127 mmol) was dissolved in H_2O (15 mL) at 40 °C and the pH value of the solution was adjusted to 1.5 with 1N HNO_3. 4,4′-Bipyridine (38.00 mg, 0.243 mmol) was then added, the pH value readjusted and the mixture stirred for 12 h at 45 °C. Following cooling at 4 °C, thin yellow needles of **6** were isolated within 1 h. The needles were filtered and washed with H_2O (5 mL). After recrystallization from H_2O, the yield was 86% (132.60 mg). $C_{72}H_{84.8}N_{32}Pd_4O_{38.4}$ (2438.52): calcd. C 35.5, H 3.5, N 18.4; found C 35.9, H 3.2, N 18.8. − ^{1}H NMR (200 MHz, D_2O, TSP, pD = 2) major peaks: δ = 10.17 (s, 2 H, arom. H3-bpz), 9.60 (d, $^3J_{\alpha,\beta}$ = 6.5 Hz, 4 H, arom. Hα-bpy), 9.24 (d, $^3J_{5,6}$ = 3 Hz, 2 H, arom. H5-bpz), 8.49 (d, $^3J_{\alpha,\beta}$ = 6.5 Hz, 4 H, arom. Hβ-bpy), 7.98 (d, $^3J_{5,6}$ = 3 Hz, 2 H, arom. H6-bpz); minor peaks: δ = 9.41 (d, $^3J_{\alpha,\beta}$ = 6.5 Hz, 4 H, arom. Hα-bpy), 9.29 (d, $^3J_{5,6}$ = 3 Hz, 2 H, arom. H5-bpz), 8.38 (d, $^3J_{5,6}$ = 3 Hz, 2 H, arom. H6-bpz), 8.35 (d, $^3J_{\alpha,\beta}$ = 6.5 Hz, 4 H, arom. Hβ-bpy).

Instrumentation: ^{1}H-NMR spectra were recorded at 20 °C with a Bruker AC 200 FT NMR spectrometer in D_2O (with TSP as internal standard). pD values (for D_2O solutions) were obtained by adding 0.4 units to the pH meter reading of the electrode. − Elemental analyses were performed with a Carlo Erba Model 1106 Strumentazione Element-Analyzer.

X-ray Crystal Structure Determinations: Intensity data for **3**, **4b**, **5b**, and **6** were collected with an Enraf−Nonius Kappa CCD[21] (Mo-K_α, λ = 0.71069 Å, graphite monochromator) with sample-to-detector distances of 26.7 (**4b**, **5b**), and 30.7 mm (**3**, **6**), respectively. They covered the whole sphere of reciprocal space by measurement of 360 frames rotating about ω in steps of 1°. The exposure times were 14 (**3**), 30 (**4b**), 45 (**5b**), and 75 s (**6**) per frame. Preliminary orientation matrices and unit cell parameters were obtained from the peaks of the first ten frames, respectively, and refined using the whole data set. Frames were integrated and corrected for Lorentz and polarization effects using DENZO.[22] The scaling as well as the global refinement of crystal parameters were performed by SCALEPACK.[22] Reflections, which were partly measured on previous and following frames, are used to scale these frames with each other. Merging of redundant reflections in part eliminates absorption effects and also reveals if crystal decay occurs. The structures were solved by standard Patterson methods[23] and refined by full-matrix least squares based on F^2 using the SHELXTL-PLUS[24] and SHELXL-93 programs.[25] The scattering factors for the atoms were those given in the SHELXTL-PLUS program. Transmission factors were calculated with SHELXL-97.[26] Hydrogen atoms were included in calculated positions and refined with isotropic displacement parameters according to the riding model, except for all protons in **4b** and the hydroxy and the four water protons in **5b**, which could be localized with difference Fourier synthesis. The anions and water molecules in **3** and **6** are disordered.[27] X-ray data are provided in Table 6.

Acknowledgments

This work was supported by the Fonds der Chemischen Industrie.

[1] J.-M. Lehn, *Supramolecular Chemistry*, VCH, Weinheim, **1995**. − P. J. Stang, *Chem. Eur. J.* **1998**, *4*, 19. − M. Fujita, K. Ogura, *Coord. Chem. Rev.* **1996**, *148*, 249. − R. W. Saalfrank, I. Bernt, *Curr. Opin. Solid State Mat. Sci.* **1998**, *3*, 407. − D. L. Caulder, K. N. Raymond, *J. Chem. Soc., Dalton Trans.* **1999**, 1185.
[2] J. A. R. Navarro, B. Lippert, *Coord. Chem. Rev.* **1999**, *185−186*, 653.
[3] M. S. Lüth, E. Freisinger, F. Glahé, B. Lippert, *Inorg. Chem.* **1998**, *37*, 5044.
[4] H. Rauter, I. Mutikainen, M. Blomberg, C. J. L. Lock, P. Amo-Ochoa, E. Freisinger, L. Randaccio, E. Zangrando, E. Chiarparin, B. Lippert, *Angew. Chem. Int. Ed. Engl.* **1997**, *36*, 1296.
[5] H. Rauter, E. C. Hillgeris, B. Lippert, *J. Chem. Soc., Chem. Commun.* **1992**, 1385. − H. Rauter, E. C. Hillgeris, A. Erxleben, B. Lippert, *J. Am. Chem. Soc.* **1994**, *116*, 616. − J. A. R. Navarro, M. B. L. Janik, E. Freisinger, B. Lippert, *Inorg. Chem.* **1999**, *38*, 426.
[6] [6a]R.-D. Schnebeck, L. Randaccio, E. Zangrando, B. Lippert, *Angew. Chem. Int. Ed.* **1998**, *37*, 119. − [6b]R.-D. Schnebeck, E. Freisinger, B. Lippert, *Angew. Chem. Int. Ed.* **1999**, *38*, 168. − [6c]R.-D. Schnebeck, E. Freisinger, B. Lippert, *J. Chem. Soc., Chem. Commun.* **1999**, 675.
[7] R.-D. Schnebeck, E. Freisinger, F. Glahé, B. Lippert, *J. Am. Chem. Soc.* **2000**. *122*, 1381.
[8] T. Suzuki, H. Kotsuki, K. Isobe, N. Moriya, Y. Nakagawa, M. Ochi, *Inorg. Chem.* **1995**, *34*, 530. − L. Carlucci, G. Ciani, D. M. Proserpio, A. Sironi, *Inorg. Chem.* **1998**, *37*, 5941. − N. Masciocchi, G. A. Ardizzoia, G. LaMonica, A. Maspero, A. Sironi, *Angew. Chem. Int. Ed.* **1998**, *37*, 3366.
[9] D. Whang, K.-M. Park, J. Heo, P. Ashton, K. Kim, *J. Am. Chem. Soc.* **1998**, *120*, 4899.
[10] D. Whang, J. Heo, C.-A. Kim, K. Kim, *Chem. Commun.* **1997**, 2361.
[11] [11a] R. Faggiani, B. Lippert, C. J. L. Lock, B. Rosenberg, *J. Am. Chem. Soc.* **1977**, *99*, 777. − [11b] R. Faggiani, B. Lippert, C. J. L. Lock, B. Rosenberg, *Inorg. Chem.* **1977**, *16*, 1192. − [11c] R. Faggiani, B. Lippert, C. J. L. Lock, B. Rosenberg, *Inorg. Chem.* **1978**, *17*, 1941. − [11d] B. Lippert, C. J. L. Lock, B. Rosenberg, M. Zvagulis, *Inorg. Chem.* **1978**, *17*, 2971.
[12] [12a] F. D. Rochon, A. Morneau, R. Melanson, *Inorg. Chem.* **1988**, *27*, 10. − [12b] F. D. Rochon, R. Melanson, *Acta Crystallogr.* **1988**, *C44*, 474.
[13] R. B. Martin *in Cisplatin: Chemistry and Biochemistry of a Leading Anticancer Drug* (Ed.: B. Lippert), VHCA and Wiley-VCH, Weinheim, **1999**, p. 183−205.
[14] D. S. Gill, B. Rosenberg, *J. Am. Chem. Soc.* **1982**, *104*, 4598.
[15] B. Rosenberg, *Biochimie* **1978**, *60*, 859. − S. J. Lippard, *Science* **1982**, *218*, 1075.
[16] P. J. Stang, D. H. Cao, S. Saito, A. M. Arif, *J. Am. Chem. Soc.* **1995**, *117*, 6273.
[17] M. Fujita, Y. J. Kwon, S. Washizu, K. Ogura, *J. Am. Chem. Soc.* **1994**, *116*, 1151.
[18] We use the term "square" in this context, because it had been introduced by Fujita and Ogura[17] as well as Stang et al.[16] For "squares" with flat organic corner stones see, e.g., ref.[3]
[19] M. Fujita, O. Sasaki, T. Mitsuhashi, T. Fujita, J. Yazaki, K. Yamaguchi, K. Ogura, *Chem. Commun.* **1996**, 1535.
[20] R. J. Crutchley, A. B. P. Lever, *Inorg. Chem.* **1982**, *21*, 2276.
[21] NONIUS BV, KappaCCD package, Röntgenweg 1, P. O. Box 811, 2600 AV Delft, Netherlands.
[22] Z. Otwinowsky and W. Minor, *Methods Enzymol.*, **1996**, *276*, 307.
[23] G. M. Sheldrick, *Acta Crystallogr.* **1990**, *A46*, 467.
[24] G. M. Sheldrick, *SHELXTL-PLUS (VMS)*, Siemens Analytical X-ray Instruments, Inc.: Madison, WI, **1990**.
[25] G. M. Sheldrick, *SHELXL-93, Program for crystal structure refinement*, University of Göttingen, Germany, **1993**.
[26] G. M. Sheldrick, *SHELXL-97, Program for the refinement of crystal structures*, University of Göttingen, Germany, **1997**.
[27] Crystallographic data (excluding structure factors) for the structure reported in this paper have been deposited with the Cambridge Crystallographic Data Centre as supplementary publication no. CCDC-137745 to CCDC-137748. Copies of the data can be obtained free of charge on application to CCDC, 12 Union Road, Cambridge CB2 1EZ, UK [Fax: (internat.) + 44-1223/336-033; E-mail: deposit@ccdc.cam.ac.uk].

Received December 15, 1999
[I99461]

NMR Solution Structure of a DNA 12/11-*mer*: d(CTCCTGTGTCTC)·d(GAGATA−AGGAG) Containing a Transplatin Interstrand G−N7/A−N1 Cross-Link

Bjørn Andersen,[a] Eloy Bernal-Méndez,[b] Marc Leng,[b] and Einar Sletten*[a]

Keywords: Oligonucleotides / Platinum / Molecular dynamics / NMR spectroscopy

The solution structure of a double-stranded DNA oligonucleotide, d(CTCCTG*TGTCTC)·d(GAGATA*–AGGAG), containing a *trans*-diammineplatinum(II) interstrand cross-link (the asterisks indicate the two cross-linked bases) has been determined by means of two-dimensional nuclear magnetic resonance (2D NMR) and NOE-restrained molecular dynamics and energy minimization refinement. The cross-linked duplex was prepared in two steps. First, *trans*-diamminedichloroplatinum(II) was reacted with the single-stranded d(CTCCTGTGTCTC), which resulted in the formation of a stable (G1,G3)-intrastrand cross-link. Then, the platinated oligonucleotide was hybridized with the partially complementary oligonucleotide d(GAGATA–AGGAG), in which the d(AT) doublet facing the intrastrand GTG cross-link replaced the d(CAC) triplet in a regular duplex. The formation of the hybrid promoted the rearrangement of the (G1,G3)-intrastrand cross-link into an interstrand cross-link. The NMR experiments were performed in 0.5 m NaCl solution. All the exchangeable and nonexchangeable proton resonances (except some H5′/H5′′ signals) of the major species could be assigned. NOESY spectra and chemical shift data indicate that the interstrand cross-link is established between G6–N7 and A18–N1. The platinated G residue is rotated about the glycosyl bond from an *anti* conformation into a *syn* conformation. The two imino protons G8–H1 and T17–H3 forming hydrogen bonds in the mismatched base pair, G8–T17, give rise to signals (upfield as expected) at δ = 10.52 and δ = 10.82. Using all the NOESY data (215 constraints) from a 0.8 mm sample, a solution structure of the cross-linked duplex has been obtained by NOE-restrained molecular dynamics/mechanics refinements. Only the central portion of the duplex deviates significantly from regular B-form geometry. The base residue T7 in the context GTG in the top strand is located in an extrahelical position. The interstrand cross-link induces a bend of 21° in the duplex.

Introduction

Recent years have witnessed the advent of oligonucleotides as tools for the modulation of gene expression. In the so-called antisense strategy, the binding of oligonucleotides to mRNA leads to inhibition of translation or RNA metabolism by two general mechanisms, namely the degradation of the targeted RNA by RNase H or the steric blocking of the cellular machinery.[1−8] Most studies in this area have dealt with RNase H-catalyzed cleavage of mRNA by phosphodiester oligonucleotides. However, a major drawback of these oligonucleotides is their rapid degradation by nucleases. They can be replaced by phosphorothioate oligonucleotides, which retain the ability to activate RNase H and are resistant to nucleases. Unfortunately, however, these are known to have side effects because of nonspecific binding to cellular proteins. An advantage of the steric blocking of cellular machinery is that chemically modified, and thus nuclease-resistant oligonucleotides can be used. However, a major constraint is that the oligonucleotide−RNA hybrids have to be sufficiently stable to avoid dissociation by the cellular machinery. Cross-linking of the oligonucleotides to their targets[1−8] can prevent such dissociation. Recently, a convenient method has been proposed for the specific and irreversible cross-linking of oligonucleotides to their targets in both cell-free and cell media. In this approach, *trans*-DDP [DDP: diamminedichloroplatinum(II)] modified oligonucleotides are used.[9]

In the reaction between *trans*-DDP and single-stranded oligonucleotides containing the triplet GNG (N being a nucleotide residue), (G1,G3)-intrastrand cross-links are formed. These intrastrand cross-links are stable as long as the oligonucleotides are single-stranded. There is, however, one exception.[10,11] It concerns intrastrand cross-links that have an adjacent C residue on the 5′ side. In the context d(CGNG) (N being A, T, or C), the following linkage isomerization occurs: *trans*-DDP [d(CGNG)−N7−G, N7−G] ⇄ *trans*-DDP [d(CGNG)−N3−C, N7−G]. Replacement of the C residue adjacent to the adduct on the 5′ side by a G, A, or T residue prevents this reaction.

Pairing of the single-stranded oligonucleotides containing a (G1,G3)-intrastrand cross-link with their complementary strands has two consequences. Firstly, the rearrangement of the (G1,G3)-intrastrand cross-link to the

[a] Department of Chemistry, University of Bergen, Allégt. 41, N-5007 Bergen, Norway
Fax: (internat.) + 47/55589490
E-mail: Einar.Sletten@kj.uib.no
[b] Centre de Biophysique Moléculaire, CNRS, Rue Charles Sadron, F-45071 Orleans Cedex 02, France
Fax: (internat.) + 33-2/38631517
Supporting information for this article is available on the WWW under http://www.wiley-vch.de/home/eurjic or from the author.

 © WILEY-VCH Verlag GmbH, D-69451 Weinheim, 2000 1434−1948/00/0606−1201 $ 17.50+.50/0

(C1,G4)-intrastrand cross-link is blocked. Secondly, another linkage isomerization reaction is triggered by the formation of the double helix, which involves rearrangement of the (G1,G3)-intrastrand cross-link into an interstrand cross-link. This rearrangement occurs irrespective of the nature of the nucleotide residues adjacent to the intrastrand cross-link.[9,12−14]

The mechanism of the rearrangement is not yet known in detail, although some points have been established.[12−14] In the interstrand cross-link, only the 5′G (and not the 3′G) of the former intrastrand cross-link is involved. The interstrand cross-linking reaction does not proceed through a solvent-associated intermediate. Cleavage of the Pt−3′G bond with formation of a monofunctional adduct can be excluded. Direct nucleophilic attack of the Pt−3′G bond by either the C residue complementary to 5′G, or the A residue if the triplet complementary to the intrastrand cross-link is replaced by the doublet d(TA) or r(UA), has been suggested. At 37 °C, the rate of the interstrand cross-linking reaction depends on several parameters, such as the shape of the double helix and the sequence of the targeted oligonucleotide. The fastest reaction (complete within a few minutes) occurs in the hybrids between platinated oligo(2′-*O*-Me)nucleotides and RNA containing the doublet UA facing the platinated triplet.

Our envisaged uses of the *trans*-DDP-modified oligonucleotides are as tools in molecular biology and as drugs for modulating gene expression. In both cases, the requisite oligonucleotides have to be designed, which implies a complete knowledge of the interstrand cross-linking reaction. Knowledge of the structures of the cross-linked duplexes is thus essential, which prompted us to undertake a systematic study of the structures of these duplexes. In this paper, we report on a structure determination of a *trans*-DDP interstrand cross-linked DNA duplex. The system investigated in detail consists of a 12/11-*mer* hybrid d(CTCCTG*TGTCTC)·d(GAGATA*−AGGAG) (the asterisks indicate the cross-linked bases), in which the lower strand differs from the regular complementary strand in that the CAC triplet complementary to the platinated GTG triplet is replaced by the doublet d(TA). The interstrand cross-linked product has been characterized by NMR spectroscopy and a combination of NOESY-restrained molecular dynamics and energy minimization refinement.

Results

Synthesis of the Cross-Linked Duplexes

A scheme showing the synthesis of a duplex incorporating an interstrand cross-link is given in Figure 1, a. The progress of the cross-linking reaction was monitored by FPLC analysis (Figure 1, b), which showed that after 9 days it had almost reached completion. The ^{1}H-NMR spectrum of the sample obtained following FPLC purification featured one set of major resonances as well as some small signals due to a minor component (< 3%) (Figure 2, a). When the spectrum was recorded a few days later, the resonances attributable to the minor component had increased to ca. 14% (Figure 2, b). The signals due to this minor species were not characterized further by NMR analysis because of a low spectral signal-to-noise ratio. Subsequently, the salt concentration was increased to 0.5 M NaCl, which led to an appreciable reduction in the amount of the minor component, its concentration returning to a level comparable to that seen in the initial spectrum (< 3%). This suggests a salt-induced shift in the conformational equilibrium in favor of the major component. The melting temperature for the cross-linked duplex in 0.150 M NaCl was found to be 62 °C, and probably a few degrees higher in 0.500 M NaCl.

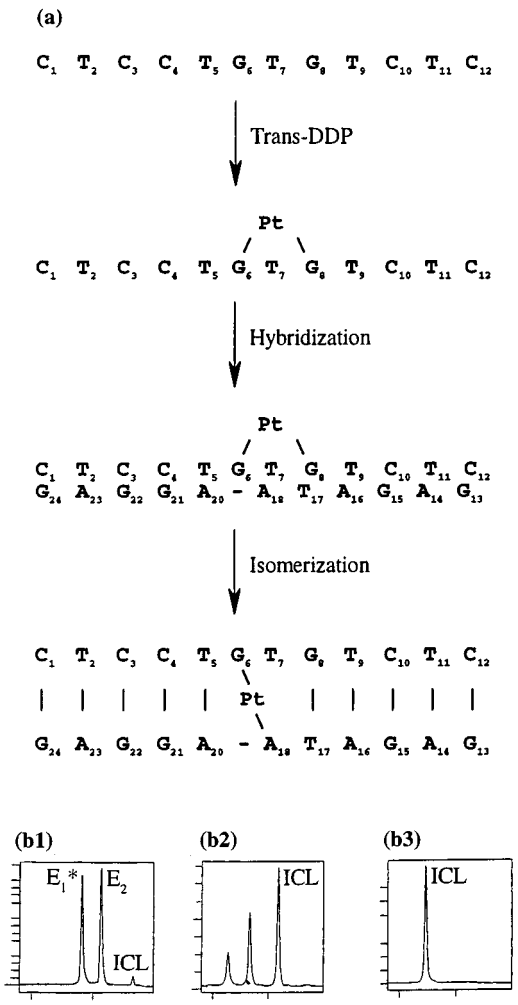


Figure 1. (a) Scheme of the cross-linking reactions; (b) FPLC elution profiles of the isomerization process from intrastrand to interstrand cross-linked (ICL) duplex: (b1) intrastrand cross-linked oligonucleotide (E_1*) mixed with its complementary sequence (E_2), (b2) a few days after mixing, (b3) FPLC-purified interstrand cross-linked (ICL) duplex

NMR Assignments

Comparison of the aromatic−H1′/H5 regions of the NOESY spectra of the platinated (Figure 3) and nonplatinated duplex (Figure 4) reveals dramatic changes in the chemical shift patterns. It is difficult to directly compare the

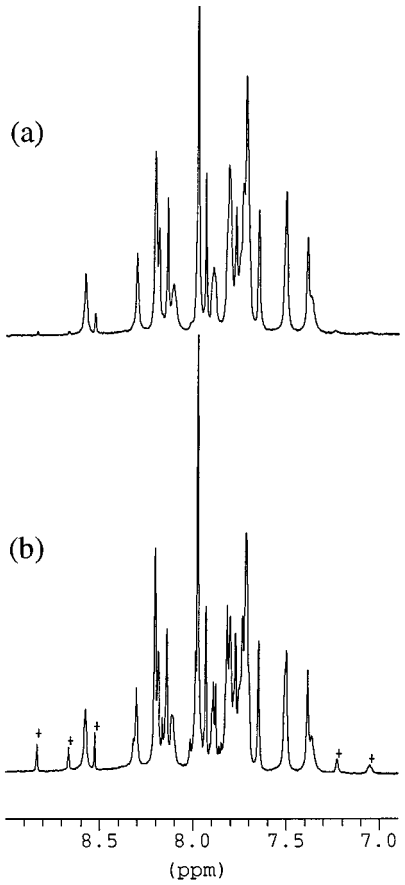


Figure 2. The downfield region of the 600 MHz ^{1}H-NMR spectrum of the *trans*-DDP cross-linked duplex d(CTCCTG* TGTCTC)·d(GAGATA*−AGGAG) (the asterisks * indicate the cross-linked bases) in D_2O at 305 K; (a) freshly prepared sample, (b) one week later; the signals attributable to the minor component are marked with +

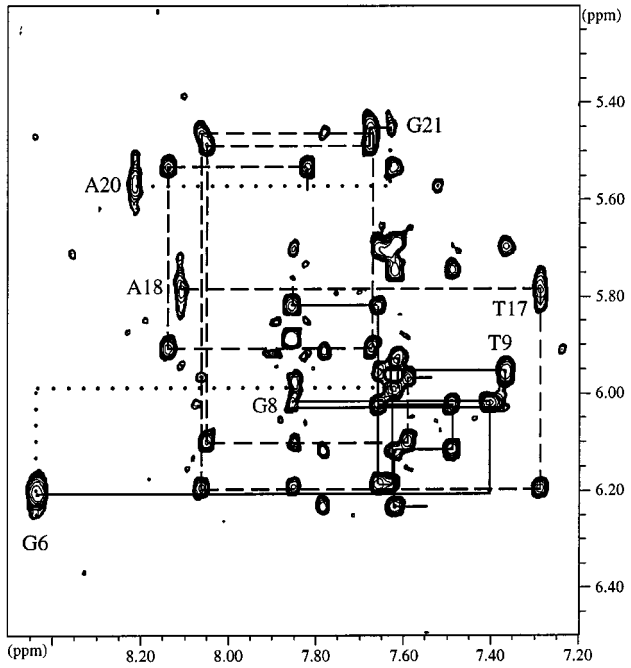


Figure 3. Contour plots of the resolution-enhanced H8/6−H1′/H5 region in the 600 MHz NOESY spectra of the *trans*-DDP cross-linked duplex d(CTCCTG*TGTCTC)·d(GAGATA*−AGGAG); the sequential connectivities are indicated with solid lines for the upper strand and broken lines for the lower strand, while absent connectivities are shown with dotted lines; the mixing time was 200 ms and the temperature 290 K

number of observed cross-peaks due to the large concentration difference, i.e. 0.8 mM and 3 mM, respectively. The non-exchangeable proton resonances were assigned following standard procedures; most of the sequential connectivities could be observed in the cross-peaks in the different spectral regions, i.e. aromatic−H1′/H3′, and aromatic−aromatic. Cross-peaks arising from traces of nonplatinated oligomers could be identified by comparison of NOESY maps of the duplex before and after platination. As expected, the 2D NOESY map of the platinated species shows a substantial downfield shift of the signal due to H8 of the cross-linked G6 residue. The chemical shift of adenine A18−H8, the cross-linked residue on the lower strand, is found in the normal range for H8 protons of nonplatinated A−N7. In the expanded portion of the downfield region of the 1D proton spectrum, two broad partially overlapping signals are observed at $\delta = 8.43$ and $\delta = 8.45$. By reference to the NOESY spectra, these resonances were assigned to the downfield shifted G6−H8 and A18−H2 protons of the platinated G and A residues, respectively. The DQF-COSY data were not of sufficient quality to yield reliable coupling constants for the sugar region due to severe overlap. The exchangeable proton resonances were assigned on the basis of the 1D spectra (Figure 5) and 2D NOESY spectra of the imino−imino and amino−aromatic regions. The chemical shifts of the assigned resonances of the platinated and non-platinated duplexes are listed in Table 1.

The NMR data for the 13/12-*mer* cross-linked duplex, which has an extra GC base pair, are almost identical to those obtained for the 12/11-*mer* (data not shown). The idea of extending the sequence was to increase the thermal stability of the duplex and thus to improve the quality of the spectral data. However, a comparison of the imino regions of the 12/11-*mer* and the 13/12-*mer* reveals only marginal improvement (data not shown).

The most prominent features in the spectra are the large downfield shifts of G6−H8 ($\delta = 8.43$) and A18−H2 ($\delta = 8.45$), which confirm that the cross-link is established between G6−N7 and A18−N1. The large intranucleotide G6−H8···H1′ crosspeak (Figure 3) corresponds to a *syn* conformation, which is probably adopted as a result of the platination. The H8/H1′ cross-peaks involving the adenine residues A18 and A20 are elongated, reflecting the rather flexible conformation at 290 K.

The connectivities involving adenine H2 protons are important in determining the global structure. The signal-to-noise level in the NOESY spectra of the nonplatinated duplex allows us to identify several H2···H1′ contacts of the type H2(n)···H1′(n), H1′(n+1), H1′(m+1), H1′(m), where n and m refer to complementary residues in a base pair. The H2(n)···H1′(m) distance in a regular Watson−Crick base pair is approximately 5.1 Å and the cross-peak correspond-

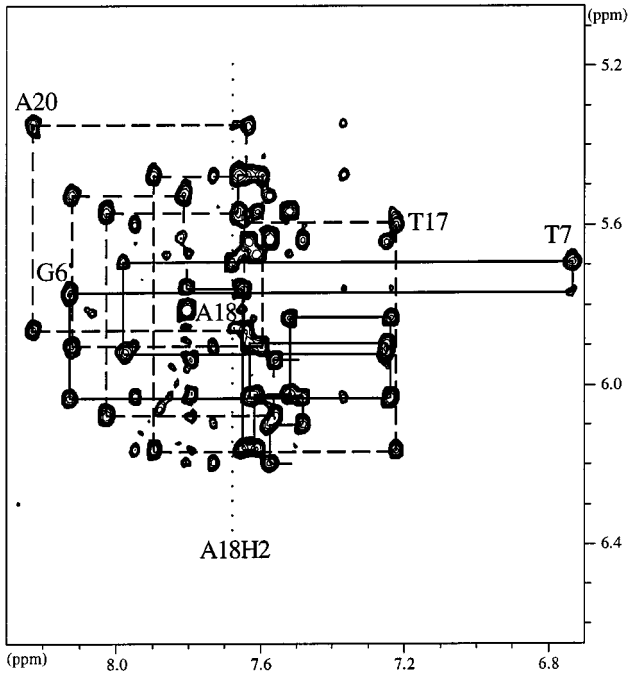


Figure 4. Contour plots of the resolution-enhanced H8/6−H1′/H5 region in the 600 MHz NOESY spectra of the nonplatinated duplex; the sequential connectivities are indicated with solid lines for the upper strand and broken lines for the lower strand, while absent connectivities are shown with dotted lines; the mixing time was 200 ms and the temperature 290 K

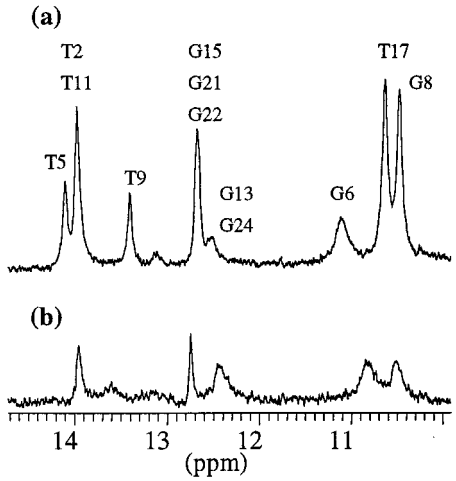


Figure 5. Imino proton resonances of the duplex d(CTCCTG*TGTCTC)·d(GAGATA*−AGGAG) at 290 K; (a) nonplatinated and (b) *trans*-DDP platinated

ing to such a long distance is not normally observed in NOESY maps. In the platinated form, H2(n)···H1′(m+1) cross-strand contacts are observed between A14/C12, A16/C10, and A23/C3.

The proton resonances of two of the thymine residues, T7 and T17, are of particular importance since these are involved in atypical duplex geometry. Thymine T7 may be located either in a bulged extrahelical position or stacked in the helix. Thymine T17 is partner in a GT mismatched base pair and thus might exhibit unusual chemical shifts. The methyl resonance of T7 is very weak, indicating a high degree of conformational motion. No cross-peaks in the aromatic−aromatic region involving T7−H6 are detected, suggesting that T7 is looped out of the double helix. The chemical shifts of the thymine T17 protons are, however, compatible with a regular B-DNA geometry.

The ^{1}H-NMR spectrum of the exchangeable protons in H_2O solution is rather noisy at 290 K (Figure 5). At lower temperatures, the situation is not improved due to extensive signal broadening at the relatively high salt concentration (0.5 M NaCl). The imino resonances of G8 and T17 are, however, easily recognized by virtue of their expected upfield positions at $\delta = 10.52$ and $\delta = 10.82$, characteristic for a mismatched base pair. Due to the low signal-to-noise level in the NOESY map, not all of the imino resonances could be assigned unambiguously.

^{31}P-NMR spectra of the nonplatinated and platinated duplexes are shown in Figure 6. It was not possible to assign the resonances on the basis of the available data. For the nonplatinated duplex, we had expected a downfield shifted resonance for the extrahelical thymine residue. However, the resonance patterns for both the nonplatinated and platinated duplexes, centered at about $\delta = -4.1$ and with no downfield shifted resonances, are indicative of a range of phosphate conformations consistent with regular DNA geometry.

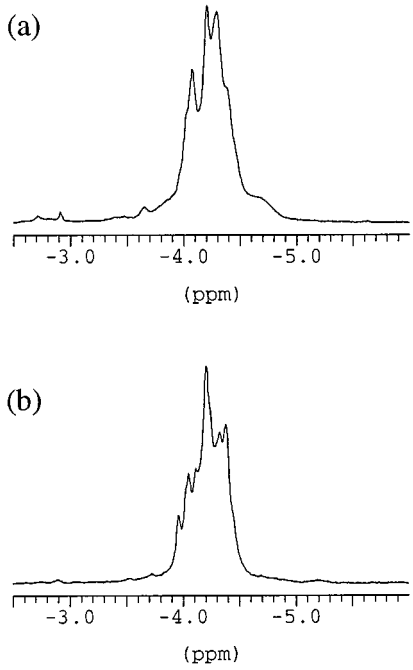


Figure 6. ^{31}P-NMR spectra of the duplex d(CTCCTG*TGTCTC)·d(GAGATA*−AGGAG) at 290 K; (a) nonplatinated and (b) *trans*-DDP platinated; shifts referenced to trimethyl phosphate

Molecular Modelling

Many cycles of subsequent interactive geometry refinements starting from regular B-DNA geometry converged at a model, the simulated NOESY spectra for which were in satisfactory agreement with the experimental spectra, as

Table 1. ^{1}H-NMR chemical shifts (ppm) for the *trans*-DDP cross-linked duplex d(CTCCTG*TGTCTC)·d(GAGATA*−AGGAG); the differences in the chemical shifts between the platinated and nonplatinated duplex are given below the chemical shifts; all shifts are referenced to the HOD resonance at δ = 4.84, T = 290 K

	H6/H8	H2/H5/CH_3	H1′	H2′	H2′′	H3′	H4′	H1/H3	Hf	Hb
C1	7.86	5.89	5.82	2.24	2.54	4.63	4.08		7.06	7.75
	0.06	0.08	0.07	0.00	0.00	0.03	0.03		0.20	0.10
T2	7.66	1.66	6.19	2.26	2.60	4.91	4.29	13.95		
	0.02	0.03	0.03	0.03	0.01	0.02	0.05	0.04		
C3	7.62	5.71	5.99	2.16	2.48	4.88	4.24		6.88	8.37
	0.03	0.04	−0.04	0.00	−0.03	0.02	0.00		0.06	0.12
C4	7.60	5.69	5.92	2.14	2.48	4.82	4.22		7.01	8.30
	0.08	0.12	0.09	0.18	0.03	0.09	0.09		0.17	0.07
T5	7.60	1.84	6.01	2.25	2.48	4.84	4.27	−		
	0.36	0.26	−0.02	0.48	0.19	−0.13	0.25	−		
G6	8.44		6.20	2.26	2.62	4.96	4.36	−	−	−
	0.31		0.43	−0.22	−0.08	0.51	0.22	−	−	−
T7	7.40	1.55	6.02	2.32	2.37	4.85	4.12	−		
	0.67	0.57	0.33	0.52	0.08	0.19	0.14	−		
G8	7.85		6.02	2.50	2.69	4.90	4.19	10.52	−	−
	−0.13		0.10	−0.24	−0.14	0.00	−0.14	0.14	−	−
T9	7.36	1.60	5.96	2.18	2.48	4.83	4.19	13.60		
	0.10	0.17	0.06	0.04	−0.02	0.06	−0.02	0.43		
C10	7.66	5.70	6.02	2.14	2.48	4.78	4.09		7.05	8.34
	0.04	0.06	−0.01	−0.01	−0.03	0.00	−0.10		0.14	0.06
T11	7.49	1.72	6.12	2.17	2.48	4.86	4.08	13.95		
	0.01	0.03	0.02	0.01	−0.02	0.00	−0.08	0.04		
C12	7.62	5.75	6.23	2.27	2.28	4.55	4.01		7.14	8.08
	0.05	0.10	0.03	0.00	0.00	0.00	0.02		0.36	−0.13
G13	7.82		5.53	2.42	2.61	4.80	4.14	12.45	−	−
	0.01		0.01	−0.04	−0.06	0.00	−0.02	0.00	−	−
A14	8.14	7.79	5.91	2.67	2.77	5.01	4.37		−	−
	0.02	0.06	0.01	0.00	−0.05	0.00	0.01		−	−
G15	7.67		5.46	2.50	2.65	4.94	4.32	12.75	−	−
	0.09		−0.02	0.08	0.09	0.01	0.01	0.17	−	−
A16	8.06	7.65	6.20	2.50	2.65	4.91	4.39		−	−
	0.16	−0.30	0.04	0.14	−0.09	−0.01	−0.01		−	−
T17	7.29	1.66	5.79	1.97	2.08	4.74	3.96	10.82		
	0.07	0.31	0.19	−0.18	−0.17	−0.09	−0.17	0.23		
A18	8.11	8.45	5.80	2.30	2.38	4.72	3.95		−	−
	0.47	0.80	−0.06	−0.14	−0.12	−0.13	−0.26		−	−
A20	8.22	7.52	5.57	2.69	2.71	5.00	4.30		−	−
	−0.01	0.15	0.21	0.09	0.06	0.07	0.03		−	−
G21	7.63		5.45	2.50	2.58	4.94	4.30	12.75	−	−
	0.02		−0.03	−0.01	−0.03	0.07	−0.01	0.17	−	−
G22	7.68		5.49	2.50	2.65	4.93	4.28	12.7	−	−
	0.02		−0.08	−0.01	−0.05	−0.03	−0.05	0.12	−	−
A23	8.05	7.85	6.10	2.60	2.86	5.00	4.40		−	−
	0.02	0.07	0.02	0.02	−0.01	0.00	0.00		−	−
G24	7.59		5.95	2.25	2.36	4.61	4.16	12.4	−	−
	0.03		0.01	0.00	0.00	0.01	0.02	0.00	−	−

judged by visual inspection. Figure 7 shows a comparison between the simulated and experimental spectra for the aromatic-H1′/H5/H3′ and aromatic-aromatic regions. All the NOESY peaks in the simulated spectra are observed in the experimental spectra, except for the cross-peaks corresponding to A18-H2G8-H8 and A20-H2G6−H8. This may be explained by partial saturation of the NOE signals involving A−H2 due to the short (2 s) relaxation delay. The overall agreement is, however, quite satisfactory. Some minor residual cross-peaks are apparent, corresponding to the H-bonded amino protons that have not been completely exchanged with deuterium, as well as a few cross-peaks that are presumably attributable to the minor component. A refinement starting from A-DNA geometry also led to an excellent fit between the simulated and experimental NOESY spectra, although the global bending for this model was larger than that in the case of a refinement starting from B-DNA.

Stereoviews of the refined structure (Figure 8) and a close-up of the central section of the duplex (Figure 9) are presented. The main feature to be noticed is the G6−N7···A18−N1 cross-link, which is accommodated within the duplex with retention of the overall B-DNA geometry. The ammonia ligands are seen to form hydrogen bonds to T5−O2 (2.70 Å) and T17−O4 (3.27 Å), respectively. In addition, both ammonia ligands are located in hydrophilic pockets and show several close contacts in the range 2.4−3.3 Å. The extra residue, thymine T7, is seen to loop out of the helix, giving it added conformational flexibility. The adenine A18 platination site could, in principle, involve either N7 or N1. Both models were tested in the refinement, but only the latter gave a reasonable fit to the NOE data. Additional support in favor of A−N1 involvement is provided by a related system where the cross-linking reaction rate is retarded when UA is replaced by the UG doublet.[13]

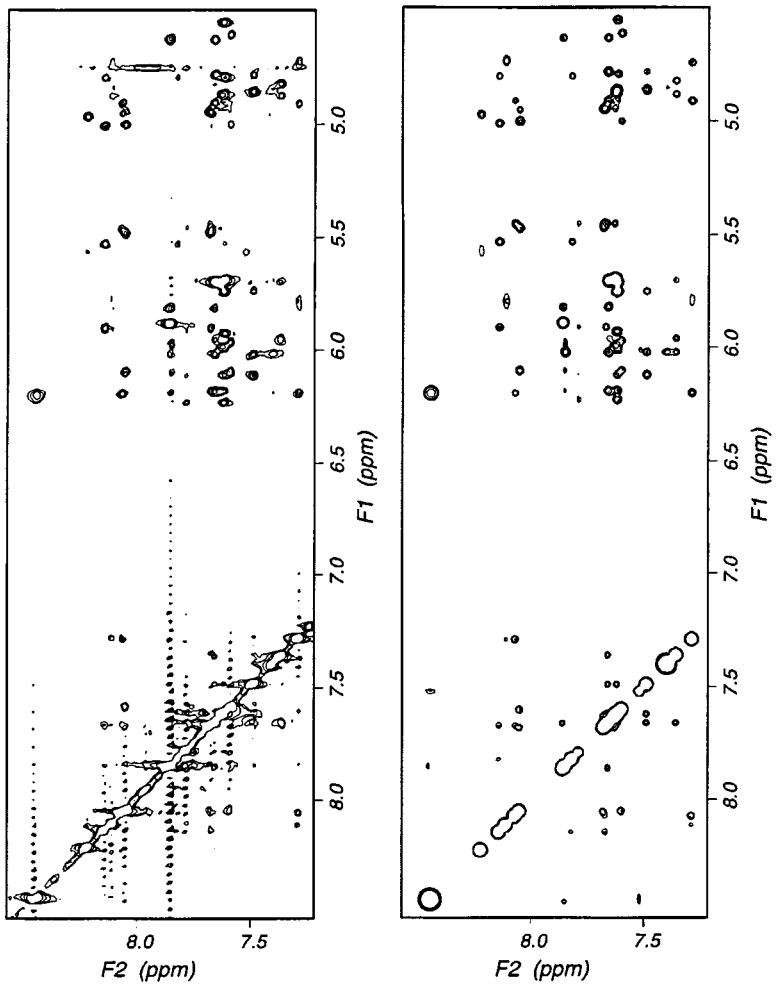


Figure 7. Expanded regions of the nonexchangeable proton 2D NOESY spectra of the *trans*-DDP cross-linked duplex d(CTCCTG*TGTCTC)·d(GAGATA*−AGGAG; left: experimental spectra: aromatic−aromatic region and aromatic−H1′/H3′ region; right: the corresponding simulated spectra

The helix is bent by 21°, as measured by the angle between the two helix axes calculated by CURVES[15] through residues 1−5 and 8−12, respectively, excluding residues G6, T7, and A18. The stacking interactions between the bases are maintained throughout the duplex except for those involving residues G6 and T7. The simulated NOESY data fit quite well with the experimental data representing the stacking region (aromatic−aromatic, Figure 7). The interplanar distances for the stacked bases were calculated by CURVES to lie in the range 2.7−3.8 Å. A complete listing of helical parameters is available as supplementary material.

Watson−Crick hydrogen-bonding is maintained for 10 of the 11 possible combinations. As expected, the platinated residues G6 and A18 are not involved in hydrogen bonding. The mismatched GT base pair, on the other hand, forms two quite regular N−H···O bonds. The chemical shifts of the two imino protons involved were observed at the expected upfield positions. The regular hydrogen-bonded base pairs have a negative propeller twist in the range −19° to −45°. Similar values have been observed in other duplex DNA oligonucleotides.[16] The mismatched base pair, G8−T17, has a positive propeller twist of 35°. The helical parameters are generally not well-defined, mainly due to a low signal-to-noise level in the 2D NOESY spectra obtained from the rather dilute (0.8 mM sample), and are not sufficiently precise for a high-quality structure determination.

Discussion

The 1,3-intrastrand cross-links between *trans*-DDP and two guanine residues separated by one base are relatively stable under single-strand conditions[10,11] and rearrange into interstrand cross-links when the platinated oligonucleotides are annealed with their complementary strands.[12−14] The different rates observed for such cross-linking reactions can be rationalized in terms of the relative positions of the attacking nucleotide residue and the platinum residue as well as the chemical nature of the attacking nucleotide residue. It is important to determine the local conformation of the double helix in these platinated species for several reasons, e.g. to establish the link between geometric factors and the rate of the interstrand cross-linking reaction.

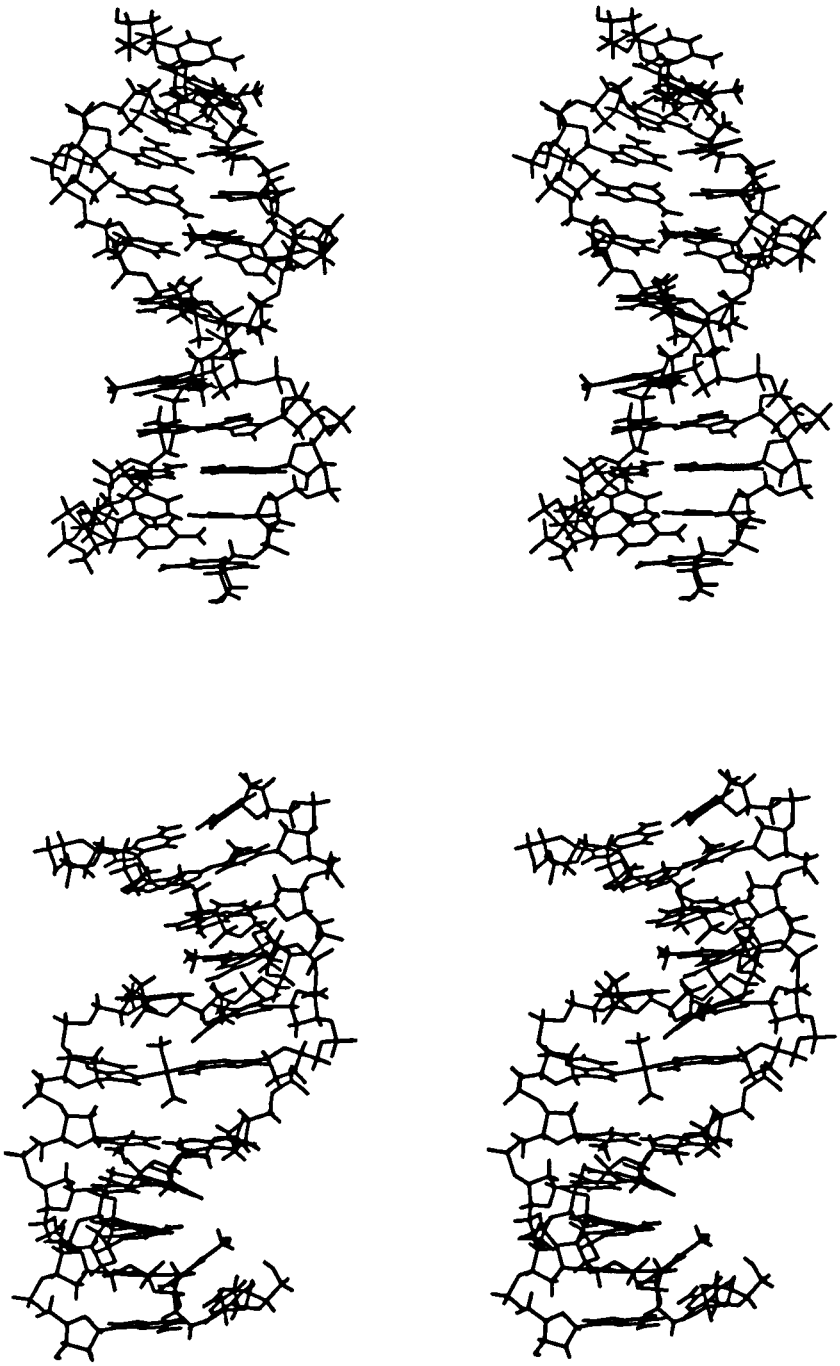


Figure 8. Stereoviews of the molecular model of the refined *trans*-DDP interstrand cross-linked duplex d(CTCCTG*TGTCTC)·d(GAGATA*−AGGAG)

The occurrence of both a major and a minor component of the cross-linked duplex, their contributions depending on time and the electrolyte concentration, indicates that a reversible conformational equilibrium is established. The minor component has not been further characterized by NMR analysis, thus the nature of these salt-induced structural changes has not been delineated. HPLC analysis and capillary electrophoretic measurements of the sample several weeks after the NMR data had been recorded revealed that the major cross-linked species was in fact accompanied by three minor constituents (3−9%).

Two broad downfield-shifted resonances at $\delta = 8.45$ and $\delta = 8.43$ were assigned to A18−H2 and G6−H8, respectively. Most of the NMR-based structural information currently available on platinum−DNA adducts pertains to *cis*-DDP, whereas only a few structural investigations of *trans*-DDP−DNA have been performed. Platination of purine N7 is predicted to induce a downfield shift of the H8 signal by ca. 0.5 ppm as a result of an inductive effect,[17] with a further contribution from conformation-dependent effects of the environment. In a study of *trans*-DDP adducts of d(GpTpG) platinated at N7, the downfield shifted G−H8

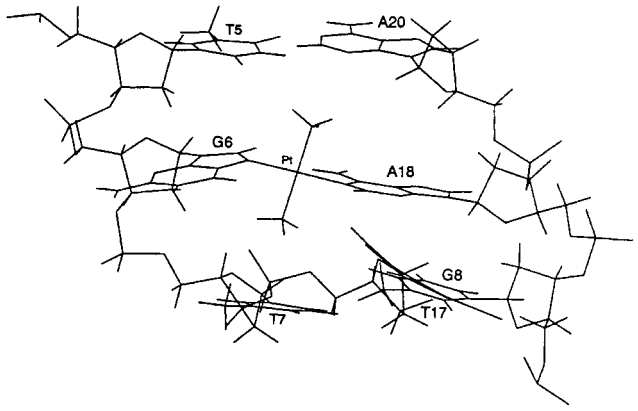


Figure 9. View of the central part of the platinated duplex

signal was observed at $\delta \approx 8.7$ (300 K).[18] In the single-stranded d(A*GG*CCT) containing the 1,3-*trans*-DDP adduct at A1−N7 and G3−N7, the signals of the aromatic protons A−H8 and G−H8 are observed at $\delta = 9.3$ and $\delta = 8.7$, respectively.[19] There is no corresponding example of an oligonucleotide *trans*-DDP-modified at A−N1, although in a study of the isomers d(GpA) and d(ApG), *cis*-DDP-modified at G−N7 and A−N1, downfield shifted A−H2 signals were observed at $\delta = 8.75$ and $\delta = 9.00$, respectively.[20]

From the NOESY spectra, it is evident that the residues adjacent to the platinated sites have a high degree of flexibility. The H8···H1′ cross-peaks involving residues A18 and A20 are especially poorly defined and provide only qualitative interatomic distance information. A sequential "walk" including *intra*- and *inter*-nucleotide connectivities in the aromatic−H1′ region can be completed for most of the residues, except for G6−H8···T7−H1′ in the upper strand and A18−H8···A20−H1′ in the lower strand. The NOESY maps for the 13/12-*mer* cross-linked duplex, which has an extra GC base pair, show essentially the same shift and connectivity pattern as for the 12/11-*mer*, thus excluding the possibility of any artifacts due to the duplex being too short.

The molecular structure of the platinated duplex shown in Figure 8 is based on NMR spectroscopy and restrained molecular dynamics and energy minimization calculations. In general, it has been observed that extrahelical pyrimidine bases tend to destack, while extrahelical purine bases stack with the nonplatinated duplexes.[21,22] However, in the NOESY spectrum of the nonplatinated duplex (Figure 4) the H6 resonance of thymine T7 in the context −GTG− is observed in an extreme upfield position, which suggests a high degree of deshielding in a base-stacked environment. In the platinated duplex, this thymine residue is looped out of the helix, although its exact location is not well-defined since T7 is involved in only a few NOE constraints. The fact that pyrimidine T7 is looped out leaves more room for the G6 residue to adopt a nonregular conformation, which may facilitate the interstrand cross-linking reaction. Kinetics experiments have shown that the rate of the interstrand cross-linking reaction is independent of the nature of the intervening base between the two cross-linked G residues in the top strand.[12−14]

The interstrand cross-link causes a local distortion of the double helix and induces a bend (21°) of its axis towards the major groove. However, it is generally accepted that the determination of global bending by NMR methods is rather inaccurate.[23] It is remarkable that the base pairs flanking the interstrand cross-links adopt a regular B-DNA conformation and that the distortion is located at the level of the cross-link. A similar conclusion has been reached in the case of duplexes containing a *cis*-DDP interstrand cross-link,[24−26] although the local distortions induced by *cis*- and *trans*-DDP are quite different.

Finally, an interesting aspect of this study is the fact that one of the amino groups of the Pt residue protrudes into the minor groove of the cross-linked duplexes (Figure 8). Both of the NH_3 ligands are seen to form hydrogen bonds to adjacent base residues (T5, T17), although one of the NH_3 ligands is less constrained and more exposed to the solvent. This suggests that the cross-linked duplexes should be able to accommodate larger nonleaving groups (L), which, in turn, may facilitate the cross-linking reaction and stabilize the platinated duplexes. Work is currently in progress with *trans* complexes of the general formula *trans*-$[Pt(NH_3)LCl_2]$.

Concluding Remarks

This work deals with structural characterization of a Pt−DNA duplex posing several nonroutine obstacles: (i) the duplex is made up of nonpalindromic sequences (giving a double set of resonances), (ii) a residue is missing from the complementary strand, (iii) the sample is dilute (0.8 mM) and furthermore contains several minor species, leading to a decreased signal-to-noise level. Thus, the task represents a real challenge to the standard NMR procedures for structure determination of oligonucleotide duplexes. In comparison with other NMR determinations of regular, platinated and nonplatinated oligonucleotides, the accuracy of the present structure is consequently expected to be lower. However, the main objective of this investigation has been achieved, i.e. to qualitatively determine the cross-linking arrangement in order to be able to suggest modifications to further speed up the cross-linking reaction rate.

Experimental Section

Sample Preparation: All the sequences were purchased from Oswell DNA Service as HPLC purified compounds. The reactions between *trans*-DDP and the pyrimidine-rich strands d(CTCCTGTGTCTC) (I) and d(CTCCTGTGCTCTC) (II) containing the GTG sites were performed as described previously.[12,14] Briefly, the single-stranded oligonucleotides ($c = 40$ μM) were incubated with 1.1 equivalents of *trans*-DDP in 10 mM $NaClO_4$/4 mM acetate buffer at pH 3.6 and

37 °C over a period of 24 h. Thereafter, the reaction mixtures were treated with thiourea (10 mM) for 10 min at 37 °C. The oligonucleotides containing a single 1,3-*trans*-{$Pt(NH_3)_2$[d(G*TG*)]} cross-link were purified by chromatography on a strongly basic anion-exchange resin on a Pharmacia FPLC system equipped with a MonoQ column, using a 0.2 to 0.7 M NaCl gradient in 10 mM NaOH. The binding of the platinum at the G residues was verified by the nonreactivity of dimethyl sulfate towards these sites.[12,14]

The platinated oligonucleotides were mixed with one equivalent of the complementary sequence, d(GAGATA−AGGAG) or d(GAGAGTA−AGGAG), respectively. Then, the duplexes (20 μM final concentration) in 500 mM NaCl, 10 mM Tris-HCl buffer (pH 7.5), and 0.5 mM EDTA were incubated at 288 K. After 9 days, the intrastrand to interstrand cross-link isomerization reactions were complete. The interstrand cross-linked duplexes were subsequently purified by chromatography on a strongly basic anion-exchange resin and then desalted on a Sep-Pak Column. The platinated 12/11-*mer* NMR sample was made up from 0.5 mL of the 0.8 mM in duplex solution in 0.5 M NaCl and 0.04 mM EDTA, and the pH was adjusted to 5.9. No buffer was added. The sample of the non-platinated duplex was dissolved in 0.55 mL of 9:1 H_2O/D_2O containing 0.520 M NaCl (pH 5.9) so that the final duplex concentration was 3.0 mM. ^{1}H-NMR spectra were recorded in H_2O solution and subsequently in D_2O after freeze-drying of the samples and redissolving them in 99.996% D_2O.

NMR Spectroscopy: The ^{1}H NMR experiments were performed on a Bruker DRX 600 instrument operating at 600 MHz for ^{1}H. In order to avoid melting of the duplexes and to obtain reasonable resolutions, all experiments were carried out at 290 K. 1D ^{1}H spectra were acquired with a total of 32 K complex points and 64 scans. For all 1D and 2D spectra, the spectral widths were 6000 Hz (in D_2O) or 13200 Hz (in H_2O) and a relaxation delay of 2 s was used. The 3-9-19 WATERGATE pulse sequence was used for water suppression.[27] The ^{1}H NOESY spectra were recorded in the pure absorption mode with quadrature detection using the States TPPI acquisition scheme.[28] A total of 2048 complex points in t_2 were collected for each of 512 t_1 increments and 80 transients were averaged for each increment. 2D NOESY spectra were acquired at four different mixing times (75, 125, 200, and 300 ms) in D_2O and in H_2O. The FIDs were processed by linear prediction routines increasing the time domain to 4 K, which significantly improves the signal-to-noise in the NOESY map.[29] DQF-COSY experiments were performed by collecting 2048 data points in t_2 and 512 data points in t_1, and the data were zero-filled to 2 K in both directions. The NMR data were processed on a Silicon Graphics INDY workstation using the program FELIX (Biosym)[30] and on a 133 MHz Pentium PC using 1D and 2D WIN-NMR (Bruker).[31] The one-dimensional ^{1}H FIDs were multiplied by an exponential window function prior to Fourier transformation. Typically, 1 Hz was added to the line widths. No baseline correction was needed. The two-dimensional NOESYs, which were used for integration, were apodized by a sinebell filter function, while assignments were made from resolution-enhanced spectra using a Gaussian function. The proton spectra were referenced to the HOD resonance at δ = 4.84 (290 K). ^{31}P-NMR spectra of the platinated and nonplatinated duplexes were acquired at 242.94 MHz. T_1 spin-lattice relaxation times were determined by the inversion recovery method.

NOE Distance-Restrained Molecular Dynamics/Mechanics Refinement: Nonexchangeable proton−proton distances were derived from initial NOE build-up rates as a function of mixing times using the cytosine H5−H6 distance of 2.46 Å as a reference. Cross-peaks were selected and integrated using WIN-NMR (Bruker). The thymine methyl (pseudo atom)−H6 distances were fixed at 3.1 Å. For all the N···H bonds, lower and upper limits of 1.7 Å and 2.0 Å, respectively, were used, while corresponding limits of 1.8 Å and 2.2 Å were used for O···H bonds. The platinum was attached to G6−N7 and A18−N1 at a fixed Pt−N distance of 2.0 Å. The square-planar coordination geometry about the metal was completed by two NH_3 ligands in *trans* positions. Charges on the metal and its NH_3 ligands were set in accordance with previous work by Kozelka et al.[32] Restrained molecular dynamics were conducted using the AMBER all-atom force field as implemented in DISCOVER (3.1) software. The calculations were carried out in vacuo with a distance-dependent dielectric constant of the form 4*r* and a force field with all 1−4 nonbonding interactions scaled by a factor of 0.5.[33]

The force constants used for the hydrogen bonds were set to 25 mol^{-1} $Å^{-2}$. For the other constraints, a force constant of 20 kcal mol^{-1} $Å^{-2}$ was applied when the relevant distances were outside of their limits. This approach is in accordance with recent work by Jourdan et al.[34] All dynamics calculations were performed on a Silicon Graphics INDY workstation using the programs INSIGHT II, DISCOVER, and NMR Refine (Biosym).[33] The calculation began with both classical A-DNA and B-DNA as modelled in INSIGHT II. The platinated guanine residue G6 was rotated into a *syn* configuration, in agreement with the derived intranucleotide G6−H8···H1′ NOE distance.

A total of 215 NOE distance constraints were used in the energy refinements of the starting models (A- and B-form DNA) using a conjugate gradient minimization algorithm. Initially, 500 cycles of energy minimization followed by 20 ps of molecular dynamics calculations at a constant temperature of 300 K were performed. The Verlet Leapfrog[35] algorithm was used to integrate the equations of motion, with an integration step of 1 fs. The average calculation frequency was 10 steps. The DISCOVER program uses Berendsens method[36] for pressure control. The molecular dynamics calculation was followed by a second run of 2000 cycles of energy refinement until an average rms gradient of 0.06 kcal mol^{-1} $Å^{-2}$ had been achieved. NMR Refine (Bruker) was used to generate the NOESY cross-peak volumes, using matrix doubling with a full relaxation matrix. T_1 leakage rates were set to 1 s^{-1}, cut-off distance to 5.5 Å, and τ_c was found to be optimal at 3.5 ns. Simulated spectra of the 200 ms NOESY experiments were calculated from these theoretical volumes using the program FELIX (Biosym). The back-calculated NOESY spectra were used to optimize the constraint file. The new constraint file was then used to create a new structure. These back-calculated refinement cycles were performed until the simulated NOESY cross-peak volumes matched the experimental data. In addition to visual matching of the cross-peak intensities, sometimes an *R*-factor, which sums the deviations between simulated and experimental cross-peaks, was calculated. However, this *R*-factor should be used with caution as a refinement parameter since intensities corresponding to short local sugar distances completely mask the intensities of weak cross-peaks that represent long-range global structure information. The program CURVES 5.3 was used to extract the helical parameters from the final structure.[15]

Acknowledgments

Financial support from the European Commission BIOMEDII program (Contract BMH4-CT97−2485) and Agence Nationale de Recherches sur le Sida is gratefully acknowledged. Thanks are ex-

tended to the Norwegian Research Council for a fellowship to B.A. We thank Dr. J. Arpalahti for carrying out additional HPLC and electrophoretic analysis.

[1] W. S. Marshall, M. H. Caruthers, *Science* **1993**, *259*, 1564−1570.
[2] C. A. Stein, Y. C. Cheng, *Science* **1993**, *261*, 1004−1012.
[3] P. S. Miller, *Prog. Nucleic Acids Res. Mol. Biol.* **1996**, *52*, 261−291.
[4] S. T. Crooke, *Med. Res. Rev.* **1996**, *16*, 319−344.
[5] S. Agrawal, *Trends Biotechnol.* **1996**, *14*, 376−386.
[6] C. Giovannangeli, C. Hélène, *Antisense Nucleic Acid Drug Dev.* **1997**, *7*, 413−421.
[7] R. W. Wagner, W. M. Flanagan, *Mol. Med. Today* **1997**, *3*, 31−38.
[8] Ciba Found. *Symp.* (Eds.: D. J. Chadwick, G. Cardew), John Wiley and Sons, Chichester, **1997**, vol. *209*.
[9] M. Boudvillain, R. Dalbies, M. Leng in *Metal Ions in Biological Systems* (Eds.: A. Sigel, H. Sigel), Marcel Dekker Inc., New York, **1996**, *33*, 87−102.
[10] K. M. Comess, C. E. Costello, S. J. Lippard, *Biochemistry* **1990**, *29*, 2102−2110.
[11] R. Dalbies, M. Boudvillain, M. Leng, *Nucleic Acids Res.* **1995**, *23*, 949−953.
[12] R. Dalbies, D. Payet, M. Leng, *Proc. Natl. Acad. Sci. USA* **1994**, *91*, 8147−8151.
[13] M. Boudvillain, M. Guerin, R. Dalbies, T. Saison-Behmoaras, M. Leng, *Biochemistry* **1997**, *36*, 2925−2931.
[14] C. Colombier, M. Boudvillain, M. Leng, *Antisense Nucleic Acid Drug Dev.* **1997**, *7*, 397−402.
[15] R. Lavery, H. Sklenar, CURVES 5.3 (http://www.ibpc.fr/UPR9080/CurForm bis.html)
[16] J. Lingbeck, M. G. Kubinec, J. Miller, B. R. Reid, G. P. Drobny, M. A. Kennedy, *Biochemistry* **1996**, *35*, 719−734.
[17] M. A. Lemaire, M. H. Fouchet, J. Kozelka, *J. Inorg. Biochem.* **1994**, *53*, 261−271.
[18] J. L. van der Veer, A. R. Peters, J. Reedijk, *J. Inorg. Biochem.* **1986**, *26*, 137−142.
[19] C. A. Lepre, K. G. Strothkamp, S. J. Lippard, *Biochemistry* **1987**, *26*, 5651−5657.
[20] F. J. Dijt, J. C. Chottard, J. P. Girault, J. Reedijk, *Eur. J. Biochem.* **1989**, *179*, 333−344.
[21] E. P. Nikonowicz, R. P. Meadows, D. G. Gorenstein, *Biochemistry* **1990**, *29*, 4193−4204.
[22] L. Joshua-Tor, D. Rabinovich, H. Hope, F. Frolow, E. Appella, J. L. Sussman, *Nature* **1988**, *334*, 82−84.
[23] V. P. Chuprina, E. Sletten, O. Y. Fedoroff, *J. Biomol. Struct. Dynam.* **1993**, *10*, 693−707.
[24] H. Huang, L. Zhu, B. R. Reid, G. P. Drobny, P. B. Hopkins, *Science* **1995**, *270*, 1842−1845.
[25] F. Paquet, C. Pérez, M. Leng, G. Lancelot, J. M. Malinge, *J. Biomol. Struct. Dynam.* **1996**, *14*, 67−77.
[26] F. Coste, J. M. Malinge, L. Serre, W. Shepard, M. Roth, M. Leng, C. Zelwer, *Nucleic Acids Res.* **1999**, *27*, 1837−1846.
[27] V. Sklenar, M. Piotto, R. Leppik, V. Saudek, *J. Magn. Reson. A* **1993**, *102*, 241−245.
[28] D. J. States, R. A. Haberkorn, D. J. Ruben, *J. Magn. Reson.* **1982**, *48*, 286−292.
[29] J. J. Led, H. Gesmar, *Chem. Rev.* **1991**, *91*, 1413−1426.
[30] *FELIX* (version 2.30) processing package, *Biosym/MSI*.
[31] *Bruker 1D WIN-NMR* (version 960901.2) and *2D WIN-NMR* (version 6.02).
[32] J. Kozelka, R. Savinelli, G. Berthier, J. P. Flament, R. Lavery, *J. Comp. Chem.* **1993**, *14*, 45−53.
[33] *BIOSYM* User Guide for *INSIGHT II* (version 2.3.5), *DISCOVER* (version 2.9.5) and *NMR Refine* (version 2.3).
[34] M. Jourdan, J. Garcia, E. Defrancq, M. Kotera, J. Lhomme, *Biochemistry* **1999**, *38*, 3985−3995.
[35] L. Verlet, *Phys. Rev.* **1967**, *159*, 98−103.
[36] H. J. C. Berendsen, J. P. M. Postma, W. F. van Gunsteren, A. DiNola, J. R. Haak, *J. Chem. Phys.* **1984**, *81*, 3684−3690.

Received December 4, 1999
[I00011]

Stability Constants and Decay of Aqua-Copper(III) – A Study by Pulse Radiolysis with Conductometric and Optical Detection

Piotr Ulanski[a] and Clemens von Sonntag*[b]

Keywords: Radicals / OH radical / Copper(III) / Copper(I) / Pulse radiolysis

Hydroxyl radicals were generated radiolytically in N_2O-saturated aqueous solutions and reacted with Cu^{2+}_{aq} ions. Pulse radiolysis with conductometric detection showed that the aqua-Cu^{III} species thus formed ($k = 3.2 \times 10^8$ dm^3 mol^{-1} s^{-1}) is uncharged at pH 5, i.e. $[Cu(OH)_3]_{aq}$, and from the changes in conductance as a function of pH it has been calculated that $Cu(OH)^{+}_{2aq}$ must have a pK value of 4.8 and $Cu(OH)^{2+}_{aq}$ a value of 3.7. At pH 2.5 there is no strong evidence for the presence of Cu^{3+}_{aq}. Aqua-$Cu(OH)_3$ decays bimolecularly to give Cu^{2+}_{aq} and H_2O_2. $Cu(OH)^{2+}_{aq}$ [and possibly also $Cu(OH)^{+}_{2aq}$] are in equilibrium with Cu^{2+}_{aq} and OH radicals [$K(Cu(OH)^{2+}_{aq}) \approx 3.7 \times 10^4$ dm^3 mol^{-1}]. Rapid electron transfer occurs from Cu^{+}_{aq} to $[Cu(OH)_3]_{aq}$ ($k = 3.5 \times 10^9$ dm^3 mol^{-1} s^{-1}).

Introduction

With the advent of pulse radiolysis in the 1960s it became possible to study the properties of transition-metal ions in unusually high oxidation states, which can be formed in aqueous solutions in reactions with the OH radical. Similarly, their lower than common oxidation states can be generated with the hydrated electron and also by the less-reducing H-atom (for a compilation of rate constants see ref.[1]; for a review see ref.[2]). In the case of Cu^{2+}_{aq} it has been shown that it is reduced at practically diffusion-controlled rates by the hydrated electron and the H-atom.[1] In the latter case a hydride is formed in the first step.[3,4] Even the less reducing superoxide radical ($E^7 = -0.3$ V)[5] is capable of reducing Cu^{2+}_{aq}.[6]

The Cu^{2+}_{aq} ion also reacts with the OH radical, although the rate of this reaction is significantly below diffusion controlled rates [Equation 1, $k_1 \approx 3 \times 10^8$ dm^3 mol^{-1} s^{-1}].[3,7–10] In neutral solution the species formed is characterized by a strong absorption at 280 nm (see Figure 8). From a high-pressure pulse-radiolysis experiment it has been concluded that in the first step a water molecule is replaced by an OH radical [Equation (1)].[10]

$$^{\bullet}OH + Cu(H_2O)^{2+}_n \rightarrow CuOH(H_2O)^{2+}_{n-1} + H_2O \quad (1)$$

Since the rate of build-up is rather slow, the primary species formed in this reaction may subsequently undergo rapid protonation/deprotonation reactions without being noticeable by changes in the UV absorption [Equations (2)–(4)].

$$Cu(H_2O)^{3+}_n \rightleftarrows CuOH(H_2O)^{2+}_{n-1} + H^+ \quad (2)$$

$$CuOH(H_2O)^{2+}_{n-1} \rightleftarrows Cu(OH)_2(H_2O)^{+}_{n-2} + H^+ \quad (3)$$

$$Cu(OH)_2(H_2O)^{+}_{n-2} \rightleftarrows Cu(OH)_3(H_2O)_{n-3} + H^+ \quad (4)$$

Thus, the species that is observed by spectrophotometry does not necessarily carry a doubly-positive charge. The absorption of the aqua-Cu^{III} intermediate varies with pH and from these data it has been deduced that it should have a pK_a value of around 3, a value that has been attributed to equilibrium (2).[3,7] Pulse radiolysis experiments with conductometric detection have indicated, however, that the intermediate observed at around pH 5 might in fact be neutral.[8,11] The rate of decay of the aqua-Cu^{III} intermediate increases with decreasing pH and decreasing Cu^{2+}_{aq} concentration, and below pH 4 no separation between the formation and disappearance was noticed. In addition, there is strong evidence that under these conditions OH radicals and the aqua-Cu^{III} intermediate must be in equilibrium.[3]

There is potentially another kind of Cu^{III} intermediate. When Cu^{+}_{aq} is reacted with H_2O_2 in the presence of methanol, a very effective chain reaction leading to the formation of formaldehyde is induced, but the fact that the chain length strongly depends on the methanol concentration has led to the conclusion that OH radicals are not the chain carrier[12,13] (for ESR experiments and a potentially different interpretation see refs.[14–17]; for the role of such intermediates in DNA cleavage see the review[18]). Because of their strong oxidative power, Cu^{III} complexes have been considered not to play a role in biological systems.[19] However, the presence of Cu^{III} has been postulated in model systems related to enzymes (refs.[20–24]). Interesting data on the properties of Cu^{III}-oligopeptide complexes have been obtained by pulse radiolysis.[25] There are also other means of generating copper(III) and this reagent is of some value in preparative organic chemistry (refs.[26,27]).

[a] Max-Planck-Institut für Strahlenchemie,
Stiftstraße 34–36, 45413 Mülheim an der Ruhr, Germany and
Institute of Applied Radiation Chemistry,
Technical University of Lodz,
Wroblewskiego 15, 93–590 Lodz, Poland
[b] Max-Planck-Institut für Strahlenchemie,
Stiftstraße 34–36, 45413 Mülheim an der Ruhr, Germany
Fax: (internat.) +49(0)208/306-3951
E-mail: vonsonntag@mpi-muelheim.mpg.de

 © WILEY-VCH Verlag GmbH, D-69451 Weinheim, 2000 1434–1948/00/0606–1211 $ 17.50+.50/0

Thus there is some interest in characterising the interesting aqua-Cu^{III} intermediate in more detail. The earlier pulse radiolysis experiments using conductometric detection were carried out in Ar-saturated solutions.[8] This is not the best condition for such an experiment. In the radiolysis of water [Equation (5)] OH radicals, hydrated electrons and H atoms are formed side by side [$G(^{\bullet}OH) \approx G(e^-_{aq}) \approx 2.8 \times 10^{-7}$ mol J^{-1}, $G(H^{\bullet}) \approx 0.6 \times 10^{-7}$ mol J^{-1}, $G(H_2O_2) = 0.7 \times 10^{-7}$ mol J^{-1}, $G(H_2) = 0.5 \times 10^{-7}$ mol J^{-1}].[28] Thus, in assessing the state of charge of the intermediate in question, the observed conductance changes have to be corrected for contributions caused by the reduction processes (formation of Cu^+_{aq} and H^+). Their assignment to $[Cu(OH)_3]_{aq}$ has been supported by a more decisive experiment.[11] In fact, such a correction can be largely avoided by saturating the solutions with nitrous oxide, which converts the hydrated electron into an OH radical [Equation (6); $k_6 = 9.7 \times 10^9$ dm^3 mol^{-1} s^{-1}].[1] Under these conditions a correction for a contribution of the H atom is minor (ca. 10%), at least when the pH is not too low, [Equation (7)], $k_7 = 2.3 \times 10^{10}$ dm^3 mol^{-1} s^{-1}.

$$H_2O \xrightarrow{\text{ionizing radiation}} {}^{\bullet}OH, e^-_{aq}, H^{\bullet}, H^+, H_2O_2, H_2 \quad (5)$$

$$e^-_{aq} + N_2O \rightarrow {}^{\bullet}OH + N_2 + OH^- \quad (6)$$

$$e^-_{aq} + H^+ \rightarrow H^{\bullet} \quad (7)$$

We have again used this approach to study the pH dependence of the stability constants of the aqua-Cu^{III} intermediates over a wide pH range (pH 2.5–5). Moreover, it will be shown that differently charged aqua-Cu^{III} may decay by different routes. Indeed, at low pH reaction (1) becomes reversible.

Results and Discussion

Determination of Stability Constants

Conductometric experiments have to be carried out at pH $\leq$ 5 in order to avoid buffering effects of Cu^{2+}_{aq} [p$K(Cu^{2+}_{aq}) \approx$ 7.2].[29] Low Cu^{2+}_{aq} concentrations have to be used in order to ensure that their reaction with the hydrated electron [$k(e^-_{aq} + Cu^{2+}_{aq} \rightarrow Cu^+_{aq}) \approx 3 \times 10^{10}$ dm^3 mol^{-1} s^{-1}][1] does not compete significantly with reaction (6). At these low Cu^{2+}_{aq} concentrations the rate of the reaction of the OH radical with Cu^{2+}_{aq} is rather slow, and very low doses per pulse (e.g. 1 $\leq$ Gy, Figure 1) have to be applied for a quantitative reaction because of the fast recombination of the OH radicals [2 $^{\bullet}OH \rightarrow H_2O_2$; $2k = 5.5 \times 10^9$ dm^3 mol^{-1} s^{-1}].[1] The conductance signal is even further reduced at high doses, since proton formation will lower the pH, an effect that also leads to a decrease in the conductance signal (cf. Figure 3).

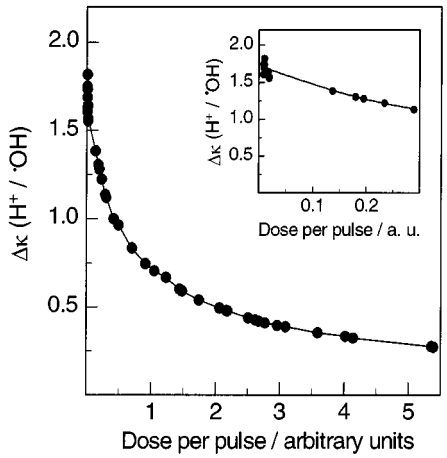


Figure 1. Pulse radiolysis of N_2O-saturated solutions of Cu^{2+}_{aq} (1×10^{-4} mol dm^{-3}), pH 5.0. The yields of conductance change (number of H^+ released per $^{\bullet}OH$ reacted) as a function of dose per pulse. One arbitrary dosimeter unit (a. u.) is approximately equivalent to 12 Gy

When the reaction of OH radicals under such conditions is followed by conductometry, the rate of increase in the conductance is proportional to the Cu^{2+}_{aq} concentration (Figure 2). From the slope of the straight line in Figure 2, a rate constant of 3.2×10^8 dm^3 mol^{-1} s^{-1} is calculated for the reaction of OH radicals with Cu^{2+}_{aq}, which compares well with the literature data obtained by optical detection (see above).

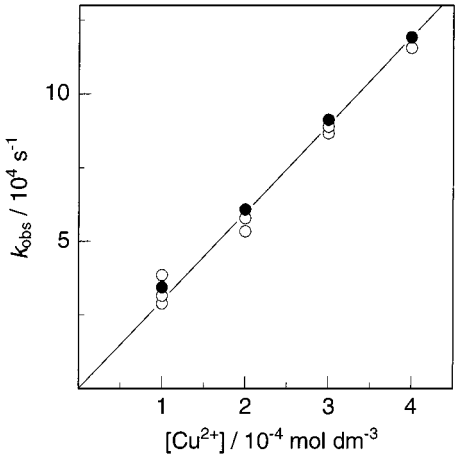


Figure 2. Pulse radiolysis of N_2O-saturated solutions of Cu^{2+}_{aq}. The rate of absorbance change at 350 nm (●; pH 5, extrapolation to zero dose) and conductance changes (○; pH 4, dose per pulse $\leq$ 1 Gy) as a function of the Cu^{2+}_{aq} concentration

In Figure 3 the proton yield per OH radical is plotted as a function of pH. These values are based upon dimethyl sulfoxide dosimetry, where one mol of OH radicals yields close to one mol of methanesulfinic acid.[30] It can be calculated from the data shown in Figure 3 that at pH 5 two mol of protons are formed per mol of OH radical reacted, i.e. the resulting aqua-Cu^{III} species must be uncharged $[Cu(OH)_3]_{aq}$, see Equation (8), which is in agreement with the earlier[8,11] conclusion.

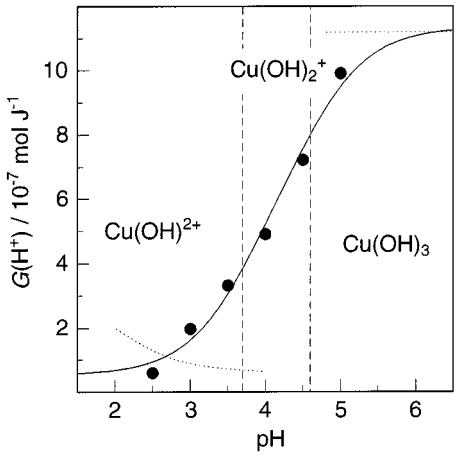


Figure 3. Pulse radiolysis of N_2O-saturated solutions of Cu^{2+}_{aq} (1×10^{-4} mol dm^{-3}). Conductance changes as a function of pH. Values extrapolated to zero dose per pulse

$$Cu^{2+}_{aq} + {}^{\bullet}OH + 2\,H_2O \rightarrow [Cu(OH)_3]_{aq} + 2\,H^+ \quad (8)$$

$$Cu^{2+}_{aq} + {}^{\bullet}OH + H_2O \rightarrow Cu(OH)^{+}_{2\,aq} + H^+ \quad (9)$$

$$Cu^{2+}_{aq} + {}^{\bullet}OH \leftrightharpoons Cu(OH)^{2+}_{aq} \quad (10)$$

Upon lowering the pH the proton yield drops, and at pH 2.5 no protons are liberated beyond those formed by the H atom with Cu^{2+}_{aq} ($Cu^{2+}_{aq} + H^{\bullet} \rightarrow Cu^{+}_{aq} + H^+$; note the dashed line in Figure 3). The experimental value at pH 2.5 is somewhat lower than this limit, which might suggest the onset of Cu^{3+}_{aq} formation. However, the relatively high background conductivity of the solution at this pH along with the low signals make the measurement conditions unfavourable. Thus, no firm conclusions can be drawn regarding the presence of the triply-charged species.

The pH range where this decrease is observed is rather narrow, although two pK values must be involved [Equations (3) and (4)].

The data can be fitted (solid line in Figure 3) using pK values at pH = 3.7 and 4.6. Our observations are in agreement with the earlier conclusion[8,11] that at pH 5 the aqua-Cu^{III} species are largely uncharged. The mono-charged species only dominates at around pH 4. In the more acidic pH range the aqua-Cu^{III} is doubly-charged and, as mentioned above, evidence for a triply-charged species at pH $\leq$ 2.5 is very weak. The difference between our results and those reported by Asmus et al.[11] only concerns the strongly acidic range. In the earlier study[11] a ten-fold higher Cu^{2+}_{aq} concentration was used and this, together with the protons, competes with N_2O for the solvated electrons. The reactions of Cu^{2+}_{aq} with the solvated electron and the H atom lead to the formation of Cu^{+}_{aq} and a proton. The reported data were corrected, but it is not stated whether the correction was only for the reduction in OH-radical yield or whether the latter effect was also corrected for in the evaluation of the conductance signals.

It is noted that the aqua-Cu^{III} species deprotonates only at much lower pH values than Cu^{2+}_{aq} (Cu^{2+}_{aq} dominates below pH 7).

A comparison can be made between the aqua-Cu^{III} and the isoelectronic aqua-Pd^{II} complex. The pK_a value of the $[Pd(H_2O)_3OH]^+$ species has been recently re-measured[31] as being close to 3.0 and the pK_a value of the neutral species must be even higher (not measurable because of the formation of polynuclear complexes). In this case the pK_a value of aqua-$Cu(OH)^{+}_{2}$ (equivalent to the neutral aqua-Pd^{II} complex) has been found at 3.7. This pK_a value is not unexpected given that the aqua-Cu^{III} ion is slightly smaller. The structure of aqua-Pd^{II} is square planar,[32] and one may therefore expect that the analogous aqua-Cu^{III} species has the same structure.

Decay of Aqua-Copper(III)

Aqua-$Cu(OH)_3$ is a highly reactive species. It decays under our experimental conditions on the millisecond time range and leads to restoration of the original conductance (Figure 4).

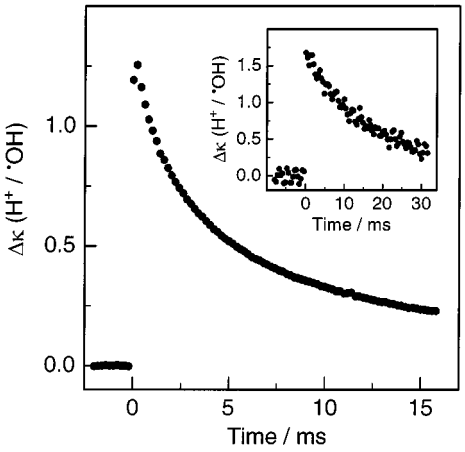


Figure 4. Pulse radiolysis of N_2O-saturated aqueous solutions of Cu^{2+}_{aq} (1×10^{-4} mol dm^{-3}) at pH 5 and a dose of 2.2 Gy (Inset: 0.1 Gy). Decay of aqua-$Cu(OH)_3$ as followed by conductance changes

At pH 5 the decay is largely bimolecular, i.e. the first half-life of decay decreases with increasing aqua-$Cu(OH)_3$ concentration. To achieve this by increasing the dose per pulse is not easy because of the slowness of the reaction of the OH radical with Cu^{2+}_{aq} (see Figure 1). However, the relevant aqua-$Cu(OH)_3$ concentration can be calculated from its maximum absorbance at 270 nm (Figure 5). These data yield a bimolecular rate constant of 1.8×10^8 dm^3 mol^{-1} s^{-1}. Similar experiments have been performed using conductometric detection. Although the dose per pulse was not known precisely in the experiments shown in the inset of Figure 5 (the estimated error is ±20%; for a possible method to determine this value exactly see ref.[33]), the approximate rate constant for the bimolecular decay of aqua-$Cu(OH)_3$ calculated from these data is $2k = 2 \times 10^8$ dm^3 mol^{-1} s^{-1}. These two sets of data agree well, but are considerably higher than the value of 4.6×10^7 dm^3 mol^{-1} s^{-1} reported earlier.[3]

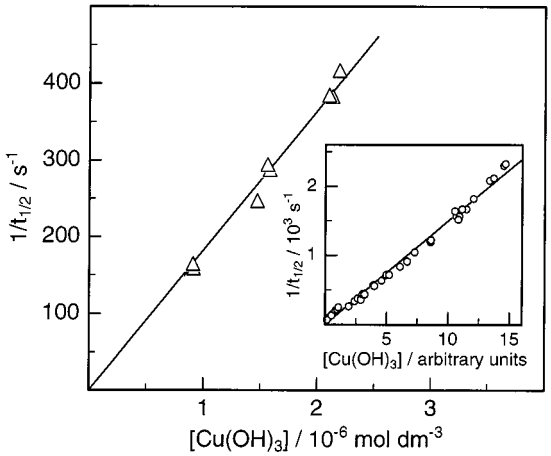


Figure 5. Pulse radiolysis of N_2O-saturated aqueous solutions of Cu^{2+}_{aq} (2×10^{-4} mol dm^{-3}) at pH 5. The reciprocal first half-lives of the decay of aqua-Cu(OH)$_3$ at 270 nm as a function of the initial $[Cu(OH)_3]_{aq}$ concentration (see text). Inset: Conductivity measurements; the initial [aqua-Cu(OH)$_3$] was taken to be proportional to the $[H^+]$ 100 μs after the pulse

It is reasonable to assume that in this bimolecular decay two Cu^{2+}_{aq} ions are reformed and one mol of H_2O_2 is thereby produced [Equation (11)].

$$2\,[Cu(OH)_3]_{aq} \rightarrow 2\,Cu^{2+}_{aq} + 4\,OH^- + H_2O_2 \quad (11)$$

This stoichiometry is indeed observed when a series of pulses of 1 Gy is given to an N_2O-saturated solution of Cu^{2+}_{aq} (2×10^{-4} mol dm^{-3}). Under these conditions the H_2O_2 concentration increases linearly with increasing dose (data not shown), and from these data a value of $G(H_2O_2) = 2.6 \times 10^{-7}$ mol J^{-1} is calculated. This value is not too far from that expected considering that Cu^{+}_{aq} [$G(Cu^{+}_{aq}) \approx 0.7 \times 10^{-7}$ mol J^{-1} under these conditions] will react rapidly with aqua-Cu(OH)$_3$ (see below) and thus will prevent the formation of H_2O_2. However, when the same experiment is carried out at the low dose rates of γ-radiolysis, only $G(H_2O_2) = 0.5 \times 10^{-7}$ mol J^{-1} is measured. Thus, reactions that consume the H_2O_2 formed must play a role in this situation and these are discussed below.

The rate of disappearance of the aqua-Cu^{III} intermediates is pH-dependent and increases as the solutions become more acidic. In addition, at low pH, build-up and decay were not clearly distinguishable.[3] It has been concluded that during this decay OH radicals are liberated [Equation (10)].[3]

A considerable drawback in the determination of equilibrium (10) by UV spectrophotometry is the fact that the reported[3,7] spectrum of the OH radical is very close to that resulting from its reaction with Cu^{2+}_{aq} at low pH. Moreover, at these low absorptions (cf. Figure 9) the signals become very noisy at the low doses required. This prevents the determination of equilibrium (10) by optical detection. However, conductometric experiments may allow some firmer conclusions to be drawn. In order to test the liberation of OH radicals, trace amounts (10^{-6} mol dm^{-3}) of dimethyl sulfoxide were added [Equation (12); $k_{12} = 7 \times 10^9$ dm^3 mol^{-1} s^{-1}].[30]

$$^{\bullet}OH + (CH_3)_2SO \rightarrow CH_3S(O)O^- + H^+ + {}^{\bullet}CH_3 \quad (12)$$

This reaction leads to the formation of methanesulfinic acid and hence contributes to a small extent to the observed conductance changes that occur immediately after the pulse, since these small amounts only scavenge ca. 9% of the primary OH radicals. However, the competition between Cu^{2+}_{aq} and dimethyl sulfoxide can become much more favourable for dimethyl sulfoxide in the long run. This is due to the fact that OH radicals liberated from the aqua-Cu^{III} intermediates will then have a chance to react with dimethyl sulfoxide in competition with a reaction with Cu^{2+}_{aq} that restores the aqua-Cu^{III} species [see Equation (10)].

This system was first tested at pH 5, where it has been shown above that very few, if any, OH radicals are liberated on the time scale of the decay of aqua-Cu(OH)$_3$, which dominates at this pH. If OH radicals had been eliminated, the conductance signal should have dropped during the bimolecular decay from two H^+ per OH radical to one H^+ per OH radical (dashed line in Figure 6). However, the former level of conductance is fully restored, confirming the above conclusions that at pH 5 no OH radicals are liberated on the pulse radiolysis time scale.

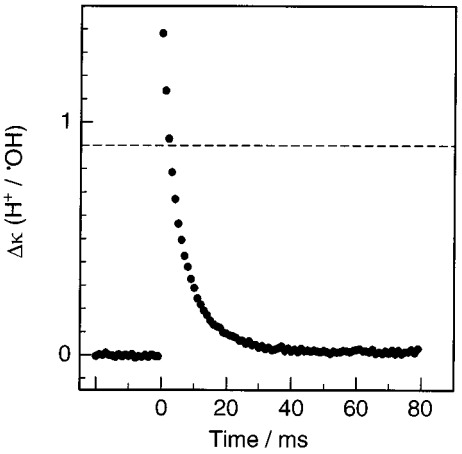


Figure 6. Pulse radiolysis of N_2O-saturated aqueous solutions of Cu^{2+}_{aq} (2×10^{-4} mol dm^{-3}) at pH 5 in the presence of dimethyl sulfoxide (10^{-6} mol dm^{-3}). The dashed line indicates the conductance change that should have been reached if aqua-Cu(OH)$_3$ had released an OH radical and the OH radicals had reacted with dimethyl sulfoxide

However, at pH 2.5, where no conductance changes are observed upon the reaction of OH radicals with Cu^{2+}_{aq}, the conductance should increase to a value of one H^+ per OH radical during the decay of the aqua-Cu^{III} intermediate when the released OH radical is scavenged by dimethyl sulfoxide. This limiting value is indicated by the dashed line in Figure 7.

From the data shown in Figure 7 it is possible to estimate the stability constant K_{10} by a simulation of the reactions that must contribute (yields of H atoms and OH radicals in N_2O-saturated solutions at this low pH [$G(H^{\bullet}) = 1.2 \times 10^{-7}$ mol J^{-1}, $G(^{\bullet}OH) = 5.0 \times 10^{-7}$ mol J^{-1}], formation of Cu^{+}_{aq}

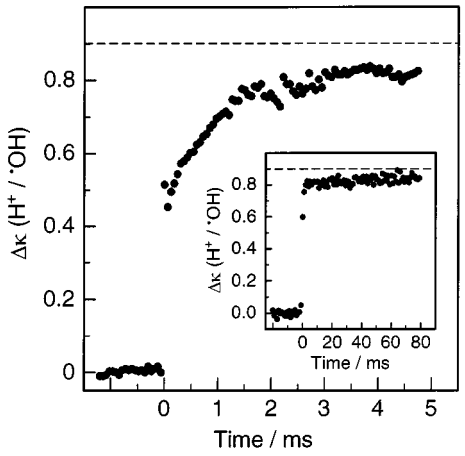


Figure 7. Pulse radiolysis of N_2O-saturated aqueous solutions of Cu^{2+}_{aq} (2×10^{-4} mol dm^{-3}) at pH 2.5 in the presence of dimethyl sulfoxide (10^{-6} mol dm^{-3}). The dashed line indicates the conductance change that should have been reached if the aqua-$Cu(OH)^{2+}$ had released an OH radical and the OH radicals had reacted with dimethyl sulfoxide

and H^+ by the H atom, bimolecular decay of Cu^+_{aq} and $Cu(OH)^{2+}_{aq}$, see below) to the observed conductivity changes, although practically no experimental variations can be made to put this value on a better footing. The experimental data are reasonably modelled by taking $k_{10} \approx 8 \times 10^3$ s^{-1}, $k_{-10} = 3 \times 10^8$ dm^3 mol^{-1} s^{-1}, i.e. $K_{10} \approx 3.7 \times 10^4$ dm^3 mol^{-1}. This value is of the same order as the values reported earlier ($K = 1.1 \times 10^4$ dm^3 mol^{-1}; at pH 3.65).[3]

The fact that OH radicals can be liberated in unimolecular reactions of aqua-Cu^{III} intermediates allows us to interpret the observation that at the low dose rates of γ-radiolysis, where reactions that are kinetically of first order will dominate, no H_2O_2 is formed at pH 2.5 and only low yields are formed at pH 5 (see above). The hydroxyl radical reacts with H_2O_2 by H-abstraction [Equation (13), $k_{13} = 2.7 \times 10^7$ dm^3 mol^{-1} s^{-1}][1] and this reaction yields the superoxide radical, which, although a peroxyl radical, is a powerful reductant[34] and readily reacts even with Cu^{2+}_{aq} [Equation (14)].[6]

$$^{\bullet}OH + H_2O_2 \rightarrow H_2O + HO^{\bullet}_2 \quad [HO^{\bullet}_2 \leftrightarrows O^{\bullet}_2{}^- + H^+;\ pK_a(HO^{\bullet}_2) = 4.8] \qquad (13)$$

$$Cu^{2+}_{aq} + O^{\bullet}_2{}^- \rightarrow Cu^+_{aq} + O_2 \qquad (14)$$

At pH 5 and with low dose rates of γ-radiolysis the yield of H_2O_2 was considerably lower than the value obtained under the high dose rate conditions of electron beam irradiation. Thus, at this pH some OH radicals must also have been liberated during the bimolecular decay of the aqua-Cu^{III} intermediates. It is hence concluded that either aqua-$Cu(OH)_3$ itself or aqua-$Cu(OH)^+_2$/aqua-$Cu(OH)^{2+}$, which are also present in lower steady-state concentrations, can liberate OH radicals [aqua-$Cu(OH)_3$ – albeit very slowly, if at all, see above].

Reaction of Aqua-$Cu(OH)_3$ with Cu^+_{aq}

In order to determine the rate of the reaction of aqua-$Cu(OH)_3$ with Cu^+_{aq} [Equation (15)] conditions were chosen where $O^{\bullet}_2{}^-$ (i.e. Cu^+_{aq}) is in a large excess in comparison with aqua-$Cu(OH)_3$. This situation can be achieved by pulse-irradiation of O_2-saturated solutions of Cu^{2+}_{aq} (1×10^{-3} mol dm^{-3}) that also contain formate ions (1×10^{-3} mol dm^{-3}). Under these conditions the OH radicals will be partially scavenged by formate [Equation (16)] and the resulting $CO^{\bullet}_2{}^-$ radicals converted by O_2 into $O^{\bullet}_2{}^-$ radicals [Equation (17)]. In addition, the solvated electrons are also converted by O_2 into $O^{\bullet}_2{}^-$ radicals, and some of the solvated electrons will also contribute to the Cu^+_{aq} yield [Equations (18) and (19)].

$$Cu^+_{aq} + [Cu(OH)_3]_{aq} \rightarrow 2\,Cu^{2+}_{aq} + 3\,OH^- \qquad (15)$$

$$^{\bullet}OH + HCO^-_3 \rightarrow H_2O + CO^{\bullet}_2{}^- \qquad (16)$$

$$CO^{\bullet}_2{}^- + O_2 \rightarrow CO_2 + O^{\bullet}_2{}^- \qquad (17)$$

$$e^-_{aq} + O_2 \rightarrow O^{\bullet}_2{}^- \qquad (18)$$

$$e^-_{aq} + Cu^{2+}_{aq} \rightarrow Cu^+_{aq} \qquad (19)$$

Under such conditions, the decay kinetics of aqua-$Cu(OH)_3$ are of (pseudo) first order. By increasing the dose per pulse, the Cu^+_{aq} concentration is raised correspondingly, and from the linear k_{obs} vs. Cu^+_{aq} concentration relationship (Figure 8) a value of $k_{15} = 3.5 \times 10^9$ dm^3 mol^{-1} s^{-1} is calculated. Thus, the expectation discussed above, namely that aqua-Cu^{III} intermediates are readily reduced by Cu^+_{aq}, has been substantiated.

In the experiments represented in Figure 8 the decay of aqua-$Cu(OH)_3$ was followed by optical detection. This required a re-determination of the absorption spectrum of aqua-$[Cu(OH)_3]_{aq}$, which is shown in Figure 9. In the present study much lower doses per pulse were used than was possible in the earlier[7] study.

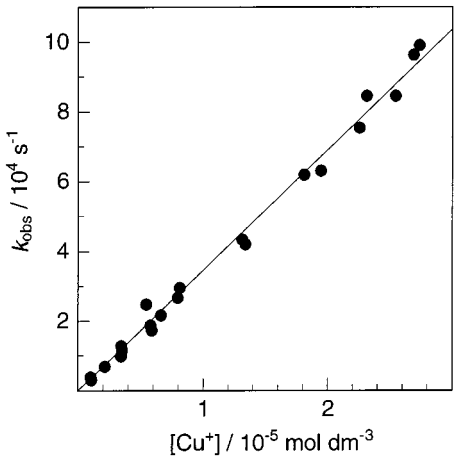


Figure 8. Pulse radiolysis of O_2-saturated aqueous solutions of Cu^{2+}_{aq} (1×10^{-3} mol dm^{-3}) containing 1×10^{-3} mol dm^{-3} of formate, pH 5.0. The observed pseudo-first-order rate constant of aqua-$Cu(OH)_3$ decay, followed as absorbance decrease at $\lambda = 300$ nm, as a function of Cu^+_{aq} concentration

It can be seen from Figure 9 that there is a considerable drop in absorbance with decreasing pH. Taking the pK

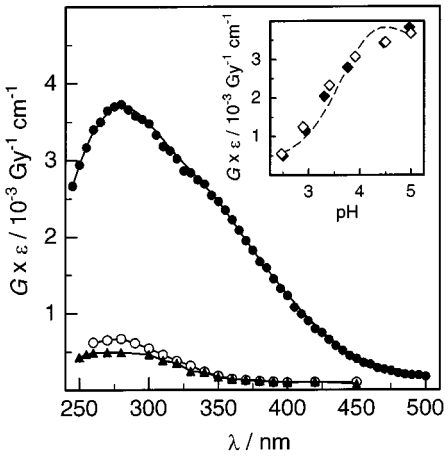


Figure 9. Pulse radiolysis of aqueous solutions of Cu^{2+}_{aq} (2×10^{-4} mol dm^{-3}). Absorption spectra (in units of $G \times \varepsilon$) recorded at 60–80 μs after a pulse of 1.8 Gy. Filled circle: N_2O-saturated solutions of pH 5.0; open circle: N_2O-saturated, pH 2.5; filled triangle: Ar-saturated, pH 2.5. Inset: Absorbance at 270 nm (in units of $G \times \varepsilon$) as a function of pH; filled square: $Cu(SO_4)/H_2SO_4$; open square: $Cu(ClO_4)_2/HClO_4$

values that were determined earlier and fixing the absorption coefficient of $Cu(OH)^{2+}_{aq}$ at 500 dm^3 mol^{-1} cm^{-1} (i.e. close to that of the OH radical),[1] the best fit (dashed line in the inset of Figure 9) is obtained with $\varepsilon[Cu(OH)^{+}_{2\,aq}]$ = 8000 dm^3 mol^{-1} cm^{-1} and ε[aqua-$Cu(OH)_3$] = 4800 dm^3 mol^{-1} cm^{-1}. The reason why the monocharged species has the highest absorption coefficient is not yet understood. In the inset in Figure 9are shown the data obtained with copper sulfate and copper perchlorate. This is a strong indication that the anion has no influence on the absorption spectra (see also ref.[3]), in particular the strong absorptions of the neutral and the monocharged species are not due to complexation by the sulfate ion.

Some experiments were also performed at pH 2.5 in Ar-saturated solutions (see filled triangle in Figure 9). Under these conditions approximately equal amounts of aqua-$Cu(OH)^{2+}$ and Cu^{+}_{aq} are formed (note the conversion of the solvated electron into an H atom at low pH). The experiments show that Cu^{+}_{aq} also absorbs in this wavelength region, but its contribution to the spectrum obtained in N_2O-saturated solutions (see open circle in Figure 9) is only small.

Experimental Section

Copper(II) sulfate pentahydrate, copper(II) perchlorate and all other chemicals were used as received. Solutions were made up in Milli-Q-filtered water (Millipore). The pH was adjusted with H_2SO_4 or with $HClO_4$. Prior to irradiation, solutions were saturated for 45 min with N_2O, which had been purified using an Oxisorb column (Messer-Griesheim), or for 20 min with O_2. γ-Irradiation was performed with a panorama ^{60}Co-γ-source (Nuclear Engineering) at a dose rate of 0.67 Gy s^{-1}. Pulse radiolysis measurements were carried out with a van de Graaff accelerator, generating 0.4 μs pulses of 2.8 MeV electrons. Details of the conductometric and optical detection systems are given elsewhere.[35,36] Dimethyl sulfoxide and thiocyanate were used as dosimeters for the conductometric and optical pulse radiolysis experiments.[30,37] In the conductometric experiments dosimetry allows the calculation of the yields (G value) of the conducting species formed, although their absolute concentrations cannot be ascertained by this method. The knowledge of the absolute concentration is only required for the evaluation of bimolecular rate constants. In principle this can be determined,[33] but for the present work it was sufficient to know the approximate valus for dose per pulse (± 20%). One dosimeter unit, as given in the figures, corresponds to approximately 12 Gy.

For the determination of H_2O_2 yields (measured spectrophotometrically with titanyl sulfate)[38] under pulse-irradiation conditions, solutions contained in a small vessel that permitted continuous N_2O-saturation were subjected to a series of electron pulses. The absorbed dose was determined using the O_2-saturated Fricke dosimeter.

Acknowledgments

We would like to thank Prof. Dr. K. Wieghardt for valuable discussions. P. U. thanks the Alexander-von-Humboldt Foundation for a stipend.

[1] G. V. Buxton, C. L. Greenstock, W. P. Helman, A. B. Ross, *J. Phys. Chem. Ref. Data* **1988**, *17*, 513–886.
[2] G. V. Buxton, R. M. Sellers, *Coord. Chem. Rev.* **1977**, *22*, 195–274.
[3] D. Meyerstein, *Inorg. Chem.* **1971**, *10*, 638–641.
[4] W. A. Mulac, D. Meyerstein, *Inorg. Chem.* **1982**, *21*, 1782–1784.
[5] P. Wardman, *J. Phys. Chem. Ref. Data* **1989**, *18*, 1637–1755.
[6] B. H. J. Bielski, D. E. Cabelli, R. L. Arudi, A. B. Ross, *J. Phys. Chem. Ref. Data* **1985**, *14*, 1041–1100.
[7] J. H. Baxendale, E. M. Fielden, J. P. Keene, in *Pulse Radiolysis* (Eds.: M. Ebert, J. P. Keene, A. J. Swallow, J. H. Baxendale), Academic Press, London, **1965**, pp. 217–220.
[8] G. C. Barker, P. Fowles, *Trans. Faraday Soc.* **1970**, *66*, 1661–1669.
[9] H. Christensen, K. Sehested, *Radiat. Phys. Chem.* **1980**, *16*, 183–186.
[10] H. Cohen, R. van Eldik, M. Masarwa, D. Meyerstein, *Inorg. Chimica Acta* **1990**, *177*, 31–34.
[11] K.-D. Asmus, M. Bonifacic, P. Toffel, P. O′Neill, D. Schulte-Frohlinde, S. Steenken, *J. Chem. Soc., Faraday Trans. I* **1978**, *74*, 1820–1826.
[12] G. R. A. Johnson, N. B. Nazhat, R. A. Saadalla-Nazhat, *J. Chem. Soc., Chem. Commun.* **1985**, 407–408.
[13] G. R. A. Johnson, N. B. Nazhat, R. A. Saadalla-Nazhat, *J. Chem. Soc., Faraday Trans. 1* **1988**, *84*, 501–510.
[14] G. V. Buxton, J. C. Green, R. M. Sellers, *J. Chem. Soc., Dalton Trans.* **1976**, 2160–2165.
[15] B. C. Gilbert, G. Harrington, G. Scrivens, S. Silvester, in *Free Radicals in Biology and Environment* (Ed.: F. Minisci), Kluwer Academic, Dordrecht, **1997**, pp. 49–62.
[16] M. R. Gunther, P. M. Hanna, R. P. Mason, M. S. Cohen, *Arch. Biochem. Biophys.* **1995**, *316*, 515–522.
[17] B. C. Gilbert, J. K. Stell, M. Jeff, *J. Chem. Soc., Perkin Trans. II* **1988**, 1867–1873.
[18] G. Pratviel, J. Bernadou, B. Meunier, *Adv. Inorg. Chem.* **1998**, *45*, 251–312 .
[19] W. Kaim, J. Rall, *Angew. Chem. Int. Ed. Engl.* **1996**, *35*, 43–60.
[20] G. R. Dyrkacz, R. D. Libby, G. A. Hamilton, *J. Am. Chem. Soc.* **1976**, *98*, 626–628.
[21] C. J. Cramer, B. A. Smith, W. B. Tolman, *J. Am. Chem. Soc.* **1996**, *118*, 11283–11287.
[22] J. A. Halfen, S. Mahapatra, E. C. Wilkinson, S. Kaderli, V. G. Young, L. Que, A. D. Zuberbühler, W. B. Tolman, *Science* **1996**, *271*, 1397–1400.
[23] S. Mahapatra, J. A. Halfen, E. C. Wilkinson, G. Pan, X. Wang, V. G. Young, J. Cramer, L. Que, W. B. Tolman, *J. Am. Chem. Soc.* **1996**, *118*, 11555–11574.

[24] F. P. Bossu, K. L. Chellappa, D. W. Margerum, *J. Am. Chem. Soc*. **1977**, *99*, 2195–2203.
[25] S. Goldstein, G. Czapski, H. Cohen, D. Meyerstein, R. van Eldik, *Inorg. Chem*. **1994**, *33*, 3255–3260.
[26] E. Balogh-Hergovich, G. Speier, *React. Kinet. Catal. Lett*. **1996**, *58*, 269–274.
[27] A. Banerjee, D. Mandal, A. Ray, P. Banerjee, G. C. Banerjee, *J. Indian Chem. Soc*. **1995**, *72*, 205–207.
[28] C. von Sonntag, *The Chemical Basis of Radiation Biology*, Taylor and Francis, London, **1987**.
[29] D. D. Perrin, *IUPAC Chem. Data Ser*. **1987**, *29*, 29–30.
[30] D. Veltwisch, E. Janata, K.-D. Asmus, *J. Chem. Soc*., *Perkin Trans. 2,* **1980**, 146–153.
[31] T. Shi, L. I. Elding, *Acta Chem. Scand*. **1998**, *52*, 897–902.
[32] R. J. Deeth, L. I. Elding, *Inorg. Chem*. **1996**, *35*, 5019–5026.
[33] H.-P. Schuchmann, D. J. Deeble, G. O. Phillips, C. von Sonntag, *Radiat. Phys. Chem*. **1991**, *37*, 157–160.
[34] C. von Sonntag, H.-P. Schuchmann in *Peroxyl Radicals* (Ed.: Z. B. Alfassi), Wiley, Chichester, **1997**, pp. 173–234.
[35] E. Bothe, E. Janata, *Radiat. Phys. Chem*. **1994**, *44*, 455–458.
[36] C. von Sonntag, H.-P. Schuchmann, *Methods Enzymol*. **1994**, *233*, 3–20.
[37] G. V. Buxton, C. R. Stuart, *J. Chem. Soc*., *Faraday Trans*. **1995**, *91*, 279–281.
[38] G. M. Eisenberg, *Ind. Eng. Chem. Anal. Ed*. **1943**, *15*, 327–328.
Received November 3, 1999
[I99392]

TRENPYPOLS: A New Water-Soluble Iron Chelator (both Fe^{III} and Fe^{II}) Involving Six-Membered Coordination Rings

Paul Baret,[a] Claude Béguin,[a] Gisèle Gellon,[a] Jean-Louis Pierre,[a] Guy Serratrice,*[a] Fabrice Thomas,[a] Jean-Pierre Laulhère,[b] and Eric Saint-Aman[c]

Keywords: Tripodal ligands / N ligands / O ligands / Thermodynamics / EPR spectroscopy / Iron

An eight-step synthesis of a new water-soluble tripodal ligand TRENPYPOLS (tris[2-(2-hydroxy-3-(2-pyridinyl)-5-sulfobenzamido)ethyl]amine) is described. TRENPYPOLS is built by connecting the TREN spacer through a tris-amide moiety to the *ortho* phenolic position of three 2-(2-hydroxyphenyl)pyridine chelating subunits, (followed by the sulfonation of the 5-positions). The three [O,N_{pyr}] bidentate subunits of TRENPYPOLS involve six-membered coordination rings. The solution coordination chemistry of the ligand and its iron complexes have been studied by means of pH potentiometric, spectrophotometric and voltammetric methods. The stability constants, log β_{110}, are 30.1 for the ferric complex and 17.7 for the ferrous complex (pFe^{III} and pFe^{II} values are 23.6 and 11.2 respectively at pH = 7.4, $[L]_{tot} = 10^{-5}$ M, $[Fe]_{tot} = 10^{-6}$ M). Comparison with the data of O-TRENSOX (8-hydroxyquinoline subunits with a 5-membered chelate ring) corroborates the usual rules concerning the influence of the chelate ring size on complexation ability. Fe^{III}-TRENPYPOLS has been tested as a single source of iron in nutritional experiments with *Arabidopsis thaliana* plant cells. The efficiency towards growth and resistance to iron chlorosis is good, comparable to that of Fe^{III}-EDTA, the most commonly used complex for in vitro cell cultures.

Introduction

Siderophores are iron-chelating agents that are excreted by microorganisms. They render iron soluble in the environment and favour the uptake of this metal.[1,2] Iron chelation, by some natural or abiotic chelators, can be used in the study of human diseases characterized by iron overload. Water-soluble iron complexes can be used to alleviate iron deficiency in plants, preventing and even reversing iron chlorosis. Natural siderophores, and most of their synthetic models, contain three catecholate or hydroxamate groups (hard donor groups) which bind the hard ferric ions, giving stable Fe^{III} octahedral complexes (Figure 1). As there has been an intense interest in the complexation of both ferrous and ferric iron for chelation therapy (Fe^{II} is hazardous and redox recycling of iron may occur in the cells[3]), for plant nutrition, and also for the development of tools for the study of iron metabolism, we have developed a promising water-soluble chelator O-TRENSOX (Figure 1).[4−7] This ligand was synthesized by connecting the TREN spacer through a tris-amide moiety to the 7 position of 8-hydroxyquinoline-5-sulfonic acid, a bidentate ligand containing both a hard phenolate oxygen and a softer pyridine nitrogen as donor groups. O-TRENSOX exhibits strong complexing ability towards the ferric cation, of the same order of magnitude as the triscatecholate (TRENCAMS)[8] and the trishydroxamate (TRENDROX)[9] analogs (Figure 1). Moreover, O-TRENSOX exhibits strong complexing ability towards the ferrous cation: as expected, [O,N_{pyr}] instead of [O,O] donor sets may allow strong complexation of both Fe^{3+} and Fe^{2+} ions. The pFe^{III} values[10] (calculated for $[Fe^{III}] = 1$ μM, [L] = 10μM at pH =7.4) shown in Figure 1 provide a direct comparison of the affinities of the ligands for Fe^{3+}. It must be emphasized that all the bidentate subunits of the usual iron chelators (and particularly those depicted in Figure 1) involve 5-membered chelate rings but few subunits involve 6- membered chelate rings. Several 1,3,5-tris(5-substituted salicylamino)cyclohexanes, which involve the unusual 6-membered coordination ring, have been synthesized and their Fe^{III} complexes structurally characterized, but no thermodynamic or kinetic data have been reported.[11]

The new water soluble ligand TRENPYPOLS incorporates three [O,N_{pyr}] bidentate subunits involving six-membered coordination rings. The solution coordination chemistry of the ligand and its iron complexes have been studied by means of pH potentiometric, spectrophotometric and voltammetric methods. The complexing ability of TRENPYPOLS has been compared to ligands involving 5-membered chelate ring. TRENPYPOLS has been tested as a single source of iron in nutritional experiments with *Arabidopsis thaliana* plant cells.

We have synthesized the first synthetic water-soluble tris bidentate iron chelator where the [O,N_{pyr}] type chelating units have been retained and incorporate a six-membered chelate ring. The so-called TRENPYPOLS (the full name of the

[a] Laboratoire de Chimie Biomimétique (LEDSS, UMR CNRS 5616), Université J. Fourier, BP 53, 38041 Grenoble Cedex 9, France
[b] CBCRB, DBMS/CB, CEA-Grenoble, 17 av. des martyrs, 38054 Grenoble Cedex 09
[c] Laboratoire d'Electrochimie Organique et de Photochimie Redox (UMR CNRS 5630), Université J. Fourier, BP 53, 38041 Grenoble Cedex 9 − France
E-mail: Guy.Serratrice@ujf-grenoble.fr

 © WILEY-VCH Verlag GmbH, D-69451 Weinheim, 2000 1434−1948/00/0606−1219 $ 17.50+.50/0

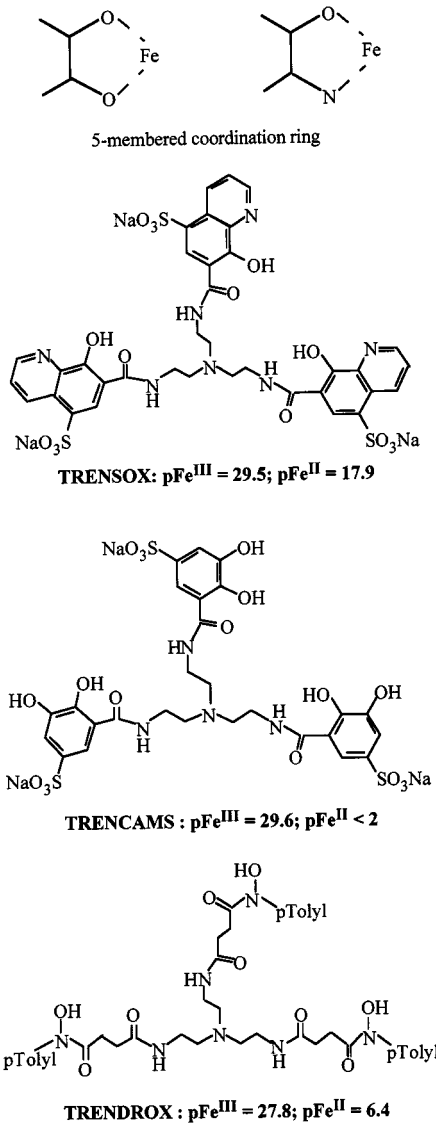


Figure 1. Iron chelators with 5-membered coordination rings

acidic form is tris[2-(2-hydroxy-3-(2-pyridinyl)-5-sulfobenzamido)ethyl]amine) is depicted in Figure 2. As in the chelators given in Figure 1, it is built by connecting the TREN spacer through a tris-amide moiety to the chelating subunits.Only a few studies of the coordination chemistry of the 2-(2-hydroxyphenyl)pyridine ligand have been reported, probably because they are difficult to prepare. Pd^{II}, Co^{III}, Ru^{II}, Ru^{III} and Cr^{III} mononuclear complexes have been described.[12−14] This ligand may be considered as an hydrolytically stable analog of salicylaldimines. It was therefore of great interest to synthesize a tripodal ligand involving three bidentate subunits of this type. This had never been realized before this work. It must be emphasized that in previous studies of the octahedral coordination involving three independent bidentate 2-(2-hydroxyphenyl)pyridine ligands, the three oxygen and the three nitrogen atoms of the coordination sphere are respectively in a *mer* arrangement, as shown in the crystal structures.[12,13] In the complex of a tripodal ligand such as TRENPYPOLS, these atoms are forced

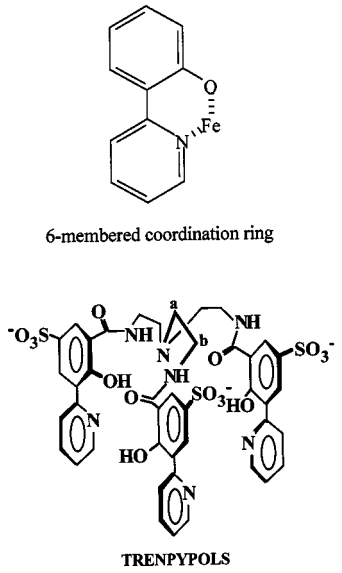


Figure 2. Structural formula of TRENPYPOLS

to be *fac*. In this paper, we report the synthesis, the iron binding properties (thermodynamic and spectroscopic studies) and the nutritional behavior for plant cells of this ligand.

Results and Discussion

Synthesis

The ligand TRENPYPOLS was prepared by sulfonation (oleum) of TRENPYPOL **9**. The methoxylated podand **8** was obtained by coupling of tris(2-aminoethylamine) (TREN) and acid chloride **7**. The key step in the preparation of **7** was the heteroaromatic coupling[15] of 2-bromopyridine and the Grignard derivative **4** of 2-bromo-6-methyl-anisole **3**. The brominated precursors **2** and **3** were prepared by slight modifications of reported procedures (Figure 3).[16,17]

Ligand Deprotonation Constants

The ligand TRENPYPOLS possesses seven deprotonation sites (three pyridinium nitrogen atoms, one tertiary ammonium nitrogen atom and three hydroxy oxygen atoms) and is denoted LH_7^+, taking into account the negative charges of the three sulfonate groups. The deprotonation constants, pK_{an}, of TRENPYPOLS were determined by potentiometric titrations of the fully protonated ligand. Analysis of the potentiometric titration curve (Figure 4a) by the SUPERQUAD program[18] yielded the pK_{an} values (σ_{fit} = 4.8) defined by Equation (1) and Equation (2) (charges omitted for clarity):

$$LH_n \rightleftarrows LH_{n-1} + H^+ \quad (1)$$

$$K_{an} = [LH_{n-1}][H^+]/[LH_n] \quad (2)$$

pK_{a1} = 10.32 ± 0.03, pK_{a2} = 10.07 ± 0.04, pK_{a3} = 9.23 ± 0.06,
pK_{a4} = 5.25 ± 0.08, pK_{a5} = 4.38 ± 0.08, pK_{a6} = 3.21 ± 0.09 and pK_{a7} = 2.77 ± 0.12

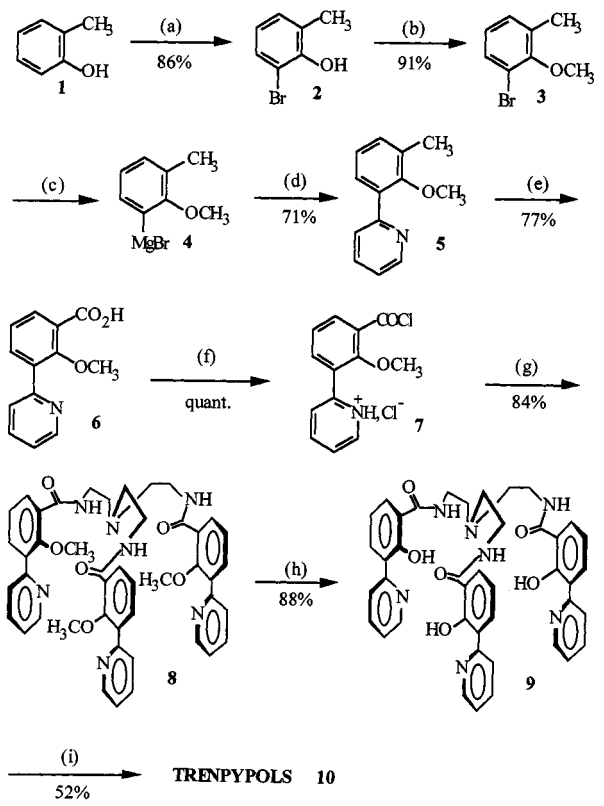


Figure 3. Synthesis of TRENPYPOLS: (a) Br_2, tBuNH$_2$, toluene, −78 °C; (b) $(CH_3)_2SO_4$, K_2CO_3, acetone reflux; (c) Mg, THF, reflux; (d) 2-bromopyridine, Ni(dppe)Cl_2 cat., THF; (e) $KMnO_4$, $NaHCO_3$, H_2O then HCl 4 N; (f) $SOCl_2$; (g) TREN, Et_3N, THF, 25 °C; (h) BBr_3, CH_2Cl_2, 0 °C; (i) H_2SO_4, oleum, 25 °C

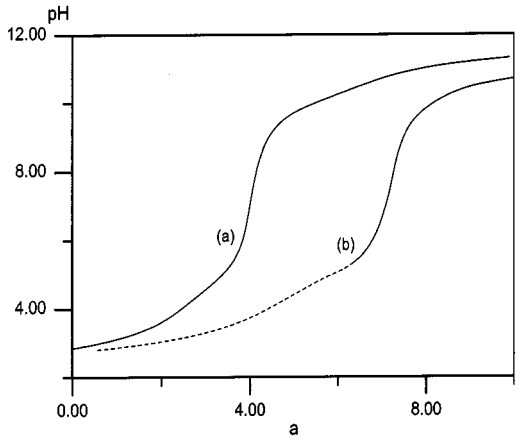


Figure 4. Potentiometric titration curves for (a) 0.5 mM ligand TRENPYPOLS; (b) TRENPYPOLS + Fe^{III} 1:1 0.5 mM (the dashed line indicates precipitation of the complex); a = mol of base added per mol of ligand. All solutions were at 25 °C and ionic strength I = 0.1 M ($NaClO_4$)

The pK_a of the tertiary ammonium nitrogen could be assigned from an ^{1}H NMR spectroscopic titration, by measuring the chemical shifts of the methylene protons H_a and H_b (see assignments in Figure 2), since they undergo a significant shift related to the deprotonation of this nitrogen. An upfield shift, as expected for a deprotonation, was observed over the pD range 4 to 6 (Figure 5) with an inflection

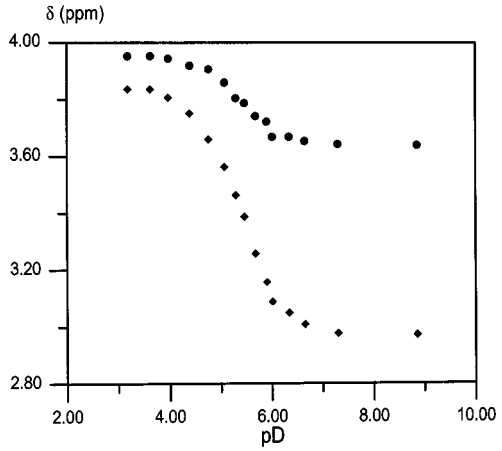


Figure 5. ^{1}H NMR chemical shifts δ (ppm) for the methylene protons H_a (◆) and H_b (●) of TRENPYPOLS in D_2O as a function of pD

point at pD 5 indicating that the value of 5.25 determined from potentiometric titration can be assigned to the tertiary amine. However, it should be noted that the pK_a values which are determined potentiometrically are macroconstants, they cannot be directly assigned to a single functional group when the pK$_a$s differ by less than 2 log units. Thus pK_{a4} is partly produced by ionization of the pyridinium nitrogens. The three lower pK_as corresponded to the pyridinium nitrogens and the three higher ones to the hydroxy groups. The range over which the determined stepwise deprotonation constants for the pyridinium nitrogens (2.77, 3.21 and 4.38) and the hydroxy groups (9.23, 10.07 and 10.32) occurs, is slightly different from the statistical factor of log 3 (0.48). This indicates that there is some cooperativity between the three arms of the tripod.

The average deprotonation constants p$K_{av(5-7)}$ for the pyridinium nitrogens is 3.4. The average deprotonation constants p$K_{av(1-3)}$ for the hydroxy groups is 9.87. In comparison with the pK_a of phenol (9.9), one would expect that the pK_a for the hydroxy groups should be less than that of phenols by about one log unit owing to the electron-withdrawing effect of the amide and sulfonate substituents. The high values for the hydroxy pK_as can be ascribed to the formation of an intramolecular hydrogen bond with the pyridyl nitrogen in each arm, which favors the protonated form and thus enhances the pK_a.

It is interesting to compare the pK_a value of 5.25 of the tertiary ammonium nitrogen with those of similar ligands based on the TREN backbone connected to the amide group and containing three bidentate units, such as 8-hydroxyquinoline (O-TRENSOX), pK_a = 6.36[7] ; 2,2′-dihydroxybiphenyl (TBPAS), pK_a = 7.1;[19] catechol (TRENCAMS), pK_a = 8.03[8]; methoxycatechol (TREN(ME)SAM), pK_a = 6.3;[20] and phenol (TRENSAM), pK_a = 8.9.[20] It has been observed that the basicity of the tertiary amine is related to its ability to form a hydrogen bond with the amide hydrogen depending on the conformation of the amide group and on the hydrogen bond networks available in the molecule. Two hydrogen bond networks may be envisaged according to Figure 6: (i) the tertiary amine deprotonates first (scheme 1) as in O-TRENSOX, TREN(ME)SAM and TRENPYPOLS, (ii) the o-hydroxy

deprotonates first as in TRENCAMS and TRENSAM (scheme 2). Scheme 1 appears more favorable for TRENPYPOLS since the hydroxy group can establish H-bonds with both the carbonyl oxygen and the second donor atom (N) leading to one five-membered ring and to two six-membered rings.

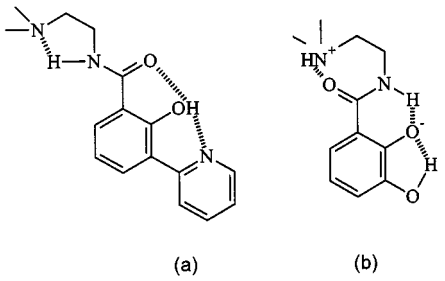


Figure 6. Deprotonation schemes of TRENPYPOLS (scheme 1) and TRENCAMS (scheme 2) showing the hydrogen bond networks

Stability Constants of the Ferric Complex

Potentiometric titrations of 1:1 solutions of ferric ion and ligand were carried out over the pH range 2.5 to 10 (Figure 4b). The titration curve has a buffer region from a (mol base per mol ligand) = 5−7 which covers a pH range of 4−5.5, indicating the formation of the FeL complex from about pH 6. However, the precipitation of the complex below pH 5 precluded the use of the titration data in the refinement program.

The spectrophotometric titration of the ferric complexes at a 1:1 metal-to-ligand molar ratio was carried out from pH 1 to 10 in order to study the Fe^{III}-TRENPYPOLS complexation equilibria as a function of pH. In addition, the equilibrium constant β_{110} was determined by spectrophotometric competition experiments. The spectra are shown in Figure 7. An increase in the pH from 1 to 3 resulted in the appearance of a charge-transfer band at λ_{max} = 470 nm (Figure 7a). The absorbance data were processed with the LETAGROP-SPEFO program.[21,22] The best fit ($\Sigma(A_{exp} - A_{calc})^2 = 2 \times 10^{-4}$) was obtained by considering the formation of the $[FeLH_5]^{2+}$ species. The values log K_{FeLH5} = 1.79 ± 0.05 and ε_{max} = 3900 M^{-1} cm^{-1} (λ_{max} = 470 nm) were obtained, where K_{FeLH5} is defined by Equation (3) and Equation (4):

$$Fe^{3+} + LH_7^+ \rightleftarrows FeLH_5^{2+} + 2\,H^+ \quad (3)$$

$$K_{FeLH5} = [FeLH_5^{2+}]\,[H^+]^2/[Fe^{3+}]\,[LH_7^+] \quad (4)$$

When the pH is raised beyond 3, the spectra exhibited one buffer region in the pH range 3.2−6 with an isosbestic point (Figure 7b), indicating the presence of only two species with different absorbance. These absorbance data were also refined with the LETAGROP-SPEFO program. The best fit [$\Sigma(A_{exp} - A_{calcd.})^2 = 3 \times 10^{-5}$] showed that deprotonation occurs via a one-proton step yielding a pK_a value of 4.50 ± 0.05 and an absorbance maximum at λ = 495 nm with ε = 2500 M^{-1} cm^{-1} for the $FeLH_{n-1}$ species according to the equilibrium shown in Equation (5):

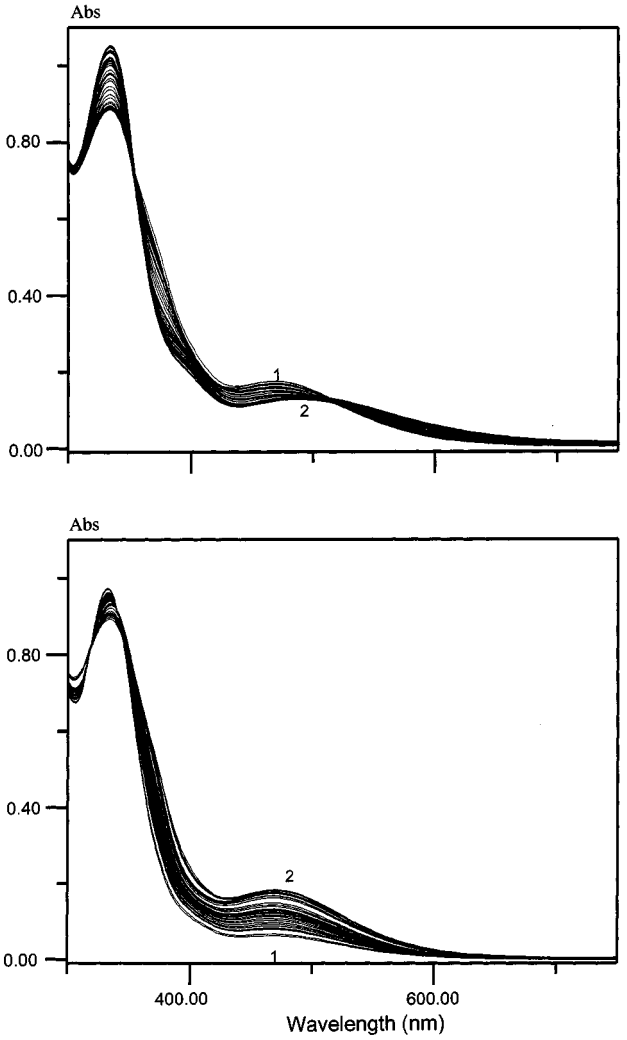


Figure 7. UV/Vis absorbance spectra of Fe^{III} -TRENPYPOLS as a function of pH; (bottom) 1: pH = 1; 2: pH = 2.5; (top) 1: pH = 3.2; 2: pH = 6; $[Fe^{3+}]_{tot}$ = $[TRENPYPOLS]_{tot}$ = 0.24 mM, I = 0.1 M ($NaClO_4$)

$$FeLH_n \rightleftarrows FeLH_{n-1} + H^+ \quad (5)$$

No spectral change was observed over the pH range 6−8.5. Beyond pH 8.5, a slight decrease in absorbance was observed suggesting the formation of hydroxo complexes.

The UV/Vis spectrum of the $[FeLH_5]^{2+}$ species exhibited features (λ_{max} = 470 nm, ε_{max} = 3900 M^{-1} cm^{-1}) that suggest a bis-salicylate coordination, involving the amide oxygen and the hydroxy oxygen atoms, as opposed to the tris-salicylate complex Fe^{III}-TRENSAM (λ_{max} = 455 nm, ε = 4800 M^{-1} cm^{-1}).[20] On raising the pH from 3 to 6, an increase of λ_{max} from 470 to 495 nm with a decrease in the molar extinction coefficient (ε = 2500 M^{-1} cm^{-1}) was observed. These parameters are consistent with a phenolato−Fe^{III} charge-transfer band. This result indicates a shift of the coordination from a salicylate to a phenolate coordination and suggests the replacement of the O(=C) → Fe^{III} bonding mode by the N_{pyr} → Fe^{III} bonding mode.

However, it should be noted that the UV/Vis absorbance dependence on the pH can only give information on the

deprotonation of the phenol group. The deprotonation constants of the $[FeLH_5]^{2+}$ complex corresponding to the ammonium nitrogen and to the three pyridinium nitrogens cannot be determined since these deprotonations do not change the phenolato−Fe^{III} charge-transfer band. It is reasonable to predict that the pK_a values for the pyridinium nitrogens are lower than that of the free ligand (i.e. < about 4). Furthermore, the potentiometric titration clearly showed that there are two deprotonation constants that are close to one another between pH 4.5 and 5. We may attribute one deprotonation to the ammonium nitrogen and the other to the phenol oxygen when compared with the value of 4.5 determined from visible spectrum.

The stability constant β_{110} of the ferric complex FeL was determined by spectrophotometric competition experiments. The constant was determined by competition against EDTA (noted Y) over the pH range 7−8. The competition equilibrium can be expressed by Equation (6) and Equation (7) (charges omitted for clarity):

$$FeL + YH + 2\,H^+ \rightleftarrows FeY + LH_3 \quad (6)$$

$$K = [FeY][LH_3]/[FeL][HY][H^+]^2 = \beta_{110}(FeY)\,K'_{a1}/\beta_{110}(FeL)\,K_{a1}\,K_{a2}\,K_{a3} \quad (7)$$

where L represents the deprotonated form of the ligand TRENPYPOLS; K_{a1}, K_{a2}, K_{a3}, the deprotonation constants of LH_3 and K'_{a1} the deprotonation constant of YH ($10^{-10.2}$).[23] The concentration of FeL was calculated from the absorbance at 500 nm where FeL is the only absorbing species. The concentrations of the other species in Equation (6) were calculated from the pH and mass balance Equations (8)−(10):

$$[Fe]_{tot} = \alpha_{FeL}\,[FeL] + \alpha_{FeY}\,[FeY] \quad (8)$$

$$[L]_{tot} = \alpha_{FeL}\,[FeL] + \alpha_{L}\,[L] \quad (9)$$

$$[Y]_{tot} = \alpha_{FeY}\,[FeY] + \alpha_{Y}\,[Y] \quad (10)$$

where α represents the usual Ringbom's coefficients.[24] Using the known formation constants of FeY (log β_{110} = 25.0),[23] the average formation constant of the Fe^{III}-TRENPYPOLS complex was determined to be log β_{110} = 30.1 ± 0.15. The pFe^{III} values have been calculated over the pH range 3−9 (or 4−9 for TRENPYPOLS and TRENCAM since the stability constants for their protonated complexes existing at pH<4 are unknown) and reported on the plot pFe = f(pH) presented in Figure 8, together with the plots calculated for other tripodal ligands based on the TREN backbone. In addition, the pFe^{III} value for TRENPYPOLS (under biologically reasonable conditions, i.e. pH = 7.4, $[L]_{tot}$ = 10^{-5} M, $[Fe]_{tot}$ = 10^{-6} M) has been calculated to be 23.6. This value is lower than those for other tripodal ligands such as TRENCAM: 27.8,[25] TRENCAMS: 29.6,[8] TRENDROX: 27.8,[9] O-TRENSOX: 29.5[7] The pFe^{III} values for the complexes involving five-membered chelate rings are significantly higher than the values for the complexes having six-membered chelate rings as in Fe^{III}-TRENPYPOLS. This result is in accordance with a general rule: an increase in the size of the chelate ring usually leads to a decrease in complex stability.[26] However, this rule had never been experimentally confirmed for octahedral complexes with tris-bidentate tripodal ligands.

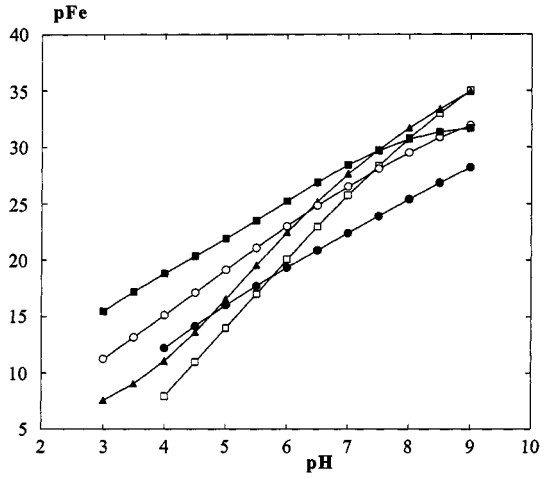


Figure 8. Plot of pFe^{III} *vs* pH for various tripodal ligands. pFe^{III} was calculated for $[L]_{tot}$ = 10^{-5} M, $[Fe^{3+}]_{tot}$ = 10^{-6} M using the known constants of TRENPYPOLS (●), O-TRENSOX[7] (■), TRENCAM[25] (□) TRENCAMS[8] (▲) and TRENDROX[9] (O).

Electron Spin Resonance

The ESR spectra of frozen aqueous solutions (with 10% glycerol) of Fe^{III}-TRENPYPOLS (Figure 9, spectra 1−5) were recorded at 100 K over the pH range 2−8. Below pH 4.8, the spectrum exhibited one single signal at g = 4.3 characteristic of a high-spin octahedral ligand field. The isotropic signal reflects a rhombic symmetry and represents a transition within the intermediate Kramer doublet (for an E/D ratio of 1/3 and a D parameter of about 0.5 cm^{-1} for this type of complex), and is large relative to the quantum of energy used in the EPR experiment. At pH above 5.8, a dissymmetric signal at g = 4.3 was observed indicating a slightly distorted rhombic geometry. The spectra resemble those of the ferric complexes with O-TRENSOX (Figure 9) in acidic (pH = 1.5, spectrum 6) and in neutral media (pH = 7.1, spectrum 7) in which the ferric ion is coordinated through a tris-salicylate mode [O(=C),O)][27] and a tris-oxinate mode $[O,N_{pyr}]^7$, respectively. These results suggest similar change of coordination for Fe^{III}-TRENPYPOLS complexes on raising the pH and are consistent with the change observed in the UV/Vis spectra.

Electrochemistry

The electrochemical behavior of the Fe^{III}-TRENPYPOLS complex, studied by cyclic voltammetry, in an aqueous electrolyte (0.1 M $NaClO_4$) buffered at pH 7 is characterized by a well-defined pair of peaks at $E^c_{1/2}$ = −0.18 V vs Ag/AgCl (0.04 V vs NHE) (ΔE_p = 0.11 V, υ = 0.1 V s^{-1}) corresponding to the quasi-reversible complexed Fe^{II}/Fe^{III} redox couple (Figure 10). Taking into account a value of $E^f_{1/2}$= 0.55 V (i.e. 0.77 V vs NHE) for the free Fe^{II}/Fe^{III} redox couple, this result shows that the complexation with TREN-

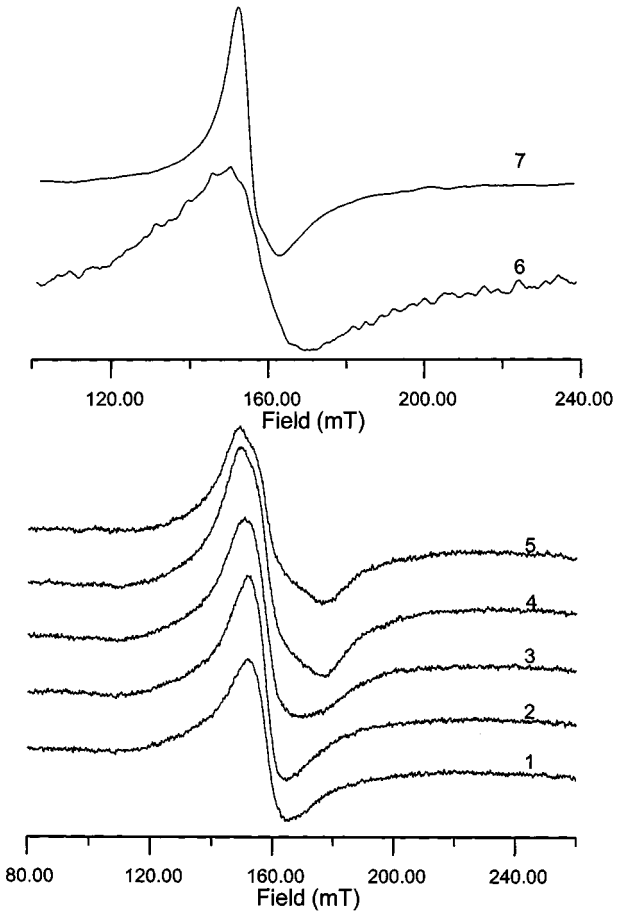


Figure 9. ESR spectra of (bottom) Fe^{III}-TRENPYPOLS (0.001 M) in frozen water-glycerol (90:10) solution at pH 4.0 (1), 4.8 (2), 5.4 (3), 5.8 (4) and 7.0 (5); (top) Fe^{III}-O-TRENSOX (0.001 M) in frozen water-glycerol (90:10) solution a pH 1.5 (6) and 7 (7).

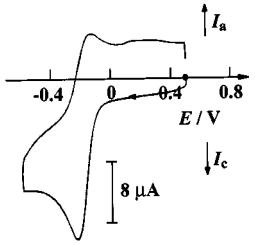


Figure 10. Cyclic voltammogram of Fe^{III}-TRENPYPOLS complex in aqueous solution (1 mM) at pH 7 with 0.1 M $NaClO_4$; v = 0.1 V s^{-1}; working electrode: glassy carbon disc (5 mm diameter).

PYPOLS leads to a strong stabilization by ca 0.73 V of the oxidized form of the redox couple. The ratio $\beta_{110}(Fe^{II}L)/\beta_{110}(Fe^{III}L)$ can be calculated from Equation (11):

$$E^c_{1/2} = E^f_{1/2} + 0.059 \log \beta_{110}(Fe^{II}L)/\beta_{110}(Fe^{III}L) \quad (11)$$

and gives $\beta_{110}(Fe^{II}L) = 17.7$ leading to a pFe^{II} value of 11.2. TRENPYPOLS appears to be a stronger ferrous ion chelator than the catecholate and hydroxamate ligands. This is a characteristic property of the $[O,N_{pyr}]$ donor set as previously observed for the ligand O-TRENSOX ($E^c_{1/2} = 0.087$ V vs NHE).[7] The difference in pFe^{II} between O-TRENSOX and

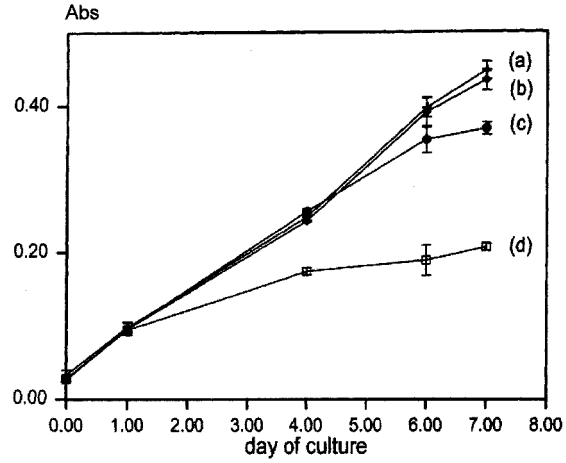


Figure 11. Growth of cells of *Arabidopsis thaliana* using Fe^{III} -TRENPYPOLS or Fe^{III} -EDTA as siderophores. A: 50 μM Fe^{III}-TRENPYPOLS; B: 50 μM Fe^{III}-EDTA; C: 5 μM Fe^{III} -TRENPYPOLS; D: without iron; 25 °C, 220 rpm, 18 hours light per day. The inoculum originated from a previous culture with 2.0 μM Fe^{III} -EDTA presenting slight symptoms of chlorosis.

TRENPYPOLS (6.7) is of the same order of magnitude as the difference between their pFe^{III} (5.9). The electrochemical behavior of the Fe^{III}-TRENPYPOLS complex has also been studied at pH 2.5 where the major species is $[FeLH_5]^{2+}$. Reduction of the complex could not be observed on the voltammograms in the accessible potential range at pH 2.5 i.e. the reduction of the complex occurs at a potential lower than −0.6 V vs Ag/AgCl (−0.38 V vs NHE). The lower reduction potential at pH 2.5 indicates that the Fe^{III} complex is more stable relative to the Fe^{II} complex at pH 2.5 than at pH 7. This suggests a change in coordination of iron as previously deduced from the UV/Vis and EPR spectra.

Plant Nutrition

TRENPYPOLS was tested as single source of iron in nutritional experiments. This was performed by comparing the growth and greening of *Arabidopdis thaliana* plant cells during cell suspension cultures. In the control experiment, iron was provided as a complex Fe^{III} -EDTA (50μM). An iron free control was cultivated in the iron free nutrient solution (MS−Fe). The assays were performed in MS−Fe supplemented with Fe^{III}-TRENPYPOLS at 5 and 50μM using 8 independent replications. The results are shown in Figure 11. Growth and resistance to chlorosis were equivalent when Fe^{III} -TRENPYPOLS was used instead of Fe^{III} -EDTA. Symptoms of chlorosis appeared when 5 μM Fe^{III} -TRENPYPOLS was used and the growth was slowed down. The efficiency of Fe^{III}-TRENPYPOLS is good, comparable to that of Fe^{III}-EDTA, the most commonly used complex for in vitro cell cultures.

Conclusion

The iron-complexing agent TRENPYPOLS is the first water-soluble tris-bidentate ligand involving three $[O,N_{pyr}]$ donor sets with 6-membered chelate rings. The solution physicochemical data (thermodynamic) of this new chelator have

been established, allowing comparisons with the usual iron chelators, with a special focus on O-TRENSOX which involves three [O,N_{pyr}] donor sets with 5-membered coordination rings. TRENPYPOLS and O-TRENSOX form a new class of Fe chelators with an affinity for both Fe^{III} and Fe^{II}. There are two important distinctions in the metal binding cavity between TRENPYPOLS and O-TRENSOX that influence the affinity of these ligands for Fe^{III} and Fe^{II}. The first, is the flexibility of the binding cavity. TRENPYPOLS provides a more flexible cavity by forming six-membered chelate rings and allowing free rotation of the pyridine ring relative to the phenol ring. O-TRENSOX forms five-membered chelate rings and prevents pyridine ring rotation through a fused ring structure. The second, is a difference in ligand pK_a values which results in a lower pFe^{III} and pFe^{II} for TRENPYPOLS. These features influence the relative Fe^{III} and Fe^{II} affinity of the two ligands as determined by their pFe values. Consequently, TRENPYPOLS has a lower Fe^{III} and Fe^{II} affinity than O-TRENSOX, but the same relative Fe^{III}/Fe^{II} selectivity ($\Delta pFe = pFe^{III} - pFe^{II}$), making it more suitable for use as a biological Fe sensor. There is always a need for biological sensors for the study of iron metabolism. They have to be able to measure the labile iron pool and the concentration of cellular free iron.[28] For this purpose, ligands with complexing abilities that are too high must be avoided since they induce perturbation in iron metabolism (uptake of iron from proteins). The pFe^{III} values of TRENPYPOLS are in a suitable range. It is envisaged that a fluorescent probe could be grafted on the ligand in order to build a new sensor, well suited to be used in conjunction with calcein, the most frequently used probe for iron to date.[28]

Experimental Section

Materials and Equipment: Solvents were distilled prior to use. The amine TREN (tris-2-aminoethyl)amine) was distilled over sodium. All other compounds were of reagent grade and were used without further purification. Fe^{III} stock solutions were prepared by dissolving appropriate amounts of ferric perchlorate hydrate (Aldrich) in standardized $HClO_4/NaClO_4$ solutions. The solutions were standardized spectrophotometrically for ferric ion by using a molar extinction coefficient of 4160 M^{-1} cm^{-1} at 240 nm.[29] − IR spectra were collected using a Perkin−Elmer 397 or Nicolet Impact 400 spectrometer. − UV/Vis absorbance spectra were recorded using 1.000 cm path length quartz cells housed in a Perkin−Elmer Lambda 2 spectrometer connected to a microcomputer. − Mass spectra were recorded on a NERMAG R 10 1 C mass spectrometer. − Microanalyses were performed by the Central Service of CNRS, Solaize (France). − Melting points were determined with a Büchi apparatus and are not corrected. − ^1H and ^{13}C NMR spectra were obtained in 5 mm tubes at 25 °C with a Bruker AM 300 or a Bruker AM 400 spectrometer. For ^1H NMR spectroscopic titrations, the ligand TRENPYPOLS was dissolved in D_2O. The pD was adjusted with DCl or NaOD solutions. pH measurements were performed with a Tacussel PHN 850 apparatus equipped with a microelectrode Radiometer XC61. pD values were calculated according to $pD = pH_{meas} + 0.4$.[30] − EPR experiments were conducted using a ESP 300E Bruker apparatus with a variable temperature unit. Spectra were treated by using the winEPR software. Each aqueous Fe^{III}-TRENPYPOLS sample (200 μL, 10^{-3} M) contained 10% glycerol. The field was scanned from 0.1 to 0.5 Tesla.

Synthesis of TRENPYPOLS (Figure 3)

2-(2-Methoxy-3-methylphenyl)pyridine (5): The Grignard reagent **4** was prepared under Argon at 0 °C, from **3** (5.05 g, 25.0 mmol) and Mg (0.65 g, 27.0 mmol) in dry THF (30 mL). It was transferred, *via* canula, to a mixture of 2-bromopyridine (3.79 g, 24.0 mmol) and $Ni(dppe)_2Cl_2$ (0.55 g, 1.00 mmol) in THF (20 mL). The mixture was then stirred overnight at room temperature. After quenching with aqueous NH_4Cl and acidification with HCl (4 M) to pH ≈ 1, THF was evaporated under vacuum. Extraction with CH_2Cl_2 (3 × 100 mL), drying on $MgSO_4$ and evaporation of the solvent gave a brown oil. Column chromatography (silica eluted with a CH_2Cl_2 + MeOH mixture (1% to 5% vol)) afforded pure **5** (3.54 g, 17.7 mmol). Yield 71%. − ^1H NMR (250 MHz, $CDCl_3$): δ = 2.35 (s, 3 H), 3.46 (s, 3 H, OCH_3), 7.12 (t, 1 H, *J* = 7.5 Hz), 7.18−7.26 (m, 2 H), 7.54 (dd, 1 H, *J* = 7.5/1.7 Hz), 7.71 (td, 1 H, *J* = 7.5 Hz, *J* = 0.7 Hz), 7.84 (broad d, 1 H, *J* = 7.5 Hz), 8.70 (ddd, 1 H, *J* = 4.9 Hz, *J* = 1.7 Hz, *J* = 0.7 Hz). − ^{13}C NMR (50 MHz, $CDCl_3$): δ = 16.1 (CH_3), 60.5 (OCH_3), 121.8 (CH), 124.2 (CH), 124.5 (CH), 128.9 (CH), 131.5 (C*q*), 131.6 (CH), 133.3 (C*q*), 136.1 (CH), 149.4 (CH), 156.3 (C*q*), 156.6 (C*q*). − MS (EI): 199 (M^+), 184, 181, 168, 154. − $C_{13}H_{13}NO$ (199.3): calcd. C 78.30, H 6.58, N 7.03; found C 77.90, H 6.57, N 6.91.

2-Methoxy-3-(2-pyridyl)benzoic Acid (6): A mixture of **5** (2 g, 10.0 mmol), $KMnO_4$ (6 g, 38.0 mmol) and $NaHCO_3$ (0.78 g, 9.3 mmol) in water (120 mL) was stirred under reflux for 3 h. MnO_2 was removed by filtration and the solution extracted with diethyl ether. The aqueous solution was acidified to pH ≈ 5 with dilute HCl and the water was evaporated under vacuum. The solid residue was treated by methanol, and inorganic salts were removed by filtration. Evaporation of methanol gave **6** as a white powder (1.77 g, 7.7 mmol), pure enough for the following step. Yield 77%. − ^1H NMR (250 MHz, CD_3OD): δ = 3.58 (s, 3 H, OCH_3), 7.22 (t, 1 H, *J* = 7.7 Hz), 7.39 (td, 1 H, *J* = 5.0 Hz, *J* = 1.6 Hz), 7.56−7.67 (m, 2 H), 7.79−7.90 (m, 2 H), 8.61 (broad d, 1 H, *J* = 4.8 Hz). − ^{13}C NMR (50 MHz, D_2O−NaOD): δ = 62.0 (OCH_3), 123.2 (CH), 124.4 (CH), 125.2 (CH), 128.8 (CH), 131.3 (CH), 133.2 (C*q*), 134.0 (C*q*), 138.0 (CH), 148.7 (CH), 153.5 (C*q*), 155.3 (C*q*), 176.3 (CO). − MS (DCI, NH_3+isobutane): 230 [M^+ + 1].

2-(3-Chloroformyl-2-methoxyphenyl)pyridinium Chloride (7): A mixture of **6** (1 g, 4.4 mmol) and distilled thionyl chloride (50 mL) was stirred under nitrogen for 4 h at room temperature. Excess $SOCl_2$ was removed under vacuum, giving **7** as a yellow powder (1.24 g, quant. yield). − ^1H NMR (200 MHz, $CDCl_3$): δ = 3.72 (s, 3 H, OCH_3), 7.56 (t, 1 H, *J* = 7.9 Hz), 8.07 (t, 1 H, *J* = 7.9 Hz), 8.25−8.35 (m, 3 H), 8.58 (t, 1 H, *J* = 7.6 Hz), 9.05 (d, 1 H, *J* = 5.1 Hz). − ^{13}C NMR (50 MHz, $CDCl_3$): δ = 63.8 (OCH_3), 125.07 (CH), 125.08 (C*q*), 125.5 (C*q*), 125.7 (CH), 128.6 (CH), 137.0 (CH), 137.7 (CH), 142.3 (CH), 145.3 (CH), 148.7 (C*q*), 157.6 (C*q*), 164.4 (CO).

Methoxylated Podand 8: A mixture of TREN (tris-2-aminoethyl)amine) (0.24 g, 16.4 mmol) and triethylamine (2.9 g, 29.0 mmol) in dry THF (10 mL) was added dropwise, under nitrogen, to a solution of acid chloride **7** (1.24 g, 4.4 mmol) in THF (50 mL). The mixture was stirred at room temperature for 12 h. Filtration and evaporation of THF afforded an orange oil which was mixed with CH_2C1_2. The solution was washed with brine then dried on Na_2SO_4. Removal of the solvent under vacuum gave a foamy material which was added to pentane. Tripodand **8** was recovered by filtration as a yellow powder (0.8 g). Yield 70%. M.p. 62−63 °C. − IR (KBr):

$\tilde{\nu}$ = 1650, 1523 cm^{-1} . − ^1H NMR (200 MHz, $CDCl_3$): δ = 2.92 (t, 6 H, *J* = 6.5 Hz, CH_2N), 3.48 (s, 9 H, OCH_3), 3.65 (td, 6 H, *J* = 6.5 Hz, $CH_2-NH-CO$), 7.26 (td, 6 H, *J* = 5.5 Hz, *J* = 3.1 Hz), 7.64−7.72 (m, 6 H), 7.75 (dd, 3 H, *J* = 7.5 Hz, *J* = 2.0 Hz), 8.03 (dd, 3 H, *J* = 7.9 Hz, *J* = 1.7 Hz), 8.16 (broad t, 3 H, NH), 8.70 (broad d, 3 H, *J* = 4.8 Hz). − ^{13}C NMR (50 MHz, $CDCl_3$): δ = 37.8 (CH_2), 53.4 ($N-CH_2$), 62.2 (OCH_3), 122.3 (CH), 124.4 (CH), 124.8 (CH), 126.9 (C*q*), 131.9 (CH), 134.1 (C*q*), 134.6 (CH), 136.3 (CH), 149.6 (CH), 155.4 (C*q*), 156.0 (C*q*), 165.6 (CO). − MS (DCI, NH_3+isobutane): 780 [M^+ + 1]. − $C_{45}H_{45}N_7O_6 \cdot 1\ H_2O$ (797.9): calcd. C 67.74, H 5.94, N 12.29; found C 67.42, H 5.83, N 12.03.

TRENPYPOL (9): Podand **8** (1.09 g, 1.4 mmol) was dissolved in dry CH_2Cl_2 (100 mL), under nitrogen at 0 °C, and BBr_3 (15 mL of a solution with 1 M CH_2Cl_2, excess) was added dropwise. The mixture was stirred for 12 h at room temperature and then concentrated under vacuum. Methanol (50 mL) was added and the mixture was stirred for 1 h and then repeatedly evaporated with methanol (5 × 100 mL). The resulting yellow precipitate was dissolved in HCl 4N and the solution was extracted with CH_2Cl_2. The aqueous solution was adjusted to pH 7−8 with $NaHCO_3$ and extracted with CH_2Cl_2. Washing with brine, drying on $MgSO_4$, evaporation of the solvent and treatment with pentane-ether gave **9**·2HCl as a yellow powder (0.964 g). Yield 85%. − IR (KBr): $\tilde{\nu}$ = 3356, 1644 cm^{-1}. − $C_{42}H_{39}N_7O_6$, $1H_2O$ (755.8): calcd. C 66.74, H 5.47, N 12.97; found C 66.68, H 5.54, N 12.66. − ^1H NMR (250 MHz, D_2O): δ = 3.77 (broad s, 6 H, CH_2N), 3.85 (broad s, 6 H, $CH_2-NH-CO$), 6.71 (t, 3 H, *J* = 7.8 Hz), 7.49 (d, 3 H, *J* = 7.6 Hz), 7.64 (m, 6 H), 7.71 (broad t, 3 H, *J* = 7.6 Hz), 8.30 (broad t, 3 H, *J* = 7.8 Hz), 8.49 (broad d, 3 H, *J* = 5.6 Hz). − ^{13}C NMR (50 MHz, DMSO): δ = 37.3 (CH_2), 52.8 ($N-CH_2$), 117.9 (CH), 119.7 (C*q*), 120.5 (C*q*), 122.3 (CH), 130.3 (CH), 131.9 (CH), 138.5 (CH), 145.2 (CH), 155.7 (C*q*), 158.9 (C*q*), 165.6 (CO). − MS (DCI, NH_3+isobutane): 738 [M^+ + 1], 567, 541, 524, 510.

TRENPYPOLS (10): Podand **9** (1 g, 1.35 mmol) was dissolved in oleum (15 mL) and the mixture was stirred for 12 h, at room temperature. The brown solution was poured onto ice and the pH was raised to 9−10 by cautious addition of 1 M NaOH. Methanol (100 mL) was added to precipitate Na_2SO_4. Filtration and concentration gave a yellow powder, containing again some Na_2SO_4; this salt was removed by repeated treatment (formation of a white precipitate, then concentration) with a mixture of methanol and diethyl ether. Evaporation of the resulting solution gave a yellow powder (tetrasodium salt, 0.74 g). Yield 52%. − IR (KBr): $\tilde{\nu}$ = 3440, 1640 cm^{-1}. − ^1H NMR (200 MHz, D_2O+NaOD): δ = 2.69 (broad s, 6 H, CH_2N), 3.36 (broad s, 6 H, $CH_2-NH-CO$), 7.06 (m, 3 H), 7.40−7.55 (m, 9 H), 8.05 (m, 3 H), 8.27 (m, 3 H). − ^{13}C NMR (50 MHz, D_2O+NaOD): δ = 36.8 (CH_2), 53.0 ($N-CH_2$), 119.0 (C*q*), 122.7 (CH), 125.9 (CH), 126.1 (C*q*), 128.8 (CH), 130.9 (CH), 132.8 (C*q*), 137.4 (CH), 148.8 (CH), 157.3 (C*q*), 170.2 (C*q*), 170.4 (CO). − MS (FAB positive mode M + 1, NBA matrix): 1066 ($C_{42}H_{35}N_7O_{15}S_3Na_4$ + 1). The molecular mass was also checked by potentiometric titration.

Potentiometric Titrations: All measurements were performed at 25 °C and the solutions were prepared with deionized and twice distilled water. The ionic strength was fixed at *I* = 0.1 M with sodium perchlorate (PROLABO puriss.). The potentiometric titrations were performed using an automatic titrator system DMS 716 Titrino (Metrohm) with a combined glass electrode (Metrohm, filled with saturated NaCl solution) and connected to an IBM Aptiva microcomputer. The electrodes were calibrated to read p[H] according to the classical method[31] (titration of 0.1 M $HClO_4$ with 0.1 M NaOH). The ligand and its Fe^{III} complex, ca 0.001 M, were titrated with standardized 0.025 M sodium hydroxide. Argon was bubbled through the solutions to exclude CO_2 and O_2. Sodium hydroxide was prepared from 0.1 M NaOH (Prolabo) and was standardized against potassium hydrogen phthalate. Carbonate content was checked by Gran's method. The titration data (108 points collected over the pH range 2.85−10.77 for the ligand solution) were refined by the nonlinear least-squares refinement program SUPERQUAD[18] to determine the deprotonation constants. The pK_{an} values were calculated from the cumulative constants determined with the program. The uncertainties in the pK_{an} values correspond to the added standard deviations (1σ) in the cumulative constants.

Spectrophotometric Experiments: The ferric complexes were studied by spectrophotometry. The UV/Vis spectrum of a solution containing equal amounts of ligand and Fe^{III} (10^{-4} M) was recorded as a function of pH over the range 1−9 (adjusted with $HClO_4$ or NaOH). An aliquot was taken from the solution after each adjustment of the pH and its spectrum was recorded. pH measurements were made with a 713 Metrohm digital pH meter equipped with a microelectrode. The ionic strength was fixed at *I* = 0.1 M with $NaClO_4$/$HClO_4$. The spectrophotometric data were analyzed using the LETAGROP-SPEFO program.[19,20]The program uses a nonlinear least-squares method to calculate the thermodynamic constants of the absorbing species and their corresponding electronic spectra. The calculations were performed using absorbance values from about 6-8 wavelengths (between 400 and 600 nm). The range of values for the residual-squares sum ($\Sigma(A_{exp}-A_{calc})^2$) of the fits was $10^{-4}-10^{-5}$.

Spectrophotometric competition experiments were carried out with Na_2H_2EDTA over the pH range 7−8. Typical solutions contained 10^{-4} M Fe^{III} ion, TRENPYPOLS and Na_2H_2EDTA. Five solutions were prepared. The samples were allowed to equilibrate for one week in the dark at 25 °C.

Electrochemical Measurements: Electrochemical experiments were carried out using a PAR model 273 potentiostat equipped with a Kipp−Zonen *x*-*y* recorder. All experiments were run at room temperature under argon in a glove-box. A standard three-electrode cell was used. An Ag/AgCl, 3M NaCl, aqueous reference electrode (+0.222 V *vs* NHE) was used. A glassy carbon disc electrode was used as the working electrode (5 mm diameter) and was polished with 1 μm diamond paste. The electrochemical behavior of the Fe^{III} -TRENPYPOLS complex was studied by cyclic voltammetry (CV) in an aqueous solution containing 0.1 M $NaClO_4$ as the supporting electrolyte and buffered with Tris-buffer for the experiments performed at pH 7 or acidified with $HClO_4$ for the experiments at pH 2. The Fe^{III} -TRENPYPOLS solutions were prepared by dissolving stochiometric amounts of ferric perchlorate and TRENPYPOLS in the electrolytic solutions.

Plant Cells Culture and Growth Measurements: Plant cells were grown in 24 well sterile cell culture plates (Nunc); each well contained an independent axenic culture (1.5 mL). Wells were inoculated at an absorbance of 0.003 (*ca* 1/12) with early stationary phase *Arabidopsis thaliana* (var. Columbia) cell suspensions. For axeny, plates were sealed with "Magic Scotch®" tape. 24 well plates were agitated at 220 rpm at 25 °C in a New Brunswik "innova" 4230 refrigerated incubator shaker. Light was supplied for 18 h a day by 2 growlux sylvania 15 W in the " photosynthesis " accessory.

The measurements of cell density were made daily as previously described.[28] The Biorad video camera system Geldoc 1000, with the "molecular analyst" software was used for quantification. Full frame images were captured in constant light conditions, i.e. white

light was adjusted so that just a few saturated pixels appeared in red in the empty optical field. In these light conditions, a reproducible relationship was found between the absorbance of wells in densitometric scanning profiles of recorded images and the amount of cells in the wells. Images of culture plates without cells were used as a baseline reference. They showed an uneven light background. This fact was compensated by the subtraction of an adapted baseline.

The medium (MS) was a modified Murashige and Skoog[32] medium; for 1 L of medium: 4.3 g macro and micro elements powder (provided by Duchefa, cat N° M0221, Haarlem Netherlands), 10 mL KH_2PO_4 (20 g/l), 0.5 mL Kinetin (0.1 g/l), 0.5 mL 2,4 D (0.2 g/l), 1 mL × 1000 vitamin solution (Duchefa M 0409) and 30 g saccharose. Iron free MS medium (MS−Fe) has the same content, made from reagent grade products, omitting the Fe^{III}-EDTA complex. The Fe^{III}-TRENPYPOLS complex was first prepared at low pH then raised to pH 5.8 with NaOH and a Tris maleate buffer, then mixed to the MS−Fe solution at the same pH. The complex was filtered using a 0.22 μm Millipore filter and sterilized. MS−Fe was autoclaved.

Acknowledgments

The authors thank Dr. Alain Deronzier (LEOPR, Grenoble, France) for the use of the laboratory facilities and Professor A. L. Crumbliss (Durham, NC) for very helpful discussions.

[1] (Ed.: G. Winkelman), *CRC Handbook of Microbial Iron Chelates*, CRC Press, Boca Raton **1991**.
[2] (Eds.: A. Sigel, H. Sigel) *Iron Transport and Storage in Microorganisms, Plants and Animals;* Metal Ions in Biological Systems, (Eds.: A. Sigel, H. Sigel), M. Dekker **1998**; vol. 35.
[3] R. R. Crichton, *Inorganic Chemistry of Iron Metabolism,* Ellis Horwood, New-York **1991**.
[4] P. Baret, C. Béguin, H. Boukhalfa, C. Caris, J.-P. Laulhère, J.-L. Pierre, G. Serratrice, *J. Am. Chem. Soc.* **1995**, *117*, 9760.
[5] C. Caris, P. Baret, C. Béguin, G. Serratrice, J.-L. Pierre, J.-P. Laulhère, *Biochem. J.* **1995**, *312,* 879.
[6] N. Rakba, C. Henry, C. Caris, I. Morel, N. Pasdeloup, P. Baret, J.-L. Pierre, P. Brissot, G. Lescoat, R. R. Crichton, *Biochem. Pharmacol.* **1998**, *55,* 1797.
[7] G. Serratrice, H. Boukhalfa, C. Béguin, P. Baret, C. Caris, J.-L. Pierre, *Inorg Chem.* **1997**, *36,* 3898.
[8] F. Thomas, C. Béguin, J.-L. Pierre, G. Serratrice, *Inorg. Chim. Acta* **1999**, *291,* 148.
[9] C. Y. Ng, S. J. Rodgers, K. N. Raymond, *Inorg. Chem.* **1989**, *28,* 2062.
[10] K. N. Raymond, G. Müller, B. F. Matzanke, *Top. Curr. Chem.* **1984,** *123,* 49.
[11] J. E. Bollinger, J. T. Mague, C. J. O′Connor, W. A. Banks, D. M. Roundhill, *J. Chem. Soc., Dalton Trans.* **1995**, 1677.
[12] P. Ganis, A. Saporito, A. Vitagliano, G. Valle, *Inorg. Chim. Acta* **1988**, *142,* 75.
[13] D. A. Bardwell, D. Black, J. C. Jeffery, E. Schatz, M. D. Ward, *J. Chem. Soc., Dalton Trans.* **1993**, 2321.
[14] C. A. Otter, D. A. Bardwell, S. M. Couchman, J. C. Jeffery, J. P. Maher, M. D. Ward, *Polyhedron* **1998**, *17,* 211.
[15] B. M. Holligan, J. C. Jeffery, M. K. Norgett, E. Schatz, M. D. Ward, *J. Chem. Soc., Dalton Trans.* **1992**, 3345.
[16] D. E. Pearson, R. D. Wysong, C. V. Breder, *J. Org Chem.* **1967**, 2358.
[17] R. A. Benkeser, W. E. Buting, *J. Am. Chem. Soc.* **1952**, *74*, 3011.
[18] P. Gans, A. Sabatini, A. Vacca, *J. Chem. Soc., Dalton Trans.* **1985**, 1195.
[19] G. Serratrice, C. Mourral, A. Zeghli, C. Béguin, P. Baret, J.-L. Pierre, *New J. Chem.* **1994**, *18*, 749. TBPAS: tris[(2,2′-dihydroxy-5,3′,5′-trisulfo-3-carboxamido-1,1′-biphényl)ethyl]amine.
[20] S. M. Cohen, M. Meyer, K. N. Raymond, *J. Am. Chem. Soc.* **1998**, *120*, 6277. TRENSAM: tris[(2-hydroxybenzoyl)-2-aminoethyl]amine, TREN(ME)SAM: tris[(2-hydroxy-3-methoxybenzoyl)-2-aminoethyl]amine.
[21] L. G. Sillen, B. Warsquist, *Arkiv. Kemi* **1969**, *31*, 377.
[22] M. Meloun, J. Havel, E. Hogfeldt, *Computation of Solution Equilibria*, Ellis Horwood, Chichester, **1988**.
[23] A. E. Martell, R. M. Smith, *Critical Stability Constants*; Plenum Press: New York, **1974**.
[24] A. Ringbom *Complexation in Analytical Chemistry*; Interscience: New York, **1963**.
[25] S. J. Rodgers, C. W. Lee, C. Y. Ng, K. N. Raymond, *Inorg. Chem*. **1987**, *26*, 1622.
[26] R. D. Hancock, A. E. Martell, *Chem. Rev.* **1989**, *89*, 1874.
[27] G. Serratrice, H. Boukhalfa, I. Gautier-Luneau, D. Luneau, P. Baret, J.-L. Pierre, *Inorg Chem*. **1999**, *38,* 840.
[28] F. Thomas, G. Serratrice, C. Béguin, SaintE. Aman, J.-L. Pierre, M. Fontecave, J.-P. Laulhère, *J. Biol. Chem*. **1999**, *274*, 13375.
[29] R. Bastian, R. Weberling, F. Palilla, *Anal. Chem.* **1956**, *28*, 459.
[30] P. K. Glasoe F. A. Long, *J. Phys. Chem*. **1960,** *64*, 188.
[31] A. E. Martell, R. J. Motekaitis, *Determination and use of stability constants;* 2nd edition, VCH Publishers: New York, **1992**.
[32] T. Murashige, F. Skoog, *Physiol. Plant*. **1962**, *15*, 473.

Received November 22, 1999
[I99416]

Binary [Hydrotris(indazol-1-yl)borato]metal Complexes, $M(Tp^{4Bo})_2$[1] with M = Fe, Co, Ni, Cu, and Zn: Electronic Properties and Solvent-Dependent Framework Structures through C−H•••π Interactions

Christoph Janiak,*[a] Savaş Temizdemir,[a] Sebastian Dechert,[b] Werner Deck,[a] Frank Girgsdies,[b] Jürgen Heinze,[c] Mario J. Kolm,[a] Tobias G. Scharmann,[b] and Oliver M. Zipffel[b]

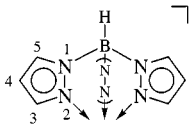
Dedicated to Prof. Dr. Heinrich Vahrenkamp on the occasion of his 60th birthday

Keywords: Boron / N ligands / UV/Vis spectroscopy / Cyclic voltammetry / Mössbauer spectroscopy / π interactions

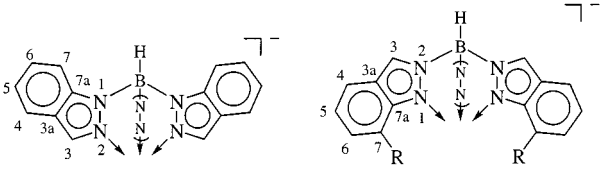
The bis[hydrotris(indazol-1-yl)borato]metal complexes $[M\{HB(C_7H_5N_2)_3\}_2]$, $M(Tp^{4Bo})_2$, with M = Fe, Co, Ni, Cu, and Zn have been synthesized and characterized by NMR, IR, UV/Vis, MS, Mössbauer spectrometry (M = Fe) and cyclic voltammetry (M = Fe, Co). The ligand field strength of the Tp^{4Bo} ligand is slightly higher than that of the normal Tp ligand. The molecular and crystal structure of the compounds with different solvents of crystallization (tetrahydrofuran, chloroform, dioxane) were elucidated by X-ray crystallography. The metal complexes exhibit the usual pseudo-octahedral D_{3d}-symmetrical geometry for two tripodal ligands with a Jahn–Teller distortion for M = Cu. The crystal packing between the molecular complexes is controlled mainly by C–H•••π interactions from the indazolyl moieties. This gives rise to large non-covalent framework structures with voids and channels ranging in volume from about 19 to 39% of the unit cell volume. The open space is filled by solvent molecules. The crystal packing and the space group depends on the type of solvent.

Introduction

The hydrotris(pyrazolyl)borate (Tp) ligand **1** was introduced into coordination chemistry by Trofimenko more than 30 years ago[2], and in various substituted forms has developed into one of the most versatile tripodal auxiliary ligands in (bio)inorganic coordination chemistry.[3−5] Particular interest is sometimes devoted to special azolyl rings, such as triazolyl,[6−9] tetrazolyl,[10] 3,5-bis(trifluoromethyl)-pyrazolyl,[11] and indazolyl.[12,13] Poly(indazolyl)borate systems are of interest because of the possible regioisomeric structures **2a** and **2b**. The latter isomer **2b** is the empirically expected form where B−N bond formation (from KBH_4 and indazole) had occurred at the least-hindered nitrogen atom N2 (by indazole numbering).[12] This isomer, however, appears only to be encountered with 7-substituted indazoles.[13−15] With unsubstituted or otherwise substituted indazoles the isomer **2a** is formed, probably because of electronic reasons. In **2a**, boron is bonded to the sterically more hindered but electronically richer nitrogen atom.[12,16,17]



1, Tp



2a, Tp^{4Bo} [1] **2b, Tp^{3Bo}**

-(N-N)- denotes the third pyrazolyl or indazolyl ring which is oriented to the rear

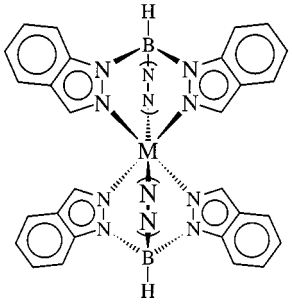
In the extension of our work on [hydrotris(triazolyl)borato]metal complexes,[6,7,9] we were interested in the electronic ligand field effect of the anellated benzo ring on the nitrogen−metal bond.[7,18] We therefore synthesized the homoleptic bis[hydrotris(indazol-1-yl)borato]metal(II) complexes $[M(\mathbf{2a})_2]$ or $[M(Tp^{4Bo})_2]$ of iron, cobalt, nickel, copper, and zinc, to compare their electronic properties with those of the analogous bis[hydrotris(pyrazolyl)borato]-metal compounds.[19−21] Furthermore, during the course of

[a] Institut für Anorganische und Analytische Chemie, Universität Freiburg,
Albertstraße 21, 79104 Freiburg, Germany
E-mail: janiak@uni-freiburg.de
[b] Institut für Anorganische und Analytische Chemie, Technische Universität Berlin,
Straße des 17. Juni 135, 10623 Berlin, Germany
[c] Institut für Physikalische Chemie, Universität Freiburg,
Albertstraße 21, 79104 Freiburg, Germany

Supporting information for this article is available on the WWW under http://www.wiley-vch.de/home/eurjic or from the author.

 © WILEY-VCH Verlag GmbH, D-69451 Weinheim, 2000 1434−1948/00/0606−1229 $ 17.50+.50/0

our studies we became interested in the crystal packing of the $M(Tp^{4Bo})_2$[1] complexes.



$[M(2a)_2]$, $[M(Tp^{4Bo})_2]$

-(N-N)- denotes the third indazolyl ring which is oriented to the rear or front, respectively

Syntheses and Properties of $[M\{HB(C_7H_5N_2)_3\}_2]$, $[M(Tp^{4Bo})_2]$ with M = Fe (4), Co (5), Ni (6), Cu (7), and Zn (8)

The hydrotris(indazol-1-yl)borato anion **2a** in the form of its potassium salt **3** reacts with transition-metal(II) salts in methanol with the formation of bis[hydrotris(indazol-1-yl)borato]metal(II) complexes [Equation (1)]. Yields were above 50%. The complexes are initially obtained as powders, but could be crystallized from tetrahydrofuran (THF), dioxane or chloroform. Crystallization proceeded either by slow solvent evaporation, cooling or overlayering of the dioxane phase with petroleum ether (30/50). The crystals of **4**−**8** quickly eliminate the incorporated $CHCl_3$ and THF solvent, when taken out of the solvent phase, with concomitant loss of crystallinity. The complexes are air-stable, but decompose in water. The tris[(indazolyl)borato]metal complexes are insoluble to slightly soluble in methanol and DMSO, and rather soluble in THF. The thermal stability of all compounds is high, their melting or decomposition point is above 300 °C (undetermined). A melting point of 446 °C had been determined for **4** by DSC.[12] The infrared spectra of the complexes are similar to each other, and to the potassium salt **3**.

$$MX_2 + 2\,KTp^{4Bo} \rightarrow [M(Tp^{4Bo})_2] + 2\,KX \qquad (1)$$

3

	M	X
4	Fe	$(SO_4)_{1/2}$
5	Co	Cl
6	Ni	Cl
7	Cu	Cl
8	Zn	O_2CCH_3

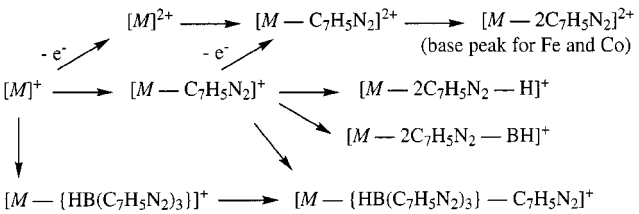
NMR Spectroscopy

The ^1H- and ^{13}C-NMR chemical shifts of the borato anion **2a** and of the diamagnetic transition-metal complexes correspond roughly to the spectrum of indazole[22] and of the tetrakis(indazol-1-yl)borato anion, $[B(C_7H_5N_2)_4]^-$,[16] and the signals were assigned accordingly. Despite its paramagnetism, the cobalt compound **5** gave a well-resolved ^1H-NMR spectrum with relatively sharp signals in a chemical shift range of over 200 ppm.[12]

The purity of the starting material **3** was checked by ^{11}B-NMR spectroscopy, and small impurities of unreacted KBH_4 as well as presumably the intermediate dihydrobis(indazolyl)borato anion, were detected.

Mass Spectrometry

The mass-spectrometric characterization shows the molecular ion for all the complexes. The Jahn−Teller-distorted Cu complex **7** gives, however, a significantly lower molecular ion intensity, and apparently also an immediate loss of one hydrogen. The most likely fragmentation for the bis[hydrotris(indazolyl)borato]metal(II) complexes involves the loss of indazolyl or indazole rings ($C_7H_5N_2$/H) and the loss of one hydrotris(indazolyl)borato ligand. The occurrence of doubly charged ions of high abundance is remarkable. The typical fragments together with their proposed fragmentation path are given in Scheme 1. For iron and cobalt, the doubly charged ion that was obtained after the loss of two indazolyl rings, $[M - 2\,(C_7H_5N_2)]^{2+}$, even represented the base peak. Figure 1 shows the mass spectrum of the iron complex **4** together with its assignment, as an example.



Scheme 1. Typical fragments in the mass spectra of the $[M\{HB(C_7H_5N_2)_3\}_2]$ complexes and proposed fragmentation path (*M in italics* = molecular complex)

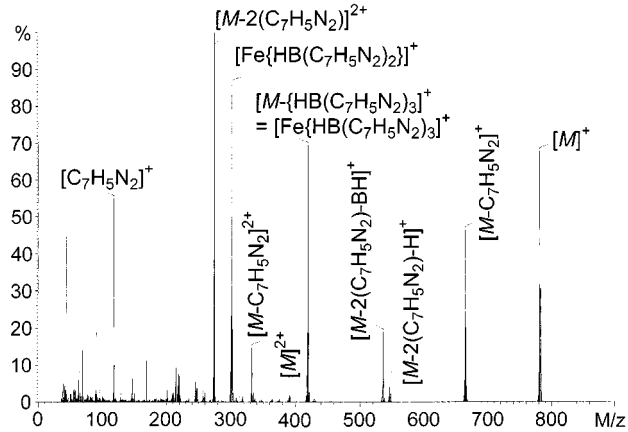


Figure 1. Mass spectrum of **4** with assignment; peak assignment was based on the calculation of the most abundant isotope combination, containing ^{56}Fe and ^{11}B; note the doubly charged ions

Optical Spectra

The positions of electronic absorption maxima and the extinction coefficients for the complexes **4**−**7** are given in Table 1 together with the assignments. The optical spectra of the complexes feature weak d-d transitions and strong metal-to-ligand charge-transfer (CT) bands. The latter start

Table 1. UV/Vis data of **4**–**7**

Complex[a]	λ [nm]	$\tilde{\nu}$ [cm^{-1}]	ε	Assignment[b]	Comparison λ [nm] for $[M\{HB(pz)_3\}_2]$ and $[M\{HB(tz)_3\}_2]$[c]	
4	493	20 280	238	$^1A_{1g} \rightarrow {}^1T_{1g}$	535[d]	526[e]
5	877	11 400	1.7	$^4T_{1g} \rightarrow {}^4T_{2g}$	901[f][g]	n.o.[e][h]
	n.o.			$(^4T_{1g} \rightarrow {}^2T_{2g}, {}^2T_{1g})$	641	n.o.
	449	22 270	75 (sh)	$^4T_{1g} \rightarrow {}^4A_{2g}$	515 (sh)	509
	425	23 530	109	$^4T_{1g} \rightarrow {}^4T_{1g}$ (P)	459	450
	404	24 810	114	$(^4T_{1g} \rightarrow {}^2A_{1g})$	n.o.	n.o.
6	776	12 890	20	$^3A_{2g} \rightarrow {}^3T_{2g}$	849[g]	
	700	14 290	11(sh)	$(^3A_{2g} \rightarrow {}^1E_g)$	760 (sh)	
	504	19 840	25	$^3A_{2g} \rightarrow {}^3T_{1g}$	570	n.a.[h]
	429	23 310	16 (sh)	$(^3A_{2g} \rightarrow {}^1T_{1g})$	522	
	389	25 710	38 (sh)	$(^3A_{2g} \rightarrow {}^1A_{1g})$	450	
	n.o., CT			$^3A_{2g} \rightarrow {}^3T_{1g}$ (P)	334	
7	633	15 790	9	$^2E_g \rightarrow {}^2T_{2g}$ (O_h)	620[g]	630[e]
				$^2B_{1g} \rightarrow {}^2B_{2g}$, ^2E_g (D_{4h})		

[a] All complexes measured in $CHCl_3$; concentrations: **4** 4.7•10^{-3} mol•l^{-1}, **5** 6.0•10^{-3} mol•l^{-1}, **6** 10.2•10^{-3} mol•l^{-1}, **7** 2.9•10^{-3} mol•l^{-1}. – [b] Term symbols are taken for octahedral complexes, thereby assuming a near to O_h site symmetry at the metal center. Although it is recognized that the actual complex symmetry is D_{3d}. Parentheses indicate spin-forbidden transitions. – [c] pz = pyrazolyl, tz = triazolyl. – [d] J. P. Jesson, S. Trofimenko, D. R. Eaton, *J. Am. Chem. Soc.* **1967**, *89*, 3158–3164. – [e] C. Janiak, *Chem. Ber.* **1994**, *127*, 1379–1385. – [f] J. P. Jesson, *J. Chem. Phys.* **1966**, *45*, 1049–1056. – [g] J. P. Jesson, S. Trofimenko, D. R. Eaton, *J. Am. Chem. Soc.* **1967**, *89*, 3148–3158. – [h] n.o. = not observed, n.a. = not available.

at 340 nm. Hence, the highest energetic spin-allowed transition for the nickel complex **6**, $^3A_{2g} \rightarrow {}^3T_{1g}$ (P), could not be observed. The spectra are related to those of the analogous bis[hydrotris(pyrazolyl)borato]- and bis[hydrotris(triazolyl)-borato]metal compounds.[18–21] Data for comparison is included in Table 1. It is evident that corresponding bands for the indazolyl complexes are shifted to lower wave length by about 25 to 70 nm for most transitions. This shift to higher energy can be correlated to a stronger ligand field of the tris(indazolyl)borato anion versus the tris(pyrazolyl)borato analog. The ligand-field strength can be quantified by the *f* value relative to H_2O (*f* = 1.00). The value *f* is calculated from $\Delta_O = f \times g$(central ion).[23] The Ni^{II} transition $^3A_{2g} \rightarrow {}^3T_{2g}$ corresponds to Δ_O = 12890 cm^{-1}. Together with $g(Ni^{2+})$ = 8900 one obtains *f* = 1.45 for hydrotris(indazolyl)borate, which is slightly larger than *f* = 1.35 for hydrotris(pyrazolyl)borate.[20] Both ligands are stronger than 2,2′-bipyridine (*f* = 1.33) or ammonia (*f* = 1.25). We note that the copper complex **7** does not follow the aforementioned hypsochromic shift.

Electrochemistry of 4 and 5

The cyclic-voltammetric investigations on the (indazolylborato)iron and -cobalt complex **4** and **5**, respectively, can be compared to the data available for the iron and cobalt analog with the hydrotris(pyrazolyl)borato and the hydrotris(triazolyl)borato ligand.[8] The results are collected in Table 2. The cyclic voltammograms for **4** and **5** are shown in Figure 2. Based on the difference of the peak potentials, ΔE_p, the iron complex **4** exhibits a reversible and fast electron transfer. The electron processes for the cobalt complex **5** are only quasi-reversible and slow. This agrees with the behavior found for the respective tris(pyrazolyl)borato derivatives. It is suggested that the slow electron transfer for cobalt is due to different spin states for Co^{II} (high spin) and Co^{III} (low spin). In comparison with the (pyrazolyl)- and (triazolyl)borato complexes, the potentials of **4** lie at intermediate values. Hence, the [(indazolyl)borato]iron complex is more difficult to oxidize than the pyrazolyl analog, but easier to oxidize than the triazolyl compound. Whereas the cobalt complex **5** is easier to oxidize than its pyrazolyl congener. This may seem contradictory at first, but the phenomena can be explained with the slightly stronger ligand field of **Tp^{4Bo}** versus **Tp** according to Scheme 2. An increase in the σ-donor and π-acceptor strength increases the ligand-field splitting. In octahedral symmetry (assumed for simplicity), the t_{2g} levels are lowered, the antibonding e_g levels raised in energy. The d^6-Fe^{II} complex **4** is low spin with the electron configuration $t_{2g}{}^6$. Thus, it becomes more difficult

Table 2. Summary of voltammetric parameters for the oxidation of $[M\{HB(azolyl)_3\}_2]$, M = Fe, Co; azolyl = pyrazolyl, triazolyl, indazolyl

Complex[a]	E_{pc}/mV[b]	E_{pa}/mV[b]	$E_{1/2}$/mV[c]	ΔE_p/mV[d]	n[e]	Remarks
$[Fe\{HB(pyrazolyl)_3\}_2]$	139	232	185.5	93	1.03	Ref.[8], reversible one-electron process
$[Fe\{HB(indazolyl)_3\}_2]$ (**4**)	490	580	530	90		Reversible one-electron process
$[Fe\{HB(triazolyl)_3\}_2]$	810	1031	920.5	221	0.67	Ref.[8], quasi-reversible one-electron process
$[Co\{HB(pyrazolyl)_3\}_2]$	−217	213	4	430	0.93	Ref.[8], quasi-reversible one-electron process
$[Co\{HB(indazolyl)_3\}_2]$ (**5**)	−110	100	0	210		Quasi-reversible one-electron process
$[Co\{HB(triazolyl)_3\}_2]$	641	811	726	170	1.27	Ref.[8], quasi-reversible one-electron process

[a] Supporting electrolyte 0.1 mol/l $[nBu_4N][ClO_4]$ or $[nBu_4N][PF_6]$; *T* = 25 °C, solvent CH_2Cl_2, complex concentration 1•10^{-3} mol/l, reference Ag/AgCl, scan rate 100 mV/s. – [b] Cathodic and anodic potentials. – [c] $E_{1/2} = (E_{pa} + E_{pc})/2$. – [d] Difference between the anodic and cathodic peak potentials, $\Delta E_p = E_{pa} - E_{pc}$. – [e] Number of transferred electrons, $n = i_{pa}/i_{pc}$.

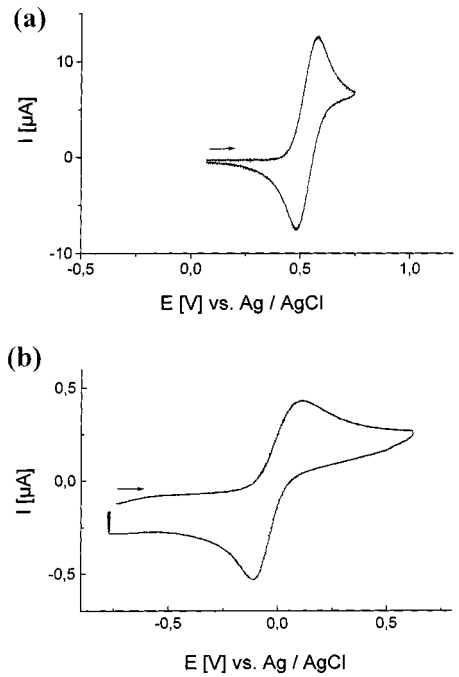
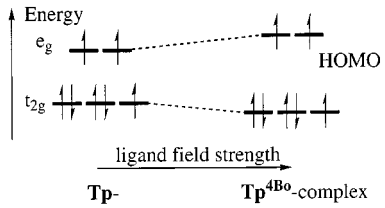


Figure 2. Cyclic voltammograms of (a) **4** and (b) **5** in CH_2Cl_2 (complex concentration 10^{-3} mol/l, 25 °C, scan rate 100 mV/s, 0.1 mol/l [nBu$_4$N][PF$_6$])



Scheme 2. The effect of an increase in ligand-field strength for Co^{II} (high spin) in O_h symmetry; from the raised e_g levels the complex becomes easier to oxidize when going from the **Tp** to the **Tp^{4Bo}** complex

to oxidize. The d^7-Co^{II} complex **5** is high spin with the electron configuration $t_{2g}^5e_g^2$. With the e_g levels raised in energy, it becomes easier to oxidize.

Mössbauer Spectroscopy of 4

Hexa-coordinated complexes of iron(II) with nitrogen donor ligands are good candidates for a temperature-induced spin crossover between the diamagnetic $^1A_{1g}$ low-spin state and the paramagnetic $^5T_{2g}$ high-spin state.[24] Also, the iron complexes of tris(pyrazolyl)borato ligands exhibit such a spin equilibrium [8,9,18,25–28] and the transition temperature was found to vary strongly with substitution on the pyrazolyl rings or the boron atom.[19,20,29] The interplay of the steric effects of substituents with the different sizes of the low- and high-spin Fe^{II} ions was demonstrated to be the decisive factor in controlling the relative stability of the spin states.[26,28] As such, we have investigated the possible spin crossover behavior of **4** by variable-temperature ^{57}Fe-Mössbauer spectroscopy. Figure 3 shows the Mössbauer spectra of **4** at three temperatures from 287 K

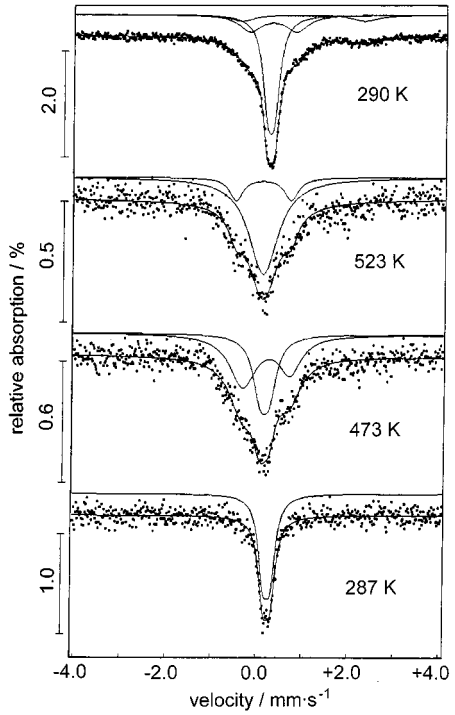


Figure 3. ^{57}Fe-Mössbauer spectra of **4** as a function of temperature; the isomer shift is scaled to the shift of α-Fe as the origin of the ordinate; the uppermost spectrum at 290 K was measured after heating the sample to 523 K and may contain some decomposition product

Table 3. Parameters of ^{57}Fe-Mössbauer spectra for the iron complex **4** (cf. Figure 3)

T/K [θ/°C]	N_{lin} [a]	$\delta^{\alpha\text{-Fe}}$[b] /mm s^{-1}	$\Gamma/2$[c] /mm s^{-1}	ΔE_Q [d] /mm s^{-1}	A_r/%[e] (A/A_Σ)
290 [17][f]	3	0.24	0.28	0.15	60
		0.28	0.61	1.02	28
		0.95	0.71	2.70	13
523 [250]	2	0.20	0.79	0.00	82
		0.20	0.38	1.21	18
473 [200]	2	0.21	0.54	-0.23	62
		0.24	0.56	1.16	38
287 [14]	1	0.34	0.26	0.16	100

[a] Number of lines used to fit the spectrum. – [b] Isomer shift refered to α-iron at room temperature. – [c] $\Gamma/2$ is half of the half-width value Γ. – [d] Quadrupole splitting. – [e]Line area relative to total area. – [f] The spectrum was measured after heating the sample to 523 K and may contain some decomposition product.

to 523 K. The corresponding Mössbauer parameters are collected in Table 3.

The initial room-temperature spectrum shows a doublet with a very small quadrupole splitting (0.16 mm s^{-1}). This, and the small positive isomer shift of 0.34 mm s^{-1}, is expected for a low-spin ($^1A_{1g}$) iron(II) complex with only a small distortion (D_{3d}) from octahedral ligand symmetry. The high-temperature spectra show a distinctly different line profile. Phenomenologically, they can be described as a broad singlet with a fine structure (shoulders). The spectra were fitted with a narrow doublet, or singlet and a wider doublet, both with a very similar isomer shift. The actual origin of the wide doublet is unclear. The small isomer shift

of 0.2 to 0.24 mm s^{-1} as well as the medium quadrupole splitting of 1.1 to 1.2 mm s^{-1} argue against iron(II) in the high-spin $^5T_{2g}$ state. Usually, for high-spin iron(II) in the quintet state an isomer shift of 0.7 to 1.2 mm s^{-1} and a large quadrupole splitting of 2.3 to 3.0 mm s^{-1} is expected.[8,24,29] Hence, we would not ascribe the fine structure to a quadrupolar relaxation phenomenon, i.e. to the onset of a spin transition. Possibly, the wide doublet may stem from partial decomposition: A second room-temperature spectrum, which was collected after heating the sample, still shows a broadened envelope around the main signal. In addition, a flat peak at positive isomer shift had emerged, which could be fitted to a doublet with an isomer shift of 0.95 mm s^{-1} and a large quadrupole splitting of 2.07 mm s^{-1}. The visual appearance of the sample was unchanged after the Mössbauer experiments.

For the bis(ligand) complex of iron with tris(pyrazolyl)borate (**1**) a transition temperature (50% low- and high-spin state) of about 133 °C was given.[26] It is suggested that the increased ligand-field strength of **2a** versus **1** may be the basis for the considerable increase in transition temperature beyond the decomposition point of the sample.

X-ray Structures of [M(Tp^{4Bo})$_2$] Complexes (M = Fe, Co, Ni, Cu, Zn) with Solvent of Crystallization

The bis[hydrotris(indazol-1-yl)borato]metal complexes could be crystallized from THF, dioxane or chloroform. The following complexes were investigated by single-crystal X-ray structure determination: **4** • 3.5 $CHCl_3$, **5** • 3.5 $CHCl_3$, **6** • 3 THF, **6** • 1.67 dioxane, **7** • 1.33 $CHCl_3$, **7** • 2.5 THF, and **8** • 1.67 dioxane. The number of solvent molecules was derived from the structure refinement. The interest in different solvents of crystallization stems from a solvent-dependent crystal packing, which became apparent in the course of these studies.

The (common) molecular structure of the M(Tp^{4Bo})$_2$ complexes for M = Fe, Co, Ni, and Zn (**4**, **5**, **6**, and **8**, respectively) is shown in Figure 4. The metal complexes exhibit the usual D_{3d}-symmetrical geometry for two tripodal ligands. In each space group found here, the metal atom occupies a center of inversion as a special position. Hence, both ligands in a complex molecule are symmetry-related. The copper compound **7** is depicted in Figure 5. The metal atoms are pseudo-octahedrally coordinated by the tris(chelate) ligand **2a**, and complex **7** exhibits the expected Jahn–Teller distortion for the d^9 ion with four short and two long Cu–N distances. The metal–nitrogen bond lengths and angles are summarized in Table 4. They are unremarkable with respect to those of other bis[tris(pyrazolyl)borato]-[30–33] and bis[tris(triazolyl)borato]metal complexes[7,18,34,35] and M–N bond lengths in general.[36] A comparison of the average M–N bond lengths from Table 4 shows the expected decrease for high-spin ions from Co to Ni, and again an increase towards Zn.[37] The rather short metal–ligand bond length for the iron compound **4** is indicative of a low-spin complex, in agreement with the Mössbauer data (see above).

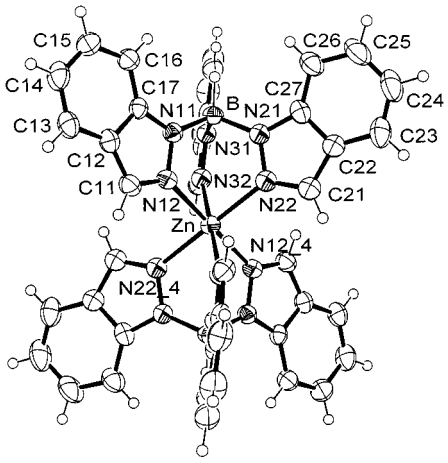


Figure 4. Molecular structure of [Zn{$HB(C_7H_5N_2)_3$}$_2$] (**8**); selected distances [Å] and angles [°]: Zn–N12 2.157(3), Zn–N22 2.156(3), Zn–N32 2.149(3); N12–Zn–N22 84.0(1), N12–Zn–N32 86.4(1), N22–Zn–N32 87.2(1), N12–Zn–N22 4 96.1(1), N32–Zn–N12 4 93.7(1), N32–Zn–N22 4 92.9(1) (see also Table 4) (symmetry-equivalent position 4 = 1 − x, −y, 1 − z)

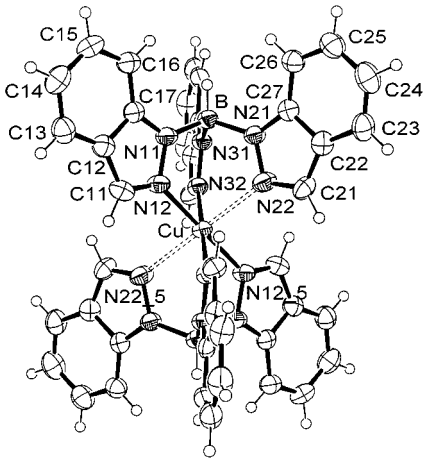


Figure 5. Molecular structure of [Cu{$HB(C_7H_5N_2)_3$}$_2$] (**7**) in **7** • 2.5 THF; selected distances [Å] and angles [°]: Cu–N12 2.043(4), Cu–N22 2.318(4), Cu–N32 2.019(3); N12–Cu–N22 86.8(1), N12–Cu–N32 87.1(1), N22–Cu–N32 85.2(1), N12–Cu–N22 5 93.3(1), N32–Cu–N12 5 92.9(1), N32–Cu–N22 5 94.9(1) (see also Table 4) (symmetry-equivalent position 5 = −x, 1 − y, −z)

One might have thought that the crystal packing of the complex molecules could be dictated by so-called face-to-face π-stacking interactions between six-membered rings of the indazolyl moieties. Such a parallel or a parallel-displaced π-stacking with a ring separation between 3.3 to 3.8 Å is an important non-covalent organization possibility in supramolecular chemistry.[38–40] Yet, the crystal packing between the molecular complexes appears to be controlled more by C–H•••π interactions from the indazolyl moieties, which is exemplified in Figure 6 and 7. Such a C–H•••π interaction between aromatic rings is referred to as a point-to-face or T-shaped arrangement.[41] Only in the structure of the nickel derivative **6** • 3 THF was a slipped face-to-face

Table 4. Selected bond lenghts and angles in the bis[hydrotris(indazol-1-yl)borato]metal complexes $M(Tp^{4Bo})_2$

Compound[a]	$Fe(Tp^{4Bo})_2$ in **4** • 3.5 $CHCl_3$[b]	$Co(Tp^{4Bo})_2$ in **5** • 3.5 $CHCl_3$[b]	$Ni(Tp^{4Bo})_2$ in **6** • 3 THF[b]	$Ni(Tp^{4Bo})_2$ in **6** • 1.67 dioxane	$Cu(Tp^{4Bo})_2$ in **7** • 1.33 $CHCl_3$[c]	$Cu(Tp^{4Bo})_2$ in **7** • 2.5 THF	$Zn(Tp^{4Bo})_2$ in **8** • 1.67 dioxane
M−N range [Å]	1.941(7)−1.972(7)	2.096(5)−2.139(5)	2.049(3)−2.066(3)	2.084(3)−2.091(4)	short: 2.002(2)−2.025(2) long: 2.357(2)−2.453(3)	short: 2.019(3) and 2.043(4) long: 2.318(4)	2.149(3)−2.157(3)
M−N average [Å]	1.958	2.117	2.058	2.087	short: 2.015 long: 2.407	short: 2.031 long: 2.318	2.154
range N−M−N chelate bite angles [°]	87.9(3)−89.5(3)	84.9(2)−86.8(2)	85.0(1)−87.7(1)	85.5(1)−87.7(1)	83.78(9)−87.66(9)	85.2(1)−87.1(1)	83.95(10)−87.15(10)
average N−M−N chelate bite angles [°]	88.6	86.1	86.5	86.9	86.0	86.4	85.8
N−M−N *cis*, except chelate [°]	90.5(3)−92.1(3)	93.2(2)−95.1(2)	92.3(1)−95.0(1)	92.3(1)−94.5(1)	92.34(9)−96.22(9)	92.9(1)−94.9(1)	92.85(10)−96.05(10)
average N−M−N *cis*, except chelate [°]	91.4	93.9	93.6	93.1	94.0	93.7	90.9

[a] Only one of the borato ligands is unique. The two borato ligands are symmetry-related through a center of inversion; special position of the metal atom. Hence, the N−M−N *trans* angles are 180.0°. − [b] Two symmetrically independent molecules in the unit cell. − [c] Three symmetrically independent molecules in the unit cell.

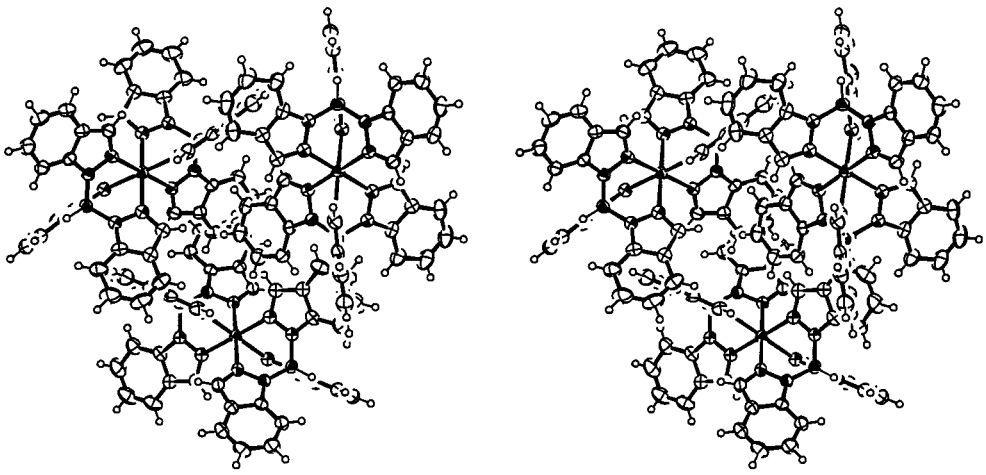


Figure 6. Stereoview of the section of the crystal structure of **4** • 3.5 $CHCl_3$ (isostructural with **5** • 3.5 $CHCl_3$) to illustrate the C−H•••π interactions between the indazolyl moieties; solvent molecules have been omitted; view approximately along *c*

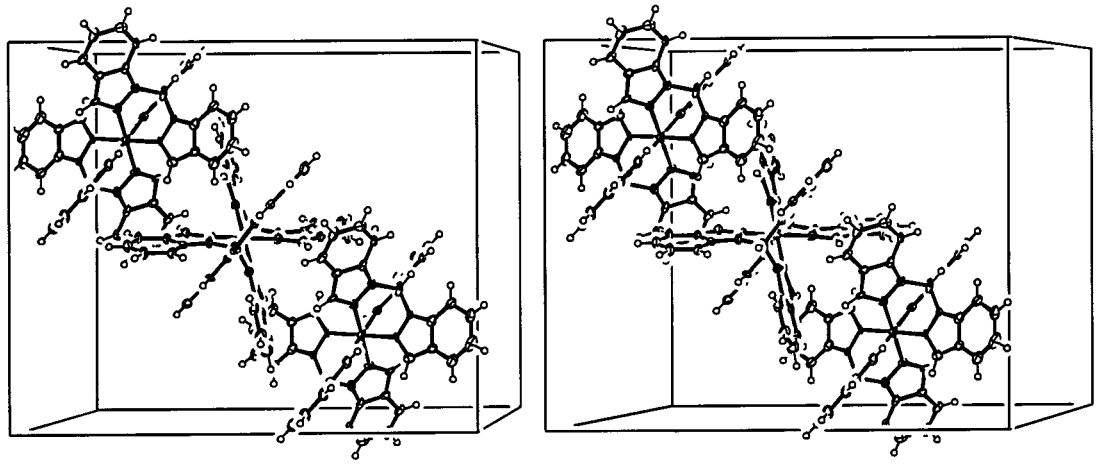


Figure 7. Stereoview of the section of the crystal structure of **8** • 1.67 dioxane (isostructural with **6** • 1.67 dioxane) to illustrate the C−H•••π interactions between the indazolyl moieties; solvent molecules have been omitted

aromatic−aromatic interaction more prominent (see Figure 9). The preference for a C−H•••π interaction can be understood when keeping in mind the fact that a parallel face-to-face geometry for aromatic rings is not necessarily attractive. For non-polarized π-systems π−π repulsion prevents a parallel π-stacking and σ−π attraction favors either a T-shaped or a displaced geometry.[42] According to the so-called Hunter−Sanders rules, a face-to-face interaction requires π-deficient and σ-positive atoms in polarized π-systems.[40,43] At the same time, a charge-charge interaction

Table 5. Potential solvent areas and C−H•••π contacts; computed with the program PLATON

Compound	**4** • 3.5 $CHCl_3$	**5** • 3.5 $CHCl_3$	**6** • 3 THF	**6** • 1.67 dioxane	**7** • 1.33 $CHCl_3$	**7** • 2.5 THF	**8** • 1.67 dioxane
Potential solvent area in solvent-free crystal lattice: volume [Å^3]/unit cell volume [Å^3]	4001.5/10362.7 ≅ 38.6%	4003.9/10490.4 ≅ 38.2%	861.3/2503.0 ≅ 34.4%	3077.7/10514.5 ≅ 29.3%	619.6/3285.3 ≅ 18.8%	1248.8/4656 ≅ 26.8%	3012.9/10536.1 ≅ 28.6%
Calculated solvent molecule volume [Å^3][a] = solvent area/number of solvent molecules (in unit cell)	4001.5/(3.5×8) = 143[a]	4003.9/(3.5×8) = 143[a]	861.3/(3×2) = 144[a]	3077.7/(1.67×9) = 205[a]	619.6/(1.33×3) = 155[a]	1248.8/(2.5×4) = 125[a]	3012.9/(1.67×9) = 201[a]
Shortest intermolecular **C−H•••C(π) contacts,** H•••C distances [Å] (and angles [°])[b][c]	2.70 (156.6)	2.77 (162.6)	2.70 (154.8)	2.81 (146.5)	2.66 (165.5)	2.89 (127.9)	2.77 (132.0)
Shortest intermolecular **ring-centroid−ring-centroid contacts** [Å] (with interplanar angle [°])[b][d]	R5−R5: 4.496 (51.3) R6−R5: 4.471 (50.0) R6−R6: 4.546 (49.7)	R5−R5: 4.803 (74.7) R6−R5: 4.435 (47.9) R6−R6: 4.493 (47.1)	R5−R5: 4.267 (7.0) R6−R5: 3.931 (6.1) R6−R6: 3.673 (6.5)	R5−R5: 4.809 (54.0) R6−R5: 4.628 (15.9) R6−R6: 4.892 (31.9)	R5−R5: 4.703 (60.7) R6−R5: 4.537 (49.8) R6−R6: 4.875 (62.2)	R5−R5: 4.942 (49.0) R6−R5: 5.190 (41.9) R6−R6: 4.913 (53.3)	R5−R5: 5.013 (57.3) R6−R5: 4.635 (24.8) R6−R6: 4.869 (31.4)
Shortest intermolecular contact (R6) **C−H•••ring-centroid** (R5 or R6) [Å][b,d]	R5: 3.18 R6: 3.08	R5: 3.03 R6: 2.66	R5: 2.96 R6: 3.15	R5: 2.85 R6: 2.79	R5: 2.70 R6: 2.65	R5: >3.4 R6: 3.08	R5: 2.87 R6: 2.76

[a] This has to be compared to an expected solvent volume for small molecules of 100−300 Å^3. − [b] A full listing of the intermolecular C−H•••π contacts [C−H•••C < 3.1 Å, C−H•••centroid < 3.4 Å (distances and angles)] and of the ring-centroid−ring-centroid contacts (< 6.0 Å) has been deposited as supporting information. − [c] The sum of the contact radii of carbon (1.70 Å) and hydrogen (1.20 Å) is 2.90 Å as given by: A.Bondi, *J. Phys. Chem.* **1964**, *68*, 441. (or covalent radius + 0.8 Å. when not given). − [d] R5 denotes the 5-membered nitrogen-containing pyrazol-type ring, R6 denotes the 6-membered anellated aryl ring of the indazolyl group.

dominates for highly charged π-systems. We suggest that delocalization of the negative ligand charge into the indazolyl rings may be the basis of a charge repulsion and C−H$^{\delta+}$−$^{\delta-}$π attraction.

The T-shaped C−H•••π interaction is found for example in the crystal structure of benzene.[44] Molecular dynamics calculations for benzene gave an optimum distance of 4.99 Å between the two ring centers in the T-shaped orientation. The theoretical interaction energy is about 10 kJ/5mol. Even at a benzene−benzene center of mass separation of 6 Å the T-shaped point-face dimer is bound by about 1.6 kJ/mol.[41,42] Table 5 summarizes the shortest intermolecular C−H•••π contacts with distances and angles. Ring-centroid−ring-centroid contacts shorter than 4.99 Å can be observed. From Figure 6 and 7 and the comparison of the interplanar angles, it is evident that the aromatic rings do not lie perpendicular to one another. Most angles are between 40 and 80° (cf. supporting information), i.e. we have tilted structures intermediate between the parallel displaced and the point-face geometry.[41] The intermolecular C−H•••π contacts start around 2.7 Å for C−H•••C and C−H•••ring centroid distances (Table 5). As such, these shortest C−H•••π contacts in the structures of **4** to **8** lie at the short end of the accepted distance range for this type of contact.[45] A full listing of the intermolecular C−H•••π contacts [C−H•••C < 3.1 Å, C−H•••centroid < 3.4 Å (distances and angles)] and of the ring-centroid−ring-centroid contacts (< 6.0 Å) can be found in the supporting information.

The solvent-incorporating structures of **4** to **8** indicate that even the very weak intermolecular C−H•••π interactions can be used to construct porous framework structures.[46] This mode of assembly gives rise to large non-covalent framework structures with voids and channels from about 19 to 39% of the unit cell volume (see Table 5). Figure 8 to 11 provide example views of these open spaces in six compounds. There, most of the potential solvent areas are built as channels. Only in the structure of **7** • 1.33 $CHCl_3$ (not shown) are cavities solely formed. The open space is filled by solvent molecules and probably based on very weak C−H•••O or C−H•••Cl hydrogen bonding. Because of the weak host−guest interactions the

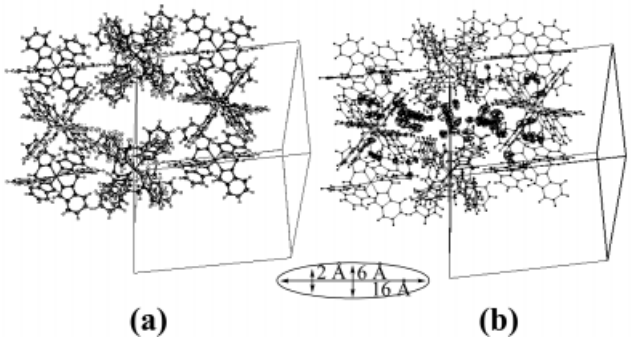


Figure 8. (a) Solvent-omitted crystal structure of **4** • 3.5 $CHCl_3$ (isostructural with **5** • 3.5 $CHCl_3$) to illustrate the channel formation along the *ab* diagonal (110 plane) and (b) the same view with a wire-frame model of the metal complexes together with the solvent molecules

solvent molecules are prone to disorder. The disorder model for the dioxane molecules in Figure 11b, which lie within the channels, is sketched in **9**. These disordered dioxane molecules give the impression of a close-packed cluster. A three-fold inversion axis ($\bar{3}$), perpendicular to the plane of projection in Figure 11 passes through them. It is suggested that the inversion axis is parallel to but does not coincide with the molecular C_2 axis bisecting the C−C bonds. The three-fold rotation wraps the molecule around with the oxygen atoms pointing outward.

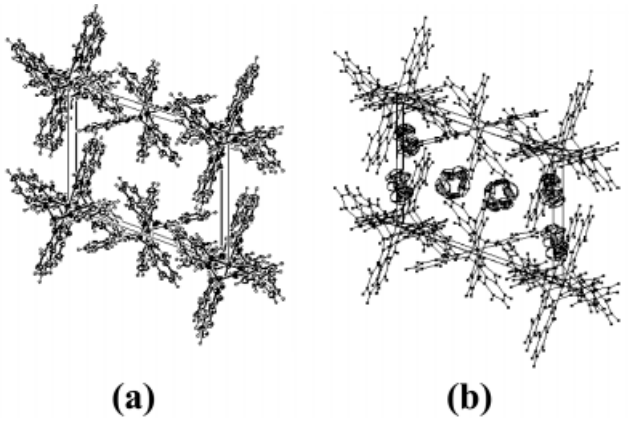


Figure 9. (a) Solvent-deleted crystal structure of **6** • 3 THF showing the channel formation along *a* and (b) the same view with a wire-frame model of the metal complexes together with the THF molecules

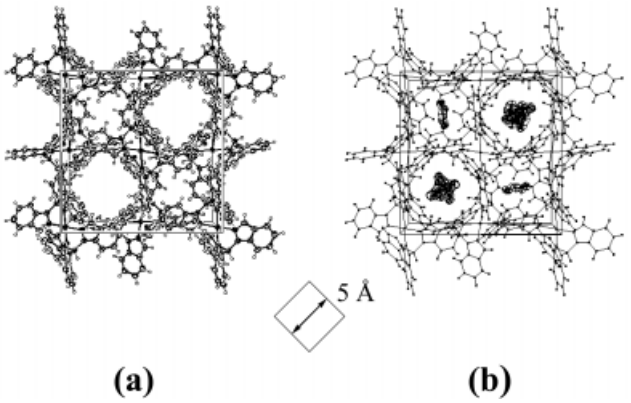


Figure 10. (a) Solvent-omitted crystal structure of **7** • 2.5 THF with the channel formation along the *c* axis and (b) the same view with a wire-frame model of the metal complexes together with the, in part, disordered solvent molecules

The calculated solvent volumes (Table 5) fall well into the expected solvent volume range of 100−300 Å^3 for small molecules. This gives some indication that the number of solvent molecules has been correctly determined within the structure refinement. The crystal packing and the space

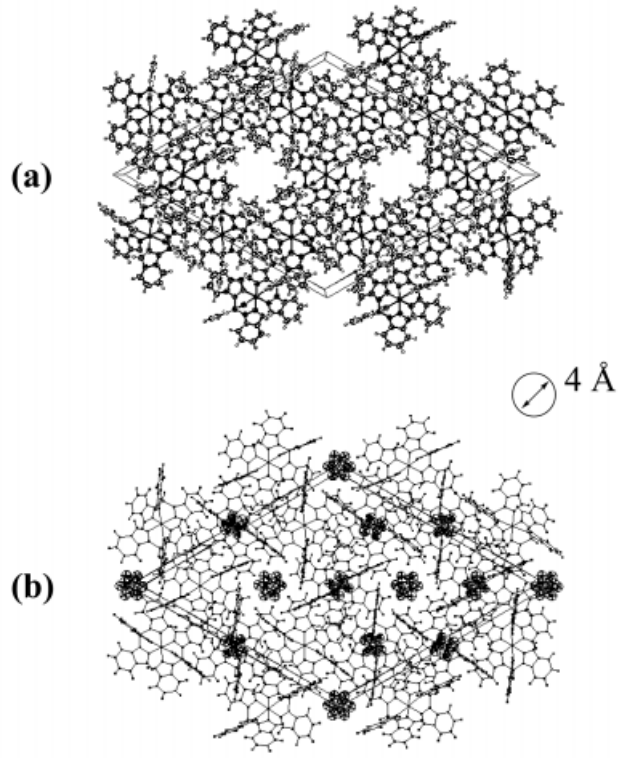
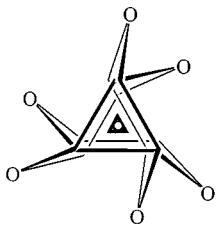


Figure 11. (a) Solvent-deleted crystal structure of **8** • 1.67 dioxane (isostructural with **6** • 1.67 dioxane) to illustrate the channel formation along *c* and (b) the same view with a wire-frame model of the metal complexes together with the disordered solvent molecules

group then depend on the type of solvent. It is well known that solvents of crystallization can have a substantial effect on the molecular and/or crystal structure of a compound.[47−49] We are currently investigating if the dioxane molecules can, at least in part, be reversibly removed from and reinserted into the framework. If so, one may envision the construction of supramolecular sensors for such small molecules in combination with a quartz crystal micro-balance.[50]



9

Conclusion

A UV/Vis-spectrometric comparison of the metal complexes shows that the tris(indazolyl)borate ligand **2a** is a somewhat stronger ligand than the long-known hydrotris(pyrazolyl)borate parent system **1**. From cyclic voltammetric studies on the iron and cobalt complexes of **2a** and **1** it is evident that the former has the effect of decreasing the energy of the t_{2g} orbitals and increasing the energy of the e_g orbitals. Unlike other homologue failed to exhibit a

temperature-induced low- to high-spin crossover before the decomposition point.

The molecular bis[hydrotris(indazolyl)borato]metal complexes can pack only loosely in the crystal leaving voids and channels which amount to as much as 38% of the unit cell volume. The voids are filled by solvent molecules. The low density packing of the molecular complexes may be due to a reluctance of the indazolyl moieties to enter into face-to-face π-stacking interactions. Instead, the crystal packing is controlled more by tilted point-face C−H•••π interactions. Most indazolyl ring planes form intermolecular angles between 40 and 80°. On the other hand, the solvent-incorporating structures of the bis[hydrotris(indazolyl)borato]metal complexes **4**−**8** indicate that even the very weak intermolecular C−H•••π interactions can be used to construct porous framework structures.

Experimental Section

The solvent, methanol, was dried with CaO by heating under reflux for 4 h under inert gas, followed by distillation. − UV/Vis spectra were obtained with a Jasco V-570, MHT-344 spectrometer in the range 1800−300 nm, and with a Polytec XDAP diode-array spectrometer with a quartz immersion probe in the range 1000−280 nm. NMR spectra were recorded with a Bruker ARX200 (200.1 MHz for ^{1}H, 50.3 MHz for ^{13}C), and calibrated against the solvent signal ([D_6]DMSO: ^{1}H NMR: δ = 2.53, ^{13}C NMR: δ = 39.5; $CDCl_3$: ^{1}H NMR: δ = 7.26, ^{13}C NMR: δ = 77.0; [D_8]THF: ^{1}H NMR: δ = 1.73, ^{13}C NMR: δ = 25.2; CD_3OD: ^{1}H NMR: δ = 3.31). The ^{11}B- and ^{10}B-NMR spectra were measured with a Bruker ARX200 (64.21 MHz for ^{11}B, 21.50 MHz for ^{10}B) relative to neat $BF_3 \bullet Et_2O$ as an external standard. A 1:2 v/v solvent mixture of [D_6]DMSO and normal DMSO was used with a sample concentration of about 130 mg/mL. Mass spectra were obtained with a Varian MAT 311A/AMD in solid-probe EI mode, at an ionization energy of 70 eV. The MS peaks listed refer to the most abundant isotope combination with ^{56}Fe, ^{59}Co, ^{58}Ni, ^{63}Cu, ^{54}Zn, and ^{11}B. Elemental analyses were carried out with a Perkin−Elmer 2400 Series II CHNS/O Analyzer. IR spectra were measured with a Nicolet Magna 750 as KBr disks.

Synthesis

Potassium Hydrotris(indazol-1-yl)borate, K[HB($C_7H_5N_2$)$_3$] (3): The potassium salt of **2a** was prepared following a general procedure by Trofimenko for tris(pyrazolyl)borate ligands:[51] KBH_4 (1.6 g, 30.0 mmol) and indazole (11.3 g, 95.9 mmol) were heated to 220 °C in a Schlenk flask that was connected to a volumetric gas measurement system. A strong gas evolution starts upon melting, and ceases towards the end of the reaction. After 4 h, 2.1 L of H_2 was evolved, which corresponds to 86.1 mmol or 96% when assuming the ideal gas law. Excess indazole was separated by sublimation (160 °C bath temperature, 1.5 mbar), to leave the product as a yellow powder (yield 10.57 g, 88%). NMR spectroscopy still showed indazole impurities that could not be removed, even after prolonged sublimation. The product was used as such for the following reactions with metal salts. M.p. 256−258 °C (ref.[12] 256−258 °C) − ^{1}H NMR (CD_3OD): 6.70−7.70 (m, 12 H, 4-, 5-, 6-, 7-H), 8.01 (s, 3 H, 3-H), the BH signal could not be observed; possibly due to its broad resonance because of quadrupolar coupling and relaxation effects from the boron atom.[52] − ^{13}C NMR (CD_3OD): δ = 113.8 (C-7), 120.3 (C-5), 121.0 (C-4), 125.7 (C-6), 125.8 (C-3a), 134.3 (C-3), 145.7 (C-7a) (the assignment of the quaternary C atoms C-3a and C-7a agrees with their lower signal intensity; the signals of the nitrogen-neighboring atoms C-3 and C-7a can be discerned by their low-field shift[7]). − ^{11}B NMR ([D_6]DMSO): δ = −3.5 (br), −9.3 (sh, assigned to the disubstituted borate), −35.6 (s, sharp signal, unchanged KBH_4). − ^{10}B NMR ([D_6]DMSO): δ = −5 (very broad with shoulder to high-field end), −35.6 (s, sharp signal, KBH_4). − MS (284 °C); *m/z* (%): 402 (4) [*M*]$^+$, 375 (4) [*M* − HCN]$^+$, 285 (20) [*M* − $C_7H_5N_2$]$^+$, 245 (12) [B($C_7H_5N_2$)$_2$]$^+$, 118 (100) [$C_7H_6N_2$]$^+$, 91 (28) [$C_7H_6N_2$ − HCN]$^+$. − IR (KBr): $\tilde{\nu}$ = 3090 cm^{-1} w, 3056 w, 3038 w (νCH), 2440 w, 2416 w, 2382 w (νBH), 1615 m (νCN), 1574 m, 1496 m, 1459 m, 1436 sh, 1400 m, 1375 sh, 1364 w, 1337 m, 1263 m, 1209 w, 1155 s, 1110 s, 1024 sh, 1010 s, 994 m, 942 m, 908 s, 855 w, 835 m, 794 w, 787 w, 779 w, 759 s, 740 s, 663 m, 656 w, 646 w, 634 w, 622w, 609 w, 600 m, 569 w, 552 w, 458 w, 429 m.

[Bis{hydrotris(indazol-1-yl)borato]metal(II) Complexes, [M{HB($C_7H_5N_2$)$_3$}$_2$]. − General Procedure: A solution of **3** (400 mg, 1.0 mmol) in CH_3OH (10 mL) was added to a solution/slurry of the metal salt (0.5 mmol) in CH_3OH (5 mL) under stirring. The precipitate formed was filtered and dried in air. The product was separated from KCl by dissolution in THF, dioxane, or chloroform, followed by filtration. Crystallization was achieved either by cooling, overlayering with petroleum ether (30/50) or slow solvent evaporation. After crystallization, the crystals contained solvent of crystallization which in the case of $CHCl_3$ or THF was rapidly lost when removed from the mother liquor.

[Fe{HB($C_7H_5N_2$)$_3$}$_2$] (4): Starting material $(NH_4)_2Fe(SO_4)_2$. Pink to red needle-shaped crystals were initially obtained from chloroform under cooling to −15 °C. After 2 d at this temperature, the needles dissolved again and red rhombic crystals formed within another day. Yield 440 mg, 95%. − M.p. 446 °C (DSC). − ^{1}H NMR ($CDCl_3$): δ = 1.59 (s, br, 1 H, BH), 6.98 (t, 3 H, *J* = 7.2 Hz, 5-H), 7.35 (overlapping d and t, 6 H, *J* = 8.4 Hz, 6-H, 7-H), 7.42 (s, 3 H, 3-H), 8.15 (d, 3 H, *J* = 8.4 Hz, 4-H); ([D_8]THF): δ = 2.55 (s, br, 1 H, BH), 6.93 (t, 3 H, *J* = 7.5 Hz, 5-H), 7.34 (overlapping d and t, 6 H, *J* = 7.8, 8.3 Hz, 6-H, 7-H), 7.48 (s, 3 H, 3-H), 8.16 (d, 3 H, *J* = 8.4 Hz, 4-H). − ^{13}C NMR ([D_8]THF): δ = 111.2 (C-7), 119.8 (C-6), 120.5 (C-5), 126.0 (C-4), 126.3 (C-3a), 143.6 (C-3), 146.6 (C-7a). − MS (469 °C); *m/z* (%): 782 (68) [*M*]$^+$, 665 (46) [*M* − $C_7H_5N_2$]$^+$, 547 (7) [*M* − 2 ($C_7H_5N_2$) − H]$^+$, 536 (19) [*M* − 2 ($C_7H_5N_2$) − BH]$^+$, 419 (69) [*M* − {HB($C_7H_5N_2$)$_3$} = Fe{HB($C_7H_5N_2$)$_3$}]$^+$, 391 (5) [*M*]$^{2+}$, 332.5 (14) [*M* − $C_7H_5N_2$]$^{2+}$, 301 (86) [Fe{HB($C_7H_5N_2$)$_2$}]$^+$, 274 (100) [*M* − 2 ($C_7H_5N_2$)]$^{2+}$, 118 (55) [$C_7H_6N_2$]$^+$. − IR (KBr): $\tilde{\nu}$ = 3110 cm^{-1} w, 3064 w, 3039 w, 2905 w (νCH), 2490 sh, 2475 m (νBH), 1623 s, 1505 m, 1461 s, 1416 vs (νCN), 1378 sh, 1362 m, 1350 s, 1330 w, 1265 m, 1216 s, 1140 vs, 1135 sh, 1123 w, 1110 s, 1016 vs, 998 m, 920 m, 912 w, 848 m, 822 s, 757 vs, 740 vs, 726 s, 680 m, 597 m, 572 w, 560 w, 499 m, 440 m. − $C_{42}H_{32}B_2FeN_{12} \bullet (THF)_2$ (926.5): calcd. C 64.82, H 5.22, N 18.14; found C 64.24, H 5.28, N 16.06.

[Co{HB($C_7H_5N_2$)$_3$}$_2$] (5): Starting material $CoCl_2 \bullet 6\,H_2O$. An initial crystallization from dioxane/petroleum ether yielded red-brown needles and a yellow solid. The brown impurity could be removed after treatment of a $CHCl_3$ solution with Al_2O_3. This changed the relative solubility of the two phases. After evaporation of $CHCl_3$ in vacuum, the remaining solid was treated again with $CHCl_3$ (5 mL) which led to the dissolution of the brown impurity leaving a citrus-yellow solid behind. The yellow solid was crystallized from hot/cold $CHCl_3$ to give initially yellow needle-shaped crystals and after longer standing yellow rhombic crystals. Yield 220 mg, 56%. − M.p. > 300 °C. − ^{1}H NMR ($CDCl_3$): δ = +111.7 (1 H, BH),

+50.2 (3 H, 7-H), +20.1 (3 H, 6-H), +10.6 (3 H, 5-H), −9.9 (3 H, 4-H), −97.8 (3 H, 3-H); ([D$_6$]DMSO): δ = + 117 (1 H, BH), + 52.2 (3 H, 7-H), + 20.8 (3 H, 6-H), + 10.8 (3 H, 5-H), − 10.3 (3 H, 4-H), −101 (3 H, 3-H); ([D$_8$]THF): δ = + 117 (1 H, BH), + 52.1 (3 H, 7-H), + 20.7 (3 H, 6-H), + 10.7 (3 H, 5-H), −10.5 (3 H, 4-H), −102 (3 H, 3-H) (corresponds to ref.[12]). − MS (438 °C); *m*/*z* (%): 785 (83) $[M]^+$, 668 (76) $[M - C_7H_5N_2]^+$, 550 (16) $[M - 2(C_7H_5N_2) - H]^+$, 422 (69) $[M - \{HB(C_7H_5N_2)_3\} = Co\{HB(C_7H_5N_2)_3\}]^+$, 392.5 (3) $[M]^{2+}$, 334 (10) $[M - C_7H_5N_2]^{2+}$, 304 (67) $[Co\{HB(C_7H_5N_2)_2\}]^+$, 275.6 (100) $[M - 2(C_7H_5N_2)]^{2+}$, 118 (33) $[C_7H_6N_2]^+$. − IR (KBr): $\tilde{\nu}$ = 3103 cm^{-1} w, 3063 w (νCH), 2498 m, 2478 m (νBH), 1623 s, 1507 s (νCN), 1462 s, 1431 m, 1412 s, 1381 m, 1367 s, 1351 s, 1321 w, 1266 s, 1217 s, 1158 s, 1148 s, 1113 s, 999 s, 947 w, 916 s, 857 m, 835 s, 826 s, 760 vs, 748 s, 728 s, 666 s, 645 w, 599 s, 434 m. − $C_{42}H_{32}B_2CoN_{12}$ (785.35): calcd. C 64.23, H 4.11, N 21.40; found C 63.86, H 3.39, N 19.81. − $C_{42}H_{32}B_2CoN_{12} \cdot 4/3\,(CHCl_3)$ (944.5): calcd. C 55.10, H 3.56, N 17.80; found C 55.63, H 3.56, N 17.89.

[Ni{HB(C$_7$H$_5$N$_2$)$_3$}$_2$] (6): Starting material anhydrous $NiCl_2$. Light pink crystals from dioxane/petroleum ether or slow evaporation of THF. Yield 250 mg, 64%. M.p. > 300 °C − ^{1}H NMR ([D$_8$]THF): δ = 2.04 (s, 1 H, 3-H), 2.44 (s, 1 H, 4-H), 3.58 (s, 1 H, 5-H) 8.79 (br, s, 1 H, 6-H), 15.09 (br, s, 1 H, 7-H). − MS (428 °C); *m*/*z* (%): 784 (11) $[M]^+$, 667 (51) $[M - C_7H_5N_2]^+$, 549 (7) $[M - 2(C_7H_5N_2) - H]^+$, 421 (29) $[M - \{HB(C_7H_5N_2)_3\} = Ni\{HB(C_7H_5N_2)_3\}]^+$, 333.5 (4) $[M - C_7H_5N_2]^{2+}$, 304 (18) $[Ni\{HB(C_7H_5N_2)_2\}]^+$, 275 (27) $[M - 2(C_7H_5N_2)]^{2+}$, 118 (100) $[C_7H_6N_2]^+$. − IR (KBr): $\tilde{\nu}$ = 3237 cm^{-1} w, 3127 w, 3110 w, 3092 w, 3063 m, 3034 w, 2968 w, 2924 w (νCH), 2850 w, 2717 w, 2675 w, 2613 w, 2563 w, 2491 m, 2471 m (νBH),1937 w, 1903 w, 1880 w, 1789 w, 1686 w, 1682 w, 1622 s (νCN), 1566 w, 1504 s, 1461 s, 1430 m, 1409 s, 1378 m, 1362 s, 1347 s, 1322 w, 1284 w, 1263 s, 1213 m, 1185 w, 1155 s, 1144 s, 1137 s, 1124 w, 1111 s, 1066 w, 1040 m, 1014 s, 1003 sh, 994 s, 973 sh, 944 w, 938 w, 913 s, 909 sh, 850 m, 832 sh, 825 s, 815 w, 778 w, 765 sh, 756 s, 741 s, 723 s, 664 s, 646 w, 641 w, 596 s, 569 w, 556 w, 431 m. − $C_{42}H_{32}B_2N_{12}Ni$ (785.1): calcd. C 64.25, H 4.11, N 21.41; found C 63.89, H 3.68, N 20.01.

[Cu{HB(C$_7$H$_5$N$_2$)$_3$}$_2$] (7): Starting material anhydrous $CuCl_2$. Dark green crystals from hot/cold $CHCl_3$ or slow evaporation of THF. Yield 350 mg, 90%. M.p. > 300 °C. − ^{1}H NMR ([D$_8$]THF): δ = 6.7 (s, br $\omega_{1/2}$ = 130 Hz), 7.8 (s, br $\omega_{1/2}$ = 113 Hz), 9.2 (s, br $\omega_{1/2}$ = 74 Hz), 11.5 (s, br $\omega_{1/2}$ = 174 Hz). − MS (446 °C); *m*/*z* (%): 788 (0.5) $[M - H]^+$, 671 (14) $[M - C_7H_5N_2 - H]^+$, 555 (30) $[M - 2(C_7H_5N_2)]^+$, 426 (5) $[M - \{HB(C_7H_5N_2)_3\} = Cu\{HB(C_7H_5N_2)_3\}]^+$, 309 (67) $[Cu\{HB(C_7H_5N_2)_2\}]^+$, 282 (100) $[Cu\{HB(C_7H_5N_2)_2\} - HCN]^+$, 118 (33) $[C_7H_6N_2]^+$. − IR (KBr): $\tilde{\nu}$ = 3119 cm^{-1} w, 3067 m, 3043w (νCH), 2497 m, 2478 m (νBH), 1625 s, 1508 s, 1467 s (νCN), 1431 m, 1412 s, 1382 m, 1366 m, 1349 s, 1268 m, 1221 s, 1212 sh, 1159 s, 1147 s, 1139 m, 1114 s, 1044 m, 1024 s, 1012 s, 999 s, 943 w, 918 s, 911 sh, 855 m, 836 m, 827 s, 761 s, 742 s, 663 s, 644 w, 599 s, 435 m. − $C_{42}H_{32}B_2CuN_{12} \cdot 1/2\,(CHCl_3)$ (849.6): calcd. C 60.08, H 3.86, N 19.78; found C 59.63, H 3.90, N 19.47.

Table 6. Crystal data for compounds **4** • 3.5 $CHCl_3$, **5** • 3.5 $CHCl_3$, **6** • 3 THF, and **6** • 1.67 dioxane

Compound	**4** • 3.5 $CHCl_3$ [a]	**5** • 3.5 $CHCl_3$ [a]	**6** • 3 THF [a]	**6** • 1.67 dioxane
Empirical formula	$C_{45.5}H_{35.5}B_2Cl_{10.5}FeN_{12}$	$C_{45.5}H_{35.5}B_2Cl_{10.5}CoN_{12}$	$C_{54}H_{56}B_2N_{12}NiO_3$	$C_{48.67}H_{45.36}B_2N_{12}NiO_{3.33}$
M [g mol^{-1}]	1200.05	1203.13	1001.44	931.97
Crystal size [mm]	0.34×0.28×0.26	0.52×0.18×0.15	0.23×0.18×0.12	0.38×0.26×0.24
Crystal description	irregular	irregular	prismatic	irregular
Crystal color	red	yellow	pink	pink
T [K]	173(2)	173(2)	163(2)	173(2)
Diffractometer	Bruker AXS CCD	Bruker AXS CCD	Enraf-Nonius CAD4	Bruker AXS CCD
Scan type, 2Θ range	ω, 3.0−52°	ω, 3.0−52	ω−2Θ, 2.9−45	ω, 2.7−52°
h; *k*; *l* range	−28, 29; −24, 24; −27, 21	−28, 25; −24, 24; −28, 28	−1, 15; −16, 17; −12, 12	−37, 36; −37, 37; −16, 9
Crystal system	monoclinic	monoclinic	triclinic	trigonal
Space group	*C*2/*c*	*C*2/*c*	*P*−1	*R*−3
a [Å]	23.5337(6)	23.2237(2)	14.187(4)	30.2345(2)
b [Å]	19.7564(5)	19.9395(3)	15.989(4)	30.2345(2)
c [Å]	22.6844(6)	23.0847(4)	11.981(4)	13.2816(2)
α [°]	90	90	109.48(4)	90
β [°]	100.7230(10)	101.0840(10)	91.36(4)	90
γ [°]	90	90	77.98(4)	120
V [Å^3]	10362.71(5)	10490.4(3)	2503.0(13)	10514.45(19)
Z	8	8	2	9
$D_{calcd.}$ [g cm^{-3}]	1.538	1.524	1.297	1.317
F(000) [electrons]	4856	4864	1052	4374
μ [mm^{-1}]	0.88	0.909	0.444	0.472
Absorption correction	SADABS	SADABS	none	SADABS
min/max transmission	0.1817/0.4537	0.5612/0.8855		0.6040/1.0000
Measured reflections	33749	35010	6883	23784
Unique reflect. for refinemt (R_{int})	10149 (0.284)	10297(0.132)	6490(0.1485)	4600 (0.1299)
Observed reflections [$I > 2\sigma(I)$]	3563	5502	2176	2799
Parameters refined	649	649	652	303
max/min Δρ≅[b][e Å^{-3}]	1.113/−0.957	1.346/−1.018	0.436/−0.571	1.105/−0.492
*R*1/*wR2*[c][$I > 2\sigma(I)$]	0.0979/0.1725	0.0842/0.1631	0.1040/0.2339	0.0699/0.1526
*R*1/*wR2*[b] (all reflections)	0.2622/0.2191	0.1702/0.2014	0.2998/0.3323	0.1331/0.1853
GOF on F^2 [c]	1.006	1.005	0.953	1.027
Weighting scheme *w*; *a*/*b*[d]	0.0465/0.0000	0.0661/60.1354	0.1550/1.9761	0.0761/39.6694

[a] Two independent molecules in the unit cell. − [b] Largest difference peak and hole. − [c] $R1 = (\Sigma||F_o| - |F_c||)/\Sigma|F_o|$; $wR2 = \{\Sigma[w(F_o^2 - F_c^2)^2]/\Sigma[w(F_o^2)^2]\}^{1/2}$ − [d] Goodness-of-fit, Gof = $\{\Sigma[w(F_o^2 - F_c^2)^2]/(n - p)\}^{1/2}$; $w = 1/[\sigma^2(F_o^2) + (a \cdot P)^2 + b \cdot P]$ where $P = [\max(F_o^2 \text{ or } 0) + 2 \cdot F_c^2]/3$.

[Zn{HB(C$_7$H$_5$N$_2$)$_3$}$_2$] (8): Starting material Zn(O$_2$CCH$_3$)$_2$ • 2 H$_2$O. White, needle-shaped crystals from dioxane/petroleum ether (diffusion method). Yield 280 mg, 71%. M.p. > 300 °C − ^{1}H NMR ([D$_6$]DMSO): δ = 7.09 (t, 1 H, *J* = 7.4 Hz, 5-H), 7.52 (t, 1 H, *J* = 7.6 Hz, 6-H), 7.63 (d, 1 H, *J* = 8.0 Hz, 7-H), 7.79 (s, 1 H, 3-H), 8.30 (d, 1 H, *J* = 8.5 Hz, 4-H); ([D$_8$]THF): δ = 7.05 (td, 1 H, *J* = 7.6, 0.8 Hz, 6-H), 7.45 (td, 1 H, *J* = 7.7, 1.1 Hz, 5-H), 7.56 (dt, 1 H, *J* = 8.1, 0.9 Hz, 7-H), 7.78 (d, 1 H, *J* = 0.9 Hz, 3-H), 8.25 (dd, 1 H, *J* = 8.7, 0.9 Hz, 4-H4). − ^{13}C NMR ([D$_8$]THF): δ = 112.9 (C-7), 121.3 (C-6), 121.8 (C-5), 123.9 (C-4), 127.7(C-3a), 134.7 (C-3), 144.6 (C-7a). − MS (441 °C); *m*/*z* (%): 790 (9) [*M*]$^+$, 673 (100) [*M* − C$_7$H$_5$N$_2$]$^+$, 555 (10) [*M* − 2 (C$_7$H$_5$N$_2$) − H]$^+$, 544 (9) [*M* − 2 (C$_7$H$_5$N$_2$) − BH]$^+$, 427 (34) [*M* − {HB(C$_7$H$_5$N$_2$)$_3$} = Zn{HB(C$_7$H$_5$N$_2$)$_3$}]$^+$, 336.5 (5) [*M* − C$_7$H$_5$N$_2$]$^{2+}$, 309 (73) [Zn{HB(C$_7$H$_5$N$_2$)$_2$}]$^+$, 278 (84) [*M* − 2 (C$_7$H$_5$N$_2$)]$^{2+}$, 118 (33) [C$_7$H$_6$N$_2$]$^+$. − IR (KBr): $\tilde{\nu}$ = 3084 cm^{-1} w, 3066 w, 3033 w (νCH), 2487 w, 2470 m (νBH), 1938 w, 1903 w, 1621 s (νCN), 1504 s, 1461 s, 1426 m, 1406 s, 1378 m, 1357 m, 1345 s, 1320 w, 1261 s, 1212 m, 1156 s, 1145 s, 1137 s, 1113 s, 1038 m, 1014 s, 995 s, 937 w, 912 m, 908 m, 842 w, 824 s, 816 s, 776 w, 755 s, 739 s, 733 s, 730 s, 686 w, 661 s, 641 w, 597 s, 568 w, 554 w, 431 m. − C$_{42}$H$_{32}$B$_2$N$_{12}$Zn (791.8): calcd. C 63.71, H 4.07, N 21.23; found C 63.48, H 3.15, N 21.01.

Electrochemical Measurements: All electrochemical experiments were carried out in specially constructed cells containing an internal drying column with highly activated alumina. The working electrode was a Pt disk sealed in soft glass (1.00 mm diameter). A Pt wire, wrapped around the glass of the working electrode, was used as the counter electrode. The reference electrode was an Ag wire on which AgCl had been deposited electrolytically. Potentials were calibrated with ferrocene (+0.352 V vs. Ag/AgCl). The measurements were performed with a Jaissle Potentiostat IMP 88 and a PAR 175 programmer.

Mössbauer Spectroscopy: ^{57}Fe-Mössbauer spectra were measured in constant acceleration modus with a triangular velocity profile [accelerator, control unit and multichannel analyzer (1024 data channels) from WISSEL]. The ^{57}Co source in an Rh matrix (AMERSHAM) had an activity of about 115 MBq. The Mössbauer transition at 14.41 keV was used for the γ-radiation. The transmission of the γ-radiation was detected by means of an NaI (Tl) scintillation counter as the detector coupled with a secondary electron multiplier (HARSHAW/ELSCINT); amplifier and energy discriminator from INTERTECHNIQUE. The experimental spectra were iteratively approximated in a least-squares fit with Lorentz functions in the thin absorber approximation (program package NORMOS).[53] Singlets were fitted with a single Lorentz curve, doublets with a symmetric or asymmetric superposition of two Lorentz functions. The spectral parameters ($\delta^{\alpha-Fe}$, Γ/2, and possibly ΔE_Q) could each be fixed or correlated in groups in the case of a multi-line fit. Fits were aimed for with largely open parameters. The $\delta^{\alpha-Fe}$ scale of the isomer shift is related to the shift of α-iron as origin of the ordinate ($\delta^{\alpha-Fe}$ = 0.11 ± 0.01 mm/s + $\delta^{Fe/Rh}$). The iron contamination in the beam, especially in the beryllium windows of the detector was taken into account with two fixed

Table 7. Crystal data for compounds **7** • 1.33 CHCl$_3$, **7** • 2.5 THF, and **8** • 1.67 dioxane

Compound	**7** • 1.33 CHCl$_3$[a]	**7** • 2.5 THF	**8** • 1.67 dioxane
Empirical formula	C$_{43.33}$H$_{33.33}$B$_2$Cl$_4$CuN$_{12}$	C$_{52}$H$_{52}$B$_2$CuN$_{12}$O$_{2.5}$	C$_{48.67}$H$_{45.36}$B$_2$N$_{12}$O$_{3.33}$Zn
M [g mol^{-1}]	949.11	970.22	938.66
Crystal size [mm]	0.40×0.38×0.18	0.5×0.4×0.2	0.32×0.32×0.21
Crystal description	irregular	prism	plate
Crystal color	dark green	dark green	colorless
T [K]	173(2)	163(2)	180(2)
Diffractometer	Bruker AXS CCD	Enraf-Nonius CAD4	Bruker AXS CCD
Scan type, 2Θ range	ω, 2.9−54	ω-2Θ, 3.4−55°	ω, 2.7−46.5°
h; *k*; *l* range	−16, 16; −15, 19 −18, 23	0, 21; 0, 21; 0, 21	−33, 33; −33, 33; −14, 14
Crystal system	triclinic	tetragonal	trigonal
Space group	*P*−1	*P*4$_2$/*n*	*R*−3
a [Å]	13.2637(3)	16.779(5)	30.3636(8)
b [Å]	15.0498(3)	16.779(5)	30.3636(8)
c [Å]	18.5660(4)	16.538(5)	13.1960(5)
α [°]	68.6800(10)	90	90
β [°]	72.8510(10)	90	90
γ [°]	88.4900(10)	90	120
V [Å^3]	3285.32(12)	4656(2)	10536.1(6)
Z	3	4	9
$D_{calcd.}$ [g cm^{-3}]	1.439	1.355	1.312
F(000) [electrons]	1453	2028	4392
μ [mm^{-1}]	0.791	0.526	0.581
Absorption correction	SADABS	none	none
min/max transmission	0.4307/0.5035		
Measured reflections	24328	5704	24730
Unique reflect. for refinemt (R_{int})	14170 (0.0578)	5346 (0.0569)	3373 (0.0636)
Observed reflection [$I > 2\sigma(I)$]	8615	2871	2601
Parameters refined	847	341	273
max/min Δρ≅[b][e Å^{-3}]	0.532/−0.630	0.696/−0.742	0.891/−0.356
*R*1/*wR*2[c][$I > 2\sigma(I)$]	0.0489/0.961	0.0662/0.1861	0.0465/0.1276
*R*1/*wR*2[b] (all reflections)	0.1004/0.1119	0.1463/0.2217	0.0631/0.1388
GOF on F^2 [c]	1.006	1.033	1.033
Weighting scheme *w*; *a*/*b*[d]	0.0256/0.0000	0.1288/0.0000	0.0819/20.9372

[a] Two independent molecules in the unit cell. − [b] Largest difference peak and hole. − [c] $R1 = (\Sigma||F_o| - |F_c||)/\Sigma|F_o|$; $wR2 = \{\Sigma[w(F_o^2 - F_c^2)^2]/\Sigma[w(F_o^2)^2]\}^{1/2}$ − [d] Goodness-of-fit, Gof = $\{\Sigma [w(F_o^2 - F_c^2)^2]/(n - p)\}^{1/2}$; $w = 1/[\sigma^2(F_o^2) + (a•P)^2 + b•P]$ where $P = [\max(F_o^2 \text{ or } 0) + 2•F_c^2]/3$.

base lines. The sample was heated under vacuum to collect the high-temperature spectra.

X-ray Structure Determinations: Data were collected with Mo-K_α radiation (λ = 0.71073 Å) and the use of a graphite monochromator. Structure solution was performed by direct methods; refinement was done by full-matrix least squares on F^2 using the SHELXTL program package (Version 5.1, Bruker AXS). All non-hydrogen positions were found and refined. The atoms were refined with anisotropic temperature factors except for the disordered dioxane solvent molecules in **6** • 1.67 dioxane and **8** • 1.67 dioxane and part of the THF solvent in **7** • 3 THF. The hydrogen atoms on the indazolyl rings and on the boron atom were placed at calculated positions, using appropriate riding models and an isotropic temperature factor of B_{eq} = 0.08 [for **8** • 1.67 dioxane B_{eq}(H) = 1.2 B_{eq}(C)]. For **6** • 1.67 dioxane and **8** • 1.67 dioxane the hydrogen position on the boron atom was found and refined. For the THF and dioxane solvent molecules no hydrogen atom positions were calculated or only on less disordered moieties. Crystal data are listed in Table 6 and 7. Graphics were computed with ORTEP3 for Windows.[54] Special computations for the crystal structure discussions were carried out with PLATON for Windows.[55] Crystallographic data (excluding structure factors) for the structures reported in this paper have been deposited with the Cambridge Crystallographic Data Center as supplementary publication No. CCDC-136881 (**4** • 3.5 $CHCl_3$), -136882 (**5** • 3.5 $CHCl_3$), -136883 (**6** • 3 THF), -136884 (**6** • 1.67 dioxane), -136885 (**7** • 1.33 $CHCl_3$), -136886 (**7** • 3 THF), -136887 (**8** • 1.67 dioxane). Copies of the data can be obtained free of charge on application to CCDC, 12 Union Road, Cambridge CB2 1EZ, UK [Fax: int. code + 44-1223/336-033; E-mail: deposit@ccdc.cam.ac.uk]. A full listing of the intermolecular C−H•••π contacts [C−H•••C < 3.1 Å, C−H•••centroid < 3.4 Å (distances and angles)] and of the ring-centroid−ring-centroid contacts (< 6.0 Å) can be found in the supporting information.

Acknowledgments

This work is supported by the Deutsche Forschungsgemeinschaft (grant Ja466/4-2, 4-3 and grant Ja466/10-1), the Fonds der Chemischen Industrie, and the Graduiertenkolleg "Unpaired Electrons" at the University of Freiburg.

[1] The abbreviation Tp^{4Bo} for hydrotris(indazol-1-yl)borate follows the suggested nomenclature by S. Trofimenko[3] to indicate the relationship to the pyrazole-derived Tp-class of ligands; "4Bo" indicates the 4,5-fusion of the benzo ring.

[2] S. Trofimenko, *J. Am. Chem. Soc.* **1967**, *89*, 3170−3177.

[3] Reviews: S. Trofimenko, *Scorpionates−Polypyrazolylborate Ligands and Their Coordination Chemistry*, Imperial College Press, **1999**. S. Trofimenko, *Chem. Rev.* **1993**, *93*, 943−980. P. K. Byers, A. J. Canty, R. T. Honeyman, *Adv. Organomet. Chem.* **1992**, *34*, 1−65. N. Kitajima, W. B. Tolman, *Prog. Inorg. Chem.* **1995**, *43*, 419. G. Parkin, *Adv. Inorg. Chem.* **1995**, *42*, 291−393. D. L. Reger, *Coord. Chem. Rev.* **1996**, *147*, 571−595. M. Etienne, *Coord. Chem. Rev.* **1997**, *156*, 201−236. C. Janiak, *Main Group Met. Chem.* **1998**, *21*, 33−49.

[4] Recent examples of inorganic Tp−metal complexes: Y. Takahashi, S. Hikichi, M. Akita, Y. Moro-oka, *Chem. Commun.* **1999**, 1491−1492. C. Janiak, L. Braun, F. Girgsdies, *J. Chem. Soc., Dalton Trans.* **1999**, 3133−3136. J. L. Kisko, T. Hascall, C. Kimblin, G. Parkin, *J. Chem. Soc., Dalton Trans.* **1999**, 1929−1935. R. L. Paul, A. J. Amoroso, P. L. Jones, S. M. Couchman, Z. R. Reeves, L. H. Rees, J. C. Jeffery, J. A. McCleverty, M. D. Ward, *J. Chem. Soc., Dalton Trans.* **1999**, 1563−1568. F. Malbosc, P. Kalck, J.-C. Daran, M. Etienne, *J. Chem. Soc., Dalton Trans.* **1999**, 271−272. C. Santini, G. G. Lobbia, C. Pettinari, M. Pellei, G. Valle, S. Calogero, *Inorg. Chem.* **1998**, *37*, 890−900. J. S. Fleming, E. Psillakis, S. M. Couchman, J. C. Jeffrey, J. A. McCleverty, M. D. Ward, *J. Chem. Soc., Dalton Trans.* **1998**, 537−543. M. H. W. Lam, Y.-Y. Tang, K.-M. Fung, X.-Z. You, W.-T. Wong, *Chem. Commun.* **1997**, 957−958. C. Janiak, S. Temizdemir, T. G. Scharmann, *Z. Anorg. Allg. Chem.* **1998**, *624*, 755−756.

[5] Recent examples of bioinorganic Tp−metal complexes: M. A. Halcrow, L. M. L. Chia, X. Liu, E. J. L. McInnes, L. J. Yellowless, F. E. Mabbs, I. J. Scowen, M. McPartlin, J. E. Davies, *J. Chem. Soc., Dalton Trans.* **1999**, 1753−1762. H. Komatsuzaki, Y. Nagasu, K. Suzuki, T. Shibasaki, M. Satoh, F. Ebina, S. Hikichi, M. Akita, Y. Moro-oka, *J. Chem. Soc., Dalton Trans.* **1998**, 511−512.

[6] C. Janiak, T. G. Scharmann, W. Günther, W. Hinrichs, D. Lentz, *Chem. Ber.* **1996**, *129*, 991−995. C. Janiak, T. G. Scharmann, P. Albrecht, F. Marlow, R. MacDonald, *J. Am. Chem. Soc.* **1996**, *118*, 6307−6308. C. Janiak, T. G. Scharmann, W. Günther, F. Girgsdies, H. Hemling, D. Lentz, *Chem. Eur. J.* **1995**, *1*, 637−644.

[7] C. Janiak, T. G. Scharmann, H. Hemling, D. Lentz, J. Pickardt, *Chem. Ber.* **1995**, *128*, 235−244.

[8] C. Janiak, T. G. Scharmann, J. C. Green, R. P. G. Parkin, M. J. Kolm, E. Riedel, W. Mickler, J. Elguero, R. M. Claramunt, D. Sanz, *Chem. Eur. J.* **1996**, *2*, 992−1000.

[9] C. Janiak, T. G. Scharmann, T. Bräuniger, J. Holubová, M. Nádvorník, *Z. Anorg. Allg. Chem.* **1998**, *624*, 769−774.

[10] C. Janiak, T. G. Scharmann, K.-W. Brzezinka, P. Reich, *Chem. Ber.* **1995**, *128*, 323−327. C. Janiak, L. Esser, *Z. Naturforsch.* **1993**, *48B*, 394−396.

[11] H. V. R. Dias, W. Jin, *Inorg. Chem.* **1996**, *35*, 3687−3694. H. V. R. Dias, W. Jin, H.-J. Kim, H.-L. Lu, *Inorg. Chem.* **1996**, *35*, 2317−2328.

[12] A. L. Rheingold, G. Yap, S. Trofimenko, *Inorg. Chem.* **1995**, *34*, 759−760.

[13] A. L. Rheingold, B. S. Haggerty, G. P. A. Yap, S. Trofimenko, *Inorg. Chem.* **1997**, *36*, 5097−5103.

[14] A. L. Rheingold, L. M. Liable-Sands, G. P. A. Yap, S. Trofimenko, *Chem. Commun.* **1996**, 1233−1234.

[15] A. L. Rheingold, B. S. Haggerty, S. Trofimenko, *Chem. Commun.* **1994**, 1973−1974.

[16] F. J. Lalor, S. M. Miller, N. Garvey, *Polyhedron* **1990**, *9*, 63−68.

[17] K. S. Siddiqi, M. A. Neyazi, S. A. A. Zaidi, *Synth. React. Inorg. Met.-Org. Chem.* **1981**, *11*, 253−265. S. A. A. Zaidi, M. A. Neyazi, *Trans. Met. Chem.* **1979**, *4*, 164−167.

[18] C. Janiak, *Chem. Ber.* **1994**, *127*, 1379−1385.

[19] J. P. Jesson, S. Trofimenko, D. R. Eaton, *J. Am. Chem. Soc.* **1967**, *89*, 3158−3164.

[20] J. P. Jesson, S. Trofimenko, D. R. Eaton, *J. Am. Chem. Soc.* **1967**, *89*, 3148−3158.

[21] J. P. Jesson, *J. Chem. Phys.* **1966**, *45*, 1049−1056.

[22] A. Fruchier, E. Alcalde, J. Elguero, *Org. Magn. Res.* **1977**, *9*, 235−236. J. Elguero, A. Fruchier, M. C. Pardo, *Can. J. Chem.* **1976**, *54*, 1329−1330.

[23] C. K. Jørgensen, *Modern Aspects of Ligand Field Theory*, Elsevier, New York, **1971**, chapter 26.

[24] Reviews: P. Gütlich, A. Hauser, H. Spiering, *Angew. Chem.* **1994**, *106*, 2109−2141; *Angew. Chem. Int. Ed. Engl.* **1994**, *33*, 2024−2054. O. Kahn, Molecular Magnetism, VCH, Weinheim, **1993**, chapter 4, p. 53ff. J. Zarembowitch, *New. J. Chem.* **1992**, *16*, 255−267. P. Gütlich, A. Hauser, *Coord. Chem. Rev.* **1990**, *97*, 1−22. H. Toftlund, *Coord. Chem. Rev.* **1989**, *94*, 67−108. E. König, *Progr. Inorg. Chem.* **1987**, *35*, 527−622. P. Gütlich, *Struct. Bonding (Berlin)* **1981**, *44*, 83−195. H. A. Goodwin, *Coord. Chem. Rev.* **1976**, *18*, 293−325.

[25] S. Zamponi, G. Gambini, P. Conti, G. G. Lobbia, R. Marassi, M. Berrettoni, B. Cecchi, *Polyhedron* **1995**, *14*, 1929−1935. T. Buchen, P. Gütlich, *Inorg. Chim. Acta* **1995**, *231*, 221−223. J.-P. Martin, J. Zarembowitch, A. Dworkin, J. G. Haasnoot, E. Codjovi, *Inorg. Chem.* **1994**, *33*, 2617−2623.

[26] F. Grandjean, G. J. Long, B. B. Hutchinson, L. Ohlhausen, P. Neill, J. D. Holcomb, *Inorg. Chem.* **1989**, *28*, 4406−4414.

[27] S. Calogero, G. G. Lobbia, P. Cecchi, G. Valle, J. Friedl, *Polyhedron* **1994**, *13*, 87−97.

[28] Y. Sohrin, H. Kokusen, M. Matsui, *Inorg. Chem.* **1995**, *34*, 3928−3934.

[29] G. J. Long, B. B. Hutchinson, *Inorg. Chem.* **1987**, *26*, 608−613.

A. Gulino, E. Ciliberto, S. Di Bella, I. Fragalà, *Inorg. Chem.* **1993**, *32*, 3759−3761. B. Hutchinson, L. Daniels, E. Henderson, P. Neill, G. J. Long, L. W. Becker, *J. Chem. Soc., Chem. Commun.* **1979**, 1003−1004. J. P. Jesson, J. F. Weiher, S. Trofimenko, *J. Chem. Phys.* **1968**, *48*, 2058−2066. J. P. Jesson, J. F. Weiher, *J. Chem. Phys.* **1967**, *46*, 1995−1996.

[30] Tp_2Fe: J D. Oliver, D. F. Mullica, B. B. Hutchinson, W. O. Milligan, *Inorg. Chem.* **1980**, *19*, 165−169.

[31] Tp_2Co: M. R. Churchill, K. Gold, C. E. Maw, Jr., *Inorg. Chem.* **1970**, *9*, 1597−1605.

[32] Tp_2Cu: A. Murphy, B. J. Hathaway, T. J. King, *J. Chem. Soc., Dalton Trans.* **1979**, 1646−1650.

[33] Tp_2Zn: K. Nakata, S. Kawabata, K. Ichikawa, *Acta Crystallogr.* **1995**, *C51*, 1092−1094.

[34] Tp'_2Fe and Tp'_2Co: C. Janiak, *Chem. Commun.* **1994**, 545−547

[35] Tp'_2Zn: C. Janiak, H. Hemling, *J. Chem. Soc., Dalton Trans.* **1994**, 2947−2952.

[36] A. G. Orpen, L. Brammer, F. H. Allen, O. Kennard, D. G. Watson, R. Taylor, *J. Chem. Soc., Dalton Trans.* **1989**, S1-S83.

[37] C. Janiak, *Moderne Anorganische Chemie* (Ed.: E. Riedel), de Gruyter, Berlin **1999**, p. 204. J. E. Huheey, E. A. Keiter, R. L. Keiter, *Inorganic Chemistry*, HarperCollins **1993**, p. 408ff.

[38] Selected recent examples: C. Janiak, S. Deblon, H.-P. Wu, M. J. Kolm, P. Klüfers, H. Piotrowski, P. Mayer, *Eur. J. Inorg. Chem.* **1999**, 1507−1521. M. P. Lightfoot, F. S. Mair, R. G. Pritchard, J. E. Warren, *Chem. Commun.* **1999**, 1945−1946. C. Bonnefous, N. Bellec, R. P. Thummel, *Chem. Commun.* **1999**, 1243−1244. S. Noro, M. Kondo, T. Ishii, S. Kitagawa, H. Matsuzaka, *J. Chem. Soc., Dalton Trans.* **1999**, 1569−1574. A. Bernardo, F. Pina, B. Escuder, E. Garcia-España, L. Godino-Salido, J. Latorre, S. V. Luis, J. A. Ramirez, C. Soriano, *J. Chem. Soc., Dalton Trans.* **1999**, 915−921. H.-P. Wu, C. Janiak, L. Uehlin, P. Klüfers, P. Mayer, *Chem. Commun.* **1998**, 2637−2638. E. Ishow, A. Gourdon, J.-P. Launay, *Chem. Commun.* **1998**, 1909−1910. N. Yoshida, H. Oshio, T. Ito, *Chem. Commun.* **1998**, 63−64.

[39] D. B. Amabilino, J. F. Stoddart, *Chem. Rev.* **1995**, *95*, 2725−2828. T. Dahl, *Acta Chem. Scand.* **1994**, *48*, 95−106.

[40] C. A. Hunter, *Chem. Soc. Rev.* **1994**, 101−109. C. A. Hunter, J. K. M. Sanders, *J. Am. Chem. Soc.* **1990**, *112*, 5525−5534.

[41] R. L. Jaffe, G. D. Smith, *J. Chem. Phys.* **1996**, *105*, 2780−2788.

[42] P. Hobza, H. L. Selzle, E. W. Schlag, *Chem. Rev.* **1994**, *94*, 1767−1785.

[43] F. Cozzi, J. S. Siegel, *Pure Appl. Chem.* **1995**, *67*, 683−689.

[44] E. G. Cox, D. W. Cruickshank, J. A. S. Smith, *Proc. R. Soc. London, Ser. A* **1958**, *247*, 1−20

[45] N. N. L. Madhavi, A. K. Katz, H. L. Carrell, A. Nangia, G. R. Desiraju, *Chem. Commun.* **1997**, 1953−1954. H.-C. Weiss, D. Bläser, R. Boese, B. M. Doughan, M. M. Haley, *Chem. Commun.* **1997**, 1703−1704. T. Steiner, M. Tamm, B. Lutz, J. van der Maas, *Chem. Commun.* **1996**, 1127−1128. P. L. Anelli, P. R. Ashton, R. Ballardini, V. Balzani, M. Delgado, M. T. Gandolfi, T. T. Goodnow, A. E. Kaifer, D. Philp, M. Pietraszkiewicz, L. Prodi, M. V. Reddington, A. M. Z. Slawin, N. Spencer, J. F. Stoddart, C. Vicent, D. J. Williams, *J. Am. Chem. Soc.* **1992**, *114*, 193−218.

[46] Other recent examples of supramolecular design involving C−H•••π interactions: B. J. McNelis, L. C. Nathan, C. J. Clark, *J. Chem. Soc., Dalton Trans.* **1999**, 1831−1834. K. Biradha, C. Seward, M. J. Zaworotko, *Angew. Chem. Int. Ed.* **1999**, *38*, 492−495.

[47] H.-P. Wu, C. Janiak, G. Rheinwald, H. Lang, *J. Chem. Soc., Dalton Trans.* **1999**, 183−190.

[48] G. Baum, E. C. Constable, D. Fenske, C. E. Housecroft, T. Kulke, *Chem. Commun.* **1998**, 2659−2660.

[49] C. Janiak, *Chem. Ber.* **1993**, *126*, 1603−1607.

[50] R. Pinalli, F. F. Nachtigall, F. Ugozzoli, E. Dalcanale, *Angew. Chem. Int. Ed.* **1999**, *38*, 2377−2380.

[51] S. Trofimenko, *Inorg. Synth.* **1970**, *12*, 99−106.

[52] R. K. Harris, *Nuclear Magnetic Resonance Spectroscopy*, Pitman, London, **1983**, chapters 5−14, pp. 138−141.

[53] R. A. Brand, University of Duisburg, Dept. of Applied Physics, **1992** (Distribution through WISSEL, Starnberg, Germany).

[54] M. N. Burnett, C. K. Johnson, *ORTEP-III*: Oak Ridge Thermal Ellipsoid Plot Program for Crystal Structure Illustrations, Oak Ridge National Laboratory Report ORNL-6895, **1996**. L. J. Farrugia, *ORTEP3 for Windows*, version 1.0.1β, University of Glasgow, Scotland, **1997**.

[55] A. L. Spek, *Acta Crystallogr.* **1990**, *A46*, C34; *PLATON* Version 29−11−98. Windows implementation: L. J. Farrugia, University of Glasgow, Scotland, **1998**.

Received November 29, 1999
[I99436]

Interplay between Metal Aminoalkoxides and β-Diketonates: Volatile Mixed-Metal Pr−Cu and Y−Cu Species without Fluorinated Ligands − Molecular Structures of $[PrCu(\eta^2\text{-thd})_3(\mu,\eta^2\text{-}OC_2H_4NMe_2)_2]$ and of $[Y_2(\eta^2\text{-thd})_4\{\mu,\eta^2\text{-}OCH(CH_2NMe_2)_2\}_2]$

Hervé Guillon,[a] Liliane G. Hubert-Pfalzgraf,*[a] and Jacqueline Vaissermann[b]

Keywords: Chemical vapor deposition / Copper / Lanthanides / β-Diketonates / Heterometallic species / Barium

The reactions between copper or lanthanide (Y, Pr) 2,2,6,6-tetramethylheptane-3,5-dionates and copper or barium aminoalkoxides were investigated in hexane. Aminoalkoxide ligands of different constraints and/or flexibility namely 2,4,6-tris(dimethylaminomethyl)phenoxide (Otamp), 2-dimethylaminoethoxide $OC_2H_4NMe_2$, 2-dimethylamino-2-propoxide $OCH(Me)CH_2NMe_2$, and 1,3-bis(dimethylamino)-2-propanol $OCH(CH_2NMe_2)_2$ were selected. Mixed-metal BaCu, PrCu, $PrCu_2$, and YCu species, as well as β-diketonatoalkoxides of barium and yttrium were isolated and characterised by analytical data, FT-IR, ^1H NMR, and ESR spectroscopy. Their thermal behaviour was investigated by TGA. The tridentate aminoalkoxide $OCH(CH_2NMe_2)_2$ was found to destabilise mixed-metal species with tetramethylheptanedionate as ancillary ligands. $[BaCu(\eta^2\text{-thd})_2(\mu,\eta^3\text{-Otamp})(\mu,\eta^{2-}\text{Otamp})(H_2O)]$, $[PrCu(\eta^2\text{-thd})_3(\mu,\eta^2\text{-}OC_2H_4NMe_2)_2]$, and $[Y_2(\eta^2\text{-thd})_4\{\mu,\eta^2\text{-}OCH(CH_2NMe_2)_2\}_2]$ were also characterised by single crystal X-ray diffraction. The latter two were volatile, whereas the volatility of the former was reduced by intramolecular hydrogen bonding. The assembling aminoalkoxide ligands ensure high coordination numbers for the heavy metals, namely seven for barium and yttrium, eight for praseodymium. The formation of the mixed-metal species improves stability toward ambient atmosphere, especially for the systems involving copper aminoalkoxides. The $[Ba(thd)\{OCH(CH_2NMe_2)_2\}_2\{OHCH(CH_2NMe_2)_2\}_2]$ species distils at 130 °C/10^{-3} Torr.

Introduction

The exploitation of the properties of anisotropic ceramics such as high T_c superconductors requires the elaboration of textured or epitaxial layers.[1] Although epitaxial layers might be obtained by sol-gel processing, this goal is more easily achieved by MOCVD techniques.[2] However, this requires appropriate precursors, namely volatile molecules which can be decomposed into the oxide within a comparable temperature range, and that are reasonably stable thermally in the container for reuse.[3] β-Diketonates are the most commonly used precursors, especially the tetramethylheptanedionate β-diketonates.[4] Besides the problems related to the use of solids as precursors, volatility and stability properties remain unsatisfactory in the case of barium, despite a large body of synthetic efforts.[5] Various liquid-source MOCVD delivery techniques that assist the transport of the precursor to the substrate and allow for maintaining the precursors at room temperature have been considered as ways to overcome the drawbacks.[6] Solubility of the precursors becomes a crucial issue for high growth rates since a solvent is an undesired ballast in a CVD process. The use of heterometallic species is an approach which reduces the number of precursors, and might improve solubility.[7] If these species are volatile, a reduction of the temperature of pyrolysis can sometimes be achieved. A large number of Ba−Cu,[8,9] Y(Ln)−Cu,[10] and a few Y−Ba[11] species of different stoichiometries have been reported. Only a few of them are volatile, they are supported by fluorinated ligands, mainly alkoxides, as assembling ligands. High Lewis acidity resulting in facile hydration or solvation and thus change in the physical properties, as well as fluoride residues in the deposits are the most common drawbacks. Aminoalkoxide ligands are often more favourable for increasing volatility than alkoxyalkoxides.[12] Schiff bases have been used recently as an alternate assembling ligand, and species such as $[M(salen)Ln(hfac)_3]$ [M = Ni, Cu; Ln = Y, Gd; H_2salen = *N*,*N*′-ethylenebis(salicylideneimine)] have been reported.[13]

We report here our investigations of the interactions between metal aminoalkoxides and tetramethylheptanedionate derivatives related to the formulation of high T_c superconductors. These were aimed at the building of mixed-metal species as well as obtaining insight into the compositions of solutions using precursors of different types.[6] The OR-type ligands, namely 2,4,6-tris(dimethylaminomethyl)-phenoxide (Otamp), 2-dimethylaminoethoxide $OR^n = OC_2H_4NMe_2$, 2-dimethylamino-2-propoxide $OR^N = OCH(Me)CH_2NMe_2$, and 1,3-bis(dimethylamino)-2-propoxide $OR'^N = OCH(CH_2NMe_2)_2$, were selected in order to cover different constraints and/or flexibility. Mixed-metal species namely $[BaCu(thd)_2(Otamp)_2(H_2O)]$, $[MCu(thd)_3(OR)_2]$

[a] Université Claude Bernard-Lyon I, IRC,
2 avenue A. Einstein, 69626 Villeurbanne Cedex, France
E-mail: hubert@univ-lyon1.fr
[b] Laboratoire de Chimie des Métaux de Transition
UMR-CNRS,
4 Place Jussieu, 75230 Paris Cedex 05, France

 © WILEY-VCH Verlag GmbH, D-69451 Weinheim, 2000 1434−1948/00/0606−1243 $ 17.50+.50/0

(M = Y, Pr, R = R^n, R'^N) and $[MCu_2(thd)_3(OR^n)_4]$ could be stabilised. By contrast, the trifunctional aminoalkoxide ligand $OCH(CH_2NMe_2)_2$ favoured the formation of volatile homometallic Y and Ba β-diketonatoalkoxides. The various species were characterised by elemental analyses, FT-IR, NMR, ESR, and TGA, and in the case of $[BaCu(\eta^2\text{-}thd)_2(\mu\text{-}Otamp)_2(H_2O)]$, $[PrCu(\eta^2\text{-}thd)_3(\mu,\eta^2\text{-}OR^n)_2]$, and $[Y(\mu,\eta^2\text{-}OR'^N)(\eta^2\text{-}thd)_2]_2$, by single crystal X-ray diffraction.

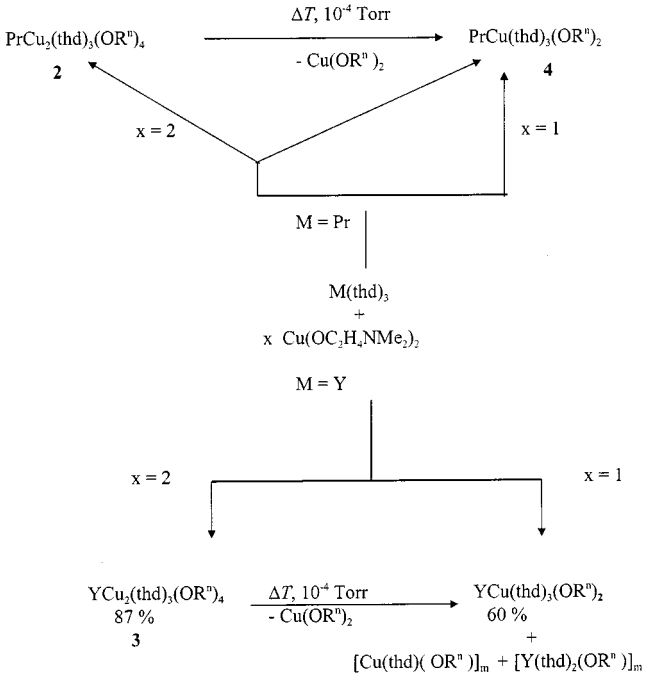
Results and Discussion

Synthesis and Characterization

Direct liquid injection MOCVD techniques are attractive for overcoming the drawbacks of the limited stability and/or volatility of solid oxide precursors such as barium derivatives.[2,6] Whereas β-diketonates are generally attractive precursors due to their commercial accessibility and easy handling, the limited solubility of the copper derivatives − as compared to the Ba and Y analogues − determines the concentration.[2c] Besides high solubility, the compounds used as sources of the metal oxide should be inert toward evolution into insoluble species during storage of the solution. This requirement is especially important for multimetallic oxides, since a unique container is generally used for convenience, and a constant stoichiometry between the different elements in solution is crucial for the composition of the multimetallic material. Previous studies have revealed the limitation encountered by mixing β-diketonates and β-oxo esters due to rapid ligand scrambling.[6−14] Copper alkoxides based on aminoalkoxide ligands are highly soluble and volatile, but quite hydrolysable.[15] The mixing of metal alkoxides and β-diketonates, namely 2,2,6,6-tetramethylheptane-3,5-dionates was expected to be more favourable despite the fact that higher susceptibility to moisture could result. The Cu−M systems (M = Y, Pr, or Ba) were investigated. Indeed, whereas yttrium is involved in the formula of superconducting YBCO materials, the praseodymium analogue is an insulator, and is thus of interest for building up heterostructures.[1]

Aryloxide-type ligands allow a great deal of control of steric hindrance, and thus solubility, volatility, and robustness toward atmosphere via the substituents in 2- and 6- positions.[12] An aryloxide with potentially chelating dimethylaminomethyl arms (Otamp) could also act as an efficient "pincer" ligand. A Ba−Cu species, $[BaCu(thd)_2(Otamp)_2(H_2O)]$ (**1**) was obtained in high yield by reaction of either Cu(thd)2 and $Ba_4O(Otamp)_6$ or $Cu(O\text{-}tamp)_2$ and $[Ba(thd)_2]_4$.

The reactions between the 2,2,6,6,-tetramethylheptane-3,5-dionates $M(thd)_3$ (M = Y or Pr) and copper 2-dimethylamino-2-propoxide $Cu(OR^N)_2$ in hexane afforded mixed-metal species $[MCu(thd)_3(OR^N)_2]$ in nearly quantitative yields by self-assembly. The same compounds were obtained using $M(thd)_2(OR^N)$, but in lower yields (ca. 60%). More complex reactions were observed with copper 2-dimethylaminoethoxide $Cu(OC_2H_4NMe_2)$. Indeed, mixed-metal β-diketonatoalkoxides of two stoichiometries, MCu and MCu_2, could be stabilised. Whereas the reaction between $Y(thd)_3$ and $Cu(OR^n)_2$ (1:2 stoichiometry) afforded only $[YCu_2(thd)_3(OR^n)_4]$ (**3**) (87% yield), for praseodymium the complexes $[PrCu_2(thd)_3(OR^n)_4]$ (**2**) and $[PrCu(thd)_3(OR^n)_2]$ (**4**) crystallised under similar conditions (35 and 45% yields, respectively). On the other hand, the yield of $[YCu(thd)_3(OR^n)_2]$, obtained by reaction of $Y(thd)_3$ and $Cu(OR^n)_2$ (1:1 stoichiometry), is reduced to ca. 60% by the formation of the homometallic species $[Cu(thd)(OR^n)]_m$ and $[Y(thd)_2(OR^n)]_m$ as by-products (established by comparison with authentic samples). The $[MCu_2(thd)_3(OR^n)_4]$ (M = Y, Pr) species are both volatile, but their sublimation (140 °C, 10^{-4} Torr) proceeds with decomposition to $[MCu(thd)_3(OR^n)_2]$ and copper aminoalkoxide. The lower stability of the MCu_2 species with respect to the MCu ones is also reflected in their sensitivity to hydrolysis and partial dissociation in solvents such as toluene. The absence of isolation of MCu_2 species in the case of the bis(2-dimethylamino-2-propoxide) ligand is probably related to its greater bulkiness. The lower stability of $[YCu(thd)_3(OR^n)_2]$ with respect to the praseodymium analogue might be due to the lower tendency of yttrium to attain octa-coordination as observed for the solid-state structure of **4** (see below) The various synthetic pathways for the aminoethoxide derivatives are summarised in Scheme 1.



Scheme 1. Synthetic routes to M−Cu (M = Y, Pr) β-diketonato-aminoethoxides ($OR'^n = OC_2H_4NMe_2$) (all reactions in hexane at room temperature)

Reactions with derivatives of the trifunctional aminoalkoxide $OR'^N = OCH(CH_2NMe_2)_2$ were also investigated. By contrast with reactions between a copper aminoalkoxide generated in situ and acetates or trifluoroacetates of alkaline-earth metals,[16] the reaction between $Y(thd)_3$ and $Ba(OR'^N)_2$, obtained in situ by alcoholysis of barium bis-

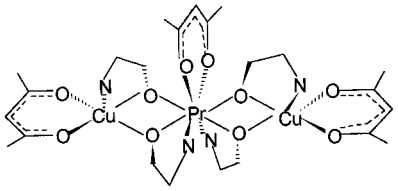
Table 1. FT-IR data (cm^{-1}) of the various compounds

Compound	υOH	δOH	υC=O, νC=C	υMO, νMN
$BaCu(thd)_2(Otamp)_2(H_2O)$	3162 m	[a]	1590 vs, 1572 vs, 1547 w, 1531 sh, 1525 vs, 1513 sh, 1511 vs, 1480 vs	598 w, 578 m, 569 m, 559 m, 525 w, 514 w, 477 m, 470 m, 456 w, 429 sh,408 m, 393 m
$PrCu_2(thd)_3(OR^n)_4$	–	–	1589 vs, 1575 vs, 1546 m 1531 s, 1502s, 1486	564 m, 502 sh, 482 m457 w, 422 w, 405 w
$PrCu(thd)_3(OR^n)_2$	–	–	1590 vs, 1554 vs, 1537 vs1515 vs, 1496 vs, 1480 m	596 m, 586 w, 510 sh, 489 sh, 473 m, 438 w, 426 w, 397 w
$YCu_2(thd)_3(OR^n)_4$	–	–	1600 sh, 1592 vs, 1577 vs, 1551 m, 1535 vs, 1530 sh, 1501 vs, 1484 vs	574 w, 507 m, 474 vs, 449 w, 430 m, 401 w
$YCu(thd)_3(OR^N)_2$	–	–	1592 vs, 1581 vs, 1572 vs, 1554 m, 1536 vs, 1505 vs, 1496 sh	570 w, 514 sh, 508 w490 m, 476 m, 442 w406 w
$PrCu(thd)_3(OR^N)_2$	–	–	1590 vs, 1578 vs, 1552 m, 1536 vs, 1504 w, 1495 vs	598 m, 509 w, 488 m,473 m, 435 w403 w
$Ba(thd)(OR'^N)(HOR'^N)$	3442 m, 3178 w	1653 w	1597 vs, 1591 vs, 1574 vs, 1531 vs, 1503 vs	588 w, 528 m, 516 w,469 m, 447 w, 400 w,387 w, 375 w
$[Y(thd)_2(OR'^N)]_2$	–	–	1594 vs, 1581 vs, 1573 vs, 1551 vs, 1538 vs, 1506 vs, 1494 vs	572 w, 527 w, 514 w, 474 m, 442 w,429 w, 408 w, 396 w

[a] Masked by the C=C and C=O absorption bands.

(trimethylsilylamide), gave no evidence of stable mixed-metal species, and $[Y(thd)_2(OR'^N)]_2$ (**8**) was isolated in nearly quantitative yields. The barium by-product, assumed to be a barium β-diketonatoalkoxide, could not be crystallised under such conditions. An adduct $[Ba(thd)(OR'^N)(R'^NOH)]$ (**7**) was however isolated by ligand exchange reactions applied to the insoluble homometallic alkoxide $Ba(OR^N)_2$. Similar observations, namely redistribution reactions, were made for the $Cu(thd)_2$–$Ba(OR'^N)_2$ system. Adduct **7** was quite air-sensitive, and attempts to make the species more robust toward ambient atmosphere by ligand exchange reactions, between the coordinated alcohol and diglyme for instance were not successful.

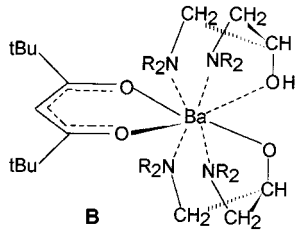
The various species were characterised by elemental analysis, FT-IR, ^{1}H-NMR, or ESR spectroscopy (Table 1). Their FT-IR spectra display strong absorption bands between 1600–1480 cm^{-1} characteristic of νC=O and νC=C vibrations of the β-diketonate ligands, other absorption bands correspond to νC–N and C–O vibrations between 1230 and 1000 cm^{-1}, and to νM–OR vibrations below 500 cm^{-1}. Compound **7** also displays absorption bands at 3178 and 3442 cm^{-1}, confirming the presence of an alcohol molecule in the metal coordination sphere. The similarity of the FT-IR spectra of the $PrCu_2$ and PrCu species suggests limited structural differences between their solid-state structures. Their FT-IR data indicate the absence of bridging thd ligands. The solid-state structure of **2** could not be solved due to disorder problems, but the cell parameters are definitely different from those of **4**. A plausible structure corresponds to **A**, in which the metal atoms are assembled by bridging alkoxide ligands where each metal centre bears a terminal η^2-thd ligand. Such a framework allows the metal atoms to reach common coordination numbers, namely eight for praseodymium and five for both copper centres. The transformation of **2** to **4** implies redistribution of one thd and OR^n ligand.



The paramagnetic praseodymium–copper and yttrium–copper species **2**, **4**, **5**, and **6** were characterised by ESR spectroscopy. The isotropic spectra at room temperature display a four line pattern centred around $<g> = 2.10$, characteristic of the coupling of the unpaired electron with copper [coupling constants A ranging from 78.6 to 92.4 G (^{63}Cu: $N = 69\%$, $I = 3/2$; ^{65}Cu: $N = 31\%$, $I = 3/2$).

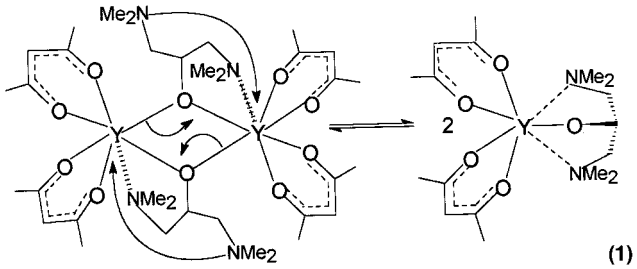
The solubility of the diamagnetic species, namely the homometallic (β-diketonato)yttrium and -barium alkoxides **7** and **8** allowed us to gain structural information by ^{1}H NMR. The poor stability of **7** under the X-ray beam at room temperature, and a destructive phase transition at lower temperature, precluded structural information in the solid state. Its molecular complexity was established by the Signer method. The value obtained in benzene accounts for a monomer. Its volatility (distillation at 130 °C/10^{-3} Torr) is in agreement with a low molecular weight, and thus a monomeric character. Its ^{1}H-NMR spectra in $CDCl_3$ are a function of the dilution, and suggest the presence of several molecular species as indicated by three resonances for the CH group of the thd ligand. The CH resonance of the aminoalkoxide at $\delta = 3.91$ is broad, suggesting fast-exchange on the NMR time scale between the aminoalkoxide and the coordinated amino alcohol molecule – each of them having the potential for different coordination modes. The signals of the CH_2NMe_2 moieties appear as a complex pattern around $\delta = 2.25$. The signal due to the OH group was found as a very broad resonance at $\delta = 5.0$. In view of the complexity of the spectra (the carbon atom in α-position

becomes asymmetric for a bidentate coordination mode) the behaviour in solution was not further investigated. Compound **7** distils as the adduct. The coordinated alcohol could not be exchanged by diglyme, dissociation of the adduct in solution is thus not very likely. Octa-coordination can be achieved for **7** when all NMe_2 donor sites are involved in interactions with the metal centre, resulting in, for instance, structure **B**. Other isomers are, however, possible, since 1,3-bis(dimethylamino)-2-propoxide can display bidentate and tridentate coordination modes and barium can quite easily adopt coordination numbers from six to eight.[4,5]



B

The ^{1}H-NMR spectra of **8** are also very complicated, and are a function of the dilution. The presence of a species in which the 1,3-bis(dimethylamino)propoxide ligand is bidentate is illustrated by the unequivalence of the protons of the CH_2 groups in α-position to the asymmetric carbon atom. The signal at $\delta = 4.21$ was attributed to an aminoalkoxide ligand displaying a symmetrical, tridentate coordination behaviour. The overall behaviour of **8** in solution can be rationalised on the basis of an equilibrium between a dimeric species **8a** (see below), having the structure found in the solid state, and a monomeric one [$Y(\eta^2\text{-thd})_2(\eta^3\text{-}OR'^N)$] (**8b**) according to Equation (1). The signals due to the thd ligands were observed at $\delta = 5.59$ and 1.05, and at $\delta = 5.67$ and 1.09 for **8a** and **8b**, respectively.



8a **8b** **(1)**

Compound **8** sublimes, although the sublimate displays small modifications in the FT-IR spectrum (with respect to **8**). Analytical and NMR data of the sublimate were identical to those of the species before sublimation. The behaviour observed in solution suggests that sublimation of **8** proceeds with partial dissociation into monomer **8b**, which might be responsible of the additional bands observed in the FT-IR at 1001, 917, 653, and 540 cm^{-1}. Yttrium is hepta-coordinated in both species **8a** and **8b**, but the Y−N coordination bonds are probably less labile in **8a** than **8b**, and this might explain the higher hydrolytic susceptibility of the compound in solution.

Molecular Structures of $[BaCu(thd)_2(Otamp)_2(H_2O)]$ and of $[PrCu(thd)_2(\mu,\eta^2\text{-}OR^n)_2]$

The structure of **1** corresponds to $[BaCu(\eta^2\text{-thd})_2(\mu,\eta^3\text{-Otamp})(\mu,\eta^2\text{-Otamp})(H_2O)]$ as depicted in Figure 1. Despite the limited number of reflections, the connectivity between the atoms could be established unambiguously. The most salient feature is the presence of a water molecule in the coordination sphere of barium. Barium and copper are clamped together by two aryloxide ligands. These display different coordination behaviours, one is bidentate (μ,η^2-), the other is tridentate (μ,η^3-). The Ba···Cu distance of 3.680(3) Å is comparable to the value reported for other Ba−Cu β-diketonatoalkoxides.[6] Barium surrounded by two NMe_2 groups (one of each Otamp ligand) and five oxygen atoms due to a chelating tetramethylheptanedionate. It is thus hepta-coordinated, with a distorted pentagonal-bipyramidal stereochemistry, the nitrogen atoms being in apical positions. Copper is five-coordinated with a tetragonal-pyramidal surrounding, and also bears a chelating tetramethylheptanedionate ligand. The Cu−O bond lengths vary from 1.89(1) to 2.11(2) Å. The longest one corresponds to Cu−O(5). The disymmetrical linkage of the thd ligand is most probably due to the elongation of the Cu−O(5) bond − with respect to the Cu−O(6) one − by Jahn−Teller effect, as commonly observed for copper.[9,17] The Ba−O distances are spread over the range 2.57(2) to 2.67(1) Å. The Ba−O(tamp) bond lengths are comparable to the values reported in the literature for aryloxides.[18] They are slightly shorter when the ligand is tridentate [Ba−O(1) 2.62(1) to compare to Ba−O(2) 2.67(1) Å and Cu−O(1) = 1.92(1) vs 1.99(1) Å for Cu−O(2)]. The Ba−N coordination bonds [2.97(2) Å av.] are longer than the Ba−O ones, but in agreement with the data reported in the literature for other barium derivatives such as $Ba_4O(Otamp)_6$ [19] or $[Ba_2Cu(thd)_4(OR^N)_2(i\text{PrOH})_2]$.[9] The Cu−N distance of 2.14(2) Å is comparable to the values observed for other Cu^{II} aminoalkoxides.[15] The short contacts between O(7)(H_2O) and two dangling nitrogen atoms of the aryloxide ligand [O(7)···N(4) 2.72 Å and O(7)···N(1) 2.79 Å, respectively] indicate the presence of intra- and intermolecular hydrogen bonding.[20] These observations are supported by a broad absorption band at 3162 cm^{-1} in the infrared spectra, and account for the poor volatility. The presence of water is most probably due to the hygroscopic phenol, as previously observed for $Pr(Otamp)_3(H_2O)_2$.[21] It also indicates that **1** is relatively stable toward hydrolysis. A number of Ba−Cu species of various stoichiometries have been reported.[8,9] Those having a 1:1 stoichiometry are usually tetranuclear species such as $[Ba_2Cu_2(\beta\text{-diket})_4(OC_2H_4OMe)_4(OHC_2H_4OMe)_2]$ (β-diket = acac, thd), in which copper is planar whereas barium is 7-coordinate.[8] The presence of one Otamp ligand acting as a tetradentate ligand and water as additional ligand allows barium to reach hepta-coordination in a monomeric unit.

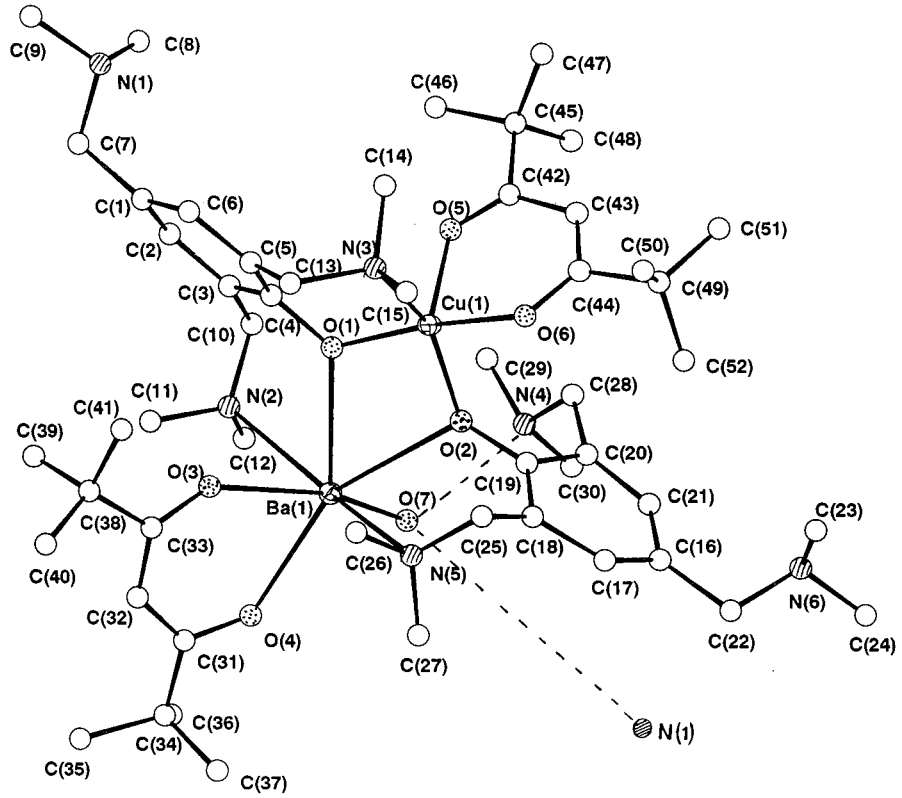


Figure 1. Molecular structure of $[BaCu(\eta^2thd)_2(Otamp)_2(H_2O)]$ showing the atom numbering scheme (dotted lines indicate H bonding)

Compound **4** is obtained by the self-assembly between $Cu(OR^n)_2$ and $Pr(thd)_3$. Its molecular structure $[PrCu(\eta^2\text{-}thd)_3(\mu,\eta^2\text{-}OR^n)_2]$ is depicted in Figure 2. Selected bond lengths and angles are collected in Table 2. From a structural point of view it can be considered as the assembly between $Pr(thd)_2(OR^n)$ and $Cu(thd)(OR^n)$ moieties. These

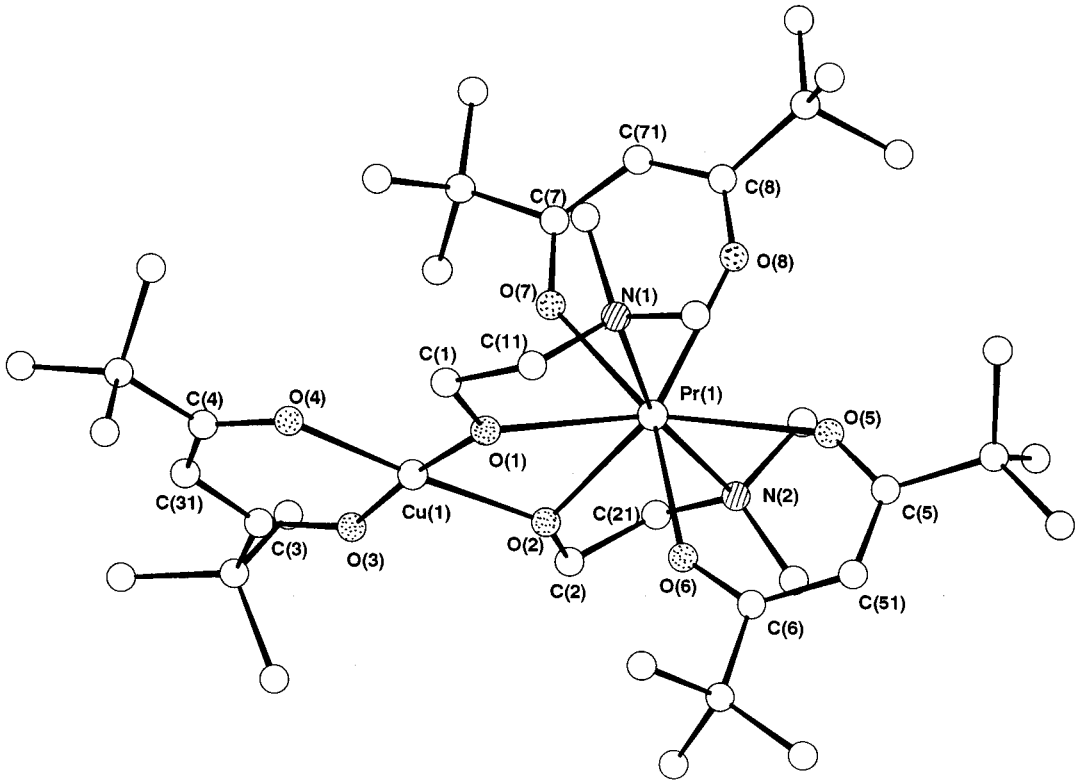


Figure 2. Crystal structure of $[PrCu(\eta^2\text{-}thd)_3(\mu,\eta^2\text{-}OC_2H_4NMe_2)_2]$

Table 2. Selected bond lengths [Å] and angles [°] for $PrCu(\eta^2\text{-thd})_3(\mu,\eta^2\text{-OR}^n)_2$

Bond lengths	
Pr(1)···Cu(1) 3.345(1)	Pr(1)−N(1) 2.701(9)
Pr(1)−O(1) 2.368(7)	Pr(1)−N(2) 2.691(9)
Pr(1)−O(2) 2.367(7)	Cu(1)−O(1) 1.896(7)
Pr(1)−O(5) 2.460(7)	Cu(1)−O(2) 1.909(7)
Pr(1)−O(6) 2.394(7)	Cu(1)−O(3) 1.910(7)
Pr(1)−O(7) 2.457(7)	Cu(1)−O(4) 1.907(7)
Pr(1)−O(8) 2.426(7)	
Angles	
O(1)−Pr(1)−O(2) 63.6(3)	O(1)−Pr(1)−O(5) 143.1(2)
O(2)−Pr(1)−O(5) 131.4(3)	O(1)−Pr(1)−O(6) 83.1(2)
O(2)−Pr(1)−O(6) 85.9(3)	O(5)−Pr(1)−O(6) 67.2(2)
O(1)−Pr(1)−O(7) 74.9(3)	O(2)−Pr(1)−O(7) 73.7(3)
O(5)−Pr(1)−O(7) 137.7(2)	O(6)−Pr(1)−O(7) 154.9(2)
O(1)−Pr(1)−O(8) 124.9(3)	O(2)−Pr(1)−O(8) 133.9(3)
O(5)−Pr(1)−O(8) 72.5(2)	O(6)−Pr(1)−O(8) 137.0(2)
O(7)−Pr(1)−O(8) 67.5(2)	O(1)−Pr(1)−N(1) 65.7(3)
O(2)−Pr(1)−N(1) 129.2(3)	O(5)−Pr(1)−N(1) 89.2(3)
O(6)−Pr(1)−N(1) 84.6(3)	O(7)−Pr(1)−N(1) 96.9(3)
O(1)−Pr(1)−N(2) 128.8(3)	O(2)−Pr(1)−N(2) 65.3(3)
O(5)−Pr(1)−N(2) 77.6(3)	O(6)−Pr(1)−N(2) 95.8(3)
O(7)−Pr(1)−N(2) 88.9(3)	O(8)−Pr(1)−N(1) 80.4(3)
O(8)−Pr(1)−N(2) 89.6(3)	N(2)−Pr(1)−N(1) 165.4(3)
O(1)−Cu(1)−O(2) 82.0(3)	O(1)−Cu(1)−O(3) 174.8(3)
O(2)−Cu(1)−O(3) 93.1(3)	O(1)−Cu(1)−O(4) 93.1(3)
O(2)−Cu(1)−O(4) 175.0(3)	O(3)−Cu(1)−O(4) 91.8(3)
Pr(1)−O(1)−Cu(1) 102.8(3)	Pr(1)−O(2)−Cu(1) 102.4(3)

units are connected by the O centre of the aminoalkoxide ligand, the pendant amino functionalities being both linked to the praseodymium atom. Praseodymium is thus eight-coordinated with a bipyramidal hexagonal geometry, in which the nitrogen atoms occupy the axial positions. Copper has a square-planar distorted surrounding. The Pr···Cu distance has a value of 3.345(1) Å, comparable to those observed for $[PrCuL(hfac)_2(O_2CCF_3)(R'^NOH)_2]$[22] [L = 2-methyl-2,4,6-tris(trifluoromethyl)-1,3-dioxane-4,6-diolato] and $[PrCu(OH)(hfac)_3(bdmmp)(bdmmpH)]$[16] [bdmmp = 2,6-bis(dimethylaminomethyl)-4-methylphenoxide]. The Pr−O bond lengths are spread over the range 2.367(1) to 2.460(7) Å, they vary according to the generalisation: Pr−μOR < Pr−O(thd), in agreement with the literature.[22−24] The Pr−N coordination bonds are considerably longer [2.695(9) Å] as reported previously.[16,21,22,25] The Cu−O bond lengths are similar for the tetramethylheptanedionate as well as the bridging alkoxide ligands [1.896(7)−1.9101(7) Å].[17] The bite angles of the thd and aminoalkoxide ligands are also similar with values of 67.3(2)° and 65.5(2)°, respectively.

Molecular Structure of $[Y_2(\eta^2\text{-thd})_4(\mu,\eta^2\text{-OR}'^N)_2]$

The structure of **8** is that of a centrosymmetric dimer $[Y_2(\eta^2\text{-thd})_4(\mu,\eta^2\text{-OR}'^N)_2]$ (Figure 3, Table 3). The yttrium atoms are hepta-coordinated, and are connected by two bridging-chelating aminoalkoxide ligands with one NMe_2 of each alkoxide ligand remaining pendant (Y···N distance of 5.22 Å). The Y···Y non-bond length has a value of 3.739(2) Å, comparable to that observed for other dinuclear yttrium species such as $[Y_2(O_2CCF_3)_6(OR'^N_2)]^{2-}$ [25], or polynuclear clusters.[12] The OR'^N ligand is generally tridentate − both NMe_2 sites interacting with the metallic centres. The only example of a μ,η^2-coordination mode is that of $Cu_2Cl_4(R'^NOH)_2$.[26] Although octa-coordination has been achieved for yttrium in β-diketonatoalkoxides such as $[Y_3(acac)_4(OC_2H_4OMe)_5]$,[27] the steric hindrance of the tetramethylheptanedionate ligands probably precludes coordination of the second N-donor site for **8**. The Y−O bond lengths are spread over the range 2.236(5) to 2.307(5) Å. These values are in agreement with the literature.[28] The Y−O−Y bridge is unsymmetrical, the intra-chelate Y−O(5′) distance being about 0.069 Å longer than Y−O(5). The Y(1)−N(1) coordination bond of 2.544(7) Å is in the range of the values observed.[25,29]The structure of **8** is related to that of $[Y(\mu,\eta^2\text{-OAc})(acac)_2(H_2O)]_2$ [30] and of $[Pr(hfac)_2(\mu,\eta^3\text{-OR}'^N)(H_2O)(THF)]_2$.[22] However, the larger ionic radius of praseodymium (1.013 Å as compared to 0.880 Å for Y) allows the metal to attain nona-coordination via a tridentate assembling coordination mode of the aminoalkoxide ligand and two additional neutral ligands.

Physical Properties: Solubility and Volatility Data

A general observation for these mixed-metal species is, as anticipated, an increase in solubility as well as a better stability toward ambient atmosphere. For instance, whereas soluble copper alkoxides are highly moisture-sensitive and the praseodymium tetramethylheptanedionate hygroscopic, **4** is air-stable. Stability to ambient atmosphere was also achieved for **1**, **5**, and **6**.

The Ba−Cu species **1** is soluble in polar, as well as non-polar media. It is stable in solvents such as diglyme (UV evidence). It is non-volatile. The TGA analysis shows a first weight loss in the 95−125 °C temperature range, due to the elimination of the water ligand. An aminophenoxide ligand is eliminated at 170−280 °C. Two identical weight losses are observed between 280−550 °C. They correspond to the elimination of the two tetramethylheptanedionate ligands. The last Otamp ligand is only partially decomposed between 550 and 970 °C. Thus, despite a quite low onset of decomposition for an aryloxide, the amount of a residue (ca. 38%) is quite higher than that expected for $BaCuO_2$ (20.9%).

The heterometallic species MCu_2 and MCu were soluble in aliphatic or aromatic hydrocarbons, or ethers such as THF or diethyl ether, but only slightly in diglyme. The M−Cu species **4**, **5**, and **6** sublime at 155 °C/10^{-4}, 130 °C/10^{-4}, and 150 °C/10^{-4} Torr, respectively. They are the first volatile Ln−Cu or Y−Cu species not supported by fluorinated ligands. It is noticeable that none of the Pr−Cu and Pr species with related aminoalkoxide ligands such as $[PrCu(OH)(hfac)_3(bdmmp)(bdmmpH)]$ and $[Pr(hfac)_2(OR'^N)(H_2O)(THF)_2]$ were volatile, despite the presence of the fluorinated diketonate in the coordination sphere.[25,26] The thermal behaviour of the novel M−Cu species was analysed by TGA under nitrogen (1 atm). The amount of

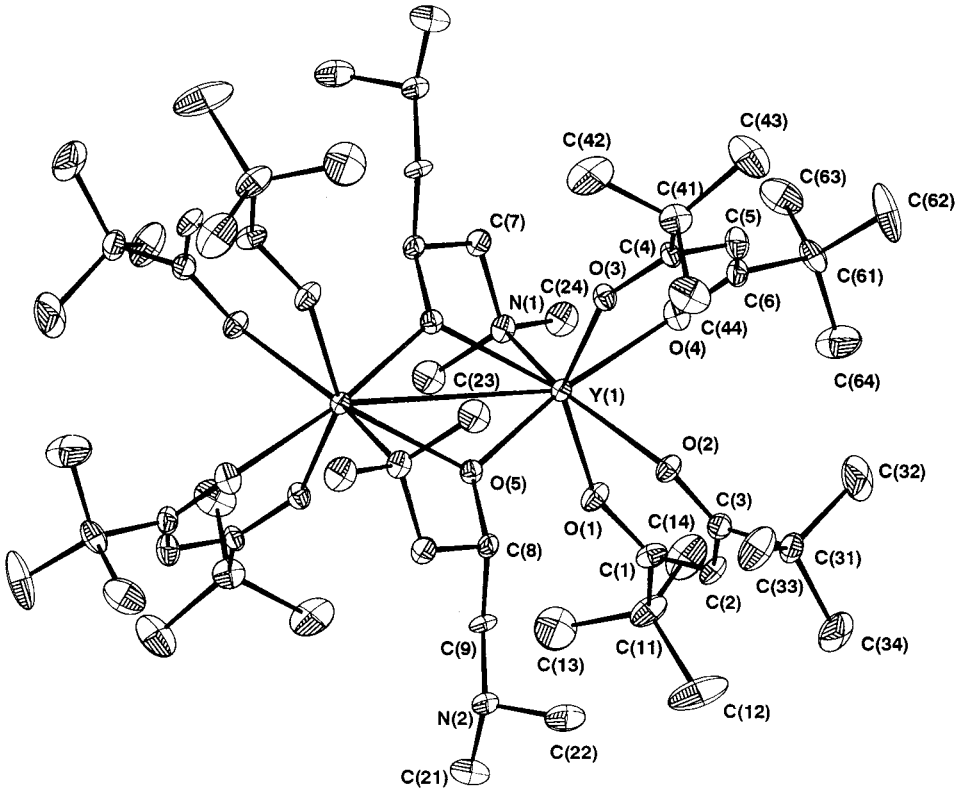


Figure 3. Molecular structure of $[Y(\eta^2\text{-thd})_2(\mu,\eta^2\text{-OR}'^{N})_2]_2$ (thermal ellipsoids at 30% probability)

Table 3. Selected bond lengths [Å] and angles [°] for $[Y(thd)_2(OR'^{N})]_2$

Bond lengths[a]			
Y(1)−Y(1′)	3.739(2)	Y(1)−O(1)	2.273(6)
Y(1)−O(2)	2.294(6)	Y(1)−O(3)	2.280(6)
Y(1)−O(4)	2.303(6)	Y(1)−O(5)	2.236(5)
Y(1)−O(5′)	2.307(5)	Y(1)−N(1)	2.544(7)
Bond angles			
O(1)−Y(1)−O(2)	74.9(2)	O(1)−Y(1)−O(3)	149.3(2)
O(2)−Y(1)−O(3)	78.8(2)	O(1)−Y(1)−O(4)	88.1(2)
O(2)−Y(1)−O(4)	83.0(2)	O(3)−Y(1)−O(4)	73.1(2)
O(1)−Y(1)−O(5)	93.3(2)	O(2)−Y(1)−O(5)	85.5(2)
O(3)−Y(1)−O(5)	100.2(2)	O(4)−Y(1)−O(5)	167.6(2)
O(1)−Y(1)−O(5′)	127.3(2)	O(2)−Y(1)−O(5′)	145.9(2)
O(3)−Y(1)−O(5′)	83.3(2)	O(4)−Y(1)−O(5′)	119.2(2)
O(1)−Y(1)−N(1)	78.5(2)	O(2)−Y(1)−N(1)	146.9(2)
O(3)−Y(1)−N(1)	118.7(2)	O(4)−Y(1)−N(1)	76.8(2)
O(5′)−Y(1)−O(5)	69.2(2)	O(5)−Y(1)−N(1)	115.6(2)
O(5′)−Y(1)−N(1)	67.2(2)	Y(1)−O(5)−Y(1′)	110.9(3)

[a] Atoms labelled with ′ are connected by an inversion centre.

residues obtained for the Y−Cu species **3** and **6** are lower than the values expected for $Y_2Cu_4O_7$ (24.3%) and $Y_2Cu_2O_5$ (21.5%), respectively. Partial sublimation has thus occurred during the TGA experiments. A similar thermal behaviour was observed for the praseodymium−copper species **2**, **4**, and **5**. The properties of the bimetallic Pr−Cu and Y−Cu species are compatible with their use in conventional as well as liquid delivery MOCVD techniques.

The homometallic species based on the OR'^{N} ligand display quite limited solubility, even in polar solvents (THF, diglyme). Both **8** and **7** are volatile. The yttrium species sublimes at 215−220 °C/10^{-3} Torr. This temperature is quite high, but in agreement with the dimeric character and thus a relatively high molecular weight.[6] The TGA profile accounts for sublimation up to 350 °C. By contrast with the barium derivative, it is air-stable in the solid state (FT-IR evidence). $[Ba(OR'^{N})(thd)(HOR'^{N})]$ distils as the adduct at 130 °C/10^{-3} Torr, it is thus one of the most volatile barium species reported to date.[4] The TGA analysis indicates a first weight loss from 120 to 245 °C, corresponding to the elimination of the coordinated alcohol. The second weight loss between 245 and 375 °C is due to the elimination of the aminoalkoxide ligand, the thd ligand is decomposed partially, leading to a $BaCO_3$ residue. Although no carbonate was observed under reduced pressure, the high moisture sensitivity of the compound is a hurdle. $[Ba(tdfnd)_2(H_2O)]_m$ and $[Ba(tdfnd)_2(diglyme)]$ [tdfndH = $C_3F_7C(O)CH_2C(O)C_3F_7$ = tetradecafluorononane-4,6-dione], which are liquid at the temperature of use and could be repeatedly transported in the vapour without decomposition, remain the most attractive Ba species for Ba oxide, along with BaF_2.[31]

Experimental Section

All reactions were performed under an inert atmosphere using Schlenk tube techniques. Solvents were dried and purified by distillation. $M(thd)_3$ (M = Y, Pr),[32] $Ba_4O(Otamp)_6$,[19] $Ba[N(SiMe_3)_2]_2$ [33] and Cu aminoalkoxides[15]were obtained according to literature methods. $Ba(OR'N)_2$ was prepared by alcoholysis of the silylamide. $Pr(thd)_2(OR^n)$ was obtained by alcoholysis of Pr silyl-

amide followed by reaction with thdH. ^{1}H- and ^{13}C-NMR, and FT-IR spectra were run with Bruker AC-200 and IR-FTS 45 spectrometers, respectively. IR spectra were obtained as Nujol mulls. ESR spectra were done with a Bruker spectrometer. Analyses were obtained from the Centre de Microanalyses du CNRS. TGA analyses were done under nitrogen with a Setaram system using a temperature ramp of 5 °C/min. FT-IR data are collected in Table 1.

$BaCu(thd)_2(Otamp)_2(H_2O)$ (1): A solution of $[Ba(thd)_2]_4$ (2.80 g, 1.39 mmol) in 20 mL of hexane was added to $Cu(Otamp)_2$ (5.50 mmol) in 20 mL of hexane. The solution turned rapidly from blue to green and was concentrated to dryness after 17 h. The crude solid was recrystallized in diethyl ether at −25 °C (4.90 g, 80%). Compound **1** was very soluble in polar and nonpolar solvents. − $C_{52}H_{92}BaCuN_6O_7$: calcd. C 56.05, H 8.32, Ba 12.33, Cu 5.70; C 56.32, H 8.42, Ba 12.35, Cu 5.70. − ESR (solid, 20 °C): $<g>$ = 2.14; $<A>$ = 106 G. − TGA (N_2, 1 atm): 95−125 °C (− H_2O), 170−280 °C (− tampOH), 280−400 °C (− thdH), 400−500 °C (− thd), 550−970 − OH, residue 38%. A similar procedure applied to $Cu(thd)_2$ (0.37 g, 0.85 mmol) and $Ba_4O(Otamp)_6$ (0.46 g, 0.2 mmol) gave **1** (0.57 g, 60%).

$MCu_2(thd)_3(OR^n)_4$ [M = Pr (2), Y(3)]: $Pr(thd)_2(OR^n)$ (1.11 g, 1.96 mmol) in 20 mL of hexane was added to $Cu(OR^n)_2$ (0.93 g, 3.88 mmol) in 10 mL of hexane. $Cu(OR^n)_2$ dissolved. Compound **2** was isolated as needles by crystallisation (1.36 g, 63%). − $C_{49}H_{97}Cu_2N_4O_{10}Pr$: calcd. C 50.28, H 8.28, Cu 10.86, N 4.78, Pr 12.04; found C 49.80, H 8.12, Cu 10.92, N 4.84, Pr 12.35. − ESR (hexane, 20 °C): $<g>$ = 2.12; $<A>$ = 79.3 G. − Crystal data (−100 °C): a = 9.806(3), b = 19.792(6), c = 31.535(7) Å, α = β = γ = 90°. − Same procedure applied to $Y(thd)_3$ (1.06 mmol, 25 mL of hexane) and $Cu(OR^n)_2$ (2.12 mmol, 10 mL of hexane) gave **3** (1.02 g, 87%). − $C_{49}H_{97}Cu_2N_4O_{10}Y$ (***mol. mass?***): calcd. C 52.63, H 8.74, Cu 11.36, N 5.01, Y 7.95; found C 52.66, H 8.7, Cu 10.50, N 4.74, Y 7.50. − ESR (hexane, 20 °C): $<g>$ = 2.10; $<A>$ = 92.4 G. − TGA (N_2, 1 atm, °C): 155−230 (− 3 × R^NOH), 230−315 (− R^NOH − 2 × thd), 315−470 (− thd), residue 19.5%.

$PrCu(thd)_3(OR)_2$ [R = R^n (4), R^N (5)] and $YCu(thd)_3(OR^N)_2$ (6): Same procedure as for **2** applied to 0.10 g of $Cu(OR^n)_2$ (0.41 mmol) in 5 mL of hexane and $[Pr(thd)_3]_2$ (0.29 g, 0.21 mmol) in 12 mL of hexane gave **4** as needles (0.37 g, 94%). − $C_{41}H_{77}CuN_2O_8Pr$: calcd. C 52.91, H 8.27, Cu 6.80, N 3.00, Pr 15.10; found C 53.88, H 8.31, Cu 6.9, N 3.13, Pr 14.600. − ESR (hexane, 20 °C): $<g>$ = 2.10; $<A>$ = 78.6 G. − TGA (N_2, 1 atm, °C): 190−235 (− 2 × R^NOH), 235−365 (− 2.5 × thd), 365−550 (− 0.5 × thd), residue 21.8%. − $[Pr(thd)_3]_2$ (0.30 g, 0.21 mmol) in 20 mL of hexane added to $Cu(OR^N)_2$ (0.12 g, 0.43 mmol) in 10 mL of hexane gave **5** (0.38 g, 92%). This could also be obtained from $Pr(thd)_2(OR^N)$ and $Cu(OR^N)_2$ (1:1 stoichiometry), but in lower yield (61%). − $C_{43}H_{81}CuN_2O_8Pr$: calcd. C 53.87, H 8.45, Cu 6.62, N 2.92, Pr 14.69; found C 53.52, H 8.42, Cu 6.95, N 2.72, Pr 15.30. − ESR (hexane, 20 °C): $<g>$ = 2.18; $<A>$ = 86.2 G. − TGA (N_2, 1 atm): 125−220 °C (− 2 × R^NOH), 220−360 (− 2 × thd), 360−600 (− thd), residue 23%. − $Y(thd)_3$ (0.69 g, 1.08 mmol) in 20 mL of hexane added to $Cu(OR^N)_2$ (0.29 g, 1.08 mmol) in 10 mL of hexane gave **6** (0.87 g, 90%). Compound **6** was also obtained by reacting $Y(thd)_2(OR^N)$ and $Cu(OR^N)_2$ (1:1) in hexane (50%). − $C_{43}H_{81}CuN_2O_8Y$: calcd. C 56.97, H 9.01, Cu 7.01, N 3.09, Y 9.81; found C

Table 4. Crystal data for **1**, **4** and **8**

	1	**4**	**8**
Empirical formula	$C_{52}H_{92}BaCuO_7N_6$	$C_{41}H_{77}CuN_2O_8Pr$	$C_{58}H_{110}O_{10}N_4Y_2$
Molecular mass	1114.2	929.7	1201.3
a [Å]	11.813(5)	16.973(5)	10.606(8)
b [Å]	20.419(7)	19.143(6)	20.511(5)
c [Å]	49.667(15)	30.225(5)	15.522(3)
α [°]	90	90	90
β [°]	90	90	98.27(4)
γ [°]	90	90	90
V [Å^3]	11980(7)	9821(5)	3341(21)
Z	8	8	2
Crystal system	orthorhombic	orthorhombic	monoclinic
Space group	*Pbca*	*Pbca*	$P2_1/n$
Linear absorption coefficient μ [cm^{-1}]	10.5	14.5	17.9
Density ρ [g·cm^{-3}]	1.23	1.26	1.19
Diffractometer	CAD4 − Enraf−Nonius	CAD4 − Enraf−Nonius	CAD4 − Enraf−Nonius
Radiation	Mo-K_α (λ= 0.71069 Å)	Mo-K_α (λ = 0.71069 Å)	Mo-K_α (λ = 0.71069 Å)
Scan type	ω/2 θ	ω/2 θ	ω/2 θ
Scan range [°]	1.0 + 0.345 tgθ	0.80 + 0.345 tgθ	0.80 + 0.345 tgθ
θ limits [°]	2−16	1−23	1−25
Temperature of measurement [°C]	163 K	room temperature	room temperature
Octants collected	h: 0−9; k: 0−15; l: 0−38	h: 0−18; k: 0−21; l: 0−33	h: 0−12; k: 0−24; l: −18−18
Number of data collected	3346	7499	6415
Number of unique data collected	2906	6811	5877
Number of unique data used for refinement	1923 $(F_o)^2 > 3\ \sigma(F_o)^2$	3311 $(F_o)^2 > 3\ \sigma(F_o)^2$	1999 $(F_o)^2 > 2\ \sigma(F_o)^2$
$R = \Sigma\|\|F_o\| - \|F_c\|\|/\Sigma\|F_o\|$	0.060	0.0407	0.0493
$R_w = [\Sigma w(\|F_o\| - \|F_c\|)^2/\Sigma w F_o^2]^{1/2}$	0.072, w = 1.0	0.0448, w = 1.0	0.0484, w =1.0
Absorption correction	DIFABS (min = 0.91, max = 1.16)	DIFABS (min = 0.87, max = 1.12)	DIFABS (min = 0.80, max = 1)
Goodness of fit s	3.5	1.8	0.94
Number of variables	280	480	335
$\Delta\rho_{min}$ [e·Å^{-3}]	−0.70	−0.33	−0.36
$\Delta\rho_{max}$ [e·Å^{-3}]	0.64	0.58	0.38

56.76, H 9.06, Cu 7.18, N 3.07, Y 9.97. − ESR (hexane, 20 °C): $<g> = 2.08$; $<A> = 92.4$ G. − Compounds **4**, **5**, and **6** are soluble in hexane, toluene, diethyl ether, and THF, and slightly soluble in diglyme.

Ba(thd)(OR′^{N})(HOR′^{N}) (7): A solution of thdH (0.43 g, 2.34 mmol) in 5 mL of THF was added to a suspension of $Ba(OR'^N)_2$ (1.07 g, 2.34 mmol) in 35 mL of THF. Rapid dissolution was observed. The solid obtained by concentrating to dryness was recrystallised in hexane to yield compound **7** (1.36 g, 95%). Dist. 120−130 °C/10^{-3} Torr. − Soluble in usual solvents (hexane, toluene, diethyl ether, THF). − $C_{25}H_{54}BaN_4O_4$: calcd. C 49.05, H 8.82, N 9.15; found C 49.03, H 8.85, N 9.10. − ^{1}H NMR ($CDCl_3$, 20 °C): δ = 5.52, 5.47, 5.44 [s, 1 H, CH(thd)], 5.0 (br, 1 H, OH), 3.91 [s, br, 2 H, CH(OR′^{N})], 2.25 (m, 32 H, CH_2NMe_2), 1.08, 1.06 and 1.02 (s, 18 H, *t*Bu). − ^{13}C{^{1}H} NMR (C_7D_8, 28 mg/mL, 20 °C): δ = 197.3 (C=O), 88.5 [CH(thd)], 67.1 [CH(OR′^{N})], 66.2 (CH_2), 45.9 (NMe_2), 41.3 [C(*t*Bu)], 29.5 [Me(*t*Bu)]. − TGA (N_2, 1 atm): 120−245 °C (− R′^{N}OH), 245−375 (− R′^{N}OH), 375−970 (decomposition of thd), residue 34%. − Crystal data (20 °C): a = 10.652(2), b = 16.006(2), c = 19.486(3) Å, α = β = 97.03(1)°, γ = 90°.

[Y(thd)$_2$(OR′^{N})]$_2$ (8): $Y(thd)_3$ (1.24 g 1.94 mmol) in 35 mL of hexane was added to a suspension of $Ba(OR'^N)_2$ (1.94 mmol, 0.83 g) in 25 mL of hexane. $Ba(OR'^N)_2$ dissolved after 15 min. Compound **8** was isolated by crystallisation (1.11 g, 96%). It sublimes at 215−220 °C/10^{-3} Torr and is only slightly soluble even in polar solvents (acetonitrile, acetone, THF). − Compound **8** could also be obtained from Ba(thd)(OR′^{N})(HOR′^{N}) (0.15 mmol) and $Y(thd)_3$ (0.15 mmol) in 15 mL of hexane (80 mg, 90%). − $C_{58}H_{110}N_4O_{10}Y_2$: calcd. C 57.99, H 9.23, N 4.66; found C 57.22, H 9.01, N 4.50. − ^{1}H NMR ($CDCl_3$, 20 °C): δ = 5.67, 5.59 [s, 4 H, CH(thd)], 4.48 (m, J = 10.9 Hz), 4.21 (quint, J = 5.6 Hz), 3.67 [sept, J = 4.1 Hz, 2 H, CH (OR′^{N}, R′^{N}OH)], 3.67 [s, br, OH (R′^{N}OH)], 2.9, 1.9 (32 H, CH_2NMe_2), 1.09, 1.05 (s, 72 H, *t*Bu). − TGA (1 atm): sublimation between 225−400 °C.

X-ray Structure Determination for 1, 4, and 8: Suitable crystals were obtained from the reaction medium for **1** and **8**, and by recrystallisation in Et_2O for **4**, and were mounted onto an Enraf−Nonius CAD-4 automatic diffractometer. The unit cell parameters and basic information about data collection and structure refinement are given in Table 4. Accurate lattice parameters and orientation matrix were obtained from least-squares refinements of the setting angles of 25 well-centred reflections. The intensities of two standard reflections monitored every hour showed no decay. Corrections for Lorentz and polarization effects were applied. Computations were performed using the PC version of CRYSTALS.[34] Scattering factors and corrections for anomalous dispersion were taken from ref.[35] Structures were solved using direct methods (SHELXS)[36] and standard Fourier techniques. All non-hydrogen atoms were refined anisotropically for **4** and **8**, and only Ba and Cu were anisotropically refined for **1**, in view of the limited number of data. In addition, only a partial structure report will be given. Hydrogen atoms were calculated and included as fixed contributors in the last refinement. Models converged for the R and R_w values in Table 4. Tables of atomic coordinates, of thermal parameters, of non-essential bond lengths and angles for the structures reported have been deposited at Cambridge Crystallographic Data Centre. CCDC reference numbers for **1**, **4**, and **8**: 137676, 137675, and 101724. Copies of the data are available free of charge on application to CCDC 12 Union Road Cambridge CB2 IEZ, UK [Fax: (internat.) + 44-1223/336-033].

Acknowledgments

This work was supported by the CEE (Grant BRE2-CT94−0742).

[1] R. Hiskes, S. A. Dicarolis, R. D. Jacowitz, Z. Lu, R. S. Feigelson, R. K. Route, J. L. Young, *J. Cryst. Growth* **1993**, *128*, 781; C. Xiaolong, L. Jingkiu, X. Sishen, Q. Zhiyu, T. Xiaoshu, X. Xianran, *Zeit. Physik. B, Condensed Mater.* **1992**, *88*, 1; I. Das, E. V. Sampathkumaran, R. Vijayaraghawan, Y. Nakazawa, M. Ishikawa, *Physica, C: Superconductivity* **1991**, *173*, 331.

[2] [2a]T. T. Kodas, *Adv. Mater.* **1989**, *6*, 180. − [2b]C. H. Stoessel, R. F. Bunshah, S. Prakash, H. R. Fetterman, *J. Supercond.* **1993**, *6*, 1. − [2c]F. Weiss, J. Lindner, J. P. Sénateur, B. Ploss, L. G. Hubert-Pfalzgraf, S. Daniele, *XIV International Conference on Chemical Vapor Deposition and EUROCVD-11*/***1997***, M. D. Allendorf, C. Bernard (Eds.), *PV 97−25*, p. 1013, The Electrochemical Society Proceeding Series, Pennington NJ, **1997**.

[3] F. Maury, *Chem. Vap. Dep.* **1996**, *2*, 113; H. Zama, S. Oda, *Jpn. J. Appl. Phys.* **1990**, 29, 1072.

[4] L. G. Hubert-Pfalzgraf, F. Labrize, C. Bois, J. Vaissermann, *Polyhedron* **1994**, *13*, 2163; R. Gardiner, D. C. Gordon, G. T. Stauf, B. A. Vaarstra, *Chem. Mater.* **1994**, *6*, 1967; R. Gardiner, D. W. Brown, P. S. Kirlin, A. L. Rheingold, *Chem. Mater.* **1991**, *3*, 1053; K. Timmer, H. A. Meimena, *Inorg. Chim. Acta* **1991**, *187*, 99; A. A. Drozdov, S. I. Trojanov, *Polyhedron*, **1992**, *11*, 2877; S. R. Drake, M. B. Hursthouse, K. M. Abdul Malik, D. J. Otway, *J. Chem. Soc., Dalton Trans.* **1993**, 2883; S. I. Trojanov, A. A. Drozdov, *Main Group Met. Chem*. **1996**, *XIX*, 547; S. R. Drake, M. B. Hursthouse, K. M. Abdul Malik, S. A. S. Miller, D. J. Otway, *Inorg. Chem.* **1993**, *32*, 4464.

[5] W. A. Wojtczak, P. F. Fleig, M. J. Hampden-Smith, *Adv. Organomet. Chem*. **1996**, *40*, 215, and refs. therein; W. A. Hermann, N. W. Huber, O. Runte, *Angew. Chem. Int. Ed.* **1994**, *34*, 5295; T. P. Hanusa, *Chem. Rev.* **1993**, *93*, 1023.

[6] [6a]L. G. Hubert-Pfalzgraf, H. Guillon, *Appl. Organomet. Chem*. **1998**, *12*, 231. − [6b]H. Dahmen, M. W. Carris, *Chem. Vap. Deposition* **1997**, *3*, 27.

[7] K. G. Caulton, L. G. Hubert-Pfalzgraf, *Chem. Rev.* **1990**, *90*, 969; V. G. Kessler, L. G. Hubert-Pfalzgraf, S. Daniele, A. Gleizes, *Chem. Mater.* **1994**, *6*, 2336; L. G. Hubert-Pfalzgraf, C. Sirio and C. Bois, *Polyhedron* **1998**, *17*, 821.

[8] N. N. Sauer, E. Garcia, K. V. Salazar, R. R. Ryan, J. A. Martin, *J. Am. Chem. Soc.* **1990**, *112*, 1524; A. P. Purdy, C. F. George, *Inorg. Chem.* **1991**, *30*, 1970; A. P. Purdy, C. F. George, J. H. Callahan, *Inorg. Chem.* **1991**, *30*, 2812; W. Bidell, H. W. Bosch, D. Veghini, H. U. Hund, J. Döring, H. Berke, *Helv. Chim. Acta* **1993**, *76*, 596.

[9] F. Labrize, L. G. Hubert-Pfalzgraf, J. Vaissermann, C. B. Knobler, *Polyhedron* **1996**, *15*, 577.

[10] W. Bidell, V. Shklover, H. Berke, *Inorg. Chem.* **1992**, *31*, 5561; W. Bidell, J. Döring, H. W. Bosch, H. U. Hund, E. Plappert, H. Berke, *Inorg. Chem.* **1993**, *32*, 502; C. Benelli, A. Caneschi, D. Gatteschi, O. Guillon, L. Pardi, *Inorg. Chem.* **1990**, *29*, 1750.

[11] F. Labrize, L. G. Hubert-Pfalzgraf, J. C. Daran, P. Tobaly, *Polyhedron* **1996**, *15*, 2707; P. Miele, J. D. Foulon, N. Hovnanian, L. Cot, *J. Chem. Soc., Dalton Trans.* **1993**, 23.

[12] L. G. Hubert-Pfalzgraf, *Coord. Chem. Rev.* **1998**, *178−180*, 967; L. G. Hubert-Pfalzgraf, *New J. Chem.*, **1995**, *19*, 727.

[13] A. Gleizes, M. Julve, N. Kuzmina, A. A. Ljkhanian, F. Thoret, I. Malkerova, J. L. Sanz, F. Senocq, *Eur. J. Inorg. Chem.* **1998**, 1169.

[14] H. Guillon, S. Daniele, L. G. Hubert-Pfalzgraf, C. Bavoux, *Inorg. Chim. Acta*, in the press.

[15] S. C. Goel, K. S. Kramer, M. Y. Chiang, W. Buhro, *Polyhedron* **1990**, *9*, 61.

[16] L. Chen, S. R. Breeze, R. J. Rousseau, S. Wang, L. K. Thompson, *Inorg. Chem.* **1995**, *34*, 454.

[17] M. Melnik, M. Kabesova, M. Koman, L. Macoskova, C. E. Holloway, *J. Coord. Chem. Rev.* **1998**, *45*, 147; C. Sirio, O. Poncelet, L. G. Hubert-Pfalzgraf, J. C. Daran, *Polyhedron* **1992**, *11*, 177.

[18] P. Miele, J. D. Foulon, N. Hovnanian, L. Cot, *Polyhedron* **1993**, *12*, 267; P. Miele, J. D. Foulon, N. Hovnanian, *Polyhedron* **1993**, *12*, 209; K. F. Tesh, T. P. Hanusa, J. C. Huffman, C. J. Huffman, *Inorg. Chem.* **1992**, *31*, 5572.

[19] K. F. Tesh, T. P. Hanusa, *J. Chem. Soc., Chem. Commun.* **1991**, 879.

[20] J. Emsley, *Chem. Soc. Rev.* **1980**, *9*, 91; P. Schuster, G. Zundel, C. Sandorfy (Eds.), *The Hydrogen Bond*, North Holland Company, Amsterdam, **1976**; B. A. Vaarstra, J. C. Huffman, P. S. Gradeff, L. G. Hubert Pfalzgraf, J. C. Daran, S. Parraud, K. Yunlu, K. G. Caulton, *Inorg. Chem.* **1990**, *29*, 3126.
[21] S. Daniele, L. G. Hubert-Pfalzgraf, J. Vaissermann, *Polyhedron* **1995**, *14*, 327.
[22] S. Wang, Z. Pang, K. D. L. Smith, Y. S. Hua, C. Deslippe, M. J. Wagner, *Inorg. Chem.* **1995**, *34*, 908.
[23] L. G. Hubert-Pfalzgraf, S. Daniele, A. Bennaceur, J. C. Daran, J. Vaissermann, *Polyhedron* **1997**, *16*, 1223.
[24] C. S. Erasmus, J. C. A. Boeyens, *Acta Crystallogr.* **1970**, *B26*, 1843; J. P. R. de Villiers, J. C. A. Boeyens, *Acta Crystallogr.* **1971**, *B27*, 692; R. A. Lalancette, M. Cefola, W. C. Hamilton, S. J. LaPlaca, *Inorg. Chem.* **1967**, *6*, 2127.
[25] S. Wang, Z. Pang, K. D. L. Smith, M. J. Wagner, *J. Chem. Soc., Dalton Trans.* **1994**, 955.
[26] J. C. Zheng, R. J. Rousseau, S. Wang, *Inorg. Chem.* **1992**, *31*, 106.
[27] O. Poncelet, L. G. Hubert-Pfalzgraf, J.-C. Daran, *Inorg. Chem.* **1990**, *29*, 2883.
[28] O. Poncelet, L. G. Hubert-Pfalzgraf, J. C. Daran, R. Astier, *J. Chem. Soc., Chem. Commun.* **1989**, 1846; S. Wang, *Inorg. Chem.* **1990**, *30*, 2252; U. Casellato, P. Guerriero, S. Tamburini, S. Sitran, P. A. Vigato, *J. Chem. Soc., Chem. Commun.* **1991**, 2145.
[29] P. Shao, D. J. Berg, G. W. Bushnell, *Inorg. Chem.* **1994**, *33*, 6334; K. Kumar, C. A. Chang, L. C. Francesconi, M. F. Malley, J. Z. Gaugoutas, M. F. Tweedle, *Inorg. Chem.* **1994**, *33*, 3567; D. Parker, K. Pulukkody, F. C. Smith, A. Batsanov, J. A. K. Howard, *J. Chem. Soc., Dalton Trans.* **1994**, 689; S. J. Mac Lain, N. E. Drysdale, *Polym. Repr.* (*Am. Chem. Soc. Div. Polym. Chem.*) **1992**, *33*, 174.
[30] O. Poncelet, L. G. Hubert-Pfalzgraf, J. C. Daran, *Polyhedron* **1990**, *9*, 1305.
[31] S. H. Shamlian, D. D. Gilliland, D. J. Cole-Hamilton, J. A. P. Nash, S. C. Thomson, S. L. Cook, *J. Mater. Chem.* **1995**, *47*, 5; B. C. Richards, S. L. Cook, D. L. Pinch, C. W. Andrews, *J. Phys. IV, Fr.* **1995**, *C5*, 407; J. A. P. Nash, S. C. Thomson, S. L. Cook, *Adv. Mater. Opt. Electron.* **1995**, *5*, 1.
[32] J. A. Cunningham, R. E. Sievers, *J. Am. Chem. Soc.* **1975**, *97*, 1586.
[33] B. A. Vaartstra, J. C. Huffman, W. E. Streib, K. G. Caulton, *Inorg. Chem.* **1991**, *30*, 121.
[34] D. J. Watkins, J. R. Carruthers, P. W. Bettridge, *Crystals User Guide*, Chemical Crystallography Laboratory, University of Oxford, U. K., **1988**.
[35] D. T. Cromer, *International Tables for X-ray Crystallography*, vol. IV, Kynoch Press, Birmingham, U. K., **1974**.
[36] G. M. Sheldrick, *SHELXS-86*, *Programm for Crystal Structure Solution*, University of Göttingen, **1986**.

Received December 9, 1999
[I99446]

Chemistry of 2*H*-Azaphosphirene Complexes, 20[‡]

Study on the Ring Formation of 2*H*-Azaphosphirene Complexes Using Sterically Demanding *C*-2,4,6-Trialkylphenyl-Substituted Aminocarbene Tungsten Complexes − Detection of a Key Intermediate

Rainer Streubel,*[a] Siegfried Priemer,[a] Frank Ruthe,[a] and Peter G. Jones[a]

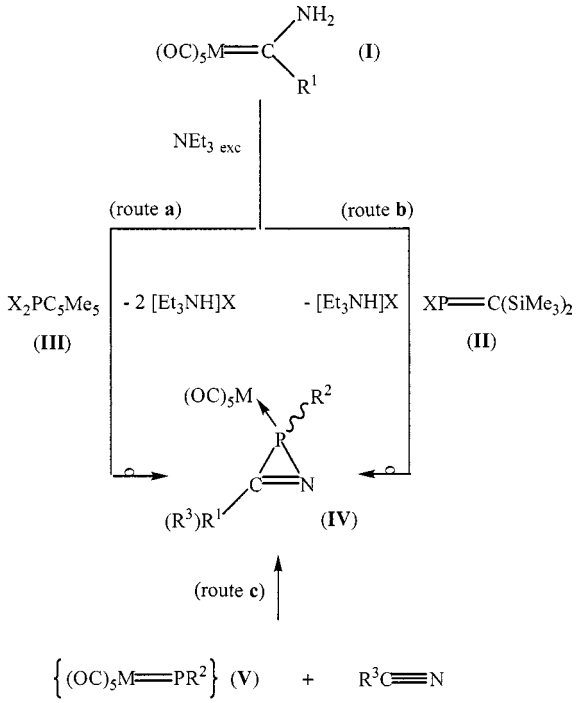
Dedicated to Professor Gerd Becker on the occasion of his 60th birthday

Keywords: Phosphorus heterocycles / 2*H*-Azaphosphirene complexes / Carbene complexes / Tungsten / Cyclizations

The synthesis of *C*-2,4,6-trialkylphenyl-substituted ethoxy- and aminocarbene tungsten complexes **1a–c** (R = Me, *i*Pr and *t*Bu) and **2a,b** (R = Me, *i*Pr) and the reaction of **2a,b** with [bis(trimethylsilyl)methylene]chlorophosphane (**3**) in the presence of triethylamine is reported. The reaction course, which finally leads to the 2*H*-azaphosphirene complexes **7a,b**, depends strictly on the steric demands of the aryl group bonded to the carbene atom; only in the case of complex **2a** was a dinuclear tungsten carbene complex formed, which was isolated and characterized by single crystal X-ray diffraction. Relative to phenyl-substituted derivatives, the 2*H*-azaphosphirene complexes **7a,b** showed enhanced reactivity towards triethylammonium chloride, furnishing the [bis(trimethylsilyl)methyl]chlorophosphane complex **8**. Condensation of **8** with complex **2a** afforded the novel dinuclear tungsten complex **9a** containing an acyclic C,N,P structural unit with a κ-C and a κ-P coordination mode; an H-bonded adduct of complex **9a** and mesitylnitrile, complex **10**, was investigated by single crystal X-ray diffraction.

Introduction

Two routes are currently known to provide access to 2*H*-azaphosphirene complexes (**IV**) (Scheme 1). The first utilises a rearrangement cascade starting from aminocarbene complexes (**I**) and either [bis(trimethylsilyl)methylene]halophosphanes (**II**) (X = Cl,[2] Br[3]) (route **a**) or alkyldihalophosphanes (**III**) (X = Cl, R = C_5Me_5[4]) (route **b**) in the presence of triethylamine. The second, a [2+1] cycloaddition reaction[5] of an electrophilic terminal phosphanediyl complex (**V**) with dialkylamino nitriles (R = R_2N) (route **c**) was detected quite recently and is especially useful for 3-donor-atom-substituted 2*H*-azaphosphirene complexes that cannot be obtained from routes **a** or **b**. Because of the increasing synthetic usefulness of 2*H*-azaphosphirene complexes as starting material for unsaturated three-,[6] four-[7] and five[5,8]-membered monocyclic and polycyclic[9] P-heterocycle complexes, we were interested in obtaining further insight into the ring forming process of 2*H*-azaphosphirene complexes based on route **a**.



Scheme 1. Routes to 2*H*-azaphosphirene metal complexes **IV** (M = Cr, Mo, W; R, R′ = alkyl, aryl)

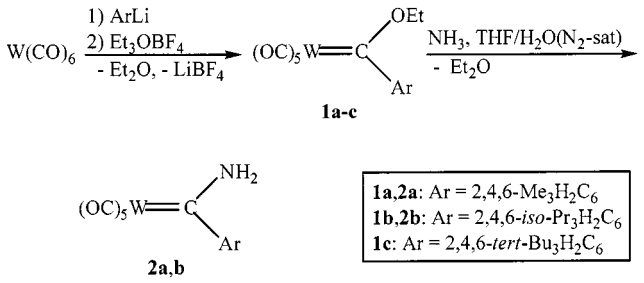
Results and Discussion

Our former investigations of the rearrangement cascade leading to 2*H*-azaphosphirene complexes (route **a**) had already shown that, in the case of a chromium complex, a transiently formed 2-aza-1-phospha-4-chroma-1,3-butadiene derivative could be trapped by addition of the NH function of [(aminobenzylidene)pentacarbonylchromium(0)] to

[‡] Part 19: Ref.[1]

[a] Institut für Anorganische und Analytische Chemie der Technischen Universität Braunschweig,
Postfach 3329, D-38023, Braunschweig, Germany
Fax: (internat.) + 49-(0)531/391-5387
E-mail: r.streubel@tu-bs.de

 © WILEY-VCH Verlag GmbH, D-69451 Weinheim, 2000 1434−1948/00/0606−1253 $ 17.50+.50/0



Scheme 2. Synthesis of carbene complexes **1a−c** and **2a,b** with sterically demanding aryl groups

the P−N double bond of the reactive intermediate, giving a dinuclear *N,N′*-PR-bridged carbene chromium complex.[2c] We suggested that this depends mainly on the lifetime of such metallaheterobutadiene intermediates, which should be enhanced by sterically demanding and thus kinetically protecting groups at either the metal or the carbene centre, especially if the rearrangement is truly intramolecular and the ligand does not dissociate prior to the formation of the three-membered ring. Therefore, we decided to investigate the rearrangement route **a** by employing sterically demanding *C*-2,4,6-trialkylphenyl-substituted aminocarbene complexes.

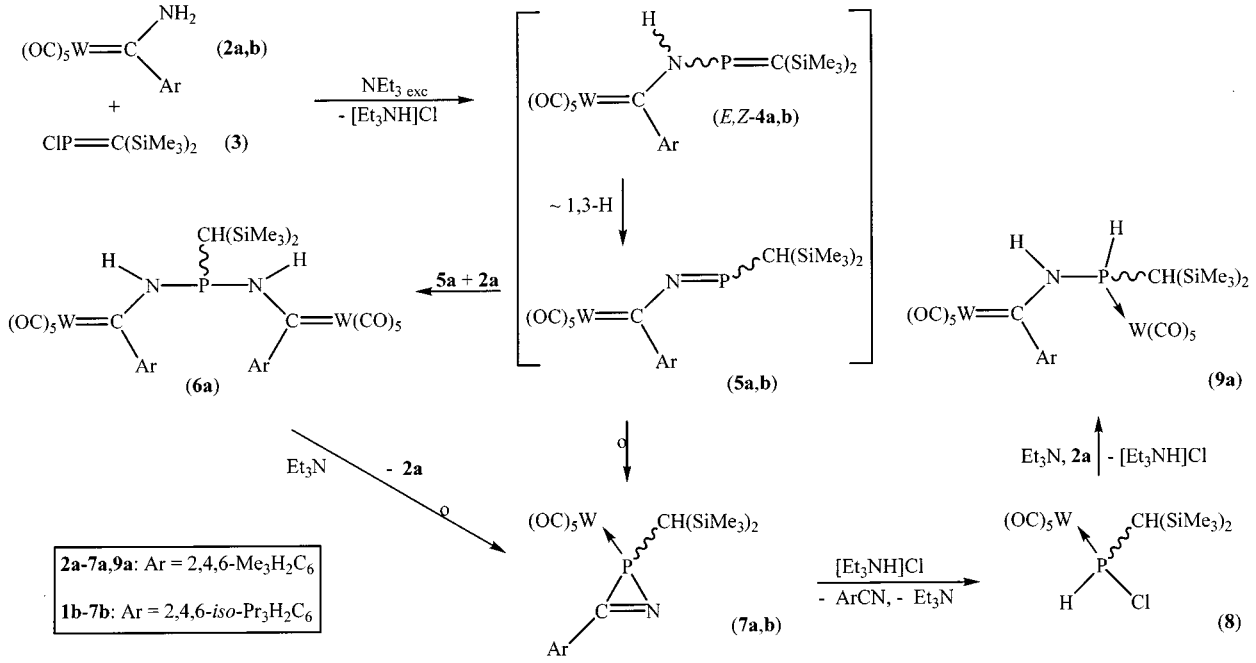
Whereas the ethoxy(aryl)carbene complexes **1a−c** were accessible by reacting aryllithium derivatives, prepared in situ, and hexacarbonyltungsten under standard conditions[10] (Scheme 2), the amino(aryl)carbene complexes **2a**,**b** were obtained only with difficulty by ammonolysis of **1a**,**b** in a 12:1 mixture of THF and a concentrated NH_3/water solution. Even after six weeks under these rather severe conditions (relative to standard procedures[10]) complex **2c** was not formed. The observation that bulky substituted alkoxy(alkyl/aryl)carbene complexes have low reaction rates and/or are remarkably inert in ether towards ammonia had already been reported; this reactivity was explained by their fourth-order reaction rate law.[10]

We therefore reacted, under standard conditions,[2] the *C*-2,4,6-trialkylphenyl-substituted aminocarbene complexes **2a**,**b** and [bis(trimethylsilyl)methylene]chlorophosphane[11] (**3**) in ether in the presence of an excess of triethylamine; the assumed reaction course is shown in Scheme 3. In the case of complex **2a** we obtained a mixture of various phosphorus-containing products, whereby the complexes **6a**, **7a**, **8** and **9a** were final products and the ^{31}P resonances of two transient species at δ = 305 and 330 were assigned to the *E*/*Z*-isomers of complex **4a** (ratio 1:1). Lowering the concentration of this reaction led to the preferred formation of complexes **8** and **9a** (ratio 1:2). It is also noteworthy that complex **6a** was only slowly transformed by base to the 2*H*-azaphosphirene complex **7a**. Whereas complexes **6a**, **8** and **9a** could be isolated in pure form by low temperature column chromatography, complex **7a** decomposed during the chromatographic separation. Nevertheless, a **7a**-enriched solution was obtained by twofold extraction of the reaction mixture with *n*-pentane at low temperature and, therefore, complex **7a** could be unambiguously characterized by ^{13}C and ^{31}P NMR spectroscopy of this solution. The nature of complexes **6a** and **9a** was also confirmed by X-ray analyses, but, to our surprise, complex **9a** crystallised only as the mesitylnitrile adduct **10**.

In the case of complex **2b**, the reaction with **3** in ether was significantly different; ^{31}P NMR spectroscopy revealed completeness of the reaction after ≈20 h, but the only phosphorus-containing product was complex **8**. Repeating the reaction in dichloromethane gave a different picture. Apart from intermediates at δ = 300 and 329 (*E*/*Z* complexes of **4b**), **7b** and **8**, another intermediate compound was formed in relatively large amounts and could be observed throughout the whole reaction, which was complete after ≈2.5 h (Figure 1). This intermediate decreased in favour of the 2*H*-azaphosphirene complex **7b** and the complex **8**, which is formed by a subsequent fast reaction of **7b** with $[Et_3NH]Cl$;[2] the marked tendency of complex **7b** to undergo this reaction is remarkable. Complex **7b** was characterized by its typical ^{31}P NMR parameters [δ = −121.7 (s, $|^1J(W,P)|$ = 303.3 Hz], but could not be isolated either by low temperature column chromatography or by an extraction procedure (see above).

The ^{31}P resonance of this new intermediate at δ = 183.3 is *not* in agreement with either a compound having a free or tungsten-coordinated $P{=}C(SiMe_3)_2$ structural unit,[12] or with analogues of complexes **6a** or **9a**. Assuming that the rearrangement cascade proceeds intramolecularly[13] two conceivable structures for this intermediate remain: complex **5b**, with the 2-aza-1-phospha-4-tungsta-1,3-butadiene moiety (or its zwitterion analogue **5b′**), and the zwitterionic complex **11** with the phosphorus atom incorporated in a three-membered ring with a partially formed P−N double bond.[14] Although the assignment of the NMR spectroscopic data to complex **5b** (**5b′**) seems more plausible, complex **11** cannot be completely excluded (Figure 2). Subsequent intramolecular rearrangements such as a nucleophilic attack of the phosphorus at the "carbene" centre in **5b**/**5b′** (thus forming complex **11**) or a shift of the pentacarbonyltungsten group in **11** from carbon to phosphorus (thus forming complex **7b**) are possible; such rearrangements, however, should be significantly hindered by bulky substituents at the "carbene" centre.

Elemental analyses and IR, MS and NMR spectroscopic data confirm unambiguously the proposed structures of the complexes **1a−c**, **2a,b**, **6a**, **7a**, **8** and **9a**. In particular, for **1a−c**, **2a,b**, **6a** and **9a** the carbene atom resonances, which are observed at low field, are of interest. In the case of the ethoxy-substituted carbene complexes, enhancement of the steric demand of the aryl substituent leads to a deshielding of the carbene atom (**1a**: δ = 334.8; **1b**: δ = 337.2; **1c**: δ = 341.2). This is just the opposite of the expected electronic influence of these aryl groups on the carbene atom. For complexes **2a**, **6a** and **9a** a deshielding of the carbene atoms was also observed [**2a**: δ = 276.2; **6a**: δ = 283.1 and 301.0 ($|^2J(P,C)|$ = 4.2 Hz); **9a**: δ = 288.3 ($|^2J(P,C)|$ = 14.3 Hz)]. Taking into account that the aryl substitution does not effect the aminocarbene resonance (**2b**: δ = 276.1), the formal substitution of an N−H function in **2a** by a PR_2 or a $PR_2W(CO)_5$ moiety influences the chemical shift of the car-



Scheme 3. Formation of 2*H*-azaphosphirene complexes **7a**,**b** and subsequent reactions

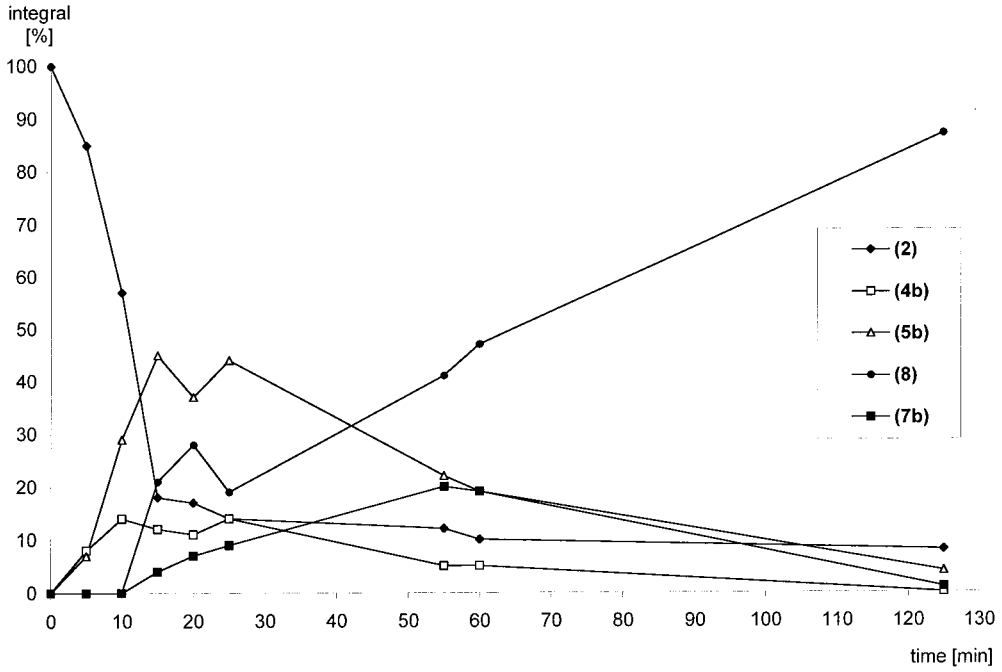


Figure 1. ^{31}P NMR monitoring of the reaction of complex **2b** with **3**

bene atoms mainly electronically. The observation of two magnetically nonequivalent carbene atoms in complex **6a** points to a remarkable intramolecular steric crowding and is so far unique.[2] This special steric situation also explains the relative stability of complex **6a** towards base-induced elimination to form complex **7a**. The P−H functions of complexes **8** and **9a** are well established by their phosphorus−proton coupling constants of $|^1J(P,H)|$ = 349.4 and 378.9 Hz, respectively. It is also remarkable that the two isotopomers of complex **8** could be distinguished by ^{31}P NMR spectroscopy (CH_2Cl_2; at 121.5 instead of 81.0 MHz) [**8**(^{35}Cl): δ = 53.23 ($|^1J(W,P)|$ = 268.38 Hz); **8**(^{37}Cl): δ = 53.3 ($|^1J(W,P)|$ = 268.80 Hz]. EI-MS experiments showed that all complexes analyzed predominantly lost carbon monoxide subsequent to the ionisation process.

The molecular structure of complex **6a**, as determined by X-ray crystallography (Figure 3), consists of two ($Me_3Si)_2HCP$-bridged amino(aryl)carbene complex moieties, which have an *E,E*-configuration of the pentacarbonyltungsten and the $(Me_3Si)_2HCP$ fragment with respect to the

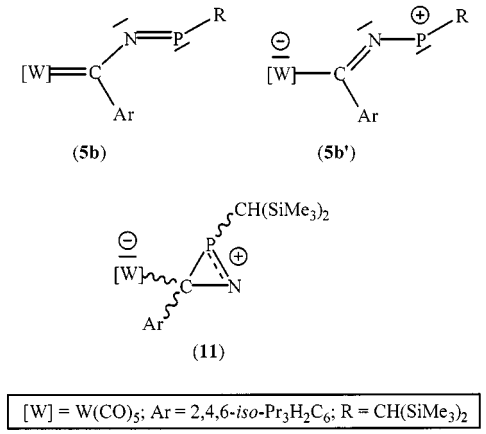


Figure 2. Plausible structures of the new intermediate in the 2*H*-azaphosphirene complex ring forming process

C−N bond, and which differ somewhat in the metal−carbon and nitrogen−phosphorus bond lengths of their nearly planar W−C−P−N skeletons [torsion angles: W(1)−C(28)−N(1)−P = −171°; W(2)−C(18)−N(2)−P = −175°]. The interplanar angle between the W−C−N and the mesityl ring plane [W(1)−C(28)−N(1)/Mes = 89.4° and W(2)−C(18)−N(2)/Mes = 81.9°] excludes any π-electron interactions between the carbene centres and the aryl rings.

The structure of complex **9a** in the mesitylnitrile adduct **10** (Figure 4) is similar with respect to the W−C−N−P subunit [W(2)−C(18)−N(1)−P = 175°] and also to the interplanar angle between the W−C−N and the mesityl ring plane [W(2)−C(18)−N(2)/Mes = 87.9°]. The freely defined hydrogen atoms at nitrogen and phosphorus adopt approximately an *E*-configuration with respect to the N−P bond. Of special interest are the dimensions of the hydrogen bond N(1)−H···N(2) unit: N−H···N = 176(7)°, N(1)···N(2) = 3.049(7) Å, N(1)−H(1) = 0.74(6) Å and N(2)···H(1) = 2.31(7) Å; a similar situation is often found for hydrogen bonds between nitriles and amides.

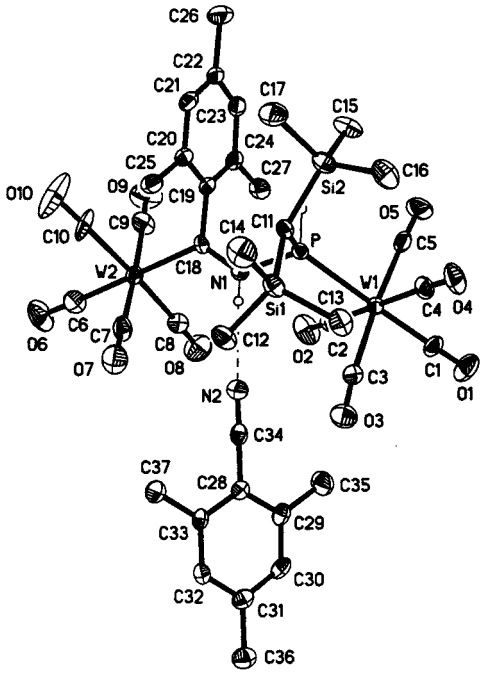


Figure 4. Molecular structure of complex **10** (ellipsoids represent 50% probability level; hydrogen atoms except P−H and N−H are omitted for clarity); selected bond lengths [Å] and angles [°]: W(1)−C(1) 2.015(7), P−W(1) 2.504(2), N(1)−P 1.769(5), P−C(11) 1.820(6), C(18)−N(1) 1.330(7), C(18)−W(2) 2.224(6), W(2)−C(6) 2.017(7); N(1)−C(18)−W(2) 126.7(4), C(18)−N(1)−P 130.1(4)

Experimental Section

General: All operations were carried out under an inert atmosphere of deoxygenated dry nitrogen. Solvents were dried according to standard procedures. − NMR spectra were recorded on a Bruker

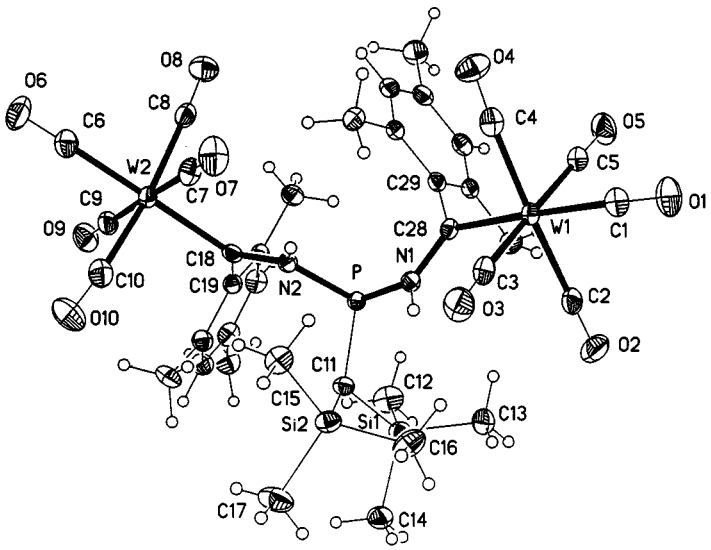


Figure 3. Molecular structure of complex **6a** (ellipsoids represent 50% probability level). Selected bond lengths [Å] and angles [°]: W(1)−C(1) 2.035(3), W(1)−C(28) 2.193(2), C(28)−N(1) 1.333(3), N(1)−P 1.7725(19), P−C(11) 1.832(2), P−N(2) 1.795(2), N(2)−C(18) 1.322(3), C(18)−W(2) 2.222(2), W(2)−C(6) 2.019(3); N(1)−C(28)−W(1) 123.89(16), C(28)−N(1)−P 127.62(16), N(1)−P−N(2) 95.59(9), C(18)−N(2)−P 126.41(17), N(2)−C(18)−W(2) 125.28(17)

AC-200 spectrometer (200 MHz for ^1H; 50.3 MHz for ^{13}C; 81 MHz for ^{31}P) using [D_3]chloroform and [D_6]benzene as solvents, the latter as internal standard, or a Bruker AMX-300 (30.4 MHz for ^{15}N) using dichloromethane as solvent and nitromethane as external standard; shifts are given relative to tetramethylsilane (^1H, ^{13}C), nitromethane (^{15}N) or 85% H_3PO_4 (^{31}P); only coupling constant magnitudes are given. − MS: Finnigan Mat 8430 (70 eV). − Elemental analyses: Carlo Erba analytical gas chromatograph. − IR: Biorad FT-IR-165; only ν(NH) and/or ν(CO) bands are given.

Preparation of {[Ethoxy(2,4,6-trimethylphenyl)carbene]pentacarbonyltungsten(0)} (1a): *n*-Butyllithium (6.25 mL, 1.6 M in *n*-hexane) was added at ambient temperature to a solution of 1-bromo-2,4,6-trimethylbenzene (2.0 g, 10 mmol) in 20 mL diethyl ether. After stirring for 70 min the reaction mixture was added to a suspension of hexacarbonyltungsten (3.5 g, 10 mmol) in 150 mL diethyl ether. The reaction mixture was stirred for 1 hour before the solvent was removed under reduced pressure (0.1 mbar). The residue was dissolved in 80 mL of water and triethyloxonium tetrafluoroborate (2.4 g, 13 mmol) was added in small portions. The mixture was extracted twice with 200 mL of *n*-pentane and the red *n*-pentane phases were filtered through a short column (SiO_2, *n*-pentane). The combined red *n*-pentane phases were concentrated under reduced pressure (0.1 mbar) and the red oily residue was purified by column chromatography (SiO_2, *n*-hexane). Removing the solvent afforded a red oil. The red oil was dissolved in 5 mL of *n*-pentane, the product precipitated at −100 °C and then dried in vacuo to give **1a** (1.95 g, 39%) as an orange powder. M.p. 80 °C (decomp.). − ^1H NMR ($CDCl_3$): δ = 1.65 [t, ^3J(H,H) = 7.10 Hz, 3 H, CH_2-CH_3], 2.17 (s, 6 H, *o*-Ar−CH_3), 2.31 (s, 3 H, *p*-Ar−CH_3), 5.14 [q, ^3J(H,H) = 7.10 Hz, 2 H, O−CH_2], 6.84 (s, 2 H, Ar−*H*3/3′). − $^{13}C\{^1H\}$ NMR ($CDCl_3$): δ = 14.1 (s, CH_2-CH_3), 19.3 (s, *o*-Ar−*C*H_3), 20.9 (s, *p*-Ar−*C*H_3), 80.7 (s, O*C*H_2), 126.4 (s, Ar−*C*2/2′), 128.8 (s, Ar−*C*3/3′), 137.5 (s, Ar−*C*4), 153.0 (s, Ar−*C*1), 198.0 (s, *cis*-*C*O), 203.7 (s, *trans*-*C*O), 334.8 (s, W=*C*R_2). − IR (KBr) $\tilde{\nu}$ = 2069 (m), 1984 (m), 1951 (s), 1921 (s), 1913 (s) cm^{-1} (CO). − MS (70 eV; ^{184}W): *m*/*z* (%) = 500 (34) [M^+], 472 (40) [M^+ − CO], 444 (31) [M^+ − 2CO], 416 (46) [M^+ − 3CO], 387 (57) [M^+ − 3CO − C_2H_5], 372 (9) [M^+ − 3CO − C_2H_5 − CH_3], 358 (100) [M^+ − 4CO − $2CH_3$]. − $C_{17}H_{16}O_6W$ (500.2): calcd. C 40.82, H 3.22; found C 41.30, H 3.24.

Preparation of {[Amino(2,4,6-trimethylphenyl)carbene]pentacarbonyltungsten(0)} (2a): Ammonia was slowly bubbled through a solution of 3 mmol of the complex **1a** in 60 mL of THF at 0 °C until it was saturated with ammonia. The reaction mixture was stirred for 20 hours at ambient temperature until a yellow colour persisted and thin liquid chromatography (SiO_2) indicated that all starting material had reacted. All volatile compounds were removed under reduced pressure (0.1 mbar) and the yellow residue, was purified by column chromatography (SiO_2, 20 °C; *n*-hexane/diethyl ether 10:1) to give **2a** (1.33 g, 94%) as a yellow powder. M.p. 163 °C (decomp.). − ^1H NMR ($CDCl_3$): δ = 2.23 (s, 6 H, *o*-Ar−*C*H_3), 2.30 (s, 3 H, *p*-Ar−*C*H_3), 6.86 (s, 2 H, Ar−*H*3/3′), 8.64 (s, br, 1 H, N*H*), 8.97 (s, br, 1 H, N*H*). − $^{13}C\{^1H\}$ NMR ($CDCl_3$): δ = 19.6 (s, *o*-Ar−*C*H_3), 20.8 (s, *p*-Ar−*C*H_3), 127.6 (s, Ar−*C*2/2′), 128.8 (s, Ar−*C*3/3′), 137.0 (s, Ar−*C*4), 149.1 (s, Ar−*C*1), 198.1 [s, ^1J(W,C) = 127.4 Hz, *cis*-*C*O], 203.2 (s, *trans*-*C*O), 276.2 (s, W=*C*R_2). − IR (KBr) $\tilde{\nu}$ = 3404 (m), 3275 (m), 3217 (m) (NH); 2065 (s), 1975 (s), 1913 (s), 1883 (s), 1861 (s) cm^{-1} (CO). − MS (70 eV); ^{184}W): *m*/*z* (%) = 471 (42) [M^+], 443 (26) [M^+ − CO], 415 (18) [M^+ − 2CO], 387 (86) [M^+ − 3CO], 359 (76) [M^+ − 4CO], 329 (100) [(M^+ − 4CO − $2CH_3$], 301 (31) [M^+ − 5CO − $2CH_3$]. − $C_{15}H_{13}NO_5W$ (471.1): calcd. C 38.24, H 2.78, N 2.97; found C 38.46, H 2.83, N 2.91.

General Procedure for the Preparation of (2,4,6-Triisopropylphenyl)- and (2,4,6-Tri-*tert*-butylphenyl)-Substituted {[Ethoxy(aryl)carbene]-pentacarbonyltungsten(0)} Complexes 1b and 1c: *n*-Butyllithium (1.6 molar in *n*-hexane, 6.25 mL) was added at −80 °C to a solution of the 1-bromo-2,4,6-trialkylbenzenes (R = *i*Pr, *t*Bu; 10 mmol) in 20 mL THF. After stirring for 90 min at −80 °C hexacarbonyltungsten (3.5 g, 10 mmol) was added in small portions to the reaction mixture, which was stirred for 18 hours and warmed up to ambient temperature before the solvent was removed under reduced pressure (0.1 mbar). The residue was dissolved in 40 mL of dichloromethane and triethyloxonium tetrafluoroborate (2.4 g, 13 mmol) was added in small portions. The solvent was removed under reduced pressure (0.1 mbar) and the residue was purified by low temperature column chromatography (SiO_2, −20 °C, *n*-hexane).

{Ethoxy[(2,4,6-triisopropylphenyl)carbene]pentacarbonyltungsten(0)} (1b): Compound **1b** (0.7 g, 12%) was obtained as a yellow orange powder. M.p. 76 °C (decomp.). − ^1H NMR ($CDCl_3$): δ = 1.04 (s, br, 6 H, *o*-Ar−CH(CH_3)$_2$), 1.21 [d, ^3J(H,H) = 6.8 Hz, 6 H, *o*-Ar−CH(CH_3)$_2$], 1.30 [d, ^3J(H,H) = 6.6 Hz, 6 H, *p*-Ar−CH(CH_3)$_2$], 1.62 (s, br, 3 H, CH_2-CH_3), 2.83 [m_c, br, 3 H, *p*-Ar−C*H*(CH_3)$_2$, *o*-Ar−C*H*(CH_3)$_2$], 5.01 (s, br, 2 H, O−CH_2), 6.94 (s, 2 H, Ar−*H*3/3′). − $^{13}C\{^1H\}$ NMR ($CDCl_3$): δ = 13.7 (s, CH_2CH_3), 21.1 [s, *o*-Ar−CH(*C*H_3)$_2$], 23.0 [s, *p*-Ar−CH(*C*H_3)$_2$], 25.2 [s, *o*-Ar−CH(*C*H_3)$_2$], 29.5 [s, *o*-Ar−*C*H(CH_3)$_2$], 33.1 [s, *p*-Ar−*C*H(CH_3)$_2$], 79.4 (s, O*C*H_2), 119.6 (s, br, Ar−*C*3/3′), 138.1 (s, br, Ar−*C*2/2′), 147.7 (s, Ar−*C*4), 149.9 (s, Ar−*C*1), 195.8 (s, *cis*-*C*O), 202.6 (s, *trans*-*C*O), 337.2 (s, W=*C*R_2). − IR (KBr) $\tilde{\nu}$ = 2069 (m), 1989 (m), 1950 (s), 1932 (s), 1905 (s), cm^{-1} (CO). − MS (70 eV; ^{184}W): *m*/*z* (%) = 584 (25) [M^+], 556 (26) [M^+ − CO], 528 (100) [M^+ − 2CO], 500 (64) [M^+ − 3CO], 472 (54) [M^+ − 4CO], 444 (74) [M^+ − 5CO], 231 (74) [($C_6H_2(C_3H_7)_3CO)^+$], 203 (5) [$(C_6H_2(C_3H_7)_3^+$], 43 (20) [$C_3H_7^+$]. − HR-MS ($C_{23}H_{28}O_6W$): calcd. 584.1397; found 584.1395 (±2 ppm).

{Ethoxy[(2,4,6-tri-*tert*-butylphenyl)carbene]pentacarbonyltungsten(0)} (1c): Compound **1c** (3.5 g, 56%) was obtained as a yellow orange powder. M.p. 82 °C (decomp.). − ^1H NMR ($CDCl_3$): δ = 1.29 [s, 9 H, *p*-Ar−C(CH_3)$_3$], 1.31 [s, 18 H, *o*-Ar−C(CH_3)$_3$], 1.77 [t, 3J(H,H) = 7.2 Hz, 3 H, CH_2CH_3], 5.03 [q, ^3J(H,H) = 7.2 Hz, 2 H, OCH_2], 7.29 (s, 2 H, Ar−H3/3′). − $^{13}C\{^1H\}$ NMR ($CDCl_3$): δ = 14.2 (s, CH_2CH_3), 31.3 [s, *p*-Ar−C(CH_3)$_3$], 34.5 [s, *o*-Ar−C(CH_3)$_3$], 34.7 [s, *p*-Ar−C(CH_3)$_3$], 38.5 [s, *o*-Ar−C(CH_3)$_3$], 80.9 (s, O*C*H_2), 122.6 (s, Ar−*C*3/3′), 137.8 (s, Ar−*C*2/2′), 149.0 (s, Ar−*C*4), 151.6 (s, Ar−*C*1), 198.3 [s, ^1J(C,W) = 129.0 Hz, *cis*-*C*O], 204.3 (s, *trans*-*C*O), 341.2 (s, W=*C*R_2). − IR (KBr) $\tilde{\nu}$ = 2069 (m), 1981 (m), 1953 (s), 1928 (s), 1910 (s) cm^{-1} (CO). − MS (70 eV; ^{184}W): *m*/*z* (%) = 626 (11) [M^+], 598 (20) [M^+ − CO], 570 (12) [M^+ − 2CO], 542 (86) [M^+ − 3CO], 513 (100) [M^+ − 3CO − C_2H_5], 485 (59) [M^+ − 4CO − C_2H_5], 273 (43) [$C_6H_2(C_4H_9)_3CO^+$], 57 (35) [$C_4H_9^+$]. − $C_{26}H_{34}O_6W$ (626.4): calcd. C 49.85, H 5.47; found C 50.07, H 5.59.

Preparation of {Amino[(2,4,6-triisopropylphenyl)carbene]pentacarbonyltungsten(0)} (2b): A concentrated solution of ammonia in water (4 mL, 50 mmol) was added at ambient temperature to a solution of **1b** (0.7 g, 1.2 mmol) in 60 mL of THF. The reaction mixture was stirred for 21 days at ambient temperature until a yellow colour persisted and thin liquid chromatography (SiO_2) indicated that all starting material was consumed. All volatile compounds were removed under reduced pressure (0.1 mbar) and the yellow residue was purified by low temperature column chromatography (SiO_2, −15 °C; *n*-hexane/diethyl ether 10:1) to give **2b** (0.6 g, 90%) as a yellow powder. M.p. 116 °C (decomp.). − ^1H NMR ($CDCl_3$):

δ = 1.17 [d, ^3J(H,H) = 6.8 Hz, 6 H, *o*-Ar−CH(CH_3)$_2$], 1.25 [d, ^3J(H,H) = 7.0 Hz, 6 H, *p*-Ar−CH(CH_3)$_2$], 1.33 [d, ^3J(H,H) = 6.8 Hz, 6 H, *o*-Ar−CH(CH_3)$_2$], 2.88 [sept, ^3J(H,H) = 7.0 Hz, 1 H, *p*-Ar−C*H*(CH$_3$)$_2$], 2.92 [sept, ^3J(H,H) = 6.8 Hz, 2 H, *o*-Ar−C*H*(CH$_3$)$_2$], 7.0 (s, 2 H, Ar-*H*3/3′), 8.64 (s, br, 1 H, N*H*), 8.97 (s, br, 1 H, N*H*). − ^{13}C{^{1}H} NMR (CDCl$_3$): δ = 23.3 [s, CH(*C*H$_3$)$_2$], 24.0 [s, CH(*C*H$_3$)$_2$], 26.4 [s, CH(*C*H$_3$)$_2$], 30.4 [s, *o*-Ar−*C*H(CH$_3$)$_2$], 34.1 [s, *p*-Ar−*C*H(CH$_3$)$_2$], 121.4 (s, Ar−*C*3/3′), 139.5 (s, Ar−*C*2/2′), 146.5 (s, Ar−*C*1), 148.6 (s, Ar−*C*4), 198.2 [s, ^1J(C,W) = 127.4 Hz, *cis*-*C*O], 202.8 (s, *trans*-*C*O), 276.1 (s, W=*C*R$_2$). − IR (KBr) ṽ = 3413 (m), 3319 (m), (NH); 2063 (s), 1971 (s), 1938 (vs), 1920 (vs), 1903 (vs) cm^{-1} (CO). − MS (70 eV; ^{184}W): *m*/*z* (%) = 555 (20) [M$^+$], 527 (8) [M$^+$ − CO], 499 (19) [M$^+$ − 2CO], 497 (19) [M$^+$ − 2CO − 2CH$_3$], 471 (85) [M$^+$ − 3CO], 469 (100) [M$^+$ − 2CO − 2CH$_3$], 203 (16) [C$_6$H$_2$(C$_3$H$_7$)$_3^+$], 43 (13) [C$_3$H$_7^+$]. − HR-MS (C$_{21}$H$_{25}$NO$_5$W): calcd. 555.1246; found 555.1240 (±2 ppm).

Preparation of *N*,*N*′-Bis{amino[(2,4,6-trimethylphenyl)carbene]pentacarbonyltungsten(0)}bis(trimethylsilyl)methylphosphane (6a), {[2-Bis(trimethylsilyl)methyl-3-(2,4,6-trimethylphenyl)-2*H*-azaphosphirene-κP}pentacarbonyltungsten(0)] (7a) and {Pentacarbonyl-[bis(trimethylsilyl)methylchlorophosphane]tungsten(0)} (8): NEt$_3$ (3.3 mL) was added at ambient temperature to a solution of complex **2a** (0.47 g, 1 mmol) and [bis(trimethylsilyl)methylene]chlorophosphane **3** (0.22 g, 1 mmol) in 10 mL of diethyl ether. The reaction mixture was stirred for 20 hours at ambient temperature until **3** was consumed (^{31}P NMR). To the yellow-orange reaction mixture was added 100 mL of pentane and the mixture then filtered. The solvent was removed under reduced pressure (0.1 mbar) and the residue was separated into two fractions by low temperature column chromatography (SiO$_2$, −20 °C; *n*-hexane/diethyl ether 15:1). Removing the solvent from the first yellow fraction under reduced pressure (0.1 mbar) gave complex **8**; similarly, the second yellow fraction gave a mixture of **6a** and **7a** as a yellow powder. The yellow powder was washed twice with 10 mL of *n*-pentane. The remaining yellow-orange residue was identified as **6a**. The solvent of the combined organic pentane phases was removed under reduced pressure (0.1 mbar) to give a yellow-orange powder, which was **7a**−enriched.

***N*,*N*′-Bis{amino[(2,4,6-trimethylphenyl)carbene]pentacarbonyltungsten(0)}bis(trimethylsilyl)methylphosphane (6a):** Compound **6a** (50 mg, 8.8%) was obtained as a yellow-orange powder. M.p. 166 °C (decomp.). − ^{1}H NMR (CDCl$_3$): δ = −0.08 [s, 9 H, Si(CH_3)$_3$], 0.32 [d, ^2J(P,H) = 4.7 Hz, 1 H, PC*H*], 0.52 [s, 9 H, Si(CH_3)$_3$], 1.07 (s, 3 H, *o*-Ar−CH_3), 2.06 (s, br, 3 H, *o*-Ar−CH_3), 2.19 (s, br, 6 H, *o*-Ar−CH_3), 2.28 (s, 3 H, *p*-Ar−CH_3), 2.50 (s, 3 H, *p*-Ar−CH_3), 6.90 (s, 1 H, Ar−*H*3/3′), 6.97 (s, 1 H, Ar-*H*3/3′), 7.03 (s, 1 H, Ar−*H*3/3′), 7.24 (s, 1 H, Ar−*H*3/3′), 9.29 (s, br, 1 H, N*H*), 9.95 (s, br, 1 H, N*H*). − ^{13}C{^{1}H} NMR (CDCl$_3$): δ = 0.9 [s, Si(*C*H$_3$)$_3$], 3.5 [s, Si(*C*H$_3$)$_3$], 17.9 (s, Ar−*C*H$_3$), 18.1 (s, Ar−*C*H$_3$), 20.5 (s, Ar−*C*H$_3$), 20.7 (s, Ar−*C*H$_3$), 20.8 [d, ^1J(P,C) = 50.5 Hz, P*C*H], 21.0 (s, Ar−*C*H$_3$), 22.5 (s, Ar−*C*H$_3$), 125.5 (s, Ar−*C*2/2′), 126.5 (s, Ar−*C*2/2′), 126.6 [d, ^4J(P,C) = 2.2 Hz, Ar−*C*2/2′], 127.5 (s, Ar−*C*2/2′), 129.0 (s, Ar−*C*3/3′), 129.1 (s, Ar−*C*3/3′), 129.2 (s, Ar−*C*3/3′), 129.9 (s, Ar−*C*3/3′), 138.1 (s, Ar−*C*4), 139.1 (s, Ar−*C*4), 146.3 [d, ^3J(P,C) = 11.9 Hz, Ar−*C*1], 147.7 [d, ^3J(P,C) = 8.8 Hz, Ar−*C*1], 197.6 [s, ^1J(W,P) = 127.4 Hz, *cis*-*C*O], 198.2 [s, ^1J(P,W) = 127.1 Hz, *cis*-*C*O], 202.2 (s, *trans*-*C*O), 202.7 (s, *trans*-*C*O), 283.1 (s, W=*C*R$_2$), 301.0 [d, ^2J(P,C) = 4.2 Hz, W=*C*R$_2$]. − ^{31}P{^{1}H} NMR (CDCl$_3$): δ = 110.3 (s). − IR (KBr) ṽ = 3324 (w), 3310 (w) (NH); 2064 (s), 1992 (m), 1984 (s), 1952 (s), 1941 (s), 1924 (s), 1913 (s), 1899 (s) cm^{-1} (CO). − MS (*pos.*-CI, NH$_3$, ^{184}W): *m*/*z* (%) = 1130 (2) [M$^+$], 661 (86) [(M + H)$^+$ −{(CO)$_5$W=C(C$_9$H$_{11}$)NH}], 469 (100) [{(CO)$_5$W=C(C$_9$H$_{11}$)NH}$^+$]. − C$_{37}$H$_{43}$N$_2$O$_{10}$PSi$_2$W$_2$ (1130.6): calcd. C 39.31, H 3.83, N 2.48; found C 39.62, H 3.95, N 2.39.

{[2-Bis(trimethylsilyl)methyl-3-(2,4,6-trimethylphenyl)-2H-azaphosphirene-κP}pentacarbonyltungsten(0)] (7a): ^{1}H NMR (C$_6$D$_6$): δ = −0.17 [s, 9 H, Si(CH_3)$_3$], 0.32 [s, 9 H, Si(CH_3)$_3$], 0.65 [d, 1 H, ^2J(P,H) = 3.6 Hz, PC*H*], 1.80 (s, 3 H, *p*-Ar−CH_3), 2.11 (s, 6 H, *o*-Ar−CH_3), 6.55 (s, 2 H, Ar-*H*3/3′). − ^{13}C{^{1}H} NMR (*n*C$_5$H$_{12}$/C$_6$D$_6$): δ = 1.8 [d, ^3J(P,C) = 2.2 Hz, Si(*C*H$_3$)$_3$], 2.3 [d, ^3J(P,C) = 3.0 Hz, Si(*C*H$_3$)$_3$], 29.2 [d, ^1J(P,C) = 25.7 Hz, P*C*H], 122.3 [d, ^2J(P,C) = 11.6 Hz, Ar−*C*1], 130.7 (s, Ar−*C*3,5), 141.9 (s, Ar−*C*2,6), 142.1 (s, Ar−*C*2,6), 144.1 (s, Ar−*C*4), 191.1 [(d, $^{(1+2)}J$(P,C) = 3.8 Hz, P*C*N], 196.7 [d, ^2J(P,C) = 8.6 Hz, *cis*-*C*O], 201.9 [d, ^2J(P,C) = 35.4 Hz, *trans*-*C*O]. − ^{31}P{^{1}H} NMR (C$_6$D$_6$): δ = −122.3 [s, ^1J(W,P) = 298.7 Hz].

{Pentacarbonyl{[bis(trimethylsilyl)methyl]chlorophosphane}tungsten(0)} (8): Compound **8** (204 mg, 37%) was obtained as a pale yellow solid. M.p. 52 °C (decomp.). − ^{1}H NMR (CDCl$_3$): δ = 0.26 [s, 9 H, Si(CH_3)$_3$], 0.34 [s, 9 H, Si(CH_3)$_3$], 1.11 [dd, ^2J(P,H) = 6.5, ^3J(H,H) = 1.5 Hz, PCH], 7.88 [dd, ^1J(P,H) = 349.4, ^1J(W,H) = 5.8, ^3J(H,H) = 1.5 Hz, 1 H, PH]. − ^{13}C{^{1}H} NMR (CDCl$_3$): δ = 0.1 [d, ^3J(P,C) = 3.0 Hz, SiMe$_3$], 2.1 [s, ^3J(P,C) = 4.3 Hz, SiMe$_3$], 24.6 [d, ^1J(P,C) = 4.8 Hz, PCH], 195.9 [d, ^1J(W,C) = 126.5, ^2J(P,C) = 6.9 Hz, *cis*-CO], 198.7 [d, ^2J(P,C) = 31.3 Hz, *trans*-CO]. − ^{31}P{^{1}H} NMR (81.0 MHz, CDCl$_3$): δ = 53.3 [d, ^1J(P,H) = 349.4, ^1J(W,P) = 268.8 Hz]. − MS (*pos.*-CI, isobutane, ^{35}Cl, ^{184}W): *m*/*z* = 550 (100) [M$^+$], 515 (56) [M − ^{35}Cl$^+$], 191 (51) [C$_7$H$_{20}$PSi$_2^+$], 73 (96) [Me$_3$Si$^+$]. − ^{31}P NMR (81.0 MHz, CDCl$_3$): δ = 53.7 [dd, ^1J(P,H) = 349.4, ^1J(W,P) = 268.8, ^2J(P,H) = 6.5 Hz]. − C$_{12}$H$_{20}$ClO$_5$PSi$_2$W (550.7): calcd. C 26.17, H 3.66; found C 26.45, H 3.80.

Preparation of *N*-{Amino[(2,4,6-trimethylphenyl)carbene]pentacarbonyltungsten(0)}-[bis(trimethylsilyl)methylphosphane]pentacarbonyltungsten(0) (9a): [Bis(trimethylsilyl)methylene]chlorophosphane **3** (0.49 g, 2.2 mmol) and 11 mL of NEt$_3$ were added at 0 °C to a solution of complex **2a** (1.10 g, 2.2 mmol) in 33 mL of diethyl ether. The reaction mixture was stirred for 70 hours at ambient temperature until **3** was consumed (^{31}P NMR) and a 1:2 mixture of **8**:**9a** was detected. The solvent was evaporated slowly to dryness under reduced pressure (0.1 mbar). The residue was extracted twice with 50 mL of *n*-pentane and filtered. The remaining residue was washed twice with 5 mL of *n*-pentane, the organic phases combined and the solvent removed under reduced pressure. The residue was separated in two fractions by low temperature column chromatography. Removing the solvent of the first yellow fraction (SiO$_2$, −20 °C; *n*-pentane) under reduced pressure (0.1 mbar) gave complex **8**. Removing the solvent of the second yellow fraction (SiO$_2$, −20 °C; *n*-pentane/diethyl ether 7:1) under reduced pressure (0.1 mbar) gave **9a**. Orange crystals of the mesitylnitrile adduct **10** were obtained by crystallisation of **9a** in the presence of mesitylnitrile in *n*-pentane.

9a: 0.44 g (40%) as an orange powder. M.p. 112 °C (decomp.). − ^{1}H NMR (C$_6$D$_6$): δ = −0.3 [d, 9 H, ^4J(P,H) = 1.1 Hz, Si(CH_3)$_3$], 0.21 [s, 9 H, Si(CH_3)$_3$], 1.33 [dd, ^3J(H^C,H^P) = 19.0 Hz, ^2J(P,H) = 3.1 Hz, 1 H, PC*H*], 1.97 (s, 3 H, Ar−CH_3), 2.10 (s, 3 H, Ar−CH_3), 2.18 (s, 3 H, Ar−CH_3), 6.45 (s, 1 H, Ar−*H*), 6.52 (s, 1 H, Ar−*H*), 6.87 [ddd, ^1J(P,H) = 378.9 Hz, ^3J(H^P,H^C) = 19.0 Hz, ^3J(H^P,H^N) = 8.0 Hz, 1 H, P*H*], 9.6 [dd, br, ^3J(H^N,P) = 27.5 Hz, ^3J(H^N,H^P) = 8.0 Hz, 1 H, N*H*]. − ^{13}C{^{1}H} NMR (C$_6$D$_6$): δ = 0.4 [d, ^3J(P,C) = 5.1 Hz, Si(*C*H$_3$)$_3$], 2.0 [d, ^3J(P,C) = 3.3 Hz, Si(*C*H$_3$)$_3$], 18.8 [d, ^1J(P,C) = 17.1 Hz, P*C*H], 19.6 (s, Ar−*C*H$_3$), 20.5 (s, Ar−*C*H$_3$),

21.6 (s, Ar−*C*H$_3$), 126.5, (s, Ar−*C*2,2′), 127.8, (s, Ar−*C*2,2′), 129.5, (s, Ar−*C*3,3′), 129.7, (s, Ar−*C*3,3′), 137.8 (s, Ar−*C*4), 145.6 [d, ^3J(P,C) = 7.4 Hz, Ar−*C*1], 195.7 [d, ^2J(P,C) = 6.6 Hz, *cis*-*C*O], 198.4 (s, *cis*-*C*O), 198.7 [d, ^2J(P,C) = 32.5 Hz, *trans*-*C*O], 202.6 [d, ^4J(P,C) = 1.9 Hz, *trans*-*C*O], 288.3 [d, ^2J(P,C) = 14.3 Hz, W=*C*R$_2$]. − ^{31}P NMR (C$_6$D$_6$): δ = 27.5 [ddd, ^1J(P,H) = 378.9 Hz, ^2J(P,H^N) = 27.5 Hz, ^2J(P,H^C) = 3.1 Hz, ^1J(P,W) = 255.5 Hz]. − IR (KBr) $\tilde{\nu}$ = 3177 (w) (NH); 2079 (m), 2065 (s), 1986(m), 1963(s), 1950 (s), 1930 (vs), 1913 (s), 1902 (s) cm^{-1} (CO). − $C_{27}H_{32}NO_{10}PSi_2W_2$ (985.4): C 32.91, H 3.27, N 1.42; found C 33.38, H 3.41, N 1.35.

Attempted Synthesis of {[2-Bis(trimethylsilyl)methyl-3-(2,4,6-triisopropylphenyl)-2*H*-azaphosphirene-κP]pentacarbonyltungsten(0)} (7b): To a solution of complex **2b** (0.05 g, 0.08 mmol) in 0.8 mL of dichloromethane were added [bis(trimethylsilyl)methylene]chlorophosphane **3** (0.02 g, 0.08 mmol) and 0.3 mL of NEt$_3$ at ambient temperature. The reaction was monitored by ^{31}P NMR spectroscopy; ^{31}P NMR signal integrals were determined ([%], relaxation time = 0) after different reaction times (t [min]).

7b: ^{31}P{^{1}H} NMR (reaction mixture, CH$_2$Cl$_2$/Et$_3$N): δ = −121.5 [s, ^1J(W,P) = 303.0 Hz].

Structure Determination of Complex 6a·CH$_2$Cl$_2$: Crystal data: $C_{38}H_{44}Cl_2N_2O_{10}PSi_2W_2$, M = 1214.50, $P\bar{1}$, a = 11.7890(10), b = 12.2501(10), c = 17.7820(14) Å, α = 83.779(3), β = 80.145(3), γ = 65.843(3)°, V = 2306.5(3) Å^3, Z = 2, $d_{calcd.}$ = 1.749 Mg/m^3, μ = 5.239 mm^{-1}, T = 143 K. The crystal (0.27 × 0.23 × 0.18 mm) was mounted in inert oil. 27513 intensities were measured (4 ≤ 2θ ≤ 60) using Mo-K_α radiation on a Bruker SMART 1000 CCD diffractometer. After absorption correction (multiple-scans) 13311 were unique (R_{int} = 0.0287) and used for all calculations (program SHELXL-97).[15] All hydrogen atoms (except rigid methyl groups) were refined with a riding model. The final $wR(F^2)$ was 0.0556 with conventional R(F) = 0.0231 for 526 parameters and 73 restraints. Highest peak 1.366, hole −1.528 e/Å^3.

Structure Determination of Complex 10: Crystal data: $C_{37}H_{43}N_2O_{10}PSi_2W_2$, M = 1130.58, $P2_1/c$, a = 14.645(2), b = 19.406(2), c = 15.262(2) Å, β = 93.51(1)°, V = 4329.5(9) Å^3, Z = 4, $d_{calcd.}$ = 1.734 Mg/m^3, μ = 5.455 mm^{-1}, T = 173 K. The crystal (0.50 × 0.40 × 0.30 mm) was mounted in inert oil. 8825 intensities were measured (6 ≤ 2θ ≤ 50) using Mo-K_α radiation on a Siemens P4 diffractometer. After absorption correction (psi-scans) 7594 were unique (R_{int} = 0.0332) and used for all calculations (program SHELXL-93).[16] All hydrogen atoms [except rigid methyl groups and freely refined (N1)−H1/(P)−H2] were refined with a riding model. The final $wR(F^2)$ was 0.0804 with conventional R(F) = 0.0336 for 507 parameters and 254 restraints. Highest peak 1.641, hole −1.806 e/Å^3. Crystallographic data (excluding structure factors) for the structures reported in this paper have been deposited with the Cambridge Crystallographic Data Centre as supplementary publication no. CCDC-138591 **(6a)** and CCDC-138592 **(10)**. Copies of the data can be obtained free of charge on application to The Director, CCDC, 12 Union Road, Cambridge, UK CB2 1EZ [Fax: (internat.) + 44-1223/336-033; E-mail: deposit@ccdc.cam.ac.uk].

Acknowledgments

Financial support by the Deutsche Forschungsgemeinschaft and the Fonds der Chemischen Industrie and HR-MS measurements by Dr. Hans-Martin Schiebel (Universität Braunschweig) are gratefully acknowledged.

[1] R. Streubel, H. Wilkens, F. Ruthe, P. G. Jones, *Chem. Commun.* **1999**, 2127−2128.
[2] [2a]R. Streubel, J. Jeske, P. G. Jones, R. Herbst-Irmer, *Angew. Chem.* **1994**, *106*, 115−117; *Angew. Chem. Int. Ed. Engl.* **1994**, *33*, 80−82. −[2b]R. Streubel, A. Ostrowski, S. Priemer, U. Rohde, J. Jeske, P. G. Jones, *Eur. J. Inorg. Chem.* **1998**, 257−261. −[2c]R. Streubel, F. Ruthe, P. G. Jones, *Eur. J. Inorg. Chem.* **1998**, 571−574. −[2d]R. Streubel, S. Priemer, F. Ruthe, P. G. Jones, D. Gudat, *Eur. J. Inorg. Chem.* **1998**, 575−578.
[3] R. Streubel, M. Hobbold, J. Jeske, P. G. Jones, *J. Organomet. Chem*. **2000**, *595*, 12−20.
[4] R. Streubel, U. Rohde, J. Jeske, F. Ruthe, P. G. Jones, *Eur. J. Inorg. Chem.* **1998**, 2005−2012.
[5] H. Wilkens, F. Ruthe, P. G. Jones, R. Streubel, *Chem. Eur. J.* **1998**, *4*, 1542−1553.
[6] [6a]A. Ostrowski, J. Jeske. P. G. Jones, R. Streubel, *J. Chem. Soc., Chem. Commun.* **1995**, 2507−2508. − [6b]R. Streubel, H. Wilkens, F. Ruthe, P. G. Jones, *Z. Anorg. Allg. Chem.* **1999**, *625*, 102−106.
[7] R. Streubel, L. Ernst, J. Jeske, P. G. Jones, *J. Chem. Soc., Chem. Commun.* **1995**, 2113−2114.
[8] [8a]R. Streubel, H. Wilkens, A. Ostrowski, C. Neumann, F. Ruthe, P. G. Jones, *Angew. Chem.* **1997**, *109*, 1549−1550; *Angew. Chem. Int. Ed. Eng.* **1997**, *36*, 1492−1493. − [8b]H. Wilkens, F. Ruthe, P. G. Jones, R. Streubel, *Chem. Commun.* **1998**, 1529−1530
[9] [9a]R. Streubel, A. Ostrowski, H. Wilkens, F. Ruthe, J. Jeske, P. G. Jones, *Angew. Chem.* **1997**, *109*, 409−413; *Angew. Chem. Int. Ed. Engl.* **1997**, *36*, 378−381. − [9b]R. Streubel, H. Wilkens, U. Rohde, A. Ostrowski, J. Jeske, F. Ruthe, P. G. Jones, *Eur. J. Inorg. Chem.* **1999**, 1567−1579. −[9c]R. Streubel, U. Schiemann, N. Hoffmann, Y. Schiemann, P. G. Jones, D. Gudat, *Organometallics* **2000**, *19*, 475−481.
[10] K. H. Dötz, H. Fischer, P. Hofmann, F. R. Kreissl, U. Schubert, K. Weiss, *Transition Metal Carbene Complexes* (Ed.: D. Seyferth), Verlag Chemie, Weinheim, **1983**.
[11] R. Appel, A. Westerhaus, *Tetrahedron Lett.* **1981**, *22*, 2159−2160.
[12] R. Appel, in *Multiple Bonds and Low Coordination in Phosphorus Chemistry*, (Eds.: M. Regitz, O. J. Scherer), Georg Thieme Verlag, Stuttgart, **1990**, p. 157−219.
[13] Investigations of the stereochemical course show that the 2*H*-azaphosphirene complex formation proceeds stereospecifically if triphenylphosphane-substituted aminocarbene complexes are used; R. Streubel, S. Priemer, J. Jeske, F. Ruthe, P. G. Jones, manuscript in preparation.
[14] E. Niecke, D. Gudat, *Angew. Chem.* **1991**, *103*, 251−270; *Angew. Chem. Int. Ed. Engl.* **1991**, *30*, 217−236.
[15] G. M. Sheldrick, *SHELXL-97, Program for crystal structure refinement*, University of Göttingen, **1997**.
[16] G. M. Sheldrick, *SHELXL-93, Program for crystal structure refinement*, University of Göttingen, **1993**.

Received January 13, 2000
[I00012]

Dimethoxyhydroxycarbenium Hexafluorometallate – Synthesis, Spectroscopic Characterization and the Crystal Structure of $(MeO)_2COH^+SbF_6^-$

Rolf Minkwitz*[a] and Frank Neikes[a]

Keywords: Carbocations / IR spectroscopy / Raman spectroscopy / NMR spectroscopy / Protonations

Dimethyl carbonate reacts in the superacidic system HF/MF_5 (M = As, Sb) with formation of $(MeO)_2COX^+MF_6^-$ (M = As, Sb; X = H, D). $(MeO)_2COH^+SbF_6^-$ crystallizes in the orthorhombic space group $Pna2_1$ (No. 33) with a = 9.668(2) Å, b = 8.340(2) Å, c = 11.135(4) Å and four formula units per cell. The unit cell contains $(MeO)_2COH^+$ cations of approximate C_s symmetry with an almost central trigonal planar CO_3 skeleton and C–O bond lengths in a range between 1.26(1) Å and 1.30(2) Å. The salt contains long O–H and Sb–F bond and an F···H contact of 1.62(9) Å. With regard to the formation of the salts, the reaction of dimethyl carbonate with the superacidic systems XF/MF_5 (X = H, D; M = As, Sb) is discussed and the Raman, IR, ^1H and ^{13}C NMR spectra of $(MeO)_2COX^+MF_6^-$ (M = As, Sb; X = H, D) are reported.

Introduction

The formulation of protonated compounds as reactive cationic intermediates is important for the explanation of reaction mechanisms. The evidence for such intermediates is of great importance in modern chemistry and can be used to confirm or deny known mechanisms. It has been shown that protonated compounds, for example, are not only short lived intermediates, but are even available in stabilized forms. A kinetic stabilization is possible due to protonation with superacids like HF/MF_5 or HSO_3F/MF_5 (M = As, Sb). This field of chemistry has been mainly developed by Olah, who was able to prove the existence of many protonated organic compounds in superacidic systems by NMR spectroscopy.[1–3]

In superacidic systems like FSO_3H/SbF_5 or HF/MF_5 (M = As, Sb) an extended spectrum of organic and inorganic species, for example element hydrides of group 15 and 16, can be protonated and stabilized.[4–14] Almost all known carbocations are mainly identified in solution by NMR spectroscopy. However, the crystal structures of protonated acetic acid, protonated carbonic acid and protonated formic acid have been investigated.[15–18] Attempts to isolate the H_2COH^+ cation failed because of the formation of the $(CH_2)O(CH_2)OH^+$ cation.[19] Substances with a CO_3 skeleton, such as the carbonate anion, the protonated carbonic acid or the monoperoxocarbonic acid anion are known and have been spectroscopically and structurally investigated.[17,20] In the row of the simplest mono-, di- and trioxocarbenium ions, we tried to isolate the dimethoxyhydroxycarbenium hexafluorometallates at low temperature in order to study their chemical behavior in acidic systems.

[a] Anorganische Chemie, Fachbereich Chemie der Universität Dortmund,
D-44221 Dortmund, Germany

Results and Discussion

Formation of $(MeO)_2COH^+$ Salts

Protonation of dimethyl carbonate by the superacidic systems HF or DF/MF_5 (M = As, Sb) gives dimethoxyhydroxycarbenium hexafluorometallates [Equation (1)].

$$(MeO)_2CO + XF + MF_5 \rightarrow (MeO)_2COX^+MF_6^- \quad (X = H, D; M = As, Sb) \quad (1)$$

The resulting colorless, moisture-sensitive salts, which are soluble in SO_2, decompose in the case of the arsenate above –38 °C, and in the case of the antimonate above –35 °C. Under inert conditions at –70 °C the salts can be stored for several weeks without decomposition. The remaining $(MeO)_2COH^+SbF_6^-$ contained crystals suitable for X-ray diffraction studies.

X-ray Crystal Structure of $(MeO)_2COH^+SbF_6^-$

Dimethoxyhydroxycarbenium hexafluoroantimonate crystallizes in the orthorhombic space group $Pna2_1$ (No. 33) with four units per cell (see Table 1).[21] Table 2 lists important bond lengths and angles and Figure 1 shows the crystal structure with atom labels. The arrangement of the $(MeO)_2COH^+SbF_6^-$ in the unit cell is shown in Figure 2. For data collection and reduction, a semiempirical correction determined from single ψ-scan data, and programs in the SHELXL package and PARST, were used.[22–25] The antimony layers were found by the Patterson method. All other atoms, including protons, were determined by difference Fourier synthesis. A final refinement with anisotropic (except H atoms) thermal parameters gave a value of R = 0.0198.

The CO bond lengths [1.26(1) Å, 1.274(8) Å and 1.30(2) Å] show no significant differences and can be compared to the lengths of the CO bonds in the dihydroxymethylcarbenium

 © WILEY-VCH Verlag GmbH, D-69451 Weinheim, 2000 1434–1948/00/0606–1261 $ 17.50+.50/0

Table 1. X-ray diffraction data of $(MeO)_2COH^+SbF_6^-$

	$(CH_3O)_2COH^+SbF_6^-$
Formula mass	326.83
Space group (no.)	$Pna2_1$ (33)
Crystal system	Orthorhombic
a, Å	9.668(2)
b, Å	8.340(2)
c, Å	11.135(4)
Volume, Å^3	897.8(4)
Density (calcd.), g cm^{-3}	2.418
Z	4
Absorption coefficient, mm^{-1}	3.148
Temperature, K	173
$F(000)$	616
Wavelength, Å	0.71069
Theta range for data collection, °	3.05 to 24.93
Index ranges	$0 \le h \le 11$, $0 \le k \le 8$, $-13 \le l \le 0$
Reflections collected/independent	780
Parameters	142
Goodness-of-fit on F^2	1.134
R[a] $[I > 2\sigma(I)]$	0.02
R[a] (all data)	0.021
Largest diff. Peak and hole, e·Å^{-3}	0.875/−0.796
Refinement method	Full matrix, least-squares on F^2

[a] $R = \Sigma||F_o| - |F_c||/\Sigma|F_o|$; Refinement method: full-matrix least-squares calculations based on F^2.

Table 2. Bond lengths [Å], selected angles (deg), and interionic distances (Å) for $(MeO)_2COH^+SbF_6^-$

	Length [Å]		Angle [deg]
Sb(1)–F(3)	1.919(3)	F(1)–Sb(1)–F(6)	90.2(2)
Sb(1)–F(4)	1.869(4)	F(2)–Sb(1)–F(5)	89.8(2)
Sb(1)–F(5)	1.868(4)	F(2)–Sb(1)–F(6)	92.4(2)
Sb(1)–F(6)	1.860(4)	F(6)–Sb(1)–F(5)	91.5(2)
O(1)–C(1)	1.26(1)	O(1)–C(1)–O(3)	122.8(11)
O(2)–C(1)	1.300(2)	O(1)–C(1)–O(2)	117.8(6)
O(3)–C(1)	1.274(8)	O(2)–C(1)–O(3)	119.4(8)
O(2)–C(2)	1.508(8)	C(1)–O(1)–H(1)	121(5)
O(3)–C(3)	1.48(1)	C(1)–O(2)–C(2)	117.2(5)
O(1)–H(1)	0.96(8)	C(1)–O(3)–C(3)	115.9(8)
O(1)···F(3)	2.570(6)		
F(3)···H(1)	1.68(8)		

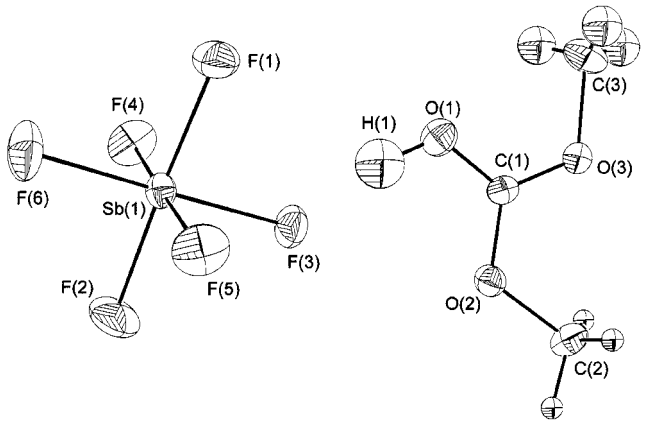


Figure 1. Projection of the asymmetric unit; thermal ellipsoids are drawn at the 50% probability level

cation and the $C(OH)_3^+$ cation as well as the almost trigonal planar CO_3 skeleton with OCO angles of 122(1)°, 117.8(6)° and 119.4(8)°.[17,18] The CO_3 skeleton geometry and the CO bond lengths, which are in a range between a single [1.508(8) Å for C(2)–O(2) and 1.48(1) Å for C(3)–O(3)] and a double CO bond [1.222(2) Å in formic acid], imply that the positive charge is delocalized. The two Me–O–C–O torsion angles [73.2(6)° and 3.1(9)°] show that the methyl groups are not located in the CO_3 plane. The O(1)···F(3) distance of 2.570(1) Å indicates a strong O(1)–H(1)···F(3) hydrogen bond,[26] which causes the Sb(1)–F(3) bond [1.919(3) Å] to be 2.7% longer than the other Sb(1)–F bonds. The maximum deviation from ideal octahedron angles in the SbF_6^- anion is 2.4°. As observed in the Raman and IR spectra the ideal octahedron structure is distorted. In the AB plane only alternating hydrogen-bonded ion pairs are formed; these planes are piled up the C axes with no contacts between adjacent planes.

Raman and IR Spectra of $(MeO)_2COX^+MF_6^-$ (X = H, D; M = As, Sb)

The infrared and Raman spectra of $(MeO)_2COD^+SbF_6^-$ are shown in Figure 3. The observed frequencies of $(MeO)_2COX^+MF_6^-$ (X = H, D; M = As, Sb) are summarized in Table 3. The assignments for the $(MeO)_2COX^+$ cation were made by a comparison with the precursor $(MeO)_2CO$ and several alkyl derivatives.[27–32] The assignments of the anions were made according to known literature data.[17,18,33]

On the condition that $(MeO)_2COX^+MF_6^-$ (X = H, D; M = As, Sb) has a C_S point symmetry, 21 (A') and 12 (A'') fundamental Raman and IR active vibrational modes are expected. Referring to the complex spectra observed, many vibrational modes are split, which could be a sign for a change to a lower symmetry in the crystal. The vibrational spectra of liquid and solid dimethyl carbonate show that, as the temperature is lowered, the observed splitting in the low-temperature spectra increases. This behavior is typical of crystal splitting in crystals of organic compounds, probably due to lattice concentration effects. The spectra become complex so that it gets difficult to assign the vibrational modes. Therefore vibrational modes are only assigned in their typical range. Without the X-ray studies and NMR spectra, the complex Raman and IR spectra could give no evidence for the existence of protonated dimethyl carbonate.

There is no denying that differences in the spectra between $(MeO)_2COH^+AsF_6^-$ and $(MeO)_2COH^+SbF_6^-$ are noticed. One possible reason for this is the crystallization in different space groups, so that varying crystalline field-splitting can be observed. Another reason might be that the influence of the anion to the vicinity of the cations differs. The measured spectra of protonated dimethyl carbonate show no further overtones, fermi resonances or combination tones in the region 1700–2900 cm^{-1}.

The antisymmetric and symmetric stretching modes of the methyl groups are observed in the region of 2960–3100 cm^{-1}. The Raman spectra of the hexafluoroantimonate anion show four different antisymmetric stretching modes at

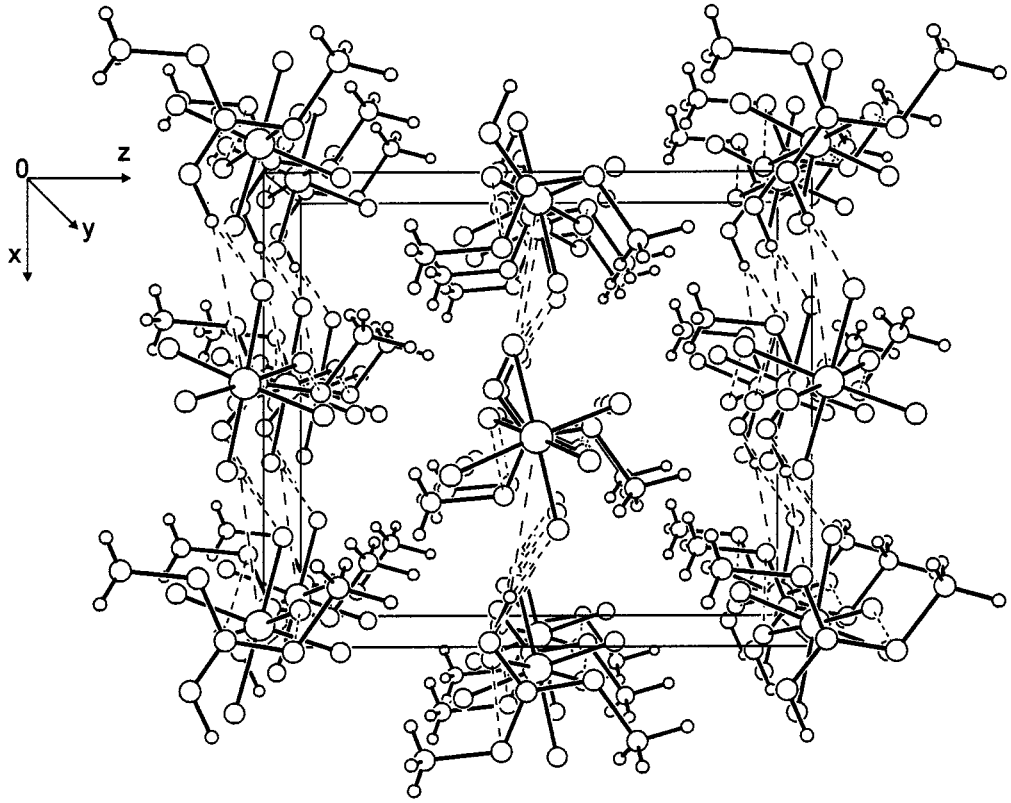


Figure 2. Projection of the $(MeO)_2COH^+SbF_6^-$ salt with contacts

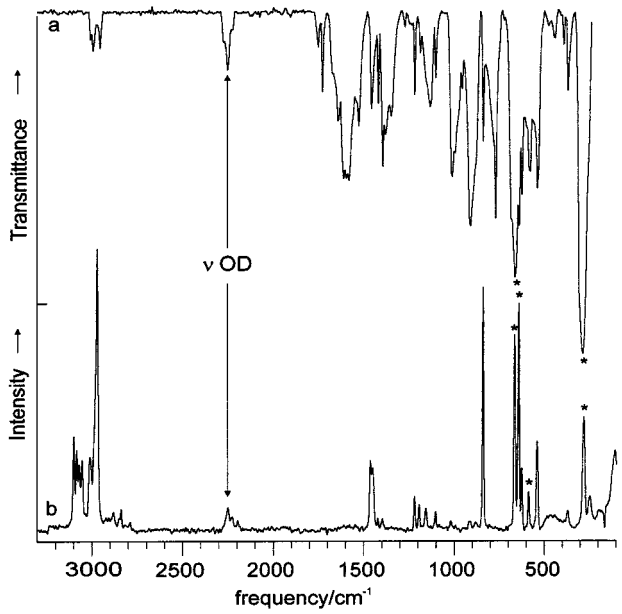


Figure 3. Infrared spectrum (trace A) and Raman spectrum (trace B) of $(MeO)_2COD^+SbF_6^-$; vibrations of the SbF_6^- anion are marked by an asterisk

3099, 3084, 3071 and 3056 cm^{-1}, but the spectra of the hexafluoroarsenate show only two modes (3090 and 3067 cm^{-1}). The same phenomenon is noticed in the area of the methyl deformation modes (1554–1349 cm^{-1}), where as many as six different frequencies are measured. Between 1220 cm^{-1} and 1153 cm^{-1} as well as between 1098 cm^{-1} and 993 cm^{-1} the rocking modes ρCH_3 are observed. A sharp Raman line and IR band is detected at 845 cm^{-1} and assigned to the CO_3 out-of-plane mode, whose position is comparable to the measured frequency in a range of 890–774 cm^{-1} for simple, complex, acidic and organic carbonate compounds.[22] The νOH absorption is observed at 3160 cm^{-1} with the H/D shifted signal at 2275 cm^{-1} (νOD) for the AsF_6^- compound and 2156 cm^{-1} for the SbF_6^- compound, which is within the expected shift range of about 900 cm^{-1}.[34]

Because of cation–anion interactions, the MF_6^- ions (M = As, Sb) do not show ideal O_h symmetry. This lowered symmetry can be seen in the spectra, where splitting of the anion vibrational modes are observed.[33]

^1H and ^{13}C NMR Spectra of $(MeO)_2COH^+MF_6^-$ (M = As, Sb)

The ^1H NMR spectra of freshly prepared $(MeO)_2COH^+MF_6^-$ (M = As, Sb) dissolved in SO_2 with TMS as external standard at –50 °C shows a singlet at δ = 4.59 (AsF_6^-) and δ = 4.63 (SbF_6^-) for the methyl groups and a singlet at δ = 11.74 (AsF_6^-) and δ = 11.8 (SbF_6^-) for the hydroxyl group. This result is comparable to the results of Olah, who observed at –80 °C a singlet at δ = 11.27 for the hydroxyl group and a singlet at δ = 4.52 for the methyl group.[35,36] The singlet for the proton of the hydroxyl group of the $C(OH)_3^+$ cation is detected at δ = 11.55; Ramsey observed a singlet at δ = 4.9 in an H_2SO_4 solution for the methyl group (Table 4).[17,37] The singlet at δ = 163 in the ^{13}C NMR (^1H coupled) is assigned to the carbon atom of the CO_3 skeleton. In the region of δ = 63 a quadruplet

Table 3. Raman and IR frequencies and their possible assignment for $(MeO)_2COX^+MF_6^-$ (X = H, D; M = As, Sb)

M = As IR	X = H Raman	M = Sb IR	X = H Raman	M = As IR	X = D Raman	M = Sb IR	X = D Raman	Possible Assignment
3162vw	3158(3)	3160vw	3158(4)					ν OH
	3090(32)	3098vw	3099(33)		3092(42)		3099(35)	ν_{as} CH_3
			3084(35)				3084(30)	ν_{as} CH_3
	3067(21)		3071(34)		3068(15)		3071(24)	ν_{as} CH_3
			3056(33)				3055(25)	ν_{as} CH_3
3038w				3047vw				ν_{as} CH_3
3016w				3019w	3016(22)	3012vw	3011(27)	ν_{as} CH_3
2990w	2986(100)			2992w	2983(100)	2994w		ν_{as} CH_3
	2977(81)	2973w	2976(100)		2968(72)	2969w	2971(100)	ν_s CH_3
				2275m	2275(8)	2256m	2251(8)	ν OD
1666vs		1660s						νCO_3
1642vs		1638s	1635(8)	1639vs		1638sh		νCO_3
				1614vs		1616s		νCO_3
						1598s		νCO_3
1585vs		1583m	1588(5)	1586vs		1585s		νCO_3
1554sh		1554m						δCH_3
			1533(6)			1529m		δCH_3
1461s	1461(18)	1458s	1464(24)	1459m	1460(30)	1460m	1463(25)	δCH_3
1446s	1453(16)		1455(18)	1447sh	1451(25)		1452(23)	δCH_3
1427s		1425s	1426(5)	1428s	1427(6)	1422m	1422(4)	δCH_3
1413s	1414(5)	1407s	1407(4)	1404s	1403(2)	1399s	1397(4)	δCH_3
		1347w	1346(6)			1349m		δCH_3
1277s		1274s		1281w		1274vw		νOCO
1219s	1221(10)	1219m	1220(13)	1220m	1221(13)	1219m	1222(12)	ρCH_3
1186s	1186(4)	1189m	1188(8)	1190w	1193(8)	1187w	1195(9)	ρCH_3
1159s	1162(5)	1153m	1159(10)		1162(8)	1157sh	1156(8)	ρCH_3
1128w		1127m		1133w		1136m		νOCO
1098vs	1098(6)	1094vs	1094(9)	1101m	1105(6)	1104m	1103(7)	ρCH_3
				1020s	1023(4)	1015vs	1019(3)	ρCH_3
993s		997m						ρCH_3
964vs	960(6)	960vs	962(8)	967m		958m		δOCO
				923vs	917(3)	915vs	918(3)	δCOD
846s	845(84)	846s	844(73)	844s	843(91)	845s	842(90)	γCO_3 out of plane
791vs		799s		796m				ρCO_3
		775s		779s	778(2)	774vs		ρCO_3
				768s				ρCO_3
632vs	631(23)	630vs	629(27)	626s	628(23)	628s	627(23)	γCO_3 in plane
608s		610s		606w				ρCO_3
			575(6)	573s				ρCO_3
565s	565(23)	563s	564(22)	568m				ρCO_3
	542(7)			547s	549(21)	544s	542(35)	τCH_3
537vs		536vs	536(19)	533vs	532(16)			τCH_3
				490s		479vw	486(4)	τCH_3
444sh		448vw	444(3)			449vw	443(5)	τCH_3
423sw				424s				τCH_3
375vs	378(23)	378m	374(4)	374sh	376(33)	374m	371(7)	τCH_3
256m		255s	252(4)	257vs				δCOC
	246(7)		242(5)		245(10)		249(12)	δCOC
202w					187(4)		196(7)	Lattice
	734(17)	664vs	665(100)		735(20)	667vs	667(73)	νMF_6^-
	721(4)		648(31)	719				νMF_6^-
701vs	702(34)	643vs	640(88)		702(48)	641vs	644(85)	νMF_6^-
	689(76)			683s	688(66)			νMF_6^-
676vs	677(50)				674(71)			νMF_6^-
593vw	595(7)		588(18)	601	598(9)	586s	586(14)	νMF_6^-
394vs	394(10)	284vs	281(37)	399	394(12)	289vs	283(41)	νMF_6^-
	366(14)				364(19)			νMF_6^-
	313(9)			318vs	311(6)			νMF_6^-

with a coupling constant of 141 Hz is observed and assigned to the methyl groups.

Experimental Section

Caution! *Avoid contact with these compounds as the hydrolysis of AsF_6^- and SbF_6^- salts forms HF, which burns the skin and causes irreparable damage. Safety precautions should be taken when using and handling these materials.*

All synthetic work and sample handling was performed by employing standard Schlenk techniques and a vacuum line (stainless steel or glass). SbF_5 (Merck) was purified by fractional distillation. The synthesis of $(MeO)_2CO$ and the drying of HF and SO_2 were carried out by known literature methods (R. Minkoite, A. Kornath, D. Savodny, *Angew. Chem. Int. Ed. Engl.* **1992**, *31*, 643–644). Reactions in HF/DF were carried out in a KEL-F reactor with a KEL-F valve.[38] Infrared spectra were recorded with a Bruker IFS 113V spectrophotometer. The spectra of dry powders were obtained on a CsI plate in a cooled IR cell.[39] The Raman spectra were recorded

Table 4. ^1H and ^{13}C NMR spectroscopic data of mono-, di- and trihydroxycarbenium ions

Ion/Precursor	^1H NMR δ [ppm] –Me	–OH	^{13}C NMR δ [ppm] –Me	CO_3
$(MeO)_2CO$[d]			–55	36
$(MeO)_2COH^+$	4.9[a]			
	4.52[b]	11.27[b]		
	4.59[c]	11.74[c]	63[c]	163[c]
$MeOC(OH)_2^+$[c]	4.47	11.55		31[d]
		11.18		
$C(OH)_3^+$[e]		11.7		167
$(MeO)_2CH^+$[f]	4.54		64.5	181
$(MeO)_2C(Me)^+$[f]	4.38		67	193
$(MeO)_3C^+$[f]	4.45		68	164

[a] Ref.[27] – [b] Ref.[37] at –80 °C. – [c] Own measurements at –60 °C with TMS as external standard. – [d] In parts per million from CS_2. – [e] Ref.[17] – [f] CD_3NO_2 as standard.

with a T64000 (ISA) using a CCD detector (EEV CCD15–11) and an Ar^+ laser tube (514.5 nm) from Spectra Physics. The spectra were recorded in a glass cell cooled with liquid nitrogen. The NMR spectra were recorded with a Bruker DPX 300 spectrometer with TMS as external standard. Single crystals were placed in Lindemann capillaries in a cooled stream of dry nitrogen, and an X-ray diffraction study was carried out at –100 °C using an Enraf Nonius Mach3 automated diffractometer.

Preparation of $(MeO)_2COX^+MF_6^-$ (M = As, Sb; X = H, D): In a 50 mL KEL-F reactor, SbF_5 (1.09 g, 5 mmol) or AsF_5 (0.85 g, 5 mmol) was dissolved in HF (3 g). The solution was frozen at –196 °C and $(MeO)_2CO$ (0.45 g, 5 mmol) was added under an inert atmosphere (N_2). The mixture was warmed to –70 °C and kept for 30 minutes. The excess HF was slowly removed under dynamic vacuum at –78 °C. The reactions with DF were made analogously to the above described synthesis.

Acknowledgments

This work was supported by the Deutsche Forschungsgemeinschaft and the Fonds der Chemischen Industrie.

[1] G. A. Olah, *Angew. Chem. Int. Ed. Engl.* **1995**, *34*, 1393.
[2] G. A. Olah, *Angew. Chem. Int. Ed. Engl.* **1973**, *12*, 173.
[3] D. Bethell, V. Gold, *Carbocation Chemistry (Studies in Organic Chemistry, 21)*, Elsevier, Amsterdam, **1985**.
[4] G. A. Olah, W. S. Tolgyesi, S. J. Kuhn, M. E. Moffat, J. J. Bastien, E. B. Baker, *J. Am. Chem. Soc.* **1963**, *85*, 1328.
[5] G. A. Olah, *Angew. Chem.* **1963**, *75*, 800.
[6] F. Seel, *Z. Anorg. Allg. Chem.* **1943**, *250*, 331.
[7] G. A. Olah, A. M. White, D. H. O'Brien, *Chem. Rev.* **1970**, *70*, 561.
[8] G. A. Olah, G. K. S. Prakash, J. Sommer, *Superacids, Wiley-Interscience,* New York, **1985**.
[9] K. O. Christe, C. J. Schack, R. D. Wilson, *Inorg. Chem.* **1975**, *14*, 2224.
[10] R. Minkwitz, D. Lennhoff, W. Sawodny, H. Härtner, *Z. Naturforsch.* **1992**, *47b*, 1661.
[11] R. Minkwitz, A. Kornath, W. Sawodny, *Angew. Chem. Int. Ed. Engl.* **1992**, *31*, 643.
[12] R. Minkwitz, A. Kornath, W. Sawodny, H. Härtner, *Z. Anorg. Allg. Chem*. **1994**, *620*, 753.
[13] K. O. Christe, *Inorg Chem*. **1975**, *14*, 2230.
[14] R. Minkwitz, V. Gerhard, *Z. Naturforsch*. **1989**, *44b*, 364.
[15] P. G. Jönsson, I. Olovsson, *Acta Cryst.* **1968**, *B24*, 559.
[16] A. Kvick, P. G. Jönsson, I. Olovsson, *Inorg. Chem.* **1969**, *8*, 2775.
[17] R. Minkwitz, S. Schneider, *Angew. Chem. Int. Ed.* **1999**, 38, 714.
[18] R. Minkwitz, S. Schneider, M. Seifert, H. Hartl, *Z. Anorg. Allg. Chem.* **1996**, *622*, 1404.
[19] R. Minkwitz, S. Schneider, H. Preut, *Angew. Chem. Int. Ed.* **1998**, *37*, 494.
[20] A. Adam, M. Mehta, *Angew. Chem. Int. Ed.* **1998**, *37*, 1387.
[21] Crystallographic data (excluding structure factors) for the structure included in this paper have been deposited with the Cambridge Crystallographic Data Centre as supplementary publication no. CCDC-138854. Copies of the data can be obtained free of charge on application to CCDC, 12 Union Road, Cambridge CB2 1EZ, UK [Fax: (internat.) + 44-1223/336-033; Email: deposit@ccdc.cam.ac.uk].
[22] M. Nardelli, *Comput. Chem.* **1983**, *7*, 95.
[23] G. Sheldrick, *SHELXS 86*, University of Göttingen, Germany, **1986**.
[24] G. Sheldrick, *SHELXL 93*, University of Göttingen, Germany, **1993**.
[25] E. Keller, *SCHAKAL, Program for the Graphic Representation of Molecular and Crystallographic Models*, Albert-Ludwig-University of Freiburg, **1988**.
[26] A. Bondi, *J. Phys. Chem.*, **1964**, 68(3), 441.
[27] B. Collingwood, H. Lee, J. K. Wilmshurst, *Aust. J. Chem.* **1966**, *19*, 1637.
[28] J. E. Katon, M. D. Cohen, *Can. J. Chem.* **1975**, *53*, 1378.
[29] D. Labrenz, W. Schröer, *J. Mol. Struct.* **1991**, *249*, 327.
[30] R. A. Pethrick, A. D. Wilson, *Spectrochimica Acta*, **1974**, *30A*, 1073.
[31] B. M. Gatehouse, S. E. Livingstone, R. S. Nyholm, *J. Chem. Soc*. **1958**, 3137.
[32] W. Behrendt, G. Gattow, M. Dräger, *Z. Anorg. Allg. Chem.* **1973**, *397*, 237.
[33] A. A. A. Emara, G. J. Schrobilgen, *Inorg. Chem.* **1992**, *31*, 1323.
[34] J. Weidlein, U. Müller, K. Dehnicke, *Schwingungsspektroskopie*, G. Thieme, Stuttgart **1982**.
[35] G. A. Olah, A. T. Ku, A. M. White, *J. Org. Chem.* **1969**, *34*, 1827.
[36] G. A. Olah, M. White, *J. Am. Chem. Soc.* **1968**, *90*, 1884.
[37] B. G. Ramsey, R. W. Taft, *J. Am. Chem. Soc.* **1966**, *88*, 3058.
[38] A. Werner, Dissertation, Universität Dortmund, **1988**.
[39] L. Bayerdorfer, R. Minkwitz, J. Jander, *Z. Anorg. Allg. Chem.*, **1972**, *392*, 137.

Received September 6, 1999
[I99318]

Protonation of the Copper(I) Form of the Blue Copper Proteins Plastocyanin and Amicyanin – A Molecular Dynamics Study

Christian Buning[a] and Peter Comba*[a]

Keywords: Blue copper proteins / Molecular dynamics / Cluster analysis / Protonated histidine / Protonation mechanism

The conformational space of the copper(I) forms of the cupredoxines amicyanin (ami) (*Paracoccus versutus*) and plastocyanin (pla) (*Populus nigra*) with a protonated histidine donor close to the C-terminus ("C-terminal histidine" ami: His96; pla: His87) was investigated with force field calculations that involve the experimentally determined structures of the protonated or unprotonated copper(I/II) forms: a setup of 36 conformers with a constrained torsional angle that involves the $C_{imidazole}$–$C_{methylene}$ (C^{γ}–C^{β}) bond (chi2; 10° increments); strain energy minimization of all constrained conformers; a 10 ps molecular dynamics search around each conformer; constrained, followed by unconstrained optimization of each of the resulting low energy structures; cluster analysis of the resulting conformations. For both cupredoxines there are two major conformers which differ in their solvent accessibility. The plastocyanin and amicyanin structures are in excellent agreement with the experimentally observed crystallographic data; the two analyses lead to the proposal for a general mechanism for the protonation of reduced blue copper proteins. This is also in agreement with the results of a conformational analysis of a complex of the protonated copper(I) form of amicyanin with phosphate.

Introduction

Blue copper proteins (cupredoxines) are relatively small metalloproteins (approximately 10–14 kDa, 100–150 amino acid residues) with a single copper center in a trigonal pyramidal coordination geometry (two histidines, a cysteine, and an axial methionine; type 1 copper center). Cupredoxines are one-electron transfer centers which are part of redox chains in plants and bacteria.[1] Among the most prominent properties are the typical intense blue color in the oxidized form [ε (≈600 nm) ≈ 5000 $L \cdot mol^{-1}cm^{-1}$; proteins with rhombic sites have increasing intensity of a second transition at ≈460 nm], attributed to charge transfer from the cysteinate donor, a small A_z hyperfine coupling in the EPR spectrum ($A_z \approx 50 \cdot 10^{-4}$ cm^{-1}), relatively high reduction potentials [≈200 to ≈680 mV vs. 150 mV for the aqueous copper(II/I) couple] and fast electron self-exchange rates [10^3 to 10^6 $M^{-1}s^{-1}$ vs. $5 \cdot 10^{-7}$ $M^{-1}s^{-1}$ for the aqueous copper(II/I) couple].[2–5] A plot of the structure of amicyanin from *Paracoccus versutus* is shown in Figure 1.

An interesting feature is that for some of the blue copper proteins the reduction potential is strongly pH-dependent, and this has been attributed to the protonation of the coordinating histidine residue close to the C-terminus ("C-terminal histidine"; His96 in amicyanin shown in Figure 1). This histidine is supposed to be the gate for electron transfer, and protonation/deprotonation (i.e. bond breakage/bond formation may then be a switch to turn off and on the electron transfer reactivity.[6]). There is experimental

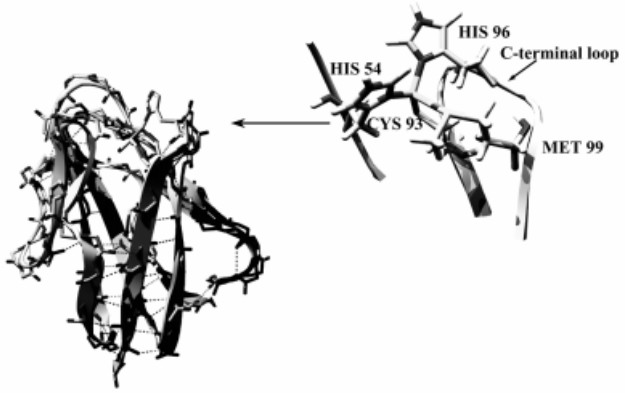


Figure 1. Representation of the tertiary structure and of the copper chromophore of amicyanin (*Paracoccus versutus*)[23]

electrochemical evidence for this protonation in plastocyanin, pseudoazurin, and amicyanin.[6–9] Structural support for the protonation has been obtained from X-ray studies of plastocyanin, pseudoazurin, and amicyanin.[10–12] [see Figure 2 for plastocyanin (His87)].

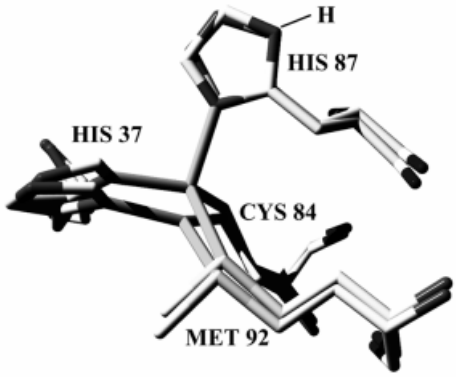


Figure 2. Overlay of the protonated and the unprotonated Cu^{I}-structures of plastocyanin[11]

[a] Anorganisch Chemisches Institut der Universität Heidelberg, Im Neuenheimer Feld 270, 69120 Heidelberg, Germany,
Fax: (internat.) +49–6221/54-6617
E-mail: comba@akcomba.oci.uni-heidelberg.de

Supporting information for this article is available on the WWW under http://www.wiley-vch.de/home/eurjic or from the author.

 © WILEY-VCH Verlag GmbH, D-69451 Weinheim, 2000 1434–1948/00/0606–1267 $ 17.50+.50/0

There are two known structures for the protonated copper(I) form of plastocyanin.[11] The major difference is the conformation of the corresponding histidine side chain. One of the structures has the protonated N^{δ} directed towards the copper center whereas in the other structure the residue is rotated around chi2 by 180° (see Table 1 for nomenclature of the torsional angles), so that the protonated N^{δ} becomes solvent accessible and forms a hydrogen bond with a water molecule. During the protonation the geometry around the copper center changes from trigonal pyramidal to trigonal planar (see Figure 2). The distance to S^{δ} from the methionine decreases from 2.9 Å to 2.5 Å in the trigonal planar form, the bond distances to S^{γ} from the cysteine and to N^{δ} from the histidine do not change significantly. The trigonal planar geometry as well as the presence of two soft donors disfavors the copper(II) oxidation state, and this leads to the observed increase of the reduction potential.

Table 1. Definition of the torsion angles

Torsion	Atom type			
ϕ	C	C^{α}	N	C
Ψ	N	C	C^{α}	N
Ω	C^{α}	N	C	C^{α}
$\chi 1$	N	C^{α}	C^{β}	C^{γ}
$\chi 2$	C^{α}	C^{β}	C^{γ}	$N^{\delta 1}$
Tor	C^{α}	C^{β}	C^{γ}	$C^{\delta 2}$

For amicyanin there are detailed kinetic studies, suggesting that two protonated forms (His96) with different structures are involved[6] (Scheme 1). The rearrangement (k_2) is slow compared to the protonation (k_1). The observed pK_a value depends on the phosphate ion concentration, suggesting that some phosphate coordination is involved. Structural information on the protonated forms is available from an EXAFS study of amicyanin at variable pH.[13] This indicates the loss of one histidine donor at low pH and a reorganization of the copper site towards a trigonal planar geometry. There are also recent X-ray studies of the protonated form of amicyanin.[10] These indicate that, for amicyanin, there are two conformers for the protonated side chain of the C-terminal histidine.

$$A \underset{k_{-1}}{\overset{[H^+]\ k_1}{\rightleftharpoons}} B \underset{k_{-2}}{\overset{k_2}{\rightleftharpoons}} C$$

Scheme 1. Three site exchange equilibrium describing the protonation of Cu^{I}-amicyanin

A pH-dependent electrochemical study of azurin (*Pseudomonas aeruginosa*) indicates that, in this cupredoxine, the coordinating histidine residues may not be protonated.[14–16] Factors that might prevent protonation are: (i) the length of the C-terminal loop: based on the observation that only those wildtype cupredoxines protonate which have two spacing amino acids between the Cys and the His[7] it was suggested that the length of the C-terminal loop is the determining factor for the protonation; (ii) the presence of the sterically demanding side chain Phe114 (azurin) in close proximity to the C-terminal His might prevent the rotation around chi2;[2,17] (iii) the absence of a proline residue next to the C-terminal His (Pro95 in amicyanin):[2,7,18] for all wildtype cupredoxines that protonate there is a Pro residue in the i-1 position with respect to the C-terminal histidine; this proline is known to interact with the protonated His of plastocyanin.[11] Recent loop-mutation studies yielded an amicyanin mutant with an azurin C-terminal loop (AmiAzu), where the coordinating C-terminal histidine may be protonated in the copper(I) form.[19] This mutant is the first cupredoxine which undergoes a protonation of the C-terminal histidine and which has more than two noncoordinating amino acids between the Cys and His donors in the C-terminal loop and no proline residue in the i-1 position which might interact with the protonated histidine side chain.

We have used molecular dynamics calculations to analyze the structural details of the protonated copper(I) forms of two blue copper proteins, plastocyanin and amicyanin, which are known to have protonated coordinating histidine groups (His96, pK_a = 6.8; His87, pK_a = 4.7, respectively). The results of the two MD calculations were also used to propose a detailed, general mechanism for the protonation of reduced cupredoxines. For amicyanin, an MD calculation of an amicyanin/phosphate complex was used to model the phosphate-dependence of the proton transfer reaction.

Computational Details

Force Field and Structural Models

DISCOVER 2.9.5.[20] with the force field AMBER[21] was used for all MM and MD calculations. The chromophore [copper(I) center and the three donor atoms of the coordinated amino acid residues (S, S, N)], the protein backbone outside a shell with a radius of 10 Å around C^{γ} of the C-terminal histidine (see Table 2), on the basis of entire amino acid residues, and the water molecules outside a shell with a radius of 7 Å were held at fixed positions. A distance-

Table 2. Amino acid sequences of the C-terminal loops of several blue copper proteins

Protein	Origin	Sequence of the C-terminal loop										
Amicyanin	*Paracoccus versutus*	**Cys**	Thr	Pro			**His**	Pro	Phe			**Met**
Plastocyanin	*Populus nigra*	**Cys**	Ser	Pro			**His**	Gln	Gly	Ala	Gly	**Met**
Pseudoazurin	*Alcaligenes faecalis*	**Cys**	Thr	Pro			**His**	Tyr	Ala	Met	Gly	**Met**
Azurin	*Pseudomonas aeroginosa*	**Cys**	Thr	Phe	Pro	Gly	**His**	Ser	Ala	Leu		**Met**

dependent dielectric constant ($\varepsilon = 1 \times r$) and a cutoff of 12 Å for the nonbonded interactions were used. The point charges were those of the AMBER force field,[21] except for the copper(I) chromophore, where the charge distribution was computed with GAUSSIAN94.[22] [Merz-Kollmann scheme; B3LYP, Dζpdf/6-31G* basis set; model compound: $Cu^{I}(SCH_3)\{S(CH_3)_2\}(Im)$ with experimental coordinates of copper(I) plastocyanin, PDB-code 6pcy[11]]. The parameters for the chromophore are [copper(I) was treated as a cation, i.e. no bonds to the donor atoms; point charge, R, ε]: Cu^{I}, 0.118, 2.4, 0.05; S_{cys}, –0.546, 4.0, 0.2; N_{His}, –0.163, 3.5, 0.16. The point charges of the entire model compound are given as supplementary material.

Conformations of the Protonated Copper(I) Form of Plastocyanin and Amicyanin

The starting structures for the conformational searches were based on experimentally determined crystallographic data; plastocyanin: *Populus nigra*, copper(I) pH = 3.8; PDB-code 6pcy;[11] amicyanin: *Paracoccus versutus*, copper(II) form;[23] the trigonal copper(I) chromophore of amicyanin was set up from this structure, based on published EXAFS data:[13] $d_{Cu-S(Cys)}$ = 2.18 Å, $d_{Cu-S(Met)}$ = 2.41 Å, $d_{Cu-N(His)}$ = 1.89 Å; assigned pH = 5.5. The copper chromophores were constrained to the experimentally observed geometries in all MD calculations. The experimentally observed water molecules were deleted from the structural data files and a solvation shell with a radius of 17 Å around C^{γ} of the C-terminal histidine (see Table 2) was constructed with a simple point charge model (SPC).

A set of 36 structures for each of the two protonated copper(I) proteins was created by a variation (10° increments) of the C^{α}–C^{β}–C^{γ}–C^{δ} torsional angle (tor) of the C-terminal histidine (see Table 1). The resulting structures were optimized (constrained angle tor, 1000 cycles, steepest descent). A 10 ps MD simulation was then performed for each of these structures (constrained angle tor, T = 600 K, 10 structures each were collected). During the MD simulation the temperature was regulated with a temperature relaxation time τ of 0.1 ps. In all calculations a time step of 1 fs was used.[24] The resulting 360 structures for each of the two copper proteins were then optimized with a constrained angle tor (10000 cycles conjugate gradient), followed by a full optimization without constraints (10000 cycles conjugate gradient).

A cluster analysis was performed for the fully energy minimized structures. The protein backbone torsions of the C-terminal loop and the side chain torsions of the protonated histidine were taken as criteria for the clustering; plastocyanin: chi1/chi2 His87, phi/psi Ala90, phi/psi Gly89, chi1/chi2 Pro86, and phi/psi Gly91; amicyanin: chi1/chi2 His96, phi/psi His96, chi1/chi2 Pro95, chi1/chi2 Pro97, and phi/psi Met99 (see Table 1 for the definition of the torsional angles and Table 2 for the amino acid sequences of the C-terminal loops of plastocyanin and amicyanin). A clustering according to these torsions allowed the definition of 12 families for amicyanin and 21 families for plastocyanin (only the highest populated clusters were examined in detail; the assignment to a cluster was based on a graphical analysis of the corresponding phi/psi plots and chi1/chi2 plots, respectively).

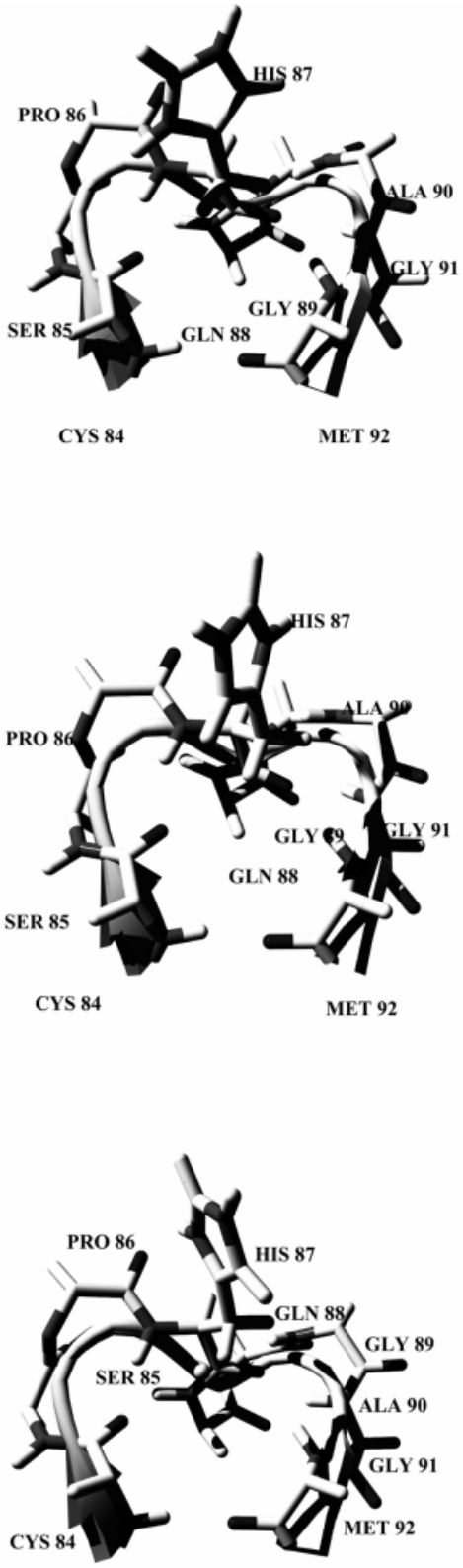


Figure 3. Representatives of the determined plastocyanin cluster: plasto1 (*top*), plasto2 (*middle*), plasto3 (*bottom*). The protein backbone of the C-terminal loop is shown plus the side chain of His 87

The Amicyanin Phosphate Complex

The structure of the protonated copper(I) amicyanin, as defined above, was used as the starting structure. Hydrogenphosphate was put in a position favorable for hydrogen bonding to N^{δ} of His96 and N–H of Arg100. The hydrogen bonds were constrained to a value of 2.5 Å. This model was energy-minimized using 10000 steps of conjugate gradient. An MD simulation at 900 K, taking 80 ps dynamics and 15 ps equilibration time was performed (τ = 0.1 ps, time step of 1 fs, see above). 80 conformations were collected and energy-minimized, using 10000 steps of conjugate gradient.

Results and Discussion

Plastocyanin

Three clusters of plastocyanin (plasto1, plasto2, plasto3) and two of amicyanin (ami1, ami2) were identified, each of which had a high population and characteristic features with respect to the histidine side chain and the C-terminal loop conformation (details of the cluster analyses are available as Supplementary Material); representative structures of the C-terminal loops are shown in Figure 3 and Figure 4, respectively. Table 3 gives detailed information on the conformation of the C-terminal loop and the protonated histidine side chain for the computed clusters and relevant experimental structures. From a comparison of the chi1/chi2 values of the three plastocyanin clusters with experimental data from X-ray studies[11] it emerges that plasto1 is very similar to the copper(I) structure at pH = 7 (deprotonated) and plasto2 is equivalent to the structure at pH = 3.8 (protonated). For plasto3 with a chi2 value of –11° there is no corresponding experimental data, and it appears that plasto3 is an intermediate between the two experimentally observed conformations. It is interesting to note here that the results of the crystallographic study of the low pH copper(I) form of plastocyanin suggest that this could be a mixture of two different conformations.[11] Thus, plasto3 might be a

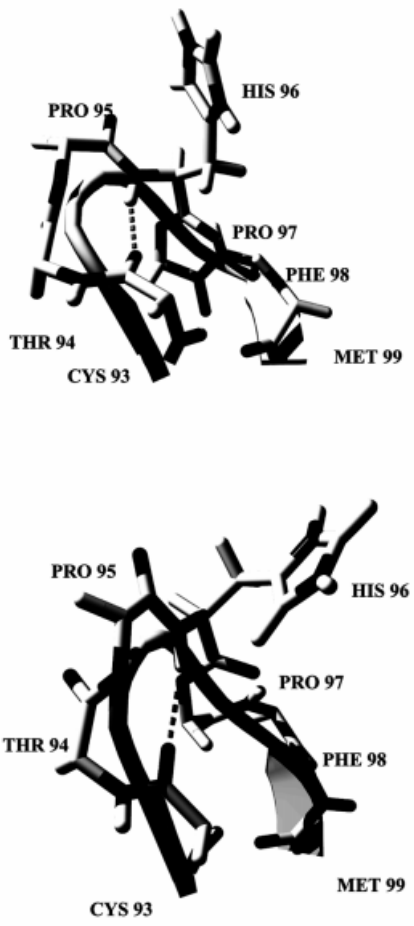


Figure 4. Representatives of the determined amicyanin cluster: ami1 (*top*), ami2 (*bottom*). The protein backbone of the C-terminal loop is shown plus the side chain of His 96 (hydrogen bonds are indicated by a dotted line)

Table 3. Comparison of the computed psi/psi torsion angles from the plastocyanin and amicyanin clusters and the chi1/chi2 angles from the protonated histidines with experimental data

		histidine	turn 1[a]		turn 2[a]		turn 3[a]	
		chi1/chi2	i+1	i+2	i+1	i+2	i+1	i+2
MD	plasto1[b]	–64°/130°	–56°/–60°	–66°/–28°	–66°/–28°	–108°/29°	–56°/–40°	–1°/–27°
MD	plasto2[b]	–59°/–71°	–61°/–47°	–48°/–40°	–48°/–40°	–117°/39°	–54°/–36°	–91°/14°
MD	plasto3[b]	–59°/–11°	–55°/–48°	–48°/–41°	–48°/–41°	–116°/25°	–55°/–37°	–87°/4°
X-ray	Plastocyanin[c]	–66°/–50°	–60°/–49°	–66°/–25°	–66°/–25°	–121°/24°	–69°/–25°	–70°/–8°
X-ray	Plastocyanin[d]	–60°/128°	–63°/–50°	–67°/–22°	–67°/–22°	–118°/14°	–67°/–29°	–70°/–8°
MD	ami1[b]	–74°/142°	–46°/–56°	–73°/–12°	–53°/–34°	–58°/–27°	–	–
MD	ami2[b]	36°/–168°	–47°/–47°	–65°/–22°	–83°/34°	–73°/–28°	–	–
X-ray	Amicyanin[e]	–49°/120°	–50°/–56°	–73°/–15°	–61°/–18°	–69°/–13°	–	–
NMR	Amicyanin[f] (A)	–	–63°/–32°	–74°/–33°	–51°/–41°	–67°/–19°	–	–
NMR	Amicyanin[f] (B)	–	–41°/107°	–2°/62°	–51°/–41°	–67°/–19°	–	–
MD	Amicyanin phosphate complex	–176°/52°	–67°/–57°	–66°/82°	–78°/57°	–100°/30°	–	–
X-ray	Pseudoazurin[g]	–52°/96°	–57°/–57°	–59°/–42°	–60°/–23°	–90°/1°	–	–

[a] Definition of the turns: plastocyanin turns 1–3: cys84-his87, ser85-gln88, gln88-gly91; amicyanin turns 1–2: cys93-his96, his96-met99; pseudoazurin turns 1–2: cys78-his81, tyr82-gly85. – [b] Median of the structures of the cluster. – [c] *Populus nigra* [Cu^{I}]; pH = 3.8 (ref.[11]). – [d] *Populus nigra* [Cu^{I}]; pH = 7 (ref.[11]). – [e] *Paracoccus versutus* [Cu^{II}] (ref.[23]). – [f] *Paracoccus versutus* [Cu^{I}] (ref.[23]). – [g] *Alcaligenes faecalis* [Cu^{I}] (ref.[12]).'

proposal for the second of these conformations at pH = 3.8.

Amicyanin

The good agreement between the computed and observed copper(I) structures of plastocyanin (see above) indicates that, based on the same MD scheme, a reasonable and accurate structural model for the protonated copper(I) form of amicyanin should be available. The cluster ami1 with a chi1/chi2 combination of –74°/142° has, in terms of the conformation of the histidine side chain, a structure that is similar to the copper(II) crystal structure.[23] In the other cluster, ami2, the protonated N^{δ} is directed towards the solvent; this conformation is similar to that of plasto2. Thus, for amicyanin there are conformations of the histidine side chain that are very similar to those of plastocyanin (see Table 3). Very recently, some experimental data on the protonated form of amicyanin became available.[10] These are in full agreement with our computed structural data.

It is instructive to extend the structural comparisons for amicyanin and plastocyanin [copper(I), unprotonated and protonated forms, experimental and computed data] to the first turn of the loop (see Table 3). A type 1 geometry is conserved in all structures. Overlay plots of all relevant structures are presented in Figure 5. The most significant structural differences for amicyanin are those of the conformations of the second turn and, for plastocyanin, those of the conformations of the third turn.

The Amicyanin/Phosphate Complex

The fact that the pK_a of amicyanin depends strongly on the phosphate anion concentration[6] suggests that an amicyanin/phosphate complex mediates the proton transfer. Published experimental data[6] indicate that the protonation rate, based on a mechanism that does not involve phosphate-protein interactions (k_1 in Scheme 1), is about two orders of magnitude faster than the diffusion-controlled limit and that, in the presence of phosphate, the proton is transferred from phosphate to the histidine nitrogen without any involvement of water molecules. A possible interpretation of these observations is that a phosphate anion binds to the positively charged Arg100 side chain. The fixed phosphate anion could then act as an anchor for protons, leading to a high local concentration. Furthermore, the Arg100-coordinated phosphate might have an ideal geometry for the stabilization of the protonated form C in Scheme 1, where the protonated N^{δ} of His96 is directed towards the solvent. There are experimental data that support a histidine/phosphate complex formation. X-ray data are available for structures which contain the motif of a phosphate or sulfate anion forming a salt bridge between a protonated histidine and a second basic amino acid.[25,26] For amicyanin, these structural and mechanistic hypotheses were examined by MD. The most favorable optimized structure of a corresponding amicyanin/phosphate complex is shown in Figure 6.

The structural model visualizes the feasibility of the discussed protonation mechanism and the stabilization of the protonated form. The hydrogen bonds between the phosphate anion and the protein are around 1.6 (± 0.1) Å (OH distances), which is at the shorter limit of the expected range. The main structural differences in the C-terminal loop of this structure, in comparison with the experimentally observed structure[23] are conformational changes at

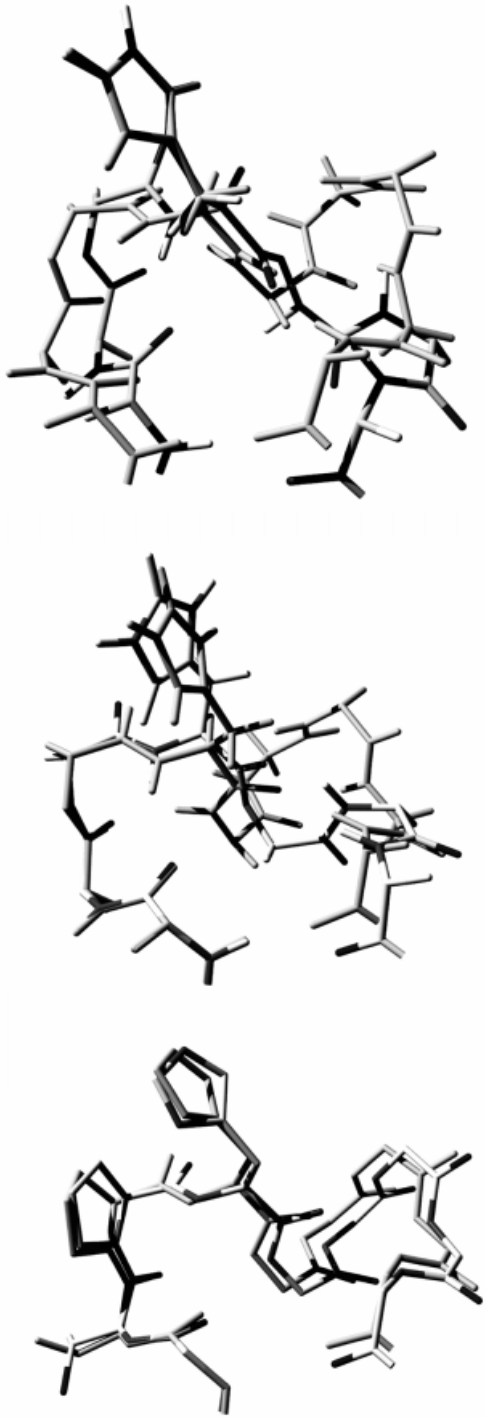


Figure 5. *Top:* Overlay of the clusters from amicyanin and plastocyanin with the protonated N^{δ} directing towards the Cu center; *middle:* Overlay of the clusters from amicyanin and plastocyanin with the N^{δ} directing into the solvent; *bottom:* Overlay of the protonated Cu^{I} structures from plastocyanin and pseudoazurin showing the protein backbone of the C-terminal loop and the side chain of the protonate histidine and the proline from the first turn

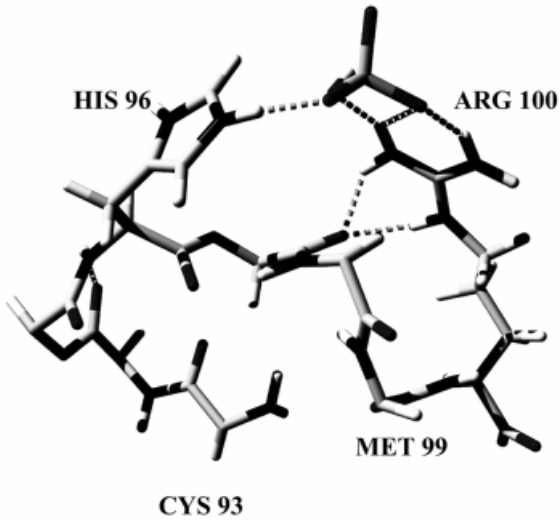


Figure 6. Calculated structure of the possible His 96-phosphate-Arg 100 complex for amicyanin from *Paracoccus versutus* (hydrogen bonds are indicated by dotted lines)

Pro95, His96, and Pro97. The conformation of His96, enforced by the coordinated phosphate anion, leads to chi1/chi2 values of –176°/52° (t/g^+). This is different from the X-ray structure of the unprotonated form[23] but one of the theoretically favored conformations (see above and Supplementary Material; g^+/g^+; g^+/g^-; t/g^+; g^-/g^+; k^-/k^-). Especially notable, however, are the phi/psi combinations for the two proline and the histidine residues (His96: 69°/100°, Pro95: –66°/82°, Pro97: –78°/57). The computed torsional angle combinations are in the ranges that are usually observed for left-handed helices (His96) or β-sheets (Pro95, Pro97), i.e., this is a reasonable conformation for the protonated C-terminal loop of the copper(I) form of amicyanin.

Conclusion

The general MD scheme used here is validated by the observation that, for plastocyanin, the experimentally observed structures are accurately reproduced. Therefore, the computed structures of the protonated copper(I) forms of amicyanin are a reliable model. The corresponding amicyanin/phosphate complex indicates how phosphate may mediate the proton transfer. All published experimental data and the computational results presented here indicate that the following steps are involved in the protonation of the C-terminal histidine in reduced blue copper proteins (see Figure 7):

(i) Decomplexation of the C-terminal histidine (structure **B**); (ii) isomerization to structure **C** with a solvent accessible histidine; (iii) protonation of the C-terminal histidine (structure **D**); (iv) isomerization to structure **E** (stabilization of the protonated structure). The rotational barrier involved in the first isomerization (**B→C**) and the solvent accessibility of structure **C** determine whether a protonation takes

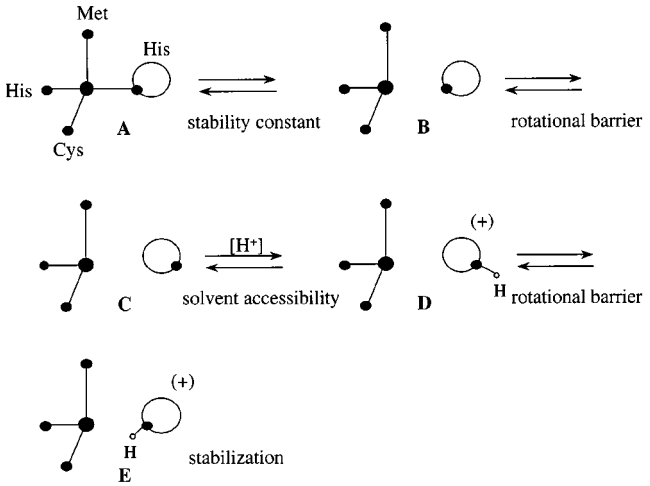


Figure 7. Schematic representation of the basic steps during the protonation of the histidine in a blue copper protein

place or not. The second rotational barrier (**D→E**) and the stabilization of structure **E** have a strong influence on the pK_a value.

Supporting Information

Details of the cluster analysis and the point charges (4 pages) are given as Supporting Information.

Acknowledgments

Generous financial support by the Volkswagen Stiftung is gratefully acknowledged. We are also grateful to Martin Frank for his help with the MD calculations and the data analyses, and to Dr. Ulf Ryde for the calculation of the point charges.

[1] C. Dennison, G. W. Canters, S. de Vries, E. Vijgenboom, R. J. van Spanning, *Adv. Inorg. Chem.* **1998**, *45*, 351–407.
[2] E. T. Adman, *Curr. Opinion Struct. Biology* **1991**, *1*, 895.
[3] G. A. Sykes, *Adv. Inorg. Chem* **1991**, *36*, 377.
[4] M. J. Sisley, R. B. Jordan, *Inorg. Chem.* **1992**, *31*, 2880–2884.
[5] P. Comba, *Coord. Chem. Rev.*, in press.
[6] A. Lommen, G. W. Canters, *J.Biol.Chem.* **1990**, 2768–2774.
[7] C. Dennison, T. Kohzuma, W. McFarlane, S. Suzuki, G. A. Sykes, *J. Chem. Soc., Chem. Commun.* **1994**, 581.
[8] C. L. Kojiro, L. Markley, *Eur. J. Biochem.* **1983**, 52–56.
[9] C. Dennison, E. Vijgenboom, W. R. Hagen, G. W. Canters, *J. Am. Chem. Soc.* **1996**, *118*, 7406–7407.
[10] Z. Zhu, L. M. Cunane, Z.-W. Chen, R. C. E. Durley, F. S. Mathews, V. L. Davidson, *Biochemistry* **1998**, *37*, 17128–17136.
[11] J. M. Guss, P. R. Harrowell, M. Murata, V. A. Norris, H. C. Freeman, *J. Mol. Biol.* **1986**, *192*, 361.
[12] E. Vakoufari, K. S. Wilson, K. Petratos, *FEBS Letters* **1994**, *347*, 203.
[13] A. Lommen, S. Wijmenga, C. W. Hilbers, G. W. Canters, *Eur. J. Biochem.* **1991**, *201*, 695.
[14] M. C. Silvestrini, M. Brunori, M. Tegoni, M. Gervais, F. Labeyrie, *Eur. J. Biochem.* **1986**, 465–472.
[15] A. F. Corin, R. Bersohn, P. E. Cole, *Biochemistry* **1983**, *22*, 2032–2038.
[16] O. Farver, Y. Blatt, I.-E. Pecht, *Biochemistry* **1982**, *21*, 3556–3561.
[17] M. V. Botuyan, A. Toy-Palmer, J. Chung, R. C. Blake II, P. Beroza, D. A. Case, H. J. Dyson, *J. Mol. Biol.* **1996**, *263*, 752.
[18] J. M. Guss, E. A. Merritt, R. P. Phizackerley, H. C. Freeman, *J. Mol. Biol.* **1996**, *262*, 686–705.

[19] C. Buning, G. W. Canters, P. Comba, C. Dennison, L. Jeuken, M. Melter, J. Sanders-Loehr, *J. Am. Chem. Soc.* **2000**, *122*, 204.
[20] *Molecular Simulations*: San Diego, California, USA.
[21] S. J. Weiner, P. A. Kollman, D. A. Case, U. C. Singh, C. Ghio, G. Alagona, S. Profeta Jr., P. Weiner, *J. Am. Chem. Soc.* **1984**, *106*, 765–784.
[22] M. J. Frisch, G. W. Trucks, A. B. Schlegel, P. M. W. Grill, B. G. Johnson, M. A. Robb, J. R. Cheeseman, T. A. Keith, G. A. Petersson, J. A. Montgomery, K. Raghavachari. M. A. Al-Laham, V. G. Zakrzcwski, J. U. Ortiz, J. B. Foresman, J. Cioslowski, B. B. Stefanov, A. Nanayakkara, C. Y. Challacombe, C. Y. Peng, P. Y. Agala, W. Chen, M. W. Wong, J. L. Andres, E. S. Replogle, R. Gomperts, R. L. Martin, D. J. Fox, J. S. Binkley, D. J. Defres, J. Baker, J. P. Stewart, M. Head-Gordon, C. Gonzales, J. A. Pople, GAUSSIAN 94, *Gaussian Inc.*, Pitsburgh, PA, **1995**.
[23] A. Romero, H. Nar, R. Huber, A. Messerschmidt, A. P. Kalverda, G. W. Canters, R. Durley, F. S. Mathews, *J. Mol. Biol.* **1994**, *236*, 1196–1211.
[24] H. J. C. Berendsen, J. P. M. Postma, W. F. van Gunsteren, A. DiNola, J. R. Haak, *J. Chem. Phys.* **1984**, *81*, 3684.
[25] E. N. Baker, *J. Mol. Biol.* **1988**, *203*, 1071.
[26] L. Chen, R. Durley, F. S. Mathews, V. L. Davidson, *Science* **1994**, 86–90.

Received September 20, 1999
[I99332]

Metal Iodides in Polyiodide Networks − The Structural Chemistry of Complex Thallium Iodides with Excess Iodine

Per H. Svensson,[a] Günther Raud,[b] and Lars Kloo*[c]

Keywords: Polyiodides / Iodine / Thallium / NMR spectroscopy

The TlI/$(R_3S)I_x$ systems (R = Me/Et, x = 3,5,7) have been investigated by means of Raman, far-IR, ^{205}Tl NMR spectroscopy and X-ray diffraction. The reaction between $(Me_3S)I_7$ and TlI results in the polyiodide compound $(Me_3S)_3I_{26}$. Raman spectra also reveal the presence of a solid thallium- and iodine-containing product. However, all attempts to structurally characterise this product were unsuccessful. The compound $(Et_3S)TlI_4$ is obtained from the reaction between $(Et_3S)I_7$ and TlI. ^{205}Tl NMR spectra show that Tl^{III} is present in the reaction mixtures of TlI/$(R_3S)I_x$ and that the peak assigned to TlI_4^- in the TlI/$(Et_3S)I_7$ system splits upon heating. This effect is reversible and indicates an equilibrium between two Tl^{III} species.

Introduction

Iodine (I_2) and the ions I^- and I_3^- can be regarded as the "building blocks" of polyiodides and by combination of these it is possible to rationalise almost all known polyiodide fragments (viz. I_5^-, I_7^-, I_8^{2-} and I_9^-). The smaller polyiodides can easily be made with many different cations. However, the larger polyiodides usually have to be stabilised with quite bulky and/or polarisable cations. Many of the larger polyiodides consist of long chains, layers or intercalated structures, which in many cases are electronically conducting and even superconducting.[1−4]

A still greater variety of iodine-rich compounds with interesting structural properties can be achieved by the incorporation of metal centres into the polyiodide structures. The inclusion of different metal compounds gives endless possibilities for structural variation. Wells' salt ($K_3Pb_2I_8{\cdot}4H_2O$) is an early example of such a substance, though not structurally characterised until 1984 by Tebbe.[5,6] Recently, several late transition metals have been incorporated into polyiodide networks.[7−11] The exchange of linear I−M−I units for I−I−I units has also been shown for M = Au.[10]

According to the literature, less, if any, effort has been devoted to heavy main-group metals in this context. These metal ions, being borderline cases between hard and soft acceptors by the hard-soft acid-base formalism, are capable of forming iodide complexes in different or sometimes mixed oxidation states.

Thallium, with its most common oxidation states +I and +III, forms several well-known, non-polyiodide compounds and complexes, such as TlI and TlI_4^-. A TlI_6^{3-} ion has not been verified, though its bromide congener $TlBr_6^{3-}$ was identified.[12] The compound TlI_3 actually consists of Tl^+ and I_3^- units.[13,14] Another less conventional property of thallium is that it is softer in the oxidation state +III than in +I. These facts indicate that the possibility of Tl^{III} oxidising I^- must be taken into account, even though the converse, iodine oxidition of Tl^I to Tl^{III}, can be induced by the right choice of ligands and reaction conditions.[14,15] Polyiodides incorporating only thallium are rather rare (TlI_3 and Tl_3I_4)[3], but they readily form $(Tl_6I_6M_x)[I_4^{2-}]$ compounds if mixed with other metals (M = Pb^{2+}, Bi^{3+}, Au^+, Ag^+).[16]

In this work, we have investigated the possibility of incorporating thallium into polyiodide networks via the reaction between Tl or TlI and the polyiodide melts of trialkylsulfonium iodide. The results have been analysed by means of X-ray diffraction, Raman, IR and ^{205}Tl NMR spectroscopy.

Results and Discussion

Spectroscopic Studies

The Raman spectrum of the reaction mixture between TlI and $(Me_3S)I_7$ (molar ratio 1:3) displays a broad peak at 176 cm^{-1}, almost identical to that of pure $(Me_3S)I_7$ (Figure 1, top). The very strong peak from the heptaiodide makes it difficult to extract any information about the reaction mixture by means of Raman and far-IR spectroscopy. However, the absence of TlI (103 cm^{-1} and 86 cm^{-1}) indicates that a reaction has taken place. The far-IR spectrum shows very similar spectral features to that of unchanged $(Me_3S)I_7$. There are some weak extra bands, but they are difficult to assign. The Raman spectrum of the solid thal-

[a] Dipartimento di Chimica Fisica ed Inorganica,
Universita di Bologna,
Viale Risorgimento 4, 40136 Bologna, Italy
[b] Inorganic Chemistry 1, Lund University,
P. O. Box 124, 22100 Lund, Sweden
[c] Inorganic Chemistry, Department of Chemistry,
Royal Institute of Technology,
10044 Stockholm, Sweden
Fax: (internat.) + 46-8/790-9349
E-mail: Larsa@inorg.kth.se

 © WILEY-VCH Verlag GmbH, D-69451 Weinheim, 2000 1434−1948/00/0606−1275 $ 17.50+.50/0

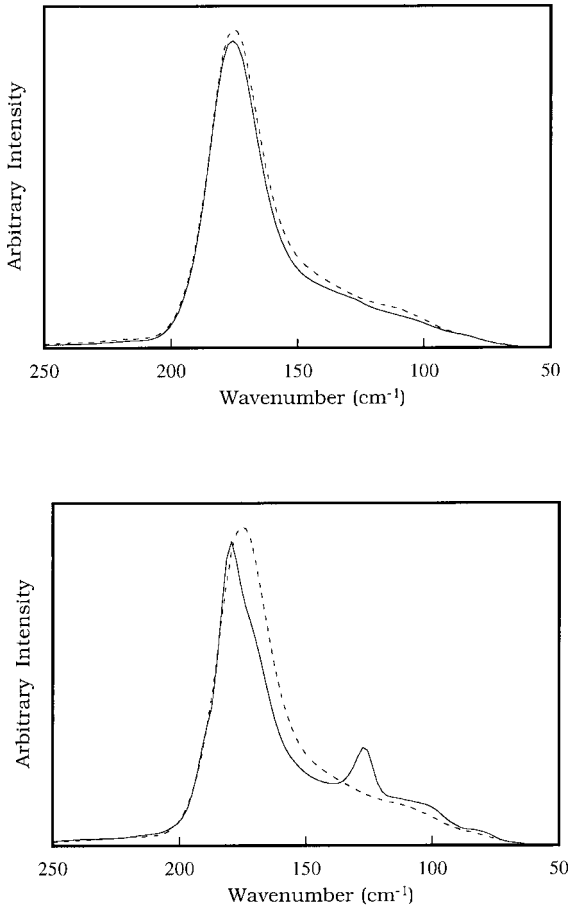


Figure 1. The Raman spectra of the reaction mixture; top: TlI and $(Me_3S)I_7$ (—), bottom: the decomposed solid product (—); (---) denotes a pure $(Me_3S)I_7$ melt

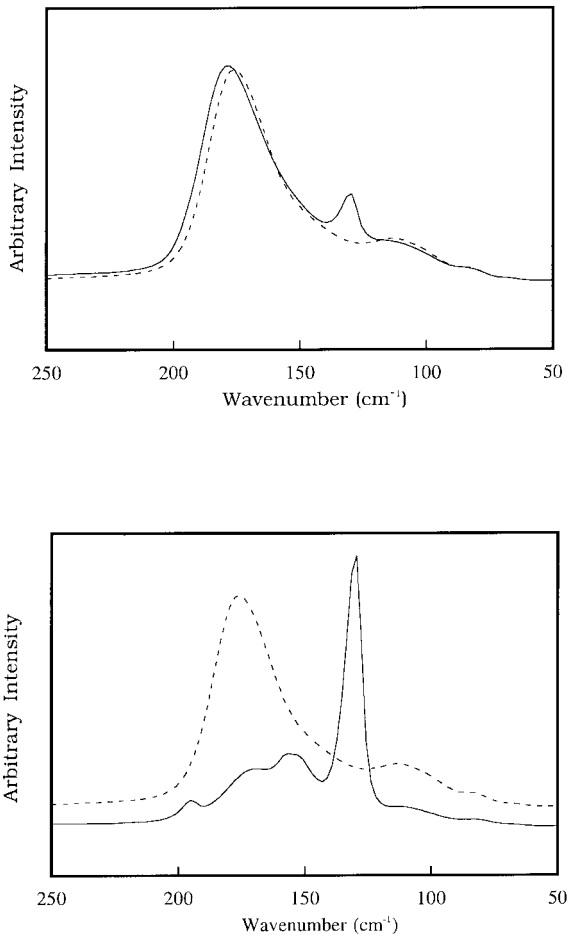


Figure 2. The Raman spectra of the reaction mixture; top: TlI and $(Et_3S)I_7$ (—), bottom: the solid product (—); (---) denotes the spectrum of pure $(Et_3S)I_7$ melt

lium-containing product separated from the reaction melt shows the same spectral features as the reaction mixture. However, if the solid product is left to decompose under ambient conditions its Raman spectrum changes (Figure 1, bottom). Two new peaks are observed at 105 and 128 cm^{-1}. The latter peak corresponds favourably to the asymmetric stretch of TlI_4^-, while the former is in the region where both TlI and triiodide ions normally give rise to spectral features.[12,17−22] This implies that the solid product has decomposed to TlI_4^- and possibly TlI or I_3^-.

The vibrational spectra of the reaction mixture from TlI and $(Et_3S)I_7$ (molar ratio 1:3) show spectral features that differ from the analogous mixture with $(Me_3S)I_7$ (Figure 2, top). The Raman spectrum displays a distinct peak at 130 cm^{-1} which is not seen in $(Me_3S)I_7$. This peak corresponds favourably with the asymmetric stretch of TlI_4^-.[12,17−22] The symmetric stretch of TlI_4^-, which should appear around 150 cm^{-1}, is probably masked by the strong polyiodide bands. The far-IR spectrum also displays differences with respect to the pure polyiodide system. These can also be assigned to TlI_4^- ions. The Raman spectra of the crystals obtained from the synthesis show that the spectral features of the polyiodides have decreased in intensity and as a consequence it is possible to identify a peak at 156 cm^{-1} corresponding to the symmetric stretch of TlI_4^- (Figure 2, bottom). A weak band at 196 cm^{-1} is also observed; it may be the overtone of the ν_1 of TlI_4^- or I_3^-, or the ν_1 of iodine. The spectral features of the crystals after some days under ambient conditions are invariant, thus indicating that the compound is stable under these conditions.

Structural Investigation

The only product that could be isolated and fully characterised from the reaction between TlI and $(Me_3S)I_7$ was found to be a polyiodide compound with no incorporation of thallium, $(Me_3S)_3I_{26}$ (**1**). However, there must be at least two different products under the chosen set of conditions: a polyiodide of the $(Me_3S)I/I_2$ system, and a thallium compound (whose spectral properties were discussed above). The structure of the thallium-containing compound could not be characterised because of its thermal instability (loss of I_2).

The structure of **1** can be described in terms of a pyramidal I_7^- ion, V/L-shaped I_5^- ions, intercalated iodine and Me_3S^+ cations (Figure 3 and Figure 4). The intramolecular I−I distances for the penta- and heptaiodides are in the range 2.75−3.29 Å (Table 1). The two independent I_5^- ions are at the limit where they may be regarded either as two I_2 molecules coordinating to an iodide ion (V-shaped) or as a

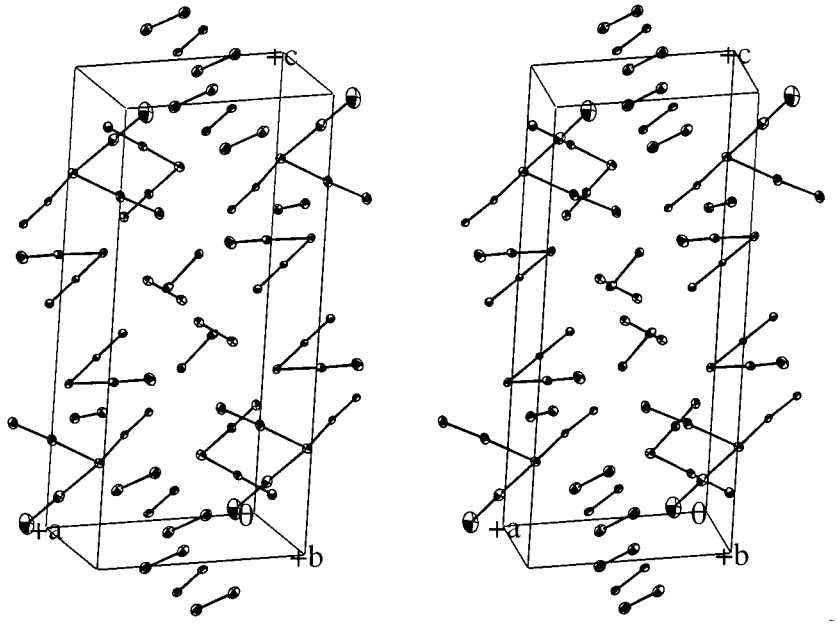


Figure 3. Stereoscopic view of the crystal structure of **1**; the cations are omitted for clarity

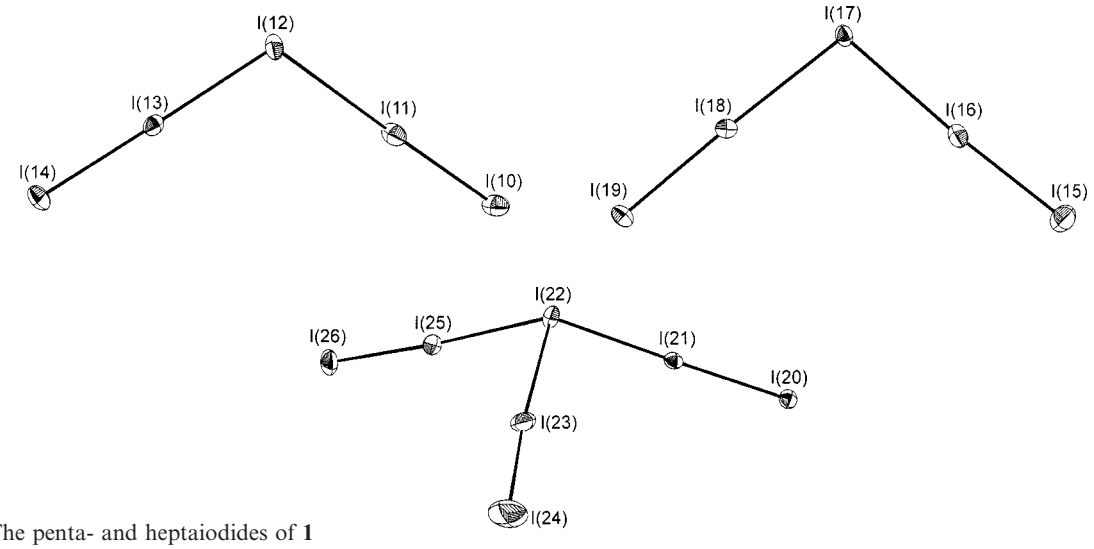


Figure 4. The penta- and heptaiodides of **1**

triiodide coordinated to an I_2 molecule (L-shaped). If the latter description is chosen, the very asymmetric triiodides I(12)−I(13)−I(14) [I(12)−I(13) 3.007(4) and I(13)−I(14) 2.843(4) Å] and I(17)−I(18)−I(19) [I(17)−I(18) 3.089(4) and I(18)−I(19) 2.805 Å] are linked to the iodine molecules I(10)−I(11) [2.751(4) Å] and I(15)−I(16) [2.790(4) Å], respectively. The triiodides are slightly bent [I(12)−I(13)−I(14) 179.3(1)° and I(17)−I(18)−I(19) 178.1(1)°].

The I_7^- anion can be described in terms of two I_2 molecules I(23)−I(24) [distance 2.748(5) Å] and I(25)−I(26) [distance 2.748(4) Å] coordinating to an asymmetric triiodide I(20)−I(21)−I(22) [distances 2.811(4) Å and 3.069(4) Å and angle 176.10(10)°]. The top angles of the "pyramid" are 94.8(1)° and 91.7(1)° [I(21)−I(22)−I(23) and I(23)−I(22)−I(25), respectively]. Consequently, with this description the formula of **1** can be written as $(Me_3S)_3[I_7(I_5)_2]\cdot 9/2I_2$. A comparison with structurally characterised pentaiodides and heptaiodides shows that the geometrical parameters of **1** are of normal magnitude.[23,24]

The intramolecular I−I distances of the intercalated I_2 units [I(1)−I(2), I(3)−I(4), I(5)−I(6), I(7)−I(8) and I(9)−I(9*)] vary from 2.73 to 2.77 Å. Pure iodine has intramolecular distances significantly shorter [2.715(6) Å in the solid state and 2.667(2) Å in the gas phase],[25,26] thus indicating a substantial charge-transfer interaction. The intermolecular I−I distances of the intercalated I_2 molecules are 3.36 Å and greater.

With the limits between intra- and intermolecular distance applied above it is easy to describe and visualise the structure of **1**. However, the situation becomes much more complicated if the limit for intramolecular distances is increased. Intermolecular I−I distances in the range 3.5−3.7 Å have been regarded as secondary bonds (van der Waals diameter of iodine 4.30 Å) and if the limit is set to 3.7 Å

in **1**, the structure instead adopts a complicated network structure.[27,28] This structure is difficult to visualise but it is possible to give a general understanding of its constitution by dividing the network into two layers. The first layer is parallel to the *ab* plane and is constructed of the pentaiodide I(10)−I(11)−I(12)−I(13)−I(14) and two of the "intercalated" iodine molecules I(5)−I(6) and I(7)−I(8) (Figures 5 and 6). The pentaiodide and the I(5)−I(6) iodine form edge-sharing, rectangular I_{16} units, while the iodine I(7)−I(8) and the "leg" of the pentaiodide I(10)−I(11) are not incorporated into the rectangular framework. The second layer is built up from I_{51} units, which are connected to each other through all edges (Figure 7). This layer intersects an equivalent layer in a chain-like manner.

The two layers are only connected to each other by I(17) which is linked to the free leg of the L-shaped pentaiodide I(10) [I(10)ΛI(17)]. Figure 8 shows how this connection ties the whole network together.

The highly crosslinked network of **1** is quite surprising considering the small cation used. There are few other polyiodides known in the literature that form extended, three-dimensional networks. All these have very bulky cations. There are some polyiodides that constitute network structures with metal centres incorporated, with the same type of cation as in **1**. These networks do not have any structural similarity with **1**, but they share the property of being highly connected and unstable under ambient conditions.[8−9]

The solid product from the reaction between TlI and $(Et_3S)I_7$ (molar ratio of 1:3) was identified as $(Et_3S)[TlI_4]$ (**2**) (Figure 9). The structure of **2** consists of tetrahedral TlI_4^- anions with Tl−I distances of 2.757(1)Å and I−Tl−I angles of 109.47(7)°, which agrees with mean values found in literature. X-ray diffraction studies on similar compounds have shown the anion to be sensitive to distortion,

Table 1. Selected bond lengths and angles for **1** and **2**

1	
I(3)−I(4)	2.736(4)
I(5)−I(6)	2.749(4)
I(7)−I(8)	2.732(4)
I(9)−I(9)	2.771(4)
I(10)−I(11)	2.744(5)
I(11)−I(12)	2.751(4)
I(12)−I(13)	3.286(4)
I(13)−I(14)	3.007(4)
I(15)−I(16)	2.843(4)
I(16)−I(17)	2.791(4)
I(17)−I(18)	3.139(4)
I(18)−I(19)	3.089(4)
I(20)−I(21)	2.805(4)
I(21)−I(22)	2.811(4)
I(22)−I(23)	3.069(4)
I(22)−I(25)	3.226(4)
I(23)−I(24)	3.290(4)
I(25)−I(26)	2.746(5)
I(1)−I(22)	2.749(4)
I(2)−I(20)	3.388(5)
I(3)−I(20)	3.517(4)
I(8)−I(14)	3.367(4)
I(4)−I(19)	3.395(4)
I(9)−I(17)	3.644(4)
I(5)−I(12)	3.424(4)
I(10)−I(17)	3.380(4)
I(6)−I(14)	3.538(5)
I(7)−I(12)	3.458(4)
1(9)−I(26)	3.356(4)
I(10)−I(11)−I(12)	3.532(5)
I(11)−I(12)−I(13)	178.78(9)
I(12)−I(13)−I(14)	112.5(1)
I(20)−I(21)−I(22)	179.3(1)
I(15)−I(16)−I(17)	176.10(10)
I(16)−I(17)−I(18)	175.1(1)
I(17)−I(18)−I(19)	100.8(1)
I(21)−I(22)−I(23)	178.1(1)
I(22)−I(23)−I(24)	94.8(1)
I(22)−I(25)−I(26)	175.7(1)
I(23)−I(22)−I(25)	176.4(1)
	91.7(1)
2	
Tl−I(1)	2.757(1)
I(1)−Tl−I(1)	109.47(7)

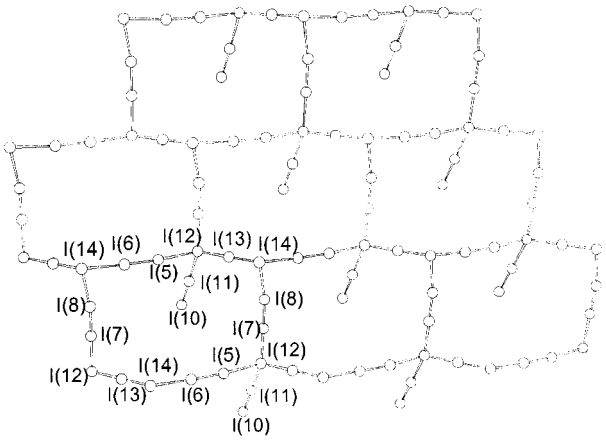


Figure 5. The I_{16} layer in the network of **1**

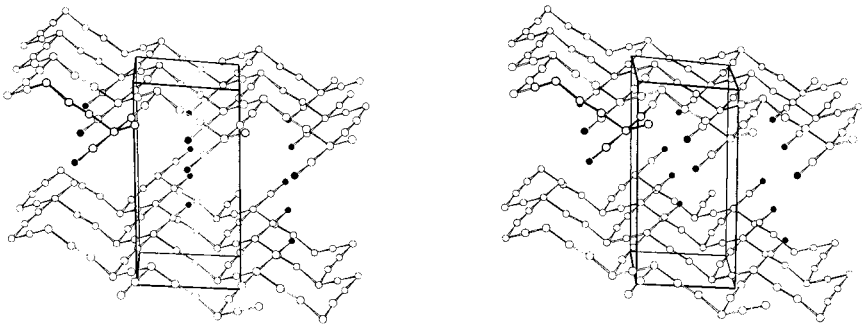


Figure 6. Stereoscopic view of the I_{16} layer in the network of **1**; the layer-connecting iodine atoms I(10) are marked black

especially by smaller cations (such as $Cs[TlI_4]$)[18] or for reasons of asymmetric coordination.[15] A directly related compound is $(Bu_4N)[TlI_4]$,[17] which shows a slight distortion of the anion, even though the ammonium cation is bulkier than Et_3S^+.

Thallium deviates from the other members of group 13, being averse to the oxidation state +III.[29] This fact, which has often been regarded as an inert-pair effect, makes Tl^{III} compounds strongly oxidising in all kinds of solvents.[29] However, the favoured Tl^{I} has to compete with the strong Lewis acidity of Tl^{III}, exemplified by the stability of the TlI_4^- complex anion. The absence of any other known Tl^{III} complexes with iodide is a consequence of thallium's reluctance to form Tl−Tl or halogen-bridged compounds, in contrast to the other elements in group 13.[29] The equilibrium between redox behaviour and complex formation, going from a weakly complex-forming Tl^{I} to a strongly complex-forming Tl^{III}, is affected by solvent properties, iodine and iodide concentration and not the least by lattice energies of the solid compounds that may be formed.[29]

In this work two iodides [TlI and $(Me_3S)I$ or $(Et_3S)I$] are present which complicates the situation even further. Not only because the iodide will interfere by "pushing the system away" from the desired Tl^{I} compounds in many solvents, but also because there is a new contribution to the lattice energy to be expected for every possible precipitate.

All these factors, summed up for the $TlI/(R_3S)I/I_2^-$ system, demand a finely tuned choice of cation size and symmetry, and stoichiometric composition of the reaction mixture. This enables a balance between the two extreme results of all parameters [Equation (1)].

$$Tl^{I}\text{/polyiodide} \leftarrow \text{choice of reaction conditions} \rightarrow Tl^{III}\text{ complex} \quad (1)$$

Reported syntheses with thallium most often lead to products to the right-hand side of Equation (1), due to the extreme stability of this complex anion.[29] Another system offering a choice between the left- and right-hand side of Equation (1) is reported by Tebbe et al.[15] Here, a crown ether is used to stabilise and increase the bulkiness of the, otherwise rare, TlI_2^+ cation. This large cation forms compounds with TlI_4^- as well as polyiodide anions. The variable in these syntheses is the iodine concentration in the solvent used.

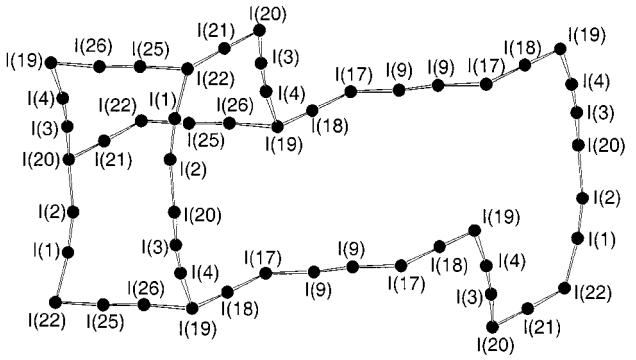


Figure 7. One of the I_{51} units that assemble the second layer

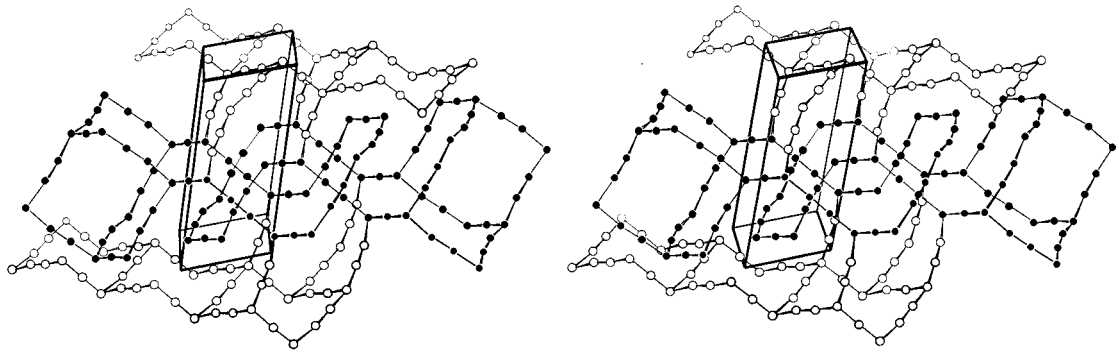


Figure 8. Stereoscopic view illustrating how the two layers are connected

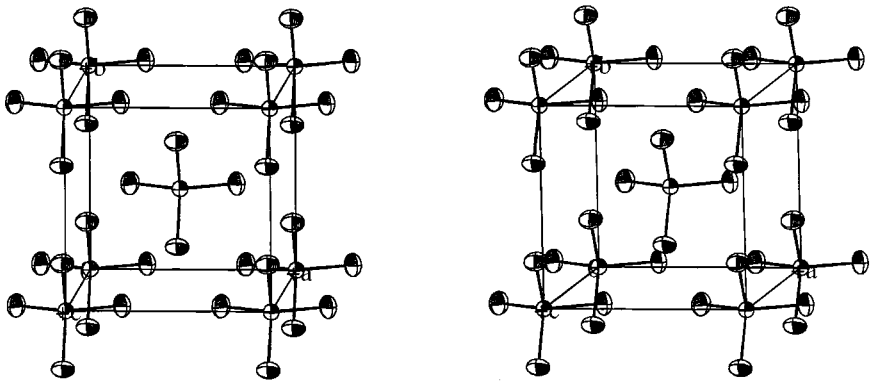


Figure 9. Stereoscopic view of the crystal structure of **2**; the cations are omitted for clarity

Under our choice of conditions, the shift in cation size going from R = Me to R = Et proved successful in the formation of both a polyiodide compound (compound **1**) and a Tl^{III} iodide complex (compound **2**). The stability of the crystalline products obey the established trends of both the Tl/I_2 and polyiodide systems: i.e. large cations (i) stabilise polyiodides[1−4] and (ii) push TlI/I towards TlI_4^-.[17,30] Following the decomposition process with Raman spectroscopy, a minor change in the I_2/I^- ratio, caused by the removal of I_2, causes compound **1** to collapse. This shifts the equilibrium towards the production of TlI_4^- [Equation (2) and (3)]. Compound **2**, on the contrary, is stable and resembles the congeners with other cations.

The oxidation of TI^{I} to Tl^{III} results in the reduction of iodine to two iodide ions. Consequently, an increase in the iodide activity is obtained [Equation (2)]. However, the complex formation of TlI_4^- requires four iodide ions [Equation (3)]. Thus, the I_2/I^- ratio is increased overall. This may explain why larger polyiodides such as $(Me_3S)_3I_{26}$ are formed by reaction with TlI.

$$Tl^{I} + I_2 \rightarrow Tl^{III} + 2\,I^- \quad (2)$$

$$Tl^{III} + 4\,I^- \rightarrow TlI_4^- \quad (3)$$

The structural and spectroscopic data obtained do not reveal which thallium species is present in the $TlI/(Me_3S)I_7$ reaction mixture.

^{205}Tl NMR Investigations

Different mixtures of TlI and $(Et_3S)I_7$ in the composition range 1:5 to 1:40 and temperature range 20 to 90 °C were investigated. Group-13 elements normally display a large chemical shift separation between the formal oxidation states +I and +III; at least as long as the ligands are relatively hard, viz. Cl^- or Br^-.

However, very soft ligands, such as I^-, have a tendency to decrease the chemical shift separation between formally Tl^{I} and Tl^{III} making unambiguous assignments of peaks in the NMR spectra more difficult. For Tl^{III} a decrease is seen for the chemical shift according to the series $Cl^- > Br^- > I^-$.[31] This series is reversed for Tl^{I} and the increase in chemical shift is coupled with growing covalency of the Tl^+-X^- bond.[31]

A mixture rich in $(Et_3S)I_7$ (1:6), preheated to 90 °C and cooled to room temperature, produces a single NMR peak at $\delta = -1414$. With the vibrational spectroscopy results in mind, this peak is assigned to TlI_4^-. Dilution with respect to $(Et_3S)I_7$ continuously shifts the frequency down to $\delta \approx -1350$ (at 1:40). The corresponding $TlI-(Me_3S)I_7$ mixtures are not liquid at room temperature and unchanged TlI can be observed visually. A 1:20 mixture displays a TlI_4^- peak at $\delta = -1368$ and a broad band (about 6 kHz) at $\delta = -1180$ assigned to TlI_3.[32]

The same features are shown by $TlI-(Et_3S)I_7$ mixtures which had not been previously treated at 90 °C. The two peaks appear at $\delta = -1400$ and -1188. A gradual increase in temperature up to 90 °C produces three spectral effects (Figure 10).

(1) The intensity of the broad band decreases and disappears after some time at 90 °C. Cooling shows that this change is reversible and suggests a simple temperature-dependent complex equilibrium.

(2) Both the broad band and the TlI_4^- peak move to more negative chemical shifts (about −1.5 ppm/°C).

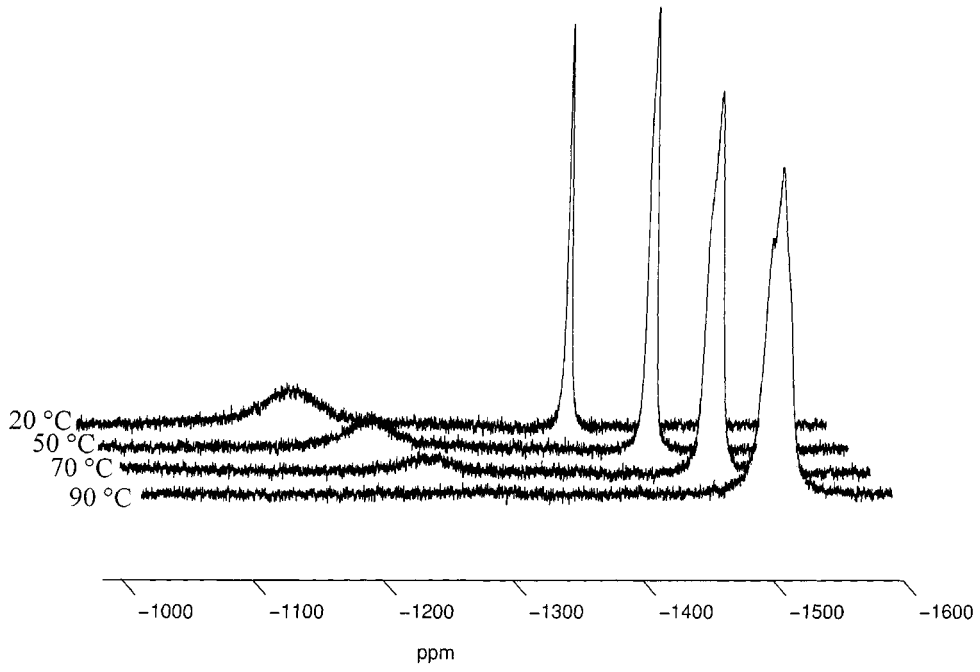


Figure 10. The ^{205}Tl NMR spectra of $TlI-(Et_3S)I_7$ with increasing temperature

(3) The peak assigned to TlI_4^- splits at higher temperatures; the new component appearing at an about 12 ppm more positive shift. This effect is reversed upon cooling, indicating a temperature-dependent equilibrium between two very similar $Tl^{III}-I^-$ species. The small difference in chemical shift and the vibrational spectroscopic data invariantly infer a Tl^{III} species of tetrahedral TlI_4^- character. The equilibrium in Equation (4) thus seems to be a logical assumption. However, recent spectroscopic and theoretical work show that the corresponding $Ga_2I_7^-$ and $In_2I_7^-$ ions only seem to be stable in solid state because of a strong tendency towards reduction of M^{III} to M^{I}.[33] Keeping in mind the easier reduction of Tl^{III} to Tl^{I}, $Tl_2I_7^-$ is a less likely species in solution. An equilibrium of the type of Equation (5) can possibly be suggested.[34]

$$2\,TlI_4^- \rightleftarrows Tl_2I_7^- + I^- \quad (4)$$

$$TlI_4^- + I_2(s) \rightleftarrows (TlI_4)^- \cdot I_2 \text{ or } TlI_3(I_3^-) \quad (5)$$

A gradual increase in temperature up to 90 °C of a $TlI-(Me_3S)I_7$ melt not preheated to 90 °C shows the features (1) and (2) (about −1 ppm/°C); however, the peak assigned to TlI_4^- surprisingly does not split at higher temperatures.

Conclusion

This work has shown that thallium does not have the same ability to be incorporated into polyiodide networks as the late transition metals (e.g. Au, Hg and Cd). A Tl/[(Me/Et)$_3$S]I_x polyiodide compound is probably formed but it is very unstable under ambient conditions and could not be detected or isolated with the methods applied. However, the polyiodide $(Me_3S)_3I_{26}$ could be isolated; which is surprising considering the small cation used. Consequently, the TlI/$(R_3S)I_x$ system indicates that it is possible to synthesise large polyiodides, even though a small cation is used, by supplying a strong Lewis acid which is not necessarily incorporated in the produced polyiodide compounds.

The Tl/[(Me/Et)$_3$S]I_x system is very complicated and the small change from Me_3S^+ to Et_3S^+ cations generate clear differences in the chemistry. In order to obtain a further understanding of which Tl species are present in the Tl/$(R_3S)I_x$ system other polyiodides with larger cations need to be investigated.

Experimental Section

Vibrational Spectroscopy: The far-infrared (far-IR) spectra were recorded with a Bio-Rad FTS 6000 FT-IR spectrometer using a resolution of 8 cm^{-1}. A globular light source was used, and a 6.25-mm Mylar beamsplitter in combination with a PE-DTGS detector produce an effective spectrum range of 50−550 cm^{-1}. The window material of the sample cells was of spectroscopic-quality polyethylene (Merck). The backscattering of the compounds was recorded using the 1064-nm radiation from an Nd:YAG laser in a Bio-Rad FT-Raman spectrometer. The radiation was recorded using a nitrogen-cooled, Ge-diode detector and 4-cm^{-1} resolution.

^{205}Tl NMR Spectroscopy: The ^{205}Tl NMR spectra of the $TlI-(R_3S)I_7$ (R = Me or Et) reaction media (1:5 to 1:40 ratios and 20−90°C) were recorded with a Varian Unity 300-MHz spectrometer operating at 172.925 MHz. A solution of 0.3 M $TlNO_3$ in water was used as standard and assigned a shift of $\delta = -7$.[35]

Synthesis of 1 and 2: The syntheses of compounds **1** and **2** were performed by direct reaction of TlI and the $(R_3S)I_7$ (R = Me or Et) melts at 90 °C. Both reactions were performed with a molar ratio of 1:3. A metal iodide/trialkylsulfonium heptaiodide ratio was chosen so that all metal iodide was dissolved in the reaction step with enough liquid polyiodide remaining to solvate the crystals produced. The latter condition is a necessary requirement for growing single crystals and for the survival of the otherwise air- and moisture-sensitive product **1**. The solid products were also examined after a few days of exposure to light and air, separated from the stabilising polyiodide melt, in order to determine the products after decomposition. A similar experiment was performed avoiding the contact with air and humidity, by sealing a tube containing the crystals and slightly heating the sample (T = 323 K) for 72 h.

Analogous syntheses starting from pure thallium metal were also performed. The products obtained were identical to those of using the TlI-based routes.

The crystalline products from the syntheses described above were recrystallised from methanol, ethanol, acetonitrile, acetone and *N*,*N*-dimethylthioformamide. In all cases, the resulting crystals observed after slow evaporation of the solvent apparently contain less iodine, i.e. they become lighter in colour than their precursors. This behaviour has previously been observed for similar compounds, most likely arising because of the effective and undesired solvation of I_2 by the solvents used. In order to minimise the loss of iodine we also recrystallised the solid compounds **1** and **2** from iodine-saturated ethanol. The latter resulted in darker crystals with a more porous habit as compared to the crystals obtained from other solvents.

X-ray Crystallographic Study: Single crystals of **1** and **2** were obtained from the reaction mixture at room temperature. The crystal data for the structures are presented in Table 2. The data for **1** were collected at 150 K, because of the tendency to lose iodine, while the data for **2** were collected at room temperature. All data were corrected for Lorentz-polarisation effects and an empirical absorption correction was applied using the Difabs (compound **1**) and ψ-scan (compound **2**) methods.[36,37] The structures were solved by the direct methods of SIR92 (**1**) and SHELXTL-PLUS (**2**) program packages.[38,39] The structure of **1** was refined on F, while the structure of **2** was refined on F^2.[40,39] The carbon and sulfur atoms of **1** were refined isotropically due to the high thermal displacement. One of the cations in **1** has the sulfur [S(1)] atom disordered in two positions. The cation of **2** is highly disordered and only the positions of the sulfur atoms were located (refined isotropically). Hydrogen atoms were placed in calculated positions for **1** (except for the disordered cation), and completely omitted in **2** because of the cation disorder. − Crystallographic data (excluding structure factors) for the structures in this paper have been deposited with the Cambridge Crystallographic Data Centre as supplementary publication nos. CCDC-134329 [for $(Me_3S)_3I_{26}$] and CCDC-34330 [for $(Et_3S)TlI_4$]. Copies of the data can be obtained, free of charge, on application to CCDC, 12 Union Road, Cambridge CB2 1EZ, UK [Fax: (internat.) + 44-1223/336033; E-mail: deposit@ccdc.cam.ac.uk].

Table 2. Crystallographic data for **1** and **2**

	1	**2**
Empirical formula	$C_9H_{27}I_{26}S_3$	$C_6H_{15}I_4STl$
M	3531.01	799.19
Crystal size [mm]	0.10×0.08×0.08	0.17×0.15×0.10
a [Å]	10.833(4)	8.680(1)
b [Å]	13.10(1)	8.680(1)
c [Å]	23.64(1)	12.294(3)
α [°]	97.77(7)	90
β [°]	97.51(5)	90
γ [°]	109.50(5)	90
V [Å^3]	3076(4)	926.3(2)
Space group	$P\bar{1}$	$I\bar{4}$
Z	2	2
D_c [gcm^{-3}]	3.811	2.870
μ [mm^{-1}]	13.18	15.47
Diffractometer	CAD4	CAD4
Radiation	Mo-K_α	Mo-K_α
Scan type	ω-2θ	ω-2θ
$2\theta_{max}$	52	50
T [K]	150	293
Total data collected	12682	786
Unique data	12367	719
R_{int}	0.076	0.047
Observed data	6672 [> 3σ(I)]	631 [> 2σ(I)]
Data/variables	287/6672	23/719
Goodness of fit	2.26	1.16
Final difference map	−3.82, 3.27	−3.04, 1.39
R	0.065	0.0543[a]
R_w	0.097	0.136[b]

[a] $R(F^2)_{obs}$. – [b] $R_w(F^2)_{obs}$.

Acknowledgments

The Swedish Natural Science Research Council and the Wenner−Gren Foundation are gratefully acknowledged for their financial support.

[1] P. Coppens in *Extended Linear Chain Compounds* (Ed.: J. S. Miller), Plenum Press, New York **1982**, vol. 1, p. 333−356.
[2] T. J. Marks, D.W. Kalina in *Extended Linear Chain Compounds* (Ed.: J. S. Miller), Plenum Press, New York **1982**, vol. 1, p. 197−331.
[3] K.-F. Tebbe in *Homoatomic Rings, Chains and Macromolecules of Main-Group Elements* (Ed.: A. L. Rheingold), Elsevier, Amsterdam **1977**, p. 551−606.
[4] B. D. Stepin, S. B. Stepina, *Usp. Khim.* **1986**, *55*, 1434−1451; *Chem. Abstr.* **1986**, *105*, 217778.
[5] H. L. Wells, *Anorg. Chem.* **1893**, *4*, 346−349.
[6] K. F. Tebbe, *Z. Kristallogr.* **1985**, *171*, 129−139.
[7] E. S. Lang, J. Strähle, *Z. Anorg. Allg. Chem.* **1996**, *622*, 981−984.
[8] H. Stegemann, K.-F. Tebbe, L. A. Bengtsson, *Z. Anorg. Allg. Chem.* **1995**, *621*, 165−170.
[9] P. H. Svensson, L. Bengtsson-Kloo, *J. Chem. Soc., Dalton. Trans.* **1998**,1425−1429.
[10] P. H. Svensson, J. Rosdahl, L. Bengtsson-Kloo, *Chem. Eur. J.* **1999**, *5*, 305−311.
[11] P. H. Svensson, L. Bengtsson-Kloo, *Inorg. Chem.* **1999**, *14*, 3390−3393.
[12] T. G. Spiro, *Inorg. Chem.* **1967**, *6*, 569−572.
[13] K. F. Tebbe, U. Georgy, *Acta. Crystallogr.* **1986**, *C42*, 1675−1678.
[14] D. F. Shriver, P. W. Atkins, C. H. Langford, *Inorganic Chemistry*, 2nd ed., Oxford University Press, Oxford, **1994**, p. 357.
[15] K.-F. Tebbe, M. El Essawi, S. A. El Khalik, *Z. Naturforsch.* **1995**, *50b*, 1429−1439.
[16] W. Stoeger, H. Schulz, A. Rabenau, *Z. Anorg. Allg. Chem.* **1977**, *432*, 5−16.
[17] J. Glaser, P. L. Goggin, M. Sandström, V. Lutsko, *Acta Chem. Scand.* **1982**, *A36*, 55−62.
[18] G. Thiele, H. W. Rotter, K. Zimmermann, *Z. Naturforsch.* **1986**, *41b*, 269−272.
[19] D. M. Adams, D. M. Morris, *J. Chem. Soc.* **1968**, 694−695.
[20] K. Arai, T. Chiba, K. Aida, *J. Inorg. Nucl. Chem.* **1981**, *43*, 2986−2988.
[21] S. P. Andrews, P. E. R. Badger, P. L. Goggin, N. W. Hurst, A. J. M. Rattray, *J. Chem. Res.* **1978**, 94−95.
[22] M. G. B. Drew, D. F. Lewis, R. A. Walton, *Inorg. Nucl. Chem. Lett.* **1970**, *6*, 163−166.
[23] *Cambridge Structural Database System*, Database V. 5.14, **1997**.
[24] *Inorganic Structural Database ICSD*, V. 5.14, Gmelin Institut, **1997**.
[25] F. van Bolhuis, P. B. Koster, T. Migchelsen, *Acta Crystallogr.* **1967**, *23*, 90−93.
[26] I. L. Karle, *J. Chem. Phys.* **1955**, *23*, 1739−1739.
[27] M. Bittner, *Präparative und röntgenographische Untersuchungen an Polyiodiden von 2,2'-Bipyridin*, Ph. D. thesis, Köln, **1994**.
[28] J. Blake, F. A. Devilliano, R. O. Gould, W-S Li, V. Lippolis, S. Parsons, C. Radek and M. Schröder, *Chem. Soc. Rev.* **1998**, *27*, 195−205.
[29] M. J. Taylor, P. J. Brothers, in *Chemistry of Aluminum, Gallium, Indium and Thallium* (Ed.: A. J. Downs), Chapman and Hall, Glasgow, **1993**, p. 111−247.
[30] F. A. Cotton, B. F. G. Johnson, R. M. Wing, *Inorg. Chem.* **1965**, *4*, 502−507.
[31] J. Glaser, *Adv. Inorg. Chem.* **1995**, *43*, 1−78.
[32] G. Ma, I. Toth, J. Glaser, to be published.
[33] M. J. Taylor, L. Kloo, unpublished results.
[34] W. Saak, S. Pohl, *Z. Anorg. Allg. Chem.* **1987**, *552*, 186−194.
[35] R. P. H. Gasser, R. E. Richards, *Mol. Phys.* **1959**, *2*, 357−361.
[36] N. Walker, D. Stuart, *Acta Crystallogr.* **1983**, *A39*, 158−163.
[37] A. C. T. North, D. C. Phillips, F. S. Mathews, *Acta Crystallogr.* **1968**, *A 24*, 351−355.
[38] A. Altomare, M. C. Burla, M. Camalli, M. Cascarano, C. Giacovazzo, A. Guagliardi, G. Polidori, *J. Appl. Crystallogr.* **1994**, *27*, 435−441.
[39] G. M. Sheldrick, *SHELXTL-PLUS*, Siemens Analytical Instruments, **1992**.
[40] *TEXSAN*, Crystal Structure Analysis Package, Molecular Structure Corporation, **1985**, **1992**.

Received September 20, 1999
[I99333]

Resolution of Secondary Phosphanes Chiral at Phosphorus by Means of Palladium Metallacycles

Joan Albert,[a] J. Magali Cadena,[a] Jaume Granell,*[a] Guillermo Muller,[a] David Panyella,[a] and Carolina Sañudo[a]

Keywords: Phosphanes / Palladium / Metallacycles / Chiral resolution / Configuration determination

The synthesis of new epimeric compounds [PdCl(C–N){(±)-PHPhR}] (C–N = (*R*)-$C_{10}H_6CHMeNH_2$ and (*R*)-$C_6H_4CHMeNH_2$, R = Me and $PhCH_2$) containing chiral secondary phosphanes is reported. Some of these diastereomers can be separated by column chromatography; subsequent reaction of these complexes with 1,2-bis(diphenylphosphanyl)-ethane (dppe) affords the free phosphanes PHBzPh and PHMePh. The configurational stability of the secondary phosphanes resolved has also been studied.

Introduction

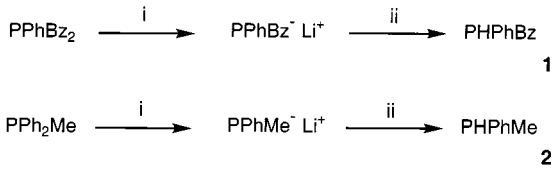
Due to the reactivity of their P−H bonds, secondary phosphanes are versatile synthons for the preparation of chiral mono- and bidentate ligands[1] but only one secondary phosphane chiral at phosphorus has been resolved to date. Six consecutive recrystallizations from acetonitrile in the presence of sodium acetylacetonate afforded the [R_P-(1*R*,2*S*,5*R*)] diastereomer of menthylmesitylphosphane in 94% optical purity.[2] The low configurational stability of P-chiral secondary phosphanes has been explained by acid-catalyzed racemization, in which the protonation of secondary phosphanes affords achiral phosphonium ions with two enantiotopic protons that can be removed at identical rates. Wild et al. have shown by ^{31}P NMR experiments that the H/D exchange between PHMePh and PDEtPh is negligible in highly purified acetonitrile in the presence of sodium acetylacetonate as a proton scavenger, showing that the resolution of secondary phosphanes may be feasible under mildly basic conditions.[3] When the phosphane is attached to metal ions, a borane or chalcogens by means of the lone pair the racemization does not occur and some diastereomers containing coordinated secondary phosphanes have been separated.[3,4] However, with the exception of the remarkable results described by Wild et al. with menthylmesitylphosphane,[2] recovery of the free optically pure ligand has not been accomplished.

Here we report the synthesis and separation of some diastereomers of compounds [PdCl($C_{10}H_6CHMeNH_2$)-(PHPhR)] (R = Me and $PhCH_2$) and the isolation of the free secondary phosphanes by the action of 1,2-bis(diphenylphosphanyl)ethane (dppe) on these cyclopalladated derivatives. The configurational stability of the secondary phosphanes resolved and the isotopic exchange between these ligands and D_2O has also been studied.

[a] Departament de Química Inorgànica, Universitat de Barcelona, Diagonal 647, 08028 Barcelona, Spain
Fax: (internat.) + 34-93/490-7725
E-mail: jgranell@kripto.qui.ub.es

Results and Discussion

(±)-Benzylphenylphosphane was synthesized by reaction of dibenzylphenylphosphane and lithium metal in tetrahydrofuran under a dry nitrogen atmosphere. After 16 h of stirring at room temperature complete cleavage of one of the CH_2−P bonds of the starting phosphane was accomplished, with formation of the benzylphenylphosphide anion. The ^{31}P NMR spectrum, under nitrogen, clearly illustrated the formation of this anion ($\delta = -37.1$) and was used to monitor the progress of the reaction. Subsequent addition of H_2O gave the secondary phosphane (±)-**1** in THF solution (Scheme 1). When methyldiphenylphosphane and lithium metal reacted in the same conditions complete cleavage of one of the Ph−P bonds of the starting phosphane was accomplished, with formation of the methylphenylphosphide anion ($\delta_P = -77.3$). Subsequent addition of H_2O gave (±)-methylphenylphosphane **(2)** in THF solution. It should be noted that these secondary phosphanes are air sensitive and careful workup under nitrogen is needed to obtain them in the free form. The separation of some diastereomers containing PHMePh or PHBzPh coordinated to iron[4b] or platinum[3][4c] has been reported but, to the best of our knowledge, these phosphanes have not been obtained in free form, optically pure.

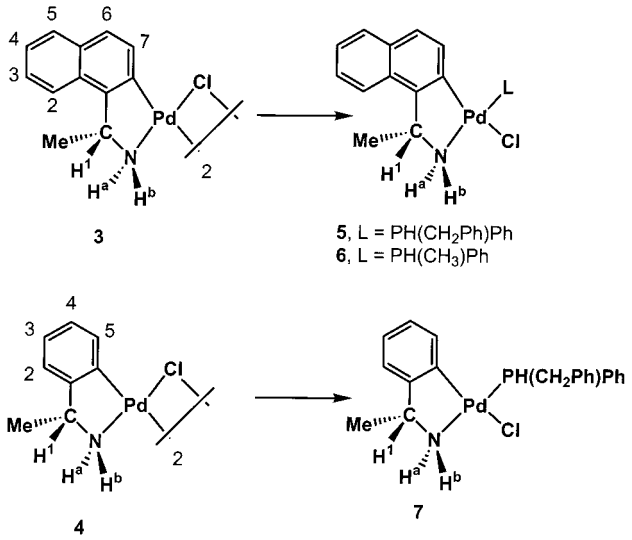


Scheme 1. i) Li, THF, room temperature, 16 h; ii) THF, room temperature, 10 min

The versatility of *ortho*-palladated derivatives of optically active N-donor ligands as resolving agents for Lewis bases has been convincingly demonstrated.[5] The optically pure cyclopalladated dinuclear compounds **3** and **4** were obtained from the optically active amines as reported.[6] Reaction of these dimers with the secondary phosphanes (±)-

 © WILEY-VCH Verlag GmbH, D-69451 Weinheim, 2000 1434−1948/00/0606−1283 $ 17.50+.50/0

PHPhR afforded the mononuclear compounds [PdCl(C−N)(PHPhR)] (**5**, **6** and **7**), as a 1:1 mixture of the diastereomers (R_C,R_P) and (R_C,S_P) (Scheme 2). All the new organometallic compounds obtained were characterized by elemental analysis and IR, ^{1}H and ^{31}P NMR spectroscopy. In some cases, 2D NMR experiments (COSY and NOESY) were carried out to complete the characterization. The high-field shift of the aromatic protons of the palladated ring in the mononuclear derivatives, due to the aromatic rings of phosphanes, indicates the *cis* disposition of the phosphorus relative to the metallated carbon atom and the chemical shift in the ^{31}P NMR spectra confirms this arrangement.[7]

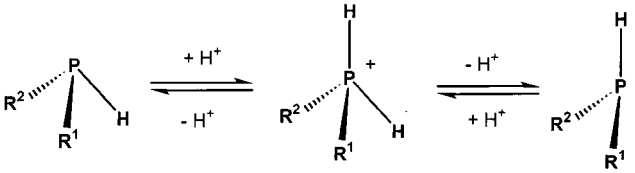


Scheme 2. L, 20 °C, $CHCl_3$ for **5** and **6** and THF for **7**

All attempts to separate the diastereomers of compounds **5**, **6** and **7** by recrystallization and all attempts to separate the diastereomers of **7** by column chromatography were unsuccessful. In contrast, the elution of compounds **5** and **6**, which contain the metallated (*R*)-(+)-1-(1-naphthyl)ethylamine, in a SiO_2 column (see Experimental Section) allowed the separation of the first diastereomer eluted **5′** and **6′**, in 45 and 63% yield, respectively (22.5 and 31.5% with respect to the total Pd), with a *de* higher than 95% in both cases [the superscripts (′) and (′′) indicate the first and the second diastereomer eluted in the column]. These results are consistent with previous reports since naphthyl adducts generally provide greater enantiomeric discrimination than their phenyl counterparts. It has been proposed that this is due to the fact that the methyl substituent of the chiral carbon atom adopts an axial disposition to avoid the unfavorable interaction with H^2 in the naphthyl adducts (see Scheme 2), and, in consequence, the five-membered metallacycle has a locked asymmetric envelope conformation. In contrast the methyl group is either axial or equatorial and this metallacycle adopts different conformations in 1-phenylethylamine derivatives.[8] The NOESY spectra of compounds **5** and **6** show that H^1 has strong negative off-diagonal peaks with H^2 and H^b and, in contrast, the methyl protons of the chiral carbon atom present only strong NOE interactions with H^a and H^1. These data confirm the axial disposition of this methyl group and the equatorial disposition of H^1 in both complexes.[9]

When a stoichiometric amount of 1,2-bis(diphenylphosphanyl)ethane was added to an ether solution of the optically pure cyclopalladated derivatives **5′** and **6′** the quantitative precipitation of the ionic compound [Pd(C−N)(dppe)]Cl took place and solutions of the enantiopure free phosphanes PHBzPh and PHMePh (^{31}P NMR : $\delta = -41.0$ or -71.7, respectively) in diethyl ether were obtained. No racemization of benzylphenylphosphane was observed when this ligand was stored in solution for 20 minutes, as verified by ^{31}P NMR spectroscopy, which showed the quantitative regeneration of the starting material **5′** from the dinuclear cyclopalladated derivative **3** and the corresponding free ligand. Three hours later significant racemization of the free phosphane was observed. In contrast, when this experiment was carried out with methylphenylphosphane, the formation of a ca. 1:1 mixture of diastereomers of **6** was observed in less than five minutes. The high configurational stability of PHBzPh is remarkable; it should be noted that an acetonitrile solution of menthylmesitylphosphane, the only secondary phosphane resolved until now, led to immediate epimerization at phosphorus in the absence of sodium acetylacetonate.[2]

Secondary phosphanes are difficult to obtain in an optically active form due to acid-catalyzed racemization, which involves the formation of an achiral phosphonium salt (see Scheme 3). In order to evaluate the tendency to protonation of the secondary phosphanes **1** and **2**, we analyzed the H/D exchange between the free phosphanes and D_2O in an NMR tube. A few drops of D_2O were added to THF solutions of the free secondary phosphanes **1** and **2** and ^{31}P NMR spectra were recorded (Figure 1). These spectra show that after 15 minutes a significant amount of PDMePh was formed, and after six hours PDMePh was the major compound. In contrast only a small amount of PDBzPh was formed after six hours. These findings suggest that the high configurational stability of PHBzPh is related to its stability against acid-catalyzed racemization, although the contribution to the racemization of other mechanisms cannot be ruled out.



Scheme 3. Acid-catalyzed racemization

The free secondary phosphanes described here are readily oxidizable and should be stored under nitrogen, although when coordinated to palladium (compounds **5** and **6**) they can be handled in air and are stable for several months. In consequence, these naphthyl cyclopalladated derivatives can also be used to store the phosphanes and to obtain them in free form when needed by reaction with dppe.

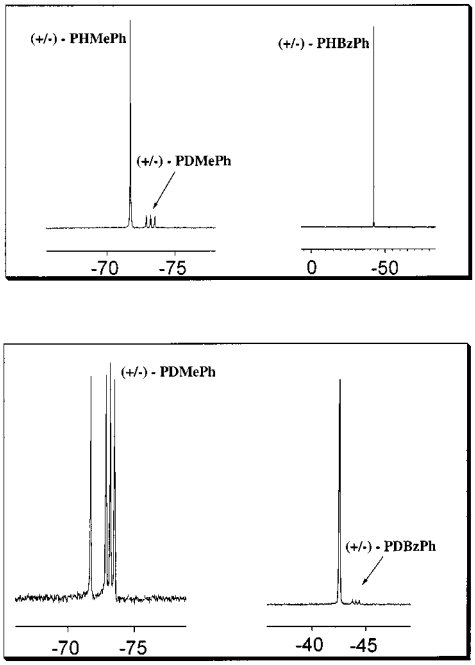


Figure 1. $^{31}P\{^{1}H\}$ NMR spectrum in THF solution of the free secondary phosphanes **1** and **2**: (a) five minutes after the addition of D_2O; (b) after six hours

Experimental Section

^{1}H NMR at 200 MHz or 500 MHz, and $^{31}P\{^{1}H\}$ at 101.26 MHz spectra were recorded on Varian Gemini 200, Varian VXR 500 and Bruker DRX 250 spectrometers, respectively. Chemical shifts (in ppm) were measured relative to $SiMe_4$ for ^{1}H and to 85% H_3PO_4 for ^{31}P. The solvents used were $CDCl_3$ for ^{1}H NMR and THF or $CHCl_3$ for ^{31}P NMR. Microanalyses were performed at the Institut de Química Bio-Orgànica de Barcelona and the Serveis Científico-Tècnics de la Universitat de Barcelona. The optical rotations of the complexes were determined at 20 °C using a Perkin−Elmer 241-MC polarimeter. Infrared spectra were recorded as KBr disks on a Nicolet 520 FT-IR spectrometer.

Materials and Synthesis: All the reactions involving free phosphanes were carried out using Schlenk techniques under a nitrogen atmosphere. All solvents were dried and degassed by standard methods. Tetrahydrofuran and diethyl ether were distilled over sodium/benzophenone, under nitrogen, before use. All chemicals were of commercial grade and used as received. Cyclopalladated compounds **3** and **4**, and $PPhBz_2$ were prepared according to procedures described elsewhere.[6,10]

Synthesis of [PdCl{(*R*)−$C_{10}H_6CHMeNH_2$}{(±)-PHBzPh}] (5): Small pieces of lithium (86.0 mg, 12.4 mmol) were added to a solution of dibenzylphenylphosphane (1.5 g, 5.2 mmol) in THF (40 mL) and the reaction mixture was stirred for 16 hours at 20 °C. The unreacted lithium was removed by decantation, and then 0.5 mL of water was added and the mixture stirred for a further 10 min. The resulting solution was dried over anhydrous Na_2SO_4 and filtered off to obtain a THF solution of (±)-PHBzPh [^{31}P NMR (101.26 MHz, $CDCl_3$): δ = −41.0 (d, J_{H-P} = 205 Hz)]. This solution was slowly added to a suspension formed by 0.24 mmol of the corresponding cyclopalladated dimer **3** in $CHCl_3$ (30 mL) until complete dissolution of the precipitate. The resulting solution was concentrated in vacuo and the solid obtained was eluted by SiO_2 column chromatography with $CHCl_3$/acetone (100:4) as eluent. Compound **5** [ca. 1:1 mixture of the diastereomers (R_C,R_P) and (R_C,S_P)] was isolated as a yellow solid. The yield of the process was 65% (160 mg) relative to the cyclopalladated compound **3**. − $C_{25}H_{25}ClNPPd$ (512.31): calcd. C 58.61, H 4.91, N 2.73; found C 58.7, H 4.8, N 2.5. − ^{31}P NMR (101.26 MHz, $CDCl_3$): δ = 26.9 (d, J_{H-P} = 362 Hz), 25.2 (d, J_{H-P} = 367 Hz).

Separation of Diastereomers 5: The 1:1 mixture of the diastereomers (R_C,R_P)- and (R_C,S_P)-**5** (100 mg) was carefully eluted at room temperature on an SiO_2 column (30 × 400 mm, 50 g SiO_2) with $CHCl_3$/acetone (100:2) as eluent. Fractions of 15 mL were collected, concentrated in vacuo and checked by ^{1}H NMR spectroscopy. The fractions were selected using the aromatic or the methylic proton signals. The first diastereomer eluted, **5′**, was obtained in 45% yield (22.5 mg), with a *de* higher than 95%, and the second diastereomer, **5′′**, was obtained in 38% yield (19 mg), with 52% diastereomeric purity.

5′: ^{1}H NMR (500 MHz, $CDCl_3$): δ = 7.88 (m, 2 H, H_{ar}), 7.67 (d, J_{HH} = 7.5 Hz, 1 H, H_{ar}), 7.59 (d, J_{HH} = 8.0 Hz, 1 H, H_{ar}), 7.47 (m, 1 H, H_{ar}), 7.40−7.30 (m, 5 H, H_{ar}), 7.19−7.12 (m, 5 H, H_{ar}), 6.97 (t, J_{HH} = 9.0 Hz, 1 H, H^7), 5.23 (sextuplet, J_{HH} = 5.5 Hz, 1 H, H^1), 5.02 (dt, J_{HH} = 6 Hz, J_{PH} = 367 Hz, 1 H, *H*P), 4.04 (br s, 1 H, H_a), 3.92 (m, 1 H, CH_2P), 3.63 (m, 1 H, CH_2P), 3.46 (br s, 1 H, H_b), 1.84 (d, $^{3}J_{HH}$ = 6.5 Hz, 3 H, *Me*). − ^{31}P NMR ($CDCl_3$): δ = 25.2 (d, J_{H-P} = 367 Hz). − $[\alpha]_D^{20}$ = +62.4 (*c* = 204 mg/100 mL, in $CHCl_3$).

5′′: ^{1}H NMR (500 MHz, $CDCl_3$): δ = 7.72−7.60 (m, 4 H, H_{ar}), 7.40−7.13 (m, 10 H, H_{ar}), 6.85 (m, 2 H, H^6, H^7), 4.91 (dt, J_{HH} = 5.6 Hz, J_{PH} = 362 Hz, 1 H, *H*P), 5.25 (q, J_{HH} = 5.8 Hz, 1 H, H^1), 4.71 (br s, 1 H, H_a), 3.57 (m, 3 H, CH_2P, H_b), 1.82 (d, $^{3}J_{HH}$ = 6.2 Hz, 3 H, *Me*). − ^{31}P NMR ($CDCl_3$): δ = 26.9 (d, J_{H-P} = 362 Hz).

[PdCl{(*R*)-$C_6H_4CHMeNH_2$}{(±)-PHBzPh}] (7): To a suspension of **4** in THF (30 mL) as starting material, the synthesis of **7** was analogous to the preparation of **5**. Compound **7** [ca. 1:1 mixture of the diastereomers (R_C,R_P) and (R_C,S_P)] was isolated as a yellow solid. The yield of the process was 30% (70 mg).

7: $C_{21}H_{23}ClNPPd$ (462.25): calcd. C 54.57, H 5.02, N 3.03; found C 54.4, H 5.2, N 3.2. − ^{1}H NMR (200 MHz, $CDCl_3$): δ = 7.90−7.70 (m, 4 H, H_{ar}), 7.50−7.30 (m, 6 H, H_{ar}), 7.20−7.10 (m, 10 H, H_{ar}), 6.95−6.85, (m, 8 H, H_{ar}), 5.05 (d, J_{HP} = 360 Hz, 2 H, *HP*), 4.10−3.50 (m, 6 H, *NH*, CH_2), 3.30 (br m, 2 H, *NH*), 1.67 (d, J_{HH} = 6.5 Hz, 3 H, *Me*), 1.60 (d, J_{HH} = 6.5 Hz, 3 H, *Me*). − ^{31}P NMR (101.26 MHz, $CDCl_3$): δ = 29.4 (d, J_{HP} = 360 Hz), 27.7 (d, J_{HP} = 362 Hz).

Synthesis of [PdCl{(*R*)-$C_{10}H_6CHMeNH_2$}{(±)-PHMePh}], 6: Small pieces of lithium (37.0 mg, 5.37 mmol) were added to a solution of methyldiphenylphosphane (0.5 mL, 2.68 mmol) in THF (20 mL) and the reaction mixture was stirred for 16 hours at 20 °C. The unreacted lithium was removed by decantation, and then 0.5 mL of water was added and the mixture stirred for a further 10 min. The resulting solution was dried over anhydrous Na_2SO_4 and filtered to obtain a THF solution of (±)-PHMePh [^{31}P NMR (101.26 MHz, $CDCl_3$): δ = −71.7 (d, J_{H-P} = 203 Hz)]. This solution was slowly added to a suspension formed of **3** (150.0 mg, 0.24 mmol) in 30 mL of $CHCl_3$ until dissolution of the precipitate. The resulting solution was concentrated in vacuo and the solid obtained was eluted by SiO_2 column chromatography with $CHCl_3$/methanol (100:3) as eluent. Compound **6** [ca. 1:1 mixture of the diastereomers (R_C,R_P) and (R_C,S_P)] was isolated as a yellow solid

in 75% yield (160 mg). – $C_{19}H_{21}ClNPPd$ (436.21): calcd. C 52.31, H 4.85, N 3.21; found C 51.3, H 4.8, N 3.1. – ^{31}P NMR ($CDCl_3$): δ = −0.8 (d, J_{H-P} = 360 Hz); −1.2 (d, J_{H-P} = 364 Hz).

Separation of Diastereomers 6.: The 1:1 mixture of the diastereomers (R_C,R_P)- and (R_C,S_P)-**6** (100 mg) was carefully eluted at room temperature on a SiO_2 column (30 × 400 mm, 30 g SiO_2) with $CHCl_3$/acetone (100:6) as eluent. Fractions of 15 mL were collected, concentrated in vacuo and checked by ^1H NMR spectroscopy. The fractions were selected using the aromatic or the methylic proton signals. The first diastereomer eluted, **6′**, was obtained in 63% yield (31.5 mg), with a *de* higher than 95%, and the second diastereomer, **6′′**, was obtained in 15% yield (7.5 mg), with 86% diastereomeric purity.

6′: ^1H NMR ($CDCl_3$): δ = 8.00 (m, 2 H, H_{ar}), 7.70 (d, J_{HH} = 6.0 Hz, 1 H, H_{ar}), 7.63 (d, J_{HH} = 8.0 Hz, 1 H, H_{ar}), 7.49−7.32 (m, 7 H, H_{ar}), 7.07 (t, J_{HH} = 8.5 Hz, 1 H, H^7), 5.28 (dq, J_{HH} = 6.0 Hz, J_{HP} = 364 Hz, 1 H, *HP*), 5.26 (sextuplet, J_{HH} = 5.5 Hz, 1 H, H^1), 4.10 (br s, 1 H, H_a), 3.46 (br s, 1 H, H_b), 1.99 (dd, J_{HH} = 6.0 Hz, J_{PH} = 11.5 Hz, 3 H, *Me*P), 1.88 (d, $^3J_{HH}$ = 6.5 Hz, 3 H, *Me*). – ^{31}P NMR ($CDCl_3$): δ = −1.2 (d, J_{H-P} = 364 Hz).

6′′: ^1H NMR ($CDCl_3$): δ = 7.75−7.60 (m, 4 H, H_{ar}), 7.43−7.20 (m, 7 H, H_{ar}), 5.07 (dq, J_{HH} = 6.0 Hz, J_{HP} = 360 Hz, 1 H, *HP*), 5.28 (sextuplet, J_{HH} = 6.2 Hz, 1 H, H^1), 4.93 (br s, 1 H, H_a), 3.45 (br s, 1 H, H_b), 1.84 (d, $^3J_{HH}$ = 6.5 Hz, 3 H, *Me*), 1.50 (dd, J_{HH} = 6.1 Hz, J_{HP} = 11.4 Hz, 3 H, *MeP*). – ^{31}P NMR ($CDCl_3$): δ = −0.8 (d, J_{H-P} = 360 Hz).

Acknowledgments

We thank the DGICYT (projects: PB 96−104 and PB97−407-C5−4) and the Comissionat per a Universitats i Recerca (project: 1997SGR 00174) for financial support. J. M. C. thanks the Agencia Española de Cooperación Internacional for a fellowship.

[1] K. M. Pietrusiewicz, M. Zablocka, *Chem. Rev.* **1994**, *94*, 1375−1411.

[2] [2a] A. Bader, M. Pabel, S. B. Wild, *J. Chem. Soc., Chem. Commun.* **1994**, 1405−1406. – [2b] A. Bader, M. Pabel, A. C. Willlis, S. B. Wild, *Inorg. Chem*. **1996**, *35*, 3874−3877.

[3] A. Bader, T. Nullmeyers, M. Pabel, G. Salem, A. C. Willis, S. B. Wild, *Inorg. Chem.* **1995**, *34*, 384−389.

[4] [4a] G. Salem, S. B. Wild, *J. Chem. Soc., Chem. Commun.* **1987**, 1378−1379. – [4b] G. T. Crisp, G. Salem, S. B. Wild, F. S. Stephens, *Organometallics* **1989**, *8*, 2360−2367. – [4c] A. Bader, G. Salem, A. C. Willis, S. B. Wild, *Tetrahedron: Asymmetry* **1992**, *3*, 1227−1230. – [4d] G. T. Crisp, G. Salem, F. S. Stephens, S. B. Wild, *J. Chem. Soc., Chem. Commun.* **1987**, 600−602. – [4e] J. Michalski, Z. Skrzypczynsky, *J. Org. Chem.* **1988**, *53*, 4549−4551. – [4f] R. de Vaumas, R. Marinetti, L. Ricard, F. Mathey, *J. Am. Chem. Soc.* **1992**, *114*, 261−266. – [4g] B. D. Zwick, M. A. Dewey, D. A. Knight, W. E. Buhro, A. M. Arif, J. A. Gladysz, *Organometallics* **1992**, *11*, 2673−2685. – [4h] T. Imamoto, T. Oshiki, T. Onozawa, T. Kusumoto, K. Sato, *J. Am. Chem. Soc.* **1990**, *112*, 5244−5252. – [4i] J. Michalski, Z. Skrzypczynsky, *J. Chem. Soc., Chem. Commun.* **1977**, 66−67.

[5] [5a] S. B. Wild, *Coord. Chem. Rev.* **1997**, *166*, 291−311. – [5b] J. Leitch, G. Salem, D. C. R. Hockless, *J. Chem. Soc., Dalton Trans.* **1995**, 649−656. – [5c] R. J. Doyle, G. Salem, A. C. Willis, *J. Chem. Soc., Dalton Trans.* **1995**, 1867−1872. – [5d] P. H. Leung, A. C. Willis, S. B. Wild, *Inorg. Chem.* **1992**, *31*, 1406. – [5e] S. Y. M. Chooi, S. Y. Siah, P. H. Leung, K. F. Mok, *Inorg. Chem.* **1993**, *32,* 4812−4818. – [5f] C. E. Barclay, G. Deeble, R. J. Doyle, S. A. Elix, G. Salem, T. L. Jones, S. B. Wild, A. C. Willis, *J. Chem. Soc., Dalton Trans.* **1995**, 57−65. – [5g] N. Gabbitas, G. Salem, M. Sterns, A. C. Willis, *J. Chem. Soc., Dalton Trans.* **1993**, 3271−3276. – [5h] V. V. Dunina, E. B. Golovan, *Tetrahedron: Asymmetry.* **1995**, *6*, 2747−2754. – [5i] M. Pabel, A. C. Willis, S. B. Wild, *Angew. Chem. Int. Ed. Engl.* **1994**, *33*, 1835−1837. – [5j] M. Pabel, A. C. Willis, S. B. Wild, *Inorg. Chem.* **1996**, *35*, 1244−1249. – [5k] V. V. Dunina, L. G. Kuz′mina, A. G. Parfyonov, Y. K. Grishin, *Tetrahedron: Asymmetry* **1998**, *9*, 1917−1921. – [5l] F. Mathey, F. Mercier, F. Robin, L. Ricard, *J. Organomet. Chem.* **1998**, *557*, 117−120. – [5m] J. Albert, J. M. Cadena, J. Granell, G. Muller, J. I. Ordinas, D. Panyella, C. Puerta, P. Valerga, *Organometallics* **1999**, *18*, 3511−3518. – [5n] J. Albert, J. Granell, J. Mínguez, G. Muller, D. Sainz, P. Valerga, *Organometallics* **1997**, *16*, 3661−3664.

[6] [6a] J. Vicente, I. Saura-Llamas, P. G. Jones, *J. Chem. Soc., Dalton Trans.* **1993**, 3619−3624. – [6b] J. Albert, J. Granell, A. Luque, J. Mínguez, R. Moragas, M. Font-Bardia, X. Solans, *J. Organomet. Chem.* **1996**, *522*, 87−95. – [6c] J. Albert, J. Granell, J. M. Cadena, *Tetrahedron: Asymmetry* **1997**, *8*, 991−994.

[7] [7a] J. Albert, M. Gómez, J. Granell, J. Sales, X. Solans, *Organometallics* **1990**, *9*, 1405−1413. – [7b] J. Albert, J. Granell, J. Sales, M. Font-Bardia, X. Solans, *Organometallics* **1995**, *14*, 1393−1404.

[8] [8a] N. W. Alcock, D. I. Humes, J. M. Brown, *J. Chem. Soc., Chem. Commun.* **1995**, 395−397. – [8b] W. McFarlane, J. D. Swarbrick, J. I. Bookham, *J. Chem. Soc., Dalton Trans.* **1998**, 3233−3238. – [8c] N. W. Alcock, J. M. Brown, D. I. Hulmes, *Tetrahedron: Asymmetry* **1993**, *4*, 743−756. – [8d] U. Berens, J. M. Brown, J. Long, R. Selke, *Tetrahedron: Asymmetry* **1996**, *7*, 285−292. – [8e] S. Y. M. Chooi, M. K. Tan, P. H. Leung, K. F. Mok, *Inorg. Chem.* **1994**, *33,* 3096−3103.

[9] B. Aw, S. Selvartnam, P. H. Leung, N. H. Rees, W. McFarlane, *Tetrahedron: Asymmetry* **1996**, *7*, 1753−1762.

[10] M. C. Browning, J. R. Mellor, D. J. Morgan, S. A. J. Pratt, L. E. Sutton, L. M. Venanzi, *J. Chem. Soc.* **1962**, 693−703.

Received October 4, 1999
[I99346]

Chiral Diphosphites as Ligands for the Rhodium- and Iridium-Catalysed Asymmetric Hydrogenation: Precatalyst Complexes, Intermediates and Kinetics of the Reaction

Oscar Pàmies,[a] Gemma Net,[a] Aurora Ruiz,*[a] and Carmen Claver[a]

Keywords: Asymmetric hydrogenation / Chiral diphosphites / Iridium / Rhodium

Rh^I and Ir^I complexes $[M(cod)PP]BF_4$ were synthesised from diphosphite ligands PP with a backbone derived from xylofuranose. They were used in the rhodium- and iridium-catalysed asymmetric hydrogenation of itaconic acid, α-acetamidocinnamic acid and methyl α-acetamidoacrylate. The kinetics of the reaction was investigated. The solution structures of the intermediates were studied by ^{31}P- and ^{1}H-HPNMR spectroscopy and a catalytic cycle is proposed.

Introduction

Most of the phosphorus ligands that have been developed for catalytic applications, particularly in asymmetric catalysis, are derivatives of aryl- or alkylphosphanes.[1] Recently, a group of less electron-rich phosphorous compounds, chelating diphosphite ligands, has received considerable attention. New reports on the use of these ligands in regio- and stereoselective hydroformylation[2] and asymmetric hydrocyanation,[3] have appeared, in which their potential utility have been demonstrated.

Very little attention has been paid to phosphites as ligands in hydrogenation, probably because of their high π-acidity, which makes the metal centre less suitable for bringing about the H_2-oxidative addition reactions. However, some catalysts based only on organyl phosphites have been applied to hydrogenation.[4] To our knowledge, only Selke et al.,[4g] Reetz et al.[4i] and Brunner et al.[4j] have reported the use of chiral diphosphites in asymmetric hydrogenation. In spite of the supposed disadvantage mentioned above and the ability to undergo hydrolysis or Arbuzov-type side reactions (starkly reduced in the case of bulky phosphites or coordinated phosphites[3b,5]), phosphites are a very attractive group of compounds for catalysis. They have many advantages, the most important of which are that they are easy to prepare from readily available starting materials and that they are less sensitive to air than phosphanes are.[3,6]

The large number of chiral diols available from asymmetric catalysis and from the chiral pool, the excellent results obtained in asymmetric hydrogenation with diphosphinites derived from D-glucose (intermediate basicity between diphosphanes and diphosphites)[7] and, more recently, with diphosphites[4i] encourage further study of the application of diphosphites in this reaction.

[a] Universitat Rovira i Virgili,
Pl. Imperial Tarraco 1, 43005 Tarragona, Spain
Fax: (internat.) + 34-977/559563
E-mail: aruiz@quimica.urv.es

Here we report the synthesis of rhodium and iridium complexes with diphosphites derived from D-(+)-xylose and their use in the asymmetric hydrogenation of acrylic acid derivatives. We also investigated the kinetics of the catalysis and the catalytic cycle. These ligands were developed by van Leeuwen and co-workers and were applied to the asymmetric hydroformylation of styrene with enantioselectivities up to 62%.[2o] These bulky diphosphites are not only derived from a readily available carbohydrate, they are also fairly robust towards hydrolysis.

Results and Discussion

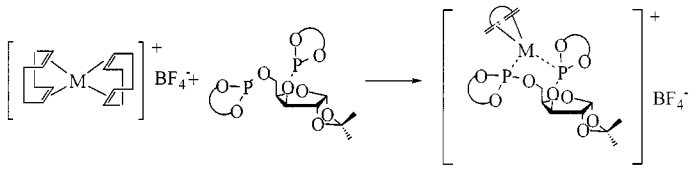
1. Synthesis of Olefinic Complexes

The reaction of the corresponding chiral diphosphites **1−3** with $[M(cod)_2]^+BF_4^-$ (M = Rh, Ir) in dichloromethane solution proceeded rapidly, with the displacement of one molecule of 1,5-cyclooctadiene ligand, even in a large excess of diphosphite ligand, to afford the cationic mononuclear complexes $[M(PP)(cod)]^+$ **4−9** (Scheme 1). These complexes were characterised by elemental analysis, ^{1}H-, ^{13}C-, and ^{31}P-NMR spectroscopy and FAB mass spectrometry.

The presence of two sets of signals in the ^{31}P-NMR spectra of all these complexes revealed the existence of two isomers in very different proportions. The relative abundance of these isomers did not change with temperature in the NMR, thereby indicating that there is no interconversion between them. The presence of isomers may be attributed to different atropisomers of the bis(phenol) moiety in the bis(phosphite) ligands, but the rapid ring inversion of the seven-membered dioxaphosphepin rings detected on the ^{31}P-NMR time scale in the free ligands and its $[HRh(PP)(CO)_2]$[2o] complexes suggest another origin for these isomers. A second, more plausible possibility is that there are different conformers for the eight-membered metal chelate ring.

Molecular mechanics calculations for complexes **4−9** were carried out. Two different conformers, **a** (boat−chair) and **b** (twist−boat−chair), which differ in the orientation

 © WILEY-VCH Verlag GmbH, D-69451 Weinheim, 2000 1434−1948/00/0606−1287 $ 17.50+.50/0



	M	diphosphite
4	Rh	1
5	Rh	2
6	Rh	3
7	Ir	1
8	Ir	2
9	Ir	3

1 $R^1 = R^2 = H$
2 $R^1 = t$Bu, R^2 = OMe
3 $R^1 = R^2 = t$Bu

Scheme 1. Synthesis of complexes $[M(cod)(PP)]^+BF_4^-$ **4−9**

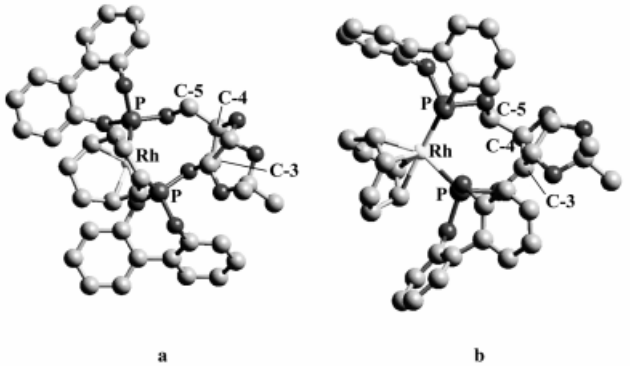


Figure 1. Conformers **a** and **b** for complex **4**

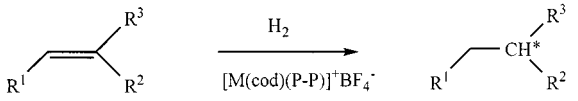
of the oxygen atom attached to C-5 in the sugar moiety, could be minimised for each complex. Figure 1 shows the minimised structures of the two conformers for complex **4**. The relative strain energies of these conformers for all complexes **4−9** are listed in Table 1. The results show that the most stable conformer is **a** for all the complexes. Their non-interconversion in VT-^{31}P NMR and the large difference in strain energy between the two conformers indicates that their transition state is extremely inaccessible.

The chemical shifts of the two different phosphorus atoms in **4−9** are in the range expected for tricoordinate P^{III} esters coordinated to Rh or Ir.[9] The rhodium−phosphorus coupling constants are very similar to those found for other $[Rh(diolefin)(PP)]^+$ complexes where PP is also a diphosphite.[4g] Coupling constants between 27 and 50 Hz can be observed between the two non-equivalent phosphorus atoms. The absence of P−P coupling in the free ligand[2o] suggests that these constants should be considered as ^2J(P−P), which means that the through-metal coupling predominates over through-backbone coupling.[9]

The characterisation by ^{13}C and ^{1}H NMR could not always be carried out because of the low intensity of some signals, partial overlapping of the spectra of mixtures of the two isomers or because the signals were too broad (especially important for product **7**). For **6**, a lowering of the temperature allowed the assignment of the ^{1}H-NMR peaks for both isomers.

2. Hydrogenation of Acrylic Acid Derivatives

The complexes $[M(cod)(PP)]^+$ (M = Rh, Ir; PP = **1**, **2**, **3**) **4−9** catalyse the asymmetric hydrogenation of itaconic acid **10** under mild conditions (5 bar, 40 °C) (Scheme 2, Table 2). In all cases, the (*R*) absolute configuration formed predominantly.



10 R^1 = H; $R^2 = CH_2COOH$; R^3 = COOH
11 R^1 = Ph; $R^2 = NHCOCH_3$; R^3 = COOH
12 R^1 = H; $R^2 = NHCOCH_3$; $R^3 = COOCH_3$

Scheme 2. Hydrogenation of acrylic acid derivatives with **4−9**

Table 1. Strain energies [kcal mol^{-1}] for conformers **a** and **b** of complexes **4−9**; experimental relative abundance (^{31}P-NMR data) in parentheses

Conformer[a]	4	5	6	7	8	9
a	484.4 (95)	380.7 (80)	237.8 (75)	404.8 (75)	297.0 (90)	153.1 (75)
b	530.1 (5)	401.0 (20)	268.9 (25)	456.6 (25)	318.9 (10)	184.5 (25)

[a] Recent investigations by our group have shown that relative strain energies between two conformers calculated by MM are very similar to those calculated with methods based on density functional theory (DFT) (see ref.[8]).

Table 2. Hydrogenation of itaconic acid **10** with $[M(cod)(PP)]BF_4$ **4−9**; M = Rh, Ir {conditions: [cat]/[itaconic acid] = 1:100; itaconic acid (2 mmol); solvent (12 mL)}

Entry	Precursor	*p* [bar]	*T* [°C]	*t* [h]	Conv. (%)	*ee* (%)
1[a]	**4**	5	40	20	20	20 (*R*)
2[a]	**5**	5	40	6	99	49 (*R*)
3[a]	**6**	5	40	6	70	45 (*R*)
4[b]	**6**	5	40	6	13	n.d.[c]
5[b]	**7**	5	40	20	100	13 (*R*)
6[b]	**8**	5	40	4	100	29 (*R*)
7[b]	**9**	5	40	4	100	35 (*R*)
8[b]	**7**	5	25	12	44	11 (*R*)
9[b]	**8**	5	25	12	68	32 (*R*)
10[b]	**9**	5	25	12	70	34 (*R*)
11[b]	**8**	1	40	4	87	47 (*R*)
12[b]	**9**	1	40	4	100	54 (*R*)
13[b]	**8**	1	25	8	70	26 (*R*)
14[b]	**9**	1	25	8	50	40 (*R*)

[a] Toluene/methanol (2:1). − [b] CH_2Cl_2/methanol (2:1). − [c] Not determined.

In contrast to the results reported by Reetz and Neugebauer,[4i] the precursors with the most hindered ligands (**2** and **3**) brought about the best conversions. The most hindered ligands, however, are also ligands with electron-donating groups, which probably enhance the rate of conversion because they favour the oxidative addition reactions in the catalytic cycle. The increase in activity with electron-donating groups in the phenyl groups is lower in the case of the iridium complexes.

The $[Rh(cod)(PP)]^+$ complexes **4−6** gave better conversions in toluene/methanol than in CH_2Cl_2/methanol (e.g., Entries 3 and 4) while the $[Ir(cod)(PP)]^+$ complexes **7−9** were more efficient in CH_2Cl_2/methanol. Within the accuracy of this experiment, there was no change in the enantioselectivities over time. This agrees with the presence of a unique catalytic species during the hydrogenation (though there is no proof for it).

The iridium complexes **7−9** were more active than their rhodium analogues, but the asymmetric inductions were lower (between 11 and 35% for the iridium compounds, between 20 and 50% for the rhodium compounds). The asymmetric inductions with precursors containing ligand **1** (Entries 1 and 5) are much lower than those with ligands **2** and **3** (Entries 2, 3, 6, and 7), as would be expected by its smaller bulkiness. The lower asymmetric induction of precursors containing ligand **1**, compared to **2** and **3**, was also observed in the hydroformylation of styrene.[2o] The change of the substituent at the *para* position of the bis(phenol) moiety showed very little effect on rate and asymmetric induction (Entries 2, 3, 6, and 7).

The high activity of the iridium complexes allowed a decrease of pressure and temperature of the reaction. Lowering the reaction temperature from 40 to 25 °C at 5 bar resulted in lower conversions but the asymmetric inductions did not change (Entries 5 vs. 8, 6 vs. 9, 7 vs. 10). Lowering the hydrogen pressure from 5 to 1 bar at 40 °C increased the asymmetric inductions (Entries 11 vs. 6, 12 vs. 7). In contrast to the observations at 5 bar, the asymmetric inductions at 1 bar are temperature-dependent. For both complexes with ligands **2** and **3**, the enantioselectivity of the reaction is decreased by a lowering of the temperature from 40 °C to 25 °C at 1 bar (Entries 11 vs. 13, 12 vs. 14). This is probably because there are different mixtures of hydride species at 1 bar and 5 bar.

Diphosphites **2** and **3** were also tested for the hydrogenation of other acrylic acid derivatives, α-acetamidocinnamic acid (**11**) and methyl α-acetamidoacrylate (**12**) (Scheme 2). The results obtained are given in Table 3.

Table 3. Hydrogenation of α-acetoamidocinnamic acid (**11**) and methyl α-acetamidoacrylate (**12**) with $[M(cod)(PP)]BF_4$ **5**, **6**, **8**, **9**; M = Rh, Ir {conditions: *T* = 40 °C, *t* = 20 h [cat]/[substrate] = 1:100; substrate (2 mmol); solvent (12 mL)}

Entry	Precursor	Substrate	*P* [bar]	Conv. (%)	*ee* (%)
1[a]	**5**	**11**	5	100	30 (*S*)
2[a]	**6**	**11**	5	100	31 (*S*)
3[b]	**8**	**11**	5	18	15 (*S*)
4[b]	**9**	**12**	5	20	19 (*S*)
5[a]	**5**	**12**	5	99	35 (*S*)
6[a]	**5**	**12**	2	100	21 (*S*)
7[c]	**5**	**12**	5	100	10 (*S*)
8[a]	**6**	**12**	5	94	33 (*S*)
9[b]	**8**	**12**	5	10	6 (*S*)
10[b]	**9**	**12**	5	9	7 (*S*)
11[b]	**8**	**12**	1	22	24 (*S*)
12[b]	**9**	**12**	1	31	35 (*S*)

[a] Toluene/methanol (2:1). − [b] CH_2Cl_2/methanol (2:1). − [c] CH_2Cl_2.

At 5 bar, the hydrogenation of **11** and **12** with the rhodium complexes **5** and **6** proceeded at a similar rate to the hydrogenation of itaconic acid (**10**), but enantiomeric excesses were lower (Entries 1, 2, 5, and 8). Lowering the pressure in the hydrogenation of **12** resulted in lower enantioselectivity (Entry 5 vs. 6). The effect was the same when the solvent was changed from toluene/methanol to CH_2Cl_2 (Entry 7 vs. 5). At 5 bar, the iridium complexes **8** and **9** were less active and enantioselective than their rhodium counterparts in the hydrogenation of **11** and **12** (Entry 1 vs. 3, 2 vs. 4; 5 vs. 9, 8 vs. 10). At 5 bar, the iridium complexes were more active and enantioselective in the hydrogenation of **11** than in that of **12** (Entries 3, 4 vs. 9, 10). The iridium compounds were unable to hydrogenate **11** at 1 bar, while they could hydrogenate **12** (Entries 11, 12) with better enantioselectivity than at 5 bar (Entries 11, 12 vs. 9, 10). However, the asymmetric induction was lower than for substrate **10** (Table 3, Entries 11, 12 vs. Table 2 Entries 11, 12).

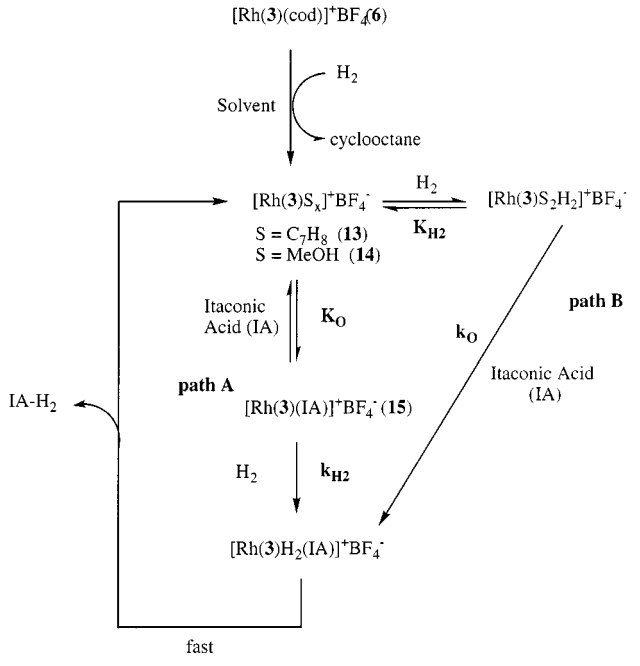
3. Catalytic Cycle Elucidation

Enantioselective hydrogenation catalysed by cationic (diolefin)(diphosphane)rhodium complexes has been thoroughly studied mechanistically. The widely accepted catalytic cycle, a result of the work of the groups of Brown, Halpern, Landis and Bosnich[10] involves the so-called alkene path, the first step of which is the hydrogenation of the diolefin coordinated to the rhodium centre, followed by the coordination of the alkene to the free site generated on the metal centre, the oxidative addition of molecular hydrogen, insertion and reductive elimination. Complexes with diphosphites do not necessarily have to follow the same se-

quence of steps, because their electronic properties are different from those of phosphanes. To identify the intermediates of the Rh-catalytic cycle of the hydrogenation of itaconic acid with phosphites and therefore to determine the sequence in the catalytic cycle, ^{1}H- and ^{31}P-HPNMR studies were carried out with the complexes of the most hindered ligand, **3**.

3.1. Characterisation Experiments of Rhodium-Cycle Intermediates

When complex [Rh(**3**)(cod)]$^+$BF$_4^-$ was dissolved in [D$_8$]toluene and kept for four hours at room temperature under 5 bar of H_2 pressure, an ABX pattern was obtained in ^{31}P HPNMR, which did not change after the system was cooled to −40 °C and then warmed up to 60 °C. The new compound was identified as [Rh(**3**)(C$_7$D$_8$)$_x$]$^+$ (Scheme 3). The stable yellow compound [Rh(**3**)(C$_7$H$_8$)$_x$]$^+$ (**13**) was isolated in a larger-scale preparative experiment in toluene. Elemental analysis and ^{1}H NMR in CCl_4 suggested that two toluene molecules was present in the compound. In general, arenes show a high tendency to form [M(η^6-arene)L$_2$]$^+$ species when L is a phosphane.[11] The (benzene)(dppe) compound was isolated as [Rh(dppe)(η^6-C$_6$H$_6$)]$^+$BF$_4^-$ · C$_6$H$_6$.[12] Compound **13** could then be formulated as [Rh(**3**)(η^6-C$_7$H$_8$)]BF$_4^-$ · C$_7$H$_8$. However, only one kind of methyl signal for toluene was detected in the ^{1}H-NMR spectrum of this complex. It appeared at δ = 2.71, in contrast to 2.37 for free toluene. There is probably a rapid exchange between them on the NMR time scale.



Scheme 3. Intermediates of the Rh catalytic cycle of the hydrogenation of itaconic acid

The two different phosphorous atoms in [Rh(**3**)(η^6-C$_7$H$_8$)]$^+$ show large P−Rh coupling constants (344.5 and 333.6 Hz), more than 100 Hz larger than in [Rh(**3**)(cod)]$^+$BF$_4^-$. These large constants may be explained by the smaller *trans* influence of the toluene rather than an olefin as ligand.

When [Rh(**3**)(η^6-C$_7$H$_8$)]$^+$BF$_4^-$ · C$_7$H$_8$ was treated with 5 bar of H_2, no formation of hydride species was detected by HPNMR as has been reported for different arene [M(η^6-arene)L$_2$]$^+$ complexes.[13]

Moreover, when the complex [Rh(**3**)(cod)]$^+$BF$_4^-$ was dissolved in [D$_8$]toluene/[D$_4$]methanol (2:1) and pressurised to 5 bar of H_2 at room temperature for four hours, the ABX pattern in the ^{31}P-HPNMR spectrum was similar. The compound could be assigned to [Rh(**3**)(CD$_3$OD)$_x$]$^+$ (Scheme 3). Cooling it to −40 °C did not change the spectrum. [Rh(**3**)(CH$_3$OH)$_2$]$^+$BF$_4^-$ (**14**) was isolated in a larger scale experiment in methanol as a stable yellow solid. The P−Rh coupling constants are also very large and similar to those obtained with the toluene complex (341.9 and 332.1 Hz). As has been reported for methanol [Rh(diphosphane)(CH$_3$OH)$_2$]$^+$ complexes,[14] the formation of hydride species was not detected by HPNMR when complex [Rh(**3**)(CH$_3$OH)$_2$]$^+$ was treated with 5 bar of H_2.

To study the coordination of itaconic acid in the cationic complex, the complex [Rh(**3**)(cod)]$^+$BF$_4^-$ was dissolved in [D$_8$]toluene and was pressurised to 5 bar at room temperature for four hours. After [Rh(**3**)(η^6-C$_7$D$_8$)]$^+$BF$_4^-$ · C$_7$D$_8$ was formed, the system was depressurised and an excess of itaconic acid in [D$_4$]methanol (2:1 with respect to [D$_8$]toluene) was added. After 17 minutes, two products, [Rh(**3**)(IA)]$^+$ (**15**) (IA denotes itaconic acid) and [Rh(**3**)(CD$_3$OD)$_2$]$^+$ were observed by ^{31}P-NMR spectroscopy. After 50 minutes, only [Rh(**3**)(IA)]$^+$ was observed in solution. Itaconic acid makes competitive or cooperative binding by α- and β-carboxylates possible. This usually results in three distinct types of complexes (for a 1:1 stoichiometry), which may coexist, where coordination takes place through the olefin and the α-carboxylate, the β-carboxylate, or both (Figure 2).[15] Despite the moderate enantiomeric excesses obtained in the asymmetric hydrogenation of itaconic acid with [Rh(**3**)(cod)]$^+$BF$_4^-$, complex [Rh(**3**)(IA)]$^+$ exists as a single isomer. Unfortunately, all attempts to isolate this compound were unsuccessful. The P−Rh coupling constants are very large (329.5 and 334.5 Hz). The P−P coupling constant is much larger than those for **13** and **14**, which could suggest that the complex has another geometry. This means that the itaconic acid is probably terdentate-coordinated through the olefin and both α- and β-carboxylates. Five-coordination is a usual geometry for itaconic acid diphosphane Rh$^{\mathrm{I}}$ complexes.[15] An IR spectrum of the solution revealed a broad carboxylic band at higher energy than in the free acid (1667 cm^{-1} vs. 1635 cm^{-1}), which supports the hypothesis about the coordination of both carboxylates. The 2D-NOESY spectrum showed cross-peaks between the olefinic protons of the itaconic acid and the *tert*-butyl groups of the ligand. This supports the hypothesis that the structure is five-coordinated.

No hydride species were observed in the ^{1}H-HPNMR spectra when a solution of complex **15** was pressurised at 5 bar of H_2.

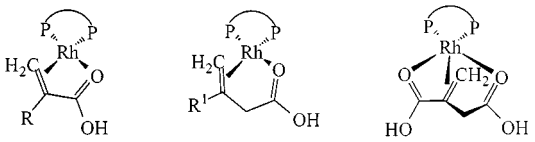


Figure 2. Possible types of coordination for itaconic acid

We can assume from the HPNMR results that the first step is the formation of $[Rh(\mathbf{3})S_2]^+$ by hydrogenation of the olefin coordinated to the rhodium centre. From this species, there are two ways in which itaconic acid can be hydrogenated (Scheme 3). The first (path A) involves the oxidative addition of the H_2 after the coordination of the alkene, while in the second (path B) the oxidative addition of H_2 takes place first.

3.2. Kinetic Study

To find out more about the mechanism of the Rh-catalyzed hydrogenation of itaconic acid at 5 bar of H_2 and 40 °C, we studied the dependence of the rate on the reaction parameters (itaconic acid concentration, H_2 pressure and Rh concentration). The formation of the hydrogenated product over time at [Rh] = 1.66 mM is depicted in Figure 3. The rate of hydrogenation increases after an initial induction period (which is independent on the H_2 pressure used), due to the hydrogenation of the coordinated cyclooctadiene. The formation of methylsuccinic acid is zero-order in substrate concentration, first-order in rhodium concentration (Table 4) and almost first-order in hydrogen pressure (Figure 4) between 5 and 11 bar. Above 11 bar, the pressure dependence of the rate is no longer linear and declines, which suggests a change in the mechanism.

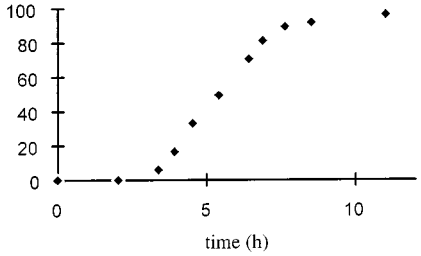


Figure 3. Variation of the conversion of itaconic acid vs. time

Table 4. Influence of the total rhodium concentration on the reaction rate at 5 bar and 40 °C

$[Rh]_T$ 10^{-3} M	k [h^{-1}]
0.83	8.1
1.66	18.9
3.33	35.6

Consequently, and due to the complexity of such a system (Scheme 3), the individual steps of the catalytic cycle had to be studied separately. K_O[IA] (Scheme 4) can be estimated from the HPNMR populations. In this way, and from the solubility of H_2 at 40 °C in toluene/methanol (2:1) ($s = 2.2 \cdot 10^{-2}$ M), which was calculated by HPNMR with CH_3CN as a standard, we can estimate K_{H2} (Scheme 4). A

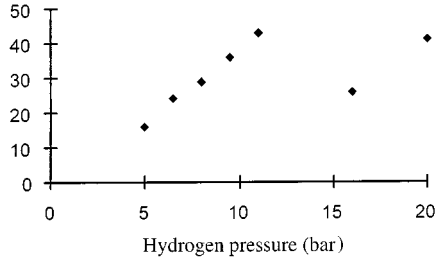
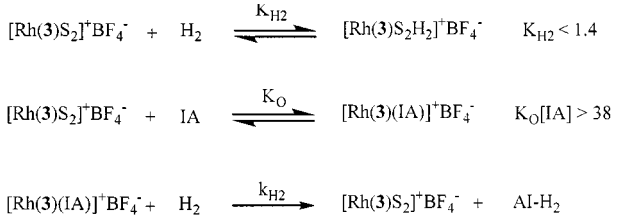


Figure 4. Dependency of the conversion of itaconic acid on H_2 pressure at 40 °C and [Rh] = 1.66 mM

sample of $[Rh(\mathbf{3})(IA)]^+BF_4^-$, generated in situ by mixing isolated $[Rh(\mathbf{3})(CH_3OH)_2]^+BF_4^-$ and 1 equiv. of itaconic acid, was charged in the HPNMR tube at 5 bar, to calculate k_{H2} by HPNMR (Scheme 4). However, the results are not conclusive because of the drop in pressure during the hydrogenation experiment.



Scheme 4. Individual steps of the catalytic cycle

From these results and the fact that the resting state observed by HPNMR at 5 bar is always complex **15**, we cannot conclude that the rate-determining step is not the addition of H_2 to the complex $[Rh(\mathbf{3})S_2]^+$, since it should have a negative order in the itaconic acid concentration. In spite of this, path B cannot be discarded because the same pattern in the rate law derived from mechanism A can be obtained from path B if the rate-determining step is the addition of IA to the complex $[Rh(\mathbf{3})S_2]^+$.

According to the improved conversion when a more basic diphosphite was used, the hydrogenation of itaconic acid with precursor **6** is in agreement with path A, where the rate-determining step is the oxidative addition after partial decoordination of IA to complex $[Rh(\mathbf{3})(IA)]^+$.

Conclusions

Complexes [M(diphosphite)(cod)]BF_4, M= Rh, Ir, with diphosphites derived from xylose, are active in the hydrogenation of some acrylic acid derivatives and achieve moderate enantioselectivities. The most basic hindered diphosphites provided better conversions and selectivities. Under the same conditions, the rhodium-catalysed hydrogenation achieved better enantioselectivities than the iridium-catalysed reaction. Kinetic studies of the Rh-catalysed hydrogenation of itaconic acid between 5 and 11 bar were consistent with a reaction rate which is zero-order in itaconic acid concentration, first-order in rhodium concentration and first-order in H_2 pressure. Despite the electronic differences between phosphanes and phosphites, the Rh-catalysed hy-

drogenation of itaconic acid with diphosphites seems to follow the same mechanism as the one proposed for diphosphanes in the hydrogenation of α-acetamidocinnamic acid.

Experimental Section

General Comments: All syntheses were performed by standard Schlenk techniques under nitrogen or argon. The complexes $[Rh(cod)_2]^+BF_4^-$,[16] $[Ir(cod)_2]^+BF_4^-$,[16] and the diphosphite ligands **1**, **2**, and **3**[2o] were prepared by previously described methods. Solvents were purified by standard procedures. All other reagents were used as commercially available. Elemental analyses were performed with a Perkin−Elmer 240 B instrument. ^{1}H-, ^{13}C{^{1}H}-, and ^{31}P{^{1}H}-NMR spectra were recorded with a Varian Gemini 300 MHz spectrometer. Chemical shifts are relative to $SiMe_4$ (^{1}H and ^{13}C) as internal standard or H_3PO_4 (^{31}P) as external standard. All assignments of NMR spectra were determined by means of COSY and HETCOR spectra. Standard pulse sequences were employed for the ^{1}H-^{2}D-NOESY.[17] EI mass spectra were obtained with an HP 5989 A spectrometer. VG-Autospect equipment was used for FAB mass-spectral analyses. The matrix was *m*-nitrobenzyl alcohol. Optical rotations were measured at 25 °C with a Perkin−Elmer 241 MC polarimeter. Hydrogenation reactions at high pressure were carried out in a home-made 100-mL stainless steel autoclave. The reaction under 1 atm of H_2 was performed in a previously described hydrogen−vacuum line.[18] The molecular mechanics calculations were carried out with the program CERIUS2 developed by Molecular Simulations (MSI)[19]and the force field UFF developed by Rappe et al.[20] Electrostatic interactions were taken into account from atomic charges generated by the Qeq method.[21]

Preparation of Rhodium Complexes. − General Procedure: The diphosphite ligand (0.1 mmol) was added to a solution of $[Rh(cod)_2]BF_4$ (40.5 mg, 0.1 mmol) in dichloromethane (2 mL). After 10 min, the desired products were obtained by precipitation with hexane.

$[Rh(1)(COD)]^+BF_4^-$ (4): (76 mg, 83%) yellow solid. − MS; *m*/*z*: 829 [M^+]. − $C_{40}H_{40}BF_4O_9P_2Rh$: calcd. C 52.42, H 4.40; found C 51.99, H 4.51. − Major conformer (95% according to ^{31}P NMR): ^{31}P NMR (121.4 MHz, $CDCl_3$, 293 K): δ = 133.4 [dd, 1 P, ^2J(P,H) = 50.0 Hz, ^1J(P,Rh) = 259.2 Hz], 139.4 [dd, 1 P, ^2J(P,H) = 50.0 Hz, ^1J(P,Rh) = 253.1 Hz]; ^{1}H NMR (300 MHz, $CDCl_3$, 293 K): δ = 1.19 (s, 3 H, CH_3), 1.42 (s, 3 H, CH_3), 2.35 (m, 8 H, CH_2), 4.01 [d, 1 H, H-2, ^3J(H2,H1) = 3.3 Hz], 4.57 (m, 1 H, H-4), 4.68 (m, 1 H, H-5′), 5.12 (m, 1 H, H-5), 5.32 (m, 1 H, H-3), 5.52 (m, 1 H, CH=), 5.69 (m, 1 H, CH=), 5.92 [d, 1 H, H-1, ^3J(H1,H2) = 3.3 Hz], 5.99 (m, 1 H, CH=), 6.04 (m, 1 H, CH=), 7.30−7.8 (m, 16 H, Ph); ^{13}C NMR (75.4 MHz, $CDCl_3$): δ = 26.5 (CH_3), 26.9 (CH_3), 28.2 (CH_2), 29.9 (CH_2), 30.0 (CH_2), 30.4 (CH_2), 63.3 (C-5), 76.7 (C-4), 81.3 (C-3), 84.4 (C-2), 105.4 (C-1), 109.0 (m, CH=), 109.9 (m, CH=), 111.0 (m, CH=), 111.9 (m, CH=,), 113.0 (CMe_2), 121.8, 122.0, 122.5, 127.0, 127.5, 127.6, 127.7, 129.4, 129.7, 130.0, 130.6, 130.8, 130.9, 131.1, 131.3, 131.5 (Ph). − Minor conformer (5% according to ^{31}P NMR): ^{31}P NMR (121.4, $CDCl_3$, 293 K): δ = 118.2 [dd, 1 P, ^2J(P,P) = 54.0 Hz, ^1J(P,Rh) = 261.2 Hz], 139.4 [dd, 1 P, ^2J(P,P) = 54.0 Hz, ^1J(P,Rh) = 256.1 Hz].

$[Rh(2)(COD)]^+BF_4^-$ (5): (107 mg, 89%) yellow solid. − MS; *m*/*z*: 1173 [M^+]. − $C_{60}H_{80}BF_4O_{13}P_2Rh \cdot 1/2\ CH_2Cl_2$: calcd. C 55.75, H 6.27; found C 56.28, H 7.01. − ^{1}H NMR (300 MHz, $CDCl_3$, 293 K): δ = 1.26 (s, 3 H, CH_3), 1.52 (m, 18 H, CH_3 *t*Bu), 1.66 (m, 21 H, CH_3, CH_3 *t*Bu), 2.35 (m, 8 H, CH_2), 3.03 (m, 1 H, H-2), 3.84 (s, 12 H, OMe), 3.92 (m, 2 H), 4.19 (m, 1 H), 4.73 (m, 1 H), 5.04 (m, 1 H, CH=), 5.29 (m, 1 H, CH=), 5.52 (m, 1 H, H-1), 6.02 (m, 2 H, CH=), 6.7−7.3 (m, 8 H, Ph). − Major conformer (80% according to ^{31}P NMR): − ^{31}P NMR (121.4 MHz, $CDCl_3$, 233 K): δ = 122.9 [dd, 1 P, $^2J_{(P,P)}$ = 52.2 Hz, $^1J_{(P,Rh)}$ = 208.2 Hz], 124.9 [dd, 1 P, ^2J(P,P) = 52.2 Hz, ^1J(P,Rh) = 214.3 Hz]. − Minor conformer (20% according to ^{31}P NMR): − ^{31}P NMR (121.4 MHz, $CDCl_3$, 233 K): δ = 114.8 [dd, 1 P, ^2J(P,P) = 27.5 Hz, ^1J(P,Rh) = 201.4 Hz], 116.9 [dd, 1 P, ^2J(P,P) = 27.5 Hz, ^1J(P,Rh) = 208.7 Hz].

$[Rh(3)(COD)]^+BF_4^-$ (6): (115 mg, 84%) yellow solid. − MS; *m*/*z*: 1277 [M^+]. − $C_{72}H_{104}BF_4O_9P_2Rh \cdot 1/2\ CH_2Cl_2$: calcd. C 61.91, H 7.52; found C 61.21, H 7.31. − ^{1}H NMR (300 MHz, $CDCl_3$, 293 K): δ = 1.27 (s, 3 H, CH_3), 1.35 (m, 36 H, CH_3 *t*Bu), 1.55 (m, 18 H, CH_3 *t*Bu), 1.70 (m, 21 H, CH_3, CH_3 *t*Bu), 2.10 (m, 2 H, CH_2), 2.40 (m, 6 H, CH_2), 3.23 (m, 1 H, H-2), 4.16 (m, 2 H), 4.83 (m, 2 H), 5.22 (m, 1 H, CH=), 5.57 (m, 1 H, H-1), 6.03 (m, 1 H, CH=), 6.11 (m, 2 H, CH=), 7.0−7.8 (m, 8 H, Ph). − Major conformer (75% according to ^{31}P NMR): − ^{31}P NMR (121.4 MHz, $CDCl_3$, 293 K): δ = 121.4 [dd, 1 P, ^2J(P,P) = 36.6 Hz, 1J(P,Rh) = 225.6 Hz], 123.6 [dd, 1 P, ^2J(P,P) = 36.6 Hz, ^1J(P,Rh) = 231.1 Hz]; ^{1}H NMR (300 MHz, $CDCl_3$, 233 K): δ = 1.36 (m, 21 H, CH_3, CH_3 *t*Bu), 1.54 (m, 12 H, CH_3, CH_3 *t*Bu), 1.67 (m, 9 H, CH_3 *t*Bu), 2.05 (m, 2 H, CH_2), 2.34 (m, 4 H, CH_2), 2.57 (m, 2 H, CH_2), 3.05 [m, 1 H, H-2, ^3J(H2,H1) = 2.3 Hz], 4.09 (m, 2 H, H-4, H-5′), 4.77 (m, 1 H, H-3), 5.04 (m, 1 H, H-5), 5.28 (m, 2 H, CH=), 5.51 [d, 1 H, H-1, ^3J(H1,H2) = 2.3 Hz], 6.25 (m, 2 H, CH=), 7.0−7.8 (m, 8 H, Ph). − Minor conformer (25% according to ^{31}P NMR): − ^{31}P NMR (121.4 MHz, $CDCl_3$, 233 K): δ = 111.2 [dd, 1 P, ^2J(P,P) = 44.5 Hz, ^1J(P,Rh) = 218.2 Hz], 113.2 [dd, 1 P, ^2J(P,P) = 44.5 Hz, ^1J(P,Rh) = 227.5 Hz]; ^{1}H NMR (300 MHz, $CDCl_3$, 233 K): δ = 1.24 (s, 3 H, CH_3), 1.36 (m, 18 H, CH_3 *t*Bu), 1.54 (m, 9 H, CH_3 *t*Bu), 1.67 (m, 9 H, CH_3 *t*Bu), 1.72 (s, 3 H, CH_3), 2.05 (m, 2 H, CH_2), 2.34 (m, 4 H, CH_2), 2.57 (m, 2 H, CH_2), 3.56 [m, 1 H, H-2, ^3J(H2,H1) = 2.5 Hz], 4.56 (m, 2 H, H-4, H-5′), 4.77 (m, 1 H, H-3), 5.04 (m, 1 H, H-5), 5.28 (m, 2 H, CH=), 5.71 [d, 1 H, H-1, ^3J(H1,H2) = 2.5 Hz], 6.25 (m, 2 H, CH=), 7.0−7.8 (m, 8 H, Ph).

Preparation of Iridium Complexes. − General Procedure: The diphosphite ligand (0.1 mmol) was slowly added to a cooled (195 K) solution of $[Ir(cod)_2]BF_4$ (49.7 mg, 0.1 mmol) in dichloromethane (2 mL). The resulting solution was stirred and the temperature was increased to 273 K. After 2 min, the desired product was obtained by precipitation with diethyl ether.

$[Ir(1)(COD)]^+BF_4^-$ (7): (88 mg, 88%) as a white solid. − MS; *m*/*z*: 919 [M^+]. − $C_{40}H_{40}BF_4IrO_9P_2$: calcd. C 47.77, H 4.01; found C 47.82, H 4.32. − Major conformer (75% according to ^{31}P NMR): ^{31}P NMR (121.4 MHz, CD_2Cl_2, 293 K): δ = 105.3 (broad, 1 P), 104 (broad, 1 P). − Minor conformer (25% according to ^{31}P NMR): ^{31}P NMR (121.4 MHz, CD_2Cl_2): δ = 104.8 (broad, 1 P), 103.5 (broad, 1 P).

$[Ir(2)(COD)]^+BF_4^-$ (8): (75 mg, 60%) as a purple solid. − MS; *m*/*z*: 1263 [M^+]. − $C_{60}H_{80}BF_4IrO_{13}P_2 \cdot 1/2\ CH_2Cl_2$: calcd. C 54.36, H 6.71; found C 54.48, H 6.66. − Major conformer (90% according to ^{31}P NMR): ^{31}P NMR (121.4 MHz, CD_2Cl_2, 253 K): δ = 113.2 [d, 1 P, ^2J(P,P) = 48.4 Hz], 113.7 [d, 1 P, ^2J(P,P) = 48.4 Hz]; ^{1}H NMR (300 MHz, CD_2Cl_2, 253 K): δ = 1.34 (s, 3 H, CH_3), 1.54 (m, 21 H, CH_3, CH_3 *t*Bu), 1.59 (m, 18 H, CH_3 *t*Bu), 2.05 (m, 3 H, CH_2), 2.19 (m, 4 H, CH_2), 2.34 (m, 1 H, CH_2), 2.92 (m, 1 H, H-2), 3.82 (s, 12 H, OMe), 4.01 (m, 1 H), 4.15 (m, 2 H), 4.81 (m, 2 H, H, CH=), 5.01 (m, 1 H, CH=), 5.43 (m, 1 H, H-1), 6.08 (m, 2 H, CH=), 6.6−7.4 (m, 8 H, Ph). − Minor conformer (10% accord-

ing to ^{31}P NMR): ^{31}P NMR (121.4 MHz, CD_2Cl_2, 253 K): δ = 114.8 [dd, 1 P, ^2J(P,P) = 49.2 Hz], 116.9 [dd, 1 P, ^2J(P,P) = 49.2 Hz].

[Ir(3)(COD)]$^+$BF$_4^-$ (9): (115 mg, 72%) as a purple solid. − MS; *m/z*: 1365 [M^+]. − $C_{72}H_{104}BF_4IrO_9P_2$: calcd. C 59.45, H 7.21; found C 58.99, H 7.30. − ^1H NMR (300 MHz, C_7D_8, 293 K): δ = 1.20−1.40 (m, 39 H, CH_3, CH_3 *t*Bu), 1.45−1.70 (m, 39 H, CH_3, CH_3 *t*Bu), 2.10 (m, 8 H, CH_2), 3.48 (m, 1 H, H-2), 3.90 (m, 1 H), 4.15 (m, 2 H), 4.50 (m, 1 H, CH=), 4.71 (m, 1 H, CH=), 5.06 (m, 1 H), 5.71 (m, 1 H, H-1), 5.80 (m, 2 H, CH=), 6.8−7.8 (m, 8 H, Ph). − Major conformer (75% according to ^{31}P NMR): ^{31}P NMR (121.4 MHz, C_7D_8, 293 K): δ = 109.76 [d, 1 P, ^2J(P,P) = 46.1 Hz], 111.23 [d, 1 P, ^2J(P,P) = 46.1 Hz]. − Minor conformer (25% according to ^{31}P NMR): ^{31}P NMR (121.4 MHz, C_7D_8, 293 K): δ = 100.18 (m, 2 P).

[Rh(3)(C_7H_8)]$^+$BF$_4^-$ · C_7H_8 (13): A 100-mL vessel was filled with a solution of **6** (0.05 mmol) in toluene (10 mL) and placed into the autoclave. The autoclave was purged three times with hydrogen and pressurised to the appropriate pressure (5 bar). After a reaction time of 3 h at room temperature, the autoclave was depressurised. The product was then obtained as a yellow solid by concentration to dryness (70 mg, quantitative). − $C_{78}H_{108}BF_4O_9P_2Rh$: calcd. C 65.00, H 7.55; found C 64.65, H 7.67. − ^1H NMR (300 MHz, C_7D_8): δ = 1.00−1.40 (m, 42 H, CH_3, CH_3 *t*Bu), 1.60−2.00 (m, 36 H, CH_3 *t*Bu), 2.71 (s, Ph−CH_3), 3.62 [dd, 1 H, H-5′, ^2J(H5′,H5) = 8.8 Hz, ^3J(H5′,H4) = 6.1 Hz], 3.92 [d, 1 H, H-2, ^3J(H2,H1) = 3.3 Hz], 4.34 [dd, 1 H, H-5, ^2J(H5,H5′) = 8.8 Hz, ^3J(H5,H4) = 12.4 Hz], 4.45 (m, 1 H, H-4), 5.26 (m, 1 H, H-3), 5.78 [d, 1 H, H-1, ^3J(H1,H2) = 3.3 Hz], 7.0−8.0 (m, 18 H, Ph). − ^{31}P NMR (121.4 MHz, C_7D_8): δ = 128.88 [dd, 1 P, ^2J(P,P) = 49.8 Hz, ^1J(P,Rh) = 344.5 Hz], 129.62 [dd, 1 P, ^2J(P,P) = 49.8 Hz, ^1J(P,Rh) = 333.6 Hz].

[Rh(3)($CH_3OH)_2$]$^+$BF$_4^-$ (14): A 10-mL Schlenk flask was filled with a solution of **13** (0.05 mmol) in methanol (10 mL). After a reaction time of 30 min at room temperature, the product was obtained as a yellow-orange solid by concentration to dryness (62 mg, quant.). − $C_{66}H_{100}BF_4O_{11}P_2Rh$: calcd. C 60.00, H 7.63; found C 60.11, H 7.87. − ^1H NMR (300 MHz, CD_3OD): δ = 1.05 (s, 3 H, CH_3), 1.32 (s, 3 H, CH_3), 1.36 (s, 18 H, CH_3 *t*Bu), 1.38 (s, 18 H, CH_3 *t*Bu), 1.62 (s, 18 H, CH_3 *t*Bu),1.90 (s, 18 H, CH_3 *t*Bu), 2.32 (s, OH), 3.17 [d, 1 H, H-2, ^3J(H2,H1) = 3.3 Hz], 3.48 (s, CH_3−O), 4.09 (m, 2 H, H-5, H-5′), 4.56 (m, 1 H, H-4), 4.74 (m, 1 H, H-3), 5.52 [d, 1 H, H-1, ^3J(H1,H2) = 3.3 Hz]. − ^{31}P NMR (121.4 MHz, CD_3OD): δ = 132.32 [dd, 1 P, ^2J(P,P) = 50.3 Hz, ^1J(P,Rh) = 341.9 Hz], 133.07 [dd, 1 P, ^2J(P,P) = 50.3 Hz, ^1J(P,Rh) = 332.1 Hz].

[Rh(3){CH_2=C(CH_2COOH)(COOH)}]$^+$BF$_4^-$ (15): Itaconic acid (6.1 mg, 0.05 mmol) was added to a solution of **14** (62 mg, 0.05 mmol) in [D_4]methanol (1 mL). After 1 h, the NMR tube was filled and the mixture analysed. − ^1H NMR (300 MHz, CD_3OD): δ = 1.04 (s, 3 H, CH_3), 1.32 (s, 3 H, CH_3), 1.35 (s, 18 H, CH_3 *t*Bu), 1.37 (s, 18 H, CH_3 *t*Bu), 1.61 (s, 18 H, CH_3 *t*Bu),1.88 (s, 18 H, CH_3 *t*Bu), 3.18 [d, 1 H, H-2, ^3J(H2,H1) = 3.6 Hz], 3.30 (s, 2 H, CH_2), 4.08 (m, 2 H, H-5, H-5′), 4.43 (m, 1 H, H-4), 4.75 (m, 1 H, H-3), 5.52 [d, 1 H, H-1, ^3J(H1,H2) = 3.6 Hz], 5.72 (m, 1 H, CH=), 6.27 (m, 1 H, CH=). − ^{13}C NMR (75.4 MHz, CD_3OD): δ = 27.1 (CH_3), 27.5 (CH_3), 32.3 (CH_3 *t*Bu), 32.4 (CH_3 *t*Bu), 32.9 (CH_3 *t*Bu), 33.2 (CH_3 *t*Bu), 33.6 (CH_3 *t*Bu), 33.8 (CH_3 *t*Bu), 38.8(CH_2), 65.2(d, C-5, *J*(C,P) = 5.8 Hz), 78.2 (dd, C-4, *J* = 10.0 Hz, *J* = 6.3 Hz), 81.4 (d, C-3, *J*(C,P) = 9.5 Hz), 84.7 (C-2), 107.9 (C-1), 114.4 (CMe_2), 129.1 (d, CH_2=, *J* = 30.6 Hz). − ^{31}P NMR (121.4 MHz, CD_3OD): δ = 138.59 [dd, 1 P, ^2J(P,P) = 79.1 Hz, ^1J(P,Rh) = 329.5 Hz], 139.86 [dd, 1 P, ^2J(P,P) = 79.1 Hz, ^1J(P,Rh) = 334.5 Hz].

Hydrogenation Experiments: The reactions were performed in a home-made autoclave. The autoclave was purged three times with H_2. In a typical run, catalytic precursor (0.02 mmol) and substrate (2 mmol) were dissolved in the appropriate mixture of solvents (12 mL) and introduced in the purged autoclave. After pressurising to the desired pressure with hydrogen and heating the autoclave to the reaction temperature, the reaction mixture was stirred. During the reaction, a number of samples were taken and analysed by NMR. After the desired reaction time, the autoclave was cooled to room temperature and depressurised. The solvent was evaporated.

Workup of the Hydrogenation Product: The following procedures were used to isolate the hydrogenation product. For methylsuccinic acid and *N*-acetylphenylalanine, the residue was dissolved in 0.5 M NaOH and separated from the insoluble catalyst by filtration. The filtrate was acidified with diluted HCl, extracted with ether, and washed with a little water. The ethereal phase was dried with sodium sulfate and concentrated to dryness. The extent of conversion was measured by ^1H-NMR spectroscopy. The enantiomeric excesses were determined by polarimetry.[22] For *N*-acetylalanine methyl ester, gas chromatography analyses were performed in a Hewlett−Packard 5890A instrument (fused silica capillary column 25 m × 0.25 mm permabond L-Chirasil-Val).

Acknowledgments

We thank the Spanish Ministerio de Educación y Cultura and the Generalitat de Catalunya (CIRIT) for financial support (PB97-0407-CO5-01) and the Generalitat de Catalunya (CIRIT) for awarding a research grant (to O. P.). We are also very much indebted to Prof. P. W. N. M van Leeuwen and Prof. B. R. James for their useful discussions and suggestions on this work.

[1] [1a] *Catalytic Asymmetric Synthesis* (Ed.: I. Ojima), VCH, Weinheim, **1993**. − [1b] *Asymmetric Catalysis in Organic Synthesis* (Ed.: R. Noyori), John Wiley Sons, New York, **1994**. − [1c] *Applied Homogeneous Catalysis with Organometallic Compounds* (Eds.: B. Cornils, W. A. Hermann), VCH, Weinheim, **1996**.

[2] [2a] S. Gladiali, J. C. Bayón, C. Claver, *Tetrahedron: Asymmetry* **1995**, *6*, 1453−1474 and references cited therein. − [2b] J. E. Babin, G. T. Whiteker, WO 93/03839, US 911, 518, **1992** (around 90% *ee*). − [2c] E. Fernández, A. Ruiz, C. Claver, S. Castillón, A. Polo, J. F. Piniella, A. Alvarez Larena, *Organometallics* **1998**, *17*, 2857−2864. − [2d] A. van Rooy, P. C. J. Kamer, P. W. N. M. van Leeuwen, *J. Organomet. Chem.* **1997**, *535*, 201−207. − [2e] J. R. Johnson, G. D. Cuny, S. L. Buchwald, *Angew. Chem. Int. Ed. Engl.* **1995**, *34*, 1760−1761. − [2f] G. D. Cuny, S. L. Buchwald, *Synlett* **1995**, 519−522. − [2g] G. D. Cuny, S. L. Buchwald, *J. Am. Chem. Soc.* **1993**, *115*, 2066−2068. − [2h] B. Moasser, W. L. Gladfelter, D. C. Roe, *Organometallics* **1995**, *14*, 3832−3838. [2i] B. Moasser, W. L. Gladfelter, *Inorg. Chim. Acta* **1996**, *242*, 125−136. [2j] G. J. H. Buisman, E. J. Vos, P. C. J. Kamer, P. W. N. M. van Leeuwen, *J. Chem. Soc., Dalton Trans.* **1995**, 409−417. − [2k] A. van Rooy, J. N. H. Debruijn, K. F. Roobek, P. C. J. Kamer, P. W. N. M. van Leeuwen, *J. Organomet. Chem.* **1996**, *507*, 69−73. − [2l] A. van Rooy, P. C. J. Kamer, P. W. N. M. van Leeuwen, K. Goubitz, J. Fraanje, N. Veldman, A. L. Spek, *Organometallics* **1996**, *15*, 835−847. − [2m] G. J. H. Buisman, L. A. van der Veen, P. C. J. Kamer, P. W. N. M. van Leeuwen, *Organometallics* **1997**, *16*, 5681−5687. − [2n] G. J. H. Buisman, L. A. van der Veen, A. Klootwijk, W. G. J. de Lange, P. C. J. Kamer, P. W. N. M. van Leeuwen, D. Vogt, *Organometallics* **1997**, *16*, 2929−2939. − [2o] G. J. H. Buisman, M. E. Martin, E. J. Vos, A. Klootwijk, P. C. J. Kamer, P. W. N. M. van Leeuwen, *Tetrahedron: Asymmetry* **1995**, *6*, 719−738. − [2p] S. Cserépi-Suzcs, I. Tóth, L. Párkányi, J. Bakos, *Tetrahedron: Asymmetry* **1998**,

9, 3135−3142. − [2q] Y. Jiang, S. Xue, Z. Li, J. Deng, A. Mi, A.S.C. Chan, *Tetrahedron: Asymmetry* **1998**, *9*, 3185−3189.

[3] [3a] M. J. Baker, P. G. Pringle, *J. Chem. Soc., Chem. Commun*. **1991**, 1292−1293. − [3b] M. J. Baker, K. N. Harrison, A. G. Orpen, G. Shaw, P. G. Pringle, *J. Chem. Soc., Chem. Commun.* **1991**, 803−804.

[4] [4a] D. J. Wink, T. J. Kwok, A. Yee, *Inorg. Chem*. **1990**, *29*, 5006−5008. − [4b] A. J. Sivak, E. L. Mutterties, *J. Am. Chem. Soc*. **1979**, *101*, 4878−4887. − [4c] L. S. Stuhl, M. Rakovski Dubois, F. J. Hirsekorn, J. R. Bleeke, A. E. Stevens, E. L. Mutterties, *J. Am. Chem. Soc*. **1978**, *100*, 2405−2410. − [4d] E. L. Mutterties, J. R. Bleeke, *Acc. Chem. Res.* **1979**, *12*, 324−331. − [4e] L. W. Grosser, *Inorg. Chem*. **1975**, *14*, 1453−1456. − [4f] H. K. A. C. Coolen, R. J. M. Nolte, P. W. N. M. van Leeuwen, *J. Organomet. Chem*. **1995**, *496*, 159−168. − [4g] R. Kadyrov, D. Heller, R. Selke, *Tetrahedron: Asymmetry* **1998**, *9*, 329−340. − [4h] R. B. Berdford, S. Castillón, P. A. Chaloner, C. Claver, E. Fernández, P. B. Hitchcock, A. Ruiz, *Organometallics* **1996**, *15*, 3990−3997. − [4i] M. T. Reetz, T. Neugebauer, *Angew. Chem. Int. Ed*. **1999**, *38*, 179−181. − [4j] H. Brunner, W. Pieronczyk, *J. Chem. Res. (S)* **1980**, 76.

[5] [5a] P. C. Nirchio, D. J. Wink, *Organometallics* **1991**, *10*, 336−340. − [5b] P. M. Lorz, W. Bertleff, M. Roeper, D. Koeffer, Eur. Pat. EP 472071, **1993**.

[6] L. H. Pignolet, *Homogeneous Catalysts with Metal Phosphine Complexes*, Plenum, New York, **1983**.

[7] [7a] R. Selke, H. G. Pracejus, *J. Mol. Catal.* **1986**, *37*, 213. − [7b] R. Selke, M. Ohff, A. Riepe, *Tetrahedron* **1996**, *52*, 15079−15102. − [7c] T. V. RajanBabu, T. A. Ayers, G. A. Halliday, K. K. You, J. C. Calabrese, *J. Org. Chem*. **1997**, *62*, 6012−6028 and references therein. − [7d] Industrial application for L-Dopa synthesis: W. Vocke, R. Hänel, F.-U. Flöter, *Chem. Tech. (Leipzig)* **1987**, *39*, 123.

[8] O. Pàmies, G. Net, A. Ruiz, C. Bo, J. M. Poblet, C. Claver, *J. Organomet. Chem*. **1999**, *586*, 125−137.

[9] [9a] *Phosphorus-31 NMR Spectroscopy in Stereochemical Analysis. Organic Compounds and Metal Complexes* (Eds.: J. V. Verkade, Louis D. Quin), VCH, **1987**. − [9b] J. Scherer, G. Huttner, M. Büchner, J. Bakos, *J. Organomet. Chem.* **1996**, *520*, 45−58.

[10] [10a] P. L. Bodgan, J. J. Irwin, B. Bosnich, *Organometallics* **1989**, *8*, 1450−1453. − [10b] J. M. Brown, P. A. Chaloner, G. A. Morris, *J. Chem. Soc., Chem. Commun.* **1983**, 664−666. − [10c] N. W. Alcock, J. M. Brown, A. E. Derome, A. R. Lucy, *J. Chem. Soc., Chem. Commun.* **1985**, 575−578. − [10d] D. G. Allen, S. B. Wild, D. L. Wood, *Organometallics* **1986**, *5*, 1009−1015. − [10e] J. M. Brown, P. J. Maddox, *J. Chem. Soc., Chem. Commun*. **1987**, 1278−1280. − [10f] J. M. Brown, P. A. Chaloner, G. A. Morris, *J. Chem. Soc., Perkin Trans. 2* **1987**, 1583−1588. − [10g] C. R. Landis, J. Halpern, *J. Am. Chem. Soc.* **1987**, *109*, 1746−1754. − [10h] J. M. Brown, P. L. Evans, *Tetrahedron* **1988**, *44*, 4905−4916. − [10i] B. M. McCulloch, J. Halpern, M. R. Thompson, C. R. Landis, *Organometallics* **1990**, *9*, 1392−1395. [10j] J.M. Brown, *Chem. Soc. Rev.* **1993**, *22*, 25−41. − [10k] C. R. Landis, T. W. Brauch, *Inorg. Chim. Acta* **1998**, *270*, 285−297. − [10l] B. F. M. Kimmich, E. Somsook, C. R. Landis, *J. Am. Chem. Soc*. **1998**, *120*, 10115−10125.

[11] [11a] E. L. Mutterties, J. R. Bleeke, E. J. Bucherer, T. A. Albright, *Chem. Rev.* **1982**, *82*, 499−525. − [11b] R. G. Gastinger, K. J. Klabunde, *Transition Met. Chem*. **1979**, *4*, 1−13. − [11c] R. Uson, L. A. Oro, C. Foces-Foces, F. H. Cano, S. García-Blanco, M. Valderrama, *J. Organomet. Chem*. **1982**, *229*, 293−304. − [11d] E. L. Mutterties, J. R. Bleeke, A. C. Sievert, *J. Organomet. Chem.* **1979**, *178*, 197−216. − [11e] R. Uson, L. A. Oro, C. Foces-Foces, F. H. Cano, A. Vegas, M. Valderrama. *J. Organomet. Chem*. **1981**, *215*, 241−253. − [11f] L. A. Oro, C. Foces-Foces, F. H. Cano, S. García-Blanco, *J. Organomet. Chem*. **1982**, *236*, 385−394. − [11g] R. Uson, L. A. Oro, D. Carmona, M. A. Esteruelas, C. Foces-Foces, F. H. Cano, S. García-Blanco, A. Vázquez de Miguel, *J. Organomet. Chem*. **1984**, *273*, 111−128. − [11h] R. Giernoth, P. Huebler, J. Bargon, *Angew. Chem. Int. Ed.* **1998**, *37*, 2473−2475.

[12] J. Halpern, *Inorg. Chim. Acta* **1981**, *50*, 11−19.

[13] R. Uson, L. A. Oro, D. Carmona, M. A. Esteruelas, C. Foces-Foces, F. H. Cano, S. García-Blanco, *J. Organomet. Chem*. **1983**, *254*, 249−260.

[14] [14a] J. Halpern, D. P. Riley, A. S. C. Chan, J. J. Pluth, *J. Am. Chem. Soc*. **1977**, *99*, 8055−8057. − [14b] D. A. Slack, I. Greveling, M. C. Baird, *Inorg. Chem*. **1979**, *8*, 3125−3132. − [14c] J. M. Brown, P. A. Chaloner, A. G. Kent, B. A. Murrer, P. N. Nicholson, D. Parker, P. J. Sidebottom, *J. Organomet. Chem*. **1981**, *216*, 263−276.

[15] [15a] J. M. Brown, D. Parker, *J. Chem. Soc., Chem. Commun.* **1980**, 342−344. − [15b] K. Achiwa, P. A. Chaloner, D. Parker, *J. Organomet. Chem.* **1981**, *218*, 249−260. − [15c] J. M. Brown, D. Parker, *J. Org. Chem*. **1982**, *47*, 2722−2730.

[16] M. Green, T. A. Kuc, S. H. Taylor, *J. Chem. Soc., A* **1971**, 2334−2337.

[17] D. J. States, R. A. Haberkorn, D. J. Ruben, *J. Magn. Reson.* **1982**, *48*, 286−292.

[18] C. Cativiela, J. Fernandez, J.A. Mayoral, E. Melendez, R. Usón, L. A. Oro, M. J. Fernandez, *J. Mol. Catal.* **1982**, 16, 19−25.

[19] *CERIUS2*, version 3.5, Molecular Simulations Inc., San Diego, USA, **1997**.

[20] [20a] L. A. Castonguay, A. K. Rappé, *J. Am. Chem. Soc*. **1992**, *114*, 5832−5842. − [20b] A. K. Rappé, C. J. Casewit, K. S. Colwell, W. A. Goddard III, W. M. Skiff, *J. Am. Chem. Soc*. **1992**, *114*, 10024−10035. − [20c] A. K. Rappe, K. S. Colwell, C. J. Casewit, *Inorg. Chem*. **1993**, *32*, 3438−3363.

[21] A. K. Rappé, W. A. Goddard-III, *J. Phys. Chem.* **1991**, *95*, 3358−3363.

[22] D. Lafont, D. Sinou, G. Descotes, *J. Organomet. Chem.* **1979**, *169*, 87−95.

Received October 11, 1999
[I99357]

"Distorted" (η^6-Arene)tricarbonylchromium Complexes: Correlation of Structural Parameters with the Electronegativity χ_G and Hammett Constants σ_p of Arene Substituents

Jean-Pierre Djukic,*[a] Françoise Rose-Munch,[b] Eric Rose,*[b] and Jacqueline Vaissermann[c]

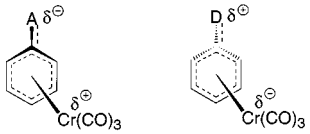
Keywords: Substituent effect / Carbonyl complexes / Chromium / Arene complexes / Structure-activity relationships

The molecular structures of 34 (η^6-arene)tricarbonylchromium complexes have been retrieved from the Cambridge Structural Data Base and investigated by focusing essentially on the distortions of the arene ligand caused by the electronic properties of the substituents connected to it. Two additional *meta*-disubstituted and one *ortho*-disubstituted arene complexes have been synthesized and their structure established by X-ray diffraction analysis. Two types of geometrical parameters have been chosen. The first one is the deviation Δ_i of the value of the endocyclic angle α_i at carbon *ipso* with respect to the ideal value α_0. The second one encompasses the chromium to *ipso*-carbon and the chromium to ring distances, d_{ipso} and d_0 respectively. It is shown that as long as no resonance effects interfere, Δ_i correlates with the group electronegativity for a wide variety of substituents whose central atom belongs to the first, second or even the third row of the periodic table. Similarly, we find that for mono-substituted arene complexes, d_{ipso} as well as d_0 correlate with the Hammett constants σ_p and σ_p^+. It is further evident that for a large variety of mono- and di-substituted (η^6-arene)tricarbonylchromium complexes, d_{ipso} correlates linearly with the σ_p^+ constant, thus indicating that d_{ipso} is a specific geometric constraint imposed by the electronic properties(e.g. inductive and mesomeric) of a given substituent connected to the arene ligand.

Introduction

The outstanding potential that (η^6-arene)tricarbonylchromium complexes bring to metal-mediated syntheses stems essentially from the stereochemical and electron-withdrawing properties of the $Cr(CO)_3$ moiety.[1] This has naturally led many groups of researchers to consider the $Cr(CO)_3$ moiety as a particularly electrophilic group which could activate a coordinated aromatic ligand toward many types of reactions that would otherwise not be feasible. It is well established that the conformational behavior of the $Cr(CO)_3$ moiety is controlled by two main parameters: first, the electronic intrinsic properties of the substituents of the arene ring and, second the steric interactions of the substituents with the metal centered rotor.[2] In the absence of any perturbing bulky group, it may be expected that electron-donating groups will favor a *syn*-eclipsed conformation of $Cr(CO)_3$ while electron-withdrawing groups will induce an *anti*-eclipsed conformation. In the solid state, the $Cr(CO)_3$ unit frequently adopts the theoretically predicted conformation although some exceptions suggest that crystal packing may impose unexpected geometries.

In a series of reports,[3] Hunter and co-workers underlined the peculiar strong distortion of complexed aromatic rings caused by π-donor substituents such as $-NR_2$. The authors investigated the possible relationship between the π-donating or π-accepting capability of a given group and the amplitude of the distortions operating over the aromatic ligand, and proposed in some cases that a π-accepting substituent **A** would induce a bending of the aromatic *ipso* carbon toward the $Cr(CO)_3$ moiety while the opposite would be observed with a π-donating substituent **D**[3a] (Scheme 1).



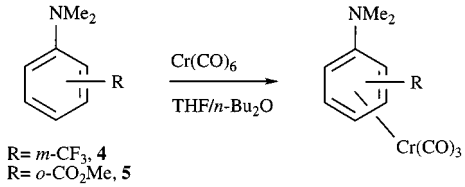
Scheme 1

This empirical model was proposed without fully considering the fact that the distortions induced by π-accepting substituents(eg. out of mean-plane folding of the arene ring toward Cr) were quite rare and small. Relevant distortions of the mean-plane in the vicinity of C_{ipso} may generally be observed only with derivatives of aniline. Therefore we decided to reinvestigate the matter by systematically analyzing the molecular structures of mono-substituted and *para*-, *meta*- and *ortho*-disubstituted (η^6-arene)$Cr(CO)_3$ complexes for their main structural properties. This was done by focusing on a set of selected structural parameters that are likely to vary depending exclusively on the electronic effects of the substituent. We show, herein, in an unprecedented manner, that these structural parameters can be correlated in a ma-

[a] UMR 7513 CNRS, Université Louis Pasteur,
4, rue Blaise Pascal, 67070 Strasbourg Cedex, France
E-mail: djukic@chimie.u-strasbg.fr
[b] UMR 7611 CNRS, Université Pierre et Marie Curie,
Case 181, 4, place Jussieu, 75252 Paris Cedex 05, France
E-mail: rose@ccr.jussieu.fr
[c] ESA 7071 CNRS, Université Pierre et Marie Curie
4, place Jussieu, 75252 Paris Cedex 05, France

 © WILEY-VCH Verlag GmbH, D-69451 Weinheim, 2000 1434–1948/00/0606–1295 $ 17.50+.50/0

jority of cases to the Hammett constants σ_p, σ_p^+, to a lesser extent to σ_p^- and to the group electronegativity χ_G of a given substituent −G, hence allowing further empirical predictions of the structure-reactivity features of any (η^6-arene)$Cr(CO)_3$ complex.



R= *m*-CF_3, **4**
R= *o*-CO_2Me, **5**

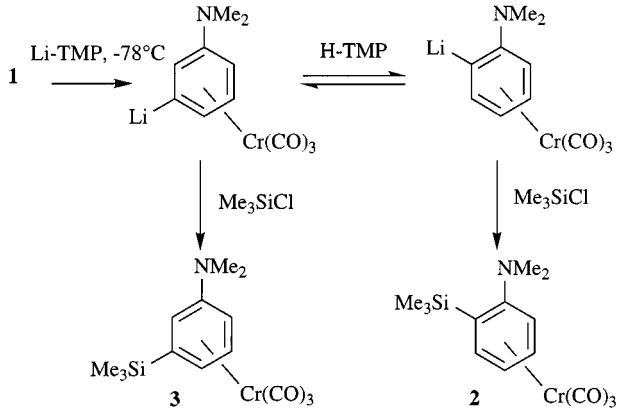
(1)

Results and Discussion

For this study, we have investigated a total of 33 X-ray structures and 1 neutron diffraction structure deposited with the Cambridge Structural Data Base (CSDB). Among these, 17 are structures of mono-substituted arene complexes, 13 are of *para*-disubstituted arene complexes and 3 are of hetero-*ortho*-disubstituted arene complexes. We have synthesized three additional complexes, two *meta*-, and one *ortho*- hetero-disubstituted arene complexes, **3**, **4**, and **5**, respectively.

Preparation of Complexes 3−5

Preparation of complex **3** was performed by sequential lithiation and silylation of **1**, (η^6-NMe_2−C_6H_5)$Cr(CO)_3$ (Scheme 2). The use of *n*BuLi as a lithiation agent afforded, after silylation, a mixture of complexes **2** and **3**[4] in a ratio of 46:54, respectively (48% overall yield). In order to optimize the yield of complex **3** we used another method of lithiation first proposed by Kündig and co-workers for (η^6-naphthalene)tricarbonylchromium.[5] 1-Lithio-2,2,6,6-tetramethylpiperidine (Li-TMP) reacted with **1** and Me_3SiCl. Complexes **2** and **3** were obtained in a ratio of 21:79 (72% overall yield). In addition, we noticed that a slight excess of 2,2,6,6-tetramethylpiperidine (H-TMP) in the basic reaction medium could cause the formation of a 50:50 mixture of complexes **2** and **3** after silylation (63% overall yield).



Scheme 2

Complex **4** was prepared by the usual method of thermolysis of $Cr(CO)_6$ in a THF/(nBu)$_2$O mixture in the presence of 1-dimethylamino-3-trifluoromethylbenzene [Equation (1)].[6] Complex **5** was obtained in a similar manner to complex **4,** by thermolysis of $Cr(CO)_6$ in presence of methyl 2-(dimethylamino)benzoate (Equation 1).

The bright orange complex was purified by the usual techniques and crystallized from a toluene/hexane solution. Single crystals of compounds **3−5** were analyzed by X-ray diffraction. It is worthy to note that the crystal system of compound **3** was found to fit the noncentrosymmetric space group $P2_12_12_1$, thus indicating that complex **3** afforded, upon crystallization, a conglomerate[7] of spontaneously resolved enantiomers (Figure 1). Acquisition and refinement data for **3−5** are provided in Table 7 in the Experimental Section of this paper. Selected interatomic distances and valence angles for compounds **3−5** are given in Table 1. Figures 1−3 display ORTEP diagrams and the atom numbering scheme for these three complexes. The three molecular structures display a significant shift of the *ipso* carbon bearing the $-NMe_2$ substituent, out of the mean-aromatic plane away from the Cr center. Compound **5** possesses a pronounced helicity due to both the distortion induced by the $-NMe_2$ group and the *ortho* relationship between the two arene substituents from which steric repulsions arise (Figure 3). The latter helicity is characterized by an absolute value of the torsion angle N−C1−C2−C9 of 15.2°.

Selection of the Structural Parameters Investigated

Although all the structures that were analyzed presented distortions of various parameters such as interatomic distances, valence angles, torsion angles, along with some unexpected conformations of the tripod, we decided to focus essentially on the variation of two elementary parameters that were expected to be sensitive to relatively independent effects. Thus, we somewhat aimed at a rationalization of the causes of arene ligand distortions through a decomposition of the overall phenomenon into a sum of independent contributions. Hence, the following parameters were selected:

1. the deviations Δ_i of the endocyclic angles α_i from the ideal α_0 value of 120.0°,

$\Delta_i = \alpha_i - \alpha_0$, and especially the one centered at C_{ipso}, e.g Δ_{ipso} (Scheme 3).

2. the chromium to C_{ipso} interatomic distance, d_{ipso}, and the distance from the Cr atom to the mean-aromatic plane, d_0 (Scheme 4).

To justify the study of the endocyclic angle, it must be recalled that with uncoordinated aromatics it is well established that the electronegativity χ_G of a given substituent -G affects the values of both the six endocyclic angles and the corresponding intracyclic $C_{Ar}-C_{Ar}$ bond lengths.[8] Several studies have shown that a linear correlation between Δ_{ipso} and χ_G, the electronegativity of the group or element,

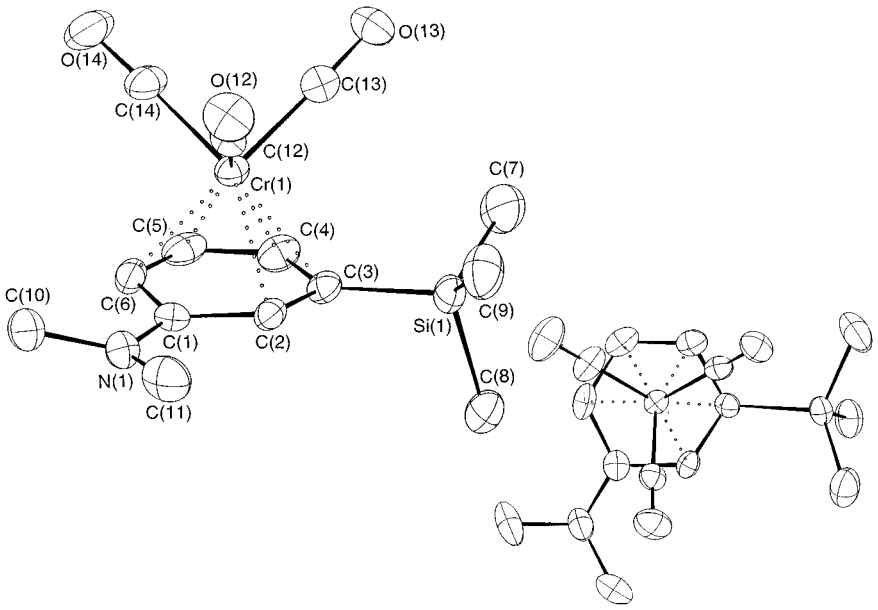


Figure 1. ORTEP diagrams and atomic numbering scheme of the molecular structure of complex **3** including a view along the Cr-ring axis

Table 1. Selected interatomic distances (Å) and valence angles (deg) for compounds **3**–**5**

compounds	**3**	**4**	**5**
interatomic distances (Å)			
Cr–C1	2.348(7)	2.41(1)	2.383(3)
Cr–C2			2.232(3)
Cr–C3	2.247(7)	2.170(1)	
Cr–C_{Ar} (aver.)	2.244	2.245	2.240
C1–C2	1.431(8)	1.39(1)	1.434(4)
C_{Ar}–C_{Ar} (aver.)	1.41	1.40	1.40
C1–N	1.355(9)	1.37(1)	1.362(4)
C3–$SiMe_3$	1.870(6)		
C3–CF_3		1.48(1)	
C2–CO_2Me			1.505(4)
angles of valence (deg)			
C6–C1–C2	115.6(6)	117.6(9)	116.6(3)
C3–C4–C5	120.2(6)	117.1(8)	118.9(3)
C2–C3–C4	117.2(6)	121.3(8)	121.9(3)

may be obtained provided that the central atom of the substituent -G connected to the arene ring belongs to the second or third row of the periodic table and/or does not show propensity to conjugate a doublet of electrons with the π-system of the considered aromatic.[9] A rationalization of the distortion of α_{ipso} by the VSEPR theory has been proposed: *a σ-electron-withdrawing substituent polarizes the localized C_{ipso}-G bonding molecular orbital, so that the bonding electron pair occupies less space in the valence shell of carbon and interacts less strongly with the two neighboring C_{ipso}–C_{ortho} σ-bonding pairs*; this causes an increase in the actual value of the internal angle α_{ipso} with respect to the value α_0, greater than that expected for a substituent having the same electronegativity as the ring; the reverse is expected with a σ-donating substituent. It has been further

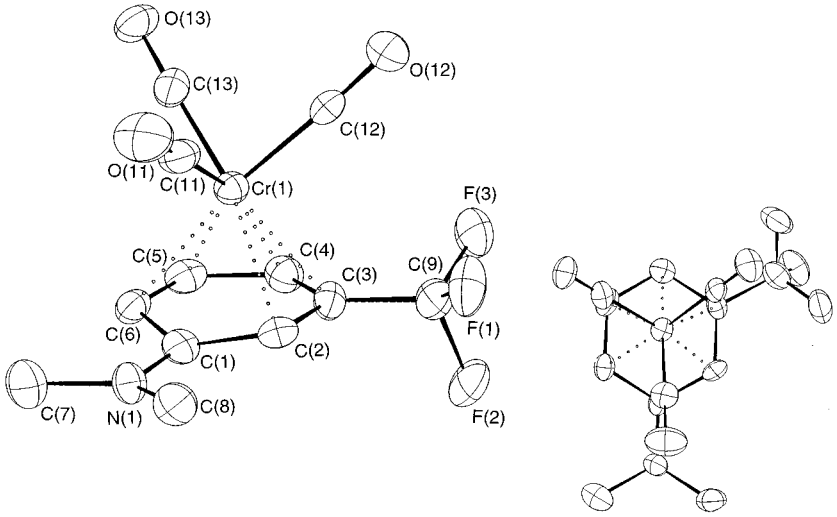


Figure 2. ORTEP diagrams and atomic numbering scheme of the molecular structure of complex **4** including a view along the Cr-ring axis

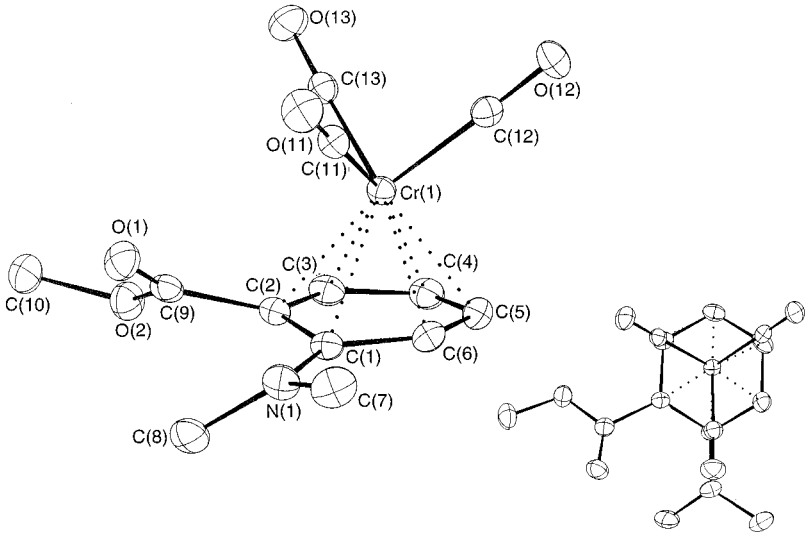
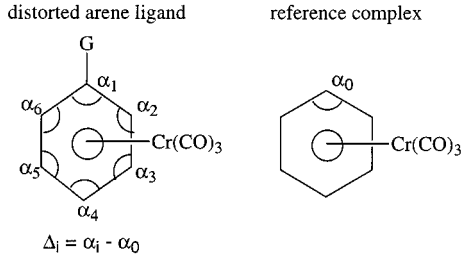
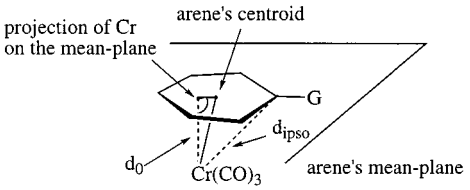


Figure 3. ORTEP diagrams and atomic numbering scheme of the molecular structure of complex **5** including a view along the Cr-ring axis



Scheme 3



Scheme 4

stressed that *if the substituent is conjugated with the ring, there is a build-up of π-electron density alongside the σ-bond and an increase of electron density within the σ-bonding molecular orbital,* in the region of the C_{ipso}−G bond, causing a decrease in the value of α_{ipso} below that of α_0. Similar trends can be expected for aromatic ligands coordinated to a $Cr(CO)_3$ moiety as it is often the π orbitals of the aromatic fragment that are involved in the interaction with molecular orbitals of $Cr(CO)_3$. The main results of the first part of our investigations are presented in the following paragraph. A preliminary and similar approach has recently been applied to a few examples of metallated (η^6-arene)$Cr(CO)_3$ σ-π complexes by Lotz and co-workers.[10]

Our interest in the study of the variation of metal-to-ring distances arose from the numerous comparative studies of the IR spectroscopic properties of substituted arene complexes. They concluded, in a convergent manner, that both the resonance and inductive electronic effects of the substituent can be readily transmitted to the CO ligands *via* the chromium center.[11] This has been shown by a net correlation between Hammett σ constants and the force constant k_{CO} of the studied carbonyl ligand C−O bond. This important fact suggested that the arene carbon σ-framework participates in the metal-ring bonding, although the metal-3d and $4p_\pi$/arene-$2p_\pi$ interaction dominates.[12] Early semi-empirical molecular orbital calculations carried out by Carroll and McGlynn[13] pointed out the importance of the ring σ-framework in the arene−Cr bonding. Recently, Phillips and co-workers studied the charge distribution in a series of poly-methyl-substituted (η^6-benzene)$Cr(CO)_3$ derivatives. They noted that with increasing methyl substitution, the major electron reorganization occurs in the arene−Cr segment of the molecule.[14] This reorganization, caused by an increase of the degree of substitution of the arene ring by methyl groups, was shown to induce an increase in the arene−Cr bond charge and order. Furthermore, it showed a progressive displacement of the bond charge from the arene ligand toward the chromium atom.

While retrieving the X-ray diffraction structural information of a large series of complexes we noticed that severe foldings of the arene ring away from the $Cr(CO)_3$ group were mostly occurring in aniline derivatives bearing $-NR_2$ groups. In a few examples, other π-electron donating or accepting substituents seemed to induce a significant folding of the ring. However, the main trend observed for complexes bearing π/σ-donor and π/σ-acceptor substituents was an increase and a decrease, respectively, in the chromium-to-*ipso*-carbon distance relative to the reference compound (η^6-benzene)$Cr(CO)_3$. This general trend somewhat rectifies and refines the empirical rule formulated by Hunter and co-workers and suggests that a folding of the arene ring is generally not necessary for the minimization of intramolecular electronic repulsions, especially in complexes bearing π-donor/acceptor substituents.

Table 2. Endocyclic angular deviations (deg) for mono-substituted arene complexes bearing a substituent -G with an electronegativity of χ_G

entry	−G compound	Δ_1 (deg)	Δ_2 (deg)	Δ_3 (deg)	Δ_4 (deg)	Δ_5 (deg)	Δ_6 (deg)	$\Sigma\Delta_i$ (deg)	σ(α) averaged	χ_G
1	−C(O)Me, **6a**	0.98	−2.24	4.93	−2.32	−2.32	−0.42	−0.29	−	2.864
2	−H, **6b**	0.0	0.0	0.0	0.0	0.0	0.0	0.0	0.09	2.176
3	$-NEt_2$, **6c**	−3.4	1.3	0.8	−1.5	2.2	−0.1	−0.7	0.3	3.011
4	$-AsPh_2$, **6d**	−1.6	1.3	−0.4	0.3	−0.1	0.7	0.2	0.3	2.161
5	−Me, **6e**	−2.5	1.2	1.8	−2.2	2.0	−0.4	−0.1	0.4	2.472
6	$-SiMe_3$, **6f**	−2.96	1.42	0.27	−0.68	0.36	1.58	−0.01	−	1.990
7	S^+(Me)(*i*Pr), **6g**	3	1	−2	1	−2	−2	−1	4	3.095[a]
8	−C(O)Ph, **6h**	−1.71	0.72	−0.38	0.53	−0.42	1.22	−0.04	−	2.681
9	$-NH_2$, **6i**	−0.9	−0.3	0.9	−1.0	0.9	−0.3	−0.7	0.2	2.992
10	−OMe, **6j**	0.7	−0.8	1.4	−1.5	2.8	−2.8	−0.2	0.4	3.543
11	$-SO_2Me$, **6k**	0.2	−0.5	−0.2	1.0	−0.3	−0.2	−0.0	0.2	2.998
12	−C≡CPh, **6l**	−0.2	−0.2	−0.9	0.8	0.9	−0.4	0.0	0.7	3.080
13	$-P(iPr)_2$, **6m**	−2.8	1.1	0.3	−0.6	0.2	1.7	−0.1	0.2	2.249
14	$-C(O)NH_2$, **6n**	−0.9	0.5	−0.5	0.6	0.3	−0.1	−0.1	0.3	2.731
15	−C(O)OMe, **6o**	−0.6	−0.3	0.6	0.0	0.3	−0.1	−0.1	0.2	2.832

[a] Approximate value taken from that established for $-S^+Me_2$

Influence of the Electronegativity of a Substituent over the Value of Endocyclic Angles: the Case of Mono-Substituted and *para*-Disubstituted (η^6-Arene)$Cr(CO)_3$ Complexes

A first approach involved the study of the angular distortion of mono-substituted (η^6-arene)$Cr(CO)_3$ complexes. Retrieval of atomic coordinates of compounds **6a**−**o**[15] from the CSDB allowed the measure of the endocyclic angles; the corresponding estimated standard deviation for the considered data were extracted from available published reports and averaged. In the cases of **6a**, **6f** and **6h**, exact values of σ(α) were not available to us. Among all the selected examples grouped in Table 2, only one complex, namely **6g**, presented a fairly high σ(α) value of 4 (entry 7, Table 2). However, this complex was considered, and the corresponding values of the endocyclic angle variations are provided.

Table 2 gives the values of Δ_i, deviations of the endocyclic angles from the ideal averaged value of 120.0 which was determined by the neutron-diffraction crystal structure of (η^6-benzene)$Cr(CO)_3$.[15b]

It can be noticed that almost all endocyclic angles deviate significantly from the ideal value. This is in contrast with observations made for uncoordinated aromatics. Indeed, it is generally observed that arene substituents cause significant distortions at the *ipso*, *ortho* and *meta* positions while *para* positions are mostly unaffected.[9] Two points can be observed: first, two related *ortho* and *meta* positions display fairly different values of $\Delta_{2,6}$ and $\Delta_{3,5}$, and second, the value of Δ_4 is often different from zero (Table 2). The presence of the $Cr(CO)_3$ tripod on the one side of the arene induces a loss of symmetry and induces distortions of the arene ring that can be characterized by the sum of the endocyclic angular deviations $\Sigma\Delta_i$. The lower values of $\Sigma\Delta_i$ are obtained for the two aniline derivatives, **6c** (−0.7) and **6i** (−0.7), the acetophenone complex **6a**, and **6g**. A negative value of $\Sigma\Delta_i$ indicates an overall decrease in the value of endocyclic angles, a possible slight change of hybridization of the orbitals of aromatic carbons and thus an actual nonplanar nature of the aromatic ligand. For the compounds considered in this table, values of $\Sigma\Delta_i$ inferior in absolute value to σ(α) correspond to an almost planar arene ligand. Deviations of atomic position from the calculated least-square mean-aromatic planes confirm the significant distortions for **6c**, **6i**, **6a**, **6g** and corroborate the information suggested by values of $\Sigma\Delta_i$. A plot of the *ipso* endocyclic distortion *versus* the electronegativity of the group as defined and calculated by Inamoto,[16] confirms that mono-substituted arene complexes follow a trend similar to that of uncoordinated arenes. Figure 4 presents a scattered distribution of data points around a mean diagonal line.

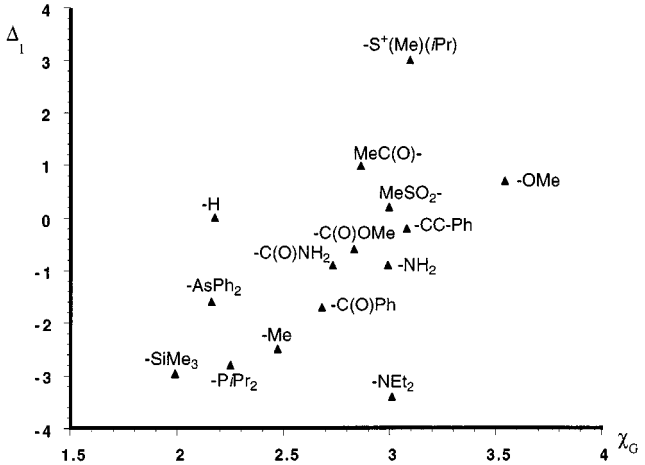


Figure 4. Graph of Δ_{ipso} (deg) *versus* χ_G for mono-substituted arene complexes

Few points are positioned out of the main statistical cloud. These data points correspond to arene complexes substituted by $-NEt_2$ (**6c**), $-S^+$(Me(iPr) (**6g**), −C(O)Me (**6a**). Strikingly, the data point corresponding to the benzene complex is found outside the statistical ascending cloud that groups together data from compounds **6f**, **6m**, **6d**, **6h**, **6n**, **6o**, **6i**, **6l**, **6k** and **6j**. This could be in part due to an underestimation of the value of χ_G for −H in aromatic compounds. It is known that the electronegativity of a given group may take significantly different values depending on

Table 3. Endocyclic *ipso*-carbon angular deviations at C1 (deg). Raw and corrected values listed with electronegativity χ_G of the group connected at C1

entry	groups, compound	Δ_1 (deg)	Δ_{1corr} (deg)	Δ_4 (deg)	$\sigma(\alpha)$	χ_{G1}
1	1-H, 4-$CH(OMe)_2$, **6p**	−0.24		−1.93		
2	1-H, 4-$CH(OEt)_2$, **6q**	−0.37		−1.11		
3	1-NMe_2, 4-$CH(OMe)_2$, **7a**	−4.0	−3.9		0.4	3.012
4	1-NMe_2, 4-$CH(OEt)_2$, **7b**	−3.0	−2.6		0.5	3.012
5	1-Cl, 4-$CH(OMe)_2$, **7c**	1.5	1.8		0.9	3.16
6	1-Cl, 4-$CH(OEt)_2$, **7d**	0.7	1.0		0.7	3.16
7	1-$SiMe_3$, 4-$CH(OMe)_2$, **7e**	−3.4	−3.1		0.4	1.990
8	1-$SiMe_3$, 4-$CH(OEt)_2$, **7f**	−4.7	−4.3		0.4	1.990
9	1-CF_3, 4-$CH(OMe)_2$, **7g**	−0.4	−0.1		0.7	2.985
10	1-CF_3, 4-$CH(OEt)_2$, **7h**	−0.5	−0.1		0.2	2.985
11	1.4-F,−F, **7i**	3.12		3.12	0.2	3.98
12	1-OCF_3, 4-NH_2, **7j**	0.6	1.5		0.2	3.486
13	1,4-OMe,−OMe, **7k**	−0.5		0.3	0.7	3.543
14	1,4-NMe_2,−NMe_2, **7l**	0.5		−0.6	0.5	3.012
15	1,4-CO_2Me,-CO_2Me, **7m**	0.0		−0.1	0.3	2.832

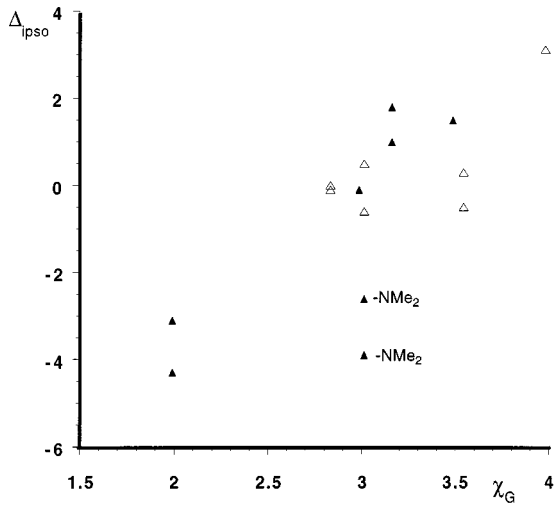


Figure 5. Graph of Δ_{ipso} (deg) *versus* χ_G for *para*-disubstituted arene complexes: (▲) compounds **7a**−**h** and **7j**; (△) compounds **7i** and **7k**−**m**

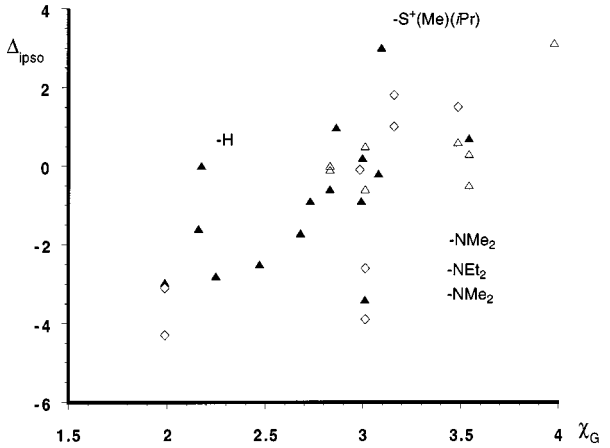


Figure 6. Graph of Δ_{ipso} (deg) *versus* χ_G for mono-substituted and *para*-disubstituted arene complexes: (▲) compounds **6a**−**o**; (△) homo-disubstituted compounds **7i**, **7k**−**m**; (◇) hetero-disubstituted compounds **7a**−**h**, **7j**

the nature of the organic or inorganic radical connected to it.[17] Therefore the plot displayed in Figure 4 must be considered as an informative qualitative picture.

We have applied a similar treatment to selected examples of hetero- and homo- *para*-disubstituted complexes bearing various types of substituents. For compounds **7a**−**h**[18] the endocyclic angular distortion at aromatic carbon 1 bearing the considered substituent located *para* to the acetal group $-CH(OR)_2$, was corrected for the distortions caused by the latter group. The correction terms applied to Δ_1 of compounds **7a**−**h** in Table 3, were extracted from the value of the *para* endocyclic angular deviations Δ_4 in the molecular structures of mono-substituted complexes **6p**−**q**. This consequently allowed the determination of approximated values of Δ_{ipso} for the following substituents: $-NMe_2$, Cl, $SiMe_3$, CF_3. A similar treatment was applied to values extracted from the molecular structure of compound **7j**[19] in order to obtain a corrected value of Δ_{ipso} for $-OCF_3$; this was carried out by applying a correction term which corresponded to the value of Δ_4 of the aniline complex **6i**. For the *para*-homo-disubstituted complexes **7i**,[20] **7k**−**m**, no corrections were applied to the values of Δ_1 and Δ_4.

A plot of these corrected and uncorrected values of Δ_{ipso} *versus* χ_G is displayed in Figure 5. A combination of the data of Table 2 and 3 allowed us to establish a new graph (Figure 6) in which it can clearly be seen that the value of the *ipso* carbon endocyclic angular deviation correlates with the Inamoto group and Pauling element[21] electronegativity χ_G, unless resonance interactions perturbe such a phenomenon as in complexes bearing $-NR_2$ (R = Me, Et), and the isolobal $-S^+RR'$ group. Electronegativities of substituents play a significant part in the overall distortion of the aromatic ring of (η^6-arene)$Cr(CO)_3$ complexes.

Correlation of Metal-to-Ring Distances with Hammett Constants in Monosubstituted (η^6-arene)$Cr(CO)_3$ Complexes: Nonlinear and Linear Correlations of the C_{ipso}−Cr and the Metal-to-Ring Mean-Plane Distances with σ_p

Metal to aromatic carbon distances have been often reported to be influenced by the "electron richness" of the

Table 4. List of values of d_{ipso}, d_0 (in Å) of mono-substituted arene complexes (η^6-G-C_6H_5)$Cr(CO)_3$ and Hammett substituent constants σ_p, σ_p^+ and σ_p^-

entry	−G, compound	d_{ipso} (Å)	$\sigma(d_{ipso})$ (Å)	d_0 (Å)	σ_p	σ_p^+	σ_p^-
1	−C(O)Me, **6a**	2.157	0.008	1.700	0.50	−	0.84
2	−H, **6b**	2.230	0.003	1.725	0.00	−	−
3	$-NEt_2$, **6c**	2.369	0.002	1.748	−0.72	−2.07	−0.43
4	$-AsPh_2$, **6d**	2.219	0.003	1.708	0.09	−	0.29
5	−Me, **6e**	2.236	0.004	1.725	−0.17	−0.31	−0.17
6	$-SiMe_3$, **6f**	2.239	0.004	1.722	−0.07	0.02	−
7	$-S^+(Me)(iPr)$, **6g**	2.140	0.05	1.671	0.90[a]	−	0.83[a]
8	−C(O)Ph, **6h**	2.193	−	1.694	0.43	0.51	0.83
9	$-NH_2$, **6i**	2.349	0.003	1.745	−0.66	−1.30	−0.15
10	−OMe, **6j**	2.264	0.005	1.740	−0.27	−0.78	−0.26
11	$-SO_2Me$, **6k**	2.172	0.002	1.682	0.72	−	1.13
12	−CCPh, **6l**	2.206	0.006	1.695	0.16	−0.03	0.30
13	$-PiPr_2$, **6m**	2.231	0.002	1.710	0.06	−	−
14	$-C(O)NH_2$, **6n**	2.210	0.002	1.699	0.36	−	0.61
15	−C(O)OMe, **6o**	2.214	0.002	1.714	0.45	0.49	0.75

[a] Approximate value taken from $-S^+Me_2$.

aromatic ring and many authors pointed out indirectly that this parameter was a sensitive probe for assessing the magnitude of electron density transfer within (η^6-arene)$Cr(CO)_3$ complexes.[19] We decided to verify whether variations of d_{ipso} and d_0 could be linked to quantified effects such as inductive or resonance effects of substituents connected to the ring. Table 4 lists the values of d_{ipso} and d_0 obtained from structural information. All standard deviations $\sigma(d_{ipso})$ were obtained from the corresponding published reports except for **6h** (entry 8, Table 4); in the case of compound **6a** (entry 1, Table 4), a geometric σ(d) value was calculated from the standard deviations of the atomic coordinates extracted from the published report. It must be noted that d_0 was determined by considering the mean-plane, including all six arene carbons, even in strongly distorted rings: in doing so we established a reliable way of "idealizing" the distortion of the arene as even in strongly distorted molecules, the p-orbital at C_{ipso} is supposedly still engaged in aromaticity[22] and in a bonding interaction with the Cr atom. In many previous reports Cr-to-ring distances were calculated without taking into account the *ipso* carbon bearing the "perturbing" substituent, thus leading to a systematic underestimation of the value of d_0.

A plot of d_{ipso} versus the Hammett constant σ_p for various substituents[23] is given in Figure 7. The constant σ_p is defined for reactions taking place at a reactive site located *para* to a substituent, a position greatly favored by both inductive and resonance effects. For a given substituent of an aromatic compound, the σ_p constant is approximately the sum of the contributions of the inductive/field parameter, *F*, and the resonance parameter, *R*.[24] As can be noticed from Figure 7, there is a clear nonlinear correlation between the two parameters d_{ipso} and σ_p. A much better result is obtained by plotting d_{ipso} versus σ_p^+. The Hammett constant σ_p^+ has been devised for substituents conjugated with a reaction center which could effectively delocalize a positive charge.[25] As a result, values of σ_p^+ for π-electron donor substituents are considerably enhanced relative to the corresponding σ_p. The former σ_p^+ Hammett constant seems more appropriate in our study as the

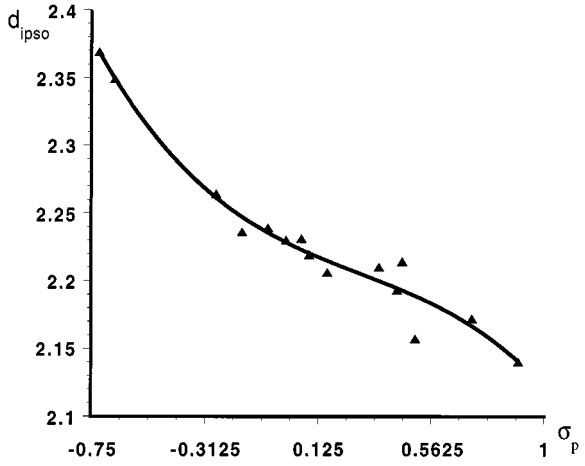


Figure 7. Plot of d_{ipso} (Å) *versus* σ_p for mono-substituted arene complexes

$Cr(CO)_3$ moiety decreases π-electron density on the aromatic ring and acts in a similar manner to an π-electron-withdrawing arene substituent inducing the creation of a positive charge in the Cr-arene segment; Kinomura and coworkers[26] have evaluated the partial charges in (η^6-benzene)$Cr(CO)_3$ to be −0.12e at benzene, +0.54e at the chromium atom, +0.15e at carbonyl carbons and −0.29e at carbonyl oxygen. Figure 8 displays a linear correlation between d_{ipso} and σ_p^+ which can be formulated by the following least-squares Equation:

$d_{ipso} = 2.23\ (\pm 0.01) - 0.07(\pm 0.01) \times \sigma_p^+$ ($n = 6$, $R = 0.955$, $\chi^2 = 0.002$).

The value of the intercept corresponds exactly to the value of d_{ipso} for the reference compound (η^6-benzene)$Cr(CO)_3$, **6b**. Figure 9 displays a plot of d_{ipso} versus σ_p^- which affords, according to expectations, a nonlinear relationship between the two parameters .

A plot of d_0 versus σ_p gives a distribution of points that strongly suggests a linear relationship between the two

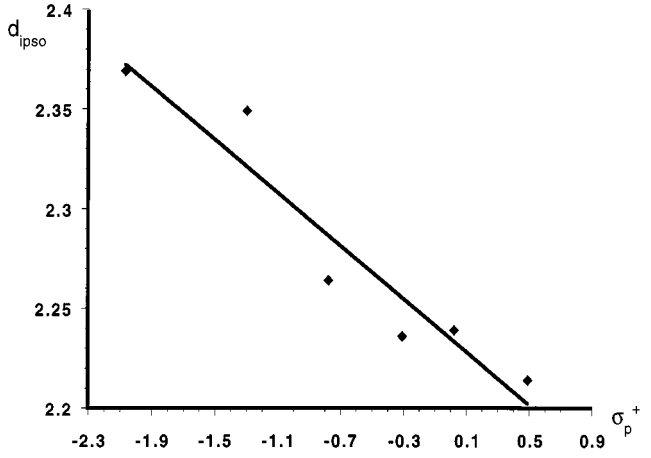


Figure 8. Plot of d_{ipso} (Å) *versus* σ_p^+ for mono-substituted arene complexes

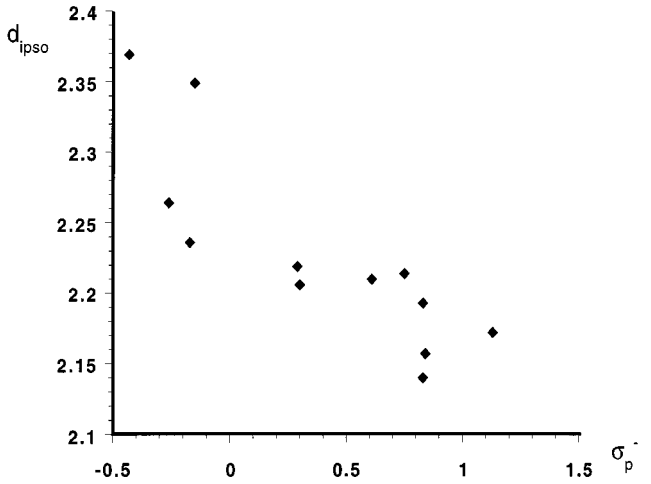


Figure 9. Plot of d_{ipso} (Å) *versus* σ_p^- for mono-substituted arene complexes

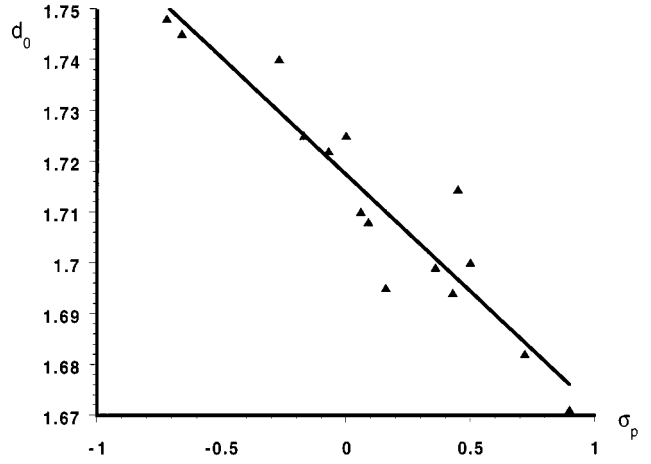


Figure 10. Plot of d_0 (Å) *versus* σ_p for mono-substituted arene complexes

parameters (Figure 10). A curve fitting carried out by the least-squares method affords the following linear relationship between d_0 and σ_p for the mono-substituted arene complexes in question:

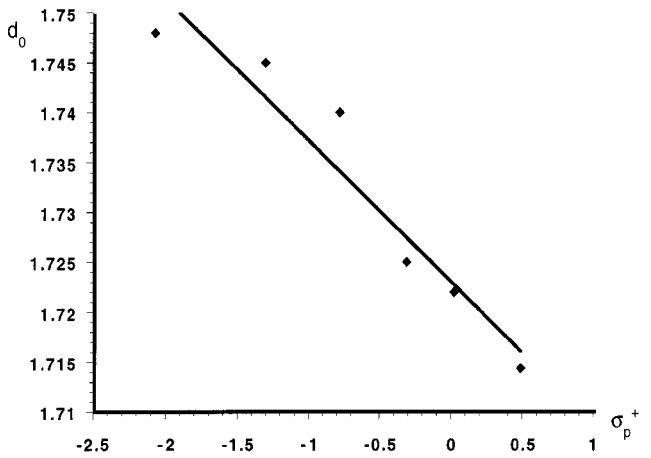


Figure 11. Plot of d_0 (Å) *versus* σ_p^+ for mono-substituted arene complexes

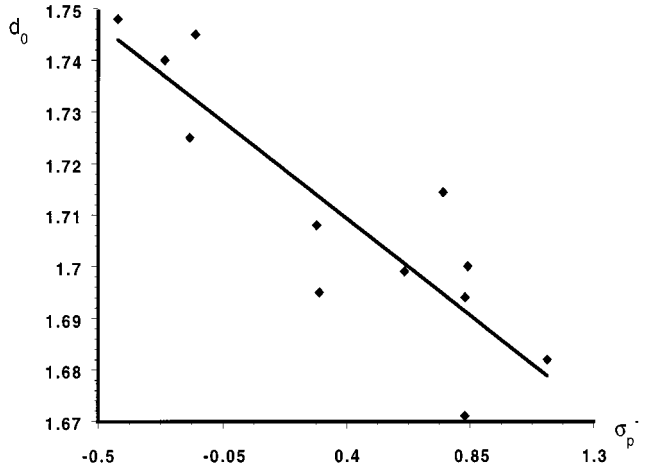


Figure 12. Plot of d_0 (Å) *versus* σ_p^- for mono-substituted arene complexes

$d_0 = 1.717(\pm 0.002) - 0.045(\pm 0.004) \times \sigma_p$, ($n = 15$, $\chi^2 = 0.0008$, $R = 0.939$).

Here the intercept is significantly lower than the value of 1.725 Å measured for the reference compound **6b**. Interestingly, plots of d_0 versus σ_p^+ (Figure 11) and σ_p^- (Figure 12) give more convincing values for the intercept, although the value of the correlation coefficient R for the expression involving σ_p^- is not optimal. The least-squares fitting carried out from the latter plots affords the following Equations:

$d_0 = 1.723(\pm 0.002) - 0.014(\pm 0.002) \times \sigma_p^+$ ($n = 6$, $\chi^2 = 7 \times 10^{-5}$, $R = 0.959$)

and

$d_0 = 1.726(\pm 0.004) - 0.041(\pm 0.007) \times \sigma_p^-$ ($n = 12$, $\chi^2 = 0.001$, $R = 0.880$).

Application of this relationship to the determination of σ_p of the two acetal groups $-CH(OMe)_2$ ($d_0 = 1.717$ Å in **6p**) and $-CH(OEt)_2$ ($d_0 = 1.709$ Å in **6q**) affords values of 0.00 and 0.17 respectively which compare satisfactorily with those established for $-CH(OMe)_2$ (σ_p value calculated

Table 5. List of values of d_{ipso} (Å) for hetero- and homo-disubstituted arene complexes and the corresponding Hammett substituent constants σ_p, σ_p^+ and σ_p^-

entry	compound	−G	$d_{ipso}(\sigma(d_{ipso}))$	σ_p	σ_p^+	σ_p^-
1	**7a**	1-NMe_2	2.382(4)	−0.83	−1.70	−0.12
		4-$CH(OMe)_2$	2.230(4)	0[a]		
2	**7b**	1-NMe_2	2.377(5)	−0.83	−1.70	−0.12
		4-$CH(OEt)_2$	2.218(5)	0.17[a]		
3	**7c**	1-Cl	2.217(7)	0.23	0.11	0.19
		4-$CH(OMe)_2$	2.213(7)	0[a]		
4	**7d**	1-Cl	2.204(4)	0.23	0.11	0.19
		4-$CH(OEt)_2$	2.203(4)	0.17[a]		
5	**7e**	1-$SiMe_3$	2.230(4)	−0.07	0.02	
		4-$CH(OMe)_2$	2.227(4)	0[a]		
6	**7f**	1-$SiMe_3$	2.240(4)	−0.07	0.02	
		4-$CH(OEt)_2$	2.233(3)	0.17[a]		
7	**7g**	1-CF_3	2.195(6)	0.54	0.61	0.65
		4-$CH(OMe)_2$	2.217(6)	0[a]		
8	**7h**	1-CF_3	2.194(2)	0.54	0.61	0.65
		4-$CH(OEt)_2$	2.207(2)	0.17[a]		
9	**7i**	1-F	2.215(4)	0.06	−0.07	−0.03
		4-F	2.215(4)	0.06	−0.07	−0.03
10	**7j**	1-OCF_3	2.199(2)	0.35		0.27
		4-NH_2	2.353(2)	−0.66	−1.30	−0.15
11	**7k**	1-OCH_3	2.262(6)	−0.27	−0.78	−0.26
		4-OCH_3	2.292(6)	−0.27	−0.78	−0.26
12	**7l**	1-NMe_2	2.322(5)	−0.83	−1.70	−0.12
		4-NMe_2	2.207(5)	−0.83	−1.70	−0.12
13	**7m**	1-CO_2Me	2.199(3)	0.45	0.49	0.75
		4-CO_2Me	2.189(3)	0.45	0.49	0.75
14	**3**	1-NMe_2	2.410(10)	−0.83	−1.70	−0.12
		3-CF_3	2.170(9)	0.54	0.61	0.65
15	**4**	1-NMe_2	2.348(7)	−0.83	−1.70	−0.12
		3-$SiMe_3$	2.247(6)	−0.07	0.02	
16	**7n**	1-*t*Bu	2.251(6)	−0.20	−0.26	−0.13
		4-C(O)OH	2.170(6)	0.45	0.42	0.77
17	**8a**	1-OH	2.33(3)	−0.37	−0.92	−0.37
		2-C(O)Me	2.15(2)	0.50		0.84
18	**8b**	1-OMe	2.28(3)	−0.27	−0.78	−0.26
		2-C(O)Me	2.24(2)	0.50		0.84
19	**8c**	1-NH_2	2.37(1)	−0.66	−1.30	−0.15
		2-Me	2.26(1)	−0.17	−0.31	−0.17
20	**5**	1-NMe_2	2.383(3)	−0.83	−1.70	−0.12
		2-C(O)OMe	2.232(3)	0.45	0.49	0.75

[a] Calculated value.

from ^{19}F NMR = 0.03) and other analogous groups such as $-CH_2OMe$ (0.01), and $-C(OMe)_3$ (−0.04). Accordingly, σ_p^+ and σ_p^- values for the two aforementioned acetal groups are estimated from the corresponding values of d_0 in **6p**−**q** as being equal to 0.43 and 0.22 for $-CH(OMe)_2$ and 1.0 and 0.41 for $-CH(OEt)_2$, respectively.

Disubstituted Arene Complexes

Values of d_{ipso} for a variety of *para*, *meta* and *ortho* disubstituted arene complexes are grouped in Table 5: *para*-disubstituted arene complexes are compounds **7a**−**m** and **7n**,[27] *meta*-disubstituted arene complexes are compounds **3**−**4**, *ortho*-disubstituted arene complexes are compounds **8a**−**b**[28] and **8c**[29] and **5**. A plot of d_{ipso} *versus* σ_p is given in Figure 13 and shows a nonlinear distribution of the data points. The largest scattering of the data points in Figure 13 is observed for the $-NMe_2$ groups in the disymmetric *para*-homodisubstituted complex **7l**, for −C(O)Me in **8a** and **8b** and for −C(O)OMe in **5**. In the three latter cases which correspond to *ortho*-disubstituted arene complexes the deviation, may be attributed to the predominant electronic effects imposed by −OH, −OMe and NMe_2 groups over the shifting of the $Cr(CO)_3$ moiety; such predominant electronic effects may induce exaggerated values of d_{ipso} for the vicinal *ortho*-position depending on the privileged direction of the shift of the chromium atom in the tripod.

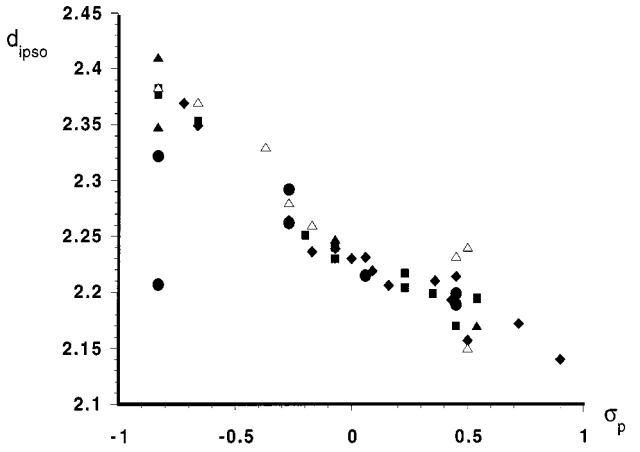


Figure 13. Plot of d_{ipso} (Å) *versus* σ_p for mono- and di-substituted arene complexes: (▲) compounds **3** and **4**; (■)compounds **7a**−**h** and **7n**; (◆) compounds **6a**−**o**; (●) compounds **7i** and **7k**−**m**; (△) compounds **8a**−**b**, **8c** and **5**

Combined values of d_{ipso} for mono- and di-substituted arene complexes (except those from **8a**−**c**, **5** and **7l**) are ploted versus σ_p in Figure 13. The shape of the plot assesses the dependency of d_{ipso} on both the inductive and resonance effects of a given aromatic substituent. It shows a relative independence towards the position and the nature of a second substituent of the arene ring (as long as it is not located at the *ortho* position).

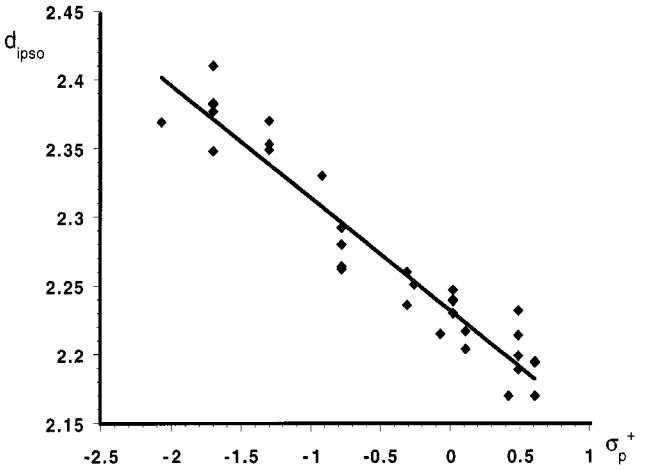


Figure 14. Plot of d_{ipso} (Å) *versus* σ_p^+ for mono- and di-substituted arene complexes having a defined value of the considered Hammett constant.

A plot of d_{ipso} *versus* σ_p^+ (Figure 14) that includes the data provided by the structures of *meta*-disubstituted arene complexes and excludes those of **8a**−**c**, **5** and **7l**, indicates now a clear linear relationship between the two parameters which is illustrated by the following linear Equation:

$d_{ipso} = 2.232(\pm 0.004) - 0.082(\pm 0.005) \times \sigma_p^+$ ($n = 33$, $\chi^2 = 0.013$, $R = 0.959$).

Table 6. List of values of d_0 (Å) for *para*-disubstituted arene complexes

entry	compound	substituents	d_0 (Å)
1	**7a**	1-NMe_2, 4-$CH(OMe)_2$	1.751
2	**7b**	1-NMe_2, 4-$CH(OEt)_2$	1.750
3	**7c**	1-Cl, 4-$CH(OMe)_2$	1.709
4	**7d**	1-Cl, 4-$CH(OEt)_2$	1.703
5	**7e**	1-$SiMe_3$, 4-$CH(OMe)_2$	1.716
6	**7f**	1-$SiMe_3$, 4-$CH(OEt)_2$	1.714
7	**7g**	1-CF_3, 4-$CH(OMe)_2$	1.702
8	**7h**	1-CF_3, 4-$CH(OEt)_2$	1.702
9	**7i**	1-F, 4-F	1.718
10	**7j**	1-OCF_3, 4-NH_2	1.743
11	**7k**	1-OCH_3,4-OCH_3	1.759
12	**7l**	1-NMe_2, 4-NMe_2	1.756
13	**7m**	1-CO_2Me, 4-CO_2Me	1.698

Here again, the value of the intercept fits the value of d_{ipso} for (η^6-benzene)$Cr(CO)_3$, **6b**.[15b] Values of σ_p^+ for the acetal groups $-CH(OMe)_2$ and $-CH(OEt)_2$ have been recalculated from the corresponding averaged values of d_{ipso} (e.g $<d_{ipso}>$) extracted from the structures of **6p−q** and **7a−h** and by applying the latter Equation. The following values were obtained and differ from those obtained from the aforementioned Equations based on the parameters d_0 of mono-substituted arene complexes: for $-CH(OMe)_2$ ($<d_{ipso}>$ = 2.223 Å), σ_p^+ = 0.11; for $-CH(OEt)_2$ ($<d_{ipso}>$ = 2.217 Å), σ_p^+ = 0.18. As for such substituents no peculiar resonance effect may be expected. The two values of σ_p^+ determined here are in our opinion more acceptable than those obtained from the previous correlation, as they are fairly close to the values reported for structurally similar groups such as $-CH_2OCH_3$ ($\sigma_p^+ = -0.05$) and $-CH_2OH$ ($\sigma_p^+ = -0.04$).[23]

Again, we find that d_{ipso} does not correlate with the σ_p^- substituent constants (graph not shown).

Values of d_0 for *para*-disubstituted complexes have been calculated in several examples and are presented in Table 6. They display a nonlinear dependence of d_0 *versus* the sum of the σ_p values for each substituent connected to the arene ligand (plot not shown here). We were not successful in establishing a simple relationship that would link d_0 either to the respective substituent electronic effects or to the molecular dipolar moment of the molecule which is presumably oriented from the arene ring to the chromium atom along the d_0 axis.[30] However, it may be noted that the value of d_0 for a given *meta*- or *para*- disubstituted arene complex is certainly significantly influenced by the values of the d_{ipso} parameter of a given substituent.

On the Prediction of the Distortions in (η^6-Arene)tricarbonylchromium Complexes

Hence, the d_{ipso} and d_0 parameters appear to be two intrinsic constraints imposed by the electronic properties of a given substituent over the geometric position of the $Cr(CO)_3$. Therefore, the main structural features of arene complexes can be predicted for mono- as well as *meta* and *para* di-substituted arene complexes regardless of the conformation of the $Cr(CO)_3$ tripod. Provided that σ_p^+ constants are established for the most common groups, it should now be possible to predict the approximate position of the Cr atom relative to the relevant C_{ipso} positions. A combination of effects related to the electronegativity, the resonance and the inductive properties of a given substituent governs the overall geometry of the arene ligand. It appears that a strong resonance effect such as that produced by amino groups emphasizes, in a rather predictable way on the basis of Hammett's σ_p^+ constants, the electronic repulsion between the Cr-centered moiety and the *ipso* position. A strong substituent resonance effect concomitantly causes a decrease of the *ipso* endocyclic angle at C_{ipso} and an increase of the related d_{ipso} value thus conceding a significant folding of the arene ligand.

Conclusion

In this article we have established that the distortions of the arene ligand in (η^6-arene)$Cr(CO)_3$ complexes are influenced by the electronegativity, the inductive and the resonance effects of arene substituents. We have shown that endocyclic angular deviations at a carbon substituted by a given substituent was generally directed by the electronegativity of the latter in the absence of perturbing resonance effects. It was shown that mesomeric effects could partially obliterate electronegativity based effects. We have also demonstrated that the chromium-to-*ipso*-carbon distance is a specific constraint imposed to the molecular spacial arrangement by the electronic properties of an arene substituent. It was established that d_{ipso} correlates linearly with σ_p^+ Hammett constants, providing us with the confirmation of a relevant participation of electrons of the σ-framework in the metal-arene ring bonding interaction and with an understanding of the role of resonance effects in the overall structural distortions. Further investigations on the possible deduction of the value of Hammett constants for uncommon organic and organometallic substituents from the structural parameters of (η^6-arene)tricarbonyl chromium complexes are currently in progress.

Experimental Section

General Remarks: All reactions were carried out under a dry nitrogen atmosphere. The complexes were, in general, stable in the solid state, in air for long periods of time. Consequently, all experiments involving arenetricarbonylchromium complexes were protected from exposure to light and oxygen. Tetrahydrofuran (THF) and di-*n*-butyl ether (DBE) were dried over sodium benzoketyl under dry nitrogen and distilled just before use. Products were separated by flash chromatography on a silica gel column (15 or 60 μm) under a dry positive nitrogen pressure. Diethyl ether (Et_2O) and petroleum ether were used as solvents for elution. − ^1H and ^{13}C NMR spectra were acquired on a Bruker AC 200 (resonance frequencies: 200 MHz for ^1H and 50 MHz for ^{13}C) spectrometer and chemical shifts were reported in parts per million downfield of Me_4Si. ^1H NMR spectra were referenced against the residual ^1H impurity of the deuterated solvent and ^{13}C NMR spectra were referenced

against the ^{13}C resonance of the solvent. − Infrared spectra (reported in cm^{-1}) were performed on Perkin−Elmer 1420 and Bruker FT spectrometers. − Elemental analyses (reported in % mass) were performed by "Le Service de Microanalyses de l'Université P. et M. Curie". The crystallographic information files (CIF) provided by the CSDB were analyzed with ORTEP-3[31] version 1.03 and ORTEX-6b[32] software. The CSDB acronyms for some of the structures of monosubstituted arene complexes studied in this paper are the following: **6a**, ACTPCR; **6b**, BZCRCO12; **6c**, ANLCRA10; **6d**, ASPHCR; **6e**, CCRTOL; **6f**, CMSICR; **6g**, CRSLFN; **6h**, DEDHAV; **6i**, KOZROG; **6j**, KOZRUM; **6k**, LEPNEZ; **6l**, RAYJAC; **6m**, RIHPED; **6n**, POLTUF.

Preparation of (η^6-*N*,*N*-Dimethyl-3-trimethylsilylaniline)tricarbonylchromium, Complex 3:[4] A solution of *n*BuLi (1.6 M, 3.0 mL, 4.8 mmol) in hexane was added dropwise to a solution of 2,2,6,6-tetramethylpiperidine (678 mg, 0.81 mL, 4.8 mmol) in THF (10 mL) at −78 °C. The resulting medium was stirred for 10 min and a solution of **1** (1.0 g, 4 mmol) in THF (10 mL) was added. The resulting mixture was stirred for an additional 30 min at −78 °C and Me_3SiCl was added (1.3 g, 1.53 mL, 12.0 mmol) dropwise. The reaction medium was slowly warmed to room temperature and extracted with Et_2O. The organic phase was washed with water and brine, dried over $MgSO_4$, filtered through Celite and the solvents removed by vacuum distillation. The yellow residue was purified by flash chromatography over silica gel. The starting substrate was first eluted (petroleum ether 100%), followed by complex **2** (Et_2O/petroleum ether = 10:90) and complex **3** (Et_2O/petroleum ether = 20:80). Recrystallization in pentane afforded complexes **2** (200 mg, 0.61 mmol, 15% yield) and **3** (739 mg, 2.25 mmol, 57% yield).

Preparation of (η^6-*N*,*N*-Dimethyl-3-trifluoromethylaniline)tricarbonylchromium, Complex 4: *N*,*N*-Dimethyl-3-trifluoromethylaniline (9.45 g, 50.0 mmol), $Cr(CO)_6$ (11 g, 50.0 mmol), THF (15 mL), nBu_2O (150 mL), 6 days. Yield of **4**: 61% (10.0 g). − M.p. 116 °C. − MS (IE); *m*/*z*: 325 (M^+). − $C_{12}H_{10}F_3NCrO_3$ (325.2): calcd. C 44.32, H 3.10, N 4.31; found C 44.26, H 3.10, N 4.19. − IR (nujol): $\tilde{\nu}$ = 1950, 1865 (C=O) cm^{-1}. − ^1H NMR (C_6D_6): δ = 4.64 (t, ^3J = 7 Hz, 1 H, H-5), 4.43 (d, ^3J = 7 Hz, 1 H, H-4), 4.41 (d, ^4J = 1.5 Hz, 1 H, H-2), 3.75 (dd, ^3J = 7 Hz ^4J = 1.5 Hz, 1 H, H-6), 1.87 (s, 6 H, NMe_2). − ^{13}C NMR ($CDCl_3$): δ = 39.7 ($(CH_3)_2$−N), 68.8−73.8−79.4−94.4 (C-2, C-4, C-5, C-6), 101.5 (q, ^2J = 30 Hz, C-3), 130.0 (q, ^1J = 120 Hz, CF_3), 133.7 (C-1), 232.9 (CO).

(η^6-*N*,*N*-Dimethyl-2-methoxycarbonylaniline)tricarbonylchromium, Complex 5: $C_{13}H_{13}O_5NCr$ (315.2): calcd: C 49.62, H 4.13, N 4.44; found C 49.82, H 4.23, N 4.48. − IR (CCl_4): $\tilde{\nu}$ = 1997, 1938 (C=O), 1735 [C(O)OMe] cm^{-1}. − ^1H NMR ($CDCl_3$): δ = 2.83 (s, 6 H, NMe_2) 3.87 (s, 3 H, OCH_3) 4.84 (t, *J* = 6 Hz, 1 H, H-4) 4.97 (d, *J* = 6 Hz, 1 H, H-6), 5.67 (t, *J* = 6 Hz, 1 H, H-5), 6.04 (d, *J* = 6 Hz, 1 H, H-3). − ^{13}C NMR ($CDCl_3$): δ = 42.7 ($N(CH_3)_2$), 52.9 (OCH_3), 76.5, 82.6, 96.6, 98.4 (C_{3-6}), 82.4 (C_2), 136.7 (C_1), 165.5 (*C*(O)OMe), 238.8 (Cr−CO).

Structural Determination of Complexes 3, 4, 5. Intensity data were collected at room temperature on an Enraf−Nonius CAD4 diffractometer using Mo-K_α radiation. Accurate cell dimensions and orientation matrices were obtained from least-square refinements of the setting angles of 25 well-defined reflections. No decay in the intensities of two standard reflections was observed during the course of the data collections. Complete crystal data, collection parameters and other significant details are listed in Table 7.

The usual corrections for Lorentz and polarization effects were applied. Computations were performed by using CRYSTALS.[33] Scattering factors and corrections for anomalous dispersion were taken from the International Table for X-ray Crystallography.[34] The structures were resolved by direct methods (SHELXS 86[35]) and refined by least squares with anisotropic thermal parameters for all nonhydrogen atoms. For compound **4**, hydrogen atoms were located on a Fourier difference map and introduced as fixed contributors in the last refinements with an overall refinable isotropic thermal parameter. The structure was refined to $R = 0.031$ with the use of 1813 reflections for 22 least-squares parameters. For compound **3**, hydrogen atoms were introduced as fixed contributors in theoretical posi-

Table 7. Acquisition and data refinement parameters for compounds **3−5**

Compound	**3**	**4**	**5**
empirical formula	$C_{14}H_{19}CrNO_3Si$	$C_{12}H_{10}CrF_3NO_3$	$C_{13}H_{13}CrNO_5$
formula mass ($g \cdot mol^{-1}$)	329.4	325.2	315.2
crystal system	orthorhombic	monoclinic	monoclinic
space group	$P2_12_12_1$	$P2_1/c$	$P2_1/n$
a (Å)	7.640(4)	11.542(3)	11.720(2)
b (Å)	11.901(3)	7.097(3)	8.791(1)
c (Å)	17.736(3)	15.920(4)	14.271(2)
β (deg)		99.23(2)	110.36(1)
V (Å^3)	1612(1)	1287(4)	1378(6)
Z	4	4	4
F(000)	688	656	648
$d_{calcd.}$ ($g \cdot cm^{-3}$)	1.36	1.68	1.52
μ (Mo-K_α) (cm^{-1})	7.69	9.07	8.25
crystal size (mm)	0.14 × 0.14 × 0.80	0.06 × 0.16 × 0.70	0.22 × 0.43 × 0.50
diffractometer	CAD4	CAD4	CAD4
monochromator	graphite	graphite	graphite
radiation	Mo-K_α(0.71070 Å)	Mo-K_α(0.71070 Å)	Mo-K_α(0.71070 Å)
T (C)	20	20	20
scan type	ω/2θ	ω/2θ	ω/2θ
2θ range (deg)	2−50	3−40	3−50
no of reflns collected	1637	1194	2414
no of reflns observed	1107 ($I > 3\sigma(I)$)	908 ($I>3\sigma(I)$)	1813 ($I>3\sigma(I)$)
R	0.0361	0.0491	0.031
R_w [a]	0.0381	0.0520	0.032
absorption correction	min. 0.81, max. 1.09	min. 0.76, max. 1.38	min. 0.87, max. 1.10
no of parameters	183	182	222

[a] $R_w = [\Sigma_i W_i(F_o - F_c)^2/\Sigma_i W_i F_o^2]^{1/2}$

tions and their coordinates were recalculated after each refinement. The structure was refined to $R = 0.036$ with the use of 1107 reflections for 183 least square parameters. Crystallographic data (excluding structure factors) for the structures reported in this paper have been deposited with the Cambridge Crystallographic Data Centre as supplementary publications no. CCDC-135688 (**4**), -135689 (**3**), -135690 (**5**). Copies of the data can be obtained free of charge on application to The Director, CCDC, 12 Union Road, Cambridge CB2 1EZ, UK [Fax: (internat.) + (1223) 336−033; E-mail: deposit@ccdc.cam.ac.uk].

Acknowledgments

We thank the CNRS for supporting this work.

[1] [1a] M. F. Semmelhack, *Ann. N.Y. Acad. Sci.* **1977**, *295*, 36−51. − [1b] G. Jaouen, *Ann. N. Y. Acad. Sci.* **1977**, *295*, 59−78. − [1c] S. G. Davies, *Organotransition Metal Chemistry, Applications to Organic Syntheses,* Pergamon Press, Oxford, U.K., **1982**, p 166. − [1d] W. E. Watts, *Comprehensive Organometallic Chemistry Pergamon Press*, Oxford, U.K., **1982**, p 1013. − [1e] A. Solladié-Cavallo, *Polyhedron* **1985**, *4*, 901−927. − [1f] V. N. Kalinin, *Russ. Chem. Rev.* **1987**, *56*, 682−700. − [1g] M. F. Semmelhack, *Comprehensive Organic Synthesis* (Ed: B. M. Trost), Pergamon Press, Oxford, U.K., **1991**, Vol. 4, p 517. − [1h] F. J. McQuillin, D. G. N. Parker, R. G. Stephenson, *Transition Metal in Organic Synthesis*, Cambridge, U.K., **1991**. − [1i] M. J. Morris, *Comprehensive Organometallic Chemistry II* (Eds: E. W. Abel, F. G. A. Stone, G. Wilkinson), Pergamon, Oxford, UK, **1994**, Vol. 5, p 471. − [1j] S. G. Davies, T. D. McCarthy, *Comprehensive Organometallic Chemistry II* (Eds: E. W. Abel, F. G. A. Stone, G. Wilkinson), Pergamon, Oxford, UK, **1995**, Vol. 12, p 1039. − [1k] F. Rose-Munch, E. Rose, *Current Org. Chem.* **1999**, *3*, 445−467.

[2] [2a] E. L. Muetterties, J. R. Bleek, E. J. Wucherer, T. A. Albright, *Chem. Rev.* **1982**, *82*, 499−525. − [2b] T. A. Albright, P. Hofmann, R. Hoffmann, *J. Am. Chem. Soc.* **1977**, *99*, 7546−7557.

[3] [3a] A. D. Hunter, L. Shilliday, W. S. Furey, M. J. Zaworotko, *Organometallics* **1992**, *11*, 1550−1560. − [3b] A. D. Hunter, V. Mozol, S. D. Tsai, *Organometallics* **1992**, **11**, 2251−2262.

[4] J. P. Djukic, F. Rose-Munch, E. Rose, F. Simon, Y. Dromzee, *Organometallics* **1995**, *14*, 2027−2038.

[5] E. P. Kündig, C. Grivet, S. Spichiger, *J. Organomet. Chem.* **1987**, *332*, C13−C16.

[6] [6a] C. A. L. Mahaffy, *J. Organomet. Chem.* **1984**, *262*, 33−38. − [6b] C. A. L. Mahaffy, P. L. Pauson, *Inorg. Synth.* **1978**, *21*, 136−140.

[7] [7a] E. L. Eliel, S. H. Wilen, *Stereochemistry of Organic Compounds*, Wiley, New York, **1994**. − [7b] A. Collet, *Comprehensive Supramolecular Chemistry* (Eds: J. L. Atwood, J. E. D. Davies, D. D. MacNicol, F. Vögtle, J. M. Lehn, D. N. Reinhoudt), Pergamon-Elsevier Science, Oxford, U.K., **1996**, Vol. 10, pp 113−149.

[8] [8a] A. Domenicano, A. Vacagio, C. A. Coulson, *Acta Crystallogr., Sect. B* **1975**, *31*, 221−234. − [8b] A. Domenicano, A. Vacagio, C. A. Coulson, *Acta Crystallogr., Sect. B* **1975**, *31*, 1630−1641. − [8c] H. Bock, K. Ruppert, C. Näther, Z. Havlas, H.-F. Herrmann, C. Arad, I. Göbel, A. John, J. Meuret, S. Nick, A. Rauschenbach, W. Seitz, T. Vaupel, B. Soulouki, *Angew. Chem. Int. Ed. Engl.* **1992**, *31*, 550−581; *Angew. Chem.* **1992**, *104*, 564.

[9] [9a] R. Norrestam, L. Schepper, *Acta Chem. Scand. A* **1981**, *35*, 91−103. − [9b] R. Norrestam, L. Schepper, *Acta Chem. Scand. A* **1978**, *32*, 889−890. − [9c] T. Maetzke, D. Zeebach, *Helv. Chim. Acta* **1989**, *72*, 624−630.

[10] R. Meyer, M. Schindehutte, P. H. van Rooyen, S. Lotz, *Inorg. Chem.* **1994**, *33*, 3605−3608.

[11] [11a] E. W. Neuse, *J. Organomet. Chem.* **1975**, *99*, 287−295. − [11b] T. E. Bitterwolf, *Polyhedron* **1988** *7*, 1377−1382. − [11c] F. van Meurs, J. M. A. Baas, H. van Bekkum, *J. Organomet. Chem.* **1976**, *113*, 353−359.

[12] [12a] J. Y. Saillard, D. Grandjean, F. Chopplin, G. Kaufmann, *J. Mol. Struct.* **1974**, *23*, 363−375. − [12b] M. F. Guest, I. H. Hillier, B. R. Higginson, D. R. Lloyd, *Mol. Phys.* **1975**, *29*, 113−128.

[13] D. G. Carroll, S. P. McGlynn, *Inorg. Chem.* **1968**, *7*, 1285−1290.

[14] L. Phillips, C. M. Barnes, M. J. Aroney, *J. Organomet. Chem.* **1997**, *539*, 121−125.

[15] [15a] **6a**: Y. Dusausoy, J. Protas, J. Besançon, J. Tirouflet, *C. R. Acad. Sci., Ser. C* **1970**, *270*, 1792−1794. − [15b] **6b**: B. Rees, P. Coppens, *Acta Crystallogr., Sect B* **1973**, *29*, 2515−2528. − [15c] **6c**: P. Le Maux, J. Y. Saillard, D. Grandjean, G. Jaouen, *J. Org. Chem.* **1980**, *45*, 4524−4526; J.Y. Saillard, D. Grandjean, P. Le Maux, J. Jaouen, *New. J. Chem.* **1981**, *5*, 153−160. − [15d] **6d**: H. J. Wasserman, M. J. Wovkulich, J. D. Atwood, M. R. Churchill, *Inorg. Chem.* **1980**, *19*, 2831−2834. − [15e] **6e**: F. van Meurs, H. van Konigsveld, *J. Organomet. Chem.* **1977**, *131*, 423−428. − [15f] **6f**: D. van der Helm, R. A. Loghry, D. J. Hanlon, A. P. Hagen, *Cryst. Struct. Commun.* **1979**, *8*, 899. − [15g] **6g**: A. Ceccon, G. Giacometti, A. Venzo, G. Zanotti, *J. Organomet. Chem.* **1981**, *205*, 61−69. − [15h] **6h**: Y. Xiaoguang, H. Jinshun, H. Jinling, *J. Struct. Chem.* **1985**, *4*, 52. − [15i] **6k**: C. F. Marcos, S. Perrio, A. M. Z. Slawin, S. E. T. Thomas, D. J. Williams, *J. Chem. Soc., Chem. Commun.* **1994**, 753−754. − [15j] **6l**: T. J. J. Muller, M. Ansorge, H. J. Lindner, *Chem. Ber.* **1996**, *29*, 1433−1440. − [15k] **6m**: W. R. Cullen, S. J. Rettig, H. Zhang, *Can. J. Chem.* **1996**, *74*, 2167−2181. − [15l] **6n**: M. M. Kubicki, P. Richard, B. Gautheron, M. Viotte, S. Toma, M. Hudecek, V. Gajda, *J. Organomet. Chem.* **1994**, *476*, 55−62. − [15m] **6o**: J. Y. Saillard, D. Grandjean, *Acta Crystallogr, Sect. B* **1976**, *32*, 2285−2289. − [15n] **6p−q**: T. M. Gilbert, C. B. Bauer, R. D. Rogers, *J. Chem. Crystallogr* **1996**, *26*, 355.

[16] N. Inamoto, S. Masuda, *Chem. Lett.* **1982**, 1003−1006.

[17] L. Komorowski, S. L. Boyd, R. J. Boyd, *J. Phys. Chem.* **1996**, *100*, 3448−3453.

[18] **7a−h**: T. M. Gilbert, A. H. Bond, R. D. Rogers, *J. Organomet. Chem.* **1994**, *479*, 73−86.

[19] **7j**: F. Rose-Munch, R. Khourzom, J. P. Djukic, E. Rose, B. Langlois, J. Vaisserman, *J. Organomet. Chem.* **1994**, *470*, 131−135.

[20] **7i**: B. R. Jagirdar, K. J. Klabunde, R. Palmer, L. J. Radanovich, T. Williams, *Inorg. Chim. Acta* **1996**, *250*, 317−326.

[21] A. L. Allred, *J. Inorg. Nucl. Chem.* **1961**, *17*, 215−221.

[22] F. Dijkstra, J. H. van Lenthe, *Int. J. Quant. Chem.* **1999**, *74*, 213−221.

[23] C. Hansch, A. Leo, R. W. Taft, *Chem. Rev.* **1991**, *91*, 165−195.

[24] C. Hansch, A. Leo, S. H. Hunger, K. H. Kim, D. Nikaitani, E. Lien, *J. Med. Chem.* **1973**, *16*, 1207−1216.

[25] H. C. Brown, Y. Okamoto, *J. Am. Chem. Soc.* **1958**, *80*, 4979−4987.

[26] F. Kinomura, T. Tamura, I. Watanabe, Y. Yokoyama, S. Ikeda, *Bull. Chem. Soc. Jpn.* **1976**, *49*, 3544−3547.

[27] **7n**: F. van Meurs, H. van Konigsveld, *J. Organomet. Chem.* **1974**, *78*, 229−235.

[28] **8a−c**: Y. Dusausoy, J. Protas, J. Besançon, J. Tirouflet, *Acta Crystallogr., Sect. B.* **1973**, *29*, 469−476.

[29] **8c**: O. L. Carter, A. T. Mc Phail, G. A. Sim., *J. Chem. Soc. A.* **1967**, 228−236.

[30] H. Lumbroso, C. Segard, B. Roques, *J. Organomet. Chem.* **1973**, *61*, 249−260.

[31] L. Farrugia, *ORTEP-3 for Windows*, *Version 1.03*, Department of Chemistry, University of Glasgow, U.K.

[32] P. McArdle, *ORTEX for Windows*, *Version 6*, UCG Crystallography Centre, Chemistry Department, University College Galway, Ireland.

[33] D. J. Watkin, J. R. Carruthers, P. W. Betteridge, *Crystals User Guide*, *Chemical Crystallography Laboratory*, University of Oxford, U.K, **1988**.

[34] *International Table for X-ray Crystallography*, Vol. IV, Kynoch Press, Birmingham, U.K., **1974**.

[35] G. M. Sheldrick, *SHELXS-86*, *Program for Crystal Structure Solution*, University of Göttingen, Germany, **1986**.

Received October 19, 1999
[I99368]

Reactions of $RSe–EMe_3$ (E = Si, Ge, Sn, Pb) with XeF_2 – RSe–F Equivalents in the Fluoroselenenylation of Acetylenes[1]

Helmut Poleschner,*[a] Matthias Heydenreich,[b] and Uwe Schilde[c]

Dedicated to Professor Egon Fanghänel on the occasion of his 65th birthday

Keywords: Xenon / Fluorine / Selenides / Acetylenes / Silicon / Germanium / Tin / Lead

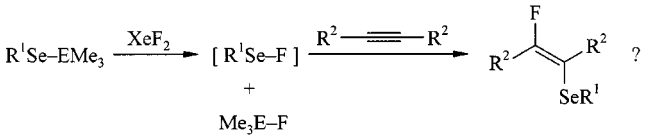
Selenides of the type $R^1Se–EMe_3$ (E = Si, Ge, Sn, Pb) react with xenon difluoride by cleavage of the Se–E bond to yield the $R^1Se–F$ intermediate and the fluorides $Me_3E–F$, whereas the Se–C bond in PhSe–*t*Bu (E = C) is stable against XeF_2. The presence of $R^1Se–F$ intermediates is confirmed by addition to acetylenes (4-octyne, 3-hexyne). Thus, the fluoroselenenylation of acetylenes gives fluoro(organylseleno)olefins in preparative yields. In the cases of E = Si, Ge, Sn, and Pb, aryl and *n*-alkyl groups are suitable as the substituent R^1. The X-ray crystal structural analysis of (*E*)-3-(*p*-carboxyphenylseleno)-4-fluorohex-3-ene – the first example of an uncharged fluoroselenoolefin synthesized from *p*-$EtO_2C–C_6H_4–Se–SnMe_3$, XeF_2, and 3-hexyne followed by an ester hydrolysis – shows that the addition of the selenenylfluoride intermediate to the acetylene proceeds via a *trans*-addition, as is known for the $R_2Se_2–XeF_2$ reagents.

Introduction

Selenium reagents are good tools for the introduction of fluorine into organic substrates. Known methods for the addition of PhSe–F equivalents to olefins and acetylenes are PhSeBr–AgF–ultra sound,[2,3] PhSeCl–AgF–MeCN,[4] *N*-phenylselenophthalimide (NPSP)–Py·9HF,[5,6] and $NPSPEt_3N·3HF$.[7] The PhSe–F intermediate was obtained exceptionally elegantly by reaction of Ph_2Se_2 with XeF_2 in a molar ratio of 1:1[8] and used in the fluoroselenenylation of olefins[8–10] and bis-selenenylation of phosphaacetylenes.[11] $PhSeF_3$ (Ph_2Se_2+3 XeF_2) reacts either by addition of $PhSeF_2/F$[9,12,13] or as the F_2 equivalent, depending on the olefin concerned,[13,14] and $PhSeF_5$ (Ph_2Se_2 + 5XeF_2) (and $PhTeF_5$) react with olefins as the F_2 equivalent.[15]

In earlier papers we reported a highly efficient synthesis of vicinal fluoro(organylseleno)olefins by fluoroselenenylation of acetylenes with $R_2Se_2–XeF_2$ reagents.[16,17] This method was shown to be useful in a very broad range concerning the acetylenes (symmetrical and unsymmetrical dialkylacetylenes, arylalkylacetylenes, terminal acetylenes, and cycloalkynes) and the applied diselenides (diaryl-, primary and secondary dialkyldiselenides, functionalized diselenides). The fluoroselenoolefins were characterized by X-ray crystal structural analysis in the form of a fluorovinyldimethylselenonium picrate as (*E*)-isomers,[17,18] and investigated in detail by ^{13}C, ^{19}F, and ^{77}Se NMR spectroscopy.[19]

Preliminary experiments showed that silyl selenides of the type $PhSe–SiR_3$ ($PhSe–SiMe_3$ and PhSe–Si*t*BuMe_2) react with XeF_2 by cleavage of the Se–Si bond to yield the PhSe–F intermediate which is added to acetylenes.[16] The high affinity of the fluorine for the silicon is the driving force responsible for the Se–Si bond breaking. However, nothing is known about the reactivity of the selenides $RSe–EMe_3$ of the higher group 14 elements, i.e., the corresponding germanium, tin, and lead selenides, with XeF_2. Therefore, the question was which of the trimethylelementorganyl selenides $R^1Se–EMe_3$ (E = C, Si, Ge, Sn, Pb) would react with XeF_2 to give the $R^1Se–F$ intermediate and $Me_3E–F$ by cleavage of the Se–E bond. Thus, the aim of the present paper is to report on our investigations of the reactions of the selenides $R^1Se–EMe_3$ (E = C, Si, Ge, Sn, Pb) with XeF_2. Aryl and *n*-alkyl groups were used as the substituents R^1. In order to prove their formation, the $R^1Se–F$ moieties were trapped with simple reactive dialkylacetylenes (3-hexyne, 4-octyne) as model compounds to give fluoro(organylseleno)olefins (Scheme 1).



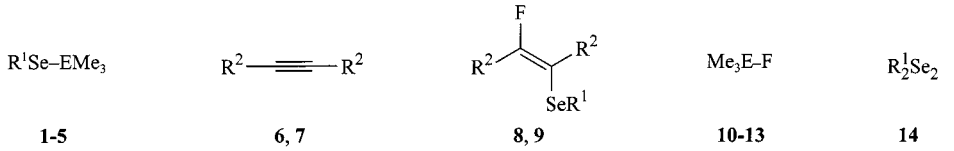
Scheme 1. Topic of the investigation

[a] Institut für Chemie, Anorganische und Analytische Chemie, Freie Universität Berlin,
Fabeckstrasse 34–36, D-14195 Berlin, Germany
Fax: (internat.) + 49(0)-30/83852424
E-mail: hpol@chemie.fu-berlin.de
[b] Institut für Organische Chemie und Strukturanalytik, Universität Potsdam,
Am Neuen Palais 10, D-14469 Potsdam, Germany
E-mail: heydenr@serv.chem.uni-potsdam.de
[c] Institut für Anorganische Chemie und Didaktik der Chemie, Universität Potsdam,
Am Neuen Palais 10, D-14469 Potsdam, Germany
Fax: (internat.) + 49(0)-331/9771473
E-mail: us@conrad.chem.uni-potsdam.de

 © WILEY-VCH Verlag GmbH, D-69451 Weinheim, 2000 1434–1948/00/0606–1307 $ 17.50+.50/0

Results and Discussion

The compounds investigated are shown below:



1-5 **6, 7** **8, 9** **10-13** **14**

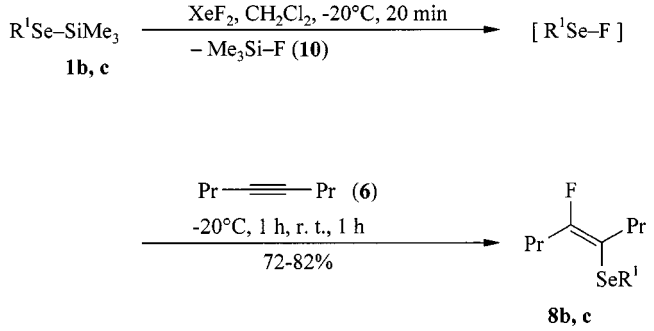
	1, 10	2, 11	3, 12	4, 13	5
E	Si	Ge	Sn	Pb	C

	6, 8	7, 9
R^2	*n*Pr	Et

	a	b	c	d	e
R^1	Me	Et	Ph	*p*-C_6H_4-CO_2Et	*p*-C_6H_4-CO_2H

Si Selenides

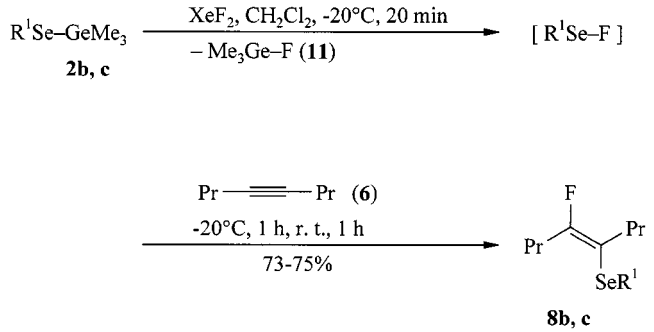
Ethylselenotrimethylsilane (**1b**) and phenylselenotrimethylsilane (**1c**) react in CH_2Cl_2 at –20 °C with one equivalent of XeF_2 to give the trimethylfluorosilane (**10**) and the $R^1Se–F$ intermediate by cleavage of the Se–Si bond. 4-Octyne (**6**) was added to the selenenyl fluoride intermediates to give the fluoroselenoolefins **8b,c** in good yields (72–82%) (Scheme 2). $Me_3Si–F$ (**10**) was identified after reaction of **1b** with XeF_2 and **6** in $CDCl_3$ by ^{19}F NMR spectroscopy. Thus, the reaction of the $R^1Se–SiMe_3$ **1** with XeF_2 takes place analogous to the synthesis of the trialkylsilyl halides $R_3Si–X$ (X = Cl, Br, I) from $PhSe–SiR_3$ and the halogens.[20]



Scheme 2. Reactions of the Si selenides

Ge Selenides

Ethylselenotrimethylgermane (**2b**) and phenylselenotrimethylgermane (**2c**) react in CH_2Cl_2 at –20 °C with XeF_2 in a molar ratio of 1:1; the intermediates are trapped with **6**.



Scheme 3. Reactions of the Ge selenides

The resulting fluoroselenoolefins **8b** and **8c** (73–75% yield) showed the cleavage of the Se–Ge bond caused by the fluorinating agent. After the reaction of **8c** with XeF_2 and **6** in $CDCl_3$, $Me_3Ge–F$ (**11**) was observed by ^{19}F NMR spectroscopy (Scheme 3).

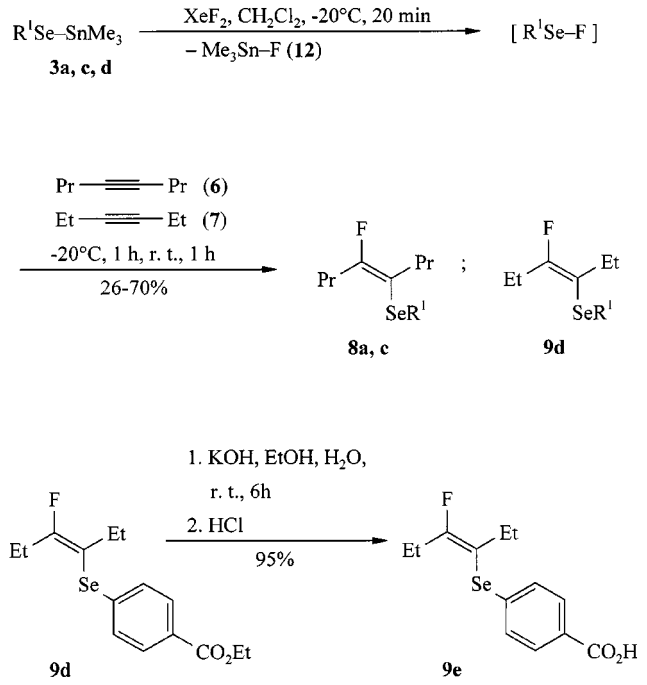
Sn Selenides

Methylselenotrimethylstannane (**3b**) and phenylselenotrimethylstannane (**3c**) react in CH_2Cl_2 at –20 °C with one equivalent XeF_2 to give trimethyltin fluoride (**12**), which precipitates immediately. The corresponding fluoroselenoolefins **8a** and **8c** (66–70% yield) were obtained after addition of **6** to this suspension (Scheme 4). The reaction of *p*-(ethoxycarbonyl)-phenylselenotrimethylstannane (**3d**) with XeF_2 and 3-hexyne (**7**) led to the formation of trimethyltin fluoride (**12**) and the adduct **9d**. Its yield was with 26%, as in the case of the corresponding *p*-CO_2Et-substituted diphenyldiselenide,[17] much smaller than with non-functionalized PhSe precursors.[16,17] $Me_3Sn–F$, which was isolated in almost quantitative yields, was confirmed by mass spectrometry and by ^{119}Sn Mößbauer spectroscopy. The resulting spectra were in good agreement with the literature.[21] The elementary composition of the ions $[M^+]$, $[M^+ – Me]$ and $[M^+ – F]$ was confirmed by high-resolution mass spectrometry. The cleavage of the Se–Sn bond by fluorination of the tin selenides **3** with XeF_2 corresponds to the reaction of $R'Se–SnR_3$ with iodine to give $R_3Sn–I$ and R'_2Se_2.[22]

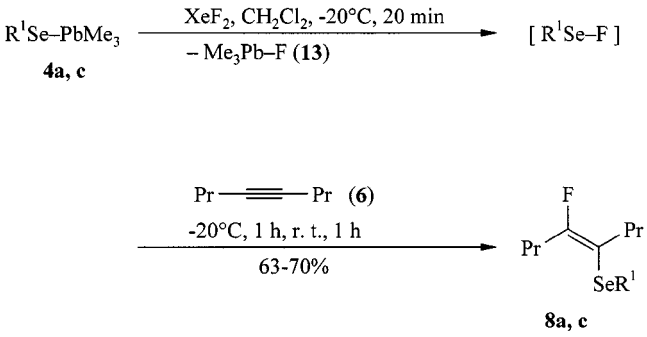
The carboxylic acid **9e** was synthesized by saponification of the carboxylic acid ester **9d**. Suitable crystals for the X-ray structural analysis could be obtained from *n*-hexane (Scheme 4).

Pb Selenides

Analogous to the tin compounds **3**, precipitation of trimethyllead fluoride (**13**) occurred during the reaction of methylselenotrimethylplumbane (**4a**) or phenylselenotrimethylplumbane (**4c**) with one equivalent XeF_2 at –20 °C in CH_2Cl_2. Subsequent reaction of the selenenyl fluoride intermediates with **6** resulted in the fluoroselenoolefins **8a** and **8c** (63–70%) (Scheme 5). $Me_3Pb–F$ (71–83%) was characterized by mass spectrometry after isolation. The elementary composition of the ions $[M^+ – Me]$ and $[M^+ – F]$ was confirmed by high-resolution mass spectrometry.



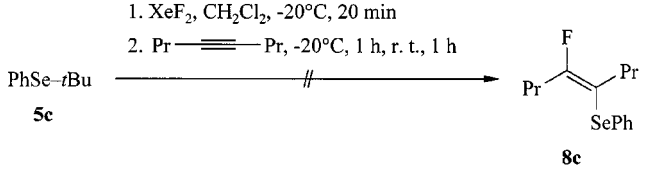
Scheme 4. Reactions of the Sn selenides



Scheme 5. Reactions of the Pb selenides

C Selenides

The reaction of *tert*-butylphenylselenide (**5c**) with XeF_2, under the conditions described above, differs from that of compounds **1-4.** The PhSe–F intermediate was not obtained and the adduct **8c** could not be obtained after treatment with **6** (Scheme 6). Cleavage of the Se–C bond by XeF_2 was not observed. This is also reported for the compound PhSe–CN.[16] However, a possible fluorination of the selenide **5c** to *t*BuPhSeF_2, in analogy to Me_2SeF_2,[23] was not investigated.



Scheme 6. Experiment with a C selenide

The mass spectra of the synthesized fluoroselenoolefins **8a–c** and **9d,e** showed the correct molecular peak with the expected isotope pattern for one Se atom. The high resolution of these peaks proved the elemental composition of these compounds. The ^{13}C NMR spectra of **8a–c** and **9d,e** agreed well with the spectra of the products obtained from the R'_2Se_2–XeF_2 reagents.[16,17] A detailed assignment and discussion of the spectra of these compounds is given in ref.[19]

X-ray Crystal Structure Analysis of 9e

Although the structure of the selenonium ion Pr(F)C=CPr(Se^+Me_2) has previously been reported,[17,18] this is the first structure of a noncharged vicinal fluoroselenoolefin. Details of the structure solution and refinement are given in the experimental section (Table 4). As can be seen from Figure 1, this compound possesses an (*E*)-configuration [torsional angles: Se–C3–C4–F –170.1(4)°; C2–C3–C4–F 3.0(9)°]. This is the most important structural information regarding the reaction course: *trans*-addition of the R^1Se–F intermediate (R^1Se–$SnMe_3$ + XeF_2) to an acetylene.

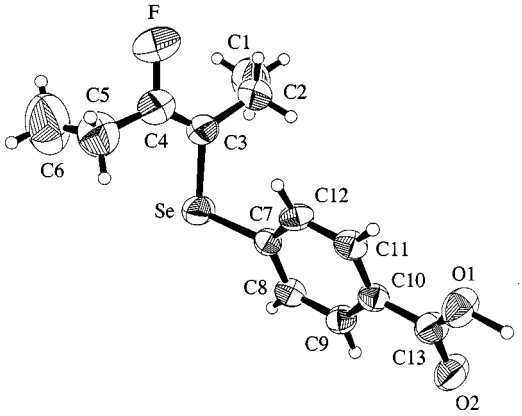
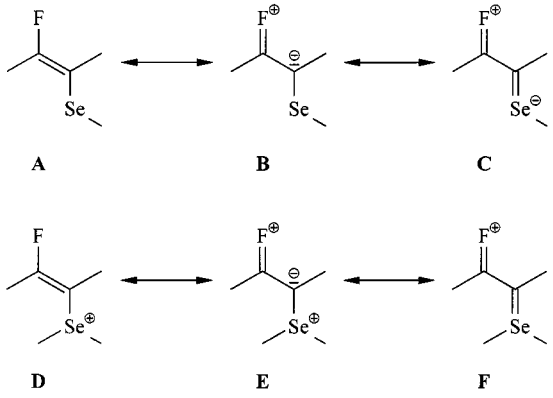


Figure 1. ORTEP plot (thermal ellipsoids 40%) of the molecular structure of the carboxylic acid **9e**; selected bond lengths [Å] and angles [°]: C1–C2 1.472(10), C2–C3 1.507(8), C3–C4 1.285(8), C4–C5 1.498(10), C5–C6 1.353(11), F–C4 1.385(7), Se–C3 1.914(5), Se–C7 1.906(4), C7–C12 1.384(6), C7–C8 1.391(6), C8–C9 1.374(7), C9–C10 1.380(6), C10–C11 1.389(6), C11–C12 1.384(6), C10–C13 1.466(6), C13–O2 1.247(6), C13–O1 1.280(5), O1–H1 1.18(5); C3–C4–F 115.6(6), C3–C4–C5 132.9(6), C4–C3–Se 117.4(5), C4–C3–C2 123.9(5), C7–Se–C3 100.3(2), Se–C3–C4–F –170.1(4), C2–C3–C4–F 3.0(9), C7–Se–C3–C2 64.4(4), C12–C7–Se–C3 23.5(4), C1–C2–C3–C4 –98.1(8), C3–C4–C5–C6 –107.8(12).

Compared with the above-mentioned selenonium ion [C–F 1.368(3) Å, C–Se 1.927(2) Å, C=C 1.328(3) Å] **9e** has a longer C–F and a shorter C–Se bond (Se–C3). The considerably shortened C=C distance in **9e** is especially noticeable. This corresponds well with the longer C–F bond and, thus, with a stronger participation of the mesomeric structure **A** against **B** and **C** in the electronic structure of the fluoroselenoolefins than of the mesomeric structure **D** against **E** and **F** in the selenonium ion. The C3–C4–C5 bond angle in **9e** is made considerably larger by the fluoro-substitution as it was found also in other fluoroolefins and the selenonium ion [133.8(2)°].[18] Both of the ethyl substituents on the C=C moiety are situated behind the π-bond plane with torsional angles of –98.1(8)° (C1–C2–C3–C4) and –107.8(12)° (C3–C4–C5–C6), respectively. The Ar–Se substituent is situated in front of the C=C plane with a torsional angle of 64.4(4)° (C7–Se–C3–C2); the Ar group is

twisted towards the C=C double bond with a torsional angle of 23.5(4)° (C12–C7–Se–C3). Obviously, in this conformation, the steric interaction between the H atoms on C2 and in the *o*-position of the aryl group is small. Two molecules are linked by two hydrogen bonds between O1 and O2 via H1 forming pairs [O1···O2 2.640(4) Å, H1···O2 1.489(11) Å, O1–H1···O2 164.55(4)°; symmetry operator 1 – *x*, 1 – *y*, –*z*].



Conclusions

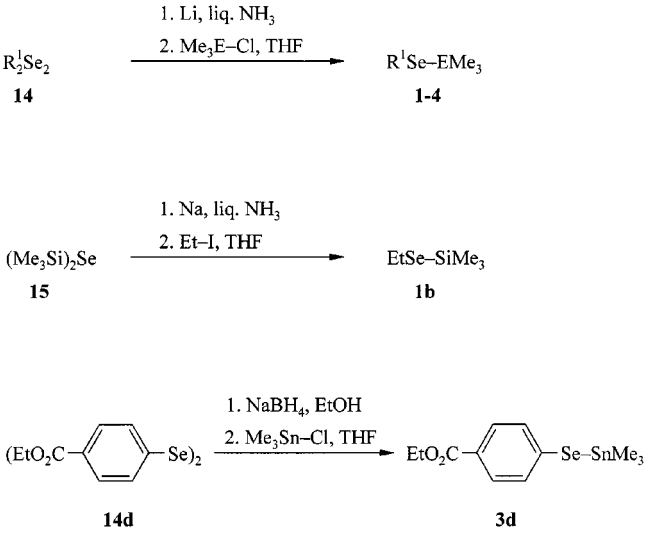
XeF_2 is able to cleave the Se–Si, Se–Ge, Se–Sn or Se–Pb bond of the selenides $R^1Se–EMe_3$ with E = Si, Ge, Sn or Pb, respectively, to give $R^1Se–F$ intermediates and $Me_3E–F$ fluorides. By contrast, the Se–C bond in PhSe–*t*Bu is not broken by XeF_2. The formation of $R^1Se–F$ intermediates is confirmed by their addition to acetylenes. The yields of the obtained fluoro(organylseleno)olefins are in the same range as in the case of $XeF_2–R^1_2Se_2$ reagents.[16,17] In this reaction the substituents R^1 can be *n*-alkyl or aryl. The reaction proceeds as a *trans*-addition of the $R^1Se–F$ intermediates to acetylenes, as is the case for $R^1_2Se_2–XeF_2$ reagents.[17,18] Comparable yields of fluoro(organylseleno)olefins from $R^1Se–EMe_3–XeF_2$ and $R^1_2Se_2–XeF_2$, and the corresponding stereochemistry of additions for the two reactions, indicate that the same reaction course is taking place in both cases.

Of further interest is whether there are other groups besides the Me_3Si and *t*BuMe_2Si moieties, for example, OH-protecting groups[24–27] such as Me_2PhSi, *i*Pr_3Si and *t*BuPh_2Si, that permit cleavage of $R^1Se–SiR_3$ by XeF_2. A further question is a possible bond cleavage by XeF_2 of other selenides of elements with a strong affinity to fluorine, e.g. compounds with Se–B, Se–Al, and Se–P bonds.

Syntheses of the Selenides $R^1Se–EMe_3$ 1–4

Different methods are known to synthesize selenides of the type $R^1Se–EMe_3$ (E = Si: PhLi/Se/Me_3SiCl,[28] Ph_2Se_2/Na(THF)/Me_3SiCl,[29,20c] Ph_2Se_2/Na(THF)/R_3SiCl(18-crown-6),[24] PhSeH/BuLi/Me_3SiCl,[20c] PhSeH/Me_3SiH/Rh-cat.[20c] and PhMgBr(Et_2O)/Se/Me_3SiCl resp. ($Me_3Si)_2Se$/Na(liq. NH_3)/RX;[30] E = Ge: $PhSeSiMe_3$/Me_3GeF[28] and Ph_2Se_2/Na(THF)/Me_3GeCl;[31] E = Sn: PhSeH/Me_3SnCl/NaOH(H_2O),[32] RSeH/Me_3SnCl/Et_3N,[33,22] Li[Al($SeMe)_4$]/Me_3SnCl,[34] Me_6Sn_2/BuLi/Se/RX (R = alkyl);[35] E = Pb. Only two patents are known: RMgBr(Et_2O)/Se/Me_3PbCl (R = Me, Ph).[36]

In this work, we report a uniform synthesis of the compounds **1–4** using the same selenium starting materials. The diselenides $R^1_2Se_2$ (**14**) were found to be most suitable, because of the possibility of their quantitative reduction to their corresponding lithium selenolates R^1SeLi in liquid ammonia with lithium. This way is superior to the reduction in the heterogeneous system Na/THF. Further reaction with the chlorides $Me_3E–Cl$ to the compounds **1–4** was carried out in THF after complete removal of the ammonia. The reaction course using the bis(trimethylsilyl)selenide (**15**) was chosen for the synthesis of ethylselenotrimethylsilane **1b** only. The reduction of the functionalized diselenide **14d** was carried out with $NaBH_4$ and subsequent stannylation in EtOH (Scheme 7).



Scheme 7. Syntheses of the selenides **1**−**4**

For $R^1Se–EMe_3$ derivatives, NMR spectroscopic data are known for only a few Ge[31a,37] and Sn compounds.[33,38] For this reason, ^{13}C and ^{77}Se NMR data of the compounds **1b**,**c**, **2b**,**c**, **3a**,**c**,**d**, **4a**,**c** and **15** are given in Table 1.

Experimental Section

The diselenides **14a**,**b**,[39] **14d**,[17] the selenides **5c**[40] and **15**[30,41] and XeF_2[42] were prepared by literature methods. **14c**, the acetylenes **6** and **7** and the chlorides $Me_3E–Cl$ (E = Si, Ge, Sn, Pb) are commercially available. – Mass spectra were recorded with Finnigan–MAT 95 and Finnigan–MAT 711 at 70 eV and 80 eV, respectively. The measurements of high-resolution spectra were carried out by the peak-match method using PFK as a reference substance. – NMR spectra were measured with a Bruker ARX 300 spectrometer in $CDCl_3$ in 5 mm sample tubes at room temperature: ^{13}C at 75.47 MHz (^{13}C reference $CDCl_3$: δ = 77), ^{19}F at 282.40 MHz (^{19}F reference $CFCl_3$: δ = 0), and ^{77}Se at 57.25 MHz (^{77}Se reference Me_2Se: δ = 0).

Reactions of $R^1Se–EMe_3$ (1–4) with XeF_2/Acetylene. – General Procedure: XeF_2 (4.1 mmol, 694 mg) was added in small portions un-

Table 1. ^{13}C and ^{77}Se NMR chemical shifts (δ) and related coupling constants (Hz) of compounds **1–4** and **15**

Compound		^{13}C Pos. 1	2	3	4	EMe_3 ($^1J_{E,C}$)	^{77}Se ($^1J_{Se,E}$)
15	$(Me_3Si)_2Se$					4.5 (52.7)	–332.4 (107.0)
1b	$EtSe–SiMe_3$	12.2 ($^1J_{Se,C}$ = 51.0)	18.6			1.7 (52.3)	–64.9 (107.3)
1c	$PhSe–SiMe_3$	125.1	136.5	128.7	126.8	1.4	85.8 (103.3)
2b	$EtSe–GeMe_3$	12.1 ($^1J_{Se,C}$ = 54.3)	18.9			2.1	–44.6
2c	$PhSe–GeMe_3$	126.1	136.4	128.7	126.7	2.2	97.3
3a	$MeSe–SnMe_3$	–4.0				–6.1 [316.6 (^{119}Sn), 288.7 (^{117}Sn)]	–287.6 [1002.2 (^{119}Sn), 957.8 (^{117}Sn)]
3c	$PhSe–SnMe_3$	126.0	136.2	128.6	126.2	–5.0 [339.2 (^{119}Sn), 324.2 (^{117}Sn)]	8.1 [969.8 (^{119}Sn), 926.5 (^{117}Sn)]
3d	p-$EtO_2C–C_6H_4Se–SnMe_3$[a]	133.8	136.0	129.4	128.3	–4.8 [341.2 (^{119}Sn), 326.0 (^{117}Sn)]	
4a	$MeSe–PbMe_3$	–3.1 ($^2J_{Pb,C}$ = 19.4)				4.7 (239.4)	–210.2 (1169.8)
4c	$PhSe–PbMe_3$	131.4	136.5	128.4	126.0	7.1 (232.3)	73.5 (1114.1)

[a] 166.2, 60.7, 14.2 (CO_2Et).

der argon to a solution of 4 mmol selenide **1–4** in 20 mL of dry CH_2Cl_2 at –20 °C and stirred for 30 min. The acetylene **6** or **7** (4 mmol) was then added and stirred for 1 h at –20 °C and for 1 h at room temperature. In the cases of **3** and **4** the precipitate $Me_3Sn–F$ (**10**) and $Me_3Pb–F$ (**11**), respectively, was separated and washed with *n*-pentane (2 × 10 mL) and the solvent was then removed under vacuum. The crude product was purified by column chromatography (10 cm silica gel, diameter 2 cm, *n*-hexane). For yields see Table 2.

Table 2. Reactions of the selenides **1–4** with XeF_2 and acetylenes **6**, **7** to the products **8**, **9**, **12** and **13**

Starting material	Products	Yields
1b, XeF_2, **6**	**8b**	0.68 g (72%)
1c, XeF_2, **6**	**8c**	0.94 g (82%)[16]
2b, XeF_2, **6**	**8b**	0.69 g (73%)
2c, XeF_2, **6**	**8c**	0.86 g (75%)
3a, XeF_2, **6**	**8a**, **12**	0.63 g (71%), 0.66 g (90%)
3c, XeF_2, **6**	**8c**, **12**	0.75 g (66%), 0.70 g (96%)
3d, XeF_2, **7**	**9d**, **12**	0.34 g (26%), 0.72 g (98%)
4a, XeF_2, **6**	**8a**, **13**	0.56 g (63%), 0.90 g (83%)
4c, XeF_2, **6**	**8c**, **13**	0.79 g (69%), 0.77 g (71%)

(*E*)-4-Fluoro-5-methylselenooct-4-ene (8a): HR-MS ($C_9H_{17}F^{80}Se$): calcd. 224.04794; found 222.04771. – ^{13}C NMR ($CDCl_3$): δ = 6.2 ($SeCH_3$), 13.3 (C-8), 13.4 (C-1), 20.2 (C-2), 21.6 (C-7), 31.6 ($^3J_{F–C}$ = 6.6 Hz, C-6), 33.0 ($^2J_{F–C}$ = 28.7 Hz, C-3), 109.2 ($^2J_{F–C}$ = 19.1 Hz, C-5), 160.5 ($^1J_{F–C}$ = 263.7 Hz, C-4).

(*E*)-4-Ethylseleno-5-fluorooct-4-ene (8b): HR-MS ($C_{10}H_{19}F^{80}Se$): calcd. 238.06359; found 238.06333. – ^{13}C NMR ($CDCl_3$): δ = 13.3 (C-1), 13.4 (C-8), 15.5 ($SeCH_2CH_3$), 19.1 ($SeCH_2CH_3$), 20.3 (C-7), 21.6 (C-2), 32.0 ($^3J_{F–C}$ = 6.7 Hz, C-3), 33.0 ($^2J_{F–C}$ = 28.8 Hz, C-6), 108.0 ($^2J_{F–C}$ = 18.8 Hz, C-4), 161.4 ($^1J_{F–C}$ = 264.3 Hz, C-5).

(*E*)-4-Fluoro-5-phenylselenooct-4-ene (8c): HR-MS ($C_{14}H_{19}F^{80}Se$): calcd. 286.06359; found 286.06381. – ^{13}C NMR ($CDCl_3$): δ = 13.4 (C-8), 13.5 (C-1), 20.3 (C-2), 21.7 (C-7), 32.4 ($^3J_{F–C}$ = 5.9 Hz, C-6), 33.2 ($^2J_{F–C}$ = 28.2 Hz, C-3), 109.7 ($^2J_{F–C}$ = 20.9 Hz, C-5), 126.3 (*p*-C), 129.1 (*m*-C), 130.3 (*o*-C), 130.8 (*i*-C), 163.3 ($^1J_{F–C}$ = 267.3 Hz, C-4).

(*E*)-3-[(*p*-Ethoxycarbonyl)phenylseleno]-4-fluorohex-3-ene (9d): HR-MS ($C_{15}H_{19}FO_2{}^{80}Se$): calcd. 330.05342; found 330.05235. – ^{13}C NMR ($CDCl_3$): δ = 11.4 (C-6), 13.4 (C-1), 14.2 (OCH_2CH_3), 24.5 ($^3J_{F–C}$ = 6.9 Hz, C-2), 25.0 ($^2J_{F–C}$ = 28.8 Hz, C-5), 60.8 (OCH_2CH_3), 109.4 ($^2J_{F–C}$ = 21.6 Hz, C-3), 128.1 (*p*-C), 128.6 (*o*-C), 130.0 (*m*-C), 138.5 (*i*-C, C–Se), 165.4 ($^1J_{F,C}$ = 269.2 Hz, C-4), 166.2 (CO_2Et).

Characterization of $Me_3E–F$ (10–13): $EtSe–SiMe_3$ (**1b**; 1 mmol, 181 mg) and $PhSe–GeMe_3$ (**2c**; 1 mmol, 274 mg) and XeF_2 (1 mmol, 169 mg) reacted with 4-octyne (**6**; 1 mmol, 110 mg) in 2 mL $CDCl_3$ as already described.

$Me_3Si–F$ (10): ^{19}F NMR ($CDCl_3$): δ = –158.2 (–159.3 ppm[43]).

$Me_3Ge–F$ (11): ^{19}F NMR ($CDCl_3$): δ = –192.1 (–190.5 ppm[44]).

$Me_3Sn–F$ (12): MS: *m*/*z* = 184 [M^+], 169 [M^+ – Me], 165 [M^+ – F]. – HR-MS ($C_3H_9F^{120}Sn$): calcd. 183.97103; found 183.97531. ($C_2H_6F^{120}Sn$) [M^+ – Me]: calcd. 168.94755; found 168.94523. ($C_3H_9{}^{120}Sn$) [M^+ – F]: calcd. 164.97262; found 164.97543. – ^{119}Sn-Mößbauer (source ^{119m}Sn in $CaSnO_3$, reference: SnO_2, sample temperature 77 K): δ = 1.357 mm/s, Δ 3.840 mm/s, Γ 0.834 mm/s (δ 1.36 mm/s, Δ 3.80 mm/s[21]).

$Me_3Pb–F$ (13): MS: *m*/*z* = 257 [M^+ – Me], 253 [M^+ – F]. – HR-MS ($C_2H_6F^{208}Pb$) [M^+ – Me]: calcd. 275.02199; found 275.02688. ($C_3H_9{}^{208}Pb$) [M^+–F]: calcd. 253.04707; found 253.04321.

(*E*)-3-(*p*-Carboxyphenylseleno)-4-fluorohex-3-ene (9e): The saponification of the ester **9d** was carried out with KOH/EtOH/H_2O, as described in ref.[17] Yield of **9e** (from 2 mmol) 0.57 g (95%), m.p. 115–117 °C (*n*-hexane). – HR-MS ($C_{13}H_{15}FO_2{}^{80}Se$): calcd. 302.02212; found 302.02003. – ^{13}C NMR ($CDCl_3$): δ = 11.4 (C-6), 13.5 (C-1), 24.6 ($^3J_{F–C}$ = 6.8 Hz, C-2), 25.1 ($^2J_{F–C}$ = 28.8 Hz, C-5), 109.3 ($^2J_{F–C}$ = 21.8 Hz, C-3), 126.8 (*p*-C), 128.6 (*o*-C), 130.7 (*m*-C), 140.4 ($^4J_{F–C}$ = 2.1 Hz, *i*-C, C–Se), 165.7 ($^1J_{F–C}$ = 269.7 Hz, C-4), 172.1 (CO_2H).

Syntheses of $R^1Se–EMe_3$ (1–4). – General Procedure: Approximately 100 mL liquid ammonia was added to 15 mmol diselenide **14**. To this stirred solution, 30 mmol (210 mg) lithium was added, until the solution was slightly blue. After evaporation of the solvent under argon the remaining NH_3 was completely removed under vacuum. To the colorless solid 50 mL dry THF was added. To this

mixture was added a solution of 30 mmol Me_3Si–Cl (3.26 g), Me_3Ge–Cl (4.60 g) or Me_3Sn–Cl (5.98 g) in 10 mL THF, or solid Me_3Pb–Cl (8.63 g), over 20 min under Ar at room temperature, and subsequently stirred for 3 h. For the Si, Ge, and Sn derivatives the THF was removed at normal pressure and the product was distilled directly from the reaction flask. It was then redistilled for further purification. For the Pb derivatives, after adding 500 mL ice water, the organic layer was separated. The aqueous phase was treated with ether (3 × 100 mL), the ether-containing phases were washed with ice water (1 × 100 mL) and dried (Na_2SO_4). After removal of the solvent the product was purified by column chromatography (5 cm silica gel, *n*-hexane). For yields see Table 3.

Table 3. Syntheses of the selenides **1–4**

$R^1Se–EMe_3$	Yield	
PhSe–$SiMe_3$ (**1c**)	4.13 g (60%)	b.p. 66–68 °C/1.3 mbar
EtSe–$GeMe_3$ (**2b**)	5.42 g (80%)	b.p. 52–55 °C/23 mbar
PhSe–$GeMe_3$ (**2c**)	6.82 g (83%)	b.p. 65 °C/0.07 mbar
MeSe–$SnMe_3$ (**3a**)	6.11 g (79%)	b.p. 65–67 °C/23 mbar
PhSe–$SnMe_3$ (**3c**)	8.16 g (85%)	b.p. 72 °C/0.09 mbar
MeSe–$PbMe_3$ (**4a**)	8.31 g (80%)	after chromatography
PhSe–$PbMe_3$ (**4c**)	10.54 g (86%)	after chromatography

Table 4. Crystal data and structure refinement for compound **9e**

Formula	$C_{13}H_{15}FO_2Se$
Molecular weight	301.21
Crystal system	Monoclinic
Space group	*P*21/*n*
Crysal size [mm]	0.798 × 0.152 × 0.152
a [Å]	14.719(2)
b [Å]	5.6667(16)
c [Å]	16.348(3)
α [°]	90.00
β [°]	92.699(13)
γ [°]	90.00
V [Å^3]	1362.1(5)
$\rho_{calcd.}$ [gcm^{-3}]	1.469
Z	4
F(000) [e]	608
μ (Mo-K_α) [mm^{-1}]	2.756
Data collection	
Diffractometer	STOE Stadi4
Radiation	Mo-K_α, 0.71071 Å graphite monochromator
T [K]	298 (2)
Scan mode	2θ/ω = 1.0
hkl range	–13/13, 0/7, 0/11
Measured reflections	2040
Unique refl. (>2σ_I)	1953
R_{int}	0.0277
Used refl.	1953
T_{min}/T_{max}	0.4872/0.5841
Refinement	
Refined parameters	175
*R*1[a] [$F_o > 4\sigma(F_o)$]	0.0393 (1098 refl.)
*wR*2[b] (all)	0.1129
GooF (all)	0.976
Weighting par. *a*,*b*[c]	0.0724/0.0169
ρ_{final} (max/min) [eÅ^{-3}]	0.408/−0.270

[a] $R1 = \Sigma||F_o| - |F_c||/\Sigma|F_o|$. – [b] $R2 = [\Sigma w(F_o^2 - F_c^2)^2/\Sigma w(F_o^2)^2]^{1/2}$. – [c] $w = 1/[\sigma^2(F_o^2) + (aP)^2 + bP]$; $P = (F_o^2 + 2F_c^2)/3$

Ethylselenotrimethylsilane (1b): Analogously to ref.[30] bis(trimethylsilyl)selenide (**15**; 50 mmol, 11.3 g) was added to a solution of Na (50 mmol, 1.15 g) in ca. 100 mL of liquid NH_3 and stirred until it decolorized. After evaporation of the ammonia under Ar, the resulting $(Me_3Si)_2NH$ was removed under vacuum at 50 °C. 50 mL of pure THF was added to the remaining Me_3Si–SeNa. To this mixture ethyl iodide (50 mmol, 7.80 g) was added over 30 min under argon and stirring. It was then stirred for a further 4 h. After filtration and washing of the NaI precipitate with 30 mL of pentane the filtrate was fractionated using a short Vigreux column. Yield of **1b** 5.93 g (65%), b.p. 32–34 °C/20 mbar.

***p*-(Ethoxycarbonyl)phenylselenotrimethylstannane (3d):** Bis[*p*-(ethoxycarbonyl)phenyl]diselenide (**14d**; 5 mmol, 2.28 g) was suspended in 40 mL EtOH under stirring at room temperature and Ar and reduced by addition of small portions of $NaBH_4$ (10 mmol, 380 mg). After stirring (30 min), a solution Me_3Sn–Cl (10 mmol, 2.00 g) in 5 mL of THF was added to this suspension and further stirred for 30 min. This mixture was taken up with 250 mL of H_2O and extracted with $CHCl_3$ (3 × 50 mL). The extract was washed with water and dried (Na_2SO_4). The product was purified by column chromatography (silica gel, *n*-hexane/ether 10:1).Yield of **3d** 2.77 g (71%).

X-ray Crystal Structure Analysis of Compound 9e: A single crystal of compound **9e** was examined with a four-circle diffractometer at room temperature in air. Intensity data were corrected for Lorentz and polarization effects. An absorption correction had to be applied with the ψ-scan technique. The structure was solved by direct methods and refined by full-matrix least-squares techniques against F^2 (see Table 4).[45] The thermal motion of all non-hydrogen atoms was treated anisotropically. The hydrogen atom at O1 was located from the difference Fourier map. All the other hydrogen atoms were calculated in idealized positions and allowed to ride on their corresponding carbon atoms. Their isotropic thermal parameters were set to 1.2 times that of the adjacent C atom.

Crystallographic data (excluding structure factors) for the structure reported in this paper have been deposited with the Cambridge Crystallographic Data Centre as supplementary publication no. CCDC-138770. Copies of the data can be obtained free of charge on application to CCDC, 12 Union Road, Cambridge CB2 1EZ, UK [Fax: (internat.) + 44-1223/336-033; E-mail: deposit@ccdc.cam.ac.uk].

Acknowledgments

H. Poleschner was encouraged by the Wissenschaftler-Integrations-Programm (WIP, 1994–1996) at the Universität Potsdam, Institut für Organische Chemie und Strukturanalytik. We thank Ms. C. Hense-Lamatsch for her committed laboratory assistance. We would like to acknowledge Dr. A. Lehmann, Bundesanstalt für Materialforschung und -prüfung (BAM), Berlin-Adlershof, and Dr. G. Holzmann, Institut für Chemie, Organische Chemie, Freie Universität Berlin, for recording the mass spectra. Also we are grateful to Dr. H. Mehner, Bundesanstalt für Materialforschung und -prüfung (BAM), Berlin-Adlershof, for recording the Mößbauer spectrum. We are indebted to Dr. D. Lentz, Institut für Chemie, Anorganische und Analytische Chemie, Freien Universität Berlin, for the synthesis of xenon difluoride.

[1] Parts of this work were presented at the 12th European Symposium on Fluorine Chemistry, Freie Universität Berlin, August/September **1998**, Abstracts of Papers p. PII-71.
[2] S. Tomoda, Y. Usuki, *Chem. Lett.* **1989**, 1235–1236.
[3] Y. Usuki, M. Iwaoka, S. Tomoda, *Chem. Lett.* **1992**, 1507–1510.

[4] J. R. McCarthy, D. P. Matthews, C. L. Barney, *Tetrahedron Lett*. **1990**, *31*, 973–976.
[5] K. C. Nicolaou, N. A. Petasis, D. A. Claremon, *Tetrahedron* **1985**, *41*, 4835–4841.
[6] C. Saluzzo, G. Alvernhe, D. Anker, G. Haufe, *Tetrahedron Lett*. **1990**, *31*, 663–666.
[7] C. Saluzzo, G. Alvernhe, D. Anker, G. Haufe, *Tetrahedron Lett*. **1990**, *31*, 2127–2130.
[8] K. Uneyama, M. Kanai, *Tetrahedron Lett*. **1990**, *31*, 3583–3586.
[9] S. A. Lermontov, S. I. Zavorin, A. N. Pushin, A. N. Chekhlov, N. S. Zefirov, P. J. Stang, *Tetrahedron Lett*. **1993**, *34*, 703–706.
[10] A. N. Chekhlov, S. A. Lermontov, S. I. Zavorin, N. S. Zefirov, *Dokl. Akad. Nauk* **1993**, *332*, 198–202; *Chem. Abstr.*, **1994**, *120*, 217957y.
[11] K. K. Laali, W. Fiedler, M. Regitz, *Chem. Commun.* **1997**, 1641–1642.
[12] A. N. Chekhlov, S. A. Lermontov, S. I. Zavorin, N. S. Zefirov, *Dokl. Akad. Nauk* **1993**, *330*, 729–732; *Chem. Abstr.* **1994**, *120*, 164387d.
[13] S. A. Lermontov, S. I. Zavorin, I. V. Bakhtin, A. N. Pushin, N. S. Zefirov, P. J. Stang, *J. Fluorine Chem.* **1998**, *87*, 75–83.
[14] A. N. Chekhlov, S. A. Lermontov, S. I. Zavorin, N. S. Zefirov, *Dokl. Akad. Nauk* **1992**, *323*, 1112–1115; *Chem. Abstr.* **1993**, *118*, 147242u.
[15] S. A. Lermontov, S. I. Zavorin, I. V. Bakhtin, N. S. Zefirov, P. J. Stang, *Phosphorus, Sulfur, Silicon* **1995**, *102*, 283–286.
[16] H. Poleschner, M. Heydenreich, K. Spindler, G. Haufe, *Synthesis* **1994**, 1043–1049.
[17] H. Poleschner, M. Heydenreich, U. Schilde, *Liebigs Ann.* **1996**, 1187–1193.
[18] H. Poleschner, U. Schilde, *Acta Cryst.* **1996**, *C52*, 644–647 and herein cited literature.
[19] H. Poleschner, M. Heydenreich, R. Radeglia, *Magn. Reson. Chem.* **1999**, *37*, 333–345.
[20] [20a] M. R. Detty, *Tetrahedron Lett*. **1979**, 4189–4192. – [20b] M. R. Detty, *J. Org. Chem.* **1980**, *45*, 924–926. – [20c] M. R. Detty, M. D. Seidler *J. Org. Chem.* **1981**, *46*, 1283–1292.
[21] K. Licht, H. Geissler, P. Koehler, K. Hottmann. H. Schnorr, H. Kriegsmann, *Z. Anorg. Allg. Chem.* **1971**, *385*, 271–288.
[22] D. W. Grant, J. L. Wardell, *J. Organomet. Chem.* **1984**, *276*, 161–166.
[23] A. M. Forster, A. J. Downs, *Polyhedron* **1985**, *4*, 1625–1635.
[24] G. Pandey, K. S. S. Poleshwar Rao, *Angew. Chem.* **1995**, *107*, 2934–2935.
[25] M. Lalonde, T. H. Chan, *Synthesis* **1985**, 817–845.
[26] T. W. Greene, P. G. M. Wuts, *Protective Groups in Organic Synthesis*, 2th. ed., Wiley, New York, **1991**, 68–86.
[27] P. J. Kocienski, *Protecting Groups,* Thieme, Stuttgart, **1994**, 28–42.
[28] J. E. Drake, R. T. Hemmings, *J. Chem. Soc., Dalton Trans.* **1976**, 1730–1734.
[29] N. Miyoshi, H. Ishii, K. Kondo, S. Murai, N. Sonoda, *Synthesis* **1979**, 300–301.
[30] M. Schmidt, E. Kiewert, H. Lux, C. Sametschek, *Phosphorus and Sulfur* **1986**, *26*, 163–167.
[31] [31a] S. Tomoda, M. Shimoda, Y. Takeuchi, *Chem. Lett.* **1989**, 1373–1376. – [31b] S. Tomoda, M. Shimoda, Y. Takeuchi, Y. Iitaka, *Chem. Lett.* **1988**, 535–538.
[32] E. W. Abel, D. A. Armitage, D. B. Brady, *J. Organomet. Chem.* **1966**, *5*, 130–135.
[33] J. D. Kennedy, W. McFarlane, *J. Chem. Soc., Dalton Trans.* **1973**, 2134–2139.
[34] J. W. Anderson, G. K. Barker, J. E. Drake, M. Rodger, *J. Chem. Soc., Dalton Trans.* **1973**, 1716–1724.
[35] A. Krief, E. Badaoui, W. Dumont, *Tetrahedron Lett.* **1993**, *34*, 8521–8522.
[36] [36a] W. L. Richardson, U. S. 3,010,980, *Chem. Abstr.* **1962**, *56*, 11620 d. – [36b] W. L. Richardson, U. S. 3,116,126, *Chem. Abstr.* **1964**, *60*, 6686 c.
[37] J. E. Drake, B. M. Glavincevski, R. E. Humphries, A. Majid, *Can. J. Chem.* **1979**, *57*, 1426–1430.
[38] B. Wrackmeyer, K. Bauer, G. Kehr, U. Dörfler, *Main Group Met. Chem.* **1995**, *18*, 1–7.
[39] H. Reinholdt in *Houben-Weyl*, 4th ed., Vol. 9, Thieme, Stuttgart, **1955**, 1086–1104.
[40] D. H. O'Brien, N. Dereu, C.-K. Huang, K. J. Irgolic, F. F. Knapp, Jr., *Organometallics* **1983**, *2*, 305–307.
[41] M. Schmidt, H. Ruf, *Z. Anorg. Allg. Chem.* **1963**, *321*, 270–273.
[42] W. Kwasnik in *Handbuch der Präparativen Anorganischen Chemie*, 3th ed., Vol. 1; (Ed.: G. Brauer), Enke, Stuttgart, **1975**, 285.
[43] [43a] F. Klanberg, E. L. Muetterties, *Inorg. Chem.* **1968**, *7*, 155–160. – [43b] S. Berger, S. Braun, H.-O. Kalinowski, ^{19}*F-NMR Spektroskopie*, Thieme, Stuttgart, **1994**, 65.
[44] R. Eujen, R. Mellies, *J. Fluorine Chem.* **1983**, *22*, 263–280.
[45] G. M. Sheldrick, *SHELX-97. Program for the Solution and Refinement of Crystal Structures*, University of Göttingen, Germany, **1997**.

Received October 29, 1999
[I99384]

Rhodium(III)-Assisted Nucleophilic Addition of Ammonia to Metal-Bound Benzyl Cyanide: Crystal Structures of *mer*-$[RhCl_3(PhCH_2CN)_3]\cdot 1/2\ C_6H_5CH_3$ and *mer*-$[RhCl_3\{PhCH_2C(NH_2)=NH\}_3]$

Vadim Yu. Kukushkin,*[a] Igor V. Ilichev,[a] Gabriele Wagner,[b] Mikhail D. Revenco,[c] Viktor H. Kravtsov,[d] and Kinga Suwinska[e]

Keywords: Nitrile complexes / Rhodium / Nucleophilic additions / Amidines / Hydrogen bonding / Clathrates

Heating of $[RhCl_3(MeCN)_3]$ in benzyl cyanide at 100 °C gives the substitution product *mer*-$[RhCl_3(PhCH_2CN)_3]$ (90% yield), whose recrystallization from an acetone/toluene mixture leads to formation of the toluene solvate *mer*-$[RhCl_3(PhCH_2CN)_3]\cdot 1/2\ C_6H_5Me$. The crystal structure of the latter, determined by X-ray single-crystal diffractometry, shows an unusual self-assembly due to intermolecular CH···Cl hydrogen bonding with concomitant clathration of toluene. Diffusion of ammonia into a solution of *mer*-$[RhCl_3(PhCH_2CN)_3]$ in neat benzyl cyanide brings about a facile rhodium(III)-assisted addition of NH_3 to the coordinated nitrile species to produce the amidine complex *mer*-$[RhCl_3\{PhCH_2C(NH_2)=NH\}_3]$ (83% yield). Both starting material and the product were characterized by elemental analyses, FAB-MS, IR and ^1H and $^{13}C\{^1H\}$ NMR spectroscopy. The crystal structure of *mer*-$[RhCl_3\{PhCH_2C(NH_2)=NH\}_3]$ provides the first example of a rhodium(III) complex with a monodentate amidine ligand.

Introduction

The application of organonitrile transition metal complexes as synthons for preparation of a great variety of new compounds by the addition of nucleophiles − such as water/hydroxide, amines with sp^3 or sp^2 nitrogen atoms or mercaptans − to the carbon atom of the nitrile group has recently been reviewed comprehensively by Michelin and colleagues.[1] Our own research in this field has so far been focused on the hydrolysis of nitriles coordinated to a Rh−Rh unit to give a novel type of metallacycle,[2] addition of ethylenediamine to $[PtCl_2(PhCN)_2]$ to afford $[Pt(NH=C(Ph)NHCH_2CH_2NH_2)_2]^{2+}$, a complex that contains two unusual seven-membered organic metallacycles bound to the same platinum(II) center,[3] and the addition of nucleophiles with concerted cyclization of cyanoguanidine that yielded a novel type of azametallacycle, *cis*-$[(PPh_3)_2Pt\{NHC(Nuc)=NC(NH_2)=NH\}][BPh_4]$[4] and facile hydrolysis of organonitriles in platinum(IV) complexes to yield $[Pt^{IV}]-NH_3$ species.[5] Furthermore, we have recently observed a reaction between platinum(IV),[6−9] rhenium(IV)[10] and rhodium(III)[11] nitrile complexes and ketoximes, aldoximes, *vic*-dioximes, or dialkylhydroxylamines which led to isolation of iminoacylated compounds containing $[M]-\{NH=C(R)ON=CR'R''\}$,[6,9−11] $[M]-\{NH=C(R)ON=C(R')-C(R')=NOH\}$[7] or $[M]-\{NH=C(R)ONR'_2\}_2]$[8] moieties.

As part of our continuing interest in ligand reactivity in general,[12−15] and in reactions of coordinated nitriles[2−11] in particular we have now studied the ammination of the rhodium(III) complex *mer*-$[RhCl_3(PhCH_2CN)_3]$ by NH_3 giving the amidine complex *mer*-$[RhCl_3\{PhCH_2C(NH_2)=NH\}_3]$; these results, along with crystal structures of both starting material and the addition product, are reported herein.

Results and Discussion

There is much current interest in the chemistry of amidine/amidato transition metal complexes as evidenced, in particular, by the large number of papers published and also by detailed reviews written on the subject.[16,17] In the vast majority of cases complexes containing $RC(NH_2)=NH$ species are prepared by direct addition of the *amidine* to a complex. Metal-assisted reactions of *coordinated organonitriles* and ammonia lead to a very attractive route for preparation of complexes containing $RC(NH_2)=NH$ ligands. Despite the isolation of the first amidine metal compound formulated as $[Pt\cdot 2MeCN\cdot 4NH_3]Cl_2$,[18] the proposal of its amidine structure[19] and the first crystallographic determination of the amidine complex, $[Pt(NH_3)_2$-

[a] Department of Chemistry, St. Petersburg State University, Universitetsky Pr. 2, 198904 Stary Petergof, Russian Federation
Fax: (internat.) + 7-812/428-6939,
E-mail: kukushkin@VK2100.spb.edu
[b] Complexo I, Instituto Superior Técnico, Av. Rovisco Pais, 1049−001 Lisbon, Portugal
[c] Department of Chemistry, State University of Moldova, MD 2009, Chisinau, Republic of Moldova
[d] Institute of Applied Physics, Academy of Sciences, MD 2028, Chisinau, Republic of Moldova
[e] Institute of Physical Chemistry of the Polish Academy of Sciences, Department of Physico-Chemistry of Supramolecular Complexes
ul. Kasprzaca 44/52, 01-224, Warzawa, Poland

 © WILEY-VCH Verlag GmbH, D-69451 Weinheim, 2000 1434−1948/00/0606−1315 $ 17.50+.50/0

$(MeC(NH_2)=NH)_2]^{2+}$,[20] this exciting chemistry was not developed much further, although additions of *substituted* amines to RCN ligands are fairly well-documented.[1] Besides the above-mentioned work[18] on the addition of NH_3 to the acetonitrile complex $[PtCl_2(MeCN)_2]$, attention should be drawn to ammination by liquid ammonia of $[Co(NH_3)_5(NCR)]^{3+}$ complexes[21] and addition of NH_3 to acetonitrile in a cationic tungsten compound.[22]

Although the kinetics and mechanisms of the reaction of metal-bound organonitriles and *primary* amines have been investigated in a limited number of cases,[1] it is generally believed[23–26] that the reaction takes place by nucleophilic attack of the amine N atom to the nitrile carbon, which is electrophilically activated by its ligation to a metal center; metal ions in high oxidation states should provide a stronger electrophilic activation towards nucleophiles thus facilitating the addition. For this study we chose a benzyl cyanide complex of rhodium(III) for the following reasons: first, it has been proved that the rhodium(III) ion provides a high degree of activation of an organonitrile. Indeed, a ca. 10^6-fold increase in the rate of base-catalyzed hydration of RCN has been reported when these species are coordinated to a Rh^{III} center.[27] Second, the electron-acceptor benzyl group of the nitrile, in contrast to the electron-donor methyl in $[RhCl_3(MeCN)_3]$, should provide an additional activation of the C atom.

The starting material for this work, *mer*-$[RhCl_3(PhCH_2CN)_3]$, was prepared in high (90%) yield by a route described earlier for phenyl- and benzyl cyanide complexes of platinum(II),[28] i.e. by heating of the easily obtained acetonitrile complex $[RhCl_3(MeCN)_3]$[29] in neat benzyl cyanide at 100 °C in an open beaker. It has been suggested that both the large excess of $PhCH_2CN$ and removal of MeCN from the reaction mixture at high temperature drive the reaction. Recrystallization of *mer*-$[RhCl_3(PhCH_2CN)_3]$ from an acetone/toluene mixture gave a toluene solvate *mer*-$[RhCl_3(PhCH_2CN)_3]\cdot 1/2\ C_6H_5CH_3$ that was characterized by X-ray single-crystal diffractometry.

The coordination polyhedron of the complex is a slightly distorted octahedron (Figure 1) with both the $PhCH_2CN$ and chloride ligands in *mer* positions. The *mer*-configuration of the rhodium(III) compound persists also in $CDCl_3$ solution as evidenced by observation of the two nonequivalent $PhCH_2CN$ species in a 1:2 ratio in ^1H and $^{13}C\{^1H\}$ NMR spectra (see Experimental Section).

The two mutually *trans* Rh–Cl bonds [Rh–Cl(1) and Rh–Cl(3)] are equal and slightly longer than the third one [Rh–Cl(2)] (Table 1) thus reflecting a higher ground-state *trans*-influence of the Cl^- ligand than the benzyl cyanide one. A higher *trans*-influence of the other nitrile, i.e. acetonitrile, was also detected in *mer*-$[RhCl_3(MeCN)_3]\cdot MeCN$,[29] while the *trans*-influence of RCN and Cl^- ligands are almost the same for (organonitrile)Pt^{II} complexes.[30–33] The geometry and bond lengths in $PhCH_2CN$ ligands (Table 1) are normal and agree well with the previously reported data on organonitrile Rh^{III} complexes.[33–41]

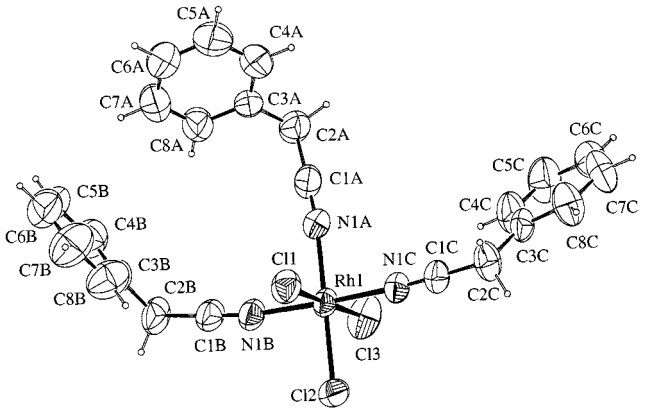


Figure 1. ORTEP drawing of *mer*-$[RhCl_3(PhCH_2CN)_3]\cdot 1/2\ C_6H_5CH_3$ with atomic numbering scheme

Table 1. Bond lengths (Å) and angles (°) in *mer*-$[RhCl_3(PhCH_2CN)_3]\cdot 1/2\ C_6H_5Me$

Rh(1)–N(1A)	2.021(4)	C(1B)–C(2B)	1.468(7)
Rh(1)–N(1B)	1.993(4)	C(2B)–C(3B)	1.520(7)
Rh(1)–N(1C)	1.982(4)	C(3B)–C(4B)	1.372(7)
Rh(1)–Cl(1)	2.326(1)	C(3B)–C(8B)	1.352(9)
Rh(1)–Cl(2)	2.302(1)	C(4B)–C(5B)	1.382(9)
Rh(1)–Cl(3)	2.326(1)	C(5B)–C(6B)	1.33(1)
N(1A)–C(1A)	1.132(6)	C(6B)–C(7B)	1.36(1)
C(1A)–C(2A)	1.456(7)	C(7B)–C(8B)	1.380(9)
C(2A)–C(3A)	1.515(7)	N(1C)–C(1C)	1.130(5)
C(3A)–C(4A)	1.373(7)	C(1C)–C(2C)	1.463(6)
C(3A)–C(8A)	1.368(7)	C(2C)–C(3C)	1.516(7)
C(4A)–C(5A)	1.390(9)	C(3C)–C(4C)	1.365(7)
C(5A)–C(6A)	1.347(9)	C(3C)–C(8C)	1.378(7)
C(6A)–C(7A)	1.353(9)	C(4C)–C(5C)	1.368(8)
C(7A)–C(8A)	1.373(8)	C(5C)–C(6C)	1.383(9)
N(1B)–C(1B)	1.125(6)	C(6C)–C(7C)	1.358(9)
		C(7C)–C(8C)	1.369(8)
Cl(1)–Rh(1)–Cl(2)	90.40(5)	C(2B)–C(3B)–C(8B)	121.8(6)
Cl(1)–Rh(1)–Cl(3)	179.03(6)	C(4B)–C(3B)–C(8B)	118.5(6)
Cl(1)–Rh(1)–N(1A)	90.62(13)	C(2C)–C(3C)–C(4C)	124.2(4)
Cl(1)–Rh(1)–N(1B)	89.89(13)	C(2C)–C(3C)–C(8C)	117.6(5)
Cl(1)–Rh(1)–N(1C)	89.20(13)	C(4C)–C(3C)–C(8C)	118.2(5)
Cl(2)–Rh(1)–Cl(3)	90.48(6)	C(3A)–C(4A)–C(5A)	120.1(6)
Cl(2)–Rh(1)–N(1A)	178.54(12)	C(3B)–C(4B)–C(5B)	120.6(6)
Cl(2)–Rh(1)–N(1B)	91.57(13)	C(3C)–C(4C)–C(5C)	121.4(5)
Cl(2)–Rh(1)–N(1C)	90.40(13)	C(4A)–C(5A)–C(6A)	120.1(7)
Cl(3)–Rh(1)–N(1A)	88.51(13)	C(4B)–C(5B)–C(6B)	119.5(7)
Cl(3)–Rh(1)–N(1B)	90.49(13)	C(4C)–C(5C)–C(6C)	119.6(6)
Cl(3)–Rh(1)–N(1C)	90.38(13)	C(5A)–C(6A)–C(7A)	120.3(7)
N(1A)–Rh(1)–N(1B)	87.39(16)	C(5B)–C(6B)–C(7B)	121.3(8)
N(1A)–Rh(1)–N(1C)	90.66(16)	C(5C)–C(6C)–C(7C)	119.6(6)
N(1B)–Rh(1)–N(1C)	177.84(18)	C(6A)–C(7A)–C(8A)	120.0(7)
Rh(1)–N(1A)–C(1A)	173.2(4)	C(6B)–C(7B)–C(8B)	118.8(8)
Rh(1)–N(1B)–C(1B)	172.2(5)	C(6C)–C(7C)–C(8C)	120.2(7)
Rh(1)–N(1C)–C(1C)	176.1(4)	C(3A)–C(8A)–C(7A)	121.2(6)
N(1A)–C(1A)–C(2A)	177.9(6)	C(3B)–C(8B)–C(7B)	121.2(7)
N(1B)–C(1B)–C(2B)	179.6(7)	C(3C)–C(8C)–C(7C)	121.0(6)
N(1C)–C(1C)–C(2C)	178.7(6)	C(2A)–C(3A)–C(4A)	121.6(5)
C(1A)–C(2A)–C(3A)	111.5(5)	C(2A)–C(3A)–C(8A)	120.2(5)
C(1B)–C(2B)–C(3B)	112.5(5)	C(4A)–C(3A)–C(8A)	118.2(6)
C(1C)–C(2C)–C(3C)	113.7(4)	C(2B)–C(3B)–C(4B)	119.6(5)

The packing diagram (Figure 2) shows that molecules of *mer*-$[RhCl_3(PhCH_2CN)_3]$ are assembled by intermolecular hydrogen bonding C(2)–H···Cl(2) between the methylene group from one molecule and the chloride from the adjacent molecule thus forming polymeric chains. The observed C(2)H···Cl(2) distances are in the range 2.84–2.85 Å indicating rather weak interactions [the combined contact radius

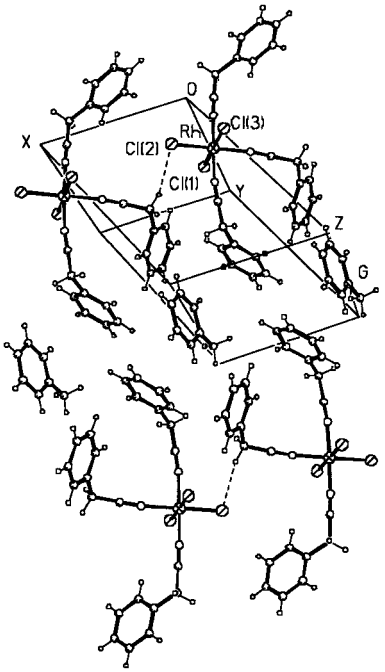


Figure 2. Packing diagram for *mer*-$[RhCl_3(PhCH_2CN)_3]\cdot 1/2\ C_6H_5CH_3$ indicating hydrogen bonding pattern

is H(1.20) + Cl(1.75) = 2.95 Å[42]].[29] Furthermore, the unit cell of *mer*-$[RhCl_3(PhCH_2CN)_3]\cdot 1/2\ C_6H_5Me$ contains half a molecule of clathrated and disordered toluene. The latter has no contacts less than the sum of the van der Waals radii with the *mer*-$[RhCl_3(PhCH_2CN)_3]$ molecule. It is worthwhile to mention that clathration of the solvent was observed in the case of the analogous complex *mer*-$[RhCl_3(MeCN)_3]\cdot MeCN$[29] that is also assembled into infinite chains by CH···Cl hydrogen bonding. These two observations together point to the need for a study on the self-assembly/clathration in similar systems. In fact, self-assembly of metal complexes by hydrogen bonding is the rapidly developing area of paramount importance for crystal engineering and material science[43−45] and it is likely − from that viewpoint − that the observation of H-bonding in the (organonitrile)Rh^{III} compounds with concomitant clathration of solvents deserves further investigations.

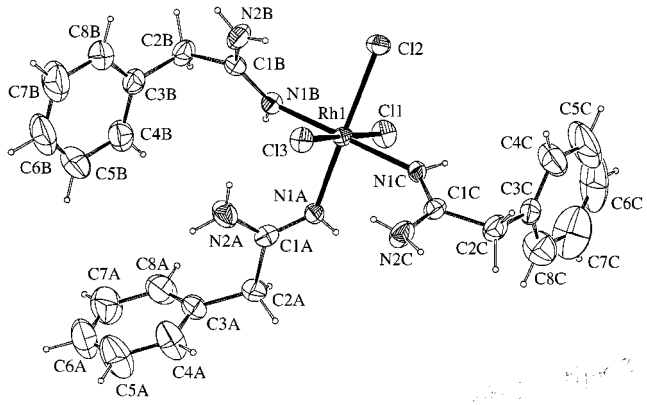


Figure 3. ORTEP drawing of *mer*-$[RhCl_3\{PhCH_2C(NH_2)=NH\}_3]$ with atomic numbering scheme

Diffusion of ammonia into a solution of *mer*-$[RhCl_3(PhCH_2CN)_3]$ in neat benzyl cyanide at 20−25 °C for one day led to the addition of NH_3 across the C≡N bond giving the rhodium(III) complex containing neutral amidine ligands *mer*-$[RhCl_3\{PhCH_2C(=NH)(NH_2)\}_3]$ which was isolated in good yield. The structure of the product of ammination has been determined by X-ray crystallography (Figure 3).

The coordination at rhodium is octahedral with small deviations from ideal geometry. The amidine species are coordinated through their imino nitrogens, adopting the *mer*-configuration which remains in $CDCl_3$ solution (see Experimental Section). The $PhCH_2C(NH_2)=NH$ ligands are in a *Z*-configuration in the solid state. Moreover, no evidence for existence of an *E*-conformation in solution can be derived from the NMR spectroscopic data. The HN=C [1.239(5)−1.285(5) Å] and H_2N−C [1.305(5)−1.330(5) Å] bonds (Table 2) lie in the normal range.[46] Hydrogen atoms from all three amidine species are involved in both *intra*-)

Table 2. Bond lengths (Å) and angles (°) in *mer*-$[RhCl_3\{PhCH_2C(NH_2)=NH\}_3]$

Rh(1)−N(1A)	1.996(3)	C(1B)−C(2B)	1.502(5)
Rh(1)−N(1B)	2.023(3)	C(2B)−C(3B)	1.467(6)
Rh(1)−N(1C)	2.018(3)	C(3B)−C(4B)	1.364(6)
Rh(1)−Cl(1)	2.313(1)	C(3B)−C(8B)	1.370(6)
Rh(1)−Cl(2)	2.367(1)	C(4B)−C(5B)	1.354(7)
Rh(1)−Cl(3)	2.355(1)	C(5B)−C(6B)	1.341(8)
N(1A)−C(1A)	1.239(5)	C(6B)−C(7B)	1.351(8)
N(2A)−C(1A)	1.323(5)	C(7B)−C(8B)	1.337(7)
C(1A)−C(2A)	1.507(5)	N(1C)−C(1C)	1.285(5)
C(2A)−C(3A)	1.466(6)	N(2C)−C(1C)	1.305(6)
C(3A)−C(4A)	1.334(7)	C(1C)−C(2C)	1.495(5)
C(3A)−C(8A)	1.354(7)	C(2C)−C(3C)	1.469(6)
C(4A)−C(5A)	1.340(8)	C(3C)−C(4C)	1.333(7)
C(5A)−C(6A)	1.332(9)	C(3C)−C(8C)	1.358(6)
C(6A)−C(7A)	1.353(9)	C(4C)−C(5C)	1.351(9)
C(7A)−C(8A)	1.350(8)	C(5C)−C(6C)	1.36(1)
N(1B)−C(1B)	1.285(5)	C(6C)−C(7C)	1.31(1)
N(2B)−C(1B)	1.330(5)	C(7C)−C(8C)	1.340(9)
N(1A)−Rh(1)−N(1C)	89.3(1)	C(7A)−C(8A)−C(3A)	121.8(6)
N(1A)−Rh(1)−N(1B)	88.7(1)	C(1B)−N(1B)−Rh(1)	134.7(3)
N(1C)−Rh(1)−N(1B)	172.1(2)	N(1B)−C(1B)−N(2B)	122.7(4)
N(1A)−Rh(1)−Cl(1)	86.6(1)	N(1B)−C(1B)−C(2B)	121.3(4)
N(1C)−Rh(1)−Cl(1)	85.0(1)	N(2B)−C(1B)−C(2B)	116.0(4)
N(1B)−Rh(1)−Cl(1)	87.3(1)	C(3B)−C(2B)−C(1B)	109.1(4)
N(1A)−Rh(1)−Cl(3)	93.3(1)	C(4B)−C(3B)−C(8B)	118.8(5)
N(1C)−Rh(1)−Cl(3)	94.0(1)	C(4B)−C(3B)−C(2B)	120.2(4)
N(1B)−Rh(1)−Cl(3)	93.7(1)	C(8B)−C(3B)−C(2B)	121.0(4)
Cl(1)−Rh(1)−Cl(3)	179.00(4)	C(5B)−C(4B)−C(3B)	120.4(5)
N(1A)−Rh(1)−Cl(2)	177.1(1)	C(6B)−C(5B)−C(4B)	118.6(6)
N(1C)−Rh(1)−Cl(2)	90.3(1)	C(5B)−C(6B)−C(7B)	122.5(6)
N(1B)−Rh(1)−Cl(2)	91.3(1)	C(8B)−C(7B)−C(6B)	118.4(6)
Cl(1)−Rh(1)−Cl(2)	90.55(4)	C(7B)−C(8B)−C(3B)	121.1(6)
Cl(3)−Rh(1)−Cl(2)	89.56(4)	C(1C)−N(1C)−Rh(1)	138.9(3)
C(1A)−N(1A)−Rh(1)	132.4(3)	N(1C)−C(1C)−N(2C)	123.2(4)
N(1A)−C(1A)−N(2A)	122.2(4)	N(1C)−C(1C)−C(2C)	123.8(4)
N(1A)−C(1A)−C(2A)	120.2(4)	N(2C)−C(1C)−C(2C)	113.0(4)
N(2A)−C(1A)−C(2A)	117.5(4)	C(3C)−C(2C)−C(1C)	114.7(4)
C(3A)−C(2A)−C(1A)	116.5(4)	C(4C)−C(3C)−C(8C)	119.2(5)
C(4A)−C(3A)−C(8A)	119.2(5)	C(4C)−C(3C)−C(2C)	119.9(5)
C(4A)−C(3A)−C(2A)	120.0(5)	C(8C)−C(3C)−C(2C)	120.9(5)
C(8A)−C(3A)−C(2A)	120.8(5)	C(3C)−C(4C)−C(5C)	119.3(7)
C(3A)−C(4A)−C(5A)	119.8(6)	C(4C)−C(5C)−C(6C)	121.0(9)
C(6A)−C(5A)−C(4A)	120.7(7)	C(7C)−C(6C)−C(5C)	118.9(9)
C(5A)−C(6A)−C(7A)	121.1(7)	C(6C)−C(7C)−C(8C)	120.9(9)
C(8A)−C(7A)−C(6A)	117.3(7)	C(7C)−C(8C)−C(3C)	120.7(7)

and *inter*molecular hydrogen bonding with chlorides thus precluding any conclusions about the "pure" ground-state *trans*-influence of $HN{=}C(NH_2)CH_2Ph$ ligands. The crystal structure of *mer*-$[RhCl_3\{PhCH_2C(NH_2){=}NH\}_3]$ is so far the only one for a rhodium(III) complex with monodentate amidines.

In conclusion, it is important to point out that *free* benzyl cyanide does not react with ammonia in $CDCl_3$ at room temperature (proved by ^1H NMR spectroscopy) or on a preparative scale (verified by a synthetic experiment) and these facts imply that the ammonia addition to *mer*-$[RhCl_3(PhCH_2CN)_3]$ is metal-assisted. To the best of our knowledge the ammination of coordinated RCN species in rhodium(III) complexes has not yet been investigated and this is the first example of its kind.

Experimental Section

Materials and Instrumentation: Solvents were obtained from commercial sources and used as received. $[RhCl_3(MeCN)_3]$ was prepared following a published method.[29] C, H and N elemental analyses were carried out by the Microanalytical Service of St. Petersburg State Technological Institute. Melting points were determined on a Kofler table. For TLC, Merck UV 254 SiO_2-plates were used. Positive-ion FAB mass spectra were obtained on a Trio 2000 instrument by bombarding 3-nitrobenzyl alcohol matrices of the samples with 8 keV (ca. 1.28×10^{15} J) Xe atoms. Mass calibration for data system acquisition was achieved using CsI. Infrared spectra (4000−400 cm^{-1}) were recorded on a BIO-RAD FTS 3000MX instrument as KBr pellets. ^1H and $^{13}C\{^1H\}$ NMR spectra were measured on a Varian UNITY 300 spectrometer at ambient temperature.

***mer*-$[RhCl_3(PhCH_2CN)_3]$:** $[RhCl_3(MeCN)_3]$ (0.1 g, 0.3 mmol) was dissolved in benzyl cyanide (1.0 mL, 8.7 mmol) and heated at 100 °C for 4 h in an open beaker. After this time the mixture was cooled to 20−25 °C and diethyl ether (20 mL) added dropwise with continuous stirring. The precipitate released was collected on a filter, washed with three portions of Et_2O (each 3 mL)and dried in air at room temperature. Yield: 0.15 g (90%); m.p. 122 °C. − TLC on SiO_2, R_f = 0.69 (eluent $CHCl_3/Me_2CO$ = 3:1, v/v). − $C_{24}H_{21}Cl_3N_3Rh$ (560.7): calcd. C 51.4, H 3.7, Cl 19, N 7.5, Rh 18.4; found C 52.3, H 3.7, Cl 18.6, N 7.5, Rh 18.5. − FAB^+-MS: *m/z* = 561 $[M]^+$, 524 $[M - Cl]^+$, 489 $[M - 2Cl]^+$, 372 $[M - 2Cl - PhCH_2CN]^+$. − IR (selected bands): $\tilde{\nu}$ = 2938 w and 2894 w ν(CH), 2316 m ν(C≡N), 1497 s and 1455 s ν(C=C), 742 s, 730 s and 695 s δ(CH) cm^{-1}. − ^1H NMR ($CDCl_3$): δ = 4.17 (s, 2 H) and 4.26 (s, 4 H, CH_2), 7.32−7.40 (m, 15 H, Ph). − $^{13}C\{^1H\}$ NMR ($CDCl_3$): δ = 25.2 (CH_2, 1C), 25.4 (CH_2, 2C), 128.1, 128.6, 129.4 (CH, 2C each) and 128.0, 128.7, 129.5 (CH, 1C each), 127.5 (C_{ipso}, 3C, Ph), 121.9 (1C) and 122.8 (2C) (C≡N). For the toluene solvate $[RhCl_3(PhCH_2CN)_3]\cdot 1/2\ C_6H_5Me$, $C_{27.5}H_{25}Cl_3N_3Rh$ (606.8): calcd. C 54.4, H 4.2, N 6.9; found C 54.9, H 4.4, N 6.6.

***mer*-$[RhCl_3\{PhCH_2C(=NH)(NH_2)\}_3]$:** A solution of *mer*-$[RhCl_3(PhCH_2CN)_3]$ (0.1 g) in benzyl cyanide (1.0 mL) in an open beaker was placed in a dessicator with 25% aqueous ammonia at the bottom and kept for 1 d at room temperature. After this time diethyl ether (20 mL) was added dropwise with continuous stirring. The precipitate formed was collected on a filter, washed with three portions of Et_2O (each 3 mL) and dried in air at room temperature. Yield: 0.09 g (83%); m.p. 170 °C. − TLC on SiO_2, R_f = 0.36 (eluent $CHCl_3/Me_2CO$ = 3:1, v/v). − $C_{24}H_{30}Cl_3N_6Rh$ (611.8): calcd. C, 47.1, H 4.9, N 13.7, Cl 17.4, Rh 16.8; found C 47.2, H 4.9, N 13.7, Cl 17.3, Rh 16.9. − FAB^+-MS: *m/z* = 612 [M], 575 $[M - Cl]^+$. − IR (selected bands): $\tilde{\nu}$ = 3490 w, 3427 m-w, 3400 m-w, 3329 m-w, 3269 m-w ν(NH), 2921 m-w ν(CH), 1650 vs, br. ν(C=N), 749 s and 702 s δ(CH) cm^{-1}. − ^1H NMR ($CDCl_3$): δ = 3.59 (s, 2 H)

Table 3. Crystal data and structure refinement

	$[RhCl_3(PhCH_2CN)_3]\cdot 1/2\ C_6H_5CH_3$	$[RhCl_3\{PhCH_2C(NH_2){=}NH\}_3]$
Empirical formula	$C_{27.5}H_{25}N_3Cl_3Rh$	$C_{24}H_{30}N_6Cl_3Rh$
Formula weight	606.77	611.80
Temperature, K	293(2)	293(2)
Wavelength (Å)	0.71073	0.71073
Crystal system, space group	Triclinic, $P\bar{1}$	Monoclinic, $C2/c$
a, Å	8.3190(4)	31.099(6)
b, Å	13.4682(7)	11.633(2)
c, Å	13.9479(8)	15.344(3)
α (°)	109.481(2)	−
β (°)	105.454(3)	105.91(3)
γ (°)	98.852(3)	−
V(Å ^{3})	1368.41(12)	5338.4(17)
Z	2	8
$\rho_{calcd.}$ (g/cm^3)	1.473	1.522
μ (Mo) (mm^{-1})	0.938	0.965
Crystal size (mm)	0.1 × 0.08 × 0.08	0.05 × 0.1 × 0.12
θ range for data collection	1.82−26.44	1.88−23.98
Index ranges	$-10 \le h \le 0$ $-16 \le k \le 16$ $-16 \le l \le 17$	$0 \le h \le 35$ $0 \le k \le 12$ $-17 \le l \le 16$
Reflections collected/unique	10079/5608 [$R_{int.}$ = 0.068]	4191/3959 [$R_{int.}$ = 0.048]
Data/restraints/parameters	5608/5/305	3959/0/343
Goodness-of-fit on F^2	1.055	0.999
Final *R* indices [$I > 2\sigma(I)$]	R_1 = 0.0524, wR_2 = 0.1243	R_1 = 0.0376, wR_2 = 0.0739
R indices (all data)	R_1 = 0.0793, wR_2 = 0.1371	R_1 = 0.0596, wR_2 = 0.0814
Largest diff. peak and hole	0.934 and −0.752	0.274 and −0.342

and 3.75 (s, 4 H, CH_2Ph), 4.78, 5.00, 5.44 and 5.62 (four s, br, NH_2), 7.09 (m, 2 H), 7.23 (m, 4 H) and 7.31 (m, 9 H, Ph), 7.63 (s, br, 3 H, =NH). – $^{13}C\{^1H\}$ NMR ($CDCl_3$): δ = 43.3 (3 C, CH_2Ph), 127.8 (2 C), 128.1 (1 C), 129.0 (2 C), 129.18 (1 C), 129.22 (1 C), 129.5 (2 C) and 133.8 (3 C, Ph), 170.1 and 171.0 (*C*=NH).

X-ray Crystallography: All crystallographic measurements were carried out with a Nonius Kappa CCD diffractometer equipped with a graphite monochromated Mo-K_α radiation source using θ rotations with 2° frames and a detector-to-crystal distance of 35 mm. The unit cell determination and integration was carried out by the program DENZO-SMN.[47] Data sets were corrected for Lorentz and polarization effects. Structures were solved using heavy-atom methods SHELXL-97.[48] All non-hydrogen atoms were refined anisotropically, whilst hydrogen atoms were fixed in the idealized position and allowed to ride. All crystallographic data and information about refinement of the two structures are given in Table 3 and bond lengths and angles in Table 1 and Table 2.

Crystallographic data (excluding structure factors) for the structures reported in this paper have been deposited with the Cambridge Crystallographic Data Centre as supplementary publications no. CCDC-137154 $C_{27.5}H_{25}N_3Cl_3Rh$ and CCDC-137155 $C_{24}H_{30}N_6Cl_3Rh$. Copies of the data can be obtained free of charge on application to CCDC, 12 Union Road, Cambridge CB2 1EZ, UK [Fax: (internat.) + 44-1223/336-033; E-mail: deposit@ccdc.cam.ac.uk].

Acknowledgments

The authors thank the INTAS for the grant 97–0166. V. Yu. K. is very much obliged to the Russian Fund for Basic Research for the grant 97–03–33626a. We thank Prof. A. J. L. Pombeiro for putting facilities at the authors disposal.

[1] R. A. Michelin, M. Mozzon, R. Bertani, *Coord. Chem. Rev.* **1996**, *147*, 299–338 and references therein.
[2] V. Yu. Kukushkin, T. Nishioka, S. Nakamura, I. Kinoshita, K. Isobe, *Chem. Lett.* **1997**, 189–190.
[3] Yu. N. Kukushkin, N. P. Kiseleva, E. Zangrando, V. Yu. Kukushkin, *Inorg. Chim. Acta* **1999**, *285*, 203–207.
[4] M. F. C. Guedes da Silva, C. M. P. Ferreira, E. M. P. R. P. Branco, J. J. R. Fraústo da Silva, A. J. L. Pombeiro, R. A. Michelin, U. Belluco, R. Bertani, M. Mozzon, G. Bombieri, F. Benetollo, V. Yu. Kukushkin, *Inorg. Chim. Acta (Topical Volume on Platinum Chemistry)* **1997**, *265*, 267–270.
[5] V. Yu. Kukushkin, I. G. Zenkevich, V. K. Belsky, V. E. Konovalov, A. I. Moiseev, E. O. Sidorov, *Inorg. Chim. Acta* **1989**, *166*, 79–84.
[6] V. Yu. Kukushkin, T. B. Pakhomova, Yu. N. Kukushkin, R. Herrmann, G. Wagner, A. J. L. Pombeiro, *Inorg. Chem*. **1998**, *37*, 6511–6517.
[7] V. Yu. Kukushkin, T. B. Pakhomova, N. A. Bokach, G. Wagner, M. L. Kuznetsov, M. Galanski, A. J. L. Pombeiro, *Inorg. Chem*. **2000**, *39*, 216–225.
[8] G. Wagner, A. J. L. Pombeiro, Yu. N. Kukushkin, T. B. Pakhomova, A. D. Ryabov, V. Yu. Kukushkin, *Inorg. Chim. Acta* **1999**, *292*, 272–275.
[9] D. A. Garnovskii, M. F. C. Guedes da Silva, T. B. Pakhomova, G. Wagner, M. T. Duarte, J. J. R. Fraústo da Silva, A. J. L. Pombeiro, V. Yu. Kukushkin, *Inorg. Chim. Acta*, in press.
[10] G. Wagner, A. J. L. Pombeiro, N. A. Bokach, V. Yu. Kukushkin, *J. Chem. Soc., Dalton Trans.* **1999**, 4083–4086.
[11] V. Yu. Kukushkin, I. V. Ilichev, G. Wagner, J. J. R. Fraústo da Silva, A. J. L. Pombeiro, *J. Chem. Soc., Dalton Trans.* **1999**, 3047–3052.
[12] J. A. Davies, C. M. Hockensmith, V. Yu. Kukushkin, Yu. N. Kukushkin, *Synthetic Coordination Chemistry: Principles and Practice*, World Scientific, Singapore–New Jersey, **1996**, pp 492.
[13] V. Yu. Kukushkin, *Coord. Chem. Rev.* **1995**, *139*, 375–407.
[14] V. Yu. Kukushkin, A. J. L. Pombeiro, *Coord. Chem. Rev.* **1999**, *181*, 147–175.
[15] V. Yu. Kukushkin, D. Tudela, A. J. L. Pombeiro, *Coord. Chem. Rev.* **1996**, *156*, 333–362.
[16] J. Barker, M. Kilner, *Coord. Chem. Rev.* **1994**, *133*, 219–300.
[17] R. C. Mehrotra, *Oximes, Guanidines and Related Species*, in *Comprehensive Coordination Chemistry* (Ed.: G. Wilkinson); Pergamon Press, Oxford, U.K., **1987**; vol. 2, pp. 276–279.
[18] L. Tschugaev, W. Lebedinski, *Compt. Rend*. **1915**, *161*, 563.
[19] for review see: Yu. N. Kukushkin, *Koord. Khim*. **1981**, *7*, 323–334 and references therein.
[20] N. C. Stephenson, *J. Inorg. Nucl. Chem*. **1962**, *24*, 801–808.
[21] D. P. Fairlie, W. G. Jackson, *Inorg. Chem*. **1990**, *29*, 140–143.
[22] S. G. Feng, J. L. Templeton, *Organometallics* **1992**, *11*, 1295–1303.
[23] R. W. Hay, in *Reactions of Coordinated Ligands* (Ed.: P. S. Braterman), vol. 2, Plenum Press, New York, **1989**, p. 280–287.
[24] E. C. Constable, *Metals and Ligand Reactivity. An Introduction to the Organic Chemistry of Metal Complexes*, VCH, Weinheim, **1995**, p. 65.
[25] A. W. Parkins, *Platinum Metals Rev.* **1996**, *40*, 169–174.
[26] B. N. Storhoff, H. C. Lewis, *Coord. Chem. Rev.* **1977**, *23*, 1–29.
[27] A. W. Zanella, P. C. Ford, *Inorg. Chem*. **1975**, *14*, 42–47.
[28] Yu. N. Kukushkin, T. B. Pakhomova, *Zh. Obstch. Khim*. **1995**, *65*, 330.
[29] O. Renn, H. Rüegger, L. M. Venanzi, J. Gallus, V. Gramlich, A. Martelletti, *Inorg. Chim. Acta* **1995**, *240*, 575–580.
[30] V. K. Belsky, V. E. Konovalov, V. Yu. Kukushkin, A. I. Moiseev, *Inorg. Chim. Acta* **1990**, *169*, 101–107.
[31] V. Yu. Kukushkin, V. K. Belsky, V. E. Konovalov, R. R. Shifrina, A. I. Moiseev, R. A. Vlasova, *Inorg. Chim. Acta* **1991**, *183*, 57–63.
[32] V. Yu. Kukushkin, I. A. Krol, Z. A. Starikova, V. M. Tkachuk, *Koord. Khim*. **1990**, *16*, 1406–1415; *Sov. Coord. Chem. (Engl. Transl.)* **1990**, *16*, 746.
[33] V. Yu. Kukushkin, V. K. Belsky, V. E. Konovalov, G. A. Kirakosyan, L. V. Konovalov, A. I. Moiseev, V. M. Tkachuk, *Inorg. Chim. Acta* **1991**, *185*, 143–154.
[34] A. Gourdon, Y. Jeannin, *Acta Cryst*., *Sect. B* **1980**, *B36*, 304–309.
[35] J. H. Merrifield, G.-Yu Lin, W. A. Kiel, J. A. Gladysz, *J. Am. Chem. Soc*. **1983**, *105*, 5811–5819.
[36] W. Lesueur, E. Solari, C. Floriani, A. Chiesi-Villa, C. Rizzoli, *Inorg.Chem*. **1997**, *36*, 3354–3362.
[37] R. Cini, G. Giorgi, E. Periccioli, *Acta Cryst., Sect. C* **1991**, *47*, 716–719.
[38] S. P. Best, A. J. Nightingale, D. A. Tocher, *Inorg. Chim. Acta* **1991**, *181*, 7–9.
[39] K. Brandt, W. S. Sheldrick *Chem. Ber*. **1996**, *129*, 1199–1206.
[40] K. Brandt, W. S. Sheldrick, *J. Chem. Soc., Dalton Trans.* **1996**, 1237–1243.
[41] F. A. Cotton, K. R. Dunbar, C. T. Eagle, L. R. Falvello, S.-J. Kang, A. C. Price, M. G. Verbruggen, *Inorg. Chim. Acta* **1991**, *184*, 35–42.
[42] A. Bondi, *J. Phys. Chem*. **1964**, *68*, 441–451.
[43] D. Braga, F. Grepioni, *Coord. Chem. Rev.* **1999**, *183*, 19–41 and references therein.
[44] J. C. Mereque Rivas, L. Brammer, *Coord. Chem. Rev.* **1999**, *183*, 43–80 and references therein.
[45] V. Yu. Kukushkin, T. Nishioka, D. Tudela, K. Isobe, I. Kinoshita, *Inorg. Chem*. **1997**, *36*, 6157–6165 and references therein.
[46] F. H. Allen, O. Kennard, D. G. Watson, L. Brammer, A. G. Orpen, R. Taylor, *J. Chem. Soc., Perkin Trans. 2* **1987**, S1–S19.
[47] Z. Otwinowski, W. Minor, in *Methods in Enzymology* (Eds.: C. W. Carter, R. M. Sweet, Academic Press, London, **1996**, vol. 276, p. 307.
[48] Sheldrick, *SHELX-97*; University of Göttingen: Göttingen, Germany, **1997**.

Received November 21, 1999
[I99419]

Titanium Complexes Containing a Disulfide-Bridged Bis(phenolato) Ligand: Synthesis and Structural Characterization of Three Different Bonding Modes

Jun Okuda,*[a] Stefan Fokken,[a] Thomas Kleinhenn,[a] and Thomas P. Spaniol[a]

Keywords: Titanium / O ligands / Bulky phenols / Lewis acids / S ligands

A series of titanium(IV) complexes containing the 2,2′-dithiobis(6-*tert*-butyl-4-methylphenolato) ligand (dtbmp) were synthesized and characterized. Treatment of titanium tetra(isopropoxide) with 2,2′-dithiobis(6-*tert*-butyl-4-methylphenol) (dtbmpH_2) gave, regardless of the molar ratio of the starting materials, a C_2-symmetric dinuclear complex [Ti_2(O*i*Pr)$_2$(μ_2-O*i*Pr)$_2$(dtbmp)]. According to the results of a single crystal X-ray analysis, the two Ti(O*i*Pr)$_2$ fragments in this complex are bridged by a dtbmp ligand and two isopropoxide ligands. The disulfide link of the dtbmp ligand is bonded to each of the titanium centers [Ti–S 2.795(1) and 2.768(1) Å], thus completing an octahedral coordination sphere around titanium. Reaction of [Ti_2(O*i*Pr)$_4$(μ_2-O*i*Pr)$_2$(dtbmp)] with Me_3SiX (X = Br, I) gave the mononuclear complex Ti(dtbmp)X_2. Crystallographic study revealed a distorted octahedral coordination with the disulfide link of the dtbmp dihapto-bonded through a relatively short Ti–S distance of 2.637(1) Å (X = Br) or 2.645(2) Å (X = I). Finally, the reaction of titanium tetra(*n*-butoxide) with dtbmpH_2 gave a C_i-symmetric dimer [Ti_2(O*n*Bu)$_2$(μ_2-O*n*Bu)$_2$(dtbmp)$_2$] that exhibits a monohapto coordination of the disulfide bridge in the dtbmp ligand with Ti–S bond lengths of 2.692(1) Å and 2.694(1) Å in the crystal.

Introduction

As precursors for homogeneous α-olefin polymerization catalysts, titanium complexes with bulky bisphenolato ligands such as the 2,2′-methylenebis(6-*tert*-butyl-4-methylphenolato) ligand (mbmp)[1] are attracting some interest as alternatives for both the *ansa*-metallocenes[2] and the chelating diamido complexes.[3] Following the remarkable finding by Kakugo et al.[1c] that in such catalyst precursors the replacement of a methylene bridge[4] by a sulfide group imparts a significant increase in the polymerization activity when activated with methylaluminoxane, crystallographic[5] and computational studies[6] have indicated that the sulfide donor plays an active role. In the putative alkyl cation, the weakly coordinating sulfide is thought to decrease the activation barrier for the olefin insertion into the alkyl−titanium bond. More recently, we noted that nine-membered chelate complexes of titanium are formed with remarkable ease with the ethylene-bridged bisphenolato ligand 2,2′-ethylenebis(6-*tert*-butyl-4-methylphenolato) ligand (ebmp).[5b,7] They copolymerize ethylene with styrene with significant incorporation of the bulky monomer styrene.[8] Since no examples for titanium complexes of 2,2′-dithiobis(6-*tert*-butyl-4-methylphenol) were known in the literature,[9] we decided to study its coordination at tetravalent titanium centers. In this contribution, we describe the synthesis and structural characterization of titanium complexes incorporating the disulfide analogue of the ebmp ligand, 2,2′-dithiobis(6-*tert*-butyl-4-methylphenolato) (dtbmp).

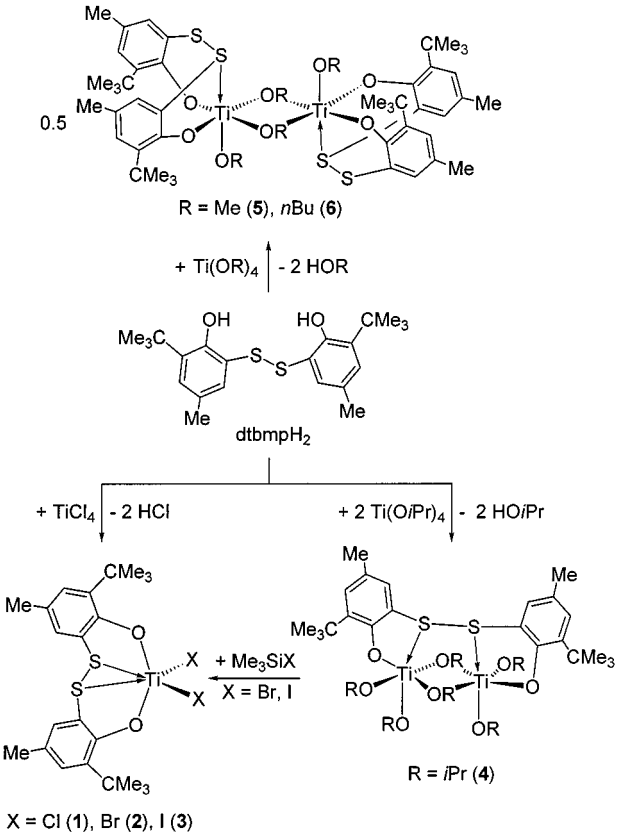
[a] Institut für Anorganische Chemie und Analytische Chemie, Johannes Gutenberg-Universität, Duesberg-Weg 10−14, D-55099 Mainz, Germany

Results and Discussion

When titanium tetrachloride was reacted with one equivalent of 2,2′-dithiobis(6-*tert*-butyl-4-methylphenol) (dtbmpH_2)[9] in hexane for 4 h, the dichloro complex Ti(dtbmp)Cl_2 (**1**) could be isolated in 78% yield as a dark red powder. Analytical, mass and ^{1}H and ^{13}C NMR spectroscopic data are consistent with a mononuclear structure with two terminal chloro ligands in which the dtbmp ligand acts as a chelating ligand. Upon complexation, all ^{1}H and ^{13}C NMR signals are shifted to lower field. In contrast to the sparingly soluble dichloro titanium complexes with the chelating bridged bisphenoxy ligands of the type [Ti{Z(OC_6H_2-4-Me-6-*t*Bu)$_2$}Cl_2] (Z = S,[5] SO,[10] and SO_2),[5b] but similar to the methylene- and ethylene-linked derivatives [Ti(mbmp)Cl_2][4a] and [Ti(ebmp)Cl_2],[7] hexane-soluble **1** appears to be mononuclear in solution.

The homologous dark red dibromo and black diiodo complexes **2** and **3** were prepared by reaction of the novel tri(isopropoxy) derivative [Ti_2(O*i*Pr)$_4$(μ_2-O*i*Pr)$_2$(dtbmp)] (**4**), described below, with an excess of Me_3SiX (X = Br, I) in ca. 40% yield. Since the analytical, mass, and ^{1}H and ^{13}C NMR spectroscopic data of **2** and **3** are similar to those of **1**, a structure analogous to that of **1** can be implied for both. Single crystals obtained by slow crystallization from pentane solutions could be analyzed by X-ray diffraction. The two complexes are isomorphous. The crystallographic data are summarized in Table 1 and an ORTEP diagram of the diiodo complex **3** is depicted in Figure 1. The molecule resides on a crystallographically imposed C_2 axis. The coordination sphere around the tetravalent titanium center can be described as strongly distorted octahedral. Whereas the two halo ligands and the two sulfur atoms of the disulfide bridge form a sort of equatorial plane [dihedral angle be-

 © WILEY-VCH Verlag GmbH, D-69451 Weinheim, 2000 1434−1948/00/0606−1321 $ 17.50+.50/0



Scheme 1

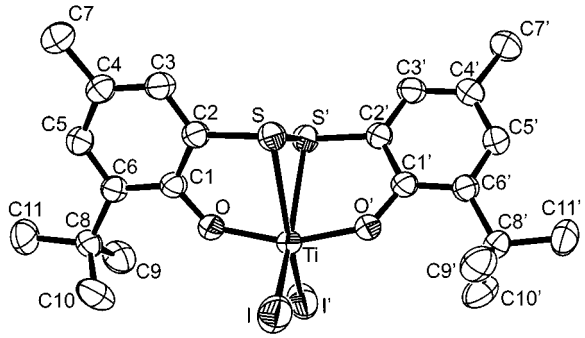


Figure 1. ORTEP diagram of the molecular structure of Ti(dtbmp)I_2 (**3**); thermal ellipsoids are drawn at 50% probability level; hydrogen atoms are omitted for the sake of clarity; selected bond lengths (Å) and angles (°): Ti−I 2.6225(6), Ti−O 1.847(2), Ti−S 2.637(1), S−S′ 2.137(2); I−Ti−I 111.00(3), O−Ti−O 158.2(1), C1−O−Ti 135.9(2), C2−S−S′ 99.8(1), S−Ti−S′ 47.82(4)

tween the TiI_2 and TiS_2 planes 12.68(2)°], the phenoxy oxygen atoms can be considered as adopting the apical sites [O−Ti−O 158.2(1)°]. While the titanium−iodine bond lengths are within the expected range of 2.65 Å,[11] the titanium−sulfur bond of 2.637(1) Å is shorter than that observed in most other tbmp titanium complexes.[5] In agreement with a stronger titanium−disulfide interaction, the sulfur−sulfur distance of 2.137(2) Å is significantly longer than that in $dtbmpH_2$ (2.086 Å).[9b] The angles at the phenoxy oxygen atoms are 135.9(2)° and are considerably smaller than the corresponding values in Ti(ebmp)Br_2[5b,7]

Table 1. Crystallographic data for **2**, **3**, **4**, and **6**

Compound	**2**	**3**	**4**	**6**
Empirical formula	$C_{22}H_{28}Br_2O_2S_2Ti$	$C_{22}H_{28}I_2O_2S_2Ti$	$C_{40}H_{70}O_8S_2Ti_2$	$C_{60}H_{92}O_8S_4Ti_2{\cdot}0.5C_6H_6$
Formula mass	596.28	690.26	838.88	1204.43
Crystal color	red	black	orange	orange
Crystal size [mm]	0.9 × 0.5 × 0.4	0.6 × 0.3 × 0.3	0.6 × 0.4 × 0.3	1.10 × 1.04 × 0.94
Crystal system	monoclinic	monoclinic	triclinic	orthorhombic
Space group	*C*2/*c*	*C*2/*c*	$P\bar{1}$	$Pna2_1$
a [Å]	14.505(6)	14.355(2)	10.249(1)	19.206(3)
b [Å]	11.949(5)	12.248(3)	13.763(1)	15.614(3)
c [Å]	14.635(5)	14.949(3)	19.018(3)	23.740(2)
α [°]	90	90	70.495(9)	90
β [°]	99.08(3)	95.55(1)	76.34(1)	90
γ [°]	90	90	77.779(8)	90
V [Å^3]	2505(2)	2616.0(9)	2431.2(5)	7119(2)
Z	4	4	2	4
$\rho_{calcd.}$ [g cm^{-3}]	1.581	1.753	1.146	1.124
μ [mm^{-1}]	3.714	2.862	0.456	0.387
F(000)	1200	1344	900	2580
$2\theta_{max}$ [°]	56	60	52	56
Index ranges	$0 \le h \le 19$	$-20 \le h \le 20$	$0 \le h \le 12$	$0 \le h \le 25$
	$-10 \le k \le 15$	$-17 \le k \le 17$	$-16 \le k \le 16$	$-20 \le k \le 18$
	$-19 \le l \le 19$	$-20 \le l \le 20$	$-22 \le l \le 23$	$-31 \le l \le 22$
Transmission (min/max)	86.68/99.96	91.91/100.00	96.73/99.85	95.39/100.00
Reflections collected	3307	7554	10039	21760
Independent reflections	3015	3781	9480	11952
	R_{int} = 0.0695	R_{int} = 0.0200	R_{int} = 0.0138	R_{int} = 0.0253
Observed with $I > 2\sigma(I)$	1742	2822	6770	9456
No. of parameters	188	174	613	730
*R*1/*wR*2/*GOF* [$I > 2\sigma(I)$]	0.0681/0.1473/1.068	0.0366/0.0910/1.083	0.0455/0.1127/1.059	0.0418/0.1097/1.071
*R*1/*wR*2/*GOF* (all data)	0.1311/0.1809/1.167	0.0564/0.1061/1.081	0.0783/0.1323/1.038	0.0589/0.1204/1.037
Resid. electron density [eÅ^{-3}]	1.183/−0.603	1.363/−1.033	0.419/−0.280	0.362/−0.259

and mononuclear nonchelating phenolato titanium complexes.[12]

Attempts to alkylate the dihalo complexes invariably resulted in the formation of dark intractable material. We suspect that the disulfide bridge is irreversibly cleaved by the reducing alkylating reagents. As anticipated, polymerization tests upon activation with MAO and ethylene were irreproducible and showed no significant activity.

When titanium tetra(isopropoxide) was reacted with one equivalent of dtbmpH_2 in toluene for three days, orange crystals of what was initially thought to be [Ti(dtbmp)(O-*i*Pr)$_2$] could be isolated. Analogous reactions of titanium tetra(isopropoxide) with methylene-, ethylene-, thio-, sulfinyl- and sulfone-bridged bisphenol all gave the di(isopropoxy) complexes [Ti{Z(OC$_6$H$_2$-4-Me-6-*t*Bu)$_2$}](O*i*Pr)$_2$ in quantitative yield.[5] However, the elemental analysis and mass spectrum of **4** indicated a dinuclear structure with only one half dtbmp ligand per titanium with a formula corresponding to [Ti$_2$(O*i*Pr)$_6$(dtbmp)]. The ^{1}H NMR spectrum has the rather striking feature of all methyl groups of the six isopropoxy groups being diastereotopic. Accordingly, the ^{13}C NMR spectrum gives rise to three inequivalent isopropyl groups. The molecule therefore does not contain any mirror plane, although the two halves of the dtbmp ligand are equivalent. This appearance is temperature independent in the range of −80 to +110 °C.

Single crystals of **4** obtained by slow cooling of a saturated solution in 2-propanol were studied by X-ray crystallography. The ORTEP diagram of the molecule is shown in Figure 2 and the crystallographic data are listed in Table 1. The results of the diffraction study reveal a dinuclear structure in which two Ti(O*i*Pr)$_2$ fragments are linked by two O*i*Pr groups and one bridging dtbmp ligand. The bulky dtbmp ligand spans the Ti$_2$(O*i*Pr)$_2$ plane so as to be located in a highly skewed way, rendering the molecule chiral. The coordination geometry around the titanium centers can be regarded as distorted octahedral. The titanium−sulfur distances with 2.7954(9) and 2.768(1) Å are clearly longer than the distance in **3**, whereas the sulfur−sulfur distance is 2.100(1) Å. The coordination mode of the disulfide fragment in **4** is comparable to that found in [(TiCl$_3$)$_2$(μ-Cl)$_2$(μ-MeSSMe)], for which titanium−sulfur distances of 2.712(3) and 2.742(3) Å and a sulfur−sulfur distance of 2.052(3) Å were reported.[13]

When equimolar mixtures of titanium tetramethoxide and tetra(*n*-butoxide) are reacted with dtbmpH_2 in toluene, orange precipitates of the dialkoxo complexes of the formula [Ti(dtbmp)(OR)$_2$] [R = Me (**5**), *n*Bu (**6**)] are formed. Based on the low solubility of **5** and **6**, a dimeric structure similar to that of [Ti{Z(OC$_6$H$_2$-4-Me-6-*t*Bu)$_2$}(O*i*Pr)$_2$]$_2$ (Z = S,[7] SO,[10] and SO$_2$[5b]) is inferred. The ^{1}H and ^{13}C NMR spectroscopic data are consistent with a C_{2h} symmetry, since two separate sets of signals for the *n*-butoxy groups are recorded. Most notably, the α-protons of the bridging group are diastereotopic and appear as two higher-order multiplets, whereas those of the terminal *n*-butoxy group give rise to a binomial triplet at 4.87 ppm with $^3J_{HH}$ = 4 Hz. The single crystal structure analysis of **6** confirmed a related dimeric structure (Table 1, Figure 3). The centrosymmetric molecule consists of two Ti{S$_2$(OC$_6$H$_2$-4-Me-6-*t*Bu)$_2$}(O*n*Bu) fragments bridged by two O*n*Bu groups in the familiar manner. The most striking feature relates to the coordination of the disulfide bridge. Only one sulfur atom is coordinated to the titanium center with a bond length of 2.692(1) and 2.694(1) Å. These distances are somewhat shorter than those in [Ti{S(OC$_6$H$_2$-4-Me-6-*t*Bu)$_2$}(O*n*Bu)$_2$]$_2$ [2.738(1) Å[5b]] and in other titanium(IV) complexes containing the tbmp ligand,[5] and may reflect a stronger titanium−sulfur bond. The other sulfur atoms of the disulfide links have a distance to the titanium of 3.828(2) and 3.832(2) Å and can be considered to be nonbonding. In agreement with this unsymmetrical bonding situation, the titanium−oxygen bonds Ti1−O4 and Ti2−O7 within the phenoxy moieties with the nonbonding

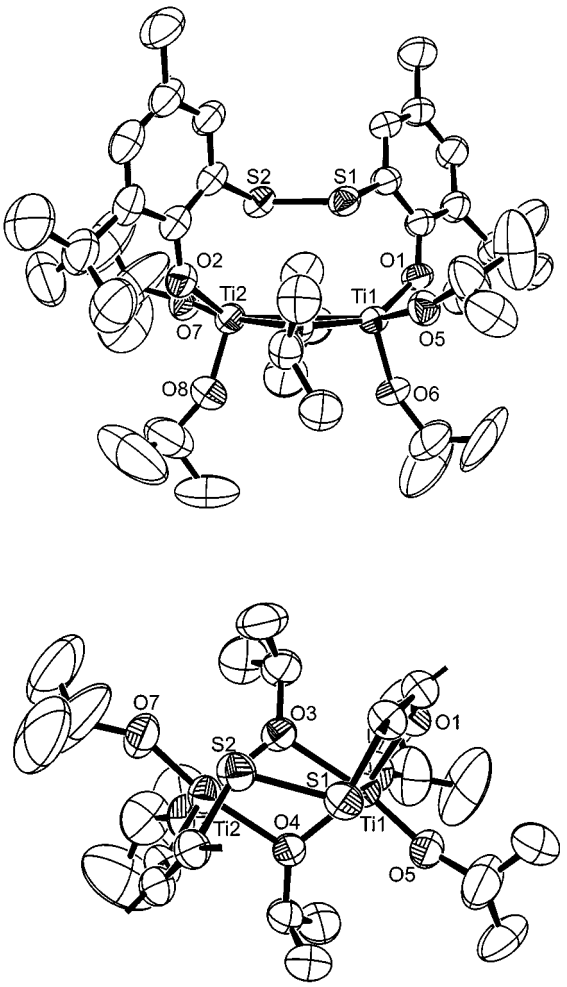


Figure 2. ORTEP diagram of the molecular structure of Ti$_2$(O*i*Pr)$_4$(μ-O*i*Pr)$_2$(dtbmp) (**4**): (a) side view; (b) top view; ring carbon atoms except those at the *ipso* and *ortho* positions have been omitted; thermal ellipsoids are drawn at 50% probability level; hydrogen atoms are omitted for the sake of clarity; selected bond lengths (Å) and angles (°): Ti1−O1 1.920(2), Ti1−O5 1.784(2), Ti1−O6 1.773(2), Ti1−O3 2.100(2), Ti1−O4 1.971(2), Ti1−S1 2.7954(9), Ti2−O2 1.923(2), Ti2−O7 1.786(2), Ti2−O3 1.972(2), Ti2−O4 2.087(2), Ti2−O8 1.779(2), Ti2−S2 2.768(1), S1−S2 2.100(1); O6−Ti1−S1 170.95(8), O3−Ti1−O5 164.97(9), O1−Ti1−O4 147.39(8), O3−Ti1−O4 72.26(7), S2−S1−Ti1 100.45(4)

sulfur atoms are significantly shorter than Ti1−O3 and Ti2−O6 and the angles at the oxygen atoms O4 and O7 are larger than those at O3 and O6. The sulfur−sulfur bond length is 2.059(2) Å and significantly shorter not only than that in **3** and **6**, but also that in dtbmpH_2. This observation can be explained by a partial sulfur−sulfur double bond character of the disulfide bridge, when only one sulfur atom is coordinated. Finally, the apparent mirror plane in the solution structure can be accounted for by a fast 1,2-shift of the titanium center from one sulfur atom to the other.

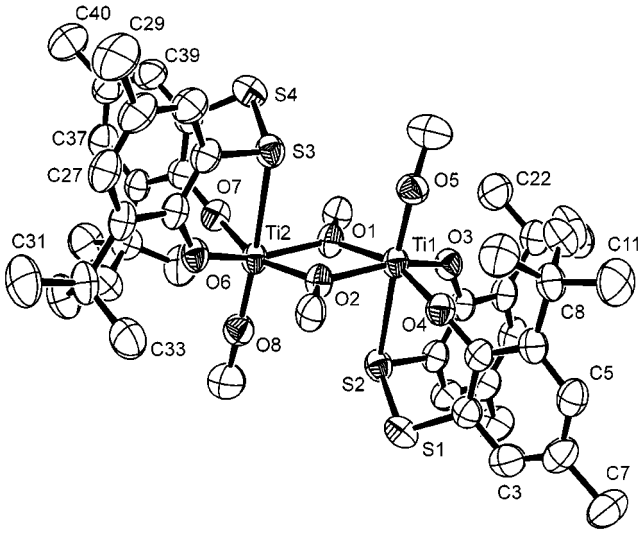


Figure 3. ORTEP diagram of the molecular structure of Ti_2(O*n*Bu)$_2$(μ-O*n*Bu)$_2$(dtbmp)$_2$ (**6**); thermal ellipsoids are drawn at 50% probability level; carbon atoms of the *n*-butoxy groups except those in the α-positions and hydrogen atoms are omitted for the sake of clarity; selected bond lengths (Å) and angles (°): Ti1−O1 2.038(3), Ti1−O2 1.997(2), Ti1−O3 1.903(2), Ti1−O4 1.855(3), Ti1−O5 1.767(3), Ti1−S2 2.692(1), Ti1−S1 3.828(2), S1−S2 2.059(2), S3−S4 2.063(2), Ti2−S3 2.694(1), Ti2−S4 3.832(2); C2−S1−S2 109.2(2), C2−S1−Ti1 76.3(1), S2−S1−Ti1 42.36(4), O1−Ti1−O2 72.91(9), O3−Ti1−O4 96.8(1) O5−Ti1−S2 171.03(9), Ti2−O1−Ti1 107.0(1), Ti1−O2−Ti2 107.5(1), C13−O3−Ti1 133.3(2), C1−O4−Ti1 153.2(3), C53−O5−Ti1 153.1(4).

In summary, we have synthesized and structurally characterized a series of tetravalent titanium complexes containing a disulfide-linked bis(phenolato) ligand dtbmp. Compared with the ethylene-bridged ligand ebmp, the coordination of the disulfide function at the tetravalent titanium center results in various coordination modes: η^2-S_2 in **2** and **3**, μ-η^1-S_2 in **4**, and η^1-S_2 in **6**. In the literature, most of the disulfide coordination chemistry is confined to that of softer late transition or coinage metals.[13] The facile reduction may, however, limit the application of titanium complexes containing the disulfide-linked bis(phenolato) ligand in polymerization catalysis.

Experimental Section

General: All experiments were performed under argon with standard Schlenk techniques. Solvents were purified, dried and distilled under argon. − ^{1}H and ^{13}C NMR: Bruker DRX 400, AC 200 or AM 400; all spectra in $CDCl_3$ at 25 °C. − Mass Spectra: Finnigan 8230. − Elemental analyses: Microanalytical laboratory of this department.

2,2′-Dithiobis(6-*tert*-butyl-4-methylphenol) (dtbmpH_2): To a solution of 2-*tert*-butyl-4-methylphenol (126 g, 767 mmol) in 120 mL of toluene was added over a period of 2 h a solution of disulfur dichloride (34.2 mL, 57.7 g, 433 mmol) in 100 mL of toluene at room temperature. The reaction mixture was stirred at 80 °C for an additional 90 min. The solvent was evaporated and the viscous, orange-brown crude product was dissolved in hot ethanol. After cooling and recrystallization from methanol in order to remove 2,2′-trithiobis(6-*tert*-butyl-4-methylphenol), yellow crystals of 2,2′-dithiobis(6-*tert*-butyl-4-methylphenol) were obtained. Yield 53.6 g (36%), m.p. 107 °C. − ^{1}H NMR: δ = 1.36 [s, 18 H, C(CH_3)$_3$], 2.18 (s, 6 H, 4-CH_3), 6.53 (s, 2 H, OH), 6.99 (d, $^4J_{HH}$ = 2 Hz, 2 H, 3-H), 7.11 (d, $^4J_{HH}$ = 2 Hz, 2 H, 5-H). − ^{13}C{^{1}H} NMR: δ = 20.5 (4-*C*H_3), 29.5 [C(*C*H_3)$_3$], 35.0 [*C*(CH$_3$)$_3$], 120.6 (C-2), 129.1 (C-4), 131.4 (C-5), 134.0 (C-3), 136.3 (C-6), 153.2 (C-1). − EI MS: *m*/*z* (%) = 390 (57) [M$^+$], 358 (82) [$C_{21}H_{26}OS_2^+$], 195 (52) [M^{2+}], 164 (100) [$C_{11}H_{16}O^+$], 149 (41) [$C_{10}H_{13}O^+$], 91 (17) [$C_7H_7^+$]. − $C_{22}H_{30}O_2S_2$ (390.6): calcd. C 67.65, H 7.74; found C 67.53, H 7.55.

Dichloro{2,2′-dithiobis(6-*tert*-butyl-4-methylphenolato)}titanium (1): To a solution of titanium tetrachloride (0.38 mL, 3.48 mmol) in 30 mL of hexane was added slowly a solution of 2,2′-dithiobis(6-*tert*-butyl-4-methylphenol) (1.36 g, 3.48 mmol) in 35 mL of hexane at room temperature. A dark red powder started to precipitate and the reaction mixture was stirred for an additional 4 h. After evaporation of the solvent, the residue was washed with 10 mL of hexane to afford 1.38 g of dark red microcrystals (78%). − ^{1}H NMR: δ = 1.49 [s, 18 H, C(CH_3)$_3$], 2.33 (s, 6 H, 4-CH_3), 7.25 (d, $^4J_{HH}$ = 1.4 Hz, 2 H, 3-H), 7.45 (d, $^4J_{HH}$ = 1.4 Hz, 2 H, 5-H). − ^{13}C{^{1}H} NMR: δ = 20.9 (4-*C*H_3), 29.5 [C(*C*H_3)$_3$], 35.4 [*C*(CH$_3$)$_3$], 122.6 (C-2), 127.8 (C-4), 132.0 (C-5), 132.2 (C-3), 137.5 (C-6), 168.0 (C-1). − EI MS: *m*/*z* (%) = 506 (27) [M$^+$], 471 (32) [M$^+$ − Cl], 194 (52) [$C_{11}H_{14}OS^+$], 91 (100) [$C_7H_7^+$]. − $C_{22}H_{28}Cl_2O_2S_2Ti$ (507.4): calcd. C 52.08, H 5.56; found C 50.98, H 5.41.

Dibromo{2,2′-dithiobis(6-*tert*-butyl-4-methylphenolato)}titanium (2): To a solution of **4** (100 mg, 119 μmol) in 15 mL pentane was added bromotrimethylsilane (97.4 μL, 715 μmol) at room temperature. After 2 d dark red crystals precipitated from the solution. Filtration and washing with 2 mL of pentane afforded the product, yield 31 mg (44%). − ^{1}H NMR: δ = 1.52 [s, 18 H, C(CH_3)$_3$], 2.33 (s, 6 H, 4-CH_3), 7.26 (d, $^4J_{HH}$ = 1.4 Hz, 2 H, 3-H), 7.45 (d, $^4J_{HH}$ = 1.4 Hz, 2 H, 5-H). − ^{13}C{^{1}H} NMR: δ = 20.9 (4-*C*H_3), 29.6 [C(*C*H_3)$_3$], 35.4 [*C*(CH$_3$)$_3$], 120.6 (C-2), 129.0 (C-4), 131.4 (C-5), 133.9 (C-3), 137.4 (C-6), 168.1 (C-1). − EI MS: *m*/*z* (%) = 596 (100) [M$^+$], 517 (78) [M$^+$ − Br], 460 (52) [M$^+$ − Br − C_4H_9], 196 (12) [$C_{11}H_{16}OS^+$]. − $C_{22}H_{28}Br_2O_2S_2Ti$ (596.3): calcd. C 44.32, H 4.77; found C 44.27, H 4.73.

Diiodo{2,2′-dithiobis(6-*tert*-butyl-4-methylphenolato)}titanium (3): To a solution of **4** (180 mg, 324 μmol) in 20 mL pentane was added iodotrimethylsilane (0.26 mL, 1.92 mmol) at room temperature. After 2 d black crystals precipitated from the solution. Filtration and washing with 5 mL of pentane afforded the product, yield 86 mg (38%). − ^{1}H NMR: δ = 1.61 [s, 18 H, C(CH_3)$_3$], 2.32 (s, 6 H, 4-CH_3), 7.30 (d, $^4J_{HH}$ = 2 Hz, 2 H, 3-H), 7.45 (d, $^4J_{HH}$ = 2 Hz, 2 H, 5-H). − ^{13}C{^{1}H} NMR: δ = 20.8 (4-*C*H_3), 29.7 [C(*C*H_3)$_3$], 35.3 [*C*(CH$_3$)$_3$], 122.8 (C-2), 129.0 (C-4), 131.2 (C-5), 131.9 (C-3), 133.7 (C-6), 168.2 (C-1). − EI MS: *m*/*z* (%) = 564 (13) [M$^+$ − I], 436 (100) [M$^+$ − 2I,], 331 (14) [M$^+$ − 2 I − 2 C_4H_9], 127 (96) [I$^+$] − $C_{22}H_{28}I_2O_2S_2Ti$ (690.3): calcd. C 38.28, H 4.09; found C 38.08, H 4.14.

Tetra(isopropoxy)di(μ-isopropoxy){μ-2,2′-dithiobis(6-*tert*-butyl-4-methylphenolato)}dititanium (4): To a suspension of 2,2′-dithiobis(6-*tert*-butyl-4-methylphenol) (1.88 g, 4.81 mmol) in 50 mL of dry 2-propanol was added titanium tetra(isopropoxide) (2.84 mL, 9.62 mmol) and the reaction mixture stirred for 2 d at room temperature. During this time the color of the solution changed from yellow to orange. The solution was concentrated to a volume of ca. 30 mL and cooled to −78 °C for 16 h to give orange crystals, yield 2.58 g (64%). − ^{1}H NMR: δ = 0.97 [d, $^3J_{HH}$ = 6.2 Hz, 6 H, CH(CH_3)$_2$], 1.00 [d, $^3J_{HH}$ = 6.2 Hz, 6 H, CH(CH_3)$_2$], 1.07 [d, $^3J_{HH}$ = 6.2 Hz, 6 H, CH(CH_3)$_2$], 1.22 [d, $^3J_{HH}$ = 6.2 Hz, 6 H, CH(CH_3)$_2$], 1.34 [d, $^3J_{HH}$ = 6.2 Hz, 6 H, CH(CH_3)$_2$], 1.40 [s, 18 H, C(CH$_3$)$_3$], 1.48 [d, $^3J_{HH}$ = 6.2 Hz, 6 H, CH(CH_3)$_2$], 2.26 (s, 6 H, 4-CH$_3$), 4.58 [sept, $^3J_{HH}$ = 6.2 Hz, 2 H, CH(CH$_3$)$_2$], 4.97 [sept, $^3J_{HH}$ = 6.2 Hz, 2 H, CH(CH$_3$)$_2$], 5.06 [sept, $^3J_{HH}$ = 6.2 Hz, 2 H, CH(CH$_3$)$_2$], 7.04 (d, $^4J_{HH}$ = 2 Hz, 2 H, 3-H), 7.38 (d, $^4J_{HH}$ = 2 Hz, 2 H, 5-H). − ^{13}C{^{1}H} NMR: δ = 20.8 (4-CH$_3$), 24.1 [CH(CH$_3$)$_2$], 24.8 [CH(CH$_3$)$_2$], 25.7 [CH(CH$_3$)$_2$], 26.1 [CH(CH$_3$)$_2$], 26.3 [CH(CH$_3$)$_2$], 26.3 [CH(CH$_3$)$_2$], 29.7 [C(CH$_3$)$_3$], 35.2 [C(CH$_3$)$_3$], 74.4 [CH(CH$_3$)$_2$], 78.5 [CH(CH$_3$)$_2$], 79.8 [CH(CH$_3$)$_2$], 118.7 (C-2), 127.0 (C-4), 131.1 (C-5), 133.8 (C-3), 137.0 (C-6), 167.2 (C-1). − EI MS: *m*/*z* (%) = 554 (2) [M$^+$ − Ti(OC$_3$H$_7$)$_4$], 436 (6) [C$_{22}$H$_{28}$O$_2$S$_2$Ti$^+$], 269 (100) [(M$^+$ − Ti(OC$_3$H$_7$)$_4$ − CH$_4$)$^{2+}$], 225 (13) [C$_{11}$H$_{13}$OS$_2^+$]. − C$_{40}$H$_{70}$O$_8$S$_2$Ti$_2$ (838.9): calcd. C 57.27, H 8.41; found C 57.08, H 9.20.

Tetramethoxybis{2,2′-dithiobis(6-*tert*-butyl-4-methylphenolato)}-dititanium (5): A mixture of 2,2′-dithio(6-*tert*-butyl-4-methylphenol) (1.68 g, 4.30 mmol) and titanium tetramethoxide (741 mg, 4.30 mmol) in 25 mL of toluene was stirred for 3 d at room temperature. After the solvent was evaporated, residual titanium tetramethoxide was removed by filtration of chloroform extracts of the reaction mixture. Evaporation of the solvent afforded a yellow powder, yield 894 mg (42%). − ^{1}H NMR: δ = 1.38 [s, 18 H, C(CH$_3$)$_3$], 2.18 (s, 6 H, 4-CH$_3$), 3.98 [br s, 3 H, OCH$_3$], 4.55 [3 H, OCH$_3$(term.)], 6.89 (d, $^4J_{HH}$ = 2 Hz, 2 H, 3-H), 7.05 (d, $^4J_{HH}$ = 2 Hz, 2 H, 5-H). − ^{13}C{^{1}H} NMR: δ = 20.7 (4-CH$_3$), 29.8 [C(CH$_3$)$_3$], 35.1 [C(CH$_3$)$_3$], 63.6, 67.1 [OCH$_3$], 119.1 (C-2), 128.2 (C-4), 128.7 (C-5), 129.0 (C-3), 129.5 (C-6), 162.8 (C-1). − EI MS: *m*/*z* (%) = 390 (65) [M/2$^+$ − 2OCH$_3$ − Ti], 195 (52) [(M/2 − 2OCH$_3$ − Ti)$^{2+}$], 164 (100) [C$_{11}$H$_{16}$O$^+$], 91 (85) [C$_7$H$_7^+$]. − C$_{48}$H$_{68}$O$_8$S$_4$Ti$_2$ (997.1): calcd. C 57.82, H 6.87; found C 59.98, H 6.83.

Tetra(*n*-butoxy){2,2′-dithiobis(6-*tert*-butyl-4-methylphenolato)}-dititanium (6): To a solution of 2,2′-dithio(6-*tert*-butyl-4-methylphenol) (917 mg, 2.35 mmol) in toluene was added titanium tetra(*n*-butoxide) (0.80 mL, 2.35 mmol). The reaction mixture was stirred for 18 h at room temperature. During this time an orange solid precipitated. Filtration and washing with 2 × 10 mL of toluene afforded orange-yellow microcrystals, yield 992 mg (73%). − ^{1}H NMR: δ = 0.44 (t, 3 H, CH$_2$CH$_2$CH$_2$CH_3), 0.86 (m, 2 H, γ-CH$_2$), 1.02 (t, 3 H, CH$_2$CH$_2$CH$_2$CH_3), 1.35 [s, 18 H, C(CH$_3$)$_3$], 1.51 (m, 2 H, γ-CH$_2$), 1.59 [m, 1 H, β-CH$_2$(term.)], 1.65 [m, 1 H, β-CH$_2$(term.)], 1.81 (m, 2 H, β-CH$_2$), 2.15 (s, 6 H, 4-CH$_3$), 4.13−4.31 (m, 2 H, OCH$_2$), 4.87 [t, $^3J_{HH}$ = 4 Hz, 2 H, OCH$_2$-(term.)], 6.84 (d, $^4J_{HH}$ = 2 Hz, 2 H, 3-H), 6.99 (d, $^4J_{HH}$ = 2 Hz, 2 H, 5-H). − ^{13}C{^{1}H} NMR: δ = 13.8, 14.1 (CH$_2$CH$_2$CH$_2$$CH_3$), 18.3, 19.1 (CH$_2CH_2$$CH_2CH_3$), 20.7 (4-$CH_3$), 30.0 [C($CH_3$)$_3$], 30.9, 34.5 (CH$_2$$CH_2CH_2CH_3$), 35.1 [$C$(CH$_3$)$_3$], 76.1, 80.1 ($CH_2CH_2CH_2CH_3$), 118.7 (C-2), 128.5 (C-4), 129.0 (C-5), 129.3 (C-3), 137.3 (C-6), 163.0 (C-1). − EI MS: *m*/*z* (%) = 582 (84) [M/2$^+$], 550 (100) [M/2$^+$ − 2 CH$_4$], 438 (99) [M/2$^+$ − 2 OC$_4$H$_9$]. − C$_{60}$H$_{92}$O$_8$S$_4$Ti$_2$ (1165.4): calcd. C 61.84, H 7.95; found C 60.89, H 7.84.

Crystal Structure Determinations of 2, 3, 4, and 6: Relevant crystallographic data are summarized in Table 1. X-ray data were collected with an Enraf−Nonius CAD4 diffractometer at 296(2) K by using Mo-K_α radiation and ω scans. Data reductions were carried out using the program system MOLEN.[15a] The structures of **2, 4,** and **6** were solved by direct methods (SHELXS-86);[15b] the structure of **3** was solved by isotypic replacement using the coordinates of **2**. All structures were refined by full-matrix least squares against F^2 (SHELXL-93).[15c] Non-hydrogen atoms were located in difference Fourier maps and refined anisotropically. All hydrogen atoms in **2** and **3** were located in difference Fourier maps and refined isotropically, whereas in **4** the hydrogen atoms of several methyl groups are included in calculated positions. In **6**, all hydrogen atoms were included into calculated positions. Four of the isopropyl groups in **4** were refined with disordered split positions. The structure of **6** also shows strong disorder of the *n*-butyl groups. Crystallographic data (excluding structure factors) for the structures included in this paper have been deposited with the Cambridge Crystallographic Data Centre as supplementary publication nos. CCDC-140742 for **2**, -140743 for **3**, -170744 for **4**, and -140745 for **6**. Copies of the data can be obtained free of charge on application to CCDC, 12 Union Road, Cambridge CB2 1EZ, UK [Fax: (internat.) + 44-1223/336-033; E-mail: deposit@ccdc.cam.ac.uk].

Acknowledgments

Generous financial support by the Fonds der Chemischen Industrie and the Deutsche Forschungsgemeinschaft is gratefully acknowledged.

[1] [1a] M. Kakugo, T. Miyatake, K. Mizunuma, *Chem. Express* **1987**, *2*, 445. − [1b] T. Miyatake, K. Mizunuma, Y. Seki, M. Kakugo, *Makromol. Chem., Rapid Commun.* **1989**, *10*, 349. − [1c] T. Miyatake, K. Mizunuma, M. Kakugo, *Makromol. Chem., Macromol. Symp.* **1993**, *66*, 203. − [1d] C. J. Schaverien, A. J. van der Linden, A. G. Orpen, *Am. Chem. Soc., Polym. Div., Polymer Prepr.* **1994**, *35*, 672. − [1e] C. J. Schaverien, A. J. van der Linden, A. G. Orpen, *J. Am. Chem. Soc.* **1995**, 117, 3008.

[2] H. H. Brintzinger, D. Fischer, R. Mülhaupt, B. Rieger, R. M. Waymouth, *Angew. Chem.* **1995**, *107*, 1255; *Angew. Chem. Int. Ed. Engl.* **1995**, *34,* 1143.

[3] G. J. P. Britovsek, V. C. Gibson, D. F. Wass, *Angew. Chem.* **1999**, *111*, 448; *Angew. Chem. Int. Ed.* **1999**, *38*, 428.

[4] [4a] J. Okuda, S. Fokken, H.-C. Kang, W. Massa, *Chem. Ber.* **1995**, *128*, 221. − [4b] C. Floriani, F. Corazza, W. Lesueur, A. Chiesi-Villa, C. Guastini, *Angew. Chem.* **1989**, *101*, 93; *Angew. Chem. Int. Ed. Engl.* **1989**, *28*, 66. − [4c] F. Corazza, C. Floriani, A. Chiesi-Villa, C. Guastini, *Inorg. Chem.* **1991**, *30*, 146.

[5] [5a] S. Fokken, T. P. Spaniol, H.-C. Kang, W. Massa, J. Okuda, *Organometallics* **1996**, *15*, 5069. − [5b] S. Fokken, Doctoral Thesis, University of Marburg, Germany, **1997**. − [5c] L. Porri, R. Ripa, P. Colombo, E. Moano, S. Capelli, S. V. Meille, *J. Organomet. Chem.* **1996**, *514*, 213.

[6] [6a] R. D. J. Froese, D. G. Musaev, T. Matsubara, K. Morokuma, *J. Am. Chem. Soc.* **1997**, *119*, 7190. − [6b] R. D. J. Froese, D. G. Musaev, K. Morokuma, *Organometallics* **1999**, *18*, 373.

[7] S. Fokken, T. P. Spaniol, J. Okuda, F. G. Sernetz, R. Mülhaupt, *Organometallics* **1997**, *16*, 4240.

[8] F. G. Sernetz, R. Mülhaupt, S. Fokken, J. Okuda, *Macromolecules* **1997**, *30*, 1562.

[9] [9a] A. H. Weinstein, *J. Org. Chem.* **1967**, *32*, 3669. − [9b] L. A. Chetkina, V. E. Zavodnik, V. K. Belskii, I. G. Arzamanova, A. P. Krysin, Y. A. Gurvich, L. I. Kuzubova, *Zh. Strukt. Khim.* **1986**, *27*, 112.

[10] J. Okuda, S. Fokken, H.-C. Kang, W. Massa, *Polyhedron* **1998**, *17*, 943.

[11] [11a] B. Tsuie, D. C. Swenson, R. F. Jordan, J. L. Petersen, *Organometallics* **1997**, *16*, 1392 [Ti−I = 2.6321(7) Å in Ti{(NSiMe$_3$)$_2$C$_6$H$_{10}$}I$_2$]. − [11b] A. J. Edwards, N. J. Burke, C.

M. Dobson, K. Prout, S. J. Heyes, *J. Am. Chem. Soc.* **1995**, *117*, 4637 [Ti−I = 2.731(3) Å in Ti{(η^5-C_5H_4)$_2$$CMe_2$$CMe_2$}$I_2$].
[12] [12a] S. L. Latesky, J. Keddington, A. K. McMullen, I. P. Rothwell, *Inorg. Chem.* **1985**, *24*, 995. – [12b] L. D. Durfee, S. L. Latesky, I. P. Rothwell, J. C. Huffman, K. Folting, *Inorg. Chem.* 1985, 24, 4569. – [12c] B. D. Steffey, P. E. Fanwick, I. P. Rothwell, *Polyhedron* **1990**, *9*, 963. – [12d] B. P. Santora, A. O. Larsen, M. R. Gagné, *Organometallics* **1998**, *17*, 3138.
[13] T. S. Lewkebandara, P. J. McKarns, B. S. Haggerty, G. P. A. Yap, A. L. Rheingold, C. H. Winter, *Polyhedron* **1998**, *17*, 1.
[14] D. Carillo, *Coord. Chem. Rev.* **1992**, *119*, 137.
[15] [15a] C. K. Fair, *MolEN*, An Interactive Structure Solution Procedure, Enraf−Nonius, Delft, **1990**. – [15b] G. M. Sheldrick, *SHELXS-86*, Program for the Solution of Crystal Structures, University of Göttingen, Germany, **1986**. – [15c] G. M. Sheldrick, *SHELXL-93*, Program for the Refinement of Crystal Structures, University of Göttingen, Germany, **1993**.

Received December 2, 1999
[I99438]

Chemoselectivity in Cyclosiloxanolate Cluster Formation: An Alkali Cation Effect?

Claudia Zucchi,[a] Manuela Mattioli,[a] Giovanna Gavioli,[a] Massimo Moret,[b] Angelo Sironi,[b] Renato Ugo,[c] Maddalena Pizzotti,[c] Olga I. Shchegolikhina,[d] and Gyula Pályi*[a]

Dedicated to Prof. Dr. Karl-Heinz Thiele (Halle-Merseburg) on the occasion of his 70th birthday

Keywords: Cations / Alkali metals / Cyclooligomerizations / Si ligands / Cluster compounds

The Cu_4 derivatives of $[EtSiO_2]Na$ have been synthesised and their cyclic voltammetry, spectroscopic behaviour and X-ray structure determination described. The changes in the alkali cation, Na^+ in place of K^+, might have a "tuning" effect in the organisation on the siloxanolate clusters resulting in a macrocyclic ($[EtSiO_2]_{12}$) ligand instead of two cyclic ($[EtSiO_2]_6$) ligands.

Introduction

Efforts at modelling[1] silica-supported transition metal catalysts[2] resulted in the discovery of reactions leading to cyclosiloxanolate clusters of higher valent transition metals.[3] This new class of metal clusters showed redox,[4] catalytic[5] and magnetic[6] features, which are interesting in their own right.

One of the most remarkable features of this chemistry is the high chemoselectivity of the organisation of these complexes.[3c,7] However, almost nothing is known about the factors which influence the architecture of the cyclosiloxanolate clusters. In this paper we report an observation which might be the first step in this direction.

Results and Discussion

It has been observed by one of our groups that the reaction of potassium ethylsiloxanolate with copper(II) chloride gives the sandwich-type complex **1** [Equation (1)].[8]

[a] Department of Chemistry, University of Modena and Reggio Emilia,
Via Campi 183, I-41100 Modena, Italy
Fax: (internat.) + 39-059/373-543
E-mail: palyi@unimo.it
[b] Department of Structural Chemistry and Inorganic Stereochemistry and CNR Centre, University of Milano,
Via Venezian 21, I-20133 Milano, Italy
Fax: (internat.) + 39-02/7063-5288
E-mail: angelo@csmtbo.mi.cnr.it
[c] Department of Inorganic and Organometallic Chemistry and CNR Centre, University of Milano,
Via Venezian 21, I-20133 Milano, Italy
Fax: (internat.) + 39-02/7066-2748
[d] A.N. Nesmeyanov Institute of Organoelement Chemistry, Russian Academy of Sciences,
28 Vavilov Street, Moscow 117813, Russia
Fax: (internat.) + 7-095/135-5085
E-mail: olga@ineos.ac.ru

$$12\ \text{"}EtSiO_2K\text{"} + 4\ CuCl_2 \rightarrow K_2\{[\text{cyclo-}(EtSiO_2)_6]_2Cu_4K_2\}\cdot 4n\text{BuOH}\ (\mathbf{1}) + 8\ KCl \quad (1)$$

Since copper(II) in earlier studies showed a tendency to also give tetrahedrally arranged Cu_4 derivatives with *only one* macrocyclic ($[RSiO_2]_{12}$) ligand, we tested whether changes in the experimental conditions would also result in tetrahedral moieties from ethylsiloxanolate anions. We therefore decided to try to change the alkali cation, which might be a "tuning" factor in the organisation of the siloxanolate clusters. In fact we observed that using sodium ethylsiloxanolate, we obtained the new complex **2** according to Equation (2)

$$12\ \text{"}EtSiO_2Na\text{"} + 4\ CuCl_2 \rightarrow Na_4[\text{cyclo-}(EtSiO_2)_{12}Cu_4]\cdot L_x\ \mathbf{(2)} + 8\ NaCl \quad (2)$$

where L_x = (**a**) 2 *n*BuOH·4NaCl; (**b**) 4 *n*BuOH. The yields observed from Equation (2) were comparable with the yields obtained with other cyclosiloxanolate clusters,[3c,7] which shows that the chemoselectivity observed in Equation (1) could *de facto* be changed by changing the alkali cation.

The new complex **2** has been characterised by elemental analysis and physical methods. Conductivity measurements showed the presence of a nondissociated cluster and relatively easy dissociation of the externally coordinated sodium ions, with λ_{eq} similar to that of other tetrahedral Cu_4 complexes.[9] Cyclic voltammetry showed a nearly reversible redox process at very negative potentials, more than 1.5 V more negative than the peak potential reported for the non-complexed Cu^{II}/Cu^0 couple.[10] This indicates a considerable stability of the complex core of **2** in solution towards dissociation, as well as survival of the reduction/oxidation process involved in the CV cycles. This behaviour seems to be

 © WILEY-VCH Verlag GmbH, D-69451 Weinheim, 2000 1434–1948/00/0606–1327 $ 17.50+.50/0

a general feature of the transition metal cyclosiloxanolate complexes.[4,9]

The medium (4000−400 cm^{-1}) and far (500−50 cm^{-1}) infrared spectra confirmed the presence of the structural elements proposed for the structure of complex **2** (C−H, Si−C, Si−O, Cu−O, Na−O interactions) indicating fairly weak Na−O interactions.

The single crystal X-ray structure determination gives a final proof for the structure of complex **2b** which, lying about the *a* Wickoff position, has a crystallographically imposed S_4 (−4) symmetry (Figure 1). The complex consists of a dodecahapto 36-membered macrocyclic ligand of formula $[(EtSiO_2)_{12}]^{12-}$ (Figure 2) binding four Cu^{2+} cations spatially arranged in a flattened tetrahedral unit. Four Na^+ cations are also loosely connected to the surface of the macrocycle leading to an overall neutral 44-membered cage. The twelve silicon and the four sodium atoms carry one exo ligand each (twelve ethyl radicals and four *n*-butyl alcohols, respectively) and the resulting "flattened spherical" moiety has a substantial lipophilic surface.

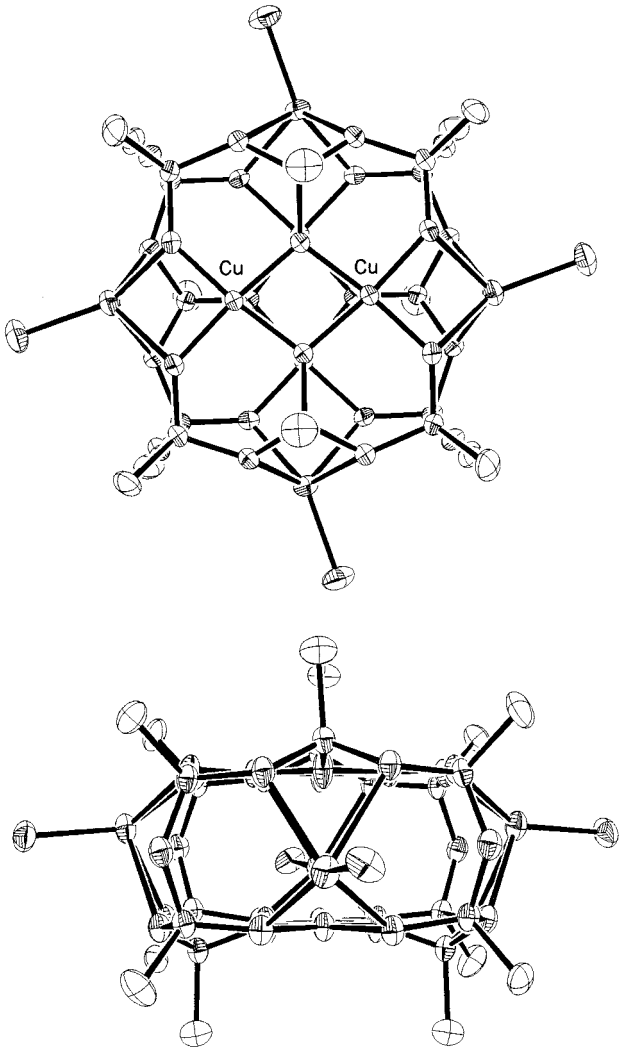


Figure 1. Two ORTEP drawings of $[(EtSiO_2)_{12}Cu_4Na_4]\cdot 4n$BuOH **(2b)**; the four disordered *n*-butyl alcohol ligands and the terminal methyl groups of the ethyl radicals are omitted for clarity; top: view down the S_4 axis; bottom: normal to the first view

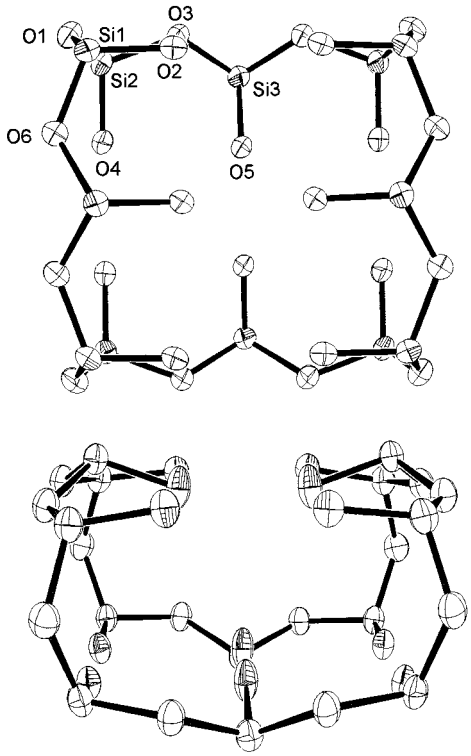


Figure 2. ORTEP drawing of the 36-membered macrocyclic cyclododeca(ethyl-siloxandodecanolate) ligand; top: view down the S_4 axis (the silicon atoms have shaded octants); bottom: almost normal to the first view (the silanolate oxygen atoms have shaded octants)

The Cu···Cu distances (≈ 3 Å) are too large to allow considerable metal−metal interactions. The coordination environment of the Cu^{2+} ions (four silanolate oxygens) is distorted square planar (as far as is allowed by the flexibility of the large ring). The Na^+ ions are coordinated to both silanolate (2) and siloxane (2) oxygens as well as to an "external" solvate butyl alcohol oxygen, thus reaching an approximately tetragonal pyramidal coordination environment.

Selected bond lengths and angles for the macrocyclic ligand are reported in Table 1; their average values ($Si-O_{silanol}$ 1.608 Å; $Si-O_{siloxane}$ 1.643 Å; Si−C 1.861 Å; $O_{siloxane}-Si-O_{siloxane}$ 106.7°; $O_{siloxane}-Si-O_{silanol}$ 109.46°; $O_{siloxane}-Si-C$ 109.2°; $O_{silanol}-Si-C$ 112.5°; Si−O−Si 128.9°) are close to those observed previously.[7,8]

The regiochemistry of the cyclododecasiloxandodecaolate ligand shows a peculiar distribution of the organic and silanol substituents with respect to each other (Figure 2). The stereospecificity of the cyclooligomerisation leading to the macrocyclic ligand is a clear indication that the metal "core" is organised first in the formation of the cyclosiloxanolate clusters, perhaps using also solvent (butyl alcohol) ligands, and this is followed by the building up of the siloxane chain from *suitably oriented* monomeric units. In the initial phase of the organisation we can thus identify the weak, but geometrically different,[11] orienting role ("template" effect) of the alkali cations. The stereochemistry of the Si_{12}-macrocycle in the present study is especially informative, especially when contrasted with the all-*cis* stereo-

Table 1. Selected bond lengths (Å) and angles (deg) for $[(EtSiO_2)_{12}Cu_4Na_4]\cdot 4n$BuOH

Cu−O(2)	1.900(2)	Cu−O(5)#1[a]	1.937(3)
Cu−O(4)#1[a]	1.939(2)	Cu−O(5)#2[b]	1.949(2)
Si(1)−O(2)	1.597(3)	Si(1)−O(1)	1.638(3)
Si(1)−O(6)	1.663(3)	Si(1)−C(1)	1.858(4)
Si(2)−O(4)	1.611(3)	Si(2)−O(1)	1.635(3)
Si(2)−O(3)	1.660(3)	Si(2)−C(2)	1.865(4)
Si(3)−O(5)	1.617(3)	Si(3)−O(6)#1[a]	1.628(3)
Si(3)−O(3)	1.635(2)	Si(3)−C(3)	1.860(5)
Na−O(7)	2.251(3)	Na−O(2)	2.322(3)
Na−O(4)#1[a]	2.402(3)	Na−O(3)	2.520(3)
Na−O(6)#1[a]	2.670(3)	C(1)−C(11A)	1.429(10)
C(1)−C(11B)	1.449(10)	C(2)−C(21)	1.558(6)
C(3)−C(31)	1.533(7)	O(7)−C(5)	1.440(5)
C(5)−C(6B)	1.508(6)	C(5)−C(6A)	1.508(6)
C(6A)−C(7A)	1.508(6)	C(6B)−C(7B)	1.508(6)
C(7A)−C(8A)	1.508(6)	C(7B)−C(8B)	1.508(6)
O(2)−Cu−O(5)#1[a]	174.11(10)	O(2)−Cu−O(4)#1[a]	90.39(10)
O(5)#1−Cu−O(4)#1[a]	95.46(10)	O(2)−Cu−O(5)#2[b]	95.55(10)
O(5)#1−Cu−O(5)#2[a][b]	78.58(11)	O(4)#1−Cu−O(5)#2[a][b]	173.88(10)
O(2)−Si(1)−O(1)	110.43(14)	O(2)−Si(1)−O(6)	110.59(13)
O(1)−Si(1)−O(6)	105.97(13)	O(2)−Si(1)−C(1)	113.46(19)
O(1)−Si(1)−C(1)	107.36(19)	O(6)−Si(1)−C(1)	108.71(17)
O(4)−Si(2)−O(1)	111.94(14)	O(4)−Si(2)−O(3)	109.54(13)
O(1)−Si(2)−O(3)	106.62(14)	O(4)−Si(2)−C(2)	112.52(16)
O(1)−Si(2)−C(2)	107.20(17)	O(3)−Si(2)−C(2)	108.80(16)
O(5)−Si(3)−O(6)#1[a]	108.53(14)	O(5)−Si(3)−O(3)	108.62(14)
O(6)#1−Si(3)−O(3)[a]	104.61(14)	O(5)−Si(3)−C(3)	111.45(19)
O(6)#1−Si(3)−C(3)[a]	112.43(19)	O(3)−Si(3)−C(3)	110.91(19)
O(7)−Na−O(2)	145.09(12)	O(7)−Na−O(4)#1[a]	116.23(12)
O(2)−Na−O(4)#1[a]	70.39(9)	O(7)−Na−O(3)	113.35(11)
O(2)−Na−O(3)	86.56(10)	O(4)#1−Na−O(3)[a]	120.90(10)
O(7)−Na−O(6)#1[a]	94.70(10)	O(2)−Na−O(6)#1[a]	120.21(10)
O(4)#1−Na−O(6)#1[a]	86.04(9)	O(3)−Na−O(6)#1[a]	59.61(8)
Si(2)−O(1)−Si(1)	132.59(16)	Si(1)−O(2)−Cu	134.61(14)
Si(1)−O(2)−Na	120.71(14)	Cu−O(2)−Na	93.48(10)
Si(3)−O(3)−Si(2)	126.20(16)	Si(3)−O(3)−Na	96.45(12)
Si(2)−O(3)−Na	121.08(14)	Si(2)−O(4)−Cu#2[b]	133.60(14)
Si(2)−O(4)−Na#2[b]	120.73(14)	Cu#2−O(4)−Na#2[b]	90.06(10)
Si(3)−O(5)−Cu#2	125.92(15)	Si(3)−O(5)−Cu#1[a]	127.63(15)
Cu#2−O(5)−Cu#1[a]	101.41(11)	Si(3)#2−O(6)−Si(1)[b]	127.83(16)
Si(3)#2−O(6)−Na#2[b]	91.12(11)	Si(1)−O(6)−Na#2[b]	120.30(13)
C(11A)−C(1)−Si(1)	119.4(5)	C(11B)−C(1)−Si(1)	120.8(5)
C(21)−C(2)−Si(2)	112.3(3)	C(31)−C(3)−Si(3)	114.8(4)
C(5)−O(7)−Na	120.4(2)	O(7)−C(5)−C(6B)	114.5(8)
O(7)−C(5)−C(6A)	111.6(5)	C(7A)−C(6A)−C(5)	113.5(8)
C(7B)−C(6B)−C(5)	106.6(11)	C(6A)−C(7A)−C(8A)	118.2(12)
C(6B)−C(7B)−C(8B)	119.5(18)		

[a] Symmetry transformations used to generate equivalent atoms: #1: $y - 1/4, -x + 1/4, -z + 1/4$. − [b] Symmetry transformations used to generate equivalent atoms: #2: $-y + 1/4, x + 1/4, -z + 1/4$.

chemistry of the Si_6[6,7,9] and Si_8[3c,12] ligands obtained in earlier studies.

Experimental Section

Starting materials were of commercial origin with the exception of the sodium ethylsilanolate, which was prepared in situ as described for the corresponding Ph derivative.[3c] − Conductivity measurements were obtained with a Conductimeter Crison mod 525 (all constant 1.02) instrument. − Cyclic voltammetric (CV) measurements were performed by Potentiostat-Galvanostat PAR 273A instrument under Ar atmosphere. − Infrared spectra were obtained by Bruker FT-IR IFS 113V spectrophotometer, using KBr pellets for the 4000−400 cm^{-1} range, and PE pellets for the 500−50 cm^{-1} range.

Preparation of the "$EtSiO_2Na$" Reagent: In a 100-mL two-necked round-bottom reaction vessel, equipped with a reflux condenser (closed with a $CaCl_2$ desiccator tube) and an Ar inlet poly(ethylsiloxane) "resin"[3c] (2.56 g, 0.03 mol) was suspended in 50 mL of dry *n*BuOH. To this suspension, under a dry, deoxygenated Ar atmosphere was added sodium hydroxide (0.60 g, 0.015 mol) in one portion while the suspension was (magnetically) stirred. Then, the reaction mixture was heated and refluxed (≈ 30 min) until it turned clear, indicating that the "resin" was completely dissolved. After the solution had cooled to room temp. metallic sodium (0.345 g, 0.015 mol), cut into small pieces, was added. After the Na had completely dissolved, the reaction mixture was again heated to reflux for an additional 30 min. This solution was used for the subsequent reaction.

Preparation of $Na_4[(EtSiO_2)_{12}Cu_4]$: The "$EtSiO_2Na$" reagent, prepared as described above, was used for the following preparation in the same reaction vessel, substituting the Ar inlet tube for a dropping funnel. A solution of anhydrous $CuCl_2$ (1.35 g, 0.01 mol), in 15 mL of dry *n*BuOH was poured into the dropping funnel and this (green) solution was then added dropwise to the solution of the "$EtSiO_2Na$" reagent during 30 min. After the first drops, the (blue) reaction mixture became turbid as a consequence of the

formation of a fine white precipitate (NaCl). After the addition was complete the dropping funnel was removed and the reaction mixture was heated to reflux under a dry Ar atmosphere for an additional 5 h. After this period the NaCl precipitate was centrifuged off while the solution was still warm, then the reaction mixture was left to cool to room temp. and the solvent was evaporated at reduced pressure and room temp. The residue was extracted with 20 mL of *n*BuOH. This extract was chilled to −30 °C. Blue crystals were obtained. Recrystallisation from *n*BuOH was repeated 2−3 times. The yield of the crude product was 2.633 g (62.4%), and that of the re-crystallised product 0.672 g (15.7%).

Crude Product: $C_{32}H_{80}Cl_4Cu_4Na_8O_{26}Si_{12}$ {[$(EtSiO_2)_{12}Cu_4Na_4$]·2*n*BuOH·4NaCl}: calcd. C 21.38, H 4.49, Cu 14.13, Na 10.22; found C 21.3, H 4.6, Cu 12.7, Na 15.5.

Recrystallised Product: $C_{40}H_{100}Cu_4Na_4O_{28}Si_{12}$ {[$(EtSiO_2)_{12}Cu_4Na_4$]·4*n*BuOH}: calcd. C 28.06, H 5.89, Cu 14.84, Na 5.37; found C 27.9, H 5.6, Cu 14.3, Na 6.2.

The deviations of the measured elemental composition from the calculated formulae are attributed to minor amounts of co-crystallised NaCl and to instability of the crystal solvates. The re-crystallised product was characterised by conductivity, cyclic voltammetry, infrared spectroscopy and X-ray single crystal diffraction.

Conductivity: Solvent: *n*BuOH, concentration 1×10^{-4} M, λ_{eq} = 10.4 Ω^{-1} cm^2 mol^{-1}.

Cyclic Voltammetry: Solvent: *n*BuOH, supporting electrolyte: 0.05 M nBu_4NClO_4 (TBAP), redox system: HMDE//Ag/AgCl//Pt, scan speed: 100 mV/s, E_{pc} = −1.78V, E_{pa} = −1.68 V, $E^0 = (E_{pc} + E_{pa})/2$ = 1.73 V.

Table 2. Crystal data and structure refinement for [$(EtSiO_2)_{12}Cu_4Na_4$]·4*n*BuOH

Empirical formula	$C_{20}H_5Cu_2Na_2O_{14}Si_6$
Formula weight	856.20
Temperature	173(2) K
Wavelength	0.71069 Å
Crystal system, space group	Tetragonal, $I4_1/a$ (No 88)
Unit cell dimensions	a = 22.814(5) Å
	b = 22.814(5) Å
	c = 14.767(3) Å
Volume	7686(3) Å^3
Z, Calculated density	8, 1.480 Mg/m^3
Absorption coefficient	1.371 mm^{-1}
F(000)	3568
Crystal size	0.1 × 0.1 × 0.1 mm
Theta range for data collection	1.64−27.03°
Limiting indices	$-22 \le h \le 29$
	$-28 \le k \le 27$
	$-17 \le l \le 18$
Reflections collected/unique	20814/3894 [R(int) = 0.0339]
Completeness to φ = 27.03	92.5%
Absorption correction	SADABS
Max. and min. transmission	1.000 and 0.904
Refinement method	Full-matrix least-squares on F^2
Data/restraints/parameters	3894/6/227
Goodness-of-fit on F^2	1.097
Final R indices [$I > 2\sigma(I)$]	$R1$ = 0.0413, $wR2$ = 0.1227
R indices (all data)	$R1$ = 0.0585, $wR2$ = 0.1309
Largest diff. peak and hole	0.623 and −0.380 e·Å^{-3}

Medium-Infrared Spectroscopy: (4000−400 cm^{-1}) (KBr pellet): $\tilde{\nu}$ = 3664 w (νO−H, assoc.); 2960 m, 2939 w, 2912 w, 2876 w, 2848 w (νC−H); 1644 m (νC−O); 1592 m, 1462 m, 1416 m, 1247 m (νC−C); 1126 s (νSi−C); 1033 s, 991 s, 954 m (νSi−O), 771 m (δC−H); 695 m (δC−C + νCu−O); 488 m, 470 w, 462 w (νSi−O skeletal + νCu−O?).

Far-Infrared Spectroscopy: (500−50 cm^{-1}) (polyethylene pellet): $\tilde{\nu}$ = 440 w (δSi−O skeletal); 364 w (νCu−O); 274 vw (δCu−O + Si−O−Si skeletal); 181 vw, 154 vw, 102 w (νNa−O).

X-ray Structure Determination of [*n*BuOH Na]$_4$[cyclo($EtSiO_2)_{12}$-Cu_4]·[2b]: A suitable crystal of **2b** was chosen and mounted, in air, on a glass fiber onto a goniometer head. Data were collected at 170 K on a Siemens SMART CCD area-detector diffractometer equipped with a Siemens LT3 cooling device. Crystal data are reported in Table 2.

Graphite-monochromated Mo-K_α (λ = 0.71073 Å) radiation was used with the generator working at 45 kV and 40 mA. Cell parameters and orientation matrix were obtained from least-squares refinement on reflections measured in three different sets of 15 frames each, in the range $0 < \varphi < 23°$. The data collection was performed by measuring 1400 frames (20 s per frame; ω scan method, Δω = 0.3°; sample-detector distance fixed at 5 cm) which, upon data reduction, afforded almost all reflections belonging to the sphere with $2\varphi < 54°$. The first 100 frames were recollected at the end to monitor crystal decay, which was not observed; an absorption correction was applied (SADABS).[13]

A total of 20814 reflections were collected (3894 unique, R_{int} = 0.0339; R_σ = 0.0283[14]). The structure was solved by direct methods (SIR97[15]) and refined with full-matrix-block least-squares (SHELX97[16]); anisotropic temperature factors were assigned to all non-hydrogen atoms except for the disordered C8A/C8B. Due to the disorder of some of the aliphatic residues hydrogen atoms were omitted from the structural model. A summary of crystal data and refinement details are reported in Table 2.

Crystallographic data (excluding structure factors) for the structure included in this paper have been deposited with the Cambridge Crystallographic Data Centre as supplementary publication no. CCDC-142093. Copies of the data can be obtained free of charge on application to CCDC, 12 Union Road, Cambridge CB2 1EZ, UK [Fax: (internat.) + 44-1223/336-033; E-mail: deposit@ccdc.cam.ac.uk].

Acknowledgments

Financial support of this work by the Italian Ministry of University and Research (MURST, ex-40%) is acknowledged.

[1] [1a] L. Markó, A. Vizi-Orosz, in *Metal Clusters in Catalysis* (Eds.: B. C. Gates, L. Guczi, H. Knözinger), Elsevier, Amsterdam, **1986**, p. 89−120. − [1b] H. H. Lamb, B. C. Gates, H. Knözinger, *Angew. Chem. Int. Ed. Engl.* **1988**, *27*, 1127−1144. − [1c] G. A. Somorjai, *Introduction to Surface Science and Catalysis*. Wiley, New York, **1994**. − [1d] G. A. Somorjai, *Chem. Rev.* **1996**, *96*, 1223−1235.

[2] [2a] G. Pályi, C. Zucchi, R. Ugo, R. Psaro, A. Sironi, A. Vizi-Orosz, *J. Mol. Catal.* **1992**, *74*, 51−59. − [2b] A. Vizi-Orosz, R. Ugo, A. Sironi, M. Moret, C. Zucchi, F. Ghelfi, G. Pályi, *Inorg. Chem.* **1994**, *33*, 4600−4603. − [2c] E. Corradi, N. Masciocchi, G. Pályi, R. Ugo, A. Vizi-Orosz, C. Zucchi, A. Sironi, *J. Chem. Soc., Dalton Trans.* **1997**, 4651−4655 and references therein.

[3] Selected references, articles: [3a] W. A. Herrmann, R. A. Anwander, V. Dufand, *Angew. Chem. Int. Ed. Engl.* **1994**, *33*, 1285−1286. − [3b] C. Zucchi, O. I. Shchegolikhina, M. Borsari, A. Cornia, G. Gavioli, A. C. Fabretti, E. Rentschler, D. Gatteschi, R. Ugo, R. Psaro, Yu. A. Pozdniakova, S. V. Lindeman, A. A. Zhdanov, G. Pályi, *J. Mol. Catal.* **1996**, *107,* 313−321. − [3c] U. Ritter, N. Winkhofer, R. Murugavel, A. Voigt, D. Stalke, H. W. Roesky, *J. Am. Chem. Soc.* **1996,** *118*, 8580−8587. − [3d] F. J. Feher, T. L. Hwang, J. J. Schwab, A. J. Shaka, J. W. Ziller, *Magn. Res. Chem.* **1997**, *35*, 730−734. − [3e] R. Murugavel, H. W. Roesky, *Angew. Chem. Int. Ed. Engl.* **1997**, *36*, 477−479. − [3f] B. Laermann, M. Lazell, M. Motevalli, A. C. Sullivan, *J. Chem. Soc., Dalton Trans.* **1997**, 1263−1264. − [3g] A. Voigt, R. Murugavel, H. W. Roesky,H. G. Schmidt, *J. Mol.*

Struct. **1997**, *437*, 49−57. − [3h] I. Abrahams, M. Lazell, H. Motevalli, S. A. A. Shah, A. C. Sullivan, *J. Organomet. Chem.* **1998**, *553*, 23−29. − [3i] V. Lorenz, A. Fischer, K. Jacob, W. Bruser, T. Gelbrich, P. G. Jones, F. T. Edelmann, *Chem. Commun.* **1998**, 2217−2218. − [3j] Y. K. Gun′ko, L. Nagy, W. Bruser, V. Lorenz, A. Fischer, S. Giessmann, F. T. Edelmann, K. Jacob, A. Vertes, *Monatshefte Chem*. **1999**, *130,* 45−54. reviews: − [3k] F. J. Fehér, T. A. Budzichowski, *Polyhedron* **1995**, *14*, 3239−3253. − [3l] R. Murugavel, A. Voigt, M. G. Walawalkar, H. W. Roesky, *Chem. Rev.* **1996**, *96*, 2205−2236. − [3m] L. King, A. C. Sullivan, *Coord. Chem. Rev.* **1999**, *189*, 19−57.

[4] G. Gavioli, M. Borsari, C. Zucchi, G. Pályi, R. Psaro, R. Ugo, O. I. Shchegolikhina, A. A. Zhdanov, *J. Organomet. Chem*. **1994**, *467*, 165−167.

[5] V. L. Kuznetsov, G. L. Elizarova, L. G. Matrienko, I. G. Latyunkhova, V. N. Kolominchuk, A. A. Zhdanov, O. I. Shchegolikhina, *J. Organomet. Chem.* **1994**, *475*, 65−72.

[6] [6a] A. Cornia, A. C. Fabretti, D. Gatteschi, G. Pályi, E. Rentschler, O. I. Shchegolikhina, A. A. Zhdanov, *Inorg. Chem*. **1995**, *34*, 5383−5387. − [6b] E. Rentschler, D. Gatteschi, A. Cornia, A. C. Fabretti, A. L. Barra, O. I. Shchegolikhina, A. A. Zhdanov, *Inorg. Chem.* **1996**, *35,* 4427−4431 − [6c] A. Cornia, A. C. Fabretti, G. Gavioli, C. Zucchi, M. Pizzotti, A. Vizi-Orosz, O. I. Shchegolikhina, Yu. A. Pozdniakova, G. Pályi, *J. Cluster Science* **1998**, *9*, 295−319 and references therein.

[7] Selected references: [7a] O. I. Shchegolikhina, A. A. Zhdanov, V. A. Igonin, Yu. E. Ovchinnikov, V. E. Shklover, Yu. T. Struchkov, *Metalloorg Khim*. **1991**, *4*, 74−84; *Engl. Transl*. **1991**, *4*, 39−44. − [7b] G. Gavioli, R. Battistuzzi, P. Santi, C. Zucchi, G. Pályi, R. Ugo, A. Vizi-Orosz, O. I. Shchegolikhina, Yu. A. Pozdniakova, S. V. Lindeman, A. A. Zhdanov, *J. Organomet. Chem*. **1995**, *485*, 257−266. − [7c] S. V. Lindeman, O. I. Shchegolikhina, Y. A. Molodtsova, A. A. Zhdanov *Acta Cryst. S. C* **1997**, 53, 305−309. − [7d] C. Zucchi, M. Mattioli, A. Cornia, A. C. Fabretti, G. Gavioli, M. Pizzotti, R. Ugo, O. I. Shchegolikhina, A. A. Zhdanov, G. Pályi, *Inorg. Chim. Acta* **1998**, *280*, 282−287.

[8] V. A. Igonin, S. V. Lindeman, Yu. T. Struchkov, Yu. A. Molodtsova, O. I. Shchegolikhina, A. A. Zhdanov, *Izv. Akad. Nauk, SSSR, Ser. Khim.* **1993**, 752−756.

[9] M. Borsari, G. Gavioli, ℓ. Zucchi, G. Pályi, R. Psaro, R. Ugo, O. I. Shchegolikhina, A. A. Zhdanov, *Inorg. Chim. Acta* **1997**, *258*, 139−144.

[10] *Encyclopaedia of Electrochemistry of the Elements*, Vol. 2 (Ed.: A. J. Bard), M. Dekker, New York, **1974**, p. 397.

[11] [11a] L. Mandolini, *Adv. Phys. Org. Chem.* ***19*86**, *22*, 1−111. − [11b] D. E. Fenton, in *Comprehensive Coordination Chemistry* (Eds.: G. Wilkinson, R. D. Gillard, J. A. McCleverty), Pergamon Press, Oxford, **1987**, Vol. 3, p. 1−80 − [11c] M. T. Reetz, *Acc. Chem. Res.* **1993**, *26*, 462−468. − [11d] R. Hoss, F. Vögtle, *Angew. Chem. Int. Ed. Engl.* **1994**, *33*, 375−384.

[12] O. I. Shchegolikhina, Yu. A. Pozdniakova, S. V. Lindeman, A. A. Zhdanov, R. Psaro, R. Ugo, G. Gavioli, R. Battistuzzi, M. Borsari, T. Rüffer, C. Zucchi, G. Pályi, *J. Organomet. Chem.* ***19*96**, *514*, 29−35.

[13] G. M. Sheldrick, *SADABS*, University of Göttingen, Germany, **1996**.

[14] $R_{int} = \Sigma|F_o^2 - F_{mean}^2|/\Sigma F_o^2$; $R_\sigma = \Sigma\sigma(F_o^2)/\Sigma F_o^2$; $R_1 = \Sigma||F_o| - |F_c||/\Sigma|F_o|$; $wR_2 = [\Sigma(F_o^2 - F_c^2)^2/\Sigma wF_o^4]^{1/2}$

[15] A. Altomare, M. C. Burla, M. Camalli, G. Cascarano, C. Giacovazzo, A. Guagliardi, A. G. G. Moliterni, G. Polidori, *J. Appl. Crystallogr.* **1999**, *32*, 115−119.

[16] G. M. Sheldrick, *SHELX97-Program for the Refinement of Crystal Structures;* University of Göttingen: Germany, **1997**.

Received December 14, 1999
[I99460]

Steric Hindrance in Substitution Reactions on Arsenic Acid by Pentaam(m)ine Complexes of Co^{III} and Cr^{III}

Gabriel González,[a] Manuel Martinez,*[a] and Elisa Rodríguez[a]

Keywords: Reaction mechanisms / Kinetics / Arsenates / Acid catalysis

The kinetics of the substitution reaction of water by $H_2AsO_4^-$ in $[M(N)_5(H_2O)]^{3+}$ (M = Co^{III}, Cr^{III}) complexes have been studied at 25 °C for a series of $(N)_5$ groups, from monodentate $(NH_3)_5$ and $(CH_3NH_2)_5$ to macrocyclic 12-methyl-1,4,7,10-tetraazacyclotridecane-12-amine (L_{13}), 6-methyl-1,4,8,11-tetraazacyclotetradecane-6-amine (L_{14}), and 10-methyl-1,4,8,12-tetraazacyclopentadecane-10-amine (L_{15}) in their *cis* (L_{13} and L_{14}, Co^{III} and Cr; L_{15}, Co^{III}) and *trans* (L_{15}, Co^{III} and Cr^{III}) water-amino geometrical arrangements around the metal ion. Equilibration rate constants were found to be too large to be interpreted as occurring through the M–OH_2 bond scission that takes place in standard substitution processes on these t_{2g}^3 and t_{2g}^6 pentaamine complexes, and were also found to be highly dependent on the acidity of the medium. The results are interpreted in view of previously studied, similar reactions, where protonation played a very important role. This role was expected for reactions occurring via As–O bond scission; that is, the data fits well with that expected for oxygen exchange reactions of the labile tetrahedral $\{AsO_4\}$ moiety. The values found are a clear indication of the differences in steric requirements of the metal-bound water attacking the tetrahedral As^V centre [i.e. for M = Co^{III}, $k^+_{\text{non acid catalysed}}$ = 93, 1.9, 0.76, and 0.44 $M^{-1}s^{-1}$ for the $(NH_3)_5$, $(CH_3NH_2)_5$, *cis*-L_{13}, and *trans*-L_{15}, respectively], as well as of electronic influences of the amines of the cobalt complex on the As^V centre when attacked by the bulk water [i.e. for M = Co^{III}, $10^3k^-_{\text{non acid catalysed}}$ = 280, 5.7, 4.4, and 4.5 s^{-1} for the $(NH_3)_5$, $(CH_3NH_2)_5$, *cis*-L_{13}, and *trans*-L_{15} respectively].

Introduction

The kinetics and mechanisms for the substitution reactions on inert Co^{III} and Cr^{III} am(m)ine complexes have been thoroughly studied both from an anation[1] and a hydrolysis[2] approach; all the mechanistic implications have already been described, and only small differences due to fine tuning are still being carried out in view of the importance of their application to other systems.[3] On the other hand, substitution reactions on labile tetrahedral oxoanions are not as well known. Few oxygen exchange studies have been carried out,[4] and very little is known about the formal metal complex substitution reactions as shown in Equation (1).[5]

$$[M(L)_5(H_2O^*)]^{n+} + EO_x^{m-} \rightleftharpoons [M(L)_5(^*OEO_{(x-1)})]^{(n-m)+} + H_2O \quad (1)$$

We have already been involved in the study of this type of reaction with H_3AsO_4 in highly acidic media.[6] These reactions are traditionally avoided[7] because of the important $[H^+]$ acceleration of the reaction rate as well as the small equilibrium displacement in kinetically measurable conditions. In our previous study, a clear $[H^+]$-catalysed path was found, its quantification was achieved, in part, thanks to the ability of Cr^{III} to form fairly stable outer-sphere complexes.[8] More recently, a study on the oxygen exchange on H_3AsO_4 with bulk water in acidic media has also been carried out;[9] an $[H^+]$-catalysed path involving a pentacoordinated As^V species has been tentatively proposed as being responsible for the important acceleration of the interchange. This is in good agreement with our previous findings. The previously undetected reaction of $[Cr(NH_3)_5(H_2O)]^{3+}$ with the $H_3AsO_4/H_2AsO_4^-$ system,[6] has been revised in view of the new instrumentation available that allows us to measure the evolution, with time, of the full spectrum at 0.8 ms intervals, even at relative high concentrations. The results obtained are discussed in view of the complete information obtained in this study.

In this paper we present the kinetic and mechanistic study of the substitution reactions shown in Equation (2).

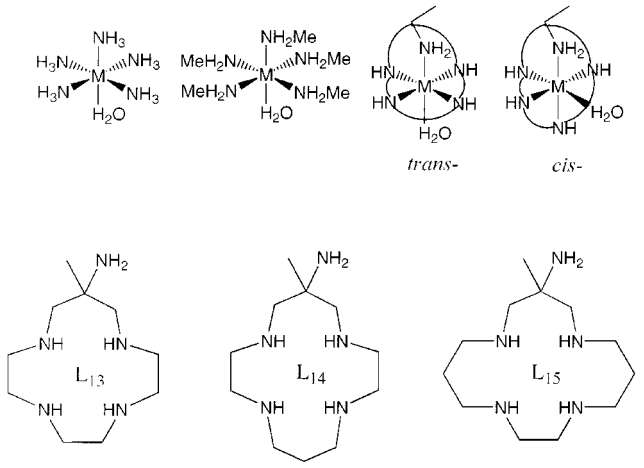
$$[M(N)_5(H_2O)]^{3+} + H_2AsO_4^-/H_3AsO_4 \rightleftharpoons [M(N)_5(H_2AsO_4)]^{2+} + H_2O/H_3O^+ \quad (2)$$

M = Co^{III} and Cr^{III}, and $(N)_5$ = $(NH_3)_5$, $(CH_3NH_2)_5$, 12-methyl-1,4,7,10-tetraazacyclotridecane-12-amine (L_{13}), 6-methyl-1,4,8,11-tetraazacyclotetradecane-6-amine (L_{14}), and 10-methyl-1,4,8,12-tetraazacyclopentadecane-10-amine (L_{15}) (Scheme 1) in highly acidic media, where all the arsenic oxoanions are present in the form of H_3AsO_4 and $H_2AsO_4^-$. For all the Co^{III} systems, no build-up of outer-sphere encounter complexes was detected, while for some of the Cr^{III} pentaamine complexes limiting kinetics were observed. As a whole, important differences have been found both for the anation and aquation reactions that could be related to the steric demands on the M^{III} centre and the electronic differences of the $(N)_5$ skeleton, as expected for an associatively activated substitution on the tetrahedral As^V centre.

[a] Departament de Química Inorgànica, Universitat de Barcelona, Diagonal 647, E-08028 Barcelona, Spain

Supporting information for this article is available on the WWW under http://www.wiley-vch.de/home/eurjic or from the author

 © WILEY-VCH Verlag GmbH, D-69451 Weinheim, 2000 1434–1948/00/0606–1333 $ 17.50+.50/0



Scheme 1

Results and Discussion

All the values of k_{obs} as a function of the different M metals, $(N)_5$ groups, acidity, and total arsenic acid concentration, $[As]_T$ are collected in the Tables of the Supporting Information. Figure 1 shows some of the plots of k_{obs} versus $[As]_T$, as a function of the acidity, found in this study. No curvature is observed for any of the Co^{III} systems, indicating that there is no build-up of any outer-sphere complex in solution. As in other chromium(III) systems,[6,8] significant curvature of the above-mentioned plots for the $(N)_5$ monodentate systems is obtained, indicating that the amount of outer-sphere complex present in solution is measurable. Finally, for the macrocyclic Cr^{III} anation reactions, again, no build-up of outer-sphere complex is observed. Furthermore, with the exception of Cr^{III}/L_{15} system, an equilibrium of the substitution reaction is observed at this $[H^+]$, with a fairly unfavourable constant for the formation of the arsenato complexes. No second-order dependence on the value of $[As]_T$ has been found for the systems studied, indicating that the involvement of dimeric arsenic species is not present under the conditions used in this study.[4]

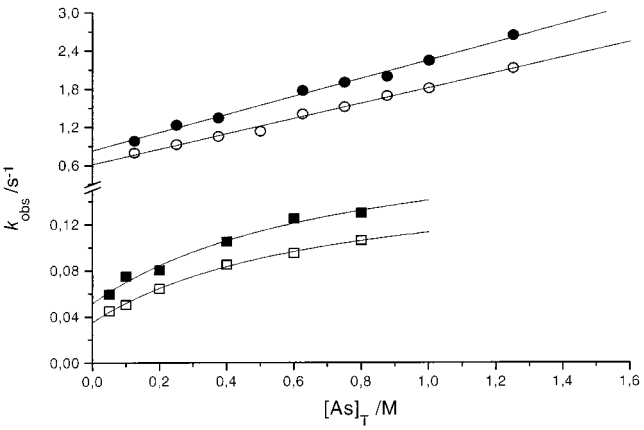


Figure 1. Selected plots of the values of k_{obs} versus $[As]_T$ at different acidities for the anation reaction of some of the complexes (T = 25 °C; $[H^+]$, $HClO_4$; I = 1.0 M, $LiClO_4$); ○: $[Co(NH_3)_5(H_2O)]^{3+}$, $[H^+]$ = 0.125 M; ●: $[Co(NH_3)_5(H_2O)]^{3+}$, $[H^+]$ = 0.175 M; □: $[Cr(MeNH_2)_5(H_2O)]^{3+}$, $[H^+]$ = 0.40 M; ■: $[Cr(MeNH_2)_5(H_2O)]^{3+}$, $[H^+]$ = 0.57 M

It is important to note that, with the exception of the Cr^{III} macrocyclic systems, even at acidities where all the arsenic and arsenato complexes in the reaction medium are present as H_3AsO_4 and $[M(N)_5(H_2AsO_4]^{2+}$, respectively, an acceleration in the equilibration reaction rate occurs on increasing the values of $[H^+]$. Taking this into account, as well as similar previously published studies,[6] a reaction scheme and a rate law such as those depicted in Scheme 2 and Equation (3) are proposed.

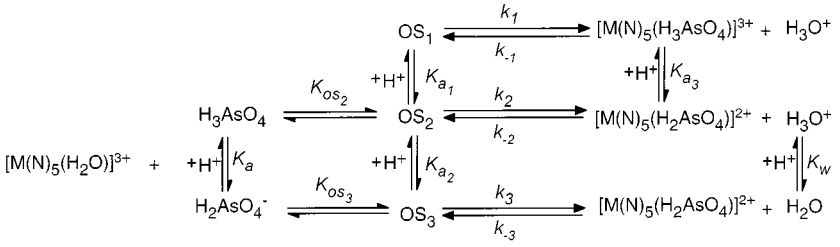
$$K_{obs} = \frac{A[As]_T}{[H^+] + K_a + B[As]_T} + C$$

$$A = k_1\left(\frac{K_{OS2}}{K_{a1}}\right)[H^+]^2\, k_2K_{OS2}[H^+] + k_3K_aK_{OS3} \qquad (3)$$

$$B = K_aK_{OS3} + K_{OS2}[H^+] + \left(\frac{K_{OS2}}{K_{a1}}\right)[H^+]^2$$

$$C = \left(\frac{k_{-1}}{K_{a3}}\right)[H^+]^2 + k_{-2}[H^+] + k_{-3}$$

Figure 2 and Figure 3 show selected plots of A and C versus $[H^+]$ for some of the systems studied. The values found for the different terms in Equation (3) at 25 °C are collected in Table 1 and Table 2. Given the fact that most of the terms turn out to be composite of rate and equilibrium constants, no attempts to measure activation parameters have been carried out. Unlike the study with $[Cr(H_2O)_6]^{3+}$ under the same conditions (Table 1), where only acid-catalysed, **1**, and protic, **2**, paths were detected,[6] in this study, important differences exist depending on the metal centre and the nature of the $(N)_5$ group of ligands. Only in the case of the Co^{III} complexes was the non-protic path **3** detected, both for anation and hydrolysis reactions, while for all the Cr^{III} and Co^{III} systems rather important contributions to the observed equilibration rate constants are that of the acid-catalysed, **1**, and protic, **2**, paths. In all, the complete set of kinetic rate constants and active reaction paths (Scheme 2) is rather complex, and highly dependent on the nature of the metal centre, the mono- or polydentate nature of the $(N)_5$ skeleton, the size of the macrocycle, and the stereoisomery of the macrocyclic ligand. Nevertheless, in all cases, given the reaction rate constants obtained in this study as well as the available substitution data on analogous $[Co(N)_5Y]^{2/3+}$ and $[Cr(N)_5Y]^{2/3+}$ systems, it is clear that the substitution processes are taking place on the As^V centre as already described for other arsenate substitution reactions.[6][7b,9] Being a tetrahedral p-block element, this process is bound to be associatively activated in character with a transition state involving a direct attack of the M-bound oxygen to the As^V centre. Scheme 3 represents such a postulated transition state, where oxygen atoms labelled with ***i*** and ***ii*** indicate possible protonation sites for reaction paths **1** and **2**, respectively. In any of both cases, the As^V centre attains a lower electron density, allowing for the entrance of the oxygen from the water bound to the cobalt complex for the anation process, or for the entrance of a bulk water molecule for the aquation (reverse) reaction. In this respect,



Scheme 2

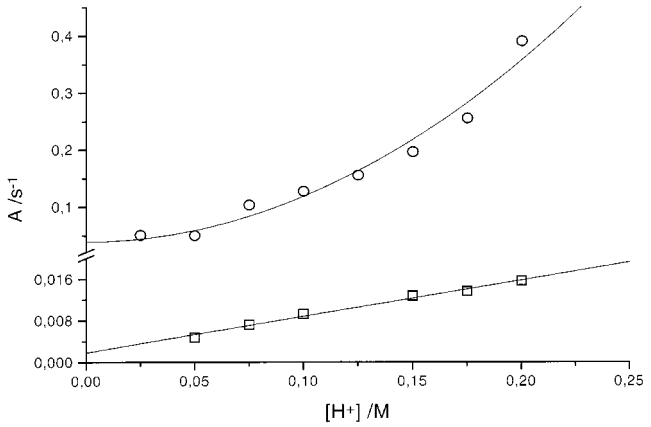


Figure 2. Plot of the values of *A* [Equation (3)] versus $[H^+]$ for the anation reactions of some of the complexes studied (T = 25 °C; $[H^+]$, $HClO_4$; I = 1.0 M, $LiClO_4$); ○: $[Co(NH_3)_5(H_2O)]^{3+}$; □: *trans*-$[CoL_{15}(H_2O)]^{3+}$

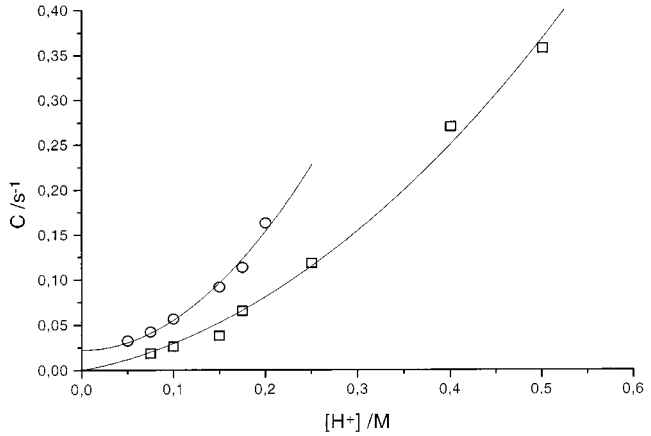
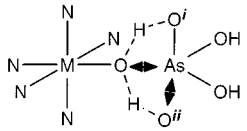


Figure 3. Plot of the values of *C* [Equation (3)] versus $[H^+]$ for the anation reactions of some of the complexes studied (T = 25 °C; $[H^+]$, $HClO_4$; I = 1.0 M $LiClO_4$); ○: *cis*-$[CoL_{15}(H_2O)]^{3+}$; □: $[Cr(NH_3)_5(H_2O)]^{3+}$

apart from obvious steric and electronic reasons affecting the magnitude of the reaction rate, the fact that some of the reaction pathways are selectively detected for some of the systems has to be looked into very carefully. Finally, the magnitude of the intrinsic errors involved due to the complex dependence of the equilibration rate constants on the acidity [Equation (2)], makes even small differences in the values very unreliable; factors of less than ca. two have to be taken with great caution specially when referring to paths **1** and **3**.



Scheme 3

Data in Table 1 indicates a clear-cut difference between chromium monodentate and macrocyclic systems. That is, while the observation of active forward path **2** and reverse path **3** in any of the substitutions studied at this $[H^+]$ is perfectly attributable to the major species existing in solution, namely H_3AsO_4 (90–98% of the total added arsenate at this $[H^+]$)[6] and *cis*-$[CrL_{13}(H_2AsO_4)]^{2+}$ (predominant at this pH, given the increase in acidity of coordinated ligands).[10] The observation of forward and reverse paths **1** and reverse path **2** seems to be a specific characteristic of monodentate pentaam(m)ine aqua complexes for these Cr^{III} derivatives {as for the already studied $[Cr(H_2O)_6]^{3+}$}.[6] In all, for the macrocyclic complexes, the active reaction paths are directly related to those involving the predominant species in solution at this pH range. Comparison of the monodentate pentaam(m)ine aqua systems clearly indicates, for the forward reaction, that the steric bulk of the entering chromium complex plays a very important role; a rate decrease of nearly one order of magnitude is observed on go-

Table 1. Values for the different rate terms in Equation (3) for the anation reactions of complexes $[Cr(N)_5(H_2O)]^{3+}$ as a function of the $(N)_5$ group (T = 25 °C; $[H^+]$ = 0.05–0.2 M $HClO_4$; I = 1.0 M $LiClO_4$); $[Cr(H_2O)_6]^{3+}$ data from ref.[6] are included for comparative purposes

$(N)_5$	Path **1**			Path **2**		Path **3**	
	$k_1(K_{OS2}/K_{a1})$ /s^{-1}	K_{OS2}/K_{a1}	k_{-1}/K_{a3} /M s^{-1}	k_2K_{OS2} /$M^{-1}s^{-1}$	k_{-2} /s^{-1}	k_3K_{OS3} /$M^{-1}s^{-1}$	k_{-3} /s^{-1}
$(NH_3)_5$	(7.3±1.0)×10^{-1}	4.9±0.1	1.0±0.1	(7.5±0.4)+10^{-1}	(2.1±0.6)×10^{-1}	---	---
$(CH_3NH_2)_5$	(1.3±0.2)×10^{-1}	2.6±0.3	(3.8±0.4)×10^{-2}	(1.4±0.4)×10^{-1}	(6.3±1.0)×10^{-2}	---	---
cis-L_{13}	---	---	---	(1.1±0.3)×10^{-1}	---	---	(1.3±0.2)×10^{-1}
trans-L_{15}	---	---	---	(3.8±0.2)×10^{-1}	---	---	---
$(H_2O)_5$	2.3±0.6	2.8±0.5	(9.6±2.1)×10^{-1}	1.1±0.4	(5.1±1.3)×10^{-1}	---	---

ing from ammine to methylamine. The electronic effect created for the more basic CH_3NH_2 ligands seems to be counterbalanced by the steric demands created on the substitution process; in this respect, the value found for K_{OS2}/K_{a1} agrees quite well with the latter assumption. A comparison of these monodentate $(N)_5$ systems with the hexaaquachromium(III) substitution studied, indicates that steric reasons have to be held responsible for the small differences in reactivity; the weaker Lewis acid character of the aqua ligand would point to the inverse of the observed effect.[11] When we move to the *cis*-L_{13} and *trans*-L_{15} $Cr^{III}/(N)_5$ systems, the most striking feature is the immediate disappearance of the acid catalysed path **1**, both for forward and reverse reactions. The values determined for k_2K_{OS2} for these two macrocyclic systems agree with the slight better steric availability of the chromium(III)-bound oxygen atom for the *trans*-L_{15} macrocyclic complex (see Scheme 1); electronic differences being at a minimum between the two macrocyclic complexes. On the one hand, it seems that the existence of a macrocyclic (including hydrogen bonding) wrapping of the Cr^{III} metal does not allow for protonation of the $[CrL_n(H_2AsO_4)]^{2+}$ final complex (Scheme 2). On the other hand, for OS_1 and OS_2, it is clear that we are not dealing with simple ion-pairing,[12] the existence of such aggregates with octahedral d^3 complexes showing larger stability constants than their d^6 analogues is a generally accepted fact.[8] Steric reasons that produce shorter $Cr–OH_2$ bond lengths for the macrocyclic systems, in spite of their shorter Cr–N bond lengths,[13] can be held responsible of a rather close approach of the arsenic acid species to the chromium-bound water oxygen. The presence of nitrogen-bound hydrogen atoms in the macrocycle are bound to produce hydrogen bonding with the available oxo groups in the H_3AsO_4 within the outer-sphere complex, deactivating protonation reaction K_{a1}. Finally, for the remarkable stability of the *trans*-$[CrL_{15}(H_2AsO_4)]^{2+}$ complex, the special capping geometry of the macrocycle (Scheme 1), with the possibility of hydrogen atoms directed to the oxo groups of the arsenate ligand, probably add up to an important increase in the stability of the complex when compared with *cis* arrangements.

With reference to cobalt data in Table 2, although monodentate and macrocyclic pentaam(m)ine complexes are still differentiable, striking differences are observed with the general trends obtained for the analogous Cr^{III} complexes, shown in Table 1. Paths **1** and **3** are operative for all the $[Co(N)_5H_2O]^{3+}/H_2AsO_4^-$ substitution processes, while path **2** is only detected for forward reactions with the macrocyclic complexes. The reactivity cannot be associated, in this case, to the dominant species in solution at this acidity (see above).

Monodentate systems have the most homogeneous reactivity pattern, as with their Cr^{III} analogues. For the equilibrium reactions, both for the acid-catalysed and the non-protic paths, the steric effect of the increased size of the Co^{III} complex is clear, the difference between $(N)_5 = (NH_3)_5$ and $(MeNH_2)_5$ rate constants being even larger than with the Cr^{III} complexes. The usual differences in M–L bond lengths for cobalt and chromium pentaamine complexes can be held responsible for the enhanced hindrance of the Co^{III} systems.[13] The preference for path **3** versus path **2** for the cobalt complexes has to be considered much more carefully. For the reverse reaction, the attack of a protonated water molecule on an As^V centre would be much less favoured for the electronically richer t_{2g}^6 Co^{III} complexes; in fact, acidity of coordinated water is higher for the $[Cr(NH_5)_5H_2O]^{3+}$ than for the $[Co(NH_5)_5H_2O]^{3+}$ complexes.[10][11a] Consequently, while attack of H_3O^+ on the tetrahedral As^V is only possible once protonation has taken place (path **1**), its attack on the non-protonated arsenato complex (path **2**) is suppressed. For the forward reactivity, the rationalisation is not so straightforward; a plausible explanation involves the (possibly complex) hydrogen bonded nature of the postulated transition state depicted in Scheme 3. Given the less positive character of the hydrogen atoms from the cobalt-bound water, the proton-receiving oxygen atoms bound to the arsenic centre must be very sensitive to the existing degree of protonation. That is, while the presence of two protons attached to oxygen atoms ***i*** and ***ii*** in Scheme 3 accelerates the reaction by enhancement of the good leaving character of one of them, the attachment of only one of such proton is not enough. Furthermore, in the latter situation,

Table 2. Values for the different rate terms in Equation (2) for the anation reactions of complexes $[Co(N)_5(H_2O)]^{3+}$ as a function of the $(N)_5$ group {T = 25 °C; $[H^+]$ = 0.05–0.2 M ($HClO_4$); I = 1.0 M $LiClO_4$}

$(N)_5$	Path **1**		Path **2**		Path **3**	
	$k_1(K_{OS2}/K_{a1})$ /s^{-1}	k_{-1}/K_{a3} /M s^{-1}	k_2K_{OS2} /$M^{-1}s^{-1}$	k_{-2} /s^{-1}	k_3K_{OS3} /$M^{-1}s^{-1}$	k_{-3} /s^{-1}
$(NH_3)_5$	8.0±0.6	(2.1±1.4)×10	---	---	(9.3±3.0)×10	(2.8±0.3)×10^{-1}
$(CH_3NH_2)_5$	1.6±0.2	1.5±0.1	---	---	1.9±0.9	(5.7±3.3)×10^{-3}
cis-L_{13}	---	(9.5±1.2)×10^{-1}	(1.3±0.1)×10^{-1}	---	(7.6±2.9)×10^{-1}	(4.4±2.7)×10^{-3}
cis-L_{14}	---	(1.3±0.1)×10^{-1}	(1.4±0.1)×10^{-1}	---	---	(6.4±2.5)×10^{-3}
cis-L_{15}	---	3.3±0.2	1.1±0.1	---	---	(2.2±0.5)×10^{-2}
trans-L_{15}	---	(4.2±0.5)×10^{-1}	(6.9±0.4)×10^{-2}	---	(4.4±0.2)×10^{-1}	(4.5±1.1)×10^{-3}

the depicted hydrogen bonding between metal-bound water and arsenate is not enough for good attack of the cobalt-bound oxygen atom on the As^V centre, only the loss of the last proton restores the reaction rate by a best hydrogen bonding interaction in the transition state.

With respect to the macrocyclic systems the situation is dramatically different. While reverse paths are the same as those found for the monodentate systems, forward path **1** is never observed, and the forward reactivity of path **3** is now shared with that from path **2**. The reasoning mentioned for the reactivity for the aquation reactions through path **1** and **3** remains valid; nevertheless, the value of the rate constants determined for the *cis*-$[CoL_{15}H_2AsO_4]^{2+}$ complex is surprisingly high. We can speculate about the fact that the increased size of the macrocycle, with shorter Co–N bond lengths than in the Cr^{III} analogues,[14] can produce a ''back-folded'' geometry of the macrocycle when a rather large $\{AsO_4\}$ tetrahedral centre is attached. Furthermore, this has to be more possible for Co^{III}, given the richer electron density of the complex that does not favour hydrogen bonding between amine protons and arsenic-bound oxygen atoms. This is contrarily to what has been said for the chromium derivatives. As for the forward reaction paths, the change in reactivity from path **1** to path **2** has to be related to the preferential nature of the interaction in the outer-sphere complex OS_2 that does not allow for reactive protonation. Thus, protonation of the OS_2 complex is prevented, even when hydrogen bonding should be less important than for the Cr^{III} analogues.[10] The value found for k_2K_{OS2} for the largest *cis*-L_{15} metal complex is definitively larger, again suggesting the possibility of a certain degree of ''back-folded'' effect in the preferential outer-sphere interaction,[12] producing a much more efficient attack on the As^V centre. With respect to the forward path **3**, the rate constant values for the *cis*-L_{13} and *trans*-L_{15} are rather important. At the moment we are not able to understand this fact, nevertheless the two systems for which k_3K_{OS3} have a definite value are those which are bound to be the less sterically demanding by themselves, and their forward rate constants are larger than those for the protic path, **2**.

Conclusions

The study carried out on the formal substitution reactions on pentaam(m)ine Cr^{III} and Co^{III} shows the ''oppressive'' array of terms typical for substitution processes taking place on tetrahedral As^V species, where the importance of protonation is evident. For the monodentate metal complexes studied, an acid catalysed path is always present, which enhances the reaction rate by the formation of a good protonated leaving group. The operation of a path with fully protonated species is only found for the chromium complexes, where fewer electrons present in the systems allows even the entrance of weak Lewis bases, as fully protonated species are, without the assistance of a good leaving group. With reference to the macrocyclic systems studied, although the same reasoning can be used for some of the reactivity, an increased influence of the steric effects are evident. In this case, not only size, but hydrogen bonding and differences in Cr^{III} and Co^{III} bond lengths, seem to be responsible for the trends observed. In all, the reactivity has proven to be extremely complex, with many factors to be accounted for. Substitution processes on p-block elements have been traditionally avoided; therefore, further studies in this field have to be carried out in order to have a good overview of the processes taking place in their reactions.

Experimental Section

Materials: $[Co(NH_3)_5(H_2O)](ClO_4)_3$, $[Cr(NH_3)_5(H_2O)](ClO_4)_3$, $[Co(CH_3NH_2)_5(H_2O)](ClO_4)_3$, $[Cr(CH_3NH_2)_5(H_2O)](ClO_4)_3$, *cis*-$[CoL_{13}(H_2O)](ClO_4)_3$, *cis*-$[CoL_{14}(H_2O)](ClO_4)_3$, *cis*-$[CoL_{15}(H_2O)](ClO_4)_3$, *trans*-$[CoL_{15}(H_2O)](ClO_4)_3$, $[Co(NH_3)_5(H_2AsO_4)](H_2AsO_4)_2$, and $[Cr(NH_3)_5(H_2AsO_4)](ClO_4)_2$ were prepared as described in the literature.[7b,12,15] $LiClO_4$ was prepared from Li_2CO_3 and recrystallized three times before use. Arsenic acid was prepared by nitric acid oxidation of As_2O_3;[16] commercially available Aldrich As_2O_5 was too impure to be used (a solution of commercial Aldrich As_2O_5 was found to produce a brown precipitate that was very difficult to eliminate, making all kinetic runs impossible).

cis-$[CrL_{13}(H_2O)](CF_3SO_3)_3$ and *trans*-$[CrL_{15}(H_2O)](ClO_4)_3$ were prepared in a similar manner to their cobalt analogues from the corresponding $[CrL_nCl](ClO_4)_2$ precursors.[15] In these cases, the base hydrolyses were carried out at pH = 9–10, and once acidified with perchloric or triflic acid, the stoichiometric amount of $AgClO_4$ was added to remove all existing chlorides in the reaction medium. On standing, the complexes are collected as orange-red solids. Occasionally, the isolated complexes were contaminated with $NaClO_4$, their recrystallisation from diluted $HClO_4$ produced analytically pure samples. The aqua complexes were characterised by their elemental analyses and UV/Vis spectra in 0.1 M $HClO_4$. – Analyses (calcd./found): *cis*-$[CrL_{13}(H_2O)](CF_3SO_3)_3 \cdot 3.5\ H_2O$: C 19.6/19.2, N 8.8/9.0; *trans*-$[CrL_{15}(H_2O)](ClO_4)_3 \cdot 2\ H_2O$: C 22.3/22.4, N 10.8/10.5. – UV/Vis (λ/nm, $\varepsilon/M^{-1}cm^{-1}$): *cis*-$[CrL_{13}(H_2O)](CF_3SO_3)_3 \cdot 3.5\ H_2O$: 486 (137), 362 (79) and *trans*-$[CrL_{15}(H_2O)](ClO_4)_3 \cdot 2\ H_2O$: 486 (61), 450 (sh), 356 (81).

cis-$[CoL_{13}(H_2AsO_4)](ClO_4)_2$, *trans*-$[CoL_{15}(H_2AsO_4)](ClO_4)_2 \cdot H_2O$, and *trans*-$[CrL_{15}(H_2AsO_4)](H_2AsO_4)_2$ were prepared as their pentaammine analogues.[17] The aqua complexes were dissolved in 3–4 M H_3AsO_4, the cherry red solution formed immediately was concentrated to a syrupy consistency. Addition of ethanol produced a red solid on standing at –30 °C. The complexes were characterised by their elemental analyses and UV/Vis spectra in solid (to avoid the fast aquation reaction) or in 2 M H_3AsO_4. – Analyses (calcd./found): *cis*-$[CoL_{13}(H_2AsO_4)](ClO_4)_2$: C 19.6/19.0, N 11.4/11.7; *cis*-$[CoL_{15}(H_2AsO_4)](ClO_4)_2 \cdot H_2O$: C 21.8/21.8, N 10.6/10.8; *trans*-$[CrL_{15}(H_2AsO_4)](H_2AsO_4)_2$: C 20.1/19.9, N 9.8/9.5. – UV/Vis in solid (λ/nm): *trans*-$[CoL_{15}(H_2AsO_4)](ClO_4)_2 \cdot H_2O$: 507; *trans*-$[CrL_{15}(H_2AsO_4)](H_2AsO_4)_2$: 509, 368. – UV/Vis in 2 M H_3AsO_4 (λ/nm, $\varepsilon/M^{-1}cm^{-1}$): *cis*-$[CoL_{13}(H_2AsO_4)](ClO_4)_2$: 500 (sh), 454 (145), 346 (132); *cis*-$[CoL_{15}(H_2AsO_4)](ClO_4)_2 \cdot H_2O$: 528 (100), 354 (139); *trans*-$[CrL_{15}(H_2AsO_4)](H_2AsO_4)_2$: 514 (73), 372 (100).

All UV/Vis spectra were recorded with an HP8452A instrument. The spectra of the final $[M(N)_5(H_2AsO_4)]^{2+}$ complexes were determined, as done[17] for the similar $[Cr(NH_3)_5(H_2AsO_4)]^{2+}$ by solution of the corresponding aqua complexes in 2 M H_3AsO_4 (the

known spectra of the characterised arsenato derivatives were used as a reference of the validity of the method).

Kinetics: The general kinetic technique has already been described.[6] All kinetic measurements were performed under pseudo-first-order conditions, with the total concentration of arsenic acid in excess over the cobalt complex. Typical M^{III} complex concentrations were within the $1–5\cdot10^{-3}$ M range. Solutions for the kinetic runs were made up from the corresponding stock solutions of $HClO_4$, metal complex, H_3AsO_4, and $LiClO_4$. Runs were carried out in a Durrum D-110 stopped-flow instrument at the desired wavelength, determined from the differences between initial and final products. Alternatively, the instrument was connected to a J&M Tidas instrument and the complete spectra were recorded and analysed; this technique allowed us to revise the anation reaction of the $[Cr(NH_3)_5(H_2O)]^{3+}$ complex, obtaining reasonable results. All the k_{obs} values were derived from the obtained absorbance versus time exponential traces using a nonlinear least-squares fitting method. All post run data fitting were done by unweighted least-squares fit to the desired equations.

Acknowledgments

Financial support from the CIRIT of the Generalitat de Catalunya (to E. R.) and the Ministerio de Educación y Cultura is gratefully acknowledged.

[1] M. C. Ghosh, P. Bhattacharya, P. Banerjee, *Coord. Chem. Rev.* **1988**, *91*, 1.
[2] F. P. Rotzinger, J. Weber, C. Daul, *Helv. Chim. Acta* **1991**, *74*, 1247.
[3] [3a] G. González, M. Martinez, E. Rodriguez, *J. Chem. Soc., Dalton Trans.* **1995**, 891. – [3b] G. González, B. Moullet, M. Martinez, A. E. Merbach, *Inorg. Chem.* **1994**, *33*, 2330. – [3c] F. Benzo, P. V. Bernhardt, G. González, M. Martinez, B. Sienra, *J. Chem. Soc., Dalton Trans. J. Chem. Soc., Dalton Trans.* **1999**, 3973.
[4] H. Gamsjäger, R. K. Murmann, *Advances in Inorganic and Bioinorganic Mechanisms* (Ed.: A. G. Sykes), **1983**, *2*, 317.
[5] [5a] M. R. Grace, P. A. Tregloan, *Inorg. Chem.* **1992**, *31*, 4524. – [5b] A. A. Holder, T. P. Dasgupta, *J. Chem. Soc., Dalton Trans.* **1996**, 2637.
[6] M. Ferrer, M. Martinez, M-A. Pitarque, *J. Chem. Soc., Dalton Trans.* **1990**, 1629.
[7] [7a] R. K. Wharton, R. S. Taylor, A. G. Sykes, *Inorg. Chem.* **1975**, *14*, 33. – [7b] T. A. Beech, N. C. Lawrence, S. F. Lincoln, *Aust. J. Chem.* **1973**, *26*, 1877. – [7c] E. E. Mercer, J. A. Hormuth, *J. Inorg. Nucl. Chem.* **1969**, 31, 2145.
[8] M. Ferrer, G. González, M. Martinez, *J. Chem. Soc., Dalton Trans.* **1990**, 2597.
[9] A. Okumura, Y. Matsumiya, K. Yamamoto, T. Ueno, M. Suzuki, S. Yamabe, *Bull. Chem. Soc. Jpn.* **1995**, *68*, 1839.
[10] R. G. Wilkins, *Kinetics and Mechanism of Reactions of Transition Metal Complexes*, 2nd ed., VCH, Weinheim, **1991**.
[11] [11a] J. Burgess, *Metal Ions in Solution*, Ellis Horwood, New York, **1978**. – [11b] K. Emerson, W. H. Graven, *J. Inorg. Nucl. Chem.* **1959**, *11*, 309.
[12] G. González, M. Martinez, *Inorg. Chim. Acta* **1995**, *230*, 67.
[13] P. V. Benrhardt, M. Martinez, X. Solans, unpublished results.
[14] [14a] G. A. Lawrance, T. W. Hambley, M. Martinez, B. W. Skelton, A. H. White *J. Chem. Soc., Dalton Trans.* **1992**, 1643. – [14b] G. A. Lawrance, T. M. Manning, M. Maeder, M. Martinez, M. A. O'Leary, W. C. Patalinhug, B. W. Skelton, A. H. White, *J. Chem. Soc., Dalton Trans.* **1992**, 1635. – [14c] G. A. Lawrance, M. Martinez, B. W. Skelton, A. H. White, *J. Chem. Soc., Dalton Trans.* **1992**, 823.
[15] M. Martinez, M. A. Pitarque, R. van Eldik, *Inorg. Chim. Acta* **1997**, *256*, 51.
[16] G. Brauer, *Handbook of Preparative Inorganic Chemistry*, 2nd edition, Academic Press, **1965**.
[17] A. Creix, M. Ferrer *Inorg. Chim. Acta* **1982**, *59*, 177.

Received July 7, 1999
[I99246]

Combined Electrochemical and EPR Studies of Manganese Schiff Base Complexes Encapsulated within the Cavities of Zeolite Y

Antonio Doménech,[a] Pilar Formentin,[b] Hermenegildo García,*[b] and María J. Sabater*[b]

Keywords: Manganese / Electrochemistry / Zeolites

Encapsulation of manganese(III) and manganese(V) Schiff base complexes within the cavities of zeolite Y has been accomplished by means of established synthetic procedures. The samples have been characterized by a combination of various analytical and spectroscopic techniques that probe either the bulk encapsulated complexes or the species present in the outermost layers of the zeolite grains. Importantly, whereas EPR measurements indicated that aerial oxidation had transformed only about 15–20% of the initially present Mn^{II} cations to Mn^{III}, electrochemical techniques revealed a predominance of Mn^{III} at the external surface. This striking result is due to the fact that electrochemical techniques specifically probe the fraction of electroactive species present in the outermost layers of the zeolite particles. In view of the fact that these complexes are the most accessible and active in heterogeneous catalytic reactions in the liquid phase, the voltammetric measurements provide important information concerning the specific evolution of the reversible Mn^{III}/Mn^{II} redox couple near the surface of the zeolite particles. Furthermore, the unequivocal electrochemical detection of intra-zeolite Mn^{V} species (not observable by EPR spectroscopy) highlights the importance of combining surface characterization tools (electrochemistry) with conventional spectroscopic techniques (IR, UV/Vis, and EPR) of the bulk particle in order to assess the differing nature and distribution of the entrapped transition metal complexes.

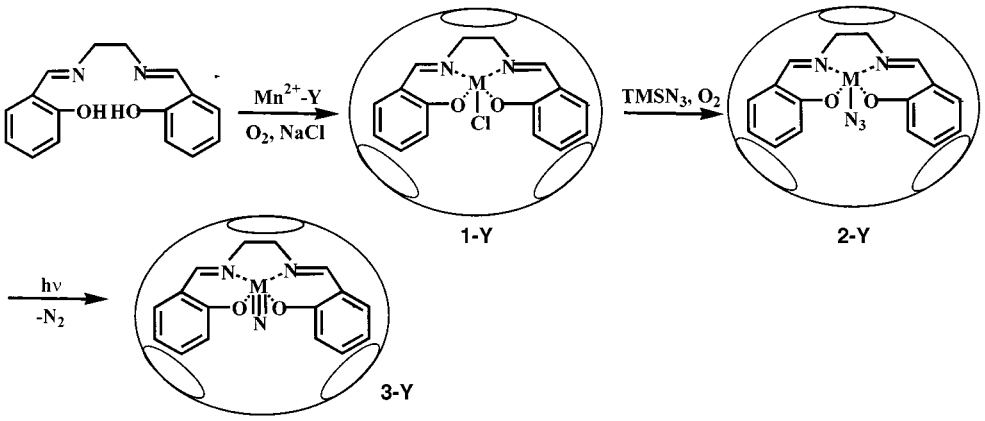
Introduction

Immobilization of transition metal complexes within the supercages of X- and Y-type zeolites has been a topic of intense research in recent years, the aim being to produce materials that combine the activity of a molecular catalyst with the sieving capability and ease of separation from the reaction mixture of a microporous solid support.[1–3] One of the most extensively studied systems has been zeolite Y encapsulated (salen)manganese(III) complexes, which have served as efficient epoxidation catalysts in both the homogeneous and heterogeneous phases.[4–7] The incorporation of such catalysts within microporous solids by so-called "ship-in-a-bottle" syntheses basically requires the manipulation of Mn^{II} salts, complex formation, and ulterior oxidation to Mn^{III} by molecular oxygen. In order to gain a detailed knowledge of these hybrid materials and to characterize the intra-zeolite complexes, a set of complementary techniques is required. Routine IR spectroscopy can give information on the intra-zeolite assembly process by probing mainly the organic ligand moiety. However, it cannot reliably distinguish between different metal oxidation states and does not give information about any residual populations of uncomplexed manganese ions that may be present. This is not the case with EPR spectroscopy and electrochemistry, since these techniques can be suitably applied to provide information on the oxidation state and redox chemistry of specific metal ions. This gives them a distinct advantage over other analytical tools. In the case under consideration here, Mn^{II} is EPR-active whereas Mn^{III} is EPR-inactive. Thus, for a given total amount of manganese, the oxidation of Mn^{II} to Mn^{III}, either complexed or uncomplexed, can be conveniently followed by monitoring the decrease in the area of the Mn^{II} EPR signal. This provides information relating to the bulk material.

On the other hand, electrochemical techniques specifically probe the fraction of electroactive species residing in the outermost layers of the zeolite grains. This is due to the fact that, on the time scale of the electrochemical measurement, the diffusion of the accompanying electrolyte that is necessary to maintain the electroneutrality of the solid only occurs to a shallow depth in the zeolite particles.[8–10] Nevertheless, the electrochemical response provides information not only on the oxidation state of the manganese ions, but also on the coordination of the metal center, since the redox potential of the complex has a distinctive value. In practice, the specific information concerning the complexes located in the external layers is very useful since, being most accessible to reagents, these complexes are the most active in heterogeneous catalysis. On the other hand, the population of complexes located at or near the external surface is also more likely to differ from that of the bulk encapsulated complexes in terms of the distribution of metal ion oxidation states. Thus, while spectroscopy gives information on the global population of complexes (i.e. those predominantly located in the internal pores), it might well be that a given catalytic activity is due almost exclusively to the distinct fraction at the outermost sites. Thus,

[a] Departamento de Química Analítica, Universidad de Valencia, Dr. Moliner, 50, 46100 Burjassot, Valencia, Spain
[b] Instituto de Tecnología Química UPV-CSIC, Universidad Politécnica de Valencia, Apartado 22012, 46071 Valencia, Spain
Fax: (internat.) + 34-96/387-7809
E-mail: hgarcia@qim.upv.es

 © WILEY-VCH Verlag GmbH, D-69451 Weinheim, 2000 1434–1948/00/0606–1339 $ 17.50+.50/0



Scheme 1. Preparation of salen-derived manganese(III) and manganese(V) Schiff base complexes in the supercages of zeolite Y

with the aim of obtaining a quantitative estimation of the amount and distribution of Mn^{II}, Mn^{III}, and Mn^{V} species through the zeolite, we have prepared various salen-derived Mn^{III} and Mn^{V} complexes in the cavities of zeolite Y. Whereas EPR measurements and electrochemical techniques were indicative of significant differences in the Mn^{II}/Mn^{III} ratio between the bulk and the external layers, Mn^{V} species were detected only by cyclic voltammetry. This study highlights the importance of combining spectroscopic techniques with surface-specific analytical tools in differentiating between different populations of entrapped complexes.

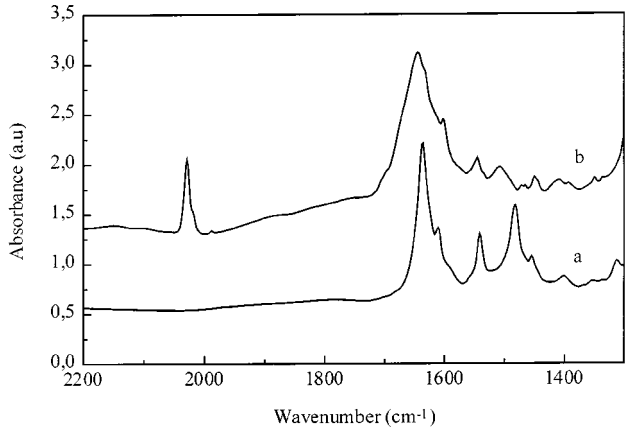


Figure 1. IR spectra of heterogeneous complexes (a) **1-Y** and (b) **2-Y**; the spectra were recorded at room temperature after heating at 100 °C and degassing at 10^{-5} mbar for 1 h

Results and Discussion

Encapsulation of the (salen)Mn complex [salen = 1,2-bis(salicylidenimino)ethylene] within the cavities of zeolite Y, to give **1-Y**, was achieved by treatment of Mn^{2+}-pre-exchanged zeolite Y (0.48% Mn^{2+}; 1 Mn^{2+} every 5 supercages) with the pre-synthesized ligand 1,2-bis(salicylideniminoethylene), followed by treatment with molecular oxygen. As we reported previously, ulterior treatment of **1-Y** with trimethylsilyl azide ($TMSN_3$) allowed access to **2-Y** (Scheme 1).[11] After removal of the excess salen ligand by Soxhlet extraction with dichloromethane, the resulting complexes **1-Y** and **2-Y** were characterized by direct comparison of their DR and IR spectra with those of the corresponding unsupported complexes (**1** and **2**), which were synthesized independently according to previously described methods.[13] The most salient spectroscopic features supporting the formation of **1-Y** were a characteristic imine stretching vibration at 1615 cm^{-1} and a band typical of metallosalen complexes at 1535 cm^{-1}. In the case of **2-Y**, an additional sharp IR absorbance due to the azide ligand at 2037 cm^{-1} confirmed the formation of this heterogenized complex (Figure 1).[11] The corresponding encapsulated nitride complex **3-Y** was obtained by photochemical denitrogenation of the (azido)metal complex **2-Y** as we have reported previously.[11] The transformation of **2-Y** into **3-Y** could be conveniently monitored by IR and Raman spectroscopies, by following the disappearance of the intense azide stretching vibration in the IR spectrum and the concomitant increase in the Raman absorption band characteristic of an Mn≡N triple bond.

The electrochemistry of the related pure complex (salen)$Mn^{III}Cl$ **1** in solution (CH_3CN, DMSO) has been thoroughly studied and essentially involves a reversible one-electron process at a formal potential close to −0.20 V vs. SCE.[8] On the other hand, the cyclic voltammogram for the parent (azido)manganese(III) complex **2**, immobilized on a polymer-film electrode and immersed in neutral aqueous or CH_3CN solution, shows a one-electron reversible couple (C_1/A_1) close to −0.25 V vs. SCE (Figure 2). In both cases, the absence of additional peaks in the +0.8 to −1.0 V potential range indicates that there is no significant dissociation of the complex.

As expected on the basis of previous literature reports, the electrochemical responses obtained for the respective zeolite-modified electrodes **1-Y** and **2-Y** have common features with the patterns and potential values observed for the species in solution and in polymer-film-modified

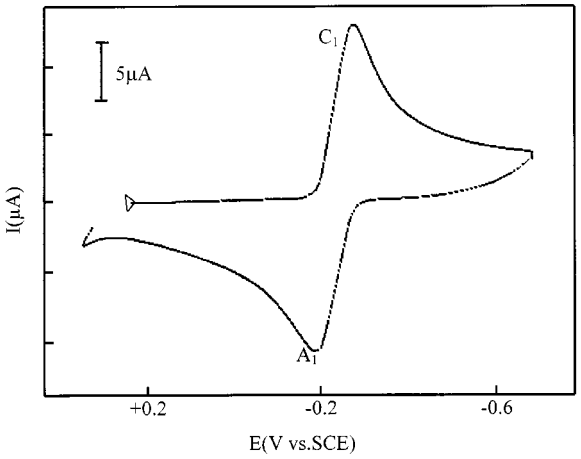


Figure 2. Cyclic voltammogram of a polymer-film-modified electrode of the (salen)MnN_3 complex immersed in H_2O (0.15 M $NaClO_4$); v = 20 mV/s

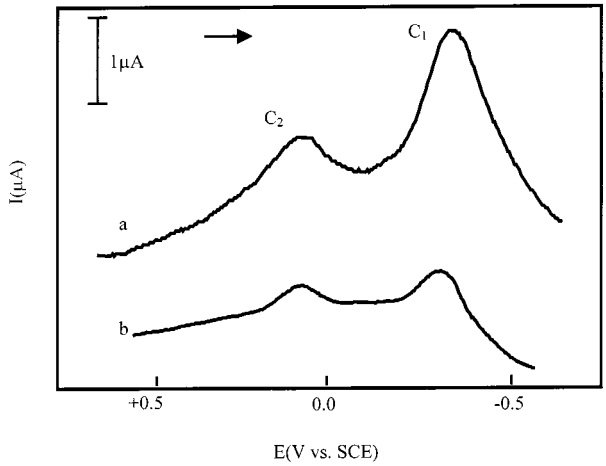


Figure 4. Differential pulse voltammograms of a zeolite-modified electrode containing **2-Y** immersed in H_2O (0.15 M $NaClO_4$); (a) first and (b) second scan; v = 10 mV/s, ΔU = 80 mV

electrodes.[14−16] In fact, both heterogeneous complexes **1-Y** and **2-Y** showed the C_1/A_1 redox couple around −0.25 V vs. SCE together with an additional cathodic peak (C_2) in the +0.3 to −0.2 potential range (Figures 3 and 4). Although comparison of the peak profiles of C_1/A_1 and C_2 suggests that they are similar, no conclusions can be drawn concerning the relative number of electrons transferred in the two processes since the populations of the relevant species are likely to be very different. The (azido)manganese(III) complex **2-Y** showed an additional two-electron oxidation process (A_3) at +0.30 V vs. SCE (Figure 3).

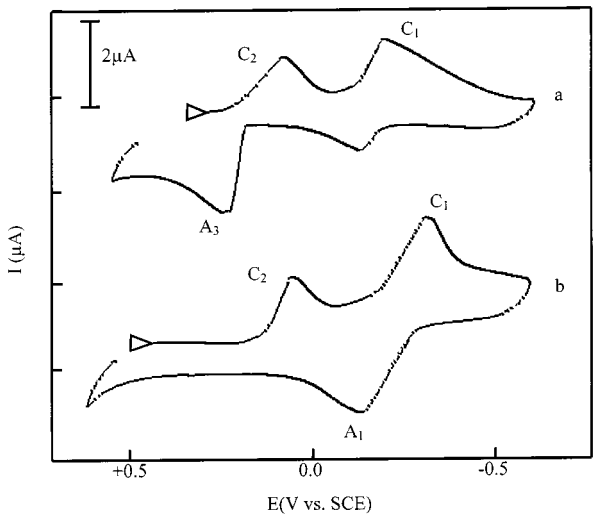


Figure 3. Cyclic voltammograms of zeolite-modified electrodes containing (a) **2-Y** and (b) **1-Y** in aqueous media (0.15 M $NaClO_4$); v = 20 mV/s

Assignment of these redox processes can be partly achieved on the basis of the electrochemical responses observed for the respective non-supported complexes. Thus, the C_1/A_1 couple clearly corresponds to redox transformations affecting those Mn(salen)X (X = Cl^-, N_3^-) complexes located in the boundary sites of the zeolite surface as indicated in eq. 1, where s represents species in the solution phase, b represents adsorbed boundary species, and M^+ is the charge-balancing cation of the salt acting as the supporting electrolyte.[14−16]

$$(salen)Mn^{III}X\,(b) + M^+(s) + e^- \rightarrow (salen)Mn^{II}X\,(b) + M^+(b) \qquad (1)$$

On the other hand, the C_2 process is also observed as a single peak in the electrochemical response of the original Mn-Y sample prior to addition of the ligand. Thus, this peak cannot correspond to any manganese Schiff base complex, but rather to other manganese species present in the outermost layers. These adventitious Mn species are most probably small oxide clusters deposited at the zeolite surface, which would not participate in the complexation.

Finally, the third redox peak A_3 can most probably be attributed to free azide ligands N_3^-. Strong support for this assignment is provided by the observations that: (i) the A_3 peak is not observed on scanning the electrochemical response of the parent complex **1-Y**, and (ii) an aqueous solution of NaN_3 shows an oxidation peak at the same potential. While azide N_3^- displacement from complex **2** by other ligands or solvent cannot be ruled out, the appearance of this specific N_3^- peak can more probably be attributed to residual traces of azido compounds employed in the synthesis of **2**.

Quantification of the Mn^{II}/Mn^{III} ratio present in electrochemically probed sites of the zeolite particle was accomplished by comparing the experimental data with theoretical voltammetric curves. These theoretical simulations were obtained by dividing the intensities of the first and second scans of the anodic peak (I'_{ap}/I''_{ap}) and assuming single reversible redox processes and equal diffusion coefficients for the species involved in the oxidation and reduction processes.[17] Although these measurements are subject to relatively large errors (25%), our estimates of the initial amount of Mn^{III} present in the non-exchanged samples was 45% for **1-Y** and 55% for **2-Y**. Furthermore, when samples of **1-Y** and **2-Y** were submitted to supplementary ion-exchange with NaCl, which supposedly replaces uncomplexed Mn^{2+} by Na^+, the proportion of Mn^{III} increased to 85% and 90% in the samples of **1-Y** and **2-Y**, respectively (the amounts of

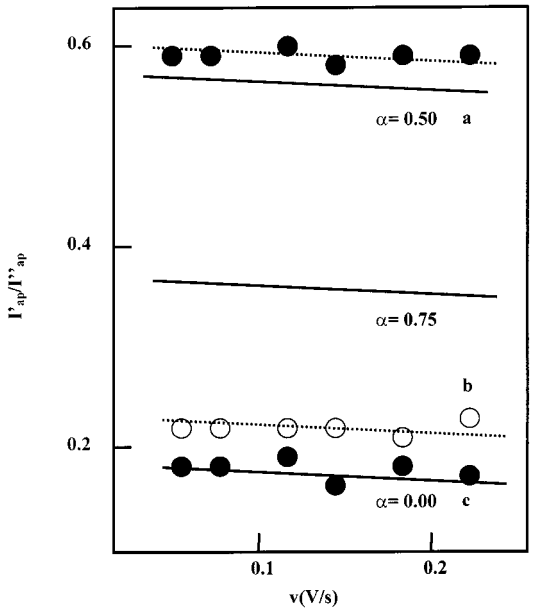


Figure 5. Comparison between theoretical and experimental plots of anodic peak intensity ratios of the first and second scans (I'_{ap}/I''_{ap}) vs. potential scan rate in CVs of different modified electrodes: (a) **2-Y** before treatment with 1 M NaCl; (b) **2-Y** after ion exchange with 1 M NaCl, and (c) pure complex **2**; the dotted lines correspond to experimental data for the supported complexes; α denotes the Mn^{II}/Mn^{III} molar fraction

Mn^{III} calculated to be present in the pure complex **2** and the supported complex **2-Y** before and after ion-exchange are represented in Figure 5).

In striking contrast, EPR measurements comparing the relative intensities of the signals before and after oxidative treatment indicated that a high proportion of the initial Mn^{II} cations of the bulk particle remained unaltered. We estimate that only about 15−20% (error 10%) of the initially present Mn^{II} cations were oxidized to Mn^{III} in both the encapsulated complexes **1-Y** and **2-Y**, reflecting the difficulty in achieving complete oxidation within the zeolite cavities.[18−20] Although absolute quantitative EPR measurements are subject to relatively large experimental errors compared to more accurate chemical analysis, we found the aforementioned ratio of oxidation states to be readily reproducible between samples examined under exactly the same conditions by EPR. Hence, this apparent contradictory result [predominant Mn^{II} by EPR but no detectable (salen)Mn^{II} complexes by cyclic voltammetry] can only be reconciled by considering that only a fraction of the total loading is really probed by cyclic voltammetry (the maximum total charge uptake was found to be 10^{-4} coulomb/mg zeolite, i.e. 10^{-9} mol e^-/mg zeolite, which roughly corresponds to 1.1% of the total complex calculated by chemical analysis). In fact, although the actual mechanisms of intrazeolite electrochemical processes remain controversial, a consensus has been reached that the electrochemical response is exclusively due to those species located in the outermost supercavities.[14−16] To obtain experimental support for the prevalence of Mn^{III} over Mn^{II} at the most exposed layers of the zeolite grains, we also measured the XPS of **1-Y**. As expected, and in accordance with the electrochemical measurements, the electronic transition at 641.7 eV, characteristic of the 2p orbital of Mn^{III} ($Mn2p_{(3/2)}$) predominated, whereas that corresponding to Mn^{II} (the characteristic satellite peak of its 2p orbital appears around 647 eV) was virtually absent.

Finally, the differential pulse voltammetric curve (DPV_s curve) of the irradiated zeolite **3-Y** featured an additional cathodic peak C_4 at +0.65 V, which, on the basis of its redox potential, could be assigned to reduction of the nitridomanganese(V) species generated photochemically from the corresponding Mn^{III} azide precursor complex (Figure 6). Since the current associated with this peak was comparable to that associated with the prior redox processes in the **2-Y** precursor, it seems reasonable to conclude that upon irradiation a significant amount of the (salen)$Mn^{III}N_3$ was transformed into the high-valent Mn^V complex, at least in the outermost layers of the particles. This interpretation is also in agreement with previous IR and Raman studies, which showed a disappearance of the N_3 stretching vibration at 2039 cm^{-1} and a concurrent appearance of the nitrido N≡M band upon irradiation.[11] We recorded an EPR spectrum of the sample under consideration here. However, in the present case, EPR spectroscopy was unable to detect the formation of any Mn^V species since the intense signal due to the residual Mn^{II} ions in the bulk zeolite completely masked any weaker signals due to the high-valent manganese complex that may have been present.

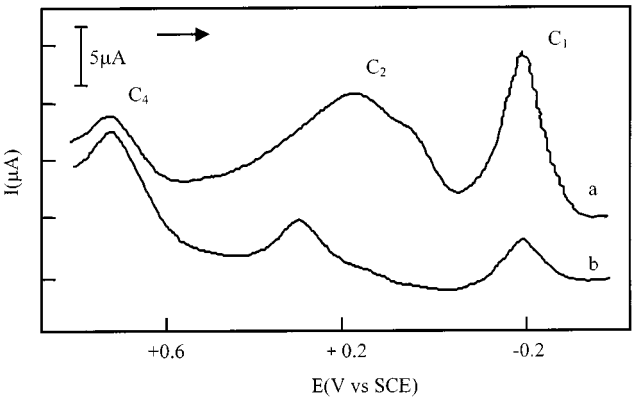


Figure 6. Differential pulse voltammograms (DPVs) for a zeolite-modified electrode containing the **3-Y** complex immersed in H_2O (0.15 M $NaClO_4$); (a) first and (b) second scan; v = 10 mV/s, ΔU = 80 mV

Conclusion

According to the data derived from the electrochemical measurements, the manganese Schiff base complexes **1-Y**, **2-Y**, and **3-Y** residing in the outermost layers of the zeolite Y particles have the oxidation state that would be expected on the basis of literature reports concerning the preparation of unsupported complexes **1**−**3**. Moreover, cyclic voltammetry and differential pulse voltammetry have confirmed the presence of coexisting Mn^{III} and Mn^V species in the supported (nitrido)manganese(V) samples **3-Y**. However, the electrochemical data relates only to a minor fraction of the bulk

(salen)Mn complexes, the total current uptake being much smaller than the amount of encapsulated complex.

In contrast, parallel EPR measurements indicated that in the bulk zeolite particles only about 20% of the Mn^{II} initially present in complexes **1-Y** and **2-Y** had been oxidized to Mn^{III}. This apparent discrepancy between electrochemical and EPR measurements indicates that the oxidation of Mn^{II} to Mn^{III} is only complete in the outermost layers, thus establishing a non-uniform distribution of manganese oxidation states through the zeolite grain.

Our work highlights the fact that, in the case of transition metal complexes encapsulated within zeolites, the catalytic behaviour could be due to a minor fraction of the total population residing in the outermost layers and having an oxidation state distinct from that of the bulk of the complex located deeper inside the zeolite particles.

Experimental Section

Preparation of Complexes 1-Y, 2-Y, and 3-Y: A mixture of 1 g of calcined and dehydrated Mn^{2+}-pre-exchanged zeolite Y (0.48% Mn^{2+}; measured by atomic absorption spectroscopy) and 0.150 g (0.56 mmol) of the previously synthesized ligand 1,2-bis(salicylideniminoethylene) was refluxed in 10 mL of dichloromethane for 12 h under nitrogen. The resulting yellow slurry was then refluxed for a further 12 h while air was bubbled through it. After filtration, the inorganic solid was subjected to Soxhlet extraction with dichloromethane for 8 h to remove excess complex and reactants. The solid was then treated with 10 mL of 1 M aq. NaCl solution for 4 h to afford the supported complex **1-Y**.

The preparation of **2-Y** was carried out by stirring 1 g of the supported complex **1-Y** with 0.02 g (0.173 mmol) of trimethylsilyl azide in 10 mL of dichloromethane for 12 h at room temperature under air bubbling. The heterogeneous complex **2-Y** thus obtained was collected by filtration and subjected to Soxhlet extraction with dichloromethane for 8 h to remove excess complex and reactants.

Sample **3-Y** was prepared through photochemical decomposition of the heterogeneous azide complex **2-Y**. The conversion could be followed by monitoring the disappearance of the characteristic IR azide stretching band and the concomitant increase of a Raman absorption at 1050 cm^{-1} assigned in the literature to the manganese(V) nitride triple bond that is progressively formed during the course of the irradiation.[11] The photolysis was carried out at room temperature in the solid state using self-supporting compressed pellets. These were irradiated through Pyrex (λ 300 nm) with light from a medium-pressure 125-W mercury lamp equipped with an outer jacket refrigerating system.

IR Spectra: FT-IR spectra of the complexes in the zeolites were recorded at room temperature using a greaseless CaF_2 cell in a Nicolet 710 FT spectrophotometer. Self-supporting wafers (ca. 10 mg) were prepared by compressing the zeolite powder at 1 $toncm^{-2}$. The samples were degassed at 100 °C and 10^{-2} Pa for 1 h prior to recording of the spectra.

EPR Spectra: Room-temperature EPR spectra were recorded with a Bruker ER200D spectrometer, working at the X-band (9.65 GHz) and using DPPH (g = 2.0036) as a reference standard. The total number of Mn^{II} ions was calculated by double integration of the signal and comparison of its area with that of the signal of the original Mn^{2+}-Y zeolite.

Electrochemical Measurements: Electrochemical measurements were performed in a conventional three-electrode cell at room temperature under argon. Cyclic voltammograms were obtained using a Newtronics 200P wave generator and an HQ 1000 potentiostat. Differential pulse voltammograms were recorded with a Metrohm E506 Polarecord.

Polymer-film electrodes were prepared as reported previously.[12a] A few μL of a dispersion of the zeolite (10 mg) in acetone (5 mL) was deposited onto the surface of a freshly polished glassy carbon electrode and the coating was allowed to dry in air at room temperature. Then, one drop of a solution of Palaroid B72 (Rohm Haas) in acetone was added and the modified electrode was dried in air. Palaroid provides a uniform thin film that exhibits good adherence and mechanical resistance.[12b]

Voltammograms of the pure complexes were recorded from 1−2 mM solutions in CH_3CN or DMSO using a freshly polished glassy carbon electrode (GCE). A platinum gauze pseudo-reference electrode was used for experiments in organic solvents, whereas a saturated calomel electrode (SCE) was used as a reference in aqueous solutions. All potentials mentioned in the text are referred to aqueous SCE. A platinum wire was used as an inert auxiliary electrode.

For experiments in organic solvents, Et_4NClO_4 (0.1 M) and Bu_4NPF_6 (0.1 M) were used as supporting electrolytes. For experiments in aqueous media, 0.15 M $NaClO_4$ was used.

XPS Measurements: XPS measurements were made at room temperature using a concentric hemispherical analyzer operated in the constant pass energy mode (50 eV). An Mg-K_α X-ray source (hν = 1253.6 eV) was used. A vacuum of ca. 5×10^{-9} Torr in the analysis chamber was maintained throughout the XPS recording. Charging effects were calibrated by analysis of the C (1s) line at 284.6 eV.

Acknowledgments

Financial support from the Spanish DGICYT (H. G., MAT97−1016-CO2) and the Generalitat Valenciana (M. J. S., GVDOC99−0203) is gratefully acknowledged.

[1] D. E. De Vos, P. Knops-Gerrits, R. F. Parton, B. M. Weckhuysen, P. A. Jacobs, R. A. Schoonheydt, *J. Incl. Phen. Mol. Recog. Chem*. **1995**, *21*, 185−213.
[2] N. Herron, *Inorg. Chem.* **1986**, *25*, 4714−4717.
[3] K. J. Balkus, A. G. Gabrielov, *J. Incl. Phen. Mol. Recog. Chem*. **1995**, *21*, 159−184.
[4] E. N. Jacobsen, W. Zhang, *J. Org. Chem.* **1991**, *56*, 2296−2298.
[5] [5a] S. B. Ogunwumi, T. Bein, *Chem. Commun.* **1997**, 901−902. − [5b] M. J. Sabater, A. Corma, A. Doménech, V. Fornés, H. García, *Chem. Commun.* **1997**, 1285−1286. − [5c] C. Bowers, P. K. Dutta, *J. Catal*. **1990**, *122*, 271−279.
[6] S. P. Varkey, C. Ratnasamy, P. Ratnasamy, *J. Mol. Catal*. **1998**, *135*, 295−306.
[7] P. Piaggio, P. McMorn, C. Langham, D. Bethull, P.C. Bulmanpage, F. E. Hancock, G. J. Hutchings, *New J. Chem*. **1998**, 1167−1169.
[8] F. Bedioui, L. Roue, J. Devinck, K. J. Balkus, Jr., *Stud. Surf. Sci. Catal*. **1994**, 917−924.
[9] L. Gaillon, N. Sajot, F. Bedioui, J. Devynck, *J. Electroanal. Chem*. **1993**, *345*, 157−167.
[10] C. Senaratne, J. Zhang, M. D. Baker, C. A. Bessel, D. L. Rolison, *J. Phys. Chem.* **1996**, *100*, 5849−5862.
[11] P. Formentín, J. V. Folgado, V. Fornés, H. García, F. Márquez, M. J. Sabater, *J. Phys. Chem. B*, submitted.
[12] [12a] A. Doménech, I. Casades, H. García, *J. Org. Chem.* **1999**, *64*, 3731−3735. − [12b] J. M. Kauffmann, T. Montenez, J. L. Vandenbalck, G. I. Patriarche, *Mikrochim. Acta* **1984**, 95−105.

[13] [13a] J. L. Leighton, E. N. Jacobsen, *J. Org. Chem.* **1996**, *61*, 389−390. − [13b] J. F. Larrow, E. N. Jacobsen, *J. Org. Chem.* **1994**, *59*, 1939−1942.
[14] F. Bedioui, E. De Boysson, J. Devynck, K. J. Balkus, Jr., *J. Chem. Soc., Faraday Trans.* **1991**, *87*, 3831−3834.
[15] F. Bedioui, L. Roué, E. Briot, J. Devynck, S. L. Bell, K. J. Balkus, Jr., *J. Electroanal. Chem*. **1994**, *373*, 19−29.
[16] [16a] C. P. Horwitz, S. E. Creager, R. W. Murray, *Inorg. Chem.* **1990**, *29*, 1006−1011. − [16b] F. Bedioui, E. Labbe, S. Gutierrez-Granados, J. Devynck, *J. Electroanal. Chem*. **1991**, *301*, 267−274.
[17] The theoretical response as a function of the relative Mn^{III}/Mn^{II} population was generated using the SIMULA (10) program. Comparison with theoretical curves is feasible since it has been observed that these plots depend on the scan rate, the Mn^{III}/Mn^{II} ratio, as well as the initial and switching potentials.
[18] Mn^{III} is EPR inactive, hence it has been quantified by assuming that the increase in this species corresponds to the decrease in Mn^{II}, as estimated from the area of the EPR signal before and after oxidative treatment.
[19] [19a] M. J. Sabater, S. García, M. Alvaro, H. García, J. C. Scaiano, *J. Am. Chem. Soc.* **1998**, *120*, 8521−8522. − [19b] P. Knops-Gerrits, D. De Vos, F. Thibault-Starzyk, P. A. Jacobs, *Nature* **1994**, *369*, 543−546.
[20] M. J. Sabater, A. Corma, J. V. Folgado, H. García, *J. Phys. Org. Chem.* **2000**, *13*, 57–62.

Received October 19, 1999
[I99367]

The Redox Behaviour of the Family $(C_{60})[Mo(CO)_2(phen)(dbm)]_n$ ($n = 1-3$) – A Comparison with the Analog $(\eta^2\text{-}C_{70})[Mo(CO)_2(phen)(dbm)]$ (phen = 1,10-Phenanthroline; dbm = Dibutyl Maleate)

Piero Zanello,*[a] Franco Laschi,[a] Arnaldo Cinquantini,[a] Marco Fontani,[a] Kaluo Tang,[b] Xianglin Jin,[b] and Lei Li[b]

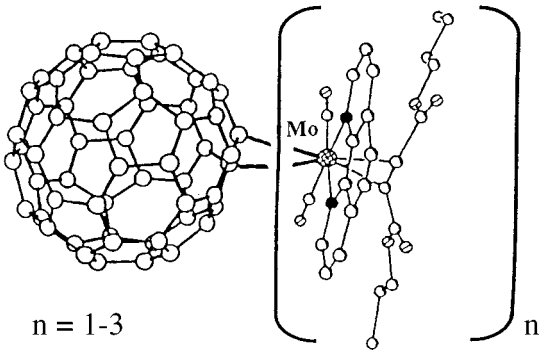
Keywords: Fullerenes / Electrochemistry / EPR spectroscopy / Molybdenum / Carbonyl complexes

The electrochemical behaviour of the series $(C_{60})[Mo(CO)_2(phen)(dbm)]_n$ (n = 1–3) has been studied in dichloromethane solution. Each member of the family displays three reversible, fullerene-centred, one-electron reductions at potential values which linearly shift towards more negative potential values by 0.15 V for each appended molybdenum fragment. Such reduction processes are in turn followed by a metal-centred reduction, which causes decomplexation of the C_{60} ligand. EPR spectra recorded on the electrogenerated monoanions $[(C_{60})\{Mo(CO)_2(phen)(dbm)\}_n]^-$ (n = 1, 2) exhibit features indicative of some interaction between the electron entering the fullerene ligand and the metallic centre(s). Comparison with the redox behaviour of the C_{70}-analog $(C_{70})[Mo(CO)_2(phen)(dbm)]$ reveals significant differences; namely that the C_{70}-analog exhibits two reversible one-electron reductions followed by a single two-electron reduction, all of these reductions being centred on the fullerene ligand. A further cathodic step centred on the metallic fragment is present, which, also in this case, causes framework destruction releasing the C_{70} ligand.

Introduction

Metallofullerenes should display a rich redox propensity because the well-known ability of fullerenes to undergo reversibly multiple one-electron transfers[1] is coupled to that of the appended metal fragments. However, only few of them have been studied from the electrochemical viewpoint[2–7] and essentially no data are available for C_{70} complexes.[2] A number of fullerenes containing exohedral multimetallic frames have been structurally characterised. They include binuclear C_{60}-Ir_2,[8,9] -Ru_2,[10] -Si_2,[11] -Fe_2,[2] -Re_2,[3] C_{70}-Ir_2,[12] trinuclear C_{60}-Ru_3,[13] -Os_3,[4] C_{70}-Ru_3,[14] tetranuclear C_{60}-Ir_4,[15] C_{70}-Pt_4,[16] pentanuclear C_{60}-Ru_5,[17] and hexanuclear C_{60}-Pt_6,[18] C_{60}-Ru_6,[17] C_{60}-Ru_5Pt,[17] and C_{70}-Ru_6[14] assemblies. Some of these multimetallic complexes are constituted with a number of identical metal fragments appended to one fullerene ligand, such as $C_{60}[Pt(PR_3)_2]_n$ ($1 \le n \le 4$)[6] and $C_{60}[S_2Fe_2(CO)_6]_n$ ($1 \le n \le 3$).[2] These derivatives have also been studied from the electrochemical viewpoint. Based on these results, we decided to perform a spectroelectrochemical study on the series $(\eta^2\text{-}C_{60})[Mo(CO)_2(phen)(dbm)]_n$ ($1 \le n \le 3$; phen = 1,10-phenanthroline; dbm = dibutyl maleate), Scheme 1.

In addition, we compared the electrochemical behaviour of $(\eta^2\text{-}C_{60})[Mo(CO)_2(phen)(dbm)]$ with that of its C_{70} analog $(\eta^2\text{-}C_{70})[Mo(CO)_2(phen)(dbm)]$. We have already reported on the mononuclear complexes $(\eta^2\text{-}C_{60})[M(CO)_2(phen)(dbm)]$ (M = Mo, W).[7]



Scheme 1

Results and Discussion

Electrochemistry and Coupled EPR Spectroscopy of $(C_{60})[Mo(CO)_2(phen)(dbm)]_n$

Figure 1 compares the cyclic voltammetric response of the three complexes $(C_{60})[Mo(CO)_2(phen)(dbm)]_n$ (n = 1–3) with that of C_{60}.

A preliminary glance shows that, as with other multimetallic fullerenes,[3,5,6] the di- and (particularly) the tri-molybdenum derivatives contain some amounts of the corresponding mono- and di-metallic precursors. These unwanted precursors do not appear to arise from the electron transfer processes, and further studies will be needed to clarify whether they originate from difficult separation or from dissociation equilibria setting up in solution. An analysis of the responses obtained by varying the scan rate, shows that in the case of $(C_{60})[Mo(CO)_2(phen)(dbm)]$, the first three

[a] Dipartimento di Chimica dell'Università di Siena, Via Aldo Moro, 53100 Siena, Italy
[b] Institute of Physical Chemistry, Peking University, Beijing 100871, P.R.China

 © WILEY-VCH Verlag GmbH, D-69451 Weinheim, 2000 1434–1948/00/0606–1345 $ 17.50+.50/0

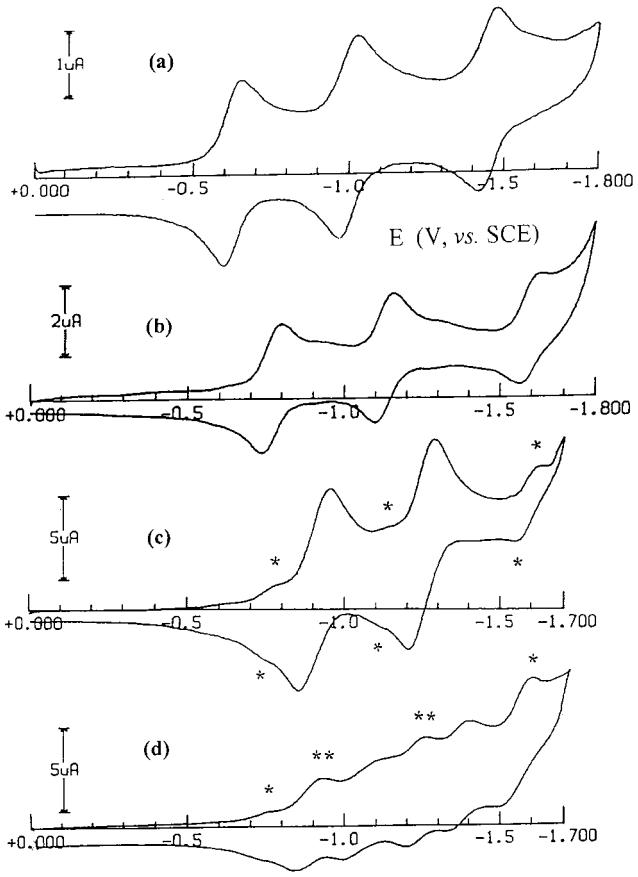


Figure 1. Cyclic voltammetric responses recorded at a platinum electrode in CH_2Cl_2 solutions containing $[NBu_4][PF_6]$ (0.2 mol dm^{-3}) and: (a) C_{60} (saturated solution); (b) $C_{60}[Mo(CO)_2(phen)(dbm)]$ ($6\cdot10^{-4}$ mol dm^{-3}); (c) $C_{60}[Mo(CO)_2(phen)(dbm)]_2$ ($5\cdot10^{-4}$ mol dm^{-3}); (d) $C_{60}[Mo(CO)_2(phen)(dbm)]_3$ ($4\cdot10^{-4}$ mol dm^{-3}); scan rate 0.2 Vs^{-1}; $T = -10$ °C

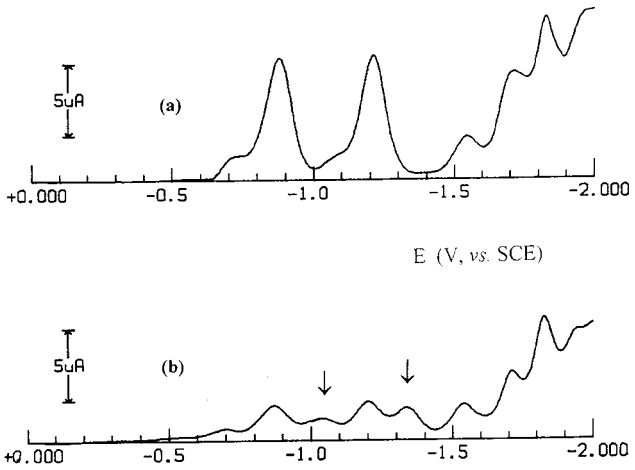


Figure 2. Differential pulse voltammograms recorded at a platinum electrode in CH_2Cl_2 solutions containing $[NBu_4][PF_6]$ (0.2 mol dm^{-3}) and: (a) $C_{60}[Mo(CO)_2(phen)(dbm)]_2$ ($5\cdot10^{-4}$ mol dm^{-3}); (b) $C_{60}[Mo(CO)_2(phen)(dbm)]_3$ ($5\cdot10^{-4}$ mol dm^{-3}); scan rate 0.004 Vs^{-1}; $T = -10$ °C; the arrows point at the processes assumed to be the first and second reduction of the tris-adduct, respectively

reversible one-electron reductions are shifted towards more negative potentials values (by about 0.15 V) with respect to those of free C_{60}, Figure 1b. A fourth reduction, not shown in Figure 1b, is also present at more negative potential values ($E_p \approx -1.9$ V). This reduction involves an ECE mechanism, in which the reduction of the Mo-fragment triggers decomplexation of $[C_{60}]^{3-}$ followed by the concomitant reduction of this trianion to the corresponding tetraanion.[7b] As Figure 1c illustrates, the insertion of the second $Mo(CO)_2(phen)(dbm)$ fragment does not substantially modify the overall reduction sequence, but results in a further cathodic shift of all the redox changes. Based on the relative peak heights of the reduction steps of the monoadduct by-product (monostarred peak-systems in Figure 1c), it seems that the second reduction of the bis-adduct triggers partial decomplexation of one Mo-fragment. Unfortunately, the interpretation of the cyclic voltammetric response of the tris-adduct illustrated in Figure 1d is less straightforward, because of the presence of excessively large amounts of mono- and bis-adducts, the reduction processes of which are labelled by single and double asterisks, respectively. By way of speculation, the reoxidation peak at about −1.0 V seems to be directly associated with the first one-electron reduction of the tris-adduct, the cathodic peak of which is partially overlapped by the second reduction of the monoadduct. Some support to such an assignment could come from the comparison between the differential pulse voltammograms of the bis- and tris- adducts shown in Figure 2, in which the first reduction of the tris-adduct seems to lie at $E_p = -1.04$ V, in between the two reductions of the bis-adduct by-product.

This being allowed, we could tentatively assign the second reversible reduction of the tris-adduct to the peak-system located at about −1.4 V. Because of the complex pattern, any attempt to assign the subsequent steps is ruled out. All the pertinent redox potentials are summarised in Table 1.

Table 1. Formal electrode potentials (V, vs. SCE) for the one-electron reductions exhibited by the metallafullerenes $(C_{60})[MoL]_n$ and $(C_{70})[MoL]$ [L = $(CO)_2(phen)(dbm)$] in dichloromethane, $T = -10$ °C

Complex	$E^{\circ\prime}_{1st}$	$E^{\circ\prime}_{2nd}$	$E^{\circ\prime}_{3rd}$	$E^{\circ\prime}_{4th}$
C_{60}	−0.63	−1.00	−1.45	−1.88
$(C_{60})[MoL]$	−0.77	−1.13	−1.60	−1.86[a]
$(C_{60})[MoL]_2$	−0.91	−1.24	−1.78	−1.92[a]
$(C_{60})[MoL]_3$	−1.04	−1.37	−	−
C_{70}	−0.61	−0.98	−1.41	−1.75
$(C_{70})[MoL]$	−0.71	−1.09	−1.51[b]	−1.82[c]

[a] Peak potential for metal-centred ECE mechanisms; measured at 0.2 Vs^{-1}. – [b] Averaged potential value for an overlapping two-electron process; see text. – [c] Peak potential for an irreversible process; measured at 0.2 Vs^{-1}.

Further support to the above assignments comes from the trend of the formal electrode potentials of the reduction processes with respect to the number of metal fragments, illustrated in Figure 3.

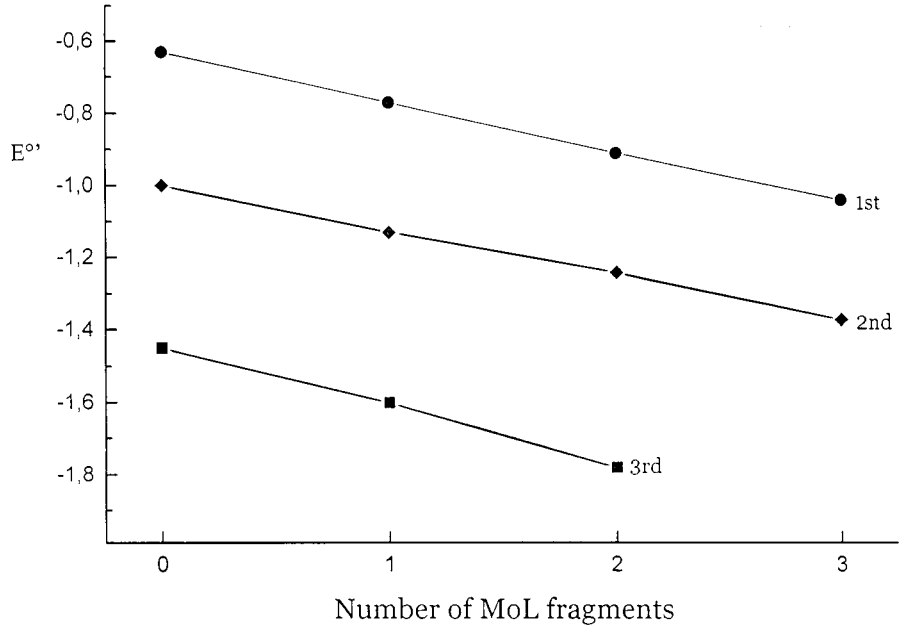


Figure 3. Plot of the formal electrode potentials of the first (1st), second (2nd), and third (3rd) fullerene centred reductions of $C_{60}[Mo(CO)_2(phen)(dbm)]_n$ vs. the number of molybdenum fragments

As it happens, for the series $C_{60}[Pt(PR_3)_2]_n$,[6] the formal electrode potentials of the first reduction increase linearly with the number of metal fragments (correlation coefficient = 1.0); the same trend substantially holds for the subsequent fullerene-centred reductions. This result points out that the electronic effects played by each metal subunit are fully additive. It should however be taken into account that the shifts of the redox potentials must arise either from the inductive effects exerted by the metal fragment(s), which can favour or disfavour the reduction processes, or from the progressive interruption of the double-bond conjugation operated by the metal coordination, which makes the reductions more difficult. This is confirmed by the examination of the redox potentials of the first one-electron reduction of the series $C_{60}[Mo(CO)_2(phen)(dbm)]_n$, $C_{60}[Pt(PEt_3)_2]_n$, and $C_{60}[S_2Fe_2(CO)_6]_n$ with respect to that of free C_{60} reported in Table 2: in spite of the fact that all complexes are η^2-6:6 coordinated, either negative or positive redox shifts occur.

Table 2. Potential shifts (in V) for the first one-electron reduction of the complexes $(C_{60})[MoL]_n$ [L = $(CO)_2(phen)(dbm)$], $C_{60}[Pt(PEt_3)_2]_n$, and $C_{60}[S_2Fe_2(CO)_6]_n$ with respect to the $[C_{60}]^{0/-}$ couple

Complex	$\Delta E^{\circ\prime}_{0/-}$	Solvent	Reference
$(C_{60})[MoL]$	−0.14	CH_2Cl_2	[a]
$(C_{60})[MoL]_2$	−0.28	CH_2Cl_2	[a]
$(C_{60})[MoL]_3$	−0.41	CH_2Cl_2	[a]
$(C_{60})[Pt(PEt_3)_2]$	−0.34	THF	6
$(C_{60})[Pt(PEt_3)_2]_2$	−0.65	THF	6
$(C_{60})[Pt(PEt_3)_2]_3$	−1.07	THF	6
$(C_{60})[Pt(PEt_3)_2]_4$	−1.45	THF	6
$(C_{60})[(S_2)Fe_2(CO)_6]$	+0.02	$1,2\text{-}Cl_2C_6H_4$	2
$(C_{60})[(S_2)Fe_2(CO)_6]_2$	+0.02	$1,2\text{-}Cl_2C_6H_4$	2
$(C_{60})[(S_2)Fe_2(CO)_6]_3$	+0.06	$1,2\text{-}Cl_2C_6H_4$	2

[a] Present work.

The X-band EPR spectrum of the monoanions $[(\eta^2\text{-}C_{60})M(CO)_2(phen)(dbm)]^-$ (M = Mo, W) electrogenerated in dichloromethane solutions have been previously discussed.[7b] As a matter of fact, the freshly electrogenerated monoanion $[(\eta^2\text{-}C_{60})Mo(CO)_2(phen)(dbm)]^-$ exhibits a well separated, broad, and unresolved axial structure having $g_{\parallel} > g\perp \neq g_{electron} = 2.0023$, Figure 4a.

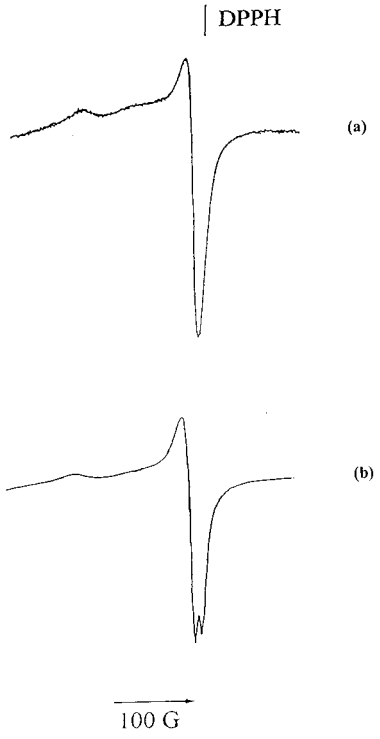


Figure 4. X-band EPR spectra of $[(\eta^2\text{-}C_{60})\{Mo(CO)_2(phen)(dbm)\}]^-$ in CH_2Cl_2 recorded at 100 K: (a) just after its electrogeneration at 250 K; (b) after exposure to air for a few seconds

Even if the low abundance of the Mo-95/97 nuclei does not allow their satellite hyperfine resolution to be detected ($I_{Mo\text{-}95}$ = 5/2; natural abundance = 15.7%; $I_{Mo\text{-}97}$ = 5/2; natural abundance = 19.5%), the width of the signal coupled to its g_i values could be interpreted as being due to a paramagnetic species possessing a partial metallic character, i.e., the fullerene based SOMO of the monoanion could have a significant contribution from the 4d-Mo AO's. In spite of the stability of the monoanion under inert atmosphere, handling the sample even for short times in air causes the appearance of a new absorption that is quite coincident with that of free $[C_{60}]^-$, Figure 4b.

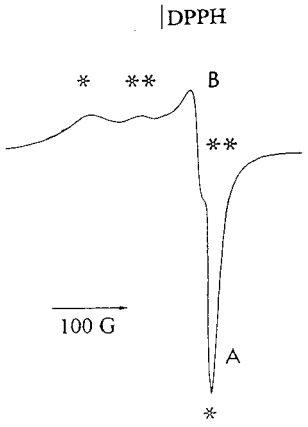


Figure 5. X-band EPR spectrum of a CH_2Cl_2 solution of the freshly electrogenerated monoanion $[(C_{60})\{Mo(CO)_2(phen)(dbm)\}_2]^-$ recorded at 100 K

Figure 5 shows the low-temperature EPR spectrum of the freshly electrogenerated monoanion $[C_{60}\{Mo(CO)_2(phen)(dbm)\}_2]^-$, and exhibits two partially overlapping signals [hereafter indicated as A (*) and B (**), respectively], both of them being resolved in axial structures with $g_{\|i} > g_{\perp i} \neq g_{electron} = 2.0023$.

Table 3. X-band EPR parameters of the electrogenerated monoanions $[(C_{60})\{MoL\}_n]^-$, [L = $(CO)_2$(phen)(dbm)] recorded at 100 K in CH_2Cl_2 solution. ($g_i = \pm 0.002$)

Monoanion	$g_{\|}$ [a]	$g_{\perp}$ [a]	$<g>$ [a][b]	g_{iso}
$[(C_{60})\{MoL\}]^-$	2.089	2.014	2.039	–
$[(C_{60})\{MoL\}_2]^-$ (A)*	2.058	1.960	1.993	–
$[(C_{60})\{MoL\}_2]^-$ (B)**	2.016	1.973	1.987	–
$[C_{60}]^-$	–	–	1.998	1.995[c]

[a] T = 100 K. – [b] $<g> = (g_{\|} + 2g_{\perp})/3$. – [c] T = 295 K; * = outer signals, ** inner signals.

The relevant best fit parameters are collected in Table 3 and can be suitably computed, taking into account an S = 1/2 Electron Spin Hamiltonian for the two axial signals. The line-shape analysis reveals that the species A and B are present in a 2:1 molar ratio. It does not seem too ventured to assume that the two paramagnetic species are geometrical isomers, with the major component likely possessing the commonest geometry in which the two Mo fragments lie at the opposite sides of C_{60}.[8,11] Also, no EPR evidence for the Mo-95/97 satellite hyperfine resolution has been gained in this case, but the spectral pattern might be interpreted in the sense that the overall SOMO likely has a contribution from either the fullerene 2p-C AO's or the two 4d-Mo AO's.

As in the case of the monoadduct, raising the temperature at the glassy-fluid transition induces disappearance of the anisotropic features, while the typical sharp signal of free $[C_{60}]^-$ anion appears as a minor species. A fast refreezing of the solution does not, however, restore the original signal, as is the case for $[(C_{60})Mo(CO)_2(phen)(dbm)]^-$,[7b] thus pointing out that $[(C_{60})\{Mo(CO)_2(phen)(dbm)\}_2]^-$ is more reactive with traces of air than $[(C_{60})Mo(CO)_2(phen)(dbm)]^-$.

Because of the multiple species present in a solution of $(C_{60})[Mo(CO)_2(phen)(dbm)]_3$, we did not attempt the EPR characterization of its monoanion.

Electrochemistry of $(\eta^2\text{-}C_{70})[Mo(CO)_2(phen)(dbm)]$

Figure 6 and Figure 7 show the cyclic voltammetric behaviour of $(C_{70})[Mo(CO)_2(phen)(dbm)]$, in comparison with that of free C_{70}, at different potential windows.

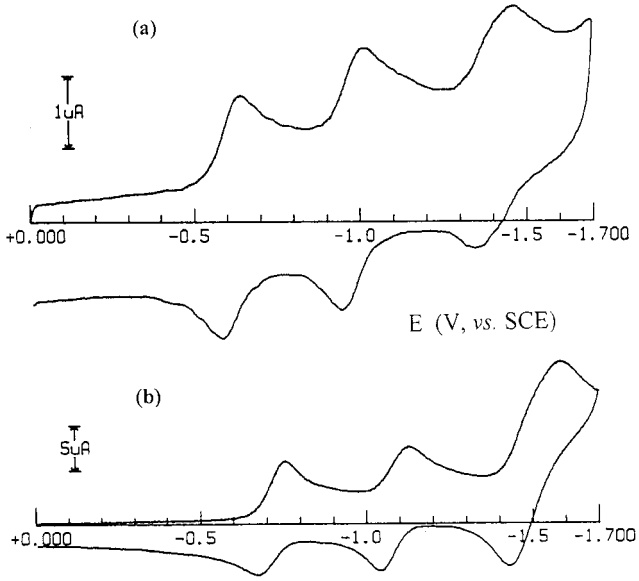


Figure 6. Cyclic voltammetric responses recorded at a platinum electrode in CH_2Cl_2 solutions containing $[NBu_4][PF_6]$ (0.2 mol dm^{-3}) and: (a) C_{70} (saturated solution); (b) $C_{70}[Mo(CO)_2(phen)(dbm)]$ ($4\cdot10^{-4}$ mol dm^{-3}); scan rate 0.2 Vs^{-1}, T = −10 °C

It is easily seen from the first three cathodic waves, Figure 6, that the presence of the Mo fragment also induces a cathodic shift of the first two C_{70}-centred one-electron reductions with respect to free C_{70}. Nevertheless, at variance with the C_{60} analog, the third cathodic process appears as an essentially overlapping two-electron step. Based on the reversibility of such processes and on the fact that the one-electron reductions of either the molybdenum fragment in $(C_{60})[Mo(CO)_2(phen)(dbm)]$ or that of the precursor $Mo(CO)_2(phen)(dbm)_2$ occur at more negative potential values (−1.9 V and −1.7 V, respectively),[7b] we are keen to assume that this closely-spaced two-electron step is due to the substantial concomitance of the third and fourth one-electron reductions of the C_{70} moiety. Finally, as far as the fourth reduction process is concerned, Figure 7, the appear-

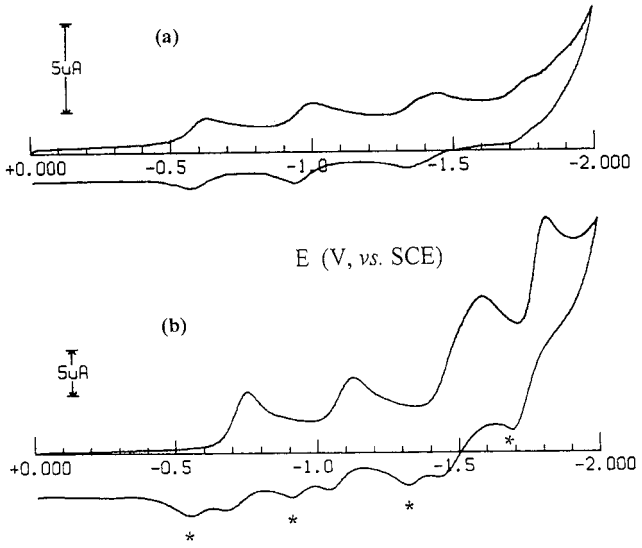


Figure 7. Cyclic voltammetric responses recorded under the same experimental conditions as for Figure 5, along a more extended potential window

ance in the back-scan of the sequential re-oxidations of the free fulleride anions (starred peaks) points out that it induces C_{70} decomplexation as a consequence of the simple EC step:

$$[M^0(\eta^2\text{-}C_{70})]^{4-} \xrightarrow{+e^-} [M^{-1}(\eta^2\text{-}C_{70})]^{5-} \xrightarrow{k} [M]^- + [C_{70}]^{4-}$$

$M = Mo(CO)_2(phen)(dbm)$

In summary, the reduction pathway of $(C_{70})[Mo(CO)_2(phen)(dbm)]$ is rather different from that of its C_{60} analogue in two respects: (i) the electronic perturbation played by the metal fragment forces the third and fourth one-electron additions to C_{70} to become concomitant; (ii) the fourth reduction involves a simple metal-centred process, whereas in the C_{60} derivative it involves the following metal-centred ECE mechanism:

$$[M^0(\eta^2\text{-}C_{60})]^{3-} \xrightarrow{+e^-} [M^{-1}(\eta^2\text{-}C_{60})]^{4-} \xrightarrow{k} [M]^- + [C_{60}]^{3-}$$

$$[C_{60}]^{3-} \xrightarrow{+e^-} [C_{60}]^{4-}$$

$M = Mo(CO)_2(phen)(dbm)$

The relevant electrochemical data are compiled in Table 1.

Finally, it is interesting to note that under the same experimental conditions, the cathodic shift induced by appending the $Mo(CO)_2(phen)(dbm)$ unit to C_{70} is lower than for C_{60}, (0.10 V vs. 0.15 V), thus suggesting that the extent to which the double bond conjugation is broken by the coordination to C_{70} should be lower than with C_{60}. Unfortunately, such a conclusion cannot be generalised because in the case of $(C_{70})[(S_2)Fe_2(CO)_6]$ and $(C_{60})[(S_2)Fe_2(CO)_6]$ the shifts with respect to the corresponding free fullerenes are −0.01 V and +0.02 V, respectively,[2] indicating that the extent of double bond saturation is higher in the C_{70} complex. Underlined that in the last case the interaction of the metal centre with the fullerene ligand is mediated by the disulfur bridge, more data on complexes bearing the same metal fragment directly bound to both C_{60} and C_{70} are needed to clarify such an electronic aspect.

Experimental Section

Material and apparatus for electrochemistry and coupled ESR measurements have been previously described.[7b] All the potential values are referred to the saturated calomel electrode (SCE). Under the present experimental conditions, the one-electron oxidation of ferrocene occurs at $E^{\circ\prime} = +0.34$ V in the temperature range from −10 °C to +10 °C, and at $E^{\circ\prime} = +0.35$ V at +20 °C. The external magnetic field H_0 for ESR spectroscopy was calibrated by using a DPPH powder sample ($g_{DPPH} = 2.0036$). Computer simulation of the ESR spectra was carried out by using the SIM14 A program.[19]

Synthesis: All the reactions were carried out under a nitrogen atmosphere with the use of standard Schlenk techniques. The preparation of $(\eta^2\text{-}C_{60})[Mo(CO)_2(o\text{-phen})(dbm)]$ has been previously reported.[7a]

$(C_{60})[Mo(CO)_2(o\text{-phen})(dbm)]_n$ (n = 2, 3): $Mo(CO)_2(o\text{-phen})(dbm)_2$ (178 mg, 0.225 mmol) was added to a solution of C_{60} (54 mg, 0.075 mmol) in benzene (25 cm^3). The mixture was heated under reflux for 2 h, and then concentrated. The resulting dark green solution was separated by column chromatography (silica gel) using benzene/THF (7:1, then 5:1, and finally 4:1) as eluent. The two main chromatography bands were collected separately, and the solvents were removed. Both the residues were washed with petroleum ether (ca. 30−60 °C) and pentane, and then dried in vacuo to give dark green powders. One is $(C_{60})[Mo(CO)_2(o\text{-phen})(dbm)]_2$ (60 mg, 44%). − Found: C 73.70, H 2.84, N 3.53; calcd.: C 73.04, H 3.07, N 3.04. − IR: $\tilde{\nu}_{max}$ = 1963 (s), 1898 (s) [νC≡O], 1689 (s) [νC=O], 1423 (m), 1159 (s), 573 (w), 525 (m) [νC_{60}]; 428(w) [ν(Mo-(η^2-C=C))], 367cm^{-1} (w) [ν(Mo−N)]. − UV/Vis (CH_2Cl_2): λ_{max} = 258 nm. − The other is $(C_{60})[Mo(CO)_2(o\text{-phen})(dbm)]_3$ (30 mg, 17%). − Found: C 71.34, H 3.05, N 3.24; calcd.: C 69.00, H 3.53, N 3.50. − IR: $\tilde{\nu}_{max}$ [cm^{-1}] = 1959 (s), 1894 (s) [νC≡O]; 1690 (s) [νC=O]; 1422 (m), 1157 (s), 570 (w), 522 (m) [νC_{60}]; 430 (w) [ν(Mo-{η^2-C=C})]; 371(w) [ν(Mo−N)]. − UV/Vis (CH_2Cl_2): λ_{max} [nm]: 258.

$(\eta^2\text{-}C_{70})[Mo(CO)_2(o\text{-phen})(dbm)]$: $Mo(CO)_2(o\text{-phen})(dbm)_2$ (39 mg, 0.05 mmol) was added to a solution of C_{70} (42 mg, 0.05 mmol) in benzene (25 cm^3). The mixture was heated under reflux for 1 h, and then concentrated. The resulting red-brown solution was separated by column chromatography (silica gel) using benzene/acetone (12:1) as eluent. The main chromatography band was collected. The solvents were removed and the residue dried in vacuo to give a red brown powder, (23 mg, 32%). Crystals were obtained by slow diffusion of pentane into a dichloromethane solution. − Found: C 81.90, H 2.55, N 1.85; calcd. for $C_{70}[Mo(CO)_2(o\text{-phen})(dbm)]$: C 82.29,; H 2.01, N 2.00}. IR: $\tilde{\nu}_{max}$ [cm^{-1}] = 1957 (s), 1890 (s) [νC≡O]; 1684(s) [ν(C=O)]; 1427 (s), 1410 (s), 1159 (s), 1131 (m), 797 (w), 674 (w), 640 (w), 573 (w), 535 (w), 456 (w) [νC_{70}]; 434 (w) [ν(Mo-{η^2-C=C})]; 367 (w) [ν(Mo−N)]. − UV/Vis (CH_2Cl_2): λmax [nm]: 238. − ^1H NMR: δ_H (Solvent $CDCl_3$ + CS_2, standard $SiMe_4$): 0.9 (t, 6 H, $CH_2CH_2CH_2CH_3$), 1.3 (m, 4 H, $CH_2CH_2CH_2CH_3$), 1.5 (m, 4 H, $CH_2CH_2CH_2CH_3$), 4.1 (t t, 4 H, O=C−O$CH_2CH_2CH_2CH_3$, s, 2 H, =C*H*), 7.8 (m,m, 2 H, $H^{3,8}$ of

phen), 7.9 (d, 2 H, $H^{5,6}$ of phen), 8.4 (m, 2 H, $H^{4,7}$ of phen), 9.0 (d,d, 2 H, $H^{2,9}$ of phen). – ^{13}C NMR: δ_C (Solvent $CDCl_3$ + CS_2): 14 (s, $CH_2CH_2CH_2CH_3$), 20 (s, $CH_2CH_2CH_2CH_3$), 31 (s, $CH_2CH_2CH_2CH_3$), 64 (s, $O{=}C{-}OCH_2CH_2CH_2CH_3$), 77 (dd, *C*=*C* of C_{70} and dbm), 124–163 (s, 41 signals comprising 6 phen and 35 C_{70} signals, 1 signal omitted), 172 (s, *C*=O)

Acknowledgments

P. Z. and his research group gratefully acknowledge the financial support of the University of Siena (ex quota 60%). K. T. and co-workers acknowledge the financial support by National Natural Science Foundation of China (Project No. 298730001).

[1] [1a]Q. Xie, E. Pérez-Cordero, L. Echegoyen, *J. Am. Chem. Soc.* **1992**, *114*, 3978. – [1b]Q. Li, F. Wudl, C. Thilgen, R. L. Whetten, F. Diederich, *J. Am. Chem. Soc.* **1992**, *114*, 3994. – [1c]C. Boudon, J.-P. Gisselbrecht, M. Gross, A. Hermann, M. Rüttimann, J. Crassous, F. Cardullo, L. Echegoyen, F. Diederich, *J. Am. Chem. Soc.* **1998**, *120*, 7860.

[2] M. D. Westmeyer, T. B. Rauchfuss, A. K. Verma, *Inorg. Chem.* **1996**, *35*, 7140.

[3] A. N. Chernega, M. L. H. Green, J. Haggitt, A. H. H. Stephens, *J. Chem. Soc., Dalton Trans.* **1998**, 755.

[4] [4a]J. T. Park, H. Song, J.-J. Cho, M.-K. Chung, J.-H. Lee, I.-H. Suh, *Organometallics* **1998**, *17*, 227. – [4b]H. Song, K. Lee, J. T. Park, M.-G. Choi, *Organometallics* **1998**, *17*, 4477.

[5] J. T. Park, J.-J. Cho, H. Song, C.-S. Jun, Y. Son, J. Kwak, *Inorg. Chem.* **1997**, *36*, 2698.

[6] S. A. Lerke, B. A. Parkinson, D. H. Evans, P. J. Fagan, *J. Am. Chem. Soc.* **1992**, *114*, 7807.

[7] [7a]K. Tang, S. Zheng, X. Jin, H. Zeng, Z. Gu, X. Zhou, Y. Tang, *J. Chem. Soc., Dalton Trans.* **1997**, 3585. – [7b]P. Zanello, F. Laschi, M. Fontani, C. Mealli, A. Ienco, K. Tang, X. Jin, L. Li, *J. Chem. Soc., Dalton Trans.* **1999**, 965.

[8] [8a]A. L. Balch, J. W. Lee, B. C. Noll, M. M. Olmstead, *J. Am. Chem. Soc.* **1992**, *114*, 10984. – [8b]A. L. Balch, J. W. Lee, B. C. Noll, M. M. Olmstead, *Inorg. Chem.* **1994**, *33*, 5238.

[9] M. Rasinkangas, T. T. Pakkanen, T. A. Pakkanen, M. Ahlgrén, J. Rouvinen, *J. Am. Chem. Soc.* **1993**, *115*, 4901.

[10] I. J. Mavunkal, Y. Chi, S.-M. Peng, G.-H. Lee, *Organometallics* **1995**, *14*, 4454.

[11] T. Kusukawa, W. Ando, *J. Organomet. Chem.* **1998**, *561*, 109 .

[12] A. L. Balch, J. W. Lee, M. M. Olmstead, *Angew. Chem. Int. Ed. Engl.* **1992**, *31*, 1356.

[13] H.-F. Hsu, J. R. Shapley, *J. Am. Chem. Soc.* **1996**, *118*, 9192.

[14] H.-F. Hsu, S. R. Wilson, J. R. Shapley, *Chem. Commun.* **1997**, 1125.

[15] M. Soimasuo, T. T. Pakkanen, M. Ahlgrén, T. A. Pakkanen, *Polyhedron* **1998**, *17*, 2073.

[16] A. L. Balch, L. Hao, M. M. Olmstead, *Angew. Chem. Int. Ed. Engl.* **1996**, *35*, 188.

[17] [17a] K. Lee, H.-F. Hsu, J. R. Shapley, *Organometallics* **1997**, *16*, 3876. – [17b] K. Lee, J. R. Shapley, *Organometallics* **1998**, *17*, 3020.

[18] P. J. Fagan, J. C. Calabrese, B. Malone, *J. Am. Chem. Soc.* **1991**, *113*, 9408.

[19] J. P. Lozos, B. M. Hoffman, C. G. Franz, *QCPE* **1973**, *243*, 11.

Received November 10, 1999
[I99399]

Synthesis and Solid-State Characterization of Isopropoxy Carboxylate Clusters of Ti^{IV}

A. Pandey,[a] V. D. Gupta,[a] and H. Nöth*[b]

Keywords: Titanium / Oxygen ligands / Alkoxy carboxylates / Structure elucidation

Reaction of $Ti(OiPr)_4$ with chloroacetic acids (1:1 and 1:2 stoichiometric ratio) in toluene gives the corresponding mono- and bis-substituted products in quantitative yield. The products $Ti(OiPr)_3(OOCR)$ (R = CH_2Cl **1a,** $CHCl_2$ **1b**, CCl_3 **1c**) are proposed to have a dimeric structure on the basis of ^1H,^{13}C NMR and IR spectroscopy. On standing in toluene, solutions of **1c** form the trinuclear species $Ti_3(\mu_3\text{-}O)(\mu_3\text{-}OiPr)_2(OiPr)_5(\mu\text{-}O_2CCCl_3)_3$ (**2**) with the three titanium atoms forming an isosceles triangle and the μ_3-O moiety at the center. On standing in toluene, solutions of **1b** form a hexanuclear product $Ti_6(\mu_3\text{-}O)_6(OiPr)_6(\mu\text{-}O_2CCHCl_2)_6$ (**3**), the structure of which consists of two stacked six-membered [Ti-μ_3-O]$_3$ rings connected by Ti–O bonds. Under comparable conditions, the *bis-substituted* product $Ti(OiPr)_2(O_2CCCl_3)_2$ (**4c**) forms the dinuclear species $Ti_2(\mu\text{-}O)(OiPr)_2(HOiPr)_2(\mu\text{-}O_2CCCl_3)_2(O_2C\text{–}CCl_3)_2$ (**5**) in which the two symmetric octahedral titanium centers are bonded to a common oxygen atom.

Introduction

Metal alkoxides [1–4] are the preferred precursors in the sol-gel process of preparing ceramic materials. However, their high hydrolytic instability needs to be overcome by the incorporation of hydroxylated nucleophilic ligands[5] such as carboxylic acids[6–15] and β-diketones[16,17] to produce new molecular precursors. Titanium oxoalkoxy carboxylates have received considerable attention in recent years. These precursors generally consist of four to six titanium atoms with one of six[6–14] types of metal-oxygen core skeletons. Recently,[18] a nonanuclear product was isolated. These highly condensed oxo species are usually generated by a secondary process i.e. esterification. For alkoxides, ether elimination[19–21] and naturally controlled hydrolysis[22] are other routes to oxo products.

Acetic acid[6–9,13,14] has been used most often for preparing the above oxoalkoxy carboxylates, perhaps because addition of acetic acid to sol-gel processes with titanium alkoxides prevents precipitation and increases the gelation time.[23] We wanted to examine the structural changes caused by gradually increasing both the acidity and steric bulk of the carboxylic acid. Therefore, we examined the reactions of chloroacetic acids with titanium isopropoxide. Initially, to produce smaller amounts of condensed/uncondensed species, these reactions were performed in excess solvent (toluene) at room temperature. Surprisingly, these toluene solutions of the simple substitution products formed oxo species on standing, which were characterized by X-ray crystallography. The extent of condensation seems to be dependent on the time the solution is left standing.

We report here the first simple di- and trinuclear oxoalkoxytitanium carboxylates. A hexanuclear species having a Ti_6O_6 core was also obtained.

Results and Discussion

Structurally characterized carboxylic acid-modified titanium alkoxides have generally been reported to contain four to six titanium atoms with one of six[6–14] metal-oxygen core skeletons. Most of these products have been obtained from either neat[9] reaction mixtures or very small solvent volumes.[12–14] Some of the products are obtained from excess solvent, but only at high temperatures[10] or under reflux[15] conditions. In excess solvent, at room temperature, the reaction of $Ti(OEt)_4$ with $(CO)_9Co_3(\mu_3\text{-}CCO_2H)$ was recently reported[11] to give the single product $Ti_6O_4(OEt)_{12}\{\mu\text{-}(CO)_9Co_3(\mu_3\text{-}CCO_2)\}_4$.

Since both the absence of solvent and high temperatures of reflux facilitate condensation *by* esterification, we have examined the reactions of $Ti(OiPr)_4$ with chloroacetic acids in solvent at room temperature (25 °C). Initially $Ti(OiPr)_4$ was dissolved in toluene and then a toluene solution of the acid was added to it dropwise while stirring.

The products of the reactions of $Ti(OiPr)_4$ with mono-, di-, and trichloroacetic acids in 1:1 stoichiometric ratio in toluene are $Ti(OiPr)_3(O_2CR)$ (R = CH_2Cl **1a**, $CHCl_2$ **1b**, CCl_3 **1c**), which were obtained in quantitative yields (Equation 1). The liberated 2-propanol was determined by chromic acid oxidation.[24]

$$Ti(OiPr)_4 + RCOOH \rightarrow Ti(OiPr)_3(OOCR) + HOiPr \quad (1)$$

The ambient-temperature ^1H NMR spectrum of **1a** shows two doublets and two septets (intensity ratio 1:2) for the *gem*-dimethyl protons corresponding to the bridging

[a] Department of Chemistry, Faculty of Science, Banaras Hindu University,
Varanasi 221005, India
[b] Institute of Inorganic Chemistry, University of Munich,
Butenandtstraße 5–13, Haus D, D-81377 Munich, Germany

 © WILEY-VCH Verlag GmbH, D-69451 Weinheim, 2000 1434–1948/00/0606–1351 $ 17.50+.50/0

and terminal isopropoxy groups respectively. The ^{13}C NMR spectrum also shows the presence of two types of isopropoxy group and one type of carboxylate group. In the IR spectrum of **1a** the difference between the antisymmetric (1580 cm^{-1}) and symmetric (1460 cm^{-1}) stretching bands of the carboxylate group ($\Delta\tilde{\nu}$ = 120 cm^{-1}) suggests[25] a bridging bidentate bonding mode. The bridging and terminal isopropoxy groups are accounted for by the bands at 1020 cm^{-1} and 1090 cm^{-1} respectively. The IR and ^{13}C NMR spectra of the products **1b** and **1c** are similar to those of **1a** but their ambient temperature ^1H NMR spectra show one doublet for the methyl protons, which is probably due to fast exchange of the O*i*Pr groups at the probe temperature. Attempts to grow single crystals of compounds **1** were not successful. Therefore, on the basis of the available spectral evidence, and in accordance with a report of Doeuff and Sanchez,[26] compounds **1** may have dimeric structures.

An attempt to crystallize **1c** by leaving the reaction mixture for two days in toluene (at –15 °C) led to a white crystalline product which was shown to be $Ti_3(\mu_3\text{-}O)(\mu\text{-}O\text{-}i\text{Pr})_2(O\text{-}i\text{Pr})_5(\mu_3\text{-}O_2C\text{–}CCl_3)_3$ (**2**) by X-ray crystallographic analysis (Equation 2).

$$3\ Ti(O\text{-}i\text{Pr})_3(OOCCCl_3) \rightarrow Ti_3O(O\text{-}i\text{Pr})_7(OOCCCCl_3)_3 + O\text{-}i\text{Pr}_2 \quad (2)$$

We were able to obtain crystalline material of **1b** from the reaction mixture of $Ti(O\text{-}i\text{Pr})_4$ with $CHCl_2COOH$ in toluene. When the mother liquor was left for a few days, a small crop of crystals was obtained, which were characterized as $Ti_6(\mu_3\text{-}O)_6(O\text{-}i\text{Pr})_6(\mu\text{-}O_2CCHCl_2)_6$ (**3**) by X-ray crystallographic analysis. The formation of this highly condensed product may also be accounted for by ether elimination (Equation 3).

$$6\ Ti(O\text{-}i\text{Pr})_3(OOCCHCl_2) \rightarrow Ti_6(O)_6(O\text{-}i\text{Pr})_6(OOCCHCl_2)_6 + 6\ O\text{-}i\text{Pr}_2 \quad (3)$$

The bis-substituted products $Ti(O\text{-}i\text{Pr})_2(O_2CR)_2$ (R = CH_2Cl **4a**, $CHCl_2$ **4b**, CCl_3 **4c**) are obtained quantitatively from the reaction of $Ti(O\text{-}i\text{Pr})_4$ with chloroacetic acids (1:2 stoichiometric ratio) according to Equation 4.

$$Ti(O\text{-}i\text{Pr})_4 + 2\ RCOOH \rightarrow Ti(O\text{-}i\text{Pr})_2(OOCR)_2 + 2\ HO\text{-}i\text{Pr} \quad (4)$$

The IR spectrum of **4c** shows four absorptions due to the carboxylate group. The two $\tilde{\nu}_{CO2}$ bands at 1766 cm^{-1} (antisymmetric) and 1377 cm^{-1} (symmetric) ($\Delta\tilde{\nu}$ = 389 cm^{-1}) were assigned as a unidentate carboxylate group while those at 1658 cm^{-1} (antisymmetric) and 1462 cm^{-1} (symmetric) ($\Delta\tilde{\nu}$ = 120 cm^{-1}) were assigned as a bridging bidentate carboxylate group. The peaks at 1015 cm^{-1} and 1089 cm^{-1} were assigned as bridging and terminal isopropoxy groups, respectively.[25] However, the ambient temperature ^1H and ^{13}C NMR spectra of **4c** were not structurally informative. The IR and the ambient temperature ^1H and ^{13}C NMR spectra of **4a** and **4b** are similar to those of **4c**. We were unable to structurally characterize **4** since we could not obtain single crystals of these compounds. As before, we tried to crystallize **4c** by leaving the reaction mixture to stand for two days, and obtained the white crystalline dinuclear species $Ti_2(\mu\text{-}O)(O\text{-}i\text{Pr})_2(HO\text{-}i\text{Pr})_2(\mu\text{-}O_2C\text{–}Cl_3)_2(O_2C\text{–}Cl_3)_2$ (**5**) (Equation 5).

$$2\ Ti(O\text{-}i\text{Pr})_4 + 4\ CCl_3COOH \rightarrow Ti_2(O)(O\text{-}i\text{Pr})_2(HO\text{-}i\text{Pr})_2(OOCCCl_3)_4 + O\text{-}i\text{Pr}_2 + 2\ HO\text{-}i\text{Pr} \quad (5)$$

The IR spectra of the volatiles from reactions (2), (3) and (5) showed strong absorptions around 1165 cm^{-1}, characteristic of isopropyl ether. No absorptions were observed in the carbonyl region. Therefore, ester formation does not appear to take place under the mild conditions of these reactions. A similar observation has been reported[10] in the reaction of $Ti(O\text{-}i\text{Pr})_4$ with $(CO)_9Co_3(\mu_3\text{-}C\text{–}CO_2H)$.

X-ray Crystallographic Structures

The X-ray structure (Figure 1, Table 1) of **2** shows the three titanium atoms sitting at the corners of an isosceles triangle with the triply bridged oxo group at the center.

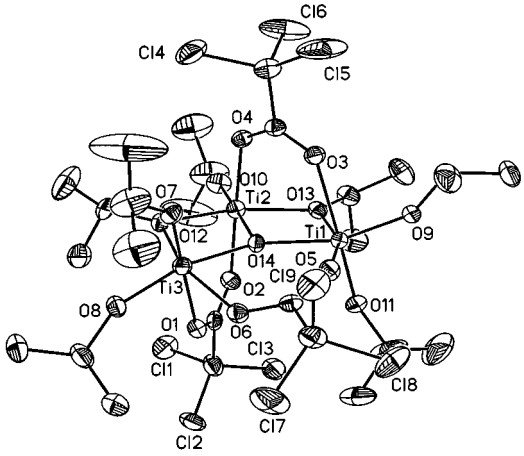


Figure 1. Molecular structure of compound **2** in ORTEP description; hydrogen atoms omitted for the sake of clarity; thermal ellipsoids represent a 25 % probability

All three trichloroacetate groups are bidentate and symmetrically bridge the three titanium centers with a propeller arrangement. All three titanium atoms are six coordinate with two of the atoms (Ti1, Ti3) in a similar coordination environment. The third titanium atom (Ti2) has one terminal O*i*Pr group, making the structure asymmetric. The bridging O*i*Pr groups are also asymmetrical with one O*i*Pr group bridging Ti1 and Ti2, and the other Ti2 and Ti3; there is no bridge between Ti1 and Ti3. This Ti_3O skeletal arrangement is the first[12] of its type reported for titanium oxo alkoxy carboxylates. It is interesting to note that if the fourth coordination site (the one generating the cubic framework) of the μ_4-O group in the structure of $Ti_4(\mu\text{-}O)(\mu_4\text{-}O)(O_2CH)_2(\mu\text{-}O\text{-}i\text{Pr})_4(O\text{-}i\text{Pr})_6$[12] was removed, a Ti_3O_3 core similar to **2** would be obtained.

The geometry around the μ_3-O group is remarkable as the sum of the angles is 360°, making it perfectly planar. The constraints of the two four-membered rings (Ti2, O13,

Table 1. Selected bond lengths [Å] and angles [°] for **2**

Bond lengths					
Ti(1)–O(11)	1.765(3)	Ti(1)–O(9)	1.783(3)	Ti(1)–O(14)	1.921(3)
Ti(1)–O(13)	2.025(3)	Ti(1)–O(5)	2.087(3)	Ti(1)–O(3)	2.276(3)
Ti(1)–Ti(2)	3.0633(13)	Ti(2)–O(10)	1.760(3)	Ti(2)–O(14)	1.920(3)
Ti(2)–O(13)	1.971(3)	Ti(2)–O(12)	1.976(3)	Ti(2)–O(4)	2.024(3)
Ti(2)–O(2)	2.056(3)	Ti(2)–Ti(3)	3.07088(12)	Ti(3)–O(7)	1.771(3)
Ti(3)–O(8)	1.780(3)	Ti(3)–O(14)	1.932(3)	Ti(3)–O(12)	2.026(3)
Ti(3)–O(6)	2.099(3)	Ti(3)–O(1)	2.261(3)	Ti(3)–O(6)	2.099(3)
Ti(3)–O(1)	2.261(3)				
Bond angles					
O(11)–Ti(1)–O(9)	101.16(13)	O(11)–Ti(1)–O(14)	100.92(13)	O(9)–Ti(1)–O(14)	157.43(13)
O(11)–Ti(1)–O(13)	96.28(13)	O(9)–Ti(1)–O(13)	105.91(12)	O(14)–Ti(1)–O(13)	76.21(11)
O(11)–Ti(1)–O(5)	91.90(13)	O(9)–Ti(1)–O(5)	91.66(12)	O(14)–Ti(1)–O(5)	82.96(11)
O(13)–Ti(1)–O(5)	158.71(11)	O(11)–Ti(1)–O(3)	177.87(13)	O(9)–Ti(1)–O(3)	80.48(12)
O(14)–Ti(1)–O(3)	77.58(11)	O(13)–Ti(1)–O(3)	81.92(11)	O(5)–Ti(1)–O(3)	89.41(11)
O(10)–Ti(2)–O(13)	102.06(14)	O(14)–Ti(2)–O(13)	77.51(11)	O(10)–Ti(2)–O(12)	102.90(14)
O(14)–Ti(2)–O(12)	77.53(11)	O(13)–Ti(2)–O(12)	155.03(12)	O(10)–Ti(2)–O(4)	94.17(13)
O(14)–Ti(2)–O(4)	88.90(11)	O(13)–Ti(2)–O(4)	87.87(11)	O(12)–Ti(2)–O(4)	91.11(12)
O(10)–Ti(2)–O(2)	89.88(13)	O(14)–Ti(2)–O(2)	87.05(12)	O(13)–Ti(2)–O(2)	91.75(12)
O(12)–Ti(2)–O(2)	87.51(12)	O(7)–Ti(3)–O(14)	100.61(13)	O(7)–Ti(3)–O(12)	98.00(13)
O(8)–Ti(3)–O(12)	103.60(13)	O(14)–Ti(3)–O(12)	76.06(11)	O(7)–Ti(3)–O(6)	91.46(13)
O(8)–Ti(3)–O(6)	93.71(12)	O(14)–Ti(3)–O(6)	83.41(11)	O(12)–Ti(3)–O(6)	158.64(11)
O(8)–Ti(3)–O(1)	81.65(13)	O(14)–Ti(3)–O(1)	78.79(11)	O(12)–Ti(3)–O(1)	82.71(11)
O(6)–Ti(3)–O(1)	87.61(11)	Ti(2)–O(12)–Ti(3)	100.24(12)	Ti(2)–O(13)–Ti(1)	100.07(12)
Ti(2)–O(14)–Ti(3)	105.70(12)	Ti(2)–O(14)–Ti(1)	105.79(12)	Ti(1)–O(14)–Ti(3)	148.52(14)

Ti1, O14 and Ti2, O14, Ti3, O12) cause the angle Ti3–O14–Ti1 (148.5°) to open up, while the other two angles (105.8°) are equal. The $Ti(2)O_6$ octahedron shares two of its edges with the other two octahedra, while the tricoordinate oxygen atom O14 is the only common point between $Ti(1)O_6$ and $Ti(3)O_6$. The three octahedra are distorted with angles ranging from 76.2° to 105.9°.

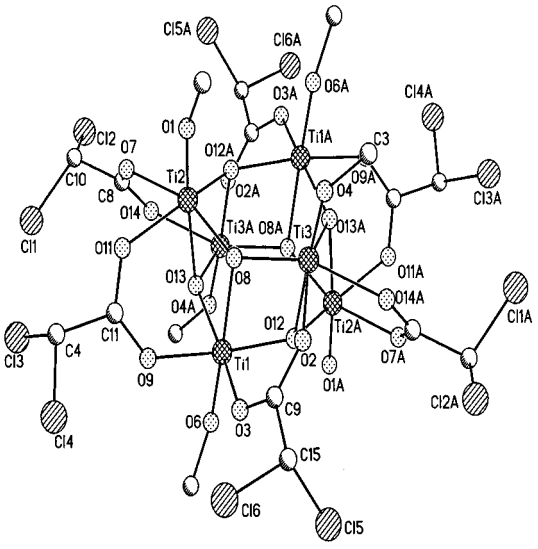


Figure 2. Stick-and-ball model of the molecular structure of the hexatitanium hexaoxo complex **3**; hydrogen atoms and the methyl carbon atoms are omitted for clarity

The X-ray crystal and molecular structure (Figure 2) of **3** shows two stacked six-membered rings consisting of alternating titanium and oxygen atoms. The rings are connected through Ti–O bonds. There is one terminal isopropoxy group attached to each titanium atom. Six dichloroacetate groups bridge the six titanium centers in a bidentate fashion, one from the upper and one from the lower ring. The angles at the alternating titanium and oxygen atoms of the hexagonal rings average 102.6° and 133.7°, respectively, showing considerable distortion in the hexagons. These angles are within the range recently reported.[12] The angles at the atoms binding the upper ring to the lower average 100.4°. While this work was in progress two oxo alkoxy carboxylates with a Ti_6O_6 core i.e. $Ti_6O_6(OiPr)_6(O_2CR)_6$ and $Ti_6O_6(OEt)_6(O_2CR)_6$ (R = H,[12] C_6H_4-*o*-OPh[15]) were reported, with their formation being attributed to ester elimination reactions. It has been ar-

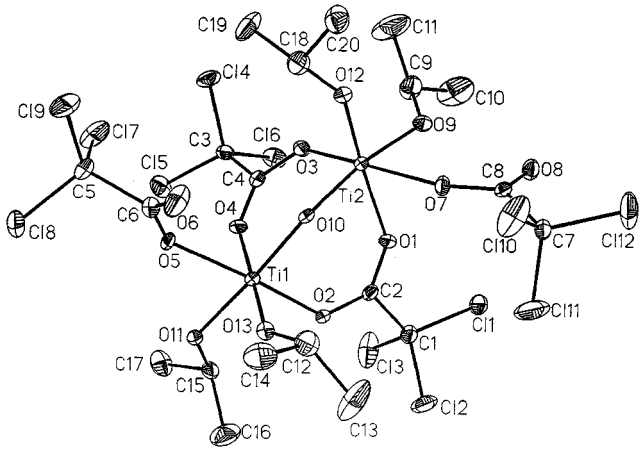


Figure 3. Molecular structure of the dititanoxane complex **5** in ORTEP description; hydrogen atoms omitted; thermal ellipsoids represent a 25 % probability

gued[12] that the sterically less demanding nature of R and increased acidity may be the reasons for the formation of highly condensed species. However, almost isostructural systems are obtained from either dichloroacetic acid (present work) or 2-phenoxybenzoic acid,[14] which does not substantiate this observation. In fact a number of oxo alkoxy carboxylates with Ti_6O_4 core, $Ti_6O_4(O_2CMe)_4(OR)_{12}$ (R = CH_2Me,[11] $CHMe_2$[14]), $Ti_6O_4(O_2CMe)_8(OR)_8$ [R = $CHMe_2$,[7] $(CH_2)_3CH_3$[9]] and $Ti_6O_4(O_2C_6H_4)_4\{\mu$-$(CO)_9Co_3(\mu_3$-$O_2CC)\}_4(OiPr)_4$[11] have been found to retain their basic structural skeleton irrespective of the steric bulk of the alkoxide and/or the carboxylic acid.

The structure of **5** (Figure 3) consists of two symmetrical, octahedral titanium centers Ti1 and Ti2 with a common μ-oxo group O10, thereby forming a novel Ti_2O core.

Each titanium atom is bound to three terminal oxygens, one each from 2-propanol, an isopropoxy and a monodentate trichloroacetate group. The two octahedrons are joined by two bridging bidentate trichloroacetate groups which are slightly distorted. The angles for the octahedrons range from 78.5° to 100.5°. Compound **5** is the first oxo alkoxy carboxylate with an alcohol attached by a dative bond. This may be due to its low nuclearity relative to other complexes. At both titanium atoms the HO*i*Pr groups are *trans* to the oxo group. The terminal groups give rise to intermolecular interactions (Cl···Cl and O–H···O contacts). Both octahedrons show a hydrogen-bonding interaction between the carbonyl oxygen of the terminal trichloroacetate group and the hydrogen of 2-propanol. Also observed are chlorine–oxygen and chlorine–titanium interactions.

Table 2. Selected bond lengths [Å] and angles [°] for **3**

Bond lengths					
Ti(1)–O(6)	1.740(5)	Ti(1)–O(13)	1.886(5)	Ti(1)–O(12)	1.891(5)
Ti(1)–O(9)	2.066(5)	Ti(1)–O(3)	2.092(6)	Ti(1)–O(8)	2.176(5)
Ti(2)–O(1)	1.747(5)	Ti(2)–O(12A)	1.899(5)	Ti(2)–O(8)	1.906(5)
Ti(2)–O(11)	2.062(5)	Ti(2)–O(7)	2.082(5)	Ti(2)–O(13)	2.156(5)
Ti(3)–O(4)	1.751(5)	Ti(3)–O(8)	1.873(5)	Ti(3)–O(13A)	1.891(5)
Ti(3)–O(2)	2.063(6)	Ti(3)–O(14A)	2.070(5)	Ti(3)–O(12)	2.180(5)
Bond angles					
O(6)–Ti(1)–O(13)	102.1(2)	O(6)–Ti(1)–O(12)	103.5(2)	O(13)–Ti(1)–O(12)	102.1(2)
O(6)–Ti(1)–O(9)	92.7(2)	O(13)–Ti(1)–O(9)	88.4(2)	O(12)–Ti(1)–O(9)	158.2(2)
O(6)–Ti(1)–O(3)	93.1(3)	O(13)–Ti(1)–O(3)	160.2(2)	O(12)–Ti(1)–O(3)	86.4(2)
O(9)–Ti(1)–O(3)	78.1(2)	O(8)–Ti(1)–O(13)	76.9(2)	O(12)–Ti(1)–O(8)	78.17(19)
O(9)–Ti(1)–O(8)	85.9(2)	O(3)–Ti(1)–O(8)	87.6(2)	O1)–Ti(2)–O(12A)	101.6(2)
O(1)–Ti(2)–O(8)	97.8(2)	O(12A)–Ti2)–O(8)	102.8(2)	O(1)–Ti(2)–O(11)	94.6(2)
O(12A)–Ti2–O(11)	158.4(2)	O(11)–Ti(2)–O(8)	88.9(2)	O(1)–Ti(2)–O(7)	95.7(2)
O(12A)–Ti2–O(7)	87.5(2)	O(11)–Ti2–O(7)	76.6(2)	O(12A)–Ti2–O(13)	77.8(2)
O(13)–Ti(2)–O(8)	77.0(2)	O(11)–Ti(2)–O(13)	87.5(2)	O(7)–Ti(2)–O(13)	89.8(2)
O(1)–Ti(2)–O(3A)	144.2(2)	O(4)–Ti(3)–O(8)	104.0(2)	O(4)–Ti3–O(13A)	100.3(2)
O(8)–Ti3–O(13A)	102.9(2)	O(4)–Ti(3)–O(2)	94.6(3)	O(2)–Ti(3)–O(8)	89.4(2)
O(4)–Ti3–O(14A)	90.9(2)	O(8)–Ti3–O(14A)	159.8(2)	O14A)–Ti3–O13A)	87.3(2)
O(2)–Ti3–O(14A)	75.8(2)	O(12)–Ti(3)–O(8)	78.5(2)	O(12)–Ti3–O(13A)	77.3(2)
O(12)–Ti3–O(14A)	87.05(19)	O(2)–Ti(3)–O(12)	87.2(2)	Ti(3)–O(8) –Ti(2)	133.3(3)
Ti(3)–O(8)–Ti(1)	100.2(2)	Ti(1)–O(8)–Ti(2)	100.2(2)	Ti(1)–O12–Ti(2A)	133.9(3)
Ti(1)–O(12)–Ti(3)	99.5(2)	Ti(3)–O12–Ti(2A)	99.9(2)	Ti(1)–O13–Ti(3A)	134.0(3)
Ti(1)–O13–Ti(2)	101.6(2)	Ti(2)–O13–Ti(3A)	101.0(2)		

Table 3. Selected bond lengths [Å] and angles [°] for **5**

Bond lengths					
Ti(1)–O(13)	1.745(5)	Ti(1)–O(10)	1.813(4)	Ti(1)–O(5)	1.960(4)
Ti(1)–O(2)	2.054(4)	Ti(1)–O(11)	2.109(4)	Ti(1)–O(4)	2.198(4)
Ti(2)–O(12)	1.740(5)	Ti(2)–O(10)	1.809(4)	Ti(2)–O(7)	1.977(4)
Ti(2)–O(3)	2.008(4)	Ti(2)–O(9)	2.111(5)	Ti(2)–O(1)	2.192(5)
Bond angles					
O(13)–Ti(1)–O(10)	97.3(2)	O(13)–Ti(1)–O(5)	100.5(2)	O(5)–Ti(1)–O(10)	98.89(19)
O(13)–Ti(1)–O(2)	94.13(19)	O(2)–Ti(1)–O(10)	91.04(18)	O(13)–Ti(1)–O(11)	97.74(19)
O(11)–Ti(1)–O(5)	83.17(17)	O(11)–Ti(1)–O(2)	82.99(17)	O(4)–Ti(1)–O(10)	86.13(18)
O(5)–Ti(1)–O(4)	82.58(18)	O(2)–Ti(1)–O(4)	82.06(18)	O(11)–Ti(1)–O(4)	78.52(17)
O(12)–Ti(2)–O(7)	97.1(2)	O(10)–Ti(2)–O(7)	98.31(19)	O(12)–Ti(2)–O(3)	94.9(2)
O(10)–Ti(2)–O(3)	91.86(19)	O(12)–Ti(2)–O(9)	96.0(2)	O(9)–Ti(2)–O(7)	83.9(18)
O(3)–Ti(2)–O(9)	82.88(19)	O(10)–Ti(2)–O(1)	86.05(18)	O(1)–Ti(2)–O(7)	81.69(18)
O(3)–Ti(2)–O(1)	85.41(19)	O(9)–Ti(2)–O(1)	79.96(17)	Ti(2)–O(10)–Ti(1)	139.6(3)

Table 4. Preparation, analytical and spectroscopic data for the complexes

Reactants [g, mol]		Product yield [g, %]	Nature	Analysis (%) (calculated values in parentheses) Ti	O*i*Pr	HO*i*Pr in volatiles
$Ti(OiPr)_4$ + $CH_2ClCOOH$ (1.220, 4.29) (0.406, 4.29)	**1a**	$Ti(OiPr)_3(OOCCH_2Cl)$ (1.352, 98.9)	Light yellow solid	15.09 (15.04)	55.51 (55.55)	0.22 (0.25)
$Ti(OiPr)_4$ + $CHCl_2COOH$ (1.251, 4.40) (0.526, 4.40)	**1b**	$Ti(OiPr)_3(OOCCHCl_2)$ (1.541, 99.9)	White solid	13.59 (13.57)	50.10 (50.15)	0.26 (0.27)
$Ti(OiPr)_4$ + CCl_3COOH (1.119, 3.94) (0.644, 3.93)	**1c**	$Ti(OiPr)_3(OOCCCl_3)$ (1.518, 99.5)	Light yellow solid	12.38 (12.33)	45.67 (45.68)	0.25 (0.24)
$Ti(OiPr)_4$ + $2CH_2ClCOOH$ (0.919, 3.23) (0.611, 6.46)	**4a**	$Ti(OiPr)_2(OOCCH_2Cl)_2$ (1.404, 98.7)	White solid	13.59 (13.56)	33.90 (33.43)	0.37 (0.39)
$Ti(OiPr)_4$ +$2CHCl_2COOH$ (0.894, 3.14) (0.812, 6.29)	**4b**	$Ti(OiPr)_2(OOCCHCl_2)_2$ (1.318, 99.3)	Light yellow solid	11.41 (11.35)	27.95 (27.96)	0.34 (0.36)
$Ti(OiPr)_4$ + $2CCl_3COOH$ (0.911, 3.20) (1.049, 6.41)	**4c**	$Ti(OiPr)_2(OOCCCl_3)_2$ (1.575, 99.9)	White solid	9.90 (9.75)	24.01 (24.03)	0.37 (0.39)

Selected bond lengths and angles for **2**, **3** and **5** are given in Table 1, Table 2 and Table 3. The Ti–O*i*$Pr_{terminal}$ distances [**2** (av. 1.772 Å), **3** (av. 1.745 Å), **5** (av. 1.742 Å)] for the three complexes are in accordance with reported[14,17] values. The Ti–HO*i*Pr (Ti1–O13, Ti2–O9) distances (av. 2.110 Å) are, as expected, longer than the isopropoxy distances. The Ti–μ-O*i*Pr lengths (av. 1.997 Å), which are present only in **2**, are shorter than the terminal Ti–O*i*Pr lengths.[12] For **2** the Ti–μ_3-O distances (av. 1.920 Å) and for **5** the Ti–μ-O distances (av. 1.811 Å) are consistent with literature[13] values.

However, for **3** the Ti–μ_3-O distances (av. 1.885 Å) are somewhat shorter than values recently reported.[12]

For **2** the distances Ti1···Ti2 and Ti2···Ti3 (av. 3.066 Å) correspond to two octahedra sharing an edge[15] while for **3** the distances from upper to lower hexagonal rings (av. 2.176 Å) are consistent with those recently reported.[10] The center of the molecule **3** is empty, resulting in a hole.

The Ti–μ-OAc distances [**2** (av. 2.115 Å), **3** (av. 2.070 Å) and **5** (av. 2.113 Å)] are also in accordance with literature values while for **5** the Ti–OAc lengths (av. 1.968 Å) are shorter than the bridging carboxylate distances.

Conclusions

The reaction of $Ti(OiPr)_4$ with chloroacetic acids in excess toluene at room temperature prevents esterification, thereby giving simple substitution products. However the propensity of the metal atoms to achieve higher coordination numbers through oxo ligands is so strong that it can even be achieved through ether elimination reactions. In this way the formation of products **2** and **5** can be accounted for. The generation of **3** from **1b** on standing in toluene suggests that the extent of the ethereal loss is directly proportional to length of time in solution. In the process significant structural changes are observed. However, due to our limited findings, no conclusions regarding effects of increasing acidity and steric bulk of carboxylic acids on the structures could be drawn.

Experimental Section

All reactions were performed under a dry argon atmosphere, using standard Schlenk and glovebox techniques. Toluene and $CDCl_3$ were dried by standard procedures. Titanium isopropoxide was obtained from $TiCl_4$ (Aldrich) by the ammonia method[27] and purified by vacuum distillation. Mono-, di- and trichloroacetic acids were distilled before use. Infrared spectra were recorded on a JASCO FT-IR-5300 as Nujol mulls between NaCl plates. ^1H and ^{13}C NMR spectra were recorded in $CDCl_3$ with a JEOL-FX 90Q spectrometer with $SiMe_4$ as internal reference. Ti was determined as TiO_2 and isopropoxy analysis by the method of Bradley[24] et al.

Synthesis

General Method for the Complexes 1a–c, and 4a–c (Table 4): A solution of the acid in toluene (ca. 20 mL) was added dropwise with stirring to a solution of $Ti(OiPr)_4$ in toluene (ca. 25 mL) over 1/2 h at room temperature (ca. 25 °C). The reaction mixture (colorless) was stirred for six hours to give a light red solution. The volatiles were removed in vacuo to give a solid residue.

1a: ^1H NMR: δ = 1.26 (d), 1.35 (d, *gem*-Me_2 of O*i*Pr), 4.80 (sept), 5.30 (sept, CH of O*i*Pr), 4.00 (s, CH_2 of the acid, 18:3:2). – ^{13}C NMR: δ = 192.91 (CO of acid), 63.43, 64.45 (CH of O*i*Pr), 41.49 (CH_2Cl of acid), 23.62, 24.32 (*gem*-Me_2 of O*i*Pr). – IR: $\tilde{\nu}$ = 1580 (ν_{as} CO_2), 1460 (ν_s CO_2), 1120 (terminal O*i*Pr), 1010 (bridging O*i*Pr).

1b: ^1H NMR: δ = 1.40 (d, *gem*-Me_2 of O*i*Pr), 4.16, 5.00 (sept, CH of O*i*Pr), 6.08 (s, CH_2 of acid, 18:3:1). – ^{13}C NMR: δ = 191.97 (CO of acid), 67.43, 68.21 (CH of O*i*Pr), 55.49 ($CHCl_2$ of acid), 23.32, 24.35 (*gem*-Me_2 of O*i*Pr). – IR: $\tilde{\nu}$ = 1589 (ν_{as} CO_2), 1460 (ν_s CO_2), 1119 (terminal O*i*Pr), 1011 (bridging O*i*Pr).

1c: ^1H NMR: δ = 1.31 (d, *gem*-Me_2 of O*i*Pr), 4.10, 5.10 (sept, CH of O*i*Pr). – ^{13}C NMR: δ = 180.97 (CO of acid), 63.43, 65.10 (CH of O*i*Pr), 86.58, (CCl_3 of acid), 23.51, 24.21 (*gem*-Me_2 of O*i*Pr). – IR: $\tilde{\nu}$ = 1658 (ν_{as} CO_2), 1460 (ν_s CO_2), 1112 (terminal O*i*Pr), 1009 (bridging O*i*Pr).

4a: ^1H NMR: δ = 1.15 (d, *gem*-Me_2 of O*i*Pr), 4.80 (sept, CH of O*i*Pr), 4.00 (CH_2 of acid) (6:1:2). – ^{13}C NMR: δ = 189.97 (CO of acid), 63.46 (CH of O*i*Pr), 43.58 (CH_2Cl of acid), 23.59 (*gem*-Me_2 of O*i*Pr). – IR: $\tilde{\nu}$ = 1769, 1654 (ν_{as} CO_2), 1378, 1460 (ν_s CO_2), 1112 (terminal O*i*Pr), 1009 (bridging O*i*Pr).

4b: ^{1}H NMR: δ = 1.40 (d, *gem*-Me_2 of O*i*Pr), 5.02 (sept, CH of O*i*Pr), 6.00 (s, CH_2 of acid) (6:1:1). – ^{13}C NMR: δ = 190.57 (CO of acid), 67.79 (CH of O*i*Pr), 57.48 ($CHCl_2$ of acid), 24.35 (*gem*-Me_2 of O*i*Pr). – IR: $\tilde{\nu}$ = 1777, 1589 (ν_{as} CO_2), 1380, 1460 (ν_s CO_2), 1110 (terminal O*i*Pr), 1010 (bridging O*i*Pr).

4c: ^{1}H NMR: δ = 1.39 (d, *gem*-Me_2 of O*i*Pr), 4.85 (sept, CH of O*i*Pr). – ^{13}C NMR: δ = 192.97, (CO of acid), 70.26 (CH of O*i*Pr), 87.81 (CCl_3 of acid), 23.29 (*gem*-Me_2 of O*i*Pr).

Ti(μ$_3$-O)(μ-O*i*Pr)$_2$(O*i*Pr)$_5$(μ-O$_2$C–CCl$_3$)$_3$ (2): A solution of Cl_3C–C(O)OH (1.295 g, 7.92 mmol) in toluene (ca. 20 mL) was added dropwise with stirring to a solution of Ti(O*i*Pr)$_4$ (2.245 g, 7.91 mmol) in toluene (ca. 25 mL) over 30 min at room temperature (30 °C). The reaction mixture (colorless) was stirred for 6 h to give a dark yellow solution. It was concentrated to half of its volume and kept at –15 °C. After 2 d, a white crystalline product (1.932 g of **2**, 65%) was obtained. – $C_{27}H_{49}Cl_9O_{14}Ti_3$ (1060.4): calcd. Ti 13.55, O*i*Pr 39.01; found Ti 13.91, O*i*Pr 38.91. – ^{1}H NMR (25 °C): δ = 1.31 (d, CH_3 of O*i*Pr), 4.11, 5.01 (sept, CH of O*i*Pr). – ^{13}C{^{1}H} NMR: δ = 180.99 (CO of acid), 90.85 (CCl_3 of acid), 63.92 (CH of O*i*Pr), 23.51, 24.21 (CH_3 of O*i*Pr). – FT-IR (Nujol): $\tilde{\nu}$ = 1658 (ν_{as} CO_2), 1460 (ν_s CO_2), 1112 (terminal O*i*Pr), 1009 (bridging O*i*Pr) cm^{-1}. – Single crystals were grown in toluene at –15° C.

Ti(O*i*Pr)$_3$(O$_2$C–CHCl$_2$ (1b) and Ti$_6$(μ$_3$-O)$_6$(O*i*Pr)$_6$(μ-O$_2$C–CHCl$_2$)$_6$ (3): White crystalline **1b** (1.110 g, 65%) was obtained by concentrating the reaction mixture of Ti(O*i*Pr)$_4$ (1.158 g, 4.07 mmol) and dichloroacetic acid (0.526 g, 4.07 mmol) in toluene by the general method. – $C_{11}H_{22}Cl_2O_5Ti_2$ (353.1): calcd. Ti 13.56, O*i*Pr 50.20; found Ti 13.89, O*i*Pr 50.01. – ^{1}H NMR (25 °C): δ = 1.42 (m, CH_3 of O*i*Pr), 4.16, 5.01 (sept, CH of O*i*Pr), 6.08 (s, CH_2 of acid). – ^{13}C{^{1}H} NMR: δ = 192.91 (CO of acid), 63.43 (CH of O*i*Pr), 55.51 ($CHCl_2$ of acid), 23.91, 24.38 (CH_3 of O*i*Pr). – FT-IR (Nujol): $\tilde{\nu}$ = 1589 (ν_{as} CO_2), 1458 (ν_s CO_2), 1120 (terminal O*i*Pr), 1006 (bridging O*i*Pr) cm^{-1}. – The mother liquor upon standing for 5 days at –15 °C gave a small batch of crystals which was shown to be **3** by X-ray crystallography.

Ti$_2$(μ-O)(HO*i*Pr)$_2$(O*i*Pr)$_2$(O$_2$C–CCl$_3$)$_2$(μ-O$_2$C–CCl$_3$)$_2$ (5): A reaction mixture comprising Ti(O*i*Pr)$_4$ (1.362 g, 4.80 mmol) and trichloroacetic acid (1.57 g, 9.60 mmol) in toluene was stirred for six hours. It was then concentrated to half of its volume and kept at –15 °C. After 2 d, a white crystalline product was obtained. – Yield: 1.651 g of **5** (72 %). – $C_{20}H_{30}Cl_{12}O_{13}Ti_2$ (999.6): calcd. Ti 9.56, O*i*Pr 23.64; found Ti 9.57, O*i*Pr 23.91. – ^{1}H NMR (25 °C): δ = 1.39 (d, CH_3 of O*i*Pr), 4.85 (sept, CH of O*i*Pr). – ^{13}C{^{1}H} NMR: δ = 192.31, 181.37 (CO of acid), 87.91 (CCl_3 of acid), 70.26 (CH of O*i*Pr), 23.29 (CH_3 of O*i*Pr). – FT-IR (Nujol): $\tilde{\nu}$ = 1787 (ν_{as} CO_2), 1378(ν_s CO_2), 1649 (ν_{as} CO_2), 1460 (ν_s CO_2) 1090 (terminal O*i*Pr), 1012 (bridging O*i*Pr) cm^{-1}. – Single crystals were obtained from toluene.

Crystallography

The structure determinations were performed using a Siemens P4 diffractometer equipped with a CCD area detector. Mo-K_α radiation (λ = 0.71013 Å) was used and the samples cooled to 193 K (**2**, **3**) and 183 K (**4**) respectively. Data reduction was achieved with the program SAINT and absorptions by SADABS (**2**, **3**) and semi-empirical methods (**4**). Computer calculations were carried out using the SHELXS-97 (Sheldrick, 1997) program package and the structures were solved by direct methods. Refinements were performed by SHELXL-97 (Sheldrick, 1997) using anisotropic thermal parameters for the non hydrogen atoms. Hydrogen atoms were placed in calculated positions and refined with a riding model. The crystallographic data for **2**, **3** and **5** are given in Table 5. Crystallographic data (excluding structure factors) for the structures reported in this paper have been deposited with the Cambridge Crystallographic Data Centre as supplementary publication no. CCDC-138443 (**2**), -138445 (**5**), -138444 (**3**). Copies of the data can be obtained free of charge on application to CCDC, 12 Union Road, Cambridge CB2 1EZ, UK [Fax: int. code + 44-1223/336-033; E-mail: deposit@ccdc.cam.ac.uk].

Table 5. Data collection for (**2**), (**3**), (**5**)

Compound	**2**	**3**	**5**
Empirical formula	$C_{27}H_{49}Cl_9O_{14}Ti_3$	$C_{30}H_{48}Cl_{12}O_{24}Ti_6$	$C_{20}H_{30}Cl_{12}O_{13}Ti_2$
Molecular mass	1060.4	1505.4	999.6
Crystal size [mm]	0.40 × 0.20 × 0.18	0.20 × 0.24 × 0.33	0.2 × 0.4 × 0.45
Crystal system	orthorhombic	monoclinic	orthorhombic
Space group	*Pbca*	*C*2/*c*	*P*2(1)2(1)(1)
a [Å]	21.990(6)	14.7192(2)	10.645(5)
b [Å]	17.628(4)	21.7216(5)	18.146(7)
c [Å]	24.323(7)	19.7550(4)	20.782(7)
α [°]	90	90	90
β [°]	90	107.230(1)	90
γ [°]	90	90	90
V [Å^3]	9429(4)	6032.7(2)	4014(3)
Z	8	4	4
ρ(calcd.) [Mg/m^3]	1.493	1.658	1.651
μ [mm^{-1}]	1.059	1.356	1.248
F(000)	4336	3024	2008
Index range	$-28 \le h \le 28$	$-15 \le h \le 15$	$-13 \le h \le 13$
	$-20 \le k \le 19$	$-23 \le k \le 23$	$-23 \le k \le 23$
	$-31 \le l \le 31$	$-21 \le l \le 21$	$-22 \le l \le 27$
2θ [°]	54.98	46.52	58.58
Temp [K]	193	193	183
Refl. collected	49114	12136	23244
Refl. unique	9668	4113	8058
Refl. observed (4σ)	5296 (2σ)	2612	6029
R(int.)	0.0574	0.0728	0.0598
No. of variables	520	320	424
Weighting scheme[a] *x*/*y*	0.0865/0.000	0.11074/0.000	0.0468/8.2523
GOOF	0.981	1.046	1.144
Final *R*(4σ)	0.0531	0.0759	0.0701
Final *wR*2	0.1357	0.1904	0.1342
Largest. resid. peak [e/Å^3]	0.960	0.909	0.833

[a] $w^{-1} = \sigma^2 F_o^2 + (xP)^2 + yP$; $P = F_o^2 + 2F_c^2)/3$.

[1] D. C. Bradley, R. C. Mehrotra, D. P. Gaur, *Metal Alkoxides*; Academic Press, New York, **1978**.
[2] D. C. Bradley, *Chem. Rev.* **1989**, *89*, 1317–1322.
[3] K. G. Caulton, L. G. Hubert-Pfalzgraf, *Chem. Rev.* **1990**, *90*, 969–995.
[4] R. C. Mehrotra, A. Singh, S. Sogani, *Chem. Rev.* **1994**, *94*, 1643–1660.
[5] C. J. Brinker, D. E. Clark, D. R. Ulrich, *Better Ceramics Through Chemistry*; North Holland; New York, **1984**.
[6] T. M. Alam, T. J. Boyle, C. D. Buchheit, R. W. Schwartz, J. W. Ziller, *Mater. Res. Soc. Symp. Proc*. **1994**, *346*, 35–40.
[7] S. Doeuff, Y. Dromzee, C. Sanchez, *C. R. Acad. Sci, Sect. 2* **1989**, *308*, 1409–1412.
[8] U. Schubert, E. Arpac, W. Glaubitt, A. Helmerich, C. Chau, *Chem. Mater.* **1992**, *4*, 291–295.
[9] S. Doeuff, Y. Dromzee, F. Taulelle,C. Sanchez, *Inorg. Chem.* **1989**, *28*, 4439–4445.
[10] X. Lei, M. Shang, T. P. Fehlner, *Organometallics* **1997**, *16*, 5289–5301.
[11] X. Lei, M. Shang, T. P. Fehlner, *Organometallics* **1996**, *15*, 3779–3781.
[12] T. J. Boyle, T. M. Alam, Cory J. Tafoya, B. L. Scott, *Inorg. Chem.* **1998**, *37*, 5588–5594.
[13] I. G. Luneau, A. Mosset, J. Galy, *Z. Kristallogr.* **1987**, *180*, 83–95.
[14] P. I. Laaziz, A. Larbot, C. Guizard, J. Durand, L. Cot, *Acta Crystallogr.* **1990**. *C46*, 2332–2334.
[15] R. Papiernik, L. G. Hubert-Pfalzgraf, J. Vaissermann,M. C. H. B. Goncalves, *J. Chem. Soc., Dalton Trans.* **1998**, 2285–2287.
[16] P. Toledano, M. In, C. Sanchez, *C. R. Acad. Sci., Sect. 2* **1991**, *313*, 1247–1253.

[17] P. D. Moran, C. E. F. Rickard, G. A. Bowmaker, R. P. Cooney, J. R. Bartlett, J. L. Woolfrey, *Inorg. Chem.* **1998**, *37*, 1417–1419.
[18] G. Kickelbick, V. Schubert, *Eur. J. Inorg. Chem.* **1998**, 159 – 164.
[19] N. Ya. Turova, N. I. Kozlova, E. P. Turevskava, T. V. Rogova, V. G. Kessler, *Mat. Res. Soc. Symp. Proc*. **1994**, *346*, 261–266.
[20] N. Ya. Turova, V. G. Kessler, S. I. Kucheiko, *Polyhedron* **1991**, *10*, 2617 –2628.
[21] V. G. Kessler, N. Ya. Turova, A. Panov, *Polyhedron* **1996**, *15*, 335–338.
[22] R. C. Mehrotra, A. Singh, *Chem. Soc. Rev.* **1996**, 1–13.
[23] S. Doeuff, M. Henry, C. Sanchez, J. Livage, *J. Non Cryst. Solids* **1987**, *89*, 206–210.
[24] D. C. Bradley, F. M. A. Halim, W. Wardlaw, *J. Chem. Soc*. **1950**, 3450–3454.
[25] K. Nakamoto, *Infrared and Raman Spectra of Inorganic and Coordination Compounds*, J. Wiley & Sons Inc., New York, London, **1963**, p. 233.
[26] S. Doeuff, C. Sanchez, *Mat. Res. Bull.* **1994**, *29*, 1–13.
[27] D. C. Bradley, R. C. Mehrotra, W. Wardlaw, *J. Chem. Soc*. **1952**, 2027 –2030.

Received April 27, 1999
[I99157]

Novel (Methyl)- and (Acetyl)palladium Complexes Containing Bis(pyrazolyl)borate Ligands – Dynamic Equilibrium between η^2 and η^1 Forms for the Complex Bp*(Me)(PCy_3)Pd [Bp* = dihydridobis(3,5-dimethylpyrazolyl)borate]

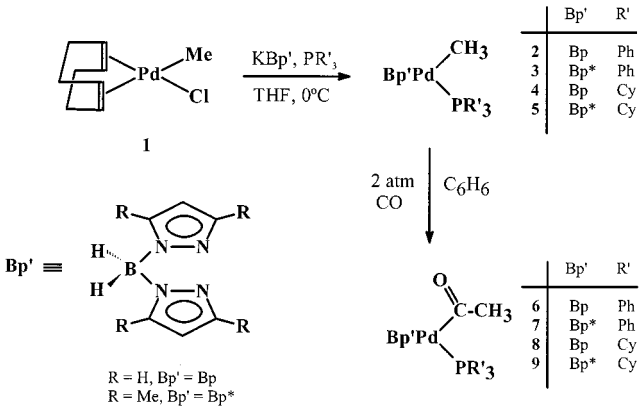
M. Mar Díaz-Requejo,[a] M. Carmen Nicasio,[a] Tomás R. Belderrain,[a] Pedro J. Pérez,*[a] M. Carmen Puerta,[b] and Pedro Valerga[b]

Keywords: Polymerisation / (Methyl)palladium complexes / Poly(pyrazolyl)borates

A series of (methyl)palladium complexes of general formula Bp′Pd(CH_3)(L) [Bp′ = Bp = dihydridobis(pyrazolyl)borate; Bp′ = Bp* = dihydridobis(3,5-dimethylpyrazolyl)borate, L = phosphane] has been synthesised. The interaction of these alkyl complexes with carbon monoxide produces the acetyl derivatives Bp′Pd(C(O)Me)(L), one of the members of this series, BpPd[C(O)Me](PPh_3), being structurally characterised by X-ray diffraction studies.

Introduction

After Brookhart's discovery of (diimine)nickel and -palladium complexes as highly efficient catalysts for olefin polymerisation,[1] the synthesis of new alkyl complexes of group-10 metals has emerged. The number of such complexes reported in the recent literature is considerable, but the catalytic capabilities towards polymerisation seem to be restricted to cationic compounds containing few, selected nitrogen-based ligands such as the above-mentioned diimine ligand.[1–3] Recently, Grubbs and co-workers have reported several neutral (aryl)(salicylaldimininato)nickel(II) complexes which act as good olefin polymerisation catalysts.[4] On the other hand, although there exist an important number of palladium complexes containing poly(pyrazolyl)borate ligands,[5] few examples of simple (alkyl)palladium(II) species have been reported.[6] The synthesis of (methyl)palladium complexes containing tris- and tetrakis-(pyrazolyl)borate has been described,[5] but, to our knowledge, there is no report on the synthesis of the analogous bis(pyrazolyl)borate derivatives. With the aim of preparing new Pd complexes bearing nitrogen donor ligands as possible olefin polymerisation catalysts, in this contribution we describe the synthesis, characterisation and chemical behaviour of several complexes of general formula Bp′Pd(Me)(PR'_3) as well as their corresponding acyl derivatives (Scheme 1).



Scheme 1

Results and Discussion

Synthesis of the Alkyl Complexes

When 1 equivalent of the KBp′ (Bp′ = Bp or Bp*) salt is added to cold (0 °C) THF solutions of Pd(Me)Cl(cod) (**1**) and PR'_3 (R′= Ph, Cy), a ligand exchange reaction takes place as shown in Scheme 1. After work up, white microcrystalline compounds **2–5** (see Table 1) are isolated in good yields. Some of these complexes are not very stable in solution at room temperature, so temperature control becomes crucial during their synthesis reactions as well as during the work up of their crystallisation solutions.

The NMR data of **2–4** are in accordance with a square-planar environment around the palladium atom, assuming that both pyrazolyl rings are bound to the metal centre. The resonances in the ^{1}H- and ^{13}C{^{1}H}-NMR spectra are well

[a] Departamento de Química y Ciencia de Materiales, Universidad de Huelva,
Carretera de Palos de la Frontera, s/n, 21819-Huelva, Spain
[b] Departamento de Ciencia de los Materiales e Ingeniería Metalúrgica y Química Inorgánica, Facultad de Ciencias, Universidad de Cádiz,
Apartado 40, Puerto Real, 11510-Cádiz, Spain

 © WILEY-VCH Verlag GmbH, D-69451 Weinheim, 2000 1434−1948/00/0606−1359 $ 17.50+.50/0

Table 1. Microanalyses and IR data for compounds **2–9**

Complex	Microanalyses [found (calcd.)] C	H	N	IR (nujol) [cm^{-1}] ν(B–H)	ν(C–N)	ν(CO)
BpPd (CH_3)(PPh_3) (**2**)	55.8 (56.6)	5.0 (4.9)	9.7 (10.6)	2250–2450	1530	
BpPd (CH_3)(PCy_3) (**3**)	54.1 (54.7)	7.4 (8.1)	9.9 (10.2)	2290–2480	1510	
Bp*Pd (CH_3)(PPh_3) (**4**)	59.1 (59.4)	5.6 (5.8)	9.0 (9.5)	2250–2490	1550	
Bp*Pd (CH_3)(PCy_3) (**5**)	58.2 (57.6)	9.0 (8.7)	10.0 (9.3)	2295–2480	1534	
BpPd ($COCH_3$)(PPh_3) (**6**)	56.0 (55.9)	5.0 (4.7)	10.0 (10.0)	2200–2428	1510	1681
BpPd ($COCH_3$)(PCy_3) (**7**)	54.1 (54.1)	7.4 (7.6)	9.8 (9.7)	2295–2429	1495	1683
Bp*Pd ($COCH_3$)(PPh_3) (**8**)	58.6 (58.6)	5.7 (5.5)	8.9 (9.1)	2200–2448	1537	1679
Bp*Pd ($COCH_3$)(PCy_3) (**9**)	56.6 (56.9)	8.0 (8.2)	8.7 (8.8)	2443–2200	1538	1677

Table 2. ^{1}H- and ^{31}P-NMR data for compounds **2–5**

Compound	^{1}H (values of *J* in Hz) PdCH_3[a]	Bp′[b] C*H*(pz)	Me(pz)	P*R*$_3$	^{31}P{^{1}H}
BpPd (CH_3)(PPh_3) (**2**)[c]	0.84 (d) (2.4)	7.68 (d) (2) 6.28 (d) (2) 6.01 t (2) 5.66 t (2)		7.60 (m) (6 H) 6.94 (m) (9 H)	39.2 (s)
BpPd (CH_3)(PCy_3) (**3**)[c]	0.81 (d) (2.5)	5.99 (m) 7.39 (d) (2) 7.56 (d) (2) 7.63 (m) 7.68 (d) (2)		2.2–0.7 (m) (33 H)	37.5 (s)
Bp*Pd (CH_3)(PPh_3) (**4**)[c]	0.78 (d) (4.3)	5.66 (s) 5.45 (s)	2.39 2.38 2.26 1.53	7.65 (m) (6 H) 6.95 (m) (9 H)	37.1 (s)
Bp*Pd (CH_3)(PCy_3) (**5**)[d]	0.79 (d) (3.1)	5.66 (br s)	2.11 2.32	2.2–0.8 (m) (33 H)	33.9 (s)

[a] *J*(HP) in parentheses. – [b] *J*(HH) in parentheses. – [c] In C_6D_6. – [d] In CD_2Cl_2.

Table 3. ^{13}C{^{1}H}-NMR data for compounds **2–5**

Compound[a]	PdCH_3	^{13}C{^{1}H}[b] Bp′ C(pz)	CH_3(pz)	P*R*$_3$
BpPd (CH_3)(PPh_3) (**2**)	–2.43 (6)	139.9 (s) 138.3 (s) 135.4 (s) 135.0 (s) 104.5 (br s) 103.9 (s)		134.7 (d) (12) 131.3 (d) (49) 129.9 (d) (2) 128.0 (d) (11)
BpPd (CH_3)(PCy_3) (**3**)	–4.6 (d) (7)	139.9 (s) 137.6 (d) (2) 135.2 (s) 134.0 (d) (2.5) 104.2 (d) (2.5) 104.1 (s)		33.6–26.4 (m)
Bp*Pd (CH_3)(PPh_3) (**4**)	–2.6 (d) (8)	105.2 (s) 104.5 (d) (3) 147.0 (d) (2.6) 146.7 (s) 144.4 (s) 143.4 (d) (2.9)	13.9 (s) 13.3 (s) 12.8 (s) 12.7 (s)	134.5 (d) (12) 132.2 (d) (49) 129.9 (d) (2.3) 128.1 (d) (11)
Bp*Pd (CH_3)(PCy_3) (**5**)	–9.86 (d) (8)	104.8 (s) 146.0 (br s) 143.1 (br s)	12.8 (s) 12.6 (s) 11.8 (br s)	35–26 (m)

[a] In C_6D_6. – [b] *J*(CP), in Hz, in parentheses.

defined (see Table 2 and Table 3). For instance, the proton signals of the Pd–CH_3 groups in the ^{13}C{^{1}H}-NMR spectra range from δ = –9.9 to δ = –2.4, each resonance splitting into a sharp doublet. The values of J_{CP} coupling constants are small (J_{CP} = 6–8 Hz), in agreement with a mutually *cis* distribution of the alkyl and phosphane ligands. The pyrazolyl rings are inequivalent since two sets of signals are observed in the ^{1}H- and ^{13}C{^{13}H}-NMR spectra. In contrast,

the ^{1}H-NMR spectrum of **5** at room temperature consists of one broad resonance for the C*H* protons (δ = 5.66) and two broad singlets for the methyl protons of the two pyrazolyl rings (δ = 2.1 and 2.3, respectively). At low temperature, –30 °C, the low-field resonance splits into two peaks centred at δ = 5.67 and 5.65, corresponding to two inequivalent C*H* protons (see Figure 1 for the VT experiment).

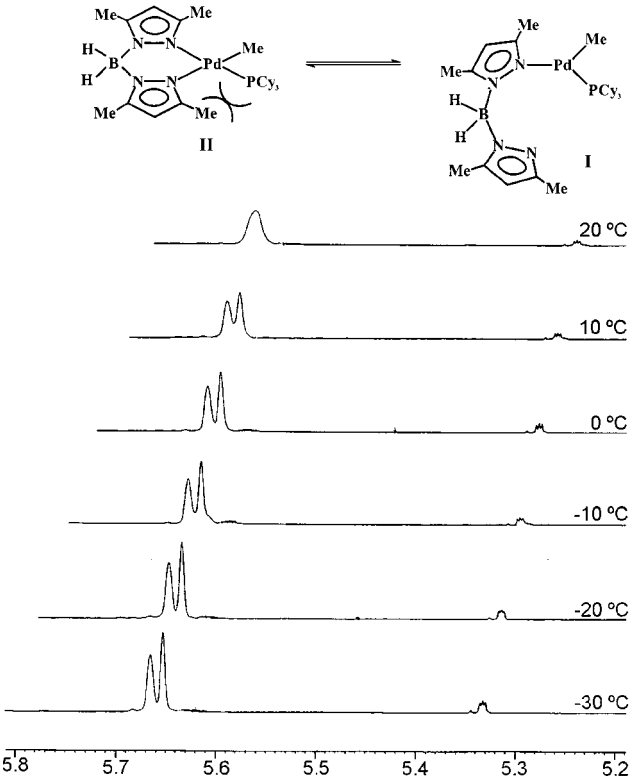


Figure 1. Variable-temperature ^{1}H-NMR spectra (CD_2Cl_2, 400 MHz) of **5** and proposed mechanism for the observed fluxionality

A phosphane exchange process cannot be responsible of the observed fluxionality, based of the following: (i) when PCy_3 is added to a solution of complex **5** in CD_2Cl_2 at room temperature, no change is observed for the resonances observed in the ^{1}H-NMR spectrum of **5**; (ii) the J_{HP} coupling constant for the methyl group remains unchanged through studied the temperature range, clearly confirming the strength of the Pd–P bond.

A possible alternative explanation for the fluxional process would invoke dissociation and re-association of one pyrazolyl ring to the Pd centre. This would be the result of steric repulsions between the methyl groups and the bulky PCy_3. Subsequently, an equilibrium between the η^2-Bp* species and an η^1-Bp* species might occur (Figure 1). Furthermore, the absence of any band in the 2100–1900 cm^{-1} range in the IR spectrum of **5** (see Table 1) indicates that no agostic interactions exist between the palladium centre and any of the B–H bonds,[7,8] making the species **I** the more reasonable proposition. An example of a process similar to the one represented in Figure 1 has been recently reported for the Rh^I complex [Rh(CO)($PMePh_2$)$_2$-($Tp^{Me2,4-Cl}$)] containing a bulky η^2-Tp ligand.[9] Etienne et al. concluded that steric effects were undoubtedly responsible of the observed structure. In addition, Ni^{II} complexes containing bulky poly(pyrazolyl)borate ligands coordinated in an η^1- fashion [e. g., Tp*t*BuNi(C_6H_5)(PMe_3)$_2$] have been described.[10,11] In the case of **5**, the existence of a 14-electron species, similar to that of structure **I**, has been proposed an intermediate in insertion-type reactions.[12] More information can be extracted from the NMR study shown in Figure 1. The calculated value of $\Delta G^{\neq}$ [13] of ca. 59.1 kJ mol^{-1} compares well with those values reported by Espinet and co-workers,[14] 45–60 kJ mol^{-1}, for exchange of pyridine groups in palladium complexes containing $P(CH_2CH_2Py)_nPh_{3-n}$ ligands.

Reaction of 2–5 with Olefin and/or CO

Our main interest in the study of these complexes was their possible application as catalysts in olefin polymerisation and/or CO/olefin copolymerisation processes. Previously, there had been examples described of the use of cationic (methyl)palladium(II) complexes for the polymerisation of ethylene and α-olefins.[1] Unfortunately, in our case, attempts to polymerise ethylene with the neutral complexes **2–5** yielded no polyethylene, even under ethylene pressure (2 atm) and the presence of phosphane scavengers like $B(C_6F_5)_3$.[15]

On the other hand, since Sen's report of palladium(II) catalysts for the CO–olefin copolymerisation reaction,[16,17] and later, Drent and co-workers' report of the perfectly alternating copolymerisation of such substrates,[18,19] the synthesis and study of new (alkyl)palladium compounds containing P–P or N–N ligands have been developed.[20,21,22] We have also tested our Bp′Pd(Me)(L) complexes as catalysts in such processes, but again, no polymer formation was observed and only the CO insertion products, Bp′Pd(COMe)(PR'_3) (**6–9**) were obtained (Scheme 1), even under CO and olefin pressure or heating conditions. These acyl derivatives **6–9** can be prepared by exposure of a solution of the corresponding alkyl complex under CO pressure (2 atm).

Spectroscopic data of the complexes **6–9** have unambiguously revealed the presence of the acyl function. Thus, the intense absorbances observed at ca. 1680 cm^{-1} in their IR spectra are attributed to ν(COR) (Table 1). In addition, in the $^{13}C\{^1H\}$-NMR spectra, the quaternary carbon atoms of the acyl moiety resonate as doublets within the range δ = 231.1–234.6 (see Table 4). Both pyrazolyl rings are inequivalent as inferred from the well-defined resonances observed in the $^{13}C\{^1H\}$-NMR spectra (see Table 5). In contrast to the observations for the other acyl derivatives, and in agreement with its alkyl precursor, complex **9**, Bp* Pd(COMe)(PCy_3) appears to also be fluxional.

A single-crystal X-ray diffraction study has been carried out on the compound BpPd(COMe)(PPh_3) (**6**). An ORTEP[22] perspective view of the molecule is depicted in Figure 2. Selected bond lengths and angles are shown in Table 6. Compound **6** has a similar geometry around the

Table 4. ^{1}H- and ^{31}P{^{1}H}-NMR data for compounds **6–9**

Compound[a]	^{1}H[b] PdCOC*H*$_3$	Bp′ C*H* (pz)	Me (pz)	P*R*$_3$	^{31}P{^{1}H}
BpPd ($COCH_3$)(PPh_3) (**6**)	1.98 (s)	7.71 (d) (2) 7.51 (d) (2) 7.42 (d) (2) 7.38 (d) (2) 6.18 (t) (2) 5.72 (t) (2)		7.74 (m) 7.50 (m) 7.45 (m)	26.7 (s)
BpPd ($COCH_3$)(PCy_3) (**7**)	2.28 (s)	7.54 (br s) 7.28 (br s) 6.11 (br s)		1.16–2.0 (m)	30.7 (s)
Bp*Pd ($COCH_3$)(PPh_3) (**8**)	2.20 (s)	5.73 (s) 5.35 (s)	2.35 (br s) 1.75 (s) 1.31 (s)	7.72 (m) 7.49 (m) 7.43 (m)	24.7 s
Bp*Pd ($COCH_3$)(PCy_3) (**9**)	2.29 (s)	5.64 (br s)	2.34 (br s) 2.21 (br s)	1.0–2.2 (m)	27.5 (s)

[a] In C_6D_6. – [b] *J*(HH), in Hz, in parentheses.

Table 5. ^{13}C{^{1}H}-NMR data for compounds **6–9**

Compound[a]	^{13}C{^{1}H} Pd–CO*C*H$_3$[b]	Bp′ *C* (pz)	Me (pz)	*C*O	P*R*$_3$[b]
BpPd ($COCH_3$)(PPh_3) (**6**)	37.9 d (20)	140.8 (s) 140.0 (s) 135.6 (s) 135.5 (s) 104.7 (s) 104.3 (s)		234.2 (s)	134.8 (d) (12) 131.4 (d) (2) 130.7 (s) 128.9 (d) (11)
BpPd ($COCH_3$)(PCy_3) (**7**)	39.1 (d) (14)	140.7 (s) 139.5 (s) 135.9 (s) 134.9 (s) 104.5 (s) 104.4 (s)		234.6 (s)	26.7 (s) 27.9 (d) (10) 30.1 (s) 34.9 (d) (21)
Bp*Pd ($COCH_3$)(PPh_3) (**8**)	37.2 (d) (16)	148.3 (s) 148.1 (s) 144.5 (s) 144.2 (s) 105.1 (s) 104.7 (s)	13.8 (s) 13.5 (s) 12.9 (s) 12.7 (s)	233.5 (s)	134.9 (d) (12) 130.9 (d) (2) 130.5 (s) 128.7 (d) (11)
Bp*Pd ($COCH_3$)(PCy_3) (**9**)	38.4 (d) (14)	146.9 (br s) 143.9 (br s) 104.9 (br s)	14.3 (br s) 12.6 (br s)	231.1 (s)	27.8 d (10) 29.9 d (20) 26.3 (s) 35.1 d (20)

[a] In C_6D_6. – [b] *J*(CP) in parentheses.

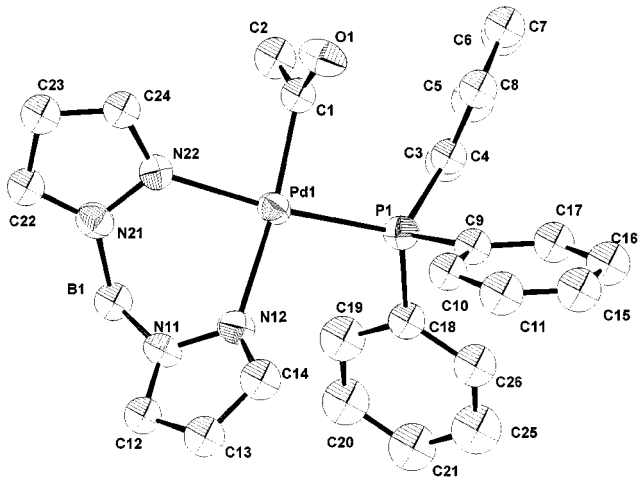


Figure 2. Molecular structure for **6**

Table 6. Selected bond lengths (Å) and angles (°) for compound **6**

Pd(1)–P(1)	2.278(3)	N(12)–Pd(1)–N(22)	87.5(3)
Pd(1)–N(12)	2.189(7)	N(12)–Pd(1)–C(1)	171.0(3)
Pd(1)–N(22)	2.107(7)	N(22)–Pd(1)–C(1)	86.1(3)
Pd(1)–C(1)	1.973(8)	P(1)–Pd(1)–N(12)	100.3(2)
		P(1)–Pd(1)–N(22)	169.4(2)
		P(1)–Pd(1)–C(1)	86.9(2)

metal centre as other palladium poly(pyrazolyl)borate complexes.[5] The molecule of **6** presents a distorted square-planar geometry in the solid state, with the values of the angles P(1)–Pd(1)–N(22) [169.4(2)°] and N(12)–Pd(1)–C(1) [171.0(3)°] slightly deviated from the ideal of 180°. The Pd–N(12) and Pd–N(22) distances [2.189(7) and 2.107(7) Å, respectively] are also in the range of those reported, for instance, in the related compound Bp*Pd(CH_2SiMe_3)(PMe_3)

[2.123(5) and 2.098(4) Å].[6] Finally, the palladium–carbon bond length found in compound **6** [1.973(8) Å] is within the range reported for the related (acyl)palladium bidentate nitrogen donor complexes [for example, 1.952(5) Å for (bpy)($MeOCC_7H_{10}COC_7H_{10}CO$)PdI[21]].

Experimental Section

All preparations were carried out using standard Schlenk techniques under nitrogen using freshly distilled and degassed solvents. Potassium bis(pyrazolyl)borates[23] and the complex (COD)-(CH_3)PdCl[24] were prepared according to literature procedures. PCy_3 and PPh_3 were purchased and used without further purification. – Infrared spectra were recorded with a Perkin–Elmer spectrophotometer, model 884. – ^{1}H- and ^{13}C-NMR spectra were recorded with a Bruker DRX400 spectrometer, chemical shifts being referred to TMS. – ^{31}P-NMR spectra were obtained with the same spectrometer using 85% aqueous H_3PO_4 as the standard. – Microanalyses were carried out by the Microanalytical Service of the Instituto de Investigaciones Químicas (Sevilla, Spain).

Synthesis of the Alkyl Derivatives Bp′(CH_3)(PR'_3)Pd [Bp′= Bp, R′ = Ph (2), Cy (3); Bp′= Bp*, R′ = Ph (4), Cy (5)]: (COD)-(CH_3)PdCl (0.5 mmol, 128 mg) was dissolved in THF (40 mL) and the corresponding phosphane ligand (0.5 mmol) was added. To the resulting solution, cooled at 0 °C, 1 equiv. of KBp′ was added and the mixture was stirred for 2 h. The solvent was removed under vacuum and the residue was extracted with THF/petroleum ether (1:1). Complexes Bp′(CH_3)(PR_3)Pd were isolated as microcrystalline white solids upon cooling of these solutions to –20 °C (75–90% yield).

Synthesis of the Acyl Derivatives (CH_3CO)Bp′(PR_3)Pd [Bp′= Bp, R′ = Ph (6), Cy (7); Bp′= Bp*, R′ = Ph (8), Cy (9)]: A typical preparation is the following: Synthesis of (MeCO)Bp*(PPh_3)Pd (**8**): Complex **4** (0.25 g, 0.43 mmol) was dissolved in dried THF (15 mL) and the resulting pale yellow solution was transferred to a pressure vessel which was charged with CO (2 atm). The reaction mixture was stirred for ca. 1 h affording a dark yellow solution. The solvent was pumped off and the crude residue investigated by NMR (C_6D_6), revealing that compound **8** was formed in almost quantitative yield. Crystallisation from petroleum ether/Et_2O (1:2) mixtures led to the isolation of complex **8** as pale yellow crystals of analytical purity (yield 75%).

Compounds **6**, **7**, **9** were obtained in a similar procedure in 65–70% yield after crystallisation. (MeCO)Bp(PPh_3)Pd (**6**) was crystallised from Et_2O/CH_2Cl_2 (1:1) mixtures; (MeCO)Bp(PCy_3)Pd (**7**) was crystallised from Et_2O solutions and (MeCO)Bp*(PCy_3)Pd (**7**) was purified by crystallisation from petroleum ether solutions.

Crystallography: A colourless crystal of $C_{26}H_{26}BN_4OPPd$ having approximate dimensions of 0.35 × 0.24 × 0.10 mm was mounted on a glass capillary and transferred to a Rigaku AFC6S diffractometer. Graphite-monochromated Mo-K_α radiation was used.

Cell constants were obtained from a least-squares refinement using the setting angles of 25 carefully centred reflections. The system was determined to be orthorhombic, space group $P2_12_12_1$ (number 19, acentric). The data were collected using the ω/2θ scan method. The intensities of three standard reflections were measured after every 100 reflections to apply the decay correction. Lorentz-polarization and absorption correction (ψ-scan method) were also applied. A summary of experimental details is shown in Table 7.

Table 7. Summary of crystal data collection and structure analysis for complex **6**

Empirical formula	$C_{26}H_{26}BN_4OPPd$
Molecular mass	558.70
Crystal size [mm]	0.35 × 0.24 × 0.10
Colour, shape	colourless, plate
Cell measurements (25 refl.)	12.6 < 2θ < 15.5°
Crystal system	orthorhombic
Space group	$P2_12_12_1$ (number 19)
Cell parameters	a = 13.849(6) Å
	b = 14.687(6) Å
	c = 12.202(5) Å
Volume	V = 2481(1) Å^3
Z	4
$\rho_{calcd.}$	1.495 g cm^{-3}
λ(Mo-K_α)	0.71069 A
μ(Mo-K_α)	8.26 cm^{-1}
F(000)	1136
Absorption correction	ψ-scan method
Transmision factors	0.715–1.000
Standards number, interval	3 refl., 100 refl.
Decay (%)	–1.00
Temperature	290(1) K
Scan method	ω/2θ
Scan Speed (ω)	4° min^{-1}
2θ interval	5° < 2θ < 50.1°
Measured reflections	2349
Unique reflections	2349
Observed reflections ($I > 3\sigma_I$)	1965
Number of parameters	172
Reflection/parameter ratio	11.42
Refinements	Full-matrix least squares on F
$R = (\|F_o\| - \|F_c\|)/\|F_o\|$	0.0434
R_w ($w = \sigma_F^2$) = $[(w(\|F_o\| - \|F_c\|)^2/wF_o^2)]^{1/2}$	0.0503
g.o.f.	1.727
Residuals peaks [e/Å^3]	+1.31, –0.53

The structure was solved by the Patterson method. The refinement was carried out on F by full-matrix least-squares methods. Pd, O and N atoms were anisotropically refined. The carbon atoms were isotropically refined, most of the hydrogen atoms (20) were included in difference Fourier and the remainder in idealised positions and were not refined. A set of 1965 observed reflections [$I > 3\ \sigma(I)$] and 172 variable parameters were used in the last cycles of refinements. The enantiomorph with slightly lower R, R_w and goodness of fit was selected. Final values of R = 0.0434 and R_w = 0.0503 were obtained. All calculations were carried out using the TEXSAN software package on a VAX 3520 computer at the "Servicio Central de Ciencia y Tecnología de la Universidad de Cádiz". Crystallographic data have been deposited with the Cambridge Crystallographic Data Center: CCDC-135559. Copies of the data can be obtained free of charge on application to CCDC, 12 Union Road, Cambridge CB2 1EZ, UK [Fax: (internat.) + 44-1223/336-033; E-mail: deposit@ccdc.cam.ac.uk].

Acknowledgments

We are grateful to the Universidad de Huelva (Plan Propio de Investigación) and Ministerio de Educación y Cultura (Acción Especial APC1998–0108) for the financial support. M. M. D.-R. thanks the Junta de Andalucía for a research studentship.

[1] L. K. Johnson, C. M. Killian, M. Brookhart, *J. Am. Chem. Soc.* **1995**, *117*, 6414.

[2] L. K. Johnson, S. Mecking, M. Brookhart, *J. Am. Chem. Soc.* **1996**, *118*, 267.
[3] S. Mecking, L. K. Johnson, L. Wang, M. . Brookhart, *J. Am. Chem. Soc.* **1998**, *120*, 888.
[4] C. Wang, S. Friedrich, T. R. Younkin, R. T. Li, R. H. Grubbs, D. A. Bansleben, M. W. Day, *Organometallics* **1998**, *17*, 3149.
[5] P. K. Byers, A. J. Canty, R. T. Honeyman, *Adv. Organomet. Chem.* **1992**, *34*, 1.
[6] E. Gutiérrez, M. C. Nicasio, M. Paneque, C. Ruiz, V. Salazar, *J. Organomet. Chem.* **1997**, *549*, 167 and references cited therein.
[7] S. Trofimenko, *Chem. Rev.* **1993**, *93*, 943.
[8] A. E. Corrochano, F. A. Jalón, A. Otero, M. M. Kubicki, P. Richard, *Organometallics* **1997**, *16*, 145 and references cited therein.
[9] F. Malbosc, P. Kalck, J.-C. Daran, M. Etienne, *J. Chem. Soc., Dalton Trans.* **1999**, 271.
[10] E. Gutiérrez, S. A. Hudson, A. Monge, M. C. Nicasio, M. Paneque, E. Carmona, *J. Chem. Soc., Dalton Trans.* **1992**, 2651.
[11] E. Gutiérrez, S. A. Hudson, A. Monge, M. C. Nicasio, M. Paneque, C. Ruiz, *J. Organomet. Chem.* **1998**, *551*, 215
[12] G. K. Anderson, R. J. Cross, *Acc. Chem. Res.* **1984**, *17*, 67.
[13] $\Delta G^{\neq}$ has been calculated by means of $\Delta G^{\neq} = RT_c[22.96+\ln(T_c/\Delta\nu)]$.
[14] J. A. Casares, P. Espinet, K. Soulantica, I. Pascual, G. Orpen, *Inorg. Chem.* **1997**, *36*, 5251.
[15] This method has been used to activate the nickel complexes reported in ref.[4]
[16] A. Sen, T. W. Lai, *J. Am. Chem. Soc.* **1982**, *104*, 3520.
[17] T. W. Lai, A. Sen, *Organometallics* **1984**, *3*, 866.
[18] E. Drent, Eur. Pat. Appl. 121965, **1984**.
[19] E. Drent, J. A. M. van Broekhoven, M. J. Doyle, *J. Organomet. Chem.* **1991**, *417*, 235.
[20] F. C. Rix, M. Brookhart, P. S. White *J. Am. Chem. Soc.* **1996**, *118*, 4746 and references cited therein.
[21] B. A. Markies, D. Kruis, M. H. P. Rietveld, K. A. N. Verkerk, J. Boersma, H. Kooijman, M. T. Lakin, A. L. Spek, G. van Koten, *J. Am. Chem. Soc.* **1995**, *117*, 5263, and references cited therein.
[22] B. Domhöver, W. Kläui, A. Kremer-Aach, R. Bell, D. Mootz, *Angew. Chem. Int. Ed.* **1998**, *37*, 21.
[23] C. K. Jonhson, *ORTEP II*, Oak Ridge National Laboratory, Tennessee, **1971**
[24] S. Trofimenko, *J. Am. Chem. Soc.* **1967**, *89*, 3170.
[25] R. E. Rülke, J. M. Ernsting, A. L. Spek, C. J. Elsevier, P. W. N. M. van Leeuwen, K. Vrieze, *Inorg. Chem.* **1993**, *32*, 5769.
Received October 14, 1999
[I99362]

Photoinduced Ligand Isomerization in Dimethyl Sulfoxide Complexes of Ruthenium(II)

Matthew K. Smith,[a] John A. Gibson,[b] Charles G. Young,[b][+] John A. Broomhead,[b][++] Peter C. Junk,[a] and F. Richard Keene*[a]

Keywords: Dimethyl sulfoxide / Isomerizations / Photochemistry / Ruthenium

Upon exposure to sunlight or UV irradiation, a DMSO solution of $[Ru(bpy)_2(DMSO)_2]^{2+}$ **(1)** (bpy = 2,2′-bipyridine; DMSO = dimethyl sulfoxide) turns rapidly from yellow to red, but subsequently slowly reverts to yellow in the dark. The photochemical sequence is explained in terms of a photopromoted linkage isomerization of the DMSO ligands from *S*- to *O*-bound, with a relaxation back to the thermodynamically stable yellow *S*-bound form in the dark by an intermolecular mechanism. The "dark" reaction has been studied by UV/Vis spectrophotometry, NMR and IR spectroscopy. The *S*-bound ligation of DMSO in the yellow cation was established by X-ray crystallographic studies of *cis*-$[Ru(bpy)_2(DMSO)_2](CF_3SO_3)_2$.

Introduction

Polypyridyl complexes of ruthenium(II) and their photochemistry have been widely studied, particularly with regard to potential application to storage of light energy and light-activated switches.[1,2] In the latter context, the development of systems which undergo reversible photoactivated chemical or structural changes are of particular interest.[3]

The complex $[Ru(bpy)_2(DMSO)_2](PF_6)_2$ {bpy = 2,2'-bipyridine, DMSO = dimethyl sulfoxide} undergoes an interesting reaction of this type. A yellow solution of the complex in DMSO rapidly turns red upon exposure to sunlight; in the dark, the solution subsequently slowly reverts to the yellow form. This process appears completely reversible as it can be performed many times on the same solution with no apparent degradation of the complex. The phenomenon appears to arise from linkage isomerization: photoactivated linkage isomerizations are known but uncommon in ruthenium chemistry,[4−6] and the present study was undertaken to elucidate aspects of the process.

[a] School of Biomedical and Molecular Sciences, James Cook University,
Townsville, Queensland 4811, Australia
Fax: (internat.) + 61-74/781-4600
E-mail: Richard.Keene@jcu.edu.au
[b] Department of Chemistry (Faculties), Australian National University,
Canberra, A.C.T. 0200, Australia
[+] Present address: School of Chemistry, University of Melbourne, Parkville, Victoria 3052, Australia.
[++] Present address: School of Chemistry, Australian Defence Force
Academy, University College (UNSW),
Canberra, A.C.T. 2600, Australia.

Results and Discussion

Synthesis and Characterization

Reactions of blue $[Ru(bpy)_2(CO_3)]$ or $[Ru(Me_2bpy)(CO_3)]$ with non-coordinating acids HX {$X^- = PF_6^-$, $CF_3SO_3^-$} in DMSO resulted in the formation of the yellow bis(dimethyl sulfoxide) complexes, $[Ru(bpy)_2(DMSO)_2]^{2+}$ and $[Ru(Me_2bpy)_2(DMSO)_2]^{2+}$, which were precipitated as the X^- salts by addition of ethanol/hexane. Microanalytical and spectroscopic data for the dimethyl sulfoxide complexes were consistent with the proposed formulations, and IR, NMR and X-ray diffraction data (vide infra) indicate the dimethyl sulfoxide ligands are *S*-bound. In DMSO solution, the complexes undergo a reversible colour change to red upon irradiation with intense sunlight (ca. 5 min) or UV radiation [0.5 h; 100 W medium-pressure Hg lamp (354 nm)].

X-ray Crystallographic Studies

The structure of $[Ru(bpy)_2(DMSO)_2](CF_3SO_3)_2$ was determined by X-ray crystallography. The Ru centre shows a distorted octahedral environment; the DMSO ligands are *S*-bound and exhibit a *cis* relationship.

Two different conformations were observed in the asymmetric unit (Figure 1); in one form the O-atom of each of the DMSO ligands was orientated towards the opposite DMSO molecule (Figure 1a), and in the other form the oxygen atoms were orientated towards the aromatic ligands (Figure 1b). The origin of this anomaly may be steric. Selected bond lengths and angles are given in Table 1. The Ru−S bond lengths [2.292−2.293 Å] are slightly longer than those observed in other DMSO-containing ruthenium species, such as $[Ru(NH_3)_5(DMSO)]^{2+}$ [2.188 Å],[7] and *cis*-

 © WILEY-VCH Verlag GmbH, D-69451 Weinheim, 2000 1434−1948/00/0606−1365 $ 17.50+.50/0

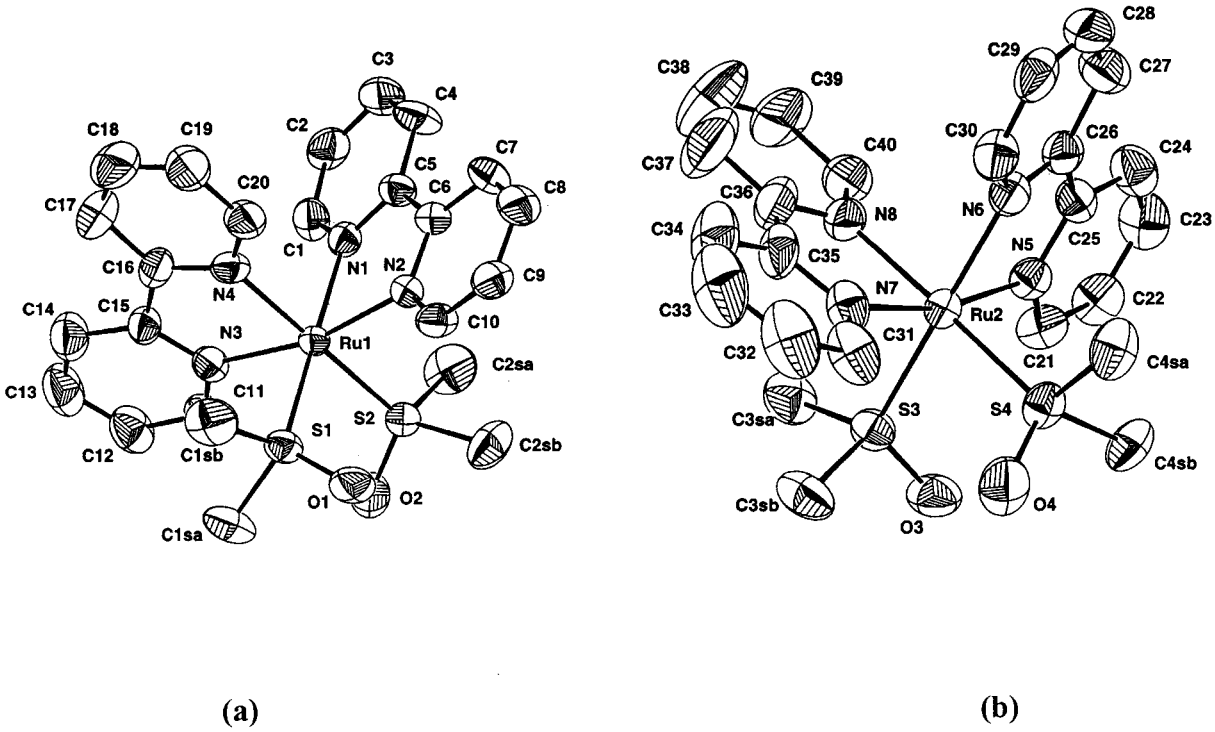


Figure 1. The two conformations (a) and (b) observed in the crystal structure of *cis*-$Ru(bpy)_2(DMSO)_2](CF_3SO_3)_2$ (thermal ellipsoids at 50% probability)

Table 1. Selected bond lengths and angles in the structure of *cis*-$[Ru(bpy)_2(DMSO)_2](CF_3SO_3)_2$

Bond	Bond length (Å)	Bonds	Angle
Ru(1)−S(1)	2.293(2)	S(1)−Ru(1)−S(2)	89.42(5)°
Ru(1)−S(2)	2.292(1)	Ru(1)−S(1)−O(1)	115.6(2)°
Ru(1)−N(1)	2.096(4)	S(3)−Ru(2)−S(4)	88.78(5)°
Ru(1)−N(2)	2.094(4)	Ru(2)−S(3)−O(3)	115.7(2)°
Ru(1)−N(3)	2.094(4)	O(1)−S(1)−C(1sa)	105.9(3)°
Ru(1)−N(4)	2.086(4)	O(1)−S(1)−C(1sb)	107.5(3)°
S(1)−O(1)	1.473(4)	O(2)−S(2)−C(2sa)	106.7(4)°
S(2)−O(2)	1.476(5)	O(2)−S(2)−C(2sb)	106.7(3)°
S(3)−O(3)	1.480(4)		
S(4)−O(4)	1.479(4)		

$[RuCl_2(DMSO)_4]$ [2.276−2.277 Å; *trans* to Cl^-].[8] This observation possibly results from competition for π-backbonding electron density exerted by the *trans* bipyridine ligands: precedence for this may be seen in the structures of complexes *cis*(Cl)-$[RuCl_2(PzH)(DMSO)_3]$ [2.281−2.286 Å, *trans* to Cl^-; 2.310Å *trans* to pyrazole (which is π-backbonding)],[9] and *trans*-$[RuCl_2(DMSO)_4]$ [2.352 Å; *trans* to DMSO ligands (which are π-backbonding)].[10] Steric interactions between the *cis*-disposed DMSO ligands may also contribute to the bond lengthening. The S−Ru−S bond angle was slightly less than 90° [89.45° and 88.93° in the two conformers].

It is noted that on the basis of steric interactions alone, O-ligation would be preferred. Accordingly, electronic and bonding factors seem to be critical in the determination of the binding mode.

Electronic Spectroscopy and Kinetic Studies

The UV/Visible absorption spectra for the yellow solution in DMSO of the freshly synthesized complex $[Ru(bpy)_2(DMSO)_2](PF_6)_2$ and the irradiated (red) solution are

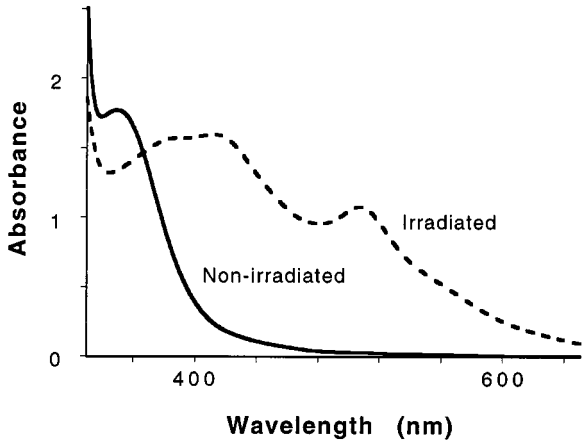


Figure 2. Absorbance spectra of $[Ru(bpy)_2(DMSO)_2](PF_6)_2$ (DMSO solution) before and after irradiation

shown in Figure 2 [λ_{max} = 348 nm, ε = 5760 $M^{-1}cm^{-1}$; λ_{max} = 507 nm, ε = 3500 $M^{-1}cm^{-1}$ and λ_{max} = 412 nm, ε = 5530 $M^{-1}cm^{-1}$, respectively]. The bathochromic shift on irradiation is consistent with a change from the "soft" *S*-bound (high field) to the "hard" *O*-bound (low field) ligands.

In DMSO solution, the red solution formed on irradiation reverted slowly in the dark to the original yellow spe-

cies. The initial light-induced reaction only occurred in DMSO, or non-coordinating solvents which contained DMSO. In other solvents the reaction proceeded not at all or to a minor extent (e.g. nitromethane, acetonitrile, dichloromethane, methanol, 1-methyl-2-pyrrolidinone), or there was an irreversible change due to the formation of a solvated species (e.g. water, *N*,*N*-dimethylformamide).[11]

The sequence observed for the "dark reaction" in DMSO solution is shown in the two segments of scan cycles (Figure 3), which illustrate a rapid initial reaction and a slower subsequent process. For the first reaction, continuous scans of the spectrum in the wavelength range 320−700 nm showed isosbestic points at λ = 440 nm and 390 nm (Figure 3a). The rate of the reaction was measured by following the time-dependence of the decay of the absorbance at 507 nm of the red complex ($t_{1/2}$ = 2.91 min. at 25 °C). The subsequent slower decay ($t_{1/2}$ = 111 min. at 25 °C) showed a different isosbestic point at 370 nm, which remained for the duration of the reaction (Figure 3b). Accordingly, the reaction proceeds via a two-step process from the red (irradiated) solution to the original yellow compound via an intermediate species.

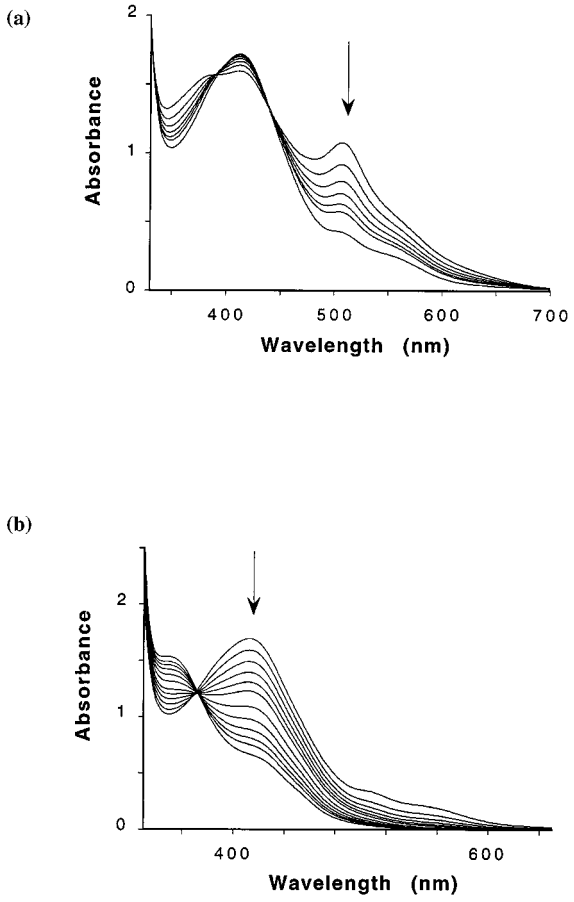


Figure 3. Absorbance spectra of $[Ru(bpy)_2(DMSO)_2](PF_6)_2$ (DMSO solution) after irradiation: (a) first 10 minute period (scan every 1 min), and (b) subsequent 285 minute period (15 min cycles)

The kinetics of the "dark" reactions which occurred after irradiation were followed using UV/Visible absorption spectral techniques over a range of temperatures. The two reactions observed were found to be pseudo-first order [plots of $\ln(A - A_{inf})$ vs. t were linear for > 3 $t_{1/2}$ in the two time domains]. The reaction rates were found to be unaffected by sample concentration, as expected.

Rate constants for the two reactions in DMSO solution at various temperatures are given in Table 2. The activation parameters for these two reactions were calculated: for the initial fast Red→Intermediate [**R**→**I**] reaction, $\Delta H^{\ddagger}$ = 58 (± 5) kJ mol^{-1} and $\Delta S^{\ddagger}$ = 83 (± 6) J mol^{-1}K^{-1}; for the slower Intermediate→Yellow [**I**→**Y**] reaction, $\Delta H^{\ddagger}$ = 92 (± 4) kJ mol^{-1} and $\Delta S^{\ddagger}$ = 162 (± 14) J mol^{-1}K^{-1}.

Table 2. Reaction rates for "dark" reactions [**I**→**Y**] for $[Ru(bpy)_2(DMSO)_2]^{2+}$ [complex concentration ca. 3−6 × 10^{-4} M]

Temp (K)	Solvent	k (s^{-1})[a] Slow Reaction	k (s^{-1})[a] Fast Reaction
25 °C (298 K)	DMSO	1.1 × 10^{-4}	4.0 × 10^{-3}
30 °C (303 K)	DMSO	2.1 × 10^{-4}	6.4 × 10^{-3}
35 °C (308 K)	DMSO	3.9 × 10^{-4}	8.7 × 10^{-3}
40 °C (313 K)	DMSO	6.9 × 10^{-4}	1.4 × 10^{-2}
45 °C (318 K)	DMSO	1.2 × 10^{-3}	1.8 × 10^{-2}
25 °C (298 K)	DMSO (50%) Nitromethane (50%)	9.1 × 10^{-5}	4.1 × 10^{-3}
25 °C (298 K)	DMSO (75%) Nitromethane (25%)	1.0 × 10^{-4}	4.2 × 10^{-3}

[a] Average of triplicate runs: estimated error ±5%.

From the structural studies reported above, the yellow form contains two *S*-bound DMSO ligands and it is highly probable that the red species formed immediately after irradiation contains two *O*-bound DMSO ligands. This may be rationalized in terms of the nature of the metal centre before and on irradiation: before irradiation, the Ru^{II} metal centre has a preference for ligands which possess the ability to backbond via ligand π-electron donation (i.e. "soft" ligands). After irradiation, however, the metal will have Ru^{III}-like character in the MLCT excited state and consequently will prefer ligands with strong σ-donating properties (i.e. "hard" ligands). Since DMSO has both "soft" (sulfur) and "hard" (oxygen) donor atoms, it is believed the DMSO switches its mode of bonding to the *O*-bound form to suit the nature of the metal. There is some precedence for this assertion: in Ru^{II} complexes involving strongly backbonding carbonyl (CO)[12] and nitrosyl (NO^+)[13] ligands, and in complexes involving Ru^{III} centres,[14,15] there is a significantly greater occurrence of *O*-bound DMSO than in the body of Ru^{II} species. In one case, Taube and coworkers have studied the kinetics of S→O isomerization on oxidation of $[Ru(NH_3)_5(DMSO)]^{2+}$.[16] More recently, an electrochemical study by Rack and Gray[17] of the system *mer*-$[RuCl_3(DMSO)(tmen)]$ {tmen = *N*,*N*,*N*',*N*'-tetramethylethylenediamine} demonstrated *S*-DMSO⇄*O*-DMSO isomerizations associated with Ru^{II}⇄Ru^{III} changes. It is probable therefore that the intermediate species observed in the "dark" reaction contains one *S*-bound and one *O*-bound DMSO ligand. This proposal is consistent with the IR analysis (see later), and is consistent with the UV/Visible spectral changes observed (Figure 3).

In principle, there are two possible mechanistic paths for the linkage isomerization reactions of *O*- to *S*-bound

DMSO; *viz.* an intermolecular substitution process in which the original DMSO ligands are replaced by solvent molecules, or an intramolecular switching mechanism involving a seven-coordinate species. There have been several investigations of linkage isomerization reactions involving the calculation of volumes of activation ($\Delta V^{\ddagger}$) which have also investigated the activation parameters $\Delta S^{\ddagger}$ and $\Delta H^{\ddagger}$.[18,19] In these mechanistic studies, for those reactions which were assigned as intramolecular in nature from the $\Delta V^{\ddagger}$ data, the corresponding $\Delta S^{\ddagger}$ values were found to be near-zero or negative, whereas a positive value indicated an intermolecular mechanism. This distinction is rationalized in terms of the increase in the number of individual molecules in going from the reactants to the transition state because of the dissociation of the ligands involved in an intermolecular process, thereby increasing the entropy of the system and resulting in a positive $\Delta S^{\ddagger}$ value. In the present system, the $\Delta S^{\ddagger}$ values for the **R→I** and **I→Y** reactions are positive, indicating that the reactions are intermolecular; i.e. the original DMSO ligands are replaced by DMSO solvent molecules during the isomerization process.

Photo-induced intramolecular linkage isomerization reactions involving tumbling mechanisms have been observed in thiocyanate-isothiocyanate, nitro-nitrito and cyanide-isocyanide conversions.[20] The reported cases of linkage isomerization involving DMSO ligands have been intermolecular[10,21,22] including Ru-DMSO systems, and it is possible that some steric or electronic factor prevents the intramolecular mechanistic path.

The rate constants of the **R→I** and **I→Y** reactions in nitromethane solutions containing 50% DMSO and 75% DMSO were comparable to those of pure DMSO solutions at 25 °C (see Table 2).

Infrared Analysis

The IR spectra of complexes containing DMSO ligands provide a means of differentiating between the *S*- and *O*-bound attachment. In ruthenium complexes, an *S*-bound DMSO exhibited a distinctive $\nu_{S=O}$ peak between 1080 and 1150 cm^{-1}, depending on the electronic nature of the other ligands in the coordination sphere. An *O*-bound form had a signal of slightly lower energy between 900 and 1000 cm^{-1}. In addition, a ν_{Ru-S} vibration occurred between 410−430 cm^{-1}, while the Ru−O signal occurred at slightly higher energy (460 to 490 cm^{-1}).[12]

The IR spectrum of yellow $[Ru(bpy)_2(DMSO)_2](PF_6)_2$ using KBr discs showed two distinct peaks which confirmed the *S*-DMSO ligation: $\nu_{S=O}$ = 1096 cm^{-1}, and ν_{Ru-S} = 425 cm^{-1}. Solid-state investigations of the red form were not possible, since a solid sample could not be isolated. Accordingly, solution IR studies were undertaken to enable assignment of the red form. A solution of the yellow complex in DMSO exhibited a peak at 1098 cm^{-1} ($\nu_{S=O}$), confirming the *S*-bound configuration remained after dissolution. Due to absorption by the DMSO solvent, the ν_{Ru-S} peak at ca. 425 cm^{-1} was obscured.

Upon irradiation of the solution and immediate measurement of its spectrum, the peak at 1098 cm^{-1} disappeared and a new absorption at 997 cm^{-1} was observed, consistent with *O*-bound DMSO. A second scan recorded ten minutes later showed this latter peak had decreased significantly, while the peak at 1098 cm^{-1} had increased slightly. A final scan five hours later showed the peak at 1098 cm^{-1} had reverted to its original intensity. This evidence indicates that, upon irradiation, the yellow solution containing the *S*-bound form converted into the *O*-bound red form. As the red species returned to the yellow form, the $\nu_{S=O}$ absorption corresponding to *O*-DMSO decreased in intensity, suggesting the DMSO ligands were reverting to the *S*-bound configuration. This decrease in intensity of this peak occurred rapidly in the first ten minutes, but slowed markedly as time progressed: this is consistent with the observations from UV/Visible spectroscopy, where the "dark" reaction of the irradiated red complex to the yellow form occurred in two stages, interpreted as a rapid conversion of the *O*-bound form rapidly to an *S*-bound/*O*-bound intermediate, which in turn slowly reverted to the fully *S*-bound form.

^{1}H NMR Spectroscopic Studies

^{1}H NMR spectral studies were also used to probe the nature of bonding changes in the DMSO ligands upon irradiation. For *S*-bound DMSO, the methyl proton resonance(s) shift downfield by up to 1 ppm from free DMSO, whereas for *O*-bound DMSO there is little shift.[21]

The aliphatic region of the spectrum of yellow $[Ru(bpy)_2(DMSO)_2](PF_6)_2$ in [D_6]dimethyl sulfoxide is shown in Figure 4a. Two peaks were observed at δ = 2.81 and 2.69, assigned as the CH_3 resonances from the *S*-bound DMSO ligands.

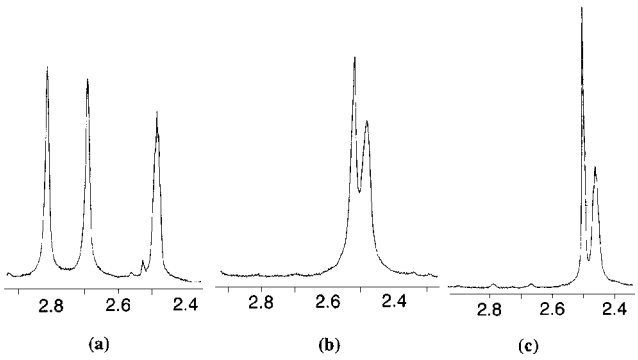


Figure 4. The 300 MHz ^{1}H NMR spectrum ([D_6]dimethyl sulfoxide solution) of the complex $[Ru(bpy)_2(DMSO)_2](PF_6)_2$: (a) before irradiation; (b) the same solution immediately after irradiation, and (c) the same solution after 5 h in the dark; ratio of integration of peaks at δ = 2.52 and 2.49 is identical in (b) and (c)

On irradiation by direct sunlight, the solution turned red and the ^{1}H NMR spectrum recorded immediately revealed the two CH_3 resonances observed in the original yellow solution had disappeared. A new resonance had developed at δ = 2.52, on the lowfield side of the solvent resonance centred at δ = 2.49 (Figure 4b), and consistent with either *O*-bound or free DMSO. When the irradiated solution was placed in the dark for five hours and the ^{1}H NMR spectrum re-measured, it was unchanged from that observed immediately after irradiation, even though the solution had

reverted completely back to the yellow form (Figure 4c). Repeating this irradiation procedure did not alter the spectrum. The loss of the peaks assigned to the *S*-bound form was established to be a consequence of the irradiation and not due to simple solvent exchange, as a freshly-prepared non-irradiated solution of the yellow complex in DMSO retained these two *S*-bound peaks for several days.

The data provide a number of insights into the photochemical sequence. The disappearance of the two resonances at $\delta = 2.81$ and 2.69 on irradiation and development of the new peak at $\delta = 2.52$ are consistent with the photoisomerization of *S*-bound form to the *O*-bound form, although the new peak is consistent with either *O*-bound or free DMSO. Following the subsequent reversion to the yellow form in the "dark" reaction, no change was observed within the aliphatic region of the spectrum: since the conversion of the *O*-bound to the *S*-bound form is known to be intermolecular (see above), the implication is that the photo-induced S→O linkage isomerization is also intermolecular. On the basis that the solvent [D_6]dimethyl sulfoxide would then be attached to the metal, no change would be expected in NMR spectra if the sequence was repeated, as was observed. This conclusion is in contrast to an earlier assessment on the system $[Ru(NH_3)_5(DMSO)]^{2+}$, where oxidation-induced S→O isomerization was thought to occur via a seven-coordinate intermediate i.e. via an intramolecular process.[16] The conclusion is also consistent with the observation that the photoreaction does not occur in the absence of DMSO and is not reversible in coordinating solvents which do not contain DMSO.

Other Systems

An attempt was made to obtain a further insight into the reaction by variation of the ligands not directly involved in the isomerization; for example, by replacement of the bpy ligands with 4,4'-dimethyl-2,2'-bipyridine (Me_2bpy), in which the substituent methyl groups are electron donating. The same general chemistry was observed, but the rate at which the photo-promoted red form reverted back to the yellow form was seen to increase relative to that of the non-methylated complex; this increase was marginal for the faster reaction (4.4×10^{-3} *cf.* 4.04×10^{-3} s^{-1}; 25 °C) but nearly double for the slower process (2.0×10^{-4} *cf.* 1.1×10^{-4} s^{-1}; 25 °C). It is not known at this stage whether the reasons for the difference are steric or electronic.

We have also observed similar photo-promoted linkage isomerizations for other ligands {such as SCN^- in the complex $[Ru(tpy)(bpy)(SCN)]^+$; tpy = 2,2':6',2''-terpyridine}[23,24] and we will report on these studies in due course.

Conclusions

The photo-induced linkage isomerization of *cis*-$[Ru(bpy)_2(DMSO)_2](PF_6)_2$ was investigated in DMSO solution. The complex contained two *S*-bound DMSO ligands (established in the solid state by X-ray crystallography) and underwent a colour change from yellow to red when irradiated with sunlight or UV light. On the basis of NMR, electronic and IR spectral studies, this was attributed to linkage isomerization from *S*- to *O*-bound DMSO. The complex subsequently slowly reverted to the yellow form in the dark in a two-step process. Kinetic studies, in association with NMR and IR spectral observations, show that these two "dark" reactions are intermolecular and involve an intermediate which is the $[Ru(bpy)_2(S\text{-DMSO})(O\text{-DMSO})]^{2+}$ species.

Experimental Section

Materials: 2,2'-Bipyridine (bpy; Aldrich), 4,4'-dimethyl-2,2'-bipyridine (Me_2bpy; Aldrich) hexafluorophosphoric acid (Aldrich), and dimethyl sulfoxide (DMSO; Aldrich, HPLC grade) were used as received. Nitromethane (BDH) was distilled over anhydrous calcium chloride before use. Trifluoromethanesulfonic acid (3 M) was distilled under vacuum and used in the short term.

Measurements: ^{1}H NMR spectra were recorded on a Varian Unity Inova-300 spectrometer in [D_6]dimethyl sulfoxide solutions at room temperature. Electronic absorption spectra were obtained using a Varian Cary 5E UV/Vis-NIR spectrophotometer in DMSO solution using 1 cm quartz cells. A Varian temperature control system was used to thermostat the kinetic studies. Infrared measurements were carried out on a Perkin−Elmer 1600 series FTIR spectrophotometer using solid KBr pressed plates, or a Presslok solution cell (32 mm diameter), comprising KBr plates and a 0.1 mm Teflon spacer. Elemental microanalyses were performed within the School of Biomedical and Molecular Sciences at James Cook University.

Syntheses: $[Ru(bpy)_2CO_3]\cdot 2H_2O$ and $[Ru(Me_2bpy)_2CO_3]$ were prepared using the literature method.[25]

$[Ru(bpy)_2(DMSO)_2](PF_6)_2$: $[Ru(bpy)_2(CO_3)]\cdot 2H_2O$ (0.05 g, 0.098 mmol) was dissolved in DMSO (0.4 mL) and HPF_6 (6 drops) added to the dark blue solution, which turned yellow. The mixture was stirred for 2 mins. to ensure the reaction went to completion. Ethanol (40 mL) and hexane (20 mL) were then sequentially added to the solution, producing a yellow precipitate. After stirring for twenty mins., the suspension was refrigerated overnight. The bright yellow crystals were collected by vacuum filtration. Yield: 0.066 g, 78%. $C_{26}H_{28}F_{12}N_4O_2P_2RuS_2$ (883.67): calcd. C 33.5, H 3.3, N 6.5, S 7.5; found C 33.7, H 3.1, N 6.3, S 6.9.

$[Ru(bpy)_2(DMSO)_2](CF_3SO_3)_2$: This complex was synthesized as described above except trifluoromethanesulfonic acid was substituted for hexafluorophosphoric acid. Yield: 0.067 g, 79%. $C_{28}H_{28}F_6N_4O_8RuS_4$ (891.86): calcd. C 36.1, H 3.23, N 6.5, S 14.7; found C 36.0, H 3.57, N 6.4, S 14.9.

$[Ru(Me_2bpy)_2(DMSO)_2](PF_6)_2\cdot[(C_2H_5)_2O]$: This compound was synthesized as for the bpy analogue, except $[Ru(Me_2bpy)_2CO_3]$ was used as the precursor. The complex was recrystallized from acetone/diethyl ether. Yield: 0.0606 g, 71%. $C_{32}H_{46}F_{12}N_4O_3P_2RuS_2$ (989.88): calcd. C 38.8, H 4.68, N 5.7; found C 39.0, H 4.71, N 6.1.

X-Ray Cystallographic Structure Determination of $[Ru(bpy)_2(DMSO)_2](CF_3SO_3)_2$: Crystals of $[Ru(bpy)_2(DMSO)_2](CF_3SO_3)_2$ were grown by slow evaporation of an ethanol/hexane solution of the complex. A unique room temperature diffractometer data set (Enraf−Nonius CAD-4 diffractometer; $T \approx 295$ K; monochromatic Mo-K_α radiation, $\lambda = 0.7107_3$Å; $2\theta/\theta$ scan mode) was measured, yielding 12314 independent reflections, 8800 with $I > 3\sigma(I)$

being considered "observed" and used in the large-block least-squares refinements. Anisotropic thermal parameters were refined for all non-hydrogen atoms. Hydrogen atoms were placed in calculated positions and were not refined. Conventional residuals R, R_w on $|F|$ are quoted, statistical weights derivative of $\sigma^2(I) = \sigma^2(I_{diff}) + 0.0004\sigma^4(I_{diff})$ being used. Neutral atom complex scattering factors were employed, and computation was by the XTAL 3.4 program system, implemented by Hall et al.[26] For crystal and refinement details see Table 3.

Table 3. Crystallographic data for *cis*-$[Ru(bpy)_2(S\text{-}DMSO)_2]/(CF_3SO_3)_2$

Formula	$C_{26}H_{28}F_6N_4O_8RuS_4$
Mol. wt.	867.84
$F(000)$	1752
a (Å)	13.405(2)
b (Å)	13.730(2)
c (Å)	18.636(5)
α (deg)	86.12(2)
β (deg)	88.09(2)
γ (deg)	78.48(1)
V (Å^3)	3352(1)
Molecules/unit cell, Z	4 (2 molecules in asymmetric unit)
Space group	Triclinic, $P\bar{1}$ (# 2)
Diffractometer	CAD4
Radiation: λ (Å)	Mo-K_α (0.71073)
2θ range, deg	2 − 50
Sigma cutoff	3σ
D_c, g cm^{-3}	1.719
μ, cm^{-1}	26.4
A* min,max	1.365, 1.800
Crystal dimensions, mm	0.74 × 0.42 × 0.84
Weighting scheme	4×10^{-4}
No. of reflections collected	12314
No. of observed reflections	8800
No. of parameters varied	884
T (K)	296
R	0.057
R_W	0.066

Crystallographic data (excluding structure factors) for the structure reported in this paper have been deposited with the Cambridge Crystallographic Centre as supplementary publication no. CCDC-134337. Copies of the data can be obtained free of charge on application to CCDC, 12 Union Road, Cambridge CB2 1EZ, UK [Fax: (internat.) + 44-1223/336-033; E-mail: deposit@ccdc.cam.ac.uk].

Kinetic Studies: Temperature-dependent kinetic studies were carried out using UV/Vis spectroscopy. Individual spectra of the yellow and red forms were obtained by measurement of a fresh solution of $[Ru(bpy)_2(DMSO)_2](PF_6)_2$ in DMSO (0.0066 g in 25 ml; $c = 3.07 \times 10^{-4}$ M) before and after irradiation for 10 min by sunlight. For the kinetic studies, the above solution of $[Ru(bpy)_2(DMSO)_2](PF_6)_2$ in DMSO was irradiated and the absorption spectra between 700 nm and 350 nm recorded in scan mode at 1 min intervals for 12 min, followed immediately by a cycle period of 15 min intervals for up to 6 h, depending on the temperature. The A_{inf} for both the **R→I** [Red→Intermediate] and **I→Y** [Intermediate→Yellow] reactions were estimated using a correlation program within Microsoft Excel software, and refined iteratively. The reactions were performed in triplicate, and agreement between the three replicates was high (within 5%).

The same procedure was repeated for $[Ru(Me_2bpy)_2(DMSO)_2](PF_6)_2$ at 25 °C.

IR Analysis: Solid state IR analyses were measured using pressed KBr discs (3 mg complex and 60 mg anhydrous KBr). Solution IR spectra (in DMSO) were obtained using a 32 mm Presslok solution cell with a 0.1 mm teflon spacer and KBr windows in absorbance mode, and the DMSO background subtracted. The spectra were recorded before and immediately after irradiation (10 mins. in sunlight). In the latter case, a second spectrum of the solution was recorded 10 mins. later, and a third after an interval of 5 h.

^{1}H NMR Spectoscopic Analysis: The ^{1}H NMR spectra of $[Ru(bpy)_2(DMSO)_2](PF_6)_2$ in $[D_6]$dimethyl sulfoxide solution were recorded on a fresh solution, then immediately after irradiation in sunlight (10 minutes with shaking in the NMR tube), and 5 h after irradiation.

Acknowledgments

The research was funded by the Australian Research Council.

[1] V. Balzani, F. Scandola, *Supramolecular Photochemistry*, Ellis Horwood, Chichester, **1991**.
[2] A. Juris, S. Barigelletti, S. Campagna, V. Balzani, P. Belser, A. von Zelewsky, *Coord. Chem. Rev.* **1998**. *84*, 85−277.
[3] A. P. de Silva, H. Q. N. Gunaratne, T. Gunnlaugsson, A. J. M. Huxley, C. P. McCoy, *Chem. Rev.* **1997**, *97*, 1515−1566.
[4] A. Del Medico, S. S. Fielder, A. B. P. Lever, W. J. Pietro, *Inorg. Chem.* **1995**, *34*, 1507−1513.
[5] A. Del Medico, P. R. Auburn, E. S. Dodsworth, A. B. P. Lever, W. J. Pietro, *Inorg. Chem.* **1994**, *33,* 1583−1584.
[6] A. Del Medico, W. J. Pietro, A. B. P. Lever, *Inorg Chim Acta* **1998**, *281*, 126−133.
[7] F. C. March, G. Ferguson, *Can. J. Chem.* **1971**, *49,* 3590−3595.
[8] A. Mercer, J. Trotter, *J. Chem. Soc. Dalton Trans.* **1975**, 2480−2483.
[9] M. M. T. Khan, N. H. Khan, R. I. Kureshy, K. Venkatasubramanian, *Polyhedron* **1992**, *11*, 431−441.
[10] E. Alessio, G. Mestroni, G. Nardin, W. M. Attia, M. Calligaris, G. Sava, S. Zorzet, *Inorg. Chem.* **1988**, *27,* 4099−4106.
[11] B. Durham, S. R. Wilson, D. J. Hodgson, T. J. Meyer, *J. Am. Chem. Soc.* **1980**,*102,* 600−607.
[12] E. Alessio, B. Milani, M. Bolle, G. Mestroni, P. Faleschini, F. Todone, S. Geremia, M. Calligaris, *Inorg. Chem.* **1995**, *34*, 4722−4734.
[13] J. E. Fergusson, C. T. Page, W. T. Robinson, *Inorg. Chem.* **1976**, *15*, 2270−2273.
[14] E. Alessio, G. Balducci, A. Lutman, G. Mestroni, M. Calligaris, W. M. Attia, *Inorg. Chim. Acta* **1993**, *203*, 205−217.
[15] E. Alessio, M. Bolle, B. Milani, G. Mestroni, P. Faleschini, S. Geremia, M. Calligaris, *Inorg. Chem.* **1995**, *34*, 4716−4721.
[16] A. Yeh, N. Scott, H. Taube, *Inorg. Chem.* **1982**, *21*, 2542−2545.
[17] J. J. Rack, H. B. Gray, *Inorg. Chem.* **1999**, *38*, 2−3.
[18] D. A. Palmer, R. van Eldik, H. Kelm, *Inorg. Chim. Acta* **1978**, *30,* 83−86.
[19] D. A. Palmer, H. Kelm, *Inorg. Chim. Acta* **1980**, *39,* 275−278.
[20] J. L. Burmeister, *Coord. Chem. Rev.* 1968, *3*, 225−245.
[21] C. V. Senoff, E. Maslowsky, R. G. Goel, *Can. J. Chem.* **1971**, *49,* 3585−3589.
[22] E. Alessio, G. Balducci, M. Calligaris, G. Costa, W. M. Attia, G. Mestroni, *Inorg. Chem.* **1991**, *30*, 609−619.
[23] N. C. Fletcher, F. R. Keene, *J. Chem. Soc., Dalton Trans.* **1998**, 2293−2301.
[24] N. C. Fletcher and F. R. Keene, unpublished work.
[25] E. C. Johnson, B. P. Sullivan, D. J. Salmon, S. A. Adeyemi, T. J. Meyer, *Inorg. Chem.* **1978**, *17,* 2211−2215.
[26] S. R. Hall, G. S. D. King, J. M. Stewart, University of Western Australia, Perth, **1995**.

Received November 12, 1999
[I99404]

Self-Assembly of Square Molecular Boxes Containing Dirhodium(II,II) Units

Sandra Lo Schiavo,*[a] Gabriella Pocsfalvi,[b] Scolastica Serroni,[a] Paola Cardiano,[a] and Pasquale Piraino*[a]

Keywords: Macrocycles / Dirhodium compounds / Porphyrins / Mass spectrometry

Dirhodium(II,II) based square molecular boxes were easily obtained by reaction of $[Rh_2(form)_2(CF_3COO)_2(H_2O)_2]$ (form = *N*,*N*′-di-*p*-tolylformamidinate) with both linear (terephthalate and oxalate) and angular [5,10-diphenyl-15,20-bis(4-carboxyphenyl)porphyrin] dicarboxylate dianions; liquid secondary ionization mass spectrometry (LSI MS) was used to establish the nuclearity of the new macrocycles. Their electrochemical properties were also investigated.

Introduction

Self-assembly of so-called "molecular squares" by means of appropriate transition metal complexes represents an attractive field of current research owing to their implication in nanotechnology. The molecular squares so far reported are mainly based on *cis*-coordinated square-planar transition metal complexes and rigid or semirigid bidentate ligands as connectors or, alternatively, on *trans* square-planar metal complexes as connectors and bidentate angular units.[1] In any case this synthetic strategy, which requires transition metal complexes with two *cis*- or *trans*-coordinated labile ligands, has been limited to the use of mononuclear transition metal complexes as building blocks.[1] Only recently have molecular squares incorporating dinuclear species as corner units have been reported.[2]

Our experience in the chemistry of dirhodium(II,II) complexes with "lantern" structures led us to plan the synthesis of molecular boxes involving dirhodium(II,II) species. These complexes, in addition to the well-known redox and axial reactivity, may exhibit equatorial reactivity too. In fact, the complex $[Rh_2(form)_2(CF_3COO)_2(H_2O)_2]$ (**1**) (form = *N*,*N*′-di-*p*-tolylformamidinate), characterized by two formamidinate and two trifluoroacetate groups symmetrically bridged in a cisoid arrangement around the Rh_2^{4+} core, exhibits a remarkable lability of the trifluoroacetate groups.[3] This leads to mild conditions for the substitution of neutral bidentate ligands at the equatorial positions without rupture of the cisoid $Rh_2(form)_2$ fragment.[4] Furthermore, complex **1** has been successfully used to synthesize a series of new mixed dirhodium(II,II) derivatives by metathetical reactions with a variety of carboxylates.[5]

These results show that **1** may be able to act as an appropriate precursor of angular building blocks, through the *cis*-$Rh_2(form)_2$ fragment, which is able to produce neutral square molecular boxes in combination with the appropriate dicarboxylate dianions as ligand connectors. The nuclearity of the boxes will depend on the dicarboxylates used: linear dicarboxylates will generate boxes with four $Rh_2(form)_2$ units at the corners, while angular ones will generate boxes with two alternating $Rh_2(form)_2$ units at the corners.

This paper deals with the synthesis and LSI MS (Liquid Secondary Ionization Mass Spectrometry) characterization of the square molecular boxes $[Rh_2(form)_2(tp)]_4$ (tp = terephthalate) (**2**), $[Rh_2(form)_2(ox)]_4$ (ox = oxalate) (**3**) and $[Rh_2(form)_2(porphy\{COO\}_2)]_2$ (**4**) [porphy$(COO)_2$] = 15,20-di-(4-carboxyphenyl)-5,10-diphenylporphyrin] incorporating the $Rh_2(form)_2$ fragment as angular units. These macrocycles represent the first examples of square molecular boxes incorporating dirhodium units as building blocks; while the manuscript was in preparation Cotton et al. anticipated the synthesis of **3**.[2]

More interestingly, looking at the redox properties of porphyrins [porphy$(COO)_2$, E = +1.1 V vs. SCE in 1,2-dichloroethane] and $[Rh_2(form)_2(CF_3COO)_2(H_2O)_2]$ [$E°(Rh_2^{4+}/Rh_2^{5+})$ = +0.59 V vs. SCE in CH_2Cl_2], **2**, **3** and **4** represent examples of multiredox molecular squares. The paper also reports a study of their redox behaviour as well as the luminescence properties of **4**.

Results and Discussion

Synthesis and Characterization

$[Rh_2(form)_2(dicarboxylate)]_4$: Treatment of $[Rh_2(form)_2(CF_3COO)_2(H_2O)_2]$ with an excess of terephthalate (tp) or oxalate (ox) disodium salts results in the formation of $[Rh_2(form)_2(tp)]_4$ (**2**) or $[Rh_2(form)_2(ox)]_4$ (**3**) in good yields. Both the compounds are green stable solids, which we were unable to obtain in a suitable crystalline form. Their solution behaviour and their spectroscopic features closely resemble those of the parent dinuclear species, **1**.[3] IR and proton NMR spectroscopic data unambiguously show that the formamidinate and carboxylate groups are coordinated

[a] Dipartimento di Chimica Inorganica, Chimica Analitica e Chimica Fisica, Università di Messina,
Salita Sperone n. 31, 98166 Vil. S. Agata, Messina, Italy
E-mail: loschiavo@chem.unime.it
[b] Centro Internazionale di Servizi di Spettrometria di Massa del C.N.R.,
Via P. Castellino 111−80131 Napoli, Italy

 © WILEY-VCH Verlag GmbH, D-69451 Weinheim, 2000 1434−1948/00/0606−1371 $ 17.50+.50/0

in the usual way, namely symmetrically bridged across the Rh_2^{4+} core. The proposed structures for **2** and **3** (Figure 1) were determined by elemental analysis and LSI MS spectrometry. Mass spectrometry using different "soft" ionisation techniques, namely LSI, ESI (electrospray ionisation) and MALDI (matrix assisted laser desorption) is currently used, in the absence of X-ray data, as a powerful tool for establishing the structure of compounds of this type.[1,6]

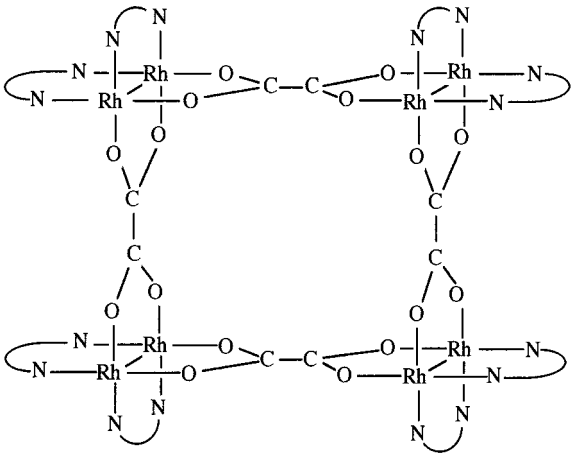


Figure 1. Proposed structure for $[Rh_2(form)_2(ox)]_4$ (**3**)

The positive ion LSI mass spectrum of **2** yields an abundant protonated molecular ion (MH^+) peak at *m/z* = 3265.5 (the *m/z* values reported here are the measured isotopically resolved, ^{12}C-containing, monoisotopic mass-to-charge ratios) corresponding to the expected $[Rh_2(form)_2(tp)]_4H^+$ composition. The loss of one or two hydrogen atoms from MH^+ can be observed with relative abundances of 50 and 15 percent to the monoisotopic molecular ion peak, respectively. This was to be found characteristic of all the three compounds investigated here. The loss of hydrogen is a frequently observed fragmentation process for molecules under conditions of liquid secondary ionization. This determines a difference in the appearance of the isotope peak cluster with respect to that theoretically expected.[7] The spectrum also shows less abundant peaks, with $[Rh_2(form)_2(tp)]_3H^+$ and $[Rh_2(form)_2(tp)]_2H^+$ compositions, at *m/z* = 2449.5 and 1633.3, respectively, which could be indicative of a systematic fragmentation of the molecule upon ionization, or, in the light of recent reports, of the presence of by-products in the sample.[2]

The LSI MS spectrum of **3** results in a base peak at *m/z* = 2961.3 (MH^+), with an isotopic distribution consistent with the expected protonated molecular ion with hydrogen loss. In this case a probe-accurate mass measurement on the MH^+ peak cluster was performed. The exact mass of the monoisotopic molecular ion peak was measured to be 2961.1581 (theoretically calculated mass is 2961.1587 for $C_{128}H_{121}N_{16}O_{16}Rh_8$ with an error of 0.2 ppm) again giving evidence for hydrogen loss. A doubly charged molecular ion (MH_2^{2+}) is also found at *m/z* = 1482.7. Analogously to the spectrum of **2**, peaks with lower abundance, corresponding to $[Rh_2(form)_2(ox)]_2H^+$ and $[Rh_2(form)_2(ox)]_3H^+$, are observed at *m/z* = 1481.2 and 2221.0, respectively.

$[Rh_2(form)_2(dicarboxylate)]_2$: We also turned our attention to self-assembly of the $Rh_2(form)_2$ fragments with functionalized porphyrins which, in the past, have been successfully used both as linear and angular connectors.[8,9] In particular we planned the synthesis of molecular boxes of lower nuclearity by combining two angular building units such as $[Rh_2(form)_2]$ and 15,20-di-(4-carboxyphenyl)-5,10-diphenylporphyrin.

$[Rh_2(form)_2(CF_3COO)_2(H_2O)_2]$ reacts with the disodium salt of 15,20-di-(4-carboxyphenyl)-5,10-diphenylporphyrin affording the complex $[Rh_2(form)_2(porphy\{COO\}_2)]_2$ (**4**) (Figure 2).

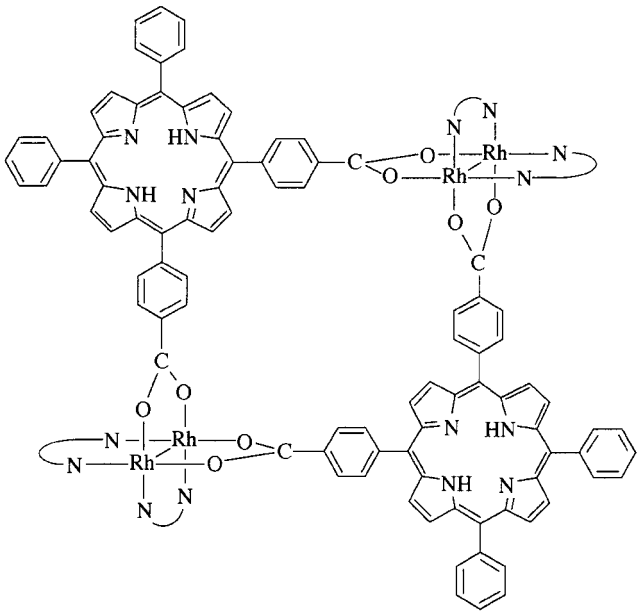


Figure 2. Proposed structure for $[Rh_2(form)_2(porphy\{COO\}_2)]_2$ (**4**)

Compound **4** is a dark red-brown microcrystalline solid very soluble in benzene and chlorinated solvents and sparingly soluble in coordinating solvents. ^1H NMR and IR spectroscopic data were consistent with the proposed structure. Even in this case LSI MS mass spectrometry was employed to assess the nuclearity of **4** (Figure 3). The mass spectrum yields the molecular ion peak (MH^+) at *m/z* = 2705.7, with a good isotopic resolution, as shown in Figure 3. No other significant peak is noted in the spectrum. The slight difference in the measured isotopic distribution with respect to the theoretical pattern of MH^+ rises from the loss of one or two hydrogen atoms from MH^+, as already observed in the mass spectra of **2** and **3**.[7]

Electrochemistry

The electrochemical data for this new family of molecular squares are collected in Table 1, together with those of the parent complex **1**, $[Rh_2(form)_4]$ and the uncoordinated porphy$(COO)_2$ ligand. The cyclic voltammograms of all the compounds are shown in Figure 4.

As shown in Figure 4a, the macrocycle **3** undergoes three reversible oxidations. A cursory look at the data reported

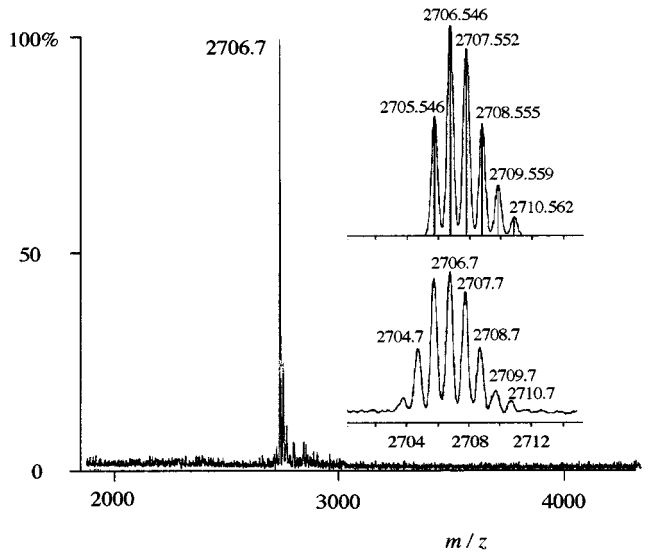


Figure 3. LSI mass spectrum of **4**, including the calculated (top) and experimental (bottom) isotopic distribution of MH^+

Table 1. Redox data; experiments were performed in argon-purged 1,2-dichloroethane solutions; all the processes are reversible except where otherwise noted; the number of exchanged electrons are reported in brackets

Compound	Oxidation (V vs. SCE)[a]		Reduction (V vs. SCE[a])
3	+0.42,[2] +0.57[2]	+1.41[4]	
2	+ 0.43[4]	+1.30[4]	
4	+0.38,[2] +1.11[b]	+1.37[b]	−1.12[2]
1[c]	+0.59[1]	+1.40[1]	
$[Rh_2(form)_4]$[c]	+0.12	+0.95	
$Porphy(COO)_2$[d]	+1.10[b]		−1.18[b]

[a] $E_{1/2}$ values are reported for reversible processes and E_{peak} values are reported for irreversible processes. – [b] Irreversible process. – [c] Data obtained in dichloromethane solution. The two one-electron reversible oxidations of **1** and $[Rh_2(form)_4]$ are due to Rh_2^{4+}/Rh_2^{5+} and Rh_2^{5+}/Rh_2^{6+} processes, respectively.[10] – [d] The oxidation and reduction processes of the uncoordinated porphyrin are centered in the π and π* molecular orbitals of the porphyrin framework, respectively.

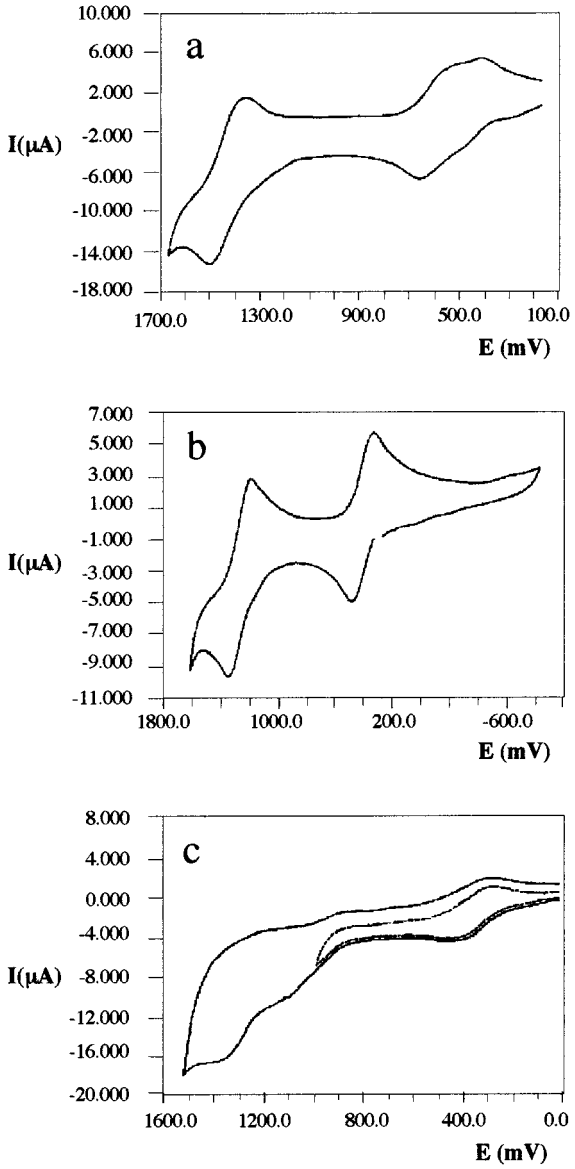


Figure 4. Cyclic voltammograms of **3** (a), **2** (b), and **4** (c); for **4** the CV obtained by scanning the potential up to +1 vs. SCE is also shown to underline the increase of the reversibility of the first process in the absence of the second and third oxidations

in Table 1 allows us to assign the first two anodic processes to the Rh_2^{4+}/Rh_2^{5+} oxidation and the third one to Rh_2^{5+}/Rh_2^{6+}. It is interesting to note that the two bielectronic Rh_2^{4+}/Rh_2^{5+} oxidation processes occur at very close potential values. These anodic processes are shifted to lower potentials with respect to that of **1** and significantly higher with respect to that of $[Rh_2(form)_4]$ as a consequence of the different electron richness of the complexes.[10] Most likely, the first dirhodium units to be oxidized are at opposite corners of the box, with no electronic interaction between them: therefore, the process at +0.42 V is best described as a two simultaneous one-electron process involving noninteracting units.[11] The CV response of **4** (Figure 4c), which does not show splitting of the Rh_2^{4+}/Rh_2^{5+} oxidation processes, supports this suggestion. The following oxidation (+0.57 V) may be assigned to two simultaneous one-electron processes involving the unoxidized Rh_2^{4+} units, whose value is displaced to more positive potential because of the interactions with the nearby Rh_2^{5+} corners. The third oxidation (+1.41 V) can be assigned to four simultaneous one-electron processes involving all the Rh_2^{5+} units and leading to Rh_2^{6+} species. This oxidation pattern suggests that the electronic interaction among Rh_2^{4+} units in the molecular square is larger than that among the Rh_2^{5+} ones.

The CV pattern of **2** (see Figure 4b) resembles that of the parent complex **1** and $[Rh_2(form)_4]$ and is significantly different from **3**. The CV and DPV experiments indicate two quantitatively identical processes, arising from two successive series of four simultaneous one-electron oxidations leading to Rh_2^{5+} and Rh_2^{6+} species, respectively. The decreased interaction between the Rh_2^{4+} units in **2** with respect to **3**, evidenced by the absence of the splitting of the Rh_2^{4+}/Rh_2^{5+} processes, reflects the larger distance between the dirhodium units.

On the basis of the assignment of the CV response given by **2** and **3** and porhy$(COO)_2$, the redox behaviour of **4** appears straightforward (Figure 4c). The first oxidation is reasonably assigned to two simultaneous Rh_2^{4+}/Rh_2^{5+} processes, the second one to the oxidation of both porphyrins, and the third one to the simultaneous Rh_2^{5+}/Rh_2^{6+} oxidation processes of the Rh_2 cores. Although a precise estimation of the exchanged electrons cannot be obtained for the second and third oxidations because of their irreversible nature, an analysis of the intensity of the cathodic peaks suggests that these processes also involve two electrons each. The irreversibility of the Rh_2^{5+}/Rh_2^{6+} process in **4** is probably a consequence of the irreversible porphyrin-based oxidation which precedes such a process. The reduction process of **4** is easily assigned as a porphyrin-based process, on the basis of the reduction behaviour of the uncoordinated porphyrin (Table 1).

Luminescence

Complexes **1**, **2**, and **3** are not emissive in fluid solution at room temperature. On the contrary, however, compound **4** exhibits a room-temperature emission with maxima at $\lambda = 648$ nm and $\lambda = 712$ nm, assigned to the porphyrin units.[12] Interestingly, such an emission is strongly reduced ($\Phi = 7 \times 10^{-5}$; $\tau < 500$ ps, which is the limit of our apparatus) with respect to the free porphyrin emission ($\Phi = 0.017$; $\tau = 10$ ns), although it is spectrally identical. The luminescence decrease can most likely be attributed to reductive electron-transfer quenching of the porphyrin excited state by the dirhodium units. This process is indeed exoergonic, by about 0.4 eV, on the basis of redox and photophysical data.[13] The rate constant of the process, calculated by taking into account the luminescence quantum yields of **4** and the free porphyrin, and the luminescence lifetime of the free porphyrin, is of the order of 10^{11} s^{-1}, in agreement with literature data concerning electron transfer at relatively short distances.[14]

Conclusions

As a final comment we would like to underline that dirhodium(II,II) compounds appear to be suitable substrates for the construction of molecular squares and, by exploiting their well-known axial reactivity, to connect these to form square channels.

Furthermore, besides providing angular building blocks, they may also be used as *exo*-bidentate building blocks linking angular species through their two axial coordination sites. This synthetic strategy opens the way to the construction of a large variety of dirhodium(II,II) based molecular boxes simply varying the angular connectors.

Experimental Section

Materials: The starting complex $[Rh_2(form)_2(CF_3COO)_2(H_2O)_2]$ was prepared according to a published procedure.[3] The 15,20-di-(4-carboxyphenyl)-5,10-diphenylporphyrin was purchased from Mid-Century Company, Illinois. All other chemicals are commercially available and were used as supplied. None of the compounds reported here are air sensitive, but all reactions were carried out under an atmosphere of dry nitrogen. Elemental analyses were performed by REDOX snc Laboratorio di Microanalisi, Cologno Monzese (Milano), Italy.

Apparatus: Infrared spectra were recorded as KBr pellets with a Perkin−Elmer FT 1720X spectrometer. Electronic absorption spectra were recorded on a Perkin−Elmer Lambda 5 UV/Visible spectrophotometer. The NMR measurements were performed with a Bruker AMX 300 spectrometer using standard pulse sequences. Liquid secondary ion mass spectrometry (LSI MS) experiments were carried out on a VG-ZAB-T (Micromass, Wythenshawe, Manchester, U.K.) four-sector mass spectrometer equipped with a 40 kV caesium ion gun. Ionization was achieved by bombardment of 30 keV of caesium ions. Samples were dissolved in chloroform. Mass spectra were obtained employing 1μL of *m*NBA matrix followed by careful addition of 1 μL sample solution on the probe. The spectra were recorded in the positive ion mode at 8 kV accelerating potential. The resolution was set to 2500 (static resolution measured at 5% valley definition), mass range was $m/z = 1500-4200$ with a scan rate 8 s $decade^{-1}$. Ions were detected by a photomultiplier detector and acquisitions were performed in continuum mode using the OPUS V3.1X software. Calibration of the mass scale was carried out on the cluster peaks of CsI. The average error was measured to be less than 0.2 Da for the entire mass range. Probe-accurate mass measurement was performed using a slow linear voltage scanning at 8000 resolution and applying polyethylene glycol as internal calibrant.

Electrochemical measurements were carried out in argon-purged 1,2-dichloroethane at room temperature with a PAR 273 multipurpose equipment interfaced to a PC. The working electrode was a glassy carbon (8 mm^2, Amel) electrode. The counter electrode was a Pt wire, and the quasi-reference electrode was an Ag wire (ferrocene was used as internal standard). The concentration of the complexes was about 5×10^{-4} M. Tetrabutylammonium hexafluorophosphate was used as supporting electrolyte and its concentration was 0.05 M. Cyclic voltammograms were obtained at scan rates of 20, 50, 200, and 500 mV/s. For reversible processes, half-wave potentials (vs. SCE) were calculated as the average of the cathodic and anodic peaks. The criteria for reversibility were the separation between cathodic and anodic peaks, the close to unity ratio of the intensities of the cathodic and anodic currents, and the constancy of the peak potential on changing scan rate. For irreversible processes, the values reported in Table 1 are the peaks estimated by differential pulse voltammetry (DPV). The number of exchanged electrons was measured with differential pulse voltammetry (DPV) experiments performed with a scan rate of 20 mV/s, a pulse height of 75 mV, and a duration of 40 ms. Experimental error on the redox potentials is ± 10 mV.

The luminescence experiments were performed in air-equilibrated dichloromethane solution at 298 K. Luminescence spectra have been obtained with a Jobin Yvon-Spex Fluoromax 2 fluorimeter. The spectra were corrected for detector response. Luminescence lifetimes were measured with an Edinburgh FL 900 time-correlated single-photon-counting spectrometer, with nitrogen discharge as the excitation pulse and using a Marquadt algorithm for pulse deconvolution. Luminescence quantum yields have been calculated by the optically diluted method,[15] using $Ru(bpy)_3^{2+}$ as quantum yield standard ($\Phi = 0.028$) in air-equilibrated aqueous solution.[16]

Experimental uncertainties on luminescence spectra, lifetimes and quantum yields are ± 2 nm, 10%, and 20%, respectively.

Syntheses

$[Rh_2(form)_2(tp)]_4$ (2): To an aqueous solution (40 mL) of disodium terephthalate (0.300 g, 1.43 mmol) was added a chloroform/acetone solution (1:3, 20 mL) of **1** (0.200 mg, 0.218 mol) and the resulting mixture left to stir for ca. 24 h. After this time the organic volatiles were removed on a rotary evaporator and the green solid was collected by filtration, washed several times with warm water and methanol and dried. The crude green solid was then dissolved in $CHCl_3$ (30 mL) and filtered through Celite. Addition of *n*-hexane (20 mL) to the filtrate afforded **2** (0.156 g, 0.048 mmol) as a green precipitate in 88% yield. − $C_{38}H_{34}N_4O_4Rh_2$: calcd. C 55.9, H 4.20, N 6.86; found C 55.64, H 4.30, N 6.88. − IR (KBr): $\nu_{asym}(CO_2)$ = 1620 (s), ν(N−C−N) = 1591 cm^{-1} (s). − UV/Vis ($CHCl_3$): λ_{max} = 520, 630. − LSI MS: *m/z* (%) = 3265.5 (100) [MH^+], 2449.5 (10) [$\{Rh_2(form)_2(tp)\}_3H^+$], 1633.3 (10) [$\{Rh_2(form)_2(tp)\}_2H^+$].

$[Rh_2(form)_2(ox)]_4$ (3): Complex **3** was prepared by following the same procedure as used for **2**. Yield 80%. − $C_{32}H_{30}N_4O_4Rh_2$: calcd. C 51.91, H 4.08, N 7.57; found C 51.95, H 4.44, N 7.26. − IR (KBr): $\nu_{asym}(CO_2)$ = 1626 (s), ν(N−C−N)= 1598 cm^{-1} (s). − UV/Vis ($CHCl_3$): λ_{max} = 625. − ^1H NMR ($CDCl_3$): δ = 2.23 (s, 12 H, CH_3), 6.80 (dd, *J* = 19.4 and 7.9 Hz, 16 H, H_{tol}), 7.41 (t, br, 2 H, N−CH−N). − LSI MS: *m/z* (%) = 2961.2 (100) [MH^+], 1482.7 [MH_2^{2+}], 2221.0 (5) [$\{Rh_2(form)_2(ox)\}_3H^+$], 1481.2 (5) [$\{Rh_2(form)_2(ox)\}_2H^+$].

$[Rh_2(form)_2(porphy\{COO\}_2)]_2$ (4): To a methanol (20 mL) mixture of 15,20-di-(4-carboxyphenyl)-5,10-diphenylporphyrin (0.120 g, 0.171 mmol) was added an aqueous solution (10 mL) of NaOH (0.015 g, 0.375 mmol). The resulting solution was stirred for ca. 30 min and then filtered. A chloroform solution (10 mL) of **1** (0.110 g, 0.121 mmol) was added dropwise to the filtrate and the resulting mixture left to stir for 24 h. During this time **4** was formed as a dark red-brown solid, which was collected by filtration and crystallized from benzene/*n*-heptane. Yield 55%. − $C_{76}H_{58}N_8O_4Rh_2$: calcd. C 67.96, H 4.32, N 8.28; found C 66.21, H 4.58, N 8.48. − IR (KBr): $\nu_{asym}(CO_2)$ = 1620 (m), ν(N−C−N) = 1594 cm^{-1} (s). − UV/Vis ($CHCl_3$): λ_{max} = 419, 515, 549, 589, 644 nm. − ^1H NMR ($CDCl_3$): δ = −2.85 (s, 2 H), 2.23 (s, 12 H), 7.11 (m, 16 H), 7.79 (m, 10 H), 8.23 (m, 8 H), 8.55 (t, br, 2 H), 8.88 (s, 8 H). − LSI MS: *m/z* (%) = 2705.9 (100) [MH^+].

Acknowledgments

We thank the Italian CNR and the MURST for financial support.

[1] M. Fujita, J. Yazaki, K. Ogura, *J. Am. Chem. Soc.* **1990**, *112*, 5645−5647; P. J. Stang, D. H. Cao, *J. Am. Chem. Soc.* **1994**, *116*, 4981−4982; P. J. Stang, D. H. Cao, S. Saito, *J. Am. Chem. Soc.* **1995**, *117*, 6273−6283; P. J. Stang, D. H. Cao, K. Chen, M. Gray, D. C. Muddiman, R. D. Smith, *J. Am. Chem. Soc.* **1997**, *119*, 5163−5168; P. J. Stang, K. Chen, *J. Am. Chem. Soc.* **1995**, *117*, 1667−1668; P. J. Stang, K. Chen, M. Arif, *J. Am. Chem. Soc.* **1995**, *117*, 8793−8797; C. Muller, J. A. Whiteford, P. J. Stang, *J. Am. Chem. Soc.* **1998**, *120*, 9827. Recent review references: B. Olenyuk, A. Fechtenkotter, P. J. Stang, *J. Chem. Soc., Dalton Trans.* **1998**, 1707−1729; M. Fujita, *Chem. Soc. Rev.* **1998**, 417−425.

[2] F. A. Cotton, L. M. Daniels, C. Lin, C. A. Murrillo, *J. Am. Chem. Soc.* **1999**, *121*, 4538−4539; J. L. Heinrich, P. A. Berseth, J. R. Long, *Chem. Commun.* **1998**, 1231−1232; P. Thuéry, M. Nierlich, B. W. Baldwin, N. Komatsuzaki, T. Hirose, *J. Chem. Soc., Dalton Trans.* **1999**, 1047−1048; H. Rauter, I. Mutikainen, M. Blomberg, C. J. L. Lock, P. Amo-Ochoa, E. Freisinger, L. Randaccio, E. Zangrando, E. Chiarparin, B. Lippert, *Angew. Chem. Int. Ed. Engl.* **1997**, *36*, 1296−1301.

[3] P. Piraino, G. Bruno, G. Tresoldi, S. Lo Schiavo, P. Zanello, *Inorg. Chem.* **1987**, *26*, 91−96.

[4] P. Piraino, G. Bruno, S. Lo Schiavo, F. Laschi, P. Zanello, *Inorg. Chem.* **1987**, *26*, 2205−2211; G. A. Rizzi, M. Casarin, E. Tondello, P. Piraino, G. Granozzi, *Inorg. Chem.* **1987**, *26*, 3406−3409; E. Rotondo, B. E. Mann, P. Piraino, G. Tresoldi, *Inorg. Chem.* **1989**, *28*, 3070−3073; E. Rotondo, G. Bruno, F. Nicolò, S. Lo Schiavo, P. Piraino, *Inorg. Chem.* **1991**, *30*, 1195−1200; P. Piraino, G. Tresoldi, S. Lo Schiavo, *Inorg. Chim. Acta.* **1993**, *203*, 101−105; G. Bruno, G. De Munno, G. Tresoldi, S. Lo Schiavo, P. Piraino, *Inorg. Chem.* **1992**, *31*, 1538−1540; S. Lo Schiavo, M. S. Sinicropi, G. Tresoldi, C. G. Arena, P. Piraino, *J. Chem. Soc., Dalton Trans.* **1994**, 1517−1522; G. Tresoldi, G. De Munno, F. Nicolò, S. Lo Schiavo, P. Piraino, *Inorg. Chem.* **1996**, *35*, 1377−1381.

[5] S. Lo Schiavo et al., manuscript in preparation.

[6] T. G. Schaaff, Y. Qu, N. Farrell, V. H. Wysocki, *J. Mass Spectrom.* **1998**, *33*, 436−443; J. Manna, C. J. Kuehl, J. A. Whiteford, P. J. Stang, D. C. Muddiman, S. A. Hofstadler, R. D. Smith, *J. Am.Chem. Soc.* **1997**, *119*, 11611−11619.

[7] K. Vekey, *Int. J. Mass Spectrom. Ion Proc.* **1990**, *97*, 265−282; K. Vekey, L. F. Zerilli, *Org. Mass Spectrom.* **1991**, *26*, 939−944.

[8] C. M. Drain, J.-M. Lehn, *J. Chem. Soc., Chem. Commun.* **1994**, 2313−2315.

[9] P. J. Stang, J. Fan, B. Olenyuk, *Chem. Commun.* **1997**, 1453−1454.

[10] S. Lo Schiavo, G. Bruno, P. Zanello, F. Laschi, P. Piraino, *Inorg. Chem.* **1997**, *36*, 1004−1012.

[11] J. B. Flanagan, S. Margel, A. J. Bard, F. C. Anson, *J. Am. Chem. Soc.* **1978**, *100*, 4248−4253.

[12] K. Kalyanasundaram, *Photochemistry of Polypyridine and Porphyrin Complexes*, Academic Press, London, UK, **1992**.

[13] The driving force Δ*E* for the reductive electron-transfer quenching has been calculated by applying the equation $\Delta E = e(E_{ox} - {}^*E_{red})$, where work terms and entropy contributions are neglected. E_{ox} is the oxidation potential of the dirhodium subunits and $^*E_{red}$ is the excited-state reduction potential of the porphyrin units in **4**. In turn, $^*E_{red}$ is obtained by the equation $^*E_{red} = E_{red} + E_{00}$, where E_{00} stands for a potential corresponding to the excited state energy, taken as the highest-energy feature of the emission spectrum.[12]

[14] M. R. Wasielewski, *Chem. Rev.* **1992**, *92*, 435−461.

[15] J. N. Demas, G. A. Crosby, *J. Phys. Chem.* **1971**, *75*, 991−1008.

[16] K. Nakamaru, *Bull. Chem. Soc. Jpn.* **1982**, *55*, 2697−2705.

Received December 10, 1999
[I99452]

Pentacarbonylhydridochromates $M^+[HCr(CO)_5]^-$: Reactivity in Organic Synthesis and Homogeneous Catalysis

Jean-Jacques Brunet[a]

Keywords: Carbonyl complexes / Hydrido complexes / Homogeneous catalysis / Hydrogenations / Reductions / Chromium

As compared to the main group hydrides (boron, aluminum, ...) and their derivatives, which are very useful *stoichiometric* reagents for selective reductions in organic synthesis, hydrides of transition metals provide the chemist with potential *catalysts* or catalyst precursors. This interesting property is enhanced by the possibility of modifying the coordination sphere, which allows access to a wide variety of hydride complexes with tunable chemical reactivities. Among these, a great variety of carbonylhydridometallates is becoming available and studies of their reactivities continuously appear in the literature. This article reviews the current state of the art as regards the synthesis and reactivity of one of the more promising and versatile carbonylhydridometallates, $[HCr(CO)_5]^-$, the simplest anionic hydride derived from hexacarbonylchromium. Its reactivity in stoichiometric reactions is considered first, and then its generation and involvement as a reactive intermediate in catalytic reactions are reviewed.

1. Introduction

The first preparation of tetracarbonylnickel by Mond in 1890[1] and of pentacarbonyliron by Berthelot[2] and Mond[3] in 1891 are among the first historic landmarks in organotransition metal chemistry.[4] Soon after, extensive work led to the development of the Fischer−Tropsch process[5] and the cobalt-catalyzed oxo process,[6] while many homogeneously catalyzed processes were devised by Reppe's group.[7] Simultaneously, increasing interest in the field of carbonylmetal compounds resulted in the preparation of carbonyl complexes of a large number of transition metals.[8] Subsequently, some derivatives of these carbonylmetal compounds were generated and characterized, including the anionic complexes or "carbonylmetallates". The latter include dianionic carbonylmetallates $[M_x(CO)_z]^{2-}$ {e.g. $[Fe(CO)_4]^{2-}$, the sodium salt of which is commercially available as the Collman reagent[9]} and carbonylhydridometallates $[HM_x(CO)_y]^-$.

From a general point of view, several potential properties of carbonylhydridometallates $[HM_x(CO)_y]^-$ are noteworthy. Firstly, they exhibit reducing properties (as either H^-- or electron-transfer agents). Secondly, they can add to unsaturated carbon−carbon double bonds, generating organometallic derivatives prone to carbon monoxide insertions, thereby allowing access to carbonylated compounds.[10] Last but not least, a great variety of derivatives is a priori available owing to the number of carbonylmetal compounds available. This interest is further increased by the possibility of formally substituting one (or two) carbon monoxide ligand(s), e.g. with phosphanes, or even with chiral phosphanes, giving rise to a wide variety of reagents with tunable reactivities.

Ten years ago, the author published an exhaustive review on the properties and applications in organic synthesis and catalysis of the versatile tetracarbonylhydridoferrates, $M^+[HFe(CO)_4]^-$, which are easily prepared from $Fe(CO)_5$.[11] A further review concerned the coordination chemistry associated with ligand substitution processes in

[a] Laboratoire de Chimie de Coordination du CNRS, UPR 8241, 205 route de Narbonne, 31077 Toulouse Cedex 4, France
E-mail: brunet@lcctoul.lcc-toulouse.fr
Fax: (internat.) + 33-5/61553003



Jean-Jacques Brunet was born in Clermont-Ferrand, France, in 1945. He attended the Faculté des Sciences and the Ecole Nationale Supérieure de Chimie de Clermont-Ferrand, where he received his Chemical Engineering degree in 1968. He obtained his PhD (These d'Etat) in 1972 at the University of Nancy under the supervision of Pr. P. Caubère. In 1985, he joined the Laboratoire de Chimie de Coordination of the CNRS (Toulouse) where he is one of the ten group leaders. His current research interests lie in organometallic chemistry and homogeneous catalysis directed towards organic synthesis, with some emphasis on both carbonylation reactions and on the functionalization of alkenes by hydroamination.

MICROREVIEWS: This feature introduces the readers to the authors' research through a concise overview of the selected topic. Reference to important work from others in the field is included.

 © WILEY-VCH Verlag GmbH, D-69451 Weinheim, 2000 1434−1948/00/0707−1377 $ 17.50+.50/0

$M^+[HFe(CO)_4]^-$.[12] The present review is devoted to the properties and applications in organic synthesis and homogeneous catalysis of the hitherto less well studied pentacarbonylhydridochromates $M^+[HCr(CO)_5]^-$, which are prepared from $Cr(CO)_6$. Some properties of these complexes have already been reported by Darensbourg et al. in 1987 in a more general review dealing with anionic transition metal hydrides.[13]

Hexacarbonylchromium, $Cr(CO)_6$, was first prepared by Job and Cassal in 1927.[14] It is a stable, nonvolatile colorless solid, and is less toxic and easier to handle than the liquid $Fe(CO)_5$.[15] Its synthesis has been improved throughout the years and it is now a commercial product.[8,16] It melts at 130 °C (dec.) and can be purified by sublimation in a static vacuum at 60−70 °C.[17] As in the carbonyliron series, several anionic carbonylchromium complexes are known, including monoanionic carbonylhydridometallates and dianionic carbonylmetallates (Scheme 1).[8]

$[HCr(CO)_5]^-$ $[Cr(CO)_5]^{2-}$

$[HCr_2(CO)_{10}]^-$ $[Cr_2(CO)_{10}]^{2-}$

$[Cr_3(CO)_{14}]^{2-}$

Scheme 1. Main carbonylchromates

The preparation procedures and structural and spectroscopic properties of $[HCr(CO)_5]^-$ salts are summarized below, and then their reactivity in stoichiometric reactions and their involvement in catalytic reactions is considered. The author is obliged to recall that the chemistry of pentacarbonylhydridochromates is largely based on the pioneering work of the groups of M. Y. and D. J. Darensbourg.

2. Preparation Procedures

2.1. Discovery

The first report of an $[HCr(CO)_5]^-$ salt was made by Behrens and Weber in 1957.[18] By protonation of $Na_2Cr(CO)_5$ with an aqueous solution of tris(*o*-phenanthroline)iron(II) sulfate, a crystalline complex could be isolated, which was formulated as $[Fe(o\text{-phen})_3][HCr(CO)_5]_2$ (elemental analysis) [Equation (1) and (2)].

$$Cr(CO)_6 + 2Na \xrightarrow{\text{liq. } NH_3} Na_2[Cr(CO)_5] + CO \quad (1)$$

$$Na_2[Cr(CO)_5] + H_2O \xrightarrow{Fe(phen)_3SO_4} [Fe(C_{12}H_8N_2)_3][HCr(CO)_5]_2 \quad (2)$$

The reaction of $[HCr(CO)_5]^-$ with water was also reported;[18,19] molecular hydrogen was liberated with formation of the hydride-bridged binuclear species $(\mu\text{-}H)[Cr_2(CO)_{10}]^-$, the structure of which was determined later.[20]

It was not until 1981 that salts of $[HCr(CO)_5]^-$ were spectroscopically characterized (IR and ^{1}H-NMR data, vide infra). Darensbourg and Deaton isolated the Et_4N^+ (26% yield) and Ph_4As^+ salts according to the above sequence [Equation (3) and (4)], followed by metathesis with Et_4NBr or Ph_4AsBr.[21]

$$Cr(CO)_6 + Na \xrightarrow{\text{liq. } NH_3} Na_2Cr(CO)_5 \xrightarrow[THF]{\text{recrist.}} [Na(THF)_x]_2Cr(CO)_5 \quad (3)$$

$$[Na(THF)_x]_2Cr(CO)_5 + MeOH \xrightarrow{CH_3CN} [Na][HCr(CO)_5] + MeONa \quad (4)$$

2.2. Preparation Procedures

Three methods have proven successful.

Firstly, a general method based on hydride/labile ligand exchange in Group 6B carbonylmetal derivatives [Equation (5)] has been reported to be feasible for M = Cr (unreported yield).[22]

$$M(CO)_5(pip) + [PPN]^+[BH_4]^- \xrightarrow{THF} [PPN]^+[HM(CO)_5]^- + pip\text{->}BH_3 \quad (5)$$

Secondly, protonation of the mononuclear dianion $[Cr(CO)_5]^{2-}$ has also been developed as a synthetic method [Equation (6) and (7)].[23]

$$Cr(CO)_5(pip) + 2\,Na[C_{10}H_8] \xrightarrow[-78°C]{THF} Na_2[Cr(CO)_5] + pip + 2\,C_{10}H_8 \quad (6)$$

$$Na_2[Cr(CO)_5] + [PPN]^+[I]^- + CH_3OH \xrightarrow[-78°C]{THF} [PPN]^+[HCr(CO)_5]^- + NaI + NaOCH_3 \quad (7)$$

70%

Thirdly, the synthesis of $[HCr(CO)_5]^-$ can be achieved by reaction of hexacarbonylchromium with hydroxide ions. Several preparations have been reported, which differ in the nature of the associated cation.

The reaction of $Cr(CO)_6$ with 2 equiv. of KOH, solubilized by cryptand 222 in THF or CH_3CN, at room temperature has been reported to quantitatively afford the $[HCr(CO)_5]^-$ derivative within minutes, as shown in a simplified manner in Equation (8).[24]

$$Cr(CO)_6 + [K(\text{crypt } 222)]^+[OH]^- \xrightarrow[\text{or } CH_3CN]{THF} [K(\text{crypt } 222)]^+[HCr(CO)_5]^- + CO_2 \quad (8)$$

Phase-transfer of hydroxide ions by a quaternary ammonium salt in a liquid−solid reaction also leads to a rapid synthesis of the $[HCr(CO)_5]^-$ derivative (75% yield), Equation (9).[25] Some amounts (≤ 20%) of the binuclear dianion $[Cr_2(CO)_{10}]^{2-}$ are also formed, which are easily separated by virtue of differences in solubility.

$$Cr(CO)_6 + [Et_4N]^+[HSO_4]^- + 15\ KOH \xrightarrow[60°C,\ 30\ min]{CH_3CN/H_2O} [Et_4N]^+[HCr(CO)_5]^- \quad (9)$$

The potassium salt $[K]^+[HCr(CO)_5]^-$ can be prepared by treatment of $Cr(CO)_6$ with KOH (7 equiv.) in a THF/MeOH/H_2O solvent mixture. Yields are in the range

60−70%, but the selectivity $[HCr(CO)_5]^-/[HCr_2(CO)_{10}]^-$ is seemingly difficult to control. Both the water content and the temperature are important factors.[26]

More recently, a rapid and useful preparation of $[K]^+[HCr(CO)_5]^-$ has been reported, which is carried out in a CH_2Cl_2/EtOH solvent mixture at room temperature [Equation (10)].[27] The advantages of this procedure are its high reproducibility (70−78% yield from each of 30 runs) and the fact that only 2 equiv. of KOH are needed, in accordance with the stoichiometry.

$$Cr(CO)_6 + 2\ KOH \xrightarrow[\text{RT, 10 min}\ \text{evaporation}]{CH_2Cl_2\text{-}EtOH} [K]^+[HCr(CO)_5]^- + KHCO_3 \quad (10)$$

70-78%

Some amounts of the bridged binuclear hydride $[K]^+[HCr_2(CO)_{10}]^-$ are also formed, which are easily eliminated (together with $KHCO_3$) by filtration of a THF solution. The purity of the thus formed potassium pentacarbonylhydridochromate can easily be verified by ^{1}H-NMR analysis since the chemical shifts of the monomeric and dimeric carbonylmetal hydrides are very different (vide infra, Table 2).

It must be noted that the chemistry of carbonylhydridochromates is characterized by the fact that the dimeric carbonylhydridochromate, $(\mu\text{-H})[Cr_2(CO)_{10}]^-$, acts as a thermodynamic sink. The monomeric hydride, $[HCr(CO)_5]^-$, reacts readily with traces of H^+ to yield the binuclear hydride according to Equation (11)−(13).

$$[HCr(CO)_5]^- + H^+ \longrightarrow H_2Cr(CO)_5 \quad (11)$$

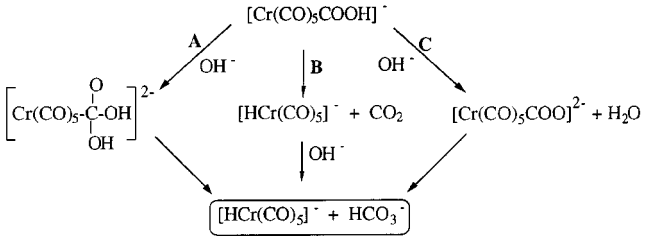
$$H_2Cr(CO)_5 \longrightarrow H_2 + Cr(CO)_5 \quad (12)$$

$$Cr(CO)_5 + [HCr(CO)_5]^- \longrightarrow (\mu H)[Cr_2(CO)_{10}]^- \quad (13)$$

As in the case of $Mo(CO)_6$ and $W(CO)_6$, the mechanism of the reaction of OH^- with $Cr(CO)_6$ is thought to involve a transient metallocarboxylic acid species [Equation (14)].[28]

$$Cr(CO)_6 + OH^- \longrightarrow [Cr(CO)_5COOH]^- \quad (14)$$

Considering the stoichiometry (2 equiv. OH^-) necessary to obtain complete conversion of the hexacarbonylmetal compound, different reaction pathways have been proposed (Scheme 2).[29]



Scheme 2. Mechanisms for the formation of $[HCr(CO)_5]^-$

In aprotic media, pathway A is considered to be the most likely, whereas pathway C should become important in aqueous alcoholic systems.[29] A different mechanism has been proposed for the in situ generation of $[HCr(CO)_5]^-$ under thermal WGSR (water gas shift reaction) conditions, i.e. under CO pressure in basic $MeOH/H_2O$ solutions at elevated temperature, as well as under photocatalyzed WGSR conditions (vide infra).

3. Main Structural and Spectroscopic Properties

3.1. Structure in the Solid State

The first solid-state characterization of a $[HCr(CO)_5]^-$ salt was performed on $[Ph_4P]^+[HCr(CO)_5]^-$.[30] The complex was found to exhibit a pseudooctahedral geometry (Figure 1), with a small *trans* effect of the hydride ligand being evident, the $Cr-C_{trans}$ distance being slightly shorter than the $Cr-C_{cis}$ distance [1.852(4) Å vs. 1.865(4) Å]. The hydride ion is located 1.66(5) Å from the chromium atom. The equatorial carbon monoxide ligands are at 90° angles to one another, but the $(CO)_{eq}-(CO)_{ax}$ bond angle is 95.4°, indicating a substantial bending of the equatorial CO ligands towards the hydride ligand. Nevertheless, this bending is less pronounced than that observed for the equatorial CO ligands in the distorted trigonal bipyramid of $[HFe(CO)_4]^-$, for which the $(CO)_{eq}-(CO)_{ax}$ bond angle is 99.1°.[31]

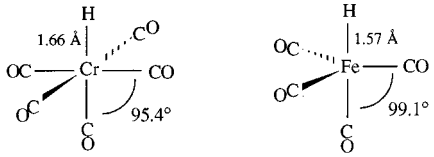


Figure 1. Comparison of solid-state geometries of $[HCr(CO)_5]^-$ and $[HFe(CO)_4]^-$

γ-Irradiated single crystals of $[PPN]^+[HCr(CO)_5]^-$ exhibit persistent anisotropic EPR spectra attributable to the free radical ($S = {}^1/_2$) anion $[Cr(CO)_5]^-$. Measurements of the *g* value and hyperfine interaction anisotropies in crystallographically aligned single crystals at 77 K are consistent with a square-pyramidal geometry for the radical.[32]

3.2. Spectroscopic Properties

3.2.1. Infrared Spectroscopy

It is well known that infrared spectroscopy is particularly useful for analyzing solutions of carbonylmetal compounds and their derivatives. The case of carbonylhydridometallates has been thoroughly studied by Darensbourg et al., whereby evidence for ion-pairing effects was found.[13]

As in the case of similar carbonylhydridometallates, e.g. $[HFe(CO)_4]^-$, no ν(M−H) band is observed. The IR spectrum of $Na^+[HCr(CO)_5]^-$ consists of one strong band (E vibration mode) at 1884 cm^{-1} (four equatorial CO ligands), one medium band ($A_1{}^1$) at 1854 cm^{-1} (CO *trans* to the hydride) with a shoulder at 1894 cm^{-1}, a weak band at 1814

cm^{-1}, and finally a very weak band at 2016 cm^{-1}.[33] Addition of HMPA to a THF solution leads to the disappearance of the band at 1814 cm^{-1} and of the shoulder at 1894 cm^{-1} (with a concomitant increase in the intensity of the 1884 cm^{-1} band), eventually giving the same spectrum as that of $PPN^+[HCr(CO)_5]^-$ (see Table 1).

Table 1. Infrared data for $[M]^+[HCr(CO)_5]^-$

M^+	Solvent	$\tilde{\nu}$(CO) [cm^{-1}] A_1^2 (vw)	E (s)	A_1^1 (m)	Ref.
Li^+	THF	2016	1885	1857	[33]
Na^+	THF	2016	1884 (1894 sh)	1854 (1814 w)	[33]
Na^+/HMPA	THF	2016	1884	1856	[33]
PPN^+	THF	2016	1884	1856	[22]
Et_4N^+	THF	2023	1892	1860	[21]
Ph_4As^+	THF	2020	1889	1860	[21]
[K-crypt]$^+$	CD_3CN	2023	1888	1857	[29]

These observations can be taken as evidence that reversible contact ion pair formation is responsible for the spectral changes. Furthermore, a change in the intensity of the A_1^1 band (CO *trans* to the hydride) has been interpreted in terms of site-specific interaction of the sodium cation with the *axial* CO oxygen atom. It must be noted that in the case of $Na^+[HFe(CO)_4]^-$ evidence has been found for a similar site-selective interaction with an *equatorial* CO oxygen atom (Figure 2).[13]

3.2.2. NMR Spectroscopy

The ^1H- (and ^2H-) NMR chemical shifts of $[HCr(CO)_5]^-$ salts invariably appear at $\delta \approx -7$ and differ considerably from those of the bridged binuclear hydride $[HCr_2(CO)_{10}]^-$ salts ($\delta \approx -20$) (Table 2). This difference is much larger than that between the corresponding mononuclear and binuclear carbonylhydridoferrates [e.g. $NaHFe(CO)_4$: $\delta_H = -8.74$; $NaHFe_2(CO)_8$: $\delta_H = -8.47$].[11]

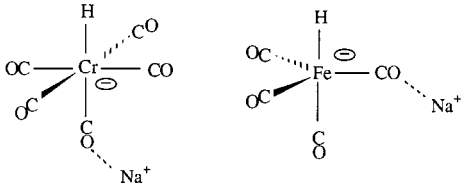


Figure 2. Comparison of Na^+ interactions in solution

Table 2. ^1H-NMR data for $[M]^+[HCr(CO)_5]^-$ and $[M]^+[HCr_2(CO)_{10}]^-$

Compound	Solvent	δ	Ref.
$[Li]^+[HCr(CO)_5]^-$	$[D_8]THF$	−6.80	[33]
$[Na]^+[HCr(CO)_5]^-$	$[D_8]THF$	−6.75	[33]
$[K]^+[HCr(CO)_5]^-$	$[D_8]THF$	−6.7	[26][27]
$[PPN]^+[HCr(CO)_5]^-$	$[D_8]THF$	−6.73	[13][33]
$[PPN]^+[HCr(CO)_5]^-$	CD_3CN	−6.92	[22]
$[Et_4N]^+[HCr(CO)_5]^-$	CD_3CN	−7.0	[21][25]
$[Ph_4As]^+[HCr(CO)_5]^-$	CD_3CN	−7.0	[21]
$[K(crypt)]^+[HCr(CO)_5]^-$	CD_3CN	−7.0	[29]
$[Na]^+[HCr_2(CO)_{10}]^-$	$[D_8]THF$	−19.17	[13][34]
$[K]^+[HCr_2(CO)_{10}]^-$	$(CD_3)CO$	−19.10	[35]
$[K]^+[HCr_2(CO)_{10}]^-$	$[D_8]THF$	−19.53	[27]
$[Et_4N]^+[HCr_2(CO)_{10}]^-$	$[D_8]THF$	−19.47	[13][34]
$[PPN]^+[HCr_2(CO)_{10}]^-$	$[D_8]THF$	−19.50	[36]

A theoretical study aimed at rationalizing the ^1H-NMR chemical shifts of these and other low-valent transition metal hydrides has recently been reported.[37] Calculations based on density functional theory and gauge-including atomic orbitals (DFT-GIAO) were in good agreement with experimental data. The negative "hydridic" shift observed for transition metal hydrides $H-ML_n$ was attributed to a paramagnetic current present in the adjacent ML_n fragment.

The ^{13}C-NMR spectrum of $[PPN]^+[HCr(CO)_5]^-$ under ambient conditions is indicative of a $CO_{cis}-CO_{trans}$ intramolecular exchange process.[22] Thus, at room temperature in CD_3CN, the five CO ligands are apparently equivalent, giving rise to just one signal (at $\delta = 228.7$), whereas at temperatures below 0 °C, two signals are observed, corresponding to four equatorial CO ligands ($\delta = 227.9$) and one axial CO ligand ($\delta = 235.1$). The same phenomenon has been observed for the $[K(crypt)]^+[HCr(CO)_5]^-$ derivative.[29]

4. Reactivity in Stoichiometric Reactions

4.1. Reactions with CO_2, CS_2, and COS

The reaction of $[HCr(CO)_5]^-$ with carbon dioxide has been studied in the context of the water gas shift reaction [Equation (15)].[38]

$$CO + H_2O \rightleftharpoons CO_2 + H_2 \quad (15)$$

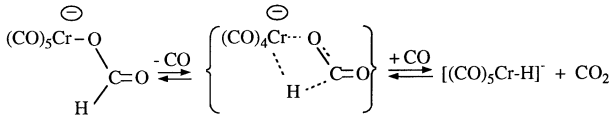
$[K(crypt\ 222)]^+[HCr(CO)_5]^-$ readily reacts with carbon dioxide or carbon disulfide in THF or CH_3CN to yield the corresponding pentacarbonylchromium formate or thioformate [Equation (16)].[24]

$$[HCr(CO)_5]^- + CX_2 \rightleftharpoons [HC(X)XCr(CO)_5]^- \quad (16)$$

The formato derivative (X = O) was shown to be identical to that prepared by the more conventional route [Equation (17)].[39]

$$[PPN]^+[Cr(CO)_5Cl]^- + TlOOCH \xrightarrow{CH_2Cl_2} [PPN^+[HC(O)OCr(CO)_5]^- + TlCl \quad (17)$$

As compared to the tungsten analogue, the pentacarbonylchromium formate exhibits two main characteristics. Firstly, it is readily decarboxylated (25−50 °C) with regeneration of $[HCr(CO)_5]^-$, and secondly, it undergoes rapid CO ligand exchange with free ^{13}CO in solution (80% incorporation within 10 min at room temp.). These observations suggest that CO lability is a requisite step for the rupture of the C−H bond of the formate ligand, leading to decarboxylation and regeneration of $[HCr(CO)_5]^-$ (Scheme 3).[24,29,40]



Scheme 3. Mechanism for the decarboxylation of $[HC(O)OCr(CO)_5]^-$

The reaction with COS proceeds instantaneously in CH_3CN, giving the addition product in which the thioformate ligand is bound to the $[Cr(CO)_6]$ moiety through its sulfur atom [Equation (18)]. This mode of binding has been established by X-ray diffraction analysis of the $[PPN][HC(O)SCr(CO)_5]$ derivative.[29,40]

$$[HCr(CO)_5]^- + COS \xrightarrow{CH_3CN} [HC(O)SCr(CO)_5]^- \quad (18)$$

Alternatively, the pentacarbonylchromium thioformate may be obtained quantitatively by reaction of the formate derivative with COS, Equation (19).[40]

$$[HC(O)OCr(CO)_5]^- + COS \xrightarrow[12h]{CH_3CN} [HC(O)SCr(CO)_5]^- + CO_2 \quad (19)$$

In contrast to its formate analogue, the thioformate complex shows no tendency for COS expulsion (owing to the greater strength of the Cr−S bond) and does not undergo ligand exchange with CO_2 or CS_2. Reaction according to Equation (19) is thus irreversible.

Ab initio calculations seem to indicate that the insertion of CO_2 into the H−Cr bond of $[HCr(CO)_5]^-$ involves an acid−base adduct (η^1-C coordination of CO_2 to the hydride), which is more stable than the reactants. The reaction pathway probably then involves a low-energy cost rearrangement into the η^2-O,H formate structure coupled with simultaneous CO dissociation.[41]

An extension of this facile insertion of CO_2 into $[HM(CO)_5]^-$ led to the catalytic synthesis of alkyl formates (vide infra, Part 5).

4.2. Reaction with Acyl Chlorides

Group 6B transition metal hydrides $[HM(CO)_4L]^-$ (M = Cr, W; L = CO or PR_3) exhibit the interesting property of reducing acyl chlorides to aldehydes without further reduction to the corresponding alcohols [Equation (20)].[42] Such selective reductions have previously been observed using $[HFe(CO)_4]^-$ [43] and $[CpV(CO)_3H]^-$.[44]

$$[PPN]^+[HCr(CO)_5]^- + RCOCl \xrightarrow[25°C]{THF} \underset{90\text{-}95\%}{RCHO} + [PPN]^+[ClCr(CO)_5]^- \quad (20)$$

These reactions are almost quantitative for both aliphatic and aromatic acyl chlorides under mild conditions. Competitive experiments involving the reduction of $PhCH_2COCl$ indicated the reactivity order: $[HW(CO)_5]^- > [HCr(CO)_5]^- > [HFe(CO)_4]^-$, which parallels their hydride-transfer abilities, as established for the reduction of non-hindered alkyl halides (vide infra).[45] Furthermore, it is noteworthy that the reductions with $[HCr(CO)_5]^-$ can be performed in the presence of other reducible functional groups such as aryl bromides, alkyl bromides, or nitroaromatics. For example, 4-bromobutyraldehyde may be obtained in 95% yield from the corresponding acyl chloride. Reduction of the bromo group requires a second equivalent of $[HCr(CO)_5]^-$.

The reagent is also useful for the delivery of deuterium to the aldehydic carbon to give RCDO-type products. Indeed, taking advantage of the facile H/D exchange with CH_3OD of the $[PPN]^+$ salt, Equation (21), the reduction of benzoyl chloride with the reagent prepared in situ from $[PPN]^+[HCr(CO)_5]^-$ and CH_3OD (2-fold molar excess) in THF affords PhCDO [Equation (22)].[46]

$$[PPN]^+[HCr(CO)_5]^- + CH_3OD \rightleftharpoons[THF] [PPN^+[CDCr(CO)_5]^- + CH_3OH \quad (21)$$

$$PhCOCl + [PPN]^+[HCr(CO)_5]^- \xrightarrow[THF]{CH_3OD} PhCDO \quad (22)$$

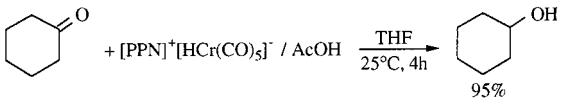
4.3. Reaction with Aldehydes and Ketones

In the course of their study on the selective reduction of acyl halides, Darensbourg et al. also discovered that $[HCr(CO)_5]^-$ is an effective reducing agent for aldehydes *under acidic conditions*.[42] Further studies allowed a determination of the scope and limitations of the stoichiometric reduction of aldehydes and ketones.[47]

$[PPN]^+[HCr(CO)_5]^-$ reacts rapidly with paraformaldehyde in THF (as shown by IR analysis) to yield methanol (98%, 0.5 h) after hydrolysis with a Brønsted acid (AcOH or H_2O). With propionaldehyde or benzaldehyde, only a sluggish reaction is observed. In contrast, rapid reductions to 1-propanol (98%, 1 h) and benzyl alcohol (90%, 1 h) are observed when the reactions are conducted in the presence of acetic acid [Equation (23)].[47]

$$RCHO + [PPN]^+[HCr(CO)_5]^- \xrightarrow[THF]{AcOH} RCH_2OH + [PPN]^+[AcOCr(CO)_4]^- \quad (23)$$
$$R = C_2H_5, C_6H_6$$

Ketones show no reaction with $[PPN]^+[HCr(CO)_5]^-$. However, in the presence of acetic acid, a range of ketones do react at room temperature in THF, cyclohexanone being more easily reduced [95%, 4 h, Equation (24)] as compared to acetophenone (45%, 72 h) and norbornanone (50%, 8 h, *endo* alcohol).



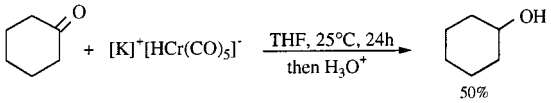
(24)

Where long reaction times are required, a drawback arises from decomposition of the reagent through H_2 elimination [Equation (25)].

$$[HCr(CO)_5]^- + AcOH \longrightarrow H_2 + [AcOCr(CO)_5]^- \quad (25)$$

With regard to the reaction mechanism, it has been shown that the reductions are not affected by the presence of an excess of the CO ligand (saturated THF solution). It was thus proposed that the ketone carbonyl group must be activated (H^+ assistance) towards nucleophilic attack by $[HCr(CO)_5]^-$. Similar K^+ assistance has been demonstrated for the reduction of ketones by hydrido(phosphane)ruthenate complexes.[48]

These conclusions are relevant to the recent observation that, in contrast to the $[PPN]^+$ salt, the potassium salt $[K]^+[HCr(CO)_5]^-$ does react with cyclohexanone *in the absence* of acid.[49] The stoichiometric reaction of $[K]^+[HCr(CO)_5]^-$ with cyclohexanone at room temperature in THF leads, after hydrolysis, to cyclohexanol (50% yield, 24 h) [Equation (26)].



(26)

However, the yield could not be increased by using longer reaction times (120 h). Spectroscopic analysis of the reaction medium prior to hydrolysis indicated that free cyclohexanol was already present. These observations were rationalized in terms of the consumption of $[HCr(CO)_5]^-$ by in situ reaction with an intermediate alkoxochromate, $[RR'CHOCr(CO)_5]^-$,[50] yielding cyclohexanol and $[Cr_2(CO)_{10}]^{2-}$. As previously proposed by Marko et al. (vide infra),[51] $[HCr(CO)_5]^-$ is thus believed to act both as a hydride and a proton donor. These hypotheses have been used to design a system for the catalytic reduction of ketones in the presence of a hydrogen-transfer agent $[KHCr(CO)_5/HCO_2H/Et_3N]$ (vide infra, Part 5).[49]

4.4. Reaction with Organic Halides

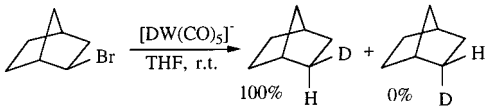
Darensbourg et al. reported a thorough study of the reactivities of anionic transition metal (Groups 6B and 8) hydrides.[52] They compared the reactivities of $[HM(CO)_4L]^-$ compounds (M = Cr, W; L = CO, PR_3) with those of $[HM(CO)_3L]^-$ analogues (M = Fe, Ru; L = CO, PR_3) in the reduction of primary, secondary, and tertiary alkyl halides. For the reaction with *n*BuBr, the following reactivity order was established [P = $P(OMe)_3$]:

$[HW(CO)_4P]^- > [HCr(CO)_4P]^- > [HW(CO)_5]^- > [CpV(CO)_3H]^- > [HCr(CO)_5]^- > [HRu(CO)_4]^- >$ *trans*-$[HFe(CO)_3P]^- >> [HFe(CO)_4]^-$ (no reaction)

This order compares well with the well-known nucleophilicity scale devised by Dessy, Pohl, and King for the series of simple transition metal carbonyl anions:[53]

$[CpFe(CO)_2]^- > [CpRu(CO)_2]^- > [CpNi(CO)]^- > [Re(CO)_5]^- > [CpW(CO)_3]^- > [Mn(CO)_5]^- > [CpMo(CO)_3]^- > [CpCr(CO)_3]^- > [Co(CO)_4]^-$

The Group 6B hydrides are efficient hydride-transfer agents towards a wide variety of C−X bonds, including tertiary centers and aromatic C−X bonds.[52] Interestingly, from a synthetic point of view, they tolerate the presence of functionalities such as nitro groups, ketones, and aldehydes. The convenient in situ method for H/D exchange allows deuterium labelling of the resulting alkane without isolation of the transition metal deuteride [Equation (27)].



(27)

The propensity for H^- transfer (vs. the SET process) could also be correlated with the propensity for $Na^+\cdots HM^-$ interaction (vs. the tendency for $Na^+\cdots OC-M^-$ interaction), whereby a useful general scale was established:

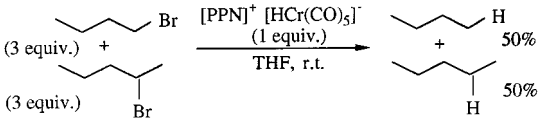
Increasing propensity for H^- transfer:

$[HFe(CO)_4]^- \rightarrow [HV(CO)_3]^- \rightarrow [HCr(CO)_5]^- \rightarrow [HW(CO)_5]^- \rightarrow [HCr(CO)_4P(OMe)_3]^- \rightarrow [HW(CO)_4P(OMe)_3]^-$.

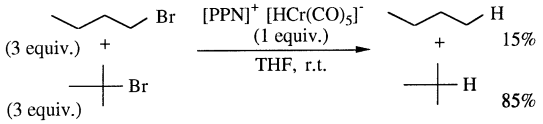
Increasing propensity for SET processes:

$[HW(CO)_4P(OMe)_3]^- \rightarrow [HCr(CO)_4P(OMe)_3]^- \rightarrow [HW(CO)_5]^- \rightarrow [HCr(CO)_5]^- \rightarrow [HV(CO)_3]^- \rightarrow [HFe(CO)_4]^-$.

As can be seen, $[HCr(CO)_5]^-$ is placed in the middle of the scale. As a matter of fact, it reacts almost equally well with primary, secondary, and tertiary alkyl bromides. However, in competition experiments it exhibits a preference for tertiary alkyl bromides [Equation (28) and (29)]. No coupling (R−R) or elimination products could be detected.[52]

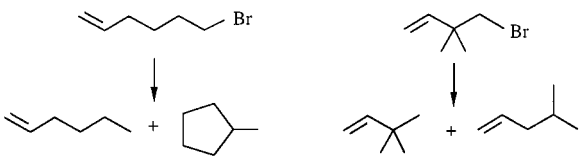


(28)



(29)

A still more interesting quantitative assessment of the competing pathways (ionic H^- transfer, S_N2, vs. radical chain mechanism, S_H2) was achieved by studying the reaction of $[HM(CO)_5]^-$ complexes with two mechanistic probes, namely 6-bromo-1-hexene and 4-bromo-3,3-dimethyl-1-butene (Scheme 4).[54]



Scheme 4. Possible reduction products from mechanistic probes

Computation of the results indicated the relative contributions of the S_N2 and S_H2 mechanisms given in Table 3.

Table 3. Relative contributions of S_N2 and S_H2 mechanisms to the reactivity of hydridometallates

Hydridometallate	S_H2 vs. S_N2 participation
$[PPN]^+[HCr(CO)_5]^-$	10% S_H2, 90% S_N2
$[PPN]^+[HW(CO)_5]^-$	0.3% S_H2, 99.7% S_N2
$[PPN]^+[HW(CO)_4P(OMe)_3]^-$	0.03% S_H2, 99.97% S_N2

Interestingly, this work also pointed out that the unrearranged reduction products arise from *both* hydride displacement of Br^- (S_N2 path) and direct trapping of the unrearranged radical $R^\cdot$ (S_H2 path).

4.5. Reactivity Towards C=C Double Bonds

No reaction was observed on stirring a THF solution of $[Et_4N]^+[HCr(CO)_5]^-$ at 50 °C under 1 atm of ethylene for 3−4 h.[21]

The reaction of $[PPN]^+[HCr(CO)_5]^-$ with a large excess of acrylonitrile results in quantitative formation of the stable insertion complex, together with large amounts of polymeric materials [Equation (30)]. The regioselectivity of the reaction was ascertained by IR, ^1H- and ^{13}C-NMR spectroscopy.[55]

$$[PPN]^+[HCr(CO)_5]^- + CH_2{=}CH\text{-}CN \xrightarrow[(20\ equiv.)]{THF} CH_3CH(CN)[PPN]^+Cr(CO)_5^- \quad (30)$$

The course of this reaction is unaffected if it is performed under CO (1 atm). Furthermore, the observed second-order kinetics and activation parameters are consistent with an associative hydride-transfer process. For the above reaction, the reactivity order of comparable hydrides $\{[HCr(CO)_5]^- < [HW(CO)_5]^- < [HW(CO)_4P(OMe)_3]^-\}$ is the same as that found for the hydride/halide displacement reactions with organic halides (vide supra).[54]

The reaction of $KHCr(CO)_5$ with *stoichiometric* amounts of α,β-unsaturated ketones and esters has recently been studied.[56] The reaction with mesityl oxide was found to proceed rapidly (within 30 min) at room temperature to selectively afford the corresponding saturated ketone without significant formation of high molecular weight products [Equation (31)]. In this reaction, $KHCr(CO)_5$ proved to be much more reactive than $KHFe(CO)_4$ or $KHCr_2(CO)_{10}$.[49]

$$Me_2C{=}CH\text{-}C(=O)Me + KHCr(CO)_5 \xrightarrow[then\ H_3O^+]{THF,\ r.t.,2h} Me_2CH\text{-}CH_2\text{-}C(=O)Me \quad (31)$$

Methyl acrylate was also found to be rapidly reduced, yielding methyl propionate within 10 min (90% yield). However, in several cases the α,β-unsaturated ketones and esters were only partially reduced to the saturated ketones and high molecular weight products were generated. Interestingly, in the case of methyl acrylate, dimethyl fumarate, and dimethyl maleate, analysis of the reaction mixture prior to hydrolysis revealed the presence of the insertion product (^1H and ^{13}C NMR) [Equation (32)].[56]

$$[K]^+[HCr(CO)_5]^- + CH_2{=}CH\text{-}C(O)OMe \xrightarrow{THF} CH_3CH(C(O)OMe)[K]^+Cr(CO)_5^- \quad (32)$$

4.6. Reactivity Towards C=N Bonds of Imines

Further to their study on the catalytic hydrogenation of imines in MeOH (vide infra, Part 5), Marko et al. reported the stoichiometric reactivity of $[Et_4N]^+[HCr(CO)_5]^-$ towards benzylideneaniline in aprotic solvents.[57]

In MeCN solution, $[Et_4N]^+[HCr(CO)_5]^-$ was found to react with *N*-benzylideneaniline at 75 °C under argon to yield the corresponding amine. Since the conversion did not exceed 50% and IR analysis indicated that the mononuclear hydride had been completely transformed into $[Cr_2(CO)_{10}]^{2-}$, the overall reaction was formulated as shown in Equation (33).[57] Under the same conditions, the binuclear hydride $[Et_4N]^+[HCr_2(CO)_{10}]^-$ proved to be practically inert.

$$PhCH{=}NPh + 2\ [HCr(CO)_5]^- \xrightarrow[75°C]{MeCN} PhCH_2NHPh + [Cr_2(CO)_{10}]^{2-} \quad (33)$$

Although the intermediate addition complex could not be observed experimentally, it was formulated as $[PhCH_2N(Ph)Cr(CO)_5]^-$. In the second step, $[HCr(CO)_5]^-$ may act as a proton donor, affording benzylaniline and the dianionic complex $[Cr_2(CO)_{10}]^{2-}$ in situ.

4.7. Miscellaneous

4.7.1. Reaction with Diselenides

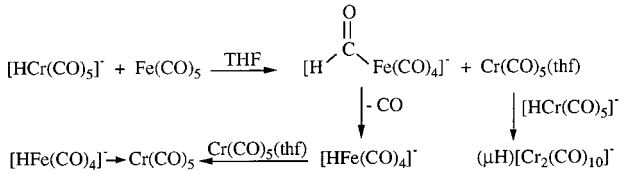
$[PPN]^+[HCr(CO)_5]^-$ reacts with dimethyl (or diphenyl) diselenide by nucleophilic cleavage of the Se−Se bond to yield the corresponding anionic chromium selenate complex [Equation (34)].[58]

$$[PPN]^+[HCr(CO)_5]^- + MeSeSeMe \xrightarrow[r.t.]{THF} \underset{96\%}{[PPN]^+[MeSeCr(CO)_5]^-} + MeSeH \quad (34)$$

4.7.2. Reaction with Electrophilic Metal Carbonyls

As part of their studies on the hydride-transfer abilities of anionic transition metal hydrides, Darensbourg et al. reported the reaction of $[HCr(CO)_5]^-$ with $Fe(CO)_5$.[59]

Whereas no reaction occurs upon mixing $[HFe(CO)_4]^-$ with $Cr(CO)_6$ (THF, room temp.), the reaction of $[HCr(CO)_5]^-$ with $Fe(CO)_5$ yields products resulting from hydride transfer. The formation of the observed products was rationalized on the basis of an ionic mechanism (Scheme 5).

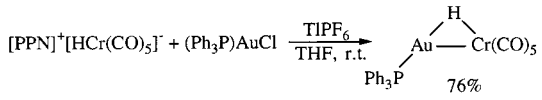


Scheme 5. Reaction of $[HCr(CO)_5]^-$ with $Fe(CO)_5$

The intermediate iron formyl complex, $[(CO)_4FeCHO]^-$, was identified on the basis of its IR and NMR characteristics.[60,61]

4.7.3. Reaction with Au^I and Ag^I Complexes

The reaction of $[HCr(CO)_5]^-$ with the gold(I) complex $(Ph_3P)AuCl$ leads to the formation of a hydrido-bridged heterobimetallic complex [Equation (35)], which has been subjected to single-crystal X-ray diffraction analysis. The three-center two-electron bond is characterized by the following distances: Au−H = 1.72(11) Å, Cr−H = 1.64(12) Å, Au−Cr = 2.770(2) Å.[62]

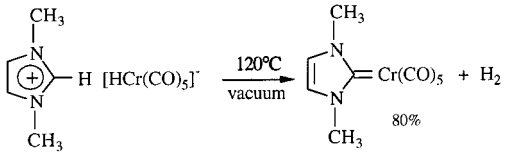


(35)

Similarly, reaction with $(Me_3P)AgI$ yields $(Me_3P)(\mu\text{-}H)AgCr(CO)_5$ in 65% yield.

4.7.4. Reaction with Imidazolium Cations

In 1968, Öfele et al. exploited the acidic nature of imidazolium salts to synthesize the first (diaminocarbene)chromium complex [Equation (36)].[63]



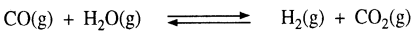
(36)

5. Reactivity in Catalytic Reactions

The pentacarbonylhydridochromate $[HCr(CO)_5]^-$ is involved as a key intermediate in several catalytic reactions, where it plays the role of a species active towards electrophiles. These are summarized below.

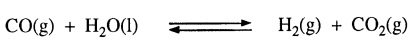
5.1. Water Gas Shift Reaction

The water gas shift reaction (WGSR) [Equation (37)] finds extensive use in industry for hydrogen enrichment of synthesis gas (CO + H_2). Current processes involve the reaction of steam with synthesis gas over iron oxide/chromium oxide or zinc oxide/copper oxide catalyst beds at high temperatures (> 300 °C).[64,65]



(37)

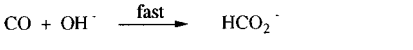
Interestingly, it has been shown that the WGSR can be carried out at lower temperatures (< 200 °C) with water present in liquid form [Equation (38)] by using homogeneous catalysts.[66] The interest in carrying out the WGSR with liquid water rather than steam stems mainly from the considerable energy saving that this would represent.[67]



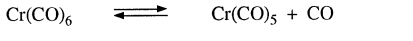
(38)

The WGSR using $Fe(CO)_5$ as a catalyst precursor has been thoroughly studied.[68] Although it soon became apparent that this catalyst was unlikely to have any practical use, due to low turnover, studies of the elementary steps of the catalytic cycle provided very useful information on the reactivity of $[HFe(CO)_4]^-$.[69]

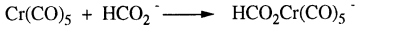
The hexacarbonyls of the Group 6B transition metals (Cr, Mo, W) have also been studied as catalyst precursors for the WGSR.[70] Indeed, it was soon recognized that, in contrast to $Fe(CO)_5$, these catalysts exhibit considerable tolerance to sulfur poisoning, an important attribute in the context of synthesis gas treatment.[71] The catalytic behavior of $Cr(CO)_6$ is representative of that of all three Group 6B hexacarbonylmetal compounds. Turnover numbers as high as 8530 mol H_2/mol $Cr(CO)_6$ per day can be achieved at 200 °C (initial CO pressure 20 bar).[67] These reactions exhibit considerably different kinetics as compared to the situation found in the case of $Fe(CO)_5$ (associative mechanism). Thus, the rate of hydrogen formation is found to be proportional to the amount of $Cr(CO)_6$ and inversely proportional to the CO pressure, and increases with base concentration. The overall kinetics led the authors to propose a dissociative mechanism based on formate decomposition [Equation (39)−(45)].[67]



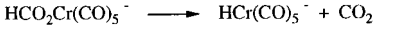
(39)



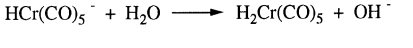
(40)



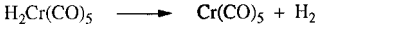
(41)



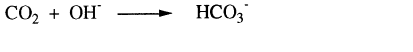
(42)



(43)



(44)



(45)

Most of these elementary steps have been studied independently.[72−76]

However, Darensbourg et al. presented compelling evidence that the *initial* mechanistic step in the *thermal* WGSR by Group 6B carbonylmetal compounds is in fact transition metal activation of CO towards attack by hydroxide ions [Equation (46)].[29][74]

$$Cr(CO)_6 + OH^- \rightleftharpoons [(CO)_5CrCOOH]^- \xrightarrow{OH^-} [(CO)_5CrH]^- + [HCO_3]^- \quad (46)$$

Once the active $[HCr(CO)_5]^-$ is formed, the formato complex $[HCO_2Cr(CO)_5]^-$ could then be generated according to Equation (43), (44), and (41).

The dissociative step [Equation (40)] is certainly involved in the photocatalyzed WGSR.[72][75] It has been shown that UV irradiation ($\lambda < 360$ nm) accelerates the conversion of $Cr(CO)_6$ into the formate complex $[HCO_2Cr(CO)_5]^-$, which is thermally activated, as evidenced by in situ IR and UV spectroscopy. The reaction is inhibited by increased CO pressure. An activation energy of 30 kJ/mol has been determined, as compared to 145 kJ/mol for the purely *thermal* WGSR.[75]

Confirmation of the dissociative mechanism [Equation (40) and (41)] is provided by the observation that $Cr(CO)_6$ is an efficient catalyst precursor for the photocatalytic decomposition of the formate ion into H_2 and CO_2 (or HCO_3^-) [Equation (47)].[76]

$$HCO_2^- + H_2O \xrightarrow[h\nu]{[Cr(CO)_6]} H_2 + HCO_3^- \quad (47)$$

5.2. Catalytic Synthesis of Alkyl Formates from Carbon Dioxide

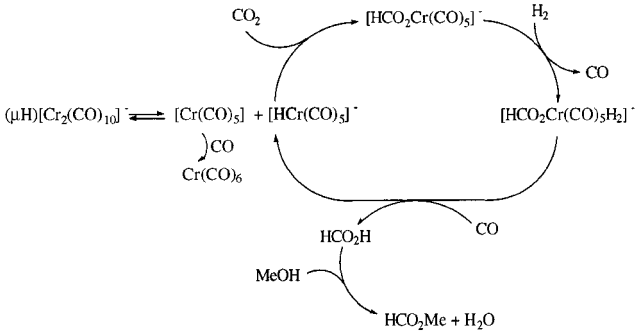
The observation that $[HCO_2M(CO)_5]^-$ complexes (M = Cr, W) undergo facile CO ligand dissociation (vide supra) led Darensbourg et al. to consider these complexes for dihydrogen binding.[77] Indeed, η^2-H_2 bonding has been evidenced (neutron diffraction studies) in some neutral Group 6B transition metal complexes such as $H_2W[P(OMe)_3]_5$.[78] Thus, $[HM(CO)_5]^-$ salts, which readily undergo insertion of CO_2 with generation of the corresponding $[HCO_2M(CO)_5]^-$ complexes, appeared to be good candidates for hydrocondensation reactions of carbon dioxide to yield alkyl formates.

Both $[PPN]^+[HCr(CO)_5]^-$ {generated in situ from $(\mu\text{-}H)[Cr_2(CO)_{10}]^-$} and the formato complex $[PPN]^+[HCO_2Cr(CO)_5]^-$ proved to be effective catalysts for the hydrogenation of CO_2 in methanol to provide methyl formate [Equation (48)]. Typical reaction conditions were a temperarure of 125 °C and loading pressures of CO_2 and H_2 of 250 psi each.

$$CO_2 + H_2 + MeOH \xrightarrow{[cat]} HCO_2Me + H_2O \quad (48)$$

Turnover numbers of 14−15 were achieved in reaction times of 24 h. These activities are higher than those reported for the same reaction using $[PPN]^+[HFe(CO)_4]^-$ or $[PPN]^+[HFe_3(CO)_{11}]^-$ as catalysts.[79]

At the end of catalytic runs, only $[HCO_2M(CO)_5]^-$ and $M(CO)_6$ could be detected by IR spectroscopy. The neutral hexacarbonylmetal compounds $M(CO)_6$ are catalytically inactive under the reaction conditions. One final point is that the catalytic activity was greatly diminished when the reactions were performed in the presence of added CO (100 psi loading pressure). On the basis of these observations, a catalytic cycle was proposed (Scheme 6). The possible formation of methyl formate through carbonylation of methanol (CO originating from the reverse of the WGSR) has been ruled out on the basis of labelling experiments. Methyl formate is formed by a rapid reaction of HCO_2H with methanol.

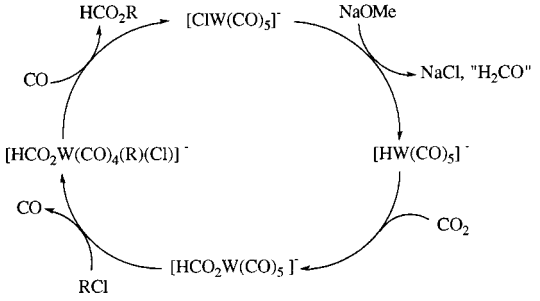


Scheme 6. Catalytic cycle for the formation of methyl formate

The catalytic synthesis of higher alkyl formates can also be performed by the reaction of alkyl halides, CO_2, and H_2 in the presence of anionic Group 6B carbonyl catalyst precursors {$[M(CO)_5Cl]^-$ or $(\mu\text{-}H)[M_2(CO)_{10}]^-$; M = Cr, W} and sodium alkoxides [Equation (49)].[80]

$$RX + CO_2 + H_2 \xrightarrow[NaY]{[cat]} HCO_2R + NaX + HY \quad (49)$$

In these reactions, terminal hydrides $[HM(CO)_5]^-$ are also involved as key intermediates in the generation of formato complexes $[HCO_2M(CO)_5]^-$. In Scheme 7, the proposed catalytic cycle is represented in the case of the tungsten complex.



Scheme 7. Catalytic cycle for the formation of alkyl formates

The intriguing steps of this catalytic cycle are the regeneration of the hydrides from the anionic carbonyl halides [activation of dihydrogen, Equation (50)], the kinetics of which have been studied, and the reaction of the formato

complexes with RX. The latter reaction has been proposed to proceed according to Equation (51)−(53).

$$[ClW(CO)_5]^- + H_2 + NaHCO_3 \longrightarrow [HW(CO)_5]^- + NaCl + H_2CO_3 \quad (50)$$

$$[HCO_2W(CO)_5]^- \rightleftharpoons [HCO_2W(CO)_4]^- + CO \quad (51)$$

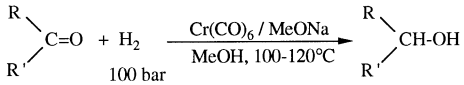
$$[HCO_2W(CO)_4]^- + n\text{BuCl} \longrightarrow HCO_2W(CO)_4(n\text{Bu})(Cl)]^- \quad (52)$$

$$HCO_2W(CO)_4(n\text{Bu})(Cl)]^- \xrightarrow{CO} [Cl(W(CO)_5]^- + HCO_2n\text{Bu} \quad (53)$$

It must be noted that such an oxidative addition of alkyl halides to $[W(CO)_5X]^-$ species [Equation (52)] is without precedent. Nevertheless, this mechanism [Equation (51)−(53)] is consistent with the experimental results.

5.3. Catalytic Hydrogenations of Aldehydes and Ketones

The first report on the use of carbonylchromium derivatives as catalysts for the hydrogenation of ketones was that of Marko et al. in 1985.[51] The hydrogenation of ketones was found to be catalyzed by $Cr(CO)_6$ in the presence of NaOMe in methanol under 100 bar H_2 at 100−120 °C [Equation (54)].



(54)

Both aliphatic and aromatic ketones could be hydrogenated in > 98% yield within 3 h (Table 4). Aromatic aldehydes were also hydrogenated, whereas aliphatic ones proved to be prone to secondary reactions.

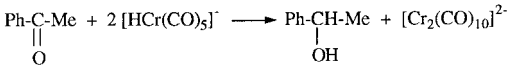
In these reactions, $Cr(CO)_6$ is a more active catalyst precursor than $W(CO)_6$, but less active than $Mo(CO)_6$, which can be used at lower temperatures.

The mechanism of this catalytic reaction has been studied.[51] The stoichiometric reaction of $[Et_4N]^+$-$[HCr(CO)_5]^-$ with acetophenone (no solvent) was monitored by GC and IR analysis. The results were interpreted in terms of Equation (55), where both H atoms involved in the reduction originate from $[HCr(CO)_5]^-$, a proposal that has been criticized,[81] but also seems to be valid for the reduction of cyclohexanone with $[K]^+[HCr(CO)_5]^-$.[49]

Table 4. Hydrogenation of carbonyl compounds in the presence of $Cr(CO)_6$/NaOMe catalyst under H_2 pressure

Carbonyl compound	Conv. to alcohol (%)[a]
acetophenone	99.8
cyclohexanone	100
acetone	100
isobutyl methyl ketone	98.8
benzaldehyde	99.6
methyl benzoate	0
4-*tert*-butylcyclohexanone	99.4[b]

[a] Ketone/$Cr(CO)_6$/NaOMe = 10:0.5:1 mmol in 4 mL MeOH, 100 bar H_2 at 20 °C, 120 °C, 3 h. − [b] *cis*/*trans* = 0.34:1.



(55)

On the basis of these results, it has been proposed that the intermediate is an alkoxocarbonylchromate.[51] Evidence supporting this hypothesis is provided by the stereochemical outcome of the hydrogenation of 4-*tert*-butylcyclohexanone (Table 4). With the catalytic system $Cr(CO)_6$/MeONa, the hydrogenation of 4-*tert*-butylcyclohexanone leads preferentially to the *trans* alcohol (75%). This observation led the authors to suggest that the primary intermediate formed from $[HCr(CO)_5]^-$ and the ketone is an alkoxocarbonylchromate $[RR'CHOCr(CO)_5]^-$. In such a complex, the bulky "$OCr(CO)_5$" group would tend to occupy the less crowded equatorial position of the 4-*tert*-butylcyclohexane ring. Reaction with a second equivalent of $[HCr(CO)_5]^-$ would then liberate the *trans* 4-*tert*-butylcyclohexanol.

In contrast, the analogous $Fe(CO)_5/Et_3N$ system furnishes only 38% *trans* 4-*tert*-butylcyclohexanol. The difference in behavior between $[HCr(CO)_5]^-$ and $[HFe(CO)_4]^-$ in the reactions with ketones stems from the fact that the former is hexacoordinate whereas the latter is only pentacoordinate. The reaction with $[HCr(CO)_5]^-$ may be regarded as a hydride transfer to the carbon atom of the ketone carbonyl group, leading to an alkoxocarbonylchromate $[RR'CHOCr(CO)_5]^-$. In contrast, the reaction with $[HFe(CO)_4]^-$ involves nucleophilic attack of the iron center, leading to an alkyliron hydride $[HFe(CO)_4(RR'CO)]^-$ with an Fe−C bond. These differences in the natures of the catalytic intermediates account for the different stereochemical outcomes in the hydrogenation of 4-*tert*-butylcyclohexanone with the chromium- and iron-based systems.

It has been proposed that in catalytic reactions, $[HCr(CO)_5]^-$ is generated through H_2 activation by the unsaturated species "$[Cr(CO)_5]$" [Equation (56)−(58)].

$$Cr(CO)_6 \rightleftharpoons Cr(CO)_5 + CO \quad (56)$$

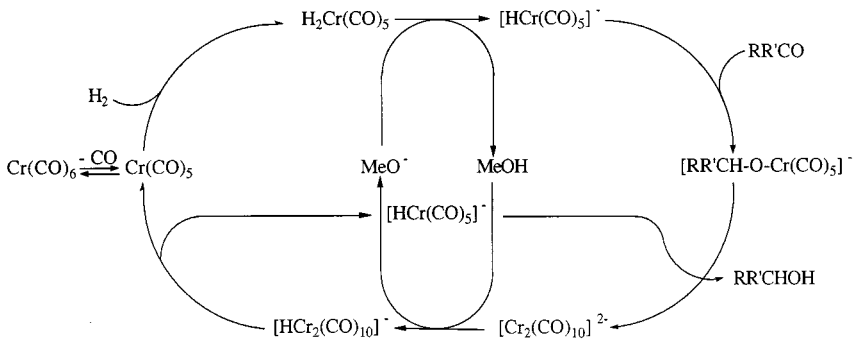
$$Cr(CO)_5 + H_2 \rightleftharpoons H_2Cr(CO)_5 \quad (57)$$

$$H_2Cr(CO)_5 + MeO^- \rightleftharpoons [HCr(CO)_5]^- + MeOH \quad (58)$$

The overall catalytic cycle is shown in Scheme 8.

The same monomeric anionic hydride is considered to be the active species when $[PPN]^+[Cr(CO)_5OAc]^-$ is used as a catalyst precursor.[81] Indeed, the acetatopentacarbonylchromate has been shown to be efficient for the hydrogenation of benzaldehyde and cyclohexanone under hydrogen pressure (47 bar, 125 °C) in THF (turnovers of 16−18 in 24 h).

With this system, generation of the active monomeric hydrido species has been proposed to occur according to Equation (59) and (60).



Scheme 8. Catalytic cycle for the hydrogenation of ketones with $Cr(CO)_6$/MeONa

$$[(CO)_5CrOAc]^- \rightleftharpoons [(CO)_4CrOAc]^- + CO \quad (59)$$

$$[(CO)_4CrOAc]^- \xrightarrow{H_2,\ CO} [HCr(CO)_5]^- + AcOH \quad (60)$$

Mechanistic models of H_2 activation by $[(CO)_4CrOAc]^-$ start with addition to generate an η^2-H_2 complex. Subsequent oxidative addition and reductive elimination would then generate $[HCr(CO)_5]^-$ and AcOH [Equation (60)]. As an alternative, the authors proposed an intramolecular ligand-assisted heterolytic cleavage, as represented in Figure 3.

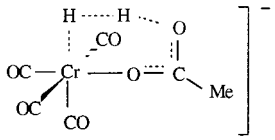
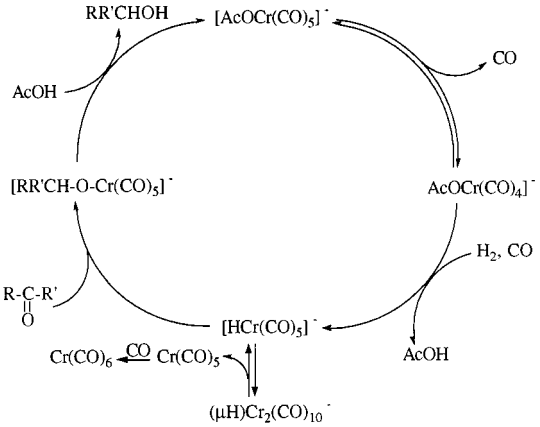


Figure 3. Intramolecular ligand-assisted heterolytic cleavage of H_2

The overall catalytic cycle is represented in Scheme 9. As a matter of fact, the hydrido binuclear complex $(\mu\text{-H})[Cr_2(CO)_{10}]^-$ ("6 o'clock position") is also an active catalyst precursor, albeit a less active one than the acetatocarbonylchromate.



Scheme 9. Catalytic cycle for the hydrogenation of ketones with $[PPN]^+[Cr(CO)_5OAc]^-$

Based on the photocatalytic decomposition of formate ion using $Cr(CO)_6$ (vide supra), in situ generation of $[HCr(CO)_5]^-$ has been used for the catalytic hydrogenation of aldehydes [Equation (61)].[82]

$$RCHO + HCO_2^- + H_2O \xrightarrow[h\nu]{Cr(CO)_6\ /\ MeOH} RCH_2OH + HCO_3^- \quad (61)$$

Typical conditions, for instance in the case of heptanal: aldehyde/HCO_2Na/$Cr(CO)_6$ = 7.2:13:0.12 mmol in 40 mL of 95% aqueous MeOH at 60 °C (60 turnovers in 100 h).

As already stated, the photocatalytic decomposition of formate ion with $Cr(CO)_6$ generates $[HCr(CO)_5]^-$.[76] In the absence of an added substrate, this decomposition reaction produces dihydrogen [Equation (62) and (63)].

$$[HCr(CO)_5]^- + H_2O \longrightarrow H_2Cr(CO)_5 + OH^- \quad (62)$$

$$H_2Cr(CO)_5 \rightleftharpoons Cr(CO)_5 + H_2 \quad (63)$$

In the presence of an aldehyde, the reactive $[HCr(CO)_5]^-$ is diverted (partially or completely) from the above WGSR cycle into an aldehyde hydrogenation cycle. On the basis of kinetic and mechanistic studies, Equation (64)−(67) have been proposed.

$$[HCr(CO)_5]^- + RCHO \rightleftharpoons [HCr(CO)_4(RCHO)]^- + CO \quad (64)$$

$$[HCr(CO)_4(RCHO)]^- \longrightarrow [Cr(CO)_4(OCH_2R)]^- \quad (65)$$

$$[Cr(CO)_4(OCH_2R)]^- + H_2O \longrightarrow [HCr(CO)_4(OCH_2R)] + OH^- \quad (66)$$

$$[HCr(CO)_4(OCH_2R)] + CO \longrightarrow RCH_2OH + Cr(CO)_5 \quad (67)$$

Replacement of one CO ligand of $[HCr(CO)_5]^-$ by the aldehyde [Equation (64)] has been proposed to account for the fact that the aldehyde hydrogenation process is inhibited by carbon monoxide.

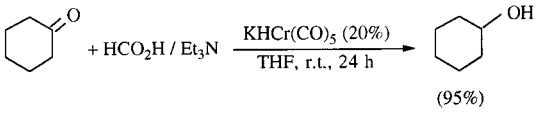
More recently, on the basis of the aforementioned stoichiometric reactivity of $KHCr(CO)_5$ with cyclohexanone (vide supra) and the hypothesis of an alkoxocarbonylchromate intermediate, a catalytic system has been designed for the transfer hydrogenation of ketones under very mild conditions.[49] In the presence of stoichiometric amounts of HCO_2H/Et_3N as a hydrogen-transfer agent, cyclohexanone was almost quantitatively (95%) reduced to cyclohexanol within 24 h using 20% $KHCr(CO)_5$ at room temp. in THF

Table 5. Transfer hydrogenation of ketones using 20% $KHCr(CO)_5$ in the presence of HCO_2H/Et_3N

Ketone	Conv. (%)[a]	Product (yield %)[b]
2-hexanone	38	2-hexanol (38)
acetophenone	25	1-phenylethanol (25)
3-methyl-2-butanone	45	3-methyl-2-butanol (45)
cyclohexanone	95	cyclohexanol (95)
4-*tert*-butylcyclohexanone	80	4-*tert*-butylcyclohexanols (80)[c]

[a] Ketone/$KHCr(CO)_5$/HCO_2H/Et_3N = 1:0.2:1:1, 24 h at room temp. in THF. – [b] GC analysis with internal standards. – [c] *cis*/*trans* = 33:67.

[Equation (68)]. Using even lower amounts of $KHCr(CO)_5$ also proved possible [e.g. 10% $KHCr(CO)_5$: 83% yield after 24 h; 5% $KHCr(CO)_5$: 70% yield after 24 h], but complete conversion of cyclohexanone was only achieved after several days.



(68)

When the catalytic reaction was performed at 0 °C, the rate was found to be lower. However, if after 24 h at 0 °C the mixture was allowed to warm to room temperature, the expected catalytic activity was restored. From reactions conducted at 60 °C, the yield of cyclohexanol remained below 50% (24 h) and did not increase further, suggesting competitive destruction of the catalytically active species.

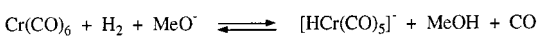
The above system was tested for the catalytic reduction of some representative ketones for 24 h at room temperature (Table 5).

As expected in the light of literature data on the reduction of ketones with hydridometallates,[47,51,83] cyclohexanones are more rapidly reduced than methyl ketones. In the case of 4-*tert*-butylcyclohexanone, the preponderant formation of the *trans* alcohol is consistent with the hypothesis of an alkoxocarbonylchromate intermediate (vide supra).

5.4. Catalytic Hydrogenation of Imines

In combination with NaOMe in methanol, all Group 6B carbonylmetal compounds catalyze the hydrogenation of *N*-benzylideneaniline into *N*-benzylaniline under ca. 100 bar hydrogen pressure at 60–160 °C.[57] Although $Mo(CO)_6$ is the most active of the three hexacarbonylmetal compounds at low temperatures, the best conversions are achieved using $Cr(CO)_6$. Typical conditions are a temperature of 120 °C, 100 bar initial H_2 loading, and a catalyst/substrate ratio of 1:50 (Table 6).

The reaction rate increases with increased H_2 pressure, while the process is inhibited by carbon monoxide. Accordingly, the active species has been suggested to be generated through the equilibrium described by Equation (69).

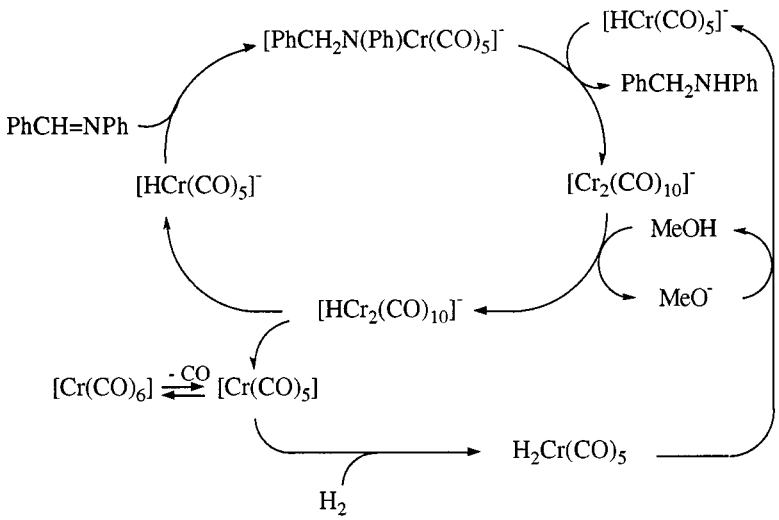


(69)

On the basis of a study of the stoichiometric reaction of $[Et_4N]^+[HCr(CO)_5]^-$ with imines (vide supra, Part 4), a catalytic cycle similar to that proposed for the hydrogenation of ketones has been suggested (Scheme 10).

6. Conclusion

The purpose of this review has been to point out the versatile properties of pentacarbonylhydridochromates



Scheme 10. Catalytic cycle for the hydrogenation of imines with $Cr(CO)_6$/MeONa

$M^+[HCr(CO)_5]^-$. These complexes are easy to prepare from $Cr(CO)_6$, and may find interesting applications as selective reducing agents in organic synthesis. As stoichiometric reagents, they have been shown to react either by H^- (or D^-) transfer or by a SET process, depending on the substrate. In comparison with similar carbonylhydridometallates, $[HCr(CO)_5]^-$ is a better H^--transfer agent than $[HFe(CO)_4]^-$ and a better electron-transfer agent than $[HW(CO)_6]^-$. As homogeneous catalysts, $M^+[HCr(CO)_5]^-$ species can be generated under various conditions and react mainly as H^--transfer agents towards electrophiles. The mechanisms of these reactions have been delineated and regeneration of the active species is generally well understood. It is to be expected that the knowledge of the different reaction pathways established for $M^+[HCr(CO)_5]^-$ species will allow extension of their application to other catalytic reactions. For instance, it is somewhat surprising that no attempted carbonylation reaction has hitherto been reported. Efforts in this area are currently underway in this laboratory.

Acknowledgments

The author is indebted to Dr. R. Mathieu for critically reading the manuscript and to B. Andrieu, R. Chauvin, O. Diallo, B. Donnadieu, P. Leglaye, J. Lienafa, and D. Neibecker who participated in the work on carbonylchromium derivatives. The Centre National de la Recherche Scientifique (France) is gratefully acknowledged for financial support.

[1] L. Mond, C. Langer, F. Quincke, *J. Chem. Soc.* **1890**, 749−753.
[2] M. Berthelot, *C. R. Acad. Sci.* **1891**, *112*, 1343−1349.
[3] L. Mond, F. Quincke, *J. Chem. Soc.* **1891**, *59*, 604−607.
[4] J. P. Collmann, L. S. Hegedus, J. R. Norton, R. G. Finke, *Principles and Applications of Organotransition Metal Chemistry*, University Science Books, Mill Valley, California, **1987**.
[5] C. D. Frohning, in *New Syntheses with Carbon Monoxide* (Ed.: J. Falbe), Springer-Verlag, New York, **1980**, p. 340−371.
[6] B. Cornils, in *New Syntheses with Carbon Monoxide* (Ed.: J. Falbe), Springer-Verlag, New York, **1980**, p. 1−225.
[7] A. Mullen, in *New Syntheses with Carbon Monoxide* (Ed.: J. Falbe), Springer-Verlag, New York, **1980**, p. 243−308.
[8] F. Calderazzo, R. Ercoli, G. Natta, *Organic Synthesis via Metal Carbonyls* (Eds.: I. Wender, P. Pino), Wiley Interscience, New York, **1968**, vol. 1, p. 1−272.
[9] J. P. Collman, *Acc. Chem. Res.* **1975**, *8*, 342−347.
[10] H. M. Colquhoun, D. J. Thompson, M. V. Twigg, *Carbonylation*, Plenum Press, New York, **1991**.
[11] J. J. Brunet, *Chem. Rev.* **1990**, *90*, 1041−1059 and references therein.
[12] J. J. Brunet, R. Chauvin, O. Diallo, F. Kindela, P. Leglaye, D. Neibecker, *Coord. Chem. Rev.* **1998**, *178−180*, 331−351.
[13] M. Y. Darensbourg, C. E. Ash, *Adv. Organomet. Chem.* **1987**, *27*, 1−50.
[14] A. Job, A. Cassal, *Bull. Soc. Chim. Fr.* **1927**, *41*, 1041−1046.
[15] G. P. Boldrini, A. Umani-Ronchi, *Synthesis* **1976**, 596−598.
[16] W. A. Herrmann, K. Öfele, C. Zybill, *Synthetic Methods of Organometallic and Inorganic Chemistry* (Ed.: W. A. Herrmann), Georg Thieme Verlag, New York, **1997**, p. 8−10.
[17] M. D. Grillone, *Inorg. Synth*. **1985**, *23*, 27−32.
[18] H. Behrens, R. Weber, *Z. Anorg. Allg. Chem.* **1957**, *291*, 122−130.
[19] H. Behrens, W. Klek, *Z. Anorg. Allg. Chem.* **1957**, *292*, 151−161.
[20] L. B. Handy, P. M. Treichel, L. F. Dahl, R. G. Hayter, *J. Am. Chem. Soc.* **1966**, *88*, 366−367.
[21] M. Y. Darensbourg, J. C. Deaton, *Inorg. Chem.* **1981**, *20*, 1644−1646.
[22] M. Y. Darensbourg, S. Slater, *J. Am. Chem. Soc.* **1981**, *103*, 5914−5915.
[23] M. Y. Darensbourg, S. Slater, *Inorg. Synth.* **1983**, *22*, 181−184.
[24] D. J. Darensbourg, A. Rokicki, M. Y. Darensbourg, *J. Am. Chem. Soc.* **1981**, *103*, 3223−3224.
[25] D. H. Gibson, F. U. Ahmed, K. R. Phillips, *Organometallics* **1982**, *1*, 679−681.
[26] M. D. Grillone, L. Palsmisano, *Transition Met. Chem.* **1989**, *14*, 81−89.
[27] J. J. Brunet, R. Chauvin, B. Donnadieu, P. Leglaye, D. Neibecker, *J. Organomet. Chem.* **1998**, *571*, 7−13.
[28] D. J. Darensbourg, J. A. Froelich, *J. Am. Chem. Soc.* **1978**, *100*, 338−340.
[29] D. J. Darensbourg, A. Rokicki, *Organometallics* **1982**, *1*, 1685−1693.
[30] M. Y. Darensbourg, R. Bau, M. W. Marks, R. R. Burch Jr., J. C. Deaton, S. Slater, *J. Am. Chem. Soc.* **1982**, *104*, 6961−6969.
[31] M. B. Smith, R. Bau, *J. Am. Chem. Soc.* **1973**, *95*, 2388−2389.
[32] R. C. Hines, K. F. Preston, J. J. Springs, A. Williams, *Organometallics* **1990**, *9*, 2298−2304.
[33] S. C. Kao, M. Y. Darensbourg, W. Schenk, *Organometallics* **1984**, *3*, 871−876.
[34] R. G. Hayter, *J. Am. Chem. Soc.* **1966**, *89*, 4376−4382.
[35] M. D. Grillone, B. B. Kedzia, *J. Organomet. Chem.* **1977**, *140*, 161−168.
[36] M. Y. Darensbourg, C. E. Ash, L. W. Arndt, C. P. Jansen, K. A. Youngdahl, Y. K. Park, *J. Organomet. Chem.* **1990**, *383*, 191−199.
[37] Y. Ruiz-Morales, G. Schreckenbach, T. Ziegler, *Organometallics* **1996**, *15*, 3920−3923.
[38] R. M. Laine, R. G. Rinker, P. C. Ford, *J. Am. Chem. Soc.* **1977**, *99*, 252−253.
[39] G. Doyle, *J. Organomet. Chem.* **1975**, *84*, 323−328.
[40] D. J. Darensbourg, A. Rokicki, *J. Am. Chem. Soc.* **1982**, *104*, 349−350.
[41] C. Bo, A. Dedieu, *Inorg. Chem.* **1989**, *28*, 304−309.
[42] S. C. Kao, P. L. Gaus, K. Youngdahl, M. Y. Darensbourg, *Organometallics* **1984**, *3*, 1601−1603.
[43] T. E. Cole, R. Pettit, *Tetrahedron Lett.* **1977**, 781−784.
[44] R. J. Kinney, W. D. Jones, R. G. Bergman, *J. Am. Chem. Soc.* **1978**, *100*, 7902−7915.
[45] S. C. Kao, M. Y. Darensbourg, *Organometallics* **1984**, *3*, 646−647.
[46] P. L. Gaus, S. C. Kao, M. Y. Darensbourg, L. W. Arndt, *J. Am. Chem. Soc.* **1984**, *106*, 4752−4755.
[47] P. L. Gaus, S. C. Kao, K. Youngdahl, M. Y. Darensbourg, *J. Am. Chem. Soc.* **1985**, *107*, 2428−2434.
[48] R. A. Grey, G. P. Pez, A. Wallo, *J. Am. Chem. Soc.* **1981**, *103*, 7536−7542.
[49] J. J. Brunet, R. Chauvin, P. Leglaye, *Eur. J. Inorg. Chem.* **1999**, 713−716.
[50] P. L. Gaus, L. M. Jones, L. A. Zamiska, *Polyhedron* **1989**, *8*, 653−657.
[51] L. Marko, Z. Nagy-Magos, *J. Organomet. Chem.* **1985**, 285, 193−203.
[52] S. C. Kao, C. N. Spillett, C. Ash, R. Lusk, Y. K. Park, M. Y. Darensbourg, *Organometallics* **1985**, *4*, 83−91.
[53] R. E. Dessy, R. L. Pohl, R. B. King, *J. Am. Chem. Soc.* **1966**, *88*, 5121−5124.
[54] C. E. Ash, P. W. Hurd, M. Y. Darensbourg, M. Newcomb, *J. Am. Chem. Soc.* **1987**, *109*, 3313−3317.
[55] M. Y. Darensbourg, B. Floris, K. A. Youngdahl, *Tetrahedron Lett*. **1989**, *30*, 1781−1784.
[56] B. Andrieu, J. J. Brunet, O. Diallo, J. Lienafa, unpublished results.
[57] J. Palagyi, Z. Nagy-Magos, L. Marko, *Transition Met. Chem*. **1985**, *10*, 336−338.
[58] W.-F. Liaw, C.-J. Liu, C.-H. Lai, *J. Chinese Chem. Soc*. **1992**, 39, 409−413.
[59] M. Y. Darensbourg, C. E. Ash, L. W. Arndt, C. P. Janzen, K. A. Youngdahl, *J. Organomet. Chem.* **1990**, *383*, 191−199.

[60] J. P. Collman, S. R. Winter, *J. Am. Chem. Soc.* **1973**, *95*, 4089−4090.
[61] C. P. Casey, S. M. Neumann, *J. Am. Chem. Soc.* **1976**, *98*, 5395−5396.
[62] M. Green, A. G. Orpen, I. D. Salter, F. G. A. Stone, *J. Chem. Soc., Dalton Trans.* **1984**, 2497−2503.
[63] K. Öfele, *J. Organomet. Chem.* **1968**, *12*, P42−P43.
[64] C. L. Thomas, *Catalytic Processes and Proven Catalysts*, Academic Press, New York, **1970**.
[65] K. Weissermel, H.-J. Arpe, *Industrial Organic Chemistry*, VCH, New York, **1993**.
[66] P. C. Ford, *Acc. Chem. Res.* **1981**, *14*, 31−37.
[67] A. D. King Jr., R. B. King, D. B. Yang, *J. Am. Chem. Soc.* **1981**, *103*, 2699−2704.
[68] R. B. King, *J. Organomet. Chem.* **1999**, *586*, 2−17, and refs. cited therein.
[69] R. G. Pearson, H. Mauermann, *J. Am. Chem. Soc.* **1982**, *104*, 500−504.
[70] R. B. King, C. C. Frazier, R. M. Hanes, A. D. King, Jr., *J. Am. Chem. Soc.* **1978**, *100*, 2925−2927.
[71] A. D. King, R. B. King, D. B. Yang, *J. Chem. Soc., Chem. Commun.* **1980**, 529−530.
[72] A. D. King Jr., R. B. King, E. L. Sailers, *J. Am. Chem. Soc.* **1981**, *103*, 1867−1868.
[73] W. A. R. Slegeir, R. S. Sapienza, R. Rayford, L. Lam, *Organometallics* **1982**, *1*, 1728−1730.
[74] D. J. Darensbourg, M. Y. Darensbourg, R. R. Burch, J. A. Froelich, M. J. Incorvia, *Adv. Chem. Ser.* **1979**, *173*, 106−120.
[75] H. Nagorski, M. J. Mirbach, M. F. Mirbach, *J. Organomet. Chem.* **1985**, *297*, 171−176.
[76] D. E. Linn, R. B. King, A. D. King, Jr., *J. Mol. Catal.* **1993**, *80*, 151−163.
[77] D. J. Darensbourg, C. Ovalles, *J. Am. Chem. Soc.* **1984**, *106*, 3750−3754.
[78] H. W. Choi, R. M. Gavin, E. L. Muetterties, *J. Chem. Soc., Chem. Commun.* **1979**, 1085.
[79] G. O. Evans, C. J. Newell, *Inorg. Chim. Acta* **1978**, *31*, L387−L389.
[80] D. J. Darensbourg, C. Ovalles, *J. Am. Chem. Soc.* **1987**, *109*, 330−3336.
[81] P. A. Tooley, C. Ovalles, S. C. Kao, D. J. Darensbourg, M. Y. Darensbourg, *J. Am. Chem. Soc.* **1986**, *108*, 5465−5470.
[82] D. E. Linn, Jr., R. B. King, A. D. King, Jr., *J. Mol. Catal.* **1993**, *80*, 165−179.
[83] K. Jothimony, S. Vanchesan, J. Kuriacose, *J. Mol. Catal.* **1985**, *32*, 11−16.

Received October 22, 1999
[I99387]

Metal-Mediated Oxidation of Tertiary Alcohols and Related Fragmentations

Karine Wietzerbin,[a] Jean Bernadou,*[a] and Bernard Meunier*[a]

Keywords: Tertiary alcohols / Oxidation / Fragmentation reactions / Metal salts / Acid catalysis / Basic catalysis / Reaction mechanisms

In contrast to the abundant literature available on the oxidation of primary and secondary alcohols, examples of oxidation of tertiary alcohols are rather rare and a general review on this topic does not exist. Therefore, this microreview will briefly describe the different existing methods, mainly metal-mediated, which consist of one or two-electron oxidations and usually lead to rearrangement, cyclization or fragmentation products. Some related data is also given for fragmentation reactions observed in basic or acid medium, or catalyzed by metal complexes without a real oxidation step.

Introduction

Primary and secondary alcohols can be easily oxidized, as exemplified by the abundant literature available on this subject.[1–6] In contrast, examples of tertiary alcohol oxidations are rather rare, and often related to a structural specificity of the substrate. In this review, we describe the different existing methods to oxidize tertiary alcohols. These reactions consist of one- or two-electron oxidation processes leading to rearrangement, cyclization or fragmentation products.

The first Part deals with 2-electron oxidations of tertiary alcohols and concerns transpositions, cyclizations and fragmentations by chromium(VI) oxides or vanadium(IV) complexes. The latter type of reaction leads to the formation of a ketone and a carbocation. The second Part is dedicated to one-electron oxidations observed with cerium(IV) and cobalt(III) derivatives. They result in fragmentation reactions yielding a ketone and a carbon radical. The third Part describes tertiary alcohols fragmentations in basic or acid

[a] Laboratoire de Chimie de Coordination du CNRS,
205 route de Narbonne, 31077 Toulouse cedex 4, France
Fax: (internat.) + 33-5/61553003
E-mail: bernadou@lcc-toulouse.fr; bmeunier@lcc-toulouse.fr



Karine Wietzerbin was born in France in 1971, and studied chemistry at the "Ecole Nationale Supérieure de Chimie" in Montpellier. In 1995 she joined the group of Bernard Meunier at the "Laboratoire de Chimie de Coordination du CNRS" in Toulouse, where she studied the mechanism of the oxidation of tertiary alcohols catalyzed by metalloporphyrins. She received a PhD for this research work in 1998. She is currently working at Eurofins Scientific (Nantes, France), where she works on food analysis using isotopic techniques.



Jean Bernadou was born in Villefranche-de-Rouergue (France) in 1947, and studied Chemistry, Pharmacy (Doctorate in Pharmaceutical Sciences in 1975) and Medicine (Doctorate in 1985) at the University Paul Sabatier of Toulouse, where he was appointed Professor of Medicinal Chemistry in 1987. His collaboration with the group of Bernard Meunier started in 1980 with his research interests in the mechanism of the action of antitumor drugs. He is currently working on biological applications of metalloporphyrins, in particular, oxidative DNA cleavage, biomimetic oxidation of drugs and characterization of reactive metal-oxo intermediates.



Bernard Meunier was born in 1947 and educated at the Universities of Poitiers (B.Sc.), Montpellier (with R. J. P. Corriu) and Orsay (with H. Felkin, ICSN-CNRS). After a period of post-doctoral study at the University of Oxford, he joined the "Laboratoire de Chimie de Coordination du CNRS" in Toulouse in 1979. His current research interests include catalytic oxidations, oxidative DNA cleavage, oxidation of pollutants, and the mechanism of action of artemisinin derivatives. He is the author of more than 230 publications and patents.

MICROREVIEWS: This feature introduces the readers to the authors' research through a concise overview of the selected topic. Reference to important work from others in the field is included.

 © WILEY-VCH Verlag GmbH, D-69451 Weinheim, 2000 1434–1948/00/0707–1391 $ 17.50+.50/0

media or catalyzed by ruthenium(II) complexes, i.e. without the need of an external oxidant. These reactions cannot be considered as genuine oxidations but they help in understanding the reactivity of tertiary alcohols under diverse conditions. The three sections are summarized in Figure 1.

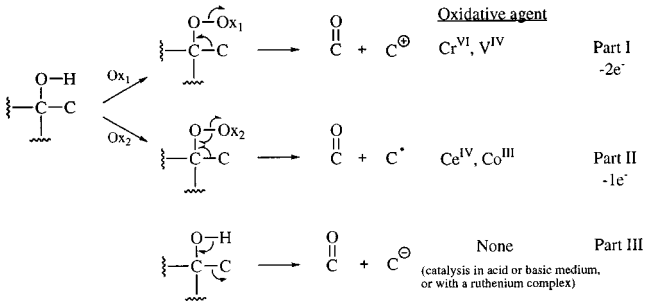


Figure 1. Modes of tertiary alcohol oxidations and fragmentations in non-oxidative media

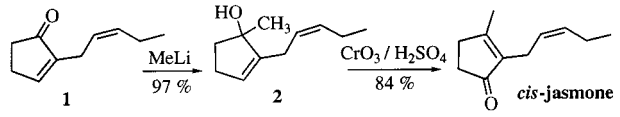
Finally, Part 4 is focused on oxidations with heme compounds. The complexity of these reactions does not allow us to classify them in one of the first three sections.

I. Two-Electron Oxidations

I.1. Oxidations Leading to Rearrangements

I.1.a. Allylic Alcohols

The ability to efficiently transpose a functional group from one carbon atom to another offers a wide degree of latitude in synthetic design of many naturally occurring compounds. For example, in 1972, the 1,3-alkylative carbonyl transposition of an α,β-unsaturated ketone *via* the oxidation of an intermediate tertiary allylic alcohol allowed Grieco[7] to prepare *cis*-jasmone (found in the essential oil of several varieties of *Jasminium*) with a reduced number of steps. The last steps of this synthesis are described in Scheme 1: The tertiary alcohol **2**, obtained by addition of methyllithium to dienone **1**, is oxidized to its transposed equivalent *cis*-jasmone using chromium trioxide in sulfuric acid (Jones reagent).[8]



Scheme 1. Last steps of formation of *cis*-jasmone

During the same period, other procedures were developed to convert tertiary allylic alcohols to α,β-unsaturated ketones. However, most of them are multi-step and indirect processes which include an initial rearrangement to a secondary alcohol, followed by oxidation to the ketone.[9,10] Moreover, the reagents used lead to a poor selectivity and low yields.

In 1976 and 1977, Babler and Coghlan,[11] and Dauben and Michno,[12] respectively, discovered a new method for 1,3-alkylative carbonyl transposition using pyridinium chlorochromate [$(ClCrO_3)^-PyH^+$] (PCC) as oxidant, which is less acidic than the Jones reagent and had been already used by Corey and Suggs[13] for oxidation of primary and secondary alcohols. The PCC oxidation of tertiary allylic alcohols (either cyclic or noncyclic), generated by 1,2-addition of organometallic reagents to α,β-unsaturated ketones, affords transposed 3-alkyl α,β-unsaturated ketones (Scheme 2). Several examples of such transpositions are reported in Table 1.[12]

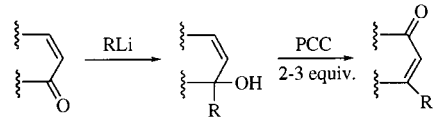
Table 1. Examples of 1,3-alkylative carbonyl transpositions by PCC (case of a starting α,β-unsaturated ketone)

Enone substrate	RLi	Allylic alcohol	Transposed enone	Yield (%)
	MeLi			94
	PhLi			90
	MeLi	 **3**	 **4**	88
	*n*BuLi	 **5**		50[a]
	PhLi	 **6**		51[b]

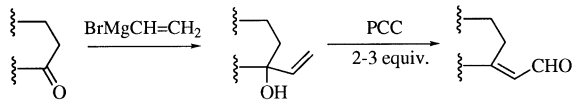
[a] 4:3 mixture of *E* and *Z* isomers, respectively. – [b] 4:1 mixture of *E* and *Z* isomers, respectively; in addition, 35% of acetophenone was also isolated.

With this method, oxidation of 1-methylcyclooct-2-en-1-ol (**3**) gives 3-methylcyclooct-2-en-1-one (**4**) in 88% yield, while the use of Jones reagent with the same compound gives a mixture of α,β- and β,γ-enones (4:3, respectively) in 48% yield. However, when the acyclic allylic alcohols **5** and **6** are oxidized, the yield is lowered due to the formation of side products generated by fragmentation reactions. For example, oxidation of 2-phenylbut-3-en-2-ol (**6**) affords acetophenone in 35% yield in addition to the transposed aldehyde.

When the initial ketone is not α,β-unsaturated, the unsaturation is conveniently introduced by reaction with an α,β-



Scheme 2. 1,3-Alkylative carbonyl transposition with PCC (case of a starting α,β-unsaturated ketone)

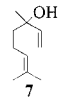


Scheme 3. 1,3-Carbonyl transposition with PCC (case of a starting saturated ketone)

unsaturated organometallic compound, e.g. vinylmagnesium bromide. Treatment of the corresponding allylic alcohol with PCC leads to an α,β-unsaturated aldehyde (Scheme 3). Such a process involves a two-carbon homologation of the starting ketone, and is equivalent to a directed aldol condensation between the latter compound and acetaldehyde. Furthermore, this is the first method described in the literature of a direct rearrangement of a tertiary allylic alcohol to an α,β-unsaturated aldehyde.

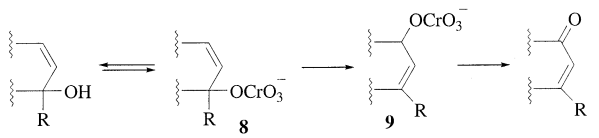
The results obtained by Dauben[12] and Babler[11] using this procedure are reported in Table 2. It is interesting to note that the 6,7-unsaturation of linalol **7** remains untouched during the oxidation process.

Table 2. Examples of 1,3-carbonyl transpositions with PCC (case of a starting saturated ketone)

Starting ketone	Allylic alcohol	Aldehyde formed	Selectivity (%)	Reference
			89	12
			83	12
			73	12
			90[a]	12
			85	11
			80-86[a]	11 + 12
			87	11

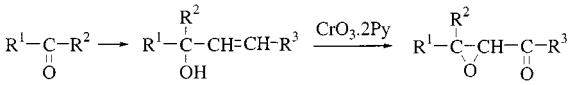
[a] 2:1 Mixture of *E* and *Z* isomers, respectively.

The mechanism proposed by Dauben and Michno[12] involves the oxidation of the substrate through its chromate ester **9**, which results from the rearrangement of the initial chromate ester **8** (Scheme 4).[12] This is consistent with the fact that formation of chromate esters from primary, secondary or tertiary alcohols is a very fast process.[14]



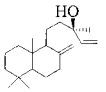
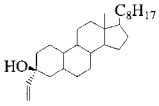
Scheme 4. Proposed mechanism for oxidation of tertiary allylic alcohols by PCC

Other chromium(VI)-oxo reagents were tested for the oxidative rearrangement of tertiary allylic alcohols and compared to PCC. Surprisingly, the use of Collins reagent ($CrO_3 \cdot 2Py$)[16] resulted in oxidative rearrangement to α-epoxy aldehydes or ketones (Scheme 5).[15]



Scheme 5. Tertiary allylic alcohol oxidation with Collins reagent

Table 3. Examples of oxidation of tertiary allylic alcohols with Collins reagent or PCC

Substrate	Oxidant	Epoxy-aldehyde[a] (% yield)	α,β-unsaturated aldehyde[b] (% yield)
			
	Collins	69	21
	PCC	–	98
			
	Collins	81	15
	PCC	–	98
			
	Collins	50	10
	PCC	–	80
			
	Collins	50	traces
	PCC	–	79
			
	Collins	70	traces
	PCC	–	72

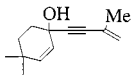
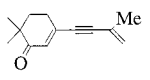
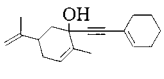
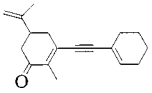
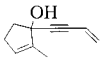
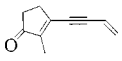
[a] 1:1 mixture of both epimers. – [b] 1:1 mixture of *E* and *Z* isomers.

The results of Table 3[15] show that for the same substrate, oxidation with Collins reagent yields mainly the α-epoxy aldehyde together with a small amount of the transposed α,β-unsaturated aldehyde, while the latter is the only product obtained with PCC as oxidant.

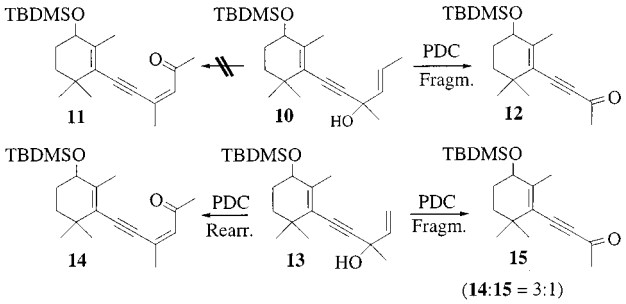
This interesting oxidative rearrangement with Collins reagent appears to be an excellent method for converting a ketone to the bis(homologous) epoxy aldehyde via a tertiary allylic alcohol.

Another chromium(VI)-amine oxidant, pyridinium dichromate [$(Cr_2O_7)^{2-}(PyH)_2^+$] (PDC),[17] was successfully used to oxidize various allylic acetylenic alcohols.[18] Prepared by addition of a lithium acetylide to an enone, the

Table 4. Examples of oxidation of enynols with PDC

Enynol substrate	Oxidation product	Yield (%)
		88
		78
		62
		90

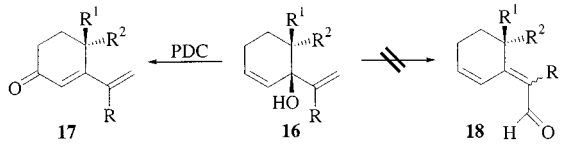
resulting enynols gave upon oxidation with PDC the transposed ketone with good to excellent yields (Table 4).[18] This PDC-induced oxidative rearrangement proceeded with complete regiospecificity since it occurred only at the olefinic site. The reaction seems to be more selective with *Z*-substituted enynols. Indeed, exposure of compound **10**, containing an *E*-double bond, to the action of PDC did not give the expected transposed product **11** (Scheme 6). Instead, ketone **12** was quantitatively produced. This product is probably the result of a vinyl hydrogen abstraction from **11**, followed by a carbon−carbon bond scission. PDC treatment of the demethylated alcohol **13** afforded a 3:1 mixture of the transposed product **14** and the fragmentation product **15**. These observations suggest that in situations where both *E*- and *Z*-vinyl hydrogen atoms are available, the rearrangement and fragmentation processes are competitive. This assumption is also consistent with the poor yields obtained by Dauben and Michno[12] for the PCC-induced oxidative rearrangement of allylic alcohols **5** and **6** (see Table 1), where the *E*-double bond could favor fragmentation reactions.



Scheme 6. Oxidation of compounds **10** and **13** with PDC

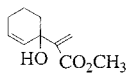
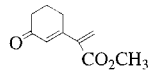
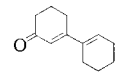
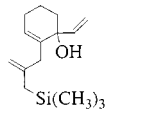
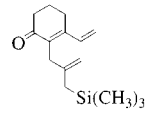
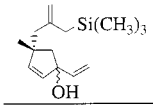
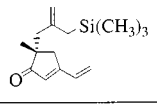
I.1.b. Bis(allylic) Alcohols

Pyridinium dichromate (PDC) was also used by Majetich et al. to oxidize dienols to dienones.[19] Their experiments established that the PDC-induced oxidative rearrangement of bis(allylic) tertiary alcohols such as **16** is regiospecific since the conjugated enone **17** is exclusively formed (Scheme 7). Several examples of these oxidations are reported in Table 5.[19]

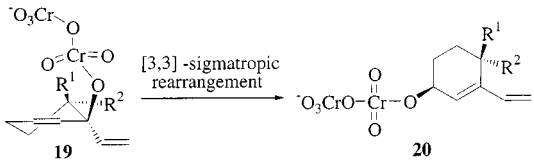


Scheme 7. Oxidation of bis-allylic alcohols with pyridinium dichromate

Table 5. Examples of oxidations of bis(allylic) tertiary alcohols with PDC

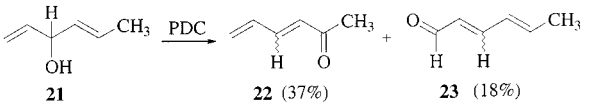
Substrate	Dienone formed	Yield (%)
		57
		62
		58
		57
		70

The regiospecificity of the [3,3]-sigmatropic rearrangement may be explained by examining the conformer **19** of the initially formed chromate ester (Scheme 8), where the Cr=O bond is above the rigid C=C double bond of the cyclohexene ring (while the exocyclic double bond is free to rotate). The rearrangement then affords the transposed chromate ester **20**, whose subsequent oxidation produces the corresponding enone.



Scheme 8. Rearrangement of the chromate ester **19** derived from **16**

This hypothesis has been supported by the oxidation of dienol **21**, in which both vinyl groups are free to rotate (Scheme 9). Treatment of **21** with PDC gave a 2:1 mixture of dienone **22** and dienal **23**, showing that the regiospecificity was lost.

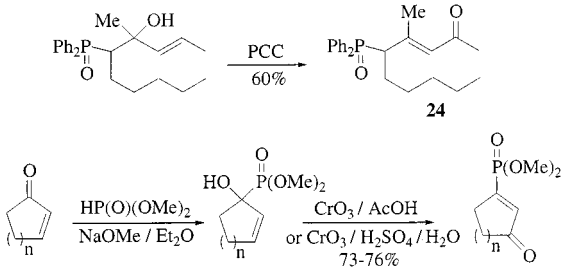


Scheme 9. Oxidation of hexan-1,4-dien-3-ol **21** with pyridinium dichromate

I.1.c. Allylic Alcohols Containing Heteroatoms

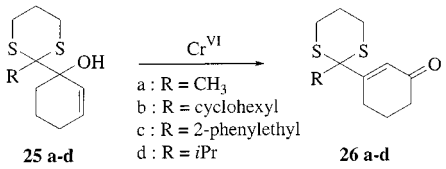
In order to extend the synthetic possibilities offered by these rearrangements, several authors attempted to use more complex substrates that would lead to attractive synthetic intermediates. They particularly focused on tertiary allylic alcohols containing heteroatoms.

Brown et al[20] and Öhler and Zbiral[21] showed that phosphorus-containing tertiary allylic alcohols could be efficiently oxidized with PCC or chromic acid (Scheme 10).[20,21]

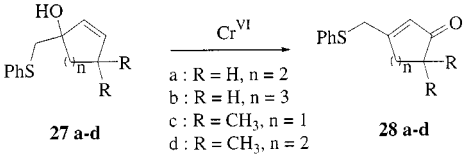


Scheme 10. Oxidations of phosphorus-containing tertiary allylic alcohols (n = 1 or 2)

Since the oxidation of sulfides to sulfoxides and sulfones with oxochromium(VI)-amine reagents is slower than the oxidation of alcohols to carbonyl compounds under the same conditions, Luzzio and Moore[22] examined the oxidative rearrangement of tertiary allylic alcohols bearing a dithianyl protecting group (general structure **25**, Scheme 11) or a (phenylthio)methyl substituent (general structure **27**, Scheme 12). This work was the continuation of early studies realized by Corey and Crouse,[23] who reported in 1968 the oxidative transposition of compounds such as **25**.



Scheme 11. Oxidation of tertiary allylic alcohols bearing a dithianyl substituent



Scheme 12. Oxidation of tertiary allylic alcohols bearing a (phenylthio)methyl substituent

In order to achieve optimal conversion, compounds **25d** and **27a** have been oxidized with different oxochromium(VI) reagents: Jones reagent, PCC, PDC, Collins reagent and 2,2′-bipyridinium chlorochromate (BPCC). The results reported in Table 6[22] established that the efficiency of conversion follows the order PCC > PDC > Collins > BPCC. The Jones reagent, which is less selective and more acidic than the oxochromium(VI)-amine complexes, led only to decomposition products.

Table 6. Oxidation of **25d** and **27a** with a series of oxochromium(VI)-amine reagents

Oxidant		Conversion (%)	
		25d	**27a**
$(ClCrO_3)^-PyH^+$	PCC	53	74
$(Cr_2O_7)^{2-}(PyH)^+$	PDC	31	62
 $ClCrO_3^-$	BPCC	<1	13
$CrO_3.2Py$	Collins	37	37

Yields could be improved by adding silica gel to the reaction medium in order to absorb the reduced chromium tars. Table 7[22] indicates the results obtained for oxidation of compounds **25a−d** to **26a−d** and of **27a−d** to **28a−d** with PCC in the presence of silica gel.

Table 7. Oxidation of **25a−d** and **27a−d** with PCC

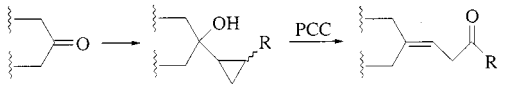
Substrate	Product	Yield(%)
25a	**26a**	28
25b	**26b**	56
25c	**26c**	62
25d	**26d**	74
27a	**28a**	75
27b	**28b**	82
27c	**28c**	83
27d	**28d**	92

In the case of the dithiane series (compounds **25a−d**), it appears that the yield increases with increasing steric hindrance of the R substituent. A possible explanation could be that as R becomes more bulky, the binding of the dithiane moiety to the unchanged reagent or reduced chromium species is disfavored, and the yields are thus increased. The ability of the dithiane moiety to bind the reduced chromium species may also explain why better yields are obtained with the (phenylthio)methyl series.

I.1.d. α-Cyclopropyl Alcohols

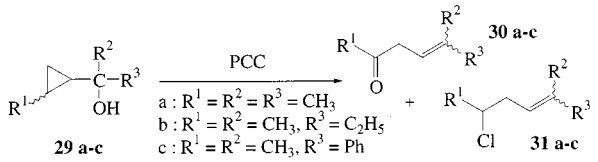
Like allylic tertiary alcohols, 2-alkylcyclopropyl carbinols are able to undergo PCC-oxidative rearrangement to give the corresponding β,γ-unsaturated ketones. The overall process is a synthetically useful method of effecting 1,4-carbonyl transposition (Scheme 13).[24] Moreover, when the tertiary alcohols used as substrates are prepared by addition of cyclopropyl organometallic reagents to ketones (as in Scheme 13), the oxidative rearrangement is also an excellent

method for converting ketones to the tris(homologous) β,γ-enones.



Scheme 13. 1,4-carbonyl transposition with PCC

The PCC-induced oxidation of tertiary 2-alkylcyclopropyl carbinols of general structure **29** (Scheme 14) yields the expected β,γ-enones **30** but also the chloro olefins **31** (48% and 15% for **30a** and **31a**, respectively). This result indicates that both the desired oxidation and the nucleophilic attack by the chloride ion take place at the homoallylic carbon atom.



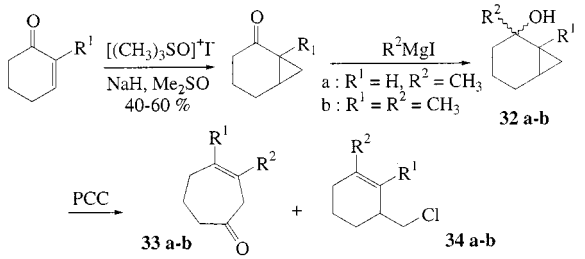
Scheme 14. Oxidation of alcohols **29a−c** with PCC

However, when the chloride ligand of the chromium complex is replaced by a tetrafluoroborate, only the desired β,γ-enone is obtained (50% for **30a**). Additionally, the use of a small amount of water together with PCC not only improved the yield of **30**, but also considerably reduced the formation of **31**. The yields obtained under these conditions are reported in Table 8.[24]

Table 8. Results of the oxidation of **29a−c** and **32a−b** with PCC in the presence of water

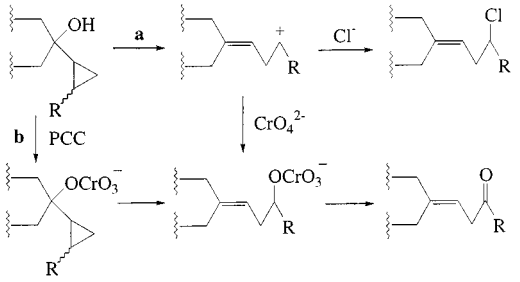
Substrate	β,γ-Enone	Yield (%)	Other products (yield, %)
29a	**30a**	60	**31a** (5)
29b	**30b**	62	**31b** (3)
29c	**30c**	57	**31c** (3)
32a	**33a**	28	**34a** (10)
32b	**33b**	30	**34b** (6)

The availability of tertiary cyclopropyl carbinols via cyclopropanation of cyclic α,β-enones followed by organometallic addition enables 1,4-carbonyl transpositions on starting ketones that already contain a cyclopropyl moiety to be performed, as depicted in Scheme 15. However, in such a process, yields are lower than above, probably because of the steric hindrance developed in these systems (Table 8, substrates **32a** and **b**).



Scheme 15. 1,4-Carbonyl transposition on α-cyclopropyl ketones

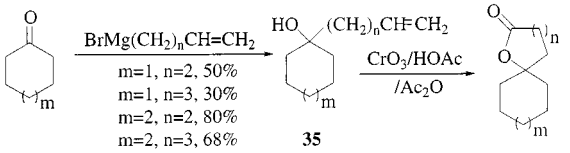
Two mechanisms have been proposed by the authors for the oxidative rearrangement of α-cyclopropyl alcohols (Scheme 16).[24] Path **a** involves a prior solvolysis of the tertiary alcohol to give a homoallylic carbocation, which then collapses in the presence of a nucleophilic species such as chloride to give a chloro olefin, or the chromate ion to give a chromate ester and then the β,γ-enone. Path **b** requires chromate ester formation prior to the rearrangement. However, path **a** appears to be more favorable for the present oxidative rearrangement since it explains the formation of chlorinated compounds.



Scheme 16. Mechanism proposed for the oxidation of 2-alkylcyclopropyl carbinols with PCC

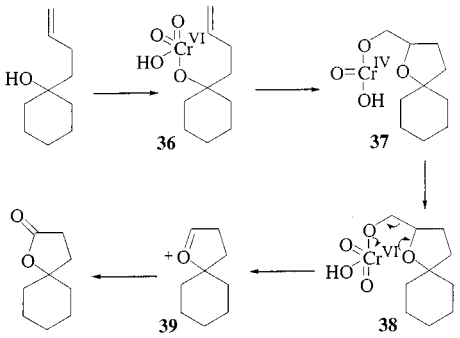
I.2. Oxidations Leading to Cyclizations

Some γ- and δ-unsaturated tertiary alcohols are able to undergo oxidative cyclizations. Treatment of tertiary alcohols of general structure **35** with the Fieser reagent CrO_3/AcOH/acetic anhydride easily gives lactones with the loss of one carbon atom (Scheme 17).[25]



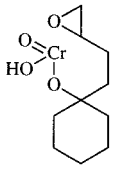
Scheme 17. Oxidative cyclization of γ- and δ-unsaturated tertiary alcohols with the Fieser reagent

The role played by the hydroxy group during the process appeared to be essential (when replaced by a methoxy or an acetoxy group, no reaction was observed). Additionally, oxidation of simple alkenes such as 1-dodecene gives only a mixture of the starting product with epoxides and acids. In an attempt to explain the cyclization process, Schlecht and Kim[25] proposed the mechanism depicted in Scheme 18. It involves the formation of the chromate ester **36**, followed by intramolecular oxidation of the double bond, which leads to the chromium(IV) ester **37**. The latter is then reoxidized to **38** by excess reagent. The oxidative fragmentation of **38** produces **39**, and then the lactone with another equivalent of oxidant.

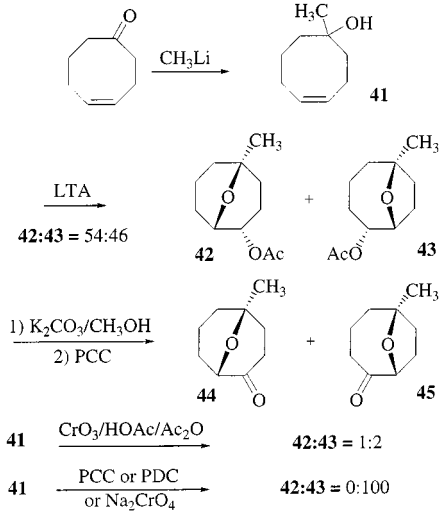


Scheme 18. Mechanism proposed for the oxidative cyclization of γ- and δ-unsaturated tertiary alcohols with the Fieser reagent

However, an alternative pathway for the transformation of **36** to **37** could proceed through the epoxy intermediate **40**, the opening of which would lead to **37**.



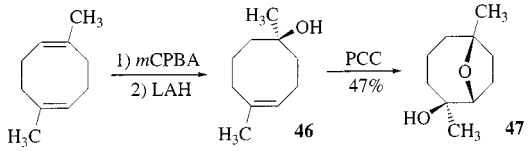
When cycloalkenols are used as the substrate, the oxidative cyclization becomes a transannular oxidative cyclization and gives β-functionalized bicyclic ethers.[26] This method is particularly convenient for preparing the oxygen-bridged bicyclic skeleton which appears in a number of biologically active natural products. Schlecht and Kim[27] observed that the oxidation of 1-methylcyclooct-4-en-1-ol (prepared from cyclooct-4-en-1-one) with lead tetraacetate (LTA) provides both acetates **42** and **43** in a ratio of 54:46, which are then converted into oxo ethers **44** and **45** by hydrolysis and oxidation (Scheme 19).



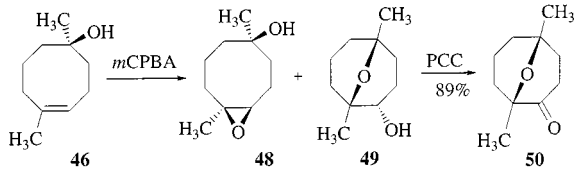
Scheme 19. Transannular cyclization of tertiary cycloalkenol

The nature of the oxidant has a great influence on the regioselectivity of the reaction since the use of the Fieser reagent instead of LTA leads to the same oxo ethers in a 1:2 ratio, while treatment with PCC, sodium chromate or PDC produces only oxo ether **45**. The cyclization process is also catalyzed by acids: the reaction rate is inhibited by addition of sodium acetate but increased in the presence of acetic acid. Additionally, no reaction occurs with the Collins reagent. These observations suggest that two different mechanisms operate depending on the nature of the oxidant. One possible mechanism involves an intermediate epoxide which undergoes internal opening by attack of the hydroxy group on one of the two carbon atoms to form two cyclic β-hydroxy ethers, subsequently oxidized to **44** and **45**. However, this mechanism does not explain the observed regioselectivity with chromium(VI) reagents. Treatment of **41** with *m*CPBA yields both the *cis*-epoxy alcohol, and a 3:2 mixture ratio of two β-hydroxy ethers corresponding to the hydrolysis products of **42** and **43** (and probably derived from the *trans*-epoxy alcohol). With either PCC or the Fieser reagent, these β-hydroxy ethers are converted into **44** and **45**, while the *cis*-epoxide gives only a complicated mixture of products under the same conditions. Consequently, the involvement of an epoxide in the course of oxidation with PCC, PDC or Na_2CrO_4 can be ruled out since it does not explain the observed regioselectivity. It seems more reasonable to postulate the formation of a chromate ester of the hydroxy group, which would be acid-catalyzed, followed by an intramolecular attack on the double bond by the tethered chromate ester moiety. In the oxidation with LTA, which occurs without selectivity, epoxide opening is likely to be involved in the mechanism. In the case of the Fieser reagent, which is a stronger oxidant than PCC, PDC and Na_2CrO_4, a contribution of both mechanisms is a reasonable assumption.

In order to obtain further information about the reaction mechanism, Schlecht and Kim studied the transannular oxidative cyclization of cyclooctenol **46**, where the methyl substituent on position 5 does not permit the further oxidation to the carbonyl, thus allowing the authors to follow the stereochemistry of the reaction.[28] The oxidation of **46** with PCC provides the β-hydroxy cyclic ether **47** exclusively (Scheme 20). The cyclization process is then not only regiospecific but also stereospecific.



Scheme 20. PCC-induced oxidative cyclization of cyclooctenol **46**



Scheme 21. Oxidation of **46** with *m*CPBA followed by PCC

As in the previous case, the action of *m*CPBA on compound **46** gives the *cis* hydroxy epoxide **48** and the cyclic

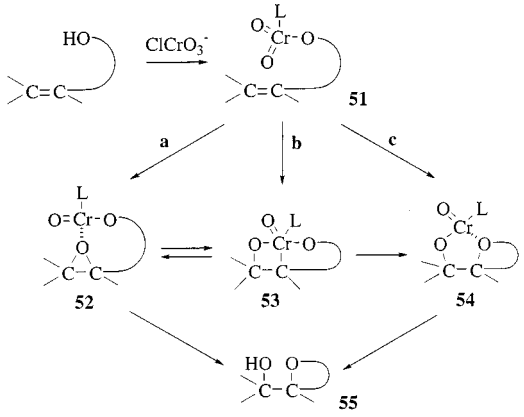
endo-β-hydroxy ether **49**, whose oxidation with PCC yields **50** (Scheme 21).

These observations are in accordance with the involvement of a chromate ester rather than an epoxide in the reaction pathway. On the basis of the *syn* configuration of the resulting product, Schlecht[28] proposed three possible mechanistic pathways after the initial step of chromate ester formation (Scheme 22):

− Pathway **a**: formation of an epoxide by an intramolecular attack of the tethered oxidant (**51** → **52** → **55** or **51** → **52** → **53** → **54** → **55**);

− Pathway **b**: formation of a metalloxetane (**51** → **53** → **54** → **55** or **51** → **53** → **52** → **55**);

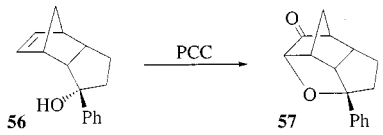
− Pathway **c**: [3+2] cycloaddition and fragmentation (**51** → **54** → **55**).



Scheme 22. Mechanism proposed for the transannular oxidative cyclization of tertiary cycloalkenols; L = Cl, O

However, the failure to convert the epoxide **52** into cyclization products upon treatment with PCC appears to rule out pathway **a** as the mechanism for the transannular oxidative cyclization.

Working with more complex substrates, where the tertiary hydroxy group was positioned in a conformationally fixed orientation with respect to the alkene group, Waddell et al.[29] obtained results which parallel those reported by Schlecht, since PCC treatment of compound **56** leads to the β-oxo ether **57** in 70% yield (Scheme 23). The process is a transannular cyclization similar to the one described by Schlecht, which probably follows the same mechanism.



Scheme 23. Oxidative cyclization of **56** with PCC

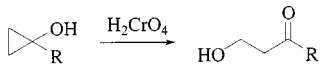
However, the strained double bond of **56** might be more reactive toward PCC than the same group in **46**. Therefore, considering a possible intermolecular attack of the double bond by the oxidant, the dicyclopentadiene was submitted to the action of PCC under the same conditions. The products proved to be only α-chloro ketones obtained in 25% yield. Consequently, the intermolecular mechanism is unlikely, and the pathway demonstrated by Schlecht may also explain the transformation of **56** to **57**.

I.3. Oxidations Leading to Fragmentations

I.3.a. Fragmentations with Chromium Oxides

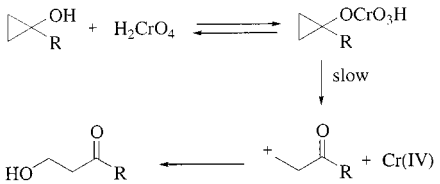
One of the first oxidative tertiary alcohol fragmentations described in the literature was reported by Barbier and Locquin in 1913.[30] They observed at that time the formation of carboxylic acids R−COOH and acetone while heating in sulfuric acid alcohols of general structure $R-CH_2-C(CH_3)_2OH$ in the presence of chromic acid. However, the reaction mechanism has been shown to involve prior dehydration of the alcohol, so that the products were in fact the result of oxidation of the intermediate olefin. This was demonstrated by Sager in 1955 by conducting kinetic studies during the oxidation of 3-ethylpentan-3-ol with chromic acid.[31]

The first example of a direct oxidation of a tertiary alcohol with chromic acid was reported by Rocek and Radkowsky in 1968.[32] They studied the oxidation of 1-methylcyclobutyl alcohol, a compound which is very reluctant to undergo dehydration[33] and whose large ring strain should favor fragmentation reactions. Although they did not identify the oxidation products, they performed kinetic measurements which revealed a first order dependence on the chromic acid concentration, thus excluding any prior dehydration. Further investigations then showed that chromic acid-induced oxidation of tertiary cyclopropanols provided β-hydroxylated ketones through ring opening (Scheme 24).[34]



Scheme 24. Oxidation of tertiary cyclopropanols with chromic acid

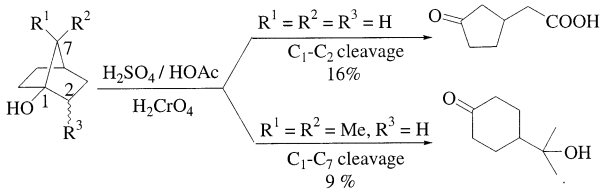
For example, 1-phenylcyclopropanol is oxidized with 43% conversion and 73% selectivity to 3-hydroxy-1-phenylpropan-1-one. Tertiary cyclopropanols are even more reactive than the corresponding secondary cyclopropanols, and the reactivity is greatly increased by alkyl substitution on the ring. This is consistent with the mechanism depicted in Scheme 25,[34] where the rate-limiting step is the formation of a carbocation by oxidative decomposition of a chromate ester of the alcohol. The reaction is then accelerated by substituents stabilizing the incipient carbocation.



Scheme 25. Reaction pathway for oxidation of tertiary cyclopropanols with chromic acid

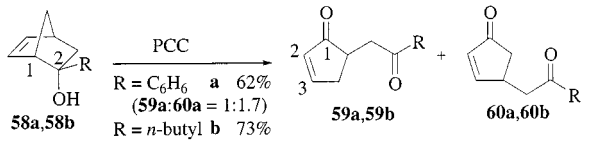
Although their conversion is low, Cawley and Spaziano showed that norbornanol derivatives are able to undergo

oxidation in a same way.[35] The C−C bond cleavage occurs on C^1-C^2 or C^1-C^7 bonds, depending on the nature of the substituents. Two kinds of product are thus obtained (Scheme 26).



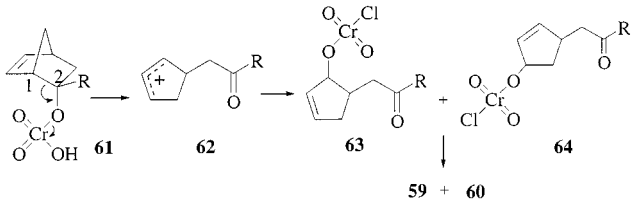
Scheme 26. Oxidation of norbornanol derivatives with chromic acid

In the same series, norbornenols of structure **58** are easily oxidized with PCC to two isomeric cyclopentenones **59** and **60** resulting from C^1-C^2 bond cleavage, the latter being the main product (Scheme 27).[29]



Scheme 27. Oxidation of **58** with PCC

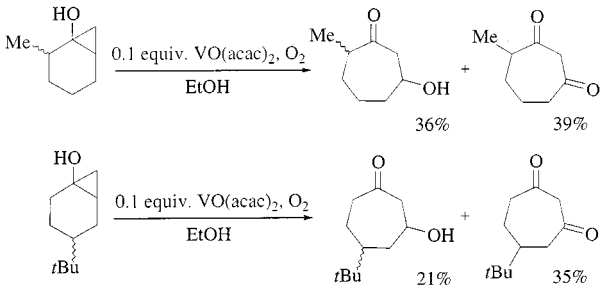
It is interesting to note that an oxidative cyclization (see section I.2) would have been reasonable given the *endo* position of the hydroxy group, but the expected highly strained 5-oxo-2,6-oxetane is not formed. The oxetane is neither a reaction intermediate, since if it were, the $O-C^2$ bond would break to give products not observed in the present case. Interestingly, PCC-induced oxidation of the *exo* isomer of **58a** leads to the same fragmentation products **59a** and **60a**. Consequently, an intramolecular oxidation of the double bond can be ruled out. The mechanism assumed for the transformation is illustrated in Scheme 28,[29] and parallels that proposed by Rocek et al.[34] in Scheme 25. It requires the formation of a chromate ester **61**, which suffers fragmentation to give the allylic carbocation **62**. Capture of **62** by a chromate species gives two new chromate esters **63** and **64**, and subsequent elimination leads to the 4- and 5-substituted cyclopentenones. It is noteworthy that this mechanism also explains the observed product ratio since **62** is not symmetric and the capture of the chromate moiety at the least hindered positive center gives **64** and the 4-substituted isomer **60** as the major product.



Scheme 28. Mechanism proposed for oxidation of **58** with PCC

I.3.b. Fragmentations with Vanadium Oxides

Bicyclic cyclopropanols undergo oxidation in the presence of catalytic amounts of vanadyl acetylacetonate $VO(acac)_2$ under oxygen to afford ring-enlarged β-hydroxy ketones and β-diketones.[36] Two examples of such reactions are represented in Scheme 29. β-Diketones are not obtained by the reaction of β-hydroxy ketones with $VO(acac)_2$, suggesting that β-diketones originate directly from the cyclopropanol systems.



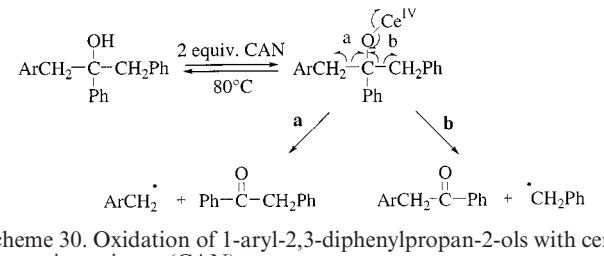
Scheme 29. Oxidation of bicyclic cyclopropanols catalyzed by vanadyl acetylacetonate

Molecular oxygen acts as the co-oxidant and reoxidizes the low valent vanadium compound formed. Nevertheless, it is possible to perform the reaction under a nitrogen atmosphere using stoichiometric amounts of $VO(acac)_2$. Although the absence of inhibition with a radical trap suggests that a radical pathway is not involved, the precise reaction mechanism is still unknown.

II. One-Electron Oxidations

II.1. Oxidative Cleavages with Ceric Ammonium Nitrate (CAN)

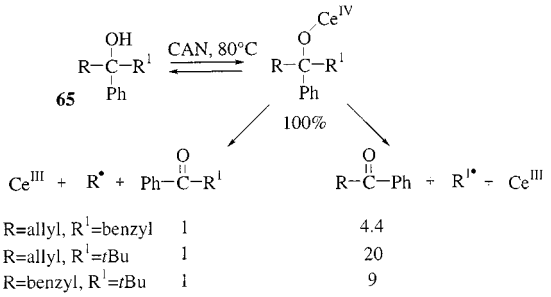
Oxidations of tertiary alcohols using ceric ammonium nitrate (CAN) as oxidant produce fragmentation products. The experiments carried out by Trahanovsky et al. on 1-aryl-2,3-diphenylpropan-2-ols showed that, in the presence of CAN, two competitive cleavages occur, producing two different ketones. The use of radical scavengers revealed the presence of aryl and benzyl radicals.[37] Therefore, the reaction likely proceeds through an intermediate $R-O-Ce^{IV}$ complex, whose homolytic cleavage affords the oxidation products (Scheme 30).



Scheme 30. Oxidation of 1-aryl-2,3-diphenylpropan-2-ols with ceric ammonium nitrate (CAN)

In order to determine whether the fragmentation regioselectivity depends on the stability of the released radicals, Trahanovsky and Macaulay investigated the oxidation of tertiary alcohols of general structure **65**, where R and R′

are allyl, *tert*-butyl or benzyl groups.[38] The relative ratios of the resulting ketones are given in Scheme 31.

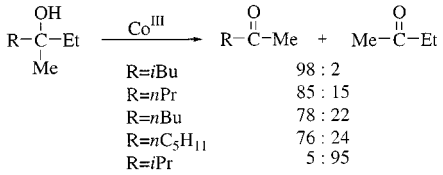


Scheme 31. Relative ratio of the ketones obtained from oxidation of **65** with CAN

It appeared that even though *tert*-butyl radical is less stable than allyl and benzyl radicals,[39] its formation was preferred. Thus, the stability of the released radicals is not the only factor controlling the selectivity of the reaction. The authors suggested that steric (release of the steric strain) or conformational factors (preventing vinyl or phenyl groups from stabilizing the incipient radicals) might play an important role during the reaction.

II.2. Cleavages with Cobalt Salts

Similarly to Ce^{IV}, Co^{III} is able to oxidize tertiary alcohols to form a ketone and a radical. Hoare and William examined the oxidation of a series of substituted tertiary alcohols in the presence of cobalt(III) perchlorate.[40,41] The results obtained and the relative ratio of the resulting ketones are indicated in Scheme 32.



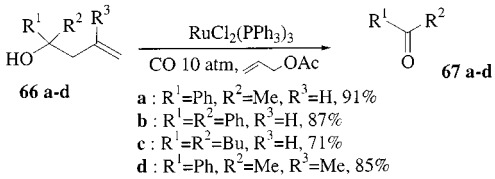
Scheme 32. Relative ratio of ketones resulting from the oxidation of alkylethylmethylcarbinols with Co^{III}

Evidence is given that the ease of elimination of the alkyl radicals increases according to the order: $Me^{\bullet} < RCH_2CH_2^{\bullet} < Et^{\bullet} < iPr^{\bullet}$. Therefore, it seems that for these simple tertiary alcohols, the fragmentation regioselectivity depends on the stability of the released radicals.

III. Fragmentations in Non-Oxidative Media

III.1. Fragmentations with Ruthenium Complexes

The selective cleavage of tertiary homoallylic alcohols has been recently investigated by Kondo et al.[42] They showed that treatment of such alcohols with allyl acetate in the presence of a ruthenium complex $[RuCl_2(PPh_3)_3]$ caused a β-allyl elimination to generate the corresponding ketone

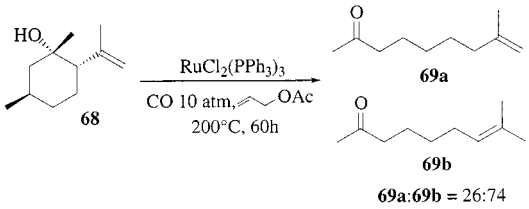


Scheme 33. Catalytic fragmentation of tertiary homoallylic alcohols with $RuCl_2(PPh_3)_3$

(Scheme 33). Thus, 2-phenylpent-4-en-2-ol (**66a**) is converted into acetophenone in 91% yield. In a same way, other derivatives bearing alkyl or aryl groups (**66b−d**) undergo a deallylation to afford various ketones **67b−d**.

Several ruthenium complexes such as $Ru_3(CO)_{12}$ or *cis*-$RuCl_2(CO)_2(PPh_3)_2$ were examined with regard to their ability to catalyze the deallylation of **66a** to **67a**. All of them show catalytic activity, and among them $RuCl_2(PPh_3)_3$ is the most efficient. In contrast, among the other transition metals examined (Pt, Pd, Ni, Rh), only the rhodium complex $[RhCl(PPh_3)_3]$ shows moderate catalytic activity (45% conversion for the deallylation of **66a** to **67a**).

A synthetic application of this procedure is illustrated in the following ring opening reaction of cyclic homoallylic alcohols (Scheme 34). Treatment of **68** with $RuCl_2(PPh_3)_3$ affords the unsaturated ketones **69a−b** in 76% yield. This catalytic system thus represents an efficient and convenient method to perform catalytic ring-opening reactions on general 2-vinylcycloalkanols.

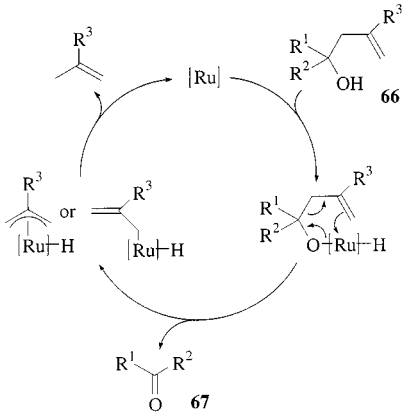


Scheme 34. Ring-opening reaction catalyzed by $RuCl_2(PPh_3)_3$

The following observations provide insight into the mechanism: (i) The treatment of a **66a** derivative bearing an acetoxy instead of the hydroxy group does not lead to **67a**. This result indicates that the first step of the reaction is the oxidative addition of a hydroxy group of **66a** to ruthenium; (ii) treatment of the saturated analogue of **66a**, i.e. 2-phenylpentan-2-ol, does not afford **67a** through propyl elimination. This suggests that the driving force of the reaction is the formation of an allylruthenium species; (iii) treatment of the secondary allylic alcohol 1-phenylbut-3-en-1-ol, which bears both a hydrogen atom and an allyl group at the β-position, yields the α,β-unsaturated ketone (1-phenylbut-2-en-1-one) from hydrogen β-elimination and not benzaldehyde from allyl elimination.

Considering all of these observations, Kondo et al. propose the mechanism depicted in Scheme 35.[42] The initial step might consist of oxidative addition of the hydroxy group of **66** to an active ruthenium center. Subsequent β-allyl elimination from the alkoxyruthenium intermediate

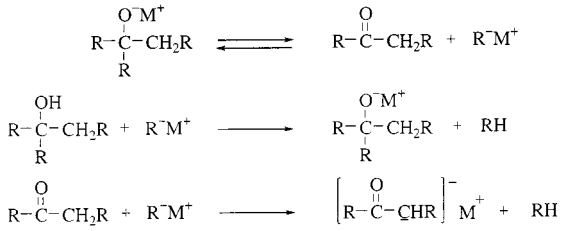
gives ketone **67** together with a (allyl)(hydrido)ruthenium species, which undergo a reductive elimination to give $R_3(CH_3)C{=}CH_2$.



Scheme 35. Proposed mechanism for the fragmentation of tertiary homoallylic alcohols with $RuCl_2(PPh_3)_3$

III.2. Alkoxide Fragmentations

Tertiary alcohols are easily cleaved in their alkoxide forms, obtained for example in the presence of metallic potassium, lithium hydride or sodium amide. At high temperatures, their oxidative fragmentation produces a ketone with elimination of a carbanion. The latter then captures a hydrogen atom from either the excess alcohol or the resulting ketone when it is an enol. The whole process is described in Scheme 36.



Scheme 36. Fragmentation of tertiary alcohols under the alkoxide form (M = metal)

In 1959, Zook et al. applied this procedure on various tertiary alcohols. The results are summarized in Table 9.[43] The experiments show that the ease of cleavage increases with the branching in the substituent R. For example, triisopropyl carbinol required a temperature of 300 °C to be cleaved to diisopropyl ketone, while 200 °C is sufficient to cleave *tert*-butyl diisopropyl carbinol, and triethyl carbinol cannot be cleaved at 335 °C (experiments 5, 6 and 8). Therefore, it seems that steric strain favors the fragmentation reaction.

Experiments 1, 2 and 3 (Table 9) carried out on diisopropylalkyl carbinols demonstrate that the ease of cleavage of primary alkyl substituents increases with increasing bulkiness of the group, the order being *n*-propyl < isobutyl < neopentyl. Additionally, primary alkyl substituents are more readily eliminated than the isopropyl group, since no trace of alkyl isopropyl ketone was detected. Phenyl and *tert*-butyl are likewise eliminated preferentially to isopropyl (experiments 4 and 5).

The nature of the metallic cation also plays an important role. The results of the experiments performed on *tert*-butyl diisopropyl carbinol showed that the temperature required for the cleavage depends on the cation used (Table 10).[43] The order of ease of cleavage is Li < Na < K, which corresponds to the order of decreasing electronegativities. This is explained by the fact that as the electronegativity of the metal decreases, the negative charge developed on the anion becomes greater and the alkoxide is then more reactive.

Table 10. Influence of the cation on the fragmentation of $(i\text{Pr})_2t\text{Bu}$-COH

Cation	Temp.(°C)	Products (%)		
		$i\text{Pr}_2t\text{BuCOH}$	$i\text{Pr}_2\text{CO}$	$i\text{PrCO}t\text{Bu}$
K	160−182	0	60	35
Na	199−215	7	52	32
Li	213−320	24	35	25

Other authors used milder conditions compared to those used by Zook et al.[44−46] For example, using potassium dimesylate $[(CH_3SOCH_2)^-K^+]$ in DMSO is a convenient way to readily cleave tertiary alcohols at room temperature. Thus, in addition to the metallic cation, the solvent chosen also has an influence on the reaction.

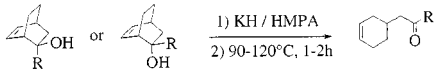
Snowden et al. have studied alkoxide cleavages, particularly with bis- and tris(homoallylic) alkoxides.[47,48] It is noteworthy that allylic homoallylic alkoxides undergo oxy-Cope rearrangement rather than fragmentation under the same conditions.[48] The authors also examined more com-

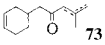
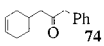
Table 9. Examples of cleavage of sodium alkoxides $R_1R_2R_3CO^-Na^+$

Exp.	Substrate			Temp.(°C)	Products (%)				
	R^1	R^2	R^3		$R^1R^2R^3COH$	R^1COR^2	R^3H	R^1COR^3	R^2H
1	*i*Pr	*i*Pr	*n*Pr	266−392	30	19	58	0	0
2	*i*Pr	*i*Pr	*i*Bu	264−362	53	37	38	0	0
3	*i*Pr	*i*Pr	*neo*P	222−240	26	35	36	0	0
4	*i*Pr	*i*Pr	Ph	242−276	13	72	70	3	3
5	*i*Pr	*i*Pr	*t*Bu	199−215	7	52	31	32	23
6	*i*Pr	*i*Pr	*i*Pr	300−312	21	20	24	−	−
7	Ph	Ph	Ph	280−320	51	23	31	−	−
8	Et	Et	Et	335	No cleavage				

plex bicyclic substrates. Thus, 2-substituted bicyclo[2.2.2]-oct-5-en-2-ols can be cleaved by heating the alkoxides at 120 °C.[49] The results obtained with such alcohols are summarized in Table 11.[49]

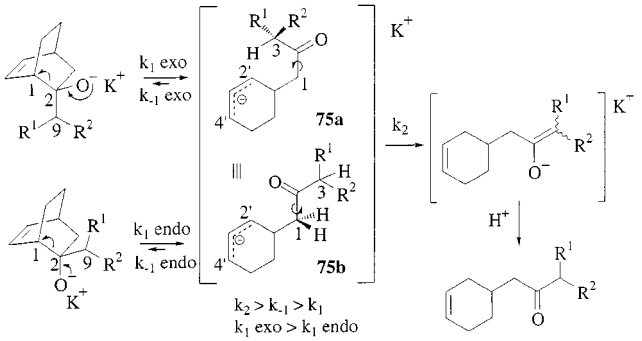
Table 11. Examples of bicyclo[2.2.2]oct-5-en-2-ols fragmentations



Exp.	Substrate	Cyclohexene formed	Yield (%)	Other products (Yield, %)
1		**70** 	68	
2		**70**	52	
3			70	
4		 **71**	67	
5		**71**	51	
6		 **72** α-β:β-γ = 1:4	74	
7		**72**	<10	 + PhOH (65) 3:1
8		 **73** α-β:β-γ = 1:4	76	
9		**73**	<10	 + PhOH (61) 3:1
10		 **74**	54	
11		**74**	<5	 + PhOH (70) 3:1

Experiments 1 to 5, in which substituents are saturated alkyl groups, demonstrate that epimeric alcohols give the same product, i.e. 1-(cyclohex-3′-enyl)alkan-2-one resulting from C^1-C^2 bond cleavage (in each case only 10% of the 2′-enyl isomer is formed). However, the *exo*-alkoxide reacts noticeably faster than its *endo* epimer. On the other hand, no epimerization of the substrate is observed during the reaction. These results are consistent with a reaction mechanism in which the rate determining step is the heterolytic cleavage of the allylic C^1-C^2 bond to form a transient allylic anion which is then irreversibly quenched by intramolecular capture of a proton on C^3 adjacent to the carbonyl group. The resulting enolate subsequently affords the ketone by external protonation (Scheme 37).[49]

The high regioselectivity with respect to the position of the cyclohexenyl double bond may be rationalized by the strong preference for intramolecular proton transfer from the C^3-position to the $C^{2'}$-position of the allylic anion (rather than the $C^{4'}$-position) via a six-membered transition state (see conformation **75a**, Scheme 36). Additionally, an intermolecular protonation would not be expected to be regioselective. The observed rate difference between the *exo*- and *endo*-epimeric alkoxides is possibly the result of stabilization of the C^1-C^2 bond in the *endo*-alkoxide by electron donation from the O-anion to the cyclic double bond.



Scheme 37. Mechanism proposed for the cleavage of bicyclo[2.2.2]-oct-5-en-2-ols in the presence of potassium hydride

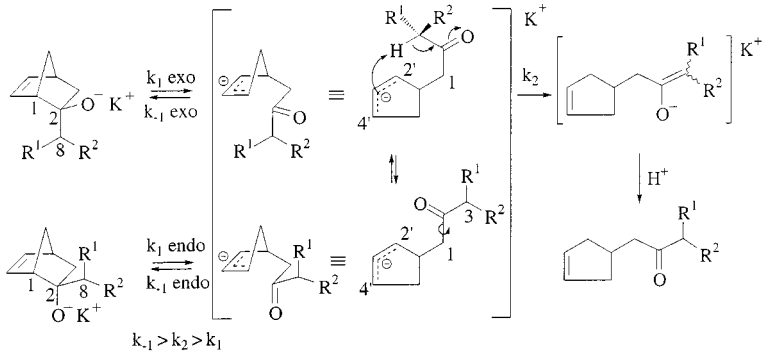
Experiments 6−11 (Table 11) were performed on substrates bearing an unsaturated C^2-substituent. In contrast with 2-alkyl-substituted alkoxides, the reaction products from these epimeric alkoxides are dependent on the substrate stereochemistry: The *exo*-alkoxides afford (4:1)-mixtures of β,γ- and α,β-unsaturated ketones via C^1-C^2 bond cleavage while the *endo*-alkoxides yield mostly the ketone resulting from C^2-C^9 bond cleavage. This marked difference between the epimeric alkoxides may be due to a strengthening of the C^1-C^2 bond in the *endo*-alkoxide caused by selective electron donation from the O-anion to the structurally rigid, cyclic double bond. In the *exo*-alkoxide, the C^2-C^9 bond may be stabilized by a similar electron donation from the O-anion to the double bond of the C^2-substituent.

Alkoxides derived from C^2-substituted norbornenols react similarly to the above compounds, producing 1-(cyclopent-3′-enyl)alkan-2-ones resulting from C^1-C^2 bond cleavage.[50] Nevertheless, an important epimerization of the substrate is observed during the reaction, suggesting that the rate determining step is the intramolecular protonation step which follows reversible C^1-C^2 bond cleavage to give the allylic anion (Scheme 38).[50]

When the substituents are unsaturated, the selectivity with regard to the cyclopentenyl double bond is decreased, indicating that an intermolecular protonation by reaction with the substrate also occurs. This is consistent with the reversibility of the first step which ensures an appreciable concentration of alkoxide during the reaction.

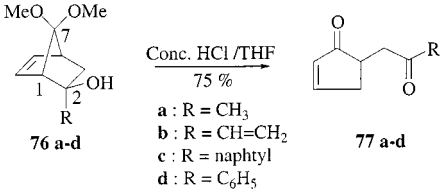
III.3. Fragmentations in Acidic Media

Norbornenols are able to undergo fragmentation, not only under basic conditions as described above, but also in acidic media. Thus, Palani et al. showed that several 7,7-dimethoxynorbornenols derivatives afford the corresponding substituted cyclopentenones through C^1-C^2 bond



Scheme 38. Mechanism proposed for the cleavage of norbornenols in the presence of potassium hydride

cleavage upon treatment with hydrochloric acid in THF (Scheme 39).[51]



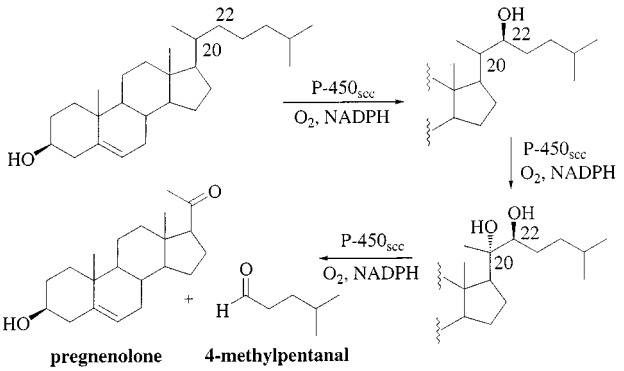
Scheme 39. Fragmentation of 7,7-dimethoxynorbornenols in acidic media

The behavior of compounds **76b** and **76c** is in remarkable contrast to that observed in basic media, since in the presence of sodium hydride the oxy Cope rearrangement products are obtained.[52] The use of hydrochloric acid is then an interesting option when the fragmentation process competes with the oxy Cope rearrangement under basic conditions.

IV. Oxidations Catalyzed by Heme-Containing Systems

IV.1. Catalysis with Cytochrome P-450

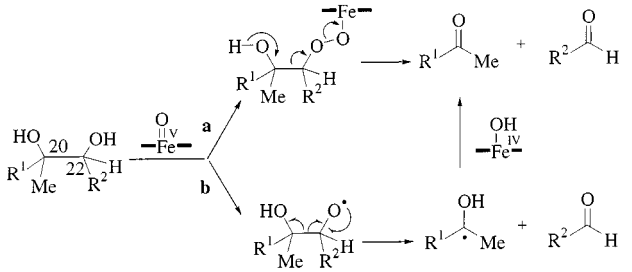
Cytochromes P-450 belong to the monooxygenase family and are able to catalyze several oxidation reactions in the presence of molecular oxygen and NADPH. Among them, alkane hydroxylations and alkene epoxidations have been widely studied.[53,54] Some of these heme-enzymes play an important role in steroids biosynthesis by catalyzing two or three successive oxidation steps, where the last one can be



Scheme 40. Cholesterol side chain cleavage catalyzed by P-450 scc/O_2/NADPH

C−C bond cleavage. These cleavages sometimes occur at carbon atoms bearing a tertiary alcohol functionality. For example, P-450$_{scc}$ (cholesterol **s**ide **c**hain **c**leavage P-450) catalyses the side chain degradation of cholesterol via two hydroxylations at C^{20} and C^{22}, followed by an oxidative cleavage of the $C^{20}-C^{22}$ bond. The whole process leads to the formation of pregnenolone and 4-methylpentanal (Scheme 40).[54−56]

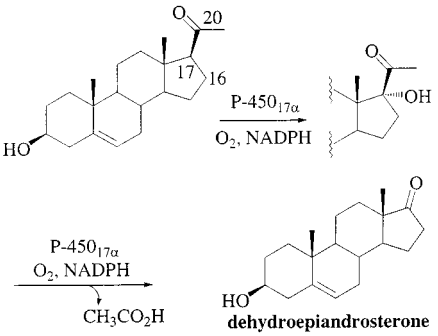
Although the first two steps are classical, the last one, where the enzyme acts as a lyase, is more original and interesting from a mechanistic point of view. The proposed mechanism is represented in Scheme 41. The active species of the catalyst is a high valent oxo-iron complex Fe=O. In the first hypothesis, the reaction pathway proceeds through the addition of the hydroxy group at C^{22} to the activated oxygen atom to form an iron-peroxo species. Deprotonation of the adjacent hydroxy group then induces the C−C bond cleavage (Scheme 41, path **a**). However, this hypothesis requires the formation of a peroxo complex with a poorly stable O−O bond, which is a thermodynamically unfavorable process. A second hypothesis involves the formation of an alkoxyl radical resulting from the abstraction of a proton and an electron at one of the hydroxy groups by the oxo-iron species. The subsequent β-fragmentation affords the oxidation products (Scheme 41, path **b**).[55,56]



Scheme 41. Mechanism of the side chain cleavage of cholesterol by P-450$_{scc}$

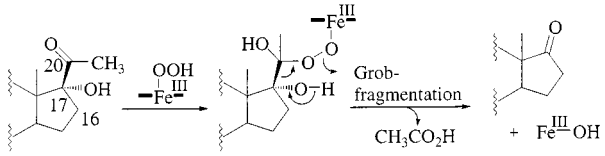
Another type of cytochrome P-450, 17α-hydroxylase-17,20-lyase or P-450$_{17\alpha}$, catalyses the pregnenolone deacetylation to form mainly dehydroepiandrosterone via an intermediate tertiary alcohol (Scheme 42).

This peculiar reaction has been widely studied by Akhtar et al.[57−59] Labeling experiments performed with $^{18}O_2$ and deuterium led to the proposal of a reaction mechanism for



Scheme 42. Deacetylation of pregnenolone by P-450$_{17\alpha}$

the last step, which is depicted in Scheme 43. Its originality lies in the nature of the active species of the catalyst, which is a Fe^{III}-hydroperoxo species. After its addition to the carbonyl group, the $C^{17}-C^{20}$ bond breaks according to a Grob-type fragmentation, releasing acetic acid. The results of the labeling experiments are in accordance with this mechanism: when hydroxypregnenolone bears a trideuteriated methyl at position 21 and reaction is performed under $^{18}O_2$, the acetic acid produced contains three deuteriums and one ^{18}O atom, whereas no labelled oxygen is incorporated into dehydroepiandrosterone.

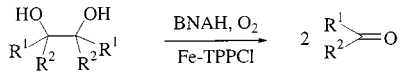


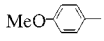
Scheme 43. Mechanism of the oxidation of hydroxypregnenolone with P-450$_{17\alpha}$

IV.2. Catalysis by Synthetic Metalloporphyrins

Synthetic metalloporphyrins are excellent biomimetic oxidation catalysts mimicking cytochrome P-450. They have been widely studied for hydroxylation and epoxidation reactions,[60] but only very few examples of tertiary alcohol oxidation have been reported in the literature up to now.

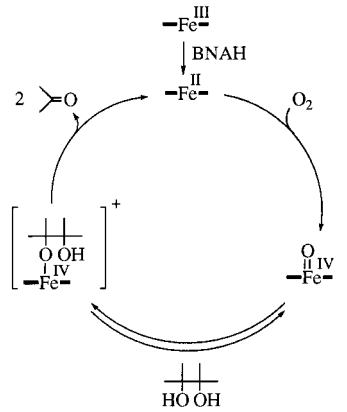
One of them concerns the oxidation of ditertiary 1,2-diols catalyzed by an iron porphyrin in the presence of molecular oxygen and 1-benzyl-3-carbamoyl-1,4-dihydropyridine (BNAH, which acts as the reducer).[61] The reaction simulates the final step of the side chain cleavage of cholesterol catalyzed by P-450$_{scc}$ (vide supra). The products formed are two ketones resulting from the cleavage of dihydroxylated C−C bond (Scheme 44).



R^1	R^2	Conv (%)	Yield (%)
	CH_3	100	95
	CH_3	100	86
		80	48
		95	91

Scheme 44. Examples of fragmentations of ditertiary 1,2-diols with the system (TPP)FeCl/BNAH/O_2

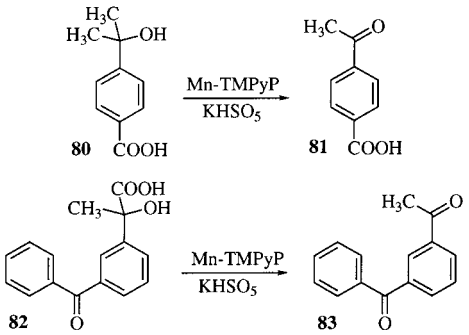
Kinetic studies enabled the authors to propose a reaction mechanism (Scheme 45) in which the active species $Fe^{IV}=O$ reacts reversibly with the diol to form a Fe^{IV}-alkoxo complex before the fragmentation. This mechanism represents an alternative to the one proposed with P-450$_{scc}$ in Scheme 41.



Scheme 45. Mechanism of the oxidation of ditertiary 1,2-diols with the system Fe−TPPCl/BNAH/O_2

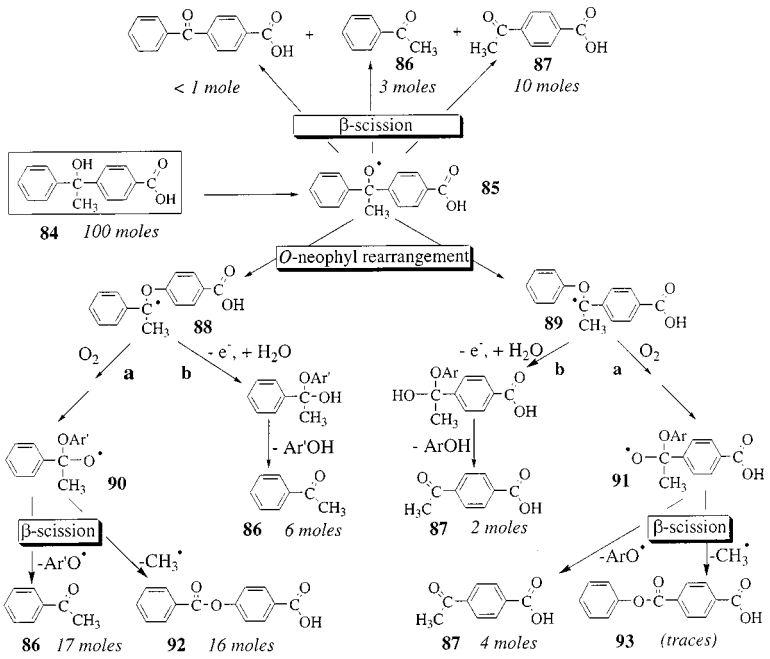
The fragmentation of ditertiary 1,2-diols can also be performed photocatalytically in the presence of a water soluble iron porphyrin and dioxygen.[62]

Recently, a catalytic system able to oxidize tertiary alcohols has been developed in our laboratory.[63] It consists of a water soluble manganese porphyrin (Mn−TMPyP) together with an oxygen atom donor, potassium monopersulfate ($KHSO_5$). The latter avoids the use of a reductant to form the active species of the catalyst. The tertiary alcohols used as substrates are the compounds **80** and **82**, whose oxidation leads respectively to the ketones **81** and **83** corresponding to the loss of a methyl or a carboxyl group (Scheme 46).



Scheme 46. Tertiary alcohols oxidation by the system Mn−TMPyP/$KHSO_5$

Labeling experiments performed with $H_2{}^{18}O$ revealed that no oxygen atom coming from water is incorporated in compound **83** (this study cannot be performed with compound **81** owing to the rapid exchange of the carbonyl oxygen atom with water). This observation suggests that **83** is formed through β-fragmentation of the alkoxyl radical of **82** resulting from the abstraction of a proton and an electron by the active species of the catalyst.



Scheme 47. Mechanism and diverse reaction pathways in oxidation of the tertiary alcohol **84** with the system Mn−TMPyP/$KHSO_5$; the number of mol is the amount of each product formed if the initial amount of **84** is 100 mol

Such a β-fragmentation of an alkoxyl radical may in fact compete with a *O*-neophyl rearrangement as has been shown in the catalytic oxidation of the tertiary alcohol **84** by the Mn−TMPyP/$KHSO_5$ system (Scheme 47).[64] Labeling experiments using $^{18}O_2$ or $H_2{}^{18}O$ under different reaction conditions demonstrate that the carbonyl oxygen atoms of acetophenone **86** and acetylbenzoic acid **87** originate either from substrate, water or dioxygen. The direct β-scission of the alkoxyl radical **85** leads to unlabelled compounds **86** and **87**. In a competitive reaction pathway, the *O*-neophyl rearrangement of **85** affords the carbon-based radicals **88** and **89** which then react with dioxygen (path **a**) or Mn^{IV}−OH/water (path **b**) to give in several steps labelled compounds **86** and **87** (the label comes either from water or dioxygen) and the unexpected esters **92** and **93** (from β-scission of the intermediate alkoxyl radicals **90** and **91**).

Conclusion

Metal-mediated oxidations of tertiary alcohols are mainly based on the use of stoichiometric or an excess of environmentally unfriendly metal oxides or metal oxy compounds (chromium oxide, ...). Consequently, this domain of tertiary alcohol oxidation is open to new catalytic methods using " green oxidants " (dioxygen, hydrogen peroxide, ...). In addition, the fragmentation reactions observed during the tertiary alcohol oxidations should be controlled by the metal center in order to ensure the product selectivity and avoid the formation of several products resulting from free-radical chemistry. Metal-controlled radical chemistry will be the future for metal-catalyzed oxidation of tertiary alcohols.

[1] T. V. Lee, in *Comprehensive Organic Synthesis* (Eds: B. M. Trost, I. Fleming, S. V. Ley), Pergamon Press, Oxford, **1991**, vol. 7, p. 291.
[2] S. V. Ley, A. Madin, in *Comprehensive Organic Synthesis* (Eds: B. M. Trost, I. Fleming, S. V. Ley), Pergamon Press, Oxford, **1991**, vol. 7, p. 251.
[3] G. Procter, in *Comprehensive Organic Synthesis* (Eds: B. M. Trost, I. Fleming, S. V. Ley), Pergamon Press, Oxford, **1991**, vol. 7, p. 305.
[4] M. Hudlicky, in *Oxidations in Organic Chemistry* (Ed.: M. Hudlicky), American Chemical Society, Washington, DC, **1990**, p. 114.
[5] J. Muzart, *Synthesis* **1993**, 11.
[6] R. A. Sheldon, J. K. Kochi, *Metal-Catalyzed Oxidations of Organic Compounds*, Academic Press, New York, **1981**.
[7] P. A. Grieco, *J. Org. Chem.* **1972**, *37*, 2363.
[8] K. Bowden, I. M. Heilbron, E. R. H. Jones, B. C. L. Weedon, *J. Chem. Soc.* **1946**, 39.
[9] B. M. Trost, J. L. Stanton, *J. Am. Chem. Soc.* **1975**, *97*, 4018.
[10] J. H. Babler, D. O. Olsen, W. H. Arnold, *J. Org. Chem.* **1974**, *39*, 1656.
[11] J. H. Babler, M. J. Coghlan, *Synth. Commun.* **1976**, *6*, 469.
[12] W. G. Dauben, D. M. Michno, *J. Org. Chem.* **1977**, *42*, 682.
[13] E. J. Corey, J. W. Suggs, *Tetrahedron Lett.* **1975**, *31*, 2647.
[14] H. Kwart, J. A. Ford, G. C. Corey, *J. Am. Chem. Soc.* **1962**, *84*, 1252.
[15] P. Sundararaman, W. Herz, *J. Org. Chem.* **1977**, *42*, 813.
[16] J. C. Collins, W. W. Hess, F. J. Frank, *Tetrahedron Lett.* **1968**, *30*, 3363.
[17] E. J. Corey, G. Schmidt, *Tetrahedron Lett.* **1979**, *5*, 399.
[18] D. Liotta, D. Brown, W. Hoekstra, R. Monahan, *Tetrahedron Lett.* **1987**, *28*, 1069.
[19] G. Majetich, S. Condon, K. Hull, S. Ahmad, *Tetrahedron Lett.* **1989**, *30*, 1033.
[20] P. S. Brown, A. B. MacElroy, S. Warren, *Tetrahedron Lett.* **1985**, *26*, 249.
[21] E. Öhler, E. Zbiral, *Synthesis* **1991**, 357.
[22] F. A. Luzzio, W. J. Moore, *J. Org. Chem.* **1993**, *58*, 2966.
[23] E. J. Corey, D. Crouse, *J. Org. Chem.* **1968**, *33*, 298.
[24] E. Wada, M. Okawara, *J. Org. Chem.* **1979**, *44*, 2952.
[25] M. F. Schlecht, H. J. Kim, *Tetrahedron Lett.* **1985**, *26*, 127.

[26] A. C. Cope, M. A. MacKervey, N. M. Weinshenker, *J. Am. Chem. Soc.* **1967**, *89*, 2932.
[27] M. F. Schlecht, H. J. Kim, *Tetrahedron Lett.* **1986**, *27*, 4889.
[28] M. F. Schlecht, H. J. Kim, *J. Org. Chem.* **1989**, *54*, 583.
[29] T. G. Waddell, A. D. Carter, T. J. Miller, *J. Org. Chem.* **1992**, *57*, 381.
[30] P. Barbier, R. Locquin, *C. R. Acad. Sc.* **1913**, *156*, 1443.
[31] W. F. Sager, *J. Am. Chem. Soc.* **1956**, *78*, 4970.
[32] J. Rocek, A. Radkowsky, *Tetrahedron Lett.* **1968**, *24*, 2835.
[33] P. Riesz, R. W. Taft, R. H. Boyd, *J. Am. Chem. Soc.* **1957**, *79*, 3724.
[34] J. Rocek, A. M. Martinez, G. E. Cushmac, *J. Am. Chem. Soc.* **1973**, *95*, 5425.
[35] J. J. Cawley, V. T. Spaziano, *Tetrahedron Lett.* **1973**, *47*, 4719.
[36] M. Kirihara, M. Ichinose, S. Takizawa, T. Momose, *Chem. Commun.* **1998**, 1691.
[37] P. M. Nave, W. S. Trahanovsky, *J. Am. Chem. Soc.* **1971**, *93*, 4536.
[38] W. S. Trahanovsky, D. B. Macaulay, *J. Org. Chem.* **1973**, *38*, 1497.
[39] D. F. McMillen, D. M. Golden, *Ann. Rev. Phys. Chem.* **1982**, *33*, 493.
[40] D. G. Hoare, W. A. William, *J. Chem. Soc.* **1962**, 965.
[41] D. G. Hoare, W. A. William, *J. Chem. Soc.* **1964**, 2552.
[42] T. Kondo, K. Kodoi, E. Nishinaga, T. Okada, Y. Morisaki, Y. Watanabe, T. Mitsudo, *J. Am. Chem. Soc.* **1998**, *120*, 5587.
[43] H. D. Zook, J. March, D. F. Smith, *J. Am. Chem. Soc.* **1959**, *81*, 1617.
[44] S. M. Partington, C. Ian, F. Watt, *J. Chem. Soc., Perkin Trans. 2* **1988**, 983.
[45] J. S. Lomas, J. E. Dubois, *J. Org. Chem.* **1984**, *49*, 2067.
[46] E. M. Arnett, L. E. Small, R. T. MacIver, J. S. Miller, *J. Org. Chem.* **1978**, *43*, 815.
[47] R. L. Snowden, S. M. Linder, B. L. Muller, K. H. Schulte-Elte, *Helv. Chim. Acta* **1987**, *70*, 1879.
[48] R. L. Snowden, S. M. Linder, B. L. Muller, K. H. Schulte-Elte, *Helv. Chim. Acta* **1987**, *70*, 1858.
[49] R. L. Snowden, K. H. Schulte-Elte, *Helv. Chim. Acta* **1981**, *64*, 2193.
[50] R. L. Snowden, *Helv. Chim. Acta* **1983**, *66*, 1031.
[51] N. Palani, T. Rajamannar, K. K. Balasubramanian, *Synlett* **1997**, 59.
[52] M. E. Jung, J. P. Hudspeth, *J. Am. Chem. Soc.* **1978**, *100*, 4309.
[53] P. R. Ortiz de Montellano, *Cytochrome P-450: Structure, Mechanism and Biochemistry*; 2nd ed., Plenum Press, New York, **1995**.
[54] M. Sono, M. P. Roach, E. D. Coulter, J. H. Dawson, *Chem. Rev.* **1996**, *96*, 2841.
[55] C. Y. Byon, M. Gut, *Biochem. Biophys. Res. Commun.* **1980**, *92*, 549.
[56] P. R. Ortiz de Montellano, in *Cytochrome P-450: Structure, Mechanism and Biochemistry* (Ed.: P. R. Ortiz de Montellano), Plenum Press, New York, **1995**, pp. 245−303.
[57] S. L. Miller, J. M. Wright, D. L. Corina, M. Akhtar, *J. Chem. Soc., Chem. Commun.* **1991**, 157.
[58] D. L. Corina, S. L. Miller, J. N. Wright, M. Akhtar, *Chem. Commun.* **1991**, 782.
[59] M. Akhtar, D. L. Corina, S. L. Miller, A. Z. Shyadehi, J. N. Wright, *Biochemistry* **1994**, *33*, 4410.
[60] B. Meunier, *Chem. Rev.* **1992**, *92*, 1411. B. Meunier, A. Robert, G. Pratviel, J. Bernadou, in *The Porphyrin Handbook* (Eds.: K. M. Kadish, K. Smith, R. Guilard), Academic Press, San Diego, **2000**, vol. 4, pp. 119−188.
[61] T. Okamoto, K. Sasaki, S. Oka, *J. Am. Chem. Soc.* **1988**, *110*, 1187.
[62] Y. Ito, K. Kunimoto, S. Miyachi, K. Kako, *Tetrahedron Lett.* **1991**, *32*, 4007.
[63] R. J. Balahura, A. Sorokin, J. Bernadou, B. Meunier, *Inorg. Chem.* **1997**, *36*, 3488.
[64] K. Wietzerbin, J. Bernadou, B. Meunier, *Eur. J. Inorg. Chem.* **1999**, 1467.

Received December 16, 1999
[I99386]

Alkali Metal Templated Assembly of an Iron Trigonal Prism

Jeremy C. Goodwin,[a] Daniel J. Price,[b] Annie K. Powell,*[c] and Sarah L. Heath*[a]

Keywords: Iron / Cluster compounds / Magnetic properties / Self-assembly / Alkali metals

A novel hexanuclear iron(III) complex $[Fe_6(C_7H_{11}NO_5)_6(\mu_2\text{-}O)_3Na][NO_3]\cdot 18H_2O$ has been synthesised from *N*-(2-hydroxypropyl)iminodiacetic acid and has been shown by X-ray crystallography to possess a prismatic structure containing a sodium ion in the core.

Introduction

Metal-directed spontaneous self-assembly has been shown to be a versatile tool in the construction of some spectacular three dimensional polymetallic architectures.[1–6] In recent years there have been several examples of the use of alkali metals to template the assembly of two dimensional metallomacrocycles[7–10] and, more recently, a three dimensional cobalt/rhenium box.[11] In the case of the metallomacrocycles, the size of the macrocycle is controlled by the radii of the templating cation. For example, with sodium Fe_6,[8,9] Cu_6[7] and Mn_6[10] wheels have been synthesised, whereas caesium promotes the synthesis of an Fe_8 wheel.[9] The metallobox formed with cobalt and rhenium is also cation selective, preferentially binding caesium over potassium. The organisation of transition metal based motifs around templating cations offers prospects for the production of tailored molecular materials and the creation of size selective host species. We have been investigating the reactions of transition metals with molecules based on the ligand heidi [H_3heidi = $N(CH_2COOH)_2(CH_2CH_2OH)$] which we have reported previously in the synthesis of polyiron(III) oxyhydroxide clusters.[12] Here we report the alkali metal templated synthesis of a new, three dimensional architecture formed with the related ligand pida [H_3pida = *N*-(2-hydroxypropyl)iminodiacetic acid], which produces an arrangement where the iron atoms form a twisted trigonal prism.

Results and Discussion

The reaction of equimolar amounts of H_3pida [*N*-(2-hydroxypropyl)iminodiacetic acid] with hydrated iron(III) nitrate and sodium hydroxide in a threefold molar excess results in the formation of **1**. An X-ray analysis of **1** reveals the formation of a beautiful three dimensional Fe_6 cage structure assembled around a central sodium cation, $[Fe_6(C_7H_{11}NO_5)_6(\mu_2\text{-}O)_3Na][NO_3]\cdot 18H_2O$, the cation of which is shown in Figure 1. The cage is formed through the interaction of three μ_2-oxide-bridged iron dimer units $\{LFe\}_2O$, linked by carboxylate bridges and templated about the central Na^+ through further carboxylate interactions. Each iron centre is in a distorted octahedral geometry consisting of a nitrogen, two carboxylate oxygens and a protonated alcohol oxygen from the ligand, a bridging μ_2-oxide and a bridging carboxylate from a symmetry related ligand. The iron-oxy core of **1** is shown in Figure 2a. The central sodium ion lies on a three fold rotation axis and is surrounded by a slightly distorted trigonal prism of oxygen atoms (Figure 2b) formed from the coordinating carboxylate oxygens of the ligand (O2, O2A, O2B, O7, O7A, O7B) with sodium to oxygen bond lengths of 2.444(3) and

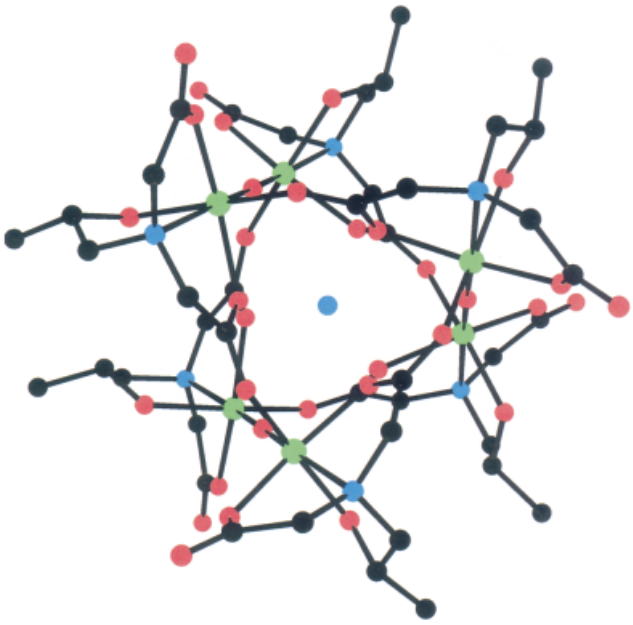


Figure 1. The cation of $[Fe_6(C_7H_{11}NO_5)_6(\mu_2\text{-}O)_3Na]^+$ **(1)** viewed down the *a* axis

[a] Department of Chemistry, University of York, Heslington, York, YO10 5DD, U.K.
Fax: (internat.) + 44-1904/432-516
E-mail: slh11@york.ac.uk, jcg105@york.ac.uk
[b] Department of Chemistry, University of Edinburgh, West Mains Road, Edinburgh, EH9 3JJ, UK
Fax: (internat.) + 44-131/650-4743
E-mail: djp01@holyrood.ed.ac.uk
[c] Institut für Anorganische Chemie, Universität Karlsruhe, Engesserstr. Geb. 30.45, D-76128 Karlsruhe, Germany
Fax: (internat.) + 49-721/608-8142
E-mail: powell@achibm6.chemie.uni-karlsruhe.de

 © WILEY-VCH Verlag GmbH, D-69451 Weinheim, 2000 1434–1948/00/0707–1407 $ 17.50+.50/0

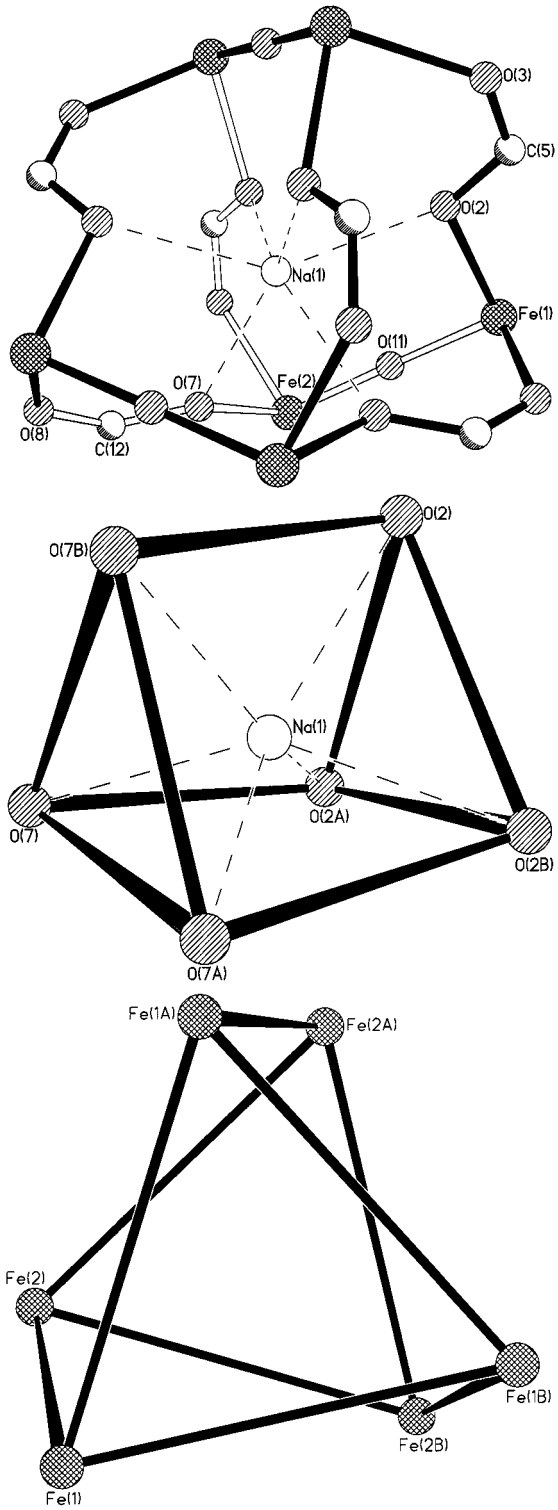


Figure 2. a) The central core of **1**; b) the coordination environment of the Na^+ cation; c) the distorted trigonal prismatic arrangement of the iron atoms

2.446(3) Å. The bridging μ_2-oxide oxygen (O11) is further away from the sodium at a distance of 2.986(3) Å. The volume of the oxygen prism, as calculated using the area of the smaller triangular face defined by O2, O2A, O2B, O7, is 14.11 $Å^3$.

The iron atoms are arranged in a much more distorted trigonal prism with the trigonal faces rotated at an angle of 27.3° to each other, as illustrated in Figure 2c. The iron atoms that form the trigonal faces of the prism are bridged by the carboxylate oxygens and are separated by distances of 5.362 Å (Fe2, Fe2A, Fe2B) and 5.365 Å (Fe1, Fe1A, Fe1B). The intra-trigonal interactions are afforded by an almost linear μ_2-oxide bridge [Fe1−O11−Fe2 = 179.1(2)°] and, consequently, the iron atoms have a much shorter separation, Fe1−Fe2 = 3.548 Å.

Reactions of equimolar equivalents of iron(III) nitrate and the barium salt of *N*-(2-hydroxypropyl)iminodiacetic acid with two equivalents of sodium hydroxide, results in the formation of the alkoxo bridged dimer $[Fe_2(C_7H_{10}NO_5)_2(H_2O)_2]$ **(2)**. The product is isostructural with the iron/heidi alkoxo bridged dimer synthesised by us previously.[12]

Preliminary magnetic studies have been performed on a powdered sample of **1** between 2 and 300 K in an applied field of 50 G. The susceptibility versus temperature is shown in Figure 3. It is clear from the product $\chi T(T)$ and the effective moment $\mu_{eff}(T)$ that **1** shows a very strong anti-ferromagnetic character, although the system does not follow a Curie-Weiss law. The room temperature net moment per iron ion is 1.83 μ_B which is much smaller than the expected value of 5.92 μ_B for isolated spin 5/2 ions implying a strong exchange coupling even at this temperature.

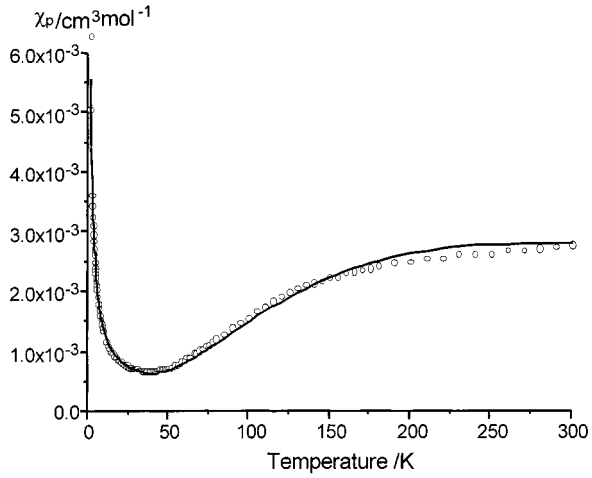


Figure 3. The molar susceptibility of **1** per unit dimer as a function of temperature (circles = experimental values, solid line = calculated for $J = -92 cm^{-1}$)

Although structurally **1** forms an Fe_6 cluster with two coupling pathways: J mediated by the μ_2-oxide bridge and J' through the carboxylate links, we expect $|J| >> |J'|$. Thus neglecting J' allows us to use a simple Heisenberg dimer model:[13]

$$\hat{H} = -2J\mathbf{S}_A \bullet \mathbf{S}_B$$

$$\chi_{dimer} = \frac{2Ng^2\mu_B^2}{k_BT}\frac{\left(e^{2x} + 5e^{6x} + 14e^{12x} + 30e^{20x} + 55e^{30x}\right)}{\left(1 + 3e^{2x} + 5e^{6x} + 7e^{12x} + 9e^{20x} + 11e^{30x}\right)}$$

where $x = J / k_BT$

The equation is often convoluted with a paramagnetic contribution from monomeric impurities (P) and a temperature independent component (C):[14]

$$\chi = (1 - P)\chi_{dimer} + 2P\chi_{monomer} + C$$

The iron(III) ion has a $^6A_{1g}$ ground term and should show Heisenberg behaviour with the temperature-independent contribution zero and the g value exactly 2.0. Fixing these and allowing the two other parameters to vary freely we obtain a good fit with $J = -82(1)$ cm^{-1} and $P = 0.4\%$.

A better fit could be obtained by allowing a nonzero temperature-independent component. This gave $J = -92(1)$ cm^{-1}, $P = 0.3\%$ and $C = 0.00032$ cm^3·mol^{-1}. In part, the problem to determine J precisely stems from the fact the J is so large, and even at room temperature the spins remain quite strongly coupled. It is interesting to note that the value of J is very sensitive to the value of C even though it is only a fraction of the estimated diamagnetic correction. Although temperature-independent behaviour may be caused by Van Vleck paramagnetism, in this case we believe that the constant (C) corresponds to a further diamagnetic correction since Pascal's constants are only approximate and no allowance had been made for the contribution of the sample capsule. We therefore conclude that the value of J for **1** is $-92(1)$ cm^{-1}. This large value of J is similar to those found in other materials where a near linear Fe−O−Fe exchange pathway is present.[15]

Conclusion

The small cavity size generated by the oxygen prism in **1** (14.11 Å^3) means that the cluster should only form in the presence of metal cations with an ionic radius similar to that of Na^+. Preliminary studies show that this may well be the case, with infrared evidence indicating that it is possible to synthesise the cluster with Ca^{2+} and Eu^{3+} templating the assembly but not with K^+, Mg^{2+} and Li^+. Hexamer formation was confirmed by the occurrence of the Fe−O−Fe asymmetric stretch at 845 cm^{-1} and the general similarity of the fingerprint region of the spectrum (1600−400 cm^{-1}). Presumably, the extra positive charge introduced by these cations will be compensated for by the presence of an additional one or two nitrate anions. The encapsulation of an ion such as Eu^{3+} or Tb^{3+} offers the possibility of creating luminescent species with long lifetimes. We are currently undertaking further characterisation of these reactions and their products.

Experimental Section

General Remarks: The magnetic behaviour of a powdered sample of **1** was measured on a Quantum Design MPMS SQUID magnetometer between 2 and 300 K in an applied field of 50 G. The molar susceptibility was corrected for diamagnetism using a value of $\chi_{dia} = -890 \times 10^{-6}$ cm^3·mol^{-1} determined from Pascal's constants. Single crystal X-ray data were collected on a Bruker SMART-CCD equipped with an Oxford Cryostream low temperature device.

***N*-(2-hydroxypropyl)iminodiacetetic Acid (pida):** DL-1-Amino-2-propanol (7.5 g, 0.1 mol), ethylbromoacetate (33.4 g, 0.2 mol) and potassium hydrogen carbonate (20.0 g, 0.2 mol) were refluxed in EtOH (50 cm^3) for 24 hours. The solid KBr formed was filtered off and the solvent removed in vacuo. The resultant pale yellow oil was refluxed in H_2O (80 cm^3) and 37% HCl (2 cm^3) for 24 hours. The solution was then reduced down to 30 cm^3 and placed in the fridge. In four days white crystals of $C_7H_{13}NO_5$ (6.12 g, 32%) formed. − $C_7H_{13}NO_5$ (191.18): calcd. C 43.98, H 6.85, N 7.33; found C 43.73, H 7.15, N 7.33. − ^{1}H NMR (250 MHz, D_2O): δ = 1.20 (d, 3 H, CH_3), 3.30 (m, 2 H, CH_2), 4.05 (s, 4 H, CH_2), 4.15 (m, 1 H, CH).

Pida Hexamer, $[Fe_6(C_7H_{11}NO_5)_6(\mu_2\text{-}O)_3Na][NO_3]\cdot 18H_2O$ (1): A solution of *N*-(2-hydroxypropyl)iminodiacetic acid (2.5 mmol) and sodium hydroxide (7.5 mmol) in water (10 cm^3) was added slowly with stirring to a solution of hydrated iron(III) nitrate (2.5 mmol) in water (10 cm^3). The pH of the resultant red solution was 2.47. Red hexagonal crystals of **(1)** formed in 59% yield after three weeks. − $C_{42}H_{104}Fe_6N_7NaO_{54}$ (1927.40): calcd. C 26.15, H 5.43, Fe 17.37, N 5.08; found C 25.94, H 4.97, Fe 17.45, N 5.24.

Pida Dimer, $[(FeC_7H_{10}NO_5)_2]\cdot 6H_2O$ (2): A solution of the barium salt of *N*-(2-hydroxypropyl)iminodiacetic acid (2.5 mmol) and sodium hydroxide (5 mmol) in water (10 cm^3) was added slowly with stirring to a solution of hydrated iron(III) nitrate (2.5 mmol) in water (10 cm^3). The pH of the resultant green solution was 2.54. Green crystals of **2** formed in 32% yield after three months. − $C_{14}H_{32}Fe_2N_2O_{16}$ (596.12): calcd. C 28.21, H 5.41, Fe 18.74, N 4.70; found C 28.14, H 5.21, Fe 18.61, N 4.94.

X-ray Crystallographic Study

Crystal Data for 1: $[Fe_6(C_7H_{11}NO_5)_6(\mu_2\text{-}O)_3Na][NO_3]\cdot 18H_2O$, red hexagonal block of dimension 0.45 × 0.33 × 0.31, M = 1927.4, trigonal, space group $P6(3)$, Z = 2, $a = b$ = 14.1386(7) Å, c = 22.3076(16) Å, U = 3861.9(4) Å^3, D_c = 1.658 g cm^{-3}, T = 150(2) K, $F(000)$ = 2004, Mo-K_α radiation (λ = 0.71073), μ = 1.217 mm^{-1}, 28695 reflections measured in the range 2.47° ≤ θ ≤ 28.29°, unique 6173 (R_{int} = 0.0514) which were used in all calculations. The structure was solved by direct methods and refined using full-matrix least-squares on F^2 to $R1$ = 0.0543, S = 0.991, for 5145 reflections with $F > 4\sigma(F)$ and 368 refined parameters, $wR2$ (all data) = 0.1411.

Crystal Data for 2: $Fe_2C_{14}H_{32}N_2O_{16}$, green needles of dimension 0.35 × 0.06 × 0.05, M = 596.12, monoclinic, space group $C2/c$, Z = 4, a = 14.0792(15) Å, b = 11.6006(12) Å, c = 14.5675(12) Å, β = 97.415(2), U = 2359.4(4) Å^3, D_c =1.678 g cm^{-3}, T = 150(2) K, $F(000)$ = 1240, Mo-K_α radiation (λ = 0.71073 Å), μ = 1.309 mm^{-1}, 6203 reflections measured in the range 2.28° ≤ θ ≤ 25.00°, 2079 unique (R_{int} = 0.091) which were used in all calculations. The structure was solved by direct methods and refined using full-matrix least-squares on F^2 to $R1$ = 0.0541, $wR2$ = 0.1396, S = 1.070, for 1698 reflections with $F > 4\sigma(F)$ and 188 refined parameters, $wR2$ (all data) = 0.1562.

Crystallographic data (excluding structure factors) for the structures reported in this paper have been deposited with the Cambridge Crystallographic Data Centre as supplementary publication nos. CCDC-137361 (**2**), CCDC-137362 (**1**). Copies of the data can be obtained free of charge on application to CCDC, 12 Union Road, Cambridge CB2 1EZ, UK [Fax: (internat.) + 44-1223/336-033; E-mail: deposit@ccdc.cam.ac.uk].

Acknowledgments

We thank the EPSRC for a studentship (JCG) and an Advanced Fellowship (DJP), the Royal Society for the provision of a University Research Fellowship (SLH). We are grateful to Dr. H. Blythe (Department of Physics, University of Sheffield) for collecting the magnetic data.

[1] A. M. Garcia, F. J. Romero Salguero, D. M. Bassani, J. M. Lehn, G. Baum, D. Fenske *Chem. Eur. J.* **1999**, *5*, 1803−1808.
[2] R. W. Saalfrank, I. Bernt, *Current Opinion In Solid State & Materials Science* **1998**, *3*, 407−413.
[3] B. Olenyuk, J. A. Whiteford, A. Fechtenkotter, P. J. Stang, *Nature* **1999**, *398*, 796−799.
[4] M. Fujita, *Chem. Soc. Rev.* **1998**, *27*, 417−425.
[5] S. Roche, C. Haslam, H. Adams, S. L. Heath, J. A. Thomas, *Chem. Commun.* **1998**, 1681−1682.
[6] J. -M. Lehn, *Supramolecular Chemistry*, VCH Weinheim, Germany, **1995**.
[7] A. J. Blake, R. O. Gould, P. E. Y. Milne, R. E. P. Winpenny, *J. Chem. Soc., Chem. Commun.* **1991**, 1453−1455.
[8] A. Caneschi, A. Cornia, A. C. Fabretti, S. Foner, D. Gatteschi, R. Grandi, L. Schenetti, *Chem. Eur. J.* **1996**, *2*, 1379−1387.
[9] R. W. Saalfrank, I. Bernt, E. Uller, F. Hampel, *Angew. Chem. Int. Ed. Engl.* **1997**, *36*, 2482−2485.
[10] G. -L. Abbati, A. Cornia, A. C. Fabretti, A. Caneschi, D. Gatteschi, *Inorg. Chem.* **1998**, *37*, 1430−1431.
[11] K. K. Klausmeyer, S. R. Wilson, T. B. Rauchfuss, *J. Am. Chem. Soc.* **1999**, *121*, 2705−2711.
[12] S. L. Heath, A. K. Powell, *Angew. Chem. Int. Ed. Engl.* **1992**, *31*, 191−193.
[13] C. J. O′Conner, *Prog. Inorg. Chem*. **1979**, *29*, 204−283.
[14] See for example: Q. Chen, J. B. Lynch, P. Gomez-Romero, A. Ben-Hussein, G. B. Jameson, C. J. O′Conner, L. Que, Jr., *Inorg. Chem*. **1988**, *27*, 2673−2681.
[15] D. M.Kurtz, Jr., *Chem. Rev.* **1990**, *90*, 585−606.

Received February 4, 2000
[I00036]

The Chemistry of New Nitrosyltungsten Complexes with Pyridyl-Functionalized Phosphane Ligands

Jürgen Baur,[a] Heiko Jacobsen,[a] Peter Burger,[a] Georg Artus,[a] Heinz Berke,*[a] and Lutz Dahlenburg[b]

Keywords: Tungsten / Hydride complexes / P ligands / N ligands / Chelates / Ligand dynamics

The coordination chemistry of pyridylphosphanes, such as 2-(6-*tert*-butylpyridyl)diphenylphosphane (Ph_2P-*tert*-Bupy) (**6**) and 2-(6-*tert*-butylpyridyl)dimethylphosphane (Me_2P-*tert*-Bupy) (**7**) towards a number of nitrosyltungsten complexes is reported. Displacement of the loosely coordinated MeCN from $[W(CH_3CN)_3(CO)_2(NO)][BF_4]$ led to the following cationic compounds incorporating mono- and bidentate coordinated phosphane ligands: *cis*,*cis*-$[W(CO)_2(NO)(Ph_2PR)(\eta^2\text{-}Ph_2PR)][BF_4]$, [R = 2-pyridyl (**9a**), 2-picolyl (**11**)], *cis*,*cis*-$[W(CO)(NO)(\eta^2\text{-}Ph_2Ppy)_2][BF_4]$ (**20**), *trans*,*trans*-$[W(CO)(NO)(\eta^2\text{-}Ph_2Ppy)_2][BPh_4]$ (**21**), *fac*-$[W(CO)_2(NO)(Me_2P\text{-py})_3][BF_4]$ (**16**), *fac*-$[W(CO)_2(NO)(Me_2P\text{-}tert\text{-Bupy})_3][BF_4]$ (**18**), *cis*,*cis*-$[W(CO)_2(NO)(Me_2Ppy)(\eta^2\text{-}Me_2Ppy)][BF_4]$ (**22**), and *cis*,*cis*-$[W(CO)_2(CH_3CN)(NO)(Me_2P\text{-}tert\text{-Bupy})_2][BF_4]$ (**23a**). The cationic complex *cis*,*mer*-$[W(CO)_3(NO)(Ph_2P\text{-}tert\text{-Bupy})_2][PF_6]$ (**14**) has been prepared by nitrosylation of *cis*/*trans*-$W(CO)_4(Ph_2P\text{-}tert\text{-Bupy})_2$ (**13**). Reactions of **9a**, **11**, **14**, **16**, and **18** with hydride transfer reagents afforded *trans*,*trans*-$HW(CO)_2(NO)(Ph_2Ppy)_2$ (**10**), *trans*,*trans*-$HW(CO)_2(NO)(Ph_2Ppic)_2$ (**12**), *trans*,*trans*-$HW(CO)_2(NO)(Ph_2\text{-}t\text{Bupy})_2$ (**15**), *cis*/*trans*-$HW(CO)_2(NO)(Me_2Ppy)_2$ (**17**), and *cis*/*trans*-$HW(CO)_2(NO)(Me_2P\text{-}tert\text{-Bupy})_2$ (**19**), respectively. Reactivity experiments with acetic acid, hydroiodic acid, carbon dioxide, and acetylenedicarboxylic acid were performed, and were found to afford *trans*-$W(CO)(NO)(Ph_2Ppy)_2(\eta^2\text{-}CH_3CO_2)$ (**24**), *trans*,*trans*-$IW(CO)_2(NO)(Ph_2Ppy)_2$ (**25**), *trans*-$W(HCO_2)(CO)_2(NO)(Ph_2Ppy)_2$ (**26**), and *trans*-$W\{\eta^2\text{-}(Z)\text{-}C(CO_2Me)=CH[C(O)OMe]\}(CO)(NO)(Ph_2Ppic)_2$ (**27**), respectively. The influence of the pyridyl substituent in **10** was probed by a comparative H/D exchange experiment in which **10** and the analogous complex $HW(CO)_2(NO)(PPh_3)_2$ were treated with MeOD. The deuterated complex *trans*,*trans*-$WD(CO)_2(NO)(Ph_2Ppy)_2$ (**28**) could be isolated. The structures of **9a**, **11**, **14**, and **20** have been determined by single-crystal X-ray diffraction analysis.

Introduction

Previously, we have demonstrated that nitrosyltungsten hydride complexes are efficient reducing agents for aldehydes and ketones, the best results being achieved in the presence of a weak acid.[1−3] Furthermore, it has been shown that O−H and N−H bonds can act as weak acid components towards weakly basic M−H bonds.[4−8] Thus, intramolecular H···H interactions may be established, which could also play an important role in the heterolytic splitting of dihydrogen.[9] The pyridylphosphane ligand offers the possibility of either abstracting a proton from an external source or of activating a dihydrogen ligand coordinated to an unsaturated metal centre.[10] Therefore, this base-promoted splitting of dihydrogen through formation of a (ligand−H^+)−(metal−H^-) intermediate is of great significance with regard to catalytic ionic hydrogenations, as recently described by Noyori.[11,12] In order to design such a bifunctional system, we set out to prepare a series of cationic nitrosyltungsten and nitrosyltungsten hydride species having basic pyridyl substituents present in their coordination spheres. Similar investigations with P,N-, P,O-, and P,S-hybrid ligands have been described previously.[13−15]

[a] Anorganisch-chemisches Institut der Universität Zürich, Winterthurerstrasse 190, 8057 Zürich, Switzerland
Fax: (internat.) + 41-1/635-46802
E-mail: hberke@unizh.ch
[b] Institut für Anorganische Chemie der Friedrich-Alexander-Universität Erlangen-Nürnberg, Egerlandstraße 1, 91058 Erlangen, Germany

Results and Discussion

Preparation of Pyridyl-Substituted Phosphane Ligands

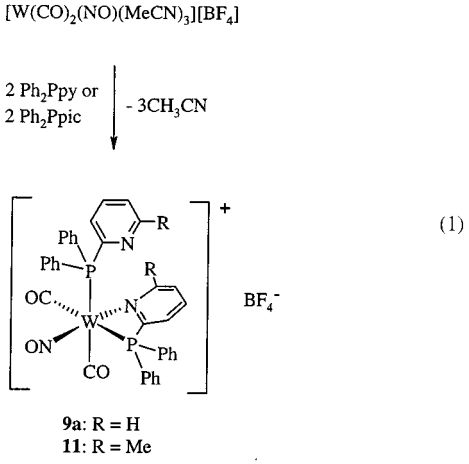
Diphenylpyridylphosphane (Ph_2Ppy)[16] and dimethylpyridylphosphane (Me_2Ppy)[17] were prepared according to literature procedures. On the other hand, new methods were developed for the synthesis of phosphanes bearing bulkier pyridyl substituents. Thus, the picolyl-substituted derivative 2-(6-methylpyridyl)diphenylphosphane (Ph_2Ppic) was synthesized by a route different from that reported in the literature[18] by adding 6-chloro-2-picoline to a solution of $LiPPh_2$, prepared from *n*-butyllithium and diphenylphosphane. For the preparation of the *tert*-butyl-substituted phosphanes, 2-(6-*tert*-butylpyridyl)diphenylphosphane (Ph_2P-*tert*-Bupy) and 2-(6-*tert*-butylpyridyl)dimethylphosphane (Me_2P-*tert*-Bupy), the starting material 2-*tert*-butyl-6-chloropyridine was synthesized according to a method described by Mariella for analogous compounds.[19]

Preparation of the Cationic Complexes

With the exception of the bulkiest phosphane, Ph_2P-*tert*-Bupy, the best yields of the cationic metal complexes were

 © WILEY-VCH Verlag GmbH, D-69451 Weinheim, 2000 1434−1948/00/0707−1411 $ 17.50+.50/0

obtained by using $[W(CH_3CN)_3(CO)_2(NO)][BF_4]$[20] as the starting material. Thus, the addition of two equivalents of Ph_2Ppy or Ph_2Ppic to $[W(CH_3CN)_3(CO)_2(NO)][BF_4]$ in dichloromethane resulted in substitution of the three acetonitrile ligands by two phosphanes, one of which coordinated in a monodentate fashion and the other in a bidentate mode, thereby affording complexes **9a** and **11**, respectively [Equation (1)]. Spectroscopic studies showed that no further phosphane coordination occurred, even in the presence of an excess of the ligand.



(1)

The variable-temperature (VT) NMR spectra of compound **9a** reveal dynamic behaviour. At room temperature, two broad resonances are observed in the ^{31}P-NMR spectrum at $\delta = 24.8$ and $\delta = -18.3$, which sharpen into two doublets below -15 °C. The energy of activation for the exchange process was estimated to be 57(2) kJ/mol by lineshape analysis. When the pyridyl groups in **9a** are replaced by picolyl groups as in complex **11**, no dynamic behaviour is observed, even at 70 °C. In order to obtain more information regarding the mechanism of the pyridyl exchange process, DFT calculations were performed on the model compound $[W(CO)_2(NO)(H_2Ppy)(\eta^2\text{-}H_2Ppy)]^+$. The energy profile of the exchange reaction, together with a systematic sketch of the reaction coordinate, is presented in Figure 1. The distance d_{N1-W} was allowed to vary from 225 pm to 395 pm; it can be seen that the energy rises smoothly from 0 kJ/mol (the reference value for the ground state) to 62 kJ/mol (the transition state) and then decreases again (see Figure 1, solid line).

More interesting still are the changes in d_{N2-W} as a function of the value of d_{N1-W} (Figure 1, dashed line). We analysed this by following the actual linear transit mode, i.e. by bringing the uncoordinated atom N1 in towards the distance for binding to the metal centre. As the N1 atom approaches (d_{N1-W} in the range from 395 pm to 325 pm), the four-membered metallacycle remains essentially intact and d_{N2-W} does not change significantly. At the transition state, two equally long d_{N-W} distances are present. If N1 is now brought closer to the metal centre, d_{N2-W} immediately takes on values around 380 pm, the distance corresponding to the uncoordinated ring. From this, it might be concluded that bond cleavage and bond formation do not occur in a

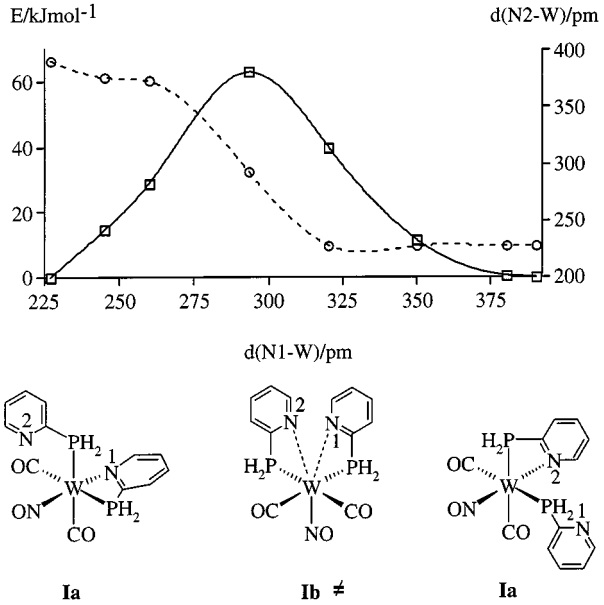


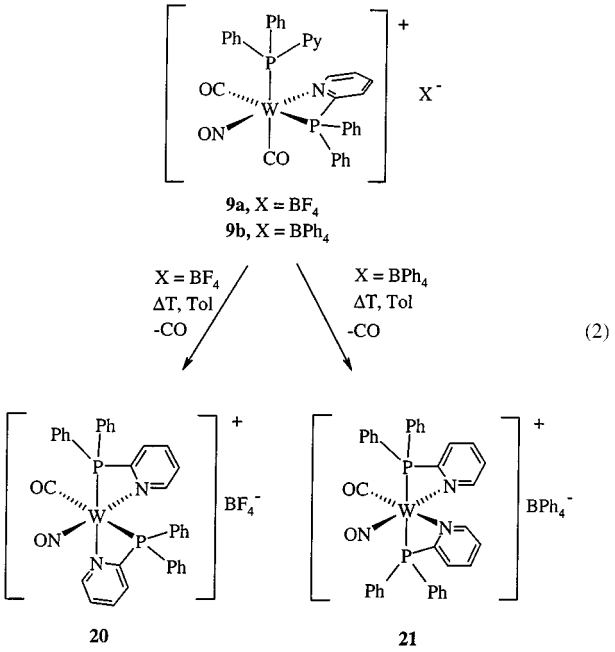
Figure 1. Energy profile for the pyridyl exchange reaction; the solid line refers to the left ordinate axis, the dashed line to the right ordinate axis

concerted fashion and one may envisage the exchange process as follows. The N2 atom of the free pyridyl unit first approaches the metal centre, which requires about two-thirds of the energy of activation. Bond cleavage then occurs, and in the transition state the two N atoms are only weakly coordinated to the tungsten centre. The formerly bound pyridyl unit rotates away to relieve steric hindrance, allowing formation of the bond between N2 and W. The calculated activation energy of 62 kJ/mol is in good agreement with the experimentally determined value of 57(2) kJ/mol. This result can thus be taken as strong evidence in favour of the suggested reaction mechanism.

Furthermore, it is noteworthy that the two pyridyl groups in complex **11** do not exchange. Taking the geometry of the transition state for **9**, replacing the H atoms in the positions α to N by methyl groups, and assuming a C−C bond length of 153 pm, it can be calculated that the two CH_3 carbon centres are separated by just 213 pm. This is within the range of the effective van der Waals radius of a methyl group (200 pm). It seems likely that the transition-state geometry of the intramolecular rearrangement of **11** does not allow the two pyridyl rings to pass each other. Thus, the exchange process is hindered for steric reasons.

When a solution of **9a** in chloroform was set aside for several hours at room temperature, the formation of small amounts of decarbonylated complex isomers with both phosphane ligands coordinated in a bidentate fashion was observed. On warming the solution to 70 °C, however, decomposition was observed by NMR spectroscopy. In order to confirm the structures of the isomers, a specific synthesis was developed [Equation (2)]. The monocarbonyl complex **20** with the phosphorus donors coordinated in a *cis* arrangement was prepared by heating a suspension of **9b** in toluene to 100 °C with slow removal of the solvent under slightly reduced pressure. A similar procedure was em-

ployed to synthesize the *trans* isomer **21**. In order to increase the solubility of the cationic species, it was necessary to replace the BF_4 anion of **9a** by BPh_4, thereby affording the analogous complex **9b**. Dissolution of **9b** with a few drops of acetonitrile in toluene, heating to 95 °C, removal of the solvent under reduced pressure, and repeating of this procedure afforded a red powder. Recrystallization from dichloromethane at −30 °C gave **21** as dark-red crystals. The ^{31}P-NMR spectrum of the product featured an AB system ($^2J_{AB}$ = 121 Hz) along with the respective tungsten satellites and characteristic J_{PW} values of 277 Hz and 299 Hz for the two P atoms located in *trans* positions.

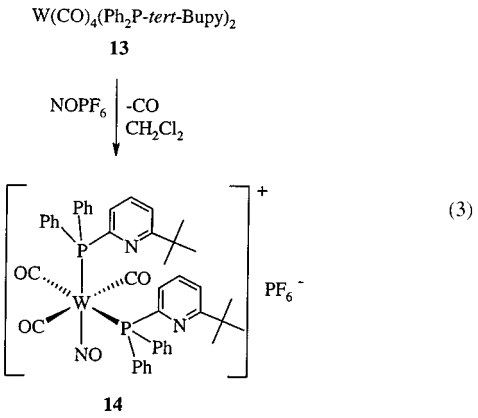


9a, X = BF_4
9b, X = BPh_4

(2)

20 **21**

A suitable reaction for preparing the cationic complex **14** bearing the bulky Ph_2P-*tert*-Bupy ligands that avoided coordination of the pyridine substituents, was found to be nitrosylation of the neutral tetracarbonyl compound **12**, Equation (3).

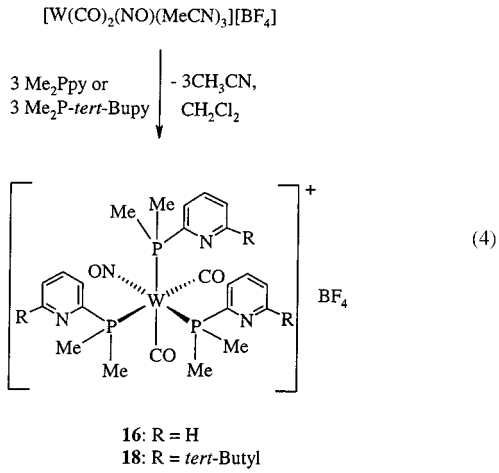


(3)

14

A 20% excess of $NOPF_6$ was found to be essential to achieve complete transformation of **13**. The crude product consisted of **14** (70%) and unidentified impurities (ca. 25%), as well as uncoordinated phosphane (5%). The collected solid was washed several times with diethyl ether and then taken up in a mixture of diethyl ether/dichloromethane. Slow evaporation of the solvents afforded bright-yellow crystals of the desired product.

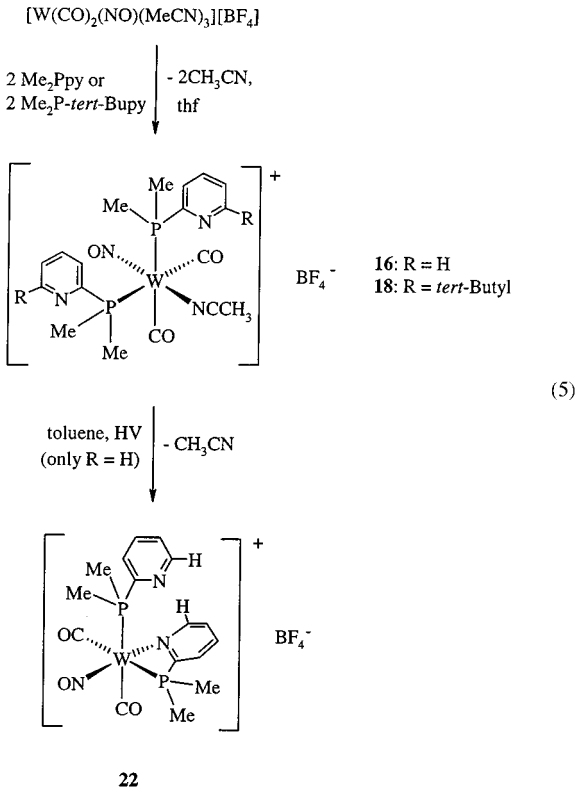
In contrast, the reaction of the more basic phosphanes Me_2Ppy or Me_2P-*tert*-Bupy with $[W(CH_3CN)_3(CO)_2(NO)][BF_4]$ in dichloromethane resulted in the substitution of three acetonitrile ligands by *P*-coordinated phosphanes [Equation (4)]. The formation of the trisubstituted complexes **16** and **18** could be observed by ^{31}P-NMR spectroscopy even after the addition of just one equivalent of the phosphane ligand to the acetonitrile complex.



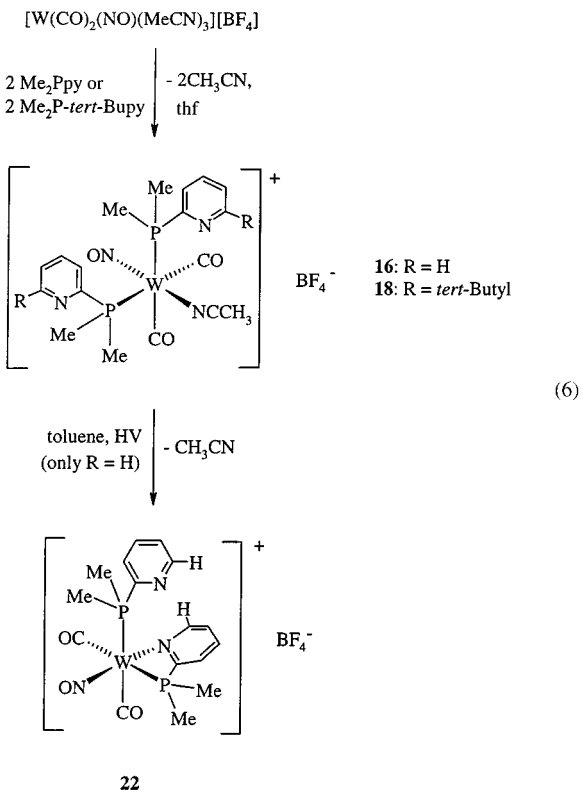
(4)

16: R = H
18: R = *tert*-Butyl

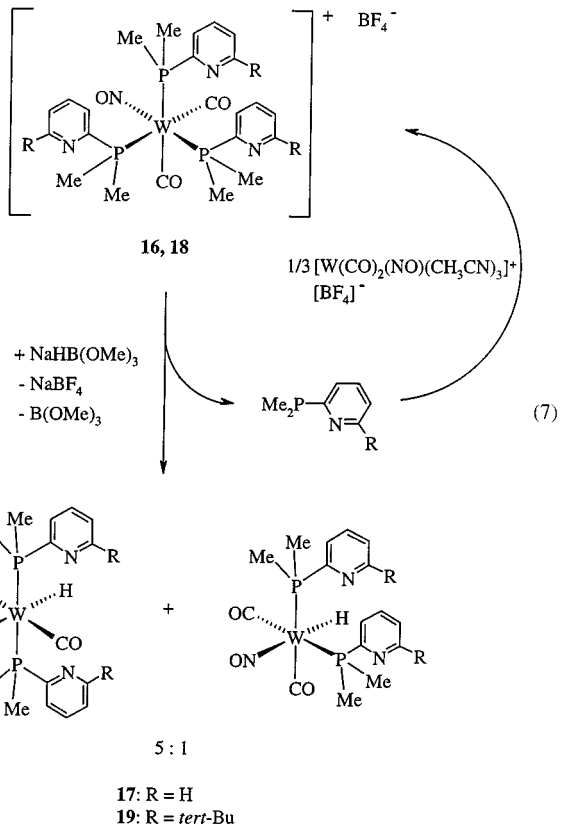
Complexes **16** and **18** were found to be very stable in air in the solid state, and only slightly moisture-sensitive in solution. When the former reaction was carried out in THF using exactly two equivalents of the phosphane, the ^{31}P-NMR spectra of the reaction mixtures showed one singlet with a J_{PW} of 254 Hz for the Me_2Ppy derivative and 257 Hz for the Me_2P-*tert*-Bupy derivative, indicating a *cis* arrangement of the two phosphanes coordinated to the tungsten centre. A further resonance of lower intensity was observed in each case, which disappeared upon addition of acetonitrile to the THF solution [Equation (5)]. Removal of the solvents in vacuo (10^{-1} mbar) afforded complex **22** with one Me_2Ppy ligand coordinated to the metal centre in a monodentate fashion and the second coordinated in a bidentate fashion, akin to the situation in complexes **9a** and **11**. With Me_2P-*tert*-Bupy ligands, however, the sterically demanding *tert*-butyl substituent prevents coordination of the pyridine ring and so complex **23a**, with one acetonitrile ligand remaining coordinated to the metal centre, is formed. In contrast to the complexes bearing less bulky phosphanes, the remaining acetonitrile ligand could not be removed from the metal coordination sphere, even at elevated temperatures. Exchange of the BF_4 anion by the more inert tetrakis[3,5-bis(trifluoromethyl)phenyl]borate (TFPB) **23b** and subsequent heating in vacuo (10^{-4} mbar) led only to slow decomposition of the complex.



(5)



(6)



(7)

Preparation of the Tungsten Hydrides

Depending on the nature of the cationic nitrosyltungsten complexes, three different hydride reagents were used to obtain the corresponding tungsten hydride compounds. For the cationic complexes **9a** and **11**, which have pyridine substituents coordinated at their metal centres, sodium bis(2-methoxyethyloxy)aluminium hydride (RedAl) was found to give the best yields, whereas for complex **14** sodium tetrahydroborate proved to be most efficient in displacing the carbonyl ligand. The resulting tungsten hydride complexes **10**, **12**, and **15** bearing diphenyl-substituted phosphanes were readily precipitated by rapid addition of ethanol to the reaction mixtures. The *tert*-butyl-substituted derivative **15** was found to be slightly more soluble than **10** and **12** and therefore had to be precipitated at low temperature to prevent further reaction of the hydride with the alcohol [Equation (6)].

Sodium hydrotrimethoxyborate was chosen for the reactions with the trisubstituted phosphane cations **16** and **18**, which afforded the tungsten hydride complexes **17** and **19**. The phosphane ligands abstracted during these reactions could not easily be removed from the products due to similar solubility properties. However, in both cases $[W(CH_3CN)_3(CO)_2(NO)][BF_4]$ proved to be an efficient phosphane scavanger affording the cationic starting complex, from which the product could simply be separated by extraction with pentane [Equation (7)].

Reactivity Studies

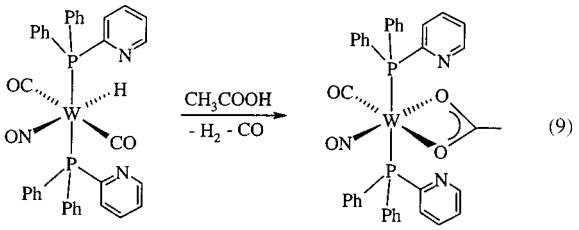
In order to assess the influence of the pyridyl substituents, complexes **10** and **12** were compared with the analog-

ous compound *trans*-$HW(CO)_2(NO)(PPh_3)_2$ prepared by Hillhouse.[21] The NMR chemical shifts and coupling constants of the carbonyl and hydride resonances, as well as the IR stretching vibrations for NO and CO, were found to be essentially identical for the three hydride complexes. Therefore, one can also expect a similar hydridic behaviour, as discussed previously by Berke et al.[22,23] for related compounds.

The reaction of **10** with HI (0.75 M in $CHCl_3$) led to the immediate evolution of hydrogen affording *trans*-$IW(CO)_2(NO)(PPh_2py)_2$ (**25**) [Equation (8)], as described for the PPh_3 derivative.

trans,trans-$HW(CO)_2(NO)(Ph_2Ppy)_2$ + HI
10
$\downarrow$ - H_2 (8)
trans,trans-$IW(CO)_2(NO)(Ph_2Ppy)_2$
25

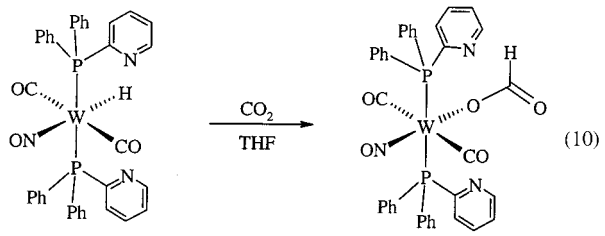
Hydrogen was also evolved when **10** was treated with glacial acetic acid in a mixture of dichloromethane and 2-propanol. Subsequent loss of one carbonyl ligand resulted in the formation of a four-membered metallacycle with the formula *trans*-$W(CO)(NO)(Ph_2Ppy)_2(\eta^2\text{-}CH_3CO_2)$ (**24**) [Equation (9)].



10 **24** (9)

The same decarbonylation reaction was also observed by Hillhouse and afforded the analogous complex bearing PPh_3 ligands.

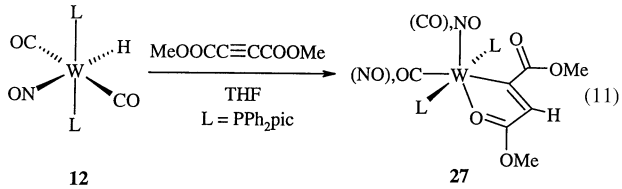
The insertion of carbon dioxide into the metal hydride bond yielding the formato complex **26** was achieved by slowly bubbling a stream of CO_2 gas through a solution of **10** in THF [Equation (10)].



10 **26** (10)

The ^{1}H-NMR resonance of the formate proton in **26** appears at $\delta = 7.06$ ($\delta = 7.08$ for the PPh_3 derivative). The oxo carbonyl resonance is seen at $\delta = 166.4$ in the ^{13}C-NMR spectrum. Identical shifts have been observed for other phosphane complexes incorporating monodentate formate ligands prepared in our laboratory, such as the analogous $P(OiPr)_3$ derivative.[24] The carbonyl intensity patterns [2050 (w), 1962 (s) cm^{-1}] in the infrared spectra are characteristic of a *trans*-dicarbonyl geometry by analogy with the PPh_3 derivative.

A further insertion experiment was performed by treating **12** with dimethyl acetylenedicarboxylate in THF. The resulting IR spectrum featured one carbonyl band at 1935 cm^{-1} indicating the loss of a single carbonyl ligand. The ^{1}H- and ^{13}C-NMR data of the resulting complex **27** were compared with those of the PMe_3 derivative.[22] However, it could not be unambiguously established which of the two isomers with regard to the positions of the NO and CO ligands had been formed [Equation (11)].

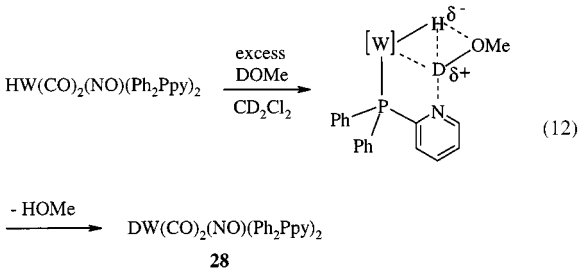


12 **27** (11)

The above reactions displayed approximately the same characteristics irrespective of whether a PPh_2py or a PPh_3 ligand was coordinated to the tungsten centre. According to the spectroscopic data and the reactivities of the tungsten hydride complexes, the pyridyl substituents seemingly have no influence on the electronic character of the hydride ligand.

Nevertheless, an H/D exchange experiment was performed in order to assess whether the basic pyridine N atom had any effect on the reactivities of the hydride complexes. The interaction of a protic alcohol function with the pyridyl substituents located in the ligand sphere could facilitate proton transfer to the hydride. In order to compare the H/D exchange rates of $HW(CO)_2(NO)(PPh_3)_2$ and $HW(CO)_2(NO)(PPh_2py)_2$ (**10**) with [D_4]methanol, a 1:1 mixture of the two complexes in CD_2Cl_2 was prepared and then a 150-fold excess of [D_4]methanol was added at 0 °C. Higher temperatures (+5 °C) led to rapid decomposition of the complexes with evolution of HD. By monitoring the reaction by ^{1}H-NMR spectroscopy for 25 min at 0 °C, it was observed that the hydride resonance of **9** at $\delta = -0.07$ completely disappeared while in the ^{31}P{^{1}H}-NMR spectra a triplet due to deuterated **9** with a PD coupling constant of $J = 3$ Hz appeared. In contrast, the analogous resonances due to $HW(CO)_2(NO)(PPh_3)_2$ did not change. After 22 hours, **10** had been completely consumed while only 30% of the PPh_3 complex had been transformed to the deuteride with partial decomposition through ligand abstraction [Equation (12)]. After a reaction time of one hour under the same conditions and further addition of [D_1]methanol to the mixture, the deuteride complex **28** readily precipitated and could be fully characterized.

Although no spectroscopic evidence was found to support the concerted mechanism proposed in Equation (12), it could be concluded from these experiments that the interaction of the protic alcohol with the pyridyl substituent is responsible for the accelerated H/D exchange.



We also carried out exploratory catalytic experiments with the hydride complexes **10** and **19** in order to investigate their activities in the ionic hydrogenation of imines. This type of catalysis has been reported for a variety of Ru, Ir, Rh, and Ti complexes. With compound **10**, we obtained the most promising results when a 5:1 mixture of isopropylisopropylideneamine and its corresponding BPh_4 salt were dissolved in a 2:1 mixture of THF/CH_2Cl_2. The amount of tungsten hydride catalyst used was 10 mol-% with respect to the imine. Stirring the reaction mixture at 70 °C for 14 hours under 60 atm of hydrogen resulted in the conversion of 35% of the imine and iminium salt to the corresponding amine and ammonium salt, respectively. The ^{31}P-NMR spectra showed one resonance corresponding to the free phosphane ligand. We conclude that about 3−4 turnovers were reached before decomposition of the catalyst occurred. Addition of the BPh_4 salt was found to be essential to initiate the reaction; no hydrogenation was observed if only the pure imine was present in solution.

When the same experiment was performed using **19** as the catalyst, an additional product could be observed in the ^1H-NMR spectrum. Reference spectra and GC-MS analysis confirmed the formation of both mono- and diisopropylamine. Further investigations using hydrogen pressures up to 100 atm and temperatures up to 90 °C led to changes in the isopropylamine/diisopropylamine ratio from 1:2 (60 °C/60 atm) up to 3:1 (90 °C/100 atm). The mechanisms of these reactions have not yet been clarified and are currently under investigation in our laboratory.

X-ray Crystal Structure Determinations

The following complexes were characterized by X-ray analysis: *cis,cis*-$[W(CO)_2(NO)(Ph_2Ppy)(\eta^2\text{-}Ph_2Ppy)][BF_4]$ (**9a**), *cis,cis*-$[W(CO)_2(NO)(Ph_2Ppic)(\eta^2\text{-}Ph_2Ppic)][BF_4]$ (**11**), *cis,mer*-$[W(CO)_3(NO)(Ph_2P\text{-}tert\text{-}Bupy)_2][PF_6]$ (**14**), and *cis,cis*-$[W(CO)(NO)(\eta^2\text{-}Ph_2Ppy)_2][BF_4]$ (**20**). In the Figures the anions of all the structures have been omitted for the sake of clarity.

Compounds **9a** (Figure 2) and **11** (Figure 3) show strongly distorted octahedra due to the formation of the four-membered metallacycle with P−W−N bond angles of approximately 64.5° in each case. The W−N(pyridyl) bond length in **11** is only slightly lengthened to 2.259(5) Å compared to 2.240 Å in **9a**. However, the steric influence of the methyl substituent in **11** is clearly apparent from the opening of the corresponding equatorial bond angles, N(1)−W(1)−C(36) in **9a** and N(2)−W(1)−C(1) in **11**, from 94.12° to 101.4(2)°.

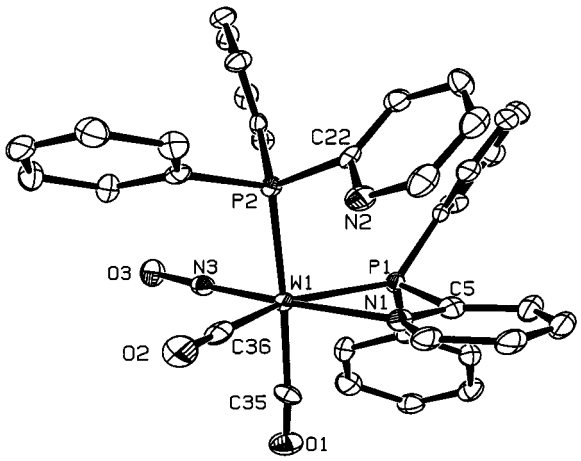


Figure 2. View of the structure of the cation of **9a**; selected bond lengths (Å) and angles (°): W(1)−N(1) 2.240, W(1)−P(1) 2.537, W(1)−P(2) 2.536, W(1)−C(36) 2.046, W(1)−N(3) 1.809, W(1)−C(35) 2.051; N(3)−W1−C(36) 95.11, N(3)−W1−C(35) 92.08, N(3)−W1−N(1) 170.70, N(3)−W1−P(2) 87.89, N(3)−W1−P(1) 106.24, C(36)−W1−C(35) 89.41, C(36)−W1−N(1) 94.12, C(36)−W1−P(2) 86.15, C(35)−W1−N(1) 86.95, C(35)−W1−P(1) 86.70, N(1)−W1−P(2) 93.80, N(1)−W1−P(1) 64.48, P(2)−W1−P(1) 97.59

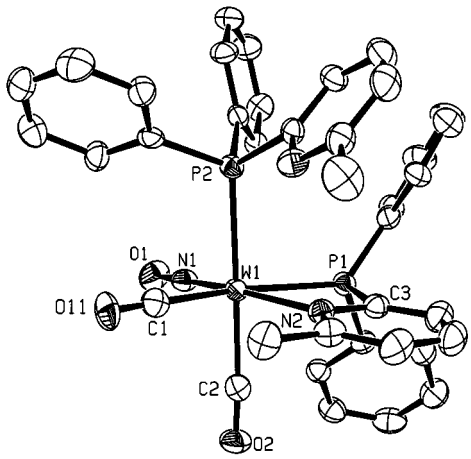


Figure 3. View of the structure of the cation of **11**; selected bond lengths (Å) and angles (°): W(1)−N(2) 2.259(5), W(1)−P(1) 2.539(2), W(1)−P(2) 2.564(1), W(1)−C(1) 2.046(7), W(1)−N(1) 1.810(5), W(1)−C(2) 2.047(6); P(1)−W(1)−P(2) 94.08(5), P(1)−W(1)−N(1) 104.1(2), P(2)−W(1)−N(1) 91.5(2), P(1)−W(1)−N(2) 64.5(1), P(2)−W(1)−N(2) 94.8(1), N(1)−W(1)−N(2) 167.3(2), P(2)−W(1)−C(1) 87.9(2), N(1)−W(1)−C(1) 89.8(2), N(2)−W(1)−C(1) 101.4(2), P(1)−W(1)−C(2) 88.2(2), N(1)−W(1)−C(2) 90.9(2), N(2)−W(1)−C(2) 83.4(2), C(1)−W(1)−C(2) 89.2(3), W(1)−P(1)−C(3) 83.6(2)

The W−N(pyridyl) bond lengths in the monocarbonyl complex **20** (Figure 4) are 2.258(3) Å for N(2) and 2.210(3) Å for N(1). The longer W−N(2) bond length can be attributed to the strong *trans* influence of the nitrosyl ligand. This effect is also manifested in the bond angles in the less strained metallacycle, 65.50(9)° for N(2)−W(1)−C(2) [cf. 64.12(9)° for N(1)−W(1)−C(1)].

In compound **14** (Figure 5), the *trans* influence of the nitrosyl ligand is also reflected in the longer phosphorus−tungsten bond length, which is 2.640(2) Å for W(1)−P(30), as compared to 2.591(2) Å for W(1)−P(10) with a carbonyl ligand coordinated in a *trans* orientation.

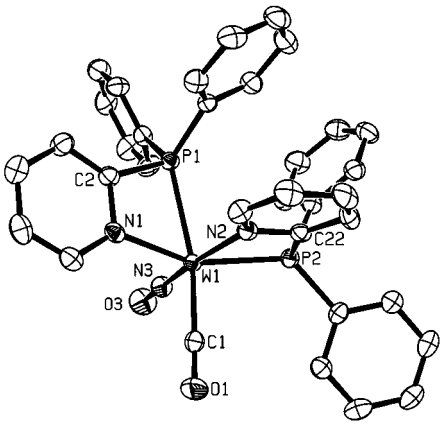


Figure 4. View of the structure of the cation of **20**; selected bond lengths (Å) and angles (°): W(1)−P(10) 2.591(2), W(1)−P(30) 2.640(2), W(1)−N(4) 1.896(7), W(1)−C(1) 1.977(8), W(1)−C(2) 2.080(9), W(1)−C(3) 2.06(1); P(1)−W(1)−P(2) 98.41(3), P(1)−W(1)−N(1) 64.12(9), P(2)−W(1)−N(1) 152.51(9), P(1)−W(1)−N(2) 84.40(8), P(2)−W(1)−N(2) 65.50(9), N(1)−W(1)−N(2) 90.7(1), P(1)−W(1)−N(3) 96.7(1), P(2)−W(1)−N(3) 105.3(1), N(1)−W(1)−N(3) 98.0(1), P(2)−W(1)−C(1) 95.0(1), N(1)−W(1)−C(1) 99.1(1), N(2)−W(1)−C(1) 90.9(1), N(3)−W(1)−C(1) 90.7(2), W(1)−P(1)−C(2) 82.5(1), W(1)−P(2)−C(22) 84.6(1), W(1)−N(1)−C(2) 108.9(3), W(1)−N(2)−C(22) 104.4(2)

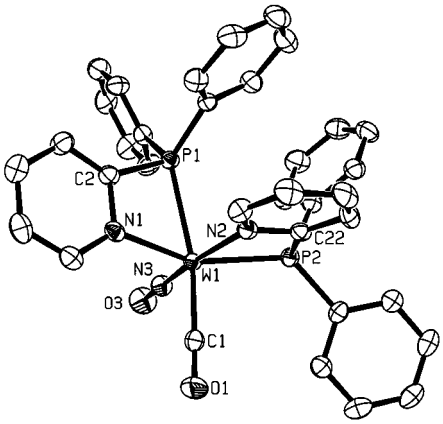


Figure 5. View of the structure of the cation of **14**; selected bond lengths (Å) and angles (°): W(1)−P(10) 2.591(2), W(1)−P(30) 2.640(2), W(1)−N(4) 1.896(7), W(1)−C(1) 1.977(8), W(1)−C(2) 2.080(9), W(1)−C(3) 2.06(1); P(10)−W(1)−P(30) 104.39(6), P(10)−W(1)−N(4) 82.0(2), P(30)−W(1)−C(1) 86.7(2), N(4)−W(1)−C(1) 87.3(3), P(10)−W(1)−C(2) 91.2(2), P(30)−W(1)−C(2) 82.5(2), N(4)−W(1)−C(2) 91.7(3), C(1)−W(1)−C(2) 93.0(3), P(10)−W(1)−C(3) 87.0(2), P(30)−W(1)−C(3) 91.5(2), N(4)−W(1)−C(3) 94.7(3), C(1)−W(1)−C(3) 90.0(4), W(1)−P(10)−C(4) 113.3(3), W(1)−P(10)−C(13) 108.3(2), W(1)−P(10)−C(19) 121.5(3), W(1)−P(30)−C(34) 108.3(2), W(1)−P(30)−C(43) 114.7(3), W(1)−P(30)−C(49) 118.3(2)

Experimental Section

General Techniques: All preparations were carried out under dry nitrogen using conventional Schlenk or glove-box techniques and dry, air-free solvents. − IR spectra were recorded with a Bio-Rad FTS-45 instrument. − ^{1}H-, ^{13}C-, and ^{31}P-NMR spectra were recorded with a Varian Gemini 200 (200 MHz for ^{1}H, 50.3 MHz for ^{13}C), a Varian Gemini 300 (300 MHz for ^{1}H, 121.5 MHz for ^{31}P, 75.4 MHz for ^{13}C), or a Bruker Avance 500 (125.8 MHz for ^{13}C). All ^{31}P-NMR spectra were proton-decoupled. The spectra were simulated using the program gNMR 4.1 (Cherwell Scientific) in the automatic iteration mode. Sodium bis(2-methoxyethyloxy)aluminium hydride (RedAl, 3.5 M in toluene) was purchased from Aldrich Chemical Co.

Sodium 3,3-Dimethyl-2-oxobutoxide (1): Sodium ribbon (15.2 g, 0.66 mol) was added to 350 mL of dry diethyl ether. A mixture of ethyl formate (48.9 g, 0.66 mol) and pinacoline (66.1 g, 0.66 mol) was then added dropwise to the reaction mixture over a period of 2 h at −30 °C. When the addition was complete, the solution was allowed to warm to room temperature and stirring was continued for a further 1 h. After evaporation of the solvent, the residual brown slurry was washed with small amounts of diethyl ether and hexane. The crude product was used in the next step without further purification. Yield: 92.4 g (0.55 mol, 83%).

6-*tert*-Butyl-3-cyano-2-pyridone (2): Sodium salt **1** (92.4 g, 0.55 mol) and cyanoacetamide (46.25 g, 0.55 mol) were dissolved in water (200 mL). Meanwhile, a solution consisting of glacial acetic acid (8 mL) and water (20 mL) was adjusted to pH = 8 by the addition of piperidine. The two solutions were then mixed and the mixture was refluxed for 2 h, cooled, and acidified with glacial acetic acid. After filtration, the brown residue was washed with water (200 mL), taken up in ethanol (200 mL), and the resulting solution was treated with activated charcoal (5 g). Evaporation of the solvent in vacuo gave the product as a white powder. Yield: 22 g (0.125 mol, 23%); m.p. 194 °C. − ^{1}H NMR (200 MHz, $CDCl_3$): δ = 12.59 (br., 1 H), 7.81 (d, $^3J_{HH}$ = 7.7 Hz, 1 H), 6.26 (d, $^3J_{HH}$ = 7.7 Hz, 1 H), 1.41 [s, 9 H, $C(CH_3)_3$]. − ^{13}C NMR (200 MHz, $CDCl_3$): δ = 164.3 (s), 162.6 (s), 148.4 (s, CH), 115.6 (s), 102.2 (s, CH), 35.9 (s, *C*Me$_3$), 28.7 [s, C(*C*H$_3$)$_3$]. − MS (EI); *m*/*z* (%): 176 [M$^+$] (22), 161 [M$^+$ − CH$_3$] (100), 134 [M$^+$ − CH$_3$ − CN − H] (12). − $C_{10}H_{12}N_2O$ (176.22): calcd. C 68.16, H 6.86, N 15.90; found C 67.89, H 6.47, N 15.82.

6-*tert*-Butyl-2-oxo-3-pyridinecarboxylic Acid (3): A solution of **2** (20.0 g, 0.11 mol) in concentrated hydrochloric acid (200 mL) was refluxed for 5 h, poured onto 200 g of ice, and washed several times with cold water. Evaporation of the water in vacuo gave the product as a white solid. Yield: 18.76 g (96 mmol, 84%); m.p. 240 °C. − ^{1}H NMR (200 MHz, $CDCl_3$): δ = 13.80 (br., 1 H), 12.40 (br., 1 H), 8.54 (d, $^3J_{HH}$ = 8 Hz, 1 H), 6.61 (d, $^3J_{HH}$ = 8 Hz, 1 H), 1.46 [s, 9 H, $C(CH_3)_3$]. − ^{13}C NMR (200 MHz, $CDCl_3$): δ = 166.1 (s), 165.4 (s), 164.0 (s), 148.1 (s, CH), 115.6 (s), 106.0 (s, CH), 36.4 (s, *C*Me$_3$), 29.3 [s, C(*C*H$_3$)$_3$]. − MS (EI); *m*/*z* (%) = 194 [M$^+$] (100), 179 [M$^+$ − CH$_3$] (76), 177 [M$^+$ − OH], 162 [M$^+$ − CH$_3$ − OH] (100). − $C_{10}H_{13}NO_3$: calcd. C 61.53, H 6.71, N 7.17; found C 61.96, H 6.30, N 7.33.

6-*tert*-Butyl-2-pyridol (4): In a 500-mL flask fitted with a cold finger, **3** (18.0 g, 92.3 mol) was heated to 315 °C for 20 min by means of a molten-metal bath. When the evolution of carbon dioxide had ceased, the residual black material was sublimed at 150 °C and a pressure of 0.1 mbar. The product was obtained in the form of white crystals. Yield: 9.4 g (62 mmol, 67%); m.p. 141 °C. − ^{1}H NMR (300 MHz, $CDCl_3$): δ = 11.76 (br., 1 H), 7.34 (m, 1 H), 6.40 (m, 1 H), 6.09 (m, 1 H), 1.34 [s, 9 H, $C(CH_3)_3$]. − ^{13}C NMR (300 MHz, $CDCl_3$): δ = 165.0 (s), 157.1 (s), 141.7 (s, CH), 117.3 (s, CH), 101.9 (s, CH), 36.4 (s, *C*Me$_3$), 29.3 [s, C(*C*H$_3$)$_3$]. − MS (EI); *m*/*z* (%): 151 [M$^+$] (100), 136 [M$^+$ − CH$_3$] (100). − $C_9H_{13}NO$ (151.21): calcd. C 71.49, H 8.67, N 9.26; found C 71.26, H 8.48, N 9.33.

2-*tert*-Butyl-6-chloropyridine (5): To a solution of **4** (9.0 g, 59.6 mmol) in refluxing phosphorus oxychloride (10 mL), phosphorus pentachloride (13.8 g) was added in small portions over a period of 30 min. The bath temperature was then increased to 160

°C and maintained at this temperature for 1 h. After cooling the mixture to room temperature and removing the solvent under reduced pressure, the residue was poured onto ice. The resulting black mixture was made strongly basic with sodium hydroxide and steam distilled to afford a pale oil. The crude product was taken up in diethyl ether and dried with Na_2SO_4. Removal of the solvent and distillation of the oil (b.p. 47 °C, 1 mbar) afforded a colourless liquid. Yield: 5.4 g (32.3 mmol, 48%). – ^{1}H NMR (300 MHz, $CDCl_3$): δ = 7.55 (m, 1 H, py), 7.22 (m, 1 H, py), 7.10 (m, 1 H, py), 1.35 [s, 9 H, $C(CH_3)_3$]. – ^{13}C NMR (300 MHz, $CDCl_3$): δ = 170.6 (s, α-C, py), 150.2 (s, α-C, py), 138.7 (s, py), 121.1 (s, py), 117.4 (s, py), 37.5 (s, *C*Me$_3$), 29.9 [s, C(*C*H$_3$)$_3$]. – MS (EI); *m*/*z* (%): 169 [M^+] (88), 154 [$M^+ - CH_3$] (100). – $C_9H_{12}NCl$ (169.66): calcd. C 63.72, H 7.13, N 8.26; found C 63.94, H 7.08, N 8.18.

2-(6-*tert*-Butylpyridyl)diphenylphosphane (6): To a solution of diphenylphosphane (2.75 g, 14.8 mmol) in THF (50 mL) at room temperature, 1.6 M *n*BuLi in THF (9.25 mL, 14.8 mmol) was added dropwise over a period of 30 min. The resulting red solution was stirred for a further 30 min and then a solution of **5** (2.5 g, 14.7 mmol) in THF (10 mL) was slowly added. The reaction mixture was stirred for a further 14 h, then quenched with ethanol (15 mL), and the solvents were evaporated under reduced pressure. The resulting pale-yellow solid was redissolved in hexane (200 mL) and this solution was treated with activated charcoal (5 g). After filtration and evaporation of the solvent, white crystals were obtained. Yield: 3.0 g (9.46 mmol, 64%). – ^{1}H NMR (300 MHz, $CDCl_3$): δ = 7.51–7.35 (m, 10 H, Ph; 1 H, py), 7.21 (m, 1 H, py), 6.97 (m, 1 H, py), 1.34 (s, 9 H, *t*Bu). – ^{31}P NMR (300 MHz, $CDCl_3$): δ = –3.4 (s). – ^{13}C NMR (200 MHz, $CDCl_3$): δ = 169.3 (d, $^1J_{CP}$ = 10 Hz, *ipso*-py), 161.6 (d, $^3J_{CP}$ = 5 Hz, *ipso*-py), 137.1 (d, $^1J_{CP}$ = 9 Hz, *ipso*-Ph), 135.6 (d, J_{CP} = 4 Hz, py), 134.2 (d, J_{CP} = 20 Hz, Ph), 128.6 (s, Ph), 128.2 (d, J_{CP} = 7 Hz, Ph), 125.0 (d, *J* = 20 Hz, py), 117.3 (s, py). – MS (FAB); *m*/*z* (%): 319 [M^+] (95), 185 [M^+ – *tert*-Bupy] (10). – $C_{21}H_{22}NP$ (319.39): calcd. C 78.97, H 6.94, N 4.39; found C 78.74, H 6.73, N 4.21.

2-(6-*tert*-Butylpyridyl)dimethylphosphane (7): To a solution of tetramethyldiphosphane (4.4 g, 36 mmol) in THF (300 mL) was added potassium metal (2.82 g, 72.1 mmol). The mixture was stirred for 1 day at 35 °C and then the unchanged potassium metal was removed. To the yellow solution of potassium dimethylphosphide was added **5** (12.1 g, 71.3 mmol). The resulting dark-red solution was stirred for 2 h, the solvent was evaporated in vacuo, and the residue was extracted with diethyl ether (3 × 50 mL). The combined dark-red extracts were distilled under reduced pressure (b.p. 62–72 °C, 0.1 mbar) to give a colourless oil (9.4 g), which proved to be an azeotropic mixture of **7** and unchanged 2-*tert*-butyl-6-chloropyridine. The ratio of the mixture was estimated from the ^{1}H-NMR spectrum to be 3:2. – ^{1}H NMR (300 MHz, $CDCl_3$): δ = 7.45 (m, py, 2 H), 7.15 (m, py, 1 H), 1.36 [d, 6 H, $^2J_{PH}$ = 2.2 Hz, $(CH_3)_2$P], 1.35 (s, 9 H, *t*Bu). – ^{31}P NMR (300 MHz, $CDCl_3$): δ = –40.6 (s).

2-(6-Methylpyridyl)diphenylphosphane (8): To a solution of diphenylphosphane (3.68 g, 19.8 mmol) in THF (70 mL) at room temperature, 1.6 M *n*-butyllithium (12.4 mL, 20.2 mmol) was added over a period of 30 min. After stirring for a further 30 min at room temperature, the red reaction mixture was cooled to 0 °C and a solution of 6-chloro-2-picoline (2.53 g, 19.8 mmol) in THF (20 mL) was added dropwise. Further stirring for 3 h at room temperature and subsequent addition of ethanol (20 mL) gave a pale-yellow solution. The solvent was evaporated under reduced pressure and the residue was extracted with hexane (400 mL). After filtration through Celite and crystallization at –30 °C, the product was obtained as large white needles. Yield: 460 mg (0.294 mmol, 77%). – ^{1}H NMR (300 MHz, $CDCl_3$): δ = 7.44 (m, 1 H, py), 7.37 (m, 10 H, Ph), 7.05 (m, 1 H, py), 6.83 (m, 1 H, py), 2.58 (s, 3 H, CH_3). – ^{31}P NMR (300 MHz, $CDCl_3$): δ = –4.4 (s). – ^{13}C NMR (300 MHz, $CDCl_3$): δ = 162.9 (d, $^3J_{CP}$ = 7 Hz, *ipso*-py), 158.9 (d, $^1J_{CP}$ = 15 Hz, *ipso*-py), 136.5 (d, $^1J_{CP}$ = 15 Hz, *ipso*-Ph), 135.8 (d, J_{CP} = 2 Hz, py), 134.0 (d, J_{CP} = 20 Hz, Ph), 128.8 (s, Ph), 128.4 (d, J_{CP} = 7 Hz, Ph), 124.8 (d, *J* = 11 Hz, py), 121.9 (s, py), 24.6 (s, CH_3). – MS (EI); *m*/*z* (%): 277 [M^+] (100), 200 [M^+ – Ph] (30), 185 [M^+ – Ph – CH_3] (12). – $C_{18}H_{16}NP$ (277.31): calcd. C 77.96, H 5.82, N 5.05; found C 78.31, H 5.56, N 4.97.

***cis*,*cis*-[W(CO)$_2$(NO)(Ph$_2$Ppy)(η^2-Ph$_2$Ppy)][BF$_4$] (9a):** To a solution of $[W(CH_3CN)_3(CO)_2(NO)][BF_4]$ (1.5 g, 3.13 mmol) in dichloromethane was added tris(2-pyridyl)phosphane (1.65 g, 6.27 mmol). After stirring the reaction mixture for 1 h at room temperature, it was concentrated to a volume of 7 mL in vacuo and diethyl ether (5 mL) was slowly added, which induced the formation of a dark-yellow oil. The residue was dissolved in dichloromethane and diethyl ether (10 mL) was again slowly added, which led to the deposition of a yellow solid. The precipitate was filtered off and washed with diethyl ether (2 × 10 mL) to give **9a** as a yellow powder. Yield: 2.2 g (2.49 mmol, 80%). – ^{1}H NMR (200 MHz, –30 °C, CD_2Cl_2): δ = 8.51–7.55 (m, Ph + py). – ^{31}P NMR (300 MHz, –30 °C, CD_2Cl_2): δ = –25.1 (d, $^2J_{PP}$ = 22 Hz, J_{PW} = 267 Hz), –18.6 (d, $^2J_{PP}$ = 22 Hz, J_{PW} = 220 Hz). – ^{13}C NMR (300 MHz, –30 °C, CD_2Cl_2): δ = 213.0 (dd, $^2J_{CP}$ = 5 × 36 Hz, CO), 207.9 (dd, $^2J_{CP}$ = 6 × 42 Hz, CO). – IR (CH_2Cl_2): $\tilde{\nu}$ = 2037 cm^{-1} (s), 1966 (s), 1676 (m). – MS (FAB); *m*/*z* (%): 796 [M^+] (80), 768 [M^+ – CO] (75). – $C_{36}H_{28}BF_4N_3O_3P_2W$ (883.24): calcd. C 48.96, H 3.20, N 4.76; found C 48.78, H 3.02, N 4.51.

***cis*,*cis*-[W(CO)$_2$(NO)(Ph$_2$Ppy)(η^2-Ph$_2$Ppy)][BPh$_4$] (9b):** A mixture of **9a** (300 mg, 0.34 mmol) and sodium tetraphenylborate (116 mg, 0.34 mmol) was stirred in THF (8 mL) for 30 min and then filtered through Celite. After removing the solvent in vacuo, the yellow oil was taken up in dichloromethane and filtered through a small pad of silica gel. The filtrate was then concentrated to a volume of 1 mL in vacuo and diethyl ether (4 mL) was added to precipitate the product as a yellow solid. The collected product was washed with pentane (3 × 5 mL) and recrystallized from CH_2Cl_2/Et_2O to give yellow crystals. Yield: 300 mg (0.25 mmol, 73%). – ^{1}H NMR (300 MHz, –30 °C, CD_2Cl_2): δ = 8.25–6.75 (m). – ^{31}P NMR (300 MHz, –30 °C, CD_2Cl_2): δ = 24.8 (d, J_{PP} = 21 Hz, J_{PW} = 267 Hz), –18.3 (d, J_{PP} = 21 Hz, J_{PW} = 219 Hz). – ^{13}C NMR (300 MHz, –30 °C, CD_2Cl_2): δ = 212.9 (dd, $^2J_{CP}$ = 5 × 36 Hz, CO), 207.5 (dd, $^2J_{CP}$ = 6 × 43 Hz, CO). – IR (CH_2Cl_2): $\tilde{\nu}$ = 2037 cm^{-1} (s), 1966 (s), 1677 (m). – MS (FAB-POS): *m*/*z* (%) = 796 [M^+] (4), 768 [M^+ – CO] (4). – $C_{60}H_{48}BN_3O_3P_2WCH_2Cl_2$ (1200.6): calcd. C 61.04, H 4.20, N 3.50; found C 60.97, H 4.17, N 3.54.

***trans*,*trans*-HW(CO)$_2$(NO)(Ph$_2$Ppy)$_2$ (10):** To a solution of **9a** (340 mg, 0.374 mmol) in THF (25 mL), sodium dihydrobis(2-methoxyethyloxy)aluminate (10.8 mL, 0.035 M in THF) was slowly added at 0 °C. After stirring for 10 min at room temperature, the reaction mixture was concentrated to a volume of 3 mL in vacuo and ethanol (8 mL) was added dropwise to precipitate the product. The mixture was filtered, and the collected yellow solid was sequentially washed with ethanol (2 × 5 mL) and diethyl ether (2 × 3 mL) to give a bright-yellow powder. Yield: 220 mg (0.276 mmol, 74%). – ^{1}H NMR (300 MHz, C_6D_6): δ = 8.44 (m, 2 H, py), 7.92 (m, 8 H, Ph), 7.64 (m, 2 H, py), 7.08–6.94 (m, 12 H, Ph), 6.84 (m, 2 H, py), 6.39 (m, 2 H, py), 0.62 (t, 1 H, J_{PH} = 22.4 Hz, J_{WH} = 31.1 Hz). – ^{31}P NMR (300 MHz, C_6D_6): δ = 30.3 (s, J_{PW} = 289 Hz). – ^{13}C

NMR (300 MHz, C_6D_6): δ = 217.2 (t, $^2J_{CP}$ = 7 Hz, CO). − IR (CH_2Cl_2): ṽ = 1935 cm^{-1} (s), 1689 (m), 1595 (m). − MS (FAB); *m*/*z* (%): 797 [M^+] (4), 769 [M^+ − CO] (20), 740 [M^+ − 2 CO] (25). − $C_{36}H_{29}N_3O_3P_2W$ (797.45): calcd. C 54.22, H 3.67, N 5.27; found C 53.96, H 3.92, N 5.04.

***cis*,*cis*-[W(CO)$_2$(NO)(Ph$_2$Ppic)(η^2-Ph$_2$Ppic)][BF$_4$] (11):** To a solution of [W(CH$_3$CN)$_3$(CO)$_2$(NO)][BF$_4$] (170 mg, 0.354 mmol) in dichloromethane (5 mL) was added 2-(6-methylpyridyl)diphenylphosphane (196 mg, 0.71 mmol). After stirring for 90 min at room temperature, the reaction mixture was concentrated to a volume of approximately 2.5 mL, whereupon diethyl ether was slowly added. The resulting yellow precipitate was collected by filtration and washed with pentane. The product could be conveniently recrystallized from CH_2Cl_2/Et_2O to give yellow crystals. Yield: 320 mg (249 mmol, 91%). − ^{1}H NMR (300 MHz, CD_2Cl_2): δ = 8.20−6.70 (m, 26 H, Ph + py), 2.40 (s, 3 H, CH_3), 2.28 (s, 3 H, CH_3). − ^{31}P NMR (300 MHz, CD_2Cl_2): δ = 23.6 (d, $^2J_{PP}$ = 21 Hz, J_{PW} = 269 Hz), −22.8 (d, $^2J_{PP}$ = 21 Hz, J_{PW} = 215 Hz). − ^{13}C NMR (300 MHz, CD_2Cl_2): δ = 211.2 (dd, $^2J_{CP}$ = 7 × 39 Hz, CO), 207.8 (dd, $^2J_{CP}$ = 6 × 42 Hz, CO), 25.4 (s, CH_3), 24.2 (s, CH_3). − IR (CH_2Cl_2): ṽ = 2036 cm^{-1} (s), 1967 (s), 1675 (m). − MS (FAB); *m*/*z* (%): 824 [M^+] (38), 796 [M^+ − CO] (30), 768 [M^+ − 2 CO] (10). − $C_{38}H_{32}BF_4N_3O_3P_2WCH_2Cl_2$ (996.23): calcd. C 47.02, H 3.44, N 4.22; found C 46.83, H 3.15, N 4.42.

***trans*,*trans*-HW(CO)$_2$(NO)(Ph$_2$Ppic)$_2$ (12):** To a solution of **9** (700 mg, 0.770 mmol) in THF (25 mL), sodium bis(2-methoxyethyloxy)dihydroaluminate (2.2 mL, 0.35 M in THF) was slowly added at 0 °C. After stirring for 1 h at room temperature, the reaction mixture was concentrated to a volume of 2 mL in vacuo, whereupon ethanol (50 mL) was added dropwise to precipitate the product. The mixture was filtered, and the collected yellow solid was sequentially washed with ethanol (2 × 10 mL) and diethyl ether (2 × 10 mL) to give a yellow powder. Yield: 355 mg (0.43 mmol, 56%). − ^{1}H NMR (300 MHz, CD_2Cl_2): δ = 7.70−7.05 (m, 26 H, Ph + py), 2.55 (s, 6 H, CH_3), −0.06 (t, 1 H, J_{PH} = 24.2 Hz, J_{WH} = 31.6 Hz). − ^{31}P NMR (300 MHz, CD_2Cl_2): δ = 31.1 (s, J_{PW} = 292 Hz). − ^{13}C NMR (300 MHz, CD_2Cl_2): δ = 215.6 (t, $^2J_{CP}$ = 6 Hz, CO), 24.5 (s, CH_3). − IR (CH_2Cl_2): ṽ = 1937 cm^{-1} (s), 1680 (m), 1592 (m). − MS (FAB); *m*/*z* (%): 826 [M^+] (12), 797 [M^+ − CO − H] (40), 769 [M^+ − 2 CO − H] (25). − $C_{38}H_{33}N_3O_3P_2W$ (825.5): calcd. C 55.29, H 4.03, N 5.09; found C 55.49, H 3.98, N 5.03.

***cis*/*trans*-W(CO)$_4$(Ph$_2$P-*tert*-Bupy)$_2$ (13):** To a solution of Ph$_2$P-*tert*-Bupy (390 mg, 1.23 mmol) in toluene (12 mL) was added tetracarbonyldi(piperidine)tungsten (280 mg, 0.60 mmol). The resulting yellow suspension was refluxed and stirred for 90 min, in the course of which homogeneity was attained. After filtration through a short pad of silica gel, the solvent was evaporated from the filtrate to afford the product as a mixture of isomers. Yield: 480 mg (0.51 mmol, 86%). The pure *trans* isomer could be isolated by column chromatography. − ^{1}H NMR (300 MHz, $CDCl_3$): δ = 7.75−7.15 (m, 26 H, Ph + py), 1.35 [s, 18 H, C(CH$_3$)$_3$]. − ^{31}P NMR (300 MHz, $CDCl_3$): δ = 29.8 (s, J_{PW} = 284 Hz). − ^{13}C NMR (300 MHz, $CDCl_3$): δ = 203.3 (t, *J* = 6 Hz, CO), 38.0 (s, *C*Me$_3$), 30.0 (s, CH_3). − IR (CH_2Cl_2): ṽ = 1890 cm^{-1} (s). − MS (FAB); *m*/*z* (%): 920 [M^+ − CH_3] (18), 850 [M^+ − 3 CO] (4), 821 [M^+ − 4 CO] (6), 503 [M^+ − 4 CO − L] (25). − $C_{46}H_{44}N_2O_4P_2W$ (934.67): calcd. C 59.11, H 4.75, N 3.00; found C 59.09, H 5.05, N 2.93.

[W(CO)$_3$(NO)(Ph$_2$P-*tert*-Bupy)$_2$][PF$_6$] (14): To a solution of **13** (190 mg, 0.203 mmol) in dichloromethane (5 mL) was added $NOPF_6$ (42 mg, 0.24 mmol). The resulting mixture was vigorously stirred, in the course of which it darkened in colour from yellow to green-orange. When the evolution of CO had ceased, a further portion of $NOPF_6$ (8.4 mg) was added and stirring was continued for 15 h. The reaction mixture was then concentrated to a volume of ca. 0.5 mL in vacuo and benzene (6 mL) was added. Concentration of this solution to a volume of 3 mL led to the separation of a green oil. The pale-yellow solution was decanted and the residue was washed with diethyl ether (2 × 4 mL). The crude product was recrystallized from CH_2Cl_2/Et_2O by slow evaporation of the solvent mixture at atmospheric pressure to give bright-yellow crystals. Yield: 109 mg (1.01 mmol, 50%). − ^{1}H NMR (300 MHz, CD_2Cl_2): δ = 7.75−6.80 (m, 26 H, Ph + py), 1.42 (s, 9 H, CH_3), 1.32 (s, 9 H, CH_3). − ^{31}P NMR (300 MHz, CD_2Cl_2): δ = 18.7 (d, $^2J_{PP}$ = 22 Hz, J_{PW} = 263 Hz), 12.5 (d, $^2J_{PP}$ = 22 Hz, J_{PW} = 178 Hz). − ^{13}C NMR (300 MHz, CD_2Cl_2): δ = 200.6 (t, $^2J_{CP}$ = 8 Hz, CO), 198.1 (dd, $^2J_{CP}$ = 8 × 34 Hz, CO), 38.5 (s, 1*C*Me$_3$), 38.6 (s, 1*C*Me$_3$), 30.1 [s, 2C(*C*H$_3$)$_3$]. − IR (CH_2Cl_2): ṽ = 2099 cm^{-1} (w), 2025 (s, sh), 1730 (m). − MS (FAB); *m*/*z* (%): 921 [M^+ − CH_3] (27), 852 [M^+ − 3 CO] (100), 561 [M^+ − 2 CO − L] (51), 533 [M^+ − 3 CO − L] (76). − $C_{45}H_{44}F_6N_3O_4P_3F_6W$ (1081.63): calcd. C 49.97, H 4.10, N 3.88; found C 49.89, H 3.99, N 3.91.

***trans*,*trans*-HW(CO)$_2$(NO)(Ph$_2$-*tert*-Bupy)$_2$ (15):** To a solution of **14** (109 mg, 0.101 mmol) and **6** (120 mg, 0.379 mmol) in THF (3 mL) was added sodium tetrahydroborate (15 mg, 0.397 mmol). Upon addition of the tetrahydroborate, the reaction mixture slowly evolved carbon monoxide and darkened in colour from yellow to dark-orange. After stirring for 30 min at 40 °C, the mixture was concentrated to a volume of 0.5 mL in vacuo and ethanol (4 mL) was added to induce precipitation of the yellow product. After filtration and washing of the collected solid with ethanol (2 × 2 mL) and pentane (2 × 2 mL), a yellow powder was obtained. Yield: 25 mg (0.038 mmol, 38%). − ^{1}H NMR (300 MHz, CD_2Cl_2): δ = 7.70−7.25 (m, 26 H, Ph + py), 1.27 (s, 18 H, CH_3), −0.18 (t, 1 H, J_{PH} = 22.5 Hz, J_{WH} = 31.0 Hz). − ^{31}P NMR (300 MHz, CD_2Cl_2): δ = 29.4 (s, J_{PW} = 287 Hz). − ^{13}C NMR (300 MHz, CD_2Cl_2): δ = 217.0 (t, $^2J_{CP}$ = 7 Hz, CO), 38.2 (s, *C*Me$_3$), 30.1 [s, C(*C*H$_3$)$_3$]. − IR (CH_2Cl_2): ṽ = 1931 cm^{-1} (s), 1685 (m), 1594 (m). − MS (FAB); *m*/*z* (%): 797 [M^+] (4), 769 [M^+ − CO] (20), 740 [M^+ − 2CO] (25). − $C_{44}H_{45}N_3O_3P_2W$ (909.66): calcd. C 58.10, H 4.99, N 4.62; found C 58.27, H 5.13, N 4.39.

[W(CO)$_2$(NO)(Me$_2$Ppy)$_3$][BF$_4$] (16): To a solution of [W(CH$_3$CN)$_3$(CO)$_2$(NO)][BF$_4$] (960 mg, 1.88 mmol) in dichloromethane (15 mL) was added Me$_2$Ppy (790 mg, 5.68 mmol) and the reaction mixture was stirred for 1 h at room temperature. It was then concentrated to a volume of 5 mL in vacuo and carefully layered with diethyl ether. After 3 d at −30 °C, orange crystals had separated. Yield: 1.26 g (1.34 mmol, 90%). − ^{1}H NMR (300 MHz, CD_2Cl_2): δ = 8.73 (m, 3 H, py), 7.83 (m, 3 H, py), 7.51 (m, 3 H, py), 7.40 (m, 3 H, py), 1.89 (m, 12 H, CH_3), 1.79 (m, 6 H, CH_3). − ^{31}P NMR (300 MHz, CD_2Cl_2): δ = −16.6 (d, $^2J_{PP}$ = 25 Hz, J_{PW} = 251 Hz), −21.9 (t, $^2J_{PP}$ = 25 Hz, J_{PW} = 165 Hz). − ^{13}C NMR (300 MHz, CD_2Cl_2): δ = 208.2 (m, CO), 15.7 [m, P(CH$_3$)$_2$]. − IR (CH_2Cl_2): ṽ = 2029 cm^{-1} (s), 1955 (s), 1683 (m). − MS (FAB): *m*/*z* (%) = 687 [M^+] (82), 548 [M^+ − L] (70), 520 [M^+ − CO − L] (79), 492 [M^+ − 2 CO − L] (22). − $C_{23}H_{30}BF_4N_4O_3P_3WCH_2Cl_2$ (942.41): calcd. C 33.56, H 3.75, N 6.52; found C 33.78, H 3.57, N 6.92.

***cis*/*trans*-HW(CO)$_2$(NO)(Me$_2$Ppy)$_2$ (17):** To THF (6 mL) was added **16** (225 mg, 0.29 mmol) and sodium hydrotrimethoxyborate. The resulting mixture was stirred for 30 min at room temperature and then the solvent was removed in vacuo. The dark-red residue

was extracted with pentane (3 × 5 mL) and the combined extracts were filtered through Celite. Evaporation of the solvent from the filtrate afforded an orange oil, which was taken up in dichloromethane (5 mL). To this solution, $[W(CH_3CN)_3(CO)_2(NO)][BF_4]$ (72 mg, 0.15 mmol) was added to trap uncoordinated Me_2Ppy. The reaction mixture was stirred for 30 min and then the solvent was evaporated in vacuo. The brown residue was extracted with pentane (3 × 5 mL) and the combined extracts were filtered through Celite and concentrated to dryness. The product was obtained as a mixture of isomers in the form of a yellow oil (*cis*/*trans* ratio, 20:80). Yield: 64 mg (0.117 mmol, 40%). − MS (FAB); *m*/*z* (%): 548 [M^+] (66), 520 [M^+ − CO] (100), 505 [M^+ − 2 CO − CH_3] (22), 492 [M^+ − 2CO] (32), 477 [M^+ − 2 CO − CH_3] (16). − $C_{16}H_{21}N_3O_3P_2W$ (549.16): calcd. C 34.99, H 3.85, N 7.65; found C 35.03, H 3.96, N 7.58. − NMR data (*cis* isomer): ^{1}H NMR (300 MHz, C_6D_6): δ = 8.22 (m, 2 H, py), 7.60 (m, 2 H, py), 6.88 (m, 2 H, py), 6.42 (m, 2 H, py), 1.62 (m, 12 H, PCH_3), 0.22 (t, 1 H, J_{PH} = 27.2 Hz, J_{WH} = 33.3 Hz). − ^{31}P NMR (300 MHz, C_6D_6): δ = −15.1 (s, J_{PW} = 251 Hz). − ^{13}C NMR (500 MHz, C_6D_6): δ = 217.1 (m, CO), 19.0 [m, $P(CH_3)_2$]. − NMR data (*trans* isomer): ^{1}H NMR (300 MHz, C_6D_6): δ = 8.42 (m, 2 H, py), 7.85 (m, 2 H, py), 7.05 (m, 2 H, py), 6.49 (m, 2 H, py), 1.89 (m, 12 H, PCH_3), −0.81 (t, 1 H, J_{PH} = 25.6 Hz, J_{WH} = 30.2 Hz). − ^{31}P NMR (300 MHz, C_6D_6): δ = −11.1 (s, J_{PW} = 280 Hz). − ^{13}C NMR (500 MHz, C_6D_6): δ = 216.9 (t, $^2J_{CP}$ = 7 Hz, CO), 20.1 [m, $P(CH_3)_2$].

[W(CO)$_2$(NO)(Me$_2$P-*tert*-Bupy)$_3$][BF$_4$] (18): To a solution of $[W(CH_3CN)_3(CO)_2(NO)][BF_4]$ (715 mg, 1.49 mmol) in dichloromethane (15 mL) was added an azeotropic mixture of Me_2P-*tert*-Bupy (1.31 g, ca. 4.5 mmol) and the reaction mixture was stirred for 18 h at room temperature. The resulting dark-orange solution was then concentrated to a volume of 2 mL, whereupon diethyl ether was added dropwise to induce precipitation of the orange product. After washing with diethyl ether (3 × 5 mL) and pentane (3 × 5 mL), the pure product was obtained as an orange solid. Yield: 1.26 g (1.34 mmol, 90%). − ^{1}H NMR (300 MHz, CD_2Cl_2): δ = 7.74 (m, 3 H, py), 7.43 (m, 3 H, py), 7.25 (m, 1 H, py), 7.07 (m, 2 H, py), 1.90 (m, 12 H, CH_3), 1.72 (m, 6 H, CH_3), 1.37 (s, 18 H, *t*Bu), 1.36 (s, 9 H, *t*Bu). − ^{31}P NMR (300 MHz, CD_2Cl_2): δ = −20.8 (d, $^2J_{PP}$ = 22.9 Hz, J_{PW} = 243 Hz), −21.9 (t, $^2J_{PP}$ = 23 Hz, J_{PW} = 158 Hz). − ^{13}C NMR (300 MHz, CD_2Cl_2): δ = 208.3 (m, CO), 38.4 [s, C, $C(CH_3)_3$], 30.2 [s, C, $C(CH_3)_3$], 16.0 [m, $P(CH_3)_2$]. − IR (CH_2Cl_2): $\tilde{\nu}$ = 2026 cm^{-1} (s), 1957 (s), 1687 (m). − MS (FAB); *m*/*z* (%): 856 [M^+] (80), 633 [M^+ − CO − L] (12), 605 [M^+ − 2 CO − L] (60). − $C_{35}H_{54}BF_4N_4O_3P_3W$ (942.41): calcd. C 44.61, H 5.78, N 5.94; found C 44.33, H 5.55, N 5.72.

***cis*/*trans*-HW(CO)$_2$(NO)(Me$_2$P-*tert*-Bupy)$_2$ (19):** Compound **19** was prepared in the same manner as described for **17** by using **18** (62 mg, 0.066 mmol) as the starting complex; (*cis*/*trans* ratio 20:80) Yield: 30 mg (0.045 mmol, 69%). − MS (FAB); *m*/*z* (%): 645 [M^+ − CH_3] (35), 632 [M^+ − CO] (25), 587 [M^+ − 2 CO − CH_3] (22). − NMR data (*cis* isomer): ^{1}H NMR (300 MHz, CD_2Cl_2): δ = −0.35 (t, 1 H, J_{PH} = 27.2 Hz, J_{WH} = 33.3 Hz), other resonances partially obscured by those of the *trans* isomer. − ^{31}P NMR (300 MHz, CD_2Cl_2): δ = −15.3 (s, J_{PW} = 251 Hz). − NMR data (*trans* isomer): ^{1}H NMR (300 MHz, CD_2Cl_2): δ = 7.7−7.2 (m, 4 H, py), 6.67 (m, 2 H, py), 2.00 (m, 12 H, PCH_3), 1.35 (s, 18 H, *t*Bu), −1.42 (t, 1 H, J_{PH} = 25.4 Hz, J_{WH} = 31.2 Hz). − ^{31}P NMR (300 MHz, CD_2Cl_2): δ = −11.4 (s, J_{PW} = 279 Hz). − ^{13}C NMR (500 MHz, CD_2Cl_2): δ = 216.6 (t, $^2J_{CP}$ = 7 Hz, CO), 38.2 (s, CMe_3), 30.1 [s, $C(CH_3)_3$], 15.3 [m, $P(CH_3)_2$].

***cis*,*cis*-[W(CO)(NO)(η^2-Ph$_2$Ppy)$_2$][BF$_4$] (20):** A suspension of **9a** (100 mg, 0.11 mmol) in toluene (10 mL) was stirred at 100 °C while the solvent was pumped off in a vacuum line to about half of the original volume over a period of 20 min. A further 5 mL of toluene was then added and the procedure was repeated. After cooling to room temperature, the solvent was decanted from the dark-orange residue and the latter was washed with THF (3 × 5 mL) and pentane (5 mL). The product could be recrystallized from CH_2Cl_2/Et_2O to give orange crystals. Yield: 68 mg (0.079 mmol, 71%). − ^{1}H NMR (300 MHz, CD_3NO_2): δ = 9.30 (m, 1 H), 8.36 (m, 1 H), 7.95 (m, 6 H), 7.74 (m, 4 H), 7.56 (m, 9 H), 7.30 (m, 3 H), 7.05 (m, 2 H), 6.48 (m, 2 H). − ^{31}P NMR (300 MHz, CD_3NO_2): δ = 2.3 (d, J_{PP} = 16 Hz, J_{PW} = 328 Hz), −12.8 (d, J_{PP} = 16 Hz, J_{PW} = 180 Hz). − ^{13}C NMR (300 MHz, CD_2Cl_2): δ = 232.5 (d, $^2J_{CP}$ = 47 Hz, CO). − IR (CH_2Cl_2): $\tilde{\nu}$ = 1920 cm^{-1} (s), 1611 (s). − MS (FAB); *m*/*z* (%): 768 [M^+] (34), 740 [M^+ − CO] (5). − $C_{35}H_{28}BF_4N_3O_2P_2W$ (855.23): calcd. C 49.15, H 3.30, N 4.91; found C 49.32, H 3.20, N 4.83.

***trans*,*trans*-[W(CO)(NO)(η^2-Ph$_2$Ppy)$_2$][BPh$_4$] (21):** To a solution of **9b** (60 mg, 0.05 mmol) in acetonitrile (1 mL) was added toluene (8 mL) and the mixture was slowly concentrated to a volume of 6 mL in vacuo at a bath temperature of 80 °C. The concentrated solution was then stirred for 2 h at 95 °C under slightly reduced pressure. After pumping off the solvent, the red residue was redissolved in acetonitrile (1 mL) and toluene (8 mL). After stirring for a further 3 h at 95 °C, the volume was reduced to 2 mL in vacuo. The mixture was filtered and a red solid was crystallized at −30 °C by layering a cold dichloromethane solution with diethyl ether and leaving the system to stand overnight. Yield: 35 mg (0.029 mmol, 59%). − ^{1}H NMR (300 MHz, CD_2Cl_2): δ = 8.2−6.7 (m, Ph + py). − ^{31}P NMR (300 MHz, CD_2Cl_2): δ = −0.5 (m, 2 P, AB system, J_{PaPb} = 121 Hz, J_{PaW} = 277 Hz, J_{PbW} = 299 Hz). − ^{13}C NMR (300 MHz, CD_2Cl_2): δ = 237.1 (m, CO). − IR (CH_2Cl_2): $\tilde{\nu}$ = 1920 cm^{-1} (s), 1625 (s). − MS (FAB); *m*/*z* (%): 768 [M^+] (18). − $C_{59}H_{48}BN_3O_2P_2W{\cdot}CH_2Cl_2$ (1172.6): calcd. C 61.46, H 4.30, N 3.58; found C 61.86, H 4.44, N 3.88.

***cis*,*cis*-[W(CO)$_2$(NO)(Me$_2$Ppy)(η^2-Me$_2$Ppy)][BF$_4$] (22):** To a solution of $[W(CH_3CN)_3(CO)_2(NO)][BF_4]$ (214 mg, 0.447 mmol) in THF (12 mL) was added Me_2Ppy (125 mg, 0.9 mmol). The transient formation of a yellow suspension could be observed before the reaction mixture became homogeneous again. After stirring overnight at room temperature, half of the solvent was evaporated in vacuo. Toluene (6 mL) was then added, stirring was continued for a further 5 min, and then the solvent was removed in vacuo. The resulting dark-yellow oil was taken up in dichloromethane (5 mL) and the product was precipitated by the slow addition of pentane. The supernatant was decanted off and the residue was washed several times with pentane to afford a yellow oil. Yield: 197 mg (0.31 mmol, 69%). − ^{1}H NMR (300 MHz, −15 °C, $C_2Cl_4D_2$): δ = 7.49 (m, 1 H, py), 7.29 (m, 1 H, py), 7.14 (m, 1 H, py), 7.00 (m, 2 H, py), 6.76 (m, 1 H, py), 6.67 (m, 1 H, py), 6.49 (m, 1 H, py), 1.53 (m, 6 H, PCH_3), 1.33 (m, 12 H, PCH_3). − ^{31}P NMR (300 MHz, −15 °C, $C_2Cl_4D_2$): δ = −9.8 (d, $^2J_{PP}$ = 25 Hz, J_{PW} = 256 Hz), −48.2 (d, $^2J_{PP}$ = 25 Hz, J_{PW} = 220 Hz). − ^{13}C NMR (300 MHz, −15 °C, $C_2D_2Cl_4$): δ = 213.0 (dd, $^2J_{CP}$ = 5 × 3 Hz, CO), 208.2 (dd, $^2J_{CP}$ = 5 × 41 Hz, CO), 15.2 [m, $P(CH_3)_2$], 11.39 [m, $P(CH_3)_2$]. − IR (CH_2Cl_2): $\tilde{\nu}$ = 2035 cm^{-1} (s), 1962 (s), 1635 (m). − MS (FAB); *m*/*z* (%): 548 [M^+] (50), 520 [M^+ − CO] (22), 492 [M^+ − 2CO] (6).

[W(CO)$_2$(CH$_3$CN)(NO)(Me$_2$P-*tert*-Bupy)$_2$][BF$_4$] (23a): To a solution of $[W(CH_3CN)_3(CO)_2(NO)][BF_4]$ (115 mg, 0.24 mmol) in THF (5 mL) was added Me_2P-*tert*-Bupy (125 mg, 0.9 mmol). After stirring the reaction mixture for 3 h at 60 °C, hexane was added to precipitate a yellow oil. The supernatant solution was decanted off

and the residue was taken up in acetonitrile (2 mL). This solution was stirred for 5 min and then the solvent was removed under high vacuum. The residual yellow oil was taken up in dichloromethane (2 mL) and precipitated once more by the slow addition of hexane. The residue was finally taken up in toluene (5 mL), filtered through Celite, and dried under high vacuum. Yield: 145 mg (0.185 mmol, 77%). − ^{1}H NMR (300 MHz, [D$_8$]toluene): δ = 7.52 (m, 4 H, py), 6.96 (m, 2 H, py), 2.26 (s, 3 H, CH_3CN), 1.70 (m, 12 H, PMe_2), 1.26 (s, 18 H, *t*Bu). − ^{31}P NMR (300 MHz, [D$_8$]toluene): δ = −12.8 (s, J_{PW} = 254 Hz). − ^{13}C NMR (300 MHz, [D$_8$]toluene): δ = 208.9 (m, CO), 38.0 (s, *C*Me$_3$), 30.1 [s, C(*C*H$_3$)$_3$], 13.4 [m, P(CH$_3$)$_2$], 2.8 (s, *C*H$_3$CN). − IR (CH_2Cl_2): $\tilde{\nu}$ = 2308 cm^{-1} (w), 2040 (s), 1967 (s), 1682 (m). − MS (FAB); *m*/*z* (%): 701 [M$^+$] (20), 660 [M$^+$ − CH_3CN] (18), 632 [M$^+$ − CO − CH_3CN] (28), 604 [M$^+$ − 2 CO − CH_3CN] (87), 544 [M$^+$ − 2 CO − CH_3CN − NO − 2 CH_3] (16). − An unidentified phosphane impurity amounting to 5% could not be removed; no elemental analysis was attempted (see text).

[W(CO)$_2$(CH$_3$CN)(NO)(Me$_2$P-*tert*-Bupy)$_2$][TFPB] (23b): A mixture of **23a** (276 mg, 0.35 mmol) and Na[TFPB] (336 mg, 0.38 mmol) was stirred for 45 min at room temperature. After evaporation of the solvent in vacuo, the residue was extracted with dichloromethane and the combined extracts were filtered through Celite. Removal of the solvent from the filtrate left the product as a yellow oil. Yield: 460 mg (0.294 mmol, 77%). − ^{1}H NMR (300 MHz, CD_2Cl_2): δ = 7.74 (br., 8 H, Ph), 7.58 (br., 4 H, Ph), 7.43 (m, 4 H, py), 7.23 (m, 2 H, py), 2.20 (s, 3 H, CH_3CN), 1.80 (m, 12 H, PMe_2), 1.35 (s, 18 H, *t*Bu). − ^{31}P NMR (300 MHz, CD_2Cl_2): δ = −13.6 (s, J_{PW} = 254 Hz). − ^{13}C NMR (300 MHz, CD_2Cl_2): δ = 207.9 (m, CO), 171.1 (d, $^3J_{CP}$ = 7 Hz, *ipso*-C, py), 162.3 (q, *ipso*-C, BPh_4), 158.1 (d, $^1J_{CP}$ = 34 Hz, *ipso*-C, py), 38.0 (s, *C*Me$_3$), 30.1 [s, C(*C*H$_3$)$_3$], 14.2 [m, P(CH$_3$)$_2$], 4.0 (s, *C*H$_3$CN). − IR (CH_2Cl_2): $\tilde{\nu}$ = 2308 cm^{-1} (w), 2040 (s), 1967 (s), 1682 (m). − MS (FAB); *m*/*z* (%): 701 [M$^+$] (20), 660 [M$^+$ − CH_3CN] (18), 632 [M$^+$ − CO − CH_3CN] (28), 604 [M$^+$ − 2 CO − CH_3CN] (87), 544 [M$^+$ − 2 CO − CH_3CN − NO − 2 CH_3] (16). − $C_{58}H_{51}BF_{24}N_4O_3P_2W$ (1564.3): calcd. C 44.93, H 3.32, N 3.58; found C 44.42, H 3.31, N 2.94.

***trans*-W(CO)(NO)(Ph$_2$Ppy)$_2$(η^2-CH$_3$CO$_2$) (24):** To a solution of **10** (30 mg, 0.038 mmol) in a mixture of dichloromethane (0.5 mL) and 2-propanol (2 mL), acetic acid (0.2 mL) was added at −30 °C. The resulting mixture was allowed to warm to room temperature, whereupon slow gas evolution was observed. After stirring for 30 min, the mixture was concentrated to a volume of 1 mL and the product was precipitated by slowly adding pentane. After subsequent washing with pentane, a red powder was obtained. Yield: 21 mg (0.025 mmol, 64%). − ^{1}H NMR (500 MHz, CD_2Cl_2): δ = 8.71 (m, 2 H, py), 7.60−7.20 (m, 26 H, Ph), 0.54 (s, 3 H, CH_3). − ^{31}P NMR (300 MHz, CD_2Cl_2): δ = 39.3 (s, J_{PW} = 308 Hz). − ^{13}C NMR (500 MHz, CD_2Cl_2): Decomposition was observed when the sample was left overnight. − IR (CH_2Cl_2): $\tilde{\nu}$ = 1894 cm^{-1} (s), 1578 (m). − MS (FAB); *m*/*z* (%): 827 [M$^+$] (2), 799 [M$^+$ − CO] (3), 768 [M$^+$ − CO(O)CH$_3$] (18). − $C_{37}H_{31}N_3O_4P_2W$ (827.47): calcd. C 53.71, H 3.78, N 5.08; found C 52.67, H 3.56, N 5.18.

***trans*-IW(CO)$_2$(NO)(Ph$_2$Ppy)$_2$ (25):** To a solution of **10** (24 mg, 0.03 mmol) in dichloromethane (0.7 mL), hydroiodic acid (0.05 mL, 0.75 M in chloroform) was added at room temperature. The colour of the solution changed from yellow to orange and gas evolution was observed. After 10 min, the solvent was removed under reduced pressure and the orange product was washed several times with pentane. Yield: 19 mg (0.021 mmol, 69%). − ^{1}H NMR (300 MHz, CD_2Cl_2): δ = 8.83 (m, 2 H, py), 7.7−7.2 (m, 26 H, Ph). − ^{31}P NMR (300 MHz, CD_2Cl_2): δ = 13.0 (s, J_{PW} = 289 Hz). − ^{13}C NMR (300 MHz, CD_2Cl_2): δ = 205.6 (t, $^2J_{CP}$ = 6 Hz, CO). − IR (CH_2Cl_2): $\tilde{\nu}$ = 2008 cm^{-1} (w), 1961 (s), 1638 (m). − MS (FAB); *m*/*z* (%): 867 [M$^+$ − 2 CO] (11), 796 [M$^+$ − I] (22), 768 [M$^+$ − I − CO] (46). − $C_{36}H_{28}IN_3O_3P_2W$ (923.34): calcd. C 46.83, H 3.06, N 4.55; found C 46.42, H 3.13, N 4.52.

***trans*-W(HCO$_2$)(CO)$_2$(NO)(Ph$_2$Ppy)$_2$ (26):** Carbon dioxide was slowly bubbled through a solution of **9** (50 mg, 0.063 mmol) in THF (4 mL) at room temperature. The colour of the solution slowly changed from yellow to orange. After 30 min, it was concentrated to a volume of 1 mL and the product was precipitated by adding diethyl ether. After washing with pentane, an orange powder was obtained. Yield: 32 mg (0.039 mmol, 60%). − ^{1}H NMR (300 MHz, CD_2Cl_2): δ = 8.80 (m, 2 H, py), 7.66−7.28 (m, 26 H, Ph), 7.06 [s, 1 H, OC(O)H]. − ^{31}P NMR (300 MHz, CD_2Cl_2): δ = 28.2 (s, $^2J_{PW}$ = 299 Hz). − ^{13}C NMR (300 MHz, CD_2Cl_2): δ = 210.4 (t, $^2J_{CP}$ = 5 Hz, CO), 166.39 [s, OC(O)H]. − IR (CH_2Cl_2): $\tilde{\nu}$ = 2050 cm^{-1} (w), 1962 (s), 1622 (br.). − MS (FAB); *m*/*z* (%): 796 [M$^+$ − OC(O)H] (18), [M$^+$ − 2 CO] (45), 768 [M$^+$ − CO − OC(O)H] (70), [M$^+$ − 2 CO − OC(O)H] (28).

***trans*-W{η^2-(*Z*)-C(CO$_2$Me)=CH[C(O)OMe]}(CO)(NO)(Ph$_2$Ppic)$_2$ (27):** To a solution of **12** (12 mg, 14.5 μmol) in [D$_8$]THF (0.7 mL) was added dimethyl acetylenedicarboxylate (2 μL, 15.5 μmol) and the reaction was monitored by ^{1}H-NMR spectroscopy. After 5 min at room temperature, the reaction was complete and a dark-red solution had been obtained. The solvent was evaporated in vacuo and the residual solid was washed several times with diethyl ether and pentane. Yield: 10 mg (10.6 μmol, 73%). − ^{1}H NMR (300 MHz, [D$_8$]THF): δ = 7.70 (m, 8 H, Ph), 7.47 (m, 2 H, py), 7.28 (m, 12 H, Ph), 7.22 (m, 2 H, py), 7.00 (m, 2 H, py), 6.89 (t, 1 H, $^4J_{PH}$ = 3.4 Hz, vinyl H), 2.92 (s, 3 H, OCH_3), 2.86 (s, 3 H, OCH_3), 2.41 (s, 6 H, pic-CH_3). − ^{31}P NMR (300 MHz, [D$_8$]THF): δ = 31.7 (s, J_{PW} = 295 Hz). − ^{13}C NMR (300 MHz, [D$_8$]THF): δ = 245.8 (t, $^2J_{CP}$ = 5 Hz, CO), 222.4 (t, $^2J_{CP}$ = 10 Hz, α-vinyl C), 183.2 (s, *C*OOMe), 179.3 (s, *C*OOMe), 160.7 (t, $^1J_{CP}$ = 30 Hz, *ipso*-C, py), 53.8 (s, OCH_3), 50.9 (s, OCH_3), 24.5 (s, CH_3); the vinylic carbon signal is obscured by aromatic resonances. − IR (CH_2Cl_2): $\tilde{\nu}$ = 1935 cm^{-1} (s), 1689 (m), 1595 (m). − MS (FAB); *m*/*z* (%): 938 [M$^+$] (2), 910 [M$^+$ − CO] (5), 798 [M$^+$ − $MeO_2CC{=}CCO_2Me$] (25).

***trans*,*trans*-WD(CO)$_2$(NO)(Ph$_2$Ppy)$_2$ (28):** To a solution of **10** (40 mg, 0.050 mmol) in dichloromethane, [D$_1$]methanol (0.5 mL) was added at 0 °C. After stirring for 1 h at exactly 0 °C, the deuterated product was precipitated from the reaction mixture by adding further [D$_1$]methanol (3 mL). The solvents were decanted and the yellow solid was dried in vacuo. Yield: 35 mg (44 μmol, 88%). − ^{2}H NMR (300 MHz, CH_2Cl_2): δ = −0.32 (br. s). − ^{31}P NMR (300 MHz, CD_2Cl_2): δ = 31.0 (t, $^2J_{PD}$ = 3 Hz). − IR (CH_2Cl_2): $\tilde{\nu}$ = 1921 cm^{-1} (s), 1628 (m); W−D not observed. − $C_{36}H_{28}DN_3O_3P_2W$ (798.45): calcd. C 54.15, H 3.53, N 5.26; found C 53.85, H 3.86, N 5.27.

X-ray Structural Determinations: Data collection for all structures was performed in a cold N_2 stream (see Table 1) with a Nicolet−Siemens P4 diffractometer in the range 2.0° ≤ φ ≤ 25.0°. The structures of complexes **9**, **11**, and **20** were solved by Patterson synthesis (SHELXS-86)[25] and refined using SHELXTL-PLUS[26] for **11** and **20** or SHELXL-93[27] for **9**. The structure of complex **14** was solved by direct methods (SIR-92,[28] SHELXTL-PLUS). Pertinent crystallographic parameters for the four structures are listed in Table 1.

Crystallographic data (excluding structure factors) for the structures reported in this paper have been deposited with the Cam-

Table 1. Experimental conditions and crystallographic data for **9a**, **11**, **14**, and **20**

	9a	**11**	**14**	**20**
Empirical formula	$C_{36}H_{28}BF_4N_3O_3P_2W$	$C_{38}H_{32}BF_4N_3O_3P_2WCH_2Cl_2$	$C_{45}H_{44}F_6N_3O_4P_3W$	$C_{37}H_{32}BCl_4F_4N_3O_2P_2WCH_2Cl_2$
Molecular mass	883.21	996.23	1081.62	1025.7
Colour	yellow	yellow	yellow	red
Cryst. size [mm]	0.2 × 0.3 × 0.3	0.25 × 0.35 × 0.40	0.15 × 0.20 × 0.35	0.25 × 0.35 × 0.35
Cryst. system	monoclinic	monoclinic	monoclinic	triclinic
Space group	$P2_1/n$	$P2_1/c$	$P2_1/c$	$P\bar{1}$
a [Å]	17.051(6)	12.160(3)	18.059(3)	12.870(3)
b [Å]	11.344(2)	10.521(4)	11.760(3)	12.938(2)
c [Å]	18.515(3)	34.088(8)	21.895(5)	13.161(3)
β [°]	107.06	96.23(2)	96.52(2)	85.98(2)
V [Å^3]	3423.7(15)	4335(2)	4691.9	2026.3(6)
Z	4	4	4	2
$D_{calcd.}$ [g/cm^3]	1.713	1.66	1.56	1.68
Radiation	Mo-K_α	Mo-K_α	Mo-K_α	Mo-K_α
T [K]	203	178	173	183
No. of rflns. collected	7489	7615	7862	7110
No. of unique rflns.	5105	8503	5528	6899
$wR2$	0.101	0.600	0.520	0.360
$R1$	5.22	4.1	5.0	2.8
goodness-of-fit	1.192	1.153	1.037	1.147

bridge Crystallographic Data Centre as supplementary publication nos. CCDC-136277−136280. Copies of the data can be obtain free of charge on application to the CCDC, 12 Union Road, Cambridge CB2 1EZ, U.K. [Fax: (internat.) + 44-1223/336003; E-mail: deposit@ccdc.cam.ac.uk].

Computational Details: The calculations utilized the Amsterdam Density Functional package ADF release 2.0.1 and release 2.3. The ADF basis set III was chosen for the main group elements, whereas W was described with a modified basis set IV with 6p functions. The self-consistent DFT calculations were based on the local exchange correlation potential of Vosko, Wilk, and Nussair,[29] with the addition of gradient corrections due to Becke[30] and Perdew[31] (NL-SCF). Relativistic effects were included using a quasi-relativistic approach.[32] The accuracy parameter for the numerical integration was set to 4.0. All molecules were fully optimized at the quantum mechanical level. Default convergence criteria[33] were employed, except for the gradients in the geometry optimizations, which were set to 0.006 hartree/Å or hartree/radian, respectively. In the transition state search, the W−N(pyridyl) distances were assumed to be equal.

Acknowledgments

We thank Dr. T. Fox for advice on the NMR investigations and the Swiss National Science Foundation for financial support.

[1] A. A. H. van der Zeijden, H. Berke, *Helv. Chim. Acta* **1992**, *75*, 513−522.
[2] A. A. H. van der Zeijden, D. Veghini, H. Berke, *Inorg. Chem.* **1992**, *31*, 5106−5116.
[3] A. A. H. van der Zeijden, H. W. Bosch, H. Berke, *Organometallics* **1992**, *11*, 2051−2057.
[4] R. H. Crabtree, *Science* **1998**, *282*, 2000−2001.
[5] R. H. Crabtree, *J. Organomet. Chem.* **1998**, *577*, 111−115.
[6] S. Park, A. J. Lough, R. H. Morris, *Inorg. Chem.* **1996**, *35*, 3001ff.
[7] H. S. Chu, C. P. Lau, K. Y. Wong, W. T. Wong, *Organometallics* **1998**, *17*, 2768−2777.
[8] E. S. Shubina, N. V. Belkova, A. N. Krylov, E. V. Vorontsov, L. M. Epstein, D. G. Gusev, M. Niedermann, H. Berke, *J. Am. Chem. Soc.* **1996**, *118*, 1105−1112.
[9] R. H. Morris, P. G. Jessop, *Coord. Chem. Rev.* **1992**, *121*, 155−284.
[10] A. Caballero, F. A. Jalon, B. R. Manzano, *Chem. Commun.* **1998**, *17*, 1879−1880.
[11] R. Noyori, T. Ikarya, A. Fujji, S. Hashiguchi, D. H. Haack, *Angew. Chem. Int. Ed. Engl.* **1997**, *36*, 285 ff.
[12] R. Noyori, S. Hashiguchi, *Acc. Chem. Res.* **1997**, *30*, 97−102.
[13] L. Dahlenburg, K. Herbst, H. Berke, *J. Organomet. Chem.* **1999**, *585*, 225−233.
[14] J. Pietsch, L. Dahlenburg, A. Wolski, H. Berke, I. L. Eremenko, D. Veghini, *J. Organomet. Chem.* **1994**, *472*, 55−70.
[15] J. Pietsch, A. Wolski, L. Dahlenburg, H. Berke, D. Veghini, I. L. Eremenko, *J. Organomet. Chem.* **1995**, *495*, 113−125.
[16] A. L. Balch, C. T. Hunt, M. M. Olmstead, J. P. Farr, A. Maisonnet, *Inorg. Chem.* **1982**, *21*, 3961.
[17] Y. Inoguchi, B. Milewski-Mahrla, H. Schmidbaur, *Chem. Ber.* **1982**, *115*, 3085−3095.
[18] P. A. A. Klusener, J. C. L. Suykerbuyk, P. A. Verbrugge, *Process for the Preparation of (Diarylphosphanyl)pyridines*, Eur. Pat. Appl. EP 499328 A2 920819, The Netherlands, **1991**.
[19] R. P. Mariella, *J. Am. Chem. Soc.* **1947**, *69*, 2670−2672.
[20] W. H. Hersh, *Inorg. Chem.* **1990**, *29*, 713−722.
[21] G. L. Hillhouse, B. L. Haymore, *Inorg. Chem.* **1987**, *26*, 1876−1885.
[22] A. A. H. van der Zeijden, C. Sontag, H. W. Bosch, V. Shklover, H. Berke, D. Nanz, W. von Philipsborn, *Helv. Chim. Acta* **1991**, *74*, 1194−1204.
[23] H. Berke, P. Burger, *Comments Inorg. Chem.* **1994**, *16*, 279−312.
[24] P. Kundel, H. Berke, *J. Organomet. Chem.* **1986**, *314*, C31−C33.
[25] G. M. Sheldrick, *Acta Crystallogr.* **1990**, *A46*, 467−473.
[26] G. M. Sheldrick, *SHELXTL-PLUS − A Program for Crystal Structure Determination*, University of Göttingen, Germany, **1994**.
[27] G. M. Sheldrick, *SHELXL-93 − A Program for Crystal Structure Refinement*, University of Göttingen, Germany, **1993**.
[28] A. Altomare, G. Cascarano, C. Giacovazzo, A. Guagliardi, M. C. Burla, G. Polidori, M. Camalli, *SIR-92*, University of Bari, **1992**.
[29] S. J. Vosko, M. Wilk, M. Nussair, *Can. J. Phys.* **1980**, *58*, 1200.
[30] A. Becke, *Phys. Rev.* **1988**, *A38*, 3098.
[31] J. P. Perdew, *Phys. Rev.* **1986**, *B33*, 8822.
[32] T. Ziegler, V. Tschinke, E. J. Baerends, J. G. Snijders, W. Ravenek, *J. Phys. Chem.* **1989**, *93*, 3050.
[33] G. te Velde, *ADF 2.1 User's Guide*, Vrije Universiteit, Amsterdam, **1996**.

Received November 12, 1999
[I99403]

Coordination Chemistry of {[Zr]−Cl−[Zr]}$^+$ Complexes[‡]

Heiko Jacobsen,[a] Thomas Brackemeyer,[b] Heinz Berke,*[a] Gerhard Erker,*[b] and Roland Fröhlich[b][‡‡]

Keywords: Bridging ligands / Cations / Density functional calculations / Zirconium

Treatment of the tris(cyclopentadienyl) cation (**1**$^+$) with zirconocene dichloride **2** gave, in almost quantitative yield, the 1:1 adduct **7**$^+$, which was isolated with $[(CH_3)B(C_6F_5)_3]^-$ as the counterion. Reaction of **1**$^+$ with the organometallic ligand Cp_3ZrCl afforded the 1:1 adduct **8**$^+$, again isolated with $[(CH_3)B(C_6F_5)_3]^-$. The X-ray analysis revealed that **7**$^+$ displays a strongly bent Zr–Cl–Zr coordination mode, in contrast to **8**$^+$, which has a tendency to linear coordination. A theoretical analysis suggests that a subtle balance between steric and electronic factors determines the geometries in such organometallic adducts.

Introduction

We have recently investigated the coordination chemistry of the tris(cyclopentadienyl) zirconium cation $[Cp_3Zr]^+$ (**1**$^+$) and determined the crystal structures of several $[Cp_3Zr-L]^+$ adducts.[1] The transition metal cation **1**$^+$ displays Lewis acid behavior and forms adducts with a variety of donor ligands, such as nitriles, isonitriles, or carbon monoxide. Further, it is known that catalytically important $[Cp_2ZrR]^+$ cations show a marked tendency to bind to their neutral $[Cp_2ZrR_2]$ precursors and related $[Cp_2ZrX_2]$ systems, yielding less active resting stages or dormant derivatives of their active metallocene catalyst systems.[2] It was tempting to find out whether the $[Cp_3Zr]^+$ cation (**1**$^+$) would react in a similar fashion as $[Cp_2ZrR]^+$ species and bind the neutral metallocene derivatives $[Cp_2ZrCl_2]$ (**2**) or $[Cp_3ZrCl]$ (**3**) despite its higher coordinative saturation.

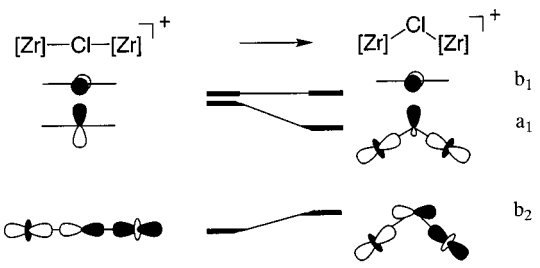
During the course of this investigation the question of the coordination geometry around the bridging Cl^- became of special interest. We were able to determine the structures of two similar {[Zr]−Cl−[Zr]}$^+$ cations, which in the solid state show very different bridging geometries. Only a few systems with unsupported $(Cp)_nZr-Cl-M$ bridges have been described in the literature. Two adducts between Cp_2ZrCl_2 and the Lewis acids AlR_3 [R = Cl, $C(CH_3)_3$] have been structurally characterized.[3] In these systems the bridging chloride and the two metal centers form Zr−Cl−M bond angles τ of 126° and 149°, respectively.

Independent of our experimental work, we initiated a theoretical study on {[Zr]−Cl−[Zr]}$^+$ cations, based on density functional theory,[4] in which we examined various coordination geometries not only around the μ-Cl bridge, but also around the Zr center. We begin the discussion with our computational work before giving an account of our experimental results and comparing theory and experiment.

Results and Discussion

Theoretical Studies

Molecular Orbital Considerations: From a molecular orbital point of view, the question of the coordination geometry of $[R_3Zr-(\mu\text{-}Cl)-ZrR_3]^+$ complexes is related to the problem of the geometries of AH_2 molecules.[5] We can analyze the bonding angle τ by considering the interaction of two cationic metal fragments $[Zr]^+$ with a Cl^- ion. The LUMO of the metal fragment is in any case a Zr-based d_{z^2}-orbital and is independent of the coordination around the transition metal center, which might be planar or trigonal pyramidal. When interacting with the p-orbitals of the chloride ion, these orbitals have the same nodal characteristics as the 1s orbital of H, and we might consider $HClH^+$ as an isolobal analog of {[Zr]−Cl−[Zr]}$^+$. The three highest occupied orbitals of such a C_{2v} symmetric moiety are shown in Scheme 1, and the bent geometry would be stabilized due to the energetic lowering of the orbital a_1.



Scheme 1. Orbital interaction diagram for bent and linear {[Zr]−Cl−[Zr]}$^+$, classified according to C_{2v} symmetry

[‡] Experimental work was carried out at the University of Münster, theoretical work at the University of Zürich.

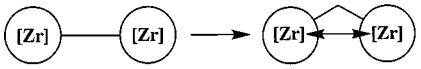
[a] Anorganisch-chemisches Institut, Universität Zürich-Irchel, Winterthurerstrasse 190, CH-8057 Zürich, Switzerland
Fax: (internat.) + 41-1/635-6802
[b] Organisch-Chemisches Institut, Universität Münster, Corrensstraße 40, D-48149 Münster, Germany
Fax: (internat.) + 49-251/833-6503
E-mail: erker@uni-muenster.de

[‡‡] X-ray structure analyses.

Supporting Information for this article is available on the WWW under http://www.wiley-vch.de/home/eurjic or from the author.

 © WILEY-VCH Verlag GmbH, D-69451 Weinheim, 2000 1434−1948/00/0707−1423 $ 17.50+.50/0

Thus, if the geometry of $\{[Zr]-Cl-[Zr]\}^+$ systems is determined by orbital interactions of the bridging fragments, we would predict a bent geometry for such molecules. The analysis is complicated, however, by the fact that the orbitals introduced above are normally not amongst the frontier orbitals of such systems. The highest occupied orbitals are usually based on ligands of the transition metal fragments. Bending also leads to an increase in steric repulsion, which then counteracts the electronic stabilization.[6]



In order to explore possible coordination geometries of $\{[Zr]-Cl-[Zr]\}^+$ systems, we choose $[ZrCl_3]^+$ (**4**$^+$) and $ZrCl_4$ (**5**) as models for the adduct-forming reaction $R_3ZrCl + [ZrR_3]^+ \rightarrow \{[Zr]-Cl-[Zr]\}^+$. From these fragments, a variety of $[Zr_2Cl_7]^+$ (**6**$^+$) complexes containing a single bridging μ-Cl^- can be constructed. Our preliminary excursion led to the conclusion that a variety of coordination modes might be realized by $\{[Zr]-Cl-[Zr]\}^+$ systems, which coexists as local minimum structures.[7a] The predictions arising from the qualitative molecular orbital arguments are met,[7b] the energetic differences between linear and bent coordination, however, are fairly small. Keeping these results in mind, we now proceed with the analysis of complexes involving the $[Cp_3Zr]^+$ cation (**1**$^+$).

Interaction of 1$^+$ with Organometallic Zirconium Chlorides: We begin with a brief introduction of the Zr fragments considered (Figure 1).

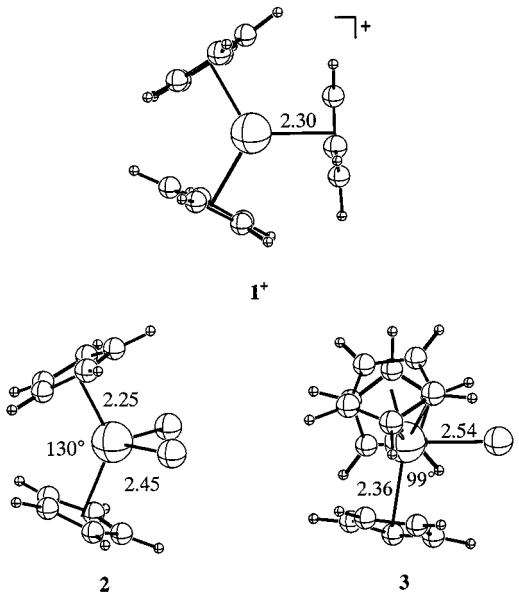


Figure 1. Optimized structures for the Zr-based building blocks **1**$^+$, **2**, and **3**

The cation **1**$^+$ has already been extensively studied.[1] An important feature is the planar coordination around the transition metal center. Whereas the structure of $[Cp_2ZrCl_2]$ (**2**) is well-known,[8] the geometry of complex $[Cp_3ZrCl]$ (**3**) has not yet been described. The system with ansa-cyclopentadienyl rings $[(CpCMe_2Cp)CpZrCl]$ that was reported by Green and co-workers[9] is similar to compound **3**. The calculated Zr−Cl bond in **3** is elongated by 0.09 Å compared to **2**, and it agrees very well with the experimental value of d(Zr−Cl) = 2.536 Å for Green′s complex. The coordination of the Cp rings deviates only slightly from a planar arrangement, resulting in $\sigma_P = 352°$, with $\sigma_P = \Sigma <$ [Cp(centroid)−Zr−Cp(centroid)].

Two coordination geometries have been calculated for the complex $[Cp_3Zr-(\mu\text{-}Cl)-ZrCp_2Cl]^+$ (**7**$^+$) (Figure 2).

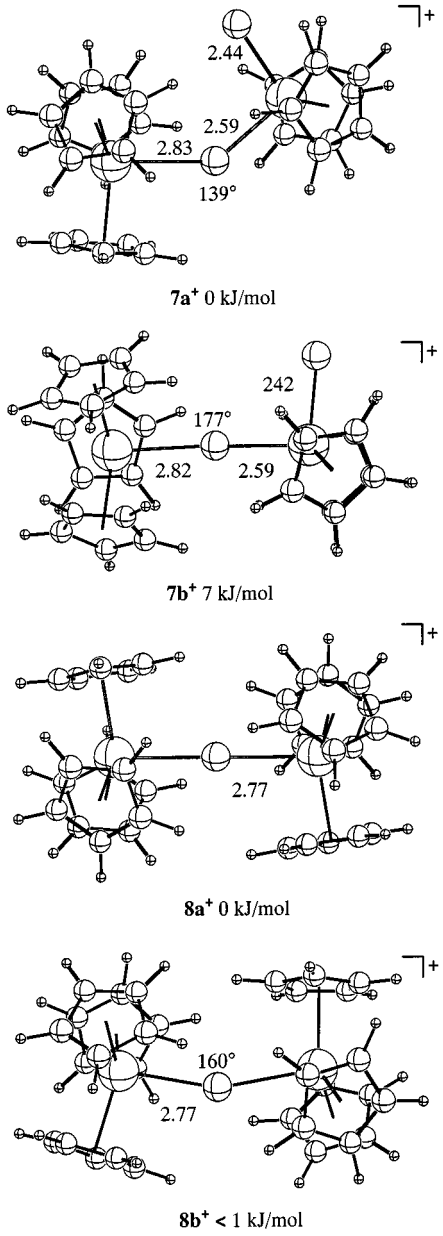


Figure 2. Optimized linear and bent geometries for the cations $[Cp_3Zr-(\mu\text{-}Cl)-ZrCp_2Cl]^+$ (**7**$^+$), and $[Cp_3Zr-(\mu\text{-}Cl)-ZrCp_3]^+$ (**8**$^+$)

The geometric features of **7a**$^+$ and **7b**$^+$ are similar but again the bent complex **7a**$^+$, with $\tau = 139°$, is energetically more stable. The bending angle τ is larger than those found for the complexes **8** but the stabilization energy for bent coordination is of the same order of magnitude and is again rather small. Two different Zr−(μ-Cl) bond lengths are ob-

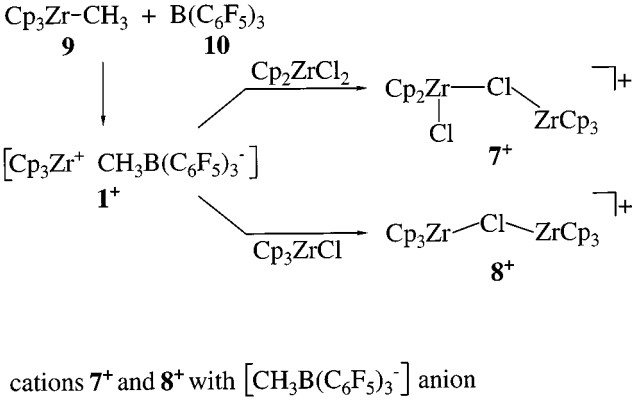
tained, again with a longer bonding contact for the metal center coordinated in a planar fashion. The σ_P values in both cases are 354°, indicating that the coordination around the $\{Cp_3Zr\}$ fragment is essentially planar.

The increase in steric bulk in $[Cp_3Zr-(\mu\text{-}Cl)-ZrCp_3]^+$ (**8**$^+$) further lowers the energy difference between a bent and a linear coordination. The two calculated geometries **8a**$^+$ and **8b**$^+$ (Figure 2) are virtually identical in energy, with a marginal preference for the linear coordination.

The potential energy hypersurface around the Zr−Cl−Zr bending mode is very shallow, and one can expect that effects due to the nature of the counterion and crystal packing will influence the molecular arrangement of **8** in the solid state. All calculations indicate that τ can take on values that vary over a larger range and are influenced by the steric bulk of the interacting fragments. The crystal structure of the $Cp_2ZrCl_2-AlR_3$ adducts further support this observation. The Zr−(μ-Cl) separation is about 0.07 Å larger than the average obtained for both Zr−Cl distances calculated for **7**$^+$. Again, the σ_P values for all $ZrCp_3$ systems amount to 353°, and are close to the ideal value of 360° for a perfectly planar coordinated Zr.

Experimental Studies

The tris(cyclopentadienyl)zirconium cation (**1**$^+$) was generated in situ by treatment of $[Cp_3ZrCH_3]$ (**9**) with the strong organometallic Lewis acid tris(pentafluorophenyl)-borane (**10**) and trapped by added zirconocene dichloride (**2**). The 1:1 adduct **7** was formed almost quantitatively (Scheme 2).



Scheme 2. Preparation of adducts **7** and **8** from the cation $[Cp_3Zr^+]$ (**1**$^+$)

Compound **7** is characterized by the occurrence of a pair of ^{1}H-/^{13}C-NMR Cp-resonances (2:3 intensity) at δ = 6.67, 6.24/118.2, 117.0 in addition to the signals of the separated $[CH_3B(C_6F_5)_3]^-$ anion. Single crystals of **7** suitable for X-ray crystal analysis were obtained from a saturated solution in dichloromethane at −30 °C. In the crystal the $[Cp_3Zr-(\mu\text{-}Cl)-ZrCp_2Cl]^+$ cation (**7**$^+$) is well separated from the $[CH_3B(C_6F_5)_3]^-$ anion (shortest B−Zr distance: 7.142 Å). The cation **7**$^+$ (Figure 3) features a Cp_3Zr subunit that is close to trigonal planar.

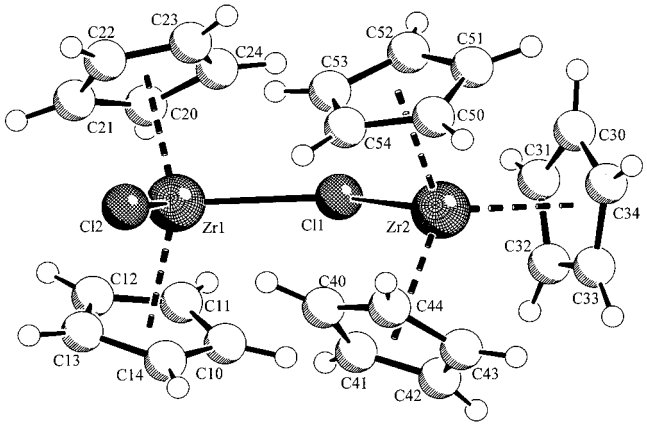


Figure 3. A view of the molecular geometry of the cation $[Cp_3Zr-(\mu\text{-}Cl)-ZrCp_2Cl]^+$ (**7**$^+$), as obtained from X−ray crystal structure analysis. Selected bond lengths [Å] and angles [°]: Zr1−Cl1 2.544(1), Zr1−Cl2 2.405(1), Zr1−C(Cp1) 2.490, Zr1−Cp1 2.187, Zr1−C(Cp2) 2.480, Zr1−Cp2 2.190, Zr2−Cl1 2.722(1), Zr2−C(Cp3) 2.596, Zr2−Cp3 2.311, Zr2−C(Cp4) 2.576, Zr2−Cp4 2.290, Zr2−C(Cp5) 2.570, Zr2−Cp5 2.281; Cl1−Zr1−Cl2 95.80(4), Cl1−Zr1−Cp1 107.4, Cl1−Zr1−Cp2 104.0, Cl2−Zr1−Cp1 107.6, Cl2−Zr1−Cp2 106.6, Cp1−Zr1−Cp2 130.2, Zr1−Cl1−Zr2 137.15(5), Cl1−Zr2−Cp3 95.2, Cl1−Zr2−Cp4 99.8, Cl1−Zr2−Cp5 100.0, Cp3−Zr2−Cp4 117.7, Cp3−Zr2−Cp5 117.7, Cp4−Zr2−Cp5 118.3. Zr−C(Cp) is the average Zr−C distance between Zr and the C atoms of the Cp ring, Zr−Cp is the distance between the calculated centroid of the Cp ring zirconium

The sum of the corresponding Cp(centroid)−Zr−Cp(centroid) angles σ_P amounts to 353.7° (Cp3−Zr2−Cp4: 117.7°, Cp4−Zr2−Cp5: 118.3°, Cp3−Zr2−Cp5: 117.7°). The zirconium atom (Zr2) is located 0.333 Å above the plane of the Cp3 to Cp5 centroids. The $[Cp_2ZrCl_2]$ donor is coordinated to the $[Cp_3Zr^+]$ cation through one of its chloride ligands (Cl1). The Zr2−Cl1 vector is oriented normal to the Cp3 to Cp5 plane. The Zr2−Cl1 bond is rather long at 2.722(1) Å, which is markedly longer than the adjacent terminal Zr1−Cl2 linkage [2.405 (1) Å] of the bent metallocene unit. The remaining bonding features at the coordinated Cp_2ZrCl_2 unit are not exceptional [angle Cl2−Zr−Cl1: 95.80(4)°]. The adduct is strongly bent at the bridging μ-chloride ligand [angle Zr1−Cl1−Zr2: 137.15(5)°], and the substituents Cl2 and Zr(2)Cp_3 are found in a *syn*-periplanar orientation at the Zr1−Cl1 bond [dihedral angles Zr2−Cl1−Zr1−Cl2 7.50(8)°].

We also synthesized the $[Cp_3Zr-Cl]$ adduct of the $[Cp_3Zr]^+$ cation. In this case the salt $[Cp_3Zr^+ CH_3B(C_6F_5)_3^-]$ (**1**) was prepared and the organometallic ligand Cp_3Zr-Cl was added to it in CH_2Cl_2 at −60 °C (Scheme 2). Workup at ambient temperature furnished the adduct complex $\{[Cp_3Zr-(\mu\text{-}Cl)-ZrCp_3]^+[CH_3B(C_6F_5)_3]^-\}$ (**8**). Complex **8** features a single ^{1}H-/^{13}C-NMR resonance at δ = 6.25 (30 H)/116.6 along with the anion methyl resonance at δ = 0.51 (3 H, broad)/10.5. Single crystals of **8** were again obtained from a saturated solution in dichloromethane at −30 °C.

The $[Cp_3Zr-(\mu\text{-}Cl)-ZrCp_3]^+$ cation (**8**$^+$) contains two Cp_3Zr units that each feature an almost trigonal pyramidal

arrangement of the three η^5 Cp ligands and the single bridging chloride around zirconium (Figure 4).

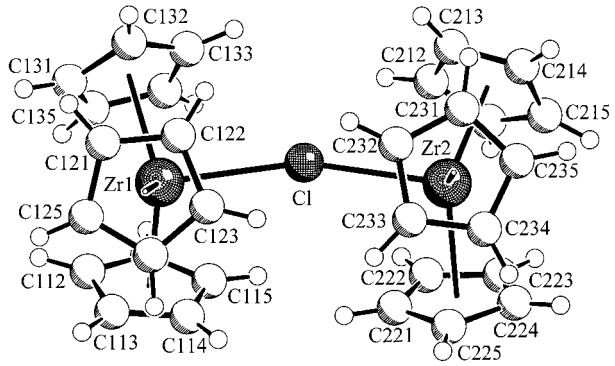


Figure 4. Molecular structure of $\mathbf{8}^+$ in the crystal. Selected bond lengths [Å] and angles [°]: Zr1−Cl 2.6918(6), Zr1−C(Cp11) 2.586, Zr−Cp11 2.296, Zr1−C(Cp12) 2.576, Zr1−Cp12 2.286, Zr1−C(Cp13) 2.586, Zr1−Cp13 2.297, Zr2−Cl 2.6893(6), Zr2−C(Cp21) 2.589, Zr2−Cp21 2.298, Zr2−C(Cp22) 2.582, Zr2−Cp22 2.291, Zr2−C(Cp23) 2.577, Zr2−Cp23 2.286; Cl−Zr1−Cp11 99.7, Cl−Zr1−Cp12 100.2, Cl−Zr1−Cp13 96.4, Cp11−Zr1−Cp12 117.5, Cp11−Zr1−Cp13 117.7, Cp12−Zr1−Cp13 117.9 Zr1−Cl−Zr2 160.88(2), Cl−Zr2−Cp21 97.9, Cl−Zr2−Cp22 99.1, Cl−Zr2−Cp23 99.8, Cp21−Zr2−Cp22 117.9, Cp21−Zr2−Cp23 117.4, Cp22−Zr2−Cp23 117.6. Nomenclature as described for Figure 3

The angle σ_P, as defined above, is 353.1° at Zr1 and 352.9° at Zr2. Again, the Zr−Cl vector is arranged almost normal to the respective Cp planes [Cp(centroid)−Zr−Cl angles at Zr1: 99.7°/100.2°/96.4°; at Zr2: 97.9°/99.1°/99.8°]. The Zr1−Cl bond length in **8** is 2.692(1) Å, which is almost identical to Zr2−Cl [2.689(1) Å], but both are slightly shorter that the $Cp_3Zr-(\mu\text{-}Cl)$ bond in **7** (see above). The Zr1−Cl−Zr2 angle in **8** is 160.88(2)°. This represents the most pronounced difference between the structures of the adducts **7** and **8**. The marked tendency of $[Cp_3Zr-(\mu\text{-}Cl)-ZrCp_3]^+$ ($\mathbf{8}^+$) towards a linear Zr−Cl−Zr structure, in contrast to the strongly bent $[Cp_3Zr-(\mu\text{-}Cl)-ZrCp_2Cl]^+$ ($\mathbf{7}^+$) framework, is in accord with the theoretical analysis and probably reflects the subtle balance of steric and electronic factors that eventually determines the structural features of such organometallic adducts of the C_{3v}-symmetrical Cp_3Zr^+ cation systems.

Comparison between Calculated Geometries and Experimental Structures

Both the X-ray crystal structure analyses, as well as the density functional calculations, result in the same molecular shape for $\mathbf{7}^+$ and $\mathbf{8}^+$. Measured and optimized bond angles are in good agreement for both cations. It is striking, however, that the calculated Zr−Cl distances are significantly overestimated by up to 0.09 Å in the calculation, as shown for $\mathbf{7}^+$ in Figure 5.

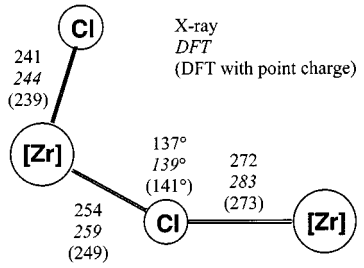


Figure 5. A comparison of the molecular framework of $\mathbf{7}^+$ obtained from crystal structure analysis and theoretical calculations

We performed additional calculations for this complex, including a negative point charge, which was located in space in close proximity to the position where the boron atom of the counterion would be found in the crystal. The Zr−Cl bonds shorten under the influence of the point charge, and are now in closer agreement to the value obtained from the X-ray structural analysis (Figure 5). The molecular environment has a significant influence on the molecular geometry of the cations for $\mathbf{7}^+$ and $\mathbf{8}^+$, especially concerning geometric parameters that are associated with the shallow potentials on the energy hypersurface.

Conclusion

In this work we have demonstrated that the tris(cyclopentadienyl)zirconium cation ($\mathbf{1}^+$) displays a similar coordination chemistry to the well studied $[Cp_2ZrR]^+$ species and is able to bind the neutral metallocene derivatives $[Cp_2ZrCl_2]$ (**2**) or $[Cp_3ZrCl]$ (**3**) as ligands. The X-ray crystal structure analyses revealed that the Zr−Cl−Zr bridging angle τ can take on values representing both a strongly bent and an almost linear coordination geometry. Our theoretical analysis suggests that a subtle balance between steric and electronic factors determines the geometries in such organometallic adducts.

Experimental Section

General Remarks: All reactions were carried out under argon using Schlenk-type glassware or in a glove-box. All solvents, including deuterated solvents used for NMR spectroscopy, were dried and distilled under argon prior to use. Tris(pentafluorophenyl)borane (**10**),[10] $[Cp_3ZrCH_3]$ (**9**),[1] $[Cp_3ZrCl]$ (**3**),[11] and $[Cp_2ZrCl_2]$ (**2**)[12] were prepared as described in the literature. − M.p. DSC 2010 (TA Instruments). − IR spectra: Nicolet-5-DXC-FT IR spectrometer; $\tilde{\nu}$ in cm^{-1}. − NMR spectra: Bruker AC-200P (^1H 200 MHz, ^{13}C 50 MHz) and Bruker AM 360 (^1H 360 MHz, ^{13}C 75 MHz) spectrometer; δ in ppm. − Elemental analyses: Foss Heraeus CHNO Rapid.

$[Cp_3Zr-(\mu\text{-}Cl)-ZrCp_2Cl]^+[CH_3B(C_6F_5)_3]^-$ (7): To a mixture of tris(η^5-cyclopentadienyl)methylzirconium (**9**) (80.0 mg, 0.27 mmol), tris(pentafluorophenyl)borane (**10**) (136 mg, 0.27 mmol) and zirconocene dichloride (**5**) (78.0 mg, 0.27 mmol) was added 15 mL of dichloromethane by means of vacuum distillation. The resulting yellow solution was allowed to warm up to room temperature with

stirring. After stirring for an additional 10 min at room temperature the solvent was removed in vacuo to yield 285 mg (97%) of the orange-yellow salt **7**. Single crystals of **7** were obtained from a saturated dichloromethane solution at −30 °C, m.p. 171 °C (DSC, decomp.). − $C_{44}H_{28}BCl_2F_{15}Zr_2$ (1106): calcd. C 47.49, H 2.55; found C 46.68, H 2.72. − IR (KBr): $\tilde{\nu}$ = 3124 cm^{-1}, 2949, 1642, 1511, 1458, 1381, 1366, 1266, 1088, 1017, 978, 966, 952, 818, 740. − ^{1}H NMR (200.13 MHz, [D$_2$]dichloromethane, 300 K): δ = 6.67 (s, 10 H, Cp-*H*), 6.24 (s, 15 H, Cp-*H*), 0.51 (br s, 3 H, B−C*H*$_3$). − ^{13}C NMR (75.47 MHz, [D$_2$]dichloromethane, 300 K): δ = 148.8 (d, $^1J_{CF}$ = 238 Hz), 137.9 (d, $^1J_{CF}$ = 243 Hz), 136.9 (d, $^1J_{CF}$ = 251 Hz) and 129.8 [br, *o*-, *p*-, *m*- and *ipso*-B(C_6F_5)$_3$], 118.8 and 117.0 (each Cp), 10.5 (s, B−CH_3).

[Cp$_3$Zr−(μ-Cl)−ZrCp$_3$]$^+$[CH$_3$B(C$_6$F$_5$)$_3$]$^-$ (8): A Schlenk flask was charged with tris (η^5-cyclopentadienyl)methylzirconium (**9**) (80.0 mg, 0.27 mmol) and tris(pentafluorophenyl)borane (**10**) (136 mg, 0.27 mmol). Dichloromethane (15 mL) was added and the resulting solution was cooled to −60 °C. At that temperature a cold solution of tris(η^5-cyclopentadienyl)chlorozirconium (**6**) (86.0 mg, 0.27 mmol) in dichloromethane (10 mL) was added. The reaction mixture was stirred for 10 min at −60 °C and then allowed to warm up to room temperature. The solvent was removed from the resulting pale yellow solution to yield 287 mg (95%) of **8**. Single crystals were obtained from a saturated dichloromethane solution at −30 °C, m.p. 159 °C (DSC, decomp.). − $C_{49}H_{33}BClF_{15}Zr_2$ (1135): calcd. C 51.83, H 2.93; found C 49.94, H 2.61. − IR (KBr): $\tilde{\nu}$ = 3125 cm^{-1}, 2959, 1642, 1510, 1458, 1366, 1267, 1087, 1010, 980, 963, 952, 845, 813, 737. − ^{1}H NMR (200.13 MHz, [D$_2$]dichloromethane, 300 K): δ = 6.25 (s, 30 H, Cp-*H*), 0.51 (br s, 3 H, B−C*H*$_3$). − ^{13}C NMR (75.47 MHz, [D$_2$]dichloromethane, 300 K): δ = 148.8 (d, $^1J_{CF}$ = 238 Hz), 137.9 (d, $^1J_{CF}$ = 243 Hz), 136.8 (d, $^1J_{CF}$ = 240 Hz) and 129.8 [br, *o*-, *p*-, *m*-, and *ipso*-B(C_6F_5)$_3$], 116.6 (Cp), 10.5 (s, B−CH_3).

Computational Details: Gradient-corrected density functional calculations were carried out with corrections for exchange and correlation according to Becke[13] and Perdew,[14] respectively (BP86). Geometries were optimized using the program system TURBOMOLE[15] within the framework of the RI-*J* approximation.[16] A triple ζ valence basis plus polarization (TZVP) was employed for all elements.[17]

X-ray Crystallographic Study: Data sets were collected with a Nonius Kappa CCD diffractometer, using a rotating anode generator FR591. Programs used: data collection: Collect;[18] data reduction: Denzo-SMN;[19] absorption correction: SORTAV;[20] structure solution: SHELXS-97;[21] structure refinement: SHELXL-97;[22] graphics: SCHAKAL.[23] X-ray crystal structure analysis of **7**: formula $C_{25}H_{25}Cl_2Zr_2 \cdot CH_3B(C_6F_5)_3 \cdot CH_2Cl_2$, M = 1190.74, 0.20 × 0.15 × 0.10 mm, a = 13.061(1), b = 13.431(1), c = 14.078(1) Å, α = 94.19(1), β = 109.85(1), γ = 104.51°, V = 2214.6(3) Å^3, $\rho_{calcd.}$ = 1.786 g cm^{-3}, μ = 8.10 cm^{-1}, empirical absorption correction (0.855 ≤ T ≤ 0.923), Z = 2, triclinic, space group $P\bar{1}$ (No. 2), λ = 0.71073 Å, T = 198 K, ω and phi scans, 23648 reflections collected (±h, ±k, ±l), [(sinθ)/λ] = 0.65 Å^{-1}, 10105 independent (R_{int} = 0.054) and 7131 observed reflections [$I \geq 2\,\sigma(I)$], 605 refined parameters, R = 0.057, wR^2 = 0.124, max. residual electron density 1.08 (−1.48) e Å^{-3}, hydrogens calculated and refined as riding atoms. X-ray crystal structure analysis of **8**: formula $C_{30}H_{30}ClZr_2 \cdot CH_3B(C_6F_5)_3$, M = 1135.45, 0.50 × 0.30 × 0.20 mm, a = 15.142(1), b = 12.601(1), c = 22.401(1) Å, β = 94.00(1)°, V = 4263.8(5) Å^3, $\rho_{calcd.}$ = 1.769 g cm^{-3}, μ = 6.55 cm^{-1}, empirical absorption correction (0.735 ≤ T ≤ 0.880), Z = 4, monoclinic, space group $P2_1/n$ (No. 14), λ = 0.71073 Å, T = 198 K, ω and phi scans, 33512 reflections collected (±h, ±k, ±l), [(sinθ)/λ] = 0.71 Å^{-1}, 12912 independent (R_{int} = 0.037) and 10797 observed reflections [$I \geq 2\,\sigma(I)$], 614 refined parameters, R = 0.035, wR^2 = 0.083, max. residual electron density 0.91 (−0.75) e Å^{-3}, hydrogens calculated and refined as riding atoms.

Structural drawings of **7**$^+$ and **8**$^+$ displaying thermal ellipsoids are provided as supporting information.

Crystallographic data (excluding structure factors) for the structures reported in this paper have been deposited with the Cambridge Crystallographic Data Centre as supplementary publication no. CCDC-137524 and 137525. Copies of the data can be obtained free of charge on application to The Director, CCDC, 12 Union Road, Cambridge CB2 1EZ, UK [Fax: (internat.) +44 (0)1223/336-033, E-mail: deposit@ccdc.cam.ac.uk].

Acknowledgments

Financial support from the Fonds der Chemischen Industrie, the Deutsche Forschungsgemeinschaft and the Swiss National Science Foundation is gratefully acknowledged.

[1] [1a] T. Brackemeyer, G. Erker, R. Fröhlich, *Organometallics* **1997**, *16*, 531−536. − [1b] T. Brackemeyer, G. Erker, R. Fröhlich, J. Prigge, U. Peuchert, *Chem. Ber.* **1997**, *130*, 899−902. − [1c] H. Jacobsen, H. Berke, T. Brackemeyer, T. Eisenblätter, G. Erker, R. Fröhlich, O. Meyer, K. Bergander, *Helv. Chim. Acta* **1998**, *81*, 1692−1709.

[2] [2a] T. Cuenca, D. T. Hardy, M. Bochmann, *J. Organomet. Chem.* **1994**, *484*, C10−C12. − [2b] S. J. Lancaster, M. Bochmann, *Angew. Chem.* **1994**, *106*, 1715−1718; *Angew. Chem. Int. Ed. Engl.* **1994**, *33*, 1634−1637.

[3] [3a] M. V. Gaudet, M. J. Zaworotko, T. S. Cameron, A. Linden, *J. Organomet. Chem.* **1989**, *367*, 267−273. − [3b] C. J. Harlan, S. G. Bott, A. R. Barron, *J. Am. Chem. Soc.* **1995**, *117*, 6465−6474.

[4] [4a] T. Ziegler, *Chem. Rev.* **1991**, *91*, 651−667. − [4b] W. Kohn, A. D. Becke, R. G. Parr, *J. Phys. Chem.* **1996**, *100*, 12974−12980. − [4c] E. J. Baerends, O. V. Gritsenko, *J. Phys. Chem. A* **1997**, *101*, 5383−5403.

[5] T. A. Albright, J. K. Burdett, M.-H. Whangboo, *Orbital Interactions in Chemistry*; John Wiley: New York, **1985**, chapter 7.3.

[6] R. L. DeKock, R. D. van Zee, T. Ziegler, *Inorg. Chem.* **1987**, *26*, 563−567.

[7] [7a] Consult the supporting information for optimized geometries and relative energies of complexes **4**$^+$, **5**, and **6**$^+$.[7b] Besides the σ_{pd}-type orbital interaction as discussed in Scheme 1, we also considered additional π_{pd}-type interactions. An overlap population analysis for a bent and a linear system, however, indicated that these secondary interactions are not dominant in determining the angular dependence of the coordination geometry around the μ-Cl bridge.

[8] [8a] H. B. Bradley, L. G. Dowell, *Anal. Chem.* **1958**, *30*, 548. − [8b] K. Prout, T. S. Cameron, R. A. Forder, S. R. Critchley, B. Denton, G. V. Rees, *Acta Crystallogr.* **1974**, *B30*, 2290−2304. − [8c] G. L. Soloveichik, T. M. Arkhireeva, V. K. Bel′skii, B. M. Bulychev, *Metalloorg. Khim.* **1988**, *1*, 226−230; *Chem. Abs.* **1989**, *110*, 173374t. − [8d] J. Y. Corey, X.-H. Zhu, L. Brammer, N. P. Rath, *Acta Crystallogr.* **1995**, *C51*, 565−567. − [8e] T. Repo, M. Klinga, I. Mutikainen, Y. Su, M. Leskelä, M. Polamo, *Acta Chem. Scand.* **1996**, *50*, 1116−1120.

[9] C. M. Diamond, M. L. H. Green, N. A. Popham, A. N. Chernega, *J. Chem. Soc., Dalton Trans.* **1993**, 2535.

[10] [10a] F. G. A. Stone, A. G. Massey, A. J. Park, *Proc. Chem. Soc.* **1963**, 212. −[10b] A. G. Massey, A. J. Park, *J. Organomet. Chem.* **1964**, *2*, 245−250.

[11] P. Etievant, B. Gautheron, G. Tainturier, *G. Bull. Chim. Fr.* **1978**, 292−298.

[12] [12a] J. J. Eisch, R. B. King, *Organomet. Synthesis*, Academic Press, New York **1965**, *1*, 75−78. − [12b] M. D. Rausch, H. B. Gordon, E. Samuel, *J. Coord. Chem.* **1971**, *1*, 141−143.

[13] [13a] A. D. Becke, *J. Chem. Phys.* **1986**, *84*, 4524−4529. − [13b] A. D. Becke, *J. Chem. Phys.* **1988**, *88*, 1053−1062. − [13c] A. D. Becke, *Phys. Rev.* **1988**, *A38*, 3098−3100.

[14] [14a] J. P. Perdew, *Phys. Rev.* **1986**, *B33*, 8822−8824. − [14b] J. P. Perdew, *Phys. Rev.* **1986**, *B34*, 7406.

[15] [15a] R. Ahlrichs, M. Bär, M. Häser, H. Horn, C. Kölmel, *Chem. Phys. Lett.* **1989**, *162*, 165−169. − [15b] O. Treutler, R. Ahlrichs, *J. Chem. Phys.* **1995**, *102*, 346−354. − [15c] R. Ahlrichs, M. von Arnim, in: *Methods and Techniques in Computational Chemistry: METECC-95* (Eds.: E. Clementi, G. Corongiu), STEF: Cagliari, **1995**, chapter 13.

[16] [16a] K. Eichkorn, O. Treutler, H. Öhm, M. Häser, R. Ahlrichs, *Chem. Phys. Lett.* **1995**, *240*, 283−290. − [16b] K. Eichkorn, O. Treutler, H. Öhm, M. Häser, R. Ahlrichs, *Chem. Phys. Lett.* **1995**, *242*, 652−670.

[17] A. Schäfer, C. Huber, R. Ahlrichs, *J. Chem. Phys.* **1994**, *100*, 5829−5835.

[18] B. V. Nonius, *Collect* **1998**.

[19] Z. Otwinowski, W. Minor, *Methods in Enzymology* **1997**, *276*, 307−326.

[20] [20a] R. H. Blessing, *Acta Crystallogr., Sect. A* **1995**, *51*, 33−37. − [20b] R. H. Blessing, *J. Appl. Cryst*. **1997**, *30*, 421−426.

[21] G. M. Sheldrick, *Acta Crystallogr., Sect. A* **1990**, *46*, 467−473.

[22] G. M. Sheldrick, *SHELXL-97*, Universität Göttingen, **1997**.

[23] E. Keller, *SCHAKAL-97*, Universität Freiburg, **1997**.

Received December 27, 1999
[I99470]

Lanthanide(III) Dodecanoates: Structure, Thermal Behaviour, and Ion-Size Effects on the Mesomorphism

Koen Binnemans,*[a] Liesbet Jongen,[a] Christiane Görller-Walrand,[a] Willem D'Olieslager,[a] Dirk Hinz,[b] and Gerd Meyer[b]

Keywords: Rare-earth compounds / Lanthanides / Metallomesogens / Liquid crystals / Metal soaps

Rare-earth salts of dodecanoic acid (lauric acid) have been prepared and characterized. The compounds have the stoichiometry $Ln(C_{11}H_{23}COO)_3$, where Ln = Y, La, Ce–Lu (except Pm). The thermal behaviour of these rare-earth dodecanoates has been investigated by hot-stage polarized optical microscopy, differential scanning calorimetry (DSC), thermogravimetry (TG), and high-temperature X-ray diffraction analysis. The compounds have a lamellar bilayer structure in the solid state, with the alkyl chains in an *all-trans* conformation normal to the ionic sublayer. The size of the trivalent lanthanide ion has proved to be a critical factor with regard to the existence of mesophases of this type of metallomesogens bearing carboxylate ligands. Thus, it was found that a mesophase can only be formed with the light lanthanide ions having large ionic radii. The mesophase stability range decreases rapidly on traversing the lanthanide series. Whereas a smectic A phase has been observed for the La^{III}, Ce^{III}, Pr^{III}, and Nd^{III} dodecanoates, no mesomorphism is apparent for the other lanthanide complexes.

Introduction

Although rare-earth containing metal soaps have long been studied,[1–15] their mesomorphism was discovered only recently. Thus, Marques et al.[16] found liquid-crystallinity in Ce^{III} soaps and, based on the textures observed by hot-stage polarized optical microscopy, the authors suggested that Ce^{III} tetradecanoate and its higher homologues formed disordered smectic mesophases, whereas more complex mesophase behaviour was observed for Ce^{III} soaps with shorter chain lengths. By high-temperature X-ray diffraction analysis, Binnemans et al.[17] identified the mesophase formed by La^{III} tetradecanoate and its higher homologues as a smectic A (SmA) phase. These compounds were found to adopt a lamellar bilayer structure. The layer spacing in the crystalline lamellar phase at moderate temperature was close to the calculated thickness of a bilayer with the *all-trans* alkyl tails *normal* to the ionic sublayer.

Since Binnemans et al.[18] observed a very pronounced effect of the contraction of the lanthanide ion radius on the transition temperatures of lanthanide-containing metallomesogens with Schiff-base ligands, we were interested in ascertaining whether a similar effect could be found for the lanthanide(III) dodecanoates. For the Schiff-base complexes, the mesophase stability range decreases on traversing the lanthanide series (broad mesophase range for the La^{III} compound → a very narrow mesophase range for the Lu^{III} compound). We have found that in the case of the lanthanide(III) dodecanoates, the ionic radius of the trivalent lanthanide ion has a critical effect on the transition temperatures in that a mesophase can only be formed with the lighter lanthanide elements. Since there have been several reports on the industrial applications of lanthanide(III) soaps as catalysts,[19,20] polymer stabilizers,[21] and photosensitizers,[22,23] as well as on their medicinal applications,[12] a good understanding of the structural properties of compounds of this type is clearly desirable.

In this paper, we report on the structures and thermal behaviour of these lanthanide(III) dodecanoates. The structures of the compounds have been studied by IR and X-ray powder diffraction analysis. Their thermal behaviour has been investigated by hot-stage polarized optical microscopy, differential scanning calorimetry (DSC), thermogravimetry (TG), and high-temperature X-ray diffraction analysis.

Results and Discussion

The dodecanoates of all the trivalent rare-earth ions other than Sc^{III} and the radioactive Pm^{III} have been synthesized. The compounds were prepared by a metathesis reaction between the sodium salt of dodecanoic acid and the appropriate rare-earth salt (hydrated nitrate or chloride) in aqueous ethanol solution (ethanol/water, 1:1). The crude soaps were recrystallized from 1-pentanol/ethanol (5:1). The yield after recrystallization ranged from 68 to 87%.

The carbon and hydrogen contents of the rare-earth soaps were determined by C/H elemental microanalysis (combustion analysis), whereas the rare-earth contents were determined by complexometric titrations with EDTA using xylenol orange as an indicator. The fatty acid contents were measured titrimetrically using a standardized NaOH solution. For all the rare-earth dodecanoates, the ratio of the

[a] Katholieke Universiteit Leuven, Department of Chemistry, Celestijnenlaan 200F, B-3001 Leuven, Belgium
Fax: (internat.) +32 16 32 79 92
E-mail: Koen.Binnemans@chem.kuleuven.ac.be
[b] Institut für Anorganische Chemie, Universität zu Köln, Greinstraße 6, D-50939 Köln, Germany

 © WILEY-VCH Verlag GmbH, D-69451 Weinheim, 2000 1434–1948/00/0707–1429 $ 17.50+.50/0

Table 1. Analysis results for the rare-earth dodecanoates

Ln^{III}	% C[a]	% H[a]	% Ln[a]	$C_{11}H_{23}COOH$/Ln	# mol H_2O
Y^{III}	61.8 (62.1)	10.1 (10.1)	12.7 (12.8)	3.04	0.5
La^{III}	57.8 (58.0)	9.3 (9.5)	18.6 (18.6)	2.93	0.5
Ce^{III}	57.3 (57.2)	9.5 (9.5)	18.5 (18.5)	3.04	1
Pr^{III}	57.7 (57.8)	9.4 (9.4)	19.0 (18.8)	2.98	0.5
Nd^{III}	57.6 (57.6)	9.4 (9.4)	19.4 (19.2)	2.96	0.5
Sm^{III}	56.6 (56.4)	9.3 (9.3)	20.1 (19.6)	3.01	1
Eu^{III}	56.3 (56.3)	9.3 (9.3)	20.4 (20.4)	2.90	1
Gd^{III}	56.5 (56.6)	9.3 (9.2)	20.8 (20.6)	2.98	0.5
Tb^{III}	56.3 (56.5)	9.3 (9.2)	20.9 (20.8)	2.98	0.5
Dy^{III}	55.7 (55.5)	9.2 (9.2)	21.3 (20.9)	3.03	1
Ho^{III}	55.9 (56.0)	9.1 (9.1)	21.9 (21.4)	2.96	0.5
Er^{III}	55.8 (55.8)	9.0 (9.1)	22.3 (21.6)	2.96	0.5
Tm^{III}	54.9 (55.1)	9.0 (9.1)	22.2 (21.5)	2.94	1
Yb^{III}	55.3 (55.4)	9.1 (9.0)	22.4 (22.2)	3.01	0.5
Lu^{III}	55.1 (55.3)	9.0 (9.0)	22.6 (22.4)	3.05	0.5

[a] The calculated values are given in brackets. For the calculations, the stoichiometries $Ln(C_{11}H_{23}COO)_3 \cdot 1/2\ H_2O$ or $Ln(C_{11}H_{23}COO)_3 \cdot H_2O$ were used, depending on the water content. The theoretically expected $C_{11}H_{23}COOH$/Ln ratio is 3.00 in all cases.

dodecanoic acid content to the rare-earth content was found to vary between 2.84 and 3.05, which is close to the theoretically expected value of 3.00 for the stoichiometry $Ln(C_{11}H_{23}COO)_3$. C, H, and Ln analyses were supportive of these findings, but also indicated that, under the reaction conditions used, the compounds could not be obtained in completely anhydrous form. Water molecules were present in all the rare-earth dodecanoates; the compounds were found to be hemihydrates, $Ln(C_{11}H_{23}COO)_3 \cdot 1/2\ H_2O$, or monohydrates, $Ln(C_{11}H_{23}COO)_3 \cdot H_2O$. The analysis results of the soaps are presented in Table 1. However, on heating, the water molecules were lost before or at the melting point and hence anhydrous lanthanide(III) dodecanoates could be obtained by cooling the melts. The water loss and the subsequent thermal decomposition of the compounds were studied by thermogravimetry in combination with DTA (heating to 1000 °C in a static air atmosphere). The TG curves show that, in general, less than 1 mol water is lost per mol of rare-earth soap. The greatest water loss is observed for Ce^{III} dodecanoate, i.e. 1.04 mol. All the rare-earth dodecanoates, with the exception of Ce^{III} dodecanoate, decompose between 360 and 380 °C. The final decomposition product is the rare-earth oxide. In the case of the Ce^{III} dodecanoate, thermal decomposition was found to commence at 200 °C. The lower thermal stability of the cerium soap may be attributed to oxidation of Ce^{III} to Ce^{IV}, which was evident from the orange colour of the ash after decomposition (CeO_2).

The lanthanide(III) dodecanoates are powders that are waxy to the touch and take on the characteristic colour of the corresponding trivalent lanthanide ion.[24] Not unexpectedly, these metal soaps have very low solubilities in water. The compounds are hydrophobic and have low wetting abilities. At room temperature, no organic solvent could dissolve appreciable quantities of these metal soaps. Their solubilities in methanol, ethanol, 1-propanol, 2-propanol, 1-butanol, 1-pentanol, 1-hexanol, 1-octanol, hexane, chloroform, dichloromethane, toluene, benzene, ethylene glycol, DMSO, DMF, and pyridine were tested. At elevated temperatures, the lanthanide(III) dodecanoates proved to be fairly soluble in the higher alcohols (1-pentanol, 1-hexanol, 1-octanol) and in the aromatic solvents (toluene, benzene). 1-Pentanol was preferred as the crystallization solvent as the product separated from solutions in this solvent as a powder rather than as a gel (as is often the case when toluene or benzene is employed). Moreover, 1-pentanol is easier to remove from the purified product than 1-hexanol or 1-octanol. The crystallinity of the product was improved when some ethanol was added to the 1-pentanol (i.e. using 1-pentanol/ethanol, 5:1).

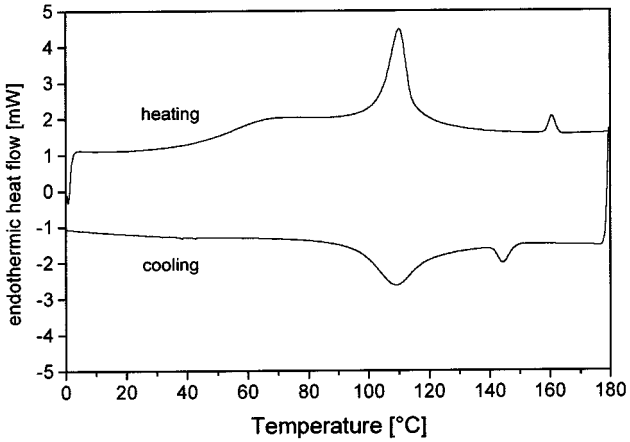


Figure 1. DSC thermogram of La^{III} dodecanoate (first heating−cooling cycle); endothermic peaks are shown pointing upwards

The melting points of the rare-earth dodecanoates $Ln(C_{11}H_{23}COO)_3$ were determined by hot-stage polarized optical microscopy, by the capillary melting technique, and by differential scanning calorimetry (DSC). Whereas in the DSC thermograms of the $Ln(C_{11}H_{23}COO)_3$ compounds with Ln = Sm−Lu, Y just a single peak is observed (corresponding to the melting point), the DSC thermograms of the dodecanoates of La^{III}, Ce^{III}, Pr^{III}, and Nd^{III} show an additional weaker peak above the melting point, indicating that these compounds form a mesophase on heating. In Figure 1, the first heating and cooling cycle in the DSC thermogram of $La(C_{11}H_{23}COO)_3$ is shown. It can be seen

that the melting peak is rather broad and shows a much higher enthalpy change than the clearing peak. Before the melting peak, a broad, weak endothermic transition is observed, which is due to the loss of water (as can be proved by thermogravimetry). In the cooling run, a slight supercooling is observed for the clearing transition. At high cooling rates (> 10 °C min^{-1}), no crystallization is observed and the samples are supercooled to a glassy state. The formation of a mesophase was also evident from the melting point determinations by hot-stage polarized optical microscopy and the capillary melting technique. Whereas the compounds showing only one peak in their DSC thermograms melted directly in a heated capillary tube to give a clear liquid (of rather low viscosity), the La^{III}, Ce^{III}, Pr^{III}, and Nd^{III} dodecanoates first melted to a highly viscous, turbid liquid and then, upon further heating, the viscosity decreased markedly and the melt became clear. Such a turbid melt is typical of a liquid-crystalline phase (i.e. a mesophase). Under the microscope, the compounds exhibited first a soft, waxy appearance and then melted to a birefringent liquid. However, it proved very difficult to obtain a good defect texture, even by cooling the isotropic liquid, as the compounds showed a very strong tendency to align homeotropically. By pressing with a needle on the cover glass it was possible to observe birefringence, but the molecules quickly re-orientated to the homeotropic alignment. The texture was suggestive of a smectic mesophase, most probably a smectic A phase (considering the presence of regions with a homeotropic alignment). It was not easy to visually observe the melting points of the mesomorphic lanthanide(III) dodecanoates owing to the high viscosities of the mesophases. The melting temperatures are thus quoted as the temperature at which the compound showed some fluidity. These temperatures are corroborated by the DSC thermograms and correspond to the maxima of the endothermic melting peaks. The clearing points were detected by hot-stage polarized optical microscopy. The transition temperatures and the corresponding enthalpy and entropy changes are listed in Table 2. For the enthalpy and entropy changes of the melting peak, the values of both the first and the second heating runs are listed. Large differences are observed between the first and the second heating runs; this is due to the fact that the evaporation enthalpy of water in the hydrated lanthanide soaps contributes to the transition enthalpy of the first heating run, whereas in the second heating run the enthalpy values are likely to be smaller owing to the fact that the samples are not completely crystalline (i.e. that they are partially amorphous). However, the enthalpy values of the clearing peak are consistent for the various compounds.

Room-temperature X-ray powder diffractograms were recorded for all of the synthesized compounds. Up to 4 peaks are observed in the low-angle region of the X-ray powder diffractograms of the solid lanthanide(III) dodecanoates, with the peak at the lowest angle showing by far the greatest intensity. The *d*-spacing values are in the ratio $1:{}^1/_2:{}^1/_3:\ \ldots\ :{}^1/_n$. These peaks correspond to the successive (00*l*) reflections and indicate the presence of a lamellar structure. Because the *d*-spacing is about twice the calculated length of the dodecanoate molecule, a bilayer structure can be postulated. The maximum average *d*-spacing of the bilayer structure was calculated for an *all-trans* conformation of the dodecanoate chain perpendicular to the metal ion base plane using Equation (1):[16]

$$d_{max} = 2d_{C-H} + 2(n-1)d_{C-C}\sin 55° + 2d_{C-O} + 2r_{Ln^{3+}} \quad (1)$$

where $n = 12$ (total number of carbon atoms), $d_{C-H} = 1.09$ Å, $d_{C-C} = 1.54$ Å, and $d_{C-O} = 1.36$ Å. For the ionic radii $r_{Ln}{}^{3+}$ of the trivalent lanthanide ions, we took the values reported by Shannon for rare-earth complexes with a coordination number of six.[25] The calculated and experimental d_{max} values, which correspond to two consecutive Ln^{III}

Table 2. Transition temperatures, enthalpies, and entropies of the rare-earth dodecanoates $Ln(C_{11}H_{23}COO)_3$

Ln^{III}[a]	Transition[b]	Temperature/°C	ΔH/kJ mol^{-1}[c]	ΔS/J K^{-1} mol^{-1}[c]
Y^{III}	Cr → I	85	114.7 (26.9)	320.4 (75.1)
La^{III}	Cr → SmA	110	63.7 (23.2)	116.3 (60.6)
	SmA → I	161	1.3	3.0
Ce^{III}	Cr → SmA	106	113.5 (30.3)	299.5 (79.9)
	SmA → I	138	0.9	2.2
Pr^{III}	Cr → SmA	98	89.6 (26.1)	241.5 (70.4)
	SmA → I	128	1.3	3.2
Nd^{III}	Cr → SmA	91	57.1 (26.5)	156.9 (72.8)
	SmA→ I	117	1.3	3.3
Sm^{III}	Cr → I	91	103.2 (21.3)	283.5 (63.5)
Eu^{III}	Cr → I	90	84.8 (20.9)	233.6 (57.6)
Gd^{III}	Cr → I	93	89.2 (20.4)	243.7 (55.7)
Tb^{III}	Cr → I	90	95.9 (17.5)	264.2 (48.2)
Dy^{III}	Cr → I	87	109.8 (20.3)	305.0 (56.4)
Ho^{III}	Cr → I	85	108.3 (23.4)	302.5 (65.4)
Er^{III}	Cr → I	84	116.6 (27.2)	326.6 (76.2)
Tm^{III}	Cr → I	83	117.9 (33.3)	331.2 (93.5)
Yb^{III}	Cr → I	81	117.5 (33.6)	331.9 (94.9)
Lu^{III}	Cr → I	78	104.9 (31.8)	298.9 (90.6)

[a] The molecular masses have been calculated assuming that the soap is anhydrous as water is lost before or at the melting point. – [b] Cr: crystalline phase; SmA: smectic A phase; I: isotropic liquid. – [c] The values are those for the first heating run, the values in brackets those for the second heating run. The values for the clearing point are the same in both heating runs.

Table 3. Calculated and experimental layer spacings d_{max} (in Å) of the rare-earth dodecanoates $Ln(C_{11}H_{23}COO)_3$ at room temperature

Ln^{III}	d_{max} (calcd.) [Å]	d_{max} (expt.) [Å]
Y^{III}	34.45	34.38
La^{III}	34.74	34.67
Ce^{III}	34.67	33.87
Pr^{III}	34.65	34.34
Nd^{III}	34.62	34.34
Sm^{III}	34.57	34.44
Eu^{III}	34.55	34.74
Gd^{III}	34.52	34.83
Tb^{III}	34.50	34.32
Dy^{III}	34.48	34.28
Ho^{III}	34.45	34.56
Tm^{III}	34.41	34.24
Yb^{III}	34.39	34.24
Lu^{III}	34.37	33.98

basal planes, are given in Table 3. Good agreement is found between the experimental and calculated values, any differences invariably amounting to less than 1% of the calculated value. As the ionic radii of the trivalent lanthanide ions decrease smoothly on traversing the lanthanide series ($r_{La}{}^{3+}$ = 1.045 Å, $r_{Lu}{}^{3+}$ = 0.861 Å for CN = 6), a corresponding decrease in the layer spacing might be expected, but this is not found experimentally. The small difference in ionic radius between La^{3+} and Lu^{3+} is outweighed by the experimental error in the determination of the *d*-values from the rather broad diffraction peaks. That the *d*-spacing does not follow the expected decrease on traversing the lanthanide series can be attributed to small variations in the conformations of the alkyl chains in the different compounds. For the calculation of the *d*-spacing, we assume an *all-trans* conformation for the alkyl chains, but random deviations can occur due to the flexibility of the alkyl chains.

The size of the lanthanide ion does have a very significant effect on the thermal behaviour of the lanthanide(III) dodecanoates. As the ionic radius of the lanthanide cation decreases, the distance between the carboxylate groups mutually opposite with respect to the plane containing the lanthanide ions also decreases. The thermal vibrations increase in amplitude at increasing temperatures and thereby induce unfavourable electrostatic interactions (repulsions) between the carboxylate groups, not only of the two opposing layers, but also between adjacent carboxylate groups within the same layer. When the repulsive forces between the negative charges are stronger than the attractive forces between the negative (carboxylate groups) and positive charges (lanthanide ions), the bilayer structure of the solid metal soap is no longer stable and breaks down. In this case, a rearrangement of the carboxylate groups and lanthanide ions to obtain a more stable solid-state structure (i.e. a crystal−crystal transition) might be expected. However, melting of the compounds is observed. The alkyl chains have sufficient thermal energy such that when the layer structure breaks down, their *all-trans* conformation is lost and they adopt a less extended conformation (which is more or less random). On melting, the metal soaps are transformed into ionic liquids with rather low viscosities. In such an ionic liquid, the total negative charge (due to the carboxylate groups) is, of course, equal to the total positive charge (due to the lanthanide ions), but the oppositely charged species can move independently of one another.

The melting points of the lanthanide(III) dodecanoates decrease over the lanthanide series; the smaller the lanthanide ion, the more unstable the layer structure becomes, and hence less thermal energy is required to break down the solid-state structure. The influence of the ion size on the melting point is also evident from the melting points of Y^{III} dodecanoate (m.p. 85 °C) and Ho^{III} dodecanoate (m.p. 85 °C), these similar values reflecting the similar ionic radii of Y^{3+} and Ho^{3+}.

A mesophase is formed when, at the melting point of the alkyl chains, the electrostatic interactions between the lanthanide ions and the carboxylate groups are still sufficiently favourable to maintain a layer structure. This is the case for the La^{III}, Ce^{III}, Pr^{III}, and Nd^{III} dodecanoates. The thermal behaviour of these compounds has been investigated by high-temperature X-ray diffraction analysis. Although the general features of the X-ray diffractograms remained the same in comparison to those of the solid compounds (except for the disappearance of the peaks of an order higher than 2), decreases in the *d*-spacings were observed at the melting points (vide infra). The X-ray diffractogram of each mesophase was consistent with a disordered smectic mesophase, indicating that the layered structure present in the solid phase is retained in the mesophase, whereas the in-plane ordering is largely lost. The loss of the in-plane ordering is reflected by the disappearance of the peak at large angles (at $2\theta \simeq 21°$, equivalent to $d \simeq 4.2$ Å) and the appearance of a much broader one, which is typical for disordered alkyl chains. Thus, the bilayer structure seen in the solid phase still represents an energetically favourable packing of the carboxylates in the mesophase. Additionally, the ratio of the peak positions in the low-angle region is $1:{}^1/_2$, indicating a one-dimensional stacking of the layers. The mesophase can be identified as a smectic A mesophase in that the layer spacing decreases slightly with increasing temperature. For a smectic C phase, an increase in layer spacing would be expected with increasing temperature.[26] The presence of an SmA phase is further supported by the homeotropically aligned regions in the optical texture observed by hot-stage polarized optical microscopy. After the clearing point, only one weak broad band is observed in the X-ray diffractograms. This is typical for the X-ray diffractogram of a liquid, indicating that the melts are isotropic. The mesophases have very high viscosities as, unlike in neutral organic molecules, the layers in the metal soaps are held together by electrostatic forces. It is difficult to shear the layers. In this sense, the mesophases can be considered as partially solid compounds, the alkyl chains exhibiting a molten behaviour, while to some extent the ionic part the structure remains intact. Consequently, sharp melting points are not observed for the lanthanide(III) dodecanoates forming a mesophase, but rather melting processes that occur over certain temperature ranges. Not all the alkyl chains melt at the same temperature. This became evident

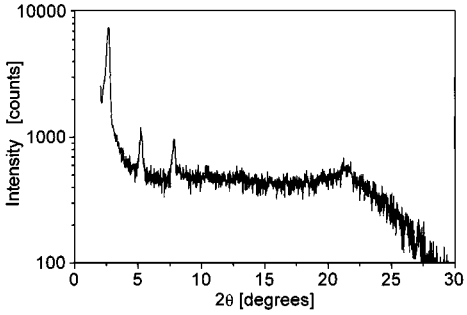


Figure 2. X-ray powder diffractogram of La^{III} dodecanoate at 50 °C

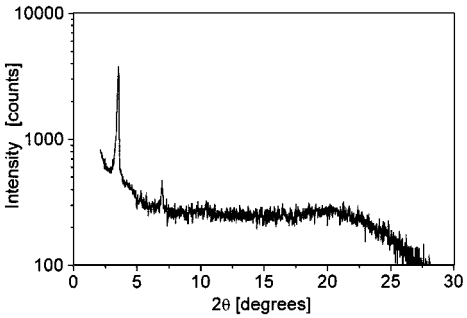


Figure 3. X-ray diffractogram of La^{III} dodecanoate in the mesophase at 135 °C

when X-ray diffractograms of the compounds forming a mesophase were recorded close to their melting points. Such X-ray diffractograms show more peaks than those of the solid phase or the mesophase and it turned out that they were in fact a superposition of these respective diffractograms. In Figure 2, the X-ray diffractogram of solid La^{III} dodecanoate at 50 °C is shown; Figure 3 shows the corresponding diffractogram of the mesophase (135 °C).

The La^{III}, Ce^{III}, Pr^{III}, and Nd^{III} dodecanoates all form mesophases, which can be identified by high-temperature X-ray diffraction analyses as smectic A phases, although some structural differences between the mesophases can be observed. For La^{III} dodecanoate, the structure of the mesophase is much closer to that of the corresponding solid compound than in the case of the Ce^{III}, Pr^{III}, and Nd^{III} compounds. This is evident from the smaller change in layer spacing upon melting of the La^{III} compound as compared with the decreases in layer spacing at the melting points of the other compounds. The change in layer spacing gradually increases from 1.28 Å for La^{III} dodecanoate, through 6.73 Å for Ce^{III} dodecanoate and 8.26 Å for Pr^{III} dodecanoate, to 8.67 Å for Nd^{III} dodecanoate (Figure 4). The decrease in *d*-value upon melting may either be due to more vigorous thermal movements of the alkyl chains giving rise to larger tilts (the average tilt remains at zero, however, and the alkyl chains are perpendicular to the layer planes) or to a curling of the chains. For Nd^{III} dodecanoate in the solid phase, the *d*-layer spacing shows a very small temperature dependence and remains virtually constant between room temperature and the melting point (Figure 5). For solid La^{III} dodecanoate, however, another phenomenon is observed: close to the melting point, a distinct decrease in the

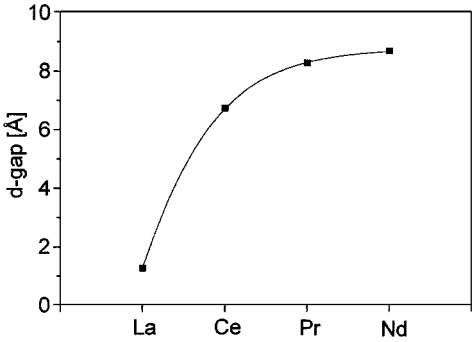


Figure 4. Variation of the change in the *d*-spacing at the melting point for the mesomorphic lanthanide(III) dodecanoates

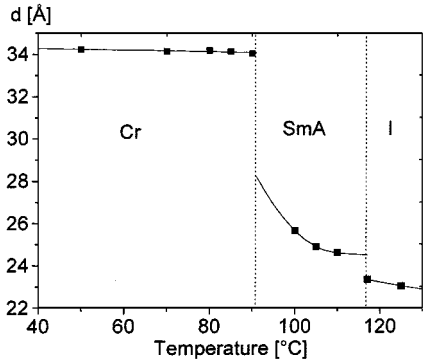


Figure 5. Evolution of the *d*-spacing of Nd^{III} dodecanoate as a function of temperature

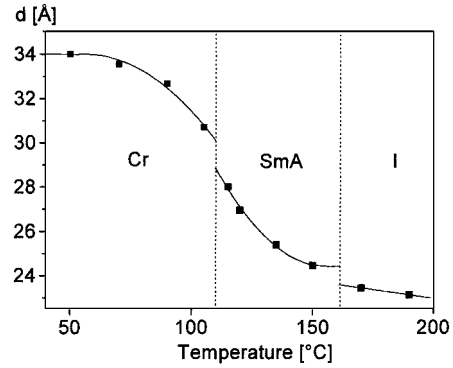


Figure 6. Evolution of the *d*-spacing of La^{III} dodecanoate as a function of temperature

layer spacing is seen (Figure 6). For Ce^{III} and Pr^{III} dodecanoate, intermediate behaviour is observed. This indicates differences in the pre-melting behaviour of the metal complexes.[27]

The layer structure is gradually lost in the compounds that form a mesophase, whereas it is lost much more abruptly in the compounds that melt without forming a mesophase. It must be emphasized that in the compounds forming a mesophase, the layer structure breaks down at the clearing point, whereas in the case of the non-mesogenic compounds total break-down of the layer structure occurs

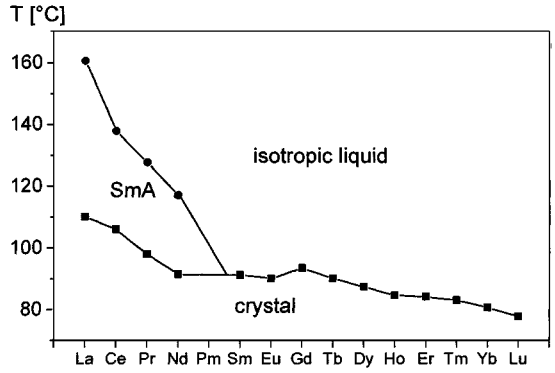


Figure 7. Phase diagram for the lanthanide(III) dodecanoates

only at the melting point. The phase diagram for the lanthanide(III) dodecanoates is shown in Figure 7.

The bilayer structure described herein is not restricted to lanthanide soaps. In fact, this mesophase structure was first described by Skoulios and Luzatti for alkali metal soaps in the "neat soap" lamellar mesophase.[28] The liquid-crystallinity of ionic metal soaps has been reviewed by Mirnaya et al.,[29] by Polishchuk and Timofeeva,[30] and by Giroud-Godquin.[31]

Although X-ray powder diffraction experiments revealed a bilayer structure for the solid lanthanide(III) dodecanoates, this technique did not give any information concerning the coordination of the lanthanide(III) ions. All that is known is that the metal ions form a layer that is sandwiched between two layers of carboxylate groups. From the stoichiometry $Ln(C_{11}H_{23}COO)_3$, it could be deduced that three carboxylate groups are present for each lanthanide ion, and that the lanthanide ions cannot be confined to one single carboxylate group (as in the case of the carboxylates of monovalent cations). We investigated the coordination around the lanthanide ion by IR spectroscopy.

The IR spectra of the various rare-earth dodecanoates proved to be all very similar. Moreover, the absorption maxima due to vibrations of the aliphatic chain of dodecanoic acid are not modified upon formation of the metal soaps. However, the IR absorptions due to the carboxyl group do change drastically. The IR spectrum of dodecanoic acid indicates the presence of a localized C=O bond and an OH bond within the COOH unit. The carbonyl (C=O) stretching vibration is observed as a very strong transition at 1700 cm^{-1}, whereas the OH stretching vibration at ca. 2660 cm^{-1} is broad due to intermolecular hydrogen bonding between two molecules of dodecanoic acid (dimeric structure). In the rare-earth dodecanoates, these transitions disappear and are replaced by the symmetric and asymmetric stretching vibrations of the carboxylate group (COO^-): ν_{symm} is seen at 1410 cm^{-1} and ν_{asymm} at 1540 cm^{-1}, giving a splitting of $\Delta\tilde{\nu} = \nu_{asymm} - \nu_{symm} =$ 130 cm^{-1}. This splitting is comparable to that seen for sodium soaps ($\Delta\tilde{\nu} = 138$ cm^{-1}), in which the metal−carboxylate bonding is essentially ionic.[16] Since in the rare-earth compounds the positions of the bands are shifted to smaller wavenumbers in comparison to the sodium soaps, there is a strong evidence to suggest that the carboxylate groups coordinate in a bidentate fashion. However, there is insufficient evidence to discriminate between a chelating bidentate or a bridging bidentate coordination mode, and even a mixture of both coordination types within the same compound cannot be ruled out. Marques et al.[16] have discussed in detail all the other transitions observed in the IR spectra of Ce^{III} carboxylates, and our results are in agreement with theirs. Recently, Corkery and Martin investigated Eu^{III} dodecanoate and Eu^{III}-doped La^{III} dodecanoate by high-resolution luminescence spectroscopy.[32] These authors found that at least two symmetrically distinct Eu^{III} sites are present in samples obtained by slow cooling of melts.

Conclusion

The lanthanide(III) dodecanoates are waxy compounds with a stoichiometry corresponding to $Ln(C_{11}H_{23}COO)_3 \cdot x\,H_2O$ ($0 \leq x \leq 1$). Water is often present in non-stoichiometric amounts, with compositions being close to the hemihydrate ($x = 0.5$) or the monohydrate ($x = 1$). TG-DTA has revealed that on heating the water molecules are lost before or at the melting point, and that cooling of the melts results in the anhydrous compounds (albeit often in a glass-like state). The X-ray powder diffraction patterns are consistent with a bilayer structure, in which an infinite layer of lanthanide ions is separated by a double layer of dodecanoate groups. The dodecanoate groups are arranged tail-to-tail. The experimentally determined layer spacing d_{max} is close to the calculated length of the dodecanoate group with the $C_{11}H_{23}$ chain in an *all-trans* conformation. The melting points of the lanthanide(III) dodecanoates decrease smoothly on traversing the lanthanide series, ranging from 110 °C for La^{III} dodecanoate to 78 °C for Lu^{III} dodecanoate. This can be attributed to an ion-size effect; the behaviour of Y^{III} dodecanoate is very similar to that of Ho^{III} dodecanoate, in accordance with the similarity of the radii of these cations. The dodecanoate salts of La^{III}, Ce^{III}, Pr^{III}, and Nd^{III} form mesophases, and the mesophase stability range decreases rapidly on traversing the lanthanide series. On the basis of hot-stage polarized optical microscopy observations and high-temperature X-ray diffraction measurements, the mesophase could be identified as a smectic A phase (SmA). The smectic phase has a very high viscosity owing to the strong electrostatic interactions between the anionic and cationic layers. Just above the melting point, the structure of the mesophase formed by La^{III} dodecanoate is close to that of the solid compound, but on proceeding towards Nd^{III} dodecanoate, the respective mesophases exhibit more liquid-like behaviour. This is reflected by the changes in *d*-spacing at the melting points. For Sm^{III} dodecanoate and the other dodecanoates, no mesomorphism is observed, not even monotropic mesomorphism. The difference in thermal behaviour between the dodecanoates of the light and heavy lanthanides can be quantitatively explained in terms of a model that takes into account the size of the lanthanide ion and the electrostatic

repulsions between the carboxylate groups. Although the present study confirms the results of earlier work on the thermal and structural properties Ce^{III} and La^{III} carboxylates,[16,17] the observation of an SmA mesophase only for the larger lanthanides $La^{III}-Nd^{III}$ is somewhat surprising and was not expected. A decrease in the mesophase stability ranges over the lanthanide series has been found for Schiff-base complexes,[18] but the lanthanide(III) dodecanoates show that small differences in ionic radius between the lanthanide ions are critical with regard to the formation or absence of a mesophase.

Experimental Section

General Remarks: Elemental analyses (CHN) were performed on a CE Instruments EA-1110 elemental analyzer. − Differential scanning calorimetry (DSC) measurements were made on a Mettler-Toledo DSC821e module. Solid samples weighing 2−5 mg were placed in aluminium pans (40 μL) with pierced lids and heated or cooled at a scan rate of 10 °C min^{-1} under a nitrogen flow. Indium metal was used as a standard to calibrate the instrument (T_m = 156.6 ± 0.3 °C, ΔH_m = 28.45 ± 0.6 J g^{-1}). − The optical textures of the mesophases were observed with an Olympus BX60 polarized optical microscope equipped with a LINKAM TMS600 hot-stage and a LINKAM TMS93 programmable temperature-controller. − High-temperature X-ray diffraction was measured on a STOE transmission powder diffractometer system STADI P with a high-temperature attachment version 0.65.1 (temperature range from room temp. to 1000 °C). Monochromatic Cu-$K_{\alpha 1}$ radiation (λ = 1.54 Å) was obtained with the aid of a curved germanium primary monochromator. Diffracted X-rays were measured by a linear position-sensitive detector (PSD). The sample was placed in a quartz capillary (outer diameter 0.3 mm, wall thickness 0.01 mm) and spun during the measurement. In general, data were collected in the range $1 \leq 2\theta \leq 30°$. − Melting points were measured on an Apotec melting-point apparatus using samples in capillaries. − Thermogravimetric curves were obtained using a Polymer Laboratories STA 1000H TG-DTA apparatus. The sample (ca. 15 mg) was heated in a static air atmosphere from 30 to 1000 °C at a rate of 10 °C min^{-1}. − FT-IR spectra were recorded on a Bruker IFS-66 spectrometer with samples in KBr pellets or as Nujol mulls. − All chemicals were used as received, without further purification. Dodecanoic acid (lauric acid) was obtained from Acros. Hydrated rare-earth nitrates were purchased from Aldrich.

Synthesis of La^{III} Dodecanoate: Dodecanoic acid (2.75 g, 13.8 mmol) was dissolved in 1:1 ethanol/water (100 mL) and converted to sodium dodecanoate by adding an equivalent amount of a standardized 0.5 M NaOH solution by means of a burette. Lanthanum nitrate hexahydrate (2.00 g, 4.6 mmol) was also dissolved in 1:1 ethanol/water (100 mL). The solution of sodium dodecanoate was then added dropwise with stirring to the solution of lanthanum nitrate at ambient temperature, which led to the immediate deposition of a white precipitate. After the addition was complete, the mixture was stirred for 1 h at ambient temperature. The precipitate was then collected by filtration through a Büchner funnel, and washed with water (3 × 100 mL), ethanol (3 × 50 mL), and acetone (3 × 50 mL) in order to remove residual traces of the lanthanum salt or of dodecanoic acid. The crude lanthanum(III) dodecanoate was dried for 24 h in vacuo at 50 °C and then recrystallized from 1-pentanol/ethanol (5:1). Crystallization was completed by placing the solution in a refrigerator. The purified soap was collected by filtration, washed with ethanol (25 mL) to remove most of the 1-pentanol, and then dried in vacuo (10^{-3} mbar) at 50 °C for at least 24 h. Lanthanum(III) dodecanoate was obtained as a white powder. Yield: 2.25 g (87%). − Elemental analysis: calcd. for $C_{36}H_{69}O_6La \cdot {}^1/_2\,H_2O$: C 58.0, H 9.5, La 18.6; found C 57.8, H 9.3, La 18.6; ratio $C_{11}H_{23}COOH$/Ln: theoretical for $La(C_{11}H_{23}COO)_3$: 3.0; found 2.93. − IR (KBr): $\tilde{\nu}$ = 1540 (s, COO^-, asymm. C−O stretch), 1410 cm^{-1} (m, COO^-, symm. C−O stretch).

All the other lanthanide(III) dodecanoates were prepared by the same method.

Analysis Procedures: − 1. Determination of Rare-Earth Content: The compound (200 mg) was dissolved in hot 0.1 M H_2SO_4 solution (15 mL). After cooling, the solution was extracted with diethyl ether to remove dodecanoic acid. An aliquot (5 mL) of the aqueous solution was transferred to a beaker by means of a volumetric pipette and its pH was adjusted to 6 by adding hexamethylenetetraamine buffer. Xylenol orange was added as an indicator and the solution was titrated with standardized 0.01 M EDTA solution until the indicator changed color from purple to yellow. Titrations were performed at 60 °C, at which temperature the color change was more easily observed. − **2. Determination of the Dodecanoic Acid Content:** The combined diethyl ether extracts containing dodecanoic acid (obtained by extracting the H_2SO_4 solution after decomposition of the soap; see above) were washed with saturated brine and then the solvent was removed under reduced pressure. The residual dodecanoic acid was redissolved in ethanol and this solution was titrated with 0.025 M NaOH solution using phenolphthalein as indicator.

Acknowledgments

K.B. is a Postdoctoral Fellow of the F.W.O. Flanders (Belgium). He thanks the F.W.O. for a "Krediet aan Navorsers". L.J. is indebted to the "Flemish Institute for the Encouragement of Scientific and Technological Research in Industry (IWT)" for financial support. Financial support by the K. U. Leuven (GOA 98/03) and by the F.W.O. Flanders (G.0243.99) is gratefully acknowledged. K. B. wishes to thank Prof. C. Görller-Walrand for providing laboratory facilities. CHN microanalyses were performed by Ms. P. Bloemen.

[1] S. N. Misra, T. N. Misra, R. C. Mehrotra, *J. Inorg. Nucl. Chem.* **1963**, *25*, 195−199.
[2] S. N. Misra, T. N. Misra, R. C. Mehrotra, *J. Inorg. Nucl. Chem.* **1963**, *25*, 201−203.
[3] R. C. Mehrotra, T. N. Misra, S. N. Misra, *J. Indian Chem. Soc.* **1966**, *43*, 61−62.
[4] M. Hasan, B. S. Sankhla, S. N. Misra, R. N. Kapoor, *J. Prakt. Chem.* **1968**, *38*, 313−319.
[5] L. D. Skrylev, V. F. Sazonova , I. I. Seifullina, *Ukrain. Khim. Zh.* **1981**, *47*, 596−599.
[6] K. N. Mehrotra, M. Chauhan, R. K. Shukla, *Monatsh. Chem.* **1989**, *120*, 1063−1068.
[7] K. N. Mehrotra, A. S. Gahlaut, M. Sharma, *J. Indian Chem. Soc.* **1987**, *64*, 309−310.
[8] K. N. Mehrotra, M. Saxena, A. Kumar, *An. Asoc. Quim. Argent.* **1990**, *78*, 319−328.
[9] K. N. Mehrotra, S. K. Upadhyaya, *Polish J. Chem.* **1991**, *65*, 1035−1042.
[10] S. K. Upadhyaya, P. S. Sharma, *J. Indian Chem. Soc.* **1993**, *70*, 735−739.
[11] K. N. Mehrotra, V. Kumari, A. Kumar, *Polish J. Chem.* **1993**, *67*, 2065−2072.
[12] L. Dobetti, P. Esposito, L. Boltri, *Eur. J. Pharm. Biopharm.* **1994**, *40*, 161−167.

[13] K. N. Mehrotra, R. K. Shukla, M. Chauhan, *Bull. Chem. Soc. Jpn.* **1995**, *68*, 1825−1831.
[14] K. N. Mehrotra , N. Sharma, *Polish J. Chem.* **1996**, *70*, 1236−1245.
[15] K. N. Mehrotra, M. Chauhan, R. K. Shukla, *Tenside Surf. Det.* **1997**, *34*, 124−127.
[16] E. F. Marques, H. D. Burrows, M. da Graça Miguel, *J. Chem. Soc., Faraday Trans.* **1998**, *94*, 1729−1736.
[17] K. Binnemans, B. Heinrich, D. Guillon, D. W. Bruce, *Liq. Cryst.* **1999**, *26*, 1717−1721.
[18] K. Binnemans, R. Van Deun, D. W. Bruce, Yu. G. Galyametdinov, *Chem. Phys. Lett.* **1999**, *300*, 509−514.
[19] S. V. Krylova, G. V. Butovskaya, V. E. Agabekov, *Kinetics and Catalysis* **1990**, *31*, 528−531.
[20] A. Oehme, U. Gebauer, K. Gehrke, M. D. Lechner, *Angew. Makromolek. Chem*. **1996**, *235*, 121−130.
[21] R. Hussain, F. Mahmood, *J. Chem. Soc., Pakistan* **1994**, *16*, 225−228.
[22] Y. Lin, *J. Rare Earths* **1996**, *14*, 98−104.
[23] R. M. Harnden, *U. S. Patent* 5,096,941 (**1992**).
[24] K. Binnemans, C. Görller-Walrand, *Chem. Phys. Lett.* **1995**, *235*, 163−174.
[25] R. D. Shannon, *Acta Cryst. A* **1976**, *A32*, 751−767.
[26] J. M. Seddon, *Structural Studies of Liquid Crystals by X-ray Diffraction*, in: *Handbook of Liquid Crystals* (Eds.: D. Demus, J. Goodby, G. W. Gray, H.-W. Spiess, V. Vill), Wiley-VCH, Weinheim, **1998**, Vol. 1, p. 635−679.
[27] G. Zerbi, G. Conti, G. Minoni, S. Pison, A. Bigotto, *J. Phys. Chem.* **1987**, *91*, 2386−2393.
[28] A. Skoulios, V. Luzzati, *Nature* **1959**, *183*, 1310.
[29] T. A. Mirnaya, V. D. Prisyazhnyi, V. A. Shcherbakov, *Russian Chem. Rev.* **1989**, *58*, 821−834.
[30] A. P. Polishchuk, T. V. Timofeeva, *Russian Chem. Rev.* **1993**, *62*, 291−321.
[31] A. M. Giroud-Godquin, *Metal-Containing Liquid Crystals*, in: *Handbook of Liquid Crystals* (Eds.: D. Demus, J. Goodby, G. W. Gray, H.-W. Spiess, V. Vill), Wiley-VCH, Weinheim, **1998**, Vol. 2B, p. 901−932.
[32] R. W. Corkery, J. P. D. Martin, *J. Lumin.* **1999**, *82*, 1−8.

Received December 28, 1999
[I99469]

New Studies on the Reactivity of Hydride-Containing Niobocene Complexes Towards Insertion and Protonation Processes

Antonio Antiñolo,*[a] Fernando Carrillo-Hermosilla,[a] Juan Fernández-Baeza,[a] Santiago García-Yuste,[a] Antonio Otero,*[a] Javier Sánchez-Prada,[a] and Elena Villaseñor[a]

Keywords: Niobium / Metallocenes / Hydrides / Dihydrogen / Protonations / Insertions

The trihydride complex [Nb(η^5-$C_5H_4SiMe_3)_2(H)_3$] **(1)** reacts with diphenylphosphane to afford the monohydride [Nb(η^5-$C_5H_4SiMe_3)_2(H)(PHPh_2)$] **(3)**. The synthesis of complex **3** has also been achieved from the initial formation of the phosphonium salt [Nb(η^5-$C_5H_4SiMe_3)_2(H)_2(PHPh_2)$]Cl **(2)** by reaction of the trihydride complex [Nb(η^5-$C_5H_4SiMe_3)_2(H)_3$] **(1)** with chlorodiphenylphosphane, followed by deprotonation of this salt in aqueous NaOH. Protonation of complex **3** at low temperature with a slight excess of CF_3COOH or CF_3COOD leads to the η^2-dihydrogen complex [Nb(η^5-$C_5H_4SiMe_3)_2(\eta^2$-$H_2)(PHPh_2)$]CF_3CO_2 **(4)** or its monodeuterated isotopomer [Nb(η^5-$C_5H_4SiMe_3)_2(\eta^2$-HD)$(PHPh_2)$]CF_3CO_2 **(5)**. When the temperature is increased to room temperature, complexes **4** and **5** transform into the *transoid* dihydrides [Nb(η^5-$C_5H_4SiMe_3)_2(H)_2(PHPh_2)$]$CF_3CO_2$ **(6)** and [Nb(η^5-$C_5H_4SiMe_3)_2(H)_2$-$(PDPh_2)$]CF_3CO_2 **(7)**, respectively. Complex **3** undergoes an insertion of CS_2 into the niobium–hydrogen bond to give the η^1-dithioformato complex [Nb(η^5-$C_5H_4SiMe_3)_2(PHPh_2)(\eta^1$-*S*-S(S)CH)] **(8)**. This complex could be detected by NMR spectroscopy but could not be isolated due to rapid conversion into the η^2-dithioformato complex [Nb(η^5-$C_5H_4SiMe_3)_2(\eta^2$-*S*,*S*-SSCH)] **(9)** by loss of the phosphane molecule. Complex **3** also reacts with CO_2 to give the η^2-formato complex [Nb(η^5-$C_5H_4SiMe_3)_2(\eta^2$-*O*,*O*-OOCH)] **(10)**; in this case the η^1-formato complex could not be detected. The reagent $ClPPh_2$ very smoothly inserts into the Nb–H bond of the complexes [Nb(η^5-$C_5H_4SiMe_3)_2(H)(L)$] [L = $PHPh_2$, CN(xylyl), CO; xylyl = 2,6-dimethylphenyl], yielding the new ionic complexes [Nb(η^5-$C_5H_4SiMe_3)_2(PHPh_2)(L)$]Cl [L = $PHPh_2$ **(11)**, CN(xylyl) **(12)**, CO **(13)**]. All the complexes described have been characterized by analytical and spectroscopic methods.

Introduction

Hydride complexes of transition metals represent one of the most important classes of compounds due to their chemical reactivity and importance in catalysis.[1] Furthermore, the chemistry of phosphorus-substituted early transition metal complexes has also recently received a great deal of attention.[2] Several groups[3,4] have found that the trihydrides [Cp_2MH_3] (M = Nb, Ta) react with chlorophosphanes PR_2Cl to afford the phosphonium salts [Cp_2MH_2-(PR_2H)]Cl. Depending on the metal (Nb or Ta) and on the nature of the phosphane substituent, deprotonation of these salts leads to hydride(phosphane) [$Cp_2MH(PR_2H)$] or hydride(phosphide) [$Cp_2MH_2(PPh_2)$] metalloligands. As part of a study of the electronic and steric influence of trimethylsilyl-substituted cyclopentadienyl ligands on the properties of niobocene complexes, we have studied the reaction of the trihydride niobocene complex [Nb(η^5-$C_5H_4SiMe_3)_2H_3$][5] with $ClPPh_2$ and the subsequent deprotonation of the phosphonium salt obtained. We have previously prepared[6] the hydride(phosphane) niobocene complexes [Nb(η^5-C_5H_4Si-$Me_3)_2(H)(PR_3)$] by heating the trihydride complex [Nb(η^5-$C_5H_4SiMe_3)_2H_3$] (**1**) in the presence of the corresponding phosphane PR_3. We have now used this method to synthesize the monohydride phosphane complex [Nb(η^5-C_5H_4Si-$Me_3)_2(H)(PHPh_2)$] (**3**) by thermal reaction of [Nb(η^5-$C_5H_4SiMe_3)_2H_3$] (**1**) with $PHPh_2$. In addition, and in keeping with our interest in dihydrogen complexes,[6,7] we report here the results for the low temperature protonation of the new monohydride complex [Nb(η^5-$C_5H_4SiMe_3)_2(H)$-$(PHPh_2)$] (**3**) and, for the first time, the deprotonation reaction of the cationic species obtained in this kind of reaction when the temperature is increased to room temperature.

Finally, the insertion of unsaturated molecules into the metal−hydride bond is considered as a fundamental chemical step in several catalytic cycles and frequently leads to reactive intermediates.[8] In connection with our recent studies of metal-promoted activation of unsaturated molecules such as heterocumulenes,[9] carbon disulfide,[10] carbon dioxide,[11] and activated alkynes,[12] we also decided to explore the reactivity of the new hydride phosphanyl complex **3** with carbon disulfide and carbon dioxide. These reactions have permitted the isolation of dithioformato- and formato-derivatives as well as the insertion of $ClPPh_2$ into the Nb−H bond of the monohydride derivatives [Nb(η^5-$C_5H_4SiMe_3)_2(H)(L)$] [L = $PHPh_2$, CN(2,6-$Me_2C_6H_3$), CO], and this has allowed us to prepare new cationic Nb^{III} species.

Results and Discussion

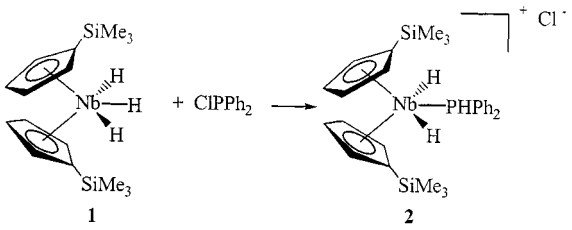
Reaction of [Nb(η^5-$C_5H_4SiMe_3)_2(H)_3$] With $ClPPh_2$

The reaction of [Nb(η^5-$C_5H_4SiMe_3)_2(H)_3$] (**1**) with $ClPPh_2$ proceeds smoothly to give quantitatively the ionic

[a] Departamento de Química Inorgánica, Orgánica y Bioquímica, Facultad de Químicas, Universidad de Castilla-La Mancha, Campus Universitario, 13071-Ciudad Real, Spain
Fax: (internat.) + 34-926/295-318
E-mail: aotero@qino-cr.uclm.es

 © WILEY-VCH Verlag GmbH, D-69451 Weinheim, 2000 1434−1948/00/0707−1437 $ 17.50+.50/0

complex $[Nb(\eta^5\text{-}C_5H_4SiMe_3)_2(H)_2(PHPh_2]Cl$ (**2**) as depicted in Equation (1).

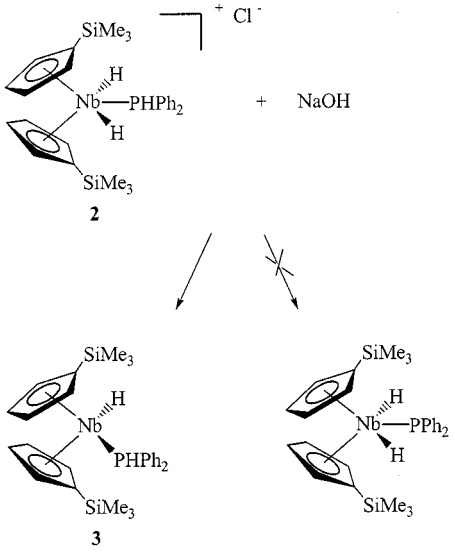


1 2 (1)

Complex **2** immediately precipitates as grey voluminous flakes after mixing Et_2O solutions of $[Nb(\eta^5\text{-}C_5H_4SiMe_3)_2(H)_3]$ (**1**) and $ClPPh_2$ at room temperature. Even at low temperature (253 K) the rate of the reaction is very fast. The low solubility of complex **2** in hydrocarbons, ethers and aromatic solvents means that the product can be isolated very easily in an analytically pure form. However, it is sufficiently soluble in acetone to allow its NMR spectrum to be recorded. The ionic nature of complex **2** was confirmed by measurement of the molar conductivity (Λ_M = 135 $\Omega^{-1}mol^{-1}$), which is in agreement with a 1:1 electrolyte.[13] Complex **2** was formed in high yield and was characterized by ^1H and ^{31}P NMR and IR spectroscopy. In the ^1H NMR spectrum ([D$_6$]acetone) only the symmetric isomer $[Nb(\eta^5\text{-}C_5H_4SiMe_3)_2(H)_2(PHPh_2)]Cl$ was observed. The cyclopentadienyl rings are equivalent and give rise to two broad resonances (see Experimental Section) for an A_2B_2 spin system in the ^1H NMR spectrum, which indicates a symmetrical disposition at the niobium centre with a rapid rotation of the phosphane moiety around the Nb−P bond. The ^1H NMR spectrum also shows a resonance due to the hydride ligands at $\delta = -2.16$ and this value is similar to those reported for the equivalent hydride ligands in $[Nb(\eta^5\text{-}C_5H_4SiMe_3)_2(H)_2(L)]PF_6$[6a] [L = P(OR)$_3$, PMe$_2$Ph] and $[M(\eta^5\text{-}C_5H_5)_2(H)_2(PR_3)]^+$.[14] The hydride ligands are equivalent and show a single resonance that appears as a doublet due to coupling with the phosphorus atom ($^2J_{HP}$ = 78.2 Hz). The signal for the hydrogen atom of the P−H group appears as a doublet at $\delta = 6.67$ ($^1J_{HP}$ = 283 Hz). The $^3J_{HH}$ value could not be observed due to the broadness of the signals. The ^{31}P NMR spectrum shows a broad doublet at $\delta = 20$ that corresponds to a second-order spin system due to the couplings $^1J_{HP}$ and $^2J_{HP}$. The IR spectrum shows a ν(P−H) band at ca. 2293 cm^{-1}, which confirms the existence of the coordinated phosphane molecule, and also a ν(Nb−H) band of medium intensity at ca. 1703 cm^{-1} (see Experimental Section).

A characteristic feature of complex **2** is the existence of two acidic centres: the P−H and the Nb−H bonds. The reaction between complex **2** and an aqueous solution of NaOH in toluene affords only the hydride(phosphane) complex **3** in good yield (75%); the corresponding phosphido complex could not be observed (Scheme 1).

The tantalum phosphido complex $Cp_2TaH_2(PPh_2)$ has been isolated by Nikonov et al. while the homologous niobium compound $Cp_2NbH_2(PPh_2)$ was not observed.[3] The



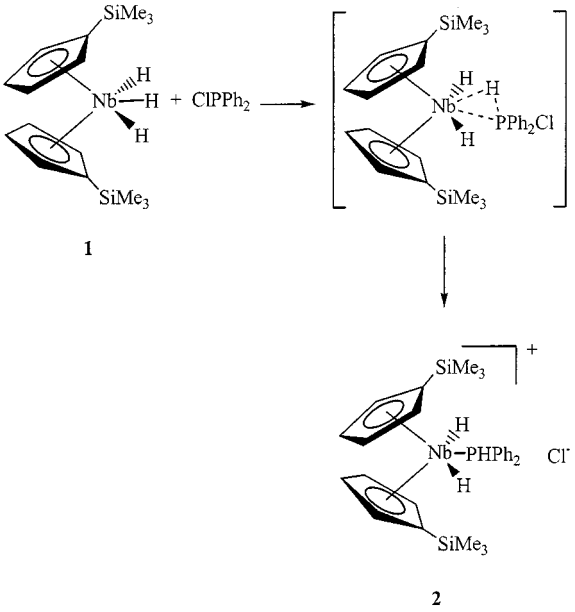
Scheme 1. Formation of **3** by reaction of **2** with NaOH

reaction was carried out in a two-phase system (water/toluene), which enabled easy extraction and isolation of the product as a red oily material. The characterization of complex **3** was performed by NMR and IR spectroscopy. The ^1H NMR spectrum shows a high-field resonance at $\delta = -7.37$ for the hydride ligand, which appears as a doublet ($^2J_{HP}$ = 29.30 Hz), whereas the P−H resonance appears as a doublet at $\delta = 6.90$ ($^1J_{HP}$ = 332 Hz). Three multiplets can also be observed that integrate for 4, 2 and 2 protons, respectively, and correspond to an AA′BB′ spin system. These signals are due to the cyclopentadienyl rings and are in accordance with an asymmetrical environment for the niobium centre (see Experimental Section). Finally, the IR spectrum shows two bands at ca. 1643 and 2281 cm^{-1}, which correspond to ν(Nb−H) and ν(P−H), respectively, and confirm the existence of the coordinated phosphane molecule.

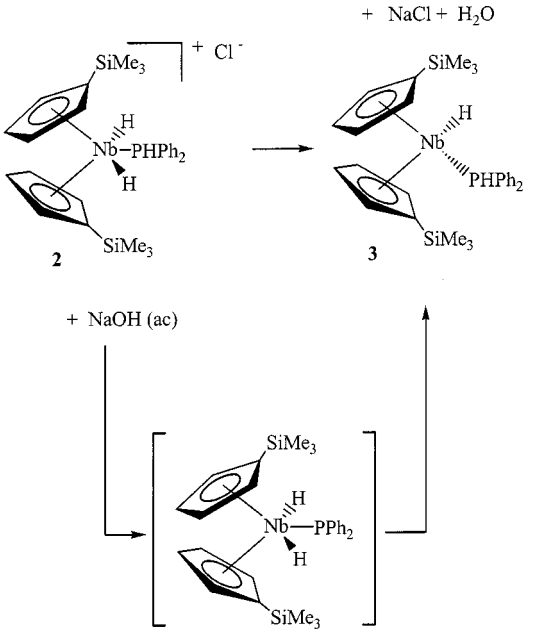
The reaction of $[Nb(\eta^5\text{-}C_5H_4SiMe_3)_2(H)_3]$ (**1**) with $ClPPh_2$ can be rationalized in terms of an insertion of the chlorophosphane into the Nb−H bond, followed by elimination of the chloride ion and rearrangement of the molecule as shown in Scheme 2. The nature of the insertion process can be considered as an interaction of the empty d-orbitals on the phosphorous with the Nb−H σ-bond, a situation that means a pentavalent phosphorus structure should be initially formed.

Deprotonation of **2** should initially occur at the more labile hydrogen atom, which is, according to the spectroscopic data, the P−H proton. This implies that deprotonation of **2** should initially produce a dihydride(phosphide) complex. However, such a complex could not be detected and probably transforms rapidly into complex **3** through a hydride shift into the vacant d-orbital at phosphorus (see Scheme 3).

Further experiments, which are described later in this paper, allowed us to confirm unequivocally that deprotonation occurs at the P−H bond. This is not unexpected



Scheme 2. Proposed reaction pathway for the formation of **2**

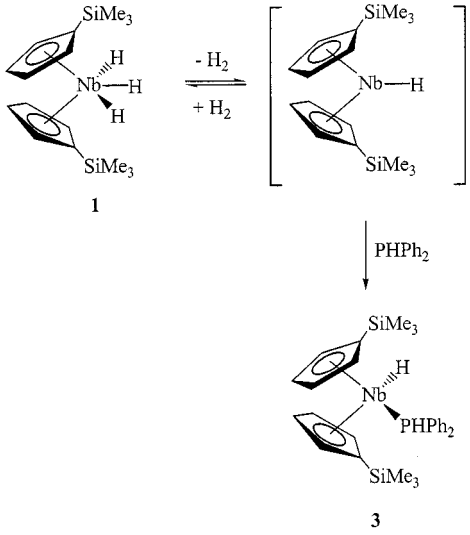


Scheme 3. Proposed reaction pathway for the deprotonation of **2**

as the P−H bond is kinetically more labile than the Nb−H bond.

Reaction of $[Nb(\eta^5\text{-}C_5H_4SiMe_3)_2(H)_3]$ With $PHPh_2$

We also prepared complex **3** in an alternative manner by reaction of $[Nb(\eta^5\text{-}C_5H_4SiMe_3)_2(H)_3]$ with $PHPh_2$. In fact, $[Nb(\eta^5\text{-}C_5H_4SiMe_3)_2(H)_3]$ (**1**) reacts slowly (3 hours) with $PHPh_2$ in THF at ca. 70 °C to afford the complex $[Nb(\eta^5\text{-}C_5H_4SiMe_3)_2(H)(PHPh_2)]$ (**3**). The initial step should be the formation of the coordinatively unsaturated 16-electron species $[Nb(\eta^5\text{-}C_5H_4SiMe_3)_2(H)]$ by thermolytic loss of H_2, followed by coordination of the phosphane ligand [Equation (2)].



(2)

The reaction is similar to that previously reported[6a,7,10] for the preparation of several families of niobocene complexes $[Nb(\eta^5\text{-}C_5H_4SiMe_3)_2(H)(L)]$ (L = π-acid ligand). Complex **3** was isolated as a spectroscopically pure, air-sensitive red oily material and the spectroscopic data are in agreement with those recorded for the complex isolated by the first method described in this paper. This one-step synthesis gives a better yield (90%) and represents a cleaner way of preparing complex **3**.

Protonation Reaction of $[Nb(\eta^5\text{-}C_5H_4SiMe_3)_2(H)(PHPh_2)]$ (3)

Complex **3** was easily protonated with CF_3COOH at low temperature to give the corresponding *cisoid* dihydrogen-containing complex **4** according to Equation (3).

$$[Cp'_2Nb(H)(PHPh_2)]\ \mathbf{(3)} + CF_3COOH \longrightarrow [Cp'_2Nb(\eta^2\text{-}H_2)(PHPh_2)]^+CF_3COO^-\ \mathbf{(4)} \quad (3)$$

When CF_3COOD is used, the monodeuterated complex **5** is obtained [Equation (4)]:

$$[Cp'_2Nb(H)(PHPh_2)]\ \mathbf{(3)} + CF_3COOD \longrightarrow [Cp'_2Nb(\eta^2\text{-}HD)(PHPh_2)]^+CF_3COO^-\ \mathbf{(5)} \quad (4)$$

These processes were carried out by adding a slight excess of CF_3COOH/D to a solution of complex **2** in $[D_6]$acetone in an NMR tube at 183 K.

The ^1H NMR spectrum of **4** at low temperature shows a dihydrogen resonance at ca. $\delta = -4.57$ that appears as a doublet due to the H-P coupling ($J_{HP} = 19.7$ Hz). The signal broadens at very low temperature but does not show decoalescence. The high-field $^1H\{^{31}P\}$ NMR spectrum of **5** at 183 K shows two triplets (1:1:1) at ca. $\delta = -4.7$ due to the existence of two different rotamers; *endo* **5a** and *exo* **5b**

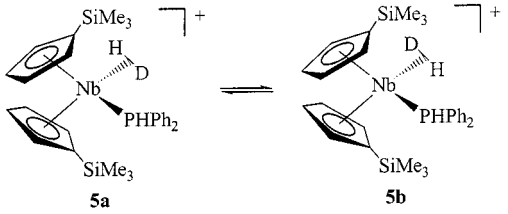


Figure 1. Rotation process of the HD coordinated molecule

(Figure 1). Both isomers show a similar J_{HD} coupling of ca. 18.20 Hz.

These rotamers exist due to the fact that the rotation of the coordinated HD molecule is frozen on the NMR time scale at this temperature.[6a,7]

When the temperature is raised, the rotamers *endo* H **5a** and *exo* H **5b** interconvert by rotation of the HD molecule. Coalescence is reached at 225 K, and at this temperature it is not possible to distinguish between the two isomers. At 263 K a single resonance (1:1:1 triplet) is observed at ca. $\delta = -4.70$ for the HD fragment (Figure 2).

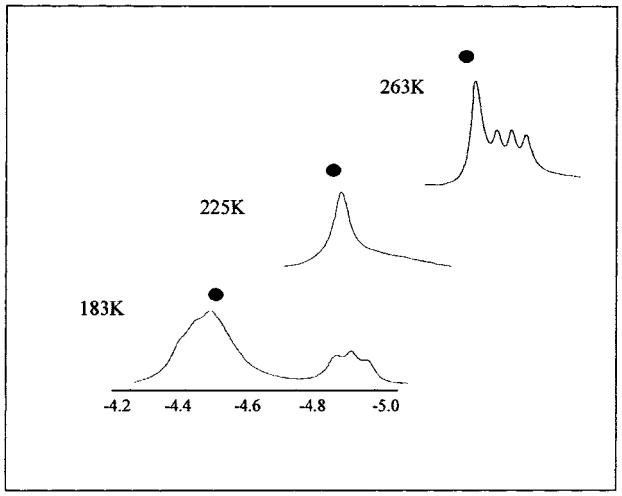
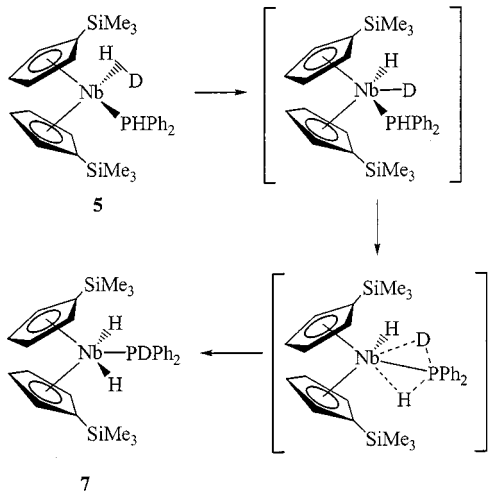


Figure 2. High-field $^1H\{^{31}P\}$ NMR spectrum (300 MHz) of **5** at variable temperature; the point denotes the presence of residual complex **4**

This phenomenon allowed the estimation of the free energy of activation of the internal rotation at the coalescence temperature ($\Delta G^{\neq} \approx 10.43$ kcal/mol K). Similar values have been observed previously for the related complexes $[Nb(\eta^5\text{-}C_5H_4SiMe_3)_2(\eta^2\text{-}HD)(PMe_2Ph)]^+$ ($\Delta G^{\ddagger} \approx 11$ kcal/mol K)[6a] and $[Nb(\eta^5\text{-}C_5H_4SiMe_3)_2(\eta^2\text{-}HD)(CNR)]^+$ ($\Delta G^{\ddagger} \approx 8-9$ kcal/mol K).[7] As a consequence of this high barrier, rotation of the HD molecule can be blocked on the NMR time scale. The value of the J_{HD} coupling constant (18.2 Hz) verifies the presence of an H−D bond and is strong evidence for the presence of a dihydrogen complex.[7] Moreover, the observation of low longitudinal-relaxation times, T_1, is very useful in providing evidence for the existence of a dihydrogen ligand. The T_1 values of the dihydrogen nuclei of **4**, $T_1(H_2)$, and the hydride ligand of complex **3**, $T_1(H)$, were determined using the method described by Crabtree et al.[15] The T_1 minima were found to be 15.8 ms at 215 K for **4** and 95 ms at 186 K for complex **3**. According to Crabtree's proposal, the H−H distance r_{H-H} in the coordinated H_2 ligand can be determined from the T_1 measurements. The observed relaxation, R_{obs}, for **4** is the sum of that due to the H−H dipole−dipole interaction (R_{H-H}) and that due to all other effects (R_O), which can be estimated using the observed relaxation for **3** [R_{obs} (3)], as a reasonable indication of the niobium and solvent contributions. From this equation we calculated $R_{H-H} = 52.68$ (μs^{-1}). Using the Morris approximation,[16] we found that $r_{H-H} = 1.16$ Å assuming rapid rotation of dihydrogen and $r_{H-H} = 0.92$ Å assuming a slow rotation. These values are in agreement with the J_{H-D} value measured for complex **5** and indicate significant stretching of the coordinated H−H bond. Similar results were found for the related compounds $[Nb(\eta^5\text{-}C_5H_4SiMe_3)_2(\eta^2\text{-}HD)(L)]^+$ [L = $P(OEt)_3$, PMe_2Ph].[6a]

After low-temperature protonation the temperature was raised to room temperature and **4** and **5** transformed into the *transoid* isomers $[Nb(\eta^5\text{-}C_5H_4SiMe_3)_2(H)_2(PHPh_2)]\text{-}CF_3CO_2$ (**6**) and $[Nb(\eta^5\text{-}C_5H_4SiMe_3)_2(H)_2(PDPh_2)]\text{-}CF_3CO_2$ (**7**), respectively, through an irreversible process. Complex **6** shows similar spectroscopic data to complex **2**, with the counterion being the only difference between the two. Complex **7** also shows very similar spectroscopic data and these are in agreement with a symmetrical disposition of the niobium centre, showing an A_2B_2 spin system in the ^1H NMR spectrum for the cyclopentadienyl ligands. Thus, the $^1H\{^{31}P\}$ NMR spectrum shows a singlet resonance at $\delta = -1.76$ due to the hydride ligands; no resonance due to a possible PH moiety is observed. Moreover, the ^{31}P NMR spectrum shows a 1:1:1 triplet resonance due to coupling with the deuterium atom ($^1J_{PD} = 34$ Hz). This signal allowed us to confirm the existence of the P−D bond for complex **7**.

The formation of complexes **6** and **7** could be considered to be the result of an oxidative addition of a coordinated dihydrogen molecule to give a *cisoid* dihydride derivative that transforms rapidly into the *transoid* isomer. According to the results obtained, the *cisoid*−*transoid* isomerization may involve the phosphorus atom, as shown in Scheme 4.



Scheme 4. Proposed reaction pathway for the formation of **7**

Isomerization of **5** may proceed by attack of the Nb−D bond at an empty d-orbital of the phosphorus atom. At the same time the P−H bond interacts with the niobium centre, thus making possible the rearrangement of the molecule to give the *transoid* derivative **7**.

When the reaction between **3** and CF_3COOH/D in acetone is performed on a Schlenk-tube scale, the only isolated products are the *transoid* dihydrides **6** and **7**. The low solubility of these complexes in hydrocarbons, ethers and aromatic solvents enabled very easy isolation of the products as colourless, analytically pure solids.

The similarity between complexes **6** and **7** and the phosphonium salt **2**, which was obtained by the reaction between trihydride **1** and $ClPPh_2$, led us to study their behaviour towards deprotonation reactions. Both complexes react with aqueous sodium hydroxide in toluene to give the previously characterized hydridophosphane **3**. This observation confirms that deprotonation of complexes **2**, **6** and **7** occurs at the P−H(P−D) bond, as discussed above.

Reaction of [Nb(η^5-$C_5H_4SiMe_3$)$_2$(H)(PHPh$_2$)] (3) with CX$_2$ (X = S, O)

Insertion of CS_2 into the Nb−H bond of [Nb(η^5-$C_5H_4SiMe_3$)$_2$(H)(PHPh$_2$)] results in the formation of an η^1-dithioformato intermediate [Nb(η^5-$C_5H_4SiMe_3$)$_2$(PHPh$_2$)(η^1-*S*-S(S)CH)] (**8**), which could not be isolated but could be detected by ^{1}H NMR spectroscopy. This complex rapidly evolves by an elimination of phosphane (due to a substitution reaction of phosphane by the noncoordinated sulfur atom) to give an η^2-dithioformato complex [Nb(η^5-$C_5H_4SiMe_3$)$_2$(η^2-*S*,*S*-SSCH)] (**9**) (Scheme 5). This complex was isolated as an air-sensitive orange solid and was previously isolated and characterized by some of us.[10]

This behaviour has previously been found in the reactions of some complexes of the type [Nb(η^5-$C_5H_4SiMe_3$)$_2$(H)(L)] with CS_2.[10]

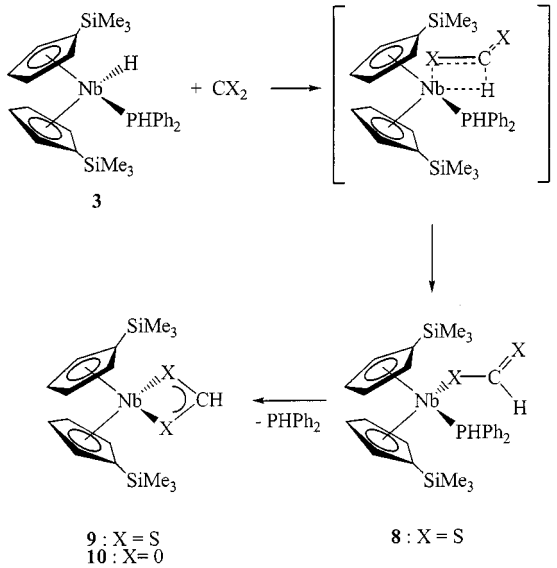
The most significant ^{1}H NMR spectroscopic data for **8** is the resonance at δ = 12.33, which corresponds to the C−H group and appears as a doublet ($^4J_{PH}$ = 2 Hz). This coupling constant confirms the presence of the coordinated phosphane. In addition, the ^{1}H NMR spectrum shows four multiplets for the cyclopentadienyl rings in accordance with an asymmetrical environment for the niobium centre.

The reaction of [Nb(η^5-$C_5H_4SiMe_3$)$_2$(H)(PHPh$_2$)] (**3**) with CO_2 in THF under 2.5 atm. of CO_2 results in the formation of the η^2-formato complex [Nb(η^5-$C_5H_4SiMe_3$)$_2$(η^2-*O*,*O*-OOCH)] (**10**) (Scheme 5) as a brown, air-sensitive oily product after appropriate workup. Complex **10** was previously prepared by some of us using different methods.[11] We have been unable to detect the η^1-formato complex due to the difficulties involved in carrying out test reactions on an NMR-tube scale. The spectroscopic data of **10** agree with those previously described.[11]

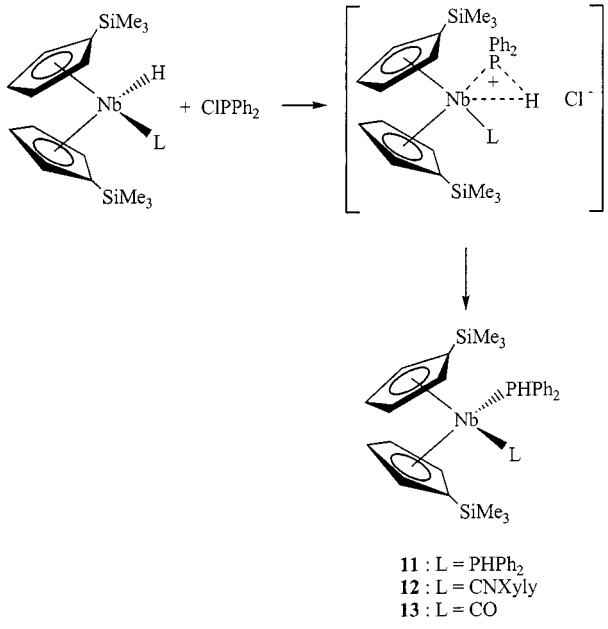
Reactivity of [Nb(η^5-$C_5H_4SiMe_3$)$_2$(H)(L)] (L = PHPh$_2$, CN(xylyl), CO) Towards ClPPh$_2$

$ClPPh_2$ very smoothly inserts into the Nb−H bond of [Nb(η^5-$C_5H_4SiMe_3$)$_2$(H)(L)] [L = $PHPh_2$, CN(xylyl), CO] to give the ionic phosphanyl complexes [Nb(η^5-$C_5H_4SiMe_3$)$_2$(PHPh$_2$)(L)]Cl [L = $PHPh_2$ (**11**), CN(xylyl) (**12**), CO (**13**)] (Scheme 6). These reactions can be rationalized in terms of an electrophilic attack of the phosphorus atom (which contains empty d orbitals) at the Nb−H bond, forming a three-centre transition state that evolves with elimination of chloride.

Complexes **11**−**13** were formed in high yield (≈ 85%) as red solids after precipitation from Et_2O. The ^{1}H NMR spectrum of **11** reveals the equivalence of the cyclopentadienyl rings, with two pseudotriplets observed at δ = 5.36 and δ = 5.50. In contrast, an asymmetrical environment for the niobium centre is observed for complexes **12**



Scheme 5. Proposed reaction pathway for the formation of **9** and **10**



Scheme 6. Insertion process of $ClPPh_2$ into an Nb−H bond

and **13**. In addition, the ^{1}H NMR spectra of **11**−**13** show a doublet resonance for the P−H moiety ($^1J_{PH} \approx 370$ Hz). The IR spectra of **11**−**13** reveal the absence of an ν(Nb−H) band and the existence of ν(P−H) at ca. 2280 cm^{-1}.

In conclusion, several aspects of the reactivity of hydride-containing niobocene species have been considered in the work described here. In particular, the reactions of $ClPPh_2$ towards hydride-niobocene complexes [Nb(η^5-$C_5H_4SiMe_3)_2(H)_3$] (**1**) and [Nb(η^5-$C_5H_4SiMe_3)_2(H)(L)$] occur through insertion of chlorophosphane into an Nb−H bond. Furthermore, the protonation reaction of **3** at low temperature gives an η^2-dihydrogen complex, which evolves at high temperature to the corresponding *transoid* dihydride species. Further work in this field is in progress.

Experimental Section

General Remarks: All operations were performed under an inert atmosphere using standard vacuum line (Schlenk) techniques. Solvents were purified by distillation from the appropriate drying agents before use. NMR spectra were obtained on a Varian Unity FT-300 and Varian Gemini FT-200 instruments. IR spectra were recorded on a Perkin−Elmer PE 883 IR spectrophotometer. Elemental analyses were performed on a Perkin−Elmer 2400 microanalyzer. [Nb(η^5-$C_5H_4SiMe_3)_2(H)_3$] was prepared as described previously.[5]

Preparation of [Nb(η^5-$C_5H_4SiMe_3)_2(H)_2(PHPh_2)$]Cl (2): [Nb(η^5-$C_5H_4SiMe_3)_2(H)_3$] (**1**) (0.30 g, 0.80 mmol) was dissolved in 40 mL of Et_2O to form a tan solution. To this solution was added $ClPPh_2$ (180 μL, 1 mmol). A colourless precipitate formed immediately. When sedimentation was complete, the colourless solution was filtered and the residue washed twice with 10 mL of Et_2O and dried in vacuo. Complex **2** was isolated as a grey solid (yield: 90%). − IR (KBr): $\nu_{(Nb-H)} = 1703$ cm^{-1}; $\nu_{(P-H)} = 2293$ cm^{-1}. − ^{1}H NMR (300 MHz, $CDCl_3$): δ = 0.08 (s, 18 H, Si*Me*$_3$), 4.76 (m, 4 H, C_5H_4), 5.86 (m, 4 H, C_5H_4), 6.67 (d, $^1J_{PH}$ = 283 Hz, 1 H, P−*H*), −2.16 (d, $^2J_{PH}$ = 78.20 Hz, 2 H, Nb−*H*), 7.33−7.45 (m, *Ph*). − ^{13}C NMR (300 MHz, $CDCl_3$): δ = −0.2 (Si*Me*$_3$), 98.0 (*C*$_5$H$_4$, *C*$_1$), 99.9 (*C*$_5$H$_4$), 97.2 (*C*$_5$H$_4$), 131.9 (s, *Ph*, *C*$_1$), 130.9 (*Ph*), 128.9 (*Ph*). − ^{31}P NMR (300 MHz, $CDCl_3$): δ = 20.00 (d, $^1J_{PH}$ = 283 Hz, *P*−H). − $C_{28}H_{39}ClNbPSi_2$ (590.45): calcd. C 56.86, H 6.60; found C 56.20, H 6.45.

Preparation of [Nb(η^5-$C_5H_4SiMe_3)_2(H)(PHPh_2)$] (3): (a) [Nb(η^5-$C_5H_4SiMe_3)_2(H)_3$] (**1**) (0.30 g, 0.80 mmol) was dissolved in 40 mL of THF to form a tan solution. To this solution was added $PHPh_2$ (0.14 mL, 0.80 mmol) by syringe. The mixture was stirred at 343 K for 4 h. The resulting red solution was evaporated to dryness. Complex **3** was isolated as a red oily material after maintaining it under vacuum for a lengthy period (yield: 95%). − (b) [Nb(η^5-$C_5H_4SiMe_3)_2(H)_2(PHPh_2)$]Cl (**2**) (0.30 g, 0.51 mmol) in 30 mL of toluene was treated with an excess (4 mL) of 0.5 M aqueous NaOH. The mixture was vigorously stirred. Within 1 h the precipitate had dissolved and the organic phase turned dark red. The toluene solution was filtered and evaporated to dryness. Complex **3** was obtained as a red oily material (yield: 75%). − IR (CsI): $\nu_{(Nb-H)} = 1643$ cm^{-1}; $\nu_{(P-H)} = 2281$ cm^{-1}. − ^{1}H NMR (300 MHz, C_6D_6): δ = 0.26 (s, 18 H, Si*Me*$_3$), 3.63 (pst, 2 H, C_5H_4), 4.03 (pst, 2 H, C_5H_4), 4.72 (m, 4 H, C_5H_4), 6.90 (d, $^1J_{PH}$ = 322 Hz, 1 H, P−*H*), −7.37 (d, $^2J_{PH}$ = 29.30 Hz, 2 H, Nb−*H*), 7.36−7.71 (m, *Ph*), 8.12 [s, 2 H, *H*$_{para}$ (*Ph*)]. − ^{13}C NMR (300 MHz, C_6D_6): δ = 0.9 (Si*Me*$_3$), 90.6 (*C*$_5$H$_4$, *C*$_1$), 91.2 (*C*$_5$H$_4$), 89.1 (*C*$_5$H$_4$), 88.7 (*C*$_5$H$_4$), 83.4 (*C*$_5$H$_4$), 134.3 (s, *Ph*, *C*$_1$), 133.3 (*Ph*), 129.0 (*Ph*), 128.3 (*Ph*). − ^{31}P NMR (300 MHz, C_6D_6): δ = −38.20 (d, $^1J_{PH}$ = 322 Hz, *P*−H).

Protonation of [Nb(η^5-$C_5H_4SiMe_3)_2(H)(PHPh_2)$] (3): Either CF_3COOH or CF_3COOD was added to a [D_6]acetone solution of [Nb(η^5-$C_5H_4SiMe_3)_2(H)(PHPh_2)$] (**3**) in a 5 mm NMR tube at 183 K, to give either the dihydrogen complex [Nb(η^5-$C_5H_4SiMe_3)_2(\eta^2$-$H_2)(PHPh_2)$]CF_3CO_2 (**4**) or its isotopomer [Nb(η^5-$C_5H_4SiMe_3)_2(\eta^2$-HD)$(PHPh_2)$]CF_3CO_2 (**5**).

Preparation of [Nb(η^5-$C_5H_4SiMe_3)_2(H)_2(PHPh_2)$]$CF_3CO_2$ (6) and [Nb(η^5-$C_5H_4SiMe_3)_2(H)_2(PDPh_2)$]$CF_3CO_2$ (7): To a solution of [Nb(η^5-$C_5H_4SiMe_3)_2(H)(PHPh_2)$] (**3**) (0.30 g, 0.55 mmol) in 30 mL of THF at 183 K was added CF_3COOH or CF_3COOD (42 μL, 0.55 mmol) by syringe. The solution was allowed to reach room temperature and stirred for 2 h. The resulting solution was evaporated to dryness. Complexes **6** and **7** were obtained as colourless solids after precipitation with Et_2O (yield: 80%).

Preparation of [Nb(η^5-$C_5H_4SiMe_3)_2(\eta^2$-*S*,*S*-SSCH)] (9): To a solution of [Nb(η^5-$C_5H_4SiMe_3)_2(H)(PHPh_2)$] (**3**) (0.30 g, 0.55 mmol) in THF (40 mL) was added CS_2 (93.1 μL, 0.55 mmol) and the reaction mixture was stirred for 1 h. The resulting solution was evaporated to dryness to give a red oily material. Complex **9** was isolated as an orange solid after precipitation from hexane (yield: 95%). − ^{1}H NMR (300 MHz, $CDCl_3$): δ = 0.22 (s, 18 H, Si*Me*$_3$), 5.05 (4 H, C_5H_4), 5.44 (4 H, C_5H_4), 4.17 (s, 1 H, SSC*H*). − ^{13}C{^{1}H} NMR (300 MHz, $CDCl_3$): δ = 0.5 (Si*Me*$_3$), 98.6 (*C*$_5$H$_4$, *C*$_1$), 103.6 (*C*$_5$H$_4$), 106.9 (*C*$_5$H$_4$), 120.0 (S*C*HS). − $C_{17}H_{27}NbS_2Si_2$ (444.12): calcd. C 45.95, H 6.08; found C, 45.81, H 5.96.

Preparation of [Nb(η^5-$C_5H_4SiMe_3)_2(\eta^2$-*O*,*O*-OOCH)] (10): A THF solution of [Nb(η^5-$C_5H_4SiMe_3)_2(H)(PHPh_2)$] (**3**) (0.30 g, 0.55 mmol) was saturated with CO_2 (2.5 atm.) in a Fischer−Porter bottle for 8 h at room temperature. The solution became increasingly dark and a brown solution was finally obtained and then evaporated to dryness. Complex **10** was obtained as an oily brown material (yield: 90%). − IR (Nujol): ν_{asym} (CO_2^-) = 1638 cm^{-1}; ν_{sym} (CO_2^-) = 1545 cm^{-1}. − ^{1}H NMR (300 MHz, C_6D_6): δ = −0.04 (s, 18 H, Si*Me*$_3$), 4.14 (m, 4 H, C_5H_4), 5.68 (m, 4 H, C_5H_4), 7.47 (s, 1 H, O_2CH). ^{13}C{^{1}H} NMR (300 MHz, C_6D_6): δ = 0.1 (Si*Me*$_3$), 107.8 (*C*$_5$H$_4$, *C*$_1$), 105.0 (*C*$_5$H$_4$), 108.1 (*C*$_5$H$_4$), 184.3 (O_2CH).

Preparation of [Nb(η^5-$C_5H_4SiMe_3)_2(PHPh_2)(L)$]Cl [L = $PHPh_2$ (11), CN(xylyl) (12), CO (13)]: To a solution of [Nb(η^5-$C_5H_4SiMe_3)_2(H)(L)$] [L = $PHPh_2$, CN(xylyl), CO] (0.55 mmol) in 40 mL of Et_2O was added $ClPPh_2$ (125 μL, 0.70 mmol) by syringe. A red-orange precipitate formed immediately. When sedimentation was complete the solution was filtered and the residue washed twice with 20 mL of Et_2O and dried in vacuo. Complexes **11**, **12** and **13** were obtained as orange or red solids. − **11:** IR (KBr): $\nu_{(P-H)}$ = 2297 cm^{-1}. − ^{1}H NMR (300 MHz, [D_6]acetone): δ = 0.05 (s, 18 H, Si*Me*$_3$), 5.36 (m, 4 H, C_5H_4), 5.50 (m, 4 H, C_5H_4), 7.87 (d, $^1J_{HP}$ = 362 Hz, 1 H, P−*H*), 7.35−7.60 (m, *Ph*), 8.12 [s, 2 H, *H*$_{para}$ (*Ph*)]. − ^{13}C NMR (300 MHz, [D_6]acetone): δ = 0.1 (Si*Me*$_3$), 102.9 (*C*$_5$H$_4$, *C*$_1$), 92.5 (*C*$_5$H$_4$), 103.7 (*C*$_5$H$_4$), 135.7 (*Ph*, *C*$_1$), 133.0 (*Ph*), 129.0 (*Ph*), 128.3 (*Ph*). − ^{31}P NMR (300 MHz, [D_6]acetone): δ = 32.00 (d, $^1J_{HP}$ = 362 Hz, *P*−H). − $C_{40}H_{48}ClNbP_2Si_2$ (774.45): calcd. C 61.98, H 6.20; found C 62.10, H 6.18.

12: IR (KBr): $\nu_{(P-H)} = 2280$ cm^{-1}; $\nu_{(CNAr)} = 2058$ cm^{-1}. − ^{1}H NMR (300 MHz, [D_6]acetone): δ = 0.17 (s, 18 H, Si*Me*$_3$), 5.36 (m, 2 H, C_5H_4), 5.55 (m, 2 H, C_5H_4), 5.65 (m, 2 H, C_5H_4), 6.11 (m, 2 H, C_5H_4), 8.70 (d, $^1J_{HP}$ = 387 Hz, 1 H, P−*H*), 7.35−7.90 (m, *Ph*),

2.31 [CN(2,6-$Me_2C_6H_3$)]. – ^{13}C NMR (300 MHz, [D_6]acetone): δ = 0.1 (SiMe_3), 100.2 (C_5H_4, C_1), 92.3 (C_5H_4), 100.0 (C_5H_4), 100.8 (C_5H_4), 102.4 (C_5H_4), 132.5 (*Ph*, C_1), 133.0 (*Ph*), 129.0 (*Ph*), 127.6 (*Ph*), 19.4 [CN(2,6-$Me_2C_6H_3$)], 248.0 [*C*N(2,6-$Me_2C_6H_3$)]. – ^{31}P NMR (300 MHz, [D_6]acetone): δ = 38.50 (d, $^1J_{HP}$ = 387 Hz, *P*–H). – $C_{37}H_{46}NNbPSi_2$ (684.00): C 66.86, H 6.93; found C 66.01, H 6.95.

13: IR (KBr): $\nu_{(P-H)}$ = 2276 cm^{-1}; $\nu_{(CO)}$ = 1940 cm^{-1}. – ^{1}H NMR (300 MHz, [D_6]acetone): δ = 0.24 (s, 18 H, SiMe_3), 5.10 (m, 2 H, C_5H_4), 5.82 (m, 2 H, C_5H_4), 5.93 (m, 2 H, C_5H_4), 6.03 (m, 2 H, C_5H_4), 7.90 (d, $^1J_{HP}$ = 381 Hz, 1 H, P–*H*), 7.35–7.60 (m, Ph), 8.12 [s, 2 H, H_{para} (*Ph*)]. – ^{13}C NMR (300 MHz, [D_6]acetone): δ = –0.5 (SiMe_3), 102.9 (C_5H_4, C_1), 97.0 (C_5H_4), 98.1 (C_5H_4), 100.6 (C_5H_4), 101.8 (C_5H_4), 131.5 (*Ph*, C_1), 131.0 (*Ph*), 129.5 (*Ph*), 128.0 (*Ph*), 250 (*C*O). – ^{31}P NMR (300 MHz, [D_6]acetone): δ = 38.00 (d, $^1J_{HP}$ = 381 Hz, *P*–H). – $C_{29}H_{37}NbOPSi_2$ (581.16): C 62.03, H 6.60; found C 61.82, H 6.68.

Acknowledgments

The authors gratefully acknowledge financial support from the Dirección General de Enseñanza Superior e Investigación Científica (Grant. No. PB-95–0023-C01-C02) of Spain.

[1] G. G. Hlatky, R. H. Crabtree, *Coord. Chem. Rev.* **1985**, 65, 1.

[2] Selected references: [2a] D. G. Dick, D. W. Stephan, *Can. J. Chem.* **1991**, 69. – [2b] J. W. Ho, R. J. Drake, D. W. Stephan, *J. Am. Chem. Soc.* **1993**, 115, 3792. – [2c] J. W. Ho, R. Rousseau, D. W. Stephan, *Organometallics* **1995**, 14, 4030. – [2d] R. T. Baker, J. C. Calabrese, R. L. Harlow, I. D. Williams, *Organometallics* **1993**, 12, 830. – [2e] E. Hey-Hawkins, M. F. Lappert, J. L. Atwood, S. G. Bott, *J. Chem. Soc., Dalton Trans.* **1991**, 939. – [2f] E. Hey-Hawkins, S. Kurtz, J. Sieger, G. Baum, *J. Organomet. Chem.* **1995**, 486, 229. – [2g] J. C. Leblanc, C. Moise, *J. Organomet. Chem.* **1989**, 364, C3. – [2h] M. Y. Chang, S. Gambarotta, F. V. Bolhuis, *Organometallics* **1988**, 7, 1864. – [2i] D. Roddick, B. D. Santarsiero, J. E. Bercaw, *J. Am. Chem. Soc.* **1985**, 107, 4670. – [2j] S. Righi, J. C. Leblanc, C. Moise, B. Nuber, *J. Chem. Soc., Chem. Commun.* **1995**, 45. – [2k] G. Bonnet, O. Lavastre, J. C. Leblanc, C. Moise, *New. J. Chem.* **1988**, 12, 551. – [2l] G. Bonnet, M. M Kubicki, C. Moise, R. Lazzaroni, P. Salvador, G. Vitulli, *Organometallics* **1992**, 1, 964.

[3] [3a] G. I. Nikonov, L. G. Kuzmina, P. Mountford, D. A. Lemenovskii, *Organometallics* **1995**, 14, 3588. – [3b] G. I. Nikonov, D. A. Lemenovskii, J. Lorberth, *Organometallics* **1994**, 13, 3127. – [3c] G. I. Nikonov, Y. K. Grishin, D. A. Lemenovskii, N. B. Kazennova, L. G. Kuzmina, J. A. K. Howard, *J. Organomet. Chem.* **1997**, 547, 183.

[4] [4a] C. Barré, M. M. Kubicki, J. C. Leblanc, C. Moise, *Inorg. Chem.* **1990**, 29, 5244. – [4b] C. Barré, P. Boudot, M. M. Kubicki, C. Moise, *Inorg. Chem.* **1995**, 34, 284. – [4c] O. Lavastre, G. Bonnet, G. Boni, M. M. Kubicki, C. Moise, *J. Organomet. Chem.* **1997**, 547, 141.

[5] A. Antiñolo, B. Chaudret, G. Commenges, M. Fajardo, F. A. Jalón, R. H. Morris, A. Otero, C. T. Schweitzer, *Chem. Commun.* **1988**, 1210.

[6] Selected references: [6a] F. A. Jalón, A. Otero, B. R. Manzano, E. Villaseñor, B. Chaudret, *J. Am. Chem. Soc.* **1995**, 117, 10123. – [6b] A. Antiñolo, M. Fajardo, F. A. Jalón, C. López-Mardomingo, A. Otero, C. Sanz-Bernabé, *J. Organomet. Chem.* **1989**, 369, 187.

[7] A. Antiñolo, F. Carrillo-Hermosilla, M. Fajardo, S. García-Yuste, A. Otero, S. Camanyes, F. Maseras, M. Moreno, A. Lledós, J. M. Lluch, *J. Am. Chem. Soc.* **1997**, 119, 6107.

[8] J. P. Collman, L. S. Hegedus, J. R. Norton, R. E. Finke, *Principles and Applications of Organotransition Metal Chemistry*, University Science Books, Mill Valley, CA, **1987**.

[9] [9a] A. Antiñolo, M. Fajardo, C. López-Mardomingo, A. Otero, Y. Mourad, Y. Mugnier, J. Sanz-Aparicio, I. Fonseca, F. Florencio, *Organometallics* **1990**, 9, 164. – [9b] A. Antiñolo, A. Otero, M. Fajardo, C. López-Mardomingo, D. Lucas, Y. Mugnier, M. Lanfranchi, M. A. Pellinghelli, *J. Organomet. Chem.* **1992**, 435, 55. – [9c] A. Antiñolo, M. Fajardo, R. Gil-Sanz, C. López-Mardomingo, P. Martin-Villa, A. Otero, M. M. Kubicki, Y. Mugnier, S. El Krami, Y. Mourad, *Organometallics* **1993**, 12, 381. – [9d] A. Antiñolo, F. Carrillo-Hermosilla, S. García-Yuste, M. Freitas, A. Otero, S. Prashar, E. Villaseñor, M. Fajardo, *Inorg. Chim. Acta* **1997**, 259, 101.

[10] [10a] A. Antiñolo, F. Carrillo, M. Fajardo, S. García-Yuste, A. Otero, *J. Organomet. Chem.* **1994**, 482, 93. – [10b] A. Antiñolo, I. del Hierro, M. Fajardo, S. García-Yuste, A. Otero, O. Blacque, M. M. Kubicki, J. Amaudrut, *Organometallics* **1996**, 15, 1966.

[11] A. Antiñolo, M. Fajardo, S. García-Yuste, I. del Hierro, A. Otero, S. El Krami, Y. Mourad, Y. Mugnier, *J. Chem. Soc., Dalton Trans.* **1995**, 3409.

[12] A. Antiñolo, F. Carrillo-Hermosilla, M. Fajardo, S. García-Yuste, M. Lafranchi, A. Otero, M. A. Pellinghelli, S. Prashar, E. Villaseñor, *Organometallics* **1996**, 15, 5507.

[13] W. J. Geary, *Coord. Chem. Rev.* **1971**, 7, 81.

[14] [14a] J. F. Leboeuf, O. Lavastre, J. C. Leblanc, C. Moise, *J. Organomet. Chem.* **1991**, 418, 359. – [14b] B. Chaudret, H. H. Limbach, C. Moise, *C. R. Acad. Sci.* Paris, 315 Ser. II **1992**, 533. – [14c] S. Sabo-Etienne, B. Chaudret, H. Abou El Makarim, J. C. Barthelat, J. P. Daudey, C. Moise, J. C. Leblanc, *J. Am. Chem. Soc.* **1994**, 116, 9335.

[15] [15a] R. H. Crabtree, M. Lavin, L. Bonneviot, *J. Am. Chem. Soc.* **1986**, 108, 4032. – [15b] D. G. Hamilton, R. H. Crabtree, *J. Am. Chem. Soc.* **1988**, 110, 4126.

[16] K. A. Earl, G. Jia, P. A. Maltby, R. H. Morris, *J. Am. Chem. Soc.* **1991**, 113 3027.

Received January 26, 2000
[I00027]

Cadmium(II) and Lead(II) Complexes with Novel Macrocyclic Receptors Derived from 1,10-Diaza-15-crown-5

David Esteban,[a] Daniel Bañobre,[a] Andrés de Blas,*[a] Teresa Rodríguez-Blas,*[a] Rufina Bastida,[b] Alejandro Macías,[b] Adolfo Rodríguez,[b] David E. Fenton,[c] Harry Adams,[c] and Jose Mahía[d]

Keywords: Cadmium / Crown compounds / Cryptands / Lead / Macrocyclic ligands

Two novel macrocycles, *N*,*N*′-bis(2-aminobenzyl)-1,10-diaza-15-crown-5 (L^1) and a non-symmetric cryptand incorporating a pyridinyl Schiff-base spacer (L^3), both derived from 1,10-diaza-15-crown-5, have been shown to act as receptors for lead(II) and cadmium(II) guests. The X-ray crystal structures reveal an *anti* conformation for the free ligand L^1, but a *syn* arrangement in the lead(II) complex, $[PbL^1](ClO_4)_2$. The corresponding cryptates of L^3 can be prepared by simple transmetallation reactions starting from the barium cryptate, showing the preference of L^3 for the heavy metal ions. The lead(II) ion, unlike cadmium(II), has been shown to be capable of acting as a template agent in the synthesis of L^3. The X-ray crystal structures of the metal cryptates allow an insight into the influence of the nature of the metal ion guest on the conformation of the macrobicyclic receptor L^3; the most significant changes are a different folding of the crown and variations in the distance between the two pivotal nitrogen atoms and the imine nitrogen atoms. The cryptand can thus expand or contract its cavity in order to accommodate the different metal ions.

Introduction

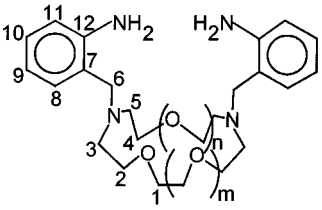
The coordination chemistry of macrocyclic ligands is currently a fascinating area of intense study for inorganic chemists. One aspect of the interest that macrocyclic ligands have promoted stems from the fact that depending on features such as the nature, number, and arrangement of the ligand donors, ligand conjugation, substitution, and flexibility, the nature of the ligand backbone, macrocyclic hole size, and the number and sizes of the chelate rings, it is possible to tailor-make different types of macrocyclic molecules for specific uses. Thus, such systems can be used as models for biological systems, to study magnetic exchange phenomena, as synthetic ionophores, to study guest−host interactions, or as therapeutic reagents for the treatment of metal intoxication. In particular, macrocycles have been widely studied as complexing agents that may be used for the selective extraction of heavy and precious metals,[1−3] an area of great interest in environmental chemistry. Furthermore, the development of new technologies in this field depends on the design of new receptors capable of binding metal ions selectively or specifically.

The direct synthesis of a free macrocycle from its organic precursors often results in a low yield of the desired cyclic product, with side reactions such as polymerization predominating. Consequently, synthetic strategies such as the use of high dilution conditions, the incorporation of a rigid group in the open-chain precursors, and the use of template agents have been developed. In a previous paper,[4] we described a synthetic route for preparing a novel family of Schiff-base cryptands derived from bibracchial lariat ethers incorporating pendant aniline moieties and various dialdehyde functions (Scheme 1; L^3, L^4, L^5, L^6). Structurally, these systems belong to the group defined as lateral macrobicycles.[5] We found that they can not be prepared by direct reaction between the organic precursors, but that barium(II) ion can act as a template, thereby allowing access to the required macrobicycles in high yields.

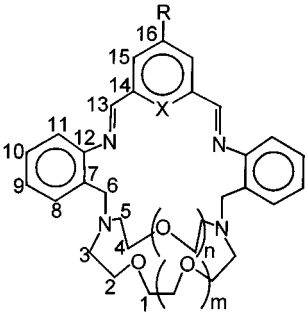
Here, we describe lead(II) and cadmium(II) complexes with the receptors L^1 and L^3 (Scheme 1), macrocycles belonging to two different structural classes, namely bibracchial lariat ethers and cryptands, respectively. The lariat ethers constitute a sub-class of macrocyclic polyethers and are characterized by the presence of one (monobracchial) or more (polybracchial) side-arms attached to pivotal atoms of the parent macrocyclic ring. The incorporation of additional donor atoms in the side arms can be used to enhance the coordination potential of these polybracchial ligands. These compounds may be regarded as having structural characteristics intermediate between those of flexible mac-

[a] Departamento Química Fundamental e Industrial, Universidade da Coruña, Campus da Zapateira s/n, E-15071 La Coruña, Spain
Fax: (internat.) +34−981/167000
E-mail: mayter@udc.es
[b] Departamento Química Inorgánica, Universidad de Santiago, Avda. de las Ciencias s/n, E-15706 Santiago de Compostela, Spain
[c] Chemistry Department, The University, Sheffield S3 7HF, U.K.
[d] Servicios Xerais de Apoio á Investigación, Universidade da Coruña, Campus da Zapateira s/n, E-15071 La Coruña, Spain

 © WILEY-VCH Verlag GmbH, D-69451 Weinheim, 2000 1434−1948/00/0707−1445 $ 17.50+.50/0



L^1: n = m = 1
L^2: n = 2, m = 1



	n	m	R	X
L^3	1	1	H	N
L^4	1	1	CH_3	C-OH
L^5	2	1	H	N
L^6	2	1	CH_3	C-OH

Scheme 1

rocyclic polyethers and relatively rigid macrobicyclic cages or cryptands.

Two issues are addressed in the present paper. Firstly, we have studied different synthetic routes and strategies for preparing lead(II) and cadmium(II) complexes with the macrobicycle L^3. Secondly, we have carried out structural studies to assess the different complexation capabilities of the two classes of macrocycles towards the heavy metal ions lead(II) and cadmium(II) as well as the influence of the nature of the metal ion guest on the conformation of the macrobicycle receptor L^3.

Results

Synthesis and Characterization of the Bibracchial Lariat Ether L^1 and its Cadmium(II) and Lead(II) Complexes

Our synthetic route to the novel bibracchial lariat ether L^1 involves two key steps, specifically *N*-binding of 2-nitrobenzyl chloride to the diaza-crown and subsequent reduction of the NO_2 groups of the resulting *N*,*N*′-bis(2-nitrobenzyl)-diaza-crown to $-NH_2$ groups with hydrazine hydrate in the presence of Pd/C as a catalyst. The synthesis can be carried out in a one-pot procedure by reducing the intermediate *N*,*N*′-bis(2-nitrobenzyl)-diaza-crown prepared in situ. In this way, better yields are obtained. Single crystals of L^1 suitable for X-ray diffraction analysis were grown by slow evaporation of the solvents from an absolute ethanol/diethyl ether (1:1) solution. As expected, the IR spectrum (KBr discs) features two bands due to a $\nu_{as}(NH_2)$ mode at 3430 and 3390 cm^{-1}, and two further bands corresponding to a $\nu_s(NH_2)$ mode at 3293 and 3275 cm^{-1}.

Reactions of the perchlorate salts $M(ClO_4)_2 \cdot n\,H_2O$ (M = Pb, Cd) with the bibracchial lariat ether L^1 yielded the complexes $[PbL^1](ClO_4)_2$ (**1**) and $[CdL^1](ClO_4)_2$ (**2**). Both were isolated as white solids. Colourless crystals of **1** suitable for single-crystal X-ray diffraction analysis were grown by allowing diethyl ether to diffuse into an acetonitrile solution of the complex. In the IR spectra (KBr discs), the amine groups give rise to $\nu_{as}(NH_2)$ and $\nu_s(NH_2)$ stretching bands at 3334 and 3277 cm^{-1} for **1** and at 3320 and 3281 cm^{-1} for **2**. Bands corresponding to the $\nu_{as}(ClO)$ stretching and $\delta_{as}(O-Cl-O)$ bending modes of the perchlorate groups appear without splitting at ca. 1100 and 625 cm^{-1}, respectively, as befits an uncoordinated anion.

The molar conductivities of the complexes at 20 °C in a ca. 10^{-3} M acetonitrile solution were measured as Λ_M = 285 $cm^2 \cdot \Omega^{-1} \cdot mol^{-1}$ for **1** and 289 $cm^2 \cdot \Omega^{-1} \cdot mol^{-1}$ for **2**. These data reveal that both complexes behave as 2:1 electrolytes in this solvent, and hence are completely dissociated.[6]

The ^1H- (Table 1) and ^{13}C-NMR spectra of the complexes were recorded in CD_3CN solution. The ^1H-NMR spectra of the complexes are clearly more complicated than that of the free lariat ether L^1. This is particularly apparent in the region $\delta = 0-4$, where signals due to the protons of the ethylenic and methylenic chains are observed. On coordination, the ligand becomes more rigid, restricting any exchange, and so the protons become non-equivalent and give rise to more signals. While the signals due to the aromatic protons are shifted downfield by ca. 0.5 ppm in the complexes, the signal due to the amine protons is shifted upfield by 0.79 ppm in **1** and by 0.04 ppm in **2** as compared to its position in the spectrum of the free ligand, thus confirming the coordination of the amine groups to the metal.

The UV/vis spectrum of the free ligand L^1, recorded in acetonitrile solution, features three absorption bands at λ_{max} = 213, 237, and 284 nm, corresponding to E_1, E_2, and B charge-transfer bands of the aromatic rings, respectively. The spectra of the complexes also feature the three expected bands, at λ_{max} = 209, 228, and 272 nm for **1**, and 213, 226, and 274 nm for **2**, shifted to lower wavelengths due to the coordination of the amine groups.

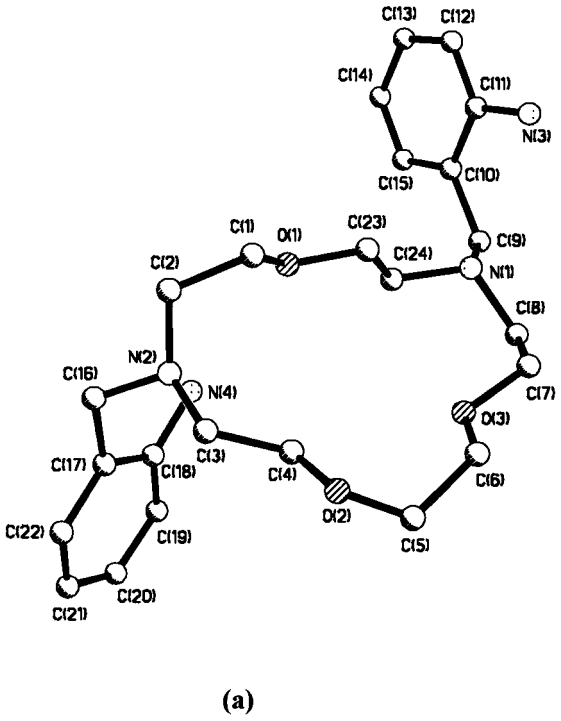
X-ray Crystal Structures of L^1 and **1**

The crystal structure of the free receptor L^1 is shown in Figure 1; selected bond lengths and angles are given in Table 2. The arms of the lariat ether are arranged on opposite sides of the crown moiety resulting in an *anti* conformation. The crystal packing is determined by intermolecular hydrogen-bonds, which involve one proton of the amine group and an oxygen atom of the neighbouring molecule. Weak intramolecular hydrogen-bonds exist between the amine groups and the pivotal nitrogen atoms, with N(pivotal)···HN(amine) bond lengths of 2.362 and 2.339 Å, N(amine)···N(pivotal) bond lengths of 2.959 and 2.894 Å, and N(amine)−H−N(pivotal) angles of 123.8° and 119.8°.

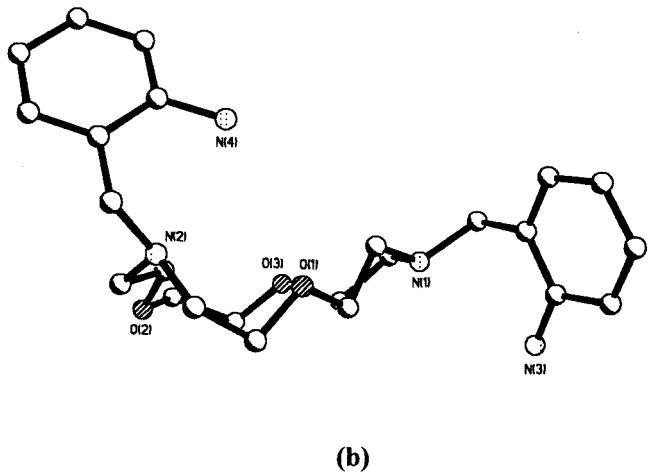
Table 1. ^{1}H-NMR data for L^1 and its complexes

[a]	NH_2	H-11	H-9	H-10	H-8	H-5	H-3	H-6	H-2	H-1	H-4
L^{1}[b]	4.99(s), 4H	6.62(d), 2H	6.57 (t), 2H	7.04 (t), 2H	6.96 (d), 2H	←2.62 (m), 8H→		←3.51 (m), 16H→			
1 [c]	4.20(s), 4H	7.12 (d), 2H	7.03 (t), 2H	7.45 (t), 2H	7.29 (d), 2H	←2.90 (m), 8H→		←3.18 (m), 16H→			
2 [d]	4.95(s), 4H	←7.16 (m), 4H→		←7.39 (t), 4H→		←2.80 -3.83 (m), 24H→					

[a] See Scheme 1 for labelling. – [b] Conditions: T = 293 K, CD_3CN, 500 MHz. Assignment supported by 2D H,H COSY, HMQC, and HMBC experiments. $J_{2,3}$ = 7.08 Hz, $J_{4,3} = J_{4,5}$ = 7.48 Hz, $J_{3,2} = J_{3,4}$ = 7.48 Hz, $J_{5,4}$ = 7.35 Hz. Chemical shifts (without assignment) of the different multiplets for crown protons are given only. – [c] Conditions: T = 293 K, CD_3CN, 200 MHz. $J_{2,3}$ = 7.33 Hz, $J_{4,3} = J_{4,5}$ = 7.32 Hz, $J_{3,2} = J_{3,4}$ = 7.81 Hz, $J_{5,4}$ = 7.81 Hz. Chemical shifts (without assignment) of the different multiplets for crown protons are given only. – [d] Conditions: T = 293 K, CD_3CN, 200 MHz. Chemical shifts (without assignment) of the different multiplets for crown and/or aromatic protons are given only.



(a)



(b)

Figure 1. X-ray crystal structure of the bibracchial lariat ether L^1 showing the atomic numbering scheme; hydrogen atoms are omitted for the sake of clarity: (a) frontal view, (b) side view

Table 2. Selected distances [Å] and angles [deg] in the bibracchial lariat ether L^1 and complex **1**

L^1			
N(1)–C(24)	1.472(3)	N(2)–C(16)	1.465(3)
N(1)–C(9)	1.476(4)	N(2)–C(3)	1.466(4)
N(1)–C(8)	1.476(4)	N(2)–C(2)	1.461(3)
N(3)–C(11)	1.389(4)	N(4)–C(18)	1.383(4)
C(24)–N(1)–C(8)	113.6(2)	C(16)–N(2)–C(3)	114.3(2)
C(8)–N(1)–C(9)	109.0(2)	N(3)–C(11)–C(10)	119.5(3)
C(24)–N(1)–C(9)	110.9(2)	N(1)–C(9)–C(10)	114.5(2)
C(2)–N(2)–C(3)	114.8(2)	N(4)–C(18)–C(17)	119.8(2)
C(2)–N(2)–C(16)	113.0(2)	N(2)–C(16)–C(17)	112.1(2)
C(23)–O(1)–C(1)	114.6(2)	C(4)–O(2)–C(5)	114.2(3)
C(7)–O(3)–C(6)	111.5(2)		
1			
Pb(1)–O(3)	2.568(5)	Pb(1)–O(2)	2.702(6)
Pb(1)–N(4)	2.652(7)	Pb(1)–O(1)	2.732(6)
Pb(1)–N(2)	2.688(7)	Pb(1)–N(1)	2.757(6)
O(3)–Pb(1)–N(4)	81.6(2)	N(2)–Pb(1)–O(2)	62.9(2)
O(3)–Pb(1)–N(2)	64.2(2)	O(3)–Pb(1)–O(1)	81.3(2)
N(4)–Pb(1)–N(2)	75.1(2)	N(4)–Pb(1)–O(1)	160.0(2)
O(3)–Pb(1)–O(2)	97.2(2)	N(2)–Pb(1)–O(1)	106.3(2)
N(4)–Pb(1)–O(2)	133.1(2)	O(2)–Pb(1)–O(1)	59.7(2)
O(3)–Pb(1)–N(1)	63.2(2)	N(4)–Pb(1)–N(1)	98.2(2)
N(2)–Pb(1)–N(1)	127.4(2)	O(2)–Pb(1)–N(1)	123.3(2)
O(1)–Pb(1)–N(1)	64.7(2)		

Figure 2 illustrates the crystal structure of the complex cation $[PbL^1]^{2+}$ of **1**, while Table 2 provides a listing of selected bond lengths and angles. Only six of the seven available donor atoms of L^1 are coordinated to the lead(II) ion with one of the aniline pendant arms uncoordinated. The metal ion lies 1.71 Å above the plane defined by the three ether oxygen atoms and is asymmetrically disposed with respect to the crown ether moiety being closer to O(3) [Pb–O(3) 2.568(5) Å] than to the other oxygen atoms [Pb–O(2) 2.702(6) Å, Pb–O(1) 2.732(6) Å]. All of these distances fall within the ranges reported for the $Pb-O_{ether}$ bonds in lead(II)–crown ether complexes.[7] The lead(II) atom lies closer to the pivotal nitrogen atom bearing the coordinating pendant arm [Pb–N(2) 2.688(7) Å] than to the pivotal nitrogen atom bearing the non-coordinating pendant arm [Pb–N(1) 2.757(6) Å]. The lead atom and the donor atoms O(3), N(1), and N(2) are essentially coplanar, with a deviation from planarity of just 0.0118 Å. This may be viewed as an equatorial plane with oxygen atoms O(2) and O(1) located 2.2017 Å and 2.4650 Å above it and the

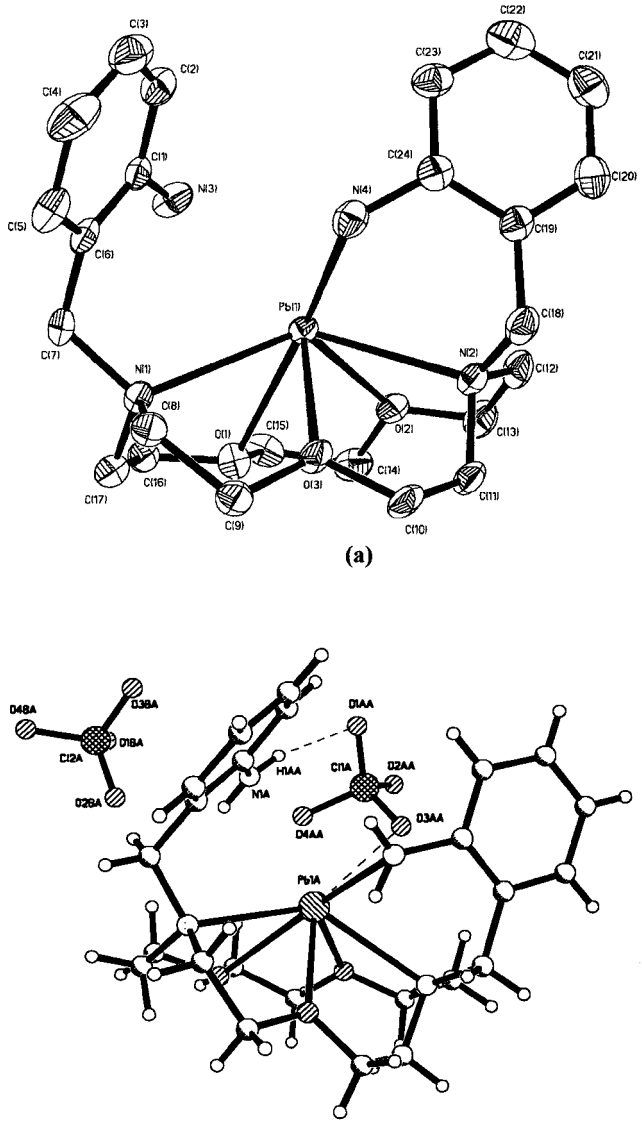


Figure 2. (a) X-ray crystal structure of the cationic complex $[PbL^1]^{2+}$ showing the atomic numbering scheme; hydrogen atoms are omitted for the sake of clarity; the ORTEP plot is drawn at a 30% probability level; (b) X-ray crystal structure of **1**

nitrogen atom N(4) lying 2.568 Å beneath it. The coordination polyhedron at the metal may be described as a dodecahedron with two unoccupied sites (Figure 3). The presence of these unoccupied sites leads to an empty zone in the coordination sphere at the metal, as indicated in Figure 3.

From a recent extensive survey of lone-pair functionality in lead(II) complexes, it has emerged that two distinct structural groups, with geometries that are holo-directed and hemi-directed, are possible. In the former group, the metal−ligand bonds can be directed to any point on the surface of an encompassing globe, whereas in the latter group there is a distinct void, or empty zone, in the global array of ligands.[8] The presence of such a void in the angular distribution of the coordination sphere about lead(II) is

Table 3. Selected distances [Å] and angles [deg] in complexes **3** and **4**

3			
Pb(1)−O(3)	2.670(6)	Pb(1)−O(1)	2.718(6)
Pb(1)−N(5)	2.703(6)	Pb(1)−O(2)	2.719(6)
Pb(1)−O(10)	2.714(8)	Pb(1)−N(4)	2.740(6)
Pb(1)−N(2)	2.744(6)		
O(3)−Pb(1)−N(5)	140.5(2)	N(5)−Pb(1)−O(2)	122.1(2)
O(3)−Pb(1)−O(10)	74.4(3)	O(10)−Pb(1)−O(2)	138.6(3)
N(5)−Pb(1)−O(10)	73.3(2)	O(10)−Pb(1)−O(1)	155.6(2)
O(3)−Pb(1)−O(1)	124.6(2)	O(3)−Pb(1)−O(2)	97.2(2)
N(5)−Pb(1)−O(1)	82.9(2)	O(1)−Pb(1)−O(2)	60.1(2)
O(3)−Pb(1)−N(4)	137.6(2)	N(5)−Pb(1)−N(4)	61.0(2)
O(10)−Pb(1)−N(4)	85.8(3)	O(1)−Pb(1)−N(4)	87.1(2)
O(1)−Pb(1)−N(4)	87.1(2)	O(2)−Pb(1)−N(4)	73.4(2)
O(2)−Pb(1)−N(4)	73.4(2)	O(3)−Pb(1)−N(2)	65.1(2)
N(5)−Pb(1)−N(2)	128.6(2)	O(10)−Pb(1)−N(2)	79.2(2)
O(1)−Pb(1)−N(2)	121.1(2)	O(2)−Pb(1)−N(2)	61.0(2)
N(4)−Pb(1)−N(2)	74.6(2)		
4			
Cd(1)−N(1)	2.349(10)	Cd(1)−N(4)	2.419(11)
Cd(1)−N(5)	2.366(9)	Cd(1)−O(3)	2.459(8)
Cd(1)−O(1)	2.374(11)	Cd(1)−O(2)	2.493(9)
Cd(1)−N(3)	2.566(10)		
N(1)−Cd(1)−N(5)	129.7(3)	N(5)−Cd(1)−O(2)	77.7(3)
N(1)−Cd(1)−O(1)	72.8(3)	O(1)−Cd(1)−O(2)	65.5(4)
N(5)−Cd(1)−O(1)	126.9(4)	N(4)−Cd(1)−O(2)	102.3(4)
N(1)−Cd(1)−N(4)	116.4(3)	O(3)−Cd(1)−O(2)	108.8(3)
N(5)−Cd(1)−N(4)	68.4(4)	N(1)−Cd(1)−N(3)	78.2(3)
O(1)−Cd(1)−N(4)	153.3(3)	N(5)−Cd(1)−N(3)	64.4(3)
N(1)−Cd(1)−O(3)	68.1(3)	O(1)−Cd(1)−N(3)	79.3(4)
N(5)−Cd(1)−O(3)	145.4(3)	N(4)−Cd(1)−N(3)	126.2(3)
O(1)−Cd(1)−O(3)	84.5(3)	O(3)−Cd(1)−N(3)	145.6(3)
N(4)−Cd(1)−O(3)	77.0(3)	O(2)−Cd(1)−N(3)	91.8(3)
N(1)−Cd(1)−O(2)	138.3(4)		

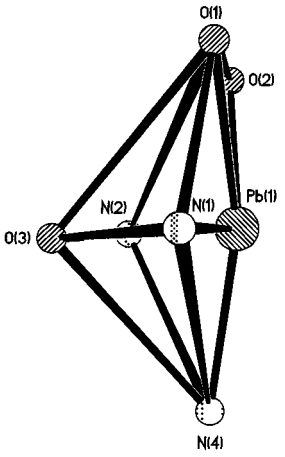


Figure 3. Coordination polyhedron of the cationic complex $[PbL^1]^{2+}$

usually taken as an indication of the presence of a stereochemically active lone pair of electrons on the lead atom.[9,10] It has also been suggested that there will be a concomitant shortening of the Pb−X bond on the side of the lead(II) away from the site of the stereochemically active lone pair.[9,11] In these hemi-directed compounds, the differences between Pb^{II}−X and Pb^{II}−*lp*-X (the latter being the distance between Pb^{II} and a ligand in the direction of the lone pair, opposite to the Pb^{II}−X direction) have been

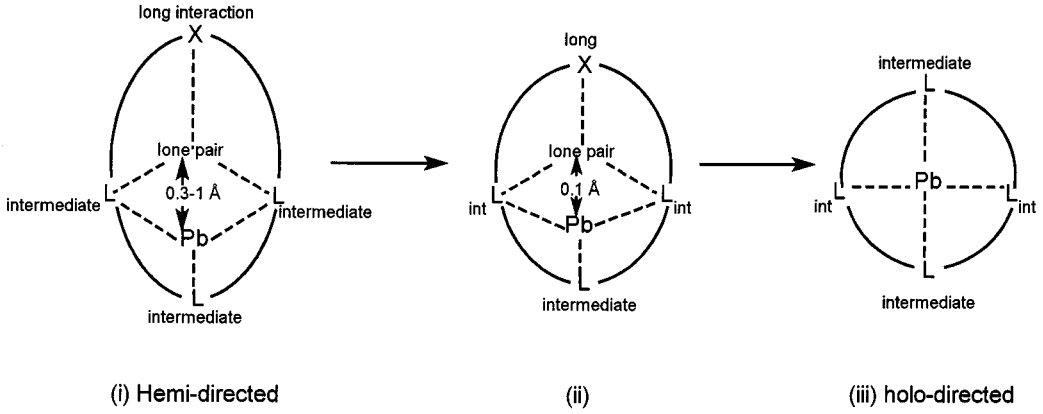


Figure 4. Hemi- and holo-direction

found to range from 0.3−1.2 Å. When the difference between these distances is small (ca. 0.1 Å), the coordination is regarded as holo-directed and the role of the lone pair becomes less clear, i.e. as to whether it exerts an effect on the stereochemistry (Figure 4). Generally speaking, hemi-directed ligand distribution is found for lead(II) compounds having coordination numbers 2−5, although lead(II) compounds having coordination numbers 6−8 have also been found to exhibit hemi-direction, particularly when harder oxygen and/or nitrogen donor atoms are available, as in the present set of ligands.[8]

Two important features of the structure of complex **1** are the empty zone in the coordination sphere about the lead(II) ion and the shortened distance between the metal and O(3) [Pb−O(3) 2.568(5) Å] relative to the other $Pb-O_{ether}$ distances. It is possible that these features may be directly attributed to a hemi-directed structure and the presence of a stereochemically active lone pair of electrons. However, this presumes that the perchlorate oxygen atoms O(3A) and O(4A) and the pendant amino nitrogen atom N(3) are distant from the lead [Pb−O(3A) 2.877, Pb−O(4A) 3.236, Pb−N(3) 2.892 Å] and thus not involved in coordination. If, however, the Pb−O(3A) and Pb−N(3) distances are considered as being long, ca. 0.3 Å in excess of the Pb−O(3) distance opposite, then the structure is close to the limit of being hemi-directed and the role of the lone pair is less clear.

Both aniline pendant arms are orientated on the same side of the macrocycle plane, resulting in a *syn* conformation, in contrast to the *anti* conformation found for free L^1. Planes containing the aromatic rings form an angle of 112.1°. Inspection of the crystal packing of **1** reveals that one of the two perchlorate anions is well-removed from the complex cation and has no interactions with neighbouring molecules. The second perchlorate anion, however, is involved in both a weak hydrogen-bonding interaction with a hydrogen atom on the non-coordinated pendant amino nitrogen atom N(3) [O(1A)···HN(3) 2.278 Å, O(1A)···N(3) 3.122 Å, O(1A)···HN(3)···N(3) 167.3°] and a weak interaction with the lead(II) atom [O(3A)···Pb 2.877 Å] (Figure 2b). This anion acts as a bridge between the metal and non-coordinated pendant amine group, thereby reinforcing the *syn* conformation present in complex **1**.

Synthesis and Characterization of Complexes of the Schiff-Base Lateral Macrobicycle L^3

Reaction of equimolar amounts of 2,6-diformylpyridine and *N*,*N*′-bis(2-aminobenzyl)-1,10-diaza-15-crown-5 (L^1) in the presence of lead(II) perchlorate in absolute ethanol under the conditions described in the Experimental Section gave the analytically pure product $[PbL^3](ClO_4)_2 \cdot EtOH$ (**3**) in 70% yield. The IR and FAB-mass spectra confirmed that condensation and [1+1] cyclization had occurred. Thus, the IR spectrum (KBr discs) of **3** features bands attributable to $\nu(C{=}N)_{imine}$ and $\nu(C{=}N)_{py}$ stretching modes at 1631 and 1583 cm^{-1}, respectively, but no bands due to carbonyl or amine vibration modes. The FAB-mass spectrum, obtained using 3-nitrobenzyl alcohol as the matrix, displays peaks at *m*/*z* (%) = 834 (37), 735 (20), and 528 (64) due to $[\mathbf{3} - (ClO_4)]^+$, $[\mathbf{3} - 2(ClO_4)]^+$, and $[L^3 + 1]^+$, respectively. Compound **3** can also be prepared by a transmetallation reaction using $[BaL^3](ClO_4)_2$ and lead(II) perchlorate; reaction in a 1:1 molar ratio in absolute ethanol solution gave **3** in 57% yield. The absence of peaks corresponding to species containing the BaL^3 fragment in the FAB-mass spectrum coupled with the presence of peaks due to $[\mathbf{3} - (ClO_4)]^+$, $[\mathbf{3} - 2(ClO_4)]^+$, and $[L^3 + 1]^+$ confirms that the transmetallation reaction has occurred and that the macrobicycle L^3 remains intact in the lead(II) complex.

^1H- and ^{13}C-NMR spectra recorded in acetonitrile solution also confirmed the integrity of the macrobicycle L^3 in this solvent; no resonances attributable to amino or aldehydic functions were seen. As expected, the signals due to the ethylenic protons of the crown moiety appear at high field as complicated multiplets as a result of the coordination of the metal by the oxygen atoms of the crown. The signals due to aromatic and pyridine protons, appearing at low field, are well-resolved and could be fully assigned. Considering the X-ray crystal structure (vide infra), two discrete signals due to the azomethine protons would be expected in the ^1H-NMR spectrum if structural integrity were to be maintained in solution. In fact, the spectrum recorded at 298 K features only one signal at δ = 9.09 (2 H) due to both of these protons. The spectrum recorded at 235 K shows a broadening of this signal, indicating a fluxional behaviour of **3** in acetonitrile solution. A striking feature of

the ^{1}H-NMR spectrum of this compound at 298 K is the rare observation of satellites attributable to proton coupling to the naturally abundant $I = 1/2$ nuclei of the metal, reflecting kinetic inertness in the complex as well as a degree of covalency in the interaction with a nearby donor atom. In the present case, the signal at $\delta = 9.09$ due to the imine protons appears as a singlet flanked by the satellites due to proton coupling to ^{207}Pb; the $^3J(^{207}\text{Pb-H}_{\text{imine}})$ coupling constant has a value of just 2.93 Hz, which corresponds with the weak $\text{Pb}-\text{N}_{\text{imine}}$ interaction observed in the crystal structure. Coupling to $I = 1/2$ metal nuclei is an emerging feature of the ^{1}H-NMR spectra of complexes containing the pyridine-2,6-diimine unit;[10,12,13] the case presented here would appear to be the third report of ^{207}Pb-^{1}H coupling in compounds of this type.

Attempted reactions between 2,6-diformylpyridine and L^1 in the presence of cadmium perchlorate under various experimental conditions yielded neither the expected cadmium complex of the Schiff-base macrobicycle L^3 nor uncoordinated L^3. In all cases, the IR spectra of the products exhibited bands attributable to $\nu(\text{C}=\text{N})_{\text{imine}}$ along with bands due to carbonyl and/or amine groups, thus indicating the presence of acyclic compounds. In contrast, a transmetallation reaction between $[\text{BaL}^3](\text{ClO}_4)_2$ and cadmium perchlorate in a 1:1 molar ratio gave rise to a yellow analytically pure product $[\text{CdL}^3](\text{ClO}_4)_2$ (**4**) in 55% yield. The FAB-mass spectrum, which features peaks due to $[\mathbf{4} - (\text{ClO}_4)]^+$, $[\mathbf{4} - 2\,(\text{ClO}_4)]^+$, and $[\text{L}^3 + 1]^+$ at *m/z* (%) = 740 (23), 641 (12), and 528 (100), respectively, and no peaks corresponding to species containing the BaL^3 fragment, provided initial evidence that the transmetallation reaction had indeed occurred and that the macrobicycle L^3 had remained intact in **4**. The IR spectrum features bands due to the C=N stretching modes of the imine and pyridine at 1641 and 1589 cm^{-1}, respectively, and bands due to the asymmetric stretching and bending modes of the perchlorate groups at 1095 and 623 cm^{-1}, respectively.

Conductivity measurements on 10^{-3} M solutions of the two cryptates in acetonitrile at 20 °C led to values of Λ_M = 291 $\text{cm}^2\Omega^{-1}\text{mol}^{-1}$ for **3** and 266 $\text{cm}^2\Omega^{-1}\text{mol}^{-1}$ for **4**, showing that both behave as 2:1 electrolytes in this solvent.[6] In the light of the X-ray crystal structure of **3** (vide infra), it is clear that its solution and solid-state structures must be different, the coordinated perchlorate anion being replaced by acetonitrile in solution.

X-ray Crystal Structure of 3

The crystal structure of the cryptate complex **3** contains the cation $[\text{PbL}^3(\text{ClO}_4)]^+$, a well-separated perchlorate anion, and a molecule of acetonitrile. Figure 5 shows a view of the structure of the cationic complex, while selected bond lengths and angles are given in Table 3. The metal ion is asymmetrically positioned in relation to the ligand cavity and only six of the eight available heteroatoms of L^3 are coordinated to it. One pivotal nitrogen atom and one imine nitrogen atom remain only weakly coordinated with long interactions [Pb−N(1) 2.857 Å, Pb−N(3) 2.837 Å]. This may possibly be linked to the influence of the lone pair as

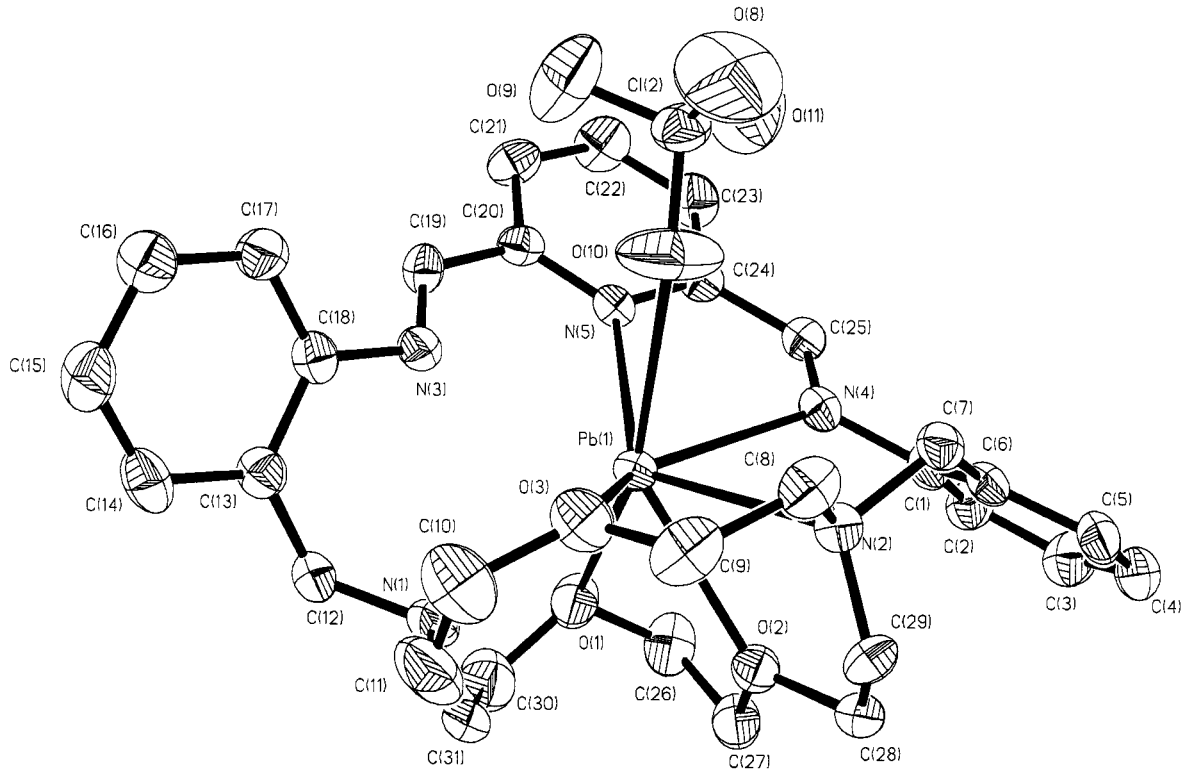


Figure 5. X-ray crystal structure of the cation of **3** with atom labelling; hydrogen atoms are omitted for simplicity; the ORTEP plot is drawn at a 30% probability level

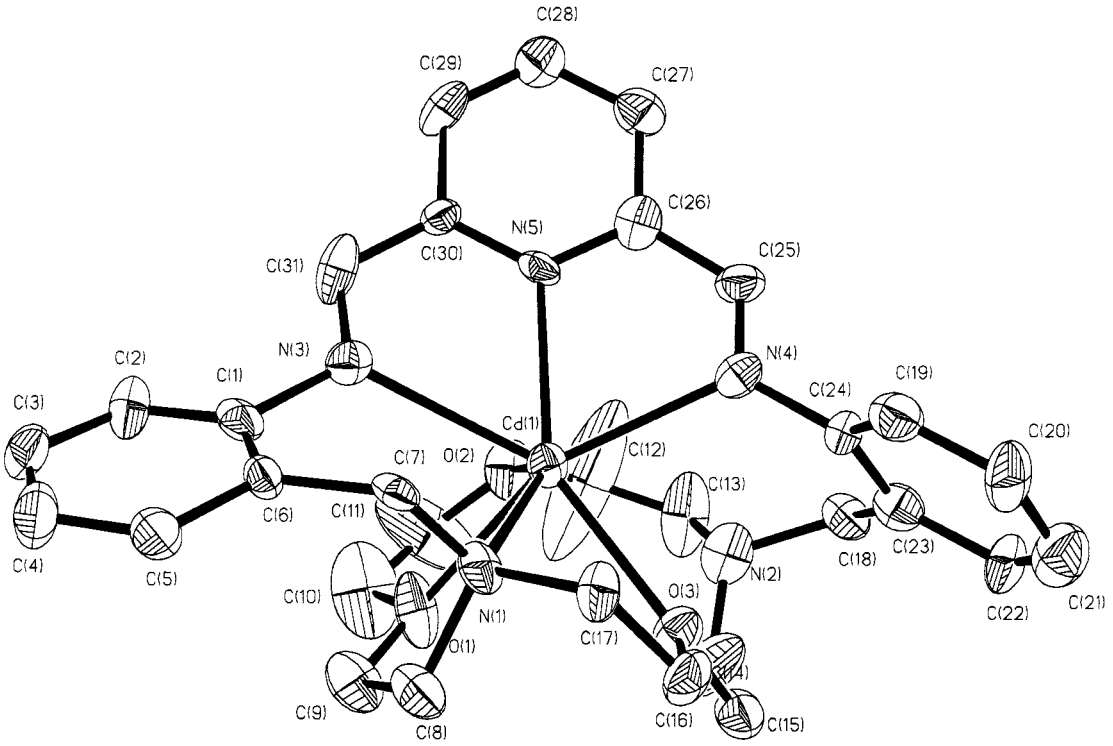


Figure 6. X-ray crystal structure of the cation of **4** with atom labelling; hydrogen atoms are omitted for simplicity; the ORTEP plot is drawn at a 30% probability level

discussed earlier. Two of the metal−oxygen bond lengths are practically equal [Pb−O(1) 2.718(6) Å, Pb−O(2) 2.719(6) Å] and slightly longer than the third [Pb−O(3) 2.670(6) Å]. These three distances fall within the range found for lead(II) crown-ether complexes;[7] the first is shorter than the corresponding distance found in compound **2**, whereas the other two are slightly longer. The distance of 2.740(6) Å for Pb−N(4) is also within the usual range found for lead(II) imine complexes,[12,14] while the Pb−N(5) distance is slightly longer than typically observed $Pb-N_{pyridine}$ distances.[15] The coordination sphere of the lead is completed by one oxygen atom of a monodentate perchlorate group and the coordination polyhedron may be described as a dodecahedron with an unoccupied site. The lateral aromatic rings of the cryptand L^3 are in different planes, which intersect at 87.2°. The pyridine ring and the two imine groups are coplanar and their plane forms dihedral angles of 52.9° with the plane containing the benzene ring bound to N(1) and 49.7° with the plane containing the other aromatic ring.

X-ray Crystal Structure of 4

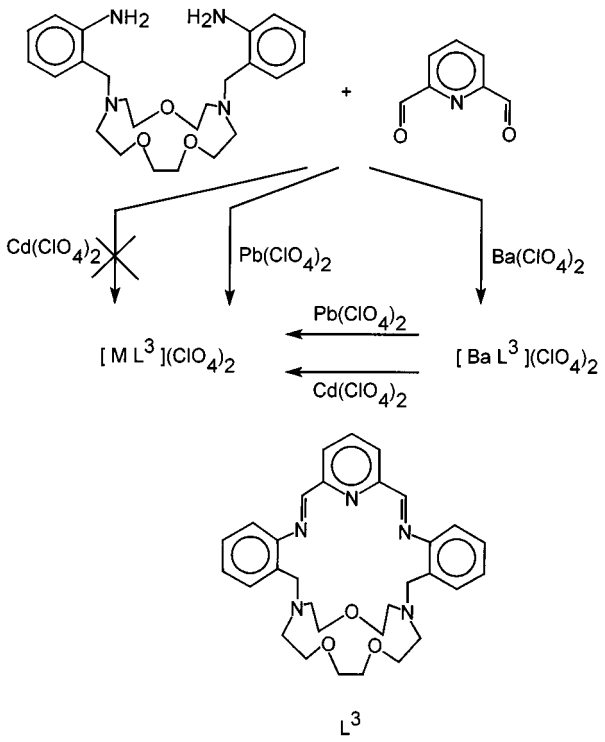
Figure 6 shows the structure of the dication $[CdL^3]^{2+}$ in crystals of $[CdL^3](ClO_4)_2$ (**4**). Selected bond distances and angles are given in Table 3. The cadmium(II) ion resides in a distorted monocapped octahedral N_4O_3 environment, bound by seven of the eight donor atoms of the macrobicyclic receptor; the pivotal nitrogen N(2) is rather distant from the metal ion [Cd−N(2) 3.134 Å] and remains uncoordinated. The bond lengths between the imine nitrogen atoms and the cadmium ion differ by 0.147 Å and fall within the range reported for similar bonds in X-ray crystal structures containing similar fragments.[14,16] The cadmium is positioned slightly closer to O(1) (2.374 Å) than to the other two oxygen atoms (2.493, 2.459 Å). As in the lead(II) cryptate **3**, the pyridine ring and the two imine groups are coplanar although in **4** this plane forms dihedral angles of 145.7° with the plane containing the benzene ring bound to N(1) and 96.9° with plane of the other aromatic ring; the lateral aromatic rings of L^3 are in different planes which intersect at 61°.

Discussion

Two points of interest emerge from the above data. The first relates to the synthetic strategies followed in preparing the lead(II) and cadmium(II) cryptates with the Schiff-base lateral macrobicycle L^3 (compounds **3** and **4**), while the second concerns the different complexation capabilities of the two types of macrocycles (lariat ether L^1 and macrobicycle L^3) towards the heavy metal ions lead(II) and cadmium(II), as well as the influence of the nature of the metal ion guest on the conformation adopted by the macrobicycle receptor L^3.

In a previous paper,[4] we reported that it proved impossible to prepare the Schiff-base lateral macrobicycle L^3 by a direct reaction between the organic precursors due to the *anti* arrangement adopted by the diamine L^1, not only in the solid state but also in solution, and that a barium cation

was required to template the reaction between L^1 and 2,6-diformylpyridine to build L^3. Herein, we have shown that the corresponding lead(II) and cadmium(II) cryptates of L^3 can be prepared by transmetallation reactions starting from the barium cryptate (Scheme 2). This indicates a coordinative preference of L^3 for these soft metal ions.



Scheme 2

The efficiencies of these soft metal ions as template agents in the synthesis of L^3 have been studied. Whereas the lead(II) ion was found to be capable of acting as an effective template in this synthesis, this was not the case with the cadmium ion. The effectiveness of lead in the templating process stems from its ability to orientate the pendant arms of the diamine L^1 in a *syn* conformation. This is evident in the X-ray crystal structure of the lead(II) complex of L^1 (**1**) and the situation is likely to be maintained in solution. An important feature of the structure of **1** is the *syn* conformation of the bibracchial macrocyclic ligand L^1, even when one pendant arm is not directly coordinated to the metal. A *syn* arrangement of L^1 has also been observed in the crystal structure of the barium complex $[BaL^1](ClO_4)_2$,[4] while an *anti* arrangement has been found in the crystal structure of the octahedral copper(II) complex $[CuL^1](ClO_4)_2$.[17] It seems likely that the disposition of the pendant arms in complexes of L^1 is related to the size of the cation present. The copper(II) cation (r_{CN4} = 0.57; r_{CN6} = 0.73 Å),[18] with a penchant for square-planar geometry, resides in the macrocyclic cavity bound by two ether oxygen and two pivotal amino nitrogen atoms. The donor atoms of the pendant arms coordinate apically so as to form an octahedral coordination sphere. The larger barium cation (r_{CN9} = 1.47 Å)[18] may be regarded as spherically symmetrical and the geometries found in its complexes are not constrained by *d*-orbital orthogonality or crystal-field stabilization energies. Consequently, in $[BaL^1](ClO_4)_2$ the barium is found in a position that allows optimal interaction with the seven ligand donor atoms and a bidentate perchlorate anion. This necessitates a *syn* orientation of the pendant arms and the overall structure resembles that of molecular clefts reported for barium complexes of bibracchial tetraimine Schiff-base macrocycles,[19–21] and for potassium and barium complexes of the related lariat ethers derived from the larger [18-aneN_2O_4] macrocyclic polyether with alcohol-bearing 2-hydroxy-1,1-dimethylethyl and [(2-hydroxyethyl)oxy]ethyl pendant arms.[22,23] The lead(II) cation is intermediate in size (r_{CN6} = 1.19 Å)[18] and its geometry is free of *d*-orbital control, as a result of which it resides above the macrocyclic cavity towards the pendant arms, one of which coordinates weakly [Pb–N(3) 2.892 Å]. It can also be suggested that the ineffectiveness of the cadmium ion as a template agent in the synthesis of the macrobicycle L^3 stems from the unsuitable conformation adopted by the diamine L^1 in the presence of this metal ion. Considering the small size of the cadmium ion (r_{CN6} = 0.95 Å) and in the light of spectroscopic characterization of the cadmium complex of the diamine L^1 (**2**), it can be stated that the metal ion lies inside the cavity of the crown in a coordination environment rather similar to that found for the copper complex;[17] L^1 must therefore adopt an *anti* arrangement.

Viewing the crystal structures of cryptates **3** and **4**, as well as that of the corresponding barium cryptate,[4] from a side perspective through the axis of the pivotal nitrogen atoms (Figure 7) allows an appraisal of the influence of the metal ion on the conformation of the macrobicycle receptor L^3. The most significant changes concern the folding of the crown, the distance between the two pivotal nitrogen atoms, and the distance between the imine nitrogen atoms. In the case of the barium cryptate (Figure 7a), the crown moiety folds in such a way that both pivotal nitrogen atoms and the two oxygen atoms of one chain form a plane (deviation from planarity 0.0425 Å). However, in neither the lead cryptate **3** nor the cadmium cryptate **4** is it possible to find a plane formed by four of the six donor atoms of the crown moiety of L^3. While the distance between the two pivotal nitrogen atoms [N(1)–N(2)] is clearly longer in the case of **4** (4.870 Å) than in the case of **3** (4.688 Å), the distance between the imine nitrogen atoms [N(3)–N(4)] is shorter in the case of **4** (4.442 Å) than in the case of **3** (4.855 Å). In both cryptates, these distances are considerably shorter than the corresponding distances in the barium cryptate, which amount to 5.389 Å and 5.002 Å, respectively. These data illustrate how the macrobicycle L^3 can either expand or contract in order to accommodate the metal ion in its cavity, in spite of the presence of a relatively rigid unsaturated chelating chain in its backbone. Some minor differences are evident from the values of the angles N(pivotal)–C–C(aryl); whereas angles N(1)–C(7)–C(6) and N(2)–C(18)–C(23) in complex **4** are practically equal, having values of 115.8(10)° and 115.3(11)°, respectively, the

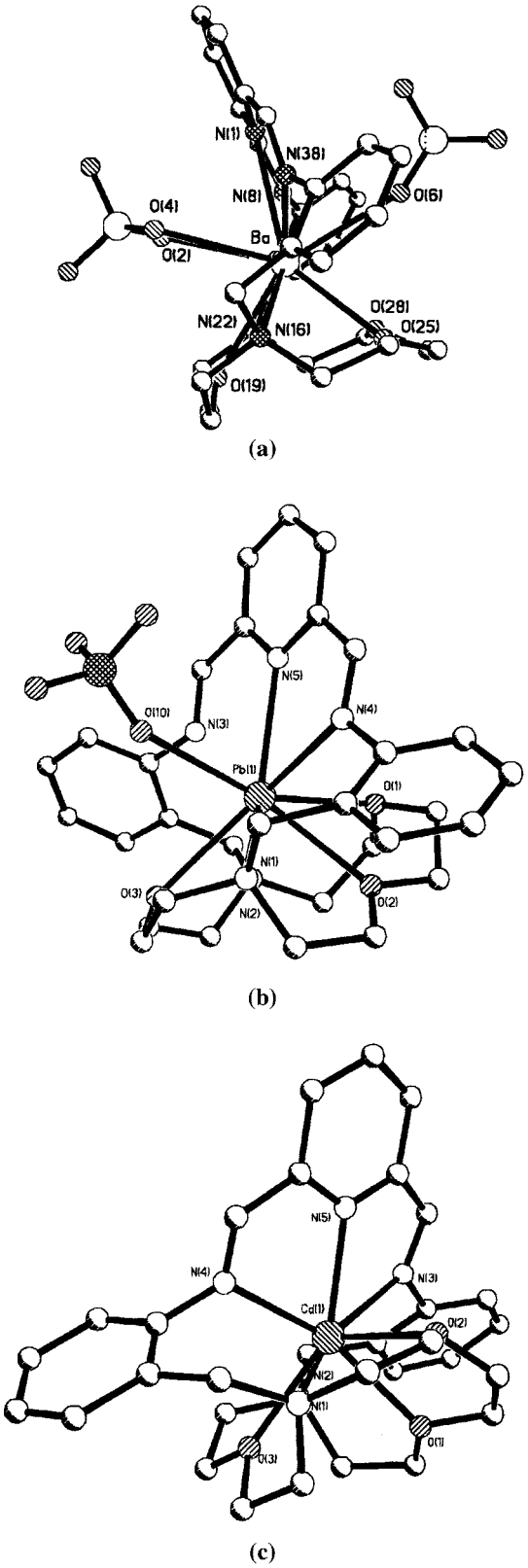


Figure 7. Side view of (a) $[BaL^3]^{2+}$(see ref.[4]), (b) $[PbL^3(ClO_4)]^+$, and (c) $[CdL^3]^{2+}$

corresponding angles in **3** have values of 114.7(7)° and 117.0(8)°.

The effect of the pyridine moiety on the arrangement of the diamine fragment in the case of lead(II) cryptate **3** can be also appreciated by comparing the X-ray crystal structure of this complex with that of the lead(II) complex with the bibracchial lariat ether L^1 (**1**). The folding of the crown moiety is clearly different in the two compounds. In **1**, the three oxygen atoms and the pivotal nitrogen N(2) form a plane (deviation from planarity 0.077 Å), with the lead(II) ion residing 1.652 Å above it, in contrast to the situation in **3**. Moreover, the distance between the two pivotal nitrogen atoms [N(1)−N(2)] is clearly longer in **1** (4.881 Å) than in **3** (4.688 Å).

Concluding Remarks

The Schiff-base lateral macrobicycle L^3 has been shown to act as a receptor for both lead(II) and cadmium(II) guests. The respective cryptates can be prepared by simple transmetallation reactions starting from the analogous barium cryptate, which highlights the preference of L^3 for the heavy metal ions. The lead(II) ion has been found to be capable of acting as a template agent in the synthesis of L^3, whereas this is not the case for the cadmium(II) ion.

The nature of the guest metal ion has been found to have a significant influence on the conformation adopted by the receptor L^3. Macrobicycle L^3 can either expand or contract to accommodate the metal ion in its cavity, in spite of the fact that its backbone incorporates a relatively rigid unsaturated chelating chain.

Experimental Section

Measurements: Elemental analyses and FAB-MS spectra were provided by the Servicios Xerais de Apoio á Investigación of the Universidade da Coruña; elemental analyses were carried out on a Carlo Erba 1180 elemental analyzer, and FAB-MS spectra were recorded on a Fisons Quatro mass spectrometer with a Cs^+ ion gun using 3-nitrobenzyl alcohol as a matrix. − ^{1}H- and ^{13}C-NMR spectra were recorded on a Bruker AC 200 F or a Bruker WM-500 spectrometer. − IR spectra were recorded from samples between KBr discs on a Perkin−Elmer 1330 spectrophotometer. − UV/vis spectra were recorded on a Uvikon 942 Plus spectrophotometer. − Melting points were measured on a Gallenkamp apparatus. − Conductivity measurements were carried out at 20 °C with a Crison Micro CM 2201 conductivimeter using 10^{-3} M solutions of the complexes in acetonitrile.

Materials: 2,6-Diformylpyridine was synthesized according to literature methods.[24,25] The barium cryptate $[BaL^3](ClO_4)_2$ was prepared as described previously.[4] All other chemicals were purchased from commercial sources and used without further purification. Solvents were of reagent grade and were purified by the usual methods.

Caution! Although we have experienced no difficulties with the perchlorate salts, these should be regarded as potentially explosive and handled with care.

Preparation of *N*,*N*′-Bis(2-aminobenzyl)-1,10-diaza-15-crown-5 (L^1): A solution of 2-nitrobenzyl chloride (1.6 g, 9.2 mmol) in acetonitrile (20 mL) was added to a stirred solution of 1,10-diaza-15-

crown-5 (1.0 g, 4.6 mmol) and Na_2CO_3 (2.4 g, 23 mmol) in acetonitrile (30 mL). The reaction mixture was stirred under reflux for 24 h. It was then filtered, the filtrate was concentrated, and the yellow oily residue was extracted with CH_2Cl_2/water. The organic phase was dried with anhydrous $MgSO_4$ and concentrated in vacuo. The resulting yellow oil was dissolved in absolute ethanol (60 mL) and Pd/C was added. Hydrazine hydrate (1.5 mL) was slowly added and the reaction mixture was heated and stirred for 24 h. It was then filtered and the solvent was removed from the filtrate in a rotary evaporator. Addition of cold diethyl ether to the oily residue led to the deposition of a white precipitate. Recrystallization from absolute ethanol/diethyl ether (1:1) gave crystals suitable for X-ray diffraction analysis. Yield: 1.2 g (61%); m.p. 92−94 °C. − $C_{24}H_{36}N_4O_3$: calcd. C 67.2, H 8.5, N 13.1; found C 66.7, H 8.5, N 13.1. − ^{13}C NMR (500 Mz, CD_3CN): δ = 54.1, 54.2 (C-3, C-1), 59.1 (C-6), 69.2, 68.3 (C-5, C-2), 70.0 (C-4), 114.9 (C-11), 116.4 (C-9), 122.9 (C-7), 128.0 (C-10), 130.1 (C-8), 148.1 (C-12). − FAB-MS: *m/z* = 429 [L^1 + 1]. − IR (KBr discs): ṽ = 3430, 3390, 3293, 3275 (NH_2), 1618, 1495, 1463, 1448 (C=C) cm^{-1}.

Preparation of the Complexes

[PbL^1](ClO$_4$)$_2$ (1): A solution of $Pb(ClO_4)_2 \cdot H_2O$ (0.11 g, 0.26 mmol) in absolute ethanol (5 mL) was added to a stirred solution of the ligand L^1 (0.12 g, 0.26 mmol) in absolute ethanol (10 mL). The reaction mixture was stirred under reflux for 6 h. During the course of the reaction, the solution became turbid and a white precipitate was deposited. This was collected by filtration, washed with absolute ethanol, and dried in air. Slow diffusion of diethyl ether into a solution of **1** in acetonitrile gave crystals suitable for X-ray crystallography. Yield: 0.15 g (73%); m.p. 268 °C (decomp.). − $C_{24}H_{36}Cl_2N_4O_{11}Pb$: calcd. C 34.5, H 4.3, N 6.7; found C 34.6, H 4.3, N 6.7. − ^{13}C NMR (200 Mz, CD_3CN): δ = 53.1, 53.2 (C-3, C-1), 56.5 (C-6), 70.0, 69.5, 68.4 (C-5, C-4, C-2), 121.4 (C-11), 123.7 (C-9), 125.1 (C-7), 131.5 (C-10), 134.6 (C-8), 142.5 (C-12). − FAB-MS: *m/z* = 735 [**1** − ClO_4], 635 [**1** − 2 ClO_4]. − IR (KBr discs): ṽ = 3334, 3277 (NH_2), 1613, 1586, 1495, 1457 (C=C), 1110, 617 (ClO_4) cm^{-1}.

[CdL^1](ClO$_4$)$_2$ (2): This white complex was prepared as described for **1** by using $Cd(ClO_4)_2$ (0.10 g, 0.26 mmol). Yield: 0.13 g (65%); m.p. 308 °C (decomp.). − $C_{24}H_{36}CdCl_2N_4O_{11}$: calcd. C 38.9, H 4.9, N 7.6; found C 39.1, H 4.6, N 7.5. − FAB-MS: *m/z* = 641 [**2** − ClO_4], 541 [**2** − 2 ClO_4]. − IR (KBr discs): ṽ = 3320, 3281 (NH_2), 1617, 1590, 1499, 1464 (C=C), 1110, 623 (ClO_4) cm^{-1}.

[PbL^3](ClO$_4$)$_2$·EtOH (3) − Method A: A solution of $Pb(ClO_4)_2 \cdot H_2O$ (0.048 g, 0.100 mmol) in absolute ethanol (5 mL) was added to a stirred solution of [BaL^3]$(ClO_4)_2$ (0.045 g, 0.050 mmol) in absolute ethanol (35 mL) and the resulting mixture was stirred under reflux for one day. During the course of the reaction, the solution became deep-yellow. It was filtered while still hot, and then the filtrate was allowed to cool to room temperature. A yellow microcrystalline precipitate formed, which was collected by filtration. Yield: 0.039 g (57%); m.p. 333 °C (decomp.). − $C_{31}H_{37}Cl_2N_5O_{11}Pb \cdot EtOH$: calcd. C 40.45, H 4.4, N 7.1; found C 40.5, H 4.5, N 7.0.

Method B: A solution of $Pb(ClO_4)_2 \cdot H_2O$ (0.122 g, 0.25 mmol) in absolute ethanol (50 mL) was added to a stirred solution of *N*,*N*′-bis(2-aminobenzyl)-1,10-diaza-15-crown-5 (0.114 g, 0.250 mmol) in absolute ethanol (120 mL). The mixture was vigorously stirred and heated while a solution of 2,6-diformylpyridine (0.036 g, 0.250 mmol) in absolute ethanol (60 mL) was added dropwise during the course of a day. After the addition was complete, the resulting pale-yellow solution was stirred under reflux for a further day. The solution was filtered while hot; upon cooling the filtrate to room temperature, a pale-yellow microcrystalline precipitate formed, which was collected by filtration. Yield: 0.170 g (70%). − $C_{31}H_{37}Cl_2N_5O_{11}Pb \cdot EtOH$: calcd. C 40.45, H 4.4, N 7.1; found C 40.7, H 4.4, N 6.9. − ^{13}C NMR (200 Mz, CD_3CN): δ = 57.8, 58.2, 58.8, 69.1, 69.6, 121.2, 129.4, 131.3, 131.8, 132.6, 133.5, 142.6, 150.1, 154.2, 164.6. − FAB-MS: *m/z* = 834 [**3** − ClO_4], 735 [**3** − 2 ClO_4]. − IR (KBr discs): ṽ = 1631 $(C=N)_{imine}$, 1583 $(C=N)_{py}$, 1490, 1456 (C=C), 1093, 623 (ClO_4) cm^{-1}. Slow diffusion of diethyl ether into a solution of **3** in acetonitrile gave crystals suitable for X-ray crystallography.

[CdL^3](ClO$_4$)$_2$ (4): A solution of $Cd(ClO_4)_2$ (0.038 g, 0.100 mmol) in absolute ethanol (5 mL) was added to a stirred solution of [BaL^3-$(ClO_4)_2$] (0.045 g, 0.050 mmol) in absolute ethanol (35 mL) and the resulting mixture was stirred under reflux for one day. During the course of the reaction, the solution became turbid and a yellow precipitate was deposited. This was collected by filtration, washed

Table 4. Crystallographic details for L^1, **1**, **3**, and **4**

	L^1	**1**	**3**	**4**
Empirical formula	$C_{24}H_{36}N_4O_3$	$C_{24}H_{36}Cl_2N_4O_{11}Pb$	$C_{33}H_{39}Cl_2N_6O_{11}Pb$	$C_{31}H_{39}Cl_2N_5O_{12}Cd$
Form. wt.	428.57	834.66	873.79	856.97
Space group	$P\bar{1}$	$P\bar{1}$	$P2(1)/c$	$P\bar{1}$
Crystal system	Triclinic	Triclinic	Monoclinic	Triclinic
Z	2	2	4	2
a [Å]	10.249(2)	8.8027(5)	17.333(5)	10.4634(9)
b [Å]	10.405(4)	10.7781(6)	13.314(4)	10.5331(8)
c [Å]	12.157(3)	16.4298(8)	16.375(6)	17.6224(14)
α [°]	86.97(4)	91.1770(10)	90	95.204(2)
β [°]	70.050(10)	105.2300(10)	93.94(2)	100.293(2)
γ [°]	78.58(3)	100.5180(10)	90	113.716(2)
V [Å^3]	1194.4(6)	1474.92(14)	3770.0(21)	1720.8(2)
$\rho_{calcd.}$ [g/cm^3]	1.192	1.879	1.716	1.654
$\mu_{calcd.}$ [mm^{-1}]	0.079	5.965	4.683	0.861
Radn. (Mo-K_α) [Å]	0.71073	0.71073	0.71073	0.71073
T [K]	293(2)	298(2)	293(2)	298(2)
Final *R* indices[a]	R_1 = 0.0660	R_1 = 0.0440	R_1 = 0.0474	R_1 = 0.0845
[$I > 2\sigma(I)$]	wR_2 = 0.1755	wR_2 =0.1025	wR_2 = 0.0971	wR_2 = 0.1883
Final *R* indices	R_1 = 0.0845	R_1 = 0.0524	R_1 = 0.0830	R_1 = 0.1862
(for all data)	wR_2 = 0.1930	wR_2 = 0.111	wR_2 = 0.1119	wR_2 = 0.2501

[a] $R_1 = \Sigma||F_o|-|F_c||/\Sigma|F_o|$ and $wR_2 = \{\Sigma[w(|F_o|^2-|F_c|^2|)^2]/\Sigma[w(F_o^4)]\}^{1/2}$.

with absolute ethanol, and dried in air. X-ray quality crystals were grown by slow diffusion of diethyl ether into a solution of **4** in acetonitrile. Yield: 0.033 g (55%); m.p. 280 °C (decomp.). − $C_{31}H_{37}CdCl_2N_5O_{11}$: calcd. C 43.9, H 4.5, N 8.2; found C 43.8, H 4.1, N 8.3. − FAB-MS: *m/z* = 740 [**4** − ClO_4], 641 [**4** − 2 ClO_4]. − IR (KBr discs): $\tilde{\nu}$ = 1641 $(C{=}N)_{imine}$, 1589 $(C{=}N)_{py}$, 1487, 1461, 1449 (C=C), 1095, 623 (ClO_4) cm^{-1}.

X-ray Crystallographic Study − Crystal Structure Determinations of L^1 and Complex 3: Macrocycle $\mathbf{L^1}$ was crystallized from absolute ethanol/diethyl ether (1:1) in the form of colourless blocks (dimensions of the selected crystal: 0.85 × 0.43 × 0.25 mm^3). Complex **3** was crystallized in the form of yellow blocks by slow diffusion of diethyl ether into an acetonitrile solution (dimensions of the selected crystal: 0.76 × 0.45 × 0.32 mm^3). X-ray data were collected at room temperature in the range $3.5 < 2\varphi < 50°$ on a Siemens P4 diffractometer by the ω-scan method. 4972 reflections were measured for L^1, 8062 for **3**, all of which were corrected for Lorentz and polarization effects and for absorption by the analysis of 10 azimuthal scans (minimum and maximum transmission coefficients 0.4373 and 0.9788 for L^1, 0.273 and 0.709 for **3**); 3218 and 4656 independent reflections, respectively, exceeded the significance level $F/\sigma(F) > 4.0$. The structure was solved by direct methods and refined by full-matrix least-squares methods on F^2. Hydrogen atoms were included in calculated positions and refined in riding mode. For L^1, convergence was reached at a final R = 0.0660, wR_2 = 0.1930; 281 parameters for all 4201 unique data, allowing for the thermal anisotropy of all non-hydrogen atoms. Minimum and maximum final electron density: −0.396 and 0.859 $eÅ^{-3}$. For **3**, convergence was reached at a final R = 0.0474, wR_2 = 0.0971; 468 parameters for all 6631 unique data, allowing for the thermal anisotropy of all non-hydrogen atoms. No residual density was found outside −0.613 and 0.648 $eÅ^{-3}$. In all cases, complex scattering factors were taken from the program package SHELXL-93[26] as implemented on a Viglen 486dx computer. Crystal data and details of the data collection and refinement are presented in Table 4.

Crystal Structure Determinations of Complexes 1 and 4: Both were crystallized in the form of yellow blocks by slow diffusion of diethyl ether into acetonitrile solutions (dimensions of the selected crystals: 0.55 × 0.25 × 0.15 mm^3 for **1** and 0.35 × 0.15 × 0.10 mm^3 for **4**). X-ray data for **1** and **4** were collected on a Siemens SMART CCD area detector single-crystal diffractometer operating at room temperature. Preliminary unit cell constants were determined from a set of 45 narrow-frame (0.3° in ω) scans. A total of 1255 frames of intensity data were collected with a frame width of 0.3° each in ω and a counting time of 10 s/frame at a crystal-to-detector distance of 4.0 cm. The collected frames were integrated using an orientation matrix determined from the narrow-frame scans and refined using Siemens SAINT software on all the observed reflections. A semiempirical absorption correction using an ellipsoidal model (maximum and minimum transmission coefficients 0.455 and 0.299) was applied for **1**, whereas an absorption correction using the SADABS program (maximum and minimum transmission coefficients 1.000 and 0.467) was applied for **4**. The integration process yielded 8176 reflections, of which 5118 were independent for **1**, and 8855 reflections, of which 5693 were independent for **4**. The structures were solved by Patterson and Fourier methods using Siemens SHELXTL-PC software[27] and refined by full-matrix least-squares methods on F^2. Hydrogen atoms were included in calculated positions and refined in riding mode. For **1**, convergence was reached at R = 0.0440, wR_2 = 0.1026; 379 parameters for all 5056 unique data, allowing for the thermal anisotropy of all non-hydrogen atoms. A final difference Fourier map showed no residual density outside −1.624 and 1.574 $eÅ^{-3}$. For **4**, convergence was reached at R = 0.0883, wR_2 = 0.1972; 460 parameters for all 5693 unique data, allowing for the thermal anisotropy of all non-hydrogen atoms; minimum and maximum final electron density: −0.829 and 1.431 $eÅ^{-3}$. Crystal data and details of the data collection and refinement are summarized in Table 4.

Crystallographic data (excluding structure factors) for the structures reported in this paper have been deposited with the Cambridge Crystallographic Data Centre as supplementary publication nos. CCDC-136178, CCDC-136179, CCDC-136180, and CCDC-136181. Copies of the data can be obtained free of charge on application to the CCDC, 12 Union Road, Cambridge CB2 1EZ, U.K. [Fax: (internat.) +44 (0)1223/336033; E-mail: deposit@ccdc.cam.ac.uk].

Acknowledgments

The authors thank the Universidade da Coruña for financial support.

[1] [1a] F. Vögtle, E. Weber (Eds.), *Host-Guest Complex Chemistry: Macrocycles*, Springer, Berlin, Heidelberg, **1985**. − [1b] R. M. Izatt, J. J. Christensen (Eds.), *Synthesis of Selective Agents (Progress in Macrocyclic Chemistry)*, Wiley, New York, **1987**, vol. 3. − [1c] J.-M. Lehn, F. Montavon, *Helv. Chim. Acta* **1978**, *61*, 67.

[2] [2a] Y. Inoue, G. W. Gokel (Eds.), *Cation Binding by Macrocycles*, Marcel Dekker, New York, **1990**. − [2b] G. W. Gokel, *Crown Ethers and Cryptands*, The Royal Society of Chemistry, Cambridge, **1991**.

[3] A. T. Yordanov, D. M. Roundhill, *Coord. Chem. Rev.* **1998**, *170*, 93.

[4] D. Esteban, D. Bañobre, R. Bastida, A. de Blas, A. Macías, A. Rodríguez, T. Rodríguez-Blas, D. E. Fenton, H. Adams, J. Mahía, *Inorg. Chem.* **1999**, *38*, 1937.

[5] According to J.-M. Lehn, *Pure & Appl. Chem.* **1980**, *52*, 2441, *lateral macrobicycles* are dissymetrical molecules structurally based on the combination of two different binding subunits, a chelating one and a macrocyclic one.

[6] W. J. Geary, *Coord. Chem. Rev.* **1971**, *7*, 81.

[7] R. D. Rogers, A. H. Bond, *Inorg. Chim. Acta* **1992**, *192*, 163.

[8] L. Shimoni-Livny, J. P. Glusker, C. W. Bock, *Inorg. Chem.* **1998**, *37*, 1853.

[9] R. D. Hancock, M. S. Shaikjee, S. M. Dobson, J. C. A. Boeyens, *Inorg. Chim. Acta* **1988**, *154*, 229.

[10] A. Bashall, M. McPartlin, B. P. Murphy, H. R. Powell, S. Waikar, *J. Chem. Soc., Dalton Trans.* **1994**, 1383.

[11] R. D. Hancock, *Perspectives in Coordination Chemistry* (Eds.: A. F. Williams, C. Floriani, A. E. Merbach), Verlag HCA, Basel, **1992**, p. 129.

[12] D. E. Fenton, R. W. Mathews, M. McPartlin, B. P. Murphy, I. J. Scowen, P. A. Tasker, *J. Chem. Soc., Dalton Trans.* **1996**, 3421.

[13] [13a] M. G. B. Drew, D. Marrs, J. Hunter, J. Nelson, *J. Chem. Soc., Dalton Trans.* **1992**, 11. − [13b] P. S. Marchetti, S. Bank, T. W. Bell, M. A. Kennedy, P. D. Ellis, *J. Am. Chem. Soc.* **1989**, *111*, 2063. − [13c] M. G. B. Drew, D. McDowell, J. Nelson, *Polyhedron* **1988**, *7*, 2229.

[14] M. G. B. Drew, O. W. Howarth, G. G. Morgan, J. Nelson, *J. Chem. Soc., Dalton Trans.* **1994**, 3149.

[15] E. C. Constable, C. Sacht, G. Palo, D. A. Tocher, M. R. Truter, *J. Chem. Soc., Dalton Trans.* **1993**, 1307, and references therein.

[16] [16a] M. G. B. Drew, J. de O. Cabral, M. F. Cabral, F. S. Esho, S. M. Nelson, *J. Chem. Soc., Chem. Commun.* **1979**, 1033. − [16b] S. M. Nelson, S. G. McFall, M. G. B. Drew, A. H. B. Othman, B. Mason, *J. Chem. Soc., Chem. Commun.* **1977**, 167. − [16c] M. G. B. Drew, S. G. McFall, S. M. Nelson, *J. Chem. Soc., Dalton Trans.* **1979**, 575. − [16d] K. R. Adam, S. Donnelly, A. J. Leong, L. F. Lindoy, B. J. McCool, A. Bashall, M. R. Dent, B. P.

Murphy, M. McPartlin, D. E. Fenton, P. A. Tasker, *J. Chem. Soc., Dalton Trans.* **1990**, 1635.
[17] C. Rodriguez-Infante, D. Esteban, R. Bastida, A. De Blas, A. Macías, A. Rodríguez, T. Rodríguez-Blas, D. E. Fenton, J. Mahía, unpublished results.
[18] R. D. Shannon, *Acta Cryst.* **1976**, *A36*, 752.
[19] H. Adams, N. A. Bailey, W. D. Carlisle, D. E. Fenton, G. Rossi, *J. Chem. Soc., Dalton Trans.* **1990**, 1271.
[20] N. A. Bailey, A.Rodriguez, C. O. Barbarin, D. E. Fenton, P. C. Hellier, P. D. Hempstead, M. Kanesato, P. B. Leeson, *J. Chem. Soc., Dalton Trans.* **1995**, 765.
[21] H. Adams, N. A. Bailey, S. R. Collinson, D. E. Fenton, C. J. Harding, S. J. Kitchen, *Inorg. Chim. Acta* **1996**, *246*, 81.
[22] K. V. Damic, R. D. Hancock, P. W. Wade, J. C. A. Boeyens, D. G. Billing, S. M. Dobson, *J. Chem. Soc., Dalton Trans.* **1991**, 293.
[23] R. Bhavan, R. D. Hancock, P. W. Wade, J. C. A. Boeyens, S. M. Dobson, *Inorg. Chim. Acta* **1990**, *171*, 235.
[24] E. P. Papadoupoulus, A. Jarrar, C. H. Issidorides, *J. Org. Chem.* **1966**, *31*, 615.
[25] D. Jerchel, J. Heider, H. Wagner, *Liebigs Ann. Chem.* **1958**, *613*, 153.
[26] G. M. Sheldrick, *SHELXL-93*, *An integrated system for solving and refining crystal structures from diffraction data*, University of Göttingen, Germany, **1993**.
[27] G. M. Sheldrick, *SHELXTL-PC*, *An integrated system for solving and refining crystal structures from diffraction data*, University of Göttingen, Germany, **1997**.

Received October 25, 1999
[I99375]

Mixed Metal Acetylides: The Pt^{II} Aryl Acetylide "$[PtC_6H_2(CH_2NMe_2)_2$-2,6-(C≡C)-4]" as a Connective Fragment

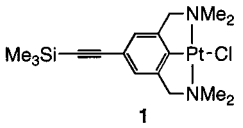
Stephan Back,[a] Robert A. Gossage,[b] Heinrich Lang,*[a] and Gerard van Koten*[b]

Keywords: Alkynes / Cyclic voltammetry / Metal-metal interactions / Conjugation / Platinum

Using $Me_3SiC{\equiv}C\{Pt\}Cl$ (**1**; $Me_3SiC{\equiv}C\{Pt\}$ = $[Pt(C_6H_2\{CH_2NMe_2\}_2$-2,6-$\{C{\equiv}CSiMe_3\}$-4]$^+$) a series of platinum monoacetylides of the type $XC{\equiv}C\{Pt\}C{\equiv}CR$ [X = $SiMe_3$: **2**, R = Ph; **3**, R = $(\eta^5$-$C_5H_4)Fe(\eta^5$-$C_5H_5)$ (abbreviated as Fc); **4**, R = C_6H_4CN-4; **5**, R = $C_6H_4(C{\equiv}CSnMe_3)$-4; X = H: **7**, R = Ph; **8**, R = Fc; **9**, R = C_6H_4CN-4] have been prepared. Studies directed towards the coordinative properties of the C_2 unit of **1** have been carried out and heterotrimetallic [μ-$(Me_3SiC{\equiv}C\{Pt\}Cl][Co_2(CO)_6]$ (**10**) could be synthesised. The successful attachment of **1** to a Ph_3PAu unit leads to linear $Ph_3PAuC{\equiv}C\{Pt\}Cl$ (**11**). Treatment of **11** with $FcC{\equiv}CSnMe_3$ produces the heterotrimetallic rigid-rod shaped complex $Ph_3PAuC{\equiv}C\{Pt\}C{\equiv}CFc$ (**13**). Cyclic voltammetric studies carried out on these Ph_3PAu-capped molecules show that the attachment of an organometallic entity on either side of the $C{\equiv}C\{Pt\}$ fragment leads to a facilitation of the Pt^{II}/Pt^{IV} oxidation.

Introduction

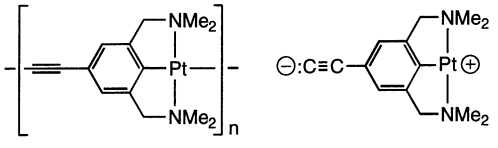
The growing interest in the application of organometallic compounds as building blocks for new materials has led to a large number of publications on their synthesis,[1] and the evaluation of theoretical aspects.[2] In particular, the assembly, chemistry, and the physical properties of a number of homo- and heterometallic acetylenic compounds have been investigated containing metals such as Re,[3] Pt,[4] Pd,[5] Ru,[6] Os,[7] Fe,[8] Rh,[9] or Ti,[10] and Au.[11] Also, a variety of tungsten carbonyl containing complexes have been studied, e.g. by McCleverty et al.[12] and other groups.[13] Many of these mixed-metal σ-acetylide compounds contain a Fc group [Fc = $(\eta^5$-$C_5H_4)Fe(\eta^5$-$C_5H_5)$] as electron "reservoir". The main features of these molecules include: (i) high and readily modified electron density at the metal centres, which should lead to (ii) facile hyperpolarisability due to interaction(s) along the π-conjugated backbone, which connects the different metals.[14] In this context, the application of ethynyl functionalised molecules such as $Me_3SiC{\equiv}C\{Pt\}Cl$ (**1**, $Me_3SiC{\equiv}C\{Pt\}$ = $[Pt(C_6H_2\{CH_2NMe_2\}_2$-2,6-$\{C{\equiv}CSiMe_3\}$-4]$^+$) seems attractive, since in this platinum containing molecule a metal centre is directly attached to a conjugated π-system, and is further stabilised by the N-donor units of the ligand framework.[15] The Pt-monochloride **1** (Scheme 1) was therefore chosen as a precursor of such heterometallic compounds.



1

Scheme 1. Precursor complex **1**

A useful property of **1** is that it possesses two chemically unique reactive sites. These can be used for building-up bi- or trimetallic systems in sequential steps. Therefore, the C≡C unit of **1** can be attached to a transition metal (TM) complex fragment in two different binding modes: (i) either *via* σ-bonding or (ii) through η^2-coordination. Both approaches are presented herein. Furthermore, the Cl ligand of **1** can be substituted by, for example, σ-acetylides. This leads to the formation of linear heterometallic monoacetylides. This structural motif can be found in long-chain molecules, such as the hypothetical molecule **A** (Scheme 2), which offers a high degree of directionality along the acetylene-arene-metal vector.



A **B**

Scheme 2. Model of a long-chain molecule showing high directionality (**A**) and its repeating unit (**B**)

Molecule **A** can be considered as being built-up from repeating units of the di-ionic substructure **B**. Thus, the attachment of the C_2 unit present in **1** to a TM complex fragment, and the substitution of Cl by a σ-acetylide group leads to the transformation of **1** into the structural type **B** molecule. Such molecules can be envisioned as model compounds of **A**. With the synthesis of these complexes, the

[a] Lehrstuhl Anorganische Chemie der Technischen Universität, Straße der Nationen 62, D-09111 Chemnitz, Germany
E-mail: heinrich.lang@chemie.tu-chemnitz.de
[b] Debye Institute, Department of Metal-Mediated Synthesis, Utrecht University,
Padualaan 8, NL-3584 CH Utrecht, The Netherlands
E-mail: g.vankoten@chem.uu.nl

 © WILEY-VCH Verlag GmbH, D-69451 Weinheim, 2000 1434−1948/00/0707−1457 $ 17.50+.50/0

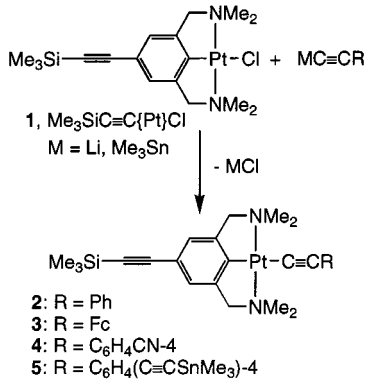
behaviour of the subunit **B** can be studied and evaluated towards its application in materials science.

Since Au is known to form very stable linear σ-acetylide complexes,[11] we choose to investigate the Ph_3PAu moiety as the terminating fragment on the 4-ethynyl unit. The formation of Pt monoacetylides containing the anionic potentially tridentate NCN "pincer" ligand (NCN = $[C_6H_3(CH_2NMe_2)_2$-2,6$]^-$) has been previously reported.[16]

Results and Discussion

Preparation of Platinum Acetylides

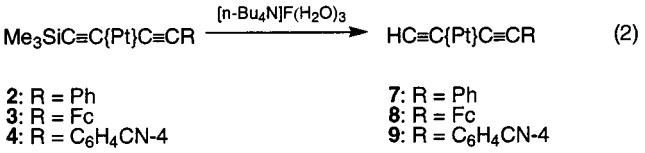
Reaction of the platinum monochloride $Me_3SiC{\equiv}C\{Pt\}Cl$ (**1**; $Me_3SiC{\equiv}C\{Pt\}$ = $[Pt(C_6H_2\{CH_2NMe_2\}_2$-2,6-$\{C{\equiv}CSiMe_3\}-4]^+$)[15] with an equimolar amount of $LiC{\equiv}CR$ {R = Ph, Fc [Fc = $(\eta^5$-$C_5H_4)Fe(\eta^5$-$C_5H_5)$], C_6H_4CN-4, $C_6H_4(C{\equiv}CSnMe_3)$-4} leads to the formation of the platinum acetylides **2**–**4** as air-stable, off-white solids (Equation 1). The rigid-rod like molecule **5** has been obtained by a procedure that uses a Me_3Sn-substituted acetylene.[17] Heterobimetallic **3** was synthesised alternatively by both routes. We tested this different approach because Cu^I catalysed reactions for the formation of Pt monoacetylides of this type have failed.[16]



(1)

The deprotection of the acetylenic unit of compounds **1**–**4** yields the mono-substituted acetylenes **7**–**9** (Equation 2).[15] The compound $HC{\equiv}C\{Pt\}Cl$ (**6**) has been described elsewhere.[15]

Analytic and spectroscopic data of compounds **1**–**9** are listed in Table 1. For comparison, the data of the previously reported Pt monochlorides **1** and **6** are included.[15]



(2)

Compounds **1**–**9** display the $\nu_{C\equiv C}$ frequencies of the acetylene units attached to the NCN system at the expected wavenumbers between 2090 and 2150 cm^{-1} in their IR spectra.[15,18] For the Pt σ-bound acetylenic units, the C≡C stretching band appears between 2070 and 2090 cm^{-1}, respectively (Table 1). These values lie in the range reported for this type of vibration.[4,16] In the ^1H NMR spectra of compounds **2**–**5** and **7**–**9**, a common general feature can be observed with respect to the chemical shift of the signals of the CH_2NMe_2 units. A comparison with the chloride-substituted Pt compounds **1** and **6** reveals that upon substitution of Cl by an acetylide, the singlet of the NMe_2 unit experiences a slight but diagnostic low-field shift, as does the resonance signal of the benzylic protons (Table 1). Both singlets appear with a set of satellites, due to the presence of spin active ^{195}Pt (I = 1/2, 33% abundance) with coupling constants ($^3J_{PtH}$) between 40 and 46 Hz (Table 1). Of particular interest in the $^{13}C\{^1H\}$ NMR spectra is the signal of the Pt-substituted carbon atom of the NCN system. Compared to its position in compound **1** (δ = 147.4) and **6** (δ = 147.6) this signal appears strongly shifted to lower field in the spectra of **2**–**5** and **7**–**9** (Table 1). The C_{ortho} resonance signal is also shifted to lower field (by around 3 ppm), when compared to **1** or **6**, respectively. This mirrors results obtained with the Pt monochloride $[PtCl(C_6H_3\{CH_2NMe_2\}_2$-2,6$)]$.[16] The carbon atoms of the

Table 1. Most representative IR, ^1H and ^{13}C $\{^1H\}$ NMR spectroscopic data of **1**–**9**

Compound $Me_3SiC{\equiv}C\{Pt\}X$ X =		IR[a]		^1H NMR ($^3J_{HH}$ [Hz])[b]		$^{13}C\{^1H\}$ NMR[b]			
		$\nu_{C\equiv C}$	$\nu_{C\equiv CPt}$	CH_3	CH_2	C_{ipso}(Pt)	$C_{ipso}(CH_2)$	$C{\equiv}CPt$	$C{\equiv}CPt$
Cl	**1**	2145	–	3.04(37)	3.96(46)	147.4	143.3	–	–
C≡CPh	**2**	2148	2077	3.18(42)	4.05(44)	169.0	145.9	108.2	135.8
C≡CFc	**3**	2144	2089	3.19(42)	4.04(40)	166.2	145.9	103.7	130.6
$C{\equiv}CC_6H_4CN$-4	**4**	2145	2071	3.19(41)	4.08(42)	168.3	145.9	107.4	133.6
$C{\equiv}CC_6H_4(C{\equiv}CSnMe_3)$-4	**5**	2148	2081	3.19(37)	4.07(39)	168.8	145.9	108.2	139.3
$HC{\equiv}C\{Pt\}X$									
Cl	**6**	2099	–	3.06(38)	3.98(45)	147.6	143.4	–	–
C≡CPh	**7**	2126	2083	3.21(43)	4.08(44)	169.1	146.0	108.2	131.1
C≡CFc	**8**	2090	2078	3.20(41)	4.07(40)	169.2	146.0	103.7	130.7
$C{\equiv}CC_6H_4CN$-4	**9**	2102	2083	3.20(40)	4.11(42)	168.4	146.0	107.7	133.6

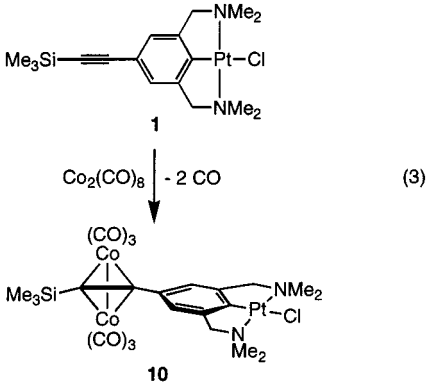
[a] Recorded in KBr [cm^{-1}]. – [b] All spectra were recorded in $CDCl_3$, with the solvent signal [rel. to $SiMe_4$ (0.00 ppm)] as internal standard.

Pt-bound acetylenic unit exhibit signals at chemical shifts that are comparable to those of other known Pt-acetylides.[4] Due to the low intensity of the C_{ipso} atom signals of the NCN unit [C(1)] and the platinum bonded acetylide ligands, ^{195}Pt-C satellites could not be detected.

The FAB mass spectra show the peak of the respective molecular ion M^+ at the expected *m/z* values as well as a typical fragmentation pattern such as *m/z* 481 $[C_{17}H_{28}N_2PtSi]^+$ or *m/z* 409 for $[C_{14}H_{19}N_2Pt]^+$.

Reactions of [4-Me$_3$SiC≡CC$_6$H$_2$(CH$_2$NMe$_2$)$_2$-2,6]PtCl (1) with Cobalt Carbonyl and Copper(I) Salts

The replacement of two CO ligands of $[Co_2(CO)_8]$ by the C_2 unit of acetylene derivatives leads to the formation of dicobaltatetrahedranes.[19] Hence, organometallic acetylides can readily yield mixed metal compounds. In order to study whether the same reactivity could be achieved with a {Pt}-substituted acetylene (i.e., with retention of the Pt−C and Pt−Cl bonds), **1** was reacted with equimolar amounts of $[Co_2(CO)_8]$ in toluene at 0 °C. This leads to the formation of the green trimetallic complex **10** in 50% isolated yield (Equation 3).

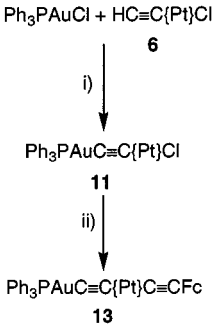


Compound **10** features a dicobaltatetrahedrane unit with the Pt-containing entity directly connected to this polyhedron. The values and pattern of the ν_{CO} frequencies resemble typical values found for $Co_2(CO)_6$ fragments.[19] The resonance signals in the ^{1}H NMR spectrum are generally slightly shifted to higher field, compared to **1**.[15] The $^{13}C\{^1H\}$ NMR spectrum displays virtually the same signal pattern as for **1**. However, the chemical shifts of the μ-C_2 unit with δ = 79.3 (C≡*C*Si) and δ = 107.6 (*C*≡CSi) experience a high-field shift of approximately 13 ppm for ≡*C*Si and a slight shift to lower field by ca. 1 ppm for *C*≡CSi. The signals assigned to the carbonyl ligands are found as a broad singlet at δ = 196.7. The FAB mass spectrum exhibits a peak for the molecular ion $[M]^+$ at *m/z* = 796. Also, the sequential loss of all six CO ligands can be observed.

The reaction of copper(I) halides with acetylene derivatives is well-known and generally yields dimeric η^2-acetylene copper(I) halides.[20] In order to investigate if the C≡C unit present in **1** can be used for the design of other bimetallic compounds, **1** has been reacted with $[CuCl]_n$ or $[Cu(NCMe)_4][BF_4]$. However, even after prolonged stirring (48 h) at low (−20 °C, CH_2Cl_2) or elevated temperatures (40−50 °C, C_6H_6), **1** did not react with $[CuCl]_n$. All spectroscopic evidence (IR, ^{1}H NMR, $^{13}C\{^1H\}$ NMR) indicated the presence of starting materials only. This mirrors results obtained earlier in a Cu^I−(Me$_3$SiC≡CPh) system.[21] This result contrasts with reports on the formation of complexes of the type $[Cu_2X_2(R'C{\equiv}CR')_2]$ [e.g. R′ = SiMe$_3$,[20] $Re(CO)_5$[22]]. In contrast to this lack of reactivity, the reaction of **1** with $[Cu(NCMe)_4][BF_4]$ led to a mixture of products that could not be separated. Moreover, the IR spectrum of the crude reaction mixture gave no indication for the occurrence of Cu^I-alkyne coordination.

Preparation of Linear Mixed Metal Compounds

Due to their stability and easy accessibility, Au^I acetylides have attracted a great deal of interest. Also, the preferred geometry and the electron-rich character of the Au^I centre makes this class of compounds attractive candidates for materials science.[11] In principle, the preparation of Au^I acetylides can be achieved by two routes: i) first a silyl-protected Pt acetylide is prepared, followed by deprotection of the C≡C functionality, and subsequent reaction of the monosubstituted acetylene with Ph_3PAuCl, or ii) treatment of HC≡C{Pt}Cl (**4**) with Ph_3PAuCl and then substitution of Cl by acetylide anions. The first route seemed to us being of little advantage because the platinum monoacetylides of this type have been reported to be sensitive to halide sources, i.e., giving rise to cleavage of the Pt-acetylide bond.[16] Therefore, the Au σ-acetylide complex **11** was synthesised first, according to well-established literature procedures (Scheme 3).[23] For comparative purposes, the gold-ferrocenyl acetylide complex $Ph_3PAuC{\equiv}CFc$ (**12**) was also prepared.



Scheme 3. Preparation of linear mixed metal (Au, Fe) complexes. i. $[CuCl]_n$, $HNEt_2$, 25 °C; ii. FcC≡CSnMe$_3$, THF, 50 °C.

Subsequently, complex **11** was reacted with FcC≡CSnMe$_3$ to form linear trimetallic **13** in virtually quantitative yield (Scheme 3). This reaction variation has been previously used in the synthesis of compound **5** (vide supra).

Experimental data with respect to the spectroscopic characterisation of complexes **11**−**13** are listed in Table 2.

The IR spectra of compounds **11**−**13** exhibit the C≡C stretching modes for the Au-bonded acetylide at typical values (Table 2).[23] The corresponding band for the Pt-bonded acetylide appears at much lower frequency than ob-

Table 2. Most diagnostic spectroscopic data (IR, $^{31}P\{^1H\}$ and $^{13}C\{^1H\}$ NMR) of **11**−**13**

Compound Ph_3PAuX X =		IR[a] C≡CAu	C≡CPt	$^{31}P\{^1H\}$ NMR[b] PPh_3	$^{13}C\{^1H\}$ NMR[b] C≡CAu
Cl		–	–	33.8	–
C≡C{Pt}Cl	**11**	2102	–	43.1	105.4, 105.7
C≡CFc	**12**	2109	–	42.9	102.5[c]
C≡C{Pt}C≡CFc	**13**	2098	1971	43.1	–[d]

[a] Recorded in KBr ($\tilde{\nu}$ [cm^{-1}]). – [b] All spectra were recorded in $CDCl_3$ with the solvent signal [rel. to $SiMe_4$ (0.00 ppm)] as internal standard. – [c] Only one signal could be detected. – [d] Due to the low solubility of **13** in any organic solvent, a $^{13}C\{^1H\}$ NMR spectrum could not be recorded.

served in compounds **2**−**5** (around 2070 cm^{-1}, Table 1). This points to a bond weakening of the Pt-centred C≡C unit, which is obviously caused by the remote presence of the Ph_3PAu fragment. The ^1H NMR spectra exhibit no change in the chemical shifts of the C≡C{Pt} fragment compared to **1** (Table 1). In the ^1H NMR spectrum of **13**, however, the resonance signals of the {Pt} unit only appear as very broad singlets. In the $^{13}C\{^1H\}$ NMR spectra of compounds **11** and **12**, the acetylenic carbon resonance signals are found at chemical shifts that are typical for gold acetylides.[11,23] Due to the low solubility of **13** in all common organic solvents, a $^{13}C\{^1H\}$ NMR spectrum could not be obtained. Compared with Ph_3PAuCl (δ = 33.8), the signal for the phosphorus atom datively bonded to Au has shifted by about 10 ppm to lower field when Cl is substituted by an acetylide anion (**11**−**13**, Table 2). This shift is characteristic for Au^I acetylides carrying organic groups and indicates that the presence of a remote Pt atom does not influence the behaviour of the $AuPPh_3$ unit in a spectroscopically noticeable manner. The FAB mass spectrum reveals the peak for the molecular ion $[M]^+$ at the expected *m*/*z* values, together with an expected fragmentation pattern. Most characteristic fragments are found at *m*/*z* = 459 $[C_{18}H_{15}AuP]^+$, *m*/*z* = 409 $[C_{14}H_{18}N_2Pt]^+$ and *m*/*z* = 210 $[C_{12}H_9Fe]^+$.

At −30 °C, crystals of the bimetallic complex **11** could be grown from a CH_2Cl_2/pentane solution. Unfortunately, these crystals were not of sufficient quality to obtain a full X-ray structural analysis (*R* = 0.1544). Nevertheless, the representation given in Figure 1 serves to corroborate the predicted linear arrangement of the metal centres in the heterobimetallic complex **11**.

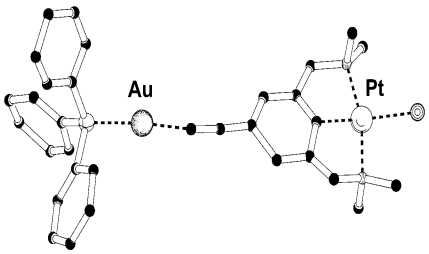


Figure 1. Structural representation of the heterobimetallic complex **11**

Electrochemical Behaviour

The mononuclear complex $Me_3SiC{\equiv}C\{Pt\}Cl$ (**1**), the heterobinuclear molecules **3**, **11**, and **12**, as well as the heterotrinuclear compound **13** have been investigated by cyclic voltammetry. The results of the electrochemical measurements are listed in Table 3. For comparative purposes, the electrochemical data of Ph_3PAuCl have been measured and these are also presented.

It appears that the reductive irreversible one-electron process for the system Au^I/Au^0 is generally shifted to a more negative potential upon substitution of the Cl ligand by acetylide (Table 3). However, the strength of the shift depends on the nature of the organometallic fragment. While for the NCN−Pt substituted acetylide a shift by approximately 0.2 V is found, the same effect for C≡CFc is larger (ca. 0.4 V). This indicates that the reduction of Au^I to Au^0 is more hampered by the presence of a Fc fragment than by the NCN−Pt unit. However, in the cyclic voltammetric experiment with the heterotrimetallic complex **13**, the Au-centred reductive process could not be detected due to the low solubility of **13** and the proximity of the edge of the electrochemical window in this system. This may also be explained by a shift of the Au^I/Au^0 reduction potential beyond this electrochemical edge. The cyclic voltammogram of **1** exhibits a concerted irreversible two-electron oxidative process that can be assigned to the system Pt^{II}/Pt^{IV}. This process is typical for Pt monochlorides of this type.[16] Upon substitution of the Cl by acetylide, as demonstrated in $Me_3SiC{\equiv}C\{Pt\}C{\equiv}CFc$ (**3**), a similar effect can be observed as in the Au^I-centred reductive process: a shift to a more negative value of the Pt^{II}/Pt^{IV} oxidation potential by ca. 0.4 V. A similar observation has been reported earlier for $PtCl[C_6H_3(CH_2NMe_2)_2$-2,6].[16] In this case, a shift of the Pt^{II}/Pt^{IV} oxidation to a more negative potential by ca. 0.2 V was reported when Cl was replaced by, e.g. $C{\equiv}CSiMe_3$. Surprisingly, the Pt-containing unit of the complexes described in the present study shows no reduction process at all. The attachment of the C≡C{Pt}Cl fragment to Ph_3PAu also leads to a shift of the Pt^{II}/Pt^{IV} oxidation to a more negative potential. As in the case of the Pt−Fc complex **3**, this indicates a facilitation of the oxidative process (Table 3). In the heterotrimetallic complex **13**, this process is shifted to a more negative value than in the bimetallic compound **11** (Table 3) but less than in complex

Table 3. Cyclic voltammetric data of compounds **11**−**13**, Ph_3PAuCl and **1** are presented for comparison; the cyclic voltammograms have been recorded in THF solutions in the presence of $[n-Bu_4N][PF_6]$ (c = 0.1 mol dm^{-3}) at 25 °C under N_2; scan-rate 100 mV s^{-1}; potentials are referenced to FcH/FcH^+ couple ($E_{1/2}$ = 0.00 V)

Compound		Oxidation $E_{1/2}$(Fc) [V]	ΔE [mV]	E_{ox}(Pt) [V]	Reduction E_{red}(Au) [V]	E_{red}(Pt) [V]
Ph_3PAuCl		−	−	−	−2.70	−
$Me_3SiC{\equiv}C\{Pt\}Cl$	**1**	−	−	0.76	−	−
$Me_3SiC{\equiv}C\{Pt\}C{\equiv}CFc$	**3**	−0.13	75	0.38	−	−
$Ph_3PAuC{\equiv}C\{Pt\}Cl$	**11**	−	−	0.53	−2.91	−
$Ph_3PAuC{\equiv}CFc$	**12**	−0.15	80	−	−3.12	−
$Ph_3PAuC{\equiv}C\{Pt\}C{\equiv}CFc$	**13**	−0.02	90	0.41	−[a]	−

[a] Due to low solubility of **13** and the proximity of the reductive process Au^I/Au^0 to the edge of the electrochemical window, a reductive process could not be observed.

3. Looking at the reversible one-electron redox process of the Fc entity, the attachment of C≡CFc to Ph_3PAu or $Me_3SiC{\equiv}C\{Pt\}$ also results in a shift to a more negative potential, with about equal magnitude. Still, the assembly of these three fragments to form complex **13** does not result in changes to the redox potential of the Fc unit with respect to the reference potential FcH/FcH^+.

It can be concluded that the stepwise increase of size and composition of the organometallic systems in the described complexes **3**−**12** induces a facilitation of the oxidative processes in each of the metal-containing subunits. This indicates that the linking of further organometallic fragments to the 4-ethynyl-substituted Pt−NCN system induces a change in the electronic system of the Pt^{II} centre. The fact that this is also induced by the remote Ph_3PAu unit suggests that the extended π-system of the $-C{\equiv}CC_6H_2(CH_2NMe_2)_2$-2,6-$Pt^+$ fragment, which also includes the coplanar coordination plane of the Pt^{II} centre, is able to conduct electronic information.

Conclusions

A series of Pt monoacetylides containing the 4-ethynyl-substituted NCN−Pt unit has been synthesised and characterised. Their use as the basis for the preparation of multimetallic systems has been shown by the assembly of $Ph_3PAuC{\equiv}C\{Pt\}C{\equiv}CFc$, **13**. Apart from the use of Li-acetylides, Me_3Sn-substituted acetylenes have been applied to the high-yield synthesis of Pt monoacetylides. The C≡C unit of $Me_3SiC{\equiv}C\{Pt\}Cl$ (**1**) can act as an η^2-coordinating ligand, as was shown by the formation of a characteristically green-coloured dicobaltatetrahedrane complex by reaction of **1** with $Co_2(CO)_8$. Electrochemical studies of these heterometallic systems revealed that the reversible oxidation of the Fc units in complexes $Me_3SiC{\equiv}C\{Pt\}C{\equiv}CFc$ (**3**) and $PPh_3AuC{\equiv}C\{Pt\}C{\equiv}CFc$ (**13**), and the irreversible Pt^{II}/Pt^{IV} oxidation are both facilitated. On the basis of these results we conclude, that the 4-ethynyl NCN unit supports electronic communication between two metal atoms through the conjugated π-system. Further work will be directed towards the construction of longer chains of repeating C≡C{Pt} units with high directionality approximating an organometallic polymer as suggested in type **A** complexes (vide supra) in a stepwise approach.

Experimental Section

General: All reactions were carried out under an atmosphere of dry nitrogen using standard Schlenk techniques. Tetrahydrofuran (THF) and diethyl ether (Et_2O) were purified by distillation from sodium/benzophenone ketyl; pentane was purified by distillation from CaH_2. − IR: Mattison Galaxy Series FTIR 5000. − NMR: Bruker AC 300 (^1H, ^{31}P, and ^{13}C); chemical shifts are reported in δ units (parts per million) downfield from tetramethylsilane with the solvent as the internal reference signal. − FAB-MS: JEOL JMS SX/SX 102A four sector mass spectrometer (10 kV accelerating voltage) at the Department of Mass Spectrometry, Bijvoet Center, Utrecht University. − MP: Büchi melting point apparatus. − Elemental analyses: H. Kolbe, Mikroanalytisches Laboratorium, Mülheim/Ruhr, Germany. − CV: Princeton Applied Research EG& G 263A analyser in a solution of $[n-Bu_4N][PF_6]$ (c = 0.1 mol dm^{-3}) in THF at 25 °C; all potentials were referenced to the ferrocene/ferrocenium couple as internal reference ($E_{1/2}$ = 0.00 V).

Remarks: The starting materials $Me_3SiC{\equiv}C\{Pt\}Cl$ (**1**),[15] $HC{\equiv}C\{Pt\}Cl$ (**6**),[15] $HC{\equiv}CC_6H_4CN$-4,[24] 1,4-$(Me_3SnC{\equiv}C)_2C_6H_4$,[25] $HC{\equiv}CFc$,[26] Ph_3PAuCl,[23] and $Me_3SnC{\equiv}CFc$[25] were prepared following published procedures. Other reagents were purchased from commercial suppliers.

Synthesis of $Me_3SiC{\equiv}C\{Pt\}C{\equiv}CPh$ (2): To a Et_2O solution (150 mL, −78 °C) of $LiC{\equiv}CPh$ (190 mg, 1.80 mmol) was added **1** (880 mg, 1.70 mmol). The mixture was allowed to warm up (25 °C) and stirred (16 h, 25 °C). All volatile material was then evaporated in vacuo and the residue was extracted with Et_2O (3 × 50 mL) and CH_2Cl_2 (3 × 40 mL). Separation from the solid residue was effected by centrifugation. The combined CH_2Cl_2 fractions were then concentrated to ca. 5 mL and addition of pentane (50 mL) yielded **2** (580 mg, 60% yield based on **1**) as off-white solid; m.p. > 200 °C. − IR (KBr): $\tilde{\nu}$ = 2148 [$\nu_{C{\equiv}C}$], 2077 [$\nu_{C{\equiv}C}$] cm^{-1}. − ^1H NMR ($CDCl_3$): δ = 0.21 (s, 9 H, SiMe_3), 3.18 s, $^3J_{HPt}$ = 42 Hz, NMe_2), 4.05 (s, $^3J_{HPt}$ = 44 Hz, 4 H, CH_2), 7.01 (s, 2 H, C_6H_2), 7.1−7.5 (m, 5 H, C_6H_5). − $^{13}C\{^1H\}$ NMR ($CDCl_3$): δ = 0.1 (SiMe_3), 55.9 (NMe_2), 79.5 (CH_2), 91.8 (Si$C{\equiv}C$), 107.2 (Si$C{\equiv}C$), 108.2 (Pt$C{\equiv}C$), 117.4 (iC/C_6H_2), 122.4 (CH/C_6H_2), 124.8 (CH/C_6H_5), 127.8 (CH/C_6H_5), 128.5 (iC/C_6H_5), 131.6 (CH/C_6H_5), 135.8 (Pt$C{\equiv}C$), 145.9 (iC/C_6H_2), 169.0 (iC/C_6H_2). − FAB-MS; m/z (rel. int.): 583 (30) [M^+], 482 (100) [$M^+ - C_8H_5$]. − $C_{25}H_{32}N_2PtSi$ (583.73): calcd. C 51.44, H 5.53, N 4.80; found C 51.32, H 5.55, N 4.73.

Synthesis of $Me_3SiC{\equiv}C\{Pt\}C{\equiv}CFc$ (3): Experimental conditions and workup were identical to those for the preparation of **2**. Experimental details: $LiC{\equiv}CFc$ (170 mg, 0.80 mmol), **1** (400 mg, 0.77 mmol), Et_2O (100 mL). Yield: 330 mg, 60% based on **1**. − Mp:

> 200 °C. − IR (KBr): $\tilde{\nu}$ = 2144 [$\nu_{C\equiv C}$], 2089 [$\nu_{C\equiv C}$] cm^{-1}. − ^1H NMR ($CDCl_3$): δ = 0.22 (s, 9 H, Si*Me*$_3$), 3.19 (s, $^3J_{HPt}$ = 42 Hz, 12 H, N*Me*$_2$), 4.04 (br s, 2 H, C_5H_4), 4.04 (s, $^3J_{HPt}$ = 40 Hz, 4 H, CH_2), 4.15 (s, 5 H, C_5H_5), 4.36 (br s, 2 H, C_5H_4), 7.01 (s, 2 H, C_6H_2). − $^{13}C\{^1H\}$ NMR ($CDCl_3$): δ = 0.1 (Si*Me*$_3$), 55.9 (N*Me*$_2$), 66.9 (*CH*/C_5H_4), 69.4 (C_5H_5), 70.0 (*iC*/C_5H_4), 70.9 (*CH*/C_5H_4), 79.5 (CH_2), 90.9 (Si*C*≡C), 103.7 (PtC≡*C*), 107.2 (SiC≡*C*), 117.3 (*iC*/C_6H_2), 122.4 (*CH*/C_6H_2), 130.6 (Pt*C*≡C), 145.9 (*iC*/C_6H_2), 166.2 (*iC*/C_6H_2). − FAB-MS; *m*/*z* (rel. int.): 692 (20) [M^+], 481 (100) [$M^+ - C_{12}H_9Fe$]. − $C_{29}H_{36}FeN_2PtSi$ (691.95): calcd. C 50.36, H 5.25, N 3.71; found C 50.48, H 5.23, N 3.97.

Synthesis of Me$_3$SiC≡C{Pt}C≡CC$_6$H$_4$CN-4 (4): Experimental conditions and workup were identical to those for the preparation of **2**. Experimental details: LiC≡CC$_6$H$_4$CN-4 (100 mg, 0.80 mmol), **1** (390 mg, 0.76 mmol), Et_2O (100 mL). Yield: 200 mg, 40% based on **1**. − Mp: > 200 °C. − IR (KBr): $\tilde{\nu}$ = 2220 [ν_{CN}], 2144 [$\nu_{C\equiv C}$], 2089 [$\nu_{C\equiv C}$] cm^{-1}. − ^1H NMR ($CDCl_3$): δ = 0.22 (s, 9 H, Si*Me*$_3$), 3.19 (s, $^3J_{HPt}$ = 41 Hz, 12 H, N*Me*$_2$), 4.08 (s, $^3J_{HPt}$ = 42 Hz, 4 H, CH_2), 7.03 (s, 2 H, C_6H_2), 7.3−7.5 (m, 4 H, C_6H_4). − $^{13}C\{^1H\}$ NMR ($CDCl_3$): δ = 0.1 (Si*Me*$_3$), 55.9 (N*Me*$_2$), 79.5 (CH_2), 92.1 (Si*C*≡C), 106.9 (SiC≡*C*), 107.4 (PtC≡*C*), 107.7 (*C*N), 117.9 (*iC*/C_6H_2), 119.7 (*iC*/C_6H_4), 122.5 (*CH*/C_6H_2), 131.5 (*iC*/C_6H_4), 131.6 (*CH*/C_6H_4), 131.9 (*CH*/C_6H_4), 133.6 (Pt*C*≡C), 145.9 (*iC*/C_6H_2), 168.3 (*iC*/C_6H_2). − FAB-MS: *m*/*z* (rel. int.): 608 (10) [M^+], 481 (100) [$C_{17}H_{27}N_2PtSi]^+$. − $C_{26}H_{31}N_3PtSi$ (608.74): calcd. C 51.30, H 5.13, N 6.90. A satisfactory elemental analysis could not be obtained.

Synthesis of Me$_3$SiC≡C{Pt}C≡CC$_6$H$_4$(C≡CSnMe$_3$)-4 (5): Compound **1** (50 mg, 0.10 mmol) and 1,4-(Me$_3$SnC≡C)$_2$C$_6$H$_4$ (90 mg, 0.20 mmol) were dissolved in THF (40 mL). The solution was stirred (10 h, 25 °C) and then concentrated to ca. 5 mL. Addition of pentane (50 mL) formed a precipitate that was separated from the supernatant solution. The residue was then dried (5 h, *vacuo*). **Note: Me$_3$SnCl is volatile and very toxic. An extra cooling trap has to be installed right after the reaction vessel.** Complex **5** (60 mg, 80% based on **1**) was obtained as off-white solid. − Mp: > 200 °C. − IR (KBr): $\tilde{\nu}$ = 2148 [$\nu_{C\equiv C}$], 2132 [$\nu_{C\equiv C}$], 2089 [$\nu_{C\equiv C}$] cm^{-1}. − ^1H NMR ($CDCl_3$): δ = 0.22 (s, 9 H, Si*Me*$_3$), 0.34 (s, $^3J_{HSn}$ = 59.8 Hz, 9 H, $SnMe_3$), 3.19 (s, $^3J_{HPt}$ = 37 Hz, 12 H, N*Me*$_2$), 4.07 (s, $^3J_{HPt}$ = 40 Hz, 4 H, CH_2), 7.02 (s, 2 H, C_6H_2), 7.29 (s, 4 H, C_6H_4). − $^{13}C\{^1H\}$ NMR ($CDCl_3$): δ = −7.7 ($SnMe_3$), 0.1 (Si*Me*$_3$), 55.9 (N*Me*$_2$), 79.5 (CH_2), 91.8 (Si*C*≡C), 93.2 (Sn*C*≡C), 107.3 (SiC≡*C*), 108.2 (PtC≡*C*), 109.7 (SnC≡*C*), 117.5 (*iC*/C_6H_2), 122.4 (*CH*/C_6H_2), 131.1 (*iC*/C_6H_4), 131.4 (*CH*/C_6H_4), 131.5 (*CH*/C_6H_4), 131.7 (*iC*/C_6H_4), 139.3 (Pt*C*≡C), 145.9 (*iC*/C_6H_2), 168.8 (*iC*/C_6H_2). − FAB-MS; *m*/*z* (rel. int.): 770 (10) [M^+], 607 (20) [$M - SnMe_3]^+$, 481 (100) [$C_{17}H_{27}N_2PtSi]^+$, 73 [$C_3H_9Si]^+$. − $C_{30}H_{40}N_2PtSiSn$ (770.53): calcd. C 46.76, H 5.23, N 3.64; found C 47.01, H 5.01, N 3.32.

Synthesis of HC≡C{Pt}C≡CPh (7): To a solution of **2** (400 mg, 0.76 mmol) in CH_2Cl_2 (100 mL), was added [*n*Bu$_4$N]F·3H$_2$O (240 mg, 0.76 mmol). After stirring (2 h, 25 °C), all volatile material was evaporated and the residue was extracted with acetone (2 × 10 mL). Separation by centrifugation and drying (*vacuo*) yielded **5** (190 mg, 50%) as a brown solid. − Mp: > 200 °C. − IR (KBr): $\tilde{\nu}$ = 3302 [$\nu_{\equiv CH}$], 2126 [$\nu_{C\equiv C}$], 2083 [$\nu_{C\equiv C}$] cm^{-1}. − ^1H NMR ($CDCl_3$): δ = 3.01 (s, 1 H, ≡C*H*), 3.21 (s, $^3J_{HPt}$ = 43.4 Hz, N*Me*$_2$), 4.08 (s, $^3J_{HPt}$ = 44 Hz, 4 H, CH_2), 7.04 (s, 2 H, C_6H_2), 7.2−7.5 (m, 5 H, C_6H_5). − $^{13}C\{^1H\}$ NMR ($CDCl_3$): δ = 55.9 (N*Me*$_2$), 75.0 (≡*C*H), 79.6 (*C*H$_2$), 85.6 (*C*≡CH), 108.2 (PtC≡*C*)[a] , 116.4 (*iC*/C_6H_2), 122.5 (*CH*/C_6H_2), 124.6 (*CH*/C_6H_5), 127.8 (*CH*/C_6H_5), 128.5 (*iC*/C_6H_5), 131.6 (*CH*/C_6H_5), 131.1 (Pt*C*≡C), 146.0 (*iC*/C_6H_2), 169.1 (*iC*/C_6H_2). − FAB-MS; *m*/*z* (rel. int.): 512 (20) [M^+], 409 (100) [$M^+ - C_8H_5$]. − $C_{22}H_{24}N_2Pt$ (511.54): calcd. C 51.66, H 4.73, N 5.48; found C 51.78, H 4.72, N 5.36.

Synthesis of HC≡C{Pt}C≡CFc (8): Experimental conditions and workup were identical to those for the preparation of **5**. Experimental details: **3** (760 mg, 1.08 mmol), [*n*Bu$_4$N]F·3H$_2$O (340 mg, 1.08 mmol), CH_2Cl_2 (30 mL). Yield: 330 mg, 60% based on **3**. − Mp: > 200 °C. − IR (KBr): $\tilde{\nu}$ = 3272 [$\nu_{\equiv CH}$], 2090 [$\nu_{C\equiv C}$], 2078 [$\nu_{C\equiv C}$] cm^{-1}. − ^1H NMR ($CDCl_3$): δ = 3.01 (s, 1 H, ≡C*H*), 3.20 (s, $^3J_{HPt}$ = 41 Hz, 12 H, N*Me*$_2$), 4.04 (t, $^3J_{HH}$ = 1.4 Hz, 2 H, C_5H_4), 4.07 (s, $^3J_{HPt}$ = 40 Hz, 4 H, CH_2), 4.15 (s, 5 H, C_5H_5), 4.36 (t, $^3J_{HH}$ = 1.4 Hz, C_5H_4), 7.02 (s, 2 H, C_6H_2). − $^{13}C\{^1H\}$ NMR ($CDCl_3$): δ = 55.9 (N*Me*$_2$), 66.9 (*CH*/C_5H_4), 69.4 (C_5H_5), 70.1 (*iC*/C_5H_4), 75.0 (*C*≡CH), 77.2 (C≡*C*H), 79.2 (*C*H$_2$), 103.7 (PtC≡*C*), 116.2 (*iC*/C_6H_2), 122.5 (*CH*/C_6H_2), 130.7 (Pt*C*≡C), 146.0 (*iC*/C_6H_2), 169.2 (*iC*/C_6H_2). − FAB-MS; *m*/*z* (rel. int.): 619 (10) [M^+], 409 (60) [$M^+ - C_{12}H_9Fe$], 210 (10) [$C_{12}H_9Fe]^+$. − $C_{26}H_{28}FeN_2Pt$ (619.46): calcd. C 50.41, H 4.56, N 4.52; found C 50.28, H 4.51, N 4.46.

Synthesis of HC≡C{Pt}C≡CC$_6$H$_4$CN-4 (9): Experimental conditions and workup were identical to those for compound **7**. Experimental details: **4** (260 mg, 0.51 mmol), [*n*Bu$_4$N]F·3H$_2$O (160 mg, 0.51 mmol), CH_2Cl_2 (30 mL). Yield: 100 mg, 40% based on **4**. − Mp: > 200 °C. − IR (KBr): $\tilde{\nu}$ = 3302 [$\nu_{\equiv CH}$], 2220 [ν_{CN}], 2102 [$\nu_{C\equiv C}$], 2083 [$\nu_{C\equiv C}$] cm^{-1}. − ^1H NMR ($CDCl_3$): δ = 3.01 (s, 1 H, ≡C*H*), 3.20 (s, $^3J_{HPt}$ = 39 Hz, 12 H, N*Me*$_2$), 4.11 (s, $^3J_{HPt}$ = 40 Hz, 4 H, CH_2), 7.05 (s, 2 H, C_6H_2), 7.3−7.5 (m, 4 H, C_6H_4). − $^{13}C\{^1H\}$ NMR ($CDCl_3$): δ = 55.9 (N*Me*$_2$), 75.3 (≡*C*H), 79.5 (s, $^3J_{CPt}$ = 38 Hz, *C*H$_2$), 85.4 (*C*≡CH), 107.4 (*C*N), 107.7 (PtC≡*C*), 116.8 (*iC*/C_6H_2), 119.7 (*iC*/C_6H_4), 122.6 (*CH*/C_6H_2), 131.7 (*CH*/C_6H_4), 132.2 (*CH*/C_6H_4), 133.6 (Pt*C*≡C), 146.0 (s, $^3J_{CPt}$ = 35.9 Hz, *iC*/C_6H_2), 168.4 (*iC*/C_6H_2). − FAB-MS; *m*/*z* (rel. int.): 536 (10) [M^+], 409 (60) [$C_{14}H_{19}N_2Pt]^+$. − $C_{23}H_{23}N_3Pt$ (536.55): calcd. C 51.49, H 4.32, N 7.83; found C 51.32, H 4.40, N 7.69.

Synthesis of [μ-(Me$_3$SiC≡C{Pt}Cl)][Co$_2$(CO)$_6$] (10): To a toluene solution (100 mL) of **1** (200 mg, 0.39 mmol), was added $Co_2(CO)_8$ (140 mg, 0.43 mmol) in one portion. After stirring (3 h, 25 °C), the solvent was reduced to ca. 10 mL and pentane (100 mL) was added. The supernatant solution was carefully decanted and the green precipitate redissolved in toluene (5 mL). Crystallisation at − 20 °C yielded **10** (140 mg, 50% based on **1**) as a green solid. − Mp: 140 °C (dec). − IR (KBr): $\tilde{\nu}$ = 2087, 2035, 2015, 1990 [ν_{CO}] cm^{-1}. − ^1H NMR ($CDCl_3$): δ = 0.40 (s, 9 H, Si*Me*$_3$), 3.11 (s, $^3J_{HPt}$ = 32 Hz, 12 H, N*Me*$_2$), 4.06 (s, $^3J_{HPt}$ = 42 Hz, 4 H, CH_2), 6.96 (s, 2 H, C_6H_2). − $^{13}C\{^1H\}$ NMR ($CDCl_3$): δ = 0.9 (Si*Me*$_3$), 54.5 (N*Me*$_2$), 79.3 (C≡*C*Si), 107.6 (*C*≡CSi), 121.0 (*CH*/C_6H_2), 132.7 (*iC*/C_6H_2), 143.2 (*iC*/C_6H_2), 147.0 (*iC*/C_6H_2), 201−204 (CO). − FAB-MS; *m*/*z* (rel. int.): 796 (20) [M^+], 768 (25) [M^+ − CO], 740 (30) [M^+ − 2 CO], 712 (20) [M^+ − 3 CO], 684 (10) [M^+ − 4 CO], 656 (20) [M^+ − 5 CO], 628 (20) [M^+ − 6 CO], 481 (100) [$C_{16}H_{27}N_2PtSi]^+$. − $C_{22}H_{27}ClCo_2N_2O_6PtSi$ (791.96): calcd. C 33.37, H 3.44, N 3.54; Si 3.55; found C 33.45, H 3.36, N 3.46; Si 3.59.

Reaction of 1 with [CuCl]$_n$. − Method A: $[CuCl]_n$ (20 mg, 0.20 mmol) and **1** (50 mg, 0.10 mmol) are stirred in C_6H_6 (30 mL, 48 h, 50 °C). − **Method B:** $[CuCl]_n$ (10 mg, 0.10 mmol) and **1** (30 mg, 0.6 mmol) are stirred in CH_2Cl_2 (30 mL, 24 h, − 20 °C).

In both cases, after removal of the solvent (in vacuo), the spectroscopic investigation (IR, ^1H NMR, $^{13}C\{^1H\}$ NMR) of the crude residue revealed the presence solely of **1**.

Reaction of 1 with [Cu(NCMe)$_4$][BF$_4$]: Compound **1** (100 mg, 0.19 mmol) and $[Cu(NCMe)_4][BF_4]$ (30 mg, 0.10 mmol) are dis-

solved in CH_2Cl_2 (30 mL]. During the course of the reaction, the solution gradually turns brown. After stirring (24 h, 25 °C),the solvent is removed (in vacuo). Spectroscopic investigation (IR, ^1H NMR, ^{13}C $\{^1H\}$ NMR) of the residue showed that a complicated mixture of compounds had been formed.

Synthesis of $Ph_3PAuC{\equiv}C\{Pt\}Cl$ (11): Compound **6** (127 mg, 0.30 mmol), Ph_3PAuCl (140 mg, 0.30 mmol) and $[CuCl]_n$ (8 mg, 0.08 mmol) were dissolved in degassed $HNEt_2$ (30 mL). After stirring (12 h, 25 °C) and evaporation (in vacuo), the residue was extracted with water (3 × 10 mL) and then with C_6H_6 (3 × 20 mL). The combined C_6H_6 extracts were evaporated and redissolved in CH_2Cl_2. The CH_2Cl_2 solution was dried over $MgSO_4$, filtered and evaporated (in vacuo). Complex **11** (170 mg, 60% based on **6**) was obtained as an off-white solid. − Mp: > 200 °C. − IR (KBr): $\tilde{\nu}$ = 2102 [$\nu_{C\equiv C}$] cm^{-1}. − ^1H NMR ($CDCl_3$): δ = 3.05 (s, $^3J_{HPt}$ = 37.8 Hz, 12 H, N*Me*$_2$), 4.09 (s, $^3J_{HPt}$ = 44 Hz, 4 H, C*H*$_2$), 6.92 (s, 2 H, C_6H_2), 7.3−7.6 (m, 15 H, C_6H_5). − $^{13}C\{^1H\}$ NMR ($CDCl_3$): δ = 54.4 (N*Me*$_2$) 77.6 (*C*H$_2$), 105.4 (C≡C), 105.7 (C≡C), 119.4 (*iC*/C_6H_2), 123.2 (s, $^3J_{PtC}$ = 33 Hz, *CH*/C_6H_2), 129.1 (d, $^3J_{PH}$ = 11 Hz, *CH*/C_6H_5), 129.8 (d, $^1J_{PH}$ = 63 Hz, *iC*/C_6H_5), 131.5 (*CH*/C_6H_5), 134.3 (d, $^2J_{PH}$ = 14 Hz, *CH*/C_6H_5) 142.9 (s, $^2J_{PtC}$ = 76 Hz, *iC*/C_6H_2), 144.8 (*iC*/C_6H_2). − ^{31}P $\{^1H\}$ NMR ($CDCl_3$): δ =43.1 (PPh_3). − FAB-MS; *m*/*z* (rel. int.): 904 (10) $[M]^+$, 868 (60) $[M - Cl]^+$, 459 (100) $[C_{18}H_{15}AuP]^+$, 401 (20) $[C_{14}H_{18}N_2Pt]^+$. − $C_{34}H_{33}AuClFeN_2PPt$ (928.17): calcd. C 42.51, H 3.68, N 3.10; found C 42.45, H 3.74, N 3.12.

Synthesis of $Ph_3PAuC{\equiv}CFc$ (12): Ph_3PAuCl (100 mg, 0.21 mmol), $FcC{\equiv}CH$ (50 mg, 0.24 mmol) and K_2CO_3 (100 mg) were dissolved in MeOH (40 mL). After stirring (12 h, 25 °C), the reaction mixture was evaporated (in vacuo). The orange residue was extracted with Et_2O (2 × 20 mL) and CH_2Cl_2 (2 × 10 mL). The combined CH_2Cl_2 extracts were concentrated to ca. 5 mL and pentane (30 mL) was added. The supernatant solution was decanted. After drying (in vacuo), **12** (120 mg, 90% based on Ph_3PAuCl) was obtained as an orange solid. − Mp: 141 °C. − IR (KBr): $\tilde{\nu}$ = 2109 [$\nu_{C\equiv C}$] cm^{-1}. − ^1H NMR ($CDCl_3$): δ = 4.11 (t, $^3J_{HH}$ = 3.6 Hz, 2 H, C_5H_4), 4.22 (s, 5 H, C_5H_5), 4.44 (t, $^3J_{HH}$ = 1.4 Hz, C_5H_4), 7.4−7.6 (m, 15 H, C_6H_5). − $^{13}C\{^1H\}$ NMR ($CDCl_3$): δ = 67.8 (*CH*/C_5H_4), 68.7 (*iC*/C_5H_4), 70.0 (C_5H_5), 102.5 (C≡C), 129.1 (d, $^3J_{PH}$ = 11 Hz, *CH*/C_6H_5), 129.9 (d, $^1J_{PH}$ = 63 Hz, *iC*/C_6H_5), 131.5 (*CH*/C_6H_5), 134.3 (d, $^2J_{PH}$ = 14 Hz, *CH*/C_6H_5). − ^{31}P $\{^1H\}$ NMR ($CDCl_3$): δ = 42.9 (PPh_3). − FAB-MS; *m*/*z* (rel. int.): 668 (90) $[M]^+$, 459 (100) $[C_{18}H_{15}AuP]^+$, 210 (10) $[C_{12}H_9Fe]^+$. − $C_{30}H_{24}AuFeP$ (668.35): calcd. C 53.91, H 3.62; found C 53.82, H 3.51.

Synthesis of $Ph_3PAuC{\equiv}C\{Pt\}C{\equiv}CFc$ (13): Compound **11** (120 mg, 0.13 mmol) and $FcC{\equiv}CSnMe_3$ (75 mg, 0.20 mmol) were dissolved in THF (20 mL). After stirring (6 h, 50 °C), the solution was concentrated to ca. 5 mL and Et_2O (40 mL) was added. The supernatant solution was decanted from the precipitate that had formed. Subsequently, this was extracted with Et_2O (2 × 10 mL) and then dried (in vacuo). Complex **13** (100 mg, 80% based on **11**) was obtained as an amber solid. − Mp: > 200 °C. − IR (KBr): $\tilde{\nu}$ = 2098 [$\nu_{C\equiv C}$], 1971 [$\nu_{C=C}$] cm^{-1}. − ^1H NMR ($CDCl_3$): δ = 3.19 (s, 12 H, N*Me*$_2$), 4.04 (br s, 2 H, C_5H_4), 4.04 (s, 4 H, C*H*$_2$), 4.15 (s, 5 H, C_5H_5), 4.36 (br s, 2 H, C_5H_4), 7.01 (s, 2 H, C_6H_2), 7.4−7.6 (m, 15 H, C_6H_5). − ^{31}P $\{^1H\}$ NMR ($CDCl_3$): δ = 43.1. − FAB-MS; *m*/*z* (rel. int.): 1078 (20) $[M^+]$, 867 (50) $[M - Fc]^+$, 668 (10) $[C_{30}H_{24}AuFeP]^+$, 459 (100) $[C_{18}H_{15}AuP]^+$, 409 $[C_{14}H_{18}N_2Pt]^+$, 210 (10) $[C_{12}H_9Fe]^+$. − $C_{44}H_{43}AuFeN_2PPt$ (1078.76): calcd. C 48.99, H 4.02, N 2.60; found C 49.12, H 4.08, N 2.68.

Acknowledgments

The authors would like to thank the Volkswagenstiftung, the Deutsche Forschungsgemeinschaft, the Fonds der Chemischen Industrie and Utrecht University (1.5 year stay of SB) for financial support. Drs. M. Lutz and A. L. Spek are thanked for the X-ray study on **11**.

[1] [1a] *Inorganic Materials* (Eds.: D. W. Bruce, D. O′Hare), Wiley, Chichester, **1992**. − [1b] S. R. Marder, J. W. Perry, *Adv. Mater.* **1993**, *5*, 804−815. − [1c] D. Astruc, *Acc. Chem. Res.* **1997**, *30*, 383−391. − [1d] P. J. Stang, B. Olenyuk, *Acc. Chem. Res.* **1997**, *30*, 502−518. − [1e] T. M. Swager, *Acc. Chem. Res.***1998**, *31*, 201−207.[1f] B. Olenyuk, A. Fechtenkötter, P. J. Stang, *Acc. Chem. Res.* **1998**, *31*, 1707−1728.

[2] [2a] D. R. Kanis, P. G. Lacroix, M. A. Ratner, T. J. Marks, *J. Am. Chem. Soc.* **1994**, *116*, 10089−10102. − [2b] D. R. Kanis, M. A. Ratner, T. J. Marks, *Chem. Rev.* **1994**, *94*, 195−242.[2c] M. B. Sponsler, *Organometallics* **1995**, *14*, 1920−1927. − [2d] P. Belazoni, N. Re, A. Sgamellotti, C. Floriani, *J. Chem. Soc.*, *Dalton Trans.* **1998**, 1825−1835. − [2e] N. Re, A. Sgamellotti, C. Floriani, *J. Chem. Soc. Dalton Trans.* **1998**, 2521−2529.

[3] [3a] M. Brady, W. Weng, Y. Zhou, J. W. Seyler, A. J. Amoroso, A. M. Arif, M. Böhme, G. Frenking, J. A. Gladysz, *J. Am. Chem. Soc.* **1997**, *119*, 775−788. − [3b] S. B. Falloon, S. Szafert, A. M. Arif, J. A. Gladysz, *Chem. Eur. J.* **1998**, *4*, 1033−1042.

[4] [4a] T. Kaharu, H. Matsubara, S. Takahashi, *J. Mater. Chem.* **1991**, *1*, 145−146. − [4b] P. Nguyen, G. Lesley, T. B. Marder, I. Ledoux, J. Zyss, *Chem. Mater.* **1997**, *9*, 406−411. − [4c] W.-Y. Wong, W.-K. Wong, P. R. Raithby, *J. Chem. Soc.*, *Dalton Trans.* **1998**, 2761−2769. − [4d] N. Ohshiro, F. Takei, K. Onitsuka, S. Takahashi, *J. Organomet. Chem.* **1998**, *569*, 195−202.

[5] [5a] P. L. Porter, S. Guha, K. Kang, C. C. Frazier, *Polymer* **1991**, *32*, 1756−1760. − [5b] M.-C. Lagunas, R. A. Gossage, A. L. Spek, G. van Koten *Organometallics* **1998**, *17*, 731−741.

[6] [6a] M. S. Khan, A. K. Kakkar, S. L. Ingham, P. R. Raithby, J. Lewis, B. Spencer, F. Wittmann, R. H. Friend, *J. Organomet. Chem.* **1994**, *472*, 247−255. − [6b] P. Steenwinkel, D. M. Grove, N. Veldman, A. L. Spek, G. van Koten, *Organometallics* **1998**, *17*, 5627−5655. − [6c] M. I. Bruce, P. Hinterding, P. J. Low, B. W. Skelton, A. H. White *J. Chem. Soc.*, *Dalton Trans.* **1998**, 467−473.

[7] [7a] N. J. Long, A. J. Martin, F. Fabrizi de Biani, P. Zanello, *J. Chem. Soc.*, *Dalton Trans.* **1998**, 2017−2021. − [7b] P. Ceroni, F. Paolucci, C. Paradisi, A. Juris, S. Raffia, S. Serroni, S. Campagna, A. J. Bord, *J. Am. Chem. Soc.* **1998**, *120*, 5480−5487. − [7c] J. Lewis, P. R. Raithby, W.-Y. Wong, *J. Organomet. Chem.* **1998**, *556*, 219−228.

[8] [8a] M. Tamm, A. Grzegorzewski, I. Brüdgam, H. Hartl, *J. Chem. Soc.*, *Dalton Trans.* **1998**, 3523−3528. − [8b] X. Gu, M. B. Sponsler, *Organometallics* **1998**, *17*, 5920−5923. − [8c] M. C. B. Colbert, J. Lewis, P. R. Raithby, M. Younus, A. J. White, D. J. Williams, N. N. Payne, C. Yellowlees, D. Beljonne, N. Chandhury, R. H: Friend, *Organometallics* **1998**, *17*, 3034−3043.[8d] T. Weyland, K. Costuas, A. Mari, J.F. Halet, C. Lapinte, *Organometallics* **1998**, *17*, 5569−5579.

[9] J.-D. Lee, L. M. Vrana, E. R. Bullock, K. J. Brewer, *Inorg. Chem.* **1998**, *37*, 3575−3580.

[10] [10a] Y. Hayashi, M. Osawa, Y. Wakatsuki, *J. Organomet. Chem.* **1997**, *542*, 241−246. − [10b] S. Back, H. Pritzkow, H. Lang, *Organometallics* **1998**, *17*, 41−44. − [10c] S. Back, R.A. Gossage, I. del Río, G. Rheinwald, H. Lang, G. van Koten, *J. Organomet. Chem.* **1999**, *582*, 126.

[11] [11a] T. E. Müller, S. W.-K. Choi, D. M. P. Mingos, D. Murphy, D. J. Williams, V. W.-W. Yam, *J. Organomet. Chem.* **1994**, *484*, 209−224. − [11b] V. W.-W. Yam, S. W.-K. Choi, *J. Chem. Soc.*, *Dalton Trans.* **1996**, 4227−4232. − [11c] I. R. Whittall, M. G. Humphrey, M. Samoc, B. Luther-Davies, *Angew. Chem.* **1997**, *109*, 386−388; *Angew. Chem. Int. Ed. Engl.* **1997**, *36*, 370−371. − [11d] R. J. Puddephatt, *Chem. Commun.* **1998**, 1055−1062.

[12] [12a] M. M. Bhadbhade, A. Das, J. C. Jefferey, J. A. McCleverty, J. A. Navas Badiola, M. D. Ward, *J. Chem. Soc.*, *Dalton Trans.* **1995**, 2769−2778. − [12b] S. Sakanishi, D. A. Bardwell, S. Couchman, J. C: Jefferey, J.A. McCleverty, M. D. Ward, *J. Organomet. Chem.* **1997**, *528*, 35−45.

[13] [13a] J. T. Liu, M.-F. Young, C. Tsai, Y. S. We, *J. Organomet. Chem.* **1998**, *564*, 257−266. − [13b] J. Mata, S. Uriel, E. Peris,

R. Lhusar, S. Houbrechts, A. Persoons, *J. Organomet. Chem.* **1998**, *562*, 197−202.
[14] M. C. B. Colbert, A. J. Edwards, J. Lewis, N. J. Long, N. A. Page, D. G. Parker, P. R. Raithby, *J. Chem. Soc*., *Dalton Trans.* **1994**, 2589−2598.
[15] S. L. James, G. Verspui, A. L. Spek, G. van Koten, *Chem. Commun*. **1996**, 1309−1310.
[16] S. Back, R. A. Gossage, M. Lutz, I. del Río, A. L. Spek, H. Lang, G. van Koten, *Organometallics* **1999**, submitted.
[17] A. Seebald, C. Stader, B. Wrackmeyer, W. Bensch, *J. Organomet. Chem.* **1986**, *311*, 233−242.
[18] J. Dale, *Properties of Acetylenic Compounds*, in: *Chemistry of Acetylenes* (Ed.: H. G. Viehe), Marcel Dekker, New York, **1969**.
[19] [19a] R. S. Dickson, P. J. Fraser, *Adv. Organomet. Chem.* **1974**, *12*, 323−377. − [19b] D. Seyferth, T. Kugita, A. L. Rheinhold, G. P. A. Yap, *Organometallics* **1995**, *14*, 5362−5366. − [19c] E. C. Constable, O. Eich, C. E. Housecroft, C. A. Johnston, *Chem. Commun.* **1998**, 2661−2662.
[20] H. Lang, S. Blau, K. Köhler, *Coord. Chem. Rev.* **1995**, *143*, 113−168 and ref. cited therein.
[21] S. Back, T. Stein, G. Rheinwald, H. Lang, *Acta Crystallogr.*, *Sect. C* **1999**, submitted.
[22] W. Beck, personal communication.
[23] M. I. Bruce, E. Horn, J. G. Matison, M. R. Snow, *Aust. J. Chem*. **1984**, *37*, 1163−1170.
[24] S. Takahashi, Y. Kuroyama, K. Sonogashira, N. Hagihara, *Synthesis* **1980**, 627−630.
[25] W. E. Davidson, M. C. Henry, *Chem. Rev.* **1967**, *67*, 73−106.
[26] J. Polin, H. Schottenberger, *Org. Synth.* **1996**, *73*, 262−269.

Received November 24, 1999
[I99427]

Structural Investigation in Solution of a Series of Five-Coordinate Bisphosphanylaryl Ruthenium(II) Complexes

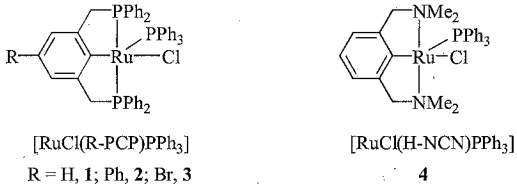
Paulo Dani,[a] Gerard P. M. van Klink,[a] and Gerard van Koten*[a]

Keywords: Ruthenium / NMR spectroscopy / NOESY / P ligands / Monoanionic terdentate *P,C,P′*-bisphosphanylaryl ligand

The structure of the ruthenium(II) complexes [RuCl{$C_6H_2(CH_2PPh_2)_2$-2,6-R-4}(PPh_3)] [R = H (**1**), Ph (**2**) or Br (**3**)] was investigated in solution using two-dimensional NMR techniques (^{1}H-^{1}H-, ^{13}C-^{1}H- and ^{31}P-^{1}H-correlation NMR spectroscopy and ^{1}H NOESY). The ^{1}H and ^{13}C NMR spectra of the complexes **1**–**3** were similar and could be completely assigned. The results of the NOESY study indicated that these complexes have a distorted square-pyramidal geometry in solution as was established for the parent complex R = H in the solid state by an X-ray crystal structure determination. The strategies used for the interpretation of the ^{1}H, ^{13}C and ^{31}P NMR spectra of these compounds and the resulting assignments form the basis for future in situ studies involving these complexes in catalytic processes.

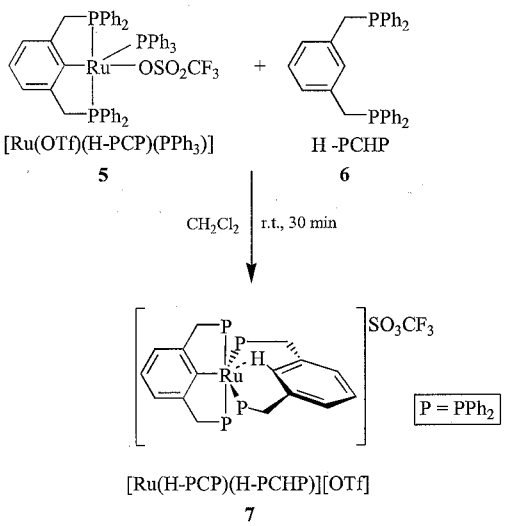
Introduction

During the last two decades a new class of organometallic species has emerged containing the metal in a terdentate monoanionic framework. In these compounds, the ligand binds to the metal through two heteroatoms (e.g. N, P, S) and an anionic carbon atom usually from an aryl fragment. Examples of this type of complexes, containing a bis-orthochelating amine[1] or phosphane,[2,3] aryl monoanion (commonly known as a "pincer" ligand) bound to a ruthenium(II) center, are presented in Scheme 1.



Scheme 1. Schematic representation of Ru−PCP and −NCN complexes

Examining the reaction behavior of these compounds revealed that [Ru(OSO_2CF_3)(H−PCP)(PPh_3)] (**5**) reacted with the parent arene $C_6H_4(CH_2PPh_2)_2$-1,3 (H−PCHP, **6**) to give **7** (see Scheme 2). In **7**, which was structurally characterized by X-ray diffraction, a neutral H−PCHP ligand is η^3-*P,H,P′* ligated to the bis-orthochelated bisphosphanylaryl ruthenium cation. Complexes like **7**, containing an aromatic C−H group coordinated to a metal center (i.e., an agostic contact),[4] are rare and are thought to be intermediates in processes leading to the formation of a metal−carbon bond (cyclometalation).[5−7]



Scheme 2. Formation of ruthenium complex **7**, containing an aryl C−H···Ru interaction

Attempts to study the structure of **7** in solution by NMR spectroscopy were hampered by a complex resonance pattern and fluxional behavior. Interpretation of the ^{1}H, ^{13}C and ^{31}P NMR patterns of **7** was further frustrated by the lack of a detailed assignment of the ^{1}H and ^{13}C NMR spectra in complexes where the PCP-type ligand had phenyl groups attached to the phosphorus atoms,[8] mainly those with geometries other than square-planar.[2,3,5,9,10] In particular, a detailed understanding of the binding mode of the H−PCHP ligand in **7** requires an accurate assignment of the aromatic region of the ^{1}H and ^{13}C NMR spectra of related complexes such as **1**−**3**. Furthermore, these PCP metal complexes have an increasing importance as novel catalysts[8b,8c,11−13] as well as materials with interesting new physico-chemical properties.[14] A detailed knowledge of the

[a] Department of Metal-Mediated Synthesis, Debye Institute, Utrecht University,
Padualaan 8, 3584 CH Utrecht, The Netherlands
Fax: (internat.) + 31-30/252-3615
E-mail: g.vankoten@chem.uu.nl

Supporting information for this article is available on the WWW under http://www.wiley-vch.de/home/eurjic or from the author.

 © WILEY-VCH Verlag GmbH, D-69451 Weinheim, 2000 1434−1948/00/0707−1465 $ 17.50+.50/0

NMR spectroscopic features of these compounds, i.e., coupling network, chemical shift and relative spatial positioning of the various nuclei, mainly the ones closer to the metal center, can play an important role in further investigations of reactivity, bonding, structure-energy relationships and in the understanding of the intimate steps of catalytic processes involving these pincer ruthenium complexes. Therefore, we set out to study in detail the NMR spectra of the [RuCl(R−PCP)PPh_3] compounds **1−3**.

Due to the presence of several aromatic rings, an obvious and nontrivial problem in compounds **1−3** is to distinguish the resonances belonging exclusively to one particular type of aromatic group. The structures of these complexes in solution were studied by ^1H, ^{13}C and ^{31}P NMR spectroscopy with the application of two-dimensional techniques (^1H-^1H-COSY, ^{13}C-^1H-COSY and ^{31}P-^1H-COSY) to allow full assignment of the ^1H and ^{13}C resonances, in particular those in the aromatic regions. Furthermore, a study of the three-dimensional structure in solution was performed by applying standard NOE techniques (^1H-NOESY). More importantly, these assignments were performed without any sort of chemical modification of the complexes studied, like, for instance, replacement of hydrogen atoms by deuterium or fluorine or NMR "silent" nuclei.

Results

The structure of [RuCl(H−PCP)(PPh_3)] (**1**) in the solid state has been determined by X-ray diffraction.[15] The local geometry around the Ru^{II} center in **1** has been described as distorted square-pyramidal (see Figure 1). The PPh_3 ligand occupies the apical position, while the other two phosphorus centers, together with the chlorine and C_{ipso} atom, form the base of the square-pyramidal arrangement. As a result, the complex has a mirror-type arrangement of the two fused five-membered chelate rings. The phosphorus center in each of the puckered chelate rings has one phenyl group equatorially and one axially (i.e., opposite to the apical PPh_3 ligand) orientated.

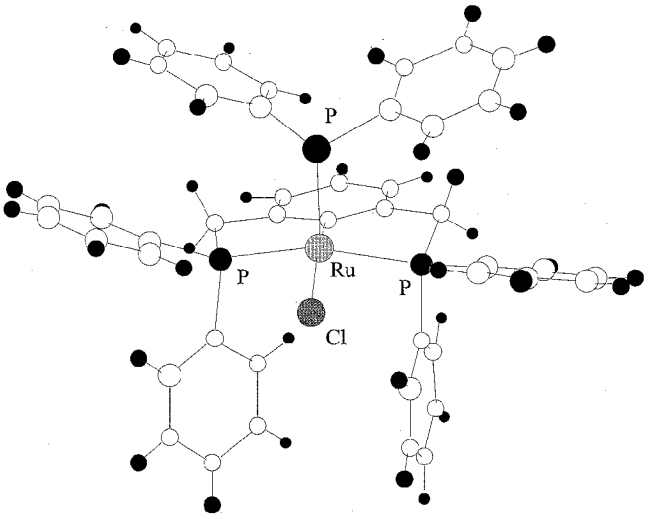


Figure 1. The molecular geometry of [RuCl(H−PCP)(PPh_3)] (**1**) in the solid state;[15] one phenyl ring from the PPh_3 ligand is omitted for clarity; the mirror-type arrangement (apparent mirror-plane) through the C_{ipso}−Ru−Cl is clearly visible

As a common feature, the ^1H NMR spectra of **1−3** contain a set of doublets of virtual triplets for the diastereotopic benzylic protons (for instance, see the abscissa in Figure 2[16]). Moreover, the $^{31}P\{^1H\}$ NMR spectra of these compounds consist of a doublet and a lower field triplet ($^2J_{pp} \approx 30$ Hz) for the R−PCP and PPh_3 phosphorus nuclei, respectively. In the $^{13}C\{^1H\}$ NMR spectra a small $^2J_{C_{ipso}-PPh_3}$ coupling constant of about 15−20 Hz is observed. These observations establish the *trans*-positioning of the R−PCP phosphorus atoms and the *cis*-arrangement of the R−PCP and PPh_3 phosphorus atoms, and suggest that the square-pyramidal structure of **1** found in the solid state exists in solution as well.

As the complexes **1−3** gave very similar results in the NMR analysis, compound **1** will be used as a representative compound for the following discussion.

^{31}P-^1H Correlation Spectroscopy (^{31}P-^1H-COSY)

The ^{31}P-^1H-COSY NMR spectra of a solution of **1** in CD_2Cl_2 allowed us to readily locate all P−Ph *ortho* protons, see Figure 2.[16] Only three cross-peaks (therefore, only three types of *ortho* protons) were observed in the aromatic region of the ^1H NMR spectrum, one for the PPh_3 ligand and the other two for the H−PCP ligand. This indicates that the four phenyl rings from the H−PCP ligand are divided into two sets of diastereotopic phenyl groups (hereafter labeled as Ph-a and Ph-b) which later could be assigned to the equatorial and axial phenyl groups, respectively (see ^1H NOESY experiments), whereas the phenyl rings of the PPh_3 ligand are equivalent. These findings imply that there is no restricted rotation about any P−Ph bond or about the Ru−PPh_3 bond. Also, no Ru−P bond dissociation-association process is operative on the NMR time scale at room temperature. Consequently, under these conditions there is a *pseudo*-molecular symmetry plane containing the C_{ipso}−Ru−P(PPh_3) atoms.

^1H-^1H Correlation Spectroscopy

In the ^1H-^1H-COSY spectrum of the ruthenium complexes **1−3** the location of protons H-3,5 (see Figure 3)[16] could easily be determined due to a cross-peak between these protons and one set of benzylic protons. The related $^4J_{HH}$ indirect coupling between these protons in the one-dimensional 300 MHz ^1H spectrum could not be observed. Interestingly, this behavior is quite general and is not restricted to cyclometalated R−PCP-type ligands. A similar phenomenon was also observed in a ^1H-^1H-COSY analysis involving related nitrogen-based ligands and can be explained by analogy with allylic systems:[17a,18a] the smaller the torsional angle between the benzyl C−H bond and the axis of the arene π-orbitals, the larger is the four-bond coupling. Therefore, the presence of this cross-peak brings interesting structural consequences because it suggests that these benzylic protons are occupying a *pseudo*-axial posi-

tion in the two fused five-membered chelate rings in relation to the ruthenium coordination plane. This idea was later confirmed by a ^{1}H NOESY experiment (see below), and it has become quite important in the structural analysis of [RuCl(H−PCP)PPh$_3$] in which the H−PCP ligand has one of the benzylic protons of each methylene carbon atom replaced by a methyl or ethyl group (i.e., the ligand has two chiral centers in the molecule).[24]

The multiplet at lowest field in the ^{1}H NMR spectrum (between δ = 7.80−7.90 for **1**), showing cross-peaks with the R−PCP phosphorus atoms in Figure 2,[16] integrates to four protons and it was observed by ^{13}C-^{1}H-COSY analysis (Figure 4)[16] to have a cross-peak with only one type of aromatic carbon atom. Therefore, it can be safely assigned as the resonance due to the four *ortho* Ph-a protons. This multiplet shows a cross-peak in the ^{1}H-^{1}H-COSY (Figure 3)[16] with protons located in a second multiplet at δ = 7.30−7.50. The nonexistence of any other cross-peak involving these two regions of the ^{1}H-^{1}H-COSY spectrum allows us to conclude that the *meta* and *para* protons of the Ph-a are overlapping and located in the multiplet at δ = 7.30−7.50.

^{13}C-^{1}H Correlation Spectroscopy

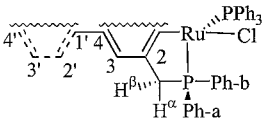
Entering the information gathered so far into normal- and long-range ^{13}C-^{1}H-correlation NMR spectra {and using the assignments of the ^{13}C{^{1}H} NMR spectrum of [RuCl(H-NCN)(PPh$_3$)] (**4**)},[1] it was possible to locate all C−H resonances as well as most of the quaternary carbons (C$_{quat}$) in the ^{1}H and ^{13}C NMR spectra of **1**−**3**. In particular, all proton and carbon resonances of the parent complexes **1** and **2** could be assigned (see Figure 4[16] for **1**). Only in the case of compound **3** could the C$_{quat}$ of the Ph-a rings not be located. Table 1 summarizes all ^{1}H and ^{13}C NMR spectroscopic data and assignments for complexes **1**−**3**.

The presence of an apparent molecular symmetry plane involving C$_{ipso}$−Ru−P(PPh$_3$)−Cl is even clearer in these ^{13}C-^{1}H-COSY NMR spectra. For instance, Figure 4[16] shows that the *ortho*-protons and -carbons of the PPh$_3$ ligand are chemically equivalent (i.e., they have identical chemical shifts) and the same conclusion can be drawn for the *meta* and *para* nuclei. Furthermore, each phenyl group of the −PPh$_2$ fragment has an individual set of resonances related to either Ph-a or Ph-b. However, the *ortho* (or *meta* or *para*) Ph-a protons and carbons appear as single resonances. The same conclusion is valid for the Ph-b group. The *ortho* and *meta* carbon nuclei as well as the C$_{quat}$ of the Ph-a and Ph-b rings give distinct *pseudo*-triplets which is the expected pattern for carbons connected to a *trans* phosphorus atom.[17b,19]

NOE Analysis

More precise information about the three-dimensional structure of species **1**−**3** in solution can be obtained from

Table 1. ^{1}H (300 MHz) and ^{13}C NMR (75 MHz) data of compounds **1**, **2** and **3** in CD_2Cl_2 (relative to internal tetramethylsilane)

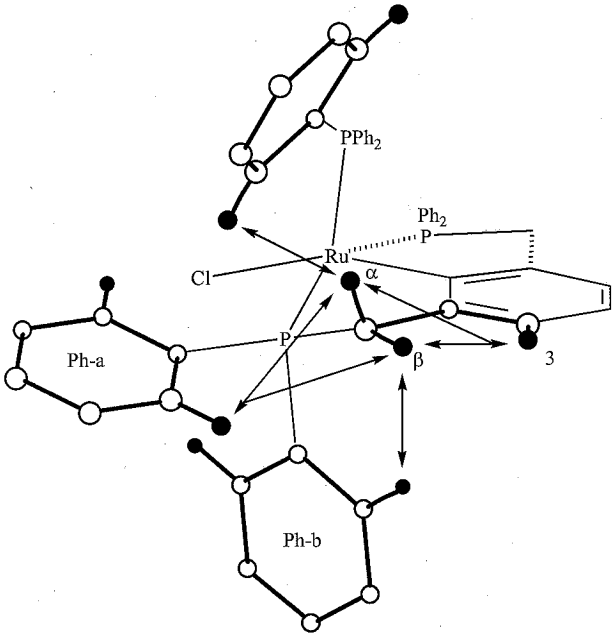


		^{1}H (δ, mult., $^2J_{HH}$, $^{vt}J_{HP}$ Hz)			^{13}C (δ, mult., J_{CP} Hz)		
		1[a]	**2**	**3**[b]	**1**	**2**	**3**
Benzylic	C−H$^{\alpha}$[c]	2.36 (bd, 16)	2.48 (bd, 16)	2.37 (bd, 16)	39.19 (vt, 15)	39.27 (vt, 16)	39.08 (vt, 15)
Groups	C−H$^{\beta}$	3.48 (dvt, 16, 6)	3.56 (dvt, 16, 6)	3.45 (dvt, 16, 6)			
	C$_{ipso}$	−	−	−	172.53 (d, 17)	173.30 (d, 16)	172.77 (d, 17)
Xylylene	C-2,6	−	−	−	151.20 (vt, 8)	151.66 (vt, 9)	152.97 (vt, 9)
Ring	C−H-3,5	6.96	7.31	7.13	123.34 (vt, 9)	121.66 (vt, 9)	125.73 (vt, 9)
	C−(R)-4	6.81	−	−	122.11 (s)	135.02 (s)	115.95 (s)
	ortho	7.84 (m)	7.88 (m)	7.85 (m)	133.15 (vt, 6)	133.11 (vt, 6)	133.10 (vt, 5)
Ph-a	*meta*	7.38	7.40	7.39	128.71 (vt, 5)	128.75 (vt, 5)	128.75 (vt, 4)
	para	7.42	7.45	7.44	130.18 (s)	130.23 (s)	130.32 (s)
	C$_{quat}$	−	−	−	134.76 (vt)	134.82	[d]
	ortho	7.11	7.18	7.11	132.81 (vt, 6)	132.84 (vt, 6)	132.71 (vt, 5)
Ph-b	*meta*	6.93	6.94	6.95	128.31 (vt, 4)	128.37 (vt, 4)	128.41 (vt, 4)
	para	7.09−7.14	7.09−7.10	7.12−7.15	129.27−129.31 (s)	129.39 (s)	129.45−129.50 (s)
	C$_{quat}$	−	−	−	136.07 (vt, 17)	135.90 (vt, 16)	[d]
	ortho	7.05	7.10	7.08	134.47 (d, 10)	134.46 (d, 10)	134.39 (d, 10)
PPh$_3$	*meta*	6.83	6.83	6.86	127.29 (d, 10)	127.29 (d, 10)	127.39 (d, 10)
	para	7.09−7.14	7.14	7.12−7.15	129.27−129.31 (s)	129.35 (s)	129.45−129.50 (s)
	C$_{quat}$	−	−	−	136.69 (dvt, ^1J = 51, ^{vt}J = 2−3)	136.55 (dm, 51)	136.35 (d, 52)
	1′	−	−	−	−	141.98 (s)	−
[b]	2′	−	7.70	−	−	126.68 (s)	−
	3′	−	7.44	−	−	128.82 (s)	−
	4′	−	7.30	−	−	126.76 (s)	−

[a] s = singlet, d = doublet, m = multiplet, b = broad and vt = virtual triplet. Non reported multiplicities are related to resonances only detected indirectly by two-dimensional techniques. − [b] See Figure at head of Table. − [c] Splittings due to the virtual triplet not resolved. − [d] One C$_{quat}$ is at δ = 134.03 and overlaps with PPh$_3$ *ortho* carbons. The other is at δ = 135.50 (vt, $^{vt}J_{CP}$ = 17 Hz). It was not possible to determine to which phenyl ring they were related to.

phase-sensitive ^{1}H NOESY measurements. The intensity of cross-peaks originating from dipolar interactions is very sensitive to the distance between the participating nuclei and they are often too weak to be detected when this distance is larger than 3 Å.[18b] A series of ^{1}H NOESY spectra was recorded. The interactions between benzylic and aromatic protons proved to be an excellent structural probe. Figure 5[16] shows this region for compound **1**. Only the benzylic protons at $\delta = 2.36$ (H^{α}) show a cross-peak with the *ortho* PPh_3 protons. This indicates that the PPh_3 ligand is in the apical position, as is observed in the solid state (Figure 1). The high-field chemical shift of H^{α} is then probably caused by a magnetic anisotropic effect originating from the PPh_3 ligand.

NOE correlation signals involving the aromatic protons H-3,5 and both benzylic protons H^{α} and H^{β} are also observed. However, the different intensities of these cross-peaks reveal that H^{β} is closer to protons H-3,5 than H^{α}. This is a clear reflection of the puckering occurring in the two fused five-membered chelate rings. The benzylic protons are not bisecting the xylylene plane. In order to be closer to H-3,5, H^{β} must be in a nearly periplanar conformation with the xylylene plane. H^{α}, on the other hand, is directed toward an *anti*-planar conformation with the same plane (Scheme 3). As a consequence, the H−PCP phosphorus atoms that are occupying the flip of an envelope conformation assumed by each one of the two fused rings, are pointing away from the PPh_3 ligand.



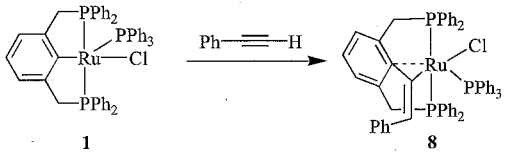
Scheme 3. Spatial interactions involving the benzylic protons in **1**

Protons H^{α} and H^{β} interact almost equally with the *ortho* protons of the Ph-a ring placing the $P-C_{quat}$ bond of Ph-a in an approximately coplanar situation with the plane formed by the $P-CH_2-C$-2 (or -6) bonds. On the other hand, the (weak) interaction between the *ortho* Ph-b protons and the H^{β} protons is consistent with a *pseudo*-axial position of the former.

The same features observed in the NOESY spectrum of **1** were also present in the spectra of complexes **2** and **3**, showing that the presence of different substituents in the *para* position relative to the metal center (H, Ph or Br for **1**, **2** or **3**, respectively) does not affect the geometry around the metal. An analysis of the NOESY spectra also showed that the structures in solution of these complexes are very similar to that found in the solid state for complex **1**.

Discussion

In the case of the unsaturated ruthenium complex $[RuCl_2(PPh_3)_3]$ it has been found in the solid state that one of the *ortho* phenyl protons is directed toward the empty coordination site, blocking this position.[20] The NMR analysis performed with complexes **1**−**3** (and the solid structure of **1** as well) did not reveal any equivalent feature. On the contrary, all Ph-a and Ph-b rings in these complexes are freely rotating and do not exhibit any preferred configuration other than being equatorial or axial, respectively. This suggests that the vacant site *trans* to the PPh_3 ligand is relatively available for the coordination of nucleophilic species. Indeed, a facile reaction between **1** and 4-phenylpyridine (4-PhPy) producing the 18-electron complex [RuCl(H−PCP)(PPh_3)L] (L = 4-PhPy) has been reported.[15] Furthermore, species in which L is either a coordinated phenyl acetylene molecule or a vinylidene substituent [L = PhC(H)=C=] are thought to be involved in the formation of ruthenium complex **8** in the reaction of **1** with phenyl acetylene (Scheme 4).[10]



Scheme 4. Reaction of **1** with phenylacetylene yielding vinylidine-substituted ruthenium complex **8**

Dissociation of PPh_3 is a common phenomenon in ruthenium complexes such as $[RuCl_2(PPh_3)_n]$ ($n = 3$ or 4).[21] However, despite the fact that the PPh_3 ligand in **1**−**3** is easily replaced by two-electron donor ligands (e.g. CO,[15] PMe_3,[15] R−PCHP[23,25]), solutions of the pure complexes did not reveal the presence of any free PPh_3. Furthermore, if intra- or intermolecular processes were operative leading to PPh_3 exchange, they would cause an interchange between the Ph-a and Ph-b protons, as well as between the benzylic protons H^{α} and H^{β}. Nevertheless, cross-peaks indicating fluxional processes were not present in any of the ^{1}H NOESY spectra recorded. Therefore, the replacement of PPh_3 in complexes **1**−**3** by the two-electron donor ligands mentioned above is most likely the result of dissociation of the PPh_3 from saturated species of these complexes.

The chemical shift of the C_{ipso} in complexes of the R−NCN ligand is sensitive toward the type of R substituent.[22] Taking the H−NCN complex as reference (i.e., R = H), downfield shifts greater than 1 ppm in the $\delta_{C_{ipso}}$ of com-

plexes containing electron-withdrawing R groups and the converse effect (i.e., upfield shifts) when electron-donating groups were present. Similar behavior was recently observed in palladium complexes of the pyridine PCP-type ligand [$C_5H_2N(CH_2PPh_2)_2$-3,5] upon coordination of Lewis acidic species to the pyridine nitrogen atom.[9c] In the case of the complexes reported here, the electronic effect of the bromo and phenyl *para* substituents on the C_{ipso} chemical shift is negligible (see Table 1) and probably reflects the buffer effect exerted by π-acidic phosphorus groups on the overall electron density of the complexes.

Conclusion

The results of the present study are currently being applied for the assignment and the understanding of more complex structures containing free and anionic PCP-type ligands, such as compound **7**,[23] ruthenium complexes containing chiral H−PCP type ligands[24] as well as other PCP-metal complexes which have recently been published. The results of these studies will be published shortly.

Experimental Section

Complexes **1, 2**[2] and **3**[25] were prepared according to literature procedures. All manipulations were performed under a dry nitrogen atmosphere using standard Schlenk techniques. Typically, ca. 30 mg of complex was dissolved in 0.7 mL of CD_2Cl_2 and then transferred to a 5 mm NMR tube provided with a glass stopper. Chemical shifts are in ppm relative to $(CH_3)_4Si$ (^1H and ^{13}C NMR spectra) or H_3PO_4 85% (^{31}P NMR spectra). CD_2Cl_2 was degassed prior to use (four times) using the freeze-pump-thaw methodology and then stored under nitrogen over molecular sieves 4 Å. ^1H, $^{13}C\{^1H\}$ and $^{31}P\{^1H\}$ NMR spectra were recorded at 298 K on a Varian Unity Inova 300 MHz spectrometer using standard pulse sequences. Except in the case of the NOESY measurements, all other two-dimensional experiments were performed in a nonphase-sensitive mode. The second pulse in the ^1H-^1H-COSY experiment was set to 45°. Normal-range ^{13}C-^1H-COSY NMR spectra were recorded considering $^1J_{HC} = 140$ Hz and for the long-range experiment the appropriate delays were adjusted for $^nJ_{HC} = 8$ Hz. T_1 times for complexes **1−3** were in the range 0.4−1.5 s. NOESY spectra were recorded with mixing times of 0.5, 1.0 and 1.5 s with a relaxation delay of 2.0 s.

1: ^1H NMR (CD_2Cl_2, 300 MHz): δ = 2.36 (bd, $^2J_{HH} = 16$ Hz, 2 H, CH_2), 3.48 (dvt, $^2J_{HH} = 16$ Hz, $^{vt}J_{HP} = 6$ Hz, CH_2), 6.81 (H-4), 6.83 (*m*-PPh_3), 6.93 (*m*-Ph-b), 6.96 (H-3,5), 7.05 (*o*-PPh_3), 7.09−7.14 (*p*-Ph-b, *p*-PPh_3), 7.11 (*o*-Ph-b), 7.38 (*m*-Ph-a), 7.42 (*p*-Ph-a), 7.84 (m, *o*-Ph-a). − $^{13}C\{^1H\}$ NMR (CD_2Cl_2, 75 MHz): δ = 39.19 (vt, $^{vt}J_{CP} = 15$ Hz, CH_2), 122.11 (s, C-4), 123.34 (vt, $^{vt}J_{CP} = 9$ Hz, C-3,5), 127.29 (d, $^3J_{CP} = 10$ Hz, *m*-PPh_3), 128.31 (vt, $^{vt}J_{CP} = 4$ Hz, *m*-Ph-b), 128.71 (vt, $^{vt}J_{CP} = 5$ Hz, *m*-Ph-a), 129.27−129.31 (s, *p*-Ph-b, *p*-PPh_3), 130.18 (s, *p*-Ph-a), 132.81 (vt, $^{vt}J_{CP} = 6$ Hz, *o*-Ph-b), 133.15 (vt, $^{vt}J_{CP} = 6$ Hz, *o*-Ph-a), 134.47 (d, $^2J_{CP} = 10$ Hz, *o*-PPh_3), 134.76 (vt, C_{quat} PPh-a), 136.07 (vt, $^{vt}J_{CP} = 17$ Hz, C_{quat} PPh-b), 136.69 (dvt, $^1J_{CP} = 51$ Hz, $^{vt}J_{CP} = 2-3$ Hz, C_{quat} PPh_3), 151.20 (vt, $^{vt}J_{CP} = 8$ Hz, C-2,6), 172.53 (d, $^2J_{CP} = 17$ Hz, C_{ipso}).

2: ^1H NMR (CD_2Cl_2, 300 MHz): δ = 2.48 (bd, $^2J_{HH} = 16$ Hz, 2 H, CH_2), 3.56 (dvt, $^2J_{HH} = 16$ Hz, $^{vt}J_{HP} = 6$ Hz, CH_2), 6.83 (*m*-PPh_3), 6.94 (*m*-Ph-b), 7.09−7.10 (*p*-Ph-b), 7.10 (*o*-PPh_3), 7.14 (*p*-PPh_3), 7.18 (*o*-Ph-b), 7.30 (4′), 7.31 (H-3,5), 7.40 (*m*-Ph-a), 7.44 (3′), 7.45 (*p*-Ph-a), 7.70 (2′), 7.88 (m, *o*-Ph-a). − $^{13}C\{^1H\}$ NMR (CD_2Cl_2, 75 MHz): δ = 39.27 (vt, $^{vt}J_{CP} = 16$ Hz, CH_2), 121.66 (vt, $^{vt}J_{CP} = 9$ Hz, C-3,5), 126.68 (s, 2′), 126.76 (s, 4′), 127.29 (d, $^3J_{CP} = 10$ Hz, *m*-PPh_3), 128.37 (vt, $^{vt}J_{CP} = 4$ Hz, *m*-Ph-b), 128.75 (vt, $^{vt}J_{CP} = 5$ Hz, *m*-Ph-a), 128.82 (s, 3′), 129.35 (s, *p*-PPh_3), 129.39 (s, *p*-Ph-b), 130.23 (s, *p*-Ph-a), 132.84 (vt, $^{vt}J_{CP} = 6$ Hz, *o*-Ph-b), 133.11 (vt, $^{vt}J_{CP} = 6$ Hz), 134.46 (d, 10), 134.82, 135.02 (s), 135.90 (vt, $^{vt}J_{CP} = 16$ Hz), 136.55 (dm, 51), 141.98 (s), 151.66 (vt, $^{vt}J_{CP} = 9$ Hz), 173.30 (d, $^2J_{CP} = 16$ Hz, C_{ipso}).

3: ^1H NMR (CD_2Cl_2, 300 MHz): δ = 2.37 (bd, $^2J_{HH} = 16$ Hz, 2 H, CH_2), 3.45 (dvt, $^2J_{HH} = 16$ Hz, $^2J_{HP} = 6$ Hz, 2 H, CH_2), 6.86 (m, 6 H, *m*-PPh_3), 6.95 (m, 4 H, *m*-PPh_2), 7.08 (m, 6 H, *o*-PPh_3), 7.11 (m, 4 H, *o*-PPh_2), 7.12−7.15 (m, 5 H, *p*-PPh_2 and *p*-PPh_3), 7.13 (2 H, CH-3,5), 7.39 (m, 4 H, *m*-PPh_2), 7.44 (m, 2 H, *p*-PPh_2), 7.85 (m, 4 H, *o*-PPh_2). − $^{13}C\{^1H\}$ NMR (CD_2Cl_2, 75 MHz): δ = 39.08 (vt, $^{vt}J_{CP} = 15$ Hz, CH_2), 115.95 (s, C−Br), 125.73 (vt, $^{vt}J_{CP} = 9$ Hz, C-3,5) 127.39 (d, $^3J_{CP} = 10$ Hz, *m*-PPh_3), 128.41 (vt, $^{vt}J_{CP} = 4$ Hz, *m*-PPh_2), 128.75 (vt, $^{vt}J_{CP} = 4$ Hz, *m*-PPh_2), 129.45−129.50 (two singlets, *p*-PPh_3 and *p*-PPh_2), 130.32 (s, *p*-PPh_2), 132.71 (vt, $^{vt}J_{CP} = 5$ Hz, *o*-PPh_2), 133.10 (vt, $^{vt}J_{CP} = 5$ Hz, *o*-PPh_2), 134.03 (m, C_{quat}-PPh_2), 134.39 (d, $^2J_{CP} = 10$ Hz, *o*-PPh_3), 135.50 (vt, $^{vt}J_{CP} = 17$ Hz, C_{quat}-PPh_2), 136.35 (d, $^1J_{CP} = 52$ Hz, C_{quat}−PPh_3), 152.97 (vt, $^{vt}J_{CP} = 9$ Hz, C-2,6), 172.77 (d, $^2J_{CP} = 17$ Hz, Ru−C_{ipso}). − $^{31}P\{^1H\}$ NMR (CD_2Cl_2, 121 MHz): δ = 36.74 (d, 2P, Br−PCP), 80.62 (t, $^2J_{PP} = 32$ Hz, 1P, PPh_3).

Acknowledgments

This work was financially supported by the Conselho Nacional de Desenvolvimento Científico e Tecnológico (CNPq), Brazil, and the Council for Chemical Sciences of the Netherlands Organization for Scientific Research (CW-NWO).

[1] J.-P. Sutter, S. L. James, P. Steenwinkel, T. Karlen, D. M. Grove, N. Veldman, W. J. J. Smeets, A. L. Spek, G. van Koten, *Organometallics* **1996**, *15*, 941−948.
[2] T. Karlen, P. Dani, D. M. Grove, P. Steenwinkel, G. van Koten, *Organometallics* **1996**, *15*, 5687−5694.
[3] G. Jia, H. M. Lee, H. P. Xia, I. D. Williams, *Organometallics* **1996**, *15*, 5453−5455.
[4] [4a] M. Brookhart, M. L. H. Green, L.-L. Wong, *Prog. Inorg. Chem.* **1988**, *36*, 1−124. − [4b] R. H. Crabtree, D. G. Hamilton, *Adv. Organomet. Chem.* **1988**, *28*, 299−338.
[5] P. Dani, T. Karlen, R. A. Gossage, W. J. J. Smeets, A. L. Spek, G. van Koten, *J. Am. Chem. Soc.* **1997**, *119*, 11317−11318.
[6] Indeed, there are claims that such intermediacy actually happens with rhodium complexes of PCP-type ligands: A. Vigalok, O. Uzan, L. J. W. Shimon, Y. Ben-David, J. M. L. Martin, D. Milstein, *J. Am. Chem. Soc.* **1998**, *120*, 12539−12544.
[7] A. C. Albéniz, G. Schulte, R. H. Crabtree, *Organometallics* **1992**, *11*, 242−249.
[8] [8a] F. Gorla, L. M. Venanzi, A. Albinati, *Organometallics* **1994**, *13*, 43−54. − [8b] F. Gorla, A. Togni, L. M. Venanzi, A. Albinati, F. Lianza, *Organometallics* **1994**, *13*, 1607−1616. − [8c] F. Caruso, M. Camalli, H. Rimml, L. M. Venanzi, *Inorg. Chem.* **1995**, *34*, 673−679. − [8d] M. E. van der Boom, M. Gozin, Y. Ben-David, L. J. W. Shimon, F. Frolow, H. B. Fraatz, D. Milstein, *Inorg. Chem.* **1996**, *35*, 7068−7073. − [8e] J. M. Longmire, X. Zhang, M. Shang, *Organometallics* **1998**, *17*, 4374−4379.
[9] [9a] S.-Y. Liou, M. Gozin, D. Milstein, *J. Am. Chem. Soc.* **1995**, *117*, 9774−9775. − [9b] S.-Y. Liou, M. Gozin, D. Milstein, *J. Chem. Soc., Chem. Commun.* **1995**, 1965−1966. − [9c] A. Weisman, M. Gozin, H.-B. Kraatz, D. Milstein, *Inorg. Chem.* **1996**, *35*, 1792−1797. − [9d] M. E. van der Boom, S.-Y. Liou, Y. Ben-David, L. J. W. Shimon, D. Milstein, *J. Am. Chem. Soc.* **1998**,

120, 6531−6541. − [9e] M. E. van der Boom, S.-Y. Liou, Y. Ben-David, M. Gozin, D. Milstein, *J. Am. Chem. Soc.* **1998**, *120*, 13415−13421.

[10] [10a] H. M. Lee, J. Yao, G. Jia, *Organometallics* **1997**, *16*, 3927−3933. − [10b] G. Jia, C. P. Lau, *J. Organomet. Chem.* **1998**, *565*, 37−48.

[11] P. Dani, T. Karlen, R. A. Gossage, S. Gladiali, G. van Koten, *Angew. Chem. Int. Ed.* **2000**, *39*, 743−745.

[12] [12a] M. Ohff, A. Ohff, M. E. van der Boom, D. Milstein, *J. Am. Chem. Soc.* **1997**, *119*, 11687−11688. − [12b] F. Liu, E. B. Pak, B. Singh, C. M. Jensen, A. S. Goldman, *J. Am. Chem. Soc.* **1999**, *121*, 4086−4087.

[13] J. M. Longmire, X. Zhang, *Tetrahedron Lett.* **1997**, *38*, 1725−1728.

[14] W. T. S. Huck, B. Snellink-Ruël, F. C. J. M. van Veggel, D. N. Reinhoudt, *Organometallics* **1997**, *16*, 4287−4291.

[15] G. Jia, H. M. Lee, I. D. Williams, *J. Organomet. Chem.* **1997**, *534*, 173−180.

[16] Figures 2 to 5 are published as supporting information and are available on the WWW under http://www.wiley-vch.de/home/eurjic.

[17] [17a] H. Günther, *NMR Spectroscopy − An Introduction*, John Wiley & Sons, New York, **1980**, p. 46. − [17b] H. Günther, *NMR Spectroscopy − An Introduction*, John Wiley & Sons, New York, **1980**, p. 123.

[18] [18a] H. Friebolin, *Basic One- and Two-Dimensional NMR Spectroscopy*, 2nd Ed., VCH, Weinheim, **1993**, p. 83. − [18b] H. Friebolin, *Basic One- and Two-Dimensional NMR Spectroscopy*, 2nd Ed., VCH, Weinheim, **1993**, p. 275.

[19] J. W. Akitt, *Practical Spectroscopy Series* **1991**, *11*, 427−483.

[20] S. J. La Placa, J. A. Ibers, *Inorg. Chem.* **1965**, *4*, 778−783.

[21] F. H. Jardine, *Prog. Inorg. Chem.* **1984**, *31*, 265−370.

[22] L. A. van de Kuil, H. Luitjes, D. M. Grove, J. W. Zwikker, J. G. M. van der Linden, A. M. Roelofsen, L. W. Jenneskens, W. Drenth, G. van Koten, *Organometallics* **1994**, *13*, 468−477.

[23] P. Dani, M. A. M. Toorneman, G. P. M. van Klink, W. J. J. Smeets, A. L. Spek, G. van Koten, manuscript in preparation.

[24] P. Dani, M. Albrecht, G. P. M. van Klink, G. van Koten, manuscript in preparation.

[25] P. Dani, B. Richter, G. P. M. van Klink, G. van Koten, manuscript in preparation.

Received December 27, 1999
[I99478]

Oxidative Stannylation with $K_6Sn_2Se_6/SnCl_2$: Synthesis and Crystal Structures of $SnCl_3$-Substituted *pseudo*-Tetrahedral Cobalt(III) Complexes

Stefanie Dehnen*[a] and Christian Zimmermann[a]

Keywords: Zintl anions / Cobalt / Oxidation / Tin / Insertions

The ternary Zintl phase $K_6Sn_2Se_6$ was recently shown to mildly oxidize Cp*-ligated Co^{II} complexes, although Sn in the formal +III oxidation state usually tends to be a reducing species. Depending on the reaction conditions, different ratios of Co^{II} and Co^{III} were observed within the product molecules. Cyclovoltammetric investigations indicated that reversible electron transfer occurred between some of the isolated molecules synthesized that way. In order to study the redox behavior of the oxidizing Sn^{III} species in the reaction system, large excesses of Sn^{II} were added to the solvent THF. A suppression of the $Co^{II} \rightarrow Co^{III}$ transition was expected if the oxidation was reversible. Herein we report the synthesis and crystal structures of $[Co_2(\mu\text{-}Cl)_3(thf)_6][CoClCp^*(SnCl_3)_2]$ (**1**) and $[Li(thf)_4][CoCp^*(SnCl_3)_3]$ (**2**) formed from reactions of $[CoClCp^*]_2$ with $K_6Sn_2Se_6$ in the presence of $SnCl_2$ in THF. The results show that oxidation could not be inhibited, indicative of irreversible redox mechanisms. Additionally, one observes the formal insertion of $SnCl_2$ units in Co–Cl bonds. For completion of the 18-electron configuration, the Cp^*Co^{III} 14-electron fragment forms sterically strained anionic structures that may in the future be relevanct as precursors for the formation of Cp*Co-coated heteroatomic aggregates. Furthermore, the cation in **1** is one of the few examples of threefold μ_2-bridged binuclear Co^{II} complexes.

Introduction

In the course of our current studies on the chemical reactivity of binary Zintl anions, we recently synthesized and structurally characterized compounds $[Co_3Cp^*_3(\mu_3\text{-}Se)_2]$, $[Co_3Cp^*_3(\mu_3\text{-}Se)_2][CoCl_2(\mu\text{-}Cl)_2Li(thf)_2]$, and $[Co_4Cp^*_4(\mu_3\text{-}Se)_4]$ which were obtained from reactions of ternary Zintl salt $K_6Sn_2Se_6$[1] with $[CoClCp^*]_2$ under different reaction conditions.[2] Due to unusual oxidation by Sn in the formal +III oxidation state, both Co^{II} and Co^{III} were observed in the mixed valence products as well as Se^{2-} ligands from $K_6Sn_2Se_6$. In order to explore whether the occurring redox processes (which have been shown to be reversible for the isolated products) – can be suppressed by addition of Sn^{II}, we treated $K_6Sn_2Se_6$ with $[CoClCp^*]_2$ in the presence of large excesses of $SnCl_2$ (see Experimental Section). The use of different ratios of Co^{II}/Sn^{II} and slightly varied reaction conditions yielded compounds $[Co_2(\mu\text{-}Cl)_3(thf)_6][CoClCp^*(SnCl_3)_2]$ (**1**) or $[Li(thf)_4][CoCp^*(SnCl_3)_3]$ (**2**) in good yields [Equation (1) or Equation (2)]. Compounds **1** and **2** were structurally characterized by single-crystal X-ray analysis.[3]

$$K_6Sn_2Se_6 + 4\ SnCl_2 + 6\ CoCl_2 + 2\ LiCp^* \xrightarrow{\text{THF}} 2\ [Co_2(\mu\text{-}Cl)_3(THF)_6][CoClCp^*(SnCl_3)_2] + 3\ K_2Se + 2\ SnSe + Li_2Se \quad (1)$$

(**1**)

$$K_6Sn_2Se_6 + 7\ SnCl_2 + 2\ CoCl_2 + 2\ LiCp^* \xrightarrow{\text{THF}} 2\ [Li(THF)_4][CoCp^*(SnCl_3)_3] + 3\ K_2Se + 3\ SnSe \quad (2)$$

(**2**)

However, instead of suppressing the oxidative effect of $K_6Sn_2Se_6$ by excess Sn^{II}, Co^{II} was again partly oxidized to Co^{III}, while $SnCl_2$ was formally inserted in Co–Cl bonds in both cases. However, the formation of the counterion $[Co_2(\mu\text{-}Cl)_3(thf)_6]^+$ is evidence of a stepwise mechanism, rather than of a direct insertion. This was possibly initialized by the partial ionization of $CoCl_2$ in THF giving $CoCl^+$ and Cl^-, followed by the aggregation of THF-solvated $CoCl^+$ with $CoCl_2$ to yield $[Co_2(\mu\text{-}Cl)_3(thf)_6]^+$, while Cl^- reacted with $SnCl_2$ to form the $SnCl_3^-$ anion. The latter finally coordinated to the Cp*-ligated Co^{III} center resulting from the oxidation reaction. Although we were not yet in the position to identify all reaction by-products with certainty, one further hint existed for the reduction of the Sn centers to Sn^{II} rather than for an oxidation to Sn^{IV}: Small $SnSe^+$ peaks were always found in the mass spectra of the primary reaction precipitates, whereas no further Sn products – such as $SnCl_4$, $SnSe_2$ or $SnCl_2$ – were observed either in the mass spectrum or in the NMR measurement of the reaction solution. Moreover, unwanted oxidation of Co^{II} by traces of oxygen in the reaction mixture can be excluded as the products are not formed by means of pure selenide donors such as K_2Se or $Se(SiMe_3)_2$ instead of $K_6Sn_2Se_6$. The observations ultimately suggest the irreversibility of the oxidation by Sn^{III} in the investigated system which correlates with the precipitation of insoluble SnSe during the reaction.

[a] Institut für Anorganische Chemie der Universität Karlsruhe (TH)
Engesserstraße, Geb. 30.45, 76128 Karlsruhe, Germany
Fax: (internat.) + 49-(0)721/608-7021
E-mail: dehnen@achibm6.chemie.uni-karlsruhe.de

 © WILEY-VCH Verlag GmbH, D-69451 Weinheim, 2000 1434–1948/00/0707–1471 $ 17.50+.50/0

A $[Co_2(\mu\text{-}Cl)_3(thf)_6]^+$ complex similar to the cation in **1** was already reported by Sobola and co-workers[4] but has, in contrast to the analog iron and nickel species,[4,5] not yet been structurally determined. The molecular structure of the complex cation in **1** is shown in Figure 1.

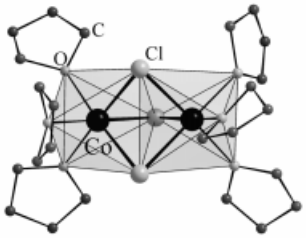


Figure 1. Molecular structure of the cation in **1** in the crystal; the drawn polyhedra illustrate the octahedral environment around the Co centers; H atoms are omitted for clarity; selected distances [pm] and angles [°]: Co−Cl 242.6(6)−248.0(6), Co−O 207.6(2)−216.0(2), Co···Co 302.4(4); Cl−Co−Cl 85.4(2)−86.8(2), O−Co−O 87.2(6)−91.4(5), O−Co−Cl(*cis*) 90.1(4)−95.5(4), O−Co−Cl-(*trans*) 175.7(4)−179.2(4)

Three oxygen atoms and three μ_2-Cl ligands surround the two Co atoms to form two face-sharing octahedra. Featuring nearly perfect octahedral angles, a slight trigonal compression results from the Co−O distances being naturally shorter than the Co−Cl bonds. The cation in **1** represents one of the few examples of octahedrally coordinated Co^{II} ions and also of threefold μ_2-bridged binuclear Co^{II} complexes. Another example is a cation coordinated terminally by 1,4,7-trimethyl-1,4,7-triazacyclononan.[6] More frequently, either the terminal ligands are negatively charged as in $[Co_2(\mu\text{-}Cl)_3(C_5Me_4R)_2]^+$ (R = Me, Et)[7,8] and thus give reason for a Co^{III} compound, or the Co^{II} complex is only doubly μ_2-Cl bridged, leading to the preferred tetrahedral coordination pattern. For instance, the latter is found in $[Co_2Cl_4(\mu\text{-}Cl)_2]^{2-}$,[9,10] in the trinuclear dianion $[\{CoCl_2\}_2\{Co(thf)_2\}(\mu_2\text{-}Cl)_4]^{2-}$ [11] or in the tetranuclear complex $[\{CoCl(thf)\}_2\{Co(thf)_2\}_2(\mu\text{-}Cl)_6]$.[12]

The anions in **1** (Figure 2) or **2** (Figure 3) are strongly related and only differ in one ligand at the Co center. Formal substitution of one $SnCl_3$ group in **2** for a Cl ligand in **1** correlates with the larger excess of $SnCl_2$ in the reaction mixture yielding **2** relative to that in the reaction leading to **1**. Both structures exhibit 18 electrons at the Co atom.

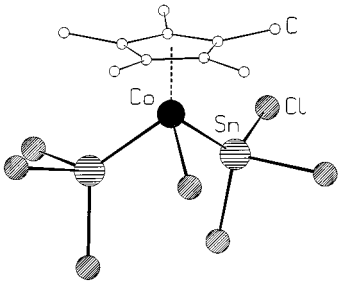


Figure 2. Molecular structure of the anion in **1** in the crystal; H atoms are omitted for clarity; selected distances [pm] and angles [°]: Co−Sn 247.4(3)−247.5(3), Sn−Cl 235.0(7)−240.3(7), Co−Cl 224.1(7), Co−C 207.1(2)−209.3(3); Sn−Co−Sn 96.2(1), Sn−Co−Cl 83.4(2)−87.2(2), Sn−Co−Cp*(*centroid*) 124.8(3)−127.1(2), Cl−Co−Cp*(*centroid*) 125.5(2), Cl−Sn−Cl 94.8(3)−97.6(3), Co−Sn−Cl 112.4(2)−125.9(2)

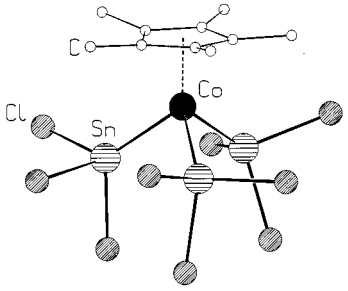


Figure 3. Molecular structure of the anion in **2** in the crystal; H atoms are omitted for clarity; selected distances [pm] and angles [°]:Co−Sn 247.1(1)−248.1(1), Sn−Cl 234.2(7)−241.1(5), Co−C 209.1(8)−215.1(7); Sn−Co−Sn 90.8(4)−93.6(4), Sn−Co−Cp*(*centroid*) 122.6(3)−125.8(3), Cl−Sn−Cl 91.3(1)−100.4(1), Co−Sn−Cl 114.1(1)−126.3(2)

In the complex anions, one Cp* ring and three further ligands *pseudo*-tetrahedrally coordinate the Co atom. Due to the steric demand of the Cp* groups, the angles around the Co center enclosed by the other ligands decrease by more than 13° with regard to the ideal tetrahedral angle of 109.47°. Steric problems that occur in the structures become clear when considering the Sn−Co−Cl angles in **1** which are narrowed even beyond orthogonal angles. In **2**, three bulky $SnCl_3$ groups inhibit this relaxation. The Sn atoms, two in **1** or three in **2**, are also placed in the center of distorted rather than ideal tetrahedra. Cl−Sn−Cl angles that are at least 9° smaller than 109.47° correspond to Cl−Sn−Co angles somewhat more obtuse than perfect tetrahedral angles. Showing similar Co−Sn bond lengths, the steric influence of the different substituents in the anions of **1** or **2** can mainly be seen from slightly elongated Co−C distances in **2** with regard to the corresponding distances in **1**.

Besides the fact that the syntheses of partly oxidized **1** and **2** suggest that the mild oxidant $K_6Sn_2Se_6$ acts irreversibly, the anions in the described products could also be relevant for another reason. Similar to other organometal-substituted tin halides, both complexes could serve to synthesize heteroatomic aggregates ligated by organometallic fragments. For example, compounds of the type $[ML_n(SnCl_3)]$ (L = Cp, CO, PR_3; R = organic group; M = Fe, Ni)[13,14] or $[(ML_n)_2(SnCl_3)_2]$ (L = Cp, CO; M = Fe, Co)[15,16] that are obtained in analogous insertion reactions (without redox processes) of either $[Cp(CO)_2Fe]Cl$, $[Co(CO)_4]Cl$ or $[NiCp(PPh_3)]Cl$ with $SnCl_2$, form organometallic saturated binary rings or cages when reacted with silylated chalcogens $E(SiMe_3)_2$ (E = S, Se, Te) or Na_2Se.[17] However, whereas the L_nM fragments of the quoted compounds contain 17 valence electrons and therefore provide only one metal−chlorine bond each for insertion of $SnCl_2$, the Cp^*Co^{III} fragments in **1** and **2** formally exhibit 14 valence electrons at the Co center. Thus, owing to the larger electronic requirements, one observes the coordination to three $SnCl_3$ units or to two $SnCl_3$ units and one Cl ligand. Whether these molecules can aggregate with silylated main-group elements, or whether the *ipso* position of two or even three $SnCl_3$ ligands at the metal center would result in a sterically overloaded product shall be further investigated.

Experimental Section

All reactions were carried out with exclusion of air and moisture, either under dry nitrogen or under argon (glove box). All solvents were dried and freshly distilled prior to use.

$[Co_2(\mu\text{-}Cl)_3(thf)_6][CoClCp^*(SnCl_3)_2]$ (1): $CoCl_2$ (26 mg, 0.20 mmol) and LiCp* (28 mg, 0.20 mmol) were stirred at room temperature for 20 min in THF (2 mL), resulting in a brown−black solution of $[CoClCp^*]_2$. After cooling down to −40 °C, $SnCl_2$ (133 mg, 0.70 mmol) in THF (1.5 mL) was added. During warming up to room temperature, the color changed to dark brown. Addition of $K_6Sn_2Se_6$ (28 mg, 0.03 mmol) at −78 °C terminated the synthesis. After 10 weeks at −40 °C, bundles of fine blue−black needle-like crystals of **1** appeared; yield: 0.071 g (0.053 mmol; 80%). − $C_{34}H_{63}Cl_{10}Co_3O_6Sn_2$ (1336.621): calcd. C 30.55, H 4.75; found C 30.52, H 4.68.

$[Li(thf)_4][CoCp^*(SnCl_3)_3]$ (2): $CoCl_2$ (78 mg, 0.60 mmol) and LiCp* (85 mg, 0.60 mmol) were stirred at room temperature for 20 min in THF (2 mL), resulting in a brown−black solution of $[CoClCp^*]_2$. A saturated solution (6 mL) of $SnCl_2$ (1.950 g, 10.28 mmol) in THF was added, causing a color change to dark blue. $K_6Sn_2Se_6$ (95 mg, 0.10 mmol) was introduced into the reaction mixture at −78 °C. After addition of 10 mL of toluene, the sample was stored at −40 °C. Within one week, large red−black cube-like crystals of **2** were found; yield: 454 mg (0.39 mmol; 65%). − $C_{26}H_{47}Cl_9CoLiO_4Sn_3$ (1164.739): calcd. C 26.81, H 4.07; found C 26.97, H 4.02.

Acknowledgments

This work was supported by the State of Baden-Württemberg (Margarete-von-Wrangell habilitation fellowship for S. D.). We gratefully acknowledge generous support from Prof. Dr. D. Fenske.

[1] C. Zimmermann, S. Dehnen, *Z. Anorg. Allg. Chem.* **1999**, *625*, 1963−1965.

[2] S. Dehnen, C. Zimmermann, *Chem. Eur. J.*, in the press.

[3] Data of the X-ray structure analyses. Mo-K_α radiation, graphite monochromator, imaging plate diffractometer STOE IPDS with rotating anode (Schneider); structure solution by direct methods and full-matrix least-squares refinement on F^2; used programs: SHELXS-86,[18] SHELXL-97.[19] − **2**: monoclinic, space group $P2_1$ (No. 4), $Z = 2$, $a = 1164.7(2)$, $b = 1408.8(3)$, $c = 1480.8(3)$ pm, $\beta = 97.40(3)°$, $V = 2572.2(9)\cdot10^6$ pm^3, $\rho_{calcd.} = 1.726$ g·cm^{-3}, $2\theta = 4-46°$, 6341 reflections measured, 4830 independent reflections [$R_{int} = 0.084$], 3772 with $I > 2\sigma(I)$, μ(Mo-K_α) = 2.641 mm^{-1}; 351 parameters (positions of nonhydrogen atoms except the partly twofold disordered atoms of the THF ligands were refined employing anisotropic displacement parameters; C and O atoms of the THF molecules were refined isotropically assuming split positions wherever necessary; H atoms were calculated for ideal positions and were not refined). Maximum peak on the final difference Fourier map: 1.129 e$^-$·Å^{-3}. $R_1 = 0.072$, $wR_2 = 0.177$. − **3**: orthorhombic, space group $Pca2_1$ (No. 29), $Z = 4$, $a = 2150.1(4)$, $b = 990.5(2)$, $c = 2006.8(4)$ pm, $V = 4273.7(15)\cdot10^6$ pm^3, $\rho_{calcd.} = 1.810$ g·cm^{-3}, $2\theta = 4-48°$, 17785 reflections measured, 6660 independent reflections [$R_{int} = 0.052$], 6238 with $I > 2\sigma(I)$, μ(Mo-K_α) = 2.705 mm^{-1}; 372 parameters (positions of nonhydrogen atoms except the partly twofold disordered atoms of the THF ligands were refined employing anisotropic displacement parameters; Cl8 and Cl9 show twofold disorder; therefore, adequate split positions were assigned; C and O atoms of the THF molecules were refined isotropically assuming split positions wherever necessary; H atoms were calculated for idealized positions and were not refined). Maximum peak on the final difference Fourier map: 1.849 e$^-$·Å^{-3}. $R_1 = 0.048$, $wR_2 = 0.133$. Crystallographic data (excluding structure factors) for the structures reported in this paper have been deposited with the Cambridge Crystallographic Data Centre as supplementary publication nos. CCDC-137021 and CCDC-137022. Copies of the data can be obtained free of charge on application to CCDC, 12 Union Road, Cambridge CB2 1EZ, UK [Fax: (internat.) + 44-1223/336-033; E-mail: deposit@ccdc.cam.ac.uk].

[4] Z. Janas, T. Lis, P. Sobota, *Polyhedron* **1992**, *11*, 3019−3023.

[5] Z. Janas, P. Sobota, T. Lis, *J. Chem. Soc., Dalton Trans.* **1991**, 2429−2434.

[6] U. Bossek, D. Nuhlen, E. Bill, T. Glaser, C. Krebs, T. Weyhermuller, K. Wieghardt, M. Lengen, A. X. Trautwein, *Inorg. Chem.* **1997**, *36*, 2834−2843.

[7] W. L. Olson, L. F. Dahl, *Acta Crystallogr., Sect. C* **1986**, *42*, 541−544.

[8] C. Couldwell, J. Hussain, *Acta Crystallogr., Sect. B* **1978**, *34*, 2444−2450.

[9] K. R. Dunbar, A. Quillevéré, S. C. Haefner, *Acta Crystallogr., Sect. C* **1991**, *47*, 2319−2321.

[10] O. K. Kireeva, B. M. Bulychev, N. R. Streltsova, V. K. Belsky, A. G. Dunin, *Polyhedron* **1992**, *11*, 1801−1807.

[11] C. v. Hänisch, D. Fenske, F. Weigend, R. Ahlrichs, *Chem. Eur. J.* **1997**, *3*, 1494−1498.

[12] P. Sobota, Z. Olejnik, J. Utko, T. Lis, *Polyhedron* **1993**, *12*, 613−616.

[13] F. Bonati, G. Wilkinson, *J. Chem. Soc. A* **1964**, 179−181.

[14] D. J. Patmore, W. A. Graham, *Inorg. Chem.* **1966**, *5*, 1405−1407.

[15] P. Hackett, A. R. Manning, *J. Chem. Soc., Dalton Trans.* **1972**, 1487−1491.

[16] F. Glockling, A. McGregor, *J. Inorg. Nucl. Chem.* **1973**, *35*, 1481−1485.

[17] [17a] K. Merzweiler, L. Weisse, *Z. Naturforsch.* **1990**, *45b*, 971−978. − [17b] K. Merzweiler, L. Weisse, *Z. Naturforsch.* **1991**, *46b*, 695−698. − [17c] K. Merzweiler, H. Kraus, L. Weisse, *Z. Naturforsch.* **1993**, *48b*, 287−290. − [17d] K. Merzweiler, H. Kraus, *Z. Naturforsch.* **1993**, *48b*, 1009−1012. − [17e] K. Merzweiler, H. Kraus, *Z. Naturforsch.* **1994**, *49b*, 425−429. − [17f] H. Kraus, K. Merzweiler, *Z. Naturforsch.* **1997**, *52b*, 635−638.

[18] G. M. Sheldrick, University of Göttingen, Germany, **1986**.

[19] G. M. Sheldrick, University of Göttingen, Germany, **1993**.

Received December 2, 1999
[I99440]

Compounds of Silicon and Homologues, 134[+] Supersilyl Compounds of Boron and Homologues, 10[++]

Tri(supersilyl)dialanyl $(t\mathrm{Bu_3Si})_3\mathrm{Al_2}^{\bullet}$ and Tetra(supersilyl)cyclotrialanyl $(t\mathrm{Bu_3Si})_4\mathrm{Al_3}^{\bullet}$ − New Stable Radicals of a Group 13 Element from Thermolysis of $(t\mathrm{Bu_3Si})_4\mathrm{Al_2}$

Nils Wiberg,*[a] Thomas Blank,[a] Wolfgang Kaim,[b] Brigitte Schwederski,[b] and Gerald Linti[c]

Keywords: Ab initio calculations / Aluminum / ESR Spectroscopy / Radicals / Silicon

The thermolysis of tetra(supersilyl)dialane $R^{*}{}_2Al–AlR^{*}{}_2$ (R^{*} = $SitBu_3$ = Supersilyl) in heptane or cyclohexane at 50 °C leads under Al–Al dissociation reversibly to monoalanyl radicals $[R^{*}{}_2Al]^{\bullet}$, which could be trapped by hydrogen or iodine (formation of $R^{*}{}_2AlH$, $R^{*}{}_2AlI$). Simultaneously, SiAl dissociation and elimination of supersilyl radicals $t\mathrm{Bu_3Si}^{\bullet}$ leads irreversibly and slowly to radicals $[R^{*}{}_2Al–AlR^{*}]^{\bullet}$, the existence of which could be established by ESR spectroscopy. The structure was clarified by ab initio calculations (nearly planar $Si_2Al–AlSi$ and linear Al–Al–Si skeleton; short Al–Al distance). By thermolyzing $R^{*}{}_2Al–AlR^{*}{}_2$ at 100 °C, the radical $[R^{*}{}_4Al_3]^{\bullet}$ (ESR spectroscopically detected) and the *tetrahedro*-tetraalane $R^{*}{}_4Al_4$ (NMR spectroscopically seen) are formed via radicals $[R^{*}{}_3Al_2]^{\bullet}$; the supersilyl radicals $t\mathrm{Bu_3Si}^{\bullet}$, formed at the same time, are stabilized by dimerization to superdisilane $R^{*}–R^{*}$ and by taking up hydrogen, giving supersilane $R^{*}–H$. According to X-ray structure analysis, the Al atoms in $[R^{*}{}_4Al_3]^{\bullet}$ are located at the corners of a triangle; one Al atom is connected with two groups R^{*}, the remaining two Al atoms each bind one substituent R^{*} in different ways.

Introduction

Unlike aluminum triorganyls R_3Al with aluminum in the oxidation state III, which were synthesized for the first time in the middle of the 19th century,[1] aluminum organyls R_mAl_n with aluminum in the oxidation state < III were unknown for a long time because of their high tendency for disproportionation into R_3Al and Al.[2,3] Therefore, dehalogenations of diorganylaluminum chlorides R_2AlCl with substituents R of *lower to medium bulkiness* like CH_2R' (R' = H, Me, Et, CMe_3, $SiMe_3$) or 2,4,6-$Me_3C_6H_2$ lead to R_3Al and Al. The results were interpreted as disproportionations of intermediately formed tetraorganyldialanes R_4Al_2.[2] According to Equation (1), the latter disproportionations may proceed via aluminum cluster compounds R_mAl_n, which are formed from starting materials with a higher *m*/*n* ratio and transform into products with a lower *m*/*n* ratio.

$$3\ R_4Al_2 \xrightarrow{-(\text{over } R_mAl_n)} 4\ R_3Al + 2\ Al\ (\text{or } 6\ R_2 + 6\ Al) \quad (1)$$

The substituents R in R_2AlCl with *higher bulkiness* like $CH(SiMe_3)_2$ or 2,4,6-$iPr_3C_6H_2$ inhibit this disproportionation. As a result of this, the dehalogenation of R_2AlCl stopped under normal conditions at the tetraorganyldialanes R_4Al_2 with aluminum in the oxidation state II.[2] Exactly the same holds for the bulky substituent Supersilyl (R^{*} = $SitBu_3$), which also allows the isolation of a dialane(4), namely tetra(supersilyl)dialane $R^{*}{}_4Al_2$ (**1**), at room temperature.[4] At higher temperatures, compound **1**, amongst others, decomposes into the *tetrahedro*-tetraalane $R^{*}{}_4Al_4$ with aluminum in the oxidation state I (and the *m*/*n* ratio decreases from 2 to 1).[4]

In this paper, two established intermediates of the mentioned dialane(4) thermolysis will be introduced, namely the dialanyl radical $R^{*}{}_3Al_2^{\bullet}$ (**2**) and the cyclotrialanyl radical $R^{*}{}_4Al_3^{\bullet}$ (**3**). The starting material $R^{*}{}_4Al_2$ (**1**) required for the thermolysis is − as was recently reported − easily prepared in quantitative yields by reaction of supersilyl sodium NaR* with aluminum trihalides AlX_3 (X = Cl, Br) in heptane at room temperature according to Equation (2):

$$6\ NaR^{*} + 2\ AlX_3 \rightarrow R^{*}{}_4Al_2\ (\mathbf{1}) + R^{*}R^{*} + 6\ NaX \quad (2)$$

Isolable reaction intermediates in the formation of the red **1** are yellow di(supersilyl)aluminum halides $R^{*}{}_2AlX$ ($AlX_3 + 2\ NaR^{*} \rightarrow R^{*}{}_2AlX + 2\ NaX$).[5] Excess supersilylsodium converts $R^{*}{}_2AlX$ into the radicals $R^{*}{}_2Al^{\bullet}$ and $R^{*\bullet}$, which, for steric reasons, cannot combine to form R_3Al, but

[+] Part 133: N. Wiberg, A. Wörner, D. Fenske, H. Nöth, J. Knizek, K. Polborn, *Angew. Chem.* **2000**, *112,* 1908−1912; *Angew. Chem. Int. Ed.* **2000**, *39*, 1838−1842.
[++] Part 9: N. Wiberg, T. Blank, A. Purath, H. Schnöckel, *Angew. Chem.* **1999**, *111*, 2745−2748; *Angew. Chem. Int. Ed.* **1999,** *38*, 2563−2565.

[a] Department Chemie der Universität München, Butenandtstraße 5−13 (Haus D), D-81377 München, Germany
[b] Institut für Anorganische Chemie der Universität Stuttgart, Pfaffenwaldring 55, D-70550 Stuttgart, Germany
[c] Institut für Anorganische Chemie der Universität Karlsruhe, Engesserstraße, Geb. 30.45, D-76128 Karlsruhe, Germany

 © WILEY-VCH Verlag GmbH, D-69451 Weinheim, 2000 1434−1948/00/0707−1475 $ 17.50+.50/0

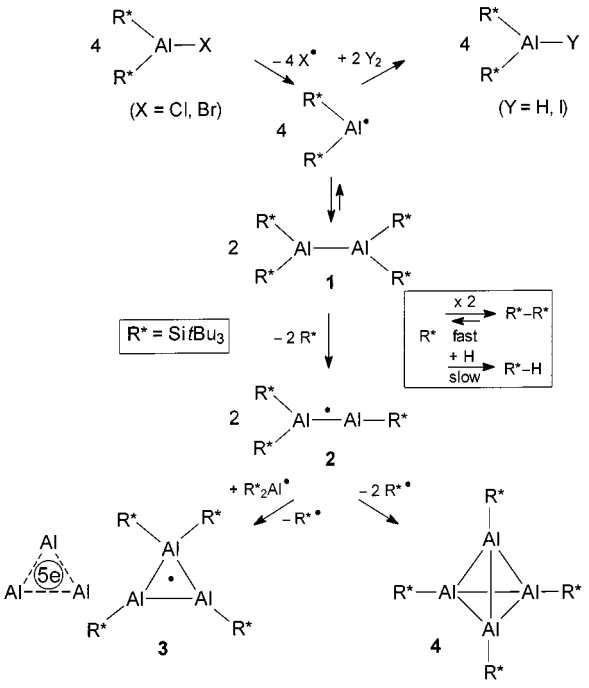
instead dimerize to $R^*_2Al-AlR^*_2$ and R^*R^* according to Equation (3) (see also Scheme 1):

$$2\,R^*_3AlX + 2\,NaR^* \rightarrow 2\,R^*_2Al^\bullet + 2\,NaX + 2\,R^{*\bullet} \rightarrow \mathbf{1} + 2\,NaX + (R^*)_2 \quad (3)$$

Formation of Dialanyl Radicals $R^*_4Al_3^\bullet$ and Cyclotrialanyl Radicals $R^*_4Al_3^\bullet$

The first step of thermolysis of **1** may involve a homolytic dissociation of the Si−Al or the Al−Al bonds (cf. Scheme 1). Mild warming of **1** in heptane or cyclohexane to 50 °C leads by fast and reversible Al−Al bond dissociation to the di(supersilyl)alanyl radical $R^*_2Al^\bullet$ in low equilibrium concentration. This is supported − as we mentioned previously[4] − by the reaction of **1** with hydrogen or iodine which leads to di(supersilyl)alane R_2AlH or di(supersilyl)aluminum iodide R^*_2AlI (cf. Scheme 1). In the absence of trapping reagents for $R^*_2Al^\bullet$ and by heating the solution to 80 °C, compound **1** slowly but irreversibly gives the tri(supersilyl)dialanyl radicals $R^*_3Al_2^\bullet$ (**2**) by Si−Al bond dissociation. The latter transforms slowly and irreversibly into the tetra(supersilyl)cyclotrialanyl radical $R^*_4Al_3^\bullet$ (**3**) and tetra(supersilyl)-*tetrahedro*-tetraalane $R^*_4Al_4$ (**4**) (Scheme 1). Thereby, compound **3** may be formed by reaction of **2** with $R^*_2Al^\bullet$, and compound **4** by reaction of **2** with itself. The simultaneously obtained supersilyl radicals $R^{*\bullet}$ dimerize to superdisilane R*−R* (cf. Scheme 1). After heating **1** in heptane or cyclohexane for 4 hours at 70 °C, the dialane(4) is completely decomposed and the black-green solution then contains **2, 3** and **4**, as well as $(R^*)_2$.

By heating the solution to 100 °C, or by heating compound **1** for 10 hours in heptane at 100 °C (reflux), the intermediately formed **2** transforms completely into **3** and red-violet **4** (cf. Scheme 1; $R^*_4Al_4$ has been prepared previously by a different method and is well characterized).[6] At the same time the superdisilane $(R^*)_2$ present in the mixture decomposes slowly into supersilyl radicals, which are then stabilized by abstracting H atoms from the chemical surroundings (formation of supersilane R*−H; cf. Scheme 1). Compound **3** crystallized after two months from a heptane solution as black-green, paramagnetic, moisture- and air-sensitive crystals. Heating **3** in heptane at higher temperatures transforms the radicals into other products, the identities of which are currently being investigated.



Scheme 1. Thermolysis of tetra(supersilyl)dialane **1**

It should be mentioned here that the heavier homologue of **2**, tri(supersilyl)digallanyl $R^*_3Ga_2^\bullet$ forms so easily that the initial stage, tetra(supersilyl)digallane $R^*_4Ga_2$, is not isolable.[7] Thermolysis of $R^*_3Ga_2^\bullet$ in heptane at 100 °C leads exclusively to tetra(supersilyl)-*tetrahedro*-tetragallane $R^*_4Ga_4$.[8] This fact supports our proposal in Scheme 1 that the tetrahedranes $R^*_4E_4$ (E = Al, Ga) are formed by reaction of $R^*_3E_2^\bullet$ with $R^*_3E_2^\bullet$, and the cyclic radicals $R^*_4E_3^\bullet$ by reaction of $R^*_3E_2^\bullet$ with $R^*_2E^\bullet$ (not present in the case of $R^*_3Ga_2^\bullet$); in fact, $R^*_4Ga_3^\bullet$ has been prepared by another route). However, other mechanisms are also imaginable. Interestingly, dilute solutions of **1** form the *tetrahedro*-tetrahedrane **4** under the action of light.

Unlike $R^*_4Al_2$ and $R^*_3Ga_2^\bullet$, tetra(supersilyl)diindane $R^*_4In_2$ thermolyzes in heptane at 100 °C within 18 hours to octa(supersilyl)dodecaindane $R^*_8In_{12}$.[9] The diindanyl $R^*_3In_2^\bullet$ and cyclotriindanyl $R^*_4In_3^\bullet$ radicals, which may be reaction intermediates, have not yet been observed by ESR spectroscopy [tetra(supersilyl)-*tetrahedro*-tetraindane $R^*_4In_4$ is not formed under these conditions].

Structure and ESR Spectrum of Dialanyl Radicals $R^*_3Al_2^\bullet$ (2)

As mentioned above, the thermolysis of **1** in heptane leads to compounds **2**, **3** and **4**. Until now, only compound **3** has been isolated as crystals from such solutions.

According to ab initio calculations at the RI-DFT level, the structure of the radical **2** is comparable to the structure of the black-blue radical $R^*_3Ga_2^\bullet$, which has previously been examined by an X-ray structure analysis.[7] Figure 1 shows the results of these calculations[10] together with selected bond lengths for $R^*_3Al_2^\bullet$ (ab initio calculation) and $R^*_3Ga_2^\bullet$ (X-ray structure analysis). Both radicals show almost a planar Si_2E-ESi skeleton (sum of angles at E1 = Al1/Ga1 359.7/359.3°); in addition, the E−E−Si skeleton is nearly linear (angles at E2 = Al2/Ga2 174.9/170.0; the E1−E2−Si3 plane is nearly orthogonal to the Si1−E1−Si2 plane). In both cases the E−E distance is comparatively short. This points to an E−E bonding order greater than one. The observed shortening of the E−E bond length in the order $R^*_3Al_2^\bullet \rightarrow R^*_3Ga_2^\bullet$ (2.537 → 2.423 Å; difference 0.114 Å) may be due to a reduction of the radius or of the charge separation in the order Al → Ga [analogously, the E−E single bond length decreases in the order $Disyl_4Al_2 \rightarrow Disyl_4Ga_2$: 2.660 → 2.541 Å; difference 0.119 Å;[2] Disyl = $CH(SiMe_3)_2$]. According to this, $R^*_3E_2^\bullet$ contains sp^2- and

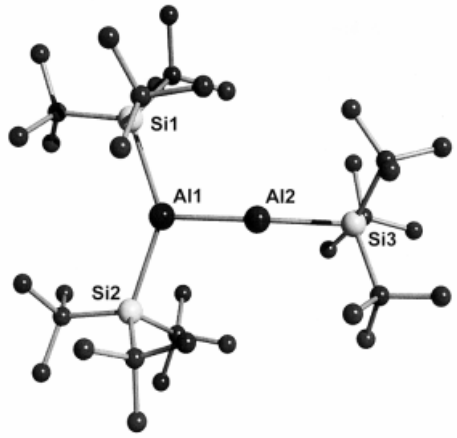


Figure 1. Structure of $R^*_3Al_2^\bullet$ (**2**) from RI-DFT calculations; selected calculated bond lengths [Å] and angles [°] (in brackets, for comparison, analogous bond lengths and angles for $R^*_3Ga_2^\bullet$; in the latter case, the mean values of two independent molecules in the cell): Al1−Al2 2.537 (2.423), Al1−Si1 2.583 (2.513), Al1−Si2 2.571 (2.499), Al2−Si3 2.562 (2.504); Al2−Al1−Si1 107.87 (109.32), Al2−Al1−Si2 109.58 (109.90), Si1−Al1−Si2 142.21 (140.44), Al1−Al2−Si3 174.90 (170.03)

sp-hybridized E atoms, which are connected via two-electron σ- and one-electron π-bonds.

The constitution of **2** is deduced from the ESR spectrum of solutions in pentane or cyclohexane. Well-resolved spectra of **2** are only obtained from alkane solutions of the dialane **1**, which always contain traces of the radical **2**, but no traces of the radical **3**.

Solutions of $R^*_2Al-A1R^*_2$ in alkanes exhibit a simple room-temperature ESR spectrum for the paramagnetic species $[R^*_2Al-A1R^*]^\bullet$. The hyperfine coupling of the unpaired electron with the two- and the three-coordinate aluminum atom (^{27}Al, nuclear spin $I = 5/2$, 100% nat. abundance) is rather similar and leads to groups of peaks with from one to six EPR lines (Figure 2a). The observed coupling constants are $a(Al1) = 2.18$ mT and $a(Al2) = 1.89$ mT; the isotropic g factor is 2.0011 (cf. Figure 1 for atom numbering and Figure 2b for simulation of the ESR spectrum). As described for a number of related radicals,[7,11,12] $[R^*_2Al-AlR^*]^\bullet$ shows a strong anisotropic broadening of the outer lines (Figure 2a). The reason for this known effect is the comparatively slow rotation of the heavy molecule in solution as a result of the large moment of inertia. Therefore, strong anisotropic contributions of the g factor and hyperfine tensors, which result from the π character of the radical electron, are not completely averaged out at room temperature. The strikingly small difference between the two ^{27}Al coupling constants does not allow a clear assignment. Obviously, the π character of the unpaired electron at the center of the two-coordinate Al atom leads to a comparatively low $a(^{27}Al)$ value, whereas the center of the three-coordinate approximately non-radical Al atom has a rather high coupling constant. The latter follows from spin polarization and from the bulkiness of the supersilyl group which may favor a large spin density. The stronger participation of s contributions is illustrated by the generally higher coupling constants for $[R^*_2Al-AlR]^\bullet$ compared to those of

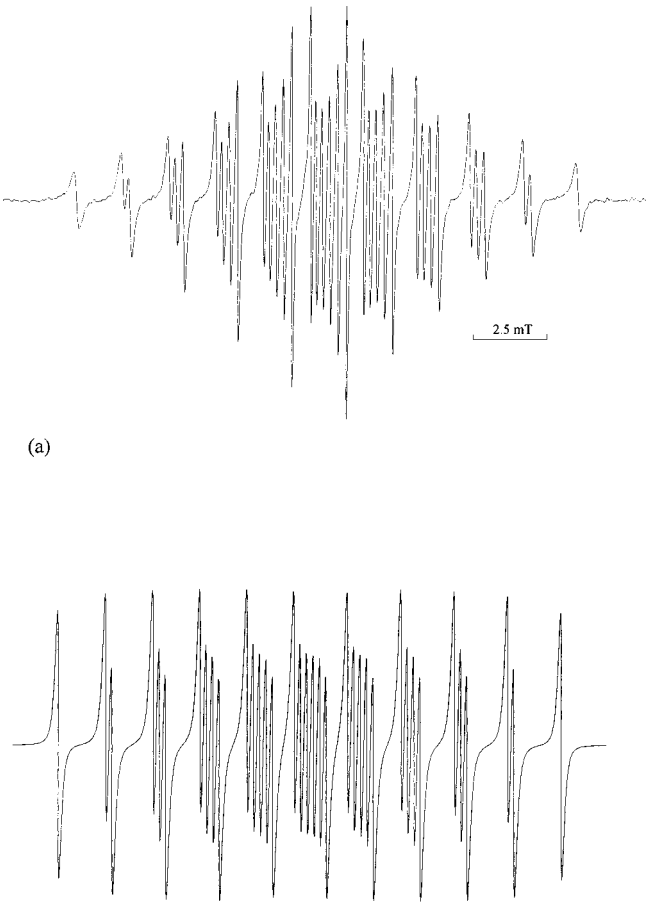


Figure 2. ESR spectrum of **2** in *n*-pentane: (a) with strong anisotropic broadening of lines, and (b) its simulation with hyperfine coupling constants $a(Al1) = 2.18$ mT and $a(Al2) = 1.89$ mT

$[R_2Al-AlR_2]^{\bullet-}$ [R′ = $CH(SiMe_3)_2$; $a(^{27}Al) = 1.11$ mT]. As the g factor differs only slightly from g (electron) = 2.0023, the radical $[R^*_2Al-AlR^*]^\bullet$ must be a π-radical. The deviation to lower g agrees with observations for the radical $[R^*_2Ga-GaR^*]^\bullet$, which shows clearer effects as a consequence of the higher spin-orbit coupling factor for gallium.[7]

Structure and ESR Spectrum of the Cyclotrialanyl Radical $R^*_4Al_3^\bullet$ (3)

The structure of the radicals $R^*_4Al_3^\bullet$ (**3**) in the black-green crystals (monoclinic; obtained from heptane) is shown in Figure 3, together with selected bond lengths and angles. According to this figure, the position of the atoms Al1 and Al3 is split. The Me groups of the *t*Bu groups at Si2 were refined in the split positions with occupancy factors of 0.5; Al1 and Al2 also have occupancy factors of 0.50. Evidently, the three Al atoms occupy the corners of a triangle with two longer sides (average Al−Al distance: 2.756 Å) and a slightly shorter base (Al−Al distance: 2.703 Å). The atom Al2 at the top of the triangle binds two supersilyl groups and each Al atom of the base is connected

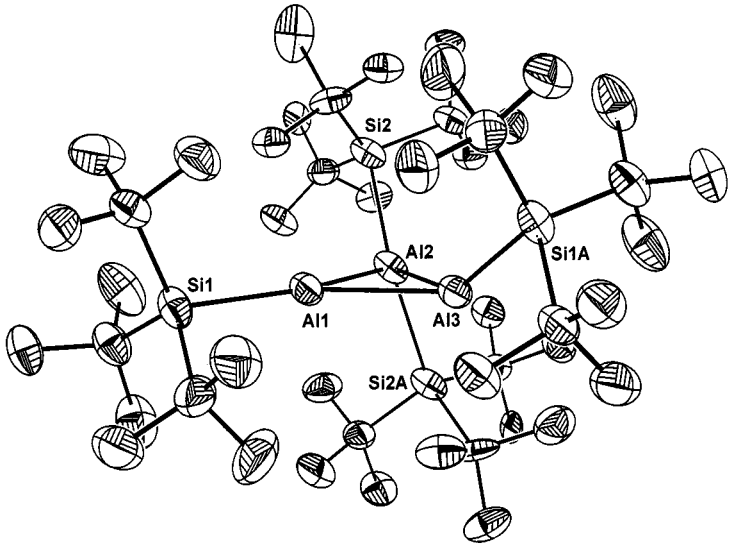


Figure 3. Structure of radicals $R^*_4Al_3^\bullet$ (**3**) in the crystal and atom numbering used (ORTEP-Plot; 25% thermal probability ellipsoids; H atoms omitted for clarity); selected distances [Å] and angles [°] in the structure of radical **3** with standard deviations (the positions of Al1 and Al2 are doubly split): Al1−Al2 2.737(2), Al1−Al3 2.703(3), Al2−Al3 2.776(2), Al1−Si1 2.519(1), Al2−Si2 2.556(1), Al3−Si3A 2.586(2); Al2−Al1−Al3 61.35(6), Al1−Al2−Al3 58.33(8), Al2−Al3−Al1 59.92(7), Si1−Al1−Al2 152.6(1), Si1−Al1−Al3 146.0(1) (angle sum at Al1 359.9), Si1A−Al3−Al2 44.5(1), Si1A−Al3−Al1 123.6(1) (angle sum at Al3 328.0), Si2−Al2−Al1 110.48(6), Si2−Al2−Al3 125.47(6), Si2A−Al2−Al1 107.66(6), Si2A−Al2−Al3 90.71(6), Si2−Al2−Si2A 137.28(8)

to only one supersilyl group. The structural data may be interpreted by assuming that the R*Al groups are more weakly bonded to R^*_2Al than to each other [cf. the Al−Al distance in $R^*_4Al_2$ (2.751 Å)].[4] If the R^*_2Al group provides one and each R*Al group two electrons for the Al_3 framework, there are 5 electrons available for the Al_3 cluster. Possibly, the radical electron acts as a π-electron for the connection of the two R*Al groups. Intuitively, one might argue that the observed geometry of **3** looks as if cyclisation of *catena*-$[R^*_2Al-R^*Al-AlR^*]^\bullet$ (a derivative of **2** with one R* exchanged by R^*_2Al) − in the course of which the connection of R*Al−AlR* becomes weather, the connection $R^*_2Al\cdots AlR^*$ becomes stronger − is stopped half way on the reaction coordinate (cf. ab initio calculations).

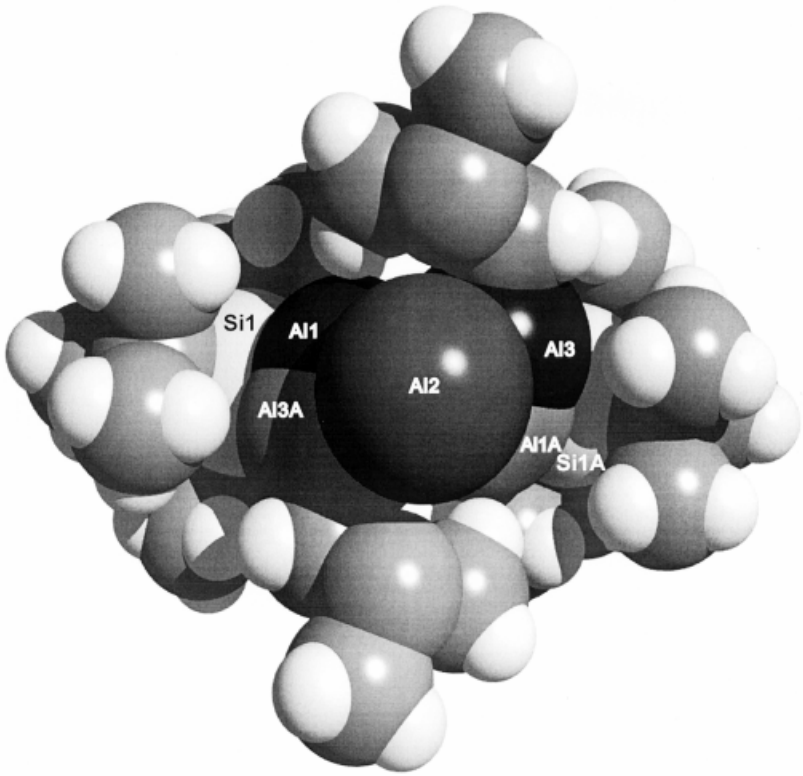


Figure 4. Space filling model of the radical **3** (Si2 and Si2A each with two *t*Bu groups are omitted for clarity)

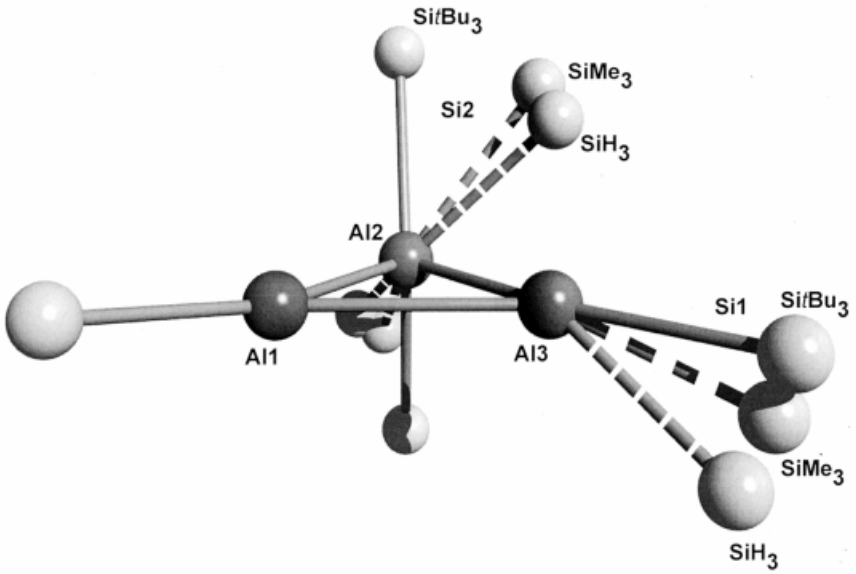


Figure 5. Structure of $R^*_4Al_3^\bullet$ with R = SiH_3, $SiMe_3$, $SitBu_3$ as derived from RI-DFT calculations;selected calculated bond lengths [Å] and angles [°] in each case for $(H_3Si)_4Al_3^\bullet$/$(Me_3Si)_4Al_3^\bullet$/$(tBu_3Si)_4Al_3^\bullet$: Al1−Al3 2.532/2.645/2.902, Al1−Al2 2.489/2.463/ 2.625, Al2−Al3 3.065/2.560/2.623, Si1−Al3 2.798/2.908/4.292; angle sum at Al1 356.80/ 349.50/360.00, angle sum at Al3 334.43/359.75/360.00

According to Figure 3, the four Si atoms of the supersilyl groups of **3** occupy the corners of a tetrahedron with five edges of roughly equal length (average Si−Si distance: 6.321 Å) and one shorter side which is connected to the atom Al2 in its center (Si−Si distance: 4.760 Å). The reason for the nearly regular tetrahedral packing of the supersilyl groups comes probably from considerable van der Waals attraction between the methyl groups of the substituents R*.[13]

The Al atoms of the Al_3 ring now fill up the interstices of the $(R^*)_4$ entity, whereby an arrangement of two planar three-coordinated atoms Al1 and Al3 and, at the same time, of a tetrahedral four-coordinated atom Al3 is obviously impossible. Consequently, in order to fill cavities in the $(R^*)_4$ entity (cf. Figure 4), one of the three-coordinated Al atoms is planar, the other one is pyramidal and the planar Si_2Al is not orthogonal to the plane of Al_3 (cf. Figure 3). Over and above that, the splitting positions of the two atoms Al1 and Al3 point to a fast structural fluctuation of the conformations of the mentioned atoms.

An ab initio calculation (RI-DFT) of the structure of radical **3** differs from the experimentally observed one in several points (cf. Figure 5); in particular, Al2 is tetrahedrally coordinated whereas Al1 and Al3 are each planar coordinated. In addition, the calculated Al1−Al3 distance is much longer than the other Al−Al bonds, contrary to the bonding situation in the experimentally observed structure of **3** (on the other hand, $R^*_4Ga_3^\bullet$ shows the predicted structure). Whether this predicted open chain structure is the global minimum was not checked, although it resulted during minimization of the energy, starting from the experimental structure. The structure of radicals $R_4Al_3^\bullet$ proved to be dependent on the bulkiness of the four substituents. Therefore, a decrease of bulkiness of the four substituents leads, according to ab initio calculations, to a bonding relation of an Al2 bonded silyl group to Al1 or Al3 (cf. Figure 5), that is a bridging position of a silyl group.

In the ESR spectrum of very dilute solutions of **1** in C_6D_{12} at 80 °C, the typical hyperfine structure of the signal for the radical **2** is observed (Figure 2a). After a few minutes this spectrum disappears. Solutions which are thermolyzed in C_6D_{12} at 80 °C for longer periods of time exhibit a low resolution ESR spectrum: many lines separated by about 1.1 mT are now seen. Obviously, two ESR signals from two different radicals overlap. After leaving this solution for a long time at room temperature, radical **2** reappears in the ESR spectrum. Finally, an ESR spectrum of a dilute solution of pure, isolated radical **3** is shown in Figure 6 (the fact that no NMR signal is detected from this solution confirms the radical character of **3**).

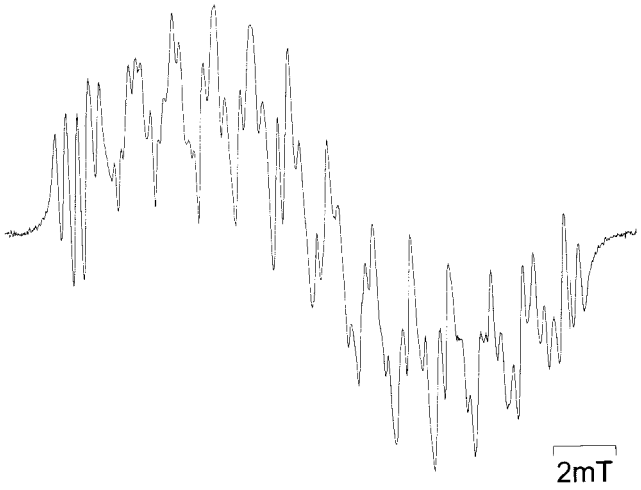


Figure 6. ESR spectrum of **3** in *n*-pentane

The resolution of the ESR spectrum of **3** at room temperature is lower and the number of lines is higher than for the ESR spectrum of **2**. Therefore, the hyperfine structure of the signal, centered at $g = 2.0053$, could not yet be analyzed completely. Besides a clearly determined small coupling

constant for one Al atom of nearly 0.3 mT, two larger and obviously different coupling constants for the second and third Al atoms of nearly 1.3 mT are determined. This assignment is in agreement with the total spectral width of 15.0 mT. According to the *g* factor and the hyperfine structure, the radical **3** is predominantly a π radical. The smaller ^{27}Al coupling constant may be associated with the four-coordinate Al center (cf. AlR_n-coordinated organic π radicals).[14,15] On the other hand, the non-equivalence of the two remaining Al centers with hyperfine coupling constants in conventional ranges is well in agreement with the results of the X-ray structure analysis of **3** (see above) and also with an equilibrium *cyclo*-**3** ⇄ *catena*-**3**, where by $R^*_4Al_3^•$ shows a cyclic structure in the solid state and a chain structure in solution.

Experimental Section

All experiments were carried out in flame-dried glass apparatus with standard Schlenk techniques under an atmosphere of dry argon or nitrogen. During all manipulations air and moisture were strictly excluded. The solvents (cyclohexane, heptane, pentane, benzene) were distilled from sodium/lead or sodium/benzophenone. For NMR spectra a JEOL GSX-270 ($^1H/^{13}C/^{29}Si$: 270.17/67.94/53.67 MHz) and a JEOL EX-400 ($^1H/^{13}C/^{29}Si$: 399.78/10.54/79.43 MHz) were available. The ^{29}Si NMR spectra were recorded with the INEPT pulse sequence using empirically optimized parameters for polarization transfer from the *t*Bu substituents. The ESR spectra were recorded with a Bruker System ESP 300.

Formation of Tri(supersilyl)dialanyl 2: In an evacuated and sealed NMR tube a solution of **1**[4] (0.020 g, 0.023 mmol) in C_6D_{12} (0.6 mL) was heated to 70 °C for 4 hours and then cooled to room temperature. After this procedure, the black-green solution was found to be free of starting material **1** (by NMR spectroscopy); however, it contained superdisilane $tBu_3Si-SitBu_3$ (identification by comparison with an authentic sample)[13] and also, according to an ESR spectrum, the radical **2** (not visible in the NMR spectrum). It did not prove possible to isolate crystals of **2** suitable for an X-ray structure analysis.

Formation of Tetra(supersilyl)cyclotrialanyl 3: A solution of **1**[4] (0.264 g, 0.308 mmol) in heptane (25 mL) was heated to 100 °C for 10 hours (reflux) and then cooled to room temperature. After this procedure, the black-green solution was found to be free of starting material **1** (by NMR spectroscopy); however, it contained supersilane tBu_3Si-H, superdisilane $tBu_3Si-SitBu_3$ and **4** [identification by comparison with an authentic samples;[6,13] δ(^1H; C_6D_{12}) = 1.148, 1.382. 1.263] and also, according to an ESR spectrum, the radical **3** (cf. Figure 6; not visible in the NMR spectrum). The area ratio of the ^1H NMR signals for tBu_3Si-H, $tBu_3Si-SitBu_3$ and $(tBu_3Si)_4Al_4$ (**4**) amounts to 6:5:4 (measured for $SitBu_3$). Consequently, besides one molecule of **4** with four silicon-bonded supersilyl groups, eleven supersilyl radicals are formed which stabilize by formation of tBu_3Si-H and $tBu_3Si-SitBu_3$. Since four tBu_3Si radicals arise during the formation of one molecule of **4** from two molecules of **1** ($2 \times \mathbf{1} \rightarrow \mathbf{4} + 4\ tBu_3Si$), $11 - 4 = 7\ tBu_3Si$ radicals must come from the formation of **3**. As two tBu_3Si radicals are produced per radical of **3** from 1.5 molecules of **1** ($1.5 \times \mathbf{1} \rightarrow \mathbf{3} + 2\ tBu_3Si$), 7 tBu_3Si radicals originate from the formation of 3.5 radicals of **3**. For the formation of 3.5 molecules of **3** and 1 molecule of **4**, therefore, $(3.5 \times 1.5) + (1 \times 2) = 7.25$ molecules of **1** are needed. Consequently, **3** and **4** are formed in yields of 70 and 30%. In another experiment dialane (0.339 g, 0.395 mmol) was heated in 25 mL cyclohexane at 80 °C for 15 hours. The solvent and all volatile components (C_6H_{12}, tBu_3Si-H) were then removed in vacuo and the remaining residue was dissolved in 10 mL heptane. After 2 months tetra(supersilyl)cyclotrialanyl **3** (0.22 g) crystallized from this solution at −25 °C as black-green cubes.

DFT Calculations: All RI-DFT calculations (AL2 and AL3) were carried out with the program package TURBOMOLE with the BP86-Functional and SV(P) basis sets.[10]

X-ray Structure Determination of 3: Stoe IPDS diffractometer, Mo-K_α radiation with λ = 0.71073 Å, graphite monochromator, image plate detector, crystal dimensions 0.15 × 0.20 × 0.28 mm, fixed on glass fiber, measurement temperature 200(2) K, $C_{48}H_{108}Al_3Si_4 \cdot 0.25C_6H_{14}$, M_r = 921.73, black-green rhombus, monoclinic space group *C*2/*c*, *a* =21.344(4), *b* = 12.794(3), *c* = 23.955(5) Å, *V* = 6514(2) Å^3, *Z* = 4, ρ_{ber} = 0.940 g·cm^{-3}, μ = 0.159 mm^{-1}, *F*(000) = 2064. − *Data collection*: 2θ =4.08 − 51.84° in $-26 \le h \le 26$, $-15 \le k \le 15$, $-29 \le l \le 29$; of 22750 reflections 6316 were independent (R_{int} = 0.068) and 4446 were observed [$F > 4\sigma(F)$], 377 parameters, R_1 = 0.0887, wR_2 = 0.2870, weighting factor $w^{-1} = \sigma^2F_0^2 + 0.194P^2$ with $P = F_0^2 + 2F_c/3$. − *Structure determination:* The structure was solved by direct methods (SHELX-97). All non-hydrogen atoms were refined anisotropically, and H atoms were included in the refinement at calculated positions with a riding model and fixed isotropic U_i values. In a distorted arrangement of four supersilyl groups the Al_3 ring is disordered embedded over the C_2 axis. In both positions of the atoms Al1 and Al2 click into free inlets of the $SitBu_3$ envelope.

Crystallographic data (excluding structure factors) for the structure reported in this paper have been deposited with the Cambridge Crystallographic Data Centre as supplementary publication no CCDC-120209. Copies of this data can be obtained free of charge on application to the Director, CCDC, 12 Union Road, Cambridge CB2 1EZ [Fax: (internat.) + 44-1223/336-033; E-mail: deposit@ccdc.cam.ac.uk].

Acknowledgments

We are grateful to the Deutsche Forschungsgemeinschaft and the Fonds der Chemische Industrie for their generous financial support. We thank Dr. A. Purath for mounting a crystal of the cyclotrialanyl.

[1] Holleman-Wiberg, *Lehrbuch der Anorganischen Chemie*, 101. Auflage, DeGruyter, Berlin, **1995**.
[2] W. Uhl, *Angew. Chem.* **1993**, *105*, 1449; *Angew. Chem. Int. Ed. Engl.* **1993**, *32*, 1386 and references cited therein.
[3] N. Wiberg, K. Amelunxen, H. Nöth, M. Schmidt, H. Schwenk, *Angew. Chem.* **1996**, *108*, 110; *Angew. Chem. Int. Ed. Engl.* **1996**, *35*, 65 and refs. cited herein.
[4] N. Wiberg, K. Amelunxen, T. Blank, H. Nöth, J. Knizek, *Organometallics* **1998**, *17*, 5431 and references cited therein.
[5] N. Wiberg, K. Amelunxen, H.-W. Lerner, H. Nöth, J. Knizek, I. Krossing, *Z. Naturforsch. B*, **1998**, *53*, 333.
[6] A. Purath, C. Dohmeier, A. Ecker, H. Schnöckel, K. Amelunxen, T. Passler, N. Wiberg, *Organometallics* **1998**, *17*, 1894.
[7] N. Wiberg, K. Amelunxen, H. Nöth, H. Schwenk, W. Kaim, A. Klein, T. Scheiring, *Angew. Chem.* **1997,** *109,* 1258; *Angew. Chem. Int. Ed. Engl.* **1997**, *36,* 1213 and references cited therein.
[8] N. Wiberg, K. Amelunxen, H.-W. Lerner, H. Nöth, W.

Ponikwar, H. Schwenk, *J. Organomet. Chem.* **1999**, *574*, 246.
[9] N. Wiberg, T. Blank, H. Nöth, W. Ponikwar, *Angew. Chem.* **1999**, *113,* 887; *Angew. Chem. Int. Ed.* **1999**, *38*, 839.
[10] Turbomole: O. Treutler, R. Ahlrichs, *J. Chem. Phys.* **1995**, *102*, 346. − Functional BP86: A. D. Becke, *Phys. Rev. A*, **1998**, *38*, 3098. − RI DFT: J. P. Peider, *Phys. Rev. B* **1996**, *33*, 8822; K. Eichkorn, O. T. Treutler, H. Ohm, M. Häser, R. Ahlrichs, *Chem. Phys. Lett.* **1995**, *242*, 612; K. Eichkorn, F. Weigend, O. Treutler, R. Ahlrichs, *Theor. Chem. Acc.* **1997**, *97*, 119.
[11] W. Uhl, U. Schütz, W. Kaim, E. Waldhör, *J. Organomet. Chem.* **1995**, *501,* 79.
[12] W. Uhl, A. Vester, W. Kaim, J. Poppe, *J. Organomet. Chem.* **1993**, *454,* 9.
[13] N. Wiberg, *Coord. Chem. Rev.* **1997**, *163*, 217.
[14] W. Kaim, *Z. Naturforsch. B* **1981,** *36*, 677.
[15] W. Kaim, *J. Organomet. Chem.* **1981,** *215*, 325.

Received December 27, 1999
[I99474]

Synthesis and Crystal Structures of Mono-Helical Complexes of Zinc(II) and Europium(III) with 1,2-Bis{[3-(2-pyridyl)pyrazol-1-yl]ethoxy}ethane

Michael H. W. Lam,*[a] Derek Y. K. Lee,[a] Sammi S. M. Chiu,[a] K. W. Man,[a] and W. T. Wong[b]

Keywords: Zinc / Europium / Helical structures / Ligand design / N ligands

A new multidentate ligand L, 1,2-bis{[3-(2-pyridyl)pyrazol-1-yl]ethoxy}ethane, has been synthesized by linking two 3-(pyridin-2-yl)pyrazoles with a 1,2-bis(ethoxy)ethyl spacer. Coordination of L with zinc(II) and europium(III) centres has led to mononuclear complexes of $[Zn(L)](ClO_4)_2$ (**1**) and $[Eu(L)Cl_2](ClO_4)$ (**2**). X-ray crystal structures of both complexes have shown that L adopted a helical coordination geometry around both metal centres. The spectroscopic properties of both complexes have also been determined. In **1**, photoluminescence was dominated by ligand centred $^1(\pi\text{-}\pi^*)$ fluorescence. In **2**, ligand-to-metal energy transfer leading to $^5D_0 \rightarrow {}^7F_n$ luminescence at the europium(III) centre was observed.

Introduction

Molecular architecture showing helical arrangement of multidentate ligands around one or more metal centres has long been one of the goals in the field of supramolecular chemistry.[1] Besides their structural elegance, molecular helices are emblems of synthetic chemists′ ability to make use of the various steric and electronic interactions within/among molecular units to engineer preferred molecular structures. While double-helical and triple-helical multinuclear (most often dinuclear) coordination complexes are the most common classes of supramolecular helix,[2,3] mononuclear molecular helices are believed to offer better control over the assembly of molecular units into desirable crystal lattices.[4] Among the various ligand systems that are capable of promoting self-assembly of mononuclear and multinuclear helical coordination complexes, oligopyridine[1b,2c−2e,2g] is the most famous and thoroughly studied one. Other ligands such as substituted bis(benzimidazolyl)pyridines,[3b,3g] substituted pyridine-2,6-dicarboxamide and pyridine-2,6-dicarboxylate,[3f,4c] as well as bis- and tris-catechol[5] are also known to induce helical coordination configurations. Recently, Ward et al.[6] has demonstrated the versatile coordination chemistry of the ligand 3-(pyridin-2-yl)pyrazole. The ease of substitution at the pyrazolyl-N^1 position provides convenient access to multidentate pyridyl-pyrazolyl ligands with the potential to induce high nuclearity supramolecular assemblies. In fact, a dicopper(I) double helicate with ligands containing two pyridyl-pyrazolyl units joined by an *o*-$CH_2C_6H_4CH_2$ spacer has been synthesized.[6h] We are particularly interested in linking two 3-(pyridin-2-yl)pyrazoles through the pyrazolyl-N^1 by a flexible carbon chain containing additional donor atoms. In this way, multidentate ligands capable of wrapping around metal centres with much greater flexibility can be formed. Compared with oligopyridine ligands, where helical configuration has to be achieved by the twisting of interannular C−C bonds between adjacent pyridine rings, the new ligand system is expected to be more energetically and sterically favourable for a helical coordination geometry. In this work we report a new, potentially hexadentate ligand formed by the linkage of two 3-(pyridin-2-yl)pyrazoles by a 1,2-ethoxyethane spacer − the 1,2-bis{[3-(2-pyridyl)pyrazol-1-yl]ethoxy}ethane (L) (Figure 1) − and its mononuclear helical complexes $[Zn(L)](ClO_4)_2$ (**1**) and $[Eu(L)Cl_2](ClO_4)$ (**2**).

Results and Discussion

Formation of the polyether-linked pyridyl-pyrazole ligand L is straightforward. Deprotonation of the pyrazolyl-

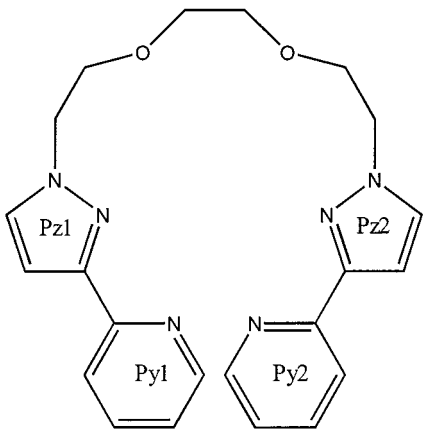


Figure 1. 1,2-Bis{[3-(2-pyridyl)pyrazol-1-yl]ethoxy}ethane (L)

[a] Department of Biology & Chemistry,
City University of Hong Kong,
Tat Chee Avenue, Kowloon, Hong Kong, China
Fax: (internat.) + 852-2788-7406
E-mail: bhmhwlam@cityu.edu.hk
[b] Department of Chemistry, The University of Hong Kong,
Hong Kong, China

 © WILEY-VCH Verlag GmbH, D-69451 Weinheim, 2000 1434−1948/00/0707−1483 $ 17.50+.50/0

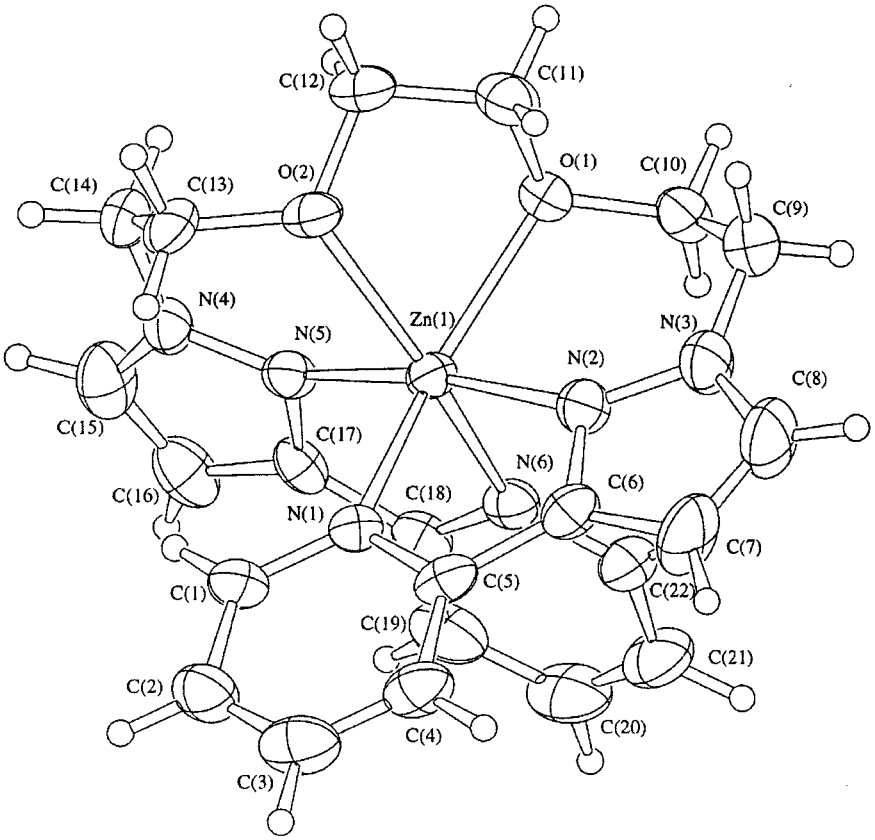


Figure 2. Perspective view of $[Zn(L)](ClO_4)_2$ (**1**)

Table 1. Selected bond lengths (Å) and angles (°) of $[Zn(L)](ClO_4)_2 \cdot H_2O$ (**1**·H_2O)

Zn(1)−O(1)	2.203(5)	Zn(1)−O(2)	2.211(5)
Zn(1)−N(1)	2.146(7)	Zn(1)−N(2)	2.081(7)
Zn(1)−N(5)	2.071(7)	Zn(1)−N(6)	2.163(7)
O(1)−Zn(1)−O(2)	74.6(2)	O(1)−Zn(1)−N(1)	153.3(2)
O(1)−Zn(1)−N(2)	80.7(2)	O(1)−Zn(1)−N(5)	104.9(2)
O(1)−Zn(1)−N(6)	101.2(2)	O(2)−Zn(1)−N(1)	97.3(2)
O(2)−Zn(1)−N(2)	106.9(2)	O(2)−Zn(1)−N(5)	82.1(2)
O(2)−Zn(1)−N(6)	156.9(2)	N(1)−Zn(1)−N(2)	77.4(3)
N(1)−Zn(1)−N(5)	99.0(3)	N(1)−Zn(1)−N(6)	95.7(2)
N(2)−Zn(1)−N(5)	170.5(3)	N(2)−Zn(1)−N(6)	94.4(3)
N(5)−Zn(1)−N(6)	77.1(3)	Zn(1)−O(1)−C(10)	115.3(5)
Zn(1)−O(1)−C(11)	109.5(5)	Zn(1)−O(2)−C(13)	116.9(5)
Zn(1)−O(2)−C(12)	113.2(5)	Zn(1)−N(1)−C(1)	127.2(6)
Zn(1)−N(1)−C(5)	113.0(6)	Zn(1)−N(2)−C(6)	114.5(6)
Zn(1)−N(2)−N(3)	135.7(6)	Zn(1)−N(5)−N(4)	136.0(6)
Zn(1)−N(5)−C(17)	115.6(6)	Zn(1)−N(6)−C(22)	128.7(6)
Zn(1)−N(6)−C(18)	112.9(6)		

N^1 of 3-(pyridin-2-yl)pyrazole by NaH followed by alkylation by 1,2-bis(chloroethoxy)ethane affords L in good yield. The coordination chemistry of 3-(pyridin-2-yl)pyrazole has been thoroughly explored by Ward et al.,[6] who have also applied a similar approach to link two 3-(pyridin-2-yl)pyrazoles by *o*-$CH_2C_6H_4CH_2$ and propyl spacers.[6h,15] In the former case, the dinuclear double helicate with copper(I) was obtained while no helical coordination geometry was observed in Fe^{II}, Cu^{II}, Zn^{II}, Ag^{I} and Pb^{II} complexes containing the latter, relatively more-flexible ligand. In our case, reacting the polyether linked L with $ZnCl_2$ or $EuCl_3 \cdot 6H_2O$ in refluxing absolute ethanol gives the hygroscopic mononuclear complexes $[Zn(L)](ClO_4)_2$ (**1**) or $[Eu(L)Cl_2](ClO_4)$ (**2**), where the two ether oxygens also participate in metal coordination. In both complexes, L acts as a hexadentate ligand resulting in a helical coordination geometry around the metal centres. The hygroscopic nature of both complexes prevented accurate elemental analysis. Therefore, the characterization relied on FAB-MS and an X-ray crystal analysis.

Perspective views of the crystal structures of complexes **1** and **2**, with atom numbering, are shown in Figure 2 and Figure 3, respectively. Selected bond lengths and angles of the two complexes are tabulated in Table 1 and Table 2. In both complexes, each symmetric unit contains one complex molecule. In $[Zn(L)](ClO_4)_2 \cdot H_2O$ (**1**·H_2O), the 22-electron zinc(II) centre is coordinated to two pyridyl-*N*, two pyrazolyl-*N* and two ether-*O* donors. The bond lengths between Zn(1)−N(1)-pyridyl and Zn(1)−N(6)-pyridyl are 2.146(7) and 2.163(7) Å, respectively. The bond lengths between Zn(1)−N(2)-pyrazolyl and Zn(1)−N(5)-pyrazolyl are 2.081(7) and 2.071(7) Å, respectively. These bond lengths are typical for zinc(II) polypyridyl and pyridyl-pyrazolyl complexes.[15] The bond lengths between Zn(1)−O(1)-ether and Zn(1)−O(2)-ether are 2.203(5) and 2.211(5) Å, respectively.

The coordination geometry at Zn(1) is a distorted octahedron with L helically wrapped around the metal centre.

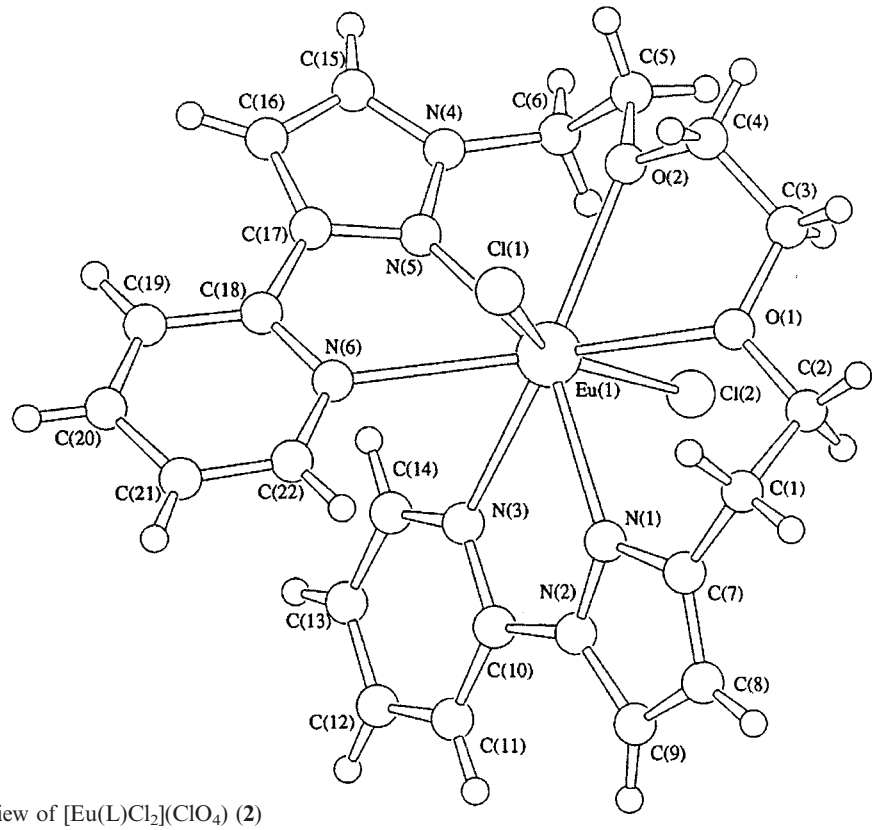


Figure 3. Perspective view of $[Eu(L)Cl_2](ClO_4)$ (**2**)

Table 2. Selected bond lengths (Å) and angles (°) of $[Eu(L)Cl_2](ClO_4)$ (**2**)

Eu(1)−Cl(1)	2.678(1)	Eu(1)−Cl(2)	2.661(1)
Eu(1)−O(1)	2.530(3)	Eu(1)−O(2)	2.507(3)
Eu(1)−N(1)	2.497(4)	Eu(1)−N(3)	2.623(4)
Eu(1)−N(5)	2.496(4)	Eu(1)−N(6)	2.648(4)
Cl(1)−Eu(1)−Cl(2)	152.30(4)	Cl(1)−Eu(1)−O(1)	74.84(8)
Cl(1)−Eu(1)−O(2)	86.13(8)	Cl(1)−Eu(1)−N(1)	91.00(9)
Cl(1)−Eu(1)−N(3)	126.18(8)	Cl(1)−Eu(1)−N(5)	101.61(9)
Cl(1)−Eu(1)−N(6)	72.35(9)	Cl(2)−Eu(1)−O(1)	77.63(8)
Cl(2)−Eu(1)−O(2)	80.42(9)	Cl(2)−Eu(1)−N(1)	84.45(10)
Cl(2)−Eu(1)−N(3)	75.73(8)	Cl(2)−Eu(1)−N(5)	95.81(9)
Cl(2)−Eu(1)−N(6)	135.28(9)	O(1)−Eu(1)−O(2)	67.3(1)
O(1)−Eu(1)−N(1)	74.1(1)	O(1)−Eu(1)−N(3)	131.5(1)
O(1)−Eu(1)−N(5)	135.7(1)	O(2)−Eu(1)−N(6)	145.7(1)
O(2)−Eu(1)−N(1)	140.7(1)	O(2)−Eu(1)−N(3)	143.6(1)
O(2)−Eu(1)−N(5)	68.4(1)	O(2)−Eu(1)−N(6)	119.6(1)
N(1)−Eu(1)−N(3)	63.6(1)	N(1)−Eu(1)−N(5)	149.7(1)
N(1)−Eu(1)−N(6)	96.5(1)	N(3)−Eu(1)−N(5)	86.9(1)
N(3)−Eu(1)−N(6)	65.3(1)	N(5)−Eu(1)−N(6)	62.3(1)
Eu(1)−O(1)−C(2)	129.2(3)	Eu(1)−O(1)−C(3)	113.7(3)
Eu(1)−O(2)−C(5)	132.4(3)	Eu(1)−O(2)−C(4)	111.1(3)
Eu(1)−N(1)−N(2)	122.3(3)	Eu(1)−N(1)−C(7)	130.9(3)
Eu(1)−N(3)−C(10)	118.9(3)	Eu(1)−N(3)−C(14)	123.1(3)
Eu(1)−N(5)−N(4)	129.4(3)	Eu(1)−N(5)−C(17)	123.6(3)
Eu(1)−N(6)−C(22)	122.2(3)	Eu(1)−N(6)−C(18)	119.7(3)

The dihedral angles between Py1/Py2 and Pz1/Pz2 are 80.64° and 79.64°, respectively.

Figure 4 shows the space filling representation of the $[Zn(L)]^{2+}$ core. The pyridine and pyrazole rings in L are nearly coplanar with interannular angles in Py1/Pz1 and Py2/Pz2 of 1.14° and 0.74°, respectively. The degree of interannular twisting is much smaller than that in found in

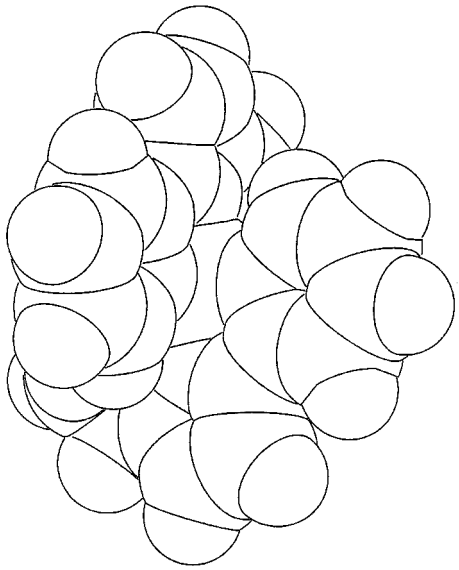


Figure 4. Space filling representation of $[Zn(L)]^{2+}$ cation with counter anions omitted

oligopyridyl helices, which normally range from 5 to 20°.[1b,16b] Presumably this is due to the presence of a flexible polyether chain in L that eases the requirement for twisting of the aromatic rings from a co-planar configuration to achieve the helical conformation.

In $[Eu(L)Cl_2](ClO_4)$ (**2**), the coordination number of the europium(III) centre is eight. The ligand L adopts a helical twist about the equatorial plane of the complex while the two coordinated chlorides occupy the apparent axial posi-

tions, although they are not exactly at 180° to each other. The bond lengths between Eu(1)−N(3)-pyridyl and Eu(1)−N(6)-pyridyl are 2.623(4) and 2.648(4) Å, respectively, and those between Eu(1)−N(1)-pyrazolyl and Eu(1)−N(5)-pyrazolyl are 2.497(4) and 2.496(4) Å, respectively. These bond lengths are typical for europium(III) pyridyl complexes.[16] The bond lengths between Eu(1)−O(1)-ether and Eu(1)−O(2)-ether are 2.530(3) and 2.507(3) Å, respectively, and those between Eu(1)−Cl(1) and Eu(1)−Cl(2) are 2.678(1) and 2.661(1) Å, respectively. The angle Cl(1)−Eu(1)−Cl(2) is 152.30(4)° and the two chlorides are evidently bent away from the two pyridine rings, probably because of steric interactions. The helical arrangement of the coordinated ligand L is more clearly demonstrated in complex **2** than in complex **1**. In **2**, the dihedral angles between Py1/Py2 and Pz1/Pz2 are 60.42° and 69.35°, respectively; the interannular angles in Py1/Pz1 and Py2/Pz2 are 7.83° and 8.58°, respectively. The degree of interannular twisting is significantly larger than that of complex **1** and is moderate compared to that found in oligopyridyl helices. Figure 5 shows the space filling representation of the $[Eu(L)Cl_2]^+$ core.

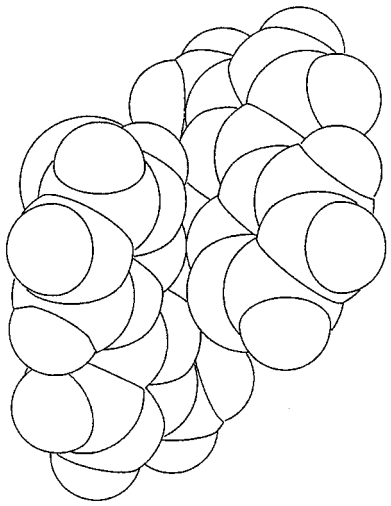


Figure 5. Space filling representation of $[Eu(L)Cl_2]^+$ cation with chlorides and counter anion omitted for clarity

Table 3. Spectroscopic and emission properties of $[Zn(L)](ClO_4)_2$ (**1**) and $[Eu(L)Cl_2](ClO_4)$ (**2**)

	UV/Vis λ/nm (ε/dm^3 mol^{-1} cm^{-1})[a]	Emission λ/nm[a],[b]
Ligand L	252 (2.4×10^4) 282 (1.3×10^4)	– –
$[Zn(L)](ClO_4)_2$ (**1**)	245 (1.27×10^4) 289 (1.35×10^4)	357
$[Eu(L)Cl_2](ClO_4)$ (**2**)	250 (5.3×10^4) 290 (4.4×10^4)	595 616 655 696

[a] In acetonitrile. – [b] At 298 K.

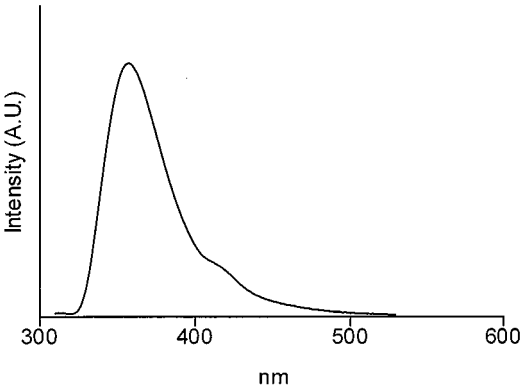


Figure 6. Room temperature emission spectra of $[Zn(L)](ClO_4)_2$ (**1**) in acetonitrile; excitation at 300 nm

Table 3 tabulates the solution spectroscopic and emission properties of complexes **1** and **2**. The UV/Visible absorption bands of both complexes are attributable to intraligand transitions. Complex **1** gives violet-blue photoluminescence in acetonitrile at room temperature (Figure 6) due to the $^1(\pi\text{-}\pi^*)$ fluorescence of the ligand. On the other hand, complex **2** produces an intense red emission in acetonitrile at room temperature. Figure 7 shows the room-temperature solution emission spectrum of **2** upon excitation at 300 nm. Emission peaks in the range 595−750 nm are characteristic of $^5D_0 \rightarrow {}^7F_n$ (n = 0 to 4) transitions at the Eu^{III} centre.[17] The observation of Eu^{III}-centred emission indicates the occurrence of energy transfer from the ligand to the metal centre **2**.

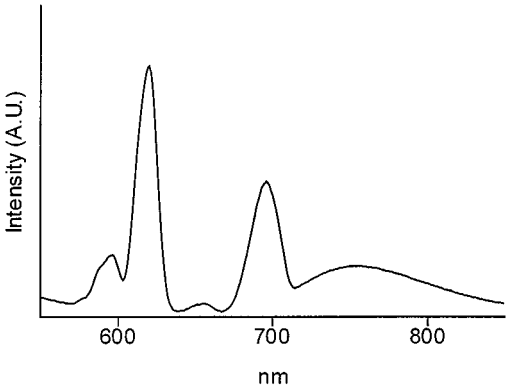


Figure 7. Room temperature emission spectra of $[Eu(L)Cl_2](ClO_4)$ (**2**) in acetonitrile; excitation at 300 nm

Conclusion

The strategy of linking two bidentate polypyridyl/pyrazolyl moieties by a flexible alkyl chain containing additional donor atoms has led to helical coordination architectures. With a 1,2-bis(ethoxy)ethyl linker, mononuclear helical complexes of $[Zn(L)]^{2+}$ and $[Eu(L)Cl_2]^+$ are obtained. Induction of a helical coordination geometry is probably assisted by the affinity of both metals for oxygen donors. An efficient ligand-to-metal energy transfer is observed in $[Eu(L)Cl_2]^+$ which leads to intense Eu^{III} centred lumines-

cence in the region 595−750 nm. This makes $[Eu(L)Cl_2]^+$ a potentially useful luminescent material in organic electroluminescent devices. Work on induction of higher nuclearity helices by L is in progress. The synthesis of analogous ligands with donor atoms other than oxygen in the linker is also being pursued.

Experimental Section

General Remarks: Europium(III) chloride hexahydrate, anhydrous zinc(II) chloride, sodium hydride (60% in mineral oil) and 1,2-bis(chloroethoxy)ethane were obtained from Aldrich. All solvents used were of analytical reagent grade (Riedel-de Haën and BDH). UV/vis spectra were measured by a Hewlett−Packard 8452A ultraviolet visible diode array spectrophotometer. Emission spectra were measured on an SFM 4800C spectrofluorometer and Perkin−Elmer LS-50B luminescence spectrometer. ^{1}H NMR spectra were measured on a Varian YH300 300 MHz NMR spectrometer. All manipulations were carried out under an N_2 atmosphere with standard Schlenk vacuum line techniques.

1,2-Bis{[3-(2-pyridyl)pyrazol-1-yl]ethoxy}ethane (L): 3-(Pyridin-2-yl)pyrazole[6a] (2.03 g, 14.0 mmol) was added to a suspension of NaH (60%, 0.56 g, 14.0 mmol) in 30 mL THF. The mixture was stirred at room temperature for 15 min. 1,2-Bis(chloroethoxy)-ethane (1.31 g, 7.0 mmol) was then added to the resultant reddish brown solution and the mixture was refluxed for 12 h. After cooling to room temperature, the mixture was filtered and the filtrate evaporated in vacuo to yield L as a light brown oil [1.9 g, 67% based on 1,2-bis(chloroethoxy)ethane]. The product was pure enough for further reaction. − ^{1}H NMR ($CDCl_3$, 300 MHz): δ = 8.61 (d, J = 4.2 Hz, 2 H, pyridyl-H^6), 7.87 (d, J = 8.1 Hz, 2 H, pyridyl-H^3), 7.69 (td, J = 8.5, 7.5 Hz, 2 H, pyridyl-H^4), 7.51 (d, J = 2.1 Hz, 2 H, pyrazolyl-H^4 or H^5), 7.18 (m, 2 H, pyridyl-H^5), 6.84 (d, J = 2.1 Hz, 2 H, pyrazolyl-H^4 or H^5), 4.33 (t, J = 5.5 Hz, 4 H, CH_2), 3.82 (t, J = 5.3 Hz, 4 H, CH_2), 3.49 (t, J = 6.3 Hz, 4 H, CH_2).

$[Zn(L)](ClO_4)_2$ (1): A mixture of anhydrous $ZnCl_2$ (0.14 g, 1.0 mmol) and L (0.40 g, 1.0 mmol) in 30 mL of absolute ethanol was refluxed for 24 h. $NaClO_4·H_2O$ (0.31 g, 2.2 mmol) was then added and the mixture was refluxed for a further 30 mins. The resultant mixture was evaporated in vacuo and the white residue was dissolved in DMF. The DMF solution was filtered into a Schlenk tube and a layer of diethyl ether was carefully laid on top of the DMF solution. The whole assembly was allowed to stand at −10 °C for two days to yield colourless crystalline $[Zn(L)](ClO_4)_2$ (**1**) (0.42 g, 62%). − MS (FAB$^+$, *m*-NBA): *m*/*z* = 569 [$M(ClO_4)^+$]. − ^{1}H NMR ([D$_6$]DMSO, 300 MHz): δ = 8.32 (d, J = 4.1 Hz, 2 H, pyridyl-H^6), 7.7 (m, 6 H, pyridyl-H^3 & H^4 and pyrazolyl-H^4 or H^5), 7.2 (m, 2 H, pyridyl-H^5), 6.6 (m, 2 H, pyrazolyl-H^4 or H^5), 4.1 (t, J = 5.4 Hz, 4 H, CH_2), 3.6 (t, J = 5.5 Hz, 4 H, CH_2), 1.98 (t, J = 6.0 Hz, 4 H, CH_2).

X-ray quality crystals of $[ZnN_6O_2C_{22}H_{24}](ClO_4)_2·H_2O$ were obtained by repeated recrystallization from DMF/Et_2O.

$[Eu(L)Cl_2](ClO_4)$ (2): The synthesis was similar to **1** except $EuCl_3·6H_2O$ (0.37 g, 1.0 mmol) was used. Layering of diethyl ether on top of a DMF solution of the reaction mixture and standing at −10 °C for three days gave colourless crystals of $[Eu(L)Cl_2](ClO_4)$ (**2**) (0.55 g, 76%). − MS (FAB$^+$, *m*-NBA): *m*/*z* = 627 [M^+]. The crystals obtained were already of a quality suitable for an X-ray crystal structure determination.

X-ray Crystallographic Study: Crystal structures of **1** and **2** were determined by X-ray diffraction using a Rigaku AFC 7R diffractometer with graphite monochromated Mo-K_α radiation and a 12-kW rotating anode generator. To avoid loss of solvent, the crystals were sealed in a layer of paraffin. Crystal data and details of measurements for complexes $[Zn(L)](ClO_4)_2·H_2O$ (**1**·H_2O) and $[Eu(L)Cl_2](ClO_4)$ (**2**) are summarized in Table 4. Absorption correlation was applied using Lorentz and polarization effects, and for absorption effects by an empirical method based on azimuthal scans of several reflections.

The structures were solved by heavy-atom Patterson Methods[7] (for **1**) and Direct Methods[8] (for **2**) and expanded using Fourier techniques.[9] Some non-hydrogen atoms were refined anisotropically, while the rest were refined isotropically by full-matrix least-squares calculations. Reliability factors were defined as $R = \Sigma(|F_o| - |F_c|)/\Sigma|F_o|$ and $R_w = [\Sigma w(|F_o| - |F_c|)^2/\Sigma w|F_o|^2]^{1/2}$. Neutral

Table 4. Crystal data for $[Zn(L)](ClO_4)_2·H_2O$ (**1**·H_2O) and $[Eu(L)Cl_2](ClO_4)$ (**2**)

	1·H_2O	**2**
Formula	$C_{22}H_{24}Cl_2N_6O_{11}Zn$	$C_{22}H_{23}Cl_3EuN_6O_6$
M	686.77	726.79
Crystal colour, habit	Colourless	colourless, block
Crystal system	Triclinic	triclinic
Space Group	$P\bar{1}$ (#2)	$P\bar{1}$ (#2)
a/Å	12.527(3)	7.564(1)
b/Å	13.008(3)	13.184(1)
c/Å	10.193(3)	14.286(1)
α/°	108.91(2)	76.24(1)
β/°	108.39(2)	89.34(1)
γ/°	98.84(2)	81.31(1)
U/Å^3	1429.3(8)	1367.4(2)
Z	2	2
Crystal dimensions/mm	0.27 × 0.34 × 0.38	0.24 × 0.25 × 0.25
F(000)	704.00	720.00
D_{calc}/g cm^{-3}	1.596	1.765
μ (Mo-*K*α) cm^{-1}	11.14	26.29
Reflection measured: total, unique	3936, 3729	4731, 4150
Maximum peak in final difference map/e Å^{-3}	0.75	0.78
Minimum peak in final difference map/e Å^{-3}	−0.61	−1.47
R	0.060	0.035
R_w	0068	0.033

atom scattering factors were taken from Cromer and Waber.[10] Anomalous dispersion effects were included in F_{calc},[11] the values for $\Delta f'$ and $\Delta f''$ were those of Creagh and McAuley.[12] The values for the mass attenuation coefficients were those of Creagh and Hubbel.[13] All calculations were performed using the teXsan[14] crystallographic software package of Molecular Structure Corporation.

Crystallographic data (excluding structure factors) for the structure(s) reported in this paper have been deposited with the Cambridge Crystallographic Data Centre as supplementary publication no. CCDC-138696 (**2**) and CCDC-138697 (**1**). Copies of the data can be obtained free of charge on application to CCDC, 12 Union Road, Cambridge CB2 1EZ, UK [Fax: (internat.) + 44-1223/336-033; E-mail: deposit@ccdc.cam.ac.uk].

Acknowledgments

We would like to acknowledge funding support from The Hong Kong Research Grants Council (CERG Grant No. 9040185) for this work.

[1] [1a] J.-M. Lehn, A. Rigault, J. Siegel, J. Harrowfield, B. Chevrier, D. Moras, *Proc. Natl. Acad. Sci. USA*, **1987**, *84*, 2565 2569. – [1b] E. C. Constable, M. G. B. Drew, M. D. Ward, *J. Chem. Soc., Chem. Commun*. **1987**, 1600–1601. – [1c] G. D. Desiraju, *Crystal Engineering: The Design of Organic Solids*, Elsevier, N. Y., 1989. – [1d] J.-M. Lehn, *Angew. Chem. Int. Ed. Engl*. **1990**, *29*, 1304–1319. – [1e] *Transition metals in Supramolecular Chemistry* (Eds.: L. Fabbrizzi, A. Poggi), Kluwer Academic, Dordecht, 1994.

[2] [2a] C. Piguet, G. Bernardinelli, A. F. Williams, *Inorg. Chem*. **1989**, *28*, 2920–2925. – [2b] C. O. Dietrich-Buchecker, J.-P. Sauvage, *Angew. Chem. Int. Ed. Engl*. **1989**, *28*, 189–192. – [2c] E. C. Constable, *Nature* **1990**, *346*, 314–315. – [2d] C. J. Cathey, E. C. Constable, M. J. Hannon, D. A. Tocher, M. D. Ward, *J. Chem. Soc., Chem. Commun*. **1990**, 621. – [2e] E. C. Constable, M. D. Ward, D. A. Tocher, *J. Chem. Soc., Dalton Trans*. **1991**, 1675–1683. – [2f] C. O. Dietrich-Buchecker, J.-P. Sauvage, *New. J. Chem*. **1992**, *16*, 277–285. – [2g] E. C. Constable, A. J. Edwards, M. J. Hannon, P. R. Raithby, *J. Chem. Soc., Chem. Commum*. **1994**, 1991–1992.

[3] [3a] A. F. Williams, C. Piguet, G. Bernardinelli, *Angew. Chem. Int. Ed. Engl*. **1991**, *30*, 1490–1492. – [3b] G. Bernardinelli, C. Piguet, A. F. Williams, *Angew. Chem. Int. Ed. Engl*. **1992**, *31*, 1622–1624. – [3c] K. T. Potts, C. P. Horwitz, A. Fessak, K. E. Nash, P. J. Toscano, *J. Am. Chem. Soc*. **1993**, *115*, 10444. – [3d] L. J. Charbonnière, A. F. Williams, U. Frey, A. E. Merbach, P. Kamalaprija, O. Schaad, *J. Am. Chem. Soc*. **1997**, *119*, 2488. – [3e] M. H. W. Lam, S. T. C. Cheung, K. M. Fung, W. T. Wong, *Inorg. Chem*. **1997**, *36*, 4618–4619. – [3f] F. Renaud, C. Piguet, G. Bernardinelli, J.-C. G. Bünzli, G. Hopfgartner, *Chem. Eur. J*. **1997**, *3*, 1646–1659. – [3g] L. J. Charbonnière, A. F. Williams, C. Piguet, G. Benardinelli, E. Rivara-Minten, *Chem. Eur. J*. **1998**, *4*, 485–493.

[4] [4a] T. Kawamoto, O Prakash, R. Ostrander, A. L. Rheingold, A. S. Borovik, *Inorg. Chem*. **1995**, *34*, 4294. – [4b] T. Kawamoto, B. S. Hammes, B. Haggerty, G. P. A. Yap, A. L. Rheingold, A. S. Borovik, *J. Am. Chem. Soc*. **1996**, *118*, 285–286. – [4c] F. Renaud, C. Piguet, G. Bernardinelli, J. –C. G. Bünzli, G. Hopfgartner, *Chem. Eur. J*. **1997**, *3*, 1660–1667.

[5] [5a] D. L. Caulder, R. E. Powers, T. N. Parac, K. N. Raymond, *Angew. Chem. Int. Ed*. **1998**, **37**, 1840–1843. – [5b] M. Albrecht, M. Schneider, *Chem. Commun*. **1998**, 137–138. – [5c] M. Albrecht, M. Schneider, R. Fröhlich, *New J. Chem*. **1998**, 753–754. – [5d] M. Albrecht, M. Schneider, H. Rottele, *Angew. Chem. Int. Ed*. **1999**, **38**, 557.

[6] [6a] A. J. Amoroso, A. M. C. Thompson, J. C. Jeffery, P. L. Jones, J. A. McCleverty, M. D. Ward, *J. Chem. Soc., Chem. Commun*. **1994**, 2751–2752. – [6b] P. L. Jones, K. J. Byrom, J. C. Jeffery, J. A. McCleverty, M. D. Ward, *Chem. Commun*. **1997**, 1361. – [6c] E. Psillakis, J. C. Jeffery, J. A. McCleverty, M. D. Ward, *J. Chem. Soc., Dalton Trans*. **1997**, 1645–1651. – [6d] D. A. Bardwell, J. C. Jeffery, P. L. Jones, J. A. McCleverty, E. Psillakis, Z. Reeves, M. D. Ward, *J. Chem. Soc., Dalton Trans*. **1997**, 2079. – [6e] K. L. V. Mann, J. C. Jeffery, J. A. McCleverty, P. Thronton, M. D. Ward, *J. Chem. Soc., Dalton Trans*. **1998**, 89–97. – [6f] P. L. Jones, J. C. Jeffery, J. P. Maher, J. A. McCleverty, P. H. Rieger, M. D. Ward, *Inorg. Chem*. **1997**, *36*, 3088. – [6g] P. L. Jones, A. J. Amoroso, J. C. Jeffery, J. A. McCleverty, E. Psillakis, L. H. Rees, M. D. Ward, *Inorg. Chem*. **1997**, *36*, 10. – [6h] J. S. Fleming, K. L. V. Mann, S. M. Couchman, J. C. Jeffery, J. A. McCleverty, M. D. Ward, *J. Chem. Soc., Dalton Trans*. **1998**, 2047–2052.

[7] PATTY: P. T. Beurskens, G. Admiraal, G. Beurskens, W. P. Bosman, S. Garcia-Granda, R. O. Gould, J. M. M. Smits, C. Smykalla, The DIRDIF program system, Technical Report of the Crystallography Laboratory, **1992**, University of Nijmegen, The Netherlands.

[8] ORIENT: P. T. Beurskens, G. Admiraal, G. Beurskens, W. P. Bosman, S. Garcia-Granda, R. O. Gould, J. M. M. Smits, C. Smykalla, The DIRDIF program system, Technical Report of the Crystallography Laboratory, **1992**, University of Nijmegen, The Netherlands.

[9] DIRDIF94: Beurskens, G. Admiraal, G. Beurskens, W. P. Bosman, R. de Gelder, R. Isreal, J. M. M. Smits, The DIRDIF-94 program system, Technical Report of the Crystallography Laboratory, **1994**, University of Nijmegen, The Netherlands.

[10] D. T. Cromer, J. T. Waber, *International Tables for X-ray Crystallography*, Vol. IV, The Kynoch Press, Birmingham, England, Table 1.2A, **1974**.

[11] J. A. Ibers, W. C. Hamilton, *Acta Crystallogr*. **1964**, *17*, 781.

[12] D. C. Creagh, W. J. McAuley, *International Tables for Crystallography*, Vol C (Ed.: A. J. S. Wilson), Kluwer Academic Publishers, Boston, Table 3.2.6.8, pp 219–222, **1992**.

[13] D. C. Creagh, J. H. Hubbell, *International Tables for Crystallography*, Vol C (Ed.: A. J. S. Wilson), Kluwer Academic Publishers, Boston, Table 3.2.4.3, pp 200–206, **1992**.

[14] teXsan: Crystal StructureAnalysis Package, Molecular Structure Corporation, **1985** & **1992**.

[15] K. L. V. Mann, J. C. Jeffery, J. A. McCleverty, M. D. Ward, *J. Chem. Soc., Dalton Trans*. **1998**, 3029–3035.

[16] [16a] R. C. Holz, L. C. Thompson, *Inorg. Chem*. **1988**, *27*, 4640. – [16b] E. C. Constable, R. Chotalia, D. A. Tocher, *J. Chem. Soc., Chem. Commun*. **1992**, 771–773.

[17] N. Sabbatini, S. Perathoner, V. Balzani, B. Alpha, J.-M. Lehn, "Antenna Effect in Eu^{3+} and Tb^{3+} cryptates", in *Supramolecularr Photochemistry*, V. Balzani Ed., NATO ASI Series, D. Reidel Publishing Company, Holland, **1987**, pp 187–206.

Received January 13, 2000
[I00006]

A General Route for the Synthesis of Triazacyclononane Functionalised with Pendant Phosphane Arms − Crystal Structures of $[NiL^1Cl(HOEt)][ClO_4]$ and $[NiL^1(NCS)_2]$ with L^1 = *N*-(Diphenylphosphanylpropyl)-1,4,7-triazacyclononane

David Ellis,[a] Louis J. Farrugia,[a] Paul A. Lovatt,[a] and Robert D. Peacock*[a]

Keywords: Macrocyclic ligands / Phosphanes / Nickel / Zinc

We present a general route for the synthesis of triazacyclononane functionalised with one, two or three pendant phosphane arms, by the free radical addition of PPh_2H to the appropriate alkene precursor *N*-[3-(diphenylphosphanyl)-propyl]-1,4,7-triazacyclononane (L^1). L^1 forms structurally characterised complexes with Zn^{II} and Ni^{II}. $[Zn_2L^1{}_2Cl_3][ClO_4]$ has a dinuclear structure in which a bridging chloride ion allows both zinc centres to be formally six-coordinate, while $NiL^1Cl(HOEt)][ClO_4]$ achieves pseudo-octahedral geometry around the nickel centre by coordinating an ethanol molecule. The ethanol molecule and the chloride ion bound to $[NiL^1Cl(HOEt)][ClO_4]$ are both labile and can be replaced by $[NCS]^-$ to give $[NiL^1(NCS)_2]$.

Introduction

The small, facially coordinating, three-nitrogen macrocycle 1,4,7-triaza-cyclononane (9[ane]N_3) has been *N*-functionalised with a wide variety of pendant arms ending in hard donor groups (−COOH, −OH, $-NH_2$, pyridyl, polypyridyl etc).[1]−[3] There are a few recent examples of functionalisation by soft donor arms, for example 4-mercaptobenzoyl,[4] $-CH_2CH_2$ SH[5] and 2-mercaptobenzyl,[6] but so far 9[ane]N_3 has not been functionalised with pendant arms ending in a phosphane group.[7]

When this work was started there were only two published examples of nitrogen macrocycles with pendant phosphane arms: 1,4,8,11-tetrakis[(diphenylphosphanyl)methyl]-1,4,8,11-tetraazacyclotetradecane which is prepared by a "one-pot" synthesis[8] which cannot be generalised, and a series of N_2O_2, N_2S_2 and NO_3 macrocycles with 2-phosphanylethyl arms.[9] Although the synthetic method used to prepare the latter series of ligands should be applicable to all nitrogen macrocycles we have not found it to be suitable in practice for 9[ane]N_3, possibly because of the high basicity of the nitrogen atoms in this ligand. Since our original communication[10] two papers have appeared reporting the synthesis of 9[ane]N_3[11] and cyclam[12] with pendant [*o*-(diphenylphosphanyl)benzyl]alkyl arms.

In view of the ubiquitous use of phosphane ligands in organometallic and coordination chemistry, and in particular the predominance of phosphane ligands in homogeneous catalysis, we have embarked upon a program designed to prepare ligands based on nitrogen macrocycles (hard ligands) bearing pendant phosphane arms. Of particular interest is the combination of three nitrogen atoms and one phosphane group giving a ligand which contains both hard and soft ligands and which is capable of forming coordinatively unsaturated complexes.

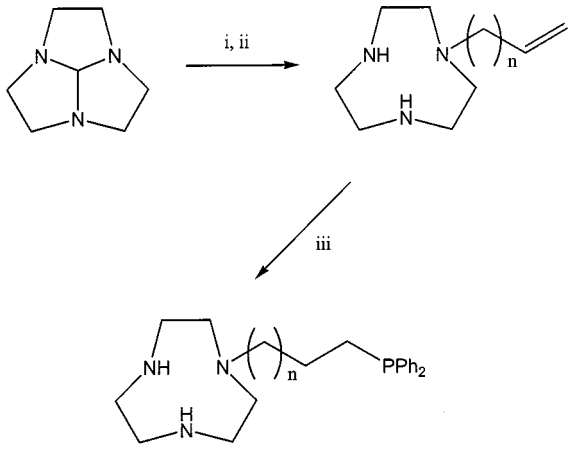
[a] Department of Chemistry, University of Glasgow, Glasgow G12 8QQ, UK
E-mail: bob@chem.gla.ac.uk

We report a general method for the preparation of phosphane pendant-arm macrocycles in which 9[ane]N_3 is functionalised with one, two or three arms. This is accomplished by free radical addition of PPh_2H to the appropriate alkene precursor. The only restriction on the method is that the arms must contain a minimum of three carbon atoms. The method is also applicable to larger nitrogen macrocycles e.g. cyclam or cyclen. A preliminary communication[10] has been published in which the crystal structure of $[Zn_2L^1{}_2Cl_3][ClO_4]$ (**3**) is described.

Results and Discussion

Preparation of the Phosphane Ligands

The pendant-arm phosphane ligands were prepared by free-radical addition of diphenylphosphane across the alkene double bond of their corresponding alkene pendant-arm derivatives (Scheme 1). The only restriction to this



Scheme 1. Reagents and conditions: L^1 (n = 1): i: allyl bromide, THF; ii: $NaOH/H_2O$; iii: PPh_2H, hν; L^2 (n = 2): i: 4-bromobut-1-ene; ii: $NaOH/H_2O$; iii: PPh_2H, hν

 © WILEY-VCH Verlag GmbH, D-69451 Weinheim, 2000 1434−1948/00/0707−1489 $ 17.50+.50/0

method is that the pendant arm must contain a minimum of three carbon atoms. The free-radical additions were accomplished in essentially quantitative yields by photolysis under strictly anaerobic conditions using a mercury lamp. The reactants were irradiated as neat liquids; *the use of solvents increased the amount of phosphane oxides in the product and was found to severely hinder the reaction rate.* Excess diphenylphosphane was removed from the reaction mixture by washing with petroleum ether (boiling range 40−60 °C) or by distillation under reduced pressure.

Free radicals are electron-deficient species and their stability decreases in the order tertiary > secondary > primary. The addition is therefore strictly *anti*-Markovnikov, since the formation of a secondary radical is preferred over the formation of a primary radical. It was originally believed that the free amine functions in L^1 and L^2 would quench the radical addition but it was soon realised that this was not the case. It was anticipated that branched alkene ligands would undergo free-radical addition with diphenylphosphane to produce racemic phosphane pendant-arm macrocycles; however, the addition reaction was extremely slow and the alkene macrocycle degraded under the photolytic conditions before any significant amount of addition was achieved. No addition products were observed for, for example, *N*-(2-methylbut-2-en-1-yl)triazacyclononane even when radical initiators such as AIBN were added.

The synthetic method is exemplified by the preparation of L^1 and L^2 and has also been used to prepare *N,N′,N′′*-tris[3-(diphenylphosphanyl)propyl]-1,4,7-triazacyclononane from *N,N′,N′′*-triallyl-1,4,7-triazacyclononane and *N*-methyl-*N′,N′′*-bis[3-(diphenylphosphanyl)propyl]-1,4,7-triazacyclononane from *N,N′*-diallyl-*N′′*-methyl-1,4,7-triazacyclononane.

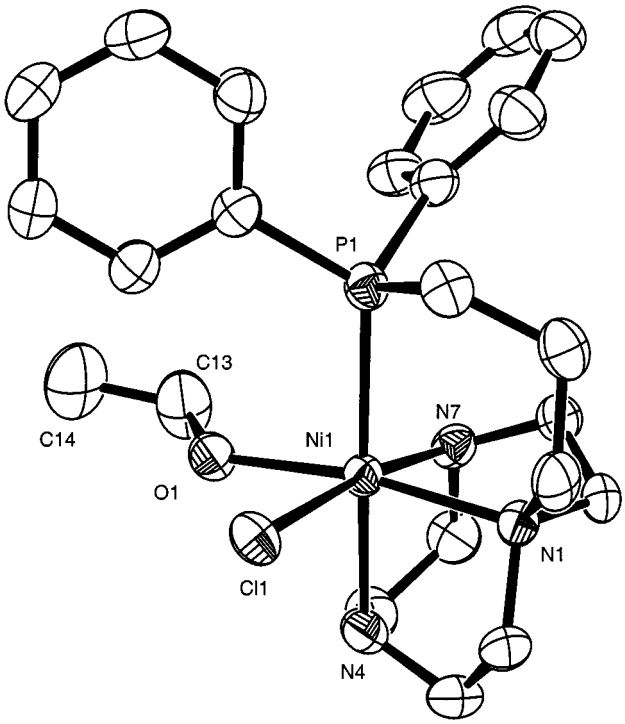


Figure 1. ORTEP for Windows[21] plot of the cation of **1** (thermal ellipsoids are drawn at 50% probability); selected bond lengths [Å] and angles [°]: Ni(1)−N(4) 2.093(3), Ni(1)−N(7) 2.094(3), Ni(1)−N(1) 2.137(3), Ni(1)−O(1) 2.171(2), Ni(1)−Cl(1) 2.438(1), Ni(1)−P(1) 2.454(1); N(4)−Ni(1)−N(7) 81.9(1), N(4)−Ni(1)−N(1) 83.7(1), N(7)−Ni(1)−N(1) 83.5(1), N(4)−Ni(1)−O(1) 86.9(1), N(7)−Ni(1)−O(1) 96.5(1), N(1)−Ni(1)−O(1) 170.6(1), N(4)−Ni(1)−Cl(1) 91.42(8), N(7)−Ni(1)−Cl(1) 172.67(8), N(1)−Ni(1)−Cl(1) 92.59(8), O(1)−Ni(1)−Cl(1) 86.18(7), N(4)−Ni(1)−P(1) 178.43(8), N(7)−Ni(1)−P(1) 97.98(8), N(1)−Ni(1)−P(1) 94.72(8), O(1)−Ni(1)−P(1) 94.56(7), Cl(1)−Ni(1)−P(1) 88.54(3), C(13)−O(1)−Ni(1) 133.8(2)

Metal Complexes

The only crystals of metal complexes which were suitable for crystallographic studies were obtained with L^1 using the perchlorate counteranion. Numerous attempts were made to form complexes of the other ligands with a variety of transition metal ions. In most cases spectroscopic evidence (UV/Vis, ^{31}P NMR) indicated that reaction had occurred.

Nickel Complexes

$[NiL^1Cl(EtOH)][ClO_4]$ (1)

Reaction of L^1 with $NiCl_2{\cdot}6H_2O$ in ethanol followed by the addition of excess $LiClO_4$ produced $[NiL^1Cl(EtOH)][ClO_4]{\cdot}H_2O$ (**1**) (Figure 1). The nickel atom is coordinated to the three amine functions and the phosphane pendant arm of L^1. An ethanol molecule and chloride ion complete the coordination sphere around the nickel centre to give a pseudo-octahedral geometry. The bonding trends in the complex are similar to those observed in the zinc dimer.[10] The longest Ni−N bond is to the nitrogen atom bearing the pendant arm and the shortest Ni−N bond is to the nitrogen atom *trans* to the phosphane group. The Ni−P bond is much longer than the average of Ni−PPh_3 bond lengths (2.321 Å) and well above the upper quartile (2.331 Å).[13]

$[NiL^1(NCS)_2]$ (2)

The addition of KSCN to $[NiL^1Cl(EtOH)]^+$ displaced the coordinated chloride ion and ethanol molecule to give a new nickel(II) complex containing two coordinated thiocyanate groups (Figure 2). The thiocyanate ion coordinates to the nickel(II) centre via the nitrogen function of the ligand. The Ni−N bonds of the macrocycle follow the same trends observed in $[NiL^1Cl(EtOH)]^+$, but the bond lengths are slightly longer in the thiocyanate complex. The Ni−P bond length in $[NiL^1(NCS)_2]$ is slightly shorter to that observed in $[NiL^1Cl(EtOH)]^+$, but is still very much longer than those observed for Ni−PPh_3. The closest reported structure related to $[NiL^1(NCS)_2]$ is the *trans*-phosphane complex $[Ni(NCS)_4\{P(CH_2CH_2CN)_3\}_2]^{2-}$ [14] in which the Ni−P bond length is 2.420Å and is only slightly longer than that in $[NiL(NCS)_2]$. The Ni−NCS bond lengths are also very similar at 2.072 and 2.068Å.

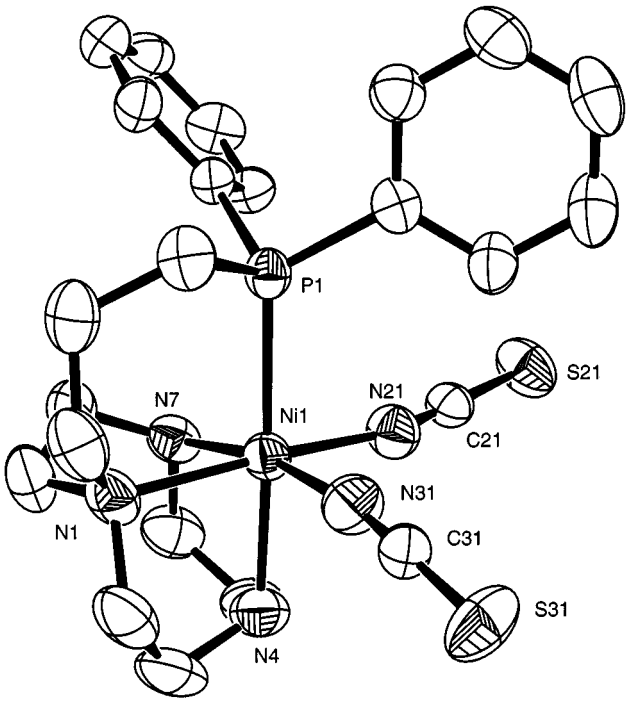


Figure 2. ORTEP for Windows[21] plot of **2** (thermal ellipsoids are drawn at 50% probability); selected bond lengths [A] and angles [°]: Ni(1)−N(31) 2.056(3), Ni(1)−N(21) 2.066(3), Ni(1)−N(4) 2.109(3), Ni(1)−N(7) 2.128(2), Ni(1)−N(1) 2.186(3), Ni(1)−P(1) 2.4165(9); N(31)−Ni(1)−N(21) 95.19(11), N(31)−Ni(1)−N(4) 89.76(11), N(21)−Ni(1)−N(4) 90.71(11), N(31)−Ni(1)−N(7) 169.03(11), N(21)−Ni(1)−N(7) 90.25(10), N(4)−Ni(1)−N(7) 80.64(10), N(31)−Ni(1)−N(1) 91.93(11), N(21)−Ni(1)−N(1) 70.32(11), N(4)−Ni(1)−N(1) 82.76(11), N(7)−Ni(1)−N(1)-81.67(10), N(31)−Ni(1)−P(1) 89.20(9), N(21)−Ni(1)−P(1) 92.61(8), N(4)−Ni(1)−P(1) 176.60(8), N(7)−Ni(1)−P(1) 100.09(7), N(1)−Ni(1)−P(1) 94.04(8), C(21)−N(21)−Ni(1) 167.2(3), C(31)−N(31)−Ni(1) 168.3(3)

Zinc Complex

[ZnL^{1}Cl(μ-Cl)ZnL^{1}Cl][ClO$_4$] (3)

Reaction of L^1 with anhydrous $ZnCl_2$ in ethanol followed by the addition of excess $LiClO_4$ precipitated [ZnL^{1}Cl(μ-Cl)ZnL^{1}Cl]ClO_4 which was recrystallised from acetonitrile. The crystal structure of the complex has been described previously.[10] It consists of a asymmetric cation in which both zinc atoms are coordinated by the three amine functions and the pendant phosphane arm of L^1. Both the zinc atoms achieve pseudo-octahedral geometry via a terminal and a bridging chloride ion.

Conclusion

We have described a general method for preparing N-macrocycles with pendant phosphane arms. The method is illustrated with the synthesis of mono-substituted L^1 and L^2 but can be used to prepare pendant-arm macrocycles in which all, or any number of, N atoms are "armed" by selective alkylation.

Experimental Section

Triazacyclononane was synthesised by the Richmond−Atkins method,[15] detosylation being effected by heating in concentrated H_2SO_4 at 115−120 °C for 36−48 h. 1,4,7-triazatricyclo-[5.2.1.0^{4,10}]decane[16] and *N*-allyltriazacyclononane[17] were prepared by published routes.

Caution: Perchlorates are potentially dangerous. Caution is advised and the handling of only small quantities is recommended.

***N*-[3-(Diphenylphosphanyl)propyl]-1,4,7-triazacyclononane (L^1):** A Schlenk tube was equipped with a magnetic stirring bar, attached to a Schlenk line and charged with *N*-allyl-1,4,7-triazacyclononane (1 g, 5.92 mmol), dissolved in dry degassed dichloromethane (5 mL). The Schlenk tube was evacuated and purged with nitrogen and diphenylphosphane (1.29 g, 1.2 mL, 6.93 mmol) was transferred to the Schlenk tube using a syringe under a strong flow of nitrogen. The contents of the flask were mixed and the dichloromethane was removed under reduced pressure. The flask was then irradiated with a 125-W Hanovia medium-pressure mercury lamp with stirring under nitrogen for 72 h. Excess diphenylphosphane was removed by washing with dry degassed petroleum ether (boiling range 40−60 °C) (2 × 5 mL). The remaining viscous oil was then left under vacuum overnight to remove any solvent and volatiles. The product was obtained in essentially quantitative yield as a very viscous yellow oil. − ^{1}H NMR (200 MHz, $CDCl_3$): δ = 1.51 (m, 2 H, −CH$_2$−C*H*$_2$−P), 1.98 (m, 2 H, −C*H*$_2$−CH$_2$−P), 2.45−2.78 (m, 14 H, N−C*H*$_2$−), 7.21−7.39 (m, 10 H, Ar−*H*). − ^{13}C NMR (51 MHz, $CDCl_3$): δ = 24.25 (d, J_{PC} = 16 Hz, N−CH$_2$CH$_2$*C*H$_2$−P), 25.69 (d, J_{PC} = 11.5 Hz, N−CH$_2$*C*H$_2$CH$_2$−P), 46.73, 46.82, 53.06 (N−*C*H$_2$−, ring), 58.73 (d, J_{PC} = 13 Hz, N−*C*H$_2$CH$_2$CH$_2$−P), 128.36, 132.68, 133.95, 138.94 (all d, aromatic). − ^{31}P NMR (81 MHz, $CDCl_3$): δ = −16.2.

***N*-[3-(Diphenylphosphanyl)butyl]-1,4,7-triazacyclononane (L^2):** The same procedure was used as described for *N*-[3-(diphenylphosphanyl)propyl]-1,4,7-triazacyclononane. Quantities used were 1.5 g (8.2 mmol) of *N*-(but-3-en-1-yl)-1,4,7-triazacyclononane, 1.68 g (1.56 mL, 9.1 mmol) of diphenylphosphane and an irradiation time of 96 h. Yield 3 g (quant.). − ^{1}H NMR (200 MHz, $CDCl_3$): δ = 1.52 (m, 4 H, N−CH$_2$CH$_2$C*H*$_2$C*H*$_2$−P), 2.05 (m, 2 H, N−CH$_2$C*H*$_2$CH$_2$CH$_2$−P), 2.47−2.70 (m, 14 H, N−C*H*$_2$−), 2.85 (b, 2 H, N−H), 7.25−7.55 (m, 10 H, Ar−*H*). − ^{13}C NMR (51 MHz, $CDCl_3$): δ = 23.63 (d, P−*C*H$_2$−, J_{PC} = 16.3 Hz), 27.83 (d, N−CH$_2$CH$_2$*C*H$_2$CH$_2$−P, J_{PC} = 11.6 Hz), 28.86 (d, N−CH$_2$*C*H$_2$CH$_2$CH$_2$−P, J_{PC} = 12.1 Hz), 43.83, 45.14, 50.67 (N−*C*H$_2$−, ring), 56.42 (N−*C*H$_2$−, arm), 128.47, 132.63, 133.85, 138.51 (all d, aromatic). − ^{31}P NMR (81 MHz, $CDCl_3$): δ = −16.43.

[NiL^{1}Cl(EtOH)][ClO$_4$]·H$_2$O (1): $NiCl_2·6H_2O$ (107 mg, 0.45 mmol) and $LiClO_4$ (240 mg, 2.25 mmol) were dissolved in degassed ethanol (20 mL) and a solution of L^1 (200 mg, 0.56 mmol) in degassed ethanol (2 mL) was added. An initial red precipitate formed which turned blue on stirring overnight. This was filtered off and recrystallised from acetonitrile/nitromethane to yield 50 mg (18%) of **1**. − $C_{23}H_{38}Cl_2N_3NiO_6P$ (613.14): calcd. C 45.1, H 6.25, N 6.85; found C 45.1, H 6.2; N 6.85.

[NiL^1(NCS)$_2$]·CH$_3$NO$_2$ (2): A solution of KNCS (20 mg, 0.21 mmol) in acetonitrile was added to a solution of **1** (27 mg, 0.045 mmol) also in acetonitrile. The resulting purple solution was left to crystallise. Crystals of **2** suitable for crystallography were obtained from nitromethane. − $C_{24}H_{33}N_6NiO_2PS_2$ (591.36): calcd. C 48.8, H 5.6, N 14.2; found C 48.7, H 5.85, N 14.9.

Table 1. Crystallographic data for **1** and **2**; $R = \Sigma(|F_o| - |F_c|)/\Sigma(F_o)$; $wR = \Sigma[w(F_o^2 - F_c^2)^2]/\Sigma[w(F_0^2)^2]^{1/4}$

	1	**2**
Empirical formula	$C_{23}H_{38}Cl_2N_3NiO_6P$	$C_{24}H_{33}N_6NiO_2PS_2$
M	613.14	591.36
Crystal system	triclinic	monoclinic
Space group	*P*−1	*C*2/*c*
a [Å]	9.8208(15)	33.195(4)
b [Å]	11.2858(16)	10.6180(10)
c [Å]	14.2217(12)	17.1470(10)
α [°]	107.142(9)	90
β [°]	105.117(9)	111.450(10)
γ [°]	102.798(12)	90
V [Å^3]	1376.0(3)	5625.1(9)
Z	2	8
D_c [gcm^{-3}]	1.480	1.397
F(000)	644	2480
μ(Mo-$K_α$) [cm^{-1}]	10.0	9.28
T [K]	292	292
No. of independent reflections	5650	9340
n in $I > nσ(I)$	4842	8119
No. used in refinement	4842	8119
No. of refined parameters	307	302
$R[I > 2σ(I)]$	0.0414	0.0508
$wR[I > 2σ(I)]$	0.1004	0.1129
Largest remaining feature in electron density map [e Å^{-3}]	+0.635 −0.296	+0.485 −0.445

[ZnL^{1}Cl(μ-Cl)ZnL^{1}Cl][ClO$_4$] (3): L^1 (203 mg, 0.57 mmol) was added to a solution of $ZnCl_2$. (68 mg, 0.5 mmol) in ethanol (20 mL) containing $LiClO_4$ (270 mg). The white precipitate was filtered, washed with ethanol and dried under vacuum. Recrystallisation from MeCN produced 111 mg (42%) of white crystals which, although of poor quality, were suitable for X-ray crystallography. − ^{1}H NMR (200 MHz, $CDCl_3$): δ = 7.77−7.37 (m, 20 H, phenyl−*H*), 2.97−1.92 (m, 40 H, CH_2 and N*H*). − ^{31}P NMR (81 MHz, CD_3CN): δ (25 °C) = −17.0, −17.3, −17.6, −19.3 (major), −27.2; δ (70 °C) = −17.0. − $C_{42}H_{60}Cl_4N_6O_4P_2Zn_2$ (1042.15): calcd. C 48.16, H 5.77, N 8.02; found C 48.23, H 6.01; N 7.65.

Crystallography: Details of the data collection and analysis of **1** and **2** are given in Table 1. Single crystals of suitable size were attached to a glass fibre using acrylic resin, and mounted on a goniometer head in a general position. Data were collected with an Enraf−Nonius TurboCAD4 diffractometer for **2** and with a Siemens P4 diffractometer for **2**, both using graphite-monochromated X-radiation (λ = 0.71073 Å). Precise unit-cell dimensions were determined by refinement of the setting angles of high-angle reflections which were flagged during data collection. Standard reflections were measured every 2 h during data collection, and a small decay of ca 7% (**1**) and 11% (**2**) was noted, and interpolated corrections were applied to the reflection data. Lorentz-polarization corrections were then applied to the reflection data. ψ-scans for **1** indicated that no absorption correction was necessary, while a semi-empirical correction was applied to **2**. The structures were solved by direct methods (SIR92).[18] All non-H atoms were allowed anisotropic thermal motion. Aliphatic CH hydrogen atoms were included at calculated positions, with C−H = 0.96 Å, while the two NH hydrogen atoms were found from difference Fourier maps and refined using a riding model. Refinement (SHELXL97)[19] was by full-matrix least squares on F^2. The weighting scheme $w = [σ^2(F_o)^2 + (AP)^2 + BP]^{-1}$ where $P = [F_o^2/3 + 2F_c^2/3]$ was used, with values of *A*, *B* = 0.0610, 0.2733 for **1** and 0.0591, 0.8873 for **2**. Counting statistics were used to estimate $σ(F_o)^2$. Neutral atom scattering factors, coefficients of anomalous dispersion and absorption coefficients were obtained from ref.[20].

Crystallographic data (excluding structure factors) for the structures reported in this paper have been deposited with the Cambridge Crystallographic Data Centre as supplementary publication nos. CCDC-132772 (**1**) and -132773 (**2**). Copies of the data can be obtained free of charge on application to CCDC, 12 Union Road, Cambridge CB2 1EZ, UK [Fax: (internat.) + 44-1223/336-033; E-mail: deposit@ccdc.cam.ac.uk].

Acknowledgments

We thank the EPSRC for financial support for D. E. (GR/J81150), and for funds towards the purchase of a diffractometer.

[1] P. K. Chaudhuri, K. Wieghardt, *Prog. Inorg. Chem.* **1987**, *35*, 329−436.
[2] P. V. Bernhardt, G. A. Lawrance, *Coord. Chem. Rev.* **1990**, *104*, 297−343.
[3] K. P. Wainwright, *Coord. Chem. Rev.* **1997**, *166*, 35−90.
[4] D. J. Evans, G. Garcia, G. J. Leigh, M. S. Newton, M. D. Santana, *J. Chem. Soc., Dalton Trans.* **1992**, 3229−3234.
[5] R. P. Hauser, V. G. Young, Jr., W. B. Tolman, *J. Am. Chem. Soc*. **1996**, *118*, 2101−2102.
[6] K. Mochizyki, F. Kesting, T. Weynermuller, K. Wieghardt, C. Butzlaff, A. X. Trautwein, *J. Chem. Soc., Chem. Commun*. **1994**, 909−910.
[7] 1,4,7-tris[(diphenylphosphanyl)methyl]-1,4,7-triazacyclononane is incorrectly depicted as the phosphane in ref.[2]
[8] H. H. Hope, M. Viggiano, B. Moezzi, P. P. Power, *Inorg. Chem*. **1984**, *23*, 2550−2552.
[9] A. Carroy, C. R. Langick, J.-P. Lehn, K. E. Matthes, D. Parker, *Helv. Chim. Acta* **1986**, *69*, 580−586.
[10] D. Ellis, L. J. Farrugia, P. A. Lovatt, R. D. Peacock, *Chem. Commun.* **1996**, 1817−1818.
[11] S. E. Watkins, X. Yang, D. C. Craig, S. B. Colbran, *J. Chem. Soc., Dalton Trans.* **1999**, 1539−1540.
[12] E. Kimura, K. Kamita, M. Hidai, *Inorg. Chim. Acta* **1996**, *246*, 151- 158.
[13] A. G. Orpen, L. Brammer, F. H. Allen, O. Kennard, D. G. Watson, R. Taylor, *J. Chem. Soc., Dalton Trans.* **1989**, S1 − S83.
[14] M. Foxman, B. H. Mazurek, *Inorg. Chem.* **1979**, *18*, 113−116.

[15] J. E. Richmond, T. J. Atkins, *J. Am. Chem. Soc*. **1974**, *96*, 2268−2270.
[16] T. J. Atkins, *J. Am. Chem. Soc.* **1980**, *102*, 6364−6369.
[17] L. J. Farrugia, P. A. Lovatt, R. D. Peacock, *Inorg. Chim. Acta* **1996**, *246*, 343−348.
[18] SIR92 − a program for automatic solution of crystal structures by direct methods: A. Altomare, G. Cascarno, C. Giacovazzo, A. Gualiardi, *J. Appl. Crystallogr.* **1994**, *27*, 435.
[19] *SHELXL97* a program for crystal structure refinement: G. M. Sheldrick, University of Göttingen, Germany, **1997**.
[20] Table 4.2.4.2, 4.2.6.8 & 6.1.1.4 from *International Tables for Crystallography, Volume C Mathematical, Physical and Chemical Tables*, Kluwer, Dordrecht, **1995**.
[21] L. J. Farrgia, *J. Appl. Crystallogr.* **1997***, 30,* 565.

Received August 11, 1999
[I99301]

Kinetic and Mechanistic Study of the H-Transfer Reduction of Dimethyl Itaconate by a Rh/TPPTS Catalyst under Biphasic Conditions: Evidence for a Rhodametallacycle Intermediate

Nathalie Tanchoux[a] and Claude de Bellefon*[a]

Keywords: H-transfer / Kinetics / Reaction mechanisms / Biphasic catalysis / Rhodium / Metallacyclobutanes

The H-transfer reduction of dimethyl itaconate under biphasic catalysis using sodium formate/water as the hydrogen source with a Rh/TPPTS complex was studied. Labelling experiments reveal that the reduction proceeds through a 1,3-hydrogen addition. Kinetic studies allow us to propose a catalytic cycle going through a rhodametallacyclobutane intermediate with a rate-determining step involving sodium formate. A formal kinetic rate law was then derived from this mechanism which accounts for the results. This work evidences the switch between the mechanism of diacid reduction and that of the corresponding esters.

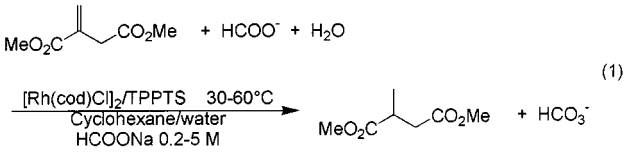
Introduction

The asymmetric hydrogenation of unsaturated substrates by either molecular hydrogen or H-transfer reduction is now one of the most important applications of homogeneous catalysis by chiral transition metal complexes.[1–4] Many studies report the use of optically pure phosphane complexes of Rh and Ru in organic[1,3] as well as in aqueous[2,5] or biphasic media.[6] The mechanisms of these reactions have been extensively studied, but very few details are known about the H-transfer reduction of α,β-unsaturated carboxylic esters using sodium formate/water in biphasic catalysis. As these reactions catalysed by chiral diphosphane complexes in aqueous medium are generally very complex, the racemic reduction of a prochiral substrate with a non-chiral monophosphane ligand was first studied. The kinetics of this reaction using dimethyl itaconate as a substrate and Rh/TPPTS as a catalytic complex were further investigated,[7] and labelling studies were undertaken in order to understand the mechanism and propose a catalytic cycle reflecting both the kinetic and mechanistic studies.

Results

Reaction

The reaction studied is the reduction of dimethyl itaconate (DMI) to dimethylmethylsuccinate (DMS) with sodium formate, catalysed by a water-soluble Rh complex in a biphasic medium (Equation 1). The catalytic system was generated by mixing the dimer $[Rh(cod)Cl]_2$ and the sodium salt of triphenylphosphanetrisulfonate (TPPTS) in an aqueous sodium formate solution.



(1)

Analysis of the organic layer by gas chromatography and mass balance calculations confirm the near quantitative (> 95%) conversion of the substrate, DMI, into the product, DMS. A side product (< 5%) was detected and identified as an isomer of DMI, 2-dimethylmesaconate (DMM), formed by the shift of the double bond from the external to the internal position. Such an isomerisation of terminal to internal olefins has been frequently reported as a side reaction in for example hydrogenations.[8–10]

Liquid–Liquid Partition Equilibrium

As the course of the reaction is more conveniently followed by analysis of the organic phase, it is primordial to correlate the measured concentrations in the organic phase to the concentrations in the aqueous phase, since the latter is where the catalytic reaction actually takes place. The concentration of species A in the aqueous and organic layers were described by the linear relationship of Equation 2.

$$P_A = \frac{C^A_{Org}}{C^A_{Aq}} \qquad (m^3_{Aq} \cdot m^{-3}_{Org}) \tag{2}$$

All the measurements of partition coefficients have already been described in a previous paper.[7] The coefficients calculated from the experimental results are given in Table 1.

[a] Laboratoire de Génie des Procédés Catalytiques,
CNRS-CPE Lyon, URA 2211,
43, boulevard du 11 novembre 1918, B.P. 2077,
69616 Villeurbanne, France
Fax: (internat.) +33-4/72431673,
E-mail: Claude.de.Bellefon@lgpc.cpe.fr

 © WILEY-VCH Verlag GmbH, D-69451 Weinheim, 2000 1434–1948/00/0707–1495 $ 17.50+.50/0

Table 1. Cyclohexane/water partition coefficients of DMI and DMS for various sodium formate concentrations at 293 K; a linear partition is observed for $0 \leq C_{Org}^{DMI} \leq 0.13$ kmol·m^{-3}

c_{HCOONa} [kmol·m$^{-3}_{Aq}$]	0	1	2.5	5
P_{DMI} [m$^3_{Aq}$·m$^{-3}_{Org}$]	1.2	2.8	4.3	11.3
P_{DMS} [m$^3_{Aq}$·m$^{-3}_{Org}$]	1.7	4	5.6	14

Kinetic Studies in a Well-Mixed Batch Reactor

The absence of mass transfer limitations in a well mixed batch reactor at 1100 rpm was previously checked.[11] A previous study[7] allowed the extraction of an activation energy of 71 kJ·mol^{-1}, in good agreement with those reported for other hydrogen transfer reductions of olefins.[12] The study also led us to propose the semi-empirical rate model of Equation 3, taking into account all the results obtained during that preliminary study.

$$r_{Aq} = \frac{kC_{Aq}^{Rh}C_{Aq}^{DMI}}{(KC_{Aq}^{DMI}+1)} \qquad (kmol.m_{Aq}^{-3}.s^{-1}) \qquad (3)$$

This model being based on preliminary results, it is only partial and does not take into account important parameters such as the concentrations of sodium formate or phosphane. More tests varying these parameters were performed in order to propose a more complete kinetic model that included the new information obtained. The range of conditions for this study is given in Table 2.

Table 2. Range of conditions for kinetic study in the batch reactor (other conditions: cyclohexane as organic phase solvent; stirring speed: 1100 rpm)

Concentration of catalyst [kmol·m$^{-3}_{Aq}$]	0.00132 to 0.005
Temperature [K]	303–313–323–333
Initial concentration of DMI in the organic phase [kmol·m$^{-3}_{Org}$]	0.024 to 0.144
Initial concentration of DMI in the aqueous phase [kmol·m$^{-3}_{Aq}$]	0.0021 to 0.013
Aqueous phase volume [10^{-6} m^3]	20 to 100
Organic phase volume [10^{-6} m^3]	10 to 20
Volume ratio α [m$^3_{Org}$·m$^{-3}_{Aq}$]	0.2 to 1
Concentration of sodium formate in the aqueous phase [kmol·m$^{-3}_{Aq}$]	0.2 to 5
TPPTS/Rh ratio	3.1 to 11.3

Formate decomposition in molecular hydrogen and sodium hydrogen carbonate has been noted, with or without substrate. This hydrogen production appears to be independent of the catalytic cycle of the DMI reduction. Tests have been performed under hydrogen pressures of 0.1 and 0.2 MPa to check for this, and no acceleration effect was noticed on the reduction rate. Thus, the DMI is not reduced by the molecular hydrogen formed from formate decomposition.

As seen in Figure 1, the observed initial reaction rate shows a first order dependence with respect to the catalyst concentration for formate concentrations of 5 and 1 kmol·m^{-3}.

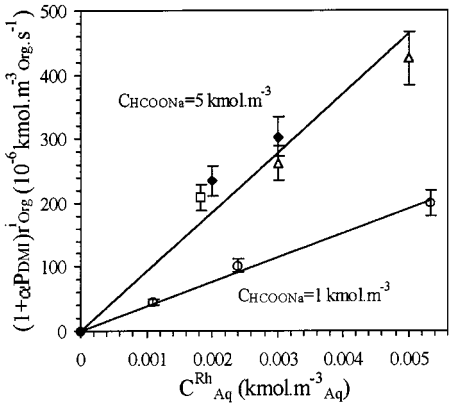


Figure 1. Influence of the catalyst concentration on the observed initial reaction rate r^i_{Org} [T = 313 K, C_{Org}^{DMI} = 0.155 kmol·m$^{-3}_{Org}$, TPPTS/Rh = 6; (◆ and ○): α = 1; (Δ): α = 0.5; (□): α = 0.45)

The influence of initial substrate concentration (Figure 2) on the observed initial rate shows an apparent zero order for the experiments carried out at a formate concentration of 1 kmol·m^{-3}, whereas it is complex for a concentration of 2.5 kmol·m^{-3} and close to an order of 1 for the most concentrated formate solution (5 kmol·m^{-3}).

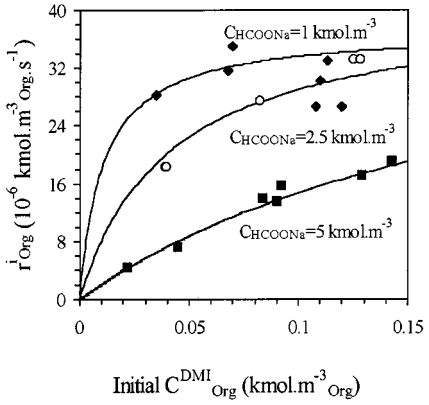


Figure 2. Influence of the initial substrate concentration on the observed initial reaction rate r^i_{Org} for different sodium formate concentrations (C_{Aq}^{Rh} = 0.002 kmol·m$^{-3}_{Aq}$, α = 1, TPPTS/Rh = 6, 313 K); the points represent the experimental data and the curves represent the semi-empirical model described by Equation 5

The effect of the phosphane on the initial rate exhibits a negative order with respect to the phosphane concentration, since the initial reaction rate decreases with increasing phosphane amounts in the aqueous phase (Figure 3).

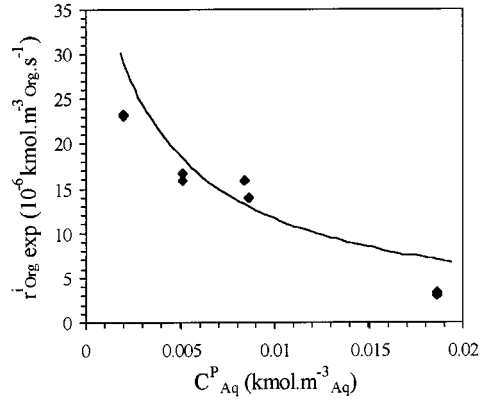


Figure 3. Influence of the phosphane concentration on the observed initial reaction rate r^{i}_{Org} (C^{DMI}_{Org} = 0.1 kmol·m$^{-3}_{Org}$, C^{Rh}_{Aq} = 0.002 kmol·m$^{-3}_{Aq}$, α = 1, C^{HCOONa}_{Aq} = 5 kmol·m$^{-3}_{Aq}$); the points represent the experimental data and the curves represent the semi-empirical model described by Equation 5

The influence of the sodium formate concentration was also studied, and it seems more complex. As shown in Figure 4, a linear increase of initial rate is observed until the formate concentration reaches 1 kmol·m$^{-3}_{Aq}$. Above this concentration, the rate decreases with increasing formate concentration. Such a complex behaviour has already been observed by Joó et al.[13] in the reduction of aldehydes by water-soluble phosphane complexes of ruthenium in biphasic medium. Joó evoked a salting-out effect due to the high formate concentration to explain this result. Formate concentration does indeed have a strong influence on the partition coefficients of the substrate and product (see Table 1).

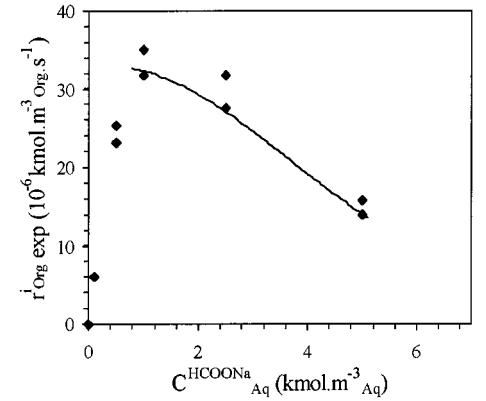


Figure 4. Influence of the sodium formate concentration on the observed initial reaction rate r^{i}_{Org} (C^{DMI}_{Org} = 0.1 kmol·m$^{-3}_{Org}$, C^{Rh}_{Aq} = 0.002 kmol·m$^{-3}_{Aq}$, α = 1, TPPTS/Rh = 6); the points represent the experimental data and the curves represent the semi-empirical model described by Equation 5

All these new results led us to propose a new semi-empirical model (Equation 4 and Equation 5), which represents all the experimental results rather well.

Knowing that $n_{DMI} = n^{DMI}_{Aq} + n^{DMI}_{Org}$, and from the mass balance in the batch reactor we can obtain

$$r_{Aq} = k\frac{C^{Rh}_{Aq}C^{DMI}_{Aq}}{\left(KC^{DMI}_{Aq} + C^{HCOO^-}_{Aq}C^{P}_{Aq}\right)} \quad (kmol.m^{-3}_{Aq}.s^{-1}) \quad (4)$$

$$-\frac{dC^{DMI}_{Org}}{dt} = r_{Org} = \frac{kC^{Rh}_{Aq}}{\left(1+\alpha P_{DMI}\right)}\frac{C^{DMI}_{Org}}{\left(\frac{K}{P_{DMI}}C^{DMI}_{Org} + C^{HCOO^-}_{Aq}C^{P}_{Aq}\right)} \quad (kmol.m^{-3}_{Org}.s^{-1}) \quad (5)$$

with α = volumetric ratio of the organic phase and the aqueous phase (m$^{3}_{Org}$·m$^{-3}_{Aq}$).

The kinetic parameters of the above model were estimated by means of a dynamic estimation and simulation software, able to perform numerical integrations using the entire concentration vs. time profiles and not only the initial rates of reaction.

As shown in Figure 2 to Figure 5 and Figure 6, the model fits rather well the experimental data except for low formate concentrations (< 1 kmol·m$^{-3}_{Aq}$). The results of the estimation are presented in Table 3.

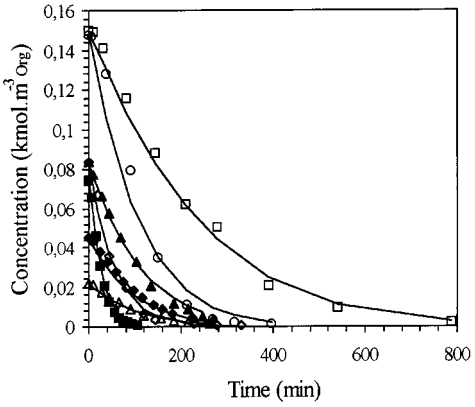


Figure 5. Concentration vs. time profiles. Comparison between experimental data (symbols) and semi-empirical model (lines). (Δ): Standard test: T = 313 K; C^{DMI}_{Org} = 0.1; C^{HCOONa}_{Aq} = 5, TPPTS/Rh = 6.3, α = 1, C^{Rh}_{Aq} = 0.002. Other tests: same with: (○) α = 0.2; (◆): α = 0.53, C^{Rh}_{Aq} = 0.005; (□): $C^{DMI}_{Org}(0)$ = 0.155, C^{HCOONa}_{Aq} = 1; (■): $C^{DMI}_{Org}(0)$ = 0.05, C^{HCOONa}_{Aq} = 2.5; (●): TPPTS/Rh = 3.1. Units: C^{DMI}_{Org} in kmol·m$^{-3}_{Org}$; C^{HCOONa}_{Aq} and C^{Rh}_{Aq} in kmol·m$^{-3}_{Aq}$; α in m$^{3}_{Org}$·m$^{-3}_{Aq}$.

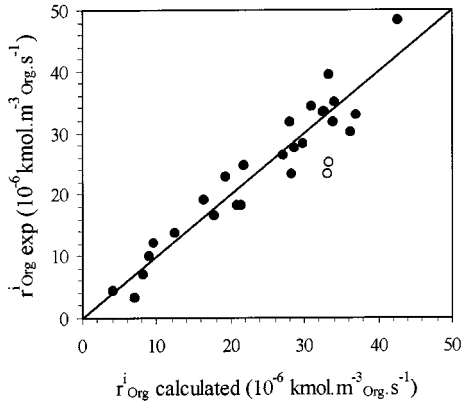


Figure 6. Calculated vs. experimental initial rates of reaction; conductions see Table 2 except for symbol (○) for which C^{HCOONa}_{Aq} = 0.5 kmol·m$^{-3}_{Aq}$

Table 3. Estimated kinetic constants and statistical analysis for the kinetic model determined from 30 experiments

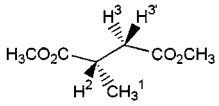
	Value[a]	Confidence interval[b]
k [$m^3_{Aq}\cdot kmol^{-1}\cdot s^{-1}$]	0.053	0.048–0.058
K [$m^{-3}_{Aq}\cdot kmol^{-1}$]	2.1	1.8–2.4

[a] WRSS: weighted residual sum of squares for the parameter estimation: 1900. – [b] Interval at 95% confidence level.

Labelling Studies

This study was completed by labelling experiments, in order to determine the chemistry occurring, and maybe obtain a better understanding of the mechanism of this reaction. Table 4 gives the regioselectivity of the deuterium distribution in the products obtained by the reduction of DMI, carried out with $D_2O/HCOO^-$ first, then with $H_2O/DCOO^-$. Deuterium was never incorporated in the methyl ester groups.

Table 4. Amount of deuterium incorporated by the dimethyl methylsuccinate



% labelled in position	H^1	H^2	H^3	$H^{3'}$
$D_2O/HCOO^-$	31±2	n.d.	58±3	47±2
$H_2O/DCOO^-$	13±3	n.d.	n.d.	n.d.

n.d.=not determined (<3%).

The extent of deuterium incorporation was determined by ^{1}H-NMR spectroscopy using the signal of the methoxy group as an internal standard (Figure 7).

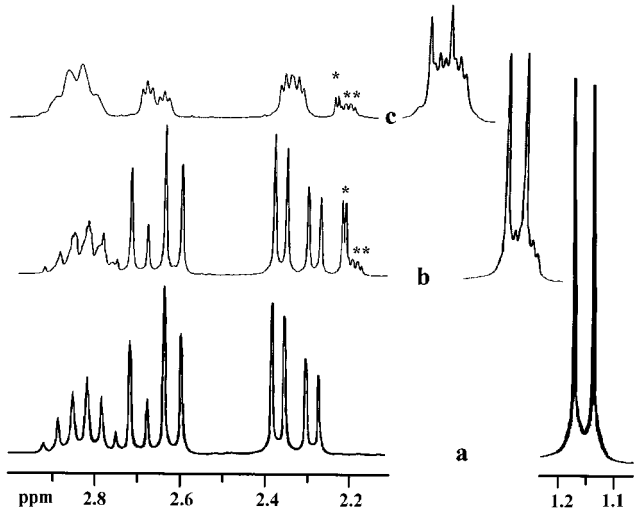


Figure 7. ^{1}H-NMR spectra of DMS (a) and of the products from reduction in $DCOONa/H_2O$ (b) and in $HCOONa/D_2O$ (c); signals of the vinylic proton in the by-product DMM: (*) **5**, (**) **6** (see Table 5)

In the case of reduction with $D_2O/HCOO^-$, the methine proton H^2 appears at δ = 2.84 as a broad multiplet (Figure 7c), showing no incorporation at this position. The two diastereotopic protons H^3 and $H^{3'}$ appear as two broad multiplets at δ = 2.33 and 2.65, corresponding to an AB system. Theses signals allowed us to determine a deuterium incorporation of 58 and 47% for each proton, respectively, i.e. a global quantitative deuterium incorporation at C^3. The methyl H^1 appears as a broad multiplet at δ = 1.14, showing a 31% deuterium incorporation at C^1. The $^{13}C\{^1H\}$-NMR spectra and DEPT sequence of the product confirmed there was no incorporation at the C^2 position. The triplet at δ = 37 corresponds to a quantitative monodeuteration –CHD in the C^3 position, confirmed by the DEPT sequence. The multiplet at δ = 16.7 shows an incorporation at the C^1 position. In the case of reduction with $H_2O/DCOO^-$, the ^{1}H-NMR spectra of DMS showed a broad multiplet at δ = 2.93 (Figure 7b) corresponding to the proton H^2, and showing no incorporation at this position. The two proton H^3 and $H^{3'}$ appeared as two doublets of doublets at δ = 2.4 and 2.72, corresponding to the coupling with the methine proton. These signals showed no deuterium incorporation at this position. The methyl appeared as a doublet and a small broad multiplet at δ = 1.21, showing 13% deuterium incorporation at C^1. The $^{13}C\{^1H\}$-NMR spectra and DEPT sequence confirmed these results. At δ = 35.7 and 37.4, two singlets showed no deuterium incorporation at C^2 and C^3, respectively. At δ = 16.7, C^1 appeared as a multiplet due to coupling with deuterium incorporated at this position.

Attempted Complex Characterization in situ

The ^{31}P-NMR spectrum of the catalytic complex in sodium formate shows broad signals centred at ca. δ = 31 and –5, probably due to a fluxional process including free TPPTS. Under catalytic conditions ([Rh] = 0.013 kmol·m^{-3}_{Aq}, TPPTS/Rh = 4), i.e. in the presence of sodium formate (3.3 kmol·m^{-3}) and DMI (0.02 kmol·m^{-3}), the NMR spectrum shows two types of compounds. The singlet at δ = 24.5 is assigned to a phosphonium according to previous reports.[14,15] It is formed by nucleophilic attack of the free TPPTS on the DMI, assisted by the Rhodium complex. Indeed, as proved in a separate experiment, the formation of the phosphonium is much slower when performed without Rhodium. Thus a yield of ca. 10%, based on TPPTS, is obtained without Rhodium, whereas a quantitative conversion of the free TPPTS is evidenced in the presence of the Rhodium complex. The change from fluxional to well defined ^{31}P spectra is thus attributed to the consumption of free TPPTS by DMI under catalytic conditions, which leads to the observation of the complex $[Rh(TPPTS)_3X]$ (X = Cl or OH)[16] based on the doublets and triplets at δ = 35.5 and 52.4 ($^1J_{Rh,P1}$ = 147 Hz, $^1J_{Rh,P2}$ = 182 Hz, and $^2J_{P1,P2}$ = 40 Hz), respectively. In water alone, under non-catalytic conditions, signals due to the complex $[Rh(TPPTS)_3(OH)]$, the phosphonium, and the TPPTS oxide are observed. A further signal at δ = 29.8 (d, $^1J_{Rh,P}$ = 145 Hz) is assigned to the cationic complex $[Rh(TPPTS)_2(cod)]^+$.[17]

Discussion

Mechanism

The results of labelling studies differ considerably from those obtained for mechanistic studies of slightly different systems, i.e. formic acid as the hydrogen source, itaconic acid as the substrate, or monophasic systems.[1–4]

The most surprising result was the absence of deuterium incorporation in the C^2 position while reducing the DMI in either a $D_2O/HCOO^-$ medium or in $H_2O/DCOO^-$. Very low incorporation of deuterium in the C^2 position has been reported recently in the H-transfer reduction of dimethyl itaconate with a Rh/diphosphane catalyst in DMSO.[18] This result indicates that the hydrogen atom incorporated in the C^2 position *must* come from the substrate dimethyl itaconate itself.

The mechanism of reduction is not likely to be close to the one proposed by Sinou[2] for the hydrogenation of DMI, as it was demonstrated that water did not play any role as a reactant, which is not the case here. Indeed, after reduction with $D_2O/HCOO^-$, the product DMS presented a 31% deuterium incorporation in the C^1 position and a complete monodeuteration in the C^3 position. As it is known that the exchange of hydrogen by deuterium in the formyl position is very slow compared to hydrogen transfer,[1] the incorporation of deuterium by the product cannot be attributed to $DCOO^-$, which is unlikely to be present in the catalytic phase.

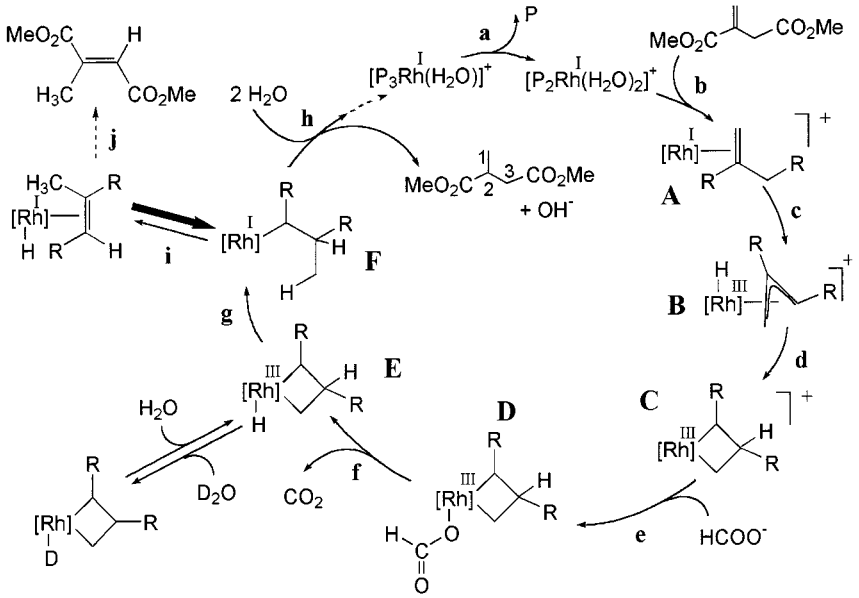
When the reduction is carried out with $H_2O/DCOO^-$, a primary kinetic isotope effect of $k_H/k_D = 2.8$ is measured. This value, in agreement with those obtained by Brunner,[1] clearly shows that the sodium formate is involved in the rate-determining step.

The only mechanism accounting for all these experimental results seems to involve going through a rhodametallocyclobutane (Scheme 1). Only this type of intermediate allows the C^2 position to remain untouched, without any incorporation of deuterium, and only partial incorporation in the methyl group when reduction is carried out with $H_2O/DCOO^-$.

The first step of the mechanism is a de-coordination of one phosphane ligand to give a Rh complex containing two phosphane equivalents. Step **b** is the coordination of the olefin to the Rh complex. Step **c** is an intramolecular oxidative addition of the olefin to the rhodium complex, which gives a π-allyl rhodium hydride. This type of intermediate is very well-known in the π-allyl mechanism of olefin isomerization with complexes of palladium[19] and rhodium.[20] The formation of the phosphonium salt may well occur by nucleophilic attack of free TPPTS at the coordinated π-allyl, which supports the view of complex B being part of the cycle.

The next step is an intramolecular rearrangement of a π-allyl rhodium hydride complex to a rhodametallacyclobutane. The formation of such a complex with addition of hydride reagents to a π-allyl rhodium complex has already been reported.[21,22] Steps **b** to **d** consist of the shift of a hydrogen atom from position 3 to position 2. The resulting sp^2 carbon (C^2) is reduced to an sp^3 carbon *intramolecularly* before any possible exchange with the reaction medium. This mechanism is the only one we could propose that explains the results of the labelling experiments.

The formate then coordinates to the metallacyclobutane intermediate. Step **f** of hydride transfer from formate to rhodium has already been postulated for the mechanism of itaconic acid reduction by hydrogen transfer,[1] although it was not possible to decide whether it occurs externally or through an intramolecular pathway. It has been shown that in this type of rhodium hydride or dihydride intermediate, scrambling always occurs.[1,23] That explains very well the partial incorporation of deuterium (13%) at the C^1 position when the reduction is carried out with $H_2O/DCOO^-$. The



Scheme 1

exchange Rh-D/H_2O must be quite slow, as the incorporation obtained in the C^1 position (31%) is close to the theoretical incorporation (33%) with $D_2O/HCOO^-$.

Step **g** is an intramolecular reductive elimination that opens the metallacyclobutane and rapidly gives a rhodium alkyl intermediate. This type of equilibrium between a metallacycle and a metal alkyl intermediate has already been seen in such reactions as C–H activation,[24–26] the metal alkyl intermediate being thermodynamically more stable than the metallacycle hydride.[26]

The final product is then recovered by hydrolysis, which explains the quantitative incorporation observed at the C^3 position when the reduction is carried out with $D_2O/HCOO^-$. This result is confirmed by the lack of incorporation at C^3 when $H_2O/DCOO^-$ is used. Hydrolysis of alkyl complexes of transition metals such as palladium (II)[27] and selective incorporation of H^+ in Rh-alkyl fragments[28] has already been reported.

The by-product, dimethylmesaconate, is formed by an isomerisation of the substrate DMS by migration of the double bond from an external to an internal position. The *cis* isomer, dimethylcitraconate, is not formed (^{13}C and ^1H NMR). A similar secondary isomerisation reaction is reported for the reduction of itaconic acid with formic acid/triethylamine.[8] Curiously, in this case, the cis isomer, i.e. citraconic acid, is formed. In the by-product, only the methyl group (position 1) incorporates deuterium (10–15% with $H_2O/DCOO^-$ and 20–25% with $D_2O/HCOO^-$), which is in accordance with the position of step **i** in the proposed mechanism.

Kinetics

Choice of the rate determining step:

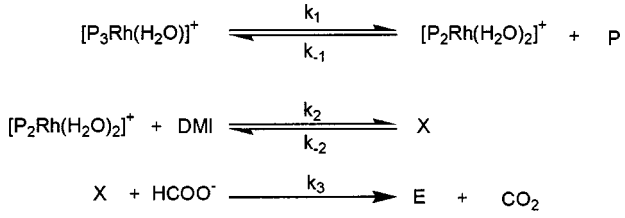
(i) The sodium formate is involved in or before the rate determining step as a primary kinetic isotope effect is noted when the reduction is carried out with $H_2O/DCOO^-$.

(ii) Hydrolysis occurs after the last rate determining step as no isotope effect is measured when the reduction is carried out with $D_2O/HCOO^-$.

(iii) Addition of sodium hydrogenocarbonate has no influence on the course of the reaction.[7] The CO_2, a product of the reaction, is not involved before the last rate determining step.

(iv) The liberation of one equivalent of phosphane ligand occurs before the last rate determining step, as addition of phosphane inhibits the reaction.

The last rate determining step is then step **f**, as it occurs after the formate coordination and before the liberation of CO_2 and the final, hydrolysis step. In addition, only the steps involving terminal products have been considered. Thus, steps **b** to **d** involving intermediates A, B, and C have been lumped in one step in the kinetics (Scheme 2), otherwise the kinetic rate law would have been more complex and would have induced more constants and larger uncertainty in their estimation. The X letter used represents intermediates A, B, and C (Scheme 2). The same process has been used for the steps **e** and **f**. The kinetic Scheme allowed us to derive a formal kinetic rate law for the formation of DMS using the Bodenstein approach for catalytic intermediates (Equation 6).



Scheme 2

$$r = k_3 \frac{C_{Aq}^{HCOO^-} C_{Aq}^{DMI} C_{Aq}^{Rh}}{\frac{k_{-2}}{k_2} + \frac{k_{-1}k_{-2}}{k_1 k_2} C_{Aq}^{P} + C_{Aq}^{HCOO^-}\left(\frac{k_3}{k_2} + \frac{k_{-1}k_3}{k_1 k_2} C_{Aq}^{P}\right) + C_{Aq}^{DMI}\left(1 + \frac{k_3}{k_1} C_{Aq}^{HCOO^-}\right)} \quad (6)$$

This rate law is in accordance with experimental results, i.e. a negative order with respect to phosphane, first order with respect to the catalyst concentration, and complex order with respect to the substrate. It was not possible, however, to take into account the influence of the sodium formate concentration. The semi-empirical model (Equation 4 and Equation 5) presents a negative order with respect to the formate concentration, whereas the formal kinetic rate law presents a positive order of between 0 and 1.

Although this expression gives a complex order with respect to formate concentration, it was not possible to take its influence into account over the whole range of concentration used for the kinetic study.

The model is in good agreement with the experiments, but it was not possible to estimate one set of kinetic parameters for both series of experiments with sodium formate concentrations of 5 and 1 $kmol \cdot m^{-3}$. In addition, as the model possesses an intrinsic inaccuracy due to constants coupling, it was not possible to determine values of intrinsic kinetic constants with a sufficient accuracy, but only ratios of constants. More tests under a wider range of conditions where kinetic constants would not be coupled need to be performed.

Conclusion and Future Work

The kinetic and mechanistic study of H-transfer reduction of dimethyl itaconate by sodium formate/water under biphasic catalysis has been presented. A complex, semi-empirical kinetic model was first validated. It exhibits complex order with respect to the substrate concentration, and inhibition by the phosphane. Numerical integration using the entire concentration vs. time profiles provided values for the kinetic parameters of this model. Labelling studies and ^1H- and ^{13}C-NMR analysis were also performed. A catalytic cycle has been proposed based on these results. A rhodametallacyclobutane intermediate best accounts for the systematic non-deuteriation of the C^2 position of the product, the reduction being carried out either by $H_2O/DCOO^-$ or $D_2O/HCOO^-$. The mechanism is also supported by the good fit between the empirical model and the formal rate law, de-

rived from the mechanistic steps, despite a poor agreement concerning the influence of sodium formate.

The main conclusion concerns the shift in the mechanism on going from diacids to their ester derivatives. Unsaturated acids reduction proceeds through a *cis*-1,2-hydrogen addition,[1,8] whereas this work shows that reduction of esters should undergo a 1,3-addition.[1] This switch in mechanism may well account for the lower optical yields observed in the enantioselective H-transfer reduction of esters compared to their corresponding acids.[8]

Experimental Section

General: ^{31}P-NMR spectra (external reference H_3PO_4 85% D_2O) were recorded on a Bruker AM 300 (121.51 MHz) and a Bruker AM 200 (81.015 MHz). ^{1}H- and ^{13}C-NMR spectra (external reference $SiMe_4$) were recorded on a Bruker AM 200 (200.13 MHz and 50.32 MHz, for ^{1}H and ^{13}C, respectively). Deuterated water (99.9 atom% D, Aldrich) and [D_2]formic acid (99+ atom%, 95% in D_2O, ACROS) for the labelling study were degassed and used without further purification. – TPPTS 30% wt in water, sodium formate (97%, Aldrich), dimethyl itaconate (97%, Aldrich), decane (99%, Aldrich), mesaconic acid (99%, Aldrich), and the catalyst precursor [Rh(cod)Cl]$_2$ (98%, Strem) were used as received. All the experiments were performed under argon or nitrogen. – Partition isotherms determination: The experimental procedure for determining partition isotherms has already been described in a previous paper.[7] – Kinetic studies in a well mixed batch reactor: All the details have already been described in a previous paper.[7] The reduction of dimethyl itaconate (DMI) was performed under a range of conditions, given in Table 2. The initial rate of reaction is calculated from the slope of concentration vs. time profiles at low conversion (< 10%).

Labelling Study/Reduction of DMI in D_2O/HCOONa: A solution of TPPTS in water (30% wt, 2 cm^3, 1.22 mmol) was evaporated. D_2O (2 cm^3) was then added to the residue, and the procedure was repeated twice. A solution of sodium formate in D_2O (5, 8 cm^3, 40 mmol) was then added to an orange slurry of [Rh(cod)Cl]$_2$ (48.9 mg, 0.2 mmol) in the solution of TPPTS in D_2O previously prepared. The mixture was stirred at room temperature for about 12 h and stored at 4 °C. The catalytic run was performed as previously described.[7] After reduction, the organic layer was separated, dried with $CaCO_3$, and the solvent was evaporated. The oily product was analysed by NMR spectroscopy. – ^{13}C NMR: δ = 16.7 (m, $^1J_{CD}$ = 19.7 Hz, C^1), 35.5 (m, C^2), 37.0 (t, $^1J_{CD}$ = 20.0 Hz, C^3), 51.5 (s, C^7), 51.8 (s, C^5), 172.1 (s, C^6), 175.5 (s, C^4). – ^{1}H NMR data for the isotopomers identified in the organic layer: **1**: δ = 1.15 (d, $^3J_{12}$ = 7.1 Hz, 3 H, H^1), 2.65 (dt, $^3J_{32}$ = 8.0 Hz, $^2J_{HD}$ = 2.3 Hz, 1 H, H^3), 2.80 (m, 1 H, H^2), 3.61, 3.63 (s, 3 H, H^5, H^7). – **2**: δ = 1.15 (d, $^3J_{12}$ = 7.1 Hz, 3 H, H^1), 2.33 (m, $^3J_{3'2}$ = 6.0 Hz, $^2J_{HD}$ = 2.3 Hz, 1 H, H$^{3'}$), 2.80 (m, 1 H, H^2), 3.61, 3.63 (s, 3 H, H^5, H^7). – **3**: δ = 1.13 (dt, $^3J_{12}$ = 7.1 Hz, $^2J_{HD}$ = 1.8 Hz, 2 H, H^1), 2.65 (dt, $^3J_{32}$ = 8.0 Hz, $^2J_{HD}$ = 2.3 Hz, 1 H, H^3), 2.80 (m, 1 H, H^2), 3.61, 3.63 (s, 3 H, H^5, H^7). – **4**: δ = 1.13 (dt, $^3J_{12}$ = 7.1 Hz, $^2J_{HD}$ = 1.8 Hz, 2 H, H^1), 2.33 (m, $^3J_{3'2}$ = 6.0 Hz, $^2J_{HD}$ = 2.3 Hz, 1 H, H$^{3'}$), 2.80 (m, 1 H, H^2), 3.61, 3.63 (s, 3 H, H^5, H^7). – **5**: δ = 2.22 (d, $^4J_{13}$ = 1.5 Hz, 3 H, H^1), 3.74, 3.70 (s, 3 H, H^5, H^7), 6.71 (broad, 1 H, H^3). – **6**: δ = 2.22 (m, $^4J_{13}$ = 1.5 Hz, $^2J_{HD}$ = 1.46 Hz, 2 H, H^1), 3.74, 3.70 (s, 3 H, H^5, H^7), 6.71 (broad, 1 H, H^3).

Labelling Study/Reduction of DMI in H_2O/DCOONa: A solution of [D_2]formic acid in D_2O (95% wt, 10 g, 0.19 mmol) was added to an aqueous solution of sodium hydroxide (10, 20 cm^3, 0.2 mmol). The mixture was then evaporated and water was added to the residue. This procedure was repeated twice to remove traces of D_2O and D^+. Water (40 cm^3) was finally added to the thus prepared [D]sodium formate. Preparation of the catalyst and realization of the kinetic tests were then performed as already described.[7] – After reduction the organic layer was separated, dried with $CaCO_3$, and the solvent was evaporated. The oily product was analyzed by NMR spectroscopy. – ^{13}C NMR: δ = 16.7 (m, $^1J_{CD}$ = 19.7 Hz, C^1), 35.7 (m, C^2), 37.4 (s, $^1J_{CD}$ = 20.0 Hz, C^3), 51.7 (s, C^7), 51.9 (s, C^5), 172.3 (s, C^6), 175.7 (s, C^4).

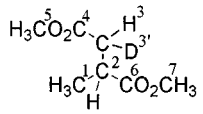
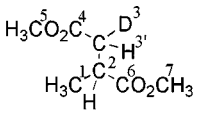
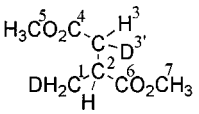
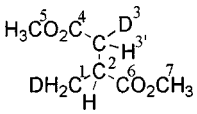
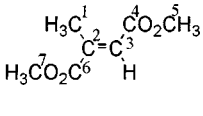
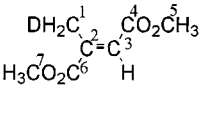
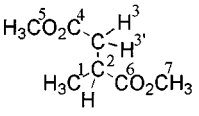
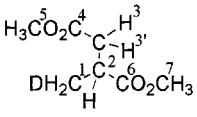
The ^{1}H-NMR data showed the presence of isotopomers **5**, **6**, **7**, and **8**. – **7**: δ = 1.16 (d, $^3J_{12}$ = 7.1 Hz, 3 H, H^1), 2.35 (dd, $^2J_{33'}$ = 16.3 Hz, $^3J_{23'}$ = 6.0 Hz, 1 H, H$^{3'}$), 2.67 (dd, $^3J_{23}$ = 8.0 Hz,1 H, H^3), 2.85 (m, 1 H, H^2), 3.61, 3.63 (s, 3 H, H^5, H^7). – **8**: δ = 1.16 (dt, $^3J_{12}$ = 7.1 Hz, $^2J_{HD}$ = 1.9 Hz, 2 H, H^1), 2.35 (dd, $^2J_{33'}$ = 16.3 Hz, $^3J_{23'}$ = 6.0 Hz, 1 H, H$^{3'}$), 2.67 (dd, $^3J_{23}$ = 8.0 Hz, 1 H, H^3), 2.85 (m, 1 H, H^2), 3.61, 3.63 (s, 3 H, H^5, H^7).

Synthesis of the By-Product DMM: A drop of sulfuric acid 98% was added to a solution of mesaconic acid (2 g, 15.3 mmol) in methanol (50 cm^3). The mixture was stirred at room temperature for 3 days. The solvent was then evaporated and the crude product obtained was characterised by ^{1}H-NMR (200 MHz, $CDCl_3$) spectroscopy. – ^{1}H NMR: δ = 2.30 (d, $^4J_{13}$ = 1.6 Hz, 3 H, H^1), 3.78, 3.82 (s, 3 H, H^5, H^7), 6.80 (q, 1 H, H^3).

Acknowledgments

The authors are grateful to the Région Rhône-Alpes, the Centre National de la Recherche Scientifique and the Rhône-Poulenc com-

Table 5. Different isotopomers/isomers present in organic layers after labelling experiments

 **1**	 **2**	 **3**	 **4**
 **5**	 **6**	 **7**	 **8**

pany for financial support. N. T. is also grateful to the Région Rhône-Alpes for a PhD grant.

[1] W. Leitner, J. Brown, H. Brunner, *J. Am. Chem. Soc.* **1993**, *115*, 152–159 and references therein.
[2] A. Bucsai, J. Bakos, M. Laghmari, D. Sinou, *J. Mol. Catal. A: Chemical* **1997**, *116*, 335–342.
[3] D. Heller, R. Kadyrov, M. Michalik, T. Freier, U. Schmidt, H. W. Krause, *Tetrahedron: Asymmetry* **1996**, *7*, 3025–3035.
[4] A. Harthun, R. Kadyrov, R. Selke, J. Bargon, *Angew. Chem. Int. Ed. Engl.* **1997**, *36*, 1103–1105.
[5] K. T. Wan, E. Davies, *Tetrahedron: Asymmetry* **1993**, *4*, 2461–2468.
[6] Y. Amrani, L. Lecomte, D. Sinou, *Organometallics* **1989**, *8*, 542–547.
[7] C. de Bellefon, N. Tanchoux, S. Caravieilhes, D. H. Schweich, *Catal. Today* **1999**, *48*, 211–219.
[8] H. Brunner, W. Leitner, *J. Organomet. Chem.* **1990**, *387*, 209–217.
[9] X. Wang, L. K. Woo, *J. Mol. Catal. A: Chemical* **1998**, *130*, 171–176.
[10] T. Karlen, A. Ludi, *Helv. Chim. Acta* **1992**, *75*, 1604–1606.
[11] C. de Bellefon, N. Tanchoux, S. Caravieilhes, *J. Organomet. Chem.* **1998**, *567*, 143–150.
[12] R. A. W. Johnstone, A. H. Wilby, *Chem. Rev.* **1985**, *85*, 129–170.
[13] A. Bényei, F. Joó, *J. Mol. Catal.* **1990**, *58*, 151–163.
[14] C. de Bellefon, E. Pollet, P. Grenouillet, *J. Mol. Catal. A: Chemical* **1999**, 145, 121–126.
[15] M. Hernandez, P. Kalck, *J. Mol. Catal. A: Chemical* **1997**, *116*, 131–146.
[16] W. A. Herrmann, J. A. Kulpe, W. Konkol, H. Bahrmann, *J. Organomet. Chem.* **1990**, *389*, 85–101.
[17] R. R. Schrock, J. A. Osborn, *J. Am. Chem. Soc.* **1971**, *93*, 2397–2407.
[18] S. Lange, W. Leitner, R. Mynott, C. Wirtz, XIth International Symposium on Homogeneous Catalysis, St. Andrews, Scotland, July **1998**, p. 73.
[19] G. W. Parshall, S. D. Ittel, *Homogeneous Catalysis: The Applications and Chemistry of Catalysis by Soluble Transition Metal Complexes*, 2nd ed., Wiley-Interscience publication, **1993**, p. 14–16.
[20] K. E. Koenig, W. S. Knowles, *J. Am. Chem. Soc.* **1978**, *100*, 7561–7564.
[21] R. A. Periana, R. G. Bergman, *J. Am. Chem. Soc.* **1984**, *106*, 7273–7274.
[22] R. A. Periana, R. G. Bergman, *J. Am. Chem. Soc.* **1986**, *108*, 7346–7355.
[23] D. J. Hardick, I. S. Blagbrough, B. V. L. Potter, *J. Am. Chem. Soc.* **1996**, *118*, 5897–5903.
[24] T. H. Tulip, D. L. Thorn, *J. Am. Chem. Soc.* **1981**, *103*, 2448–2450.
[25] W. D. Jones, F. J. Feher, *J. Am. Chem. Soc.* **1984**, *106*, 1650–1663.
[26] R. H. Crabtree, *Chem. Rev.* **1985**, *85*, 245–269.
[27] S. Ganguly, D. Roundhill, *Organometallics* **1993**, *12*, 4825–4832.
[28] C. Detellier, G. Gelbard, H. B. Kagan, *J. Am. Chem. Soc.* **1978**, *100*, 7556–7561.

Received August 27, 1999
[I99314]

Mercaptocalixarenes as Mercury(II) Extractors: Synthesis, Structural Analysis and Extraction Properties of Lipophilic Dimercaptocalix[4]arenes

Photon Rao,[a] Olivier Enger,[a] Ernest Graf,[a] Mir Wais Hosseini,*[a] André De Cian,[b] and Jean Fischer[b]

Keywords: Calixarenes / Cyclophanes / Macrocycles / Mercury / S ligands

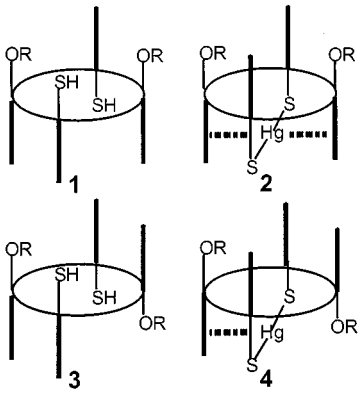
Lipophilic calix[4]arene derivatives that contain two O–C_{12} alkyl chains and two SH groups at the lower rim were synthesized and characterized in the 1,2- and partial-cone conformations. Both conformers were treated with Hg^{2+} and formed neutral mononuclear Hg^{2+} complexes, in which the cation was linearly coordinated to two sulfur atoms. The lipophilic dimercaptocalixarenes were shown to extract Hg^{2+} cations exclusively and efficiently from an aqueous phase into chloroform.

Introduction

The presence of toxic heavy metals in aqueous reservoirs is an important environmental issue.[1] In particular, the mercury(II) cation represents an environmental danger to a variety of living organisms, including mammals,[2] due to its toxicity. Because of the use of mercury derivatives in fungicides and insecticides, Hg^{2+} cations are present in our environment at a rather high level.[3] Since the extraction of heavy metal cations such as Hg^{2+} from aqueous solutions into organic phases may be a possible alternative for water purification, the design of selective extractors for heavy metals appeared to us to be an interesting challenge.

The affinity of mercury for sulfur-containing ligands has been well established.[4] Based on this observation, calixarene derivatives bearing pendent sulfur atoms,[5] and thiacrown ethers[6] have been used as extractors for Hg^{2+} cations. In this context, we and others have been working on sulfur-containing calixarene derivatives such as di-[7] and tetramercaptocalix[4]arenes,[8,9] in which two and four OH groups were replaced by two or four SH functions, respectively as well as mercaptoparacyclophane[10] and thiacalix[4]arenes.[11,12]

We have previously demonstrated that di-[7] and tetramercaptocalix[4]arenes[9] were able to form mono- and binuclear mercury complexes, respectively, in which the calix unit adopted the 1,3-alternate conformation. The cation was therefore strongly coordinated to two thiolate centres, and experienced other interactions with two aromatic rings, thus fulfilling its "2 + 4" coordination requirements. With this insight, the ligand **1**, composed of the *p-tert*-butylcalix[4]arene backbone bearing two SH and two OC_{12} groups, was designed. The two alkyl chains were introduced in order to increase the lipophilicity of the Hg^{2+} complex **2** (Scheme 1).



Scheme 1

In this contribution we report the synthesis of **1** and **3**, and their Hg^{2+} complexes **2** and **4**, respectively, as well as the extraction of mercury from water into chloroform by conformers **1** and **3**.

Results and Discussion

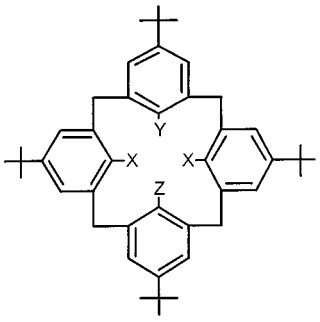
Synthesis

The synthetic strategy used to prepare **1** was based on dithiacarbamoylation of *p-tert*-butylcalix[4]arene **5**[13] at the 1- and 3-positions, followed by transformation of the remaining two OH groups into ether fragments by treatment with bromododecane. Thermal rearrangement of the $OCSNMe_2$ fragments into the $SCONMe_2$ groups was then accomplished by the Newman–Kwart method,[14] and finally, the reductive deprotection of the sulfur atoms using $LiAlH_4$ yielded the desired mercapto derivatives **1** and **3** (Scheme 2 and 3).

Thiacarbamoylation of *p-tert*-butylcalix[4]arene with $(Me)_2NCSCl$ in the presence of K_2CO_3 in refluxing acetone for 24 h yielded 5–10% of the trisubstituted derivative, as

[a] Laboratoire de Chimie de Coordination Organique, Université Louis Pasteur (UMR CNRS 7513), 67000 Strasbourg, France
E-mail: hosseini@chimie.u-strasbg.fr
[b] Laboratoire de Cristallochimie et Chimie Structurale, Université Louis Pasteur (UMR CNRS 7513), 67000 Strasbourg, France

 © WILEY-VCH Verlag GmbH, D-69451 Weinheim, 2000 1434–1948/00/0707–1503 $ 17.50+.50/0



1 or **3** X = O-$(CH_2)_{11}$-CH_3, Y = Z = SH
5 X = Y = Z = OH
6 or **10** X = OH, Y = Z = $OCSNMe_2$
7 or **11** X = O-$(CH_2)_{11}$-CH_3, Y = Z = $OCSNMe_2$
8 or **12** X = O-$(CH_2)_{11}$-CH_3, Y = $OCSNMe_2$, Z = $SCONMe_2$
9 or **13** X = O-$(CH_2)_{11}$-CH_3, Y = Z = $SCONMe_2$

Scheme 2

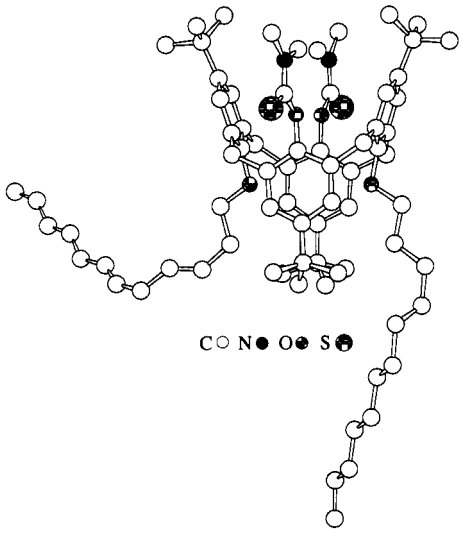
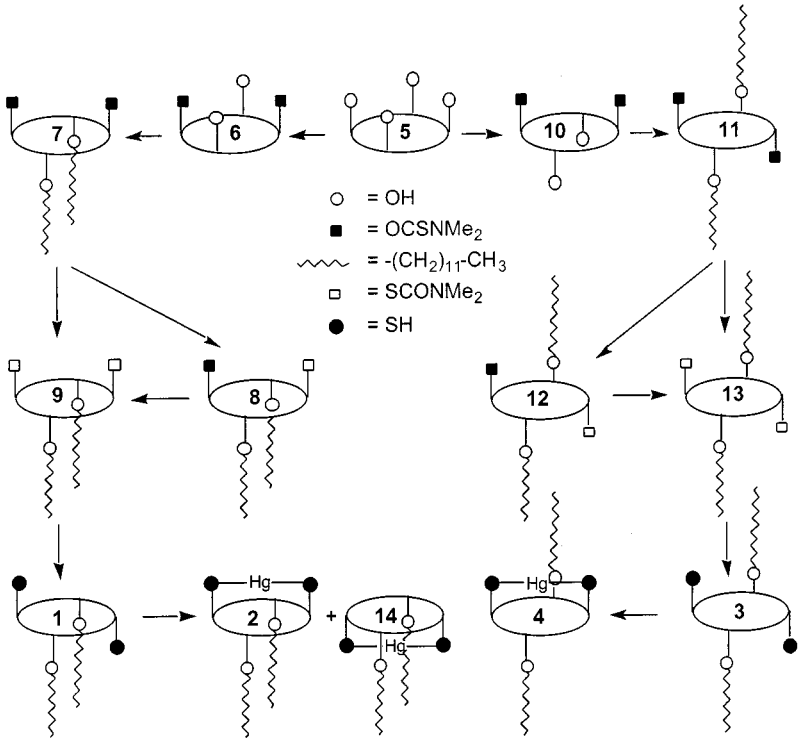


Figure 1. X-ray structure of the disubstituted compound **7** in the 1,3-alternate conformation; for the sake of clarity, H atoms are not represented; selected average bond lengths and angles: $d_{C=S}$ = 1.66 Å, d_{C-N} = 1.33 Å, d_{C-OPh} = 1.36 Å, d_{N-CH3} = 1.45 Å, OCS angle = 124.5°, NCS angle = 125.5°, NCO angle = 110.05°

well as the disubstituted conformers **6** (13%) and **10** (40%), non interconvertible at room temperature. While the treatment of **6** with bromododecane in the presence of NaH in refluxing THF afforded the tetrasubstituted compound **7** in the 1,3-alternate conformation in quantitative yield after 24 h, surprisingly, under the same conditions, the reaction of **10** afforded the compound **11** in the 1,2-alternate conformation. Both compounds **7** (Figure 1) and **11** (Figure 2) were characterized in the solid state by single-crystal X-ray diffraction methods.

The thermal rearrangement of **7** was performed in vacuum on the melt at 340 °C, and yielded the mono-rearranged compound **8** (50%), the bis-rearranged compound **9** (25%) and the unchanged starting material **7** (25%). Subsequently, compound **8** could be rearranged in 20% yield to **9** under similar conditions. Attempts to increase the yield



Scheme 3

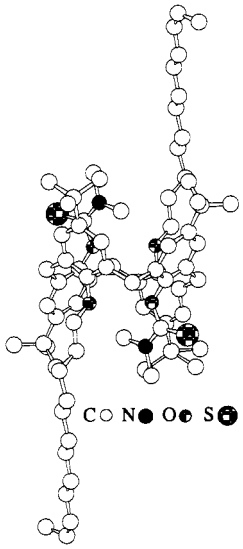


Figure 2. X-ray structure of compound **11** in the 1,2-alternate conformation; for the sake of clarity, H atoms are not represented; selected bond lengths and angles: $d_{C=S}$ = 1.66 Å, d_{C-N} = 1.32 Å, d_{C-OPh} = 1.36 Å, d_{N-CH_3} = 1.47 Å, OCS angle = 123.8°, NCS angle = 126.4°, NCO angle = 109.7°

by performing the reaction in refluxing ditolyl ether failed.[8] Reductive deprotection of **9** was performed using $LiAlH_4$ in refluxing THF, yielding the dimercapto compound **1** (80%) in the partial cone conformation. On the other hand, performing the same sequence of reactions on **11** afforded **12** (40%), the bis-rearranged derivative **13** (20%), and the starting compound **11** (40%). As before, **12** could be rearranged into **13** under the same conditions in 15% yield. Compound **13**, in the 1,2-alternate conformation, was transformed into the desired compound **3** in 74% yield by treatment with $LiAlH_4$ in refluxing THF. The final structural assignment of both **1** and **3** was based on 2D-ROESY NMR data.

Complexation

In order to isolate the mercury complexes **2** and **4**, compounds **1** and **3** were treated with mercuric acetate in refluxing THF for 30 min. For the Hg^{2+} complex **2** that formed with compound **1**, the calix unit was in the 1,3-alternate conformation, whereas in the case of the complex **4** formed with compound **3**, the calix unit was found to be in the partial cone conformation (Scheme 1). These two conformations for the calix backbone were established by 2D-ROESY as well as by ^{199}Hg-NMR experiments. Mercury resonances were observed at $\delta = -1375$ for **2** and at $\delta = -1294$ for **4**. These values are close to the one observed previously ($\delta = -1394$) for the bis(binuclear) mercury complex formed with tetramercaptocalix[4]arene,[9] in which the 1,3-alternate conformation was established by X-ray crystallography. The difference in the chemical shifts observed for **2** and **4** may be rationalized in terms of the Hg^{2+}−aromatic interactions. Indeed, based on previous observations, the rather negative chemical shift value observed may be attributed to the local environment of the metal centre in both **2** and **4** complexes, where the Hg^{2+} cation is completely and half-sandwiched between two aromatic rings, respectively. The observation of a ^{199}Hg-NMR signal at $\delta = -1054$ for the (*p-tert*-butyl−Ph−S)$_2$Hg complex supports the above explanation, because in that case, no Hg^{2+}−aromatic interactions would be present.

Extraction

In this contribution, we report only some preliminary investigations dealing with the extraction of heavy metal cations. The extraction ability of both compounds **1** and **3** was studied under the following conditions: A 5-mL $CHCl_3$ solution of **1** or **3** (mM concentration) was stirred for 30 min in the presence of a 5-mL 95% aqueous acetic acid solution containing $Hg(OAc)_2$ (mM concentration). Aliquots were taken from the aqueous phase, and the amount of mercury remaining was determined by colourimetric titration with dithizon (see Table 1).

Table 1. Extraction of M^{2+} by **1** and **3**

	(mM)[a]	M^{2+}	[M^{2+}] (mM)[b]	%[c]
1	2.8	Hg^{2+}	1.5	100
1	2.8	Hg^{2+}	3.0	87
1	2.8	Hg^{2+}	10.0	34
3	2.8	Hg^{2+}	10.0	34
1	2.8	Pb^{2+}	11.0	none[d]
1	2.8	Cd^{2+}	10.0	none[d]
3	3.0	Pb^{2+}	11.0	none[d]
3	3.0	Cd^{2+}	10.0	none[d]

[a] A solution of the ligand prepared in $CHCl_3$. − [b] A solution of $M(OAc)_2$ in 95% aqueous acetic acid. − [c] Determined (accuracy 0.05 mM) by titrating the aqueous layer after extraction with a solution of dithizon. − [d] Also confirmed by ^{1}H NMR which shows only the presence of the free ligand after the removal and evaporation of the $CHCl_3$ layer.

The nature of the complexes formed between ligands **1** or **3** and mercury cation under extraction conditions was investigated in the following manner: A biphasic mixture composed of a $CHCl_3$ solution containing either the ligand **1** or **3** in mM concentration, an aqueous phase containing 5% acetic acid, added in order to avoid the hydrolysis of the mercuric salt, and $Hg(OAc)_2$ in mM concentration, was stirred at room temperature. As expected, it was found that Hg^{2+} cations were extracted from the aqueous phase into the organic layer. After removal of the organic phase and evaporation of the $CHCl_3$, the nature of the extracted complexes was elucidated by ^{1}H NMR ($CDCl_3$, 25 °C), which showed that in both cases the extracted complexes were identical to the prepared and independently identified complexes **2** and **4**, respectively. However, in the case of ligand **1**, a small amount of another complex showing a rather high symmetry was detected by ^{1}H NMR. This compound was separated by preparative thin layer chromatography and was investigated by mass spectrometry in the FAB^+ mode, and showed a peak at 1216.8 (100%) identical to that observed for mercury complexes **2** and **4**. Furthermore, performing ^{1}H NMR ($CDCl_3$, 25 °C) on the isolated complex, demonstrated that it was the other possible complex **14** (Scheme 3), where the calix unit adopts the cone conformation. However, in marked contrast with complex **2**, where

the calix unit, by adopting the 1,3-alternate conformation, allows both the coordination of the metal cation to two thiolate centres as well as metal−π interactions through the formation of the sandwich complex, in the case of **14** only the coordination of the metal cation to two thiolate groups is possible. This fact may explain the formation of **14** in rather low yield.

When compound **1** (2.8 mM) was present in excess with respect to Hg^{2+} (1.5 mM), 100% of the cation was extracted into chloroform, indicating the high affinity of **1** for mercury cations (see Table 1). On the other hand, in the case of a slight (3.0 mM) or a large (10.0 mM) excess of Hg^{2+} cations, 87% and 34% extraction was observed, respectively. Interestingly, under the same conditions, no extraction of Cd^{2+} or Pb^{2+} cations was observed using **1** or **3**, demonstrating the remarkable selectivity of both compounds **1** and **3** for the Hg^{2+} cations with respect to cadmium and lead cations. The latter observation demonstrates the validity of the design of selective extracting agents for mercury cations.

Conclusions

In conclusion, the synthesis of two new mercaptocalix[4]-arene derivatives bearing long alkyl chains was achieved. Both compounds were shown to efficiently and selectively extract the Hg^{2+} cation from acidic aqueous solution into chloroform. Both compounds showed remarkable selectivity towards Hg^{2+} cation with respect to Cd^{2+} and Pb^{2+} cations. A systematic study of the extraction ability of the reported compounds is currently under investigation.

Experimental Section

General: ^{1}H-, ^{13}C- and ^{199}Hg-NMR spectra were recorded with Bruker WP 200SY and AM 400 instruments operating at 200.13, 50.32, and 71.66 MHz, respectively. ^{1}H-NMR peak positions are reported relative to $CHCl_3$ (δ = 7.26). ^{13}C-NMR peak positions are reported relative to $CDCl_3$ (δ = 77. 0). ^{199}Hg-NMR peak position are reported relative to $CH_3S-Hg-SCH_3$ as external reference. Mass spectra (FAB^+) were recorded in nitrobenzyl alcohol.

Procedure for the Preparation of Compounds 6 and 10: To a slurry of **5**[13] (16.00 g, 25 mmol) in acetone (600 mL), K_2CO_3 (13.8 g, 100 mmol) was added, and the mixture was heated under reflux for 30 min. Then, a solution of *N*,*N*-dimethylthiocarbamoyl chloride (12.5 g, 100 mmol) in acetone (20 mL) was added and refluxing was continued for a further 16 h. Volatile components were removed under vacuum, and the contents of the flask was diluted with water (50 mL) and acidified to pH = 2 by careful addition of dilute aqueous H_2SO_4. The solid thus obtained was extracted with CH_2Cl_2 (5×100 mL) and the removal of the solvent left a crude material which was purified by column chromatography (SiO_2, CH_2Cl_2), and yielded 13% (2.7 g) of **6** and 40% (8.1 g) of **10**.

Compound 6: M.p. > 350 °C. − ^{1}H NMR (200 MHz, $CDCl_3$): δ = 1.00 (s, 18 H), 1.32 (s, 18 H), 3.13 (s, 12 H), 3.49 (s, 12 H), 3.48 (d, *J* = 15 Hz, 4 H), 3.82 (d, *J* = 15 Hz, 4 H), 4.79 (s, 2 H), 6.88 (s, 4 H), 7.07 (s, 4 H). − ^{13}C NMR (50 MHz, $CDCl_3$): δ = 31.1, 31.8, 33.7, 34.0, 34.1, 38.4, 43.6, 125.5, 126.1, 128.0, 132.2, 142.5, 146.6, 148.9, 150.6, 186.8. − MS (FAB^+); *m*/*z* (%): 823.3 (100) [$M^{\cdot+}$], 734.2 (90) [M^+ − $OCSN(Me)_2$]. − $C_{50}H_{66}N_2O_4S_2{\cdot}H_2O$ (841.23): calcd. C 71.39, H 8.15; found C 71.53, H 7.95.

Compound 10: M.p. > 350 °C. − ^{1}H NMR (200 MHz, $CDCl_3$): δ = 1.28 (s, 18 H), 1.32 (s, 18 H), 1.71 (s, 12 H), 3.21 (s, 12 H), 3.63 (d, *J* = 15 Hz, 4 H), 4.00 (d, *J* = 15 Hz, 4 H), 4.81 (s, 2 H), 7.06 (s, 4 H), 7.26 (s, 4 H). − ^{13}C NMR (50 MHz, $CDCl_3$): δ = 31.4, 31.8, 34.0, 34.4, 36.7, 43.4, 125.0, 126.4, 133.1, 142.8, 147.3, 149.1, 149.8, 184.7. − MS (FAB^+); *m*/*z* (%): 823.3 (100) [M^+].

General Procedure for the Preparation of Compounds 7 and 11: To a slurry of either compound **6** or **10** (0.50 g, 0.6 mmol) in THF (50 mL) was added NaH (0.20 g, 8.3 mmol) followed by bromododecane (2.0 mL, 8.7 mmol), and the mixture heated under reflux for 8 h. Volatile components were removed under vacuum, and the reaction mixture quenched by dropwise addition of water (5 mL). After acidification with dilute aqueous H_2SO_4, the solid was extracted in CH_2Cl_2. Volatile components were again removed under vacuum, and the crude material was purified by column chromatography (SiO_2, CH_2Cl_2/hexane: 1:1) affording **7** or **11** in quantitative yields.

Compound 7: ^{1}H NMR (200 MHz, $CDCl_3$): δ = 0.89 (t, *J* = 6.6 Hz, 6 H), 1.15−1.35 (m, 36 H), 1.50−1.65 (m, 4 H), 2.16 (s, 6 H), 3.39 (s, 6 H), 3.51 (t, *J* = 8 Hz, 4 H), 3.60 (d, *J* = 2.2 Hz, 2 H), 3.71 (d, *J* = 15 Hz, 4 H), 6.87 (s, 4 H), 7.09 (s, 4 H). − ^{13}C NMR (50 MHz, $CDCl_3$): δ = 14.1, 22.6, 25.7, 26.1, 29.3, 29.5, 29.6, 29.7, 31.4, 31.6, 31.8, 33.9, 34.0, 38.2, 38.6, 43.4, 71.1, 126.0, 126.8, 132.5, 134.4, 143.3, 145.8, 148.6, 155.8, 185.9. − MS (FAB^+); *m*/*z* (%): 1159.7 (100) [M^+]. − $C_{74}H_{114}N_2O_4S_2$ (1159.86): calcd. C 76.63, H 9.91, N 2.42; found C 76.76, H 9.80, N 2.38.

Compound 11: ^{1}H NMR (200 MHz, $CDCl_3$): δ = 0.87 (t, *J* = 6.6 Hz, 6 H), 1.11−1.37 (m, 40 H), 1.32 (s, 18 H), 1.34 (s, 18 H), 1.42 (s, 6 H), 3.13 (s, 6 H), 3.32 −3.52 (m, 6 H), 3.82−3.95 (m, 6 H), 6.91 (d, *J* = 2.2 Hz, 2 H), 7.09 (d, *J* = 2.2 Hz, 2 H), 7.28 (d, *J* = 2.2 Hz, 2 H), 7.35 (d, *J* = 2.2 Hz, 2 H). − ^{13}C NMR (50 MHz, $CDCl_3$): δ = 14.1, 22.6, 25.5, 29.2, 29.5, 30.2, 31.5, 31.7, 31.8, 34.0, 34.2, 37.2, 39.3, 43.2, 74.2, 125.1, 125.3, 125.5, 125.8, 132.7, 133.3, 133.4, 134.8, 145.1, 147.0, 147.5, 154.0, 184.7. − MS (FAB^+); *m*/*z* (%): 1159.7 (100) [M^+]. − $C_{74}H_{114}N_2O_4S_2$ (1159.86): calcd. C 76.63, H 9.91, N 2.42; found C 76.57, H 9.76, N 2.36

Compounds 8 and 9: In a round-bottomed flask, compound **7** (0.21 g, 0.18 mmol) was heated under vacuum to 340 °C for 3 h. The reaction mixture was purified by column chromatography (SiO_2, CH_2Cl_2) affording 50% (0.10 g) of the mono-rearranged compound **8** and 25% (0.05 g) of the bis-rearranged compound **9**, along with 25% (0.06 g) of the starting material **7**.

Compound 8: ^{1}H NMR (200 MHz, $CDCl_3$): δ = 0.90 (t, *J* = 6.6 Hz, 6 H), 1.26 (s, 58 H), 1.32 (s, 18 H), 1.66 (s, 3 H), 2.70−3.00 (m, 6 H), 3.29 (s, 3 H), 3.35−3.50 (m, 4 H), 3.72 (d, *J* = 17 Hz, 2 H), 3.87 (d, *J* = 17 Hz, 2 H), 6.87 (d, *J* = 2.2 Hz, 2 H), 7.02 (s, 2 H), 7.02 (d, *J* = 2.2 Hz, 2 H), 7.19 (s, 2 H). − ^{13}C NMR (50 MHz, $CDCl_3$): δ = 14.1, 14.2, 22.8, 25.9, 29.0, 29.4, 29.7, 30.1, 31.4, 31.7, 31.8, 32.0, 34.0, 34.2, 34.3, 36.6, 38.7, 39.7, 42.5, 43.5, 70.6, 77.4, 122.7, 125.5, 126.4, 128.0, 128.6, 133.0, 134.2, 134.8, 144.2, 146.4, 146.9, 148.9, 150.3, 155.0, 167.4, 184.4. − MS (FAB^+); *m*/*z* (%): 1160.0 (100) [$M^{\cdot+}$].

Compound 9: ^{1}H NMR (200 MHz, $CDCl_3$): δ = 0.90 (t, *J* = 6 Hz, 6 H), 1.10−1.40 (m, 40 H), 1.26 (s, 18 H), 1.30 (s, 18 H), 2.60−2.80 (br. s, 6 H), 2.80−3.30 (br. s, 6 H), 3.35−3.45 (m, 4 H), 3.89 (s, 8

H), 7.00 (s, 4 H), 7.12 (s, 4 H). − ^{13}C NMR (50 MHz, $CDCl_3$): δ = 14.2, 21.0, 22.0, 25.9, 29.2, 29.4, 29.7, 30.0, 31.0, 31.4, 31.7, 34.0, 34.3, 36.7, 42.5, 71.1, 123.0, 126.1, 127.9, 134.5, 144.0, 146.3, 149.5, 150.0, 168.0. − MS (FAB^+); *m/z* (%): 1160.0 (100) [$M^{\cdot+}$].

Compounds 12 and 13: In a round-bottomed flask, compound **11** (0.1 g, 0.08 mmol) was heated under vacuum to 340 °C for 3 h. The reaction mixture was purified by column chromatography (SiO_2, CH_2Cl_2) affording 40% (0.04 g) of the mono-rearranged compound **12** and 20% (0.02 g) of the bis-rearranged compound **13**, along with 40% (0.04 g) of the starting material **11**.

Compound 12: ^{1}H NMR ($CDCl_3$, 200 MHz): δ = 0.8−1.5 (m, 88 H), 2.74 (s, 6 H), 3.1−4.1 (m, 10 H), 4.54 (d, *J* = 12 Hz, 2 H), 6.88−7.43 (m, 8 H).

Compound 13: ^{1}H NMR ($CDCl_3$, 200 MHz): δ = 0.8−0.9 (m, 6 H), 1.0−1.4 (m, 88 H) 2.6−4.0 (m, 10 H), 4.2−4.6 (m, 2 H), 6.84, − 7.38 (m, 8 H).

Compound 1: To a solution of **9** (0.08 g, 0.07 mmol) in dry THF (10 mL) was added $LiAlH_4$ (0.02 g, 0.5 mmol) and the solution was heated under reflux for 3 h. After cooling, the reaction mixture was quenched by dropwise addition of H_2O, and acidified to pH = 2 with aqueous 10% H_2SO_4. The crude product was extracted with CH_2Cl_2 (20 × 2 mL). After removal of the solvent, the crude material was purified by column chromatography (SiO_2; CH_2Cl_2/hexane, 75:25) affording the desired compound **1** in 80% yield (0.06 g). − ^{1}H NMR (500 MHz, $CDCl_3$): δ = 0.90 (t, *J* = 6 Hz, 6 H), 1.04 (s, 18 H), 1.20−1.45 (m, 40 H), 1.32 (s, 9 H), 1.35 (s, 9 H), 2.15 (s, 1 H), 3.37 (s, 1 H), 3.48 (d, *J* = 3.2 Hz, 2 H), 3.63 (dd, *J* = 7.2 Hz, 4 H), 3.85−4.00 (m, 6 H), 6.60 (d, *J* = 2.5 Hz, 2 H), 7.11 (s, 2 H), 7.15 (d, *J* = 2.5 Hz, 2 H), 7.43 (s, 2 H). − ^{13}C NMR (50 MHz, $CDCl_3$): δ = 14.2, 22.8, 26.6, 29.4, 29.7, 30.9, 31.3, 31.5, 32.0, 33.8, 34.0, 34.3, 34.9, 40.6, 75.5, 125.0, 125.6, 128.5, 130.3, 130.7, 130.8, 140.0, 140.5, 141.7, 143.6, 145.7, 146.7, 154.1. − MS (FAB^+); *m/z* (%): 1016.8 (100) [$M^{\cdot+}$], 829.6 (60). − HRMS ($C_{68}H_{104}O_2S_2$): calcd. 1016.7478; found 1016.7474.

Compound 3: To a solution of **13** (0.05 g, 0.043 mmol) in dry THF (10 mL) was added $LiAlH_4$ (0.02 g, 0.5 mmol) and the solution was heated under reflux for 3 h. After cooling, the reaction mixture was quenched by dropwise addition of H_2O, and acidified to pH = 2 with aqueous 10% H_2SO_4. The crude product was extracted with CH_2Cl_2 (20×2 mL). After removal of the solvent, the crude material was purified by column chromatography (SiO_2; CH_2Cl_2/hexane, 75:25) affording the desired compound **3** in 74% yield (0.04 g). − ^{1}H NMR (200 MHz, $CDCl_3$): δ = 0.89 (t, *J* = 6.6 Hz, 6 H), 1.10−1.40 (m, 40 H), 1.24 (s, 18 H), 1.33 (s, 18 H), 2.84 (s, 2 H), 3.40 (t, *J* = 6.6 Hz, 4 H), 3.70 (d, *J* = 14 Hz, 4 H), 4.24 (d, *J* = 14 Hz, 4 H), 7.08 (s, 4 H), 7.19 (s, 4 H). − ^{13}C NMR (50 MHz, $CDCl_3$): δ = 15.0, 24.0, 27.2, 30.0, 30.2, 30.3, 30.8, 32.7, 32.8, 33.0, 35.5, 74.8, 125.3, 127.4, 128.0, 134.6, 143.2, 145.0, 155.0, 157.5.

General Procedure for the Preparation of Complexes 2 and 4: To a THF solution (1.0 mL) of the dithiol **1** or **3** (0.010 g, 0.01 mmol), excess $Hg(OAc)_2$ (0.10 g, 0.3 mmol) was added and the mixture stirred for 30 min. After evaporation of the solvent, the residue was extracted with CH_2Cl_2 (5×4 mL). After removal of the solvent, the crude mixture was purified by column chromatography (SiO_2) using as eluent 10−20% CH_2Cl_2/hexane in the case of the complex **2** and 20−40% CH_2Cl_2/hexane in the case of the complex **4**. Whereas complex **2** was obtained in quantitative yield (0.012 g), complex **4** was isolated in 74% yield (0.009 g).

Complex 2: ^{1}H NMR (200 MHz, $CDCl_3$): δ = 0.90 (t, *J* = 6 Hz, 6 H), 1.28 (s, 18 H), 1.31 (s, 58 H), 3.56 (t, *J* = 8 Hz, 4 H), 4.05 (d, *J* = 15 Hz, 4 H), 4. 17 (d, *J* = 15 Hz, 4 H), 7.11 (s, 4 H), 7.32 (s, 4 H). − ^{13}C NMR (50 MHz, $CDCl_3$): δ = 14.0, 22.8, 26.1, 29.5, 29.6, 29.7, 29.8, 31.4, 31.7, 31.9, 34.2, 43.3, 72.0, 126.5, 132.0, 134.1, 145.0, 154.5. − ^{199}Hg NMR (72 MHz, $CDCl_3$): δ = −1375. − MS (FAB^+); *m/z* (%): 1216.8 (75) [M^+, $C_{68}H_{102}HgO_2S_2$], 1159.9 (25) [M^+ − isobutene], 1016.1 (25) [M − Hg]$^+$, 829.6 (55) [M^+ − Hg − $O(CH_2)_{11}CH_3$].

Complex 4: ^{1}H NMR (200 MHz, $CDCl_3$): δ = 0.88 (t, *J* = 6.6 Hz, 3 H), 0.89 (t, *J* = 6.6 Hz, 3 H), 1.20 (s, 18 H), 1.26 (s, 54 H), 1.95 (dd, *J* = 9.4 Hz, *J* = 7.2 Hz, 4 H), 3.13 (t, *J* = 8 Hz, 2 H), 3.54 (d, *J* = 12 Hz, 2 H), 3.95 (t, *J* = 7.0 Hz, 2 H), 4.07 (d, *J* = 16 Hz, 2 H), 4.33 (d, *J* = 16 Hz, 2 H), 5.29 (d, *J* = 12 Hz, 2 H), 6.92 (d, *J* = 2 Hz, 2 H), 7.23 (s, 2 H), 7.25 (d, *J* = 2 Hz, 2 H), 7.40 (s, 2 H). − ^{13}C NMR(50 MHz, $CDCl_3$): δ = 14.2, 22.7, 25.7, 26.4, 29.4, 29.7, 31.3, 31.6, 31.8, 32.0, 34.1, 34.3, 35.0, 44.6, 71.0, 124.8, 125.2, 125.6, 130.9, 134.2, 134.7, 144.7, 147.9. − ^{199}Hg NMR (72 MHz, $CDCl_3$): δ = −1294. − MS (FAB^+); *m/z* (%): 1216.8 (40) [M^+, $C_{68}H_{102}HgO_2S_2$], 829.6 (30) [M^+ − Hg − $O(CH_2)_{11}CH_3$].

Complex 14: ^{1}H NMR (200 MHz, $CDCl_3$): δ = 0.88 (t, *J* = 2.5 Hz, 6 H), 0.89 (s, 18 H), 1.20 −1.40 (m, 40 H), 1.32 (s, 18 H), 3.45 (d, *J* = 13 Hz, 4 H), 3.92 (t, *J* = 8 Hz, 4 H), 5.40 (d, *J* = 13 Hz, 4 H), 6.73 (s, 4 H), 7.18 (s, 4 H). − MS (FAB^+); *m/z* (%): 1216.8 (100) [M^+], 829.5 (87) [M^+ − Hg − $O(CH_2)_{11}CH_3$].

Crystal Structures: X-ray structure determinations of single crystals were performed with an Enraf−Nonius Kappa CCD. For all computations the Nonius OpenMoleN package[15] was used. Absorption corrections were partially integrated in the data reduction procedure. Both structures were solved using direct methods and refined against |*F*|. Hydrogen atoms were introduced as fixed contributors when a residual electron density was observed near their expected positions. Crystallographic data (excluding structure factors) for structures reported have been deposited with the Cambridge Crystallographic Data Centre as supplementary publication no. CCDC-138614 and -138615. Copies of the data can be obtained free of charge on application to CCDC, 12 Union Road, Cambridge, CB2 1EZ, UK [Fax: (internat.) + 44-1223/336-033; E-mail: deposit@ccdc.cam.ac.uk].

Crystallographic Data for 7: Colourless crystals, 173 K, $C_{74}H_{114}N_2O_4S_2$, *M* = 1159.87, triclinic, *a* = 14.2423(5), *b* = 15.5842(5), *c* = 19.1515(4) Å, α = 107.436(9), β = 91.359(9), γ = 118.149(9), *V* = 3506 (1) Å^3, space group *P*−1, *Z* = 2, $D_{calcd.}$ = 1.10 gcm^{-3}, Mo-K_α graphite kappa CCD, μ = 0.117 mm^{-1}, 6192 data with $I > 3\sigma(I)$, *R* = 0.078, *Rw* = 0.092.

Crystallographic Data for 11: Colourless crystals, 173 K, $C_{74}H_{114}N_2O_4S_2$, *M* = 1159.87, triclinic, *a* = 10.0750(4), *b* = 13.6749(6), *c* = 13.7344(6) Å, α = 107.099(9) Å, β = 90.294(9) Å, γ = 101.117(9) Å, *V* = 1749.8(4) Å^3, space group *P*−1, *Z* = 1, $D_{calcd.}$ = 1.10 gcm^{-3}, Mo-K_α graphite kappa CCD, μ = 0.117 mm^{-1}, 3575 data with $I > 3\sigma(I)$, *R* = 0.079, *Rw* = 0.102.

Extraction: In a 1.5-cm diameter tube, a $CHCl_3$ solution (5 mL, 2.8−3.0 mM) of the dithiol **1** or **3** was layered with a water/acetic acid (95:5) solution of $M(OAc)_2$ (5 mL, 1.5−11.0 mM, M = Hg, Cd, Pb), and the biphasic system was stirred vigorously at 26 °C for 45 min. Continued stirring beyond this period (up to 24 h) failed to show any additional extraction for any of the metals studied. An aliquot (25−100 μL, depending on the expected residual concentration of the metal ion) was taken from the top aqueous layer and added to a solution of dithizon[16] (300 mM) in $CHCl_3$, and the absorbance (*A*) measured at 480 nm. The metal concentration (*C*) was determined from the standard *A* versus *C* plot.

Determination of Standard (*A*/*C*) Plot for Metal Salts: Aliquots (10−60 μL) in 10-μL increments were withdrawn from a 95% aqueous acetic acid solution of the metal acetate [$M(OAc)_2$, 10 mM], and added to a solution of dithizon (300 mM, 10 mL) in $CHCl_3$ in a stoppered volumetric flask. After shaking the contents of the flask for 2 min, the absorption at 480 nm was measured and plotted against the concentration to yield a straight line. The unknown concentration of the metal salt was determined following the corresponding absorbance from the *A*/*C* plot with an accuracy of 0.05 mM.

Acknowledgments

We thank the CNRS and the Institut Universitaire de France (IUF) for financial support. P. R. thanks the French Embassy in New Delhi for a scholarship.

[1] J. S. Thayer, *Environmental Chemistry of Heavy Elements*, VCH, Weinheim, **1995**.
[2] G. J. Grant, *Encycl. Inorg. Chem*. **1995**, *4*, 2136−2145.
[3] R. B. Martin, *Encycl. Inorg. Chem*. **1995**, *4*, 2185−2196.
[4] A. Müller, E. Diemann, *Compr. Coord. Chem*. **1995**, *2,* 515−550; K. Brodersen, H.-U. Hummel, *Compr. Coord. Chem*. **1995**, *5*, 1047−1097.
[5] A. T. Yordanov, O. M. Falana, H. F. Koch, D. M. Roundhill, *Inorg. Chem*. **1997**, *36*, 6468−6471; A. T. Yordanov, D. M. Roundhill, *New J. Chem.* **1996**, *20*, 447−451; A. T. Yordanov, O. M. Falana, H. F. Koch, D. M. Roundhill, G. J. Lumetta, B. P. Hay, *Chem. Commun*. **1998**, 503−504.
[6] R. M. Izatt, R. E. Terry, L. D. Hansen, A. G. Avondet, J. S. Bradshaw, N. K. Dalley, T. E. Jensen, J. J. Christensen, *Inorg. Chim. Acta* **1978**, *30*, 1−8.
[7] X. Delaigue, M. W. Hosseini, A. De Cian, N. Kyritsakas, J. Fischer, *J. Chem. Soc., Chem. Commun*. **1995**, 609−610.
[8] C. G. Gibbs, C. D. Gutsche, *J. Am. Chem. Soc.* **1993**, *115*, 5338−5339, C. G. Gibbs, P. K. Sujeeth, J. S. Rogers, G. G. Stanley, M. Krawiec, W. H. Watson, C. D. Gutsche, *J. Org. Chem*. **1995**, *60*, 8394−8402.
[9] X. Delaigue, J. McB. Harrowfield, M. W. Hosseini, A. De Cian, J. Fischer, N. Kyritsakas, *J. Chem. Soc., Chem. Commun*. **1994**, 1579−1580.
[10] X. Delaigue, M.W. Hosseini, *Tetrahedron Lett.* **1993**, *34*, 8111−8112.
[11] H. Kumagai, M. Hasegawa, S. Miyanari, Y. Sugawa, Y. Sato, T. Hori, S. Ueda, H. Kamiyama, S. Miyano, *Tetrahedron Lett.* **1997**, *38*, 3971−3972; T. Sone, Y. Ohba, K. Moriya, H. Kumada, K. Ito, *Tetrahedron Lett.* **1997**, *38*, 10689−10692.
[12] H. Akdas, L. Bringel, E. Graf, M. W. Hosseini, G. Mislin, J. Pansanel, A. De Cian, J. Fischer, *Tetrahedron Lett*. **1998**, *39*, 2311−2314; G. Mislin, E. Graf, M. W. Hosseini, A. De Cian, J. Fischer, *Chem. Commun.* **1998**, 1345−1346; G. Mislin, E. Graf, M. W. Hosseini, A. Bilyk, A. K. Hall, J. McB. Harrowfield, B. W. Skelton, A. H. White, *Chem. Commun.* **1999**, 373−374; G. Mislin, E. Graf, M. W. Hosseini, A. De Cian, J. Fischer, *Tetrahedron Lett*. **1999**, *40*, 1129−1132.
[13] C. D. Gutsche, M. Iqbal, *Org. Synth.* **1989**, *68*, 234−237.
[14] M. S. Newman, H. A. Karnes, *J. Org. Chem.* **1966**, *31*, 3980−3984; Y. Ting, W. Verboom, L. G. Groenen, J.-D. van Loon, D. N. Reinhoudt, *J. Chem. Soc., Chem.Commun.* **1990**, 1432−1433.
[15] *OpenMoleN*, Interactive Structure Solution, Nonius B.V., Delft, The Nederlands, **1997**.
[16] S. Alegret, M. Blanco, J.-M. Paulis, *Anal. Chim. Acta* **1985**, *177*, 285−289.

Received October 11, 1999
[I99354]

Multicomponent Polyanions, 49

A Potentiometric and (^{31}P, ^{51}V) NMR Study of the Aqueous Molybdovanadophosphate System

Anna Selling,*[a] Ingegärd Andersson,[a] John H. Grate,[b] and Lage Pettersson[a]

Keywords: Polyoxometalates / Phosphorus / Vanadium / Potentiometry / Formation constants

The equilibrium speciation of the quaternary system H^+/MoO_4^{2-}/HVO_4^{2-}/HPO_4^{2-} in aqueous 0.600 M Na(Cl) at 25 °C and 90 °C was studied by pH potentiometry and ^{31}P (202.5 MHz) and ^{51}V (131.6 MHz) NMR spectrometry. The study focused on solutions containing the oxoanion components in the ratios (Mo + V)/P = 12:1 and Mo/V ≥ 3.8, in the pH range 0–5, wherein Keggin anions of the formula $[H_zMo_{12-x}V_xPO_{40}]^{(3+x-z)-}$ with x = 1–3 are the predominant species. Formation constants (log β) and pK_a values for Keggin anions with x = 1–3 were determined from ^{31}P and ^{51}V resonance chemical shift data, ^{31}P resonance intensity data, and pH potentiometric data with the multidata least squares calculation program LAKE. The $[Mo_{11}VPO_{40}]^{4-}$ anion does not protonate, $[Mo_{10}V_2PO_{40}]^{5-}$ anions can be monoprotonated, and $[Mo_9V_3PO_{40}]^{6-}$ anions can be triprotonated. The six most intense ^{31}P NMR resonances of $[H_zMo_9V_3PO_{40}]^{(6-z)-}$ could be followed over the pH range studied. It was also possible to assign some ^{31}P resonances to a specific isomer of $[Mo_9V_3PO_{40}]^{6-}$.

Introduction

Speciation and structures in aqueous heteropoly- and isopolyoxometalate systems have been studied at Umeå University by potentiometric [H^+] titrations and multinuclear NMR spectrometry. Data obtained by these methods were used in the least-squares calculation program LAKE,[1] which can consider different types of data simultaneously; it thus proved possible to determine speciation and formation constants in complicated systems. These methods were applied in this study for characterising Keggin molybdovanadophosphate anions, $[H_zMo_{12-x}V_xPO_{40}]^{(3+x-z)-}$, in the aqueous H^+/MoO_4^{2-}/HVO_4^{2-}/HPO_4^{2-} system.[2] Keggin molybdovanadophosphates are dioxygen-regenerable oxidants capable of mediating a variety of catalytic oxidation reactions,[3] such as Wacker-like aqueous palladium-catalysed oxidations of olefins to carbonyls.[4] Understanding the nature of the aqueous Keggin molybdovanadophosphates is essential to rational development of this chemical process and motivated the present study. We therefore studied acidic, aqueous molybdovanadophosphate solutions containing the oxoanion components in the ratio (Mo + V)/P = 12:1, in which the Keggin molybdovanadophosphates, $[H_zMo_{12-x}V_xPO_{40}]^{(3+x-z)-}$, are formed as the predominant species.

[a] Department of Inorganic Chemistry, Umeå University
SE-90187 Umeå Sweden
Fax: (internat.) +46-90/786 9195
E-mail: anna.selling@chem.umu.se
[b] Catalytica Inc.,
430 Ferguson Drive, Mountain View, California 94043, U.S.A.

The α-Keggin structure, first reported by Keggin in 1933,[5] is the structure encountered most frequently by far. Rotation of each M_3O_{13} group in turn by π/3 gives the β-, γ-, δ-, and ε-structures.[6,7] These are increasingly disfavoured, in this order, by increasing internal electrostatic repulsions of the M atoms. Some β-structures and, recently, one γ-structure[8] have been reported for XM_{12}^{VI} species, but we are unaware of any δ- and ε-structures. β-Structures become more likely when the internal electrostatic repulsions are decreased, either by the substitution of M^{VI} by lower-valence M atoms or by the reduction of M^{VI} atoms.

In the parent α-Keggin $[Mo_{12}PO_{40}]^{3-}$ structure, which has T_d symmetry, all Mo sites are equivalent by symmetry, so that one isomorphous substitution of V for Mo results in a single α-$[Mo_{11}VPO_{40}]^{4-}$ structure. By isomorphous substitution of two, three, or four V for Mo, 5, 13, or 27 positional α-Keggin isomers and an increasing number of β-isomers can be formed.[7] Consequently, the present study was restricted to solutions containing Keggin molybdovanadophosphates with $x \leq 3$ to somewhat simplify this complicated system.

The binary H^+/HVO_4^{2-},[9–11] H^+/MoO_4^{2-},[12] and H^+/HPO_4^{2-} [13] and the ternary H^+/HVO_4^{2-}/HPO_4^{2-},[13] H^+/MoO_4^{2-}/HPO_4^{2-},[14,15] and H^+/MoO_4^{2-}/HVO_4^{2-} [16,17] subsystems in 0.6 M Na(Cl) at 25 °C have all been previously characterised and are used in the present study of the quaternary system. The present study was extended to a higher temperature, 90 °C, to assess the effect of temperature on speciation. Many applications of Keggin molybdovanadophosphates in oxidation reactions[4] are performed at such elevated temperatures.

 © WILEY-VCH Verlag GmbH, D-69451 Weinheim, 2000 1434–1948/00/0707–1509 $ 17.50+.50/0

Our ^{31}P- and ^{51}V-NMR characterisation of the isomeric Keggin decamolybdodivanadophosphate ions, $x = 2$, at 25 °C and 90 °C, and their individual pK_a values, has already been reported.[18] Many of the conclusions presented herein for the Keggin nonamolybdotrivanadophosphates, $x = 3$, rely substantially, by analogy, on the findings presented in that report. Some preliminary results from the present study were presented earlier at an international workshop.[19]

Notations and Designations

The polyanion formation constants are reported with H^+, MoO_4^{2-}, HVO_4^{2-}, and HPO_4^{2-} as the components, and equilibria are written according to Equation (1).

$$p\,H^+ + q\,MoO_4^{2-} + r\,HVO_4^{2-} + s\,HPO_4^{2-} \rightleftarrows [(H^+)_p(MoO_4^{2-})_q(HVO_4^{2-})_r(HPO_4^{2-})_s]^{p-2(q+r+s)} \quad (1)$$

The resulting polyanions will, for brevity, sometimes be denoted by their (p,q,r,s) integers and formation constants are reported as $\beta_{p,q,r,s}$. The potentiometric $[H^+]$-titration data establish only the composition, that is, (p,q,r,s), of the various polyanions. Their actual ionic formulae are related to their (p,q,r,s) values by loss of water, Equation (2).

$$[(H^+)_p(MoO_4^{2-})_q(HVO_4^{2-})_r(HPO_4^{2-})_s]^{p-2(q+r+s)} \rightleftarrows [H_{(p+r+s-2w)}Mo_qV_rP_sO_{(4q+4r+4s-w)}]^{p-2(q+r+s)} + w\,H_2O \quad (2)$$

Complementary structural information, such as NMR and X-ray data, is required to establish the formulae. Compositions given in brackets, as in $[HMo_9V_3PO_{40}]^{5-}$, designate the ionic formulae of discrete Keggin ions. To designate Keggin structures without regard to protonation state and charge, the abbreviated form Mo_9V_3P is sometimes used.

Compositions given in braces, as in $\{Na_5HMo_9V_3PO_{40}\}$, designate the macroscopic elemental compositions of certain solutions and solids of Keggin salts. This designation rigorously specifies the known mole ratios of Na, Mo, V, and P present. In the solids and in the majority of solutions, Mo, V and P are present in exactly the Keggin proportions, (Mo + V) = 12 P, and are predominantly incorporated into Keggin anions. The macroscopic composition in braces therefore corresponds, essentially, to the average Keggin anion formula and the countercations present to balance its average anionic charge. These average formulae in braces can have nonintegral ratios of the elements.

To designate the positional isomers of α and β Keggin species, the recommended IUPAC numbering schemes are used.[20] Like Pope[21] and most other authors, however, we indicate the vanadium positions in Keggin molybdovanadophosphates by the lowest possible numbers (1,*a*,*b* for α-$[Mo_9V_3PO_{40}]^{6-}$ isomers), not by the highest possible numbers (12,*c*,*d*) as in the recommended IUPAC schemes. In this paper, all references to dissymmetric positional isomers refer to both enantiomers together.

The acidity measurements are on the concentration scale, where pH = $-\log [H^+]$, *not* on the activity scale, where pH = $-\log \{H^+\}$. We will, for simplicity, use pH instead of $-\log [H^+]$. For brevity, the total concentrations of molybdenum, vanadium, and phosphorus are often denoted by Mo, V, and P.

Results and Discussion

Equilibrium Analysis

Since the present study focused on solutions containing the oxoanion components in the ratio (Mo + V)/P = 12:1, in the pH range 0−5, the predominant oxoanion species present were the Keggin anions, $[H_zMo_{12-x}V_xPO_{40}]^{(3+x-z)-}$. Figure 1 maps the solutions, in (Mo/V) vs. pH space, for which data were collected.

The equilibrium calculations were simplified by the use of data only from solutions with Mo/V ≥ 3.8, and in these solutions only $[H_zMo_{12-x}V_xPO_{40}]^{(3+x-z)-}$ species with $x =$

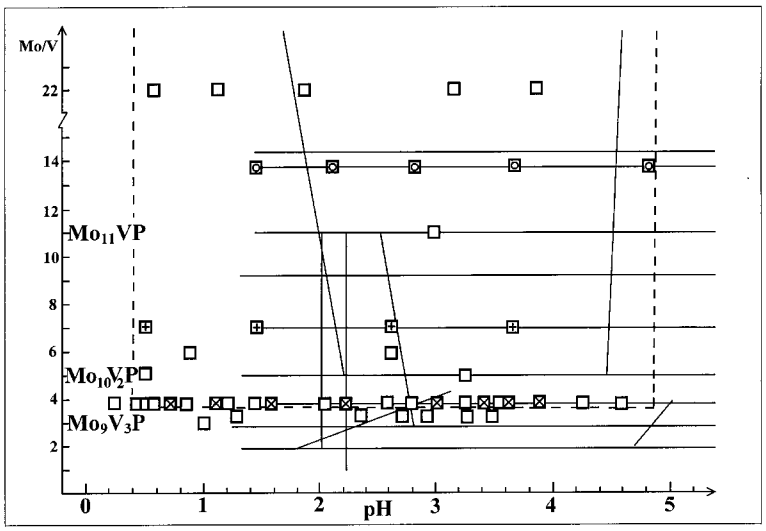


Figure 1. Mo/V ratios and pH values of Keggin molybdovanadophosphate solutions for which experimental data were collected by EMF titrations (continuous lines) from ^{31}P- and ^{51}V-NMR spectroscopy (□). Note the break in the Mo/V scale. The data used in the equilibrium calculations is from solutions within the dashed lines. NMR data from the points marked with ○, +, and X are included in the distribution diagrams of Figures 3, 4, and 5, respectively

Table 1. Polyhedral structures of the thirteen positional isomers of α-$[Mo_9V_3PO_{40}]^{6-}$ with their designation, symmetry point group, statistically predicted abundance in these α-isomers, and ^{31}P NMR resonance assignment (Figure 8). The VO_6 octahedra are shaded. Statistically predicted abundance 1 is for the α-isomers only. Statistically predicted abundance 2 is found for both the α- and β-isomers when approx. 17% of phosphorus is bound in β-isomers (see text)

Polyhedral Structure	Designation (enantiomer)	Symmetry	Statistical Abundance 1	Assignment ^{31}P	Statistical Abundance 2	Integral
	α-1,4,9	C_{3v}	1.82 %	Resonance 1	1.5 %	0.8 %
	α-1,2,3	C_{3v}	1.82 %	Resonance 2	1.5 %	2.7 %
	α-1,2,4 (α-1,3,9)	C_1	10.9 %	Resonance 3	9.1 %	28 %
	α-1,2,6 (α-1,3,7)	C_1	10.9 %		9.1 %	
	α-1,4,8 (α-1,5,9)	C_1	10.9 %		9.1 %	
	α-1,4,6	C_S	5.46 %	Resonance 4	4.5 %	5.2 %
	α-1,2,8 (α-1,3,5)	C_1	10.9 %	Resonance 5	9.1 %	20 %
	α-1,4,7 (α-1,6,9)	C_1	10.9 %		9.1 %	
	α-1,2,10	C_S	5.46 %		4.5 %	
	α-1,2,11 (α-1,3,11)	C_1	10.9 %		9.1 %	
	α-1,5,8	C_S	5.46 %		4.5 %	
	α-1,5,7 (α-1,6,8)	C_1	10.9 %		9.1 %	
	α-1,6,12 (α-1,7,10)	C_3	3.61 %		3.0 %	

1−3 are present. Solutions with Mo/V < 3.8 contain $[H_zMo_8V_4PO_{40}]^{(7-z)-}$ species and, at lower Mo/V, even higher V-content species. ^{31}P- and ^{51}V-NMR data from solutions with Mo/V < 3.8 were collected to help in assigning resonances and obtaining accurate relative abundances (by resonance integration) for the isomeric Mo_9V_3P species.

α-Keggin compositions with $x \geq 2$ can exist as positional isomers. Table 1 shows the polyhedral structures, symmetries, and statistically predicted relative abundances for the α-isomers of Mo_9V_3P. We were able to track the pH dependence of the ^{31}P resonances of the more abundant, but not all, Mo_9V_3P isomers at 25 °C. Figure 2 shows the ^{31}P chemical shifts of six Mo_9V_3P resonances plotted against pH over the range 0−6, along with the ^{31}P chemical shift vs. pH dependence for $[Mo_{11}VPO_{40}]^{4-}$ and the $Mo_{10}V_2P$ isomers determined previously.[18]

Equilibrium calculations were directed at identifying the Keggin compositions, $[H_zMo_{12-x}V_xPO_{40}]^{(3+x-z)-}$, present and for determining their formation constants, for x = 1−3. The equilibrium analysis of this system is complicated by two factors. First, the Keggin species exist in solution as equilibrium distributions over compositions of varying x, centred on the solution bulk composition. Consequently, it is not possible to EMF titrate species that have one x composition in the near absence of species of higher and lower x compositions. (The exception is $[Mo_{11}VPO_{40}]^{4-}$ (x = 1), which is present only as the single α-isomer, which remains unprotonated up to pH < 0, and does not significantly disproportionate at equilibrium into x = 0 and x = 2 species.[18]) Second, compositions with $x \geq 2$ exist as equilibrium mixtures of isomers, each with its own pK_a, which cannot be individually EMF titrated. Consequently, EMF titration data for solutions containing $Mo_{10}V_2P$ and Mo_9V_3P compositions manifest simultaneous titrations of numerous species.

The data from EMF titrations at different Mo/V ratios allow the calculations to distinguish the titration of the abundance-weighted average x = 2 species from the titration of the abundance-weighted average x = 3 species. Only the NMR chemical shifts vs. pH data (equivalent to spectrometric titrations) allow the titration curves, and thus the pK_a values and formation constants, of individual isomeric

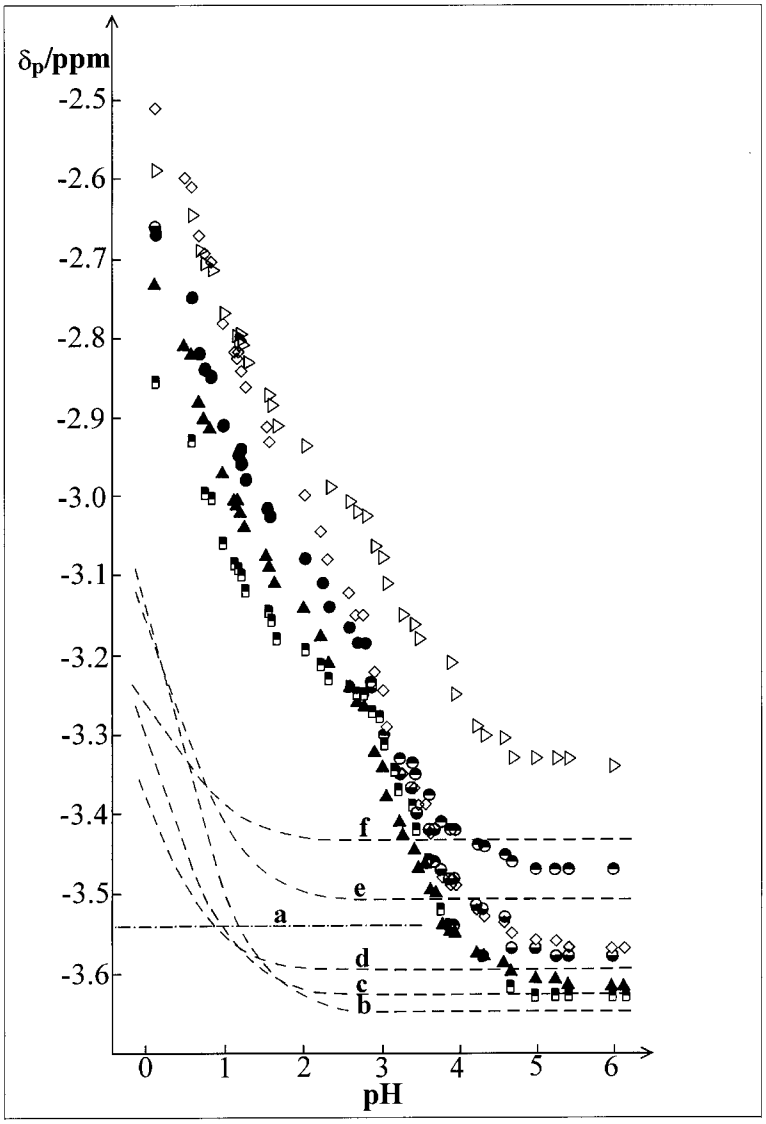


Figure 2. ^{31}P chemical shifts, at 25 °C, of the most intense Keggin Mo_9V_3P isomers, plotted as a function of pH. The dashed dotted line (a) shows the chemical shift of $[Mo_{11}VPO_{40}]^{4-}$ and the dashed curves (b−f) show the chemical shifts of the $Mo_{10}V_2P$ isomers: **b**: α-1,4; **c**: α-1,2 + α-1,5; **d**: α-1,6 + α-1,11; **e**, **f**: β-4,10 and β-4,11[18]

species to be distinguished. For the $Mo_{10}V_2P$ composition, it proved possible to resolve and track the ^{31}P- and ^{51}V-NMR resonances of the different isomers against pH sufficiently to assign the resonances to isomeric structures, to determine the pK_a values of the monoprotonated anions, and to evaluate their relative abundances.[18] Those data have been used to calculate the individual formation constants of $[H_zMo_{10}V_2PO_{40}]^{(5-z)-}$ species where $z = 0$, 1, as described below. As mentioned earlier, it was not possible to resolve and track the resonances of all the significant Mo_9V_3P isomers over pH, either by ^{31}P- or ^{51}V-NMR, and only "average" pK_a values and formation constants for these isomers could be determined.

To establish the formation constants for the $[H_zMo_{12-x}V_xPO_{40}]^{(3+x-z)-}$ compositions, the EMF potentiometric and NMR data were extensively evaluated with the LAKE multimethod least-square program, as described below. The "best" model obtained is reported in Table 2.

The determination of the formation constants began with the evaluation of the combined EMF and NMR integral data for solutions with the oxoanion component ratios (Mo+V)/P ≥ 11.8. At Mo/V ratios above or at 13.75, α-$[Mo_{11}VPO_{40}]^{4-}$ is strongly favoured over compositions with higher vanadium content, and is the only molybdovanadophosphate species present at pH < 2. Because this composition contains so much more P and Mo than in the $Mo_{11}VP$ Keggin composition, some molybdophosphate species are also present in these solutions. Since the formation constants of the species in the molybdophosphate system were previously determined in the same ionic medium,[15] the formation constant of α-$[Mo_{11}VPO_{40}]^{4-}$ could be determined accurately.

Table 2. The formation constants of $[Mo_{11}VPO_{40}]^{4-}$, $[H_zMo_{10}V_2PO_{40}]^{(5-z)-}$ (z = 0, 1), and $[H_zMo_9V_3PO_{40}]^{(6-z)-}$ (z = 0, 1, 2, 3), based on EMF data, NMR integral data for the molybdovanadophosphate species and the ^{31}P chemical shift data for the $Mo_{10}V_2P$ species and the most intense Mo_9V_3P resonance. The formation constants reported for the $Mo_{10}V_2P$ and Mo_9V_3P compositions are each the abundance-weighted average formation constants over all the isomeric species with that composition

NMR symbol	(p,q,r,s) notation	Formula	log β ± (3σ)	pK_a
Δ	22,11,1,1	$Mo_{11}VPO_{40}^{4-}$	141.5 (2)	
○	21,10,2,1	$Mo_{10}V_2PO_{40}^{5-}$	146.9 (3)	
	22,10,2,1	$HMo_{10}V_2PO_{40}^{4-}$	147.2 (3)	0.3
◇	20,9,3,1	$Mo_9V_3PO_{40}^{6-}$	147.1 (3)	
	21,9,3,1	$HMo_9V_3PO_{40}^{5-}$	150.2 (3)	3.1
	22,9,3,1	$H_2Mo_9V_3PO_{40}^{4-}$	151.7 (3)	1.5
	23,9,3,1	$H_3Mo_9V_3PO_{40}^{3-}$	152.2 (3)	0.5

By next expanding the evaluation to include data from solutions in which $Mo_{10}V_2P$ species are also present, but in which Mo_9V_3P species are still absent, the formation constants for the $Mo_{10}V_2P$ compositions were determined. In addition to the combined EMF and NMR integral data for such solutions, this evaluation also included the chemical shift vs. pH data for the ^{51}V resonance of the α-1,2-$[H_zMo_{10}V_2PO_{40}]^{(5-z)-}$ (z = 0, 1) isomer. This isomer was chosen as a surrogate for the average $Mo_{10}V_2P$ composition, as its pK_a (0.26) is midway between the most extreme pK_a values of the $Mo_{10}V_2P$ isomers (0.04 for α-1,6 + α-1,11 and 0.48 for α-1,4).[18] The formation constants so determined for $[Mo_{10}V_2PO_{40}]^{5-}$ and $[HMo_{10}V_2PO_{40}]^{4-}$ are essentially the abundance-weighted average formation constants for the manifold of $Mo_{10}V_2P$ isomers. (They are strictly this average except to the extent that the surrogate pK_a differs from the actual average pK_a.)

The solutions whose data were used to determine formation constants for the $Mo_{10}V_2P$ compositions included solutions with the oxoanion component ratios (Mo + V)/P ≥ 11.8, as above, but at pH > 2. Above pH = 2, $[Mo_{11}VPO_{40}]^{4-}$ is partly (pH = 2−4) or completely (pH > 4) disproportionated to molybdophosphate species and $Mo_{10}V_2P$ species at equilibrium. Figure 3 shows a phosphorus distribution diagram for solutions of this composition over the entire pH range of this study, 0−5. Experimental points from the ^{31}P-NMR integral data are included in Figure 3, showing that the fit of experimental data to the calculated formation constants is good.

Also among the solutions containing $Mo_{10}V_2P$ species, but not Mo_9V_3P species, that were used to determine the $Mo_{10}V_2P$ formation constants, were solutions with the oxoanion components in the Keggin ratio (Mo + V)/P = 12.0 and with the Mo/V ratio decreased to above or equal to 7 (average composition $Mo_{10.5}V_{1.5}P$). Figure 4 shows a calculated phosphorus distribution diagram as a function of pH and experimental ^{31}P NMR integral data points for solutions of this composition, with Mo/V = 7.

After the evaluation was expanded to include EMF, NMR integral, and shift data from solutions with the Mo/V ratio decreased to above or at 3.8 (average composition

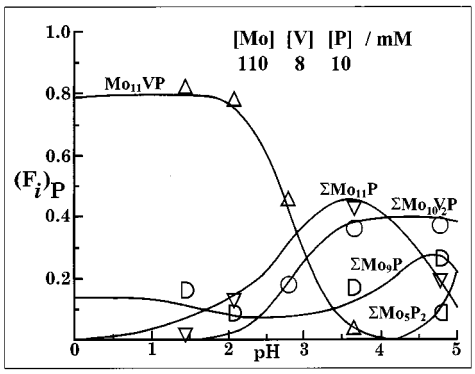


Figure 3. Distribution diagram of phosphorus-containing species as a function of pH in a solution with the oxoanion components in the ratio (Mo + V)/P = (11 + 0.8):1 = 11.8 and 10 mM P. $(F_i)_P$ is the fraction of the total phosphorus. At this ratio, some well-known molybdophosphate species, $Mo_{11}P$, Mo_9P, and Mo_5P_2, are present. The symbols represent experimental ^{31}P-NMR integral data

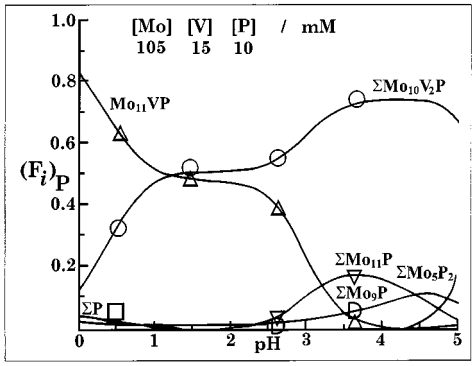


Figure 4. Distribution diagram of phosphorus-containing species as a function of pH in a solution with oxoanion components in the ratio (Mo + V)/P = (10.5 + 1.5):1 and 10 mM P. The symbols represent experimental ^{31}P-NMR integral data

$Mo_{9.5}V_{2.5}P$), the formation constants for the Mo_9V_3P compositions were determined. The final calculation is a simultaneous variation of all constants in which all kinds of data with Mo/V ≥ 3.8 are used, and the result is shown in Table 2. Only the ^{31}P chemical shift data vs. pH for the highest intensity Mo_9V_3P resonance (▲ in Figure 2) were included. A model with four $[H_zMo_9V_3PO_{40}]^{(6-z)-}$ compositions (z = 0,1,2,3) gave the best explanation of included data. (For the manifold of Mo_9V_3P isomers, the pH dependence of the chemical shift of the most intense ^{31}P resonance was taken as a surrogate for the abundance-weighted average pH dependence.)

The pK_a values for the highest intensity Mo_9V_3P ^{31}P-NMR resonance (▲ in Figure 2) were also determined in a LAKE calculation in which only the chemical shift vs. pH data were used. These pK_a values (pK_{a3} = 3.18, pK_{a2} = 1.66, pK_{a1} = 0.56) agree well with the three pK_a values determined by equilibrium in Table 2 (pK_{a3} = 3.1, pK_{a2} = 1.5, pK_{a1} = 0.5).

Figure 5 shows a distribution diagram of phosphorus, as a function of pH, at a Mo/V = 3.8 ratio, based on the results showed in Table 2. In this figure, each of the protonation states is plotted individually with dotted lines and the solid lines show the sums of "homonuclear" species.

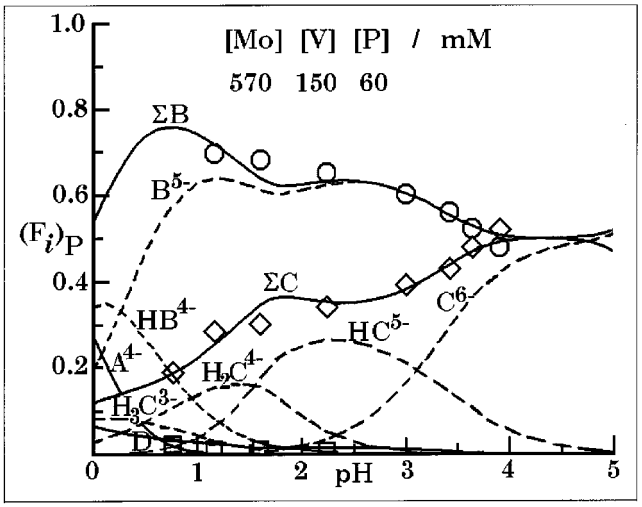


Figure 5. Distribution diagram of phosphorus-containing species as a function of pH in a solution with the oxoanion components in the ratio (Mo + V)/P = (9.5 + 2.5):1 and 60 mM P. Each of the protonation states is plotted individually with dotted lines and the solid lines show the sums of "homonuclear" species. $\mathbf{A^{4-}}$ = $[Mo_{11}VPO_{40}]^{4-}$; $\mathbf{B^{5-}}$ = $[Mo_{10}V_2PO_{40}]^{5-}$; $\mathbf{HB^{4-}}$ = $[HMo_{10}V_2PO_{40}]^{4-}$; $\mathbf{\Sigma B}$ = B^{5-} + HB^{4-}; $\mathbf{C^{6-}}$ = $[Mo_9V_3PO_{40}]^{6-}$; $\mathbf{HC^{5-}}$ = $[HMo_9V_3PO_{40}]^{5-}$; $\mathbf{H_2C^{4-}}$ = $[H_2Mo_9V_3PO_{40}]^{4-}$; $\mathbf{H_3C^{3-}}$ = $[H_3Mo_9V_3PO_{40}]^{3-}$; $\mathbf{\Sigma C}$ = C^{6-} + HC^{5-} + H_2C^{4-} + H_3C^{3-}; **D** = H_3PO_4. The symbols represent experimental ^{31}P-NMR integral data

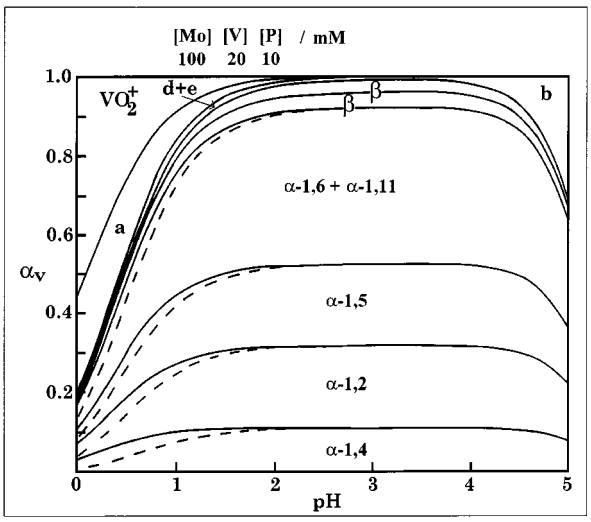


Figure 6. Diagram showing the cumulative distribution of vanadium-containing species, α_V, as a function of pH in solutions; the oxoanion components appear in the ratio (Mo + V)/P = (10 + 2):1, at P = 10 mM. The area between a solid curve and the dashed curve below it represent the protonated species, $[HMo_{10}V_2PO_{40}]^{4-}$. **a**: $[Mo_{11}VPO_{40}]^{4-}$; **b**: $[Mo_9V_3PO_{40}]^{6-}$; **d**: $[H_2Mo_9V_3PO_{40}]^{4-}$; **e**: $[H_3Mo_9V_3PO_{40}]^{3-}$

NMR integral data have an error of about 5−10%, which can explain the disparity between the model and the experimental data in the figure. In this solution $Mo_{10}V_2P$ species contain 40−50% of the total amount of vanadium and 60−70% of phosphorus over almost the entire pH range.

The relative abundances of the $[Mo_{10}V_2PO_{40}]^{5-}$ isomers, determined previously,[18] and the abundance-weighted average formation constant determined in this study (Table 2) were used for calculating the formation constants of the individual $[Mo_{10}V_2PO_{40}]^{5-}$ isomers; these are reported in Table 3. The pK_a values determined for the conjugate, monoprotonated $[HMo_{10}V_2PO_{40}]^{4-}$ isomers[18] were used for the determination of their formation constants (Table 3).

Table 3. Individual formation constants for the $[H_zMo_{10}V_2PO_{40}]^{(5-z)-}$ (z = 0, 1) isomers, calculated from the abundance-weighted average formation constants for the composition, their relative abundances among themselves (NMR integral data), and their pK_a values; the latter data is from ref.[18]

(*p,q,r,s*) notation	Formula	IUPAC notation	log β	pK_a
21,10,2,1	$Mo_{10}V_2PO_{40}^{5-}$		146.93	
		α-1,4	145.97	
		α-1,2	146.25	
		α-1,5	146.25	
		α-1,6+α-1,11	146.53	
		β	145.53	
		β	145.41	
22,10,2,1	$HMo_{10}V_2PO_{40}^{4-}$		147.19	0.26
		α-1,4	146.45	0.48
		α-1,2	146.51	0.26
		α-1,5	146.51	0.26
		α-1,6+α-1,11	146.57	0.04
		β	145.88	0.35
		β	145.74	0.33

Figure 6 shows a calculated vanadium distribution diagram, distinguishing between the individual $Mo_{10}V_2P$ isomers, for solutions containing the oxoanion components in the (Mo + V)/P = (10 + 2):1 ratio. Comparison between different total concentrations shows that a decrease in concentration gives a decrease in the pH stability range of the $Mo_{10}V_2P$ compositions as well. This is especially pronounced at the acidic end of the pH range, where the $Mo_{10}V_2P$ composition dissociates VO_2^+ and reconstitutes as $[Mo_{11}VPO_{40}]^{4-}$. This equilibrium decomposition of $Mo_{10}V_2P$ and Mo_9V_3P compositions to $[Mo_{11}VPO_{40}]^{4-}$ with increasing acidity in the pH region where they become monoprotonated (pH ≈ 1 and less) can also be discerned in the distribution diagrams of Figure 5 and 6. Similarly, Figure 5 shows that the Mo_9V_3P compositions decompose to $[Mo_{10}V_2PO_{40}]^{5-}$ with increasing acidity in the pH region where they become protonated. The decomposition of Keggin molybdovanadophosphates, dissociating VO_2^+ and redistributing to lower vanadium-content Keggin species, is favoured by: (1) decreasing Keggin ion concentrations, favouring dissociative equilibria, (2) increasing acidity, and (3) increasing vanadium content in the Keggin composition. It is also favoured by (4) reduction of vanadium(V) to vanadium(IV), in which case VO^{2+} is dissociated.

Assignments of NMR Resonances to Mo_9V_3P Isomers

In the previous study,[18] it proved possible to completely assign the ^{31}P and ^{51}V resonances of α-$[Mo_{11}VPO_{40}]^{4-}$, of all five of the α-$Mo_{10}V_2P$ isomers, and of the couple of β-$Mo_{10}V_2P$ isomers existing in detectable concentrations in the equilibrium solutions. The assignments of the resonances to the α-isomers relied on a number of factors:

– The ability to resolve the ^{31}P and ^{51}V resonances and to track them over pH

– Interpretations based on comparisons of the relative intensities of the resonances to the statistically predicted relative abundances of the α-isomers[28]

– The expected relative magnitudes of the ^{51}V chemical shift changes of the different isomers in response to their protonation

– The expected relative pK_a values of the monoprotonated anions

– The expected broader ^{51}V resonance line width of the α-(1,2) isomer with corner-sharing V-octahedra[21]

– Correlations between the ^{31}P and ^{51}V resonances based on these factors

It did not prove possible to make a similar complete assignment of the detected ^{31}P and ^{51}V resonances of the individual Mo_9V_3P isomers. The ^{51}V resonances proved too broad and overlapping, at 131.5 MHz, to be resolved and to be tracked over the pH range. The ^{31}P resonances of only six of the most abundant Mo_9V_3P isomers could be resolved and tracked over pH, at 202.5 MHz (Figure 2). Nonetheless, partial assignments of the ^{31}P and ^{51}V resonances to structural motifs of the Mo_9V_3P isomers did prove possible. These interpretations depended substantially on analogy to the more definitive assignments of the ^{31}P and ^{51}V resonances of the $Mo_{10}V_2P$ isomers. This analysis focused on the spectra of solutions with the oxoanion components in the (Mo + V)/P = (9 + 3):1 ratio at pH ≥ 4.5. The ^{31}P spectrum of such a solution (120 mM P) at pH = 5.96 at 25 °C showed that about 87% of the phosphorus was present in the Mo_9V_3P species, with the balance distributed in essentially equal amounts between the $Mo_{10}V_2P$ species and the Mo_8V_4P species. (See Figure 8 and the discussion of the ^{31}P spectrum below.) At pH ≥ 4.5, all the $Mo_{10}V_2P$ and Mo_9V_3P isomers are fully deprotonated, so that protonation effects on their chemical shifts could be avoided when they were compared.

^{51}V NMR Spectra

The ^{51}V resonances of vanadium oxoanions have narrower line widths, and are therefore better resolved, at higher temperature. Our previous study[18] determined that the relative abundances of the $Mo_{10}V_2P$ isomers are approximately the same at 25 and 90 °C. This is also expected to be the case for the Mo_9V_3P isomers. Consequently, our analysis of the ^{51}V resonances of the $[Mo_9V_3PO_{40}]^{6-}$ species focused on spectra of solutions at 90 °C. However, even at this higher temperature, and with resolution enhancement algorithms, it was not possible to resolve the ^{51}V resonances of all the isomers.

The 13 α-isomers of the $[Mo_9V_3PO_{40}]^{6-}$ composition (Table 1) will, by symmetry, exhibit 30 potentially resolvable ^{51}V-NMR resonances. Table 4 shows the 30 inequivalent vanadium environments among the 13 α-isomers. Many of these inequivalent vanadium environments are obviously very similar, so it is expected that many of their resonances would have very close chemical shifts and are not resolved.

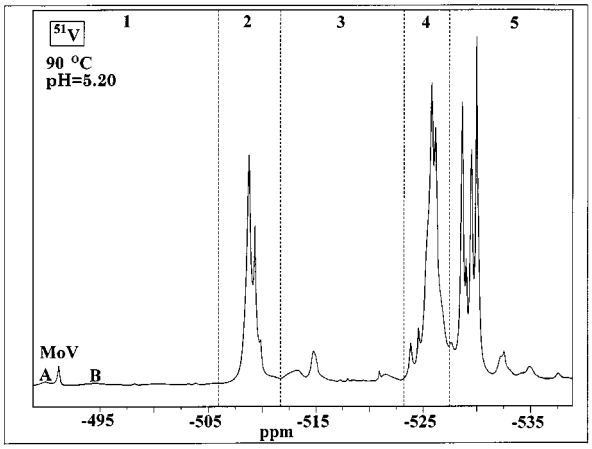


Figure 7. The ^{51}V spectrum of a solution containing the oxoanion components in the ratio (Mo + V)/P = (9 + 3):1 (120 mM P) at 90 °C, at which temperature the pH = 5.20. The chemical shift regions 1–5 are discussed in the text

Figure 7 shows the ^{51}V spectrum of a solution containing the oxoanion components in the ratio (Mo + V)/P = (9 + 3):1 (120 mM P) at pH = 5.20 at 90 °C. By analogy to the ^{51}V resonances of the α-$[Mo_{10}V_2PO_{40}]^{5-}$ isomers,[18] five regions of the spectrum, divided as shown in Figure 7, were assigned to five distinct types of vanadium environments within the $[Mo_9V_3PO_{40}]^{6-}$ isomers, as described below.

α-1,4-$[Mo_{10}V_2PO_{40}]^{5-}$, the sole $Mo_{10}V_2P$ α-isomer in which the two vanadium octahedra are edge-sharing, is distinguished by the most downfield ^{51}V resonance of the $[Mo_{10}V_2PO_{40}]^{5-}$ isomers, 16 ppm downfield from the nearest other $[Mo_{10}V_2PO_{40}]^{5-}$ resonance, at δ = −509.75 at 90 °C. By analogy, region 2, at δ = −506 to −512 in the Mo_9V_3P spectrum at 90 °C (Figure 7), is assigned to pairs of vanadium octahedra that are edge-sharing, but are separated from the third vanadium octahedron in the Keggin structure.

By analogy to the α-1,4-$[Mo_{10}V_2PO_{40}]^{5-}$ resonance's chemical shift being distinctly far downfield from the resonances of other $[Mo_{10}V_2PO_{40}]^{5-}$ isomers, the most downfield resonances of the Mo_9V_3P isomers, in region 1, are assigned to isomers in which all three vanadium octahedra are mutually edge-sharing in a V_3O_{13} unit. The narrow resonance labelled MoV in Figure 7 is known to be that of the molybdovanadate species $[Mo_4V_2O_{19}]^{4-}$.[16,17] In this region, there are two minor resonances, marked A and B, of Mo_9V_3P species. However there is only one α-Mo_9V_3P isomer (α-1,4,9) where all three vanadium octahedra are mutually edge-sharing. The furthest downfield resonance, A, is tentatively assigned to the vanadium atoms of α-1,4,9-$[Mo_9V_3PO_{40}]^{6-}$. The very broad resonance B might arise from a β-isomer in which all three vanadium octahedra are mutually edge-sharing. This could be the β-10,11,12 or the β-1,4,9 isomer, in which the mutually edge-sharing V_3O_{13} unit or a mutually edge-sharing Mo_3O_{13} unit, respectively, in the α-1,4,9 structure is rotated by π/3, or possibly both isomers.

Table 4. The 30 possible ^{51}V NMR resonances of the 13 α-$[Mo_9V_3PO_{40}]^{6-}$ isomers. The VO_6 octahedra are shaded and the octahedron(s) responsible for the resonance is/are in dark colour. The table reports the statistically predicted relative intensities of the resonances and the regions of the spectrum in which the specific resonance is thought to appear (see Figure 7)

Polyhedral Structure	Designation	Statistical Abundance	Region	Polyhedral Structure	Designation	Statistical Abundance	Region
	α-1,4,9	1.82 %	1		α-1,2,8	3.63 %	4
	α-1,2,3	1.82 %	4		α-1,2,8	3.63 %	4
	α-1,2,4	3.63 %	2		α-1,2,8	3.63 %	5
	α-1,2,4	3.63 %	3		α-1,2,11	3.63 %	4
	α-1,2,4	3.63 %	4		α-1,2,11	3.63 %	4
	α-1,2,6	3.63 %	2		α-1,2,11	3.63 %	5
	α-1,2,6	3.63 %	3		α-1,2,10	3.64 %	4
	α-1,2,6	3.63 %	4		α-1,2,10	1.82 %	5
	α-1,4,6	3.64 %	2		α-1,5,8	1.82 %	5
	α-1,4,6	1.82 %	5		α-1,5,8	3.64 %	5
	α-1,4,7	3.63 %	2		α-1,5,7	3.63 %	5
	α-1,4,7	3.63 %	2		α-1,5,7	3.63 %	5
	α-1,4,7	3.63 %	5		α-1,5,7	3.63 %	5
	α-1,4,8	3.63 %	2		α-1,6,12	3.61 %	5
	α-1,4,8	3.63 %	2				
	α-1,4,8	3.63 %	5				

α-1,2-$[Mo_{10}V_2PO_{40}]^{5-}$, the sole $Mo_{10}V_2P$ α-isomer in which the two vanadium octahedra are corner-sharing, exhibits the next most downfield ^{51}V resonance of the $[Mo_{10}V_2PO_{40}]^{5-}$ isomers, at δ = −526.10 at 90 °C. By analogy, region 4 at δ = −523 to −527 in the Mo_9V_3P spectrum at 90 °C (Figure 7) is assigned to pairs of vanadium octahedra that are corner-sharing, but are separated from the third vanadium octahedron in the Keggin structure. The α-isomer with three mutually corner-sharing vanadium octahedra (α-1,2,3) could be expected to have its resonance in this region (but see below).

The resonances in region 3, between region 2 of edge-sharing vanadium octahedra pairs and region 4 of corner-sharing vanadium octahedra pairs, are consequently assigned to individual vanadium octahedrons that are positioned between the two others, edge-sharing with one and corner-sharing with the other. Since edge-sharing with another vanadium octahedron has such a strong downfield effect on the chemical shift, the two resonances that are both the most downfield and the most intense within region 3 are reasonably assigned to these "in-between" vanadium octahedrons in the α-1,2,4 and α-1,2,6 isomers. The more upfield and more minor resonances within region 3 may be the "in-between" vanadium octahedrons in the β-isomers. It is also possible that the resonance of the α-1,2,3 isomer (with *three* mutually corner-sharing vanadium octahedra) may be downfield of region 4, in region 3.

The α-1,2-$Mo_{10}V_2P$ isomer is also unique among the α-$Mo_{10}V_2P$ isomers in having a distinctively broad resonance line width.[18] This is expected for corner-sharing vanadium octahedra, as revealed by Leparulo-Loftus and Pope's study of isostructural tungstovanadates, including α-Keggin decatungstodivanadophosphate isomers, and is supported by the theoretical explanation provided in that report.[21] It also was a key factor, but not an isolated factor, in the complete assignment of the ^{51}V resonances of the $Mo_{10}V_2P$ isomers. By an extensive evaluation of line widths of the resonances in the major intensity regions 2, 4, and 5 by line shape

Table 5. The statistically predicted relative abundance of the α-$[Mo_{10}V_2PO_{40}]^{5-}$ isomers and their actual relative abundance by ^{51}V resonance intensities. The statistically predicted relative intensities of groups of ^{51}V resonances of the α-$[Mo_9V_3PO_{40}]^{6-}$ isomers, grouped by type of vanadium environment, and the actual relative intensities among the regions of the spectrum assigned to these groups, as shown in Figure 7. The last column gives, as a percentage, the disparity between the actual relative intensities and those statistically predicted

Isomers	Statistical abundance	Integral ^{51}V	Disparity %
$Mo_{10}V_2P$			
α-1,4 (pair of edge-sharing V)	18.2%	13.3%	73%
α-1,2 (pair of corner-sharing V)	18.2%	23.3%	128%
α-1,5 + α-1,6 + α-1,11 (separated V)	63.7%	63.3%	99%
Mo_9V_3P			
Region 1 (edge-sharing V_3O_{13} units)	1.8%	0.7%	39%
Region 2 (pairs of edge-sharing V)	25.4%	20.5%	81%
Region 3 (V edge-sharing to another V and corner-sharing to a third V)	7.3%	4.9%	67%
Region 4 (pairs of corner-sharing V)	27.2%	37.0%	136%
Region 5 (V separated from other V)	38.1%	37.0%	97%

analysis, the resonances in region 4 were determined to have broader line widths than the resonances in these other regions. This further supports the assignment of the resonances in region 4 to corner-sharing vanadium octahedra. The resonances in region 3, assigned to the "in-between" vanadium octahedrons that are corner-sharing with another vanadium octahedron, have visually broad line widths, as seen in Figure 7.

The three α-$Mo_{10}V_2P$ isomers, and the one detected β-$Mo_{10}V_2P$ isomer with separated vanadium octahedra have resonances with narrow line widths at $\delta = -528$ to -529 at 90 °C.[18] By analogy, region 5 in the Mo_9V_3P spectrum, upfield of $\delta = -527$ at 90 °C (Figure 7) and comprising narrow resonances closely grouped between $\delta = -528$ and -530, is assigned to the isolated vanadium octahedrons within the Mo_9V_3P isomers.

This assignment of the resonances by chemical shift region to five different types of vanadium environments found in the Mo_9V_3P isomers accords well with the expected relative abundances of these environments in the α-isomers. The statistically predicted relative abundances of the 30 inequivalent vanadium environments among the α-isomers are listed in Table 4. A direct comparison of the resonance intensities, integrated region-by-region, with these statistically predicted relative abundances of the different types of vanadium environments among the α-isomers is complicated by two factors. First, this analysis ignores the presence of β-isomers. Second, it assumes that the 13 α-isomers are all of equal stability, so their distribution is governed solely by the statistics of their structural degeneracies. The results of this comparison are presented below after these complicating factors are discussed.

As discussed in the introduction, β structures become more likely as molybdenum(VI) in the parent Keggin molybdophosphate ion, $[Mo_{12}PO_{40}]^{3-}$, is increasingly substituted by vanadium(V). In the previous work, no β-isomer of $[Mo_{11}VPO_{40}]^{4-}$ was detected, and about 10% of the total vanadium in the $Mo_{10}V_2P$ species was present in β-isomers.[18] Therefore, more than 10% of the total vanadium in the Mo_9V_3P species is expected to be present in β-isomers in this case. The ^{31}P spectrum (Figure 8) of the solution, at 25 °C, whose ^{51}V spectrum, at 90 °C, is shown in Figure 7, indicates that about 17% of the P in the Mo_9V_3P species is present in β-isomers. (See discussion below.)

The ^{51}V resonances of similar vanadium environments (edge- or corner-sharing with another vanadium octahedron, separated, etc.) are expected to have similar chemical shifts whether in an α- or a β-isomer, and to appear in the same region of the spectrum. This is the case for the ^{51}V resonances of the deprotonated $Mo_{10}V_2P$ isomers.[18] In the ^{51}V NMR spectrum at 90 °C, two β-$[Mo_{10}V_2P_{40}]^{5-}$ were detected. One, assigned to the β-4,11 isomer with separated vanadium octahedra, has the chemical shift $\delta = -528.8$ and is overlapped by the resonances of the α-isomers with separated vanadium octahedra. The other, assigned to the β-4,10 isomer with corner-sharing vanadium octahedra, the assignment being based in part on its relatively broad line width, characteristic of corner-sharing vanadium octahedra, has its chemical shift at $\delta = -526.7$, nearest to the α-1,2-$[Mo_{10}V_2P_{40}]^{5-}$ isomer with corner-sharing vanadium octahedra. The chemical shifts for these β-isomers are within the designated regions (Figure 7) for separated (region 5) and corner-sharing (region 4) vanadium octahedra.

Accordingly, the presence of β-isomers should not compromise the assignments of the spectral regions to the various types of vanadium environments. However, to the extent that certain structural relationships among the vanadium octahedra (edge- or corner-sharing with another vanadium, separated, etc.) are more conducive to stabilising β-structures than others, the distribution of the types of vanadium environments determined by resonance integration region-by-region will be skewed by their distribution among only the α-isomers.

The previous study revealed that the α-isomers of $[Mo_{10}V_2P_{40}]^{5-}$ are not of equal stability.[18] While their relative abundances in solution approximate their statistically predicted relative abundances, there are some significant deviations. Table 5 lists the α-$Mo_{10}V_2P$ isomers with their type of vanadium environment and compares the statistically predicted relative abundances of the types of vanadium environments with their relative abundances in the deprotonated α-isomers, (only) determined by their resonance intensities. The α-1,4 isomer, with edge-sharing vanadium octahedra, is substantially less abundant than predicted by

statistics. In contrast, the α-1,2 isomer, with corner-sharing vanadium octahedra, is substantially more abundant than predicted by statistics. The total abundance of the remaining α-isomers, with spread (separated) vanadium octahedra, closely agrees with their total statistically predicted abundance.

Table 5 also lists the types of vanadium environments of the Mo_9V_3P isomers, assigned by spectral region, and compares the statistically predicted relative abundances of these types of vanadium environments among the α-Mo_9V_3P isomers, with their relative abundances determined by region-by-region integration of the spectrum shown in Figure 7. This comparison shows that the relative abundances of the types of vanadium environments approximate their statistically predicted relative abundances, but with discrepancies directly analogous to those found for the $Mo_{10}V_2P$ isomers. The abundance of pairs of edge-sharing vanadium octahedra (region 2) is substantially less than statistically predicted. The abundance of pairs of corner-sharing vanadium octahedra (region 4) is substantially greater than statistically predicted. The abundance of isolated vanadium octahedrons separated from others (region 5) closely agrees with the statistics.

The abundance of isomers in which all three vanadium octahedra are mutually edge-sharing in a V_3O_{13} unit (region 1) is even more depressed relative to the statistically predicted abundance of the α-1,4,9 isomer than the abundance of pairs of edge-sharing vanadium octahedra (region 2) relative to their statistical prediction. This appears directionally consistent, but it must be noted that it is difficult to obtain accurate integrated intensities for such weak resonances as in region 1.

In view of this analogy to the relative abundances of the $Mo_{10}V_2P$ isomers, the assignment of the ^{51}V resonances of the Mo_9V_3P isomers by chemical shift region to the different types of vanadium environments appears well supported by the region-by-region integration of their resonance intensities.

^{31}P-NMR Spectra

The ^{31}P-NMR resonances of Mo_9V_3P species proved to be difficult to assign to specific isomers. Our examination of the ^{31}P-NMR resonances of the Keggin $[Mo_9V_3PO_{40}]^{6-}$ species focused on the spectra of solutions at 25 °C. Contrary to their ^{51}V-NMR resonances, the ^{31}P resonances of these Keggin oxoanions have narrower line widths and are better resolved at 25 °C than at higher temperatures.

Figure 8 shows the ^{31}P spectrum of the same solution, at 25 °C, whose ^{51}V spectrum at 90 °C is shown in Figure 7. (Its pH at 25 °C is 5.96.) The ^{31}P spectrum allows an assessment of the relative amounts of the $Mo_{(12-x)}V_xP$ compositions present. Resonances can be readily sorted by x of the $Mo_{(12-x)}V_xP$ compositions, when their relative intensities in solutions of various Mo/V ratios are observed.[18] Region A in Figure 8 contains resonances of Mo_8V_4P species, which comprise approx. 6.4% of the total phosphorus in solution. Some minor Mo_8V_4P resonances, further upfield among the resonances in region B of Figure 8, are unresolved. On the

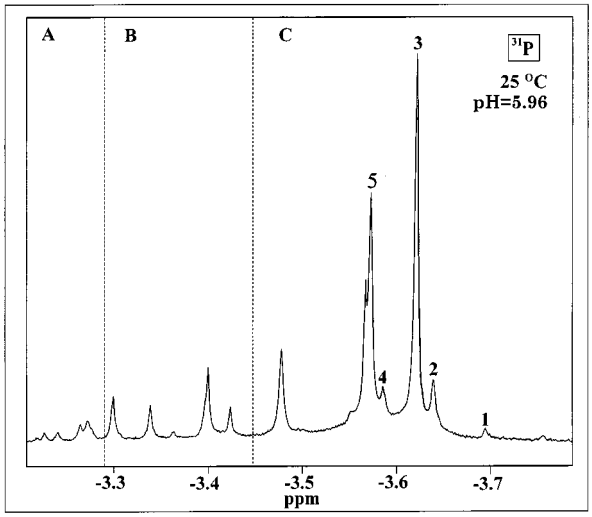


Figure 8. The ^{31}P spectrum of the same solution whose ^{51}V spectrum is shown in Figure 7, but at 25 °C, at which temperature the pH is 5.96. The chemical shift regions, A, B, and C are discussed in the text

basis of the overall composition of the solution, corresponding to the average composition Mo_9V_3P, it is concluded that an essentially equal amount of the total phosphorus in the solution is present as $Mo_{10}V_2P$ species, whose resonances are among the Mo_9V_3P resonances in region C of Figure 8.[18] Consequently, about 87% of the total phosphorus in this solution is present in Mo_9V_3P species.

A partial assignment of the ^{31}P resonances of Mo_9V_3P species proved possible by analogy to what was learned previously from the full assignment of the ^{31}P resonances of the $Mo_{10}V_2P$ isomers.[18] The resonances of the α- and β-$[Mo_{10}V_2PO_{40}]^{5-}$ isomers appear in separate chemical shift groups. This can be seen in Figure 2 from the chemical shift vs. pH curves of the $Mo_{10}V_2P$ species at pH > 3 where all the species are completely deprotonated. The resonances of the five α-isomers (all within the three resolved resonances labelled b, c, and d in Figure 2) appear closely grouped at distinctly higher field than the resonances detected for the two β-isomers (e and f in Figure 2), which also have a broader spread in chemical shifts. Figure 2 also shows that, at pH > 5 where the Mo_9V_3P species are completely deprotonated, four of the six most intense ^{31}P resonances are closely grouped in the same chemical shift region as the resonances of the five α-$[Mo_{10}V_2PO_{40}]^{5-}$ isomers. (Only the most intense phosphorus resonances are plotted in Figure 2, as only they could be tracked as a function of pH as the various resonances converged and diverged.) These four high-field, more intense Mo_9V_3P resonances, and the minor resonances in the same chemical shift region are confidently assigned to α-$[Mo_9V_3PO_{40}]^{6-}$ isomers.

The most downfield $[Mo_9V_3PO_{40}]^{6-}$ resonance plotted in Figure 2, which is downfield of even the most downfield detected β-$[Mo_{10}V_2PO_{40}]^{5-}$ resonance, appears on this basis to be a β-$[Mo_9V_3PO_{40}]^{6-}$ isomer. Similarly, the most downfield resonance in region C of Figure 8 has a chemical shift between the two detected β-$[Mo_{10}V_2PO_{40}]^{5-}$ resonances, but its intensity, greater than that of any resonance

in region B, is more consistent with an α-isomer. There is probably no distinct chemical shift border between the resonances of the 13 α-isomers and 43 β-isomers of Mo_9V_3P composition.

To get an approximation of the relative amounts of α- and β-Mo_9V_3P isomers, we considered the resonances in region C to be α-Mo_9V_3P isomers, subtracting the contribution from $Mo_{10}V_2P$ isomers, and the resonances in region B to be β-Mo_9V_3P isomers. The integrated resonance intensities over these regions indicate approximately 17% β- and 83% α-Mo_9V_3P isomers. Table 1 lists two columns of statistically predicted abundances of the α-Mo_9V_3P isomers. The first (1) gives the statistically predicted distribution of the α-isomers among the total α-isomers, as if only α-isomers were present (total 100%). The second (2) gives the statistically predicted distribution of the α-isomers among the total α-isomers, corrected for only 83% of the total phosphorus being present in α-isomers (total 83%). This second "predicted relative abundance" distribution was used for comparing individual ^{31}P resonance intensities, as a percentage of the total intensity of the ^{31}P resonances of Mo_9V_3P (regions B + C, corrected for the $Mo_{10}V_2P$ contribution), to the predicted percentage relative abundance of the isomers (see below).

A partial assignment of the ^{31}P resonances in region C of Figure 8 to specific α-$[Mo_9V_3PO_{40}]^{6-}$ isomers is based on their relative intensities and a trend revealed by the assignment of the ^{31}P resonances of the α-$[Mo_{10}V_2PO_{40}]^{5-}$ isomers.[18] The ^{31}P resonances of the unprotonated α-$[Mo_{10}V_2PO_{40}]^{5-}$ isomers reflect, in chemical shift order from upfield to downfield, decreasing polarity in the charge distribution surrounding the phosphorus. The more the vanadium atoms are separated in the Keggin structure, decreasing the charge polarity, the lower the field of the chemical shift. On this same basis, the α-$[Mo_9V_3PO_{40}]^{6-}$ isomers have been ordered in Table 1, from top-to-bottom, in the expected chemical shift order, from upfield to downfield.

The α-$[Mo_9V_3PO_{40}]^{6-}$ isomer with the most unbalanced charge distribution, expected to be most upfield, is the α-1,4,9 isomer (at the top of Table 1), with a predicted relative abundance of 1.5%. The most upfield significant resonance in Figure 8, labelled 1, contains 0.8% of the total phosphorus of regions B and C. The next resonance, labelled 2 in Figure 8, contains 5.4% of the total phosphorus in regions B and C. The α-1,2- and α-1,5-$[Mo_{10}V_2PO_{40}]^{5-}$ species also appear at this chemical shift,[18] unresolved, and contribute to about half of this integrated relative intensity. Thus, approx. 2.7% of the total phosphorus intensity may be assigned to the α-1,2,3 isomer. A comparison with the two most unbalancedly charged α-$[Mo_{10}V_2PO_{40}]^{5-}$ isomers shows that the integral of α-1,4,9 should be underestimated and α-1,2,3 overestimated. One would expect to find these two resonances well separated, since vanadium atoms are connected by sharing oxygen either in a corner or on an edge.

The next downfield, resolved resonance in Figure 8, labelled 3, which is the most intense resonance in the spectrum, has a total relative intensity of approx. 31% over regions B and C. This resonance overlaps the resonances of α-1,6- and α-1,11-$[Mo_{10}V_2PO_{40}]^{5-}$, which should contribute approx. 2.7% to this integrated relative intensity, leaving approx. 28% for Mo_9V_3P species. The three α-Mo_9V_3P isomers which appear next in the charge distribution order (Table 3), α-1,2,4, α-1,2,6 and α-1,4,8, have very similar charge distributions (unique in having all vanadium octahedra connected in series, but not all mutually connected as in the preceding two isomers in Table 1). Their predicted statistical abundance of 27.3% makes assignment of the resonance labelled 3 plausible. Examination of this resonance by curve fitting shows that it is composed of two resonances in a 2:1 ratio. According to charge distribution, the α-1,2,4 and α-1,2,6 isomers with a pair of edge-sharing vanadium octahedra and a third corner-sharing vanadium octahedron are more alike in charge than the α-1,4,8 isomer in which the third vanadium octahedron is separated from the other two.

The next downfield resonance (labelled 4 in Figure 8) is expected to be that of the α-1,4,6 isomer. Its relative intensity over regions B and C, 5.2%, agrees well with the predicted statistical abundance of 4.5%. The still next downfield resonance (labelled 5 in Figure 8), with a relative intensity of approx. 20% of the total phosphorus in regions B and C, agrees well with the sum of the predicted statistical abundances (18.2%) of the next two expected α-1,2,8 and α-1,4,7 isomers.

Beyond this, the remaining ^{31}P resonances could not be assigned to Mo_9V_3P species with any confidence. At increasingly downfield chemical shift, above $\delta = -3.5$, it becomes less and less certain whether the resonances arise from α-isomers or β-isomers or both. We can note that the α-1,6,12-$[Mo_9V_3PO_{40}]^{6-}$ isomer, with the most balanced internal charge distribution among the α-Mo_9V_3P species, is expected to have the most downfield chemical shift among the α-$[Mo_9V_3PO_{40}]^{6-}$ species. With a very low predicted statistical abundance (Table 1), however, its resonance could not be clearly assigned.

Experimental Section

Concentrated Molybdovanadophosphate Solutions and Solids: Molybdovanadophosphate sodium salt solutions were prepared by the method developed at Catalytica.[22] Free molybdovanadophosphoric acid solutions were prepared by the method developed by Onoda and Otake,[23] with modifications.[22] The solutions 0.30 M $\{Na_5Mo_{10}V_2PO_{40}\}$, 0.317 M $\{H_{4.9}Mo_{10.1}V_{1.9}PO_{40}\}$, 0.10 M $\{Na_4Mo_{11}VPO_{40}\}$, and 0.30 M $\{H_4Mo_{11}VPO_{40}\}$, and the solids $\{Na_5Mo_{10}V_2PO_{40}\} \cdot 13.6\ H_2O$, $\{H_5Mo_{10}V_2PO_{40}\} \cdot 10.1\ H_2O$, $\{Na_4Mo_{11}VPO_{40}\} \cdot 12.4\ H_2O$, and $\{H_4Mo_{11}VPO_{40}\} \cdot 21.5\ H_2O$ are those whose preparations were previously described.[18] A solution of 0.30 M $\{Na_5HMo_9V_3PO_{40}\}$, also used in the present studies, was prepared by neutralisation of 0.30 M $\{Na_3H_3Mo_9V_3PO_{40}\}$. These solutions were prepared as described below. Raw material sources were the same as for the previously reported preparations.[18]

Solution of 0.30 M $\{Na_3H_3Mo_9V_3PO_{40}\}$: In a 12 L Morton flask equipped with an electric heating mantle, efficient reflux condenser, and high torque overhead mechanical stirrer, granular V_2O_5 (4.50

mol, 818.46 g) was suspended in 3.5 L of distilled water, and the mixture was heated to about 60° C. Granular anhydrous Na_2CO_3 (4.50 mol, 476.95 g) was slowly added in portions to the rapidly stirred mixture, causing CO_2 liberation and dissolution of the V_2O_5 to give an essentially homogeneous solution. The solution was heated at reflux for 1 h. The solution was then dark blue-green due to dissolved V^{IV} which was originally present in the V_2O_5. Approximately 1 mL of 30% H_2O_2 was added dropwise, causing the dark blue-green colour to fade, leaving a slightly turbid, pale-tan sodium metavanadate solution. The solution was maintained at reflux for an additional 60 min to ensure the decomposition of excess peroxide and it was then cooled to room temp. The solution was filtered to remove the small amount (< 0.2 g) of brown solid, which contained almost all the iron and silica impurities originally present in the V_2O_5. The clear sodium metavanadate solution (orange coloured owing to small amounts of decavanadate species present at this very high vanadate concentration) was then returned to the Morton flask, diluted with 4.0 L of distilled water; then MoO_3 (27.00 mol, 3886.38 g) was added with rapid stirring. The mixture was heated to about 60 °C and H_3PO_4 (3.00 mol, 344.25 g, 85.4% w/w) was added. The mixture was heated at reflux and thereby converted into a clear, dark, burgundy-red solution. After 3 h at reflux, the homogenous solution was cooled to room temp and was volumetrically diluted with distilled water to a total volume of 10.00 L, giving 0.30 M $\{Na_3H_3PMo_9V_3O_{40}\}$.

Solution of 0.30 M $\{Na_5HMo_9V_3PO_{40}\}$: Granular Na_2CO_3 (0.15 mol, 15.90 g) was slowly added to $\{Na_3H_3PMo_9V_3O_{40}\}$ (0.15 mol, 0.500 L, 0.30 M) with rapid stirring. The resulting solution was boiled for 1.5 h, cooled to room temp, and volumetrically diluted with distilled water to 0.500 L, giving 0.30 M $\{Na_5HMo_9V_3PO_{40}\}$.

Solutions for Potentiometric and Quantitative NMR Studies: Stock solutions of the components (HCl, Na_2MoO_4, $NaVO_3$, and NaH_2PO_4) were prepared as previously described, from the same source materials.[13,18] The solutions for the potentiometric and NMR studies were prepared by mixing of the stock solutions of the components, from the concentrated molybdovanadophosphate solutions (listed above), and/or from the solid Keggin molybdovanadophosphoric acids and sodium salts (listed above) in the same manner as previously described.[18] Boiled distilled water was used to prepare all the solutions. After the components were mixed, the molybdovanadophosphate solutions required up to 24 h at 25 °C to reach equilibrium. For measurements at 90 °C, see ref.[18]

Ionic Medium: The pH potentiometry at 25 °C and the NMR studies at 25 °C and 90 °C were all conducted on solutions of the ionic 0.6 M Na(Cl), to maintain constant activity coefficients. Since anion equilibria are studied, the cation concentration in the ionic medium was kept constant, 0.600 M Na^+, and the Cl^- concentration was varied to provide the balance of counteranions not provided by the molybdate, vanadate, and phosphate oxoanion species. This is the same medium referred to in previous studies as 0.6 M Na(Cl).

pH Potentiometry: Titrations were conducted at 25.0 ± 0.1 °C with an automated potentiometric titrator. Free H^+ concentrations were determined by measurement of the EMF of the cell given below, with an Ingold type 201-NS glass electrode, an Ag/AgCl reference electrode prepared according to Brown,[24] and a Wilhelm bridge.[25] Cell: − Ag,AgCl | 0.6 M NaCl || equilibrium solution | glass electrode +

The free H^+ concentration was calculated from the measured EMF, E (in mV), by Equation (3), where the last term is the liquid junction potential in acid solutions for the 0.6 M Na(Cl) medium and the Wilhelm-type bridge used.

$$E = E_0 + 59.157\log[H^+] - 76[H^+] \quad (3)$$

The constant E_0 was determined before and after each titration with separate solutions of known $[H^+]$. A fluoropolymer-encased magnetic bar was used to stir the solution in the titration vessel. The solution was protected from atmospheric carbon dioxide by a stream of argon gas. The argon was sparged through 10% NaOH solution to remove any acid impurities, 10% H_2SO_4 solution to remove any alkaline impurities, and, finally, a 0.6 M NaCl medium before introduction to the titration vessel.

pH Potentiometric Data: A total of 42 titrations covering the ranges of pH from 1.3 to 5.2, Mo/V ratios from 2 to 22, and (Mo + V)/P ratios from 11.5 to 15.4 were performed, and 187 selected points were used in the calculations. The solid lines in Figure 1 show the EMF titrations over (Mo/V) vs. pH space, and show that the titrations were done at constant pH with varying Mo/V ratios, at a constant Mo/V ratio with varying pH, and at simultaneously varied pH and Mo/V ratio. The total concentration of phosphorus was varied between 8 and 20 mM. To confirm that solutions reached equilibrium, pH titrations were done in both directions, acidic towards neutral and neutral towards acidic. The titration data used in the calculations were restricted to Mo/V ratios greater than 3.8 (corresponding to $x \leq 2.5$ in the average Keggin composition $[Mo_{12-x}V_xPO_{40}]^{(3+x)-}$), to avoid solutions containing Mo_8V_4P anions. The data used in the calculations were also restricted to pH > 1.3, as data from titrations at lower pH values were not considered accurate enough.

NMR Measurements: The ^{31}P- and ^{51}V-NMR measurements were obtained on a Bruker AM500 spectrometer at 202.5 and 131.6 MHz, respectively. The probe temperature was thermostatted at 25.0 ± 0.5 °C or 90.0 ± 1.0 °C. The field frequency stabilisation was locked to deuterium by insertion of the 8 mm sample tubes into 10 mm tubes containing D_2O. The samples were spinning in all experiments.

The spin-lattice relaxation times (T_1) were evaluated with the Bruker software inversion recovery method and were determined for the different Keggin species to approx. 30 s for ^{31}P and just a few ms for ^{51}V. For determining the relative abundances of species from their resonance intensities, spectra were recorded quantitatively with the relaxation delay set to at least $5 \cdot T_1$, and the free induction decay (FID) was multiplied by an exponential line-broadening function (LB = 1), with the Bruker software, to improve the signal/noise ratio. A Gaussian-Lorentzian double apodization was applied to the FID, also with the Bruker software, to enhance resolution to obtain more accurate chemical shifts of overlapping resonances. Chemical shifts are reported relative to external $VOCl_3$ and external 85% H_3PO_4, with positive chemical shifts (δ) corresponding to higher frequency.

In acid solutions the α-$[Mo_{11}VPO_{40}]^{4-}$ ion was used as internal ^{31}P and ^{51}V chemical shift standard to determine the chemical shifts with high accuracy and precision. In the more neutral solutions, the chemical shifts of the fully deprotonated $[Mo_{10}V_2PO_{40}]^{5-}$ isomers had a constant "plateau" vs. pH and could be used as internal ^{31}P and ^{51}V chemical shift standards. The ^{31}P chemical shifts are dependent on the concentration of Keggin ions, and 10 mM Keggin ions was used as the reference state for chemical shifts.[18]

NMR solutions were collected from titrations and from separately prepared solutions ("point solutions") corresponding to points in a hypothetical pH titration. After equilibration, the pH values in these point solutions were measured with a combination electrode, ORION Research 81-03 ROSS or INGOLD U402-M6-S7/100. The

electrodes were calibrated with solutions of known $[H^+]$ in 0.6 M Na(Cl). Due to the long relaxation time of ^{31}P resonances in Keggin species, the phosphorus concentrations were sometimes as high as 120 mM, which improves the signal/noise ratio in the spectra and facilitates the determination of chemical shifts with fewer scans.

NMR Data for the Calculations: Integrals from 44 NMR spectra ($0.44 < pH < 4.78$), shown with as □ in Figure 1, and 67 shift values from different spectra ($0 < pH < 6.13$) were used in the calculations. The total concentration of phosphorus was varied between 8 and 60 mM for integral data and between 8 and 120 mM for chemical shift data. Mo_8V_4P species appear in acid solutions with a Mo/V ratio of 3 ($x = 3$ in the average Keggin ion composition). NMR data used in the calculations were, in the same way as titration data, restricted to Mo/V ratios above 3.8, to avoid solutions containing Mo_8V_4P anions, and to thereby simplify the calculations.

The ^{31}P resonances are much better resolved than the ^{51}V resonances at 25 °C. Consequently, we mainly used the integral data from ^{31}P spectra, and not from ^{51}V spectra, in the calculations. In the more neutral solutions, however, the ^{31}P resonances were severely overlapped, so that it was not possible to obtain reliable integral values. For this reason, the NMR data used in the calculations were restricted to those obtained at $pH \leq 4.8$.

Computer Programs: Resonance intensities were computed by integration with the Bruker software, or, for overlapping resonances, by line shape analysis with the programs NMR*i*,[26] UXNMR/P version 1.1, and WIN-NMR version 950901.0, with the chemical shifts determined by resolution enhancement (see above) as input. Using these programs, it is possible to obtain integral values with errors less than 10%. The mathematical analysis of combined $[H^+]$-EMF data, and ^{31}P-NMR shift and integral data, was accomplished with the least-squares program LAKE.[1] LAKE is capable of treating multimethod data simultaneously; this considerably refines the equilibrium analysis. Compositions, (*p,q,r,s*), and formation constants, $\beta_{p,q,r,s}$, are varied so that the error squares sum, $U = \Sigma(W_i \Delta A_i)^2$ is minimised. The complex, or set of complexes, with the lowest U value forms the model that best explains the experimental data. A_i can be either the total concentration of components, free species concentrations, NMR peak integrals, chemical shifts or a combination of these. W_i are weighting factors that are subjectively set to give different types of data appropriate contributions to the results. In the present study, we used weighting factors that give NMR peak integrals and shift values a predominant contribution to the sum of residuals. Calculation and plotting of distribution diagrams were performed with the program SOLGASWATER.[27]

Acknowledgments

Financial support from Catalytica Inc. and the Swedish Natural Science Research Council (NFR) for the work at University of Umeå is hereby gratefully acknowledged.

[1] N. Ingri, I. Andersson, L. Pettersson, A. Yagasaki, L. Andersson, K. Holmström, *Acta Chem. Scan.* **1996**, *50*, 717−734.

[2] The ionic formulae of these Keggin anions are more commonly written as $[H_zPMo_{12-x}V_xO_{40}]^{(3+x-z)-}$). We usually denote the composition of a solution species by the stoichiometric integers of the components used in our potentiometric study of its equilibrium formation. We also find it convenient to use our standard order − H, Mo, V, P − when writing ionic formulae.

[3] C. L. Hill, C. M. Prosser-McCartha, *Coord. Chem. Rev.* **1995**, *143*, 407−455.

[4] J. H. Grate, D. R. Hamm, S. Mahajan, in: *Polyoxometallates: From Platonic Solids to Anti-retroviral Activity* (Eds.: M. T. Pope, A. Müller), Kluwer, Dordrecht, **1994**, pp. 281−305.; J. H. Grate, D. R. Hamm, S. Mahajan, in: *Catalysis of Organic Reactions* (Eds.: J. R. Kosak, T. A. Johnson) Marcel Dekker, New York, **1984**, chapter 16, p. 213.; International Applications published under the Patent Cooperation Treaty, Publication Numbers, WO 91/13851, WO 91/13853, and WO 91/13854, published 19 September, **1991**.

[5] J. F. Keggin, *Nature* **1933**, *131*, 908−909; *Proc. Roy. Soc., Ser. A.* **1934**, *144*, 75−100.

[6] L. C. W. Baker, J. S. Figgis, *J. Am. Chem. Soc.* **1970**, *92*, 3794−3797.

[7] M T. Pope, *Heteropoly and Isopoly Oxometalates*; Springer-Verlag, New York, **1983**, pp. 23−27.

[8] A. Tézé, J. Canny, L. Gurban, R. Thouvenot, G. Hervé, *Inorg. Chem.* **1996**, *35*, 1001−1005.

[9] L. Pettersson, B. Hedman, I. Andersson, N. Ingri, *Chem. Scr.* **1983**, *22*, 254−264.

[10] L. Pettersson, B. Hedman, A.-M. Nenner, I. Andersson, *Acta Chem. Scand* **1985**, *A 39*, 499−506.

[11] K. Elvingson, M. Fritzsche, D. Rehder, L. Pettersson, *Acta Chem. Scand.* **1994**, *48*, 878−885.

[12] A. Yagasaki, I. Andersson, L. Pettersson, *Inorg. Chem.* **1987**, *26*, 3926−3933.

[13] A. Selling, I. Andersson, L. Pettersson, C. M. Schramm, S. L. Downey, J. H. Grate, *Inorg. Chem.* **1994**, *33*, 3141−3150.

[14] L. Pettersson, I. Andersson, L.-O. Öhman, *Inorg. Chem.* **1986**, *25*, 4726−4733. This study was carried out in 3.0 M $NaClO_4$, but the speciation is essentially the same as in 0.6 M Na(Cl) (ref.[15]).

[15] L. Pettersson, I. Andersson, manuscript in preparation.

[16] O. W. Howarth, L. Pettersson, I. Andersson, *Chem. Soc. Dalton Trans.* **1989**, 1915−1923.

[17] O. W. Howarth, L. Pettersson, I. Andersson, *Chem. Soc. Dalton Trans.* **1991**, 1799−1812.

[18] L. Pettersson, I. Andersson, A. Selling, J. H. Grate, *Inorg. Chem.* **1994**, *33*, 982−993.

[19] L. Pettersson, in: *Polyoxometallates: From Platonic Solids to Anti-retroviral Activity* (Eds.: M. T. Pope, A. Müller), Kluwer, Dordrecht, **1994**; pp. 27−40.

[20] Y. Jeannin, M. Fournier, *Pure Appl. Chem.* **1987**, *59*, 1529−1548.

[21] M. A. Leparulo-Loftus, M. T. Pope, *Inorg. Chem.* **1987**, *26*, 2112−2120.

[22] J. H. Grate, D. R. Hamm, R. J. Saxton, Internations Patent Application Publication Number WO 91/13681, 1991; J. H. Grate, *J. Mol. Catal. A* **1996**, *114*, 93−101.

[23] T. Onoda, M. Otake, U.S. Patent 4,156,574, 1979.

[24] A. S. Brown, *J. Am. Chem. Soc.* **1934**, *56*, 646−647.

[25] W. Forsling, S. Hietanen, L.-G. Sillén, *Acta Chem. Scand.* **1952**, *6*, 901−909.

[26] C. L. Dumoulin, G. C. Levy, *J. Mol. Struct.* **1984**, *113*, 299−310.

[27] G. Eriksson, *Anal. Chim. Acta* **1979**, *112*, 375−383.

[28] The statistically predicted relative abundances correspond to the α isomers′ degeneracies, and are reported herein as percentages of the total of their degeneracies. The degeneracy of each isomer equals the number of ways x vanadium can be substituted for x molybdenum in the parent T_d α-$[Mo_{12}PO_{40}]^{3-}$ structure, to provide that α-$[Mo_{(12-x)}V_xPO_{40}]^{(3+x)-}$ isomer. For dissymmetric isomers, the degeneracies of their enantiomorphs are added together.

Received November 1, 1999
[I99390]

Neutral Trichlorooxorhenium(V) Complexes Containing New Heterofunctionalized Phosphane Ligands of the Type PN_2 and PNO

João D. G. Correia,[a] Ângela Domingos,[a] and Isabel Santos*[a]

Keywords: Rhenium / P ligands / Chelates / Radiopharmaceuticals

The new heterofunctionalized phosphane [(1*R*,2*R*)-*N*-(2-aminocyclohexyl)]-2-(diphenylphosphanyl)benzamide (**L¹**), *N*-(2-aminoethyl)-2-(diphenylphosphanyl)benzamide (**L²**) and 2-(diphenylphosphanyl)-*N*-(2-hydroxyethyl)benzamide (**L³**) were synthesized by reaction of *N*-[2-(diphenylphosphanyl)-benzoyloxy]succinimide (**3**) in dichloromethane with (1*R*,2*R*)-(–)-diaminocyclohexane, ethylenediamine and ethanolamine, respectively. Reactions of $[Re(O)Cl_4]^-$ with **L¹**, **L²** and **L³**, at a 1:1 metal/ligand molar ratio gave neutral trichlorooxorhenium(V) complexes of the type $[Re(O)Cl_3\{\kappa^2\text{-L}\}]$ [L = **L¹** (**4**), **L²** (**5**), **L³** (**6**)]. The characterization of the compounds involved IR, ^{1}H- and ^{31}P-NMR spectroscopy, and X-ray crystallographic analysis for **L¹**, **5** and **6**. The Re atom is six-coordinate in complexes **4**–**6**, with an oxo ligand, three chloride ligands and a neutral bidentate heterofunctionalized phosphane ligand.

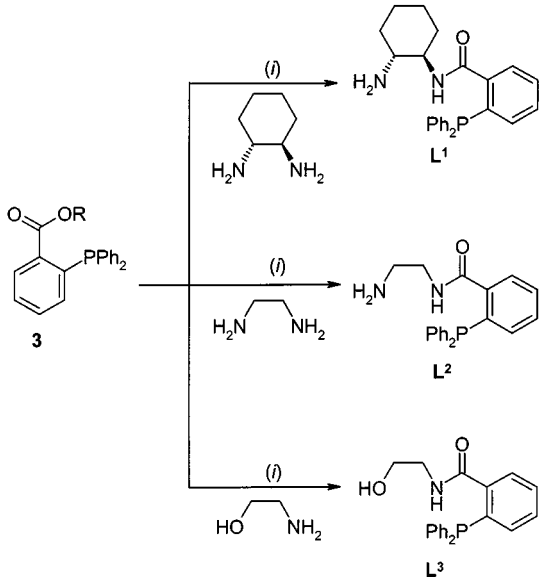
Introduction

The continuous demand for more sensitive and specific probes for targeting diseased organs or physiological functions in Nuclear Medicine, both in the diagnostic or therapeutic field, has led to an increasing interest in the development of receptor-binding radiopharmaceuticals.[1] Due to its physico-chemical properties and widespread availability, ^{99m}Tc is still the most used radionuclide for diagnosis, and both ^{186}Re and ^{188}Re appear as interesting radionuclides for the development of radiopharmaceuticals with therapeutic potential.[2] For the metal centre in the oxidation state (V) and an $[M{=}O]^{3+}$ core, the use of a bifunctional tetradentate or a tridentate ligand, and a bifunctional unidentate coligand ([3+1] approach) are among the most popular strategies for the design and preparation of new, more specific radiopharmaceuticals.[3] Due to its σ-donor and π-acceptor properties, phosphanes are known to stabilize complexes of rhenium and technetium with the metal centre in different oxidation states.[4,5] A number of heterofunctionalized phosphane-containing ligands have previously been described and used to stabilize the core $[M{=}O]^{3+}$ (M = Re, Tc).[6–8] However, they are all either bidentate, with PN, PO or PS donor sets [6–8] or tetradentate.[9] We have synthesized new tridentate PNO- and PN_2-type ligands, with potential tridentate character, with the aim of designing new radiopharmaceuticals using the [3+1] approach. Surprisingly, we observed that, depending on the reaction conditions, these ligands are very versatile in terms of coordination mode and charge. Indeed, they can act as neutral, mono- or dianionic bi/tridentate chelates.[10] In this paper we report on the synthesis and characterization of the new heterofunctionalized phosphane ligands as well as on the preparation of Re^V adducts where the ligands coordinate to the metal centre in a bidentate and neutral fashion.

Results and Discussion

Synthesis and Characterization of the Ligands

The heterofunctionalized phosphane ligands **L¹**, **L²** and **L³** were synthesized as depicted in Scheme 1. The activation of 2-(diphenylphosphanyl)benzoic acid with *N*-hydroxysuccinimide was achieved in good yield (94%) by a slight modification of a reported method.[11] Reaction of *N*-[2-(diphenylphosphanyl)benzoyloxy]succinimide (**3**) in CH_2Cl_2 at room temperature with (1*R*,2*R*)-(−)-diaminocyclohexane, ethylenediamine and ethanolamine afforded, after appropriate workup, **L¹** (89%), **L²** (74%) and **L³** (87%), respectively.



Scheme 1. Synthesis of the Ligands **L¹**, **L²**, and **L³**; R = *N*-succinimido; (*i*) dichloromethane, room temperature

[a] Departamento de Química, ITN,
Estrada Nacional 10, 2686-953 Sacavém Codex, Portugal
E-mail: isantos@itn1.itn.pt

 © WILEY-VCH Verlag GmbH, D-69451 Weinheim, 2000 1434–1948/00/0707–1523 $ 17.50+.50/0

The IR spectra of $\mathbf{L^1}$ and $\mathbf{L^2}$ exhibit $\nu(NH_2)$ stretching bands at 3220 cm^{-1} and 3320 cm^{-1}, respectively, and for $\mathbf{L^3}$ the IR spectrum shows a strong band at 3310 cm^{-1} which is assigned to ν(OH). In all the spectra a strong band appears at 1630 cm^{-1} due to ν(C=O). In the ^{1}H-NMR spectra of $\mathbf{L^1}$ a doublet appears at δ = 5.71 due to the NH of the amide group. For $\mathbf{L^2}$ and $\mathbf{L^3}$ the signals of these groups appear as broad singlets at δ = 6.23 and 6.27, respectively.

Unlike $\mathbf{L^1}$, where a multiplet at δ = 1.89, assigned to the protons of the amine group, is observed, the ^{1}H-NMR spectrum of $\mathbf{L^2}$ does not present any signal for this group. For $\mathbf{L^3}$, no resonance signal is observed for the hydroxy group. The ^{31}P-NMR spectra of $\mathbf{L^1}$, $\mathbf{L^2}$, and $\mathbf{L^3}$ show only one peak at δ = −10.5, −9.3 and −9.9, respectively. $\mathbf{L^3}$ decomposed slightly in solution on standing, leading to the corresponding phosphane oxide, as indicated by the new ^{31}P-NMR signal which appears at δ = 36.6.[12]

Single colorless crystals of $\mathbf{L^1}$, suitable for X-ray diffraction analysis, were obtained from a mixture of dichloromethane/hexane. $\mathbf{L^1}$ crystallizes in the monoclinic acentric space group $P2_1$ with three crystallographically independent molecules in the asymmetric unit. The three independent molecules are labelled similarly, being distinguished by the first digit of the atom label.

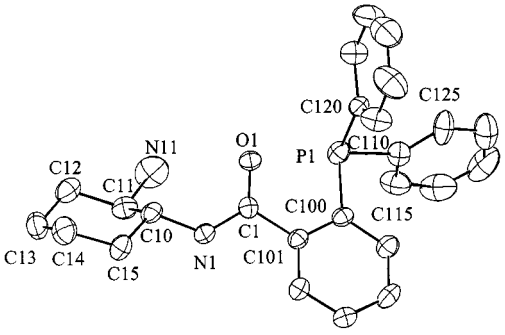
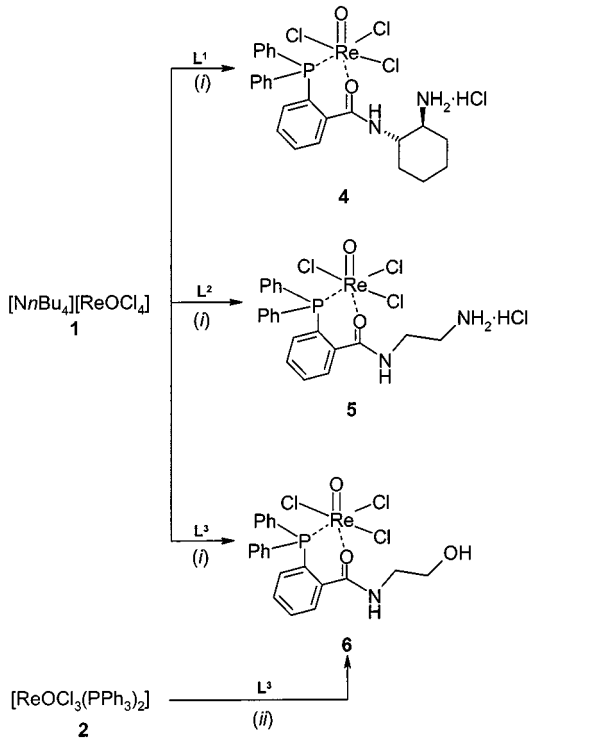


Figure 1. ORTEP drawing of ligand $\mathbf{L^1}$ with the atom numbering scheme; thermal ellipsoids are drawn at the 30% probability level; selected mean bond lengths [Å] and angles [°]: C(1)−O(1) 1.231(8), N(1)−C(1) 1.329(9), N(1)−C(10) 1.448(9), C(11)−N(11) 1.449(11), C(1)−C(101) 1.498(10), P(1)−C(100) 1.848(8), P(1)−C(110) 1.838(9), P(1)−C(120) 1.837(8), av. $(C-C)_{cyclohex}$ 1.51(1), av. $(C-C)_{Phenyl}$ 1.37(2); N(1)−C(1)−O(1) 123.3(7), O(1)−C(1)−C(101) 120.7(7), N(1)−C(1)−C(101) 116.1(7), C(10)−N(1)−C(1) 124.5(6)

Figure 1 shows an ORTEP view of one molecule with the atom numbering scheme as well as selected bond lengths and angles. Within two standard deviations the three molecules can be considered chemically equivalent, presenting similar molecular dimensions. The packing of the molecules forms a network of hydrogen bonds involving the amide N−H group and the carbonyl oxygen atoms. The shortest intermolecular distances are 2.887 Å for O(1) and N(2′) (x, y, $-1 + z$), 2.862 Å for O(2) and N(3′) ($1 - x$, $-0.5 + y$, $1 - z$) and 2.858 Å for O(3) and N(1′) ($2-x$, $y + 0.5$, $-z$) (the average N···O contact distance is 2.929 Å for the hydrogen bonds "C=O···H−N").[13] The cyclohexane ring shows the usual chain conformation.



Scheme 2. Synthesis of the complexes **4**−**6**; (*i*) MeOH, room temperature; (*ii*) dichloromethane, room temperature

Synthesis and Characterization of the Complexes

Reactions of $\mathbf{L^1}$, $\mathbf{L^2}$ and $\mathbf{L^3}$ with [nBu$_4$N][Re(O)Cl$_4$] (**1**) in methanol, at a 1:1 molar ratio, at room temperature, afforded the new unusual neutral trichlorooxorhenium(V) complexes **4**−**6** (Scheme 2). To the best of our knowledge, several compounds containing the "Re(O)Cl$_3$" moiety are known. However, this unit is stabilized either by diphosphanes or by neutral monodentate ligands.[14]−[16] When a heterofunctionalized phosphane ligand such as (2-hydroxyphenyl)diphenylphosphane (PO) is used, deprotonation occurs with formation of the monoanionic complex [Re(O)Cl$_3$(PO)]$^-$.[7c] Phosphane-containing peptides (PN$_2$O donor set) were studied, and deprotonation was also observed. In this case, the ligands coordinate in a dianionic and tetradentate fashion.[9b] Thus, the neutral behavior of our ligands and the observed coordination mode are not very common, probably as a result of the influence of the type of substituents attached to the amide nitrogen atom.

Complex **6** was also obtained by stoichiometric reaction of $\mathbf{L^3}$ with [Re(O)Cl$_3$(PPh$_3$)$_2$] (**2**) in CH$_2$Cl$_2$. After evaporation of the solvent, complexes **4** and **5** were obtained as light blue and pale green solids, respectively. Complex **6**, unlike **4** and **5**, precipitated from its reaction mixture and, upon appropriate workup, was obtained as a dark green solid in an almost quantitative yield. Complexes **4**−**6** are stable towards air and moisture and almost insoluble in most organic solvents and water. Complexes **5** and **6** are moderately soluble in acetonitrile, whereas **4** is insoluble in this solvent. Complex **4** is moderately soluble in tetrahydrofuran and dimethyl sulfoxide but tends to decompose in these solvents. The characterization of **4**−**6** has been done

by elemental analysis, IR, ^{1}H- and ^{31}P-NMR spectroscopy, and by X-ray crystallographic analysis in the case of **5** and **6**.

The IR spectra of complexes **4**–**6** exhibit Re=O stretching vibrations at 1000 cm^{-1}. These values are in the normal range as those found for monooxorhenium complexes (945–1067 cm^{-1}).[17] The C=O stretching vibration of the carbonyl group appears at 1570, 1590 and 1590 cm^{-1} for **4**, **5** and **6**, respectively. These values are lower in energy (by ca. 40–60 cm^{-1}) relative to the corresponding free ligands, confirming the coordination of the carbonyl group to the metal centre. In addition, all the complexes display IR absorptions typical of ν(Re–Cl) at 320 cm^{-1} and at 315 cm^{-1}; and absorptions of coordinated phosphane ligands, in particular two strong absorption bands at 750 cm^{-1} and at 697 cm^{-1}, associated with C–H and C–C out-of-plane bending vibrations in monosubstituted benzene rings.[18]

Due to the low solubility of all complexes their NMR spectra were run either in CD_3CN or in $(CD_3)_2SO$. The ^{31}P-NMR spectra of **5** and **6** in CD_3CN show only one resonance signal, which appears at δ = −15.4 and −16.5, respectively. These resonance signals are shifted slightly upfield in $(CD_3)_2SO$, and appear at δ = −18.1 for both complexes. When compared with those of the free ligands, the resonance signals found for **5** and **6** are shifted upfield (ca. 6 ppm). For complex **4**, it was only possible to run the ^{31}P-NMR spectrum in $(CD_3)_2SO$ and, in this solvent, the initial blue solution turned green within seconds. Two resonance signals are observed in the spectrum at δ = −17.2 and 32.9. The resonance signal at δ = −17.2 compares well with the value of δ = −18.1 found for complexes **5** and **6** in the same solvent, and led us to assign the signal to adduct **4**. An upfield shift (about 7.6 ppm) relative to the resonance signal of the free ligand [−9.6 ppm in $(CD_3)_2SO$], is observed for the resonance signal of **4**. This also compares well with the shift found for complexes **5** and **6**. The resonance at δ = 32.9 is assigned to the phosphane oxide of the ligand.[12] This result confirms that $(CH_3)_2SO$ is able to oxidise aromatic tertiary phosphanes coordinated to oxoRe complexes by oxygen transfer, as previously reported.[19] In order to confirm the presence of phosphane oxide signals in this region of the spectrum, **L^1** was oxidized with hydrogen peroxide in a parallel experiment. The ^{31}P-NMR spectrum of the resulting product in $(CD_3)_2SO$ reveals only one resonance signal at δ = 32.0.

The ^{1}H-NMR spectra of **5** and **6** present three sets of multiplets assigned to the protons of the aromatic rings. Two of the multiplets integrate for one proton each and the third for twelve protons. The chemical shifts are comparable in both complexes and the protons are slightly deshielded with respect to those of the free **L^2** and **L^3**. The remaining signals observed in the spectra are due to the amide and to the ethylene protons of the coordinated heterofunctionalized phosphane ligands. In both complexes the amide proton signal is significantly shifted downfield relative to those of the free ligands and this is certainly due to the more acidic character of this proton after the coordination of **L^2** and **L^3** to the rhenium atom through the carbonyl group.

As mentioned above, complex **4** decomposed in $(CD_3)_2SO$ yielding partially the oxidised form of the ligand. However, in the phenyl and amide region of the ^{1}H-NMR spectrum, we could easily identify some resonance signals that correspond to the remaining adduct **4**. In fact, we observe signals at δ = 11.16 (1 H, d, NH), 8.71 (1 H, t, aromatic), 8.11 (1 H, s, br., aromatic) and 7.19 (1 H, m, aromatic). The pattern, the chemical shifts and type of splitting compare very well with what is observed in the spectrum of complex **5**, in the same solvent. The region of the cyclohexyl protons is quite complicated and the assignment of the resonance signals of **4** is not possible.

Crystal Structures of Complexes 5 and 6

The X-ray crystallographic analysis on a poor-quality crystal of **5** did not provide an adequate data set for an accurate determination of the structure of this complex. It was not possible to refine the structure with acceptable *R* values (R_1 = 0.0925, wR_2 = 0.1946) and with sufficient accuracy. However, it was possible to unambiguously define the connectivities of the atoms around the Re atom (Figure 2), and to confirm that the molecular structure of complex **5** is analogous to that of **6**.

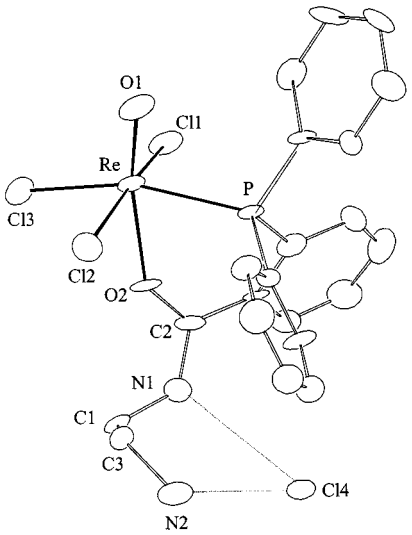


Figure 2. ORTEP drawing of complex **5** with the atom numbering scheme; thermal ellipsoids are drawn at the 30% probability level

Compound **5** crystallized from boiling acetonitrile as dark green crystals in the triclinic space group $P\bar{1}$ with cell parameters *a* = 9.840(2) Å, *b* = 12.000(3) Å, *c* = 13.604(3) Å, α = 66.12(2)°, β =86.01(2)°, γ = 68.30(1)°, *V* = 1358.7(5) Å^3, *Z* = 2, D_c = 1.788 gcm^{-3}. Besides a disordered acetonitrile molecule of solvent in the lattice, a residual peak of electron density of the order of 18 eÅ^{-3} was found which refined properly as a chloride ion. The chloride ion is hydrogen-bonded to the two nitrogen atoms of the molecule: to the amide N(1) atom [N(1)···Cl(4) 3.073 Å] and to the amine N(2) atom [N(2)···Cl(4) 3.273 Å]. The molecular structure of **6** as well as selected bond lengths and angles are shown in Figure 3.

The overall geometry around the six-coordinate rhenium atom is described as an highly distorted octahedron, as can

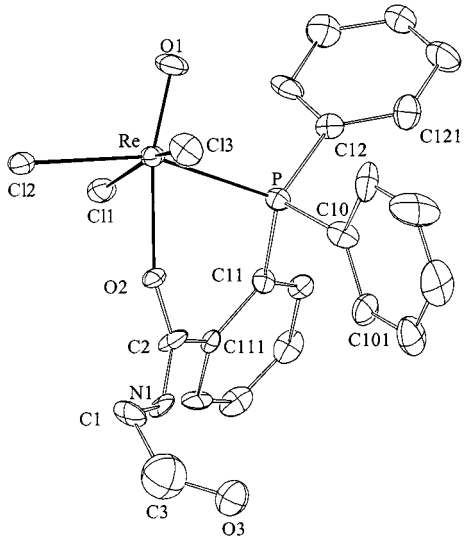


Figure 3. ORTEP drawing of complex **6** with the atom numbering scheme; thermal ellipsoids are drawn at the 30% probability level; selected mean bond lengths [Å] and angles [°]: Re−O(1) 1.659(10), Re−O(2) 2.133(10), Re−Cl(1) 2.367(5), Re−Cl(2) 2.377(4), Re−Cl(3) 2.355(4), Re−P 2.425(5), C(2)−O(2) 1.26(2), N(1)−C(2) 1.28(2), N(1)−C(1) 1.46(2), av. P−C 1.82(2); O(1)−Re−O(2) 167.2(5), O(1)−Re−Cl(1) 97.6(4), O(1)−Re−Cl(2) 107.5(4), O(1)−Re−Cl(3) 95.5(4), O(1)−Re−P 93.1(4), Cl(1)−Re−Cl(3) 166.1(2), Cl(2)−Re−Cl(3) 85.9(2), Cl(1)−Re−P 89.0(2), Cl(2)−Re−P 159.3(2), O(2)−Re−Cl(1) 85.3(4), Cl(3)−Re−P 94.9(2), Re−O(2)−C(2) 141.0(13), O(2)−C(2)−N(1) 121(2), O(2)−Re−P 74.5(3), C(2)−N(1)−C(1) 124.1(14), N(1)−C(2)−C(111) 118(2)

be seen by the bond angles around the Re atom. With the axial direction being defined along the Re=O bond, three equatorial positions are occupied by the chloride ions, whereas the fourth equatorial position is occupied by the phosphorous atom of the ligand. The equatorial plane deviates from planarity (atomic deviations from −0.091 to 0.087 Å), and the Re atom is displaced 0.34 Å towards the multiply bonded oxygen. The bidentate chelate forms a non-planar six-membered ring through the phosphorus and the carbonyl oxygen atoms bonded to the metal centre. The oxygen atom of the carbonyl group coordinates to the axial position *trans* to Re=O [O(1)−Re−O(2), 167.2(5)°].

As far as we are aware, this is the first structural characterization of an Re^V neutral adduct complex of the type $[Re(O)Cl_3(\kappa^2\text{-L})]$. For comparison, we have complexes with neutral monodentate ligands or with monoanionic bidentate ligands. The Re−O(1) bond length [1.659(10) Å] in **6** compares well with the values found in $[Re(O)Cl_3(Ph_3PO)(PPh_3)]$ [1.669(4)Å],[15] $[Re(O)Cl_3(PPh_3)(DMF)]$ [1.664(4) Å],[16] and in the anionic monooxorhenium(V) compound $[Re(O)Cl_3(PO)]^-$ [1.669(6) Å; PO = (2-hydroxyphenyl)diphenylphosphane].[7c] This distance in **6** is slightly shorter than the corresponding values 1.692(7) and 1.69(1) Å found in $[Re(O)(PN)_2(OEt)]$ and in the orthorhombic form of $[Re(O)(PN)_2Cl]$ [PN = (2-aminophenyl)diphenylphosphane], respectively.[6b]

The Re−P bond length [2.425(5) Å] compared well with the value found in the anionic monooxorhenium(V) compound $[Re(O)Cl_3(PO)]^-$ [2.422(2) Å] but is shorter than in $[Re(O)Cl_3(Ph_3PO)(PPh_3)]$ [2.506(2) Å], $[Re(O)(PN)_2(OEt)]$ [av. 2.494(3) Å] and in $[Re(O)(PN)_2Cl]$ [av. 2.450(5) Å].[7c,6b,15]

The Re−Cl bond length [av. Re−Cl, 2.366(5) Å] compares well with that found in $[Re(O)Cl_3(PO)]^-$ [av. 2.380(3) Å], but is shorter than in the Re^V complex containing two PN phosphane ligands $[Re(O)(PN)_2Cl]$ [2.422(6) Å].[6b,7c]

The shorter Re−P and Re−Cl bond lengths in complex **6**, relative to the corresponding bond lengths in the complexes mentioned above, are most likely due to steric factors, chelating mode of the ligands and nature of the atoms involved in the coordination with the rhenium centre. The *trans*-Re−O(2) (oxygen atom of the carbonyl group of the ligand) distance [2.133(10)Å] compares well with the value found in $[Re(O)Cl_3(PPh_3)(DMF)]$ [2.133(4)Å] for the bond between the oxygen atom of DMF and the metal centre.[16a] This bond length is considerably longer than that between the amide oxygen atom of MAG_1 (mercaptoacetyl glycine) and the rhenium atom in the complex $[Re(O)(MAG_1Et)_2]$ [2.051(5)Å].[16b] This difference is probably due to the different nature of the donor atoms of the ligands involved in the coordination sphere of the metal centre.

The severe problem of disorder in the terminal C(3)−O(3)H atoms prevents any discussion or comparison of bond lengths within the group, as can be seen by the large standard deviations. Nevertheless, we can say that there is no short intermolecular interaction involving the O(3) atom. An intermolecular interaction involving Cl(2)···N(1) atoms (distance of 3.272 Å) is observed in the packing of the molecules in the crystalline state.

Concluding Remarks

New tridentate heterofunctionalized phosphane ligands have been synthesised and fully characterized. No deprotonation of these ligands occurs under mild conditions when they react with $[nBu_4N][Re(O)Cl_4]$. The new complexes formed are the neutral trichlorooxorhenium(V) adducts $[Re(O)Cl_3\{\kappa^2\text{-L}\}]$, which are rare examples of oxo complexes stabilized by neutral heterofunctionalized phosphane ligands. The rhenium atom is six-coordinate in an octahedral configuration with the oxo function *trans* to the oxygen atom of the carbonyl group and with the phosphorous atom in the equatorial position.

Experimental Section

General Procedures: All chemicals were of reagent grade. Ethylenediamine and ethanolamine were purchased from Aldrich and distilled prior to use. (1*R*,2*R*)-(−)-diaminocyclohexane was purchased from Aldrich and was used as received. The reactions were performed in air unless otherwise indicated. 2-(Diphenylphosphanyl)-benzoic acid and the complexes $[nBu_4N][Re(O)Cl_4]$ (**1**) and $[Re(O)Cl_3(PPh_3)_2]$ (**2**) were prepared as reported in the literature.[20−22] ^1H- and ^{31}P-NMR spectra were recorded with a Varian Unity 300-MHz spectrometer; ^1H chemical shifts were referenced with the residual solvent resonance relative to tetramethylsilane and the ^{31}P chemical shifts were measured with an external H_3PO_4 solution

(85%) as a reference. Chemical shifts are given in ppm. The NMR samples were prepared in $CDCl_3$, CD_3CN or $(CD_3)_2SO$. Infrared spectra were recorded in the range 4000−200 cm^{-1} with a Perkin−Elmer 577 spectrometer using KBr pellets. Elemental analyses were performed with a Perkin−Elmer automatic analyser.

***N*-[2-(Diphenylphosphanyl)benzoyloxy]succinimide (3):** 2-(Diphenylphosphanyl)benzoic acid (1.00 g, 3.27 mmol) and *N*-hydroxysuccinimide (0.75 g, 6.54 mmol) were dissolved in dichloromethane (20 mL) at room temperature, and a solution of dicyclohexylcarbodiimide (1.35 g, 6.54 mmol) in dichloromethane was added dropwise. The reaction was complete after 3 h (TLC: ethyl acetate/hexane, 50:50). The formed urea was separated by filtration through a pad of Celite wetted with dichloromethane, and the filtrate concentrated to dryness. The resulting white residue was chromatographed on an appropriate column of silica gel with 20−35% ethyl acetate/hexane (gradient), to afford a white yellowish solid, which was further recrystallized from dichloromethane/hexane to give **3** in an analytical pure form. Yield 1.24 g (94%). − ^{1}H NMR ($CDCl_3$): δ = 2.81 (4 H, s, CH_2), 6.99 (1 H, m aromatic), 7.19−7.32 (9 H, m, aromatic), 7.45 (3 H, m, aromatic), 8.31 (1 H, m, aromatic). − ^{31}P NMR($CDCl_3$): δ = −4.4. − IR (KBr): $\tilde{\nu}$ = 1760 cm^{-1} (vs, C=O). − $C_{23}H_{18}NO_4P{\cdot}0.5CH_2Cl_2$ (445.8): calcd. C 63.31, H 4.30, N 3.14; found C 63.77, H 4.63, N 3.23.

[(1*R*,2*R*)-*N*-(2-Aminocyclohexyl)]-2-(diphenylphosphanyl)benzamide (L^1): *N*-[2-(Diphenylphosphanyl)benzoyloxy]succinimide (0.89 g, 2.20 mmol), dissolved in dichloromethane (10 mL), was added dropwise to a solution of (1*R*,2*R*)-(−)-diaminocyclohexane (0.50 g, 4.40 mmol) in the same solvent (25 mL). The reaction was complete after 3 h, as indicated by the TLC (ethyl acetate/hexane, 50:50). The mixture was washed with 25 mL of water and the organic phase was separated. The aqueous phase was extracted with dichloromethane (2 × 30 mL). The organic phases were collected, dried with $MgSO_4$, filtered and concentrated to dryness. The resulting viscous oil was recrystallized from dichloromethane/hexane, affording colourless crystals of $\mathbf{L^1}$. Yield 0.79 g (89%). − ^{1}H NMR ($CDCl_3$): δ = 0.85 (1 H, m, cyclohexyl), 1.17 (4 H, m, cyclohexyl), 1.65 (3 H, s, br., cyclohexyl), 1.89 (2 H, m, NH_2), 2.15 (1 H, m, C*H*NH_2), 3.60 (1 H, m, C*H*NH), 5.71 (1 H, d, NH), 6.92 (1 H, m, aromatic), 7.19−7.40 (12 H, m, aromatic), 7.62 (1 H, m, aromatic). − ^{31}P NMR($CDCl_3$): δ = −10.5. − ^{31}P NMR [$(CD_3)_2SO$]: δ = −9.6. − IR (KBr): $\tilde{\nu}$ = 3220 cm^{-1} (m, NH_2), 1630 cm^{-1} (vs, C=O). − $C_{25}H_{27}N_2OP$ (402.5): calcd. C 74.61, H 6.76, N, 6.96; found C 73.75, H 6.55, N 6.89.

***N*-(2-Aminoethyl)-2-(diphenylphosphanyl)benzamide (L^2):** *N*-[2-(Diphenylphosphanyl)benzoyloxy]succinimide (0.70 g, 1.74 mmol), dissolved in dichloromethane (10 mL), was added dropwise to a solution of ethylenediamine (0.25 mL, 3.70 mmol) in the same solvent. After 2 h (TLC: ethyl acetate/hexane, 50:50), the white precipitate was removed by filtration through a pad of Celite and the filtrate was concentrated to dryness. The resulting yellowish viscous oil was dissolved in the minimum amount of ethanol and water was added dropwise until no more white solid precipitated. The solid was recovered by filtration, washed twice with water and dried under vacuum, yielding $\mathbf{L^2}$ in an analytical pure form. Yield 0.45 g (74%). − ^{1}H NMR ($CDCl_3$): δ = 2.68 (2 H, t, CH_2), 3.30 (2 H, q, CH_2), 6.23 (1 H, s, br., NH), 6.92 (1 H, m, aromatic), 7.23−7.39 (12 H, m, aromatic), 7.59 (1 H, m, aromatic). − ^{31}P NMR ($CDCl_3$): δ = −9.3. − ^{31}P NMR (CD_3CN): δ = −8.6. − IR (KBr): $\tilde{\nu}$ = 3320 cm^{-1} (m, NH_2), 1630 cm^{-1} (vs, C=O). − $C_{21}H_{21}N_2OP{\cdot}H_2O$ (366.4): calcd. C 68.84, H 6.33, N 7.65; found C 69.61, H 6.08, N 8.17.

2-(Diphenylphosphanyl)-*N*-(2-hydroxyethyl)benzamide (L^3): *N*-[2-(Diphenylphosphanyl)benzoyloxy]succinimide (3.30 g, 8.20 mmol), dissolved in dichloromethane (20 mL), was added dropwise to a solution of ethanolamine (1.08 mL, 19.60 mmol) in the same solvent (45 mL). After 3 h (TLC: ethyl acetate/hexane, 50:50), the white solid, which precipitated, was eliminated by filtration through a pad of Celite and the filtrate was concentrated to dryness. The resulting yellowish viscous oil afforded a white solid after drying for several hours under vacuum. The compound was washed with water and recovered by filtration. After drying, $\mathbf{L^3}$ was obtained in an analytical pure form. Yield 2.50 g (87%). − ^{1}H NMR ($CDCl_3$): δ = 3.39 (2 H, q, CH_2), 3.59 (2 H, t, CH_2), 6.27 (1 H, s, br., NH), 6.94 (1 H, m, aromatic), 7.24−7.39 (12 H, m, aromatic), 7.59 (1 H, m, aromatic). − ^{31}P NMR ($CDCl_3$): δ = − 9.9. − ^{31}P NMR (CD_3CN): δ = − 8.4. − IR (KBr): $\tilde{\nu}$ = 3310 cm^{-1} (m, OH), 1630 cm^{-1} (vs, C=O). − $C_{21}H_{20}NO_2P$ (349.1): calcd. C 72.18, H 5.77, N 4.01; found C 71.74, H 6.56, N 4.25.

[{(1*R*,2*R*)-*N*-(2-Aminocyclohexyl)}-2-(diphenylphosphanyl)benzamide]trichlorooxorhenium(V), [Re(O)(κ^2-L^1)Cl_3]·HCl (4): $\mathbf{L^1}$ (0.068 g, 0.17 mmol), dissolved in MeOH (5 mL), was added dropwise to a solution of **1** (0.10 mg, 0.17 mmol) in MeOH (10 mL). The reaction turned brown immediately and within a few minutes turned green. After 3 h at room temperature, the solution was concentrated to dryness giving an highly viscous oil. After washing several times with dichloromethane, a light blue solid precipitated, which was vacuum-dried. Yield 0.066 g (52%). − ^{31}P NMR: [$(CD_3)_2SO$]: δ = −17.2, 32.9. − IR (KBr): $\tilde{\nu}$ = 1570 cm^{-1} (vs, C=O), 1000 cm^{-1} (vs, Re=O), 320 cm^{-1} (m, Re−Cl). − $C_{25}H_{28}Cl_4N_2O_2PRe$ (747.5): calcd. C 40.17, H 3.78, N 3.75; found C 40.18, H 3.68, N 3.81.

[*N*-(2-Aminoethyl)-2-(diphenylphosphanyl)benzamide]trichlorooxorhenium(V), [Re(O)(κ^2-L^2)Cl_3]·HCl (5): Compound **5** was prepared in a similar manner to **4**. $\mathbf{L^2}$ (0.20 g, 0.58 mmol) and **1** (0.34 g, 0.58 mmol) were allowed to react to form a light green solid, **5**. Yield 0.23 g (58%). Single crystals of poor quality for X-ray crystallographic analysis were obtained by recrystallization of **5** from boiling acetonitrile. − ^{1}H NMR (CD_3CN): δ = 2.98 (2 H, s, br., CH_2), 3.45 (2 H, s, br, CH_2), 7.16 (1 H, m, aromatic), 7.52−7.80 (12 H, m, aromatic), 8.68 (1 H, t, br., aromatic), 11.48 (1 H, s, br., NH). − ^{1}H NMR [$(CD_3)_2SO$]: δ = 2.82 (2 H, m, CH_2), 3.26 (2 H, m, CH_2), 7.09 (1 H, m, aromatic), 7.48−7.66 (8 H, m, aromatic), 7.84 (2 H, m, aromatic), 8.08 (2 H, s, br., aromatic), 8.54 (1 H, m, aromatic), 11.42 (1 H, s, br., NH). − ^{31}P NMR (CD_3CN): δ = −15.4. − ^{31}P NMR [$(CD_3)_2SO$]: δ = −18.1. − IR (KBr): $\tilde{\nu}$ = 1590 cm^{-1} (vs, C=O), 1000 cm^{-1} (vs, Re=O), 320 cm^{-1} (s, Re−Cl). − $C_{21}H_{22}Cl_4N_2O_2PRe$ (691.9): calcd. C 36.42, H 3.20, N 4.05; found C 36.02, H 2.60, N 3.74.

Trichloro[2-(diphenylphosphanyl)-*N*-(2-hydroxyethyl)benzamide]-oxorhenium(V), [Re(O)(κ^2-L^3)Cl_3] (6). − Method a: $\mathbf{L^3}$ (0.10 g, 0.29 mmol), dissolved in MeOH (5 mL), was added dropwise to a solution of **1** (0.17 g, 0.29 mmol) in MeOH (10 mL). The reaction turned dark green immediately, then violet-blue and finally bright green. A dark green solid precipitated which was then isolated by filtration, washed 3 times with MeOH and vacuum-dried. Complex **6** was obtained in an almost quantitative yield. − **Method b:** A suspension of complex **2** (0.092 g, 0.11 mmol) in dry dichloromethane (25 mL) was treated with $\mathbf{L^3}$ (0.040 g, 0.11 mmol) under an inert atmosphere. Within a few minutes a green reaction mixture was obtained. After 1 h, a dark green solid started to precipitate. The reaction was allowed to proceed for 18 h. The solid was then isolated by filtration and washed 3 times with dry dichloromethane. Single crystals, suitable for X-ray crystallographic analysis, were

Table 1. Crystal data and structure refinement of **L[1]** and **6**

	L[1]	**6**
Empirical formula	$C_{25}H_{27}N_2OP$	$C_{21}H_{20}Cl_3NO_3PRe{\cdot}CH_3CN$
M	402.46	698.95
Crystal size [mm]	0.70 × 0.54 × 0.18	0.34 × 0.12 × 0.11
Crystal system	monoclinic	orthorhombic
Space group	$P2_1$	$P2_12_12_1$
a [Å]	12.808(2)	8.0460(8)
b [Å]	15.193(2)	10.7286(10)
c [Å]	18.105(3)	30.116(3)
β [°]	106.544(14)	
V [Å^3]	3377.2(9)	2599.7(4)
Z	6	4
T [K]	293(2)	293(2)
D_c [g cm^{-3}]	1.187	1.786
μ(Mo-K_α) [mm^{-1}]	0.140	5.071
F(000)	1284	1360
No. reflections measured	6386	4566
No. unique reflections	6180 (0.0325)[a]	4311 (0.0972[a])
$R1$[b]	0.0670	0.0702
wR_2[b]	0.1085	0.0836

[a] Value of *R*(int). – [b] The values were calculated for data with $I > 2\sigma(I)$ only.

obtained by recrystallization from boiling CH_3CN. Yield 0.040 g (55%). – ^{1}H NMR (CD_3CN): δ = 3.16 (2 H, m, CH_2), 3.38 (2 H, t, CH_2), 7.14 (1 H, m, aromatic), 7.51–7.81 (12 H, m, aromatic), 8.03 (1 H, t, br., aromatic), 9.08 (1 H, s, br., NH). – ^{1}H NMR [$(CD_3)_2SO$]: δ = 3.09 (2 H, m, CH_2), 3.26 (2 H, m, CH_2), 7.06 (1 H, m, aromatic), 7.46–7.88 (12 H, m, aromatic), 8.23 (1 H, m, aromatic), 10.92 (1 H, s, br., NH). – ^{31}P NMR (CD_3CN): δ = −16.5. – ^{31}P NMR: [$(CD_3)_2SO$]: δ = – 18.1. – IR (KBr): $\tilde{\nu}$ = 3250 cm^{-1} (w, OH), 1590 cm^{-1} (vs, C=O), 1000 cm^{-1} (vs, Re=O), 315 cm^{-1} (s, Re–Cl). – $C_{21}H_{20}Cl_3NO_3PRe$ (657.9): calcd. C 38.34, H 3.06, N 2.13; found C 37.97, H 2.90, N 1.97.

X-ray Crystallographic Analysis: A colourless crystal of **L[1]** and a dark green crystal of **6** were fixed inside thin-walled glass capillaries. Data were collected at room temperature with an Enraf–Nonius CAD-4 diffractometer with graphite-monochromatized Mo-K_α radiation, using an ω-2θ scan mode. Unit cell dimensions were obtained by least-squares refinement of the setting angles of 25 reflections with 16.6° < 2θ < 24.0° for **L[1]**, and 16.2° <2θ< 29.7° for **6**. A summary of the crystallographic data is given in Table 1. Data were corrected[23] for Lorentz polarization effects, for linear decay (no decay was observed for **L[1]**, and a decay of 16.7% was observed for **6**) and for absorption by empirical corrections based on ψ scans. The structures were solved by Patterson methods[24] and subsequent difference Fourier techniques and refined by full-matrix least-squares procedures on F^2 using SHELXL93[25]. For **6**, an acetonitrile solvent molecule of crystallization was also located in the Fourier difference map. During the isotropic refinement of **6** the terminal C(3)–O(3) atoms showed rather large thermal parameters and were found to be disordered over two different positions with 0.52 and 0.48 occupancies. All the non-hydrogen atoms were refined with anisotropic thermal motion parameters, with isor restraints being applied to the disordered atoms. The contributions of the hydrogen atoms were included in calculated positions [except that of the disordered O(3)H atom]. The absolute configuration of both crystals studied were determined by refinement of the Flack parameters, and the refined models proved to be the correct enantiomorphs. A final Fourier difference synthesis was featureless for **L[1]**, and revealed residual electron densities of +1.11 and −1.27 e.Å^{-3} for **6** without any chemical meaning. Atomic scattering factors and anomalous dispersion terms were taken as in ref.[25] The ORTEP drawings were made with ORTEP II[26] and all calculations were performed with a Decα 3000 computer. A summary of the crystal data and of the refinement procedures is given in Table 1. Crystallographic data (excluding structure factors) for the structures reported in this paper have been deposited with the Cambridge Crystallographic Data Centre as supplementary publication no. CCDC-137148 (**L[1]**) and -137149 (**6**). Copies of the data can be obtained free of charge on application to CCDC, 12 Union Road, Cambridge CB2 1EZ, UK [Fax: int. code + 44-1223/336-033; E-mail: deposit@ccdc.cam.ac.uk].

Acknowledgments

J. D. G. C. would like to thank the Fundação para a Ciência e Tecnologia (National Foundation for Science and Technology) for a PRAXIS XXI postdoctoral fellowship.

[1] [1a] S. Jurisson, D. Berning, Wei Jia, Dangshe Ma, *Chem. Rev.* **1993**, *93*, 1137. – [1b] K. E. Britton, *Eur. J. Nucl. Med.* **1998**, *25*, 1671. – [1c] L. Thunus, R. Lejeune, *Coord. Chem. Rev.* **1999**, *184*, 125.

[2] [2a] J. R. Dilworth, S. J. Parrott, *Chem. Soc. Rev.* **1998**, *27*, 43. – [2b] B. Joahnnsen, H. Spies, *Top. Curr. Chem.* **1996**, *176*, 79 and references therein. – [2c] K. Hashimoto, K. Yoshihara, *Top. Curr. Chem.* **1996**, *176*, 275 and references therein.

[3] [3a] S. S. Jurisson, J. D. Lydon, *Chem. Rev.* **1999**, *99*, 2205. – [3b] S. Liu, D. S. Edwards, *Chem. Rev.* **1999**, *99*, 2235.

[4] Davidson, C. J. L. Lock in *Comprehensive Coordination Chemistry*, vol. 4 (Eds:. H. G. Wilkinson, R. D. Gillard, J. A. McCleverty), Pergamon Press, Oxford, **1987**.

[5] F. Refosco, F. Tisato, A. Moresco, A. Cagnolini, G. Bandoli, C. Bolzati *in Technetium and Rhenium in Chemistry and Nuclear Medicine*, vol. 4 (Eds.: M. Nicolini, G. Bandoli, U. Mazzi), S. G. Editorali, Padova, **1995**, p. 133.

[6] [6a] F. Refosco, C. Bolzati, A. Moresco, G. Bandoli, A. Dolmella, U. Mazzi, M. Nicolini, *J. Chem. Soc., Dalton Trans.* **1991**, 3043. – [6b] F. Refosco, F. Tisato, G. Bandoli, C. Bolzati, A. Dolmella, A. Moresco, M. Nicolini, *J. Chem. Soc., Dalton Trans.* **1993**, 605. – [6c] F. Tisato, F. Refosco, C. Bolzati, A. Cagnolini, S. Gatto, G. Bandoli, *J. Chem. Soc., Dalton Trans.* **1997**, 1421.

[7] [7a] C. Bolzati, F. Refosco, F. Tisato, G. Bandoli, A. Dolmella, *Inorg. Chim. Acta* **1992**, *201*, 7. – [7b] F. Refosco, F. Tisato, G. Bandoli, E. Deutsch, *J. Chem. Soc., Dalton Trans.* **1993**, 2901. – [7c] C. Bolzati, F. Tisato, F. Refosco, G. Bandoli, A. Dolmella, *Inorg. Chem.* **1996**, *35*, 6221.

[8] [8a] J. R. Dilworth, A. J. Hutson, S. Morton, M. Harman, M.

B. Hursthouse, J. Zubieta, C. M. Archer, J. D. Kelly, *Polyhedron* **1992**, *11*, 2151. – [8b] N. de Vries, J. Cook, A. G. Jones, A. Davidson, *Inorg. Chem.* **1991**, *30*, 2662. – [8c] F. Tisato, F. Refosco, G. Bandoli, C. Bolzati, A. Moresco, *J. Chem. Soc., Dalton Trans.* **1994**, 1453.

[9] [9a] F. Tisato, F. Refosco, A. Moresco, G. Bandoli, A. Dolmella, C. Bolzati, *Inorg. Chem.* **1995**, *34*, 1779. – [9b] M. Santimaria, U. Mazzi, S. Gatto, A. Dolmella, G. Bandoli, M. Nicolini, *J. Chem. Soc., Dalton Trans.* **1997**, 1765.

[10] J. D. G. Correia, Â. Domingos, I. Santos, unpublished results.

[11] G. W. Anderson, J. E. Zimmerman, F. M. Callahan, *J. Am. Chem. Soc.* **1964**, *86*, 1839.

[12] D. G. Gorenstein, D. O. Shah in *Phosphorous-31 NMR, Principles and Applications* (Ed.: D. O. Gorenstein), Academic Press, Orlando, **1984**, p. 549.

[13] G. Gilli in *Fundamentals of Crystallography* (Ed.: C. Giacovazzo), International Union of Crystallography, Oxford University Press, **1992**, p. 465.

[14] J. E. Fergusson, *Coord. Chem. Rev.* **1966**, *1*, 459.

[15] J. C. Bryan, M. C. Perry, J. B. Arterburn, *Acta Crystallogr.* **1998**, *C54*, 1607.

[16] [16a] V. S. Sergienko, M. A. Porai-Koshits, V. E. Mistryukov, K. V. Kotegov, *Sov. J. Coord. Chem. (Engl. Transl.)* **1975**, *1*, 33. – [16b] B. Noll, S. Noll, P. Leibnitz, H. Spies, P. E. Schulze, W. Semmler, B. Johannsen, *Inorg. Chim. Acta* **1997**, *255*, 399.

[17] W. A. Nugent, J. M. Mayer, *Metal-Ligand Multiple Bonds*, Wiley-Interscience, John Wiley & Sons, New York, **1988**.

[18] K. Nakamoto, *Infrared Spectra of Inorganic and Coordination Compounds*, Wiley-Interscience, John Wiley & Sons, New York, **1970**.

[19] J. C. Bryan, R. E. Stenkamp, T. H. Tulip, J. M. Mayer, *Inorg. Chem.* **1987**, *26*, 2283.

[20] J. E. Hoots, T. B. Rauchfuss, D. A. Wrobleski, *Inorg. Synth.* **1982**, *21*, 175.

[21] R. Alberto, R. Schibli, A. Egli, P. August Schubiger, W. A. Herrmann, G. Artus, U. Abram, T. A. Kaden, *J. Organomet. Chem.* **1995**, *493*, 119.

[22] G. W. Parshall, *Inorg. Synth.* **1977**, *17*, 110.

[23] C. K. Fair, *MOLEN*, Enraf−Nonius, Delft, The Netherlands, **1990**.

[24] G. M. Sheldrick, *SHELXS-86*, *Program for the Solution of Crystal Structures*, University of Göttingen, Germany, **1986**.

[25] G. M. Sheldrick, *SHELXL-93*, *Program for the Refinement of Crystal Structure*, University of Göttingen, Germany, **1993**.

[26] C. K. Johnson, *ORTEPII*, *Report ORNL-5138*, Oak Ridge National Laboratory, Oak Ridge, TN, USA, **1976**.

Received November 19, 1999
[I99415]

Synthesis, Crystal Structure, Magnetic Properties and ^{57}Fe Mössbauer Spectroscopy of the New Trinuclear $[Fe_3(4\text{-}(2'\text{-hydroxyethyl})\text{-}1,2,4\text{-triazole})_6(H_2O)_6](CF_3SO_3)_6$ Spin Crossover Compound

Yann Garcia,[a] Philippe Guionneau,[b] Georges Bravic,[b] Daniel Chasseau,[b] Judith A. K. Howard,[c] Olivier Kahn†,[b] Vadim Ksenofontov,[a] Sergei Reiman,[a] and Philipp Gütlich*[a]

Dedicated to Professor Arndt Simon on the occasion of his 60th birthday

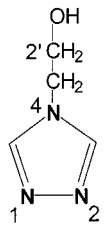
Keywords: Iron / Spin crossover / Trinuclear complex / Hydrogen bonds / Mössbauer spectroscopy

$[Fe_3(hyetrz)_6(H_2O)_6](CF_3SO_3)_6$ [hyetrz = 4-(2′-hydroxyethyl)-1,2,4-triazole] represents the first structurally characterized iron(II) spin crossover compound for which the structure has been solved above and below room temperature in both spin states. The compound crystallizes in the trigonal system, space group $R\bar{3}$, a = 12.763(1) Å, β = 67.144(1)°, V = 1684.3(1) Å^3, Z = 6 at 120 K. At 330 K the space group is retained and a = 13.0183(3) Å, β = 67.376(3)°, V = 1805.8(1) Å^3. The molecular structure consists of trinuclear Fe^{II} entities linked together by an unprecedented three-dimensional network of hydrogen bonds. This compound shows a gradual spin crossover behavior centered around room temperature, which has been followed by temperature-dependent magnetic susceptibility measurements as well as by ^{57}Fe Mössbauer spectroscopy. The nature of the spin crossover behavior is discussed on the basis of the structural features.

Introduction

One of the appealing aspects of the phenomenon of spin crossover between high-spin (HS) and low-spin (LS) states resides in the occurrence of bistability, i.e. the possibility of observing two electronic states in a given range of external perturbation.[1−3] In this respect, Fe^{II} spin crossover compounds have been widely investigated.[4−7] For an assembly of spin crossover molecules governed by the thermodynamical regime, the perturbation may be caused by the temperature and then bistability leads to the occurrence of thermal hysteresis, which endows the system with a memory effect.[1] A challenging field of research concerns the design of new Fe^{II} polynuclear spin crossover materials exhibiting strong inter-site interactions. A strategy towards obtaining such compounds consists of linking the active sites by chemical bridges to give extended or polymeric structures.[8] Extensive research efforts have been directed towards Fe^{II} polymeric chain compounds containing 4-R-substituted derivatives of 1,2,4-triazole, because of the favorable characteristics of their spin crossover behavior.[8−17] Such behavior generally involves very abrupt transitions, as well as important thermal hysteresis effects accompanied by a pronounced thermochromic response, making them the compounds of choice for various applications in molecular electronics[3,8,9,18] or as temperature sensors.[8,14,17] So far, no crystal structure is available for these materials although several Cu^{II} structures have been solved.[19−21]

Oligomers are generally used as model systems for the polymers because they are better defined from a crystallographic point of view and the physical properties can be easily correlated to the structural data. This is also the case for the Fe^{II} linear trinuclear compounds containing 4-R-substituted 1,2,4-triazole as ligands. Several crystal structures of these model compounds have been solved[22−24] or have been studied by EXAFS spectroscopy.[25] It was with this goal in mind that we decided to investigate the structure and magnetic properties of the new trinuclear compound of formula $[Fe_3(hyetrz)_6(H_2O)_6](CF_3SO_3)_6$ with hyetrz = 4-(2′-hydroxyethyl)-1,2,4-triazole (see Scheme 1).



Scheme 1. 4-(2′-hydroxyethyl)-1,2,4-triazole (hyetrz)

[a] Institut für Anorganische Chemie und Analytische Chemie, Universität Mainz,
Staudingerweg 9, 55099 Mainz, Germany
E-mail: P.guetlich@uni-mainz.de
[b] Institut de Chimie de la Matière Condensée de Bordeaux, Laboratoire des Sciences Moléculaires, UPR CNRS No. 9048, 33608 Pessac, France
[c] Durham Crystallography Group, Chemistry Department, Durham University,
Durham, DH1 3LE, UK

 © WILEY-VCH Verlag GmbH, D-69451 Weinheim, 2000 1434−1948/00/0707−1531 $ 17.50+.50/0

This ligand was selected in order to increase the dimensionality through hydrogen bonding interactions. The compound shows a spin crossover behavior centered around room temperature. Its crystal structure has been solved in its LS and HS states. In addition, the dynamic character of the spin crossover behavior has been evidenced by ^{57}Fe Mössbauer spectroscopy.

Results

Description of the Structure of $[Fe_3(hyetrz)_6(H_2O)_6](CF_3SO_3)_6$

An atomic displacement ellipsoid plot of the molecule is represented in Figure 1 and relevant information on bond lengths and bond angles is given in Table 1.

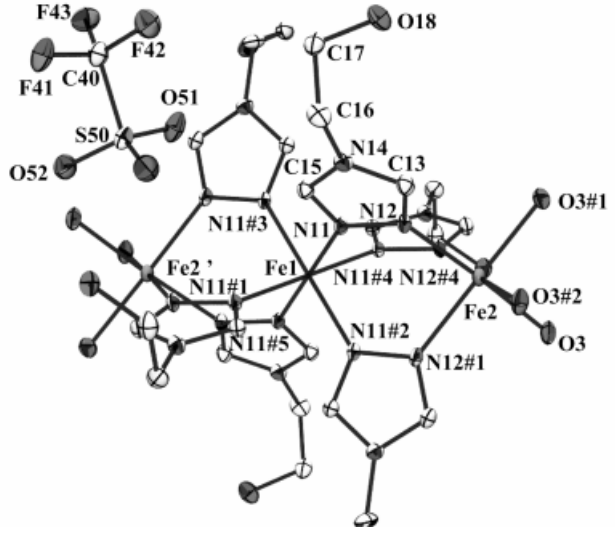


Figure 1. Atomic displacement ellipsoid view (50% probability) of the molecule of $[Fe_3(hyetrz)_6(H_2O)_6](CF_3SO_3)_6$ at 120 K. Hydrogen atoms have been omitted for clarity. Labeled atoms are generated by the following symmetry operations: #1 *z*, *x*, *y*; #2 *y*, *z*, *x*; #3 $-x$, $-y$, $-z$; #4 $-z$, $-x$, $-y$; #5 $-y$, $-z$, $-x$

Table 1. Selected bond lengths [Å] and angles [°] of $[Fe_3(hyetrz)_6(H_2O)_6](CF_3SO_3)_6$ at 120 K and 330 K. Estimated standard deviations are given in parentheses

	T = 120 K	T = 330 K
Fe1−Fe2	3.7833(2)	3.8325(3)
Fe1−N11	2.003(1)	2.169(3)
Fe2−N12	2.161(2)	2.176(5)
Fe2−O3	2.124(2)	2.113(6)
N11−Fe1−N11#1[a]	91.67(6)	89.2(2)
N11−Fe1−N11#4	88.33(6)	90.8(2)
N12−Fe2−N12#1	88.69(6)	92.1(2)
N12−Fe2−O3#1	88.57(6)	87.0(2)
N12−Fe2−O3#2	93.39(6)	91.2(2)
O3−Fe2−O3#1	89.44(6)	89.8(2)

[a] Labeled atoms are generated by the following symmetry operations: #1 *z*, *x*, *y*; #2 *y*, *z*, *x*; #4 $-z$, $-x$, $-y$.

The title compound crystallizes in the trigonal space group $R\bar{3}$. The asymmetric unit contains one trifluoromethanesulfonate anion, one hyetrz ligand, one water molecule, one iron(II) ion, which is labeled as Fe1 and located at the origin (occupancy factor of 1/6), and another iron(II) ion, Fe2, which lies at the special position $x = y = z$ (occupancy factor of 1/3). Thus, the crystalline unit contains one $[Fe_3(hyetrz)_6(H_2O)_6]^{6+}$ cation and six trifluoromethanesulfonate anions. The third iron(II) ion of the cation, labeled as Fe2′, is the homolog of the Fe2 ion by the center of inversion on which the Fe1 ion lies. Three of the hyetrz ligands, which are homologous to one other by the 3-fold symmetry, act as bidentate ligands linking Fe1 to Fe2 through the nitrogen atoms N11 and N12. The three other hyetrz ligands, which are homologous to the former by the center of inversion, link Fe1 to Fe2′. Finally, the water molecules, linked to Fe2 and Fe2′, complete the extremities of the trinuclear unit.

The Fe1 and Fe2 ions present octahedral surroundings. The environment of Fe1 is very regular as the six Fe1−N distances are all equal by symmetry. At 120 K, these bond lengths of 2.003(1) Å correspond to the expected values for an Fe^{II} ion in the LS state.[26] The adjacent N−Fe1−N bonds form an angle of 91.67(6)° when the nitrogen atoms are homologous by the 3-fold symmetry and an angle of 88.33(6)° when the nitrogen atoms are homologous by the center of symmetry. At 330 K, the Fe1−N distances are much longer [2.169(1) Å] and correspond to a HS state.[26] The N−Fe1−N angles are slightly different [89.2(2)° and 90.8(2)° respectively]. The environment of Fe2 is heterogeneous as this ion is bonded to three oxygen atoms and three nitrogen atoms, with only one atom of each species being crystallographically independent. The Fe2−N bond lengths are 2.161(2) Å at 120 K [2.176(5) Å at 330 K] and the Fe2−O bond lengths were found to be 2.124(2) Å at 120 K [2.113(6) Å at 330 K]. Thus, the Fe2 ions are in the HS state whatever the temperature and only the central iron(II) ion shows spin crossover behavior. The increase of the Fe1−N bond length from 120 K to 330 K is equal to 0.166 Å, which is larger than the relatively weak increase (0.143 Å) found for $[Fe_3(etrz)_6(H_2O)_6](CF_3SO_3)_6$.[22] At 330 K, peripheral iron(II) octahedra become more compressed and regular. One can see this effect in a more pronounced way from the side of the oxygen atoms. This is a consequence of the increasing volume of the central iron(II) ion on going from the LS to the HS state. The Fe−Fe intramolecular distance significantly increases with temperature (see Table 1).

The least square planes through the triazole ligands form angles of 60°. This characteristic has already been observed for instance in the linear trinuclear compounds with the related ligand 4-ethyl-1,2,4-triazole (etrz), $[M^{II}_3(etrz)_6(H_2O)_6](CF_3SO_3)_6$ [M = Fe (HS and LS),[22] Mn,[27] Zn[28]], where a $C3_2$ symmetry is present. The *N*1,*N*2−1,2,4-triazole bridging ligands are all identical by symmetry and link the Fe^{II} ions with Fe−N−N bond angles of 127.59(8)° and 122.66(8)° in the LS state and of 125.7(2)° and 122.8(2)° in the HS state. All 1,2,4-triazole rings are planar; the deviation from the least-squares plane through the ring atoms is smaller than 0.002(1) Å.

The crystal packing is built from the translation of the cation contained in the unit cell and thus, by symmetry, all

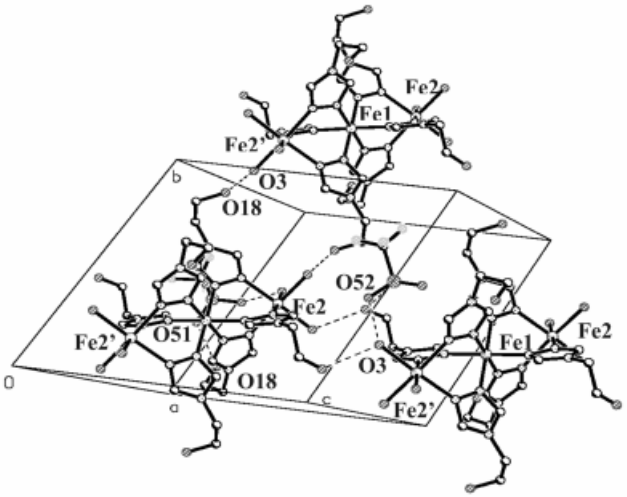


Figure 2. View of the intermolecular interactions between the trinuclear units of [Fe_3(hyetrz)$_6$(H_2O)$_6$](CF_3SO_3)$_6$ at 120 K

Table 2. Relevant interatomic distances (up to 3 Å) and angles of the hydrogen bonding interactions in [Fe_3(hyetrz)$_6$(H_2O)$_6$](CF_3SO_3)$_6$. Estimated standard deviations are given in parentheses

D −H···A	D−H	H···A	D···A	D−H···A
120 K				
O3−H31O18 (−*z*, −*x*, −1 − *y*)	0.81(3)	1.89(3)	2.700(2)	176(3)
O3−H32O52#3[a]	0.83(3)	2.01(3)	2.829(2)	171(3)
O18−H181O51#5	0.78(3)	1.95(3)	2.730(2)	173(3)
330 K				
O3−H31O18(−*z*, −*x*, −1 − *y*)	*	*	2.72(1)	*
O3−H32O52#3	*	*	2.83(1)	*
O18−H181O51#5	*	*	2.75(1)	*

[a] At 330 K, the hydrogen atoms could not be localized. Labeled atoms are generated by the following symmetry operations: #3. −*x*, −, −*z*; #5: −*y*, −*z*, −*x*.

the cations are parallel to each other. They are aligned along the *a*, *b*, and *c* directions. This crystal packing is very different from the packing of [Fe_3(iptrz)$_6$(H_2O)$_6$](tosylate)$_6$ · 2 H_2O (iptrz = 4-isopropyl-1,2,4-triazole) where the adjacent entities are perpendicular to each other in one direction.[24]

The water molecules are all coordinated to an iron(II) ion, and no free water molecules have been found in the network. This characteristic has already been observed in the structures of the trinuclear compounds [Fe_3(etrz)$_6$(H_2O)$_6$](CF_3SO_3)$_6$ [22] and [Fe_3(iptrz)$_6$(H_2O)$_6$]I_6.[29] However, this lack of supplementary water molecules does not imply the absence of a hydrogen-bonding network. Figure 2 displays a view of the intermolecular interactions at 120 K and Table 2 gives the relative bond lengths and angles.

Hydrogen-bonding through the oxygen atoms of the sulfonate groups of the triflate anions (O3···O52 #3) links the coordinated water molecules. These anions are also linked by hydrogen-bonding to the hydroxy groups of the ethyl chain in the 4-position of the triazole ligands (O18···O51 #5). The trinuclear units are not isolated. Indeed, they are linked to each other by hydrogen-bonding interactions. These are situated between the water molecules and the hydroxy groups of the triazole ligands (O3···O18; −*y*, −*z*, −*x*). The related O···O distances do not vary with temperature (Table 2).

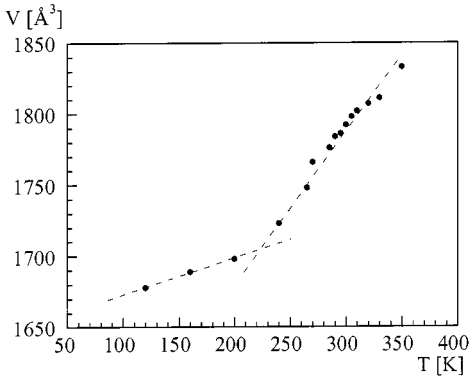


Figure 3. Temperature dependence of the cell volume of [Fe_3(hyetrz)$_6$(H_2O)$_6$](CF_3SO_3)$_6$

No intramolecular interaction between different hydroxy groups of the same trinuclear unit has been detected. This situation is in contrast to the structure of the Cu^{II} linear chain compound [Cu(hyetrz)$_3$](ClO_4)$_2$ · 3 H_2O, where hydrogen bonding between hydroxy groups arising from different *N*1,*N*2−1,2,4-triazole bridges were found.[20]

Temperature Dependence of the Cell Parameters

The symmetry of the cell is the same on both sides of the spin transition. The crystal system implies a strict isotropy of the thermal contraction. Figure 3 shows the temperature dependence of the cell volume from 120 K to 350 K. Within this range, the volume variation of 7.3% and the differential dV/VdT of 3.44 10^{-4} K^{-1} are comparable to the average value calculated for a series of mononuclear iron(II) spin crossover compounds (6.5% and ≈ 3.5 10^{-4} K^{-1}).[30] Two different domains can be defined in this curve: a first one from 350 K to 225 K where the volume contraction (5.6%, 5.6 10^{-4} K^{-1}) corresponds to the contributions of the spin transition and the thermal contraction, and a second one from 225 K to 120 K where the volume decrease is only due to the thermal contraction (1.7%, 1.6 10^{-4} K^{-1}). In the first domain, we can roughly estimate the volume variation due to the spin transition by subtracting the contribution due to the thermal variation with the hypothesis that the behavior is the same as in the second domain. Such a value, $\Delta V_{SC} \approx 90$ Å^3, is very similar to the volume contraction due to the spin crossover found in previously published mononuclear compounds, $\Delta V_{SC} \approx 80-90$ Å.[30,31]

Magnetic Properties

The magnetic behavior of [Fe_3(hyetrz)$_6$(H_2O)$_6$](CF_3SO_3)$_6$ is shown in Figure 4 in the form of a $\chi_M T$ vs. T plot, χ_M being the molar magnetic susceptibility and T being the temperature. At 77 K the $\chi_M T$ value is 7.40 cm^3 K mol^{-1}, which is about the value expected for two iron(II) ions in the HS state. The value of $\chi_M T$ remains constant upon heating up to 235 K, after which it increases progressively reaching a value of 10.92 cm^3 K mol^{-1} at 360 K, which corresponds to the expected value for three iron(II) ions in

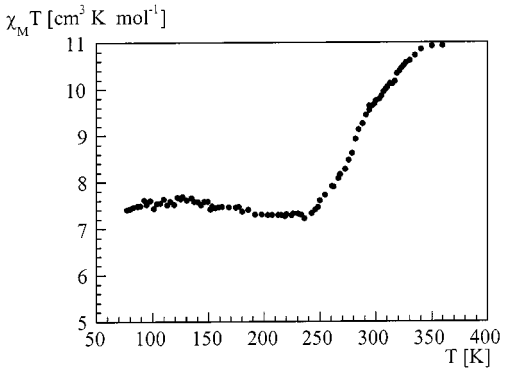


Figure 4. Evolution of $\chi_M T$ vs. T for $[Fe_3(hyetrz)_6(H_2O)_6](CF_3SO_3)_6$

the HS state. A similar magnetic behavior has been observed upon cooling for this gradual transition. The transition temperature $T_{1/2}$, for which 50% of the sites involved in the conversion are HS and 50% are LS, is equal to 290 K. The temperature range in which 80% of central iron(II) ions change spin state (ΔT_{80}) is 70 K. This value has to be compared with the 40 K found for $[Fe_3(etrz)_6(H_2O)_6](CF_3SO_3)_6$.[22]

The assumption of negligible magnetic exchange between second-neighbor iron(II) ions is justified in view of the study of the *N*1,*N*2−1,2,4-triazole triply-bridged $Fe^{II}-Fe^{II}-Fe^{II}$ [22] and $Co^{II}-Co^{III}-Co^{II}$ [32] trinuclear clusters, where the central metal ion is diamagnetic, and no magnetic interactions could be detected between the paramagnetic terminal metal ions.

Optical Measurements

Since this compound is highly thermochromic, the Fe^{II} spin transition has been studied optically using a specially designed device.[12,13] This technique provides an accurate determination of the transition temperature although it does not give any information regarding the percentage of Fe^{II} ions involved in the spin transition. A similar ST behavior as found by magnetic measurements has been observed, with $T_{1/2} = 292$ K.

Mössbauer Measurements

^{57}Fe Mössbauer spectra were recorded at several temperatures between 4.2 K and 293 K. Parameters derived from least-squares fitting are listed in Table 3.

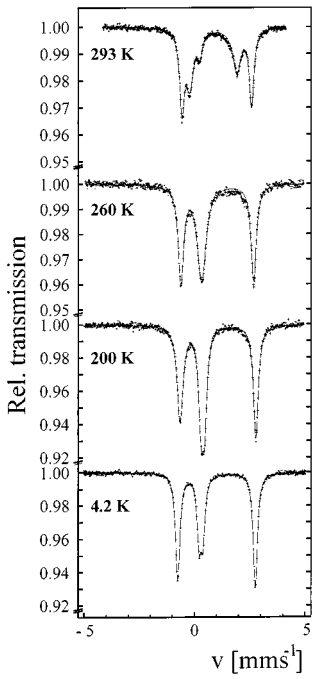


Figure 5. Selected ^{57}Fe Mössbauer spectra of $[Fe_3(hyetrz)_6(H_2O)_6](CF_3SO_3)_6$ recorded at different temperatures

As can be seen from Figure 5, the spectrum measured at 4.2 K shows the expected structure for a trinuclear iron(II) 1,2,4-triazole compound with two iron(II) ions in the HS state and one in the LS state with a relative intensity 1:2. The outer two lines refer to the quadrupole doublet arising from the two peripheral iron(II) ions in the HS state. The signal in the middle represents the poorly resolved quadrupole doublet of the central iron(II) ion in the LS state. The small splitting of the LS doublet indicates that the local environment of the central iron(II) ion is not symmetric, which is not seen in the crystal structure at 120 K. On heating the sample up to 200 K, the spectrum remains essentially the same, with the difference observed between the intensities of the LS and HS doublets being attributed to the known difference of the Debye−Waller factors for the two species. The Debye−Waller factor for the LS state is generally larger (by ca. 20%) than that for the HS state and shows a different temperature dependence for the two states. The consequence of this situation is that the area fractions of the Mössbauer resonance lines do not reflect exactly the actual concentrations of the two states; the LS

Table 3. ^{57}Fe Mössbauer parameters of $[Fe_3(hyetrz)_6(H_2O)_6](CF_3SO_3)_6$

T [K]	δ [mm s^{-1}]	ΔE_Q [mm s^{-1}]	Γ [mm s^{-1}]	rel. area [%]	Spin state
4.2[a]	0.301 ± 0.001	0.172 ± 0.002	0.125 ± 0.004	34.5 ± 0.7	LS
	1.007 ± 0.001	3.510 ± 0.001	0.132 ± 0.002	65.5 ± 0.4	HS
200	0.383 ± 0.007	0.162 ± 0.004	0.182 ± 0.003	45.5 ± 1.3	LS
	1.071 ± 0.001	3.426 ± 0.003	0.144 ± 0.003	54.5 ± 1.8	HS
260	0.331 ± 0.004	−	0.234 ± 0.013	45.0 ± 1.9	LS
	1.039 ± 0.002	3.289 ± 0.004	0.145 ± 0.003	55.0 ± 2.1	HS
293	0.253 ± 0.008	−	0.128 ± 0.014	24.2 ± 1.2	LS
	1.016 ± 0.002	3.152 ± 0.003	0.123 ± 0.003	47.7 ± 3.5	HS
	0.858 ± 0.004	2.133 ± 0.008	0.226 ± 0.007	28.0 ± 2.3	HS

[a] The temperature of the ^{57}Co(Rh) source was 4.2 K.

state rather is overestimated due to the higher tightness of binding in the LS iron complex molecules as compared to the HS complex molecules. At 260 K, the HS doublet attributed to the external iron(II) ions remains the same but the HS doublet of the central iron(II) ion is not distinguishable while the spin crossover occurs at this temperature (cf. Figure 3 and Figure 4). An unusual broadening of the lines of the LS doublet is observed, which is most likely due to the dynamic nature of the spin crossover behavior. At room temperature the spectrum shows two additional lines attributed to the LS and HS species of the central iron(II) ion with an approximate intensity ratio of 1:1, indicating that the transition temperature $T_{1/2}$ is near to 290 K [the peak in the middle refers to the LS state of the central iron(II) ion, the two neighboring signals constitute the HS quadrupole doublet of the central iron(II) ion, and the outer two signals are the quadrupole doublet of the two peripheral iron(II) ions]. Because the relaxation phenomenon is still present at room temperature, the lines of the new HS species together with the remainder of the LS species are about twice as broad as the lines of the external Fe^{II} ions. In the present study, we have restricted ourselves to a qualitative approach to the relaxation phenomenon. For a quantitative analysis, the ^{57}Fe Mössbauer relaxation spectra in the spin crossover region should be fitted using the corresponding relaxation theory,[33] which is a very elaborate task and is beyond the scope of this study. At room temperature, one notices that the isomer shift and the quadrupole splitting of the central and the peripheral iron(II) ions in the HS state do not coincide (see Table 3). This is clear from the fact that the first coordination spheres are different, namely the presence of only nitrogen atoms for the central iron(II) ion and mixed nitrogen-oxygen surroundings for peripheral iron(II) ions. This, of course, gives rise to different electric field gradients and thus different electric quadrupole interactions for the two inequivalent iron sites.

The Mössbauer experiment at 4.2 K was also carried out in an external magnetic field of 5 T directed parallel to the γ-ray beam. The obtained spectrum (Figure 6) exhibits two groups of sextets with the following hyperfine parameters:

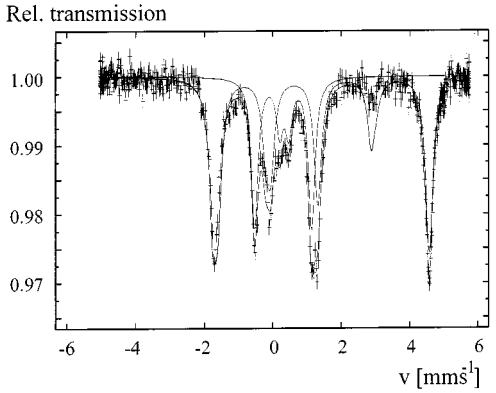


Figure 6. ^{57}Fe Mössbauer spectrum of [Fe_3(hyetrz)$_6$(H_2O)$_6$](CF_3SO_3)$_6$ recorded at 4.2 K in an external magnetic field of 5 T parallel to the direction of the γ rays

H_{LS} = 5.16 T, δ_{LS} = 0.307 mm s^{-1}, ΔEQ_{LS} = −0.03 ± 0.01 mm s^{-1}, φ_{LS} = 0°; H_{HS} = 13.1 T, δ_{HS} = 1.004 mm s^{-1}, ΔEQ_{HS} = −3.51 ± 0.01 mm s^{-1}, φ_{HS} = 87.3°. φ_{LS} and φ_{HS} characterize the polar angles between the principal axis V_{ZZ} of the electrical field gradient and the local magnetic field H at the iron nuclei of LS and HS states. Analyzing the values of the hyperfine parameters, one can conclude the following. Negative signs of the quadrupole splitting on both states indicate that the orbital singlet is the ground state. This means that the three octahedra are elongated along the trigonal axes of the trinuclear unit. This conclusion is in agreement with the structural data obtained at 120 K. In the LS state the iron nuclei only "see" the external magnetic field. Because of the spatial averaging for the powder sample the effective value of the polar angle φ_{LS} is zero. In the HS state, the external magnetic field induces slow spin-lattice relaxation and the effective field on the iron nuclei is a superposition of both external and internal fields. The internal magnetic field is nearly perpendicular to the direction of V_{ZZ} (φ_{HS} = 87.3°), which apparently coincides with the axial axis of the trinuclear unit. It is noteworthy that the deviation of the magnetic field axis from the nearly perpendicular V_{zz} axis almost coincides with the deviation of 3° found between the parts containing oxygen and nitrogen atoms of the peripheral irregular octahedra of the trinuclear unit.

Discussion and Conclusion

In this paper we have described the molecular structure as well as the magnetic properties of a new linear trinuclear iron(II) spin crossover compound. The spin transition regime is centered in the room temperature region. The crystal structure has been solved above and below the transition temperature. If we compare the hyetrz ligand with its homolog, the etrz ligand, the chain in the 4-position of the 1,2,4-triazole has been functionalized by the introduction of a hydroxy group. This substituent has been selected for its potential to be linked by hydrogen bonding interactions to other entities of the network. Therefore, we can expect an increase in the intermolecular interactions in comparison to the trinuclear compound formed with the etrz ligand, [Fe_3(etrz)$_6$(H_2O)$_6$](CF_3SO_3)$_6$.[22] This has been borne out experimentally, because a molecular assembly of linear trinuclear entities linked by an unprecedented three-dimensional network of hydrogen bonds has been discovered for the title compound. The hydroxy groups play the role of bridges between the trinuclear units by hydrogen bonding with the water molecules coordinated to metal ions. Besides, the triflate anions allow the strengthening of the interactions, by hydrogen bonding with the water molecules and the alcohol groups.

Regarding the magnetic properties, a weak cooperative spin crossover behavior was observed. This can be understood if one considers the isolated molecule where only the central metal ion undergoes the spin crossover. However, surprisingly, the ST curve of this material is less abrupt than

the one found for $[Fe_3(etrz)_6(H_2O)_6](CF_3SO_3)_6$, as given by the comparison of the ΔT_{80} values for these two compounds. This could indicate that the presence of intermolecular interactions by hydrogen bonding would not have a favorable effect on the cooperativity developed by such trinuclear systems. A loss of cooperativity in this way has already been observed for the linear trinuclear compounds $[Fe_3(iptrz)_6(H_2O)_6](CF_3SO_3)_6$ and $[Fe_3(iptrz)_6(H_2O)_6]$-(tosylate)$_6 \cdot 2\,H_2O$.[24] The tosylate derivative, which presents a less cooperative spin crossover behavior, shows a crystal structure in which the trinuclear units are linked to the anions and the noncoordinated water molecules by hydrogen bonding. This network, assumed to be more flexible than the one found for the triflate derivative (which does not include any lattice water molecules) was taken as being responsible for the less cooperative behavior of the observed transition. This hypothesis could also be valid for $[Fe_3(hyetrz)_6(H_2O)_6](CF_3SO_3)_6$. It is interesting to note that the transition temperature, which is 203 K for $[Fe_3(etrz)_6(H_2O)_6](CF_3SO_3)_6$, is now 290 K for the title compound. Thus, a pronounced shift of $T_{1/2}$ towards higher temperatures has been observed. This behavior can be directly attributed to the introduction of hydrogen bonds into the network, a property that apparently increases the ligand field strength at the central iron ion. This stabilization of the LS state by hydrogen bonding has already been reported for other ST compounds; for instance the case for the Fe^{II} linear chain compound [Fe(hyetrz)$_3$](3-nitrophenylsulfonate)$_2$.[14,17] The dehydrated material shows a spin crossover behavior at low temperature whereas the hydrated material is LS at room temperature. Thus, in this case, the inclusion of water molecules through hydrogen bonding stabilizes the LS state. Such an effect has also been observed in the mononuclear spin crossover complex [Fe(2-pic)$_3$]Cl$_2 \cdot$ Sol with 2-pic = 2-picolylamine, where the system with Sol = H_2O still exhibits thermal spin crossover although with a very large hysteresis, but the system with Sol = $2{\cdot}H_2O$ shows LS behavior up to room temperature.[34]

Pronounced relaxation effects have been evidenced by ^{57}Fe Mössbauer spectroscopy for $[Fe_3(hyetrz)_6(H_2O)_6](CF_3SO_3)_6$ by virtue of considerable resonance line broadening. Clear evidence of the dynamic nature of the spin crossover behavior was revealed from the very beginning of the spin transition (260 K). This is in contrast with $[Fe(2\text{-pic})_3](PF_6)_2$ ($T_{1/2}$ = 178.5 K) where relaxation effects were only found below 200 K, which is near to the completion of the spin transition.[33] In addition, intersystem crossing dynamics in the solid state for this mononuclear compound were found to be very similar to other Fe^{II} compounds in solution. In the case of trinuclear compounds, the analogy with liquids is much more reasonable because the spin crossover entities are more isolated from each other in comparison to mononuclear compounds. In this case we are dealing with a diluted system. For this reason one could consider trinuclear systems as good candidates for the study of the dynamics of the spin crossover interconversion in the solid state. To the best of our knowledge, the title compound is the first to exhibit such pronounced features of relaxation in the solid state.[33,35]–[39] This is probably related to its very high transition temperature,[37] or to the simultaneous onset of molecular motions and spin crossover behavior. In other words, these two latter processes may be interconnected. Having learned that Fe^{II} trinuclear compounds could exhibit relaxation effects, we cannot exclude that this could also be responsible for the broadening of the lines of the LS doublet at 242 K for $[Fe_3(iptrz)_6(H_2O)_6]$(tosylate)$_6$ with iptrz = 4-isopropyl-1,2,4-triazole.[24] This effect could also be present for other Fe^{II} spin crossover compounds like, for example, $[Fe\{HB(trz)_3\}_2]$ with HB(trz)$_3$ = hydrotris(1,2,4-triazolyl)borate.[40]

Mössbauer experiments performed in the presence of an external magnetic field could allow us to confirm the structural data. This technique could, in future, provide structural information for other Fe^{II} trinuclear compounds for which the crystal structure is not yet available.[23,24] We intend to revisit this aspect in a subsequent paper.

Table 4. Crystallographic data of $[Fe_3(hyetrz)_6(H_2O)_6](CF_3SO_3)_6$ at 120 K and 330 K

Formula	$C_{30}H_{54}F_{18}Fe_3N_{18}O_{30}S_6$	$C_{30}H_{54}F_{18}Fe_3N_{18}O_{30}S_6$
Molecular weight	1848.52	1848.52
T [K]	120	330
Color	purple	colorless
Dimensions [mm^3]	$0.5 \times 0.25 \times 0.25$	$1.6 \times 0.80 \times 0.80$
Space group	$R\bar{3}$ (no. 148)	$R\bar{3}$ (no. 148)
a, b, c [A]	12.7363(1)	13.0183(3)
α, β, γ [°]	67.144(1)	67.376(3)
V [A^3]	1684.3(1)	1805.8(1)
Z	1	1
$\rho_{calcd.}$ [g cm^{-3}]	1.82	1.70
Device	SMART CCD	SMART CCD
λ [A], Mo-K_α	0.71073	0.71073
μ [cm^{-1}]	9.68	9.02
Collected Reflections	18135	4608
Obs. Uniq. Reflections	2586	1976
Rint	0.019	0.049
Parameters	195	165
$R(F)$[a]	0.022	0.063
$wR(F)^2$ [a]	0.056	0.174
S	1.07	1.04

[a] $R(F) = \Sigma||F_o|-|F_c|| / \Sigma|F_o|$ for $F_o > 4\sigma(F_o)$, $wR(F^2) = [\Sigma w(F_o^2 - F_c^2)^2/\Sigma wF_o^2]^{1/2}$, $w = 1/(\sigma^2(F_o^2) + 0.035F^2)$; $S = (\Sigma_i\, w_i\, \Delta\Phi^2)/(n - m)$.

Experimental Section

Starting Materials: Commercially available solvents, monoformyl hydrazine, triethylorthoformate, 2-ethanolamine, and iron(II) triflate were used without further purification.

Synthesis of [Fe_3(hyetrz)$_6$(H_2O)$_6$](CF_3SO_3)$_6$: The ligand 4-(2′-hydroxyethyl)-1,2,4-triazole (hyetrz) was prepared as described previously.[20] A solution of hyetrz (1.06 mmol, 0.12 g) in water (10 mL) was added to a solution of $Fe(CF_3SO_3)_2 \cdot 6\,H_2O$ (0.54 mmol, 0.25 g) in water (20 mL). The volume of the solution was reduced to 15 mL. After two weeks, the mauve compound crystallized upon slow evaporation of the colorless solution at room temperature. The crystals were filtered off, washed with water and dried under ambient air. Yield: 17%. IR: $\tilde{\nu}_{am}(SO_3^-) = 1279\ cm^{-1}$.

Physical Measurements: Magnetic susceptibilities were measured in the temperature range 77−400 K with a fully automated Manics DSM-8 susceptometer equipped with an Oxford instruments DN170 continuous-flow cryostat and a Bruker BE15f electromagnet operating at ca. 0.8 Tesla. Data were corrected for magnetization of the sample holder and for diamagnetic contributions, which were estimated from the Pascal constants. − Optical measurements were carried out using the device described previously[12,13] with a heating rate of 1 K min^{-1} in the temperature range 77−400 K. Mössbauer spectra were recorded in transmission geometry with a Co/Rh source kept at liquid helium temperature and a conventional spectrometer operating in the constant-acceleration mode. The samples were sealed in a Plexiglass sample holder and mounted in a helium-bath cryostat. The cryostat was equipped with a superconductor solenoid operating with a field of 5T. The spectra were fitted to Lorentzian-shaped lines using a nonlinear iterative minimization routine (MOSFUN).

Crystallographic Data Collection and Structure Determination: Experimental and crystal data are reported in Table 4. The single crystals appear pink at 293 K and purple at 120 K. This color is due to the $^1A_{1g} \rightarrow {}^1T_{1g}$ d-d transition of LS Fe^{II} occurring at 520 nm. The color of the compound changes to colorless upon heating to ca. 330 K. This is due to the fact that the spin-allowed d-d transition of lowest energy of the compound in the HS state, $^5T_{2g} \rightarrow {}^5E_g$, occurs at the limit of the visible and IR regions. The structural properties have been investigated from 120 K to 330 K with a Bruker Smart diffractometer associated with an Oxford Cryo-System nitrogen open cryostat. A first sample was cooled to 120 K at a rate of 2 K min^{-1}. 3024 frames were collected using ω scans in 0.2° steps with a 10 s time exposure per frame. Complete data collection was also performed at 293 K and at 310 K but no coherent data could be obtained and the structure could not be solved. A second crystal was used to collect the data at 330 K where the spin crossover is almost complete. Unfortunately, the single crystals melt at this temperature after around four hours, which did not allow us to finish the data collection. The same strategy of data collection as at 120 K was used but only the first 770 frames could be used, which nevertheless gave enough unique observed reflections (1976 observed reflections for 165 refined parameters). Finally, a third crystal was used to determine the cell parameter evolution from 120 K to 330 K. The computing data reduction was performed using the SAINT package including absorption correction using the SADABS program.[41] Such a correction slightly improved the internal R factor (decrease of 1.5%). The crystal structures were solved and refined with SHELXTL.[42] The full-matrix least square refinement of the atomic parameters was based on F^2. All the non-hydrogen atoms were refined with anisotropic thermal parameters. The crystal structure at 330 K is clearly not very accurate, mainly due to the very large thermal motion. Hydrogen atoms were placed using difference Fourier maps at 120 K and their atomic positions were refined, while it was not possible to locate them at 330 K.

Crystallographic data have been deposited at the Cambridge Crystallographic Data Centre as supplementary publication no CCDC-134366 for the structure at 330 K and CCDC-134367 for the structure at 120 K. Copies of the data can be obtained free of charge on application to CCDC, 12 Union Road, Cambridge CB21EZ, UK [Fax: (+44) 1223/336-033; E-mail: deposit@ccdc.cam.ac.uk].

Acknowledgments

This work was partly funded by the TMR Research Network ERB-FMRX-CT98-0199 entitled "Thermal and Optical Switching of Molecular Spin States (TOSS)". P. G. and Y. G. also express their thanks to the Fonds der Chemischen Industrie and the Materialwissenschaftliches Forschungszentrum der Universität Mainz for financial support.

[1] O. Kahn, J. P. Launay, *Chemtronics* **1988**, *3*, 140.
[2] J. Zarembowitch, O. Kahn, *New. J. Chem.* **1991**, *15*, 181.
[3] O. Kahn, *Molecular Magnetism*, VCH, New York, **1993**.
[4] H. A. Goodwin, *Coord. Chem. Rev.* **1976**, *18*, 293.
[5] P. Gütlich, *Struct. Bonding (Berlin)* **1981**, *44*, 83.
[6] P. Gütlich, A. Hauser, H. Spiering, *Angew. Chem. Int. Ed. Engl.* **1994**, *33*, 2024 and references therein.
[7] [7a]P. Gütlich, J. Jung, *J. Mol. Struct.* **1995**, *347*, 21. − [7b]P. Gütlich, J. Jung, H. A. Goodwin, *NATO ASI Series C*, Kluwer, Dordrecht, The Netherlands, **1996**, p. 327. − [7c]P. Gütlich, J. Jung, *Nuovo Cimento Soc. Ital. Fis. D* **1996**, *18*, 107. − [7d]P. Gütlich, *Mol. Cryst. Liq. Cryst.* **1997**, *305*, 17. − [7e]P. Gütlich, H. Spiering, A. Hauser, in: *Inorganic Electronic Structure and Spectroscopy* (Eds.: E. I. Solomon, A. B. P. Lever), John Wiley & Sons, Inc., **1999**, p. 575.
[8] [8a]O. Kahn, E. Codjovi, Y. Garcia, P. J. van Koningsbruggen, R. Lapouyade, L. Sommier, *Symp. Ser.* **1996**, *644*, 298. − [8b]O. Kahn, C. Jay-Martinez, *Science* **1998**, *279*, 44. − [8c]O. Kahn, Y. Garcia, J. F. Letard, C. Mathonière, NATO ASI Series, Kluwer, Dordrecht, The Netherlands, **1998**, p. 127.
[9] O. Kahn, J. Kröber, C. Jay, *Adv. Mater.* **1992**, *4*, 718.
[10] J. Kröber, E. Codjovi, O. Kahn, F. Grolière, C. Jay, *J. Am. Chem. Soc.* **1993**, *115*, 9810.
[11] J. Kröber, J. P. Audière, R. Claude, E. Codjovi, O. Kahn, J. G. Haasnoot, F. Grolière, C. Jay, A. Bousseksou, J. Linares, F. Varret, A. Gonthier-Vassal, *Chem. Mater.* **1994**, *6*, 1404.
[12] O. Kahn, E. Codjovi, *Phil. Trans. R. Soc. London* **1996**, *A354*, 359.
[13] E. Codjovi, L. Sommier, O. Kahn, C. Jay, *New J. Chem.* **1996**, *20*, 503.
[14] Y. Garcia, P. J. van Koningsbruggen, E. Codjovi, R. Lapouyade, O. Kahn, L. Rabardel, *J. Mater. Chem.* **1997**, *7*, 857.
[15] P. J. van Koningsbruggen, Y. Garcia, E. Codjovi, R. Lapouyade, O. Kahn, L. Fournès, L. Rabardel, *J. Mater. Chem.* **1997**, *7*, 2069.
[16] Y. Garcia, P. J. van Koningsbruggen, R. Lapouyade, L. Rabardel, O. Kahn, M. Wierczorek, R. Bronisz, Z. Ciunik, M. F. Rudolf, *C. R. Acad. Sci. Paris* **1998**, *IIc*, 523.
[17] Y. Garcia, P. J. van Koningsbruggen, R. Lapouyade, L. Fournès, L. Rabardel, O. Kahn, V. Ksenofontov, G. Levchenko, P. Gütlich, *Chem. Mater.* **1998**, *10*, 2426.
[18] C. Jay, F. Grolière, O. Kahn, J. Kröber, *Mol. Cryst. Liq. Cryst.* **1993**, *234*, 255.
[19] V. P. Sinditskii, V. I. Sokol, A. E. Fogel'zang, M. D. Dutov, V. V. Serushkin, M. A. Porai-Koshits, B. S. Svetlov, *Russ. J. Inorg. Chem.* **1987**, *32*, 1149.
[20] Y. Garcia, P. J. van Koningsbruggen, G. Bravic, P. Guionneau, D. Chasseau, G. L. Cascarano, J. Moscovici, K. Lambert, A. Michalowicz, O. Kahn, *Inorg. Chem.* **1997**, *36*, 6357.
[21] Y. Garcia, Ph.D. thesis, University of Bordeaux I (France), **1999**.

[22] [22a] G. Vos, R. A. Le Fèbre, R. A. G. de Graaff, J. G. Haasnoot, J. Reedijk, *J. Am. Chem. Soc.* **1983**, *105*, 1682. – [22b] G. Vos, R. A. G. de Graaff, J. G. Haasnoot, A. M. van der Kraan, P. de Vaal, J. Reedijk, *Inorg. Chem.* **1984**, *23*, 2905.
[23] M. Thomann, O. Kahn, J. Guilhem, F. Varret, *Inorg. Chem.* **1994**, *33*, 6029.
[24] J. J. A. Kolnaar, G. van Dijk, H. Kooijman, A. L. Spek, V. G. Ksenofontov, P. Gütlich, J. G. Haasnoot, J. Reedijk, *Inorg. Chem*. **1997**, *36*, 2433.
[25] A. Michalowicz, J. Moscovici, B. Ducourant, D. Cracco, O. Kahn, *Chem. Mater.* **1995**, *7*, 1833.
[26] E. König, *Prog. Inorg. Chem*. **1987**, *35*, 527.
[27] A. L. Spek, G. Vos, *Acta Cryst.* **1983**, *C39*, 990.
[28] G. Vos, J. G. Haasnoot, G. C. Verschoor, J. Reedijk, P. E. L. Schaminee, *Inorg. Chim. Acta* **1985**, *105*, 31.
[29] J. J. A. Kolnaar, Ph.D. Thesis, University of Leiden, **1998**.
[30] P. Guionneau, J. F. Létard, D. S. Yuffit, D. Chasseau, J. A. K. Howard, A. E. Goeta, O. Kahn, *J. Mater. Chem*. **1999**, *4*, 985.
[31] M. Mikami, M. Konno, Y. Saito, *Chem. Phys. Lett*. **1979**, *63*, 566.
[32] L. Antolini, A. C. Fabretti, D. Gatteschi, A. Giusti, R. Sessoli, *Inorg. Chem.* **1991**, *30*, 4858.
[33] P. Adler, H. Spiering, P. Gütlich, *Inorg. Chem.* **1987**, *26*, 3840.
[34] M. Sorai, J. Ensling, K. M. Hasselbach, P. Gütlich, *Chem. Phys.* **1977**, *20*, 197.
[35] H. R. Chang, J. K. McCusker, H. Toftlund, S. R. Wilson, A. X. Trautwein, H. Winkler, D. N. Hendrickson, *J. Am. Chem. Soc.* **1990**, *112*, 6814.
[36] E. König, *Struct. Bonding (Berlin)* **1991**, *76*, 51.
[37] A. Bousseksou, C. Place, J. Linares, F. Varret, *J. Magn. Magn. Mat.* **1992**, *104*, 225.
[38] G. Lemercier, A. Bousseksou, M. Verelst, F. Varret, J. P. Tuchagues, *J. Magn. Magn. Mat.* **1995**, *150*, 227.
[39] P. J. Kunkeler, P. J. van Koningsbruggen, J. P. Cornelissen, A. M. van der Horst, A. M. van der Kraan, A. L. Spek, J. G. Haasnoot, J. Reedijk, *J. Am. Chem. Soc.* **1996**, *118*, 2190.
[40] C. Janiak, T. G. Scharmann, J. C. Green, R. P. G. Parkin, M. J. Kolm, E. Riedel, W. Mickler, J. Elguero, R. M. Claramunt, D. Sanz, *Chem. Eur. J.* **1996**, *2*, 992.
[41] *SMART Version 4.050*. Siemens Analytical X-ray Instruments, Madison WI, U.S.A., **1995**.
[42] G. M. Sheldrick, *SHELXTL-Plus. Release 4.1*. Siemens Analytical X-ray Instruments Inc., Madison WI, U.S.A, **1991**.

Received November 24, 1999
[I99424]

Pseudotetrahedral Organocobalt(III) Compounds Containing Specific Coordination Sites for Brønsted Acids

Mario Roberto Meneghetti,[c] Mary Grellier,[a] Michel Pfeffer,*[a] André De Cian,[b] and Jean Fischer[b]

Keywords: Cobalt / Acids / Hydrogen bonds / Organometallic receptors / N ligands

Transmetallation of the lithiated derivative 2,6-bis[dimethyl(amino)methyl]phenyllithium with the cobalt(III) centre of the dimer bis[(η^5-cyclopentadienyl)cobalt(iodo)(μ-iodo)] has been found to afford the organocobalt compound [CoI{2-(Me_2NCH_2)-6-($Me_2NH^+CH_2$)C_6H_3}(η^5-C_5H_5)]I, **3**, in which the potentially terdentate (pincer) ligand is bound to Co through the formerly lithiated aryl carbon atom and one NMe_2 unit only, whilst the second NMe_2 group is protonated by HI. In the presence of aqueous KPF_6, **3** has been found to undergo both substitution of the iodide bound to Co by a water molecule and deprotonation of the Me_2NH group to afford [CoI{2,6-(Me_2NCH_2)$_2$$C_6H_3$}(η^5-$C_5H_5$)($H_2O$)]$PF_6$, **4a**. It was found that the water ligand in **4a** could be substituted by neutral ligands such as PMe_2Ph as well as by Brønsted acids such as HCl, HI, HF, or HOAc to afford the compounds [CoX{2-(Me_2NCH_2)-6-($Me_2NH^+CH_2$)C_6H_3}(η^5-C_5H_5)]PF_6, **5a**–**d**, where X = Cl, I, F, or OAc, respectively. Crystal structure analyses of some representative examples of these compounds, including **4a**, have shown unambiguously that an intramolecular hydrogen bond is present between X and the proton of the Me_2NH^+ unit. ^{1}H-NMR evidence that this interaction persists in solution has been found for compounds **4a**, **5a**, **5c**, and **5d**.

Introduction

We have recently shown that organometallic compounds of Co^{III} containing a metallacyclic unit may readily be synthesized by transmetallation reactions of lithiated tertiary amines.[1] Such reactions have afforded a wide variety of stable pseudotetrahedral organocobalt compounds in which the cobalt is a stereogenic centre. While investigating the scope of this procedure, we became interested in ascertaining whether other lithiated polydentate amino derivatives could be used to extend the synthetic potential to other organocobalt compounds with a view to varying the nature of the resulting compounds. Thus, we first attempted to synthesize derivatives using the well-known "pincer" ligand [2,6-(Me_2NCH_2)$_2$$C_6H_3$]$^-$ = N^C^N, the chemistry of which with transition metals has been extensively studied by van Koten et al.[2]

This ligand usually bonds to a metal centre through an aryl−M σ bond, but it is also capable of donating a further two electron pairs to the metal through N coordination. The potentially terdentate "pincer" ligand has been shown to be extremely flexible in its coordination and bonding modes (see Figure 1). Its use has led to the isolation and characterization of bis(amino)aryl metal complexes of both main group and transition metals, which exhibit novel reactivities and structural features.[3] Consequently, although it was reasonable to assume that the lithiated derivative of the "pincer" ligand would interact with a Co^{III} centre, we could not predict a priori the type of structure that would be formed.

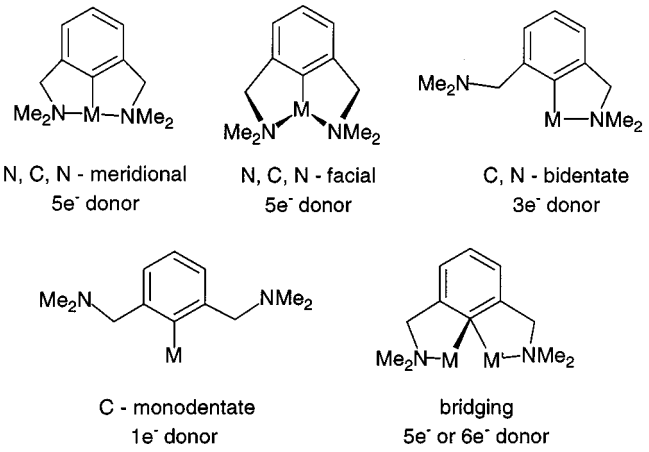


Figure 1. Encountered bonding modes of the pincer ligand

Prior to our work, we were aware of only one cobalt(II) complex, namely Co[2,6-(Me_2NCH_2)$_2$$C_6H_3$]X(L) (X = Cl, Br, I; L = py, PPh_3),[4] in which this "pincer" ligand is coordinated to Co through one aryl carbon and the two nitrogen atoms in a meridional geometry (see Figure 2). Its structure was deduced on the basis of ESR studies and it

[a] Laboratoire de Synthèses Métallo-Induites, UMR 7513 du CNRS, 4, rue Blaise Pascal, F-67000 Strasbourg, France
[b] Laboratoire de Cristallochimie et Chimie Structurale, UMR 7513 du CNRS, 4, rue Blaise Pascal, F-67000 Strasbourg, France
[c] Address [a] or permanent address: Laboratory of Molecular Catalysis, IQ/UFRGS, Av. Bento Gonçalves, 9500 Porto Alegre, Brazil

 © WILEY-VCH Verlag GmbH, D-69451 Weinheim, 2000 1434−1948/00/0707−1539 $ 17.50+.50/0

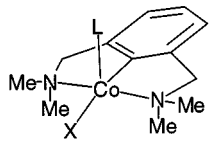


Figure 2. Proposed structure of $Co^{II}[C_6H_3(CH_2NMe_2)_2$-2,6]XL

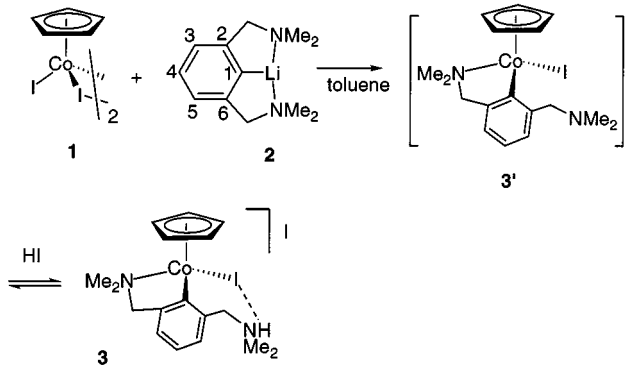
proved to be isostructural with the related Ni^{III} compound $Ni[C_6H_3(CH_2NMe_2)_2$-2,6]Br_2.[5]

We describe herein the synthesis of a number of novel aryl Co^{III} complexes in which the "pincer" ligand is coordinated to the cobalt centre through the carbon and one nitrogen atom while significant intramolecular H-bonding interactions are in evidence between the third anionic ligand and the protonated non-coordinated NMe_2 unit.

Results

1. Synthesis of the Organometallic Complexes

We have recently shown that *ortho*-lithiated N-containing ligands (LiC^N) can be readily transmetallated with $[CpCoI_2]_2$, thereby generating a series of stable organocobalt complexes of the type CpCo(C^N)I. However, we found that when any lithiated aryl compound substituted at its 2-position by CH_2NMe_2 and at its 6-position by another substituent (Me, OMe, or F) was used, the expected product was not obtained.[1] Nevertheless, in marked contrast, reaction of the lithiated "pincer" ligand **2** with $[CpCoI_2]_2$ (**1**) in toluene at room temperature afforded the organocobalt compound **3** as a green powder in good yield (see Scheme 1).



Scheme 1

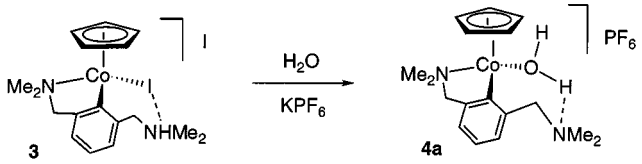
Complex **3** was found to be very soluble in acetone, THF, and chlorinated solvents, quite soluble in C_6H_6, sparingly soluble in Et_2O and MeOH, and insoluble in alkanes. Analytical samples of this complex were obtained by slow diffusion of *n*-hexane into a CH_2Cl_2 solution. It proved to be stable towards air, both in the solid-state and in solution (2 days in $CDCl_3$).

Compound **3** has been fully characterized by ^{1}H- and ^{13}C-NMR spectrometry, IR spectroscopy, and X-ray analysis (see below). The ^{1}H- and ^{13}C-NMR spectra in $CDCl_3$ feature resonances consistent with a diamagnetic Co^{III} complex associated with the relevant organic fragments. From the ^{1}H-NMR spectrum of **3**, it can be concluded that only one of the NMe_2 units is diastereotopic, giving rise to two signals at $\delta = 3.16$ and 2.31. A broad singlet at $\delta = 2.93$ can be assigned to the second NMe_2 unit. This latter chemical shift is at rather low field compared to the signals of non-coordinated NMe_2 groups in related molecules, which usually appear at around $\delta = 2.1-2.3$.[6,7]

Since both combustion analyses and ^{1}H-NMR spectra suggested that **3** was actually a 1:1 adduct of $[CoI\{C_6H_3(CH_2NMe_2)(CH_2NMe_2)$-2,6$\}(\eta^5$-$C_5H_5)]$, **3′**, and HI, we propose that some hydroiodic acid was produced during the synthesis of **3′**, which then protonated the non-coordinated NMe_2 group. Addition of an excess of HI to a $CDCl_3$ solution of **3** in an NMR tube led to splitting of the aforementioned broad signal resulting in two doublets at $\delta = 3.02$ and 2.82 with $^3J_{H-H} = 5.64$ Hz, as well as to the appearance of a well-defined broad singlet at $\delta = 10.0$. These signals can be assigned to the methyl groups and the acidic proton, respectively, of the protonated Me_2NH^+ group. Thus, it would seem that in solution **3** is in equilibrium with **3′** and HI according to Scheme 1; in the presence of excess of HI, this equilibrium is shifted completely towards **3**. The same phenomenon was evident from the ^{13}C-NMR spectra. On treatment of **3** with HI, a broad signal at $\delta = 42.03$ was transformed into two signals at $\delta = 44.17$ and 40.69, corresponding to the two diastereotopic methyl groups of the Me_2NH^+ unit.

2. Reaction of 3 with Water (Synthesis of 4a)

By washing a solution of **3** in CH_2Cl_2 several times with water and combining the aqueous extracts, a new complex, **4a**, was obtained (Scheme 2). This could be isolated as a red powder following the addition of KPF_6.



Scheme 2

IR spectroscopy confirmed the presence of a water molecule in the complex through the appearance of an intense, sharp absorption at 3575 cm^{-1}. Combustion analysis clearly revealed that one water molecule was present and, significantly, that hydroiodic acid was no longer incorporated. By NMR spectrometry, two distinct diastereotopic NMe_2 groups were observed in $CDCl_3$ solution. It is remarkable that the NMe_2 group coordinated to the cobalt centre displays chemical shifts separated by more than 2.0 ppm, whereas for the second NMe_2 group the chemical shift difference is just 0.65 ppm.

3. Reactions of 4a with Phosphanes and Brønsted Acids

3.1 Reaction with PMe_2Ph

It was found that the water ligand in **4a** could be substituted by a phosphane (PMe_2Ph) to quantitatively afford **4b** as a violet powder. The ^{1}H-NMR spectrum of **4b** features

the expected signals with two singlets due to a coordinated NMe_2 unit at $\delta = 2.89$ and 2.23 and a singlet at $\delta = 2.34$ due to the "free" amine. Additionally, two discrete AB spin systems for the CH_2 groups are observed. In the presence of traces of hydrochloric acid, the "free" NMe_2 unit of **4b** is protonated to give **6**, which could be isolated as a red powder. In its ^{1}H-NMR spectrum, **6** exhibits a signal at $\delta = 9.25$ attributable to the H^+ of the Me_2NH^+ group, and a broad unresolved peak due to the methyl groups of the Me_2NH^+ unit, which appears further downfield ($\delta = 3.37$) compared to the corresponding signal of the unprotonated amine. Moreover, in the IR spectrum a typical absorption band for an $N-H^+$ unit is observed at 2704 cm^{-1}.

3.2 Reactions with Brønsted Acids

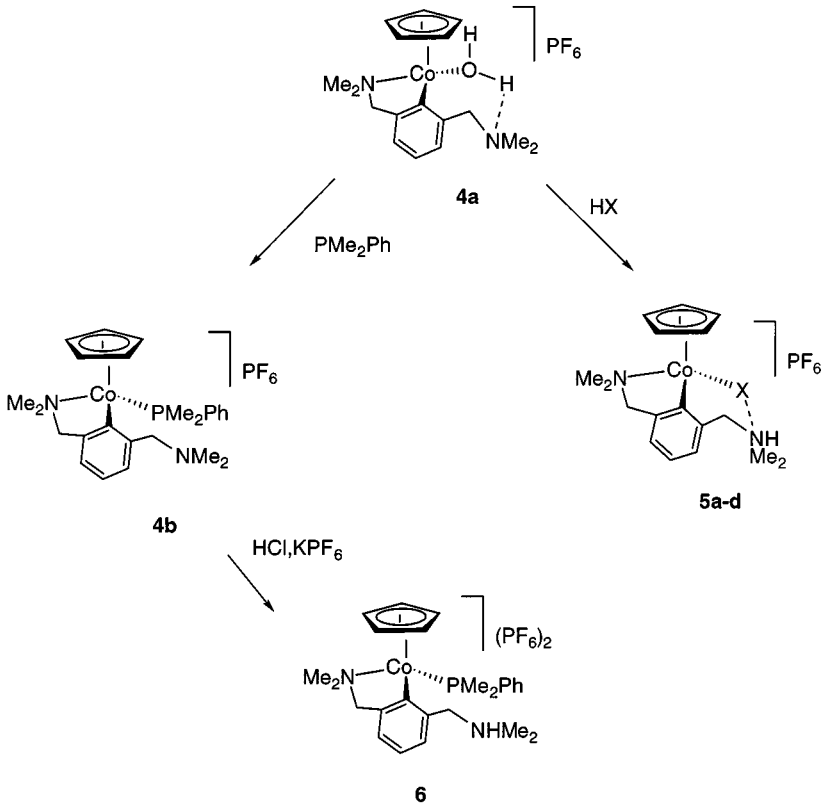
3.2.1 Reaction with HCl (Synthesis of 5a)

In order to find out why the aquo complex **4a** was obtained, we tried to expand this series of compounds by employing related ligands. We found that neither primary or secondary amines nor alcohols led to adducts analogous to **4a**, i.e. no products of substitution of the water molecule by these OH- or NH-containing ligands were obtained. However, we have found that a series of Brønsted acids are capable of substituting the water ligand in **4a** to afford stable organocobalt compounds, and that such reactions occur without any hydrolysis of the Co−C bond of the complex (see Scheme 3). Thus, treatment of **4a** with HCl afforded **5a** as a red-violet powder. This substitution was best achieved using ammonium chloride as a source of HCl with **4a** in methanol.

The ^{1}H-NMR spectrum of **5a** is similar to that of **4a** in that the large chemical shift difference ($\Delta\delta \approx 2.0$ ppm) for the NMe_2 unit coordinated to the cobalt is again apparent and the protonated NMe_2 group is also diastereotopic ($\Delta\delta \approx 0.5$ ppm). Furthermore, the effect of "HCl coordination" versus "H_2O coordination" on the cobalt centre can easily be detected. In **5a**, both the CH_2 and NMe_2 protons of the non-coordinating CH_2NMe_2 unit are very much deshielded as compared to those of the corresponding unit in **4a** (see Experimental Section). The coordinated hydrochloric acid gives rise to a broad signal at $\delta = 9.48$. In the IR spectrum a typical absorption for the M_2N-H^+ group is seen at 2692 cm^{-1}.

3.2.2 Reaction with HI (Synthesis of 5b)

The reaction of **4a** with HI (derived from NH_4I) furnished **5b** as a green powder of a similar hue as **3**. The IR spectrum of **5b** confirmed the presence of an Me_2NH^+ group through the appearance of an absorption band at 2697 cm^{-1}. The ^{1}H-NMR spectrum of **5b** provides strong evidence that this compound has a different magnetic environment compared to **4a** and **5a**, with the $\Delta\delta$ of the diastereotopic Me groups of the NMe_2-Co unit being comparable to that in **3** (0.6 ppm). The acidic proton of the Me_2NH^+ group could be observed as a broad feature at $\delta = 9.33$, but the J_{H-H} between H^+ and NMe_2 in this group was not detectable. It seems likely that the structure of **5b** is similar to that observed in **3**, i.e. with the same ligands about the cobalt centre, and most likely the same electronic interac-



Scheme 3

tion between the iodo ligand and the Me_2NH^+ unit (see below).

3.2.3 Reaction with HF (Synthesis of 5c)

Compound **5c** could easily be obtained in good yield by treatment of **4a** with 40% aq. HF. The IR spectrum of **5c** features a large, prominent absorption band at 2260 cm^{-1} due to the stretching vibration of an $N-H^+$ bond. In order to unambiguously confirm that this band was indeed due to a stretching mode of an $N-H^+$ unit, a H/D exchange experiment using D_2O was carried out. Under these conditions, a new absorption at 1800 cm^{-1} was observed, while the absorption at 2260 cm^{-1} disappeared, thus confirming our assignment. This significant shift to lower frequency for the ν_{sN-H} band of a tertiary ammonium salt[8] may be explained in terms of a hydrogen-bonding interaction between NH^+ and F, which would increase the $N-H^+$ bond length and consequently decrease the associated stretching frequency. Moreover, the ν_{sN-H}/ν_{sN-D} ratio (1.25) gives an additional indication of the existence of a strong hydrogen bond between N−H and F in **5c**.[9]

The ^{1}H-NMR spectrum of **5c** displays the same trends as observed for the previous complexes. This feature suggests that the structures are closely related, i.e. the water ligand in **4a** is merely replaced by HCl and HF to form **5a** and **5c**, respectively. The large Δδ chemical shift difference (2.43 ppm) for the NMe_2-Co unit is strongly indicative of interactions akin to those found in **4a** and **5a**. Some interesting features of the ^{1}H-NMR spectrum of **5c** arise from the presence of the F atom: (i) the signal of the NH^+ proton is located at δ = 11 and shows a sizable J_{H-F} coupling constant (89 Hz);[10] (ii) the highfield resonating methyl group of the NMe_2 unit directly coordinated to the cobalt centre displays a $^4J_{H-F}$ coupling (6.90 Hz); (iii) the two methyl groups of the non-coordinated NMe_2 unit display a $^4J_{H-F}$ coupling (≈ 4.1 Hz), proving the existence of bonding interactions between N−H and F−Co.

3.2.4 Reaction with CH_3COOH (Synthesis of 5d)

Treatment of **4a** with an excess of CH_3COOH in methanol led to the formation of **5d** in very good yield. The IR spectrum of **5d** features a series of overtones consistent with the presence of an Me_2NH^+ group (2700−2400 cm^{-1}) and a typical C=O absorption band at 1634 cm^{-1}. The ^{1}H-NMR spectrum of **5d** also shows a large Δδ chemical shift difference (2.24 ppm) for the NMe_2 unit coordinated to Co, as observed for **4a**, **5a**, and **5c**.

4. X-ray Crystal Structure Analysis of 3, 4a, 5a, and 5d

In order to obtain more structural information on this series of novel complexes, X-ray diffraction studies on some representative compounds have been undertaken. In Table 1, selected geometrical parameters for the complexes **3**, **4a**, **5a**, and **5d** are presented. ORTEP representations of the cationic parts of these salts are depicted in Figures 3−6, while crystallographic data is collected in Table 2. Despite the rather different ^{1}H-NMR data observed for these compounds, their molecular geometries display several analo-

Table 1. Selected bond distances and angles in complexes **3**, **4a**, **5a**, and **5d**

Bond lengths [Å]		Bond angles [°]	
Compound 3			
Co−Cp#[a]	1.731(2)	N1−Co−C14	83.2(2)
Co−C(Cp)$_{av}$	2.106(8)	N1−Co−I1	98.9(2)
Co−I1	2.598(1)	I1−Co−C14	97.0(2)
Co−N1	2.067(6)	Cp^a−Co−N1	127.8(5)
Co−C14	1.966(5)	Cp^a−Co−C14	122.7(5)
N1−C8	1.52(1)	Cp^a−Co−I1	118.6(6)
C8−C9	1.50(1)	Co−N1−C8	103.0(5)
C9−C14	1.387(8)	N1−C8−C9	106.6(6)
N2−HO1	0.88(1)	C8−C9−C14	118.1(6)
N2I1	3.43(1)	C9−C14−Co	110.4(4)
		C6−N1−Co−I1	19.1(5)
		N2−HO1−I1	170(1)
		C14−C13−C15−N2	92.6(6)
4a			
Co−Cp#[a]	1.719(6)	N1−Co−C14	82.6(2)
Co−C(Cp)$_{av}$	2.090(6)	N1−Co−O1	94.1(2)
Co−O	1.977(4)	O−Co−C14	91.2(2)
Co−N1	2.029(4)	Cp^a−Co−N1	128.2(6)
Co−C14	1.951(5)	Cp^a−Co−C14	124.0(1)
N1−C8	1.494(8)	Cp^a−Co−O	124.6(3)
C8−C9	1.474(8)	Co−N1−C8	103.0(3)
C9−C14	1.404(8)	N1−C8−C9	107.9(8)
N2HO1	1.74(1)	C8−C9−C14	115.1(6)
N2O	2.588(8)	C9−C14−Co	110.7(6)
		C6−N1−Co−O	12.6(4)
		N2−HO1−O	168(1)
		C14−C13−C15−N2	−65.4(7)
5a			
Co−Cp#	1.71(1)	N1−Co−C14	82.8(1)
Co−C(Cp)$_{av}$	2.089(4)	N1−Co−Cl	96.8(1)
Co−Cl	2.2832(9)	Cl−Co−C14	95.9(1)
Co−N1	2.074(3)	Cp^a−Co−N1	125.5(8)
Co−C14	1.964(3)	Cp^a−Co−C14	128.7(6)
N1−C8	1.487(5)	Cp^a−Co−Cl	120.9(2)
C8−C9	1.490(5)	Co−N1−C8	120.9(2)
C9−C14	1.406(5)	N1−C8−C9	107.5(3)
N2Cl	3.028(8)	C8−C9−C14	116.4(3)
N2−H01	1.08(7)	C9−C14−Co	110.7(2)
ClH01	1.99(2)	N2−H01Cl	158.1(4)
N2Cl	3.02(8)	C6−N1−Co−Cl	14.6(6)
		C14−C13−C15−N2	−77.5(4)
5d			
Co−Cp#	1.71(8)	N1−Co−C14	82.5(3)
Co−C(Cp)$_{av}$	2.082(9)	N1−Co−O1	96.4(2)
Co−O1	1.992(5)	O1−Co−C14	93.3(3)
Co−N1	2.010(6)	Cp^a−Co−N1	131.0(2)
Co−C14	1.936(7)	Cp^a−Co−C14	122.9(5)
N1−C8	1.48(1)	Cp^a−Co−O1	119.9(4)
C8−C9	1.51(1)	Co−N1−C8	102.9(4)
C9−C14	1.37(1)	N1−C8−C9	105.7(6)
O1−C18	1.31(1)	C8−C9−C14	115.8(7)
O2−C18	1.20(1)	C9−C14−Co	110.3(5)
N2O1	2.72(2)	O1−C18−O2	123.8(9)
N2−H01	0.92(2)	O1−C18−C19	114.0(8)
O1H01	1.80(2)	O2−C18−C19	122.1(8)
		N2−H01O1	173.0(3)
		C7−N1−Co−O1	16.4(4)
		C14−C13−C15−N2	−67.9(7)

[a] Cp# centroid of cyclopentadienyl ring.

gies, at least as far as the "CpCo(pincer)" fragments of the molecules are concerned.

In all cases, the cobalt atoms are found in a distorted octahedral (pseudotetrahedral) environment. The metal coordination sphere comprises a η^5-C_5H_5 ligand and the "pincer" coordinated through the central aryl carbon atom and the nitrogen atom of one NMe_2 unit only. The final coordination site at Co is occupied by an iodide, a water molecule, a chloride, or an acetate group coordinated through an oxygen atom, respectively (throughout this section these ligands will be denoted as "X").

The bite angles of the five-membered chelated rings, N1−Co−C14, and the distances Co−centroid Cp, Co−C14, and Co−N1 are similar in all the complexes. The chelate ring (note that comparable distances and angles have recently been reported for related organocobalt species)[1,11] appears to display a somewhat unfavourable orientation of the N1−C6 bond with respect to the Co−X bonds, which are more or less eclipsed; the torsion angle C6−N1−Co−X is in the range 12.6° to 19.3°. This geometry leads to a puckering of the five-membered chelate ring, which may minimize the steric interactions of the CH_2NMe_2 unit, the N of which does not interact with the Co or the Cp ring (see Figures 3, 5, and 6). However, this NMe_2 unit is positioned in such a way that it resides at a suitable distance from the X groups.

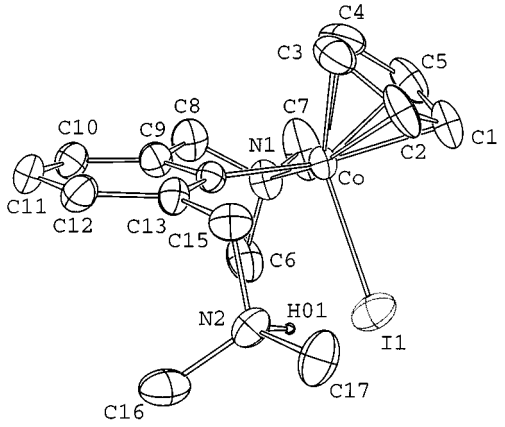


Figure 3. ORTEP view of the cation of **3** [CoI{C_6H_3(CH_2NMe_2)-($CH_2NMe_2H^+$)-2,6}(η^5-C_5H_5)]I

In complexes **3** (Figure 3), **5a**, and **5d**, these nitrogen atoms are protonated and the N−H bond of the $NHMe_2^+$ unit points towards the group X. On the other hand, in compound **4a** the lone pair on the NMe_2 group is oriented towards one O−H vector of the water coordinated to Co. These interactions lead to rather short N···X distances in all four cases. In **3**, however, the N2···I1 distance amounts to 3.43 Å, which is 0.2 Å shorter than the sum of the relevant van der Waals radii and corresponds to the upper range for hydrogen bonds between I and NH^+.[12]

In **4a**, the N2···O distance measures 2.59 Å, which is indicative of significant hydrogen-bonding between the water

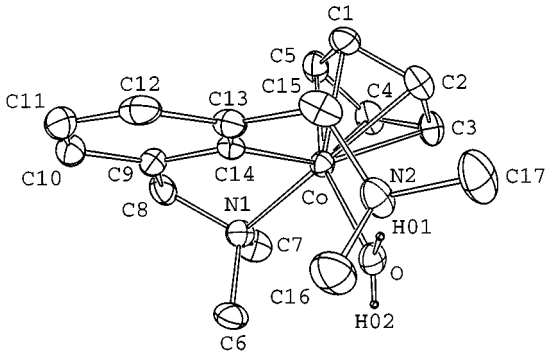


Figure 4. ORTEP view of the cationic part of **4a** [Co{C_6H_3-(CH_2NMe_2)(CH_2NMe_2)-2,6}(η^5-C_5H_5)(H_2O)]PF_6

coordinated to Co and the nitrogen lone pair (Figure 4). This N2···O distance falls at the short end of the range of distances reported for similar types of hydrogen bonds; the O···N distances in O−H···N systems are more typically in the range 2.68−2.79 Å.[13]

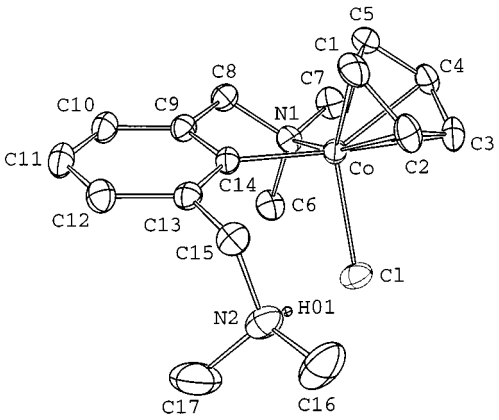


Figure 5. ORTEP view of the cationic part of **5a** [CoCl{C_6H_3-(CH_2NMe_2)($CH_2NMe_2H^+$)-2,6}(η^5-C_5H_5)]PF_6

In the crystal structure of compound **5a** (Figure 5), the N···Cl distance [3.02(8) Å] is also shorter than is typically found for related intermolecular interactions.[12] It is noteworthy that in this case the proton attached to the nitrogen atom could be located [(N2−H = 1.08(7) Å; N−H···Cl = 158.1(4)°].

Related intramolecular N−H···Cl interactions have recently been described for ruthenium compounds built-up from simple tridentate ligands bearing two distal pyridine bases uncoordinated to the Ru; such compounds, in which the pyridine ligands are protonated, display intramolecular N···Cl distances analogous to that reported here.[14]

Finally, the O···N distance in **5d** (Figure 6) amounts to 2.72 Å, at the short end of the range for N−H···O systems (2.81−3.04 Å).[12] Here, too, the hydrogen atom was successfully located (N2−H = 0.92 Å). These structural data are indicative of a significant hydrogen bond in this molecule as well, as the N2−H···O angle is very close to 180° [173.0(3)°].[12] Note that in this latter complex the N···O distance is significantly longer than in **4a** (see above), which

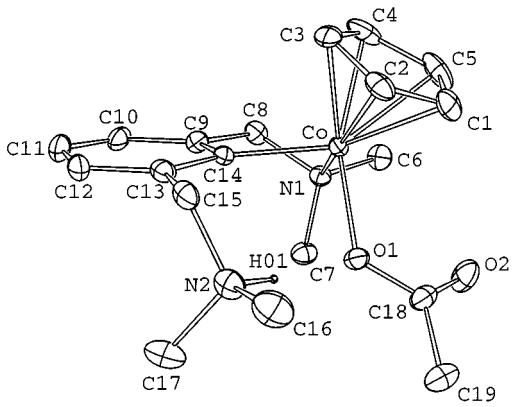
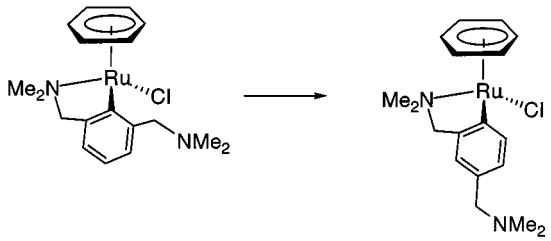


Figure 6. ORTEP view of the cationic part of **5d** [Co(CH_3COO)-{$C_6H_3(CH_2NMe_2)(CH_2NMe_2H^+)$-2,6}($\eta^5$-$C_5H_5$)]$PF_6$



Scheme 4

rules out the possibility of considering the aquo complex as an association between OH^- and an NH^+ unit.

It thus appears that the CH_2NMe_2 unit is remarkably flexible in adapting its orientation to the nature of the ligand attached to Co, although in all cases the nitrogen atom points towards the ligand X.

This latter behaviour is in marked contrast to that exhibited by some recently reported organoruthenium compounds incorporating the same pincer ligand. Indeed, Steenwinkel et al.[15] have shown that the pincer ligand in two such Ru^{II} compounds also interacts with Ru through the central carbon atom and just one nitrogen atom of an NMe_2 unit. However, in these compounds, in contrast to what we have seen in our cobalt complexes, the lone pair of the non-coordinated NMe_2 unit appears to be oriented away from the metal *and* from a chloride/phosphane ligand, respectively. In fact, these complexes proved to be unstable and isomerized to two compounds (see Scheme 4) in which the ruthenium atoms had migrated from the central carbon to carbons *ortho* and *para* to the two CH_2NMe_2 groups through a sequence of intramolecular C−H activation reactions. The driving force for this rearrangement most probably stems from the increased steric bulk of the non-coordinated CH_2NMe_2 moiety, which must interact with the arene ligand.

The stabilities of our complexes may thus be interpreted in terms of some extra stabilization of the organocobalt molecule owing to the presence of a hydrogen bond, a feature that is not possible in their ruthenium analogues. We have checked that treatment of the corresponding ruthenium complex by an acid such as HCl does not lead to any such intramolecular hydrogen bond; instead, we only observed extensive decomposition of the organoruthenium complex. We may thus view the cobalt complexes as dimetallacyclic species, in which five-membered and pseudo seven-membered chelated rings are present about the cobalt atom.

5. Behaviour of the Co-Pincer Compounds in Solution

A common feature of the structures of the four compounds is an intramolecular interaction between an NH^+ unit and X in **3**, **5a**, and **5d**, and between N and H−O in **4a**. In addition to these close contacts, puckering of the five-membered chelate rings of all complexes appears to result in an unfavourable orientation with respect to the Co−X vectors of the molecules. This latter phenomenon has also been observed in the related ruthenium compounds.[15] A reasonable explanation for this is that this ring puckering minimizes the steric interaction between the non-coordinated NMe_2 unit and the arene moiety of the Ru derivatives. A driving force behind adoption of the same conformation of the related organocobalt metallacycles in our compounds might also be a minimization of the steric interaction between the Cp ring and the NMe_2 group. However, it is evident from the chemical shifts of the NMe_2 unit of the five-membered chelate that we can unequivocally identify two different types of compounds.

The Δδ of the diastereotopic NMe_2 group coordinated to Co is very much dependent on the conformation of the five-membered chelate ring. We have seen previously in related metallacyclic compounds that when the conformation of this chelate ring is such that one N−Me bond and a Co−X bond are eclipsed (X = PR_3, for instance), then the Δδ of the two NMe_2 groups is usually greater than 1.6 ppm. Thus, in the ^{1}H-NMR spectrum of compound **3**, in which the hydrogen bond between $N-H^+$ and I is likely to be the weakest of the series studied, this Δδ is 0.85 ppm. A value of the same order of magnitude is observed for **4b**, **5b**, and **6**, for which no such hydrogen bond can be invoked. It is interesting to note that the Ru analogues of our compounds,[15] in which no hydrogen bonds are present, display analogous Δδ values (0.1−0.5 ppm). On the other hand, for the other compounds, Δδ is equal to or larger than 2.0 ppm, which can be taken as strong evidence that the conformation of the five-membered chelate is maintained in solution. Since this conformation is thermodynamically not the most stable, one may infer from these results that the strength of the intramolecular hydrogen bond[10] is sufficient to prevent a conformational change of the organocobalt chelate ring, which would lead to staggered N−Me and Co−X bonds in solution (see Figure 7).

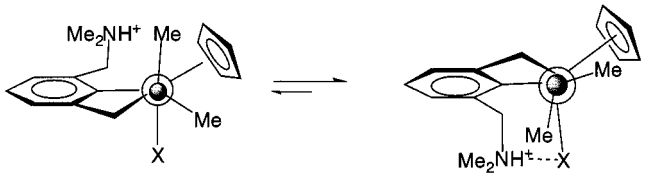


Figure 7. Newman projection along the N−Co vector of the complexes **5** showing the relationship between the intramolecular NHX interaction and the degree of ring puckering

Conclusion

We have synthesized an organometallic compound possessing a coordination site at which Brønsted acids can be accommodated. This behaviour is seemingly specific to Co^{III} since analogous ruthenium(II) compounds, despite their close structural analogies, are not capable of similar interactions with acids. It would also seem to be a specific feature of the metallated ligand since our previous closely related organocobalt complexes consisting of N^C chelates do not display such behaviour. Further work is currently in progress with the aim of defining the scope of this behaviour with different acid derivatives and extending the range of pseudo terdentate ligands that may exhibit analogous behaviour.

Experimental Section

General: All reactions were performed in Schlenk flasks under oxygen-free, dry nitrogen. Solvents were dried and distilled under nitrogen, toluene from sodium and CH_2Cl_2 from P_2O_5. − IR spectra were recorded from samples in KBr on a Bruker IFS-66 spectrometer. − Elemental analyses were performed by the Service Central d'Analyse de l'Université Louis Pasteur (Strasbourg). − ^{1}H-NMR spectra were recorded at 300.13 MHz, ^{13}C{^{1}H}-NMR spectra at 75.47 MHz, and ^{31}P{^{1}H}-NMR spectra at 121.51 MHz on a Bruker FT instrument (AC-300) and were externally referenced to TMS. Chemical shifts (δ) and coupling constants (*J*) are expressed in ppm and Hz, respectively.

The starting materials $[CpCoI_2]_2$ [16] and $Li[C_6H_3(CH_2NMe_2)_2]$ [17] were prepared according to published methods.

[CoI{2-(Me_2NCH_2)-6-($Me_2NH^+CH_2$)C_6H_3}(η^5-C_5H_5)]I (3): To a stirred suspension of $[CpCoI_2]_2$ (1.511 g, 2.00 mmol) in toluene (100 mL) at 0 °C was slowly added 2,6-bis[dimethyl(amino)methyl]-phenyllithium (**2**) (0.79 g, 4.00 mmol). The resulting green suspension was stirred for 16 h at room temperature and then the volatiles were completely removed in vacuo. The residue was taken up in CH_2Cl_2/MeOH (98:2) and the resulting solution was stirred for 30 min and then filtered. The filtrate was concentrated to a volume of 30 mL and hexane was slowly added. The green solid thus formed was washed with hexane and dried in vacuo to give **3** as green crystals. Yield: 0.88 g (50%). − IR (KBr): $\tilde{\nu}$ = 2733 cm^{-1} (ν_s Me_2N-H^+). − ^{1}H NMR ($CDCl_3$): δ = 10.01 (br. s, 1 H, NH^+), 7.97 (d, $^3J_{H-H}$ = 7.44, 1 H, Ar), 7.08 (t, $^3J_{H-H}$ = 7.14, 1 H, Ar), 6.90 (d, 1 H, Ar), 5.07 (s, 5 H, C_5H_5), 5.09 and 4.98 (AB spin system, $^2J_{H-H}$ = 13.17, 2 H, CH_2N), 3.94 and 3.39 (AB spin system, $^2J_{H-H}$ = 13.20, 2 H, CH_2N-Co), 3.16 and 2.31 (2 s, 6 H, $Co-NMe_2$), 2.93 (br. s, 6 H, NMe_2H^+). − ^{13}C{^{1}H} NMR ($CDCl_3$): δ = 153.9, 149.8, 142.1, 128.9, 125.2, 122.1 (C_6H_3), 85.1 (C_5H_5), 75.7 (CH_2N-Co), 64.1 (CH_2N), 58.9 and 58.5 ($Co-NMe_2$), 42.0 (br. s, NMe_2). − $C_{17}H_{25}CoI_2N_2$ (570.1): calcd. C 35.81, H 4.42, N 4.91; found C 33.67, H 4.23, N 4.38.

[2,6-(Me_2NCH_2)$_2$Co{C_6H_3(CH_2NMe_2)}(η^5-C_5H_5)(H_2O)]PF_6 (4a): A solution of **3′** (0.44 g, 1.00 mmol) in CH_2Cl_2 (20 mL) was washed several times with water (10 mL). The combined red aqueous solutions were then treated with excess KPF_6, which led to the immediate deposition of a red-brown solid. After stirring for 15 min, the solid was collected by filtration, washed with hexane, recrystallized from acetone/hexane, and dried in vacuo to give **4a** as brown-red crystals. Yield: 0.28 g (60%). − IR (KBr): $\tilde{\nu}$ = 3575 cm^{-1} (ν_s H−OH). − ^{1}H NMR ([D$_6$]acetone): δ = 7.25 (d, $^3J_{H-H}$ = 6.93, 1 H, Ar), 7.16 (t, $^3J_{H-H}$ = 7.32, 1 H, Ar), 7.09 (d, 1 H, Ar), 5.49 (s, 5 H, C_5H_5), 4.64 and 3.65 (AB spin system, $^2J_{H-H}$ = 12.24, 2 H, CH_2NMe_2), 4.40 and 3.69 (AB spin system $^2J_{H-H}$ = 13.90, 2 H, CH_2N-Co), 3.49 and 1.34 (2 s, 6 H, NMe_2-Co), 2.20 (br. s, 6 H, NMe_2).[18] − ^{13}C{^{1}H} NMR ([D$_6$]acetone): δ = 158.0, 152.1, 130.2, 125.3, and 122.7 (C_6H_3), 85.4 (C_5H_5), 76.7 (CH_2N-Co), 67.7 (CH_2N), 58.4 and 49.2 (NMe_2-Co), 43.0 (NMe_2). − $C_{17}H_{26}CoF_6N_2OP$ (478.3): calcd. C 42.69, H 5.48, N 5.86; found C 43.02, H 5.43, N 5.84.

[Co{2,6-(Me_2NCH_2)$_2$$C_6H_3$}($\eta^5$-$C_5H_5$)($PMe_2Ph$)]$PF_6$ (4b): To a solution of **4a** (0.48 g, 1.00 mmol) in CH_2Cl_2 (10 mL) was added PMe_2Ph (0.17 mL, 1.20 mmol). After 3 h, *n*-hexane (100 mL) was added, which led to the deposition of a dark-violet solid. The solid was collected by filtration and dried in vacuo to give **4b** as a red-violet powder. Yield: 0.46 g (77%). − ^{1}H NMR ([D$_6$]acetone): δ = 7.70−7.40 (m, 5 H, PPh), 7.29 (d, $^3J_{H-H}$ = 7.32, 1 H, Ar), 7.08 (t, 1 H, Ar), 6.81 (d, $^3J_{H-H}$ = 7.08, 1 H, Ar), 5.91 (s, 5 H, C_5H_5), 3.44 and 3.33 (AB spin system, $^2J_{H-H}$ = 12.18, 2 H, CH_2N), 3.44 and 3.33 (AB spin system, $^2J_{H-H}$ = 14.40, 2 H, CH_2N), 2.89 and 2.23 (2 s, 6 H, NMe_2-Co), 2.34 (s, 6 H, NMe_2), 2.21 and 1.97 (2 d, $^2J_{H-P}$ = 9.51 and $^2J_{H-P}$ = 10.26, 6 H, PMe_2). − ^{31}P{^{1}H} NMR ([D$_6$]acetone): δ = 12.8 (s, PMe_2Ph), −143.6 (sept., PF_6, $^1J_{P-F}$ = 707.0). − ^{13}C{^{1}H} NMR ([D$_6$]acetone): δ = 151.4 (d, $^2J_{C-P}$ = 35.77), 150.1, 149.4, 131.2, 124.6, 122.9 (C_6H_3), 135.5 (d, $^1J_{C-P}$ = 60.98), 131.3, 129.6 (d, $^2J_{C-P}$ = 8.41) (PPh), 88.2 (C_5H_5), 74.3 (CH_2N-Co), 67.5 (CH_2N), 60.0 and 55.2 (NMe_2-Co), 45.0 (NMe_2), 22.2 and 15.3 (2 d, $^1J_{C-P}$ = 31.69 and $^1J_{C-P}$ = 33.67) (PMe_2). − $C_{25}H_{35}CoF_6N_2P_2$: (598.4): calcd. C 50.18, H 5.89, N 4.68; found C 50.62, H 5.75, N 4.38.

[CoCl{2-(Me_2NCH_2)-6-($Me_2NH^+CH_2$)C_6H_3}(η^5-C_5H_5)]PF_6 (5a): To a solution of **4a** (0.48 g, 1.00 mmol) in MeOH (20 mL) was added excess NH_4Cl. After 7 h, the volatiles were removed. The residue was redissolved in CH_2Cl_2 and this solution was filtered. The brown filtrate was concentrated and the residue was recrystallized from acetone/hexane and dried in vacuo to give **5a** as dark, red-violet crystals. Yield: 0.40 g (81%). − IR (KBr): $\tilde{\nu}$ = 2692 cm^{-1} (ν_s Me_2N-H^+). − ^{1}H NMR ([D$_6$]acetone): δ = 9.48 (br. s, 1 H, NH^+), 7.41 (d, $^3J_{H-H}$ = 6.90, 1 H, Ar), 7.18 (t, $^3J_{H-H}$ = 7.14, 1 H, Ar), 7.12 (d, $^3J_{H-H}$ = 6.45, 1 H, Ar), 5.46 (s, 5 H, C_5H_5), 5.07 and 4.60 (AB spin system, $^2J_{H-H}$ = 12.63, 2 H, CH_2N), 4.60 and 3.72 (AB spin system, $^2J_{H-H}$ = 14.05, 2 H, CH_2N), 3.50 and 1.51 (2 s, 6 H, NMe_2-Co), 3.21 and 2.68 (2 br. s, 6 H, NMe_2). − ^{13}C{^{1}H} NMR ([D$_6$]acetone): δ = 157.4, 152.6, 143.0, 132.2, 125.2, 123.4 (C_6H_3), 86.6 (C_5H_5), 76.7 (CH_2N-Co), 66.3 (CH_2N), 58.6 and 52.4 (NMe_2-Co), 43.4 and 39.8 (2 br. s, NMe_2). − $C_{17}H_{25}ClCoF_6N_2P$ (496.7): calcd. C 41.10, H 5.07, N 5.64; found C 42.10, H 5.00, N 5.40.

[CoI{2-(Me_2NCH_2)-6-($Me_2NH^+CH_2$)C_6H_3}(η^5-C_5H_5)]PF_6 (5b): To a solution of **4a** (0.48 g, 1.00 mmol) in MeOH (20 mL) was added excess NH_4I. After 7 h, the volatiles were removed. The residue was redissolved in CH_2Cl_2 and this solution was filtered. The green filtrate was concentrated and the residue was recrystallized from CH_2Cl_2/hexane. The solid was collected by filtration, washed with hexane, further recrystallized from acetone/hexane, and dried in vacuo to give **5b** as a green powder. Yield: 0.46 g (78%). − IR (KBr): $\tilde{\nu}$ = 2697 cm^{-1} (ν_s Me_2N-H^+). − ^{1}H NMR ([D$_6$]acetone): δ = 9.33 (br. s, 1 H, NH^+), 7.92 (d, $^3J_{H-H}$ = 7.38, 1 H, Ar) 7.04 (t, 1 H, Ar), 6.97 (d, 1 H, Ar), 5.34 (s, 5 H, C_5H_5), 5.10 and 5.00 (AB spin system, $^2J_{H-H}$ = 13.11, 2 H, CH_2NH), 3.98 and 3.42 (AB spin system, $^2J_{H-H}$ = 13.32, 2 H, CH_2N-Co), 3.19 and 2.55 (2 s,

6 H, NMe_2−Co), 2.98 (br. s, 6 H, $HNMe_2$). − $^{13}C\{^1H\}$ NMR ([D$_6$]acetone): δ = 156.0, 152.0, 142.9, 129.8, 124.7, 122.6 (C_6H_3), 86.0 (C_5H_5), 75.1 (CH_2N−Co), 66.5 (CH_2N), 58.6 and 57.9 (NMe_2−Co), 42.5 (br. s, NMe_2). − $C_{17}H_{25}CoF_6IN_2P$ (588.2): calcd. C 34.71, H 4.28, N 4.76; found C 33.91, H 4.16, N 4.96.

[CoF{2-(Me_2NCH_2)-6-($Me_2NH^+CH_2$)C_6H_3}(η^5-C_5H_5)]PF_6 (5c): To a solution of **4a** (0.48 g, 1.00 mmol) in acetone (20 mL) was added 40% aq. HF (0.3 mL). After 3 h, the mixture was filtered, the filtrate was concentrated, and the residue was crystallized from hexane. The solid was collected by filtration, washed with hexane, recrystallized from acetone/hexane, and dried in vacuo to give **5c** as a brown powder. Yield: 0.39 g (82%). − IR (KBr): $\tilde{\nu}$ = 2260 cm^{-1} (ν_s Me_2N-H^+). − ^{1}H NMR ([D$_6$]acetone): δ = 11.00 (br. d, $^1J_{H-F}$ = 89.14, 1 H, NH^+), 7.37 (d, $^3J_{H-H}$ = 6.66, 1 H, Ar), 7.21 (t, $^3J_{H-H}$ = 7.17, 1 H, Ar), 7.17 (d, $^3J_{H-H}$ = 6.90, 1 H, Ar), 5.44 (s, 5 H, C_5H_5), 5.20 and 4.41 (AB spin system, $^2J_{H-H}$ = 12.87, 2 H, CH_2NH^+), 4.43 and 3.71 (AB spin system, $^2J_{H-H}$ = 14.07, 2 H, CH_2N−Co), 3.64 and 1.21 (s and d, $^4J_{H-F}$ = 6.90, 6 H, NMe_2−Co), 3.04 and 2.26 (2 d, $^4J_{H-F}$ = 4.05 and $^4J_{H-F}$ = 4.29, 6 H, NMe_2H^+). − $^{13}C\{^1H\}$ NMR ([D$_6$]acetone): δ = 153.0, 143.7, 148.5, 130.7, 125.3, 123.4 (C_6H_3), 85.2 (C_5H_5), 76.4 (CH_2N−Co), 66.4 (CH_2NH^+), 58.4 and 47.9 (NMe_2−Co), 43.3 and 39.9 (NMe_2H^+). − $C_{17}H_{25}CoF_7N_2P$ (480.3): calcd. C 42.51, H 5.25, N 5.83; found C 42.09, H 5.74, N 5.72.

[Co(CH_3COO){2-(Me_2NCH_2)-6-($Me_2NH^+CH_2$)C_6H_3}(η^5-C_5H_5)]PF_6 (5d): To a solution of **4a** (0.48 g, 1.00 mmol) in acetone (20 mL) was added acetic acid (0.2 mL). After 3 h, the mixture was filtered, the filtrate was concentrated, and the residue was crystallized from hexane. The solid was collected by filtration, washed with hexane, recrystallized from acetone/hexane, and dried in vacuo to give **5d** as brown crystals. Yield 0.44 g (85%). − IR (KBr): $\tilde{\nu}$ = overtones between 2700−2400 cm^{-1} (ν_s Me_2N-H^+), 1638 cm^{-1} (ν_s C=O). − ^{1}H NMR ([D$_6$]acetone): δ = 10.70 (br. s, 1 H, NH^+), 7.42 (d, $^3J_{H-H}$ = 6.69, 1 H, Ar), 7.24 (t, $^3J_{H-H}$ = 7.38, 1 H, Ar), 7.16 (d, $^3J_{H-H}$ = 6.66, 1 H, Ar), 5.40 (s, 5 H, C_5H_5), 5.18 and 4.57 (AB spin system, $^2J_{H-H}$ = 12.87, 2 H, CH_2NH^+) 4.38 and 3.68 (AB spin system, $^2J_{H-H}$ = 13.83, 2 H, CH_2N−Co), 3.51 and 1.27 (2 s, 6 H, NMe_2−Co), 3.31 and 2.64 (2 s, 6 H, Me_2NH^+), 1.96 (s, 3 H, CH_3COO). − $^{13}C\{^1H\}$ NMR ([D$_6$]acetone): δ = 178.0 (COO), 158.6, 153.2, 143.6, 131.3, 125.4, 123.6 (C_6H_3), 85.7 (C_5H_5), 76.7 (CH_2N−Co), 66.6 (CH_2NH^+), 57.5 and 48.6 (NMe_2−Co), 43.8 and 40.1 (NMe_2H^+), 24.0 (CH_3COO). − $C_{19}H_{28}CoF_6N_2O_2P$ (520.3): calcd. C 43.86, H 5.42, N 5.38; found C 43.05, H 4.99, N 5.27.

[Co{2-(Me_2NCH_2)-6-($Me_2NH^+CH_2$)C_6H_3}(η^5-C_5H_5)(PMe_2Ph)]-(PF_6)$_2$ (6): To a solution of **4b** (0.48 g, 0.50 mmol) in CH_2Cl_2 (20 mL) was added 10% aq. HCl (0.3 mL), which led to the immediate separation of a light-red solid. After 3 h, this solid was col-

Table 2. X-ray diffraction data

Complex	**3**	**4a**	**5a**	**5d**
Crystal data				
Formula	$C_{17}H_{25}CoI_2N_2$	$C_{17}H_{26}CoN_2O{\cdot}PF_6$	$C_{17}H_{25}ClCoN_2{\cdot}PF_6$	$C_{19}H_{28}CoN_2O_2{\cdot}PF_6$
M_r	570.14	478.31	496.75	520.34
Crystal system	monoclinic	orthorhombic	orthorhombic	orthorhombic
Space group	$P2_1$	$Pbca$	$Pca2_1$	$Pna2_1$
a [Å]	11.1104(3)	12.542(1)	15.2698(3)	15.246(2)
b [Å]	7.1910(2)	15.172(1)	6.9796(1)	7.557(1)
c [Å]	12.7706(3)	21.880(1)	19.4307(2)	19.646(4)
β [°]	100.635(1)			
V [Å^3]	1002.78(8)	4163.5(8)	2070.87(9)	2263(1)
Z	2	8	4	4
Colour	green	orange	dark red	violet
Crystal dim. [mm]	0.20 × 0.15 × 0.10	0.16 × 0.12 × 0.10	0.20 × 0.20 × 0.15	0.40 × 0.40 × 0.20
$D_{calcd.}$ [gcm^{-3}]	1.89	1.53	1.59	1.53
F(000)	548	1968	1016	1072
μ [mm^{-1}]	3.933	0.963	1.093	0.896
Min. and max. trans.				0.8940/1.0000
Data collection				
T [K]	294	173	173	294
λ [Å]	0.71073	0.71073	0.71073	0.71073
Radiation	Mo-K_α graphite-monochromated	Mo-K_α graphite-monochromated	Mo-K_α graphite-monochromated	Mo-K_α graphite-monochromated
Diffractometer	CCD	CCD	CCD	Enraf Nonius MACH3
Scan mode	θ scans	θ scans	θ scans	θ/2θ
hkl limits	$-13 \le h \le 11$ $-8 \le k \le 8$ $-14 \le l \le 14$	$0 \le h \le 13$ $0 \le k \le 16$ $0 \le l \le 24$	$-9 \le h \le 9$ $-19 \le k \le 19$ $-23 \le l \le 23$	$0 \le h \le 9$ $0 \le k \le 18$ $0 \le l \le 24$
limits [°]	2.5/25.36	2.5/23.25	2.5/29.56	2.5/26.28
No. of data meas.	6291	22289	18396	2647
No. of data with $I > 3\sigma(I)$	1751	1986	2325	1481
Weighting scheme	$4F_o^2/[\sigma^2(F_o^2) + 0.0064\ F_o^4]$	$4F_o^2/[\sigma^2(F_o^2) + 0.0004\ F_o^4] + 1.0$	$4F_o^2/[\sigma^2(F_o^2) + 0.0064\ F_o^4]$	$4F_o^2/[\sigma^2(F_o^2) + 0.0036\ F_o^4]$
No. of variables	198	253	288	283
R	0.031	0.046	0.039	0.036
R_w	0.050	0.057	0.048	0.044
GoF	1.059	1.121	1.043	1.068
Largest peak in final difference [eÅ^{-3}]	0.803	0.476	0.328	0.290

lected by filtration and washed with hexane. It was then stirred with saturated aqueous KPF_6 solution for 1 h, filtered off, washed with hexane, recrystallized from acetone/hexane, and dried in vacuo to give **6** as a light-red powder. Yield 0.18 g (62%). − IR (KBr): $\tilde{\nu}$ = 2704 cm^{-1} (ν_s Me_2N-H^+). − ^1H NMR ([D$_6$]acetone): δ = 9.25 (br. s, 1 H, NH^+), 7.95−7.45 (m, 5 H, PPh), 7.63 (d, $^3J_{H-H}$ = 7.14, 1 H, Ar), 7.28 (t, 1 H, Ar), 7.03 (d, 1 H, Ar), 5.94 (s, 5 H, C_5H_5), 4.92 and 4.58 (AB spin system, $^2J_{H-H}$ = 14.02, 2 H, CH_2NH^+), 3.80 and 3.08 (AB spin system, $^2J_{H-H}$ = 14.56, 2 H, CH_2N-Co), 3.37 (ps. s, 6 H, Me_2NH^+), 2.86 and 2.02 (s and d, $^4J_{H-P}$ = 1.38, 6 H, NMe_2-Co), 2.25 and 1.58 (2 d, $^2J_{H-P}$ = 9.63 and $^2J_{H-P}$ = 10.17, 6 H, PMe_2). − $^{31}P\{^1H\}$ NMR ([D$_6$]acetone): δ = 13.0 (s, PMe_2), −143.5 (sept., $^1J_{P-F}$ = 708.0). − $^{13}C\{^1H\}$ NMR ([D$_6$]acetone): δ = 156.2 (d, $^2J_{C-P}$ = 25.82), 151.5, 144.0, 126.5, 126.0, 124.4 (C_6H_5), 134.8 (d, $^1J_{C-P}$ = 37.56), 131.5, 131.5 (d, $^2J_{C-P}$ = 16.43), 129.9 (d, $^3J_{C-P}$ = 9.38) (PPh), 89.1 (C_5H_5), 75.3 (CH_2N-Co), 64.8 (CH_2NH^+), 59.7 and 54.8 (NMe_2-Co), 44.2 (NMe_2H^+), 21.2 and 15.2 (2 d, $^2J_{C-P}$ = 32.86, PMe_2).

X-ray Data and Structure Determinations for 3, 4a, 5a, and 5d: Single crystals suitable for X-ray diffraction analysis were obtained as described above. In the case of **3**, **4a**, and **5a**, data were collected on a Nonius KappaCCD diffractometer, while for **5d** a Nonius MACH3 machine was used. All four data collections were performed using Mo-K_α graphite-monochromated radiation (λ = 0.7107 Å), φ and ω scans for **3**, **4a**, and **5a**, and θ/2θ scans for **5d**. Absorption corrections were computed from the psi scans of 7 reflections for **5d**, while for **3**, **4a**, and **5a** these corrections were partially included in the data reduction procedure. The structures were solved using direct methods and refined against |*F*|. Hydrogen atoms were introduced in structure factor calculations as fixed contributors by their computed coordinates [*d*(C−H) = 0.95 Å, *B*(H) = 1.3*Beqv Å^2 of the attached carbon atom] except for the NH protons of **3**, **5a**, and **5d** and the water protons of **4a**, which were located in difference Fourier maps. The absolute structures of **3**, **4a**, and **5d** were determined by refinement of Flack's *x* parameter. For all computations, the Nonius OpenMoLeN package[19] was used. Crystal data and results for all four compounds are given in Table 2.

Crystallographic data (excluding structure factors) for the structures reported in this paper have been deposited with the Cambridge Crystallographic Data Centre as supplementary publication nos. CCDC-132438 (**3**), -132439 (**4a**), -132440 (**5a**), and -132441 (**5d**). Copies of the data can be obtained free of charge on application to the CCDC, 12 Union Road, Cambridge CB2 1EZ, U.K. [Fax: (internat.) +44 (0)1223/336033; E-mail: deposit@ccdc.cam.ac.uk].

Acknowledgments

Financial support of this work through a grant to M.M. by the French/Brazilian exchange program CAPES−COFECUB (project 188/96) is gratefully acknowledged.

[1] M. Pfeffer, M. R. Meneghetti, M. Grellier, J. Dupont, J. Fischer, *Organometallics* **1999**, *18*, 5560−5570.
[2] G. van Koten, *Pure & Appl. Chem.* **1989**, *61*, 1681−1684.
[3] P. H. M. Rietveld, D. Grove, G. van Koten, *New J. Chem.* **1997**, *21*, 751−771.
[4] A. A. H. van der Zeijden, G. van Koten, *Inorg. Chem.* **1986**, *25*, 4723−4725.
[5] D. M. Grove, G. van Koten, R. Zoet, N. W. Murrell, J. A. Welch, *J. Am. Chem. Soc.* **1983**, *105*, 1379−1380.
[6] S. Toyota, T. Futawaka, H. Ikida, M. Oki, *J. Chem. Soc., Chem. Commun.* **1995**, 2499−2500.
[7] C. A. Olazàbal, F. P. Gabbaï, A. H. Cowley, C. I. Carrano, C. M. Mokry, M. R. Bond, *Organometallics* **1994**, *13*, 421−423.
[8] D. H. Williams, I. Fleming, *Spectroscopic Methods in Organic Chemistry*, McGraw-Hill Book Company, London, **1989**, Table 2.5, p. 43.
[9] G. A. Jeffrey, *An Introduction to Hydrogen Bonding*, Oxford University Press, Oxford, **1997**.
[10] E. Peris, J. C. Lee Jr., J. R. Rambo, O. Eisenstein, R. H. Crabtree, *J. Am. Chem. Soc.* **1995**, *117*, 3485−3491.
[11] H. Werner, L. Xiaolan, K. Peters, H. G. von Schering, *Chem. Ber./Recueil* **1997**, *130*, 565−570.
[12] F. A. Cotton, G. Wilkinson, *Advanced Inorganic Chemistry*, 5th ed., John Wiley & Sons, New York, **1988**, p. 90−94.
[13] N. N. Greenwood, A. Earnshaw, *Chemistry of the Elements*, Pergamon Press, Oxford, **1984**, p. 57−69.
[14] S. M. Redmore, C. E. F. Rickard, S. J. Webb, L. J. Wright, *Inorg. Chem.* **1997**, *36*, 4743−4748.
[15] P. Steenwinkel, S. L. James, R. A. Gossage, D. M. Grove, H. Kooijman, W. J. J. Smeets, A. L. Spek, G. van Koten, *Organometallics* **1998**, *17*, 4680−4693.
[16] D. M. Roe, P. M. Maitlis, *J. Chem. Soc. (A)* **1971**, 3173−3175.
[17] P. Steenwinkel, S. L. James, D. M. Grove, N. Veldman, A. L. Spek, G. van Koten, *Chem. Eur. J.* **1996**, *2*, 1440−1445.
[18] Coordinated water was not observed by ^1H-NMR spectroscopy at room temperature.
[19] *OpenMoleN*, Interactive Structure Solution, Nonius B.V., Delft, The Netherlands, **1997**.

Received November 26, 1999
[I99432]

Biomimetic Zinc Complexes With A New Tripodal Nitrogen-Donor Ligand: Tris[2-(1-methyl-4-tolylimidazolyl)phosphane] ($Pim^{Me,pTol}$)

Wolfgang Kläui,*[a] Claudia Piefer,[a] Gerd Rheinwald,[b] and Heinrich Lang[b]

Dedicated to Prof. Dr. H. Vahrenkamp on the occasion of his 60th birthday

Keywords: Bioinorganic chemistry / Carbonic anhydrase / Zinc / N ligands / Tripodal ligands

The new potentially threefold-chelating ligand tris[2-(1-methyl-4-tolylimidazolyl)]phosphane ($Pim^{Me,pTol}$) has been prepared. The *p*-tolyl substituents on the imidazole rings form a shielded hydrophobic cavity. The first X-ray-structure analysis of this ligand system confirms the proposed structure. The reaction of $Pim^{Me,pTol}$ with ZnX_2 salts (X = Cl, Br, I, NO_3) yields monomeric Zn^{II} complexes. The X-ray crystal structures of $[Pim^{Me,pTol}ZnCl]_2(ZnCl_4)$ and $[Pim^{Me,pTol}ZnNO_3]NO_3$ prove that the Zn^{2+} centres are in a tetrahedral environment with threefold *N*-imidazole coordination. This arrangement mimics the active centre of carbonic anhydrase (CA).

Introduction

Zinc is an essential element in biological systems.[1] Its first biological function was found in the enzyme carbonic anhydrase (CA), a hydrolase which catalyses the hydration of carbon dioxide at physiological pH, according to (Equation 1).

$$CO_2 + 2\,H_2O \overset{CA}{\rightleftharpoons} HCO_3^- + H_3O^+ \quad (1)$$

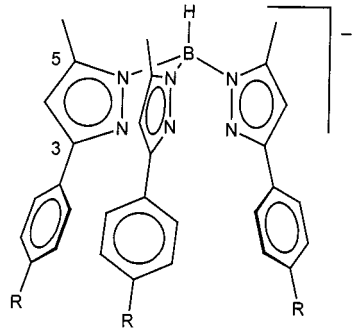
In the absence of a catalyst, this apparently simple reaction is extremely slow. However, it is imperative to nearly all living organisms that this reaction is fast. CA accelerates the rate of hydration of CO_2 10^7-fold.[2] In order to understand the essential structure and reaction characteristics of bioinorganic systems, small molecular model complexes are a convenient approximation. One model system for CA is based on sterically demanding tris(pyrazolyl)hydroborate (Tp) ligands **A**. This type of ligand forms zinc(II) complexes with structural and functional properties similar to those of the active site of CA. An essential prerequisite for the successful application of such systems is the introduction of bulky groups R, such as *tert*-butyl[3], phenyl[4], *p*-cumyl[5] or *p*-tolyl,[6] in the 3-position of the pyrazolyl rings. The presence of these sterically demanding substituents inhibits the formation of bis-ligand complexes $[Zn(Tp)_2]$ and it forces coordination numbers smaller than six. Whereas *tert*-butyl substituents reduce the coordination number exclusively to four, aryl substituents enable Zn^{II} to extend its coordination sphere to five.[7] In addition, the aryl groups form a hydrophobic pocket around the zinc ion. The hydrophobic surrounding should help the coordinated water in complexes $[TpZnOH_2]$ to become acidic at physiological pH. While with this, the importance of steric factors in CA model systems has been established, it remains unclear whether the negative charge of the Tp ligands is required to stabilise biomimetic zinc complexes. One of the main problems in this context is the sensitivity of Tp ligands toward hydrolysis.

Tris(imidazolyl)phosphane ligands are neutral and hydrolytically stable analogues of the Tp ligands to which they are sterically and electronically very similar. Zinc complexes of tris[2-(4,5-diisopropyl)imidazolyl]phosphane[8] and tris[2-(4,5-di-*n*-propyl)imidazolyl]phosphane[9] have been synthesised. It turned out that these complexes are remarkably different in their efficiency in catalysing the CO_2/HCO_3^- equilibrium. Unfortunately the 1,3-tautomerism in the imidazole rings makes it difficult to assess the geometry of the catalytically active zinc complexes. Knowing that the histidyl-imidazol *N*-ligation to metal ions is ubiquitous in nature, further development of zinc coordination chemistry with other imidazole-derived ligands is obviously desirable.

Until now two tris(imidazolyl)phosphane ligands of type **B** have been prepared (Scheme 1).[10] They have 1,4- rather than 4,5-substituted imidazole rings. While in Tp ligands **A** the 5-methyl groups serve as a protecting unit for the hydrolytically sensitive B−N bonds, the 1-alkyl substituent in **B** is only necessary to suppress the 1,3-tautomerism in the imidazole. These tripodal ligands of type **B** have been described only with bulky alkyl substituents in the 1-position as well as in the 4-position. This can be attributed to the fact that the synthesis of substituted imidazole rings is relatively difficult. Thus, only very few zinc-containing enzyme model complexes incorporating substituted imidazole *N*-donor groups have been reported.

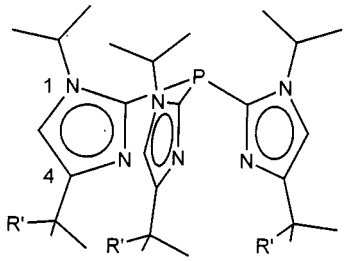
[a] Institut für Anorganische und Strukturchemie I, Heinrich-Heine-Universität Düsseldorf,
Universitätsstraße 1, 40225 Düsseldorf, Germany
Fax: (internat.) + 49-(0)2/111-2287
E-mail: klaeui@uni-duesseldorf.de
[b] Lehrstuhl für Anorganische Chemie, Technische Universität Chemnitz,
Straße der Nationen 62, D-09107 Chemnitz, Germany

 © WILEY-VCH Verlag GmbH, D-69451 Weinheim, 2000 1434−1948/00/0707−1549 $ 17.50+.50/0



A

R = H, CH_3, $CH(CH_3)_2$



B

R' = H, CH_3

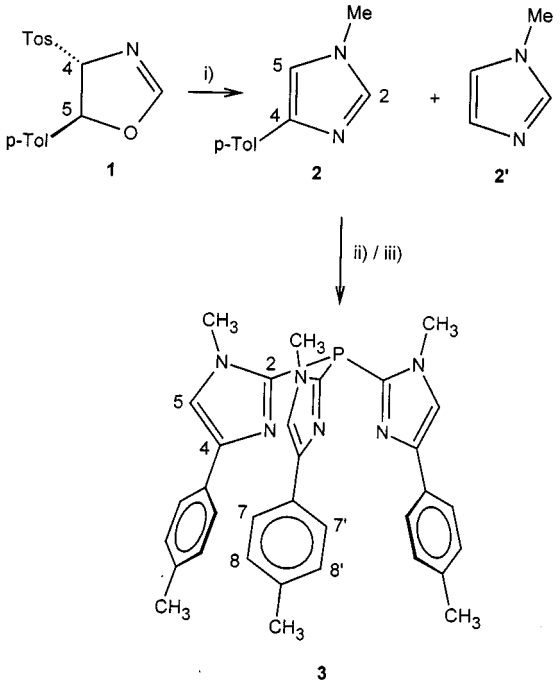
Scheme 1. Schematic structures of aryl-substituted tris(pyrazolyl)-borate ligands and of bulky 1,4-dialkyl-substituted tris(imidazolyl)-phosphane ligands

We describe here the synthesis of the new tripodal *p*-tolyl-substituted tris(imidazolyl)phosphane ligand $Pim^{Me,pTol}$ (**3**) and its reaction behaviour towards Zn^{II} salts in order to develop model systems which can mimic CA enzyme characteristics. This ligand is the first ligand of its type with aryl substituents in the 4-position of the imidazole rings. The aryl substituents were expected to play the same role as in the analogous Tp ligands, i.e. they should form a sterically demanding and hydrophobic cavity around the zinc ion. A bulky isopropyl substituent in the 1-position as in the known ligands $Pim^{iPr,iPr}$ and $Pim^{iPr,tBu}$ [10] seems unnecessary. We have chosen the small methyl group to keep the solubility in protic solvents as high as possible.

Results and Discussion

Synthesis and Spectroscopic Characterisation

The well-established way of preparing tris(imidazolyl)-phosphanes of type **B**[11] was not suitable for synthesising the desired ligand $Pim^{Me,pTol}$ (**3**). Because of the difficulty of introducing an aryl substituent into the imidazole ring regiospecifically, we applied an alternative route, via oxazolines **1**, to prepare the 1,4-disubstituted imidazoles **2**.[12] The mechanism of this reaction did not exclude, a priori, the formation of the second regioisomer **2′**. The isomer **2** as the only product could be confirmed by 2D NMR experiments.[13] Flash chromatography of the reaction mixture afforded crude 1-methyl-4-tolylimidazole in an acceptable yield. In the following step, the imidazole was lithiated in the 2-position and then treated with PCl_3 in THF at −78 °C (Scheme 2) yielding **3** as a colourless solid after crystallisation from dichloromethane/hexane.

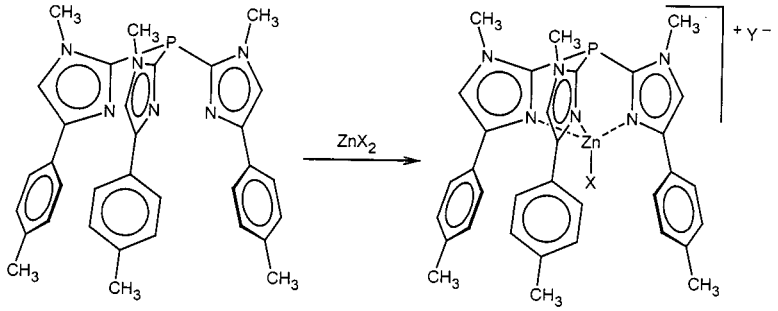


Scheme 2. Synthesis and schematic structure of the aryl-substituted tris(imidazolyl)phosphane ligand $Pim^{Me,pTol}$ (**3**); i) $MeNH_2$ in benzene, autoclave, T = 120 °C, ii) *n*BuLi, THF, −78 °C; iii) PCl_3, THF

The ^1H NMR spectrum of **3** shows C_{3v} symmetry with an $[AB]_2$-system at δ = 7.43 for the *p*-tolyl protons. The doublet at δ = 7.18 ($^3J_{HH}$ = 8 Hz) of the $[AB]_2$-system is assigned to the *m*-protons of the *p*-tolyl group and the doublet at δ = 7.68 ($^3J_{HH}$ = 8 Hz) is assigned to the protons in the *o*-position on the basis of correlated $^1H,^{13}C$ HMBC NMR spectra. The singlet at δ = 7.38 can be assigned to the proton in the 5-position of the substituted imidazole ring and the singlet at δ = 3.76 can be assigned to the protons of the $N-CH_3$ group. In the $^{31}P\{^1H\}$ NMR spectrum of **3** the ^{31}P signal appears at δ = −57.9 as a singlet. The EI mass spectrum of **3** exhibits the peak for the molecular ion at the expected *m/z* value together with a characteristic fragmentation pattern.

The zinc(II) complexes $[Pim^{Me,pTol}ZnX]Y$ were prepared in high yield by stirring the tris(imidazolyl)phosphane **3** with ZnX_2 salts in THF (X = NO_3, Cl, Br) or in ethanol (X = I), under reflux (Scheme 3). The complexes **4a**−**4d** form colourless solids and can be crystallised from acetonitrile or nitromethane to yield analytically pure colourless crystals.

The ^1H NMR spectra of the zinc complexes **4a**−**4d** also show a signal pattern corresponding to C_{3v} symmetry. The signal of the proton in the 5-position of the imidazole ring



4	X	Y
a	Cl	½ $ZnCl_4$
b	Br	Br
c	I	I
d	NO_3	NO_3

Scheme 3. Synthesis and schematic structures of the zinc complexes [$Pim^{Me,pTol}ZnX$]Y (**4a−d)**

is shifted to lower field and split into a doublet (**4a:** δ = 7.53, $^4J_{PH}$ = 4 Hz; **4b:** δ = 7.49, $^4J_{PH}$ = 4 Hz; **4c:** δ = 7.46, $^4J_{PH}$ = 5 Hz; **4d:** δ = 7.56, $^4J_{PH}$ = 4 Hz) when compared to the signal in the free ligand **3**. Upon coordination to Zn^{II}, the ^{31}P signal for complexes **4a−4d** is shifted to higher field (**4a:** δ = −113.7; **4b:** δ = δ = −118.2; **4c:** δ = −119.4; **4d:** δ = −117.8). A similar shift has also been reported for the ^{31}P signal of ligands of type **B** in Cu^I complexes, e.g. [$Pim^{iPr,iPr}CuCH_3CN$][BF_4].[10b] The FAB mass spectra of the Zn^{II} complexes **4a−4d** exhibit the peak for the molecular ion at the expected *m/z* value together with a characteristic fragmentation pattern.

Solid State Structure of 3, 4a and 4d

Crystals of **3** suitable for an X-ray crystal structure determination were obtained by slow evaporation of an acetone solution. It crystallises in the monoclinic space group *Cc* with four independent molecules per unit cell. Crystals of the complexes **4a** and **4d** were grown by diffusion of hexane into a nitromethane solution. Both complexes crystallise in the triclinic space group $P\bar{1}$. The structure of **4a** contains two independent cationic molecules and three solvent molecules of nitromethane per unit cell. The two independent cationic molecules differ only within the ranges of standard deviations, except for one Zn−N distance and some torsion angles.[14] Crystals of **4d** contain one strongly disordered nitromethane molecule. The solid-state structure of the ligand **3** is shown in Figure 1, the structure of the cation [$Pim^{Me,pTol}ZnCl$]$^+$ of **4a** in Figure 2 and the structure of [$Pim^{Me,pTol}ZnNO_3$]$^+$ of **4d** is presented in Figure 3. Selected bond length, angles and torsion angles are given in Table 1. The structure of the free ligand **3** is the first solid-state structure reported for a tris(imidazolyl)phosphane ligand.

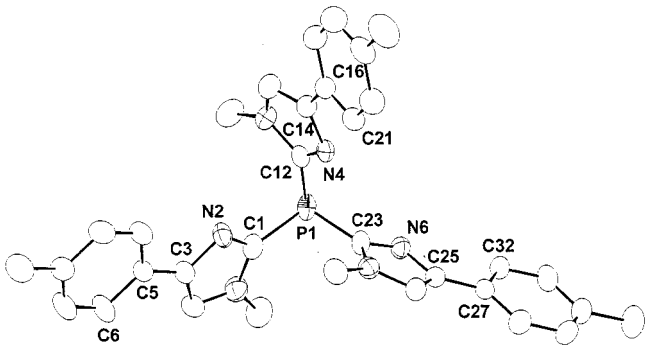


Figure 1. ZORTEP plot[25] (50% probability) of $Pim^{Me,pTol}$ (**3**)

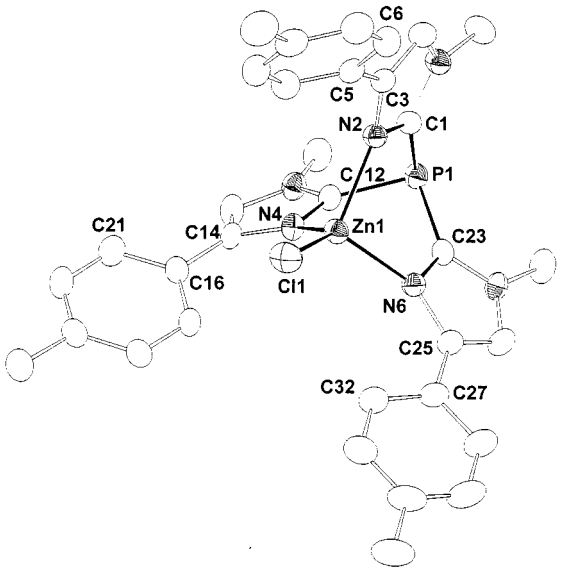


Figure 2. ZORTEP plot[25] (50% probability) of [$Pim^{Me,pTol}ZnCl$]$^+$ in **4a**

Figure 1 shows a trigonal pyramidal environment of P(1) with P−C σ-bond lengths and C−P−C bond angles comparable to those of aromatic phosphanes such as tri-*o*-tolylphosphane[15] or tri-*m*-tolylphosphane.[16] The P−C σ-bond lengths of **3** (1.813−1.841 Å) are similar to those found for tri-*o*-tolylphosphane[15] (1.830−1.837 Å) or tri-*m*-tolylphosphane[16] (1.829−1.838 Å). Only one C−P−C bond angle [96.8(2)°] is smaller than those found for tri-*o*-tolylphosphane[15] (101.6−103.4°) or tri-*m*-tolylphosphane[16] (100.6−102.2°). The small deviation of the N−C−C−C bond torsion angles of **3** (Table 1) from 0° or 180°, respectively, indicates that the *p*-tolyl rings are nearly coplanar with the imidazolyl-system in the free ligand.

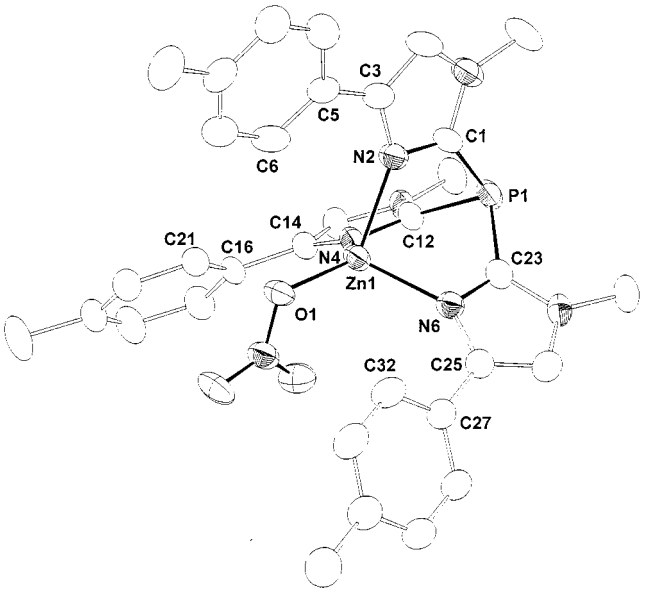


Figure 3. ZORTEP plot[25] (50% probability) of $[Pim^{Me,pTol}ZnNO_3]^+$ in **4d**

Table 1. Selected bond distances (Å), angles (°) and torsion angles (°) for $Pim^{Me,pTol}$ (**3**), $[Pim^{Me,pTol}ZnCl]^+$ in **4a**, and $[Pim^{Me,pTol}ZnNO_3]^+$ in **4d**

	3	**4a**	**4d**
Zn(1)−N(6)		2.074(3)	2.025(2)
Zn(1)−N(4)		2.057(3)	2.026(2)
Zn(1)−N(2)		2.062(3)	2.092(2)
P(1)−C(1)	1.841(5)	1.818(4)	1.817(3)
P(1)−C(12)	1.824(5)	1.824(4)	1.825(3)
P(1)−C(23)	1.813(5)	1.812(4)	1.828(3)
N(4)−Zn(1)−N(2)		95.75(12)	93.97(9)
N(6)−Zn(1)−N(2)		99.89(11)	95.44(9)
N(6)−Zn(1)−N(4)		90.29(12)	100.23(9)
C(1)−P(1)−C(12)	96.8(2)	97.36(16)	95.61(13)
C(1)−P(1)−C(23)	103.5(2)	98.71(17)	97.29(14)
C(12)−P(1)−C(23)	102.2(2)	97.57(16)	100.42(13)
N(2)−C(3)−C(5)−C(6)	179.5(5)	141.5(4)	−15.0(5)
N(4)−C(14)−C(16)−C(21)	−15.1(7)	146.5(5)	29.4(4)
N(6)−C(25)−C(27)−C(32)	5.9(6)	14.0(6)	−35.6(5)
Zn(1)−Cl(1)/−O(1)		2.1725(10)	1.9592(19)

The structures of the two cationic Zn^{II} complexes **4a** and **4d** reveal a slightly distorted tetrahedral coordination environment of Zn^{II} with threefold *N*-imidazolyl coordination. The Zn(1)−Cl(1) bond length in **4a** [2.1725(10)Å] does not differ significantly from that of the other known tris(imidazolyl)phosphanezinc chloride complex chloro{tris[2-(4,5-diisopropylimidazolyl)phosphane]}zinc chloride [2.170(2)-Å].[17] The Zn(1)−O(1) bond length [1.9592(19)Å] pertaining to the coordinating NO_3 in **4d** is similar to the Zn−O distances in the nitrato complex tris[2-(1-isopropyl-4-*tert*-butylimidazolyl)phosphane]zinc nitrate [1.986(4)-Å].[10a] The nitrate ligand in complex **4d** acts as a monodentate ligand[18] unlike the coordinating nitrate in tris[2-(1-isopropyl-4-*tert*-butylimidazolyl)phosphane]zinc nitrate which shows an anisobidentate coordination mode. This is surprising in view of the different steric bulk of the *p*-tolyl and *tert*-butyl groups. We expected that the less bulky *p*-tolyl groups would allow for bidentate coordination of the nitrate ligand. The N−Zn−N bond angles in both **4a** (90.3−99.9°) and **4d** (94.0−100.2°) are smaller than the tetrahedral angle. These angles do not differ significantly from previously reported values for tris(imidazolyl)phosphanes, e.g. chloro{tris[2-(4,5-diisopropylimidazolyl)phosphane]}-zinc chloride[17] or $[Pim^{iPr,tBu}ZnX]^+$ (X = OH, I, NO_3).[10a] The three Zn−N bond lengths in the structure **4a** are equal (mean: 2.064 Å) and are very similar to the Zn−N bond lengths in **4d** (2.025−2.092 Å) and $[Pim^{iPr,tBu}ZnX]^+$ (X = OH, I, NO_3).[10a] It is worth mentioning that the Zn−N bond lengths and N−Zn−N bond angles in the analogous hydrotris(pyrazolyl)borate complexes $[Tp^{Me,Ph}ZnNO_3]$[4a] and $[Tp^{Me,Ph}ZnCl]$,[19] do not differ significantly from those found for tris(imidazolyl)phosphanes. The P−C bond lengths of **4a** (mean: 1.818 Å) and **4d** (mean: 1.823 Å) are equivalent within the standard deviation and show no significant differences to those found for the free ligand **3**. The C−P−C bond angles of **4a** (97.4−98.7°) and **4d** (95.6−100.4°) are slightly smaller than the C−P−C bond angles of the free ligand **3** (96.8−103.5°). This suggests that the tridentate coordination of **3** to Zn^{II} induces no significant strain on the ligand independent of the coordinating anion. The natural bite of the ligand seems to be ideally tailored to the tris-chelating coordination of Zn^{II}. The already mentioned N−C−C−C torsion angles of **4a** and **4d** (Table 1) vary a bit more than those observed for **3**. This small deviation from coplanarity can be interpreted as being caused by weak interactions of the coordinating anion with the *p*-tolyl substituents.

Conclusion

We have synthesised the new *p*-tolyl-substituted tris(imidazolyl)phosphane ligand $Pim^{Me,pTol}$ (**3**) and prepared a variety of stable Zn^{II} complexes. $Pim^{Me,pTol}$ (**3**) is the first tris(imidazolyl)phosphane ligand with a hydrophobic cavity formed by three aryl substituents. The geometry of its zinc complexes (bond lengths, angles, bite of the ligand) is similar to the geometry of the tris(pyrazolyl)borate zinc complexes. A comparison of the X-ray structure analyses of the free ligand $Pim^{Me,pTol}$ (**3**) and the two complexes $[Pim^{Me,pTol}ZnCl]_2ZnCl_4$ (**4a**) and $[Pim^{Me,pTol}ZnNO_3]NO_3$ (**4d**) reveals that the tris(imidazolyl)phosphane ligand hardly changes its bond angles upon metal coordination. The natural bite angle of the ligand is obviously ideally suited for zinc ion complexation. The orientation of the *p*-tolyl groups in the Zn^{II} complex **4d** shows that the hydrophobic cavity can adjust to the nonspherical shape of the nitrate ligand. The cavity seems deep and wide enough to allow access of an additional small molecule. This aspect is probably important to the mimicry of carbonic anhydrase activity. We think that the $Pim^{Me,pTol}$ ligand **3** is more suitable for reaction in protic solvents than the $Tp^{R,R'}$ ligands with their B−N bonds that are inherently sensitive to hydrolysis.

Experimental Section

General Remarks: The compounds 5-tolyl-4-tosyloxazoline[12] and tris[2-(1-methyl-4-tolylimidazolyl)phosphane[10b] **3** were synthesised according to the literature procedures for analogous systems. Ethanol was purified and degassed by standard procedures. All other solvents and reagents were used without further purification. ^{1}H NMR spectra, ^{31}P NMR spectra and ^{13}C NMR spectra were recorded on a Bruker DRX 200 spectrometer, the 2D NMR spectra were recorded on a Bruker DRX 500 spectrometer. The chemical shifts (δ) are reported in ppm with the solvent signal as reference. The EI-mass spectra were recorded on a double focussing mass spectrometer, model 311 A Varian MAT, ionisation energy 70 eV. The FAB mass spectra were recorded on a mass spectrometer Finnigan, Model MAT 8200, with an NBA matrix.

5-Tolyl-4-tosyloxazoline (1): Prepared according to a literature procedure[12] with tosylmethyl isocyanide (25.0 g, 128 mmol), tolylaldehyde (15.4 g, 128 mmol) and finely powdered sodium cyanide (0.4 g, 8 mmol) in 100 mL of dry ethanol. Yield: 38 g (90%) as a colourless crystalline solid. − ^{1}H NMR ($CDCl_3$): δ = 2.39 (s, 3 H, tolyl C*H*$_3$), 2.49 (s, 3 H, tosyl C*H*$_3$), 5.07 (dd, $^3J_{HH}$ = 6 Hz, $^4J_{HH}$ = 2 Hz, 1 H, oxazoline C^5 *H*), 6.05 (d, $^3J_{HH}$ = 6 Hz, 1 H, oxazoline C^4 *H*), 7.24 (s, 5 H, tosyl C_6H_4, oxazoline C^2 *H*), 7.42 (d, $^3J_{HH}$ = 8 Hz, 2 H, $C_6H_2H_2CH_3$), 7.88 (d, $^3J_{HH}$ = 8 Hz, 2 H, $C_6H_2H_2CH_3$).

1-Methyl-4-tolylimidazole, Im^{Me,pTol} (2): A suspension of 5-tolyl-4-tosyloxazoline (102 g, 310 mmol) in 250 mL of benzene was stirred under nitrogen in a 500 mL autoclave fitted with an inlet tube and a PTFE insert. The hole device was cooled to −78 °C. Then, dry methylamine (39.9 g, 1.28 mol) was condensed into the autoclave which was subsequently heated with stirring to 120 °C. After 20 h a red orange mixture was obtained and flash chromatography (ethyl acetate/dichloromethane, 4:1) afforded crude 1-methyl-4-tolylimidazole (15 g, 87 mmol; 28% relative to **1**) which was recrystallized from diethyl ether as colourless flakes. − ^{1}H NMR ($CDCl_3$): δ = 2.39 (s, 3 H, $C_6H_4CH_3$), 3.74 (s, 3 H, NC*H*$_3$), 7.16 (d, $^4J_{HH}$ = 1 Hz, 1 H, imidazolyl C^5*H*), 7.22 (d, $^3J_{HH}$ = 8 Hz, 2 H, *m*-*H* of *p*-tolyl), 7.49 (s, 1 H, imidazolyl C^2*H*), 7.69 (d, $^3J_{HH}$ = 8 Hz, 2 H, *o*-*H* of *p*-tolyl). − ^{13}C{^{1}H} NMR ($CDCl_3$): δ = 21.6 (s, $C_6H_4CH_3$), 33.9 (d, *J* = 3 Hz, N*C*H$_3$), 115.9 (s, imidazole *C*^{2} H), 125.1 (s, 2C, *p*-tolyl *C*$^{7,7'}$H), 129.7 (s, 2C, *p*-tolyl *C*$^{8,8'}$H), 131.9 (s, *p*-tolyl *C*), 136.7 (s, *p*-tolyl *C*), 138.8 (d, *J* = 2 Hz, imidazole *C*^{5}H), 142.8 (s, imidazole *C*^{4}). − MS (EI): *m*/*z* (%) = 172 (100) [M$^+$], 157 (16) [M$^+$ − CH_3], 130 (21) [M$^+$ − CH_3 − NCH], 103 (16) [$C_8H_7^+$], 77 (12%) [$C_6H_5^+$].

Tris[2-(1-methyl-4-tolylimidazolyl)]phosphane, Pim^{Me,pTol} (3): The procedure for Pim^{iPr,iPr} [10b] was modified by using THF as solvent instead of diethyl ether and replacing the THF with dichloromethane before adding the ammonia solution. Preparation of **3** from 1-methyl-4-tolylimidazole (15 g, 87 mmol), *n*-butyllithium (62 mL, 99 mmol, 1.6 M in hexane), freshly distilled PCl_3 (4.2 g, 30 mmol) and 150 mL of THF. Yield: 7.4 g (14 mmol; 45% rel. to PCl_3) of tris[2-(1-methyl-4-tolylimidazolyl)]phosphane as a colourless solid after recrystallization from dichloromethane/hexane. − ^{1}H NMR ($CDCl_3$): δ = 2.38 (s, 9 H, $C_6H_4CH_3$), 3.76 (s, 9 H, NC*H*$_3$), 7.18 (d, $^3J_{HH}$ = 8 Hz, 6 H, $C_6H_2H_2CH_3$), 7.38 (s, 3 H, imidazole C^5 *H*), 7.68 (d, $^3J_{HH}$ = 8 Hz, 6 H, $C_6H_2H_2CH_3$). − ^{13}C{^{1}H} NMR ($CDCl_3$): δ = 21.7 (s, $C_6H_4CH_3$), 35.2 (m, N*C*H$_3$), 121.0 (s, imidazole *C*^{2}P), 125.2 (s, 2C, *p*-tolyl *C*$^{7,7'}$H), 129.6 (s, 2C, *p*-tolyl *C*$^{8,8'}$H), 131.7 (s, *p*-tolyl *C*), 136.8 (s, *p*-tolyl *C*), 141.1 (d, *J* = 11 Hz, imidazole *C*^{5}H), 143.5 (d, *J* = 9 Hz, imidazole *C*^{4}). − ^{31}P{^{1}H} NMR ($CDCl_3$): δ = −57.9. − MS (EI): *m*/*z* (%) = 544 (13) [M$^+$], 372 (16) [P($N_2C_{11}H_{11}$)$_2^+$ − H], 359 (76) [P($N_2C_{11}H_{11}$)$_2^+$ − CH_2], 202 (20) [$PN_2C_{11}H_{11}^+$], 173 (52) [Im$^{Me,pTol+}$ + H], 130 (30) [Im$^{Me,pTol+}$ − CH_3 − NCH].

Bis[chloro{tris[2-(1-methyl-4-tolylimidazolyl)]phosphane}zinc] Tetrachlorozincate, [Pim^{Me,pTol}ZnCl]$_2$ZnCl$_4$ (4a): A stirred solution of Pim^{Me,pTol} (546 mg, 1.00 mmol) in 40 mL of THF was treated with $ZnCl_2$ (126 mg, 0.925 mmol) in THF. The reaction mixture was heated under reflux for 30 min then stirred for an additional 12 h at 25 °C. The complex precipitated as a colourless powder, which was collected by filtration and washed with 30 mL of THF. Drying under vacuum afforded **4a** (0.37 g, 0.25 mmol; 82% rel. to $ZnCl_2$). − ^{1}H NMR (CD_3NO_2): δ = 2.37 (s, 9 H, *p*-tolC*H*$_3$), 4.12 (s, 9 H, NC*H*$_3$), 7.25 (d, $^3J_{HH}$ = 8 Hz, 6 H, $C_6H_2H_2CH_3$), 7.53 (d, $^4J_{PH}$ = 4 Hz, 3 H, imidazolyl C^5*H*), 7.61 (d, $^3J_{HH}$ = 8 Hz, 6 H, $C_6H_2H_2CH_3$). − ^{31}P NMR (CD_3NO_2): δ = −113.7. − MS (FAB): *m*/*z* (%) = 643 (83) [Pim^{Me,pTol}ZnCl]$^+$, 472 (14) [P($N_2C_{11}H_{11}$)$_2$ZnCl]$^+$, 438 (5) [P($N_2C_{11}H_{11}$)$_2$Zn]$^+$, 373 (6) [P($N_2C_{11}H_{11}$)$_2^+$], 202 (3) [$PN_2C_{11}H_{11}^+$] 77 (36) [$C_6H_5^+$].

Bromo{tris[2-(1-methyl-4-tolylimidazolyl)]phosphane}zinc Bromide, [Pim^{Me,pTol}ZnBr]Br (4b): This compound was prepared according to the procedure described for [Pim^{Me,pTol}ZnCl]$_2$ZnCl$_4$ (**4a**) with **3** (273 mg, 0.501 mmol) and $ZnBr_2$ (113 mg, 0.502 mmol). Yield: 0.31 g (80%) of **4b** as a colourless powder. − ^{1}H NMR (CD_3NO_2): δ = 2.38 (s, 9 H, *p*-tolC*H*$_3$), 4.22 (s, 9 H, NC*H*$_3$), 7.24 (d, $^3J_{HH}$ = 7 Hz, 6 H, $C_6H_2H_2CH_3$), 7.49 (d, $^4J_{PH}$ = 4 Hz, 3 H, imidazolyl C^5 *H*), 7.55 (d, $^3J_{HH}$ = 7 Hz, 6 H, $C_6H_2H_2CH_3$). − ^{31}P{^{1}H} NMR (CD_3NO_2): δ = −118.2. − MS (FAB): *m*/*z* (%) = 689 (25) [Pim^{Me,pTol}ZnBr]$^+$, 518 (5) [P($N_2C_{11}H_{11}$)$_2$ZnBr]$^+$, 438 (3) [P($N_2C_{11}H_{11}$)$_2$Zn]$^+$.

Iodo{tris[2-(1-methyl-4-tolylimidazolyl)]phosphane}zinc Iodide, [Pim^{Me,pTol}ZnI]I (4c): This compound was prepared according to the procedure described for [Pim^{Me,pTol}ZnCl]$_2$ZnCl$_4$ (**4a**) with **3** (273 mg, 0.501 mmol), ZnI_2 (159 mg, 0.498 mmol) and ethanol as solvent. Yield: 0.36 g (84%) of **4c** as a colourless powder. − ^{1}H NMR (CD_3NO_2): δ = 2.37 (s, 9 H, *p*-tolC*H*$_3$), 4.23 (s, 9 H, NC*H*$_3$), 7.24 (d, $^3J_{HH}$ = 7 Hz, 6 H, $C_6H_2H_2CH_3$), 7.46 (d, $^4J_{PH}$ = 5 Hz, 3 H, imidazolyl C^5*H*), 7.50 (d, $^3J_{HH}$ = 8 Hz, 6 H, $C_6H_2H_2CH_3$). − ^{31}P{^{1}H} NMR (CD_3NO_2): δ = −119.4. − MS (FAB): *m*/*z* (%) = 735 (100) [Pim^{Me,pTol}ZnI]$^+$, 564 (18) [P($N_2C_{11}H_{11}$)$_2$ZnI]$^+$, 438 (23) [P($N_2C_{11}H_{11}$)$_2$Zn]$^+$, 373 (26) [P($N_2C_{11}H_{11}$)$_2^+$].

Nitrato{tris[2-(1-methyl-4-tolylimidazolyl)]phosphane}zinc Nitrate, [Pim^{Me,pTol}ZnNO$_3$]NO$_3$ (4d): This compound was prepared according to the procedure described for [Pim^{Me,pTol}ZnCl]$_2$ZnCl$_4$ (**4a**) with $Zn(NO_3)_2{\cdot}6H_2O$ (298 mg, 1.00 mmol). Yield: 0.67 g (92%) of **4d** as colourless powder. − ^{1}H NMR (CD_3CN): δ = 2.40 (s, 9 H, *p*-tolC*H*$_3$), 4.10 (s, 9 H, NC*H*$_3$), 7.30 (d, $^3J_{HH}$ = 8 Hz, 6 H, $C_6H_2H_2CH_3$), 7.48 (d, $^3J_{HH}$ = 8 Hz, 6 H, $C_6H_2H_2CH_3$), 7.56 (d, $^4J_{PH}$ = 4 Hz, 3 H, imidazolyl C^5*H*). − ^{31}P{^{1}H} NMR (CD_3CN): δ = −117.8. − MS (FAB): *m*/*z* (%) = 670 (100) [Pim^{Me,pTol}ZnNO$_3$]$^+$, 438 (18) [P($N_2C_{11}H_{11}$)$_2$Zn]$^+$, 373 (16) [P($N_2C_{11}H_{11}$)$_2^+$], 202 (11) [$PN_2C_{11}H_{11}^+$], 77 (94) [$C_6H_5^+$], 51 (69) [$C_4H_3^+$].

X-ray Crystallographic Study: For all compounds Pim^{Me,pTol} (**3**), [Pim^{Me,pTol}ZnCl]$_2$ZnCl$_4$ (**4a**), and [Pim^{Me,pTol}ZnNO$_3$]NO$_3$ (**4d**) data collection was carried out using a Bruker Smart CCD system. All data were corrected for absorption using SADABS.[20] The structures were solved using direct methods [SHELX-97[21] (**3**) and (**4a**), SIR-97[22] (**4d**)] and refined using least-squares methods (SHELX-97). Before the final refinement of **4d** the electron density of a strongly disordered nitromethane molecule was treated with PLATON[23] using the built-in SQUEEZE routine.[24] Crystal data for **3**, **4a** and **4d** are summarised in Table 2. Requests concerning the

Table 2. Crystallographic data for $Pim^{Me,pTol}$ (**3**), $[Pim^{Me,pTol}ZnCl]_2[ZnCl_4]\cdot 3CH_3NO_2$ (**4a**) and $[Pim^{Me,pTol}ZnNO_3]NO_3$ (**4d**)

	3	**4a**	**4d**
Crystal shape	rectangular rod	triclinic	triangular plates
Crystal colour	colourless	colourless	colourless
Crystal size (mm^3)	$1.2 \times 0.3 \times 0.1$	$0.45 \times 0.25 \times 0.2$	$0.4 \times 0.4 \times 0.08$
Empirical formula	$C_{33}H_{33}N_6P$	$C_{69}H_{75}Cl_6N_{15}O_6P_2Zn_3$	$C_{33}H_{33}N_8O_6PZn$
Formula weight	544.62	1681.19	734.01
Crystal system	Monoclinic	Triclinic	Triclinic
Space group	*Cc*	$P\bar{1}$	$P\bar{1}$
a (Å)	6.4913(3)	11.3536(2)	10.6721(6)
b (Å)	24.1876(12)	17.99740(10)	11.2203(6)
c (Å)	18.7098(10)	19.6392(2)	17.9169(10)
α (°)	90	94.1396(9)	106.3791(12)
β (°)	94.0140(10)	105.9953(5)	92.2410(11)
γ (°)	90	95.8169(9)	114.1669(11)
V ($Å^3$)	2930.4(3)	3816.66(8)	1848.47(18)
Z	4	2	2
d (calc, g/cm^3)	1.234	1.463	1.319
Type of diffractometer	Bruker Smart CCD	Bruker Smart CCD	Bruker Smart CCD
Radiation used (λ, Å)	Mo-K_α (0.71073)	Mo-K_α (0.71073)	Mo-K_α (0.71073)
Monochromator	Graphite	Graphite	Graphite
Data-collecting mode	ω-scans	ω-scans	ω-scans
Linear absorption coefficient (mm^{-1})	0.127	1.247	0.760
Temperature (K)	173(2)	173(2)	173(2)
Max., min. transmission	0.949229, 0.456016	0.754681, 0.637147	0.846095, 0.727768
Total reflections	6746	30943	14790
Independent reflections	3341	20075	9666
Unique reflections [$I \geq 2\sigma(I)$]	2716	12210	5514
R(int)	0.1170	0.0338	0.0361
Scan range	$1.68 \leq \theta \leq 29.99°$	$1.49 \leq \theta \leq 30.44°$	$1.20 \leq \theta \leq 30.22°$
Index ranges	$-8 \leq h \leq 2$ $-33 \leq k \leq 34$ $-11 \leq l \leq 26$	$-11 \leq h \leq 15$ $-25 \leq k \leq 24$ $-27 \leq l \leq 22$	$-8 \leq h \leq 14$ $-15 \leq k \leq 15$ $-24 \leq l \leq 25$
F(000)	1152	1728	760
R,[a] R_w [$I > 2\sigma(I)$][b]	0.0599, 0.1495	0.0544, 0.1236	0.0549, 0.1062
R indices (all data)	0.0757, 0.1644	0.1074, 0.1474	0.1110, 0.1249
Maximum d/s	0.727	3.475	0.694
Maximum e-density ($e\cdot Å^{-3}$)	0.362	1.342	0.618
Minimum e-density ($e\cdot Å^{-3}$)	−0.541	−1.304	−0.372
Used reflections	3341	20075	9666
L.S. restraints	2	11	0
Refined parameters	367	921	448
Goodness-of-fit on F^2	1.068	1.015	0.954

[a] $R = \Sigma(||F_o| - |F_c||)/\Sigma|F_o|$. – [b] $R_w = [\Sigma(w(F_o^2 - F_c^2)^2)/\Sigma(wF_o^4)]^{1/2})$, $S = [\Sigma\, w(F_o^2 - F_c^2)^2]/(n - p)^{1/2})$, n = number of reflections, p = parameters used, w calc of (**3**): $w = 1/[\sigma^2(F_o^2) + (0.0966P)^2 + 0.0000P]$, w(calc) of (**4a**): $w = 1/[\sigma^2(F_o^2) + (0.0592P)^2 + 2.8419P]$, w(calc) of (**4d**): $w = 1/[\sigma^2(F_o^2) + (0.0484P)^2 + 0.0000P]$, where $P = (F_o^2 + 2F_c^2)/3$

X-ray crystal structure section should be addressed to one of the authors (Dr. Gerd Rheinwald).

Crystals of **3** with X-ray quality were obtained by evaporation of an acetone solution. The selected crystal was a colourless rectangular rod with dimensions of $1.2 \times 0.3 \times 0.1$ mm^3 and data collection proceeded at 173 K.

X-ray quality colourless triangular plates of **4a** were grown by diffusion of hexane into a nitromethane solution at 293 K. A crystal of dimensions $0.45 \times 0.25 \times 0.2$ mm^3 was selected and data collection proceeded at 173 K.

Colourless triclinic crystals of **4d** suitable for an X-ray study were also grown by diffusion of hexane into a nitromethane solution at 293 K. A crystal of dimensions $0.4 \times 0.4 \times 0.08$ mm^3 was selected and data collection proceeded at 173 K.

All crystals were prepared and handled under perfluoropolyalkyl ether (ABCR GmbH & Co KG, viscosity 1600 cSt.).

Crystallographic data (excluding structure factors) for the structures reported in this paper have been deposited with the Cambridge Crystallographic Data Centre as supplementary publication nos. CCDC-137726 **(3)**, -137727 **(4a)** and -137728 **(4d)**. Copies of the data can be obtained free of change on application to CCDC, 12 Union Road, Cambridge CB2 1EZ, UK [Fax: (internat.) + 44-1223/336-033; E-mail: deposit@ccdc.cam.ac.uk].

Acknowledgments

Financial support for this work was provided by the Deutsche Forschungsgemeinschaft and the Fonds der Chemischen Industrie. We thank Dr. Peters for measuring the 2D HMBC NMR spectra and for helpful discussions.

[1] [1a] B. L. Vallee, A. Galdes, *Adv. Enzymol.* **1982**, *56*, 283−430. – [1b] B. L. Vallee, in *Zinc Enzymes* (Ed.: T. G. Spiro), Wiley, New York, **1983**. – [1c] *Zinc Enzymes* (Ed.: I. Bertini, C. Luchinat, W. Maret, M. Zeppezauer), Birkhäuser, Boston, **1983**.
[2] R. G. Khalifah, *J. Biol. Chem.* **1971**, *246*, 2561−2573.
[3] R. Alsfasser, S. Trofimenko, A. Looney, G. Parkin, H. Vahrenkamp, *Inorg. Chem.* **1991**, *30*, 4098−4100.
[4] [4a] K.-W. Yang, Y.-Z. Wang, Z.-X. Huang, *Polyhedron* **1997**, *16*, 109−112. – [4b] A. L. Rheingold, R. L. Ostrander, B. S. Haggerty, S. Trofimenko, *Inorg. Chem.* **1994**, *33*, 3666−3676.
[5] M. Ruf, H. Vahrenkamp, *Inorg. Chem.* **1996**, *35*, 6571−6578.

[6] W. Kläui, U. Schilde, M. Schmidt, *Inorg. Chem.* **1997**, *36* 1598−1601.
[7] [7a] A. Looney, G. Parkin, R. Alsfasser, H. Vahrenkamp, *Angew. Chem.* **1992**, *104*, 57−58; *Angew. Chem. Int. Ed. Engl.* **1992**, *31*, 92−93. − [7b] U. Hartmann, H. Vahrenkamp, *Chem. Ber.* **1994**, *127*, 2381−2385.
[8] [8a] J. Huguet, R. S. Brown, *J. Am. Chem. Soc.* **1980**, *102*, 7571−7572. − [8b] R. S. Brown, N. J. Curtis, J. Huguet, *J. Am. Chem. Soc.* **1981**, *103*, 6953−6959.
[9] H. Slebocka-Tilk, J. L. Cocho, Z. Frakman, R. S. Brown, *J. Am. Chem. Soc.* **1984**, *106*, 2421−2431.
[10] [10a] C. Kimblin, W. E. Allen, G. Parkin, *J. Chem. Soc., Chem. Commun.* **1995**, 1813−1815. − [10b] T. N. Sorrell, W. E. Allen, P. S. White, *Inorg. Chem.* **1995**, *34*, 952−960.
[11] [11a] T. N. Sorrell, W. E. Allen, *J. Org. Chem.* **1994**, *59*, 1589−1590. − [11b] T. N. Sorrell, W. E. Allen, in *Inorganic Synthesis* **1998**, *32*, John Wiley & Sons. 66−70.
[12] D. A. Horne, K. Yakushijin, G. Büchi, *Heterocycles* **1994**, *39*, 139−153.
[13] The product has been identified on the basis of correlated $^{1}H,^{1}H$ NMR and $^{1}H,^{13}C$ HMBC NMR spectra.
[14] These differences were attributed to packing effects.
[15] T. S. Cameron, B. Dahlèn, *J. Chem. Soc., Perkin 2* **1975**, *2*, 1737−1751.
[16] T. S. Cameron, K. D. Howlett, K. Miller, *Acta Cryst.* **1978**, *B34*, 1639−1644.
[17] R. J. Read, M. N. G. James, *J. Am. Chem. Soc.* **1981**, *103*, 6947−6952.
[18] The nitrate ligand has been classified as binding to a single metal centre by three different coordination modes: i) bidentate, ii) anisobidentate, and iii) monodentate. See: G. J. Kleywegt, W. G. R. Wiesmeijer, G. J. Van Driel, W. L. Driessen, J. Reedijk, J. H. Noordik, *J. Chem. Soc., Dalton Trans.* **1985**, 2177−2184.
[19] F. Hartmann, W. Kläui, A. Kremer-Aach, D. Mootz, A. Strerath, H. Wunderlich, *Z. Anorg. Allg. Chem.* **1993**, *619*, 2071−2076.
[20] Inc.: W. I. Madison, in *Area-Detector Absorption Correction*, Siemens Industrial Automation, **1996**.
[21] G. M. Sheldrick, in *SHELX97. Programs for Crystal Structure Analysis* (Release 97−2), University of Göttingen, Germany **1997**.
[22] A. Altomare, M. C. Burla, M. Camalli, G. L. Cascarano, C. Giacovazzo, A, Guagliardi, A. G. G. Moliterni, G. Polidori, R. Spagna, *J. Appl. Cryst.* **1999**, *32*, 115−121.
[23] A. L. Spek, in *PLATON. A Multipurpose Crystallographic Tool*, Utrecht University, Utrecht, The Netherlands **1999**.
[24] P. van der Sluis, A. L. Spek, *Acta Cryst.* **1990**, *A46*, 194−201.
[25] L. Zsolnai, G. Huttner, University of Heidelberg **1994**.

Received December 6, 1999
[I99444]

Base Control of Electron-Transfer Reactions of Manganese(III) Porphyrins

Ikuo Nakanishi,[a] Shunichi Fukuzumi,*[a] Jean-Michel Barbe,[b] Roger Guilard,*[b] and Karl M. Kadish*[c]

Keywords: Electron transfer / Kinetics / Manganese / Metalloporphyrins / Quinones

Homogeneous electron-transfer kinetics for the reduction of four different manganese(III) porphyrins using different reductants were examined in deaerated acetonitrile, and the resulting data were evaluated in light of the Marcus theory of electron transfer to determine electron-exchange rate constants between manganese(III) and manganese(II) porphyrins. The investigated compounds are represented as (P)MnCl, where P = the dianion of dodecaphenylporphyrin (DPPX; X = H_{20}, $Cl_{12}H_8$, or F_{20}) or tetraphenylporphyrin (TPP). The electron transfer from semiquinone radical anion derivatives to $(P)Mn^{III}Cl$ leads to formation of the corresponding Mn^{II} complex, $[(P)Mn^{II}Cl]^-$. The electron-exchange rate constants derived from the electron-transfer rate constants decrease with an increasing degree of nonplanarity of the porphyrin macrocycle and follow the order: (TPP)MnCl (3.1×10^3 $M^{-1}\cdot s^{-1}$) > ($DPPH_{20}$)MnCl (1.1×10^{-2} $M^{-1}\cdot s^{-1}$) > ($DPPCl_{12}H_8$)MnCl (3.5×10^{-4} $M^{-1}\cdot s^{-1}$) > ($DPPF_{20}$)MnCl (4.3×10^{-6} $M^{-1}\cdot s^{-1}$). The coordination of two molecules of pyridine (py) or DMSO to ($DPPH_{20}$)MnCl to form $[(DPPH_{20})Mn(py)_2]^+$ or $[(DPPH_{20})Mn(DMSO)_2]^+$ enhances the rate of electron-transfer reduction. This indicates that there is a significant decrease in the reorganization energy upon axial ligand coordination of pyridine or DMSO.

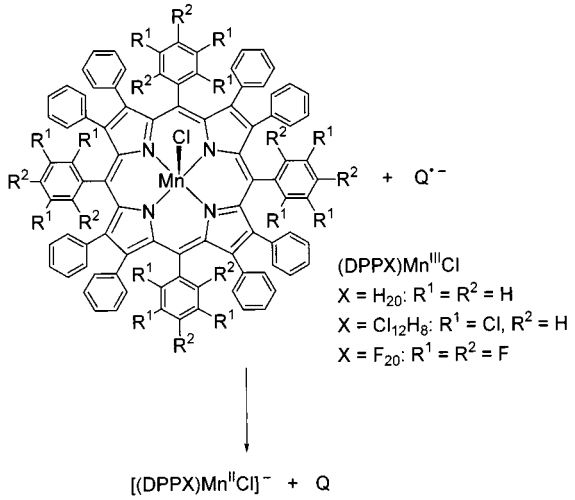
Introduction

Metalloporphyrins have been utilized as important electron carriers in a variety of biological and chemical redox systems, since electron-transfer reactions of metalloporphyrins can be finely tuned by the metal, the porphyrin macrocycle and the axial ligands.[1] The axial ligand has merited special attention among the factors which control the rates of electron-transfer reactions of metalloporphyrins, since the redox properties of metalloporphyrins can be finely tuned by the addition of an external base ligand. Although there seems to be no need to accelerate further the electron-transfer reactions of metalloporphyrins, which are normally fast, the rates of electron transfer of some metalloporphyrins are known to be relatively slow because of the large reorganization energy associated with the electron transfer.[1] In this context, we have recently reported that the rates of metal-centered electron-transfer oxidation of $(OETPP)Fe^{III}(R)$ (OETPP = the dianion of octaethyltetraphenylporphyrin and R = σ-bonded axial ligand such as Ph), which has a saddle-shaped nonplanar porphyrin macrocycle, are much slower than those of $(OEP)Fe^{III}(R)$ (OEP = the dianion of octaethylporphyrin), which has a planar porphyrin macrocycle, and this can be associated with the large reorganization energies upon electron-transfer oxidation of the metal center of the nonplanar porphyrins.[2] It has also been shown that the slow electron transfer of a nonplanar iron(III) porphyrin is significantly accelerated by axial coordination of pyridine due to the decreased reorganization energy upon electron-transfer oxidation.[2] Such nonplanar conformations of porphyrins have been suggested as being related to their functions in biological systems.[3−8]

We report herein the effects of conformational distortions of the porphyrin ring on the electron-transfer kinetics for reduction of (P)MnCl, where P represents either the dianion of tetraphenylporphyrin (TPP), which is planar, or the dianion of dodecaphenylporphyrins (DPPX, X = H_{20}, $Cl_{12}H_8$, F_{20}) which are known to adopt a nonplanar conformation.[3,9−11] Manganese is an essential metal in several biological systems which are involved in electron-transfer reactions,[12] and extensive efforts have therefore been devoted to elucidating electron-transfer processes in synthetic manganese porphyrins.[13−18] The detailed kinetics for the electron-transfer reduction of (P)MnCl by the semiquinone radical anion ($Q^{\bullet -}$) in Equation (1) enables us to compare the reorganization energies λ for reduction of manganese porphyrins with a planar macrocycle, as in (TPP)MnCl, and a nonplanar macrocycle, as in (DPPX)MnCl.[19] We also report the acceleration in the rate of electron-transfer reduction of ($DPPH_{20}$)MnCl upon axial coordination of pyridine or DMSO, and this data should provide valuable insights into those factors which control the electron-transfer reactivities of metalloporphyrins.

[a] Department of Material and Life Science,
Graduate School of Engineering, Osaka University, CREST,
Suita, Osaka 565−0871, Japan
Fax: (internat.) +81-6-6879−7368
E-mail: fukuzumi@ap.chem.eng.osaka-u.ac.jp
[b] LIMSAG, UMR 5633, Université de Bourgogne,
Faculté des Sciences "Gabriel",
6 Boulevard Gabriel, F-21100 Dijon, France
Fax: (internat.) +33-3-8039−6117
E-mail: roger.guilard@u-bourgogne.fr
[c] Department of Chemistry, University of Houston,
Houston TX 77204−5641, USA
Fax: (internat.) +1−713−743−2745
E-mail: kkadish@uh.edu

 © WILEY-VCH Verlag GmbH, D-69451 Weinheim, 2000 1434−1948/00/0707−1557 $ 17.50+.50/0



(1)

Results and Discussion

Slow Electron-Transfer Reduction of Nonplanar Manganese Porphyrins

The one-electron reduction potentials (E^0_{red}) of (P)MnCl determined by the cyclic voltammetry (CV) measurements[16] are shown in Table 1.

Table 1. Rate constants (k_{et}) and free energy changes (ΔG^0_{et}) for electron-transfer reduction of (P)MnCl with semiquinone radical anion ($Q^{\bullet -}$) in deaerated MeCN or deaerated DMSO at 298 K, their one-electron reduction potentials (E^0_{red}, V vs. SCE) and electron self-exchange rate constants (k_{ex}) of (P)MnCl/[(P)MnCl]$^-$

(P)MnCl	E^0_{red} [a] [V]	ΔG^0_{et} [eV]	k_{et} [b] [M^{-1} s^{-1}]	k_{ex} [c] [M^{-1} s^{-1}]
(TPP)MnCl	−0.22[d]	−0.28	5.4×10^7	3.1×10^3
$(DPPH_{20})$MnCl	−0.36	−0.14	1.3×10^4	1.1×10^{-2}
$(DPPH_{20})$MnCl	−0.36	−0.22[e]	4.1×10^4	6.6×10^{-3}
$[(DPPH_{20})Mn(py)_2]Cl$	−0.41	−0.09	1.9×10^6	1.5×10^3
$[(DPPH_{20})Mn(py)_2]Cl$	−0.41	−0.17[e]	5.8×10^6	8.4×10^2
$[(DPPH_{20})Mn(DMSO)_2]Cl$	−0.40	−0.10	2.3×10^6	1.6×10^3
$(DPPCl_{12}H_8)$MnCl	−0.15	−0.35	8.6×10^4	3.5×10^{-4}
$(DPPF_{20})$MnCl	0.04	−0.54	2.0×10^5	4.3×10^{-6}

[a] Determined in PhCN unless otherwise noted, 0.1 M TBAP, scan rate = 0.1 V s^{-1}. See ref.[16] The experimental error is within ±0.005 V. – [b] The experimental error is within ±5%. – [c] Determined using Equations 3–5. – [d] Determined in MeCN, 0.1 M TBAP, scan rate = 0.1 V s^{-1}. – [e] Electron-transfer reduction by methyl-*p*-benzosemiquinone radical anion ($MeQ^{\bullet -}$).

The CV measurements on (TPP)MnCl were performed in both MeCN and PhCN. The E^0_{red} value in MeCN (−0.22 V) is essentially the same as that in PhCN (−0.23 V). In spite of the electron-withdrawing effect of the additional phenyl groups in $DPPH_{20}$, the E^0_{red} value of $(DPPH_{20})$MnCl (−0.36 V) is more negative than that of (TPP)MnCl (−0.22 V). This may be ascribed to the stronger Mn^{III}–N binding of the nonplanar conformation of the $DPPH_{20}$ ligand than the planar TPP ligand. Since the E^0_{red} value of $(DPPF_{20})$MnCl remained unchanged after addition of excess Cl^- (0.1 M), there should be no dissociation of Cl^- after reduction of Mn^{III} to Mn^{II}.

Semiquinone radical anions are employed as one-electron reductants whose oxidation potentials[20] are low enough to reduce each Mn^{III} porphyrin to its Mn^{II} form [Equation (1)]. These reducing agents were prepared by comproportionation of the *p*-benzoquinone derivatives with the corresponding hydroquinone dianions, which were generated by reaction of the hydroquinones with tetra-*n*-butylammonium hydroxide.[21] The rates of electron transfer from the semiquinone radical anion to (TPP)MnCl or (DPPX)MnCl were measured by monitoring the increase in absorbance of the Mn^{II} Soret band {e.g. at 488 nm for $[(DPPH_{20})Mn^{II}Cl]^-$ in Figure 1a} using a stopped-flow technique.

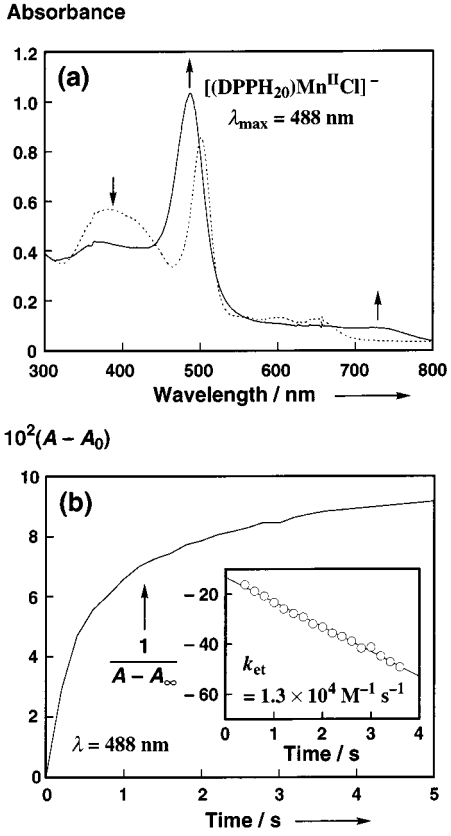


Figure 1. (a) Spectral changes upon addition of $Q^{\bullet -}$ (2.0×10^{-5} M) to a deaerated MeCN solution of $(DPPH_{20})$MnCl (2.0×10^{-5} M) at 298 K; (b) time course of the absorption change at 488 nm in the reaction of $(DPPH_{20})$MnCl (8.3×10^{-5} M) with $Q^{\bullet -}$ (8.3×10^{-5} M) in deaerated MeCN at 298 K; inset: the second-order plot

The electron-transfer rates obey second-order kinetics when the initial concentrations of (P)MnCl and the semiquinone radical anion are equal (Figure 1b). The observed second-order rate constants k_{et} of the electron-transfer reactions are listed in Table 1, which also lists the free-energy change of electron transfer from the semiquinone radical anion to (P)MnCl (ΔG^0_{et}). The ΔG^0_{et} values were calculated from the one-electron reduction potentials of (P)MnCl (E^0_{red}) and the one-electron oxidation potentials of the semiquinone radical anions (E^0_{ox}), which are equivalent to the one-electron reduction potentials of the corresponding quinones[20] by Equation (2), where F is the Faraday constant.

$$\Delta G^0_{et} = F(E^0_{ox} - E^0_{red}) \quad (2)$$

It was confirmed that the k_{et} value for electron transfer from the semiquinone radical anion ($Q^{\bullet-}$) to $(DPPF_{20})MnCl$ in the presence of 0.1 M tetrabutylammonium chloride (1.8×10^5 $M^{-1}\cdot s^{-1}$) is essentially the same as the k_{et} value in the absence of excess Cl^- (2.0×10^5 $M^{-1}\cdot s^{-1}$). This indicates that no dissociation of Cl^- is involved in the electron-transfer reduction of $(DPPF_{20})MnCl$.

The self-exchange rate constants (k_{ex}) of (P)MnCl/[(P)MnCl]$^-$ can be determined from k_{et} and the self-exchange rate constants (k_{ex}') of $Q^{\bullet-}$/Q by using the Marcus equations [Equation (3) and Equation (4)],[22] where K_{et} is the equilibrium constant for electron transfer, f is a correction factor (generally close to 1), and Z is the collision frequency, taken as 1×10^{11} $M^{-1}\cdot s^{-1}$. The self-exchange rate constants (k_{ex}') of $Q^{\bullet-}$/Q was previously determined as 8.1×10^7 $M^{-1}\cdot s^{-1}$ from the linewidth variation of the EPR spectrum of semiquinone radical anion ($Q^{\bullet-}$) in the presence of various concentrations of *p*-benzoquinone (Q) in PhCN at 298 K.[23] The K_{et} values are obtained from the ΔG^0_{et} values by using Equation (5). The k_{ex} values of (P)MnCl/[(P)MnCl]$^-$ thus obtained are listed in Table 1.

$$k_{ex} = k^2_{et}/(k_{ex}' K_{et} f) \quad (3)$$

$$\ln f = (\ln K_{et})^2/4[\ln(k_{ex}\, k_{ex}'/Z^2)] \quad (4)$$

$$K_{et} = \exp(-\Delta G^0_{et}/RT) \quad (5)$$

The k_{ex} values depend significantly on the type of porphyrin macrocycle and decrease in the order: (TPP)MnCl (3.1×10^3 $M^{-1}\cdot s^{-1}$) > $(DPPH_{20})MnCl$ (1.1×10^{-2} $M^{-1}\cdot s^{-1}$) > $(DPPCl_{12}H_8)MnCl$ (3.5×10^{-4} $M^{-1}\cdot s^{-1}$) > $(DPPF_{20})MnCl$ (4.3×10^{-6} $M^{-1}\cdot s^{-1}$). Hence, the electron-transfer rate at a given free energy change of electron transfer should also decrease in this order. This is clearly shown as the plots of lg k_{et} values vs. ΔG^0_{et} in Figure 2, which includes the data for other semiquinone radical anions used as reductants. The dependence of lg k_{et} on ΔG^0_{et} is given by Equation (6) which is derived from Equations 3−5.[22] The reorganization energy of electron transfer (λ) corresponds to the average of each component, λ_{11} for the electron self-exchange of Q/$Q^{\bullet-}$ and λ_{22} of (P)MnCl/[(P)MnCl]$^-$ [Equation (7)]. The fit of the curves to the Marcus theory of adiabatic outer-sphere electron transfer [Equation (6) and Equation (7)][22] indicates that the rate variations at a given ΔG^0_{et} value arise from the difference in the λ value given in Figure 2 and not from the nonadiabaticity.

$$\Delta G^{\ddagger} = (\lambda/4)(1 + \Delta G^0_{et}/\lambda)^2 \quad (6)$$

$$\lambda = (\lambda_{11} + \lambda_{22})/2 \quad (7)$$

The significantly small k_{ex} value of $(DPPF_{20})MnCl$ (4.3×10^{-6} $M^{-1}\cdot s^{-1}$) as compared with that of (TPP)MnCl (3.1×10^3 $M^{-1}\cdot s^{-1}$) may be related to differences in the conformation of the porphyrin macrocycles. The crystal structure of $(DPPF_{20})MnCl$ reveals a nonplanar conformation of the macrocycle because of peripheral congestion of the porphyrin.[16] The Mn^{III} center is located inside the curved

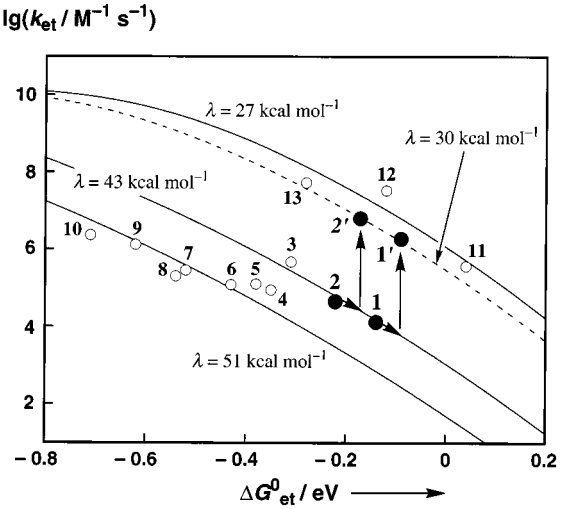


Figure 2. Dependence of lg k_{et} on ΔG^0_{et} for the electron-transfer reductions of the (P)MnCl derivatives by semiquinone radical anions in deaerated MeCN at 298 K; the numbers refer to the system: **1**: $(DPPH_{20})MnCl/Q^{\bullet-}$; **1′**: $[(DPPH_{20})Mn(py)_2]^+/Q^{\bullet-}$; **2**: $(DPPH_{20})MnCl/MeQ^{\bullet-}$; **2′**: $[(DPPH_{20})Mn(py)_2]^+/MeQ^{\bullet-}$; **3**: $(DPPH_{20})MnCl/2,6\text{-}Me_2Q^{\bullet-}$; **4**: $(DPPCl_{12}H_8)MnCl/Q^{\bullet-}$; **5**: $(DPPF_{20})MnCl/ClQ^{\bullet-}$; **6**: $(DPPCl_{12}H_8)MnCl/MeQ^{\bullet-}$; **7**: $(DPPCl_{12}H_8)MnCl/2,6\text{-}Me_2Q^{\bullet-}$; **8**: $(DPPF_{20})MnCl/Q^{\bullet-}$; **9**: $(DPPF_{20})MnCl/Q^{\bullet-}$; **10**: $(DPPF_{20})MnCl/Q^{\bullet-}$; **11**: (TPP)MnCl/2,5-$Cl_2Q^{\bullet-}$; **12**: (TPP)MnCl/$ClQ^{\bullet-}$; **13**: (TPP)MnCl/$Q^{\bullet-}$; 2,6-$Me_2Q$ = 2,6-dimethyl-*p*-benzoquinone, MeQ = methyl-*p*-benzoquinone, Q = *p*-benzoquinone, ClQ = chloro-*p*-benzoquinone, 2,5-Cl_2Q = 2,5-dichloro-*p*-benzoquinone; the solid and dashed lines are drawn based on the Marcus theory of electron transfer [Equation (6)and Equation (7)] using the λ values shown in the figure (see text)

surface of the nonplanar porphyrin macrocycle with a Mn^{III}−N distance of 1.99(1) Å.[16a] The strong binding of Mn^{III} to the nonplanar porphyrin causes a major bond-reorganization on the reduction of Mn^{III} to Mn^{II} and this is accompanied by a metal out-of-plane displacement since an electron is added to the $d_{x^2-y^2}$ orbital which directly interacts with the pyrrole nitrogen orbitals. Hence, the greater the nonplanarity of the porphyrin ligand, the stronger seems to be the binding of Mn^{III} to the ligand, the larger is the reorganization energy of the electron-transfer reduction and the smaller is the k_{ex} value, as was experimentally observed in the present study.

Effects of Axial Coordination on Electron Transfer

The slow electron-transfer reduction of nonplanar manganese porphyrins can be accelerated by axial coordination of a base since the addition of a nitrogenous base such as pyridine (py) to five-coordinate metalloporphyrins often results in substantial changes in the redox reactivities.[1,2,24,25] The addition of pyridine to an MeCN solution of $(DPPH_{20})MnCl$ results in a significant change in the UV/vis spectrum, as shown in Figure 3.

These changes can be analyzed by Equation (8), which is derived by assuming that *n* molecules of pyridine coordinate to $(DPPH_{20})MnCl$.

$$\lg[(A_0 - A)/(A - A_\infty)] = n\lg[py] + \lg K \quad (8)$$

In this Equation A_0 is the absorbance of $(DPPH_{20})MnCl$ in the absence of pyridine, A_∞ is the absorbance of the fully

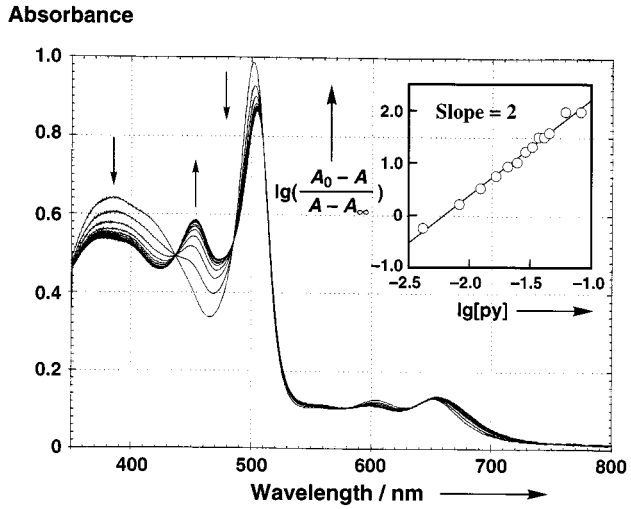


Figure 3. Spectral changes upon addition of py (4.1×10^{-3} M, each) to a deaerated MeCN solution of $(DPPH_{20})Mn^{III}Cl$ (1.8×10^{-5} M) at 298 K; inset: plot of $\lg[(A_0 - A)/(A - A_\infty)]$ vs. lg[py]; A_0, A, A_∞: absorbance at 452 nm

formed complex with pyridine, A is the absorbance of the equilibrium mixture, and K is the formation constant. The slope, n, in such plot gives the number of molecules of pyridine coordinated. The plot of $\lg[(A_0 - A)/(A - A_\infty)]$ vs. lg[py] (inset in Figure 3) indicates that two molecules of pyridine coordinate to $(DPPH_{20})MnCl$ to form the six coordinate complex $[(DPPH_{20})Mn(py)_2]^+$ (λ_{max} = 477 nm) and a lg$K$ value of 4.0 is calculated under the given experimental conditions [Equation (9)].

$$(DPPH_{20})Mn^{III}Cl + 2py \overset{K}{\rightleftharpoons} [(DPPH_{20})Mn^{III}(py)_2]Cl \quad (9)$$

The addition of pyridine to the $(DPPH_{20})MnCl$/reductant system results in a significant increase in the rate of electron transfer from the reductant to $(DPPH_{20})MnCl$. Most electron-transfer rates of (DPPX)MnCl in the presence of pyridine were so rapid so as to fall outside the stopped-flow range. Thus, the least reactive systems in Table 1, i.e. the $(DPPH_{20})MnCl/Q^{\bullet-}$ and $(DPPH_{20})MnCl/MeQ^{\bullet-}$ systems were chosen to determine the effect of pyridine on the electron-transfer rate. The electron-transfer rate constant k_{et} increases with an increase in the pyridine concentration to reach a constant value as shown in Figure 4.

The acceleration of the rate of electron transfer by the binding of pyridine may be ascribed to the much faster electron-transfer rate-constant for the six-coordinate complex ($k_{et(6)}$), $[(DPPH_{20})Mn(py)_2]^+$, than that for the five-coordinate complex ($k_{et(5)}$), $(DPPH_{20})MnCl$, as shown in Scheme 1. The $k_{et(6)}$ value for electron transfer from $Q^{\bullet-}$ to $[(DPPH_{20})Mn(py)_2]^+$ of 1.9×10^6 $M^{-1}\cdot s^{-1}$ was determined from the constant value in Figure 4 and is two orders of magnitude larger than the $k_{et(5)}$ value (1.3×10^4 $M^{-1}\cdot s^{-1}$) as shown in Table 1. Similarly, the $k_{et(6)}$ value for electron transfer from $MeQ^{\bullet-}$ to $[(DPPH_{20})Mn(py)_2]^+$ was determined from the data in Figure 4 to be 5.8×10^6 $M^{-1}\cdot s^{-1}$, which is also two orders of magnitude larger than the $k_{et(5)}$ value (4.1×10^4 $M^{-1}\cdot s^{-1}$).

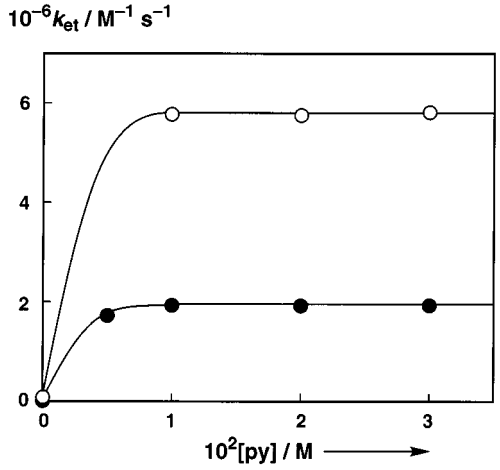
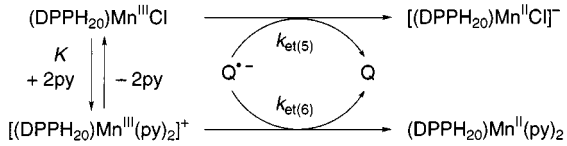


Figure 4. Plot of k_{et} vs. [py] for the electron transfer from $Q^{\bullet-}$ (filled circles; 9.1×10^{-6} M) or $MeQ^{\bullet-}$ (open circles; 9.1×10^{-6} M) to $(DPPH_{20})MnCl$ (9.1×10^{-6} M) in the presence of py in deaerated MeCN at 298 K



Scheme 1. Base-catalyzed electron transfer

The one-electron reduction potential might be expected to shift in a negative direction by the axial ligand coordination of pyridine when the electron-transfer reduction becomes energetically less favorable. However, the reduction of $[(DPPH_{20})Mn(py)_2]^+$ occurs at $E^0_{red} = -0.41$ V vs. SCE which is only slightly more negative than the E^0_{red} value (−0.36 V) of the five-coordinate complex $(DPPH_{20})MnCl$ (Table 1). Such a small negative shift of the reduction potential by coordination of pyridine cannot account for the large acceleration in the rate of electron transfer for the six-coordinate complex as compared to the five coordinate complex, as shown by the arrows along the curve with a constant λ value in Figure 2. Thus, the acceleration in the rate of electron transfer upon axial coordination of pyridine results from a significant decrease in the reorganization energy associated with the electron-transfer reduction of $[(DPPH_{20})Mn(py)_2]^+$. This is shown by the vertical arrows in Figure 2 where the dependence of k_{et} for the electron-transfer reduction of $[(DPPH_{20})Mn(py)_2]^+$, using a λ value of 30 kcal mol^{-1}, is given by the dashed line. The λ value becomes close to the value for the planar porphyrin (27 $kcal\cdot mol^{-1}$ for TPPMnCl). The acceleration effect of pyridine on the rates of electron transfer for the other (DPPX)MnCl complexes could not be determined quantitatively because of the fast electron-transfer rates for $[(DPPX)Mn(py)_2]^+$ which are beyond the detection limit of a stopped-flow technique, but such a rate-acceleration effect of pyridine indicates a significant decrease in the reorganization energy upon the axial ligand-coordination of the base. The k_{ex} values of $[(DPPH_{20})Mn(py)_2]^+$ (1.5×10^3 $M^{-1}\cdot s^{-1}$) determined from the k_{et} value using Equation (3)

and Equation (4) is five orders of magnitude larger than that of $(DPPH_{20})MnCl$ (Table 1).

We have also examined the rates of electron-transfer reduction of $(DPPH_{20})MnCl$ by $Q^{\bullet-}$ in deaerated DMSO. The UV/vis spectrum of the Mn^{III} complex in DMSO is similar to that in pyridine, suggesting that the six-coordinate complex $[(DPPH_{20})Mn(DMSO)_2]^+$ (λ_{max} = 480 nm) is formed in DMSO. The rate of electron-transfer from $Q^{\bullet-}$ to the Mn^{III} complex in DMSO was determined to be 2.3×10^6 $M^{-1}\cdot s^{-1}$, which is essentially the same as that of $[(DPPH_{20})Mn(py)_2]^+$ (1.9×10^6 $M^{-1}\cdot s^{-1}$). Addition of one mol of pyridine to a deaerated DMSO solution of Mn^{III} complex resulted in little acceleration of the electron-transfer reduction of the Mn^{III} complex by $Q^{\bullet-}$ (2.7×10^6 $M^{-1}\cdot s^{-1}$). These results indicate that the rates of electron-transfer reduction of the six-coordinate Mn^{III} porphyrins are much faster than those of the five-coordinate Mn^{III} porphyrins because of the smaller reorganization energies in the six-coordinate complex upon electron transfer than the five-coordinate complex, as observed in the case of the electron-transfer oxidation of (OETPP)Fe(R).[2]

Experimental Section

Materials: The synthesis and characterization of (P)MnCl (P = TPP or DPPX where X = H_{20}, $C_{12}H_8$ or F_{20}) have been reported in the literature.[16,19] *p*-Benzoquinone derivatives (2,6-Me_2Q: 2,6-dimethyl-*p*-benzoquinone; MeQ: methyl-*p*-benzoquinone; Q: *p*-benzoquinone; ClQ: chloro-*p*-benzoquinone; 2,5-Cl_2Q: 2,5-dichloro-*p*-benzoquinone) as well as the corresponding hydroquinones were purchased from Tokyo Chemical Industry Co., Ltd., and recrystallized from ethanol prior to use. Tetra-*n*-butylammonium hydroxide (TBAOH: 1.0 M in methanol) was purchased from Aldrich and used as received. Acetonitrile (MeCN) and benzonitrile (PhCN) were purchased from Wako Pure Chemical Ind. Ltd., and purified by successive distillation over CaH_2 and P_2O_5 according to standard procedures.[26] Tetra-*n*-butylammonium perchlorate (TBAP) was purchased from Sigma Chemical Co., recrystallized from ethanol, and dried under vacuum at 40 °C prior to use.

Spectral and Kinetic Measurements: Typically, a 3.0 μL aliquot of semiquinone radical anion ($Q^{\bullet-}$: 0.02 M) in MeCN was prepared by comproportionation between *p*-benzoquinone (Q: 0.01 M) and hydroquinone (QH_2: 0.01 M) in the presence of 0.02 M TBAOH[21] and then added to a quartz cuvette (10 mm i.d.) which contained $(DPPH_{20})MnCl$ (2.0×10^{-5} M) in deaerated MeCN (3.0 mL). This led to an electron transfer from $Q^{\bullet-}$ to $(DPPH_{20})MnCl$. The UV/visible spectral changes associated with this electron transfer were monitored with the use of a Hewlett Packard 8453 diode array spectrophotometer. The same procedure was used to follow reactions of other manganese porphyrins. The binding of pyridine or DMSO to $(DPPH_{20})MnCl$ in MeCN was monitored by measuring the UV/vis spectral changes as a function of the ligand concentration. All measurements were carried out in a dark cell compartment using deaerated conditions. It was confirmed that the monitoring light did not affect the thermal rates.

Kinetic measurements for electron transfer from $Q^{\bullet-}$ to (P)MnCl were carried out using a Union RA-103 stopped-flow spectrophotometer under deaerated conditions. Typically, deaerated MeCN solutions of (P)MnCl and $Q^{\bullet-}$ were transferred to the spectrophotometric cell by means of a glass syringe which had earlier been purged with a stream of argon. The rates of the electron transfer (k_{et}) were followed by monitoring an increase in the absorbance due to the reduced porphyrin product, $[(P)MnCl]^-$ (e.g. at 488 nm for $[(DPPH_{20})MnCl]^-$), under second-order conditions where the initial concentrations of (P)MnCl and $Q^{\bullet-}$ are the same. In each case, it was confirmed that the k_{et} values derived from at least five independent measurements which agreed within an experimental error of ±5%. Second-order rate constants were determined by a least-squares curve fit using a Macintosh personal computer. The second-order plots of $(A_\infty - A)^{-1}$ vs. time (A_∞ and A are the final absorbance and the absorbance at the reaction time, respectively) were linear for three or more half-lives with the correlation coefficient, $\rho > 0.999$.

Cyclic Voltammetry: The redox potentials of (P)MnCl in PhCN or MeCN containing 0.1 M TBAP as supporting electrolyte were determined at room temperature by cyclic voltammetry under deaerated conditions using a three electrode system and a BAS 100B electrochemical analyzer. The working and counter electrodes were platinum while $Ag/AgNO_3$ (0.01 M) was used as the reference electrode. All potentials are reported as V vs. SCE. The $E_{1/2}$ value of ferrocene used as a standard is approximately 0.37 V vs. SCE in PhCN or MeCN under our solution conditions.[27]

Acknowledgments

This work was partially supported by an International Scientific Research Program (No. 11694079) and a Grant-in-Aid for Scientific Research Priority Area (Nos. 11133232 and 11136229) from the Ministry of Education, Science, Culture and Sports, Japan. R. G. acknowledges support from the CNRS. K. M. K. also acknowledges support from the Robert A. Welch Foundation (Grant E-680).

[1] S. Fukuzumi, *The Porphyrin Handbook* (Eds.: K. M. Kadish, K. M. Smith, R. Guilard), Academic Press, San Diego, CA, **1999**, Vol. 8, 115−151.
[2] S. Fukuzumi, I. Nakanishi, K. Tanaka, T. Suenobu, A. Tabard, R. Guilard, E. Van Caemelbecke, K. M. Kadish, *J. Am. Chem. Soc.* **1999**, *121*, 785−790.
[3] W. R. Scheidt, Y. J. Lee, *Struc. Bonding (Berlin)* **1987**, *64*, 1−70.
[4] [4a] H.-C. Chow, R. Serlin, C. E. Strouse, *J. Am. Chem. Soc.* **1975**, *97*, 7230−7237. − [4b] R. Serlin, H.-C. Chow, C. E. Strouse, *J. Am. Chem. Soc.* **1975**, *97*, 7237−7242.
[5] [5a] S. Gentemann, C. J. Medforth, T. P. Forsyth, D. J. Nurco, K. M. Smith, J. Fajer, D. Holten, *J. Am. Chem. Soc.* **1994**, *116*, 7363−7368. − [5b] K. M. Barkigia, M. D. Berber, J. Fajer, C. J. Medforth, M. W. Renner, K. M. Smith, *J. Am. Chem. Soc.* **1990**, *112*, 8851−8857.
[6] T. L. Horning, E. Fujita, J. Fajer, *J. Am. Chem. Soc.* **1986**, *108*, 323−325.
[7] R. G. Alden, M. R. Ondrias, J. A. Shelnutt, *J. Am. Chem. Soc.* **1990**, *112*, 691−697.
[8] K. M. Barkigia, L. Chantranupong, K. M. Smith, J. Fajer, *J. Am. Chem. Soc.* **1988**, *110*, 7566−7567.
[9] J. A. Shelnutt, C. J. Medforth, M. D. Berber, K. M. Barkigia, K. M. Smith, *J. Am. Chem. Soc.* **1991**, *113*, 4077−4087.
[10] J. Takeda, T. Ohya, M. Sato, *Inorg. Chem.* **1992**, *31*, 2877−2880.
[11] C. J. Medforth, J. D. Hobbs, M. R. Rodriguez, R. J. Abraham, K. M. Smith, J. A. Shelnutt, *Inorg Chem.* **1995**, *34*, 1333−1341.
[12] [12a] K. M. Faulkner, S. I. Liochev, I. Fridovich, *J. Biol. Chem.* **1994**, *269*, 23471−23476. − [12b] P. R. Gardner, D. D. H. Nguyen, C. W. White, *Arch. Biochem. Biophys.* **1996**, *325*, 20−28. − [12c] M. Hoshino, Y. Nagashima, H. Seki, M. De Leo, P. C. Ford, *Inorg. Chem.* **1998**, *37*, 2464−2469.
[13] B. Meunier, *Chem. Rev.* **1992**, *92*, 1411−1456.

[14] [14a] L. O. Spreer, A. C. Maliyackel, S. Holbrook, J. W. Otvos, M. Calvin, *J. Am. Chem. Soc.* **1986**, *108*, 1949−1953. − [14b] A. C. Maliyackel, J. W. Otvos, M. Calvin, L. O. Spreer, *Inorg. Chem.* **1987**, *26*, 4133−4135. − [14c] M. Schappacher, R. Weiss, *Inorg. Chem.* **1987**, *26*, 1189−1190. − [14d] R. S. Czernuszewicz, Y. O. Su, M. K. Stern, K. A. Macor, D. Kim, J. T. Groves, T. G. Spiro, *J. Am. Chem. Soc.* **1988**, *110*, 4158−4165. − [14e] K. R. Rodgers, H. M. Goff, *J. Am. Chem. Soc.* **1988**, *110*, 7049−7060. − [14f] J. T. Groves, M. K. Stern, *J. Am. Chem. Soc.* **1988**, *110*, 8628−8638. − [14g] R. D. Arasasingham, T. C. Bruice, *Inorg. Chem*. **1990**, *29*, 1422−1427. − [14h] R. J. Balahura, R. A. Kirby, *Inorg. Chem.* **1994**, *33*, 1021−1025.

[15] K. M. Kadish, M. Sweetland, J. S. Cheng, *Inorg. Chem*. **1978**, *17*, 2795−2797.

[16] [16a] R. Guilard, K. Perié, J.-M. Barbe, D. J. Nurco, K. M. Smith, E. Van Caemelbecke, K. M. Kadish, *Inorg. Chem.* **1998**, *37*, 973−981. − [16b] K. Perie, J. M. Barbe, P. Cocolios, R. Guilard, *Bull. Soc. Chim. Fr.* **1996**, *133*, 697−702.

[17] [17a] X. H. Mu, F. A. Schultz, *Inorg. Chem.* **1992**, *31*, 3351−3357. − [17b] X. H. Mu, F. A. Schultz, *J. Electroanal. Chem.* **1993**, *353*, 349−355. − [17c] D. Feng, F. A. Schultz, *Inorg. Chem.* **1988**, *27*, 2144−2149. − [17d] X. H. Mu, F. A. Schultz, *Inorg. Chem.* **1990**, *29*, 2877−2879.

[18] K. M. Kadish, D. G. Davis, *Ann. N. Y. Acad. Sci.* **1973**, *206*, 495−503.

[19] S. Fukuzumi, I. Nakanishi, J.-M. Barbe, R. Guilard, E. Van Caemelbecke, N. Guo, K. M. Kadish, *Angew. Chem.* **1999**, *111*, 1017−1019; *Angew. Chem. Int. Ed.* **1999**, *38*, 964−966.

[20] S. Fukuzumi, S. Koumitsu, K. Hironaka, T. Tanaka, *J. Am. Chem. Soc.* **1987**, *109*, 305−316.

[21] S. Fukuzumi, T. Yorisue, *Bull. Chem. Soc. Jpn.* 1992, *65*, 715−719.

[22] [22a] R. A. Marcus, *Annu. Rev. Phys. Chem.* **1964**, *15*, 155−196. − [22b] R. A. Marcus, *Angew. Chem.* **1993**, *105*, 1161−1172; *Angew. Chem. Int. Ed. Engl.* **1993**, *32*, 1111−1121.

[23] ESR linewidth analysis: [23a] R. Chang, *J. Chem. Educ.* **1970**, *47*, 563−568. − [23b] K. S. Cheng, N. Hirota, *Investigation of Rates and Mechanisms of Reaction, Vol. VI* (Ed.: G. G. Hammes), Wiley, New York, **1974**, 565−636. − [23c] I. Nakanishi, S. Itoh, T. Suenobu, S. Fukuzumi, *Chem. Commun.* **1997**, 1927−1928. − [23d] S. Fukuzumi, I. Nakanishi, T. Suenobu, K. M. Kadish, *J. Am. Chem. Soc.* **1999**, *121*, 3468−3474.

[24] [24a] K. M. Kadish, *Iron Porphyrins, Part 2* (Eds.: A. B. P. Lever, H. B. Gray), Addison-Wesley, Reading, MA, **1982**, 161−249. − [24b] K. M. Kadish, L. A. Bottomley, *Inorg. Chem.* **1980**, *19*, 832−836. − [24c] F. A. Walker, J. A. Barry, V. L. Balke, G. A. McDermott, M. Z. Wu, P. F. Linde, *Adv. Chem. Ser.* **1981**, *201*, 377−416.

[25] D. Lançon, P. Cocolios, R. Guilard, K. M. Kadish, *Organometallics* **1984**, *3*, 1164−1170.

[26] D. D. Perrin, W. L. F. Armarego, D. R. Perrin, *Purification of Laboratory Chemicals*; Pergamon Press, Elmsford, NY, **1966**.

[27] C. K. Mann, K. K. Barnes, *Electrochemical Reactions in Nonaqueous Systems*, Marcel Dekker, Inc., New York, **1990**.

Received December 10, 1999
[I99450]

Substitution Behaviour of an Alkylcobaltamine Complex − Evidence for a Limiting Dissociative Mechanism

Carlos Dücker-Benfer,[a] Mohamed S. A. Hamza,[a][+] Conrad Eckhardt,[a] and Rudi van Eldik*[a]

Keywords: Cobalt / High-pressure chemistry / Kinetics / Isomerization / Amine complexes

The substitution behaviour of pentaamminemethylcobalt(III) with ethylenediamine (en) was studied in detail in aqueous ammonia solution. The displacement of four ammonia ligands by two ethylenediamine (en) chelates was followed by a subsequent slow *cis* to *trans* rearrangement of the bis(ethylenediamine)(amine)methyl complex. The dependence of the substitution reaction on [en], [NH_3], temperature and pressure was studied, and the observed kinetic traces could be fitted to the sum of two exponentials. The rate law for both reaction steps showed saturation kinetics with respect to [en] and [NH_3], and the activation parameters confirmed the operation of a limiting dissociative reaction mechanism under all conditions. For the first substitution reaction, $k_{sat.}(en)_{10\ °C}$ = 1.8 ± 0.4 s^{-1}, $k_{sat.}(NH_3)_{10\ °C}$ = 1.7 ± 0.3 s^{-1} and $\Delta V^{\#}_{15\ °C}$ = +14 ± 1 $cm^3 \cdot mol^{-1}$, for the second substitution reaction, $k_{sat.}(en)_{10\ °C}$ = 0.55 ± 0.12 s^{-1}, $k_{sat.}(NH_3)_{10\ °C}$ = 0.58 ± 0.10 s^{-1} and $\Delta V^{\#}_{15\ °C}$ = +24 ± 1 $cm^3 \cdot mol^{-1}$. The subsequent isomerization reaction was also studied in detail, and a complete set of activation parameters confirm the operation of a dissociative mechanism for the *cis* to *trans* rearrangement for which $k_{iso25\ °C}$ = (1.48 ± 0.07) × 10^{-3} s^{-1}; $\Delta H^{\#}$ = 115 ± 5 $kJ \cdot mol^{-1}$; $\Delta S^{\#}$ = + 86 ± 16 $J \cdot K^{-1} \cdot mol^{-1}$and $\Delta V^{\#}$ = +14.2 ± 0.6 $cm^3 \cdot mol^{-1}$.

Introduction

The lability and substitution mechanism of Co^{III} complexes can largely be controlled by the nature of spectator ligands. In terms of a classical example involving complex-formation reactions of $[Co(NH_3)_5H_2O]^{3+}$, displacement of the four in-plane coordinated ammonia ligands by a porphyrin macrocycle, results in a large increase in lability of the coordinated solvent molecule in the axial position *trans* to the remaining amine ligand.[1] Such a modification not only enhances the lability of coordinated water, but also causes a changeover in the ligand substitution mechanism from a dissociative interchange (I_d) to a limiting dissociative (D) mechanism. Similarly, the introduction of a strong σ-donor ligand, such as a methyl group, *trans* to the coordinated solvent molecule is also expected to cause a significant increase in lability, and maybe even a changeover in substitution mechanism. [2−7]

Such effects have been observed in the past for model Rh^{III} complexes of the type *trans*-$[Rh(dmg)_2(R)(L)]$ (dmg = dimethylglyoximate; R = Me, CH_2Cl, CH_2CF_3; L = H_2O), which exhibit different substitution rates and substitution mechanisms depending on the σ-donor properties of R.[3] The introduction of several metal−carbon bonds through a ligand such as Cp* (pentamethylcyclopentadienyl) on aquated Rh^{III} not only causes an increase in the water exchange rate constant for $[Rh(Cp^*)(H_2O)_3]^{2+}$ by 11 orders of magnitude relative to $[Rh(H_2O)_6]^{3+}$, but also a changeover from an I_a water exchange mechanism for the hexaqua ion to an I_d mechanism for the Cp* complex, as supported by the significantly different volumes of activation reported for the water exchange reactions.[2,8]

Cobalt complexes with a metal−carbon σ-bond can mimic the reactivity and mechanistic behaviour of B_{12} coenzymes. Compounds that have been studied include *trans*-$[Co(dmg)_2(R)(L)]$ (R = CH_3, *i*-C_3H_7, 5′-deoxyadenosyl; L = NH_3, pyridine (py), 2-NH_2py, 5,6-dimethylbenzimidazole, MeOH, Me_2S, etc.) and many Schiff base complexes.[4,5,7,9−26] The simplest model for the B_{12} coenzyme was recently synthesized by Kofod and consists of a Co^{III} metal centre surrounded by five ammonia ligands and one methyl group.[27] The X-ray structure shows a large increase in the length of the Co−N bond *trans* to the metal−carbon bond compared to those of the equatorial positions.[28] An interesting question is to what extent the introduction of a single metal−carbon σ-bond affects the substitution behaviour of this Co^{III} complex.

We have undertaken a detailed kinetic study of the reaction of $[Co(NH_3)_5(CH_3)]^{2+}$ with ethylenediamine (en), and could identify the rapid stepwise formation of *cis*-$[Co(en)_2(NH_3)(CH_3)]^{2+}$ and the subsequent slower isomerization to the stable *trans*-$[Co(en)_2(NH_3)(CH_3)]^{2+}$ complex. All rate and activation parameters could be resolved and strongly support the operation of a limiting dissociative (D) mechanism for all reaction steps.

[a] Institute for Inorganic Chemistry, University of Erlangen-Nürnberg,
Egerlandstraße 1, D-91058 Erlangen, Germany
E-mail: vaneldik@chemie.uni-erlangen.de
[+] On leave from the Department of Chemistry,
Ain Shams University, Cairo, Egypt

 © WILEY-VCH Verlag GmbH, D-69451 Weinheim, 2000 1434−1948/00/0707−1563 $ 17.50+.50/0

Results and Discussion

Preliminary Observations

The pentaamminemethyl complex is stable in solution only in the presence of a large excess of NH_3 (>3 M). In less concentrated ammonia, the complex undergoes slow decomposition due to hydrolysis and Co−C bond breakage, accompanied by the formation of the hexaammine complex and Co^{III} hydroxides. It was also observed that the pentaamminemethyl complex is sensitive to light and easily undergoes a photo-induced cleavage of the Co−C bond.

Experiments with monodentate ligands such as thiourea and derivatives, various substituted amines and thiocyanate, did not show significant spectral changes under the selected conditions, indicating that only weak complex formation occurred with these nucleophiles in the presence of the high concentration of ammonia. This is most probably due to the strong *trans* labilizing effect of the cobalt−carbon bond and the competition with the excess ammonia in solution. The reaction with cyanide leading to the formation of $[Co(CN)_5(CH_3)]^{3-}$ was recently reported by Kofod,[28] but the reaction was not studied kinetically. We therefore employed bidentate ligands that would lead to thermodynamically more stable products as a result of the chelate effect. Preliminary experiments were successful with bipyridine, phenanthroline or ethylenediamine (en). Of these, only en was soluble enough in water to perform kinetic measurements under pseudo-first-order conditions.

Important to note is that the pH had to be higher than 9.3, the pK_a of NH_4^+. At lower pH, protonation of ammonia reduces its coordination ability and therefore the stability of the complex. A pH of ca. 11 proved to be most convenient, since ethylenediamine then acts simultaneously as a nucleophile and as a buffer.

Application of the rapid scan technique revealed an increase in absorbance between 250 and 620 nm (Figure 1), and absorbance−time plots at several wavelengths exhibited good fits for the sum of two exponentials. Following this fast reaction, a slow subsequent step could be observed which then led to the final UV/Vis spectrum of *trans*-$[Co(en)_2(NH_3)(CH_3)]^{2+}$ (see Figure 2). Important to note is that in the presence of a high NH_3 concentration in solution, the formation of the amine complex was observed in the UV/Vis spectra, but when the NH_3 concentration was systematically decreased, the shoulder around 300 nm, which was assigned to the *trans*-amine complex,[28] disappeared. The final spectrum of the slower reaction at low $[NH_3]$ was identical to that of the *trans*-$[Co(en)_2(H_2O)(CH_3)]^{2+}$.[28] Only at high $[NH_3]$ (ca. 3 M) can the equilibrium be shifted to form the *trans* amine complex. This finding clearly demonstrates the high degree of *trans*-labilization caused by the methyl group at this position. The observed spectral changes (Figure 2) can be explained in terms of the *cis* to *trans* isomerization of $[Co(en)_2(NH_3)(CH_3)]^{2+}$, which followed the fast ligand-substitution reactions.

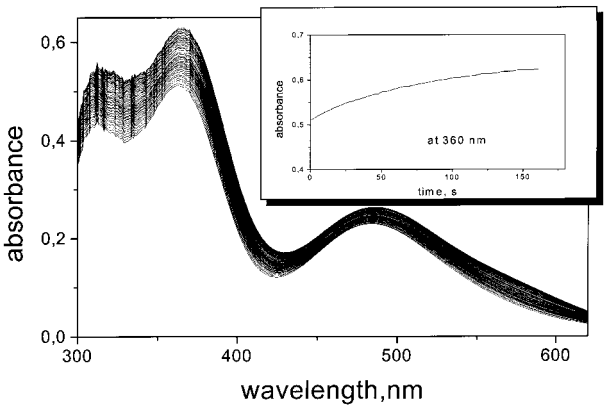


Figure 1. Repetitive-scan spectra for the reaction of $[Co(NH_3)_5(CH_3)]^{2+}$ with ethylenediamine; conditions: $[Co^{III}]$ = 2.5 mM, [en] = 0.2 M, $[NH_3]$ = 0.3 M, integration time for each spectrum 20 ms, total time 163.8 s, time between two spectra 2.64 and 4.64 s (two time bases), pH = 11 (not buffered); inset: the absorbance vs. time trace at 360 nm at room temperature

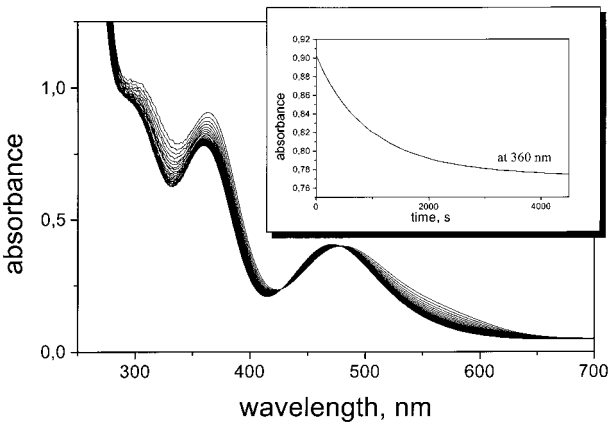


Figure 2. Repetitive-scan spectra recorded for the *cis* to *trans* isomerization of $[Co(en)_2(NH_3)(CH_3)]^{2+}$; conditions: [en] = 0.2 M, $[NH_3]$ = 0.3 M, 20.0 °C, time between two spectra 120 s, total time 38 min, pH ≈ 11(not buffered); inset: the absorbance vs. time trace at 360 nm

Ligand Substitution Mechanism

A study of the ethylenediamine concentration dependence of the fast reactions at a fixed 3 M ammonia concentration, revealed a decrease in k_{obs} for both reaction steps with increasing [en] as shown in Figure 3. Limiting rate constants of 1.8 ± 0.4 and 0.55 ± 0.12 s^{-1} at 10 °C were found for the first and second reaction steps, respectively, at high ethylenediamine concentrations. Under these conditions ([en] = 0.9 M) the effect of the ammonia concentration on the observed rate constants was studied (see Figure 4), and the values of $k_{obs(1)}$ again decreased with increasing $[NH_3]$ to reach a limiting value of 1.7 ± 0.3 s^{-1} (at 10 °C) at high ammonia concentration. The value of $k_{obs(2)}$ remains practically constant over the selected concentration range with a value of 0.58 ± 0.10 s^{-1} at high ammonia concentration. These limiting values are in excellent agreement with those reported for the dependence on [en] in Figure 3. At low

$[NH_3]$, the kinetic traces can only be fitted with a single exponential and no value for $k_{obs(2)}$ could be determined.

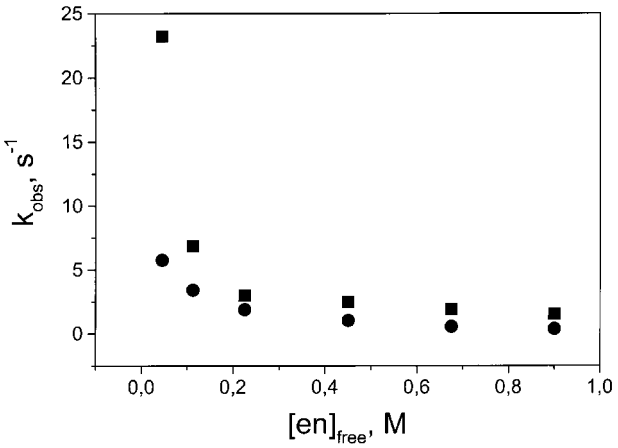


Figure 3. Plot of the observed rate constant (k_{obs}) vs. [en] at a constant $[NH_3]$ of 3 M at 10 °C, pH = 11, I = 0.5 M (NO_3^- medium); the filled squares are for the first ($k_{obs(1)}$) and the filled circles for the second ($k_{obs(2)}$) substitution reactions, respectively; $[en]_{free}$ is given as total [en] − $[enH^+]$

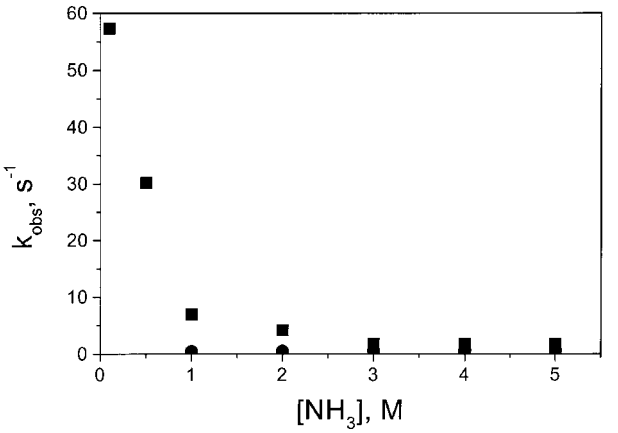


Figure 4. Plot of the observed rate constant (k_{obs}) vs. $[NH_3]$ at a constant [en] of 2 M at 10 °C, pH = 11, I = 0.5 M (NO_3^- medium); the filled squares are for the first ($k_{obs(1)}$) and the filled circles for the second ($k_{obs(2)}$) substitution reactions, respectively; $[NH_3]$ is given as total concentration

The temperature dependence of the reactions was measured under limiting concentration conditions, i.e. high concentrations of en and NH_3, over a rather limited temperature range due to the high ammonia concentration present in solution. The activation parameters could not be determined accurately and are therefore not reported. The pressure dependence of the reactions was measured under similar conditions and the results are summarized in Figure 5. Both $k_{obs(1)}$ and $k_{obs(2)}$ decrease significantly with increasing pressure. All rate and activation parameters are summarized in Table 1. The observed concentration dependences, as well as the reported activation volumes, strongly support the operation of a dissociative mechanism for both subsequent ligand-substitution processes. The unusual dependence of k_{obs} on $[NH_3]$ and [en] was also found by Malin et al. and Henderson et al. for substitution reactions of iron complexes, and a dissociative character was proposed for the mechanisms.1[29−31]

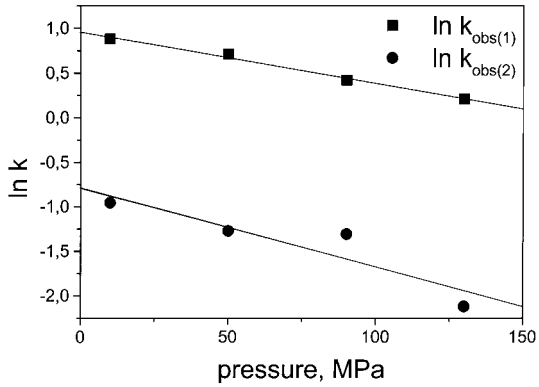
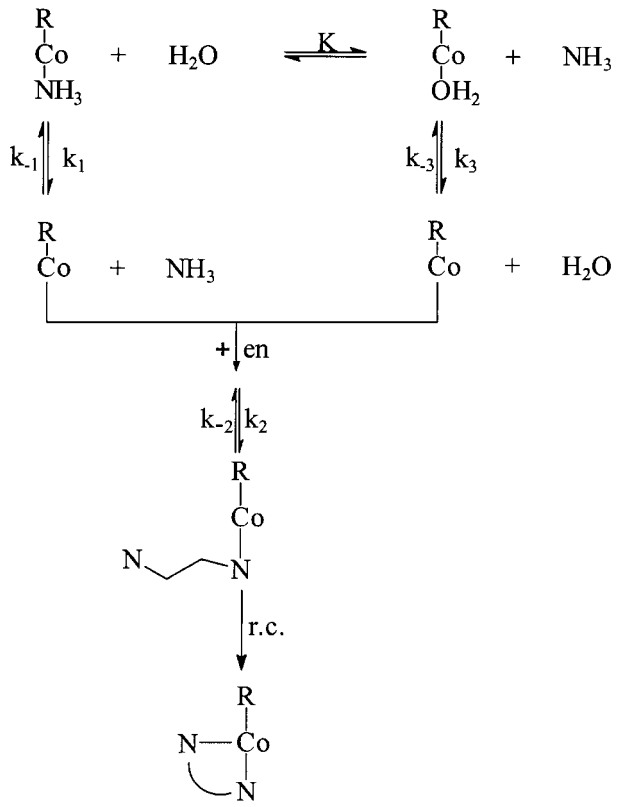


Figure 5. Pressure dependence of the observed rate constants for the two complex formation reactions $[Co(NH_3)_5(CH_3)]^{2+}$ with ethylenediamine, measured under limiting concentration conditions; conditions: [en] = 0.9 M, $[NH_3]$ = 3 M, temp. 15 °C, pH = 11, I = 0.5 M (NO_3^- medium)



Scheme 1

The first substitution reaction can be described by the mechanism outlined in Scheme 1.

As mentioned in the introduction, it is generally accepted that the metal−carbon bond in $[Co(NH_3)_5(CH_3)]^{2+}$ will induce a significant *trans*-labilization effect and cause a rapid spontaneous aquation reaction. The aquation equilibrium will be controlled by the concentration of ammonia in solution, for which the overall equilibrium constant can be ex-

Table 1. Rate and activation parameters for the reaction of $[Co(NH_3)_5(CH_3)]^{2+}$ with ethylenediamine (en) in ammonia solution

	k ($\times 10^3$) [s^{-1}]	$k_{sat}(NH_3)$[a] [s^{-1}]	$k_{sat}(en)$[a] [s^{-1}]	$\Delta H^{\#}$ [$kJ \cdot mol^{-1}$]	$\Delta S^{\#}$ [$J \cdot mol^{-1}K^{-1}$]	$\Delta V^{\#}_{15\,°C}$ [$cm^3 \cdot mol^{-1}$]
k_1	–	1.7 ± 0.3	1.8 ± 0.4	–	–	+14 ± 1
k'_1	–	0.58 ± 0.10	0.55 ± 0.12	–	–	+24 ± 1
k_{iso}[b]	1.48 ± 0.07	–	–	115 ± 5	+86 ± 16	+14.2 ± 0.6

[a] k_{sat} was measured under limiting conditions, i.e. for $k_{sat}(NH_3)$, $[NH_3]$ = 5 M and [en] = 2 M; for k_{sat}(en), $[NH_3]$ = 3 M and [en] = 2 M at 10 °C; pH = 11, I = 0.5 M (NO_3^- medium). – [b] k_{iso} was measured at 25 °C in nonbuffered solution.

pressed by $K = [Co-H_2O][NH_3]/[Co-NH_3]$. It has been suggested that this equilibration involves the five-coordinate $[Co(NH_3)_4(CH_3)]^{2+}$ species, which can react with either water or ammonia in the absence of another nucleophile. In the presence of ethylenediamine, the five-coordinate intermediate can be scavenged by en to form the 1:1 *trans*-$[Co(NH_3)_4(en)(CH_3)]^{2+}$ product species. This species is stabilized by a ring-closure reaction of ethylenediamine, accompanied by the loss of an amine ligand. The operation of a limiting D mechanism was also supported by the presence of five-coordinate species that are stabilized by the Co–C bond among the Co^{III} complexes of bis(salicylaldehyde)ethylenediamine and bis(acetylacetonato)ethylenediamine prepared by Costa and co-workers [9,32,33] and among the Co^{III} porphyrin pentacoordinated complexes.[34] Application of steady-state conditions to the five-coordinate intermediate $[Co(NH_3)_4(CH_3)]^{2+}$, results in the following expression for k_{obs}, where $f_{Co-NH3} = [NH_3]/(K+[NH_3])$ and $f_{Co-H2O} = K/(K+[NH_3])$.

$$k_{obs} = \frac{k_1 k_2 f_{Co-NH_3}[en] + k_3 k_2 f_{Co-H_2O}[en] + k_{-1} k_{-2}[NH_3] + k_{-2} k_{-3}[H_2O]}{k_{-1}[NH_3] + k_{-3}[H_2O] + k_2[en]}$$

This rate law can account for the decrease in k_{obs} with increasing $[NH_3]$ and [en].[29–31] The [en] dependence in Figure 3 was studied at a fixed and high $[NH_3]$, under which conditions this equation simplifies to

$$k_{obs} = \frac{k_1 k_2 f_{Co-NH_3}[en] + k_3 k_2 f_{Co-H_2O}[en] + k_a}{k_b + k_2[en]}$$

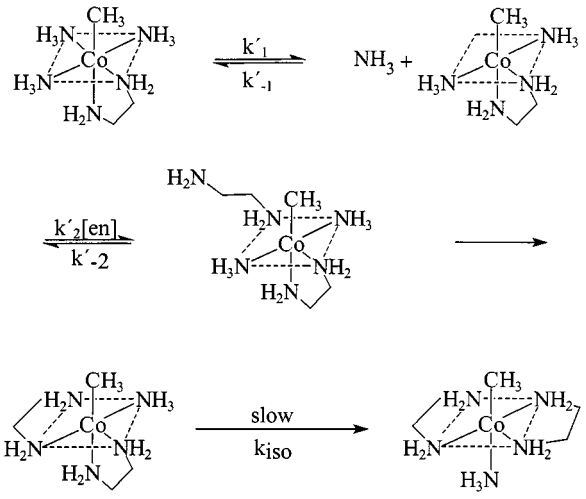
and reaches the limiting value

$$k_{obs} = k_1 f_{Co-NH_3} + k_3 f_{Co-H_2O} = \frac{k_1[NH_3] + k_3 K}{K + [NH_3]}$$

at high [en]. At high $[NH_3]$, this expression simplifies to $k_{obs} = k_1$. Furthermore, this expression can also account for the $[NH_3]$ dependence studied at high [en] (see Figure 4), from which the limiting rate constant found at high $[NH_3]$ must again be k_1. Thus under limiting conditions of high $[NH_3]$ and [en], the rate-determining step involves the dissociation of NH_3 from $[Co(NH_3)_5(CH_3)]^{2+}$. This accounts for the decrease in k_{obs} with increasing $[NH_3]$, since the aqua complex is expected to be much more labile than the corresponding amine complex. Extrapolation to $[NH_3] = 0$ results in $k_{obs} = k_3 \geq 60\ s^{-1}$, i.e. at least 50 times larger than k_1.

It follows that the suggested reaction mechanism and the given rate law can, in a qualitative way, account for the observed concentration dependences and the limiting rate constants reached at high NH_3 and en concentrations. A detailed fit of the data is limited by the complexity of the rate law. The activation parameters in Table 1 determined under limiting concentration conditions also support the dissociative nature of the substitution process.

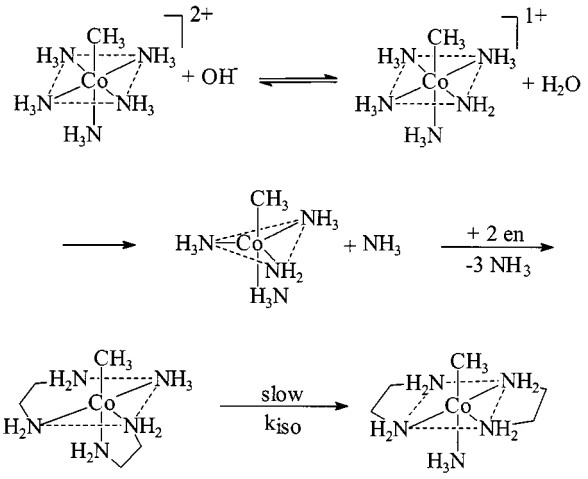
The subsequent formation of the 1:2 complex *cis*-$[Co(en)_2(NH_3)(CH_3)]^{2+}$ is about three to five times slower than the formation of the 1:1 complex, and it was more difficult to extract accurate data from the kinetic traces. The overall observed trends are very similar to those of the first substitution process, and we therefore suggest a similar mechanism for the attack of the second en ligand. This reaction must involve the displacement of a *cis* ligand, i.e. one of the three remaining amine ligands, since the *trans* position is occupied by en. The *cis*-labilization effect of the methyl group is expected to be much smaller, and therefore also the release of NH_3 in this position should also be slower than in the first reaction. The weaker labilization may also account for the absence of a clear $[NH_3]$ dependence, i.e. a lower $[NH_3]$ is still sufficient to stabilize the amine complex such that the equilibration with the aqua complex (see Scheme 1) does not have to be included in this case. The reaction steps can be summarized as shown in Scheme 2, from which it follows that k'_1 will be the rate-determining step under limiting [en] conditions and repre-



Scheme 2

sents the dissociation of an equatorial amine ligand. The five-coordinate intermediate rapidly reacts with a second en ligand, followed by a ring-closure reaction to produce *cis*-$[Co(en)_2(NH_3)(CH_3)]^{2+}$. The reported activation volume for the second substitution process (Table 1) also supports the operation of a limiting dissociative mechanism. Subsequently, the slow *cis* to *trans* isomerization of the latter complex occurs (see further Discussion).

The volumes of activation found for the subsequent substitution reactions under limiting concentration conditions, viz. $+14 \pm 1$ and $+24 \pm 1$ $cm^3 \cdot mol^{-1}$, are significantly positive in line with a limiting D mechanism. The value for the first reaction is close to the value reported for the dissociation of NH_3 in various octahedral complexes.[35–37] Since the *trans* influence of the methyl group already labilizes the $Co-NH_3$ bond in the ground state, as seen from X-ray structure analysis,[28] the volume increase required to dissociate NH_3 in the transition state will be significantly smaller than the partial molar volume of ammonia, viz. 24.85 $cm^3 \cdot mol^{-1}$.[38,39] The significantly higher value found for the second reaction step is surprising. This value may suggest that not only ammonia is labilized in the *cis* position, but also the ethylenediamine chelate. Partial ring-opening could, along with the dissociation of ammonia, account for the larger volume of activation. Alternatively, the more positive volume of activation found for the second substitution reaction may be due to the operation of a conjugate-base mechanism under the selected conditions. Earlier studies have demonstrated that base hydrolysis reactions proceeding by means of a conjugate base mechanism are characterized by large positive volumes of activation as a result of conjugate base formation and the subsequent ligand dissociation step.[40–44] For this reason we have checked the base concentration dependence of the substitution reactions, and the results are reported in Figure 6. The first substitution process is significantly accelerated by base, whereas the second substitution reaction hardly shows any base concentration dependence. The suggested conjugate base mechanism which could account for the acceleration observed for the first substitution process is outlined in Scheme 3.



Scheme 3

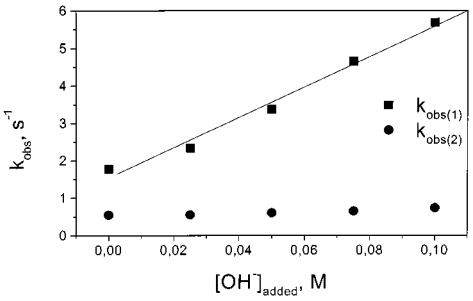


Figure 6. Plot of the observed rate constant (k_{obs}) vs. added $[OH^-]$ for the reaction of $[Co(NH_3)_5(CH_3)]^{2+}$ with ethylenediamine; conditions: [en] = 0.9 M, $[NH_3]$ = 3 M, temp. 10 °C, pH ≈ 11, I = 0.5 M (NO_3^- medium)

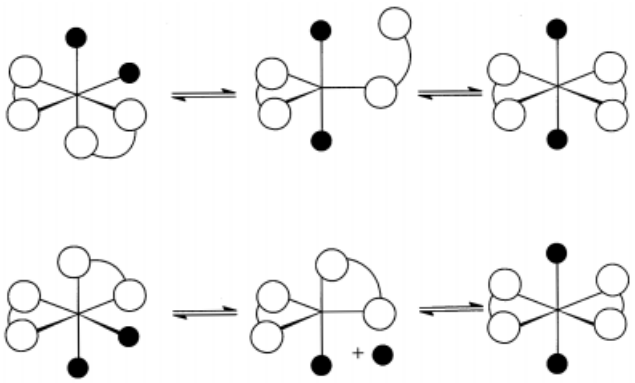
It follows from the data in Figure 6 that under the experimental conditions (pH ≈ 11, [en], $[NH_3]$) selected for the pressure dependence study, no significant contribution from base catalysis exists, and we can therefore rule out this possible explanation for the larger activation volume for the second substitution process.

cis–trans Isomerization Mechanism

The third and slower reaction step was assigned to the formation of the *trans* complex. The isomerization was followed as a subsequent reaction of the *cis*-complex rapidly produced on dissolving the pentaammine complex in a solution of en and NH_3. It was characterized by UV/Vis spectra with sharp isosbestic points at 427 and 492 nm, new bands formed at 358 and 466 nm, and a shoulder at 290 nm (see Figure 2). The positions of these bands shifted slightly to 363 and 470 nm when $[Co(NH_3)_5(CH_3)](NO_3)_2$ was dissolved in water without the addition of NH_3. This suggests that a water molecule occupies the trans position in the absence of NH_3.

The final spectrum is identical to the one published for the isolated and X-ray characterized *trans*-$[Co(en)_2(NH_3)(CH_3)](S_2O_6)$ complex.[28] The rate of the isomerization reaction was studied over a [en] range of 0.3 to 2.2 M, at a fixed $[NH_3]$ of 0.2 M. Absorbance–time traces were recorded and could be fitted with a single exponential. The rate of the *cis–trans* rearrangement was found to be independent of [en], with an average value of $(1.48 \pm 0.07) \times 10^{-3}$ s^{-1} for k_{iso} at 25 °C. The solutions were not buffered during these measurements. The activation parameters measured in the unbuffered solution, $\Delta H^{\#}$(iso) = 115 ± 5 $kJ \cdot mol^{-1}$, $\Delta S^{\#}$(iso) = 86 ± 16 $J \cdot mol^{-1} \cdot K^{-1}$ and $\Delta V^{\#}$(iso) = $+14.2 \pm 0.6$ $cm^3 \cdot mol^{-1}$, are all consistent with a limiting dissociative mechanism.

As known from a series of *cis-trans* isomerization reactions of cobalt complexes of the type $Co(en)_2XY$, the mechanism is in most cases a mixture of D or I type of reactions. In earlier papers isomerization mechanisms were discussed in terms of the possible reactions outlined in Scheme 4.[40,45]



Scheme 4

The main question that arises from Scheme 4 is how to distinguish between the two possible reaction paths that both involve ligand dissociation and will result in a positive volume of activation. It is not clear whether a square pyramidal or a trigonal bipyramidal intermediate is involved. On the one hand, we have the strong *trans* influence on the coordination site opposite to the carbon atom, as seen in the bond lengths of the solid state structure of $[Co(NH_3)_5(CH_3)](NO_3)_2$ [28] and in the fast Co^{III} substitution kinetics on the stopped-flow time scale. On the other hand, there are also the *cis* effects of both the methyl and the bidentate ligand which will weaken the $Co-NH_3$ bond and can therefore open another reaction path. It was necessary to keep the $[NH_3]$ at a low level in these reactions. At higher $[NH_3]$, the reaction was suppressed and the *cis* to *trans* rearrangement could no longer be observed. This is in line with the suggested rate-determining dissociation of NH_3. At high NH_3 concentration, the vacant coordination site will again be readily occupied by ammonia, and isomerization will be prevented. At low $[NH_3]$, competition between the free dangling end of en and NH_3 as entering ligands is at play. Once the second nitrogen donor of en is bound to the Co centre, the chelate effect prevails and stabilizes the *trans* product. The volume of activation data are also typical for the dissociation of NH_3 in the rate determining step.[35–37]

Under these circumstances we favour the reaction path involving the dissociation of NH_3 and the formation of the trigonal bipyramidal intermediate, since it readily provides the correct path for the isomerization reaction. The dissociation (ring-opening) of the en ligand may occur on a rapid time scale, but does not lead to isomerization of the complex due to an efficient ring-closure reaction.

This suggestion differs from what was suggested earlier for the isomerization of $[Co^{III}(en)_2(L)H_2O]$ complexes, where L is NH_3, Cl^-, Br^- or OH^-. The authors found that the reaction path is influenced by the strength of the Co–L bond relative to the strength of the Co–en bond.[45] However, in these studies the strong *trans* effect of the carbon donor, which will labilize any bond in that position, was not present.

To rule out the possible participation of a conjugate base mechanism during the *cis* to *trans* isomerization, the added base concentration was varied in a series of experiments. Only the loss of the isosbestic points and a general decrease in absorbance could be observed, suggesting that other processes interfere under such conditions.

Conclusions

The mechanism of ligand substitution in $[Co(NH_3)_5(CH_3)]^{2+}$ is strictly dissociative. The large volume increase found when going to the transition state can be accounted for in terms of only intrinsic volume effects. The high values of either $+14\ cm^3 \cdot mol^{-1}$ for the first or $+24\ cm^3 \cdot mol^{-1}$ for the second step strongly support the limiting dissociative character of the substitution process.

The $[Co(NH_3)_5(CH_3)]^{2+}$ cation is not favoured to be used as model for B_{12} chemistry due to the necessary presence of high ammonia concentrations and an unfavourable pH. The mechanistic understanding of the labilizing *trans* effect is important in terms of recent reports in the literature describing an interest in the activation of inert metal centres such as Co^{III}, Rh^{III}, and Ir^{III} complexes.[2,3,8,46–49] One major interest is the understanding of the electronic vs. steric tuning effects in simple substitution reactions, to enhance the understanding of catalytic cycles, and to synthesize specially designed complexes to be used as highly reactive and selective catalysts. In that respect, the final product of the substitution process reported here, *trans*-$[Co(en)_2(NH_3)(CH_3)]^{2+}$, may be a potential model for the vitamin B_{12} coenzyme and related systems.

Experimental Section

Methylhydrazine, cobalt(II) nitrate hexahydrate, ethylenediamine (en), sodium nitrate and ammonia solutions were all purchased from Aldrich or Merck and used as received, except for en which was distilled and stored under nitrogen before use. Pentaamminemethylcobalt(III) nitrate was prepared according to the method of Kofod,[27] but oxygen was bubbled through the reaction mixture for 4 h instead of exposure to air. The complex was stored under nitrogen in the dark. The purity of the complex was checked by elemental analysis and ^1H NMR and UV/Vis spectroscopy.[27,28] – All solutions for the kinetic measurements were freshly prepared with Millipore water in the dark before use. 10% of the total concentration of en was protonated with nitric acid to use en-enH$^+$ as buffer. – The NMR measurements were performed on a Bruker Avance DRX 400 WB NMR spectrometer. – UV/Vis spectra were recorded on either a Cary 1 or a Shimadzu UV-2101PC spectrophotometer. – Kinetic measurements for the fast substitution reactions were performed on an Applied Photophysics BioSX 18 MV instrument connected to a diode-array detector (TIDAS 200–620 nm, J&M, Aalen, Germany) to measure complete spectra on a ms time scale. The *cis* to *trans* rearrangement was followed as a subsequent slower step after mixing the complex and en solutions in a tandem cuvette or a pill box cell. In this case, no buffer was used. Kinetic measurements at elevated pressure were performed on a home-made high-pressure stopped-flow apparatus for the fast reactions or in a home-made high-pressure cell combined with a Shimadzu UV-2101PC spectrophotometer for the slower isomerization step.[50,51]

Acknowledgments

The authors gratefully acknowledge financial support from the Deutsche Forschungsgemeinschaft, Fonds der Chemischen Industrie, and the Alexander von Humboldt Foundation for a fellowship to M. S. A. H.

[1] J. G. Leipoldt, R. van Eldik, H. Kelm, *Inorg. Chem.* **1983**, *22*, 4146−4149.
[2] L. Dadci, H. Elias, U. Frey, A. Hörnig, U. Koelle, A. E. Merbach, H. Paulus, J. S. Schneider, *Inorg. Chem.* **1995**, *34*, 306−315.
[3] C. Dücker-Benfer, R. Dreos, R. van Eldik, *Angew. Chem. Int. Ed. Engl.* **1995**, *34*, 2245−2247.
[4] B. D. Gupta, K. Qanungo, V. Singh-Shobini, *Ind. J. Chem.* **1998**, *37A*, 707−711.
[5] R. Dreos-Garlatti, G. Tauzher, G. Costa, *Inorg. Chim. Acta* **1984**, *82*, 197−200.
[6] R. Dreos-Garlatti, G. Tauzher, G. Costa, *Inorg. Chim. Acta* **1986**, *121*, 27−32.
[7] J. M. Pratt, R. G. Thorp, *Adv. Inorg. Chem. Rad. Chem* **1969**, *12*, 375−427.
[8] M. S. Eisen, A. Haskel, H. Chen, M. M. Olmstead, D. P. Smith, M. F. Maestre, R. H. Fisch, *Organometallics* **1995**, *14*, 2806−2812.
[9] A. Bigotto, G. Costa, G. Mestroni, G. Pellizer, A. Puxeddu, E. Reisenhofer, L. Stefani, G. Tauzher, *Inorg. Chim. Acta Rev.* **1970**, *1*, 41−49.
[10] N. Bresciani-Pahor, M. Forcolin, L. G. Marzilli, L. Randaccio, M. F. Summers, P. J. Toscano, *Coord. Chem. Rev.* **1985**, *63*, 1−125.
[11] N. Bresciani-Pahor, M. Calligaris, L. Randaccio, L. G. Marzilli, M. F. Summers, P. J. Toscano, J. Grossmann, D. Liotta, *Organometallics* **1985**, *4*, 630−636.
[12] K. L. Brown, D. Chernoff, D. J. Keljo, R. G. Kallen, *J. Am. Chem. Soc.* **1972**, *94*, 6697−6704.
[13] K. L. Brown, D. Lyles, M. Pencovici, R. G. Kallen, *J. Am. Chem. Soc.* **1975**, *97*, 7338−7346.
[14] K. L. Brown, S. Satyanarayana, *J. Am. Chem. Soc.* **1992**, *114*, 5674−5684.
[15] J. E. Byrd, W. K. Wilmarth, *Inorg. Chim. Acta. Rev.* **1971**, *2*, 7−18.
[16] A. L. Crumbliss, W. K. Wilmarth, *J. Am. Chem. Soc.* **1970**, *92*, 2593−2594.
[17] R. Dreos, E. Herlinger, G. Tauzher, S. Vuano, G. Nardin, L. Randaccio, *Organometallics* **1998**, *17*, 2366−2369.
[18] R. Dreos-Garlatti, G. Tauzher, G. Costa, M. Green, *Inorg. Chim. Acta* **1981**, *50*, 95−99.
[19] R. Dreos-Garlatti, G. Tauzher, *Inorg. Chim. Acta* **1988**, *142*, 107−111.
[20] R. J. Guschl, T. L. Brown, *Inorg. Chem.* **1973**, *12*, 2815−2819.
[21] M. Kumar, E. Natarajan, P. Neta, *J. Phys. Chem.* **1994**, *98*, 8024−8029.
[22] P. Moore, *Pure Appl. Chem.* **1985**, *57*, 347−354.
[23] S. J. Moore, R. J. Lachicotte, S. T. Sullivan, L. G. Marzilli, *Inorg. Chem.* **1999**, *38*, 383−390.
[24] L. Randaccio, S. Geremia, R. Dreos-Garlatti, G. Tauzher, F. Asano, G. Pellizer, *Inorg. Chim. Acta* **1992**, *194*, 1−8.
[25] T. Sakurai, J. P. Fox, L. L. Ingraham, *Inorg. Chem.* **1971**, *10*, 1105−1106.
[26] L. M. Hansen, P. N. V. Pavan Kumar, D. S. Marynick, *Inorg. Chem.* **1994**, *33*, 728−735.
[27] P. Kofod, *Inorg. Chem.* **1995**, *34*, 2768−2770.
[28] P. Kofod, P. Harris, S. Larsen, *Inorg. Chem.* **1997**, *36*, 2258−2266.
[29] H. E. Toma, J. M. Malin, E. Giesbrecht, *Inorg. Chem.* **1973**, *12*, 2084−2089.
[30] J. M. Malin, H. E. Toma, E. Giesbrecht, *J. Chem. Educ.* **1977**, *54*, 385−386.
[31] R. A. Henderson, K. E. Oglieve, *J. Chem. Soc., Chem. Commun.* **1994**, 1961−1962.
[32] S. Brückner, M. Calligaris, G. Nardin, L. Randaccio, *Inorg. Chim. Acta* **1969**, *3*, 308−312.
[33] M. F. Summers, L. G. Marzilli, N. Bresciani-Pahor, L. Randaccio, *J. Am. Chem. Soc.* **1984**, *106*, 4478−4485.
[34] J. S. Summers, J. L. Petersen, A. M. Stolzenberg, *J. Am. Chem. Soc.* **1994**, *116*, 7189−7195.
[35] U. Spitzer, R. van Eldik, *Inorg. Chem.* **1982**, *21*, 4008−4014.
[36] K. Bal Reddy, R. van Eldik, *Inorg. Chem.* **1991**, *30*, 596−598.
[37] I. Maciejowska, R. van Eldik, G. Stochel, Z. Stasicka, *Inorg. Chem.* **1997**, *36*, 5409−5412.
[38] R. H. Stokes, *Aust. J. Chem.* **1975**, *28*, 2109−2114w.
[39] D. A. Palmer, H. Kelm, *Inorg. Chem.* **1977**, *16*, 3139−3143.
[40] G. A. Lawrance, D. R. Stranks, *Acc. Chem. Res.* **1979**, *12*, 403−409.
[41] Y. Kitamura, R. van Eldik, H. Kelm, *Inorg. Chem.* **1984**, *23*, 2038−2043.
[42] R. van Eldik, Y. Kitamura, C. P. Piriz Mac-Coll, *Inorg. Chem.* **1986**, *25*, 4252−4256.
[43] Y. Kitamura, G. A. Lawrance, R. van Eldik, *Inorg. Chem.* **1989**, *28*, 333−338.
[44] T. Poth, H. Paulus, H. Elias, R. van Eldik, A. Grohmann, *Eur. J. Inorg. Chem.* **1999**, 643−650.
[45] N. Serpone, D. G. Bickley, *Prog. Inorg. Chem.* **1972**, *17*, 391−566.
[46] R. Boca, H. Elias, *Polyhedron* **1996**, *15*, 2425−2431.
[47] U. Kölle, W. Kläui, *Z. Naturforsch.* **1991**, *46B*, 75−83.
[48] U. Kölle, *Coord. Chem. Rev.* **1994**, *135/136*, 623−650.
[49] U. Kölle, R. Görissen, T. Wagner, *Chem. Ber.* **1995**, *128*, 911−917.
[50] R. van Eldik, W. Gaede, S. Wieland, J. Kraft, M. Spitzer, D. A. Palmer, *Rev. Sci. Instrum.* **1993**, *64*, 1355−1357.
[51] F. K. Fleischmann, E. G. Conze, D. R. Stranks, H. Kelm, *Rev. Sci. Instrum.* **1974**, *45*, 1427−1429.

Received December 27, 1999
[I99472]

Contribution to the Chemistry of Boron, 245[‡]

Deprotonation of *B*,*B*′-Di-*tert*-butyl-*B*,*B*′-difluorenyldiborane(4) and the Structure of the Di-*tert*-butyl-difluorenylidenediborate(2−) Anion

Ralf Littger,[a] Heinrich Nöth*[a] and Max Suter[a]

Dedicated to Prof. Dr. D. Walther on the occasion of his 60th birthday

Keywords: Boranes / Borates / Deprotonation / Anions / Alkali metals

In contrast to the deprotonation of the diorganyl(fluorenyl)-boranes tBu$_2$B(fl-H) and Me$_2$B(fl-H), which cannot be achieved uniformly, the deprotonation of B$_2$(tBu)$_2$(fl-H)$_2$ in THF proceeds smoothly to give the anion B$_2$(tBu)$_2$(fl)$_2^{2-}$. The isolated salts have been identified as [Na(thf)$_n$]$_2$[B$_2$$tBu_2(fl)_2$] and [Na(thf)(OEt$_2$){Na(OEt$_2$)$_2$}][B$_2$$tBu_2(fl)_2$]. The X-ray structure of the latter compound reveals a longer B–B bond [1.744(9) Å] than that in the parent compound B$_2$(tBu$_2$)(fl-H)$_2$ [1.687(7) Å]. One sodium center is coordinated to the five-membered ring of one fluorenylidene substituent, while the other is coordinated to three C atoms of one of the six-membered rings. This results in a rather asymmetric structure. Each sodium center is also coordinated by two ether ligands.

Introduction

We have recently reported on the synthesis, molecular structures,[2] and synthetic potential[3] of the alkali and alkaline earth metal salts of bis(dimethylamino)difluorenyldiborane(4),[4] (Me$_2$N)$_2$B$_2$(fl-H)$_2$ (fl-H = fluorenyl = C$_{13}$H$_9$). A common feature of these compounds is a bent metallocene-type structure, in which the metal cations (Li, K, or Ca) are complexed by the two fluorenylidene ligands of the [(Me$_2$N)$_2$B$_2$(fl)$_2$]$^{2-}$ unit. The two fluorenylidene ligands are connected by a diborane(4)-*ansa*-bridge. The boron centers of (Me$_2$N)$_2$B$_2$(fl-H)$_2$ are shielded electronically by N−B π-bonding. Thus, in the dianion [(Me$_2$N)$_2$B$_2$(fl)$_2$]$^{2-}$, the lone pairs on the dimethylamino groups and the π-systems of the deprotonated fluorenyl substituents compete for the vacant p$_z$ orbitals at the boron centers. The π-interactions of the fluorenylidene substituents with the boron centers are, however, reduced by the complexation of the countercations, resulting in larger angles between the planes at the boron atoms and the planes of the fluorenylidene substituents than one might observe in the free dianions. Our interest has now been drawn to how substitution of the dimethylamino groups of [(Me$_2$N)$_2$B$_2$(fl)$_2$]$^{2-}$ by non-π-donor ligands affects the degree of π-interaction between the anionic fluorenyl groups and the boron centers and how this influences the ligand capacity of the [R$_2$B$_2$(fl)$_2$]$^{2-}$ unit (R = organyl group). To answer these questions, we have synthesized di-*tert*-butyl-difluorenyldiborane(4), (tBu)$_2$B$_2$(fl-H)$_2$, and have studied its deprotonation by sodium. For comparison purposes, we have also investigated the deprotonation of some related monoboranes, specifically fluorenyldimethylborane, Me$_2$B(fl-H), and di-*tert*-butyl-fluorenylborane, tBu$_2$B(fl-H).

Synthesis

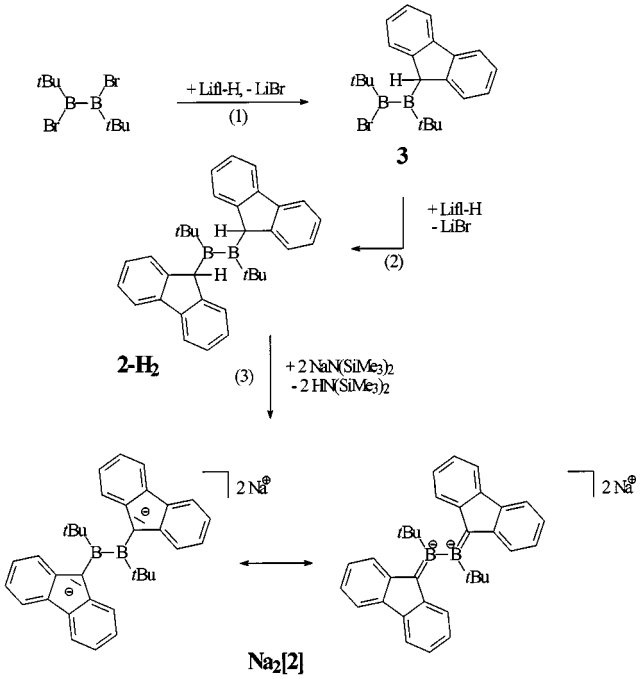
In order to obtain a stable difluorenyl-diorganyldiborane(4), we decided to replace the dimethylamino groups of (Me$_2$N)$_2$B$_2$(fl-H)$_2$ (**1**-H$_2$) by *tert*-butyl groups. This group is known[5,6] to be sufficiently bulky to prevent redox disproportionation, which occurs in diborane(4) compounds that lack adequate electronic shielding. Indeed, di-*tert*-butyl-difluorenyldiborane(4) (**2**-H$_2$) could be readily prepared by the stepwise substitution of the bromine atoms of dibromo-di-*tert*-butyldiborane(4)[7] by the fl$^-$ anion. Unexpectedly, however, MeO substitution of (tBu)$_2$B$_2$(OMe)$_2$, which has been successfully employed for the preparation of the tetraalkyldiborane(4) derivatives (tBu)$_2$B$_2$(tBu)R (R = Me,[5] CH$_2$SiMe$_3$,[5] CH$_2$CMe$_3$[6]) and (tBu)$_2$B$_2$(CH$_2$CMe$_3$)$_2$,[6] did not work in the present case. No reaction occurred between (tBu)$_2$B$_2$(OMe)$_2$ and fluorenyllithium. On the other hand, (tBu)$_2$B$_2$(fl-H)Br (**3**), could be obtained almost quantitatively from the reaction of (tBu)$_2$B$_2$Br$_2$ with one equivalent of fluorenyllithium [Scheme 1, (1)]. The reaction of pure **3** with a further equivalent of fluorenyllithium also proceeded quantitatively [Scheme 1, (2)], as shown by the ^{11}B-NMR spectrum of the reaction mixture. The diborane(4) compounds **2**-H$_2$ and **3** were isolated as colorless solids. At room temperature, they were found to be stable in solution as well as in the solid state.

The syntheses of di-*tert*-butyl-fluorenylborane (**4**-H) and fluorenyl-dimethylborane (**5**-H) proved to be straightfor-

[‡] Part 244: Ref.[1]

[a] Department of Chemistry, Inorganic Chemistry, University of Munich,
Butenandtstraße 5−13, Haus D, 81377 München, Germany

 © WILEY-VCH Verlag GmbH, D-69451 Weinheim, 2000 1434−1948/00/0707−1571 $ 17.50+.50/0

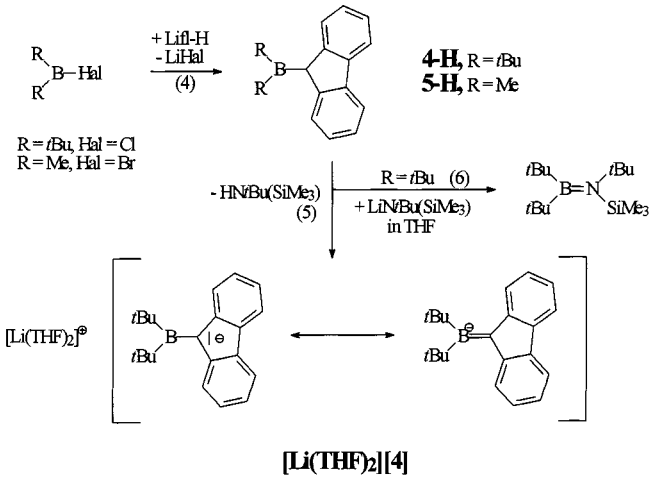


Scheme 1

ward. These compounds could be obtained by treating fluorenyllithium with one equivalent of tBu$_2$BCl or Me$_2$BBr, respectively [Scheme 2, (4)], and were isolated as colorless, crystalline solids. Other diorganyl-fluorenylboranes, R$_2$B(fl-H) (R = Et, Ph), have been reported previously.[8]

boron atoms in this compound. The disodium salt of the dianion [**2**]$^{2-}$ was isolated as an orange solid as a THF solvate [Na(thf)$_x$]$_2$[**2**] and was characterized by multinuclear NMR spectroscopy. The dimetallation of **2**-H$_2$ was further confirmed by performing a single-crystal X-ray structure analysis on the related solvate [Na(thf)(OEt$_2$)][Na(OEt$_2$)$_2$][**2**].

The lithium monoborate, containing the anion [tBu$_2$B(fl)]$^-$ ([**4**]$^-$) is the main product of the reaction between tBu$_2$B(fl-H) (**4**-H) and one equivalent of LiNtBu(SiMe$_3$) in tetrahydrofuran solution [Scheme 2, (5)]. The ^{11}B-NMR spectrum of the reaction mixture not only shows a signal due to this anion (δ = 77.9), but further signals at δ(^{11}B) = 87.9 [tBu$_2$B(fl-H)] and 54.0 [possibly tBu$_2$B−NtBu(SiMe$_3$), 8%] and minor signals in the region δ(^{11}B) = +10.0 to 0.0 (tetracoordinated borates, 5%). The lithium salt [Li(thf)$_2$][**4**] was recovered as a 4:1 mixture with fluorenyllithium. All attempts to separate these compounds by crystallization were unsuccessful. The formation of fluorenyllithium leads us to believe that the fluorenyl ligand of **4**-H is substituted by the amide [NtBu(SiMe$_3$)]$^-$ in a competing reaction [Scheme 2, (6)]. This hypothesis is supported by the ^{11}B-NMR signal at δ(^{11}B) = 54.0, which is consistent with an amino-diorganylborane tBu$_2$B−NtBu(SiMe$_3$), a compound that could be formed through such a substitution reaction [cf. the ^{11}B resonance of Me$_2$B−NtBu(SiMe$_3$): δ(^{11}B) = 56.2].[9] The deborylation of alkylboranes upon treatment with strong bases is well known for Et$_2$B(Cp),[10,11] a compound akin to **4**-H.



Scheme 2

On treatment with two equivalents of NaN(SiMe$_3$)$_2$ in tetrahydrofuran solution, **2**-H$_2$ is doubly deprotonated [Scheme 1, (3)]. According to the ^{11}B-NMR spectrum of the reaction mixture, the dianion [(tBu)$_2$B$_2$(fl)$_2$]$^{2-}$ (**2**$^{2-}$) is the main product (90%). Unidentified boron species give rise to signals in the region δ (^{11}B) = +5 to −20 (altogether 10%). This indicates that the steric shielding of the boron centers of **2**-H$_2$ is insufficient to completely suppress the nucleophilic attack of Li(H)fl. On the other hand, the double deprotonation of the sterically less shielded **1**-H$_2$ is quantitative as a result of the additional electronic shielding of the

The lithium salt [Li(thf)$_2$][**4**] has been characterized by multinuclear NMR spectroscopy. Its data are especially interesting with regard to the interpretation of the NMR data of the title dianion [**2**]$^{2-}$. These will be discussed later.

The deprotonation of Me$_2$B(fl-H) (**5**-H) which contains a sterically and electronically poorly shielded boron center is difficult. As yet, we have been unable to extract any useful information from the NMR spectra of the reaction mixture generated when **5**-H is treated with alkali metal amides or sodium metal. From the reaction of Et$_2$B(fl-H) with Na[BHEt$_3$], a compound claimed[8] to be [Na(digly-

me)$_{1.5}$][Et_2B(fl)] has been isolated. However, its NMR data are not compatible with a tricoordinated boron atom (vide infra).

NMR Spectra

The NMR-spectroscopic data of compounds **3**, **2**-H_2, **4**-H, **5**-H, Na_2[**2**], and [Li(thf)$_2$][**4**] are reported in the Experimental Section. The ^{11}B-NMR resonance of **2**-H_2 at $\delta(^{11}B) = 102.5$ is indicative of a tetraalkyldiborane(4) compound.[5,6] However, only a single, albeit broad resonance at $\delta(^{11}B) = 92.9$ is observed for the two different boron atoms of **3**, this chemical shift being intermediate between those of the resonances of the corresponding symmetric species **2**-H_2 [$\delta(^{11}B) = 102.5$] and (tBu)$_2B_2Br_2$ [$\delta(^{11}B) = 88.0$].[7] The asymmetric structure of **3** is, however, reflected in its ^{1}H- and ^{13}C-NMR spectra, which show discrete signals due to the two different *tert*-butyl groups. The fluorenyl substituents of both **3** and **2**-H_2 give rise to double sets of signals. In the case of **3**, all the nuclei of the single fluorenyl group are chemically inequivalent, but the two fluorenyl substituents of **2**-H_2 should be equivalent. At the present time, the question as to whether the observed inequivalence is due to hindered rotation about the B−B bond and/or about the B−C_{fl} bonds remains unclear. Most probably, the barrier associated with rotation about the B−B bond is higher than that for rotation about the B−C bond and hence diastereomers arise. Indeed, diastereomers have been found for much less sterically demanding substituted diborane(4) derivatives, such as (Me_2N)$_2B_2i$Pr$_2$ and (Me_2N)$_2B_2$(benzyl)$_2$ (room temperature, 400 MHz).[12]

The NMR data of the monoboranes **4**-H and **5**-H are unexceptional: **4**-H shows two sets of signals due to the two *tert*-butyl groups in the ^{1}H- and ^{13}C-NMR spectra and a single set of signals due to the fluorenyl substituent. This corresponds to a preferred conformation in which the plane of the fluorenyl substituent is oriented perpendicular to the plane at the boron center, with hindered rotation about the B−C_{fl} bond. The two methyl groups of **5**-H are chemically equivalent and the observation of one set of signals due to the fluorenyl group indicates free rotation about the B−C_{fl} bond. This difference between **4**-H and **5**-H (one signal in the ^{1}H- and ^{13}C-NMR spectra due to the *B*-methyl groups for the latter) can therefore be attributed purely to steric factors.

The boron atoms in the disodium salt Na_2[**2**] [$\delta(^{11}B) = 74.0$] are better shielded by 28 ppm than in the protonated **2**-H_2 [$\delta(^{11}B) = 102.5$]. This can be rationalized in terms of a strong π interaction between the deprotonated fluorenyl substituents and the boron centers. Even larger shielding effects have been observed in other cases, e.g. $\Delta\delta = 43.2$ for the couple Mes_2B-CH_3 [$\delta(^{11}B$, THF) = 83.6]/[$Mes_2B-CH_2]^-$ [$\delta(^{11}B$, THF) = 40.4] (Mes = 2,4,6-trimethylphenyl)[13] and $\Delta\delta = 38.6$ for the couple Mes_3B/[$Mes_2B-(3,5\text{-}Me_2)C_6H_2CH_2]^-$.[14] We assume that the negative charges in Na_2[**2**] are not only stabilized by the boron centers, but by the π system of the fluorenyl substituents as well. Such additional stabilization is naturally not possible for a CH_2^- group, even less so for a $PhCH^-$ group. In this context, it seems unlikely that the anion of [Na(diglyme)$_{1.5}$][Et_2B(fl)][8] has the structure of a deprotonated trialkylborane with a trigonal-planar coordinated boron atom. For the system Et_2B(fl-H) [$\delta(^{11}B$, THF) = 50.9]/[$Et_2B(fl)]^-$ [$\delta(^{11}B$, THF) = −25.5], a shielding difference of $\Delta\delta^{11}B = 76.4$ has been reported. However, the ^{11}B resonance for [$Et_2B(fl)]^-$ would be consistent with a tetracoordinated borate anion (dimeric species?).[15]

Compared to the corresponding resonances in Na_2[(Me_2N)$_2B_2$(fl)$_2$], Na_2[**1**],[2] the ^{13}C nuclei of the fluorenyl substituents are seen to be deshielded in Na_2[(tBu)$_2B_2$(fl)$_2$], Na_2[**2**], on average by 2.4 ppm (see Table 1), thus indicating a stronger π interaction between the fluorenyl substituents and the boron centers in the latter compound.

Even more deshielded are the C atoms in fluorenylidene(tetramethylpiperidino)borane,[17] tmp−B=fl (tmp = 2,2,6,6-tetramethylpiperidyl), a compound related to Na_2[**2**] containing a true B=C_{fl} double bond. In this case, one observes a $\Delta\delta(^{13}C)$ value of 2.3 ppm (average for C2 to C13) compared to Na_2[**2**].

Despite the partial B=C_{fl} double-bond character in Na_2[**2**], the fluorenyl substituents give rise to single sets of signals in the ^{1}H- and ^{13}C-NMR spectra. This indicates that the rotation about the B−C_{fl} bond is still a fast process on the NMR time scale. On the other hand, the signals due to C-2,13, C-4,11, and 5-,10-H are significantly broader, showing the onset of coalescence.

The ^{11}B resonance of [Li(thf)$_2$][**4**] is shifted to higher field by just 8.4 ppm compared with that of protonated **4**-H. This is surprising as deprotonation of the fluorenyl substituents in the related **2**-H_2/[**2**]$^{2-}$ system leads to a downfield shift in the resonance of the ^{11}B nuclei by 28 ppm. In comparison with Na_2[**2**], the ^{13}C-NMR signals of the fluorenyl substituents in [Li(thf)$_2$][**4**] are upfield shifted by an average of 2.6 ppm (see Table 2). These observations are consistent with a lesser degree of B−C_{fl}-π interaction in the monoborane case, with more electron density residing in the fluorenyl system. This complies with a noncoplanar orientation of the plane of the fluorenyl substituent and the plane about the boron center in [**4**]$^-$ due to the presence of the two bulky *tert*-butyl substituents at the boron atom. The small difference in shielding can then readily be explained in terms of an essentially perpendicular arrangement of the fl-H and fl$^-$ group with respect to the tBu$_2$B moiety.

The ^{1}H- and ^{13}C-NMR data of [Li(thf)$_2$][**4**] are strongly solvent-dependent. In C_6D_6 solution, the ^{13}C nuclei of the central five-membered ring (C-1, C-2,13, C-7,8) of the fluorenyl substituent are better shielded by 4.5 ppm (average) than in THF solution (see Table 2). On the other hand, the protonated benzoid ^{13}C nuclei of the fluorenyl substituent are deshielded by 2.4 ppm (average) in C_6D_6 solution. The same is true for the ^{1}H nuclei, which are deshielded by 0.53 ppm (average) in C_6D_6 solution as compared to their resonances in THF solution. This behavior is not unusual for alkali metal fluorenides and can be explained in terms of a solvent dependency of the formation of contact ion

Table 1. Comparison of the ^{13}C-NMR data of the fluorenyl substituents of Li_2[fl−$(CH_2)_2$−fl], Na_2[**1**], Na_2[**2**], and tmp−B=fl

Solvent	$Li_2[(CH_2)_2(fl)_2]$[16] [D_8]THF	Δ	Na_2[**1**][2] THF	Δ	Na_2[**2**] THF	Δ	tmp−B=fl[17] $CDCl_3$
C-2,13	135.9	+5.2	141.1	+4.9	146.0	−1.9	144.1
C-7,8	123.4	+2.3	125.7	+4.5	130.2	+3.5	133.7
C-4,11	118.9	+1.7	120.6	+1.9	122.5	+2.3	124.8
C-6,9	118.9	+0.8	119.7	+1.3	121.0	−1.2	119.8
C-3,12	114.8	+3.7	118.5	−0.4	118.1	+2.9	121.0
C-5,10	107.2	+3.5	110.7	+2.1	112.8	+8.1	120.9
Δ		+2.9		+2.4		+2.3	

Table 2. Comparison of the ^{13}C-NMR data of the fluorenyl group of [Li(thf)$_2$][**4**] (solvent-dependent) with those of the fluorenyl groups of Na_2[**2**]

Solvent	[Li(thf)$_2$][**4**] C_6D_6	Δ	[Li(thf)$_2$][**4**] THF	Δ	Na_2[**2**] THF
C-2,13	137.4	+4.7	142.1	+3.9	146.0
C-7,8	122.0	+4.4	126.4	+3.8	130.2
C-4,11	121.6	−1.2	120.4	+2.1	122.5
C-6,9	121.5	−2.3	119.2	+1.8	121.0
C-3,12	120.3	−2.0	118.3	−0.2	118.1
C-5,10	112.6	−3.9	108.7	+4.1	112.8
C-1	100.7		105.2		n.b.
Δ				+2.6	

pairs (CIPs) and solvent-separated ion pairs (SSIPs).[18] In the poorly solvating solvent C_6D_6, CIPs are formed between [Li(thf)$_2$]$^+$ and [**4**]$^-$. The cation [Li(thf)$_2$]$^+$ is located above the five-membered ring of the fluorenyl substituent, polarizing the π electrons towards this central ring, thereby accounting for the enhanced shielding of the central ^{13}C nuclei and the deshielding of the nuclei of the peripheral carbon atoms. In the strongly solvating solvent THF, an equilibrium exists between CIPs and SSIPs, as a result of which the polarizing effect of the cation [Li(thf)$_2$]$^+$ towards the fluorenyl substituent is somewhat diminished.

Molecular Structures

In order to obtain further information on the degree of C_{fl}−B-π bonding in the dianion [**2**]$^{2-}$, an X-ray structure determination of [Na(thf)(Et$_2$O)][Na(Et$_2$O)$_2$][**2**] was performed. The protonated compounds **2**-H_2 (Figure 1) and **4**-H were also subjected to X-ray structure analyses for comparison purposes. To the best of our knowledge, the crystal structure of **2**-H_2 represents the first solid-state structure of a noncyclic tetraalkyldiborane(4). A structure useful for making comparisons is that of the cyclic diborane(4) derivative [−B(Me)−B(Me)−C(SiMe$_3$)$_2$−Si(Me)$_2$−C(SiMe$_3$)$_2$−], in which all the atoms connected to the diborane(4) unit are C(sp^3) atoms.[19] The most striking feature of **2**-H_2 is that the planes at B1 and B2 are arranged perpendicularly to one another (C1−B1−C27/C14−B2−C31 = 89.2°). Normally, the planes at the boron atoms in diborane(4) derivatives form angles in the range 60−80°. The orthogonal orientation of the planes at the boron atoms in **2**-H_2 can be attributed to the presence of the sterically demanding *tert*-butyl groups in this compound. Despite the bulky substitution of **2**-H_2, the B1−B2 distance is quite short at 1.688(8) Å and, indeed, is the shortest yet found for a neutral tetraorganyldiborane(4). Comparable diborane(4) derivatives are Mes_2B−BMesPh [1.706(12) Å],[20] Mes_2B−BMes(CH_2SiMe_3) [1.71(2) Å],[20] Mes_2B_2[$CH(SiMe_3)_2$]$_2$ [1.739(7) Å],[21] and the afore-mentioned diboracyclopentane [1.729(8), 1.709(9) Å].[19] The two fluorenyl substituents of **2**-H_2 show significantly different B−C_{fl} bond lengths [B1−C1 = 1.609(6) Å, B2−C14 = 1.641(6) Å] and two different orientations with respect to the diborane(4) unit, as indicated by the dihedral angles C31−B2−C14−H14a = 171.6° and C27−B1−C1−H1a = 9.4°. For the trialkylborane **4**-H (Figure 2), a B−C_{fl} distance of 1.612(8) Å is found. The most significant feature of the molecular structure of **4**-H is the perpendicular arrangement of the plane at the boron center and the plane of the fluorenyl substituent (C1−C14−C18/C1 to C13 = 89.0°), which has already been established on the basis of ^{1}H- and ^{13}C-NMR data.

We were unable to obtain single crystals of a THF solvate of Na_2[**2**] from THF or THF/hexane mixtures. However, crystals suitable for X-ray crystallography were formed when [Na(thf)$_x$]$_2$[**2**] (Figure 3) was crystallized from diethyl

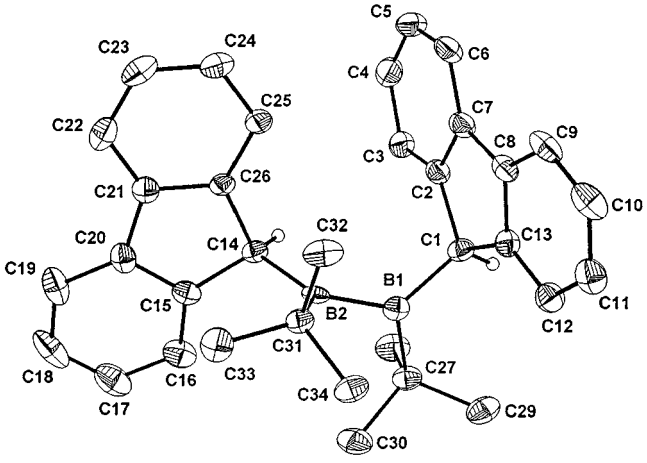


Figure 1. Molecular structure of (*t*Bu)$_2$B$_2$(fl-H)$_2$ (**2**-H_2); thermal ellipsoids are drawn at a 25% probability level; hydrogen atoms, except those on atoms C-1 and C-14, have been omitted for the sake of clarity; selected bond lengths [Å]: B1−B2 1.687(7), B1−C1 1.609(6), B2−C14 1.641(6), B1−C27 1.615(6), B2−C31 1.586(6); selected angles [°]: B2−B1−C1 124.1(3), B2−B1−C27 120.4(4), C1−B1−C27 115.1(4), B1−B2−C14 116.2(3), B1−B2−C31 121.6(3), C14−B2−C31 122.2(3), C1−B2−C27/C14−B1−C31 89.3, C1−B2−C27/C1 to C13 81.5, C14−B1−C31/C14 to C26 82.8

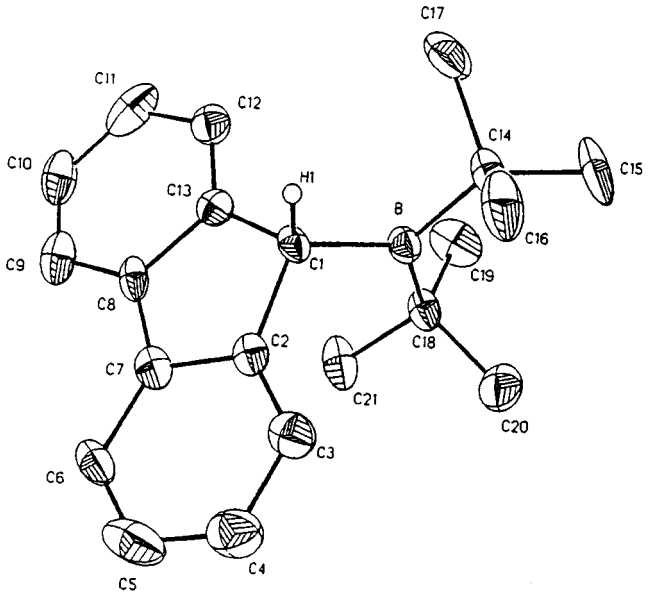


Figure 2. Molecular structure of tBu$_2$B(fl-H) (**4**-H); thermal ellipsoids are shown at a 25% probability level; hydrogen atoms, except that on atom C-1$_a$ have been omitted for the sake of clarity; selected bond lengths [Å]: B−C1 1.616(3), B−C14 1.594(3), B−C18 1.607(4); selected angles [°]: C1−B−C14 113.6(2), C1−B−C18 120.7(2), C14−B−C18 125.7(2), C1−C14−C18/C1 to C13 89.0

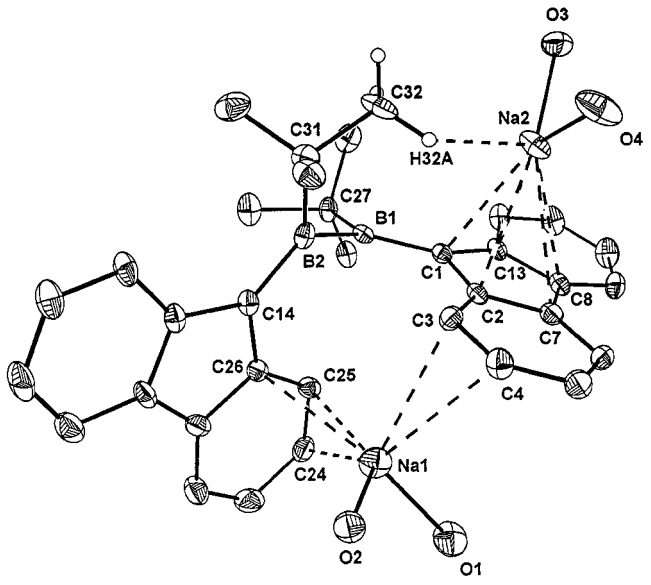


Figure 3. Molecular structure of [Na(thf)(OEt$_2$)][Na(OEt$_2$)$_2$][**2**]; thermal ellipsoids are shown at a 25% probability level; carbon atoms of the ether ligands and hydrogen atoms, except those at atom C-32, have been omitted for the sake of clarity; selected bond lengths [Å]: B1−B2 1.744(9), B1−C1 1.529(8), B1−C27 1.615(9), B2−C14 1.533(9), B2−C31 1.626(9), Na1−C25 2.720(6), Na1−C3 2.818(6), Na1−C26 2.822(6), Na1−C4 2.987(7), Na1−C24 3.071(7), Na1−O1 2.301(6), Na1−O2 2.329(5), Na2−C13 2.599(6), Na2−C1 2.671(6), Na2−C8 2.898(6), Na2−C2 2.912(6), Na2−C7 3.075(7), Na2−O4 2.242(6), Na2−O3 2.250(5), Na2−H32A 2.495; selected angles [°]: B2−B1−C1 121.6(5), B2−B1−C27 115.6(5), C1−B1−C27 122.8(5), B1−B2−C14 121.0(5), B1−B2−C31 116.0(5), C14−B2−C31 122.9(5), C27−B2−C1/C31−B1−C14 82.1, C27−B2−C1/C1 to C13 13.8, C31−B1−C14/C14 to C26 12.7, O1−Na1−O2 109.4(2), O3−Na2−O4 96.4(2)

ether at −20 °C. The structure determination confirmed the dimetallation of **2**-H$_2$ by sodium. The absence of protons at the fluorenyl carbon atoms bonded to the boron atoms is evident from the sum of the bond angles about these atoms (C1: 359.7°; C14: 360.0°). The dianion [**2**]$^{2-}$ and the two sodium cations form a monomeric contact ion triple. The sodium cations are complexed by one (Na2) or both (Na1) fluorenyl substituents of the dianion and by two additional ether molecules.

The angles between the planes at the boron atoms and the planes of the fluorenyl substituents are 12.7° and 13.8°, respectively. In the related dimetallated derivatives of **1**-H$_2$, the corresponding angles are 40.2 and 49.4°. The B−C$_{fl}$ distances in Na$_2$[**2**] are 10 pm shorter [1.529(8) and 1.533(9) Å] than those in the protonated **2**-H$_2$. These distances are also significantly shorter than those in (Me$_2$N)$_2$B$_2$Ph$_2$, a related compound with a B−C$_{sp2}$ bond (average B−C distance = 1.585 Å), but shorter than those in the analogous M$_2$[**1**] compounds (M$_2$ = Li$_2$, K$_2$, Ca) (average B−C$_{fl}$ distance of 1.547 Å). Together with the almost coplanar arrangement of the planes at the boron atoms and the fluorenyl planes, this gives an additional indication of significant B−C$_{fl}$-π bonding in Na$_2$[**2**].

The B−C$_{fl}$ distances in Na$_2$[**2**] are best compared with the B−C distance of 1.52(1) Å[22] in the anion [Mes$_2$B−(3,5-Me$_2$)C$_6$H$_2$CH$_2$]$^-$, as the boron atom has a similar acidity and the negative charge is also stabilized by an organic π system. In Na$_2$[**2**], steric repulsion between the fluorenyl substituents and the *tert*-butyl groups connected to the same boron atom is to be expected, and this indeed becomes apparent on comparing the pairs of angles B1−C1−C2/B1−C1−C13 = 122.5°/134.7° and B2−C14−C26/B2−C14−C15 = 122.5°/133.9° (see Figure 4). The two fluorenyl substituents are forced apart by the *tert*-butyl group connected to the same boron atom. This most probably accounts for the fact that the B−C$_{fl}$ distances in Na$_2$[**2**] are longer than they would be in a sterically less strained system. The two planes form an angle of 82.1°. Like the similar planes in the C$_2$BB starting material **2**-H$_2$, these are oriented almost perpendicularly to one another. The B−B distance in the dianion is 1.744(9) Å, which is 5.7 pm *longer* than the B−B distance in the parent protonated compound **2**-H$_2$ [1.687(7) Å]. An even more elongated B−B bond [1.859(8) Å] occurs in the less twisted (43°) diborane(4) unit of the related Li$_2$[Mes$_2$B$_2${C(SiMe$_3$)$_2$}$_2$].[23]

It is interesting to compare the rather unusual coordination modes of Na2 and especially of Na1 in Na$_2$[**2**] (Figure 4) with those observed in other fluorenyl sodium compounds.

Na2 is bonded in an asymmetric η^5 mode to the central five-membered ring of the fluorenyl substituent C1 to C13 (see Figure 4, top). It is not located centrally above the fluorenyl substituent, but is rather shifted towards C13 and C1, resulting in shorter contacts between Na2 and these carbon atoms [Na2−C13 = 2.599(6) Å, Na2−C1 = 2.671(6) Å]. A similar shift and similar Na−C distances have been reported for monomeric Nafl·PMDTA.[24] In both cases, the two shortest Na−C contacts are those to C1 and one of its neighbors. The coordination sphere about Na2 is completed by two ether molecules (one molecule of tetrahydrofuran

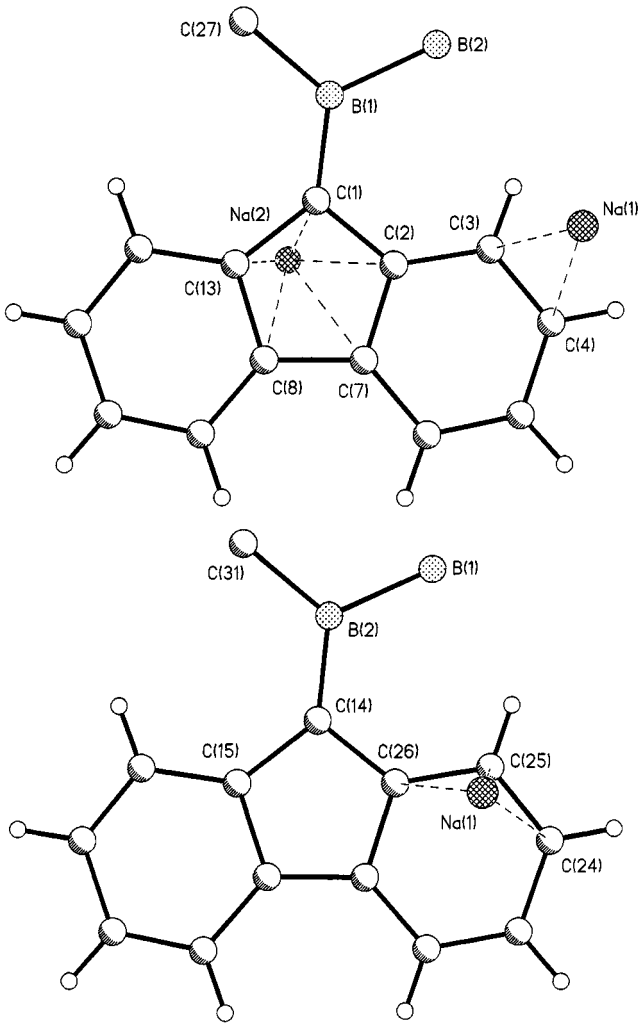


Figure 4. Plots showing the positions of the sodium cations Na1 and Na2 in $[Na(thf)(OEt_2)][Na(OEt_2)_2]$[**2**] with respect to the planes of the fluorenyl substituents C1 to C13 (top) and C14 to C26 (bottom); distances between the sodium cations and the fluorenyl planes [A]: Na2−(C1 to C13) 2.401, Na1−(C1 to C13) 2.642, Na1−(C14 to C26) 2.673

and one molecule of diethyl ether) and there is a weak interaction (Na2−H32a = 2.495 Å) between Na2 and a methyl group of the *tert*-butyl substituent bonded to B2. In contrast to monomeric $[Na(thf)(OEt_2)][Na(OEt_2)_2]$[**2**], solvates of fluorenylsodium in which the sodium cation is also coordinated to the fluorenyl anion and two donor atoms are either polymeric, such as $[Na(fl)\cdot TMEDA]_\infty$, or oligomeric, such as $[Na(fl)\cdot TMPDA]_4$. A monomeric solvate of fluorenylsodium is only formed with the tridentate PMDTA ligand.[24]

Na1 interacts with both fluorenyl substituents of the dianion $[\mathbf{2}]^{2-}$. The fluorenyl substituents do not coordinate Na1 through the carbon atoms of the central five-membered rings as has been observed for alkali metal compounds of the analogous dianion $[\mathbf{1}]^{2-}$. Such a di-η^5 coordination is impossible in the case of $[\mathbf{2}]^{2-}$ because of the almost perpendicular orientation of the planes at the boron atoms and the small angles between the planes at the boron atoms and the planes of the fluorenyl substituents. Na1 is coordinated by the benzoid carbon atoms of the fluorenyl substituents instead. It shows three contacts to the fluorenyl substituent C14 to C26 with Na−C distances of Na1−C25 = 2.720(6) Å, Na1−C26 = 2.822(6) Å, and Na1−C24 = 3.071(7) Å, and two contacts to the fluorenyl substituent C1 to C13 with Na−C distances of Na1−C3 = 2.818(6) Å and Na1−C4 = 2.987(7) Å (see Figure 4). If Na1 is projected perpendicularly onto the fluorenyl plane defined by the carbon atoms C1 to C13, it can be seen that this cation lies outside of the area of this fluorenyl substituent (see Figure 4, bottom). This coordination is strongly reminiscent of that of one of the sodium atoms in the cyclic tetramer $[Na(fl)\cdot TMPDA]_4$, in which the Na−C distances measure 3.025(5) and 3.032(5) Å.[24] Similar "out-of-ring coordination" has been observed in the dipotassium salt $[K(DME)]_2$[**1**].[2] The coordination sphere of Na1 is completed by two molecules of diethyl ether. The average Na−O distance is 2.315 Å, 7 pm longer than for Na2; the O−Na−O angle is 13° wider for Na1 (O1−Na1−O2 = 109.4°) compared to that at Na2 (O3−Na2−O4 = 96.4°).

Conclusion

The present study has again shown that the quantitative deprotonation of alkylboranes is not easily achieved. Even in the case of the compounds **2**-H_2 and **4**-H, in which the boron centers are sterically very shielded, the action of the weak nucleophilic bases $NaN(SiMe_3)_2$ and $LiNtBu(SiMe_3)$ leads to products in which significant numbers of boron atoms are tetracoordinated. As expected, the dianion $[\mathbf{2}]^{2-}$ displays a higher degree of C−B-π bonding than the related dimethylamino derivative $[\mathbf{1}]^{2-}$, as has been established on the basis of the following criteria: the B−C_{fl} bond lengths are shorter, the angles between the planes at the boron atoms and the planes of the corresponding fluorenyl substituents are smaller, and NMR studies show the ^1H and the ^{13}C nuclei of the fluorenyl substituents to be more deshielded. In $[\mathbf{2}]^{2-}$, the π system is not delocalized over the C_{fl}−B−B−C_{fl} unit as might be expected for an isoelectronic butadiene system. This is obvious as the planes at the boron atoms adopt an almost perpendicular arrangement. Therefore, $[\mathbf{2}]^{2-}$ is best described as a system in which two borylated carbanions are connected by a B−B single bond without B−C-π bond character. The question remains as to why butadiene-like structures are not realized for $[\mathbf{2}]^{2-}$ and the related anion $[Mes_2B_2\{C(SiMe_3)_2\}_2]^{2-}$, i.e. whether this is due to steric reasons or also due to the electronic situation.

Experimental Section

General: All manipulations were carried out under N_2 using Schlenk techniques. Solvents were dried by standard procedures. Commercial chemicals were purified prior to use as necessary; $(tBu)_2B_2Br_2$,[25] $(tBu)_2BCl$,[26] Me_2BBr,[27] Li(fl),[28] $NaN(SiMe_3)_2$, and $LiNtBu(SiMe_3)$[29] were prepared according to literature procedures. − NMR: Bruker AC-P 200 (^{11}B), Jeol EX 400 (^1H, ^{13}C);

standards: ext. $BF_3{\cdot}Et_2O$ (^{11}B), int. TMS or C_6D_6 (^1H, ^{13}C). – IR: Perkin–Elmer 325. – MS: Varian CH7 (70 eV). – X-ray structure determinations: Siemens P4 or Nicolet R3m diffractometer, Mo-K_α radiation, graphite monochromator.

1-Bromo-1,2-di-*tert*-butyl-2-(1-fluorenyl)diborane(4) (3): A suspension of fluorenyllithium (0.69 g, 4.01 mmol) in toluene (20 mL) was added dropwise to a solution of (tBu$_2$)B$_2$Br$_2$ (1.18 g, 3.99 mmol) in toluene (25 mL) at −78 °C. The mixture was allowed to warm to room temperature, stirred for 6 h, and then the insoluble material (0.32 g) was removed by centrifugation. The solution was concentrated to dryness, the residue was redissolved in hexane (12 mL), and this solution stored for 20 h at −20 °C. A colorless solid separated, which was filtered off, washed with cold hexane, and dried in vacuo. – Yield: 0.40 g of **3** (26%); m.p. 92–93 °C. – $C_{21}H_{27}B_2Br$ (381.0): calcd. C 66.21, H 7.14; found C 64.74, H 6.37. – MS (70 eV); *m*/*z* (%): 380 (100) [$M^{\bullet+}$], 233 (45) [$M^{\bullet+}$ − B(fl-H)Br], 165 (56) [fl-H]. – ^{11}B NMR (64.2 MHz, $CDCl_3$): δ = 92.9 ($h_{1/2}$ = 940 Hz). – ^1H NMR (400 MHz, $CDCl_3$): δ = 7.84, 7.78, 7.50, 7.45 [d, 1 H, ^3J(H,H) = 7.3 Hz; d, 1 H, ^3J(H,H) = 7.3 Hz; d, 1 H, ^3J(H,H) = 6.8 Hz; d, 1 H, ^3J(H,H) = 7.3 Hz, 3-,6-,9-,12-H], 7.32 (m, 4 H, 4-,5-,10-,11-H), 4.57 (s, 1 H, 1-H), 1.29, 0.37 [2 s, 2 × 9 H, 2 C(CH_3)$_3$]. – ^{13}C NMR (100.6 MHz, $CDCl_3$): δ = 147.1, 143.9 (C-2,13), 142.2, 140.5 (C-7,8), 126.7, 126.6, 126.5, 126.3, 126.1, 125.8 (C-3,4,5,10,11,12), 120.4, 119.9 (C-6,9), 49.3 (C-1), 30.1, 29.3 [*C*(CH$_3$)$_3$], 27.5, 26.2 [C(*C*H$_3$)$_3$].

1,2-Di-*tert*-butyl-1,2-bis(1-fluorenyl)diborane(4) (2-H$_2$): A suspension of fluorenyllithium (0.40 g, 2.32 mmol) in toluene (15 mL) was slowly added to a stirred solution of **3** (0.87 g, 2.28 mmol) in toluene (10 mL) at −78 °C. The mixture was allowed to warm to room temperature, stirred for 20 h, and then the insoluble material was separated by centrifugation. The solution was then concentrated to dryness in vacuo and the residue was redissolved in hexane (10 mL). Storing this solution for 3 d at −25 °C gave colorless, microcrystalline **2**-H$_2$, which was filtered off, washed with cold hexane (3 mL), and dried in vacuo for several hours. – Yield: 0.44 g of **2**-H$_2$ (41%); m.p. 138–139 °C. – $C_{34}H_{36}B_2$ (466.3): calcd. C 87.58, H 7.78; found C 85.47, H 7.57. – MS (70 eV); *m*/*z* (%): 466 (11) [$M^{\bullet+}$], 409 (5) [$M^{\bullet+}$ − C(CH$_3$)$_3$], 301 (91) [$M^{\bullet+}$ − $C_{13}H_9$], 233 (34) [$M^{\bullet+}$/2], 176 (77) [B(fl-H)], 165 (100) [fl-H]. – ^{11}B NMR (64.2 MHz, C_6D_6): δ = 102.5 ($h_{1/2}$ = 2250 Hz). – ^1H NMR (400 MHz, C_6D_6): δ = 7.76 [d, 2 H, ^3J(H,H) = 7.3 Hz, 6-H], 7.68 [d, 2 H, ^3J(H,H) = 7.3 Hz, 9-H], 7.57 [d, 2 H, ^3J(H,H) = 6.4 Hz, 3-H], 7.28 (pseudo-t, 2 H, 5-H), 7.19 (pseudo-t, 2 H, 10-H), 7.14 (pseudo-t, 2 H, 4-H), 7.04 (pseudo-t, 2 H, 11-H), 6.35 (m, very broad, 12-H), 4.66 (s, 2 H, 1-H), 0.75 [s, 18 H, C(CH_3)$_3$]. – ^{13}C NMR (100.6 MHz, C_6D_6): δ = 147.2, 145.6 (C-2,13), 142.9, 142.6 (C-7,8), 127.0 (C-4), 126.4 (C-5,10,11,12), 125.6 (C-3), 120.6 (C-6), 120.3 (C-9), 50.5 (C-1), 32.5 [*C*(CH$_3$)$_3$], 28.7 [C(*C*H$_3$)$_3$]. The ^1H and ^{13}C NMR resonances were assigned on the basis of ^1H-^1H-COSY and ^1H-^{13}C-HETCOR NMR experiments.

Di-*tert*-butyl-(1-fluorenyl)borane (4-H): A suspension of fluorenyllithium (2.14 g, 12.43 mmol) in toluene (30 mL) was slowly added to a stirred solution of tBu$_2$BCl (1.99 g, 12.40 mmol) in toluene (20 mL) at −78 °C. The mixture was allowed to warm to room temperature, in the course of which a brown-red color developed. After stirring for a further 20 h at room temperature, the insoluble material was separated by centrifugation and this solid was extracted with toluene (10 mL). The toluene solutions were combined and concentrated to dryness in vacuo. The residue (3.31 g) was redissolved in hexane (15 mL) and storage of this solution at −25 °C led to the deposition of large, colorless needles (0.50 g). Concentration of the mother liquor and further storage at −25 °C furnished a second crop of crystals (1.32 g). – Yield: 1.82 g of **4**-H (51%); m.p. 70–72 °C. – $C_{21}H_{27}B$ (290.3): calcd. C 86.90, H 9.38; found C 83.69, H 7.77. – ^{11}B NMR (64.2 MHz, C_6D_6): δ = 86.3 ($h_{1/2}$ = 670 Hz). – ^1H NMR (400 MHz, C_6D_6): δ = 7.75 [d, 2 H, ^3J(H,H) = 7.3 Hz, 6-,9-H], 7.28 [pseudo-t, ^3J(H,H) = 7.3 Hz, 2 H, 4-,11-H or 5-,10-H], 7.23 [d, 2 H, ^3J(H,H) = 6.8 Hz, 3-,12-H], 7.18 [pseudo-t, 2 H, ^3J(H,H) = 7.3 Hz, 4-,11-H or 5-,10-H], 4.41 (s, 1 H, 1-H), 1.24, 0.53 [2 s, 2 × 9 H, 2C(CH_3)$_3$]. – ^{13}C NMR (100.6 MHz, C_6D_6): δ = 147.9 (C-2,13), 143.2 (C-7,8), 126.8, 126.2 (C-4,5,10,11), 124.4 (C-3,12), 120.6 (C-6,9), 48.8 (C-1), 30.3, 29.9 [*C*(CH$_3$)$_3$], 28.6, 27.6 [C(*C*H$_3$)$_3$].

(1-Fluorenyl)dimethylborane (5-H): A suspension of fluorenyllithium (3.37 g, 19.6 mmol) in toluene (20 mL) was added dropwise to a stirred solution of Me_2BBr (2.37 g, 19.6 mmol) in toluene (20 mL) at −78 °C. The mixture was allowed to warm to ambient temperature, stirred for a further 3 d, and then the insoluble material (1.75 g) was separated by centrifugation. This solid was extracted with toluene (7 mL) and the toluene solutions were combined. Removal of all volatile compounds in vacuo left a red oil (3.45 g), heating of which at 110–130 °C/10^{-3} Torr resulted in the formation of very thin, colorless needles. – Yield: 2.79 g of **5**-H (69%); m.p. 49–50 °C. – $C_{15}H_{15}B$ (206.1): calcd. C 87.42, H 7.34; found C 86.67, H 7.87. – ^{11}B NMR (64.2 MHz, C_6D_6): δ = 83.8 ($h_{1/2}$ = 310 Hz). – ^1H NMR (400 MHz, C_6D_6): δ = 7.74 [d, 2 H, ^3J(H,H) = 7.3 Hz, 6-,9-H], 7.22 (m, 6 H, 3-,4-,5-,10-,11-,12-H), 4.29 (s, 1 H, 1-H), 0.53 (s, 6 H, CH_3). – ^{13}C NMR (100.6 MHz, C_6D_6): δ = 145.4 (C-2,13), 142.1 (C-7,8), 126.8, 126.3 (C-4,5,10,11), 124.8 (C-3,12), 120.5 (C-6,9), 53.8 (C-1), 13.0 (CH$_3$).

[Na(thf)$_x$]$_2$[(tBu)$_2$B$_2$(fl)$_2$] {[Na(thf)$_x$]$_2$[2]}: A solution of NaN(SiMe$_3$)$_2$ (0.31 g, 1.69 mmol) in tetrahydrofuran (7 mL) was added dropwise to a stirred solution of **2**-H$_2$ (0.41 g, 0.88 mmol) in tetrahydrofuran (10 mL) at room temperature. During the addition of the base, the color of the reaction mixture turned orange. Stirring was continued for 20 h and then the deep-red mixture was concentrated to dryness in vacuo. On treating the residue with hexane (10 mL), an orange powder formed, which was collected by filtration (0.28 g), washed with hexane (3 mL), and dried in vacuo. ^{11}B-, ^1H-, and ^{13}C-NMR spectroscopy showed the product to be a THF solvate of the disodium salt [Na(thf)$_x$]$_2$[**2**]. Crystals of the solvate [Na(thf)(OEt$_2$)][Na(OEt$_2$)$_2$][**2**] suitable for X-ray crystallography were obtained by recrystallizing the orange powdery [Na(thf)$_x$]$_2$[**2**] from diethyl ether at −20 °C. – ^{11}B NMR (64.2 MHz, THF/C_6D_6): δ = 72.0 ($h_{1/2}$ = 4100 Hz). – ^1H NMR (400 MHz, THF/C_6D_6): δ = 8.27 [d, 4 H, ^3J(H,H) = 8.3 Hz, 6-,9-H], 7.88 [d, 4 H, ^3J(H,H) = 7.3 Hz, 3-,12-H], 6.77 [(at +55 °C, t), 4 H, 4-,11-H], 6.60 (pseudo-t, 4 H, broad, 5-,10-H), 1.44 [s, 18 H, C(CH_3)$_3$]. – ^{13}C NMR (100.6 MHz, THF/C_6D_6): δ = 146.0 (broad, C-2,13), 130.2 (C-7,8), 122.5 (broad, C-4,11), 121.0 (C-6,9), 118.1 (C-3,12), 112.8 (C-5,10); (C-1) and [*C*(CH$_3$)$_3$] could not be detected; 34.7 [C(*C*H$_3$)$_3$].

Reaction of 4-H with LiN(tBu)(SiMe$_3$): A solution of LiNtBu(SiMe$_3$) (0.51 g, 3.37 mmol) in tetrahydrofuran (15 mL) was added dropwise to a solution of **4**-H (0.96 g, 3.31 mmol) in tetrahydrofuran (15 mL) at room temperature. The mixture was stirred for 1 d, in the course of which a deep-red color developed. After removing all volatile material in vacuo, a dark-red resinous residue (1.88 g) remained. Addition of hexane (20 mL) produced an orange powder (0.75 g), which was collected by filtration, washed with hexane (5 mL), and dried in vacuo. ^1H-, ^{13}C-, and ^{11}B-NMR spectroscopy showed this powder to consist of a 4:1 mixture of [Li(thf)$_2$][**4**] and fluorenyllithium. The powder proved to be very soluble in THF and benzene and moderately soluble in hexane. Separation of the

Table 3. Crystallographic data for the structures of **2**-H_2, **4**-H, and [Na(thf)(Et_2O)][$Na(Et_2O)_2$][**2**] and details relating to data collection and structure refinement

	2-H_2	**4**-H	[Na(thf)(Et_2O)][$Na(Et_2O)_2$][**2**]
Empirical formula	$C_{34}H_{36}B_2$	$C_{21}H_{27}B$	$C_{50}H_{72}B_2Na_2O_4$
Molecular mass	466.28	290.24	804.68
Crystal size [mm]	0.35 × 0.20 × 0.35	0.6 × 0.4 × 0.4	0.50 × 0.45 × 0.42
Crystal system	Orthorhombic	Monoclinic	Monoclinic
Space group	$P2_12_12_1$	$P2(1)/c$	$P2(1)/n$
a [Å]	9.269(2)	13.967(3)	12.282(4)
b [Å]	14.470(3)	14.502(3)	25.00(1)
c [Å]	20.579(8)	8.999(2)	16.04(1)
β [°]	90	90.119(4)	103.15(4)
V [Å^3]	2760.1(15)	1822.9(7)	4796(5)
Z	4	4	4
ρ(calcd.) [Mg/mm^3]	1.122	1.058	1.114
μ [mm^{-1}]	0.062	0.058	0.083
F(000)	1000	632	1744
Index range	$-1 \le h \le 10$	$-17 \le h \le 17$	$0 \le h \le 12$
	$-1 \le k \le 16$	$-18 \le k \le 18$	$-1 \le k \le 25$
	$-22 \le l \le 23$	$8 \le l \le 12$	$-16 \le l \le 16$
2θ [°]	4.0 to 47.0	5.34 to 57.88	3.08 to 43.00
T [K]	203	193(2)	173
Refl. collected	5285	10492	6033
Refl. unique	4073	3397	5404
Refl. observed (4σ)	2451	2085	2766
No. of variables	325	208	559
GooF	0.88	0.987	1.085
R	0.0551	0.0599	0.0729
$wR2$	0.0663	0.1714	0.1580
[e/Å^3]	0.25	0.223	0.297

two components by fractional crystallization could not be achieved. − **NMR Data for [Li(thf)$_2$][4]:** ^{11}B NMR (64.2 MHz, THF/C_6D_6): δ = 77.9 ($h_{1/2}$ = 950 Hz). − ^{1}H NMR (400 MHz, THF/C_6D_6): δ = 7.76 [d, 2 H, ^3J(H,H) = 7.3 Hz, 6-,9-H], 7.19 [d, 2 H, ^3J(H,H) = 8.3 Hz, 3-,12-H], 6.71 [pseudo-t, 2 H, ^3J(H,H) = 7.1 Hz, 4-,11-H], 6.35 [pseudo-t, 2 H, ^3J(H,H) = 7.3 Hz, 5-,10-H], 1.15 [s, 18 H, C(CH_3)$_3$]. − ^{13}C NMR (100.6 MHz, THF/C_6D_6): δ = 142.1 (C-2,13), 126.4 (C-7,8), 120.4 (C-4,11), 119.2 (C-6,9), 118.3 (C-3,12), 108.7 (C-5,10), 105.2 (C-1), 31.0 [C(CH$_3$)$_3$], 30.3 [C(CH$_3$)$_3$]. − ^{1}H NMR (400 MHz, C_6D_6): δ = 8.27 [d, 2 H, ^3J(H,H) = 7.8 Hz, 6-,9-H], 7.61 [d, 2 H, ^3J(H,H) = 8.3 Hz, 3-,12-H], 7.25 [pseudo-t, 2 H, ^3J(H,H) = 7.6 Hz, 4-,11-H], 6.99 [pseudo-t, 2 H, ^3J(H,H) = 7.3 Hz, 5-,10-H], 2.66 (m, 8 H, THF), 1.35 [s, 18 H, C(CH_3)$_3$], 1.04 (m, 8 H, THF). − ^{13}C NMR (100.6 MHz, C_6D_6): δ = 137.4 (C-2,13), 122.0 (C-7,8), 121.6 (C-4,11), 121.5 (C-6,9), 120.3 (C-3,12), 112.6 (C-5,10), 100.7 (C-1), 67.6 (THF), 30.9 [C(CH$_3$)$_3$], 29.4 [C(CH$_3$)$_3$], 25.0 (THF). − **NMR Data for Fluorenyllithium:** ^{1}H NMR (400 MHz, THF/C_6D_6): δ = 7.85 (d, 2 H, 6-,9-H), 7.24 (d, 2 H, 3-,12-H), 6.75 (pseudo-t, 2 H, 4-,11-H), 6.37 (pseudo-t, 2 H, 5-,10-H), 5.87 (s, 1 H, 1-H). − ^{13}C NMR (100.6 MHz, THF/C_6D_6): δ = 138.0 (C-2,13), 123.4 (C-7,8), 119.4 (C-4,11), 118.9 (C-6,9), 116.5 (C-3,12), 108.4 (C-5,10), 81.4 (C-1).

X-ray Structure Determination: Single crystals were coated with perfluoroether oil and mounted on glass fibres. They were cooled to −80 °C on the goniometer head. Cell dimensions were determined by automatically centering reflections taken from rotation photographs. Data collections were performed in the ω/2θ mode with variable scan speeds and adjusted scan widths. After data reduction (Lorentz and polarization correction), direct methods were applied for structure solution. The model was initially refined after atom assignment with isotropic temperature parameters, and then the positions of the atoms were refined using an anisotropic description. Hydrogen atom positions were calculated and included in the final calculation with fixed isotropic thermal parameters as riding on the respective C-atoms. Selected crystallographic data and data related to the structure solution and refinement are summarized in Table 3. Programs used: SHELXTL and SHELXL-93. Crystallographic data (excluding structure factors) for the structure reported in this paper have been deposited with the Cambridge Crystallographic Data Centre as supplementary publication no. CCDC-143688 to -143690. Copies of the data can be obtained free of charge on application to the CCDC, 12 Union Road, Cambridge CB2 1EZ, U.K. [Fax: (internat.) + 44-1223/336-033; E-mail: deposit@ccdc.cam.ac.uk].

Acknowledgments

We thank the Fonds der Chemischen Industrie and Chemetall GmbH for support of this work. Thanks are also due to Mr. P. Mayer for recording many NMR spectra, and to the team in the microanalytical laboratory for performing the analyses.

[1] W. Lippert, H. Nöth, W. Ponikwar, T. Seifert, *Eur. J. Inorg. Chem.* **1999**, 817−824.
[2] R. Littger, N. Metzler, H. Nöth, M. Wagner, *Chem. Ber.* **1994**, *127*, 1901−1908.
[3] R. Littger, H. Nöth, M. Thomann, M. Wagner, *Angew. Chem.* **1993**, *105*, 275−277; *Angew. Chem. Int. Ed. Engl.* **1993**, *32*, 295−297.
[4] H. Nöth, M. Wagner, *Chem. Ber.* **1991**, *124*, 1963−1972.
[5] W. Biffar, H. Nöth, H. Pommerening, *Angew. Chem.* **1980**, *92*, 63−64; *Angew. Chem. Int. Ed. Engl.* **1980**, *19*, 56.
[6] K. Schlüter, A. Berndt, *Angew. Chem.* **1980**, *92*, 64−65; *Angew. Chem. Int. Ed. Engl.* **1980**, *19*, 57.
[7] H. Pommerening, Ph.D. Thesis, University of Munich, **1979**.
[8] P. Paetzold, B. Boeke, *Chem. Ber.* **1976**, *109*, 1011−1016.
[9] H. Nöth, W. Tinhof, B. Wrackmeyer, *Chem. Ber.* **1974**, *107*, 518.
[10] H. Grundke, P. I. Paetzold, *Chem. Ber.* **1971**, *104*, 1136−1146.
[11] E. Herberich, B. Schmidt, U. Englert, *Organometallics* **1995**, *14*, 471−480.

[12] R. Littger, Ph.D. Thesis, University of Munich, **1996**.
[13] M. M. Olmstead, P. P. Power, K. J. Weese, *J. Am. Chem. Soc*. **1987**, *109*, 2541−2542.
[14] B. G. Ramsey, L. M. Isabelle, *J. Org. Chem*. **1981**, *46*, 179.
[15] H. Nöth, B. Wrackmeyer, *NMR Spectroscopy of Boron Compounds*, vol. 14 (*NMR Basic Principles and Applications*; Eds.: P. Diehl, E. Fluck, R. Kosfeld), Springer Publ., Heidelberg, Berlin, New York, **1978**.
[16] B. Becker, V. Enkelmann, K. Müller, *Angew. Chem*. **1989**, *101*, 501−503; *Angew. Chem. Int. Ed. Engl*. **1989**, *28*, 458.
[17] B. Glaser, H. Nöth, *Chem. Ber*. **1986**, *119*, 3253−3267.
[18] [18a] U. Edlund, *Org. Magn. Reson*. **1979**, *12*, 661−666. – [18b] J. B. Grutzner, J. M. Lawlor, L. M. Jackman, *J. Am. Chem. Soc*. **1972**, *94*, 2306−2315.
[19] U. Englert, R. Finger, P. Paetzold, B. Redenz-Stormanns, Z. Pawelec, W. Wojnowski, *Organometallics* **1995**, *14*, 1507−1509.
[20] A. Moezzi, M. M. Olmstead, R. A. Bartlett, P. P. Power, *Organometallics* **1992**, *11*, 2383−2388.
[21] A. Berndt, see reference [18] in: A. Moezzi, M. M. Olmstead, R. A. Bartlett, P. P. Power, *Organometallics* **1992**, *11*, 2383−2388.
[22] R. A. Bartlett, P. P. Power, *Organometallics* **1986**, *5*, 1916−1917.
[23] M. Pilz, J. Allwohn, P. Willershausen, W. Massa, A. Berndt, *Angew. Chem*. **1990**, *102*, 1085−1087; *Angew. Chem. Int. Ed. Engl.* **1990**, *29*, 1030−1032.
[24] S. Corbelin, J. Kopf, E. Weiss, *Chem. Ber*. **1991**, *124*, 2417−2422.
[25] H. Pommerening, Dissertation, University of Munich, **1979**.
[26] U. Höbel. H. Nöth, H. Prigge, *Chem. Ber.* **1986**, *119*, 325−327.
[27] H. Nöth, H. Vahrenkamp, *J. Organomet. Chem.* **1968**, *11*, 399−405.
[28] M. Wagner, Dissertation, University of Munich, **1992**.
[29] C. R. Krüger, H. Niederprüm, *Inorg. Synth*. **1966**, *8*, 15−19.

Received December 30, 1999
[I99477]

Synthesis and Properties of Dinuclear Complexes with a Photochromic Bridge: An Intervalence Electron Transfer Switching "On" and "Off"

Sandrine Fraysse,[a] Christophe Coudret,*[a] and Jean-Pierre Launay*[a]

Keywords: Photochromism / Metallacycles / Molecular devices / Electron transfer

Two cyclometallated $Ru(bpy)_2(pp)$ units (bpy = 2,2′-bipyridine; pp = 2-phenylpyridine) were grafted via ethynyl spacers onto the photochromic cores of the norbornadiene or dithienylethene families, to give the bimetallic ruthenium(II) complexes **1** and **2a**, respectively. Two aspects of these compounds were studied: (i) photoisomerization (norbornadiene to quadricyclane for **1**, open form to closed form of the dithienylethene core for **2a**), and (ii) intervalence transitions in the mixed-valence ruthenium(II–III) state, with determination of the metal–metal electronic coupling (V_{ab}) by Hush's equation. Moderate metal–metal electronic coupling (0.068 eV) was found for **1**, but **1** cannot be isomerized into the quadricyclane form. On the other hand, **2a** can be reversibly photoisomerized to the closed form **2b**. An iodine(III) reagent, the triflate salt of bis(pyridyl)phenyliodonium, was used for the oxidation of **2a** and **2b**. During these oxidations, an intervalence band due to intramolecular electron transfer between ruthenium(II) and ruthenium(III) was detected for **2b**, but not for **2a**. This switching "on" or "off" of the intervalence transition is rationalized with extended Hückel calculations. Finally, the molecular orbital calculation explains the observed tendency of the closed form **2b** to reopen upon oxidation.

Introduction

Switching at the molecular scale is one of the great challenges of molecular electronics.[1a] It is important to devise molecules able to reproduce one of the most important functions of electronic devices, that is, the ability to change in a controlled manner between a "conducting" and a "nonconducting" state, which is a prerequisite for the realization of logical functions. Ideally, such molecules should be used in nanometric-scale devices involving a unique molecule, and experiments along these lines are in progress.[1b–1d] However, due to the difficulty of experiments dealing with unique molecules, one has to rely, for some time still, on more conventional studies involving a (noninteracting) ensemble of molecules in solution, probed by spectroscopic methods. An important issue is the ability to transfer electrons intramolecularly between clearly identified sites.

Intramolecular electronic coupling between two redox sites can be probed by the intervalence transition occurring in the near-infrared for the mixed-valence state.[2] Hush's equation[3] allows the intensity of this transition to be used to estimate the electronic coupling term V_{ab}, that is, the efficiency of the bridge at mediating electron transfer between the distant redox sites.

In the search for molecules able to show a switching effect, we have tried to introduce as bridging ligand a photochromic moiety exhibiting two states ("on" and "off") with respect to electronic coupling. Symmetrical photochromic cores were selected to preserve the formal "exchangeability" of the two metallic centers. The association of photochromism and intervalence electron transfer is schematically represented in Figure 1a.

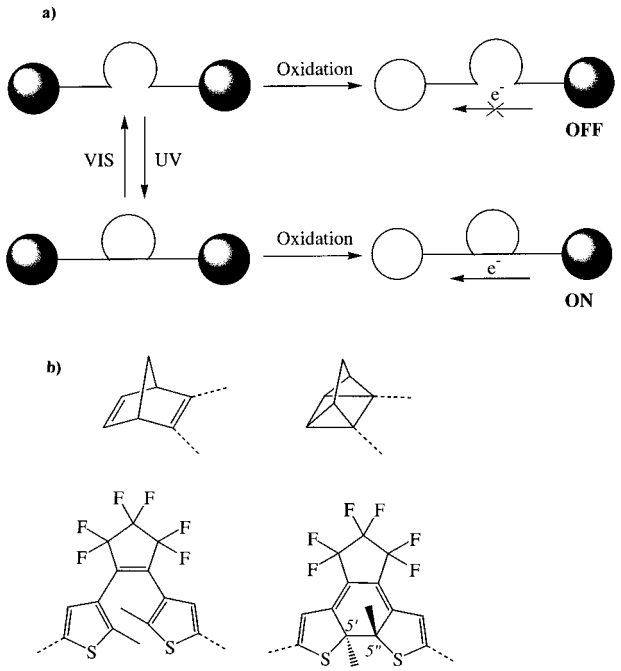


Figure 1. (a) Principle of the association of a switching moiety with intervalence electron transfer; (b) photochromic processes considered in the present paper; in the case of dithienylethene derivatives, the nomenclature **Na** and **Nb** will be used for the open and closed forms, respectively

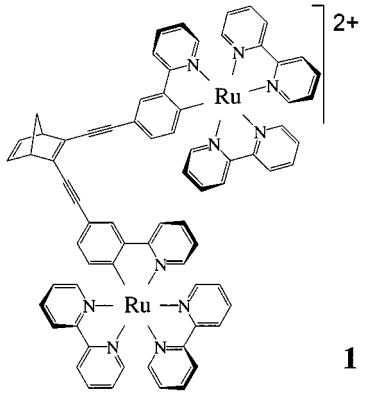
A previous attempt used the norbornadiene/quadricyclane isomerization in a bis(pentaammineruthenium) complex of dicyanonorbornadiene.[4] Extinction of the intervalence band occurred in the dicyanoquadricyclane complex, but the photoreaction was not reversible and the

[a] Centre d'Elaboration de Matériaux et d'Etudes Structurales, CNRS,
29 rue Jeanne Marvig, 31055 Toulouse Cedex, France
Fax: (internat.) + 33-5/62257999
E-mail: coudret@cemes.fr
launay@cemes.fr

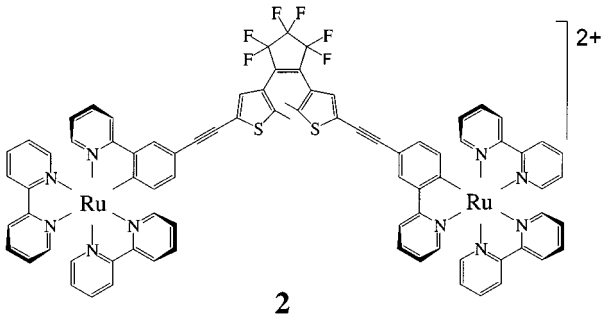
 © WILEY-VCH Verlag GmbH, D-69451 Weinheim, 2000 1434–1948/00/0707–1581 $ 17.50+.50/0

ruthenium−nitrile bond was not stable enough for further studies.

In other respects, as photochromic moieties, systems of the dithienylethene family, discovered by Irie et al,[5] exhibit several attractive characteristics: good stability, reversibility, high quantum yield, separated absorption spectra for the two forms, resistance to fatigue after multiple cycling. Their interest (particularly when the central double bond is locked by a perfluorocyclopentene cycle), was recognized by Lehn et al.[6] who described several associations of such photochromic parts with redox groups and their peculiar electrochemical and nonlinear optical properties. Thus, complex functions were obtained, involving the association of photochromism and electrochromism, that is, the sensitivity to two different stimuli.[6]



1



2

Scheme 1. Target molecules; **2** is represented as the open form **2a**

The redox sites we report on here are cyclometalated ruthenium complexes (Scheme 1). Cyclometalation has been shown to confer stability on the complexes, and, furthermore, strong electronic coupling, resulting in intense intervalence transitions, occurs.[2a,7,8] Strictly speaking, the coupling depends also on the nature of the spacer, but it turns out that most cyclometalated compounds associated with spacers such as phenylene units, or combinations of ethynyl units and aromatic groups are efficient for electron transfer. In the present paper, we report on our use of analogues of $[Ru(bpy)_3]^{2+}$, where one 2,2′-bipyridine is formally replaced by a deprotonated 2-phenylpyridine ligand.[9] We have recently shown how this easily functionalized cyclometalated complex could be used as an organometallic synthon.[9,10] Gram quantities are easily prepared and the corresponding chemistry has proved to be flexible and versatile. It is, in particular, possible to introduce ethynyl residues, which are efficient conjugated spacers, for example in tolane derivatives.[11] Such a "building block" approach involving a palladium-catalyzed cross-coupling reaction constitutes a very convergent synthesis of conjugated dinuclear complexes.

The present paper describes the properties of binuclear complexes with cyclometalated units as terminal groups, and with photochromic bridges such as norbornadiene or dithienylethene (Figure 1b). Their photochemistry in the homovalent $Ru^{II}-Ru^{II}$ state was studied. Note that the transformations expected are opposite: in the case of norbornadiene, photoisomerization drives the system from a conjugated state ("on") to a nonconjugated one ("off"), while the reverse is true when cyclization of the dithienylethene moiety occurs.

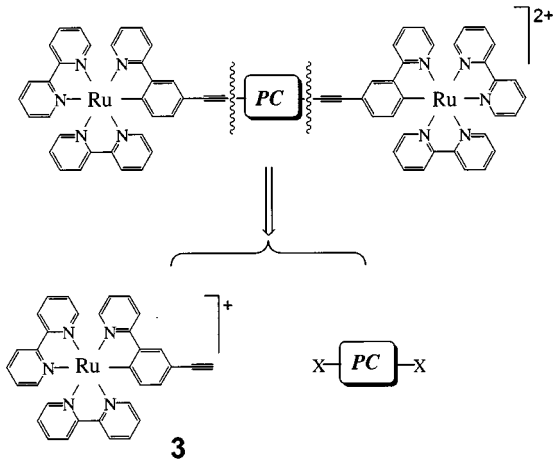
Results and Discussion

Syntheses

The general retrosynthetic route we adopted relies on extensive use of a palladium-catalyzed ethynylation reaction, which involves cross-coupling between a substituted acetylene and an electrophilic sp^2-hybridized carbon atom.[12] The disconnection we selected, outlined in Scheme 2, is mostly based on the fact that a ruthenium complex bearing a protected ethynyl group was readily available. While keeping the synthesis highly convergent, this also enabled us to circumvent some reactivity problems due to the use of the brominated ruthenium complex precursor.[10]

Organometallic Synthon

Two complexes, with an acetylene group protected by a trimethylsilyl (TMS) or by a 2-hydroxypropan-2-yl (POH) group, were available.[9] However, fluoride-induced desilylation of the TMS-protected compound was always accompanied by extensive decomposition of the cyclometalated part. On the other hand, the easily purified POH-protected alkyne **4** was found to be quantitatively deprotected with



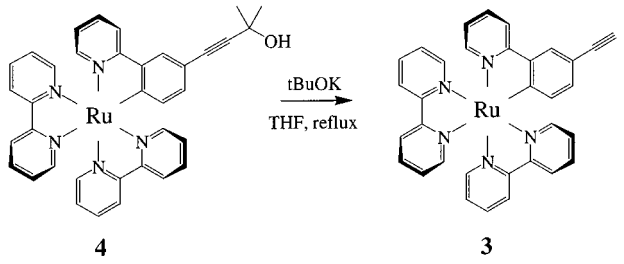
3

Scheme 2. General retrosynthetic route (PC = photochromic unit)

*t*BuOK in refluxing THF. No purification was found to be necessary, apart from removal of potassium salts and anion metathesis, thereby unnecessary exposure to air could be avoided (Scheme 3).

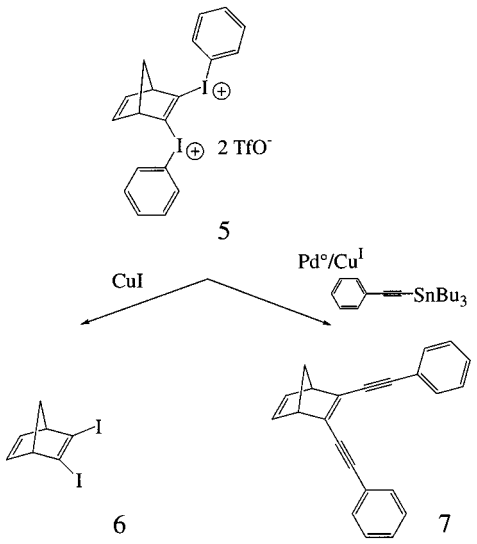
Photochromic Synthons

To use low reaction temperatures for the final cross coupling, we focused our attention on iodinated precursors of the photochromic core.



4 3

Scheme 3. Organometallic synthon

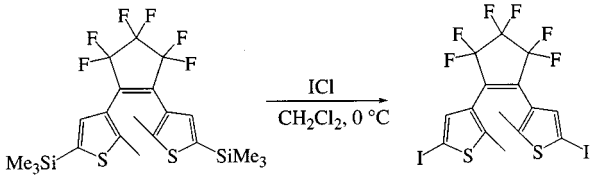


Scheme 4. Norbornadiene precursor **6** and model compound **7**

For the norbornadiene precursor, we thought of the bis(iodonium) derivative **5**, recently described by Stang and Zhdankin (Scheme 4).[13] This compound is easily prepared and can undergo either copper-mediated nucleophilic substitutions yielding dihalo- or dicyanonorbornadiene,[14] or palladium/copper ethynylation with an alkynylstannane, affording a family of new enediyne-containing molecules.[15]

Only two reports were found in which the dithienylperfluorocyclopentene photochromic group is used as a synthon (i.e., a diboronic acid[6e]or a dibromide[16]): the usual strategy is to prepare the derivatives by the interaction of a suitably substituted 3-lithiothiophene and perfluororocyclopentene in the final step.[5,6a−6d]

A convenient precursor of the diiodinated synthon **9** is the bis(5-trimethylsilyl) derivative of 1,2-bis(2′-methylthien-3′-yl)perfluorocyclopentene (**8**), the synthesis of which was described by Irie.[16] In marked contrast to the difficulty of the analogous bromination reaction,[16] the electrophilic trimethylsilyl *ipso* substitution with ICl as iodinating agent smoothly afforded the previously unknown diiodo derivative **9** in virtually quantitative yield. (Scheme 5).



8 9

Scheme 5. Dithienylethene precursor

Crystallization from acetonitrile afforded crystals suitable for an X-ray study; an ORTEP diagram is given in Figure 2.

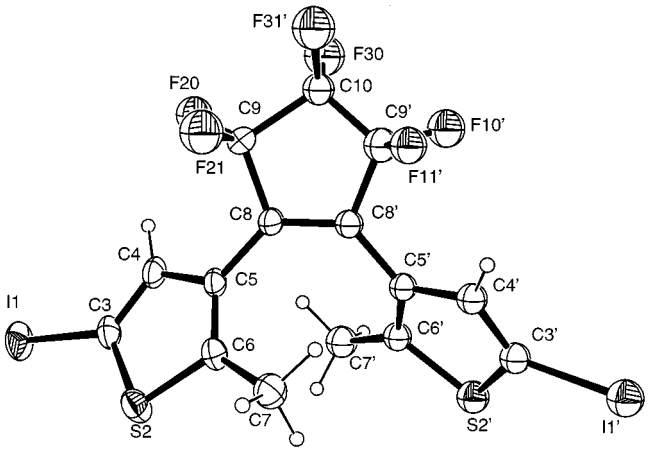


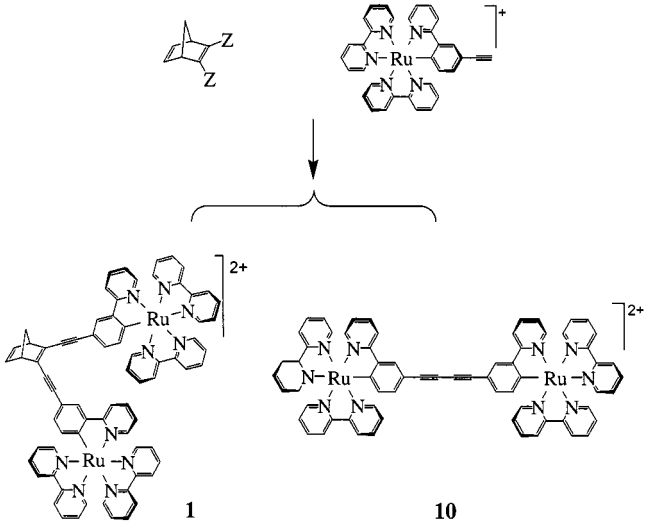
Figure 2. ORTEP plot of **9** with 30% probability displacement ellipsoids; the atoms with a superscript prime are related to those without superscript by a crystallographic twofold axis running though the middle of the C(8)−C(8′) bond; the nonplanar perfluorocyclopentene ring is partially disordered and only one conformer is shown here for clarity (bond lengths in Å, torsion angle in °): I1−C3 2.072(5), C3−C4 1.351(7), C4−C5 1.438(6), C5−C6 1.368(7), C3−S2 1.706(6), S2−C6 1.732(5), C5−C8 1.465(6), C8−C8′ 1.362(8); C6−C5−C8−C8′ 42(1)

Compound **9** exhibits pseudo-C_2 symmetry. The general conformation is transoid, that is, the methyl groups of the thiophene rings are above and below the plane of the perfluorocyclopentene ring, as Irie et al. observed for the related 1,2-bis(2,5-dimethyl-3-thienyl)perfluorocyclopentene.[17] This conformation is adapted for the cyclization reaction which can occur with relatively small movements.[17] The angle between the thiophene rings and the perfluorocyclopentene ring is 42°. The perfluorocyclopentene ring is not strictly planar, and thus the molecule exists in two conformations with statistical disorder (only one is shown in Figure 2). The bond lengths are in agreement with an electronic structure made up of two thiophene rings linked essentially by a single bond to perfluorocyclopentene. There appears to be little or no conjugation between the three rings.

Final Coupling

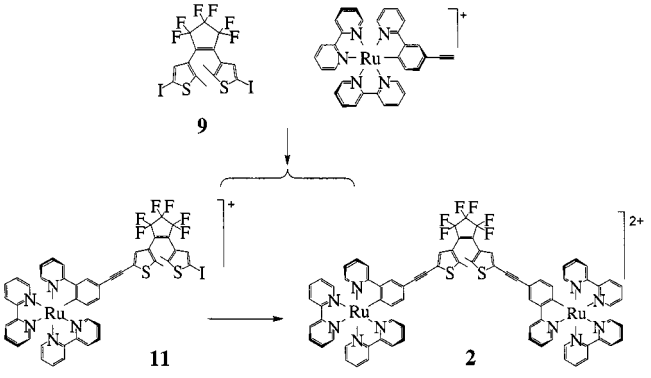
In the case of norbornadiene derivatives, difficulties were experienced in the stannylation of the alkyne functionality,[18,19] so we attempted a direct coupling with the bis(iodinane) **5**. Dinuclear complexes were readily obtained.

Unfortunately, a careful mass-spectrometry analysis showed that the desired complex **1** was systematically contaminated with the butadiyne derivative **10**, resulting from an oxidative coupling reminiscent of the Glaser reaction, despite drastic precautions against atmospheric oxygen contamination. Suspecting the iodinane **5** to be the necessary oxidizer,[20] we thought of using the expectedly less reactive diiodonorbornadiene **6**. Adapting literature coupling conditions to this substrate,[21] we were able to prepare the desired complex **1** in 40% yield (Scheme 6).



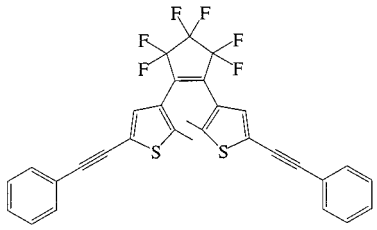
Scheme 6. Norbornadiene dinuclear complexes

In the case of the dithienylethene derivative, ethynylation occurred at room temperature in DMF under Sonogashira's conditions with $Pd(PPh_3)_4$ as catalyst source,[10,22] yielding the dinuclear complex **2**, albeit in moderate yield (20%). The major by-product was the mononuclear complex **11** (30%) which could be, if needed, converted into the dinuclear complex **2** by the same reaction conditions (Scheme 7).



Scheme 7. Dithienylethene complexes

All the dinuclear complexes were purified by preparative thin layer chromatography on silica, with a mixture of toluene and acetonitrile as eluent. However, it was found that crude complexes had to be deposited in CH_2Cl_2 to get proper separation (vide infra). These complexes, isolated as hexafluorophosphates, were identified by conventional analytical techniques.[23]



12a

Scheme 8. Model compound **12a**

Finally, for comparison purposes, the model compound **12a** (Scheme 8), in which the conjugated part is similar to the one of **2a**, was synthesized from **9** and phenylacetylene.[24]

Electrochemistry and Intervalence Electron Transfer in the Native Forms 1 and 2a

The cyclic voltammograms of **1** and **2a** exhibit a single reversible oxidation wave at 0.50 and 0.53 V (MeCN) vs SCE, respectively, corresponding to the oxidation of both ruthenium(II) sites. However, as in similar complexes with large metal−metal separations, this does not preclude the generation of appreciable concentrations of the mixed valence $Ru^{II}-Ru^{III}$ form during partial oxidation.[2] Conproportionation constants (K_c) for the equilibria between the $Ru^{II}-Ru^{II}$, $Ru^{III}-Ru^{III}$ and $Ru^{II}-Ru^{III}$ (mixed valence forms) were obtained by differential pulse voltammetry. K_c was found to be 13 for **1** and to be 11 for **2a**, corresponding to ca. 65% of the mixed-valence form at half-oxidation. These K_c values compare well with the ones observed for complexes of similar length.[2c]

An estimation of the electronic coupling parameter V_{ab} from the intervalence band characteristics is possible through Hush's Equation [Equation (1)][3,25] where $\bar{\nu}$ is the band position, $\Delta\bar{\nu}_{1/2}$ is the full width at half-maximum, and ε_{max} is the maximum extinction coefficient, while R_{MM} is the metal−metal distance.

$$V_{ab} = \frac{2.05\ 10^{-2}\sqrt{\bar{\nu}\ \Delta\bar{\nu}_{1/2}\ \varepsilon_{max}}}{R_{MM}} \quad (1)$$

In the case of **1**, the progressive oxidation (either chemical or electrochemical) revealed an intervalence transition in the 1300−2000-nm range. After correction for the conproportionation equilibrium, and deconvolution of the mixed-valence spectrum to extract the profile of the intervalence transition, according to a method already published,[2a,2d] the intervalence band parameters were obtained (Table 1). The V_{ab} parameter is found to be 0.068 eV. It is interesting to compare this with the similar complex with dicyanonobornadiene as a bridge and pentaammineruthenium as end groups, for which the coupling (0.023 eV) was three times less.[4] This shows the advantage of cyclometalated units as redox groups.

In the case of **2a** (where ruthenium atoms are initially in oxidation states II−II), the progressive oxidation to the

Table 1. Intervalence band parameters for compounds **1** and **2b**

Compound	K_c	$\tilde{\nu}$ [cm^{-1}]	$\Delta\tilde{\nu}_{1/2}$ [cm^{-1}]	ε [mol^{-1} L cm^{-1}]	R_{MM} [Å]	V_{ab} [eV]
1	13±2	5500±200	5000±300	3460±200	11.1	0.068±0.005
2b	12±2	7400±500	5000±300	1400±100	23.4	0.025±0.003

III−III fully oxidized form could be achieved easily and was found to be reversible. During oxidation, a band near 850 nm kept appearing; it is assigned to a ligand-to-metal charge transfer transition. No intervalence band was observed, regardless of the oxidation method [electrochemical with concentration, $c = 4 \cdot 10^{-4}$ M, or chemical with bis(pyridyl)phenyliodonium triflate with concentration, $c = 6 \cdot 10^{-5}$ M, see below].

Photochemistry

Photoisomerizations were undertaken for complexes **1** and **2a**, with the aim of generating either a less conjugated form (norbornadiene to quadricyclane isomerization of **1**) or a more conjugated form (photocyclization of the dithienylethene derivative **2a**).

In the case of **1**, irradiations at 254 and 365 nm either in methanol or acetonitrile, monitored by ^{1}H-NMR spectroscopy, did not produce isomerization to quadricyclane. Experiments on the simpler compound 1,2-bis(phenylethynyl)-norbornadiene (**7**) did not result in photoisomerization either. Thus, it seems that for norbornadiene, the extension of conjugation due to the phenylethynyl parts is responsible for the lack of photochemical reactivity, probably by quenching the excited state of the norbornadiene part. Such negative effects of the conjugation length were described elsewhere.[26]

Irradiation of **2a** in MeCN or CH_3OH at different wavelengths (405, 313, 365, and 254 nm) was first followed by UV/Vis spectroscopy. A broad band appeared at 670 nm, which corresponds to the photocyclized isomer, according to similar examples.[6b][6e] The highest intensity at the photostationary state was obtained with 254-nm irradiation, and all following studies were performed at this wavelength. Since the other bands in the UV/Vis spectra did not disappear (see below), another technique was necessary to measure the degree of conversion into the closed form. We found that for concentrations of ca. $2 \cdot 10^{-4}$ mol L^{-1} it was possible to monitor the reaction (in CD_3OD) by both UV/Vis and ^{1}H-NMR spectroscopy, in the latter case the signals of the methyl protons closest to the newly created bond were used. During irradiation, the sharp singlet at $\delta = 1.98$, corresponding to methyl protons of the open form **2a**, decreased and was progressively replaced by a signal at $\delta = 2.21$, attributed to the methyl protons of the closed form. The relative integration of the two methyl signals showed that a photostationary state was reached after two hours of irradiation, the closed form **2b** concentration reaching 75% of the initial complex content. Since conversions up to 100% were reported for similar systems,[6] the incomplete isomerization in our case is probably related to the persistence of an absorption for the closed form at all wavelengths, due to the organometallic part. Thus, in contrast to other photochromic compounds of this family, it is not possible to find a wavelength for which only the open form **2a** would be excited.

Since the photochemical ring closure of **2a** was not complete, a purification step was necessary to obtain the spectroscopic behavior of the pure closed form **2b**. However, the conditions described above, involving thin-layer chromatography with a toluene/acetonitrile mixture as eluent failed; the two isomers migrated as a single and stretched spot. It was recently shown[27] that chromatographic elution of ionic compounds was made difficult because of some streaking of the bands. This was attributed to partial ion exchange between the ion pairs and the stationary phase. To force this equilibrium toward ion-pairing, and since dichloromethane gave the best results as deposition solvent, we chose to saturate the TLC plate with an excess of KPF_6. Despite their relatively small structural differences, separation of the two isomers **2a** and **2b** could be achieved: elution with a dichloromethane/ethyl acetate/pyridine mixture revealed a pink band (**2a**) followed by a blue band (**2b**) which migrated slightly more slowly (R_F = 0.40 and 0.34 for **2a** and **2b**, respectively). The ^{1}H-NMR spectrum of the blue product (Figure 3) agreed with structure **2b**, and showed, in particular, the displacement of the thiophene protons upon cyclization.

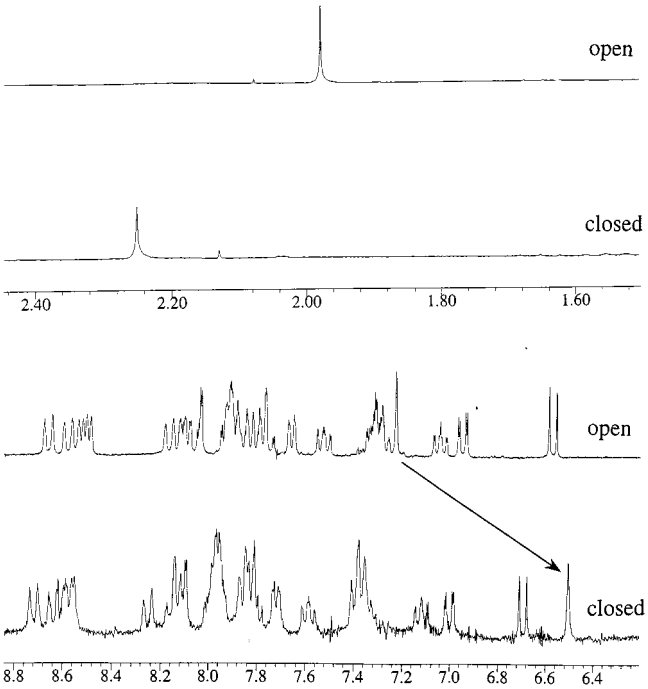


Figure 3. ^{1}H-NMR spectra of the open form **2a** and the closed form **2b** of the bis(ethynylcyclometalated) dithienylethene complex; the arrow shows the displacement of the thiophene protons

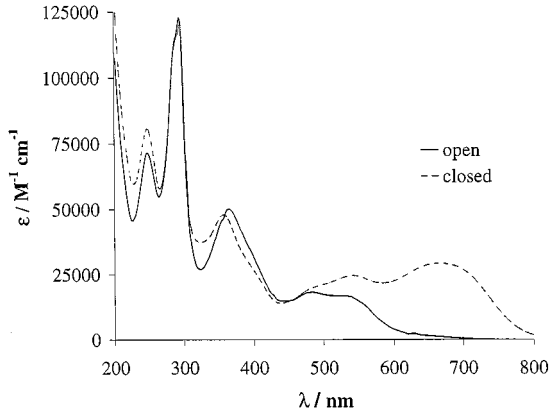


Figure 4. UV/Vis spectra of the open form **2a** and the closed form **2b** of the bis(ethynylcyclometalated) dithienylethene complex

The closed form did not revert thermally when kept for several hours in the dark. The back-reaction, that is, ring reopening, could be observed when irradiation was performed in the red part of the spectrum, with an incandescence lamp with a Kodak red filter excluding radiation below 600 nm.

The UV/Vis spectra of **2a** and **2b** are shown in Figure 4. Upon photocyclization, the UV/Vis spectrum is modified mainly in the red region, with the broad 670-nm peak rising. In the rest of the spectrum, only weak changes are observed, with a small decrease of some bands (see Figure 4). The extinction coefficient at 670 nm for the closed form is 29700 mol^{-1} L cm^{-1}. This high value can be related to the presence of donor substituents,[28] in our case the cyclometalated ruthenium(II) units, and also to the length of the conjugated system.

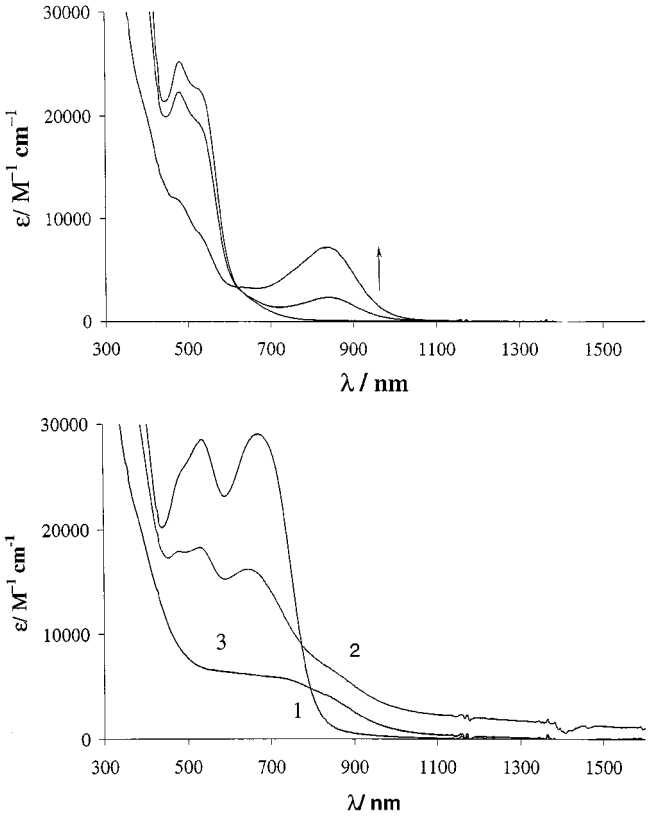


Figure 5. Spectra obtained during oxidation with bis(pyridyl)-phenyliodonium; top: *open* form **2a**; bottom: *closed* form **2b** exhibiting an intervalence absorption in the 1000−1500 nm range; total concentration: $5.7 \cdot 10^{-5}$ mol·L^{-1}; path length: 1 cm; 1: initial spectrum; 2: spectrum at half-oxidation; 3: spectrum of the fully oxidized solution

Electrochemistry and Intervalence Transition of 2b

The closed form **2b** gives rise to a single oxidation wave at 0.52 V (MeCN) vs SCE, corresponding to the oxidation of both ruthenium atoms. Differential pulse voltammetry yields $K_c = 12$.

The oxidation of **2b**, particularly by controlled-potential electrolysis, was not a simple process. During oxidation, the characteristic band of the closed form of the photochromic core, near 670 nm, decreased, suggesting a major alteration of the structure. Furthermore, after complete oxidation, a reduction by hydrazine did not restore the characteristic color and spectrum of **2b** in its reduced form, but instead a spectrum very close to the one of **2a**. Thus, during oxidation, a ring reopening occurred, and the final product was the oxidized form of **2a**.[29] (Incidentally, the same oxidation-induced ring reopening was also observed with the mononuclear **11b** complex.)

We found that the reopening during electrolysis was in fact a relatively slow reaction (half-reaction time ca. 5−10 min), consecutive to the oxidation step. Thus, it was conceivable to quench it with a faster oxidation procedure than controlled-potential electrolysis, the latter being limited by mass transport between the electrode and the bulk solution. After systematic search of chemical oxidation procedures, we chose an oxidation by the triflate salt of bis(pyridyl)phenyliodonium, formally containing iodine(III).[30] Interestingly, in our case, this reagent reacted instantaneously, did not generate acidic species (which would be harmful for the cyclometalated moieties), and the by-products are merely iodobenzene and pyridine. Finally, both the reagent and by-product (iodobenzene) are almost nonabsorbent in the visible and near-IR regions.

Upon chemical oxidation of pure **2b**, obtained from chromatography, we observed the decrease of the 670-nm band and the rising and subsequent decay of a weak absorption in the near-infrared, behavior characteristic of intervalence transitions (Figure 5, bottom). [The decrease of the 670-nm band comes from the fact that the ruthenium(II) donor groups, which increase the extinction coefficient of the closed form, [28] are no longer present.] In a control experiment, no near-IR absorption was obtained by oxidation of the monometallic complex **11a**, neither with the open form itself nor with the closed form **11b**; this suggests that the near-IR absorption in **2b** is indeed linked to the bimetallic nature of the complex.

To obtain the parameters for Hush's equation, after correction for the conproportionation equilibrium ($K_c = 12$), the spectrum was deconvoluted according to a procedure already described,[2d] to separate the intervalence band from the tail of the nearby more intense band located near 900 nm. Although no true maximum was observed for the

intervalence band, spectral simulation showed that a band exists. Additional evidence for an intervalence absorption was provided by the reproducibility of the results, and the typical increase followed by a decrease upon oxidation. The resulting parameters of the intervalence band are reported in Table 1. With the use of R_{MM} = 23.4 Å, from molecular modeling methods,[31] V_{ab} = 200 cm^{-1} (0.025 eV). By contrast, as said above, nothing was observed in the case of **2a** (Figure 5, top).

To understand the electronic mechanism of the coupling, an extended Hückel evaluation of V_{ab} in both **2a** and **2b** was performed. We showed elsewhere that this method is sufficient for obtaining realistic values of the electronic coupling and that it allows qualitative discussions.[2a] The geometries of **2a** and **2b** were first minimized by molecular mechanics.[31] Then molecular orbitals were computed by the extended Hückel method,[32] and V_{ab} was obtained from the "dimer splitting" procedure.[2a] For **2b**, a coupling of 0.021 eV was obtained versus 0.003 eV for **2a**. The former value is consistent with the observed coupling, while the latter explains the disappearance of the intervalence transition, since a 7-fold reduction in V_{ab} should result in a ca. 50-fold (i.e., 7^2) reduction in the extinction coefficient. In chemical terms, for **2a**, the useful part of the bridge (ignoring sulfur contributions) is made up of a nonconjugated octatriene, while in **2b**, it can be considered to be a conjugated octatetraene. Interestingly, values of V_{ab} in the 0.02-eV range have already been observed for conjugated systems with four double bonds and metal−metal distances near 20 Å.[2d] A more complete discussion of the spatial extension and properties of the orbitals involved in the electron transfer for such compounds is given elsewhere.[33]

The extended Hückel calculation also rationalizes the behavior of **2b** upon oxidation. While in **2a**, the ruthenium d orbitals are well separated from other molecular orbitals with mainly ligand character, so that the oxidation is truly metal-centered, in **2b**, a filled orbital of the ligand has moved up and appears at an energy very close to metal orbitals. Thus, although the oxidation bears primarily on the metal (as shown by the electrochemical behavior: **2a** is oxidized reversibly at 0.53 V, while the model compound **12a** is oxidized *irreversibly* at 1.04 V[24]), it is relatively easy to partially depopulate a *ligand* orbital by oxidation. Because this ligand orbital is bonding between carbon atoms C-5′ and C-5" (see Figure 1b), its depopulation should favor the reopening. In this respect, the oxidation process is somewhat analogous to the photochemical excitation.

Conclusion

The general synthetic strategy of using palladium-catalyzed ethynylation reactions between a substituted acetylene and an electrophilic sp^2-hybridized carbon atom proved to be versatile and could be adapted for the present purpose. Compounds with two redox groups linked by a photoisomerizable bridge were obtained, but their behavior differed markedly with respect to the bare photochromic parts. In particular, the extension of conjugation could suppress photoisomerization (**1**) or make it nonquantitative (**2a**), probably because the additional conjugated parts and the redox groups can act as energy sinks. Such an effect was also reported elsewhere.[26]

Despite these difficulties, we found two interesting features associated with the same molecule (**2a/2b**): full photoinduced electron transfer between two metal units, and reversible photochromism. The intervalence transition could be switched completely "on" or "off". The order of magnitude of the electronic coupling in both forms was correctly reproduced by an extended Hückel calculation. Compounds **2a** and **2b** allowed a fundamental study of switching (in the electrical sense) at the molecular level.

Experimental Section

Starting Materials: Reagents were of commercial grade. THF was dried with Na/benzophenone, CH_2Cl_2 with CaH_2, and MeCN with molecular sieves. Amines were used as received. Preparative TLC plates were purchased from Merck. Compound **4** was synthesized according to ref.[9] Octafluorocyclopentene was purchased from Interchim. Bis(iodonium)norbornadiene (**5**), diiodonorbornadiene (**6**), bis(phenylethynyl)norbornadiene (**7**) were synthesized according to literature procedures. For **8**, the procedure in ref.[16] was adapted: Octafluorocyclopentene was added to a ca. 0.2 M solution of 4-lithio-5-methyl-2-trimethylsilylthiophene in THF at −80 °C, and the mixture was allowed to warm up over 5 h. Compound **8** was obtained after chromatography (SiO_2, pentane) and recrystallization (MeCN), the yield was 50% on a gram scale. All the reactions and handling of the compounds sensitive to UV light were carried out in the dark.

Perfluoro-1,2-bis(2-iodo-5-methylthien-4-yl)cyclopentene (9): A solution of **8** (150 mg, 0.29 mmol) and iodine monochloride (190 mg, 1.17 mmol) in CH_2Cl_2 (10 mL) was stirred at −5 °C for 2 h. After solvent evaporation, the residue was purified by column chromatography (basic Al_2O_3, pentane) to give 165 mg of **9** as a waxy solid in 90% yield. M.p. 96 °C. − ^{1}H NMR: (250 MHz, $CDCl_3$, 20 °C, TMS): δ = 7.2 (s, 1 H), 1.9 (s, 3 H). − $^{13}C\{^1H\}$ NMR ($CDCl_3$, 250 MHz, 20 °C): δ = 147.7 (C-5′), 136.0,(C-3′), 135.2 (C-2′), 126.6 (C-4′), perfluorocyclopentene (multiplets) 111.7, 115.7, 119.9, 14.3 (CH_3). − ^{19}F NMR (CD_3OD, 200 MHz, 20 °C, external CF_3COOH as reference): δ = −31.7 to −31.9 (m, 2 F), −53.5 to −53.6 (m, 1 F). − MS (CI, NH_3); *m/z* (%): 620.0 (100). − $C_{15}H_8S_2F_6I_2{\cdot}CH_3CN$ (619.8): calcd. C 30.88, H 1.68, S 9.70; found C 30.86, H 1.50, S 9.53.

Ethynylcyclometalated Compound 3: A solution of **4** (150 mg, 0.19 mmol) and potassium *tert*-butoxide (25 mg, 0.22 mmol) in 5 mL of dry, oxygen-free THF was stirred at reflux temp. for 2 h. After the solvent was cooled and removed, the residue was taken up in dichloromethane and the filtered solution was concentrated, yielding **3** as an amorphous solid. The reaction was quantitative. − ^{1}H NMR (250 MHz, CD_3CN, 20 °C, TMS): δ = 3.27 (s, 1 H), 6.47 (d, *J* = 7.8 Hz, 1 H), 6.91 (dd, *J* = 7.7, 1.6 Hz, 1 H), 6.9 (td, *J* = 6.0, 1.4 Hz, 1 H), 7.21−7.26 (m, 3 H), 7.43 (td, *J* = 7.0, 1.2 Hz, 1 H), 7.60 (dd, *J* = 4.0, 1.0 Hz, 2H), 7.69−7.87 (m, 7 H), 7.96−8.08 (m, 3 H), 8.33 (dd, *J* = 8.0, 3.0 Hz, 2 H), 8.40 (d, *J* = 8.1 Hz, 1 H), 8.46 (d, *J* = 8.1 Hz, 1 H). − MS (FAB, NBA); *m/z* (%): 592 (100) $[M - PF_6]^+$. − $C_{33}H_{24}N_5PF_6Ru$ (736): calcd. C 53.81, H 3.28, N 9.51; found C 53.78, H 3.76, N 8.71.

Bis(ethynylcyclometallated) Norbornadiene Complex 1: Diiodonorbornadiene (30.9 mg 0.09 mmol), $Pd(PPh_3)_4$ (10 mg, 0.05 equiv.), CuI (10 mg, 0.3 equiv.) and finally 1 mL of diisopropylamine were added to 2 mL of a DMF solution containing 0.19 mmol of **3**. The solution was stirred at room temp under argon for 10 h. The solvent was then removed in vacuo and the crude product was purified by chromatography on a silica gel preparative plate (eluent: toluene/acetonitrile 60:40), with desorption by a concentrated solution of ammonium hexafluorophosphate in MeCN). Yield: 59 mg (40%). − ^{1}H NMR: (250 MHz, CD_3CN, 20 °C, TMS): δ = 2.17−2.19 (m, 1 H), 2.30−2.32 (m, 1 H), 3.70 (br. s, 2 H), 6.51 (d, *J* = 7.9 Hz, 2 H), 6.85−6.97 (m, 6 H), 7.10−7.25 (m, 6 H), 7.40−7.53 (m, 4 H), 7.58−7.86 (m, 14 H), 7.94 (sd, *J* = 1.5 Hz, 2 H), 7.97−8.03 (m, 6 H), 8.29−8.35 (m, 4 H), 8.38 (d, *J* = 8.2 Hz, 2 H), 8.46 (d, *J* = 8.2 Hz, 2 H). − MS (ES); *m/z*: 1417 $[M - PF_6]^+$, 859 $[M - 2PF_6 - (Ru(bpy)_2)]^+$, 790 $[M - 2PF_6 - (Ru(bpy)_2) - Cp]^+$, 636 $[M - 2PF_6]^{2+}$. − $C_{73}H_{52}N_{10}P_2F_{12}Ru_2{\cdot}3H_2O$ (1615): calcd. C 54.28, H 3.62, N 8.67; found C 54.21, H 3.88, N 8.09.

Mono- and Bis(ethynylcyclometalated) Dithienylethene Complexes in Their Open Forms 11a and 2a: The reaction was carried out with 55.8 mg (0.09 mmol) of **9** and was worked up in a manner identical to that described above for the synthesis of **1**. Yield 32 mg (20%) of **2a** and 33 mg (30%) of **11a**.

11a: ^{1}H NMR: (250 MHz, CD_3OD, 20 °C, TMS): δ = 1.96 (s, 3 H), 1.99 (s, 3 H), 6.56 (d, *J* = 7.7 Hz, 1 H), 6.95 (dd, *J* = 7.7, 1.7 Hz, 1 H), 7.04 (td, *J* = 6.7, 1.1 Hz, 1 H), 7.20 (s, 1 H), 7.28−7.35 (m, 4 H), 7.42 (d, *J* = 5.5 Hz, 1 H), 7.52 (td, *J* = 7.8, 1.6 Hz, 1 H), 7.65 (dd, *J* = 5.1, 1.0 Hz, 1 H), 7.72−7.97 (m, 6 H), 8.04 (sd, *J* = 1.9 Hz, 1 H), 8.08−8.13 (m, 2 H), 8.18 (d, *J* = 7.9 Hz, 1 H), 8.52 (dd, *J* = 8.4, 3.7 Hz, 2 H), 8.58 (d, *J* = 7.9 Hz, 1 H), 8.66 (d, *J* = 8.1 Hz, 1 H). − ^{19}F NMR (CD_3OD, 200 MHz, 20 °C, external CF_3COOH as reference): δ = −31.7 to −31.9 (m, 2 F), −53.5 to −53.6 (m, 1 F). − MS (ES); *m/z*: 1084.1 $[M - PF_6]^+$. − UV/Vis (MeCN): λ_{max} (ε, $M^{-1}{\cdot}cm^{-1}$) = 482 (12300), 364 (30800), 294 (81100), 248 (62000) nm. − $C_{48}H_{31}N_5PF_{12}S_2IRu{\cdot}2EtOH$ (1321.5): calcd. C 47.28, H 3.28, N 5.30; found C 47.94, H 2.97, N 5.31.

2a: ^{1}H NMR (250 MHz, CD_3OD, 20 °C, TMS): δ = 1.98 (s, 6 H), 6.57 (d, *J* = 7.9 Hz, 2 H), 6.96 (dd, *J* = 7.9, 1.6 Hz, 2 H), 7.04 (td, *J* = 6.4, 1.0 Hz, 2 H), 7.24 (s, 2 H), 7.26−7.37 (m, 6 H), 7.52 (td, *J* = 6.4, 1.2 Hz, 2 H) 7.65 (dd, *J* = 5.1, 1.0 Hz, 2 H), 7.72−7.96 (m, 14 H), 8.01 (sd, *J* = 1.6 Hz, 2 H), 8.08−8.19 (m, 6 H), 8.52 (dd, *J* = 8.2, 3.9 Hz, 4 H), 8.58 (d, *J* = 8.1 Hz, 2 H), 8.66 (d, *J* = 7.9 Hz, 2 H). − ^{19}F NMR (CD_3OD, 200 MHz, 20 °C, external CF_3COOH as reference): δ = −31.7 to −31.9 (m, 2 F), −53.5 to −53.6 (m, 1 F). − MS (ES); *m/z*: 1693 $[M - PF_6]^+$, 774 $[M - 2PF_6]^{2+}$. − UV/Vis in MeOH: λ_{max} (ε, $M^{-1}{\cdot}cm^{-1}$) = 480 (20600), 366 (50000), 295 (139000), 247 nm (84100). − $C_{81}H_{54}N_{10}P_2F_{18}S_2Ru_2{\cdot}6H_2O$ (1944): calcd. C 50.00, H 3.42, N 7.20; found C 49.86, H 3.14, N 6.93.

Bis(ethynylcyclometalated) Dithienylethene Complex in Its Closed Form 2b: Compound **2a** was converted into **2b** on a preparative scale as follows: An efficiently stirred solution of **2a** (16 mg) in 10 mL of acetonitrile or methanol was irradiated in a quartz vessel with two standard TLC-visualization UV lamps at 254 nm for 12 to 24 h. To the resulting mixture, 0.05 mL of hydrazine and 5 mg of NH_4PF_6 were added, and the solution was concentrated to dryness. The solid was dissolved in dichloromethane and subjected to preparative TLC chromatography on silica gel plates previously immersed in a saturated aqueous KPF_6 solution for 1 h and then dried in an oven overnight. Elution of the plate (eluent: dichloromethane/ethyl acetate/pyridine, 100:100:1) was carried out with careful protection from light. Washing of the silica with a mixture of dichloromethane/ethanol/triethylamine (91:8:1) readily provided desorption of the band corresponding to **2b** (6.5 mg).

2b: ^{1}H NMR (250 MHz, CD_3OD, 20 °C, TMS): δ = 2.21 (s, 6 H), 6.46 (s, 2 H), 6.65 (d, *J* = 7.4 Hz, 2 H), 6.80 (d, *J* = 7.5 Hz, 2 H), 7.04−7.10 (m, 2 H), 7.24−7.40 (m, 6 H), 7.48−7.59 (m, 2 H), 7.68 (d, *J* = 4.5 Hz, 2H), 7.74−8.00 (m, 14 H), 8.03−8.13 (m, 6 H), 8.21 (d, *J* = 7.9 Hz, 2 H), 8.46−8.61 (m, 6 H), 8.68 (d, *J* = 8.1 Hz, 2 H). − UV/Vis in MeOH: λ_{max} (ε, $M^{-1}{\cdot}cm^{-1}$) = 670 (29700), 545 (24800), 358 (48500), 295 (123000), 248 nm (82000). − $C_{81}H_{54}N_{10}P_2F_{18}S_2Ru_2{\cdot}10H_2O$ (2016): calcd. C 48.22, H 3.70, N 6.94; found C 48.31, H 3.47, N 6.49.

X-ray Crystal Structure of 9: Crystals were obtained by cooling of a saturated solution in acetonitrile, and were mounted on an Enraf Nonius Kappa CCD diffractometer. Mo-K_α (λ = 0.71073 Å) radiation was used and the temperature was 293 K. The space group was monoclinic *C*2/*c*; *a* = 20.7183(5) Å, *b* = 9.0480(5) Å, *c* = 11.9644(4) Å, β = 120.987(2)°, *V* = 1922.8(9) Å^3, *Z* = 4. Structure determination was performed with direct methods (SIR 92),[34] from 2470 reflections, of which 1810 with $I > 3\sigma(I)$ were used for refinement against F^2 (CRYSTALS).[35] Non-hydrogen atoms were treated anisotropically except for disordered atoms (C10 and F). H atoms (isotropic) were placed from difference Fourier maps and were not refined. Final values: *R* = 5.17%, *Rw* = 7.26%; residual electron density: −0.8, +1.2 e/Å^3. Drawings were made with ORTEP III.[36] Crystallographic data (excluding structure factors) for the structure reported in this paper were deposited at the Cambridge Crystallographic Data Centre as supplementary publication no. CCDC-136201. Copies of the data can be obtained free of charge on application to CCDC, 12 Union Road, Cambridge CB2 1EZ (UK) [Fax: (internat.) + 44-1223/336-033; E-mail: deposit@ccdc.cam.ac.uk].

Photochemistry: For analytical investigations, photochemical irradiations of **2a** were performed in 2-mm or 1-cm quartz cells placed in front of either a standard TLC-visualization UV lamp (365 and 254 nm), or an optical system combining a medium-pressure Mercury lamp and interference filters (405, 365, and 313 nm). For the reopening reaction of **2b**, an incandescence lamp with a red filter was used. The solutions were stirred either with a small magnetic bar (1-cm cells), or by the cell being turned upside down every minute (2-mm cells incompletely filled under argon to imprison a bubble). Concentrations were in the 10^{-5} mol L^{-1} range (1-cm cells). For the combined UV/Vis/NMR experiment in CD_3OD at 254 nm, the concentration was $2{\cdot}10^{-4}$ mol L^{-1} (2-mm cells). After irradiation of the photostationary state, the solution (ca. 0.6 mL) was transferred to the NMR tube. Preparative photochemistry took place in a quartz vessel as described above.

Electrochemistry: Electrochemical techniques were performed with an AUTOLAB PC-controlled potentiostat. The reference electrode was a saturated calomel electrode (SCE) isolated from the solution by a double frit system. The solvent was acetonitrile and the supporting electrolyte was 0.1 M tetrabutylammonium hexafluorophosphate. For cyclic voltammetry, the working electrode was a Pt disk (diameter 1 mm), and the scan rate 0.1 $V{\cdot}s^{-1}$. Differential pulse voltammetry was performed with a Metrohm rotating platinum electrode (1000 rev/min) with pulses of 70 ms duration and 25 mV amplitude. For controlled potential electrolysis, the working electrode was a platinum grid, and the anodic and cathodic compartments were separated by a additional frit.

Iodine(III) Reagent: The reported preparation[30] starts from iodobenzene diacetate. However, the commercial reagent gave unsatis-

factory results. Thus, it was prepared from iodobenzene, acetic anhydride, and hydrogen peroxide according to ref.[37] Then iodobenzene diacetate was converted into the triflate salt of bis(pyridyl)-phenyliodonium by reaction with trimethylsilyl trifluoromethanesulfonate.[30] The obtained whitish solid was kept under argon at −20 °C.

For oxidation experiments, in a typical run, a $5.7\cdot10^{-5}$ mol L^{-1} solution of **2a** in anhydrous MeCN was prepared. A volume of 2.5 mL of this solution was started with, and the oxidation was performed in a 1-cm cell by addition of a solution of the iodine(III) reagent ($3.0\cdot10^{-2}$ mol·L^{-1} in MeCN) with a micropipette. Full oxidation was found to occur for 26 μL, at which the spectrum of the $Ru^{III}-Ru^{III}$ species was obtained. In a second experiment, half the above quantity (i.e., 13 μL) was added, and the absorption spectrum, corresponding to the mixed-valence species in conproportionation equilibrium, was immediately recorded. For the closed form **2b**, oxidation was performed as above on 1 mL of a $2.6\cdot10^{-4}$ M solution in a 5-mm cell.

Calculations: Compounds **2a** and **2b** were minimized[31] with the universal force field[38] modified with the following parameters: 350 kcal mol^{-1} $Å^{-2}$ and 2.05 Å for Ru−N bonds, 350 kcal mol^{-1} $Å^{-2}$ and 2.02 Å for Ru−C bonds. Since the energy was almost insensitive to a rotation around the acetylenic bonds, the thiophene rings and the phenyl groups were made coplanar to avoid rotational disorder. This gave molecules with only one element of symmetry, a C_2 axis. Molecular orbitals were computed by the extended Hückel method, with the CACAO program[32] with Ru(4d) orbital energies set at −11.0 eV. The V_{ab} parameters were extracted from the energy splitting between two orbitals with strong weights on metal atoms and opposite symmetries with respect to the C_2 axis of the molecules. Due to the low symmetry around the metal sites, it turned out that for each molecules *two* such couples of orbitals were found: one corresponding to an interaction propagating through the phenyl ring of the phenylpyridine ligand, and another corresponding to an interaction through the pyridine ring. Since the two couplings V_{phen} and V_{pyr} were of the same order of magnitude, they were combined by Equation (2).

$$V_{ab} = \sqrt{V_{phen}^2 + V_{pyr}^2} \quad (2)$$

Acknowledgments

We thank J. C. Cobas, J. Cruces and F. Sardina for providing a free copy of the NMR software MestRe-C 1.5.1 (http://qobrue.usc.es/jsgroup/MestRe-C/MestRe-C.html), Christine Viala for technical help, Robert Weiss for precious advice, Jean-Claude Micheau and Véronique Pimienta for photochemical experiments, Catherine Romero for UV/Vis measurements, André Gourdon for the resolution of the X-ray structure, and MENRT for a thesis grant to S. F.

[1] [1a] For an overview of molecular electronics see, for instance: *Molecular Electronics: Science and Technology* (Eds.: A. Aviram, M. Ratner), *Annals NY Acad. Sci.* **1998**, *852*, and references therein. – [1b] C. Joachim, J. K. Gimzewski, *Chem. Phys. Lett.* **1997**, *265*, 353. – [1c] A. Gourdon, H. Tang, in *Molecular Electronics: Science and Technology* (Eds.: A. Aviram, M. Ratner), *Annals NY Acad. Sci.* **1998**, *852*, p. 219. – [1d] V. J. Langlais, R. R. Schlittler, H. Tang, A. Gourdon, C. Joachim, J. K. Gimzewski, *Phys. Rev. Lett*. **1999**, *83*, 2809.

[2] [2a] C. Patoux, J.-P. Launay, M. Beley, S. Chodorowski-Kimmes, J.-P. Collin, S. James, J.-P. Sauvage, *J. Am. Chem. Soc.* **1998**, *120*, 3717. – [2b] C. Patoux, C. Coudret, J.-P. Launay, C. Joachim, A. Gourdon, *Inorg. Chem.* **1997**, *36*, 5037. – [2c] A.-C. Ribou, J.-P. Launay, M. L. Sachtleben, H. Li, C. W. Spangler, *Inorg. Chem.* **1996**, *35*, 3735. – [2d] A.-C. Ribou, J.-P. Launay, K. Takahashi, T. Nihira, S. Tarutani, C. W. Spangler, *Inorg. Chem*. **1994**, *33*, 1325. – [2e] C. Creutz, *Progr. Inorg. Chem*. **1983**, *30*, 1, and references therein.

[3] N. S. Hush, *Progr. Inorg. Chem.* **1967**, *8*, 391; N. S. Hush, *Coord. Chem. Rev.* **1985**, *64*, 135.

[4] P. Lainé, V. Marvaud, A. Gourdon, J.-P. Launay, R. Argazzi, C.-A. Bignozzi, *Inorg. Chem.* **1996**, *35*, 711.

[5] M. Irie, M. Mohri, *J. Org. Chem.* **1988**, *53*, 803. M. Hanazawa, R. Sumiya, Y. Horikawa, M. Irie, *J. Chem. Soc., Chem. Commun.* **1992**, 206; M. Irie, O. Miyatake, K. Uchida, *J. Am. Chem. Soc.* **1992**, *114*, 8715.

[6] [6a] S. L. Gilat, S. H. Kawai, J.-M. Lehn, *J. Chem. Soc., Chem. Commun.* **1993**, 1439. – [6b] S. L. Gilat, S. H. Kawai, J.-M. Lehn, *Chem. Eur. J.* **1995**, *1*, 275. –[6c] S. H. Kawai, S. L. Gilat, R. Ponsinet, R.; J.-M. Lehn, *Chem. Eur. J.* **1995**, *1*, 285. – [6d] S. H. Kawai, S. L. Gilat, J.-M. Lehn, *Eur. J. Org. Chem*. **1999**, 2359. – [6e] G. M. Tsivgoulis, J.-M. Lehn, *Chem. Eur. J.* **1996**, *2*, 1399.

[7] M. Beley, S. Chodorowski-Kimmes, J.-P. Collin, P. Lainé, J.-P. Launay, J.-P. Sauvage, *Angew. Chem. Int. Ed. Engl*. **1994**, *33*, 1775.

[8] J.-P. Sutter, D. M. Grove, M. Beley, J.-P. Collin, N. Veldman, A. L. Spek, J.-P. Sauvage, G. Van Koten, *Angew. Chem. Int. Ed. Engl*. **1994**, *33*, 1282.

[9] C. Coudret, S. Fraysse, J.-P. Launay, *Chem. Commun.* **1998**, 663.

[10] S. Fraysse, C. Coudret, J.-P. Launay, *Tetrahedron Lett.* **1998**, *39*, 7873.

[11] M. Magoga, C. Joachim, *Phys. Rev. B* **1997**, *56*, 4722.

[12] *Metal-Catalysed Cross-coupling Reactions* (Eds.: F. Diederich, P. J. Stang), Wiley-VCH, Weinheim, **1998**, chapter 5.

[13] P. Stang, V. Zhdankin, *J. Am. Chem. Soc*. **1991**, *113*, 4571.

[14] P. Stang, A. Schwarz, T. Blume, V. Zhdankin, *Tetrahedron Lett.* **1992**, *33*, 6759.

[15] P. Stang, A. Schwarz, V. Zhdankin, *Synthesis* **1993**, 35.

[16] T. Saika, M. Irie, T. Shimidzu, *J. Chem. Soc., Chem. Commun.* **1994**, 2123.

[17] S. Kobatake, T. Yamada, K. Uchida, N. Kato, M. Irie, *J. Am. Chem. Soc*. **1999**, *121*, 2380.

[18] B. P. Warner, S. L. Buchwald, *J. Org. Chem.* **1994**, *59*, 5822.

[19] J. K. Stille, J. H. Simpson, *J. Am. Chem. Soc.* **1987**, *109*, 2138.

[20] A related example of a Glaser-like reaction involving an organic halide as oxidizer was reported: M. E. Wright, C. K. Lowe-Ma, *Organometallics* **1990**, *9*, 347.

[21] R. Durr, S. Cossu, O. De Lucchi, *Synth. Commun.* **1997**, *27*, 1369.

[22] K. Sonogashira, Y. Tohda, N. Hagihara, *Tetrahedron Lett.* **1975**, *50*, 4467.

[23] Due to the chirality of the organometallic group (Λ or Δ configuration), the complexes are obtained as mixtures of stereoisomers such as ΛΛ, ΔΔ and ΔΛ for **2a**. However, the chiral centers are generally sufficiently far apart for their steric interaction to be negligible, so that the chirality of the two metal centers can be considered to be independent. Moreover, in similar examples involving $Ru(bipy)_2$-like terminal units, no consequences of the chirality of the metal centers were reported, neither on the NMR spectra (J. Bolger, A. Gourdon, E. Ishow, J.-P. Launay, *Inorg. Chem*. **1996**, *35*, 2937), nor on the electrochemical and spectroscopic behavior (M. J. Powers, T. J. Meyer, *J. Am. Chem. Soc.* **1980**, *102*, 1289; A. C. Benniston, V. Goulle, A. Harriman, J.-M. Lehn, B. Marczinke, *J. Phys. Chem.* **1994**, *98*, 7798). See also the review: R. J. Crutchley, *Adv. Inorg. Chem.* **1994**, *41*, 273, and references therein. Thus, the stereochemical aspects are not considered in the rest of this paper.

[24] ^1H NMR (250 MHz, CD_3OD, 20 °C) of **12a**: δ = 2.02 (s, 3 H), 7.34 (s, 1 H), 7.40−7.46 (m, 3 H), 7.58−7.60 (m, 2 H). Electrochemistry: irreversible oxidation at 1.04 V vs SCE in MeCN. Colorless "open" compound **12a** undergoes photocyclization upon irradiation with UV light, to give the "closed" cobalt-blue isomer **12b**. For a $1.6\cdot10^{-5}$ M solution in MeCN, the photostationary state is reached within 25 s (cf. 30 s for **8**). UV/Vis in MeCN: λ_{max} (nm) (ε [M^{-1} cm^{-1}]): *open* form (**12a**): 306 (61250); *closed* form (**12b**): 604 (21900).

[25] In this expression, V_{ab}, $\bar{\nu}$, and $\Delta\bar{\nu}_{1/2}$ are in cm^{-1}, ε_{max} in mol^{-1} L cm^{-1}, and R_{MM} is in Å. The proportionality factor

0.0205 comes from (i) the definition of the oscillator strength f in terms of experimental quantities, (ii) the relation of f with the transition moment μ_{tr} (P. W. Atkins, *Physical Chemistry*, 4th ed., Oxford University Press, Oxford, **1990**, pp. 503−504), and (iii) the expression of μ_{tr} in the particular case of intervalence transitions, according to Hush.[3] The literal expression of this factor is $[3\,h\,C\,\varepsilon_0(\ln 10)/4\,\pi^2\,N_A\,e^2]^{1/2}\,(\pi/\ln 2)^{1/4}$ where h is Planck's constant, C is the velocity of light, ε_0 is the permittivity of a vacuum, N_A is Avogadro's number, and e is the elementary charge; a value of $6.513\cdot10^{-12}$ is obtained in SI units. Converted into the more common non-SI units, the result is $6.513\cdot10^{-12} \times (1000)^{1/2}\cdot10^8$, i.e., 0.0205.

[26] A. T. Bens, D. Frewert, K. Kodatis, C. Kryschi, H.-D. Martin, H. P. Trommsdorff, *Eur. J. Org. Chem*. **1998**, 2333.

[27] J. Lacour, S. Torche-Haldimann, J. J. Jodry, C. Ginglinger, F. Favarger, *Chem. Commun.* **1998**, 1733; J. Lacour, S. Barchéchath, J. J. Jodry, C. Ginglinger, *Tetrahedron Lett.* **1998**, *39*, 567.

[28] M. Irie, K. Sakemura, M. Okinaka, K. Uchida, *J. Org. Chem.* **1995**, *60*, 8305.

[29] A related example of ring opening upon oxidation was described: C. Pac, *Pure Appl. Chem.* **1986**, *58*, 1249. C. Pac, *J. Photochem. Photobiol. A* **1987**, *41*, 37. It involves a photoinduced oxidation of a strained carbocycle (cyclobutane) by a sensitizer, resulting in bond cleavage in the former. For another case of ring reopening by photoinduced electron transfer, see: T. Carell, R. Epple, V. Gramlich, *Angew. Chem. Int. Ed. Engl*. **1996**, *35*, 620.

[30] R. Weiss, J. Seubert, *Angew. Chem. Int. Ed. Engl.* **1994**, *33*, 891.

[31] *Cerius2*, Biosym/Molecular Simulations, San Diego, CA, USA.

[32] *CACAO PC Version 4.0*, July **1994**. C. Mealli, D. M. Proserpio, *J. Chem. Educ*. **1990**, *67*, 399.

[33] J.-P. Launay, S. Fraysse, C. Coudret, *Mol. Cryst. Liq. Cryst*., in press.

[34] A. Altomare, G. Cascarano, G. Giacovazzo, A. Guagliardi, M. C. Burla, G. Polidori, M. Camalli, "SIR92 − a program for automatic solution of crystal structures by direct methods", *J. Appl. Crystallogr*. **1994**, *27*, 435.

[35] D. J. Watkin, C. K. Prout, J. R. Carruthers, P. W. Betteridge, R. I. Cooper, *CRYSTALS Issue 11*, Chemical Crystallography Laboratory, University of Oxford, Oxford (UK).

[36] *ORTEP III*: L. J. Farrugia, *J. Appl. Crystallogr*. **1997**, *30*, 565.

[37] K. H. Pausacker, *J. Chem. Soc.* **1953**, 107.

[38] A. K. Rappé, C. J. Casewit, K. S. Colwell, W. A. Goddard, W. M. Skiff, *J. Am. Chem. Soc*. **1992**, *114*, 10024.

Received January 5, 1999
[I00009]

Properties of Chalcogen−Chalcogen Bonds, 23[+]

Novel Mesityltellurium Cations from Selenenation and Tellurenation Reactions of Dimesityl Telluride in the Presence of the $Br_2/AgSbF_6$ Reagent

Jörg Jeske,[a] Wolf-Walther du Mont,*[a] Frank Ruthe,[a] Peter G. Jones,[a] Laura M. Mercuri,[b] and Paola Deplano[b]

Dedicated to Professor Brigitte Sarry on the occasion of her 80th birthday

Keywords: Tellurium / Cations / Hypervalency / Secondary interactions / Selenium / Xerox process

The reaction of dimesityl telluride (**2**) with bis(pentafluorophenyl) diselenide (**1**), Br_2 and $AgSbF_6$ provides small amounts of crystalline $[Mes_2TeSeC_6F_5][SbF_6]$ (**3**). The main products, however, are $[Mes_2TeTeMes][SbF_6]$ (**4**) and $MesSeC_6F_5$ (**5**). Reactions of **2** with Br_2 and $AgSbF_6$ provide – depending on the stoichiometric ratio – **4** and $[Mes_3Te][SbF_6]$ (**6**) or $[Mes_2TeBr][SbF_6]$ (**7**). **2**, Mes_2Te_2, Br_2 and $AgSbF_6$ provide **4** in a fair yield. Addition of **2** to **4** leads to the tritellurium salt $[Mes_5Te_3][SbF_6]$ (**8**). Cation–anion interactions due to the α-heteroatom electrophilicity of RSe-, RTe- and Br-substituted telluronium salts are followed by structure determinations of **3**, **4**, **6**, **7** and **8** and by Raman-spectroscopic observations of the Te–Te vibrations in compounds **4** and **8**.

Introduction

In the course of the Xerox process, undesired residual charges can persist after exposure of amorphous Se/Te alloys to light. These residual charges may be due to charge separation by formation of chalcogenonium cations (with 3 covalent bonds) and chalcogenolate anions (with only 1 covalent bond) in the solid sate, as depicted schematically in Scheme 1 for tellurium chains.[1]

Such polar defects in Se/Te alloys should be metastable with respect to thermal reactions (i.e. collapsing of the ion pairs) leading to "classical" chalcogen chains involving only di-coordinated selenium and tellurium. We propose an alternative, namely that persistent "-onium" and "-ate" functionalities might interact with each other in a nonclassical way (Scheme 2), leading to structural moieties related to Böttcher's hypervalent polytellurides.[2−4] As organic model compounds for such interactions and as novel "isomers" of the stable diaryl tellurides that might mimic unusual soft−soft interactions, telluronium tellurolates Ph_3Te^+ TeR^- were studied with respect to their existence, structure and mode of decomposition.[5] These compounds exist in the solid state as dimers of ion pairs exhibiting weak cation−anion tellurium−tellurium interactions. At room temperature, the orange-red solids decompose into the more stable diaryl tellurides, accompanied by small amounts of the related ditellurides and biphenyl [Equation (1)]. Telluronium selenolates are slightly more stable than the tellurolates, but they exhibit similar structures and decomposition pathways.

$$(Ph_3TeER)_2 \rightarrow Ph_2Te + PhTeER + R_2E_2 + Ph_2$$
$$ER = p\text{-}CH_3C_6H_4Te,\ p\text{-}CH_3C_6H_4Se^{[5]} \quad (1)$$

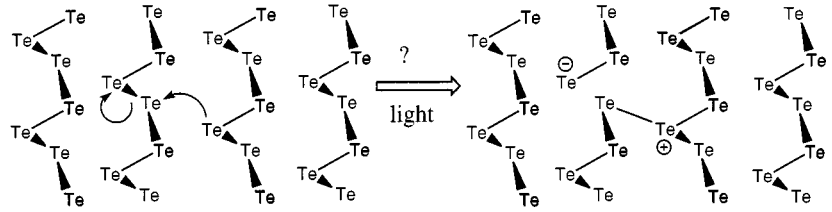
Intuitively, and from comparison with homonuclear cation−anion interactions by (n→σ*) overlap in iodophosphonium ions,[6] we expect that the cation−anion interactions and the colour of $[Ph_3TeER]_2$ (E = Se, Te) would be determined by n(E) → σ*(C−Te) interactions. These would also explain the VSEPR-consistent coordination geometries of the Te and Se atoms of the dimers of ion pairs.[5] The coordination geometries of pyramidal (3-Te-8) and hypervalent square-pyramidal (5-Te-12) tellurium atoms allow the application of extended (n→σ*) interactions (4 orthogonal 3-center-4-electron systems), involving p orbitals of the anions as donor functions and σ* (C−Te) energy levels as acceptors, as a qualitative bonding model. These cation−anion interactions, however, are much weaker than Te−Te contacts within "nonclassical" polytellurides[2−4,7] and polytellurium dications.[8]

Calculations on $[R_3TeER]_n$ (R = H, Me; n = 1, 2) on the basis of the experimental Te···Te and Te···Se distances,

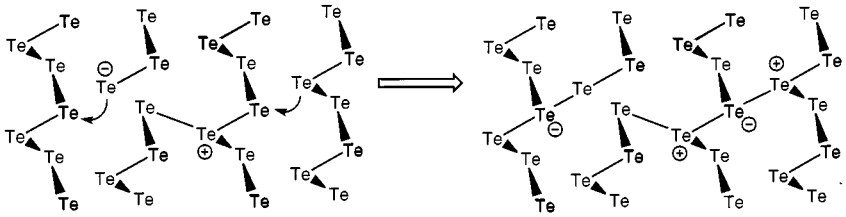
[+] Part 22: Ref.[21]

[a] Institut für Anorganische und Analytische Chemie der Technischen Universität Braunschweig
Postfach 3329, 38023 Braunschweig, Germany
Fax: (internat.) + 49-(0)531/391-5387
E-mail: w.du-mont@tu-bs.de
[b] Dipartimento di Chimica Inorganica ed Analitica, Università di Cagliari,
Cittadella di Monserrato, 90131 Monserrato-Cagliari, Italy
Fax: (internat.) + 39-070/675-4499
E-Mail: deplano@vaxca1.unica.it

 © WILEY-VCH Verlag GmbH, D-69451 Weinheim, 2000 1434−1948/00/0707−1591 $ 17.50+.50/0



Scheme 1. The valence-alternation model ($2C_2^0 \rightarrow C_3^+ + C_1^-$) for localised gap states in lone-pair semiconductors applied to tellurium (Kastner−Adler−Fritzsche model)[1]



Scheme 2. "Classic" (8-Te-3 and 8-Te-1) (left) and "hypervalent" (8-Te-3 and 10-Te-3) (right) version of the Kastner−Adler−Fritzsche model

however, do not indicate a positive contribution of Te−Te and Te−Se orbital overlap to the overall energy.[9] The poor acceptor properties of R_3Te^+ towards RTe^- and RSe^- reflect the relative strength (a kind of "*trans* effect") of Te−C bonds, which do not offer low-lying σ* levels to facilitate the attack of donating nucleophiles.[10] Atoms that are more weakly bonded to the telluronium centre, however, would encourage the attack of donating nucleophiles, as shown by the increased electrophilicity of hypothetical $TeI_3^+$and $MeTeI_2^+$ cations relative to R_3Te^+ cations in Me_3Te^+ $MeTeI_4^-$ [11] and $(Ph_3Te^+)_2$ TeI_6^{2-}.[12] For this reason, we decided to synthesise telluronium ions containing one "soft" chalcogen atom adjacent to the formally positively charged tellurium atom of the cation. As an electron-withdrawing substituent we chose the pentafluorophenylseleno group. As further substituents, mesityl groups were selected to enhance crystallisation. An initial experiment explored whether bis(pentafluorophenyl) diselenide (**1**) would add oxidatively to dimesityl telluride (**2**) yielding an, as yet unknown, compound of the type $R_2Te(SeR')_2$ (formally regarded as an adduct of a $[R_2TeSeR']^+$ cation with a RSe^- anion). ^{77}Se- and ^{125}Te-NMR spectra of the reaction mixture, however, did not provide evidence for the presence of the compound $Mes_2Te(SeC_6F_5)_2$.[13] To elucidate whether the failure of the desired oxidative addition of **1** to the diaryl telluride **2** was really due to thermal instability of $Mes_2Te(SeC_6F_5)_2$ (and not to kinetic factors), we then attempted to generate an $[R_2TeSeR']^+$ cation by an independent route.

Reactions

Triorganylperoxonium ions $[R_2OOR]^+$,[13] -disulfonium ions $[R_2SSR]^+$,[14,15] related organoselenium cations such as $[(MeSe)_2SeMe]^+$ [15] and $[Ph_2Se_6]^{2+}$ [16] and oxytelluronium cations $[R_2TeOTeR_2]^{2+}$,[17,18] are well-known species; corresponding selenotelluronium salts $[R_2TeSeR']^+$ X^-, however, have not yet been reported in the literature,[5,12] Such compounds will undergo reductive elimination when the counterion X^- is a good nucleophile towards the $R'Se^+$ group. Salts of the type $[RR'TeTeR']^+$ X^- have been proposed as reactive intermediates when dialkyl ditellurides were activated by alkyl halides for one-pot reactions with carbon nucleophiles.[19] Oxidation of molecules that contain two R_2Te functions in the presence of poorly nucleophilic counteranions has led to a number of cyclic dications with $[R_2Te-TeR_2]^{2+}$ moieties;[20] in the presence of two R_2Se donor functions, hypervalent species with dicationic $[RR'Se-TeR''_2-SeRR']^{2+}$ functions have been generated.[20]

For the generation of $(Mes_2TeSeC_6F_5)^+$ SbF_6^- (**3**) we chose the oxidation of bis(pentafluorophenyl) diselenide (**1**) in the presence of dimesityl telluride (**2**), and SbF_6^- as a poorly nucleophilic counteranion. On addition of few drops of the $Ag[SbF_6]$ solution in CH_2Cl_2 to the mixture of **1**, **2**, and Br_2, the solution became deep red; precipitation of AgBr occurred only after addition of the complete amount of $Ag[SbF_6]$. Crystallisation by diffusion of hexane first provided very dark crystals of a novel compound **4**, which did not contain selenium. Spectroscopic and analytical data and a crystal-structure determination confirmed that **4** is unexpectedly a dimesityl(mesityltelluro)telluronium salt $[Mes_2TeTeMes][SbF_6]$.[21] At a later stage of the crystallisation procedure, a small amount of the originally desired orange-brown selenotelluronium salt **3** and further crystals of black **4** were isolated. An NMR investigation of the remaining oil revealed the presence of mesityl pentafluorophenyl selenide (**5**) [$\delta^{77}Se = +370$, $^3J(^{77}Se, ^{19}F) = \pm 11$ Hz]. Unexpected products **4** and **5** indicated cleavage of the Te−C bonds (loss of a mesityl group of **2**) and formation of a new Se−C bond by attachment of a mesityl group to selenium providing **5** [Equation (2)]. To gain more insight into the loss of a mesityl group from **2**, we treated **2** with 1/2 Br_2 and $Ag[SbF_6]$ only. This reaction also provided crystals of compound **4**; however, these black crystals were ac-

companied by a small amount of greenish crystals of $[Mes_3Te][SbF_6]$ (**6**) [Equation (3)]. This "aryl scrambling" could be associated with a disproportionation by aryl transfer between two R_2Te^+ cations or within an $[R_2Te-TeR_2]^{2+}$ dication, with an aryl cation transfer from R_2Te^{2+} to R_2Te providing R_3Te^+ and RTe^+, the latter being trapped by coordination with R_2Te. A somewhat related formal tellurium analogue to the pinacol−pinacolone rearrangement had previously been discussed when the rearrangement of Wöhler's "α-base $R_2Te(OH)_2$" into the "β-base"[22] was recognised as an alkyl transfer between tellurium atoms.

$$(C_6F_5)_2Se_2 + Mes_2Te + Br_2 + 2\ AgSbF_6 \rightarrow (Mes_2TeSeC_6F_5)SbF_6$$

1 **2** **3**

$$+ (Mes_2TeTeMes)SbF_6 + MesSeC_6F_5 + 2\ AgBr \quad (2)$$

4 **5**

$$2\ \mathbf{2} + Br_2 + 2\ AgSbF_6 \rightarrow \mathbf{4} + (Mes_3Te)SbF_6 + 2\ AgBr \quad (3)$$

6

The observed partial decomposition of **2** upon oxidation with $Br_2/AgSbF_6$ into **4** and **6** would correspond to a dismutation $2\ R_2Te \rightarrow R_3Te^+ + RTe^-$,[6] if the cation of **4** were formally regarded as an adduct of the tellurolate anion $MesTe^-$ with the dication Mes_2Te^{2+}. Carrying out the bromination of **2** with *one* equivalent of Br_2 (Mes_2Te/Br_2, 1:1) and adding one equivalent of $AgSbF_6$ allowed the isolation of the bromotelluronium salt $[Mes_2TeBr][SbF_6]$ (**7**) as yellow crystals [Equation (4)]. In the absence of the diselenide **1**, mesityl group transfer between **7** or the intermediate dication $[Mes_2Te]^{2+}$ and **2**, provided Mes_3Te^+ (the cation of compound **6**), whereas coordination of the remaining $MesTe^+$ moiety with **2** then led to stable **4** [Equation (5)]. In the presence of diselenide **1**, mesityl group transfer to the arylseleno group provided **5**, the remaining $MesTe^+$ moiety was again coordinated by **2** furnishing stable **4**. The latter type of reaction can indeed be verified using Mes_2Te_2, Br_2, $AgSbF_6$ and **2**: this synthesis is an excellent large-scale preparation of compound **4** [Equation (5)].[21] The isolation of compound **4** was favoured by its extremely low solubility; no solution-NMR data of **4** could be obtained.

$$\mathbf{2} + Br_2 + AgSbF_6 \rightarrow (Mes_2TeBr)SbF_6 + AgBr \quad (4)$$

7

$$2\ \mathbf{2} + Mes_2Te_2 + Br_2 + AgSbF_6 \rightarrow 2\ \mathbf{4} + 2\ AgBr \quad (5)$$

However, on addition of one further equivalent of **2** to suspended **4**, the black precipitate dissolved and provided the soluble novel [bis(dimesityltelluronio)mesityl tellurolate(II)] hexafluoroantimonate, $Mes_5Te_3SbF_6$ (**8**). The cation of **4** was obviously still coordinatively unsaturated and by adding one more equivalent of **2** "saturated" **8** was obtained, which contains a hypervalent central tellurium atom [Equation (6)]. This addition of **2** to **4** forming **8** is closely related to the well-known addition of I^- to I_2 to give I_3^-, which contains a hypervalent central iodine atom. Related homonuclear trichalcogen moieties with linearly coordinated central hypervalent sulfur or selenium atoms have been known since the detection of trithiapentalenes,[23] the tris(selenocyanate) monoanion and related species.[24] A related tetracationic system with approximately linear Se−Se···Se arrangements is formed by the interaction of one molecule of 1,2-bis(3-methyl-2-selenoxo-4-imidazolinyl)ethane ("ebis") with two $[(ebis)_2]^{2+}$ dications.[25] An organotellurium anion with an approximately linear triiodide-like Te_3 moiety related to **8**[21] was detected only recently.[26]

$$\mathbf{2} + \mathbf{4} \rightarrow [(Mes_2Te)_2TeMes]SbF_6 \quad (6)$$

8

Spectroscopic and Structural Studies

Comparison of Selenotelluronium Salt 3 and Tellurotelluronium Salt 4

The description of the ditelluronium cation in **4** as a mesitylenetellurenyl cation $MesTe^+$, stabilised by the coordinating Lewis base **2**, is supported by the nature and extent of the various intermolecular interactions of the cations of **4** and of the closely related compound **3** with their SbF_6^- counteranions in the solid state. In solid **4** two cations and two anions form cyclic molecular dimers through secondary Te···F interactions,[21] in solid **3** similar sequences of Te···F and Se···F interactions lead to polymeric chains of cations and anions (Figure 1−4).

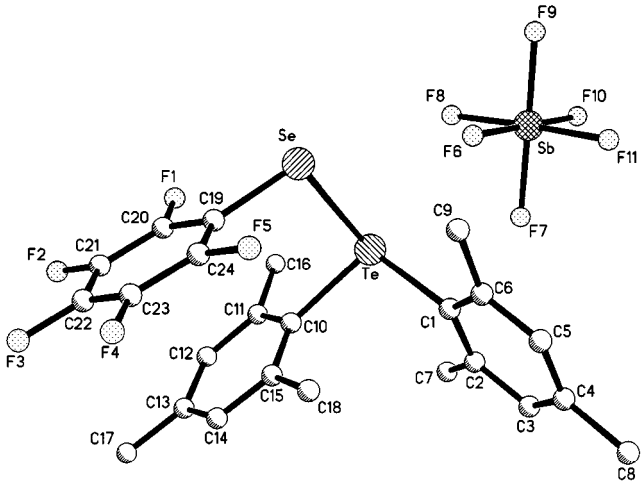


Figure 1. Molecular structure of **3** (cation−anion contacts neglected); selected distances [pm] and angles [°]: Te−C(10) 211.5(3), Te−C(1) 213.3(4), Se−C(19) 190.1(4), Te−Se 257.55(5), Sb−F(6) 189.1(2), Sb−F(7) 187.9(2), Sb−F(11) 185.8(2); C(10)−Te−C(1) 101.80(13), C(10)−Te−Se 96.10(9), C(19)−Se−Te 101.30(11)

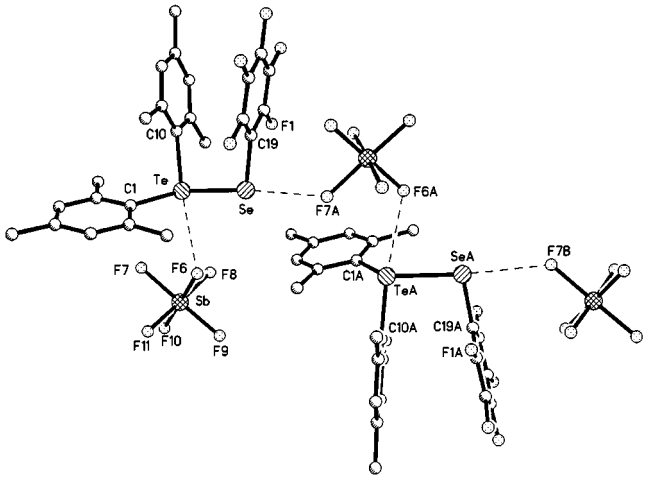


Figure 2. Cation−anion interactions in solid **3**; selected distances [pm] and angles [°]: Te−F(6) 296.2(2), Se−F(7)#1 301.1(2); C(10)−Te−F(6) 173.84(10), C(1)−Te−F(6) 81.28(10), Se−Te−F(6) 77.76(5), C(19)−Se−F(7)#1 84.25(12)

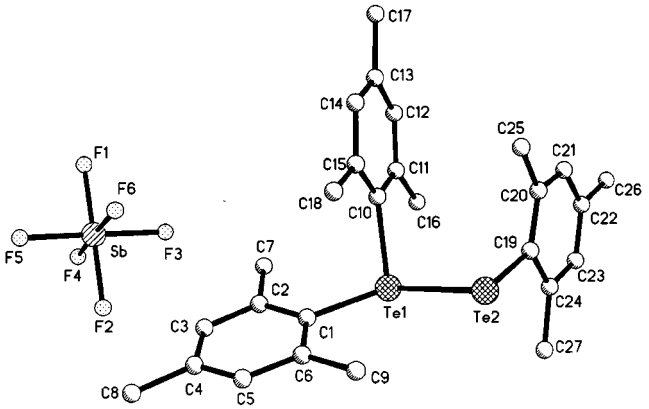


Figure 3. Molecular structure of **4** (cation−anion contacts neglected); selected distances [pm] and angles [°]: Te(1)−C(1) 214.1(4), Te(1)−C(10) 212.7(4), Te(2)−C(19) 213.1(5), Te(1)−Te(2) 276.45(5), Sb−F(1) 187.2(3), Sb−F(2) 186.7, Sb−F(5) 183.9(3); C(1)−Te(1)−Te(2) 112.76(12), C(10)−Te(1)−Te(2) 95.34(11), C(19)−Te(2)−Te(1) 86.18(12)

The coordination geometry of all chalcogen atoms in **3** and **4** can be described as pseudo-trigonal-bipyramidal, when secondary Te···F and Se···F contacts are taken into consideration. When Te1 is considered as the central atom (*one* lone pair of electrons, 10-Te-4[27]), the neighbouring F atom adopts an apical position (C10−Te−F6 in **3**: 173.8°, C10−Te1−F1 in **4**: 175.6°), and the neighbouring "two-coordinated" chalcogen atom is equatorial. Regarding the Se atom in **3**, the gradual transition from two-coordination towards a "T-type" surrounding (10-Se-3[27]) can be recognised from the nearly linear arrangement Te−Se···F (Te−Se−F7A 173.8°, Te−Se−C19 101.3°, C19−Se−F7A 84.2°). For the "two-coordinated" Te atom in **4** the geometric features of a typical "T-type" structure (Te1−Te2−F2 168.3°, Te1−Te2−C19 86.2°, C19−Te2−F2 83°) are fully expressed. The typical T-type geometry is associated with a short contact between the "two-coordinated" Te atom and a fluorine atom of the counterion. This Te···F contact of

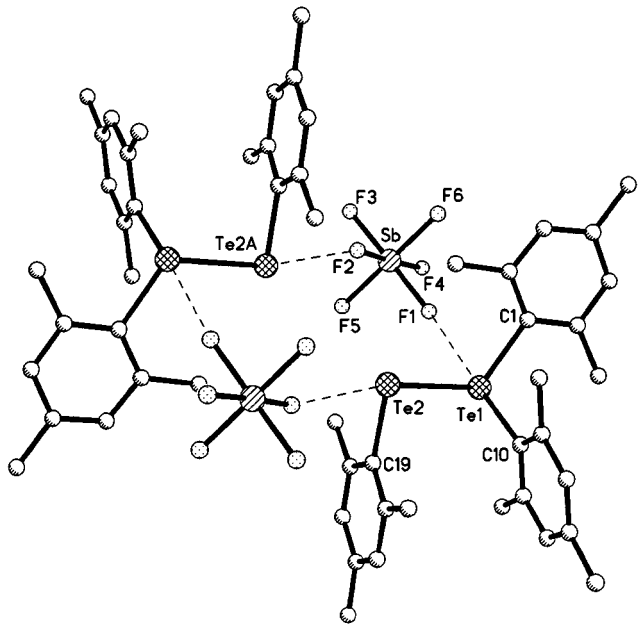
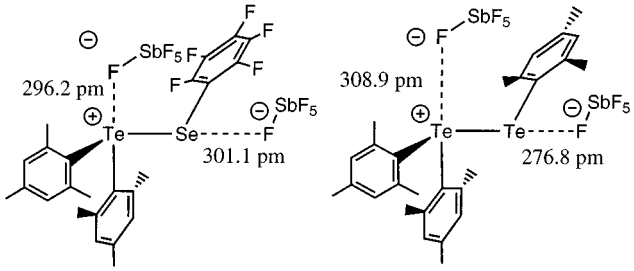


Figure 4. Intermolecular interactions within dimers of **4**; selected distances [pm] and angles [°]: Te(1)−F(1) 308.9(3), Te(2)−F(2A) 276.8(3); C(10)−Te(1)−F(1) 175.65(12), Te(2)−Te(1)−F(1) 88.94(6), Te(1)−Te(2)−F(2A) 168.27(9), C(19)−Te(2)−F(2A) 83.01(14)

the Te atom in the α-position to the telluronium centre of **4** (Te2···F2A 276.8 pm) is significantly shorter than the Te···F contact from the telluronium centre that bears the formal +1 charge (Te1−F1 308.9 pm) and is also shorter than the Se···F contact in **3** (**3**: Se···F7A 301.1 pm). The latter contact is longer (weaker) than the Te···F contact involving the telluronium centre, which is the predominant type of cation−anion interaction (Te···F6 296.2 pm) of the selenotelluronium salt; i.e. **3** is "the normal case" whereas **4** exhibits the unusual short Te···F contact involving the formally uncharged tellurium atom. This rather strong F→Te donor−acceptor interaction also coincides with a slight lengthening of the Te−Te bond in **4** (Mes_2Te_2: d = 270 pm;[28] **4**: d = 276.45 pm) and with a bathochromic shift of the Te−Te vibration mode in the Raman spectrum of **4** (143 cm^{-1}) compared with uncharged Me_2Te_2 [$\tilde{\nu}$(Te−Te) = 181 cm^{-1}] (Scheme 3).[29]



Scheme 3. Cation−anion interactions in **3** and **4**

Weakening of Te···Te bonds is to be expected when the F→Te donation leads to partial population of the σ* orbital of the Te−Te bond. The extent of the latter interaction al-

lows the prediction that the Te atom involved, in the α-position to the telluronium centre, will have acceptor properties as a Lewis acid. Following this, **4** can be understood as a type of arenetellurenyl cation (RTe^+) that is coordinated but not yet coordinatively saturated by one diaryl telluride nucleophile.[10,30] The bridging of the cations of **3** and **4** by the SbF_6^- anions through donor−acceptor interactions correlates well with the expansion of the bridging Sb−F bonds of the anions [**3**: *d*(Sb−F) between 185.8 ppm (terminal) and 189.1 pm (bridging); **4**: *d*(Sb−F) between 183.9 (terminal) and 187.2 pm (bridging)]. As a test of the electrophilicity of **4**, the reaction of **4** with another molecule of **2** as a nucleophile was carried out. This led to the detection of the hypervalent cation **8**.[21]

Structures of Trimesityltelluronium Salt 6 and Bromodimesityltelluronium Salt 7

The propeller-like conformation of the cation of **6** with angles C−Te−C close to tetrahedral (104−109°) is very similar to that of the known compound Mes_3TeI.[31] Te···F contacts are very long (363−367 pm), i.e. cations and anions are well separated (Figure 5, 6).

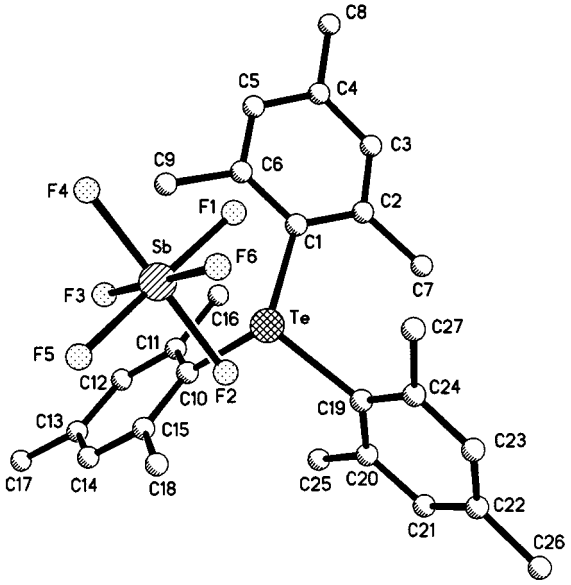


Figure 5. Molecular structure of **6**; selected distances [pm] and angles [°]: Te−C(1) 213.5(3), Te−C(10) 213.1(3), Te−C(19) 213.7(3), Te−F(1) 366.9(2), Te−F(2) 363.7(2), Te−F(3) 366.3(2) Sb−F(1) 187.3(2), Sb−F(4) 186.2(2); C(1)−Te−C(10) 104.42(11), C(1)−Te−C(19) 109.25(12), C(19)−TeC(19) 104.57(12)

The solid bromodimesityltelluronium salt **7** contains two independent ion pairs within the asymmetric unit. Since the fluorine atoms of both anions are disordered (they were refined on two different positions, see Figure 6), only a qualitative description of the cation−anion interactions can be given. The bromotelluronium salt **7** can be regarded as closely related to **3** and **4**: They contain telluronium cations with rather "soft" heteroatoms adjacent to the formally charged tellurium centre, offering two choices for cation−anion interactions. The shortest Te···F distances in **7** range from 262 to 324 pm, i.e., they are comparable to the Te···F distance of **3** and to that involving the formally charged telluronium centre of **4**. The coordination spheres of the Te atoms of **7** can be regarded as pseudo-trigonal-bipyramidal, with two carbon atoms and the lone pair in equatorial positions and an apical Te−F contact. The bromine atoms of the cations of **7** participate in the cation−anion interaction network by exhibiting contacts to (disordered) fluorine atoms of the SbF_6^- anions [Br(2)−F(3A) and Br(2)−F(3′A), depicted in Figure 6]. These Br···F distances, being shorter than the Se···F distances in **3**, indicate a certain Lewis acidity of the bromine atoms, a general property of heavy α-heteroatoms adjacent to onium centres.[5,12,21]

Compounds R_2TeBr_2 generally exist as molecular (10-Te-4) species with two apical Te−Br bonds, even when R is a very good electron-withdrawing substituent.[31] Being closer to an ideal 2c−2e bond, the Te−Br bond of **7** is significantly shorter than the apical Te−Br bonds of $(C_6F_5)_2TeBr_2$.[32]

Description of the Tritellurium Cation 8

Trialkyldisulfonium cations $[R_2SSR]^+$ do not tend to valence-shell expansion of sulfur by cation−anion interactions[14] or by addition of a second dialkyl sulfide nucleophile. The purple-black compound **4**, however, reacted in a straightforward manner with **2**, providing the novel brown-red "pentaaryltritelluranium" salt **8**. Due to its moderate solubility, a full set of solution-NMR data of **8** could be collected. The two Mes_2Te groups within the cation of **8** are NMR-equivalent; their ^{125}Te-NMR signal [$\delta(^{125}Te) = +854$] and the ^{125}Te-NMR signal of the central MesTe moiety of **8** [$\delta(^{125}Te) = +388$] are broadened to a somewhat different extent, and the Te−Te NMR coupling cannot be resolved. Dynamic exchange equilibria in solution were confirmed by addition of a small amount of **2** to a solution of **8**: from such a mixture, one averaged signal from free and coordinated **2** [$\delta(^{125}Te) = +842$] and a further signal from the unaffected central MesTe moiety [$\delta(^{125}Te) = +385$] were resolved. The related tritelluride anion $Ph_3Te_3^-$ [26] is also kinetically labile in solution. Crystalline **8**[21] contains $Mes_5Te_3^+$ cations, SbF_6^- anions and CH_2Cl_2. The cation contains an approximately linear Te_3 backbone. The two Te−Te distances are slightly different (Te1−Te2 304.9 pm, Te3−Te1 297.9 pm); they are both significantly longer in comparison with Te−Te single bonds such as those of **4** (Figure 7) or Mes_2Te_2. The average Te−Te distance of **8** (301.5 pm) is similar to that of $Ph_3Te_3^-$ (302.5 pm),[32] shorter than the typical Te−Te distances of linear Te−Te−Te moieties of "nonclassical" inorganic polytellurides, for instance the Te_5^{4-} ion within solid NaTe: *central*: *d*(TeTe) = 308 pm; *terminal*: *d*(TeTe) = 282 pm.[2,33] From the vibrational spectra of solid **8**, a strong Raman emission at 102 cm^{-1} can be assigned to the symmetric Te_3 stretching mode (Figure 8). The analogy of the position of this Raman emission to that of a slightly asymmetric triiodide anion is clear.[34,35] However, it is surprising, that the antisymmetric vibration is apparently not resolved in the IR spectrum.

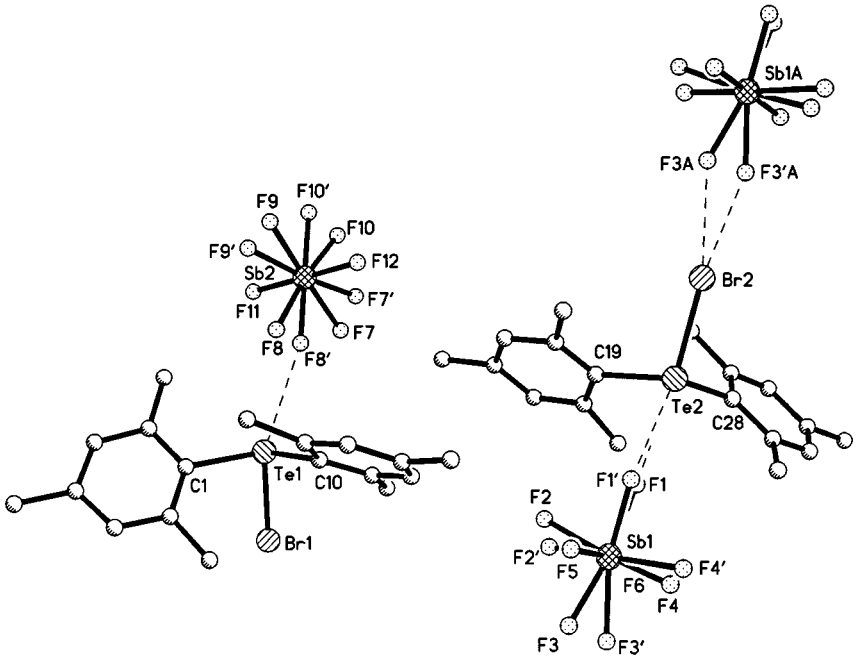


Figure 6. Structures of the two independent ion pairs and anion disorder of **7**; selected distances [pm] and angles [°], ion pair 1: Te(1)−C(1) 211.6(11), Te(1)−C(10) 212.9(10), Te(1)−Br(1) 250.9(2), Te(1)−F(8) 324(2), Te(1)−F(8′) 293(2); C(1)−Te(1)−C(10) 106.8(4), C(1(Te(1)−Br(1) 91.6(3), C(10)−Te(1)−Br(1) 101.8(3); ion pair 2: Te(2)−C(28) 213.9(12), Te(2)−C(19) 213.1(11), Te(2)−Br(2) 247.9(2), Te(2)−F(1) 262(2), Te(2)−F(1′) 266(2), Br(2)−F(3A) 269(2), Br(2)−F(3′A) 280(2); C(28)−Te(2)−C(19) 106.4(4), C(28)−Te(2)−Br(2) 93.4, C(19)−Te(2)−Br(2) 100.5(3)

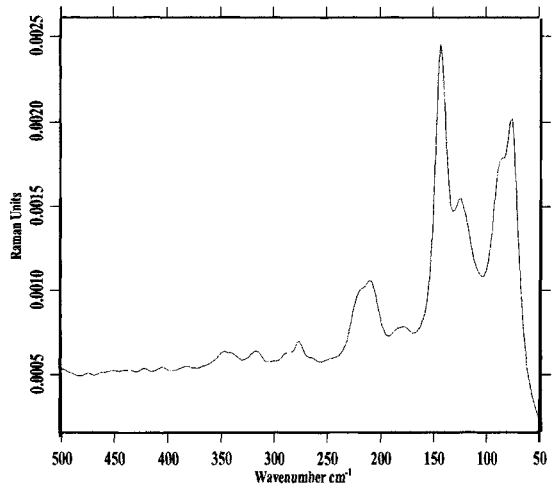


Figure 7. Raman emissions of solid **4**

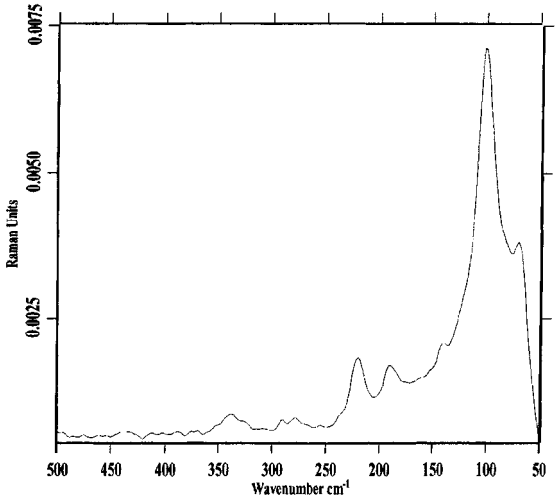
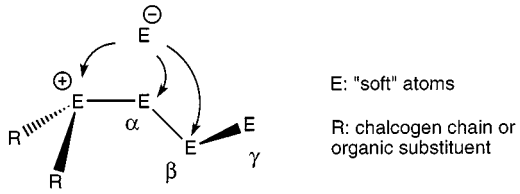


Figure 8. Raman emissions of solid **8**

A strong IR absorption at 289 cm^{-1} is observed in **8** and **4** (in the latter the band is less symmetric showing a shoulder at approximately 278 cm^{-1}). This band seems to confirm the presence of SbF_6 anions (it is present in all the samples containing this anion that we have investigated including $AgSbF_6$), while the vibrations expected in the Raman spectrum appear as weak peaks in **8** and **4**, the Raman spectra being dominated by the strong inter-tellurium vibrations. Surprisingly, to the best of our knowledge, a strong IR absorption at 289 cm^{-1} has not been reported previously in spite of numerous vibrational studies involving SbF_6 anions.[36] An (unassigned) strong IR absorption at 275 cm^{-1} has been reported for solid $[Cp_2ReCl_2](SbF_6)_3$.[37] For an SbF_6 anion in an octahedral structure, three Raman-active vibrations [$\nu_1(A_{1g})$ (668 cm^{-1}), ν_2 (E_g) (558 cm^{-1}) and ν_5 (F_{2g}) (294 cm^{-1})] and two infrared-active vibrations [$\nu_3(F_{1u})$ (669 cm^{-1}), ν_4 (F_{1u})(350 cm^{-1})] are expected.[38] The sixth vibration ν_6 (F_{2u}) calculated at 294 cm^{-1}, is predicted to be inactive in both the infrared and Raman spectra, but should become infrared-active in those structures that have lower symmetry than O_h.[39] We suggest that the band at 289 cm^{-1} is due to ν_4, and the presence of a shoulder at 278 cm^{-1} in **4** could be associated to ν_6, whose activity is related to the lowering of the symmetry as a result of the observed distortions in this anion (Figure 7).

The formation of nonclassical linear Te_3 moieties has been described theoretically as the hypothetical addition of Te^{2-} ions to Te_2^{2-} ions,[2,4] The above reaction of nucleophile **2** with electrophile **4** furnishing **8** is the first well-defined addition of two 8e⁻-tellurium species to form a linear 10e⁻-Te_3 species.[21,26] This model reaction provides an experimental approach to understanding how cationic defects in solid selenium−tellurium alloys (Scheme 1 and 2) may be stabilised by acceptor−donor interaction of adjacent two-coordinate tellurium atoms with tellurium atoms of neighbouring tellurium chains. However, it should be noted that soft heteroatoms (such as Se and Te) in β- and γ-positions from the onium centre can also exhibit certain Lewis-acidic properties (Scheme 4).



Scheme 4. Sites of nucleophilic attack in chalcogen cations

As in the stabilisation of onium-like cationic defects ("C-3") above, masking of the *negative* charges ("C-1") (Scheme 1) by local formation of hypervalent anionic Te_3 moieties (such as those in $LiTe_3$, $Ph_3Te_3^-$ or $NaTe_3$ [2,4,26,33,40]) will contribute to the stabilisation of anionic defects in tellurium.

Experimental Section

^{77}Se- and ^{125}Te-NMR spectra were run with a Bruker AM 200 spectrometer (38.2 MHz for ^{77}Se and 63.1 MHz for ^{125}Te) using CH_2Cl_2 as a solvent, if not otherwise specified. *J* values are given in Hz. − Raman spectra (resolution ± 4 cm^{-1}) were recorded with a Bruker RFS 100 FTR spectrometer (Nd:YAG laser excitation, 1064 nm). The solid samples, in the form of powders or crystals, were packed into glass capillary tubes and then fitted into the compartment designed for use with a 180° scattering geometry. The power level of the laser source was in the range of 70−150 mW. − Far-FTIR spectra (500−50 cm^{-1}) were recorded with a Bruker IFS 55 spectrometer (as polyethylene pellets). − Mass spectra were determined with Finnegan MAT 8430 and 4315 spectrometers [EI, 70 eV, CI, or FAB with *o*-nitrobenzylamine (NBA)]. − Melting points were determined with a Kofler hot-stage microscope and all values are uncorrected. − Elemental analyses were carried out by the Analytisches Laboratorium des Instituts für Anorganische und Analytische Chemie, Technische Universität Braunschweig. Solvents were dried by distillation under nitrogen from the appropriate drying agent, glassware was flame-dried and cooled under a stream of nitrogen.

3: A solution of $AgSbF_6$ (0.68 g, 2.0 mmol) in 10 mL of dichloromethane was added to a stirred mixture of Mes_2Te (1.1 g, 2.0 mmol), $(C_6F_5Se)_2$ (0.49 g, 1.0 mmol) and Br_2 (0.08 g, 0.50 mmol), dissolved in 30 mL dichloromethane. Upon addition of the first drops of the $AgSbF_6$ solution, the reaction mixture adopted an intense red colour. Precipitation of silver bromide occurred after all the $AgSbF_6$ had been added. After 30 min, the silver bromide was removed by filtration and a layer of 40 mL of hexane was carefully added to the red-brown solution. Within 18 h, the two phases had mixed by diffusion and black crystals (compound **4**) had separated from the mixture. The supernatant liquid was decanted and all volatiles were removed under vacuum until an oily residue remained. This residue was dissolved in a small amount of dichloromethane and a layer of hexane was again carefully added to the solution. Another crop of **4** (black crystals) was accompanied by a small amount of orange-brown crystals [m.p. 154 °C (dec.)] which were identified by X-ray crystallography as the desired compound **3**. Correct elemental analytical data were not obtained. Attempts to purify crude **3** by fractional crystallisation led to isolation of a further amount of **4**, which appeared to be a decomposition product of crude **3**. Evaporation of the solvents from the remaining slightly yellowish mother liquor furnished a viscous oil. ^{77}Se-NMR spectra and EI mass spectra allowed to the detection of mesityl (pentafluorophenyl) selenide (**5**) and bis(pentafluorophenyl) diselenide (**1**) in the the oily residue. − ^{77}Se NMR of the mixture: δ = 370 [$^3J(^{77}Se,^{19}F)$ = 11.0 Hz, $(C_6F_5)_2Se_2$ = **1**], 176 [$^3J(^{77}Se,^{19}F)$ = 14.3 Hz, C_6F_5−Se−Mes = **5**]. − EI-MS of the mixture; *m*/*z* (%): 494 (50) [$(C_6F_5)_2Se_2^+$], 366 (84) [C_6F_5−Se^+−Mes], 247 (100) [C_6F_5−Se^+], 119 (35) [Mes^+].

4: Bromine (0.12 g, 0.75 mmol) was added to a solution of Mes_2Te (0.55 g, 1.5 mmol) and Mes_2Te_2 (0.49 g, 0.75 mmol) in 30 mL of dichloromethane, at room temperature. Subsequently, silver hexafluoroantimonate (0.50 g, 1.5 mmol), dissolved in 5 mL of dichloromethane, was added to the mixture. The colour of the solution turned from brown to deep red and precipitation of silver bromide began. Stirring was continued in the dark for 1 h for the reaction to reach completion. After removal of the precipitate by filtration, hexane was added to the brown solution. **4** separated from the solution as a brown-violet powder (0.94 g; 74%) that melted at 189 °C (dec.). Black single crystals suitable for X-ray diffraction[21] were obtained with help of the diffusion method (dichloromethane solution/hexane). Crystalline **4** was only slightly soluble in dichloromethane (intensely greenish-brown solution) and in methanol (colourless solution). − $C_{27}H_{33}F_6SbTe_2$ (848.5): calcd. C 38.22, H 3.92; found C 38.37, H 4.03. − ^{1}H NMR (CD_2Cl_2): δ = 7.05 (2 H), 2.34 (6 H), 2.32 (3 H). − ^{125}Te NMR: no signal observed due to low solubility. − Raman: $\tilde{\nu}$ = ν(Te−Te) 143 cm^{-1}. − FAB-MS (NBA), positive mode; *m*/*z* (%): 741 (5) [$Mes_3Te_3^+$], 613 (40) [$Mes_3Te_2^+$], 494 (22) [$Mes_2Te_2^+$], 368 (100) [Mes_2Te^+], 248 (24) [$MesTe^+$−H], 119 (70) [Mes^+]; negative mode; *m*/*z* (%): 494 (7) [$Mes_2Te_2^-$], 472 (2.5) [$Sb_2F_{12}^-$], 235 (100) [SbF_6^-], 216 (2) [SbF_5^-], 197 (2) [SbF_4^-]. − FT-IR: $\tilde{\nu}$ = 341 (2.8), 321 (2.8), 289 (10), 278 sh, 218 (3.4) 62 (2.2) cm^{-1}. − FT-Raman: $\tilde{\nu}$ = 210 (4.0), 143 (10.0), 124 (5.0), 85 (shoulder), 76 (8.0) cm^{-1}.

7: A solution of 1 mmol of Mes_2TeBr_2 was prepared by oxidation of Mes_2Te (0.37 g, 1.0 mmol), dissolved in 10 mL of dichloromethane, with a solution of bromine (0.16 g, 1.00 mmol) in 5 mL of dichloromethane at 0 °C. Addition of silver hexafluoroantimonate (0.38 g, 1.0 mmol) led to a deep red solution and to the precipitation of AgBr, which was removed by filtration after continued stirring for 15 min. Upon addition of 35 mL of hexane to the red solution, a yellow precipitate separated from the yellowish supernatant solution. In order to remove the remaining amounts of silver bromide from the yellow crude product, the latter was again treated with 5 mL of dichloromethane and the undissolved solid (AgBr) was removed by filtration. Precipitation by addition of 10 mL of hexane provided 0.54 g (79%) of yellow **7** (m.p. 148 °C, dec.). − $C_{18}H_{22}BrF_6SbTe$ (681.6): calcd. C 31.72, H 3.25; found C 30.98, H

3.25. − ^{1}H NMR (CD_2Cl_2): δ = 7.16 (2 H), 2.52 (6 H), 2.39 (3 H). − ^{125}Te NMR (CH_2Cl_2/C_6D_6): δ = 1128. − FAB-MS (NBA), positive mode; *m/z* (%): 617 (8) [$Mes_3Te_2^+$], 520 (45) [NBA(Mes_2Te^+ − H], 447 (45) [Mes_2TeBr^+], 368 (85) [Mes_2Te^+], 248 (40) [$MesTe^+$ − H], 119 (100) [Mes^+].

8: A solution of **8**, prepared by slight warming of a mixture of $Mes_2TeTeMes\ SbF_6$ (**4**) (0.43 g, 0.50 mmol) and Mes_2Te (**2**) (0.25 g, 0.70 mmol) in 2 mL of dichloromethane, was kept at −18 °C in order to obtain crystals that were suitable for X-ray diffraction.[21] After separation of the clear brownish-red needles from the solution by filtration, the solvent-containing single crystals decomposed under vacuum into a brown powder of **8** (0.45 g, 74%) which melted at 169 °C (dec.). The given yield and analytical data concern the solvent-free final product. **8** was fairly soluble in dichloromethane; addition of hexane to such a solution led to a precipitate of **4**. − $C_{45}H_{55}F_6SbTe_3$ (1214): calcd. C 44.50, H 4.56; found C 44.64, H 4.48. − ^{1}H NMR (CD_2Cl_2): δ = 7.04 (2 H), 2.32 (6 H), 2.30 (3 H). − ^{125}Te NMR (CH_2Cl_2/C_6D_6): δ = 854, 388; after addition of a 20% excess of **1**: δ = 842, 385. − FAB-MS (NBA), positive mode; *m/z*: 741 (2) [$Mes_3Te_3^+$], 613 (40) [$Mes_3Te_2^+$], 494 (14) [$Mes_2Te_2^+$], 368 (100) [Mes_2Te^+], 248 (20) [$MesTe^+$−H], 119 (55) [Mes^+]; negative mode; *m/z*: 494 (7) [$Mes_2Te_2^-$], 472 (3) [$Sb_2F_{12}^-$], 235 (100) [SbF_6^-], 216 (2) [SbF_5^-], 197 (2) [SbF_4^-]. − FT-IR: $\tilde{\nu}$ = 326 (3.2), 289 (10.0), 204 (3.8), 100 (shoulder), 78 (4.6) cm^{-1}. − FT-Raman: $\tilde{\nu}$ = 220 (2.0), 189 (1.9), 141 (2.5), 102 (10.0), 78 (shoulder), 70 (5.2) cm^{-1}.

Crystal Structure Determination of 3: Empirical formula: $C_{24}H_{22}F_{11}SbSeTe$, M = 847.73; orthorhombic, space group *Pbca*, a = 1452.73(12) pm, b = 1583.6(2) pm, c = 2405.6(2) pm; V = 5.5341(9) nm^3; Z = 8; $d_{calcd.}$ = 2.035 Mg m^{-3}; μ = 3.433 mm^{-1}, T = 173 K. An orange prism (0.62 × 0.42 × 0.20 mm) was mounted in an inert oil. 6933 intensities were measured (2θ = 6−50°, ω-scans; $-17 < h < 6$, $-18 < k < 0$, $-28 < l < 0$) using Mo-K_α radiation (graphite monochromator) with a Siemens P4 diffractometer. After absorption correction (ψ-scans; min. and max. transmission: 0.516, 1.000), 4877 reflections were unique (R_{int} = 0.0190) and used for all calculations (program SHELXL-93[41]). The structure was solved by direct methods and refined anisotropically by full-matrix least squares on $|F|^2$. Rigid methyl groups were employed, all other protons were refined using a riding model. The final $wR(F^2)$ was 0.0576, with conventional $R(F)$ 0.0268 for 349 parameters and 267 restraints (highest peak 754, deepest hole −463 e/nm^3).

Crystal Structure Determination of 6: Empirical formula: $C_{27}H_{33}F_6SbTe$, M = 720.88; orthorhombic, space group *Pbca*, a = 1616.55(10) pm, b = 1738.52(12) pm, c = 1985.6(2) pm; V = 5.5804(7) nm^3; Z = 8; $d_{calcd.}$ = 1.716 Mg m^{-3}, μ = 2.067 mm^{-1}, T = 173 K. A green prism (0.62 × 0.60 × 0.55 mm) was mounted in an inert oil. 4908 intensities were measured (2θ = 6−50°, ω-scans; $-19 < h < 6$, $-20 < k < 0$, $-0 < l < 23$) using Mo-K_α radiation (graphite monochromator) with a Siemens P4 diffractometer. After absorption correction (ψ-scans; min. and max. transmission: 0.821, 0.948), 4908 reflections were unique (R_{int} = 0.0190) and 4906 were used for all calculations (program SHELXL-93).[41] The structure was solved by direct methods and refined anisotropically by full-matrix least squares on $|F|^2$. Rigid methyl groups were employed, all other protons were refined using a riding model. The final $wR(F^2)$ was 0.0509, with conventional $R(F)$ 0.0242 for 326 parameters and 249 restraints (highest peak 344, deepest hole −488 e/nm^3).

Crystal Structure Determination of 7: Empirical formula: $C_{36}H_{44}Br_2F_{12}Sb_2Te_2$, M = 1363.23; monoclinic, space group $P2_1/n$, a = 1144.2(2) pm, b = 1210.3(2) pm, c = 3171.8(5) pm; V = 4.3860(13) nm^3; Z = 4; $d_{calcd.}$ = 2.064 Mg m^{-3}, μ = 4.434 mm^{-1}, T = 143 K. A yellow cut needle (0.80 × 0.42 × 0.38 mm) was mounted in an inert oil. 8158 intensities were measured (2θ = 6−50°; ω-scans; $-13 < h < 6$, $0 < k < 14$, $-37 < l < 37$; data are composed of independent set plus some Friedel pairs) using Mo-K_α radiation (graphite monochromator) with a Stoe STADI-4 diffractometer. After absorption correction (ψ-scans; min. and max. transmission: 0.460, 0.764), 7722 reflections were unique (R_{int} = 0.0498) and 7703 were used for all calculations (program SHELXL-93).[41] The structure was solved by direct methods and refined anisotropically by full-matrix least squares on $|F|^2$. Rigid methyl groups were employed, all other protons were refined using a riding model. The final $wR(F^2)$ was 0.1982, with conventional $R(F)$ 0.0675 for 457 parameters and 24 restraints (highest peak 1849, deepest hole −1561 e/nm^3).

Crystallographic data (excluding structure factors) for the structures reported in this paper have been deposited with the Cambridge Crystallographic Data Centre as supplementary publication no. CCDC-121862 (**3**), -100165 (**4**),[21] -121863 (**6**), -121964 (**7**), -100165 (**8**).[21] Copies of the data can be obtained free of charge on application to CCDC, 12 Union Road, Cambridge CB2 1EZ, UK [Fax: (internat.) + 44-1223/336-033; E-mail: deposit@ccdc.cam.ac.uk).

Acknowledgments

We thank the Deutsche Forschungsgemeinschaft, the Fonds der Chemischen Industrie, and the INTAS/RFBR program (95−126) for financial support.

[1] M. Kastner, D. Adler, H. Fritzsche, *Phys. Rev. Lett.* **1976**, *37*, 1504−1507; R. A. Street, N. F. Mott, *Phys. Rev. Lett.* **1975**, *35*, 1293.
[2] P. Böttcher, *Angew. Chem.* **1988**, *100*, 781−794; *Angew. Chem. Int. Ed. Engl.* **1988**, *27,* 759.
[3] M. G. Kanatzidis, *Angew. Chem.* **1995**, *107*, 2281−2283; *Angew. Chem. Int. Ed. Engl.* **1995**, *34*, 2109−2111.
[4] Q. Liu, N. Goldberg, R. Hoffmann, *Chem. Eur. J.* **1996**, *2*, 390−397.
[5] W.-W. du Mont, J. Jeske, P. G. Jones, *Angew. Chem.* **1996**, *108*, 2822−2824; *Angew. Chem. Int. Ed. Engl.* **1996**, *35*, 2653−2655.
[6] M. Bätcher, W.-W. du Mont, S. Pohl, W. Saak, *Phosphorus Sulfur Silicon Relat. Elem.* **1990**, *49/50*, 147−150; W.-W. du Mont, F. Ruthe, *Coord. Chem. Rev.* **1999**, *189*, 101−133.
[7] B. Schreiner, K. Dehnicke, K. Moczek, D. Fenske, *Z. Anorg. Allg. Chem.* **1993**, *619*, 1414.
[8] J. Beck, *Coord. Chem. Rev.* **1997**, *163*, 55−70.
[9] C. Janiak, Universität Freiburg, EHT and PM3 calculations, personal communication.
[10] I. Haiduc, R. B. King, M. G. Newton, *Chem. Rev.* **1994**, *94*, 301−326.
[11] F. Einstein, J. Trotter, C. Williston, *J. Chem. Soc. A* **1967**, 2018−2023.
[12] J. Jeske, Dissertation TU Braunschweig, **1997**; W.-W. du Mont, J. Jeske, P. G. Jones, VII. Int. Conf. on the Chemistry of Selenium and Tellurium, Vaalsbroek Castle (NL)/Aachen (D), **1997** (Abstract); *Phosphorus Sulfur Silicon Relat. Elem.* **1999**, *136−138*, 305−308; J. Beck, A. Fischer, *Z. Anorg. Allg. Chem.* **1995**, *621*, 1042.
[13] G. A. Olah, G. Rasul, Burrichter, M. Hachoumy, G. K. Surya Prakash, R. I. Wagner, K. O. Christe, *J. Am. Chem. Soc.* **1997,** *119,* 9571−9573.
[14] T. P. Hilditch, S. Smiles, *J. Chem. Soc.* **1907**, *91*, 1394−1399; R. Minkwitz, H. Prenzel, H. Pritzkow, *Z. Naturforsch.* **1987**, *B42*, 750−755.

[15] R. Laitinen, R. Steudel, R. Weiss, *J. Chem Soc., Dalton Trans.* **1986**, 1095−1100.
[16] R. Faggiani, R. J. Gillespie, J. W. Kolis, *J. Chem. Soc, Chem. Commun.* **1987,** 592.
[17] F. L. Gilbert, T. M. Lowry, *J. Chem. Soc.* **1928,** 3179−3189; P. Nylen, *Z. Anorg. Allg. Chem.* **1941**, *246*, 227−242.
[18] K. Kobayashi, N. Deguchi, E. Horn, N. Furukawa, *Angew. Chem.* **1998**, *110*, 1031−1033; *Angew. Chem. Int. Ed.* **1998**, *37*, 1026−1028.
[19] V. A. Potapov, S. V. Amosova, V. Yu. Shestakova, A. R. Zhnikin, B. V. Petrov, *Recl. Trav. Chim. Pays-Bas* **1996**, *215*, 441−442.
[20] H. Fujihara, T. Ninoi, R. Akaishi, T. Erata, N. Furukawa, *Tetrahedron Lett.* **1991,** *32*, 4537; H. Fujihara, H. Ishitani, Y. Takaguchi, N. Furukawa, *Chem. Lett.* **1995**, 571−572
[21] J. Jeske, W.-W. du Mont, P. G. Jones, *Angew. Chem.* **1997**, *109*, 2304−2306; *Angew. Chem. Int. Ed. Engl.* **1997**, *36*, 2219−2221.
[22] H. D. K. Drew, *J. Chem. Soc.* **1929,** 560−569.
[23] S. Bezzi, M. Mammi, C. Garbagli, *Nature* **1958**, *182*, 247.
[24] O. Foss, *Pure Appl. Chem.* **1970**, *24*, 31.
[25] F. Bigoli, P. Deplano, F. A. Devillanova, A. Girlando, V. Lippolis, M. L. Mercuri, M. A. Pellingghelli, E. F. Trogu, *Inorg. Chem.* **1996**, *35*, 5403−5406.
[26] A. C. Hillier, S. Y. Liu, A. Sella, M. R. J. Elsegood, *Angew. Chem.* **1999**, *111*, 2918−2920, *Angew. Chem. Int. Ed. Engl.* **1999**, *38,* 2745−2747.
[27] (10-Te-4) means: 10 valence electrons at the central Te atom, that contains 4 substituents: C. W. Perkins, J. C. Martin, A. J. Arduengo III., W. Lau, A. Alegria, J. K. Kochi, *J. Am. Chem. Soc.* **1980**, *102*, 7753.
[28] A. Edelmann, S. Brooker, N. Bertel, M. Noltemeyer, H. W. Roesky, G. M. Sheldrick, F. T. Edelmann, *Z. Naturforsch.* **1992**, *B47*, 305−309.
[29] C. W. Sink, A. B. Harvey, *J. Mol. Struct.* **1969,** *4*, 203; W. R. McWhinnie, P. Thavornyutikarn, *J. Organomet. Chem.* **1972**, *35*, 149−154.
[30] S. Hauge, O. Vikane, *Acta Chem. Scand., Ser A* **1983**, *27,* 723; W.-W. du Mont, H.-H. Meyer, S. Kubiniok, S. Pohl, W. Saak, *Chem. Ber.* **1992***, 125*, 761−766.
[31] M. Wieber, R. Habersack, *Phosphorus Sulfur Silicon* **1995,** *106***,** 233−241.
[32] N. W. Alcock, W. D. Harrison, *J. Chem. Soc., Dalton Trans.* **1984**, 869; D. Naumann, L. Ehmanns, K.-F. Tebbe, W. Crump, *Z. Anorg. Allg. Chem.* **1993***, 619*, 1269−1276.
[33] P. Böttcher, R. Keller, *J. Less-Common Met.* **1985**, *109*, 311−321.
[34] P. Deplano, F. A. Devillanova, J. R. Ferraro, M. L. Mercuri, V. Lippolis, E. F. Trogu, *Appl. Spectrosc.* **1994**, *48*, 1236.
[35] P. Deplano, J. R. Ferraro, M. L. Mercuri, E. F. Trogu, *Coord. Chem. Rev.* **1999**, *188*, 71−95.
[36] J. Passmore, T. S. Cameron, P. D. Boyle, G. Schatte, T. Way, *Can. J. Chem*. **1996**, *74*, 1671, and references therein.
[37] P. Gowik, T. M. Klapötke, I. Torniepoth-Oetting, *Chem. Ber.* **1989**, *122*, 2273.
[38] K. Nakamoto, in "*Infrared and Raman Spectra of Inorganic and Coordination Compounds*", 4th ed., John Wiley & Sons, Inc., New York, **1986**.
[39] G. M. Begun, A. C. Ruthenberg, *Inorg. Chem*. **1967**, *6*, 2212.
[40] D. Y. Valentine, O. B. Cavin, H. L. Yakel, *Acta Crystallogr. B* **1977**, *33*, 1389−1396.
[41] G. M. Sheldrick, *SHELXL-93, A Program for Crystal Structure Refinement*, Göttingen, **1993.**

Received January 20, 2000
[I00020]

Synthesis and Structural Characterisation of a New Form of Bis(acyclovir)(ethylenediamine)platinum(II) − Correlation between the Puckering of the Carrier Ligand and the Canting of the Nucleobases

Renzo Cini,[a] Sabina Grabner,[b] Natasa Bukovec,[b] Leonardo Cerasino,[c] and Giovanni Natile*[c]

Keywords: Acyclovir / Platinum / Atropisomerism / Antitumor agents / Nucleobases

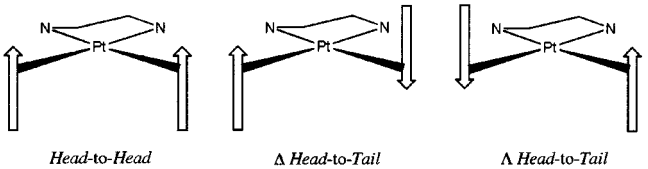
A new conformer of the $[Pt(en)(acv)_2]^{2+}$ cation (en = ethylenediamine; acv = acyclovir = 9-[(2-hydroxyethoxy)methyl]guanine) has been prepared by slow crystallisation of the $[Pt(en)(acv)_2]SO_4 \cdot 2.5H_2O$ salt. X-ray diffraction studies have shown that the guanine moieties have a *Head-to-Head* conformation (*HH*) with the two C(8)-H vectors pointing towards the same side with respect to the platinum coordination plane; the dihedral angles formed by the purine planes and the coordination plane are 58.3(2)° and 41.5(2)°, respectively. There is a correlation between the canting of the purine bases (right or left handed) and the puckering of the ethylenediamine chelate ring (δ or λ). Right-handed canting is associated with λ puckering of the chelate ring and left-handed canting with δ puckering of the chelate ring, so that in both cases one of the two purines forms an O(6)···H–N hydrogen bond with a "quasi equatorial" NH of the ethylenediamine. The "quasi equatorial" character of the NH appears to be a common feature for intramolecular H-bonds between guanine bases and *cis*-amines. The purine not involved in the H-bond has the six-membered ring portion leaning towards the *cis* purine rather than towards the *cis* amine and may give rise to a weak O(6)···Pt attractive interaction. Such an interaction is supported by density functional (DFT) molecular orbital calculations carried out on the model systems $[Pt(NH_3)_4(CH_2O)]^{2+}$ and *Head-to-Tail* *cis*-$[Pt(NH_3)_2\{N(=CH_2)–C(=CH_2)–C(=O)–NH_2\}_2]^{2+}$. The exocyclic chains linked to N(9) each have two different orientations, and all four are stretched away from the metal centre as well as from the purine N(1)H and N(2)H_2 protons. The acv and the en NH protons are instead involved in H-bonds with the sulfate anion.

Introduction

Combination drug chemotherapy has enjoyed much success in the treatment of cancer. This is attributed to the fact that development of resistant cell lines is delayed or prevented and that synergistic interactions between chemotherapeutic agents with different mechanisms of interactions can occur.[1] Observations of this kind have spawned the idea of binding two different cytotoxic moieties within the same molecule, i.e. the creation of multifunctional drugs,[2] and this has become a leading strategy in current studies.

The report that cisplatin was found to be an effective topical treatment in mice[3] prompted some investigators to explore the possibility that platinum(II) or palladium(II) complexes containing antiviral nucleosides might act in a synergistic fashion.[4−6] The prototype complex $[Pt(NH_3)_2(acv)_2](NO_3)_2$ appeared to be equally inhibitory as compared to acv when both were assayed against HSV-1 (KOS). Moreover the complex was not cytotoxic to normal cells at the highest concentration tested (400 mg/cm^3). The reason for such a dramatic decrease in toxicity of $[Pt(NH_3)_2(acv)_2](NO_3)_2$, when compared with the precursor $[Pt(NH_3)_2Cl_2]$, is not fully understood.

In a previous paper we reported the X-ray crystal structure of this multifunctional complex in which the two ammines had been replaced by a chelating ethylenediamine.[7] The two guanine bases adopted the usual *Head-to-Tail* conformation (*HT*) with the two purines tilted over the coordination plane and forming O(6)···H−N H-bonds with the *cis* amine groups. We have now succeeded in crystallising a second conformer of the same complex in which the two guanines are arranged in the very rare *Head-to-Head* (*HH*) conformation (see Scheme 1). To the best of our knowledge this is the only metal *cis*-bis(nucleobase) complex containing identical ligands that has been crystallised in its two possible rotamers to date.



Scheme 1. Representations of the *Head-to-Tail* and *Head-to-Head* orientations of the two guanines with respect to the Pt/N_4 coordination plane

[a] Dipartimento di Scienze e Tecnologie Chimiche e dei Biosistemi, Università di Siena, via E. Bastianini 12, I-53100 Siena, Italy
[b] Department of Chemistry, University of Ljubljana, Askerceva 5, SI-1000 Ljubliana, Slovenia
[c] Dipartimento Farmaco-Chimico, Università di Bari, via E. Orabona 4, I-70125 Bari, Italy
E-mail natile@farmchim.uniba.it

 © WILEY-VCH Verlag GmbH, D-69451 Weinheim, 2000 1434−1948/00/0707−1601 $ 17.50+.50/0

The results of this investigation are reported here. The discussion will concentrate on the structural motifs induced by platinum coordination and their relevance to the primary lesion responsible for the cytotoxicity of platinum drugs to tumour cells, which involves the cross-linking of two adjacent guanine bases on one strand of the DNA double helix.[8−11]

Results

The preparation of the complex cation was given in the previous paper concerning a *Head-to-Tail* conformer.[7] Comparison of the FTIR spectra of the complex and of free acv indicates that binding of Pt(II) to N(7) shifts bathochromically the carbonyl frequency, ν[C(6)=O], which occurs at 1717 cm^{-1} for uncomplexed acv and at 1685 cm^{-1} for the complexed species. Platinum complexation also shifts the frequencies of ν[C(8)−N(7)] and δ[C(8)−H] from 1483 to 1498 cm^{-1}, respectively, as observed in related cases.[12] The typical absorptions for a free SO_4^{2-} ion are identified at 1071 and 630 cm^{-1}.[13]

Only one set of proton resonances [C(8)H: δ = 8.18; N(9)CH_2: δ = 5.43; OCH_2CH_2: δ = 3.55 and 3.49; N(*E*)CH_2: δ = 2.77] was observed suggesting free rotation of the two guanine bases around the Pt−N(7) bonds as proposed earlier for similar bifunctional platinum complexes.[14] The ^{195}Pt spectrum showed a signal at δ = −2664 which is in the expected chemical shift range for bifunctional *cis*-DDP complexes.

The complex cation and the proximal sulfate anion for the [Pt(en)(acv)$_2$]SO_4·2.5H_2O salt (**1**) are depicted in Figure 1, selected geometrical parameters are listed in Table 1 and Table 2.

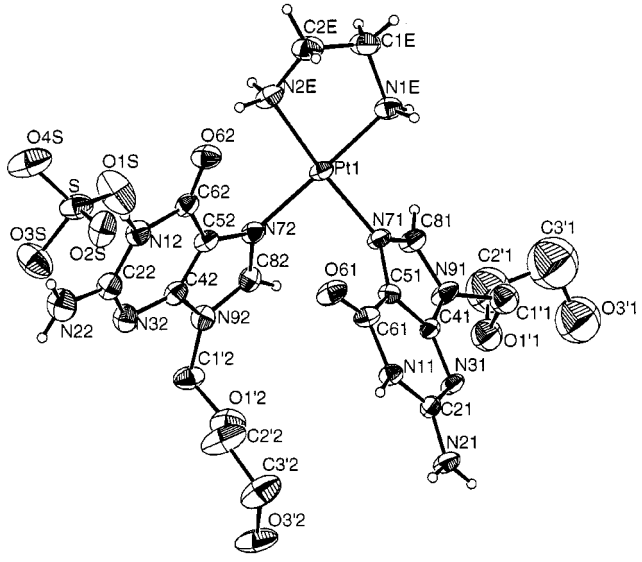


Figure 1. Drawing of the complex molecule and of the sulfate anion from the original set of coordinates; the ellipsoids represent 30% probability

Table 1. Selected bond lengths [Å] for [Pt(en)(acv)$_2$]SO_4·2.5H_2O (**1**)

Vector	Length	Vector	Length
Pt(1)−N(1*E*)	2.021(8)	Pt(1)−N(2*E*)	2.030(7)
Pt(1)−N(71)	2.024(7)	Pt(1)−N(72)	2.037(7)
N(1*E*)−C(1*E*)	1.506(12)	N(2*E*)−C(2*E*)	1.484(13)
C(1*E*)−C(2*E*)	1.485(15)		
O(61)−C(61)	1.213(10)	O(62)−C(62)	1.224(11)
N(11)−C(21)	1.383(11)	N(12)−C(22)	1.375(13)
N(11)−C(61)	1.399(10)	N(12)−C(62)	1.400(11)
N(21)−C(21)	1.335(11)	N(22)−C(22)	1.341(12)
N(31)−C(21)	1.316(11)	N(32)−C(22)	1.322(13)
N(31)−C(41)	1.341(10)	N(32)−C(42)	1.369(12)
N(71)−C(81)	1.288(11)	N(72)−C(82)	1.299(11)
N(71)−C(51)	1.393(11)	N(72)−C(52)	1.397(11)
N(91)−C(81)	1.356(11)	N(92)−C(82)	1.360(12)
N(91)−C(41)	1.386(11)	N(92)−C(42)	1.375(11)
N(91)−C(1′1)	1.491(16)	N(92)−C(1′2)	1.483(12)

Table 2. Selected bond angles [deg] for [Pt(en)(acv)$_2$]SO_4·2.5H_2O **(1)**

Vectors	Angles	Vectors	Angles
N(1*E*)−Pt(1)−N(2*E*)	83.4(3)		
N(1*E*)−Pt(1)−N(71)	91.8(3)	N(2*E*)−Pt(1)−N(72)	95.4(3)
N(1*E*)−Pt(1)−N(72)	177.6(3)	N(2*E*)−Pt(1)−N(71)	174.8(3)
N(71)−Pt(1)−N(72)	89.5(3)		
C(1*E*)−N(1*E*)−Pt(1)	111.8(6)	C(2*E*)−N(2*E*)−Pt(1)	108.2(6)
C(51)−N(71)−Pt(1)	128.5(6)	C(52)−N(72)−Pt(1)	130.5(6)
C(81)−N(71)−Pt(1)	125.7(6)	C(82)−N(72)−Pt(1)	123.3(6)
N(1*E*)−C(1*E*)−C(2*E*)	108.1(8)	N(2*E*)−C(2*E*)−C(1*E*)	109.8(9)
C(21)−N(11)−C(61)	125.9(7)	C(22)−N(12)−C(62)	125.1(8)
C(21)−N(31)−C(41)	112.3(7)	C(22)−N(32)−C(42)	110.9(9)
C(51)−N(71)−C(81)	105.8(7)	C(52)−N(72)−C(82)	105.7(7)
C(41)−N(91)−C(81)	106.4(7)	C(42)−N(92)−C(82)	106.1(8)
C(41)−N(91)−C(1′1)	122.7(10)	C(42)−N(92)−C(1′2)	126.4(8)
C(81)−N(91)−C(1′1)	124.4(10)	C(82)−N(92)−C(1′2)	127.0(8)
N(21)−C(21)−N(11)	117.2(8)	N(22)−C(22)−N(12)	116.6(9)
N(31)−C(21)−N(11)	123.1(8)	N(32)−C(22)−N(12)	124.2(9)
N(31)−C(21)−N(21)	119.7(8)	N(32)−C(22)−N(22)	119.2(10)
N(31)−C(41)−C(51)	129.3(8)	N(32)−C(42)−C(52)	129.2(9)
N(31)−C(41)−N(91)	125.1(7)	N(32)−C(42)−N(92)	123.7(9)
C(51)−C(41)−N(91)	105.6(7)	C(52)−C(42)−N(92)	107.0(8)
C(41)−C(51)−N(71)	109.3(7)	C(42)−C(52)−N(72)	108.9(7)
C(41)−C(51)−C(61)	119.2(8)	C(42)−C(52)−C(62)	119.3(8)
N(71)−C(51)−C(61)	131.4(8)	N(72)−C(52)−C(62)	131.8(9)
O(61)−C(61)−N(11)	120.7(8)	O(62)−C(62)−N(12)	118.3(8)
O(61)−C(61)−C(51)	129.2(8)	O(62)−C(62)−C(52)	130.7(9)
N(11)−C(61)−C(51)	110.1(7)	N(12)−C(62)−C(52)	111.0(9)
N(71)−C(81)−N(91)	112.8(8)	N(72)−C(82)−N(92)	112.4(8)

Platinum Coordination Sphere

The platinum(II) centre has the usual square-planar geometry, the donors being the two nitrogen atoms from ethylenediamine and the N(7) atoms from the two guanine moieties, as recently found for a different salt of the same cation, [Pt(en)(acv)$_2$][PF_6]$_{1.5}$$Cl_{0.5}$·$H_2O$ (**2**),[7] in which, however, the two purine bases have the usual *HT* conformation. The metal centre does not show any appreciable deviation from the plane defined by the donors. The N(1*E*)−Pt−N(2*E*) bond angle is 83.4(3)° in perfect agreement with the values previously reported for the Pt(en) group present in other complexes (ref.[7] and references therein). A strict similarity between the present structure and that of **2** also exists for the N(7)−Pt−N(7) bond angle between the two acv ligands: 89.5(3)° and 90.7(6)° for **1** and **2**, respectively. However, it must be noted that the N(*E*)−Pt−N(7) angles be-

tween *cis* donors are significantly different in the present structure [91.8(3)° and 95.4(3)°, respectively] while they are equal in complex **2** with an *HT* conformation of the acv ligands. The bond lengths for Pt−N(*E*) [2.025(7) Å (average)] and for Pt−N(7) [2.030(7) Å (average)] are in good agreement with previous values for other platinum(II) complexes (ref.[7] and references therein).

The orientation of the two acv ligands with respect to the coordination plane is *HH*, with the C(8)−H vectors pointing towards the same side of the plane. The dihedral angles formed by the two purine systems with the coordination plane are significantly different: 58.3(2)° and 41.5(2)° for acv(1) and acv(2), respectively. It should be noted that the O(6) atom of acv(2) forms a strong intramolecular hydrogen bond with the *cis* amine [N(2*E*)···O(62) = 2.83(2) Å; N−H···O = 153(1)°]. In contrast, the O(61) atom from purine(1) is not involved in any intramolecular hydrogen bond. The different intramolecular contacts found for the two purine systems are reflected by the difference between the Pt−N(7)−C(5) and Pt−N(7)−C(8) bond angles, which is 7.2(6)° for acv(2) and 2.8(6)° for acv(1). Therefore, probably for geometrical reasons, the pseudo macrocycle formed by the O(62)···H−N(2*E*) H-bond linking acv(2) and N(2*E*) requires an opening rather than a narrowing of the Pt−N(7)−C(5) angle. There is also the possibility that the acv(1) ligand, not involved in an H-bond with the *cis*-amine, can feel a Pt···O(61) attractive interaction. This possibility is supported by DFT molecular orbital calculations (see following section) even though the Pt···O(61) contact distance of 3.474(6) Å is rather large [greater than the sum of the Van der Waals radii for Pt (1.8 Å) and O (1.5 Å)][15] and the values of the Pt−N(7)−C(5) and Pt−N(7)−C(8) angles [128.5(6)° and 125.7(6)°, respectively] are equal within two times the estimated standard deviations [it should be recalled, however, that in general the Pt−N(7)−C(5) angle is 4−10° greater than Pt−N(7)−C(8)].[7]

Acyclovir Ligand

The bond lengths and angles relevant to the two guanine systems are in good agreement with those previously reported for other acyclovir complexes (ref.[5,7] and references therein, and ref.[16]). The purine systems are planar, the largest deviations from the least-squares plane defined by the endocyclic atoms being that of N(32) [0.029(8) Å]. The linkages with exocyclic atoms, C(2)−N(2) and C(6)−O(6), have considerable double bond character as can be seen from the bond lengths of 1.338(11) and 1.218(10) Å (averages), respectively.

The aliphatic chains linked to N(9) are stretched away from the coordination sphere, as found for the *HT* conformer **2**. They do not interact intramolecularly with the N−H of the guanine and ethylenediamine systems. Both chains are affected by an extensive statistical disorder (see Experimental Section) which was refined to an acceptable degree of accuracy to permit a reliable analysis of the respective conformations.

The values of the glycosidic torsion angles C(4)−N(9)−C(1′)−O(1′) (χ) are 102(1)° and −101(2)° for acv(1), and −96(1)° and −56(2)° for acv(2). Therefore, all the orientations around N(9)−C(1′) can be described as *gauche*. Interestingly, the values for acv(1) are significantly different from those found for the free ligand [74.4(5)−90.5(6)°][17] and for all Pt−acv complexes so far reported [ref.[16] and references therein]. The N(9)−C(1′)−O(1′)−C(2′) torsion angles (φ) are 107(2)° and −82(3)° for acv(1), and 66(2)° and −64(3)° for acv(2); this *gauche* conformation was also found in the *HT* conformer **2**.[7] The C(1′)−O(1′)−C(2′)−C(3′) torsion angles (γ) are 68(3)° and −94(3)° for acv(1) and 174(1)° and −163(2)° for acv(2), therefore the conformations are *gauche* and *trans*, respectively. The conformations previously reported for this torsion angle were mostly *trans*. Finally, the O(1′)−C(2′)−C(3′)−O(3′) (ω) angles are 73(3)° and −43(4)° for acv(1) and −48(3)° and 69(3)° for acv(2), in agreement with the *gauche* conformation also found for free acv and the previously reported Pt−acv complexes.[5,7]

Ethylenediamine Ligand

The C−N [1.495(12) Å, average] and C−C [1.485(15)] bond lengths and the bond angles around the N and C atoms are in agreement with the typical sp^3 hybridisation of these atoms and with the values reported previously.[7] The five-membered chelate ring is puckered as shown by the deviations of C(1*E*) [−0.06(1) Å] and C(2*E*) [0.51(1) Å] from the least-squares plane of the donors. Both the λ and δ conformations for the Pt(en) chelate ring are present because of the inversion symmetry operation of the *C*2/*c* space group.

Crystal Packing

The sulfate anion has hydrogen bonds with the N(1) and N(2) atoms of acv(2) [N(12)···O(1*S*) = 2.84(3) Å, N−H···O = 161(1)°; N(12)···O(8*S*) = 2.67(2) Å, N−H···O = 165(1)°; N(22)···O(3*S*) = 2.98(2) Å, N−H···O = 160(1)°]. The sulfate anion at (x + 0.5, y + 0.5, z) interacts with the C(8)−H and the N(1*E*)−H groups [C(8)···O(2*S*) = 3.14(2) Å, C−H···O = 134(1)°; N(1*E*)···O(2*S*) = 2.96(2) Å, N−H···O = 170(1)°]. The water molecule O(1 W) (−x, y, −z + 0.5) interacts with N(11) [N···O = 2.85(1) Å, N−H···O = 174(1)°] whereas O(2 W) (−x + 0.5, y − 0.5, −z + 0.5) interacts with N(2*E*) [N···O = 3.03(1) Å, N−H···O = 143(1)°]. Other hydrogen bonds involve the exocyclic chain of the acv moieties and the water molecules, i.e. O(3′1) and O(2 W) (−x + 0.5, y + 0.5, −z + 0.5), O(3′2) and O(3 W) (−x − 0.5, −y + 0.5, −z + 1), and O(3′C) and O(8*S*) (x, y + 1, z) for which the O···O distances are 2.70(2), 2.77(2), and 2.67(1) Å, respectively.

Short contact distances are found between O(3′2), O(3′C) (−x, −y + 1, −z + 1) and C(82) [3.13(2) Å], between O(1′B) (x, y − 1, z) and C(2*E*) [3.39(2) Å], and between O(1′) and O(1′2) (−x, −y + 1, −z + 1) [3.13(1) Å], suggesting a significant repulsive interaction between these

atoms. The attractive and repulsive contacts, which involve several atoms of the exocyclic chains, explain the disorder of the chains themselves and justify the model refined in this work (see Experimental Section).

Finally, an important role for the crystal packing of the present structure is played by the stacking interactions between the purine systems (Figure 2). The shortest interatomic distance is between C(52) and N(32) ($-x$, $-y$, $-z$ + 1) [3.46(1) Å].

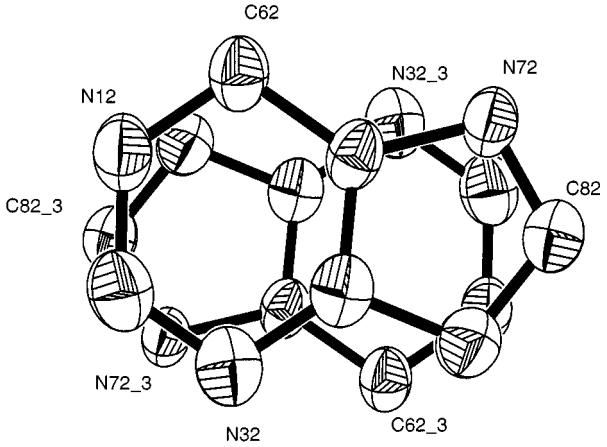


Figure 2. View of the two purine systems from acyclovir(2) which are involved in the strongest stacking interaction; the view is perpendicular to the planes

Molecular Orbital Analysis

The geometry optimized structure for $[Pt(NH_3)_4(CH_2O)]^{2+}$ is reported in Figure 3.

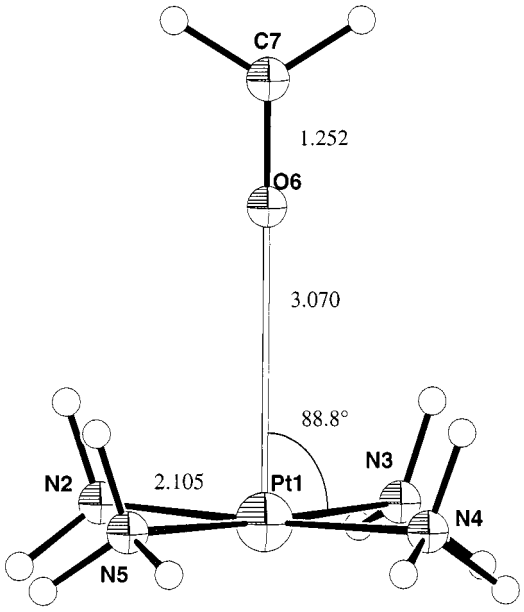


Figure 3. Geometry-optimized structure for $[Pt(NH_3)_4(CH_2O)]^{2+}$

The Pt···O equilibrium distance is 3.070 Å, significantly smaller than the sum of the Van der Waals radii of the two atoms (3.20−3.30 Å).[15] This suggests that an overall attractive interaction between $Pt(NH_3)_4{}^{2+}$ and the CH_2O molecule is operative. The analysis of the MO′s shows that the HOMO for $[Pt(NH_3)_4(CH_2O)]^{2+}$ is composed mostly of *z*-type atomic orbitals from Pt, O and C atoms [Pt: $5d_z^2$ (0.814), $6p_z$ (0.115), and $6d_z^2$ (0.199); O: $2p_z$ (−0.157) and 3s (0.190); C: $2p_z$ (0.120)]. Therefore a covalent interaction exists between the Pt atom and the carbonyl moiety which is assisted by electrostatic and/or hydrogen bonding contributions. In this system, the initial $[Pt(NH_3)_4]^{2+}$ species has an overall positive charge of 2; moreover the O−Pt−N and Pt−N−H (*syn* to O) bond angles (88.8° and 108.4°, respectively) are indicative of weak intramolecular N−H···O hydrogen bonds (N···O = 3.68 Å, N−H···O = 112.3°).

The computed C−O bond length is 1.241 Å in the free molecule and 1.252 Å in the complex molecule. This small lengthening effect might be related to the back donation from the filled Pt $5d_z^2$ orbital to the empty O 3s orbital. The energy of the complex formation for the formal reaction between $[Pt(NH_3)_4]^{2+}$ and CH_2O to form $[Pt(NH_3)_4(CH_2O)]^{2+}$ is −33.942 kcal·mol^{-1}.

The system $[PtCl_4]^{2-}$ and CH_2O was also analyzed. Starting from an initial interatomic Pt···O distance of 2.0 Å the geometry optimization leads to dissociation of the two components. Therefore the electrostatic repulsive interaction between $[PtCl_4]^{2-}$ and the electron rich O atom prevails on the covalent Pt−O linkage. For this latter system, the lack of hydrogen bond interactions is also in favour of dissociation.

The single point calculation on the *HT* isomer of *cis*-$[Pt(NH_3)_2\{N(=CH_2)-C(=CH_2)-C(=O)-NH_2\}_2]^{2+}$ (see Experimental Section) showed that one of the filled frontier orbital consists mostly of Pt $5d_z^2$ (ca. 0.130) and O $2p_z$ (ca. 0.160). The Pt−O distances {from X-ray diffraction on the *HT* *cis*-$[Pt(NH_3)_2(acv)_2]^{2+}$} are 3.320 and 3.409 Å.[18a] Therefore, a covalent interaction between the Pt centre and the O=C function might exist in both the *HT* isomer of *cis*-$[Pt(NH_3)_2(acv)_2]^{2+}$ (compound **3**, ref.[18a]) and *HH* $[Pt(en)(acv)_2]^{2+}$ (present work), although in the latter case the dihedral angle between the acyclovir and platinum-coordination planes is significantly smaller than 90°, and O(6) comes less close to the *z* axis. Intermolecular interactions and/or interligand interactions, related to the canting of the two nucleobases, may be responsible for the deviation of acv1 from orthogonality

Discussion

Nucleobase rotation has been intensively studied for purine complexes of general formula *cis*-$A_2Pt(II)$ (with A_2 = two monodentate or a bidentate amine).[11] The results obtained from these studies are meaningful with regard to the formation and stability of the bifunctional adduct formed in the reaction of the antitumor drug *cis*-$[PtCl_2(NH_3)_2]$ with DNA. Favourable or unfavourable interactions between nucleobases and between these and the carrier ligand are crucial as far as the formation and stability of a given bifunctional adduct are concerned.

In general, for nonbulky carrier ligands (these comprise all primary amines and most of the secondary amines), the rate of rotation of the guanine bases is fast on the NMR

time scale and therefore a single set of signals, which is the average of several possible conformers, is observed. This applies not only to the case of two untethered nucleotides, but also to guanines linked by a phosphodiester chain.[19] Under these circumstances a valuable help in the understanding of factors determining the stability of a given conformation can come from the structural characterisation of various conformers isolated in the solid state. Usually, however, only one of the stable conformers is obtained.

The use of acyclovir as a platinum-coordinating guanine base has been particularly fortunate since it has allowed the crystallisation of three different conformers of the *cis*-$[PtA_2(acv)_2]^{2+}$ species [$A_2 = (NH_3)_2$ or en], all of them possible models of the cisplatin−DNA bifunctional adducts. Two conformers have already been reported,[7,18a] both of which have the guanine base in the most common *HT* arrangement. Such an orientation of the two guanines is favoured by the electrostatic interaction between the two base dipoles. In one case (compound **3**)[18a] the two bases are nearly perpendicular to the coordination plane [dihedral angles of 81.0(4)° and 76.8(4)°]. This positioning of the bases optimises the dipole−dipole interaction but excludes the possibility of H-bond formation between the O(6) of the purine and the *cis* amine group. Interestingly, there was an indication of a possible attractive interaction between the O(6) atoms of the two guanines and the platinum centre. This possibility has been confirmed by the theoretical investigation reported in the present paper.

In the second *HT* conformer (compound **2**)[7] the two purines are tilted over the coordination plane [angles between the purine and the coordination plane of 50.5(3)° and 54.3(3)°]. The tilting of the bases decreases the stabilisation due to the interaction between the base dipoles but allows the formation of H-bonds between the O(6) of the purines and the *cis* amine groups. Interestingly, the two *HT* conformers characterised in the solid state correspond to the two energy minima deduced both from experimental results[20] and theoretical investigations for this type of adduct.[21]

By crystallisation of the same cation under slightly different experimental conditions a new conformer has been obtained (compound **1**). It has the two purines arranged in the rare *HH* conformation; a detailed description of the structure has been given in the previous section. While in the *HT* conformers the two nucleobases within each conformer had comparable inclinations with respect to the coordination plane (difference between dihedral angles $\leq 4°$), in the case of the *HH* conformer the inclination is very different for the two purines (difference between dihedral angles of 17°). The purine with the smaller dihedral angle has the O(6) forming an H-bond with the *cis* amine; such an H-bond is precluded for the second purine which, however, could have O(6) interacting with the platinum centre.

A DFT molecular-orbital analysis carried out on the model system $[Pt(NH_3)_4(CH_2O)]^{2+}$ (C_{2v} symmetry), gave indications of a covalent bonding interaction between the Pt and O atoms. The atomic orbitals mostly involved in this interaction are Pt $5d_z^2$ and $6d_z^2$, and O $2p_z$. The optimized geometry for the $[Pt(NH_3)_4(CH_2O)]^{2+}$ molecule converges to a Pt−O distance of 3.070 Å, a value much shorter than the sum of the Van der Waals radii. The bond formation energy for the formal reaction between $[Pt(NH_3)_4]^{2+}$ and CH_2O is −33.942 kcal·mol^{-1}. A similar DFT molecular-orbital analysis carried out on the *HT cis*-$[Pt(NH_3)_2\{N(=CH_2)-C(=CH_2)-C(=O)-NH_2\}_2]^{2+}$ also gave indications of a covalent bonding interaction between the Pt and O atoms, even though the Pt−O distances were set at 3.320 and 3.409 Å (geometrical parameters of compound **3**). Therefore, it can be concluded that even at long Pt−O distances such as those found in *HT* $[Pt(NH_3)_2(acv)_2]^{2+}$ [18a] and for one acyclovir in *HH* $[Pt(en)(acv)_2]^{2+}$ (present work) an attractive Pt−O interaction may also exist. Such an attractive interaction appears to be weaker in the latter case, where not only is acv1 far from being orthogonal to the coordination plane and the Pt···O distance is longer but also the Pt−N7−C5 angle has failed to become smaller than the Pt−N7−C8 angle (this was the case for the former complex). Moreover, it has to be noted that, for previously reported platinum complexes of guanine derivatives, Pt···O contact distances as short as 3.526(7) Å[18b] and 3.39(1) Å[18c] were found.

There is a correlation between the canting of the purine bases (right or left handed) and the puckering of the ethylenediamine chelate ring (δ or λ). Right-handed canting is associated with λ puckering of the chelate ring and left-handed canting with δ puckering of the chelate ring, so that in both cases one purine forms an H-bond with a "quasi equatorial" NH. Therefore, the H-bond between O(6) of the guanine and the NH of the *cis* carrier ligand appears to be preferentially formed with NH protons having a "quasi equatorial" character than with protons of the "quasi axial" type. This is true for both the *HH* conformation (only one guanine forming the H-bond, present work) and the *HT* conformation (both guanines forming H-bonds, ref.[7]).

It is also likely that in the case of chiral carrier ligands such as 1,2-diaminocyclohexane (DAC) and 2,3-diaminobutane (DAB) the effect of chirality is transmitted from the carrier ligands to the coordinated nucleobases via the stereochemistry of the hydrogen atoms on the coordinated amino nitrogens. Recent results on modifications of natural DNA and synthetic oligodeoxyribonucleotide duplexes by *cis*-$[PtCl_2(DAB)]$ complexes were consistent with the distortion induced in the platinated DNA being determined by hydrogen-bond formation between the carbonyl oxygen of the guanine residues and the "quasi equatorial" hydrogens of the *cis* diamine in the 1,2-d(GpG) intrastrand cross-link.[22]

Experimental Section

Starting Materials: Ethylenediamine, K_2PtCl_4, and Ag_2SO_4 were purchased from Fluka, and acyclovir (acv) was a gift of LEK, Pharmaceutical Works, Slovenia. [PtCl(dmso)(en)]Cl was prepared following the method by Romeo et al.[23]

Preparation of the Complex: $[Pt(en)(acv)_2](SO_4)\cdot 2.5H_2O$ was synthesized by mixing 0.50 mmol of Ag_2SO_4 and 0.50 mmol of [PtCl(dmso)(en)]Cl in 10 mL of water and stirring the solution for 24 h at 60 °C. After filtration 1.00 mmol of acv was added. This mixture was stirred at 50 °C for 24 h and then the solvents evaporated in the open air. Colourless crystals suitable for X-ray analysis were obtained from the solution in a few days. – $C_{18}H_{35}N_{12}O_{12.5}PtS$: calcd. C 25.5, H 4.2, N 19.9; found C 26.0, H 3.9, N 20.1.

Physical Measurements: Infrared spectra in the range 4000–370 cm^{-1} were recorded as nujol mulls on a Perkin–Elmer System 2000 FT spectrophotometer. NMR spectra were recorded on a Bruker Avance DPX 300 (^1H at 300.131 MHz, ^{195}Pt at 64.325 MHz) spectrometer. Sample concentration was 18 mg in 0.6 mL of D_2O (99.9% deuterium). Acetonitrile was used as internal reference [$\delta(^1H) = 2.00$; $\delta(^{13}C) = 1.3$; $\delta(^{15}N) = -135.8$ relative to nitromethane]. ^{195}Pt chemical shifts are referenced to H_2PtCl_6 which was recorded separately. The sample temperature was set at 302 K and controlled to approximately ±0.5 K. *ID spectra:* ^1H: 10 ppm sweep width, 32 k time domain, zero filling to 64 k; ^{195}Pt: 64.4 kHz sweep width, 1368 time domain, 100 k scans, line broadening of 50 Hz prior to FT.

X-ray Structure Analysis[24]

Data Collection: A colourless needle of **1** of dimensions 0.30 × 0.10 × 0.05 mm was selected under a polarising microscope, and then mounted on a glass fibre. The data were collected with a Siemens P4 automatic four-circle diffractometer. Graphite-monochromatized Mo-K_α radiation ($\lambda = 0.71073$ Å) was employed. Accurate cell constants (Table 3) were determined by full-matrix least-squares refinement of the values of 28 carefully centred randomly selected reflections in the range $10 \leq 2\theta \leq 33°$. The data were collected at 295 K and then corrected for Lorentz-polarization and absorption effects (ψ-scan technique based on at least three reflections). The collected reflections totalled 4751, 3365 of which were independent with $I > 2\sigma(I)$. The space group (*C*2/*c*, no. 15) is in agreement with the systematic extinctions. Three standard reflections were monitored periodically (97 reflections) during the data collection; no appreciable decay was observed.

Table 3. Selected crystal data and structure refinement for $[Pt(en)(acv)_2]SO_4\cdot 2.5H_2O$ **(1)**

Parameters	Value
Empirical formula	$C_{18}H_{35}N_{12}O_{12.50}PtS$
Formula weight	846.73
Temperature/K	293(2)
Wavelength/Å	0.71073
Crystal system, space group	Monoclinic, *C*2/*c* (no. 15)
Unit cell dimensions	
a/Å	23.479(2)
b	11.2710(10)
c	22.691(3)
β/deg	101.16(1)
Volume /Å^3	5891.2(11)
Z, Calculated density /Mg·m^{-3}	8, 1.909
Absorption coefficient/mm^{-1}	4.916
Reflections collected/unique	4475/4355 [*R*(int) = 0.0106]
Refinement method	Full-matrix least-squares on F^2
Data/restraints/parameters	4355/9/442
Final *R* indices [$I > 2\sigma(I)$, 3365 refls.]	*R*1, 0.0414; *wR*2, 0.0993
R indices (all data)	*R*1, 0.0613; *wR*2, 0.1095

Structure Solution and Refinement: The structure was solved with the Patterson and Fourier techniques. The difference-Fourier map computed after a twelve-cycles refinement at the isotropic level showed three new peaks in the proximity of three atoms of the exocyclic chains of both the acyclovir molecules. This was interpreted as a statistical disorder and the six new peaks were assigned as oxygen and carbon atoms, namely O(1′B), C(1′B) and C(2′B), and O(1′C), O(3′C) and C(2′C). On the basis of the peak height, the occupancies of the new atoms were fixed at 0.4 and 0.3, respectively, whereas those of the atoms O(1′1), C(1′1), and C(2′1) and O(1′2), O(3′2), and C(2′2) were fixed at 0.60 and 0.70, respectively. At the same stage of refinement four new peaks appeared close to the oxygen atoms [O(1*S*)–O(4*S*)] of the sulfate anion in agreement with a statistical disorder also for this part of the structure. The new peaks were assumed as possible positions for oxygen atoms [whose symbols were assigned as O(5*S*)–O(8*S*)]. The occupancies of the two sets of oxygen atoms were fixed at 0.5 each.

Three broad peaks from the Fourier-difference map were assigned to oxygen atoms of three water molecules whose occupancies are 1, 1, and 0.5, respectively, in agreement with the elemental analysis of the sample and with the analysis of the crystal packing and the hydrogen bonding scheme. The bond lengths for the atoms of the exocyclic chains of acyclovir were restrained as follows: C–O = 1.45 ± 0.02 Å; C–C = 1.52 ± 0.02 Å. The hydrogen atoms for the whole structure were included through the HFIX and AFIX options of SHELX97,[25] excluding the hydrogen atoms for the exocyclic chain of acyclovir and those of the water molecules, which were not included at all. The hydrogen atoms were allowed to ride on the atoms to which they are linked. At the final refinement stage the hydrogen atoms and all the atoms of the disordered chain from acyclovir(1) were treated as isotropic. All the other atoms were refined anisotropically. The thermal parameters for the H-atoms were restrained to be 1.2 times the U_{eq} values of the atoms to which they are bound. All the calculations were carried out with the SHELX 97,[25] PARST 97[26] and XPMA-ZORTEP[27] and ORTEP 3[28] computer programs implemented on Pentium machines.

Molecular Orbital Analysis and Computational Methods: All the calculations were performed with the GAUSSIAN94/DFT package[29] implemented on an Origin 2000 SG machine located at CINECA (Interuniversity Computing Center), Bologna, Italy. Geometry optimizations and energy calculations were obtained by using the B3LYP method[30] and the LANL2DZ basis set.[29] This consists of 6–31G-like functions for nontransition metal atoms, excluding the Cl atom for which the basis set 6–31G**[20] was used, and a valence double-zeta basis set for 3*s*, 3*p*, 3*d* and 4*s* electrons and orbitals along with an effective core potential (Hay and Wadt[31]) for the metal. All the geometrical parameters were fully optimized without symmetry constraints, unless otherwise specified. Other details are as those reported in ref.[32]. The systems investigated were CH_2O, $[Pt(NH_3)_4]^{2+}$, $[Pt(NH_3)_4(CH_2O)]^{2+}$, $[PtCl_4]^{2-}$ and $[PtCl_4]^{2-}\cdots CH_2O$. The starting structures for the metal-containing molecules have planar coordination geometries.

Finally, a single-point DFT calculation was carried out for the molecule *HT cis*-$[Pt(NH_3)_2\{N(=CH_2)-C(=CH_2)-C(=O)-NH_2\}_2]^{2+}$ as a model for *HT cis*-$[Pt(NH_3)_2$-(Guanine)$_2]^{2+}$. The coordinates for the nonhydrogen atoms were those from the *HT cis*-$[Pt(NH_3)_2(acv)_2]^{2+}$ complex reported in ref.[18a]. The hydrogen atoms were introduced in calculated positions by using the HyperChem 5.0 package;[33] whereas molecular drawings were obtained through XPMA-ZORTEP.[27] and ORTEP 32.[28] packages. All graphic calculations were performed on Pentium machines.

Acknowledgments

R. C. thanks Mr. F. Berrettini for the X-ray data collection at Centro Interdipartimentale di Analisi e Determinazioni Strutturali (CIADS) and Centro di Calcolo Interuniversitario dell'Italia Nord-Orientale (CINECA), Bologna, for the grant proj. n° 99/1522−5. The authors also thanks the Universities of Bari and Siena (Contribution ex 60%), the Ministero dell'Università e della Ricerca Scientifica e Tecnologica, MURST (Cofin. 1988 n° 9803021072), the Consiglio Nazionale delle Ricerche, CNR (Roma) and the EC (COST Chemistry projects D8/0009/97 and D8/0012/97 to G.N.).

[1] V. T. De Vita, Jr., in *Cancer* (Eds.: V. T. De Vita Jr., S. Hellman, S. A. Rosenberg), Lippincott, Philadelphia, PA, 257, 1985; B. Rosenberg, *Cancer* (Amsterdam), **1985**, *55*, 2303.
[2] M. A. Khaled, R. D. Morin, F. Benington, J. P. Daugherty: *Cancer Chemother. Pharmacol*. **1984**, *13*, 73.
[3] M. B. Snyder, L. D. Saravolatz, N. Markowitz, D. Pohlod, S. G. Ward, R. C. Taylor, *J. Antimicrob. Chemother*. **1987**, *19*, 815.
[4] E. Dubler, M. Grüter-Heini, G. Hänggi, M. Knoepfel, H. Schmalle, EUROBIC II, *Florence, 30 August−3 September*, **1994**, abstr. 110.
[5] L. Cavallo, R. Cini, J. Kobe, L. G. Marzilli, G. Natile, *J. Chem. Soc., Dalton Trans.* **1991**, 1867.
[6] M. Coluccia, A. Boccarelli, C. Cermelli, M. Portolani, G. Natile, *Metal Based Drugs*, **1995**, *2*, 249.
[7] S. Grabner, J. Plavec, N. Bukovec, D. Di Leo, R. Cini, G. Natile, *J. Chem. Soc., Dalton Trans.* **1998**, 1447.
[8] S. E. Sherman, S. J. Lippard, *Chem. Rev.* **1987**, *87*, 1153.
[9] J. Reedijk, A. M. J. Fichtinger-Shepman, A. T. van Oosterom, P. van de Putte; *Struct. Bond*. **1987**, *67*, 53.
[10] E. R. Jamieson, S. J. Lippard, *Chem. Rev.* **1999**, *99*, 2467.
[11] S. O. Ano, Z. Kuklenyik, L. G. Marzilli, Structure and Dynamics of Pt Anticancer Drug Adducts from Nucleotides to Oligonucleotides as Revealed by NMR Methods. *Cisplatin: Chemistry and Biochemistry of a leading Anticancer Drug* (Ed.: B. Lippert), Verlag Helvetica Chimica Acta, Zürich, **1999**, 27−35.
[12] H. A. Tajmir-Riahi, T. Theophanides, *Can. J. Chem.* **1983,** *61,* 1813.
[13] K. Nakamoto, *Infrared and Raman Spectra of Inorganic and Coordination Compounds*, John Wiley & Sons, inc., New York, **1997***, pt. B*, p. 80.
[14] A. T. M. Marcelis, H. -J. Korte, B. Krebs, J. Reedijk, *Inorg. Chem.* **1982**, *21,* 4059; R. E. Cramer, P. L. Dahlstrom, *Inorg. Chem.* **1985**, *24*, 3420; *J. Am. Chem. Soc.* **1979**, *101*, 3679; Y. Xu, G. Natile, F. P. Intini, L. G. Marzilli, *J. Am. Chem. Soc.* **1990**, *112*, 8177.
[15] A. Bondi*, J. Phys. Chem*., **1964**, *68*, 441.
[16] Á. García-Raso, J. J. Fiol, F. Bádenas, R. Cons, Á. Terrón, M. Quirós, *J. Chem. Soc., Dalton Trans.* **1999**, 167.
[17] G. I. Birnbaum, M. Cygler, D. Shugar, *Can. J. Chem.* **1984**, *62*, 2646.
[18] [18a] A. Sinur, S. Grabner, *Acta Crystallogr., Sect. C* **1995**, *51*, 1769. − [18b] H. Shollhorn, G. Raudaschl-Sieber, G. Muller, U. Thewalt, B. Lippert, *J. Am. Chem. Soc.* **1985**, *107*, 5932. − [18c] S. E. Sherman, D. Gibson, A. H.-J. Wang, S. J. Lippard, *Science* **1985**, *230*, 412.
[19] S. O. Ano, F. P. Intini, G. Natile, L. G. Marzilli, *J. Am. Chem. Soc*. **1998**, *120*, 12017. L. G. Marzilli, S. O. Ano, F. P. Intini, G. Natile, *J. Am. Chem. Soc*. **1999**, *121*, 9133.
[20] B. L. Heyl, K. Shinozuka, S. K. Miller, D. G. VanDerveer and L. G. Marzilli, *Inorg. Chem.* **1985**, *24*, 661.
[21] J. Kozelka, Computational Studies on Platinum Antitumor Complexes and Their Adducts with Nucleic Acid Constituents. *Cisplatin: Chemistry and Biochemistry of a leading Anticancer Drug* (Ed.: B. Lippert), Verlag Helvetica Chimica Acta, Zürich, **1999**, 537−556.
[22] J. Molina, C. Hofr, L. Maresca, G. Natile, V. Brabec, *Biophys. J.* **2000**, *78*, 2008.
[23] R. Romeo, D. Minniti, S. Lanza, *Inorg. Chim. Acta*, **1997**, *22*, 87.
[24] Crystallographic data (excluding structure factors) for the structure reported in this paper have been deposited with the Cambridge Crystallographic Data Centre as supplementary publication no. CCDC-138638. Copies of the data can be obtained free of charge on application to CCDC, 12 Union Road, Cambridge CB2 1EZ, UK [fax (internat.): + 44-1223/336-033; E-mail: deposit@ccdc.cam.ac.uk].
[25] G. M. Sheldrick, *SHELX 97, Program for the Refinement of Crystal Structures*, University of Göttingen, **1997**.
[26] M. Nardelli, *PARST 97, A System of Computer Routines for Calculating Molecular Parameters from Results of Crystal Structure Analyses*, University of Parma, **1997**.
[27] L. Zsolnai, *XPMA-ZORTEP 98*, University of Heidelberg, **1998**.
[28] C. K. Johnson, M. N. Burnett, *ORTEP-3 for Windows*, Oak Ridge National Laboratory: **1998**. 32-bit Implementation by L. J. Farrugia, University of Glasgow.
[29] M. J. Frisch, G. W. Trucks, H. B. Schlegel, P. M. W. Gill, B. G. Johnson, M. A. Robb, J. R. Cheeseman, T. Keith, G. A. Petersson, J. A. Montgomery, K. Raghavachari, M. A. Al-Laham, V. G. Zakrzewski, J. V. Ortiz, J. B. Foresman, J. Cioslowski, B. B. Stefanov, A. Nanayakkara, M. Challacombe, C. Y. Peng, P. Y. Ayala, W. Chen, M. W. Wong, J. L. Andres, E. S. Replogle, R. Gomperts, R. L. Martin, D. J. Fox, J. S. Binkley, D. J. Defrees, J. Baker, J. P. Stewart, M. Head-Gordon, C. Gonzalez, J. A. Pople, Gaussian, Inc., Pittsburgh PA, **1995**.
[30] A. D. Becke, *J. Chem. Phys.* **1988**, 88, 1053; C. Lee, W. Yang, R. G. Parr, *Phys. Rev.* **1988**, B37, 785.
[31] P. J. Hay, W. R. Wadt, *J. Chem. Phys.* **1985**, 82, 299.
[32] R. Cini, A. Cavaglioni, *Inorg. Chem.* **1999**, 38, 3751; R. Cini, *J. Biomol. Struct. & Dyn.* **1999**, 16, 1225.
[33] *HyperChem Release 5 for Windows*, Hypercube, Inc. Scientific Software, 1115 NW 4th Street Gainsville, Florida, 32601−4256, **1998**.

Received January 21, 2000
[I00023]

Linear and Bent Oxo-Bridged Dimers of Ruthenium Pyrazole Nitrosyls

D. Scott Bohle*[a] and Elizabeth S. Sagan[a]

Dedicated to Professor Heinrich Vahrenkamp on the occasion of his 60th birthday

Keywords: Pyrazole complexes / Nitrosyl complexes / Oxo-bridged complexes / Ruthenium / N ligands

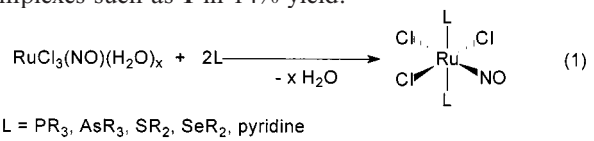
The nitrosylation of $RuCl_3 \cdot (H_2O)_x$ in thionyl chloride affords anhydrous $[RuCl_3(NO)]$ which, when treated with a variety of ligands L, gives $[RuCl_3(L)_2(NO)]$. For L = 3,5-dimethylpyrazole (dmpH) it is possible to isolate and characterize the corresponding monomeric complex **1** as well as unusual oxo-bridged dimeric products with nitrosyl ligands *trans* to the oxo ligand with either a linear geometry, as in *trans*-$O[RuCl_2(NO)(dmpH)_2]$ **(2)** and $[Cl_4(NO)Ru]O[Ru(NO)(dmpH)_4]$ **(4)**, or with a bent geometry, as in *trans*-$O[RuCl(NO)(dmpH)(\mu\text{-dmp})]_2$ **(3)**. These compounds have been characterized by elemental analysis and vibrational and NMR spectroscopy, as well as by single crystal X-ray diffraction. Collectively the structural and spectroscopic data support a delocalized π-bonding model across the linear ON–Ru–O–Ru–NO framework.

Introduction

Although ruthenium is renowned for its propensity to form robust adducts of nitric oxide,[1] the majority of these compounds contain relatively soft ligands which favor low formal oxidation states. Thus, to the best of our knowledge there are no reported examples of ruthenium nitrosyl complexes with either terminal oxo or nitrido ligands. Even the number of such complexes where the oxygen or nitrogen atom bridges two centers is very small,[2,3] and there has been surprisingly little research into this area of chemistry. The recognition of the critical role nitric oxide has in biological signal transduction,[4,5] and the increasingly frequent observed interaction of iron proteins with nitric oxide,[6] spur considerable current interest in its coordination chemistry. Nitrosyl derivatives of the oxo-bridged diiron proteins, and related model iron or ruthenium compounds, is a surprisingly sparse area of chemistry and many issues of their stereochemistry, electronic structure, and spectroscopy need to be examined in detail. Herein we describe: (i) the facile synthesis of several examples of mononuclear and oxo-bridged dinuclear ruthenium pyrazole complexes; (ii) the X-ray diffraction structures of three of these derivatives which contain both linear and bent Ru−O−Ru bonds; and (iii) the characterization of these new derivatives. Taken together these results allow us to assess the degree of synergistic π-acceptance and π-donation across the ON−Ru−O−Ru−NO framework.

Results and Discussion

A common synthon in ruthenium(II) nitrosyl chemistry is "$RuCl_3(NO)$" which is readily obtained by passing NO through alcoholic solutions of $RuCl_3 \cdot (H_2O)_x$.[7] Although this solid can be isolated as a trihydrate, it is frequently used directly for reactions with excess ligands L (L = tertiary phosphanes and arsanes, thioethers, or selenyl ethers)[8−10] to give the diamagnetic complexes $[RuCl_3(NO)L_2]$ [Equation (1)]. In these cases the $[RuCl_3(NO)L_2]$ product can usually be isolated in high yield by simple filtration of the product from the ethanol solution; there are no reports of other hydrated or oxo-bridged products being isolated from this one-pot approach. With amines and nitrogen bases this strategy has considerably less general utility; for example, although pyridine, acetonitrile, 2,2′bipyridine, and 1,10-phenanthroline add to $[RuCl_3(NO)]$ to give six-coordinate products, the reaction with ammonia, 3,5-dimethylpyrazole or {[tris(3,5-dimethylpyrazolyl)borate]$^-$ = DMTPZ} under the conditions in Equation 1 leads to mixtures of products and low general yields of the desired product.[8,11] In the case of 3,5-dimethylpyrazole this is due to the formation of the oxo-bridged diruthenium products to be described below. In the case of DMTPZ, however, the low yields (ca. 9%) for $[(DMTPZ)RuCl_2(NO)]$ isolated from the reaction of commercial $[RuCl_3(NO)]$ and Tl(DMTPZ), are in part due to hydrolysis of the DMTPZ to give mono-pyrazole complexes such as **1** in 14% yield.[11]



(1)

L = PR_3, AsR_3, SR_2, SeR_2, pyridine

A simple solution to these problems is to dehydrate $RuCl_3 \cdot (H_2O)_x$ by performing the nitrosylation reaction in thionyl chloride. To this end we have modified a method devised by Demant et al. where $RuCl_3 \cdot (H_2O)_x$ is nitrosylated in thionyl chloride [Equation (2)] and the resulting product is filtered off and used directly.[12] When anhydrous $[RuCl_3(NO)]$ is prepared in this manner, and then treated

[a] Department of Chemistry University of Wyoming,
Laramie, WY 82071−3838, USA
Fax: (internat.) + 1-307/766-2807
E-mail: bohle@uwyo.edu

 © WILEY-VCH Verlag GmbH, D-69451 Weinheim, 2000 1434−1948/00/0707−1609 $ 17.50+.50/0

with excess 3,5-dimethylpyrazole in toluene at reflux [Equation (3)], the major product is *mer*-$[RuCl_3(NO)(dmpH)_2]$ **(1)**, which is isolated in 87% yield after chromatography on silica. This product is identical by IR and NMR spectroscopy to that isolated in low yield by Onishi.[11] A trace second product of this reaction is the known bright yellow $[RuCl_3(dmpH)_3]$.[13−15]

$$RuCl_3(H_2O)_x \xrightarrow[-\,x\,SO_2,\,-\,2x\,HCl]{NO,\ SOCl_2(solvent)} RuCl_3(NO) \qquad (2)$$

$$RuCl_3(NO) \xrightarrow[\Delta,\ T = 105\ ^\circ C,\ 22\ h]{2LH,\ toluene} \mathbf{1} \qquad (3)$$

LH = 3,5-dimethylpyrazole

The brick red mononuclear complex **1** has a relatively labile coordination sphere as it is readily converted into a range of other derivatives by hydrolysis or by treating it with an excess of a coordinating ligand, i.e. the reaction of **1** and triphenylphosphane in ethanol at reflux gives $[RuCl_3(NO)(PPh_3)_2]$ in high yield. When **1** is heated to reflux in wet benzene it rapidly hydrolyzes to give mainly the golden colored, oxo-bridged dimer **2** [Equation (4)] and a trace of the oxo and pyrazolato bridged dimer **3**. When **1** is treated with one equivalent of a silver salt there is the rapid formation of a silver chloride precipitate, but the only product isolated from this type of reaction is unchanged starting material, **1**, in ca. 60% yield. Chelating anions such as dibenzyldithiocarbamate also react rapidly with **1** at ambient temperatures to give a mixture of isomers with the formula $[RuCl(Bz_2NCS_2)_2(NO)]$.

$$\underset{\mathbf{1}}{RuCl_3(NO)(LH)_2} \xrightarrow[\Delta,\ T = 76\ ^\circ C]{H_2O,\ (benzene)} \underset{\mathbf{2}}{ON\text{-}Ru\text{-}O\text{-}Ru\text{-}NO} \quad + \mathbf{3}\ (trace) \qquad (4)$$

Under forcing conditions for the reaction of $RuCl_3(NO)\cdot(H_2O)_x$ with 3,5-dimethylpyrazole it is possible to isolate in good yield the mixed μ-oxo; di(μ-pyrazolato) bridged complex, **3** by the addition of excess sodium hydroxide and heating the solution at reflux in ethanol for 16 hours [Equation (5)]. This complex is also formed as a minor product of the synthesis of the linear oxo-bridged complex **2** from the hydrolysis of **1** in benzene. Finally the asymmetric linear complex $[Cl_4(ON)RuORu(NO)(dmpH)_4]$ **(4)** is a minor product of the reaction of thermolyzed $RuCl_3(NO)\cdot(H_2O)_x$ with 3,5-dimethylpyrazole, and can be separated from the major product of this reaction (compound **1**) by column chromatography. Although this product contains formal $16e^-$ and $20e^-$ centers, $\{(ON)RuCl_4\}^{-1}$ and $\{(ON)Ru(dmpH)_4\}^{+3}$, respectively, this distinction rests upon the presence of protons on the 3,5-dimethylpyrazole ligands. In light of the hydrogen bonding observed in the solid state, described below, these formal assignments should not be taken too seriously.

$$RuCl_3(NO)(H_2O)_2 \xrightarrow[EtOH\ \Delta,\ T = 76\ ^\circ C\ 16\ hours]{LH/NaOH} \mathbf{3} \qquad (5)$$

4

Single crystal X-ray crystallography has been used to characterize these derivatives: critical crystallographic parameters are collected in Table 1, views of the four molecules are shown in Figure 1−4, and selected geometrical parameters are collected in Table 2. With the exception of the disordered solvent in **2** the bond lengths and angles are determined precisely and allow for meaningful comparisons. In each case the Ru−NO fragments are linear with short metal−nitrogen bond lengths and a ruthenium geometry close to an ideal octahedron. Overall the ruthenium chloride bonds in these compounds have similar lengths, with the exception of Ru−Cl(1) in **1**, where the chloride *trans* to the nitrosyl is significantly shorter than the others. On average the ruthenium−nitrogen distances to the pyrazole ligands are similar for the terminal pyrazoles, which in turn are slightly longer than the bridging pyrazoles in **3**. This trend is also seen in $[\{(p\text{-cymene})Ru(\mu_2\text{-}OH)\}_2(\mu\text{-pyrazolato})]BF_4$ where the ruthenium−nitrogen bond lengths are 2.078(3) Å.[16]

As can be seen from the ORTEP representations of **2, 3**, and **4** in Figure 1−4 the planes defined by the pyrazole rings adopt an orientation which allow for relatively short N−H···Cl interactions in the solid state. In particular the linear, oxo-bridged dimers have short chlorine−hydrogen interactions: compound **2** has Cl(1)−HN(6) = 2.398(4) Å, Cl(2)−HN(8) = 2.392(4) Å, Cl(3)−HN(2) = 2.435(3) Å, and Cl(4)−HN(4) = 2.371(4) Å, while **4** has Cl(1)−HN(4) = 2.397(2) Å, Cl(2)−HN(6) = 2.330(2) Å, Cl(3)−HN(10) = 2.392(4) Å, and Cl(4)−HN(8) = 2.354(2) Å. On the other hand, in the mononuclear complex **1** and the bent oxo-bridged dimer **3**, the chloride−hydrogen separations are much longer; in **1** Cl(1)−HN(3) = 2.748(2) Å, and Cl(2)−HN(5) = 2.690(4) Å, while in **3** these separations are Cl(1)−HN(10) = 2.757(2) Å, and Cl(2)−HN(8) = 2.791(3) Å. Correlated with these structural observations are variations in the frequencies of the N−H stretching bands, ν(N−H) between 3598 cm^{-1} in **4** to 3140 cm^{-1} in **2**.

Characteristic vibrational and electronic spectroscopic data for these compounds are collected in Table 3. The nitrosyl stretching frequencies clearly fall into the region for linear nitrosyls, and all of the oxo-bridged dimers

Table 1. Crystallographic data and refinement parameters

Compound	**1**	**2**	**3**	**4**
Empirical formula	$C_{10}H_{16}Cl_3N_5ORu$	$C_{20}H_{32}N_{10}Cl_4O_3Ru_2{\cdot}C_2H_5OH$	$C_{20}H_{30}N_{10}Cl_2O_3Ru_2$	$C_{20}H_{32}N_{10}Cl_4O_3Ru_2$
Mass (g mol^{-1})	429.7	849.63	731.58	804.56
Color; Habit	Red; Block	Orange; Prism	Burgundy; Prism	Orange; Prism
Crystal size (mm)	0.58 × 0.22 × 0.1	0.45 × 0.36 × 0.04	1.26 × 0.46 × 0.36	0.48 × 0.20 × 0.12
Crystal system	Monoclinic	Monoclinic	Monoclinic	Monoclinic
Space group	$P2_1/n$	$C2/c$	$P2_1/n$	$P2_1/c$
a (Å)	12.103(2)	37.41(1)	10.407(2)	16.250(2)
b (Å)	11.088(2)	10.665(3)	19.166(5)	10.640(1)
c (Å)	12.641(2)	18.911(5)	15.240(3)	19.637(4)
β (°)	109.50(2)	112.46(1)	108.14(1)	96.67(1)
Volume (Å ^{3})	1599.1(4)	6972(4)	2889(1)	3372.3(7)
Z	4	8	4	4
Density (Mg m^{-3})$_c$	1.785	1.609	1.682	1.752
μ (mm^{-1})	1.483	1.215	1.271	1.412
22 Range (°)	4.04 to 50.00	4.0 to 50.0	3.5 to 50.0	4.2 to 50.0
Index ranges h	$-1 \le h \le 14$	$-44 \le h \le 1$	$-1 \le h \le 12$	$-1 \le h \le 19$
k	$-1 \le k \le 13$	$-11 \le k \le 1$	$-1 \le k \le 22$	$-1 \le k \le 12$
l	$-15 \le l \le 14$	$-18 \le l \le 20$	$-18 \le l \le 17$	$-23 \le l \le 23$
Obs. Reflections	2814	4515	5081	5920
Final R (obs.)	$R = 0.032$	$R = 0.067$	$R = 0.046$	$R = 0.037$
	$R_w = 0.086$	$R_w = 0.178$	$R_w = 0.121$	$R_w = 0.095$
Goodness-of-fit	1.03	0.987	1.085	1.065
Data-to-parameter ratio	15.5:1	12.0:1	15.2:1	15.6:1
Largest diff. peak	0.58 e Å^{-3}	1.41 e Å^{-3}	0.84 e Å^{-3}	0.75 e Å^{-3}
Largest diff. hole	−0.72 e Å^{-3}	−1.18 e Å^{-3}	−1.3 e Å^{-3}	−1.1 e Å^{-3}

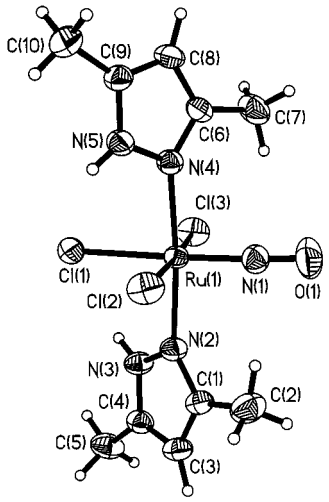


Figure 1. ORTEP view of $[RuCl_3(NO)(dmpH)_2]$ **(1)** showing all hydrogen atoms in calculated positions and all heavy atoms as 30% thermal ellipsoids

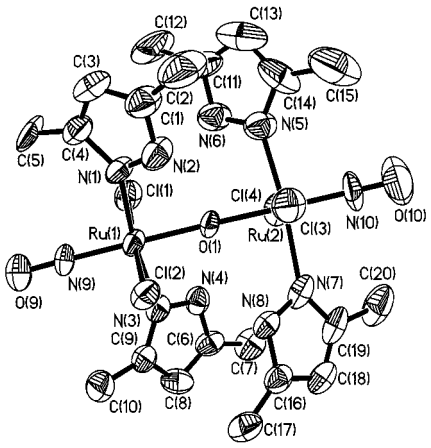


Figure 2. ORTEP view of $O[RuCl_2(NO)(dmpH)_2]_2$ **(2)** showing non-hydrogen atoms as 30% thermal ellipsoids

2−**4** have lower ν(NO) frequencies than does the mononuclear complex **1**. In the case of complex **2** there is a single, strong and relatively broad ν(NO) band at 1809.1 cm^{-1} in the infrared spectrum and this is assigned as the asymmetric nitrosyl stretch across the ON−Ru−O−Ru−NO framework. In the Raman spectrum a single weak band at slightly higher energy (1821 cm^{-1}) is observed for **2**, and this is assigned as a symmetric nitrosyl stretch for the dinuclear framework. For complexes **3** and **4** both ν(NO) modes are IR active and in both cases are split by ca. 28 cm^{-1}, a value significantly higher than found for **2**. The similarity in splitting is somewhat surprising in light of the different ruthenium environments in the case of **4** and the C_2 symmetry present in **3**. The Ru−O−Ru framework also has a strong IR active $\nu(Ru{-}O{-}Ru)_{asym}$ at 791.7 cm^{-1} as well as a Raman active $\nu(Ru{-}O{-}Ru)_{sym}$ mode at 334 cm^{-1} for the linear dimer **2**. As shown in Figure 5, the low energy Raman spectra for **1**−**4** contain numerous common bands including a strong band 589−602 cm^{-1} and weaker bands at 441−448 cm^{-1}, 359−365 cm^{-1}, and 282−291 cm^{-1}. For the bent oxo-bridged dimer **3** there is a unique weak band at 495 cm^{-1} which may be due to either the $\nu(Ru{-}O{-}Ru)_{sym}$ band or to the bridging pyrazole. In **4** it is difficult to assign a unique band to the $\nu(Ru{-}O{-}Ru)_{sym}$ mode.

The electronic spectra for the oxo-bridged dimers are dominated by three bands, with the lowest energy band being relatively weak and broad and generally observed as a shoulder to the stronger UV bands. For the oxo-bridged dimer **3**, the two most prominent UV bands are at lower energies than for either of the linear oxo-bridged dimers **2** or **4**. For the mononuclear complex **1** the intense red color

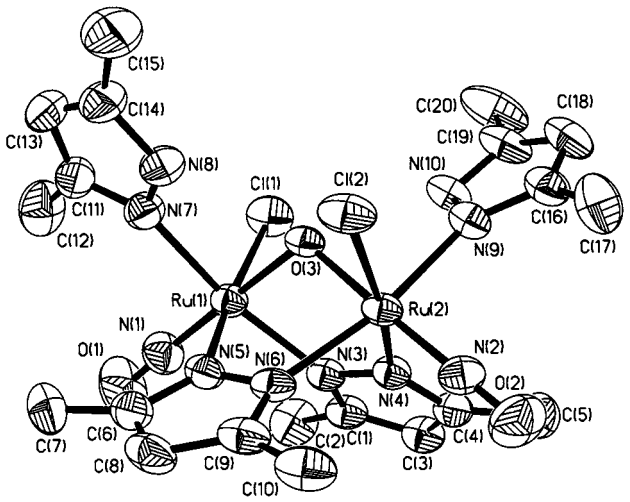


Figure 3. ORTEP view of $O[RuCl_2(NO)(dmpH)(dmp)]_2$ **(3)** with non-hydrogen atoms represented as 30% thermal ellipsoids

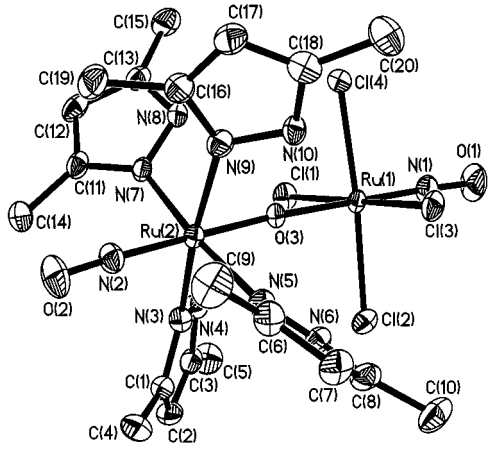


Figure 4. ORTEP view of $[Cl_4(NO)Ru]O[Ru(NO)(dmpH)_4]$ **(4)** with hydrogen atoms omitted and all other atoms represented as 30% thermal ellipsoids

is due to a comparatively strong low energy band at 538 nm. All of the new complexes described in this paper are clearly diamagnetic at room temperature and give sharp ^1H and ^{13}C NMR spectra with no indication of fluxional exchange broadening. In each case the solution spectra indicate that the structures determined by X-ray diffraction correspond to those in solution. The electrochemistry of species **1**−**4** is dominated by irreversible reductions at circa −0.9 V. In the cyclic voltammetry experiments no return wave is seen, even at relatively fast sweep rates (2000 mV s^{-1}) and the oxidative sweep indicates numerous new by-products from these processes.

There are surprisingly few well-characterized metallonitrosyl complexes with either bridging or terminal oxo ligands. This might be attributable to the widely perceived notion that the oxo ligand and strong π-accepting ligands such as a nitrosyl have differing preferences for a metal's oxidation state and environment. In terms of group 8 transition metals there are several early reports of oxo-bridged ruthenium nitrosyl dimers $Ru_2N_6O_{15}$ stemming from the addition of nitric oxide to RuO_4.[2,3] More recently, an oxo-bridged osmium porphyrin nitrosyl complex has been serendipitously isolated and structurally characterized from the reaction of [Os(OEP)(CO)] and ClNO.[17] Other examples of the ON−M−O−M−NO framework can be found for Ir, μ_2-$O[Ir(NO)(PPh_3)_2]_2$,[18,19] and its oxidative-addition products,[20,21] as well as more numerously for molybdenum.[22−25] In general the iridium examples are similar to those described here for ruthenium in the that the nitrosyl is *trans* to the oxo-ligand, while in the case of molybdenum the nitrosyls are *cis* to the oxo bridge. This trend may be due to the use of polyhapto chelate ligands in the molybdenum examples; in these cases the ancillary ligand is required to occupy the *trans* position. It remains an open question whether an oxo-bridged molybdenum nitrosyl dimer with a less constrained coordination sphere would

Table 2. Selected geometric parameters for crystallographically characterized compounds

	$RuCl_3(NO)(LH)_2$ **1**	$O[RuCl_2(NO)(LH)_2]_2$ **2**	$O[RuCl(LH)(\mu_2\text{-}L)(NO)]_2$ **3**	$O[RuCl_4(NO)][Ru(LH)_4(NO)]$ **4**
Ru−O (Å)		Ru(1) 1.917(6) Ru(2) 1.885(6)	Ru(1) 1.910(3) Ru(2) 1.913(3)	Ru(1) 1.940(2) Ru(2) 1.873(2)
Ru−O−Ru (°)		178.9(4)	116.35(13)	176.6(2)
O−Ru−NO (°)		Ru(1) 179.6(4) Ru(2) 179.0(4)	Ru(1) 178.1(2) Ru(2) 178.2(2)	Ru(1) 177.67(14) Ru(2) 179.27(14)
Ru−NO (Å)	1.735(3)	Ru(1) 1.734(9) Ru(2) 1.721(10)	Ru(1) 1.747(4) Ru(2) 1.752(4)	Ru(1) 1.731(3) Ru(2) 1.759(3)
Ru−N−O (°)	177.5(3)	Ru(1) 178.5(10) Ru(2) 177.1(13)	Ru(1) 177.7(5) Ru(2) 179.6(4)	Ru(1) 176.2(3) Ru(2) 177.0(3)
Ru−Cl (Å)	Cl(1) 2.3389(9) Cl(2) 2.3625(9) Cl(3) 2.3812(9)	Cl(1) 2.388(3) Cl(2) 2.369(3) Cl(3) 2.381(4) Cl(4) 2.371(4)	Cl(1) 2.3978(13) Cl(2) 2.3988(11)	Cl(1) 2.385(1) Cl(2) 2.398(1) Cl(3) 2.401(1) Cl(4) 2.377(1)
Ru−N_{pz} (Å)	N(2) 2.096(3) N(4) 2.102(3)	N(1) 2.087(9) N(3) 2.067(10) N(5) 2.090(10) N(7) 2.090(10)	N(3) 2.074(4) N(4) 2.058(3) N(5) 2.064(4) N(6) 2.061(4) N(7) 2.095(4) N(9) 2.102(4)	N(3) 2.081(3) N(5) 2.085(3) N(7) 2.082(3) N(9) 2.080(3)

Table 3. Characteristic spectroscopic data for key compounds

Compound	Vibrational bands[a] ν(NO)	ν(NH)	ν(RuORu)	Electronic bands nm(log{ε})
1	1883.4 (s) IR	3387.8 (m) 3329.9 (m)	–	538 (1.77) 430 (189) 296 (3.36) 264 (3.34)
2	1809.1 (s) IR 1821 (w) RA	3219.0 (m) 3140 (m)	791.7 (s) IR 744 (m) RA	520 (shoulder) 343 (4.35) 264 (3.95)
3	1829.4 (s) IR 1802.4 (s) IR 1821 (m) RA 1795 (w) RA	3208.4 (m)	715.5 (s) IR 680.9 (m) RA	520 (2.50) 396 (3.35) 293 (4.24)
4	1818.2 (s) IR 1790.2 (s) IR	3598 (w) 3248(m)	792.2 (s) IR 786.1 (m) RA	450 (shoulder) 343 (4.72) 264 (4.33)

[a] All vibrational frequencies are given in cm^{-1} and measured in KBr for infrared bands (IR) or as a neat powder for the Raman active bands (RA).

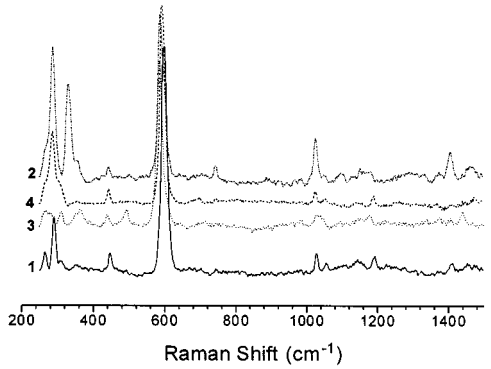


Figure 5. Raman spectra of compounds **1**–**4** measured as powders with 648 nm excitation radiation; **1** (bottom, solid line), **2** (top, dash double dotted line), **3** (second from bottom, dotted line ·····), and **4** (dashed line)

adopt a *cis* or *trans* oxo geometry. Thus there is little intrinsically incompatible with coordination of oxo and nitrosyl ligands within a single coordination sphere.

Attempts to prepare sulfur-bridged analogues to **2**–**4** have been unsuccessful. Thus when **1** is treated with hydrogen sulfide under the conditions which lead to hydrolytic dimerization to give **2**, there is rapid formation of an amorphous black powder that is completely insoluble in most solvents. This solid still contains a strong sharp nitrosyl stretching band at 1785 cm^{-1} in the IR and analyzes for RuS_4NO contaminated with some pyrazole species. Thus, excess hydrogen sulfide results not only in the loss of the *trans* chloride in **1**, but also the two remaining chlorides and the two 3,5-dimethylpyrazole ligands. In an attempt to control the stoichiometry of the sulfur substitution reaction more carefully, compound **1** was treated with $S(SiMe_3)_2$ in benzene at reflux. However under these conditions **1** was quantitatively recovered unchanged.

Complexes **2**–**4** have the potential of a "push-pull" in the bonding along the ON–Ru–O–Ru–NO framework. In this overly simplified model the nitrosyls act as π-accepting ligands while the oxo is a π-donor ligand. In higher oxidation states the bridging-oxo ligand is known to mediate strong ruthenium–ruthenium interactions as evidenced by reversible electrochemistry and by the strong coupling observed in the magnetic susceptibility of $[(bipy)_2ClRuORuCl(bipy)_2]^{n+}$ (n = 2 or 3).[26] In the qualitative molecular-orbital scheme proposed by Weaver et al.[26] two *p*-type lone pairs of the oxygen can π–bond with the six t_{2g} orbitals based on the two ruthenium to give pairs of π-bonding, nonbonding, and antibonding orbitals, as well as the two d_{xy} ruthenium orbitals. These π-orbital pairs are degenerate in the linear D_{4h}-symmetric complexes and are closely spaced for D_{2h}-symmetric species such as **2**. Regardless of the local symmetry, this molecular orbital scheme leads to no net stabilizing interaction for ruthenium(II) oxo-bridged dimers since the t_{2g} set is full. This correlates with the general absence of linear oxo-bridged complexes of d^6 metal centers. However, once a nitrosyl ligand is introduced into the *trans* position to the oxo-bridge there will be strong backbonding interactions between the filled π^* and π_{NB} orbitals and the accepting π^* orbitals of the nitrosyl ligands. In a qualitative sense these interactions should be stronger than in the parent complex because the energy match between the π^* and π_{NB} and the π^*_{NO} will be better since the former orbitals are of higher energy. In addition, the overlap between these orbitals will probably increase due to the spatial extension of these orbitals towards the nitrosyl. Thus in these qualitative terms the net π-interaction for the ON–Ru–O–Ru–NO fragment is expected to be highly stabilizing in a linear geometry, and stabilized to a similar extent in a bent Ru–O–Ru geometry.

The structural consequences of possible π-delocalization over the oxo-ruthenium-nitrosyl framework are expected to be manifested most strongly in the trends in the ruthenium–oxygen distances for the bridged oxo ligand. Thus the ruthenium–oxygen bonds in **2**–**4** might be expected to be shorter than those in related complexes which lack a strong π-accepting ligand *trans* to the bridging oxo group. There are few direct comparison complexes where oxo ligands bridge two ruthenium(II) d^6 centers. However there is little significant difference between the two Ru–O bond lengths in linear bridged **2** or **4** and the bent species **3**. There is a significant difference between the

ruthenium−oxygen bond lengths in the asymmetric linear bridged species **4** where the Ru(1)−O(3) for the $RuCl_4(NO)$ group, formally with a −1 charge, is 0.067(2) Å longer than Ru(2)−O(3) for the $Ru(LH)_4(NO)$ group which formally has a charge of +3. Note however that all of these bond lengths are about 0.05 and 0.1 Å longer than the ruthenium−oxygen bond lengths in linear Ru^{III} and Ru^{IV} oxo-bridged dimers found in the CCDB.[27] The Ru−O−Ru bending found in **3** is similar to that found in structurally characterized carboxylato, oxo-bridged ruthenium dimers where the mean ruthenium−oxygen−ruthenium bond angle is 122.3 °.[27]

For the nitrosyl stretching frequencies the formation of the oxo-bridge results in an 80 cm^{-1} decrease in the two ν(NO) bands, and this suggests increased Ru−NO back-bonding in all three of the oxo-bridged complexes. Correlated with this trend are the Ru−O bond lengths which range between 1.873(2) and 1.940(2) Å, values which are ca. 0.20 Å shorter than for the many nonchelating Ru^{II}−OR bond lengths in the CCDB. On the other hand these bond lengths are ca. 0.05−0.1 Å longer than for structurally characterized high-valent, oxo-bridged ruthenium dimers which typically contain electronegative ligands *trans* to the oxo-bridge. The ν(Ru−O−Ru) stretching frequencies for **2**−**4** are also lower than for high-valent species. For example, in $K_4Ru_2OCl_{10}$ $\nu(Ru-O-Ru)_{asym}$ = 888 cm^{-1} and $\nu(Ru-O-Ru)_{sym}$ = 259 cm^{-1}, and have a difference $\nu_{asym}-\nu_{sym}$ = 629 cm^{-1}.[28] For **2** the values are ν_{asym} = 791.7 cm^{-1} and ν_{sym} = 343 cm^{-1}, with a difference $\nu_{asym}-\nu_{sym}$ = 449 cm^{-1}. The ν_{asym} frequency is at the low end of the reported range for these modes, and this correlates with the small difference between the two Ru−O−Ru stretching modes.[29,30]

Although the most well understood receptor for nitric oxide is the heme protein soluble guanylate cyclase,[31,32] a diverse array of other physiological sinks for nitric oxide have been proposed.[33] In many cases the critical protein/nitric oxide interaction is the binding of nitric oxide to enzymatically active metals such as the diiron site in bacterioferritin,[34] the oxo-bridged diiron center in hemerythrin[35] or methane monooxygenase hydroxylase,[36] the [2Fe-2S] iron-sulfur cluster in mammalian ferrochelatase,[37] or the [4Fe-4S] cluster in HiPIP.[38] In these cases the new nitrosylated ferroproteins have markedly different redox, structural, and kinetic properties as compared to the parent protein, and a current major interest in metallobiochemistry is understanding how nitrosylation mediates these effects. For the oxo-bridged diiron proteins, nitrosylation of the iron(s) can potentially result in the introduction of the nitric oxide *cis* or *trans* to the oxo bridge. Although in most cases the specific coordination geometry of these nitrosylated diiron sites is not known, our work suggests that *trans* coordination geometries may be thermodynamically favored.

Conclusion

In all of the chemistry described in this paper the nitrosyl and oxo-ligands retain a rigorous *trans* geometry; there is no indication of either isomerization or the presence of isomers where these two ligands are *cis*. However, other isomers or related complexes may very well be accessible with a judicious choice of conditions or with other ligand sets. The *trans* arrangement of the oxo-bridge and nitrosyl allows for some π-delocalization as evidenced by the spectroscopic and structural results.

Experimental Section

General: The instrumentation, methods, apparatus, and experimental techniques have been described in detail in previous papers.[39] 3,5-Dimethylpyrazole and thionyl chloride were purchased from Aldrich and used as provided. Ruthenium(II)nitrosyl trichloride was either synthesized by a variation of the method of Demant et al.[12] or the solid was purchased from Strem Chemicals. In general the pyrazole complexes are stable towards aerial oxidation and hydrolysis and thus they can be stored, chromatographed, and handled in the open. Electrochemistry experiments were performed with a BAS-50 W potentiostat with a platinum disk electrode, a silver auxiliary electrode, and a silver/silver chloride reference electrode. All experiments were performed in dry oxygen-free dichloromethane at room temperature with 0.1 M $[N(n\text{Bu})_4][PF_6]$ backing electrolyte.

Anhydrous $RuCl_3(NO)$: Commercial hydrated ruthenium trichloride (321 mg) was suspended in 10 mL thionyl chloride in a Fisher−Porter bottle and the vessel flushed with nitrogen before pressurizing with nitric oxide to 2.76 bar (40 psi). This mixture was then heated at 65 °C for 12 hours during which time the original black suspension dissolved to give a deep red solution from which a fine red solid precipitated upon cooling to room temperature. After flushing the head space of the reactor with nitrogen, dry carbon tetrachloride (30 mL) was added and the solution filtered to give 350 mg (95%) of red product. − IR (Nujol): ν(NO) = 1894 cm^{-1}. − Cl_3NORu (237.43): calcd. Cl 44.79, N 5.90; found Cl 44.95, N 5.71.

***mer*-$[RuCl_3(NO)(dmpH)_2]$ (1):** $RuCl_3NO$ (0.07 g), prepared by treating $RuCl_3$ with nitric oxide in thionyl chloride, in dry toluene (20 mL) was treated with 3,5-dimethylpyrazole (1.4 g) at reflux for 22 h. During this period, and upon subsequent cooling, a deep-red precipitate formed, which was filtered and washed with copious quantities (50 mL) of ethanol, and subsequently with water, ethanol, and hexanes. The yield of this crude material, which is mostly **1** and a small quantity of bright yellow $[RuCl_3(dmpH)_3]$, was 122 mg. Final purification was achieved by column chromatography on silica gel (20 cm × 4 cm column, with chloroform as the eluent) to elute first the deep red-purple $[RuCl_3(NO)(dmpH)_2]$, which was recovered in a final yield of 87% (111 mg) by addition of ethanol and concentrating the solution on a rotary evaporator to remove the chloroform. Elution with acetone/chloroform (4:50) gave traces of a bright yellow compound, which was subsequently identified as $[RuCl_3(dmpH)_3]$.[14,15] $RuCl_3(NO)(dmpH)_2$: UV/Vis (CH_2Cl_2): λ_{max} (log ε[M^{-1} cm^{-1}]) = 538 (1.77) nm, 430 (1.89), 296 (3.36), 264 (3.34). − ^1H NMR (22 °C, $CDCl_3$): δ = 10.74 (s, 1 H, N−*H*), 5.99 (s, 1 H, C−*H*), 2.61 (s, 3 H, C*H*$_{3'}$), 2.37 (s, 3 H, C*H*$_{3'}$). − ^{13}C NMR (22 °C, $CDCl_3$) δ = 153.8, 143.1(s, *C*−CH_3), 108.0(s, *C*−H), 14.7, 11.4 (s, C−*C*H_3). − IR (KBr): ν(NH) = 3387.8 (m) cm^{-1}, 3329.9 (m); ν(NO) = 1883.4 (s); with additional bands at 1569 (m), 1276.8 (m), 1186.2 (w), 1157.3 (w), 1056.9 (m), 823.6 (w), 792.7 (m), 655.8 (m), 569 (w), 505.3 (m) cm^{-1}. − $C_{10}H_{16}Cl_3N_5ORu$

(429.73): calcd. C 27.95, H 3.75, N 16.30; found C 28.15, H 3.95, N 16.10. − M.p. 248 °C(dec). This complex is also a by-product of the addition of 3,5-dimethylpyrazole to the direct nitrosylation product of $RuCl_3{\cdot}(H_2O)_x$ in ethanol, followed by chromatographic separation. Crystals suitable for X-ray diffraction were grown by vapor-phase diffusion of 2-propanol into a chloroform solution of **1** at −20 °C.

***trans*-O[RuCl$_2$(NO)(dmpH)$_2$] (2):** $RuCl_3(NO)(dmpH)_2$ (**1**; 41 mg) in 20 mL (wet) benzene was heated at reflux for 16 hours in the open air. The resulting red-orange solution was cooled and the benzene removed on a rotary evaporator. The red crystalline solid was taken up in dichloromethane and chromatographed on a 30 × 2 cm silica column with dichloromethane. The first yellow-orange fraction was collected and recrystallized by the addition of an equal volume of ethanol and concentration to 20 mL. The resulting flaky orange-yellow solid was filtered and washed with ethanol and hexane and dried to give **2** (32 mg, 83%). Further elution of the column with dichloromethane gave 5 mg of the bent oxo-pyrazolato complex **3**. − UV/Vis (CH_2Cl_2): λ_{max} (log ε[M^{-1} cm^{-1}]) = 520 (shoulder) nm, 343 (4.35), 264 (3.95). − ^{1}H NMR (22 °C, $CDCl_3$): δ = 12.15 (s, 1 H, N-*H*), 5.67 (d, $^4J_{HH}$ = 1.14 Hz, 1 H, C−*H*), 2.59, 2.05 (s, 3 H, C$H_{3'}$). − ^{13}C NMR (22 °C, $CDCl_3$): δ = 151.2, 142.4 (s, *C*−CH_3), 106.3 (s, *C*−H), 14.0, 10.7(s, C−*C*H_3). − IR (KBr): ν(NH) = 3219 (s) and 3140 (w) cm^{-1}; ν(NO) = 1809.1 (s); $\nu(RuORu)_{as}$ = 791.7 (s); with additional bands at 1570.9 (m), 1473.4 (w), 1409.9 (m), 1377.1 (w), 1276.8 (m), 1191.9 (m), 1151.4 (w), 1056.9 (m), 746.4 (w), 690.5 (m), 582.5 (m), 446.5 (w) cm^{-1}. − $C_{20}H_{32}Cl_4N_{10}O_3Ru_2$ (804.56): calcd. C 29.86, H 4.01, N 17.41; found C 30.08, H 4.01, N 17.32. Crystals suitable for X-ray diffraction were grown by vapor-phase diffusion of ethanol into a dichloromethane solution of **2**.

***trans*-O[RuCl(NO)(dmpH)(μ-dmp)]$_2$ (3):** In a 100 mL Fisher−Porter pressure bottle $RuCl_3{\cdot}(H_2O)_x$ (0.118 g) was suspended in 30 mL absolute ethanol and sealed with a stainless steel pressure head. The solution and apparatus was purged for 30 minutes with a stream of nitrogen and then pressurized with 2.76 bar (40 psi) of nitric oxide at ambient temperature. After 5 hours the pressure was brought back to 2.76 bar (40 psi) and the mixture was allowed to stir for a total of 20 hours at room temperature during which time the color changed from a deep red-black to pink. Following the release of NO pressure the solution and apparatus was purged for an additional 40 minutes with a stream of nitrogen and the uniform ethanol solution of "$RuCl_3(NO)$" was transferred to a 100 mL round bottom flask to which was added 3,5-dimethylpyrazole (2.5 equiv., 0.137 g) and sodium hydroxide (1 equiv., 0.023 g) in 1 mL water. The resulting darkened solution was heated at reflux for 16 hours and then cooled to give a copious deep red precipitate of product. After filtration and successive washes with ethanol, water, and ethanol the burgundy-colored product was dried in a vacuum desiccator. Recrystallization from dichloromethane/ethanol gave **3** (0.124 g, 61%). − UV/Vis (CH_2Cl_2): λ_{max} (log ε[M^{-1} cm^{-1}]) = 520 (2.50) nm, 396 (3.35), 293 (4.24). − ^{1}H NMR (22 °C, $CDCl_3$): δ = 11.87 (s, 1 H, N−*H*), 5.88 and 5.73 (s, 1 H, C−*H*), 2.59, 2.58, 2.17, and 2.06 (s, 3 H, C$H_{3'}$). − ^{13}C NMR (22 °C, $CDCl_3$): δ = 152.9, 142.7 [s, *C*−CH_3(pyrazole)], 150.8 [s, *C*−CH_3(pyrazolate)], 108.5 and 107.2 (s, *C*−H), 14.6, 11.3 [s, C−*C*H_3(pyrazole)], 13.7, 13.8 [s, C−*C*H_3(pyrazolate)]. − IR (KBr): ν(NH) = 3208.4 (m); ν(NO) = 1829.4 (s) and 1802.4 (s); $\nu(RuORu)_{as}$ = 715.5 (s) cm^{-1}; with additional bands at 1565.1 (m), 1534.3 (w), 1473.4 (m), 1444.6 (m), 1419.5 (s), 1380 (m), 1353 (w), 1271 (m), 1187.1 (m), 1148.5 (m), 1016.3 (m), 788.8 (m), 775.3 (m), 649 (w), 580.5 (m), 496.6 (w), 440.7 (w) cm^{-1}. − $C_{20}H_{30}Cl_2N_{10}O_3Ru_2$ (731.64): calcd. C 32.84, H 4.13, N 19.15; found C 32.96, H 4.17, N 19.10. Crystals suitable for X-ray diffraction were grown by vapor-phase diffusion of ethanol into a dichloromethane solution of **3**.

[Cl$_4$(NO)Ru]O[Ru(NO)(dmpH)$_4$] (4): Hydrated ruthenium trichloride (1.1 g) was suspended in 50 mL ethanol in a 100 mL Fisher−Porter bottle, and was nitrosylated with 2.76 bar (40 psi) of nitric oxide pressure for 20 hours. During this period the initially black-red suspension became a uniform pale red color. After releasing the excess nitric oxide pressure and flushing the solution with nitrogen, the pale-red solution was transferred to a 100 mL round bottom flask and the solvent removed at room temperature. The resulting solid was heated to 86 °C under a water aspirator vacuum for 45 minutes and the red-black residue was then taken into an inert atmosphere box under nitrogen. This solid was suspended in 30 mL dry ethanol and allowed to react with 3,5-dimethylpyrazole (1.53 g) for 3 hours at reflux. This solution was cooled to room temperature to give a copious red precipitate and a black solution, which was then filtered and washed with ethanol and hexane to give 1.39 g of red solid. This crude product was a mixture of **1**, **2**, **3**, and **4**, which was separated by column chromatography on silica gel (20 × 5 cm column) with dichloromethane used to elute **1** (69%) and **2**(18%). Chloroform was used to elute **3** (trace) as a purple band, which was followed by a slow moving orange band **4**. The asymmetrical linear oxo-bridged product was separated by eluting with 5:1 chloroform/acetone and isolated by the addition of 20 mL ethanol followed by concentration and crystallization on the rotary evaporator. Filtration followed by successive washes with ethanol and hexane gave 25 mg (12%) of red-orange crystals UV/Vis (CH_2Cl_2): λ_{max} (log ε[M^{-1} cm^{-1}]) = 450 (shoulder) nm, 343 (4.72), 264 (4.33). − ^{1}H NMR (22 °C, $CDCl_3$): δ = 12.49 (s, 1 H, N−*H*), 5.91(s, 1 H,C−*H*), 2.39, 1.93 (s, 3 H, C$H_{3'}$). − ^{13}C NMR (22 °C, $CDCl_3$): δ = 150.6, 145.3 (s, *C*−CH_3), 107.1 (s, *C*−H), 12.8, 11.8 (s, C−*C*H_3). − IR (KBr): ν(NH) = 3598 (w), and 3148 (m) cm^{-1}; ν(NO) = 1818.2 (s) and 1790.2 (s); $\nu(RuORu)_{as}$ = 792.2 (s); with additional bands at 1569.9 (m), 1473 (w), 1409.3 (m), 1376 (w), 1284.4 (m), 1184.2 (m), 1060.2 (m), 711.6 (m), 655.2 (w), 579.5 (m) cm^{-1}. − $C_{20}H_{32}Cl_4N_{10}O_3Ru_2$ (804.56): calcd. C 29.86, H 4.01, N 17.41; found C 29.69, H 4.24, N 17.12. Crystals suitable for X-ray diffraction were grown by vapor-phase diffusion of ethanol into a dichloromethane solution of **4**.

X-ray Crystallographic Study

X-ray diffraction data were collected at room temperature for single crystals of compounds $[RuCl_3(NO)(dmpH)_2]$ **(1)**, $[O\{RuCl_2(NO)(dmpH)_2\}_2]$ **(2)**, $[O\{RuCl_2(NO)(dmpH)(\mu\text{-dmp})\}_2]$ **(3)**, and $[Cl_4(ON)RuORu(NO)(dmpH)_4]$ **(4)** on a Siemens P4 Diffractometer equipped with a molybdenum tube [$\lambda(K_{\alpha1})$ = 0.70926 Å; $\lambda(K_{\alpha2})$ = 0.71354 Å] and a graphite monochromator. In each case the diffraction data were measured using ω scans. The intensities of three standard reflections monitored every 100 reflections during the respective data collections indicated negligible crystal decomposition. The structures were solved by direct methods and refined by full-matrix least-squares techniques on F^2 using structure solution programs from the SHELXTL program.[40] Important crystallographic parameters are collected in Table 1.

Crystallographic data (excluding structure factors) for the structure(s) reported in this paper have been deposited with the Cambridge Crystallographic Data Centre as supplementary publication no. CCDC 139381−139384, for **1**−**4** respectively. Copies of the data can be obtained free of charge on application to CCDC, 12

Union Road, Cambridge CB2 1EZ, UK [Fax: (internat.) + 44-1223/336-033; E-mail: deposit@ccdc.cam.ac.uk].

Acknowledgments

We gratefully acknowledge financial support from the DOE, (Grant DE-FCO2−91ER) and Professor Keith Carron of this department for the generous use of his laser Raman spectrometer.

[1] W. P. Griffith, *The Chemistry of the Rarer Platinum Metals*, Interscience Publishers, New York, **1967**.
[2] D. Scargill, J. M. Fletcher, *Proc. Chem. Soc. (London)* **1961**, 251.
[3] F. S. Matrin, J. M. Fletcher, P. G. M. Brown, B. M. Gatehouse, *J. Chem. Soc.* **1959**, 76.
[4] R. F. Furchgott, *Angew. Chem. Int. Ed.* **1999**, 38, 1871−1880.
[5] I. J. Ignarro, *Angew. Chem. Int. Ed.* **1999**, 38, 1882−1892.
[6] S. Pfeiffer, B. Mayer, B. Hemmens, *Angew. Chem. Int. Ed.* **1999**, 38, 1715−1731.
[7] J. M. Fletcher, I. L. Jenkins, F. M. Lever, F. S. Martin, A. R. Powell, R. Todd, *Inorg. Nucl. Chem.* **1955**, 1, 378−401.
[8] M. B. Fairy, R. J. Irving, *J. Chem. Soc. (A)* **1966**, 475−479.
[9] R. E. Townsend, K. J. Coskran, *Inorg. Chem.* **1971**, 10, 1661−1664.
[10] J. E. Fergusson, C. T. Page, *Aust. J. Chem.* **1976**, 29, 2159−2165.
[11] M. Onishi, *Bull. Chem. Soc. Jpn.* **1991**, 64, 3039−3045.
[12] U. Demant, W. Willing, U. Muller, K. Dehnicke, *Z. Anorg. Allg. Chem.* **1986**, 532, 175−183.
[13] J. Soucek, *Coll. Czech. Chem. Commun.* **1962**, 27, 1645−1650.
[14] F. Kralik, J. Vrestal, *Coll. Czech. Chem. Commun.* **1962**, 27, 1651−1657.
[15] F. Kralik, J. Vrestal, *Coll. Czech. Chem. Commun.* **1961**, 26, 1298−1304.
[16] D. Carmona, A. Mendoza, J. Ferrer, F. J. Lahoz, L. O. Oro, *J. Organometal. Chem.* **1992**, 431, 87−102.
[17] L. Cheng, C. Li, H.-S. Chung, M. A. Khan, G. B. Richter-Addo, *Organometallics* **1998**, 17, 3853−3864.
[18] P. Carty, A. Walker, M. Mathew, G. J. Palenik *J. Chem. Soc., Chem. Commun.* **1969**, 1374−1375.
[19] G. S. Brownlee, P. Carty, D. N. Cash, A. Walker, *Inorg. Chem.* **1975**, 14, 323−327.
[20] F. W. B. Einstein, D. Sutton, P. L. Vogel, *Inorg. Nucl. Chem. Lett.* **1976**, 12, 671−675.
[21] P.-T. Cheng, S. C. Nyburg, *Inorg. Chem.* **1975**, 14, 327−329.
[22] H. Adams, N. A. Bailey, G. Denti, J. A. McCleverty, J. M. A. Smith, A. Wlodarczyk, *J. Chem. Soc., Dalton Trans.* **1983**, 2287−2292.
[23] D. Sellmann, B. Seubert, F. Knock, M. Moll, *Z. Anorg. Allg. Chem.* **1991**, 600, 95−108.
[24] P. Legzdins, P. J. Lundmark, E. C. Phillips, S. J. Rettig, J. E. Veltheer, *Organometallics* **1992**, 11, 2991−3003.
[25] A. Wlodarczyk, J. P. Maher, S. Coles, D. E. Hibbs, M. H. B. Hursthouse, K. M. A. Malik, *J. Chem. Soc., Dalton Trans.* **1997**, 2597−2605.
[26] T. R. Weaver, T. J. Meyer, S. A. Adeyemi, G. M. Brown, R. P. Eckber, W. E. Hatfield, E. C. Johnson, R. W. Murray, D. Untereker, *J. Am. Chem. Soc.* **1975**, 97, 3039−3048.
[27] Cambridge Structural Database, Version 2.3.7, **1998**. Cambridge Crystallographic Data Centre, Cambridge, England.
[28] J. S. Filippo, R. L. Grayson, H. J. Sniadoch, *Inorg. Chem.* **1976**, 15, 269−274.
[29] J. A. Baumann, T. J. Meyer, *Inorg. Chem.* **1980**, 19, 345−350.
[30] W. P. Griffith, *J. Chem. Soc. (A)* **1969**, 211−218.
[31] J. N. Burstyn, A. E. Yu, E. A. Dierks, B. K. Hawkins, J. H. Dawson, *Biochemistry* **1995**, 34, 5896−5903.
[32] L. J. Ignarro, *Seminars in Hematology* **1989**, 26, 63−76.
[33] J. S. Stamler, D. J. Singel, J. Loscalzo, *Science* **1992**, 258, 1898−1902.
[34] N. E. Le Brun, S. C. Andrews, G. R. Moore, A. J. Thomson, *Biochem. J.* **1997**, 326, 173−179.
[35] J. Springborg, P. C. Wilkins, R. G. Wilkins, *Acta Chem. Scand.* **1989**, 43, 967−974.
[36] D. E. Coufal, P. Tavares, A. S. Pererira, B. H. Hyunh, S. J. Lippard, *Biochemistry* **1999**, 38, 4504−453.
[37] V. M. Sellers, M. K. Johnson, H. A. Dailey, *Biochemistry* **1996**, 35, 2699−2704.
[38] M. W. Foster, J. A. Cowan, *J. Am. Chem. Soc.* **1999**, 121, 4093−4100.
[39] D. S. Bohle, C.-H. Hung, B. D. Smith, *Inorg. Chem.* **1998**, 37, 5798−5806.
[40] G. M. Sheldrick, SHELXTL, Version 5.03/Iris, Universtität Göttingen, **1994**.

Received February 2, 2000
[I00035]

Peroxovanadium(V) Complexes of L-Lactic Acid as Studied by NMR Spectroscopy

Licínia L. G. Justino,[a] M. Luísa Ramos,[a] M. Madalena Caldeira,[a] and Victor M. S. Gil*[a]

Keywords: Vanadium / Peroxo complexes / L-Lactic acid / Multinuclear NMR spectroscopy

A multinuclear (^{1}H, ^{13}C, ^{17}O, ^{51}V) 1D and 2D NMR study of the complexation of L-lactic acid with vanadium(V) and hydrogen peroxide shows that four peroxo complexes are formed in aqueous solution in the pH range 1–7. Two isomeric 2:2:1 (metal:ligand:peroxo) complexes, together with a 2:2:2 species, are found over the entire pH range. At pH values below 2 an additional 1:1:1 complex is formed. The acid was found in all cases to act as a bidentate ligand through the carboxylic and the adjacent hydroxyl groups. To the best of our knowledge, this is the first report of dinuclear peroxovanadium complexes in which one of the metal centres is an oxovanadium centre (2:2:1 species).

Introduction

Over the past few years increasing attention has been paid to the chemistry of peroxovanadium(V) complexes. This interest is mainly due to the important role of these complexes in biological systems and their application in oxidation reactions. Peroxovanadium(V) complexes have been found to have antitumour[1] and insulin mimetic activities,[2,3] and have been studied as functional models for the vanadium haloperoxidase enzymes.[4,5] These enzymes catalyse the oxidation of halides by hydrogen peroxide and are thought to be involved in the biosynthesis of a large number of marine natural products, many of them with potent antifungal, antibacterial, antiviral (e.g. HIV) and antineoplastic properties.[6] In addition, a large variety of oxidation reactions can be efficiently performed by peroxovanadium(V) complexes. These complexes have been shown to hydroxylate benzene and other aromatics, epoxidise and hydroxylate alkenes and allylic alcohols and oxidise sulfides and primary and secondary alcohols.[7]

Previously, the vanadium(V) complexes that form with several α-hydroxycarboxylic acids were the object of a multinuclear NMR study carried out by this group.[8–10] In view of the interest in peroxovanadium(V) compounds and the need to know their structures in order to fully understand both their chemistry and biochemistry, we have now extended our previous work to the more complex systems involving hydrogen peroxide. This paper deals with the peroxo complexes that form when hydrogen peroxide is added to a mixture of a vanadate(V) salt and L-lactic acid in aqueous solution. Our intention was to investigate these species with respect to their number, stoichiometries, structures and stability by NMR spectroscopy. This technique has been intensively used in the study of vanadium(V)/hydrogen peroxide systems, both in the presence and absence of other ligands,[11–18] and has proved to be successful in the structural characterisation of the species present in solution.

A previous ^{51}V NMR study[17] revealed that a monoperoxovanadium complex of L-lactic acid is formed at pH 1. This species was characterised as being octahedral with a 1:1:1 stoichiometry (metal:ligand:peroxo). No additional studies of this system using NMR or other techniques were found in the literature.

Results and Discussion

Vanadium(V) undergoes very complex hydrolysis and polymerization reactions in aqueous solution, forming a large variety of products depending on the concentration, pH and ionic strength.[19,20] In the presence of hydrogen peroxide and a ligand such as an α-hydroxycarboxylic acid, new equilibria are established and, as a consequence, additional species can be formed, namely peroxovanadates, oxo complexes and peroxo complexes. The formation of peroxo complexes will result, therefore, from competition between several equilibria.

^{1}H, ^{13}C, ^{17}O and ^{51}V NMR spectra of V^{V}-L-lactic acid–H_2O_2 were obtained for D_2O solutions of the complexing species (concentrations ranging from 0.15 M to 2.0 M), with various molar ratios (H_2O_2:metal from 5:1 to 1:1 and metal:ligand from 3:1 to 1:3), and for different pH* values (1–9.5). Figure 1 shows a typical ^{1}H NMR spectrum of this system obtained for the pH* range 2–7. In this spectrum, signals due to several complexes, free ligand and degradation products (mainly acetaldehyde and acetic acid) are observed. The observation of distinct signals for both bound and free ligand is a consequence of slow ligand exchange on the NMR time scale.

Figure 1 also illustrates, through the presence of several L-lactic acid oxo complexes,[8,10] the various competing equilibria in which the ligand is involved.

[a] Department of Chemistry, University of Coimbra, 3000 Coimbra, Portugal

 © WILEY-VCH Verlag GmbH, D-69451 Weinheim, 2000 1434–1948/00/0707–1617 $ 17.50+.50/0

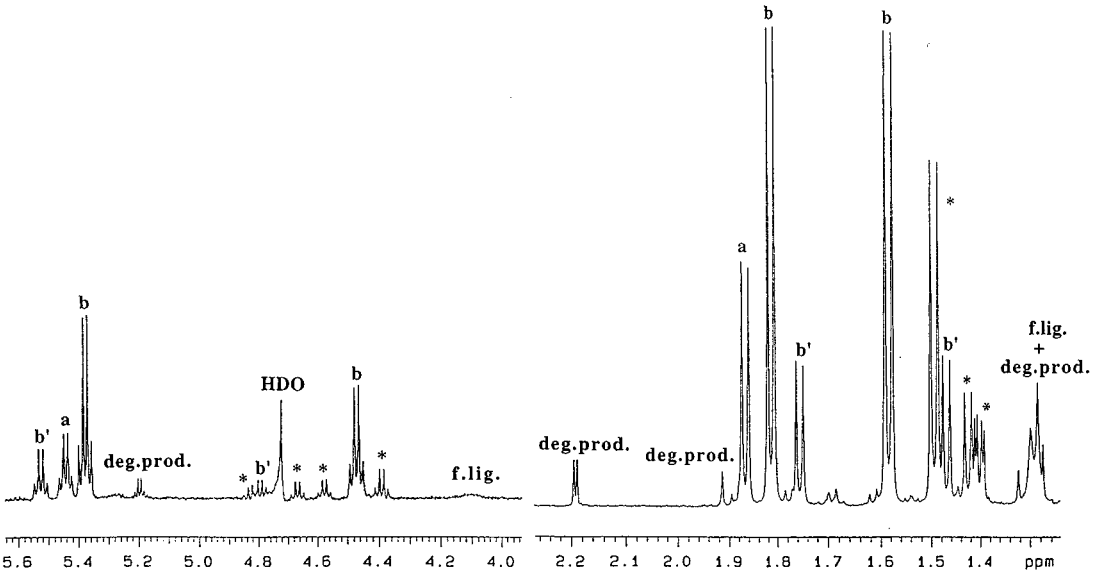


Figure 1. ^{1}H NMR spectrum (499.824 MHz) of a 0.05 M:0.05 M:0.05 M solution in D_2O of V^V−L-lactic acid−H_2O_2, pH* = 4.0, temp. 298 K, approximately 3 hours after preparing the solution, (*): oxo complexes.

Three peroxo complexes, **a**, **b** and **b′**, are formed in the pH* region between 2 and 7. Their concentrations relative to the other species present in solution are at a maximum in the pH* range 2−5. ^{51}V NMR results show that at higher pH* values the metal is essentially involved in the formation of peroxovanadates. At pH* values below 2, besides **a**, **b** and **b′**, an additional complex is formed: species **c**.

Dinuclear Complexes

The ^{1}H NMR spectra of complexes **b** and **b′** show the occurrence of two different sets (A_3X spectra) of ligand signals for each complex. Attributing two sets of signals to one complex is based on the observation that the two doublets due to the methyl protons have equal intensities, irrespective of concentration and pH* conditions. These observations suggest that both complexes **b** and **b′** have two ligand molecules in different magnetic environments. Complex **a**, on the other hand, shows only one set of signals for the ligand, suggesting either the existence of only one ligand molecule in the complex or that all the ligand molecules present are magnetically equivalent. Similarly, the ^{13}C NMR spectra show the occurrence of two sets of ligand signals for complexes **b** and **b′** and only one set for complex **a**.

Table 1 shows the ^{1}H and ^{13}C NMR parameters at pH* 4 for complexes **a**, **b** and **b′**. HETCOR and homonuclear decoupling experiments were performed in order to assign the proton and carbon shifts of complexes **b** and **b′**.

The ^{1}H and ^{13}C chemical shifts observed for the ligand on complexation indicate which groups are bound to the metal. The high frequency shifts observed for the carboxylic carbon nucleus and the adjacent carbinol carbon and proton nuclei in complexes **a**, **b** and **b′** are a clear indication that those groups are involved in complexation.

An analysis of Table 1 and Figure 1 shows that one of the ligand molecules in each one of the complexes **b** and **b′** undergoes significantly smaller ^{1}H shifts on complexation (0.15−0.68 ppm) than the other (0.44−1.41 ppm). In fact, while one set of signals for each complex is found near to those of the oxo complexes, the other is found at higher frequencies.

The metal to ligand molar ratio has no significant effect on the relative concentrations of the three peroxo complexes **a**, **b** and **b′**, which indicates that these complexes have similar metal:ligand stoichiometries. Simple calculations involving metal and ligand (CH_3 protons) signal intensities lead to the conclusion that the three peroxo complexes are n:n (metal:ligand) species.

The formation of peroxovanadium(V) complexes of L-lactic acid strongly depends on the hydrogen peroxide:metal molar ratio. Those species are present only if this ratio is equal to or smaller than 2. If greater than 2 equivalents peroxide to metal is used, peroxovanadates are the main species in solution. When equal molar amounts of hydrogen peroxide and vanadium(V) are used, the peroxo complexes are the major species present immediately after preparation of the solution. If the ratio is 2, the major species initially formed is the diperoxovanadate $[VO(OO)_2(H_2O)_n]^-$. Over time, as the peroxide concentration decreases due to disproportionation catalysed by vanadium(V),[13] the concentration of the peroxovanadates decreases and the concentration of L-lactic acid peroxo complexes increases. These results suggest that no more than one peroxide ion is involved for each metal centre. This conclusion is supported by ^{51}V NMR results. ^{51}V chemical shifts in vanadium complexes are known to be sensitive to the coordination number and to the nature of the ligands. For α-hydroxycarboxylic acids, such as L-lactic acid, ^{51}V signals at approximately $\delta = -595$ have been attributed to monoperoxo species which have a seven-coordinate VO^{3+} metal centre.[21] Figure 2 shows a ^{51}V NMR spectrum where three signals ascribed to complexes **a**, **b** and **b′** are observed at approximately $\delta = -595$, indicating that these complexes have monoperoxovanadium(V) centres. However, two additional signals attributed to

Table 1. ^{1}H and ^{13}C NMR parameters for V^{V} + L-lactic acid + H_2O_2 at pH* = 4.0 (^{1}H) and pH* = 4.2 (^{13}C) (298K)

	δ_H [ppm][a]	J_{HH} [Hz]	δ_C [ppm][a]
L-lactic acid			
	1.32 (CH_3)	6.8	21.43 (CH_3)
	4.13 (CH)		69.46 (CH)
			182.89 (CO_2H)
V^{V}+L-lactic acid+H_2O_2			
complex **a**			
δ	1.87 (CH_3)	7.1	19.88 (CH_3)
Δδ	0.55		−1.55
δ	5.45 (CH)		80.39 (CH)
Δδ	1.32		10.93
δ			188.44 (CO_2H)
Δδ			5.55
complex **b**			
δ	1.82, 1.59 (CH_3)	6.8, 6.8	21.49, 19.24 (CH_3)
Δδ	0.50, 0.27		0.06, −2.19
δ	5.38, 4.47 (CH)		80.73, 84.69 (CH)
Δδ	1.25, 0.34		11.27, 15.23
δ			187.09, 186.50[b] (CO_2H)
Δδ			4.20, 3.61
complex **b**′			
δ	1.76, 1.47 (CH_3)	6.8, 7.1	23.03,[c] (CH_3)
Δδ	0.44, 0.15		1.60
δ	5.54, 4.81 (CH)		84.30, 85.88 (CH)
Δδ	1.41, 0.68		14.84, 16.42
δ			186.72[b,c] (CO_2H)
Δδ			3.83

[a] δ Values relative to TMS, using *tert*-butyl alcohol (δ_H 1.2, δ_C 31.2) as internal reference. − [b] The oblique line refers to the possibility of a reverse assignment. − [c] Not observed due to its superposition with more intense signals.

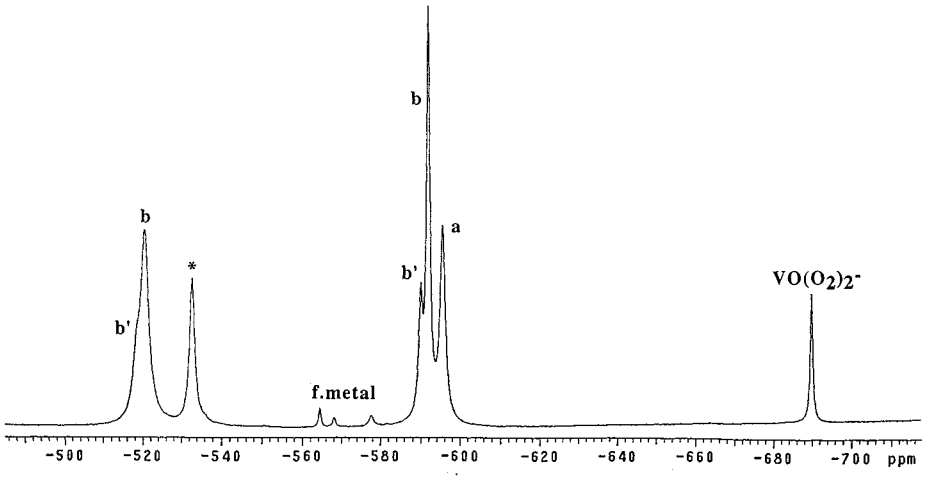


Figure 2. ^{51}V NMR spectrum (131.404 MHz) of a 0.05 M:0.05 M:0.05 M aqueous (30% D_2O) solution of V^{V}−L-lactic acid−H_2O_2, pH* = 4.5, temp. 298 K, approximately 24 hours after preparing the solution, (*): oxo complex.

the complexes **b** and **b**′ are observed at approximately δ = −520 (Figure 2 and Table 2).

The assignment of the two signals at δ = −518.6 and −520.4 was made possible by a time-dependent ^{51}V NMR study, which shows that the disappearance of the signal due to complex **a** is followed by the appearance of two sets of signals, each with two peaks of equal intensity. By combining these data with the information provided by ^{1}H NMR spectra, the two ^{51}V signals of greater intensity can be attributed to complex **b** and the two weaker signals to complex **b**′. We note that in the meantime part of the hydrogen peroxide has

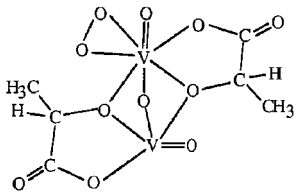
Table 2. ^{51}V NMR chemical shifts for V^{V}+L-lactic acid+H_2O_2 at 298K

	δ_V [ppm][a]
V^{V} + L-lactic acid + H_2O_2	
complex **a** (pH* 4.0)	−595.9
complex **b** (pH* 4.0)	−520.4, −592.2
complex **b**′ (pH* 4.0)	−518.6, −590.6
complex **c** (pH* 1.1)	−546.0

[a] δ Values relative to $VOCl_3$ as external reference.

disproportionated and signals due to free metal can consequently be detected. ^{51}V chemical shifts at −520 ppm are not, however, expected for peroxo complexes, but for five-coordinate oxovanadium(V) complexes.[21]

These results, together with the previously mentioned observations concerning the ^{1}H NMR data, suggest that **b** and **b′** are probably isomers of stoichiometry 2:2:1 (metal:ligand:peroxo). Several hypotheses could be advanced for the structure of these complexes, depending on the groups involved in V−O−V bridges and on the possible arrangements of the oxo and peroxo groups. We choose to propose an equatorial position (relative to the axial V=O) for the peroxo group in a bipyramidal pentagonal geometry on the basis of the solid state structures found by X-ray diffraction for most peroxovanadium complexes.[7] In addition, OH bridging is expected to be preferred to CO_2H bridging, as found for numerous peroxovanadium complexes.[1,22,23] Accordingly, structure **1** (Scheme 1) can be proposed. The occurrence of two complexes can be explained by considering apical or equatorial positions for the V=O group in the oxovanadium centre.



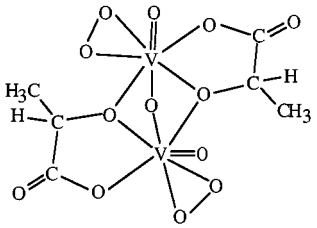
1

Scheme 1

The two ligands and the two vanadium centres in **1** are clearly magnetically nonequivalent, one ligand spectrum showing a smaller shift on complexation and two ^{51}V signals arising, characteristic of oxovanadium(V) and peroxovanadium(V) centres. This kind of dinuclear peroxovanadium complex, in which one of the metal centres is an oxovanadium centre, has not been previously reported.

Regarding complex **a**, its ^{51}V chemical shift indicates a monoperoxo seven-coordinate metal centre,[21] similar to the peroxovanadium centres of complexes **b** and **b′**. Since a 1:1:1 species would require two water molecules bound to the metal, a 2:2:2 species, which does not have this requirement, is expected to be favoured. Based on these considerations, and on the fact that the ^{1}H and ^{13}C NMR results require that the two ligand molecules are magnetically equivalent, we propose structure **2** (Scheme 2) for complex **a**. A similar structure has been found by X-ray diffraction for the complex $K_2[\{VO(O_2)(L\text{-}tartH_2)\}_2(\mu\text{-}H_2O)]\cdot 5H_2O$.[23] Additional support for this proposal is provided by the kinetic behaviour observed for the three peroxo complexes. Over time, complex **a**, which has two peroxovanadium centres, will convert into complexes **b** and **b′** by losing one of the peroxo groups. This was confirmed by some experiments which showed that the addition of hydrogen peroxide to **b** and **b′** lead to the formation of **a**.

Some support for the proposed structures comes from the (natural abundance) ^{17}O NMR spectra. Although no signals due to V−O−V bridges and the peroxo groups could be detected, resonances due to terminal V=O atoms are consistent with the presence of two equivalent V=O groups in complex **a** and two nonequivalent V=O groups in complex **b** (complex **b′** is too weak to be detected by ^{17}O NMR). Thus, two signals at δ = 1179.0 and δ = 1188.8 are found for complexes **a** and **b**, respectively, in accordance with reported values for other peroxovanadium(V) complexes.[24] In addition, a signal at δ = 1054.5 is detected for complex **b**, which is in the region of V=O oxygen signals due to oxovanadium complexes with L-lactic acid (δ = 1094.9 and 1067.8).



2

Scheme 2

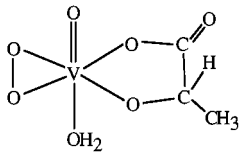
Mononuclear Complexes

The ^{51}V NMR spectra recorded for solutions at pH* 1 having a hydrogen peroxide:metal molar ratio equal to or smaller than 2 and metal:ligand molar ratios from 0.5 to 2 show, besides the signals of the complexes **a**, **b**, **b′** and $[VO(OO)_2(H_2O)_n]^-$ (δ = −690.3),[12] the signal of the monoperoxo cation $[VO(OO)(H_2O)_n]^+$ (δ = −536.3),[11,12] the peaks of the two major oxovanadium complexes of L-lactic acid (δ = −533.3 and −542.4)[8,10] and a signal at δ = −546.0. The latter is attributed to a new peroxovanadium(V) complex, species **c**. This species is especially favoured if the hydrogen peroxide:metal molar ratio is equal to 1. Over time, complex **c** disappears and the oxo complexes become the dominant species.

The ^{1}H NMR spectra of the same solutions show the peaks of complexes **a**, **b**, **b′**, those of one of the oxo complexes and a broad dominant signal at δ = 1.39 which coincides with the chemical shift of the CH_3 protons of the other oxo complex. However, the corresponding CH signal is not observed. Over time, as complex **c** disappears, the CH signal of the oxo complex becomes visible and the peak at δ = 1.39 becomes a well defined doublet. These results suggest that the ligand is involved in a rapid (on the NMR time scale) exchange process between species **c** and one of the oxo complexes, leading to extreme broadening of the CH signals (they are not observed) and to the coalescence of the CH_3 resonances into a broad signal. Because of rapid degradation of complex **c**, it was not possible to obtain any ^{13}C NMR spectra of this species.

Based on the ^{51}V chemical shift, which is typical of six-coordinated species,[21] we can propose **c** as being a six-coordinated complex having a 1:1:1 (metal:ligand:peroxo) stoichiometry. A 1:2:1 species would mean the metal is

seven coordinate. The ligand will probably be bound in the equatorial plane, as found by X-ray diffraction for the complex $VO(OO)(C_5H_4NCOO)(H_2O)_2$.[25] The remaining position in the coordination shell would be occupied by one water molecule. A possible structure for **c** is **3** (Scheme 3), which has been previously proposed by other authors.[17]



3

Scheme 3

Conclusion

In the presence of hydrogen peroxide and L-lactic acid, vanadium(V) forms several complexes in aqueous solution, L-lactic acid peroxovanadium complexes among them. The aim of the present study was to obtain information on the latter by using multinuclear NMR spectroscopy.

Four peroxo complexes were found to form under the conditions of this study. At low-intermediate pH (2−7), three dimeric complexes are formed, two of them (2:2:1 species) being the result of partial degradation (loss of one peroxide unit) of a bis(peroxide) complex (2:2:2 species). Dimeric 2:2:2 peroxovanadium complexes have been characterised by X-ray diffraction for other α-hydroxycarboxylic acids, such as citric,[1] DL-malic[22] and L-tartaric acids.[23] At very low pH (below 2) a 1:1:1 species is detected in addition to these complexes. This latter result is consistent with the tendency of vanadium ions to undergo depolymerization in very acidic media.

Experimental Section

Analytical grade ammonium vanadate(V) and commercially available L-lactic acid and hydrogen peroxide (35%) were used. Vanadate, lactic acid and hydrogen peroxide stock solutions were prepared. The hydrogen peroxide stock solution was prepared immediately prior to use. The concentrations of the vanadate and acid solutions were established by weight. Prior to use, the D_2O lactic acid solution was heated in boiling water for 2 hours to accomplish depolymerization. The samples were prepared by adding the appropriate amounts of the stock vanadate, lactic acid and hydrogen peroxide solutions. The pH was adjusted (cautiously, to reduce the possibility of drastic local disturbances of equilibria that may be slow to disappear) by addition of solutions of DCl and NaOD; the pH* values quoted are the direct pH-meter readings (room temperature) after standardization with aqueous (H_2O) buffers. The ^1H and ^{13}C NMR spectra were obtained on a Varian UNITY-500 NMR spectrometer (at 499.824 and 125.692 MHz, respectively). The residual water signal was reduced by using the Presat sequence. The ^{13}C spectra were recorded using proton-decoupling techniques with suppression of the nuclear Overhauser effect. The methyl signal of *tert*-butyl alcohol was used as internal reference for ^1H (δ = 1.2) and ^{13}C (δ = 31.2) relative to TMS. The ^{51}V and ^{17}O spectra were obtained on the same spectrometer (131.404 and 67.792 MHz, respectively) using $VOCl_3$ (δ = 0) and D_2O (δ = 0) as external references for ^{51}V and ^{17}O shifts, respectively. Typically, spectral widths of 30000 Hz, acquisition times of 1 s, pulse delays of 10 s and 5000 pulses were used when recording ^{13}C spectra. For ^{51}V and ^{17}O spectra, the corresponding parameters were 80000 and 100000 Hz, 0.04 and 0.02 s, 0.01 and 0 s, about 16000 and 4×10^6 pulses, respectively. The 2D NMR spectra, HETCOR,[26] were also recorded on the Varian UNITY-500 NMR spectrometer.

Acknowledgments

This work has been supported by "Fundação para a Ciência e a Tecnologia", of the Portuguese Ministry of Science and Technology (Project PRAXIS QUI-63/96). The authors are also indebted to the referees for some suggestions.

[1] C. Djordjevic, M. Lee, E. Sinn, *Inorg. Chem.* **1989**, *28*, 719−723 and references therein.
[2] A. Shaver, J. B. Ng, D. A. Hall, B. S. Lum, B. I. Posner, *Inorg. Chem.* **1993**, *32*, 3109−3113.
[3] B. I. Posner, R. Faure, J. W. Burgess, A. P. Bevan, D. Lachance, G. Zhang-Sun, I. G. Fantus, J. B. Ng, D. A. Hall, B. S. Lum, A. Shaver, *J. Biol. Chem.* **1994**, *269*, 4596−4604.
[4] G. J. Colpas, B. J. Hamstra, J. W. Kampf, V. L. Pecoraro, *J. Am. Chem. Soc.* **1994**, *116*, 3627−3628.
[5] G. J. Colpas, B. J. Hamstra, J. W. Kampf, V. L. Pecoraro, *J. Am. Chem. Soc.* **1996**, *118*, 3469−3478.
[6] A. Butler, J. V. Walker, *Chem. Rev.* **1993**, *93*, 1937−1944.
[7] A. Butler, M. J. Clague, G. E. Meister, *Chem. Rev.* **1994**, *94*, 625−638.
[8] M. M. Caldeira, M. L. Ramos, N. C. Oliveira, V. M. S. Gil, *Can. J. Chem.* **1987**, *65*, 2434−2440.
[9] M. M. Caldeira, M. L. Ramos, A. M. Cavaleiro, V. M. S. Gil, *J. Mol. Struct.* **1988**, *174*, 461−466.
[10] V. M. S. Gil, *Pure and Appl. Chem.* **1989**, *61*, 841−848.
[11] A. T. Harrison, O. W. Howarth, *J. Chem. Soc., Dalton Trans.* **1985**, 1173- 1177.
[12] N. J. Campbell, A. C. Dengel, W. P. Griffith, *Polyhedron* **1989**, *8*, 1379−1386.
[13] J. S. Jaswal, A. S. Tracey, *Inorg. Chem.* **1991**, *30*, 3718−3722.
[14] A. S. Tracey, J. S. Jaswal, *J. Am. Chem. Soc.* **1992**, *114*, 3835−3840.
[15] J. S. Jaswal, A. S. Tracey, *J. Am. Chem. Soc.* **1993**, *115*, 5600−5607.
[16] V. Conte, F. Di Furia, S. Moro, *J. Mol. Catal.* **1994**, *94*, 323−333.
[17] V. Conte, F. Di Furia, S. Moro, *J. Mol. Catal. A* **1995**, *104*, 159−169.
[18] M. S. Reynolds, A. Butler, *Inorg. Chem.* **1996**, *35*, 2378−2383.
[19] C. F. Baes, R. E. Mesmer, *The Hydrolysis of Cations*, Wiley; New York, **1976**, pp. 201−210 and refs therein.
[20] E. Heath, O. W. Howarth, *J. Chem. Soc., Dalton Trans.* **1981**, 1105−1110.
[21] D. Rehder, C. Weidemann, A. Duch, W. Priebsch, *Inorg. Chem.* **1988**, *27*, 584−587.
[22] C. Djordjevic, M. Lee-Renslo, E. Sinn, *Inorg. Chim. Acta* **1995**, *233*, 97−102.
[23] P. Schwendt, P. Svancárek, L. Kuchta, J. Marek, *Polyhedron* **1998**, *17*, 2161- 2166.
[24] M. Postel, C. Brevard, H. Arzoumanian, J. G. Riess, *J. Am. Chem. Soc.* **1983**, *105*, 4922−4926.
[25] H. Mimoun, L. Saussine, E. Daire, M. Postel, J. Fischer, R. Weiss, *J. Am. Chem. Soc.* **1983**, *105*, 3101−3110.
[26] A. D. Bax, G. A. Morris, *J. Magn. Reson.* **1981**, *42*, 51−59; A. D. Bax, *J. Magn. Reson.* **1983**, *53*, 517−520; J. A. Wilde, P. H. Bolton, *J. Magn. Reson.* **1984**, *59*, 343−346.

Received November 3, 1999
[I99393]

Dinuclear Aminotroponiminate Compounds Containing Two Dialkyl Aluminum Substituents

Stephan Schulz,*[a] Martin Nieger,[a] Heike Hupfer,[a] and Peter W. Roesky*[b]

Keywords: Aluminum / Aminotroponiminate / Coordination chemistry / N Ligands

Reaction of the *n*-propyl-bridged bis(aminotroponimine) H_2[(*i*Pr)TP] with various dialkylaluminum hydrides R_2AlH, in hexane, led to novel bimetallic compounds of composition [$(R_2Al)_2${(*i*Pr)TP}] (R = Me, Et, *i*Bu). Depending on the size of the substituents R bound to the Al centers the complexes crystallize either in a cisoid (R = Me) or a transoid (R = *i*Bu) conformation. The steric crowding at the aluminum centers is also observed in solution.

Introduction

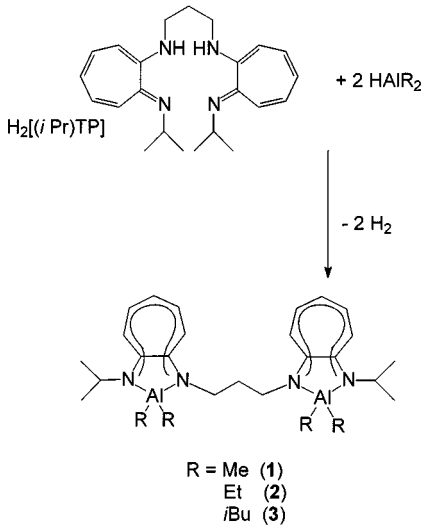
Organoaluminum compounds have attracted much attention due to their varied applications including, for example, organic syntheses, industrial catalytic processes, and chemical vapor deposition (CVD) processes.[1] Aluminum alkyls are employed as activators of group 4 complexes in Ziegler−Natta catalysis or related systems, and are known to act themselves as ethylene oligomerization and polymerization catalysts.[2] Recently, several classes of dialkylaluminum-substituted compounds, which include bidentate, monoanionic, and nitrogen-based ligands, including amidinates,[3] guadinates,[4] and aminotroponiminates,[5,6] were reacted with activators such as $[HNMe_2Ph][B(C_6F_5)_4]$, $B(C_6F_5)_3$ or $[Ph_3C][B(C_6F_5)_4]$ to give aluminum cations. These cations, with weak counterion interactions, were used for the catalytic olefin polymerization.[3−5,7] Recent reports from our laboratory have described the preparation and characterization of monobridged aminotroponiminates as nitrogen-based ligands.[8] The tris(methylene)-bridged dianionic ligand 1,3-di[2-(isopropylamino)troponiminate]propane $[(i\text{Pr})\text{TP}]^{2-}$ was shown to coordinate in a chelating mode to various lanthanide ions.[8] Depending on the size of the lanthanide ion, products of composition [{(*i*Pr)TP}LnCl(THF)]$_2$ (Ln = La, Nd) or [{(*i*Pr)TP}LnCl]$_2$ (Ln = Er, Yb, Lu), in which the central atom has either a sevenfold (La, Nd) or a sixfold (Er, Yb, Lu) coordination sphere, were obtained.[8−10] Our interest in the coordination behavior of $[(i\text{Pr})\text{TP}]^{2-}$ with smaller metal ions than the lanthanides in the oxidation state +3 led us to group 13 metals. It has been demonstrated that in gallium and indium compounds of composition [{(*i*Pr)TP}MCl] (M = In, Ga), the structure reveals a chiral fivefold coordination sphere of the ligands around the center metal.[11] Analogous to the lanthanide complexes, the $[(i\text{Pr})\text{TP}]^{2-}$ ligand also coordinates in a chelating mode to indium and gallium.

Herein we report on the reaction of the neutral ligand H_2[(*i*Pr)TP] with various dialkylaluminum hydrides R_2AlH. We focused our attention mainly on the coordination behavior of $[(i\text{Pr})\text{TP}]^{2-}$ and its dependence on the size of the alkyl substituents.

Results

The bimetallic aluminum complexes [$(R_2Al)_2${(*i*Pr)TP}] [R = Me (**1**), Et (**2**), *i*Bu (**3**)] were synthesized by reactions of the neutral ligand H_2[(*i*Pr)TP][8] with the corresponding dialkyl aluminum hydrides R_2AlH in hexane (Scheme 1). Upon cooling **1**−**3** were obtained as yellow crystalline solids with fairly high sensitivity towards air and moisture.

The new complexes were characterized by standard analytical/spectroscopic techniques. Furthermore, the solid-state structures of **1** (Figure 1) and **3** (Figure 2) were investigated by single crystal X-ray diffraction. X-ray quality



Scheme 1. Reaction of H_2[(*i*Pr)TP] with various dialkylaluminum hydrides R_2AlH

[a] Institut für Anorganische Chemie der Universität Bonn, Gerhard-Domagk-Straße 1, D-53121 Bonn, Germany
Fax: (internat.) + 49-228/735-327
E-mail: stephan@ac4010se.chemie.uni-bonn.de
[b] Institut für Anorganische Chemie der Universität Karlsruhe, Engesserstraße Geb. 30.45, D-76128 Karlsruhe, Germany
Fax: (internat.) + 49-721/661-921
E-mail: roesky@achibm6.chemie.uni-karlsruhe.de

 © WILEY-VCH Verlag GmbH, D-69451 Weinheim, 2000 1434−1948/00/0707−1623 $ 17.50+.50/0

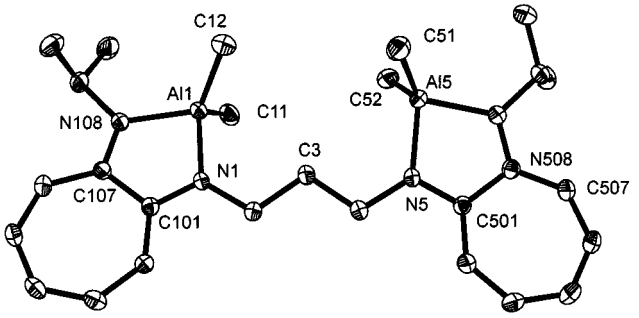


Figure 1. Perspective ORTEP view of the molecular structure of **1**; thermal ellipsoids are drawn to encompass at 50% probability; selected distances [pm] and angles [°]: Al(1)−N(1) 190.3(2), Al(1)−N(108) 191.0(2), Al(1)−C(11) 196.5(3), Al(1)−C(12) 196.8(3), N(1)−C(101) 134.4(3), N(108)−C(107) 134.5(3), N(5)−Al(5) 190.4(2), Al(5)−N(508) 191.4(2), Al(5)−C(51) 197.0(3), Al(5)−C(52) 196.7(3), N(5)−C(501) 134.9(3), N(508)−C(507) 133.5(3); N(1)−Al(1)−N(108) 84.0(1), N(1)−Al(1)−C(11) 112.0(1), N(108)−Al(1)−C(11) 114.5(1), N(1)−Al(1)−C(12) 115.4(1), N(108)−Al(1)−C(12) 112.9(1), C(11)−Al(1)−C(12) 114.5(1), N(5)−Al(5)−N(508) 84.0(1), N(5)−Al(5)−C(51) 114.7(1), N(508)−Al(5)−C(51) 112.0(1), N(5)−Al(5)−C(52) 112.0(1), N(508)−Al(5)−C(52) 113.3(1), C(51)−Al(5)−C(52) 116.6(1)

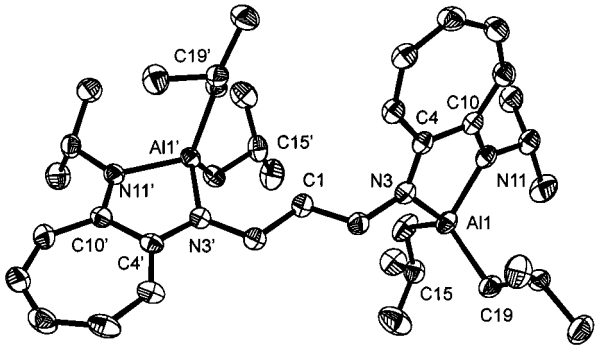


Figure 2. Perspective ORTEP view of the molecular structure of **3**; thermal ellipsoids are drawn to encompass at 50% probability; selected distances [pm] and angles [°]: Al(1)−N(3) 191.6(2), Al(1)−N(11) 191.7(2), Al(1)−C(19) 198.2(2), Al(1)−C(15) 198.4(2), N(3)−C(4) 133.9(2), N(11)−C(10) 134.0(2), Al(1′)−N(3′) 189.8(2), Al(1′)−N(11′) 191.8(2), Al(1′)−C(19′) 198.2(2), Al(1′)−C(15′) 198.2(2), N(3′)−C(4′) 133.7(2), N(11′)−C(10′) 134.0(2); N(3)−Al(1)−N(11) 83.2(1), N(3)−Al(1)−C(19) 111.7(1), N(11)−Al(1)−C(19) 111.4(1), N(3)−Al(1)−C(15) 111.3(1), N(11)−Al(1)−C(15) 116.1(1), N(3′)−Al(1′)−N(11′) 83.2(1), N(3′)−Al(1′)−C(19′) 112.1(1), N(11′)−Al(1′)−C(19′) 112.0(1), N(3′)−Al(1′)−C(15′) 111.9(1), N(11′)−Al(1′)−C(15′) 114.5(1)

crystals were grown either from hot hexane (**1**) or from pentane at −30 °C (**3**). In contrast to all other known structures in which the $[(i\text{Pr})\text{TP}]^{2-}$ ligand coordinates in a chelating fashion, **1** and **3** only show a metal-bridging coordination mode. Since the cisoid arrangement of both metal atoms in **1** suggests that a chelating coordination of the ligand might be possible, Me_2AlH was reacted with an excess of $H_2[(i\text{Pr})\text{TP}]$ at elevated temperature to force the ligand to coordinate in a chelating fashion. However, even under these reaction conditions only **1** was obtained. In contrast to **1** the two metal centers of **3** are located in a transoid conformation in the solid state which is mainly caused by the increased steric demand of the *i*Bu substituents of the aluminum atoms. Thus, **1** features a noncrystallographic C_2 symmetry through C3 (parallel to the planes of the seven-membered rings) whereas **3** has a noncrystallographic C_2 symmetry through C1. The heterocyclic five-membered ring systems (N, Al, N, C, C) are essentially planar with an average deviation from the least-square plane of 2 pm (**1**) and 1 pm (**3**). The four-coordinate aluminum centers in both **1** and **3** adopt a distorted tetrahedral geometry. The N−Al−N angles are 84.0(1)°, 84.0(1)° (**1**) and 83.2(1)°, 83.2(1)° (**3**). The larger steric demand of the *i*Bu substituents in **3** compared to Me in **1** leads to a slight decrease of the N−Al−N angle, while the C−Al−C angles are increased [114.5(1)°, 116.6(1)° (**1**) and 118.1(1)°, 118.1(1)° (**3**)]. The Al−N distances [190.3(2) pm to 191.4(2) pm (**1**); 191.6(2) pm, 191.7(2) pm (**3**)] are typical for four-coordinate Al, e.g. $[(i\text{Pr})_2\text{ATI}]AlMe_2$ [191.5(1) pm] and $[(i\text{Pr})_2\text{ATI}]AlH_2$ (ATI = aminotroponiminate) [188.2(4) pm, 188.6(4) pm] have similar bond lengths.[5] The $C_{ring}-N$ distances [av. 134.3(3) pm (**1**); 133.9(2) pm and 134.0(2) pm (**3**)] are similar to the values observed for $[(i\text{Pr})_2\text{ATI}]H$ [131.4(3) pm and 134.2(3) pm] and $[(i\text{Pr})_2\text{ATI}]AlMe_2$ (av. 133.8 pm).[5]

For compound **1** one sharp $Al-CH_3$ signal is observed in the ^1H and ^{13}C NMR spectra ($\delta = -0.25$ and $\delta = -6.1$, respectively). Due to the nonequivalence of the Al−αH in **2** and **3**, a splitting of the Al−αH resonance is seen in the ^1H NMR spectra [Al−C*H*$_2$: $\delta = 0.35$ and 0.36 (**2**); $\delta = 0.36$ and 0.38 (**3**)] but not in the ^{13}C NMR spectra [e.g. Al−*C*H$_2$: $\delta = 2.9$ (**2**); $\delta = 25.4$ (**3**)]. The ^1H and ^{13}C NMR spectra also point to a symmetrical coordination of the $[(i\text{Pr})\text{TP}]^{2-}$ anion in solution. The signals of the isopropyl C*H* of **1**−**3** are well-resolved into a septet and show only a slight high-field shift [$\delta = 3.50$ (**1**), 3.51 (**2**) and 3.54 (**3**)] compared to that of the free ligand $H_2[(i\text{Pr})\text{TP}]$ ($\delta = 3.55$).[8] This is in sharp contrast to comparable lanthanide alkyl compounds of composition $[\{(i\text{Pr})\text{TP}\}\text{Ln}-\text{R}]$ [Ln = La, Lu; R = $CH(SiMe_3)_2$, CH_2SiMe_3)] in which the isopropyl C*H* signal is strongly downfield shifted {$\delta = 3.67$ $[\{(i\text{Pr})\text{TP}\}_2LaCH(SiMe_3)_2]$;[8] $\delta = 3.93$ $[\{(i\text{Pr})\text{TP}\}_2LuCH_2SiMe_3]$[10]}. Besides the NMR investigations all new compounds were also characterized by elemental analyses and IR and EI mass spectroscopy. Compounds **1**−**3** show molecular ion peaks as well as characteristic fragmentation patterns.

Conclusions

In conclusion, it can be emphasized that the reactions of $H_2[(i\text{Pr})\text{TP}]$ with various aluminum alkyl compounds R_2AlH lead to bimetallic complexes of composition $[(R_2Al)_2\{(i\text{Pr})\text{TP}\}]$ (R = Me, Et, *i*Bu). In contrast to other complexes of group 3, 13 and the lanthanide metals the TP ligand does not bind in a chelating fashion; instead, a metal-bridging coordination is observed. Obviously, due to the smaller ion radius of the aluminum(III) center, bis(aminotroponiminate) complexes cannot be formed. Depending on the steric size of the alkyl groups bound to Al either a cisoid or a transoid conformation of $[(R_2Al)_2\{(i\text{Pr})\text{TP}\}]$ is observed in the solid state. In summary, our results extend

the series of the few known bimetallic complexes of group 13 elements such as salen complexes.[12−15]

Experimental Section

General: All manipulations were performed in a glovebox under an N_2 atmosphere or with standard Schlenk techniques. Solvents were dried over sodium/potassium and degassed prior to use. *i*Bu_2AlH was purchased from Aldrich and used as received. Me_2AlH,[16] Et_2AlH[17] and H_2[(*i*Pr)TP][8] were prepared by literature methods. − A Bruker AMX 300 spectrometer was used for NMR spectroscopy. ^1H and $^{13}C\{^1H\}$ NMR spectra were referenced to internal C_6D_5H (^1H: δ = 7.154; ^{13}C: δ = 128.0). − Infrared spectra were recorded in Nujol between KBr plates with a Nicolet Magna 550 and are reported in wave numbers. − Mass spectra were recorded at 70 eV on Varian MAT 711 spectrometer in the electron ionisation mode. − Melting points were observed in sealed capillaries and were not corrected. − Elemental analyses were performed at the Mikroanalytisches Labor der Universität Bonn.

[$(Me_2Al)_2$[(*i*Pr)TP]] (1): Me_2AlH (0.12 g, 2.00 mmol) was dissolved in hexane (20 mL). At ambient temperature a solution of H_2[(*i*Pr)TP] (0.36 g, 1.00 mmol) in hexane (30 mL) was added, immediately followed by gas evolution and precipitation of a yellow solid. After the gas evolution had stopped, the suspension was heated under reflux for 10 min, until the solid had dissolved. Cooling to −10 °C gave **1** as yellow crystals (0.45 g, 95%). Single crystals were formed from a solution of hot hexane. (60 °C to 25 °C within 8 h). M.p. 128 °C. − ^1H NMR (300 MHz, C_6D_5H, 25 °C): δ = −0.25 (s, 12 H, Al−CH_3), 1.17 [d, $^3J_{H-H}$ = 6.4 Hz, 12 H, CH(CH_3)$_2$], 2.12 (m, 2 H, CH_2−CH_2−CH_2), 3.18 (m, 4 H, CH_2−CH_2−CH_2), 3.50 [dsept, $^3J_{H-H}$ = 6.4 Hz, $^5J_{H-H}$ = 0.7 Hz 2 H, C*H*(CH_3)$_2$], 6.21 (t, $^3J_{H-H}$ = 9.3 Hz, 2 H, H_{ring}), 6.31 (d, J_{H-H} = 11.4 Hz, 2 H, H_{ring}), 6.36 (d, J_{H-H} = 11.1 Hz, 2 H, H_{ring}), 6.71−6.84 (m, 4 H, H_{ring}). − $^{13}C\{^1H\}$ NMR (80 MHz, C_6D_5H, 25 °C): δ = −6.1 (Al−CH_3), 22.9 [CH(CH_3)$_2$], 27.6 (CH_2−CH_2−CH_2), 44.8 (CH_2−CH_2−CH_2), 47.6 [CH(CH_3)$_2$], 113.5 (C_{ring}), 114.0 (C_{ring}), 119.7 (C_{ring}), 136.8 (C_{ring}), 136.9 (C_{ring}), 161.4 (N−C_{ring}), 162.1 (N−C_{ring}). MS (EI, 20 eV): *m*/*z* (%) = 476 (2) [M^+], 461 (64) [$M^+ - CH_3$], 389 (100) [$M^+ - Al - 4CH_3$], 208 (7) [$M^+/2 - 2CH_3$]. − IR (nujol): ṽ = 2362, 2337, 1511, 1259, 1095, 1018, 798, 721 cm^{-1}. − $C_{27}H_{42}Al_2N_4$(476.6): calcd. C 68.04, H 8.88, N 11.76; found C 67.93, H 8.82, N 11.71.

[$(Et_2Al)_2$[(*i*Pr)TP]] (2): Et_2AlH (0.17 g, 2.00 mmol) was dissolved in hexane (20 mL) and added at ambient temperature to a solution of H_2[(*i*Pr)TP] (0.36 g, 1.00 mmol) in hexane (30 mL). After the gas evolution had stopped the solution was heated under reflux for 15 min. Cooling to −30 °C gave **2** as a yellow solid (0.45 g, 85%). M.p. 111 °C. − ^1H NMR (300 MHz, C_6D_5H, 25 °C): δ = 0.35 (q, $^3J_{H-H}$ = 8.2 Hz, 4 H, CH_2Al), 0.36 (q, $^3J_{H-H}$ = 8.1 Hz, 4 H, CH_2Al), 1.18 [d, $^3J_{H-H}$ = 6.4 Hz, 12 H, CH(C*H*$_3$)$_2$], 1.33 (t, $^3J_{H-H}$ = 8.1 Hz, 12 H, C*H*$_3$$CH_2$Al), 2.13 (m, 2 H, CH_2−CH_2−CH_2), 3.27 (m, 4 H, CH_2−CH_2−CH_2), 3.51 [dsept, $^3J_{H-H}$ = 6.4 Hz, $^5J_{H-H}$ = 0.8 Hz, 2 H, C*H*(CH_3)$_2$], 6.21 (t, $^3J_{H-H}$ = 9.3 Hz, 2 H, H_{ring}), 6.33 (d, J_{H-H} = 11.4 Hz, 2 H, H_{ring}), 6.43 (d, J_{H-H} = 11.0 Hz, 2 H, H_{ring}), 6.71−6.87 (m, 4 H, H_{ring}). − $^{13}C\{^1H\}$ NMR (80 MHz, C_6D_5H, 25 °C): δ = 2.9 (CH_2Al), 10.2 (*C*$H_3$$CH_2$Al), 22.7 [CH(*C*$H_3$)$_2$], 27.0 ($CH_2$−*C*$H_2$−$CH_2$), 44.8 (*C*$H_2$−$CH_2$−*C*$H_2$), 47.5 [*C*H($CH_3$)$_2$], 113.4 ($C_{ring}$), 114.1 ($C_{ring}$), 119.8 ($C_{ring}$), 136.8 ($C_{ring}$), 136.9 ($C_{ring}$), 161.8 (N−$C_{ring}$), 162.5 (N−$C_{ring}$). − MS (EI, 20 eV): *m*/*z* (%) = 532 (4) [M^+], 503 (100) [M^+ − Et], 389 (70) [M^+ − Al − 4Et]. − IR (nujol): ṽ = 1595, 1511, 1423, 1274, 1234, 1160, 1043, 989, 962, 881, 731, 630, 576 cm^{-1}. − $C_{31}H_{50}Al_2N_4$ (532.7): C 69.89, H 9.46, N 10.52; found C 69.63, H 9.39, N 10.50.

[$(iBu_2Al)_2${(*i*Pr)TP}] (3): In a procedure similar that for **2**, compound **3** was obtained as a yellow solid (0.45 g, 70%) at −30 °C. Single crystals were formed from a pentane solution at −30 °C. M.p. 113 °C (dec). − ^1H NMR (300 MHz, C_6D_5H, 25 °C): δ = 0.36 (d, $^3J_{H-H}$ = 6.8 Hz, 4 H, CH_2Al), 0.38 (d, $^3J_{H-H}$ = 6.9 Hz, 4 H, CH_2Al), 1.12 [d, $^3J_{H-H}$ = 6.3 Hz, 12 H, (C*H*$_3$)$_2$CHCH_2Al], 1.14 [d, $^3J_{H-H}$ = 6.3 Hz, 12 H, (C*H*$_3$)$_2$CHCH_2Al], 1.23 [d, $^3J_{H-H}$ = 6.5 Hz, 12 H, NCH(*C*H_3)$_2$], 2.01 [sept, 2 H, $^3J_{H-H}$ = 6.5 Hz, 4 H, (CH_3)$_2$C*H*CH_2Al], 2.16 (m, 2 H, CH_2−CH_2−CH_2), 3.30 (m, 4 H, CH_2−CH_2−CH_2), 3.54 [dsept, $^3J_{H-H}$ = 6.4 Hz, $^5J_{H-H}$ = 0.6 Hz, 2 H, NC*H*(CH_3)$_2$], 6.23 (t, $^3J_{H-H}$ = 9.3 Hz, 2 H, H_{ring}), 6.34 (d, J_{H-H} = 11.5 Hz, 2 H, H_{ring}), 6.45 (d, J_{H-H} = 11.1 Hz, 2 H, H_{ring}), 6.76 (m, 2 H, H_{ring}), 6.93 (m, 2 H, H_{ring}). − $^{13}C\{^1H\}$ NMR (80 MHz, C_6D_5H, 25 °C): δ = 22.7 [CH(*C*H_3)$_2$], 25.4 (CH_2Al), 26.6 (CH_2−*C*H_2−CH_2), 27.5 [(CH_3)$_2$*C*HCH_2Al], 28.8 [(*C*H_3)$_2$CHCH_2Al], 29.0 [(*C*H_3)$_2$CHCH_2Al], 45.0 (*C*H_2−CH_2−*C*H_2), 47.6 [*C*H(CH_3)$_2$], 113.8 (C_{ring}), 114.6 (C_{ring}),

Table 1. Crystallographic details for [$(Me_2Al)_2$[(*i*Pr)TP]] (**1**) and [$(iBu_2Al)_2$[(*i*Pr)TP]] (**3**)

	1	3
Formula	$C_{27}H_{42}Al_2N_4$	$C_{39}H_{66}Al_2N_4$
Formula weight	476.6	644.9
Space group	$P2_1/c$ (Na 14)	$P\bar{1}$ (No. 2)
a, pm	735.04(2)	1165.11(4)
b, pm	1873.28(6)	1270.21(5)
c, pm	2005.54(5)	1493.67(6)
α,°		91.630(2)
β, °	98.250(2)	112.803(2)
γ, °		101.484(2)
V, 10^6 pm^3	2732.92(13)	1983.28(13)
Z	4	2
T, K	123(2)	123(2)
Radiation	Mo-K_α (λ = 0.71073 Å)	Mo-K_α (λ = 0.71073 Å)
μ, mm^{-1}	0.128	0.103
Reflections collected	24437	30770
Unique reflections	4804 [R_{int} = 0.050]	9450 [R_{int} = 0.040]
Parameters	302	406
*R*1 for $I > 2\sigma(I)$	0.054	0.053
w*R*2 (all data)	0.134	0.148

119.9 (C_{ring}), 136.9 (C_{ring}), 137.0 (C_{ring}), 161.7 (N−C_{ring}), 162.2 (N−C_{ring}). − MS (EI, 20 eV): *m*/*z* (%) = 644 (0.03) [M^+], 587 (100) [M^+ − *i*Bu], 389 (31) [M^+ − 4*i*Bu], 322 (14) [M^+/2]. − IR (Nujol): $\tilde{\nu}$ = 2360, 2337, 1594, 1511, 1421, 1274, 1223, 1172, 1052, 727, 667, 619 cm^{-1}. − $C_{39}H_{66}Al_2N_4$ (644.9): C 72.63, H 8.37, N 8.69; found C 72.58, H 8.34, N 8.68.

X-ray Structure Solution and Refinement: Crystallographic data are summarized in Table 1. Figure 1 shows the ORTEP diagram of the solid state structure of **1** and Figure 2 that of **3**. Data were collected on a Nonius Kappa-CCD diffractometer. Structures of **1** and **3** were solved by direct methods (SHELXS-97)[18] and refined by full-matrix least-squares on F^2. All non-hydrogen atoms were refined anisotropically and hydrogen atoms by a riding model (SHELXL-97).[19]

Crystallographic data (excluding structure factors) for the structures reported in this paper have been deposited with the Cambridge Crystallographic Data Centre as supplementary publication nos. CCDC-138108 (**1**) and CCDC-138109 (**3**). Copies of the data can be obtained free of charge on application to CCDC, 12 Union Road, Cambridge CB21EZ, UK [Fax: (internat.) + (44)-1223/336-033; E-mail: deposit@ccdc.cam.ac.uk].

Acknowledgments

This work was supported by the Deutsche Forschungsgemeinschaft, the Fonds der Chemischen Industrie and the BMBF. Additionally, generous support from Prof. Dr. D. Fenske and Prof. Dr. E. Niecke is gratefully acknowledged.

[1] [1a] J. J. Eisch, in *Comprehensive Organometallic Chemistry*, 2nd ed. (Eds.: I. Abel, F. G. A Stone, G. Wilkinson), Pergamon Press, Oxford, U.K., **1995**, Vol. 1, pp 431−502.[1b] J. J. Eisch, in *Comprehensive Organometallic Chemistry*, 2nd ed (Eds.: I. Abel, F. G. A Stone, G. Wilkinson), Pergamon Press, Oxford, U.K., **1995**, Vol. 11, pp 277−311, and references therein.[1c] W. S. Rees, Jr., in *CVD of Nonmetals*, VCH, Weinheim, **1996**.[1d] A. C. Jones, P. O'Brian, in *CVD of Compound Semiconductors: Precursor Synthesis, Development and Applications*, VCH, Weinheim, **1997**.

[2] G. J. P. Britovsek, V. C. Gibson, D. F. Wass, *Angew. Chem.* **1999**, *111*, 448−468; *Angew. Chem. Int. Ed.* **1999**, *38*, 428−447, and references therein.

[3] M. P. Coles, R. F. Jordan, *J. Am. Chem. Soc.* **1997**, *119*, 8125−8126.

[4] S. L. Aeilts, M. P. Coles, D. C. Swenson, R. F. Jordan, *Organometallics* **1998**, *7*, 3265−3270.

[5] H. V. R. Dias, W. Jin, R. E. Ratcliff, *Inorg. Chem.* **1995**, *34*, 6100−6105.

[6] E. Ihara, V. G. Young, R. F. Jordan, *J. Am. Chem. Soc.* **1998**, *120*, 8277−8278.

[7] C. E. Radzewich, M. P. Coles, R. F. Jordan, *J. Am. Chem. Soc.* **1998**, *120*, 9384−9385.

[8] P. W. Roesky, *Inorg. Chem.* **1998**, *37*, 4507−4511.

[9] P. W. Roesky, M. R. Bürgstein, *Inorg. Chem.* **1999**, *38*, 5629−5632.

[10] P. W. Roesky, *J. Organomet. Chem.* in press.

[11] M. R. Bürgstein, N. P. Euringer, P. W. Roesky, *Dalton. Trans.* **2000**, 1045−1048.

[12] P. Wei, T. Keizer, D. A. Atwood, *Inorg. Chem.* **1997**, *36*, 4060−4065.

[13] P. Wei, T. Keizer, D. A. Atwood, *Inorg. Chem.* **1999**, *38*, 3914−3918.

[14] D. A. Atwood, J. A. Jegier, M. P. Remington, D. Rutherford, *Aust. J. Chem.* **1996**, *49*, 1333−1338.

[15] M. S. Hill, P. Wei, D. A. Atwood, *Polyhedron* **1998**, *17*, 811−819.

[16] T. Wartik, H. I. Schlesinger, *J. Am. Chem. Soc*. **1953**, *75*, 835−839.

[17] K. Ziegler, H. G. Gellert, H. Lehmkuhl, W. Pfohl, K. Zosel, *Liebigs Ann. Chem*. **1960**, *629*, 1−13.

[18] G. M. Sheldrick SHELXS-97, Program for Structure Solution: *Acta Crystallogr. Sect. A* **1990**, *46*, 467−473.

[19] G. M. Sheldrick SHELXL-97, Program for Crystal Structure Refinement, Universität Göttingen, **1997**.

Received December 20, 1999
[I99468]

Fe^{III}-Hydroperoxo and Peroxo Complexes with Aminopyridyl Ligands and the Resonance Raman Spectroscopic Identification of the Fe−O and O−O Stretching Modes

A. Jalila Simaan,[a] Susanne Döpner,[b] Frédéric Banse,[a] Sophie Bourcier,[c] Guy Bouchoux,[c] Alain Boussac,[d] Peter Hildebrandt,*[b] and Jean-Jacques Girerd*[a]

Keywords: Iron / Peroxides / Nonheme iron models / Raman spectroscopy

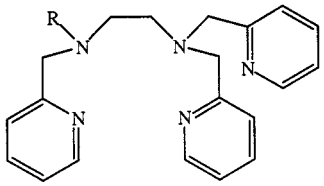
Nonheme Fe^{III}-hydroperoxo and Fe^{III}-peroxo complexes with aminopyridyl-type ligands have been prepared and characterized by UV/Vis, EPR, mass and Resonance Raman (RR) spectroscopy. The $Fe^{III}(OOH)$ species are low-spin and exhibit a deep purple color due to the ligand-to-metal charge transfer (LMCT) band centered at ca. 550 nm. The RR spectra of the $Fe^{III}(OOH)$ complexes display two bands at ca. 620 and 800 cm^{-1} that are assigned to the respective Fe–O and O–O stretching modes on the basis of the characteristic H/D and $^{16}O/^{18}O$ frequency shifts. Upon deprotonation, $Fe^{III}(O_2)$ species are obtained which possess a high-spin configuration of nearly axial symmetry and a LMCT transition in the near infrared (ca. 750 nm). The frequencies of the Fe–O and O–O stretching modes at ca. 465 and 820 cm^{-1}, as well as their respective $^{16}O/^{18}O$ shifts of –16 and –45 cm^{-1}, indicate an η^2 coordination geometry for the $Fe^{III}(O_2)$ complex.

Introduction

The currently proposed mechanism for catalytic oxygenation by cytochrome P450 involves an Fe^{III}-peroxo intermediate that leads, upon protonation, to a ferryl species which is able to insert an oxygen atom into a C−H bond.[1] Whereas the Fe^{III}-peroxo species has been observed during the enzymatic reaction cycle, identification of the ferryl species has not yet been possible due to its high reactivity.[2] For nonheme systems such as bleomycin,[3] a ferryl species may also be implied, although in this case experimental proof has not yet been presented either. Specifically, the intermediate state denoted as "activated bleomycin" has been recently shown to be $(BLM)Fe^{III}(OOH)$.[4] In order to understand the reactivity of such nonheme hydroperoxoiron species, several chemical models have been prepared and studied.[5−14]

A well-known example of a nonheme Fe^{III}-peroxo complex is $[(EDTA)Fe^{III}(O_2)]^{3-}$.[15,16] Spectroscopic studies demonstrated a side-on coordination of the peroxo group in this complex. We recently reported the formation of a new type of nonheme Fe^{III}-peroxo complex using the ligand [*N*-methyl-*N*,*N*′,*N*′-tris(2-pyridylmethyl)ethane-1,2-diamine] (trispicMeen).[17] This Fe^{III}-peroxo species was obtained by deprotonation of the Fe^{III}-hydroperoxo complex.[8,11] Analogous species were obtained by Jensen et al.[14] RR spectroscopic studies by Ho et al.[18] indicated an η^2-coordination of the peroxo group in $[(N4py)Fe^{III}(O_2)]^+$.

The present study is dedicated to the RR spectroscopic characterization of the hydroperoxo and peroxo species of Fe^{III} complexes formed with trispicMeen as well as of the corresponding Fe^{III} complexes involving the ligands [*N*,*N*′,*N*′-tris(2-pyridylmethyl)ethane-1,2-diamine] (trispicen) and [*N*,*N*,*N*′,*N*′-tetrakis(2-pyridylmethyl)ethane-1,2-diamine] (TPEN) (Scheme 1).



R = H trispicen
R = Me trispicMeen
R = CH_2Py TPEN

Scheme 1. Ligands used in this study

Results and Discussion

The starting materials for preparing the hydroperoxo and peroxo species are Fe^{II} complexes. For the complex with the trispicMeen ligand, [(trispicMeen)FeCl]Cl was used as starting material.[17] The structure of the related species

[a] Laboratoire de Chimie Inorganique, UMR CNRS 8613, Université Paris-Sud, 91405 Orsay, France
[b] Max-Planck-Institut für Strahlenchemie, D-45470 Mülheim/Ruhr, Germany
[c] Laboratoire des Mécanismes Réactionnels, UMR CNRS 7651, Ecole Polytechnique, 91128 Palaiseau, France
[d] Section de Bioénergétique, URA CNRS 2096, CEA Saclay, 91191 Gif-sur-Yvette, France

 © WILEY-VCH Verlag GmbH, D-69451 Weinheim, 2000 1434−1948/00/0707−1627 $ 17.50+.50/0

[(trispicMeen)FeCl]BPh_4 has been recently determined.[11] For the complexes with the ligand trispicen, [(trispicen)-FeCl]PF_6 served as starting material. In the case of the TPEN ligand, the parent complex was prepared in THF and isolated as a yellow powder, the analysis of which corresponds to [(TPEN)Fe]$Cl_2 \cdot 0.5H_2O$. The yellow color and the magnetic susceptibility, measured as a function of temperature,[19] demonstrate a ferrous high-spin state which may be indicative of the coordination of chloride to Fe^{II}, i.e. [(TPEN)FeCl]$Cl \cdot 0.5H_2O$. In MeOH, an orange color was obtained and the UV/Vis spectrum was identical to that of [(TPEN)Fe]$(ClO_4)_2$ in the same solvent, suggesting dissociation of the chloride ligand in solution to give the $[(TPEN)Fe]^{2+}$ complex. The structure of [(TPEN)-Fe]$(ClO_4)_2$ has been previously published.[20]

UV/Visible Absorption Spectroscopy

The species containing the $Fe^{III}OOH$ unit absorb around 550 nm (Table 1) as already reported for [(trispicMeen)-$Fe(OOH)]^{2+}$.[8] Upon deprotonation, [(trispicMeen)Fe-$(O_2)]^+$ is formed which gives an absorption band at much lower energy (740 nm, Table 1).[14,17] The same observations were made for the corresponding transformation of $[(TPEN)Fe(OOH)]^{2+}$ to $[(TPEN)Fe(O_2)]^+$ (Figure 1). These bands are attributed to LMCT transitions from the HO_2^- or O_2^{2-} groups to Fe^{III}.

Table 1. Characteristics of the LMCT band in MeOH for the different complexes

Complex	λ_{max} (ε/м$^{-1}$.cm^{-1})	ref.
Hydroperoxo		
$[(trispicMeen)Fe(OOH)]^{2+}$	537 nm (1000)	[8][11]
$[(trispicen)Fe(OOH)]^{2+}$	531 nm (950)	this work
$[(TPEN)Fe(OOH)]^{2+}$	541 nm (900)	this work
Peroxo		
$[(trispicMeen)Fe(O_2)]^+$	740 nm (500)	[17]
$[(TPEN)Fe(O_2)]^+$	755 nm (450)	this work

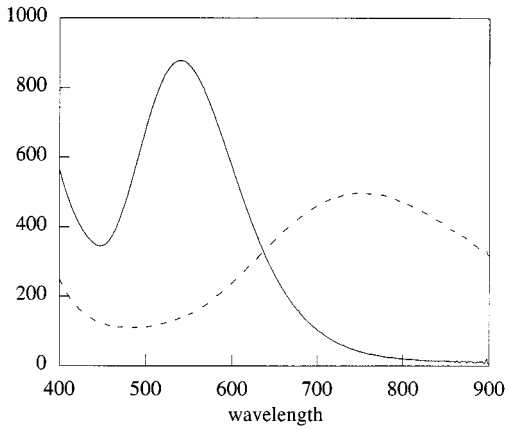


Figure 1. UV/Vis spectra of $[(TPEN)Fe^{III}(OOH)]^{2+}$ (1 мм in MeOH, 100 equiv. of H_2O_2) before ( ) and after addition of three equiv. of NEt_3 (− − −) measured at ambient temperature; the bands at 541 nm and 755 nm are attributed to the LMCT transitions of $[(TPEN)Fe^{III}(OOH)]^{2+}$ and $[(TPEN)Fe^{III}(O_2)]^+$, respectively

The formation of the purple complex [(trispicen)-$Fe(OOH)]^{2+}$ in MeOH was monitored by UV/Vis spectroscopy. Upon addition of base, the purple color disappeared although we failed to trap the putative $[(trispicen)Fe(O_2)]^+$ species.

EPR Spectroscopy

The $Fe^{III}OOH$ species display EPR spectra that are typical for ferric low-spin (LS) states. At 100 K, the g values of $[(trispicen)Fe(OOH)]^{2+}$ and $[(trispicMeen)Fe(OOH)]^{2+}$ were observed at 2.19, 2.14, 1.96 and at 2.19, 2.12, 1.95, respectively.[8,11] For $[(TPEN)Fe(OOH)]^{2+}$, we have found resonances at 2.22, 2.15, 1.967 (Figure 2).

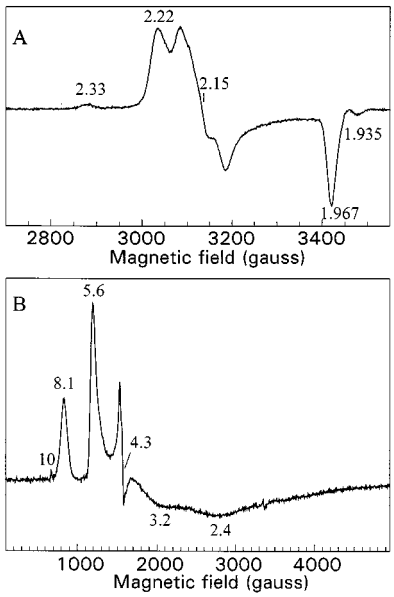
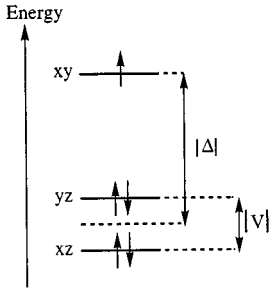


Figure 2. A: EPR spectrum of $[(TPEN)Fe^{III}(OOH)]^{2+}$ in MeOH measured at 15 K; B: EPR spectrum of $[(TPEN)Fe^{III}(OOH)]^{2+}$ in MeOH at 4 K in the presence of three equivalents of NEt_3; the signal at $g = 4.3$ corresponds to a degradation product

It is possible to describe the g values for a LS Fe^{III} by using the model of Griffith[21] as presented by Taylor,[22] which takes into account the spin-orbit coupling and distortion from octahedral geometry. These effects lift the six-fold degeneracy of the $^2T_{2g}$ ground state and three well-separated Kramers doublets are obtained. This corresponds to a lifting of the orbital degeneracy, as indicated in Scheme 2, where the rhombic and axial distortion energies are denoted by V and Δ, respectively.



Scheme 2. Splitting of the T_{2g} orbitals due to distorsions

Table 2. EPR g_{max}, g_{inter}, g_{min} values for $Fe^{III}OOH$ $s = 1/2$ units; parameters of the Griffith−Taylor model of the g tensor: *a, b, c* are the coefficients of the wavefunctions; $\Sigma = a^2 + b^2 + c^2$; V is the rhombic distorsion energy; Δ is the axial distorsion energy; both are in units of λ, the spin-orbit coupling constant

complex	$-g_{min}$, g_z	g_{max}, g_y	$-g_{inter}$, g_x	*a*	*b*	*c*	Σ	V/λ	Δ/λ
(BLM)Fe(OOH)	−1.94	2.26	−2.17	0.072	0.052	0.993	0.993	3.04	−8.74
$[(trispicMeen)Fe(OOH)]^{2+}$	−1.95	2.19	−2.12	0.055	0.039	0.992	0.988	4.05	−11.31
$[(trispicen)Fe(OOH)]^{2+}$	−1.96	2.19	−2.14	0.053	0.041	0.994	0.993	2.86	−11.19
$[(TPEN)Fe(OOH)]^{2+}$	−1.967	2.22	−2.15	0.056	0.040	0.999	1.002	3.98	−11.29

At 100 K, only the lowest doublet is populated. The two wave functions of the ground Kramers doublet are written as:

$$|+> = a\,|\xi\alpha> - i\,b\,|\eta\alpha> - c\,|\zeta\beta> \quad (1)$$

$$|-> = -a\,|\xi\beta> - i\,b\,|\eta\beta> - c\,|\zeta\alpha> \quad (2)$$

where $|\xi\alpha>$, $|\eta\alpha>$, $|\zeta\beta>$ refer to the states with the unpaired electron in the d_{yz}, d_{xz}, and d_{xy} orbital, respectively. The associated g values are given by:[22]

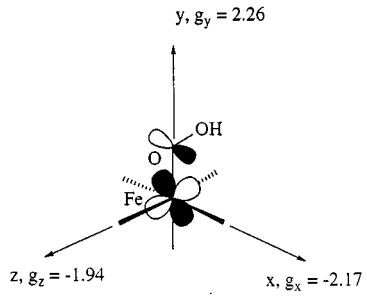
$$g_z = 2[(a + b)^2 - c^2] \quad (3)$$

$$g_y = 2[(a + c)^2 - b^2] \quad (4)$$

$$g_x = 2[a^2 - (b + c)^2] \quad (5)$$

These equations were used to evaluate the constants a, b, and c assuming that $g_x\,g_y\,g_z$ is positive. This assumption, originally suggested by Veselov et al.,[23] appears to be justified in view of the chemical meaning of the results. The a, b and c values were calculated from the experimental g values. As described by Taylor[22] we selected the axes such that $|V| < (2/3)\,|\Delta|$. The results are presented in Table 2.

For $(BLM)Fe^{III}OOH$, values of $g_z = -1.94$, $g_y = 2.26$, and $g_x = -2.17$ were found corresponding to $a = 0.072$, $b = 0.052$, and $c = 0.993$ with $V/\lambda = 3.04$ and $\Delta/\lambda = -8.74$. These values imply that the hole (and hence the unpaired electron) is in an orbital which has predominantly d_{xy} character, and that this orbital is strongly destabilized. The d_{xz} and d_{yz} orbitals would be lower in energy, with the d_{xz} being the lowest. Based on an ENDOR study of activated bleomycin, Veselov et al.[23] suggested, by comparison with LS hemes, that the axis of g_{max} (y from the calculation above) is perpendicular to the conjugated pyrimidine plane and parallel to the Fe-peroxo axis. This conclusion is not in contradiction with the above discussion and leads to the following proposal for the orientation of the g tensor (Scheme 3).



Scheme 3. Nature of the singly occupied T_{2g} orbital and orientation of the g tensor

The values for $[(trispicMeen)Fe(OOH)]^{2+}$ are similar to those of $(BLM)Fe^{III}OOH$ with $g_z = -1.95$, $g_y = 2.19$, $g_x = -2.12$, $a = 0.055$, $b = 0.039$, $c = 0.992$, $V/\lambda = 4.05$, $\Delta/\lambda = -11.31$. Thus, in analogy to bleomycin, it is concluded that in this model complex the unpaired electron is also in a d_{xy} type orbital. Note that the axial perturbation is stronger in the model complexes than in the activated bleomycin. This different behavior may be due to the stronger π-acceptor capability of the ligand in the model complexes so that the interaction between the d_{xy} type orbital and the π* orbital of OOH becomes stronger.

The $Fe^{III}-O_2$ species are high spin ($S = 5/2$) with resonances at $g = 7.5$ and 5.9 as determined for $[(trispicMeen)Fe(O_2)]^+$.[17] The $g = 7.5$ signal can be interpreted as arising from the upper Kramers doublet with $E/D = 0.08$ for $D < 0$, whereas the $g = 5.9$ signal may arise from the intermediate Kramers doublet.[17] The complex $[(TPEN)Fe(O_2)]^+$ displays resonances at $g = 10$, 8.1, 5.6, 3.2, 2.4 (Figure 2). These signals are due to the different Kramers doublets with $E/D = 0.10$ for $D < 0$. The $g = 10$ signal is tentatively assigned to the ground doublet whereas the signals at $g = 5.6$ and $g = 2.4$ may originate from the intermediate doublet. The $g = 8.1$ and $g = 3.2$ may then be attributed to the upper doublet. These findings suggest that $[(trispicMeen)Fe(O_2)]^+$ and $[(TPEN)Fe(O_2)]^+$ have similar structures.

Mass Spectrometry

$[(TrispicMeen)Fe(OOH)]^{2+}$ and $[(trispicMeen)Fe(O_2)]^+$ have been detected by Electrospray Ioniation Mass Spectrometry.[11,17] After addition of three equivalents of Et_3N to a purple 10^{-3} M solution of $[(TPEN)Fe(OOH)]^{2+}$ in methanol, the ESI-MS spectrum (Figure 3) exhibits a major peak at $m/z = 512.3$ which can be attributed to $[(TPEN)Fe^{III}(O_2)]^+$. Among the other peaks detected, those at $m/z = 425.3$ and 542.3 are assigned to $(TPENH^+)$ and $([(TPEN)Fe^{III}(OMe)_2]^+)$, respectively. The peak at $m/z = 512.3$ disappears after 10 min, which parallels the disappearance of the blue color of the solution.

Resonance Raman Spectroscopy

Excitation in resonance with the LMCT transitions should provide a preferential enhancement of the vibrational modes originating from the iron-(hydro)peroxo entities, which is indeed confirmed by the present experiments. The RR spectra of the hydroperoxo complexes were recorded with excitation at 568 nm. The spectral regions be-

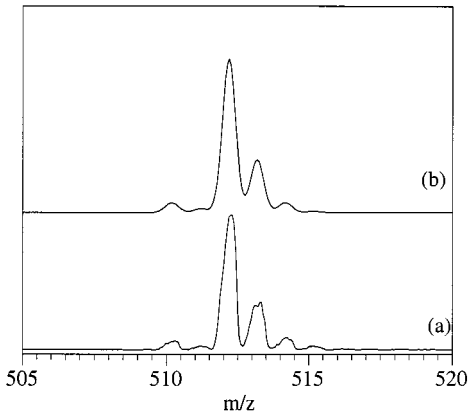


Figure 3. EI-MS features of $[(TPEN)Fe^{III}(O_2)]^+$ at m/z = 512.3: a) experimental spectrum; b) calculated spectrum

tween 570 and 640 cm^{-1} and 710 and 880 cm^{-1}, which are expected to include the iron−oxygen and oxygen−oxygen stretching modes, respectively, are shown in Figure 4 for the $[(trispicMeen)Fe(OOH)]^{2+}$ complex. The former region displays two bands at 617 cm^{-1} and 632 cm^{-1} that are possible candidates for the Fe−O stretching. The 617 and 632 cm^{-1} bands are not detected in the spectrum of the parent state, i.e. prior to the addition of H_2O_2, implying that both bands originate from the $[(trispicMeen)Fe(OOH)]^{2+}$ complex or derivatives thereof. The dominant band at 617 cm^{-1} shifts to lower wavenumbers 613 and 600 cm^{-1} upon H/D exchange and ^{18}O-labeling, respectively (Table 3). These shifts are consistent with the calculated values obtained from a simple two-body oscillator model for the Fe−OOH moiety of the presumed hydroperoxo complex.

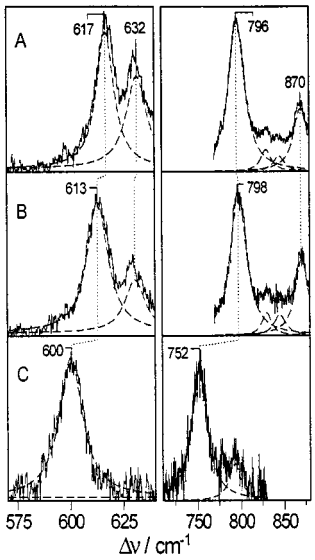


Figure 4. RR spectra of $[(trispicMeen)Fe(OOH)]^{2+}$ obtained with 568 nm excitation. (A) natural abundance, complex prepared with H_2O_2; (B) deuterated, complex prepared with D_2O_2; (C) ^{18}O-labeled, complex prepared with $H_2{}^{18}O_2$; the regions of the iron−oxygen and oxygen−oxygen stretching modes are displayed in the left and right panels, respectively; the dotted lines represent the fitted Lorentzian bandshapes.

Therefore, the band at 617 cm^{-1} is assigned to the Fe−O stretching mode of the $[(trispicMeen)Fe(OOH)]^{2+}$ complex. The second band in this region at 632 cm^{-1} remains essentially unchanged upon deuteration. The intensity of this band relative to the 617 cm^{-1} band reveals some variations in the different samples and, moreover, increases with time along with the decomposition of $[(trispicMeen)Fe(OOH)]^{2+}$. Samples which have been measured four hours after complex preparation show a broad band centered at ca. 630 cm^{-1} whereas no band can be detected at 617 cm^{-1}. We therefore attribute the band at 632 cm^{-1} to a degradation product of $[(trispicMeen)Fe(OOH)]^{2+}$. Note that this band is hardly detectable in the ^{18}O-labeled complex, which may be due to a relatively small contribution of this degradation product in the sample. The Fe−O frequency at 617 cm^{-1} is in agreement with the value found by Que and co-workers for $[(N4py)Fe(OOH)]^{2+}$ and $[(TPA)Fe(OOH)]^{2+}$.[12,13]

The O−O stretching mode is expected between ca. 770 and 850 cm^{-1}.[12,13] This part of the spectrum also includes a band at 870 cm^{-1} originating from the O−O stretching mode of H_2O_2 (Figure 4). In the deuterated solvent, this band reveals a small shift of 1 cm^{-1} as previously noted.[15] The strongest band in this region, at 796 cm^{-1}, is unambiguously assigned to the O−O stretching mode of $[(trispicMeen)Fe(OOH)]^{2+}$ since it shifts to lower wavenumber (752 cm^{-1}) in the ^{18}O-labeled sample (Table 3), which confirms the predictions for a hydroperoxo complex. Upon H/D exchange this mode reveals a similar shift to that for H_2O_2.[15]

The complex $[(TPEN)Fe(OOH)]^{2+}$ shows essentially the same RR spectra as $[(trispicMeen)Fe(OOH)]^{2+}$ (Figure 5) with nearly identical frequencies for the Fe−O and O−O stretching modes (Table 3). These similarities with $[(trispicMeen)Fe(OOH)]^{2+}$ indicate that the additional pyridyl arm of the TPEN ligand is not involved in the coordination to iron. In contrast, in the RR spectrum of $[(trispicen)Fe(OOH)]^{2+}$ both the Fe−O and the O−O modes are observed at higher frequencies than in $[(trispicMeen)Fe(OOH)]^{2+}$ and $[(TPEN)Fe(OOH)]^{2+}$ (Table 3). Furthermore, the isotopic shifts are also larger. These differences could be related to a different geometry of the FeOOH unit in $[(trispicen)Fe(OOH)]^{2+}$ as a consequence of the reduced steric hindrance upon replacement of the tertiary amino group by a secondary amino group (i.e. R = H vs. R = CH_2py in Scheme 4).

For the investigation of the blue peroxo complexes, excitation at 647 nm, albeit not in rigorous resonance with the LMCT transition, provides a preferential enhancement of the modes associated with the iron peroxo group. In the O−O stretching region, the RR spectrum of $[(trispicMeen)Fe(O_2)]^+$ displays a new band at ca. 819 cm^{-1} which shifts down to 776 cm^{-1} in the ^{18}O-labeled complex but remains unchanged upon H/D exchange so that it is unambiguously assigned to the O−O stretching mode (Figure 6). A careful inspection reveals an asymmetric shape of the 819 cm^{-1} band both in nondeuterated and deuterated solvents but not of the 776 cm^{-1} band of the ^{18}O-labeled species. A band-fitting analysis of the 819 cm^{-1} peak affords a strong band at 819 and a weaker one at 827 cm^{-1}

Table 3. Frequencies of the iron−oxygen and oxygen−oxygen modes of the various iron hydroperoxo and iron peroxo complexes; the accuracies of the frequencies (given in cm^{-1}) are ca. 0.3 cm^{-1} for the hydroperoxo species and ca. 1.0 cm^{-1} for the individual band components of the composite peaks in the peroxo complexes; the abbreviations H/D and $^{16}O/^{18}O$ denote the H/D and $^{16}O/^{18}O$ isotopic shifts

Complex	ν_{Fe-O}	ΔH/D	$\Delta^{16}O/^{18}O$	ν_{O-O}	ΔH/D	$\Delta^{16}O/^{18}O$
Hydroperoxo						
$[(trispicMeen)Fe(OOH)]^{2+}$	617.2	−4.1	−17.0	796.4	+1.2	−44.7
$[(TPEN)Fe(OOH)]^{2+}$	617.2	−3.7	n.d.[a]	795.9	+2.0	n.d.[a]
$[(trispicen)Fe(OOH)]^{2+}$	624.8	−7.1	−22.6	800.7	+0.2	−50.5
Peroxo						
$[(trispicMeen)Fe(O_2)]^{+}$	470	0.0	−16	819	−	−
	−	−	−	−	0.0	−45[b]
	−	−	−	827	−	−
$[(TPEN)Fe(O_2)]^{+}$	470	n.d.[a]	n.d.[a]	817	−	−
	−	−	−	−	n.d.[a]	n.d.[a]
	−	−	−	824	−	−

[a] n.d.: not determined. − [b] The $^{16}O/^{18}O$ shifts refer to shifts of the peak maxima.

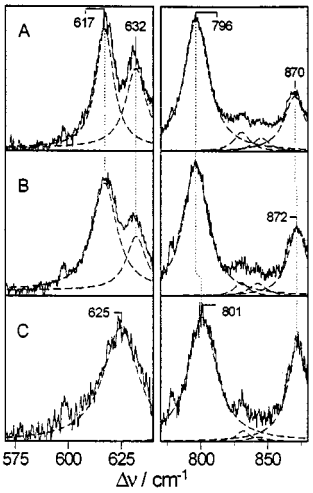
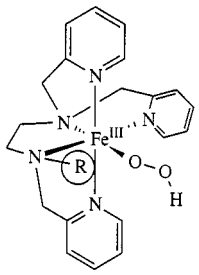


Figure 5. RR spectra of $[(trispicMeen)Fe(OOH)]^{2+}$, $[(TPEN)Fe(OOH)]^{2+}$ and $[(trispicen)Fe(OOH)]^{2+}$ obtained with excitation at 568 nm; the regions of the iron-oxygen and oxygen-oxygen stretching modes are displayed in the left and right panels, respectively; the dotted lines represent the fitted Lorentzian bandshapes



Scheme 4. Proposed structure for the FeOOH complex indicating the possible steric hindrance between the alkyl substituent and the hydroperoxo group

(Table 3). These band components are also found in the $[(TPEN)Fe(O_2)]^{+}$ complex, albeit with slightly different frequencies and relative intensities (Figure 7).

A comparable heterogeneity is observed for the iron−oxygen stretching of $[(trispicMeen)Fe(O_2)]^{+}$ and $[(TPEN)Fe(O_2)]^{+}$ which is attributable to the composite bands centered at 470 cm^{-1} (Figure 6). These bands are not affected by H/D exchange but shift to lower wavenumber by ca. 16 cm^{-1} in the ^{18}O-labeled complex. The relatively

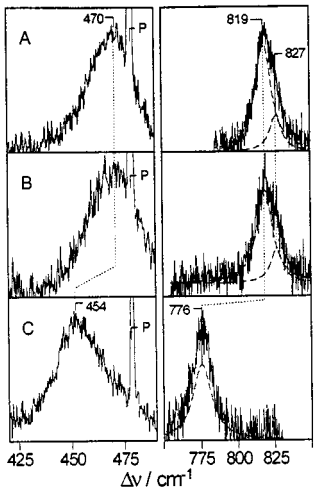


Figure 6. RR spectra of $[(trispicMeen)Fe(O_2)]^{+}$ obtained with excitation at 647 nm: (A) natural abundance, complex prepared with H_2O_2; (B) deuterated, complex prepared with D_2O_2; (C) ^{18}O-labeled, complex prepared with $H_2{}^{18}O_2$; the regions of the iron-oxygen and oxygen-oxygen stretching modes are displayed in the left and right panels, respectively; the dotted lines represent the fitted Lorentzian bandshapes; the sharp peak labeled P originates from a plasma line of the laser

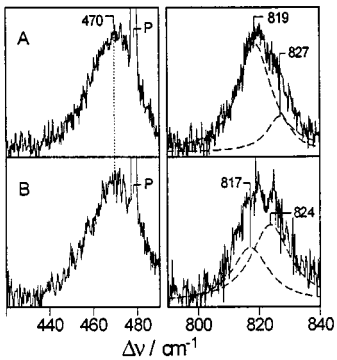


Figure 7. RR spectra of $[(trispicMeen)Fe(O_2)]^{+}$ and $[(TPEN)Fe(O_2)]^{+}$ obtained with excitation at 647 nm; the regions of the iron−oxygen and oxygen−oxygen stretching modes are displayed in the left and right panels, respectively; the dotted lines represent the fitted Lorentzian bandshapes; the sharp peak labelled P originates from a plasma line of the laser

low frequencies of the Fe−O stretches are related to the spin configuration in the peroxo complexes. Whereas the LS configuration in the hydroperoxo complexes allows for the formation of a relatively strong Fe−O bond corresponding to a high Fe−O stretching frequency, the HS configuration of the peroxo complexes leads to a weakening of the Fe−O bond which is reflected by the substantially lower Fe−O stretching frequency.[13]

Both the Fe−O and O−O stretching frequencies and their $^{18}O/^{16}O$ shifts indicate a side-on structure of the iron-peroxo moiety, in agreement with previous findings for Fe^{III} peroxo complexes ligated by EDTA and N4py.[15,16,18] The coexistence of two closely spaced O−O stretching modes, as well as the asymmetric profile of the Fe−O stretching peak, may indicate two conformers which subtly differ in structural details.

Conclusion

All Fe^{III} compounds studied in this work form LS hydroperoxo complexes. Whereas the trispicMeen and TPEN derivatives reveal very similar spectroscopic properties, $[(trispicen)Fe(OOH)]^{2+}$ exhibits somewhat higher Fe−O and O−O stretching frequencies, indicating slightly different molecular structures. This compound evidently also displays a different reactivity since no peroxo complex could be detected at room temperature. It may be that the lifetime of this species is too short due to the sensitivity to oxidation of the secondary amine NH group of the trispicen ligand. In the peroxo complexes of the other compounds, the Fe^{III} adopts an HS configuration. However, the anisotropy of this $S = 5/2$ state depends on the auxiliary ligand. Whereas complexes with N4py and EDTA ligands lead to a rhombic state, a more axial state is found for the Fe^{III}-peroxo complexes formed with trispicMeen and TPEN ligands. Regardless of these differences, the present RR spectroscopic data indicate an η^2-coordination of the peroxo groups in the trispicMeen and TPEN complexes as well, implying that side-on coordination represents a structural motif that is largely independent of the type of auxiliary ligand.

Experimental Section

General: All manipulations were carried out using standard Schlenk techniques. Starting materials were purchased from Acros. Solvents were purchased from Merck and used without further purification. $^{18}O_2H_2$ was provided as a 2% aqueous solution from Leman. − UV/Vis: Varian Cary 5E equipped with a temperature controller. − MS: Quattro II (Micromass, Manchester, UK) triple quadrupole electrospray mass spectrometer. Typical optimized values for the source parameters were: capillary: 2.5 kV, counter electrode: 0.4 kV, cone voltage: 15 to 30 V, source temperature: 80 °C, RF lens: 0.7 V, skimmer lens offset: 5 V. − EPR spectra were recorded on a Bruker ESP 300 E spectrometer. For low-temperature studies, an Oxford Instruments continuous-flow helium cryostat and a temperature control system were used. Magnetic susceptibility measurements in the 10−300 K temperature range were carried out with a MPMS5 SQUID susceptometer (Quantum Design Inc.). The calibration was made at 298 K using a palladium reference sample furnished by Quantum Design Inc.

RR Measurements: RR experiments were carried out at ambient temperature using an U1000 spectrograph (ISA) equipped with 1200 lines/mm gratings and a liquid-nitrogen cooled CCD camera. The spectral bandwidth was 2.8 cm^{-1} and the increment per data point was ca. 0.2 cm^{-1}. The wavenumber stability of the monochromator was 0.1 cm^{-1}. The 568- and 647-nm lines of a Kr^+ laser, with a power 25 and 50 mW, respectively, at the sample were used for excitation. Further details of the experimental set-up are given elsewhere.[24] The samples with concentrations corresponding to an optical density of 1.4 at the excitation wavelength were prepared directly prior to the experiments. RR measurements were carried out by using a rotating cuvette to avoid photodecomposition. Under these conditions the samples were stable for ca. 30 min (Fe−O−O−H) and 10 min (Fe−O−O). The integrity of samples during the RR experiments was checked by comparing the consecutively measured RR spectra obtained with an integration time of 1 s. For improvement of the signal-to-noise ratio, the individual spectra were finally combined. The sum spectra obtained in this way represent measurements of a total accumulation time of between 10 and 40 s. After removal of the structureless background by polynomial subtraction, the spectra were analyzed by a band-fitting procedure using Lorentzian lineshapes.[25]

Synthesis of the Ligands: The trispicen, trispicMeen, and TPEN ligands were prepared according to previously described procedures.[8,11,20]

Syntheses of the Complexes: The complexes $[(TPEN)Fe](PF_6)_2$, $[(TPEN)Fe](ClO_4)_2$, $[(trispicMeen)FeCl]PF_6$ and [(trispicMeen)-FeCl]Cl were prepared as previously described.[8,17,20]

Synthesis of the Complex $[(TPEN)Fe]Cl_2 \cdot 0.5H_2O$: A solution of $FeCl_2 \cdot 4H_2O$ (0.49 mmol) in dry THF under argon was added to a solution of TPEN (0.51 mmol) in dry THF. The immediate yellow precipitate was collected by filtration (yield = 80%). − ESI MS: m/z = 240.2 $[\{(TPEN)Fe\}^{2+}]$, 515.1 $[\{(TPEN)FeCl\}^{+}]$ − UV/Vis (MeOH, 300 K): λ_{max} = 417 nm (ε = 10500 $M^{-1}.cm^{-1}$) − $C_{26}H_{28}Cl_2FeN_6 \cdot 0.5H_2O$ (560.31): calcd. C 55.73, H 5.22, N 15.0; found C 55.76, H 5.16, N 14.39.

Synthesis of the Complex $[(trispicen)FeCl]PF_6$: A solution of $FeCl_2 \cdot 4H_2O$ (0.30 mmol) in ethanol was added to a solution of trispicen (0.31 mmol) in ethanol. A yellow powder was obtained after addition of NH_4PF_6 (0.31 mmol) and collected by filtration (yield = 56%). − UV/Vis (MeOH, 300 K): λ_{max} = 395 nm (ε = 1900 $M^{-1}.cm^{-1}$).

[1] M. Sono, M. P. Roach, E. D. Coulter, J. H. Dawson, *Chem. Rev.* **1996**, *96*, 2841−2887.
[2] D. E. Benson, K. S. Suslick, S. G. Sligar, *Biochemistry* **1997**, *36*, 5104−5107.
[3] J. Stubbe, J. W. Kozarich, W. Du, D. E. Vanderwall, *Acc. Chem. Res.* **1996**, *29*, 322−330.
[4] J. W. Sam, X. J. Tang, J. Peisach, *J. Am. Chem. Soc.* **1994**, *116*, 5250−5256.
[5] C. Nguyen, R. J. Guajardo, P. K. Mascharak, *Inorg. Chem.* **1996**, *35*, 6273−6281.
[6] I. Lippai, R. S. Magliozzo, J. Peisach, *J. Am. Chem. Soc.* **1999**, *121*, 780−784.
[7] M. Lubben, A. Meetsma, E. C. Wilkinson, B. Feringa, L. Que, Jr, *Angew. Chem. Int. Ed. Engl.* **1995**, *34*, 1512−1514.
[8] I. Bernal, I. M. Jensen, K. B. Jensen, C. J. McKenzie, H. Toftlund, J. P. Tuchagues, *J. Chem. Soc., Dalton Trans.* **1995**, 3667−3675.

[9] C. Kim, K. Chen, J. Kim, L. Que, Jr, *J. Am. Chem. Soc.* **1997,** *119*, 5964−5965.
[10] M. E. de Vries, R. M. La Crois, G. Roelfes, H. Kooijman, A. L. Spek, R. Hage, B. L. Feringa, *Chem. Commun.* **1997**, 1549−1550.
[11] P. Mialane, A. Novorojkine, G. Pratviel, L. Azéma, M. Slany, F. Godde, A. J. Simaan, F. Banse, T. Kargar-Grisel, G. Bouchoux, J. Sainton, O. Horner, J. Guilhem, L. Tchertanova, B. Meunier, J. J. Girerd, *Inorg. Chem.* **1999**, *38*, 1085−1092.
[12] R. Y. N. Ho, G. Roelfes, B. L. Feringa, L. Que, Jr, *J. Am. Chem. Soc.* **1999**, *121*, 264−265.
[13] G. Roelfes, M. Lubben, K. Chen, R. Y. N. Ho, A. Meetsma, S. Genseberger, R. M. Hermant, R. Hage, S. K. Mandal, V. G. Young, Jr, Y. Zang, H. Kooijman, A. L. Spek, L. Que, Jr, B. L. Feringa, *Inorg. Chem.* **1999**, *38*, 1929−1936.
[14] K. B. Jensen, C. J. McKenzie, L. P. Nielsen, J. Z. Pedersen, H. M. Svendsen, *Chem. Commun.* **1999**, 1313−1314.
[15] S. Ahmad, J. D. McCallum, A. K. Shiemke, E. H. Appelman, T. M. Loehr, J. Sanders-Loehr, *Inorg. Chem.* **1988**, *27*, 2230−2233.
[16] F. Neese, E. I. Solomon, *J. Am. Chem. Soc.* **1998**, *120*, 12829−12848.
[17] A. J. Simaan, F. Banse, P. Mialane, A. Boussac, S. Un, T. Kargar-Grisel, G. Bouchoux, J. J. Girerd, *Eur. J. Inorg. Chem.* **1999**, 993−996.
[18] R. Y. N. Ho, G. Roelfes, R. Hermant, R. Hage, B. L. Feringa, L. Que, Jr, *Chem. Commun.* **1999**, 2161−2162.
[19] The magnetic susceptibility of a solid sample of [(TPEN)Fe]Cl_2 $0.5H_2O$ has been measured as a function of temperature . It clearly shows an $S = 2$ state from 300 K down to 10 K.
[20] H. R. Chang, J. K. McCusker, H. Toftlund, S. R. Wilson, A. X. Trautwein, H. Winkler, D. N. Hendrickson, *J. Am. Chem. Soc*. **1990**, *112*, 6814−6827.
[21] J. S. Griffith, *The Theory of Transition Metal Ions,* Cambridge University Press, London, **1961.**
[22] C. P. S. Taylor, *Biochim. Biophys. Acta* **1977**, *491*, 137−149.
[23] A. Veselov, H. Sun, A. Sienkiewicz, H Taylor, R. M. Burger, C. P. Scholes, *J. Am. Chem. Soc.* **1995**, *117*, 7508.
[24] H. Wackerbarth, U. Klar, W. Günther, P. Hildebrandt, *Applied Spectroscopy* **1999**, *53*, 283−291.
[25] S. Döpner, P. Hildebrandt, A. G. Mauk, H. Lenk, W. Stempfle, *Spectrochim. Acta* **1996**, *A51*, 573−584.

Received July 26, 1999
[I99276]

Structure, Equilibrium and Ribonuclease Activity of Copper(II) and Zinc(II) Complexes Formed with a Dinucleating Bis-Imidazole Ligand

Tamás Gajda,*[a,b] Roland Krämer,[b] and Attila Jancsó[a]

Keywords: Enzyme models / Hydrolyses / Phosphodiesters / Copper / Zinc

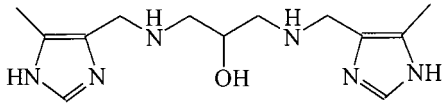
The syntheses, crystal structures, solution equilibria and ribonuclease activity are reported for copper(II) and zinc(II) complexes of a new potentially dinucleating, bis-imidazole ligand *N*,*N*′-bis(5-methylimidazol-4-ylmethyl)-1,3-diaminopropan-2-ol (**bimido**). The zinc(II) ion in [Zn(bimido)Cl]NO_3 is coordinated in a slightly distorted square pyramidal environment, with the four N atoms of bimido in the basal positions and the Cl^- ion in the axial one. The two copper(II) ions in $[Cu_2(bimido_{-1H})(DPP)(ClO_4)(CH_3OH)]ClO_4 \cdot 1/2\ H_2O$ (DPP = diphenyl phosphate) are bridged by the deprotonated alkoxo group of bimido and by the phosphate group of DPP in a 1,3-bridging mode. Depending on the [M]/[L] ratio, the ML and M_2L_{-2H} species are present in solution in the neutral pH range, having analogous structures as described above for the crystalline complexes. The zinc(II)-bimido (2/1) system, in a 65% EtOH-H_2O mixed solvent, shows an important increase of hydrolytic activity, parallel with the formation of the Zn_2L_{-2H} species, with a sigmoidal pH-rate profile modelling both steps of RNA hydrolysis. The k_{cat} value for the transesterification of 2-hydroxypropyl-*p*-nitrophenyl phosphate by Zn_2L_{-2H}, determined from saturation kinetic measurements (T = 298 K), corresponds to a maximum rate acceleration (k_{cat}/k_{uncat}) of ca. 10^4. The observed pseudo-first order rate constant for the hydrolysis of uridine 2′,3′-cyclic monophosphate, under nearly physiological conditions (T = 310 K, pH = 8, $[Zn_2L_{-2H}]$ = 3.6 mM, $k_{obs} = 2 \cdot 10^{-5}\ s^{-1}$) reflects a higher hydrolytic activity of Zn_2L_{-2H} towards this biologically relevant substrate (k_{obs}/k_{uncat} indicates ca. 10^4 fold rate acceleration). The proposed mechanisms include bifunctional Lewis-acid and general base catalysis.

Introduction

The fundamental role of the imidazole moiety in the active centre of a large number of metalloproteins is well established. During the past two decades a wide variety of imidazole-containing ligands have been investigated to mimic structural features of these enzymes, but less attention was devoted to functional mimicking. The presence of an imidazole moiety in the catalytic centres of enzymes is often related to hydrolytic reactions. Phosphoesterases are responsible for the hydrolysis of phosphate esters and are involved in a number of biological processes. Nucleases are an important class of these enzymes and are used in the repair and hydrolysis of DNA and RNA, as well as in viral defence (restriction enzymes).

Low molecular weight functional model complexes of phosphoesterases have attracted great interest due to their possible application in biotechnology, molecular biology and chemotherapy. A number of metalloenzymes that hydrolyse phosphate esters are activated by two or more cooperating metal ions.[1] The possible cooperative effect of the bimetallic core on the hydrolysis of phosphoesters has inspired a number of model studies dealing with dinuclear complexes.[2−14] Mechanistic features of some low molecular weight model complexes show notable similarities to the mechanism proposed for certain dinuclear phosphoesterases,[2] in particular the μ-1,3 bridging of the phosphoester substrate combined with nucleophilic attack of metal-bound hydroxide. Although important rate acceleration of phosphate ester hydrolysis has been demonstrated in many cases, only a few reflect on the catalytic centres of the native phosphoesterases, from both a structural and functional point of view.

As an extension of our study on coordination chemistry of the imidazole ring,[14−17] we report here the syntheses, crystal structures, solution equilibria and ribonuclease activity of copper(II) and zinc(II) complexes formed with a new multidentate, bis-imidazole ligand *N*,*N*′-bis(5-methylimidazol-4-ylmethyl)-1,3-diaminopropan-2-ol (bimido, Scheme 1).



Scheme 1. Schematic structure of bimido

Our aim was to design a dinucleating imidazole ligand which provides a relatively open coordination environment for the bound metal ions and an alkoxo-bridge which holds them relatively close to each other, allowing the metal-metal cooperation in the binding and the hydrolysis of phosphoesters. In the presence of an excess of metal ([Zn]/[L] = 2/1), the zinc(II)-bimido system was indeed found to be an

[a] Department of Inorganic and Analytical Chemistry, University of Szeged
6701 Szeged, P.O. Box 440, Hungary,
Fax: (internat.) +36/62-420-505,
E-mail: tamas.gajda@chem.u-szeged.hu
[b] Anorganisch-Chemisches Institut der Universität, Wilhelm-Klemm Straße 8, 48149 Münster, Germany
Supporting information for this article is available on the WWW under http://www.wiley-vch.de/home/eurjic or from the author.

 © WILEY-VCH Verlag GmbH, D-69451 Weinheim, 2000 1434−1948/00/0707−1635 $ 17.50+.50/0

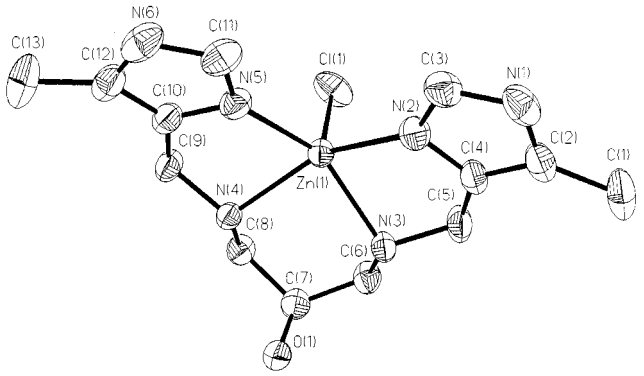


Figure 1. ORTEP view (50%) of **1** with the atom-labelling scheme. Hydrogen atoms and nitrate ions are omitted for clarity

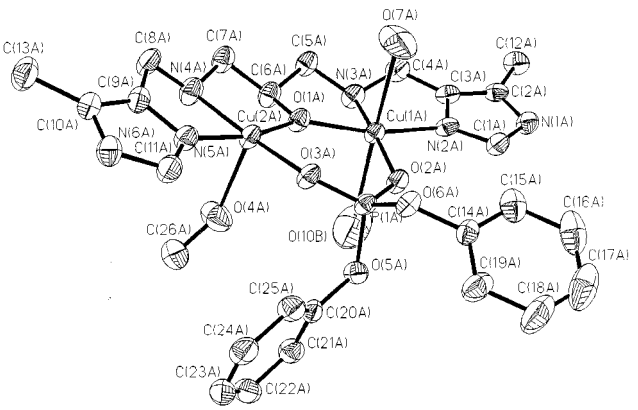


Figure 2. ORTEP view (30%) of **2** with the atom-labelling scheme. Hydrogen atoms and perchlorate ions (except of O(7A) and O(10B)) are omitted for clarity

efficient accelerator, modelling both steps of RNA hydrolysis: transesterification of 2-hydroxypropyl-*p*-nitrophenyl phosphate (hpnp) and hydrolysis of uridine 2′,3′-cyclic monophosphate (2′,3′-cUMP).

Results and Discussion

Description of the Crystal Structures

a. [Zn(bimido)Cl]NO_3 (1)

The molecular structure of **1** is shown in Figure 1, selected bond lengths and angles are given in Table 1. The zinc(II) ion in complex **1** is coordinated in a slightly distorted square pyramidal environment, with the four N atoms of bimido in the basal positions and the Cl^- ion in the axial one. The zinc(II) ion is displaced by 0.527(1) Å from the least-square plane defined by N(2), N(3), N(4) and N(5). The O(1) oxygen of the alcohol is not coordinated to the metal ion. Several hydrogen bonds between the hydrogens on O(1), N(1), N(3) and the nitrate oxygens stabilise the crystal structure. In addition, two complex molecules are linked by a moderately strong hydrogen bonding interaction between the hydrogen on N(6) and O(1) (-x, y-1/2, -z+1/2) with an N(6)−O(1) bond length of 2.802 Å.

The penta-coordinated zinc(II) ion is less common in biological systems, but may be relevant to the catalytic reaction intermediates.[18] Although several square pyramidal zinc(II) complexes are known for linear or cyclic tetraaza ligands,[19] only a few examples can be found for imidazole derivatives.[20]

The average Zn−N_{im} distance (2.05 Å) is considerably shorter than the corresponding distance of the secondary amines (2.15 Å). The former value (Zn−N_{im}) is also somewhat shorter than the corresponding distance in the only available square pyramidal zinc(II) complex with basal imidazole coordination (2.08 Å).[20]

The largest distortion in complex **1** from the ideal square pyramidal structure is in the N2−Zn−N5 angle, which is 101.2° (Δ = 15.2°). This is due to the presence of the two fused 5-membered chelate rings in complex **1**, having N−Zn−N angles less than 80°.

Table 1. Selected interatomic bond lenghts (Å) and angles (°) for [Zn(bimido)Cl]NO_3 (**1**)

Zn−N(2)	2.072(2)	Zn−N(4)	2.167(2)
Zn−N(3)	2.132(2)	Zn−N(5)	2.031(2)
Zn−Cl(1)	2.261(1)		
N(2)−Zn−N(3)	79.35(8)	N(4)−Zn−N(5)	78.34(8)
N(2)−Zn−N(4)	151.74(8)	N(2)−Zn−Cl(1)	108.92(7)
N(2)−Zn−N(5)	101.17(8)	N(3)−Zn−Cl(1)	102.60(7)
N(3)−Zn−N(4)	86.53(8)	N(4)−Zn−Cl(1)	97.95(7)
N(3)−Zn−N(5)	148.02(8)	N(5)−Zn−Cl(1)	107.25(7)

b. [Cu_2(bimido$_{-1H}$)(DPP)(ClO_4)(CH_3OH)]ClO_4·1/2H_2O (2)

The complex crystallises with two identical dinuclear cations, four perchlorates and a lattice water per unit cell. The molecular structure of **2** is shown in Figure 2, while selected bond lengths and angles are provided in Table 2. The dinuclear complex consists of two distinct copper(II) centres, one is five (4+1) coordinated, the other is six (4+2) coordinated and they are doubly bridged by the alkoxide oxygen of bimido and by the phosphate oxygens of DPP in a 1,3-bridging mode. The five coordinated Cu(2) has a slightly distorted square-pyramidal geometry. The basal plane of Cu(2) is determined by the N(1), N(2), O(1) atoms of bimido in addition to the O(2) oxygen of DPP, while a non-

Table 2. Selected interatomic bond lenghts (Å) and angles (°) for [Cu_2(bimido$_{-1H}$)(DPP)(ClO_4)(CH_3OH)]ClO_4·1/2 H_2O (**2**)

Cu(1)−O(1)	1.901(4)	Cu(2)−O(1)	1.881(4)
Cu(1)−O(2)	1.915(4)	Cu(2)−O(3)	1.916(4)
Cu(1)−N(2)	1.929(5)	Cu(2)−N(4)	2.001(5)
Cu(1)−N(3)	1.999(5)	Cu(2)−N(5)	1.921(5)
Cu(1)−O(7)	2.540(7)	Cu(2)−O(4)	2.361(6)
Cu(1)−O(10)[a]	2.57(1)	Cu(1)···Cu(2)	3.493(2)
O(1)−Cu(1)−O(2)	98.5(2)	O(1)−Cu(2)−O(3)	97.4(2)
O(1)−Cu(1)−N(2)	165.1(2)	O(1)−Cu(2)−N(5)	166.7(2)
O(2)−Cu(1)−N(2)	94.8(2)	O(3)−Cu(2)−N(5)	94.1(2)
O(1)−Cu(1)−N(3)	84.3(2)	O(1)−Cu(2)−N(4)	85.9(2)
O(2)−Cu(1)−N(3)	171.6(2)	O(3)−Cu(2)−N(4)	173.3(2)
N(2)−Cu(1)−N(3)	83.5(2)	N(5)−Cu(2)−N(4)	82.0(2)
O(1)−Cu(1)−O(7)	85.5(2)	O(1)−Cu(2)−O(4)	88.9(2)
O(2)−Cu(1)−O(7)	89.7(3)	O(3)−Cu(2)−O(4)	99.8(2)
N(2)−Cu(1)−O(7)	87.9(3)	N(5)−Cu(2)−O(4)	95.9(2)
N(3)−Cu(1)−O(7)	98.4(3)	N(4)−Cu(2)−O(4)	86.0(3)
		Cu(2)−O(1)−Cu(2)	134.9(2)

[a] Symmetry transformation: $x + 1$, y, z.

deprotonated methanol oxygen is coordinated in the apical position (Cu−O = 2.359 Å). The six coordinated Cu(1) has the same donors in the tetragonal plane (N(3), N(4), O(1) and O(3)), but both axial positions are occupied by loosely bound perchlorate oxygens with a Cu−O distance of ≈ 2.54 Å. As a result, the $Cl(1)O_4^-$ perchlorate ion bridges two neighbouring dinuclear complexes, forming an infinite chain within the crystal. This structural motif has been found in only a few dicopper complexes.[21b] In fact, the oxygen atoms of the methanol and perchlorate ion interact weakly with the metallic orbitals, as a result of the Jahn−Teller effect. The lattice water occupies a special position ($x = 0.5$, $y = 0.5$, $z = 0.5$). The interatomic distances between the water oxygen (O(15)) and the other non-hydrogen atoms are all ≥ 3.88 Å.

The bond lengths in the tetragonal planes of the copper ions ($Cu-N_{im}$ = 1.927 and 1.920, $Cu-N_{am}$ = 1.997 and 2.002, $Cu-O_{alc}$ = 1.901 and 1.880, $Cu-O_P$ = 1.915 and 1.917 Å) are similar for the two metal centres. The Cu−N distances are, however, considerably shorter (Δ = 0.05−0.15 Å) relative to the structurally similar tri- or tetrasubstituted (benz)imidazole derivatives of 1,3-diamino-2-propanol.[21] This is probably due to the less distorted tetragonal plane in **2**. On the other hand, the Cu−O distances are typical as compared with the related dinuclear complexes.

The Cu(1)−Cu(2) distance and the Cu(1)−O(1)−Cu(2) angle in **2** are 3.493 Å and 134.9°, respectively. These relatively large values are due to the constraint caused by the fused 5-membered chelate rings of the ligand backbone and are in the range obtained for similar complexes of substituted 1,3-diamino-2-propanol ligands.[21,22] The metal-metal separation and the μ-1,3 bridging fashion of the phosphodiester DPP in **2** is related with many dinuclear metallo-phosphoesterases.[1][2a] The double Lewis activation of phosphodiester achieved in this way is certainly a key feature concerning the observed hydrolytic activity of **2** (see later).

The least square calculation revealed only minor distortion of the basal plane of Cu(2), but the donor atoms are considerably deviated (average deviation 0.133 Å) from the best plane of Cu(1). As a consequence of the different geometry, only Cu(2) is deplaced considerably (0.1 Å towards O(4)) from its basal plane. The angle between the two least-square planes of the copper(II) centres is 9.4(1)° and between the best plane of the Cu_2O_3P unit and the basal plane of Cu(2) is 7.8(1)°. These facts result in an essentially planar structure of the complex cation.

Finally, several hydrogen bonds, e.g. between N(6)−H and O(11); N(3) −H and O9 ($x + 1$, y, z); O(4) −H and O8 ($x + 1$, y, z), stabilise the crystal structure.

Complex Formation in Aqueous Solution

The determined protonation and complex formation constants are listed in Table 3 together with some derived data. The two imidazole rings of bimido have pK values that are ca. one log unit higher than that of the structurally similar *N*,*N*′-bis(imidazol-4-ylmethyl)-1,2-ethanediamine[23] (bimeda, pK = 3.21 and 4.26), probably due to the electron-donating methyl groups on the imidazole rings.

Table 3. Logarithmic formation constants for copper(II) and zinc(II) complexes of bimido (T = 298 K, I = 0.1 M ($NaClO_4$) in water and I = 0.05 M (sodium benzenesulfonate) in a 65% (w/w) ethanol−water mixture); $\beta_{pqr} = [M_pL_qH_r]/[M]^p[L]^q[H]^r$, with estimated errors in parentheses (last digit)

pqr	water		65% (w/w)
zinc(II)	copper(II)	zinc(II)	EtOH−H_2O
011	9.055(4)		8.49(1)
012	16.586(4)		15.20(1)
013	21.722(6)		19.35(2)
014	26.074(6)		22.87(2)
111	13.83(5)	−	14.43(2)
110	9.63(1)	18.97(1)	10.97(1)
11−1	0.10(1)	7.81(1)	1.19(3)
21−2	−	−	−0.37(1)
21−3	−	−	−10.38(3)
pK_{11-1}^{110}	9.53	11.16	9.86
$\log K_{ML,corr}$	−16.44	−7.10	−11.90
pK_{21-3}^{21-2}	−	−	10.01
NP[a](FP[b])	366(0.005cm^{-3})	340(0.004cm^{-3})	723(0.008cm^{-3})

[a] NP:number of experimental points. − [b] FP: fitting parameter.

In the presence of zinc(II) the same species are formed in both [Zn]/[L] = 1/1 and 1/2 systems. Complex formation starts at pH 4, with the formation of the 3N-coordinated MLH species (Figure 3A). The succeeding ZnL complex is the unique species in the neutral pH region. Its formation at slightly acidic pH suggests 4N coordination in this complex, which is, in fact, proven by X-ray analysis. At higher pH further base consumption is observed (pK = 9.53) which can be assigned to the deprotonation of a metal-bound water molecule (the formation of a metal-coordinated alkoxide anion is less likely due to steric reasons).

In the presence of the copper(II) ion ([Cu]/[L] = 1/1 or 1/2) only the CuL and CuL_{-1H} complexes are detected in the whole pH range. The formation of the CuL species is complete at pH 4. This fact, together with the spectroscopic parameters determined for this complex ($g_\perp$ = 2.057, $g_{//}$ = 2.221, $A_{//}$ = 0.0190 T, g_o = 2.112, A_o = 0.0079 T, λ_{max}^{d-d} = 570 nm), strongly suggest a 4N coordination in the equatorial plane of copper(II) in CuL. The presence of imidazole rings in bimido results in a rather high stability. The basicity corrected stability constants of the ML complex ($\log K_{ML,corr} = \log \beta_{110} - \log \beta_{014} = -7.1$ and −16.44 for Cu^{II} and Zn^{II}, respectively) are ca. 2−4 orders of magnitude higher than those of the 1,4,8,11-tetraazaundecane.[24] Similarly, the existence of the fused chelates causes significant stabilisation relative to the complexes of the strongly related 4-aminomethylimidazole (e.g. $\log K_{CuL2,corr}$ = −11.0,[25] $\Delta \log K_{corr}$ = 3.9). The deprotonation, leading to the CuL_{-1H} species, occurs at pK = 11.16. The observed slight change in the EPR parameters during this process (g_o = 2.109, A_o = 0.00806 T) indicates only minor variations in the coordination sphere of copper(II), i.e. deprotonation of the non-coordinating imidazole-N1 nitrogen. The observed high pK value agrees well with those obtained for analogous systems.[17]

Our intention was to achieve dinuclear complexes of bimido, but the solubility of the complexes formed at 2/1

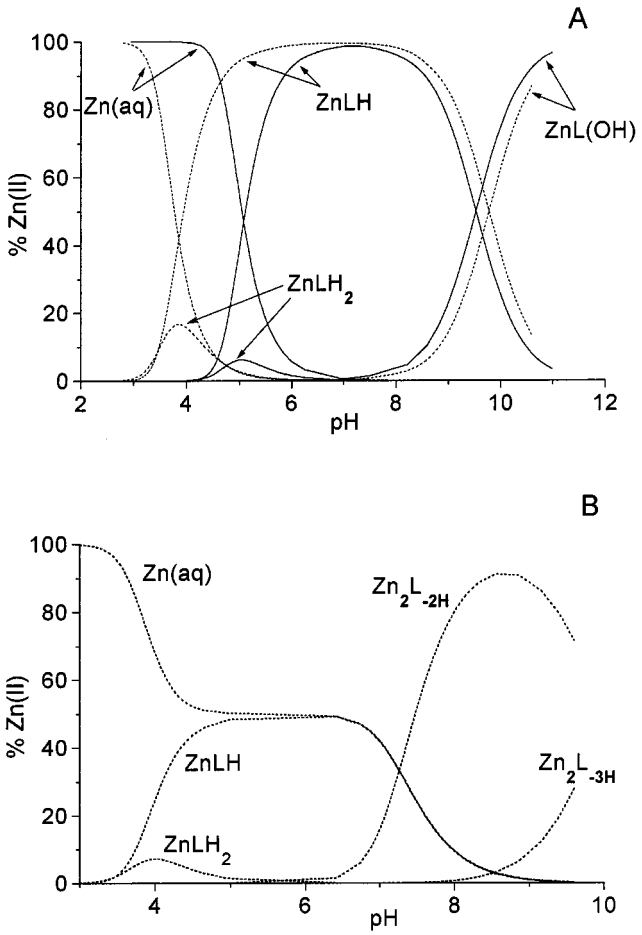


Figure 3. Species distribution curves in the zinc(II)-bimido system at metal-to-ligand ratio 1/1 (A) and 2/1 (B) in water (solid line) and in a 65% (w/w) EtOH-H_2O mixture (dotted line); [Zn] = 3 mM (A) and 1 mM (B)

metal-to-ligand ratio was found to be very sensitive to the solvent used and the background electrolyte. A relatively sharp and well-resolved ^{1}H NMR spectrum can be obtained by dissolving the crystalline complex **2** in [D_6]DMSO (see supporting information, Figure S1). The signals related to the ligand are spread over a 150 ppm range. The occurrence of the spectrum strongly supports the presence of the dinuclear unit in solution too, allowing magnetic interaction between the metal centres.[26] In the aqueous solution of copper(II)-bimido ([Cu]/[L] = 2/1) system, without background electrolyte, two strongly overlapping deprotonations are observed pH-metrically between pH 6 and 8, accompanied by the decrease in EPR signal intensity and by a red shift of the *d-d* transition (see supporting information, Figure S2). This indicates the rearrangement of the donor groups in the equatorial plane of copper(II) and the formation of magnetically coupled metal centres. Although no further information is available, the Cu_2L_{-2H} complex formed between pH 6−7, probably has an analogous structure to the crystallographically determined dinuclear complex **2** (the formation of protonation isomers, as in the case of zinc (see later), cannot be ruled out). However, in the presence of any common background electrolyte precipitation is observed preventing further study.

Complex Formation in a 65% (w/w) Ethanol-Water Mixed Solvent

In the case of the zinc(II)-bimido ([Zn]/[L] = 2/1−1/2) system, solubility problems are overcome by using a 65% (w/w) ethanol-water solvent mixture. This solution is clear in the whole pH range and thus it is suitable for equilibrium and kinetic measurements (see also the experimental section). The pK values of bimido are lower than those obtained in aqueous solution (Table 3), according to the somewhat lower permittivity of the solvent. Since the association is more favoured in this medium than in water, the stability of the ZnLH and ZnL complexes, reflected by the basicity corrected stability constants (Table 3), is considerably higher.

At a 2/1 metal-to-ligand ratio, two deprotonations (one per zinc(II) ion) are observed between pH 6.5−8, in a strongly overlapping manner, forming the M_2L_{-2H} species (Figure 3B). A similar observation is mentioned above for copper(II), but in the present case the deprotonation processes take place at higher pH values of ca. 0.7 units. With increasing pH, a further deprotonation is observed (pK = 10.0).

The ^{1}H NMR spectrum of the ZnL species is changed significantly relative to that of the free ligand (Figure 4).

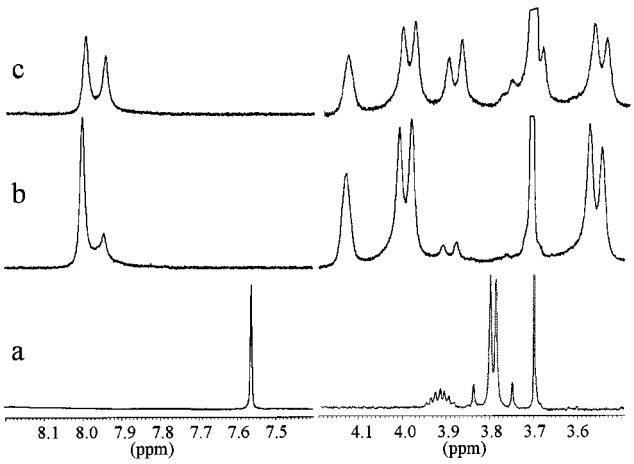


Figure 4. Selected regions of the ^{1}H NMR spectra measured in the zinc(II)-bimido system in 65% CD_3OD - D_2O at pH = 8.6 with the variaton of the metal to ligand ratio. [bimido] = 0.005 M (a) and 0.002 M (b, c). [Zn] = 0.0 M (a), 0.0022 M (b) and 0.004 M (c)

The hydrogens of CH_2, linked to the imidazole rings, become strongly inequivalent and all signals shift upon the coordination. The increasing metal-to-ligand ratio at pH 8.5 induces further characteristic changes on the spectra. A new set of peaks appears, indicating the formation of a complex, Zn_2L_{-2H} according to the pH-metric results, which is in a slow exchange on the NMR timescale. Kinetically inert complexes may originate from the formation of either imidazolate- or alkoxo-bridged metal centres. The chemical shift of the imidazole C2−H protons is, however, weakly influenced by the deprotonation. Metal-promoted

Table 4. ^{1}H NMR chemical shifts and determined coupling constants (see below the table) for the different species formed in the bimido-zinc(II) system at pH = 8.6 in 75% CD_3OD - D_2O

species	C2−H(im), 2 H	C*H*−OH, 1 H	CH_2−im, 2 H+2 H	CH_2−CH, 2 H+2 H	CH_3−im, 6 H
free lig.	s, 7.56	m, 3.92 [a]	m, 3.81, 3.78 [b]	m, 3.27, 3.09 [a],[c]	s, 2.21
ZnL	s, 8.00	m, 4.13	m, 3.99, 3.56 [b]	m, 3.27, 3.09 [c]	s, 2.22
Zn_2L_{-2H}	s, 7.93	m, 3.75	m, 3.88, 3.70 [b]	m, − [d], 2.97 [c]	s, 2.13
	s, 7.98	m, 4.13	m, 3.98, 3.55 [b]	m, 3.26, 3.08 [c]	s, 2.22

[a] Three bond couplings between C*H*−OH and the two inequivalent CH_2−CH hydrogens: ^3J = 4.7 and 7.4 Hz. − [b] Two bond couplings between the inequivalent CH_2-im hydrogens: ^2J = 13.4, 14.0, 15.0 and 13.8 Hz, respectively. − [c] Two bond couplings between the inequivalent CH_2−CH hydrogens: ^2J = 12.2, 11.7, 11.2 and 12.0 Hz, respectively. − [d] Chemical shift could not be determined due to the overlapping with the broad solvent signal.

proton loss of the neutral imidazole ring i.e. formation of an imidazolate-bridge, induces an important (more than 1 ppm) shift[14,16] which is not comparable with the presently observed 0.06 ppm. On the other hand, notable changes appear on the signals of the 2-hydroxypropyl unit, especially concerning the central CH group (Table 4). These facts suggest, that the new set of peaks is related to an alkoxo-bridged dinuclear complex. This complex probably has an analogous structure with the crystallographically determined dinuclear complex **2**. Such a structural motif has recently been found in a dinuclear zinc(II) complex of a four substituted 1,3-diamino-2-propanol derivative.[27] Complex **2** and Zn_2L_{-2H} are different, however, in their protonation states. The second deprotonation in Zn_2L_{-2H} can be assigned to the proton loss of a metal-bound water molecule.

However, as can be seen from Figure 4. only ca. 45% of the ligand is transformed into the above-mentioned complex at a two-fold metal excess and at pH 8.6, while 55% of the ligand remains as a fast exchanging species. A simple explanation of this behaviour would be the presence of 27.5% free metal ion beside the Zn_2L_{-2H} and ZnL complexes. In the absence of the ligand, however, a well defined $Zn(OH)_2$ precipitate can be observed above pH 7.0 even at a 0.3 mM metal concentration, which prevents any accurate pH-metric or kinetic study. Since the solution of zinc(II)-bimido complexes ([Zn]/[L] = 2/1) is clear even at a 7 mM metal concentration, the only plausible explanation for the above observation is the presence of protonation isomers, i.e. two complexes with the same Zn_2L_{-2H} composition. One of them is the above-mentioned alkoxo-bridged complex $Zn_2(L_{-1H})(OH)$ which is in a slow exchange. In the other isomer the metal ions are chelated by two nitrogens and both deprotonations are related to the metal-bound water molecules ($Zn_2L(OH)_2$) . The ^{1}H NMR signals of this species is only slightly shifted relative to those of the ZnL complex, since the ligand in both cases coordinates to the metal ion(s) by its four nitrogen donors.

Protonation isomers are generally in a fast mutual exchange but in the present case, the protonation of the alkoxide anion induces rearrangement of the coordination sites, which slows the entire process. The $Zn_2L(OH)_2$ complex remains in a fast mutual exchange with ZnL and L.

The further deprotonation around pH 10 results in the formation of Zn_2L_{-3H} species, which is probably better described as $Zn_2(L_{-1H})(OH)_2$.

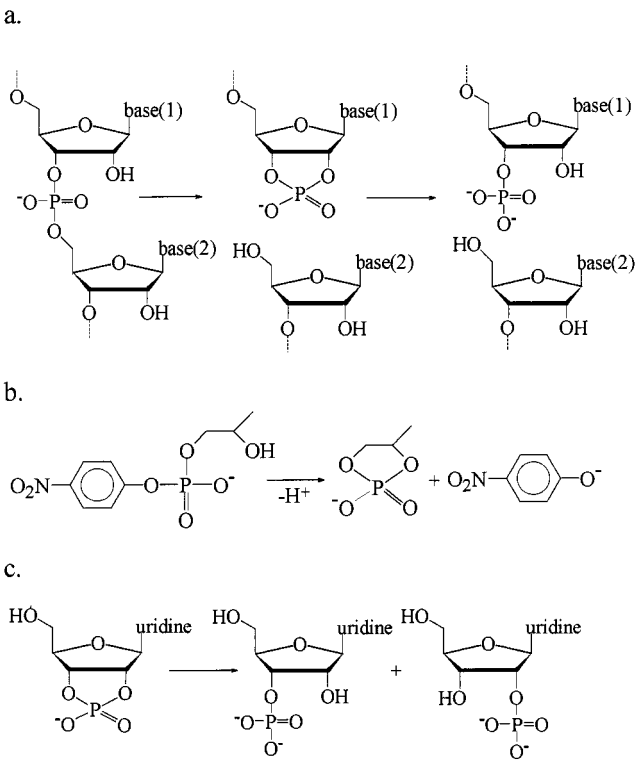
Kinetic Study

The hydrolytic cleavage of RNA is a two-step process: the first step is a transesterification forming a cyclic phosphoester, while the second step is the ring opening.

The hydrolytic activity of the above systems is tested by modelling both steps of RNA hydrolysis i.e. transesterification of hpnp and hydrolysis of 2′,3′-cUMP (Scheme 2).

Hydrolytic Activity of the Copper(II)-bimido Complexes

The pH-rate profiles of the transesterification of hpnp and hydrolysis of cUMP, having sigmoidal character, are



Scheme 2. The two-step process of RNA hydrolysis (a) and the used model substrates: b. 2-hydroxypropyl-*p*-nitrophenyl phosphate (hpnp) and c. uridine 2′,3′-cyclic monophosphate (2′,3-cUMP). Base(1) and base(2) indicate organic base constituents of RNA

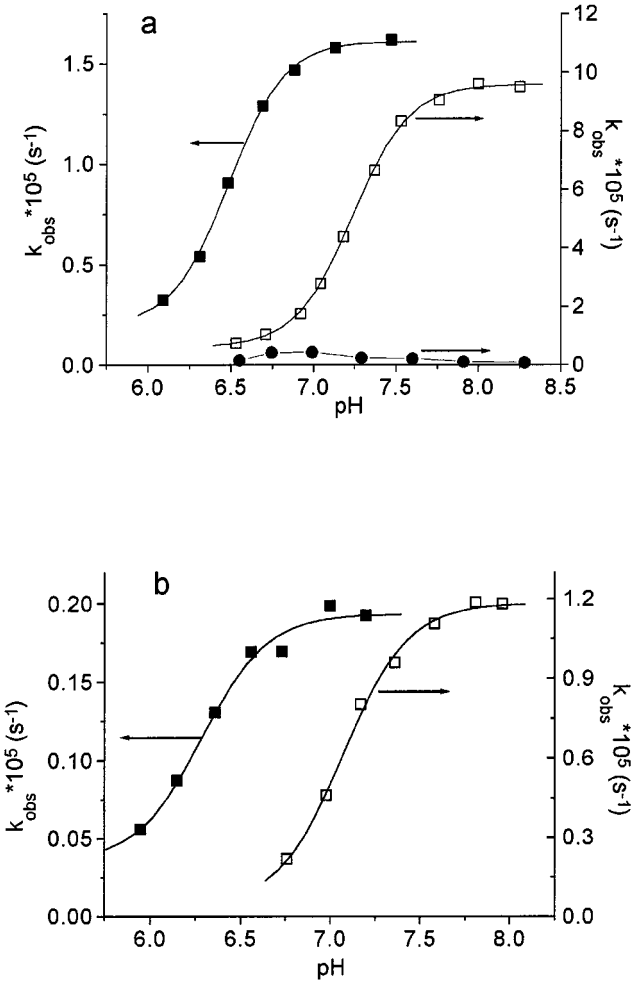


Figure 5a−b. The effect of pH on the observed kinetic data. − a) (■) transesterification of hpnp by the copper(II)-bimido complexes (T = 298 K, 0.51·[Cu] = [L] = 5·10^{-4} M, 0.01 M MES or HEPES, [hpnp] = 5.4·10^{-4} M); (□) transesterification of hpnp by the zinc(II)-bimido complexes (65% (w/w) EtOH-H_2O, T = 298 K, I = 0.05 M, 0.52·[Zn] = [L] = 5.6·10^{-4} M, [hpnp] = 5.4·10^{-4} M); (•) transesterification of hpnp by the zinc(II)-ion alone (65% (w/w) EtOH-H_2O, T = 298 K, I = 0.05 M, [Zn] = 3.0·10^{-4} M, [hpnp] = 9.8·10^{-4} M). − b) (■) hydrolysis of cUMP by the copper(II)-bimido complexes (T = 310 K, 0.51·[Cu] = [L] = 5.1·10^{-4} M, 0.01 M MES or HEPES, [cUMP] = 50 μM); (□) hydrolysis of cUMP by the zinc(II)-bimido complexes (65% (w/w) EtOH-H_2O, T = 310 K, I = 0.05 M, 0.52·[Zn] = [L] = 2.1·10^{-3} M, [cUMP] = 50 μM)

shown in Figure 5. In both cases, the observed rate increases between pH 6−7.5, which is parallel with the formation of the Cu_2L_{-2H} species (see also Figure S2), implying its active role in the reaction. However, due to the absence of background electrolyte, a detailed kinetic study was not performed.

Transesterification of hpnp by the Zinc(II)-Bimido Complexes

The pH-rate profile of the transesterification of hpnp shows a sigmoidal shape again (Figure 5,a). The increasing activity between pH 6.5−8 is parallel with the pH-metrically observed deprotonations at a 2/1 metal-to-ligand ratio (Figure 3.b). The pseudo-first order rate constant levels off between pH 8−8.8 and decreases at higher pH (not shown). The pK value determined from the kinetic data (pK = 7.24) agrees well with the pH-metric results. For comparative purposes, we also studied the hydrolytic activity of the zinc(II) solution in the absence of bimido (Figure 5,a). Due to the formation of a $Zn(OH)_2$ precipitate above pH 7, the observed rate constants are relatively uncertain. Nevertheless, the free zinc(II) induced rate enhancement is negligible relative to that of zinc(II)-bimido system. All these facts suggest that the hydrolytic activity is related to the Zn_2L_{-2H} species, although no distinction can be made concerning the two protonation isomers since their ratio is independent from pH and concentration. The uncatalysed reaction of hpnp at pH 8 is relatively slow ($k_{obs,uncat}$ = 1.3·10^{-7} s^{-1}, half lifetime 62 days) under the conditions used. However, in the presence of 0.54 mM Zn_2L_{-2H} complex at pH 8, the half lifetime decreases to 2 hours. Three turnovers are observed without significant loss of activity at pH 8 when a 3-fold excess of hpnp is present over the dinuclear complex (0.5 mM).

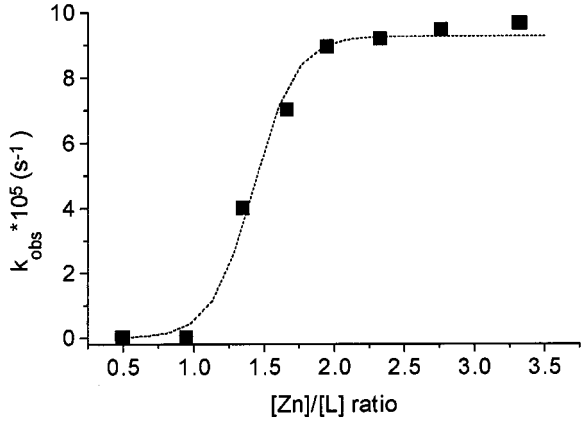


Figure 6. Dependence of the rate of transesterification on the [Zn]/[bimido] ratio at constant bimido concentration; pH = 7.98, [bimido] = 5.6·10^{-4} M

Figure 6 shows the observed pseudo-first order rate constants as a function of the [Zn]/[bimido] ratio at constant ligand concentration. The rate is negligible up to equimolar conditions, it sharply increases between a 1/1 and 2/1 ratio and finally levels off at a higher metal excess (where precipitation occurred). This observation provides further argument that the observed activity is a result of the Zn_2L_{-2H} species.

At a constant metal-to-ligand ratio and at pH 7.98, the rate of transesterification linearly depends on the concentration of the Zn_2L_{-2H} complex between 0.2 mM < [Zn] < 2 mM (Figure 7). The second order rate constant (k_2) determined from the slope of this plot is 0.186 M^{-1}s^{-1}. This value is 2.5 times higher than that of the hydroxide ion induced transesterification ($k_{2,OH}$ = 0.0745 M^{-1}s^{-1}), determined between pH 8.8−10.9 in water (in a 65% EtOH-H_2O mixture precipitation occurred using CAPS buffer).

The rate of transesterification is also measured as a function of the substrate concentration (Figure 8). At higher hpnp concentration, saturation kinetics is observed, implying that the transesterification proceeds through pre-equi-

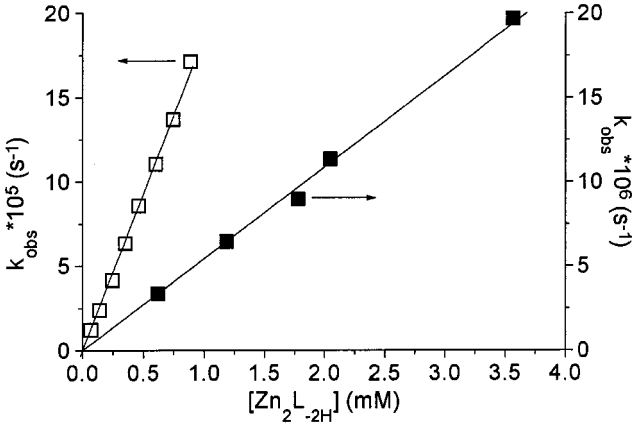


Figure 7. Dependence of the observed pseudo-first order rate constant on the concentration of $[Zn_2L_{-2H}]$ complex. – (□) transesterification of hpnp (65% (w/w) EtOH-H_2O, T = 298 K, I = 0.05 M, 0.52·[Zn] = [L], pH = 7.98, [hpnp] = $5\cdot10^{-4}$ M); (■) hydrolysis of cUMP (65% (w/w) EtOH-H_2O, T = 310 K, I = 0.05 M, 0.52·[Zn] = [L], [cUMP] = 50 μM)

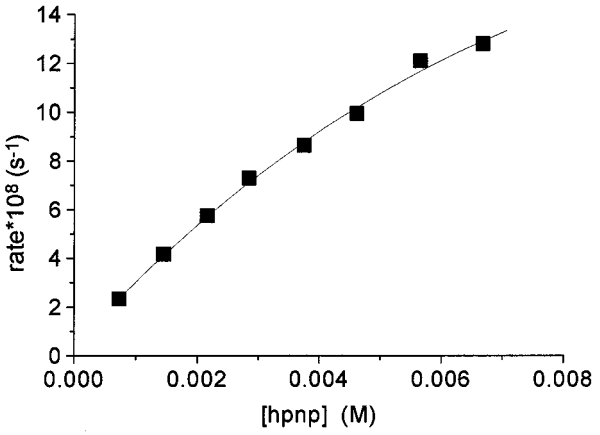
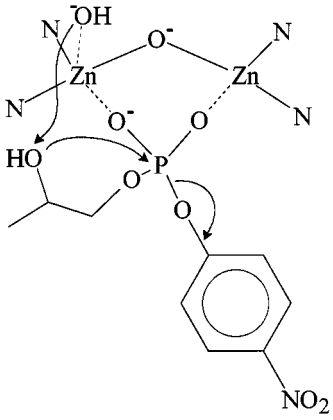


Figure 8. Saturation kinetic experiments for the transesterification of hpnp (65% (w/w) EtOH-H_2O, T = 298 K, I = 0.05 M, 0.52·[Zn] = [L] = $2.1\cdot10^{-4}$ M, pH = 7.98)

libration of an active (catalyst-substrate) complex. The Michaelis-Menten constant (K_M), determined by nonlinear parameter fitting, is 9.1 mM (K_{ass} = $1/K_M$ =110 M^{-1}) and the first order catalytic rate constant (k_{cat}) is $1.52\cdot10^{-3}$ s^{-1}. These values indicate the moderate binding affinity of hpnp to the dinuclear Zn_2L_{-2H} species, but high catalytic activity of this complex. As far as we are aware, the above k_{cat} value is the highest value reported to date for transesterification of hpnp by a zinc(II) complex.

The above experimental data, together with the crystal structure of complex **2**, provide some information on the possible mechanism of the transesterification. The pH-rate profile levels off between pH 8–8.8 (Figure 5.a) parallel with the concentration distribution of the Zn_2L_{-2H} species (Figure 3.b). This means that general base catalysis, activating the nucleophilic β-OH group, is provided mainly by the metal-bound hydroxide ion. However, the second order rate constant of the transesterification by the dinuclear zinc(II) complex is 2.5-fold higher than $k_{2,OH}$. This implies a bifunctional mechanism for the transesterification, since the nucleophilicity of the metal-bound hydroxide ion is considerably lower than that of the free OH^- ion. Thus, additional Lewis-acid activation, or in other words metal coordination of the phosphate group, should be considered. Based on the crystal structure of the dinuclear complex **2**, this probably occurs in a μ-1,3 bridging fashion (Scheme 3). In most cases, such double Lewis-activation is the key feature of highly active dinuclear complexes.[2,7,8,28]



Scheme 3. The proposed mechanism for hpnp transesterification by the alkoxo-bridged dinuclear complex

Since bridging alkoxide anions are not considered to be active as (general-)base catalysts,[2,4,6,8] the proposed mechanism should be valid for both protonation isomers. Due to the constant ratio of the protonation isomers, no experimental data are available for their individual activity. An overview of the literature data indicates, however, higher hydrolytic activity of rigidly pre-organised bimetallic cores,[2,29] allowing direct metal-metal cooperation, as compared with the more flexible dinuclear complexes. This would suggest the predominance of the $Zn_2(L_{-1H})(OH)$ isomer in the hydrolytic processes.

Hydrolysis of 2′,3′-cUMP

The use of *p*-nitrophenyl phosphates to mimic natural phosphoesterases is not fully justified, since in contrast to biological phosphoesters, the 4-nitrophenolate leaving group does not require electrophilic stabilisation. To mimic the second step of RNA hydrolysis we use the biologically more relevant 2′,3′-cUMP, which provides a direct analogy to the natural process (Scheme 2).

The pH-rate profile of 2′,3′-cUMP hydrolysis by the dinuclear zinc complex (Figure 5.b) shows similar sigmoidal behaviour as the hpnp transesterification. A pK value of 7.06 can be determined from the kinetic data which is somewhat smaller than the previously determined pK = 7.24. This difference is due to the four-fold increase in the metal concentration and the higher temperature (310 K) used in present case. 2′,3′-cUMP is highly resistant to hydrolysis. The second order rate constant[30] for the hydroxide-catalysed hydrolysis at 37 °C is ca. $6.5\cdot10^{-3}$ $M^{-1}s^{-1}$. Based on this value, the approximate parameters for the autohydrolysis at pH 8 are $k_{obs,uncat}$ = $1–2\cdot10^{-9}$ s^{-1} and the half-life time is ca. 11–22 years. In the presence of a 3.6 mM dinuclear zinc(II) complex the half-life time of 2′,3′-cUMP is 10

hours at pH 8. Thus, a 3.6 mM zinc complex provides ca. $1-2\cdot10^4$-fold rate acceleration, which is the highest value reported to date for the 2′,3′-cUMP hydrolysis promoted by a dinuclear zinc(II) complex. On the other hand, Komiyama′s dinuclear zinc(II) complex[4] hydrolyses ApA with a comparable rate and thus, although no numerical data is given, it probably provides a faster hydrolyses for cyclic monophosphates. We also tested the activity of the dinuclear zinc(II)-bimido complex towards the hydrolysis of UpU. In the presence of a 4 mM dinuclear species and at 310 K, ca. 5% conversion is achieved after 3 days. This suggests an accelerated reaction but the rate is too small for accurate measurement.

The rate of hydrolysis shows first order dependence on the concentration of the Zn_2L_{-2H} species (Figure 7) between 1.2 mM < [Zn] < 7.2 mM. The second order rate constant determined from the slope is 0.0054 M^{-1} s^{-1}. This value is close to that of the hydroxide ion (ca. 0.0065 M^{-1} s^{-1}).

The mechanism of the hydrolysis by the dinuclear complex is probably similar (as depicted in Scheme 3) to the hpnp transesterification. In the present case, however, the metal-bound hydroxide ion may act either as a general base (deprotonating the attacking water molecule) or as a direct nucleophile.

Experimental Section

Materials: Zinc(II) perchlorate (Fluka) solutions were standardised complexometrically. pH metric titrations were performed by Titrisol NaOH standard solution (Merck). HEPES, HEPPS, CHES, CAPS (Aldrich) and MES and 2′,3′-cUMP (Sigma) were used without further purification. The barium salt of 2-hydroxypropyl-*p*-nitrophenyl phosphate (hpnp) was prepared according to the literature procedure[31].

Synthesis of *N,N′*-Bis(5-methylimidazol-4-ylmethyl)-1,3-diaminopropan-2-ol·4 HCl (Bimido): 5-Methylimidazole-4-carboxaldehyde (1.67 g, 15 mmol) and 1,3-diamino-2-propanol (0.7 g, 7.5 mmol) were dissolved in 60 mL of dry methanol. To this solution 1.2 g of sodium borohydride were added in small portions while stirring. After 3 h at room temperature, the reaction was completed by refluxing for 1 h. The methanol solution was then acidified by concentrated hydrochloric acid. The precipitate was filtered , the solution was reduced to 2−3 mL and 30 mL of methanol was added. The precipitate was filtered off again. The solution was evaporated to dryness by codistillation with absolute ethanol. The crude product was recrystallised twice from methanol. Yield: 2 g, 63%. The structure and purity was confirmed by NMR spectroscopy and potentiometry. ^{1}H NMR (D_2O): δ = 8.63 (s, 2 H, C2−H(im)), 4.43 (s, 4 H, CH_2−im), 4.34 (m, ^3J = 4.0 and 11.3 Hz, 1 H, C*H*−OH), 3.30 and 3.16 (m, ^2J = 15.8 Hz, ^3J = 4.0 and 11.3 Hz, 2 H + 2 H, CH_2−CH) and 2.36 (s, 6 H, CH_3-im). No other signal was detected.

pH-metric Measurements: The complex formation equilibria were investigated by potentiometric titrations using an automatic titration set including a Dosimat 665 (Metrohm) autoburette, an Orion-710A precision digital pH-meter and an ORION ROSS 8103BN type combined glass electrode. The experimental procedure referring to the aqueous solution (0.1 M $NaClO_4$, and T = 298±0.1) was described in detail earlier.[15–17]

In 65% (w/w) ethanol-water mixture the zinc(II)-bimido ([Zn]/[L] = 2/1−1/2) solution was clear between pH 2−10 when only buffer was present, but gave slight precipitation using any common inorganic background salt. To avoid this precipitation sodium benzenesulfonate (0.05 M) was used as a background salt and a clear solution, in the used concentration ([Zn] = $0.4-7.0\cdot10^{-3}$ mol dm^{-3}) and pH range, was obtained. The pH-meter was calibrated by standard aqueous buffer solutions (pH = 4.01 and 7.0, Mettler−Toledo) and the actual pH in the mixed solvent was then determined by subtracting 0.24 units from the pH-meter reading according to the method of Bates.[32] The ionisation constant of water determined under the used conditions (pK_w = 14.92±0.02) is in good agreement with that of extrapolated value from the literature data.[33]

The protonation and the complex formation constants were calculated as the average of 4 and 8 independent titrations (50−80 data points per titration), respectively. The metal-to-ligand ratios were varied from 2:1 to 1:2 with metal-ion concentrations between $5\cdot10^{-4}$ and $4\cdot10^{-3}$ mol dm^{-3}. The species formed in the systems were characterised by the following general equilibrium process

$$pM + qL + rH \rightleftarrows M_pL_qH_r$$

(charges are omitted for simplicity; M denotes the metal ion and L the non-protonated ligand molecule) and the concentration stability constants of these species were calculated by the computer program PSEQUAD.[34]

X-ray Crystallography: The crystals suitable for X-ray analysis were obtained by the following ways:

[Zn(bimido)Cl]NO_3 (1): Bimido·4 HCl (66 mg, 0.15 mmol) dissolved in 5 mL of dry methanol was neutralised with 4 equivalents of NaOH (in MeOH). $Zn(NO_3)_2\cdot6H_2O$ (44.6 mg, 0.15 mmol) was then added. The solution was heated to 50 °C and gently concentrated to 2−3 mL. After slowly cooling the solution to room temperature, colourless crystals were obtained in 2−3 days. Anal. calculated for $C_{13}H_{22}ClN_7O_4Zn$: C 35.38, H 4.99, N 22.22; found C 35.08, H 4.91, N 22.42.

[Cu_2(bimido$_{-1H}$)(DPP)(ClO_4)(CH_3OH)]ClO_4·1/2 H_2O (2): In a similar way, bimido·4 HCl (66 mg, 0.15mmol) in 5 mL dry methanol was mixed with 6 equivalents of NaOH (in MeOH), diphenylphosphonic acid (32.7 mg, 0.15 mmol) and $Cu(ClO_4)_2\cdot6H_2O$ (111.2 mg, 0.3 mmol). After a similar treatment as in **1**, deep blue crystals were obtained. Anal. calculated for $C_{26}H_{36}Cl_2Cu_2N_6O_{14.5}P$: C 34.94, H 4.03, N 9.41; found C 35.06, H 4.08, N 9.34.

X-ray data were collected on a STOE IPDS diffractometer using Mo-K_α-radiation (λ = 0.71073 Å) at 213 K with sample-to-plate distance of 70 mm and a scan range from 100 to 301° (**1**) and from 5 to 205° (**2**), with an exposure time of 4 min per 1.5° increment for **1** and 1.3° for **2**. The structures were solved using the direct method[35] and refined[36] by full-matrix least square by minimising the function $\Sigma w(|F_0|-|F_c|)^2$, where F_0 and F_c are the observed and calculated structure factors. Anisotropic thermal parameters were used for all non-hydrogen atoms except for the lattice water oxygen in **2**. Hydrogen atoms were included in the refinement using the riding model. The isotropic thermal parameters for the methyl and hydroxyl protons were refined with 1.5 times, for all other hydrogen atoms with 1.2 times, U_{eq} of the attached atom. H atoms of the lattice water in **2** were not found. The residual electron density on the final difference Fourier map was relatively low for **1**

Table 5. Crystallographic data, details of data collection and structure analysis for complexes **1** and **2**

	1	**2**
empirical formula	$C_{13}H_{22}ClN_7O_4Zn$	$C_{26}H_{36}Cl_2Cu_2N_6O_{14.5}P$
M_r	441.19	893.56
crystal size (mm)	0.24×0.32×0.48	0.16×0.20×0.32
crystal system	monoclinic	triclinic
space group	$P2_1/c$	$P\bar{1}$
a (Å)	11.311(2)	7.290(1)
b (Å)	13.299(3)	13.430(3)
c (Å)	12.816(3)	18.090(4)
α, deg	90.00	92.37(3)
β, deg	103.43(3)	97.02(3)
γ, deg	90.00	99.38(3)
V (Å^3)	1865.26	1730.9(6)
density calcd. (g cm^{-1})	1.571	1.714
Z	4	2
T (K)	213(2)	213(2)
Θ range for data collection	4.05−26.05°	4.71−26.12°
index ranges	$-13\leq h\leq 12$, $-16\leq k\leq 16$, $-15\leq l\leq 15$	$-8\leq h\leq 8$, $-16\leq k\leq 16$, $-22\leq l\leq 22$
μ (mm^{-1})	1.490	1.506
F(000)	885	914
reflections collected/unique	14864/3657 [R(int) = .00752]	13672/6281 [R(int) = .1060]
number of parameters	235	466
final R indices (all data)[a]	R_1 = 0.0305, $wR2$ = 0.0750	R_1 = 0.1033, $wR2$ = 0.1956
final R indices [$I>2\sigma(I)$]	R_1 = 0.0314, $wR2$ = 0.0836	R_1 = 0.0657, $wR2$ = 0.1656
weighting scheme[b]	$1/[\sigma^2(F_o^2) + (0.0328P)^2 + 1.34P]$	$1/[\sigma^2(F_o^2) + (0.0897P)^2 + 2.83P]$
goodness of fit on F^2	1.046	1.050
diff. Fourier peaks, min/max	−0.32/0.33	−0.67/1.56

[a] $R_1 = \Sigma \mid |F_o| - |F_c| \mid / \Sigma |F_0|$, $wR_2 = [\Sigma w(F_o^2 - F_c^2)^2/\Sigma w(F_o^2)^2]^{1/2}$. − [b] $P = [\max(F_o^2,0) + 2F_c^2]/3$

(0.33/−0.32 e/Å^3), while in case of **2** the two highest peaks were found to be 1.56 and 0.85 e/Å^3, associated with Cl(1). The thermal parameters of the complex cation in **2** were well behaved, but those of the perchlorate ions and lattice water were relatively large. Attempts to improve the model for the disordered Cl(1) perchlorate ion resulted in a lower final agreement index and residual electron density, but a higher thermal parameter for one of the disordered perchlorate oxygen and thus were unsatisfactory. Further data collection parameters and information related to the structure refinement are collected in Table 5.

Crystallographic data (excluding structure factors) for the structures reported in this paper have been deposited with the Cambridge Crystallographic Data Center as supplementary publication no. CCDC-127400 (**1**) and CCDC-135915 (**2**). Copies of the data can be obtained free of charge on application to CCDC, 12 Union Road, Cambridge CB2 1EZ, UK (Fax:+44−1223/336−033; E-mail: deposit@ccdc.cam.ac.uk).

NMR Spectroscopic Measurements: The ^{1}H NMR spectroscopic measurements were performed on a Bruker AM-360 spectrometer, operating at room temperature. The chemical shifts have been given as relative shifts from DSS (the sodium salt of 4,4-dimethyl-4-silapentane-1-sulfonate) using dioxane as the internal reference (3.7 ppm from DSS).

Kinetic Measurements. − Transesterification of hpnp: The reaction was followed in 65% (w/w) ethanol-water ($I \approx 0.05$ M with 0.02 M buffer (HEPES, HEPPS or CHES) and 0.03 M sodium benzenesulfonate). The increase in the absorbance maximum at 400 nm of the *p*-nitrophenolate anion (ε = 18900) was monitored. The pK of *p*-nitrophenol and the buffers were determined independently for our conditions (pK = 8.04±0.01 (hpnp), 7.13±0.01 (HEPES), 7.56±0.01 (HEPPS), 8.80±0.01 (CHES)). The initial concentration of hpnp varied from 0.4 mM to 7 mM. The initial slope method (≤ 4% conversion) was used to determine the pseudo first order rate constants. The reported data are the average of triplicate measurements (reproducibility ≤ 10%).

Hydrolysis of 2′,3′-cUMP: Kinetic data were measured by hydrolysing the 2′,3′-cUMP in a 65% (w/w) ethanol-water mixture (buffer concentration 0.05 M) in the presence of zinc(II)-bimido complexes at 310 K and by analysing the unchanged substrate and products (uridine-2′-phosphate, uridine-3′-phosphate and a small amount of uridine) by HPLC . The pH of the reaction solutions were measured at 298 K, before initiation of the hydrolysis. The initial substrate concentration was $5\cdot10^{-4}$ mol dm^{-3}. Ten aliquots of the reaction solutions were periodically taken up in each run. The progress of the reaction was stopped by mixing 0.1 mL aliquot with equal amount of eluent used for HPLC (0.025 moldm^{-3} acetate buffer, pH = 4.3, containing 0.1 mol dm^{-3} ammonium chloride). The sample was then injected into the HPLC column. The chromatographic separations were carried out on a Merck HPLC system. The column was a Lichrospher 100 RP-18 (150 × 4 mm i.d.), 5 mm particle size (Merck). The UV detection was carried out at 260 nm. The hydrolysis was followed for c.a. three half-lives, by observing the disappearance of uridine-2′,3′-cyclic monophosphate. In all cases pseudo first-order kinetics were observed. The rate constants (k_{obs}) were obtained from the plots of the ratio of the peaks area: [substrate]/([substrate]+[product]) (A_t) *vs* time fitted by the standard exponential model ($A_t = A_0\exp(-k_{obs}\cdot t)$), using a nonlinear least-squares treatment. The reported data are the average of duplicate measurements (reproducibility ≤ 10%).

Acknowledgments

T. G. thanks the Alexander von Humboldt Foundation for a research fellowship. This work was supported by the Deutsche Forschungsgemeinschaft and by the Hungarian Research Foundation (Project No. T025114).

[1] [1a] W. N. Lipscomb, N. Sträter, *Chem. Rev.* **1996**, *96*, 2375−2433. − [1b] D. E. Wilcox, *Chem. Rev.* **1996**, *96*, 2435−2458.

[2] For reviews on dinuclear functional models see: [2a] R. Krämer, T. Gajda, *Perspectives on Bioinorganic Chemistry*, vol. 4 (Ed.:R.

W. Hay, J. R. Dilwoth, K. Nolan), JAI Press Inc., **1999**, pp. 207−240. − [2b] J. Chin, *Curr. Opin. Biol*. **1998**, *1*, 514−521. − [2c] N. H. Williams, B. Takasaki, M. Wall, J. Chin, *Acc. Chem. Res.* **1999**,*32*,485−493.

[3] W. H. Chapman Jr., R. Breslow, *J. Am. Chem. Soc.* **1995**, *117*, 5462−5469.

[4] M. Yashiro, A. Ishikubo, M. Komiyama, *J. Chem. Soc., Chem. Commun.* **1995**, 1793−1794.

[5] P. Molenveld, S. Kapsabelis, J. F. J. Engbersen, D. N. Reinhoudt, *J. Am. Chem. Soc.* **1997**, *119*, 2948−2949.

[6] T. Koike, M. Inoue, E. Kimura, M. Shiro, *J. Am. Chem. Soc.* **1996**, *118*, 3091−3099.

[7] D. Wahnon, R. C. Hynes, J. Chin, *J. Chem. Soc., Chem. Commun.* **1994**, 1441−1442.

[8] M. Wall, R. C. Hynes, J. Chin, *Angew. Chem.* **1993**, *105*, 1696−1697; *Angew. Chem. Int. Ed. Engl.* **1993**, *32*, 1633−1635.

[9] M. J. Young, J. Chin, *J. Am. Chem. Soc.* **1995**, *117*, 10577−10578.

[10] S. Liu, A. D. Hamilton, *Bioorg. Med. Chem. Lett.* **1997**, *7*, 1779−1784.

[11] S. Liu, Z. Lou, A. D. Hamilton, *Angew. Chem.* **1997**, *109*, 2794−2796; *Angew. Chem. Int. Ed. Engl.* **1997**, *36*, 2678−2680.

[12] [12a] P. Hurst, B. K. Takasaki, J. Chin, *J. Am. Chem. Soc*. **1996**, *118*, 9982−9983. − [12b] K. Matsumura, M. Komiyama, *J. Biochem.* **1997**, *122*, 387−394.

[13] P. Molenveld, J. F. Engbersen, H. Kooijman, A. L. Spek, D. N. Reinhoudt, *J. Am. Chem. Soc.* **1998**, *120*, 6726−6737.

[14] I. Török, T. Gajda, B. Gyurcsik, G. K. Tóth, A. Péter, *J. Chem. Soc., Dalton Trans.* **1998**, 1205−1212.

[15] T. Gajda, B. Henry, J.-J. Delpuech, *J. Chem. Soc., Dalton Trans.* **1993**, 1301−1306.

[16] T. Gajda, B. Henry, J.-J. Delpuech, *Inorg. Chem.* **1995**, *34*, 2455−2460.

[17] T. Gajda, B. Henry, A. Aubry, J.-J. Delpuech, *Inorg. Chem*. **1996**, *35*, 586−593.

[18] T. P. E. Auf der Heyde, L. R. Nassimbeni, *Acta Crystallogr. Sect. B*, **1984**, *B40*, 582−589.

[19] see for example N. W. Alcock, A. Berry, P. Moore, *Acta Crystallogr. Sect. C*, **1984**, *C48*, 16−17.

[20] E. E. Bernarducci, P. K. Bharadwaj, R. A. Lalancette, K. Krogh-Jespersen, J. A. Potenza, H. J. Schugar, *Inorg. Chem.* **1983**, *22*, 3911−3920.

[21] [21a] V. McKee, M. Zvagulis, J. D. Dagdigian, M. G. Patch, C. A. Reed, *J. Am. Chem. Soc*. **1984**, *106*, 4765−4772. − [21b] J. H. Satcher, Jr., M. W. Droege, T. J. R. Weakley, R. T. Taylor, *Inorg. Chem*. **1995**, *34*, 3317−3328. − [21c] H. Nie, S. M. J. Aubin, M. S. Mashuta, R. A. Porter, J. F. Richardson, D. N. Hendrickson, R. M. Buchanan, *Inorg. Chem.* **1996**, *35*, 3325−3334.

[22] [22a] W. Mazurek, B. J. Kennedy, K. S. Murray, M. J. O′Connor, J. R. Rodgers, M. S. Snow, A. G. Wedd, P. R. Zwack, *Inorg. Chem*. **1985**, *24*, 3258−3264. − [22b] Y. Nishida, S. Kida, *J. Chem. Soc., Dalton Trans.* **1986**, 2633−2640. − [22c] M. Mikuriya, Y. Hatano, E. Asato, *Chem. Lett*. **1996**, 849−850. − [22d] S. T. Frey, N. M. Murthy, S. T. Weintraub, L. K. Tomphson, K. D. Karlin, *Inorg. Chem.* **1997**, *36*, 956−957. − [22e] T. N. Sorrel, C. J. O′Connor, O. P. Anderson, J. H. Reibenspies, *J. Am. Chem. Soc.* **1985**, *107*, 4199−4206.

[23] D. W. Gruenwedel, *Inorg. Chem.* **1968**, *7*, 495−501.

[24] D. C Weatherburn, E. J. Billo, J. P. Jones, D. W. Margerum, *Inorg. Chem.* **1970**, *9*, 1557−1559.

[25] P. Huber, R. Griessen, H. Sigel, *Inorg. Chem*. **1971**, *10*, 945−947.

[26] V. Clementi, C. Luchinat, *Acc. Chem. Res.* **1998**, *31*, 351−361.

[27] S. J. Brundenell, L. Spiccia, D. C. R. Hockless, E. R. T. Tiekink, *J. Chem. Soc., Dalton Trans.* **1999**, 1475−1481.

[28] N. H. Williams, J. Chin, *Chem. Commun.* **1996**, 131−132.

[29] J. S. Seo, N.-D. Sung, R. C. Hynes, J. Chin, *Inorg. Chem.* **1996**, *35*, 7472−7473.

[30] H. I. Abrash, C.-C. S. Cheung, C. Davis, *Biochemistry* **1967**, *6*, 1298−1308.

[31] D. M. Brown, D. A. Usher, *J. Chem. Soc.* **1965**, 6558−6565.

[32] R. G. Bates *Determination of pH*, 2nd ed., John Wiley & Sons, New York, **1964**, pp. 226−227.

[33] E. M. Wooley, D. G. Hurkot, L. G. Hepler, *J. Phys. Chem.* **1970**, *74*, 3908−3916.

[34] L. Zékány, I. Nagypál, in *Computational Methods for the Determination of Formation Constants*, Ed. D. J. Leggett, Plenum, New York, **1991**.

[35] G. M. Sheldrick, SHELXS-86, Program for Crystal Structure Solution; Universität Göttingen, **1986**.

[36] G. M. Sheldrick, SHELXL-97, Program for Crystal Structure Refinement; Universität Göttingen, **1997**.

Received October 25, 1999
[I99377]

Synthesis and Coordination of the New Chiral Tridentate O,N,O Ligand 2,6-Bis[(1*S*,2*S*,5*R*)-(−)-menthyl]pyridine to Molybdenum(VI) and Vanadium(V) Oxo Complexes: Crystal Structures of [(2,6-Bis{(−)-menthyl}pyridine)MoO_2] and [(2,6-Bis{(−)-menthyl}pyridine)$VO]_2$(μ-O)

Stéphane Bellemin-Laponnaz,[a] Karl S. Coleman,[a] Peter Dierkes,[a] Jean-Pierre Masson,[a] and John A. Osborn*[a]

Keywords: Molybdenum / Vanadium / Chiral ligands / Oxo complexes / Homogeneous catalysis

The novel tridentate chiral ligand 2,6-bis{(–)-menthyl}-pyridine (**1**), was readily prepared from the reaction of 2,6-dilithiopyridine with (–)-menthone. Reaction of **1** with $VO(OiPr)_3$ and $[MoO_2(acac)_2]$ resulted in the formation of the new metal-oxo complexes $[VO(ONO)]_2$(μ-O) (**2**) and $[MoO_2(ONO)]$ (**3**) [ONO = (**1** – 2 H)]. Both metal-oxo compounds **2** and **3** have demonstrated the ability to catalyze the asymmetric oxidation of prochiral olefins with *t*BuOOH as the oxidant. The compounds **1**–**3** have been fully characterized by ^1H, ^{13}C and ^{51}V (where appropriate) NMR spectroscopy, mass spectrometry, microanalysis and IR spectroscopy. Furthermore, the molecular structures of **2** and **3** have been determined by single-crystal X-ray diffraction.

Introduction

Vanadium(V) and molybdenum(VI) compounds[1,2] are of great importance in catalytic reactions involving oxidation processes. Nature makes use of both of these metal centers in oxidation reactions, for example in vanadium bromoperoxidases[3] and molybdenum oxotransferase enzymes.[4] Our interest in this area lies mainly in the development of new asymmetric oxidation catalysts[5,6] using novel tridentate chiral ligands possessing nitrogen and oxygen donor atoms. It has previously been demonstrated that asymmetric tridentate bis-alkoxy nitrogen donor ligands can be used in epoxidation reactions,[7,8] as well as oxo transfer reactions to sulfides,[9] with peroxides as the co-oxidant. However, in the former case, selectivity appears to be lower than in other known systems, while in the latter, the nature of the catalytically active species remains uncertain. Dioxomolybdenum(VI) complexes containing achiral pyridine alkoxy ligands have also been shown to have great potential in the oxidation of terminal olefins with molecular oxygen.[10,11] Herein we describe the synthesis of the novel tridentate chiral ligand 2,6-bis{(−)-menthyl}pyridine (**1**) and its coordination to vanadium and molybdenum to give the new asymmetric oxo complexes $[VO(ONO)]_2$(μ-O) **(2)** and $[MoO_2(ONO)]$ **(3)** {ONO = 2,6-bis{(−)-menthyl}-pyridine}. The molecular structures of **2** and **3** are presented and their potential as asymmetric epoxidation catalysts discussed.

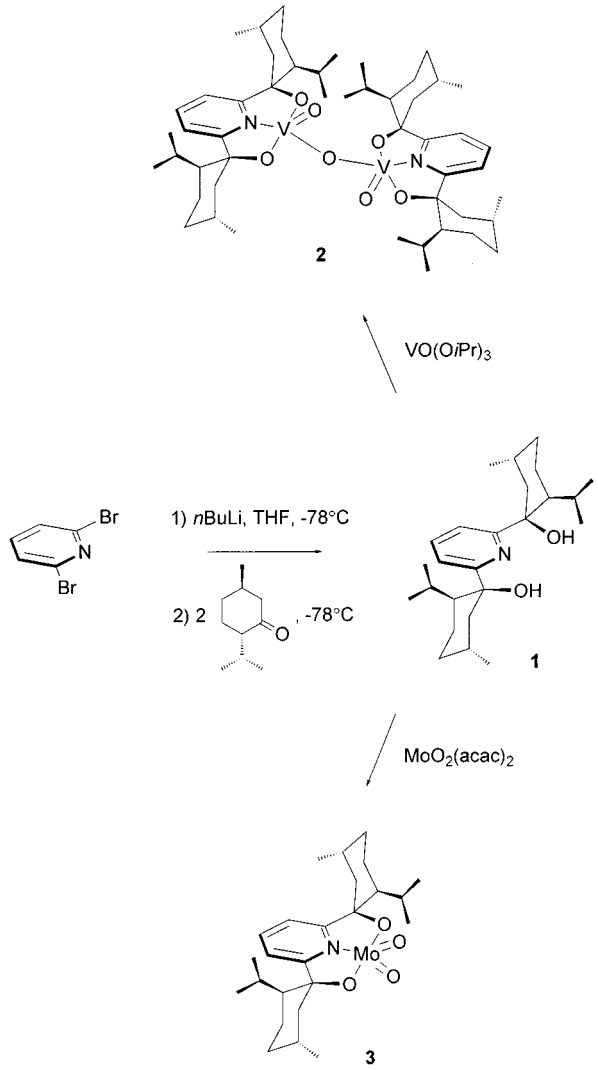
[a] Laboratoire de Chimie des Métaux de Transition et de Catalyse, UMR 7513 au CNRS, Institut Le Bel, Université Louis Pasteur, 4, rue Blaise Pascal, 67070 Strasbourg Cedex, France
E-mail: osborn@chimie.u-strasbg.fr
Fax: (internat.) + 33-388/416-171

Results and Discussion

The new chiral ligand 2,6-bis{(−)-menthyl}pyridine (**1**), characterized by ^1H and ^{13}C NMR spectroscopy, mass spectrometry and microanalysis, is readily prepared by the reaction of 2,6-dilithiopyridine with (−)-menthone. Reaction of the chiral pyridine-diol ligand **1** with $VO(OiPr)_3$ or $MO_2(acac)_2$ resulted in displacement of the weakly coordinated O*i*Pr or acac ligands to give the corresponding vanadium(V) and molybdenum(VI) oxo complexes $[VO(ONO)]_2$(μ-O) **(2)** and $[MoO_2(ONO)]$ **(3)** {ONO = 2,6-bis{(−)-menthyl}pyridine} in high yield (Scheme 1).

It was evident from the ^1H and ^{13}C NMR spectroscopic data that coordination of the C_2 symmetric ligand **1** to vanadium, to give complex **2**, resulted in two nonequivalent menthol moieties. Crystallographic analysis of a suitable crystal showed the complex to be dimeric in the solid state. The molecular structure of $\mathbf{2}\cdot C_6H_{12}$ is shown in Figure 1 and the selected bond lengths and bond angles are given in Table 1. Two five-coordinate vanadium atoms are bridged by an oxygen atom to form the binuclear asymmetric unit of the cell. The binuclear unit of **2** appears to be somewhat unique when compared to other V^V-V^V dimeric oxo complexes[12−14] as the two independent V atoms, V(1) and V(2), contain different coordination geometries. V(1) appears to possess a slightly distorted square pyramidal arrangement of ligands with the oxo ligand in the apical position and the metal center displaced 0.40 Å above the equatorial plane. However, V(2) is best approximated by a trigonal bipyramidal arrangement with the oxo and bridging oxo ligand in the equatorial plane (Figure 1). However, one could argue that V(1) is simply a more distorted trigonal bipyramidal arrangement of ligands than V(2). The V=O distances [V(1)−O(2) = 1.575(5) Å, V(2)−O(5) = 1.600(5) Å]

 © WILEY-VCH Verlag GmbH, D-69451 Weinheim, 2000 1434−1948/00/0707−1645 $ 17.50+.50/0



Scheme 1. Synthesis of complexes **2** and **3**.

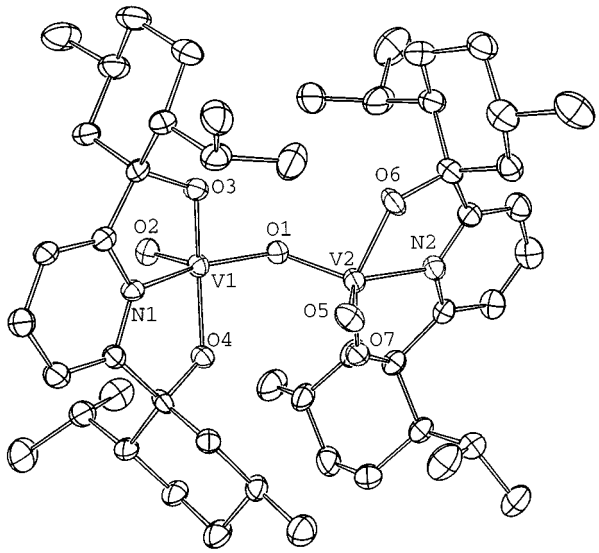


Figure 1. Molecular structure of [(2,6-Bis{(−)-menthyl}pyridine)-VO]$_2$(μ-O)·C_6H_{12} (**2**).

Table 1. Selected bond lengths (Å) and angles (deg) for **2**·C_6H_{12} and **3**·C_6H_{14}

2·C_6H_{12}		**3**·C_6H_{14}	
Bond Lengths			
V(1)−O(1)	1.810(4)	Mo(1)−O(1)	1.763(7)
V(1)−O(2)	1.575(5)	Mo(1)−O(2)	2.438(9)
V(1)−O(3)	1.834(4)	Mo(1)−O(3)	1.694(9)
V(1)−O(4)	1.845(4)	Mo(1)−O(4)	1.911(7)
V(1)−N(1)	2.056(5)	Mo(1)−O(5)	1.916(8)
V(2)−O(1)	1.770(4)	Mo(1)−N(1)	2.17(1)
V(2)−O(5)	1.600(5)	Mo(2)−O(1)	2.426(8)
V(2)−O(6)	1.846(5)	Mo(2)−O(2)	1.754(7)
V(2)−O(7)	1.836(5)	Mo(2)−O(6)	1.692(8)
V(2)−N(2)	2.104(6)	Mo(2)−O(7)	1.924(7)
		Mo(2)−O(8)	1.908(8)
		Mo(2)−N(2)	2.187(9)
Bond Angles			
O(1)−V(1)−N(1)	152.7(2)	O(1)−Mo(1)−O(2)	73.6(3)
O(1)−V(1)−O(2)	107.7(2)	O(1)−Mo(1)−O(3)	105.5(4)
O(1)−V(1)−O(3)	97.0(2)	O(1)−Mo(1)−O(4)	105.6(4)
O(1)−V(1)−O(4)	97.2(2)	O(1)−Mo(1)−O(5)	99.9(4)
N(1)−V(1)−O(2)	99.5(2)	O(1)−Mo(1)−N(1)	155.6(4)
O(2)−V(1)−O(3)	104.0(2)	O(2)−Mo(1)−O(3)	177.4(4)
O(2)−V(1)−O(4)	104.6(2)	O(2)−Mo(1)−O(4)	79.5(3)
V(1)−O(1)−V(2)	128.2(3)	O(2)−Mo(1)−O(5)	82.8(3)
O(1)−V(2)−N(2)	121.5(2)	O(2)−Mo(1)−N(1)	82.3(3)
O(1)−V(2)−O(5)	109.6(2)	O(3)−Mo(1)−O(4)	98.5(4)
O(1)−V(2)−O(6)	100.9(2)	O(3)−Mo(1)−O(5)	98.8(5)
O(1)−V(2)−O(7)	99.3(2)	O(3)−Mo(1)−N(1)	98.7(4)
N(2)−V(2)−O(5)	128.8(2)	O(4)−Mo(1)−O(5)	143.1(4)
O(5)−V(2)−O(6)	98.0(2)	O(4)−Mo(1)−N(1)	72.9(4)
O(5)−V(2)−O(7)	96.6(2)	Mo(1)−O(1)−Mo(2)	105.9(3)
O(6)−V(2)−O(7)	149.3(2)	Mo(1)−O(2)−Mo(2)	105.7(3)

are characteristic of a double bond; however, the difference between the two values is intriguing and may be a consequence of the different coordination geometries of the two metal centers. The bridging oxo bond is unsymmetrical with V(1)−O(1) = 1.810(4) Å and V(2)−O(1) = 1.770(4) Å and the V(1)−O1−V(2) angle is 128.3(3)°, a rare example of a complex having a V−O−V angle near to 120°.[12] The two terminal oxygen atoms are *trans*-directed lying on opposite sides of the VOV plane (Figure 1). The remaining ligand-to-metal bonds are unexceptional.

The ^{1}H and ^{13}C NMR spectra of **3** showed, as expected, one set of resonances for the two menthol groups on the chiral pyridine-diol ligand suggesting the formation of a C_2-symmetric five-coordinate molybdenum dioxo complex. This was confirmed by solution IR spectroscopy which showed two sharp bands of equal intensity at 938 and 918 cm^{-1} for the symmetric and asymmetric stretch of the molybdenum-dioxo unit. However, interestingly, the IR spectrum in the solid state suggests that the molybdenum complex is oligomeric as no sharp or clear Mo=O stretches are observed. This was confirmed by a crystallographic analysis of a suitable crystal of **3**·C_6H_{14}, which revealed two independent five-coordinate mononuclear complexes that are weakly associated by two Mo=O···Mo interactions to give an essentially "binuclear" structure. The molecular structure of **3**·C_6H_{14} is shown in Figure 2, and selected bond lengths and bond angles are given in Table 1. A sim-

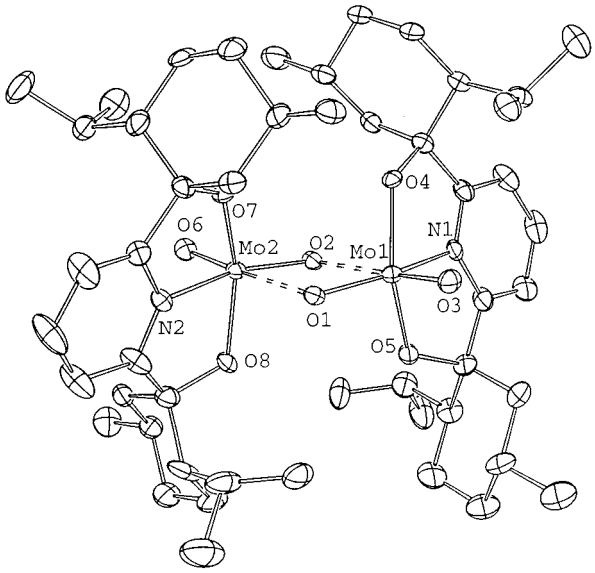


Figure 2. Molecular structure of [(2,6-Bis{(−)-menthyl}pyridine)-MoO_2]·C_6H_{14} (**3**).

ilar interaction can be seen in the structure of $[MoO_2(C_5H_3N\text{-}2,6\text{-}(CH_2O)_2)]_n$[15] where the Mo=O···Mo interaction in this case leads to a "linear" polymeric structure, with the sixth site in the distorted octahedral coordination sphere occupied by an oxo atom of an adjacent molecule. The "dimer" formation of **3** in the solid state provides a new structural type for dioxomolybdenum(VI) complexes. Typically, five-coordinate dioxomolybdenum(VI) complexes have been found to be monomeric[7,16] or polymeric.[15] Complex **3** has a distorted octahedral stereochemistry containing *cis*-oxo groups with the Mo=O unit of the second molecule *trans* to the oxo group. The terminal Mo=O distances [1.694(9) Å, 1.692(8) Å] are similar to other known Mo=O distances.[17] The Mo=O moiety that is found to interact with the second metal center is slightly longer [1.763(7) Å, 1.754(7) Å] than the other Mo=O bond lengths;[17] however, the distances are still short enough to suggest that the Mo=O bond retains much of its double bond character. The Mo···O interactions [2.438(9) Å, 2.426(8) Å] are too large to be considered a formal bond, but are in line with the Mo···O=Mo distance found in the polymeric complex $[MoO_2(C_5H_3N\text{-}2,6\text{-}(CH_2O)_2)]_n$ (2.518(3) Å). However, the Mo···O=Mo angles in **3** [105.88(3)°, 105.72(3)°] are considerably smaller than in the polymeric structure [151.7(2)°].[15] The remaining chiral pyridine-diol ligand bonds to the molybdenum center are unexceptional.

Conclusion

We have demonstrated the facile two-step synthesis of a new, inexpensive, chiral pyridine-diol ligand **1** and its coordination to both V^V and Mo^{VI} metal centers to form the metal oxo complexes **2** and **3**. Preliminary studies show that both complexes **2** and **3** (1 mol-%) are active in the catalytic asymmetric epoxidation of 1-hexene in conjunction with *t*BuOOH: 50% conversion into the epoxide has been observed for both metal complexes with an enantiomeric excess of up to 25%. Further work is underway to optimize the selectivity of this reaction and to test the versatility of complexes **2** and **3**. The coordination properties of the asymmetric ligand **1** to other metal centers will also be investigated further.

Experimental Section

General Remarks: Unless otherwise specified, all reagents were purchased from commercial suppliers and used without purification. All experiments were carried out using dried solvents and under a nitrogen or argon atmosphere, using a Schlenk line or a Vacuum Atmospheres glovebox equipped with a Dri-Train HE-493 inert atmosphere purifier. − ^1H (300 MHz) and $^{13}C\{^1H\}$ (75 MHz) NMR spectra were recorded on a Bruker AC300 NMR spectrometer and referenced to Me_4Si; ^{51}V (105 MHz) NMR spectra were recorded on a Bruker AM400 NMR spectrometer and referenced to $VOCl_3$. − FTIR spectra were recorded using a Perkin−Elmer Model FTIR-1600 spectrometer on KBr discs. − Mass spectrometry and elemental analyses were carried out by the corresponding facilities at the Chemistry Research Center at the Université Louis Pasteur, Strasbourg.

Synthesis of 2,6-Bis{(−)-menthyl}pyridine (1): To a solution of *n*BuLi (69.0 mmol, 43.50 mL, 1.6 M in hexane) in 100 mL of THF was added dropwise a solution of 2,6-dibromopyridine (7.50 g, 31.5 mmol) in 50 mL of THF at −100 °C. After 1 hour at −100 °C and 3 hours at −78 °C, a solution of (−)-menthone (11.55 g, 75.0 mmol) in 25 mL of THF was added slowly. The mixture was then left to warm to room temperature overnight. Distilled water (500 mL) was then added and the organic phase extracted with 2 × 150 mL of diethyl ether. The collected organic phases were washed with a solution of $NaHCO_3$, dried over $MgSO_4$ and the solvents removed under vacuum to afford a yellow oil. This yellow oil was purified by the preparation of the pyridinium salt by reaction with the resolving agent D-(1*S*)-(+)-camphor-10-sulfonic acid. Thus, a solution of D-(1*S*)-(+)-camphor-10-sulfonic acid (7.31 g, 31.5 mmol) in 100 mL of acetonitrile was added to the yellow oil. After reduction of the volume to 40 mL, 250 mL of diethyl ether was added. The flask was then cooled to −25 °C and colorless crystals formed overnight. The crystals were collected, washed with cold diethyl ether and dried under vacuum (8.80 g). Finally, the crystals were dissolved in CH_2Cl_2 and washed with an aqueous solution of $NaHCO_3$. The solution was then dried over $CaSO_4$ and the solvent removed to afford **1** as a colorless oil (4.0 g, 30%), which was shown to be optically pure by chiral HPLC (Chiralcel OD column). − ^1H NMR (300 MHz, $CDCl_3$): δ = 0.66 [d, ^3J = 6.9 Hz, 6 H, CH_3 (menthone)], 0.81 [d, ^3J = 6.8 Hz, 6 H, CH_3 (ment.)], 0.90 [d, ^3J = 6.4 Hz, 6 H, CH_3 (ment.)], 0.95−1.30 [m, 4 H, CH_2 (ment.)], 1.40−2.00 [m, 16 H, CH, CH_2 (ment.)], 4.2 (very broad, OH), 7.33 [d, ^3J = 7.8 Hz, 2 H, CH (arom.)], 7.70 [t, ^3J = 7.8 Hz, 1 H, CH (arom.)]. − $^{13}C\{^1H\}$ NMR (75 MHz, $CDCl_3$): δ = 18.5 [2 CH_3 (ment.)], 21.6 [2 CH_2 (ment.)], 22.2 [2 CH (ment.)], 23.4 [2 CH (ment.)], 27.2 [2 CH_3 (ment.)], 28.4 [2 CH_3 (ment.)], 35.1 [2 CH_2 (ment.)], 50.0 [2 CH_2 (ment.)], 49.6 [2 CH (ment.)], 78.0 (2 C−OH), 117.1 [2 C (arom.)], 137.4 [C (arom.)], 163.7 [2 C (arom.)]. − IR (KBr): $\tilde{\nu}$ = 3462 (s br), 2952 (s), 2868 (s), 1580 (w), 1577 (m), 1456 (s), 1386 (m), 1366 (m), 1294 (w), 1264 (w), 1165 (m), 1160 (m), 1094 (w), 1058 (m), 1023 (w), 978 (w), 948 (m), 910 (w), 891 (w), 852 (w), 807 (m), 756 (m), 714 (w), 671 (w), 641 (w), 516 (w) cm^{-1}. − MS (EI +): *m*/*z* = 387.3 [M^+]. − $C_{25}H_{41}NO_2$ (387.61): calcd. C 77.47, H 10.66, N 3.61; found C 77.36, H 10.45, N 3.62.

Synthesis of [(2,6-Bis{(−)-menthyl}pyridine)VO]$_2$(μ-O) (2): Ligand **1** (0.120 g, 0.31 mmol) was dissolved in CH_2Cl_2 (5 mL), treated with [VO(O*i*Pr)$_3$] (0.073 g, 0.30 mmol) and stirred for 2 hours at room temperature. The solvent was then removed under vacuum and the resulting solid redissolved in ether (3 mL). Distilled water (5 μL) was then added and the solution left to crystallize overnight at 4 °C. The resulting yellow crystals were collected and dried under vacuum (120 mg, 86%). − ^{1}H NMR (300 MHz, $CDCl_3$): δ = 0.73 [d, ^3J = 6.9 Hz, 6 H, CH_3 (menthone)], 0.81 [d, ^3J = 6.9 Hz, 6 H, CH_3 (ment.)], 0.87 [d, ^3J = 6.7 Hz, 6 H, CH_3 (ment.)], 0.90 [d, ^3J = 6.6 Hz, 6 H, −CH_3 (ment.)], 1.09 [d, ^3J = 6.8 Hz, 12 H, CH_3 (ment.)], 1.20−2.20 [m, 30 H, CH_2, CH (ment.)], 2.65 [m, 2 H, CH (ment.)], 7.14 [d, ^3J = 7.6 Hz, 2 H, CH (arom.)], 7.16 [d, ^3J = 7.7 Hz, 2 H, CH (arom.)], 7.88 (dd, ^3J = 7.7 Hz 2 H, CH (arom.)]. − ^{13}C {^{1}H} NMR (75 MHz, $CDCl_3$): δ = 19.0 [CH_3 (ment.)], 19.4 [CH_3 (ment.)], 21.4 [CH_2 (ment.)], 22.0 [CH_2 (ment.)], 22.4 [CH (ment.)], 22.7 [CH (ment.)], 23.9 [CH (ment.)], 24.2 (CH (ment.)], 28.3 [CH_3 (ment.)], 35.5 [CH_2 (ment.)], 50.7 [CH_2 (ment.)], 51.7 [CH (ment.)], 99.2 [C (ment.)], 99.7 [C (ment.)], 117.0 [CH (arom.)], 117.3 [CH (arom.)], 141.6 [CH (arom.)], 175.7 [C (arom.)]. − ^{51}V NMR (105 MHz, $CDCl_3$): δ = −533 ($\nu_{1/2}$ = 163 Hz). − IR (KBr): $\tilde{\nu}$ = 3069 (w), 2949 (s br), 2865 (s br), 1600 (m), 1579 (m), 1466 (s), 1384 (w), 1365 (w) 1296 (m), 1205 (w), 1144 (w), 1057 (w), 976 (s), 949 (s), 900 (w), 864 (w), 808 (m), 761 (s), 714 (s), 596 (m), 530 (m), 516 (m) cm^{-1}. − MS (CI (−)]: *m*/*z* (%) = 469.3 (100) 1/2 [M + H]$^-$. − $C_{50}H_{78}N_2O_7V_2$ (921.05): calcd. C 65.20, H 8.54; found C 66.11, H 8.48.

Synthesis of [(2,6-Bis{(−)-menthyl}pyridine)MoO$_2$] (3): [MoO_2(acac)$_2$] (0.820 g, 2.51 mmol) was dissolved in MeOH (40 mL) and treated with ligand **1** (1.00 g, 2.58 mmol). The solution was then refluxed for 30 mins and, upon cooling, a white precipitate was formed. The reaction mixture was filtered and the white solid dried in vacuo (0.900 g, 70%). − ^{1}H NMR (300 MHz, $CDCl_3$): δ = 0.78 [d, ^3J = 6.8 Hz, 6 H, CH_3 (menthone)], 0.93 [d, ^3J = 6.3 Hz, 6 H, CH_3 (ment.)], 0.95 [d, ^3J = 6.7 Hz, 6 H, CH_3 (ment.)], 1.01−2.01 [m, 18 H, CH_2, CH (ment.)], 7.34 [d, ^3J = 7.7 Hz, 2 H, CH (arom.)], 8.14 (dd, ^3J = 7.7 Hz, 1 H, CH (arom.)]. − ^{13}C {^{1}H} NMR (75 MHz, $CDCl_3$): δ = 18.9 [CH_3 (ment.)], 21.8 [CH_2 (ment.)], 22.1 [CH (ment.)], 23.9 [CH (ment.)], 28.4 [CH_3 (ment.)], 34.9 [CH_2 (ment.)], 50.1 [CH_2 (ment.)], 51.1 [CH (ment.)], 98.9 [C (ment.)], 118.4 [CH (arom.)], 143.7 [CH (arom.)], 173.3 [C (arom.)]. − IR (KBr): $\tilde{\nu}$ = 3071 (w), 2950 (s br), 1605 (m), 1578 (m), 1469 (s), 1384 (m), 1363 (m), 1297 (s), 1205 (m), 1173 (m), 1145 (m), 1106 (w), 1093 (w), 1062 (s), 1030 (m) 1010 (m), 978 (s), 936 (s br), 860 (s), 835 (m), 802 (m), 759 (m), 708 (s), 674 (w), 626 (w), 588 (m), 552 (m), 515 (s), 478 (m), 373 (w) cm^{-1}. − IR (CH_2Cl_2): $\tilde{\nu}$ = 938 ($\nu_{(Mo=O)}$, symmetric), 918 ($\nu_{(Mo=O)}$, asymmetric) cm^{-1}. − MS (EI +): *m*/*z* = 515.2 [M$^+$]. − $C_{25}H_{39}MoNO_4$ (513.52): calcd. C, 58.47, H 7.65, N 2.73; found C 58.53, H 7.77, N 2.89.

X-ray Crystallographic Study: The oxo complexes **2**·C_6H_{12} and **3**·C_6H_{14} were crystallized by slow diffusion of cyclohexane and hexane, respectively, layered onto a solution of the complex in dichloromethane. The intensity data were obtained at 173 K with graphite monochromated Mo-K_α radiation (λ = 0.71073 Å) on a Nonius Kappa CCD diffractometer. The structures were solved using direct methods and refined against $|F|$. Hydrogen atoms were introduced as fixed contributors. For all computations the Enraf−Nonius MolEN package was used.[18] Additional data collection and refinement parameters are presented in Table 2.[19] The absolute configuration of each compound was determined and confirmed: Flack parameters were 0.08(3) for **2**·C_6H_{12} and 0.03(7) for **3**·C_6H_{14}.

Table 2. Crystal data and summary of intensity data collection and structure refinement of **2**·C_6H_{12} and **3**·C_6H_{14}

Emperical formula	**2**·C_6H_{12} $C_{50}H_{78}N_2O_7V_2\cdot C_6H_{12}$	**3**·C_6H_{14} $C_{50}H_{78}N_2O_8Mo_2\cdot C_6H_{14}$
fw	1005.23	1113.25
space group	$P2_1$	$P2_12_12_1$
a/Å	13.091(1)	14.026(1)
b/Å	15.574(1)	16.512(1)
c/Å	15.019(1)	24.694(1)
α/°	90	90
β/°	111.54(1)	90
γ/°	90	90
V/Å^3	2848.2(3)	5719.0(8)
Z	2	4
*ρ*calc/g cm^{-3}	1.17	1.29
μ/mm^{-1}	0.363	0.476
diffractometer	KappaCCD	KappaCCD
T/K	173	173
scan type	phi scans	phi scans
no. of data meas.	21383	25775
no. of data used	3469	3359
criterion	$I > 3\sigma(I)$	$I > 3\sigma(I)$
no. of variables	603	613
R[a]	0.041	0.050
R_w[b]	0.061	0.074
Flack × param	0.08(3)	0.03(7)
largest peak (eÅ^{-3})	0.400	0.486
GOF[c]	1.221	1.048

[a] $R = \Sigma||F_o| - |F_c||/\Sigma|F_o|$. − [b] $R_w = [\Sigma w(|F_o| - |F_c|)^2/\Sigma w(F_o^2)]^{1/2}$. − [c] GOF = $[\Sigma w(|F_o| - |F_c|)^2/(N_o - N_v)]^{1/2}$.

Acknowledgments

We gratefully acknowledge the support of this work by the Centre National de la Recherche Scientifique and we would like to thank Nathalie Gruber, Dr. André De Cian and Prof. Jean Fischer for X-ray analyses and Dr. Marie-Thérèse Youinou for helpful discussions. K. S. C. also wishes to thank the European Commission and P. D. the Deutsche Forschungsgemeinschaft for their support.

[1] T. Hirrao, *Chem. Rev.* **1997**, *97*, 2707−2714.
[2] R. H. Holm, *Chem. Rev.* **1987**, *87*, 1401−1449.
[3] R. Wewer, M. B. E. Kreenn, in *Vanadium in Biological Systems* (Ed.: N. D. Chasteen), Kluwer Academic Publishers, Dordrecht, **1990**.
[4] B. E. Schultz, S. F. Gheller, M. C. Muetterties, M. J. Scott, R. H. Holm, *J. Am. Chem. Soc*. **1993**, *115*, 2714−2722.
[5] A. Butler, M. U. Clague, G. E. Meister, *Chem. Rev.* **1994**, *94*, 625−635.
[6] V. Conte, F. DiFuria, C. Licini, *Appl. Catal. A*. **1997**, *157*, 335−361.
[7] J. M. Hawkins, J. C. Dewan, K. B. Sharpless, *Inorg. Chem.* **1986**, *25*, 1501−1503.
[8] J. M. Hawkins, K. B. Sharpless, *Tetrahedron Lett.* **1987**, *28*, 2825−2828.
[9] C. Bolm, F. Bienwald, *Angew. Chem. Int. Ed. Engl.* **1995**, *34*, 2640−2642.
[10] W. A. Hermann, G. M. Lobmaier, T. Priermeier, M. R. Mattner, B. Scharbert, *J. Mol Cat. A* **1997**, *117*, 455−469.
[11] B. Scharbert, G. Lobmaier, W. A. Hermann, DE Patent Appl. 4,447,231 (Cl B01J31/16).
[12] J. Dai, S. Akiyama, M. Munakata, M. Mikuriya, *Polyhedron* **1994**, *13*, 2495−2499.
[13] S. Dutta, P. Basu; A. Chakravorty, *Inorg. Chem*. **1993**, *32*, 5343−5348.
[14] U. Casellato, P. A. Vigato, R. Graziani, M. Vidali, F. Milani, M. M. Musiani, *Inorg. Chim. Acta*. **1982**, *61*, 121−128.
[15] J. M. Berg, R. H. Holm, *Inorg. Chem*. **1983**, *22*, 1768−1771.
[16] J. M. Berg, R. H. Holm, *J. Am. Chem. Soc*. **1984**, *106*, 3035−3036.

[17] A. G. Orpen, L. Brammer, F. H. Allen, O. Kennard, D. G. Watson, R. Taylor, *J. Chem. Soc., Dalton Trans.* **1989**, S1.
[18] *OpenMolEN*, *Interactive Structure Solution,* B. V. Nonius Delft, The Netherlands, **1997**.
[19] Crystallographic data (excluding structure factors) for the structure(s) included in this paper have been deposited with the Cambridge Crystallographic Data Centre as supplementary publication no. CCDC-137162 (**2**·C_6H_{12}) and -137163 (**3**·C_6H_{14}). Copies of the data can be obtained free of charge on application to CCDC, 12 Union Road, Cambridge CB2 1EZ, UK [Fax: (internat.) + 44-1223/336-033; E-mail: deposit@ccdc.cam.ac.uk].

Received December 30, 1999
[I99476]

Mononuclear Ruthenium and Hetero-Tetranuclear Ruthenium-Silver Complexes Containing the Unsymmetrical Bidentate Ligands $R_2P(CH_2)_nER'_2$ (n = 1, 2; E = P, As) as Chelating or Bridging Units

Guido Fries,[a] Birgit Weberndörfer,[a] Kerstin Ilg,[a] and Helmut Werner*[a]

Dedicated to Professor Gerhard Roewer on the occasion of his 60th birthday

Keywords: Arene complexes / Heteronuclear complexes / Ruthenium / Silver / Unsymmetrical chelating ligands

The chelate complexes [(*p*-cym)RuCl(κ²-$Ph_2PCH_2CH_2As$*t*Bu_2)]PF_6 (**3**), [(arene)RuCl(κ²-$Ph_2PCH_2CH_2PR_2$)]PF_6 (**4**, **7**, **8**) and [(*p*-cym)RuCl(κ²-*i*Pr_2PCH_2As*t*Bu_2)]PF_6 (**11**) were prepared either from [(arene)RuCl(NCMe)$_2$]PF_6 (**1**, **5**) or from [(arene)$RuCl_2$]$_2$ (**2**, **6**), in the presence of NH_4PF_6 or $AgPF_6$. The stepwise reaction of [(*p*-cym)$RuCl_2$]$_2$ (**2**) with Ph_2P-CH_2CH_2P*t*Bu_2 and $AgPF_6$ gave the hetero-tetranuclear compound [{(*p*-cym)RuAg(μ-Cl)$_2$(μ-P^1_{Ru},P^2_{Ag}-$Ph_2P^1CH_2CH_2P^2$-*t*Bu_2)}$_2$]$(PF_6)_2$ (**9**), the structure of which was determined by an X-ray crystal structure analysis. The bidentate As,O donor $Ph_2P(O)CH_2CH_2As$*t*Bu_2 also reacted with **2**, in the presence of $AgPF_6$, to afford the chelate complex [(*p*-cym)RuCl-{κ²(*As*,*O*)-$Ph_2P(O)CH_2CH_2As$*t*Bu_2}]PF_6 (**10**), which was also characterized crystallographically.

Introduction

In the search for new, possibly hemilabile, bidentate ligands, we recently described a simple and fairly general one-pot synthesis for unsymmetrical 1,2-bis(phosphanyl)-ethanes and 1-arsanyl-2-phosphanylethanes with and without a stereogenic center.[1] In an initial attempt, we tested the coordination properties of one of the new ligands, $Ph_2PCH_2CH_2P$*i*Pr_2, towards ruthenium(II) and prepared a series of octahedral complexes including [Ru{κ²(*O*,*Cl*)-OC_6Cl_5}$_2$($Ph_2PCH_2CH_2P$*i*Pr_2)] in which the pentachlorophenolate anions behave as chelating ligands.[1,2] In the last decade the chemistry of (arene)ruthenium(II) complexes has attracted a great deal of attention[3] and so we became interested in finding out whether the compounds $Ph_2PCH_2CH_2PR_2$ and $Ph_2PCH_2CH_2AsR_2$, even with bulky substituents R such as *tert*-butyl or cyclohexyl, could also bind to an [(arene)RuCl]$^+$ fragment in a chelating fashion. The present paper reports the preparation of several complexes of the general type [(arene)RuCl(L−L′)]PF_6, and describes the isolation and structural characterization of a novel dicationic tetranuclear Ru_2Ag_2 compound in which two $Ph_2PCH_2CH_2P$*t*Bu_2 ligands bridge the Ru^{II} and Ag^{I} metal centers.

Results and Discussion

The preparation of the chelate complexes **3**, **4** and **7**, **8** (see Scheme 1) can be achieved by two different routes, using either the cationic bis(acetonitrile)ruthenium(II) compounds **1** and **5**[4] or the well-known (arene)ruthenium dichloride dimers **2** and **6** as the starting materials. While **1** and **5** react quite smoothly with the new unsymmetrical 1,2-bis(phosphanyl)- or 1-arsanyl-2-phosphanylethanes in acetonitrile at room temperature to give the half-sandwich-type complexes **3**, **4** and **7**, **8**, respectively, the dimers **2** and **6** are somewhat less reactive and only in the presence of NH_4PF_6 or $AgPF_6$, in dichloromethane as solvent, do they afford the products in good yields.

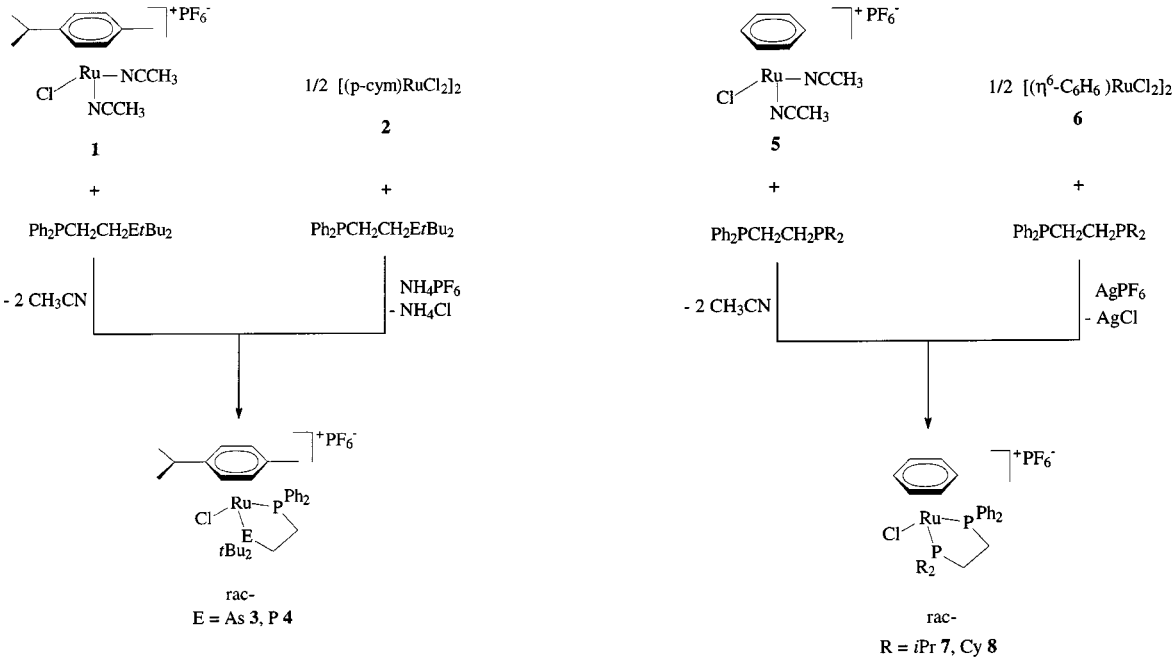
Compounds **3**, **4** and **7**, **8** are orange, air-stable solids that are soluble in polar solvents such as CH_2Cl_2, THF, methanol, or acetone, and which have been characterized both by elemental analysis and conductivity measurements. Compared to the free ligands $Ph_2PCH_2CH_2PR_2$ and $Ph_2PCH_2CH_2As$*t*Bu_2, the resonances in the ^{31}P-NMR spectra of **3**, **4**, **7**, and **8** are shifted to significantly lower fields, the difference in the chemical shifts being 50−90 ppm.

The unusual tetranuclear complex **9** (Scheme 2) is obtained if the reaction of **2** with $Ph_2PCH_2CH_2P$*t*Bu_2 is carried out in the presence of $AgPF_6$ instead of NH_4PF_6. In contrast to **4**, which also contains $Ph_2PCH_2CH_2P$*t*Bu_2 as a ligand, the ^{31}P-NMR spectrum of **9** displays, besides the signal for the PF_6^- anion, a doublet at δ = 28.0 and two doublet of doublets at δ = 68.0 and 67.9, which arise from the coupling of the ^{31}P nuclei of the P*t*Bu_2 unit with the silver isotopes ^{107}Ag and ^{109}Ag, respectively. The resulting coupling constants $J(^{31}P^{107}Ag)$ = 643.0 Hz and $J(^{31}P^{109}Ag)$ = 743.3 Hz are considerably larger than in a variety of (phosphane)silver(I) complexes.[5] Similar $J(^{31}P^{107}Ag)$ and $J(^{31}P^{109}Ag)$ values (657.5 and 758.8 Hz) have recently been observed for the tris(pyrazolyl)borato compound [{HB[3,5-$(CF_3)_2$pz]$_3$}Ag(PPh_3)] where the coordination number of Ag^{I} is four.[6]

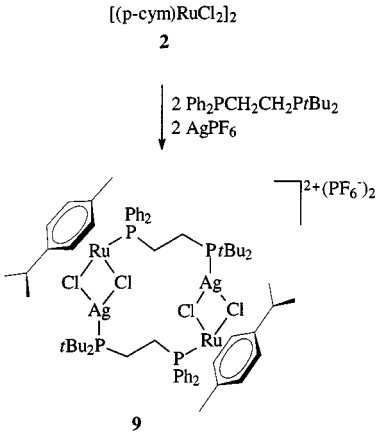
The result of the X-ray crystal structure analysis of the cation of **9** is shown in Figure 1. The coordination sphere around the two ruthenium centers in the centrosymmetric dimer corresponds to that of a half-sandwich-type molecule

[a] Institut für Anorganische Chemie der Universität Würzburg
Am Hubland, 97074 Würzburg, Germany

 © WILEY-VCH Verlag GmbH, D-69451 Weinheim, 2000 1434−1948/00/0707−1651 $ 17.50+.50/0



Scheme 1



Scheme 2

with the tridentate *p*-cymene, the phosphorus atom of the PPh_2 unit and the two chlorine atoms Cl1 and Cl2 occupying the six coordination sites. The geometry around the two silver centers is distorted trigonal-planar, one angle (Cl1−Ag2−P2A) being nearly 120° while the two others (Cl2−Ag2−P2A and Cl1−Ag2−Cl2) deviate significantly from the value expected for an sp^2-hybridized metal atom. The distance Ag2−P2A of 2.3592(1) Å is somewhat shorter than in the anionic species $[Cl(C_6Cl_5)_2Pt(\mu\text{-}Cl)Ag(PPh_3)]^-$ [2.395(2) Å][7] and in the neutral compounds $[(PPh_3)_2Ag(\mu\text{-}Cl)_2OsCl_2(\mu\text{-}Cl)_2Ag(PPh_3)_2]$ [2.452(3) and 2.455(3) Å][8] and $[(PPh_3)_2Ag(\mu\text{-}Cl)_2Co(\mu\text{-}Cl)_2Ag(PPh_3)_2]$ (2.43−2.47 Å).[9] The most remarkable feature, however, is the short bond length Ag2−Cl2 [2.4707(18) Å], which is not only much shorter than the distance Ag2−Cl1 [2.7261(19) Å] but also differs from the Ag−Cl bond lengths found in other chloride-bridged silver-metal complexes.[7,8,9] In contrast to the distances Ag2−Cl1 and Ag2−Cl2, the bond lengths Ru1−Cl1 and Ru1−Cl2 are almost identical [2.4234(17) and 2.4432(18) Å] and only slightly longer than those in the mononuclear compounds $[(arene)RuCl_2(L)]$.[10] We note that quite recently a tetranuclear Ru_2Ag_2 complex has been reported in which an $Ag(\mu\text{-}iPr_2PCH_2CH_2PiPr_2)Ag$ fragment is linked to two phenylethynyl ligands, each of which is σ-bonded to one ruthenium center.[11]

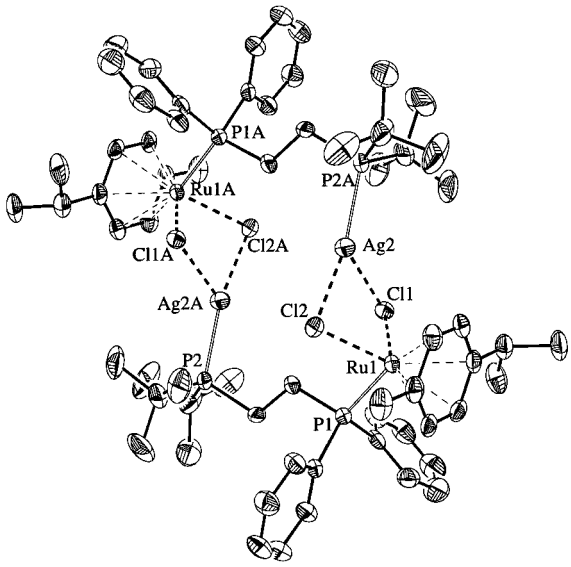


Figure 1. Molecular structure (ORTEP plot) of **9**; the PF_6^- ions are omitted for clarity; selected bond lengths [Å] and angles [°]: Ru1−P1 2.3608(17), Ru1−Cl1 2.4234(17), Ru1−Cl2 2.4432(18), Ag2−Cl1 2.7261, Ag2−Cl2 2.4707(18), Ag2−P2A 2.3592(19); P1−Ru1−Cl1 84.50(6), P1−Ru1−Cl2 88.28(6), Cl1−Ru1−Cl2 87.31(6), Ru1−Cl1−Ag2 82.70(5), Ru1−Cl2−Ag2 87.88(6), Cl1−Ag2−P2A 121.69(6), Cl2−Ag2−P2A 157.48(6), Cl1−Ag2−Cl2 80.39(5)

The observation that not only the 1,2-bis(phosphanyl)-ethanes $Ph_2PCH_2CH_2PR_2$ (R = *i*Pr, *t*Bu, Cy) but also the As,P counterpart $Ph_2PCH_2CH_2AstBu_2$ is easily oxidized to

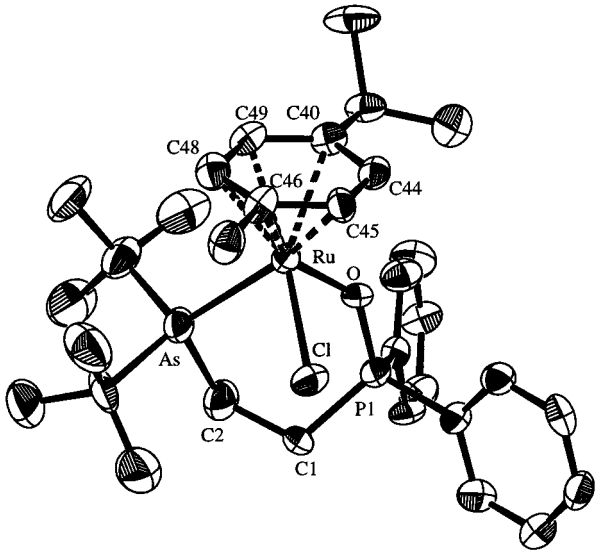
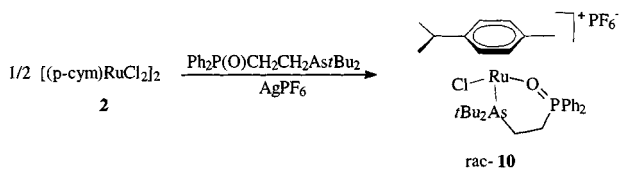


Figure 2. Molecular structure (ORTEP plot) of **10**; the PF_6^- ion is omitted for clarity; selected bond lengths [Å] and angles [°]: Ru−As 2.5490(11), Ru−O 2.141(5), Ru−Cl 2.386(2), P1−O 1.510(5), Ru−C40 2.215(7), Ru−C44 2.201(8), Ru−C45 2.198(8), Ru−C46 2.212(7), Ru−C48 2.171(8), Ru−C49 2.176(7); As−Ru−O 83.49(13), As−Ru−Cl 87.67(6), Cl−Ru−O 88.19(14), Ru−O−P1 135.7(3), Ru−As−C2 111.7(2), As−C2−C1 116.2(6), P1−C1−C2 110.0(6), O−P1−C1 113.9(3)

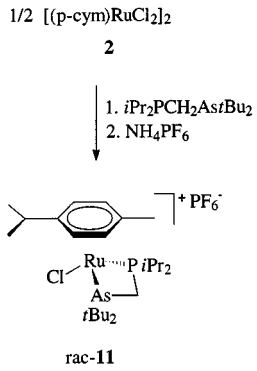
the corresponding oxide $Ph_2P(O)CH_2CH_2AstBu_2$, prompted us to use this molecule as a ligand in (arene)ruthenium(II) chemistry. Treating a solution of the oxide $Ph_2P(O)CH_2CH_2AstBu_2$, generated in situ from the precursor $Ph_2PCH_2CH_2AstBu_2$ and molecular oxygen, with a solution of **2** in CH_2Cl_2, in the presence of one equivalent of $AgPF_6$, leads to the formation of the PF_6 salt of the cationic complex **10** (Scheme 3) in which the oxophosphorane forms a six-membered chelate ring with the metal center. The dark-red solid is air-stable and readily soluble in THF, nitromethane and methanol. The resonance in the ^{31}P-NMR spectrum of **10** appears at $\delta = 53.8$ and is shifted by ca. 17 ppm upfield compared to the corresponding signal for **3**. In the latter compound the nonoxidized ligand $Ph_2PCH_2CH_2AstBu_2$ is coordinated to the ruthenium center rather than $Ph_2P(O)CH_2CH_2AstBu_2$.

The molecular structure of the cation of **10** is shown in Figure 2. The single crystals, which were grown from a solution in methanol, contained only one enantiomer of the cationic (arene)ruthenium complex in which, owing to the calculated structural parameter x of −0.025(15), the asymmetric metal center possesses the (*R*) configuration.[12] In analogy to the situation in **9**, the coordination geometry around the ruthenium center is pseudo-octahedral with the arsenic, the oxygen and the chlorine atoms bonded opposite to the tridentate *p*-cymene ligand. The distance Ru−Cl [2.386(2) Å] is ca. 0.05 Å shorter than the two Ru−Cl bond lengths in **9** but quite similar to the Ru−Cl distances found in other cationic (arene)(chloro)ruthenium(II) complexes.[13] The Ru−As bond length [2.5490(11) Å] is slightly longer than the average Ru−As distance in the neutral compounds *trans*-$[RuI_2(AsMe_2Ph)_4]$ [2.458−2.504 Å][14] and $[RuCl_2(CO)_2(AsPh_3)_2]$ [2.4927(6) Å, 2.4855(6) Å],[15] where six monodentate ligands are bonded to the ruthenium(II) ion. The distances Ru−O and P1−O are nearly the same as in the related cations $[(p\text{-cym})RuCl\{\kappa^2(P,O)\text{-}Ph_2P(O)CH_2PPh_2\}]^+$ and $[(p\text{-cym})RuCl\{\kappa^2(P,O)\text{-}Ph_2P(O)CH(CH_3)PPh_2\}]^+$, which were quite recently prepared by Faller et al. and structurally characterized as the SbF_6^- salts.[16]



Scheme 3

To compare the ligand behavior of 1-arsanyl-2-phosphanylethanes and (arsanyl)(phosphanyl)methanes, the reaction of the starting material **2** with $iPr_2PCH_2AstBu_2$ was also carried out. After heating the two substrates in ethanol, the cationic complex $[(p\text{-cym})RuCl\{\kappa^2\text{-}iPr_2PCH_2AstBu_2\}]^+$ with chloride as the counterion was formed, which upon salt metathesis with NH_4PF_6 gave **11** in 80% yield (Scheme 4). Similarly to **3**, compound **11** is a yellow air-stable solid that is soluble in polar solvents and, in nitromethane, shows the conductivity of a 1:1 electrolyte. The chemical shift of the singlet resonance in the ^{31}P-NMR spectrum of **11** indicates a chelate coordination of the unsymmetrical bidentate As,P ligand to the ruthenium center.[17] In agreement with the structural proposal, the ^{1}H-NMR spectrum of **11** displays two signals at $\delta = 3.41$ and 3.22 for the CH_2 protons of the $AsCH_2P$ unit and, due to P−H and H−H couplings, these are split into doublets of doublets.



Scheme 4

Conclusions

The work presented in this paper has shown that 1,2-bis(phosphanyl)ethanes as well as 1-arsanyl-2-phosphanylethanes, regardless of the bulk of the PR_2 or AsR_2 units, prefer to coordinate to a cationic $[(arene)RuCl]^+$ fragment in a chelating fashion. Only in the presence of silver(I) as an additional metal center was a heteronuclear Ru_2Ag_2 complex isolated and, in this case, the unsymmetrical bidentate ligand $Ph_2PCH_2CH_2PtBu_2$ binds in a bridging mode. Although four-membered chelate rings are generally less favored than five-membered rings, the methane derivat-

ive iPr$_2$PCH$_2$AstBu$_2$, like Ph$_2$PCH$_2$CH$_2$AstBu$_2$, generates a chelate complex with [(p-cym)RuCl]$^+$ as a building block.

Experimental Section

All operations were carried out under argon using Schlenk techniques. The starting materials **1**, **5**,[4] **2** and **6**[18] as well as the ligands iPr$_2$PCH$_2$AstBu$_2$,[19] Ph$_2$PCH$_2$CH$_2$AstBu$_2$ and Ph$_2$PCH$_2$CH$_2$PR$_2$ (R = iPr, tBu, Cy)[1,2] were prepared as described in the literature. − NMR: Bruker AC 200 and AMX 400. − Conductivity measurements (in nitromethane): Schott conductometer CG 851. − Melting points determined by DTA.

1. Preparation of [(p-cym)RuCl(κ^2-Ph$_2$PCH$_2$CH$_2$AstBu$_2$)]PF$_6$ (3): (a) A solution of 120 mg (0.2 mmol) of **1** in 3 mL of CH$_3$CN was treated dropwise with a solution of 97 mg (0.2 mmol) of Ph$_2$PCH$_2$CH$_2$AstBu$_2$ in 3 mL of CH$_3$CN at room temperature. A change of color from yellow to orange occurred. The solution was concentrated to dryness in vacuo, the residue was washed with 5 mL of pentane and dried. An orange microcrystalline solid was obtained; yield 128 mg (65%). − (b) A suspension of 133 mg (0.2 mmol) of **2** in 5 mL of CH$_2$Cl$_2$ was treated with 177 mg (0.4 mmol) of Ph$_2$PCH$_2$CH$_2$AstBu$_2$ and stirred for 2 h at room temperature. A solution of 72 mg (0.4 mmol) of NH$_4$PF$_6$ in 3 mL of CH$_2$Cl$_2$ was added and the resulting reaction mixture was stirred for 2 h and then filtered. The filtrate was concentrated to dryness in vacuo, the residue was washed with 10 mL of ether and dried. An orange microcrystalline solid was obtained; yield 216 mg (60%); m.p. 145 °C (dec.). − Conductivity Λ = 74.3 cm^{2}Ω^{-1}mol^{-1}. − ^{1}H NMR (400 MHz, CD$_2$Cl$_2$): δ = 7.65−7.30 (m, 10 H, C$_6$H$_5$), 6.50 [d, 1 H, J(HH) = 5.8 Hz, 1 × H of C$_6$H$_4$], 6.37, 5.85 [both d, 1 H each, J(HH) = 6.2 Hz, 2 × H of C$_6$H$_4$], 5.64 [d, 1 H, J(HH) = 5.8 Hz, 1 × H of C$_6$H$_4$], 3.28−3.23 (br m, 1 H, 1 × H of PCH$_2$CH$_2$As), 2.76 [sept, 1 H, J(HH) = 7.0 Hz, CH$_3$C$_6$H$_4$CH(CH$_3$)$_2$], 2.50−2.43, 2.31−2.22, 1.91−1.82 (each br m, 3 H, 3 × H of PCH$_2$CH$_2$As), 1.52, 1.36 (both s, 9 H each, AsCCH$_3$), 1.35, 1.30 [both d, 3 H each, J(HH) = 7.0 Hz, CH$_3$C$_6$H$_4$CH(CH_3)$_2$], 1.04 [s, 3 H, CH_3C$_6$H$_4$CH(CH$_3$)$_2$]. − ^{13}C NMR (100.6 MHz, CD$_2$Cl$_2$): δ = 135.5 [d, J(PC) = 42.9 Hz, *ipso*-C of C$_6$H$_5$], 134.0 [d, J(PC) = 8.6 Hz, C$_6$H$_5$], 133.1 [d, J(PC) = 58.2 Hz, *ipso*-C of C$_6$H$_5$], 131.8 [d, J(PC) = 8.6 Hz, C$_6$H$_5$], 131.6 [d, J(PC) = 5.7 Hz, C$_6$H$_5$], 131.6 (s, C$_6$H$_5$), 129.6 [d, J(PC) = 9.5 Hz, C$_6$H$_5$], 129.0 [d, J(PC) = 10.5 Hz, C$_6$H$_5$], 126.1 [d, J(PC) = 5.7 Hz, C$_6$H$_4$], 98.4, 92.3, 89.7, 89.0 (all s, C$_6$H$_4$), 86.2 [d, J(PC) = 8.6 Hz, C$_6$H$_4$], 46.7, 42.0 (both s, AsCCH$_3$), 32.0 (s, AsCCH$_3$), 30.6 [s, CH$_3$C$_6$H$_4$$C$H(CH$_3$)$_2$], 30.1 (s, As$CCH_3$), 29.8 [d, J(PC) = 35.3 Hz, PCH$_2$CH$_2$As], 22.8, 20.8 [both s, CH$_3$C$_6$H$_4$CH(CH$_3$)$_2$], 19.3 [d, J(PC) = 8.6 Hz, PCH$_2$$CH_2$As], 15.3 [s, CH$_3C_6H_4$CH(CH$_3$)$_2$]. − ^{31}P NMR (162.0 MHz, CD$_2$Cl$_2$): δ = 71.1 (s, Ph$_2$P), −144.3 [sept, J(FP) = 710.6 Hz, PF$_6^-$]. − C$_{32}$H$_{46}$AsClF$_6$P$_2$Ru (818.1): calcd. C 46.98, H 5.67; found C 46.43, H 5.15.

2. Preparation of [(p-cym)RuCl(κ^2-Ph$_2$PCH$_2$CH$_2$PtBu$_2$)]PF$_6$ (4): (a) In an analogous way to that described for **3** [method (a)] using 174 mg (0.4 mmol) of **1** and 127 mg (0.4 mmol) of Ph$_2$PCH$_2$CH$_2$PtBu$_2$ as starting materials. Yield 203 mg (75%). − (b) In an analogous way to that described for **3** [method (b)] using 162 mg (0.3 mmol) of **2**, 191 mg (0.5 mmol) of Ph$_2$PCH$_2$CH$_2$PtBu$_2$ and 86 mg (0.5 mmol) of NH$_4$PF$_6$ as starting materials. Orange microcrystalline solid; yield 287 mg (70%); m.p. 152 °C (dec.). − Conductivity Λ = 61.8 cm^{2}Ω^{-1}mol^{-1}. − ^{1}H NMR (400 MHz, CD$_2$Cl$_2$): δ = 7.68−7.35 (m, 10 H, C$_6$H$_5$), 6.45, 6.18, 5.95, 5.46 [all d, 1 H each, J(HH) = 6.2 Hz, C$_6$H$_4$], 3.31−3.19 (br m, 2 H, PCH_2CH$_2$P), 2.81−2.77 (br m, 1 H, PCHCH$_3$), 2.60−2.42 (br m, 3 H, PCH$_2$CH_2P and PCHCH$_3$), 2.20 [s, 3 H, CH_3C$_6$H$_4$CH(CH$_3$)$_2$], 1.60−1.10 [m, 24 H, CH$_3$C$_6$H$_4$CH(CH_3)$_2$ and PCCH$_3$]. − ^{13}C NMR (100.6 MHz, CD$_2$Cl$_2$): δ = 136.0 [d, J(PC) = 11.4 Hz, C$_6$H$_5$], 132.8 (m, C$_6$H$_5$), 131.0 [d, J(PC) = 2.9 Hz, C$_6$H$_5$], 129.8 [d, J(PC) = 41.0 Hz, C$_6$H$_5$], 128.8, 128.3 [both d, J(PC) = 10.5 Hz, C$_6$H$_5$], 125.8, 102.9 (both s, C$_6$H$_4$), 93.0 [d, J(PC) = 3.8 Hz, C$_6$H$_4$], 92.2 [d, J(PC) = 2.9 Hz, C$_6$H$_4$], 91.9, 90.3 [both d, J(PC) = 6.7 Hz, C$_6$H$_4$], 36.8 [dd, J(P^{1}C) = 25.7, J(P^{2}C) = 14.3 Hz, PCH$_2$CH$_2$P], 35.2 [dd, J(P^{1}C) = 31.9, J(P^{2}C) = 10.0 Hz, PCH$_2$$CH_2$P], 31.3 [s, CH$_3C_6H_4$$C$H(CH$_3$)$_2$], 28.5 [d, J(PC) = 25.7 Hz, PCCH$_3$], 27.7 [d, J(PC) = 20.0 Hz, PCCH$_3$], 22.4 [s, CH$_3$C$_6$H$_4$CH(CH$_3$)$_2$], 21.7 [d, J(PC) = 2.9 Hz, PCCH$_3$], 20.9 [s, CH$_3$C$_6$H$_4$CH(CH$_3$)$_2$], 20.7 [d, J(PC) = 3.9 Hz, PCCH$_3$], 20.2 [s, CH$_3$C$_6$H$_4$CH(CH$_3$)$_2$]. − ^{31}P NMR (162.0 MHz, CD$_2$Cl$_2$): δ = 85.2 [d, J(PP) = 33.1 Hz, tBu$_2$P], 78.3 [d, J(PP) = 33.1 Hz, Ph$_2$P], −144.9 [sept, J(FP) = 709.5 Hz, PF$_6^-$]. − C$_{32}$H$_{46}$ClF$_6$P$_3$Ru (774.2): calcd. C 49.65, H 5.99; found C 49.64, H 5.76.

3. Preparation of [(η^6-C$_6$H$_6$)RuCl(κ^2-Ph$_2$PCH$_2$CH$_2$PiPr$_2$)]PF$_6$ (7): (a) In an analogous way to that described for **3** [method (a)], by using 163 mg (0.4 mmol) of **5** and 129 mg (0.4 mmol) of Ph$_2$PCH$_2$CH$_2$PiPr$_2$ as starting materials. Yield 207 mg (77%). − (b) A suspension of 273 mg (0.6 mmol) of **6** in 8 mL of CH$_3$CN was treated with 361 mg (1.1 mmol) of Ph$_2$PCH$_2$CH$_2$PiPr$_2$ and 258 mg (1.1 mmol) of AgPF$_6$ and stirred for 2 h at 60 °C. Upon cooling to room temperature, the solvent was removed in vacuo and the residue was extracted with 10 mL of CH$_2$Cl$_2$. The extract was then concentrated to dryness in vacuo, the residue was washed with 10 mL of ether and dried. An orange microcrystalline solid was obtained; yield 570 mg (75%); m.p. 148 °C (dec.). − Conductivity Λ = 69.8 cm^{2}Ω^{-1}mol^{-1}. − ^{1}H NMR (400 MHz, CD$_2$Cl$_2$): δ = 7.78−7.12 (m, 10 H, C$_6$H$_5$), 5.86 (s, 6 H, C$_6$H$_6$), 2.70−1.83 (br m, 6 H, PCH$_2$CH$_2$P and PCHCH$_3$), 1.37 [dd, 6 H, J(PH) = 15.8, J(HH) = 7.9 Hz, PCHCH_3], 1.28 [dd, 3 H, J(PH) = 15.1, J(HH) = 7.2 Hz, PCHCH_3], 1.22 [dd, 3 H, J(PH) = 14.4, J(HH) = 7.0 Hz, PCHCH_3]. − ^{13}C NMR (100.6 MHz, CD$_2$Cl$_2$): δ = 135.5 [d, J(PC) = 47.8 Hz, *ipso*-C of C$_6$H$_5$], 133.9, 133.3 [both d, J(PC) = 9.2 Hz, C$_6$H$_5$], 131.6, 129.9 [both d, J(PC) = 10.2 Hz, C$_6$H$_5$], 129.2, 129.1 [both d, J(PC) = 11.1 Hz, C$_6$H$_5$], 93.4 [d, J(PC) = 2.0 Hz, C$_6$H$_6$], 31.6 [d, J(PC) = 24.4 Hz, PCHCH$_3$], 26.6 [d, J(PC) = 26.4 Hz, PCHCH$_3$], 26.6 [dd, J(P^{1}C) = 35.6, J(P^{2}C) = 8.1 Hz, PCH$_2$CH$_2$P], 21.3 [dd, J(P^{1}C) = 30.0, J(P^{2}C) = 10.7 Hz, PCH$_2$$CH_2$P], 20.6 (s, PCH$CH_3$), 19.7 [d, J(PC) = 2.0 Hz, PCHCH$_3$], 19.4 (s, PCHCH$_3$), 18.8 [d, J(PC) = 3.0 Hz, PCHCH$_3$]. − ^{31}P NMR (162.0 MHz, CD$_2$Cl$_2$): δ = 86.9 [d, J(PP) = 32.7 Hz, iPr$_2$P], 70.0 [d, J(PP) = 32.7 Hz, Ph$_2$P], −144.3 [sept, J(FP) = 710.6 Hz, PF$_6^-$]. − C$_{26}$H$_{34}$ClF$_6$P$_3$Ru (690.0): calcd. C 45.26, H 4.97; found C 44.98, H 5.06.

4. Preparation of [(η^6-C$_6$H$_6$)RuCl(κ^2-Ph$_2$PCH$_2$CH$_2$PCy$_2$)]PF$_6$ (8): (a) In an analogous way to that described for **3** [method (a)], by using 120 mg (0.3 mmol) of **5** and 119 mg (0.3 mmol) of Ph$_2$PCH$_2$CH$_2$PCy$_2$ as starting materials. Yield 270 mg (78%). − (b) In an analogous way to that described for **7** [method (b)], by using 225 mg (0.5 mmol) of **6**, 370 mg (0.9 mmol) of Ph$_2$PCH$_2$CH$_2$PCy$_2$ and 227 mg (0.9 mmol) of AgPF$_6$ as starting materials. Orange microcrystalline solid; yield 520 mg (75%); m.p. 131 °C (dec.). − Conductivity Λ = 71.6 cm^{2}Ω^{-1}mol^{-1}. − ^{1}H NMR (400 MHz, CD$_2$Cl$_2$): δ = 7.72−7.18 (m, 10 H, C$_6$H$_5$), 5.92 (s, 6 H, C$_6$H$_6$), 2.84−2.72 (m, 2 H, PCH_2CH$_2$P), 2.42−2.23 (m, 2 H, PCH$_2$CH_2P), 2.20−1.15 (br m, 22 H, CH and CH$_2$ of C$_6$H$_{11}$). − ^{13}C NMR (100.6 MHz, CD$_2$Cl$_2$): δ = 135.5 [d, J(PC) = 48.6 Hz, *ipso*-C of C$_6$H$_5$], 133.8, [d, J(PC) = 9.5 Hz, C$_6$H$_5$], 132.0, 131.9 [both d,

J(PC) = 2.9 Hz, C_6H_5], 131.7 [d, J(PC) = 9.5 Hz, C_6H_5], 130.4 [d, J(PC) = 54.3 Hz, *ipso*-C of C_6H_5], 129.9 [d, J(PC) = 9.5 Hz, C_6H_5], 129.1 [d, J(PC) = 10.5 Hz, C_6H_5], 93.3 (s, C_6H_6), 42.9 [d, J(PC) = 21.9 Hz, CH of C_6H_{11}], 37.1 [d, J(PC) = 25.7 Hz, CH of C_6H_{11}], 30.7, 30.0, 29.9, 29.8 (all s, CH_2 of C_6H_{11}), 29.4 [d, J(PC) = 4.8 Hz, CH_2 of C_6H_{11}], 28.1 [d, J(PC) = 13.4 Hz, CH_2 of C_6H_{11}], 27.4 [d, J(PC) = 9.5 Hz, CH_2 of C_6H_{11}], 27.7, 27.1 [both d, J(PC) = 10.5 Hz, CH_2 of C_6H_{11}], 26.6 [dd, $J(P^1C)$ = 35.3, $J(P^2C)$ = 6.7 Hz, P*C*$H_2$$CH_2$P], 26.2 [d, J(PC) = 10.5 Hz, CH_2 of C_6H_{11}], 20.3 [dd, $J(P^1C)$ = 30.5, $J(P^2C)$ = 10.5 Hz, PCH_2*C*H_2P]. – ^{31}P NMR (162.0 MHz, CD_2Cl_2): δ = 79.2 [d, J(PP) = 30.5 Hz, Cy_2P], 70.2 [d, J(PP) = 30.5 Hz, Ph_2P], −142.1 [sept, J(FP) = 710.6 Hz, PF_6^-]. – $C_{32}H_{42}ClF_6P_3Ru$ (770.1): calcd. C 49.91, H 5.50; found C 49.46, H 5.86.

5. Preparation of [(*p*-cym)RuAg(μ-Cl)$_2$(μ-P^1_{Ru},P^2_{Ag}-Ph$_2$P^{1}CH$_2$-CH$_2$P^2*t*Bu$_2$)]$_2$(PF$_6$)$_2$ (9): A solution of 245 mg (0.4 mmol) of **1** and 286 mg (0.8 mmol) of $Ph_2PCH_2CH_2Pt$Bu$_2$ in 5 mL of CH_2Cl_2 was stirred for 1 h and then treated dropwise with a solution of 198 mg (0.8 mmol) of $AgPF_6$ in 3 mL of CH_2Cl_2. After 1 h of stirring at room temperature, the resulting reaction mixture was filtered. The filtrate was concentrated to dryness in vacuo, the residue was washed with 10 mL of pentane and dried. A red microcrystalline solid was obtained; yield 701 mg (95%); m.p. 204 °C (dec.). – ^{1}H NMR (400 MHz, CD_2Cl_2): δ = 7.78 (m, 4 H, C_6H_5), 7.58 (m, 6 H, C_6H_5), 5.44, 5.25 [both d, 4 H, J(HH) = 5.0 Hz, C_6H_4], 2.63−2.52 (m, 2 H, PC$H_2$$CH_2$P), 2.22 [sept, 1 H, J(HH) = 7.0 Hz, $CH_3C_6H_4CH(CH_3)_2$], 1.33−1.19 (br m, 2 H, PCH_2CH_2P), 1.04 [s, 3 H, $CH_3C_6H_4CH(CH_3)_2$], 0.98 [d, 18 H, J(PH) = 15.0 Hz, $PCCH_3$], 0.77 [d, 3 H, J(HH) = 6.8 Hz, $CH_3C_6H_4CH(CH_3)_2$], 0.73 [d, 3 H, J(HH) = 7.0 Hz, $CH_3C_6H_4CH(CH_3)_2$]. – ^{13}C NMR (100.6 MHz, CD_2Cl_2): δ = 132.9 [d, J(PC) = 9.5 Hz, C_6H_5], 132.5 [d, J(PC) = 3.5 Hz, C_6H_5], 129.7 [d, J(PC) = 44.8 Hz, *ipso*-C of C_6H_5], 129.7 [d, J(PC) = 9.5 Hz, C_6H_5], 108.8, 95.6 [both s, C_6H_4], 91.4 [d, J(PC) = 3.8 Hz, C_6H_4], 86.4 [d, J(PC) = 4.8 Hz, C_6H_4], 34.2 [dd, $J(P^1C)$ = 11.0, $J(P^2C)$ = 5.2 Hz, P*C*CH_3], 31.0 [s, $CH_3C_6H_4CH(CH_3)_2$], 29.4 [d, J(PC) = 6.7 Hz, PC*C*H_3], 25.4 [dd, $J(P^1C)$ = 21.5, $J(P^2C)$ = 15.7 Hz, P*C*$H_2$$CH_2$P], 21.2, 17.8 [both s, $CH_3C_6H_4CH(CH_3)_2$ and $CH_3C_6H_4CH(CH_3)_2$], 13.9 (m, PCH_2CH_2P). – ^{31}P NMR (162 MHz, CD_2Cl_2): δ = 68.0 [dd, $^1J(^{109}AgP)$ = 743.3 Hz, J(PP) = 39.2 Hz, tBu$_2$P], 67.9 [dd, $^1J(^{107}AgP)$ = 643.0 Hz, J(PP) = 39.2 Hz, tBu$_2$P], 28.0 [d, J(PP) = 39.2 Hz, Ph_2P], −144.3 [sept, J(FP) = 710.8 Hz, PF_6^-]. – $C_{64}H_{92}Ag_2Cl_4F_{12}P_6Ru_2$ (1835): calcd. C 41.89, H 5.05, Ag 11.76; found C 41.87, H 5.33, Ag 11.63.

6. Preparation of [(*p*-cym)RuCl{κ^2(As,O)-Ph$_2$P(O)CH$_2$CH$_2$-As*t*Bu$_2$}]PF$_6$ (10): A solution of 214 mg (0.5 mmol) of $Ph_2PCH_2CH_2Ast$Bu$_2$ in 10 mL of CH_2Cl_2 was treated with oxygen for ca. 10 min at room temperature and then added to a solution of 165 mg (0.3 mmol) of **1** in 4 mL of CH_2Cl_2. After 1 h of stirring, a solution of 132 mg (0.5 mmol) of $AgPF_6$ in 3 mL of CH_2Cl_2 was added dropwise. The resulting reaction mixture was stirred for 20 min and then filtered. The filtrate was concentrated to dryness in vacuo, the residue was washed twice with 4 mL of cold methanol and dried. A dark-red microcrystalline solid was obtained; yield 199 mg (45%); m.p. 131 °C (dec.). – ^{1}H NMR (200 MHz, CD_2Cl_2): δ = 7.75−7.26 (m, 10 H, C_6H_5), 6.53 [d, 1 H, J(HH) = 5.8 Hz, 1 × H of C_6H_4], 6.39, 5.89 [both d, 1 H each, J(HH) = 6.4 Hz, 2 × H of C_6H_4], 5.62 [d, 1 H, J(HH) = 6.1 Hz, 1 × H of C_6H_4], 3.30−3.20 (br m, 1 H, 1 × H of PCH_2CH_2As), 2.74 [sept, 1 H, J(HH) = 7.1 Hz, $CH_3C_6H_4CH(CH_3)_2$], 2.52−2.46, 2.35−2.21, 1.89−1.82 (all br m, 3 H, PCH_2CH_2As), 1.51, 1.34 (both s, 9 H each, $AsCCH_3$), 1.33, 1.30 [both d, 3 H each, J(HH) = 7.1 Hz, $CH_3C_6H_4CH(CH_3)_2$], 1.10 [s, 3 H, $CH_3C_6H_4CH(CH_3)_2$]. – ^{13}C NMR (50.3 MHz, CD_2Cl_2): δ = 142.5 [d, J(PC) = 43.9 Hz, *ipso*-C of C_6H_5], 135.0 [d, J(PC) = 8.4 Hz, C_6H_5], 134.3 [d, J(PC) = 52.2 Hz, *ipso*-C of C_6H_5], 132.8 [d, J(PC) = 8.4 Hz, C_6H_5], 131.6 [d, J(PC) = 5.8 Hz, C_6H_5], 131.5 (s, C_6H_5), 129.4 [d, J(PC) = 9.5 Hz, C_6H_5], 129.0 [d, J(PC) = 10.5 Hz, C_6H_5], 125.8 [d, J(PC) = 4.7 Hz, C_6H_4], 97.4, 92.6, 89.9, 89.1 (all s, C_6H_4), 87.2 [d, J(PC) = 8.7 Hz, C_6H_4], 46.5, 42.3 (both s, As*C*CH_3), 32.3 (s, AsC*C*H_3), 30.4 [s, $CH_3C_6H_4CH(CH_3)_2$], 31.8 [d, J(PC) = 30.3 Hz, P*C*$H_2$$CH_2$As], 30.1 (s, $AsCCH_3$), 22.5, 21.3 [both s, $CH_3C_6H_4CH(CH_3)_2$], 20.3 [d, J(PC) = 6.6 Hz, PCH_2CH_2As], 14.8 [s, $CH_3C_6H_4CH(CH_3)_2$]. – ^{31}P NMR (81 MHz, CD_2Cl_2): δ = 53.8 [s, Ph_2P(O)], −144.2 [sept, J(FP) = 710.8, PF_6^-]. – $C_{32}H_{46}AsClF_6OP_2Ru$ (834.1): calcd. C 46.08, H 5.56; found C 45.56, H 5.15.

7. Preparation of [(*p*-cym)RuCl(κ^2-*i*Pr$_2$PCH$_2$As*t*Bu$_2$)]PF$_6$ (11): A solution of 32 mg (0.1 mmol) of **2** in 5 mL of ethanol was treated with a solution of 67 mg (0.2 mmol) of iPr$_2$PCH$_2$AstBu$_2$ in 5 mL of ethanol and the mixture stirred under reflux for 24 h. Upon cooling to room temperature, 17 mg (0.1 mmol) of NH_4PF_6 was added to the reaction mixture. After 10 min of stirring, the solvent was removed in vacuo, the residue was washed three times with 10 mL of pentane and dried. A yellow solid was obtained; yield 75 mg (80%); m.p. 86 °C. – Conductivity Λ = 70.2 $cm^2\Omega^{-1}mol^{-1}$. – ^{1}H NMR (400 MHz, $CDCl_3$): δ = 6.34 [d, 1 H, J(HH) = 5.3 Hz, 1 × H of C_6H_4], 6.14 [d, 1 H, J(HH) = 5.8 Hz, 1 × H of C_6H_4], 6.08 [d, 1 H, J(HH) = 5.9 Hz, 1 × H of C_6H_4], 5.28 [d, 1 H, J(HH) = 5.3 Hz, 1 × H of C_6H_4], 3.41 [dd, 1 H, J(PH) = 15.0, J(HH) = 9.9 Hz, 1 × H of PCH_2As], 3.22 [dd, 1 H, J(PH) = 14.8, J(HH) = 9.9 Hz, 1 × H of PCH_2As], 2.57, 2.65, 2.77 [all m, 1 H each, P*C*HCH_3 and $CH_3C_6H_4C$*H*$(CH_3)_2$], 2.19 [s, 3 H, $CH_3C_6H_4CH(CH_3)_2$], 1.56 [dd, 3 H, J(PH) = 16.1, J(HH) = 7.3 Hz, $PCHCH_3$], 1.46, 1.40 (both s, 9 H each, $AsCCH_3$), 1.32 [dd, 3 H, J(PH) = 11.4, J(HH) = 7.2 Hz, $PCHCH_3$], 1.29 [dd, 3 H, J(PH) = 10.8, J(HH) = 6.9 Hz, $PCHCH_3$], 1.27 [dd, 3 H, J(PH) = 9.7, J(HH) = 7.3 Hz, $PCHCH_3$], 1.25 [d, 3 H, J(HH) = 7.1 Hz, $CH_3C_6H_4CHCH_3$], 1.19 [d, 3 H, J(HH) = 7.0 Hz, $CH_3C_6H_5CHCH_3$]. – ^{13}C NMR (100.6 MHz, $CDCl_3$): δ = 124.0 [d, J(PC) = 5.7 Hz, C_6H_4], 95.4, 88.3, 88.1 (all s, C_6H_4), 84.4 [d, J(PC) = 7.6 Hz, C_6H_4], 82.9 (s, C_6H_4), 45.6 [d, J(PC) = 6.7 Hz, As*C*CH_3], 39.4 (s, As*C*CH_3), 31.8 (s, $AsCCH_3$), 31.7 [d, J(PC) = 19.0 Hz, PCH_2As], 29.4 [s, $CH_3C_6H_4CH(CH_3)_2$], 28.4 (s, AsC*C*H_3), 27.0, 27.2 [both d, J(PC) = 17.9 Hz, P*C*HCH_3], 22.4 [s, $CH_3C_6H_4CH(CH_3)_2$], 18.8, 19.0, 19.8, (all s, $PCHCH_3$), 17.5 [d, J(PC) = 2.9 Hz, $PCHCH_3$], 17.3 [s, $CH_3C_6H_4CH(CH_3)_2$]. – ^{31}P NMR (162 MHz, $CDCl_3$): δ = 19.3 (s, P*i*Pr$_2$), −142.1 [sept, J(FP) = 710.6 Hz, PF_6^-]. – $C_{25}H_{48}AsClF_6P_2Ru$ (736.0): calcd. C 40.80, H 6.57; found C 40.53, H 6.29.

X-ray Structure Determination of Compounds 9 and 10:[20] Single crystals of **9** were grown from acetone/methanol at 25 °C and those of **10** from methanol at 25 °C. Crystal data collection parameters for these structures are presented in Table 1. The data were collected with an Enraf−Nonius CAD4 diffractometer (**9**) and with a Stoe IPDS diffractometer using monochromated Mo-K_α radiation (λ = 0.71073 Å). Intensity data were corrected for Lorentz and polarization effects. The structures were solved by direct methods (**10**) with SHELXS-97.[21] All structures were refined by full-matrix least-squares procedures on F^2 using SHELXL-97.[22] The positions of all hydrogen atoms were calculated according to ideal geometry and were refined by employing the riding method. For **10** the Flack parameter was refined to a value of −0.025(15)[12] and the extinction coefficient was refined to 0.00116(10).

Table 1. Crystal data for complexes **9** and **10**

	9	**10**
Formula	$C_{64}H_{92}Ag_2Cl_4F_{12}P_6Ru_2$	$C_{32}H_{46}AsClF_6OP_2Ru$
M	1834.9	834.1
Crystal system	triclinic	orthorhombic
Space group	*P*($\bar{1}$) (no. 2)	*Pna*2 (1) (no.33)
a [Å]	10.383(4)	19.770(4)
b [Å]	14.144(5)	12.180(2)
c [Å]	15.424(6)	14.510(3)
α [°]	95.67(2)	90
β [°]	108.36(2)	90
γ [°]	103.54(2)	90
V [Å^3]	2053.3(14)	3494(1)
Temperature [K]	193(2)	173(2)
Z	2	4
D_c [g cm^{-3}]	1.560	1.586
μ [mm^{-1}]	1.146	1.614
No. reflections measured	8514	18919
No. unique reflections (R_{int})	7202 (0.0352)	6072 (0.0882)
$R1$[a]	0.0810	0.0408
$wR2$[b]	0.1270	0.0774

[a] $R = \Sigma|F_o - F_c|/\Sigma F_o$ [for $F_o > 2\,\sigma(F_o)$] for the number of observed reflections [$I > 2\sigma(I)$], respectively. – [b] $wR_2 = [\Sigma w(F_o^2 - F_c^2)^2/\Sigma w(F_o^2)^2]^{1/2}$; $w^{-1} = [\sigma^2(F_o^2) + (0.0452\,P)^2 + 7.7438P]$ (**9**), $[\sigma^2(F_o^2) + (0.0111P)^2 + 0.0000P]$ (**10**), where $P = (F_o^2 + 2F_c^2)/3$; for all data reflections, respectively.

Acknowledgments

This work was supported by the Deutsche Forschungsgemeinschaft (SFB 347) and the Fonds der Chemischen Industrie. We are grateful to the latter in particular for a Ph.D. scholarship (to K. I.). Moreover, we thank S. Link for committed collaboration during an advanced study course. We also thank Dr. W. Buchner and Mrs. M.-L. Schäfer for NMR measurements, Mrs. R. Schedl and Mr. C. P. Kneis for elemental analysis and DTA measurements. Generous support by the BASF AG and the Degussa-Hüls AG is also gratefully acknowledged.

[1] G. Fries, J. Wolf, M. Pfeiffer, D. Stalke, H. Werner, *Angew. Chem.* **2000**, *112*, 575–577; *Angew. Chem. Int. Ed.* **2000**, *39*, 564–566.

[2] G. Fries, Dissertation, Universität Würzburg, **2000**.

[3] [3a]H. Le Bozec, D. Touchard, P. H. Dixneuf, *Adv. Organomet. Chem.* **1989**, *29*, 163–247. – [3b]M. A. Bennett, in: *Comprehensive Organometallic Chemistry*, vol. 7 (Eds.: E. W. Abel, F. G. A. Stone, G. Wilkinson), Pergamon, New York, **1995**, chapter 9. – [3c]R. Noyori, S. Hashiguchi, *Acc. Chem. Res.* **1997**, *30*, 97–102.

[4] [4a]D. E. Fogg, B. R. James, *J. Organomet. Chem*. **1993**, *462*, C21–C23. – [4b]F. B. McCormick, D. D. Cox, W. B. Gleason, *Organometallics* **1993**, *12*, 610–612.

[5] R. J. Lancashire, in: *Comprehensive Coordination Chemistry*, vol. 5 (Eds.: G. Wilkinson, R. D. Gillard, J. A. McCleverty), Pergamon, New York, **1987**, p. 800.

[6] H. V. Rasika Dias, W. Jin, H.-J. Kim, H.-L. Lu, *Inorg. Chem.* **1996**, *35*, 2317–2328.

[7] R. Uson, J. Fornies, M. Tomas, I. Ara, J. M. Casas, *Polyhedron* **1992**, *11*, 1783–1787.

[8] P. D. Robinson, C. C. Hinckley, M. Matusz, P. A. Kibala, *Polyhedron* **1987**, *6*, 1695–1698.

[9] P. Braunstein, D. G. Kelly, Y. Dusausoy, D. Bayeul, M. Lanfranchi, M. Tiripicchio, *Inorg. Chem.* **1994**, *33*, 233–242.

[10] [10a] M. R. J. Elsegood, D. A. Tocher, *Polyhedron* **1995**, *14*, 3147–3156. – [10b] P. D. Smith, A. H. Wright, *J. Organomet. Chem.* **1998**, *559*, 141–147. – [10c] S. Serron, S. P. Nolan, Y. A. Abramov, L. Brammer, J. L. Petersen, *Organometallics* **1998**, *17*, 104–110. – [10d] D. K. Gupta, A. N. Sahay, D. S. Pandey, N. K. Jha, P. Sharma, G. Espinosa, A. Cabrera, M. C. Puerta, P. Valerga, *J. Organomet. Chem*. **1998**, *568*, 13–20.

[11] I. de los Rios, M. J. Tenorio, M. C. Puerta, P. Valerga, *Organometallics* **1998**, *17*, 3356–3363.

[12] [12a] S. Freitag, R. Herbst-Irmer, L. Lameyer, D. Stalke, *Organometallics* **1996**, *15*, 2839–2841. – [12b] H. D. Flack, *Acta Crystallogr., Sect. A* **1983**, *39*, 876–881. – [12c] G. Bernadinelli, H. D. Flack, *Acta Crystallogr., Sect. A* **1985**, *41*, 500.

[13] [13a] G. Henig, M. Schulz, H. Werner, *Chem. Commun.* **1997**, 2349–2350. – [13b] J. Bank, P. Steinert, B. Windmüller, W. Wolfsberger, H. Werner, *J. Chem. Soc., Dalton Trans.* **1996**, 1153–1159. – [13c] I. de los Rios, M. J. Tenorio, M. A. J. Tenorio, M. C. Puerta, P. Valerga, *J. Organomet. Chem.* **1996**, *525*, 57–64. – [13d] I. S. Thorburn, S. J. Rettig, B. R. James, *J. Organomet. Chem.* **1985**, *296*, 103–114.

[14] N. J. Holmes, W. Levason, M. Webster, *J. Chem. Soc., Dalton Trans.* **1997**, 4223–4229.

[15] A. A. Batista, J. Zukerman-Schpector, O. M. Porcu, S. L. Queiroz, M. P. Araujo, G. Oliva, D. H. F. Souza, *Polyhedron* **1994**, *13*, 689–693.

[16] J. W. Faller, B. P. Patel, M. A. Albrizzio, M. Curtis, *Organometallics* **1999**, *18*, 3096–3104.

[17] H. Werner, M. Manger, U. Schmidt, M. Laubender, B. Weberndörfer, *Organometallics* **1998**, *17*, 2619–2627.

[18] M. A. Bennett, A. K. Smith, *J. Chem. Soc., Dalton Trans.* **1974**, 233–241.

[19] J. Wolf, M. Manger, U. Schmidt, G. Fries, D. Barth, B. Weberndörfer, D. A. Vice, W. D. Jones, H. Werner, *J. Chem. Soc., Dalton Trans.* **1999**, 1867–1875.

[20] Crystallographic data (excluding structure factors) for the structures of **9** and **10** have been deposited with the Cambridge Crystallographic Data Centre as supplementary publication nos. CCDC-140027 (**9**) and -140028 (**10**). Copies of the data can be obtained free of charge on application to CCDC, 12 Union Road, Cambridge CB2 1EZ, UK [Fax: (internat.) + 44-1223/336-033; E-mail: deposit@ccdc.cam.ac.uk).

[21] G. M. Sheldrick, *Acta Crystallogr., Sect. A* **1990**, *46*, 467.

[22] G. M. Sheldrick, *Program for Crystal Structure Refinement*, Universität Göttingen, **1996**.

Received February 8, 2000
[I00040]

A Structurally Characterised Pair of Dicobalt(III) Peroxo/Superoxo Complexes with C_2-Symmetrical Tetrapodal Pentadentate Amine Ligands, and Some Reactivity en route

Stefan Schmidt,[a] Frank W. Heinemann,[a] and Andreas Grohmann*[a]

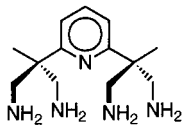
Dedicated to Professor Martin A. Bennett on the occasion of his retirement

Keywords: N ligands / Cobalt / Peroxo complexes / Superoxo complexes / Sulfito complexes

The tetrapodal pentaamine ligand 2,6-bis(1′,3′-diamino-2′-methylprop-2′yl)pyridine (pyN_4, **1**) provides square-pyramidal coordinated cobalt(II) building blocks, which have been used in the synthesis of the singly-bridged dicobalt(III) μ_2-η^1:η^1-peroxo and superoxo complexes $[(\mathbf{1})Co–O_2–Co(\mathbf{1})]^{4+/5+}$, isolated as the chloride, bromide, and mixed chloride/dithionate and bromide/dithionate salts. The peroxo complex is accessible by the classical route involving oxygenation of $[(pyN_4)Co^{II}]$, but has also been obtained from a cobalt(III) precursor in air, which implies that the pentaamine **1** acts as a multi-electron reductant. Oxidation of the peroxo complex with chlorine generated in situ from an HCl/H_2O_2 mixture (H_2O_2 derived from partial peroxo complex hydrolysis) generates the superoxo complex. Both cations have highly symmetrical solid state structures, locked in transoid Co–O–O–Co conformations by two pairs of intramolecular hydrogen bonds. Each involves two protons in the equatorial $Co(NH_2R)_4$ plane of one half of the molecule and the bridge oxygen atom in the other half. A significant difference between the two structures is the orientation of the O_2 bridge, which is coplanar with the pyridine rings of the coordination caps in the peroxo complex and at right angles in the superoxo complex. The reactivities of the complexes in acidic and basic media have been explored, and the mononuclear bromo complex $[(\mathbf{1})CoBr]^{2+}$ was isolated in one of the products. Dithionite, intended as an external reducing agent in the reaction of $Na_3[Co^{III}(CO_3)_3]$ with **1**, instead yields the *S*-sulfito complex cation $[(\mathbf{1})Co(SO_3)]^+$, by disproportionation of $S_2O_4^{2-}$ to give SO_3^{2-} and S^{2-}. All complexes have been characterised by ^1H, ^{13}C NMR, IR, Raman, UV/Vis, and EPR spectroscopy (as applicable), elemental analysis and X-ray structure determination, and the cyclic voltammetry parameters of the peroxo/superoxo pair of complexes have been determined.

Introduction

With a view to creating an active ligand periphery for octahedrally coordinating transition metal ions, we recently introduced a tetrapodal pentadentate amine ligand with an NN_4 donor set (pyN_4, **1**).[1] This ligand acts as a highly symmetrical square-pyramidal coordination cap,[2] and derivatisation of the equatorial NH_2 groups[3] is aimed at creating a functional environment for a monodentate "substrate" at the sixth coordination site. Judicious choice of functional groups should allow for the fine-tuning of secondary interactions between the substrate and the ligand periphery (such as hydrogen bonding, interaction with an electrochemically active centre, π,π-stacking, etc.) and thus enable the modulation of substrate reactivity.[4] An alternative approach is to link pyN_4 coordination caps through suitable bridges so as to create polynucleating ligands,[5] which can bind two or more metal centres having "labile" coordination sites in close proximity.



1

Mononuclear cobalt(III) complexes of the parent ligand **1** that have been isolated so far have a chloro,[1] an OH,[6] or a CH_3[7] ligand at the sixth coordination site. The kinetic inertness and the known reactivity of Co^{III} amine complexes with respect to Mannich-type transformations of the coordinated ligands[8,9] led us to further explore this class of complexes. Dinuclear complexes with a suitable bridge linking two $[M(pyN_4)]^{n+}$ fragments have two adjacent $M(H_2NR)_4$ planes, which opens up the possibility of connecting the two coordination caps. In the case of M = Co, a readily introduced bridge can be derived from dioxygen.

Peroxo and superoxo amine complexes of cobalt(III) have been the subject of scientific investigations for at least 150 years,[10–12] the first detailed study being that of Frémy in 1852. He noted that aqueous ammonia solutions containing cobalt(II) salts turn dark upon exposure to air. He isolated

[a] Institut für Anorganische Chemie,
Universität Erlangen-Nürnberg,
Egerlandstraße 1, D-91058 Erlangen, Germany
E-mail: grohmann@anorganik.chemie.uni-erlangen.de

 © WILEY-VCH Verlag GmbH, D-69451 Weinheim, 2000 1434–1948/00/0707–1657 $ 17.50+.50/0

and analysed the brown compound $[Co_2(NH_3)_{10}O_2](SO_4)_2 \cdot 3H_2O$ and found that it evolved oxygen when redissolved in water.[13,14] Work by Maquenne and Vortmann followed, recording facile oxidation of the brown material, which led to a "class of dark green compounds".[15,16] Werner and Mylius were the first in 1898 to describe the brown products as ammine complexes containing two cobalt atoms linked by an O_2 bridge, $[(NH_3)_5Co-O-O-Co(NH_3)_5]^{4+}$ $(X^-)_4$, and to assign the general formula $[(NH_3)_5Co-O-O-Co(NH_3)_5]^{5+}$ $(X^-)_5$ to the green products.[17] Both assignments were confirmed after structural techniques became available.

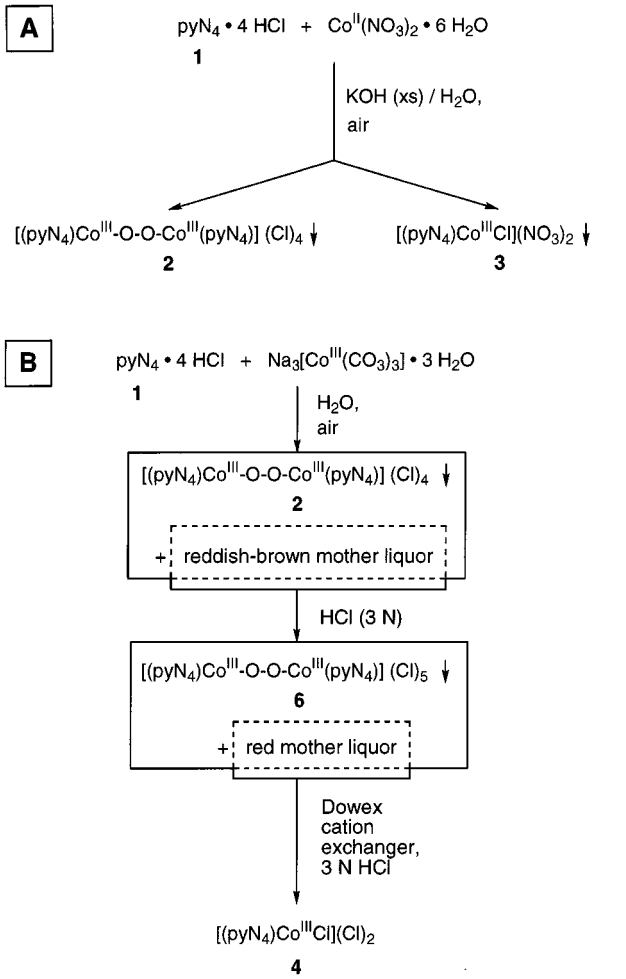
Structural analogues of these prototypes with chelating amine ligands were subsequently prepared. The potential of these and similar complexes as oxygen carriers for a variety of applications was soon recognized[18–20] and has been actively investigated to this day.[21–23] The literature on singly-bridged dinuclear peroxo and superoxo amine complexes of cobalt(III) is extensive, and the structures of a large number of peroxo complexes have been determined. The structural characterisation of superoxo complexes has, by contrast, been accomplished much less frequently, and there is little precedent in the literature where the parameters of singly-bridged peroxo and superoxo cobalt(III) complexes with otherwise identical ligands have been compared.[24–26] For these reasons, we chose to investigate the formation and structure of dinuclear cobalt(III) complexes of **1** with a dioxygen-derived bridging group, as well as some peripheral reactions, and present results in this contribution.

Results and Discussion

Simplicio and Wilkins showed that oxygen uptake by ammoniacal cobalt(II) solutions is due mainly to the reaction of the pentakis(ammine) aqua complex $[Co(NH_3)_5(H_2O)]^{2+}$, whereas the bis(aqua) and tris(aqua) complexes $[Co(NH_3)_4(H_2O)_2]^{2+}$ and $[Co(NH_3)_3(H_2O)_3]^{2+}$ are virtually inert.[27,28] While such species do add oxygen when the nitrogen donor atoms are incorporated into chelate ligands, oxygenation is clearly enhanced as a consequence of an increasing number of ammine or amino groups coordinated to cobalt.[11] A variety of chelating pentaamines, including an early example of a tetrapodal pentadentate ligand,[29,30] have been investigated in this context, and a number of μ-peroxo complexes thus obtained have been structurally characterised. Synthesis usually involves oxygenation of aqueous solutions of cobalt(II) salts in the presence of a ligand.[31–41] As described below, this method was successful with the pentaamine ligand **1**, but we also found an alternative route which uses dioxygen from air, a cobalt(III) starting material, and no apparent reducing agent.

[(1)Co−O−O−Co(1)]Cl$_4$ (2)

Procedure A: The peroxo-bridged dinuclear tetrachloride **2** was obtained as a brown microcrystalline precipitate from a cooled aerated aqueous solution containing stoichiometric quantities of **1**·4HCl[1] and $Co(NO_3)_2 \cdot 6H_2O$ (see Scheme 1, Part **A**). An excess of potassium hydroxide was used to neutralise the acid form of the amine ligand, resulting in a basic reaction medium. No attempt was made to optimise the yield (9%), which may increase with longer reaction times. A significant amount of a red crystalline material identified as $[(\mathbf{1})CoCl](NO_3)_2$ **3**, precipitated from the filtrate upon standing for several days. Compound **2** may be recrystallised from water to give the hydrate $[(\mathbf{1})Co-O-O-Co(\mathbf{1})]Cl_4 \cdot 3H_2O$, as indicated by elemental analysis. Solubility in other polar protic solvents, such as methanol and DMSO, is also high. Contrary to the observations with other dicobalt(III) peroxo complexes,[12] **2** does not release dioxygen upon heating the solid in vacuo (145 °C, 12 h), and the material is recovered unchanged. The IR spectrum of **2** has bands characteristic of the pyN_4 coordination cap. An intense absorption in the Raman spectrum at 800 cm^{-1} is assigned to the O−O stretching vibration, in agreement with data obtained for related complexes.[21,42] Compound **2** is diamagnetic, and its ^{1}H NMR spectrum ([D$_6$]DMSO, room temp.) resembles that recorded for the mononuclear chloro complex $[(\mathbf{1})CoCl](Cl)(ClO_4) \cdot H_2O$,[1] with two signals of triplet and doublet multiplicity in the intensity ratio 1:2 for the pyridine ring protons. The Co−O−O−Co unit is not expected to be linear. Hence, ro-



Scheme 1. Preparation of dicobalt(III) peroxo and superoxo complexes of the pentaamine ligand **1**

tation around the Co−O bond must be fast on the NMR time scale as the spectrum shows all amine and methylene groups to be equivalent. The geminal protons in these groups are, however, diastereotopic, and each gives rise to a set of two well-resolved resonances. The assignment of the exocyclic CH_3 protons is straightforward. The ^{13}C NMR spectrum mirrors the diagnosis of fast rotation of the {(pyN_4)Co} fragments in solution, and supports the assumption of highly symmetrical coordination caps. The UV/Vis spectrum of **2** has an intense band at 295 nm. Such a band is due to the $\pi_\sigma^*(O_2^{2-}) \rightarrow d_z^2(Co)$ LMCT transition.[43] In solution spectra, it has been suggested to be typical of *trans*-μ_2-η^1:η^1-dicobalt(III) peroxo complexes in which the Co−O−O−Co unit is planar (dihedral angle of 180°).[34,37] Bands at ca. 325 nm and ca. 375 nm, which would indicate a nonplanar arrangement of the Co−O−O−Co unit in solution, are absent.[34,37] However, in the light of our NMR spectral data which imply conformational nonrigidity of the Co−O−O−Co unit in solution, the observed UV/Vis spectrum more likely reflects primarily the symmetrical ligand field of the pyN_4 ligand, whereas a ligand field of lower symmetry is expected to produce a two-band spectrum.[44] The cyclic voltammogram of **2** has a quasi-reversible redox wave associated with the peroxo/superoxo system at $E_{1/2} = +0.40$ V (vs. NHE; solvent: DMSO; for other conditions see Experimental Section).[45] Two irreversible one-electron waves are recorded at $E_{1/2} = -1.11$ V and $E_{1/2} = -1.67$ V, respectively, which we assign to the sequential reduction of the cobalt(III) centres to cobalt(II).[33,36]

Procedure B: We fortuitously found an alternative synthesis of **2** when we wished to repeat the preparation of the mononuclear complex [(**1**)CoCl](X)$_2$ (X = Cl: **4**). The published procedure[1] requires that all manipulations be carried out under a blanket of dinitrogen, allowing the isolation of red [(**1**)CoCl](Cl)$_2$ as the primary product. Performing the reaction between $Na_3[Co(CO_3)_3]\cdot 3H_2O$ and **1**·4HCl in air under otherwise identical conditions (including a water/methanol solvent mixture) gave a brown microcrystalline precipitate which was found to be the dinuclear peroxo-bridged tetrachloride **2** (isolated yield accounts for 18% of **1**; see Scheme 1, Part **B**). The mother liquor was basic. Compound **2** did not precipitate quantitatively, owing to its marked solubility in water. Workup of the mother liquor allowed the sequential isolation of the superoxo complex [(**1**)Co−O−O−Co(**1**)]Cl$_5$ **(6)**, and the mononuclear chloro complex [(**1**)CoCl](Cl)$_2$ **(4)** (see below). The NMR, IR, Raman and UV/Vis spectroscopic data of **2** obtained according to procedure **B** are identical to the data determined for the product prepared by route **A**. Addition of an excess of sodium dithionate to an aqueous solution of **2** gave single crystals of [(**1**)Co−O−O−Co(**1**)](S_2O_6)-$Cl_2\cdot 6H_2O$ **(5)** which were suitable for an X-ray structure analysis.

[(1)Co−O−O−Co(1)]Cl$_5$ (6)

In Procedure **B** (see above and Scheme 1, Part **B**), a reddish-brown filtrate remained after the isolation of precipitated peroxo complex **2**, still containing a sizeable amount of this complex in solution. Acidification of this filtrate with hydrochloric acid and reaction overnight produced a green crystalline precipitate and a red solution. The ESR spectrum of the isolated crystalline material (DMSO, 120 K) has a Zeeman splitting factor of $g = 2.0269$, which is in agreement with the formulation of the product as a singly-bridged dicobalt(III) superoxo complex. Hyperfine coupling with the ^{59}Co nucleus is not observed.[26,46] Elemental analysis of a recrystallised sample showed that the product was a bridged superoxo complex [(**1**)Co−O−O−Co(**1**)]Cl$_5$, **6** (isolated yield accounts for 14% of **1**). Further support comes from the Raman spectrum of a solid sample (dispersant: KBr) which shows a strong absorption at 1075 cm^{-1}, in a region typical of ν(O−O str) of other bridged superoxo complexes.[21,42] The UV/Vis spectrum has bands of varying intensity at 208, 307, 464, and 698 nm and is thus in good qualitative agreement with the spectrum reported for $[(NH_3)_5Co-O-O-Co(NH_3)_5]Cl_5\cdot 4H_2O$.[47] As expected, the cyclic voltammogram of the superoxo complex (determined for the mixed chloride hexafluorophosphate salt [(**1**)Co−O−O−Co(**1**)]Cl$_2$(PF_6)$_3$) corresponds to that of the peroxo complex **2** (above). The red filtrate of this reaction provided, upon workup, the desired mononuclear complex **4** (yield accounts for 19% of **1**). Partial anion exchange of **6** with sodium dithionate gave single crystals of [(**1**)Co−O−O−Co(**1**)](S_2O_6)$_2$Cl·10H_2O **(7)**, which were suitable for X-ray structure analysis.

The superoxo complex was also formed when sulfuric acid was used instead of hydrochloric acid for the acidification of the reaction mixture, as long as the reaction was performed on the chloride salt **2**. Alternatively, the superoxo complex formed when the perchlorate salt [(**1**)Co−O−O−Co(**1**)](ClO_4)$_4$ was reacted with HCl. The superoxo complex did not form when the perchlorate salt was treated with H_2SO_4. Instead, the colour of the solution turned orange, indicating the formation of a mononuclear species, presumably the aqua complex [(**1**)Co(OH_2)]$^{3+}$. Aqueous hydrogen peroxide alone showed no reaction with either the chloride or the perchlorate salt. When allowed to react with the chloride salt **2**, a mixture of hydrogen peroxide and hydrochloric acid produced the superoxo complex much faster (as judged by the change of colour from brown to green) than hydrochloric acid alone.

Our conclusions from these observations are as follows: (i) Unlike Procedure **A**, the reduction equivalents required for the generation of the peroxo bridge in Procedure **B** cannot originate from the metal precursor as this already contains cobalt in the +3 oxidation state. Methanol as reductant cannot be excluded at this stage (see, however, below) but we have no indications for the formation of formaldehyde which would be the likely oxidation product. Alternatively, a decomposition pathway may operate by which a certain amount of pentaamine ligand **1** is oxidised, with concomitant formation of cobalt(II), which is subsequently reoxidised upon reaction with aerial dioxygen.[48] This would explain the moderate yields of **2**, **4** and **6** obtained from

these reactions (only about 50% of **1** is accounted for in the products); (ii) The chloride ion and water are unlikely reductants for Co^{III}, on the grounds that the redox potentials of the half-reactions $2\ Cl^- \rightarrow Cl_2 + 2\ e^-$ and $2\ H_2O \rightarrow O_2 + 4\ H^+ + 4\ e^-$ are too high for Co^{III} to accomplish either oxidation and be reduced in the presence of amine ligand. While experimental evidence indicates that $Na_3[Co(CO_3)_3]\cdot 3H_2O$ reacts with aqueous HCl in the absence of other ligands to form the hexaaqua complex $[Co^{III}(H_2O)_6]^{3+}$ (which is a powerful oxidant in aqueous solution, generating O_2, H^+, and $[Co^{II}(H_2O)_6]^{2+}$), it is unlikely that in the presence of the chelating amine ligand, cobalt(II) can originate from this reaction. We have no experimental data to support the notion that in our system of peroxo and superoxo complexes, the O_2 bridge derives from dioxygen generated internally, by a Co^{III}/Co^{II} redox reaction as indicated above. In the original preparation of the mononuclear chloro complex **6** under an inert atmosphere,[1] formation of the peroxo complex was not observed. Impurities or decomposition products in the starting material, $Na_3[Co(CO_3)_3]\cdot 3H_2O$, might act as a source of cobalt(II), but batches were freshly prepared, and elemental analyses indicated the correct composition; (iii) For the transformation of **2** into **6** upon addition of hydrochloric acid, we postulate HCl-induced decomposition of **2** and liberation of hydrogen peroxide[48] (Equations 1a–c). At a critical HCl concentration, mixtures of H_2O_2 and HCl are known to form Cl_2,[49] which acts as an oxidising agent on the peroxo complex **2** and produces the superoxo complex **6** (Scheme 1, Part **B**). This assumption is supported by the fact that neither hydrogen peroxide alone nor a combination of chloride-free acid and non-halide salt of the peroxo complex will produce the superoxo complex. In a separate experiment, a brown aqueous solution of **2** reacted immediately with gaseous chlorine or its solution in water to give a green precipitate. The formation of cobalt(III) superoxo complexes by reaction of the corresponding peroxo complexes with halogens has been described in the literature.[11,26]

$$[(pyN_4)Co^{III}\text{-}O\text{-}O\text{-}Co^{III}(pyN_4)]\,(Cl)_4 + 2\ HCl \xrightarrow{\mathbf{2}} 2\ [(pyN_4)Co^{III}Cl](Cl)_2 + H_2O_2 \quad (1a)$$

$$H_2O_2 + 2\ HCl \longrightarrow Cl_2 + 2\ H_2O \quad \text{(at critical [HCl])} \quad (1b)$$

$$2\ [(pyN_4)Co^{III}\text{-}O\text{-}O\text{-}Co^{III}(pyN_4)]\,(Cl)_4 + Cl_2 \xrightarrow{\mathbf{2}} 2\ [(pyN_4)Co^{III}\text{-}O\text{-}O\text{-}Co^{III}(pyN_4)]\,(Cl)_5 \quad (1c)$$
(**4**)

$$3\ [(pyN_4)Co^{III}\text{-}O\text{-}O\text{-}Co^{III}(pyN_4)]\,(Cl)_4 + 4\ HCl \longrightarrow 2\ [(pyN_4)Co^{III}\text{-}O\text{-}O\text{-}Co^{III}(pyN_4)]\,(Cl)_5 + 2\ [(pyN_4)Co^{III}Cl](Cl)_2 + 2\ H_2O \quad (1d)$$

[(1)Co–O–O–Co(1)]Br_4 (8) and [(1)Co–O–O–Co(1)]Br_5 (10)

For clarification of the circumstances surrounding the formation of **2** from a cobalt(III) precursor in air, some of the reactions described above were repeated in the absence of methanol with the methanol-free salt **1**·5HBr, or with the hydrobromide/methanol solvate **1**·4HBr·MeOH, and with a variation of pH. The methanol-free hydrobromide was prepared from the methanol solvate by ion exchange chromatography (Dowex 50W×2, eluent: 3 N HBr). The reaction of equimolar quantities of **1**·5HBr and $Na_3[Co(CO_3)_3]\cdot 3H_2O$ under a blanket of nitrogen in degassed water gave an orange solution, which upon exposure to air, deposited the tetrabromide salt **8** as a greenish-brown crystalline material in an isolated yield accounting for 21% of **1**. The solubility of the tetrabromide **8** in water is far lower than that of the tetrachloride **2**, making precipitation near-quantitative. The mother liquor contained the mononuclear bromo complex [(**1**)CoBr](Br)$_2$ **(9)** as the only other isolated product. Repeating the reaction with **1**·4HBr·MeOH and a water/methanol (1:1 v/v) solvent mixture under otherwise identical conditions gave essentially the same results. A further experiment combined **1**·4 HBr·MeOH (10 mmol), $Na_3[Co(CO_3)_3]\cdot 3H_2O$ (10 mmol), and HBr (10 mmol) in a water/methanol solvent mixture, the reaction being carried out in air (see Experimental Section). The tetrakis(hydrobromide) salt provides four equivalents of acid, while sodium tris(carbonato)cobaltate contains six equivalents of base. We reasoned that further addition of acid would make more cobalt(III) available for complexation. After reaction, the mixture was found to be at pH 7, and the peroxo complex **8** was isolated in the highest yield recorded in this series of experiments (accounting for 56% of **1**). Workup of the mother liquor provided the bromo complex **9** in a yield accounting for 22% of **1**. An experiment with additional HBr (pH after the reaction was 4) gave, instead of the peroxo complex, the bromo complex **9** as the exclusive product. Heating an authentic sample of **9** at reflux under a stream of air for an extended period of time (12 h), in the presence or absence of methanol, did not produce the dinuclear peroxo complex; rather, **9** was partially transformed into the aqua complex [(**1**)Co(H_2O)]Br_3, as indicated by ^1H NMR and IR spectroscopy.[50] Finally, the superoxo complex **10** was obtained as green microcrystals from a suspension of peroxo complex **8** in 3 N HBr in an isolated yield of 65% relative to **8**. From the mother liquor was isolated the bromo complex **9** as the only other product. The IR, Raman, NMR and UV/Vis spectroscopic parameters of **8** and **10** (as applicable) are similar to those determined for the corresponding chloride salts **2** and **6**. Addition of excess sodium dithionate to an aqueous solution of **8** gave single crystals of [(**1**)Co–O–O–Co(**1**)](S_2O_6)$Br_2\cdot 6H_2O$ (**11**), and partial anion exchange of **9** with NH_4PF_6 (carried out in a similar manner) gave single crystals of [(**1**)CoBr]-Br(PF_6)$\cdot H_2O$ (**12**). Both batches of crystals were suitable for X-ray structure analysis.

Our conclusions from the observed reactivity are as follows: (i) Methanol as a possible reductant may be excluded; (ii) The addition of one extra equivalent of acid increases the yield of peroxo complex **8** markedly. Products containing close to 80% of the initially employed pentamine ligand **1** were isolated, making the involvement of **1** as a *one*-electron reductant questionable; (iii) The action of bromide ion as reductant in the formation of the peroxo complex may be excluded since only the aqua complex is generated in a control experiment. Moreover, the generated bromine should induce further oxidation, leading to the superoxo complex, which is not observed; (iv) The yield of superoxo complex from the reaction of the peroxo complex with HBr corresponds exactly to the theoretical value expected on the basis of Equation 1d. This observation suggests that processes analogous to those described by Equations 1a−1c for the chloride salt operate for the bromide salt: the acid-induced decomposition of one third of the peroxo complex yields hydrogen peroxide which oxidises bromide ion to bromine, which in turn oxidises the remaining two thirds of peroxo complex.[11]

Overall, the most likely explanation for the observed reactivity is that the polyamine ligand **1** acts as a multiple-electron donor, depending on the reaction conditions. We are currently seeking to identify a specific ligand oxidation product. An amino acid ester has previously been suggested to be the electron source in the preparation of a bridging peroxo cobalt(III) dimer from a cobalt(III) precursor in air.[48]

The reactivity of the described peroxo and superoxo complexes with varying pH may be summarised as follows: Once generated, the peroxo complexes may be transformed into bridged superoxo and mononuclear species upon addition of a suitable acid. In aqueous alkaline solution (pH $\geq$ 12), the peroxo complexes are stable for hours without noticeable decomposition, while the superoxo complexes react with aqueous ammonia to reform the peroxo complexes. Similar reactivity has been documented for a number of O_2-bridged dicobalt(III) complexes with other polyamine ligands.[11]

[(1)CoSO$_3$]Br (13)

With a view to studying the effect of an external reducing agent on the generation of the peroxo complex **8** from $Na_3[Co(CO_3)_3]\cdot 3H_2O$ and **1**·4HBr·MeOH in air, we reacted two equivalents each of the cobaltate and the pentaamine ligand in the presence of one equivalent of sodium dithionite in water, which contained an excess of $NaHCO_3$ ($Na_2S_2O_4$ has been used to decompose $Co^{II}-O_2$ adducts, but the product(s) deriving from the dithionite ion have never been identified[27]). The only isolated products of this reaction were a finely divided black solid (which tested positive for S^{2-} and is presumably Co_2S_3) and an orange-brown microcrystalline precipitate identified as the *S*-sulfito complex [(**1**)CoSO$_3$]Br (**13**) by elemental and X-ray structural analysis (yield accounts for 39% of the pentaamine ligand **1**). The formation of Co_2S_3 and **13** in the presence of dithionite implies disproportionation of the latter, a reaction known to occur in basic solution,[51] particularly in the presence of heavy metal salts having a propensity to form sulfides (Equation 2). There is no indication of the intermediacy of a cobalt(II) species in the formation of **13**.[52] The observed formation of **13** contrasts with the classical synthesis of cobalt(III) *S*-sulfito amine complexes, in which the SO_3^{2-} ligand is introduced in the form of sodium disulfite ($Na_2S_2O_5$), which hydrolyses rapidly on dissolving in water to give an equilibrium mixture of $SO_2/HSO_3^-/SO_3^{2-}$.[53,54] Cobalt(III) *S*-sulfito amine complexes have been studied in detail because of the particularly strong kinetic and structural *trans* effect exerted by the SO_3^{2-} ligand,[53,55−59] a phenomenon which causes some of the compounds to have unusual catalytic[60] and redox properties.[52,60]

$$3\,S_2O_4^{2-} + 6\,OH^- \longrightarrow 5\,SO_3^{2-} + S^{2-} + 3\,H_2O \qquad (2)$$

Solid State Structures

Structural details of the square-pyramidally coordinated {(pyN_4)Co} fragment have been described elsewhere,[1,6,7] and the corresponding bond lengths and angles in compounds **5**, **7**, **12** and **13** are given in Table 1 for reference. Parameters that quantify distortions (if any) of the ligand cap are listed in Table 2. The structures of **3** and **11** have been determined and deposited with the Cambridge Structural Database but will not be discussed, as their parameters are similar to those of [(**1**)CoCl](Cl)(ClO_4)·H_2O[1] and **5**, respectively. The discussion addresses the salient structural features of the cations in **5**, **7**, **12** and **13**, especially the conformation of and intramolecular hydrogen bonding in the O_2-bridged dinuclear complexes.

[(**1**)Co−O−O−Co(**1**)](S_2O_6)$Cl_2\cdot 6H_2O$ (**5**)

The cation (Figure 1) contains two virtually undistorted octahedral cobalt(III) centres and lies on a twofold crystallographic rotation axis which passes through the midpoint of the O−O bond. The 4+ charge on the cation is consistent with the assignment of the bridging group as peroxide, and the Co−O [1.883(3) Å] and O−O bond lengths [1.467(5) Å] as well as the Co−O−O angle [110.7(3)°] are all within the range of values found for other Co(N_5) peroxo complexes.[37] The dihedral angle Co1−O1−O1A−Co1A is 177.5(2)°. The Co−O−O−Co core is virtually coplanar with the pyridine ring N11···C15, the best planes being at an angle of 4.62(3)°. As a consequence of the inherent molecular symmetry, the two CoN_4 units are parallel and adopt an eclipsed conformation with respect to each other (Figure 2a). Relevant nonbonded distances within the (N_4)Co−O−O−Co(N_4) subunit are listed in Table 3. The Co−N bond *trans* to the O_2^{2-} group (1.928(4) Å) is significantly shorter than the equatorial bonds (on average 1.950 Å), both values being similar to the corresponding bond lengths in the pentaamine peroxo complex [(trenen)-Co−O−O−Co(trenen)](ClO_4)$_4$ [trenen = *N*,*N*,*N*′-tris(2-

Table 1. Selected bond lengths [Å] and angles [°] for compounds **5**, **7**, **12** and **13** with estimated standard deviations in parentheses; see also Table 3

Bond or angle	**5**	**7**	**12**	**13**
Co1−N11	1.928(4)	1.928(2)	1.934(5)	1.997(3)
Co1−N12	1.945(3)	1.958(2)	1.964(4)	1.968(4)
Co1−N13	1.950(3)	1.949(2)	−	1.978(4)
Co1−N14	1.950(3)	1.955(2)	−	1.973(4)
Co1−N15	1.956(3)	1.946(2)	1.960(5)	1.968(4)
Co1−X[a]	1.883(3)	1.915(2)	2.422(1)	2.226(1)
N11−Co1−X[a]	177.7(1)	177.11(8)	179.6(2)	179.2(1)
N11−Co1−N12	90.7(1)	91.74(9)	91.2(2)	88.5(2)
N11−Co1−N13	92.4(1)	88.1(1)	−	91.6(1)
N11−Co1−N14	92.2(2)	93.10(9)	−	91.0(1)
N11−Co1−N15	91.2(2)	90.5(1)	90.2(2)	89.7(2)
X−Co1−N12[a]	90.1(1)	89.21(9)	89.0(1)	91.9(1)
X−Co1−N13[a]	89.7(1)	89.18(9)	−	89.1(1)
X−Co1−N14[a]	87.1(1)	85.98(9)	−	88.7(1)
X−Co1−N15[a]	86.7(1)	92.21(9)	89.5(1)	89.6(1)
N12−Co1−N13	88.8(2)	90.6(1)	−	88.4(2)
N12−Co1−N15	91.8(1)	91.8(1)	90.8(2)	90.7(2)
N13−Co1−N14	91.6(1)	90.2(1)	−	92.2(2)
N14−Co1−N15	87.6(2)	87.6(1)	−	88.7(2)
N12−Co1−N12A	−	−	88.2(3)	−
N15−Co1−N15A	−	−	90.2(3)	−
Co1−N11−C11	119.6(3)	119.6(2)	118.8(5)	119.9(3)
Co1−N11−C15	120.3(3)	119.9(2)	119.7(5)	119.7(3)
N11−C11−C18	116.7(4)	117.6(2)	118.6(6)	116.6(3)
N11−C15−C22	116.6(4)	117.0(2)	118.3(6)	116.8(4)
C12−C11−C18	123.0(3)	122.3(2)	121.9(7)	122.5(4)
C14−C15−C22	122.4(4)	122.7(2)	121.8(7)	123.0(4)
C11−C18−C19	112.9(4)	112.9(3)	112.9(6)	111.8(4)
C15−C22−C23	112.7(4)	112.3(2)	111.7(7)	112.2(4)
C11−C18−C16	110.4(4)	106.5(3)	108.8(4)	111.3(4)
C15−C22−C21	109.6(4)	111.0(2)	110.1(4)	109.5(4)
C16−C18−C19	106.5(3)	107.6(3)	107.2(4)	106.8(4)
C21−C22−C23	106.8(4)	107.2(2)	107.1(5)	107.1(4)
C16−C18−C17	111.5(4)	109.6(3)	−	110.5(4)
C16−C18−C16A	−	−	112.0(6)	−
C21−C22−C20	111.6(4)	111.1(2)	−	110.7(4)
C21−C22−C21A	−	−	110.5(7)	−
C18−C16−N12	113.0(3)	111.7(2)	113.8(5)	114.2(4)
C22−C21−N15	113.5(4)	113.3(2)	113.1(5)	114.0(4)
C16−N12−Co1	118.5(3)	118.7(2)	118.6(3)	118.0(3)
C21−N15−Co1	118.4(3)	118.2(2)	118.5(3)	118.7(3)

[a] **5**: X = O1; **7**: X = O1; **12**: X = Br1; **13**: X = S1.

Table 2. Intramolecular angles [°] and distances [Å] quantifying the slight distortions of the ligand cap in complexes **5, 7** and **13** (with estimated standard deviations in parentheses); compound **12** does not show these distortions owing to crystallographically imposed symmetry; see footnote and text for definitions of angles

Bond or angle	**5**	**7**	**13**
ε[a]	4.07(5)	5.5(5)	6.0(5)
ζ[b]	2.5(2)	1.8(2)	4.1(3)
η[c]	2.3(2)	2.9(1)	5.4(2)
d(C16···C21)[d]	5.085(6)	5.019(5)	5.124(7)
d(C17···C20)[d]	4.922(6)	5.017(4)	4.884(7)

[a] Angle ε between the least-squares planes defined by the pyridine ring (N11, C11, C12, C13, C14, C15) and the quaternary and methyl carbon atoms C18/C19/C22/C23. − [b] Angle ζ between the least-squares planes defined by the equatorial nitrogen atoms N12/N13/N14/N15 and the methylene carbon atoms C16/C17/C20/C21. − [c] Angle η subtended by the lines N11···C13 and N11−Co1 at N11. − [d] This distance is 5.032(8) Å in **12**.

aminoethyl)ethane-1,2-diamine][37] and, incidentally, the mononuclear hydroxo species [(**1**)Co(OH)](ClO$_4$)$_2$.[6] This contrasts with a marked *trans* influence of the peroxo ligand

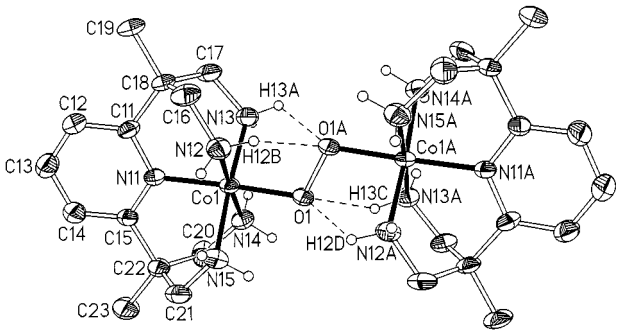


Figure 1. Molecular structure of the peroxo complex cation in **5** with thermal ellipsoids at the 50% probability level; only the hydrogen atoms in the Co(NH$_2$R)$_4$ planes are shown, and intramolecular hydrogen bonds are indicated by dashed lines

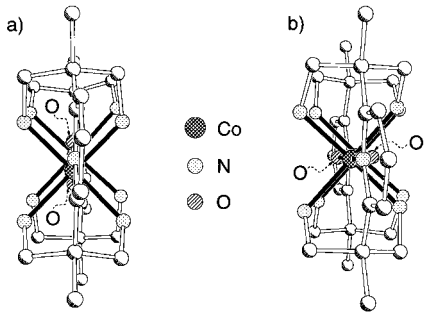


Figure 2. Views along the Co−Co vector of the peroxo (a) and superoxo (b) complex cations in **5** and **7**, respectively, illustrating the eclipsed conformations of the pyN$_4$ coordination caps; relative to the pyridine rings, the O$_2$ bridge is coplanar in (a), and positioned at right angles in (b)

Table 3. Characteristic angles (°), bonded and nonbonded distances (Å) within the (N$_4$)Co−O−O−Co(N$_4$) subunits of **5** and **7** with estimated standard deviations in parentheses

Angle or distance	**5**	**7**
Co1−O1−O1A−Co1A	177.5(2)	180
Co1−O1−O1A	110.7(3)	116.5(2)
Co1−O1	1.883(3)	1.915(2)
O1−O1A	1.467(5)	1.325(3)
Co1···O1A	2.765(3)	2.771(2)
Co1···Co1A	4.497(2)	4.576(1)
O1···N12	2.709(4)	2.720(3)
O1···N13	2.704(4)	2.712(3)
O1···N14	2.640(5)	2.639(3)
O1···N15	2.635(5)	2.782(3)
O1···N12A	2.767(5)	2.872(3)
O1···N13A	2.747(5)	3.845(3)
O1···N14A	3.846(5)	3.726(3)
O1···N15A	3.851(5)	2.921(3)
N12···N(x)	x = 15A: 4.359(6)	x = 14A: 4.411(4)
N13···N(x)	x = 14A: 4.435(6)	x = 15A: 4.637(4)

found in the structures of other CoN$_5$ complexes, where the Co−N(*trans*) bond can be up to 3% longer than the other Co−N bonds.[37,61]

In the solid state, the central Co−O−O−Co moiety of **5** is locked in a transoid conformation by four intramolecular hydrogen bonds indicated as dashed lines in Figure 1, defining the "triangular" arrangement N12−H12B···O1A···H13A−N13 and its symmetry-related counterpart [averaged distances and angles: d(N···O) = 2.76 Å; (N−H···O) =

126°]. Similar triangular intramolecular hydrogen bonding with planar Co−O−O−Co units has been found in the complexes [(en)(dien)Co−O−O−Co(dien)(en)]$(ClO_4)_4$,[62] [(tren)(NH_3)Co−O−O−Co(NH_3)(tren)]$(SCN)_4\cdot 2H_2O$[63] and [(papd)Co−O−O−Co(papd)]$(S_2O_6)(NO_3)_2\cdot 4H_2O$[34] (papd = 1,5,8,11,15-pentazapentadecane), and the adopted solid state conformations of bis[pentaaminecobalt(III)] peroxo cations have been discussed in terms of the balance of such intramolecular hydrogen-bonding interactions and lattice energy effects.[34] Intramolecular hydrogen bonding which significantly *distorts* the Co−O−O−Co core of a dicobalt(III) peroxo species from planarity has been described for $[(NH_3)_5Co-O-O-Co(NH_3)_5](SO_4)_2\cdot 4H_2O$,[25] and most recently also for a complex with carbohydrate-derived ligands.[64]

[(**1**)Co−O−O−Co(**1**)]$(S_2O_6)_2Cl\cdot 10H_2O$ (**7**)

Figure 3 shows the molecular structure of the cation, which formally consists of two essentially undistorted octahedral cobalt(III) centres linked by an O_2^- bridge, with an inversion centre at the midpoint of the O−O bond. The superoxo nature of the bridge is evident from the 5+ charge on the cation and the significantly shorter O−O bond length [1.325(3) Å] relative to **5**. This value and the Co−O distance [1.915(2) Å] and Co−O−O angle [116.5(2)°] are similar to the corresponding values determined for other $Co(N_5)$ superoxo complexes.[24,26,36,65] Molecular symmetry requires the Co−O−O−Co unit to be planar and, in the same way as in **5**, implies that the CoN_4 "squares" are parallel and adopt an eclipsed orientation (Figure 2b). It can be seen from Table 3 that, while the metal centres in **7** are further apart than in **5**, the other nonbonded distances within the (N_4)Co−O−O−Co(N_4) framework are similar in both structures. Also, the Co−N bond lengths in **7** are virtually identical to those in **5**. Most significantly, the bond *trans* to the *superoxo* bridge in **7** has the same length (within experimental error) as the bond *trans* to the *peroxo* bridge in **5** and is significantly shorter than the equatorial bonds. In the two previously characterised pairs of cobalt(III) peroxo/superoxo complexes with otherwise identical ligands,[24−26] the $Co-N_{trans}$ distance decreased markedly on going from peroxide to superoxide. It should be noted at this point that the coordination geometry imposed by the pyN_4 ligand does not necessarily obscure the *trans*-influence of ligands at the sixth site. A strong *trans*-influence is apparent in the structure of $[(\mathbf{1})Co(CH_3)]S_2O_6$,[7] and still discernible in the structure of **13** (below).

The most striking difference between the structures of **5** and **7** in the solid state is that, while the peroxo group is coplanar with the pyridine rings in **5**, the superoxo group in **7** is orientated at essentially right angles to them [87.0(2)°, which is the angle between the best planes defined by Co−O−O−Co and the pyridine ring N11···C15, respectively). The intramolecular hydrogen-bonding in **7** is again triangular, but this time involves nitrogen atoms on either diaminopropyl sidearm of the pyN_4 coordination cap [N12−H12B···O1A···H15A−N15 and its symmetry equivalent; averaged distances and angles: d(N···O) = 2.90 Å; (N−H···O) = 107°]. It is assumed that the different hydrogen-bonding requirements[26,66] of the bridging groups in either salt, as well as electrostatic effects due to the different sets of counterions, are responsible for the change in the solid state conformation upon oxidation. Density functional theory-based calculations are currently being performed[67] in order to gain insight into the electronic structures of the adopted geometries.[43,65]

[(**1**)CoBr]Br$(PF_6)\cdot H_2O$ (**12**) and [(**1**)Co(SO_3)]Br$\cdot 3H_2O$ (**13**)

The coordination cap of the cation in **12** (Figure 4a) is perfectly regular, owing to a crystallographic mirror plane which contains the pyridine ring. Distances and angles are similar to the values observed for **5** and **7** (Table 1), and also to those of the related chloro complex [(**1**)CoCl](Cl)$(ClO_4)\cdot H_2O$.[1] The $Co-N_{ax}$ bond in **12** is again slightly shorter [1.934(5) Å] than the four $Co-N_{eq}$ bonds [1.960(5) and 1.964(4) Å]. The Co−Br bond length at 2.422(1) Å lies in the range of values for this bond in other bromocobalt(III) complexes.[68][69] The molecular structure of the *S*-sulfito complex cation in **13** is shown in Figure 4b. The coordination cap is essentially regular (Table 1). The sulfito ligand shows rotational disorder, which may be a consequence of mismatched intra-cation hydrogen bonding between the protons on the equatorial N_4 donor set and the three trigonally disposed sulfito oxygen atoms. Two preferred orientations of the sixth ligand (with occupancy factors of 75% and 25%) have been refined. The Co−S bond length is 2.226(1) Å and thus ident-

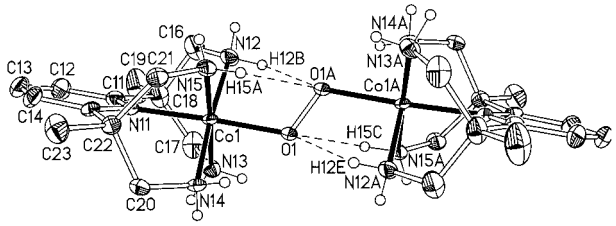


Figure 3. Molecular structure of the superoxo complex cation in **7** with thermal ellipsoids at the 50% probability level; only the hydrogen atoms in the $Co(NH_2R)_4$ planes are shown, and intramolecularhydrogen bonds are indicated by dashed lines

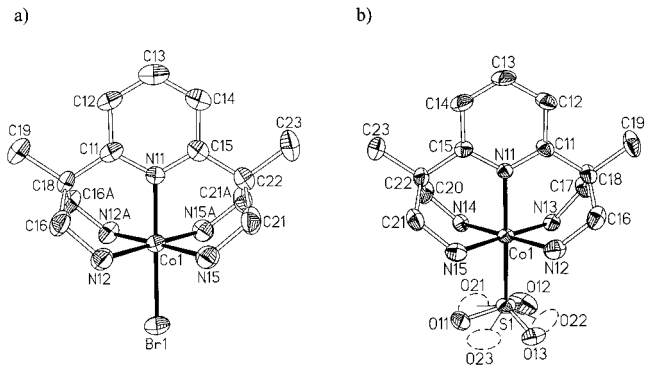


Figure 4. Molecular structures of the mononuclear cations in **12** (a) and **13** (b), with ellipsoids at the 50% probability level; hydrogen atoms have been omitted for clarity; the other resolvable orientation of the *S*-sulfito ligand in **13** is indicated by dashed ellipsoids

ical to the value in the related complex $[(en)_2(NH_3)Co(SO_3)]ClO_4$ [2.227(2) Å].[57] In contrast to the situation in complexes **5**, **7** and **12**, there is a noticeable structural *trans*-influence of the sixth ligand in **13**, as is evident from $Co-N_{ax}$ and $Co-N_{eq}$(av) bond lengths of 1.997(3) Å and 1.972(4) Å, respectively. This influence of the *S*-sulfito ligand in **13** is, however, not as pronounced as in a *trans*-ammine-bis(ethylenediamine)cobalt complex, where the difference between axial and averaged equatorial bond lengths is 0.11 Å.[57]

Conclusion

The work presented here extends the series of known cobalt(III) complexes of the type $[(\mathbf{1})CoX]^{n+}$, in which the tetrapodal pentaamine ligand **1** acts as a highly symmetrical square pyramidal coordination cap. While the preparation of mononuclear complexes with $X = Br^-$, H_2O is straightforward, it is unusual for $X = SO_3^{2-}$, which involves the disproportionation of dithionite ion to SO_3^{2-} and S^{2-}. Singly-bridged dinuclear μ_2-η^1:η^1-peroxo and -superoxo complexes $[(\mathbf{1})Co-O_2-Co(\mathbf{1})]^{4+/5+}$ are accessible by established methods [oxygenation of a cobalt(II) precursor/oxidation of the peroxo complex thus formed]. The peroxo complex may, however, be obtained in a better yield from a cobalt(III) precursor in air, which implicates the pentaamine **1** as a multi-electron reductant under the chosen conditions. The most significant solid-state structural difference between peroxo and superoxo complex is the orientation of the O_2 bridge relative to the pyridine rings of the coordination caps. Both complexes have parallel $Co(NH_2R)_4$ units in an eclipsed conformation on either side of the O_2 bridge. The peroxo complex is stable in basic aqueous solution and thus represents an attractive template for Mannich-type reactions which may, by analogy to the preparation of "sepulchrates" pioneered by Sargeson, lead to molecules with an encapsulated Co−O−O−Co spine. Work to this end is currently in progress.

Experimental Section

Materials and Instrumentation: Manipulations were performed in air unless otherwise stated. Reagents were AR grade or better and were purchased from Merck, Fluka, and Aldrich. Compounds **1**·4HCl[1] and **1**·4HBr·MeOH[70] were prepared as described previously. IR (KBr discs) and UV/Vis spectra (solvent: water) were recorded on Perkin−Elmer 16PC FT-IR and Shimadzu UV-3101 PC instruments, respectively. Cyclic voltammograms were recorded using an EG & G potentiostat PAR model 264A and a conventional three-electrode configuration consisting of a glassy carbon working electrode, a platinum auxiliary electrode and a platinum reference electrode (scan rate: 20 mV s^{-1}). NMR spectra were measured on a JEOL JNM-EX 270 spectrometer, and mass spectra were obtained on a JEOL MSTATION 700 spectrometer. Elemental analyses were performed using Carlo Erba Elemental Analysers 1106 and 1108. The ESR spectrum (DMSO glass, 120 K) was obtained on a Bruker ESP 300E instrument. Raman spectra were measured with a laser spectrophotometer (Coherent Inova 90) using argon-ion excitation at 514 nm over the region 400−3400 cm^{-1}.

X-ray Crystallography: Crystal data for compounds **5, 7**, **12** and **13** are given in Table 4, and selected distances and angles are listed in Table 1−3. The structures of the cations are presented in Figure 1, Figure 3, and Figure 4. Data for compounds **3** and **11** have been deposited (CCDC) but are not discussed. All structures were solved by direct methods and refined by full-matrix least-squares procedures on F^2 using either SHELXTL 5.03[71] (**7**, **12**) or SHELXTL 5.1.[72] The hydrogen atoms of **5** and **12** were geometrically positioned and allowed to ride on their carrier atoms during refinement; their isotropic displacement parameters were tied to those of the adjacent atoms by a factor of 1.2 or 1.5. For **7** and **13**, hydrogen atom positions were obtained from a difference Fourier synthesis and refined with a common fixed isotropic displacement parameter. Hydrogen atoms for the solvate water molecules of **5**, **12**, and **13** were not included.

Crystallographic data (excluding structure factors) for the structures reported in this paper have been deposited with the Cambridge Crystallographic Data Centre as supplementary publication nos. CCDC-137875 (**3**) − -137880 (**13**). Copies of the data can be obtained free of charge on application to CCDC, 12 Union Road, Cambridge CB2 1EZ, UK [Fax: (internat.) + 44-1223/336-033; E-mail: deposit@ccdc.cam.ac.uk]

[(1)Co−O−O−Co(1)]Cl_4 (2). − Procedure A: The preparation was carried out in air and essentially followed the procedure given by Mori et al.[73] To a solution of **1**·4HCl (3.00 g, 7.55 mmol) in water (3 mL) was added a solution of KOH (1.70 g, 30.3 mmol) in water (2 mL). This solution was added slowly (pipette) with stirring to a filtered solution of $Co^{II}(NO_3)_2·6H_2O$ (2.20 g, 7.55 mmol) in water (5 mL). In the course of the addition, the mixture turned brown, and a turbidity appeared. The mixture was cooled to 5 °C, and reacted with a stream of compressed air from the immersed tip of a Pasteur pipette for 90 min. A solution of $NaNO_3$ (0.88 g, 10 mmol) in water (1.5 mL) was then added, and bubbling of the ice-cooled solution continued for 30 min., after which time a microcrystalline brown precipitate had formed. This was filtered over a glass frit (porosity G4), washed with cold water (2 mL), then with ethanol (3 mL) and diethyl ether (3 mL), and dried in vacuo. After recrystallization from a small amount of warm water (4 mL) the isolated yield of single crystals was 0.56 g (0.71 mmol, 9.3%). The crystals were suitable for X-ray crystallography. − IR (KBr): $\tilde{\nu}$ = 3442 cm^{-1} (s), 3194vs, 2968m, 2934m, 2880w, 1606m, 1468m, 1394m, 1384m, 1167m, 1102m, 1037m, 762m, 560m. − ^1H NMR ([D_6]DMSO, room temp.): δ = 8.19 [AB_2, 3 lines, ^3J(HH) = 8.07/8.07 Hz, 2 H, H^4], 7.72 [AB_2, 2 lines, ^3J(HH) = 8.07 Hz, 4 H, $H^{3,5}$], 5.47 [br. m, 8 H, −N*H*H−], 5.27 [br. m, 8 H, −NH*H*−], 2.93 [br. m, 8 H, −C*H*H−], 2.28 [br. m, 8 H, −CH*H*−], 1.47 (s, 12 H, $-CH_3$); (D_2O, room temp.): δ = 8.06 [AB_2, 3 lines, ^3J(HH) = 7.34/8.07 Hz, 2 H, H^4], 7.65 [AB_2, 2 lines, ^3J(HH) = 8.07 Hz, 4 H, $H^{3,5}$], 2.78 [d, ^2J(HH) = 12.47 Hz, 8 H, −C*H*H−], 2.38 [d, ^2J(HH) = 13.20 Hz, 8 H, −CH*H*−], 1.43 (s, 12 H, $-CH_3$). − ^{13}C NMR ([D_6]DMSO, room temp.): δ = 165.83 (s, C2/6), 140.39 (s, C4), 120.37 (s, C3/5), 47.09 (s, >C<), 44.96 (s, $-CH_2-$), 21.55 (s, $-CH_3$). − UV/Vis (water): λ max (ε) = 293 (19 707). − $C_{26}H_{50}Cl_4Co_2N_{10}O_2·3H_2O$ (848.5): calcd. C 36.81, H 6.65, N 16.51; found C 37.01, H 6.58, N 16.79.

Procedure B: The preparation was carried out in air. To a mixture of **1**·4HCl (3.27 g, 8.23 mmol) and $Na_3[Co(CO_3)_3]·3H_2O$[74] (2.98 g, 8.23 mmol) was added a mixture of water and methanol (1:1, 100 mL) in one portion, which resulted in immediate foaming (evolution of CO_2). The mixture was heated at reflux until CO_2 evolution ceased. Upon standing at room temperature, a microcrys-

Table 4. Crystallographic data for compounds **5**, **7**, **12** and **13**

	5	**7**	**12**	**13**
Empirical formula	$C_{26}H_{62}Cl_2Co_2N_{10}O_{14}S_2$	$C_{26}H_{70}ClCo_2N_{10}O_{24}S_4$	$C_{13}H_{27}Br_2CoF_6N_5OP$	$C_{13}H_{31}BrCoN_5O_6S$
Formula weight	991.74	1188.47	633.12	524.33
Crystal system	monoclinic	triclinic	monoclinic	triclinic
Space group (no.)	*C*2/c (no. 15)	$P\bar{1}$ (no. 2)	$P2_1/m$ (no. 11)	$P\bar{1}$ (no. 2)
a [Å]	27.206(11)	9.859(2)	10.873(1)	8.227(2)
b [Å]	7.802(1)	9.940(2)	7.980(1)	9.891(2)
c [Å]	22.011(2)	13.437(2)	13.193(2)	13.595(2)
α [°]	90	72.83(1)	90	104.84(1)
β [°]	119.26(2)	89.03(2)	110.93(1)	94.23(1)
γ [°]	90	72.77(1)	90	100.16(1)
Z	4	1	2	2
V [Å^3]	4076(2)	1198.1(4)	1069.2(2)	1044.3(4)
$\rho_{calcd.}$ [g cm^{-3}]	1.616	1.647	1.967	1.667
Diffractometer	Siemens P4	Siemens P4	Siemens P4	Siemens P4
λ[Å][a]	0.71073	0.71073	0.71073	0.71073
Crystal size [mm^3]	0.40 × 0.40 × 0.20	0.60 × 0.40 × 0.35	0.90 × 0.38 × 0.10	0.65 × 0.50 × 0.40
T [°C]	293(2)	200(2)	295(2)	200(2)
Absorption correction	–	Psi-scan	Psi-scan	Psi-scan
T_{min}/T_{max}	–	0.653/0.945	0.018/0.064	0.072/0.138
Scan	ω	ω	ω	ω
2Θ range	$4 \le 2\Theta \le 54$	$4 \le 2\Theta \le 56$	$4 \le 2\Theta \le 54$	$4 \le 2\Theta \le 54$
Measured reflections	10137	6670	3290	5487
Unique reflections	4417	5685	2509	4524
Observed reflections[b]	2527	4732	1859	3405
μ(Mo-K_α) [mm^{-1}]	1.122	1.014	4.681	2.873
Refined parameters	253	409	158	347
Data/parameter ratio	17.5	13.9	15.9	13.0
*wR*2 (all data)[c]	0.1455	0.1232	0.1712	0.1256
*R*1 (obs. data)[d]	0.0560	0.0461	0.0601	0.0506
ρ_{fin}(max/min) [e Å^{-3}]	0.810/−0.873	0.766/−1.553	1.142/−1.657	0.836/-1.515
Weighting scheme[e]	$k = 0.0563/l = 0$	$k = 0.0708/l = 0.6384$	$k = 0.1093/l = 0.8048$	$k = 0.0715/l = 0.2747$

[a] Mo-K_α, graphite monochromator. – [b] With $F_o \ge 4\,\sigma(F)$. – [c] $wR2 = (\{\Sigma[w(F_o^2 - F_c^2)^2]\}/\{\Sigma[w(F_o^2)^2]\})^{0.5}$. – [d] $R1 = \Sigma||F_o| - |F_c||/\Sigma|F_o|$ for $F > 4\sigma(F)$. – [e] $w = 1/[\sigma^2(F_o^2) + (k{\cdot}P)^2] + l{\cdot}P$ and $P = (F_o^2 + 2F_c^2)/3$.

talline green−brown material precipitated, leaving a reddish brown filtrate. The solid was collected by filtration, washed repeatedly with small volumes of methanol and dried in vacuo (0.61 g, 0.73 mmol, 17.7% relative to **1**). – IR (KBr): $\tilde{\nu}$ = 3430 cm^{-1} (s), 3186s, 3094s, 2964w, 2938w, 2878w, 1605s, 1467s, 1394w, 1276w, 1206w, 1164m, 1102m, 1040m, 816w, 763m, 560w, 482w. – $C_{26}H_{50}Cl_4Co_2N_{10}O_2{\cdot}1.5H_2O{\cdot}0.5CH_3OH$ (837.5): calcd. C 38.01, H 6.62, N 16.72; found C 38.32, H 7.03, N 17.12.

[(1)Co−O−O−Co(1)]Cl$_5$ (6): The filtrate obtained as under B above (100 mL) was acidified with hydrochloric acid (3 N, 5 mL), and stirred overnight at room temperature. A green precipitate formed which was collected by filtration, washed with small volumes of methanol, and dried in vacuo (0.69 g, 0.59 mmol, 14% relative to **1**). An anion exchange with NH_4PF_6 was carried out in order to obtain analytically pure material. – IR (KBr): $\tilde{\nu}$ = 3627 cm^{-1} (w), 3426w, 3083m, 1607m, 1472m, 1441w, 1220w, 1178w, 1112w, 1032w, 938vs, 764w, 740w, 559s. – ESR (DMSO, 120 K): *g* = 2.0269. – UV/Vis (water): λ max (ε) = 698 (1720), 464 (360), 307 (28940), 208 (42520). – $C_{26}H_{50}Cl_2Co_2F_{18}N_{10}O_2P_3{\cdot}H_2O$ ([(**1**)Co−O−O−Co(**1**)] $Cl_2(PF_6)_3{\cdot}H_2O$, 1176): calcd. C 26.55, H 4.46, N 11.91; found C 26.53, H 4.39, N 11.82.

[(1)CoCl]Cl$_2$ (4): The mother liquor obtained in the preparation of **6** (100 mL) was loaded on a Dowex 50WX2 cation exchange column (∅ 15 mm, length 250 mm). Gradient elution with HCl gave an orange−red fraction (3 N HCl, 300 mL). Reducing its volume to ca. 50 mL on a rotary evaporator induced precipitation of a microcrystalline pink solid, which was collected, washed with small volumes of an ethanol/diethyl ether mixture (1:1), and diethyl ether, and dried in vacuo (0.74 g, 1.6 mmol, 19.2% relative to **1**). – IR (KBr): $\tilde{\nu}$ = 3394 cm^{-1} (s), 3199s, 3086s, 2970w, 2882w, 1603s, 1470m, 1396w, 1289w, 1261w, 1214w, 1171m, 1104m, 1042m, 826w, 774w. – ^{1}H NMR ([D$_6$]DMSO, room temp.): δ = 8.19 [AB$_2$, 3 lines, ^3J(HH) = 7.66/7.90 Hz, 1 H, H^4], 7.69 [AB$_2$, 2 lines, ^3J(HH) = 7.90 Hz, 2 H, H^{3,5}], 6.46 [br. m, 4 H, −N*H*H−], 5.23 [br. m, 4 H, −NH*H*−], 2.74 [br. m, 4 H, −C*H*H−], 2.25 [br. m, 4 H, −CH*H*−], 1.47 (s, 6 H, $-CH_3$). – ^{13}C NMR ([D$_6$]DMSO, room temp.): δ = 165.18 (s, C2/6), 140.98 (s, C4), 121.00 (s, C3/5), 47.16 (s, >C<), 44.16 (s, $-CH_2-$), 21.33 (s, $-CH_3$). – $C_{13}H_{25}Cl_3CoN_5{\cdot}0.75C_2H_5OH{\cdot}H_2O$ (469.2): calcd. C 37.12, H 6.77, N 14.93; found C 37.49, H 7.04, N 15.27.

[(1)CoBr]Br$_2$ (9). – Procedure A: The preparation was carried out in air. To a mixture of **1**·4HBr·MeOH (6.07 g, 10.0 mmol) and $Na_3[Co(CO_3)_3]{\cdot}3H_2O$ (3.62 g, 10.0 mmol) was added a mixture of water and methanol (50:50 v/v, 180 mL) in one portion, which resulted in immediate foaming. After CO_2 evolution had subsided, hydrobromic acid (1.0 N, 10 mL) was added. The mixture was heated at reflux until CO_2 evolution ceased. The mixture (still hot) was filtered to remove unchanged $Na_3[Co(CO_3)_3]$, and a brown crystalline material precipitated on standing at room temperature, leaving a reddish brown mother liquor. The solid was removed by filtration and washed with methanol ([(**1**)−Co−O−O−Co−(**1**)]$Br_4{\cdot}3H_2O$, 2.85 g, 55.5% relative to **1**). The filtrate was loaded on a Dowex 50WX2 cation exchange column (∅ 15 mm, length 250 mm). Gradient elution with HBr gave a red−violet fraction (3 N HBr, 300 mL). Reducing its volume to ca. 50 mL on a rotary evaporator induced precipitation of a microcrystalline purple solid, which was collected, washed with small volumes of an ethanol/diethyl ether mixture (50:50 v/v), and dried in vacuo (1.23 g, 2.24 mmol, 22.4% relative to **1**).

Procedure B: [(**1**)−Co−O−O−Co−(**1**)]Br_4·3H_2O (0.30 g, 0.29 mmol) was suspended in hydrobromic acid (3 N, 25 mL) and stirred for one hour. Over this period the colour of the suspension changed from brown to green. The precipitate was collected by filtration, washed with small volumes of an ethanol/diethyl ether mixture (50:50 v/v) and dried in vacuo ([(**1**)−Co−O−O−Co−(**1**)]Br_5, 0.20 g, 65% relative to **1**), leaving a reddish violet filtrate. Reducing the volume of the filtrate to ca. 50 mL on a rotary evaporator induced precipitation of a microcrystalline reddish purple solid, which was collected, washed with a small amount of ethanol/diethyl ether (50:50 v/v) and dried in vacuo. As elemental analysis was not yet satisfactory, and in order to obtain single crystals suitable for X-ray crystallography, an anion exchange was carried out with NH_4PF_6. − IR (KBr): $\tilde{\nu}$ = 3671 cm^{-1} (m), 3596m, 3421w, 3304m, 3181m, 3088m, 2951w, 1595s, 1470m, 1400w, 1284w, 1210w, 1170m, 1104m, 1034m, 846vs, 741w, 559vs, 415w. − ^{1}H NMR ([D_6]DMSO, room temp.): δ = 8.21 [AB_2, 3 lines, ^3J(HH) = 7.90/7.66 Hz, 1 H, H^4], 7.71 [AB_2, 2 lines, ^3J(HH) = 7.93 Hz, 2 H, $H^{3,5}$], 5.40 [br. m, 8 H, −NH_2], 2.76 [br. m, 4 H, −C*H*H−], 2.26 [br. m, 4 H, −CH*H*−], 1.46 (s, 6 H, −CH_3). − ^{13}C NMR ([D_6]DMSO, room temp.): δ = 165.06 (s, C2/6), 141.11 (s, C4), 121.22 (s, C3/5), 46.77 (s, >C<), 44.12 (s, −CH_2−), 21.27 (s, −CH_3). − $C_{13}H_{25}Br_2CoF_6N_5P$·$H_2O$ ([(**1**)CoBr]$BrPF_6$·H_2O, 633.1): calcd. C 24.66, H 4.30, N 11.06; found C 24.86, H 4.00, N 11.09.

[(1)CoSO$_3$]Br (13): Manipulations were performed under nitrogen in deoxygenated solvents using standard Schlenk techniques. To a mixture of **1**·4HBr·MeOH (0.61 g, 1.0 mmol) and $Na_3[Co(CO_3)_3]$·3H_2O (0.36 g, 1.0 mmol) was added water (25 mL) in one portion (with stirring), which resulted in immediate foaming (evolution of CO_2). After CO_2 evolution had ceased, a solution of $Na_2S_2O_4$ (0.1 g, 0.5 mmol) and $NaHCO_3$ (0.17 g, 2.0 mmol) in water (10 mL) was added, and the mixture stirred overnight. Precipitated Co_2S_3 was removed by filtration, and the hydrogen sulfide which evolved after acidification identified by its smell. The volume of the mother liquor was reduced until an orange−brown precipitate appeared, and the suspension then kept at 4 °C overnight in order to complete precipitation. The microcrystalline material was collected by filtration, washed repeatedly with small volumes of ethanol and dried in vacuo (0.22 g, 39% relative to **1**). The volume of the mother liquor was reduced further, and storage at 4 °C produced a small batch of single crystals suitable for X-ray structural analysis. Anion exchange of the major fraction with NH_4PF_6 in dilute aqueous ammonia gave crystalline material which analysed correctly for C, H, and N, and was used for IR and NMR spectroscopic characterization. − IR (KBr): $\tilde{\nu}$ = 3471 cm^{-1} (s), 3329s, 3227s, 2975w, 2890w, 1670w, 1606m, 1471m, 1402w, 1283w, 1206w, 1109s, 1082s, 1025m, 984vs, 840vs, 770w, 740w, 638m, 558s, 510w. − ^{1}H NMR ([D_6]DMSO, room temp.): δ = 8.26 [AB_2, 3 lines, ^3J(HH) = 7.90/7.90 Hz, 1 H, H^4], 7.80 [AB_2, 2 lines, ^3J(HH) = 7.90 Hz, 2 H, $H^{3,5}$], 3.99 [br. m, 8 H, −NH_2], 2.65 [br. m, 4 H, −C*H*H−], 2.15 [br. m, 4 H, −CH*H*−], 1.40 [br. s, 6 H, −CH_3]. − ^{13}C NMR ([D_6]DMSO, room temp.): δ = 166.02 (s, C2/6), 140.24 (s, C4), 120.09 (s, C3/5), 45.29 (s, >C<), 44.34 (br. s, −CH_2−), 21.12 (s, −CH_3). − $C_{13}H_{25}CoF_6N_5O_3PS$·2$H_2O$ (571.4): calcd. C 27.33, H 5.12, N 12.26, S 5.61; found C 27.51, H 5.46, N 12.19, S 5.44.

Acknowledgments

We thank Professor D. Sellmann for generous support of this work and Professor S. Schneider, Dr. G. Brehm and Dr. M. Niegl for the measurement of the Raman spectra. Financial support from the Deutsche Forschungsgemeinschaft is gratefully acknowledged.

[1] A. Grohmann, F. Knoch, *Inorg. Chem.* **1996**, *35*, 7932−7934.
[2] C. Dietz, F. W. Heinemann, J. Kuhnigk, C. Krüger, M. Gerdan, A. X. Trautwein, A. Grohmann, *Eur. J. Inorg. Chem.* **1998**, 1041−1049.
[3] C. Dietz, F. W. Heinemann, A. Grohmann, *Eur. J. Inorg. Chem.* **1999**, 2147−2156.
[4] C. Dietz, S. Schmidt, F. W. Heinemann, A. Grohmann, in *Selective Reactions of Metal-Activated Molecules* (Eds.: H. Werner, P. Schreier), Vieweg, Braunschweig, **1998**, p. 217−221.
[5] S. Schmidt, W. Bauer, F. W. Heinemann, H. Lanig, A. Grohmann, *Angew. Chem.* **2000**, *112*, 950−953; *Angew. Chem. Int. Ed.* **2000**, *39*, 913−916.
[6] T. Poth, H. Paulus, H. Elias, R. van Eldik, A. Grohmann, *Eur. J. Inorg. Chem.* **1999**, 643−650.
[7] A. Grohmann, F. W. Heinemann, P. Kofod, *Inorg. Chim. Acta* **1999**, *286*, 98−102.
[8] A. M. Sargeson, *Pure Appl. Chem.* **1986**, *58*, 1511−1522.
[9] Sargeson, Geue and co-workers very recently reported the synthesis of of 2,2′-dimethyl-2,2′-iminodimethylenebis(1,3-propanediamine), which is structurally similar to **1**: B. Fabius, R. J. Geue, R. G. Hazell, W. G. Jackson, F. Krebs Larsen, C. J. Qin, A. M. Sargeson, *J. Chem. Soc., Dalton Trans.* **1999**, 3961−3972.
[10] C. Bianchini, R. W. Zoellner, *Adv. Inorg. Chem.* **1997**, *44*, 263−339.
[11] S. Fallab, P. R. Mitchell, *Adv. Inorg. Bioinorg. Mechan.* **1984**, *3*, 311−377.
[12] A. G. Sykes, J. A. Weil, *Progr. Inorg. Chem.* **1970**, *13*, 1−106.
[13] E. Frémy, *Ann. Chem. Pharm.* **1852**, *83*, 227−249.
[14] E. Frémy, *Ann. Chem. Pharm.* **1852**, *83*, 289−317.
[15] L. Maquenne, *C. R. Hebd. Seances Acad. Sci.* **1883**, *96*, 344−345.
[16] G. Vortmann, *Monatsh. Chem.* **1885**, *6*, 404−445.
[17] A. Werner, A. Mylius, *Z. Anorg. Chem.* **1898**, *16*, 245−267.
[18] E. C. Niederhoffer, J. H. Timmons, A. E. Martell, *Chem. Rev.* **1984**, *84*, 137−203.
[19] D. H. Busch, in *Oxygen Complexes and Oxygen Activation by Transition Metals* (Eds.: A. E. Martell, D. T. Sawyer), Plenum Press, New York, **1988**, p. 61−85.
[20] A. E. Martell in *Oxygen Complexes and Oxygen Activation by Transition Metals* (Eds.: A. E. Martell, D. T. Sawyer), Plenum Press, New York, **1988**, p. 87−106.
[21] D. Ramprasad, A. G. Gilicinski, T. J. Markley, G. P. Pez, *Inorg. Chem.* **1994**, *33*, 2841−2847.
[22] A. G. Kolchinski, B. Korybut-Daszkiewicz, E. V. Rybak-Akimova, D. H. Busch, N. W. Alcock, H. J. Clase, *J. Am. Chem. Soc.* **1997**, *119*, 4160−4171.
[23] N. D. Rosso, B. Szpoganicz, A. E. Martell, *Inorg. Chim. Acta* **1999**, *287*, 193−198.
[24] The N_5 donor set in refs.[24,25] is $(NH_3)_5$: W. P. Schaefer, R. E. Marsh, *Acta Cryst.* **1966**, *21*, 735−743.
[25] W. P. Schaefer, *Inorg. Chem.* **1968**, *7*, 725−731.
[26] The N_5 donor set is (en)(dien): D. D. Dexter, C. N. Sutherby, M. W. Grieb, R. C. Beaumont, *Inorg. Chim. Acta* **1984**, *86*, 19−31.
[27] J. Simplicio, R. G. Wilkins, *J. Am. Chem. Soc.* **1969**, *91*, 1325−1329.
[28] R. G. Wilkins, in *Bioinorganic Chemistry* (Eds.: R. Dessy, J. Dillard, L. Taylor), American Chemical Society, Washington, **1971**, vol. 100, p. 111−134.
[29] S. Takano, Y. Yano, W. Tagaki, *Chem. Lett.* **1981**, 1177−1180.
[30] S. Tamagaki, Y. Kanamaru, M. Ueno, W. Tagaki, *Bull. Chem. Soc. Jpn.* **1991**, *64*, 165−174.
[31] J. H. Timmons, A. Clearfield, A. E. Martell, R. H. Niswander, *Inorg. Chem.* **1979**, *18*, 1042−1047.
[32] J. H. Timmons, R. H. Niswander, A. Clearfield, A. E. Martell, *Inorg. Chem.* **1979**, *18*, 2977−2982.
[33] W. R. Harris, G. L. McLendon, A. E. Martell, R. C. Bess, M. Mason, *Inorg. Chem.* **1980**, *19*, 21−26.
[34] M. Zehnder, U. Thewalt, *Z. Anorg. Allg. Chem.* **1980**, *461*, 53−60.
[35] C. J. Raleigh, A. E. Martell, *J. Coord. Chem.* **1985**, *14*, 113−117.

[36] P. V. Bernhardt, G. A. Lawrance, T. W. Hambley, *J. Chem. Soc., Dalton Trans.* **1990**, 235−241.
[37] B. M. Gatehouse, G. McLachlan, L. L. Martin, R. L. Martin, L. Spiccia, *Aust. J. Chem.* **1991**, *44*, 351−359, and references therein.
[38] N. F. Curtis, W. T. Robinson, D. C. Weatherburn, *Aust. J. Chem.* **1992**, *45*, 1663−1680.
[39] A. Bencini, A. Bianchi, S. Cabani, N. Ceccanti, P. Paoletti, M. R. Tinè, *J. Chem. Soc., Dalton Trans.* **1993**, 695−702.
[40] M. Maeder, H. R. Mäcke, *Inorg. Chem.* **1994**, *33*, 3135−3140.
[41] D. A. Buckingham, W. G. Jackson, P. A. Marzilli, A. M. Sargeson, *Aust. J. Chem.* **1999**, *52*, 185−204.
[42] C. G. Barraclough, G. A. Lawrance, P. A. Lay, *Inorg. Chem.* **1978**, *17*, 3317−3322.
[43] E. I. Solomon, F. Tuczek, D. E. Root, C. A. Brown, *Chem. Rev.* **1994**, *94*, 827−856.
[44] S. Fallab, M. Zehnder, *Helv. Chim. Acta* **1984**, *67*, 392−398.
[45] D. T. Richens, A. G. Sykes, *J. Chem. Soc., Dalton Trans.* **1982**, 1621−1624.
[46] D. L. Duffy, D. A. House, J. A. Weil, *J. Inorg. Nucl. Chem.* **1969**, *31*, 2053−2058.
[47] V. M. Miskowski, J. L. Robbins, I. M. Treitel, H. B. Gray, *Inorg. Chem.* **1975**, *14*, 2318−2321.
[48] G. J. Gainsford, W. G. Jackson, A. M. Sargeson, *Aust. J. Chem.* **1986**, *39*, 1331−1336.
[49] *Gmelins Handbuch der Anorganischen Chemie*, Gmelin-Institut, Verlag Chemie, Weinheim, **1966**, "Sauerstoff", System-No. 3, "Lieferung 7", 8th ed.; "Wasserstoffperoxid"; p. 2295−2297.
[50] A sharp singlet (^{1}H NMR, [D$_6$]DMSO) at δ = 6.28 which disappears upon addition of D_2O and a new band in the IR spectrum of medium intensity at 755 cm^{-1} [ν(OH, wag)] are assigned to the aqua ligand: G. Socrates, *Infrared Characteristic Group Frequencies*, Second ed. Wiley, Chichester, **1994**, p. 222.
[51] *Gmelins Handbuch der Anorganischen Chemie*, Gmelin-Institut, Verlag Chemie, Weinheim, **1960**, "Schwefel", System-No. 9, "Teil B − Lieferung 2", 8th ed.; p. 387−396.
[52] A redox decomposition in aqueous solution leading to Co^{II} and an $HSO_3^{\cdot}$ free radical species has been suggested for sulfito cobalt(III) complexes: M. A. Thacker, K. L. Scott, M. E. Simpson, R. S. Murray, W. C. E. Higginson, *J. Chem. Soc., Dalton Trans.* **1974**, 647−651.
[53] H. Siebert, G. Wittke, *Z. Anorg. Allg. Chem.* **1973**, *399*, 43−51.
[54] A. C. Dash, A. K. Patnaik, A. N. Acharya, *Transition Met. Chem.* **1998**, *23*, 45−55.
[55] E. N. Maslen, C. L. Raston, A. H. White, J. K. Yandell, *J. Chem. Soc., Dalton Trans.* **1975**, 327−329.
[56] R. C. Elder, M. J. Heeg, M. D. Payne, M. Trkula, E. Deutsch, *Inorg. Chem.* **1978**, *17*, 431−440.
[57] C. L. Raston, A. H. White, J. K. Yandell, *Aust. J. Chem.* **1980**, *33*, 1123−1128.
[58] K. J. Schneider, R. van Eldik, A. Roodt, J. G. Leipoldt, *Inorg. Chim. Acta* **1986**, *122*, 1−5.
[59] M. D. Johnson, R. J. Balahura, *Inorg. Chem.* **1992**, *31*, 808−809.
[60] A. M. Al-Ajlouni, P. C. Paul, E. S. Gould, *Inorg. Chem.* **1998**, *37*, 1434−1437.
[61] A. E. Martell, *Acc. Chem. Res.* **1982**, *15*, 155−162.
[62] J. R. Fritch, G. G. Christoph, W. P. Schaefer, *Inorg. Chem.* **1973**, *12*, 2170−2175.
[63] U. Thewalt, M. Zehnder, S. Fallab, *Helv. Chim. Acta* **1977**, *60*, 867−873.
[64] T. Tanase, T. Onaka, M. Nakagoshi, I. Kinoshita, K. Shibata, M. Doe, J. Fujii, S. Yano, *Inorg. Chem.* **1999**, *38*, 3150−3159.
[65] V. M. Miskowski, B. D. Santarsiero, W. P. Schaefer, G. E. Ansok, H. B. Gray, *Inorg. Chem.* **1984**, *23*, 172−176.
[66] F. R. Fronczek, W. P. Schaefer, R. E. Marsh, *Acta Crystallogr., Sect. B* **1974**, *30*, 117−121.
[67] M. Hennemann, T. Clark, A. Grohmann, to be published.
[68] I. Bernal, J. Cetrullo, W. G. Jackson, *Inorg. Chem.* **1993**, *32*, 4098−4101.
[69] O. Börtin, *Acta Chem. Scand. A* **1976**, *30*, 475−476.
[70] S. Schmidt, L. Omnès, F. W. Heinemann, J. Kuhnigk, C. Krüger, A. Grohmann, *Z. Naturforsch.* **1998**, *53b*, 946−954.
[71] SHELXTL 5.03 for Siemens Crystallographic Research Systems, Siemens Analytical X-ray Instruments, Inc., Madison, USA, **1995**.
[72] SHELXTL 5.1, Bruker AXS, Inc., Madison, USA, **1998**.
[73] M. Mori, J. A. Weil, M. Ishiguro, *J. Am. Chem. Soc.* **1968**, *90*, 615−621.
[74] H. F. Bauer, W. C. Drinkard, *Inorg. Synth.* **1966**, *8*, 202−204.

Received December 17, 1999
[I99466]

Ion Chemistry in XH_4/Allene (X = Ge, Si) Gaseous Mixtures − Formation of X−C Bonds

Paola Benzi, Lorenza Operti,* Roberto Rabezzana

Eur. J. Inorg. Chem. **2000**, 505−512

Due to a correction error, some columns of Table 6 on page 510 remained misaligned rendering the table incomprehensible. The correct version is given below.

Table 6. Reactions of $Si_3H_5^+$, $Si_4H_7^+$,$SiC_2H_n^+$, and $SiC_3H_n^+$ ions with allene and silane in a SiH_4/C_3H_4 mixture

Reactants	Product Ions and Rate Constants (k_{exp})[a]	Σk_{exp}	k_L[b]	Efficiency[c]
$Si_3H_5^+ + C_3H_4$	$Si_3CH_5^+$ (0.93), $Si_3CH_9^+$ (0.90), $Si_3C_3H_5^+$ (2.6)	4.4	10.38	0.43
$Si_4H_7^+ + C_3H_4$	$Si_3C_3H_5^+$ (0.46), $Si_4CH_7^+$ (0.80), $Si_4CH_{11}^+$ (0.78), $Si_4C_3H_7^+$ (1.6)	3.6	9.96	0.36
$SiC_2H_3^+ + C_3H_4$	$SiC_3H_3^+$ (0.50), $SiC_3H_5^+$ (0.76), $SiC_5H_5^+$ (1.3)	2.6	11.35	0.23
$SiC_2H_5^+ + C_3H_4$	$SiC_2H_3^+$ (2.4), $SiC_3H_5^+$ (0.90), $SiC_3H_7^+$ (0.67), $SiC_5H_7^+$ (1.5)	5.5	11.26	0.49
$SiC_3H_5^+ + C_3H_4$	$SiC_4H_5^+$ (1.1), $SiC_4H_7^+$ (0.39)	1.5	10.85	0.14
$SiC_3H_6^+ + C_3H_4$	$SiC_4H_6^+$ (0.74), $SiC_4H_8^+$ (0.32), $SiC_5H_7^+$ (0.97), $SiC_6H_9^+$ (2.2)	4.2	10.82	0.39
$SiC_3H_6^+ + SiH_4$	$Si_2C_3H_8^+$ (0.95)	0.95	10.38	0.092
$SiC_3H_7^+ + C_3H_4$	$SiC_3H_5^+$ (0.15), $SiC_4H_7^+$ (1.6), $SiC_4H_9^+$ (0.66), $SiC_5H_7^+$ (1.1), $SiC_6H_9^+$ (1.3), $SiC_6H_{10}^+$ (0.25)	5.1	10.80	0.47
$SiC_3H_7^+ + SiH_4$	$Si_2C_3H_9^+$ (0.38)	0.38	10.36	0.037

[a] Rate constants are expressed as 10^{-10} $cm^3molecule^{-1}s^{-1}$; experiments were run at 333 K; uncertainty is within 20%. − [b] Rate constants have been calculated according to the Langevin theory calculating polarizability of C_3H_4 as in ref.[19], and taking polarizability of SiH_4 from ref.[20] − [c] Efficiency has been calculated as the ratio $\Sigma k_{exp}/k_L$.

The Editors
[C I99284]

 © WILEY-VCH Verlag GmbH, D-69451 Weinheim, 2000 1434−1948/00/0707−1669 $ 17.50+.50/0

Cyclopropenylium−Borate Betaines: Opening an Organometallic Route to Neutral Carbocation-Like Compounds

Sabine Venne-Dunker,[a] Wolfgang Ahlers,[a] Gerhard Erker,*[a] and Roland Fröhlich[a][+]

Keywords: Cyclopropenylium cation / Group-4 metallocenes / Alkynyl coupling / Insertions / Zirconium / Boron

Treatment of bis(propynyl)zirconocene (**5**) with a stoichiometric quantity of $B(C_6F_5)_3$ leads to C–C coupling of the alkynyl ligands to form the zirconocene–(μ-hexadiyne)–borate betaine complex **11**. This apparently is in an endothermic equilibrium with a methylenecyclopropene-type isomer **13**, formed by intramolecular alkyne insertion into the (sp^2-carbon)–zirconium linkage, which is very effectively trapped by added scavenger reagents such as organic nitriles or isonitriles, to yield the stable unsaturated three-membered ring products **14** or **15**, respectively. Subsequent hydrolysis removes the zirconocene moiety from the product, but the newly formed (sp^2-carbon)–$B(C_6F_5)_3$ linkage remains intact. The resulting products **16** and **17** formally contain a central methylenecyclopropene framework, but their structural properties point to a substantial π-delocalization, that indicates a pronounced participation of an enamino-substituted cyclopropenylium–borate betaine resonance structure. The description of the neutral betaine compounds **16** and **17** as approaching cyclopropenylium cation-type compounds that have their counteranion covalently bonded to them, is further supported by the observation of low activation barriers of the rotation around the exocyclic C3–C4 bond [$\Delta G^{\neq}_{CCrot}$ (330 K) = 17.5 ± 0.5 kcal mol^{-1} for **17a**] and around the C5–N linkage [$\Delta G^{\neq}_{CNrot}$ (306 K) = 14.5 ± 0.5 kcal mol^{-1} for **16a**]. The neutral cyclopropenylium–betaine compound **17a** shows a carbocation-like chemical reactivity, and inserts *tert*-butyl isocyanide to yield the ring-expanded four-membered carbocyclic product **21**.

Introduction

Cyclopropenylium cations $C_3R_3^+$ (**1**) represent the smallest members of the carbocyclic arenes. The many reported examples of this class of compounds profit from the marked thermodynamic stabilization provided by aromaticity, but kinetically the reactivity features of many cyclopropenylium systems appear to be largely governed by their ionic nature, and hence by electrostatic effects.[1] It would be interesting to see how the cyclopropenylium arenes would behave in the absence of their positive charge. In principle, this could be achieved by covalently attaching a suitable anion as a

[a] Organisch-Chemisches Institut der Universität Münster, Corrensstraße 40, 48149 Münster, Germany
Fax: (internat.) + 49-(0)251/833-6503
E-mail: erker@uni-muenster.de
[+] X-ray crystal structure analyses





Sabine Venne-Dunker (top left) studied chemistry at the Universität Münster where she did her diplom thesis in Prof. Erker's group. Since October 1998 she has been carrying out work for her doctoral thesis on the synthesis of novel Group-4 and -5 metal complexes and their catalytic application.

Wolfgang Ahlers (top right) also studied chemistry at the Universität Münster and did his doctoral dissertation in Prof. Erker's group. He received his doctoral degree in 1997. He then joined the BASF company in Ludwigshafen, where he currently does catalysis research in the Ammoniaklaboratorium.

Gerhard Erker (bottom left) studied chemistry at the Universität Köln. In 1973 he received his doctoral degree at the Universität Bochum, where he worked with Professor Wolfgang R. Roth in physical organic chemistry. After a stay as a DFG postdoctoral fellow with Professor Maitland Jones, Jr. at Princeton University (carbene chemistry) he did his habilitation at Bochum (1981). He was a Heisenberg fellow at the Max-Planck-Institut für Kohlenforschung in Mülheim a. d. Ruhr (1984–1985), then a C3-Professor at the Institut für Organische Chemie in Würzburg, and since 1990 he has been a C4-Professor at Münster. His major research interests are in the areas of reaction mechanisms, the synthesis of unusually structured organic compounds, organometallic chemistry, and catalysis.

Roland Fröhlich (bottom right) studied chemistry at the universities of Münster and Köln and received his doctoral degree in 1982. After postdoctoral studies at the Institute for Crystallography of the Universität Karlsruhe he worked as a sales and application manager for Enraf Nonius. Since 1993 he is a senior scientist at the Universität Münster being responsible for the X-ray laboratory of the Institut für Organische Chemie. Since 1994 he is also a docent for X-ray Crystallography at the University of Jyväskylä, Finland.

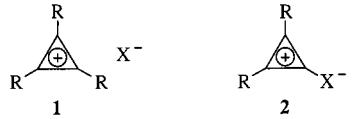




MICROREVIEWS: This feature introduces the readers to the authors' research through a concise overview of the selected topic. Reference to important work from others in the field is included.

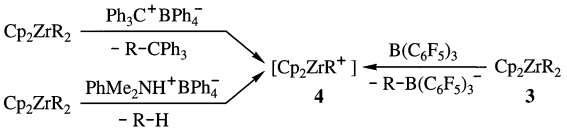
 © WILEY-VCH Verlag GmbH, D-69451 Weinheim, 2000 1434−1948/00/0808−1671 $ 17.50+.50/0

substituent to the cyclopropenylium core. Such a construction would result in the formation of a cyclopropenylium betaine **2**, a system that is neutral overall, but may be highly polarized and function chemically as a cyclopropenylium system without the electrostatic effects of the otherwise dominating positive charge, provided of course that the right combination of substituents and the internal anion moiety is used (Scheme 1).



Scheme 1. Design of a cyclopropenylium betaine **2**, a potential carbocyclic three-membered ring arene without a featured positive charge

It is well established that dialkylzirconocene complexes are easily converted into [$^{R}Cp_2ZrR^+$] cations by treatment with a variety of electrophilic reagents.[2] The reaction of $^{R}Cp_2ZrR_2$, generated in situ, with methylalumoxane is mostly used for a direct generation of the [$^{R}Cp_2ZrR^+$] species, serving as a very active homogeneous metallocene Ziegler catalyst for α-olefin polymerization.[3] Treatment of a variety of $^{R}Cp_2ZrR_2$ starting materials with either a suitable Lewis acid [e.g. $B(C_6F_5)_3$] or Brønsted acid [e.g. $PhMe_2NH^+$ BPh_4^-], or a stable carbenium ion [e.g. Ph_3C^+ BPh_4^-] has invariably resulted in the formation of stable and isolable [$^{R}Cp_2ZrR^+$] cations, albeit generally carrying σ-ligands R with sp^3-carbon atoms bonded to the transition metal center.[4] The observation of some unusual chemistry taking place with alkynyl zirconocene cations [$Cp_2Zr-C\equiv C-R^+$], generated by the Lewis acid route mentioned above, has led to the development of a simple organometallic route to a variety of examples of cyclopropenylium−betaine systems **2**, to the best of our knowledge representing the first examples of their kind. The development of this synthetic entry is reviewed in this article, along with a description of the structural features and some chemistry of the unique cyclopropenylium−borate betaines prepared by our new reaction (Scheme 2).

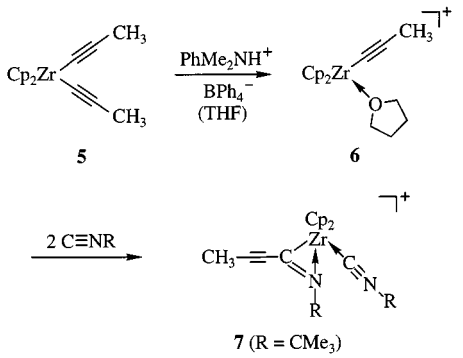


Scheme 2. Methods of [Cp_2ZrR^+] cation generation used in this study

Results and Discussion

(Propynyl)zirconocene Cation Prepared by a Protonation Route

Bis(propynyl)zirconocene (**5**) was synthesized by treatment of zirconocene dichloride with two molar equivalents of propynyllithium.[5] The X-ray crystal structure analysis of **5** revealed a Zr−C(sp) σ-bond length of 2.249(3) Å, which is only slightly shorter than the documented Zr−C(sp^3) bond length in $Cp_2Zr(CH_3)_2$ [2.277(5) Å], thus indicating that there is probably no extensive propargyl π-interaction of the −C≡C−R unit with the 16-electron metallocene moiety in **5**.[5] Treatment of **5** with the Brønsted acid *N*,*N*-dimethylanilinium tetraphenylborate in THF, furnished the (σ-propynyl)zirconocene cation−THF adduct **6**. This turned out to be a very reactive and sensitive complex, but we were able to characterize it chemically by means of an alkyl isocyanide insertion reaction. *tert*-Butyl isocyanide inserts into the Zr−C(sp) σ-bond of **6** to form an (η^2-iminoacyl)zirconocene cation complex, which takes up another equivalent of the isonitrile reagent to form the stable product **7** that was isolated and characterized by X-ray diffraction (see Scheme 3 and Figure 1).[6]



Scheme 3. Generation and reaction of a THF-stabilized (σ-alkynyl)zirconocene cation

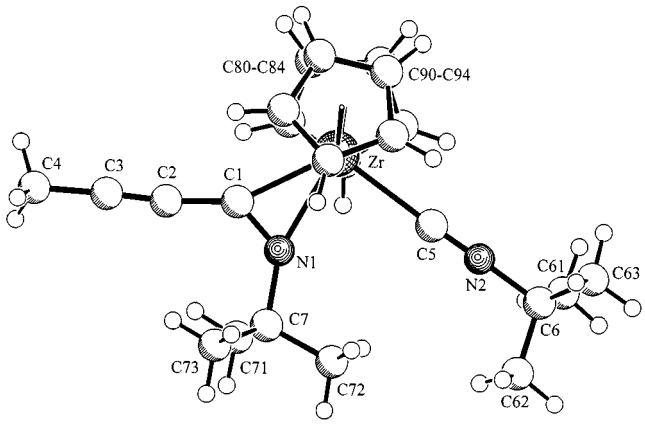
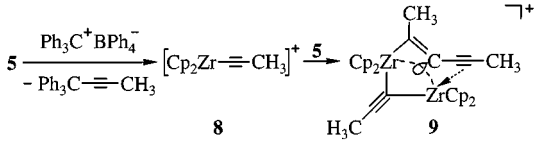


Figure 1. Molecular structure of **7** (cation only); selected bond lengths [Å] and angles [°]: Zr−C1 2.194(3), Zr−N1 2.229(3), Zr−C5 2.350(4), Zr−C(Cp) 2.501(4), C1−N1 1.264(4), C1−C2 1.412(5), C2−C3 1.191(5), C3−C4 1.453(5), N1−C7 1.499(4), C5−N2 1.148(4), N2−C6 1.464(4); C1−Zr−C5 117.36(12), C1−Zr−N1 33.20(11), N1−Zr−C5 84.17(11), Zr−C1−N1 74.9(2), Zr−C1−C2 153.7(3), Zr−N1−C1 71.9(2), Zr−N1−C7 158.8(2), Zr−C5−N2 177.3(3), C1−C2−C3 173.0(4), C2−C3−C4 177.2(4), C2−C1−N1 131.3(3), C1−N1−C7 129.0(3), C5−N2−C6 176.1(4)

(Propynyl)zirconocene Cation Generated by the Trityl Cation Route Leads to a Stable Planar-Tetracoordinated Carbon Compound

Treatment of bis(propynyl)zirconocene (**5**) with trityl tetraphenylborate led to the abstraction of a σ-C≡C−CH_3 ligand (to yield $Ph_3C-C\equiv C-CH_3$) and generation of the donor-ligand free [$Cp_2Zr-C\equiv C-CH_3^+$] cation (**8**). In contrast with the analogous [$Cp_2Zr-CH_3^+$] cation, complex **8**



Scheme 4. Formation of a stable planar-tetracoordinated carbon compound from (propynyl)zirconocene cation

is not stable under the typical reaction conditions of its generation, but instantaneously reacts with one equivalent of the bis(propynyl)zirconocene starting material.[7] Rapid carbon−carbon coupling ensues, with formation of a μ-hexadiyne ligand. The resulting dinuclear cation complex **9** contains a bridging μ-propynyl ligand and an unsymmetrically bridging μ-hexadiyne moiety (Scheme 4). The latter contains a planar-tetracoordinated carbon atom[8] (C2 in Figure 2) that features short bonds to two adjacent carbon atoms [C1−C2 1.317(8) Å, C2−C3 1.400(8) Å] as well as to the two zirconium centers [C2−Zr1 2.530(5) Å, C2−Zr2 2.434(6) Å, the sum of the bond angles at C2 is 360.0°]. The C1−C2 bond represents a C=C double bond, and the Zr1−C2−Zr2 linkage is to be regarded as a three-center two-electron bonding situation. Thus, the bonding features at carbon atom C2 are as expected for a stable *anti*-van't Hoff/LeBel compound that contains stabilizing metal substituents. Complex **9** represents just another example of an increasing number of isolated and structurally characterized examples of such types of very stable but unusually structured carbon compounds.[8b][8c]

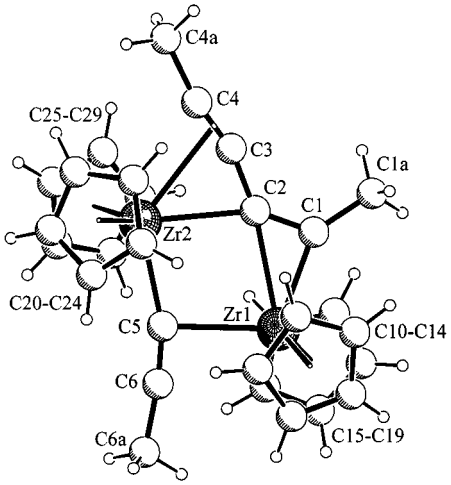
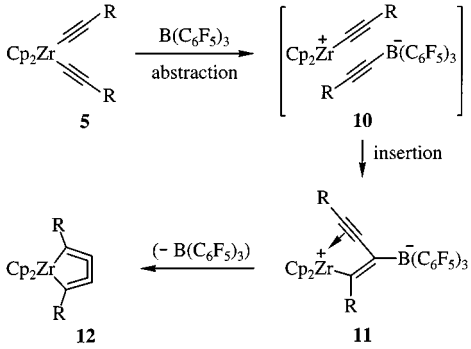


Figure 2. Molecular structure of the "*anti*-van't Hoff/LeBel compound" **9**

Reactions of Bis(alkynyl)zirconocenes with $B(C_6F_5)_3$, the Unexpected Formation of Carbocyclic Three-Membered Ring Products by Unsymmetrical Alkynyl Dimerization

We have found that a variety of bis(alkynyl)zirconocenes **5** are converted into their substituted (η-butadiyne)$ZrCp_2$ isomers **12** by treatment with catalytic amounts of the strong organometallic Lewis acid $B(C_6F_5)_3$.[9,10] The likely intermediate of the catalytic C−C coupling reaction is **11**. Several examples of such zirconocene−(μ-RC_4R)−borate betaines were isolated from the stoichiometric reaction of a



Scheme 5. Products formed in the reaction of bis(alkynyl)zirconocenes with $B(C_6F_5)_3$

variety of bis(alkynyl)zirconocenes [as well as bis(alkynyl)-hafnocenes] with $B(C_6F_5)_3$.[9,11] It is likely that the $B(C_6F_5)_3$ reagent abstracts a σ-alkynyl ligand from the metallocene to form the ion pair **10**. Subsequent rapid alkyne insertion of the $R-C\equiv C-B(C_6F_5)_3^-$ unit into the (sp-C)−Zr σ-bond of the very reactive [$Cp_2Zr-C\equiv C-R^+$] cation moiety then results in carbon−carbon coupling to directly yield the observed metallocene−(μ-diyne)−borate betaine system **11** (see Scheme 5).

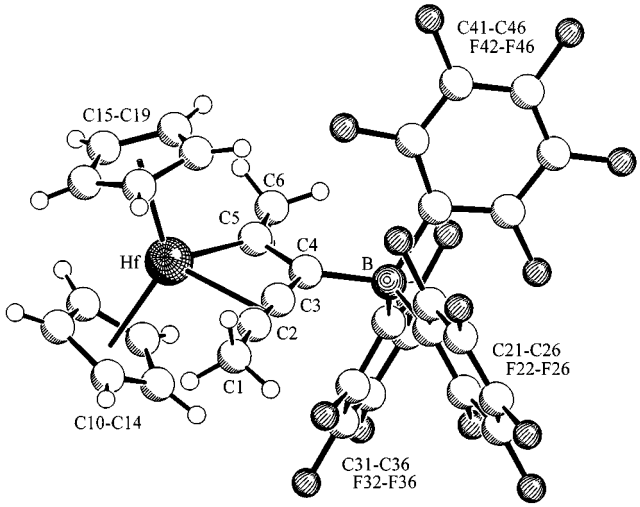


Figure 3. A view of the molecular structure of the metallocene−(μ-hexadiyne)−borate betaine **11′**

The hafnocene−(μ-hexadiyne)−borate betaine **11′** was characterized by X-ray diffraction (see Figure 3).[11,12] It shows the presence of a planar μ-C_4Me_2 ligand that bridges between hafnium and boron. The (sp^2-C)-to-hafnium σ-bond (C5−Hf in Figure 3) amounts to 2.150(10) Å. The C4−B bond length is 1.63(2) Å. The C4−C5 bond [1.412(13) Å] is in the range for a carbon−carbon double bond, whereas the adjacent C2−C3 bond is much shorter at 1.220(14) Å. The Hf−(C2≡C3) unit represents one of the rare examples of a structurally characterized (η^2-alkyne) group-4 metallocene moiety. The characteristic Hf−C2 and Hf−C3 bond lengths were found to be 2.671(11) Å and 2.310(10) Å, respectively.

In the crystal, the borate unit is chiral, exhibiting a $-B(C_6F_5)_3$ propeller geometry. This chirality element is persistent in many examples of the complexes **11** in solution

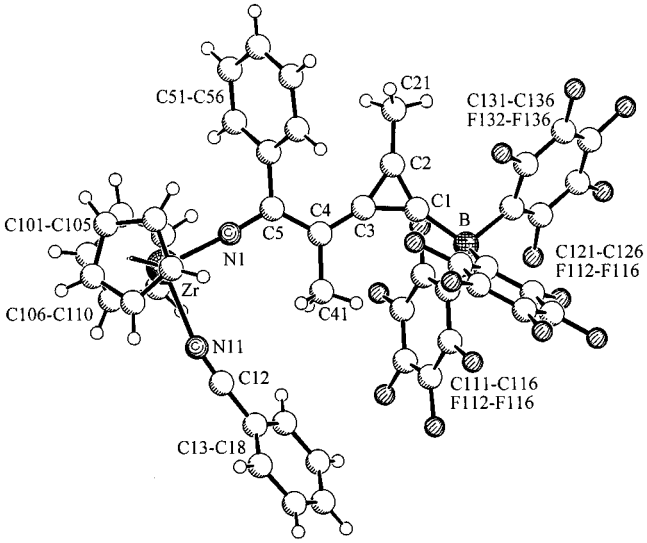
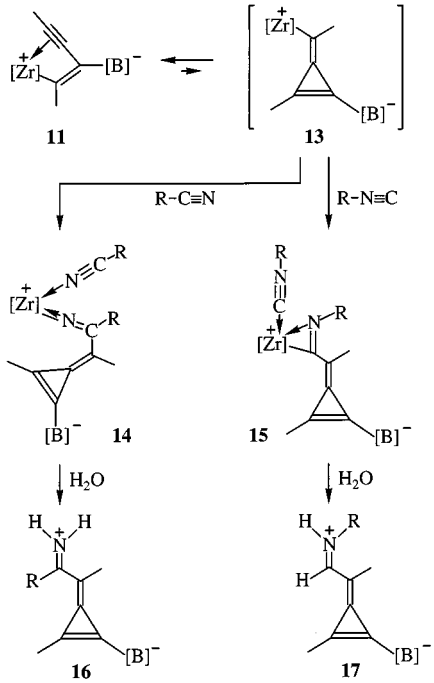


Figure 4. Molecular structure of complex **14**

on the NMR time scale. This gives rise, at sufficiently low temperature, to the observed typical NMR signals for diastereotopic pairs of Cp ligands. From the coalescence of the ^{1}H-NMR Cp resonances the Gibbs activation energies of the borate-propeller enantiomerization were obtained. The $\Delta G^{\neq}_{enant}$ values showed a marked dependence on the steric bulk of the substituents R attached at the μ-C_4 ligand (see Scheme 5) [e.g.: M = Zr, R = CH_3: $\Delta G^{\neq}_{enant}$ (292 K) = 14.3 kcal mol^{-1}; R = cyclohexyl: $\Delta G^{\neq}_{enant}$ (323 K) = 16.4 kcal mol^{-1}].[11]

A most unusual reaction took place when the zirconocene−(μ-hexadiyne)−borate betaine complex **11** was treated with benzonitrile. A rapid reaction ensued which resulted in the consumption of two molar equivalents of the nitrile reagent with formation of product **14**.[9] The X-ray crystal structure analysis (see Figure 4) showed that an unsaturated three-membered ring was formed with typical bond lengths of 1.335(3) Å (C1−C2), 1.394(3) Å (C2−C3), and 1.423(3) Å (C1−C3). The exocyclic unsaturated C3−C4 linkage features a bond length of 1.366(3) Å, and the newly formed bond (C4−C5 in Figure 4) amounts to 1.427(3) Å. The central C_4 framework of **14** in principle features a methylenecyclopropene-type structure, although a marked tendency for π-delocalization is noticed upon comparison with unperturbed methylenecyclopropene examples. The Zr−N=CR_2 unit is almost linear [Zr−N−C 173.4(2)°], and exhibits a marked heteroallene character [Zr−N 1.955(2) Å, N=C 1.299(2) Å].[13] The second benzonitrile unit is just coordinated to zirconium, and stabilizes the electron-deficient metallocene cation substructure in the dipolar arrangement of complex **14** [Zr−N≡C angle 166.5(2)°, Zr−N 2.289(2) Å, N≡C 1.142(3) Å].

The formation of a methylenecyclopropene unit from **11** can be formulated by a reaction sequence initiated by an intramolecular insertion of the coordinated alkyne moiety into the adjacent (sp^2-C)−Zr σ-bond. Compound **13**, the methylenecyclopropene isomer of **11**, is formed in situ and may be present in an equilibrium situation, although the



Scheme 6. Trapping of the in situ generated zirconium−(methylenecyclopropene)−borate betaine **13** with nitriles and isonitriles {[Zr] = Cp_2Zr; [B] = $B(C_6F_5)_3$; substituents used for **14** and **16**: R = C_6H_5 (**a**), *p*-$C_6H_4OCH_3$ (**b**), *p*-$C_6H_4N(CH_3)_2$ (**c**), *p*-$C_6H_4CO_2CH_3$ (**d**); for **15** and **17**: R = $C(CH)_3$ (**a**)}

unsaturated three-membered ring isomer formation must be quite endothermic (by > 20−30 kcal mol^{-1}). Nevertheless, it appears that the high energy isomer **13**, which is present in only a minute equilibrium concentration, being too low for direct detection, is very efficiently trapped, e.g. by the added nitrile to yield the stable product **14**. The overall stabilization of the eventually observed product comes from the C−C and N−Zr bond formation. A variety of differently substituted nitriles have successfully been used as scavengers of **13**. Other typical insertion reagents have been used as well, such as isonitriles,[14] in which case the stable (η^2-iminoacyl)Zr derivatives **15** are obtained in good yield (see Scheme 6).[15] The structure of a typical example (**15a**), derived from $Cp_2Zr(C{\equiv}C{-}C_3H_7)_2$, $B(C_6F_5)_3$, and *tert*-butyl isocyanide, is depicted in Figure 5.

Hydrolysis removes the zirconocene unit efficiently from the framework of **14** and **15**.[16,17] The borate group remains, and we have isolated the iminium−borate betaine systems **16** and **17**, respectively, in good yield (see Scheme 6) with a variety of substituent combinations. The X-ray crystal structures were determined for a number of representative examples, which revealed the remarkable structural features of this class of compounds (see Scheme 7 and Table 1). From the data compiled in Table 1 and Figure 6 it becomes apparent that compounds **16** are characterized by a very pronounced bond lengths equilibration of the C1-to-C5 core. The C1−C2 bond length is uniformly at ca. 1.35 Å. The C1−C3 bond length is ca. 1.40 Å, and the C2−C3 bond typically adopts an intermediate value of 1.37 Å. This marked bond length equilibration effect also extends to the C3−C4 linkage, which at 1.39 Å is clearly below the ex-

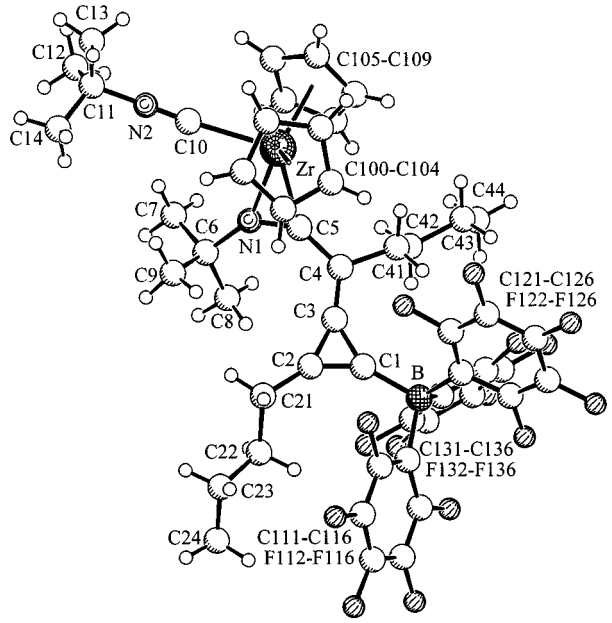
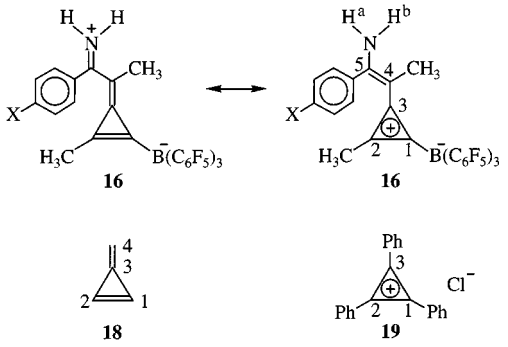


Figure 5. Molecular structure of **15a**; selected bond lengths [Å] and angles [°]: B−C1 1.609(5), C1−C2 1.328(4), C1−C3 1.432(4), C2−C3 1.417(5), C2−C21 1.474(5), C3−C4 1.353(4), C4−C41 1.523(4), C4−C5 1.430(4), C5−N1 1.277(4), N1−C6 1.482(4), C5−Zr 2.219(3), N1−Zr 2.197(3), Zr−C10 2.351(3), C10−N2 1.137(4), N2−C11 1.457(4); B−C1−C2 150.6(3), B−C1−C3 147.4(3), C2−C1−C3 61.6(2), C1−C2−C3 62.8(2), C1−C2−C21 145.9(4), C21−C2−C3 151.2(3), C1−C3−C2 55.6(2), C2−C3−C4 159.0(3), C3−C4−C41 117.7(3), C3−C4−C5 124.7(3), C41−C4−C5 116.7(3), C4−C5−N1 142.1(3), C4−C5−Zr 144.6(2), N1−C5−Zr 72.3(2), C5−N1−C6 135.7(3), C5−N1−Zr 74.1(2), C5−Zr−N1 33.6(1), C5−Zr−C10 118.2(1), N1−Zr−C10 84.6(1), Zr−C10−N2 175.1(3), C10−N2−C11 176.7(4)



Scheme 7. Resonance structures of **16** [X = H (**a**), OCH_3 (**b**), $N(CH_3)_2$ (**c**), CO_2CH_3 (**d**)]

Table 1. C−C bond lengths [Å] of the molecular core of typical examples of the compounds **16**; all compounds were prepared starting from bis(propynyl)zirconocene, see also Scheme 7

Compound	X	C1−C2	C1−C3	C2−C3	C3−C4	C4−C5
a	H	1.341(3)	1.399(3)	1.372(3)	1.396(3)	1.383(3)
b	OCH_3	1.345(3)	1.399(3)	1.376(3)	1.395(3)	1.377(3)
c	$N(CH_3)_2$	1.348(3)	1.405(3)	1.376(3)	1.393(3)	1.383(3)
d	CO_2CH_3	1.356(3)	1.405(3)	1.387(3)	1.393(3)	1.380(3)

pected $C(sp^2)-C(sp^2)$ single bond value, almost matching the C4−C5 bond length at ca. 1.38 Å (see Table 1). These values are quite atypical for a methylenecyclopropene framework, when compared with the typical C−C distances

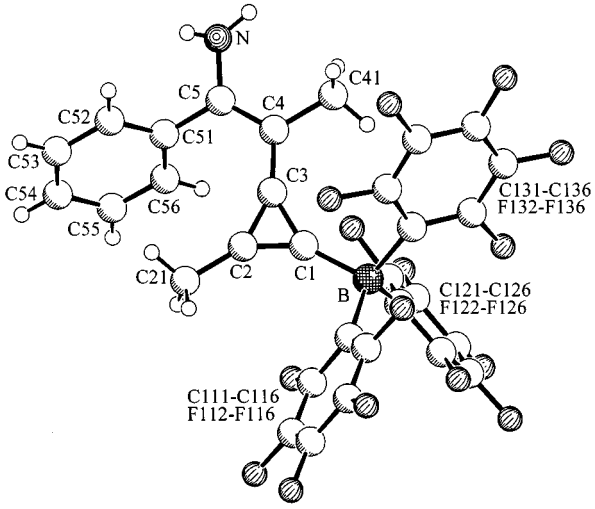


Figure 6. A view of the molecular structure of **16a**; selected bond lengths [Å] and angles [°]:C1−C2 1.341(3), C1−C3 1.399(3), C1−B 1.623(3), C2−C3 1.372(3), C2−C21 1.479(3), C3−C4 1.396(3), C4−C5 1.383(3), C4−C41 1.509(4), C5−N 1.339(3), C5−C51 1.477(4); C2−C1−C3 60.1(2), C2−C1−B 150.6(2), C3−C1−B 149.3(2), C1−C2−C3 62.1(2), C1−C2−C21 148.7(2), C3−C2−C21 149.2(2), C1−C3−C2 57.9(2), C2−C3−C4 154.2(2), C4−C3−C1 147.8(2), C3−C4−C5 118.8(2), C3−C4−C41 119.8(2), C5−C4−C41 121.4(2), C4−C5−N 121.0(3), N−C5−C51 116.0(2), C4−C5−C51 123.0(2)

in e.g. the parent hydrocarbon methylenecyclopropene itself (C1−C2 1.323 Å, C1−C3 1.441 Å, C3−C4 1.332 Å).[18]

The observed structural π-bond delocalization probably indicates a pronounced contribution of a cyclopropenylium-type structure in the framework of compounds **16** (and of **17**, see below). The triphenylcyclopropenylium cation shows a C−C bond length of 1.373 Å inside the three-membered ring,[1] a value about which the three C1-to-C3 bond lengths of compounds **16** are closely centered (see above). Thus, compounds **16** may be structurally regarded as being very closely related to cyclopropenylium betaines bearing an enamino substituent at carbon atom C3. These unique compounds, therefore, may structurally be regarded as cyclopropenylium compounds that are devoid of their +1 charge, because they carry their counter anion covalently bonded to them.

A mandatory consequence of a description of compounds **16** and **17** as substituted cyclopropenylium betaines is that the rotational barrier about the exocyclic C3−C4 partial π-bond is low, thus allowing for a rapid *cis*/*trans* isomerization of the substituents at C2 and C4 of the framework. It must be noted that none of the *cis* isomers (e.g. *cis*-**16** or *cis*-**17**) can directly result from our synthetic scheme (see Scheme 6). Consequently, any appearance of a respective product that exhibits the former alkynyl substituents −R in a relative *cis* orientation at positions C2 and C4 at the planar central carbon framework must be considered an indication of a subsequent isomerization reaction involving rotation about the C3−C4 linkage under the applied, very mild reaction conditions. Such a *cis* product, namely the *N*-*tert*-butyl-substituted cyclopropenylium betaine *cis*-**17a**, obtained by *tert*-butyl isocyanide trapping of the metallocene−borate betaine **13a** followed by hydrolysis, was

characterized structurally.[17] Compound *cis*-**17a** exhibits the typical tendency of C−C-bond length leveling in the central C_5 unit that is characteristic of the members of this larger family of compounds (see Figure 7).

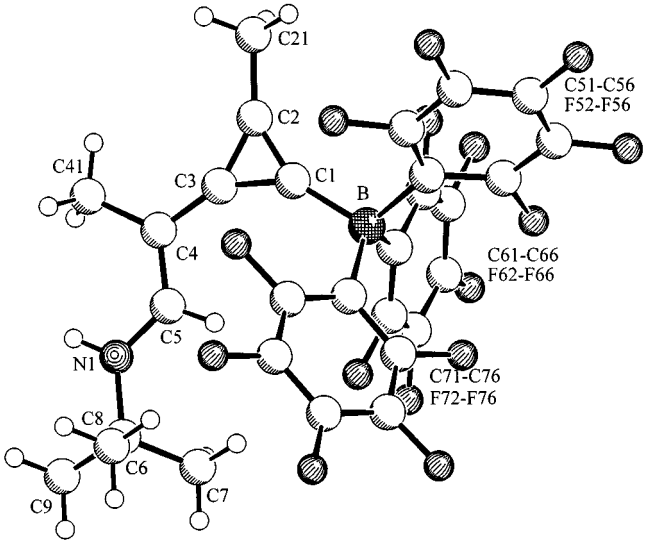
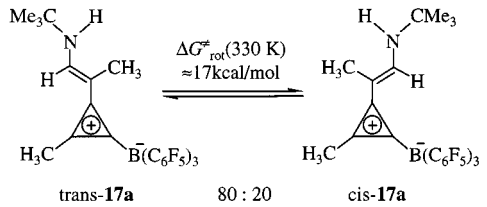


Figure 7. Molecular structure of the cyclopropenylium−borate betaine compound *cis*-**17a**; selected bond lengths [Å] and angles [°]: C1−C2 1.350(6), C1b−C2b 1.356(6), C1−C3 1.416(5), C1b−C3b 1.399(6), C1−B 1.611(6), C1b−B1b 1.610(6), C2−C3 1.383(6), C2b−C3b 1.374(6), C3−C4 1.388(6), C3b−C4b 1.394(6), C4−C5 1.380(6), C4b−C5b 1.370(6), C5−N1 1.316(5), C5b−N1b 1.325(5), N1−C6 1.484(6), N1b−C6b 1.475(6); B−C1−C2 153.5(4), B1b−C1b−C2b 152.0(4), B−C1−C3 145.3(4), B1b−C1b−C3b 147.1(4), C2−C1−C3 59.9(3), C2b−C1b−C3b 59.8(3), C1−C2−C3 62.4(3), C1b−C2b−C3b 61.7(3), C1−C3−C2 57.7(3), C1b−C3b−C2b 58.6(3), C1−C3−C4 149.1(4), C1b−C3b−C4b 149.2(4), C2−C3−C4 153.1(4), C2b−C3b−C4b 152.3(4), C3−C4−C5 116.2(4), C3b−C4b−C5b 116.5(4), C4−C5−N1 125.8(4), C4b−C5b−N1b 126.4(4), C5−N1−C6 126.0(4), C5b−N1b−C6b 125.4(4)

The rotation around the C3−C4 bond in **17a** is indeed kinetically very facile in solution. Compound **17a**, dissolved in [D_5]bromobenzene, exhibits typical NMR signals of the two isomers *trans*- and *cis*-**17a** in solution (Scheme 8). The compounds are present in a ca. 80:20 ratio at 270 K. Raising the temperature results in a broadening of the signals, of e.g. the methyl substituents, and eventually to coalescence. From the dynamic NMR behavior of the complex pair, *trans*-**17a** and *cis*-**17a**, a Gibbs activation energy of $\Delta G^{\neq}_{CCrot}$ (330 K) = 17.0 ± 0.4 kcal mol^{-1} was obtained. Microscopically this value probably corresponds to the activation barrier of rotation around the C3−C4 [C(sp^2)−C(sp^2)] linkage in the compound **17a**. The observed value of 17 kcal mol^{-1} [17] is much lower than expected for a normal C=C double bond rotation, which



Scheme 8. Facile rotational *trans*/*cis* isomerization of the compound **17a**

strongly supports the interpretation that these complexes behave as neutral three-membered ring aromatic cyclopropenylium betaine systems.

The *trans*/*cis* isomerization was observed for several other examples of this general class of compounds.[12] As a consequence of the pronounced cyclopropenylium betaine character the rotation around the enamine C5−NH_2 bond in the complexes listed in Table 1 is fast. Invariably, values close to $\Delta G^{\neq}_{CNrot}$(306 K) ≈ 14.5 ± 0.5 kcal mol^{-1} were observed, almost independent of the arene substituents X (see Scheme 7).[12][16b,17]

First Reactions of the Cyclopropenylium−Borate Betaines

Carbenium ions react with a variety of soft neutral carbon nucleophiles by carbon−carbon coupling. The reaction with isonitriles is a typical example that may ultimately lead to products derived from intermediately formed iminium ions.[19] It is expected that the neutral betaine systems **16** and **17** should typically undergo similar reactions due to the incipient carbenium ion character of their cyclopropenylium cation-type substructural unit, and this has indeed been observed when some of the cyclopropenylium betaines were treated with alkyl isocyanide reagents.

The cyclopropenylium−borate betaine **17a** reacted rapidly with one molar equivalent of *tert*-butyl isocyanide in methanol solution to selectively yield the product **21** (see Scheme 9 and Figure 8).[17] The insertion and ring expansion is likely to be initiated by nucleophilic attack of the isonitrile to the cyclopropenylium C2 position of the betaine starting material (to generate **20**). This is probably followed by C−C σ-bond migration to the in situ formed imi-

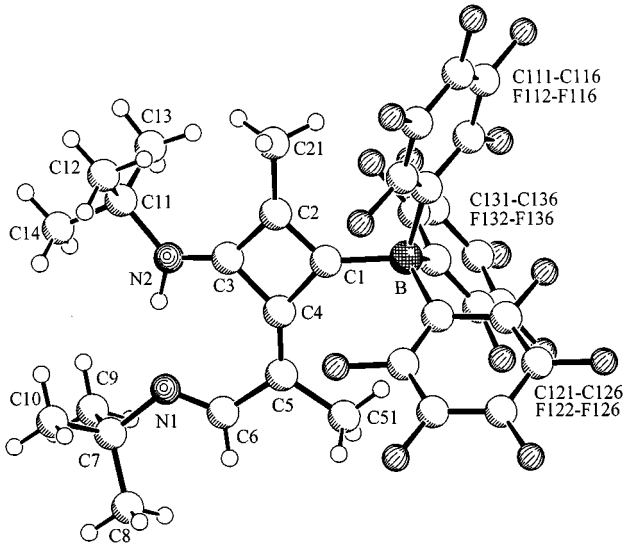
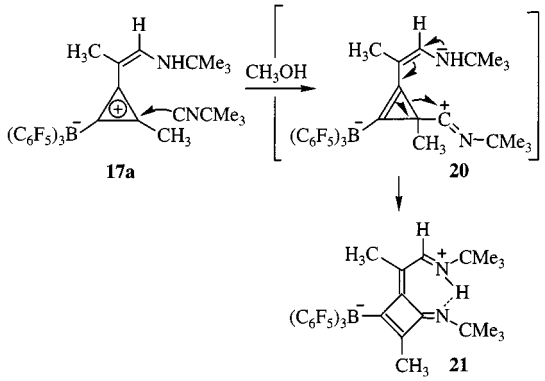


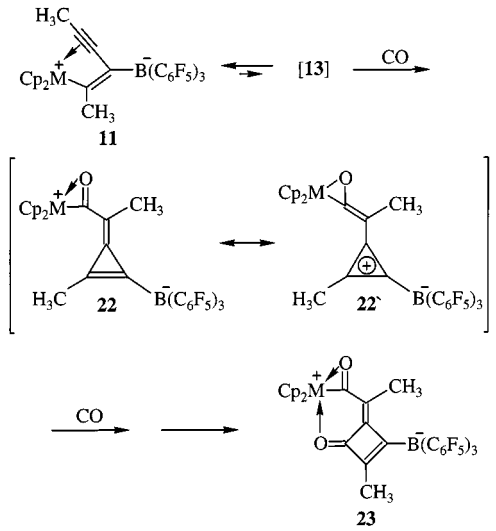
Figure 8. Molecular structure of the isonitrile insertion product **21**; selected bond lengths [Å] and angles [°]: B−C1 1.631(3), C1−C2 1.383(3), C1−C4 1.506(3), C2−C3 1.454(3), C3−N2 1.290(3), C3−C4 1.481(3), N2−C11 1.495(3), C4−C5 1.340(3), C5−C6 1.475(3), C6−N1 1.265(3), N1−C7 1.490(3); B−C1−C2 132.9(2), B−C1−C4 134.6(2), C1−C2−C3 92.2(2), C1−C4−C3 86.4(2), C2−C1−C4 91.5(2), C2−C3−C4 89.8(2), C2−C3−N2 140.6(2), C3−N2−C11 128.3(2), C1−C4−C5 138.3(2), C3−C4−C5 135.3(2), C4−C5−C6 124.4(2), C5−C6−N1 127.1(2), C6−N1−C7 121.3(2)



Scheme 9. Ring expansion reaction of **17a** upon treatment with an isonitrile

noacyl cation to give the favored expanded conjugated bis-(imine) product **21** directly.

The isonitrile insertion product was characterized by X-ray diffraction.[12,17] This has revealed the presence of the unsaturated central four-membered ring structure. One of the C=N functionalities is a part of this structure, and the other is attached to it. There is a bridging hydrogen between the two imino nitrogen atoms (^{1}H NMR: δ = 9.98), and the borate counter anion is again covalently bonded to the framework. In contrast to the markedly delocalized π-system of the cyclopropenylium betaine systems (**16** and **17**, see above), compound **21** contains clearly alternating single and double bonds around its completely unsaturated perimeter.



Scheme 10. Reaction of the betaine complex **11** with carbon monoxide

A related reaction probably takes place upon treatment of the betaine complex **11** with carbon monoxide (Scheme 10). It seems that initially the high-lying methylenecyclopropene intermediate **13** is trapped by C−C bond-forming insertion as usual, in this case giving rise to the formation of the corresponding (η^2-acyl)zirconocene product **22**. Its resonance structure **22′**, which consequently reacts rapidly by further CO uptake under the reaction conditions to eventually yield the methylenecyclobutenone complex **23**, seems to provide a favored description of the cyclopropenylium features of this neutral organometallic product. The product, **23**, was characterized spectroscopically,[12] and shows a variety of characteristic features similar to the closely related compound **21**.

Conclusions

We have found a simple way to make a number of examples of a new variety of unsaturated three-membered ring compounds.[20] Our organometallic route, which combines coupling of two acetylides at the zirconocene template [upon treatment with a stoichiometric quantity of the strong organometallic Lewis acid tris(pentafluorophenyl)-borane], with trapping of its methylenecyclopropene isomer and subsequent hydrolysis, makes compounds **16** and **17** readily available in high yield. These compounds show a pronounced cyclopropenylium−borate betaine character, with regard to their structural properties in the solid state and their typical dynamic features in solution. Thus, it seems that such compounds represent the first series of examples that may be regarded as cyclopropenylium ions bearing their counter anion covalently bonded to their three-membered ring framework. Their structural, dynamic and, as shown in first examples, chemical behavior is the same as would be expected for the smallest carbocyclic arenes, the cyclopropenylium cations, but without the dominating effects of the charge. In some respect, systems such as **16** or **17** might be suited to the study and development of some "carbenium ion chemistry without the charge". Now that first examples have become available by easily accessible organometallic pathways, the development of the chemistry of neutral variants of a variety of charged organic species as parts of such simple betaine systems may become feasible.[21]

Acknowledgments

Financial support by the Fonds der Chemischen Industrie and the Deutsche Forschungsgemeinschaft is gratefully acknowledged.

[1] D. Wendisch, *Methoden Org. Chem. (Houben-Weyl)* **1971**, vol. IV/3, p. 749−763; W. E. Billups, A. W. Moorehead, *The Chemistry of the Cyclopropyl Group* (Ed.: Z. Rappoport), Wiley, NewYork, **1987**, p. 1558−1569; R. Breslow, R. Haynie, J. Mirra, *J. Am. Chem. Soc.* **1959**, *81*, 247−248; R. Breslow, J. Posner, *Org. Synth.* **1967**, *47*, 62−68; A. W. Krebs, *Angew. Chem.* **1965**, *77*, 10−22; *Angew. Chem. Int. Ed. Engl.* **1965**, *4*, 10−22.

[2] R. F. Jordan, *Adv. Organomet. Chem.* **1991**, *32*, 325−387; M. Bochmann, *J. Chem. Soc., Dalton Trans.* **1996**, 255−270.

[3] H. J. Sinn, W. Kaminsky, *Adv. Organomet. Chem.* **1980**, *18*, 99−149.

[4] [4a] A. G. Massey, A. J. Park, F. G. A. Stone, *Proceedings Chem. Soc*. **1963**, 212−213; A. G. Massey, A. J. Park, *J. Organomet. Chem.* **1964**, *2*, 245−250; X. Yang, C. L. Stern, T. J. Marks, *J. Am. Chem. Soc.* **1991**, *113*, 3623−3625; X. Yang, C. L. Stern, T. J. Marks, *J. Am. Chem. Soc.* **1994**, *116*, 10015−10031. − [4b] M. Bochmann, A. J. Jaggar, J. C. Nicholls, *Angew. Chem.* **1990**, *102*, 830−832; *Angew. Chem. Int. Ed. Engl.* **1990**, *29*, 780−782. − [4c] J. C. W. Chien, W.-M. Tsai, M. D. Rausch, *J. Am. Chem. Soc.* **1991**, *113*, 8570−8571.

[5] G. Erker, W. Frömberg, R. Mynott, B. Gabor, C. Krüger, *Angew. Chem.* **1986**, *98*, 456−457; *Angew. Chem. Int. Ed. Engl.*

1986, *25*, 463−465; W. Frömberg, doctoral dissertation, Univ. Würzburg, **1986**.

[6] W. Ahlers, G. Erker, R. Fröhlich, *J. Organomet. Chem.* **1998**, *571*, 83−89.

[7] W. Ahlers, B. Temme, G. Erker, R. Fröhlich, F. Zippel, *Organometallics* **1997**, *16*, 1440−1444.

[8] [8a] R. Hoffmann, R. W. Alder, C. F. Wilcox, Jr., *J. Am. Chem. Soc.* **1970**, *92*, 4992−4993; R. Hoffmann, *Pure Appl. Chem.* **1971**, *28*, 181−194; J. B. Collins, J. D. Dill, E. D. Jemmis, Y. Apeloig, P. von R. Schleyer, R. Seeger, J. A. Pople, *J. Am. Chem. Soc.* **1976**, *98*, 5419−5427; K. Sorger, P. von R. Schleyer, *J. Mol. Struct.* **1995**, *338*, 317−346. − [8b] D. Röttger, G. Erker, *Angew. Chem.* **1997**, *109*, 840−856; *Angew. Chem. Int. Ed. Engl.* **1997**, *36*, 812−827; G. Erker, *Chem. Soc. Rev.* **1999**, 28, 307−314. − [8c] A. Gunale, D. Steiner, D. Schweikart, H. Pritzkow, A. Berndt, W. Siebert, *Chem. Eur. J.* **1998**, *4*, 44−52, and references cited in these articles.

[9] B. Temme, G. Erker, R. Fröhlich, M. Grehl, *Angew. Chem.* **1994**, *106*, 1570−1572; *Angew. Chem. Int. Ed. Engl.* **1994**, *33*, 1480−1482.

[10] U. Rosenthal, A. Ohff, W. Baumann, R. Kempe, A. Tillack, V. V. Burlakow, *Angew. Chem.* **1994**, *106*, 1678−1680; *Angew. Chem. Int. Ed. Engl.* **1994**, *33*, 1605−1607. V. V. Burlakow, A. Ohff, C. Lefeber, A. Tillack, W. Baumann, R. Kempe, U. Rosenthal, *Chem. Ber.* **1995**, *128*, 967−971; Review: A. Ohff, S. Pulst, C. Lefeber, N. Punlecke, P. Arndt, V. V. Burlakow, U. Rosenthal, *Synlett* **1996**, 111−118.

[11] W. Ahlers, B. Temme, G. Erker, R. Fröhlich, T. Fox, *J. Organomet. Chem.* **1997**, *527*, 191−201.

[12] W. Ahlers, doctoral dissertation, Univ. Münster, **1997**.

[13] G. Erker, W. Frömberg, C. Krüger, E. Raabe, *J. Am. Chem. Soc.* **1988**, *110*, 2400−2405; G. Erker, W. Frömberg, J. L. Atwood, W. E. Hunter, *Angew. Chem.* **1984**, *96*, 72−73, *Angew. Chem. Int. Ed. Engl*. **1984**, *23*, 68−69.

[14] R. D. Adams, D. F. Chodosh, *Inorg. Chem.* **1978**, *17*, 41−48. Review: L. D. Durfee, I. P. Rothwell, *Chem. Rev.* **1988**, *88*, 1059−1079. See also: B. Temme, G. Erker, *J. Organomet. Chem.* **1995**, *488*, 177−182.

[15] B. Temme, G. Erker, R. Fröhlich, M. Grehl, *J. Chem. Soc., Chem. Commun.* **1994**, 1713−1714.

[16] [16a] G. Erker, W. Ahlers, R. Fröhlich, *J. Am. Chem. Soc.* **1995**, *117*, 5853−5854. − [16b] S. Venne-Dunker, diplom thesis, Univ. Münster, **1998**.

[17] W. Ahlers, G. Erker, R. Fröhlich, F. Zippel, *Chem. Ber./Recueil* **1997**, *130*, 1079−1084.

[18] W. E. Billups, L.-J. Lin, E. W. Casserly, *J. Am. Chem. Soc.* **1984**, *106*, 3698−3699; S. W. Staley, T. D. Norden, *J. Am. Chem. Soc.* **1984**, *106*, 3699−3700.

[19] S. Lehnhoff, M. Goebel, R. M. Karl, R. Klösel, J. Ugi, *Angew. Chem.* **1995**, *107*, 1208−1211; *Angew. Chem. Int. Ed. Engl.* **1995**, *34*, 1104−1107; M. Passerini, *Gazz. Chim. Ital.* **1921**, *51*, 126−129; Reviews: H. M. Walborsky, M. P. Periasamy, *The Chemistry of Triple-Bonded Functional Groups, Part 2; The Chemistry of Functional Groups* (Eds.: S. Patai, Z. Rappoport), Wiley, New York, **1983**, chapter 20: "Recent Advances in Isocyanide Chemistry"; I. Ugi, "Isocyanide Chemistry", *Organic Chemistry, a Series of Monographs* (Ed.: A. T. Blomquist), Academic Press, New York, **1971**, vol. 20.

[20] For remotely related cationic examples see e.g.: T. Eicher, A. Löschner, *Z. Naturforsch.* **1966**, *21B*, 295−297; T. Eicher, A. Hansen, *Tetrahedron Lett.* **1967**, *44*, 4321−4326. Review: T. Eicher, J. L. Weber, *Top. Curr. Chem.* **1975**, *57*, 1−109.

[21] Details of the X-ray crystal structure analyses of complexes **16b−d** (see Table 1), that were not published previously, were deposited with the Cambridge Crystallographic Data Centre as supplementary publications no. CCDC-137521 to -137523. Copies of the data can be obtained free of charge on application to CCDC, 12 Union Road, Cambridge CB2 1EZ, UK [Fax: int. code + 44-1223/336-033, E-mail: deposit@ccdc.cam.ac.uk].

Received December 8, 1999
[I99447]

The Structure Chemistry of Boron-Rich Solids of the Alkali Metals

Barbara Albert[a]

Keywords: Alkali metals / Boron / Borides / Carbaborides / Polyhedral frameworks

The electronic situation of boron atom frameworks in boron-rich solids is not easy to understand. Attempts to describe such compounds according to known bonding theories such as the Lipscomb or Zintl–Klemm approaches, are not completely unambiguous. To gain further insight and to create a solid experimental basis for the development of a conclusive bonding concept for non-molecular boron-rich compounds, it is essential to investigate metal borides in which the number of electrons transferred from the metal atoms to the boron atom framework appears to be well-defined. Alkali metal borides and carbaborides are such compounds, and it is the aim of this work to provide additional knowledge on their existence and crystal structures. Focussing on the crystal structures of alkali metal borides and carbaborides that are characterised by frameworks of interconnected boron atom polyhedra; it can be shown that there exist convincing geometrical similarities between boron-rich molecules and polyhedral entities in extended networks. This allows for the comparison between the bonding of boron-rich molecules with that of boron-rich solids.

Introduction

The chemistry of alkali metal borides has been covered by several reviews of Hagenmuller and Naslain and coworkers, that were published between 1967 and 1977.[1−3] At that time, it seemed likely that only three representatives of binary alkali metal borides had been synthesised in form of mono-phasic samples. These compounds were described as "NaB_6",[4] "NaB_{15}",[5,6] and "KB_6".[7,8] Unfortunately, the high-temperature synthesis conditions necessary to react boron and alkali metals usually do not lead to highly-crystalline products. The existence and crystal structures of the known boron-rich compounds of the alkali metals remained somehow unclear because in the sixties the technique of crystal structure solution and refinement based on powder diffractometry was still very young.

The lithium−boron(−carbon) system has been investigated by several groups. Boron-rich compounds like Li_3B_{14},[9−11] Li_2B_6,[9,12,13] and LiB_{13}[14] were found, as well as the lithium boride carbide LiBC.[9,15] Most of these borides were characterised by single-crystal X-ray diffraction. The formulae of these compounds were derived from the localisation and occupancies of the lithium ions in the crystal structures because it is very difficult to determine the exact composition of compounds consisting of light elements only. This was made even more difficult by certain disorder phenomena concerning the lithium atom positions. Therefore, it can be considered a real break-through, that due to the efforts of Nesper and von Schnering and coworkers we now know at least three well-defined representatives in the lithium−boron(−carbon) system. Other compounds which were described as "$LiB_{10.85}$",[16] "Li_2B",[17] "LiB",[18] "Li_5B_4", "Li_3B",[19,20] "Li_7B_6",[21] "LiB_2",

[a] Institut für Anorganische und Analytische Chemie,
Justus-Liebig-Universität,
Heinrich-Buff-Ring 58, 35392 Giessen, Germany
Fax: (internat.) + 49-641/993-4109
E-mail: barbara.albert@anorg.chemie.uni-giessen.de



Barbara Albert studied chemistry at the Rheinische Friedrich-Wilhelms-Universität in Bonn, Germany. She received her PhD in 1995, working with solid-state chemist Professor Dr. Martin Jansen. Thanks to a Feodor-Lynen-stipend from the Alexander von Humboldt foundation, Bonn, she spent a post-doctoral year in the group of Professor Dr. A. K. Cheetham at the Materials Research Laboratory, University of California, Santa Barbara, U.S.A., where she worked on Gismondine type (P) zeolites and their structural characterisation via powder diffractometry. From 1996 to 1998, she received a Lise-Meitner-stipend from the Land Nordrhein-Westfalen. Hereby enabled to develop her own research projects, she began to synthesise, characterise, and investigate new boron-rich compounds. In 1997, her habilitation project was awarded by the Ministry of Education and Science in Nordrhein-Westfalen with the Bennigsen-Foerder-award for young scientists and artists and in 1999 with the ADUC award. Since 1998, Barbara Albert has a C1 position as a scientific assistant with Professor Dr. J. Beck at the Justus-Liebig-Universität in Giessen.

MICROREVIEWS: This feature introduces the readers to the authors' research through a concise overview of the selected topic. Reference to important work from others in the field is included.

 © WILEY-VCH Verlag GmbH, D-69451 Weinheim, 2000 1434−1948/00/0808−1679 $ 17.50+.50/0

"LiB_{10}",[22] and "LiB_3"[23] (in historical order) have not proven to give reproducible results with regard to their identity and properties.

Due to their well-defined oxidation state in chemical compounds, alkali metals are especially appropriate as reaction partners of boron to investigate the electronic situation of the boron framework in the resulting boron-rich solids. Today, modern powder diffractometry and solid-state NMR spectroscopy allow us to re-address the characterisation of alkali metal boron-rich compounds. It is necessary to carefully analyse the structure and electron count of boron atom polyhedra in well-defined compounds, in order to obtain a plausible description of the chemical bonding in boron-rich solids. An investigation into the geometrical similarities between the polyhedral entities in molecules and in solids is advisable before a comparison between the bonding situation in the two types of structures can be made. In this review, the chosen experimental system is that of the alkali metal boron-rich compounds. New compounds such as Na_3B_{20},[24,25] NaB_5C,[26] Na_2B_{29},[27] and KB_5C[28] will be described and put into context with what is known from earlier work on alkali metal borides and carbaborides. The electronic situation of these compounds will be compared with that of boron-rich molecules.

One question that is of great interest is: Does a monovalent sodium or potassium hexaboride exist? "NaB_6" and "KB_6" should be discussed on a new experimental basis. This point is very important for the discussion of the bonding in boron-rich solids. It should help to decide whether Lipscomb's bonding concept[29,30] developed for boron-rich molecules is applicable for non-molecular structures.

If hexaborides of type M^IB_6 do exist, the electronic analogy between octahedral $[B_6H_6]^{2-}$ molecules and octahedral $[B_6]^{2-}$ entities in the framework of boron-rich solids like CaB_6 cannot be made. According to the traditional picture which was first introduced by Longuet-Higgins and de V. Roberts[31] and which is depicted in Figure 1, each octahedron in the framework needs twenty electrons for stabilisation. Fourteen of these are needed to fill the molecular orbitals of the B_6 unity (multicentre bonds), and six (+6 from the bonding partners) are needed for the conventional 2electron-2center bonds directed outwardly towards neighbouring octahedra (the latter are comparable to the B−H bonds in the $[B_6H_6]^{2-}$ molecular anion). Eighteen electrons are provided by the six boron atoms, the missing two electrons have to be transferred from the cation to the framework. If the cation can provide even more electrons, like for example in LaB_6, the extra electron is obviously not needed for the bonding orbitals of the boron atom framework. This is shown by the high electrical conductivity that is observed for LaB_6. However, if the cations provide fewer electrons, the polyhedral arrangement should be destabilised. So, how could this be possible if compounds such as "NaB_6" or "KB_6" with an octahedral framework existed?

The correlation between crystal structure and electron count in similar compounds containing, for example, silicon or tin instead of boron, has been discussed before .[32−34]

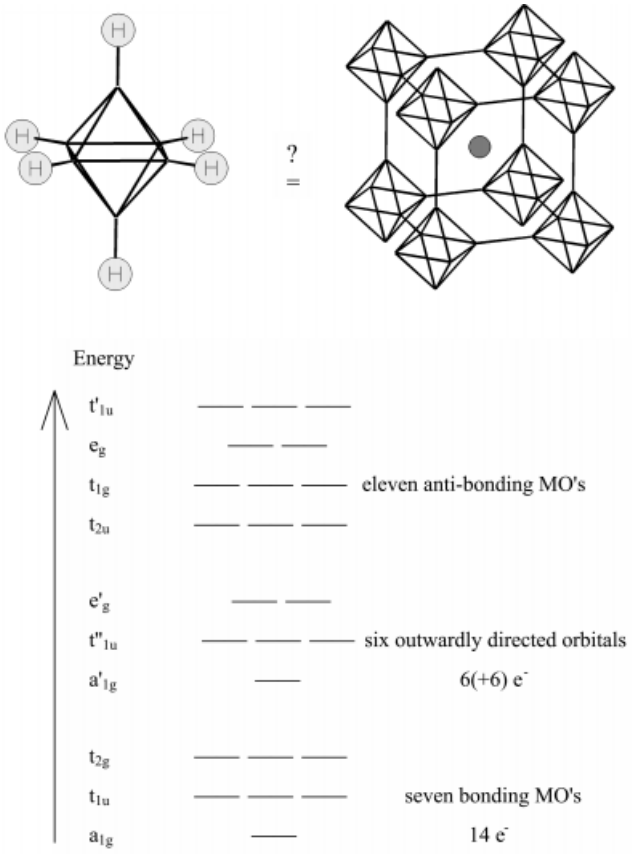


Figure 1. Cartoon showing a molecular $[B_6H_6]^{2-}$ anion (left) and the hexaboride structure model (right), bottom: MO scheme for the B_6 entity

The Alkali Metal Borides

Moissan (1892) and Kroll (1918) were the first to find indications for the existence of alkali metal borides when investigating "impure" samples of boron.[35,36] Forty years later, Hofmann[37] and later, Lipp[38] attempted to synthesise Li-B alloys, but they did not get well-defined compounds.

The first mono-phasic sample of an alkali metal boride described in the literature is a sodium boride synthesised by Hagenmuller and Naslain in 1963.[4] The formula "NaB_6" was assigned to the crystalline powder obtained by a high-temperature reaction from the elements. Today, we know the exact composition of this compound to be Na_3B_{20}.[24,25] It can be synthesised from the elements in arc-welded tantalum tubes lined with inner crucibles made of pyrolytic boron nitride at temperatures around 1050 °C. Its crystal structure recently was solved from high-resolution X-ray powder data and will be described below.

Since 1964, different groups have investigated both the lithium−boron and the potassium−boron systems. For the latter, only one representative could be synthesised in form of a crystalline powder, "KB_6".[7,8] It was obtained only from the α-rhombohedral modification of boron and its powder diffraction pattern suggested close similarity of the

crystal structure with that of the well-known alkaline earth hexaborides (Ca, Sr, Ba).[39−44] Alkaline earth hexaborides contain a boron atom framework of three-dimensionally interconnected octahedra and divalent metal ions in 24-fold coordination spheres between the octahedra (Figure 1, top right). However, recent results concerning "KB_6" using electron energy loss spectroscopy and solid-state NMR spectroscopy suggested the presence of a third element in this compound.[45] Therefore, it seems highly probable that no binary compound in the potassium−boron system has ever been prepared until now. With regard to the lithium−boron system, in 1964 the existence of "$LiB_{3.7-4.1}$" was suggested by Lipp.[38] Since then, most other lithium borides which have been described could not be characterised to a satisfying extent. Fortunately, about fifteen years ago Nesper and von Schnering and co-workers succeeded in growing single crystals of Li_3B_{14} and Li_2B_6.[9−13] Li_3B_{14} contains a boron atom framework of interconnected B_8 and B_{10} cages. For Li_2B_6, a boron atom arrangement similar to that of the alkaline earth hexaborides was found with two cations instead of one between the slightly distorted octahedra.

The first alkali metal boride that was obtained in the form of small single crystals was described as "NaB_{16}",[4] later the formula was corrected to "NaB_{15}".[5,6] Its crystal structure was published in 1970.[5] In fact, the analysis for these crystals published in the original paper already indicated a slightly different composition. This was confirmed by a recent reinvestigation of the crystal structure, using the combined capacity of different spectroscopic and diffraction techniques. These included X-ray and neutron powder diffractometry, ^{23}Na MAS-NMR spectroscopy, single crystal investigations, and electron microscopy. The actual phase composition is Na_2B_{29} and its crystal structure is characterised by a framework consisting of interconnected boron atom icosahedra and additional interstitial boron atoms.[27]

In conclusion, we now know of at least four examples of alkali metal borides which are well-defined in terms of their composition and crystal structures, and they are Li_2B_6,[13] Li_3B_{14},[11] Na_3B_{20},[24,25] and Na_2B_{29}.[27] Rubidium or caesium borides have not been obtained yet.

Alkali Metal Carbaborides

The alkali metal−boron−carbon system has not been investigated until recently, except for one compound discovered by Nesper and von Schnering and co-workers during their search for lithium borides, LiBC.[9,15] The crystal structure of LiBC is similar to that of hexagonal boron nitride, exhibiting planar 6^3-B/C-nets. The layers are stacked along the *c* axis with lithium ions in the centres of the formed hexagonal B/C prisms. Within the sheets and in between them, a colouring scheme characterised by strictly alternating B/C ordering is observed, similar to that found recently for another layer-type compound, CaB_2C_2.[46]

Formerly unknown carbaborides with three-dimensionally extended boron/carbon frameworks were discovered recently, NaB_5C and KB_5C.[26,28] These compounds, which are the first known representatives of ternary sodium and potassium B/C compounds, were obtained by a high-temperature reaction from the elements in form of monophasic crystalline powders without a detectable phase deviation. Their crystal structures resemble those of the alkaline earth hexaborides, carbon being statistically distributed at the boron atom positions of the octahedral framework. In fact, KB_5C is isoelectronic with the well-known CaB_6 and has similar properties.

At present, three representatives of the system alkali metal−carbon−boron are known. These are LiBC, NaB_5C, and KB_5C.

Crystal Structures of the Boron-Rich Compounds of Alkali Metals

The crystal structures of NaB_5C, KB_5C, Li_2B_6,[13] Na_3B_{20}, Li_3B_{14},[11] and Na_2B_{29} are shown in Figure 2.[47]

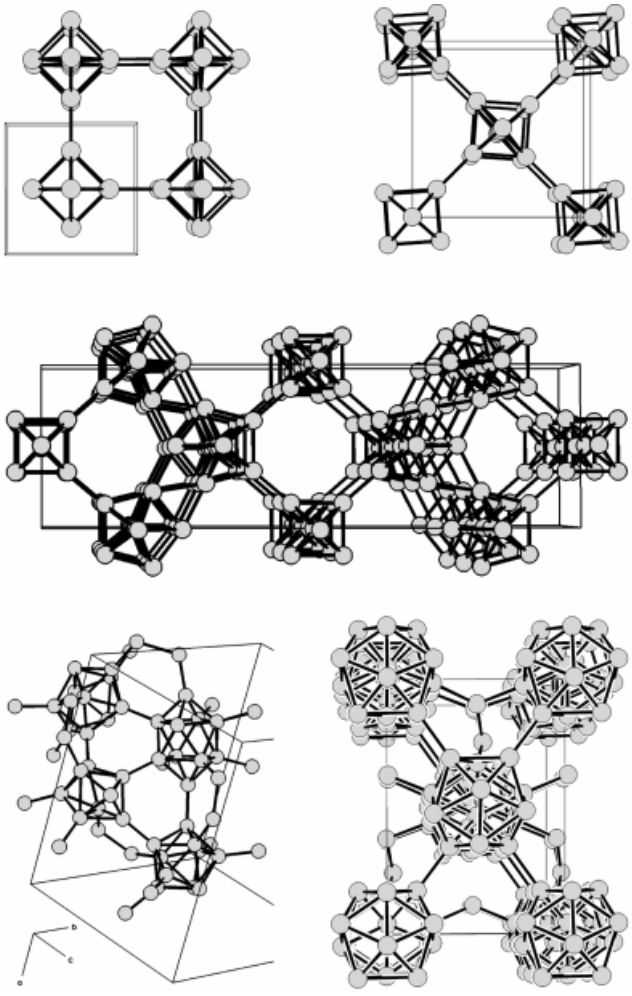


Figure 2. Perspective views of the unit cells of NaB_5C (top left), Li_2B_6 (top right, view along [001]), Na_3B_{20} (middle, view along [001]), Li_3B_{14} (bottom left, only a portion of the unit cell contents is shown for reasons of clarity), and Na_2B_{29} (bottom right, view along [010])

Table 1. Structure data on boron-rich solids of the alkali metals

Compound	ref.	Space group	Lattice parameters [pm,°]
Li_2B_6	[9,12,13]	*P*4/*mbm*, no. 127	597.5, 418.9
Li_3B_{14}	[9,10,11]	*I*-42*d*, no. 122	1076.4, 894.7
LiBC	[9,15]	$P6_3/mmc$, no. 194	275.2, 705.8
Na_3B_{20}	[24,25]	*Cmmm*, no. 65	1869.5, 570.1, 415.1
Na_2B_{29}	[27]	*I*1*m*1, no. 7	585.9, 1039.9, 833.2, 90.4
NaB_5C	[26,28]	*Pm*-3*m*, no. 221	409.3
KB_5C	[28]	*Pm*-3*m*, no. 221	412.8

Structural data of these phases is summarised in Table 1. The crystal structures of alkali metal boron-rich compounds are characterised by non-metal frameworks consisting of different polyhedra that are three-dimensionally interconnected. Metal ions are localised in the cavities between the polyhedra. The interatomic distances are shorter than the intramolecular distances within the polyhedra. This is a well-known phenomenon and occurs due to the deficiency of electrons in the multicentre bonds in the boron atom clusters relative to the 2electron-2center bonds between them. Table 2 gives the averaged different inter- and intramolecular B-B distances for alkali metal borides.

The polyhedra observed in these compounds are as follows: octahedra in NaB_5C, KB_5C, and Li_2B_6,[13] octahedra and pentagonal bipyramids in Na_3B_{20}, dodecahedra and bicapped quadratic antiprisms in Li_3B_{14},[11] and icosahedra in Na_2B_{29}. Most of these polyhedra are slightly distorted, this will be discussed later.

In the cubic carbaborides, the B/C framework maintains the high symmetry of the hexaboride structure, whereas in Na_3B_{20} a less symmetric but otherwise very similar arrangement of polyhedra is present in which two-thirds of the octahedra are replaced by pentagonal bipyramids. Ribbons of these pentagonal bipyramids run parallel to the b axis of the unit cell. These ribbons are formed because only four of the seven boron atoms of a pentagonal bipyramid form 2electron-2centre bonds with four neighbouring polyhedra (two octahedra, two pentagonal bipyramids), similar to the hexaboride structure. Each of the remaining three boron atoms per polyhedron shows close contact to two boron atoms of neighbouring polyhedra. The boron atom coordination spheres of the sodium cations are 20-fold and 24-fold, respectively. This is shown in Figure 3.

The 24-fold coordination sphere is very similar to that of the cations in the carbaborides.

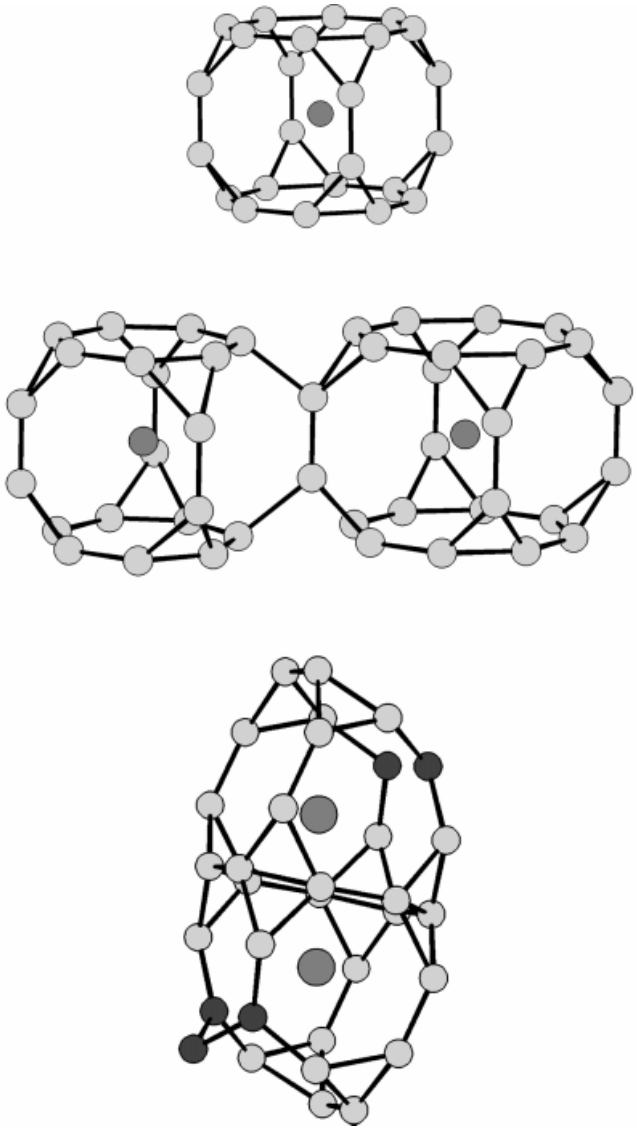


Figure 3. Sections of the structures of NaB_5C (top), Na_3B_{20} (middle), and Na_2B_{29} (bottom); sodium atoms are light grey, boron atoms are dark gray (polyhedral) and black (interstitial)

Na_2B_{29} was formerly known as "NaB_{15}", and the slight difference in the two types of sodium atoms with respect to their boron atom coordination sphere, eventually led to the proper compositional description of this compound (Figure 3, bottom). Using ^{23}Na-MAS triple quantum NMR spectroscopy the presence of two types of sodium atoms

Table 2. Inter- and intramolecular B−B distances for solids and intramolecular B−B distances for molecules

Polyhedron	Molecule: mean intrapolyhedral B−B distance [pm]	Solid: mean intrapolyhedral B−B distance [pm]	Solid: mean interpolyhedral B−B distance [pm]
$[B_6]$	$K_2[B_6H_6]$:[50] 172	Li_2B_6:[13] 176	171
	$[N(CH_3)_4]_2[B_6H_6]$:[63] 169	Na_3B_{20}: 177	172
$[B_7]$	$[(C_5H_5N)_2CH_2][B_7Br_7]$:[51] 174	Na_3B_{20}: 180	171
$[B_8]$	$[Zn(NH_3)_4][B_8H_8]$:[52] 177	Li_3B_{14}:[11] 180	174
$[B_{10}]$	$[N(C_2H_5)_3H]_2[B_{10}H_{10}]$:[53] 178.5	Li_3B_{14}:[11] 181.5	174
$[B_{12}]$	$[N(CH_3)_4]_2[B_{12}H_{12}]CH_3CN$:[54] 178.5	Na_2B_{29}: 182	177

with distinct boron atom environments was detected. The different coordination spheres of the sodium atoms are as a result of the presence of two types of interstitial boron atoms close to a single type of sodium atom in one case, and the presence of only one type of interstitial boron atom close to the second type of sodium atom in the other. The coordination sphere of Na1 includes 20 neighbouring boron atoms with a mean Na−B distance of 284 pm, whereas Na2 coordinates 21 boron atoms with a mean distance of 286 pm. Due to the loss of symmetry, the crystal structure of "NaB_{15}" = Na_2B_{29} originally described in the orthorhombic crystal system, had to be refined in the monoclinic crystal system.

Polyhedra in Boron-Rich Solids and Molecules

In order to compare the bonding situation of boron atom polyhedra in solids with that in molecules, it is first necessary to compare their geometric situations. Boron atom cages have been found in the *closo*-hydroborates $[B_nH_n]^{2-}$ with $n = 5-12$.[48] For such compounds with $n = 6$, 8, 9, 10, 11, and 12, single crystal X-ray structure determinations have been performed and the overall regularity of these polyhedra was confirmed. Homoatomic polyhedra in boron-rich systems are always isohedral containing only $n = 3$ polygons (deltahedra), as can be seen in Figure 4.

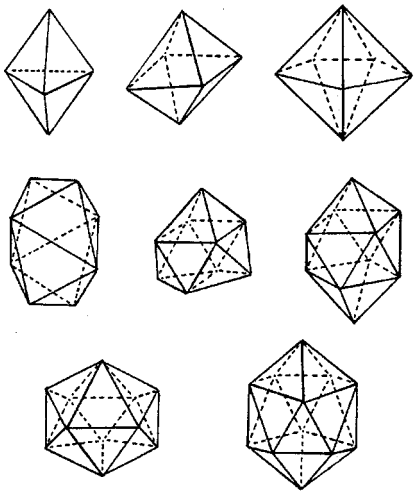


Figure 4. Polyhedra in *closo*-hydroborates according to Barton[48]

However, these polygons do not necessarily have to be regular. In principle, the octahedron and icosahedron are regular (Platonic) solids, the trigonal and pentagonal bipyramids have been described as semi-regular (Catalan) solids.[49] Less regular is the $n = 8$ cluster, which is a bisdisphenoid called a triangulated dodecahedron, the $n = 9$ and $n = 10$ cluster are monocapped and bicapped antiprisms, the $n = 11$ polyhedron is called an octadecahedron. Five of these polyhedra known from *closo*-hydroborates and their derivatives, can also be found in alkali metal boron-rich solids, the octahedron, pentagonal bipyramid, dodecahedron, bicapped antiprism, and the icosahedron. Data on the B-B bond lengths are given in Table 2 already indicate a comparability of the polyhedral entities in solids and molecules. Their similarity can be appreciated in Figure 5, where the same polyhedra extracted from the crystal structure descriptions of $K_2[B_6H_6]$,[50] $[(C_5H_5N)_2CH_2][B_7Br_7]$,[51] $[Zn(NH_3)_4][B_8H_8]$,[52] $[N(C_2H_5)_3H]_2[B_{10}H_{10}]$,[53] and [N-

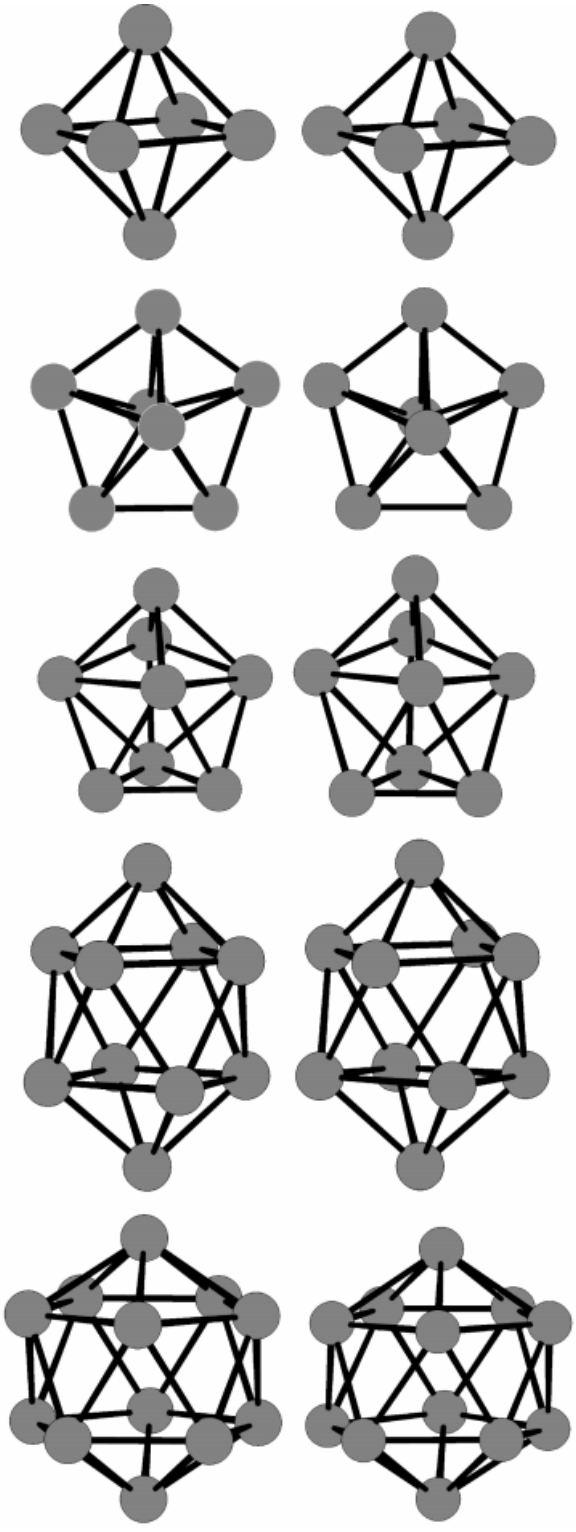


Figure 5. Comparison of the polyhedra found in *closo*-hydroborates (left, top to bottom: $K_2[B_6H_6]$, $[(C_5H_5N)_2CH_2][B_7Br_7]$, $[Zn(NH_3)_4][B_8H_8]$, $[N(C_2H_5)_3H]_2[B_{10}H_{10}]$, $[N(CH_3)_4]_2[B_{12}H_{12}]$-$(CH_3CN)$ and alkali metal borides (right, top to bottom: Na_3B_{20}, Li_3B_{14}, Na_2B_{29})

Table 3. Degree of polyhedral distortion (r.m.s.) for different boron cages in molecules and solids

Polyhedron	Point group	Molecule: r.m.s.	Solid: r.m.s.
$[B_6]$	O_h	$K_2[B_6H_6]$:[50] 0, $[N(CH_3)_4]_2[B_6H_6]$:[63] 0	KB_5C: 0 Na_3B_{20}: 0.0155 Li_2B_6:[13] 0.0128
$[B_7]$	D_{5h}	$[(C_5H_5N)_2CH_2][B_7Br_7]$:[51] 0.0502	Na_3B_{20}: 0.0820
$[B_8]$	D_{2d}	$[Zn(NH_3)_4][B_8H_8]$:[52] 0	Li_3B_{14}:[11] 0.0170
$[B_{10}]$	D_{4d}	$[N(C_2H_5)_3H]_2[B_{10}H_{10}]$:[53] 0.0042	Li_3B_{14}:[11] 0.0465
$[B_{12}]$	I_h	$[N(CH_3)_4]_2[B_{12}H_{12}]CH_3CN$:[54] 0.0045	Na_2B_{29}: 0.0506

$(CH_3)_4]_2[B_{12}H_{12}]CH_3CN$[54] are compared with those extracted from alkali metal borides.

Deviations from the ideal (which in principle cannot exist: by definition, an octahedron is an ideal octahedron or it is not an octahedron[55]) are quantified using the Program SYMMOL,[56] which is based on the idea, that symmetry can be treated "as a continuous property rather than a discrete ("yes or no") one".[57] Table 3 summarises a comparison between molecular boron atom cages and cages cut out from extended boron atom frameworks, by giving the r.m.s. (root mean square) values which characterise the degree of distortion of the polyhedra. These values are always higher than zero when crystallographic symmetry is not present.

Besides the first trivial case (top, crystallographic symmetry is already O_h), it is obvious that the polyhedra are more distorted in compounds with extended frameworks than in molecules. However, the "ideal" symmetry of the polyhedra is clearly determined even for the more distorted entities and the deviations from regular polyhedra are quite small.

Conclusions

At present, the alkali metal−boron system and the alkali metal−boron−carbon system are characterised by the proven existence of seven representatives. By crystal structure analyses of these compounds, a class of well-defined boron-rich solids has been established. These compounds are especially useful in the analysis of the bonding situation in electron-deficient polyhedral *frameworks*. Lipscomb's concept is usually applicable in describing the bonding situation in electron-deficient boron-rich *molecules*. It states that for molecular B_n *closo*-cages, the electronic demand necessary to stabilise the polyhedral arrangement is $2n + 2$, according to the traditional counting scheme (Rudolph−Williams−Wade rules[58−60]). Even if we have to remind ourselves that there exist other concepts to describe boron-rich compounds (for example Mingos' rules[61]) and of known exceptions from Lipscomb's predictions (for example B_9Br_9[62] and $Li_{1.8}B_{14}$[9−11]), the conclusions which can be drawn from the experimental findings summarised in this review are as follows. The analysis of the crystal structures of alkali metal borides and carbaborides reveals geometrical similarities between polyhedra in boron-rich solids and boron-rich molecules, which suggest a comparability of their bonding situation. Consequently, each octahedral B_6 entity which is part of an extended framework should need $2n + 2$ (= 14) electrons plus six electrons for the interpolyhedral contacts, as it was suggested 45 years ago by Longuet-Higgins and de V. Roberts. Within their limitations, the evidence described above confirm the applicability of this concept, since compounds correctly described by the formulas NaB_6 and KB_6 were found not to exist. Instead, we discovered NaB_5C and KB_5C, for which the electron count is fulfilled.

Acknowledgments

I would like to thank Professor Dr. J. Beck, Bonn, for his support, and K. Schmitt and K. Hofmann, Giessen, for their enthusiastic help. Financial support from the DFG (AL536/1-1), Dr. Otto Röhm Gedächtnisstiftung, and the Fonds der Chemischen Industrie is gratefully acknowledged.

[1] R. Naslain, J. Etourneau, P. Hagenmuller, *Alkali Metal Borides* in: *Boron and Refractory Borides* (Ed.: V. I. Matkovich) Springer, Berlin **1977**.
[2] R. Naslain, J. Etourneau, P. Hagenmuller, *Electron Techn.* **1970**, *3*, 35.
[3] P. Hagenmuller, R. Naslain, M. Pouchard, C. Cros, *Chem. Soc. Spec. Publ.* **1967**, *22*, 207.
[4] P. Hagenmuller, R. Naslain, *C.R. Acad. Sci.* **1963**, *257*, 1294.
[5] R. Naslain, J. S. Kasper, *J. Solid State Chem.* **1970**, *1*, 150.
[6] R. Naslain, A. Guette, P. Hagenmuller, *J. Less-Com. Met.* **1976**, *47*, 1.
[7] R. Naslain, J. Etourneau, *Compt. Rend.* **1966**, *263(6)*, 484.
[8] R. Naslain, J. Etourneau, P. Hagenmuller, *Bull. Soc. Chim. Fr.* **1967**, *7*, 2529.
[9] G. Mair, Dissertation, Universität Stuttgart, **1984**.
[10] G. Mair, R. Nesper, H. G. von Schnering, *Mater. Sci. Monogr. B (React. Solids, Part B)* **1985**, *28*, 861.
[11] G. Mair, R. Nesper, H. G. von Schnering, *J. Solid State Chem.* **1988**, *75*, 30.
[12] M. Wörle, Dissertation, ETH Zürich, **1995**.
[13] G. Mair, H. G. von Schnering, M. Wörle, R. Nesper, *Z. Anorg. Allg. Chem.* **1999**, *625*, 1207.
[14] M. Kobayashi, I. Higashi, H. Matsuda, K. Kimura, *J. Alloys Comp.* **1995**, *221*, 120.
[15] M. Wörle, R. Nesper, G. Mair, M. Schwarz, H. G. von Schnering, *Z. Anorg. Allg. Chem.* **1995**, *621*, 1153.
[16] D. R. Secrist, *J. Am. Ceram. Soc.* **1967**, *50*, 520.
[17] S. D. James, L. E. DeVries, *J. Electrochem. Soc.* **1976**, *123*, 321.
[18] V. P. Sorokin, P. I. Gavrilov, E. V. Levakov, *Russ. J. Inorg. Chem.* **1977**, *22*, 329.
[19] F. E. Wang, M. A. Mitchell, R. A. Sutula, J. R. Holden, L. H. Bennett, *J. Less-Comm. Met.* **1978**, *61,* 237.
[20] M. A. Mitchell, R. A. Sutula, *J. Less-Com. Met.* **1978**, *57*, 161.
[21] S. Dallek, D. W. Ernst, B. F. Larrick, *J. Electrochem. Soc.* **1979**, *126*, 866.
[22] I. I. Serebryakova, V. I. Lyashenko, V. D. Levandovskii, *Powder Metallurgy Met. Ceram.* **1994**, *33*, 49.

[23] A. Meden, J. Mavri, M. Bele, S. Pejovnik, *J. Phys. Chem.* **1995**, *99*, 4252.
[24] B. Albert, *Angew. Chem.* **1998**, *110*, 1135.
[25] B. Albert, K. Hofmann, *Z. Anorg. Allg. Chem.* **1999**, *625*, 709.
[26] B. Albert, K. Schmitt, *Chem. Commun.* **1998,** 2373.
[27] B. Albert, K. Hofmann, C. Fild, H. Eckert, M. Schleifer, R. Gruehn, *Chem. Eur J.*, accepted for publication.
[28] B. Albert, K. Schmitt, *Chem. Mat.* **1999**, *11*, 3406.
[29] W. N. Lipscomb, *Boron Hydrides*, Benjamin, New York **1963**.
[30] W. H. Eberhardt, B. Crawford, W. N. Lipscomb, *J. Chem. Phys.* **1954**, *22*, 989.
[31] H. C. Longuet-Higgins, M. de V. Roberts, *Proc. R. Soc. London Ser.* **1954**, *A 224*, 336.
[32] H. G. v. Schnering, *Angew. Chem.* **1981**, *93*, 44.
[33] N. Wiberg, H.-W. Lerner, H. Nöth, W. Ponikwar, *Angew. Chem.* **1999**, *111*, 1176.
[34] H. G. V. Schnering, M. Somer, M. Kaupp, W. Carrillo-Cabrera, M. Baitinger, A. Schmeding, Y. Grin, *Angew. Chem.* **1998**, *110*, 2507.
[35] H. Moissan, *Comp. Rend.* **1892**, *114*, 319.
[36] W. Kroll, *Z. Anorg. Allg. Chem.* **1912**, *102*, 1.
[37] H. Hofmann, Dissertation, Universität Stuttgart **1959**.
[38] A. Lipp, Deutsches Patent 1 255 093, **1964**.
[39] H. Moissan, P. Williams, *Compt. Rend.* **1897**, *125*, 629.
[40] M. von Stackelberg, F. Neumann, *Z. Physik. Chem.* **1932**, *B19*, 314.
[41] L. Pauling, S. Weinbaum, *Z. Kristallogr.* **1934**, *87*, 181.
[42] T. Ito, T. Kasukawa, I. Higashi, Y. Satow, *Proc. 11th Int. Symp. Boron, Borides and Related Compounds, JJAP Series* **1994**, *10*, 11.
[43] H. R. Ott, M. Chernikov, E. Felder, L. Degiorgi, E. G. Moshopouou, *Z. Phys.* **1997**, *B102*, 337.
[44] L. W. Rupp, P. H. Schmidt, *J. Phys. Chem. Solids* **1969**, *30*, 1059.
[45] B. Albert, K. Schmitt, C. Fild, H. Eckert, in preparation.
[46] B. Albert, K. Schmitt, *Inorg. Chem.* **1999**, *38*, 6159.
[47] R. Hundt, Program KPLOT, Bonn, Germany, **1979**.
[48] L. Barton, *Top. Curr. Chem.* **1982**, *100*, 169.
[49] A. F. Wells, *Structural Inorganic Chemistry*, 5th Ed., Clarendon Press, Oxford, **1984**.
[50] I. Y. Kuznetsov, D. M. Vinitskii, K. A. Solntsev, N. T. Kuznetsov, *Russ. J. Inorg. Chem.* **1987**, *32*, 1803.
[51] A. Franken, H. Thomson, W. Preetz, *Z. Naturforsch.* **1996**, *51b*, 744.
[52] L. J. Guggenberger, *Inorg. Chem.* **1969**, *8,* 2771.
[53] K. Hofmann, B. Albert, *Z. Naturforsch.,* accepted for publication.
[54] K. Hofmann, B. Albert, *Z. Kristallogr., Suppl.* **2000**, *17*, 58.
[55] R. Hoppe, personal communication.
[56] T. Pilati, A. Forni, *J. Appl. Crystallogr.* **1998**, *31*, 503.
[57] H. Zabrodsky, S. Peleg, D. Avnir, *J. Am. Chem. Soc.* **1993**, *115*, 8278.
[58] K. Wade, *Adv. Inorg. Radiochem.* **1976**, *18*, 1.
[59] R. W. Rudolph, *Acc. Chem. Res.* **1976**, *9*, 446.
[60] R. E. Williams, *Adv. Inorg. Chem. Radiochem.* **1976**, *18*, 67.
[61] D. M. P. Mingos, *Acc. Chem. Res.* **1984**, *17*, 311.
[62] H. Binder, R. Kellner, K. Vaas, M. Hein, F. Baumann, M. Wanner, R. Winter, W. Kaim, W. Hönle, Y. Grin, U. Wedig, M. Schultheiss, R. K. Kremer, H. G. v. Schnering, O. Groeger, G. Engelhardt, *Z. Anorg. Allg. Chem.* **1999**, *625*, 1059.
[63] R. Schaeffer, Q. Johnson, G. S. Smith, *Inorg. Chem.* **1965**, *4*, 917.

Received December 3, 1999
[I99441]

Biomimetic Catalysis with an Immobilised Chiral Rhodium(III) Complex

Kurt Polborn[a] and Kay Severin*[a]

Keywords: Heterogeneous catalysis / Molecular imprinting / Hydrogenations / Transition states / Rhodium

An organometallic transition state analogue for the asymmetric reduction of acetophenone with a Cp*Rh complex has been synthesised and structurally characterised (**3**). This complex has a chiral *N*,*N*′-chelate ligand with a styrene side chain to allow its incorporation into organic polymers. The remaining coordination site is occupied by a methylphenylphosphinato ligand. This ligand acts as a pseudosubstrate which mimics acetophenone. The conformation and configuration of **3** in the crystal are in excellent agreement with the postulated transition structure. Following the protocol of molecular imprinting, complex **3** was co-polymerised with ethylene glycol dimethacrylate in the presence of a porogen. The resulting polymer **P3** was ground and sieved and the phosphinato ligand was substituted with a chloro ligand to generate a shape-selective cavity in proximity to the catalytically active metal centre. When tested for its ability to catalyse the reduction of acetophenone and related substrates the imprinted polymer **P3** showed a significantly higher activity than a control polymer **P2** without a cavity. Excellent enantioselectivities (up to 95% *ee*) were obtained, with the catalyst **P3** being more selective than the respective control catalyst **P2** (Δee = 2–9%). Competition experiments with acetophenone and a second co-substrate have revealed that the cavity generated with the phosphinato ligand is specific for acetophenone.

Introduction

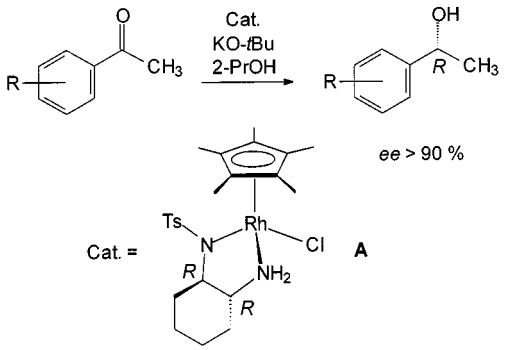
Modern organometallic catalysts display high activities, some of which can rival those of metalloenzymes.[1] Nevertheless there is a fundamental difference in how the selectivity and activity is controlled in these systems. For (homogeneous) organometallic catalysts these parameters are mainly determined by the nature of the metal ion and the first coordination sphere.[2] For metalloenzymes, on the other hand, ligands of the second coordination sphere, that is, functional groups in the vicinity of the catalytically active centre, are crucial for chemical transformations. A well-defined microenvironment allows for the molecular recognition between enzyme and substrate and/or transition state and is thus the basis for high selectivity.

In recent years several approaches for manipulating the microenvironment of synthetic organometallic catalysts in a controlled fashion have been described. For example, catalytically active metal complexes have been covalently attached to organic host molecules (e.g. cyclodextrins)[3] or embedded into porous inorganic materials (e.g. zeolites).[4] However, most of these strategies either require substantial synthetic efforts or the obtained catalysts are rather unspecific. Recently, we have reported an alternative approach which combines the technology of molecular imprinting[5] with organometallic chemistry: a transition metal catalyst, having a polymerisable side chain, is co-polymerised with an organic crosslinking monomer. During the polymerisation a pseudosubstrate is coordinated to the catalytically active centre. Selective removal of the pseudosubstrate generates a complementary, shape selective cavity. The realisation of this concept was demonstrated for the Ru^{II}-catalysed transfer hydrogenation of benzophenone.[6] Here we describe the synthesis of a highly active and selective *chiral* Rh^{III} catalyst for the asymmetric reduction of acetophenone, obtained by molecular imprinting with a defined transition-state analogue (TSA).[7,8]

Results and Discussion

The asymmetric transfer hydrogenation of ketones and imines, catalysed by chiral complexes of the late transition metals has received considerable attention in recent years.[9] In particular, chiral (arene)Ru^{II} catalysts have been shown to be highly selective. Excellent results have also been obtained with the Cp*Rh complex **A** (Scheme 1): for the reduction of acetophenone and derivatives with 2-propanol in the presence of base an enantiomeric excess of more than 90% *ee* was observed.[10]

All experimental data for this reaction point to a cyclic transition state with a hydrogen bond from the carbonyl O-



Scheme 1. Asymmetric transfer hydrogenation of aromatic ketones with a chiral rhodium(III) catalyst[10a]

[a] Institut für Anorganische Chemie der Ludwig-Maximilians-Universität, Butenandtstraße 5–13, D-81377 München, Germany
E-mail: kse@cup.uni-muenchen.de

 © WILEY-VCH Verlag GmbH, D-69451 Weinheim, 2000 1434–1948/00/0808–1687 $ 17.50+.50/0

atom to the adjacent amine group. Theoretical investigations on related Ru-catalysed reactions have provided additional evidence for such a geometry (Figure 1).[11] We propose a phosphinato complex as a TSA for the asymmetric reduction of acetophenone.

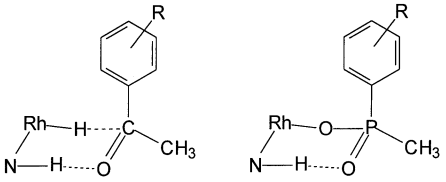
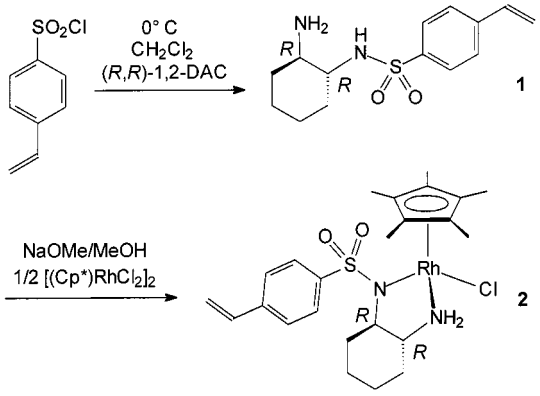


Figure 1. Postulated transition structure for the Rh^{III}-catalysed transfer hydrogenation of aromatic ketones (left); transition-state analogue with a phosphinato ligand (right)

Here we describe the synthesis and the structure of a polymerisable $CpRh^{III}$ catalysts with a methylphenylposphinato ligand. To allow catalysts of this kind to be incorporated into organic polymers we have synthesised a ligand with a styrene instead of a tolyl side chain. This was accomplished by condensation of (1*R*,2*R*)-1,2-diaminocyclohexane with *p*-styrylsulfonyl chloride (**1**). The rhodium complex **2** was obtained in good yields by reaction of **1** with $[Cp^*RhCl_2]_2$ in the presence of NaOMe (Scheme 2). The ^1H NMR spectrum of **2** shows only one set of signals ($CDCl_3$). This indicates that the synthesis is completely diastereoselective.

The structure of the racemic[12] complex **2** in the crystal is depicted in Figure 2. The coordination around the rhodium



Scheme 2. Synthesis of complex **2**

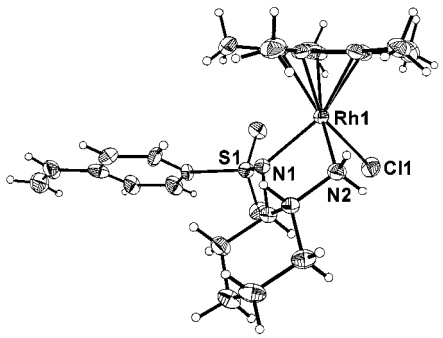
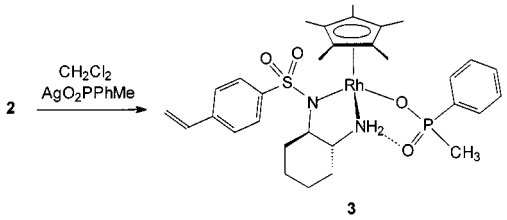


Figure 2. Structure of one enantiomer[12] of **2** in the crystal; selected bond length [Å] and angles [°]: Rh(1)−Cl(1) 2.416(2), Rh(1)−N(1) 2.152(4), Rh(1)−N(2) 2.120(4); N(2)−Rh(1)−N(1) 79.0(2), N(2)−Rh(1)−Cl(1) 82.23(13), N(1)−Rh(1)−Cl(1) 89.65(12)

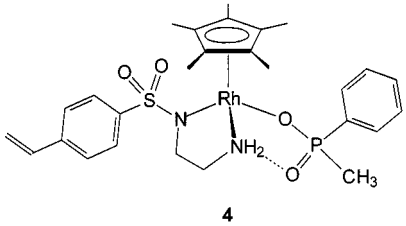
atom can be described as distorted octahedral with a bidentate, monoanionic amine ligand. The structure is similar to that found for the Cp*Rh complex **A**.[10a] Importantly, they have the same relative configuration of the rhodium atom with respect to the chiral ligand. The same relative configuration is also observed for structurally related (arene)Ru^{II} complexes.[13]

Substitution of the chloro ligand with the pseudosubstrate − the phosphinato ligand − is achieved by reaction of **2** with silver methylphenylphosphinate (Scheme 3). The resulting complex **3** has four stereogenic centres: the two carbon atoms of the amine ligand, the rhodium atom and the phosphorous atom. Four stereoisomers, which should be distinguishable by NMR spectroscopy, are thus expected. Again, however, the NMR spectra show only one set of signals ($CDCl_3$). This points to the fact that the configuration of the metal atom, as well as that of the phosphorous atom is controlled by the ligand, meaning that the chiral information is transferred with high efficiency from the ligand to the metal atom and the pseudosubstrate.



Scheme 3. Synthesis of complex **3**

It is important to note that the free phosphinato ligand is optically inactive. To determine the configurational stability of the phosphinato ligand coordinated to the rhodium atom we have synthesised complex **4** which bears an achiral chelate ligand. NMR experiments with this complex have shown that the configurational stability of the phosphinato ligand in **4** is very low. Most likely, the same is true for complex **3**.



The result of a single crystal analysis of racemic[12] **3** is shown in Figure 3. As is the case for compound **2**, the metal atom in **3** has the opposite configuration to that of the ligand. The coordination of the phosphinato ligand corresponds exactly to the postulated transition state: a monodentate coordination to the rhodium atom and a hydrogen bond to the adjacent amine group is observed. Based on quantum chemical calculations about the transition state of related (arene)Ru(aminoalcoholate) complexes Andersson et al. have predicted a strong preference for an almost planar H−Ru−N−H unit, with an energetic minimum obtained for H−Ru−N−H = 10°.[11a] Remarkably, this is exactly the value found for the corresponding angle in com-

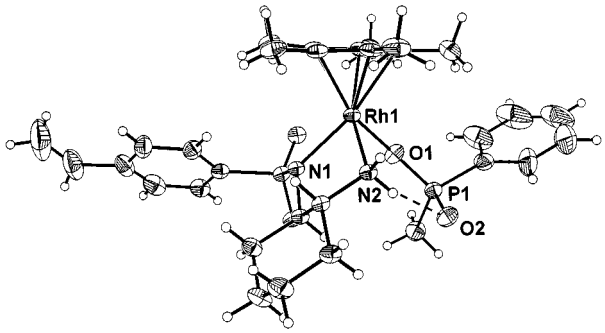
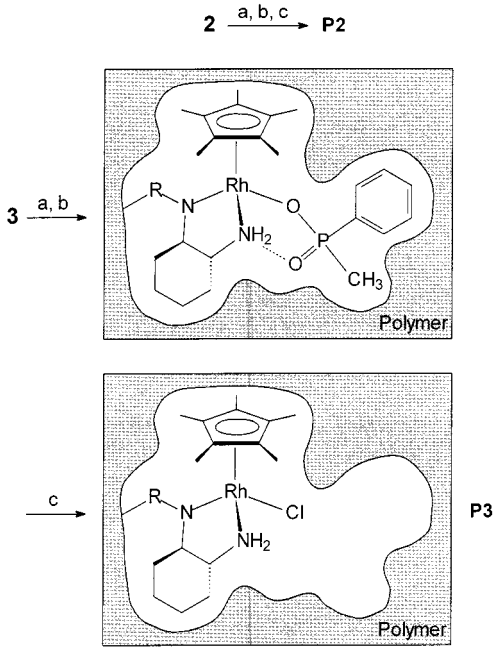


Figure 3. Structure of one enantiomer[12] of **3** in the crystal; selected bond length [Å] and angles [°]: Rh(1)−O(1) 2.131(2), Rh(1)−N(1) 2.142(4), Rh(1)−N(2) 2.120(4), P(1)−O(2) 1.489(3), P(1)−O(1) 1.504(3); N(2)−Rh(1)−N(1) 78.52(12), N(2)−Rh(1)−O(1) 88.59(12), N(1)−Rh(1)−O(1) 86.83(12)

plex **3** in the crystal (O1−Rh1−N2−H = 9.9°). From experiments with the homogeneous catalyst **A** it was observed that the reduction of acetophenone gives *R*-1-phenylethanol with high selectivity.[10a] For the transition structure a *syn*-configuration of the aryl group of the phosphinato ligand and the Cp* ring is therefore predicted. And indeed, this is the geometry which is observed for **3**. These results confirm that **3** is an excellent analogue for the transition state of the asymmetric reduction of acetophenone.

Immobilisation of the catalyst precursors **2** and **3** was achieved by co-polymerisation with ethylene glycol dimethacrylate (EGDMA) in the presence of a porogen ($CHCl_3$/MeOH, 4:1). The combination of EGDMA and $CHCl_3$ has previously been shown to be well suited for imprinting studies.[6,14] 2,2′-Azobis(4-methoxy-2,4-dimethylvaleronitrile) (V-70) was employed as the thermal initiator. The polymers **P2** and **P3** were ground and sieved to obtain a uniform particle size (25−100 μm). The orange powders were subsequently stirred in a solution of benzyltriethylammonium chloride in methanol (0.1 M), a procedure which selectively cleaves off the phosphinato ligand.[15] Therefore, both polymers have an almost identical chemical composition. Contrary to polymer **P2**, the molecularly imprinted polymer (MIP) **P3** has shape-selective cavities in proximity to the catalytically active centre of the rhodium complexes (Scheme 4).

To test the activity and enantioselectivity of the polymeric catalysts **P2** and **P3** we investigated the reduction of acetophenone with 2-propanol in the presence of KOH. For reactions with 1 mol-% **P2** after 6 h (*R*)-1-phenylethanol was obtained with 93% *ee* in 41% yield (Table 1). In the presence of the imprinted polymer **P3** the yield was increased to 81% with an optical purity of 95% *ee*. A similar increase in activity (the initial turnover frequencies differ by more than a factor of two) and selectivity (Δee = 2−8%) was observed for sterically related monohalogenated substrates. A significant difference in the enantioselectivity (Δee = 9%) was also detected in reactions with the more bulky substrate 1-acetonaphthone. These results show that the cavity generated by molecular imprinting has a pronounced effect on the activity of the immobilised catalyst. Furthermore, the expected decrease in selectivity of the heterogeneous catalyst **P2** as compared to the homogeneous version **A** is nearly abolished with the MIP catalyst **P3**. The increased enantioselectivity of **P3** (Δee = 2−9%) is most likely the result of additional space around the catalytically active rhodium complexes. The contribution of chiral cavities is less probable due to the low configurational stability of the pseudosubstrate. Overall, the imprinted catalyst **P3** displays an activity and selectivity which can compete with the homogeneous catalyst **A**[10] and which is higher than the values obtained with other homogeneous Cp*Rh catalysts.[10b,16] Compared to supported catalysts for the transfer hydrogenation of acetophenone, **P3** occupies a top position.[8a,17,18]



Scheme 4. Synthesis of the control polymer **P2** and the imprinted polymer **P3**: a) EGDMA, $CHCl_3$/CH_3OH, V-70, 24 h, 35 °C; b) 4 h, 65 °C; c) $[NEt_4]Cl$, CH_3OH

Table 1. Transfer hydrogenation of aromatic ketones in the presence of the imprinted catalyst **P3** and the control catalyst **P2**

Catalyst	Ketone	Time [h]	Yield [%]	*ee* [%][a]
P3 (**P2**)	Acetophenone	6	81 (41)	95 (93)
P3 (**P2**)	*p*-Fluoroacetophenone	6	71 (36)	93 (90)
P3 (**P2**)	*o*-Fluoroacetophenone	6	85 (52)	84 (76)
P3 (**P2**)	*m*-Fluoroacetophenone	3	98 (75)	94 (92)
P3 (**P2**)	*m*-Chloroacetophenone	3	98 (69)	94 (92)
P3 (**P2**)	1-Acetonaphthone	6	52 (24)	83 (74)

[a] In all cases the main isomer has the configuration *R*.

The substrate specificity was determined in competition experiments. The kinetics of the reduction of a mixture of acetophenone and a second substrate in the presence of **P2** or **P3** was investigated (ketone1/ketone2/catalyst = 50:50:1). Aliphatic and aromatic ketones, which differ in size and reactivity, were chosen as co-substrates. A comparison of the initial reaction rates revealed that in *all* cases the imprinted polymer **P3** displays a higher selectivity for

Table 2. Substrate selectivity of the polymeric catalysts **P2** and **P3**

Co-substrate	Selectivity[a] P3	Selectivity[a] P2
Cyclohexanone	$3.8\ 10^{-1}$	$3.1\ 10^{-1}$
2-Adamantanone	1.4	1.1
Benzophenone	$1.4\ 10^{1}$	8.9
α-Tetralone	4.2	3.7
2-Acetylnaphthalene	$8.9\ 10^{-1}$	$7.7\ 10^{-1}$

[a] The selectivity is calculated by dividing the initial rate of 1-phenylethanol formation by the initial rate of product formation for the reduction of the co-substrate.

acetophenone than the control polymer **P2** (Table 2), although the substrate selectivity is lower than that found for the immobilised ruthenium complexes previously described.[6] In accordance with the molecular structure determined for **3**, these kinetic studies prove that the methylphenylphosphinato ligand represents an excellent pseudosubstrate for acetophenone and leaves a *specific* and *shape-selective* imprint in the polymeric matrix.

Conclusions

We have shown that heterogeneous catalysts for the asymmetric transfer hydrogenation of aromatic ketones are available by immobilisation of the chiral rhodium complexes **2** and **3**, both of which were structurally characterised. The microenvironment of the polymeric catalyst **P3** was modified in a controlled fashion by molecular imprinting with the organometallic TSA **3**. As a result an enhanced activity combined with an excellent enantioselectivity was observed for the reduction of acetophenone and related substrates. Kinetic experiments have revealed that the cavity generated by imprinting is specific for acetophenone.

The concept presented in this paper for the construction of shape selective cavities in proximity to the catalytically active centre of organometallic catalysts is very simple and flexible. The results prove that this method is suitable for generating heterogeneous catalysts with a superior performance in asymmetric reactions even when optically inactive pseudosubstrates are employed. It appears likely that this methodology is applicable to other catalysts and reactions. Research along these lines may ultimately lead to tailor-made organometallic catalysts with enzyme-like characteristics.

Experimental Section

General: The synthesis of all complexes as well as the transfer hydrogenation was performed under an atmosphere of dry nitrogen, using standard Schlenk techniques. Solvents were freshly distilled over an appropriate drying agent and stored under nitrogen prior to usage. EGDMA was washed with NaOH (1 M) and saturated NaCl solution and dried with Na_2SO_4. After filtration the monomer was distilled under reduced pressure. The azo initiator V-70 was obtained from Wako Chemicals. AgO_2PPhMe was obtained as a white precipitate by reaction of KO_2PPhMe with $AgNO_3$. The synthesis of $[Cp^*Rh(NH_2CH_2CH_2NSO_2C_8H_7)Cl]$ was carried out analogously to that of **2** using the achiral ligand $NH_2CH_2CH_2NHSO_2C_8H_7$.[6b] 4-Vinyl-benzenesulfonyl chloride[18] and $[Cp^*RhCl_2]_2$[19] were prepared according to literature procedures. The ^1H, ^{13}C and ^{31}P NMR spectra were recorded on a JEOL EX 400 or a GSX 270 spectrometer with the solvent as the internal standard. All spectra were recorded at room temperature; exceptions are indicated. The GC analysis was performed with a Varian 3800 spectrometer using a CP-Cyclodextrin-B-2,3,6-M-19 column (50 m).

Synthesis of Ligand 1: A solution of *p*-styrylsulfonyl chloride (816 μL) in CH_2Cl_2 (30 mL) was added slowly (1 h) to a solution of (*R*,*R*)-1,2-diaminocyclohexane (1.84 g, 16.1 mmol) in CH_2Cl_2 (20 mL) at 0 °C. The mixture was warmed to room temperature, filtered and the solvent was removed under reduced pressure. The product was purified by flash chromatography with EtOAc/MeOH (3:2) and crystallised from CH_2Cl_2/hexane. Yield: 730 mg (16%, referred to the amine), m.p. 105−107 °C. − ^1H NMR (270 MHz, $CDCl_3$): δ = 1.04−1.26 (m, 4 H, CH_2), 1.57−1.95 (m, 4 H, CH_2), 2.37−2.46 (m, 1 H, CHN), 2.63−2.72 (m, 1 H, CHN), 3.04 (s, br, 3 H, NH_2, NH), 5.41 (d, ^3J = 11 Hz, 1 H, CH=CH_2), 5.87 (d, ^3J = 18 Hz, 1 H, CH=CH_2), 6.73 (dd, ^3J = 11 Hz, ^3J = 18 Hz, 1 H, CH=CH_2), 7.51 (d, ^3J = 8 Hz, 1 H, C_6H_4), 7.85 (d, ^3J = 8 Hz, 1 H, C_6H_4). − ^{13}C NMR (68 MHz, $CDCl_3$):δ = 24.8, 25.0, 32.7, 35.5 (CH_2), 54.8, 60.3 (NCH), 117.3, 126.8, 127.5, 135.5, 139.9, 141.7 (C_6H_4−CH=CH_2). − $C_{14}H_{20}N_2O_2S\cdot 1/3H_2O$ (286.39): calcd. C 58.72, H 7.27, N 9.78; found C 58.91, H 7.67, N 9.70.

Synthesis of Complex 2: A solution of (1*R*,2*R*)-*N*-(*p*-styrylsulfonyl)-1,2-diaminocyclohexane (280 mg, 1.0 mmol) and NaOMe (1.0 mmol, 2.37 M in MeOH) in CH_2Cl_2/MeOH (20 mL, 1:1) was added slowly to a solution of $[Cp^*RhCl_2]_2$ (309 mg, 0.5 mmol) in CH_2Cl_2 (20 mL). After stirring for 2 h the solvent was removed under reduced pressure and the product was extracted with CH_2Cl_2 (30 mL). After addition of hexane (20 mL) the solvent was removed under reduced pressure to give a yellow powder which was dried in vacuo. Yield: 451 mg (79%), m.p. 225−227 °C (dec.). − ^1H NMR (270 MHz, $CDCl_3$): δ = 0.81−1.98 (m, 7 H, CH_2), 1.74 (s, 15 H, Cp*), 2.23−2.30 (m, 3 H, NCH, CH_2), 2.99−3.02 (m, 1 H, NH), 3.38−3.42 (m, 1 H, NH), 5.27 (d, ^3J = 11 Hz, 1 H, CH=CH_2), 5.77 (d, ^3J = 18 Hz, 1 H, CH=CH_2), 6.70 (dd, ^3J = 11 Hz, ^3J = 18 Hz, 1 H, CH=CH_2), 7.39 (d, ^3J = 8 Hz, 2 H, C_6H_4), 8.02 (d, ^3J = 8 Hz, 2 H, C_6H_4). − ^{13}C NMR (101 MHz, $CDCl_3$): δ = 9.7 (CH_3, Cp*), 24.6, 24.9, 34.6, 36.3 (CH_2), 63.5, 64.4 (NCH), 94.0 (d, $^1J_{RhC}$ = 8 Hz, C, Cp*) 115.1, 125.9, 128.3, 136.4, 139.0, 145.4 (C_6H_4−CH=CH_2). − $C_{24}H_{34}ClN_2O_2RhS\cdot H_2O$ (570.97): calcd. C 50.49, H 6.36, N 4.91; found C 50.77, H 6.09, N 4.82.

Synthesis of Complex 3: A suspension of **2** (111 mg, 0.20 mmol) and AgO_2PPhMe (58 mg, 0.22 mmol) in CH_2Cl_2 (10 mL) was stirred for 96 h at room temperature. The solid products were removed by filtration and the solvent was reduced to a volume of 2 mL. After addition of hexane the solvent was removed in vacuo to give an orange powder which was dried in vacuo. Yield: 119 mg (86%), m.p. 148−150 °C (dec.). − ^1H NMR (270 MHz, $CDCl_3$): δ = 0.61−1.57 (m, 6 H, CH_2), 1.33 (d, $^2J_{PH}$ = 14 Hz, 3 H, PCH_3), 1.48 (s, 15 H, Cp*), 1.84−2.07 (m, 3 H, NCH, CH_2), 2.29−2.37 (m, 1 H, NCH), 5.20 (d, ^3J = 11 Hz, 1 H, CH=CH_2), 5.68 (d, ^3J = 17 Hz, 1 H, CH=CH_2), 6.60 (dd, ^3J = 11 Hz, ^3J = 17 Hz, 1 H, CH=CH_2), 7.26−7.30 (m, 5 H, PPh, C_6H_4), 7.66−7.77 (m, 4 H, PPh, C_6H_4). − ^{13}C NMR (101 MHz, $CDCl_3$): δ = 9.5 (CH_3, Cp*), 18.8 (d, $^1J_{PC}$ = 99 Hz, PCH_3), 24.4, 24.6, 33.9, 35.0 (CH_2), 63.3, 63.8 (NCH), 93.7 (d, $^1J_{RhC}$ = 9 Hz, C, Cp*) 115.5, 125.9,

Table 3. Crystallographic data of **2** and **3**

	2	**3**
Empirical formula	$C_{24}H_{34}ClN_2O_2RhS$	$C_{31}H_{42}N_2O_4PRhS{\cdot}0.5{\cdot}CH_2Cl_2$
Molecular weight [g mol^{-1}]	552.95	715.07
Crystal size	0.10 × 0.20 × 0.30	0.20 × 0.33 × 0.53
Crystal system	Monoclinic	Monoclinic
Space group	$P2_1/c$	$P2_1/c$
a [Å]	9.500(1)	9.1575(1)
b [Å]	12.525(3)	14.569(4)
c [Å]	21.364(5)	26.831(5)
β [°]	94.52(2)	93.578(13)
Volume [Å^3]	2534(1)	3572(1)
Z	4	4
Density [g cm^{-3}]	1.449	1.329
Absorption coefficient [mm^{-1}]	0.884	0.691
Θ range [°]	2.15 to 23.99	2.62 to 23.98
Index ranges	−7 → 10, −0 → 14, −24 → 24	−10 → 0, −16 → 0, −30 → 30
Reflections collected	4240	5976
Independent reflections	3965 (R_{int} = 0.0390)	5586 (R_{int} = 0.0314)
Absorption correction	Semi-empirical	Semi-empirical
Max. and min. transmission	0.9990 and 0.8758	0.9999 and 0.9333
Weights	$w = 1/(\sigma^2(F_0^2) + (0.0332P)^2 + 4.3928P]$; $P = (F_0^2 + 2F_c^2)/3$	$w = 1/(\sigma^2(F_0^2) + (0.0598P)^2 + 2.6744P]$; $P = (F_0^2 + 2F_c^2)/3$
Data/restraints/parameters	3122/8/323	4680/21/394
Goodness-of-fit on F^2	1.201	1.159
Final R indices [$I>2\sigma(I)$]	$R1$ = 0.0407, $wR2$ = 0.0866	$R1$ = 0.0391, $wR2$ = 0.1043
R indices (all data)	$R1$ = 0.0602, $wR2$ = 0.1020	$R1$ = 0.0500, $wR2$ = 0.1125
Largest diff. peak/hole [eÅ^{-3}]	0.487/−0.390	0.848/−0.457

126.9 (C_6H_4−CH=CH_2), 127.8−130.5 (m, PPh), 135.8, 139.6, 146.9 (C_6H_4−CH=CH_2). − ^{31}P NMR (109 MHz, $CDCl_3$):δ = 40.0. − $C_{31}H_{42}N_2O_4PRhS{\cdot}H_2O$ (690.64): calcd. C 53.91, H 6.42, N 4.06; found C 54.04, H 6.75, N 3.93.

Synthesis of Complex 4: The synthesis of **4** was carried out analogously to that of **3** using [Cp*Rh($NH_2CH2CH2NSO_2C_8H_7$)Cl] (100 mg, 0.20 mmol) and AgO_2PPhMe (58 mg, 0.22 mmol). Yield: 109 mg (86%), m.p. 120−122 °C (dec.). − ^{1}H NMR (270 MHz, CD_3OD): δ = 1.34 (d, $^2J_{PH}$ = 14 Hz, 3 H, PCH_3), 1.66 (s, 15 H, Cp*), 2.46−2.50 (m, 2 H, CH_2), 2.62−2.66 (m, 1 H, CH_2), 5.34 (d, ^3J = 11 Hz, 1 H, CH=CH_2), 5.89 (d, ^3J = 18 Hz, 1 H, CH=CH_2), 6.77 (dd, ^3J = 11 Hz, ^3J = 18 Hz, 1 H, CH=CH_2), 7.39−7.82 (m, 9 H, PPh, C_6H_4). − ^{13}C NMR (68 MHz, CD_3OD): δ = 8.2 (CH_3, Cp*), 17.8 (d, $^1J_{PC}$ = 99 Hz, PCH_3), 45.7, 50.3 (CH_2), 94.5 (d, $^1J_{RhC}$ = 9 Hz, C, Cp*) 115.5−142.7 (m, C_6H_4−CH=CH_2, PPh). − ^{31}P NMR (109 MHz, CD_3OD):δ = 31.0. − $C_{27}H_{36}N_2O_4PRhS{\cdot}H_2O$ (636.54): calcd. C 50.95, H 6.02, N 4.40; found C 51.37, H 6.07, N 4.10.

Synthesis of Polymer P2: A freshly prepared mixture of V-70 (15 mg) and EGDMA (4.95 mmol) was added to a solution of **2** (50 μmol) in $CHCl_3$/MeOH (467 μL, 4:1) in a 4 mL screw-cap vial. The orange solution was sonicated (1 min) and degassed with nitrogen (2 min). The vial was closed and tempered at 35 °C (24 h) and then at 65 °C (3 h). The obtained polymer was ground, sieved (particle size: 25−100 μm) and stirred in a solution of benzyltriethylammonium chloride in MeOH (0.1 M). The polymer was isolated, washed with MeOH (4 × 40 mL) and dried in vacuo. The synthesis of the polymer **P3** was performed analogously to that of **P2** using complex **3** (50 μmol).

X-ray Crystallographic Investigations: An Enraf Nonius CAD 4 diffractometer was employed for data collection using Mo-K_α radiation (T = 295 K). The structures were solved by direct methods (SHELXS86) and were refined by means of the full-matrix least-squares procedures using SHELXL93 (Table 3). All non-hydrogen atoms were refined anisotropically. For the hydrogen atoms a riding model was employed. The styryl groups of **2** is disordered. Restraints were used for parts of the aromatic ring. Compound **3** crystallizes together with 0.5 molecules of dichloromethane. The solvent molecules are disordered and restraints were used for the refinement.

Crystallographic data (excluding structure factors) for the structures reported in this paper have been deposited with the Cambridge Crystallographic Data Centre as supplementary publication no. CCDC-136894 (**2**) and CCDC-136895 (**3**). Copies of the data can be obtained free of charge on application to CCDC, 12 Union Road, Cambridge CB2 1EZ, UK [Fax: (internat.) +44-1223/336-033; E-mail: deposit@ccdc.cam.ac.uk].

Transfer Hydrogenations: A suspension of **P2** (20.2 mg, this corresponds to 1.0 μmol Rh if a quantitative incorporation is assumed) in 2-propanol containing 1.2 μmol KOH were stirred for 15 min at 33 °C. The reaction was started by addition of the substrate in 2-propanol. The initial concentration of the substrate was 0.1 M (0.5 M for competition experiments) with a total volume of 1 mL. Samples were removed at the times indicated, quenched with 2-propanol/EtOAc (3:1), filtered and analysed by capillary GC (CP-cyclodextrin-B-2,3,6-M-19 column by Chrompack, 50 m). For competition experiments the course of the reaction was analysed for the first 12 min. Reactions with the imprinted polymer **P3** were performed simultaneously and under identical conditions.

Acknowledgments

K. S. thanks Prof. Dr. W. Beck (LMU München) for his generous support and E. Karaghiosoff for technical assistance. Financial funding from the Bayerischer Habilitations-Förderpreis (K. S.) is gratefully acknowledged.

[1] A turnover frequency (TOF) of more than 10^5 h^{-1} was observed for ruthenium(II)-catalysed hydrogenations or for the alkene polymerisation with metallocene catalysts: [1a] H. Doucet, T. Ohkuma, K. Murata, T. Yokozawa, M. Kozawa, E. Katayama, A. F. England, T. Ikariya, R. Noyori, *Angew. Chem.*

1998, *110*, 1792−1796; *Angew. Chem. Int. Ed.* **1998**, *37*, 1703−1707. − [1b] H.-H. Brintzinger, D. Fischer, R. Mühlhaupt, B. Rieger, R. Waymouth, *Angew. Chem*. **1995**, *107*, 1255−1283; *Angew. Chem. Int. Ed. Engl*. **1995**, *34*, 1143.

[2] Exceptions are organometallic Lewis acids, the reactivity of which is often influenced by the second coordination sphere. For example see: E. P. Kündig, C. M. Saudan, G. Bernardinelli, *Angew. Chem.* **1999**, *111*, 1298−1301; *Angew. Chem. Int. Ed.* **1999**, *38*, 1220−1223.

[3] [3a] M. T. Reetz, S. R. Waldvogel, *Angew. Chem*. **1997**, *109*, 870−873; *Angew. Chem. Int. Ed. Engl*. **1997**, *36*, 865−867. − [3b] M. T. Reetz, C. Frömbgen, *Synthesis* **1999**, *9*, 1555−1557. − [3c] R. Breslow, S. D. Dong, *Chem. Rev.* **1998**, *98*, 1997−2011.

[4] [4a] J. M. Thomas, *Angew. Chem*. **1999**, *111*, 3800−3843; *Angew. Chem. Int. Ed.* **1999**, *38*, 3588−3628. − [4b] E. J. Creyghton, R. S. Downing, *J. Mol. Cat. A* **1998**, *134*, 47−61.

[5] [5a] K. Haupt, K. Mosbach, *Trends Biotech.* **1998**, *16*, 468−475. − [5b] G. Wulff, *Angew. Chem*. **1995**, *107*, 1958−1979; *Angew. Chem. Int. Ed. Engl.* **1995**, *34*, 1812−1832. − [5c] *Molecular and Ionic Recognition with Imprinted Polymers* (Eds.: R. A. Bartsch, M. Maeda Oxford University Press, New York, **1998**.

[6] [6a] K. Polborn, K. Severin, *Chem. Commun.* **1999**, 2481−2482. − [6b] K. Polborn, K. Severin, *Chem. Eur. J.*, submitted for publication.

[7] Strategies to design catalysts with the help of TSAs have been summarised: [7a] P. A. Brady, J. K. M. Sanders, *Chem. Soc. Rev.* **1997**, *26*, 327−336. − [7b] J. K. M. Sanders, *Chem. Eur. J.* **1998**, *4*, 1378−1383. − [7c] M. E. Davies, A. Katz, W. R. Ahmad, *Chem. Mater.* **1996**, *8*, 1820−1839.

[8] Mosbach and Lemaire have utilised classical coordination compounds to obtain catalytically active polymers by molecular imprinting. The pseudosubstrate complexes were prepared in situ prior to polymerisation and were not further characterised: [8a] P. Gamez, B. Dunjic, C. Pinel, M. Lemaire, *Tetrahedron Lett*. **1995**, *36*, 8779−8782. − [8b] F. Locatelli, P. Gamez, M. Lemaire, *J. Mol. Catal. A* **1998**, *135*, 89−98. − [8c] J. Matsui, I. A. Nicholls, I. Karube, K. Mosbach, *J. Org. Chem.* **1996**, *61*, 5414−5417.

[9] [9a] M. J. Palmer, M. Wills, *Tetrahedron: Asymmetry* **1999**, *10*, 2045−2061. − [9b] R. Noyori, S. Hashiguchi, *Acc. Chem. Res.* **1997**, *30*, 97−102.

[10] [10a] K. Murata, T. Ikariya, R. Noyori, *J. Org. Chem*. **1999**, *64*, 2186−2187; related Rh^{III}- and Ir^{III} catalysts with *N*-*p*-toluenesulfonyl-1,2-diphenylenediamine ligands have been described: [10b] K. Mashima, T. Abe, K. Tani, *Chem. Lett.* **1998**, 1199−1200. − [10c] J. Mao, D. C. Baker, *Org. Lett.* **1999**, *1*, 841−843.

[11] [11a] D. A. Alonso, P. Brandt, S. J. M. Nordin, P. G. Andersson, *J. Am. Chem. Soc.* **1999**, *121*, 9580−9588. − [11b] M. Yamakawa, H. Ito, R. Noyori, *J. Am. Chem. Soc.* **2000**, *122*, 1466−1478.

[12] To obtain single crystals of **2** and **3** complexes with a racemic ligand (*R*,*R* and *S*,*S*) were employed.

[13] [13a] K.-J. Haak, S. Hashiguchi, A. Fujii, T. Ikariya, R. Noyori, *Angew. Chem.* **1997**, *109*, 297−300; *Angew. Chem. Int. Ed. Engl.* **1997**, *36*, 285−288. − [13b] S. Hashiguchi, A. Fujii, J. Takehara, T. Ikariya, R. Noyori, *J. Am. Chem. Soc.* **1995**, *117*, 7562−7563.

[14]] [14a] J. Matsui, Y. Miyoshi, O. Doblhoff-Dier, T. Takeushi, *Anal. Chem.* **1995**, *67*, 4404−4408. − [14b] B. Sellergren, K. J. Shea, *J. Chromatogr.* **1993**, *635*, 31−49. − [14c] G. Vlatakis, L. I. Andersson, R. Müller, K. Mosbach, *Nature* **1993**, *361*, 645−647.

[15] Upon addition of benzyltriethylammonium chloride to a solution of **3** a quantitative exchange of the phosphinato is observed. This was shown by in situ NMR experiments (^{31}P, ^{1}H).

[16] D. Carmona, F. J. Lahoz, R. Atencio, L. A. Oro, M. P. Lamata, F. Viguri, E. San José, C. Vega, J. Reyes, F. Joó, A. Kathó, *Chem. Eur. J.* **1999**, 1544−1564.

[17] [17a] D. J. Bayston, C. B. Travers, M. E. C. Polywka, *Tetrahedron Asymmetry* **1998**, *9*, 2015−2018. − [17b] R. ter Halle, E. Schulz, M. Lamaire, *Synlett* **1997**, 1257−1258. − [17c] E. Breysse, C. Pinel, M. Lemaire, *Tetrahedron: Asymmetry* **1998**, *9*, 879−900.

[18] H. Kamogawa, A. Kanzawa, M. Kadoya, T. Naito, M. Nanasawa, *Bull. Chem. Soc. Jpn.* **1983**, *56*, 762−765.

[19] C. White, A. Yates, P. M. Maitlis, *Inorg. Synth.* **1992**, *29*, 228−230.

Received February 29, 2000
[I00077]

Reactivity of the Anionic Carbonyltrirhenium Cluster $[Re_3(\mu\text{-}H)_3(\mu_3\text{-}ampy)(CO)_9]^-$ − Synthesis of Neutral Phosphane and Alkenyl Derivatives

Javier A. Cabeza,*[a] Fabrizia Grepioni,*[b] Angela Llamazares,[a] Víctor Riera,[a] and Rajiv Trivedi[a]

Keywords: Rhenium / Cluster compounds / Hydrido complexes / Phosphanes / Alkynes / Insertions

Protonation of the trinuclear anionic rhenium cluster $[HNEt_3][Re_3(\mu\text{-}H)_3(\mu_3\text{-}ampy)(CO)_9]$ (**1**) (Hampy = 2-amino-6-methylpyridine) with $[HOEt_2][BF_4]$ at low temperature leads to dihydrogen and the neutral unsaturated dihydride derivative $[Re_3(\mu\text{-}H)_2(\mu_3\text{-}ampy)(CO)_9]$. The low thermal stability of this compound (it undergoes decomposition above 5 °C) has prevented its isolation as a pure solid. The compound $[Re_3(\mu\text{-}H)_3(CO)_{12}]$ is the major product obtained when the protonation of **1** is carried out under CO. Protonation of **1** in the presence of phosphanes or alkynes gives the neutral derivatives $[Re_3(\mu\text{-}H)_2(\mu_3\text{-}ampy)(PR_3)(CO)_9]$ (**2**: R = Ph; **3**: R = *p*-tolyl) or $[Re_3(\mu_3\text{-}H)(\mu_3\text{-}ampy)(\mu\text{-}RC{=}CHR')(CO)_9]$ (**4**: R = R′ = Ph; **5**: R = R′ =Et; **6a**: R = Ph, R′ = H; **6b**: R = H, R′ = Ph). In **2** and **3**, the phosphane ligand is in an equatorial position on an Re atom of the NH-bridged Re–Re edge, *cis* to a hydride ligand and far away from the other hydride ion. In compounds **4**–**6**, the alkenyl ligand, which arises from the insertion of the corresponding alkyne into an Re–H bond, is attached to two metal atoms in a $\mu\text{-}\eta^1{:}\eta^2$ fashion, spanning the same Re–Re edge as the NH fragment of the ampy ligand. The hydride ligand of compounds **4**–**6** coordinates in a triply bridging fashion, capping the Re_3 triangle. Compounds **4**–**6** represent the first examples of trirhenium clusters containing alkenyl ligands.

Introduction

Until now, few carbonyl cluster compounds (three or more metal atoms connected by metal−metal bonds) of rhenium are known,[1] in comparison to those known for ruthenium and osmium.[2] This is undoubtedly due to the lack of a convenient rhenium cluster precursor. In fact, with few exceptions,[3] the cluster compounds made from $[Re_2(CO)_{10}]$, the most readily available carbonylrhenium complex, can only be isolated in medium to low yield.[4−6] For example, $[Re_3(\mu\text{-}H)_3(CO)_{12}]$, which is isoelectronic with the most important ruthenium and osmium starting clusters $[M_3(CO)_{12}]$ (M = Ru, Os), is prepared from $[Re_2(CO)_{10}]$ either by hydrogenation[4a] or treatment with $Na[BH_4]$ followed by acidification,[5d,5e] but both procedures are rather tedious and the yields are only moderate. Moreover, $[Re_3(\mu\text{-}H)_3(CO)_{12}]$ is kinetically very stable and most of its reactions require high temperatures (which promote changes in cluster and/or ligand integrity, often leading to mixtures of products)[1] or derivatization to the more reactive $[Re_3(\mu\text{-}H)_3(CO)_{10}(MeCN)_2]$.[7] Ciani, D'Alfonso and co-workers have extensively studied the derivative chemistry of the anionic unsaturated cluster $[Re_3(\mu\text{-}H)_4(CO)_{10}]^-$,[1] but its best preparation requires a high pressure hydrogenation (100 atm) of $[Re_3(\mu\text{-}H)_2(CO)_{12}]^-$,[8] which is made by deprotonation of $[Re_3(\mu\text{-}H)_3(CO)_{12}]$.[9] In addition, the unsaturated cluster $[Re_4(\mu_3\text{-}H)_4(CO)_{12}]$, which can be made by hydrogenation of $[Re_2(CO)_{10}]$,[4a] is so reactive that its reactions are generally not very selective, often leading to mixtures of many products.[10]

We have recently reported that the anionic carbonyltrirhenium cluster $[HNEt_3][Re_3(\mu\text{-}H)_3(\mu_3\text{-}ampy)(CO)_9]$ (**1**) (Hampy = 2-amino-6-methylpyridine) can be prepared in fair yield (70%) from $[Re_4(\mu_3\text{-}H)_4(CO)_{12}]$, Hampy and triethylamine.[10] It should be noted that in carbonylruthenium cluster compounds, as for example $[Ru_3(\mu\text{-}H)(\mu_3\text{-}ampy)(CO)_9]$,[11] face-bridging 2-aminopyridinato ligands help maintain the cluster integrity and provide reaction pathways of low activation energy.[12] In fact, over a hundred carbonylruthenium clusters containing μ_3-2-aminopyridinato ligands have already been prepared,[2a] including some efficient catalyst precursors for alkyne hydrogenation,[13] dimerization[14] and polymerization[14] reactions.

All the above-mentioned data prompted us to study the reactivity of compound **1**. We have already investigated the synthesis of tetranuclear Re_3Au clusters by reactions of **1** with gold complexes.[15] We now report its protonation reaction as well as the preparation of some neutral phosphane and alkenyl derivatives. The latter represent the first examples of trirhenium clusters containing alkenyl ligands.

Results and Discussion

Protonation Reaction of Compound 1

Compound **1** was found to be very stable toward nucleophilic reagents. No reaction was observed when **1** was

[a] Departamento de Química Orgánica e Inorgánica, Instituto de Química Organometálica "Enrique Moles", Universidad de Oviedo, 33071 Oviedo, Spain
E-mail: jac@sauron.quimica.uniovi.es
Fax: (internat.) + 34-985/103446
[b] Dipartimento di Chimica, Universitá di Sassari, via Vienna 2, 07100 Sassari, Italy
E-mail: grepioni@ssmain.uniss.it

 © WILEY-VCH Verlag GmbH, D-69451 Weinheim, 2000 1434−1948/00/0808−1693 $ 17.50+.50/0

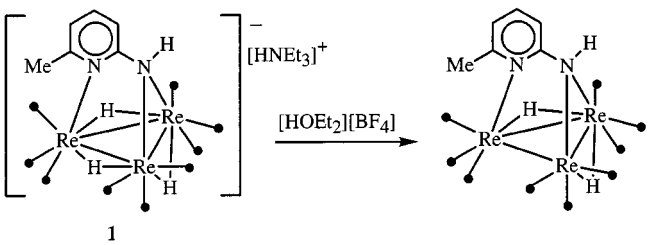
treated with phosphane, nitrile or alkyne reagents in THF at reflux temperature. Its anionic character and the fact that it is a saturated 48-electron trinuclear cluster may account (at least in part) for its stability toward nucleophilic reagents.

Interestingly, an instantaneous reaction was observed when compound **1** was treated with $[HOEt_2][BF_4]$: The color changed from colorless to yellow, a gas was evolved and drastic changes were observed in the IR spectrum of the solution. Unfortunately, no pure products could be isolated from this reaction, regardless of the solvent (THF, dichloromethane, acetonitrile) and the ratio of the reactants.

In order to obtain some insight of this reaction, the protonation was subsequently monitored by ^1H NMR spectroscopy at low temperature. A single product was observed upon mixing the reagents in CD_2Cl_2 at −78 °C, characterized by two uncoupled hydride resonances of equal intensity at $\delta = -7.85$ and -8.53, in addition to a set of resonances due to the ampy ligand. This compound remained unchanged upon warming the solution to 5 °C but, unfortunately, it decomposed to other products above this temperature.

These data suggest that the protonation of compound **1** results in the release of dihydrogen and in the formation of the neutral species $[Re_3(\mu\text{-}H)_2(\mu_3\text{-ampy})(CO)_9]$. The asymmetric structure proposed for this species in Scheme 1 is in agreement with the observation of two hydride resonances in the ^1H NMR spectrum. Its coordinative unsaturation (46-electron) may be responsible for its low thermal stability. Although the use of coordinating solvents (THF, acetonitrile) did not lead to the isolation of solvated derivatives as pure products, some phosphane and alkyne derivatives could be isolated carrying out the protonation in the presence of the appropriate ligands (vide infra). The structures of these derivatives are also in agreement with that proposed for $[Re_3(\mu\text{-}H)_2(\mu_3\text{-ampy})(CO)_9]$ in Scheme 1.

Treatment of a solution of compound **1** in dichloromethane with $[HOEt_2][BF_4]$ under carbon monoxide led to a transient color change of the initial colorless solution to pale yellow, but it returned to colorless within a few seconds. An appropriate workup of this solution allowed the isolation of $[Re_3(\mu\text{-}H)_3(CO)_{12}]$ as the major carbonyl complex of the reaction mixture. This result, which may seem of little relevance, is indeed quite interesting, since it reveals that in carbonylrhenium cluster chemistry the triply bridging ampy ligand can be removed under mild conditions and, therefore, it should not be expected to maintain the trinuclear cluster integrity as efficiently as it does in ruthenium cluster chemistry.[11−14]



1

Scheme 1. Protonation of compound **1**

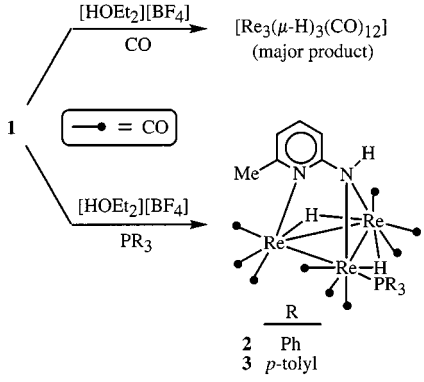
Neutral Phosphane Derivatives of Compound 1

Protonation of a dichloromethane solution of complex **1** with $[HOEt_2][BF_4]$ in the presence of triphenylphosphane (1:1:1 mol ratio) led to the immediate formation of the yellow neutral derivative $[Re_3(\mu\text{-}H)_2(\mu_3\text{-ampy})(PPh_3)(CO)_9]$ (**2**). Its formulation was clearly evidenced by its microanalysis and spectroscopic data. Its ^1H NMR spectra shows two hydride resonances, one as a doublet of doublets ($\delta = -9.50$, $J = 12.3$ and 1.6 Hz) and the other as a small doublet ($\delta = -9.92$, $J = 1.6$ Hz), indicating that the compound has two hydride ligands which couple slightly to each other (1.6 Hz) and that only one of them couples to the phosphorus atom ($J = 12.3$ Hz). As this J_{P-H} coupling value is typical of a *cis* arrangement of hydride and phosphane ligands in trinuclear metal clusters,[16] and as no coupling is observed between the other hydride ion and the phosphorus atom, we propose the structure depicted in Scheme 2 for this complex. No crystals of compound **2** suitable for an X-ray diffraction study could be obtained.

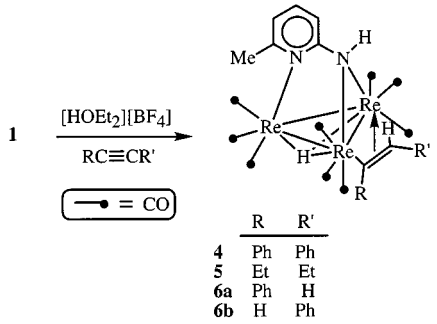
As the structure proposed for compound **2**, although reasonable, is not unambiguous, we decided to prepare an analogous derivative, containing a different phosphane ligand, in an attempt to obtain X-ray diffraction-quality crystals. The compound $[Re_3(\mu\text{-}H)_2(\mu_3\text{-ampy})\{P(p\text{-tolyl})_3\}(CO)_9]$ (**3**) was made by a similar procedure as that used for **2**. Its analytical and spectroscopic data indicate that it is isostructural with complex **2**, but, unfortunately, it could not be crystallized.

It seems clear that compounds **2** and **3** are formed upon coordination of the corresponding phosphane to the unsaturated species that results when complex **1** is protonated and dihydrogen is released.

The number of previously described phosphane derivatives of trirhenium clusters is very small, and most of them are simple phosphane-substituted derivatives of carbonyl hydrido clusters.[1,17] The anionic formimidoyl complex $[Re_3(\mu\text{-}H)_3(\mu\text{-}CH{=}NC_6H_{11})(PMe_2Ph)(CO)_9]^-$ is the only previous example of a trirhenium cluster containing both N-donor and P-donor ligands.[18]



Scheme 2. Protonation of compound **1** in the presence of CO and phosphane ligands



Scheme 3. Synthesis of neutral alkenyl derivatives

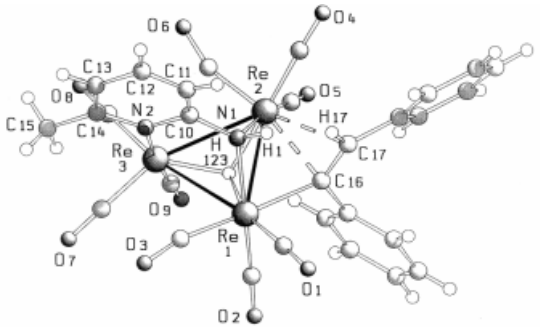


Figure 1. Molecular structure of $[Re_3(\mu_3\text{-}H)(\mu_3\text{-ampy})(\mu\text{-PhC=CHPh})(CO)_9]$ (**4**); selected bond lengths [Å]: Re(1)−Re(2) 2.853(2), Re(1)−Re(3) 3.018(2), Re(2)−Re(3) 3.054(2), Re−H(123) 1.88, 1.88, 1.90, Re(1)−C(16) 2.20(2), Re(2)−C(16) 2.30(2), Re(2)−C(17) 2.45(2), Re(1)−N(1) 2.16(2), Re(2)−N(1) 2.17(2), Re(3)−N(2) 2.27(2), mean $Re-C_{(CO)}$ 1.914, mean C−O 1.165

Neutral Alkenyl Derivatives of Compound 1

Protonation of compound **1** with $[HOEt_2][BF_4]$ in the presence of diphenylacetylene, 3-hexyne or phenylacetylene led to the neutral alkenyl derivatives $[Re_3(\mu_3\text{-}H)(\mu_3\text{-ampy})(\mu\text{-RC=CHR}')(CO)_9]$ (**4**: R = R′ = Ph; **5**: R = R′ = Et; **6a**: R = Ph, R′ = H; **6b**: R = H, R = Ph) (Scheme 3). Compounds **4** and **5** were obtained as pure products, but the isomeric compounds **6a** and **6b** were obtained as an inseparable mixture. These results suggest that the reaction is quite general since it works well for internal, terminal, aryl- and alkylalkynes, giving a mixture of two isomers when the alkyne used is not symmetric. In these compounds, the alkenyl ligands arise from the coordination of the corresponding alkyne to the unsaturated species formed by protonation of compound **1**, followed by a migratory insertion of the alkyne into a Re−H bond.

The compounds were characterized by analytical and spectroscopic methods. All have similar IR and NMR spectra, indicating that they have a common structure. The most relevant features of their ^1H NMR spectra are (a) the presence of a resonance due to the vinyl hydrogen atom in the range δ = 6−3, as observed for many complexes of other metals containing bridging alkenyl ligands,[13,14] and (b) the observation of only one hydride resonance as a small doublet (J = 3.0 Hz in all cases except for **6b**, which was observed as a singlet). Decoupling experiments revealed that such a doublet arises from the coupling of the hydride with the hydrogen atom of the NH fragment of the ampy ligand (which is observed as a broad singlet in the ^1H NMR spectrum at room temperature). The fact that the hydride ligand signal of **6b** is observed as a singlet suggests that its structure may differ from that of the other alkenyl derivatives, but we have been unable to investigate this matter further because compounds **6a** and **6b** were always obtained as a mixture.

The analytical and spectroscopic data of these alkenyl derivatives were not sufficient to unequivocally assign the positions of the hydride and alkenyl ligands in the clusters. Therefore, an X-ray diffraction study was required. None of the compounds crystallized well, nonetheless, in the case of compound **4**, we managed to obtain crystals of sufficient quality for the diffraction experiment. The molecular structure of compound **4** is shown in Figure 1, together with the labeling scheme and selected bond length parameters. The ampy ligand coordinates to the Re_3 triangle in a capping mode, previously observed in many trinuclear clusters.[10−16] The alkenyl ligand spans the same Re−Re edge as the amido fragment of the ampy ligand. The carbonyl ligands are bound to the cluster in a terminal fashion, three to each Re atom. Although the hydride location could not be directly obtained from the diffraction data, calculations with the program XHYDEX[19] revealed a minimum energy position for the hydride ligand in a triply bridging site, capping the metal triangle as shown in Figure 1 and Scheme 3. Triply bridging hydrides are frequently observed in carbonylrhenium clusters.[1]

The reactions leading to compounds **4**−**6** can be regarded as pioneering processes in the so far unreported field of the reactivity of carbonyltrirhenium clusters with unsaturated hydrocarbons. In fact, compounds **4**−**6** are the first examples of trirhenium clusters containing alkenyl ligands.

Experimental Section

General: Solvents were dried with sodium diphenyl ketyl (hydrocarbons) or calcium hydride (dichloromethane) and distilled under nitrogen prior to use. The reactions were carried out under nitrogen, using Schlenk vacuum-line techniques, and were routinely monitored by solution IR spectroscopy (carbonyl stretching region) and by spot TLC (silica gel). − Compound **1** was prepared by a published procedure,[10] all other reagents were purchased as analytically pure samples. − IR spectra were recorded with a Perkin−Elmer FT 1720-X spectrophotometer, using 0.1-mm CaF_2 cells. − ^1H and $^{31}P\{^1H\}$ NMR spectra were run at room temperature with Bruker AC-200 and AC-300 instruments, being referenced to internal $SiMe_4$ (for ^1H: δ = 0) or external aqueous 85% H_3PO_4 (for ^{31}P: δ = 0). − Microanalyses were obtained from the University of Oviedo Analytical Service.

Protonation of Compound 1: A 5-mm NMR tube was charged under nitrogen with compound **1** (0.012 g) and CD_2Cl_2 (0.5 mL) and immersed in a bath kept at −78 °C. Addition of $[HOEt_2][BF_4]$ (2 μL) to the cold solution led to a color change from colorless to yellow. The tube was quickly transferred to the NMR probe, previously cooled at −80 °C. The resonances of a pure product were observed at δ = −8.53 (s, 1 H, μ-H), −7.85 (s, 1 H, μ-H), 2.78 (s, 3 H, ampy-Me), 6.44 (s, br, 1 H, ampy-N*H*), 6.76 (d, 7.6 Hz, 1 H, ampy-C*H*), 6.87 (d, 7.6 Hz, 1 H, ampy-C*H*), 7.50 (t, 7.6 Hz, 1 H, ampy-C*H*) ppm. This product could not be isolated.

Protonation of Compound 1 under Carbon Monoxide: A solution of compound **1** (0.025 g, 0.024 mmol) in dichloromethane (10 mL) was treated with $[HOEt_2][BF_4]$ (3.5 μL, 0.025 mmol) while the solution was kept under carbon monoxide. The initially colorless solution changed to pale yellow upon addition of the acid, but it soon returned to colorless. After being stirred for 3 h, the IR spectrum of the solution showed the presence of $[Re_3(\mu\text{-}H)_3(CO)_{12}]$. The solvent was removed under reduced pressure and the residue was extracted into hexane (3 × 5 mL). The extract was concentrated to dryness to give a colorless solid which was found to be $[Re_3(\mu\text{-}H)_3(CO)_{12}]$ (IR, ^{1}H NMR). The fraction insoluble in hexane contained $[HNEt_3][BF_4]$ and Hampy among other minor products (IR, ^{1}H NMR).

$[Re_3(\mu\text{-}H)_2(\mu_3\text{-ampy})(PPh_3)(CO)_9]$ (2): $[HOEt_2][BF_4]$ (3 μL, 0.021 mmol) was added to a dichloromethane solution (10 mL) of compound **1** (0.023 g, 0.022 mmol) and PPh_3 (0.006 g, 0.023 mmol). The color changed from colorless to yellow. The solution was stirred for 2 h and concentrated to dryness. The solid residue was extracted with toluene (3 × 5 mL). The extract was concentrated to dryness and the residue was crystallized from dichloromethane/hexane to give compound **2** as a yellow solid (0.015 g, 58%). − $C_{33}H_{24}N_2O_9PRe_3$ (1182.16): calcd. C 33.53, H 2.05, N 3.37; found C 33.64, H 2.13, N 3.16. − IR (CH_2Cl_2): $\tilde{\nu}$ = 2049 (m), 2017 (vs), 1949 (m), 1938 (m), 1923 (m) cm^{-1}. − ^{1}H NMR ($CDCl_3$): δ = −9.92 (d, *J* = 1.6 Hz, 1 H, μ-H), −9.50 (dd, 12.3 and 1.6 Hz, 1 H, μ-H) 2.59 (s, 3 H, ampy-Me), 4.88 (s, br, 1 H, ampy-N*H*), 5.59 (d, *J* = 7.7 Hz, 1 H, ampy-C*H*), 6.51 (d, *J* = 7.7 Hz, 1 H, ampy-C*H*), 6.87 (t, *J* = 7.7 Hz, 1 H, ampy-C*H*), 7.5−7.1 (m, 15 H, 3 Ph). − ^{31}P{^{1}H} NMR ($CDCl_3$): δ = 1.4 (s).

$[Re_3(\mu\text{-}H)_2(\mu_3\text{-ampy})\{P(p\text{-tolyl})_3\}(CO)_9]$ (3): This compound was prepared as described above for compound **2**. Reagents: **1** (0.021 g, 0.020 mmol), P(*p*-tolyl)$_3$ (0.007 g, 0.022 mmol), $[HOEt_2][BF_4]$ (3 μL, 0.021 mmol). Yellow solid (0.014 g, 57%). − $C_{36}H_{30}N_2O_9PRe_3$ (1224.24): calcd. C 35.32, H 2.47, N 2.29; found C 35.54, H 2.66, N 2.12. − IR (CH_2Cl_2): $\tilde{\nu}$ = 2049 (m), 2017 (vs), 1949 (m), 1940 (m), 1919 (m) cm^{-1}. − ^{1}H NMR ($CDCl_3$): δ = −9.93 (d, *J* = 1.3 Hz, 1 H, μ-H), −9.50 (dd, *J* = 11.0 and 1.3 Hz, 1 H, μ-H), 2.40 (s, 9 H, 3 Me), 2.57 (s, 3 H, ampy-Me), 4.87 (s, br, 1 H, ampy-N*H*), 5.63 (d, *J* = 7.7 Hz, 1 H, ampy-C*H*), 6.51 (d, *J* = 7.7 Hz, 1 H, ampy-C*H*), 6.86 (t, *J* = 7.7 Hz, 1 H, ampy-C*H*), 7.6−7.2 (m, 12 H, 3 C_6H_4). − ^{31}P{^{1}H} NMR ($CDCl_3$): δ = −0.77 (s).

$[Re_3(\mu_3\text{-}H)(\mu_3\text{-ampy})(\mu\text{-PhC=CHPh})(CO)_9]$ (4): $[HOEt_2][BF_4]$ (5 μL, 0.035 mmol) was added to a dichloromethane solution (10 mL) of compound **1** (0.035 g, 0.034 mmol) and diphenylacetylene (0.007 g, 0.039 mmol). The color changed from colorless to orange. The solution was stirred for 1 h and was concentrated to dryness. The solid residue was extracted with toluene (2 × 5 mL). The extract was concentrated to dryness and the residue was crystallized from dichloromethane/hexane to give compound **4** as an orange solid (0.024 g, 64%). − $C_{29}H_{19}N_2O_9Re_3$ (1098.10): calcd. C 31.72, H 1.74, N 2.55; found C 32.00, H 1.82, N 2.43. − IR (CH_2Cl_2): $\tilde{\nu}$ = 2055 (w), 2027 (vs), 2016 (s), 1956 (m), 1946 (sh), 1924 (sh) cm^{-1}. − ^{1}H NMR ($CDCl_3$): δ = −6.10 (d, *J* = 3.0 Hz, 1 H, μ_3-H), 2.88 (br, 1 H, ampy-N*H*), 3.06 (s, 3 H, ampy-Me), 4.86 (s, 1 H, alkenyl-C*H*), 7.6−6.5 (m, 12 H, 2 Ph + 2 ampy-C*H*).

$[Re_3(\mu_3\text{-}H)(\mu_3\text{-ampy})(\mu\text{-EtC=CHEt})(CO)_9]$ (5): This compound was prepared as described above for compound **4**. Reagents: **1** (0.060 g, 0.059 mmol), 3-hexyne (8 μL, 0.070 mmol), $[HOEt_2][BF_4]$ (9 μL, 0.063 mmol). Orange solid (0.038 g, 64%). − $C_{21}H_{19}N_2O_9Re_3$ (1002.01): calcd. C 25.17, H 1.91, N 2.80; found C 25.20, H 2.01, N 2.72. − IR (CH_2Cl_2): $\tilde{\nu}$ = 2055 (w), 2028 (vs), 2009 (s), 1958 (m), 1937 (sh), 1926 (m) cm^{-1}. − ^{1}H NMR ($CDCl_3$): δ = −8.97 (d, *J* = 3.0 Hz, 1 H, μ_3-H), 1.25 (m, 6 H of 2 Et), 2.30 (m, 2 H of Et), 2.77 (q, *J* = 6.2 Hz, 2 H of Et), 3.07 (s, 3 H, ampy-Me), 4.31 (br, 1 H, ampy-N*H*), 5.68 (t, *J* = 6.1 Hz, 1 H, alkenyl-C*H*), 6.80 (d, *J* = 7.6 Hz, 1 H, ampy-C*H*), 6.87 (d, *J* = 7.6 Hz, 1 H, ampy-C*H*), 7.46 (t, *J* = 7.6 Hz, 1 H, ampy-C*H*).

$[Re_3(\mu_3\text{-}H)(\mu_3\text{-ampy})(\mu\text{-PhC=CH}_2)(CO)_9]$ (6a) and $[Re_3(\mu_3\text{-}H)(\mu_3\text{-ampy})(\mu\text{-HC=CHPh})(CO)_9]$ (6b): These compounds were prepared as a 1:1 mixture, as described above for compound **4**. Reagents: **1** (0.025 g, 0.024 mmol), phenylacetylene (3 μL, 0.026 mmol), $[HOEt_2][BF_4]$ (4 μL, 0.028 mmol). Orange solid (0.012 g, 49%). − $C_{23}H_{15}N_2O_9Re_3$ (1022.01): calcd. C 27.03, H 1.48, N 2.74; found C 27.32, H 1.66, N 2.55. − IR (CH_2Cl_2): $\tilde{\nu}$ = 2056 (w), 2026 (vs), 2017 (s), 1957 (m), 1941 (sh), 1936 (sh) cm^{-1}. − Selected ^{1}H NMR ($CDCl_3$) data for **6a** (extracted from the spectrum of the mixture): δ = −6.36 (d, *J* = 3.0 Hz, 1 H, μ_3-H), 2.06 (s, 1 H, alkenyl-C*H*), 3.06 (s, 1 H, alkenyl-C*H*). − Selected ^{1}H NMR ($CDCl_3$) data for **6b** (extracted from the spectrum of the mixture): δ = −7.69 (s, 1 H, μ_3-H), 4.74 (d, *J* = 5.0 Hz, 1 H, alkenyl-C*H*), 7.19 (d, *J* = 5.0 Hz, 1 H, alkenyl-C*H*).

Crystal Structure of Compound 4: X-ray diffraction data was collected at room temperature with a Nonius CAD-4 diffractometer equipped with a graphite monochromator [λ(Mo-K_α) = 0.71073 Å]. Crystal data and details of measurement: $C_{29}H_{19}N_2O_9Re_3$, *M* = 1098.06, monoclinic $P2_1/n$, *a* = 11.450(4), *b* = 24.150(8), *c* = 12.344(4) Å, β = 116.89(3)°, *V* = 3044(1) Å^3, *Z* = 4, *F*(000) = 2016, D_c = 2.396 g cm^{-3}, μ = 11.954 mm^{-1}, measured refl.s 4218, unique refl.s = 4199, 209 parameters, R_1[on *F*, 2401 $I > 2\sigma(I)$] = 0.0641, R_w(on F^2, all data) = 0.1757, GoF = 0.998. The structure was solved by direct methods followed by difference Fourier syntheses and full-matrix least-squares refinement on F^2, using SHELXL97.[20a] Due to decay of the poorly diffracting crystal, the resulting data set contained a limited number of reflections with sufficient intensity; rigid constraints were applied to the phenyl groups and only rhenium and oxygen atoms were treated anisotropically. Absorption correction was applied by azimuthal scanning of high χ reflections (min.−max. absorption correction 0.67−1.00). H atoms bound to C atoms were added in calculated positions and were refined riding on their respective C atoms. The H atom bound to the N atom was directly located from a Fourier map and was not refined. The position of the hydride H atom was calculated using the program XHYDEX[19] and its coordinates were included in the Fourier calculations but not refined. Visual inspection of space filling diagrams of the molecule also allowed approximate location of the hydride H atom position, since a suitable niche was found in accordance with the calculated position. The program SCHAKAL97[20b] was used for the molecular graphical representation. Crystallographic data (excluding structure factors) for compound **4** have been deposited with the Cambridge Crystallographic Data Centre as supplementary publication no. CCDC-140540. Copies of the data can be obtained free of charge on application to CCDC, 12 Union Road, Cambridge CB2 1EZ, UK [Fax: (internat.) + 44-1223/336-033, E-mail: deposit@ccdc.cam.ac.uk].

Acknowledgments

This work has been supported by the Spanish DGES (grant PB95−1042 to J. A. C.), the University of Sassari (F. G.), and the Spanish Ministerio de Educación y Cultura (postdoctoral fellowships to A. L. and R. T.).

[1] For comprehensive reviews on carbonylrhenium cluster chemistry, see: [1a] J. M. O'Connor, in *Comprehensive Organometallic Chemistry II* (Eds.: E. W. Abel, F. G. A. Stone, G. Wilkinson), Pergamon, Oxford, U. K., **1995**, vol. 6 (Ed.: C. P. Casey), p. 173. – [1b] T. J. Henly, *Coord. Chem. Rev.* **1989**, *93*, 269.

[2] For comprehensive reviews on carbonylruthenium and -osmium cluster chemistry, see: [2a] A. J. Deeming, in *Comprehensive Organometallic Chemistry II* (Eds.: E. W. Abel, F. G. A. Stone, G. Wilkinson), Pergamon, Oxford, U. K., **1995**, vol. 7 (Eds.: D. F. Shriver, M. I. Bruce), p. 684. – [2b] A. K. Smith, in *Comprehensive Organometallic Chemistry II* (Eds.: E. W. Abel, F. G. A. Stone, G. Wilkinson), Pergamon, Oxford, U. K., **1995**, vol. 7 (Eds.: D. F. Shriver, M. I. Bruce), p. 836. – [2c] M. P. Cifuentes, M. G. Humphrey, in *Comprehensive Organometallic Chemistry II* (Eds.: E. W. Abel, F. G. A. Stone, G. Wilkinson), Pergamon, Oxford, U. K., **1995**, vol. 7 (Eds.: D. F. Shriver, M. I. Bruce), p. 908.

[3] M. I. Bruce, P. J. Low, *J. Organomet. Chem.* **1996**, *519*, 221.

[4] [4a] H. D. Kaesz, S. A. R. Knox, J. W. Koepke, R. B. Saillant, *J. Chem. Soc., Chem. Commun.* **1971**, 447. – [4b] R. B. Saillant, G. Barceló, H. D. Kaesz, *J. Am. Chem. Soc.* **1970**, *92*, 5739. – [4c] R. J. Johnson, H. D. Kaesz, *Inorg. Synth.* **1978**, *18*, 60. – [4d] S. R. Wang, S. L. Wang, C. P. Cheng, C. S. Yang, *J. Organomet. Chem.* **1992**, *431*, 215.

[5] [5a] B. T. Huie, S. W. Kirtley, C. B. Knobler, H. D. Kaesz, *J. Organomet. Chem.* **1981**, *213*, 45. – [5b] R. Bau, B. Fontal, H. D. Kaesz, M. R. Churchill, *J. Am. Chem. Soc.* **1967**, *89*, 6374. – [5c] H. D. Kaesz, B. Fontal, R. Bau, S. W. Kirtley, M. R. Churchill, *J. Am. Chem. Soc.* **1969**, *91*, 1021. – [5d] M. A. Andrews, S. W. Kirtley, H. D. Kaesz, *Inorg. Synth.* **1977**, *17*, 66. – [5e] D. K. Huggins, W. Fellmann, J. M. Smith, H. D. Kaesz, *J. Am. Chem. Soc.* **1964**, *86*, 4841.

[6] [6a] G. Ciani, V. G. Albano, A. Immirzi, *J. Organomet. Chem.* **1976**, *121*, 237. – [6b] A. Bertolucci, M. Freni, P. Romiti, G. Ciani, A. Sironi, V. G. Albano, *J. Organomet. Chem.* **1976**, *113*, C61. – [6c] A. Bertolucci, G. Ciani, M. Freni, P. Romiti, V. G. Albano, A. Albinati, *J. Organomet. Chem.* **1976**, *117*, C37. – [6d] M. Freni, P. Romiti, G. D'Alfonso, *J. Organomet. Chem.* **1977**, *140*, 195.

[7] R. D. Adams, J. E. Cortopassi, S. B. Falloon, *Organometallics* **1992**, *11*, 3794.

[8] T. Beringhelli, G. Ciani, G. D'Alfonso, H. Molinari, A. Sironi, *Inorg. Chem.* **1985**, *24*, 2666.

[9] M. R. Churchill, P. H. Bird, H. D. Kaesz, R. Bau, B. Fontal, *J. Am. Chem. Soc.* **1968**, *90*, 7135.

[10] J. A. Cabeza, A. Llamazares, V. Riera, R. Trivedi, F. Grepioni, *Organometallics* **1998**, *17*, 5580.

[11] P. L. Andreu, J. A. Cabeza, V. Riera, Y. Jeannin, D. Miguel, *J. Chem. Soc., Dalton Trans.* **1990**, 2201.

[12] J. K. Shen, F. Basolo, P. Nombel, N. Lugan, G. Lavigne, *Inorg. Chem.* **1996**, *35*, 755.

[13] [13a] J. A. Cabeza, J. M. Fernández-Colinas, A. Llamazares, *Synlett* **1995**, 579. – [13b] J. A. Cabeza, I. del Río, J. M. Fernández-Colinas, V. Riera, *Organometallics* **1996**, *15*, 449.

[14] P. Nombel, N. Lugan, F. Mulla, G. Lavigne, *Organometallics* **1994**, *13*, 4673.

[15] J. A. Cabeza, V. Riera, R. Trivedi, F. Grepioni, *Organometallics*, in press.

[16] [16a] P. L. Andreu, J. A. Cabeza, V. Riera, C. Bois, Y. Jeannin, *J. Chem. Soc., Dalton Trans.* **1990**, 3347. – [16b] P. L. Andreu, J. A. Cabeza, M. A. Pellinghelli, V. Riera, A. Tiripicchio, *Inorg. Chem.* **1991**, *30*, 4611

[17] [17a] T. Beringhelli, G. D'Alfonso, M. Freni, G. Ciani, A. Sironi, H. Molinari, *J. Chem. Soc., Dalton Trans.* **1986**, 2691. – [17b] S. R. Wang, S. L. Wang, C. P. Cheng, C. S. Yang, *J. Organomet. Chem.* **1992**, *431*, 215. – [17c] C. J. Adams, M. I. Bruce, B. W. Skelton, A. H. White, *J. Organomet. Chem.* **1993**, *447*, 91.

[18] T. Beringhelli, G. D'Alfonso, M. Freni, G. Ciani, M. Moret, A. Sironi, *J. Organomet. Chem.* **1990**, *399*, 291.

[19] A. G. Orpen, *XHYDEX, a Program for Locating Hydrides*, Bristol University, Bristol, UK, **1980**.

[20] [20a] G. M. Sheldrick, *SHELXL97 Program for Crystal Structure Determination*, University of Göttingen, Göttingen, Germany, **1997**. – [20b] E. Keller, *SCHAKAL97 Graphical Representation of Molecular Models*, University of Freiburg, Freiburg, Germany, **1997**.

Received February 22, 2000
[I00065]

Calcium Ions Affect the Exchange Network but not the Structure of a Small Peptide (Melanostatin) in Solution: A ^{1}H and ^{13}C NMR Spectroscopic Study

Elena Gaggelli,*[a] Nicola D'Amelio,[a] Nicola Gaggelli,[a] and Gianni Valensin[a]

Keywords: Calcium / Melanostatin / Peptides / Exchange rates / NMR spectroscopy

The interaction of calcium ions with the peptide hormone melanostatin (Pro–Leu–Gly–NH_2) was investigated by ^{1}H and ^{13}C NMR spectroscopy in [D_6]DMSO containing H_2O (1%). Chemical shifts, spin-lattice relaxation rates, ^{1}H NOESY maps and the temperature coefficients of the amide ^{1}H NMR chemical shifts were measured at increasing concentrations of calcium. A 1:1 complex with the metal coordinated to the carbonyl moieties of Pro and Gly (K_d = 17 ± 2 mM^{-1}) was shown to be the major species in solution, although evidence was also provided for the occurrence of a minor species with the metal bound to the Leu carbonyl and with different stoichiometry. Upon metal complexation, substantial changes in the intrinsic chain flexibility of the peptide and in the exchange rates between water and amide protons were detected.

Introduction

Calcium ions are widely recognized as being central to a complex intra-cellular messenger system that mediates a wide range of biological processes. Binding selectivity, allowance for irregular bond lengths and angles and the diffusion-limited reaction on-rates make calcium a suitable binder for most biomolecules, especially peptides and proteins. The relatively high concentration of calcium in extracellular fluids (close to 1 mM) has prompted investigations of its possible role in mediating interactions of flexible peptides with their macromolecular targets.[1,2] Indeed, calcium was shown to favor the interaction of carnosine with human serum albumin,[1,2] and enhance the stability of the "active" conformation in oxytocin,[3] vasopressin,[3] and bradykinin.[4] Here we show that calcium modifies the rate of exchange of an amide proton in an intrinsically flexible small peptide (melanostatin) through the intervention of the metal hydration-sphere rather than as a consequence of exposure to water of a solvent-shielded proton.

Melanostatin (MIF, melanocyte-stimulating hormone release inhibiting factor), an important tri-peptide hormone (Pro-Leu-Gly−NH_2), was chosen because of the slow exchange rate measured for the Leu-amide proton[5−8] and its biological relevance. MIF, first discovered in rat hypothalamus,[9] is generated by the enzymatic cleavage of oxytocin, and is believed to modulate dopamine-receptors in the central nervous system[10] and to inhibit the release of the melanocyte-stimulating hormone.[11,12]

All NMR spectroscopic experiments were carried out in carefully deoxygenated [$^{2}H_6$]-dimethyl sulfoxide ([D_6]DMSO) containing 555 mM H_2O (1%). This mixture was considered because it mimics critical biochemical functions, which take place away from bulk water, where molecules with hydrophilic moieties retain solvating water.

[a] Department of Chemistry, University of Siena,
Via A.Moro, Siena 53100, Italy
Fax: (internat.) + 39-0577/234-254
E-mail: gaggelli@unisi.it

Results and Discussion

Before the addition of calcium, the NMR spectroscopic features of melanostatin were typical of small flexible peptides showing no intramolecular structuring and motional averaging among different conformations. However, as previously observed,[5−8] the Leu-amide proton was found to exchange slowly with cosolvent water. Beyond the relatively large temperature coefficient of the amide ^{1}H NMR chemical shift (Table 1), a negative cross peak in NOESY and ROESY spectra was detected. While a NOESY negative cross peak may also arise from a true dipolar interaction, the negative sign in the ROESY spectrum demonstrates the occurrence of exchange only. The ratio of the cross peak to the Leu−NH diagonal peak intensity decreases almost linearly with increasing values of the mixing time, t_m (Figure 1). The surprisingly high temperature coefficient had been previously interpreted in terms of a solvent-shielded ("caged") but not hydrogen-bonded amide proton.[5−8] The remaining amide hydrogens display temperature coefficients typical of solvent-exposed protons. However, the negative cross peaks in the NOESY and ROESY spectra show slow exchange between the *syn* and *anti* protons of Gly−NH_2.

Table 1. ^{1}H NMR chemical shifts and temperature coefficients of amide protons measured for melanostatin 2.5 mM in [D_6]DMSO/water in the absence and in the presence of [Ca^{2+}] = 25 mM

Peak	δ (ppm)	Δδ/ΔT (ppm/K)[a] [Ca^{2+}] = 0 mM	[Ca^{2+}] = 25 mM
Gly−NH	8.21	−0.0050	−0.0048
Leu−NH	8.09	−0.0022	−0.0019
Gly−NH_2 (*anti*)	7.23	−0.0044	−0.0026
Gly−NH_2 (*syn*)	7.03	−0.0040	−0.0034

[a] Errors in the calculated coefficients were evaluated at ±2−3%.

 © WILEY-VCH Verlag GmbH, D-69451 Weinheim, 2000 1434−1948/00/0808−1699 $ 17.50+.50/0

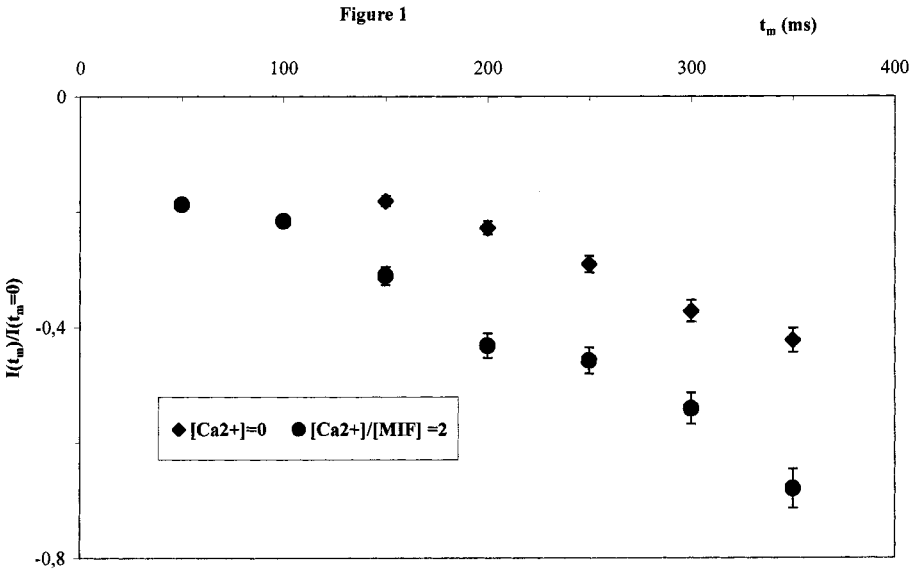


Figure 1. Intensities of the Leu−NH-water normalized exchange cross peak vs. the mixing time measured in NOESY experiments on melanostatin 2.5 mM in [D_6]DMSO/water (1%) in the absence and in the presence of Ca^{2+} 25 mM; T = 298 ± 0.1 K

Upon addition of calcium up to a ratio of [Ca^{2+}]/[MIF] = 20, several spectroscopic features were observed demonstrating formation of a 1:1 complex that substantially modifies the exchange network of the peptide with bulk water.

^{1}H and ^{13}C NMR Chemical Shifts

Both carbonyls (Figure 2 and Figure 3) and amide protons (Figure 4) were selectively affected allowing identification of the metal coordinating groups and evaluation of the dissociation constant of the complex. The Pro- and Gly-carbonyls were the most affected by the metal ion and were therefore assigned as the binding groups. It is interesting to note that two ^{13}C resonances were resolved for the Leu-carbonyl in the bound state, where the less intense of the two shifted downfield substantially. These findings seem to suggest the occurrence of a minor species, in slow chemical exchange with the major one, where the Leu-carbonyl is bound to calcium together with the Gly- or, alternatively, the Pro- carbonyls.

The titration of chemical shifts was preferably accomplished by using ^{1}H NMR spectroscopic data on amide protons that allowed several points to be obtained in a reasonable time. The exponential curves, shown in Figure 4, could be fitted to the following 1:1 binding equation [Equation (1)]with the standard regression procedure already described[13,14]

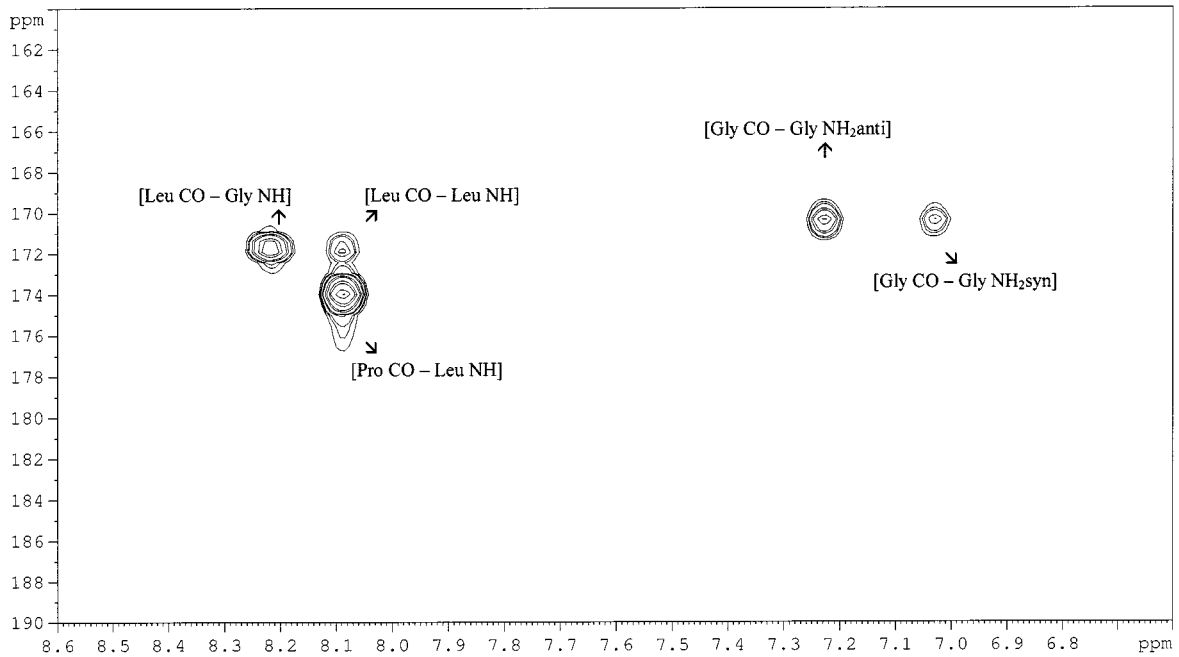


Figure 2. Low-field region of the HMBC spectrum of melanostatin 2.5 mM in [D_6]DMSO/water (1%); T = 298 ± 0.1 K

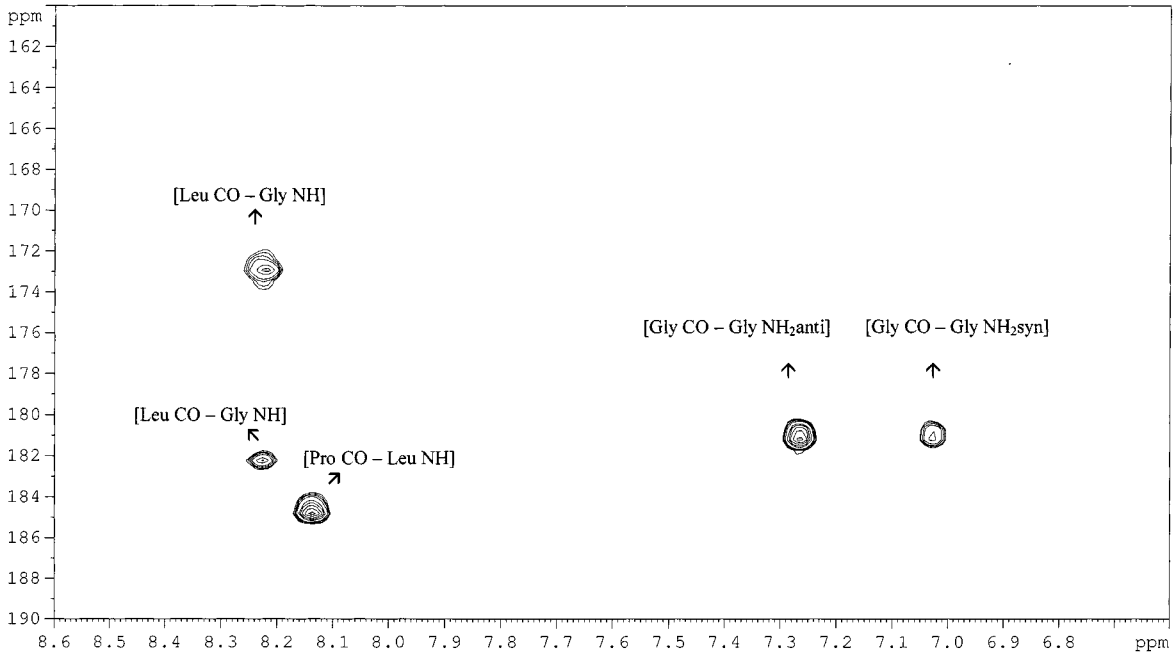


Figure 3. Low-field region of the HMBC spectrum of melanostatin 2.5 mM − Ca^{2+} 25 mM in [D_6]DMSO/water (1%); T = 298 ± 0.1 K

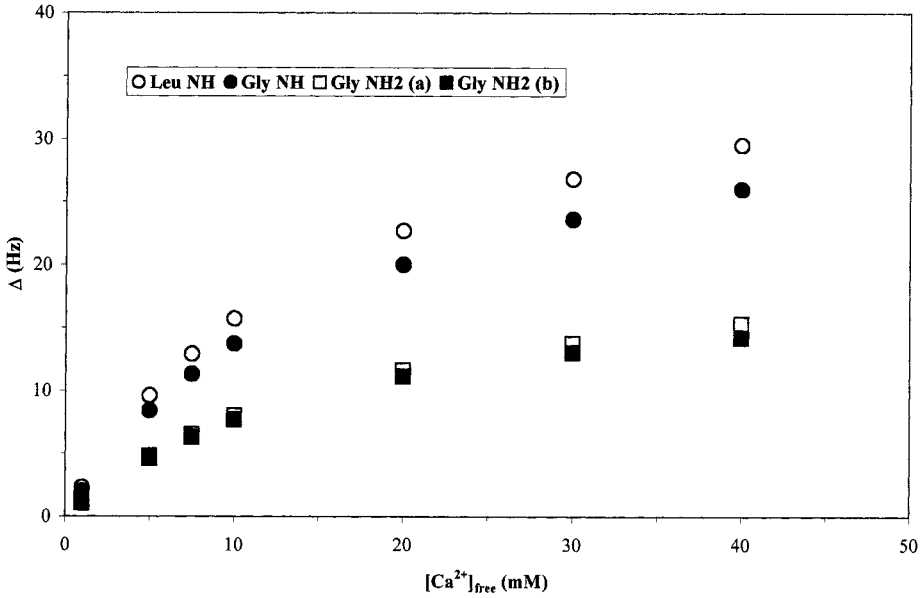


Figure 4. ^{1}H NMR downfield chemical shift changes of amide protons of melanostatin 2.5 mM in [D_6]DMSO/water (1%) vs. calcium concentration; T = 298 ± 0.1 K

$$\Delta = \Delta_0 \frac{[Ca^{2+}]_{free}}{K_d + [Ca^{2+}]_{free}} \quad (1)$$

$$\frac{\bar{\upsilon}}{[MIF]_{total}} = \frac{n}{K_d} - \frac{\bar{\upsilon}}{K_d} \quad (2)$$

where Δ is the actual change in chemical shift, Δ_0 the same change in chemical shift at the *plateau*, and K_d is the dissociation constant from the metal complex. By considering all data, K_d values in the range 0.15−0.20 mM were obtained at constant ionic strength (I = 150 mM). A Scatchard plot (not shown) was also obtained by using the experimental chemical shifts for Leu-NH and the relation shown in Equation (2)[13] where $\tilde{\upsilon}$ is the molar concentration ratio [MIF]/[Ca^{2+}] × Δ/Δ_0, $\tilde{\upsilon}/[MIF]_{total} = \Delta/(\Delta_0 - \Delta)[Ca^{2+}]_{total}$ and n is the stoichiometry of the complex. The slope and intercept from the graph of $\tilde{\upsilon}/[MIF]_{total}$ vs. $\tilde{\upsilon}$ are −5550.1 ± 11.1 and 5820.4 ± 10.6, respectively. As a consequence, the estimated values of K_d and n are ≈0.18 mM and 1, respectively. The fact that the 1:1 complex shows up as the predominant species in solution does not exclude the occurrence of different complexes in fast exchange on the NMR timescale.

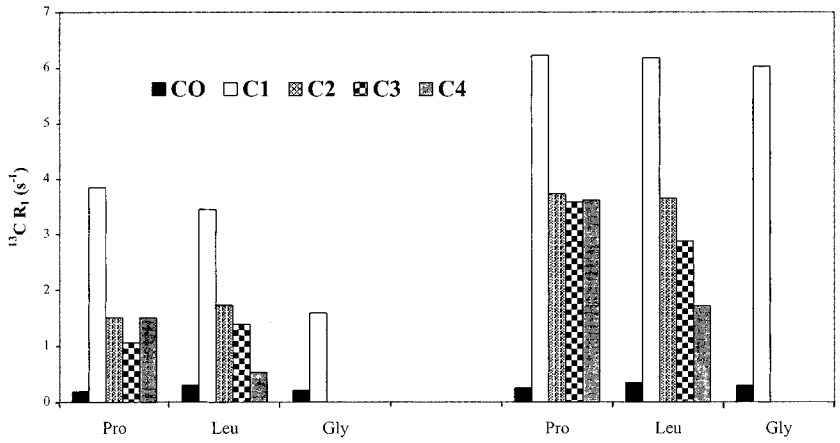


Figure 5. ^{13}C NMR spin-lattice relaxation rates of melanostatin 2.5 mM in [D$_6$]DMSO/water (1%) (left) and melanostatin 2.5 mM – Ca^{2+} 25 mM in [D$_6$]DMSO/water (1%) (right). T = 298 ± 0.1 K. Rates of protonated carbons were normalized with the number of attached protons.

^{1}H and ^{13}C NMR Spin-Lattice Relaxation Rates

Measuring ^{13}C spin-lattice relaxation rates at [Ca^{2+}]/[MIF] = 2 (Figure 5) provided the following information. In the free state, the backbone α carbons (C1 in Figure 5) display different normalized rates (R_1/n_H, where n_H is the number of protons attached to the considered carbon) and the Pro and Leu residues are characterized by the expected internal flexibility. In the calcium complex all relaxation rates are faster and, moreover, the backbone carbons are relaxed with similar rate constants and flexibility somehow reduced. The largest enhancement of relaxation rate is therefore measured for the Gly-methylene that, in the free state, was modulated by effective correlation times shorter than the other backbone carbons.

In the same manner all proton spin-lattice relaxation rates were progressively enhanced by increasing the concentration of calcium (the effect on amide protons is shown in Figure 6). In ^{13}C NMR spectroscopy the spin-lattice relaxation rates are usually determined by the dipole-dipole interaction with attached protons at a fixed distance (r_{CH} = 0.109 nm). This differs from the case of the ^{1}H nuclear spin where relaxation mainly occurs by dipole–dipole interactions with all other surrounding protons either at fixed or time-dependent distances [Equation (3)][15,16]

$$R_{1i} = \sum_{j\neq i}\rho_{ij} + \sum_{j\neq i}\sigma_{ij} + \rho_i^* \qquad (3)$$

where ρ_i* accounts for eventual mechanisms other than the dipole–dipole and ρ_{ij} and σ_{ij} are given by Equation (4)[16,17] where the interaction between any two protons i and j is averaged among all the accessible N configurations, the kth one of them being characterized by the internuclear distance r_k and the existential probability P_k. All other terms have the usual meaning: γ_H is the proton magnetogyric ratio, ω_H is the proton Larmor frequency, h is the reduced Planck constant and τ_c is the motional correlation

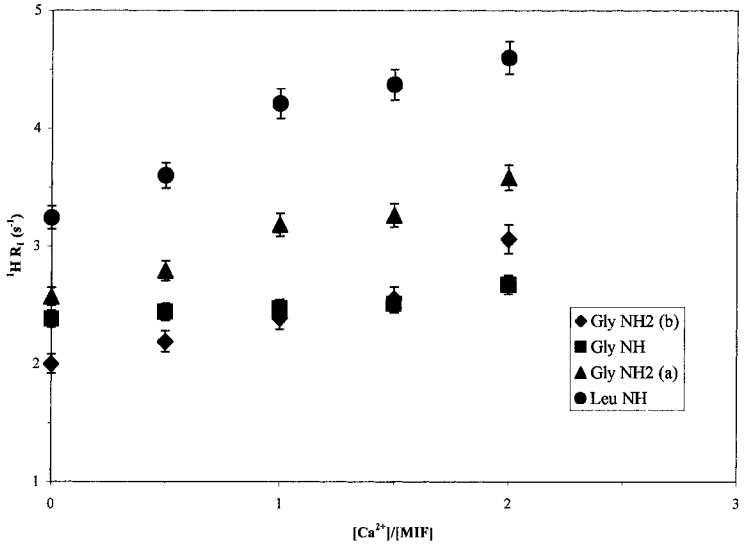


Figure 6. ^{1}H NMR spin-lattice relaxation rates of amide protons of melanostatin 2.5 mM in [D$_6$]DMSO/water (1%) vs. calcium concentration; T = 298 ± 0.1 K

$$\rho_{ij} = \frac{1}{10}\gamma_H^4\hbar^2\left\{\frac{3\tau_c}{1+\omega_H^2\tau_c^2} + \frac{6\tau_c}{1+4\omega_H^2\tau_c^2} + \tau_c\right\}\sum_{k=1}^{N}\frac{P_k}{r_k^6}$$

$$\sigma_{ij} = \frac{1}{10}\gamma_H^4\hbar^2\left\{\frac{6\tau_c}{1+4\omega_H^2\tau_c^2} - \tau_c\right\}\sum_{k=1}^{N}\frac{P_k}{r_k^6} \quad (4)$$

time. As a consequence, while the calcium-induced enhancement of ^{13}C relaxation rates can be suitably interpreted in terms of lengthened effective correlation times (vide infra), the same may not hold for protons, where changes in the number of interacting protons, internuclear distances or in ρ_i* may also be effective.

Selective (R_1^{sel}) and double selective ($R_1^{i,k}$) proton spin-lattice relaxation rates were therefore measured in order to better delineate the observed calcium induced effects. It is in fact well known that[15,18]

$$R_{1i}^{sel} = \sum_{j\neq i}\rho_{ij} + \rho_i^*$$

$$R_{1i}^{i,k} = \sum_{j\neq i}\rho_{ij} + \rho_i^* + \sigma_{ik} \quad (5)$$

Table 2. ^1H NMR relaxation rates of amide protons measured for melanostatin 2.5 mM in [D_6]DMSO/water in the absence and in the presence of [Ca^{2+}] = 25 mM

Peak	[Ca^{2+}] = 0 mM R_1/R_1^{sel}	$\sigma_{ij}\{H_j\}$ (s^{-1})	[Ca^{2+}] = 25 mM R_1/R_1^{sel}	$\sigma_{ij}\{H_j\}$ (s^{-1})
Gly−NH	1.36	----	1.09	----
Leu−NH	1.10	0.14 {Leu H_α}	1.01	−0.22 {Leu Hα}
Gly−NH_2 (*anti*)	0.59	−1.62 {Gly−NH_2}	0.62	−1.42 {Gly−NH_2}
Gly−NH_2 (*syn*)	0.64	−1.58 {Gly−NH_2}	0.66	−1.36 {Gly−NH_2}

Once measured, the new parameters (shown in Table 2) were used to delineate the effects of calcium on motional correlation times and ρ_i* through the evaluation of the ratio of nonselective to selective relaxation rates as well as on any dipole−dipole relaxation term of a proton pair σ_{ik} [Equation (6)]

$$\frac{R_{1i}}{R_{1i}^{sel}} = \frac{\sum_{j\neq i}\rho_{ij} + \sum_{j\neq i}\sigma_{ij} + \rho_i^*}{\sum_{j\neq i}\rho_{ij} + \rho_i^*} \quad (6)$$

$$\sigma_{ik} = R_{1i}^{i,k} - R_{1i}^{sel} = \sigma_{ki} = R_{1k}^{i,k} - R_{1k}^{sel}$$

The decrease of R_1/R_1^{sel} confirms that binding to calcium implies slowing down of molecular motions although different ρ_i* contributions to the relaxation pathway in the free and metal-bound states may also occur. As in the case of spin-lattice relaxation of carbons, the most affected is Gly-H_α which is thus verified to experience the largest reduction in mobility. The two obtained dipolar relaxation terms, $\sigma_{NH_2(a)-NH_2(b)}$ (−1.42 s^{-1} in the free and −1.34 s^{-1} in the metal-bound state) and $\sigma_{LeuNH-LeuH_\alpha}$, (+0.14 s^{-1} in the free and +0.05 s^{-1} in the metal-bound state), suggest that intramolecular chemical exchange provides the main relaxation mechanism for the Gly-NH_2 protons (negative σ's are obtained at each correlation time) and again that the motional correlation time in the bound state may be longer than in the free state; the dipolar relaxation rate, σ, in fact decreases and eventually becomes negative at increasing τ_c. However, any change in conformation yielding longer distances may reduce the observed rate. It is concluded that proton relaxation rates strongly suggest that binding to calcium reduces the motional flexibility of melanostatin, although other effects, namely a change in the relaxation mechanism and/or in internuclear distances, cannot be ruled out.

Temperature Dependence of Amide ^1H Chemical Shifts

The surprisingly high temperature coefficient of Leu-NH (Table 1) has been previously noticed and interpreted in terms of a solvent shielded but not hydrogen-bonded amide proton. The other three protons display coefficients typical of solvent exposed protons. However, upon addition of calcium, all coefficients are progressively enhanced, especially that of the low field Gly-NH_2 proton (from −4.4 ppb/K to −2.6 ppb/K).

^1H 2D NOESY Experiments

NOESY experiments were run for the free and calcium-bound peptide at several mixing times, t_m, in the range 50−600 ms. Beyond the positive ones, the following proton pairs displayed negative exchange cross peaks in the free state with increasing volumes at increasing t_m:

(i) the *syn* and *anti* protons within the Gly-NH_2 moiety;

(ii) Leu-NH and the residual water signal (Figure 1).

This last cross peak was analyzed by considering the following exchange matrix governing the mixing process [Equation (7)][19]

$$\hat{L} = \begin{pmatrix} \left(-R_{NH}^{sel} - \rho_{NH}^* - x_{H_2O}k\right) & -x_{MIF}\left(\sigma_{NH-H_2O} - k\right) \\ -x_{H_2O}\left(\sigma_{NH-H_2O} - k\right) & \left(-R_{H_2O}^{sel} - \rho_{H_2O}^* - x_{MIF}k\right) \end{pmatrix} \quad (7)$$

where the x are mol fractions and k is the exchange rate. By considering that $R_{NH}^{sel} >> R_{H_2O}^{sel}$, ρ_{NH}* << R_{NH}^{sel}, ρ_{H_2O}* << R_{NH}^{sel}, $x_{H_2O} >> x_{MIF}$, $\sigma_{NH-H_2O} << k$, Equations 8−10 were obtained for diagonal and cross peak coefficients as a function of the mixing time[19]

$$a_{NH}(t_m) = x_{MIF}e^{-\delta t_m}\left\{\cosh(Dt_m) - \frac{\delta}{D}\sinh(Dt_m)\right\}$$

$$a_{NH-H_2O}(t_m) = x_{MIF}\frac{k}{D}e^{-\delta t_m}\sinh(Dt_m) \quad (8)$$

with

$$\delta = \frac{1}{2}\left(R_{NH}^{sel} + k\right)$$

$$D = \frac{1}{\sqrt{2}}\left(R_{NH}^{sel} + k\right) \quad (9)$$

It follows that the ratio between the intensities of cross- and diagonal peaks is given by:

$$\frac{I_{NH-H_2O}}{I_{NH}} = \frac{k\sqrt{2}}{R_{NH}^{sel} + k} \frac{\sinh\left\{\frac{1}{\sqrt{2}}\left(R_{NH}^{sel} + k\right)t_m\right\}}{\cosh\left\{\frac{1}{\sqrt{2}}\left(R_{NH}^{sel} + k\right)t_m\right\} - \frac{\sqrt{2}}{2}\sinh\left\{\frac{1}{\sqrt{2}}\left(R_{NH}^{sel} + k\right)t_m\right\}} \quad (10)$$

which is an almost linear function of I_c/I_d vs. t_m at constant values of k and R_{NH}^{sel}. Interestingly, as shown in Figure 1, in the calcium-bound state the intensity of the water-Leu-NH cross peak at any value of t_m was rather enhanced, while that of the other exchange peak was reduced. Analysis of the reported equation allowed two inferences, (i) $k > R$ determines that the intensity ratio almost uniquely depends upon t_m; (ii) $k < R$ yields enhancements of the intensity ratio when increasing either k or R, or both. However, the effect of increasing k (at constant R) can be calculated to overwhelm that of increasing R (at constant k). This seems to suggest that the main, but not the only, cause of the observed phenomena is to be sought in a substantial change in the proton exchange rates between the involved environments.

Conclusion

Melanostatin is a small flexible molecule that, upon binding to calcium, undergoes several NMR spectroscopically detectable changes. The main species is a 1:1 complex with Pro- and Gly- carbonyls bound to the metal ion with $K_d \approx 0.16$ mM. Minor species bound through the Leu-carbonyl were also detected (Figure 7 and Figure 8). Metal chelation brings about a sizeable increase in effective motional correlation times, modulating reorientational motions of almost all carbon-proton and proton-proton dipole-dipole vectors as deduced by the enhanced ^{13}C and ^{1}H NMR relaxation rates. Moreover, the degrees of internal flexibility are reduced and the peptide is somehow forced to assume a single conformation. The most interesting feature of the complex is the change in the intensities of exchange cross peaks. It may be speculated that in the free state, reorientational motions transiently destroy the interaction with water. In the metal-bound state the Leu-amide proton enters the proton exchange network of the flexible coordination sphere of calcium. It is hydrogen-bonded to a coordinated water molecule that rapidly exchanges with bulk solvent. That this might be the case is ratified by the enhanced temperature coefficient of the involved amide proton. In the same way the large increase in the same coefficient of the low-field Gly-amide proton suggests that the same occurs for one of the NH_2 protons, thus reducing the rate of intramolecular exchange connected to damped rotation around the C−N bond. For better delineation of structure and dynamics, the motional correlation time of the calcium complex was calculated by considering the following:

(i) the ^{13}C NMR spin lattice relaxation rates ($\tau_c = 0.11 \pm 0.07$ ns at 298 K)

(ii) the proton dipolar relaxation rate $\sigma_{LeuNH-LeuH\alpha}$ at two different frequencies ($\tau_c = 0.14 \pm 0.08$ ns at 298 K).

$\tau_c = 0.12$ ns was then used to evaluate $r_{LeuNH-LeuH\alpha}$ at 0.261 ± 0.012 nm. Other constraints were not necessary to generate the models of the complexes (shown in Figure 7 and Figure 8) by using the AMBER force field within the HYPERCHEM software package. In this figure, four of the low conformational energy structures are superimposed onto the major complex, in order to show that the structure of the Leu side chain is ill-defined; whereas the rest of the molecule is structurally well defined, especially around the

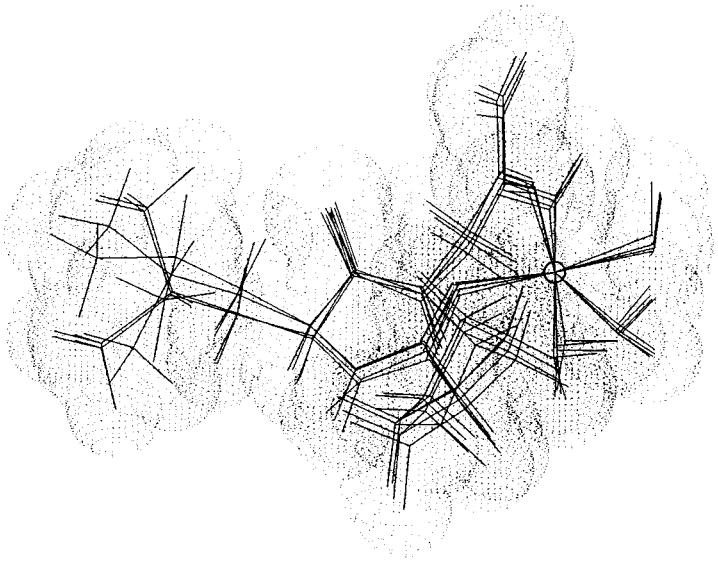


Figure 7. Superimposed stick models of four low energy structures of the main calcium-melanostatin 1:1 complex in [D_6]DMSO/water (1%); the calcium ion is circled and highlighted

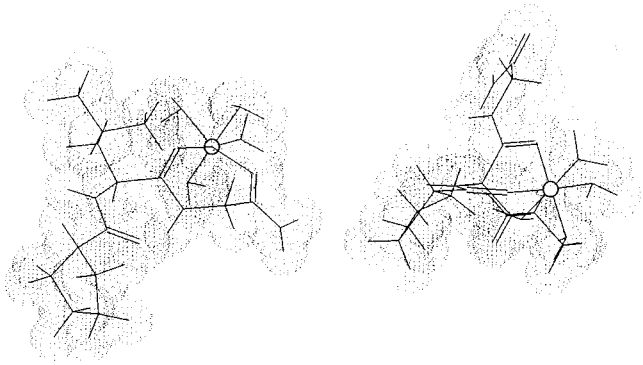


Figure 8. Stick models of low energy structures of the minor calcium-melanostatin 1:1 complexes in [D_6]DMSO/water (1%); calcium ions are circled and highlighted

metal ion (the RMSD value, calculated over the backbone atoms, was 0.06 nm).

The observed phenomena may be relevant for the biological role of calcium. Exchange of amide protons in proteins and peptides is in fact closely related to secondary and tertiary structures in solution, being the three-dimensional arrangement of any biological molecule ultimately associated with water. Backbone and side-chain hydration is a dominant factor in the stabilization of the structure, and in the process of backbone folding. It also plays an essential role in substrate binding and the mechanism of peptide and protein mediated reactions. Water diminishes charge-charge interactions and, in many proteins, has the integral role of filling cavities. Water molecules surround the molecular surface and the exchange with bulk water determines the kinetics of substrate binding or aggregation processes.

NMR 1D or 2D methods have been thoroughly exploited in discriminating solvent shielded vs. solvent exposed exchangeable protons in proteins and peptides. Exchange rates of individual amide protons in the range from reciprocal milliseconds to reciprocal months have been determined. Changes in the exchange network of backbone and side-chain protons have been consequently interpreted as demonstrating structural changes following either binding of substrates, cofactors, metal ions etc. or induced aggregation. What has been observed for melanostatin leads us to conclude that exchange rates may also be modulated by the intervention of hydration spheres of coordinated metal ions.

Experimental Section

MIF was obtained from Sigma Chemical Co. Purity of the peptide was assessed from NMR spectra and no further purification was required. Calcium perchlorate, also obtained from Sigma Chemical Co., was dried over P_2O_5 for several hours before use. Solutions were made in [D_6]DMSO containing water (1%) and were carefully deoxygenated through a freezing-sealing-thawing procedure. NMR spectroscopic experiments were carried out at 4.7 T (Varian VXR 200) and 14.1 T (Bruker Avance 600) at temperatures controlled to ± 0.1 K. Chemical shifts were referenced to internal [D_4]-trimethylsilylpropane sulfonate ([D4]TSP). NOESY experiments were carried out with standard pulse sequences at different values of the mixing time (in the range 50−600 ms). ROESY experiments were obtained at mixing times in the range 50−100 ms with the r.f. strength for the spin-lock field at values < 3.5 kHz. 2D ^{1}H-^{13}C shift correlation methods were used to detect and assign ^{13}C NMR spectra at relatively low concentration. Both ^{1}H-detected heteronuclear multiple-quantum coherence (HMQC) and ^{1}H-detected multiple-bond heteronuclear multiple-quantum coherence (HMBC) spectra were obtained with standard pulse sequences. Proton spin-lattice relaxation rates were measured with inversion recovery pulse-sequences using either non-selective, single-selective or double-selective π pulses. The rates were calculated with regression analysis of the initial decay curves of longitudinal magnetization components leading to errors in the range ±3%. Two sets of calcium titrations were performed at constant ionic strength (I = 150 mM). An approximate measure of K_d was obtained in the first set without maintaining a constant concentration of MIF.. In the second set, the peptide was added to Ca^{2+} solution to maintain a constant concentration of MIF in each NMR sample. Standard regression analysis was used to fit curves to the data by using the following equation:

$$\Delta = \Delta_0 [Ca^{2+}]_{free}/\{K_d + [Ca^{2+}]_{free}\}$$

The experimental calcium concentration was corrected thus:

$$[Ca^{2+}]_{free} = [Ca^{2+}]_{total} - [MIF]\ \Delta/\Delta_0$$

where Δ/Δ_0 is the fractional change in the chemical shift of the observed proton.[13,14]

[1] E. Gaggelli, G. Valensin, *J. Chem. Soc., Perkin Trans. 2* **1990**, 401−406.
[2] E. Gaggelli, N. Gaggelli, G. Valensin, A. Maccotta, *Bull. Magn. Reson.* **1992**, *14*, 302−306.
[3] M. Delfini, E. Gaggelli, G. Valensin, *Curr. Top. Pept. Prot. Res.* **1994**, *1*, 375−385.
[4] E. Gaggelli, N. D'Amelio, A. Maccotta, G. Valensin, *Eur. J. Biochem.* **1999**, *262*, 268−276.
[5] L. L. Reed, P. L. Johnson, *J. Am. Chem. Soc.* **1973**, *95*, 7523−7524.
[6] R. Deslauriers, R. Walter, I. C. P. Smith, *FEBS Letters* **1973**, *37*, 27−32.
[7] J. R. Garbow, C. A. McWherter, *J. Am. Chem. Soc.* **1993**, *115*, 238−244.
[8] Y. U. Sasidhar, M. M. Dhingra, A. Saran, *Indian J. Biochem. Biophys.* **1990**, *27*, 69−75.
[9] R. M. Nair, A. J. Kastin, A. V. Schally, *Biochem. Biophys. Res. Comm.* **1971**, *43*, 1376−1381.

[10] R. K. Mishra, S. Chius, P. Chiu, C. P. Mishra, *Methods Find. Exp. Clin. Pharmacol.* **1983**, *5*, 203−233.
[11] A. V. Schally, A. J. Kastin, *Endocrinology* **1966**, *79*, 768−772.
[12] M. E. Celis, S. Taleisnik, R. Walter, *Proc. Natl. Acad. Sci. USA* **1971**, *68*, 1428−1433.
[13] J. Reuben, *J. Am. Chem. Soc.* **1973**, *95*, 3534−3539.
[14] C. K. Vishwanath, K. R. K. Easwaran, *Biochemistry* **1981**, *20*, 2018−2023.
[15] R. Freeman, H. D. W. Hill, B. L. Tomlinson, L. D. Hall, *J. Chem. Phys.* **1974**, *61*, 4466−4473.
[16] J. H. Noggle, R. E. Schirmer, *The Nuclear Overhauser Effect* Academic Press, New York, **1971**.
[17] J. Tropp, *J. Chem. Phys.* **1980**, *72*, 6035−6043.
[18] L. D. Hall, H. D. W. Hill, *J. Am. Chem. Soc.* **1976**, *98*, 1269−1270.
[19] J. Jeener, B. H. Meier, P. Bachmann, R. R. Ernst, *J. Chem. Phys.* **1979**, *71*, 4546−4553.

Received November 11, 1999
[I99374]

Synthesis, Structural Characterisation and Electrochemical Studies of Neutral Alkenylcarbyne Tungsten Complexes Bearing Chelating Bidentate and Tridentate Phosphanes

Lei Zhang,[a,b] M. Pilar Gamasa,[a] José Gimeno,*[a] M. Fátima C. Guedes da Silva,[b,c] Armando J. L. Pombeiro,[b] Claudia Graiff,[d] Maurizio Lanfranchi,[d] and Antonio Tiripicchio[d]

Keywords: Carbyne complexes / Alkenylcarbyne / Tungsten / Electrochemistry / Phosphanes

Neutral alkenylcarbyne complexes [X = SCN; *n* = 1 (**2a**), 4 (**2b**). X = OCN; *n* = 1 (**2c**), 4 (**2d**)] were prepared by reaction of the acetonitrile complexes [*n* = 1 (**1a**), 4 (**1b**)] with M[OCN] or M[SCN] (M = Na, K, Bu_4N), and were fully characterised. The synthesis of complex **3**, containing the tridentate phosphane triphos [triphos = $PPh(CH_2CH_2PPh_2)_2$], is also described. The structures of **2b** and **3** were determined by X-ray diffraction methods. In both complexes, the coordination of the W atom was octahedral, with the N-bonded thiocyanate (**2b**) or the chlorine (**3**) anions *trans* to the alkenylcarbyne group. The W–N and W–Cl bond lengths were significant longer than the average found in the literature; this indicates the remarkable *trans* influence of the alkenylcarbyne moiety. The electrochemical behaviour of complexes **2a**–**d** and **3**, as well as that of the related compounds **D** (**2e**: X = F, *n* = 4), (**2f**: X = Cl, *n* = 1), (**2g**: X = $S_2P(OEt)_2$, *n* = 1) and **A** (**4**: *n* = 1) was investigated by cyclic voltammetry (CV) and controlled potential electrolysis (CPE) in aprotic media and at a Pt electrode. They underwent irreversible anodic and cathodic processes, the former usually being multi-electronic in the time scale of CPE and involving anodically induced proton dissociation from the alkenylcarbynes. These ligands behave as remarkably strong π-electron acceptors and from the linear relationship between the oxidation potential of the first anodic wave and the electrochemical P_L ligand parameter, it was possible to estimate, for the first time for a carbyne-containing metal centre, that is, the site {(dppe)$(CO)_2$W≡C–R}, the values of the electrochemical electron richness (E_s) and the polarisability (β) parameters. These values indicate that this site has low electron richness and low polarisability; this is accounted for by the extensive π-electron acceptance of the alkenylcarbyne ligand. P_L was also estimated for the $S_2P(OEt)_2^-$ ligand, which was shown to act as a rather strong net electron releaser.

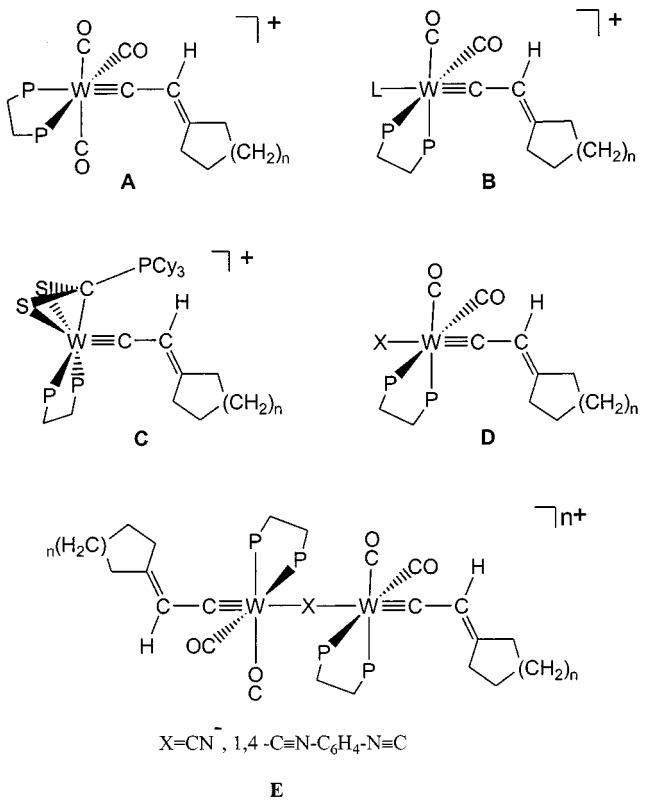
Introduction

We have recently reported a systematic methodology for the synthesis of Fischer-type alkenylcarbyne tungsten complexes, which has led to the preparation of a large series of cationic **A**, **B** (L = PMe_3, MeCN), and **C**, and neutral **D** [X = F, Cl, Br, I, CN, κ^1-(*S*)-$S_2P(OEt)_2$] derivatives[1−3] (Scheme 1). Furthermore, we have also studied[3] the synthesis and electrochemical behaviour of dinuclear complexes containing cyanide and diisocyanide bridging ligands **E** [X = CN, 1,4-$(CN)_2C_6H_4$], which are readily generated from the reaction of the labile cationic complexes **B** (L = MeCN) with complexes **D** (X = CN) or the bidentate diisocyanide ligand 1,4-$(CN)_2C_6H_4$. Complexes **E** are unusual examples of dimetallic species bearing long π-conjugated electronic chains involving two terminal α,β-unsaturated carbyne moieties. Molecular systems of this type, containing metallic fragments and extended organic π-systems linked by metal−carbon multiple bonds, are attracting increasing interest. Continuing our work in this field, we were interested to explore the synthesis of novel carbyne complexes displaying related conjugated electronic systems. Since electrochemical studies on metal−carbyne derivatives are rather scarce,[3−8] the synthesis of novel complexes would provide further study subjects for developing the knowledge on the electrochemical behaviour of these types of derivatives, as well as on the electron donor/acceptor character of such ligands, and on the electronic properties of their binding metal centres.

We now report the synthesis and electrochemical studies of novel neutral derivatives of type **D** [dppe = κ^2-(*P,P*)-$Ph_2P(CH_2)_2PPh_2$; X = κ-(N)-SCN; *n* = 1 (**2a**), 4 (**2b**). X =

[a] Instituto Universitario de Química Organometálica "Enrique Moles" (Unidad Asociada al CSIC), Departamento de Química Orgánica e Inorgánica, Facultad de Química, Universidad de Oviedo,
E-33071 Oviedo, Spain
Fax: (internat.) +34-985/103446
E-mail: jgh@sauron.quimica.uniovi.es
[b] Centro de Química Estrutural, Complexo I, Instituto Superior Técnico,
Av. Rovisco Pais, P-1049-001 Lisbon, Portugal
Fax: (internat.) + 351-21/8464455,
E-mail: pombeiro@alfa.ist.utl.pt
[c] Universidade Lusófona de Humanidades e Tecnologias,
Av. Campo Grande 376, P-1749-024 Lisbon, Portugal
[d] Dipartimento di Chimica Generale ed Inorganica, Chimica Analitica, Chimica Fisica, Università di Parma, Centro di Studio per la Strutturistica Diffrattometrica del CNR,
I-43100 Parma, Italy
Fax: (internat.) + 39-0521/905557
E-mail: tiri@unipr.it

 © WILEY-VCH Verlag GmbH, D-69451 Weinheim, 2000 1434−1948/00/0808−1707 $ 17.50+.50/0



Scheme 1

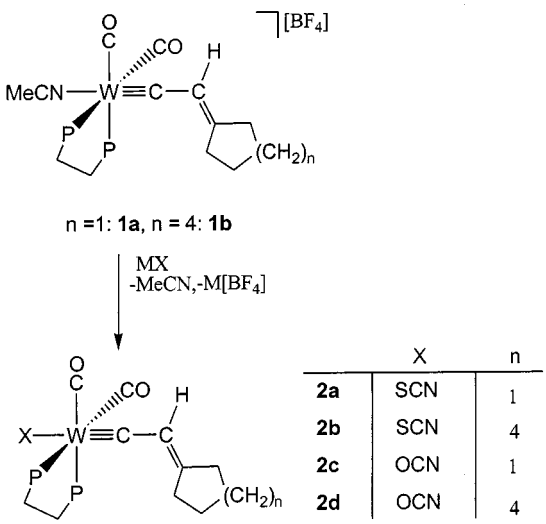
OCN; n = 1 (**2c**), 4 (**2d**)] and **3** (Schemes 2 and 3). The molecular structures of complexes **2b** and **3** were determined by X-ray diffraction. Electrochemical studies by cyclic voltammetry and of controlled potential electrolysis of these and related alkenylcarbyne complexes are also reported.

Results and Discussion

Synthesis and Characterisation of Complexes 2a−d

Complexes **2a−d** were prepared by the reaction of the labile acetonitrile complexes **1a**,**b** with an equimolar amount of KSCN or NaOCN in MeOH (Scheme 2). Alternatively, complexes **2a**,**b** were also formed from the treatment of **1a**,**b** with [Bu_4N][SCN] in CH_2Cl_2. After the resulting solutions were worked up, the desired carbyne complexes were isolated (80−90% yield) as yellow air-stable solids (see Experimental Section) and were characterised by elemental analysis and IR spectroscopy and ^{1}H-, ^{31}P{^{1}H}-, and ^{13}C{^{1}H}-NMR spectroscopy. In addition, the structure of **2b** was determined by X ray diffraction (see below).

The IR spectra (CH_2Cl_2) of **2a−d** contained two strong ν(CO) absorptions (Table 1), as expected for the presence of the *cis*-dicarbonyl arrangement, as also observed for the analogous halide derivatives.[1] Furthermore, IR spectra of **2a**,**b** displayed a very strong absorption at 2064 cm^{-1}, assigned to the CN stretching vibration of the SCN group in accord with most of the N-bonded thiocyanato complexes.[9] This coordination mode was confirmed by the X-



	X	n
2a	SCN	1
2b	SCN	4
2c	OCN	1
2d	OCN	4

Scheme 2

ray diffraction structural determination of **2b** (vide infra). Similarly, IR spectra of **2c**,**d** showed another strong absorption at 2212 cm^{-1}, as expected for ν_a(NCO) [consisting mainly of ν(CN) vibration].[9] Since the majority of the cyanato complexes are reported to be N-bonded, we tentatively assigned this linkage to complexes **2c**,**d**. Although the ν_s(NCO) vibration for such a type of linkage is expected to appear in the 1370−1300 cm^{-1} range,[10−11] only a weak band at 1335−1338 cm^{-1} was observed. Other pseudohalide N-bonded Fischer type carbyne complexes have been reported.[12]

The ^{31}P{^{1}H}-NMR spectra (Table 1) of **2a−d** displayed single resonances at ca. δ = 40, indicating the chemical equivalence of the phosphorus atoms of dppe in accordance with the proposed *trans* pseudohalide−carbyne arrangement. J(P-W) values of ca. 228 Hz are similar to those found for the analogous halide derivatives.[1] The ^{1}H-NMR spectra (Table 1) showed a broad signal at δ 4.97−5.00 for the alkenyl proton resonance (=C$_\beta$H−) of the cyclopentenyl derivatives (n = 1, **2a**,**c**), which was shifted to a higher field (δ 4.65−4.68) in cyclooctenyl analogues (n = 4, **2b**,**d**). ^{13}C{^{1}H}-NMR spectra (Table 2) were also consistent with the expected resonances in accord with the proposed formulations. In particular, the spectra showed typical carbyne carbon resonances as triplet signals at δ = 273.0−279.0 [^2J(C−P) = 10.0−10.6 Hz], in addition to the resonances for the C$_\beta$ and C$_\gamma$ nuclei of the alkenylcarbyne chain and the *cis*-dicarbonyl ligands, which appeared as a virtual doublet of doublets. The carbon resonance of the OCN group appeared as a singlet signal at δ 145.0, while that of the SCN group was overlapped by those of the aromatic groups.

We have reported[3] that the analogous cyanide carbyne derivatives of type **D** (X= CN; n = 1, 4) (Scheme 1) reacts with complexes **1a**,**b**, affording cyanide-bridged bis(alkenylcarbyne) dinuclear complexes of type **E** (X= CN) (Scheme 1). All attempts directed to the formation of analogous dinuclear μ-NCO and μ-NCS bridging complexes from the reactions of **2a−d** with a stoichiometric amount

Table 1. Selected IR and $^{31}P\{^1H\}$- and ^1H NMR data for the neutral alkenylcarbyne tungsten complexes **2a**–**d** and **3**

Complexes	IR[a] ν(CO)	ν(CN)	$^{31}P\{^1H\}$[b][c]	^1H[b] $C_\beta H$
2a	2001 (s), 1932 (vs)	2064 (vs)[d]	41.2 s (229.6)	4.97 s,br
2b	2000 (s), 1932 (vs)	2064 (vs)[d]	41.1 s (228.8)	4.65 s,br
2c	1997 (vs), 1927 (vs)	2212 (vs)[e]	39.8 s (227.9)	5.00 s,br
2d	1996 (vs), 1927 (vs)	2212 (vs)[e]	39.7 s (228.3)	4.68 s,br
3	1897 (vs)		84.1 t (8.6,[f] 201.0) 48.2 d (8.6,[f] 294.0)	4.94 s,br

[a] Spectra recorded in CH_2Cl_2, ν (cm^{-1}). Abbreviations: s, strong; vs, very strong. – [b] Spectra recorded in $CDCl_3$, δ in ppm, *J* in Hz. Abbreviations: s, singlet; d, doublet; t, triplet; br, broad. – [c] In parenthesis, *J*(P–W). – [d] ν(SCN). – [e] ν(OCN). – [f] *J*(P–P).

Table 2. Selected $^{13}C\{^1H\}$ NMR data for the neutral alkenylcarbyne tungsten complexes **2a**–**d** and **3**

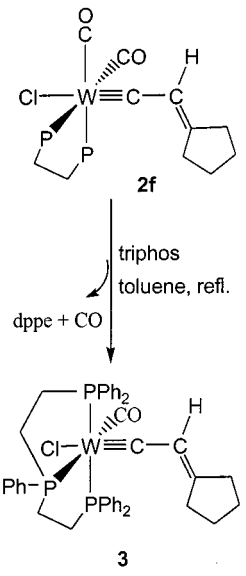
Complexes[a]	C_α [b]	C_β	C_γ[c]	CO[b]	YCN (Y=S,O)
2a	273.0 t (10.2)	[d]	162.6 t (3.2)	213.1 vdd (43.4, 6.8)	[d]
2b	273.1 t (10.3)	135.2 s	161.1 t (3.2)	213.3 vdd (43.5, 6.9)	[d]
2c	279.0 t (10.6)	[d]	164.5 t (3.3)	212.9 vdd (39.7, 6.1)	145.0 s
2d	278.8 t (10.0)	135.0 s	162.8 t (3.3)	212.9 vdd (40.1, 7.1)	145.0 s
3	270.6 dt (9.7, 8.8)	[d]	156.1 s	233.7 dt (88.0, 41.0)	

[a] Spectra recorded in $CDCl_3$, δ in ppm, *J* in Hz. Abbreviations: s, singlet; d, doublet; t, triplet; dd, doublet of doublet; dt, doublet of triplet; m, multiplet; v, virtual. – [b] Within parenthesis, ^2J(C–P). – [c] Within parenthesis, ^4J(C–P). – [d] Overlapped by aromatic carbon atoms.

of **1a**,**b** or the labile acetone complex *fac*-$[W(CO)_3(dppe)(Me_2CO)]$[1a,13] were unsuccessful. In all the cases, the starting complexes were recovered unchanged.

Synthesis and Characterisation of Complex 3

The reaction of an equimolar mixture of **2f**[1a] and triphos $[PPh(CH_2CH_2PPh_2)_2]$ in refluxing toluene led to the formation of **3**, which was isolated (75% yield) as an orange air-stable solid (Scheme 3). The reaction was monitored by IR spectroscopy in the carbonyl region and was allowed to proceed until the absorptions of the starting *cis*-dicarbonyl complex disappeared. The ^{31}P-NMR spectrum of the resulting solution revealed the presence of free dppe.



Scheme 3

Analytical and spectroscopic data (IR and NMR) of **3** supported this formulation and the structure was confirmed by an X-ray diffraction study (see below). Significantly, the IR spectrum (CH_2Cl_2) (Table 1), showed a strong ν(CO) absorption at 1897 cm^{-1} and the $^{13}C\{^1H\}$-NMR spectrum (Table 2) displayed the expected resonances for the alkenylcarbyne moiety and the carbonyl group. Thus, carbon carbyne resonances appeared as a doublet of triplet signal at δ = 270.6, characteristic of the AB_2X spin system with ^2J(C–P) values of 9.7 and 8.8 Hz arising from the presence in the *cis* positions of two sets of inequivalent phosphorus atoms of the triphos ligand. Carbonyl resonances appeared at δ = 233.7 [dt, ^2J(C–P) = 88.0 and 41.0 Hz], revealing the presence of one *trans* and two *cis* phosphorus nuclei. The $^{31}P\{^1H\}$-NMR spectrum (Table 1) was consistent with the triphos arrangement around the metal centre, showing the resonances typical of an AB_2 system [δ = 84.1 (t) and 48.2 (d), *J*(P–W) = 201 and 294 Hz, respectively]. The ^1H-NMR spectrum showed aromatic and proton resonances of the triphos as well as those of the alkenylcarbyne group (see Experimental Section).

X-ray Crystal Structures of Complexes 2b and 3

The structures of complexes **2b** and **3** are shown in Figure 1 and Figure 2 together with the atom numbering scheme. Selected bond lengths and angles are given in Table 3 and Table 4, respectively.

In both complexes, the W atom was coordinated as a distorted octahedron, with the two apical positions occupied by the C atom from the alkenylcarbyne ligand and by the N atom of the isothiocyanate group (**2b**) or by the Cl atom (**3**). In **2b** the coordination was completed by two P atoms from a chelating dppe ligand and by two carbonyl

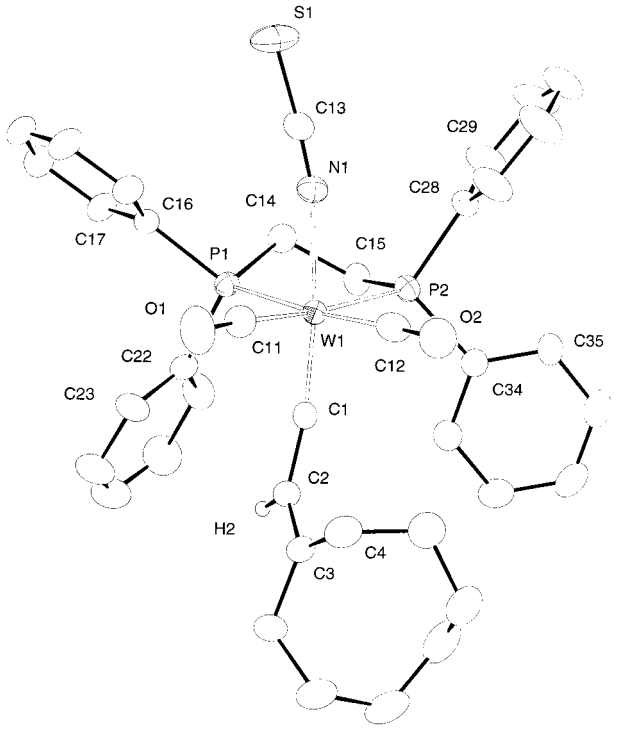


Figure 1. ORTEP view of the molecular structure of complex **2b**, with the atom-numbering scheme, the thermal ellipsoids are drawn at the 30% probability level

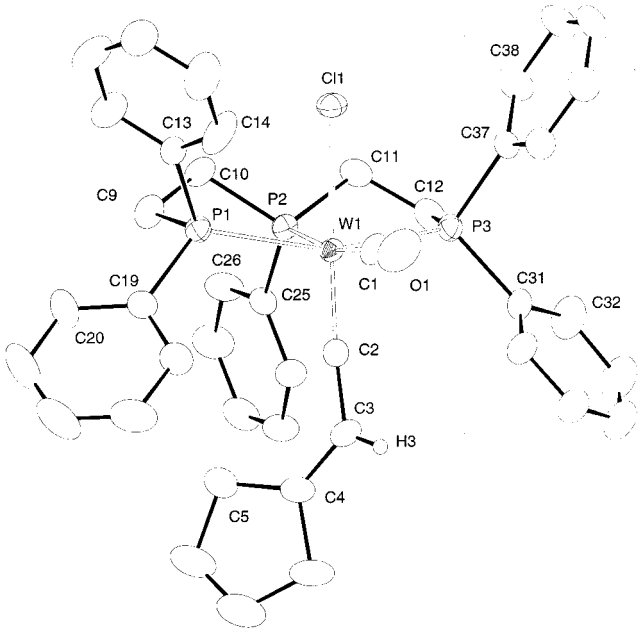


Figure 2. ORTEP view of the molecular structure of complex **3**, with the atom-numbering scheme, the thermal ellipsoids are drawn at the 30% probability level

groups, whereas in **3** the coordination was completed by three P atoms from the triphos ligand and by a carbonyl group. In **2b** the W atom was only slightly, 0.0780(4) Å, displaced from the mean plane through the four equatorial atoms pointing towards the carbyne carbon atom, whereas in **3** this deformation was much more enhanced, the W atom being displaced by 0.3535(3) Å. The W≡C bond

Table 3. Selected bond lengths [Å] and angles [°] for complex **2b**

W(1)−C(1)	1.848(5)	W(1)−N(1)	2.200(5)
W(1)−P(2)	2.533(1)	W(1)−P(1)	2.538(1)
S(1)−C(13)	1.627(7)	N(1)−C(13)	1.158(8)
C(1)−C(2)	1.427(7)	C(2)−C(3)	1.354(8)
C(3)−C(4)	1.510(11)	C(3)−C(10)	1.516(9)
C(4)−C(5)	1.515(11)	C(9)−C(10)	1.519(10)
C(5)−C(6)	1.538(11)	C(8)−C(9)	1.514(13)
C(6)−C(7)	1.523(14)	C(7)−C(8)	1.515(13)
P(1)−C(22)	1.826(6)	P(1)−C(14)	1.841(6)
P(1)−C(16)	1.834(6)	P(2)−C(28)	1.831(6)
P(2)−C(34)	1.836(6)	P(2)−C(15)	1.840(6)
O(1)−C(11)	1.141(8)	O(2)−C(12)	1.148(8)
C(1)−W(1)−N(1)	173.6(2)	C(13)−N(1)−W(1)	168.8(5)
C(1)−W(1)−C(11)	87.6(2)	C(1)−W(1)−C(12)	91.2(2)
C(11)−W(1)−C(12)	87.4(3)	C(11)−W(1)−N(1)	88.0(2)
C(12)−W(1)−N(1)	93.2(2)	C(1)−W(1)−P(2)	97.3(2)
C(11)−W(1)−P(2)	175.0(2)	C(12)−W(1)−P(2)	93.6(2)
N(1)−W(1)−P(2)	87.0(1)	C(1)−W(1)−P(1)	92.4(2)
C(11)−W(1)−P(1)	98.8(2)	C(12)−W(1)−P(1)	173.0(2)
N(1)−W(1)−P(1)	83.7(1)	P(2)−W(1)−P(1)	79.99(5)
C(2)−C(1)−W(1)	171.5(4)	C(3)−C(2)−C(1)	127.0(6)
C(2)−C(3)−C(4)	120.7(6)	C(2)−C(3)−C(10)	119.8(7)
C(4)−C(3)−C(10)	119.5(6)	N(1)−C(13)−S(1)	176.4(6)
C(3)−C(4)−C(5)	113.7(7)	C(4)−C(5)−C(6)	116.8(7)
C(5)−C(6)−C(7)	115.9(7)	C(8)−C(7)−C(6)	116.5(8)
C(7)−C(8)−C(9)	116.5(8)	C(10)−C(9)−C(8)	114.7(7)
C(3)−C(10)−C(9)	117.7(7)	O(2)−C(12)−W(1)	177.9(6)
O(1)−C(11)−W(1)	176.9(6)		

Table 4. Selected bond lengths [Å] and angles [°] for complex **3**

W(1)−C(2)	1.821(5)	W(1)−P(3)	2.473(2)
W(1)−P(2)	2.485(2)	W(1)−P(1)	2.488(2)
W(1)−Cl(1)	2.572(1)	C(2)−C(3)	1.446(7)
C(3)−C(4)	1.346(8)	W(1)−C(1)	2.009(6)
P(1)−C(19)	1.835(6)	P(3)−C(12)	1.856(6)
P(1)−C(13)	1.838(5)	P(3)−C(31)	1.854(6)
P(1)−C(9)	1.865(6)	P(3)−C(37)	1.833(5)
P(2)−C(25)	1.826(5)	P(2)−C(11)	1.841(5)
P(2)−C(10)	1.829(5)	C(9)−C(10)	1.527(8)
C(11)−C(12)	1.541(8)	C(4)−C(5)	1.501(8)
C(4)−C(8)	1.518(8)	C(7)−C(8)	1.466(11)
C(5)−C(6)	1.486(9)	C(6)−C(7)	1.405(12)
C(2)−W(1)−C(1)	87.9(2)	C(2)−W(1)−P(3)	97.6(2)
C(1)−W(1)−P(3)	96.3(2)	C(2)−W(1)−P(2)	102.0(1)
C(1)−W(1)−P(2)	169.7(2)	P(3)−W(1)−P(2)	79.95(6)
C(2)−W(1)−P(1)	100.9(2)	C(1)−W(1)−P(1)	100.6(2)
P(3)−W(1)−P(1)	155.18(5)	P(2)−W(1)−P(1)	80.22(6)
C(2)−W(1)−Cl(1)	177.3(1)	C(1)−W(1)−Cl(1)	90.3(2)
P(3)−W(1)−Cl(1)	80.53(5)	P(2)−W(1)−Cl(1)	79.65(5)
P(1)−W(1)−Cl(1)	81.36(5)	C(3)−C(2)−W(1)	172.9(4)
C(4)−C(3)−C(2)	128.7(6)	O(1)−C(1)−W(1)	178.0(5)
C(3)−C(4)−C(5)	127.1(5)	C(7)−C(8)−C(4)	105.0(7)
C(3)−C(4)−C(8)	125.4(6)	C(6)−C(7)−C(8)	110.4(7)
C(5)−C(4)−C(8)	107.6(6)	C(7)−C(6)−C(5)	109.2(8)
C(6)−C(5)−C(4)	105.5(6)		

lengths were 1.848(5) Å in **2b** and 1.821(5) Å in **3**, comparable to those found in analogous alkenyl−carbyne complexes.[1] As expected, a remarkable alkenylcarbyne *trans* influence can be envisaged: (a) The value of the W−N bond length in **2b**, 2.200(5) Å, is longer than the average (2.148 Å) found for 12 hexacoordinate tungsten complexes with terminal N-bonded thiocyanate ligands, and (b) The W−Cl bond length in **3**, 2.572(1) Å, is much longer than the average (2.388 Å) found for 80 hexacoordinate tungsten complexes with terminal chloride ligands. (From the Cam-

bridge Crystallographic Data Base). It is noteworthy that the W−P bond lengths in **2b** with the dppe ligand, 2.533(1) and 2.538(1) Å, are significantly longer than those found in **3** with the triphos ligand, 2.488(2), 2.485(2), and 2.473(2) Å.

Electrochemical Studies

The electrochemical behaviour of the alkenylcarbyne complexes **2a**−**2d**, **3** and, for comparative purposes, of the related compounds **2e**,[2] **2f**,[1a] **2g**,[1b] and **4**,[1a] in 0.2 mol dm^{-3} [NBu_4][BF_4]/NCMe (or THF), was studied by cyclic voltammetry (CV) and controlled potential electrolysis (CPE), at a Pt (or vitreous C) disk or a Pt-gauze electrode, respectively.

Table 5. Cyclic voltammetric data for the alkenylcarbyne complexes **2a**−**d**, **2e**−**g** (Type D: Scheme 1), **3** and **4** (n = 1; Type A: Scheme 1)

Compound	X	n	$^{I}E_{p/2}^{ox}$ ($^{I}E_{1/2}^{ox}$)[a]	$^{II}E_{p}^{ox}$ ($^{II}E_{1/2}^{ox}$)[a]	E_p^{red}
2a	SCN	1	1.04	1.20[b]	−1.93
2b	SCN	4	1.06	1.23[b]	−1.98
2c	OCN	1	0.85	(1.02)[b]	−2.17
2d	OCN	4	0.85	(1.01)[b]	−2.19
2e[c]	F	4	0.92	1.34	−1.57
					−1.93
2f[c]	Cl	1	0.82	1.33[b]	−2.22[d]
2g[c]	$S_2P(OEt)_2$	1	0.69	−	−1.61[e]
					−2.07
3		1	(0.32)	0.59	−
4[c]		1	1.78	−	−1.08

[a] Potentials (peak potential E_p or half-peak potential $E_{p/2}^{ox}$ for the irreversible processes, or, in brackets, half-wave potential $E_{1/2}^{ox}$ for the reversible ones) in Volt ± 0.02 vs. SCE measured in 0.2 mol dm^{-3} [NBu_4][BF_4]/NCMe at a scan rate of 0.2 V s^{-1}, at a Pt disc (d = 0.5 mm) electrode, unless stated otherwise. [b] With a decreasing current intensity, relatively to the first anodic wave, upon increasing scan rate. [c] Included for comparison (electrochemical behavior investigated in this study): **2e**,[2] **2f**,[1a] **2g**,[1b] **4**.[1a] − [d] In THF. − [e] Broad and with a relatively low current-intensity.

Complexes **2** and **4** underwent, by CV (Table 5), one irreversible anodic wave (I) ($^{I}E_{p/2}^{ox}$ in the range 0.7−1.1 V vs. SCE for **2**, or 1.78 V for **4**), $^{I}E_{p/2}^{ox}$ which was usually followed, at a higher potential (ca. 1.0−1.3 V for **2**), by a second one (II) which was, however, not detected for **4**, conceivably being buried under the solvent/electrolyte discharge. An irreversible cathodic wave was also detected at E_p^{red} in the range −1.6 to −2.2 V (**2**) or −1.08 V (**4**).

For the triphos complex **3**, with just a single CO ligand, the first anodic wave (which corresponds to a single-electron reversible oxidation) was observed at the lowest oxidation potential ($^{I}E_{1/2}^{ox}$ = 0.32 V) when compared with those of **2** (dicarbonyl complexes) or **4** (tricarbonyl compound), in agreement with the known[14] strong π-electron acceptance of the CO ligand(s) with resulting enhancement of the oxidation potential of the corresponding complexes. In fact, the oxidation potential of the first anodic wave clearly reflects the net π-acceptor minus σ-donor character of the ligands, as measured by the electrochemical P_L ligand parameter[14] (the stronger that character, the higher the P_L).

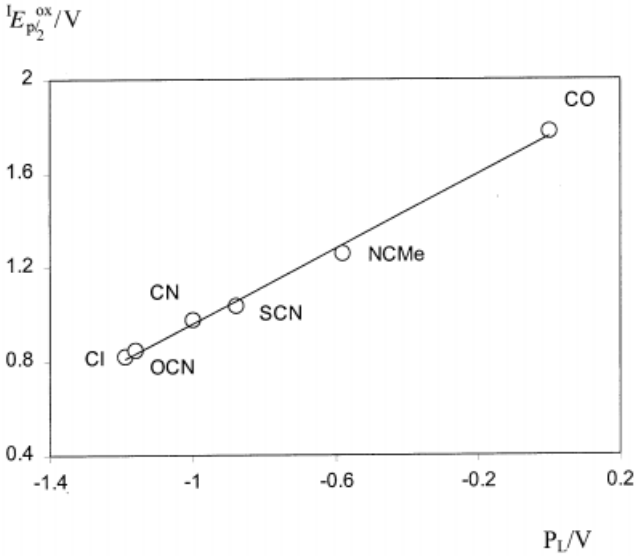


Figure 3. Plot of $^{I}E_{p/2}^{ox}$ for complexes **D** [n = 1; X = SCN (**2a**), OCN (**2c**), Cl (**2f**), or CN[3]], **A** [n = 1 (**4**)], and **1a**[3], vs. the electrochemical P_L ligand (X or L)[14] parameter. $^{I}E_{p/2}^{ox}$ = 0.80 P_L + 1.76 (correlation coefficient r = 0.998)

This is shown by the linear plot of $^{I}E_{p/2}^{ox}$ vs. P_L (Figure 3), for the series of complexes with a common alkenylcarbyne (n = 1), namely the neutral complexes [Type **D**; X = SCN (**2a**), OCN (**2c**), Cl (**2f**) or CN] and the cationic complexes **4** (Type **A**) and **1a** in which P_L refers to the variable ligand (X or L) coordinated to the common metal centre. The $^{I}E_{p/2}^{ox}$ values for the cyano- and the acetonitrile complexes were previously reported[3] and are included for comparative purposes.

A lowering of the net σ-electron-donor minus π-electron-acceptor ability of the X or L ligand (or, in other words, an increase of its net π-electron-acceptor minus σ-electron-donor character) results in stabilisation of the HOMO of the complex and therefore in an anodic shift of the oxidation potential. Hence, the values of the oxidation potential of complexes **2** with the anionic X ligand follow the order $Cl^- < OCN^- < CN^- < SCN^-$ (with corresponding P_L ligand values of −1.19, −1.16, −1.00 or −0.88 V[14]) and are significantly lower than that, $^{I}E_{p/2}^{ox}$ = 1.26 V,[3] of the acetonitrile complex, and much less anodic than that, $^{I}E_{p/2}^{ox}$ = 1.78 V, of the carbonyl analogue **4**, and are also in close agreement with the increasingly higher P_L values for ligating NCMe and CO (−0.58 and 0.0 V, respectively[14]). The tricarbonyl complex **4** with an alkenylcarbyne ligand exhibited a much higher oxidation potential than that of the related tetracarbonyl [$W(CO)_4$(dppe)] ($E_{1/2}^{ox}$ = 1.02 V),[3] indicating that the ligating alkenylcarbyne behaves as a much stronger net π-electron-acceptor minus σ-electron-donor than carbonyl. This is also the reason why the other alkenylcarbyne complexes with the strong electron-donating SCN^- ligand were still oxidized at a potential higher than that of [$W(CO)_4$(dppe)]. The carbyne ligands in *trans*-[$ReX(\equiv CCH_2R)(dppe)_2$][$BF_4$] (X = F or Cl; R = alkyl, aryl or ester) have also been shown[4] to behave as more efficient π-electron acceptors than CO.

The above linear plot corresponds to the expression [Equation (1)] proposed by C. J. Pickett et al.[14] that relates the oxidation potential of the members of a series of 18-electron octahedral complexes $[M_sL]$ (with a common $\{M_s\}$ site) with P_L for the variable L ligand. E_s is a measure of the electron richness of the metal site, and is expressed by the oxidation potential of the carbonyl complex $[M_s(CO)]$ (the higher E_s, the lower the electron richness is), and β is a measure of the polarisability of the metal site.

$$E^{ox}[M_sL] = E_s + \beta \cdot P_L(L) \quad (1)$$

Therefore, from the intercept and the slope of the plot of Figure 3, one can estimate these parameters for the common metal site of our study, $\{M_s\}$ =

$$\{(dppe)(CO)_2W{\equiv}CCH{=}\overline{CCH_2CH_2CH_2CH_2}\},$$

as E_s = 1.76 V and β = 0.80. This is the first time such parameters have been estimated for a metal site with a carbyne ligand and it is noteworthy to mention that the electron richness of this centre is rather low, even lower than that (E_s = 1.50 V) of $\{M(CO)_5\}$ (M = Cr, Mo or W),[14,15] on account of the very strong π-electron acceptor character of the alkenylcarbyne ligand and of the two carbonyls.

Moreover, the polarisability is also low [e.g., for $\{M(CO)_5\}$ (M = Cr, Mo, or W), β = 1.0−0.9[14,16]], indicating a high capacity of the alkenylcarbyne ligand to "buffer" changes in the energy of the HOMO of the complex upon replacement of the *trans* ligand, conceivably as a result of extensive delocalization of the HOMO along the carbyne ligand. Such a propensity, exhibited by strong π-electron-acceptor ligands is known for other cases such as the rhenium carbonyl centre $\{Re(CO)(dppe)_2\}^+$ with a much lower β (0.62)[17] than that of the related chloride site $\{ReCl(dppe)_2\}$ (β = 3.4).[18]

This study also provided an opportunity to investigate the electronic coordination properties of a S-bonded ligand. In spite of the relevance of S-bonded ligands in coordination chemistry, the P_L of these ligands have virtually never been determined. From the above plot, it was possible to estimate the P_L value for the ligand $S_2P(OEt)_2^-$ as −1.34 V. Hence, this ligand behaves as a slightly stronger net electron donor than Cl^- and NCO^- (P_L = −1.19 or −1.16 V, respectively),[14] and is a much more effective electron releaser than NCS^- (P_L = −0.88 V[14]).

The anodic processes of the alkenyl−carbyne complexes of this study are commonly multi-electronic on the time scale of CPE and involve anodically induced proton loss. This has also been observed[3] for the related complexes **D** (X = CN; *n* = 1 or 4) (Scheme 1), **1a** and **1b**. Hence, CPE of, for example, **2f** at the first anodic wave (I) consumes ca. 3 Faradays/mol and generates ca. 2 mol H^+/mol complex measured by potentiometric acid−base titration of the electrolysed solution, whereas a total of ca. 4 Faradays/mol and ca. 4 mol H^+/mol complex was measured upon exhaustive CPE at the peak potential of the second anodic wave (II).

As a result of the oxidation of the complex, the Brönsted acidity of the alkenylcarbyne ligand is enhanced and proton loss occurs not only from the W≡C−CH= group but also from the carbocyclic moiety. Although we could postulate the formation of, for example, vinylidene or allenylidene species, we unfortunately did not succeed in the attempted isolation and full characterisation of the products derived from CPE.

The aminocarbyne (CNH_2) and the isocyanide (CNH) ligands at *trans*-$[ReCl(CNH_n)(dppe)_2][BF_4]_{n-1}$ (*n* = 2 or 1)[6] and *trans*-$[FeH(CNH)(dppe)_2][BF_4]$,[19] as well as some aminocarbenes in complexes of Pd^{II} or Pt^{II} [20] are also anodically activated toward proton extrusion, but the less acidic carbynes CCH_2R (R = alkyl, aryl or ester) in *trans*-$[ReX(\equiv C-CH_2R)(dppe)_2][BF_4]$ (X = F or Cl)[4] do not undergo such a reaction upon single-electron oxidation of their complexes; this oxidation is fully reversible on the time scale of the CV.

The proton loss is also in agreement with the detection, by CV (cathodic sweep) of the electrolysed solution, of an irreversible and broad cathodic wave, usually at ca. −0.5 V, assigned to H^+ reduction. This cathodic wave was also observed in the cyclic voltammetric study of the complexes, upon reverse of the anodic scan (run at a sufficiently low scan rate) following the oxidation waves. When the Pt electrode was replaced with a vitreous carbon one, that cathodic wave underwent an extensive cathodic shift (e.g., to ca. −1.2 V for **2g**) in agreement with the expected overpotential required for H^+ reduction at vitreous carbon.

The involvement of more than one electron with coupled H^+ extrusion in the anodic CV processes, at sufficiently low scan rates, was also corroborated by the enhancement of their current functions $i_p^{ox}\ C^{-1}\ v^{-1/2}$ (i_p^{ox}, anodic peak current; C, concentration; *v*, scan rate) upon (i) a decrease of the scan rate (e.g., by a factor of ca. 2−2.5 for **2a**, **2b** or **2f**, from v = 10 V s^{-1} to 0.050 V s^{-1}) and (ii) addition of pyridine. (e.g., by a factor of ca. 2, for a fivefold molar excess of base, for **2f** at v = 0.2 V s^{-1}). In the absence of base and at sufficiently high scan rates, the extent of deprotonation is lowered due to the restricted duration of the assay, and the first anodic wave tends to that of a single-electron process, for example, the current function of **2f** approaches that of the one-electron oxidation of *trans*-$[ReCl(N_2)(dppe)_2]$ at scan rates above ca. 5 Vs^{-1}.

Concluding Remarks

Our studies on the chemistry of α,β-unsaturated carbyne Fischer-type tungsten complexes[1–3] were extended (Scheme 1) by the work reported here on novel mononuclear complexes of type **D** (X = NCS, NCO; *n* = 1,4) (**2a−d**) (Scheme 2) and the analogous monocarbonyl derivative **3** (Scheme 3) containing the tridentate phosphane $PPh(CH_2CH_2PPh_2)_2$ (triphos). These complexes are further examples of the synthetic potential of the acetonitrile precursor complexes **1** for the preparation of the relatively scarcely known unsaturated carbyne complexes. Special features of these complexes are the following: (a) They have a conjugated π-system of C≡N and C=C bonds, bridged by

a metal carbyne M≡C moiety. In recent years, there has been an increasing interest in metal complexes with extended π-conjugated systems, since they can be used as components of molecular materials with enhanced electrical conductivities and nonlinear (NLO) properties.[21] (b) As shown by the X-ray crystal structure determinations, the bond lengths W−Cl and W−NCS in complexes **2a** and **3**, respectively, are longer than the average values; this indicates that the alkenylcarbyne group has a *trans* influence. (c) Such an influence conceivably results from the extensive π-electron-acceptor ability of these carbyne ligands, as shown by electrochemical studies which also indicate, for the first time, that such ligands have a remarkable lowering effect on both the electron richness and polarisability of the metal sites which they belong to. These features confirm the above proposed extended π-electron delocalisation along the alkenylcarbyne−metal−*trans*-ligand framework. (d) The alkenylcarbyne ligand is susceptible to anodically-induced deprotonation; the potential synthetic use of this towards the formation of novel multiple metal−carbon bonded species should be further explored.

Experimental Section

General: The reactions were carried out under dry nitrogen by Schlenk techniques. All solvents were dried by standard methods and were distilled under nitrogen before use. The precursor complexes **1a**,**b** and **2f** as well as **2e**, **2g**, and **4** were prepared by literature methods.[1a,1b,2] NaOCN, KSCN, [NBu_4]SCN, triphos [$PhP(CH_2CH_2PPh_2)_2$] (Aldrich) were used as received. − Infrared spectra were recorded on a Perkin−Elmer 1720-XFT spectrometer. − Mass spectra (FAB) were recorded on a VG-Autospec spectrometer, operating in the positive mode; 3-nitrobenzyl alcohol (NBA) was used as the matrix. − The conductivities were measured at room temp, in ca. 10^{-3} mol dm^{-3} acetone solutions, with a Jenway PCM3 conductivimeter. − The C, H, and N analyses were carried out with a Perkin−Elmer 240-B microanalyzer. − ^{1}H-, ^{13}C-, and ^{31}P-NMR spectra were run on a Bruker AC200 spectrometer at 200 MHz (^{1}H), 81 MHz (^{31}P) or 50.3 MHz (^{13}C) and a Bruker AC300 spectrometer at 300 MHz (^{1}H), 121.5 MHz (^{31}P) or 75.5 MHz (^{13}C). The spectral references were tetramethylsilane (TMS) for ^{1}H and ^{13}C, and 85% H_3PO_4 for ^{31}P-NMR measurements. All spectra were recorded with $CDCl_3$ as solvent. − Selected IR and ^{1}H-, ^{13}C{^{1}H}-, and ^{31}P{^{1}H}-NMR spectroscopic data are collected in Table 1 and 2.

Synthesis of 2a (X = SCN; *n* = 1), 2b (X = SCN; *n* = 4), 2c (X = OCN; *n* = 1), 2d (X = OCN; *n* = 4): An equiv. of KSCN (0.019 g) or NaOCN (0.013 g) was added to an orange solution of **1a** (0.172 g) or **1b** (0.180 g) (0.2 mmol) in 40 mL of methanol. The mixture was stirred at room temperature for a few hours. The reactions were followed by IR spectroscopy. The resulting solution was evaporated to dryness when no more starting material was detected. The residue was extracted with CH_2Cl_2 and filtered. Removal of the solvent in vacuo gave the desired compounds **2a−d** as yellow solid in very high yield. **2a**,**b** were prepared similarly from [Bu_4N]SCN in CH_2Cl_2. Yield: **2a**, 0.139 g, 88%; **2b**, 0.167 g, 90%; **2c**, 0.142 g, 92%; **2d**, 0.147 g, 90%.

2a: IR [KBr, ν(SCN); ν(CO)]: 2057 (vs); 1989 (vs), 1920 (vs). − ^{1}H NMR ($CDCl_3$): δ = 1.48 (m, 4 H, 2 CH_2), 1.96 (m, 2 H, CH_2), 1.99 (m, 2 H, CH_2), 2.60 [m, 2 H, $P(CH_aH_b)_2P$], 2.80 [m, 2 H, $P(CH_aH_b)_2P$], 7.37−7.73 (m, 20 H, 2 PPh_2). − ^{13}C NMR ($CDCl_3$): δ = 25.6 (s, CH_2), 26.2 (s, CH_2), 27.6 [m, $P(CH_2)_2P$], 31.5 (s, CH_2), 34.3 (s, CH_2), 128.3−135.5 (m, $C_β$, 2 PPh_2). − $C_{36}H_{33}NO_2P_2SW$: calcd. C 54.8, H 4.2, N 1.8; found C 55.2, H 4.2, N 1.6.

2b: IR [KBr, ν(SCN); ν(CO)]: 2056 (vs); 1984 (vs), 1911 (vs). − ^{1}H NMR ($CDCl_3$): δ = 1.40 (m, 6 H, 3 CH_2), 1.47 (m, 2 H, CH_2), 1.70 (m, 2 H, CH_2), 1.80 (m, 2 H, CH_2), 2.32 (m, 2 H, CH_2), 2.60 [m, 2 H, $P(CH_aH_b)_2P$], 2.80 [m, 2 H, $P(CH_aH_b)_2P$], 7.18−7.73 (m, 20 H, 2 PPh_2). − ^{13}C NMR ($CDCl_3$): δ = 25.5 (s, CH_2), 26.7 (s, CH_2), 26.8 (s, CH_2), 26.9 (s, CH_2), 27.0 (s, CH_2), 27.6 [m, $P(CH_2)_2P$], 31.6 (s, CH_2), 35.7 (s, CH_2), 128.3−132.5 (m, 2 PPh_2). − MS (FAB, *m*/*z*) [M^+ − 2 CO] = 775, [M^+ − SCN] = 773. − $C_{39}H_{39}NO_2P_2SW$: calcd. C 56.3, H 4.7, N 1.7; found C 55.8, H 4.6, N 1.5.

2c: IR [KBr, ν(OCN); ν(CO)]: 2209 (vs); 1986 (s), 1914 (s). − ^{1}H NMR ($CDCl_3$): δ = 1.47 (m, 4 H, 2 CH_2), 1.97 (m, 2 H, CH_2), 2.00 (m, 2 H, CH_2), 2.60 [m, 2 H, $P(CH_aH_b)_2P$], 2.80 [m, 2 H, $P(CH_aH_b)_2P$], 7.36−7.74 (m, 20 H, 2 PPh_2). − ^{13}C NMR ($CDCl_3$): δ = 25.6 (s, CH_2), 26.1 (s, CH_2), 27.3 [m, $P(CH_2)_2P$], 31.8 (s, CH_2), 34.1 (s, CH_2), 128.2−135.6 (m, $C_β$, OCN, 2 PPh_2). − $C_{36}H_{33}NO_3P_2W$: calcd. C 55.9, H 4.3, N 1.8; found C 55.5, H 4.5, N 2.0.

2d: IR [KBr, ν(OCN); ν(CO)]: 2211 (vs); 1987 (s), 1916 (s). − ^{1}H NMR ($CDCl_3$): δ = 1.41 (m, 6 H, 3 CH_2), 1.48 (m, 2 H, CH_2), 1.71 (m, 2 H, CH_2), 1.78 (m, 2 H, CH_2), 2.34 (m, 2 H, CH_2), 2.60 [m, 2 H, $P(CH_aH_b)_2P$], 2.80 [m, 2 H, $P(CH_aH_b)_2P$], 7.33−7.72 (m, 20 H, 2 PPh_2). − ^{13}C NMR ($CDCl_3$): δ = 25.6 (s, CH_2), 26.8 (s, CH_2), 26.9 (s, CH_2), 27.0 (s, 2 CH_2), 27.4 [m, $P(CH_2)_2P$], 31.5 (s, CH_2), 35.8 (s, CH_2), 128.3−135.4 (m, OCN, 2 PPh_2). − $C_{39}H_{39}NO_3P_2W$: calcd. C 57.4, H 4.8, N 1.7; found C 57.5, H 4.5, N 1.8.

Synthesis of 3: A yellow solution of **2f** (0.383 g, 0.5 mmol) and an equiv. amount of $PhP(CH_2CH_2PPh_2)_2$ (0.267 g) in 50 mL of toluene was stirred under reflux for 24 h. The resulting orange solution was evaporated to dryness and the residue was washed with diethyl ether (3 × 10 mL) to remove the dppe. Drying in vacuo gave the desired compound **3** as an orange solid in good yield (0.339 g, 75%). − IR [KBr, ν(CO)]: 1874 (s). − ^{1}H NMR ($CDCl_3$): δ = 1.39 (m, 4 H, 2 CH_2), 1.84 (br, 2 H, CH_2), 1.97 (br, 2 H, CH_2), 2.14 (m, 2 H, PCH_2), 2.55 (m, 4 H, 2 PCH_2), 3.39 (m, 2 H, PCH_2), 7.14−7.78 (m, 25 H, Ph, 2 PPh_2). − ^{13}C NMR ($CDCl_3$): δ = 26.4 (m, PCH_2), 27.0 (s, CH_2), 27.6 (s, CH_2), 31.8 (s, CH_2), 34.4 (m, PCH_2), 34.5 (s, CH_2), 128.3−140.4 (m, $C_β$, Ph, 2 PPh_2). − MS (FAB, *m*/*z*) [M^+ − CO] = 847, [M^+ − CO − Cl − H] = 810, [M^+ − C_5H_8] = 807, [M^+ − Cl − C_5H_{10}] = 770, [M^+ − CO − C_7H_9] = 754, [M^+ − CO − Cl − C_6H_8] = 731. − $C_{42}H_{42}ClOP_3W$: calcd. C 57.7, H 4.8; found C 58.0, H 4.8.

Crystal Structure Determination of 2b and 3: The intensity data were collected at room temp on a Philips PW 1100 (**2b**) and on a Siemens AED (**3**) single-crystal diffractometer with graphite-monochromated Mo-$K_α$ radiation and the θ/2θ scan technique. Final unit cell parameters were obtained from a least-squares refinement of 24 (**2b**) and 28 (**3**) reflections. Crystallographic and experimental details for both structures are summarised in Table 6. Data were corrected for Lorentz and polarisation effects in the usual manner. A correction for absorption was made for both complexes [maximum and minimum value for the transmission coefficient was 1.000 and 0.5754 (**2b**) and 1.000 and 0.6493 (**3**)].[22]
Both structures were solved by Patterson and Fourier methods and refined by full-matrix least-squares procedures (based on F_o^2) with

Table 6. Experimental data for the X-ray diffraction studies of complexes **2b** and **3**

Empirical formula	$C_{39}H_{39}NO_2P_2SW$	$C_{42}H_{42}ClOP_3W$
Formula mass	831.6	875.0
Temperature	293(2) K	293(2) K
Wavelength	0.71073 Å	0.71073 Å
Crystal system	Monoclinic	Monoclinic
Space group	$P2_1/c$	$P2_1/n$
Unit-cell dimensions	a = 10.784(3)Å	a = 11.174(4)Å
	b = 18.611(5)Å	b = 17.800(5)Å
	c = 18.425(4)Å	c = 19.148(5)Å
	β = 91.61(2)°	β = 96.07(6)°
Volume	3696(2) Å^3	3787(2) Å^3
Z	4	4
Density (calculated)	1.494 Mg/m^3	1.535 Mg/m^3
Absorption coefficient, μ	3.301 mm^{-1}	3.280 mm^{-1}
F(000)	1664	1752
Crystal size	0.18 × 0.27 × 0.22 mm	0.21 × 0.34 × 0.35 mm
θ range (deg)	3.07−30.02	3.05−28.05
Index ranges	$-15 \le h \le 15$	$-14 \le h \le 12$
	$0 \le k \le 26$	$-21 \le k \le 23$
	$0 \le l \le 25$	$-25 \le l \le 16$
Reflections collected	11062	9408
Independent reflections	10771 (R_{int} = 0.0555)	9157 (R_{int} = 0.0364)
Obs. refl [$I > 2\sigma(I)$]	7039	4981
Refinement method	Based on F^2	Based on F^2
Data/restr./param.	10771/0/422	9157/0/445
Goodness-of-fit on F^2	1.820	0.887
Final R indices [$I > 2\sigma(I)$][a]	$R1$ = 0.0410, $wR2$ = 0.1009	$R1$ = 0.0366, $wR2$ = 0.0916
R indices (all data)[a]	$R1$ = 0.1018, $wR2$ = 0.1500	$R1$ = 0.0822, $wR2$ = 0.1041
Largest diff. peak and hole	2.521 and −2.284 eÅ^{-3}	1.336 and −1.812 eÅ^{-3}

[a] $R1 = \Sigma|F_o - F_c|/|\Sigma(F_o)$, $wR2 = \{\Sigma[w(F_o^2 - F_c^2)^2]/\Sigma[w(F_o^2)^2]\}^{1/2}$.

anisotropic thermal parameters in the last cycles of refinement for all the non-hydrogen atoms. The hydrogen atoms were introduced into the geometrically calculated positions and were refined riding on the corresponding carbon atoms. In the final cycles of refinement a weighting scheme $w = 1/[\sigma^2F_o^2 + (0.0730\,P)^2 + 0.5625\,P]$ (**2b**) and $w = 1/[\sigma^2F_o^2 + (0.0627\,P)^2]$ (**3**) where $P = (F_o^2 + 2\,F_c^2)/3$ was used. All calculations were carried out on the DIGITAL AlphaStation 255 computers of the "Centro di Studio per la Strutturistica Diffrattometrica del CNR," Parma, with the SHELX-97 systems of crystallographic computer programs.[23]

Electrochemical Measurements: The electrochemical experiments were carried out either on an EG&G PAR 273 A potentiostat/galvanostat connected to a 386-SX personal computer through a GPIB interface, or on an EG&G PAR 173 potentiostat/galvanostat and an EG&G PARC 175 Universal programmer. Cyclic voltammetry (CV) was undertaken in a two-compartment three-electrode cell, at a platinum- or vitreous carbon disc (d = 0.5 mm) working electrode, probed by a Luggin capillary connected to a silver-wire pseudo-reference electrode; a platinum or tungsten auxiliary electrode was employed. Controlled-potential electrolyses (CPE) were carried out in a three-electrode H-type cell with a platinum-gauze working and counter electrodes in compartments separated by a glass frit; a Luggin capillary, probing the working electrode, was connected to a silver-wire pseudo-reference electrode. The oxidation potentials of the complexes were measured by cyclic voltammetry in 0.2 mol dm^{-3} [NBu$_4$][BF$_4$]/NCMe (or THF), in the presence of ferrocene as the internal standard, and the redox potential values are quoted relative to the SCE by using the [Fe(η^5-C$_5$H$_5$)$_2$]$^{0/+}$ couple ($E_{1/2}^{ox}$ = 0.42 or 0.545 V vs SCE, in 0.2 mol dm^{-3} [NBu$_4$][BF$_4$]/NCMe or THF, respectively). The use, as reference electrode, of the SCE or other electrode in aqueous medium, was avoided due to the sensitivity of the systems to water. The CPE experiments were monitored regularly by CV, thus assuring that no significant potential drift occurred along the electrolyses.

The acid−base titrations of the electrochemically oxidised solutions were carried out as indicated before,[20] with a solution of NaOH in CH$_3$OH which was standardised by titration against benzoic acid in the organic solvent (thymol blue was used as the indicator). The results presented were corrected for background effects by performing, in each case, the titration of the blank solution of 0.2 mol dm^{-3} [NBu$_4$][BF$_4$] which was electrolysed under identical conditions to those used for the corresponding complex solution.

Supplementary Material: The supplementary material for both structures includes the lists of atomic coordinates for the non-H atoms, calculated coordinates for the hydrogen atoms, and anisotropic thermal parameters. The details of the crystal structure investigations are deposited at the Cambridge Crystallographic Data Centre as supplementary publications nos. CCDC-130866 (**2b**) and CCDC-130867 (**3**). Copies of the data can be obtained free of charge on application to CCDC, 12 Union Road, Cambridge CB2 1EZ, UK [Fax: (internat.) + 44 (0)1223/336 033, E-mail: deposit@ccdc.cam.ac.uk.

Acknowledgments

This work was supported by the DGICYT (Project PB93-0325, Spain), the E. C. (Human Capital Mobility programme. Project: ERBCHRXCT 940501), and the PRAXIS XXI Programme (Portugal). L. Z. is grateful for the financial support from the Spanish Ministerio de Educación y Ciencia (visiting researcher grant), Agencia Española de Cooperación Internacional (Spain, doctoral fellowship) and the Fundaçao para a Ciência e a Tecnologia (Portugal, postdoctoral PRAXIS XXI grant).

[1] [1a] L. Zhang, M. P. Gamasa, J. Gimeno, R. J. Carbajo, F. López-Ortiz, M. Lanfranchi, A. Tiripicchio, *Organometallics* **1996**, *15*, 4274−4284. − [1b] L. Zhang, M. P. Gamasa, J. Gimeno, A. Galindo, C. Mealli, M. Lanfranchi, A. Tiripicchio, *Organometallics* **1997**, *16*, 4099−4108.

[2] R. J. Carbajo, F. López-Ortiz, L. Zhang, *Magn. Reson. Chem.* **1998**, *36*, 807−814.

[3] L. Zhang, M. P. Gamasa, J. Gimeno, R. J. Carbajo, F. López-Ortiz, M. Lanfranchi, A. Tiripicchio, M. F. C. Guedes da Silva, A. J. L. Pombeiro, *Eur. J. Inorg. Chem.* **2000**, 341−350.
[4] S. S. P. R. Almeida, A. J. L. Pombeiro, *Organometallics* **1997**, *16*, 4469−4478.
[5] A. J. L. Pombeiro, *New J. Chem.* **1997**, *21*, 649.
[6] M. A. N. D. A. Lemos, M. F. C. Guedes da Silva, A. J. L. Pombeiro, *Inorg. Chim. Acta* **1994**, *226*, 9−16.
[7] A. J. L. Pombeiro, J. McCleverty, *Molecular Electrochemistry of Inorganic. Bioinorganic and Organometallic Compounds*, NATO ASI Series; Kluwer Academic Publishers, Dordrecht, **1993**, pp. 331−344.
[8] F. R. Kreissl, *Transition Metal Carbyne Complexes*, NATO ASI Series; Kluwer Academic Publishers, Dordrecht, **1993**.
[9] K. Nakamoto, *Infrared and Raman Spectra of Inorganic and Coordination Compounds, 4th ed.*, Wiley-Interscience Publication, New York, **1986**, p. 283.
[10] Y. Wang, J. J. R. Fraústo da Silva, A. J. L. Pombeiro, M. A. Pellinghelli, A. Tiripicchio, *J. Organomet. Chem.* **1993**, *454*, 211−216.
[11] J. Kohout, M. Hvastijova, J. Gazo, *Coord. Chem. Rev.* **1978**, *27*, 141−172.
[12] [12a] G. A. Carriedo, G. Sánchez, V. Riera, C. Bois, Y. Jeannin, D. Miguel, *J. Chem. Soc., Dalton Trans.* **1990**, 3355−3362. − [12b] E. O. Fischer, D. Wittmann, D. Himmelreich, U. Schubert, K. Ackermann, *Chem. Ber.* **1982**, *115*, 3141−3151. − [12c] E. O. Fischer, D. Wittmann, D. Himmelreich, R. Cai, K. Ackermann, D. Neugebauer, *Chem. Ber.* **1982**, *115*, 3152−3166.
[13] W. A. Schenk, H. Muller, *Chem Ber.* **1982**, *115*, 3618−3630.
[14] J. Chatt, C. T. Kan, G. J. Leigh, C. J. Pickett, D. R. Stanley, *J. Chem. Soc., Dalton Trans.* **1980**, 2032−2038.
[15] C. J. Pickett, D. Pletcher, *J. Chem. Soc., Dalton Trans.* **1975**, 879−886.
[16] G. Facchin, M. Mozzon, R. A. Michelin, M. T. A. Ribeiro, A. J. L. Pombeiro, *J. Chem. Soc., Dalton Trans.* **1992**, 2827−2835.
[17] A. J. L. Pombeiro, *Inorg. Chim. Acta* **1985**, *103*, 95−103.
[18] A. J. L. Pombeiro, C. J. Pickett, R. L. Richards, *J. Organomet. Chem.* **1982**, *224*, 285−294.
[19] S. S. P. R. Almeida, M. F. C. Guedes da Silva, J. J. R. Fraústo da Silva, A. J. L. Pombeiro, *J. Chem. Soc., Dalton Trans.* **1999**, 467−472.
[20] R. Bertani, M. Mozzon, R. A. Michelin, F. Benetollo, G. Bombieri, T. J. Castilho, A. J. L. Pombeiro, *Inorg. Chim. Acta* **1991**, *189*, 175−187.
[21] [21a] D. W. Bruce, D. O'Hare, *Inorganic Materials*, Wiley, New York, **1992**. − [21b] M. H. Chisholm, *Angew. Chem. Int. Ed. Engl.* **1991**, *30*, 673−674. − [21c] H. Lang, *Angew. Chem. Int. Ed. Engl.* **1994**, *32*, 547−550.
[22] N. Walker, D. Stuart, *Acta Crystallogr., Sect. A* **1983**, *39*, 158−166. F. Ugozzoli, *Comput. Chem.* **1987**, *11*, 109.
[23] G. M. Sheldrick, *SHELX-97*, Program for the solution and the refinement of crystal structures, Universität Göttingen, Germany, **1997**.

Received December 10, 1999
[I99451]

Chiral Quadridentate Ligands Derived from Amino Acids and Some Zinc Complexes Thereof

Nicole Niklas,[a] Olaf Walter,[b] and Ralf Alsfasser*[a]

Dedicated to Prof. Dr. Heinrich Vahrenkamp on the occasion of his 60th birthday

Keywords: Bioinorganic chemistry / Zinc / Amino acids / Chiral ligands / Tripodal ligands

A series of three new quadridentate ligands was synthesized by reaction of the haloacetylated amino acid esters L-BrAc–Phe–OMe (**4a**), L-BrAc–Lys(Z)–OMe (**4b**), and ClAc–Gly–OEt (**4c**), respectively, with bis(picolyl)amine (bpa, **5**). The obtained products L-bpaAc–Phe–OMe (**3a**), L-bpaAc–Lys(Z)–OMe (**3b**), and bpaAc–Gly–OEt (**3c**) were treated with $Zn(OTf)_2$ (OTf = $CF_3SO_3^-$) to yield the trigonal-bipyramidal complexes [(L-bpaAc–Phe–OMe)ZnOTf](OTf) (**6a**), [(L-bpaAc–Lys(Z)–OMe)ZnOTf](OTf) (**6b**), and [(bpaAc–Gly–OEt)ZnOTf](OTf) (**6c**). Crystal structures of **6c** and the hydrolysis product [(L-bpaAc–Phe–OMe)-(H_2O)ZnOTf]$(OTf)_2$ (**7a**) are reported. The results suggest the formation of a chiral pocket at the metal center provided by the benzyl substituent in the L-phenylalanine derivative **7a**. This observation is further supported by ^{1}H-NMR and circular dichroism spectroscopic data. These methods indicate a significant ordering effect within the ligands upon metal coordination as well as interactions between the first coordination spheres and their chiral environments provided by the L-phenylalanine and L-lysine moieties of **3a** and **3b**, respectively. Our results are discussed with respect to the development of chiral building blocks for transition metal catalysts and biomimetic assemblies.

Introduction

Apart from their importance in biological systems, amino acids are versatile building blocks for a variety of fascinating synthetic molecular and supramolecular assemblies such as peptide nucleic acids (PNAs),[1] dendrimers,[2] micelles,[3] or de novo designed peptides[4] and proteins.[5,6] The scope of accessible amino acid side-chain functionalities has been tremendously broadened by organic chemists who have developed different methods for the enantioselective synthesis and processing of artificial amino acids carrying, for example, aromatic rings,[7] sugars,[8] or organic cofactors such as pyridoxamine[9] and flavine.[10] The latter two examples illustrate the potential of nonnatural amino acids as catalytically active components for the design of new materials.

Catalytically active amino acid derivatives are attractive targets not only for organic chemists but also for coordination chemistry. There is a still growing interest in metal complexes as enantioselective catalysts for organic conversions such as oxidations,[11,12] carbon−carbon bond formations,[13] or hydrolytic cleavage reactions.[14,15] Metal complexes of synthetic amino acids with covalently attached synthetic polydentate chelators are interesting building blocks for polyfunctional catalysts. They are chiral and have a powerful potential for combinatorial catalyst screening.[16,17] However, only a few examples of suitable ligands have been described in the literature. Those include bifunctional chelating reagents[18−20] developed for pharmaceutical applications, conjugates of lysine with EDTA or EDTA-related ligands,[21−23] as well as a bipyridine-modified alanine.[24] The only example of an acyclic tridentate amine ligand connected to an amino acid is a terpyridine derivative of cysteine, which has not been isolated as a monomer.[25,26]

Work in our laboratories has focused on the development and investigation of Werner-type coordination compounds with synthetic amino acids carrying well-defined metal binding sites.[27−29] In this report we present ligands derived from glycine, L-phenylalanine, and L-lysine. Zinc complexes have been prepared and investigated by X-ray crystallography, NMR, and circular dichroism spectroscopy. Characteristics of the compounds are the availability of suitable coupling positions for further derivatization, the interplay between the metal center and its chiral environment, as well as the availability of open coordination sites for metal-centered reactions.

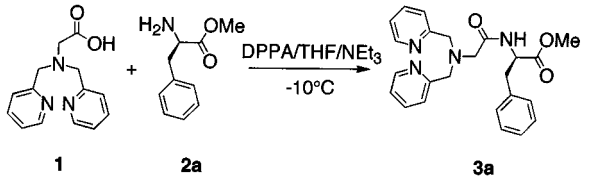
Results

Ligand Synthesis

Our initial approach involved applying carboxylate-substituted tridentate amines in standard amide coupling reac-

[a] Institute for Inorganic Chemistry,
University of Erlangen-Nürnberg,
Egerlandstraße 1, 91058 Erlangen, Germany
Fax: (internat.) + 49-(0)9131/852-7387
E-mail: alsfassr@anorganik.chemie.uni-erlangen.de
[b] ITC-CPV, Forschungszentrum Karlsruhe,
Postfach 3640, 76021 Karlsruhe

 © WILEY-VCH Verlag GmbH, D-69451 Weinheim, 2000 1434−1948/00/0808−1723 $ 17.50+.50/0

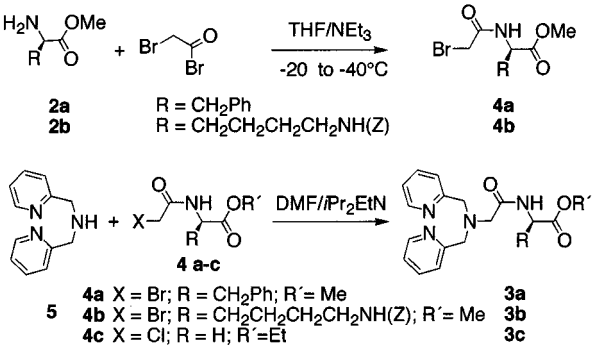


Scheme 1. Azide coupling strategy for the synthesis of the ligand **3a**

tions with the N-termini of amino acids (Scheme 1). The triamine used was the bis(picolyl)glycine **1**, which was prepared according to a procedure described by Que et al.[30] for the synthesis of iron complexes. Different methods were examined for coupling **1** to the amino group of L-phenylalanine methyl ester. Attempts to prepare the acid chloride by reaction of bis(picolyl)glycine with thionyl chloride failed. Formation of an amide bond by the intermediate formation of a mixed anhydride with isobutyl chlorofomate[31] also proved unsuccessful. The desired ligand L-bpaAc−Phe−OMe (**3a**) was finally obtained from **1** and phenylalanine methyl ester (**2a**) by the application of diphenylphosphoryl azide at low temperature in THF (Scheme 1).[31] However, purification of the product was difficult and the method afforded only poor yields (below 10%).

Since the coupling strategies described above were not satisfactory we changed our approach. The method employed involves bromoacetylation of an appropriate amino acid ester followed by nucleophilic substitution (Scheme 2). This coupling method has been shown to be very useful for the synthesis of polyfunctional chelating ligands. Typical examples include polyazamacrocycle−protein conjugates[32] for pharmaceutical applications and a phenylalanine−triazacyclononanetriamide derivative that served as a model for peptide organization at transition-metal templates.[33] Applications are not limited to metal-peptide derivatives, as exemplified by the synthesis of a hexadentate open-chain ligand by Sargeson et al.[34]

Scheme 2 illustrates our synthesis of L-bpaAc−Phe−OMe (**3a**) and the analogous ligand L-bpaAc−Lys(Z)−OMe (Z = benzyloxycarbonyl) (**3b**). L-Phe−OMe (**2a**) and L-Lys(Z)−OMe (**2b**) were treated with bromoacetyl bromide to yield the respective products L-BrAc−Phe−OMe (**4a**) and L-BrAc−Lys(Z)−OMe (**4b**). The synthesis of **4a** has been reported earlier in a communication by Fairlie et al.[33] but no experimental details were



Scheme 2. Haloacetyl strategy for the synthesis of the ligands **3a**−**c**

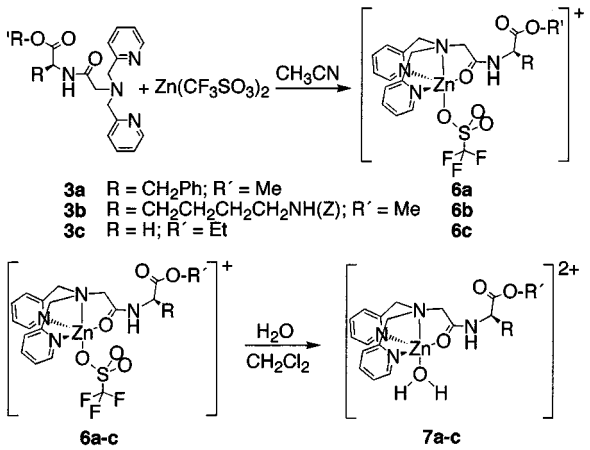
given. Subsequent reaction of **4a** and **4b** with bis(picolyl)-amine (bpa, **5**) resulted in the formation of the desired chiral ligands **3a** and **3b**.

We have also prepared the nonchiral glycine derivative **3c** (Scheme 2) for comparative studies concerning the role of the chiral ligand environments provided by **3a** and **3b**. The starting material for this synthesis was commercially available (chloroacetyl)glycine. It turned out that the yields of its reaction with **5** (ca. 50%) are significantly lower than those obtained after bromide substitution even if both steps of the bromoacetyl bromide route are considered (overall yield ca. 80%). All three ligands were conveniently purified by flash column chromatography and obtained as spectroscopically pure (^{1}H NMR) yellow oils, which were further characterized by FD-MS.

Complexes

The amino acid ligands **3a**−**c** readily react with nonaqueous zinc triflate [$Zn(OTf)_2$] in dry acetonitrile (Scheme 3). Single crystals suitable for X-ray crystallographic characterization were obtained for [(bpaAc−Gly−OEt)ZnOTf]OTf (**6c**) (Figure 1). The initially formed triflate complexes **6a**−**c** are extremely moisture-sensitive and hygroscopic. Their hydrolysis products **7a**−**c** are readily obtained in the presence of moisture from solvents or air. Single crystals of the aquo complex [(L-bpaAc−Phe−OMe)(H_2O)Zn](OTf)$_2$ (**7a**, Figure 2) were obtained from dichloromethane/ethyl ether solutions of **6a**, which were exposed to air. Accordingly, it is difficult to obtain samples that do not show at least trace amounts of water in their NMR spectra. C,H,N elemental analysis data are also consistent with the presence of various amounts of water. However, the monocations [LZnOTf]$^+$ are the dominant species observed by FAB mass spectrometry for all complexes.

It is interesting to note that the glycine derivative **6c** was found to be the least moisture-sensitive whereas we were not able to obtain a dry sample of the L-bpaAc−Lys(Z)−OMe complex **6b**. Purification of the latter was further complicated because the compound always separates as an oil regardless of the solvent applied, thereby



Scheme 3. Synthesis and structures of the zinc complexes **6a**−**c** and **7a**−**c**

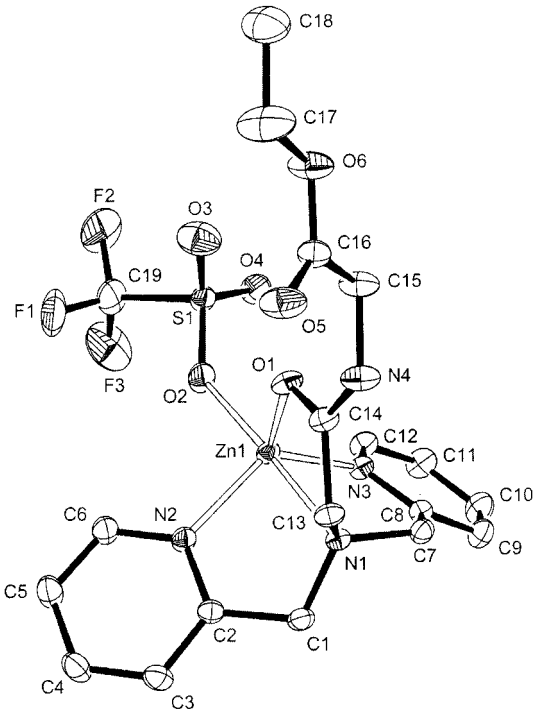


Figure 1. X-ray structure of the cation $[(bpaAc-Gly-OEt)(OTf)Zn]^+$ (**6c**, H atoms omitted for clarity)

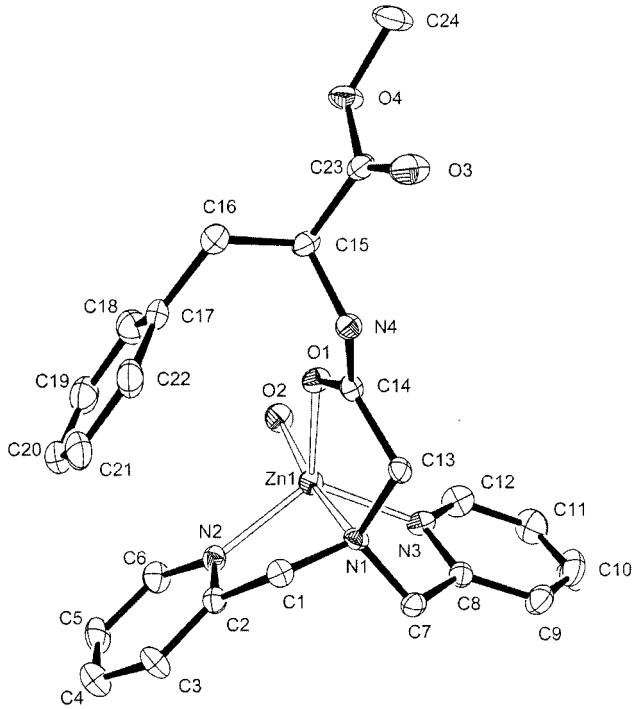


Figure 2. X-ray structure of the cation $[(bpaAc-Phe-OMe)(H_2O)Zn]^{2+}$ (**7a**, H atoms omitted for clarity)

preventing recrystallization. The oil solidified as a white foam upon drying under vacuum and this was characterized by NMR, IR, and circular dichroism spectroscopy, as well as by FAB-MS. The spectroscopic properties of this compound compare well with those of complexes **7a** and **7c** thus ensuring a correct interpretation of the data, which are consistent with the formulation **7b** given in Scheme 3.

Table 1. Selected bond lengths [Å] and angles [°] for the complexes **6c** and **7a**

	6c	**7a**
Zn(1)−O(2)	2.0145(18)	1.990(3)
Zn(1)−O(1)	2.0197(I8)	2.054(2)
Zn(1)−N(2)	2.039(2)	2.046(3)
Zn(1)−N(3)	2.060(2)	2.057(3)
Zn(1)−N(1)	2.1883(19)	2.189(3)
O(2)−Zn(1)−O(1)	99.29(9)	92.52(12)
O(2)−Zn(1)−N(2)	97.06(8)	105.96(15)
O(1)−Zn(1)−N(2)	113.13(8)	113.12(11)
O(2)−Zn(1)−N(3)	102.36(8)	101.59(15)
O(1)−Zn(1)−N(3)	116.84(8)	113.91(11)
N(2)−Zn(1)−N(3)	121.80(8)	123.42(13)
O(2)−Zn(1)−N(1)	176.93(8)	170.40(13)
O(1)−Zn(1)−N(1)	80.68(7)	78.45(10)
N(2)−Zn(1)−N(1)	80.18(8)	80.87(11)
N(3)−Zn(1)−N(1)	80.32(8)	79.48(12)

Solid-State Structures

The mononuclear cation of [L-bpaAc−Gly−OEt)Zn-(OTf)](OTf) (**6c**) is shown in Figure 1. Selected bond lengths and angles are summarized in Table 1. A slightly distorted trigonal bipyramidal coordination environment at Zn^{2+} is observed with one triflate anion and the bridging tertiary amine nitrogen atom occupying the axial positions (N−Zn−O = 177°). The two pyridine N atoms and the amide oxygen atom of the amino acid ligands are bound in the trigonal plane. A comparison with zinc complexes of tris(picolyl)amine[35] and bis(picolyl)glycine,[36] respectively, confirms that the equatorial pyridine N−Zn bonds (204−206 pm), as well as the longer axial N−Zn bond (219 pm) are typical for tripodal quadridentate ligands derived from bis(picolyl)amine. In contrast, all Zn−N bonds are equal in trigonal-bipyramidal[37] and octahedral[38] zinc complexes of the tridentate bis(picolyl)amine ligand itself. The amide and triflate O−Zn distances in **6** (CO: 202 pm; OTf: 201 pm) are in excellent agreement with those found for carboxylate O−Zn bonds in bis(picolyl)glycine complexes.[36]

Facile exchange of a triflate ligand is an expected property of the complexes **6a**−**c**. When a sample of [(L-bpaAc−Phe−OMe)Zn(OTf)](OTf) (**6a**) in CH_2Cl_2/Et_2O was exposed to moist air overnight, crystals of the dicationic aquo complex $[(L\text{-}bpaAc-Phe-OMe)(H_2O)Zn](OTf)_2$ (**7a**, Figure 2 and Table 1) were obtained. A slight tetragonal distortion of its trigonal bipyramidal geometry is evident from the 170° angle between the coordinated water molecule, Zn^{2+}, and the tertiary amine nitrogen atom. The axial oxygen ligand is tilted towards the amide oxygen atom [**7a**: $H_2O-Zn-O$ = 92°/H_2O-Zn-N(equatorial) = 102−106° compared with **6**: OTf−Zn−O = 99° OTf−Zn−N(equatorial) = 97−102°].

As can be seen from Figure 1 and 2 the ester functions of the ligands are noncoordinating and available for further derivatization. An interesting feature of the chiral phenyl-

alanine ligand in **7a** is the orientation of its phenyl ring. The ring covers one side of the open coordination site between the amide oxygen atom and one of the pyridine rings with its center located 4.5 Å away from the metal center. The possible formation of a chiral pocket is an important difference between **3a**/**3b** and comparable ligands developed by Canary et al.[39,40] These authors have synthesized chiral derivatives of tris(picolyl)amine by derivatization of the bridging methylene groups of the ligands leading to complexes in which the bulky substituents are always pointing away from the metal center.

The solid-state IR spectra (KBr pellets) of our compounds are consistent with the X-ray crystallographic results. Binding of the amide oxygen atom is evident from a red shift of the amide IR vibrations in the complexes compared with the free ligands [1672 (**3a**) → 1641 (**7a**); 1668 (**3b**) → 1637 (**7b**); 1674 (**3c**) → 1641 (**7c**)]. The spectra of all complexes exhibit signals for the triflate anions between 1200 and 1300 cm^{-1}. These values are typical for noncoordinating $CF_3SO_3^-$ and are consistent with the formulations **7a**−**7c**. A broad OH band at 3000 cm^{-1} was always observed.

NMR Spectra

The solid-state structure of **7a** suggests that the chiral environment provided by the phenylalanine moiety may influence the accessibility of the open coordination site of the metal centers. It is important for reactivity studies to probe this structural feature in solution. We selected diamagnetic Zn^{2+} complexes as a starting point for our investigations since they allow the application of NMR spectroscopy to compare solution and solid-state structures. The assignment of the ^{1}H-NMR signals of **7a**−**c** ($CDCl_3$ solutions) is based on comparison with the free ligands, the bromoacetylated compounds, and the starting materials, as well as ^{1}H-^{1}H and ^{1}H-^{13}C COSY spectra.

As may be expected the pyridine proton resonances are shifted to lower frequencies upon coordination of the metal ion. The two rings are equivalent in the free ligands **3a**−**c**, as well as in [(bpa-Gly−OEt)(H_2O)Zn]($OTf)_2$ (**7c**). A different pattern is observed in the spectra of the chiral complexes **7a** and **7b**. These compounds show two inequivalent pyridine rings with partially overlapping signals as a consequence of the chiral carbon center. The observed splitting is a clear indication of the structural rigidity induced by metal coordination.

A very sensitive probe for changes in the environment are the methylene proton resonances, which are shown in Figure 3. Unfortunately, some of the signals overlap with those of the methyl esters and α-CH groups but they are unambiguously assignable based on ^{1}H-^{1}H and ^{1}H-^{13}C COSY experiments as well as integration. The C(O)−CH_2 groups are observed as singlets in the ligands **3a**−**3c**. Their corresponding signals of the chiral complexes **7a** and **7b** are split into two doublets. The pyridine-CH_2 protons are diastereotopic in the chiral ligands **3a** and **3b** and their signals appear as AB systems with geminal coupling constants of ca. 14 Hz. These signals are further split in the

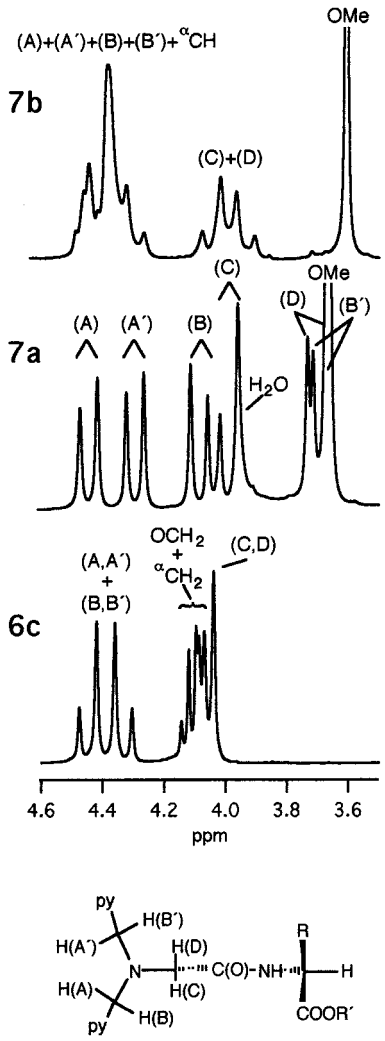


Figure 3. ^{1}H-NMR spectra of the zinc complexes **6c**, **7a**, and **7b** in $CDCl_3$

spectra of the complexes **7a** and **7b** since the two pyridine rings become inequivalent.

Most interesting is the ^{1}H-NMR spectrum of the phenylalanine derivative **7a**. Six doublets are observed for the six methylene protons. Two of them are observed at a significantly higher field (δ = 3.7) than expected if the other two complexes **7b** and **7c** are considered as a reference. The ^{1}H-^{1}H COSY spectrum confirms that one of these signals can be assigned to the C(O)−CH_2 group, whereas the other corresponds to a pyridine−methylene bridge. We interpret the observed high-field shift as an effect of the aromatic ring current of the phenyl ring, which is situated between one pyridine ring and the amide function (Figure 2). A corresponding high-field shift is also observed for the phenyl protons in **7a**, which are observed at rather unusual values of δ = 6.62 (H4) and δ = 6.92 (H3,5). The NMR spectra thus confirm the importance of specific interactions between the benzyl group of phenylalanine and the metal coordination sphere in **7a**.

Exchange of the coordinated triflate by water from air is also evident from NMR spectroscopy. For the extremely hygroscopic free ligands in $CDCl_3$ we occasionally observe

a signal at $\delta = 2$, which is assignable to H_2O. This signal is shifted to significantly lower fields in the complexes with values ranging up to $\delta = 5.6$ in the spectrum of [(L-bpa-Lys−OMe)(H_2O)Zn](OTf)$_2$ (**7b**). The position depends on the water content and moves towards $\delta = 2$ for higher H_2O concentrations. This is consistent with a fast equilibrium between coordinated and noncoordinated water molecules. It is interesting to note that the urethane H signals of the benzyloxycarbonyl protecting groups in **3b** and **7b** are sensitive to the presence of water and shift to slightly higher fields if the compounds are not rigorously dry. All other signals, including the amide H resonance, are invariant in $CDCl_3$ under all experimental conditions relevant for this work.

Circular Dichroism

Ordering phenomena of chiral molecules and supramolecules in solution are conveniently probed by circular dichroism spectroscopy.[41]–[49] A particular advantage of the method is its applicability where UV/Vis spectra are not very informative. The electronic absorption spectra of the bromoacetylated amino acids **4a** and **4b**, (chloroacetyl)glycine, the ligands **3a**−**3c**, as well as the zinc complexes **7a**−**7c** in methanol, show only a broad band at 260 nm, which is largely obscured by the slope of a strong absorption below 200 nm. In contrast, the CD spectra of [(L-bpaAc−Phe−OMe)(H_2O)Zn](OTf)$_2$ (**7a**, Figure 4a) and [(L-bpaAc−Lys−OMe)(H_2O)Zn](OTf)$_2$ (**7b**, Figure 4b) measured in methanol (10^{-3} M) have very distinct features that further support the data obtained from NMR and X-ray crystallographic studies.

The parent amino acids L-Lys−OMe and L-Phe−OMe display only one band at 210 nm (Lys) and 220 nm (Phe), respectively. The signal observed for phenylalanine is stronger and may be assigned to the π-π* transition of the phenyl ring. Bromoacetylation of ε-(benzyloxycarbonyl)lysine methyl ester results in a new signal with a negative Cotton effect at 225 nm and a positive Cotton effect at 245 nm. A shoulder at 245 nm is also well-resolved in the corresponding phenylalanine derivative. This feature disappears in the spectra of the two ligands **3a** and **3b** and a new band with a positive Cotton effect is observed at 260 nm. We assign this band to π-π* transitions of the pyridine rings in agreement with interpretations given by Canary et al.[40] Upon complexation with Zn^{2+} the sign of the pyridine signal changes and the band is shifted to slightly longer wavelengths. It is evident from Figure 4b that the intensity of the 220-nm band is significantly smaller for the ligand **3a** than for the other phenylalanine derivatives discussed in our study. This may be a consequence of the higher flexibility of L-bpaAc−Phe−OMe compared with either **2a**, **4a**, or **7a**. However, we do not have an obvious explanation for this behavior at the present stage of our investigations.

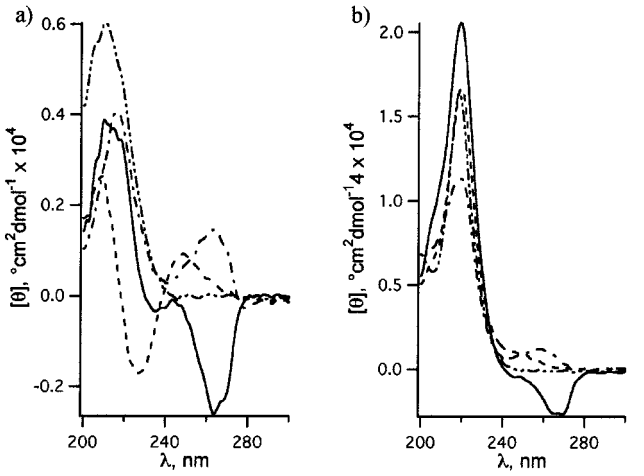


Figure 4. Circular dichroism spectra (10^{-3} M in methanol) of: (a) the L-lysine derivatives Lys(Z)−OMe (**2b**; − · · −), BrAc−Lys(Z)−OMe (**4b**; − −), bpaAc−Lys(Z)−OMe (**3b**; − · −), and [(bpaAc−Lys(Z)−OMe)(H_2O)Zn](OTf)$_2$ (**7b**, —); (b) the L-phenylalanine derivatives Phe−OMe (**2a**; − · · −), BrAc−Phe−OMe (**4a**; − −), bpaAc−Phe−OMe (**3a**; − · −), and [(bpaAc−Phe−OMe)(H_2O)Zn](OTf)$_2$ (**7a**; —)

Discussion

The ligands **3a**−**c** are quadridentate and readily bind zinc(II) to yield stable compounds that are soluble in a variety of solvents ranging from methanol to chloroform. A labile coordination site is available in the trigonal-bipyramidal triflate complexes **6a**−**c**. This is illustrated by the facile ligand exchange observed in the presence of moisture (air), which results in the formation of **7a**−**c**. We have designed our ligands with two features in mind. One is the availability of a functional group for further derivatization. This requirement is met by the presence of a noncoordinating ester function in the complexes **6a**−**c** and **7a**−**c**. No indication was found in the solid state or in solution for an interaction between this group and the metal center. Furthermore, the protected ε-amino group of lysine in bpa-Lys(Z)−OMe (**3b**) may be useful as an additional site for modifications.

Our second objective was to find a chiral noncoordinating environment provided by the ligands. The three amino acid derivatives used in the present study are well suited for comparative studies concerning interactions between the coordinated metal center and its noncoordinating environment since their side chains represent achiral and chiral, as well as aliphatic and aromatic substituents. In the solid-state structure of **7a** the phenyl ring of L-phenylalanine is oriented towards the open coordination site at Zn^{2+} (Figure 2) covering one side of the complex between a pyridine ring and the coordinated amide group. The NMR- and CD-spectroscopic studies presented in this report provide evi-

dence for a significant organization of the chiral environment upon metal complexation in **7a** and **7b** in solution. This is of particular interest for applications of the ligands and complexes in molecular recognition and reactivity studies.

Conclusions

The ligands **3a**−**c** are useful new building blocks for the synthesis of polyfunctional transition-metal complexes based on the chiral pool provided by natural amino acids. They bind tightly and in a well-defined manner to metal ions but offer sufficient flexibility and accessible open coordination sites for metal-ion reactivity. The amino acid side chains cover one side of the complexes such that the complexes **7a** and **7b** are promising candidates for enantioselective molecular recognition and hydrolysis studies. Our concept allows a facile and systematic modification of the properties of metal complexes by variation of the amino acid. The lysine derivative **7b** is particularly interesting for further modifications at the ε-amino group of the ligand. We are currently investigating this possibility in order to extend our building-block approach.

Experimental Section

General Methods: Spectra were recorded with the following instruments: UV/Vis: Cary 1G Spectrophotometer. − Circular Dichroism: Jasco J710 Spectropolarimeter. − IR: Mattson Polaris FT IR. − ^{1}H and ^{13}C NMR: Bruker Avance DPX 300. All chemical shifts are referenced to TMS as internal standard, with high-frequency shifts recorded as positive. − All reactions were carried out under dry nitrogen. The following workup was performed under ambient laboratory conditions unless stated otherwise. The bis(picolyl)glycine **1**[30] and bis(picolyl)amine **5**[52,53] were synthesized according to published procedures. L-Lys(Z)−OMe·HCl (**2b**) was purchased from Nova Biochem, L-Phe−OMe·HCl (**2a**) from Bachem. Absolute solvents (THF, CH_2Cl_2, Et_2O, DMF, CH_3CN) were purchased from Fluka and stored under nitrogen. Ethyl acetate and hexane were reagent grade (Roth). All solvents were used without further purification. Silca gel Merck type 9385 (230−400 mesh, 60 Å) from Aldrich was used for flash column chromatography. Eluents were optimized by TLC on silica gel 60 F254 sheets (0.2 mm layer) from Riedel-de Haën. All other chemicals including ClAc−Gly−OEt and deuterated solvents were obtained from Aldrich. Triethylamine was distilled under N_2 prior to use.

Diphenylphosphoryl Azide (DPPA) Coupling

bpaAc−Phe−OMe (3a): Freshly distilled NEt_3 (1.00 mL, 7.00 mmol) was added in one portion to a stirred suspension of **2a** × HCl (166 mg, 0.77 mmol) under N_2 in 10 mL of absolute THF. Stirring was continued for 30 min, the mixture filtered to remove NEt_3 × HCl and the resulting clear solution cooled to −10 °C using an ice/salt bath. This solution was added in one portion with stirring to another THF (10 mL) solution containing **1** (150 mg, 0.70 mmol) at −10 °C. DPPA (0.17 mL, 0.77 mmol) was added slowly followed by dropwise addition of NEt_3 (0.11 mL, 0.77 mmol). Care was taken to keep the temperature at or below −10 °C. The stirred reaction mixture was kept at −10 °C for another 30 min and the resulting solution was then allowed to warm up to room temperature. Stirring was continued overnight, all the solvent was removed under vacuum and the residue was treated with 10 mL of $CHCl_3$. Cooling to −20 °C afforded a solid, which was filtered off and discarded. The filtrate was concentrated to dryness and the solid obtained was redissolved in a minimum amount of AcOEt. This solution was purified by flash column chromatography on silica gel. Impurities eluted with AcOEt and the product was obtained with yields below 10% by subsequent elution with pure methanol.

Bromoacetylated Amino Acid Esters

BrAc−Phe−OMe (4a): L-Phe−OMe·HCl (10.00 g, 46.40 mmol) was suspended in 200 mL of THF. Triethylamine (12.93 mL, 92.80 mmol) was added with stirring and the mixture was cooled to −10 °C in an ice/salt bath. Bromoacetyl bromide (4.04 mL, 46.40 mmol) was dissolved in 50 mL of THF and the solution was added dropwise to the cold suspension over a period of 2 h. The mixture was stirred for another 2 h without further cooling. Insoluble $HNEt_3Br$ was filtered off and the solvent removed in a vacuum. The crude yellow solid obtained after removal of all THF was redissolved in the minimum amount of ethyl acetate. Colorless needles of the product **4a** (13.46 g, 44.86 mmol, 96.7%) were obtained after addition of hexane and storage in a refrigerator (−20 °C) overnight. The compound was collected on a sintered-glass filter, dried under vacuum, and characterized by FAB-MS, ^{1}H-NMR and ^{13}C-NMR spectroscopy. − FAB-MS (nitrobenzyl alcohol); *m/z*: 300 [M^+], 240 [M^+ − COOMe]. − ^{1}H NMR (300 MHz, $CDCl_3$): δ = 3.15 (m, 2 H, $^{\beta}CH_2$), 3.74 (s, 3 H, OCH_3), 3.84 (s, 2 H, Br−CH_2), 4.85 (m, 1 H, $^{\alpha}CH$), 6.83 (s, br, 1 H, NH), 7.12 (m, 2 H, H2-Ph + H6-Ph), 7.28 (m, 3 H, H3-Ph + H4-Ph + H5-Ph). − ^{13}C NMR (75 MHz, $CDCl_3$): δ = 28.6 (Br−C), 37.7 ($^{\beta}C$), 52.5 (OCH_3), 53.7 ($^{\alpha}C$), 127.3, 128.7, 129.3 (C2-Ph + C3-Ph + C4-Ph + C5-Ph + C6-Ph), 135.9 (C1-Ph), 165.2, 171.3 [C(O)-ester + C(O)-amide]. − IR (KBr): $\tilde{\nu}$ = 1734 cm^{-1} (COOMe), 1645 (amide I), 1537 (amide II). − Circular Dichroism (10^{-3} M in methanol): λ, nm ([θ] × 10^4 °cm^2dmol^{-1}) = 219 (+1.67), 244 (shoulder, +0.11).

BrAc−Lys(Z)−OMe (4b): L-Lys(Z)−OMe·HCl (5.02 g, 15.20 mmol) was suspended in 150 mL of THF and cooled to −30 °C in a methanol/dry ice bath. Triethylamine (4.22 mL, 30.40 mmol) was added and the mixture stirred for 30 min. Bromoacetyl bromide (1.32 mL, 15.20 mmol) was dissolved in 50 mL of THF and the solution added dropwise to the cold suspension over a period of 2.5 h. The mixture was stirred for another 1.5 h at −30 °C. Insoluble $HNEt_3Br$ was filtered off and the solvent removed by rotary evaporation. The crude brown solid obtained after removal of all THF was redissolved in 50 mL of hot ethyl acetate and the solution left at −20 °C overnight. The product precipitated as a colorless solid, which was filtered off and dried under vacuum. A second crop was obtained after addition of hexane and subsequent cooling. The fractions were combined (5.51 g, 13.27 mmol, 87.3%) and characterized by FAB-MS, ^{1}H-NMR and ^{13}C-NMR spectroscopy. − FD-MS ($CDCl_3$); *m/z*: 415 [M^+]. − ^{1}H NMR (300 MHz, $CDCl_3$): δ = 1.38 (m, 2 H, $^{\gamma}CH_2$), 1.52 (m, 2 H, $^{\delta}CH_2$), 1.81 (m, 2 H, $^{\beta}CH_2$), 3.18 (m, 2 H, $^{\varepsilon}CH_2$), 3.75 (s, 3 H, OCH_3), 3.87 (s, 2 H, Br−CH_2), 4.57 (m, 1 H, $^{\alpha}CH$), 4.89 (m, 1 H, NH-Z), 5.09 (s, 2 H, CH_2-Z), 7.35 (m, 5 H, Ph-Z), 7.02 (d, 1 H, $^3J_{HH}$ = 7.3 Hz, NH). − ^{13}C NMR (75 MHz, $CDCl_3$): δ = 22.2 ($^{\gamma}C$), 28.7 (Br−C), 29.4 ($^{\delta}C$), 31.7 ($^{\beta}C$), 40.47 ($^{\varepsilon}C$), 52.6 (OCH_3 + $^{\alpha}C$), 66.7 (CH_2-Z), 128.1, 128.1, 128.4, 128.5 (Z-C2-Ph + Z-C3-Ph + Z-C4-Ph + Z-C5-Ph + Z-C6-Ph), 136.6 (Z-C1-Ph), 156.5 [Z-C(O)], 165.6, 172.2 [C(O)-ester + amide]. − IR (KBr): $\tilde{\nu}$ = 1740 cm^{-1} (COOMe), 1698 (Z-urethane), 1646 (amide I), 1540 (amide II). − Circular Dichroism

(10^{-3} M in methanol): λ, nm ([θ] × 10^4 °cm^{2}dmol^{-1}) = 209 (+0.26), 227 (−0.17), 248 (+0.09).

Ligands

General Procedure: Equimolar amounts of bis(picolyl)amine (**5**), the respective haloacetylated amino acid ester, and ethyldiisopropylamine (DIPEA) were dissolved in DMF. The solution was stirred for 20 h at room temperature. All solvents were removed by rotary evaporation. Ethyl acetate was added, resulting in the precipitation of the ammonium halide salt, which was filtered off and discarded. The filtrate was concentrated to dryness yielding a brown oil, which was purified by silica gel column chromatography using CH_2Cl_2/MeOH (11:1) as eluent. A small yellow fraction containing some of the haloacetylated amino acid ester starting material eluted first. The product was eluted next as a broad light yellow (yellow in the case of **3a**) fraction. A third yellow fraction, which was well separated from the product, was usually not collected. The solution containing the desired product was concentrated to dryness by rotary evaporation and the resulting light yellow oil dried under vacuum.

bpaAc−Phe−OMe (3a): 9.00 g (29.98 mmol) of **4a**, 5.91 g (29.98 mmol) of bpa, 5.20 mL (29.98 mmol) of DIPEA, 100 mL of DMF, 100 mL of AcOEt. Yield: 10.17 g (24.31 mmol, 81%). − $C_{24}H_{26}N_4O_3$ (418.5 g/mol): FD-MS ($CDCl_3$); *m/z*: 418 [M^+]. − ^{1}H NMR (300 MHz, $CDCl_3$): δ = 2.00 (H_2O), 3.12−3.29 (ABX, 2 H, $^{\beta}CH_2$), 3.26 [s, 2 H, C(O)−CH_2], 3.69 (s, 3 H, OCH_3), 3.73, 3.85 (2 × d, 4 H, $^2J_{HH}$ = 14.2 Hz, 2 × py-CH_2), 4.90 (m, 1 H, $^{\alpha}CH$), 7.18 (m, 9 H, 5 × H-Ph + H3-py + H5-py), 7.56 (m, 2 H, H4-py), 8.52 (d, 2 H, $^3J_{HH}$ = 4.9 Hz, H6-py), 9.05 (d, 1 H, $^3J_{HH}$ = 8.0 Hz, NH). − ^{13}C NMR (75 MHz, $CDCl_3$): δ = 37.5 ($^{\beta}C$), 52.1 (OCH_3), 53.1 ($^{\alpha}C$), 57.6 [C(O)−CH_2], 60.1 (py-CH_2), 122.3, 122.9 (C3-py + C5-py), 126.80, 128.4, 129.2 (C2-Ph + C3-Ph + C4-Ph + C5-Ph + C6-Ph), 136.5 (3 C, 2 × C4-py + C1-Ph), 149.1 (C6-py), 158.2 (C2-py), 171.2, 172.1 [C(O)-ester + C(O)-amide]. − IR (film on NaCl): $\tilde{\nu}$ = 1745 cm^{-1} (COOMe), 1672 (amide I), 1513 (amide II). − Circular Dichroism (10^{-3} M in methanol): λ, nm ([θ] × 10^4 °cm^{2}dmol^{-1}) = 221 (+1.13), 257 (+0.05), 265 (+0.13).

bpaAc−Lys(Z)−OMe (3b): 1.83 g (4.41 mmol) of **4b**, 877 mg (4.41 mmol) of bpa, 0.77 mL (4.41 mmol) of DIPEA, 50 mL of DMF, 30 mL of AcOEt. Yield: 1.67 g (3.13 mmol, 71%). − $C_{29}H_{35}N_5O_5$ (533.6 g/mol): FD-MS ($CDCl_3$); *m/z*: 534 (M^+). − ^{1}H NMR (300 MHz, $CDCl_3$): δ = 1.39 (m, 2 H, $^{\gamma}CH_2$), 1.51 (m, 2 H, $^{\delta}CH_2$), 1.85 (m, 2 H, $^{\beta}CH_2$), 3.12 (m, 2 H, $^{\varepsilon}CH_2$), 3.35 [s, 2 H, C(O)−CH_2], 3.67 (s, 3 H, OCH_3), 3.78, 3.86 (2 × d, 4 H, $^2J_{HH}$ = 9.7 Hz, 2 × py-CH_2), 4.60 (m, 1 H, $^{\alpha}CH$), 5.06 (s, 2 H, Z-CH_2), 5.21 (m, 1 H, Z-NH), 7.14 (dd, 2 H, H5-py), 7.32 (m, 7 H, Z-Ph + H3-py), 7.60 (dd, 2 H, H4-py), 8.53 (d, 2 H, $^3J_{HH}$ = 4.56 Hz, H6-py), 9.22 (d, 1 H, $^3J_{HH}$ = 7.3 Hz, NH). − ^{13}C NMR (75 MHz, $CDCl_3$): δ = 22.7 ($^{\gamma}C$), 29.3 ($^{\delta}C$), 31.7 ($^{\beta}C$), 40.7 ($^{\varepsilon}C$), 51.7, 52.0 (OCH_3 + $^{\alpha}C$), 57.8 [C(O)−CH_2], 60.5 (py-CH_2), 66.4 (Z-CH_2), 122.4, 123.1 (C3-py + C5-py), 128.0, 128.1, 128.3, 128.4 (Z-C2-Ph + Z-C3-Ph + Z-C4-Ph + Z-C5-Ph + Z-C6-Ph), 136.6 (2 C, Z-C1-Ph + C4-py), 149.2 (C6-py), 156.4, 158.3 [C(O)-Z + C2-py], 171.5, 172.8 [C(O)-ester + C(O)-amide]. − IR (film on NaCl): $\tilde{\nu}$ = 1741 cm^{-1} (COOMe), 1718 (Z-urethane), 1668 (amide I), 1529 (amide II). − Circular Dichroism (10^{-3} M in methanol): λ, nm ([θ] × 10^4 °cm^{2}dmol^{-1}) = 216 (+0.40), 263 (+0.15).

bpaAc−Gly−OEt (3c): 7.87 g (43.81 mmol) of ClAc−Gly−OEt; 8.72 g (43.81 mmol) of dpa, 7.65 mL (43.81 mmol) of DIPEA, 100 mL of DMF, 100 mL of AcOEt. Yield: 6.04 g (17.60 mmol, 40%). − $C_{18}H_{22}N_4O_3$ (342.4 g/mol): FD-MS ($CDCl_3$); *m/z*: 342 [M^+]. − ^{1}H NMR (300 MHz, $CDCl_3$): δ = 1.24 (t, 3 H, $^3J_{HH}$ = 7.1 Hz, OCH_2CH_3), 2 (H_2O), 3.37 [s, 2 H, C(O)−CH_2], 3.90 (s, 4 H, py-CH_2), 4.08 (d, 2 H, $^3J_{HH}$ = 5.9 Hz, $^{\alpha}CH_2$), 4.18 (q, 2 H, $^3J_{HH}$ = 7.1 Hz, OCH_2CH_3), 7.16 (dd, 2 H, H5-py), 7.35 (d, 2 H, H3-py), 7.63 (m, 2 H, H4-py), 8.55 (d, 2 H, H6-py), 9.07 (m, 1 H, NH). − ^{13}C NMR (75 MHz, $CDCl_3$): δ = 14.1 (OCH_2CH_3), 41.0 ($^{\alpha}C$), 57.9 [C(O)−CH_2], 60.2 (py-CH_2), 61.1 (OCH_2CH_3), 122.4 (C3-py), 123.3 (C5-py), 136.6 (C4-py), 149.2 (C6-py), 158.3 (C2-py), 169.8, 171.8 [C(O)-ester + C(O)-amide]. − IR (film on NaCl): $\tilde{\nu}$ = 1747 cm^{-1} (COOEt), 1674 (amide I), 1525 (amide II).

Zn Complexes

General Procedure: Solid $Zn(OTf)_2$ was added in one portion to a stirred solution of 1 equiv. of the respective ligand in CH_3CN. Stirring was continued overnight at room temp. followed by removal of all solvent under vacuum. CH_2Cl_2 was added to the residue and the resulting suspension left in a refrigerator (−20 °C) overnight. Unchanged $Zn(OTf)_2$ precipitated and was filtered off. In the case of **7b** the solvent was removed by rotary evaporation and the residue dried under vacuum. Further purification was not possible since the compound did not precipitate but rather separated as an oil from common organic solvents. Accordingly, the reported yield refers to the crude product. The two other complexes (**6c** and **7a**) were purified by addition of Et_2O to the clear CH_2Cl_2 filtrate and recrystallization at −20 °C. These complexes precipitated overnight as colorless microcrystalline solids. Yields are reported for recrystallized samples. It is evident from C,H,N analysis and NMR data that the bpaAc−Gly−OEt complex **6c** was isolated without significant amounts of coordinated water whereas the same workup affords the corresponding aquo complex **7a** for bpaAc−Phe−OMe. Single crystals suitable for X-ray structure analysis of **6c** and **7a** were obtained by slow recrystallization of the pure complexes from CH_2Cl_2/Et_2O at −20 °C under dry nitrogen over a period of several weeks.

[(bpaAc−Gly−OEt)(OTf)Zn](OTf) (6c): 426 mg (1.24 mmol) of **5**, 416 mg (1.24 mmol) of $Zn(OTf)_2$, 10 mL of CH_3CN, 10 mL of CH_2Cl_2. Yield: 573 mg (0.81 mmol, 65%). − $C_{20}H_{22}F_6N_4O_9S_2Zn$ (705.9 g/mol): calcd. C 34.03, H 3.14, N 7.94; found C 33.85, H 3.25, N 7.74. − FAB-MS (nitrobenzyl alcohol); *m/z*: 555 (**3c**-ZnOTf$^+$), 407 (**3c**-Zn$^+$). − ^{1}H NMR (300 MHz, $CDCl_3$): δ = 1.21 (t, 3 H, $^3J_{HH}$ = 7.1 Hz, OCH_2CH_3), 4.04 [s, 2 H, C(O)−CH_2], 4.10 (m, 4 H, $^{\alpha}CH_2$, OCH_2CH_3), 4.34, 4.44 (2 × d, 4 H, $^2J_{HH}$ = 5.6 Hz, 2 × py-CH_2), 7.63 (m, 4 H, H5-py + H3-py), 8.05 (m, 2 H, H4-py), 8.92 (d, 2 H, H6-py), 9.03 (m, 1 H, NH). − ^{13}C NMR (75 MHz, $CDCl_3$): δ = 13.9 (OCH_2CH_3), 42.4 ($^{\alpha}C$), 56.2 [C(O)−CH_2], 57.8 (py-CH_2), 61.8 (OCH_2CH_3), 120.2 (q, $^1J_{CF}$ = 301.9 Hz, OTf^-), 125.3, 125.9 (C3-py, C5-py), 141.9 (C4-py), 149.2 (C6-py), 154.3 (C2-py), 167.5, 174.3 [C(O)-ester + C(O)-amide]. − IR (KBr): $\tilde{\nu}$ = 1747 cm^{-1} (COOEt), 1641 (amide I), 1245 (CF_3SO_3), 1218 (CF_3SO_3).

[(bpaAc−Phe−OMe)(H_2O)Zn](OTf)$_2$ (7a): 743 mg (1.77 mmol) of **3a**, 643 mg (1.77 mmol) of $Zn(OTf)_2$, 15 mL of CH_3CN, 15 mL of CH_2Cl_2. Yield: 964 mg (1.20 mmol, 68%). − $C_{26}H_{28}F_6N_4O_{10}S_2Zn$ (800.0 g/mol): calcd. C 39.03, H 3.53, N 7.00; found C 38.94, H 3.53, N 6.82. − FAB-MS (nitrobenzyl alcohol); *m/z*: 631 (**3a**-ZnOTf$^+$), 481 (**3a**-Zn$^+$). − ^{1}H NMR (300 MHz, $CDCl_3$): δ = 2.84, 3.23 (ABX, 2 H, $^{\beta}CH_2$), 3.66 (s, 3 H, OCH_3), 3.67 [d, 1 H, $^2J_{HH}$ = 16.8 Hz, py-CH(A′)*H*(B′)], 3.70 [d, 1 H, $^2J_{HH}$ = 16.8 Hz, C(O)−CH(C)*H*(D)], 3.98 [d, 3 H, $^2J_{HH}$ = 16.8 Hz, C(O)−C*H*(C)H(D) + H_2O], 4.08 [d, 1 H, $^2J_{HH}$ = 16.8 Hz, py-CH(A)*H*(B)], 4.29 [d, 1 H, $^2J_{HH}$ = 16.8 Hz, py-CH(*A′*)H(B′)], 4.44 [d, 1 H, $^2J_{HH}$ = 16.8 Hz, py-CH(*A*)H(B)], 4.99 (m, 1 H, $^{\alpha}CH$), 6.62 (dd, 1 H, H4-Ph), 6.98 (dd, 2 H, H3,5-Ph), 7.19 (d, 2 H, H2,6-Ph),

Table 2. Details of crystal structure analyses

Compound	**6c**	**7a**
Empirical formula	$C_{20}H_{21}F_6N_4O_9S_2Zn$	$C_{26}H_{26}F_6N_4O_{10}S_2Zn \cdot H_2O$
Molecular mass	704.90	816.01
Temperature	200(2) K	200(2) K
Wavelength [Å]	0.71073	0.71073
Crystal system	monoclinic	monoclinic
Space group	$P2_1/n$	$P2_1$
a [Å]	15.4015(8)	13.8284 (18)
b [Å]	9.2332(5)	9.4051(19)
c [Å]	21.0333(11)	14.290(3)
β [°]	108.1050(10)	106.426(18)
Volume [Å^3]	2843.0(3)	1782.7(6)
Z	4	2
Calculated density	1.647 Mg/m^3	1.520 Mg/m^3
Absorption coefficient	1.104 mm^{-1}	0.896 mm^{-1}
F(000)	1428	832
Crystal size [mm]	0.4 × 0.2 × 0.2	0.25 × 0.15 × 0.15
θ range [°]	1.96−28.36	1.54−28.30
Index ranges	$-20 \le h \le 20$ $-12 \le k \le 11$ $-28 \le l \le 27$	$-18 \le h \le 18$ $-12 \le k \le 12$ $-18 \le l \le 18$
Reflections collected/unique	28766/6920	19429/8552
Refinement method	based on F^2	based on F^2
Data/restr./parameters	6920/0/388	8552/1/473
Goodness-of-fit on F^2	1.087	0.886
Final R indices [$I > 2\sigma(I)$]	$R1$ = 0.0410 $wR2$ = 0.1135	$R1$ = 0.0423 $wR2$ = 0.0697
R indices (all data)	$R1$ = 0.0549 $wR2$ = 0.1203	Rl = 0.1026 $wR2$ = 0.0806
Largest diff. peak and hole	0.874 and −1.065 eÅ^{-3}	0.361 and −0.411 Å^{-3}

7.62 (m, 4 H, H3-py + H5-py), 8.01, 8.08 (2 × m, 2 H, H4-py), 8.83, 8.85 (2 × m, 2 H, H6-py), 9.02 (d, 1 H, $^3J_{HH}$ = 8.6 Hz, NH). − ^{13}C NMR (75 MHz, $CDCl_3$): δ = 37.87 ($^{\beta}$C), 52.74 (OCH_3), 55.28 ($^{\alpha}$C), 56.04 [C(O)−CH_2], 57.58, 57.68 (py−CH_2), 120.21 (q, $^1J_{CF}$ = 317 Hz, OTf$^-$), 125.12, 125.36, 125.73 (2 × C3-py + 2 × C5-py), 126.42, 128.01, 129.74 (C2-Ph + C3-Ph + C4-Ph + C5-Ph + C6-Ph), 135.76 (C1-Ph), 141.71, 141.79 (2 × C4-py) 148.97, 149.04 (2 × C6-py), 154.25, 154.30 (2 × C2-py), 169.78, 173.46 [C(O)-ester + amide]. − IR (KBr): $\tilde{\nu}$ = 1749 cm^{-1} (COOMe), 1633 (amide I), 1284 (CF_3SO_3), 1245 (CF_3SO_3). − Circular Dichroism (10^{-3} M in methanol): λ, nm ([θ] × 10^4 °cm^{2}dmol^{-1}) = 219 (+2.05), 246 (−0.05), 265 (−0.26), 270 (−0.26).

[(bpa-Lys(Z)−OMe)(H_2O)Zn](OTf)$_2$ (7b): 131 mg (0.25 mmol) of **3b**, 91 mg (0.25 mmol) of Zn(OTf)$_2$, 10 mL of CH_3CN, 5 mL of CH_2Cl_2. Yield: 161 mg (0.19 mmol, 76%). − FAB-MS (nitrobenzyl alcohol); *m/z*: 746 (**3b**-ZnOTf$^+$), 596 (**3b**-Zn$^+$). − ^{1}H NMR (300 MHz, $CDCl_3$): δ = 1.20 (m, 2 H, $^{\gamma}CH_2$), 1.46 (m, 2 H, $^{\delta}CH_2$), 1.73 (m, 2 H, $^{\beta}CH_2$), 3.07 (m, 2 H, $^{\varepsilon}CH_2$), 3.67 (s, 3 H, OCH_3), 3.93, 4.04 [2 × d, 2 H, $^2J_{HH}$ = 17.4 Hz, C(O)−CH_2], 4.38 (m, 5 H, 2 × py-CH_2 + $^{\alpha}$CH), 5.07 (s, 2 H, CH_2-Z), 5.21 (m, 1 H, NH-Z), 7.35 (m, 5 H, Ph-Z), 7.54 (m, 4 H, 2 × H3-py + 2 × H5-py), 8.00 (m, 2 H, 2 × H4-py), 8.80 (m, 3 H, 2 × H6-py + NH). − ^{13}C NMR (75 MHz, $CDCl_3$): δ = 22.4 ($^{\gamma}$C), 29.0 ($^{\delta}$C), 30.5 ($^{\beta}$C), 40.4 ($^{\varepsilon}$C), 52.6 (OCH_3), 53.9 ($^{\alpha}$C), 56.9 [C(O)−CH_2], 58.8 (py-CH_2), 67.9 (Z-CH_2), 120.1 (q, $^1J_{CF}$ = 323 Hz, OTf$^-$), 125.1, 125.6 (C3-py + C5-py), 127.8, 128.0, 128.5 (5 C, Z-C2-Ph + Z-C3-Ph + Z-C4-Ph + Z-C5-Ph + Z-C6-Ph), 136.8 (2 C, Z-C1-Ph), 141.4 (C4-py), 148.6 (C6-py), 154.0 (C2-py), 156.8 [C(O)-Z], 170.6, 173.3 [C(O)-ester + C(O)-amide]. − IR (KBr): $\tilde{\nu}$ = 1745 cm^{-1} (COOMe), 1708 (Z-urethane), 1637 (amide I), 1283 (CF_3SO_3), 1253 (CF_3SO_3). − Circular Dichroism (10^{-3} M in methanol): λ, nm ([θ] × 10^4 °cm^{2}dmol^{-1}) = 213 (+0.37), 235 (−0.03), 264 (−0.26), 269 (−0.26).

X-ray Data Collection and Structure Refinement Details: Crystal data and experimental conditions are listed in Table 2. The molecular structures are illustrated in Figures 1 and 2. Selected bond lengths and bond angles with standard deviations in parentheses are presented in Table 1. Intensity data were collected with a Siemens SMART 5000 CCD-Diffractometer with graphite-monochromated Mo-K_α radiation (λ = 0.71073 Å). The exposure time was 10 s per frame collected with the ω-scan technique (Δω = 0.3°). The collected reflections were corrected for Lorentz, polarization and absorption effects. The structures were solved by direct methods and refined by full-matrix least-squares methods on F^2.[54]−[56] Non-hydrogen atoms were refined with anisotropic thermal parameters in both structures. The hydrogen atoms of the coordinated water molecule and the amide hydrogen atom of **7a** were localized from the difference electron density map and refined with isotropic thermal parameters. All other hydrogen atoms were fixed in geometrically calculated positions and isotropically refined. Details of the crystal structure determinations have been deposited at the Cambridge Crystallographic Data Centre as supplementary publication nos. CCDC-140521 (**6c**) and -140522 (**7a**). Copies of the data can be obtained free of charge on application to CCDC, 12 Union Road, Cambridge CB2 1EZ, U.K. [Fax: (internat.) + 44-1223/336-033; E-mail: deposit@ccdc.cam.ac.uk].

Acknowledgments

The authors gratefully acknowledge financial support from the Deutsche Forschungsgemeinschaft. We thank Prof. Rudi van Eldik who generously let us share his equipment, laboratory space, and

funding. We also thank Dr. Reiner Waibel at the Institute for Pharmacy and Food Chemistry, University of Erlangen, for his help with the circular dichroism measurements.

[1] E. Uhlmann, A. Peyman, G. Breipohl, D. W. Will, *Angew. Chem.* **1998**, *110*, 2954−2983.
[2] D. K. Smith, F. Diederich, *Chem. Eur. J.* **1998**, *4*, 1353−1361.
[3] X. Cha, K. Ariga, T. Kunitake, *J. Am. Chem. Soc.* **1996**, *118*, 9545−9551.
[4] T. Lescrinier, C. Hendrix, L. Kerremans, J. Rozenski, A. Link, B. Samyn, A. van Aerschot, E. Lescrinier, R. Eritja, J. van Beeumen, P. Herdewijn, *Chem. Eur. J.* **1998**, *4*, 425−433.
[5] N. Voyer, J. Lamothe, *Tetrahedron* **1995**, *51*, 9241−9284.
[6] J. P. Schneider, J. W. Kelly, *Chem. Rev.* **1995**, *95*, 2169−2187.
[7] T. Hohsaka, D. Kajihara, Y. Ashizuka, H. Murakami, M. Sisido, *J. Am. Chem. Soc.* **1999**, *121*, 34−40.
[8] E. Graf von Roedern, E. Lohof, G. Hessler, M. Hoffmann, H. Kessler, *J. Am. Chem. Soc.* **1996**, *118*, 10156−10167.
[9] B. Imperiali, R. S. Roy, *J. Am. Chem. Soc.* **1994**, *116*, 12083−12084.
[10] T. Carell, J. Butenandt, *Angew. Chem.* **1997**, *109*, 1590−1593.
[11] G. Strukul, *Angew. Chem.* **1998**, *110*, 1256−1267.
[12] G. G. Melikyan, *Aldrichim. Acta* **1998**, *31*, 50−64.
[13] M. Shibasaki, H. Sasai, T. Arai, *Angew. Chem.* **1997**, *109*, 1290−1310.
[14] A. Blasko, T. C. Bruice, *Acc. Chem. Res.* **1999**, *32*, 475−484.
[15] N. H. Williams, B. Takasaki, M. Wall, J. Chin, *Acc. Chem. Res.* **1999**, *32*, 485−493.
[16] J.-M. Lehn, *Chem. Eur. J.* **1999**, *5*, 2455−2463.
[17] B. Jandeleit, D. J. Schaefer, T. S. Powers, H. W. Turner, W. H. Weinberg, *Angew. Chem.* **1999**, *111*, 2648−2689.
[18] D. E. Reichert, J. S. Lewis, C. J. Anderson, *Coord. Chem. Rev.* **1999**, *184*, 3−66.
[19] W.-W. V. Yam, K.-W. K. Lo, *Coord. Chem. Rev.* **1999**, *184*, 157−240.
[20] Z. Guo, P. J. Sadler, *Angew. Chem.* **1999**, *111*, 1610−1630.
[21] F. Ruan, Y. Chen, P. B. Hopkins, *J. Am. Chem. Soc.* **1990**, *112*, 9403.
[22] F. Ruan, Y. Chen, K. Itoh, T. Sasaki, P. B. Hopkins, *J. Org. Chem.* **1991**, *56*, 4347.
[23] K. Shah, T. M. Rana, *Synth. Commun.* **1996**, *26*, 2695−2702.
[24] B. Imperiali, S. L. Fisher, *J. Am. Chem. Soc.* **1991**, *113*, 8527−8528.
[25] B. Cuenod, A. Schepartz, *Tetrahedron Lett.* **1991**, *33*, 3325.
[26] B. Cuenod, A. Schepartz, *Science* **1993**, *259*, 510.
[27] R. Alsfasser, R. van Eldik, *Inorg. Chem.* **1996**, *35*, 628−636.
[28] B. Geißer, R. Alsfasser, *Eur. J. Inorg. Chem.* **1998**, 957−963.
[29] B. Geißer, A. Ponce, R. Alsfasser, *Inorg. Chem.* **1999**, *38*, 2030−2037.
[30] D. D. Cox, S. J. Benkovic, L. M. Bloom, F. C. Bradley, M. J. Nelson, L. Que, D. E. Wallick, *J. Am. Chem. Soc.* **1988**, *110*, 2026−2032.
[31] M. Bodanszky, A. Bodanszky, *The Practice of Peptide Synthesis*, Springer Verlag, Berlin, **1994**.
[32] D. Parker, *Chem. Soc. Rev.* **1990**, *19*, 271−291.
[33] A. A. Watson, A. C. Willis, D. P. Fairlie, *Inorg. Chem.* **1997**, *36*, 752−753.
[34] P. M. Angus, A. J. Elliot, A. M. Sargeson, A. C. Willis, *J. Chem. Soc., Dalton Trans.* **1999**, 1131−1136.
[35] C. S. Allen, C.-L. Chuang, M. Cornebise, J. W. Canary, *Inorg. Chim. Acta* **1995**, *239*, 29−37.
[36] A. Abufarag, H. Vahrenkamp, *Inorg. Chem.* **1995**, *34*, 2207−2216.
[37] J. Wirbser, H. Vahrenkamp, *Z. Naturforsch.* **1992**, *47b*, 962−968.
[38] J. Glerup, P. A. Goodson, D. J. Hodgson, K. Michelsen, K. M. Nielsen, H. Weihe, *Inorg. Chem.* **1992**, *31*, 4611−4616.
[39] J. W. Canary, C. S. Allen, J. M. Castagnetto, Y. Wang, *J. Am. Chem. Soc.* **1995**, *117*, 8484−8485.
[40] J. W. Canary, C. S. Allen, J. M. Castagnetto, Y.-H. Chiu, P. J. Toscano, Y. Wang, *Inorg. Chem.* **1998**, *37*, 6255−6262.
[41] G. Snatzke, *Angew. Chem.* **1968**, *80*, 15−26.
[42] L. Velluz, M. Legrand, *Angew. Chem.* **1965**, *77*, 842−850.
[43] P. Xie, M. Diem, *J. Am. Chem. Soc.* **1995**, *117*, 429−437.
[44] M. T. Werth, S.-F. Tang, G. Formicka, M. Zeppezauer, M. K. Johnson, *Inorg. Chem.* **1995**, *34*, 218−228.
[45] D. R. Benson, B. R. Hart, X. Zhu, M. B. Doughty, *J. Am. Chem. Soc.* **1995**, *117*, 8502−8510.
[46] M. Y. Ogawa, A. B. Gretchikhine, S. D. Soni, S. M. Davis, *Inorg. Chem.* **1995**, *34*, 6423.
[47] R. P. Bonomo, S. Pedotti, G. Vecchio, E. Rizzarelli, *Inorg. Chem.* **1996**, *35*, 6873−6877.
[48] R. P. Houser, M. P. Fitzsimons, J. K. Barton, *Inorg. Chem.* **1999**, *38*, 1368−1370.
[49] R. E. Austin, R. A. Maplestone, A. M. Sefler, K. Liu, W. N. Hruzewicz, C. W. Liu, H. S. Cho, D. E. Wemmer, P. A. Bartlett, *J. Am. Chem. Soc.* **1997**, *119*, 6461−6472.
[50] L. Grondahl, N. Sokolenko, G. Abbenate, D. P. Fairlie, G. R. Hanson, L. R. Gahan, *J. Chem. Soc., Dalton Trans.* **1999**, 1227−1234.
[51] R. Winter, F. Noll, *Methoden der Biophysikalischen Chemie*, Teubner, Stuttgart, **1998**.
[52] F. Hojland, H. Toftlund, S. Yde-Andersen, *Acta Chem. Scand.* **1983**, *A37*, 251−257.
[53] J. K. Romary, R. D. Zachariasen, J. D. Barger, H. Schiesser, *J. Chem. Soc. C* **1968**, 2884.
[54] Siemens Area Detector Absorption Correction, Siemens.
[55] G. M. Sheldrick, *SHELX-97*; Universität Göttingen, **1997**.
[56] L. Zsolnai, *xpma, zortep*, Universität Heidelberg, **1997**.

Received December 2, 1999
[I99439]

Reactions of UCl_4 with *t*Bu-Calix[4, 5, and 6]arenes: The First "Non-Uranyl" Calixarene Complexes of Uranium

Pascal C. Leverd*[a] and Martine Nierlich[a]

Keywords: Alkoxides / Calixarenes / Uranium

The reactions of UCl_4 with *t*Bu-calix[4, 5, and 6]arenes (*t*Bu-calix[*n*]arene = $H_nL[n]$) were used to isolate $[\{UCl(L[4])\}_3O]$ (**1**), $[\{U(L[5])\}_2O]^{2-}$ (**2**), and $[U(H_3L[6])_2]$ (**4**). The dianionic species **2** could be oxidized to its U^{VI} homologue $[\{U(L[5])\}_2O]$ (**3**). In contrast to **1**–**3** that are located around a μ-oxo bridge, **4** can be viewed as a homoleptic alkoxide. **1**–**4** are the first "non-uranyl" calixarene complexes of uranium to be reported.

Introduction

Calixarenes are made of phenolic units linked by methylene bridges into a macrocyclic arrangement.[1] For reasons linked with environmental needs and with the management of nuclear waste solutions, the actinide complexes of these potential polyalkoxide ligands have always attracted special attention from coordination chemists.[2] Research has particularly focussed on the complexes of the uranyl cation $[UO_2]^{2+}$,[3] partly because the special coordination requirements of this cation was thought to be particularly suited to the geometry of calixarenes. However, apart from the work on uranyl cations, surprisingly few complexes of the 5f-metals have been fully characterized. In fact, the thorium compound $[Th_4(HL[8])(H_2L[8])(dmso)_4(OH)_3(OH_2)]$ ($H_nL[n]$ = *t*Bu-calix[*n*]arene, dmso = Me_2SO) is the only "non-uranyl" actinide complex of this family of macrocycles whose crystal structure is available, to date, in the literature.[4] In an attempt to widen the scope of calixarene coordination chemistry to the complexes of uranium at lower oxidation states, we set out to study the reactions of UCl_4 with *t*Bu-calix[4, 5, and 6]arenes. We report herein the synthesis and the X-ray characterization of $[\{UCl(L[4])\}_3O]$ (**1**), $[\{U(L[5])\}_2O]^{2-}$ (**2**), $[\{U(L[5])\}_2O]$ (**3**), and $[U(H_3L[6])_2]$ (**4**). Complexes **1**−**4** are the first "non-uranyl" calixarene complexes of uranium to be reported.

Results and Discussion

When UCl_4 is treated with $H_4L[4]$ or $H_5L[5]$ in pyridine, the pale green solution turns slowly to red. After a few hours of heating the two components at 333 K, the dark red colour turns to black, in the case of $H_4L[4]$, and to a very dark red in the case of $H_5L[5]$. The solutions were allowed to stand, and after a few days, crystals suitable for X-ray crystallography were isolated. The structures were solved and revealed that $[\{UCl(L[4])\}_3O]$ (**1**) and $[\{U(L[5])\}_2O]^{2-}$ (**2**) had been produced by the reaction.

$$3\ UCl_4 + 3\ H_4L[4] \xrightarrow[H_2O]{\text{pyridine}} [\{UCl(L[4])\}_3O] + 12[HNC_5H_5]Cl$$

$$2\ UCl_4 + 2\ H_5L[5] \xrightarrow[H_2O]{\text{pyridine}} [HNC_5H_5]_2[\{U(L[5])\}_2O] + 8[HNC_5H_5]Cl$$

The formation of oxo-alkoxide species such as **1** and **2** is often observed in the process of synthesizing homoleptic alkoxide complexes.[5] The presence of the oxygen atom is usually explained by the hydrolysis of the intermediates by even traces of water or by a number of other possible mechanism e.g. elimination of ether. In our case, the extreme sensitivity of uranium alkoxide to moisture and the absence of any evidence for the chemical transformation of the calixarenes seems to indicate that water is present in the reaction mixture. The syntheses of **1** and **2** were nonetheless very reproducible, and starting from $H_4L[4]$ and $H_5L[5]$, we never managed not to obtain the oxo species. We are currently investigating the reaction of UCl_4 with the sodium salts of calixarenes, which should help to keep the reaction mixture rigorously dry.

Complex **1** is a trinuclear cluster organized around a μ_3-oxo bridge (Figure 1). The two-electron donor O(5) located on the C_3 axis binds the three metal cations in an almost planar fashion (±0.085 Å). This triangular geometry is often encountered in uranium chemistry, and the U(1)−O(5) bond length of 2.224(2) Å is not exceptional when compared to those of other clusters described in the literature.[6] The calixarene is fully deprotonated and all its phenolate groups form σ bonds with the metal center [U−O between 2.042(9) and 2.217(8) Å]. One of the oxygen atoms of the macrocycle [O(2)] helps to maintain the geometry of the cluster by bridging two adjacent uranium atoms [U−O 2.549(8) Å]. One unchanged chloride ligand is still present on each metal cation [U−Cl 2.645(4) Å]. All three U−Cl bonds point in a direction nearly parallel to the C_3 axis. The U−O and U−Cl bond lengths compare well with those found in the literature.[7] Large U−O−C angles of terminal

[a] CEA-Saclay, Service de Chimie Moléculaire,
Bât. 125, 91191 Gif sur Yvette, France
Fax: (internat.) + 33-1/69086640
leverd@drecam.cea.fr

 © WILEY-VCH Verlag GmbH, D-69451 Weinheim, 2000 1434−1948/00/0808−1733 $ 17.50+.50/0

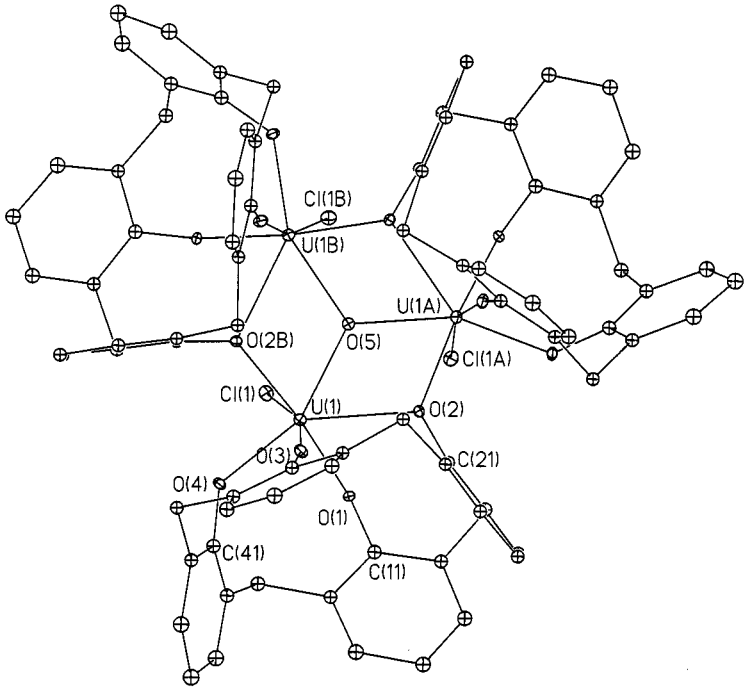


Figure 1. X-ray structure of complex **1** projected along the C_3 axis; all *t*Bu groups and hydrogen atoms or solvent molecules have been omitted for clarity; selected bond lengths [Å] and angles [°] with estimated standard deviations in parentheses: U(1)−O(1) 2.042(9), U(1)−O(2) 2.217(8), U(1)−O(3) 2.08(1), U(1)−O(4) 2.111(9), U(1)−O(5) 2.224(2), U(1)−Cl(1) 2.645(4), U(1)−U(1A) 3.831(2), U(1)−O(2B) 2.549(8); U(1)−O(5)−U(1A) 118.9(2), O(5)−U(1)−Cl(1) 80.9(4), U(1)−O(1)−C(11) 172.3(9), U(1)−O(2)−C(21) 120.4(7), U(1)−O(2A)−C(21A) 132.8(8), U(1)−O(3)−C(31) 171.0(9), U(1)−O(4)−C(41) 130.8(7)

alkoxide ligands are usually interpreted in terms of π-electron donation from the oxygen lone-pair orbitals to the metal ion.[8] These angles range between 130.8(7) and 172(3)° in **1**, which could be associated with substantial π-donation from at least two phenolate groups of the macrocycle [O(1) and O(3)]. However, in the case of bulky ligands such as calixarenes, it seems difficult to draw a line between steric requirements and electronic properties. The three cations share 17 electrons donated by the ligands, formally making **1** a mixed valence complex, with two of its metal centers in the oxidation state +VI and one in +V. Nonetheless, no difference could be observed in the environment of the three metal cations due to the presence of the C_3 axis of symmetry. The remaining electron is therefore likely to be equally shared by the three equivalent cations.[9] After $[U_2(O\mathit{t}Bu)_9]$ (+IV and +V) and $[\{(THF)U(OPh)_3(\mu_2\text{-}OPh)(\mu_3\text{-}O)(UO_2)(THF)\}_2]$ (+V and +VI), **1** is only the third mixed-valence uranium alkoxide to be described.[8][6b] Each metal cation is coordinated by seven donor atoms: The geometry around the uranium center is a distorted capped trigonal prism [O(1)−O(3)−O(2) and O(5)−Cl(1)−O(2B) define the faces of the prism, while O(4) is the cap]. The "$U_3Cl_3(\mu_3\text{-}O)(\mu_2\text{-}OR)_3$" core results from the arrangement of three such polyhedrons sharing an edge [O(5)−O(2) and its symmetry equivalents]. One molecule of pyridine is present in each calix[4]arene cavity. Whereas fused "double calixarenes" are well-known species in coordination chemistry and have been successfully used in the synthesis of metal networks,[10] **1** is the first example of a fused "triple calixarene" (Figure 2).[11] Complex **1** organizes three cone-shaped cavities and directs them in three directions of space that are separated by an angle of 120°. These three macrocycles are occupied by guest pyridine molecules in the solid state. If an adequate inclusion spacer was found to link these cavities, **1** could represent a unique paramagnetic building block for the design of new supramolecular two-dimensional networks. The other potential interest of **1** is the study of the reactivity that could take place around the remaining chloride anions. The example of $[cis\text{-}Cl_2W(L[4])]$ has already proven that a rich chemistry could be built around the displacement of the halide ligands of a metal calixarene complex.[12]

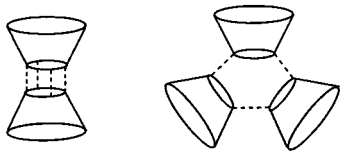


Figure 2. Schematic representation of the fused "double" and "triple" calixarenes

Complex **2** is a dinuclear complex located around a μ_2-oxo bridge (Figure 3). The two-electron donor, O(6), sits on the inversion center of the molecule and binds the two metal cations in a perfectly linear fashion. The U−O−U moiety is then sandwiched between two fully deprotonated *t*Bu-calix[5]arene units. Such a linear mode of binding [U(1)−O(6) 2.0969(9) Å] is commonplace in uranium chem-

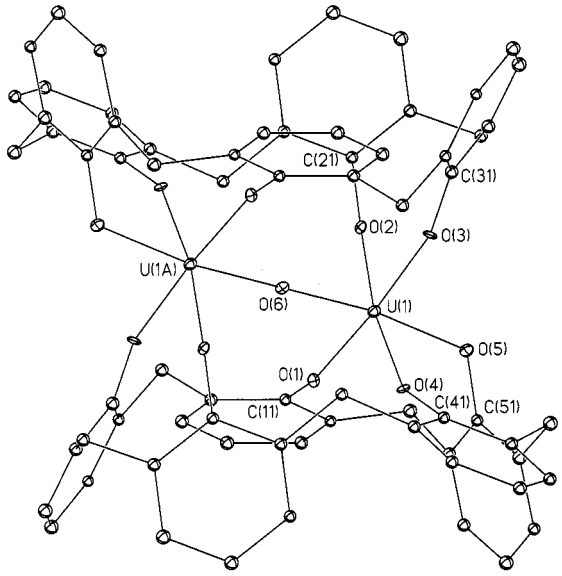


Figure 3. X-ray structure of complex **2**; all *t*Bu groups, hydrogen atoms, and solvent molecules have been omitted for clarity; respective selected bond lengths and mean bond lengths [Å] and angles [°] with estimated standard deviations in parentheses for **2** and **3**: U(1)−O(1) 2.141(9), 2.159(6); U(1)−O(2) 2.158(9), 2.112(6); U(1)−O(3) 2.110(9), 2.112(6); U(1)−O(4) 2.155(9), 2.154(6); U(1)−O(5) 2.186(9), 2.143(6); U(1)−O(6) 2.0969(9), 2.078(6); U(1)−O(1)−C(11) 152.0(8), 153.0(6); U(1)−O(2)−C(21) 142.4(8), 149.1(6); U(1)−O(3)−C(31) 160.8(8), 155.6(6); U(1)−O(4)−C(41) 156.0(7), 154.4(6); U(1)−O(5)−C(51) 120.9(7), 123.6(5)

istry.[13] The geometry around the metal center is distorted octahedral [minimum and maximum O−U−O angles equal 83.0(4) and 96.3(4)°, respectively] with each $L[5]^{5-}$ ligand binding the first uranium cation with three of its phenolate groups and the second metal cation with the other two. Of the 6 pyridine molecules found in the lattice, four were found to form pyridinium dimers (N−HN bond length of 2.98 Å). One of the pyridine molecules of the dimer is included in the cavity of the macrocycle. Such inclusion of a cation in the aromatic cavity of a calixarene is a common feature in calixarene chemistry.[14] The presence of two organic cations in the lattice implies that **2** is in fact a dianionic complex of U(+V). The broad paramagnetic signals observed in the NMR spectrum and the typical dark-red color further confirm the valency deduced from the X-ray analysis. Whereas numerous examples of U^V homoleptic alkoxides are reported in the literature,[15] it seems that mixed oxo-alkoxides such as **2** have not yet been described for this particular oxidation state. If molecules of the type $[OU(OR)_3]$ have been mentioned briefly by Bradley, they have not been well characterized by today's standards.[16] Complex **2** is also a unique example of a "double calixarene" made by the fusion of two cone-shaped calix[5]arenes. While such species are well known for the calix[4]arenes, they are more unusual for the larger macrocycles. To the best of our knowledge, the uranyl dimer $[\{UO_2(H_2L[6])\}_2]$ is the only other such compound present in the literature.[17] The closest related compound is $[Eu_2(H_2L[5])_2(dmso)_4]$, a bimetallic lanthanide complex held together by two *t*Bu-calix[5]arenes, but where the macrocycle is not in the cone conformation.[18]

As a powder or as a solution, **1** slowly decomposes to insoluble products when exposed to air. Conversely, a solution of **2** in a mixture of pyridine and acetone immediately oxidizes and turns to a light red. This solution slowly deposits beautiful single crystals among other uncharacterized decomposition products. The crystal structure was solved and revealed $[\{U(L[5])\}_2O]$ (**3**), the U^{VI} homologue of **2**.

$$[HNC_5H_5]_2[\{U(L[5])\}_2O] \xrightarrow[O_2]{\text{pyridine}} [\{U(L[5])\}_2O] + \text{decomposition products}$$

The geometry of **3** is similar to that of **2**, and no shortening of the U−O distances is observed, however the oxidation state is unambiguously confirmed by the diamagnetic NMR spectrum and by the lighter color of the complex. A pyridine molecule occupies the cavity of the calixarene in the solid state. Complex **3** is stable when exposed to air as a solid powder but slowly decomposes in the various solvents we used. The possibility of oxidizing U^V alkoxides into their U^{VI} derivatives by means of alcoholysis has been known for a long time, however the latter are strong oxidizing species that can also be used as intermediates in the synthesis of lower oxidation state complexes.[19] The oxidation of **2** to **3** does not lead to changes in the coordination geometry of the metal center and is a good example of the robustness conferred to the complex by the bridging macrocycle.

While the reactions of $H_4L[4]$ and $H_5L[5]$ with UCl_4 bear some resemblance in the kinds of oxo compounds they deliver, the reaction of $H_6L[6]$ does not follow the same pathway. When UCl_4 is treated with $H_6L[6]$ in pyridine, the pale green solution never turns to red. After hours of heating a mixture of the two reagents in pyridine under reflux, a change of color was eventually observed. Although the NMR spectrum of the mixture indicates that a reaction had possibly taken place,[20] we never managed to isolate a complex at this stage of the procedure. However, when the reaction mixture was exposed to air, the brown-green color immediately turned to a bright red. The solution was allowed to stand and after a few days, crystals suitable for X-ray crystallography were isolated. The structure was solved and revealed that $[U(H_3L[6])_2]$ (**4**) had been formed among other uncharacterized decomposition products.

$$UCl_4 + 2\,H_6L[6] \xrightarrow[O_2]{\text{pyridine}} [U(H_3L[6])_2] + \text{decomposition products}$$

Complex **4** is a U(+VI) complex, where two $H_3L[6]$ ligands coordinate the metal cation through three successive phenolate groups (Figure 4). The metal cation is the center of inversion of the complex. Its coordination geometry is thus a distorted octahedron [minimum and maximum O−U−O angles equal 85.6(3) and 94.4(3)°, respectively] with classical U−O bond lengths. Complex **4** can be viewed as an homoleptic uranium alkoxide. These are known since the early days of the Manhattan project, which started 5f-metal coordination chemistry.[21] However, only a few of

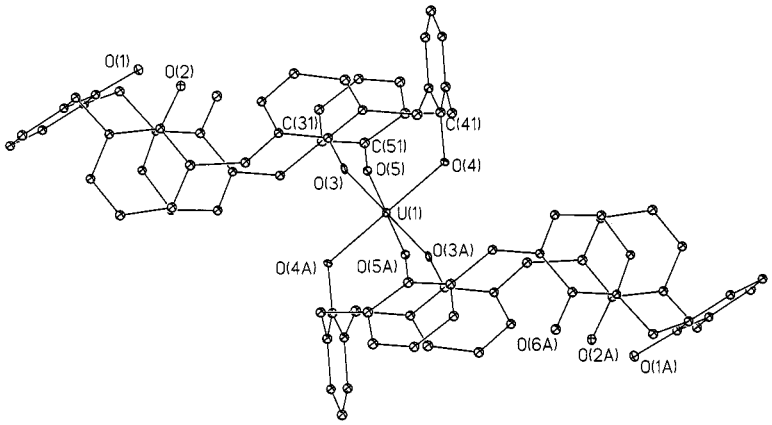


Figure 4. X-ray structure of complex **4**; all *t*Bu groups, hydrogen atoms, and solvent molecules have been omitted for clarity; selected bond length [Å] and angles [°] with estimated standard deviations in parentheses: U(1)−O(3) 2.10(1), U(1)−O(4) 2.132(8), U(1)−O(5) 2.112(9); U(1)−O(3)−C(31) 164.3(7), U(1)−O(4)−C(41) 126.(8), U(1)−O(5)−C(51) 169.1(8)

these compounds have been characterized by means of X-ray diffraction,[8,15a,15c,22] and none of them is a U^{VI} complex.[23] Complex **4** is the first "$U(OR)_6$" complex to be characterized by single-crystal X-ray diffraction. Its coordination geometry is close to the octahedral one of [$U(OTeF_5)_6$].[24] The conformation of the calixarene is 1,2,3-alternate, with the aromatic faces bearing the phenolic groups defining the first partial cone, and the three corresponding to the phenolate groups defining the second. This conformation is commonplace for the uncoordinated calix[6]arene derivatives, but had, to the best of our knowledge, never been encountered among the crystal structures of their metal complexes.[25] The fusion of two 1,2,3-alternate calix[6]arene affords a molecule with four aromatic cavities (Figure 5). In the solid state, all these half-cones are filled by pyridine molecules, thus **4** is the host to four molecular guests.

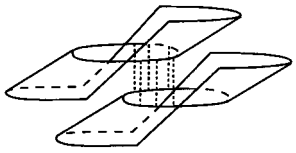


Figure 5. Schematic representation of **4** emphasizing its four half-cone cavities

In conclusion, the reactions of UCl_4 with H_4L[4], H_5L[5], and H_6L[6] enabled us to synthesize **1**, **2**, and **4**, the three first "non-uranyl" calixarene complexes of uranium. Complex **2** oxidizes to yield its U^{VI} equivalent **3** when exposed to air. The oxidation state of the metal ion in **1**−**4** is +V or +VI. If **1**−**3** contain μ-oxo bridges, **4** can be seen as a homoleptic uranium alkoxide. The isolation of **1**−**4** represents an exceptional example of the diversity of uranium compounds, and of the various molecular architectures that can be obtained from ring-size variation of a large polyalkoxide ligand. This reinforces the idea that a rich chemistry can be built at the boundary between macrocycle, supramolecular, and coordination chemistries.

Experimental Section

All NMR spectra were performed with a Bruker DPX-200. − Elemental analyses were performed at Analytische Laboratorien, D-51789 Lindlar, Germany. − Unless specified, all reactions were performed in a glove box under dry N_2. H_4L[4], H_5L[5], and H_6L[6] were dried under vacuum for 12 h at 323 K prior to use. Pyridine was dried with K (***Caution!***) and distilled prior use.

Synthesis of 1: UCl_4 (0.050 g, 0.130 mmol) was treated with H_4L[4] (0.085 g, 0.130 mmol) in pyridine (20 mL) at 333 K for 12 h. The black solution obtained was filtered and concentrated under vacuum (10 mL). It was then left standing overnight to afford a black microcrystalline powder that was filtered off, washed with cold pyridine and dried in vacuo to afford [{UCl(L[4])}$_3$O] · 2 (NC_5H_5) (0.018 g, 0.006 mmol, 14%). − ^{1}H NMR: δ = 20.12, 16.08, 11.36, 11.11, 9.60, 9.21, 9.00, 6.20, 5.63, 3.59, 3.38, 1.91, 1.87, 1.77, 1.68, 1.65, 1.61, 1.58, 1.55, 1.48, 1.23, 1.09, −0.13, −0.21, −0.34, −4.00, −14.23.[9] − $C_{142}H_{166}Cl_3N_2O_{13}U_3$ (2927.9): calcd. C 58.25, H 5.67, N 0.96; found C 58.03, H 5.75, N 0.93.

Synthesis of 2: UCl_4 (0.050 g, 0.130 mmol) was treated with H_5L[5] (0.107 g, 0.130 mmol) in pyridine (20 mL) at 333 K for 12 h. The dark red solution obtained was filtered and concentrated under vacuum (10 mL). It was then left standing overnight to afford a red microcrystalline powder that was filtered off. This powder was slowly recrystallized in pyridine to afford [HNC_5H_5]$_2$-[{U(L[5])$_2$O] · 4 (NC_5H_5) as beautiful single crystals (0.029 g, 0.011 mmol, 17%). − ^{1}H NMR: δ = 14.04 (br., 8 H, ArH), 8.81 (br., 4 H, ArH), 7.95 (br., 8 H, ArH), 6.39 (br., 8 H, Ar−CH_2−Ar), 4.68 (br., 8 H, Ar−CH_2−Ar), 1.63 (36 H, *t*Bu), 1.34 (18 H, *t*Bu), 0.97 (36 H, *t*Bu), −1.22 (br., 4 H, Ar−CH_2−Ar). − $C_{140}H_{162}N_6O_{11}U_2$ (2579.5): calcd. C 65.18, H 6.28, N 3.26; found C 65.24, H 6.49, N 3.33.

Synthesis of 3: Compound **2** (0.020 g, 0.008 mmol) was dissolved in a 50% mixture of pyridine and acetone (2 mL) at room temperature, and briefly exposed to air. The light-red solution thus obtained was left standing overnight to afford a red microcrystalline powder that was filtered off. This powder was slowly recrystallized in pyridine to afford a mixture of [{U(L[5])$_2$O] · 2.5 (NC_5H_5) as small monocrystals (0.007 g, 0.003 mmol, 37%) and microcrystalline H_5L[5]. Successive recrystallization in various solvents did not afford **3** in its elementally pure form. − ^{1}H NMR: δ = 9.11, 8.60,

8.23, 6.99, 6.74 (5 × 4 H, ArH), 6.61, 4.70 (br., 2 × 8 H, Ar−CH_2−Ar), 4.10 (br., 4 H, Ar−CH_2−Ar), 1.62 (36 H, *t*Bu), 1.26 (18 H, *t*Bu), 0.95 (36 H, *t*Bu).

Synthesis of 4: UCl_4 (0.050 g, 0.130 mmol) was treated with $H_6L[6]$ (0.256 g, 0.260 mmol) in pyridine (10 mL) at room temperature for 10 min and then briefly exposed to air. The red solution thus obtained was concentrated under vacuo (2 mL) and left standing for two weeks to deposit a red microcrystalline powder that was filtered off, washed with pentane, and dried in vacuo to afford $[U(H_3L[6])] \cdot 2\,(NC_5H_5)$ (0.030 g, 0.013 mmol, 10%). − 1H NMR: δ = 12.00 (br., 6 H, OH), 8.59, 8.45, 8.24, 7.72, 7.22, 6.88 (6 × 4 H, ArH), 6.73, 5.93, 4.31 (br., 3 × 8 H, Ar−CH_2−Ar), 1.55 (36 H, *t*Bu), 1.46 (18 H, *t*Bu), 1.17 (18 H, *t*Bu), 0.80 (36 H, *t*Bu). − $C_{142}H_{172}N_2O_{12}U$ (2335.4): calcd. C 73.02, H 7.36, N 1.20; found C 72.70, H 7.61, N 0.98.

X-ray Crystallographic Studies: Crystal data collection was performed with a Nonius Kappa CCD diffractometer equipped with a fiber glass collimator. Copies of the crystallographic data of **1**, **2**, **3**, and **4** can be obtained free of charge on application to CCDC, 12 Union Road, Cambridge CB2 1EZ, UK [Fax: (internat.) + 44 1223/336-033; E-mail: deposit@ccdc.cam.ac.uk].

Crystal Data of $1 \cdot 11.5\,(NC_5H_5)$: $C_{189.5}H_{213.5}N_{11.5}Cl_3O_{13}U_3$ (3680.7), 0.24 × 0.20 × 0.18 mm, trigonal, *P*−3*c*1, *Z* = 4, *a* = 21.576(3), *b* = 21.576(3), *c* = 45.517(9) Å, α = 90, β = 90, γ = 120°, *V* = 18350(5) Å^3, $\rho_{calcd.}$ = 1.333 g·cm^{-3}, *F*(000) = 7460, $2\theta_{max}$ = 60.58°, graphite-monochromated Mo-K_α radiation (λ = 0.71073 Å), μ_{Mo} = 2.744 cm^{-1}, *T* = 123 K. The structure was solved by direct methods,[26] and refined on F^2.[27] Of the 26624 reflections measured, 8902 were found to be independent (R_{int} = 0.123), 4419 of which were considered as observed [$I > 2\sigma(I)$] and were used in the refinement of the 427 parameters, leading to a final R_1 of 0.0844 and a R_{all} of 0.1942. wR_{obs} and wR_2 were found to be 0.1681 and 0.2369, respectively. Hydrogen atoms were introduced in the calculation as riding on calculated positions. The goodness-of-fit parameter *S* was 1.134 and the maximum residual density 0.960 eÅ^{-3}. Crystallographic data (excluding the structure factors) have been deposited with the Cambridge Crystallographic Data Centre as supplementary publication no. CCDC-140041.

Crystal Data of $[HNC_5H_5]_2[2] \cdot 4\,(NC_5H_5)$: $C_{140}H_{162}N_6O_{11}U_2$ (2580.8), 0.24 × 0.18 × 0.18 mm, monoclinic, *P*2(1)/*n*, *Z* = 2, *a* = 12.580(3), *b* = 19.950(4), *c* = 25.120(5) Å, α = 90, β = 98.74(3), γ = 90°, *V* = 6231(2) Å^3, $\rho_{calcd.}$ = 1.376 g·cm^{-3}, *F*(000) = 2632, $2\theta_{max}$ = 41.48°, graphite-monochromated Mo-K_α radiation (λ = 0.71073 Å), μ_{Mo} = 2.657 cm^{-1}, *T* = 123 K. The structure was solved by direct methods,[26] and refined on F^2.[27] Of the 35322 reflections measured, 6267 were found to be independent (R_{int} = 0.094), 3006 of which were considered as observed [$I > 2\sigma(I)$] and were used in the refinement of the 280 parameters, leading to a final R_1 of 0.0659 and a R_{all} of 0.1739. wR_{obs} and wR_2 were found to be 0.1110 and 0.1506, respectively. Solvent pyridine molecules were constrained to regular hexagons. Uranium and oxygen atoms were considered anisotropic. All the other atoms were considered as isotropic in order to keep a reasonable data/parameters ratio. Hydrogen atoms were introduced in the calculation as riding on calculated positions. The goodness-of-fit parameter *S* was 0.995 and the maximum residual density 0.705 eÅ^{-3}. Crystallographic data (excluding the structure factors) have been deposited with the Cambridge Crystallographic Data Centre as supplementary publication no. CCDC-140042.

Crystal Data of $[3]_2 \cdot 5\,(NC_5H_5)$: $C_{245}H_{285}N_5O_{22}U_4$ (4603.9), 0.18 × 0.18 × 0.12 mm, monoclinic, *P*2(1)/*n*, *Z* = 4, *a* = 26.907(5), *b* = 28.012(6), *c* = 31.015(6) Å, α = 90, β = 107.16(3), γ = 90°, *V* = 22336(8) Å^3, $\rho_{calcd.}$ = 1.369 g·cm^{-3}, *F*(000) = 9336, $2\theta_{max}$ = 41.64°, graphite-monochromated Mo-K_α radiation (λ = 0.71073 Å), μ_{Mo} = 2.955 cm^{-1}, *T* = 123 K. The structure was solved by direct methods[26] and refined on F^2.[27] Of the 171260 reflections measured, 22846 were found to be independent (R_{int} = 0.0682), 15455 of which were considered as observed [$I > 2\sigma(I)$] and were used in the refinement of the 1455 parameters, leading to a final R_1 of 0.0473 and a R_{all} of 0.0889. wR_{obs} and wR_2 were found to be 0.0982 and 0.1158, respectively. Uranium and oxygen atoms were considered anisotropic. All the other atoms were considered as isotropic in order to keep the number of parameters smaller than 1500. Above this value our refinement software is unable to operate. Hydrogen atoms were introduced in the calculation as riding on calculated positions (*U* = 1.2 times that of the corresponding atom). Solvate molecules of pyridine were refined as regular hexagons. The goodness-of-fit parameter *S* was 1.084 and the maximum residual density 1.226 eÅ^{-3}. The latter was located in the center of the thermally agitated solvent molecule bearing N(5). Crystallographic data (excluding the structure factors) have been deposited with the Cambridge Crystallographic Data Centre as supplementary publication no. CCDC-140040.

Crystal Data of $4 \cdot [HNC_5H_5]_2Cl_2 \cdot 10\,(NC_5H_5)$: $C_{192}H_{224}Cl_2N_{12}O_{12}U$ (3200.7), 0.18 × 0.12 × 0.12 mm, triclinic, *P*−1, *Z* = 1, *a* = 15.770(3), *b* = 16.680(3), *c* = 17.380(4) Å, α = 84.24(3), β = 72.78(3), γ = 87.35(3)°, *V* = 4344(2) Å^3, $\rho_{calcd.}$ = 1.224 g·cm^{-3}, *F*(000) = 1682, $2\theta_{max}$ = 41.90°, graphite-monochromated Mo-K_α radiation (λ = 0.71073 Å), μ_{Mo} = 1.027 cm^{-1}, *T* = 123 K. The structure was solved by direct methods,[26] and refined on F^2.[27] Of the 14651 reflections measured, 8598 were found to be independent (R_{int} = 0.156), 4672 of which were considered as observed [$I > 2\sigma(I)$] and were used in the refinement of the 482 parameters, leading to a final R_1 of 0.0918 and a R_{all} of 0.1829. wR_{obs} and wR_2 were found to be 0.1984 and 0.2613, respectively. Solvent pyridine molecules were constrained to regular hexagons. Uranium, chlorine, and oxygen atoms were considered anisotropic, as well as the carbon atoms of the non-disordered methyl of the *t*Bu groups. All the other atoms were considered as isotropic in order to keep a reasonable data/parameters ratio. Hydrogen atoms were introduced in the calculation as riding on calculated positions. The goodness-of-fit parameter *S* was 1.095 and the maximum residual density 0.848 eÅ^{-3}. Crystallographic data (excluding the structure factors) have been deposited with the Cambridge Crystallographic Data Centre as supplementary publication no. CCDC-140043.

[1] C. D. Gutsche, in: *Calixarenes Revisited* (Ed. J. F. Stoddart), Monographs in Supramolecular Chemistry, Royal Society of Chemistry, Cambridge, **1998**.

[2] [2a] L. Cecille, *Radioactive Waste Management and Disposal*, Elsevier, London, New York, **1991**. − [2b] L. Cecille, M. Casarci, L. Pietrelli, *New Separation Chemistry Techniques for Radioactive Waste and other Specific Applications*, Elsevier, London, New York, **1991**. − [2c] C. Wieser, C. B. Dieleman, D. Matt, *Coord. Chem. Rev.* **1997**, 165, 93−161. − [2d] J.-C. Bünzli, J. M. Harrowfield, in: *Calixarenes, A Versatile Class of Macrocyclic Compounds* (Eds.: J. Vicens, V. Böhmer), Kluwer Academic Publishers, Dordrecht, **1991**, pp. 211−231.

[3] [3a] K. Araki, N. Hashimoto, H. Otsuka, T. Nagasaki, S. Shinkai, *Chem. Lett*. **1993**, 829−832. − [3b] O. M. Falana, H. F. Koch, D. M. Roundhill, G. J. Lumetta, B. P. Hay, *Chem. Commun*. **1998**, 503−504. − [3c] J. M. Harrowfield, *Gazz. Chim. Ital.* **1997**, 127, 663−671. − [3d] P. Thuéry, M. Nierlich, M. I. Ogden, J. M. Harrowfield, *Supramol. Chem.* **1998**, 9, 297−303. − [3e] P. C. Leverd, P. Berthault, M. Lance, M. Nierlich, *Eur. J. Inorg. Chem.* **1998**, 1859−1862. − [3f] P. D. Beer, M. G. B. Drew, D. Hesek, M. Kan, G. Nicholson, P. Schmitt, P. D. Sheen, G. Williams, *J. Chem. Soc., Dalton Trans.* **1998**, 2783−2786.

[4] J. M. Harrowfield, M. I. Ogden, A. H. White, *J. Chem. Soc., Dalton Trans.* **1991**, 2625−2632.
[5] R. C. Mehrotra, A. Singh, *Chem. Soc. Rev.* **1996**, 1−13.
[6] [6a] F. A. Cotton, D. O. Marler, W. Schwotzer, *Inorg. Chim. Acta* **1984**, 95, 207−209. − [6b] A. J. Zozulin, D. C. Moody, R. R. Ryan, *Inorg. Chem*. **1982**, 3083−3086. − [6c] P. Charpin, G. Folcher, M. Nierlich, M. Lance, D. Vigner, A. Navaza, C. De Rango, *Acta Crystallogr.* **1990**, C46, 1778−1781. − [6d] P. C. Leverd, T. Arliguie, M. Ephritikhine, M. Nierlich, M. Lance, J. Vigner, *New J. Chem.* **1993**, 769−771.
[7] [7a] W. G. Van Der Sluys, A. P. Sattelberger, *Chem. Rev.* **1990**, 90, 1027−1040. − [7b] T. J. Marks, *Science* **1982**, 217, 989−997. − [7c] M. Ephritikhine, *New J. Chem.* **1992**, 451−469. − [7d] F. T. Edelmann, Y. K. Gun'ko, *Coord. Chem. Rev.* **1997**, 163−237.
[8] F. A. Cotton, D. O. Marler, W. Schwotzer, *Inorg. Chem*. **1984**, 23, 4211−4215.
[9] The EPR study, magnetic susceptibility measurements, and full interpretation of the NMR spectrum of **1** will be the subject of a future paper.
[10] M. W. Hosseini, A. De Cian, *Chem. Commun*. **1998**, 727−733.
[11] Mention is made of a trinuclear complex of uranyl with *t*Bu-calix[6]arene in ref.[3c], but the detailed experimental results have, as far as we are aware, remained unpublished.
[12] L. Giannini, G. Guillemot, E. Solari, C. Floriani, N. Re, A. Chiesi-Villa, C. Rizzoli, *J. Am. Chem. Soc*. **1999**, 2797−2807.
[13] J.-C. Berthet, J.-F. Le Maréchal, M. Nierlich, M. Lance, J. Vigner, M. Ephritikhine, *J. Organomet. Chem*. **1991**, 408, 335−341.
[14] P. C. Leverd, P. Berthault, M. Lance, M. Nierlich, *Eur. J. Org. Chem.* **2000**, 133−139.
[15] [15a] F. A. Cotton, D. O. Marler, W. Schwotzer, *Inorg. Chim. Acta* **1984**, 85, L31−L32. − [15b] P. G. Eller, P. J. Vergamini, *Inorg. Chem*. **1983**, 3184−3189. − [15c] P. C. Blake, M. F. Lappert, R. G. Taylor, J. L. Atwood, H. Zhang, *Inorg. Chim. Acta* **1987**, 139, 13−20.
[16] D. C. Bradley, R. N. Kapoor, B. C. Smith, *J. Inorg. Nucl. Chem*. **1962**, 24, 863−867.
[17] P. Thuéry, M. Lance, M. Nierlich, *Supramol. Chem.* **1996**, 7, 183−185.
[18] L. J. Charbonnière, C. Balsiger, K. J. Schlenk, J.-C. Bünzli, *J. Chem. Soc., Dalton Trans.* **1998**, 505−510.
[19] R. G. Jones, E. Bindsschadler, D. Blume, G. Karmas, G. A. Martin, J. R. Thirtle, F. A. Yeoman, H. Gilman, *J. Am. Chem. Soc.* **1956**, 78, 6030−6032.
[20] When UCl_4 is treated with two equivalents of H_6L[6] in pyridine in NC_5D_5 at 333 K in an NMR tube, broad peaks appear at δ = 12.00, 7.90, 4.05, 1.45, and −4.00, indicative of the formation of a paramagnetic compound.
[21] [21a] R. G. Jones, G. Karmas, G. A. Martin, H. Gilman, *J. Am. Chem. Soc.* **1956**, 78, 4285−4290. − [21b] D. C. Bradley, A. K. Chatterjee, A. K. Chatterjee, *J. Inorg. Nucl. Chem*. **1959**, 12, 71−78.
[22] [22a] W. G. Van Der Sluys, C. J. Burns, J. C. Huffman, A. P. Sattelberger, *J. Am. Chem. Soc.* **1988**, 110, 5924−5925. − [22b] W. G. Van Der Sluys, A. P. Sattelberger, W. E. Streib, J. C. Huffman, *Polyhedron* **1989**, 8, 9, 11247−1249. − [22c] S. R. Sofen, K. Abu-Dari, D. P. Freyberg, K. N. Raymond, *J. Am. Chem. Soc.* **1978**, 7882−7887.
[23] Mention of the crystal structure of $[U(OMe)_6]$ is made in; E. A. Cuellar, S. S. Miller, T. J. Marks, E. Weitz, *J. Am. Chem. Soc*. **1983**, 105, 4580−4589, but the experimental results have, to the best of our knowledge, remained unpublished.
[24] L. K. Templeton, D. H. Templeton, N. Bartlett, K. Seppelt, *Inorg. Chem*. **1976**, 15, 11, 2720−2722.
[25] [25a] S. G. Bott, A. W. Coleman, J. L. Atwood, *J. Chem. Soc., Chem. Commun*. **1986**, 610−611. − [25b] G. D. Andreetti, G. Calestani, F. Ugozzoli, A. Arduini, E. Ghidini, A. Pochini, R. Ungaro, *J. Incl. Phenom*. **1987,** 5, 123−126. − [25c] L. M. Engelhardt, B. M. Furphy, J. M. Harrowfield, D. L. Kepert, A. H. White, F. R. Wilner, *Aust. J. Chem*. **1988**, 41, 1465−1476. − [25d] J. M. Smith, S. G. Bott, *Chem. Commun*. **1996**, 377−378. − [25e] F. J. Parlevliet, A. Olivier, W. G. J. de Lange, P. C. J. Kamer, H. Kooijman, A. L. Speck, P. W. N. M. van Leeuwen, *Chem. Commun*. **1996**, 583−584. − [25f] S. Blanchard, L. Le Clainche, M.-N. Rager, B. Chansou, J.-P. Tuchagues, A. F. Duprat, Y. Le Mest, O. Reinaud, *Angew. Chem. Int. Ed.* **1998**, 37, 19, 2732−2735.
[26] G. M. Sheldrick, *SHELXS 86, A Program for the Solution of Crystal Structures*, University of Göttingen, Germany, **1990**.
[27] G. M. Sheldrick, *SHELXL 93, A Program for the Refinement of Crystal Structures*, University of Göttingen, Germany, **1993**.

Received February 10, 2000
[I00044]

Unsaturated Hetero Chains, IX[+]

1:1- and 2:1-Copper(II) Complexes From Primary *N*-Acylamidines

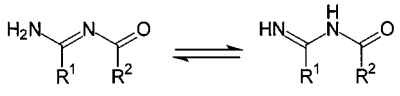
Jan K. Eberhardt,[a] Roland Fröhlich,[a][++] Sabine Venne-Dunker,[a][++] and Ernst-Ulrich Würthwein*[a]

Keywords: *N*-Acylamidines / Copper(II) complexes / N ligands / O ligands

Four different types of six-membered chelate Cu^{II} complexes **2**–**5** have been synthesized from copper(II) salts and primary *N*-acylamidines ($H_2N–CR^1=N–CR^2=O$) **1**. The twofold positively charged complexes **2**–**4** contain two neutral ligands around the Cu^{II} ion. In the 1:1 compound **2** the copper(II) ion is four coordinate, leading to a distorted square coordination. The 2:1 compounds **3** and **4** show similar structural properties; the approximate square plane of the complexes is complemented by one or two loose apical contacts to the triflate counter ions. In the centrosymmetric, neutral 2:1 complex **5**, two anionic ligands interact with the central Cu^{II} ion, leading to an approximate square-planar coordination of the Cu^{II} ion. The structural versatility of these *N*-acylamidine complexes is discussed in terms of counter ion and solubility influences. All complexes have been completely characterized, including X-ray diffraction analysis.

Introduction

In order to investigate the fundamental properties of oligonitriles we initiated a thorough research program concentrating on the complex-forming ability of these new oligomers.[1] In a recent paper we reported the synthesis and structural properties of two palladium(II) complexes of differently substituted tetrameric *N*-acylated and *N*-thioacylated oligonitriles.[2] The formation of six-membered chelate rings involving either two nitrogen atoms or one nitrogen and one sulfur atom were characteristic features of these complexes. We are now focussing on the copper(II) complexes of small donor substituted model oligonitriles, the *N*-acylamidines **1**. They also offer coordination sites for the formation of six-membered chelates, namely the oxygen atom of the acyl functionality and the nitrogen atom of the amino group. In case of *N*-acylamidines **1** containing a $-NH_2$ (primary *N*-acylamidines) or a -NHR group (secondary *N*-acylamidines) tautomerism involving 1,3 proton shifts may be expected (isomers **A** and **B**).



A **B**

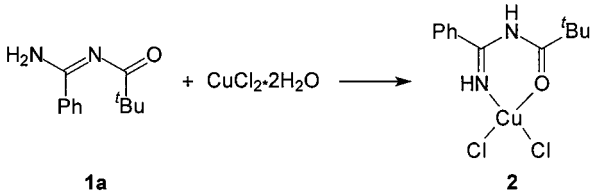
However, spectroscopic studies[3] as well as X-ray diffraction determinations[4] indicate the predominance of the *N*-acylamidine structures **A** in solution and in the solid phase. The second tautomer **B**, with the two protons on different nitrogen atoms, plays only a minor role in the equilibrium.

In this paper we present four different copper(II) complexes representing three different types of primary *N*-acylamidine complexes. To the best of our knowledge, there is only one report of a metal complex with a simple primary *N*-acylamidine in the literature; in 1978, the preparation and X-ray structure determination of a 2:1 nickel complex involving an anionic *N*-acylamidine ligand was reported by an Italian group.[5] *N*-Acylamidines may be considered to be aza analogues of enaminones (3-aminopropenones); several metal complexes of these ligands are known.[6]

Results

Depending on the reaction conditions, we were able to synthesize and characterize spectroscopically and by X-ray diffraction three different types of *N*-acylamidine copper(II) complexes.

If *N*-pivaloyl benzamidine (**1a**) and $Cu^{II}Cl_2 \cdot 2\,H_2O$ are dissolved in an equimolar ratio in acetonitrile, dark green crystals **2** are obtained in 67.5% yield after careful precipitation using diethyl ether.



1a **2**

The new compound **2** was studied by X-ray analysis. Crystalline **2** forms a mononuclear 1:1 complex, including 1.5 molecules of acetonitrile, with a *cis*-$CuCl_2$ unit. Complexation at the oxygen atom and nitrogen atom N(5) (crystallographic numbering) of neutral **1a** by the copper ion leads to the six-membered chelate ring of metal complex **2**

[+] Part VIII: Ref.[2]
[++] X-ray diffraction analyses.

[a] Institut für Organische Chemie der Westfälischen Wilhelms-Universität Münster,
Corrensstraße 40, D-48149 Münster, Germany
Fax: (internat.) + 49-(0)251/833-9772

 © WILEY-VCH Verlag GmbH, D-69451 Weinheim, 2000 1434–1948/00/0808–1739 $ 17.50+.50/0

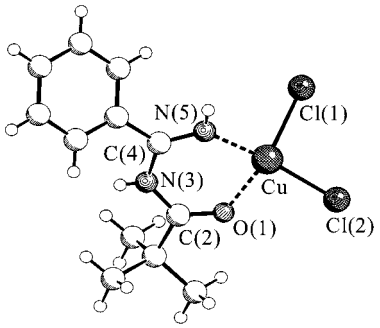


Figure 1. Molecular structure of **2**; selected bond parameters: bond lengths [Å]: Cu−Cl(1) 2.2786(7), Cu−Cl(2) 2.2167(7), Cu−O(1) 2.0245(15), Cu−N(5) 1.932(2), O(1)−C(2) 1.225(3), C(2)−N(3) 1.355(3), N(3)−C(4) 1.385(3), C(4)−N(5) 1.271(3); bond angles [°]: Cl(1)−Cu−Cl(2) 96.41(3), N(5)−Cu−O(1) 85.35(7), N(5)−Cu−Cl(1) 90.77(6), O(1)−Cu−Cl(2) 91.76(5), O(1)−C(2)−N(3) 122.3(2), C(2)−N(3)−C(4) 127.2(2), N(5)−C(4)−N(3) 120.6(2); torsional angles [°]: N(5)−Cu−O(1)−C(2) 12.22 (0.24), Cl(2)−Cu−O(1)−C(2) −176.89 (0.24), Cl(1)−Cu−O(1)−C(2) −71.69 (0.27), Cu−O(1)−C(2)−N(3) −10.17 (0.40), O(1)−C(2)−N(3)−C(4) −2.82 (0.43), C(2)−N(3)−C(4)−N(5) 9.31 (0.41), N(3)−C(4)−N(5)−Cu −2.43 (0.40), O(1)−Cu−N(5)−C(4) −5.61 (0.26)

(Figure 1). The organic section of the chelate ring is rather flat, with the copper atom well in the plane of the ligand. One of chlorides is also located in the plane; the other chloride, however, is positioned far below the plane (see Figure 1), resulting in a strongly tetrahedrally deformed square planar coordination geometry around copper(II) (sum of angles: 364.29°). Coordination bond lengths are 1.932(2) to N, 2.205(2) to O and 2.217(1) and 2.279(1) Å to chlorine. The N−Cu−O bond angle amounts to 85.35°.

Due to complexation, the amino group of the ligand is transformed into an imine moiety by a formal 1,3-shift of one of the amino hydrogen atoms to nitrogen atom N(3). The lone pair of the sp^2 hybridized imine-type nitrogen atom N(5) acts as the coordination site; thus, a conjugated 6π/5z ligand is present in the complex, carrying a central planar sp^2 amino group. This ligand may also be understood as a combination of a ketiminato and a ketono donor connected by an amino group, as can be seen from the rather similar C=N and C=O bond lengths [1.271(3) versus 1.225(3) Å]. The same applies to the C−N bonds [1.355(3) and 1.385(3) Å]. The phenyl ring is twisted out of the plane of the complex by around 40°, possibly due to packing effects rather than intramolecular steric strain. The IR spectra (KBr) show two broad absorptions at 3400 and 3200 cm^{-1}, which are assigned to the =NH and −NH stretching vibrations (isomer **B**); in contrast, the free ligand shows bands at 3320 and 3160 cm^{-1}, which are attributed to the unsymmetrical and symmetrical NH_2 stretching vibrations (isomer **A**). UV absorptions of low intensity are observed at 464 and 391 nm due to d→d transitions at the metal ion, causing the green-yellow color of solutions of **2**.

The reaction of two equivalents of either *N*-(4-methylbenzoyl) benzamidine (**1b**) or *N*-pivaloyl benzamidine (**1a**) with one equivalent of $Cu(CF_3SO_3)_2$ in acetonitrile leads to the formation of the respective copper(II) complexes **3** (Figure 2) and **4** (Figure 3). Crystallization was achieved by

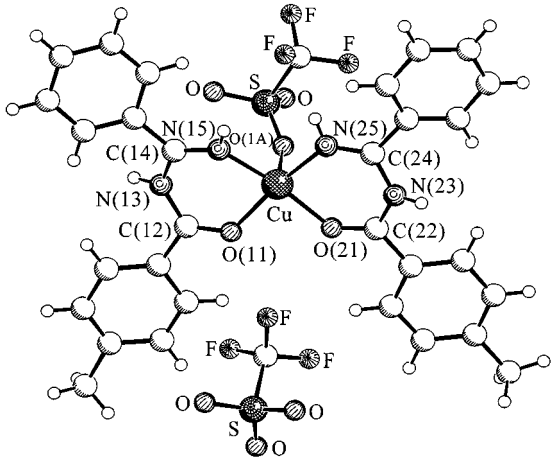
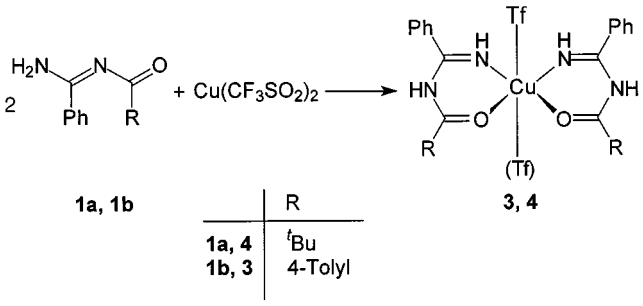


Figure 2. Molecular structure of **3**; selected bond parameters: bond lengths [Å]: Cu−O(1A) 2.282(4), Cu−O(11) 1.944(4), Cu−O(21) 1.956(4), Cu−N(15) 1.936(5), Cu−N(25) 1.930(5), O(11)−C(12) 1.243(7), C(12)−N(13) 1.375(8), N(13)−C(14) 1.383(8), C(14)−N(15) 1.295(7), O(21)−C(22) 1.247(7), C(22)−N(23) 1.363(8), N(23)−C(24) 1.373(8), C(24)−N(25) 1.267(8); bond angles [°]: N(25)−Cu−N(15) 95.5(2), N(15)−Cu−O(11) 88.00(19), N(25)−Cu−O(21) 88.3(2), O(11)−Cu−O(21) 86.90(17), N(25)−Cu−O(1A) 96.2(2), N(15)−Cu−O(1A) 95.19(19), C(12)−O(11)−Cu 127.5(4), O(11)−C(12)−N(13) 122.2(5), C(12)−N(13)−C(14) 126.3(5), N(15)−C(14)−N(13) 120.1(5), C(14)−N(15)−Cu 127.1(4), C(22)−O(21)−Cu 129.4(4), O(21)−C(22)−N(23) 121.9(6), C(22)−N(23)−C(24) 127.5(5), N(25)−C(24)−N(23) 121.1(6), C(24)−N(25)−Cu 130.0(5); torsional angles [°]: O(1A)−Cu−O(11)−C(12) −69.69 (0.49), N(15)−Cu−O(11)−C(12) 25.40 (0.49), Cu−O(11)−C(12)−N(13) −9.00 (0.81), O(11)−C(12)−N(13)−C(14) −18.51 (0.91), C(12)−N(13)−C(14)−N(15) 16.49 (0.88), N(13)−C(14)−N(15)−Cu 12.44 (0.79), O(11)−Cu−N(15)−C(14) −26.95 (0.50), O(1A)−Cu−N(15)−C(14) 66.00 (0.51), N(25)−Cu−O(21)−C(22) 9.41 (0.50), Cu−O(21)−C(22)−N(23) −3.20 (0.84), O(21)−C(22)−N(23)−C(24) −10.72 (0.98), C(22)−N(23)−C(24)−N(25) 13.73 (0.98), N(23)−C(24)−N(25)−Cu −2.65 (0.86), O(21)−Cu−N(25)−C(24) −6.34 (0.53)

adding surplus of diethyl ether, yielding metal complexes **3** (83.5% yield, from **1b**) and **4** (91.2% yield, from **1a**).



Both compounds **3** and **4** were analyzed by X-ray diffraction. Both complexes consist of two neutral *N*-acylamidines in their C=NH tautomeric form **B** (analogously to **2**) complexing a central copper(II) ion (mononuclear 2:1 complexes); the two counter ions are in close vicinity to the doubly positively charged complex (see below). As in **2**, conjugated six-membered chelate rings are formed by coordination of the oxygen atoms and terminal nitrogen atoms of the *N*-acylamidines (isomer **B**) to copper (II). In both complexes *cis* O−Cu−O and *cis* N−Cu−N coordination is observed. A fifth (and in **4**, a sixth as well) coordination

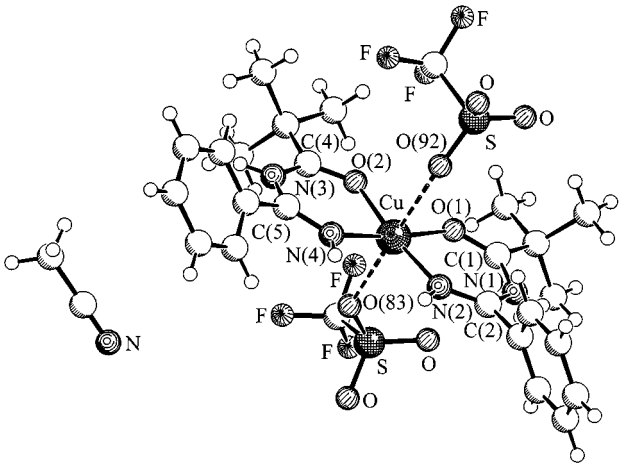


Figure 3. Molecular structure of **4**; selected bond parameters: bond lengths [Å]: Cu−N(2) 1.923(2), Cu−O(2) 1.9447(16), Cu−O(1) 1.9479(18), Cu−N(4) 1.951(2), Cu−O(83) 2.4028(19), C(1)−O(1) 1.226(3), C(1)−N(1) 1.372(3), C(2)−N(2) 1.270(3), C(2)−N(1) 1.388(3), C(4)−O(2) 1.226(3), C(4)−N(3) 1.363(3), C(5)−N(4) 1.279(3), C(5)−N(3) 1.393(3); bond angles [°]: N(2)−Cu−O(1) 88.20(8), O(2)−Cu−O(1) 86.09(7), N(2)−Cu−N(4) 97.26(9), O(2)−Cu−N(4) 88.15(8), N(2)−Cu−O(83) 96.14(9), O(2)−Cu−O(83) 88.04(8), O(1)−C(1)−N(1) 122.0(2), N(2)−C(2)−N(1) 121.9(2), O(2)−C(4)−N(3) 122.5(2), N(4)−C(5)−N(3) 121.1(2), C(1)−O(1)−Cu 131.00(17), C(5)−N(4)−Cu 129.13(18), C(1)−N(1)−C(2) 126.3(2), C(2)−N(2)−Cu 129.71(19), C(4)−N(3)−C(5) 126.8(2), C(4)−O(2)−Cu 130.73(17); torsion angles [°]: N(1)−C(1)−O(1)−Cu −7.45 (0.36), N(2)−Cu−O(1)−C(1) 8.29 (0.22), O(2)−Cu−O(1)−C(1) −175.87 (0.22), N(4)−Cu−O(1)−C(1) 151.03 (0.60), N(3)−C(5)−N(4)−Cu 6.76 (0.35), N(2)−Cu−N(4)−C(5) 178.13 (0.22), O(2)−Cu−N(4)−C(5) 2.69 (0.22), O(1)−C(1)−N(1)−C(2) −2.64 (0.39), N(2)−C(2)−N(1)−C(1) 9.47 (0.40), N(1)−C(2)−N(2)−Cu −6.03 (0.38), O(2)−Cu−N(2)−C(2) −37.27 (0.81), O(1)−Cu−N(2)−C(2) −1.21 (0.24), O(2)−C(4)−N(3)−C(5) 5.05 (0.39), N(4)−C(5)−N(3)−C(4) −12.82 (0.38), N(3)−C(4)−O(2)−Cu 8.66 (0.36), N(2)−Cu−O(2)−C(4) −150.95 (0.63), N(4)−Cu−O(2)−C(4) −10.83 (0.22), O(83)−Cu−O(2)−C(4) 82.55 (0.22)

site of copper is loosely occupied by an oxygen atom of a $CF_3SO_3^-$ anion, although the corresponding Cu−O distances are substantially longer (see below). In compound **3**, the copper atom is five-coordinate, having an approximately flat square-pyramidal geometry, in compound **4** the central ion is six-coordinate, forming an elongated octahedral or square-bipyramidal geometry, as is known for other copper(II) complexes. Coordination bond lengths in **3** are: Cu−N: 1.930(5),1.936(5); Cu−O: 1.944(4), 1.956(4), 2.282 (4) Å (to $CF_3SO_3^-$). Coordination bond lengths in **4** are: Cu−N: 1.923(2), 1.951(2); Cu−O: 1.945(2), 1.948(2), 2.403(2), 2.560(2) Å (both to $CF_3SO_3^-$).

The IR absorptions in the NH_2 region are similar to those of **2** (3400 and 3220 cm^{-1}). Low intensity d→d transitions at 627 nm (**3**) and 626 nm (**4**) cause the blue color of the complexes.

A third type of a *N*-acylamidine copper(II) complex is obtained by treating $Cu(SO_4) \cdot 5\,H_2O$ with *N*-pivaloylpivalamidine (**1c**). $Cu(SO_4) \cdot 5\,H_2O$ and **1c** are mixed in aqueous ethanol, the solution is extracted with cyclohexane. The solvent is removed and the solid is recrystallized from acetonitrile. Metal complex **5** is obtained in 41.9% yield (calculated for **1c**) as violet needles (Figure 4).

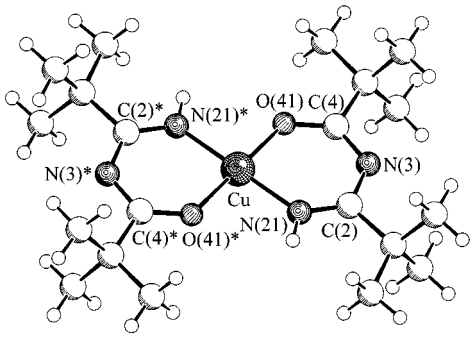
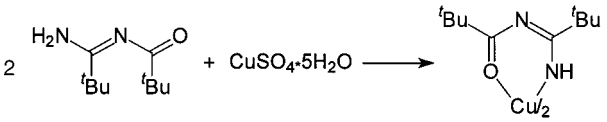


Figure 4. Molecular structure of **5**; selected bond parameters: bond lengths [Å]: Cu−N(21) 1.905(2), Cu−N(21)* 1.905(2), Cu−O(41)* 1.917(2), Cu−O(41) 1.917(2), C(2)−N(21) 1.287(4), C(2)−N(3) 1.348(4), N(3)−C(4) 1.329(4), C(4)−O(41) 1.275(4); bond angles [°]: N(21)−Cu−N(21)* 180.0(2), N(21)−Cu−O(41)* 90.5(1), N(21)*−Cu−O(41)* 89.5(1), N(21)−Cu−O(41) 89.5(1), N(21)*−Cu−O(41) 90.5(1), N(21)−C(2)−N(3) 125.1(3), C(2)−N(21)−Cu 128.2(2), C(4)−N(3)−C(2) 122.8(3), O(41)−C(4)−N(3) 127.3(3), C(4)−O(41)−Cu 126.8(2); torsion angles [°]: N(3)−C(2)−N(21)−Cu 2.30 (0.47), O(41)−Cu−N(21)−C(2) 1.53 (0.28), N(21)−C(2)−N(3)−C(4) −3.81 (0.49), C(2)−N(3)−C(4)−O(41) −0.27 (0.50), N(3)−C(4)−O(41)−Cu 5.39 (0.47), N(21)−Cu−O(41)−C(4) −5.12 (0.26)



1c **5**

In this type of 2:1 mononuclear complex two anionic *N*-acylamidines **1c** are bound to Cu^{II}, forming a neutral six-membered bis-chelate. Interestingly, the O−Cu−O and N−Cu−N units are now in a *trans* arrangement, forming the planar copper(II) complex with centric symmetry. The Cu−N [1.905(2)] and Cu−O bonds [1.917(2) Å] are rather similar in length; compared to the complexes **2**−**4** with neutral *N*-acylamidines as ligands, these bonds are shorter by about 0.05 Å as a consequence of the formally anionic ligands. As in **2**−**4** effective cyclic conjugation is indicated by the bond lengths of the ligands. However, compared to **2**−**4**, the C=O/C=N bonds in **5** are longer and the N−C−N bonds around carbon atom C(3) are shorter, resulting in a much less pronounced bond alternation.

As expected, there is only one IR signal in the NH region at 3330 cm^{-1}, occurring as a very strong, sharp absorption from the N−H stretching vibration (compare ref.[7]). The UV spectra of **5** are in sharp contrast to those of **3** and **4**; the low intensity d→d transition at 561 nm causes the purple color of the solutions and indicate stronger interactions between the ligand and the copper(II) ion than in **3** and **4**.

Discussion

As exemplified by these three types of copper(II) complexes, primary *N*-acylamidines (**1**) are rather versatile ligands for metal complexation. This is mainly due to the NH_2 groups which allow on the one hand the use of primary *N*-acylamidines as neutral ligands (isomer **B** in com-

pounds **2**−**4**), and on the other as anionic (compound **5**; see also ref.[5]) or even dianionic ligands.[8] Tautomerism between isomers **A** and **B** is important in view of the thermodynamics of the complex formation since migration of one proton to the central nitrogen atom allows the formation of a favorable cyclic conjugated six-membered chelate. Correspondingly, tertiary *N*-acylamidines carrying dialkylamino groups, which lack this possibility, are much weaker ligands compared to the primary compounds **1**.[1]

The formation of the different types of complexes obviously depends on the counter ion of the copper(II) salts employed. Independent of the stoichiometry used, ligand **1a** forms a 1:1 (**2**) and a 2:1 (**4**) complex from an acetonitrile solution if one uses copper(II) chloride and copper(II) triflate respectively. Both complexes are obtained by precipitation using diethyl ether. The solubility of the salts and complexes seems to play the important role in controlling the products. Under the conditions mentioned above, no deprotonation takes place and one obtains complexes of the neutral ligands. In contrast, reaction of the aliphatically substituted ligand **1c** in aqueous ethanol yields the neutral complex **5** containing the anionic ligand after repeated extraction with cyclohexane as nonpolar solvent. Most likely, the extraction of the highly hydrophobic complex shifts the complexation equilibrium towards the observed uncharged product, even in the absence of an additional base.

Finally, this series of closely related Cu^{II} complexes is a good demonstration of the versatility of this d^9 ion, giving *N*-acylamidine complexes with coordination numbers four, five and six, including regular square planar (**5**), tetrahedrally distorted planar (**2**), square pyramidal (**3**) and elongated octahedral (**4**) coordination; in all cases four short N−Cu/O−Cu bonds are formed. In the latter two cases, one or two long apical O−Cu contacts to the counter ions are also observed.

Experimental Section

Materials and Methods: Compounds **1a, 1b**, and **1c** were prepared as previously described.[9] Commercially available solvents (p. a. quality) were used without further purification. − CHN analyses were performed with a DiaCHN 240 (Perkin−Elmer). − IR spectra were recorded on a Perkin−Elmer PE 298 spectrophotometer as KBr pellets. − UV/Vis-spectra were recorded using a Cary 1 Bio spectrophotometer (Varian). − ^{1}H- and ^{13}C-NMR spectra were obtained using a Bruker WM 300 and a Bruker AMX 400 spectrometer. The MS (ESI) spectra were recorded using a Quattro LC-Z mass spectrometer (Micromass).

$CuCl_2$-Complex of *N*-Pivaloylbenzamidine (2): Compound **1a** (20 mg, 0.100 mmol) is treated at room temperature with $CuCl_2 \cdot 2\,H_2O$ (17 mg, 0.100 mmol) in acetonitrile (2 mL). After stirring for 5 min a clear, green solution is formed. After some time, diethyl ether (12 mL) is carefully added to form an upper layer. After five days green crystals of **2** are collected (27 mg, 0.067 mmol, 67% yield). − IR (KBr): $\tilde{\nu}$ = 3400 cm^{-1} (br, NH), 3200 (br, NH), 3050 (m, $CH_{arom.}$), 2960 (s, $CH_{aliph.}$), 2850 (w, $CH_{aliph.}$), 1650 (vs, C=O), 1570 (s, $C{=}C_{arom.}$), 1480 (s), 1390 (w), 1370 (m), 1360 (m), 1280 (w), 1220 (m), 1180 (s), 1100 (w), 1060 (m), 1020 (w), 990 (w), 960 (w), 870 (m), 840 (m), 810 (m), 780 (m), 750 (s), 700 (s). − UV/Vis (acetonitrile): λ_{max} [nm] (ε) = 464 (212), 391 (136), 273 sh (10082), 245 (13274), 197 (25444). − ^{1}H NMR (400.13 MHz, CD_3CN): δ = 2.08 (s), 3.97 (br), 6.38 (br), 6.81 (br), 9.71 (br). − MS (ESI, acetonitrile): *m/z* (%) = 506.0 (3) [$C_{24}H_{32}N_4O_2CuCl^+$], 470.1 (20) [$C_{24}H_{31}N_4O_2Cu^+$], 328.0 (2) [$C_{12}H_{15}N_2OCu^+$], 235.5 [$C_{24}H_{32}N_4O_2Cu^{2+}$], 205.0 (100) [$C_{12}H_{17}N_2O^+$]. − $C_{12}H_{16}Cl_2CuN_2O \cdot 1.5$ MeCN (400.29).

X-ray Diffraction Analysis of $2 \cdot 1.5$ MeCN: ($C_{12}H_{16}Cl_2CuN_2O \cdot 1.5$ MeCN),[10] the green single crystal was analyzed using a Nonius KappaCCD diffractometer with Mo-K_α radiation (λ=0.71073 Å) using a graphite monochromator at 293(2) K. Crystal system: monoclinic, space group *C*2/c (No. 15) with cell parameters a = 15.371(1) Å, b = 12.046(1) Å, c = 21.670(1) Å, β = 106.70(1)°, V = 3843.2(4) Å^3, $\rho_{calcd.}$ = 1.384 Mg/m^3, Z = 8. Crystal size: 0.20 × 0.10 × 0.10 mm. 18292 reflections were collected leading to 5718 independent and 4061 observed [$I > 2\sigma(I)$] reflections. Absorption coefficient μ = 1.420 mm^{-1}, absorption correction via SORTAN (0.764 ≤ T ≤ 0.871). 217 refined parameters. Non-hydrogen atoms were refined anisotropically. H-Atoms were geometrically positioned (riding model). $R(F)$ = 0.0451, $wR(F^2)$ = 0.1080; residual electron density: 0.519 and −0.517 eÅ^{-3}.[11]

$Cu(CF_3SO_2)_2$ Complex of *N*-(4-Methylbenzoyl)benzamidine (3): Compound **1b** (24 mg, 0.100 mmol) is treated at room temperature with of $Cu(CF_3SO_2)_2$ (18 mg, 0.050 mmol) in acetonitrile (1.5 mL). After stirring for 2 min a clear, blue solution is formed. After some time, diethyl ether (12 mL) is carefully added to form an upper layer. After three days blue crystals of **3** are collected (35 mg, 0.042 mmol, 83.5% yield). − IR (KBr): $\tilde{\nu}$ = 3440 cm^{-1} (br, NH), 3220 (s, NH), 3030 (m, $CH_{arom.}$), 2900 (sh, $CH_{aliph.}$), 1640 (vs, C=O), 1600 (s, $C{=}C_{arom.}$), 1560 (m), 1500 (sh), 1480 (s), 1440 (w), 1380 (m), 1270 (vs), 1220 (vs), 1180 (m), 1160 (s), 1120 (m), 1020 (s), 940 (w), 880 (w), 830 (w), 780 (w), 740 (s), 700 (m). − UV/Vis (acetonitrile): λ_{max} [nm] (ε) = 627 (102), 465 (42), 267 (24430), 216 sh (14974), 195 (42734). − ^{1}H NMR (300.13 MHz, CD_3CN): δ = 2.32 (br), 7.19 (s), 7.62 (br), 9.62 (br). − MS (ESI, acetonitrile): *m/z* (%) = 538.1 (20) [$C_{30}H_{27}N_4O_2Cu^+$], 269.5 (12) [$C_{30}H_{28}N_4O_2Cu^{2+}$], 239.0 (100) [$C_{15}H_{15}N_2O^+$]. − $C_{32}H_{28}CuF_6N_4O_8S_2$ (838.26): calcd. C 45.85 H 3.37 N 6.68; found C 45.34 H 3.49 N 6.42.

X-ray Diffraction Analysis of 3: ($C_{32}H_{28}CuF_6N_4O_8S_2$),[10] the blue single crystal was analyzed using a Nonius KappaCCD diffractometer with Mo-K_α radiation (λ = 0.71073 Å) using a graphite monochromator at 198(2) K. Crystal system: monoclinic, space group $P2_1$ (No. 4) with cell parameters a = 10.329(1) Å, b = 16.902(1) Å, c = 10.676(1) Å, β = 109.96(1)°, V = 1751.9(3) Å^3, $\rho_{calcd.}$ = 1.589 Mg/m^3, Z = 2. Crystal size: 0.20 × 0.20 × 0.10 mm. 14055 reflections were collected leading to 5497 independent and 4390 observed [$I > 2\sigma(I)$] reflections. Absorption coefficient μ = 0.831 mm^{-1}, absorption correction via SORTAN (0.852 ≤ T ≤ 0.922). 486 refined parameters. Non-hydrogen atoms were refined anisotropically. H-Atoms were geometrically positioned (riding model). $R(F)$ = 0.0566, $wR(F^2)$ = 0.1301; Flack parameter 0.007(17); residual electron density: 0.905 and −0.717 eÅ^{-3}.[11]

$Cu(CF_3SO_2)_2$ Complex of *N*-Pivaloylbenzamidine (4): Compound **1a** (20 mg, 0.100 mmol) is treated at room temperature with $Cu(CF_3SO_2)_2$ (18 mg, 0.050 mmol) in acetonitrile (1.5 mL). After stirring for 2 min a clear, blue solution is formed. After some time, diethyl ether (12 mL) is carefully added to form an upper layer. After five days blue crystals of **4** are collected (37 mg, 0.046 mmol, 91.2% yield). − IR (KBr): $\tilde{\nu}$ = 3400 cm^{-1} (br, NH), 3240 (s, NH), 3090 (w, $CH_{arom.}$), 2960 (s, $CH_{aliph.}$), 2860 (sh, $CH_{aliph.}$), 1660 (vs,

C=O), 1570 (w), 1490 (s, C=$C_{arom.}$), 1400 (w), 1380 (m), 1280 (s), 1240 (vs), 1220 (s), 1180 (m), 1160 (s), 1020 (s), 850 (w), 780 (w), 750 (m). − UV/Vis (acetonitrile): λ_{max} [nm] (ε) = 626 (67), 249 (24350), 200 (39544). − ^{1}H NMR (300.13 MHz, CD_3CN): δ = 2.35 (br), 4.58 (br), 7.20 (s), 7.49 (br), 9.60 (br). − MS (ESI, acetonitrile): *m/z* (%) = 620.1 (10) [$C_{24}H_{32}N_4O_2CuCF_3SO_3^+$], 470.1 (70) [$C_{24}H_{31}N_4O_2Cu^+$], 235.5 (62) [$C_{24}H_{32}N_4O_2Cu^{2+}$], 205.0 (100) [$C_{12}H_{17}N_2O^+$]. − $C_{28}H_{35}CuF_6N_5O_8S_2$ (811.27): calcd. C 41.45 H 4.35 N 8.63; found C 40.99 H 3.92 N 7.83

X-ray Diffraction Analysis of 4 · MeCN: ($C_{28}H_{35}CuF_6N_5O_8S_2$),[10] the blue single crystal was analyzed using a Nonius KappaCCD diffractometer with Mo-K_α radiation (λ = 0.71073 Å) using a graphite monochromator at 223(2) K. Crystal system: orthorhombic, space group *Pbca* (No. 61) with cell parameters *a* = 14.032(1) Å, *b* = 21.886(1) Å, *c* = 23.673(1) Å, *V* = 7270.1(7) Å^3, $\rho_{calcd.}$ = 1.482 Mg/m^3, *Z* = 8. Crystal size: 0.20 × 0.20 × 0.15 mm. 62323 reflections were collected leading to 8343 independent and 5919 observed [$I > 2\sigma(I)$] reflections. Absorption coefficient μ = 0.798 mm^{-1}, absorption correction via SORTAN (0.857 ≤ *T* ≤ 0.890). 464 refined parameters. Non-hydrogen atoms were refined anisotropically. H-Atoms were geometrically positioned (riding model). *R*(*F*) = 0.0453, *wR*(F^2) = 0.1069; residual electron density: 0.620 and −0.522 eÅ^{-3}.[11]

Cu^{II} Complex of *N*-Pivaloylpivalamidine (5): An excess of $Cu(SO_4) \cdot 5\,H_2O$ is suspended in 50% aqueous ethanol at room temperature. The saturated solution (2.0 mL) is mixed with a solution of **1c** (92 mg, 0.500 mmol) dissolved in ethanol (2.0 mL). About 1 g of $Cu(SO_4) \cdot 5\,H_2O$ is added. After stirring for 10 min, the mixture is filtered and the mother-liquor is extracted with cyclohexane (3 × 2 mL). The solvent is removed in vacuo. The precipitate is recrystallized from acetonitrile and affords **5** [45 mg, 0.105 mmol, 41.9% yield (calcd. for **1c**)] as violet needles. − IR (KBr): $\tilde{\nu}$ = 3330 (vs, NH), 2920 (vs, $CH_{aliph.}$), 2900 (s, $CH_{aliph.}$), 2820 (m, $CH_{aliph.}$), 1550 (vs, C=O), 1470 (vs.), 1450 (s), 1420 (s), 1380 (m), 1300 (s), 1330 (m), 1230 (sh), 1220 (s), 1200 (sh), 1020 (w), 930 (m), 870 (s), 800 (m), 760 (s), 740 (sh). − UV/Vis (acetonitrile): λ_{max} [nm] (ε) = 561 (12), 300 sh (3018), 252 (11162), 209 (10508), 192 (13290). − ^{1}H NMR (300.13 MHz, [D_8]toluene): δ = 1.25 (s), 1.67 (s), 4.96 (br), 5.80 (br). − MS (ESI, acetonitrile, cations): *m/z* (%) = 431.2 (85) [$C_{20}H_{39}CuN_4O_2^+$], 215.5 (5) [$C_{20}H_{40}CuN_4O_2^{2+}$], 185.0 (100) [$C_{10}H_{21}N_2O^+$]. − MS (ESI, acetonitrile, anions): *m/z* (%) = 464.2 (100) [$C_{20}H_{38}N_4O_2CuCl^-$], 219.0 (18) [$C_{10}H_{20}N_2OCl^-$]. − $C_{20}H_{38}CuN_4O_2$ (430.10): calcd. C 55.85 H 8.91 N 13.03; found C 56.39 H 9.13 N 13.34. −

X-ray Diffraction Analysis of 5: ($C_{20}H_{38}CuN_4O_2$),[10] the violet single crystal was analyzed using a Nonius KappaCCD diffractometer with Mo-K_α radiation (λ = 0.71073 Å) using a graphite monochromator at 198(2) K. Crystal system: monoclinic, space group $P2_1/n$ (No. 14) with cell parameters *a* = 5.952(1) Å, *b* = 18.286(3) Å, *c* = 11.469(1) Å, β = 96.55(1)°, *V* = 1240.1(3) Å^3, $\rho_{calcd.}$ = 1.152 Mg/m^3, *Z* = 2. Crystal size: 0.30 × 0.10 × 0.10 mm. 7240 reflections were collected leading to 2782 independent and 1900 observed [$I > 2\sigma(I)$] reflections. Absorption coefficient μ = 0.899 mm^{-1}, absorption correction via SORTAN (0.774 ≤ *T* ≤ 0.915). 130 refined parameters. Non-hydrogen atoms were refined anisotropically. H-Atoms were geometrically positioned (riding model). *R*(*F*) = 0.0534, *wR*(F^2) = 0.1222; residual electron density: 0.549 and −0.364 eÅ^{-3}.[11]

Acknowledgments

We thank Mrs. B. Wibbeling for data collection and technical assistance. Financial support by the Deutsche Forschungsgemeinschaft (Sonderforschungsbereich 424) and the Fonds der Chemischen Industrie (Frankfurt) is gratefully acknowledged.

[1] The results described in this paper are part from the Diploma Thesis of J. K. Eberhardt, University of Münster, **1999**.
[2] N. C. Aust, A. Beckmann, R. Deters, R. Krämer, L. Terfloth, S. Warzeska, E.-U. Würthwein, *Eur. J. Inorg. Chem*. **1999**, 1189−1192.
[3] S.-O. Chua, M. J. Cook, A. R. Katritzky, *J. Chem. Soc., Perkin Trans. 2* **1974**, 546−552.
[4] J. Prigge, R. Fröhlich, E.-U. Würthwein, unpublished X-ray diffraction analyses.
[5] J. C. J. Bart, I. W. Bassi, M. Calcaterra, M. Peroni, *Inorg. Chim. Acta* **1978**, *28*, 201−210.
[6] See for example: G. E. Gurr, *Acta Cryst., B* **1968**, *24*, 1511−1518.
[7] K. Hiraki, Y. Kinoshita, J. Kinoshita-Kawashima, H. Kamano, *J. Chem. Soc., Dalton Trans.* **1996**, 291−298.
[8] M. J. Carney, P. J. Walsh, F. J. Hollander, R. G. Bergman, *Organometallics* **1992**, *11*, 761−777.
[9] M. Buhmann, Diploma Thesis, Universität Münster, **1989**; A. Guzman, M. Romero, F. X. Talamas, R. Villena, R. Greenhouse, J. M. Muchowski, *J. Org. Chem*. **1996**, *61*, 2470−2483.
[10] Crystallographic data (excluding structure factors) for the structure reported in this paper have been deposited with the Cambridge Crystallographic Data Centre as supplementary publications no. CCDC-137212 (**2**), CCDC-137213 (**3**), CCDC-137114 (**4**), and CCDC-137215 (**5**). Copies of the data can be obtained free of charge on application to CCDC, 12 Union Road, Cambridge, CB2 1EZ, UK [Fax: (internat.) + 44−1223/336-033; E-mail: deposit@ccdc.cam.ac.uk].
[11] Programs used: Data collection: Collect: Nonius B. V., 1994. − Data reduction: Denzo-SMN: Z. Otwinowski, W. Minor, *Methods in Enzymology* **1997**, *276*, 307−326. − Absorption correction: SORTAN: R. H. Blessing, *Acta Cryst*. **1995**, *A51*, 33−37; *J. Appl. Cryst*. **1997**, *30*, 421−426. − Structure solution: SHELXS-86 and SHELXS-97: G. M. Sheldrick, *Acta. Cryst*. **1990**, *A46*, 467−473. − Structure refinement: SHELXL-97: G. M. Sheldrick, Universität Göttingen, **1997**. − Graphics: SCHAKAL: E. Keller, Universität Freiburg, **1997**.

Received December 27, 1999
[I99473]

Coordination Compounds of *tripod*Co^{II} and *tripod*Co^{I} − Selective Substitution and Redox Behaviour

Rolf Rupp,[a] Gottfried Huttner,*[a] Peter Kircher,[a] Rainer Soltek,[a] and Michael Büchner[a]

Dedicated to Prof. Jürgen Wolfrum on the occasion of his 60th birthday

Keywords: Tripod ligands / Cobalt(I/II) / Ligand substitution / Alkyne / Redox behaviour

The five-coordinate *tripod*Cobalt(II) compound [*tripod*-$Co^{II}Cl_2$] (**2**) [*tripod* = $CH_3C(CH_2PPh_2)_3$] undergoes selective substitution of its chlorine groups on activation with KPF_6 in the first substitution step and by $TlPF_6$ in the second. Compounds of the type [*tripod*$Co^{II}LL'$]$^{2+}$ with two nitrile (**3**$^{2+}$) or isonitrile (**5**$^{2+}$) ligands are obtained by this route. Compounds [*tripod*$Co^{II}L_2$] containing two equal ligands L are also accessible from Co^{II}_{aq} as the starting material. The syntheses of [*tripod*$Co^{II}(CNR)_2$]$^{2+}$ (**5**$^{2+}$) and [*tripod*$Co^{II}X_2$] (X = CN, NCO, NCS) (**6**) are reported. Different routes to *tripod*Co^{I} derivatives are described. Depending on the nature of the co-ligands, four-coordinate − [*tripod*Co^{I}NCO] (**7**) − or five-coordinate − [*tripod*$Co^{I}(CNR)_2$]$^{+}$ (**5**$^{+}$) − compounds are obtained. Several high-yield syntheses of [*tripod*Co^{I}-alkyne]$^{+}$ (**8**$^{+}$) compounds are reported. The compounds are characterised by the usual analytical and spectroscopic techniques including X-ray analysis of selected examples.

Introduction

An extensive chemistry has been described for the *tripod*cobalt template $[CH_3C(CH_2PPh_2)_3Co]^{n+}$ (n = 0−3).[1−4] Stable compounds [*tripod*CoL_m]$^{n+}$ have been characterised with cobalt in all four of its formal oxidation states of Co^0 to Co^{III}.[1−4] The standard entry into *tripod*-cobalt chemistry is by reaction of the *tripod* ligand with cobalt(II) salts in the presence of co-ligands L, which will generally produce the five-coordinate species [*tripod*$Co^{II}L_2$]. In specific cases, due to electron transfer between the co-ligand and the metal centre, *tripod*cobalt(I) derivatives e.g. [(*tripod*cobalt(I) iodide][2a] or *tripod*cobalt(III) derivatives e.g. [*tripod*cobalt(III) catecholate]$^{+}$ [4] may also be accessible by this route. While many compounds [*tripod*cobalt(II)L_2]$^{n+}$ and a number of compounds [*tripod*cobalt(I)L_2]$^{+}$ or [*tripod*cobalt(I)L] are known, almost nothing is known about the possible exchange of co-ligands in such species by selective substitution reactions.

Exchange of the η^2-acetato ligand in [*tripod*cobalt(II) acetate]$^{+}$ [3a] with an allylic ligand and the substitution of one chloride ligand in [*tripod*cobalt(II)Cl_2][2b,3b] by neutral donor ligands[2b,3c] appear to be the only examples of selective substitution reactions in *tripod*cobalt(II) chemistry. As far as *tripod*Co^{I} chemistry is concerned, the extensive work of J. Ellermann et al. has shown that the carbonyl groups in [*tripod*$Co^{I}(CO)_2$]$^{+}$ − which is obtained from $Co_2(CO)_8$ as the starting material − undergo substitution reactions under photolytic conditions.[2c−2e] The possibility of exchanging the chloride ligand in [*tripod*Co^{I}Cl] has only recently been reported as a selective entry into *tripod*Co^{I} chemistry.[2f]

It is apparent that in order to further develop the chemistry of the *tripod*cobalt template, it is necessary to develop more general methods of substitution processes. In view of the many cases where reversible reductions or oxidations of [*tripod*$Co^{II}L_2$]$^{n+}$ compounds have been documented by cyclic voltammetry, it is also necessary to find preparative methods which allow selective change in the oxidation state of the metal centre. Such methods would be especially useful with respect to *tripod*Co^{I} chemistry since *tripod*Co^{II} compounds are more easily accessible than the corresponding *tripod*Co^{I} species.

We report here on the stepwise selective subsitution of the chloro ligands in [*tripod*$CoCl_2$] (**1**) by two different donor ligands L and L′ to produce [*tripod*$Co^{II}LL'$]$^{n+}$ (n = 0, 2). Compounds of the type [*tripod*$Co^{II}L_2$]$^{n+}$, on the other hand, are easily accessible by standard methods, with the synthesis of such compounds [L = RNC, RCN (n = 2); CN^-, OCN^-, SCN^- (n = 0)] being reported. Upon reduction, these compounds [*tripod*$Co^{II}L_2$] produce [*tripod*$Co^{I}L_2$] or [*tripod*Co^{I}L] depending on the nature of L. With nitriles as co-ligands L, the cobalt(I) species [*tripod*$Co^{I}(NCR)_2$]$^{+}$ are highly reactive and react with alkynes to produce [*tripod*$Co^{I}(\eta^2$-alkyne)]$^{+}$, which may also be obtained from [*tripod*Co^{I}Cl] and alkyne upon activation with $TlPF_6$.[2f]

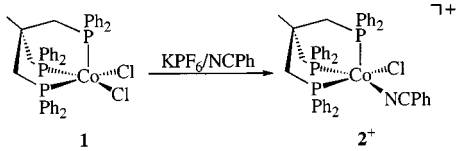
Results and Discussion

Stepwise Substitution Leading to [tripod$Co^{II}LL'$]

[*tripod*$CoCl_2$] (**1**)[2b,3b] undergoes selective substitution of one of its two chloro ligands by neutral two-electron donors upon activation with KPF_6[2b] or $NaBPh_4$.[3c]

[a] Anorganisch-Chemisches Institut der Universität Heidelberg
Im Neuenheimer Feld 270, D-69120 Heidelberg, Germany
Fax: (internat.) + 49-(0)6221/545707
E-mail: g.huttner.@indi.aci.uni-heidelberg.de

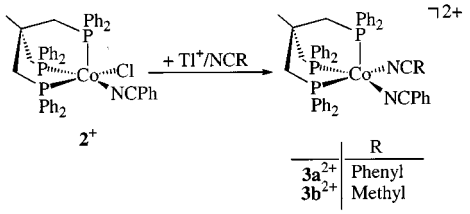
 © WILEY-VCH Verlag GmbH, D-69451 Weinheim, 2000 1434−1948/00/0808−1745 $ 17.50+.50/0



Scheme 1

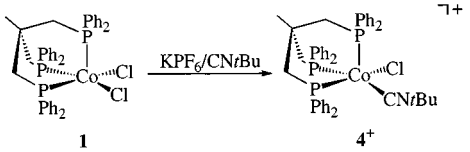
The benzonitrile derivative $\mathbf{2}^+$ (Scheme 1) is obtained by a procedure analogous to the one reported for the synthesis of [*tripod*Co^{II}(Cl)(NCMe)]$^+$.[2b] Analytical and spectroscopic data (Tables 3 and 4) confirm its identity. The remaining chloride group in $\mathbf{2}^+$ may be replaced in a second substitution step upon activation with $TlPF_6$.

While compounds such as $\mathbf{3a}^{2+}$, with two identical nitrile substituents, might also be obtained by more standard methods[3d], the synthesis of compound $\mathbf{3b}^{2+}$, containing two different nitrile donors relies on the selective stepwise substitution process described (Scheme 2). Both compounds are fully characterised (Tables 3 and 4).



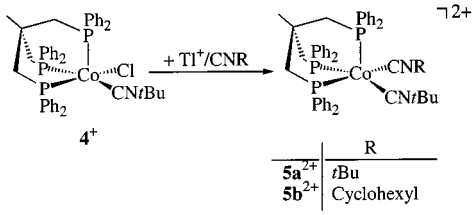
Scheme 2

It had been found by L. Sacconi et al. that **1** undergoes selective substitution of one chloro group by cyclohexyl isocyanide upon activation with $NaBPh_4$.[3c] Analogously, in the presence of KPF_6, **1** reacts with *t*BuNC to produce the monosubstituted product $\mathbf{4}^+$ (Scheme 3, for analytical and spectroscopic data see Tables 3 and 4).



Scheme 3

Only when activated with $TlPF_6$ will the remaining chloride group in $\mathbf{4}^+$ undergo substitution, producing $\mathbf{5}^{2+}$ (Scheme 4, for analytical and spectroscopic data see Tables 3 and 4).

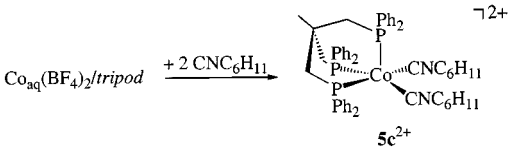


Scheme 4

Compounds such as $\mathbf{5a}^{2+}$, containing two identical isonitrile ligands, may directly be obtained from **1** by using a 2:1 molar ratio of $TlPF_6$/**1** in the presence of two equivalents of the corresponding isonitrile. An excess of isonitrile has to be avoided since it leads to partial decoordination of the *tripod* ligand. Decomplexation is apparent from the corresponding ^{31}P-NMR spectra, which generally, even for the necessarily paramagnetic *tripod*Co^{II} compounds, show well resolved signals for the coordinated phosphorus donors around $\delta = 34$ and the signal of a decoordinated *tripod* phosphorus donor at $\delta = -27$.

One Step Formation of [tripod$Co^{II}L_2$]

Compounds such as $\mathbf{5a}^{2+}$ are easily accessible by the standard procedure of treating a mixture of $Co^{II}_{aq}(BF_4)_2$/*tripod* in $EtOH/CH_2Cl_2$ with two equivalents of an isonitrile. Since no single crystals suitable for X-ray analysis had been obtained for the PF_6^- salts of either $\mathbf{5a}^{2+}$ or $\mathbf{5b}^{2+}$, this synthetic procedure was applied with cyclohexyl isocyanide as the co-ligand to give the salt of $\mathbf{5c}^{2+}$, in the hope it would produce crystals suitable for X-ray analysis (Scheme 5).



Scheme 5

The formation of $\mathbf{5c}^{2+}$ under these reaction conditions is clear from the mass spectrum of its salt, which shows a prominent peak for [*tripod*$Co(CNC_6H_{11})_2]^+$ ($m/z = 901$) independent of the anion used. Crystals were obtained after metathesis with KPF_6 in acetone and crystallisation of the metathesis product from acetone by vapour phase diffusion of Et_2O. Structural analysis of these crystals clearly reveals the structure of $\mathbf{5c}^{2+}$ (Figure 1 and 2; Table 1 and 6).

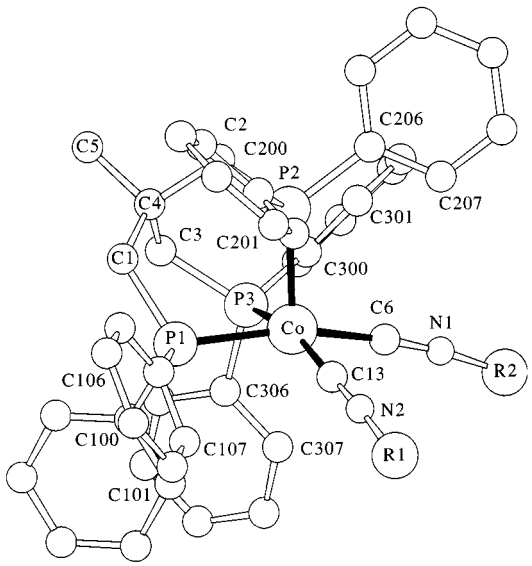


Figure 1. X-ray structure of $\mathbf{5c}^{2+}$ ($R^1 = R^2 = C_6H_{11}$)

The crystal structure was unexpectedly found to contain $PO_2F_2^-$ counterions. Formation of this type of counterion from PF_6^- has been reported in several cases.[5] The water necessary for this hydrolysis reaction may come from the cobalt(II)$_{aq}$ starting material as well as from water in the acetone solvent used for crystallisation. There are two crys-

Table 1. Bond lengths [pm], bond angles [°] and torsion angles [°] for the [*tripod*CoL$_n$]$^{m+}$ compounds **5c**$^{2+}$[(PF$_2$O$_2$)$^-$]$_2$, **5a**$^+$(PF$_2$O$_2$)$^-$, **6a**, **6c**, and **7a** (standard deviations in units of the least significant digit given in each case)

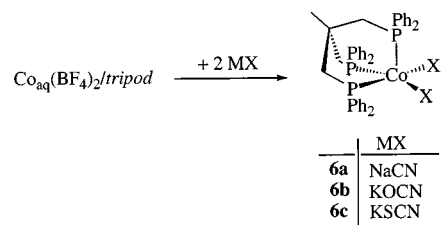
Compound[b]	**5a**$^+$(PF$_2$O$_2$)$^-$ [a] L = CN*t*Bu *n* = 2; *m* = 1	**5c**$^{2+}$[(PF$_2$O$_2$)$^-$]$_2$ L = CNC$_6$H$_{11}$ *n* = 2; *m* = 2	**6a** L = CN *n* = 2; *m* = 0	**6c** L = NCS *n* = 2; *m* = 0	**7a** [a] L = NCO *n* = 1; *m* = 0
Co−P1	219.9(2)	224.1(2)	221.3(2)	219.8(4)	223.2(1)
Co−P2	222.1(2)	229.5(2)	228.9(2)	229.4(4)	221.9(1)
Co−P3	219.9(2)	224.1(2)	224.1(2)	220.5(4)	221.8(1)
Co−L1	184.4(7)	187.1(7)	188.6(1)	190.6(1)	192.8(2)
Co−L2	182.6(6)	187.5(7)	191.1(1)	190.8(1)	−
P1−Co−P2	88.24(3)	88.7(7)	90.8(1)	92.84(1)	91.6(3)
P2−Co−P3	96.01(3)	95.8(8)	90.4(1)	91.10(1)	92.9(3)
P1−Co−P3	90.07(3)	87.4(7)	89.2(1)	89.58(2)	90.7(4)
P1−Co−L1	90.2(5)	93.2(3)	87.4(3)	92.7(3)	124.9(2)
P1−Co−L2	161.7(5)	165.7(3)	167.1(3)	151.4(3)	−
P2−Co−L1	110.6(5)	100.6(3)	116.2(3)	99.1(3)	121.9(2)
P2−Co−L2	106.1(5)	105.2(2)	101.5(3)	115.3(3)	−
P3−Co−L1	154.5(4)	163.6(2)	153.3(3)	169.4(3)	125.2(2)
P3−Co−L2	90.2(4)	87.7(3)	94.4(3)	85.5(3)	−
L1−Co−L2	84.5(3)	87.8(3)	83.86(4)	87.6(3)	−
C4−C1−P1−Co	31.4	24.9	26.6	13.3	28.4
C4−C2−P2−Co	32.0	37.9	26.7	12.9	30.0
C4−C3−P3−Co	22.1	21.9	27.9	10.3	29.8
Hz−P1−C100−C101[c]	−17.6	−8.0	−8.2	21.1	−34.7
Hz−P1−C106−C107[c]	−42.4	−26.8	59.3	70.2	−0.5
Hz−P2−C200−C201[c]	−27.6	−2.6	9.9	16.9	−27.3
Hz−P2−C206−C207[c]	−9.2	13.2	5.8	27.4	1.6
Hz−P3−C300−C301[c]	−63.4	−80.0	−41.0	40.4	−46.8
Hz−P3−C306−C307[c]	−11.5	−5.8	−2.0	17.3	5.5

[a] For the sake of comparison the structure was inverted with respect to the deposited data. − [b] For **5a**$^+$, **5c**$^{2+}$ the designators L1 and L2 refer to the ligands labelled by R1 and R2 respectively in Figures 2 and 3. For **6a** and **6c** L1 refers to the ligand designated by C6N6 and L2 to the one designated by C7N7 in each case (Figures 2 and 3). − [c] In order to define the rotation of the phenyl groups with respect to the idealised C_3 axis of the [*tripod*Co] entity the following procedure was adopted: a vector vertical to the P1−P2−P3 plane and pointing towards the observer with respect to the projections given in Figures 2 and 3 is fixed at the individual phosphorus atoms. Its end point is called Hz. The torsion angles given refer to this convention.

tallographically independent anions in the unit cell of **5c**$^{2+}$, both of which show disorder (see Experimental Section). In contrast to the anions, the cations of **5c**$^{2+}$ are not affected by disorder problems. The idealised square pyramidal structure of **5c**$^{2+}$ is apparent from Figure 1 and 2 and Table 1. It is assumed that **5a**$^{2+}$ and **5b**$^{2+}$ adopt the same type of geometry.

Compound **5c**$^{2+}$ can only obtained by the described route if the amount of isonitrile used does not exceed the stoichometric limit. If an excess of isonitrile is used, mixtures of compounds are obtained having at least partial replacement of the phosphorus donors by isonitrile ligands.

With cyanide as an isoelectronic anionic equivalent of RNC, the risk of replacing the phosphorus donors by cyanide ligands is even higher as it has been found that aqueous solutions of NaCN may completely replace the *tripod* and the co-ligands in [*tripod*CoL$_2$].[3e,6] Nevertheless, under controlled conditions, the cyano derivative **6a** is accessible by the standard procedure (Scheme 6).



	MX
6a	NaCN
6b	KOCN
6c	KSCN

Scheme 6

The cyanide ligands in **6a** may be viewed as isoelectronic equivalents of isonitriles analogous to compounds such as **5**$^{2+}$; they may also be seen as pseudo-halide ligands analogous to **1**. This latter classification leads to the question of whether other pseudo-halide derivatives may be accessible by the same type of procedure. It is in fact found that NCO$^-$ and NCS$^-$ form the corresponding pseudo-halide derivatives **6b** and **6c**. The compounds are isolated as microcrystalline powders (**6b**: green; **6c**: brown) with the analytical and spectroscopic data being in agreement with the assigned formulations (Table 3 and 4). The structures of **6a** and **6c** have been solved by X-ray crystallography (Figure 2 and Figure 3; Tables 1; 6 and 7).

Both compounds show an idealised square-pyramidal coordination of the cobalt centre with one of the phosphorus donors (P2, Figure 2 and 3; Table 1) occupying the apical position and with the other two phosphorus donors and the two co-ligands forming the base of the pyramid. Comparison of the three structures of the type [*tripod*Co^{II}L$_2$] reported in this paper (**5c**$^{2+}$, **6a**, **6c**; Table 1; Figure 2 and 3) shows that the apical Co−P bond is longer (229 pm) than the equatorial Co−P bonds (220−224 pm). The P−Co−P angles are, by virtue of being part of the chelate cage, close to 90° in each case. The L−Co−L angles spanned by the coordinated atoms of the co-ligands are found in the narrow range of 84−88° (Table 1). The P−Co−L angles fall into two classes. The angles referring to ligands which are in an idealised *trans* position to each other show values be-

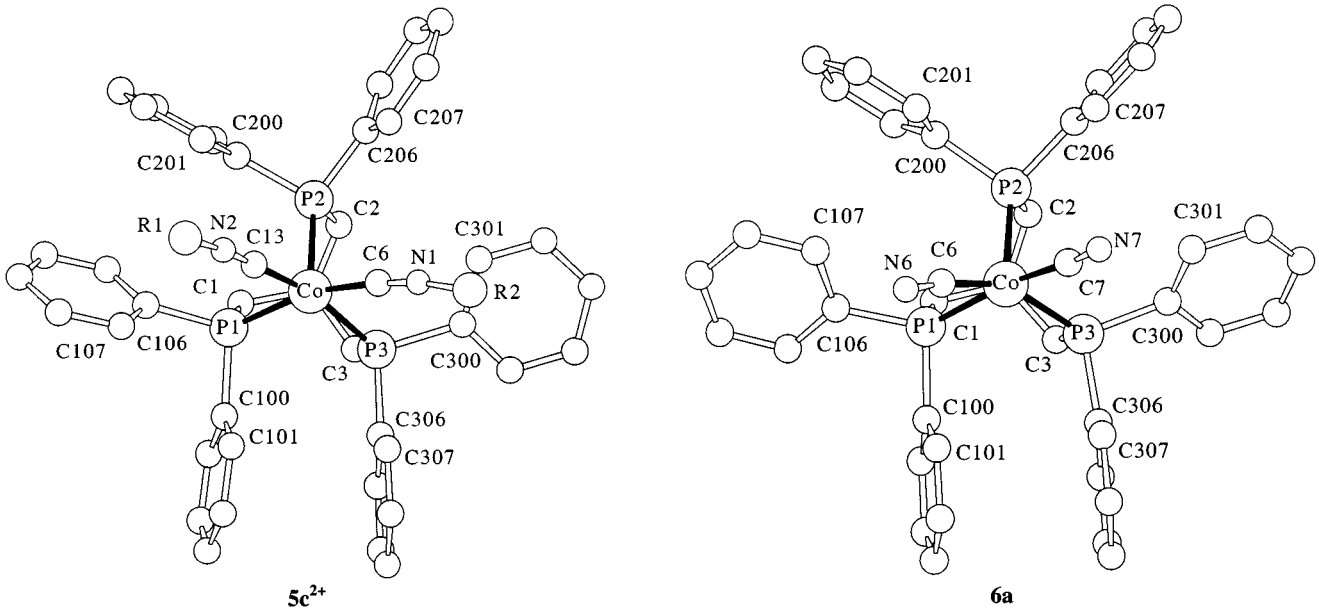


Figure 2. X-ray structure of compounds $\mathbf{5c}^{2+}$ ($R^1 = R^2 = C_6H_{11}$) and **6a**; projection onto the P1−P2−P3 plane

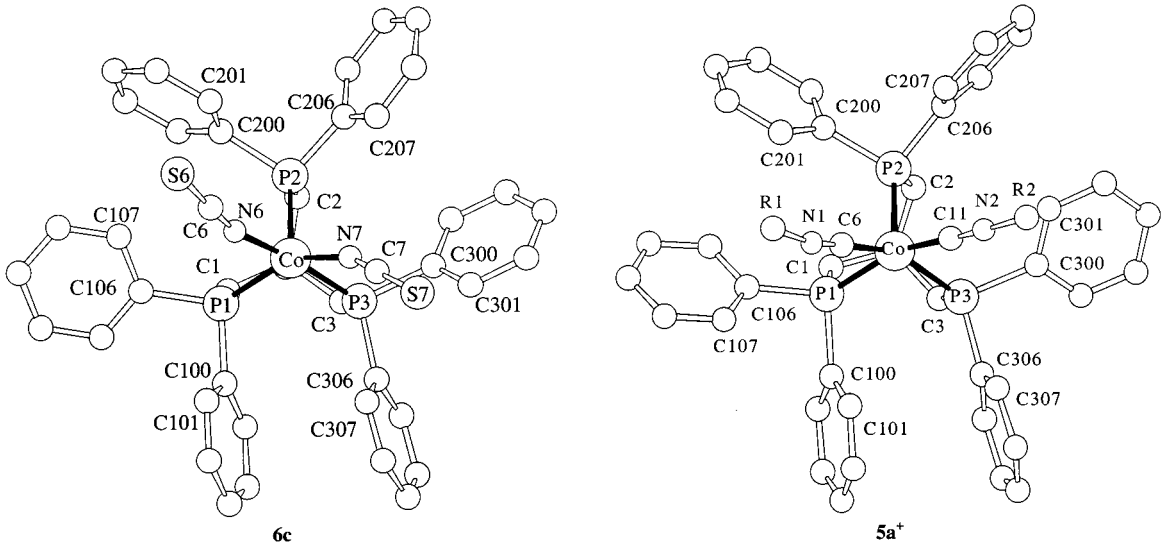


Figure 3. X-ray structure of compounds **6c** and $\mathbf{5a}^{+}$ ($R^1 = R^2 = t$Bu); projection onto the P1−P2−P3 plane.

tween 151° and 169° (Table 1) while angles referring to mutual idealised *cis* positions are in a range between 86° and 116°. The deviations from the idealised square-pyramidal geometry are thus substantial. Nevertheless the Co−P bond described as axial is definitely the longest one in each case. The scheme used to label the atoms refers to the standard used in many other publications referring to the structure of *tripod*Co compounds.[7] It is such that the torsion angles of the chelate scaffolding (C4−Ci−Pi−Co; Table 1; Figure 2 and 3) are positive throughout. The rotational position of the phenyl groups (Hz−Pi−Cj−Ck; Table 1; Figure 2 and 3) shows a common trend for all three compounds $\mathbf{5c}^{2+}$, **6a**, **6c**. Two of the phenyl groups at P1 and P3 (labels C100 and C306, Figure 2 and 3, Table 1) are oriented such that they are almost parallel to the idealised C_3 axis of the *tripod*Co fragment, while the other two phenyl groups at these phosphorus atoms are tilted with respect to this axis. The phenyl groups at the axial phosphorus centre P2 tilt to a lesser degree (Figure 2 and 3; Table 1) and may well be close to being parallel to the idealised C_3 axis.

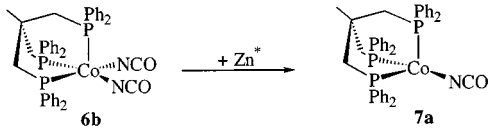
tripodCo^{I} Complexes

Starting from Co^{II} Precursors

*tripod*Co^{I} complexes should be accessible from *tripod*Co^{II} compounds, irrespective of whether their cyclovoltammetric reduction is reversible or not. In the case of a reversible reduction one would expect the reduction product to have the same composition as the Co^{II} starting material as well as a similar structure. An irreversible reduction, on the other hand, does not necessarily mean that the compound decomposes to a complex mixture of products, it only means that the product will have a structure and possibly con-

stitution which is different from the starting material. Preparative reduction has therefore been conducted for [*tripod*CoL_2] species whose cyclovoltammograms show reversible reductions, such as **5a**$^{2+}$ and **6a**, as well as those which show irreversible ones, such as **6b/c** (Tables 3 and 4).

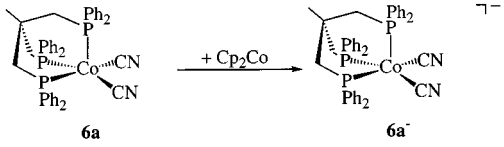
An example of a [*tripod*$Co^{II}L_2$] compound which undergoes irreversible reduction but still selectively produces a specific *tripod*Co^{I} compound is [*tripod*$Co^{I}Cl_2$] (**1**) which is preparatively reduced to [*tripod*$Co^{I}Cl$].[2a,2b,2f] With this in mind the pseudo-halide derivatives **6b/c**, which show an irreversible reduction step in their cyclovoltammograms, may well be expected to selectively produce [*tripod*Co^{I}] derivatives upon preparative reduction. This expectation is born out by the successful synthesis of **7a** from **6b** using activated zinc powder as the reductant (Scheme 7).



Scheme 7

Brown **6b** produces green **7a** which is obtained as a microcrystalline powder (analytical and spectroscopic data in Tables 3 and 4). Crystals of **7a** are obtained by vapour diffusion of petroleum ether (boiling range 40−60 °C) into its CH_2Cl_2 solutions. The coordination around the Co^{I} centre of **7a** can be described as a trigonally distorted tetrahedron (Figure 4; Table 1) as is characteristic of compounds [*tripod*$Co^{I}L$].[2a,2b,2n] Compound **7a** is found to be paramagnetic with two unpaired electrons per formula unit. This is to be expected if the coordination environment around the d^8-Co^{I} centre of **7a** is an idealised tetrahedron. Two of the P−Co−P angles are about 90°; the P−Co−L angles are found to be around 120°. The rotational position of the phenyl groups closely correspond to a C_3-symmetric arrangement with three of these groups being almost parallel to the idealised C_3 axis and the three other ones (Figure 4; Table 1) being inclined in similar extents in this direction in a propeller type arrangement.

Since the five-coordinate Co^{II} compound **6b** forms the four-coordinate Co^{I} species **7a** it is clear why the cyclovoltammetric reduction is irreversible. Clearly, a rapid ligand dissociation process is initiated when **6b** undergoes one-electron reduction. With **6a** the electrochemical behaviour is the reverse of the one found for **6b**. Compound **6a** undergoes reversible reduction while its oxidation is irreversible whereas **6b** is reversibly oxidised with the reduction being irreversible. Reduction of **6a** by Cp_2Co is predicted to produce the five-coordinate compound [*tripod*$Co^{I}(CN)_2]^-$, **6a**$^-$ (Scheme 8).



Scheme 8

The salt containing **6a**$^-$ as the anion and Cp_2Co^+ as the cation is obtained as a microcrystalline red-brown material. It has not been possible to obtain it in an analytically pure form. On the other hand FAB-MS spectra clearly demonstrate its composition from [*tripod*$Co^{I}(CN)_2]^-$ (m/z = 737) and Cp_2Co^+ (m/z = 189). The presence of cyano ligands is indicated by a weak IR absorption at 2100 cm^{-1}. The corresponding broad and weak absorption is not shifted by much compared to the starting compound **6a**. The observed bands should be composed of an envelope of two vibration modes (sym. and antisym.) which are not individually resolved. The ^{31}P-NMR spectra of **6a**$^-$ show a signal characteristic for an η^3-coordinated *tripod* ligand at δ = 31.

Since the Cp_2Co^+ salt of **6a**$^-$ could not be isolated as an analytically pure compound an alternative synthesis of **6a**$^-$ was tested. [*tripod*^{I}Co$(CO)_2]^+$, which is known to undergo carbonyl substitution under photochemical activation[2c−2e] reacts with NaCN to also produce **6a**$^-$. The reaction is,

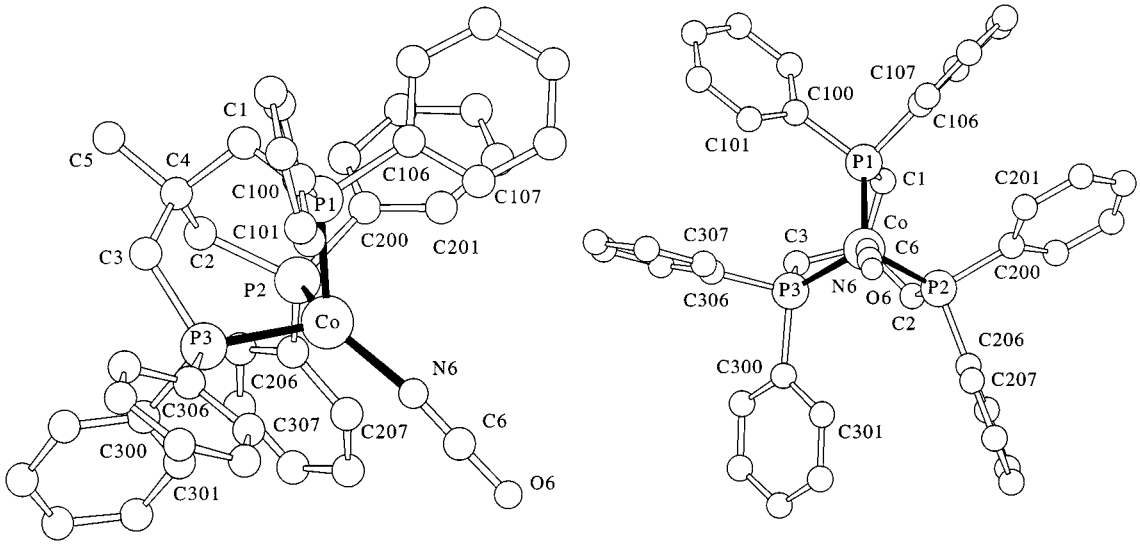
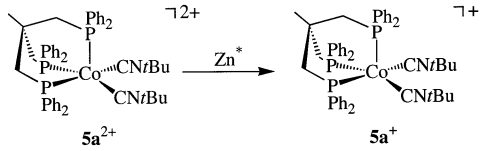


Figure 4. X-ray structure of compound **7a**

however, not as clean as the one starting from **6a**. The product obtained from [*tripod*$Co^{I}(CO)_2]^+$, while showing the FAB^- signal of $\mathbf{6a}^-$ (m/z = 737), is found to be contaminated by species in which the ligand groups of the *tripod* ligand are partially decoordinated (^{31}P NMR: $\delta = -27$).

If cyanide is viewed as a pseudo-halide species, the five-coordination of $\mathbf{6a}^-$ is in contrast to the four-coordination of **7a**. In view of the backbonding properties of the cyanide ligand the five-coordination of $\mathbf{6a}^-$ corresponds to the five-coordination of [*tripod*$Co^{I}(CO)_2]^+$. This latter view leads to the expectation that the reduction of the isonitrile derivatives $\mathbf{5}^{2+}$ might produce stable Co^{I} derivatives, since isonitrile ligands have more in common with carbonyl ligands than their isoelectronic relatives CN^-.[8] The reversible cyclovoltammetric reduction of $\mathbf{5a}^{2+}$ is mirrored by the straightforward preparative reduction of $\mathbf{5a}^{2+}$ to $\mathbf{5a}^+$ by activated zinc powder (Scheme 9).



Scheme 9

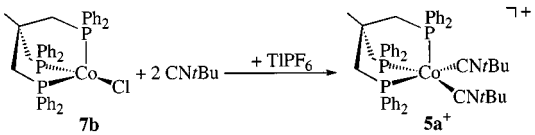
Compound $\mathbf{5a}^+$ is isolated as its PF_6^- salt after chromatography on SiO_2 as a microcrystalline powder with almost the same orange yellow colour as characteristic for starting material $\mathbf{5a}^{2+}[(PF_6)^-]_2$. The cyclovoltammogram observed for $\mathbf{5a}^+$ is the same as the one observed for $\mathbf{5a}^{2+}$ with the reduction wave of $\mathbf{5a}^{2+}$ corresponding to the oxidation wave of $\mathbf{5a}^+$ (Table 3, Experimental Section). Compound **5a**(PF_6) is a diamagnetic salt showing well-resolved NMR spectra (Experimental Section). This may be taken as a further proof of the five-coordination of its cobalt centre since four-coordination would lead to paramagnetism (see **7a**). Single crystals were grown by dissolving **5a**(PF_6) in CH_2Cl_2 and allowing Et_2O to diffuse into this solution. After several trials, a few crystals suitable for X-ray crystallography could be obtained. These crystals were found to contain a $PF_2O_2^-$ counterion instead of the PF_6^- counterion of the starting material due to hydrolysis during the crystallisation experiments. While the counterion shows disorder, in the crystal the cation $\mathbf{5a}^+$ is completely ordered (see Experimental Section).

The structure of the cation of $\mathbf{5a}^+$ is very similar to the structure of $\mathbf{5c}^{2+}$ (not taking into account the different substituents of the isonitrile ligands: $\mathbf{5c}^{2+}$: $C_6H_{11}NC$; $\mathbf{5a}^+$: C_4H_9NC), Figure 2 and 3). The idealised square-pyramidal coordination around the cobalt centres is evident from Figure 2 as well as from the data in Table 1. Co−P and Co−L bond lengths are longer in the Co^{II} compound $\mathbf{5c}^{2+}$ as compared to those in the Co^{I} species $\mathbf{5a}^+$. Arguments based on ionic radii would lead one to expect the contrary. Models based on covalent bonding characterise $\mathbf{5a}^+$ as an electron-precise 18-electron compound with the maximum number of valence electrons involved in bonding whereas $\mathbf{5c}^{2+}$ has a 17-electron configuration and thus one bonding electron less than $\mathbf{5a}^+$. The observed shortening of the bond lengths when going from the 17-electron compound $\mathbf{5c}^{2+}$ to the 18-electron species $\mathbf{5a}^+$ is thus easily understood. There is only one other pair of *tripod*Co derivatives for which the structure of the Co^{I} and the Co^{II} form is known. [*tripod*Co(η^3-allyl]$^{m+}$ (m = 0, 1) exists in the two different oxidation states Co^{I} and Co^{II}.[2n,3b] [With modified tripodal ligands such as $P(CH_2CH_2PPh_2)_3$ other structurally characterised pairs of Co^{I}/Co^{II} redox couples are known.][3l,3k] The same regularities observed for $\mathbf{5a}^+/\mathbf{5c}^{2+}$ are found for [*tripod*Co(η^3-allyl]$^{m+}$ (m = 0, 1).[2n,3b] The Co−P bonds in the Co^{II} species are some 8 pm longer than the ones in the Co^{I} derivative. The difference between the lengths of the basal and apical Co−P bonds is apparent for the cobalt(II) species (Co−P_{apical}: 230 pm; Co−P_{basal}: 221 pm) while these bonds are almost equal for the Co^{I} compound (215−217 pm).[2n,3b] A similar trend is evident when comparing the Co−P distances of $\mathbf{5c}^{2+}$ and $\mathbf{5a}^+$ (Table 1).

While isonitriles RNC are strongly backbonding ligands, nitriles RCN are far less so.[8] While the isonitrile derivative [*tripod*$Co^{II}(CNR)_2]^{2+}$ ($\mathbf{5a}^{2+}$) produces the stable five-coordinate Co^{I} reduction product $\mathbf{5a}^+$, the corresponding nitrile derivatives [*tripod*$Co^{II}(RCN)_2]^{2+}$ ($\mathbf{3}^{2+}$) are expected to produce less stable Co^{I} species since charge delocalisation into the nitrile ligand will not help to stabilise these compounds to a great extent. Nevertheless, compounds $\mathbf{3}^{2+}$ have been found to undergo reversible reduction[3d] indicating that relatively long lived five-coordinate species $\mathbf{3}^+$ are produced. One-electron reduction is not immediately followed by a ligand-dissociation step. This is in contrast to the behaviour of the five-coordinate isocyanate derivative [*tripod*$Co^{II}(NCO)_2]$ (**6b**) which produces the four-coordinate [*tripod*$Co^{I}(NCO)]$ (**7a**) upon reduction. When [*tripod*$Co^{II}(NCMe)_2](BF_4)_2$[3d] is treated with activated zinc powder, a blue solution is immediately obtained from the green solution of the starting material. When the excess zinc powder is filtered off, this solution turns brown. No single compound could be isolated from these solutions and it remains speculative whether the blue or brown colour is due to [*tripod*$Co^{I}(RCN)_2]^+$.

Starting from Co^{I} Precursors

It was felt that starting from appropriate Co^{I} compounds might solve the problem of producing nitrile derivatives of *tripod*Co^{I}. The corresponding synthetic procedure was tested with the synthesis of the isonitrile compound $\mathbf{5a}^+$ from [*tripod*$Co^{I}Cl]$ (**7b**) (Scheme 10).



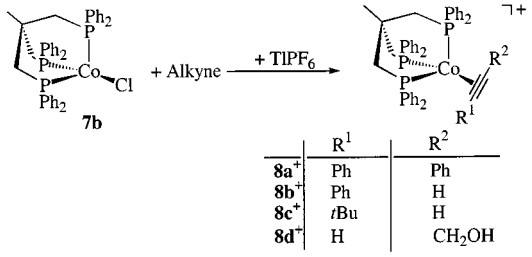
Scheme 10

Since it is known that $\mathbf{5a}^+$ is a stable compound (see above) one should be able to isolate it if the procedure works. When a beige suspension of **7b** in THF is treated with $TlPF_6$, a white precipitate of TlCl forms leading to a yellow solution of [*tripod*$Co^{I}L_n]^+$ where L should be a THF

ligand. When this mixture is treated with two equivalents of *t*BuNC, an immediate colour change is observed and **5a**$^{+}$(PF$_6$)$^{-}$ is obtained in good yield. The analytical and spectroscopic data of the product correspond to those obtained when **5a**$^{+}$ is prepared from **5a**$^{2+}$ by reduction (see above). The propensity of [*tripod*CoCl] to produce compounds [*tripod*CoL$_2$]$^{+}$ when activated by Tl^{+} had already been used for the synthesis of such compounds where L$_2$ is a diene or a heterodiene ligand.[2f] The reaction principle therefore appears to be quite general and the reaction of **7b** with nitriles should produce nitrile derivatives of *tripod*Co^{I} (**3**$^{+}$). On addition of nitriles to the suspensions prepared from **7b** and TlPF$_6$ (see above), an immediate colour change from yellow to brown is observed. The brown products could, however, not be isolated and their formulation as **3**$^{+}$ may be erroneous. An argument for this formulation is the observation that such brown solutions are also obtained when **3**$^{2+}$ is reduced by activated zinc powder (see above).

The fact that the brown compounds cannot be isolated as such shows that they are reactive species which by themselves should be able to undergo ligand substitution processes. As a test for this hypothesis the brown solutions were treated with tolane since it is known that [*tripod*Co^{I}(η^2-alkyne)] compounds are stable isolable species.[2g,2h] The salt of **8a**$^{+}$ is obtained by this procedure in yields around 90% (Table 2 and 5). Compound **8a**$^{+}$ had been obtained by L. Sacconi et al.[2g] who used the in situ reduction of Co^{II} salts by 2-propanol in the presence of *tripod* and tolane as their preparative method. The yields obtained by this procedure are not given in the literature but reproduction of these syntheses resulted in yields around 30%.[2i]

The sequence of **7b** → **3b**$^{+}$ → **8a**$^{+}$ is successful. It shows that alkynes are excellent probes for trapping kinetically



Scheme 11

labile *tripod*Co^{I} intermediates (Scheme 11). Such intermediates are of course also formed when solutions of **7b** are treated with Tl^{+} and, as expected, such solutions react with alkynes to produce the corresponding [*tripod*Co^{I}(η^2-alkyne)] complexes **8**$^{+}$ as well.

The reaction is also tolerant to terminal alkynes (**8b**$^{+}$, **8c**$^{+}$) and OH substituents on the alkyne ligand (**8d**$^{+}$).

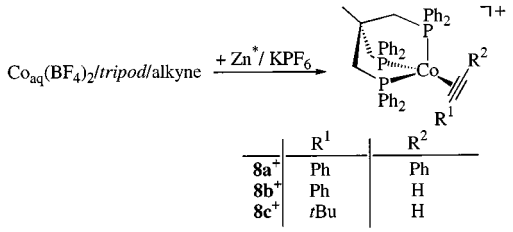
Based on the observation made by L. Sacconi et al.[2g] that compounds **8a**$^{+}$ and **8b**$^{+}$ are obtained from a mixture of Co(ClO$_4$)$_{2aq}$/*tripod*/alkyne with 2-propanol as the reductant it is reasonable to test this type of reaction by using a more conventional reductant instead of 2-propanol. A mixture of Co$^{II}_{aq}$(BF$_4$)$_2$ and *tripod* reacts with alkynes when treated with activated zinc powder as reductant (Scheme 12).

It is found that this synthetic procedure works well, with apparently almost quantitative formation of **8**$^{+}$; yields of the isolated pure compounds are only reduced by loss during chromatographic work up. This simple reaction protocol is also tolerant to terminal alkynes (**8b**$^{+}$, **8c**$^{+}$) while alcoholic groups are not tolerated. The 18-electron compounds **8**$^{+}$ show well-resolved NMR spectra (Table 5). All groups of signals in their ^{1}H-, ^{13}C-, and ^{31}P-NMR spectra

Table 2. Syntheses, yields and properties of compounds **2**−**8** (see Experimental Section)

Compound	Method	Co-ligand	Colour	Yield [%]	Melting point [°C][a]
2PF$_6$		104 mg benzonitrile	orange-brown	75	170
3a(PF$_6$)$_2$	A	208 mg benzonitrile	dark-green	85	170
	B	208 mg benzonitrile	dark-green	79	
3b(PF$_6$)$_2$	A	43 mg acetonitrile	green	74	165
4PF$_6$		84 mg *tert*-butyl isonitrile	green	82	185
5a(PF$_6$)$_2$	A	84 mg *tert*-butyl isonitrile	red-orange	76	210
	B	168 mg *tert*-butyl isonitrile	red-orange	82	
5b(PF$_6$)$_2$	A	110 mg cyclohexyl isonitrile	red-orange	70	200
5aPF$_6$	C	168 mg *tert*-butyl isonitrile	red-orange	59	180
	D	168 mg *tert*-butyl isonitrile	red-orange	51	
6a		98 mg NaCN	claret	94	
6b		164 mg KOCN	brown	71	175
6c		196 mg KSCN	beige	59	170
7a			brown-green	89	170
8PF$_6$	G	178 mg diphenylethyne	dark-green	91	175
	H	178 mg diphenylethyne		88	
8PF$_6$	G	102 mg phenylethyne	green	77	161
	H	102 mg phenylethyne		61	
8PF$_6$	G	82 mg 2,3-dimethylbutyne	green	59	155
	H	82 mg 2,3-dimethylbutyne		51	
8PF$_6$	G	57 mg propynol	dark-green	66	140

[a] Decomposition.



	R^1	R^2
8a$^+$	Ph	Ph
8b$^+$	Ph	H
8c$^+$	*t*Bu	H

Scheme 12

can be unequivocally assigned (Table 5). The coordination of both of the carbon atoms of the alkyne ligand is clear from the ^{13}C-NMR signals relating to these atoms. The η^2 coordination of the alkynes in compounds of the type **8**$^+$ is also indicated by comparison with a structurally analysed example.[2n] There is only one ^{31}P-NMR signal for each compound **8**$^+$. In any static structure with a C_2-symmetric alkyne, the juxtaposition of the C_3-symmetric P3−Co entity and the C_2-symmetric alkyne with the coinciding C_2 and C_3 axes give a minimum of two different phosphorus environments, and generally three different types of environment for the phosphorus atoms will exist. A single ^{31}P-NMR peak, observed for all compounds **8**$^+$, indicates that the alkynes rotate around the constitutional C_3 axis of the *tripod*Co template such that all the different environments are averaged in the time domain of the NMR experiment. Rapid rotation of the co-ligands around the idealised C_3 axis of the *tripod*Co template with only one ^{31}P-NMR signal being apparent − where a static structure would lead to at least two signals − is often observed.[2f]

Compounds **8**$^+$ are diamagnetic, which means that the alkyne acts as a 4-electron donor ligand, so that **8**$^+$ are 18-electron compounds. Oxidation of **8**$^+$ occurs at potentials above 1000 mV (vs. SCE, Table 5) and is irreversible throughout. This means that the formal oxidation products **8**$^{2+}$ are unstable. Reduction, on the other hand, is reversible or at least quasireversible for all compounds **8**$^+$ (Table 5) occurring between −600 and −800 mV (vs. SCE). The neutral reduction products **8** are formal 19-electron compounds. Their stability is thus unexpected. This may be explained by the argument that alkynes are known to act as rather flexible donor molecules, which may supply between two and four electrons.[8] In this sense the extra electron would be localised on the alkyne ligands. Any attempts to isolate the neutral compounds **8** have been unsuccessful so far.

No distinct reaction product could be obtained from Co$^{II}_{aq}$(BF$_4$)$_2$/*tripod* with HC≡C−CH$_2$OH as the alkyne and activated zinc powder as the reductant, while the reaction based on **7b** as the starting material gave the corresponding alkyne derivative **8d**$^+$ in high yield. When Me$_3$SiC≡CH is used as the alkyne, both types of reaction failed to produce an isolable η^2-alkyne compound of the type **8**$^+$. By the appropriate colour change (yellow to green with **7b** as the starting material and red-brown to green with Co$^{II}_{aq}$ as the starting compound) the production of an η^2-alkyne derivative **8**$^+$ is indicated in each case. However, on evaporation of the solvent the green-brown species decomposes to produce a grey residue from which no compounds can be extracted showing any indication (MS, ^{31}P NMR) of the presence of species of the type **8**$^+$. With TMSC≡CTMS the observations are again different. Independent of which reaction methodology is applied, no colour change is observed. With its TMS substituents, the alkyne is too bulky to enter the reaction pocket of the *tripod*cobalt template. If the alkyne substituents were to bend backwards as they do with coordinated alkynes (C≡C−R = 140°[2h]) TMSC≡CTMS might possibly fit into the pocket. However, bending will only start to occur when the coordinatively unsaturated metal and the alkyne triple bond are close enough to each other. This appears to be impossible with the small [*tripod*M]$^+$ reaction pocket and the bulky TMSC≡CTMS alkyne. If the *tripod*Co entity is seen as a protective group for protecting alkynes from undergoing standard organic transformations the observed selective response to the bulkiness of the alkyne substituents might find its application in organic synthesis.

Conclusion

The chlorine groups of [*tripod*Co^{II}(Cl)$_2$] (**1**) may be substituted in a stepwise manner by two different donor ligands to produce [*tripod*Co^{II}LL′]$^{2+}$. A broader range of preparative methods exists for the synthesis of compounds [*tripod*Co^{II}L$_2$]$^{n+}$ (n = 0, 2) with two equal donor ligands (L = RCN, RNC, CN$^-$, OCN$^-$, SCN$^-$).

Cobalt(II) derivatives [*tripod*Co^{I}L$_2$] (L = RNC) or [*tripod*Co^{I}L] (L = NCO$^-$, alkyne) are available by different routes starting from the *tripod*Co^{I} precursors [*tripod*Co^{I}(CO)$_2$]$^+$ or [*tripod*Co^{I}Cl]. They are also accessible from Co^{II} precursors using Co$^{II}_{aq}$ under reducing conditions.

Experimental Section

General Remarks: Unless otherwise noted, all manipulations were carried out under argon by means of standard Schlenk techniques. All solvents were dried by standard methods and distilled under argon (PE 40/60 = petroleum ether, boiling range 40−60 °C).[9] The zinc powder (Merck) used in some of the reactions was activated by stirring it under argon with a magnetic bar for 12 h. For ultrasonic activation of reaction mixtures an ultrasonic bath (Bender & Hobein, Laboson 200) was used. *tripod*Co^{II}Cl$_2$ was prepared in accordance with a literature procedure.[3i] All other chemicals were obtained from commercial suppliers and used without further purification. The solvents [D$_6$]acetone, CDCl$_3$, and CD$_2$Cl$_2$ used for NMR-spectroscopic measurements were degassed by three successive freeze-pump-thaw cycles and dried over 4-Å molecular sieves. − NMR: Bruker Avance DPX 200 operating at 200.12 MHz (^{1}H), 50.323 MHz (^{13}C{^{1}H}), 81.015 MHz (^{31}P{^{1}H}) T = 303 K, unless stated otherwise; chemical shifts (δ) in ppm with respect to [D$_6$]acetone (^{1}H: δ = 2.05; ^{13}C: δ = 29.8, 206.2), CDCl$_3$ (^{1}H: δ = 7.27; ^{13}C: δ = 77.0) and CD$_2$Cl$_2$ (^{1}H: δ = 5.32; ^{13}C: δ = 53.8) as internal standards. ^{31}P chemical shifts (δ) are in ppm with respect to 85% H$_3$PO$_4$ (^{31}P: δ = 0) as external standard. − IR: Bruker IFS-66, KBr disks. − EPR: Bruker ESP 300E (X-band, external standard diphenylpicrylhydrazyl). All measurements were carried

out at 20 °C in a standard cavity ER 4102St. − Magnetic measurements: Sherwood Scientific Magnetic Susceptibility Balance MSB, MK I, JM Alfa # 9997 (Sherwood Scientific Ltd.), calibration with $HgCo(SCN)_4$. All measurements were carried out at 20 °C. − UV/Vis: Perkin−Elmer Lambda 19. − Fast-atom bombardment (FAB): Finnigan MAT 8230, xenon, matrix: 4-nitrobenzyl alcohol. − HR-MS (FAB): JEOL JMS 700, matrix: 4-nitrobenzyl alcohol. − Elemental analyses: Microanalytical Laboratory of the Organisch-Chemisches Institut, Universität Heidelberg. − Melting points (not corrected): Gallenkamp MFB-595 010. − Photochemical activation: mercury high-pressure lamp (Hanau, TQ 150), Duran glass apparatus. − Cyclic voltammetry: Metrohm Universal Meß- und Titriergefäß, Metrohm GC electrode RDE 628, platinum electrode, SCE electrode, Princeton Applied Research potentiostat Model 273, 10^{-3} M in 0.1 M n-Bu_4NPF_6/CH_2Cl_2. Reactions described as reversible show a square-root dependence of current versus scan speed in the range of 50 to 800 mVs^{-1}.

General Procedure for the Synthesis of [*tripod*Co^{II}(Cl)(L)]PF_6 Complexes (L = NCPh: 2; L = CN*t*Bu: 4): [*tripod*$CoCl_2$] (**1**) (753 mg, 1 mmol) was dissolved in acetone (15 mL) to give a green-blue solution. The appropriate co-ligand (Table 2, 1 mmol) and KPF_6 (185 mg, 1 mmol) was added to the solution. While stirring the reaction mixture for 15 min, a colour change was observed − orange-brown in the case of nitriles and green in the case of isonitriles. The solvent was evaporated in vacuo and the residue dissolved in CH_2Cl_2. The solution was filtered to remove KCl. The solvent was evaporated again and the residue washed with Et_2O (5 × 5 mL). Removal of the solvent afforded **2**PF_6 and **4**PF_6. For analytical data of the compounds see Table 3 and Table 4.

General Procedure for the Synthesis of [*tripod*Co^{I}LL′]$(PF_6)_2$ Complexes from Compounds [*tripod*Co^{II}(Cl)(L)]PF_6

Method A [L = L′ = NCPh ($3a^{2+}$); L = NCPh, L′ = NCMe ($3b^{2+}$); L = CN*t*Bu ($5a^{2+}$); L = CN*t*Bu, L′ = CNCy ($5b^{2+}$)]: The appropriate [*tripod*Co^{II}(Cl)(L)]PF_6 compound (L = NCPh: **2**PF_6; L = CN*t*Bu: **4**PF_6, 1 mmol) and $TlPF_6$ (349 mg, 1 mmol) were dissolved in THF (20 mL). The appropriate co-ligand L′ (Table 2, 1 mmol) dissolved in THF (5 mL) was added to the suspension and the reaction mixture treated in an ultrasonic bath for 5 min. During this time the reaction mixture changed its colour − orange-brown to green in the case of nitriles, green to red-orange in the case of isonitriles. The solvent was evaporated in vacuo and the residue dissolved in CH_2Cl_2. The solution was filtered to remove TlCl. The solvent was evaporated again, the residue dissolved in THF (1 mL) and precipitated with Et_2O (5 × 5 mL). Removal of the solvent afforded **3a**$(PF_6)_2$, **3b**$(PF_6)_2$, **5a**$(PF_6)_2$, and **5b**$(PF_6)_2$. For analytical data of the compounds see Table 3 and 4.

Method B [L = NCPh ($3a^{2+}$); L = CN*t*Bu ($5a^{2+}$)]: 1 mmol (753 mg) of [*tripod*$Co(Cl)_2$] (**1**) and 2 mmol (700 mg) of $TlPF_6$ were dissolved in 20 mL of THF. 2 mmol of the appropriate ligand L (Table 2), dissolved in 5 mL of THF, was added to the reaction mixture which was then treated in an ultrasonic bath for 15 min. During this procedure the reaction mixture changed its colour − blue-green to green in the case of the nitrile and to red-orange in the case of the isonitrile. The solvent was evaporated in vacuo and the residue dissolved in CH_2Cl_2. The solution was filtered to remove the TlCl produced. The solvent was evaporated again, the residue dissolved in 1 mL of THF and precipitated with 5 mL of Et_2O five times. Removal of the solvent afforded **3a**$(PF_6)_2$ and **5a**$(PF_6)_2$. For analytical data of the compounds see Table 3 and 4.

Preparation of [*tripod*Co^{I}(CN*t*Bu)$_2$]PF_6 {[5a(PF_6)]}

Method C: Freshly prepared [*tripod*CoCl][2f] (**1**) (718 mg, 1 mmol) and $TlPF_6$ (349 mg, 1 mmol) were suspended in THF (20 mL) to give a yellow solution while a fine white powder precipitated. *tert*-Butyl isocyanide (168 mg, 2 mmol), dissolved in THF (5 mL), was added dropwise to the suspension and the reaction mixture treated in an ultrasonic bath for 10 min. During this time the reaction mixture changed its colour from brown-orange to red-orange. The solvent was evaporated in vacuo and the residue dissolved in CH_2Cl_2. The solution was filtered to remove $TlPF_6$. The solvent was evaporated and the residue purified by chromatography on SiO_2 (ICN 32-63, 60 Å) with a solvent mixture of Et_2O/CH_2Cl_2 (5:1) to give the PF_6 salt of [*tripod*Co(CN*t*Bu)$_2$]$^+$. − MS-FAB: 849 [*tripod*Co(CN*t*Bu)$_2$]$^+$. − ^{1}H NMR ($CDCl_3$): 1.37 (s, 18 H, *ligand*-CH_3), 1.58 (br., 4 H, *tripod*-CH_3), 2.77 (br., 6 H, CH_2), 7.16−7.74 (m, 30 H, aromatic H). − ^{13}C NMR ($CDCl_3$): 25.9 (s, *ligand*-CH_3), 30.5 (m, CH_2), 38.6 (s, *ligand*-C_q), 38.9 (m, *tripod*-CH_3), 39.3 (s,

Table 3. Analytical data for compounds **2**$^+$ to **7**

Compound	IR: $\tilde{\nu}$ [cm^{-1}]	EPR[a]	$\mu_{eff.}$ [B. M.][b]	Cyclovoltammetry potential [mV][a]
2PF_6	PF: 840 vs NC: 2255 w	g_1 = 2.14 ($A_1 \approx$ 24 G) g_2 = 2.10 ($A_2 \approx$ 30 G)	2.0	−
3a$(PF_6)_2$	PF: 840 vs NC: 2325 w	$g \approx$ 2.1	2.0	−
3b$(PF_6)_2$	PF: 840 vs NC: 2320, 2285 w	$g \approx$ 2.1	2.0	−
4PF_6	PF: 840 vs CN: 2185 vs	$g \approx$ 2.1	1.9	−
5a$(PF_6)_2$	PF: 840 vs CN: 2120, 2190 vs	$g \approx$ 2.1	2.0	$E_{1/2}$ = 120, ΔE = 150 E_p^a = 1600; ΔE_{Fc} = 140
5b$(PF_6)_2$	PF: 840 vs CN: 2110 vs	$g \approx$ 2.1	1.9	−
6a	CN: 2096, 2101 w	g = 2.10 (A = 22 G)	1.8	$E_{1/2}$ = −1076, ΔE = 110 E_p^a = 840; ΔE_{Fc} = 105
6b	OCN: 2230, 2210 s	g_1 = 2.12 ($A_1 \approx$ 23 G) g_2 = 2.10 ($A_2 \approx$ 30 G)	2.1	$E_{1/2}$ = 325, ΔE = 120 E_p^c = −1255; ΔE_{Fc} = 140
6c	SCN: 2100, 2070 s	g_1 = 2.14 ($A_1 \approx$ 24 G) g_2 = 2.11 ($A_2 \approx$ 31 G)	2.1	$E_{1/2}$ = 500, ΔE = 120 E_p^c = −995; ΔE_{Fc} = 210
7a	OCN: 2200 s	−	2.9	−

[a] All measurements were performed in CH_2Cl_2 solutions at 20 °C at scan speeds of 200 mVs^{-1}. − [b] Magnetic balance MSB MK I, 20 °C, see Experimental Section.

Table 4. Analytical data for compounds $\mathbf{2}^+$ to **7**

Compound	Mass spectrometry (*m*/*z*)	HR-FAB (*m*/*z*) calculated/*found*	Elemental analysis calculated/*found*
2PF_6	821 [M^+] 718 [M^+ − NCPh]	−	C: 55.94/*56.28* H: 4.41/*4.97* N: 1.33/*0.71*[a]
3a$(PF_6)_2$	683 [*tripod*Co^+]	−	C: 55.99/*56.13* H: 4.19/*4.23* N: 2.37/*2.35*
3b$(PF_6)_2$	683 [*tripod*Co^+]	−	C: 50.93/*51.22* H: 4.11/*4.67* N: 2.33/*2.52*[a]
4PF_6	767 [M^+ − Cl] 718 [M^+ − CN*t*Bu]	−	C: 58.33/*58.80* H: 5.12/*5.93* N: 1.48/*2.41*
5a$(PF_6)_2$	849 [M^+] 766 [M^+ − CN*t*Bu]	849.3006/*849.3085*	[b]
5b$(PF_6)_2$	875 [M^+] 792 [M^+ − CN*t*Bu] 767 [M^+ − CNCy]	875.3223/*875.3244*	[b]
6a	736 [M^+] 709 [M^+ − CN] 683 [M^+ − 2 CN]	−	C: 70.21/*70.34* H: 5.39/*5.52* N: 3.81/*3.93*
6b	767 [M^+]	−	C: 67.27/*65.99* H: 5.12/*5.07* N: 3.64/*3.54*
6c	799 [M^+]	−	C: 59.73/*58.17* H: 4.67/*4.50* N: 3.16/*3.11*[a]
7a	726 [M^+]	−	C: 69.52/*69.54* H: 5.42/*5.54* N: 1.93/*1.93*

[a] One CH_2Cl_2 solvate molecule per formula unit. − [b] Due to varying contents of solvent molecules in the crystals elemental analysis was not satisfactory.

tripod-C_q), 123.4−133.8 (aromatic C), 156.1 (s, CN). − ^{31}P NMR ([D_6]acetone): δ = −144.2, (sept, $^1J_{PF}$ = 713 Hz), 32.4. − IR: ṽ [cm^{-1}] = 840 (vs, PF_6), 2140 (vs, CN). − HR-FAB (calculated/*found*): 849.30066/*849.3085*. − Cyclovoltammetry (CH_2Cl_2): $E_{1/2}$ = 125 mV, Δ*E* = 140 mV; E_p^a = 1600 mV, ΔE_{Fc} = 110 mV. − Elemental analysis [calculated for composition as found by X-ray analysis of the same batch **5a**$(PF_2O_2^-) \cdot 0.4\ Et_2O \cdot 0.25\ CH_2Cl_2$]: calcd. C 61.57, H 5.77, N 2.82; found C 60.22, H 6.14, N 3.62.

Method D: $Co_{aq}(BF_4)_2$ (342 mg, 1 mmol) and *tripod* (624 mg, 1 mmol) were dissolved in CH_2Cl_2/ethanol (1:1, 30 mL) to give a brown-red solution. A five-fold excess of zinc powder and *tert*-butyl isocyanide (168 mg, 2 mmol), dissolved in THF (5 mL), were added dropwise. The reaction mixture was treated in an ultrasonic bath for 5 min. The solvent was removed in vacuo, the residue dissolved in CH_2Cl_2 and filtered to remove $ZnCl_2$ and excess zinc powder. The solvent was evaporated, the residue dissolved in THF and treated with a three-fold excess of KPF_6. The solvent was removed in vacuo, the residue dissolved in CH_2Cl_2 and filtered to remove excess KPF_6 and KBF_4. The solvent was evaporated and the residue purified by chromatography on SiO_2 (ICN) with a solvent mixture of Et_2O/CH_2Cl_2 (5:1) to give the PF_6 salt of [*tripod*$Co^I(CNtBu)_2]^+$ (**5a**PF_6). For analytical data see above.

Preparation of [*tripod*$Co^{II}(CN)_2$] (6a): $Co_{aq}(BF_4)_2$ (342 mg, 1 mmol) and *tripod* (624 mg, 1 mmol) were dissolved in CH_2Cl_2/EtOH (1:2, 30 mL) to give a brown-red solution. NaCN (98 mg, 2 mmol), dissolved in ethanol/water (1:1, 20 mL), was added dropwise to give a claret solution. The solvent was removed in vacuo, the residue dissolved in CH_2Cl_2 and filtered to remove $NaBF_4$. Concentration afforded **6a** as claret powder. Single crystals suitable for X-ray analysis were obtained by vapour diffusion of Et_2O into a CH_2Cl_2 solution of **6a**.

Generation of [*tripod*$Co^I(CN)_2]^-$ (6a$^-$). − Method E: Compound **6a** (739 mg, 1 mmol) and Cp_2Co (189 mg, 1 mmol) were dissolved in 20 mL of THF. The colour of the solution changed from claret to brown. The solvent was evaporated and the residue washed with Et_2O (5 × 5 mL). − MS-FAB: FAB-positive: 189 [Cp_2Cp^+]; FAB-negative: 739 [*tripod*$Co^I(CN)_2]^-$. − ^{31}P NMR (CD_2Cl_2): δ = 32.4. − IR: ṽ [cm^{-1}] = 2100 (w, CN).

Method F: [*tripod*$Co^I(CO)_2]PF_6$[2c] (885 mg, 1 mmol) and NaCN (98 mg, 2 mmol) were suspended in THF (50 mL). The suspension was irradiated for 3 h. During this time a colour change from claret to brown was observed. The solvent was removed in vacuo and the brown residue washed Et_2O (5 × 5 mL). MS-FAB: FAB-negative: 739 [*tripod*$Co(CN)_2]^-$. − ^{31}P NMR (CD_2Cl_2): δ = 32.4. − IR: ṽ [cm^{-1}] = 2100 (w, CN).

General Procedure for the Synthesis of [*tripod*$Co^{II}(NCX)_2$] Complexes [X = O (6b); X = S (6c)]: $Co_{aq}(BF_4)_2$ (342 mg, 1 mmol) and *tripod* (624 mg, 1 mmol) were dissolved in CH_2Cl_2/ethanol (1:2, 30 mL) to give a brown-red solution. The appropriate salt KX (Table 2, 2 mmol), dissolved in solvent (methanol in the case of **6b**, Et_2O in the case of **6c**, 20 mL), was added. The solvent was removed in vacuo, the residue dissolved in CH_2Cl_2 and filtered to remove KBF_4. The solvent was evaporated and the residue washed with Et_2O at 0 °C (5 × 5 mL). For analytical data of the compounds see Table 3 and 4.

Preparation of [*tripod*Co^INCO] (7a): [*tripod*$Co^{II}(NCO)_2$] (**6b**) (767 mg, 1 mmol) was dissolved in THF (20 mL) and a five-fold excess of zinc powder added. The reaction mixture was treated in an ultrasonic bath for 5 min. The solvent was removed in vacuo, the residue dissolved in CH_2Cl_2 and filtered. After concentration, **7a** was obtained as microcrystalline brown-green powder. Single

crystals suitable for X-ray analysis were obtained by vapour diffusion of Et_2O into a solution of **7a** in CH_2Cl_2. For analytical data of the compound see Table 3 and 4. The product corresponds in all its properties to the one obtained by an independent method.[2d]

General Procedure for the Synthesis of the PF_6 Salts of [*tripod*Co^{I}(η^2-alkyne)]$^+$ ($8a^+-8d^+$). – Method G: Freshly prepared [*tripod*CoCl][2f] (**1**) (718 mg, 1 mmol) and $TlPF_6$ (349 mg, 1 mmol) were suspended in THF (20 mL) to give a yellow solution while a fine white precipitate was formed. The appropriate alkyne (Table 2, 1 mmol) was added to the suspension and the reaction mixture treated in an ultrasonic bath for 10 min. During this procedure the reaction mixture changed its colour to green. The solvent was evaporated in vacuo and the residue dissolved in CH_2Cl_2. The solution was filtered to remove TlCl. The solvent was evaporated again and the residue (except $8d^+$) purified by chromatography on SiO_2 (ICN 32-63, 60 Å) with a solvent mixture of Et_2O/CH_2Cl_2 (5:1) to produce the PF_6 salts of $8a^+-8c^+$. In the case of $8d^+$ the solvent was evaporated and the residue was washed with Et_2O (5 × 5 mL). For analytical data of the compounds see Table 5.

Method H: $Co_{aq}(BF_4)_2$ (342 mg, 1 mmol) and *tripod* (624 mg, 1 mmol) were dissolved in CH_2Cl_2/EtOH (1:1, 30 mL) to give a brown-red solution. The appropriate alkyne (Table 2, 1 mmol) and a five-fold excess of zinc powder were added. The reaction mixture was treated in an ultrasonic bath for 5 min. The solvent was removed in vacuo, the residue dissolved in CH_2Cl_2 and filtered to remove $ZnCl_2$ and excess zinc powder. The solvent was evaporated, the residue dissolved in THF and treated with a three-fold excess of KPF_6. The solvent was removed in vacuo, the residue dissolved in CH_2Cl_2 and filtered to remove excess KPF_6 and KBF_4. The solvent was evaporated again and the residue purified by chromatography on SiO_2 (ICN 32-63, 60 Å) with a solvent mixture of Et_2O/CH_2Cl_2 (5:1) to produce the PF_6 salts of $8a^+-8c^+$. Analytical data of the compounds: Table 5.

X-ray Crystallographic Study: The measurements were carried out with a Siemens P4 four-circle diffractometer (**6a**) or a Nonius–Kappa CCD diffractometer ($5c^{2+}$, $5a^+$, **6b**, and **7a**), all using graphite-monochromated Mo-K_α radiation. In case of the Siemens P4 four-circle diffractometer measurements, the intensities of three reference reflections (measured every 100 reflections) remained constant throughout the data collection, thus indicating crystal and electronic stability. The data collected with the Siemens P4 diffractometer were corrected by standard methods including experimental absorption correction. The data from the Nonius–Kappa CCD device were processed by the standard Nonius software.[10] All calculations were performed using the SHELXT PLUS software package. Structures were solved by direct methods with the SHELXS-97 program and refined with the SHELXL-97 program.[11,12] Graphical handling of the structural data during solution and refinement was performed with XPMA.[13] Atomic coordinates and anisotropic thermal parameters of the non-hydrogen atoms were refined by full-matrix least-squares calculations. Table 6 and Table 7 compile the data for the structure determinations. The geometry of the counterion $PO_2F_2^-$ of $5c^{2+}[(PO_2F_2)^-]_2$ as found in this analysis is rather inaccurate due to disorder problems but is in overall agreement with the literature data.[5] This disorder could be resolved by the split-atom technique such that at one of these positions two different rotational positions were sufficient, whereas at the other position three to four rota-

Table 5. Analytical data for compounds $8a^+$ to $8d^+$

Compound	**8a**PF_6	**8b**PF_6	**8c**PF_6	**8d**PF_6
^{1}H{^{31}P} NMR	[D_6]acetone	CD_2Cl_2	$CDCl_3$	CD_2Cl_2
tripod-CH_3	1.83 br., 3 H	1.93 br., 3 H	1.89 br., 3 H	1.92 br., 3 H
tripod-CH_2	2.90 br., 6 H	2.64 br., 6 H	2.57 br., 6 H	2.60 br., 6 H
aromat. H	7.03–7.57 m, 40 H	7.06–7.59 m, 35 H	7.01–7.65 m, 30 H	7.04–7.52 m, 30 H
≡C–H	–	10.38 q, J_{PH} = 6 Hz, 1 H	9.84 br., 1 H	9.84 br., 1 H
ligand-CH_3	–	–	1.40 br. s, 9 H	–
≡C–CH_2	–	–	–	2.35 br., 2 H
^{31}P NMR	[D_6]acetone	CD_2Cl_2	$CDCl_3$	CD_2Cl_2
PPh_2	38.9 s	40.0 s	37.8 s	42.3 s
PF_6	−144.2, $^1J_{PF}$ = 713 Hz	−144.2, $^1J_{PF}$ = 713 Hz	−144.2, $^1J_{PF}$ = 713 Hz	−144.2, $^1J_{PF}$ = 713 Hz
^{13}C {^{1}H } NMR[a]	CD_2Cl_2	CD_2Cl_2	[b]	CD_2Cl_2
tripod-CH_3	36.9 m	36.6 br.	–	36.7 br.
tripod-CH_2	33.7 m	33.4 p-t, *J* = 13 Hz	–	33.9 p-t, *J* = 12 Hz
tripod-C_q	39.5 s	40.1 s	–	40.4 s
aromat. C	123.6–137.5 m	129.1–135.2 m	–	129.1–133.8 m
C≡*C*–C	178.3 s	174.6 s	–	177.9 s
C≡*C*–H	–	165.8 s	–	159.5 bs
≡C–*C*H_2	–	–	–	65.1 b
IR: $\tilde{\nu}$(PF) [cm^{-1}]	845	845	845	835
Mass spectrometry (*m/z*)	861 [M^+]	785 [M^+]	765 [M^+]	737 [M^+]
Cyclovoltammetry:	$E_{1/2}$ = −610	$E_{1/2}$ = −715[d]	$E_{1/2}$ = −790	$E_{1/2}$ = −730
	ΔE = 195	ΔE = 150	ΔE = 65	ΔE = 90
Potential [mV][c]	E_p^a =1210	E_p^a = 1110	E_p^a =1110	E_p^a =1025
	ΔE_{Fc} = 130	ΔE_{Fc} = 140	ΔE_{Fc} = 100	ΔE_{Fc} = 120
UV/Vis	370 (2260)	370 (930)	470 (460)	350 (6710)
[nm] ($lmol^{-1}cm^{-1}$)[c]	460 (1010)	610 (580)	600 (580)	440 (1980)
	590 (760)			580 (1105)
Elemental analysis:	C: 65.61/*65.36*	C: 63.24/*63.12*	C: 57.90/*57.29*[e]	C: 59.74/*59.42*
calculated/*found*	H: 4.91/*5.21*	H: 4.87/*5.16*	H: 5.16/*5.41*	H: 4.90/*5.41*
HR-FAB (*m/z*):	861.2379/*861.2366*	–	765.2379/*765.2426*	–
calculated/*found*		–		–

[a] CH_3, CH_2, CH, and C carbon atoms were determined in a 135° DEPT experiment. – [b] No satisfying ^{13}C-NMR spectra could be obtained due to disintegration of the compound during the measurement. – [c] All measurements were performed in CH_2Cl_2 at 20 °C. – [d] Quasi-reversible reduction. – [e] Calculated for one CH_2Cl_2 solvate per formular unit.

Table 6. Crystal data for compounds $\mathbf{5}^{2+}$, $\mathbf{5}^{+}$, and **6a**

Compound	$\mathbf{5a}^{+}(PF_2O_2)^{-}$ [a]	$\mathbf{5c}^{2+}[(PF_2O_2)^{-}]_2$ [b]	**6a** [c]
Empirical formula	$C_{51}H_{57}CoF_2N_2O_2P_4$	$C_{55}H_{61}CoN_2O_4F_4P_5$	$C_{43}H_{39}CoN_2P_3$
Molecular mass	950.85	1103.89	735.60
Crystal system	monoclinic	orthorhombic	orthorhombic
Space group	$P2_1$ (No. 4)[12]	*Pbcn* (No. 60)[12]	*Pbca* (No. 61)[12]
Lattice constants	a = 1256.9(3) pm	a = 3676.6(7) pm	a = 1684.3(5) pm
	b = 1657.6(3) pm	b = 1449.3(3) pm	b = 1903.4(6) pm
	c = 1285.2(3) pm	c = 2057.7(4) pm	c = 2221.5(8) pm
	β = 99.50(3)°	β = 90°	β = 90°
Cell volume	3561×10^6 pm^3	10938×10^6 pm^3	7122×10^6 pm^3
Molecular units per cell	Z = 2	Z = 8	Z = 8
Density (calculated)	1.260 g cm^{-3}	1.358 g cm^{-3}	1.372 g cm^{-3}
Temperature	200 K	200 K	200 K
Measuring device	Nonius Kappa CCD	Nonius Kappa CCD	Siemens Nicolet-Syntex
Number of reflections for cell refinement			25
Scan range	4.1 ° < 2φ < 50.0 °	3.0 ° < 2φ < 50.0 °	3.7 ° < 2φ < 45.1 °
Method	ω scan, Δω = 1.0 °	ω scan, Δω = 1.0 °	ω scan, Δω = 0.6 °
Scan speed	15 s/frame	12 s/frame	6 < dω/dt < 29.3 ° min^{-1}
Measured reflections	47755	163249	4708
Unique reflections	9294	9628	4678
Observed reflections ($I \geq 2\sigma$)	7768	6005	2479
Number of parameters refined	602	625	361
Maximum of residual electron density	1.18×10^{-6} e pm^{-3}	1.27×10^{-6} e pm^{-3}	0.59×10^{-6} e pm^{-3}
Agreement factors	R_1 = 0.070	R_1 = 0.086	R_1 = 0.082
(F^2 refinement)	R_w = 0.200	R_w = 0.285	R_w = 0.199

[a] Anions are disordered (see X-ray Crystallographic Study). The crystal specimen analysed was found to contain 0.25 CH_2Cl_2 and 0.4 Et_2O per $\mathbf{5a}^{+}$.These solvate molecules as a whole occupy distinct positions within the crystal, but show rotational disorder. – [b] About disorder of the anions see X-ray Crystallographic Study. The crystal specimen analysed was found to contain 0.5 EtOH per $\mathbf{5c}^{2+}$. – [c] One of the CN ligands shows disorder with respect to the Co–C–N bond angle.

Table 7. Crystal data for compounds **6c** and **7a**

Compound	**6c**[a]	**7a**
Empirical formula	$C_{43}H_{39}CoN_2P_3S_2$	$C_{42}H_{39}CoNOP_3$
Molecular mass	799.78	725.63
Crystal system	monoclinic	monoclinic
Space group	$P2_1/n$ (No. 14) [12]	*Cc* (No. 9) [12]
Lattice constants	a = 928.6(2) pm	a = 1212.3(2) pm
	b = 2698.0(5) pm	b = 1639.4(3) pm
	c = 1701.4(3) pm	c = 1822.6(4) pm
	β = 100.97(3)°	β = 100.51(3)°
Cell volume	4185×10^6 pm^3	3562×10^6 pm^3
Molecular units per cell	Z = 4	Z = 4
Density (calculated)	1.368 g cm^{-3}	1.353 g cm^{-3}
Temperature	200 K	200 K
Measuring device	Nonius Kappa CCD	Nonius Kappa CCD
Scan range	3.9 ° < 2φ < 50.0 °	4.2 ° < 2φ < 52.0 °
Method	ω scan, Δω = 1.0 °	ω scan, Δω = 2.0 °
Scan speed	30 s/frame	5 s/frame
Measured reflections	45160	24740
Unique reflections	7133	7017
Observed reflections ($I \geq 2\sigma$)	1788	6245
Number of parameters refined	226	437
Maximum of residual electron density	1.17×10^{-6} e pm^{-3}	0.43×10^{-6} e pm^{-3}
Agreement factors	R_1 = 0.093	R_1 = 0.035
(F^2 refinement)	R_w = 0.250	R_w = 0.072

[a] The crystal specimen analysed was found to contain 0.75 CH_2Cl_2 per molecule **6c**.

tional positions had to be taken into account in order to reproduce the electron-density distribution. The $PO_2F_2^-$ counterion in $\mathbf{5a}^{+}(PO_2F_2)^{-}$ is also disordered. Refinement in a split-atom model with the phosphorus atom, the two oxygen atoms, and one fluorine atom in just one position and the second fluorine atom equally distributed over two positions gave a satisfactory agreement. Crystallographic data (excluding structure factors) for the structures reported in this paper have been deposited with the Cambridge Crystallographic Data Centre as supplementary publication no. CCDC-135321 to -135325. Copies of data can be obtained free of charge on application to CCDC, 12 Union Road, Cambridge, Cambridge CB2 1EZ, UK [Fax: (internat. code) + 44-1223/336-033; E-mail: deposit@ccdc.cam.ac.uk].

Acknowledgments

We are indebted to the Deutsche Forschungsgemeinschaft (SFB 247) and the Fonds der Chemischen Industrie for financial support. One of us (R. R.) is indebted to the Graduiertenkolleg "Selektivität

in der organischen und metallorganischen Synthese und Katalyse'' for a scholarship. The unselfish cooperation of Dr. J. Groß and Mr. T. Jannack (mass-spectrometric measurements), Mr. D. Günauer (cyclic voltammetry), Mrs. A. Dittes, Mrs. C. Vetter, Mrs. E. Weiß, and Mr. F. Liebscher (elemental analysis) is gratefully acknowledged.

[1] Cobalt(0): F. Cecconi, C. A. Ghilardi, S. Midollini, S. Moneti, A. Orlandini, M. Bacci, *J. Chem. Soc., Chem. Commun.* **1985**, 731−733.

[2] Cobalt(I): [2a] L. Sacconi, S. Midollini, *J. Chem. Soc., Dalton Trans.* **1972**, 1213−1216. − [2b] K. Heinze, G. Huttner, L. Zsolnai, P. Schober, *Inorg. Chem.* **1997**, *36*, 5457−5469. − [2c] J. Ellerman, J. F. Schindler, *Z. Naturforsch.* **1975**, *30b*, 914−919. − [2d] J. Ellermann, J. F. Schindler, *Chem. Ber.* **1976**, *109*, 1095−1105. − [2e] J. Ellermann, J. F. Schindler, *J. Organomet. Chem.* **1975**, *94*, 201−212. − [2f] R. Rupp, A. Frick, G. Huttner, P. Rutsch, U. Winterhalter, A. Barth, P. Kircher, L. Zsolnai, *Eur. J. Inorg. Chem.* **2000**, 523−536. − [2g] C. Bianchini, P. Dapporto, A. Meli, L. Sacconi, *J. Organomet. Chem.* **1980**, *193*, 117−126. − [2h] R. Rupp, G. Huttner, H. Lang, E. R. Hovestreydt, M. Büchner, *Eur. J. Inorg. Chem.*, submitted. − [2i] V. Körner, Ph. D. Thesis, Universität Heidelberg, **1996**. − [2j] C. A. Ghilardi, C. Mealli, S. Midollini, V. I. Nefedov, A. Orlandini, L. Sacconi, *Inorg. Chem.* **1980**, *19*, 2454−2462. − [2k] D. L. DuBois, D. W. Meek, *Inorg. Chem.* **1976**, **15**, 3076−3088. − [2l] M. Di Vaira, L. Sacconi, *Angew. Chem.* **1982**, *94*, 338−351; *Angew. Chem. Int. Ed. Engl.* **1982**, *27*, 330. − [2m] A. Barth, G. Huttner, M. Fritz, L. Zsolnai, *Angew. Chem.* **1990**, *102*, 956−958; *Angew. Chem. Int. Ed. Engl.* **1990**, *29*, 929. − [2n] V. Sernau, G. Huttner, J. Scherer, O. Walter, *Chem. Ber.* **1996**, *129*, 243−245. − [2o] V. Sernau, G. Huttner, J. Scherer. L. Zsolnai, T. Seitz, *Chem. Ber.* **1995**, *128*, 193−195.

[3] Cobalt(II): see for example ref.[2b] − [3a] V. Sernau, G. Huttner, M. Fritz, L. Zsolnai, O. Walter, *J. Organomet. Chem.* **1993**, *453*, C23−C29. − [3b] P. Dapporto, S. Midollini, L. Sacconi, *Inorg. Chem.* **1975**, *14*, 1643−1650. − [3c] C. A. Ghilardi, S. Midollini, L. Sacconi, *J. Organomet. Chem.* **1980**, *186*, 279−287. − [3d] A. Asam, B. Janssen, G. Huttner, L. Zsolnai, O. Walter, *Z. Naturforsch., B: Chem. Sci.* **1993**, *48*, 1707−1714. − [3e] R. Soltek, Diploma, Universität Heidelberg, **1994**. − [3f] S. Vogel, A. Barth, G. Huttner, T. Klein, L. Zsolnai, R. Kremer, *Angew. Chem.* **1991**, *103*, 325−327; *Angew. Chem. Int. Ed. Engl.* **1991**, *30*, 303. − [3g] S. Vogel, G. Huttner, C. Emmerich, *Z. Naturforsch.* **1993**, *48b*, 353−362. − [3h] C. Bianchini, D. Masi, C. Mealli, A. Meli, M. Sabat, *Gazz. Chim. Ital.* **1986**, *116*, 201−206. − [3i] K. Heinze, G. Huttner, O. Walter, *Eur. J. Inorg. Chem.* **1999**, *4*, 593−600. − [3j] V. Körner, S. Vogel, G. Huttner, L. Zsolnai, O. Walter, *Chem. Ber.* **1996**, *129*, 1107−1113. − [3k] A. Orlandini, L. Sacconi, *Cryst. Struct. Commun.* **1975**, *4*, 157−161. − [3l] C. A. Ghilardi, L. Sacconi, *Cryst. Struct. Commun.* **1975**, *4*, 149−152.

[4] Cobalt(III): see for example literature cited in: [4a] C. Bianchini, D. Masi, C. Mealli, *Inorg. Chem.* **1987**, *26*, 3683−3693. − [4b] S. Vogel, G. Huttner, L. Zsolnai, *Z. Naturforsch.* **1993**, *48b*, 641−652. − [4c] K. Heinze, G. Huttner, L. Zsolnai, A. Jacobi, P. Schober, *Chem. Eur. J.* **1997**, *3*, 732−743. − [4d] P. Barbaro, C. Bianchini, K. Linn, C. Mealli, A. Meli, F. Vizza, F. Laschi, P. Zanello, *Inorg. Chim. Acta* **1992**, *198−200*, 31−56.

[5] S. Kitagawa, M. Kondo, S. Kawata, S. Wada, M. Maekawa, M. Munakata, *Inorg. Chem.* **1995**, *34*, 1455−1465.

[6] K. Heinze, G. Huttner, L. Zsolnai, *Chem. Ber./Recueil* **1997**, *130*, 1393.

[7] S. Beyreuther, J. Hunger, G. Huttner, S. Mann, L. Zsolnai, *Chem. Ber.* **1996**, *129*, 745 and literature cited therein.

[8] H. Werner, *Angew. Chem.* **1990**, *102*, 1109; *Angew. Chem. Int. Ed. Engl.* **1990**, *29*, 1077.

[9] *Organikum*, Deutscher Verlag der Wissenschaften, Berlin, **1990**.

[10] *DENZO-SMN, Data processing software*, Nonius **1998**; http://www.nonius.com

[11] [11a] G. M. Sheldrick, *SHELXS 97, Program for Crystal Structure Solution*, University of Göttingen, **1997**; http://shelx.uni-ac.gwdg.de/shelx/index.html − [11b] G. M. Sheldrick, *SHELXL 97, Program for Crystal Structure Refinement*, University of Göttingen, **1997**; http://shelx.uni-ac.gwdg.de/shelx/index.html

[12] *International Tables for X-ray Crystallography*, vol.4, Kynoch Press, Birmingham, U. K., **1974**.

[13] L. Zsolnai, G. Huttner, *XPMA*, http://www.rzuser.uni-heidelberg.de/v54/xpm.html, Universität Heidelberg, **1994**.

Received October 21, 1999
[I99371]

Heterometallic Nitrido-Carbonyl Clusters − Synthesis and Characterization of $[Fe_5MN(CO)_{14}(C_5H_5)]^{2-}$, $[Fe_3M_3N(CO)_{18}]^{3-}$ (M = Mo, W) and $[HFe_5MoN(CO)_{16}]^{2-}$ and Solid-State Structures of $[Fe_5MoN(CO)_{14}(C_5H_5)]^{2-}$, $[Fe_5WN(CO)_{14}(C_5H_5)]^{2-}$, and $[Fe_3Mo_3N(CO)_{18}]^{3-}$

Roberto Della Pergola,*[a] Massimiliano Branchini,[b] Alessandro Fumagalli,[c] Luigi Garlaschelli,[b] Mario Manassero,*[d] and Mirella Sansoni[d]

Keywords: Iron / Molybdenum / Tungsten / Nitrides / Interstitial atoms / Cluster

The anionic clusters $[Fe_5MN(CO)_{14}Cp]^{2-}$ [M = Mo (**1**) or W (**2**)] were synthesized from $[Fe_4N(CO)_{12}]^-$ and $[MCp(CO)_3]^-$ in refluxing acetonitrile. The clusters $[Fe_3M_3N(CO)_{18}]^{3-}$ [M = Mo (**3**) or W (**4**)] were prepared by reaction of $[Fe_4N(CO)_{12}]^-$ with $[M_2(CO)_{10}]^{2-}$ under the same conditions. The molybdenum-containing anions **1** and **3** are obtained in higher yields than **2** and **4**. The reaction of the tetranuclear iron cluster with $[Mo(\eta^6\text{-}Me_3C_6H_3)(CO)_3]$ affords a mixture of $[Fe_3Mo_3N(CO)_{18}]^{3-}$ and $[HFe_5MoN(CO)_{16}]^{2-}$ (**5**). The solid state structures of the clusters **1**, **2** and **3** have been determined; they consist of six metal atoms, arranged in octahedral metal cages encapsulating a μ_6-N ligand. The cyclopentadienyl ligand is bound to Mo in **1** and to W in **2**; these anions have three edge-bridging carbonyl groups and eleven terminal carbonyl groups. The cluster **3** possesses three molybdenum atoms in a *fac* arrangement, and the carbonyl ligands are all terminal, or asymmetrically bridging. Inspection of the interatomic distances suggests that molybdenum interacts preferentially with the carbonyl and the nitrido ligands, whereas the iron atoms bind strongly with the other metal centres. The solid state structure of **5** could not be fully resolved owing to crystal disorder. Analytical and spectroscopic data (infrared and ^{1}H NMR) are all consistent with the proposed formula.

Introduction

The interest in heterometallic clusters is still growing, and several examples of their application in catalysis can be found in the literature.[1] In homogeneous catalysis, mixed metal species are preferred, due to the presence of polar metal−metal bonds which can tune electron density at the metal centres, thus modifying the reactivity of the coordinated ligands.[2] In the field of heterogeneous catalysis, mixed-metal species can be exploited for the formation of bimetallic particles which are extraordinarily uniform in their morphology and composition.[3] In this context, the stability of the cage due to the interstitial atoms can avoid sinterization during the absorption to the support and the decarbonylation. Heterometallic species often have unusual structures of remarkable stability due to the preference of the two elements for different chemical sites within the cluster.[4] In these compounds, the HOMO−LUMO gap can be small, and the frontier orbitals can be filled/depleted without decomposition. Therefore, heterometallic clusters with an odd number of valence electrons, and possibly displaying unusual magnetic properties, are not uncommon.[5]

For these reasons, we are studying the reactions of $[Fe_4N(CO)_{12}]^-$ with carbonyl complexes of different transition metals, aiming for the preparation of iron-based mixed-metal clusters stabilized by a nitrido ligand.[6,7] The interstitial atom plays an essential role in these syntheses, limiting the fragmentation of the starting material and directing the reconstruction of *closo* polyhedra. In order to prove the generality of this approach, and to expand this kind of chemistry as much as possible, we turned our investigations to the metals of groups 6, 7 and 10. We describe here the synthesis and characterization of several bimetallic species containing molybdenum or tungsten. These organometallic species may suggest a new approach to the preparation of transition metal nitrides,[8] which are widely investigated for their catalytic properties.[9]

[a] Dipartimento di Scienze dell' Ambiente e del Territorio, Università di Milano-Bicocca
Piazza della Scienza 1, 20126 Milano, Italy
rpergola@mailserver.unimi.it
Fax: (internat.) + 39-02/236-2748
[b] Dipartimento di Chimica Inorganica, Metallorganica ed Analitica and Centro del CNR Università di Milano, via G. Venezian 21, 20133 Milano, Italy
[c] Dipartimento di Biologia Strutturale e Funzionale, Università degli studi dell'Insubria, via J. H. Dunant 3, 21100 Varese, Italy
[d] Dipartimento di Chimica Strutturale e Stereochimica Inorganica and Centro del CNR − Università di Milano via G. Venezian 21, 20133 Milano, Italy
E-mail: m.manassero@csmtbo.mi.cnr.it

 © WILEY-VCH Verlag GmbH, D-69451 Weinheim, 2000 1434−1948/00/0808−1759 $ 17.50+.50/0

Results

Syntheses

$[Fe_5MoN(CO)_{14}(C_5H_5)]^{2-}$ (1) and $[Fe_5WN(CO)_{14}(C_5H_5)]^{2-}$ (2)

The carbido dianion $[Fe_4C(CO)_{12}]^{2-}$ reacts with a large variety of metal complexes acting as Lewis acids, to give metal-cage expansion.[10] In contrast, the nitrido species $[Fe_4N(CO)_{12}]^-$, because of the low specific charge, reacts only after reduction, possibly through the labilization of a carbonyl ligand.[11] Under these conditions, the nitride reagent is partially destroyed, and the iron carbonyl fragment can contribute to the construction of larger metal cages. We have already exploited this approach to obtain $[Fe_6N(CO)_{15}]^{3-}$ [6] and $[Fe_5RhN(CO)_{15}]^{2-}$.[7] While attempting the synthesis of heterometallic species containing molybdenum or tungsten, we tested first nucleophilic anionic metal complexes, such as $[M_2(CO)_{10}]^{2-}$ or $[M(CO)_3(C_5H_5)]^-$ (M = Mo or W).[12] The reaction of $[Fe_4N(CO)_{12}]^-$ with $[Mo(CO)_3(C_5H_5)]^-$ was performed in MeCN, with both reagents as their tetraethylammonium salts in a 2:1 molar ratio. Since the process of cluster growth cannot be described by a simple balanced chemical equation, the best conditions were empirically determined to obtain the maximum yield and the simplest way of purification. Indeed, when the tetranuclear iron cluster was completely consumed (after ca. 18 h) we detected formation of the new cluster species $[Fe_5MoN(CO)_{14}(C_5H_5)]^{2-}$ (**1**), together with the known compound $[Fe_6N(CO)_{15}]^{3-}$ [6] and a large amount of unreacted $[Mo(CO)_3(C_5H_5)]^-$. The anion **1** was separated by extraction with methanol and recovered by addition of a bulky cation. The reaction with $[W(CO)_3(C_5H_5)]^-$ proceeds exactly the same way, usually requiring more time to be completed, with lower yields. Frequently, the final products **1** and **2** are slightly contaminated by traces of the $[M(CO)_3(C_5H_5)]^-$ reagents.

$[Fe_3Mo_3N(CO)_{18}]^{3-}$ (3) and $[Fe_3W_3N(CO)_{18}]^{3-}$ (4)

The reaction of $[Fe_4N(CO)_{12}]^-$ with $[Mo_2(CO)_{10}]^{2-}$ or $[W_2(CO)_{10}]^{2-}$ (both as $[NEt_4]^+$ salts in a 1:1 molar ratio) is much more rapid and selective than above, yielding mainly $[Fe_3M_3N(CO)_{18}]^{3-}$. In this case the difference of reactivity between molybdenum and tungsten is relevant: the reaction with $[Mo_2(CO)_{10}]^{2-}$ in refluxing MeCN is completed within 1 h while the tungsten derivative requires more than 5 h, even in EtCN where the boiling temperature is ca. 15 °C higher. At the end, the soluble minor impurities can be extracted in methanol, leaving behind a residue which is analytically pure according to elemental analyses. Crystals of the salt $[NEt_4]_3$**3** were grown from acetonitrile/diisopropyl ether,[13] but, unfortunately, were unsuitable for an X-ray determination; we had to prepare many different salts by cation exchange with tetraalkylammonium halides. The same metathesis proved unsuccessful for tungsten, and therefore we could only obtain the parameters of the unit cell of $[NEt_4]_3$**4**, which was isomorphous with $[NEt_4]_3$**3**, thus confirming its formula. The infrared spectra of **3** and **4** are almost superimposable, suggesting that the two compounds are also isostructural in solution.

$[HFe_5MoN(CO)_{16}]^{2-}$ (5)

The trianion **3** can be also obtained in slightly lower yields from the reaction between $[Fe_4N(CO)_{12}]^-$ and a large excess of $[Mo(CO)_3(Me_3C_6H_3)]$ in refluxing THF. In this case, the new dianion **5** is formed as a by-product; it can be separated by selective extraction with methanol, and then precipitated in a microcrystalline form by the addition of bulky organic cations. Crystals of the $[PPh_4]^+$ and $[N(PPh_3)_2]^+$ salts, both unsuitable for X-ray analysis, were obtained by this method after crystallization from THF/2-propanol. The salt $[PPh_4]_2$**5** allowed a partial structural determination, which unambiguously showed an octahedral metallic framework with a Mo:Fe ratio of 1:5.[14] Several alternative procedures have been unsuccessfully tested to selectively obtain **5** or the hypothetical Fe−W−N analogue; they include the reaction between $[Fe_4N(CO)_{12}]^-$ and the neutral complexes $[M(CO)_3(NCEt)_3]$ or the reaction between the same iron cluster and the bimetallic anions $[HFeM(CO)_9]^-$.[15]

Solid-State Structures

Molecular structures of $[Fe_5Mo(CO)_{14}(C_5H_5)]^{2-}$ and $[Fe_5W(CO)_{14}(C_5H_5)]^{2-}$

The solid-state structures of the two anions have been determined from their $[PPh_4]^+$ salts. $[PPh_4]_2$**1** and $[PPh_4]_2$**2**·C_4H_8O crystallize in different space groups, owing to the presence of one molecule of crystallization (THF) in the latter. However, the two clusters **1** and **2** have almost identical molecular geometries, with strikingly similar structural parameters. Relevant bond lengths and angles are presented in Table 1, and the structure of **1** is shown in Figure 1. The six metal atoms define an octahedron with an interstitial nitrogen atom. The cyclopentadienyl ligand is bound to molybdenum (or tungsten in **2**).

The clusters possess three edge-bridging ligands, the remainder being terminal. The disposition of the carbonyl groups strictly recalls that found in the heterometallic species $[Fe_5M'N(CO)_{15}]^{2-}$ (M′ = Rh or Ir).[7] This similarity is not unexpected considering that the "$M(C_5H_5)^-$" and the "$M'(CO)^-$" fragments are isoelectronic (12 valence electrons). As such, the four anions can be envisaged as adducts (from the stoichiometric and electronic point of view) between the well-known square pyramidal $[Fe_5N(CO)_{14}]^-$ cluster (74 valence electrons)[16] and the $[M-L]^-$ fragments, thus representing a nice example of the relationship between *nido* and *closo* cluster cages.[17]

The average bond lengths (Å) and angles (°) for the metal cage and the ligand environment are collected in Table 2. From the intermetallic distances in **1**, the covalent radii of iron and molybdenum can be estimated as $r_{Fe} = 1.32$ and $r_{Mo} = 1.52$ Å. The metal−nitrogen bond lengths also differ by 0.19 Å, suggesting that the interstitial ligand does not

Table 1. Selected interatomic distances (Å) and angles (°) for $[Fe_5MoN(CO)_{14}(C_5H_5)]^{2-}$ **(1)** and $[Fe_5WN(CO)_{14}(C_5H_5)]^{2-}$ **(2)**, with estimated standard deviations in parentheses

	(**1**, M = Mo)	(**2**, M = W)
M−Fe(1)	2.860(1)	2.839(1)
M−Fe(2)	2.847(1)	2.845(1)
M−Fe(3)	2.850(1)	2.825(1)
M−Fe(4)	2.800(1)	2.818(1)
Fe(1)−Fe(2)	2.566(1)	2.562(1)
Fe(1)−Fe(4)	2.701(1)	2.684(1)
Fe(1)−Fe(5)	2.634(1)	2.654(1)
Fe(2)−Fe(3)	2.663(1)	2.668(1)
Fe(2)−Fe(5)	2.675(1)	2.646(1)
Fe(3)−Fe(4)	2.687(1)	2.690(1)
Fe(3)−Fe(5)	2.608(1)	2.591(1)
Fe(4)−Fe(5)	2.637(1)	2.589(1)
M−N	2.075(3)	2.059(2)
Fe(1)−N	1.870(3)	1.874(2)
Fe(2)−N	1.888(2)	1.870(2)
Fe(3)−N	1.883(3)	1.882(2)
Fe(4)−N	1.871(3)	1.878(2)
Fe(5)−N	1.909(3)	1.893(2)
M−C(12)	2.060(5)	2.062(3)
M−C(13)	2.139(3)	2.069(3)
M−C(15)	2.279(5)	2.289(4)
M−C(16)	2.276(6)	2.277(3)
M−C(17)	2.306(6)	2.299(3)
M−C(18)	2.372(6)	2.343(3)
M−C(19)	2.328(5)	2.331(3)
Fe(1)−C(1)	1.750(5)	1.758(3)
Fe(1)−C(2)	1.734(5)	1.738(3)
Fe(1)−C(14)	1.928(4)	1.958(3)
Fe(2)−C(3)	1.756(4)	1.767(3)
Fe(2)−C(4)	1.752(4)	1.753(3)
Fe(2)−C(14)	1.994(5)	1.944(3)
Fe(3)−C(5)	1.769(4)	1.775(3)
Fe(3)−C(6)	1.753(5)	1.767(3)
Fe(3)−C(10)	2.252(5)	2.240(3)
Fe(3)−C(12)	2.123(5)	2.067(3)
Fe(4)−C(7)	1.754(4)	1.766(3)
Fe(4)−C(8)	1.766(4)	1.762(3)
Fe(4)−C(13)	1.948(4)	2.040(3)
Fe(5)−C(9)	1.717(5)	1.761(3)
Fe(5)−C(10)	1.856(5)	1.837(3)
Fe(5)−C(11)	1.782(4)	1.824(3)
M−C(12)−O(12)	144.8(4)	143.6(2)
M−C(13)−O(13)	138.2(3)	142.7(2)
Fe(3)−C(12)−O(12)	129.2(4)	129.9(2)
Fe(4)−C(13)−O(13)	135.3(3)	130.6(2)
Fe(5)−C(10)−O(10)	152.9(4)	153.3(3)
Fe(5)−C(11)−O(11)	168.1(5)	157.3(3)

Table 2. Average interatomic distances (in Å) and angles in the nitride clusters **1**−**3**; (t = terminal, br = bridging, Cp = cyclopentadienyl)

	1 (M = Mo)	**2** (M = W)	**3** (M = Mo)
Fe−M	2.840	2.832	2.845
Mo−Mo			3.145
Fe−Fe	2.646	2.636	2.609
Fe−N	1.884	1.879	1.945
M−N	2.075	2.059	2.104
Fe−C_t	1.76	1.77	1.78
Mo−C_t			1.93
Fe−C_{br}	2.00	2.00	
M−C_{br}	2.10	2.07	
M−C_{Cp}	2.31	2.31	
C_t−O_t	1.16	1.15	1.16
C_{br}−O_{br}	1.18	1.17	
Fe−C_t−O_t	172°	172°	171°
Mo−C_t−O_t			176°
Fe−C_{br}−O_{br}	136°	135°	
M−C_{br}−O_{br}	142°	143°	

interact preferentially with iron or molybdenum. However, the $Fe(CO)_3$ vertex opposite to the MoCp group shows the longest Fe(5)−N separation (1.909 Å), which could be indicative of an excess of electron density on iron [contributed by the three terminal ligands CO(9), CO(10) and CO(11)]. In agreement with this, the CO(10) and CO(11) ligands show some deviation from linearity, and short nonbonding contacts with Fe(3) and Fe(4). CO(12) and CO(13), spanning Fe−Mo edges, are asymmetric; if the different dimensions of Mo and Fe, and the M−C−O angles are taken into account, the two carbonyl groups appears to interact more strongly with the molybdenum centres.

In the Fe−W cluster the cage undergoes a small, but significant, contraction and the distances are all shorter by about 0.01 Å. As a consequence, the apparent metallic radii in **2** are r_{Fe} = 1.32 and r_w = 1.51 Å. The difference between the W−N and the Fe−N bond lengths is only 0.18 Å, slightly smaller than expected, suggesting a negligible preference of nitrogen for tungsten.

Also, the parameters for the outer ligands are very similar in the two homologous clusters, and, indeed, the only relevant difference in their ligand architecture is a more marked tilting of CO(11) in **2** toward a bridging coordination.

Molecular structure of $[Fe_3Mo_3N(CO)_{18}]^{3-}$

The molecular structure of this trianion was determined on the mixed salt $[NMe_3(CH_2Ph)]_2[NEt_4]$**3**. The anion is depicted in Figure 2, and the relevant structural parameters are listed in Table 3. Compound **3** also has an octahedral metallic framework, with the three molybdenum atom in a *fac* arrangement. The architecture of the eighteen carbonyl ligands can be viewed as a perturbation of the idealized high symmetry system having three terminal ligands for each metal atom. In the real situation, many iron-bound CO groups are tilted toward molybdenum in order to compensate the different number of valence electrons. As a result, the average M−C−O angle is much smaller for Fe than Mo (171 vs. 176°). Nevertheless, only CO(18) can be classified as a bridging, though asymmetric, ligand. This description is also in keeping with the solution infrared spectrum, which shows a high-lying band at 1820 cm^{-1} indicative of semibridging ligands, overlapping a very weak band (at 1748 cm^{-1}) attributable to "true" bridging ligands.

The octahedral metal cage of **3** is heavily distorted, showing short Fe−Fe [2.609 Å] and very long Mo−Mo [3.145 Å] separations. The Mo−Mo bond lengths in **3** are quite unusual for octahedral clusters, but are well within the range observed for Mo−Mo single bonds.[18,19] The covalent radii of the metal atoms are, therefore, r_{Fe} = 1.30 and r_{Mo} = 1.57 Å, a difference of 0.27 Å. The average Fe−Mo interaction is 2.845 Å, which matches the sum of the apparent radii. However, when examining the metal−ligand bond

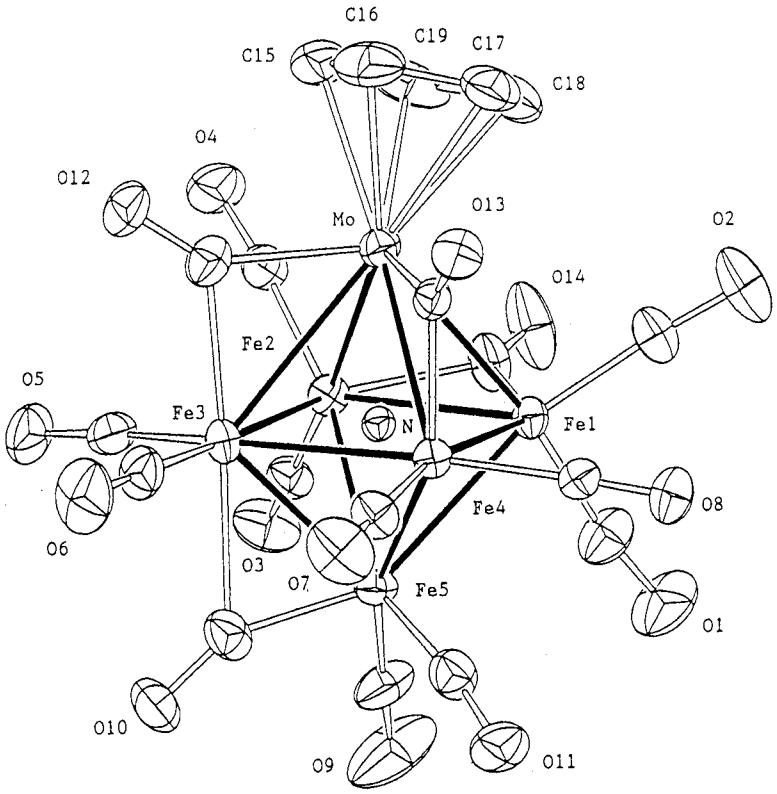


Figure 1. The solid state structure of $[Fe_5MoN(CO)_{14}(C_5H_5)]^{2-}$; ellipsoids are drawn at the 30% probability level; the carbon atoms of the carbonyl ligands are labelled as the oxygen to which they are attached

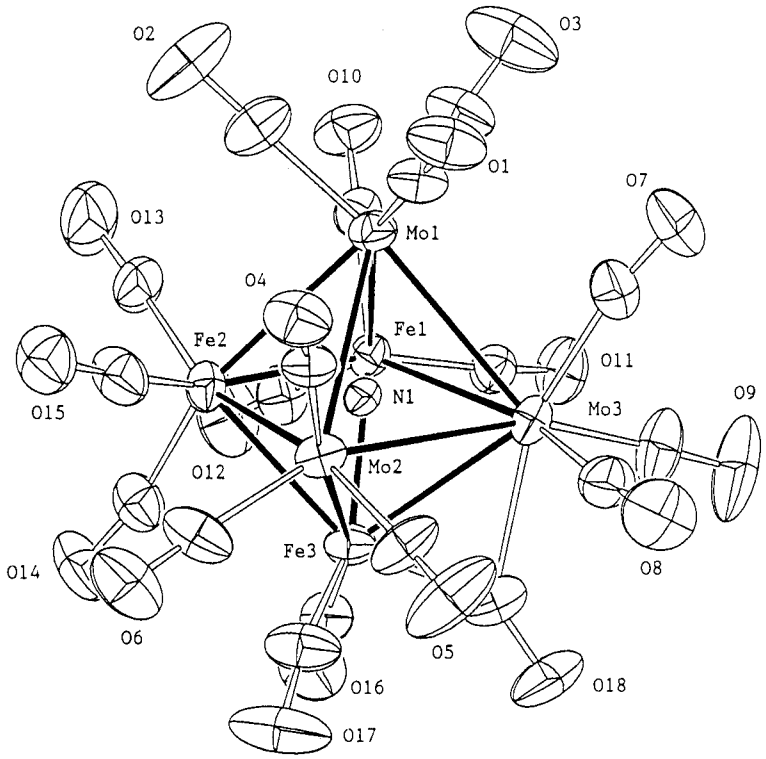


Figure 2. The solid state structure of $[Fe_3Mo_3N(CO)_{18}]^{3-}$

lengths, the difference between Mo and Fe appears much smaller: 0.14 Å for the metal−CO distances, and 0.16 Å for the metal−nitrogen separations. For example, the Mo−N bond lengths average 2.104 Å and the Fe−N 1.945 Å. On that basis, it appears that the three molybdenum atoms bind much more efficiently with the ligands (both external and interstitial), whereas iron would rather reinforce the bonds within the metal cages.

Table 3. Selected interatomic distances (Å) and angles (°) for $[Fe_3Mo_3N(CO)_{18}]^-$ **(3)** with estimated standard deviations in parentheses

Mo(1)−Mo(2)	3.143(1)
Mo(1)−Mo(3)	
Mo(1)−Fe(1)	2.852(1)
Mo(1)−Fe(2)	2.921(1)
Mo(2)−Mo(3)	3.212(1)
Mo(2)−Fe(2)	2.801(1)
Mo(2)−Fe(3)	2.825(1)
Mo(3)−Fe(1)	2.892(1)
Mo(3)−Fe(3)	2.779(1)
Fe(1)−Fe(2)	2.557(1)
Fe(1)−Fe(3)	2.620(1)
Fe(2)−Fe(3)	2.649(1)
Mo(1)−N	2.102(4)
Mo(2)−N	2.109(4)
Mo(3)−N	2.101(3)
Fe(1)−N	1.950(4)
Fe(2)−N	1.956(3)
Fe(3)−N	1.928(4)
Mo(1)−C(1)	1.915(6)
Mo(1)−C(2)	1.921(7)
Mo(1)−C(3)	1.910(8)
Mo(2)−C(4)	1.900(6)
Mo(2)−C(5)	1.895(6)
Mo(2)−C(6)	1.943(7)
Mo(3)−C(7)	1.973(7)
Mo(3)−C(8)	1.925(7)
Mo(3)−C(9)	1.944(7)
Mo(3)−C(18)	2.333(8)
Fe(1)−C(10)	1.804(7)
Fe(1)−C(11)	1.764(6)
Fe(1)−C(12)	1.769(6)
Fe(2)−C(13)	1.750(8)
Fe(2)−C(14)	1.801(7)
Fe(2)−C(15)	1.735(7)
Fe(3)−C(16)	1.769(6)
Fe(3)−C(17)	1.759(8)
Fe(3)−C(18)	1.893(6)
Mo(3)−C(18)−O(18)	133.3(5)°
Fe(3)−C(18)−O(18)	145.2(6)°

Experimental Section

All the solvents were purified and dried by conventional methods and stored under nitrogen. All the reactions were carried out under an oxygen-free nitrogen atmosphere using standard Schlenk techniques.[20] $[NEt_4][Fe_4N(CO)_{12}]$,[21] $[NEt_4][M(CO)_3(C_5H_5)]$,[22] $[NEt_4]_2[M_2(CO)_{10}]$[23] and $[Mo(CO)_3(Me_3C_6H_3)]$[24] were prepared by literature methods. Infrared spectra in solution were recorded on a Perkin−Elmer 16 PC FT-IR spectrophotometer, using calcium fluoride cells previously purged with N_2. Elemental analyses were carried out by the staff of Laboratorio di Analisi of the Dipartimento di Chimica Inorganica, Metallorganica e Analitica. ^1H NMR spectra were recorded on a Bruker AC200 spectrometer. Yields refer to the starting iron nitride.

Synthesis of $[PPh_4]_2[Fe_5MoN(CO)_{14}(C_5H_5)]$: $[NEt_4][Fe_4N(CO)_{12}]$ (0.32 g, 0.45 mmol) and $[NEt_4][Mo(CO)_3(C_5H_5)]$ (0.08 g, 0.22 mmol) were dissolved in MeCN (20 mL) and refluxed for 18 h. The solvent was evaporated in vacuum, and the residue suspended in MeOH (20 mL). The solid left undissolved (which consisted of $[NEt_4]_3[Fe_6N(CO)_{15}]$ and decomposition products) was removed by filtration, and solid $[PPh_4]Br$ (1 g) was added. The precipitate was collected by filtration, washed with 2-propanol and dried. The dark red solid was extracted from the frit with the minimum amount of THF and layered with 2-propanol to give dark crystals of $[PPh_4]_2[Fe_5MoN(CO)_{14}(C_5H_5)]$. Elemental analyses of the product material are satisfactory. Yield 0.14 g; 20%.

The salt $[PPh_4]_2$**1** is insoluble in MeOH or 2-propanol, sparingly soluble in THF, and very soluble in acetone or MeCN. − IR (MeCN): ν(CO) = 2002m, 1943vs, 1745mw cm^{-1}. − ^1H NMR (CD_3CN): δ = 4.59 (s, 5 H, C_5H_5), 7.9 (m, 40 H, $[PPh_4]^+$).

Synthesis of $[PPh_4]_2[Fe_5WN(CO)_{14}(C_5H_5)]$THF: $[NEt_4][Fe_4N(CO)_{12}]$ (0.51 g, 0.72 mmol) and $[NEt_4][W(CO)_3(C_5H_5)]$ (0.16 g, 0.35 mmol) were dissolved in MeCN (30 mL) and refluxed for 24 h. The mixture was worked-up as above. Typical yields are as low as 5−10%. − $C_{71}H_{53}Fe_5NO_{15}P_2W$ (1685.2): calcd. C 50.60, H 3.17, N 0.83; found C 51.4, H 3.0, N 0.6. Elemental analysis confirms the presence of one molecule of clathrated THF. − IR (MeCN): ν(CO) = 2020w, 2000w, 1958vs, 1946sh, 1811m, 1784mw, 1725mw cm^{-1}. − ^1H NMR (CD_3CN): δ = 4.73 (s, 5 H, C_5H_5), 7.9 (m, 40 H, $[PPh_4]^+$).

Synthesis of $[NEt_4]_3[Fe_3Mo_3N(CO)_{18}]$: $[NEt_4][Fe_4N(CO)_{12}]$ (0.24 g, 0.34 mmol) and $[NEt_4]_2[Mo_2(CO)_{10}]$ (0.22 g, 0.30 mmol) were dissolved in MeCN (20 mL) and refluxed for 1 h. The solvent was then evaporated in vacuum, and the residue suspended in MeOH (20 mL). The solid residue was collected by filtration, washed with 2-propanol and then dried. The black solid was extracted from the frit with the minimum amount of MeCN and layered with diisopropyl ether to give black crystals of $[NEt_4]_3[Fe_3Mo_3N(CO)_{18}]$. Yield 0.12 g, 26%.

Salts of **3** are usually insoluble in alcohols or THF, sparingly soluble in acetone and very soluble in MeCN. − IR (MeCN): ν(CO) = 2006 vw, 1931 vs, 1822 w,br 1748 w cm^{-1}. − $C_{42}H_{60}Fe_3Mo_3N_4O_{18}$ (1364.3): calcd. C 36.98, H 4.43, N 4.11; found C 37.2, H 4.5, N 4.3.

Crystals of the mixed salt used for X-ray analysis were obtained from an incomplete metathesis reaction between $[NEt_4]_3$**3** and $[NMe_3(CH_2Ph)]Cl$ in MeCN.

Synthesis of $[NEt_4]_3[Fe_3W_3N(CO)_{18}]$: $[NEt_4][Fe_4N(CO)_{12}]$ (0.24 g, 0.34 mmol) and $[NEt_4]_2[W_2(CO)_{10}]$ (0.31 g, 0.34 mmol) were dissolved in EtCN (20 mL) and refluxed for 4 h. The solvent was then evaporated in vacuo and the black residue treated as above. − IR (MeCN): ν(CO) = 2007 vw, 1933 vs, 1821 w,br 1759 w cm^{-1}.

Synthesis of $[PPh_4]_2[HFe_5MoN(CO)_{16}]$: $[NEt_4][Fe_4N(CO)_{12}]$ (0.55 g, 0.78 mmol) and $[Mo(CO)_3(Me_3C_6H_3)]$ (1.04 g, 3.47 mmol) were dissolved in THF (20 mL) and refluxed for 5 h. The solvent was evaporated in vacuum, and the residue washed repeatedly with toluene (4 × 10 mL). It was than suspended in MeOH (20 mL). Solid $[NEt_4]Br$ was added and the mixture was stirred for 0.5 h. Addition of water induced complete precipitation. The solid was collected by filtration, washed with water and dried. Impure $[NEt_4]_2[HFe_5MoN(CO)_{16}]$ was extracted from the frit with THF leaving the insoluble $[NEt_4]_3$**3** behind (yield 18%).

Pure $[PPh_4]_2$**5** was obtained by metathesis. The THF was evaporated in vacuo, the residue was dissolved in MeOH and $[PPh_4]Br$ was added. The microcrystalline solid was collected by filtration, washed with 2-propanol, dried and dissolved in the minimum amount of THF. Crystals were obtained by layering with 2-propanol. Yield 21%. − IR (THF): ν(CO) = 1959 vs, 1880m,br 1799 m cm^{-1}. − ^1H NMR (CD_3CN): δ = −19.77. − $C_{64}H_{41}Fe_5MoNO_{16}P_2$ (1517.2): C 50.67, H 2.72, N 0.92; found C 50.3, H 2.7, N 0.9.

X-ray Data Collection and Structure Determination: Crystal data and other experimental details are summarized in Table 4. The dif-

Table 4. Crystallographic data and collection parameters for compounds $[PPh_4]_2$**1**, $[PPh_4]_2$**2**·OC_4H_8 and $[NMe_3(CH_2Ph)]_2[NEt_4]$**3**

Compound	$[PPh_4]_2$**1**	$[PPh_4]_2$**2**·OC_4H_8	$[NMe_3(CH_2Ph)]_2[NEt_4]$**3**
Empirical formula	$C_{67}H_{45}Fe_5MoNP_2O_{14}$	$C_{71}H_{53}Fe_5NO_{15}P_2W$	$C_{46}H_{52}Fe_3Mo_3N_4O_{18}$
Mass	1525.2	1685.2	1404.3
Space group	*P*1(bar) (no.2)	*C*2/*c* (no.15)	*P*1(bar) (no.2)
a/Å	11.297(2)	41.244(4)	12.018(2)
b/Å	12.712(2)	15.135(1)	13.164(2)
c/Å	23.993(4)	21.907(2)	18.270(2)
α/°	99.70(1)		77.87(1)
β/°	99.89(1)	97.32(1)	89.73(1)
γ/°	106.87(1)		75.80(1)
V/Å^3	3160(1)	13563(2)	2751(1)
Z	2	8	2
D_c/g cm^{-3}	1.603	1.650	1.696
μ (Mo-K_α)/cm^{-1}	14.2	28.8	14.9
Final *R* and R_w indices[a]	0.037, 0.047	0.023, 0.030	0.044, 0.052

[a] $R = [\Sigma(|F_o - k|F_c||)/\Sigma F_o]$, $R_w = [\Sigma w(F_o - k|F_c|)^2/\Sigma wF_o^2]^{1/2}$, $w = 1/[\sigma(F_o)]^2$, $\sigma(F_o) = [\sigma^2(F_o^2) + (0.04F_o^2)^2]^{1/2}/2F_o$.

fraction experiments were carried out on a Siemens SMART CCD area-detector diffractometer at room temperature using Mo-K_α radiation (λ = 0.71073 Å) with a graphite crystal monochromator in the incident beam. Cell parameters and orientation matrices were obtained from the least-squares refinement of 150 (for $[PPh_4]_2$**1**), 278 (for $[PPh_4]_2$**2**·OC_4H_8), and 100 {for $[NMe_3(CH_2Ph)]_2[NEt_4]$**3**} reflections measured in three different sets of 15 frames each, in the range $3 < \theta < 23°$. At the end of the data collection the first 50 frames, containing 416 reflections (for $[PPh_4]_2$**1**), 894 reflections (for $[PPh_4]_2$**2**C_4H_8O), and 249 reflections (for $[NMe_3(CH_2Ph)]_2[NEt_4]$**3**) were recollected to monitor crystal decay, which was not observed, so that no time-decay correction was needed. The collected frames were processed with the software SAINT,[25] and an absorption correction was applied (SADABS)[26] to the 34144 collected reflections of $[PPh_4]_2$**1** {13768 of which are unique with $R_{int} = 0.0224$ [$R_{int} = \Sigma|F_o^2 - F_{mean}^2|/\Sigma F_o^2$]}, the 76667 collected reflections of $[PPh_4]_2$**2**·C_4H_8O (16514 of which are unique with $R_{int} = 0.0263$), and the 29939 collected reflections of $[NMe_3(CH_2Ph)]_2[NEt_4]$**3** (11983 of which are unique with $R_{int} = 0.0436$).

The calculations were performed on an AST Power Premium 486/33 computer using the Personal Structure Determination Package[27] and the physical constants tabulated therein. Scattering factors and anomalous dispersion corrections were taken from ref.[28] The structures were solved by SHELXS direct methods (contained in the Personal SDP)[27] and refined by full-matrix least-squares minimizing the function $\Sigma w(F_o - kF_c)^2$ (refinement on *F*).

In $[NMe_3(CH_2Ph)]_2[NEt_4]$**3** one of the two $[NMe_3(CH_2Ph)]^+$ cations is partially disordered, with four phenylic carbon atoms split into eight peaks, four with occupancy factors of 0.60, and four with occupancy factors of 0.40. These eight atoms were refined with isotropic thermal parameters. All the other non-hydrogen atoms were refined with anisotropic thermal parameters. The hydrogen atoms bound to the eight disordered carbon atoms were ignored. All the other hydrogen atoms were placed in their ideal positions (C−H = 0.97 Å, B = 1.15 times that of the carbon atom to which they are attached) and not refined. In the final difference Fourier maps, maximum residuals were 0.82(7) e Å^{-3} at 0.84 Å from Fe(2) in $[PPh_4]_2$**1**, 0.57(6) e Å^{-3} at 1.04 Å from C(222) (a carbon atom of a $[PPh_4]^+$ cation) in $[PPh_4]_2$**2**·C_4H_8O, and 1.36(9) e Å^{-3} at 1.08 Å from Fe(2) in $[NMe_3(CH_2Ph)]_2[NEt_4]$**3**.

Crystallographic data (excluding structure factors) for the structure(s) included in this paper have been deposited with the Cambridge Crystallographic Data Centre as supplementary publication nos. CCDC-135691 (**1**), CCDC-135692 (**2**), and CCDC-135693 (**3**). Copies of the data can be obtained free of charge on application to CCDC, 12 Union Road, Cambridge CB2 1EZ, UK [Fax: (internat.) + 44-1223/336-033; Email: deposit@ccdc.cam.ac.uk].

Acknowledgments

This work was funded by cofinanziamento MURST (Italy).

[1] *Catalysis by Di- and Polynuclear Metal Cluster Compounds* (Eds.: R. D. Adams, F. A. Cotton), Wiley-VCH, New York, **1998**.
[2] [2a] M. Garland, *Organometallics* **1993**, *12*, 535−543 − [2b] R. D. Adams, T. S. Barnard, *Organometallics* **1998**, *17*, 2885−2890 − [2c] V. Ferrand, G. Süss-Fink, A. Neels, H. Stoeckli-Evans, *J. Chem. Soc., Dalton Trans.* **1998**, 3825−3831.
[3] [3a] M. S. Nashner, A. I. Frenkel, D. Somerville, W. Hills, J. R. Shapley, R. G. Nuzzo, *J. Am. Chem. Soc.* **1998**, *120*, 8093−8101 − [3b] D. S. Shephard, T. Maschmeyer, G. Sankar, J. M. Thomas, D. Ozkaya, B. F. G. Johnson, R. Raja, R. D. Oldroyd, R. G. Bell, *Chem. Eur. J.* **1998**, *4*, 1214−1224.
[4] L. J. Farrugia, *Adv. Organomet. Chem.* **1990**, *31*, 301−391.
[5] J. Sinzig, L. J. de Jongh, A. Ceriotti, R. Della Pergola, G. Longoni, M. Stener, K. Albert, N. Rosch, *Phys. Rev Lett.* **1998**, *81*, 3211−3214.
[6] R. Della Pergola, C. Bandini, F. Demartin, E. Diana, L. Garlaschelli, P. L. Stanghellini, P. Zanello, *J. Chem. Soc., Dalton Trans.* **1996**,747−754.
[7] R. Della Pergola, A. Cinquantini, E. Diana, L. Garlaschelli, F. Laschi, P. Luzzini, M. Manassero, A. Repossi, M. Sansoni, P. L. Stanghellini, P. Zanello, *Inorg. Chem.* **1997**, *36*, 3761−3771.
[8] S. Alconchel, F. Sapiña, D. Beltrán, A. Beltrán, *J. Mater. Chem.* **1998**, *8*, 1901−1909.
[9] [9a] A. York, *Chem. Brit.* **1999**, *35*, 25−27; − [9b] M. K. Neylon, S. Choi, H. Kwon, K. E. Curry, L. T. Thompson, *Appl. Catal. A.-General* **1999**, *183*, 253−263 − [9c] C. C. Yu, S. Ramanathan, S. T. Oyama, *J. Catal.* **1999**, *173*, 10−16.
[10] M. Tachikawa, R. L. Geerts, E. L. Muetterties, *J. Organomet. Chem.* **1981**, *213*, 11−24.
[11] P. Zanello, F. Laschi, A. Cinquantini, R. Della Pergola, L. Garlaschelli, M. Cucco, F. Demartin, T. R. Spalding, *Inorg. Chim. Acta* **1994**, *226*, 1−8.
[12] C.-K. Lai, W. G. Feighery, Y. Zhen, J. D. Atwood, *Inorg. Chem.* **1989**, *28*, 3929−3930.
[13] Orthorhombic, space group *Aba*2 (no. 41) *a* = 31.393(6) *b* = 47.534(8) *c* = 21.885(4) Å, *V* = 32658 Å^3, *Z* = 24. The structure solution was incomplete, because of cation disorder.
[14] Monoclinic, space group $P2_1/n$ (n. 14) *a* = 11.492(2) *b* = 14.845(3) *c* = 19.149(3) Å β = 100.78(2)°, *V* = 3209 Å^3, *Z* = 2. The structure solution was incomplete, because of ligand disorder.
[15] L. W. Arndt, C. J. Bischoff, M. Y. Darensbourg, *Inorg. Synth.* **1989**, *26*, 335−338.

[16] R. Hourihane, T. R. Spalding, G. Ferguson, T. Deeney, P. Zanello, *J. Chem. Soc., Dalton Trans.* **1993**, 43−46.
[17] K. Wade, *Adv. Inorg. Chem. Radiochem.* **1976**, *18*, 1−66.
[18] C. P. Gibson, J.-S. Huang, L. F. Dahl, *Organometallics* **1986**, *5,*1676−1681 and refs. therein.
[19] C. P. Gibson, L. F. Dahl, *Organometallics* **1988**, *7*, 543−552.
[20] I. F. Shriver, M. A. Dredzon, *The Manipulation of Air-Sensitive Compounds*, 2nd ed. **1986**, Wiley New York.
[21] D. E. Fjare, W. L. Gladfelter, *Inorg. Chem.* **1981**, *20*, 3533−3539.
[22] P. Braunstein, R. Bender, J. Jud, *Inorg. Synth.* **1989**, *26*, 341−345.
[23] [23a] R. G. Hayter, *J. Am. Chem. Soc.* **1966**, *88*, 4376−4382 − [23b] J. K. Ruff, W. J. Schlientz, *Inorg. Synth.* **1974**, *15*, 84−89.
[24] B. Nicholls, M. C. Whiting, *J. Chem. Soc.* **1959**, 551−556.
[25] SAINT, Reference manual, Siemens, Energy and Automation, Madison, WI, **1994−1996**.
[26] G. M. Sheldrick, SADABS, Empirical Absorption Correction Program, University of Gottingen, **1997**.
[27] [27a] B. A. Frenz, *Comput. Phys.* **1988**, *2*, 42 (− [27b] *Crystallographic Computing 5,* Oxford University Press: Oxford, UK, **1991**; Chapter 11, p. 126.
[28] *International Tables for X-ray Crystallography*, Vol.4, Kynoch Press, Birmingham, **1974**.

Received October 25, 1999
[I99376]

Trimeric Anions in $KTeO_2F$

Ulrich Keßler[a] and Martin Jansen*[a]

Keywords: Tellurium / Lone pair / Lewis acids / Solid-state structures / Anions

$KTeO_2F$ was prepared by solid state reaction from KF and TeO_2 at 350 °C. The structure has been determined by single crystal X-ray analysis [$P2_1/n$, $Z = 12$, $a = 1177.8(2)$ pm, $b = 1499.0(3)$ pm, $c = 619.5(2)$ pm, $\beta = 94.11(2)$ °, $R_1 = 0.0266$, $wR_2 = 0.0604$]. A characteristic feature of the structure is the presence of trimeric anions $Te_3O_6F_3^{3-}$ in which the tellurium atoms are bridged by oxygen atoms. The lone pairs are stereoactive leading to pseudotrigonal bipyramidal coordination at the tellurium atoms. Additional weak bonding interactions link these trimeric anions resulting in a layered structure.

Introduction

Acid base reactions between acidic oxides and basic (alkali) metal oxides are well-known and have lead to anions ranging from discrete *ortho* anions like sulfate to polymeric anions with chainlike (Na_3SbO_4[1]), layered (Li_3InO_3[2]) or framework ($NaGaO_2$[3]) structures. When reacting acidic oxides with basic fluorides one can generally expect the resulting fluorooxides to differ in two aspects from the pure oxo compounds. Firstly, the coordination numbers attainable should be higher, and secondly, the fluorooxo compounds should show a higher tendency to form polymeric anions.

The preparation of such fluorooxo compounds can be challenging because the desired products may tend to undergo dismutation reactions.

In the course of our investigations on reactions of fluorides with chalcogen dioxides we have solved the crystal structures of KSO_2F[4] and $KSeO_2F$.[5] Both compounds had been the subject of spectroscopic (IR, Raman)[6–8] and theoretical[8] studies leading to ambiguous results concerning the bonding situations in the complex anions. On the one hand, Seel and Boudier[7] interpreted the IR spectrum of KSO_2F in terms of discrete SO_2F^- anions containing a S–F single bond. On the other, Paetzold and Aurich[6] deduced a weakened S–F and Se–F bond with concomitant interionic bridging from the analysis of the spectra of KSO_2F and $KSeO_2F$, respectively. This weakened S–F bond was also postulated by Kornath et al.[8] who performed quantum mechanical calculations (RHF niveau). Although the crystal structures of KSO_2F and $KSeO_2F$ are closely related (they are both isopunctual) the fluorosulfite anion is discrete containing a S–F single bond, while the fluoroselenite shows weak intermolecular bonding through an asymmetric fluorine bridge, thus linking the SeO_2F^- units to chains.

We here report on the synthesis and characterization of $KTeO_2F$ representing the end member of the KEO_2F series (E = chalcogen).

Results and Discussion

Synthesis and Crystal Structure

$KTeO_2F$ has been obtained by the solid state reaction of potassium fluoride and tellurium dioxide at 350 °C in closed silver crucibles. A colourless crystalline solid that is sensitive to moist air was obtained. Its crystal structure has been solved by single crystal structure analysis (Table 1 and Table 2).

The main feature of the structure of $KTeO_2F$ is the presence of unprecedented trimeric anions $Te_3O_6F_3^{3-}$ in which the tellurium atoms are linked by oxygen atoms forming a six-membered puckered ring (Figure 1). The coordination of the crystallographically independent tellurium atoms by oxygen and fluorine atoms is pseudotrigonal bipyramidal. The terminal oxygen atoms occupy equatorial positions and the fluorine atoms axial positions. The bridging oxygen atoms link an equatorial with an axial vertex of the trigonal bipyramids. The deviations of the bond lengths and angles from perfect trigonal bipyramids can be understood on the basis of the VSEPR model.[9]

These trimeric units are linked by additional oxygen–tellurium interactions to chains running along the crystallographic *c* axis. These oxygen–tellurium contacts [282.2(3) pm] are much shorter than the sum of the van der Waals radii[10] [360 pm; r_{vdW}(Te): 210 pm, r_{vdW}(O): 150 pm] and must be considered as weakly bonding. Further interionic bridging is accomplished by fluorine–tellurium contacts [309.2(3) pm] similarly linking the trimers along the *b* axis [sum of van der Waals radii:[10] 360 pm; r_{vdW}(F): 150 pm]. Thus the anions form weakly bonded corrugated layers in the *bc* plane (Figure 2). The coordination spheres of the tellurium atoms Te1 and Te2 are extended by these intermolecular interactions to strongly distorted pseudooctahedra. The additional ligands are the terminal oxygen and fluorine atoms of Te3. The calculation of the valence

[a] Max-Planck-Institut für Festkörperforschung,
Heisenbergstraße 1, 70569 Stuttgart, Germany
Fax: (internat.) + 49-(0)711/689-1502
E-mail: martin@jansen.mpi-stuttgart.mpg.de

 © WILEY-VCH Verlag GmbH, D-69451 Weinheim, 2000 1434–1948/00/0808–1767 $ 17.50+.50/0

Table 1. Data collection and refinement parameters of $KTeO_2F$

Crystal data[a]	
Space group (No.)	$P2_1/n$ (14)
a [pm]	1177.8(2)
b [pm]	1499.0(3)
c [pm]	619.5(2)
β [°]	94.11(2)
V [10^6 pm^3]	1090.9(5)
Z	12
ρ_X [g cm^{-3}]	3.976
μ [mm^{-1}]	9.16
Crystal size [mm]	ca. 0.1 × 0.05 × 0.2
Diffractometer	Smart CCD
Radiation	Mo-K_α
Monochromator	Graphite
Detector distance [mm]	30
Rotation range [°]	3 × 180
Rotation step width [°]	0.3
$2\theta_{max}$ [°]	75.08
Reflections measured	$-20 \le h \le 20$, $-25 \le k \le 25$, $-10 \le l \le 10$
Number of reflections	22026
Completeness of data set	99.2%
Absorption correction	semiempirical (SADABS)
Min./max. transmission	0.151/0.276
Number of unique reflections	5726
R_{int}, R_σ	0.0511, 0.0364
Number of parameters	136
Number of reflections $F_o > 4\sigma(F_o)$	4748
R_1 [$F_o > 4\sigma(F_o)$], R_1 (all)	0.0266, 0.0362
wR_2, a, b	0.0604, 0.0292, 0.000
Goof	0.960
$\Delta\rho_{max}$, $\Delta\rho_{min}$ [10^{-6} e pm^{-3}]	0.98, −1.87 (64 pm from Te3, 35 pm from Te3)

[a] Further details of the crystal-structure investigation may be obtained from the Fachinformationszentrum Karlsruhe, D-76344 Eggenstein-Leopoldshafen, Germany, on quoting the depository number CSD-411068.

Table 2. Selected interatomic distances [pm] and angles [°]

Te1−O1	180.6(3)	Te2−O2	180.1(3)	Te3−O3	181.5(3)
Te1−O4	191.9(3)	Te2−O6	190.9(3)	Te3−O5	188.4(3)
Te1−O5	209.1(3)	Te2−O4	207.8(3)	Te3−O6	207.2(3)
Te1−F1	211.0(3)	Te2−F2	209.3(2)	Te3−F3	208.2(2)
Te1−O3	282.2(3)	Te2−F3	309.2(3)		
O1−Te1−O4	99.0(2)	O2−Te2−O6	97.8(2)	O3−Te3−O5	102.3(2)
O1−Te1−O5	87.6(2)	O2−Te2−O4	92.9(1)	O3−Te3−O6	93.6(2)
O1−Te1−F1	86.1(1)	O2−Te2−F2	87.3(2)	O3−Te3−F3	88.8(2)
O4−Te1−O5	87.9(1)	O6−Te2−O4	90.9(2)	O5−Te3−O6	89.7(2)
O4−Te1−F1	87.5(2)	O6−Te2−F2	85.7(2)	O5−Te3−F3	81.9(1)
O5−Te1−F1	171.5(1)	O4−Te2−F2	176.5(1)	O6−Te3−F3	171.6(1)
K1−F2	254.5(3)	K2−O2	267.6(3)	K3−O1	278.3(3)
K1−F3	256.3(3)	K2−F1	267.9(3)	K3−F2	280.0(3)
K1−O1	261.4(3)	K2−F2	272.5(3)	K3−O3	281.3(3)
K1−O2	264.0(3)	K2−O5	280.3(3)	K3−F1	288.7(3)
K1−F1	264.1(3)	K2−O3	285.9(3)	K3−O5	308.0(3)
K1−O4	296.8(3)	K2−O6	288.6(3)	K3−O4	309.5(3)
		K2−F3	303.7(3)	K3−O2	309.7(3)
		K2−F3	318.4(3)	K3−O1	313.2(3)
				K3−O1	322.1(3)

sums[11,12] gives support to assuming weak bonding contributions of these intermolecular Te−O/Te−F contacts since this leads to virtually equal valence sums for the three different tellurium atoms (Te1: 4.12, Te2: 4.17, Te3: 4.17).

The three potassium atoms are coordinated by six, eight and nine oxygen and fluorine atoms, respectively. K1 is situated between two layers and is coordinated by three ligands from each layer. K2 and K3 are located in voids within the layers that are formed by the anions, and are coordinated by six and seven ligands from that layer and two ligands from an adjacent layer. These electrostatic interactions of potassium with oxygen or fluorine hold together the anionic layers along the a axis.

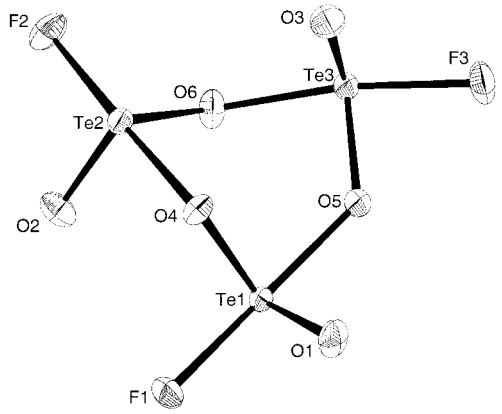


Figure 1. Trimeric cyclic anion $Te_3O_6F_3^{3-}$

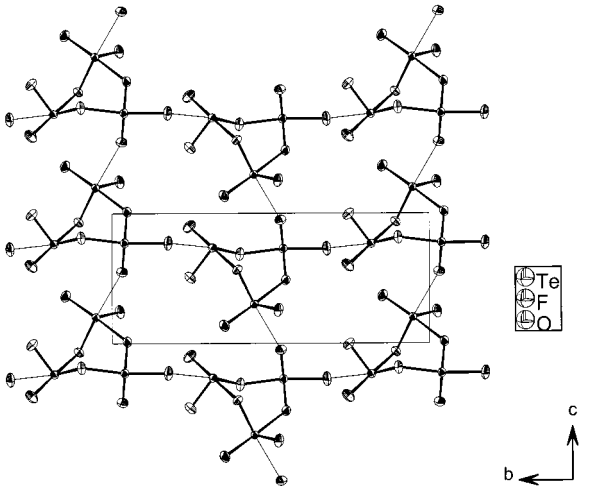


Figure 2. View along [100] showing the association of $Te_3O_6F_3^{3-}$-trimers building infinite layers

When comparing the structures of $KTeO_2F$ and its homologues one observes an increase in coordination number of the chalcogen atom as one would expect when moving from KSO_2F (C.N. 3) via $KSeO_2F$ (C.N. 3 + 1) to $KTeO_2F$ [C.N. 4 (Te3) and C.N. 4 + 1(Te1, Te2)]. However, the tendency towards intermolecular interactions through fluorine bridges, as exhibited by the selenium compound, is not continued. Instead polymerization is accomplished almost exclusively through oxygen atoms.

Since $KTeO_2F$ is the first fluorooxotellurite whose structure has been determined, it is interesting to compare it to those of pure oxotellurites. In contrast to, for example, the oxide adducts of SiO_2 or P_2O_5 in which the silicon and phosphorus atoms are fourfold coordinated, and which contain vertice-sharing tetrahedra like in the binary oxides, the tellurium-oxygen network is significantly changed when reacting TeO_2 with alkali metal oxides. The fourfold coor-

dination (pseudotrigonal bipyramidal) of the tellurium atoms is partly ($K_2Te_4O_9$, $K_2Te_2O_5$)[13] or fully (K_2TeO_3)[14] reduced to threefold pseudotetrahedral coordination. However, the structure of $KTeO_2F$ shows that, upon fluoride addition to tellurium dioxide, both the fourfold coordination of the tellurium atoms and the linkage scheme of the polyhedra (bridging oxygen atoms link equatorial and axial vertices) are preserved. It will be interesting to obtain structural information on other fluoride adducts of TeO_2 which contain more fluoride than $KTeO_2F$. Preliminary X-ray investigations on $Rb_2TeO_2F_2$[15] indicate the existence of discrete pseudotrigonal bipyramidal $TeO_2F_2^{2-}$ anions, thus confirming the preservation of the tellurium coordination when adding fluoride to TeO_2.

Vibrational Spectroscopy and Thermal Analysis

The vibrational spectra of $KTeO_2F$ are given in Table 3. For a twelve-atom molecule of C_1 symmetry, 30 absorptions are expected though additional absorptions could be present due to combination vibrations, overtones or factor group splitting. No assignment was made because of the complexity of the spectra. Theoretical studies appear to be necessary in order to reach an unambiguous assignment of the absorptions. However, the spectra do not agree with the spectra given by Milne[16] who has claimed to have synthesized $KTeO_2F$.

Table 3. Infrared and Raman spectra of $KTeO_2F$ [cm^{-1}]

IR	Raman	IR	Raman
817 (vs)	817 (vs)		360 (w)
793 (vs)	795 (vs)	343 (vs)	341 (vw, sh)
	767 (w)	330 (vs)	332 (w)
752 (w)		317 (s)	322 (w, sh)
736 (w)	737 (w)		312 (w)
	709 (m)	300 (m, sh)	304 (m)
692 (vs)	690(m)	291 (m, sh)	294 (w, sh)
682 (vs)			285 (w)
662 (vs)	660 (w)	263 (w)	269 (w)
610 (w)	609 (w, sh)	232 (m)	225 (w)
587 (m)	586 (s)	210 (m)	209 (m)
460 (s)	453 (m)	194 (w)	199 (m)
439 (m, sh)	440 (w, sh)	175 (vw, sh)	173 (m)
	412 (w)	157 (w)	162 (w, sh)
393 (m)			151 (w)
368 (s)	375 (w)		

DTA measurements show one endothermic signal at 376 °C indicating the melting point.

Conclusion

$KTeO_2F$ can be synthesized by standard solid-state techniques from KF and TeO_2. The crystal structure represents a new structure type, the characteristic feature of which is the presence of trimeric anions $Te_3O_6F_3^{3-}$. The tellurium atoms exhibit pseudotrigonal bipyramidal coordination; they are linked by oxygen atoms forming a puckered six-membered ring. The trimeric anions are linked to layers by secondary bonding interactions.

When compared to the homologous sulfur and selenium compounds, $KTeO_2F$ shows both expected and unexpected features. While the increase in coordination number agrees with the trend known from KSO_2F and $KSeO_2F$, the bridging by oxygen atoms in $KTeO_2F$ is different from the weak bridging by fluorine atoms in $KSeO_2F$.

In contrast to the significant change of the tellurium coordination when basic oxides are reacted with TeO_2, the characteristic pseudotrigonal bipyramidal coordination of the tellurium atoms is preserved upon fluoride addition to tellurium dioxide.

Experimental Section

Synthesis: The handling of all substances was performed under carefully dried argon by standard Schlenk techniques or in an argon filled drybox (< 0.1 ppm H_2O).

KF (Merck, p. a., > 99%) was finely ground and dried in vacuum at 200 °C before use. It was then stored in sealed glass ampoules.

TeO_2 was prepared following a literature method[17] by oxidation of powdered tellurium (Merck, 99%) with nitric acid (Baker, p.a., 65%) and subsequent thermal decomposition of the basic nitrate $Te_2O_3(OH)(NO_3)$. It was stored in sealed glass ampoules.

Single-phase $KTeO_2F$ was prepared by heating a compacted stoichiometric mixture of KF and TeO_2, in a closed silver crucible encapsulated in duran glass, under argon to 350 °C for 14 days. This was then cooled to room temperature at 10 °C/h. The powder diffraction measurements of the samples were performed in sealed glass capillaries of 0.1 mm diameter. Single crystals were obtained from mixtures containing 2% KF in excess and heating for 30 days. Crystals suitable for structure determination were selected in a drybox and sealed into glass capillaries of 0.3 mm diameter.

X-ray Diffraction Analysis: Powder diffraction measurements were carried out on a powder diffractometer (STOE StadiP) with a linear position sensitive detector using Cu-$K_{\alpha 1}$ radiation (Ge monochromator). Silicon was used as an external standard. Indexing of the powder pattern yielded a monoclinic cell. Systematic absences indicated the space group $P2_1/n$ (No. 14).

Precession photographs of the single crystal used for structure determination proved the unit cell dimensions and the space group. The intensity data collection was carried out with a Smart CCD system (Bruker AXS) using Mo-K_α radiation (graphite monochromator). The data were corrected semi-empirically for absorption (SADABS[18]) improving the residual value R_{int} from 0.0866 to 0.0511. The tellurium and potassium atoms were found by the Patterson method (SHELXS-97[19]), and oxygen and fluorine atoms by a subsequent difference Fourier synthesis (SHELXL-97[20]). The distinction between oxygen and fluorine was made by chemical arguments [bond lengths, valence sums, most electronegative ligand in apical position (Bent's rule)]. Fluorine in the bridging position was tested but this assignment was rejected because the displacement parameters of the bridging atoms were larger than those of the terminal ligands. Moreover, the final difference Fourier map showed the largest peaks at the terminal apical oxygen atoms and the R-values were significantly larger (wR_2 = 0.0825). The structure refinement converged at R_1 = 0.0266, wR_2 = 0.0604. Further information on the structure determination is given in Table 1 and structural parameters are listed in Table 2.

Vibrational spectroscopy: Infrared spectra were recorded on a Bruker IFS113v with a DTGS detector using CsI pellets prepared in a drybox.

Raman spectra were recorded on a Dilor multichannel XY system (microscope technique, Kr laser, 647.1 nm, ca. 10 mW). The samples were sealed in melting point capillaries.

Thermal Analysis: Combined DTA/TG measurements were performed on a Netzsch STA 409 in an argon atmosphere using corundum crucibles.

Acknowledgments

This work was supported by the Deutsche Forschungsgemeinschaft and the Fonds der Chemischen Industrie. We thank Dr. J. Nuß, MPI für Festkörperforschung, for the single crystal data collection and Prof. Dr. J. Weidlein, University of Stuttgart, for the recording of the Raman spectrum.

[1] B. Schwedes, R. Hoppe, *Z. Anorg. Allg. Chem.* **1972**, *393*, 136−148.
[2] F. Stewner, R. Hoppe, *Z. Anorg. Allg. Chem.* **1970**, *374*, 239−258.
[3] E. Vielhaber, R. Hoppe, *Z. Anorg. Allg. Chem.* **1969**, *369*, 14−32.
[4] U. Keßler, M. Jansen, *Z. Anorg. Allg, Chem.* **1999**, *625*, 385−388.
[5] C. Feldmann, M. Jansen, *Chem. Ber.* **1994**, *127*, 2173−2176.
[6] R. Paetzold, K. Aurich, *Z. Anorg. Allg. Chem.* **1965**, *335*, 281−288.
[7] F. Seel, J. Boudier, *Z. Anorg. Allg. Chem.* **1966**, *342*, 173−176.
[8] A. Kornath, F. Neumann, R. Ludwig, *Inorg. Chem.* **1997**, *36*, 5570−5573.
[9] R. J. Gillespie, Angew. Chem. **1967**, *79*, 885−896.
[10] A. Bondi, *J. Phys. Chem.* **1964**, *68*, 441−451.
[11] I. D. Brown, D. Altermatt, *Acta Cryst.* **1985**, *B41*, 244−247.
[12] N. E. Brese, M. O′Keeffe, *Acta Cryst.* **1991**, *B47*, 192−197.
[13] C. R. Becker, S. L. Tagg, J. C. Huffman, J. W. Zwanziger, *Inorg. Chem.* **1997**, *36*, 5559−5564.
[14] L. Andersen, V. Langer, A. Strömberg, D. Strömberg, *Acta Cryst.* **1989**, *B45*, 344−348
[15] U. Keßler, M. Jansen, work in progress.
[16] J. Milne, *Inorg. Chem.* **1978**, *17*, 3592−3596.
[17] H. Marshall, *Inorg. Synth.* **1950**, *3*, 143−145.
[18] Bruker AXS, *SADABS*, Part of Smart CCD Software.
[19] G. M. Sheldrick, *SHELXS-97*, Crystal Structure Solution Program, University of Göttingen, **1997**.
[20] G. M. Sheldrick, *SHELXL-97*, Crystal Structure Refinement Program, University of Göttingen, **1997**.

Received January 20, 2000
[I00021]

Synthesis, Crystal Structure and Spectral Characterization, of a New Phase of Tris(phthalocyaninato)dibismuth(III), $Bi_2(Pc)_3$

Karim Benihya,[a] Mireille Mossoyan-Déneux,*[a] Friedemann Hahn,[b] Nancy Boucharat,[a] and George Terzian[a]

Keywords: Bismuth / Phthalocyanines / Triple-decker compounds / Sandwich complexes / IR spectroscopy / UV/Vis spectroscopy

Direct-template synthesis and purification of a new phase of the triple-decker bismuth(III) phthalocyanine $Bi_2(Pc)_3$, prepared from bismuth acetate and phthalonitrile, are described. X-ray analysis shows a triple-decker molecular structure involving three phthalocyanine rings and two bismuth atoms that are 3.838(9) Å apart. The coordination polyhedron is a distorted square anti-prism. The average distances between the bismuth(III) and the isoindolic nitrogens are 2.336 Å and 2.726 Å, respectively, for the external saucer-shape ring and the more planar inner ring. The intramolecular distance between two neighbouring $4N_{iso}$ mean-planes is 3.17 Å, the inner Pc ring being rotated by 38.3° with respect to the peripheral ones. The shortest intermolecular distance between two carbon atoms in the crystal packing is 3.284 Å. This black phase is a regular stack of phthalocyanine rings that have their π system all overlapping. UV/Visible and FT-IR spectra are discussed in relation to the molecular structure and fully characterize this triple-decker compound.

Introduction

Heavy metal phthalocyanines have interesting electronic properties in the solid state. Rare-earth phthalocyanines and lead phthalocyanine Pb(Pc) have been studied intensively,[1−5] but only recently have some reports been published on phthalocyanine complexes with vicinal element: bismuth.[6,7] H. Isago and Y. Kagaya reported the synthesis, spectral characterization, and redox potential of bromo and chloro(phthalocyaninato) bismuth (III) complexes.[8,9] R. Kubiak et al. described the crystal structure of a bismuth phthalocyanine-bismuth iodide complex with formula $(Bi(Pc))_4(Bi_4I_{16})$,[10] and the synthesis and structure of an iodine-doped bismuth(III) diphthalocyanine $Bi(Pc)_2I_{1.5}$.[11] G. Ostendorp and H. Homborg described the synthesis, structure, and electrochemical and spectral properties of a bisphthalocyanine $Bi(Pc)_2,CH_2Cl_2$.[12] Bismuth(III) is very close to lanthanoids (III) in its ionic radius[13] and its ability to coordinate a large number of atoms.[14] Rare earth phthalocyanines have been investigated as monophthalocyanines,[15] bisphthalocyanines $Ln(Pc)_2$ [15−18] (double-decker compounds), or trisphthalocyanines $Ln_2(Pc)_3$ [19−21] (triple-decker compounds), because all these compounds can have many applications in electronic and display devices. Among all these complexes, the more recently studied are the triple-decker compounds, particularly the mixed ligand phthalocyanine-porphyrin lanthanide molecules.[22−25] Some homoleptic triple-decker sandwich molecules built with three phthalocyanine macrocycles have been reported: (Pc)M(Pc)M(Pc) synthetized by K. Kasuga et al.[26] with M = Y, Nd, Gd, Er, and Lu; (Pc)Lu(CRPc)Lu(Pc) with CRPc = crown-ether-substituted phthalocyanine,[27] synthesized by N. Ishikawa and Y. Kaizu who introduced the crown-ether at the periphery of the macrocycle to give these compounds greater solubility, and the $M_2(obPc)_3$ (obPc = 2,3,9,10,16,17,23,24-octabutoxyphthalocyanine, M = ytterbium, dysprosium,[28] lanthanum and lutetium[29]) synthesized by K. Takahashi et al. The only reported triple-decker phthalocyanine complexes built around a metal without any f orbitals are the indium complex[30] and, very recently, a red-violet phase of bismuth triple-decker phthalocyanine,[31] both obtained by J. Janczak et al. In this report, we present the preparation of a black phase of the same molecule $Bi_2(Pc)_3$, and discuss its crystal and molecular structures, as well as its characterization by FT-IR and UV/Visible spectroscopies.

Results and Discussion

Synthesis and Characterization

All the preparations of triple-decker rare earth phthalocyanine complexes reported in the literature are long, or include many steps.[26,27] Their purification is performed through precipitation and/or extraction with various solvents, and repeated chromatographic procedures on alumina. Janczak and Kubiak have proposed a new method[32] that allowed them to synthesize indium(III) triple-decker phthalocyanine. However, they could not obtain the $Bi_2(Pc)_3$ complex by this method since the oxidation potential of the reaction $Bi \rightarrow Bi^{3+}$ is too high. For the synthesis

[a] Université de Provence, Laboratoire de chimie de coordination, case D22,
Av. de l'escadrille Normandie-Niemen, 13397 Marseille Cedex 20, France
Fax: (internat.) +33-4/91028959
E-mail: Mireille.Mossoyan-Deneux@LCC.u-3mrs.fr
[b] STOE & CIE GmbH,
Hilpertstraβe 10, D-64295 Darmstadt, Germany

 © WILEY-VCH Verlag GmbH, D-69451 Weinheim, 2000 1434−1948/00/0808−1771 $ 17.50+.50/0

of $Bi_2(Pc)_3$ they used a mixture of Bi_2Se_3 and phthalonitrile, pressed into pellets, heated at 220 °C for 24 h[31]. Our preparation method of the tris (phthalocyaninato) dibismuth(III), presented here, is very fast and simple. A mixture of bismuth acetate with a large excess of phthalonitrile was heated to 310 °C during 30 min. The obtained black powder was washed with organic solvents, and placed under reflux in an aqueous solution of NaOH for 30 min. $Bi_2(Pc)_3$ is not soluble in any of the usual solvents (water, acetone, alcohol), and is very slightly soluble in DMF or DMSO, as well as aromatic solvents like chloronaphthalene or quinoline, but not enough to recrystallize. Attempts to obtain sublimed crystals or powder by vacuum sublimation with a very slight stream of nitrogen were unsuccessful. Instead, while using the tubular oven, a very thin metallic mirror (probably metallic bismuth) was deposited on the cold wall of the quartz tube. Further away a dark blue layer, characterized as $H_2(Pc)$ by its IR spectrum, and still further needles of phthalonitrile were also found. This shows the instability of our compound, which is moreover photosensitive: slow decomposition at room temperature was observed when solutions were left in daylight whereas solid samples or dissolved samples kept in the dark at 4−10 °C, remained unchanged over several years. Contact with dilute acids led to demetallation, yielding $H_2(Pc)$. Thus $Bi_2(Pc)_3$, like Pb(Pc), appears to be a labile metallophthalocyanine.

Crystal Structure

Figure 1 shows the triple-decker structure of the molecule. We named the internal macrocycle A, and the two external macrocycles B and B′. The centre of the square formed by the four pyrrolic nitrogens of cycle A (Ct_A) form a crystallographically-imposed inversion centre of the molecule, so that the two macrocycles B and B′ are equivalent. The coordinates of each atom of the B′ ring are deduced from those of the corresponding atom of the B ring by inversion operation: $C(x, y, z) \rightarrow C'(-x, -y + 1, -z)$.

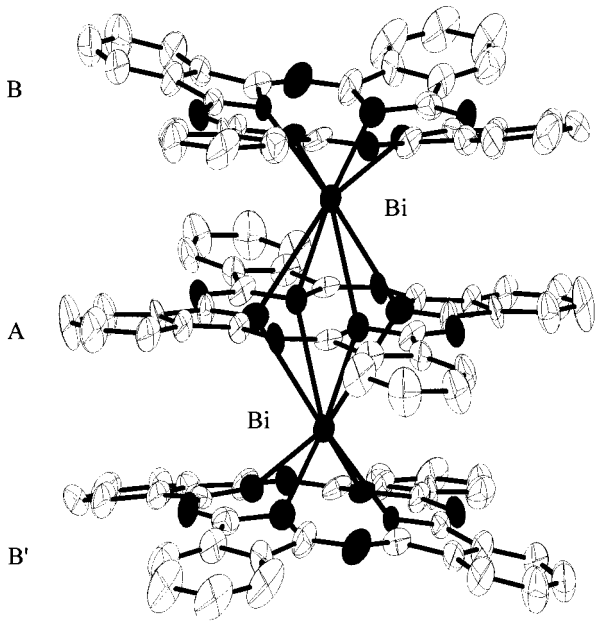


Figure 1. ORTEP drawing of $Bi_2(Pc)_3$ viewed along the *b* axis, with thermal ellipsoids shown at the 50% probability level. H atoms are omitted for clarity. The internal macrocycle is named A and the two external macrocycles B and B′

Figure 2,a is a view of the molecule along the Bi−Bi′ axis, and Figure 2,b shows this split molecule with the three macrocycles projected along the Bi−Bi′ axis, with the numbering scheme, and the staggering angles between the macrocycles. The distances between each bismuth and the centres (Ct) of the squares formed by the four pyrrolic nitrogens of the cycles A (Ct_A), B (Ct_B), and B′ (Ct_B') are indicated at the right of the scheme. As in all the other triple-decker compounds,[30,31,33] the metallic ions are not equidistant from Ct_A and Ct_B: the distance from the metallic ion is 1.918(0) Å for Ct_A and 1.247(1) Å for Ct_B or $Ct_{B'}$. The larger distance to ring A reflects the fact that the benzopyrrolic nitrogens (N_{iso}) of this macrocycle are bridging the two bismuth(III) atoms Bi and Bi′. Interestingly, these bridging nitrogens are not equivalent; selected bond lengths and angles characterizing the coordination polyhedron are given in Table 1: N11 and N9′ are closer to Bi than to Bi′, and N9 and N11′ are closer to Bi′: N11−Bi = 2.695(8) Å, N11−Bi′ = 2.774(10) Å, N9−Bi′ = 2.693(11) Å, N9−Bi = 2,740(10) Å, while the four $Bi-N_{iso}$ bonds lengths of the cycles B or B′ are equivalent (mean length = 2.34 Å). The mean rotational angles between the macrocycles A and B, and between B and B′, measured on the more external benzene carbon atoms, are 38.3° and 0.5°, respectively. The distance between the two bismuth atoms in the molecule is 3.839(0) Å, and the distance between the two centres (Ct_A) and (Ct_B) of the macrocycles is 3.17 Å. We found many distances for pyrrolic carbon atoms between neighbouring A and B planes shorter than 3.3 Å. For example: C25′−C48 = 3.275 Å, C1−C40 = 3.262 Å, C41−C8 = 3.220 Å, C48−C9 = 3.289 Å. These distances are shorter than the van der Waals distance (3.4 Å) for aromatic carbon atoms, so that adjacent phthalocyanine planes are interacting by their π orbitals. The two mean-planes $4N_{iso\ B}$ and $4N_{iso\ B'}$ are strictly parallel on account of symmetry. The angle between these two mean-planes and the $4N_{iso\ A}$ plane is approximately 3.10° (±1.94). Thus, the coordination polyhedron is a distorted square anti-prism. We note that the hole at the centre of the macrocycle B (and B′) is slightly larger than the hole at the centre of the macrocycle A (the distances between N3 and N7 and between N1 and N5 are both 3.95 Å, while the distance between N11 and N11′ is 3.90 Å and between N9 and N9′ is 3.85 Å).

The deviations from the $4N_{iso\ A}$ plane and the $4N_{iso\ B}$ mean-plane for each atom of the asymmetric unit of the molecule are shown on Figure 2,b. Benzopyrrole cycles are numbered I, II, III, IV, V, and VI. We named the 5-membered and the 6-membered ring of benzopyrrole I as I5 and I6, respectively, and the 5-membered and the 6-membered ring of benzopyrrole II as II5 and II6, and so on. The macrocycles B and B′ are slightly convex, the four mean-planes of the pyrrole rings making dihedral angles of 6.26 (I), 6.67 (II), 10.46 (III), and 8.12° (IV) with the $4N_{iso\ B}$ mean-plane

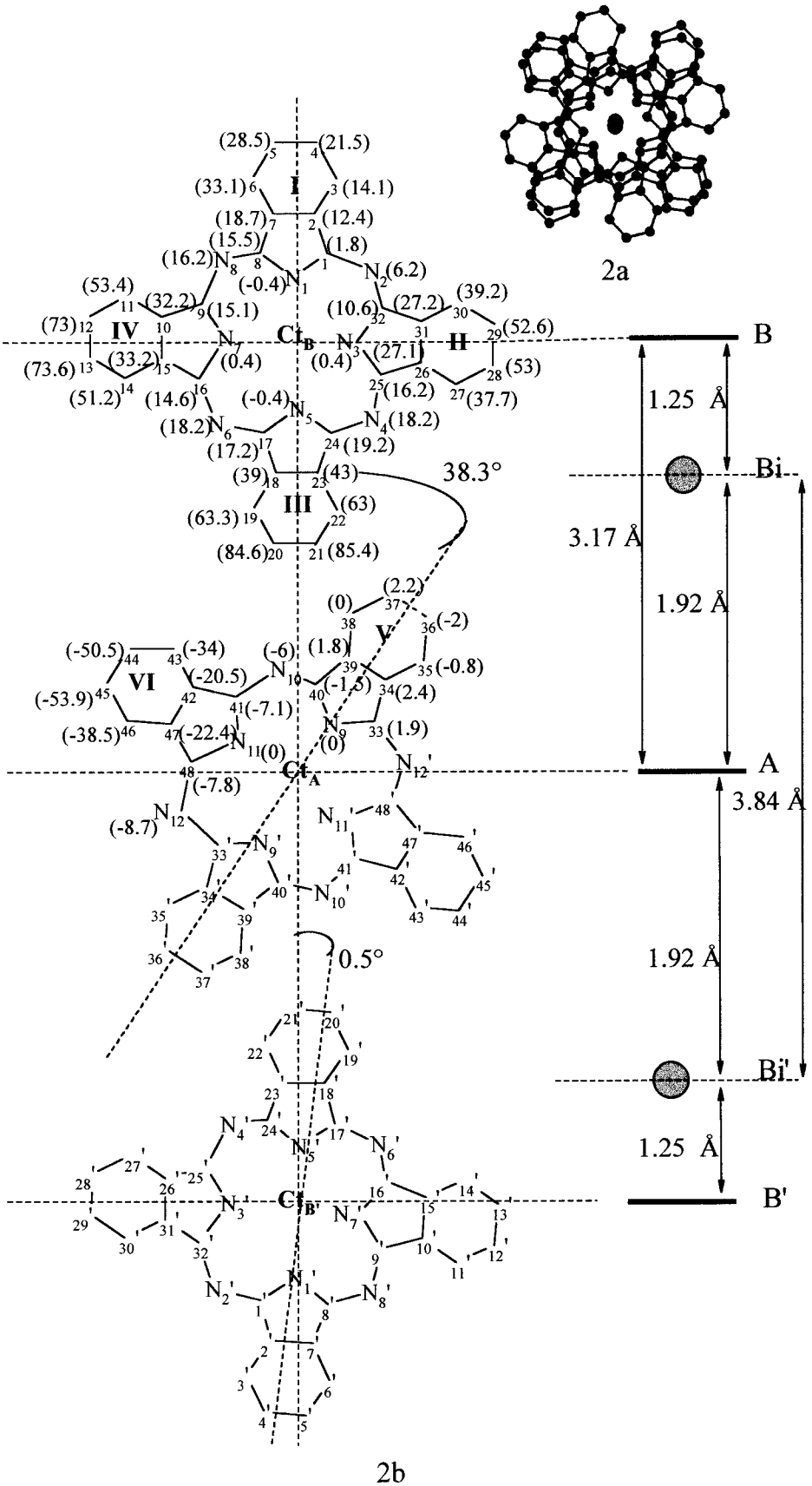


Figure 2. 2a) ORTEP drawing of $Bi_2(Pc)_3$ viewed along the Bi−Bi′ axis. − 2b) Split molecule of $Bi_2(Pc)_3$ with the three phthalocyanine rings projected along the Bi−Bi′ axis showing the numbering scheme and the staggering angles between the macrocycles. The deviation of each atom from the $4N_{iso\ A}$ and $4N_{iso\ B}$ mean-planes, respectively, are indicated in parentheses for the asymmetric unit

Table 1. Selected bond lengths (Å) and angles (deg) for $Bi_2(Pc)_3$

Bond lengths (Å)		Angles (deg)			
Bi−N1	2.339(10)	N1−Bi−N3	72.8(4)	N3−Bi−N11	149.4(3)
Bi−N3	2.348(9)	N1−Bi−N5	115.7(3)	N5−Bi−N7	74.5(4)
Bi−N5	2.330(9)	N1−Bi−N7	73.6(4)	N5−Bi−N9	147.7(3)
Bi−N7	2.326(11)	N1−Bi−N9	85.0(3)	N5−Bi−N11	137.7(3)
Bi−N9	2.740(10)	N1−Bi−N11	90.1(3)	N7−Bi−N9	137.4(3)
Bi−N11	2.695(8)	N3−Bi−N5	72.8(4)	N7−Bi−N11	82.3(3)
Bi−N9′	2.693(11)	N3−Bi−N7	115.3(4)	N9−Bi−N11	60.8(3)
Bi−N11′	2.774(10)	Bi−N9−Bi′	89.9(3)	Bi−N11−Bi′	89.1(4)
Bi−Bi′	3.838(9)	N3−Bi−N9	91.9(3)		
Bi−Bi	8.036(9)				

Table 2. Dihedral angles (deg) between $4N_{iso}$ mean-planes and pyrrolic cycles, and between pyrrole and benzene rings labelled 5 and 6, respectively

Mean-planes			Angles (deg)	
A	B	C	A−B	B−C
$4N_{isoB}$	I_5	I_6	6.26	1.75
$4N_{isoB}$	II_5	II_6	6.67	1.24
$4N_{isoB}$	III_5	III_6	10.46	0.53
$4N_{isoB}$	IV_5	IV_6	8.12	1.77
$4N_{isoA}$	V_5	V_6	0.92	1.52
$4N_{isoA}$	VI_5	VI_6	5.54	2.08

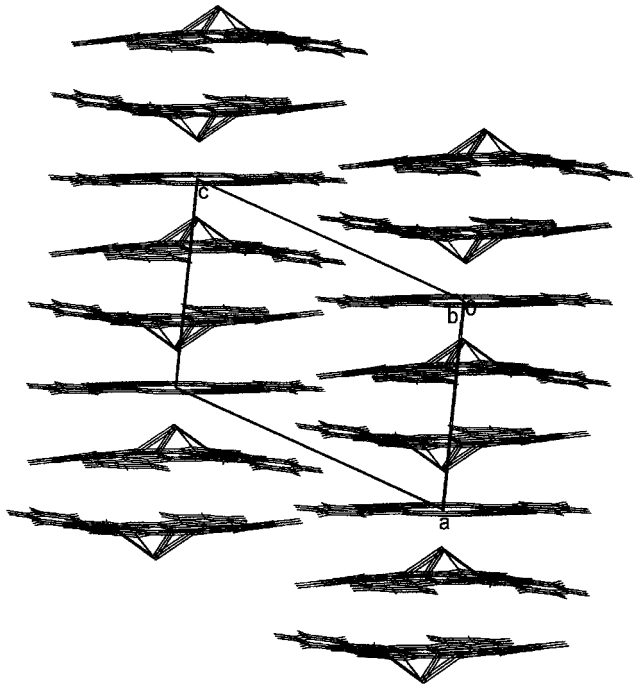


Figure 3. Projection along the *b* axis showing the columnar structure of the stacking of $Bi_2(Pc)_3$ molecules

(Table 2). Nevertheless, each benzopyrrole is nearly planar: all the angles between the pyrrole and benzene mean-planes are smaller than 1.8°. The most planar benzopyrrole (III) shows the greatest deviation from the mean-plane $4N_{iso\ B}$, and has the furthest external carbon atoms (C30 and C31) from the $4N_{iso\ B}$ mean-plane. Cycle A is nearly perfectly planar, but the benzopyrroles V and V′ are more coplanar than cycles VI and VI′, which spread slightly up and down from the $4N_{iso\ A}$ plane. The two mean-planes of the pyrrole rings make dihedral angles of 0.92 and 5.54° (±3.02) (V and VI). Dihedral angles between the pyrrole and benzene mean-planes are 1.52 (V) and 2.08° (VI).

Figure 3 shows the relative position of successive molecules in the stacking, viewed along the b axis. The stacking axis is the a axis. The closest atoms of two successive molecules in the stack lie at the distance of 3.284 Å (C4−C16). That distance is also lower than the van der Waals distance for aromatic carbon atoms. Adjacent external macrocycles of two neighbouring molecules in the stacking are also interacting by their π orbitals, so that all the phthalocyanine macrocycles are in interaction. The closest atoms in two neighbouring stacks, in the direction of the c axis, are C44 and C21, and lie at the distance of 3.497 Å apart. We have a columnar structure, in which $Bi_2(Pc)_3$ molecules are stacked segregatively, with the π orbitals of all the macrocycles interacting with each other along the column. Such a structure favours a good electrical conductivity, but since $Bi_2(Pc)_3$ is a closed-shell molecule, we think that this compound cannot be an electrical conductor without partial oxidation. Electrical properties of this triple-decker complex are currently being studied.

Similar to the comparisons made for lanthanoid phthalocyanines in the literature,[15,34,35] Table 3 compares our structure with those of double-decker compounds $Bi(Pc)_2,CH_2Cl_2$,[12] and $Bi(Pc)_2I_{1.5}$,[11] and with that of the bismuth monophthalocyanine-bismuth iodide complex.[10] The later contains a $BiPc^+$ moiety, and has the shortest distances for Bi−Ct (1.14 Å) and $Bi-N_{iso}$ (2.27 Å). In $Bi(Pc)_2,CH_2Cl_2$ the bismuth atom is nearly equidistant (1.48 and 1.50 Å) from the centres of the two $4N_{iso}$ mean-planes with a $Bi-N_{iso}$ length mean value of 2.47 Å, while in $Bi(Pc)_2I_{1.5}$, the Bi^{III} atom is not equidistant from the two Pc macrocycles (1.337 Å and 1.938 Å), and the structure shows alternating short and long $Bi-N_{iso}$ bond lengths (2.34 Å and 2.76 Å, respectively). The distance between the $4N_{iso}$ mean-planes that we observe for our triple-decker compound (3.17 Å) is intermediate between those of the two double-decker complexes $Bi(Pc)_2,CH_2Cl_2$ and $Bi(Pc)_2I_{1.5}$ (2.98 Å and 3.275 Å, respectively), in which the phthalocyanine macrocycles are oxidized. The benzopyrrole cycles of our complex have the same dimensions as those of the bisphthalocyanine, except the $N_{iso}-C_\alpha$ lengths that are longer in the triple-decker complex and the $C_\delta-C_\delta$ and $C_\beta-C_\beta$ bond lengths that are shorter.

It is very interesting to compare the structure of this black phase with the red-violet phase obtained by J. Janczak et al.[31] It is well-known that metallophthalocyanines crystallize in different phases depending of the crystallization method.[36] Generally, the molecular structure is only slightly affected but the stacking is different. In our case too, the molecular data of the two phases look very similar (Table 4), but there are some differences, principally in the stacking. The two molecules are alike with nearly the same coordination polyhedron, but the distances $Bi-N_{iso\ A}$ are slightly longer in the red-violet phase (2.747 Å) than in the black phase (2.726 Å). The staggering angle is equal to

Table 3. Comparison of the geometrical parameters for the black phase of $Bi_2(Pc)_3$ with those of other bismuth phthalocyanine complexes: the red-violet triple-decker phase,[31] the double-decker,[11−12] and monophthalocyanine[10] structures, reported in the literature

Compound Reference	$Bi_2(Pc)_3$ This work	$Bi_2(Pc)_3$ [31]	$Bi(Pc)_2,CH_2Cl_2$ [12]	$Bi(Pc)_2I_{1.5}$ [11]	$Bi(Pc)^+$ [10]
M−Ct_A (Å)	1.92	1.92	1.48	1.94	
M−Ct_B (Å)	1.25	1.25	1.5	1.34	1.14
M−$N_{iso\ A}$(Å)	2.72*[a]	2.75*[a]		2.76*[a]	
M−$N_{iso\ B}$(Å)	2.34*[a]	2.33*[a]	2.47*[a]	2.38*[a]	2.27*[a]
Rotation angle (deg)					
A−B	38.3	36.4	45	39.4	
B−B′	0.5	0	−	−	
Distance between planes (Å)	3.17	3.10	2.98	3.27	
Distance N−C (Å)					
$N_{iso\ A}-C_{\alpha A}$[b]	1.40*[a]				
$N_{iso\ B}-C_{\alpha B}$	1.40*[a]	1.39*[a]	1.36*[a]		1.38*[a]
$N_{aza\ A}-C_{\alpha A}$	1.34*[a]				
$N_{aza\ B}-C_{\alpha B}$	1.33*[a]	1.32	1.33*[a]		1.32*[a]
Distance C−C (Å)					
$C_\alpha-C_\beta$[c]	1.46*[a]		1.46*[a]		
$C_\beta-C_\gamma$[d]	1.38*[a]		1.38*[a]		
$C_\gamma-C_\delta$[e]	1.38*[a]	1.38*[a]	1.38*[a]		1.39*[a]
$C_\delta-C_\delta$	1.37*[a]		1.39*[a]		
$C_\beta-C_\beta$	1.37*[a]		1.38*[a]		

[a] Distances with asterisk (*) are mean distances. − [b] C_α = C1, C8, C9, C16, C17, C24, C25, C32, C33, C40, C41 and C48. − [c] C_β = C2, C7, C10, C15, C18, C23, C26, C31, C34, C39, C42 and C47. − [d] C_γ = C3, C6, C11, C14, C19, C22, C27, C30, C35, C38, C43 and C46. − [e] C_δ = C4, C5, C12, C13, C20, C21, C28, C29, C36, C37, C44 and C45.

Table 4. Crystallographic data for $Bi_2(Pc)_3$. Black and red-violet phases are compared

	Black phase (this work)	Red-violet phase[31]
Formula	$Bi_2C_{96}H_{48}N_{24}$	$(C_{32}H_{16}N_8)Bi_2$
Cryst. size, mm	0.03 × 0.04 × 0.08	0.14 × 0.12 × 0.07
Colour	black	red-violet
Cryst. syst.	triclinic	triclinic
Mol. wt	1955.6	1955.54
Space group	$P\bar{1}$	$P\bar{1}$
a, Å	11.2179(5)	11.217(2)
b, Å	13.6180(6)	13.616(3)
c, Å	14.8834(8)	14.931(3)
α, deg	107.756(5)	107.7(3)
β, deg	99.725(5)	100.14(3)
γ, deg	112.932(4)	112.82(3)
V, Å^3	1883.8	1887.4(7)
Z	1	1
d_{calcd}	1.724	1.721
Diffractometer	STOE IPDS	
Radiation	(graphite monochromator) Mo-K_α, 0.71073 Å	
μ mm^{-1}	4.53	4.726
Scan mode	φ scan	
Scan step, deg	0.5	
Scan time, min/deg	12	
Scan total, deg	180	
2θ limits, deg	2.9 ≤ 2θ ≤ 48.4	2 ≤ 2θ ≤ 52.2
No. of data measured	6255	11996
No. of refined parameters	550	
Unique reflections	3572	6499
R_{int}(SHELXL-93):	0.0747	
Unique data with[$F_0 > 4\sigma(F_0)$]	2026	
R_1	0.0398	0.0611
wR_2	0.0617	0.0720
Goodness-of-fit	0.619	1.005

36.4° in the red-violet phase and 38.3° in the other. The major difference between the two phases is found, as we have said, in the stacking. The red-violet phase is constituted of molecules stacked back to back along the stacking axis without interaction between the π orbitals of adjacent molecules, with the shortest intermolecular distances between the overlapping phthalocyaninato ring planes being 3.56 Å. Such an alternating of short and long distances be-

tween the phthalocyanines rings along the stack does not favour good electrical conductivity. In the black phase, the shortest interatomic distances between two adjacent molecules is 3.284 Å, while there are many interatomic distances between two adjacent (Pc) rings in the same molecule shorter than 3.3 Å. So the black phase appears as a regular stack of phthalocyanines rings which have their π systems in interaction with each other, and that structure favours good conductivity.

Infrared Spectroscopy

Literature on the vibrational spectroscopy of triple-decker Pc complexes is poor. The site of one-electron oxidation in several lanthanide porphyrin-phthalocyanine triple-decker complexes was studied by resonance Raman spectroscopy[22] and some mixed phthalocyaninato-porphyrinato europium(III) triple-decker complexes were characterized by IR and Raman spectroscopies.[25] Previous studies[37–44] on monophthalocyanines have separated and assigned the frequencies of the vibrations (strongly coupled in the macrocyclic ligand). Janczak recently reported IR and far IR spectra of $In_2(Pc)_3$ compared with those of $In(Pc)_2$. [37] Figures 4 and 5 show the far and middle infrared spectra, respectively, of our complex (a), compared with the well-known spectra (b)[1,40] of lead monophthalocyanine Pb(Pc). Isago et al.[8] reported that spectra of Bi(Pc)X (X = Cl, Br) in the middle IR region, resemble those of Pb(Pc). In both spectra of $Bi_2(Pc)_3$, (middle and far infrared) we observe the same absorptions at nearly the same frequencies as in the Pb(Pc) spectra. We attribute these absorptions to the vibrations of the two parts of $Bi_2(Pc)_3$ constituted by one bismuth ion and one macrocycle B or B′, which have the same structure as Pb(Pc). We note some supplementary absorptions in each group of vibrations that we attribute to the vibrations of the moiety formed by the two bismuth atoms and the macrocycle A.

Analysis of the Far Infrared Spectra

Far and middle IR spectra of $In_2(Pc)_3$ were reported recently.[37] The far IR spectrum is slightly more complicated than that of $Bi_2(Pc)_3$, while the middle IR spectra are very similar. Due to the fact that Bi atom is heavier than In, many bands are shifted to lower frequencies for the $Bi_2(Pc)_3$ spectrum. Five bands or groups of bands are characteristic of phthalocyanine ring deformations. They lie around 625, 560–600, 490, 430–440, and 350 cm^{-1}, nearly at the same frequencies for Pb(Pc) and $Bi_2(Pc)_3$. A more thorough examination of the spectra shows that the bands for $Bi_2(Pc)_3$ are larger and less resolved than the corresponding ones in Pb(Pc). Expansions of some of these bands followed by a deconvolution are shown on Figure 5,(I) and Figure 5,(II). The group centred at 625 cm^{-1} contains only one band at 626 cm^{-1} with a shoulder at 617 cm^{-1} in the spectrum of Pb(Pc), and three bands at 626, 617, and 622 cm^{-1} in the spectrum of $Bi_2(Pc)_3$ [Figure 5,(II)]. We assigned the two first bands to the deformation of the phthalocyanine rings B and B′, and the absorption at 622 cm^{-1} to the deformation of ring A. In Figure 4, the two bands at 279 and 154 cm^{-1} for $Bi_2(Pc)_3$ have the same intensity ratio and the same wavenumber difference as the two bands at 271 and 147 cm^{-1} for Pb(Pc). We assign these two bands, respectively, to the symmetric and asymmetric stretching modes of $N_{iso}-Bi-N_{iso}$ for B and B′ rings, and to the symmetric and asymmetric stretching modes of $N_{iso}-Pb-N_{iso}$, by reference to previous work.[44,47] We equally note two supplementary bands at 223 and 94 cm^{-1} in the spectrum of

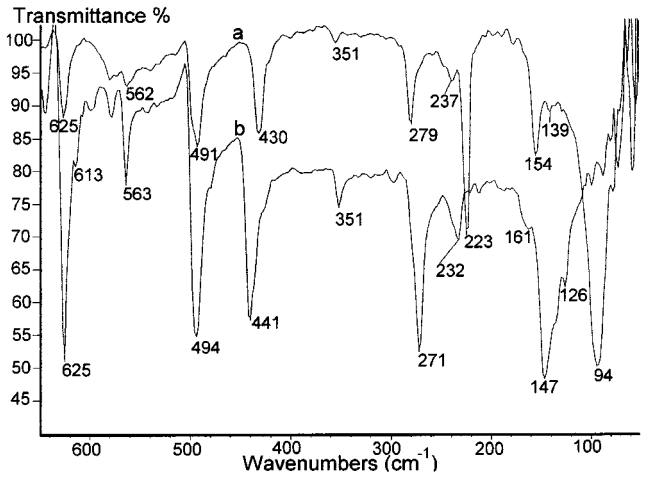


Figure 4. Far infrared spectrum of $Bi_2(Pc)_3$ (a) compared to that of Pb(Pc) (b)

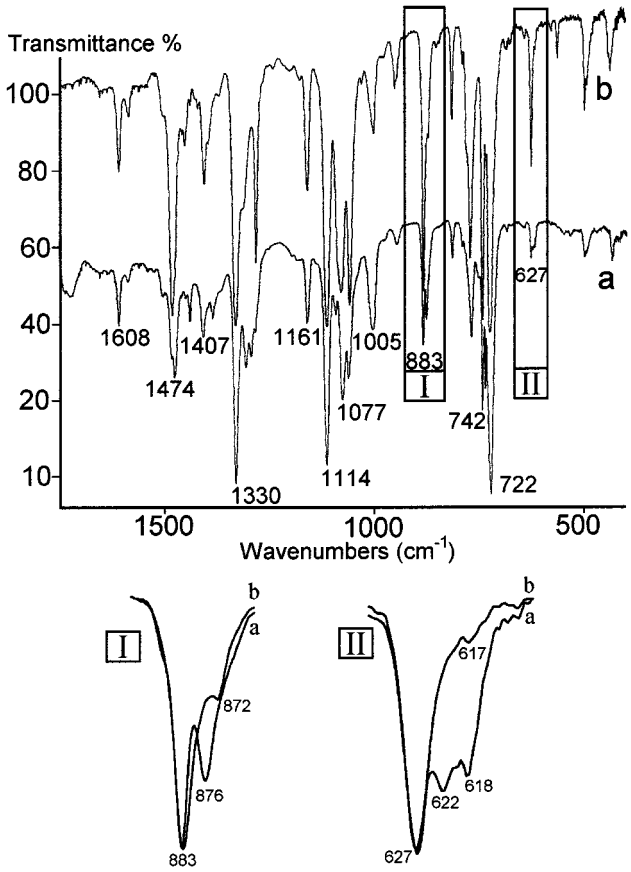


Figure 5. Middle infrared spectrum of $Bi_2(Pc)_3$ (a) compared to that of Pb(Pc) (b). I and II are expansions of the group of bands centred at 625 cm^{-1} and 883 cm^{-1}, respectively

$Bi_2(Pc)_3$. We assign these two new bands to the symmetric and asymmetric stretching modes of $N_{iso}-Bi-N_{iso}$ of macrocycle A. Their frequencies are lower than those of the same modes in the B macrocycle. This is in accordance with the bond lengths difference: 2.34 Å for the $Bi-N_{iso}$ distance of macrocycle B and B′, and 2.72 Å for the $Bi-N_{iso}$ distance of macrocycle A.

Analysis of Spectra in the Middle Infrared

The band, which lies at 883 cm^{-1} in both the spectra of Pb(Pc) and $Bi_2(Pc)_3$, is described in the literature as a metal-dependant vibration of the macrocycle.[39] This band, extended in Figure 5,(I), presents a new band at 876 cm^{-1} in the $Bi_2(Pc)_3$ spectrum, at the low wavenumbers side beyond a shoulder at 872 cm^{-1} which is evident in both spectra. We still consider this new band as a metal-dependant vibration of macrocycle A. Other supplementary bands assigned to macrocycle A are visible at 1294, 1306, and 1474 cm^{-1} in the area of the C−C stretching modes. A small band at 1385 cm^{-1} becomes very intense when the sample is allowed to age in dark at 4−10 °C for several months. The initial IR spectrum is restored when the aged sample is placed under reflux in an aqueous solution of 0.2 M NaOH.

In conclusion of this paragraph, we consider that the new bands assigned to macrocycle A, and particularly the bands related to the $Bi-N_{iso}$ vibrations, are a typical fingerprint of homoleptic triple-decker phthalocyanine complexes.

UV/Visible Spectroscopy

UV/Visible spectroscopy was largely used for the study and the characterization of rare earth triple-decker phthalocyanines. The spectra of $M_2(Pc)_3$ (M = Ln, In) are characterized by the presence of a large absorption band around 640 nm, with a shoulder or a little band more or less separated at larger wavelengths.[19,21,2,37] These two bands (Q_2 and Q_1, respectively) are due to an intramolecular π-π* interaction among the ligands, and are dependant on the distance between cycles in the triple-decker complex.[26,29] Theoretical studies[20,27] on $Lu_2(Pc)_3$ were compared with the experimental spectrum of (Pc)Lu(CRPc)Lu(Pc), which shows two major bands at 633 (Q_2) and 716 (Q_1) nm. The most intense band (633 nm) was assigned to an exciton coupling state, in which all the transitions moments in the Pc planes are in the same direction, the second (716 nm) was attributable mainly to a charge resonance state between two outer Pc′s. Two shoulder bands were observed at 580 and 550 nm. The former was assigned to a vibronic band associated with the 633 nm intense band, and the later attributed to another electronic excitation. In the B band region a broad band was observed at 330 nm.

We recorded the UV/Visible spectrum of $Bi_2(Pc)_3$ in pyridine (Figure 6, a), DMF (b), and DMSO (c). At the same concentration, spectra in pyridine and DMSO are similar. In DMF the spectrum is identical with that recorded in pyridine, but there is an hypsochromic shift of 43 nm ±3 for all the bands observable in the studied wavelength field. DMSO and pyridine are both molecules which are known

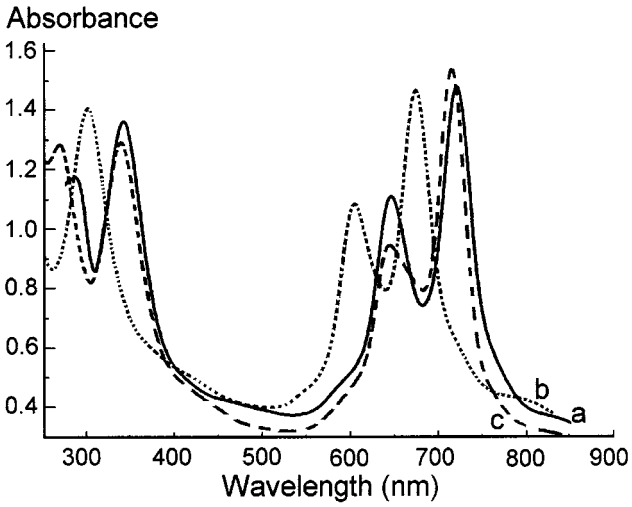


Figure 6. UV/Visible spectra of $Bi_2(Pc)_3$ in pyridine (a), DMF (b), and DMSO (c)

to coordinate strongly in apical position the metal of the monophthalocyanines. DMF has the same behaviour, but is a weaker ligand. In all our spectra, the Q band exhibits splitting in Q_1 and Q_2 bands. In pyridine Q_1 lies at 718 nm and Q_2 at 644 nm. In disagreement with the observations reported about the spectra of $Ln_2(Pc)_3$ and that of $In_2(Pc)_3$,[37] the most intense band is Q_1 at 718 nm, while Q_2 at 644 nm is smaller. Another remark refers to the value of the Q band splitting, which is reported to decrease as the interplanar distance increases.[20,28] For (Pc)Lu(CRPc)Lu(Pc) this splitting value is 83 nm with a interplanar distance fixed at 2.9 Å. As our interplanar distance is measured by the crystallographic study (3.17 Å), we expected a splitting value significantly smaller than 83 nm. The difference in the position of Q_1 and Q_2 bands is 74 nm. Nevertheless, K. Takahashi et al.[29] reported that as the interplanar distance lengthens, the intensity of Q_1 decreases, and that of Q_2 increases. One important difference with these results is the inversion of the intensities of the Q_1 and Q_2 bands. The B band region is more complicated and varies with the solvent. Some authors[48,49] have described, in addition to the B band, two other bands at lower wavelengths, the N band resulting mainly from a transition $b_{2u}(\pi) \rightarrow e_g(\pi^*)$, and the L band resulting from a combination of $a_{2u}(\pi) \rightarrow e_g(\pi^*)$ and $b_{2u}(\pi) \rightarrow e_g(\pi^*)$ transitions. In pyridine, the B and N bands are visible at 342 nm and 288 nm, respectively. In DMSO, the B band also lies at 342 nm, while the N band shifts to 272 nm, and the L band appears at 235 nm.

Conclusion

We have prepared a black phase of the tris(phthalocyaninato)dibismuth(III), $Bi_2(Pc)_3$, by a direct and fast template synthesis from bismuth acetate and phthalodinitrile. X-ray crystal analysis shows a triple-decker structure with two bismuth cations sandwiched between three phthalocyaninato ligands, the central macrocycle being rigorously planar, and the two external macrocycles convex. These latter are al-

most superimposable, while the central ligand is rotated by about 38.3° in relation to the peripheral Pc rings. The four Bi−N bond lengths involving isoindole nitrogens of the external phthalocyanines (mean: 2.34 Å) are shorter than those involving isoindole nitrogens of the central plane (mean: 2.72 Å). The distance between $4N_{iso}$ mean-planes in the molecule is 3.17 Å, and the shortest distance between two atoms belonging to two neighbouring molecules is 3.28 Å. This structure is closely related to that described by J. Janczak and R. Kubiak for a red-violet phase of $Bi_2(Pc)_3$, but the stacking is more compact and more regular in the black phase. The infrared spectra of $Bi_2(Pc)_3$ compared with that of Pb(Pc) allowed us to distinguish some deformations typical of the internal macrocycle from those of the peripheral ones. Particularly, the symmetric and asymmetric stretching modes of the $N_{iso}-Bi-N_{iso}$ groups related to the isoindole nitrogens of the central ring are identified, and differentiated from the similar groups belonging to the external rings. That differentiation is proposed as a typical fingerprint of homoleptic triple-decker phthalocyanine complexes having a similar structure. The UV/Visible spectrum of $Bi_2(Pc)_3$ is similar to all those published for $Ln_2(Pc)_3$ compounds, with the Q band split into two bands, Q_1 and Q_2. Nevertheless, we observe an inversion of the intensities of these bands, Q_1 being significantly more intense than Q_2. The presentation of these results which associates a complete crystallographic structure and the UV/Visible spectrum may be the first step for a theoretical study of the excited electronic states of $Bi_2(Pc)_3$.

Experimental Section

General Remarks: The FT-IR spectra were recorded on either a Nicolet 20 SXB spectrometer with 2 cm^{-1} resolution, or a Perkin−Elmer spectrum 1000 with 1 cm^{-1} resolution, using KBr pellets (1%) on 4000−400 cm^{-1} range and polyethylene pellets (10%) on 400−80 cm^{-1} range. UV/Visible Spectra were recorded on an Unicam UV 4 spectrometer using 10^{-4} M solution concentrations.

Synthesis and Purification: Bismuth acetate was prepared in the laboratory from bismuth nitrate·$5H_2O$ (R.P. Prolabo) using the classic method of preparation of metallic acetates,[50] by dissolving metals or metallic salts in a minimum quantity of hot concentrated nitric acid and subsequent addition of acetic anhydride (puriss. p.a. Fluka AG). Bismuth acetate (1.9 g, 5 mmol) and phthalonitrile (6.5 g, 50 mmol, puriss 99% Fluka chemica) were ground, and placed in a long glass tube, one end of which was sealed and welded with a glass rod. This reaction vessel was placed in a tubular oven at 240 °C and the extremity of the glass rod, which is out of the oven, is fixed in a chuck of a stirring shaft. The reaction mixture was rapidly heated to 310 °C during 30 min. When the reaction tube was taken out of the oven immediately after the end of the reaction and then kept at room temperature, the crude product contained many crystals. The obtained powder was washed with organic solvents in the following sequence: acetone, ethanol, benzene, acetone, dimethylformamide, chloronaphthalene, then quinoline, benzene and finally washed with ethanol and dried. The product was poured in an aqueous solution of NaOH 0.2 M and placed under reflux for 30 min. The solution was filtered and rinsed with hot distilled water until complete neutralisation of the filtrate. After washing with ethanol the product was dried at 60 °C (yield ca. 63%). This washing procedure produced a shiny black crystalline powder. Very little crystals were selected and manipulated under binocular lens at the magnifying power ×64.

Chemical Analysis: The demetallation of $Bi_2(Pc)_3$, by contact with acidic solutions was used for a chemical analysis giving the number of phthalocyanine macrocycles for one bismuth. $Bi_2(Pc)_3$ (833 mg, 0.426 mmol) was heated under reflux in 20 mL of a 35% HCl solution for two hours. The hydrolysis produced insoluble $H_2(Pc)$ and a soluble salt of bismuth (chloride or oxychlorides). Filtration, repeated washing procedures, and drying led to 665 mg (1.29 mmol) of $H_2(Pc)$ characterized by IR spectroscopy. An identical hydrolysis procedure was performed from 755.8 mg (0.38 mmol) of $Bi_2(Pc)_3$. The filtrate and the washing solutions together were made up to 500 mL with the addition of distilled water. The content of bismuth of the resulting solution, determined by AAS led to 0.76 mmol of elemental bismuth. Then we obtained 3 mol of $H_2(Pc)$ and 2 mol of bismuth for each mol of starting $Bi_2(Pc)_3$. That confirmed the high purity of our product.

X-ray Crystallographic Study:[51] One of the largest crystals (0.03×0.04×0.08 mm) obtained from the crude product after washing was picked out and stuck on a glass needle. Data collection and analysis were performed using STOE IPDS V2.78 Software on a STOE IPDS diffractometer. The crystal is a weak scatterer because of its size. By inspecting the reciprocal space with RECIPE program, reflections from three crystal domains could be detected. Reflections of all domains were integrated simultaneously with TWIN, which showed that the volume ratio of the domains was 16:11:1. All crystal systems shared a nearly common c^* axis in the reciprocal space. For the structure solution, the intensity data set of the biggest domain was employed. The structure was refined with isotropic-, then anisotropic temperature factors by full-matrix least-squares techniques using the SHELXL 97 program. The hydrogen atoms of the phenyl groups were located with geometrical correlation, and their thermal parameters were fixed. The final unweighted and weighted agreement factors converged to $R_1 = 0.0398$ and $wR_2 = 0.0617$; a goodness-of-fit calculation resulted in a value of 0.619. The drawing preparations were made by using the graphic program of the SHELXTL package. Crystal data details are given in Table 4.

[1] A. Ahmad, R. A. Collins, *J. Phys. D: Appl. Phys.* **1991**, *24*, 1894−1897.
[2] K. Kumazawa, M. Yamanaka, *Jpn. J. Appl. Phys.* **1991**, *30*, 530−531.
[3] H. Tada, K. Saiki, A. Koma, *Surf. Sc.* **1992**, *268*, 387−396.
[4] L. Ottaviano, L. Lozzi, S. Santucci, S. Di Nardo, M. Passacantando, *Surf. Sc.* **1997**, *392*, 52−61.
[5] N. Papageorgiou, J. C. Mossoyan, M. Mossoyan-Déneux, G. Terzian, E. Janin, M. Göthelid, L. Giovanelli, J. M. Layet, G. Le Lay, *Applied Surf. Science* to be published.
[6] A. W. Snow, N. L. Jarvis, *J. Am. Chem. Soc.* **1984**, *106*, 4706−4711.
[7] R. B. Freas, J. E. Campana, *Inorg. Chem.* **1984**, *23*, 4654−4658.
[8] H. Isago, Y. Kagaya, *Bull. Chem. Soc. Jpn.* **1994**, *67*, 383−389.
[9] H. Isago, Y. Kagaya, *Bull. Chem. Soc. Jpn.* **1994**, *67*, 3212−3215.
[10] R. Kubiak, K. Ejsmont, *J. Mol. Struct.* **1999**, *474*, 275−281.
[11] J. Janczak, R. Kubiak, F. Hahn, *Inorg. Chim. Acta.* **1998**, *281*, 195−200.
[12] G. Ostendorp, H. Homborg, *Z. Anorg. Allg. Chem.* **1996**, *662*, 873−880.
[13] R. D. Shannon, *Acta Crystallogr., Sect. A* **1976**, *32*, 751−767.

[14] R. D. Rogers, A. H. Bond, S. Aguinaga, *J. Am. Chem. Soc.* **1992**, *114*, 2960−2967.
[15] A. De Cian, M. Moussavi, J. Fischer, R. Weiss, *Inorg. Chem.* **1985**, *24*, 3162−3167.
[16] P. N. Moskalev, I. S. Kirin, *Russ. J. Phys. Chem.* **1972**, *46*, 1019−1022.
[17] G. C. S. Collins, D. J. Schiffrin; *J. Electroanal. Chem.* **1982**, *139*, 335−369.
[18] M. Mossoyan-Déneux, D. Benlian, A. Baldy, M. Pierrot, *Mol. Cryst. Liq. Cryst. Inc. Nonlin. Opt.* **1988**, *156*, 247−256.
[19] M. M′Sadak, J. Roncali, F. Garnier, *J. Chim. Phys.* **1986**, *83*, 211−216.
[20] N. Ishikawa, Y. Kaizu, *J. Phys. Chem.* **1996**, *100*, 8722−8730.
[21] M. M′Sadak, J. Roncali, F. Garnier, *J. Electroanal. Chem.* **1985**, *189*, 99−111.
[22] T-H. Tran-Thi, T. A. Mattioli, D. Chabach, A. De Cian, R. Weiss, *J. Phys. Chem.* **1994**, *98*, 8279−8288.
[23] D. Chabach, A. De Cian, J. Fischer, R. Weiss, M. El Malouli Bibout, *Angew. Chem. Int. Ed. Engl.* **1996**, *35*, 898−899.
[24] J. Jiang, R. L. C. Lau, T. W. D. Chan, T. C. W. Mak, D. K. P. Ng, *Inorg. Chim. Acta.* **1997**, *255*, 59−64.
[25] D. P. Arnold, J. Jiang, *Chem. Lett.* **1999**, *6*, 483−484.
[26] K. Kasuga, M Ando, H. Morimoto, M. Isa, *Chem. Lett.* **1986**, 1095−1098.
[27] N. Ishikawa, Y. Kaizu, *Chem. Phys. Lett.* **1994**, *228*, 625−632.
[28] K. Takahashi, Y. Tomita, Y. Hada, K. Tsubota, M. Handa, K. Kasuga, K. Sogabe, T. Tokii, *Chem. Lett.* **1992**, 759−762.
[29] K. Takahashi, J. Shimoda, M. Itoh, Y. Fuchita, H. Okawa, *Chem. Lett.* **1998**, 173−174.
[30] J. Janczak, R. Kubiak, *J. Chem. Soc., Dalton Trans.* **1993**, 3809−3812.
[31] J. Janczak, R. Kubiak, *Polyhedron* **1999**, *18*, 2775−2780.
[32] R. Kubiak, J. Janczak, *J. Alloys Compd.* **1993**, *200*, L7−L8
[33] D. Chabach, M. Lachkar, A. De Cian, J. Fischer, R. Weiss, *New J. Chem.* **1992**, *16*, 431−433.
[34] J. W. Buchler, A. De Cian, J. Fischer, M. Kihn-Botulinski, H. Paulus, R. Weiss, *J. Am. Chem. Soc.* **1986**, *108*, 3652−3659.
[35] M. Moussavi, A. De Cian, J. Fisher, R. Weiss, *Inorg. Chem.* **1986**, *25*, 2107−2108.
[36] F. Iwatsu, T. Kobayashi, N. Uyeda, *J. Phys. Chem.* **1980**, *84*, 3223−3230.
[37] J. Janczak, *Pol. J. Chem.* **1998**, *72(8)*, 1871−1878
[38] A. N. Sidorov, I. P. Kotlyar, *Opt. Spectr.* **1961**, *11*, 92−96.
[39] H. F. Shurvell, L. Pinzuti, *Can. J. Chem.* **1966**, *44*, 125−136.
[40] T. Kobayashi, F. Kurokawa, N. Uyeda, E. Suito, *Spectrochim. Acta* **1970**, *26A*, 1305−1311.
[41] T. Kobayashi, F. Kurokawa, N. Uyeda, E. Suito, *Spectrochim. Acta* **1970**, *26A*, 1313−1322.
[42] F. Cariati, F. Morazzoni, M. Zocchi, *J. Chem. Soc., Dalton Trans.* **1978**, 1018−1024.
[43] F. Morazzoni, F. Cariati, G. Micera, *Spectrochim. Acta* **1980**, *36A*, 867−870.
[44] W. Kalz, H. Homborg; *Z. Naturforsch* **1983**, *38b*, 470−484.
[45] H. Homborg, W. Kalz; *Z. Naturforsch* **1984**, *39b*, 1490−1499.
[46] G. Terzian, B. Moubaraki, M. Mossoyan-Déneux, D. Benlian, *Spectrochim. Acta* **1989**, *45*,675−677.
[47] W.J. Kroenke, M. E. Kenney, *Inorg. Chem.* **1964**, *3*, 696−698.
[48] M .S. Haghighi, H. Homborg, *Z. Anorg. Allg. Chem.* **1994**, *620*, 1278−1284.
[49] A. Henrikson, B. Roos, M. Sundbom, *Theoret. Chim. Acta (Berl.)* **1972**, *27*, 303−313.
[50] H. Shirai, H. Tsuiki, E. Masuda, T. Koyama, K. Hanabusa, N. Kobayashi, *J. Phys. Chem.* **1991**, *95*, 417−423.
[51] T. A. Stephenson, S. M. Morehouse, A. R. Powell, J. P. Heffer, G. Wilkinson, *J. Chem. Soc.* **1965**, *6*, 3632−3640.
[52] Crystallographic data for the structure reported in this paper have been deposited with the Cambridge Crystallographic Data Center as supplementary publication no. CCDC-117152. Copies of the data can be obtained free of charge on application to CCDC, 12 Union Road, Cambridge CB2 1EZ, U.K. [Fax: (internat.) +44-1223-336033; E-mail: deposit@ccdc.cam.ac.uk]

Received October 26, 1999
[I99378]

Structure and Magnetic Properties of Tetrakis(3,4,5-trimethoxyphenyl)porphinatomanganese(III) 2,3,5,6-Tetrafluoro-7,7,8,8-tetracyanoquinodimethenide: The First Example of an Isolated $[TCNQF_4]^{\bullet -}$

Mitchell T. Johnson,[a] Atta M. Arif,[a] and Joel S. Miller*[a]

Keywords: Cyanocarbon / Magnetic ordering / Crystal structure / Fluorocarbon / Electron transfer salts / Organic magnets

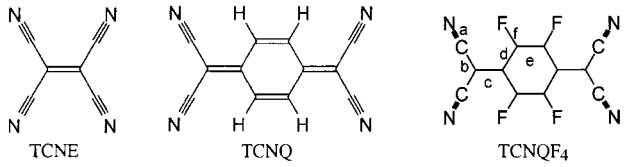
The crystal structure of *meso*-tetrakis(3,4,5-trimethoxyphenyl)porphinatomanganese(III) 2,3,5,6-tetrafluoro-7,7,8,8-tetracyanoquinodimethenide, $[MnT(MeO)_3PP][TCNQF_4]\cdot 3$-($o$-$C_6H_4Cl_2$), $\mathbf{1}\cdot 3C_6H_4Cl_2$, provides the first example of a non-dimeric $[TCNQF_4]^-$ that is stabilized by *trans*-μ-coordination to Mn^{III}. Compound $\mathbf{1}\cdot 3C_6H_4Cl_2$ crystallizes in the monoclinic $C2/c$ space group [a = 16.9486(10) Å, b = 25.7170(14) Å, c = 19.4009(12) Å, β = 107.091(4)°, V = 8082.8(8) Å^3, T = 200 K, Z = 4, $R(F_o)$ = 0.0547]. The $[TCNQF_4]^-$ formulation was confirmed from the crystal structure data, as well as the ν_{CN} absorption at 2196 and 2165 cm^{-1} in the IR spectrum. The $[TCNQF_4]^-$ moiety is planar with a methylene-carbon–ring-carbon distance of 1.41 Å, which is 0.038 Å longer than that for $TCNQF_4$. $\mathbf{1}\cdot 3C_6H_4Cl_2$ forms 1-D zigzag chains of alternating $\mathbf{1}^+$ and $[TCNQF_4]^-$, where the Mn^{III} atoms are bound in a *trans*-μ-fashion with Mn–N and intrachain Mn···Mn distances of 2.321(3) Å and 12.685 (4) Å, respectively. The MnNC angle and the dihedral angle between the $[TCNQF_4]^-$ and the mean MnN_4 planes are 135.9(2)° and 46.4°, respectively, with the phenyl rings rotated 80° with respect to the mean porphyrin plane. The magnetic susceptibility of $\mathbf{1}\cdot 2.3C_6H_4Cl_2$ can be calculated from the Curie–Weiss expression with θ = –37 K (T > 250 K) and θ′ = +29 K (75 < T < 200 K) with an observed minimum in $\chi T(T)$, typical of ferrimagnets, at 215 ± 10 K. At 2 T the magnetization is 14.900 emuOe/mol or 89% of 16.755 emuOe/mol expected for an S_{Tot} = 2 – 1/2 = 3/2 system. The intrachain antiferromagnetic coupling, J/k_B, is –71 K (–49 cm^{-1}; –61 meV) based on a fit to the Seiden expression for noninteracting chains comprised of alternating quantum (S = 1/2) and classical (S > 1/2) spins, and the Hamiltonian $H = -2JS_a\cdot S_b$. Compound $\mathbf{1}\cdot 2.3C_6H_4Cl_2$ ferrimagnetically orders at 7.3 K [based on the maxima in the 10 Hz χ′(T) data]. Hysteresis is observed at 2 K with coercive field, H_{cr}, of 17.1 kOe and remnant magnetization of 7.200 emuOe/mol; hysteresis is not observed at 5 K. This compound also displays metamagnetic behavior at 2 K above a critical field of 20.2 kOe. The frequency-dependent transitions observed in the χ′(T) and χ"(T) a.c. data are attributed to the transition to a spin glass or superparamagnetic state.

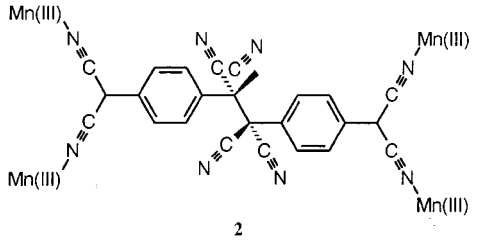
Introduction

Magnetically ordered molecular solids continue to attract attention worldwide, with a focus on new means of attaining a high degree of connectivity between spin-containing moieties.[1] Two classes of organic-based magnets exist; those with active and those with passive organic ligands. Passive organic ligands position the metal-ion-based spin sites to modulate the spin exchange, while active organic ligands contribute spins to the magnetic moment in addition to positioning the metal-ion-based spin sites.[1d,1e] In a few cases organic ferromagnets lacking metal ions have been prepared.[1g,1i] The magnetic ordering temperatures T_c can range up to 400 K for active-organic magnets containing metal-ion-based spins, but only up to 1.48 K for metal-ion-free systems.[1d,1e] Active ligands are rare and have been limited to strong electron acceptors, e.g. cyanocarbons [tetracyanoethylene (TCNE)],[1a–1e] chloranil,[2] and nitronyl nitroxides.[1f,1j,3] [Mn(porphyrin)][TCNE] (TCNE = tetracyanoethylene) form a family of organic-based ferrimagnets with magnetic ordering temperatures as high as 28 K.[1a,4] Several related ferrimagnets based on the antiferromagnetic coupling of S = 5/2 $Mn^{II}(hfac)_2$ (Hhfac = hexafluoroacetylacetone) and S = 1/2 nitroxides,[1f,1j] as well as S = 5/2 Mn^{II} and S = 1/2 Cu^{II} sites have been reported.[3] To date systematic approaches aimed at understanding and subsequently controlling the magnetic behavior of this class of 1-D coordination polymers has primarily focused on making the TCNE electron-transfer salts of substituted manganese(II) porphyrins.[1a,4,5] These ongoing studies have identified a correlation between a decrease of the $MnNC_{TCNE}$ angle and an increase in the intrachain magnetic coupling.[5a,6] This is attributed to increasing the magnetic coupling by increasing the σ overlap of the d_z2 and π* orbitals.[6] More recently, we have sought to alter the radical anionic bridging ligand from $[TCNE]^-$ to identify its effect on magnetic behavior. This had led to the observation that the chloranil radical anion can also stabilize magnetic ordering for this class of organic magnets.[2] Replacement of TCNE with TCNQ (TCNQ = 7,7,8,8-tetracyano-*p*-quinodimethane) is an obvious approach, but, to date, structurally characterized materials have been elusive.[7] An exception is the reaction of TCNQ with *meso*-tetrakis(2,4,6-trimethylphenyl)porphyrinatomanganese(II), which unexpectedly forms the diamagnetic μ_4-σ-$[TCNQ]_2^{2-}$ linkage, **2**.[8] In addition to TCNQ, we identified perfluoro-TCNQ, $TCNQF_4$, as a potential acceptor to stabilize magnetic ordering for this class of magnets.

[a] Department of Chemistry, 315 S. 1400 E. RM Dock, University of Utah,
Salt Lake City, UT 84112–0850, USA
Fax: (internat.) + 1-801/581-8433
E-mail: jsmiller@chemistry.utah.edu

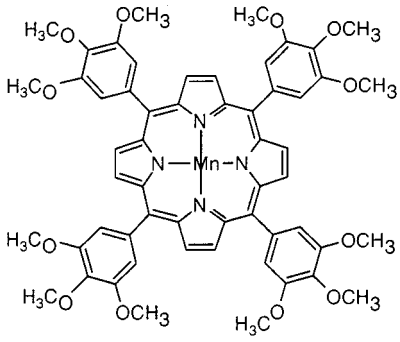
 © WILEY-VCH Verlag GmbH, D-69451 Weinheim, 2000 1434–1948/00/0808–1781 $ 17.50+.50/0





2

$TCNQF_4$[9] is a very strong acceptor[10] that was sought as a component in molecule-based conductors.[10b,11] Although easily reduced to form stable $[TCNQF_4]^-$ in solution, in contrast to $[TCNQ]^-$, these solids always possessed strong diamagnetic $[TCNQF_4]_2^{2-}$ dimers which did not support the formation of segregated 1-D conducting chains. Likewise, replacement of TCNE with $TCNQF_4$ to stabilize ferromagnetic ordering for the $[Fe^{III}(C_5Me_5)_2]^+[TCNE]^-$ ferromagnet, led to the formation of diamagnetic $[TCNQF_4]_2^{2-}$ dimers that did not stabilize magnetic ordering.[12] $[TCNQF_4]^-$ could form the diamagnetic μ_4-σ-$[TCNQF_4]_2^{2-}$ linkage analogous to **2**; hence the larger substituted manganese(II) porphyrin, *meso*-tetrakis(2,4,6-trimethoxyphenyl)-porphyrinatomanganese(II), $Mn^{II}T(MeO)_3PP$ **(1)**, and herein we report the synthesis, structure and bulk magnetic properties of $[Mn^{III}T(MeO)_3PP][TCNQF_4]\cdot xC_6H_4Cl_2$, $\mathbf{1}\cdot xC_6H_4Cl_2$.



$Mn^{II}T(MeO)_3PP$

Results and Discussion

The reaction of $TCNQF_4$ and $Mn^{II}T(MeO)_3PPpy$ in 1,2-$C_6H_4Cl_2$ forms $[Mn^{III}T(MeO)_3PP][TCNQF_4]\cdot 3C_6H_4Cl_2$, $\mathbf{1}\cdot 3C_6H_4Cl_2$. The ν_{CN} IR absorptions at 2196 (m) and 2165 (s) cm^{-1} are too low in energy for $TCNQF_4$ [i.e. 2225 cm^{-1}],[12,13] and too high in energy for $[TCNQF_4]^{2-}$ [i.e. 2168 (s) and 2133 (s) cm^{-1}].[12] These values are comparable to 2195 ± 1 (s) and 2177 ± 2 (s) characteristic of $[TCNQF_4]_2^{2-}$,[12,13] but the lower value is sufficiently different to suggest a different bonding mode for $[TCNQF_4]^-$.

The solvent content of the sample used for magnetic measurements was determined to be 2.3 solvent molecules per formula unit by TGA heating at a rate of 15 °C/min starting from 38 °C. Weight loss was observed immediately and all three solvent molecules were lost by 130 °C, after which decomposition was observed as a steady weight loss to 400 °C. The mass spectra showed the effluent of the TGA contains only solvent. Other solvents were also tried, but only *o*-$C_6H_4Cl_2$ gave an identical IR spectrum to the magnetic material.

X-ray Crystal Structure

$\mathbf{1}\cdot 3C_6H_4Cl_2$ (Figure 1) is composed of alternating chains of $[MnTPP]^+$ cations and $[TCNQF_4]^-$ anions. The three 1,2-dichlorobenzene solvent molecules fill the voids of the structure and are the only source of disorder. This disorder is observed in the 1,2-$C_6H_4Cl_2$ which occupies two positions that are related by a C_2 symmetry operation.

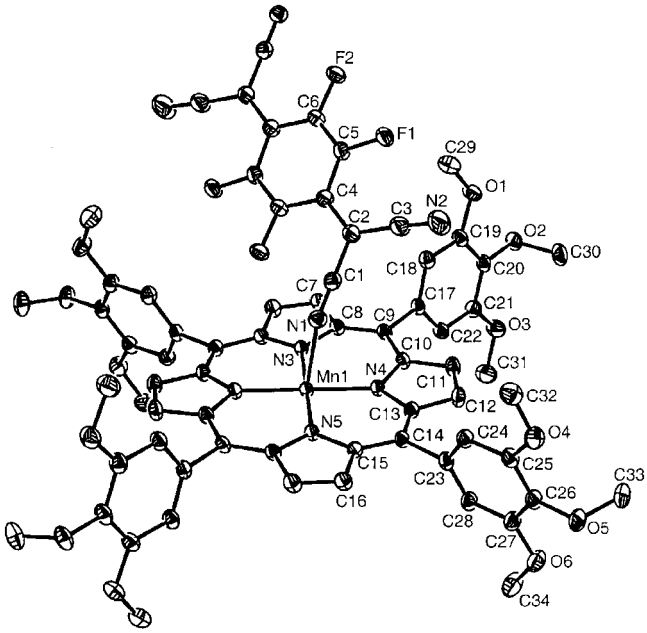
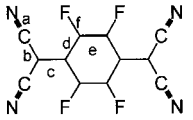


Figure 1. ORTEP drawing (50% probability level) and atom labeling diagram; the three solvent molecules are omitted for clarity

The $[MnT(MeO)_3PP]^+$ cations lie on crystallographic inversion centers with Mn at the center. The Mn^{III} atoms lie at the inversion center with $Mn–N_{por}$ distances averaging 2.004 Å, consistent with typical $[MnTPP]^+$ distances.[2,4,5a–5c,8,14] The trimethoxyphenyl-substituent plane is rotated 80° from the mean porphyrin plane.

The $TCNQF_4$ is essentially planar with a small deviation of the dicyanomethylene moiety which is twisted from the benzenoid ring plane by 5°. The $C_F–C_F$, $C_F–C_C$, and $C_C–C_{CN}$ distances are 1.352(4), 1.410(4), and 1.410(4) Å, respectively, which differ from $TCNQF_4^0$ by 0.02, 0.03, and 0.04 Å, respectively,[10b,12,15] but are comparable to the values for reduced $TCNQF_4$ as $[TCNQF_4]_2^{2-}$.[10,13,16] The bond lengths for $\mathbf{1}\cdot 3C_6H_4Cl_2$ are summarized along with other reported structures for $[TCNQF_4]^n$, Table 1. The key bond length that best describes the oxidation state of the $TCNQF_4$ is the distance *c*. This quinone-type bond in-

Table 1. Summary of the chemically different bond lengths for structurally characterized $[TCNQF_4]^n$ (n = 0, 1–, 2–)



Distances[a] in $[TCNQF_4]^n$ (n = 0, 1–, 2–)	a (Å)	b (Å)	c (Å)	d (Å)	e (Å)	f (Å)	ref.
n = 0							
$TCNQF_4$	1.140	1.437	1.372	1.437	1.334	1.336	[10b]
$[Fe(C_5H_5)_2]_2[TCNQF_4]_3$	1.149	1.439	1.373	1.438	1.331	1.334	[12]
$[NMe_4][TCNQF_4]\cdot 0.5TCNQF_4$	1.15	1.46	1.35	1.43	1.32	1.33	[15b]
$[benzotrithiphene]_2[TCNQF_4]$	1.144	1.410	1.369	1.429	1.339	1.328	[15e]
[*N*-(2-OHNp)pyreneamine][$TCNQF_4$]	1.144	1.437	1.378	1.439	1.342	1.335	[15f]
$[Dithianthrene(OEt)_4][TCNQF_4]$	1.141	1.431	1.385	1.436	1.339	1.337	[15g]
[DMQtT][$TCNQF_4$]	1.138	1.423	1.380	1.440	1.339	1.327	[15c]
n = 1–							
$[Mn^{III}T(MeO)_3PP][TCNQF_4]$	1.142	1.414	1.410	1.410	1.352	1.348	[f]
[MePhen][$TCNQF_4$][b]	1.140	1.423	1.410	1.413	1.346	1.348	[16l]
[Tempo][$TCNQF_4$][b]	1.139	1.428	1.403	1.419	1.338	1.352	[16h]
[Bis(benzo)TTF][$TCNQF_4$][b]	1.143	1.424	1.411	1.415	1.351	1.352	[16i]
$[(CH_2)_6TSeF][TCNQF_4]$[b]	1.142	1.430	1.405	1.413	1.360	1.349	[16j]
[TTF][$TCNQF_4$][b,g]	1.171	1.539	1.332	1.439	1.318	1.283	[16k]
$[Fe(C_5H_5)_2]_2[TCNQF_4]_3$[b]	1.148	1.423	1.418	1.418	1.345	1.364	[12]
$[Fe(C_5H_5)_2]_2]$ $[TCNQF_4]$[b]	1.140	1.435	1.429	1.420	1.360	1.349	[12]
$[Me_2Phen][TCNQF_4]$[b]	1.144	1.429	1.415	1.415	1.353	1.354	[16g]
[*N*-BuPhen][$TCNQF_4$][b]	1.144	1.417	1.413	1.410	1.350	1.346	[16d]
$[Cp_2Mo_2(SMe)_4][TCNQF_4]$[c,d]	1.139	1.429	1.397	1.410	1.365	1.337	[16f]
$[W(n\text{-}C_5H_4Bu t)_2(C_3S_5)][TCNQF_4]$[d]	1.145	1.423	1.393	1.421	1.340	1.331	[15d]
$[Cp_2Modmid][TCNQF_4]$[d]	1.146	1.418	1.425	1.412	1.362	1.338	[16e]
$[Cp_2Wdmid][TCNQF_4]$[d]	1.15	1.42	1.42	1.423	1.362	1.333	[16e]
$[Cp_2Modmit][TCNQF_4]$[d]	1.14	1.42	1.44	1.40	1.37	1.35	[16e]
$[Cp_2Wdmit][TCNQF_4]$[d]	1.14	1.42	1.414	1.420	1.358	1.341	[16e]
$[Cp_2Modsit][TCNQF_4]$[d]	1.15	1.43	1.42	1.43	1.33	1.35	[16e]
$[Cp_2Wdsit][TCNQF_4]$[d]	1.14	1.43	1.42	1.41	1.37	1.34	[16e]
$[Fe(C_5Me_5)_2][TCNQF_4]$[b]	1.149	1.425	1.418	1.412	1.356	1.347	[12]
$[NMe_4][TCNQF_4]\bullet 0.5TCNQF_4$[b]	1.135	1.142	1.42	1.40	1.35	1.35	[15b]
n = 2–							
$[Fe(C_5H_5)_2]_2[TCNQF_4]$	1.154	1.403	1.457	1.398	1.373	1.359	[16a]

[a] Distances are averaged if more than one was reported. – [b] $[TCNQF_4]_2^{2-}$ – [c] $TCNQF_4$'s in dimer are offset by ca. 45°; diamagnetic. – [d] $[\sigma\text{-}TCNQF_4]_2^{2-}$. – [f] This work. – [g] Not plotted in Figure 2 as the unusual deviation of the reported bond length with respect to the other compounds in this table.

creases as the negative charge increases for $[TCNQF_4]^n$. This increase in negative charge is also evidenced by the contraction of bond d and a lengthening of bond e. When the bond length for c is plotted for each of the compounds (Figure 2) the separations of the 0, 1– and 2– species can easily be distinguished, and **1**·$3C_6H_4Cl_2$ clearly lies in the 1– regime.

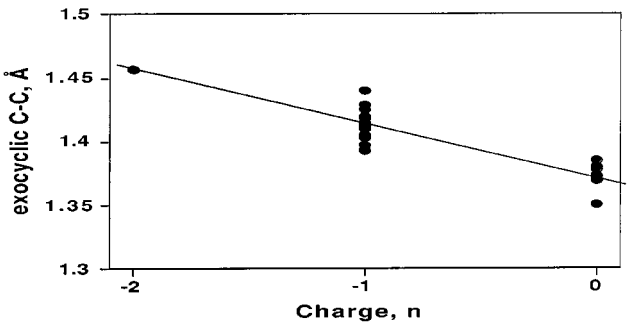


Figure 2. Bond length correlations with bond c (see Table 2) in various $[TCNQF_4]^n$ (n = 0, 1–, 2–)

This semi-quinoid-type character also causes the ring *ipso* angles to differ from the ideal 120° to 123° about F and 113° about $C(CN)_2$. The internal F angle is 118° and the external F angle is 119°. The internal C1–C2–C3 angle in 113°, while the C1–C2–C4 and C3–C2–C4 angles are 123° and 124°, respectively. Hence, in accord with the IR data (vide supra) $[TCNQF_4]^-$ must be present. $[TCNQF_4]^-$ is *trans*-μ bonded to two Mn^{III} atoms with a distance of 2.321(3) Å and an $MnNC_{TCNF4}$ angle of 135.9(2)°. The MnN_{TCNF4} distance is in the range noted for $[TCNE]^-$ analogs;[2,4,5a–5c,8,14] however, this angle is smaller than that observed for [Mn(porphyrin)][TCNE] systems, namely, the MnNC angle which range from 140° to 165°. This is presumably due to the additional space to be filled from the larger acceptor. The dihedral angle between the mean MnN_4 and the mean $[TCNQF_4]^-$ planes is 46.4°. This is in the range of those observed for the [Mn(porphyrin)][TCNE] class of compounds that range from ca. 33.4 to 89.4°.[2,4,5a–5c,8,14] The intrachain Mn···Mn separation is 12.685 Å, which, as expected due to the larger length of $[TCNQF_4]^-$ with respect to $[TCNE]^-$, exceeds the range of

intrachain Mn···Mn separations (i.e. 8.587 to 10.376 Å).[2,4,5a–5c,8,14] The interchain Mn···Mn separations of 16.959, 18.759, and 23.663 Å are also larger than those observed for the $[TCNE]^-$ electron transfer salts which is attributed to the larger spin-bearing ligand used; this is also consistent with the $[Mn^{III}TPP][chloranil]$ magnet.[2]

In the solid state $\mathbf{1}\cdot 3C_6H_4Cl_2$ forms parallel 1-D chains comprised of alternating S = 2 cations and S = 1/2 anions. All chains are identical and possess a zigzag motif (Figure 3). This is a result of the $TCNQF_4$'s aligning *cis* with respect to each other about the manganese center. These uniform chains are arranged into offset layers giving rise to two different interchain Mn···Mn distances as depicted in Figure 3. This zigzag motif is observed for the first time for this $[Mn(porphyrin)]^+$ family of magnets; however, the effect of the structural arrangement on the magnetic properties is uncertain at present.

Magnetic Behavior

The magnetic susceptibility, χ, of $\mathbf{1}\cdot 2.3C_6H_4Cl_2$ in the range 2 to 300 K can be fit to the Curie-Weiss expression, $\chi \propto 1/(T-\theta)$, with $\theta = -37$ K ($T > 250$ K), and an effective θ',[5b] of 29 K ($75 < T < 200$ K), Figure 4.

This θ'-value is markedly lower than the values observed in [Mn(porphyrin)][TCNE] uniform chain systems which range from 42 to >200 K.[1a,5] The room temperature effective moment, μ_{eff} [$\equiv(8\chi T)^{1/2}$], value is 4.81 μ_B which is slightly lower than the predicted value of 5.20 μ_B for an uncoupled S = 1/2, S = 2 system. The $\chi T(T)$ plot have a minimum at 215 ± 10 K (see Figure 4) characteristic of ferrimagnetically coupled systems.[17] The position of this minimum is responsible for the observed lower room temperature χT values. With decreasing temperature $\chi T(T)$ reaches a maximum at 9 K with a value of 10.2 emuK/mol, due to saturation, and then decreases rapidly. The $\chi T(T)$

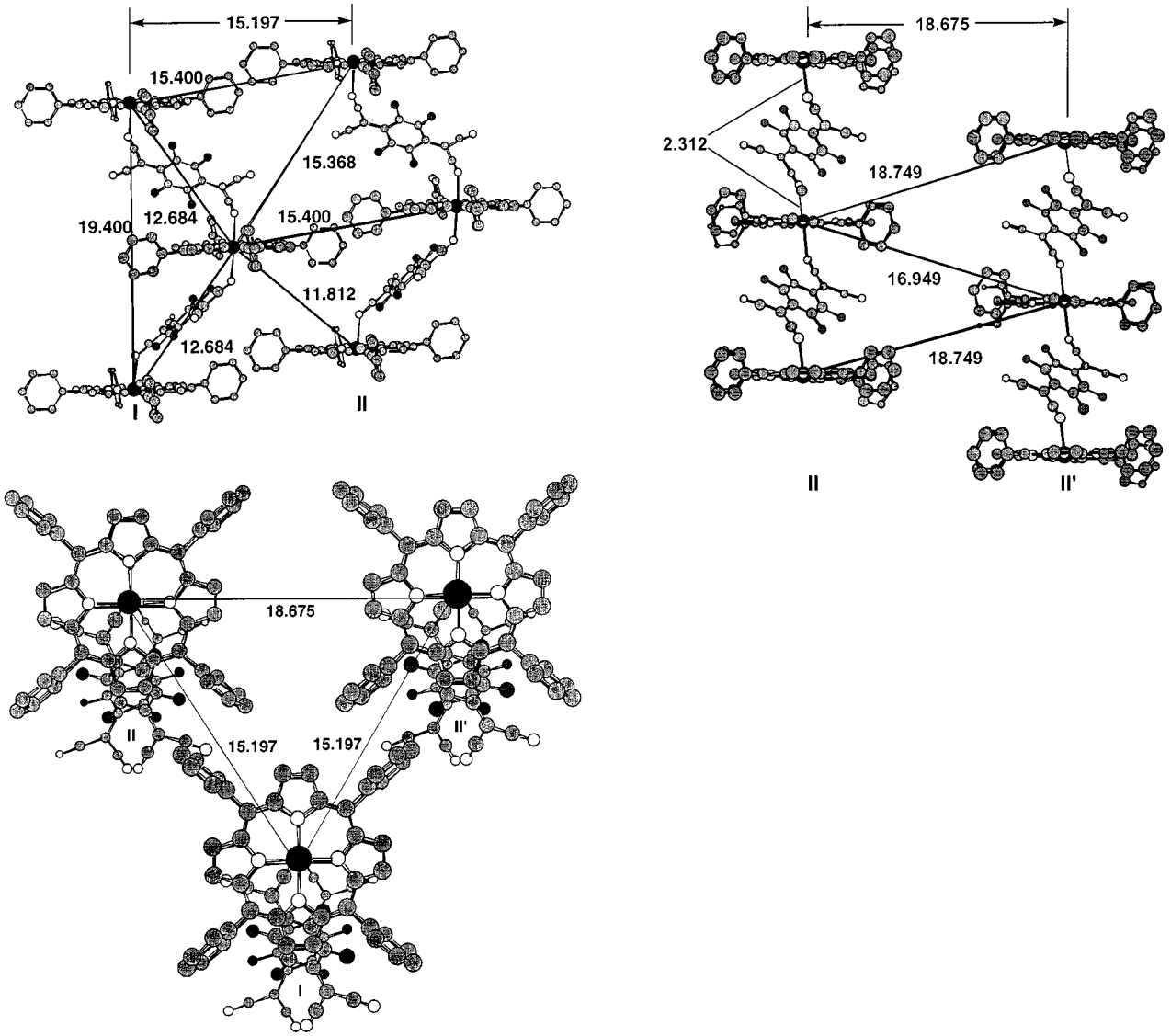


Figure 3. Views of intra- and interchain interactions among the unique chains: **I**, **II**, and **III** for $[MnT(MeO)_3PP][TCNQF_4]\cdot 3C_6H_4Cl_2$

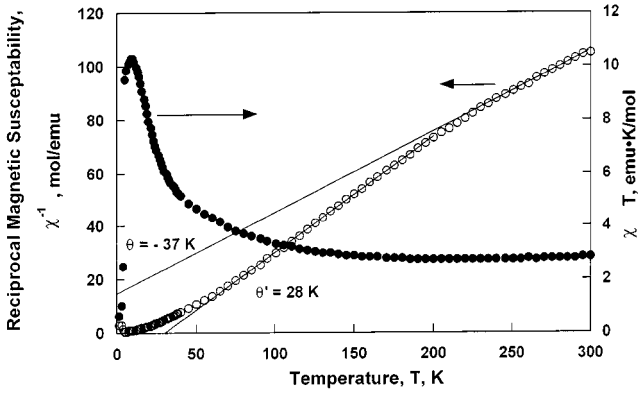


Figure 4. $\chi^{-1}(T)$ (o), and the $\chi T(T)$ (•) fit to the Seiden model (solid line) with $J/k_B = -71$ K (49 cm^{-1}) for $H = -2J\boldsymbol{S}_i\cdot\boldsymbol{S}_j$.for polycrystalline **1**·2.3$C_6H_4Cl_2$; the sample was cooled to 2 K in zero field, then the field (1000 Oe) was turned on and data was measured whilst warming to 300 K

data above 150 K can be fit to the Seiden model[18] for non-interacting chains comprised of alternating $g = 2$ quantum $S = 2$ and classical $S = 1/2$ spins, with $J/k_B = -71$ K (–49 cm^{-1}; –61 meV) for $H = -2J\mathbf{S}_i\cdot\mathbf{S}_j$, Figure 4. The deviation below 150 K is attributed to the onset of three-dimensional interactions and exceeds the values predicted by the model. Below 47 K, however, the slope of the calculated $\chi T(T)$ data begins to rise faster than the experimental data. This type of crossover has not been observed before in this family of magnets, but may be attributed to short correlation lengths. These short correlation lengths are also manifested in the lowered maximum of the $\chi T(T)$ data.

Antiferromagnetic behavior is also evident from the saturation magnetization. The isothermal magnetization at 2 K increases rapidly with the application of a small field, quickly rising to near saturation, M_s (see Figure 5). At 2 T the magnetization is 14.900 emuOe/mol or 89% of 16.755 emuOe/mol expected for an $S_{Tot} = 2 - 1/2 = 3/2$ system. This is substantially lower than that expected from ferromagnetic coupling, i.e. 27.925 emuOe/mol for an $S_{Tot} = 2 + 1/2 = 5/2$ system. At 2 K metamagnetic behavior is observed (field-induced changeover from an antiferromagnetic ground state to a ferromagnetic ground state) with a critical field of ca. 20.2 kOe, Figure 5. Similar field-dependent behavior was observed for [MnTPP][TCNE], which exhibits a

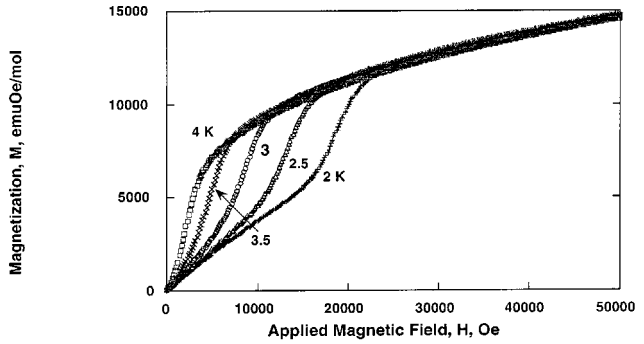


Figure 5. The magnetization curves taken at 2, 2.5, 3, 3.5, and 4 K for **1**·2.3$C_6H_4Cl_2$ displaying the disappearance of the metamagnetic behavior as the temperature is increased; the inset displays a critical field of 20.2 kOe taken from the 2 K saturation data.(solid line)

critical field of ca. 30 kOe at 2.25 K corresponding to a spin-flop transition.[19]

The field-induced crossover from an antiferromagnetic ground state to a ferromagnetic ground state is not observed above 4 K. Sample-independent hysteresis with a large coercive field of 17.1 kOe is observed at 2 K (Figure 6), but is not observed at 5 K. The 2 K remnant magnetization is 7.200 emuOe/mol. The field-cooled and zero-field-cooled data $M(T)$ data at 0.1, 1, and 10 Oe, show a bifurcation at 5.4 K (Figure 7); however, this is not a good measure of T_c since the bifurcation can begin at higher temperatures and not be observable with so few data points.

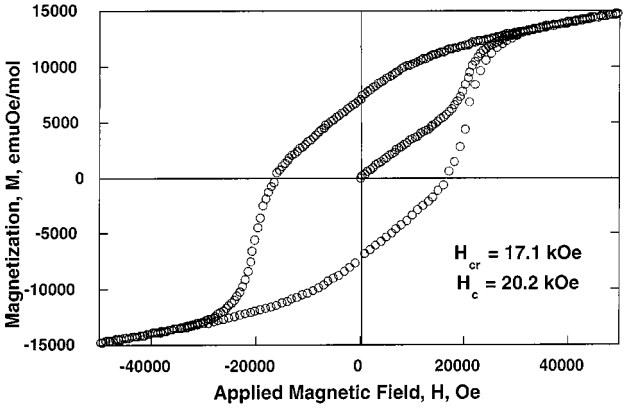


Figure 6. The observed hysteresis for **1**·2.3$C_6H_4Cl_2$ taken at 2 K; the sample was frozen in mineral oil and cooled in zero applied field

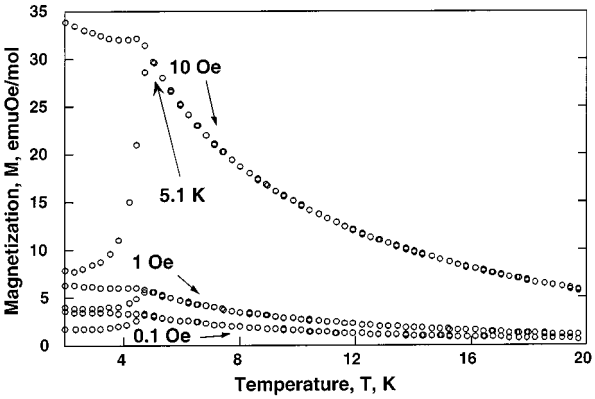


Figure 7. The field cooled and zero-field-cooled data for **1**·2.3$C_6H_4Cl_2$ displaying bifurcation at fields of 0.1, 1.0, and 10 Oe

In addition to dc measurements, the susceptibility was determined in an applied ac field of 1000 Oe (<0.05 dc field) at several frequencies and the resulting data are consistent with long-range ferromagnetic order. A peak in the real part of the 10 Hz ac susceptibility $\chi'(T)$ at 7.3 K is a better measure of T_c (Figure 8). An out-of-phase component, $\chi''(T)$, characteristic of a noncompensated moment is present with a peak at 6.3 K. There are also large frequency dependencies of both $\chi'(T)$ and $\chi''(T)$. The frequency dependence of $\chi'(T)$, ϕ [$= (T_{1000\ Hz} - T_{10\ Hz})/\{T_{10\ Hz}[\log(1000/10)]\}$], is 0.17 which is characteristic of the material being a

spin glass or superparamagnetic state.[20] The broad nature of the $\chi'(T)$ and $\chi''(T)$ peaks suggests that more than one transition is occurring.

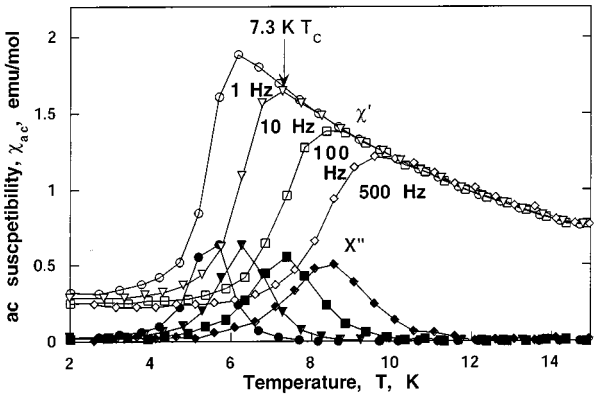


Figure 8. The dispersive, χ', and absorptive, χ'', components of the a.c. susceptibility measured at 1, 10, 100 and 500 Hz for **1**·2.3$C_6H_4Cl_2$; the 7.3 K absorption in the 10 Hz frequency data is defined as T_c; the sample was cooled to 2 K in zero field and data was taken upon warming

Experimental Section

Synthesis: All manipulations were carried out in a Vacuum Atmospheres DriLab under nitrogen. All glassware was oven dried at 110 °C and immediately pumped into the DriLab. The solvents were dried from appropriate drying agents under nitrogen. 3,4,5-Trimethoxybenzaldehyde (Acros) was used as received. $H_2T(MeO)_3PP$ was synthesized by modified literature methods,[21] The $MnT(MeO)_3PPCl$ was prepared by refluxing the free base in DMF with $Mn(OAc)_2{\cdot}4H_2O$ (Acros) and shaking with brine. $Mn^{II}T(MeO)_3PPpy$ was prepared by literature methods.[22] $TCNQF_4$, a gift from O. Webster, was recrystallized prior to use.

$[Mn^{III}T(MeO)_3PP][TCNQF_4]$·x*o*-$C_6H_4Cl_2$: This compound was prepared by adding a filtered solution of $TCNQF_4$ (12 mg, 0.043 mmol) dissolved in hot 1,2-dichlorobenzene (10 mL) to a filtered solution of $Mn^{II}T(MeO)_3PPpy$ (32 mg, 0.043 mmol) in hot 1,2-dichlorobenzene (5 mL). The resulting solution was allowed to stand for three weeks, and the black crystals (11 mg) formed were collected by vacuum filtration. Identical material can be obtained by refluxing $Mn^{II}T(MeO)_3PPpy$ and $TCNQF_4$ for 10 min and letting the solution cool to room temperature. Upon addition of hexane, a black precipitate can be collected on a fritted glass disc with a yield of approximately 70%. The black filtrate was washed with hexane (2 × 5 mL), then stored under nitrogen. – IR: ν_{CN} = 2196(m) and 2165(s) cm^{-1}.

X-ray Structure Determination: Isolation of crystals suitable for X-ray diffraction is described above. The crystal, in the mother liquor, was mounted on a glass fiber covered in oil, mounted on the goniometer and rapidly cooled in a stream of liquid nitrogen at 200 K. Data was collected at 200 K with a Nonius Kappa CCD-based X-ray diffractometer system operated at 2000 W power. The cell constants and an orientation matrix for the data collection were obtained by least-squares refinement of 6707 reflections; the key crystallographic information is given in Table 2. The crystal structure was solved by direct methods using SHELXL97.[23] Non-hydrogen atoms were refined anisotropically. Only one of the three solvent molecules is disordered, which was detected through the use of difference electron maps which illustrated a second orientation of the solvent. These two orientations were fit with the aid of a graphics workstation and the model was refined. The bonds and angles for this solvent were restrained to a standard geometry throughout the refinement.

Table 2. Summary of the crystallographic data for $[MnT(MeO)_3PP][TCNQF_4]{\cdot}3C_6H_4Cl_2$

Chemical formula	$C_{86}H_{64}Cl_6F_4MnN_8O_{12}$
M_r, Dalton	1745.09
Space group	*C*2/*c*
a	16.9486(10) Å
b	25.7170(14) Å
c	19.4009(12) Å
β	107.091(4)°
V	8082.8(8) $Å^3$
Z	4
T	200 K
λ	0.71073 Å
ρ_{calcd}	1.434 $g{\cdot}cm^{-3}$
μ_{calcd}	0.439 mm^{-1}
$R(F_o)$[a]	0.0547
$R_w(F_o)$[b]	0.1340

[a] $\Sigma(|F_o| - |F_c|) / \Sigma|F_o|$. – [b] $\Sigma w(|F_o| - |F_c|)^2 / \Sigma w|F_o|^2$.

Crystallographic data (excluding structure factors) for the structure reported herein have been deposited with the Cambridge Crystallographic Data Centre as supplementary publication no. CCDC-129223. Copies of the data can be obtained free of charge on application to The Director, CCDC, 12 Union Road, Cambridge CB2 1EZ, UK [Fax: (internat.) + 44-1223/336-033; E-mail: deposit@ccdc.cam.ac.uk).

Physical Methods: The magnetic susceptibility was determined as previously reported.[2] The diamagnetic correction for the 2.3 equiv. of the 1,2-$C_6H_4Cl_2$ solvate (as determined by TGA) was calculated using Pascal's constants to be -951×10^{-6} emu/mol.

The thermal properties were studied on a TA Instruments Model 2050 thermogravimetric analyzer (TGA, ambient to 1000 °C) placed in a Vacuum Atmospheres DriLab under argon, to retain the integrity of air- and water-sensitive samples. Samples were placed in an aluminum pan and heated to 450 °C at 15 °C/min under a continuous flow of nitrogen (10 mL/min).

The infrared spectra were recorded on a BioRad FTS 40 FTIR in the range of 650 to 4000 cm^{-1} on NaCl discs as a mineral oil mull.

Acknowledgments

The authors gratefully acknowledge the support from the National Science Foundation (Grant Nos. CHE9320478 and CHE9807669) as well as helpful discussions with Dr. D. K. Rittenberg.

[1] Recent reviews: [1a] J. S. Miller, A. J. Epstein, *Chem. Commun.* **1998**, 1319. – [1b] W. Plass, *Chem. Zeit* **1998**, *32*, 323. – [1c] J. S. Miller, A. J. Epstein, *Adv. Chem. Ser.* **1995**, *245*, 161. – [1d] J. S. Miller, A. J. Epstein, *Chem. Eng. News* **1995**, *73(*#40), 30. – [1e] J. S. Miller, A. J. Epstein, *Angew. Chem. Int. Ed. Engl.* **1994**, *33,* 385; *Angew. Chem.* **1994**, *106,* 399. – [1f] D. Gatteschi, *Adv. Mater.* **1994**, *6,* 635. – [1g] M. Kinoshita, *Jap. J. Appl. Phys.* **1994**, *33*, 5718. – [1h] O. Kahn, *Molecular Magnetism*, VCH Publishers, Inc. **1993**. – [1i] R. Chiarelli, A. Rassat, Y. Dromzee, Y. Jeannin, M. A. Novak, J. L. Tholence, *Phys. Scrip.* **1993**, *T49*, 706. – [1j] A. Caneschi, D. Gatteschi, *Progr. Inorg. Chem.* **1991**, *37*, 331.

[2] E. J. Brandon, B. M. Burkhart, R. D. Rogers, J. S. Miller, *Chem. Eur. J.* **1998**, *4*, 1938.

[3] K. Inoue, H. Iwamura, T. Iwamura, T. Hayamizu, Y. Ohashi, *J. Am. Chem. Soc.* **1996**, *118*, 1803. H. Iwamura, K. Inoue, K. Hayamizu, *Pure Appl. Chem.* **1996**, *68*, 243. K. Inoue, T. Hayamizu, T. Iwamura, *Mol. Cryst., Liq. Cryst.* **1995**, *273*, 67.

[4] D. K. Rittenberg, J. S. Miller, *Inorg. Chem* **1999**, *38*, 4838.

[5] [5a] J. S. Miller, E. J. Brandon, in *NATO ARW Supramolecular Engineering of Synthetic Metallic Materials: Conductors and Magnets* (Eds.: J. Veciana, C. Rovira, D. Amabilino) **1998**, *C518*, 197. – [5b] E. J. Brandon, D. K. Rittenberg, A. M. Arif, J. S. Miller, *Inorg. Chem.* **1998**, *37*, 3376. – [5c] E. J. Brandon, A. M. Arif, B. M. Burkhart, J. S. Miller, *Inorg. Chem.* **1998**, *37*, 2792. D. K. Rittenberg, K-i. Sugiura, Y. Sakata, I. A. Guzei, A. L. Rheingold, J. S. Miller, *Eur. J. Chem.* **1999**, *5*, 1874. E. J. Brandon, A. M. Arif, J. S. Miller, K-i. Sugiura, B. M. Burkhart, *Cryst. Eng.* **1998**, *1*, 97. K-i.Sugiura, S. Mikami, T. Tanaka, M. Sawada, J. L. Manson, J. S. Miller, Y. Sakata, *Chem. Lett.* **1997**, 1071. A. Böhm, C. Vazquez, R. S. McLean, J. C. Calabrese, S. E. Kalm, J. L. Manson, A. J. Epstein, J. S. Miller, *Inorg. Chem.* **1996**, *35,* 3083. – [5d] K. Nagai, L. Jiang, T. Iyoda, A. Fujishima, K. Hashimoto, *Thin Solid Films* **1998**, *331*, 165; K. Greisar, M. A. Athanassopoulou, Z. Tomkowicz, *Mol. Cryst., Liq. Cryst.* **1997**, *306*, 57; K. Griesar, M. A. Athanassopoulou, E. A. Soto Bustamante, Z. Tomkowicz, A. J. Zaleski, W. Haase, *Adv. Mater.* **1997**, *9*, 45; K. Nagai, T. Iyoda, A. Fujishima, K. Hashimoto, *Solid. State. Commun.* **1997**, *102*, 809.

[6] E. J. Brandon, C. Kollmar, J. S. Miller, *J. Am. Chem. Soc.* **1998**, *120,* 1822.

[7] H. Winter, E. Dormann, R. Gompper, R. Janner, S. Kothrade, B. Wagner, H. Naarmann, *J. Mag. Mater.* **1995**, *140–144*, 1443; H. Winter, M. Klemen, W. Dormann, R. Gompper, R. Janner, S. Kothrade, B. Wagner, *Mol. Cryst., Liq. Cryst.* **1995**, *273*, 111; M. Klemen, C. Wachter, H. Winter, W. Dormann, R. Gompper, D. Hermann, *Mol. Phys.* **1997**, *90*, 407.

[8] S. Mikami, K-i. Sugiura, J. S. Miller, Y. Sakata, *Chem. Lett.* **1999**, 413.

[9] R. C. Wheland, E. L. Martin, *J. Org. Chem.* **1975**, *40*, 3101.

[10] [10a] M. D. Ward, *Electroanal. Chem.* **1989**, 16, 182. – [10b] T. Emge, M. Maxfield, D. Cowan, T. J. Kistenmacher, *Mol. Cryst., Liq. Cryst.* **1981**, *65*, 161.

[11] Z. S. Li, S. Matsuzaki, M. Onomichi, M. Sano, G. Saito, *Syn. Met.* **1986**, *16*, 71; X. Wu, Z. Hu, *Syn. Met.* **1995**, *70*, 1169.

[12] J. S. Miller, J. H. Zhang, W. M. Reiff, *Inorg. Chem.* **1987**, *26*, 600.

[13] D. A. Dixon, J. C. Calabrese, J. S. Miller, *J. Phys. Chem.* **1988**, *93,* 2284.

[14] [14a] V. W. Day, B. R. Sults, E. L. Tasset, R. S. Marianelli, L. J. Boucher, *Inorg. Nucl., Chem. Lett.* **1975**, *11*, 505. – [14b] B. Cheng, F. Cukiernik, P. Fries, J-C. Marchon, W. R. Scheidt, *Inorg. Chem.* **1995**, *34*, 4627. – [14c] R. Guildard, K. Perié, J-M. Barbe, D. J. Nurco, K. M. Smith, E. V. Caemelbecke, K. M. Kadish, *Inorg. Chem.* **1998**, *37*, 973. – [14d] J. T. Landrum, K. Hatano, W. R. Scheidt, C. A. Reed, *J. Am. Chem. Soc.* **1980**, *102*, 6729. – [14e] C. L. Hill, M. M. Williamson, *Inorg. Chem.* **1985**, *24*, 2834, 3024. [14f] E. B. Fleischer, *Acc. Chem Res.* **1970**, *3*, 105. – [14g] W. R. Scheidt, C. A. Reed, *Chem. Rev.* **1981**, *81*, 543. – [14h] P. Turner, M. J. Gunter, T. W. Hambley, A. H. White, B. W. Skelton, *Inorg. Chem.* **1992**, *31*, 2297.

[15] [15a] I. V. Jourdain, M. Fourmigué, J. Amaudrut, *Organometallics* **1999,** *18*, 1834. – [15b] T. Sugimoto, K. Ueda, M. Tsujii, H. Fujita, N. Hosoito, N. Kanehisa, Y. Shibamoto, Y. Kai, *Chem. Phys. Lett.* **1996**, *249*, 304. – [15c] S. Hotta, H. Kobayashi, *Syn. Met.* **1994**, *66*, 117. – [15d] I. V. Jourdain, M. Fourmigué, F. Guyon, J. Amaudrut, *J. Chem. Soc. Dalton Trans.* **1998**, 483. – [15e] T. Sugano, T. Hashida, A. Kobayashi, H. Kobayashi, M. Kinoshita, *Bull. Chem. Soc. Jpn.* **1988**, *61*, 2303. – [15f] N. Hoshino-Miyajima, I. Luneau, T. Mitani, Y. Maruyama, *Bull. Chem. Soc. Jpn.* **1994**, *67,* 622. – [15g] S. Friederichs, J. Kudnig, G. Klar *Z. Naturforsch. Teil B*, **1996**, *51*, 1295.

[16] [16a] D. A. Dixon, J. C. Calabrese, J. S. Miller, *J. Phys. Chem.* 1**989**, *93*, 2284. – [16b] Y. Nakamura, H. Iwamura, *Bull. Chem. Soc. Jpn.* **1993,** *66*, 3724. – [16c] R. Metzger, N. Heimer, D. Gundel, H. Sixl, R. Harms, H. Keller, D. Nothe, D. Wehe, *J. Chem. Phys.* **1982**, *77*, 6203. – [16d] D. Stein, H. Sitzmann, R. Boese, E. Dormann, H. Winter, *J. Organomet. Chem.* **1991**, *412*, 143. – [16e] M. Fourmigué, B. Domereq, I. Jourdain, P. Molinie, F. Guyon, and J. Amaudrut, *Chem. Eur. J.* **1998**, 4, 1714. – [16f] M. Fourmigué, V. Perrocheau, R. Clerac, C. Coulon, *J. Mater. Chem.* **1997**, *7*, 2235. – [16g] Z. G. Soos, H. J. Keller, K. Ludolf, J. Queckborner, D. Wehe, S. Flandrois, *J. Chem. Phys*, **1981**, *76*, 5287. – [16h] S. Nakatsuji, A. Takai, K. Nishikawa, Y. Morimoto, N. Yasuoka, K. Suzuki, T. Enoki, H. Anzai, *Chem. Commun.* **1997**, *182*, 275. – [16i] T. J. Emge, W. A. Bryden, F. M. Wiygul, D. O. Cowen, T. J. Kistenmacher, *J. Chem. Phys.* **1982**, *77*, 3188. – [16j] T. J. Emge, D. O. Cowen, A. N. Bloch, T. J. Kistenmacher, *Mol. Cryst., Liq. Cryst.* **1983**, *95*, 191. – [16k] F. M. Wygul, T. J. Emge, T. J. Kistenmacher, *Mol. Cryst., Liq. Cryst.* **1982**, *90* 163. – [16l] J. S. Miller, unpublished.

[17] E. Coronado, M. Drillon, R. Georges, in *Research Frontiers in Magnetochemistry*, O'Connor, C. J., Ed., World Scientific, **1993**, 26; D. Beltran, M. Drillon, E. Coronado, R. Georges, *Stud. in Inorg Chem.* **1983**, *3*, 589; M. Drillon, E. Coronado, D. Beltran, R. Georges, *Chem. Phys.* **1983**, *79*, 449; M. Verdaguer, M. Julve, A. Michalowicz, O. Kahn, *Inorg. Chem.* **1983**, *22*, 2624; M. Drillon, J. C. Gianduzzo, R. Georges, *Phys. Lett. A*, **1983**, *96A*, 413.

[18] J. Seiden, *J. Physique Lett.* **1983***, 44,* L947.

[19] P. Zhou, B. G. Morin, A. J. Epstein, R. S. McLean, J. S. Miller, *J. Appl. Phys.* **1993**, *73*, 6569.

[20] J. A. Mydosh, *Spin Glasses*, Francois and Taylor, Washington, D.C., **1993**.

[21] A. D. Adler, F. R. Longo, J. D. Finarelli, J. Goldmacher, J. Assour, L. Korsakoff, *J. Org. Chem.* **1967**, *32*, *476*.

[22] W. Xiaotai, S. D Gray, L. K. Woo, *Inorg. Chem.* **1998**, *37*, 5.

[23] G. M. Sheldrick, J. Chen, SHELX97–2 *Programs for Crystal Structure Analysis (Release 97–2)*, Universität Göttingen, **1998**.

Received October 25, 1999
[I99379]

Reaction of a Zirconocene(butadiene)borate-Betaine Single-Component Ziegler Catalyst with Trimethylphosphane

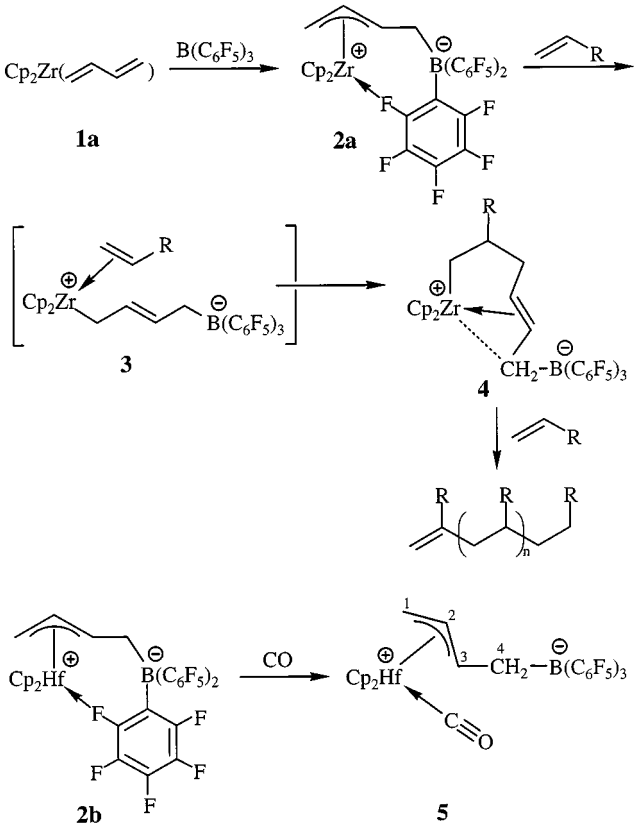
Marc Dahlmann,[a] Roland Fröhlich,[a][+] and Gerhard Erker*[a]

Keywords: Zirconium / Metallocenes / Borates / (Butadiene)zirconocene / Phosphanes

Trimethylphosphane adds to the zirconocene–$[C_4H_6B(C_6F_5)_3]$ betaine complex **2a** regioselectively by an overall inversion pathway, with opening of the internal ZrF–C_{Ar} bond and formation of the $Cp_2Zr(PMe_3)[C_4H_6B(C_6F_5)_3]$ adduct **6**. Complex **6** was characterized by X-ray diffraction. The betaine complex **6** contains a $-CH_2B(C_6F_5)_3$-substituted π-allyl ligand with characteristic bonding parameters of C1–C2: 1.402(8) Å, C2–C3: 1.373(7) Å, Zr–C1: 2.443(5) Å, Zr–C2: 2.526(4) Å, and Zr–C3: 2.681(4) Å.

Introduction

Tris(pentafluorophenyl)borane adds to (butadiene)zirconocene (**1**) to yield the $Cp_2Zr[C_4H_6B(C_6F_5)_3]$ betaine **2a** (Scheme 1). Complex **2** and its substituted Group-4 metallocene analogues are active single-component homogeneous Ziegler catalysts.[1] In addition, complex **2** and its congeners insert one equivalent of an α-olefin under selected reaction conditions to selectively form the primary product **4** of the initiative sequence leading into the catalytic cycle of the olefin polymerization process.[2,3] From a detailed kinetic study it is known that a reactive (η^2-alkene)(σ-allyl)metallocene-type intermediate (**3**) is formed in a preceding equilibrium step, followed by rate-determining alkene insertion into the Zr−C σ-bond.[4] The intermediate **3** cannot be observed directly because of its rapid subsequent CC-coupling reaction.[5] Therefore, we tried to model the structural chemistry of this first step by the addition of a suitable non-olefin two-electron donor ligand. THF added to **2a** with opening of the ZrF coordination, but we could not obtain crystals of the addition product that were suited for an X-ray crystal structure analysis.[1b,6,7] A carbon monoxide addition product to the hafnium homolog **2b** was characterized by X-ray diffraction, but turned out to be the wrong regioisomer (**5**) in comparison with the pathway probably followed in the alkene insertion reaction.[1a,8] We have now prepared and structurally characterized the PMe_3 adduct to the $Cp_2Zr[C_4H_6B(C_6F_5)_3]$ betaine, and found that its coordination characteristics may potentially resemble a structural situation expected at an early stage of the alkene addition reaction.



Scheme 1

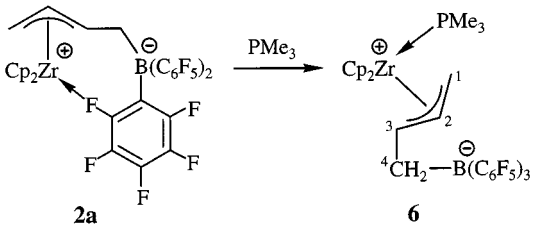
Results and Discussion

The betaine complex $Cp_2Zr[C_4H_6B(C_6F_5)_3]$ (**2a**) was generated in situ by treatment of (butadiene)zirconocene (**1**)[9] with the organometallic Lewis acid tris(pentafluorophenyl)-borane[10,11] in toluene. If care is taken to ensure that the two components are employed in a 1:1 ratio, then the formation of **2a** is close to quantitative, and it is not necessary to isolate the resulting metallocene−borate betaine complex, and the toluene solution of **2a** can be used directly to carry out subsequent reactions.

The addition of a four-fold excess of trimethylphosphane resulted in an instantaneous formation of the 1:1 addition product **6**, of the phosphane to the zirconium complex

[a] Organisch-Chemisches Institut der Universität Münster, Corrensstraße 40, D-48149 Münster, Germany
Fax: (internat.) + 49-(0)251/8336503
E-mail: erker@uni-muenster.de
[+] X-ray crystal-structure analysis.

 © WILEY-VCH Verlag GmbH, D-69451 Weinheim, 2000 1434−1948/00/0808−1789 $ 17.50+.50/0



Scheme 2

(Scheme 2). The $Cp_2Zr(PMe_3)[C_4H_6B(C_6F_5)_3]$ complex (**6**) crystallized in pure form from the reaction mixture at −20 °C, and was isolated in > 90% yield as a pale yellow crystalline material. Since the product was poorly soluble once it was precipitated, solutions of **6**, generated in situ in a deuterated solvent, were used for some of the NMR spectroscopic characterization.

The ^{1}H-NMR spectrum reveals that the PMe_3 addition complex **6** is chiral. It shows the signals of a pair of diastereotopic Cp-ligands at δ = 4.88 and 4.64. Each signal is split into a doublet by coupling with the phosphorus nucleus of the coordinated PMe_3 ligand (J_{PH} = 2 Hz).[12] Consequently, a ^{31}P-NMR resonance is observed for **6** at δ = 1.25, which is markedly shifted to a higher δ value relative to free trimethylphosphane (δ = −62.1). Coordination of the PMe_3 donor ligand to zirconium has opened the ZrF interaction that was characteristic of the starting material **2a** (^{19}F NMR: δ = −213 for the ZrF−C_6H_4[B] unit).[1a] In **6**, only a set of three ^{19}F-NMR resonances is observed in the typical $RB(C_6F_5)_3^-$ range. A distorted (π-allyl)Zr moiety is retained in complex **6** as judged from the characteristic ^{1}H- and ^{13}C-NMR chemical shifts (see Table 1). The regiochemical preference of the PMe_3 addition, leading to a "$-CH_2B-$ inside" (as found in **5**) or "$-CH_2B-$ outside" structure[8a] (as formulated for **6** in Scheme 2) cannot be deduced from the NMR data of the obtained product. We were able to answer this question by an X-ray crystal structure analysis of **6**.

The single crystals obtained from the preparation of **6** (see above) were suitable for an X-ray crystal-structure analysis. The betaine complex exhibits a pseudo-tetrahedral coordination environment around the central zirconium atom. In the front sector of the bent metallocene wedge one finds the C_4H_6[B] moiety, coordinated to the metal center through its carbon atoms C1−C3, and the PMe_3 ligand.

Table 1. A comparison of selected NMR data of the complexes **2a** and **6**

^{1}H NMR[a]						
	1-H	1-H′	2-H	3-H	4-H	4-H′
2a	1.85	1.47	5.88	5.23	2.56	2.25
6	1.43	0.49	3.79	4.00	3.29	2.06
^{13}C NMR[a]						
	C-1		C-2	C-3		C-4
2a	52.7		131.3	123.8		28.5
6	44.1 (J_{PC}=12 Hz)		109.6	117.1 (J_{PC}=7 Hz)		32.5

[a] In [D_8]toluene at 303 K (**2a**) or 298 K (**6**).

Table 2. A comparison of selected bond lengths (in Å) between the complexes **2a**, **6**, and **5**

Compound (M)	**2a** (Zr)[a]	**6** (Zr)	**5** (Hf)[a]
C1−C2	1.414(9)	1.402(8)	1.399(8)
C2−C3	1.342(8)	1.373(7)	1.369(8)
C3−C4	1.521(8)	1.499(7)	1.497(7)
C4−B	1.633(9)	1.665(6)	1.675(8)
M−C1	2.339(5)	2.443(5)	2.396(5)
M−C2	2.494(6)	2.526(4)	2.514(5)
M−C3	2.710(5)	2.681(4)	2.742(5)
M−X	2.423(3)[b]	2.705(1)[c]	2.246(7)[d]

[a] From ref.[1a]. − [b] Zr···F. − [c] Zr−P. − [d] Hf−CO.

The substituted allyl unit is coordinated in a η^3-fashion, but it is distorted toward a σ,π-type coordination geometry, as it is often observed for (allyl)zirconocene complexes.[13] However, this distortion in **6** is much less pronounced than it was, for instance, in the metallacyclic betaine complex **2a** (see Table 2). In **6** the *d*(Zr−C2) − *d*(Zr−C3) bond lengths difference [Δ(ZrC2/3)] amounts to only 0.155 Å, whereas Δ(ZrC2/3) = 0.216 Å was observed for complex **2a**.

The addition of the phosphane ligand has resulted in a cleavage of the ZrF−C interaction that was typical for the betaine system **2a**,[14] and has led to a conformational change of the $C_4H_6B(C_6F_5)_3$ chain. In **6**, rotation around the C3−C4 vector has oriented the C4−$B(C_6F_5)_3$ unit away from the metallocene moiety [θC2−C3−C4−B = −95.4(5)°] to minimize steric interaction between these two bulky groups.

The PMe_3 ligand was added to the bent metallocene from a position oriented as far away as possible from the bulky $-CH_2-B(C_6F_5)_3$ end of the 1-3η-$C_4H_6-B(C_6F_5)_3$ ligand (see Figure 1). It is found attached at the front side of the bent metallocene wedge in a position close to the CH_2-terminus of the $-CH_2$-borane-substituted π-allyl ligand.[15] The Zr−P bond length is 2.705(1) Å. The $Me_3P-ZrCp_2L$ unit attains a staggered-like conformational arrangement of groups along the P−Zr vector. In **6**, the bond angles at phosphorus show a systematic deviation from an ideal tetrahedron: the three H_3C-P angles are markedly smaller [101.6(3)°, 101.9(4)°, 102.6(3)°] than the adjacent C−P−Zr angles [115.7(2)°, 116.1(2)°, 116.7(2)°]. This is probably due to steric interactions, and indicates the importance of steric factors governing the regiochemistry of the adduct formation in complexes of types **6** (Figure 1) and **5** (see Scheme 1).[16]

Conclusions

The ZrF bond in the metallocene betaine complex **2a** is rather weak, estimated at ca. 8 kcal mol^{-1} bond dissociation energy from dynamic ^{19}F-NMR spectroscopy.[1b] Therefore, it is not surprising, that the zirconium−fluorine linkage in **2a** is rapidly cleaved by the addition of typical 2-electron donor ligands such as carbon monoxide or trimethylphosphane. The small CO ligand can apparently be added from the sterically less favorable side to yield the

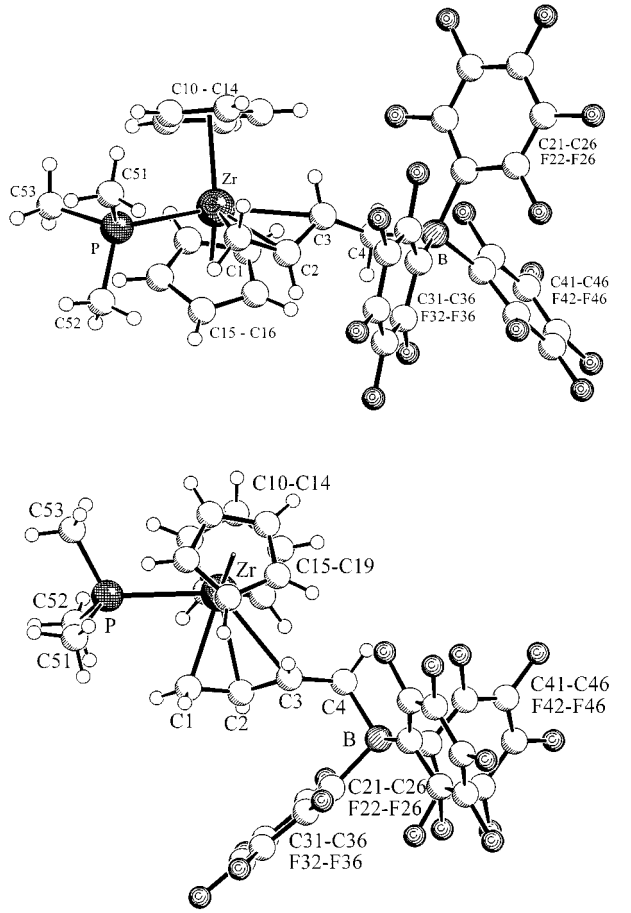


Figure 1. Two projections of the molecular structure of complex **6**; selected bond lengths [Å] and angles [°]: Zr−C1 2.443(5), Zr−C2 2.526(4), Zr−C3 2.681(4), Zr−C4 3.768(5), Zr-P 2.705(1), C1−C2 1.402(8), C2−C3 1.373(7), C3−C4 1.499(7), C4−B 1.665(6), B−C21 1.649(7), B−C31 1.665(6), B−C41 1.650(7), P−C51 1.832(6), P−C52 1.821(7), P−C53 1.829(6); Zr−C1−C2 76.9(3), Zr−C2−C1 70.4(3), Zr−C2−C3 81.1(3), Zr−C3−C2 68.6(2), Zr−C3−C4 126.4(3), C1−Zr−C2 32.7(2), C1−Zr−C3 57.3(2), C2−Zr−C3 30.4(2), C1−C2−C3 125.2(5), C2−C3−C4 123.2(4), C3−C4−B 114.9(4), C4−B−C21 115.8(4), C4−B−C31 104.1(4), C4−B−C41 107.6(4), C21−B−C31 110.3(4), C21−B−C41 104.9(4), C31−B−C41 114.4(4), C1−Zr−P 70.5(1), Zr−P−C51 116.7(2), Zr−P−C52 115.7(2), Zr−P−C53 116.1(2), C51−P−C52 101.9(4), C51−P−C53 102.6(3), C52−P−C53 101.6(3)

"$-CH_2-B(C_6F_5)_3-$ inside" regioisomer **5**,[1a] but the addition of the sterically more demanding PMe_3 ligand already leads to the exclusive observation of a typical stereochemical inversion pathway. Addition of the phosphane takes place *trans* to the ZrF bond in the σ-ligand plane at the front sector of the bent metallocene wedge, leading to the selective formation of the observed regioisomer **6**, however, it is unclear whether this product formation is thermodynamically or kinetically controlled.

The involvement of a (σ-allyl)(π-olefin)metallocene betaine-type intermediate, such as **3** (see Scheme 1) in the course of the alkene insertion/polymerization sequence starting from **2**, has been indirectly demonstrated by kinetic measurements. These have shown that the typical metallocene−allyl-inversion process of **2a**, followed by dynamic NMR spectroscopy, is markedly slower in pure toluene ($\Delta G^{\ddagger}_{inv}$ = 19.8 kcal mol^{-1}) than in the presence of added propene ($\Delta G^{\ddagger}_{inv}$ = 16.5 kcal mol^{-1}).[4] The allyl inversion process must proceed through a (σ-allyl)-metallocene-type intermediate,[17] in the presence of the alkene this means by involvement of **3**. The observed allyl inversion barrier ($\Delta G^{\ddagger}_{inv}$) is lowered because the essential reactive intermediate is stabilized by π-alkene coordination, and so is the preceding transition state, according to the Hammond postulate.[18] Since the addition reactions to **2** respond very sensitively to steric interferences, it may be that an alkene adds to **2a** in a manner very similar to PMe_3, namely from the less hindered side adjacent to the unsubstituted allyl side. This potentially leads to a stereochemical inversion at the metal center upon replacing the weak F−C(Ar) coordination to zirconium. The resulting PMe_3 adduct **6**, that we obtained and structurally characterized, may therefore, potentially resemble the structural situation during the alkene addition reaction to the metallocene betaine system at an early stage on the reaction coordinate.

Experimental Section

Reactions were carried out under argon using Schlenk-type glassware or in a glove-box. Solvents were dried and distilled under argon prior to use. For additional general information, including a list of spectrometers and instruments used for physical characterization, see ref.[1b] (Butadiene)zirconocene[9] and $B(C_6F_5)_3$[10] were prepared according to literature procedures. For this study, the betaine complex **2a** (see below) was generated in situ and spectroscopically shown to be identical to the previously isolated material.

Reaction of 2a with Trimethylphosphane. − Preparation of 6. − a) NMR Experiment: For its spectroscopic characterization, complex **6** was generated in situ in [D_8]toluene. A solution of 8 mg (29.0 μmol) of (butadiene)zirconocene (**1**) in 0.4 mL of [D_8]toluene was added dropwise to a solution of 15 mg (29.3 μmol) of $B(C_6F_5)_3$ in 0.2 mL of [D_8]toluene at ambient temperature in a vial inside the glove-box. The reaction mixture was kept for 30 min at ambient temperature; during this time a small fraction of the betaine **2a** precipitated. The clear supernatant solution was transferred to an NMR tube and sealed with a septum. Trimethylphosphane (0.02 mL) was syringed into the solution. After mixing, a pale yellow solution of **6** was obtained that was used for some of the spectroscopic characterization.

b) Formation of 6 on a Preparative Scale: A solution of 54 mg (105 μmol) of $B(C_6F_5)_3$ in 3 mL of toluene was added dropwise at ambient temperature to a solution of 29 mg (105 μmol) of (butadiene)-zirconocene in 6 mL of toluene. After 30 min trimethylphosphane (0.13 mL, 420 μmol) was added and the mixture stirred for 20 min at room temperature. The pale yellow solution was kept for 1 d at −20 °C. The product crystallized as yellow needles, which were collected by filtration, washed with toluene (4 mL), and dried in vacuo to yield 85 mg (93%) of **6**, m.p. 234 °C (decomp.). The isolated product shows a low solubility in toluene. Single crystals from this preparation were used for the X-ray crystal structure analysis of **6**: formula $C_{35}H_{25}BF_{15}PZr \times 2\ C_7H_8$, M = 1047.82, light yellow crystal 0.30 × 0.20 × 0.10 mm, a = 32.936(1), b = 15.360(1), c = 21.055(1) Å, β = 113.93(1)°, V = 9736.1(8) Å^3, $\rho_{calcd.}$ = 1.430 g cm^{-3}, μ = 3.49 cm^{-1}, empirical absorption correction via SORTAV (0.903 ≤ T ≤ 0.966), Z = 8, monoclinic, space group $C2/c$ (No. 15), λ = 0.71073 Å, T = 198 K, ω and φ scans, 28280 reflections

collected ($\pm h$, $\pm k$, $\pm l$), [(sinθ)/λ] = 0.62 Å^{-1}, 9810 independent (R_{int} = 0.041) and 7840 observed reflections [$I \geq 2\,\sigma(I)$], 607 refined parameters, R = 0.076, wR^2 = 0.234, max. residual electron density 3.55 (−0.56) e Å^{-3}, beside the localized toluene molecules there is probably a further solvent molecule around 0,y,1/4. Even with strong geometrical constraints a chemical meaningful description is not possible and therefore this electron density is not taken into account in the final refinement, hydrogens calculated and refined as riding atoms.

Data set was collected with Nonius Kappa CCD diffractometer, equipped with a rotating anode generator, Nonius FR591. Programs used: data collection COLLECT (Nonius B.V., 1998), data reduction Denzo-SMN (Z. Otwinowski, W. Minor, *Methods in Enzymology*, **1997**, *276*, 307−326), absorption correction SORTAV (R. H. Blessing, *Acta Cryst.* **1995**, *A51*, 33−37; R. H. Blessing, *J. Appl. Cryst.* **1997**, *30*, 421−426), structure solution SHELXS-97 (G. M. Sheldrick, *Acta Cryst.* **1990**, *A46*, 467−473), structure refinement SHELXL-97 (G. M. Sheldrick, Universität Göttingen, 1997), graphics SCHAKAL (E. Keller, Universität Freiburg, 1997).

Crystallographic data (excluding structure factors) for the structure reported in this paper has been deposited with the Cambridge Crystallographic Data Centre as supplementary publication no. CCDC-138789. Copies of the data can be obtained free of charge on application to The Director, CCDC, 12 Union Road, Cambridge CB2 1EZ, UK [Fax: (internat.) +44(1223)336−033, E-mail: deposit@ccdc.cam.ac.uk].

^{1}H NMR (599.9 MHz, [D$_8$]toluene, 298 K): δ = 4.88, 4.64 (each d, J_{PH} = 2.0 Hz, each 5 H, C_5H_5), 4.00 (m, 1 H, 3-H), 3.79 (ddd, 2× ^3J = 14.5 Hz, ^3J = 8.5 Hz, 1 H, 2-H), 3.29 (br d, J = 11.3 Hz, 1 H, 4-H), 2.06 (partially under solvent signal, 1 H, 4-H′), 1.43 (m, 1 H, 1-H), 0.49 (ddd, ^2J = 5.0 Hz, ^3J = 14.5 Hz, ^3J = 5.0 Hz, 1 H, 1-H′), 0.40 [d, $^2J_{PH}$ = 7.2 Hz, 9 H, P(CH$_3$)$_3$]. − ^{13}C NMR (150.8 MHz, [D$_8$]toluene, 298 K): δ = 149.1 [d, $^1J_{CF}$ = 240 Hz, *o*-B(C$_6$F$_5$)$_3$], 138.6 [d, $^1J_{CF}$ = 250 Hz, *p*-B(C$_6$F$_5$)$_3$], 137.4 [d, $^1J_{CF}$ = 250 Hz, *m*-B(C$_6$F$_5$)$_3$], 117.1 (d, J_{PC} = 7 Hz, CH, C-3), 109.6 (CH, C-2), 105.2, 104.5 (each CH, C_5H_5), 44.1 (d, J_{PC} = 12 Hz, CH$_2$, C-1), 32.5 (CH$_2$, C-4), 15.8 [d, $^1J_{PC}$ = 23 Hz, CH$_3$, P(CH$_3$)$_3$], *ipso*-C of B(C$_6$F$_5$)$_3$ not detected. − GHSQC[19] (599.9 MHz, [D$_8$]toluene, 298 K): δ = 4.88/105.2; 4.64/104.5 (each C_5H_5/C_5H_5), 4.00/117.1 (3-H/C-3), 3.79/109.6 (2-H/C-2), 3.29/32.5 (4-H/C-4), 2.06/32.5 (4-H′/C-4), 1.43/44.1 (1-H/C-1), 0.49/44.1 (1-H′/C-1), 0.40/15.8 (P(CH_3)$_3$/P(CH_3)$_3$). − ^{19}F NMR (564.3 MHz, [D$_8$]toluene, 298 K): δ = −167.1 (t, 2× $^3J_{FF}$ = 21 Hz, 6F, *m*-F), −163.7 (t, $^3J_{FF}$ = 21 Hz, 3F, *p*-F), −132.6 (d, $^3J_{FF}$ = 21 Hz, 6F, *o*-F). − ^{31}P NMR (202.6 MHz, [D$_8$]toluene, 298 K): δ = 1.25. − IR (KBr): $\tilde{\nu}$ = 3137 (w), 2964 (w), 2918 (w), 1641 (m), 1512 (vs), 1459 (vs), 1294 (m), 1271 (m), 1147 (m), 1080 (s), 977 (s), 959 (s), 819 (s), 808 (s), 801 (s), 758 (m), 682 (m) cm^{-1}. − $C_{35}H_{25}BF_{15}PZr$ (863.6): calcd. C 48.68, H 2.92; found C 48.97, H 3.19.

Acknowledgments

Financial support from the Fonds der Chemischen Industrie, the Bundesminister für Bildung und Wissenschaft, Forschung und Technologie (BMBF), and the Deutsche Forschungsgemeinschaft is gratefully acknowledged.

[1] [1a] B. Temme, G. Erker, J. Karl, H. Luftmann, R. Fröhlich, S. Kotila, *Angew. Chem.* **1995**, *107*, 1867−1869; *Angew. Chem. Int. Ed. Engl.* **1995**, *34*, 1755−1757. − [1b] J. Karl, G. Erker, R. Fröhlich, *J. Am. Chem. Soc.* **1997**, *119*, 11165−11173. − [1c] See also: G. Kehr, R. Fröhlich, B. Wibbeling, G. Erker, *Chem. Eur. J.* **2000**, *6*, 258−266.

[2] B. Temme, J. Karl, G. Erker, *Chem. Eur. J.* **1996**, *2*, 919−924. J. Karl, G. Erker, *Chem. Ber./Recueil* **1997**, *130*, 1261−1267. J. Karl, G. Erker, *J. Mol. Catal.* **1998**, *128*, 85−102.

[3] For related systems see e.g.: R. F. Jordan, D. F. Taylor, *J. Am. Chem. Soc.* **1989**, *111*, 778−779. R. F. Jordan, R. E. LaPointe, P. K. Bradley, N. Baenziger, *Organometallics* **1989**, *8*, 2892−2903. R. F. Jordan, D. F. Taylor, N. C. Baenziger, *Organometallics* **1990**, *9*, 1546−1557. A. S. Guram, R. F. Jordan, D. F. Taylor, *J. Am. Chem. Soc.* **1991**, *113*, 1833−1835. A. S. Guram, R. F. Jordan, *Organometallics* **1991**, *10*, 3470−3479. Z. Guo, D. C. Swenson, R. F. Jordan, *Organometallics* **1994**, *13*, 1424−1432. Y. W. Alelyunas, N. C. Baenziger, P. K. Bradley, R. F. Jordan, *Organometallics* **1994**, *13*, 148−156. C. Pellecchia, A. Grassi, A. Zambelli, *J. Chem. Soc., Chem. Commun.* **1993**, 947−949. C. Pellecchia, A. Grassi, A. Immirzi, *J. Am. Chem. Soc.* **1993**, *115*, 1160−1162. C. Pellecchia, A. Immirzi, A. Zambelli, *J. Organomet. Chem.* **1994**, *479*, C9−C11. C. Pellecchia, A. Immirzi, D. Pappalardo, A. Peluso, *Organometallics* **1994**, *13*, 3773−3775. C. Pellecchia, A. Grassi, A. Zambelli, *Organometallics* **1994**, *13*, 298−302.

[4] J. Karl, M. Dahlmann, G. Erker, K. Bergander, *J. Am. Chem. Soc.* **1998**, *120*, 5643−5652.

[5] For related d^0-metallocene π-alkene complexes see e.g.: Z. Wu, R. Jordan, *J. Am. Chem. Soc.* **1995**, *117*, 5867−5868. C. P. Casey, S. L. Hallenbeck, D. W. Pollock, C. R. Landis, *J. Am. Chem. Soc.* **1995**, *117*, 9770−9771. M. V. Galakhov, G. Heinz, P. Royo, *J. Chem. Soc., Chem. Commun.* **1998**, 17−18. C. P. Casey, D. W. Carpenetti II, H. Sakurai, *J. Am. Chem. Soc.* **1999**, *121*, 9483−9484.

[6] M. Dahlmann, Dissertation, Universität Münster, **1999**.

[7] For related metallocene-betaine-THF adducts see: M. Dahlmann, G. Erker, M. Nissinen, R. Fröhlich, *J. Am. Chem. Soc.* **1999**, *121*, 2820−2828.

[8] [8a] K. Tatsumi, A. Nakamura, P. Hofmann, P. Stauffert, R. Hoffmann, *J. Am. Chem. Soc.* **1985**, *107*, 4440−4451 and references cited therein. − [8b] G. Fachinetti, G. Fochi, C. Floriani, *J. Chem. Soc., Dalton Trans.* **1977**, 1946−1950. F. Fachinetti, C. Floriani, H. Stoeckli-Evans, *J. Chem. Soc., Dalton Trans.* **1977**, 2297−2302. G. Erker, F. Rosenfeldt, *J. Organomet. Chem.* **1980**, *188*, C1−C4.

[9] [9a] H. Yasuda, Y. Kajihara, K. Mashima, K. Nagasuna, K. Lee, A. Nakamura, *Organometallics* **1982**, *1*, 388−396. G. Erker, J. Wicher, K. Engel, F. Rosenfeldt, W. Dietrich, C. Krüger, *J. Am. Chem. Soc.* **1980**, *102*, 6344−6346. G. Erker, J. Wicher, E. Engel, C. Krüger, *Chem. Ber.* **1982**, *115*, 3300−3310. − [9b] Reviews: G. Erker, C. Krüger, G. Müller, *Adv. Organomet. Chem.* **1985**, *24*, 1−39. H. Yasuda, K. Tatsumi, A. Nakamura, *Acc. Chem. Res.* **1985**, *18*, 120−126.

[10] A. G. Massey, A. J. Park, F. G. A. Stone, *Proc. Chem. Soc. London* **1963**, 212. A. G. Massey, A. J. Park, *J. Organomet. Chem.* **1964**, *2*, 245−250. A. G. Massey, A. J. Park, *Organometallic Syntheses*, R. B. King, J. J. Eisch, Eds., Elsevier, New York, **1986**, Vol. 3, p. 461−462.

[11] For related reactions see e.g.: X. Yang, C. L. Stern, T. J. Marks, *J. Am. Chem. Soc.* **1994**, *116*, 10015−10031.

[12] B. E. Bosch, G. Erker, R. Fröhlich, O. Meyer, *Organometallics* **1997**, *16*, 5449−5456.

[13] D. J. Brauer, C. Krüger, *Organometallics* **1982**, *1*, 207−210. G. Erker, K. Engel, U. Dorf, J. L. Atwood, W. E. Hunter, *Angew. Chem.* **1982**, *94*, 915−916; *Angew. Chem. Int. Ed. Engl.* **1982**, *21*, 914−915. G. Erker, K. Berg, C. Krüger, G. Müller, K. Angermund, R. Benn, G. Schroth, *Angew. Chem.* **1984**, *96*, 445−446; *Angew. Chem. Int. Ed. Engl.* **1984**, *23*, 455−456. E. J. Larson, P. C. Van Dort, J. S. Dailey, J. R. Lakanen, L. M. Pederson, M. E. Silver, J. C. Huffman, S. O. Russo, *Organometallics* **1987**, *6*, 2141−2146. G. Erker, K. Berg, K. Angermund, C. Krüger, *Organometallics* **1987**, 6, 2620−2621. E. J. Larson, P. C. Van Dort, J. R. Lakanen, D. W. O′Neill, L. M. Pederson, J. J. McCandless, M. E. Silver, S. O. Russo, J. C. Huffman, *Organometallics* **1988**, *7*, 1183−1187. G. Erker, *Angew. Chem.* **1989**, *101*, 411−426; *Angew. Chem. Int. Ed. Engl.* **1989**, *28*, 397−412.

[14] Steric hindrance, as present in Cp$_2$*Zr[C$_4$H$_6$B(C$_6$F$_5$)$_3$] leads to similar structural features: J. Karl, G. Erker, R. Fröhlich, *J. Organomet. Chem.* **1997**, *535*, 59−62.

[15] H. H. Brintzinger, L. S. Bartell, *J. Am. Chem. Soc.* **1970**, *92*, 1105−1107. W. Lauher, R. Hoffmann, *J. Am. Chem. Soc.* **1976**,

98, 1729−1742. J. C. Green, *Chem. Soc. Rev.* **1998**, *27*, 263−271.

[16] After submission of this paper, a very similar structure of the PMe_3 stabilized *ansa*-metallocene complex [Zr{$Me_2C(\eta$-$C_5H_4)_2$}(η^3-$C_4H_6B(C_6F_5)_3$)PMe_3] with bond lengths Zr−C1 2.464(5) Å, Zr−C2 2.527(5) Å, Zr−C3 2.613(6) Å, C1−C2 1.410(8) Å, C2−C3 1.384(8) Å, and Zr−P 2.748(2) Å (atom numbering scheme analogous as in Figure 1) was reported in the literature: J. C. Green, M. L. H. Green, G. C. Taylor, J. Saunders, *J. Chem. Soc., Dalton Trans.* **2000**, 317−327.

[17] E. G. Hoffmann, R. Kallweit, G. Schroth, K. Seevogel, W. Stempfle, G. Wilke, *J. Organomet. Chem*. **1975**, *97*, 183−202.

[18] G. S. Hammond, *J. Am. Chem. Soc*. **1955**, *77*, 334−338. See also: D. Fàrcasiu, *J. Chem. Educ.* **1975**, *52*, 76−79.

[19] S. Braun, H.-O. Kalinowski, S. Berger, *150 and More Basic NMR Experiments*, VCH, Weinheim, **1998** and references cited therein.

Received January 14, 2000
[I00015]

Addition and Coupling Reactions of Zirconocene Cation Complexes that Contain a Pendant η^2-Formaldiminium Side Chain

Jörg Pflug,[a] Gerhard Erker,*[a] Gerald Kehr,[a][+] and Roland Fröhlich[a][++]

Keywords: Metallocenes / Cations / Phosphanes / Alkenes / Insertions / Zirconium / C−H activation

The pendant (η^2-formaldiminium)zirconocene cation complex **3** is generated by treatment of the $(Cp–CMe_2NMe_2)CpZrMe_2$ precursor **1** with $B(C_6F_5)_3$. The formation of **3** proceeds with C–H activation and methane evolution. Addition of the phosphanes PPh_2R (R = Ph, CH_3 and cyclopropyl) leads to the stable adducts **6a–c**, in which the Zr–CH_2–N three-membered ring structure of the (η^2-formaldiminium)Zr subunit is retained. The reactive complex **3** readily inserts benzophenone into the Zr–CH_2(N) linkage to yield the carbon–carbon coupling product **7**. α-Olefins also insert into the reactive Zr–C bond of **3**. Exposure of **3** to ethene at a low temperature (–50 °C) results in the formation of the labile metallacyclic mono-alkene-insertion product **8**, that is characterized spectroscopically. Styrene and 4-*tert*-butylstyrene undergo a clean [2,1]insertion into the Zr–C bond of **3** to selectively yield the isomerically pure mono-insertion products **9a** and **9b**, respectively, that exhibit their aryl substituents in the α-position adjacent to the zirconium center. In each case a single stereoisomer is formed that contains a σ-π-structured η^3-benzylic coordination of the chain end, exhibiting the *meso*-allyl position oriented *cis* to the substituted Cp ring at the resulting metallacyclic framework. Complex **9b** was characterized by X-ray crystal-structure analysis.

Introduction

Alkylzirconocene cations[1] are known to readily undergo alkene insertion;[2] this reaction is the basis for their action as active Ziegler polymerization catalysts.[3] However, they can also undergo C−H activation reactions if suitable reagents are brought in the vicinity of the $[Zr]^+–CH_3$ moiety.[4] Such behavior is observed when the amino-functionalized metallocene $(Cp–CMe_2NMe_2)CpZr(CH_3)_2$ (**1**)[5] is treated with the alkyl abstractor $B(C_6F_5)_3$ (Scheme 1).[6] The alkylzirconocene cation **2** which is generated in situ, is not stable under the reaction conditions but rapidly reacts further by proton abstraction from the pendant $N–CH_3$ group to form **3** with methane evolution. The product **3** probably contains a strong nitrogen−zirconium interaction and thus might be viewed as a η^2-formaldiminium complex. The three-membered ring structure is confirmed for the isonitrile adduct **4** by X-ray diffraction.[4] The Zr(η^2-CH_2=NR_2^+) moiety can also be recognized spectroscopically by a characteristically increased $^1J_{CH}$ coupling constant of the CH_2 group inside the three-membered metallacycle[7] [**4**: $^1J_{CH}$ = 153 Hz (N−CH_2−Zr), 138 Hz (N−CH_3); **3**: $^1J_{CH}$ = 152 Hz (N−CH_2−Zr), 139 Hz (N−CH_3)]. The ^{15}N-NMR chemical shift also seems to correspond to the coordinative situation at the pendant nitrogen functionality:[4,8] A ^{15}N-NMR resonance (in $[D_2]$dichloromethane) of δ = −338 is observed for the starting material **1**, whereas markedly decreased ^{15}N-NMR shift values are observed for the (η^2-formaldiminium)zirconocene cations **3** [$\delta(^{15}N) = -358$] and **4** [$\delta(^{15}N) = -375$], respectively. We have studied the behavior of the reactive complex **3**[9] towards a variety of reagents, including phosphanes, organic carbonyl compounds, and alkenes. Representative examples of the reaction of the (η^2-formaldiminium)zirconium cation system with such reagents are described in this article.

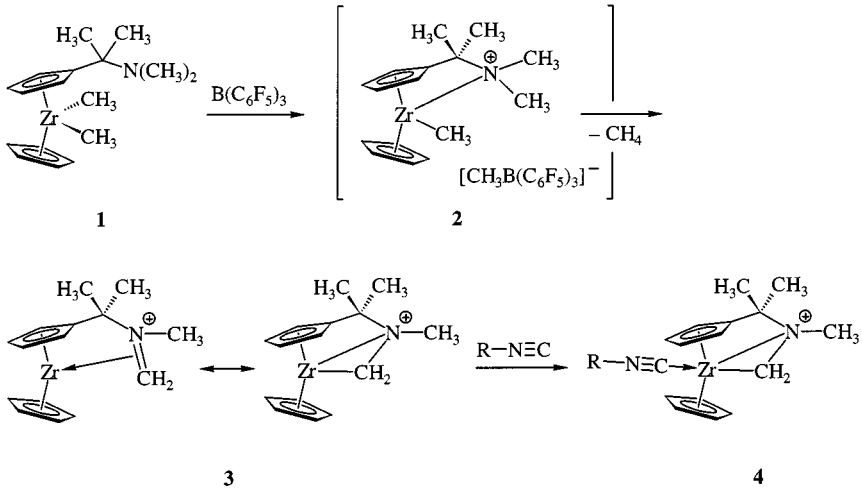
Results and Discussion

The pendant (η^2-formaldiminium)Zr cation complex **3** was generated in situ by treatment of its immediate precursor **1** with $B(C_6F_5)_3$ in $[D_2]$dichloromethane at −50 °C.[4] The phosphanes PPh_3 (**5a**), $P(Me)Ph_2$ (**5b**), and P(cyclopropyl)Ph_2 (**5c**) were added to samples of this solution. The corresponding phosphane addition products[10] (**6a−c**, respectively) were formed instantaneously (Scheme 2). Upon addition of pentane and after warming to room temperature, they separated from the reaction mixture as dark-colored oils and were each isolated in a ca. 50% yield.

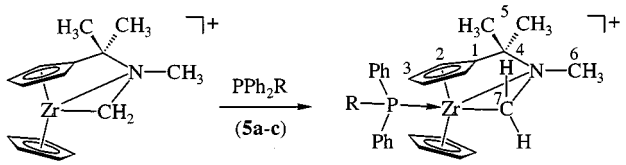
The cationic (triphenylphosphane)zirconium complex **6a** shows a ^{31}P-NMR resonance signal at δ = 31.2. The phosphane coordination results in a $^3J_{PH}$ coupling (1.5 Hz) of the Cp hydrogen atoms (Table 1).[11] The chiral metallocene complex exhibits two pairs of diastereotopic C_5H_4 NMR resonances at δ = 6.19, 5.93, 5.68, 4.58 (^{1}H) and δ = 113.0, 108.8, 107.2, 96.9 (^{13}C), as well as the signals of a pair of diastereotopic methyl groups [δ = 1.61, 1.01 (^{1}H); 25.3, 17.6 (^{13}C)] bonded to carbon atom C-4 (see Scheme 2), and the methylene hydrogen atoms at C-7 (see Table 1). All three complexes **6a−c** show ^{15}N-NMR resonance signals at δ ≈ −376. This is very characteristic for a bonding situation

[a] Organisch-Chemisches Institut der Universität Münster, Corrensstraße 40, 48149 Münster, Germany
Fax: (internat.) + 49-(0)251/833-6503
E-mail: erker@uni-muenster.de
[+] NMR spectroscopy.
[++] X-ray crystal-structure analysis.
Supporting information for this article is available on the WWW under http://www.wiley-vch.de/home/eurjic or from the author.

 © WILEY-VCH Verlag GmbH, D-69451 Weinheim, 2000 1434−1948/00/0808−1795 $ 17.50+.50/0



Scheme 1. Formation of **3** by a C−H abstraction route (complexes **3** and **4** with $[CH_3B(C_6F_5)_3]^-$ anion, R = $-C(CH_3)_3$)



3 R = Ph (**a**), CH_3 (**b**), cyclopropyl (**c**) **6a-c**

Scheme 2. Formation of the phosphane adducts **6** (complexes **4** and **6** with $[CH_3B(C_6F_5)_3]^-$ anion)

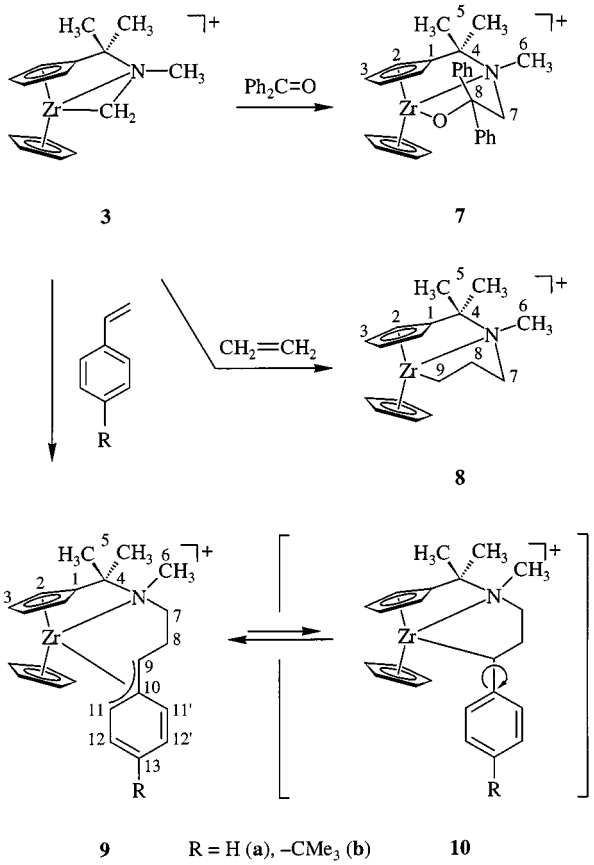
Table 1. Selected NMR data of the complexes **6** (in CD_2Cl_2 at ambient temperature)

Complex	**6a**	**6b**	**6c**
Cp (^{1}H)	5.88	5.94	6.02
($^3J_{PH}$)	(1.5 Hz)	(1.5 Hz)	(1.5 Hz)
(N)CH_2 (^{1}H)	1.89, 1.64	1.89, 1.43	1.79, 1.24
($^2J_{HH}$)	(9.4 Hz)	(9.5 Hz)	(m)
($^3J_{PH}$)	(4.8, 1.9 Hz)	(4.7, 2.0 Hz)	(m)
(N)CH_2 (^{13}C)	46.8	45.9	46.7
($^2J_{PC}$)	(15.5 Hz)	(15.7 Hz)	(15.8 Hz)
($^1J_{CH}$)	[a]	(155, 146 Hz)	[a]
(N)CH_3 (^{13}C)	44.5	44.7	44.6
($^1J_{CH}$)	[a]	(138 Hz)	[a]
(N)CH_3 (^{15}N)	−376	−377	−376

[a] Not determined.

where the forminium nitrogen atom retains a strong bonding contact with the central metal atom. The presence of a (Zr−N−CH_2) three-membered ring is further indicated by the rather large $^1J_{CH}$ coupling constants (155 and 146 Hz). They are much larger than the $^1J_{CH}$ value of the adjacent N(CH_3) group (138 Hz). We thus conclude that phosphane addition to the zirconium atom in **3** does not lead to the opening of the (Zr−N−CH_2) three-membered ring structure of the cationic organometallic C−H activation product. The (η^2-formaldiminium)zirconocene unit is still intact in the complexes **6a**−**c**.

We then treated **3** with benzophenone.[12] As expected, a rapid reaction takes place. The spectra of the isolated product (57% yield) indicated that carbon−carbon coupling between the *N*-methylene group and the carbonyl carbon atom had taken place − i.e. the ketone inserts into the Zr−CH_2(N) σ bond of the starting material **3**, to yield the new cation complex **7**. The former carbonyl carbon atom (C-8 in Scheme 3) now shows a ^{13}C-NMR shift of δ = 81.0,[13] and the C-7 resonance signal is at δ = 66.8. Both values indicate that carbon−carbon coupling has taken place and that the three-membered ring was opened. The most remarkable feature of the new complex **7** is that it is chiral. This is evident from the NMR-spectroscopic obser-



9 R = H (**a**), –CMe_3 (**b**) **10**

Scheme 3. Insertion reactions of **3** (all complexes with $[CH_3B(C_6F_5)_3]^-$ anion)

vation of diastereotopic methyl groups at C-4 [δ = 1.65, 1.50 (^{1}H); 25.5, 22.5 (^{13}C)], diastereotopic hydrogen atoms at C-7 (δ = 3.90, 3.57), diastereotopic phenyl groups at C-8 and diastereotopic pairs of the C-2-H and C-3-H C_5H_4-methine moieties [δ = 6.45, 6.37, 6.23, 6.17 (^{1} H); 125.9, 107.5, 106.7, 104.9 (^{13}C)]. The chirality of **7** may result from the internal coordination of the nitrogen atom to the zirconium center, or from the internal ion pairing by $CH_3B(C_6F_5)_3^-$ anion coordination to the metal center. The available spectroscopic data [^{15}N-NMR resonance signals at δ = −339 in CD_2Cl_2, −344 in C_6D_6/[D_8]THF (1:1); $CH_3B(C_6F_5)_3^-$ resonance signals at δ = 0.40 (^{1}H NMR) and 9.4 (^{13}C NMR)] are inconclusive. Without an X-ray crystal-structure analysis it was not possible to decide, with conclusive certainty, between these two possibilities. Tentatively, we assigned complex **7** a structure with a weak intramolecular metal−nitrogen interaction.

Complex **3** readily inserts a variety of reactive α-olefins, such as ethene, propene, 1-butene or 1-decene at low temperature (−50 °C). In each case a single mono-insertion product was formed regioselectively[14,15] (regular [1,2]addition was observed[3] to give the β-alkyl-substituted products in the latter cases). However, all these products rapidly decomposed upon warming to 0 °C with the formation of as yet unidentified product mixtures. Due to this thermal instability these products could not be isolated, and we have limited ourselves to briefly describing the spectroscopic characterization of the ethene-mono-insertion product **8** (for further data see the Supporting Information).

The ethene-insertion product **8** was generated by treatment of **4** with gaseous C_2H_4 at −50 °C in [D_2]dichloromethane and directly characterized by NMR spectroscopy at a low temperature. The NMR spectra show that a C_3H_6 chain connects Zr and N in **8** [^{13}C: δ = 53.4 ($^1J_{CH}$ = 144 Hz, C-7), 14.3 (124 Hz, C-8), and 46.8 (132 Hz, C-9)]. The insertion product **8** is chiral {NMR signals of diastereotopic pairs of C_5H_4 methine groups at δ = 118.4, 117.1, 110.2, 106.9 (^{13}C) and 7.40, 6.44, 6.37, 6.33 (^{1} H); of methyl substituents at C-4 [δ = 1.48, 1.28 (^{1}H); 24.9, 20.9 (^{13}C)] and of hydrogen atoms at the connecting $-CH_2-CH_2-CH_2-$ chain} (see the Experimental Section for details). We assume that the chirality of the molecular framework of complex **8** is due to a (weak) intramolecular nitrogen−zirconium interaction. The corresponding ^{15}N-NMR resonance of **8** is found at δ = −349 (in [D_2]dichloromethane at 223 K).

We then treated the cation **3** with styrene and 4-*tert*-butylstyrene, respectively. The corresponding mono-insertion products **9a**, **9b** are rather stable and can be isolated as solid materials in 70−80% yield. Single crystals of the *p*-*tert*-butylstyrene insertion product **9b** could be obtained. Complex **9b** was characterized by an X-ray crystal-structure analysis (see Figure 1).

The solid-state structure of **9b** shows that a new carbon−carbon bond has been formed between the (N)−CH_2 methylene and the styrene =CH_2 group [C7−C8: 1.514(6) Å]. The adjacent alkyl-substituted benzyl subunit is η^3-coordinated to the zirconium center through the benzylic methine carbon atom and two of the arene carbon atoms, the *ipso*-C and one of the *ortho*-arene carbon atoms.[16] The corresponding C−C bond lengths inside the π-allyl moiety are 1.430(6) Å (C9−C10) and 1.410(5) Å (C10−C11). The (π-allyl)zirconocene unit is *syn*-substituted at C9 [angle C8−C9−C10 123.5(4)°]. As expected, the η^3-benzylic moiety is rather unsymmetrically bonded to the zirconium center[17] with Zr−C9 being much shorter [2.389(4) Å] than Zr−C10 [2.604(4) Å] and Zr−C11 [2.654(4) Å]. The partial π coordination of the arene ring in **9b** results in a slight bond alternation in the remaining framework [C11−C12 1.405(6) Å, C12−C13 1.374(6) Å, C13−C12A 1.423(6) Å, C12A−C11A 1.351(6) Å, C11A−C10 1.424(5) Å].

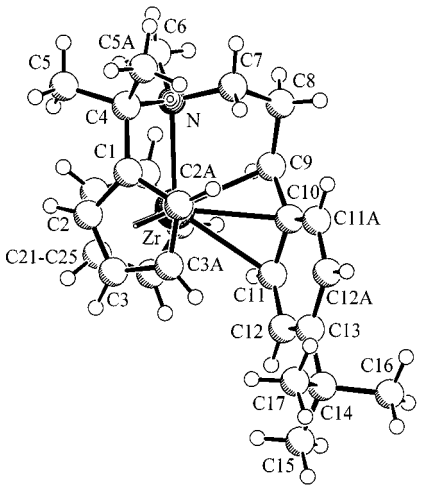


Figure 1. Molecular structure of complex **9b**; selected bond lengths [Å] and angles [°]: Zr−C1 2.461(4), Zr−C2 2.467(4), Zr−C2A 2.501(4), Zr−C3 2.541(4), Zr−C3A 2.560(4), Zr−N 2.498(3), Zr−C9 2.389(4), Zr−C10 2.604(4), Zr−C11 2.654(4), C1−C4 1.502(6), C4−N 1.554(6), N−C7 1.497(5), C7−C8 1.514(6), C8−C9 1.502(6), C9−C10 1.430(6), C10−C11 1.410(5), C10−C11A 1.424(5), C11−C12 1.405(6), C11A−C12A 1.351(6), C12−C13 1.374(6), C12A−C13 1.423(6); C1−C4−N 100.2(3), C4−N−C7 111.1(3), C4−N−Zr 98.4(2), Zr−N−C7 104.8(2), N−C7−C8 111.6(3), C7−C8−C9 111.3(4), C8−C9−Zr 115.8(3), C8−C9−C10 123.5(4), C9−C10−C11 117.6(4), C9−C10−C11A 126.3(4), C9−C10−Zr 65.3(2), C11−C10−Zr 76.4(2), C11A−C10−Zr 122.8(3), C10−C11−C12 121.8(4), C12−C11−Zr 125.4(3)

The Zr−N distance in **9b** is found at 2.498(3) Å. This is clearly within bonding distance,[18] but is substantially longer than that found in e.g. complex **4** [2.312(8) Å].[4] The nitrogen atom in **9b** is a distorted tetrahedron [bond angles C7−N−C4 111.1(3)°, C7−N−C6 107.4(3)°, C6−N−C4 113.9(3)°, Zr−N−C7 104.8(2)°, Zr−N−C6 120.7(3)°, and Zr−N−C4 98.4(2)°, sum of bond angles 656.3° vs. 656.8° of an ideal tetrahedron]. The formation of a small-ring Cp−CMe_2−N−Zr substructure introduces some strain into complex **9b**, which results in a slight distortion of the (η^5-C_5H_4R)Zr coordination [Zr−C(Cp) bond lengths ranging from 2.461(4)/2.467(4) Å through 2.501(4) Å to 2.541(4)/2.560(4) Å].

In principle, this general structural arrangement could have led to the formation of two stereoisomeric [2,1]insertion products[19] of the styrene reagents into the Zr−C(H_2) bond of **3**; however, in the crystal only the stereoisomer with the "tip" of the σ,π-benzyl unit pointing toward the substituted (η⁵-C_5H_4)−CMe_2−(N) ring (*cis* isomer) is observed.

Only a single isomer of **9b** is seen by NMR spectroscopy in solution. Complex **9b** is also chiral in solution. The NMR spectrum shows two pairs of diastereotopic C_5H_4-methine groups (^{13}C-NMR resonances at δ = 124.8, 109.0, 106.9, 101.9; ^{1}H: δ = 5.96, 5.81, 4.66, 4.07), two diastereotopic methyl groups at C-4 [δ = 25.1, 22.5 (^{13}C); δ = 1.45, 1.33 (^{1}H)], and pairs of diastereotopic CH_2 hydrogen atoms at C-7 and C-8 (see the Experimental Section for details). The ^{15}N-NMR resonance of complex **9b** occurs at δ = −352. At low temperature (233 K), the four CH carbon resonances of the arene ring in **9b** are clearly distinguished [^{13}C: δ = 88.7 (C11), 124.0 (C11′), 133.6 (C12), 133.5 (C12′); ^{1}H: δ = 5.46 (11-H), 7.06 (11′-H), 7.30 (12-H), 7.73 (12′-H)]. The $^1J_{CH}$ coupling constant of the C-11-H unit is markedly smaller (150 Hz) than the related arene C-11′/C-12/C-12′-H $^1J_{CH}$ coupling constants, which are all in the typical arene 157−159 Hz range. The ^{13}C-NMR chemical shifts of the remaining carbon atoms of the (σ,π-allyl)Zr subunit of the substituted (η³-benzyl)Zr moiety of **9b** are seen at δ = 135.6 (C-10) and 69.6 ($^1J_{CH}$ = 141 Hz, C-9). The 9-H ^{1}H-NMR signal is located at δ = 3.82.

Complex **9b** shows temperature-dependent NMR spectra of the arene methine signals originating from the substituted styrene reagent. Raising the temperature leads to the broadening of the 11-H/11′-H and 12-H/12′-H pairs of resonances and coalescence. We assume that this dynamic behavior is due to equilibration of the stable σ,π-coordinated η³-arene complex **9b** with a reactive η¹-benzyl-type intermediate[16,20] (**10b**, see Scheme 3), which allows rapid rotation around the C(sp^2)−C(sp^3) σ bond on the NMR time scale, leading to the observed averaging of the pairs of CH resonances. From the 12-H/12′-H ^{1}H-NMR coalescence a Gibbs activation energy of $\Delta G^{\neq}$(278 K) = 10.7 ± 0.4 kcal mol^{-1} is obtained for this dynamic intramolecular equilibration process of complex **9b**.[21]

Styrene insertion into the Zr−C-7 bond of **3** proceeds analogously. Only the [2,1]insertion product is formed,[19] i.e. the regioisomer **9a** that features the arene substituent at the α-carbon atom adjacent to the metal center. This regiochemistry of the insertion reaction allows for the stabilization of the product by distorted η³-benzylic arene coordination. This extra stabilization is likely to be the reason for the observed regiochemistry because there is evidence in the literature that rate-determining insertion in homogeneous metallocene Ziegler chemistry is preceded by a reversible alkene coordination/dissociation equilibrium,[22] which is a prerequisite of such a thermodynamic control of the regiochemistry. Styrene insertion also leads to a single stereoisomer **9a**. We again assume *cis* arrangement of the η³-benzyl stereogenic unit with the substituted Cp ring.

Experimental Section

The reactions were carried out under argon using Schlenk-type glassware or in a glovebox. Solvents were dried and distilled under argon prior to use. − ^{15}N-NMR spectra (60.7 MHz) were recorded with a Varian Unity Plus 600 NMR spectrometer by using a GHMBC pulse sequence (^nJ(^{15}N,^{1}H) = 5 Hz, n = 3, 4). The ^{15}N chemical shift is given with respect to a 2% [^{15}N]benzamide/0.2% $Cr(acac)_3$ sample in DMSO [δ(^{15}N) = −279.3, relative to neat CH_3NO_2, δ(^{15}N) = 0; Ξ(^{15}N) = 10.1367 MHz]. (For additional general information see ref.[4]) The preparation of **3** was described by us previously.[4] Complex **1**[5] and $B(C_6F_5)_3$[6] were prepared as described in the literature.

Reaction of 3 with Triphenylphosphane. − Preparation of 6a: A cold solution (−50 °C) containing **1** (150 mg, 0.45 mmol) in 5 mL of dichloromethane was added to a solution of $B(C_6F_5)_3$ (228 mg, 0.45 mmol) in 5 mL of dichloromethane at −50 °C. The mixture was stirred for 30 min to generate **3**. Triphenylphosphane (117 mg, 0.45 mmol) was then added. The mixture was kept at −50 °C for 15 min and then warmed to room temperature. The product was precipitated as a dark brown oil by the dropwise addition of pentane (5 mL). The supernatant organic phase was decanted. The remaining oil was washed with pentane (5 mL). Pentane (7 mL) was then added and the product stirred overnight to give a solid, which was collected to yield 266 mg of **6a** (54%), m.p. 102 °C (dec. at 212 °C). − ^{1}H NMR ([D_2]dichloromethane, 599.99 MHz): δ = 7.59 (m, 3 H, Ph-*p*-H), 7.54 (m, 6 H, Ph-*m*-H), 7.36 (m, 6 H, Ph-*o*-H), 6.19, 5.93, 5.68, 4.58 (m, each 1 H, C_5H_4), 5.88 (d, $^3J_{PH}$ = 1.5 Hz, 5 H, Cp-H), 2.56 (s, 3 H, 6-H), 1.89 (dd, $^3J_{PH}$ = 4.8 Hz, $^2J_{HH}$ = 9.4 Hz, 1 H, 7-H), 1.64 (dd, $^3J_{PH}$ = 1.9 Hz, $^2J_{HH}$ = 9.4 Hz, 1 H, 7-H), 1.61, 1.01 (s, each 3 H, 5-H, 5-H), 0.50 [br s, 3 H, $B(C_6F_5)_3$-CH_3]. − ^{13}C NMR ([D_2]dichloromethane, 150.84 MHz): δ = 134.0 (d, $^2J_{PC}$ = 19.5 Hz, C-*o*-Ph), 131.7 (C-*p*-Ph), 129.7 (d, $^3J_{PC}$ = 9.0 Hz, C-*m*-Ph), 117.0 (C-1), 113.0, 108.8, 107.2, 96.9 (C_5H_4), 108.2 (C-Cp), 58.6 (C-4), 46.8 (d, $^2J_{PC}$ = 15.5 Hz, C-7), 44.5 (C-6), 25.3, 17.6 (C-5, C-5′); 148.6 [dm, $^1J_{CF}$ = 232 Hz, *o*-$B(C_6F_5)_3$], 137.8 [dm, $^1J_{CF}$ = 241 Hz, *p*-$B(C_6F_5)_3$], 136.8 [dm, $^1J_{CF}$ = 250 Hz, *m*-$B(C_6F_5)_3$], 128.5 [br, *ipso*-$B(C_6F_5)_3$], 10.0 [$B(C_6F_5)_3$-CH_3]; C-*ipso*-Ph resonance not observed. − ^{15}N,^{1}H GHMBC ([D_2]dichloromethane, 60.72/599.99 MHz, 223 K): δ = −376.3/1.61, −376.3/1.01 (N/5-H, N/5′-H). − ^{31}P NMR ([D_2]dichloromethane, 81.02 MHz): δ = 31.2. − $C_{52}H_{38}BF_{15}NPZr$ (1095): calcd. C 57.05, H 3.50, N 1.28; found C 56.10, H 3.75, N 1.15.

Reaction of 3 with Methyldiphenylphosphane. − Preparation of 6b: Analogously as described above a sample of **1** (150 mg, 0.45 mmol) (in 5 mL of dichloromethane) was treated at −36 °C with $B(C_6F_5)_3$ (228 mg, 0.45 mmol) (in 5 mL of dichloromethane), and with methyldiphenylphosphane (89 mg, 0.45 mmol) after 15 min. After workup, as described above, the yield was 237 mg (51%) of complex **6b**, m.p. 199 °C (dec.). − ^{1}H NMR ([D_2]dichloromethane, 599.99 MHz): δ = 7.59 (m, 1 H, Ph-*p*-H), 7.56 (m, 2 H, Ph-*m*-H), 7.51 (m, 1 H, Ph-*p*-H), 7.50 (m, 2 H, Ph-*m*-H), 7.35 (m, 2 H, Ph-*o*-H), 7.21 (m, 2 H, Ph-*o*-H), 6.17, 5.97, 5.80, 4.33 (m, each 1 H, C_5H_4), 5.94 (d, $^3J_{PH}$ = 1.7 Hz, 5 H, Cp−H), 2.52 (s, 3 H, 6-H), 2.05 (d, $^2J_{PH}$ = 6.6 Hz, 3 H, PCH_3), 1.89 (dd, $^2J_{HH}$ = 9.5 Hz, $^3J_{PH}$ = 4.7 Hz, 1 H, 7-H), 1.61, 1.01 (s, each 3 H, 5-H, 5′-H), 1.43 (dd, $^2J_{HH}$ = 9.5 Hz, $^3J_{PH}$ = 2.0 Hz, 1 H, 7-H′), 0.50 [br s, 3 H, $B(C_6F_5)_3$-CH_3]. − ^{13}C {GATED} NMR ([D_2]dichloromethane, 150.84 MHz): δ = 134.9 (d, $^1J_{PC}$ = 36.0 Hz, C-*ipso*-Ph), 133.4 [C-*ipso*-Ph (from GHMBC)], 133.0 (d, $^2J_{PC}$ = 11.2 Hz, C-*o*-Ph), 131.9 (C-*p*-Ph), 131.4 (d, $^2J_{PC}$ = 10.1 Hz, C-*o*-Ph), 131.2 (C-*p*-Ph), 129.8 (d, $^3J_{PC}$ = 9.2 Hz, C-*m*-Ph), 129.5 (d, $^3J_{PC}$ = 9.2 Hz, C-*m*-Ph),

112.6 (C-1), 108.3, 107.0, 106.5, 96.7 (C_5H_4), 107.5 (C-Cp), 58.7 (C-4), 45.9 (d, $^1J_{PC}$ = 15.7 Hz, $^1J_{CH}$ = 146 Hz, $^1J_{CH}$ = 155 Hz, C-7), 44.7 ($^1J_{CH}$ = 138 Hz, C-6), 25.3 ($^1J_{CH}$ = 128 Hz), 17.3 ($^1J_{CH}$ = 128 Hz) (C-5, C-5′), 15.0 ($^1J_{PC}$ = 24.0 Hz, $^1J_{CH}$ = 132 Hz, P*C*H$_3$); 148.6 [dm, $^1J_{CF}$ = 239 Hz, *o*-B(C_6F_5)$_3$], 137.8 [dm, $^1J_{CF}$ = 240 Hz, *p*-B(C_6F_5)$_3$], 136.8 [dm, $^1J_{CF}$ = 245 Hz, *m*-B(C_6F_5)$_3$], 10.5 [B(C_6F_5)$_3$-*C*H$_3$]; *ipso*-B(C_6F_5)$_3$ signal not observed. − ^{15}N,^{1}H GHMBC ([D$_2$]dichloromethane, 60.72/599.99 MHz): δ = −376.7/1.61, −376.7/ 1.01 (N/5-H, N/5-H′). − $C_{47}H_{36}BF_{15}NPZr$ (1033): calcd. C 54.66, H 3.51; found C 54.65, H 3.71.

Reaction of 3 with Cyclopropyl(diphenyl)phosphane. − Preparation of 6c: Complex **3** was generated analogously as described above by treatment of **1** (150 mg, 0.45 mmol) with B(C_6F_5)$_3$ (228 mg, 0.45 mmol) in 3 mL of dichloromethane at −36 °C. Cyclopropyl-(diphenyl)phosphane (101 mg, 0.45 mmol) was added. The mixture was kept at −36 °C for 15 min and then warmed to room temperature. After workup, as described above, the yield was 243 mg (51%) of **6c**, m.p. 195 °C (decomp.). − ^{1}H NMR ([D$_2$]dichloromethane, 599.99 MHz): δ = 7.57 (m, 2 H, Ph-*p*-H), 7.53 (m, 4 H, Ph-*m*-H), 7.34 (m, 4 H, Ph-*o*-H), 6.11, 5.95, 5.86, 4.90 (m, each 1 H, C_5H_4), 6.02 (d, $^3J_{PH}$ = 1.4 Hz, 5 H, Cp−H), 2.47 (s, 3 H, 6-H), 1.79 (m, 1 H, 7-H), 1.61, 1.03 (s, each 3 H, 5-H, 5′-H), 1.43 (m, 1 H, PC*H*), 1.24 (m, 1 H, 7-H′), 1.14 (m, 2 H, P*c*C*H*$_2$), 0.50 [br s, 3 H, B(C_6F_5)$_3$-C*H*$_3$], 0.34 (m, 2 H, P*c*C*H*$_2$). − ^{13}C NMR ([D$_2$]dichloromethane, 150.84 MHz): δ = 133.5 (d, $^2J_{PC}$ = 10.9 Hz, C-*o*-Ph), 133.4 (d, $^2J_{PC}$ = 10.7 Hz, C-*o*-Ph), 131.8 (C-*p*-Ph), 131.6 (C-*p*-Ph), 129.5 (d, $^3J_{PC}$ = 9.0 Hz, C-*m*-Ph), 129.4 (d, $^3J_{PC}$ = 9.2 Hz, C-*m*-Ph), 112.4 (C-1), 107.9, 107.0, 106.8, 96.8 (C_5H_4), 107.5 (C-Cp), 58.7 (C-4), 46.7 (d, $^2J_{PC}$ = 15.8 Hz, C-7), 44.6 (C-6), 25.4, 17.0 (C-5, C-5′), 14.2 (s, P*C*H), 8.3 (d, $^1J_{PC}$ = 29.2 Hz, P*C*H), 5.7 (br, P*c*C*H*$_2$), 5.4 (d, $^2J_{PC}$ = 4.1 Hz, P*c*C*H*$_2$); 148.6 [dm, $^1J_{CF}$ = 239 Hz, *o*-B(C_6F_5)$_3$], 137.8 [dm, $^1J_{CF}$ = 240 Hz, *p*-B(C_6F_5)$_3$], 136.8 [dm, $^1J_{CF}$ = 245 Hz, *m*-B(C_6F_5)$_3$], 10.2 [B(C_6F_5)$_3$-*C*H$_3$]; *ipso*-B(C_6F_5)$_3$ and C-*ipso*-Ph signals not observed. − ^{15}N,^{1}H GHMBC ([D$_2$]dichloromethane, 60.72/599.99 MHz): δ = −376.2/1.61, −376.2/1.03 (N/5-H, N/5′-H). − $C_{49}H_{38}BF_{15}NPZr$ (1059): calcd. C 55.58, H 3.62, N 1.32; found C 55.70, H 3.50, N 1.31.

Reaction of 3 with Benzophenone. − Preparation of 7: A cold solution (−30 °C) containing **1** (150 mg, 0.45 mmol) in 3 mL of bromobenzene was treated with a solution of B(C_6F_5)$_3$ (228 mg, 0.45 mmol) in 6 mL of bromobenzene at −30 °C. The mixture was stirred for 15 min to generate **3**. Benzophenone (81 mg, 0.45 mmol) was then added. After 15 min at −30 °C, the red mixture was warmed to room temperature and the product was precipitated as a red oil by the addition of pentane (6 mL). The organic phase was decanted off. The residue was washed 4 times with pentane (3 mL each) and dried in vacuo to yield 265 mg (58%) of **7**, m.p. 213 °C (dec.). − ^{1}H NMR ([D$_2$]dichloromethane, 599.99 MHz, 223 K): δ = 7.71 (m, 2 H, Ph-*o*-H), 7.48 (m, 2 H, Ph-*m*-H), 7.35 (m, 1 H, Ph-*p*-H), 7.22 (m, 2 H, Ph-*o*-H), 7.11 (m, 3 H, Ph-*m*-H, Ph-*p*-H), 6.45, 6.37, 6.23, 6.17 (C_5H_4), 6.11 (s, 5 H, Cp-H), 3.90 (d, $^2J_{HH}$ = 13.8 Hz, 1 H, 7-H), 3.57 (d, $^2J_{HH}$ = 13.8 Hz, 1 H, 7-H), 2.41 (s, 3 H, 6-H), 1.65, 1.50 (s, each 3 H, 5-H, 5′-H), 0.40 [br s, 3 H, B(C_6F_5)$_3$-C*H*$_3$]. − ^{13}C NMR ([D$_2$]dichloromethane, 150.84 MHz, 223 K): δ = 147.0, 143.9 (each C-*ipso*-Ph), 128.3, 128.3 (each C-*m*-Ph), 127.3, 126.7 (C-*p*-Ph), 125.5, 124.4 (C-*o*-Ph), 125.9, 107.5, 106.7, 104.9 (C_5H_4), 125.0 (C1), 114.2 (C-Cp), 88.4 (C-8), 66.6 (C-7), 61.0 (C-4), 41.7 (C-6), 25.5, 22.5 (C-5, C-5′), 147.7 [dm, $^1J_{CF}$ = 241 Hz, *o*-B(C_6F_5)$_3$], 137.0 [dm, $^1J_{CF}$ = 250 Hz, *p*-B(C_6F_5)$_3$], 135.9 [dm, $^1J_{CF}$ = 247 Hz, *m*-B(C_6F_5)$_3$], 128.1 [br, *ipso*-B(C_6F_5)$_3$], 9.4 [B(C_6F_5)$_3$-C*H*$_3$]. − ^{15}N,^{1}H GHMBC ([D$_2$]dichloromethane, 60.72/599.99 MHz, 223 K): δ = −339.2/1.65, −339.2/1.50 (N/5-H, N/5-H). − $C_{47}H_{33}BF_{15}NOZr$ (1014.8): calcd. C 55.63, H 3.28, N 1.38; found C 55.52, H 3.47, N 1.46.

Treatment of 3 with Ethene. − Generation of 8: The insertion reaction was carried out as an NMR-spectroscopic experiment. A sample of **1** (11 mg, 29 μmol) was dissolved in 0.5 mL of [D$_2$]dichloromethane and this mixture was added at −50 °C to solid B(C_6F_5)$_3$ (15 mg, 29 μmol). The formation of **3** was monitored by NMR spectroscopy. Gaseous ethene (2 mL) was then introduced into the solution. The NMR-spectroscopic analysis at −50 °C revealed the clean formation of **8**. − ^{1}H NMR ([D$_2$]dichloromethane, 599.99 MHz, 223 K): δ = 7.40 (m, 1 H, 2′-H), 6.58 (s, 5 H, Cp-H), 6.44, 6.33 (m, each 1 H, 3-H, 3′-H), 6.37 (m, 1 H, 2-H), 3.38 (pt, 1 H, 7-H), 2.36 (m, 1 H, 9-H), 2.29 (m, 1 H, 7-H′), 2.27 (s, 3 H, 6-H), 2.02 (m, 1 H, 8-H), 1.75 (m, 1 H, 9-H′), 1.54 (m, 1 H, 8-H′), 1.48, 1.28 (s, each 3 H, 5-H, 5′-H), 0.39 [br s, 3 H, (C_6F_5)$_3$BC*H*$_3$]. − ^{13}C {GATED} NMR ([D$_2$]dichloromethane, 150.84 MHz, 223 K): δ = 121.8 (C-1), 118.4 ($^1J_{CH}$ = 177 Hz), 110.2 ($^1J_{CH}$ = 177 Hz) (C-3, C-3′), 117.1 ($^1J_{CH}$ = 175 Hz, C-2′), 115.2 ($^1J_{CH}$ = 175 Hz, C-Cp), 106.9 ($^1J_{CH}$ = 173 Hz, C-2), 63.1 (C-4), 53.4 ($^1J_{CH}$ = 144 Hz, C-7), 46.8 ($^1J_{CH}$ = 132 Hz, C-9), 41.2 ($^1J_{CH}$ = 139 Hz, C-6), 24.9 ($^1J_{CH}$ = 129 Hz), 20.9 ($^1J_{CH}$ = 129 Hz) (C-5, C-5′); 14.3 ($^1J_{CH}$ = 124 Hz, C-8), 147.7 [dm, $^1J_{CF}$ = 238 Hz, *o*-B(C_6F_5)$_3$], 137.0 [dm, $^1J_{CF}$ = 254 Hz, *p*-B(C_6F_5)$_3$], 135.9 [dm, $^1J_{CF}$ = 242 Hz, *m*-B(C_6F_5)$_3$], 127.8 [br, *ipso*-B(C_6F_5)$_3$], 9.5 [B(C_6F_5)$_3$-*C*H$_3$]. − ^{15}N,^{1}H GHMBC ([D$_2$]dichloromethane, 60.72/599.99 MHz, 223 K): δ = −348.9/1.48, −348.9/1.28 (N/5-H, N/5′-H).

Reaction of 3 with Styrene. − Preparation of 9a: A cold solution (−36 °C) containing **1** (150 mg, 0.45 mmol) in 3 mL of dichloromethane was added to solid B(C_6F_5)$_3$ (228 mg, 0.45 mmol). The mixture was stirred for 30 min to generate **3**. Styrene (47 mg, 0.45 mmol) was then added. After 45 min at −36 °C, the mixture was warmed to room temperature and the product was precipitated as a red oil by the dropwise addition of pentane (9 mL). The organic phase was carefully decanted. The remaining oil was washed with pentane (3 × 3 mL). Pentane (9 mL) was then added and the product stirred overnight to give a pale red solid, which was collected to yield 334 mg (79%) of **9a**, m.p. 211 °C (dec.). − ^{1}H NMR ([D$_2$]dichloromethane, 599.99 MHz): δ = 7.57 (m, 2 H, 12-H, 12′-H), 7.21 (t, $^3J_{HH}$ = 6.0 Hz, 13-H), 6.35 (s, 5 H, Cp-H), 5.97, 5.85, 4.71, 4.27 (m, each 1 H, C_5H_4), 3.92 (pd, 1 H, 9-H), 3.62 (m, 1 H, 7-H), 2.78 (m, 1 H, 8-H), 2.69 (m, 1 H, 7-H′), 2.42 (s, 3 H, 6-H), 2.35 (m, 1 H, 8-H′), 1.50, 1.39 (s, each 3 H, 5-H, 5-H′), 0.50 [br s, 3 H, B(C_6F_5)$_3$-C*H*$_3$]; remaining Ph-H signals not observed because of a dynamic process. − ^{1}H NMR ([D$_2$]dichloromethane, 599.99 MHz, 223 K): δ = 7.63 (t, $^3J_{HH}$ = 8.0 Hz, 1 H, 12′-H), 7.42 (t, $^3J_{HH}$ = 8.0 Hz, 1 H, 12-H), 7.15 (t, $^3J_{HH}$ = 8.0 Hz, 1 H, 13-H), 7.07 (d, $^3J_{HH}$ = 8.0 Hz, 1 H, 11′-H), 5.49 (d, $^3J_{HH}$ = 8.0 Hz, 1 H, 11-H), 6.31 (s, 5 H, Cp-H), 5.95, 5.82, 4.62, 4.19 (m, each 1 H, C_5H_4), 3.87 (m, 1 H, 9-H), 3.54 (m, 1 H, 7-H), 2.72 (m, 1 H, 8-H), 2.64 (m, 1-H, 7-H′), 2.36 (s, 3 H, 6-H), 2.29 (m, 1 H, 8-H′), 1.45, 1.33 (s, each 3 H, 5-H, 5′-H), 0.39 [br s, 3 H, B(C_6F_5)$_3$-C*H*$_3$]. − ^{13}C {GATED} NMR ([D$_2$]dichloromethane, 150.84 MHz, 223 K): δ = 138.4 (C-10), 139.3 ($^1J_{CH}$ = 162 Hz, C-12), 134.7 ($^1J_{CH}$ = 160 Hz, C-12′), 125.9, 109.3, 106.2, 102.0 (C_5H_4), 124.1 ($^1J_{CH}$ = 162 Hz, C-13), 123.6 ($^1J_{CH}$ = 160 Hz, C-11′), 118.6 (C-1), 112.1 (C-Cp), 88.2 ($^1J_{CH}$ = 150 Hz, C-11), 70.0 ($^1J_{CH}$ = 145 Hz, C-9), 63.4 (C-7), 61.5 (C-4), 40.8 (C-6), 25.1, 22.6 (C-5, C-5′), 23.8 (C-8), 147.6 [dm, $^1J_{CF}$ = 240 Hz, *o*-B(C_6F_5)$_3$], 137.2 [dm, $^1J_{CF}$ = 259 Hz *p*-B(C_6F_5)$_3$], 135.8 [dm, $^1J_{CF}$ = 240 Hz, *m*-B(C_6F_5)$_3$], 127.8 [br, *ipso*-B(C_6F_5)$_3$], 9.5 [B(C_6F_5)$_3$-*C*H$_3$]. − ^{15}N,^{1}H GHMBC ([D$_2$]dichloromethane, 60.72/599.99 MHz): δ = −352.7/1.50,

−352.7/1.39 (N/5-H, N/5′-H). − Coalescence: 12-H and 12′-H: $\Delta G^{\neq} = 10.6 \pm 0.5$ kcal/mol ($T_C = 268$ K, $\Delta\nu = 126$ Hz; $[D_2]$dichloromethane). − $C_{42}H_{31}BF_{15}NZr$ (936.7): calcd. C 53.85, H 3.34, N 1.50; found C 54.00, H 3.28, N 1.23.

Reaction of 3 with 4-*tert*-Butylstyrene. − Preparation of 9b: Analogously as described above, complex **1** (150 mg, 0.45 mmol) was treated with $B(C_6F_5)_3$ (228 mg, 0.45 mmol) in dichloromethane (−36 °C) and after 15 min with 4-*tert*-butylstyrene (72 mg, 0.45 mmol). After 30 min at −36 °C, the mixture was warmed to room temperature. After workup as described above, the yield was 321 mg (72%) of complex **9b**. Single crystals of **9b** suitable for the X-ray crystal structure analysis were obtained by allowing diethyl ether vapor to diffuse into a solution of **9b** in dichloromethane at −36 °C; m.p. 124 °C. − ^{1}H NMR ($[D_2]$dichloromethane, 599.99 MHz): δ = 7.60 (br m, 2 H, 12′-H, 12-H), 6.34 (s, 5 H, Cp-H), 5.98, 5.83, 4.73, 4.16 (m, each 1 H, C_5H_4), 3.86 (pd, 1 H, 9-H), 3.62 (m, 1 H, 7-H), 2.77 (m, 1 H, 8-H), 2.67 (m, 1 H, 7-H′), 2.40 (s, 3 H, 6-H), 2.34 (m, 1 H, 8-H′), 1.50, 1.38 (s, each 3 H, 5-H, 5′-H), 1.34 (s, 9 H, 15-H), 0.50 [br s, 3 H, $B(C_6F_5)_3$-CH_3]; remaining Ph-H signals not observed because of a dynamic process. −^{1}H NMR ($[D_2]$dichloromethane, 599.99 MHz, 233 K): δ = 7.73 (d, $^3J_{HH}$ = 7.5 Hz, 1 H, 12′-H), 7.30 (d, $^3J_{HH}$ = 8.7 Hz, 1 H, 12-H), 7.06 (d, $^3J_{HH}$ = 7.5 Hz, 1 H, 11′-H), 6.31 (s, 5 H, Cp-H), 5.96, 5.81, 4.66, 4.07 (m, each 1 H, C_5H_4), 5.46 (d, $^3J_{HH}$ = 8.7 Hz, 1 H, 11-H), 3.82 (pd, 1 H, 9-H), 3.55 (m, 1 H, 7-H), 2.72 (m, 1 H, 8-H), 2.64 (m, 1 H, 7-H′), 2.35 (s, 3 H, 6-H), 2.28 (m, 1 H, 8-H′), 1.45, 1.33 (s, each 3 H, 5-H, 5′-H), 1.29 (s, 9 H, 15-H), 0.42 [br s, 3 H, $B(C_6F_5)_3$-CH_3]. − ^{13}C {GATED} NMR ($[D_2]$dichloromethane, 150.84 MHz, 233 K): δ = 147.6 (C-13), 135.6 (C-10), 133.6 ($^1J_{CH}$ = 159 Hz, C-12), 133.5 ($^1J_{CH}$ = 157 Hz, C-12′), 124.8 ($^1J_{CH}$ = 175 Hz), 109.0 ($^1J_{CH}$ = 174 Hz), 106.9 ($^1J_{CH}$ = 175 Hz), 101.9 ($^1J_{CH}$ = 173 Hz) (C_5H_4), 124.0 ($^1J_{CH}$ = 159 Hz, C-11′), 118.9 (C-1), 112.1 ($^1J_{CH}$ = 175 Hz, C-Cp), 88.7 ($^1J_{CH}$ = 150 Hz, C-11), 69.6 ($^1J_{CH}$ = 141 Hz, C-9), 63.6 ($^1J_{CH}$ = 136 Hz, C-7), 61.5 (C-4), 40.8 ($^1J_{CH}$ = 138 Hz, C-6), 34.4 (C-14), 30.6 ($^1J_{CH}$ = 126 Hz, C-15), 25.1 ($^1J_{CH}$ = 127 Hz), 22.5 ($^1J_{CH}$ = 128 Hz) (C-5, C-5′), 24.1 ($^1J_{CH}$ = 126 Hz, C-8), 148.6 [dm, $^1J_{CF}$ = 234 Hz, *o*-$B(C_6F_5)_3$], 137.8 [dm, $^1J_{CF}$ = 239 Hz, *p*-$B(C_6F_5)_3$], 136.8 [dm, $^1J_{CF}$ = 248 Hz, *m*-$B(C_6F_5)_3$], 128.7 [br, *ipso*-$B(C_6F_5)_3$], 9.9 [$B(C_6F_5)_3$-CH_3]. − ^{15}N,^{1}H GHMBC ($[D_2]$dichloromethane, 60.72/599.99 MHz): δ = −352.4/1.45, −352.4/1.33 (N/5-H, N/5′-H). − Coalescence: 12-H and 12′-H: $\Delta G^{\neq} = 10.7 \pm 0.5$ kcal/mol ($T_C = 278$ K, $\Delta\nu = 258$ Hz; $[D_2]$dichloromethane) − $C_{46}H_{39}BF_{15}NZr$ (992.8): calcd. C 55.65, H 3.96, N 1.41; found C 55.44, H 4.14, N 1.34. −

X-ray Crystal Structure Analysis of 9b: Empirical formula $C_{46}H_{39}BF_{15}NZr$, M = 992.8, yellow crystal 0.25 × 0.20 × 0.20 mm, a = 12.881(1) Å, b = 13.411(1) Å, c = 13.406(1) Å, α = 87.51(1)°, β = 63.99(1)°, γ = 86.67(1)°, V = 2077.4(3) Å^3, $\rho_{calcd.}$ = 1.587 g cm^{-3}, μ = 3.68 cm^{-1}, empirical absorption correction via ψ scan data (0.914 ≤ T ≤ 0.930), Z = 2, triclinic, space group $P\bar{1}$ (No. 2), λ = 0.71073 Å, T = 223 K, ω/2θ scans, 8809 reflections collected (+h, ±k, ±l), [(sinθ)/λ] = 0.62 Å^{-1}, 8420 independent (R_{int} = 0.063) and 6020 observed reflections [$I \geq 2\,\sigma(I)$], 584 refined parameters, R = 0.053, wR^2 = 0.141, max. residual electron density 0.92 (−0.90) e Å^{-3}, hydrogen atoms calculated and refined as riding atoms. The data set was collected with a Nonius MACH3 diffractometer, equipped with a rotating anode generator Nonius FR591. Programs used: data collection EXPRESS (Nonius B.V., **1994**); data reduction MolEN (K. Fair, Enraf Nonius B.V., **1990**); structure solution SHELXS-97 (G. M. Sheldrick, *Acta Crystallogr.* **1990**, *A46*, 467−473), structure refinement SHELXL-97 (G. M. Sheldrick, Universität Göttingen, **1997**); graphics (with unsystematical numbering schemes) SCHAKAL (E. Keller, Universität Freiburg, **1997**). Crystallographic data (excluding structure factors) for the structure reported in this paper have been deposited with the Cambridge Crystallographic Data Centre as supplementary publication CCDC-138759. Copies of the data can be obtained free of charge on application to CCDC, 12 Union Road, Cambridge CB2 1EZ, UK [Fax: (internat.) + 44-1223/336-033, E-mail: deposit@ccdc.cam.ac.uk].

Supporting Information Available: Additional spectroscopic details and characterization of additional reaction products of **3** with organic carbonyl compounds and alkenes. Supporting information for this article is available on the WWW under http://www.wiley-vch.de/home/eurjic or from the author.

Acknowledgments

Financial support from the Fonds der Chemischen Industrie and the Deutsche Forschungsgemeinschaft is gratefully acknowledged.

[1] R. F. Jordan, W. E. Dasher, S. F. Echols, *J. Am. Chem. Soc.* **1986**, *108*, 17118−17119. R. F. Jordan, C. S. Bajgur, R. Willet, B. Scott, *J. Am. Chem. Soc.* **1986**, *108*, 7410−7411. R. F. Jordan, *Adv. Organomet. Chem*. **1991**, *32*, 325−387.
[2] P. Cossee, *J. Catal*. **1964**, *3*, 80−88. E. J. Arlmann, P. Cossee, *J. Catal*. **1964**, *3*, 99−100.
[3] M. Aulbach, F. Küber, *Chem. Unserer Zeit* **1994**, *28*, 197−208. H.-H. Brintzinger, D. Fischer, R. Mülhaupt, B. Rieger, R. M. Waymouth, *Angew. Chem*. **1995**, *107*, 1255−1283; *Angew. Chem. Int. Ed. Engl*. **1995**, *34*, 1143−1171. M. Bochmann, *J. Chem. Soc., Dalton Trans.* **1996**, 255−270. W. Kaminsky, *J. Chem. Soc., Dalton Trans.* **1998**, 1413−1418. A. L. McKnight, R. M. Waymouth, *Chem. Rev.* **1998**, *98*, 2587−2598.
[4] J. Pflug, A. Bertuleit, G. Kehr, R. Fröhlich, G. Erker, *Organometallics* **1999**, *18*, 3818−3826.
[5] A. Bertuleit, C. Fritze, G. Erker, R. Fröhlich, *Organometallics* **1997**, *16*, 2891−2899. A. Bertuleit, M. Könemann, L. Duda, G. Erker, R. Fröhlich, *Top. Catal*. **1999**, *7*, 37−44.
[6] [6a] A. G. Massey, A. J. Park, F. G. A. Stone, *Proceedings Chem. Soc*. **1963**, 212. A. G. Massey, A. J. Park, *J. Organomet. Chem*. **1964**, *2*, 245−250. A. G. Massey, A. J. Park in *Organometallic Synthesis* (Eds.: R. B. King, J. J. Eisch), Elsevier, New York, **1986**, vol. 3, p. 461−462. − [6b] X. Yang, C. L. Stern, T. J. Marks, *J. Am. Chem. Soc.* **1994**, 116, 10015−10031. See also: B. Temme, G. Erker, J. Karl, H. Luftmann, R. Fröhlich, S. Kotila, *Angew. Chem.* **1995**, *107*, 1867−1869; *Angew. Chem. Int. Ed. Engl*. **1995**, *34*, 1755−1757.
[7] For additional organometallic examples that show this spectroscopic effect see e.g.: K. Kropp, V. Skibbe, G. Erker, C. Krüger, *J. Am. Chem. Soc.* **1983**, *105*, 3353−3354. G. Erker, *Acc. Chem. Res.* **1984**, *17*, 103−109. G. Erker, R. Schlund, C. Krüger, *J. Chem. Soc., Chem. Commun.* **1986**, 1403−1404. G. Erker, U. Hoffmann, R. Zwettler, P. Betz, C. Krüger, *Angew. Chem.* **1989**, *101*, 644−645; *Angew. Chem. Int. Ed. Engl*. **1989**, *28*, 630−631. U. Blaschke, G. Erker, M. Nissinen, E. Wegelius, R. Fröhlich, *Organometallics* **1999**, *18*, 1224−1234. H. C. Strauch, K. Bergander, G. Kehr, R. Fröhlich, G. Erker, *Eur. J. Inorg. Chem.* **1999**, 1461−1466.
[8] See for a comparison: H. G. Alt, K. Föttinger, W. Milius, *J. Organomet. Chem*. **1999**, *572*, 21−30.
[9] For remotely related systems see e.g.: H. H. Karsch, K.-A. Schreiber, M. Reisky, *Organometallics* **1998**, *17*, 5052−5060.
[10] See for a comparison: R. F. Jordan, P. K. Bradley, N. C. Baenziger, R. E. LaPointe, *J. Am. Chem. Soc*. **1990**, *112*, 1289−1291. Z. Hou, T. L. Breen, D. W. Stephan, *Organometallics* **1993**, *12*, 3158−3167. T. L. Breen, D. W. Stephan, *J. Am. Chem. Soc*. **1995**, *117*, 11914−11921.
[11] G. Erker, U. Dorf, C. Krüger, K. Angermund, *J. Organomet. Chem*. **1986**, *301*, 299−312. B. E. Bosch, G. Erker, R. Fröhlich, O. Meyer, *Organometallics* **1997**, *16*, 5449−5456.
[12] For other examples of ketone addition products to reactive Zr−C bonds see: G. Erker, K. Engel, J. L. Atwood, W. E. Hunter, *Angew. Chem.* **1983**, *95*, 506−507; *Angew. Chem. Int.*

Ed. Engl. **1983**, *22*, 494−495; G. Erker, U. Dorf, *Angew. Chem.* **1983**, *95*, 800; *Angew. Chem. Int. Ed. Engl*. **1983**, *22*, 777−778. R. F. Jordan, W. E. Dasher, S. F. Echols, *J. Am. Chem. Soc*. **1986**, *108*, 1718−1719. See also: H. C. Strauch, G. Erker, R. Fröhlich, M. Nissinen, *Eur. J. Inorg. Chem.* **1999**, 1453−1459.

[13] See for a comparison: F. Rosenfeldt, G. Erker, *Tetrahedron Lett.* **1980**, *21*, 1637−1640; *J. Organomet. Chem*. **1982**, *224*, 29−42. G. Erker, U. Dorf, P. Czisch, J. L. Petersen, *Organometallics* **1986**, *5*, 668−676.

[14] R. F. Jordan, D. F. Taylor, *J. Am. Chem. Soc*. **1989**, *111*, 778−779. R. F. Jordan, R. E. LaPointe, P. K. Bradley, N. Baenziger, *Organometallics* **1989**, *8*, 2892−2903. R. F. Jordan, D. F. Taylor, N. C. Baenziger, *Organometallics* **1990**, *9*, 1546−1557. A. S. Guram, R. F. Jordan, D. F. Taylor, *J. Am. Chem. Soc*. **1991**, *113*, 1833−1835. A. S. Guram, R. F. Jordan, *Organometallics* **1991**, *10*, 3470−3479. C. Pellecchia, A. Grassi, A. Zambelli, *J. Chem. Soc., Chem. Commun*. **1993**, 947−949. C. Pellecchia, A. Grassi, A. Immirzi, *J. Am. Chem. Soc.* **1993**, *115*, 1160−1162. Z. Guo, D. C. Swenson, R. F. Jordan, *Organometallics* **1994**, *13*, 1424−1432. Y. W. Alelyunas, N. C. Baenziger, P. K. Bradley, R. F. Jordan, *Organometallics* **1994**, *13*, 148−156. C. Pellecchia, A. Immirzi, A. Zambelli, *J. Organomet. Chem*. **1994**, *479*, C9−C11. C. Pellecchia, A. Immirzi, D. Pappalardo, A. Peluso, *Organometallics* **1994**, *13*, 3773−3775. C. Pellecchia, A. Grassi, A. Zambelli, *Organometallics* **1994**, *13*, 298−302. B. Temme, J. Karl, G. Erker, *Chem. Eur. J.* **1996**, *2*, 919−924. J. Karl, G. Erker, *Chem. Ber./Recueil* **1997**, *130*, 1261−1267; *J. Mol. Catal*. **1998**, *128*, 85−102. M. Dahlmann, G. Erker, M. Nissinen, R. Fröhlich, *J. Am. Chem. Soc*. **1999**, *121*, 2820−2828.

[15] For a remotely related system see e.g.: Y. Sun, W. E. Piers, G. P. A. Yap, *Organometallics* **1997**, *16*, 2509−2513. Y. Sun, R. E. v. H. Spence, W. E. Piers, M. Parvez, G. P. A. Yap, *J. Am. Chem. Soc.* **1997**, *119*, 5132−5143. X. Song, M. Bochmann, *J. Organomet. Chem*. **1997**, 545−546; 597−600. H. van der Heijden, B. Hessen, A. G. Orpen, *J. Am. Chem. Soc.* **1998**, *120*, 1112−1113.

[16] F. A. Cotton, M. D. La Prade, *J. Am. Chem. Soc*. **1968**, *90*, 5418−5422. F. A. Cotton, T. J. Marks, *J. Am. Chem. Soc*. **1969**, *91*, 1339−1346. J. R. Blecke, R. R. Burch, C. L. Coulman, B. C. Schardt, *Inorg. Chem*. **1981**, *20*, 1316−1318. R. R. Burch, E. L. Muetterties, V. W. Day, *Organometallics* **1982**, *1*, 188−197. E. Carmona, J. M. Martin, M. Paneque, M. L. Poveda, *Organometallics* **1987**, *6*, 1757−1765. J. D. Debad, P. Legzdins, S. A. Lumb, S. J. Rettig, R. J. Batchelor, F. W. B. Einstein, *Organometallics* **1999**, *18*, 3414−3428.

[17] D. J. Brauer, C. Krüger, *Organometallics* **1982**, *1*, 207−210. G. Erker, K. Engel, U. Dorf, J. L. Atwood, W. E. Hunter, *Angew. Chem*. **1982**, *94*, 915−916; *Angew. Chem. Int. Ed. Engl.* **1982**, *21*, 914. G. Erker, K. Berg, C. Krüger, G. Müller, K. Angermund, R. Benn, G. Schroth, *Angew. Chem*. **1984**, *96*, 445−446; *Angew. Chem. Int. Ed. Engl.* **1984**, *23*, 455−456. E. J. Larson, P. C. Van Dort, J. S. Dailey, J. R. Lakanen, L. M. Pederson, M. E. Silver, J. C. Huffman, S. O. Russo, *Organometallics* **1987**, *6*, 2141−2146. G. Erker, K. Berg, K. Angermund, C. Krüger, *Organometallics* **1987**, *6*, 2620−2621. E. J. Larson, P. C. Van Dort, J. R. Lakanen, D. W. O'Neill, L. M. Pederson, J. J. McCandless, M. E. Silver, S. O. Russo, J. C. Huffman, *Organometallics* **1988**, *7*, 1183−1187. G. Erker, *Angew. Chem*. **1989**, *101*, 411−426; *Angew. Chem. Int. Ed. Engl.* **1989**, *28*, 397−412. B. E. Hauger, P. J. Vance, T. J. Prins, M. E. Wemple, D. A. Kort, M. E. Silver, J. C. Huffman, *Inorg. Chim. Acta* **1991**, *187*, 91−97.

[18] A. G. Orpen, L. Brammer, F. H. Allen, O. Kennard, D. G. Watson, R. Taylor, *J. Chem. Soc., Dalton Trans.* **1989**, S1−S83.

[19] For other stoichiometric and catalytic examples of styrene [2,1]insertion reactions see e.g.: C. Pellecchia, D. Pappalardo, L. Olivia, A. Zambelli, *J. Am. Chem. Soc*. **1995**, *117*, 6593−6594. A. Zambelli, C. Pellecchia, A. Proto, *Macromol. Symp.* **1995**, *89*, 373−382. E. Boring, M. Sabat, M. G. Finn, R. N. Grimes, *Organometallics* **1998**, *17*, 3865−3874.

[20] E. G. Hoffmann, R. Kallweit, G. Schroth, K. Seevogel, W. Stempfle, G. Wilke, *J. Organomet. Chem*. **1975**, *97*, 183−202.

[21] M. L. H. Green, L.-L. Wong, A. Seela, *Organometallics* **1992**, *11*, 2660−2668, and references cited therein.

[22] [22a] J. Karl, M. Dahlmann, G. Erker, K. Bergander, *J. Am. Chem. Soc.* **1998**, *120*, 5643−5652. − [22b] For partially related studies see e.g. M. Brookhart, A. F. Volpe, D. M. Lincoln, I. T. Horváth, J. M. Millar, *J. Am. Chem. Soc.* **1990**, *112*, 5634−5636. C. P. Casey, S. L. Hallenbeck, D. W. Pollock, C. R. Landis, *J. Am. Chem. Soc.* **1995**, *117*, 9770−9771. Z. Wu, R. F. Jordan, *J. Am. Chem. Soc.* **1995**, *117*, 5867−5868. M. V. Galakhov, G. Heinz, P. Royo, *J. Chem. Soc., Chem. Commun*. **1998**, 17−18. C. P. Casey, D. W. Carpenetti II, H. Sakurai, *J. Am. Chem. Soc.* **1999**, *121*, 9483−9484.

Received January 18, 2000
[I00016]

Carboxylation of Acetophenone with Zinc(II) Alkoxides/CO_2 Systems: A Mechanistic Study

Michael Kunert,[a] Michael Bräuer,[a] Olaf Klobes,[b] Helmar Görls,[c] Eckhard Dinjus,*[b] and Ernst Anders[a]

Dedicated to Professor Dirk Walther on the occasion of his 60th birthday

Keywords: Zinc / Carbon dioxide fixation / Carboxylato complexes / CH-acidic substrates / Ab initio calculations

The crystal structures of the homoleptic dimer zinc(II) 2,6-di-*tert*-butylphenoxide (**1b**) and of the corresponding monomer **1b/**$(DMSO)_2$ are presented. The structural motif of **1b** is a Zn–O–Zn–O four-membered ring. The bulky phenoxide ligands led to a coordination number of only three for the zinc atom. Monomer **1b/**$(DMSO)_2$ crystallized as a four-coordinated monomer with a highly distorted tetrahedral geometry around the zinc center. ^{13}C NMR investigations reveal details for the reaction of CO_2 with a series of alkoxide zinc(II)/solvent systems [2,6-dimethylphenoxide zinc(II) (**1a**), zinc(II) 2,6-di-*tert*-butylphenoxide (**1b**), zinc(II) 2,6-diphenylphenoxide (**1c**), zinc(II) 4-*tert*-butylphenoxide (**1d**), and zinc(II) 2-pyridylcarbinolato (**2**)]. The interpretation of the ^{13}C NMR signals agree with ab initio calculations of a model zinc(II) phenoxide/CO_2 system. Experimentally, the carboxylation of acetophenone as a representative for CH-acidic substrates was carried out with specific zinc(II) phenoxide/CO_2 systems. The reactions resulted in yields of ca. 40% of benzoyl acetic acid. The role of the soluble zinc(II) phenylcarbonate intermediate is discussed with respect to the subsequent CO_2 transfer reaction.

Introduction

Several investigations intermediate into the mechanism of the activation of CO_2 by Zn^{II} complexes are documented.[1,2,5] Some of the fundamental understanding was obtained from the investigation of the mechanism of the copolymerization of CO_2 and epoxides.[1,3,5] However, the number of soluble zinc(II) compounds which are amenable to mechanistic investigations is limited. A synthesis first reported by Caulton allows for the preparation of soluble homoleptic zinc(II) alkoxide compounds (Figure 2).[4] The majority of the compounds prepared by this method are monomeric zinc(II) alkoxide structures.[4,5]

Darensbourg reported on the copolymerization process of cyclohexene oxide and CO_2 using zinc(II) phenoxides at 80 °C and a pressure of 55 bar.[5] NMR investigations revealed a shift of the carbon peak of CO_2 (170 ppm). This was demonstrated for the reaction of CO_2 with zinc(II) 2,4,6-trimethylphenoxide in pyridine at room temperature. The insertion of CO_2 into only one metal phenoxide group was proposed. This is in agreement with the X-ray structure of the dimeric $[Cd(S_2CO\text{-}2,6\text{-}Ph_2C_6H_3)]_2(\mu\text{-}O\text{-}2,6\text{-}Ph_2C_6H_3)_2$ obtained from the reaction of CS_2 with the corresponding cadmium(II) phenoxide (cf. Figure 7).[6]

In this paper new results concerning the activation and the transfer of CO_2 mediated by homoleptic zinc(II) alkoxide complexes are reported. The carboxylation of acetophenone to give benzoyl acetic acid at ambient temperature is described (Figure 1). This represents a novel application of easily accessible zinc complexes.

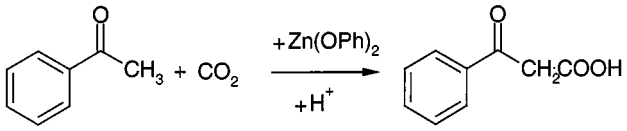


Figure 1. Carboxylation of acetophenone

Results and Discussion

1. Crystal Structure of Zinc(II) 2,6-Di-*tert*-butylphenoxide and Zinc(II) 2,6-Di-*tert*-butylphenoxide/$(DMSO)_2$

X-ray structures of zinc(II) phenoxides thus far reported indicate the preference of monomeric complexes which contain solvent molecules or phosphane ligands in the coordination polyhedron.[1,4,5,7] In the case of dimeric structures, there are heteroleptic compounds such as alkyl(alkyloxy) zinc(II), alkyl(aryloxy) zinc(II) compounds or $\{Zn[\mu\text{-}OCEt_3)[N(SiMe_3)_2]\}_2$.[8] For the zinc(II) 2,4,6-tris-*tert*-butylphenoxide in THF solution, an aggregation to a stereochemically rigid dimer has been reported by Caulton by means of cryoscopic molecular weight determination.[4]

[a] Institut für Organische Chemie und Makromolekulare Chemie der Friedrich-Schiller-Universität,
Humboldtstraße 10, D-07743 Jena, Germany
[b] Forschungszentrum Karlsruhe, Institut für Technische Chemie, Bereich Chemisch-Physikalische Verfahren,
Postfach 3640, 76021 Karlsruhe, Germany
[c] Institut für Anorganische und Analytische Chemie der Friedrich-Schiller-Universität,
August-Bebel-Straße 2, D-07743 Jena, Germany

 © WILEY-VCH Verlag GmbH, D-69451 Weinheim, 2000 1434–1948/00/0808–1803 $ 17.50+.50/0

We now report on the X-ray structure of a homoleptic dimeric zinc(II) 2,6-di-*tert*-butylphenoxide complex crystallized from pentane (Figure 3).[9] The synthesis was performed in THF or toluene under an argon atmosphere, as previously described (Figure 2).[4,5]

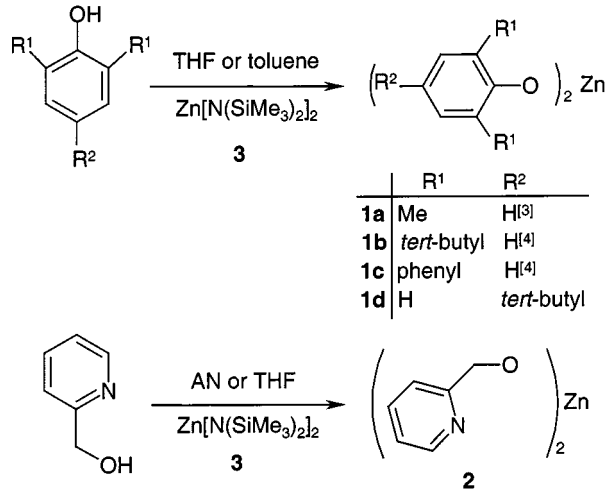


Figure 2. Synthesis of zinc(II) alkoxides

This complex contains a central four-membered Zn−O−Zn−O ring (Figure 3). The metal cation is coordinated in a distorted trigonal planar geometry. The Zn−O bond lengths of the bridging Zn−O−Zn moiety [(Zn1−O2 (1.941(1) Å, Zn1−O4(1.975(1) Å, Zn2−O2(1.980(1) Å, Zn2−O4(1.949(1) Å] are significantly larger than the terminal bonds [Zn1−O1 1.831(1) Å) and Zn2−O3 1.839(1) Å].

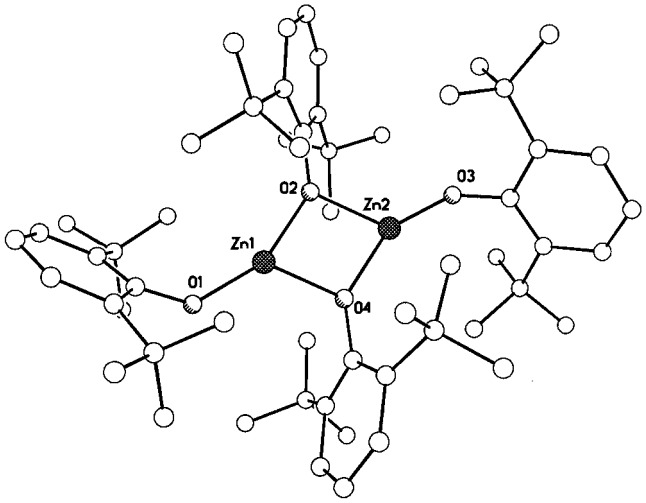


Figure 3. X-ray structure of the dimer of **1b**. Selected distances [Å] and bond angels [°]: Zn1−O1 1.831(2), Zn1−O2 1.941(2), Zn1−O4 1.975(2), Zn2−O3 1.839(2), Zn2−O2 1.980(2), Zn2−O4 1.949(2), Zn1−Zn2 2.9484(6), O1−C1 1.377(4), O3−C29 1.359(4), O2−C15 1.404(4), O4−C43 1.405(4), O1−Zn1−O2 150.5(1), O1−Zn1−O4 125.3(1), O2−Zn1−O4 82.6(1), O4−Zn2−O2 82.3(1)

The terminal zinc O(aryl) distances are equal within the experimental error to those found for the monomeric zinc complexes 2,6-di-*tert*-butylphenoxide−ZnL with L = $MePh_2$ and PCy_3 [Zn−O 1.845(4) and Zn−O 1.869 (3) Å].[7] In these complexes, the zinc atom is also coordinated in an analogous trigonal planar fashion. In the monomeric Zn^{II} phenoxide/(oxygen or nitrogen donor ligand)$_2$ structures which are reported, and also in the structure of **1b**/$(DMSO)_2$ (Figure 4), the zinc atom prefers a distorted tetrahedral coordination.[4,5,10] Also in these cases, the Zn−O bond lengths are in the range of Zn−O 1.846(11) [2,6-diisopropylphenoxide−zinc(II)/$(THF)_2$] to Zn−O 1.908(1) Å [**1b**/$(DMSO)_2$]. They are slightly longer than those of the bridged Zn−O bonds in the homoleptic dimeric structure. In heteroleptic dimeric zinc(II) compounds, the Zn−O distances [e.g. Zn−O 1.970(1) Å,[8a] 1.930(3) Å,[8b] 2.075(2) Å[8c]] are comparable to the bridging Zn−O bonds in **1b**. In general, the addition of solvent molecules to an unsolvated species leads to a ca. 0.1 Å shorter Zn−O(aryl) distance, which is easily understood in terms of electrostatic effects. In the dimeric structure, the oxygen interacts with two zinc centers.

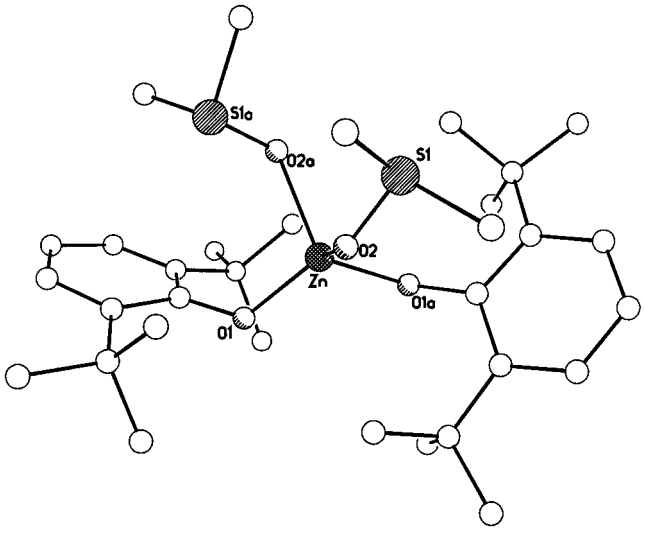


Figure 4. X-ray structure of the monomer of **1b**/$(DMSO)_2$. Selected distances [Å] and bond angels [°]: Zn−O1 1.907(1), Zn−O2 2.044(1), O1−C1 1.341(2), O1−Zn−O2 123.52(4), O1−Zn−O1a 108.77(6), O1−Zn−O2a 104.43(4), O2−Zn−O2a 93.04(7)

2. Reactivity of CO_2 with Zinc(II) Phenoxides in DMSO

The reaction of CO_2 with zinc(II) alkoxides has been studied by means of NMR spectroscopy in order to characterize the structure of a soluble phenoxide zinc(II)/CO_2 intermediate. Such an activated CO_2 is an essential prerequisite to enable the carboxylation of CH-acidic compounds at room temperature. We performed ^{13}C and ^{1}H NMR investigations in [D6]DMSO, [D7]DMF and [D5]pyridine before and after addition of CO_2. A typical NMR experiment is depicted in Figure 5 and 6 (see also Table 1).

After the addition of $^{13}CO_2$ and warming at 40 °C for 6 hours, the spectrum showed the ^{13}C chemical shifts of **1a.** Relative to these ^{13}C NMR signals, a downfield shift of the signals for the phenoxide *para*- and *ortho* carbons of 5.5 and 2.2 ppm (from δ = 113 to δ = 119 and from δ = 126 to δ = 128, respectively) was observed. This was accompanied by an upfield shift of the signal for the *ipso* carbon atom of 7.2 ppm (from δ = 163 to δ = 155). Physically dissolved $^{13}CO_2$ has a chemical shift of δ = 124. Apart from the

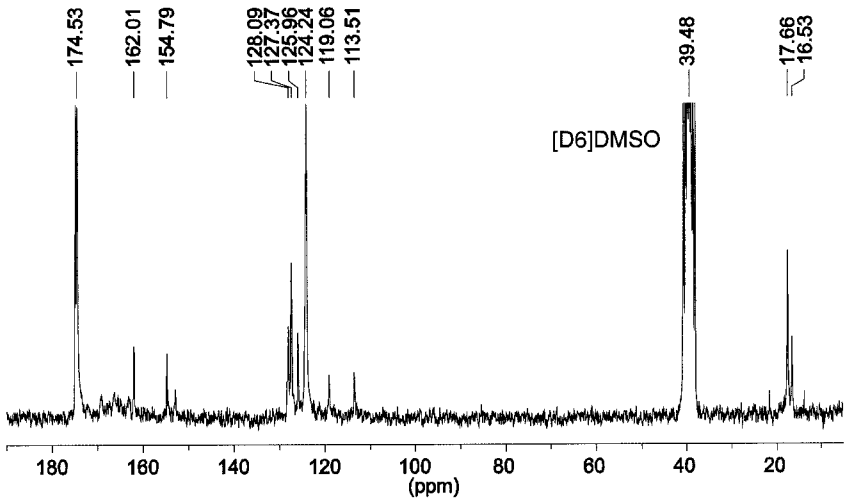


Figure 5. ^{13}C NMR spectra of **1a** in [D_6]DMSO after the addition of $^{13}CO_2$ and 6 h at 40 °C

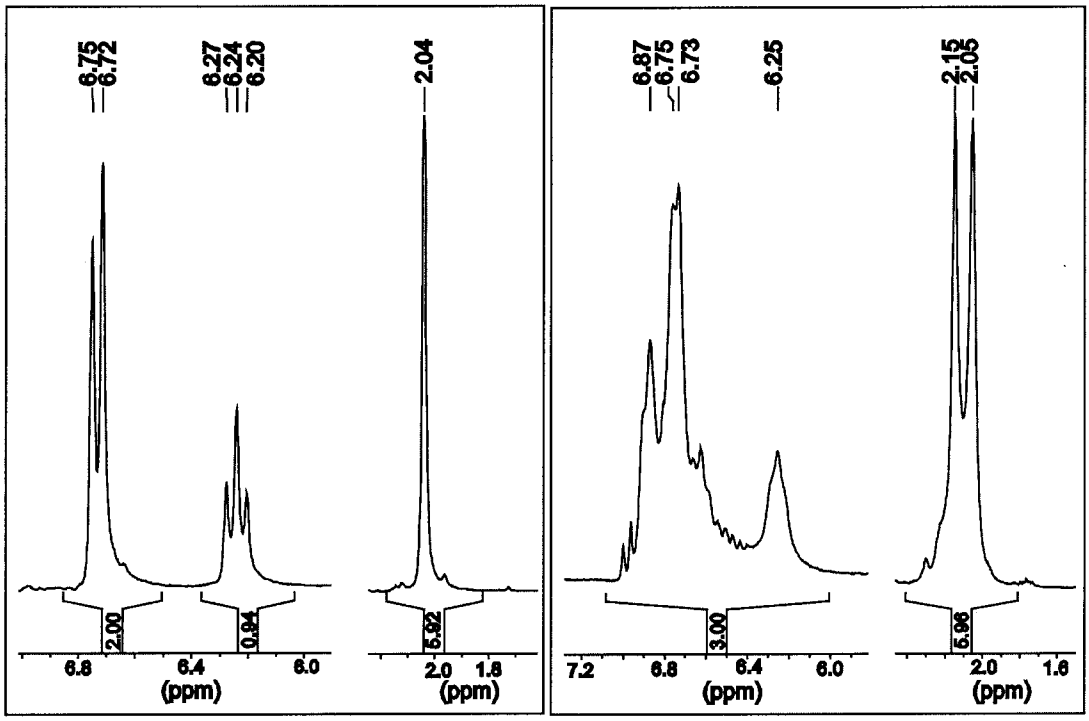


Figure 6. ^1H NMR spectra of **1a** in [D_6]DMSO and after the addition of $^{13}CO_2$ and 6 h at 40 °C

chemical shifts of the phenyl ring carbon atoms, an intense signal was detected at $\delta = 174.3$. After the addition of $^{13}CO_2$, the ^1H NMR spectrum showed a multiplet for the phenoxide hydrogen atoms and a signal at $\delta = 2.15$ in addition to the signal for the methyl hydrogen atom of **1a**. The integration of these two methyl signals suggests a 1:1 molar ratio. This is in agreement with the structure of a 2,6-diphenylphenoxide/CS_2 cadmium(II) complex and the results of the ^{13}C NMR investigations reported by Darensbourg (Figure 7).[5,6]

In contrast to Darensbourg's results, a reaction of the sterically hindered **1b** with CO_2 could be observed in DMSO.[4] The NMR spectrum is similar to that of 2,6-dimethylphenoxide zinc(II) (Table 1). Darensbourg proposed that the initiation process of the copolymer synthesis was the epoxide ring opening, because CO_2 showed no reactivity with sterically hindered zinc(II) phenoxide complexes. With our result we have found a new argument for a CO_2 insertion into the Zn−O bond as the first step of the mechanism of these reaction.

In agreement with the results of Darensbourg, **1a** and **1b** do not react with CO_2 in pyridine.[5] Also in the case of **1c** in various solvents (DMSO, DMF, pyridine, THF) and of **1d** in pyridine (**1d** is only soluble in pyridine) no such reactions were observed by ^{13}C NMR investigations. On further warming of **1d** to 60 °C, a white powder precipitated and an NMR experiment could not be performed. The product was isolated and washed with pentane. It was insoluble in

Table 1. Comparison of calculated and experimental ^{13}C chemical shifts of metal phenoxide systems

molecule	C_{CO2} δ values	C_{ipso} δ values	C_{para} δ values
I[a]		166.8	117.2
II[a]	135.2	169.7	120.9
III[a]	149.5	154.8	133.3
IV[a]	170.7	157.1	132.4
NaOPh[a]		180.4	113.5
NaO_2COPh[a]	173.5	163.0	129.7
NaOPh[b]		170.5	112.4
1a[b]		163.4	113.6
1a/$^{13}CO_2$ [c]	174.8	162.0/154.7	113.5/119.0
1b[b]		166.1	112.4
1b/$^{13}CO_2$ [c]	174.5	165.9/153.6	112.2/120.1
1c[b]		161.1	115.9
1d[d]		165.7	118.8

[a] GIAO-SCF (B3LYP/6−311+G*) calculated ^{13}C chemical shifts (δ, ppm relative to TMS = 0.0 ppm) on the Hartree−Fock optimized geometries (RHF/6−311+G*). − [b] Exp. in [D_6]DMSO. −[c] Exp. in [D_6]DMSO and 40 °C. − [d] Exp. in [D_5]pyridine.

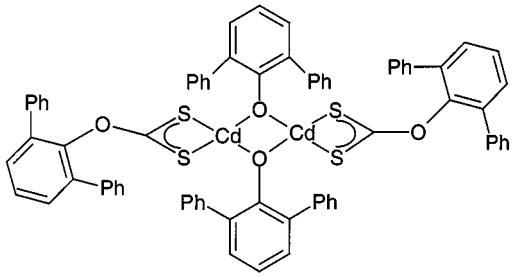


Figure 7. $[Cd(S_2CO\text{-}2,6\text{-}Ph_2C_6H_3)]_2(\mu\text{-}O\text{-}2,6\text{-}Ph_2C_6H_3)_2$ [6]

water and reacted with dilute HCl (gas evolution). In the MS measurement, both the phenol and CO_2 could be detected. We presumed that the complete reaction of CO_2 with both Zn−O(aryl) bonds of the phenoxide leads to an insoluble phenylcarbonate zinc(II). The formation of a soluble alkoxide zinc(II)/CO_2 complex is dependent on the solvent which is used and the steric demand of the phenol ligands.

In the case of the (2-pyridylcarbinolato)zinc(II) complex **2**, no signal was found in the region of δ = 170, but in pyridine a markedly broadened signal at δ = 156 was observed. Additionally, the broadened signals for the carbon atoms of the ring indicated an equilibrium reaction of the complex with CO_2. In order to get insight into the mechanism of this CO_2 insertion, quantum mechanical calculations on the model system zinc(II) phenoxide were carried out.

3. Ab initio Calculations

Darensbourg has shown a significant binding of various solvent molecules to the zinc center of phenoxide zinc(II) compounds in solution even at ambient temperature.[5] Unfortunately, computational limitations prevented us from considering the effects of microsolvation and thus explicit solvent molecules were not included in the model. However, as will be shown, our calculations agree well with the experimental data, thus verifying the validity of our approach. An analogous reaction mechanism for carbonic anhydrase was previously proposed for the activation of carbon dioxide.[11]

Due to the considerable size of the molecular geometry, optimizations were restricted to the HF/G-311+G* level of theory. All geometries were fully optimized and the nature of the stationary points characterized by harmonic frequency analysis. B3LYP/G-311+G* single point calculations were performed on the optimized geometries in order to introduce electron correlation into the energy calculation. The Gaussian94 set of programs was used.

The proposed mechanism is depicted in Figure 8. One of the electron lone pairs of the zinc-bonded oxygen interacts with the carbon of CO_2 to form the electrostatic encounter complex **II** (−2.79 kcal mol^{-1}). This facilitates the nucleophilic attack, leading to the intermediate product **III** (6.92 kcal mol^{-1}) which can rearrange to form the more stable insertion product **IV** (3.24 kcal/mol). This energy profile suggests a reversibility of the reaction.

The calculated stability of the encounter complex in solution must be questioned because electrostatic interactions in general decrease in the presence of solvent molecules.

The calculated Zn−O distance (1.78 Å) is found to be 0.15 Å shorter than the terminal Zn−O distances in the X-ray structure (cf. Figure 3). Considering the absence of dative solvent molecules in the calculated structure this fact is not surprising. In a previous study on the corresponding sodium compounds, the deviations from the experimental structures were in the range of 0.3−0.4 Å.[12] The choice of the model and the level of theory can therefore be considered to be satisfactory. The most important structural features are summarized in Figure 8. For the structures **I**−**IV**, we calculated the ^{13}C chemical shifts (Table 1). The RHF/6−311+G* level of theory on the formerly optimized geometries were used, following the guidelines reported by Chesseman et al.[13] Analogous results could be calculated in the case of the formation of the sodium phenyl carbonate.

These data allow for the verification of the ^{13}C NMR interpretation, summarized in the second part of this study. The peak at ca. 174 ppm can be assigned unambiguously to the inserted CO_2 carbon of the carbonate structure **IV**. There is also an upfield shift of the ^{13}C NMR signal of the *ipso* carbon atom and a downfield shift of the signal for the phenoxide *para* carbon, when following the reaction course from the zinc(II) phenoxide to zinc(II) phenylcarbonate.

In the case of the reaction of **2** with CO_2, the broadened signal at δ = 156 is an indicative of the existence of an equilibrium between the reactants and/or intermediate products such as **III** and **IV**.

4. Carboxylation of Acetophenone

The carboxylation of CH-acidic substrates (e.g. acetone or acetophenone) with an alkaline phenoxide solvent system was first carried out by Bottachio et al.[14] He postulated the formation of phenol and an enolate which is stabilized by the appropriate solvent in a very complex equilibrium. In a successive step, the enolate reacts with CO_2 to give the alkaline salt of the carboxylic acid. Walther et al.

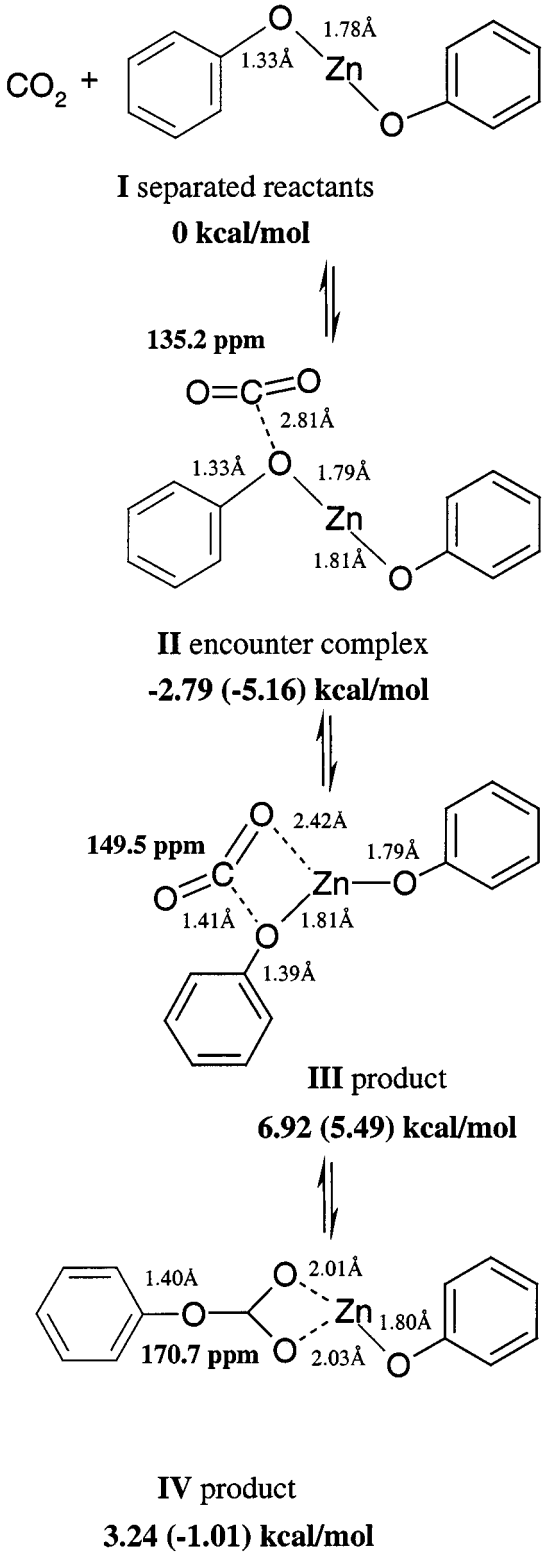


Figure 8. Quantum mechanical calculations on the model system phenoxide zinc(II)/CO_2 [geometries, relative energies, ^{13}C chemical shifts (δ, ppm relative to TMS) - B3LYP/6−311+G*//RHF/6−311+G* level of theory, HF results in parentheses]

postulated the activation of CO_2 by NaOPh/solvent complexes.[15] They obtained particularly high yields of carboxylic acids with a NaOPh/solvent ratio of 4−5:1 at room temperature. The use of magnesium enolates or carbamates had also been reported for these reactions.[16]

In our investigations, the carboxylation of acetophenone was carried out with zinc(II) alkoxide complexes (Table 2)

Table 2. Yield of the carboxylation of acetophenone in DMSO to afford benzoyl acetic acid

Complex	Yield [%]		
	25 °C	40 °C	80 °C
Zinc(II) 2,6-dimethylphenoxide (**1a**)	33	46	32
Zinc(II) 2,6-di-*tert*-butylphenylphenoxide (**1b**)	24	37	25
Zinc(II) 2,6-diphenylphenoxide (**1c**)	4	23	<1
Zinc(II) 4-*tert*-butylphenoxide (**1d**)	0	0	0
(2-Pyridylcarbinolato)zinc(II) (**2**)	<1	<1	<1
Bis(trimethylsilylamido)zinc(II) (**3**)	5	4, 16[a]	8

[a]In THF.

The ligand, the solvent and the temperature were varied. Best results were obtained using **1a** and **1b** at a temperature of 40 °C in DMSO. Comparable yields resulted in cases for which a molar ratio of 3:1 of the zinc(II) complexes to acetophenone was applied. The lower yield of benzoyl acetic acid observed at a reaction temperature of 80 °C indicates a plausible but unwanted decarboxylation. A further explanation for the decreasing yield could be the formation of an insoluble phenylcarbonate zinc(II), which would limit the transfer of the CO_2 at this temperature.

The use of **1c** in DMSO for the reaction led to a lower yield of the benzoyl acetic acid. This can be explained both by a complete reaction of CO_2 to a zinc(II) 2,6-diphenylphenylcarbonate and by a poor solubility of the insertion product. In the case of **1d** dissolved in pyridine, the addition of CO_2 led to a precipitation of the previously described "white powder". After addition of acetophenone, no benzoyl acetic was detected.

Solvent dependence: For **1a**−**1c** dissolved in pyridine, the detection of a reaction with $^{13}CO_2$ in the NMR investigations and also the carboxylation failed. It worth noting that although the starting $Zn[N(SiMe_3)]_2$ **3** does not undergo an insertion reaction with CO_2, the amide **3** also enabled the carboxylation of acetophenone. The model reaction requires a zinc(II) complex which is soluble in the presence of CO_2. Reaction of the phenoxide zinc(II) complexes with acetophenone (i.e. without CO_2) was not observed in our NMR investigations. Our experiments revealed no indication of the formation of acetophenolate zinc(II) and phenol. The charge on the carbon of the activated complexes (natural charge of **III**: q_c = 0.9974 and of **IV**: q_c = 0.9947) allows no statement about the preference of the two product structures as a potential reactant towards acetophenone. At present we presume that the reaction of the zinc(II) complex, CO_2 and acetophenone is a concerted reaction, in which one of the structures **III** or **IV** plays a dominant role (cf. Figure 8).

On the other hand, (2-pyridylcarbinolato)zinc(II), (hydroxypyridinato)zinc(II) and (2,6-di-*tert*-butylbenzoato)-zinc(II) are inactive for the carboxylation of acetophenone (20 °C, 40 °C; DMSO, pyridine). Thus, the carboxylation of CH-acidic compounds requires a well optimized zinc(II)

complex with a specific ligand design. An important property of this complex is an acceptable solubility (this requires bulky ligands). A relative low coordination number of the metal center is assumed to be decisive, too.

However, we have found a new reaction of zinc(II) alkoxides with CO_2 and acetophenone under remarkably mild conditions.

Experimental Section

The syntheses of **1a−1c** were performed under an argon atmosphere as previously described.[4,5]

Zinc(II) 2,6-Dimethylphenoxide {Zn[(OC$_6$H$_3$)(CH$_3$)$_2$]$_2$} (1a): The procedure was modified by adding Zn{N(Si(CH$_3$)$_3$)$_2$}$_2$ (7.0 g, 18 mmol) in THF (80 mL) to a solution of sublimed 2,6-dimethylphenol (4.4 g, 36 mmol) in THF (100 mL). It was heated at reflux for 4 h. After cooling to room temperature, a white powder precipitated. The THF was removed in vacuo and the resulting solid was washed twice with pentane (50 mL) and dried in vacuo to yield a colorless powder. − Yield 5.7 g (83%), $C_{16}H_{18}O_2Zn$ (307.70): calcd. C 62.5, H 5.9; found C 60.55, H 6.20 (It is not possible to remove the ether ligand completely). − IR (KBr, disk): $\tilde{\nu}$ = 3026, 2918 [ν(C−H)], 1594, 1474, 1410 [ν(C=C)], 1200 [ν(C−O)], 760 cm^{-1} [δ(C−H)]. − ^{1}H NMR ([D$_6$]DMSO, 25 °C, TMS): δ = 2.03 (s, 6 H, C*H$_3$*), 6.22 (t, 1 H, C*H$_2$ para*), 6.82 (d, 2 H, C*H$_2$ meta*). − ^{13}C NMR ([D$_6$]DMSO, 25 °C, TMS): δ = 113.6 (*C*H, *para*), 125.9 (*C*H, *ortho*), 127.6 (*C*H, *meta*), 163.5 (*C*−O, *ipso*).

Zinc(II) 2,6-Di-*tert*-butylphenoxide {Zn[(OC$_6$H$_3$)(C(CH$_3$)$_3$)$_2$]$_2$} (1b): To a solution of sublimed 2,6-di-*tert*-butylphenol (7.5 g, 36 mmol) in THF or pentane (40 mL) was added a solution of Zn{N(Si(CH$_3$)$_3$)$_2$}$_2$ (7.0 g, 18 mmol) in THF or pentane (80 mL). The solution was stirred for 4 h. The THF was then removed in vacuo and the resulting solid was washed twice with pentane (50 mL) and dried in vacuo to yield a colorless powder. After 3 days the product turned pale yellow. − Yield 6.2 (72%), $C_{28}H_{42}O_2Zn$ (476.02): calcd. C 70.65, H 8.89; found C 68.20, H 8.76. − IR (KBr, disk): $\tilde{\nu}$ = 3080, 2959 [ν(C−H)], 1468, 1426 [ν(C=C)], 1226 [ν(C−O)], 749 cm^{-1} [δ(C−H)]. − ^{1}H NMR ([D$_6$]DMSO, 25 °C, TMS): δ = 1.38, 1.40 (overlapping singlets, 19 H, C*H$_3$*), 6.27, 6.73 (t, 1 H, C*H$_2$ para*), 6.91, 7.07(d 2 H, C*H$_2$ meta*). − ^{13}C NMR ([D$_6$]DMSO, 25 °C, TMS): δ = 30.5, 31.3 (*C*H$_3$, *tert*-butyl) 34.7, 35.1 (*C*, *tert*-butyl) 112.4 (*C*H, *para*), 123.9, 124.4 (*C*H, *ortho*), 139.4 (*C*H, *meta*), 166.1 (*C*−O, *ipso*).

Zinc(II) 2,6-Diphenylphenoxide {Zn[(OC$_6$H$_3$)(C$_6$H$_5$)$_2$]$_2$} (1d): The synthesis and isolation are identical to those for the previous zinc phenoxides. Sublimed 2,6-diphenylphenol (8.9 g, 36 mmol) and Zn{N(Si(CH$_3$)$_3$)$_2$}$_2$ (7.0 g, 18 mmol) were used for the reaction. Yield 9.3 g (93%), $C_{36}H_{26}O_2Zn(THF)_2$ (700.19): calcd. C 75.48, H 6.05; found C 73.89, H 5.73. − IR (KBr, disk): $\tilde{\nu}$ = 3050, 3023 [ν(C−H)], 1594, 1496, 1459, 1429 [ν(C=C)], 1224 [ν(C−O)], 762, 746, 703 cm^{-1}[δ(C−H)]. − ^{1}H NMR ([D$_4$]THF, 25 °C, TMS): δ = 7.1 (t, 1 H, C*H*), 7.3−7.7 (m, 1 H, C*H*). − ^{13}C NMR ([D$_4$]THF, 25 °C, TMS): δ = 115.9 (*C*H, *para*), 126.4 (*C*H, *para*), 126.4, 128.5, 129.0, 130.4, 132.9, (*C*H, *ortho*, *meta*), 142.5, 161.1 (*C*−O, *ipso*).

Zinc(II) 4-*tert*-Butylphenoxide {Zn[(OC$_6$H$_3$)(C(CH$_3$)$_3$)]$_2$} (1c): The synthesis and isolation are identical to those for the previous zinc phenoxides. After addition of Zn{N(Si(CH$_3$)$_3$)$_2$}$_2$ (7.0 g, 18 mmol) in THF (30 mL) to a solution of sublimed 4-*tert*-butylphenol (5.4 g, 36 mmol) in THF (80 mL) a white powder precipitated directly. Yield 12.2 (93%), $C_{20}H_{26}O_2Zn$ (363.80): calcd. C 66.0, H 7.2; found C 64.9, H 7.3. − IR (KBr, disk): $\tilde{\nu}$ = 2964, 2870 [ν(C−H)], 1600, 1514, 1460 [ν(C=C)], 1244 [ν(C−O)], 828 cm^{-1}[δ(C−H)]. − ^{1}H NMR ([D$_6$]pyridine, 25 °C, TMS): δ = 1.2 (m, 9 H, C*H$_3$*), 7.2 (s, 4 H, C*H*). − ^{13}C NMR ([D$_6$]pyridine, 25 °C, TMS): δ = 31.9 (*C*H$_3$, *tert*-butyl) 33.7 (*C*, *tert*-butyl) 118.8 (*C*H, *para*), 126.6 (*C*H, *ortho*, *meta*), 165.7 (*C*−O, *ipso*).

(2-Pyridylcarbinolato)zinc(II) {Zn[(OCH$_2$)(C$_5$H$_4$N)]$_2$} (2): To a solution of 2-(hydroxymethyl)pyridine (2.8 g, 26 mmol) in acetonitrile (80 mL), a solution of Zn{N(Si(CH$_3$)$_3$)$_2$}$_2$ (5.0 g, 13 mmol) in acetonitrile was added. From the stirred solution a white powder precipitated. The acetonitrile was removed by decanting and the resulting product washed twice with acetonitrile (50 mL), dried in vacuo to yield a colorless powder. Yield 3.3 g (90%), $C_{12}H_{12}N_2O_2Zn$ (281.62): calcd. C 51.18.0, N 9.95, H 4.29; found C 51.24, N 10.24, H 4.50. − IR (KBr, disk): $\tilde{\nu}$ = 3057, 2809, [ν(C−H)], 1607, 1568, 1483, 1441 [ν(C=C), ν(N=C)], 1094 cm^{-1} [ν(C−O)]. − ^{1}H NMR ([D$_3$]acetonitrile, 25 °C, TMS): δ = 3.7 (s, 2 H, C*H$_2$*), 6.32 (t, 1 H, C*H*), 6.48 (d, 1 H, C*H*), 6.85 (t, 1 H, C*H*), 7.54 (d, 1 H, C*H*). − ^{13}C NMR ([D$_3$]acetonitrile, 25 °C, TMS): δ = 64.3 (*C*H$_2$) 120.7 (*C*H, *meta*) 122.4 (*C*H, *ortho*), 137.2, 148.6 (*C*H, *para*), 161.0 (*C*−*C*H$_2$, *ipso*).

Crystallization of the Dimeric 1b and Monomeric 1b/(DMSO)$_2$: A saturated solution of zinc(II) 2,6-di-*tert*-butylphenoxide in pentane or DMSO, respectively, was allowed to cool to room temperature and then filtered to separate from crystallites. Colorless crystals suitable for X-ray structure determination were grown in the filtrate after a few days. − The intensity data were collected on a Nonius KappaCCD diffractometer, using graphite-monochromated Mo-K_α radiation. Data were corrected for Lorentz and polarization effects, but not for absorption.[17] − The structures were solved by direct methods (SHELXS[18]) and refined by full-matrix least squares techniques against F_o^2 (SHELXL-97[19]). For the compounds zinc(II) 2,6-di-*tert*-butylphenoxide/(DMSO)$_2$ the hydrogen atoms were located by difference Fourier synthesis and refined isotropically. The hydrogen atoms of the compound zinc(II) 2,6-di-*tert*-butylphenoxide were included at calculated positions with fixed thermal parameters. All nonhydrogen atoms were refined anisotropically. XP (SIEMENS Analytical X-ray Instruments, Inc.) was used for structure representations.[20]

NMR Experiments: Samples of zinc(II) complexes (**1a−1c, 2, 3**) in aprotic polar solvents (0.1 M) were transferred into a NMR tube with a Young-valve system under an argon atmosphere. After measurement of both the ^{13}C NMR and the ^{1}H NMR spectrum, the solution was saturated thoroughly with CO_2 or $^{13}CO_2$ and reexamined. After this, the probe was heated for 6 h at 40 °C and the measurements were repeated at room temperature. A Bruker AC200 NMR spectrometer was used.

Carboxylation of Acetophenone: In a typical carboxylation run, {Zn[(CH$_3$)$_2$(OC$_6$H$_3$)]$_2$} (0.10 g, 0.3 mmol) was dissolved in the polar aprotic solvent (20 mL) and saturated with CO_2. Acetophenone (0.04 g, 0.3 mmol) was then added to the solution. Afterwards, CO_2 was passed through the solution for six hours at the reaction temperature. A 1:1 mixture of water/methanol (100 mL) was added to the reaction solution.

Separation and Quantitative Analysis of the Product Mixture: Phenol, acetophenone and benzoyl acetic acid were analyzed by HPLC (Gynkotec System): The method was developed by modifying a previously described procedure (Burtscher et al.).[21] Column: Nucleosil 5 C18, (Macherey−Nagel & Co.), injection volume: 20 μL, solvent A: 50% 0.01M phosphate buffer KH_2PO_4 (Merck

analytical grade), solvent B: 50% acetonitrile, flow rate: 0.8 mL min^{-1}, isothermal at 298 K, program: isocratic, wavelength: 295 nm. The retention times are 4.2 min for benzoyl acetic acid and 7.0 min for acetophenone. The quantitative analysis was carried out by an external standard method. On the basis of a stock solution of acetophenone (6.1×10^{-4} g mL^{-1}) and benzoyl acetic acid (6.2×10^{-4} g mL^{-1}), a dilution series was measured. The calibration line was determined by linear regression (acetophenone: correction factor 1.051, variation coefficient 0.30%; benzoyl acetic acid: correction factor 1.108, variation coefficient 0.22%).

The carboxylation reaction was performed three times for each solvent and was analyzed twice via HPLC. The results, shown in Table 2, are averaged values of these three reactions.

Acknowledgments

Financial support from the Deutsche Forschungsgemeinschaft (Collaborative Research Center 436, University of Jena, Germany), the Fonds der Chemischen Industrie (Germany), the Thüringer Ministerium für Wissenschaft, Forschung und Kultur (Erfurt, Germany) and the Max-Planck-Gesellschaft is gratefully acknowledged. We thank Dr. T. Zevaco (Karlsruhe, Germany) for useful discussions.

[1] D. J. Darensbourg, M. Holtcamp, *Coord. Chem. Rev.* **1996**, *153*, 155−174; M. Ruf, H. Vahrenkamp, *Chem. Ber.* **1997**, *130*, 975−980.

[2] R. Alsfasser, M. Ruf, S. Trofimenko, H. Vahrenkamp, *Chem. Ber.* **1993**, *126*, 703−710; R. Walz, K. Weis, M. Ruf, H. Vahrenkamp, *Chem. Ber.* **1997**, *130*, 975−980; E. Kimura, *Tetrahedron* **1992**, *48*, 6175−6217; E. Kimura, *Progress in Inorganic Chemistry*, edited by K. D. Karlin, John Wiley & Sons, **1994**, *41*, 443−491; E. Kimura, T. Koike, M. Shinoya, *Structure and Bonding,* **1997**, *89*, 1−28; K. Nakata, M. K. Uddin, K. Ogawa, K. Ichikawa, *Chemistry Letters* **1997**, 991−992; P. Ghosh, G. Parkin, J. Chem. Soc., *Dalton Trans.*, **1998**, 2281−2283.

[3] S. Inoue, M. Kobayashi, H. Koinuma, T. Tsuruta, *Macromol. Chem.* **1972**, *155*, 61−73; S. Inoue, M. Kobayashi, H. Koinuma, T. Tsuruta, *Macromol. Chem.* **1972**, *155*, 61−73; W. Kuran, S. Pasynkiewicz, J. Skupinska, *Macromol. Chem.* **1977**, *178*, 47−54; W. Kuran, S. Pasynkiewicz, J. Skupinska, *Macromol. Chem.* **1977**, *178*, 2149−2158; W. Kuran, T. Listos, *Macromol. Chem. Phys.* **1994**, *195*, 977−984; A. Rokicki, U.S. Patent, 4.782.445; H.-N. Sun, U.S. Patent, 4.789.727; H.-N. Sun, U.S. Patent, 4.783.445; M. Cheng, E. B. Lobkovsky, W. Kuran, T. Listos, *Macromol. Chem. Phys.* **1994**, *195*, 1011−1015; P. Gorecki, W. Kuran, *J. Polymer. Lett. Ed.* **1985**, *23*, 299; G. W. Coates, *J. Am. Chem. Soc.* **1998**, *120*, 11018−11019.

[4] R. L. Geerts, J. C. Huffman, K. G. Caulton, *Inorg. Chem.* **1986**, *25*, 1803−1805.

[5] D. J. Darensbourg, M. W. Holtcamp, *Macromolecules* **1995**, *28*, 7577−7579; D. J. Darensbourg, M. W. Holtcamp, G. E. Struck, M. S. Zimmer, S. A. Niezzgoda, P. R. Rainey, J. B. Robertson, J. D. Draper, J. H. Reibensies, *J. Am. Chem. Soc.* **1999**, *121*, 107−116.

[6] D. J. Darensbourg, S. A. Niezgoda, J. D. Draper, J. H. Reibenspies, *J. Am. Chem. Soc.* **1998**, *120*, 4690−4698.

[7] D. J. Darensbourg, M. S. Zimmer, P. Rainey, D. L. Larkins, *Inorg. Chem.* **1998**, *37*, 2852−2853.

[8] [8a] M. Parvez, G. L. Bergstresser, H. G. Richey, *Acta Cryst.* **1992**, *C48*, 641−644. − [8b] S. C. Goel, M. Y. Chiang, W. E. Buhro, *Inorg. Chem.* **1990**, *24*, 4646−4652. − [8c] J. T. B. H. Jastrzebski, J. Boersma, G. van Koten, W. J. J. Smeets, A. L. Spek, *Recl. Trav. Chim. Pays-Bas.* **1988**, *107*, 263−266. − [8d] P. A. Schaaf, E. Wissing, J. Boersma, W. J. J. Smeets, A. L. Spek, G. Koten, *Organometallics* **1993**, *12*, 3624−3629. − [8e] F. H. van der Steen, J. Boersma, A. L. Spek, G. van Koten, *Organometallics* **1991**, *10*, 2467−2480.

[9] Crystal data for 2,6 di-*tert*-butylphenoxide zinc(II): $C_{56}H_{84}O_4Zn_2 \times 0.5\ C_5\ H_{12}$, M_r = 988.05 $gmol^{-1}$, colorless prism, size $0.32 \times 0.30 \times 0.28$ mm^3, monoclinic, space group $P2_1/c$, a = 22.8849(5), b = 12.2669(4), c = 21.7376(6) Å, β = 114.162(1)°, V = 5567.7(3) $Å^3$, T = −90 °C, Z = 4, $\rho_{calcd.}$ = 1.179 gcm^{-3}, μ (Mo-K_α) = 9.04 cm^{-1}, $F(000)$ = 2132, 14729 reflections in $h(-25/25)$, $k(-13/0)$, $l(-24/24)$, measured in the range $2.05° \leq \Theta \leq 23.25°$, completeness Θ_{max} = 96.7%, 7969 independent reflections, R_{int} = 0.0471, 5715 reflections with $F_o > 4\ \sigma(F_o)$, 593 parameters, 4 restraints, $R1_{obs}$ = 0.043, wR^2_{obs} = 0.114, $R1_{all}$ = 0.084, wR^2_{all} = 0.175, GOOF = 0.914, largest difference peak and hole: 0.606/−0.502 e $Å^{-3}$.

[10] Crystal data for 2,6-di-*tert*-butylphenoxide zinc(II)/$(DMSO)_2$: **1b**/$(DMSO)_2$: $C_{32}H_{54}O_4S_2Zn$, M_r = 632.24 $gmol^{-1}$, colorless prism, size $0.36 \times 0.34 \times 0.32$ mm^3, monoclinic, space group $C2/c$, a = 14.4358(2), b = 14.7357(2), c = 17.1059(3) Å, β = 107.142(1)°, V = 3477.15(9) $Å^3$, T = −90 °C, Z = 4, $\rho_{calcd.}$ = 1.208 gcm^{-3}, μ (Mo-K_α) = 8.58 cm^{-1}, $F(000)$ = 1360, 4547 reflections in $h(-10/16)$, $k(-16/11)$, $l(-18/18)$, measured in the range $2.13° \leq \Theta \leq 23.28°$, completeness Θ_{max} = 96.2%, 2452 independent reflections, R_{int} = 0.012, 2377 reflections with $F_o > 4\ \sigma(F_o)$, 285 parameters, 0 restraints, $R1_{obs}$ = 0022, wR^2_{obs} = 0.065, $R1_{all}$ = 0.023, wR^2_{all} = 0.071, GOOF = 1.021, largest difference peak and hole: 0.227/−0.278 e $Å^{-3}$.

[11] S. Lindskog, J. E. Coleman, *Proc. Natl. Acad. Sci. U.S.A.* **1973**, *70*, 2505; J. E. Coleman, J. *Biol. Chem.* **1967**, *242*, 5212; S. Lindskog, in *Carbonic Anhydrase*, Ed.: S. Lindskog, Wiley, New York **1983**, p. 77.

[12] T. Kremer, P. v. R. Schleyer, *Organometallics* **1997**, *16*, 737−746.

[13] J. R. Chesseman, G. W. Trucks, T. A. Keith, M. J. Frisch, *J. Chem. Phys.* **1996**, *104*, 5497−5509.

[14] G. Bottaccio, G. P. Chiusoli, *Chem. Commun.* **1966**, *24*, 618; G. Bottaccio, G. P. Chiusoli, M. Felicioli, *Gaz. Ch. Ital.* **1973**, *103*, 105−116; G. Bottaccio, G. P. Chiusoli, E. Alneri, M. Marchi, G. Lana, (Montedison S. p. A.) DE 2612577 C2, **1976**; G. Bottaccio, M. Marchi, G. P. Chiusoli, *Gaz. Ch. Ital.* **1976**, *106*, 831−841; G. Bottaccio, M. Marchi, *Gaz. Ch. Ital.* **1977**, *107*, 499−500.

[15] D. Walther, U. Ritter, S. Geßler, J. Sieler, M. Kunert, *Z. Anorg. Allg. Chem.* **1994**, *620*, 101−106; M. unert, M. Nauck, J. Sieler, E. Dinjus, *Chem. Ber.* **1997**, *130*, 1461−1465.

[16] M. Stiles, *J. Am. Chem. Soc.* **1959**, *81*, 2598−2599; H. L. Finkbeiner, G. W. Wagner, *J. Org. Chem*, **1963**, *28*, 215−217; N. M. Matsumura, Y. S. Sakaguchi, T. O. Ohba, H. Inoue, *J. Chem. Soc., Chem. Commun.* **1980**, 326−327.

[17] Z. Otwinowski, W. Minor, "Processing of X-ray Diffraction Data Collected in Oscillation Mode", in: Methods in Enzymology, vol. 276, *Macromolecular Crystallography, Part A*, edited by C.W. Carter & R.M. Sweet, pp. 307−326, Academic Press, **1997**.

[18] G. M. Sheldrick, *Acta Crystallogr. Sect. A* **1990**, *46*, 467−473.

[19] G. M. Sheldrick, *SHELXL-97*, University of Göttingen, Germany, **1993**.

[20] Crystallographic data (excluding structure factors) for the structures reported in this paper have been deposited with the Cambridge Crystallographic Data Centre as supplementary puplication no. CCDC-136058 and CCDC-136059. Copies of the data can be obtained free of Charge on application to CCDC, 12 Union Road, Cambridge CB2 1EZ, UK [Fax: (internat.)+44-1223/336.033; E-mail:deposit@ccdc.cam.ac.uk].

[21] E. Burtscher, H. Bider, R. Concin, O. Bobleter, *J. Chrom.* **1982**, *252*, 167−175.

Received October 27, 1999
[I99381]

Intramolecular Stabilization of Carbene Complexes $(CO)_4W{=}C(NRR')Si(aryl)_2X$ (X = H, CMe=CHMe, NEt_2) by Interaction of the Metal Center with the Silicon Substituent X

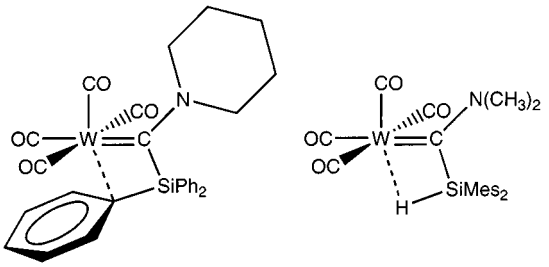
Matthias Schwarz,[a] Guido Kickelbick,[a] and Ulrich Schubert*[a]

Keywords: Carbene complexes / Density functional calculations / Agostic interactions / Three-center bonds / Silicon / Tungsten

The degree of intramolecular stabilization by the substituent X in the carbene complexes $(CO)_4W{=}C(NRR')Si(aryl)_2X$ was investigated by density functional calculations and reactivity studies. Calculations carried out for $(CO)_4W{=}C(NH_2)SiH_2X$ (X = H, Ph, Me, CMe=CHMe) or $(CO)_4W{=}C(NH_2)OMe$ show that the agostic Si–H interaction in $(CO)_4W{=}C(NH_2)SiH_3$ transfers as much electron density to the metal as the π–interaction of the olefinic group in $(CO)_4W{=}C(NH_2)SiH_2CMe{=}CHMe$. An agostic interaction is not observed if the silicon atom is replaced by a carbon atom. Interaction of the phenyl group in $(CO)_4W{=}C(NH_2)SiH_2Ph$ is much weaker and can be described as a weak π–interaction. Owing to the agostic Si–H interaction, $(CO)_5W{=}C(NHR)SiHMes_2$ (R = Me, Et) does not eliminate $HSiR'_3$ upon thermolysis, as observed in the corresponding complexes $(CO)_5W{=}C(NHR)SiR'_3$, but instead gives the 16-electron complex $(CO)_4W{=}C(NHR)SiHMes_2$. When the complexes $(CO)_5W{=}C(NMe_2)SiPh_2CMe{=}CHMe$ or $(CO)_5W{=}C(NHMe)SiPh_2NEt_2$ are thermolyzed or photolyzed, CO is eliminated and either the olefinic or amino group coordinates intramolecularly to the empty coordination site. The corresponding reaction was not observed when the stable 16-electron complexes $(CO)_4W{=}C(NR_2)SiPh_3$ were allowed to react with olefins or tertiary amines respectively. The X-ray structure analysis of $(CO)_4W{=}C(NMe_2)SiPh_2CMe{=}CHMe$ is reported.

Introduction

Stable 16-electron carbene complexes $(CO)_4M{=}C(NR_2)SiR'_3$ (M = Cr, Mo, W) were previously obtained by thermal or photochemical CO cleavage from the corresponding 18-electron complexes $(CO)_5MC(NR_2)SiR'_3$.[1] These complexes are stabilized by intramolecular interaction of one of the silicon substituents with the metal center. In $(CO)_4W{=}C(NMe_2)SiHMes_2$ (Mes = 2,4,6-$C_6H_2Me_3$), the Si−H group interacts with the tungsten atom,[1c] and with one of the phenyl groups in $(CO)_4W{=}C(NC_5H_{10})SiPh_3$ (Scheme 1).[1a] In the $SiPh_3$ derivative, the $W-C_{phenyl}$ distances indicate that the *ipso* carbon atom is mainly involved in the interaction with the metal atom. The intramolecular interactions result in severe distortions of the bond angles at the carbene carbon atom (W−C−Si bond angle of 87.8(6)° in $(CO)_4W{=}C(NMe_2)SiHMes_2$ and of 101.2(4)° in $(CO)_4W{=}C(NC_5H_{10})SiPh_3$).



Scheme 1

[a] Institut für Anorganische Chemie, Technische Universität Wien,
Getreidemarkt 9, A-1060 Wien, Austria

Despite the agostic interactions in the silylcarbene complexes, the coordination site is still accessible. Reaction of $(CO)_4W{=}C(NMe_2)SiR_3$ (SiR_3 = $SiPh_3$, $SiPh_2Me$) with CO, phosphanes, phosphites or isonitriles quantitatively yielded the 18-electron carbene complexes *cis*-$(CO)_4LW{=}C(NMe_2)SiR_3$ (L= CO, RNC, PR_3, $P(OR)_3$).[1b][1d] The latter complexes showed no tendency towards eliminating a ligand. However, addition of acetonitrile or pyridine to $(CO)_4W{=}C(NMe_2)SiPh_2Me$ was reversible, i.e. the complexes *cis*-$(CO)_4LW{=}C(NMe_2)SiPh_2Me$ (L = MeCN, C_5H_5N) eliminated L on evaporation of the reaction solutions, and the 16-electron complexes were re-formed. No adduct formation was observed when triethylamine, olefins or acetylenes were added to solutions of the 16-electron complex $(CO)_4W{=}C(NMe_2)SiPh_2Me$.[1d]

16-Electron carbene complexes are postulated as key intermediates in many reactions of Fischer-type carbene complexes. The stable analogues allow us to study how intramolecular interactions influence the stability and hence the reactivity of electron-deficient carbene complexes and how such interactions are controlled by electronic and steric effects. If these are properly tuned, a coordination site at the metal could be reversibly opened and protected during the reaction. In this paper, we report theoretical and experimental results of intramolecular interactions in silyl-substituted 16-electron carbene complexes.

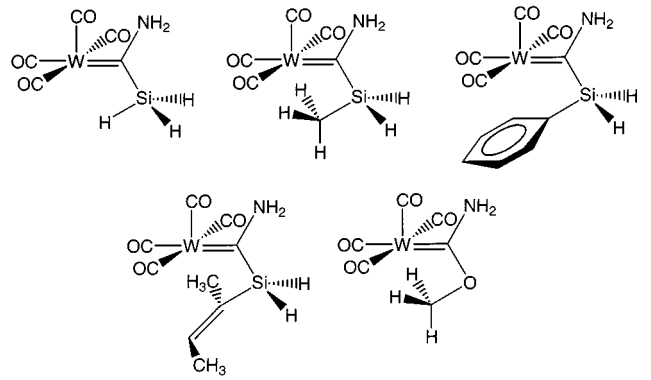
Results and Discussion

Theoretical Calculations

To examine the nature of the intramolecular interaction and the role of steric and electronic factors in the silyl-sub-

 © WILEY-VCH Verlag GmbH, D-69451 Weinheim, 2000 1434−1948/00/0808−1811 $ 17.50+.50/0

stituted 16-electron carbene complexes $(CO)_4W{=}C(NC_5H_{10})SiPh_3$ [1a] and $(CO)_4W{=}C(NMe_2)SiMes_2H$,[1c] we carried out density functional calculations on these and related compounds, with the NR_2 replaced by NH_2 and the SiR_3 groups replaced by SiH_2R (R = H, Ph, Me, CMe=CHMe) or OMe (Scheme 2).



Scheme 2

The first question was whether steric crowding at the carbene carbon atom or the electronic interaction between the tungsten center and the substituents on silicon cause the small W−C−Si angles observed in the structurally investigated complexes. Therefore, the bulky substituents at the nitrogen and silicon atoms were substituted by hydrogen atoms. Geometrical optimization of the model structures were carried out from two starting points, the crystallographically determined structures (if known) on the one hand, and artificial structures with the bond angles around the carbene carbon atom set at 120°, on the other. In both cases, the optimizations gave very similar minimum structures, which should therefore correspond to the global minimum. This was also indicated by a frequency analysis, where no imaginary frequencies were observed. Structural parameters of the optimized structures are given in Table 1. The obtained bond lengths and angles are in good agreement with the experimental values from X-ray structure analyses. The fact that the geometry optimizations without the bulky ligands achieved the geometries of the real complexes allows us to conclude that steric reasons for the distorted arrangement around C(carbene) can be excluded. Instead, electronic reasons should be the driving force for the agostic interactions and associated structural phenomena.

The orbital responsible for the intramolecular interaction between the 16-electron tungsten carbene fragment and a donating group is the empty metal d_z^2-orbital. Stabilization of the empty coordination site can be achieved by either an agostic interaction with a suitable σ-bond or by interaction with π-orbitals of an organic substituent such as a phenyl or olefinic group.

Geometry optimization of $(CO)_4W{=}C(NH_2)SiH_3$ showed that one Si−H bond is preferentially located in the W−C−Si plane, as is observed in the solid-state structure of $(CO)_4W{=}C(NMe_2)SiMes_2H$. This conformation gives the best interaction of the Si−H bond with the empty d_z^2-orbital at the tungsten atom as shown in the electron density plot (Figure 1). The plot shows that both the H and the Si atom participate in a delocalized occupied orbital. Thus, the Si−H bond acts as an intramolecular electron donor which results in charge transfer from Si−H to the metal,

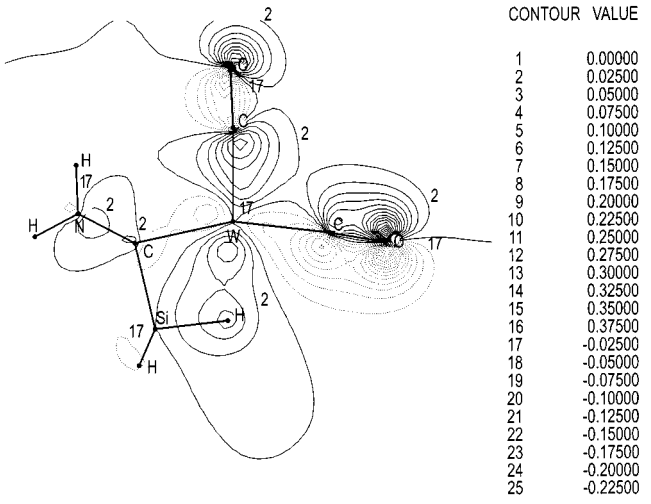


Figure 1. Contour plot of the calculated electron density for the molecular orbital participating to the greatest extent in the agostic interaction in the W=C−Si−H plane of $(CO)_4W{=}C(NH_2)SiH_3$.

Table 1. Selected parameters of the optimized structures of $(CO)_4W{=}C(NH_2)X$ (distances in pm and angles in deg; C_c = carbene carbon atom). In the $SiMeH_2$ and OMe derivative, the orientation of the methyl group was fixed (see Text)

	X = SiH_3	$SiMeH_2$	OMe	$SiPhH_2$	$Si(CMe{=}CHMe)H_2$
W−C_c	209.9	212.1	218.9	212.2	214.4
C_c−Si	185.3	189.6	C_c−O: 137.8	187.9	191.0
C_c−N	134.0	134.5	134.5	134.4	134.1
Si−C	−	187.4	O−C: 146.9	187.1	190.3
Si−H	153.3, 146.9, 146.9	147.4, 147.6	−	147.5, 147.5	148.5, 149.4
W−C_c−Si	89.2	110.0	W−C_c−O: 122.33	105.3	103.3
W−C_c−N	140.2	130.6	128.3	131.6	132.3
C_c−Si−H	96.5, 116.9, 116.9	107.9, 111.1	−	110.9, 111.0	110.5, 115.2
C_c−Si−C	−	106.6	115.7	104.3	95.5
W−C_c−Si−H	0.0	−	−	−	−
W−C_c−Si−C	−	−14.4	W−C_c−O−C: 3.1	0.4	−12.9
C_{CO}−W−C_c−N	0.0	4.0	0.8	−0.3	20.7
W···H	207.7	−	−	−	−
W···C	W···Si: 277.0	319.9	322.9	290.9	263.3, 270.8
Natural charge on W	−0.54	−0.33	−0.33	−0.37	−0.46

i.e. an increase in the natural charge on the metal center (−0.54) compared to systems where no such interaction is present (Table 1).

The agostic interaction has interesting structural consequences, such as an increase in the bond length of the agostic Si−H bond (153.3 pm) as compared to the other two Si−H bonds (146.9 pm). The bending of the agostic Si−H bond ($C_{carbene}$−Si−H 96.5°, compared to 116.9° of the other two hydrogen atoms) also reflects the extraordinary bonding situation in the W−C−Si−H moiety. Furthermore, the W−$C_{carbene}$−Si angle is very small (89.2°) and the W−H distance rather short (207.7 pm). The calculated structural parameters correspond very well with the corresponding values observed in the solid-state structure of $(CO)_4W{=}C(NMe_2)SiMes_2H$ [W−$C_{carbene}$−Si 87.8(6)°, W−H 210(10) pm, Si−H 150(10) pm].[1c]

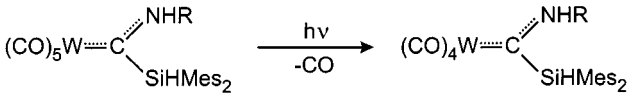
The WH interaction is restricted to the cases where the hydrogen atom is bound to silicon. This was confirmed by density functional calculations on $(CO)_4W{=}C(NH_2)SiMeH_2$ and $(CO)_4W{=}C(NH_2)OMe$ in which only the conformers with the methyl group pointing into the empty coordination site of the tungsten atom were considered (Scheme 2). In both compounds, the carbon-bonded hydrogen atoms could approach the W center with much less geometric distortion around $C_{carbene}$ than in $(CO)_4W{=}C(NH_2)SiH_3$. Nevertheless, an agostic interaction was not observed due to the fact that in the optimized structures (in which rotation of the CH_3 group was allowed) the CH_3 group was oriented in such a way that the C−H bond located in the W=C−Si plane was pointing away from the W atom.

Another possible means of stabilizing the 16-electron fragment are intramolecular π-interactions. In the investigated complexes, this was achieved either by an interaction of the *ipso* C atom of a phenyl substituent at silicon or by the coordination of the double bond of a butenyl substituent. The calculations revealed that the interaction of the SiPh substituent with the tungsten atom does not lead to a large transfer of electron density to the metal center and thus is a rather weak interaction. Interaction with the butenyl substituent is much stronger, as expected. This is also reflected in the relatively long W−C_{ipso} distance of 290.0 pm in $(CO)_4W{=}C(NH_2)SiPhH_2$ compared to the W−C_{olefin} distances of 263.3 pm and 270.8 pm in $(CO)_4W{=}C(NH_2)Si(CMe{=}CHMe)H_2$ (see also the X-ray structure analysis of **7** described below). The calculated W−C distances between the metal and the olefin in $(CO)_4W{=}C(NH_2)Si(CMe{=}CHMe)H_2$ differ by approximately 20 pm from the values in the X-ray structural analysis (W−C(81) 246.9(7) pm, W−C(82) 252.3 pm). One reason for these observations is that substitution of the bulky phenyl groups at silicon by H atoms in the calculation has a more significant effect, due to the bulkiness of the butenyl group, than in other substitution patterns. The charge on the tungsten atom in the butenyl derivative (−0.46) is close to that of the SiH_3 substituted compound with an efficient agostic interaction. The butenyl derivative corresponds to the many known alkenyl-substituted carbene complexes in which the olefinic group is connected to the carbene carbon by carbon and/or nitrogen atoms (see below).

Thermal Decomposition of $(CO)_5W{=}C(NHR)SiHMes_2$

We wanted to test whether the agostic Si−H interaction affects reactions of silyl carbene complexes in which the silyl group is involved. Contrary to the corresponding NHR-substituted alkyl or arylcarbene complexes, the silylcarbene complexes $(CO)_5W{=}C(NHR)SiR_3$ (SiR_3 = $Si(aryl)_3$, $SiPh_2Me$) undergo a thermally[2] or photochemically[3] induced fragmentation reaction that quantitatively yields $HSiR_3$ and the isonitrile complexes $(CO)_5WCNR$.

When solutions of the SiR_2H-substituted complexes $(CO)_5W{=}C(NHR)SiHMes_2$ (R = Me, Et) (**1a,b**)[4] were photolyzed, this fragmentation was not observed. The spectroscopic data clearly showed that the 16-electron complexes $(CO)_4W{=}C(NHR)SiHMes_2$ (**2a,b**) were formed instead (Equation 1). The complexes **2a,b** are relatively stable. On heating, they gave **1a,b** and $W(CO)_6$, but no isonitrile complex.



1a,b **2a,b**

The complexes **2a,b** showed the same spectroscopic features as previously observed for NR_2-substituted 16-electron carbene complexes. The ν(CO) bands in the IR spectra were shifted to lower wavenumbers relative to **1a,b**, the ν(SiH) band was no longer observed, and the SiH signal in the ^1H NMR spectrum was shifted to higher field. The SiH coupling constants (**2a**: 104 Hz, **2b**: 105 Hz) were the same as previously observed in $(CO)_4W{=}C(NMe_2)SiHMes_2$ (106 Hz) as a result of a strong agostic W···H···Si interaction (see above). The configuration of the amino group was assigned (only the *Z* isomer is formed) on the basis of the chemical shifts of the alkyl substituents.[5]

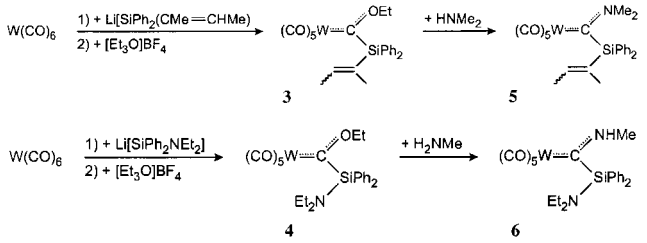
These results show that the agostic interaction of the Si−H group with the metal center blocks the fragmentation reaction of the silylcarbene ligand (i.e. the cleavage of $HSiR_3$) that is observed in the absence of this interaction.

Intramolecular Stabilization of Silyl Carbene Complexes by Stronger Interactions

Although we did not observe the addition of amines or olefins to the empty coordination site of the stable 16-electron complexes $(CO)_4M{=}C(NR_2)SiR_3$,[1d] we anticipated that such groups could interact with the metal center when they were part of the silyl substituent.

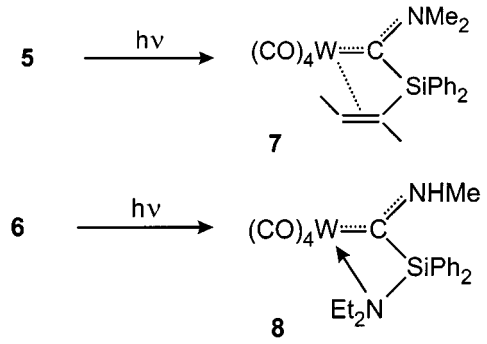
The ethoxy(silyl)carbene complexes $(CO)_5W{=}C(OEt)SiPh_2X$ (**3**: X = CMe=CHMe; **4**: X = NEt_2) were prepared by the Fischer route starting from $W(CO)_6$ and $LiSiPh_2X$, followed by alkylation of the formed anionic acyl complex with $[Et_3O]BF_4$ (Equation 2 and 3). The 2-butenyl-substituted complex **3** was obtained with the (*Z*)- and (*E*)-butenyl groups in a 3:1 ratio. For the synthesis of **4**, an excess of

$[Et_3O]BF_4$ has to be avoided, because otherwise the amino group is cleaved.



Reaction of **3** with Me_2NH and of **4** with $MeNH_2$ resulted in the formation of the corresponding amino(silyl)-carbene complexes **5** and **6** in high yields (Equation 2 and 3). Surprisingly, the ratio of the (*Z*/*E*) isomers of **5** (different configuration of the butenyl group) changed from 3:1 in the ethoxy-substituted complex **3** to 10:1 in the amino-substituted complex **5**. The (*E*/*Z*) isomers of **6** (relative to the C(carbene)−N bond) were formed in equal portions, according to the NMR spectroscopic data.

When ether solutions of **5** or **6** were irradiated with UV light, CO was evolved, and the thermally stable tetracarbonyl complexes **7** and **8** were obtained in high yields (Equation 4 and 5). The spectroscopic data clearly showed that the olefinic group in **7** and the amino group in **8** are coordinated to the metal center.



Comparison of the NMR chemical shifts and the coupling constants of the butenyl group in **5** and **7** showed clear differences caused by π-coordination in **7**. The =CH signal in **7** is shifted to higher field by 1.2 ppm, while the signals of the CH_3 groups are shifted to lower field. Due to the weakening of the C=C bond by π-coordination, the ^4J(HCCCH) and ^5J(HCCCCH) couplings were only observed in **5**, but not in **7**. In the ^{13}C NMR spectrum of **7**, the carbon atoms of the C=C bond were strongly shifted to higher field relative to **5**, as expected. In the (aminosilyl)-carbene complex **8**, the $N-CH_2$ protons became diastereotopic upon coordination to the metal. The quadruplet observed in the ^1H NMR spectrum of the pentacarbonyl complex **6** was therefore split to a multiplet in **8**.

Only one isomer was observed for both **7** and **8**. Only the isomer with the *Z* configuration of the butenyl group was formed for **7**. The *E* isomer either gives no stable complex or is isomerized during irradiation. Comparison of the chemical shift of the NMe group and the ^3J(HNCH) coupling constant with complexes of known configuration did not allow an unequivocal determination of the geometry along the C(carbene)−N bond in **8**. Since the (*E*/*Z*) ratio in the pentacarbonyl complex was 1, and the yield of **8** was larger than 50%, isomerization must have occurred during irradiation. Photochemical isomerization of the amino group in aminocarbene complexes was previously observed for $(CO)_4W=C(NHCH_2CH=CH_2)Tol$[6] and theoretically explained for $(CO)_5Cr=C(NMe_2)Ph$.[7] The same photochemical process was found to be responsible for the isomerization of the ethoxy group in $(CO)_5W=C(OEt)SiPh_3$ and the CO elimination in $(CO)_5W=C(NC_4H_8)SiPh_3$.[8]

The ν(CO) bands in the IR spectra of **7** and **8** had the typical pattern of *cis*-$(CO)_4WLL'$ complexes with local C_{2v} symmetry. The spectra clearly showed that the electron density at the metal increases in the order **2a** < **7** < **8** (Table 2). However, the similarity of the IR spectra of **2a** and **7** indicates that intramolecular interaction of the η^2-coordinated SiH group and the π-alkenyl substituent with the tungsten atoms are electronically comparable. This is in agreement with the density functional calculations discussed above. Similar results were previously found in competition experiments between $HSiR_3$ and olefins for coordination to unsaturated metal centers.[9]

Table 2. Comparison of the ν(CO) bands of the complexes **2a**, **7** and **8** (petroleum ether or pentane solutions)

2a	2027(m)	1947(s)	1937 (vs)	1895(s)
7	2024(s)	1938(sh,s)	1928(vs)	1894(s)
8	1995(m)	1940(vs)	1915(vs)	1845(m)

The molecular structure of **7** was determined by an X-ray structure analysis (Figure 2, Table 3). The alkenyl group coordinates in a π fashion despite the relatively short spacer (C(5), Si) tethering it to the metal. In other structurally characterized alkenyl-substituted tungsten carbene complexes, such as $(CO)_4W=C(NHCH_2CH=CH_2)Tol$,[6] $(CO)_4W=C(OEt)(CH_2)_nCH=CHR$ (n = 2, 3)[10] or related cyclopentenyl derivatives,[11] the linkage between the olefinic group and the metal atom is longer, and therefore the bonding situation is less strained. That coordination of the C=C bond occurs at all is probably due to the strong distortion of the W−C(carbene)−Si (98.0(3)°) and the C(carbene)−Si−C(81) angle (93.1(3)°). Similarly large distortions have been observed in the structurally characterized 16-electron silylcarbene complexes;[1a,1c] they would hardly be possible in silicon-free systems.

Although the W−CO and W−C(carbene) bond lengths and angles around the tungsten atom in **7** are very similar to $(CO)_4W=C(NHCH_2CH=CH_2)Tol$,[6] the W−C(olefin) interaction in **7** is less optimal. The observed W−C(81)/C(82) distances [246.9(7) and 252.3(8) pm] are significantly longer and less symmetric than the corresponding distances in the known alkenyl-substituted complexes mentioned above (238−251 pm).

The geometry of *cis*-olefin carbene complexes can be characterized by the torsional angles α and β (Scheme 3). The angle α represents the dihedral angle between the car-

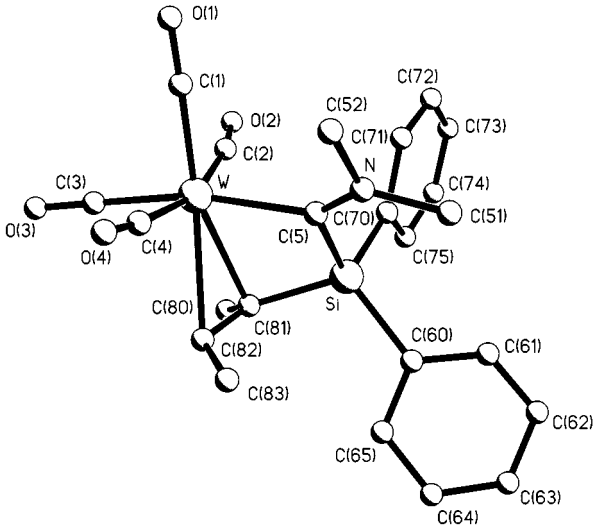
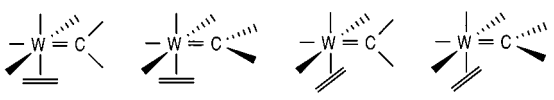


Figure 2. Molecular structure of **7**. Important distances (in pm) and angles (in deg): W−C(1) 198(1), W−C(2) 204(1), W−C(3) 199(1), W−C(4) 203(1), W−C(5) 220.4(8), W−C(81) 246.9(7), W−C(82) 252.3(8), C(5)−N 131.1(9), C(5)−Si 190.7(7), Si−C(81) 187.7(8). C(1)−W−C(5) 98.1(3), C(2)−W−C(5) 96.84, C(3)−W−C(5) 167.5(3), C(4)−W−C(5) 94.4(3), C(2)−W−C(4) 164.5(4), W−C(5)−N 136.4(6), W−C(5)−Si 98.0(3), C(5)−Si−C(81) 93.1(3), Si−C(81)−C(82) 121.6(6).

Table 3. Summary of crystal data, data collection and structure analysis of **7**

Chemical formula	$C_{23}H_{23}NO_4SiW{\cdot}1.5C_6H_6$
Formula weight	706.53
Crystal size [mm]	0.27 × 0.22 × 0.17
T [K]	293
Crystal system	monoclinic
Space group	$P2_1/c$
a [pm]	1199.96(2)
b [pm]	1040.48(2)
c [pm]	2566.30(2)
β [°]	91.824(1)
Volume × 10^6 [pm^3], Z	3202 pm^3, 4
D_c [g cm^{-3}]	1.465
μ (Mo-K_α) [mm^{-1}]	3.678
θ range [°]	1.59−24.99
Reflections collected	17950
R_{int}	0.1537
No. independent reflections	5643
Final R [$I > 2\sigma(I)$]	R_1 = 0.054, wR_2 = 0.097
Maximum difference Fourier peaks e/Å^{-3}	1.28
Weighting Scheme	$w=1/[\sigma^2(F_o^2) + 0.36P]$ with $P = (F_o^2 + 2F_c^2)/3$

bene plane (plane of the carbene carbon atom and the atoms directly bonded to it) and the plane $C_{carbene}$,W,C=$C_{centroid}$, and β the dihedral angle between the olefin plane (W,C(81),C(82)) and the plane $C_{carbene}$,W,C=$C_{centroid}$.



Scheme 3

According to Extended-Hückel calculations,[12] the (90,0) conformation is the most favorable, and the (0,0) conformation the least favorable. The calculated energy difference between both conformations is 16.2 kcal/mol for $(CO)_4(C_2H_4)W{=}CH_2$. The conformation of **7** (34.4, 73.8) is clearly between the two extremes, but close to that of $(CO)_4W{=}C(NHCH_2CH{=}CH_2)Tol$ (25.7, 77.0). Thus, a similar mutual orientation of the carbene and olefin planes is reached owing to the strong angular distortions within the carbene ligand of **7**. This geometry is obviously maintained in solution. While only three signals are observed for the carbonyl ligands in the ^{13}C NMR spectra of **2** and **8**, the chemical inequivalence of all CO ligands in **7** is a consequence of the observed geometry. Contrary to the alkenyl substituent in **7**, the amino substituent in **8** has no preferred orientation in its interaction with the metal, and therefore the complex appears to be more fluxional.

Conclusions

The 16-electron carbene complexes $(CO)_4M{=}C(NR_2)SiR'_2H$ are stabilized by a strong agostic interaction of the Si−H group with the metal center. In contrast, the stabilization of $(CO)_4M{=}C(NR_2)SiPh_3$ can be traced back to a weak η^1-coordination of the phenyl group by π-interaction. Theoretical calculations indicate that electron transfer to the metal by the agostic Si−H interaction is of a similar magnitude to the π-coordination of an olefinic ligand. The agostic Si−H interaction is strong enough to inhibit the previously observed thermal elimination of $HSiR'_3$ from $(CO)_5M{=}C(NHR)SiR'_3$. Heating the complexes $(CO)_5W{=}C(NHR)SiR'_2H$ results in CO cleavage instead; the resulting 16-electron complexes $(CO)_4W{=}C(NHR)SiR'_2H$ are stabilized by the W···H···Si interaction.

When the group X in $(CO)_5W{=}C(NR_2)SiR'_2X$ is an olefinic or amino substituent, it is coordinated to the metal center once a CO ligand is eliminated. While external olefins or tertiary amines did not coordinate to the vacant coordination site of the 16-electron complexes $(CO)_4W{=}C(NR_2)SiR'_3$, *intra*molecular coordination of the same groups results in stable complexes. The interaction of the substituent X in $(CO)_4W{=}C(NR_2)SiR'_2X$ with the metal center can thus be tuned from a very weak π-type bonding for X = Ph to a rather strong agostic bond for X = H, a classic π-bond for X = $CR{=}CR_2$, or a Lewis acid/base interaction for X = NR_2.

Experimental Section

All operations were performed in an atmosphere of dry and oxygen-free N_2, using dried and nitrogen-saturated solvents. A high pressure Hg lamp (Heraeus TQ 150) was used for the photochemical reactions. − Column chromatography was performed with silica (Woelm, 0.063−0.200 mm mesh) as the stationary phase, from which oxygen was removed by heating in vacuo and storage under N_2. − IR spectra: Perkin−Elmer 283, CaF_2-cuvettes. − ^1H NMR and ^{13}C NMR spectra: Bruker AC 250.

Computational Methods: Calculations were carried out at the gradient corrected density functional level by using the local spin density approximation,[13] combined with Becke's gradient correction[14] and Lee, Yang and Parr's correlation functional (B3LYP),[15] implemented in the GAUSSIAN94[16] package. The effective core potential of Hay and Wadt[17] implemented in the GAUSSIAN94 package (LANL2DZ) was used for the tungsten atom. Silicon atoms were described by the same potential with additional polarization functions (α(Si) = 0.45). Carbon, nitrogen and oxygen atoms were described with the [6/1/1/1/4/1] basis set of Dunning.[18] The natural bond orbital formalism [19] was applied for the population analysis. The contour plots were prepared with the program MOLDEN.[20]

$(CO)_4W{=}C(NHR)SiHMes_2$ (2a,b): A solution of **1a** (330 mg) or **1b** (340 mg, 0.55 mmol)[4] in diethyl ether (120 mL) was irradiated at −20 °C with UV light. A slight stream of argon was passed through the solution to expel CO and thus to prevent the back reaction. The volume of the solution was kept at 120 mL by occasionally adding ether. The reaction was monitored by IR spectroscopy. Irradiation was stopped and the solvent removed in vacuo when the CO bands of **2** no longer increased in intensity. The oily residue was dissolved in a minimum amount of petroleum ether/ether (2:1) and chromatographed on silica at −20 °C with the same solvent mixture. Unreacted **1** was eluted first, followed by an orange red zone of **2**. After elution, the solvent was removed and the orange red product powder washed with small amounts of pentane at 0 °C.

2a: Yield 241 mg (73%). − IR (pentane): ν_{NH} = 3234(w), ν_{CO} = 2027 (m), 1947 (s), 1937 (vs), 1895 (s) cm^{-1}. − ^1H NMR (C_6D_6): δ = −2.61 [s, *J*(*Si*H) = 104 Hz, ^1J(WH) = 35 Hz, 1 H, W···H···Si], 2.01 (s, 6 H, *p*-CH_3), 2.26 (s, 12 H, *o*-CH_3), 2.64 [d, ^3J(HNCH) = 4.5 Hz, 3 H, *Z*-NCH_3], 6.58 (s, 4 H, C_6H_2), 8.37 (br s, 1 H, NH). − ^{13}C NMR (C_6D_6): δ = 20.9 (*p*-CH_3), 23.5 (*o*-CH_3), 44.6 (*Z*-NCH_3), 203.7 [^1J(WC) = 128 Hz, *eq*/*cis*-CO], 214.8, 218.4 (*eq*/*trans*- + ax/*cis*-CO), 288.7 (C_{Carben}).

2b: Yield 235 mg (69%). − IR (diethyl ether): ν_{CO} = 2020 (m), 1925 (vs, br), 1890 (s) cm^{-1}. − ^1H NMR (C_6D_6): δ = −2.54 [s, *J*(*Si*H) = 105, ^1J(WH) = 35 Hz, 1 H, W···H···Si], 0.84 [t, ^3J(HCCH) = 7.5 Hz, 3 H, CH_2-CH_3], 2.02 (s, 6 H, *p*-CH_3), 2.32 (s, 12 H, *o*-CH_3), 3.23 (m, 2 H, Z/N−CH_2), 6.58 (s, 4 H, C_6H_2), 8.76 (br s, 1 H, NH). − ^{13}C NMR (C_6D_6): δ = 12.7 (CH_2-CH_3), 21.0 (*p*-CH_3), 23.6 (*o*-CH_3), 52.9 (*Z*-NCH_2), 203.8 (eq/*cis*-CO), 214.8, 218.4 (eq/trans- + ax/*cis*-CO), 286.3 ($C_{Carbene}$).

$(CO)_5W{=}C(OEt)SiPh_2CMe{=}CHMe$ (3): To a solution of *E*/*Z*-$Ph_2ClSi-CMe{=}CHMe$ (1.97 g, 7.22 mmol) in THF (30 mL), Li (250 mg, 36.0 mmol) was added in small pieces. The solution turned dark red after 10 min and was stirred for additional 4 h at room temperature. The solution was then filtered into a dropping funnel and added dropwise over 1.5 h to a suspension of $W(CO)_6$ (2.11 g, 6.0 mmol) in diethyl ether (200 mL) at −78 °C. The solution was allowed to warm to 0 °C and stirred at this temperature for 2 h. After cooling to −50 °C, $[Et_3O]BF_4$ (5 g) was added, and the mixture was stirred at 0 °C for 1 h. All steps of the reaction were monitored by IR spectroscopy. The solution was then filtered and the solvent removed in vacuo. The product complex was extracted from the residue with several 20 mL portions of petroleum ether (until the added solvent remained colorless). The combined solutions were concentrated to 15 mL and chromatographed on silica at −15 °C with a petroleum ether/ether (50:1) mixture). Elution of the red zone and removal of the solvent resulted in a red oil. Yield 2.64 g (59%). − IR (petroleum ether): ν_{CO} 2070 (s), 1960 (sh, vs), 1950 (vs, br) cm^{-1}. − ^1H NMR (C_6D_6): δ = 1.10 [t, ^3J(HCCH) = 7.1 Hz, 3 H, *trans*-OCH_2CH_3], 1.13 [t, ^3J(HCCH) = 7.1 Hz, 3 H, *cis*-OCH_2CH_3], 1.41 [d, ^3J(HCCH) = 7.1 Hz, 3 H, *trans*-$CHCH_3$], 1.42 [d, ^{3}J(HCCH) = 7.1 Hz, 3 H, *cis*-$CHCH_3$], 1.78 [d, ^4J(HCCCH) = 11.4 Hz, 3 H, *trans*-$SiCCH_3$], 1.79 [d, ^4J(HCCCH) = 1.4 Hz, 3 H, *cis*-$SiCCH_3$], 4.74 [q, ^3J(HCCH) = 7.1 Hz, 2 H, *trans*-OCH_2], 4.77 [q, ^3J(HCCH) = 7.1 Hz, 2 H, *cis*-OCH_2], 6.23 (m, *cis*/*trans*-CH, 1 H), 7.00−7.80 (m, 10 H, Ph). − ^{13}C NMR (C_6D_6): δ = 14.3 (*cis*-OCH_2CH_3), 14.4 (*trans*-OCH_2CH_3), 14.8 (*trans*-$CHCH_3$), 20.4 (*cis*-$CHCH_3$), 25.6 (*cis*-$SiCCH_3$), 27.2 (*trans*-$SiCCH_3$), 85.0 (*cis*-OCH_2), 85.1 (*trans*-OCH_2), 127−145 (Ph and C=C), 197.7 [^1J(WC) = 127 Hz, *cis*/*cis*-CO], 197.8 (*trans*/*cis*-CO), 206.1 (*cis*/*trans*-CO), 206.2 (trans/trans-CO), 400.3 (*cis*-$C_{Carbene}$), 402.3 (*trans*-$C_{Carbene}$). − ^{29}Si NMR (C_6D_6): δ = −18.0 [^2J(WC*Si*) = 12.9 Hz].

$(CO)_5W{=}C(OEt)SiPh_2NEt_2$ (4): To a solution of $Ph_2ClSiNEt_2$[21] (1.80 g, 6.2 mmol) in THF (30 mL), Li (180 mg, 25.9 mmol) was added in small pieces at 0 °C. The solution was stirred for 4 h at 0 °C, filtered into a dropping funnel cooled to 0 °C and then added dropwise within 1 h to a suspension of $W(CO)_6$ (1.62 g, 4.6 mmol) in diethyl ether (200 mL) at −78 °C. The solution was allowed to warm to 0 °C and stirred at this temperature for 2 h. After cooling to −50 °C, $[Et_3O]BF_4$ (437 mg, 2.3 mmol) was added, and the mixture was stirred at 0 °C for 1 h. Then more $[Et_3O]BF_4$ (two portions of 50 mg, together 0.52 mmol) were added. All steps of the reaction were monitored by IR spectroscopy. The solution was then filtered and the solvent removed in vacuo. The residue was extracted with benzene (30 mL), filtered and dried in vacuo. Dark red oil; yield 1.74 g (60%). − IR (diethyl ether): ν_{CO} 2065 (s), 1970 (s), 1955 (vs), 1935 (vs, br) cm^{-1}. − ^1H NMR (C_6D_6): δ = 0.90 [t, ^3J(HCCH) = 7.1 Hz, 6 H, NCH_2CH_3], 1.14 [t, ^3J(HCCH) = 7.1 Hz, 3 H, OCH_2CH_3], 2.90 [q, ^3J(HCCH) = 7.1 Hz, 4 H, NCH_2), 4.77 [q, ^3J(HCCH) = 7.1 Hz, 2 H, OCH_2], 7.10−7.80 (m, 10 H, Ph). − ^{13}C NMR (C_6D_6): δ = 14.5 (OCH_2CH_3), 14.9 (NCH_2CH_3), 41.0 (NCH_2), 85.1 (OCH_2), 128.2, 130.2, 134.3, 136.7 (Ph), 198.0 [^1J(WC) = 128 Hz, *cis*-CO], 206.5 (*trans*-CO), 404.5 ($C_{Carbene}$). − ^{29}Si NMR (C_6D_6) δ = −22.0.

$(CO)_5W{=}C(NMe_2)SiPh_2CMe{=}CHMe$ (5): A stream of dry diethylamine was passed through a solution of **3** (1.86 g, 3.01 mmol) in diethyl ether (150 mL). Over 1 h, the dark red solution turned yellow. The progress of the reaction was monitored by IR spectroscopy. The solution was concentrated in vacuo, re-dissolved in petroleum ether/ether mixture (10 mL, 10:1) and chromatographed on silica at −15 °C. First, a small red zone containing **3** was eluted with petroleum ether, and then a yellow zone containing the product with petroleum ether/ether (20:1). A yellow solid was obtained after removal of the solvent. Yield 1.32 g (71%). M.p. 109 °C. − IR (petroleum ether): ν_{CO} 2060 (m), 1972 (w), 1933 (vs, br), 1925 (sh, vs) cm^{-1}. − ^1H NMR (C_6D_6): δ = 1.57 [dq, ^3J(HCCH) = 7.1, ^5J(HCCCH) = 1.4 Hz, 3 H, *cis*-$CHCH_3$], 1.64 [dq, ^4J(HCCCH) = 1.5, ^5J(HCCCH) = 1.4 Hz, 3 H, *cis*-$SiCCH_3$], 2.57 (s, 3 H, *trans*-*E*-NCH_3), 2.68 (s, 3 H, *cis*-*E*-NCH_3), 3.35 (s, 3 H, *trans*-*Z*-NCH_3), 3.41 (s, 3 H, *cis*-*Z*-NCH_3), 5.95 [qq, ^3J(HCCH) = 7.1 Hz, ^4J(HCCCH) = 1.5 Hz, 1 H, *cis*-CH), 7.10−7.60 (m, 10 H, Ph). − ^{13}C NMR (C_6D_6): δ = 20.7 ($CHCH_3$), 24.4 ($SiCCH_3$), 54.0 (*E*-NCH_3), 58.6 (*Z*-NCH_3), 127−145 (Ph, C=C), 199.1 [^1J(WC) = 127 Hz, *cis*-CO], 203.7 (*trans*-CO), 291.3 [^1J(WC) = 86 Hz, $C_{Carbene}$]. − ^{29}Si NMR (C_6D_6): δ = −19.6. − $C_{24}H_{23}NO_5SiW$ (617.39): calcd. C 46.69, H 3.75, N 2.27; found C 46.74, H 3.69, N 2.28.

$(CO)_5W{=}C(NHMe)SiPh_2NEt_2$ (6): A stream of dry methylamine was passed through a solution of **4** (1.50 g, 2.52 mmol) in diethyl ether (150 mL). Over 15 min, the dark red solution turned yellow.

The progress of the reaction was monitored by IR spectroscopy. The solution was concentrated in vacuo and re-dissolved in a petroleum ether/ether mixture (20 mL, 10:1). On cooling to −30 °C, a yellow precipitate was obtained which was separated and dried in vacuo. Yield 1.48 g (95%). − IR (diethyl ether): ν_{CO} 2070 (s), 1975 (s), 1935 (vs), 1925 (vs, sh) cm^{-1}. − ^1H NMR (C_6D_6): δ = 0.68 [t, ^3J(HCCH) = 7.1 Hz, 6 H, *E*-NCH_2CH_3], 0.81 (t, ^3J(HCCH) = 7.1 Hz, 6 H, *Z*-NCH_2CH_3], 2.01 [d, ^3J(HNCH) = 5.0 Hz, 3 H, *E*-NCH_3], 2.59 [q, ^3J(HCCH) = 7.1 Hz, 4 H, *E*-NCH_2], 2.82 [q, ^3J(HCCH) = 7.1 Hz, 4 H, *Z*-NCH_2], 3.03 [d, ^3J(HNCH) = 4.3 Hz, 3 H, *Z*-NCH_3], 7.10−7.80 (m, 10 H, Ph), 9.35 (br s, 1 H, *Z*-NH), 9.63 (br s, 1 H, *E*-NH). − ^{13}C NMR (C_6D_6): δ = 14.7 (NCH_2CH_3), 40.6 (NCH_2), 42.1 (*E*-NCH_3), 45.2 (*Z*-NCH_3), 200.0 (*cis*-CO), 204.0 (*trans*-CO), 287.3 ($C_{Carbene}$). − ^{29}Si NMR (C_6D_6): δ = −13.1.

$(CO)_4W{=}C(NMe_2)SiPh_2CMe{=}CHMe$ (7): A solution of **5** (0.72 g, 1.22 mmol) in diethyl ether (150 mL) was irradiated with UV light at −20 °C. A light stream of argon was passed through the reaction solution to expel liberated CO. The reaction was monitored by IR spectroscopy and stopped when all bands of **5** had disappeared (about 2 h). The solution was concentrated in vacuo, and the residue washed with petroleum ether at −20 °C. Orange red crystals were obtained after drying in vacuo. Yield 0.67 g (93%). − IR (petroleum ether): ν_{CO} 2024 (s), 1938 (sh, s), 1928 (vs), 1894 (s) cm^{-1}. − ^1H NMR (C_6D_6): δ = 2.11 [d, ^3J(HCCH) = 6.4 Hz, 3 H, $CHCH_3$], 2.32 (s, 3 H, $SiCCH_3$), 2.68 (s, 3 H, *E*-NCH_3), 3.08 (s, 3 H, *Z*-NCH_3), 4.75 [q, ^3J(HCCH) = 6.4 Hz, 1 H, CH], 7.00−7.50 (m, 10 H, Ph). − ^{13}C NMR (C_6D_6): δ = 27.8 ($SiCCH_3$), 28.4 ($CHCH_3$), 54.1 (*E*-NCH_3), 54.9 (*Z*-NCH_3), 84.4 (CH), 98.3 ($SiCCH_3$), 207.1, 209.7 [^1J(WC) = 125 Hz, *eq*/*cis*-CO], 214.2 [^1J(WC) = 130 Hz, *eq*/*trans*-CO], 216.5 [^1J(WC) = 155 Hz, *ax*/*cis*-CO], 291.4 [^1J(WC) = 82 Hz, $C_{Carbene}$]. − ^{29}Si NMR (C_6D_6): δ = −35.8. − $C_{23}H_{23}NO_4SiW$ (589.38): calcd. C 46.87, H, 3.93, N 2.38; found C 47.04, H 4.25, N 2.29.

$(CO)_4W{=}C(NHMe)SiPh_2NEt_2$ (8): A solution of **6** (1.40 g, 2.26 mmol) in diethyl ether (150 mL) was irradiated with UV light at −20 °C. A light stream of argon was passed through the reaction solution to expel liberated CO. The reaction was monitored by IR spectroscopy and stopped when all bands of **6** had disappeared (about 3 h). The solution was concentrated in vacuo, re-dissolved in a petroleum ether/ether mixture (10 mL, 20:1) and chromatographed on silica at −15 °C with the same solvent mixture. First, a yellow zone of **6** (re-formed by decomposition of **8**) was eluted, and then, with a 2:1 mixture of petroleum ether and ether mixture, an orange red zone containing the product. An orange red oil was obtained after removal of the solvent. Yield 0.83 g (62%). − IR (petroleum ether): ν_{CO} 1995 (m), 1940 (vs), 1915 (vs), 1845 (m) cm^{-1}. − ^1H NMR (C_6D_6): δ = 0.65 [t, ^3J(HCCH) = 7.1 Hz, 6 H, NCH_2CH_3], 1.71 [d, ^3J(HNCH) = 4.3 Hz, 3 H, NCH_3], 2.86, 3.06 (m, 4 H, NCH_2), 7.20−7.80 (m, 10 H, Ph), 8.58 (br s, 1 H, NH). − ^{13}C NMR (C_6D_6): δ = 13.8 (NCH_2CH_3), 51.4 (NCH_2), 52.3 (NCH_3), 209.9 [^1J(WC) = 130 Hz, *eq*/*cis*-CO], 217.3 [^1J(WC) = 165 Hz, *ax*/*cis*-CO], 224.1 [^1J(WC) = 128 Hz, *eq*/*trans*-CO], 302.3 (C_{Carben}). − ^{29}Si NMR (C_6D_6): δ = −6.0.

X-ray Structure Analysis of 7: (see also Table 3) Selected crystals were sealed in a glass capillary and mounted on a Siemens SMART diffractometer with a CCD area detector. Graphite-monochromated Mo-K_α radiation (71.073 pm) was used for all measurements. The crystal-to-detector distance was 5.85 cm. A hemisphere of data was collected by a combination of three sets of exposures at 293 K. Each set had a different φ angle for the crystal, and each exposure took 20 s and covered 0.3° in ω. The data were corrected for polarization and Lorentz effects, and an empirical absorption correction (SADABS) was applied. The cell dimensions were refined with all unique reflections. The structure was solved by direct methods (SHELXS86). Refinement was carried out with the full-matrix least-squares method based on F^2 (SHELXL93) with anisotropic thermal parameters for all nonhydrogen atoms. Hydrogen atoms were inserted in calculated positions and refined riding with the corresponding atom. Crystallographic data (excluding structure factors) for the structure reported in this paper have been deposited at the Cambridge Crystallographic Data Centre as supplementary publication no. CCDC 140737. Copies of the data can be obtained free of charge on application to CCDC, 12 Union Road, Cambridge CB2 1EZ, UK (Fax: (internat.) +44−1223/336−033; E-mail: deposit@ccdc.cam.ac.uk).

Acknowledgments

We thank the Fonds zur Förderung der wissenschaftlichen Forschung (FWF), Vienna, for supporting this work.

[1] [1a] U. Schubert, W. Hepp, J. Müller, *Organometallics* **1986**, *5*, 173. [1b] W. Hepp, U. Schubert, *J. Organomet. Chem.* **1990**, *385*, 221. [1c] U. Schubert, M. Schwarz, F. Möller, *Organometallics* **1994**, *13*, 1554. [1d] U. Schubert, M. Schwarz, *Inorg. Chim. Acta* **1994**, *220*, 73.
[2] W. Hepp, U. Schubert, *J. Organomet. Chem.* **1987**, *321*, 317.
[3] M. Schwarz, *Ph. D. Thesis*, University of Würzburg, **1997**.
[4] U. Schubert, P. Wülfert, S. Mock, *J. Organomet. Chem.* **1993**, *459*, 55.
[5] E. Moser, E. O. Fischer, *J. Organomet. Chem.* **1968**, *13*, 387; **1969**, *16*, 275.
[6] C. P. Casey, A. J. Shusterman, N. W. Vollendorf, K. J. Haller, *J. Am. Chem. Soc*. **1982,** *104*, 2417.
[7] T. F. Block, R. F. Fenske, *J. Organomet. Chem.* **1977**, *139*, 235
[8] A. D. Rooney, J. J. McGarvey, K. C. Gordon, R.-A. McNicholl, U. Schubert, W. Hepp, *Organometallics* **1993**, *12*, 1277.
[9] S. B. Duckett, R. N. Perutz, *J. Chem. Soc., Chem. Commun.* **1991**, 28.
[10] C. A. Toledano, J. Levisalles, M. Rudler, H. Rudler, J.-C. Daran, Y. Jeannin, *J. Organomet. Chem.* **1982**, *228*, C7. C. A. Toledano, H. Rudler, J.-C. Daran, Y. Jeannin, *J. Chem. Soc., Chem. Commun.* **1984**, 574.
[11] C. A. Toledano, A. Parlier, H. Rudler, J.-C. Daran, Y. Jeannin, *J. Chem. Soc.* **1984**, 576, C. Alvarez-Toledano, A. Parlier, H. Rudler, M. Rudler, J.-C. Daran, C. Knobler, Y. Jeannin, *J. Organomet. Chem.* **1987**, *328*, 357.
[12] F. Volatron, O. Eisenstein, *J. Am. Chem. Soc.* **1986**, *108*, 2173.
[13] S. H. Vosko, L. Wilk, M. Nusair, *Canadian J. Phys.* **1980**, *57*, 1200.
[14] A. D. Becke, *J. Chem. Phys.* **1993**, *98*, 5648.
[15] C. Lee, W. Yang, R. G. Parr, *Phys. Rev. B* **1988**, *37*, 785.
[16] *Gaussian 94*, M. J. Frisch, G. W. Trucks, H. B. Schlegel, P. M. W. Gill, B. G. Johnson, M. W. Wong, J. B. Foresman, M. A. Robb, M. Head-Gordon, E. S. Replogle, R. Gomperts, J. L. Andres, K. Raghavachari, J. S. Binkley, C. Gonzalez, R. L. Martin, D. J. Fox, D. J. Defrees, J. Baker, J. J. P. Stewart, J. A. Pople, *Gaussian*, Inc., Pittsburgh PA, **1995**.
[17] P. J. Hay, W. R. Wadt, *J. Chem. Phys.* **1985**, *82*, 270, 299.
[18] T. H. Dunning, Jr., *J. Chem. Phys.* **1989**, *90*, 1007.
[19] *NBO Version 3.1*, E. D. Glendening, A. E. Reed, J. E. Carpenter, F. Weinhold, A. E. Reed, L. A. Curtiss, *Chem. Rev.* **1988**, *88*, 899.
[20] G. Schaftenaar, J. H. Noordik, *J. Comput.-Aided Mol. Design* **2000**, *14*, 123.
[21] K. Tamao, E. Nakajo, Y. Ito, *Tetrahedron.* **1988**, *44*, 3997.

Received February 21, 2000
[I00069]

Superexchange Interactions through Quasi-Linear End-to-End Azido Bridges: Structural and Magnetic Characterisation of a New Two-Dimensional Manganese–Azido System $[Mn(DENA)_2(N_3)_2]_n$ (DENA = diethylnicotinamide)

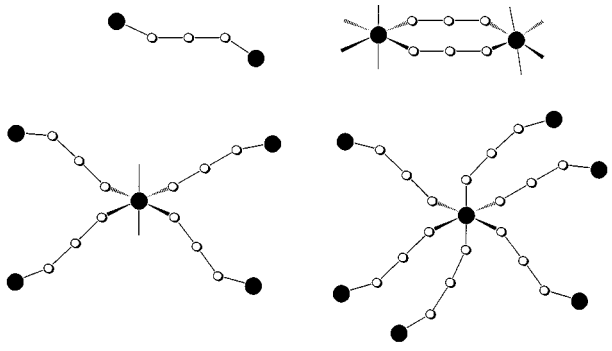
Mohamed A. S. Goher,[a] Morsy A. M. Abu-Youssef,[a] Franz A. Mautner,[b] Ramon Vicente,[c] and Albert Escuer*[c]

Keywords: Manganese / Two-dimensional systems / Azido bridges

Reaction of sodium azide with manganese(II) and diethylnicotinamide (DENA) leads to the two-dimensional system *trans*-$[Mn(DENA)_2(N_3)_2]_n$. The compound crystallises in the *P*2/*c* (monoclinic) group. Structural determination shows layers of manganese atoms bridged by means of single $\mu_{1,3}$-azido bridges. The polymeric structure is achieved by means of two different $\mu_{1,3}$-azide bridges, one of them with Mn–N–N bond angles of 148.4(2)°, whereas the second nonequivalent azido bridge has the unusual feature of quasi-linear coordination with Mn–N–N bond angles of 171.7(2)°. Molecular orbital calculations and susceptibility data show antiferromagnetic interaction and similar constant coupling values for the two superexchange pathways, in spite of the structural differences. Susceptibility, magnetisation, and EPR properties are compared with related azido systems.

Introduction

Manganese-azide compounds in which the azide ligand acts as a bridge exclusively in the end-to-end coordination mode (EE) have recently been developed. The number of reported compounds is limited to seven, but there is an exceptional versatility of topologies and magnetic properties: one dinuclear system has a single quasi-linear EE bridge,[1] there are three chains with double EE azido bridges,[2,3] two 2-D systems[4,5] and one 3-D compound,[6] in which each of the manganese atoms is coordinated to the four neighbouring manganese atoms by means of four single EE bridges, and, finally, one 3-D system with each manganese atom octahedrally surrounded by six EE bridges. 1[7]



Scheme 1. Basic units found to date for Mn^{II}/end-to-end azide systems

[a] Chemistry Department, Faculty of Science, Alexandria University, P.O.Box. 426, Ibrahimia, Alexandria 21321, Egypt
[b] Institut für Physikalische und Theoretische Chemie, Technische Universität Graz, A-8010 Graz, Austria
[c] Departament de Química Inorgànica, Universitat de Barcelona, Diagonal 647, 08028 Barcelona, Spain
E-mail: aescuer@kripto.qui.ub.es

Magnetically, all of them show antiferromagnetic interactions, even the quasi-linear EE bridge. The magnetic properties for the two general cases of single[6b] or double[2] EE bridge correlate with the bond structural parameters (mainly bond angles) that determine the overlap of the MO of the bridge with the adequate AO of the manganese atoms. Interest in this kind of compound was reinforced by the characterisation of long-range magnetic ordering with spontaneous magnetisation below T_C = 28 K for the 2-D $[Mn(4\text{-acpy})_2(N_3)_2]_n$ system, (4-acpy = 4-acetylpyridine).[8a]

The EE bridge has also been found in other kinds of 1-D, 2-D honeycombs, or 3-D alternating systems together with a second kind of bridge, such as the end-on azido bridge (EO)[2,6b,8] or other ligands such as 4,4'-bipyridine[9] or bipyrimidine.[10] However, in these cases, the intrinsic difficulties in determining the *J* values makes it difficult to correlate the magnitude of the coupling with structural data.[10c]

Following our research on compounds of this kind, we studied the derivative obtained from the reaction of manganese(II) with diethylnicotinamide (DENA) and sodium azide. The new two-dimensional system *trans*-$[Mn(DENA)_2(N_3)_2]_n$ was structurally characterised; this compound consists of well-isolated layers in which the manganese atoms are bridged by four azido ligands (two pairs of nonequivalent bridges) in the EE mode, showing the expected antiferromagnetic coupling. One of these nonequivalent EE bridges shows quasi-linear Mn–N–N–N–Mn coordination, with Mn–N–N bond angles of 171.7°, far from the preferred bond angles derived from the sp^2 arrangement of the terminal nitrogen atoms of the ligand. It should be emphasised that constrained linear $\mu_{1,3}$-coordination for azido bridges has been found only recently through the use of systems in which the two paramagnetic ions are placed in rigid cryptand ligands.[1]

 © WILEY-VCH Verlag GmbH, D-69451 Weinheim, 2000 1434–1948/00/0808–1819 $ 17.50+.50/0

In this paper we present the synthesis, structural characterisation, magnetic behaviour (focusing our attention on the exceptional linear azido bridge), and EPR data for $[Mn(DENA)_2(N_3)_2]_n$, together with a comparison with the previously reported end-to-end manganese–azido systems.

Results and Discussion

Crystal Structure of $[Mn(DENA)_2(N_3)_2]_n$ (1)

The structure of **1** consists of 2D manganese–azido sheets. A labelled ORTEP plot of the asymmetric unit is shown in Figure 1 Manganese atoms are placed in a centrosymmetric octahed al environment. The coordination polyhedron is formed by two DENA and four azido ligands coordinated in a *trans* arrangement, elongated along the axis defined by the pyridinic ligands, Mn–N(1) = 2.291(3) and similar Mn–N azido distances Mn–N(11) = 2.210(3) and Mn–N(21) = 2.225(3) Å. Each azido ligand acts as a bridge to the next manganese atom in the end-to-end coordination mode, allowing a two-dimensional polymer in the *bc* plane (Figure 2). Whereas the bond angle Mn–N(21)–N(22) = 148.4(2)° lies in the normal range for this kind of compound,[2,7] Mn–N(11)–N(12) = 171.7(2)° shows a quasi-linear coordination which has to date only been reported for systems with strong sterical constraints, such as cryptand compounds. The Mn–azido–Mn torsion angle, defined as the Mn–N(11)–N(12)–N(11C)–Mn(1C) dihedral angle, is 180°, whereas Mn–N(21)–N(22)–N(21A)–Mn(1A) has a torsion angle value of 166.7(2)°. Due to these asymmetric bond angles and the Mn–N_3–Mn torsion angle, the planes defined by the neighbouring manganese atom and the four bonded N (azido) atoms show a low dihedral angle of 5.6°. Minimum Mn–Mn intraplane distances are 6.553(3) Å and 6.695(3) Å, whereas the shorter interplane distance is 14.153 Å (*x* axis of the cell) due to the large space occupied by the pyridine ligands which isolate the manganese–azide layers (Figure 2). The general trends of the structure of **1** is similar to that of the two-dimensional compounds with 4-acetylpyridine or methylisinicotinate ligands;[4,5] the most significant differences are the more asymmetric Mn–N–N and Mn–N···N–Mn bond angles (Table 1).

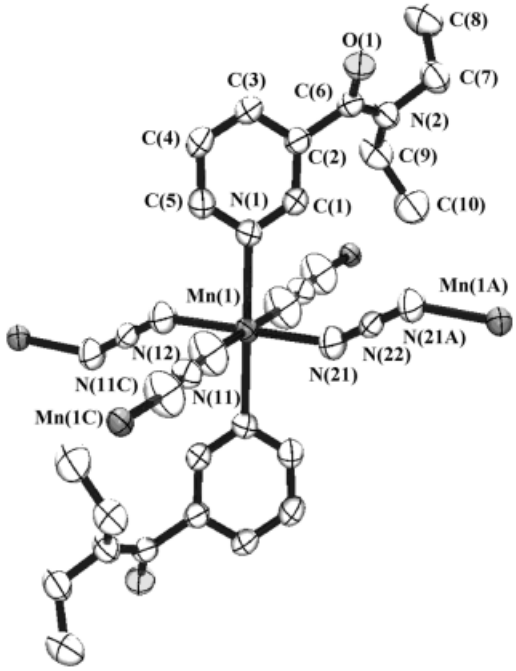


Figure 1. ORTEP drawing of $[Mn(DENA)_2(N_3)_2]_n$; ellipsoids at 50% probability level

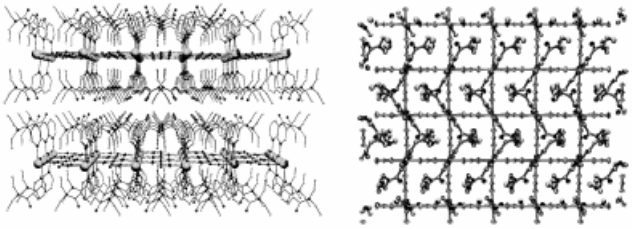


Figure 2. View of the $[Mn(DENA)_2(N_3)_2]_n$ compound along the (0 0 1) direction, to show the large interplane separation induced by the large pyridinic ligand (left); view along the (1 0 0) direction, showing the quadratic manganese–azide network

Table 1. Comparative structural and magnetic data for the three two-dimensional manganese–EE azide systems structurally characterised to date. "Angl. mean planes" refers to the angle between the MnN_4 (*N*-azide) planes; intersheet *d* is the minimum Mn–Mn interplane distance; ΔHpp is the EPR linewidth at room temperature; T_C indicates the ordering temperature, if present.

	L = DENA	L = 4-acpy	L = Me-*i*-nic
Mn–N–N	148.4°/171.7°	129.0°/151.6°	128.3°/149.7°
Mn–N···N–Mn	180°/166.7°	100.4°	96.8°
Angle's mean planes	5.65°	83.3°	84.9°
Intersheet *d* [Å]	14.153	11.563	12.424
J [cm^{-1}]	–3.42	–3.83	–2.24
ΔHpp [*G*]	30	30	46
T_C	$T_C < 2$	28 K	$T_C < 2$
ref.	this study	[4, 8a]	[5]

Superexchange Mechanism

Structural date enable two different superexchange pathways to be proposed, one through the azido bridge, with Mn–N–N bond angles of 148.4° (J_1), and a second through the azido bridge, with Mn–N–N bond angles of 171.7° (J_2). Previous MO calculations[6b] on the single azido bridge for manganese(II) systems (d^5 configuration) show that when the bond angle increases and approaches 180°, the interaction through the dz^2 orbitals of the paramagnetic centres and the nonbonding π orbitals of the bridge decreases, tending to zero for the 180° bond angle, whereas the overlap between the d*xz* and d*yz* atomic orbitals and the π orbitals of the bridge increases to the maximum interaction at 180°. In our case, we performed the MO calculations for the experimental bond angles, according to the molecular simulation previously proposed, and using as input parameters the experimental Mn–N(azide), N–N bond lengths and the experimental Mn–N–N and M–N–N–N–Mn bond and tor-

sion angles. The results of the calculations,[11] plotted in the Δ^2 form (Δ gap between the antibonding symmetric and antisymmetric combinations derived from each magnetically active atomic orbital of the manganese atoms, according to the Hoffmann model),[12] indicate that the superexchange through the N(11)–N(12)–N(11C) bridge occurs mainly through the two d*xz* and d*yz* interactions, whereas the dz^2 pathway contribution is negligible due to its quasi-orthogonal position with respect to the nonbonding π orbitals of the bridge (Figure 3). For the second N(21)–N(22)–N(21A) bridge, the lower bond angle enhances the overlap of the dz^2 orbitals with the π MO of the azido group, but the d*xz* interaction simultaneously decreases (Figure 3). Calculation of the $\Sigma\Delta^2$ affords the 0.104 and 0.102 eV^2 values for each bridge, indicating that the antiferromagnetic contributions for the two different bridges are accidentally similar. The main consequence is that the reported compound is assumed to be a structurally alternating 2-D system due to the two nonequivalent bridges, but magnetically the system may be studied as a homogeneous plane.

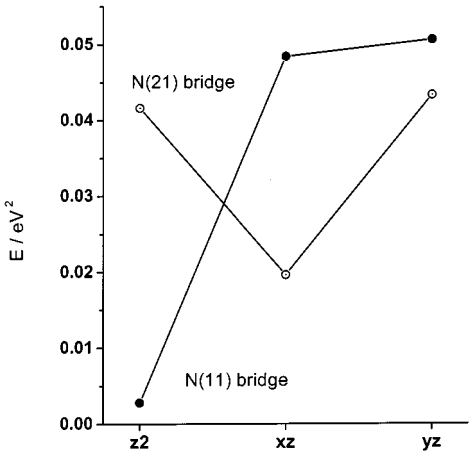


Figure 3. Contribution of each of the three active superexchange pathways for the two different EE bridges of $[Mn(DENA)_2(N_3)_2]_n$

It is remarkable that EE bridges with M–N–N bond angles close to 180° are unusual. To date the only structural and magnetic data for this kind of system was obtained from Mn–N–N–N–Mn units encapsulated in cryptand cavities to force the quasi-linear coordination of the bridge. The magnetic interaction, which was consistent with the theoretical model, was moderately antiferromagnetic.[1]

Magnetic Properties

Susceptibility measurements were performed under a 100 G field in the 300–2 K temperature range. The susceptibility plot shows a maximum placed at 44 K, whereas $\chi_M \cdot T$ decreases continuously on cooling, from 3.87 cm^3 K mol^{-1} at 300 K, and tending to zero at low temperature (Figure 4). This behaviour corresponds to moderate antiferromagnetic coupling and the low temperature shape indicates that canting-like long-range interactions are not effective even at 2 K. Magnetisation measurements at 2 K in the range ±5 T also show behaviour that is normal for an antiferromagnet (Figure 5). Structural data suggest that two *J* superexchange coupling constants are required to fit the susceptibility data, but the above MO calculations show that J_1 is roughly equal to J_2 and so the data were treated as for a homogeneous system. The susceptibility data in the 300–30 K range were fitted with the high-temperature expansion series of Lines[13] for a quadratic-layer Heisenberg antiferromagnet, derived from $H = \Sigma_{nn}(-JS_iS_j)$, where Σ_{nn} runs over all pairs of nearest spins *i* and *j*. The best-fit parameters were $J = -3.42(1)$ cm^{-1}, $g = 2.01$, $R = 9 \cdot 10^{-5}$. The *J* value and the position of the maximum agree with the value obtained from the simplified expression[13] $kT_{max}/|J| = 1.12\ S\ (S + 1) + 0.10$, from which a $J = -3.1$ cm^{-1} value is expected.

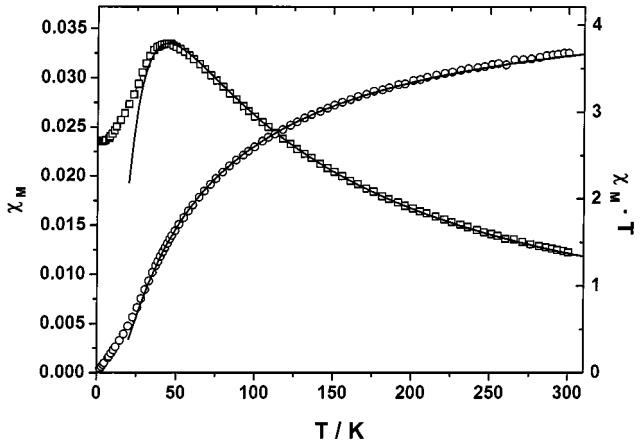


Figure 4. χ_M (dot centered circles) and $\chi_M \cdot T$ (dot centered squares) vs *T* plots for a polycrystalline sample of $[Mn(DENA)_2(N_3)_2]_n$;the solid lines show the best fit under the conditions described in the text

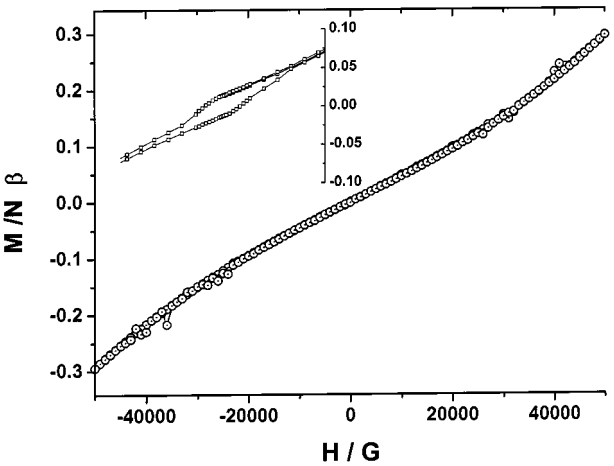


Figure 5. Magnetisation at 2.5 K vs applied field for $[Mn(DENA)_2(N_3)_2]_n$, compared with the related compound $[Mn(Meinc)_2(N_3)_2]_n$ which shows spontaneous magnetisation as a consequence of the structural differences (inset, range ±1.5 T)

This *J* value is comparable with the reported data for the two similar systems with the same topology (Table 1). The main difference between these systems is shown by $[Mn(4\text{-}acpy)_2(N_3)_2]_n$, which shows an ordered phase with a T_C of

28 K, as a consequence of the J value and the angle between the mean Mn equatorial planes, which may induce a canting phenomenon.[4][8a] $[Mn(Me\text{-}i\text{-}nic)_2(N_3)_2]_n$ has a lower J value, which should shift T_C to low temperature. Finally, for the compound reported in this paper, the quasi-parallel main axis of the coordination octahedron of the manganese atoms avoids the canting possibility.

The EPR spectrum consists of a sharp isotropic line centred at $g = 2.00$. Linewidth mainly depends on two factors: superexchange narrowing and dipolar broadening. When structural data, which show Mn···Mn intraplane distances greater than 6.5 Å are included, dipolar effects, if present, should be extremely weak, whereas the relatively high constant coupling of –3.4 cm^{-1} has a strong effect in narrowing the linewidth. The experimental spectrum shows a linewidth of 30 G, similar to the 4-acetylpyridine compounds ($J = -3.8$ cm^{-1}) and lower than the linewidth observed for the methylisonicotinate system ($J = -2.2$ cm^{-1}); this confirms the above assumptions. The dipolar broadening mechanism[14] for a two-dimensional manganese system is an anisotropic property which follows the $a + b\,(1 - \cos^2\theta)^2$ law, i.e., the maximum linewidth appears when the spectrum is measured parallel to the plane and it has the minimum linewidth at the 54.3° magic angle. The possible effects of dipolar broadening were checked in a single-crystal EPR experiment at room temperature, but for all the orientations of the crystal, the spectra were practically identical, showing a minor change in the linewidth between 28–33 G. In recent experiments[3] with the one-dimensional system $[Mn(3,5\text{-lut})_2(\mu_{1,3}\text{-}N_3)_2]_n$ (3,5-lut = 3,5-dimethylpyridine), in which the intrachain Mn···Mn distance is 5.140–5.159 Å, dipolar effects were found (linewidth variation between 40–90 G), but the greater Mn···Mn distance for the DENA compound is experimentally at the upper limit and makes this effect nondetectable.

Experimental Section

General: Infrared spectra (4000–400 cm^{-1}) were recorded in KBr pellets on a Nicolet 520 FTIR spectrophotometer. – Magnetic measurements were carried out with a Quantum Design instrument with a SQUID detector, working in the temperature range 300–2 K. The magnetic field was 100 G for the study of the low-temperature phenomena. Magnetisation measurements were recorded in the ±5 T range of external magnetic field. Diamagnetic corrections were estimated from Pascal Tables. – EPR spectra were recorded at X-band frequency with a Bruker ES200 spectrometer equipped with an Oxford liquid-helium cryostat for variable temperature work.

Synthesis of the Compound: The title complex $[Mn(DENA)_2(N_3)_2]_n$ (**1**) was synthesised by the dropwise addition of 5 mL of an aqueous solution of NaN_3 (0.42 g, 6.5 mmol) to an ethanolic solution mixture, about 30 mL, of manganese chloride trihydrate (0.59 g, 3 mmol) and 1.43 g (8 mmol) of *N*,*N*-diethylnicotinamide. The final clear solution was kept in a refrigerator for several weeks to produce well-formed crystals of the complex. Yield: 0.94 g (ca. 63%). – $C_{20}H_{28}MnN_{10}O_2$ (495.46): calcd. C, 48.4; H 5.7, Mn 11.1, N 28.3, O 6.5; found: C 48.3, H 5.6, Mn 11.2, N 28.5, O 6.4.

IR Spectra: The IR spectrum of the title complex $[Mn(DENA)_2(N_3)_2]_n$ shows bands attributable to the *N*,*N*-diethylnicotinamide ligand at normal frequencies [ν(C=O) at 1627 cm^{-1} (vs)]. In the 2000–2100 cm^{-1} region the complex shows a very strong and broad band, assigned to the asymmetric stretching azide group vibrations [$\nu_{as}(N_3)$] centred at 2092 cm^{-1} (vs). This band appears at normal frequencies; it was compared with that of the linear Mn–N_3–Mn cryptand system previously reported, (2200 cm^{-1}). In the region 1280–1360 cm^{-1} two bands could be attributed to the [$\nu_s(N_3)$] mode: 1378 cm^{-1} (ms) and 1336 cm^{-1} (m). In the far infrared region, two bands attributable to the ν(Mn–N_3) mode around 386 and 374 cm^{-1} and two bands due to the ν[Mn–N(L)] mode around 256 and 236 cm^{-1} were observed.

Crystal Structure Determination and Refinement of the Structure: Single-crystal X-ray data for $[Mn(DENA)_2(N_3)_2]_n$ were collected

Table 2. Crystal data and structure refinement for $[Mn(DENA)_2(N_3)_2]_n$ (**1**)

Empirical formula	$C_{20}H_{28}MnN_{10}O_2$
Formula mass	495.46
Crystal system	monoclinic
Space group	*P*2/*c* (no. 13)
a [Å]	14.153(5)
b [Å]	6.695(3)
c [Å]	13.066(5)
α [°]	90.00
β [°]	101.29(3)
γ [°]	90.00
V [Å^3]	1214.1(8)
Z	2
T [°C]	25(2)
λ(Mo-K_α) [Å]	0.71069
d_{calc} [g cm^{-3}]	1.355
μ(Mo-K_α) [mm^{-1}]	0.581
Max. transmission	1.000
Min. transmission	0.555
Max. peak in final diff. synthesis [eÅ^{-3}]	0.667
Min. peak in final diff. synthesis [eÅ^{-3}]	–0.244
R[a]	0.0492
$R^2\omega$≅[b]	0.1349

[a] $R(F_o) = \Sigma||F_o| - |F_c||/\Sigma|F_o|$. – [b] $R\omega(F_o)^2 = (\Sigma\{\omega[(F_o)^2 - (F_c)^2]^2\}/\Sigma\{\omega[(F_o)^2]^2\})^{1/2}$.

Table 3. Selected bond lengths [A] and angles [°] for **1**

Mn(1)–N(11)	2.210(3)
(1)–N(21)	2.225(3)
Mn(1)–N(1)	2.291(3)
N(11)–N(12)	1.145(3)
N(21)–N(22)	1.159(3)
C(6)–O(1)	1.236(3)
C(6)–N(2)	1.347(4)
N(1)–Mn(1)–N(1B)	180.0
N(11)–Mn(1)–N(11B)	180.0
N(21B)–Mn(1)–N(21)	180.0
N(1)–Mn(1)–N(11)	90.75(9)
N(1)–Mn(1)–N(11B)	89.25(9)
N(1)–Mn(1)–N(21)	91.2(1)
N(1)–Mn(1)–N(21B)	88.8(1)
N(11)–Mn(1)–N(21)	93.3(1)
N(11)–Mn(1)–N(21B)	86.7(1)
N(11B)–Mn(1)–N(21B)	93.3(1)
Mn(1)–N(11)–N(12)	171.7(2)
Mn(1)–N(21)–N(22)	148.3(2)
N(11)–N(12)–N(11C)	180.0
N(21)–N(22)–N(21A)	178.9(4)

with a modified STOE four-circle diffractometer. Crystal size: 0.50 × 0.34 × 0.24 mm. The crystallographic data, conditions maintained for the intensity data collection and some features of the structure refinement are listed in Table 2. Graphite-monochromated Mo-$K\alpha$ radiation (λ = 0.71069 Å) was used to collect the data set; the ω-scan technique was employed. The accurate unit-cell parameters were determined from automatic centering of 34 reflections ($8.5° < \theta < 12.9°$) and were refined by least-squares methods. 3318 reflections (2531 independent reflections, R_{int} = 0.0370) were collected in the range $2.94° < \theta < 26.50°$. An intensity decay of 6% for control reflections (–1 –2 0; 0 –2 1; 5 0 2), measured after every set of 100 reflections, was observed during data collection. Corrections were applied for Lorentz-polarization effects, for intensity decay, as well as for absorption, using the DIFABS[15] computer program. The structure was solved by direct methods with the SHELXS-86[16] computer program, and was refined by full-matrix least-squares methods on F^2 with the SHELXL-93[17] program as incorporated in the SHELXTL/PC V 5.03[18] program library, and the graphics program PLUTON.[19] All non-hydrogen atoms were refined anisotropically. The hydrogen atoms were fixed geometrically with the HFIX utility[18] (i.e., hydrogen atoms riding with idealized geometrical values on their parent carbon atoms with fixed distances: CH = 0.93 Å, CH_2 = 0.97 Å and CH_3 = 0.96 Å). Selected bond parameters are given in Table 3.

Atomic positional and thermal parameters, lists of bond lengths and angles, and F_o/F_c values are available as supplementary material from one of the authors (F. A. M.). Crystallographic data (excluding structure factors) for the structure reported in this paper have been deposited with the Cambridge Crystallographic Data Centre as supplementary publication No. CCDC-127494. Copies of the data can be obtained free of charge on application to CCDC, 12 Union Road, Cambridge CB2 1EZ, U. K. [Fax: (int.) +44–1223/336 033; E-mail: deposit@ccdc.cam.ac.uk].

Molecular orbital calculations and magnetic susceptibility properties were explored for the new two-dimensional system *trans*-$[Mn(DENA)_2(N_3)_2]_n$ (DENA = diethylnicotinamide). The compound shows an unusual alternating of the azide bridges with Mn–N–N bond angles of 171.7(2)° and 148.4(2)°. The antiferromagnetic interaction has been correlated with the structural data.

Acknowledgments

This research was partially supported by the CICYT (Grant PB96/0163) and OENB (Grant 6630). F. A. Mautner and M. A. M. Abu-Youssef thank Prof. C. Kratky and Dr. Belaj (University of Graz) for the use of experimental equipment.

[1] A. Escuer, C. J. Harding, Y. Dussart, J. Nelson, V. McKee, R. Vicente, *J. Chem. Soc., Dalton Trans.* **1999**, 223.
[2] A. Escuer, R. Vicente, M. A. S. Goher, F. A. Mautner, *Inorg. Chem.* **1998**, *37*, 782.
[3] M. A. M. Abu-Youssef, A. Escuer, D. Gatteschi, M. A. S. Goher, F. A. Mautner, R. Vicente, *Inorg. Chem.* **1999**, *38*, 5716.
[4] A. Escuer, R. Vicente, M. A. S. Goher, F. A. Mautner, *Inorg. Chem.* **1995**, *34*, 5707.
[5] A. Escuer, R. Vicente, M. A. S. Goher, F. A. Mautner, *J. Chem. Soc., Dalton Trans.* **1997**, 4431.
[6] [6a] M. A. S. Goher, F. A. Mautner, *Croat. Chem. Acta* **1990**, *63*, 559. – [6b] A. Escuer, R. Vicente, M. A. S. Goher, F. A. Mautner, *Inorg. Chem.* **1996,** *35*, 6386**.**
[7] F. A. Mautner, R. Cortés, L. Lezama, T. Rojo, *Angew. Chem. Int. Edit. Engl.* **1996**, *35*, 78.
[8] [8a] A. Escuer, R. Vicente, F. A. Mautner, M. A. S. Goher, *Inorg. Chem.* **1997**, *36*, 3440. – [8b] M. A. S. Goher, N. A. Al-Salem, F. A. Mautner, *J. Coord. Chem.* **1998**, *44*, 119.
[9] H. Y. Shen, D. Z. Liao, Z. H. Jiang, S. P. Yan, B. W. Sun, G. L. Wang, X. K. Yao, H. G. Wang, *Chem. Lett.* **1998**, 469.
[10] [10a] G. De Munno, M. Julve, G. Viau, F. Lloret, J. Faus, D. Viterbo, *Angew. Chem. Int. Ed. Engl.* **1996**, *35*, 1807. – [10b] R. Cortés, L. Lezama, J. L. Pizarro, M. I. Arriortua, T. Rojo, *Angew. Chem. Int. Ed. Engl.* **1996**, *35*, 1810. – [10c] J. Curely, F. Lloret, M. Julve, *Phys. Rev. B* **1998**, *58*, 11465.
[11] C. Mealli, D. M. Proserpio, CACAO program (Computed Aided Composition of Atomic Orbitals), *J. Chem. Educ.* **1990**, *67*, 399.
[12] P. J. Hay, J. C. Thibeault and R. Hoffmann, *J. Am. Chem. Soc.* **1975**, *97*, 4884.
[13] M. E. Lines, *J. Phys. Chem. Solids* **1970**, *31*, 101.
[14] A. Bencini, D. Gatteschi, *EPR of Exchange Coupled Systems*, Springer-Verlag, Berlin Heidelberg **1990**, Chap. 10 and references therein.
[15] N. Walker, D. Stuart, *Acta Crystallogr.* **1983**, *A39*, 158.
[16] G.M. Sheldrick, *SHELXS-86*, Program for the Solution of Crystal Structure. University of Gottingen, Germany, **1986**.
[17] G.M. Sheldrick, *SHELXL-93*, Program for the Refinement of Crystal Structure. University of Gottingen, Germany, **1993**.
[18] *SHELXTL 5.03* (PC-Version), Program library for the Solution and Molecular Graphics. Siemens Analytical Instruments Division, Madison, WI, **1995**.
[19] A. L. Spek, *PLUTON-92*, University of Utrecht, 3584, CH Utrecht, The Netherlands **1992**.

Received June 24, 1999
[I99230]

Palladium-Catalyzed Reactions for the Synthesis of Fine Chemicals, 14[+]

Control of Chemo- and Regioselectivity in the Palladium-Catalyzed Telomerization of Butadiene with Methanol − Catalysis and Mechanism

Frank Vollmüller,[a] Jochen Krause,*[b] Susanne Klein,[b] Wolfgang Mägerlein,[c] and Matthias Beller*[c]

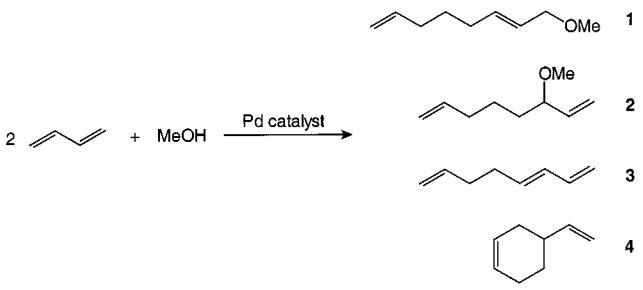
Keywords: Palladium / Butadiene / Telomerization / Homogeneous catalysis

The palladium-catalyzed telomerization reaction of butadiene with methanol has been examined with the aim of controlling the chemoselectivity (telomerization vs. dimerization products) and regioselectivity (linear vs. branched telomerization product) of the reaction. We have shown that the reaction temperature, ligand-to-metal ratio and ratio of substrates exert a large influence on the selectivity of the reaction. Selectivities of up to 97% for the desired linear telomerization product **1** can be achieved below 50 °C by employing both low PPh_3/Pd and butadiene/methanol ratios. Mono(phosphane)palladium(0)–diallyl ether complexes, Ar_3P–Pd[$(CH_2=CHCH_2)_2O$] (**5**), serve as new catalysts for the reaction. In order to gain a mechanistic understanding of the observed selectivity effects, we synthesized the phosphane(octadienyl)palladium(II) complexes **7a** and **9a** as model compounds for key reaction intermediates and examined their stoichiometric reactions with the methoxide nucleophile. Based on our results, we propose an extension of the known telomerization mechanism that accounts for the observed selectivity effects.

Introduction

An important ecological requirement of todays chemical processes is to produce a desired compound with high selectivity whilst, as far as possible, avoiding waste or by-products. Therefore, the possibility of controlling the product selectivity in a chemical reaction is of great interest. This control can be achieved, for example, by employing an appropriate catalyst or by adjusting the crucial reaction parameters.

During the course of our studies with regard to palladium-catalyzed C−C coupling reactions we became interested in the telomerization of butadiene, since this reaction assembles simple starting materials in a 100% atom-efficient manner to give valuable functionalized octadienes. These compounds are useful as intermediates in the total synthesis of several natural products,[2] as well as in industry, as precursors for plasticizer alcohols,[3] solvents, corrosion inhibitors and nonvolatile herbicides.[4] The telomerization reaction is the dimerization of two molecules of a 1,3-diene in the presence of an appropriate nucleophile HX,[5] e.g. alcohols,[6] water,[7] amines,[8] carboxylic acids[9] and others,[10] to give substituted octadienes (1-substituted 2,7-octadiene, 3-substituted 1,7-octadiene). Of these the 1-substituted 2,7-octadiene (*n*-product) is the major isomer formed for most nucleophiles. Due to the fact that they are readily available and cheap,[11] butadiene and methanol are attractive starting materials for this reaction, reacting to yield 1-methoxyocta-2,7-diene (**1**) (Scheme 1). As previous studies have shown,[6j] the major by-products include the 3-substituted octa-1,7-diene **2** (iso product), 1,3,7-octatriene (**3**) (formed by the linear dimerization of butadiene) and, less importantly, 4-vinylcyclohexene (**4**) (formed by the Diels−Alder reaction of two molecules of butadiene).



Scheme 1

Although the mechanism of the palladium-catalyzed telomerization reaction has been carefully examined,[12] de-

[+] Part 13: Ref.[1]

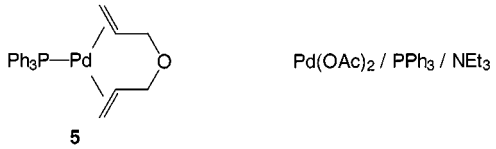
[a] Clariant Deutschland GmbH, Division Feinchemikalien, Industriepark Höchst,
65916 Frankfurt am Main, Germany
Fax: (internat) + 49-(0)69/30517562
E-mail: frank.vollmueller@clariant.com
[b] Clariant Deutschland GmbH, Division Feinchemikalien, Werk Griesheim
Postfach 831251, 65916 Frankfurt am Main, Germany
Fax. (internat) + 49-(0)69/386411
E-mail: jochen.krause@clariant.com
[c] Institut für Organische Katalyseforschung an der Universität Rostock e.V.
Buchbinderstraße 5−6, 18055 Rostock, Germany
Fax: (internat) + 49-(0)381/4669324
E-mail: matthias.beller@ifok.uni-rostock.de

 © WILEY-VCH Verlag GmbH, D-69451 Weinheim, 2000 1434−1948/00/0808−1825 $ 17.50+.50/0

tailed investigations focusing on the control of product selectivity in this process have not yet been carried out. In this paper, we describe the important factors determining the chemo- and regioselectivity, i.e. reaction temperature, ligand-to-metal ratio and butadiene-to-methanol ratio. New mono(phosphane)palladium(0) complexes **5**[13] were successfully employed as catalysts. The observed effects are rationalized mechanistically by a modified reaction mechanism for the butadiene telomerization reaction.

Results and Discussion

The examined telomerization reaction of butadiene with methanol is shown in Scheme 1.[14] Either (diallyl ether)(triphenylphosphane)palladium(0) (**5**)[13] or mixtures of palladium(II) acetate and triphenylphosphane (sometimes in combination with triethylamine) were used as the catalysts (Figure 1).



5

Figure 1

Compound **5** is representative of a new class of palladium(0) complexes in which only *one* phosphane ligand is coordinated to the palladium center. Compound **5** represents a stable analogue of an intermediate in the catalytic cycle of the reaction (vide infra, Schemes 2 and 5) and, as such, is well suited for our investigations, since it does not need to be activated (e.g. by ligand dissociation, reduction, etc.) before entering the catalytic cycle. For reasons of industrial applicability we have also included Pd^{II} precursor complexes in our studies due to the great availability of $Pd(OAc)_2$. It has already been reported that Pd^{II} precursors are rapidly reduced to the catalytically active Pd^0 species if a base, e.g. NEt_3, is present in the reaction mixture.[15] Thus, 100 equivalents NEt_3 (relative to Pd) were added to the runs in which the Pd^{II} precursor complex was used. Initial experiments showed that the content of NEt_3 in the reaction does not influence the chemo- nor the regioselectivity of the telomerization. Therefore, for the selectivity studies it was less important if the applied catalyst precursor was a Pd^0 or a Pd^{II} compound.

Selectivity Studies

The product selectivity of the palladium-catalyzed telomerization is largely influenced by temperature, ratio of starting materials and concentration of the phosphane ligands. Table 1 summarizes the influence of the reaction temperature.

The chemoselectivity, i.e. the discrimination between telomerization products (**1**, **2**) and the linear dimerization product 1,3,7-octatriene (**3**), remains excellent (95%) up to 50 °C (Entries 1−3, Table 1) but drops to 77% at 90 °C (Entry 4; Table 1). Thus, the high catalytic activity at elevated temperatures [turnover frequency (TOF) = 21000 h^{-1}: Entry 4, Table 1] is at the expense of the chemoselectivity. Above 100 °C, the Diels−Alder reaction of butadiene to yield 4-vinylcyclohexene becomes increasingly significant. On the other hand, the regioselectivity, i.e. the discrimination between both telomers **1** and **2**, remains high (≥ 95%) throughout the whole temperature range examined. Obviously, the side reaction leading to the undesired octatriene **3** becomes more important at temperatures above 50 °C, whereas the side reaction leading to the undesired iso telomer **2** is influenced by temperature to a much lesser extent. For palladium-catalyzed reactions in general, the ligand-to-metal ratio is one of the most critical reaction parameters. Typically, the variation of the ligand-to-palladium ratio influences the stability and the activity of the palladium catalyst but has a less pronounced effect on the reaction selectivity. Interestingly, in the case of the butadiene telomerization reaction the P/Pd ratio does not only influence the catalyst stability and activity but also dramatically affects the regioselectivity of the reaction. This effect was observed for both catalyst systems shown in Figure 1. The results of the catalytic runs with 1, 2, 3, 10 and 50 equivalents of phosphane (with respect to palladium) are shown in Table 2.

Firstly, the influence of the ligand-to-metal ratio on the selectivity was studied at −10 °C. The telomerization reaction was carried out using the palladium(0) complex **5** without any additional triphenylphosphane (P/Pd = 1:1: Entry 1, Table 2), as well as in the presence of 1 equiv. of triphenylphosphane (P/Pd = 2:1: Entry 2, Table 2). In both cases

Table 1. Influence of the reaction temperature on the product selectivity

Entry	Ratio butadiene/ methanol	Catalyst	Catalyst concentration [mol-%]	Temp. [°C]	Reaction time [h]	Conversion [%]	TON **1** + **2** + **3**	TOF [h^{-1}]	Yield **1** + **2** [%]	Yield **3** [%]	Chemoselectivity (**1** + **2**) [%]	Regioselectivity [%] (*n*/iso)
1	2:1	**5**	7×10^{-2}	−10	6	64	914	152	63	1	98	97.3 (36:1)
2	1:2	**5**	2.5×10^{-2}	30	2.5	36	1376	556	34	0.4	95	97.3 (36:1)
3	2:1	**5**	4×10^{-3}	50	2	27	6750	3375	26	1	96	95.8 (23:1)
4	2:1	**5**	1×10^{-3}	90	0.5	11	10500	21000	8.5	2	77	95.0 (19:1)

Table 2. Variation of the palladium to phosphane ratio

Entry	Ratio butadiene/ methanol	Catalyst	Catalyst concentration [mol-%]	Temp. [°C]	Reaction time [h]	Additives	Conversion [%]	TON **1** + **2** + **3**	Yield **1** + **2** [%]	Yield **3** [%]	Chemoselectivity (**1** + **2**) [%]	Regioselectivity [%] (*n*/iso)
1	2:1	**5**	7×10^{-2}	−10	6	–	64	914	63	1	98	97.3 (36:1)
2	2:1	**5**:1 PPh_3	5×10^{-2}	−10	6	–	29	560	28	0.3	97	92.3 (12:1)
3	1:2	**5**	4×10^{-3}	50	2	–	35	8500	34	0	97	97.0 (32:1)
4	1:2	$Pd(OAc)_2$ 3 PPh_3	1×10^{-2}	50	2.5	100 equiv. NEt_3	63	6200	61	1	97	96.6 (28:1)
5	1:2	$Pd(OAc)_2$ 3 PPh_3	1.8×10^{-3}	90	2.5	100 equiv. NEt_3	58	30280	49.5	5	85	95.0 (19:1)
6	1:2	$Pd(OAc)_2$ 10 PPh_3	1×10^{-3}	50	16	100 equiv. NEt_3	23	23000	22	1	> 99	94.1 (16:1)
7	1:2	$Pd(OAc)_2$ 10 PPh_3	1.8×10^{-3}	90	2.5	100 equiv. NEt_3	73	38890	62	8	85	93.3 (14:1)
8	2:1	$Pd(OAc)_2$ 50 PPh_3	5×10^{-4}	50	16	100 equiv. NEt_3	14	28000	13	< 1	> 99	87.5 (7:1)
9	2:1	$Pd(OAc)_2$ 50 PPh_3	5×10^{-4}	90	16	100 equiv. NEt_3	40	70000	30	5	75	85.7 (6:1)

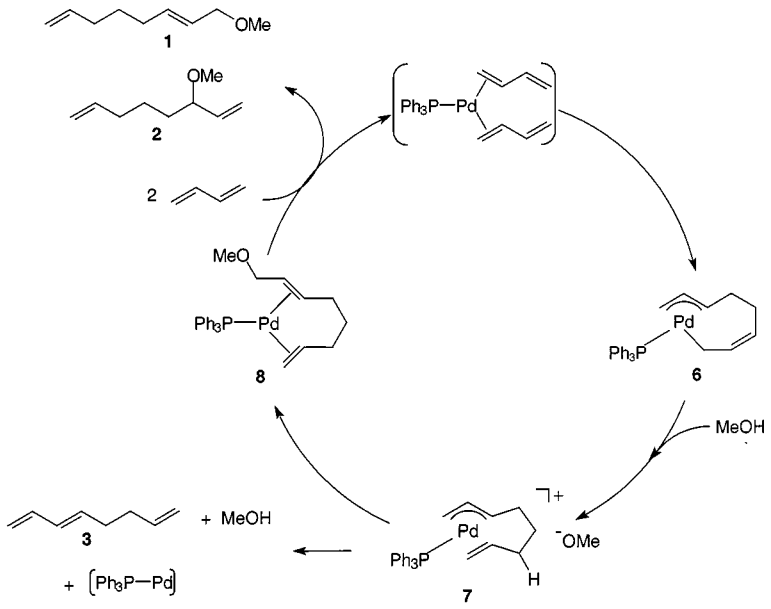
the chemoselectivity towards the telomerization products **1** and **2** was ≥ 97%; however, the *n*/iso ratio changed dramatically. With a P/Pd ratio of 1 the linear isomer **1** was produced in a 36:1 ratio relative to the branched isomer **2**. With a P/Pd ratio of 2 the ratio of **1** to **2** decreased to 12:1. Telomerization reactions using palladium(II) as the pre-catalyst do not yield any telomerization products at −10 °C. At 50 °C, in the presence of the palladium(0) complex **5** (i.e. P/Pd = 1: Entry 3, Table 2), **1** and **2** were still produced with both a high chemoselectivity of 97% and a high *n*/iso ratio of 32:1. On changing to $Pd(OAc)_2$ with 3 equiv. of triphenylphosphane (Entry 4, Table 2), the *n*/iso ratio drops slightly to 28:1, while the chemoselectivity remains excellent (97%). A further increase in the amount of triphenylphosphane at this temperature reduces the regioselectivity, thus the *n*/iso ratio decreases to 16:1 (P/Pd = 10:1: Entry 6; Table 2) and to 7:1 (P/Pd = 50:1: Entry 8, Table 2). However, the chemoselectivity (97−99%) is not affected to any significant extent by the change in the P/Pd ratio. When the telomerization reaction was carried out at 90 °C, both the chemo- and the regioselectivity were influenced by the P/Pd ratio. In the presence of 3 equiv. and 10 equiv. of triphenylphosphane (Entries 5 and 7, Table 2) the chemoselectivity decreases to 85%, and to 75% in the presence of 50 equiv. of the ligand (Entry 9, Table 2). The main side-product observed at 90 °C is 1,3,7-octatriene (**3**). In addition, the *n*/iso selectivity decreases with an increase in the reaction temperature and with an increasing P/Pd ratio. Hence, at 90 °C the linear-to-branched ratio decreases from 19:1 (3 equiv. PPh_3: Entry 5, Table 2) to 14:1 (10 equiv. PPh_3: Entry 7, Table 2). With 50 equiv. of triphenylphosphane the *n*/iso ratio was 6:1 (Entry 9, Table 2), similar to the run at 50 °C (Entry 8; Table 2).

In general, the ratio of telomerization products to dimerization products (chemoselectivity) decreases above a certain temperature (50 °C) and is not really affected by the P/Pd ratio. On the other hand, the regioselectivity is predominantly influenced by the amount of ligand present! The best regioselectivity using triphenylphosphane as the ligand is obtained with a ligand-to-palladium ratio of 1:1 below 50 °C (*n*/iso > 32:1; Entries 1 and 3, Table 2) while a *n*/iso ratio below 6:1 (Entries 8 and 9, Table 2) seems to be the borderline selectivity at high P/Pd ratios.

It is interesting to note that the established reaction mechanism ("Jolly mechanism") for the telomerization of butadiene and methanol (Scheme 2) does not explain the observed changes in regioselectivity.[12e]

It is proposed that in the presence of palladium(0) species two molecules of butadiene couple to form the $PPh_3-Pd-(\eta^1,\eta^3$-octadiendiyl) complex **6**. Protonation by methanol at the C-6 atom of the C_8 chain leads to the $PPh_3-Pd-(\eta^2,\eta^3-C_8H_{13})$ species **7**. In the following step the methoxide ion adds to either allylic terminus C-1 or C-3 of the C_8 chain resulting in the formation of the telomers **1** (via **8**) or **2**, respectively. The formation of 1,3,7-octatriene (**3**) occurs as a side reaction by hydrogen abstraction (C-4) from **7**.

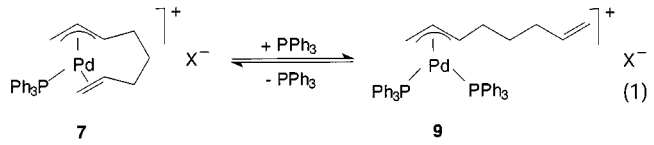
The regioselectivity-determining step of the process is the nucleophilic attack of methanol or methoxide ion on the (π-allyl)mono(phosphane)palladium complex **7**. The nucleophilic attack at the C-1 atom is favored for steric reasons, while the attack at the C-3 atom is electronically favored.[16] Moreover, the linear telomer is the thermodynamically more stable product due to the internal double bond, whereas the branched isomer with the terminal double bond is less stable. However, our control experiments with various mixtures of **1** and **2** reveal that the telomerization reaction does not proceed under thermodynamic control at the described reaction conditions, since product formation is not reversible. We propose that the major reason for the selective formation of the linear telomer **1** is the energetically favored formation of a trigonal planar (1,6-diene)palladium complex [LPd(1,6-diene)]. The branched telomer has a 1,7-diene structure which would give rise to a (1,7-diene)-palladium complex. As demonstrated by us, the stability of trigonal planar (1,6-diene)palladium complexes [LPd(1,6-



Scheme 2

diene)] is much higher than those with a 1,7-diene ligand.[13a,13c]

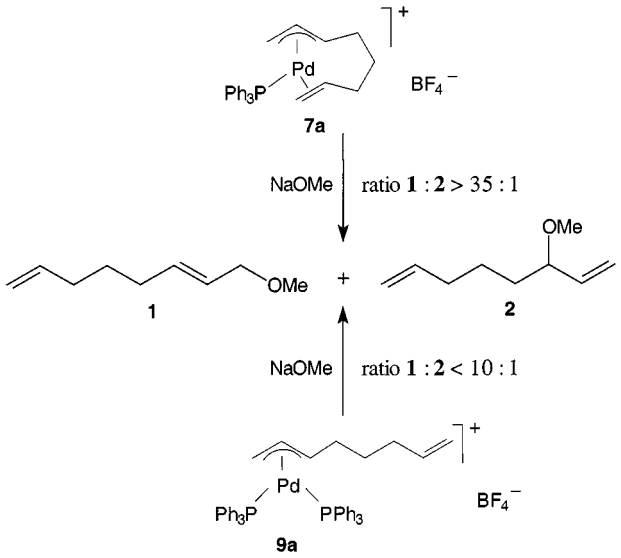
Due to the large influence of the P/Pd ratio on the regioselectivity, we postulate that (π-allyl)bis(phosphane)palladium complexes of type **9** (X = MeO^-) are involved as additional intermediates in the catalytic cycle [Equation (1)].



In complex **9**, nucleophilic attack at the C-1 allylic terminus does not give rise to an energetically favored chelating 1,6-diene coordination of the C_8 chain since coordination of both C−C double bonds is not possible at the P_2Pd^0 moiety. Hence, the greater preference for the linear telomer is less pronounced when compared with **7**. In an attempt to prove this hypothesis, we prepared the (octadienyl)palladium complex **7a** (X = BF_4^-)[12a,17] and reacted it with triphenylphosphane to obtain **9a** (X = BF_4^-). We then investigated the reactions of both **7a** and **9a** with sodium methoxide.

Proceeding from our observation that (diallyl ether)palladium complexes **5** catalyze the telomerization reaction even at low temperatures, we treated **5** with an excess of butadiene at −20 °C and obtained **6** in a quantitative yield.[17] Addition of tetrafluoroboric acid or tetrakis[3,5-bis(trifluoromethyl)phenyl]boric acid[18] in diethyl ether produced the respective cationic complexes of type **7**. The compound with the latter anion has the advantage of a high solubility in organic solvents and is therefore especially suitable for further investigations. On treatment with two equivalents of triphenylphosphane in THF, followed by the addition of pentane, the bis(phosphane)palladium complex **9a** was isolated in a quantitative yield. When excess phosphane was used, the nucleophilic attack of triphenylphosphane on the π-allyl group occurred with concomitant precipitation of tetrakis(triphenylphosphane)palladium.

In order to compare the regioselectivity of the nucleophilic attack of the methoxide anion on **7a** (X = BF_4^-) and **9a** (X = BF_4^-), each complex was treated with a threefold excess of sodium methoxide in THF/methanol (Scheme 3).



Scheme 3

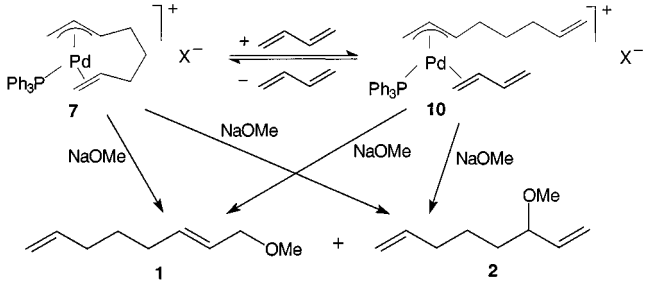
In the case of **7a**, the mixture turned black after a few minutes at room temperature due to the precipitation of palladium metal. GC analysis of the product mixture showed that products **1** and **2** were formed in a ratio > 35:1. The reaction of **9a** with sodium methoxide required slight heating (30 °C) to complete the reaction. GC analysis indicated a ratio of 1:2 < 10:1. Hence, attack of the meth-

Table 3. Variation of the ratio of butadiene to methanol

Entry	Ratio butadiene/ methanol	Catalyst	Catalyst concentration [mol-%]	Temp. [°C]	Reaction time [h]	Conversion [%]	TON **1** + **2** + **3** [%]	Yield **1** + **2** [%]	Yield **3** [%]	Chemoselectivity (**1** + **2**) [%]	Regioselectivity [%] (*n*/iso)
1	2:1	$Pd(OAc)_2$ 3 PPh_3	2×10^{-3}	50	16	43	21500	41	2	95	90.0 (9:1)
2	2:1	$Pd(OAc)_2$ 3 PPh_3	5×10^{-4}	90	16	27	48000	18	6	75	93.8 (15:1)
3	2:1	$Pd(OAc)_2$ 10 PPh_3	2×10^{-3}	50	16	34	17000	33	1	97	87.5 (7:1)
4	2:1	$Pd(OAc)_2$ 10 PPh_3	5×10^{-4}	90	16	35	70000	23	12	66	92.9 (13:1)
5	1:6	$Pd(OAc)_2$ 3 PPh_3	1×10^{-3}	90	16	43	39000	36	3	84	95.5 (21:1)

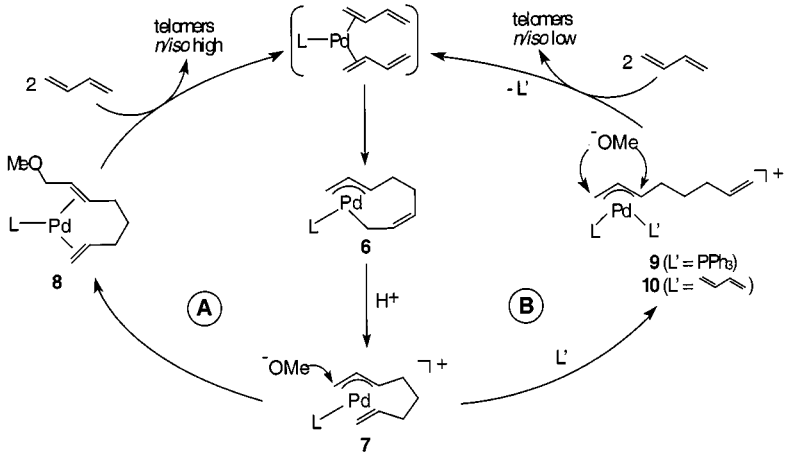
oxide ion on the C-1 allylic terminus in **9a** is less favored than in **7a**, but it is still preferred relative to the C-3 allylic terminus − probably for steric reasons.[16] From these studies it can be concluded that an excess of triphenylphosphane in the telomerization reaction mixture leads to the formation of allylbis(phosphane)palladium complexes of type **9**, which are responsible for a lower *n*/iso ratio of the telomerization products.

Additional support for our selectivity model comes from the fact that the concentration of butadiene also effects the regioselectivity of the attack of methanol on the (allyl)palladium complex. In general, experiments were carried out with a butadiene-to-methanol ratio of 1:2. Apart from this mixture, reactions with a stoichiometric ratio of starting materials and either a large excess of butadiene or methanol were studied. The results are summarized in Table 3.



Scheme 4

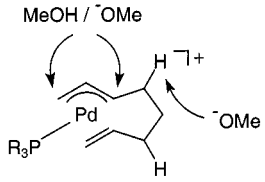
Indeed, we observed that variation in the ratio of starting materials significantly influences the regioselectivity. With increasing concentration of butadiene the yield of the linear telomer **1** decreases (compare Table 2 and 3). More specifically, at 50 °C with a stoichiometric butadiene to methanol ratio, the *n*/iso selectivity is only 9:1 (3 equiv. PPh_3: Entry 1, Table 3) and 7:1 (10 equiv. PPh_3: Entry 3, Table 3), respectively. In contrast, the *n*/iso selectivity totals 28:1 (3 equiv. PPh_3: Entry 4, Table 2) and 16:1 (10 equiv. PPh_3: Entry 6, Table 2) using a reaction mixture that contains a butadiene-to-methanol ratio of 1:2. The same trend holds true at a reaction temperature of 90 °C. In addition, it is shown that employing an excess of methanol, larger than 2:1, has only a small additional positive influence on the regioselectivity (compare Entry 5, Table 2 and Entry 5, Table 3). The influence of the butadiene concentration on the regioselectivity of the telomerization reaction was also observed by Beger et al.,[6b] but has not yet been explained. We suggest that the decrease in regioselectivity with increasing butadiene concentration is due to the loss of the coordination of the internal olefin in **7**. As shown in Scheme 4, the formation of a new intermediate **10** is proposed in the presence of excess butadiene. As stated before, the regioselectivity of the nucleophilic attack on **10** is no longer deter-



Scheme 5

mined by the formation of the favorable complex **8** with a chelating 1,6-diene ligand. Thus, an excess of butadiene has an analogous effect as an excess of phosphane.

The ratio of butadiene to methanol also influences the chemoselectivity of the reaction. Up to 12% of 1,3,7-octatriene (**3**) is produced when stoichiometric amounts of butadiene and methanol are combined at 90 °C (3 equiv. PPh_3: Entry 2; 10 equiv. PPh_3: Entry 4, Table 3). The chemoselectivity is much better at higher methanol concentrations (Entry 5, Table 2 and Entry 5, Table 3). This significant increase in **3** makes it likely that the telomers **1** and **2** result not only from an attack of the corresponding methoxide ion which is produced upon protonation of **6**, but also by the intermolecular reaction of methanol with **7**. While methanol is believed to react only as a nucleophile yielding the telomers, the methoxide anion can react either as a nucleophile or as a base to yield 1,3,7-octatriene (Figure 2). As a result the formation of 1,3,7-octatriene becomes more likely at lower methanol concentrations.



7

Figure 2

Conclusions

In this paper we described a detailed study of the palladium-catalyzed telomerization of butadiene with methanol concerning the control of chemo- and regioselectivity. The selective formation of the linear telomer 1-methoxyocta-2,7-diene (**1**) is influenced by the reaction temperature, the ligand-to-metal ratio and the stoichiometry of the starting materials. By careful optimization of these parameters, *n*/iso selectivities > 35:1 are realized at a low P/Pd ratio of 1:1 and high methanol-to-butadiene ratios in the absence of other coordinating species (regioselectivity up to 97%). *A second phosphane ligand bound to the palladium center dramatically reduces the regioselectivity for **1**.* With regard to chemoselectivity, the best results are obtained at low temperatures and high methanol-to-butadiene ratios (chemoselectivity up to 98%). In contrast to the regioselectivity, the chemoselectivity does not depend significantly on the P/Pd ratio.

All our results from the catalysis tests are in general agreement with the previously described mechanism proposed by Jolly. However, in order to explain the observed influences of the P/Pd ratio and the butadiene/Pd ratio on the selectivity we propose an extended mechanistic outline for telomerizations which contains two different reaction pathways (Scheme 5): pathway A going through **7** and **8** (with an energetically favored 1,6-diene C_8-ligand structure) leading to a high *n*/iso selectivity, and pathway B with **9** and **10** as intermediates which react with a lower *n*/iso selectivity as compared with **7**.

A comparison of the reactivity of the isolated complexes **7a** and **9a** with methoxide shows unequivocally that the main principle which governs the *n*/iso selectivity is the internal coordination of the olefinic side-chain. *These results appear to be of general relevance to telomerization reactions with other nucleophiles,* e.g. *this explains why the telomerization of butadiene with acetic acid yields comparably low n/iso ratios.* Thus, it is foreseeable that telomerizations with other oxygen nucleophiles or amines may be controlled by applying the same set of parameters, which we have presented here.

Another result of our work is the discovery that (diallyl ether)mono(phosphane)palladium complexes **5** react with butadiene below 0 °C to give complexes **6**. This allows extremely easy access to the catalytic intermediates of the butadiene telomerization reaction. Furthermore, (diallyl ether)mono(phosphane)palladium complexes are also efficient catalysts for the reaction of butadiene and methanol even at −10 °C. It is likely that these Pd^0 complexes will find use in other catalytic reactions.

Acknowledgments

This work has been performed at the TU München and the former Central Research of Hoechst AG. We thank Prof. Dr. K. Kühlein for his continuing support and Drs. K.-J. Haack, H. Geissler, S. Bogdanovic, R. Fischer, G. Stark and M. Hateley for valuable discussions.

[1] A. Zapf, M. Beller, *Chem. Eur. J.*, in press.

[2] [2a] J. Tsuji, H. Yasuda, T. Mandai, *J. Org. Chem.* **1978**, *43*, 3606. – [2b] J. Tsuji, Y. Kobayashi, T. Takahasi, *Tetrahedron Lett.* **1980**, *21*, 483.

[3] N. Yoshimura, M. Tamura (Kuraray Co. Ltd.), US 4.356.333, **1981**; *Chem. Abstr.* **1982**, *96*, 103630s.

[4] J. Falbe, H. Bahrmann, W. Lipps, D. Mayer, in: *Ullmann's Encyclopedia of Industrial Chemistry*, vol. A1 (Eds.: W. Gerhartz, Y. S. Yamamoto, F. T. Campbell, R. Pfefferkorn, J. F. Rounsaville), VCH, Weinheim, **1985**, p. 279.

[5] For reviews on telomerization reactions see: [5a] W. Keim, A. Behr, M. Röper, in: *Comprehensive Organometallic Chemistry*, vol. 8 (Eds.: G. Wilkinson, F. G. A. Stone, E. W. Abel), Pergamon Press, Oxford, **1982**, p. 372. – [5b] A. Behr, in: *Aspects of Homogeneous Catalysis*, vol. 5 (Ed.: R. Ugo), D. Reidel Publishing Company, Dordrecht, Boston, Lancaster, **1984**, p. 3. – [5c] R. F. Heck, *Palladium Reagents in Organic Syntheses*, Academic Press, London, **1985**. – [5d] J. M. Takacs, in: *Comprehensive Organometallic Chemistry II*, vol. 12 (Eds: E. W. Abel, F. G. A. Stone, G. Wilkinson), Pergamon Press, Oxford, **1995**, p. 785. – [5e] J. Tsuji, *Palladium Reagents and Catalysts: Innovations in Organic Synthesis*, John Wiley & Sons, Chichester, **1995**, p. 422. – [5f] N. Yoshimura, in: *Applied Homogeneous Catalysis with Organometallic Compounds*, vol. 1 (Eds. B. Cornils, W. A. Herrmann) VCH, Weinheim, **1996**, p. 351.

[6] [6a] S. Takahashi, T. Shibano, N. Hagihara, *Tetrahedron Lett.* **1967**, 2451. – [6b] J. Beger, H. Reichel, *J. Prakt. Chem.* **1973**, *315*, 1067. – [6c] J. Beger, C. Duschek, H. Füllbier, W. Gaube, *J. Prakt. Chem.* **1974**, *316*, 26. – [6d] D. Commereuc, Y. Chauvin, *Bull. Soc. Chim. Fr.* **1974**, 652. – [6e] M. Perree-Fauvet, Y. Chauvin, *Tetrahedron Lett.* **1975**, 4559. – [6f] P. Grenouillet, D. Neibecker, J. Poirier, I. Tkatchenko, *Angew. Chem.* **1982**, *94*, 796; *Angew. Chem. Int. Ed. Engl.* **1982**, *21*, 767. – [6g] R. M. Hanes (National Distillers and Chemical Corporation), US 4.642.392, **1987**; *Chem. Abstr.* **1987**, *107*, 133904x. – [6h] R.

M. Hanes (National Distillers and Chemical Corporation), US 4.831.183, **1989**; *Chem. Abstr.* **1987**, *107*, 133904x. – [6i] G. B. Jacobsen, H. L. Pelt, B. J. Schaart (Dow Chemical Benelux), WO 91 / 09822, **1989**; *Chem. Abstr.* **1991**, *115*, 158514y. – [6j] R. Patrini, M. Lami, M. Marchionna, F. Benvenuti, A. M. Raspolli Galletti, G. Sbrana, *J. Mol. Catal.* **1998**, *129*, 179. – [6k] F. Benvenuti, C. Carlini, M. Marchionna, R. Patrini, A. M. Raspolli Galletti, G. Sbrana, *J. Mol. Catal.* **1999**, *140*, 139. – [6l] M. Basato, L. Crociani, F. Benvenuti, A. M. Raspolli Galletti, G. Sbrana, *J. Mol. Catal.* **1999**, *145*, 313.

[7] [7a] K. E. Atkins, W. E. Walker, R. M. Manyik, *J. Chem. Soc., Chem. Commun*. **1971**, 330. – [7b] T. Maeda, Y. Tokitoh, N. Yoshimura (Kuraray Co. Ltd.), EP 296.550, **1987**; *Chem. Abstr.* **1989**, *110*, 173469c. – [7c] Y. Tokitoh, N. Yoshimura (Kuraray Co. Ltd.), EP 287.066, **1988**; *Chem. Abstr.* **1989**, *110*, 78070g. – [7d] K. Wada, K. Sato, Y. Kasori, Y. Misu (Mitsubishi Kasei Corp.), EP 361.304, **1989**; *Chem. Abstr.* **1990**, *113*, 131562j. – [7e] M. Röper, W. Bertleff, D. Köffer (BASF AG), DE 3.806.305, **1989**; *Chem. Abstr.* **1990**, *112*, 98016p. – [7f] A. Thome, W. Bertleff (BASF AG), US 5.043.487, **1990**; *Chem. Abstr.* **1991**, *114*, 121472m. – [7g] T. Maeda, Y. Tokitoh, N. Yoshimura (Kuraray Co. Ltd.), US 5.100.854, **1990**; *Chem. Abstr.* **1989**, *110*, 173469c. – [7h] Y. Tokitoh, T. Higashi, K. Hino, M. Murasawa, N. Yoshimura (Kuraray Co. Ltd.), EP 436.226, **1990**; *Chem. Abstr.* **1991**, *115*, 158508z. – [7i] D. L. Packett (Union Carbide Corp.), US 5.169.981, **1991**; *Chem. Abstr.* **1993**, *118*, 191171u. – [7j] C. Miyazawa, T. Mori, H. Kameo, S. Isogai (Mitsubishi Kasei Corp.), EP 605.735, **1993**; *Chem. Abstr.* **1994**, *120*, 133838x. – [7k] E. Monflier, P. Bourdauducq, J.-L. Courturier (Elf Atochem S. A.), US 5.345.007, **1993**; *Chem. Abstr.* **1994**, *121*, 179094a. – [7l] J. R. Livingston (Exxon Chemical Patents Inc.), US 5.302.750, **1993**; *Chem. Abstr.* **1994**, *121*, 86253m. – [7m] T. Mori, H. Kameo, S. Isogai, S. Saita (Mitsubishi Chemical Cap.), US 5.583.271, **1995**; *Chem. Abstr.* **1996**, *125*, 142108q. – [7n] E. Monflier, P. Bourdauducq, J. L. Couturier, J. Kervennal, A. Mortreux, *Appl. Catal.* **1995**, *131*, 167. – [7o] E. Monflier, P. Bourdauducq, J. L. Couturier, J. Kervennal, I. Suisse, A. Mortreux, *Catal. Lett.* **1995**, *34*, 201. – [7p] E. Monflier, P. Bourdauducq, J. L. Couturier, J. Kervennal, A. Mortreux, *J. Mol. Catal.* **1995**, *97*, 29.

[8] For aliphatic amines see: [8a] S. Takahashi, T. Shibano, N. Hagihara, *Bull. Chem. Soc. Jpn.* **1968**, *41*, 454. – [8b] J. Beger, F. Meier, *J. Prakt. Chem.* **1980**, *322*, 69. – [8c] U. M. Dzhemilev, G. A. Tolstnikov, A. G. Telin, M. Y. Dolomatov, E. G. Galkin, G. A. Tolstnikov, *Izv. Akad. Nauk SSSR, Ser. Khim.* **1980**, 163; *Chem. Abstr.* **1980**, *92*, 197776m. – [8d] C. Moberg, *Tetrahedron Lett.* **1981**, *22*, 4827. – [8e] T. Antonsson, A. Langlet, C. Moberg, *J. Organomet. Chem.* **1989**, *363*, 237. – For anilines see: [8f] K. Takahashi, A. Miyake, G. Hata, *Bull. Chem. Soc. Jpn.* **1972**, *45*, 1183. – For ammonia see: [8g] J. Tsuji, M. Takahashi, *J. Mol. Catal.* **1981**, *10*, 107. – [8h] T. Prinz, W. Keim, B. Drießen-Hölscher, *Angew. Chem.* **1996**, *108*, 1835; *Angew. Chem. Int. Ed. Engl.* **1996**, *35*, 1708. – For amino alcohols see: [8i] A. Groult, A. Guy, *Tetrahedron* **1983**, *39*, 1543. For amino acids see: [8j] U. M. Dzhemilev, R. N. Fakhretdinov, A. G. Telin, *Zh. Org. Khim.* **1986**, *22*, 1610; *Chem. Abstr.* **1987**, *107*, 154706z. – For hydrazines see: [8k] A. G. Telin, R. N. Fakhretdinov, U. M. Dzhemilev, *Izv. Akad. Nauk SSSR, Ser. Khim.* **1986**, 2474. – For hydroxylamines see: [8l] R. N. Fakhretdinov, A. G. Telin, U. M. Dzhemilev, *Izv. Akad. Nauk SSSR, Ser. Khim.* **1986**, 2254. – For phthalimides see: [8m] Y. Inoue, M. Taguchi, M. Toyofuku, H. Hashimoto, *Bull. Chem. Soc. Jpn.* **1984**, *57*, 3021. – [8n] M. I. Zakharkin, V. V. Guseva, D. D. Sulaimankulova, E. A. Petrushkina, *Zh. Org. Khim.* **1987**, *23*, 1654. – For formamides see: [8o] Y. Inoue, M. Taguchi, M. Toyofuku, H. Hashimoto, *Bull. Chem. Soc. Jpn.* **1984**, *57*, 3021.

[9] Acetic acid: [9a] W. E. Walker, R. M. Manyik, K. E. Atkins, M. L. Farmer, *Tetrahedron Lett.* **1970**, 3817. – [9b] D. Rose, H. Lepper, *J. Organomet. Chem.* **1973**, *49*, 473. – Phthalic acid: [9c] R. Fletcher (British Petroleum Company Ltd.), GB 1.505.317, **1976**; *Chem. Abstr.* **1978**, *89*, 90137q. – [9d]W. Keim, A. Durocher, P. Voncken, *Erdöl, Kohle, Erdgas, Petrochem. Brennst.-Chem.* **1976**, *29*, 31. –

[10] For silanols see: [10a] N. Hagihara, S. Takahashi, T. Shibano (Jpn. Pat. 7.700.006), **1977**; *Chem. Abstr.* **1977**, *86*, 189198k. – [10b] M. Capka, P. Svoboda, J. Hetflejs, *Coll. Czech. Chem. Commun.* **1973**, *38*, 1242. – For nitroalkanes see: [10c] T. Mitsuyasu, M. Hara, J. Tsuji, *J. Chem. Soc., Chem. Commun.* **1971**, 345. – [10d] T. Mitsuyasu, J. Tsuji, *Tetrahedron* **1974**, *30*, 831. – [10e] W. Keim, A. Köhnes, T. Röthel, D. Enders, *J. Organomet. Chem.* **1990**, *382*, 295. – For 1,3-dicarbonyl compounds see: [10f] W. Keim, D. Schwarzer, D. Vogt, *Chem.-Ing.-Tech.* **1995**, *67*, 903.

[11] The current industrial price for butadiene is in the range of 0.55−0.65 DM/kg; mixtures of butadiene with other C_4 olefins are even cheaper.

[12] [12a] R. Benn, P. W. Jolly, R. Mynott, B. Raspel, G. Schenker, K.-P. Schick, G. Schroth, *Organometallics* **1985**, *4*, 1945. – [12b] R. Benn, P. W. Jolly, T. Joswig, R. Mynott, K.-P. Schick, *Z. Naturforsch.* **1986**, *41b*, 680. – [12c] A. Döhring, P. W. Jolly, R. Mynott, K.-P. Schick, G. Wilke, *Z. Naturforsch.* **1981**, *36b*, 1198. – [12d] P. W. Jolly, R. Mynott, B. Raspel, K.-P. Schick, *Organometallics* **1986**, *5*, 473. – [12e] P. W. Jolly, *Angew. Chem.* **1985**, *97*, 279; *Angew. Chem. Int. Ed. Engl.* **1985**, *24*, 283. – [12f] A. Behr, G. v. Ilsemann, W. Keim, C. Krüger, Y.-H. Tsay, *Organometallics* **1986**, *5*, 514.

[13] [13a] J. Krause, Dissertation, Düsseldorf, **1993**. – [13b] J. Krause, K.-J. Haack, G. Cestaric, R. Goddard, K.-R. Pörschke, *Chem. Commun.* **1998**, 1291. – [13c] J. Krause, G. Cestaric, K.-J. Haack, K. Seevogel, W. Storm, K.-R. Pörschke, *J. Am. Chem. Soc.* **1999**, *121*, 9807.

[14] 37 mg (0.14 mmol) of triphenylphosphane and 11 mg (0.05 mmol) of palladium(II) acetate were dissolved in 56 g (1.75 mol) of methanol under argon. The mixture was transferred into a cooled (dry ice) autoclave (Parr model 4561). Subsequently, 54 g (1.00 mol) of butadiene was condensed into the autoclave and the vessel was heated to the reaction temperature. After the reaction was complete, the autoclave was cooled down and the remaining butadiene was recondensed. The conversion was determined by the mass difference of butadiene. The yields of telomerization products were determined by GC (with dodecane as an internal standard) using an HP 6869A gas chromatograph. In order to isolate the octadienyl ethers, the reaction mixture was distilled in vacuo.

[15] R. McCrindle, G. Ferguson, G. J. Arsenault, A. J. McAlees, D. K. Stephenson, *J. Chem. Res. Synop.* **1984**, 360.

[16] [16a] B. Åkermark, S. Hansson, B. Krakenberger, A. Vitagliano, K. Zetterberg, *Organometallics* **1984**, *3*, 679.– [16b] B. Åkermark, A. Vitagliano, *Organometallics* **1985**, *4*, 1275.– [16c] B. Åkermark, K. Zetterberg, S. Hansson, B. Krakenberger, A. Vitagliano, *J. Organomet. Chem.* **1987**, *335*, 133.

[17] **{(1,2,3,7,8-η)-2,7-Octadienyl}(triphenylphosphane)palladium(II) Tetrafluoroborate (7a), {(1,2,3-η)-2,7-Octadienyl}bis(triphenylphosphane)palladium(II) Tetrafluoroborate (9a):** $[Pd(\eta^2,\eta^2\text{-}C_6H_{10}O)(PPh_3)]$ (**5**) (233 mg, 0.50 mmol) was suspended in 8 mL (96 mmol) of butadiene at −78 °C. After warming up to −20 °C, the yellow mixture was stirred for 1 h. Butadiene was removed in vacuo and the remaining light yellow solid was washed with two 5-mL portions of cold pentane. The obtained analytically pure (η^1,η^3-octadienediyl)palladium complex **6** was suspended in 8 mL of diethyl ether at −78 °C. A stoichiometric amount of HBF_4 (68 μL, 0.50 mmol of a 54% solution in diethyl ether) was added to yield a clear yellow solution. After warming to −20 °C and removal of the solvent in vacuo, **7a** was obtained as a yellow powder in a quantitative yield. Complex **9a** was synthesized by slowly adding PPh_3 (52 mg, 0.20 mmol), dissolved in 3 mL of THF, to a solution of **7a** (56 mg, 0.10 mmol) in 3 mL of THF at −60 °C. After stirring the yellow solution for 1 h at −20 °C, pentane (3 mL) was added and **9a** precipitated as a light gray solid which was isolated by filtration in a quantitative yield. The hydrogen atoms were labeled as described in ref.[12a] The ^{13}C-NMR signals were assigned by means of a C,H-COSY experiment. – **7a:** ^{1}H NMR (400 MHz, [D$_8$]THF, −50 °C): δ = 7.50−7.30 (m, 15 H, H_{Ph}), 5.54 [pseudo-sext, ^3J(1-H,4-H) = ^3J(1-H,5-H) = 12.7 Hz, ^3J(1-H,2-H) = 6.7 Hz, 1 H, 1-H], 5.05 (m, 1 H, 12-H), 4.66 (m, 1 H, 5-H), 4.27 [dd, ^3J(2-H,1-H) = 6.7 Hz, ^3J(2-H,P) = 3 Hz, 1 H, 2-H), 3.99 [pseudo-t, ^3J(13-H,12-H) = ^3J(13-H,P) = 8.6 Hz, 1 H, 13-H], 3.54 (m, 1 H, 14-H), 3.20 (m, 1 H, 4-H), 2.49 (m, 2 H, 7-H, 11-H), 2.38 (m, 1 H, 8-H), 2.09 (m, 1 H, 9-H), 1.45 (m, 1 H, 6-H), 0.97 (m, 1 H, 10-H). – ^{13}C{^{1}H} NMR (101 MHz, [D$_8$]THF, −50 °C): δ = 135−129 (C_{Ph}), 117.7 (C-2), 113.1 (C-7), 101.6 (C-3), 82.2 (C-8), 78.1 (C-1), 33.4 (C-5), 29.6 (C-4), 29.1 (C-6). – ^{31}P{^{1}H} NMR (162 MHz, [D$_8$]THF, −50 °C): δ = 24.94. – **9a:** ^{1}H NMR (400 MHz, [D$_8$]THF, −50 °C): δ = 7.50−7.10 (m, 30 H,H_{Ph}), 5.91 [pseudo-sext, ^3J(1-H,4-H) = ^3J(1-H,5-H) = 12.7 Hz, ^3J(1-H,2-H) = 6.7 Hz, 1 H, 1-H],

5.46 [pseudo-sext, ^3J(12-H,14-H) = 16.5 Hz, ^3J(12-H,13-H) = ^3J(12-H,10/11-H) = 6.7 Hz, 1 H, 12-H], 4.75 (m, 2 H, 13-H, 14-H), 4.48 (m, 1 H, 5-H), 3.53 (m, 2 H, 2-H, 4-H), 1.63, 1.50 (m, 6 H, 6-H to 11-H). – $^{31}P\{^1H\}$ NMR (162 MHz, [D$_8$]THF, −50 °C): AB spin system: δ_A = 24.68; δ_B = 24.26; $^2J(P_A,P_B)$ = 41.6 Hz.

[18] M. Brookhart, B. Grant, A. F. Volpe, Jr., *Organometallics* **1992**, *11*, 3920.

Received June 7, 1999
[I99208]

Redox Chemistry of $[Co_4(CO)_3(\mu_3\text{-}CO)_3(\mu_3\text{-}C_7H_7)(\eta^5\text{-}C_7H_9)]$ – Reversible Carbon–Carbon Coupling versus Metal Cluster Degradation

Hubert Wadepohl,*[a] Stefan Gebert,[a] Hans Pritzkow,[a] Domenico Osella,*[b] Carlo Nervi,[c] and Jan Fiedler[d]

Dedicated to Professor Heinrich Vahrenkamp on the occasion of his 60th birthday

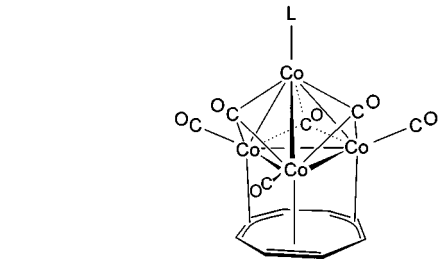
Keywords: Carbocycles / Clusters / Cobalt / Electrochemistry / Facial ligands

Chemical reduction of the tetracobalt cluster complex $[Co_4(CO)_3(\mu_3\text{-}CO)_3(\mu_3\text{-}C_7H_7)(\eta^5\text{-}C_7H_9)]$ **(3)**, followed by addition of $[PPh_4]Br$, gives the complex $[\{Co_4(CO)_3(\mu_3\text{-}CO)_3(\mu_3\text{-}C_7H_7)\}_2\{\mu\text{-}\eta^4\text{:}\eta^4\text{-}(C_7H_9)_2\}]^{2-}$ as a mixture of two diastereomers $[\mathbf{4A}]^{2-}$ and $[\mathbf{4B}]^{2-}$ in high yield. The crystal structure of $[\mathbf{4A}]^{2-}[PPh_4]_2\cdot 1.5C_7H_8$ has been determined and confirms the reductive coupling of two Co_4 cluster coordinated apical cycloheptadienyl rings to form a bridging bicycloheptyl-3,5,3′,5′-tetraene ligand. Reduction of **3** with $Li[HBEt_3]$ and subsequent treatment with aqueous $[NnBu_4]Cl$ results in the formation of $[Co_4(CO)_3(\mu_3\text{-}CO)_3(\mu_3\text{-}C_7H_7)(C_7H_{10})]^-$ $[\mathbf{5}]^-$. Addition of $[(\eta\text{-}C_6H_6)Ru(NCMe)_3][BF_4]_2$ after the borohydride reduction gives $[Ru(\eta\text{-}C_6H_6)Co_3(CO)_3(\mu_3\text{-}CO)_3(\mu_3\text{-}C_7H_7)]$ **(6)**, a product derived from reductive Co_4 cluster degradation. A detailed electrochemical and spectro-electrochemical study of the redox behaviour of **3** and $[\mathbf{4}]^{2-}$ has been carried out. The complex potential current response of **3** is rationalized in terms of the formation of the radical anion $[\mathbf{3}]^-$ as the primary intermediate, which may be reversibly reduced further to give the much more stable $[\mathbf{3}]^{2-}$ and then $[\mathbf{3}]^{3-}$. Dimerization of $[\mathbf{3}]^-$ to give $[\mathbf{4}]^{2-}$ occurs by formation of a new carbon–carbon bond between the apical C_7H_9 ligands. The two redox-active moieties in $[\mathbf{4}]^{2-}$ behave as independent, non-interacting redox centres. The oxidized form **4** is unstable and dissociates back to **3** almost quantitatively, thus completing a redox cycle characteristic of a "molecular battery". The homogeneous rate constant for dimerization has been evaluated as k_{DIM} ($2\ [\mathbf{3}]^- \rightarrow [\mathbf{4}]^{2-}$) = 0.30 ± 0.05 $mM^{-1}\ s^{-1}$.

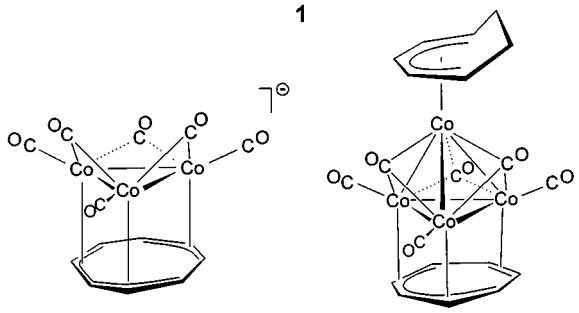
Introduction

Two contrasting statements are frequently made concerning the consequences of an electron transfer to or from a molecular metal cluster complex:[1] (i) behaviour of the cluster as an "electron sponge", i.e. the ability to add or lose electrons without any great effect on the framework, and (ii) a rearrangement of the metal core, upon reduction typically involving cleavage of metal–metal bonds. This is usually attributed to the frontier orbitals of the cluster being generally nonbonding or antibonding with respect to the metal–metal interactions. However, as shown, for example, by the frequently observed labilization of ligands[2] at the periphery of the cluster, metal–ligand bonding may also be affected by the electron–transfer process.[3]

Recently, we have reported on the redox behaviour of a series of tetracobalt cluster complexes with a cyclooctatetraene ligand in the unusual facial (μ_3) coordination mode.[4] On chemical reduction, cluster complexes of the



1



2 **3**

[a] Anorganisch-chemisches Institut der Ruprecht-Karls-Universität,
Im Neuenheimer Feld 270, D-69120 Heidelberg, Germany
E-mail: bu9@ix.urz.uni-heidelberg.de
[b] Dipartimento di Scienze e Tecnologie Avanzate, Università del Piemonte Orientale "A. Avogadro",
Corso T. Borsalino 54, I-15100 Alessandria, Italy
E-mail: osella@ch.unito.it
[c] Dipartimento di Chimica IFM, Università di Torino,
Via P. Giuria 7, I-10125 Torino, Italy
[d] The J. Heyrovský Institute of Physical Chemistry, Academy of Sciences of the Czech Republic,
Dolejskova 3, 18223 Prague 8, Czech Republic

 © WILEY-VCH Verlag GmbH, D-69451 Weinheim, 2000 1434–1948/00/0808–1833 $ 17.50+.50/0

type $[Co_4(CO)_3(\mu_3\text{-}CO)_3(\mu_3\text{-}C_8H_8)(L)]$ [**1a**, L = η^4-C_8H_8; **1b**, L = η^4-C_6H_8; **1c**, L = η^4-diphenylfulvene; **1d**, L = $(CO)_2$][5] are degraded to give the trinuclear cluster anion $[Co_3(CO)_3(\mu_2\text{-}CO)_3(\mu_3\text{-}C_8H_8)]^-$ $[\mathbf{2}]^-$ in high yield. This behaviour follows the general pattern outlined above, but is nevertheless in marked contrast to that of the parent binary carbonyl cluster, $[Co_4(CO)_{12}]$. Here, reduction usually leads to a complete breakdown of the cluster.[6] The trinuclear anion $[Co_3(CO)_{10}]^-$, a close analogue of $[\mathbf{2}]^-$, is quite unstable and can only be obtained from $[Co_4(CO)_{12}]$ under very special conditions.[7]

We report herein on the reduction of $[Co_4(CO)_3(\mu_3\text{-}CO)_3(\mu_3\text{-}C_7H_7)(\eta^5\text{-}C_7H_9)]$ **(3)**,[5] a cluster complex with a facial cycloheptatrienyl ligand. It is shown that the reduction chemistry of this complex is fundamentally different from that of **1**, despite the fact that these systems are isoelectronic and structurally similar.

Results

Preparative and Spectroscopic Investigations

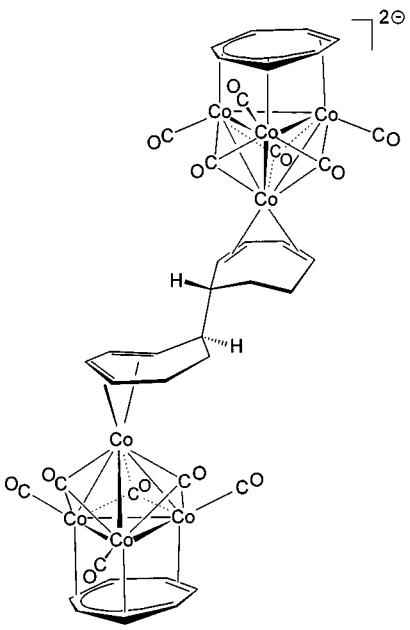
Treatment of $[Co_4(CO)_3(\mu_3\text{-}CO)_3(\mu_3\text{-}C_7H_7)(\eta^5\text{-}C_7H_9)]$ **(3)** with either $Li[HBEt_3]$, LiPh, $Na_2[Fe(CO)_4]$, or cobaltocene, followed by addition of $[PPh_4]Br$ and precipitation with methanol gave a >80% yield of the complex $[\{Co_4(CO)_3(\mu_3\text{-}CO)_3(\mu_3\text{-}C_7H_7)\}_2\{\mu\text{-}(C_7H_9)_2\}][PPh_4]_2$ as a mixture of two diastereomers, $[\mathbf{4A}]^{2-}[PPh_4]_2$ and $[\mathbf{4B}]^{2-}[PPh_4]_2$. Complete separation of the two isomers proved to be impossible on a preparative scale. Repeated crystallization from methanol/THF or nitromethane led to an enrichment in one diastereomer in the solid (up to an 86:14 ratio). This complex, $[\mathbf{4A}]^{2-}[PPh_4]_2$, was finally obtained in pure form as a small batch of single crystals by layering a CH_2Cl_2 solution of the 86:14 isomeric mixture with toluene. Isomer $[\mathbf{4B}]^{2-}[PPh_4]_2$ was only obtained about 80% pure (containing 20% $[\mathbf{4A}]^{2-}[PPh_4]_2$) from the pooled mother liquors.

Column chromatography of the supernatant solution that was left after the first precipitation with methanol gave a second anion, $[Co_4(CO)_3(\mu_3\text{-}CO)_3(\mu_3\text{-}C_7H_7)(C_7H_{10})]^-$ $[\mathbf{5}]^-$, which was obtained as the $[PPh_4]^+$ salt in very low yield (about 1%). In another experiment, where the reaction product of **3** and $Li[HBEt_3]$ was treated with aqueous $[NnBu_4]Cl$, $[\mathbf{5}]^-$ was isolated after recrystallization from ethanol as the $[NnBu_4]^+$ salt in 26% yield.

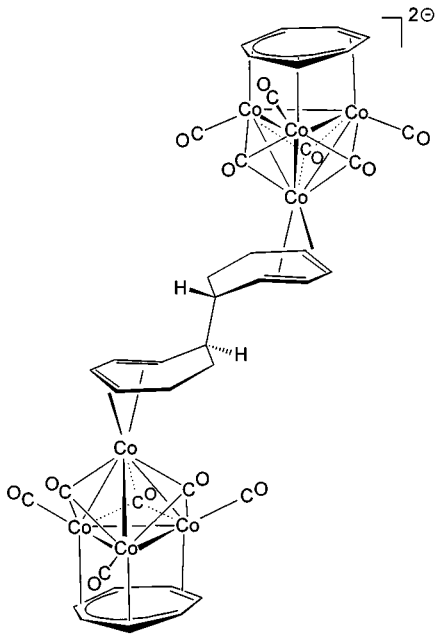
The course of the reaction of **3** with $Li[HBEt_3]$ was found to be unaffected by changing the stoichiometric ratio (1−4 equivalents of the reducing agent were used). NMR analysis of the initial reduction product (in $[D_8]$THF) showed only minor resonances in the region $-2 \leq \delta \leq 10$.

In order to trap any more highly reduced species, a THF solution of complex **3** was first treated with $Li[HBEt_3]$. The resulting material was then reacted with $[(\eta\text{-}C_6H_6)Ru(NCMe)_3][BF_4]_2$ in CH_2Cl_2. From this reaction, the dark-brown cluster complex $[Ru(\eta\text{-}C_6H_6)Co_3(CO)_3(\mu_3\text{-}CO)_3(\mu_3\text{-}C_7H_7)]$ **(6)** was isolated in 18% yield after column chromatography. On monitoring the reaction by IR spectroscopy, a rapid decrease in the ν_{CO} bands attributable to the starting material **3** was observed following the addition of the $Li[HBEt_3]$ solution, which was accompanied by a concomitant increase of new broad features at 1950 (sh), 1926 (vs), 1700 (sh), and 1675 (s) cm^{-1}. The formation of **6** was seen to be complete within a few minutes after the addition of one equivalent of the ruthenium reagent.

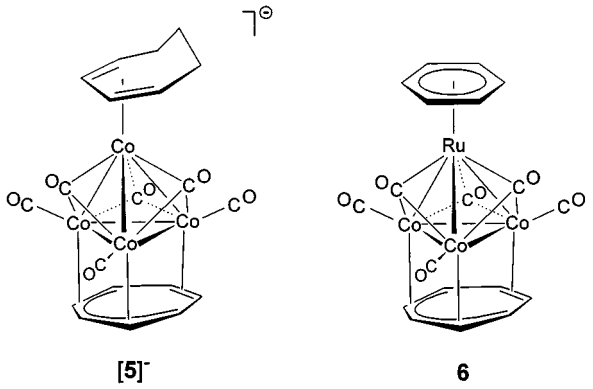
The cluster anions $[\mathbf{4A}]^{2-}$, $[\mathbf{4B}]^{2-}$, and $[\mathbf{5}]^-$, as well as the neutral complex **6**, were characterized by spectroscopic



$[\mathbf{4A}]^{2-}$



$[\mathbf{4B}]^{2-}$



[5]⁻ **6**

methods, and by a crystal structure analysis of $[\mathbf{4A}]^{2-}[PPh_4]_2$. The infrared ($\nu_{CO}$) spectra of all the anions are quite similar; they consist of two broad features in the characteristic regions for terminal (around 1930 cm^{-1}) and triply-bridging carbonyls (around 1680 cm^{-1}). Compared to the neutral starting material, the CO stretches are shifted by about 50−60 cm^{-1} to lower frequencies. Due to the broad absorptions, a distinction between the individual species cannot be made. The IR bands of the Co_3Ru complex **6** also appear at slightly lower wavenumbers (about 10−20 cm^{-1}) than those of the Co_4 cluster **3**. ^1H and ^{13}C NMR spectroscopic data for $[\mathbf{4A}]^{2-}$ and $[\mathbf{4B}]^{2-}$ are collected in Table 1 and Table 2, along with the corresponding data for $[\mathbf{5}]^-$.

The spectra of **6** are very simple, with just two singlets appearing in both the ^1H (δ = 3.20, 5.35) and ^{13}C NMR spectra (δ = 59.8, 95.6). Due to the low solubility and the long relaxation times of the carbonyls, no ^{13}C resonances were detected for these ligands in **6**.

Molecular Structure of $[\mathbf{4A}]^{2-}$

An X-ray crystal structure determination was carried out on a single crystal of $[\mathbf{4}]^{2-}[PPh_4]_2 \cdot 1.5C_7H_8$, containing the diastereomer $[\mathbf{4A}]^{2-}$. Details of the structure determination are given in the Experimental Section. The crystal structure arises from a packing of octanuclear cluster dianions $[\{Co_4(CO)_3(\mu_3\text{-}CO)_3(\mu_3\text{-}C_7H_7)\}_2\{\mu\text{-}\eta^4\text{:}\eta^4\text{-}(C_7H_9)_2\}]^{2-}$ and tetraphenylphosphonium cations, which are interspersed by a total of three molecules of toluene per unit cell as a solvent of crystallization. Due to the rather poor quality of the single crystals, coupled with inherent disorder in some parts of the structure, the accuracy of the structure determination is limited.

A view of the $[\mathbf{4A}]^{2-}$ molecule is presented in Figure 1. Salient bond lengths are given in Table 3. The complex di-

Table 1. ^1H NMR spectroscopic data (δ, in CD_2Cl_2) for $[\{Co_4(CO)_3(\mu_3\text{-}CO)_3(\mu_3\text{-}C_7H_7)\}_2\{\mu\text{-}(C_7H_9)_2\}]^{2-}$ $[\mathbf{4}]^{2-}$ and $[Co_4(CO)_3(\mu_3\text{-}CO)_3(\mu_3\text{-}C_7H_7)(C_7H_{10})]^-$ $[\mathbf{5}]^-$

Complex	μ_3-C_7H_7	η^4:η^4-$C_{14}H_{18}$	
$[PPh_4]_2[\mathbf{4A}]^{2-}$	3.48 (s, 14 H)	CH_2:	1.1 (m, 4 H), 1.9 (m, 4 H)
		(CH)bridgehead:	1.4 (m, 2 H)
		(CH)diene (H-1, H-4):	3.28 (m, 2 H), 3.4 (m, 2 H)[a]
		(CH)diene (H-2, H-3):	5.3 (m, 2 H),[a] 5.48 (m, 2 H)
$[PPh_4]_2[\mathbf{4B}]^{2-}$	3.44 (s, 14 H)	CH2:	1.1 (m, 4 H), 1.9 (m, 4 H)
		(CH)bridgehead:	1.4 (m, 2 H)
		(CH)diene (H-1, H-4):	3.3−3.4 (m, 4 H)[a]
		(CH)diene (H-2, H-3):	5.3 (m, 2 H),[a] 5.54 (m, 2 H)
$[PPh_4][\mathbf{5}]^-$	3.50 (s, 7 H)	CH2:	1.41 (m, 4 H), 1.95 (m, 2 H)
		(CH)diene (H-1, H-4):	3.4 (m, 2 H)[a]
		(CH)diene (H-2, H-3):	5.49 (m, 2 H)

[a] Resonances partially obscured by solvent or C_7H_7 resonance.

Table 2. $^{13}C\{^1H\}$ NMR spectroscopic data (δ, in CD_2Cl_2) for $[\{Co_4(CO)_3(\mu_3\text{-}CO)_3(\mu_3\text{-}C_7H_7)\}_2\{\mu\text{-}(C_7H_9)_2\}]^{2-}$ $[\mathbf{4}]^{2-}$ and $[Co_4(CO)_3(\mu_3\text{-}CO)_3(\mu_3\text{-}C_7H_7)(C_7H_{10})]^-$ $[\mathbf{5}]^-$; signal multiplicities (due to coupling to ^1H) were determined by DEPT (135°) spectra and are given as even (e) or odd (o)

Complex	μ_3-C_7H_7	η^4:η^4-C14H18		CO
$[PPh_4]_2[\mathbf{4A}]^{2-}$	56.0 (e)	CH_2:	28.2 (o), 28.5 (o)	202.5, 280.8
		(CH)bridgehead:	45.5 (e)	
		(CH)diene (C-1, C-4):	70.2 (e), 72.5 (e)	
		(CH)diene (C-2, C-3):	100.4 (e), 100.5 (e)	
$[PPh_4]_2[\mathbf{4B}]^{2-}$	56.0 (e)	CH_2:	26.9 (o), 28.5 (o)	205.5, 280.3
		(CH)bridgehead:	45.9 (e)	
		(CH)diene (C-1, C-4):	70.3 (e), 73.6 (e)	
		(CH)diene (C-2, C-3):	99.7 (e), 100.9 (e)	
$[PPh_4][\mathbf{5}]^-$	56.3(e)	CH_2:	24.2 (o), 28.0 (o)	[a]
		(CH)diene (C-1, C-4):	70.1 (e)	
		(CH)diene (C-2, C-3):	100.2 (e)	

[a] Not detected.

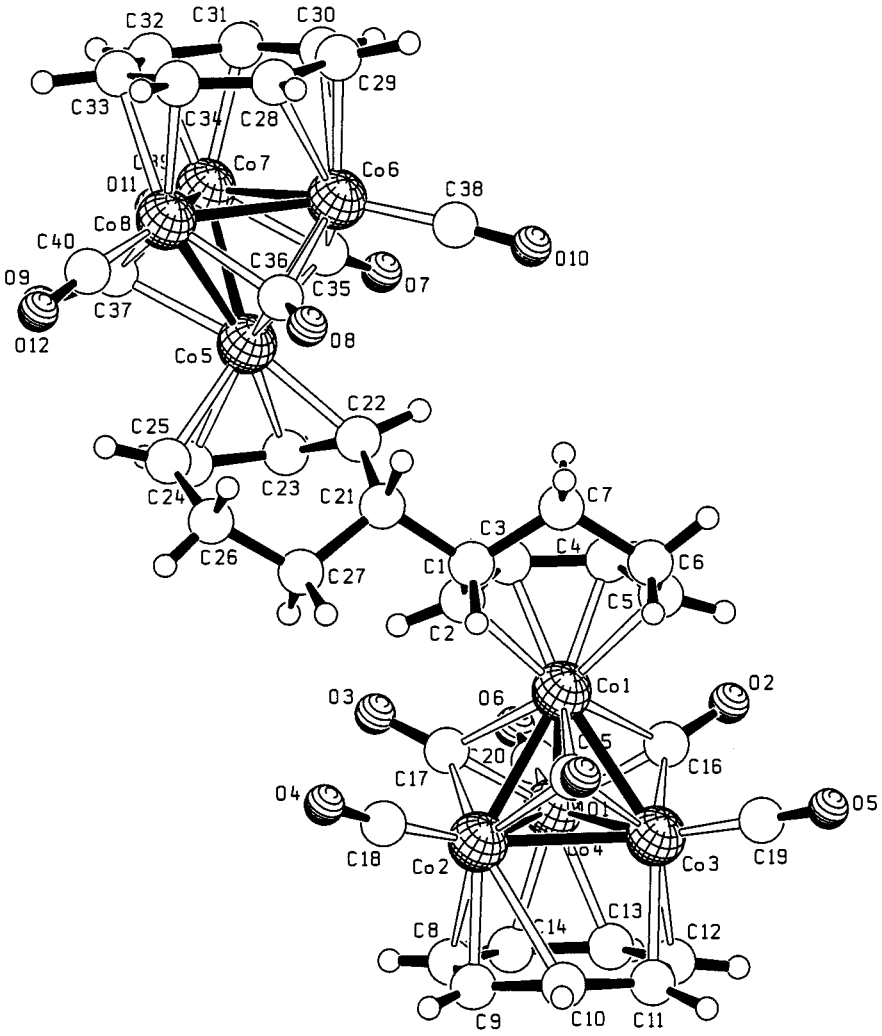


Figure 1. Molecular structure of $[\{Co_4(CO)_3(\mu_3\text{-}CO)_3(\mu_3\text{-}C_7H_7)\}_2\{\mu_2\text{-}\eta^4\text{:}\eta^4\text{-}(C_7H_9)_2\}]^{2-}$ $[\mathbf{4A}]^{2-}$ in the crystals of $[\mathbf{4A}]^{2-}[PPh_4]_2$; only one of the two disordered μ_3-C_7H_7 rings bonded to Co6, Co7, and Co8 is shown

anions $[\mathbf{4A}]^{2-}$ consist of two essentially identical subunits of the composition $[Co_4(CO)_3(\mu_3\text{-}CO)_3(\mu_3\text{-}C_7H_7)(C_7H_9)]$, which are fused together through a carbon−carbon bond involving C1 and C21 of the apical C_7H_9 ligands.[8] This results in a bridging bicyclic ring system, where both cyclohepta-1,3-diene moieties are η^4-coordinated to a $[Co_4(CO)_3(\mu_3\text{-}CO)_3(\mu_3\text{-}C_7H_7)]$ cluster unit. With respect to the bridging ligand, the two Co_4 clusters adopt an *anti* arrangement. The molecule has approximate C_2 symmetry, with the diad bisecting the bond C1−C21.

Electrochemical Investigations

The anodic cyclic voltammetric (CV) response of the cluster complex $[Co_4(CO)_3(\mu_3\text{-}CO)_3(\mu_3\text{-}C_7H_7)(\eta^5\text{-}C_7H_9)]$ **(3)** in THF solution at a glassy carbon (GC) electrode is similar to those previously reported for the butterfly structure $[Co_4(CO)_{10}(RC_2R)]$,[9] for the binary carbonyls $[Co_4(CO)_{12}]$[10] and $[Co_2(CO)_8]$,[11] and for the organometallic derivatives $[Co_3(CO)_9(CR)]$[12] and $[Co_2(CO)_6(RC_2R)]$.[13] A multi-electron oxidation peak is observed at +0.70 V, followed by an electrochemical response typical of an insoluble material adsorbed onto the electrode, and finally by anodic stripping of metallic Co from the GC electrode. This kind of oxidation process has been described in detail elsewhere[13b] and will not be considered further here. In this study, we focus on reduction processes. The relevant half-wave potentials are summarized in Table 4.

At high scan rates, the cathodic CV response of **3** in THF solution shows two subsequent one-electron processes, centred at $E_{1/2}(A/A') = -0.57$ V and $E_{1/2}(B/B') = -1.22$ V (Figure 2).

The two peak couples, which correspond to the redox processes $\mathbf{3}/[\mathbf{3}]^-$ (A/A′) and $[\mathbf{3}]^-/[\mathbf{3}]^{2-}$ (B/B′), are electrochemically and chemically reversible. The peak heights are similar to that of the peak due to an equimolar solution of decamethylferrocene (Fc*) added as an internal standard. However, as the scan rate is lowered, chemical complications arise. By switching the potential at −1.00 V, the first one-electron reduction peak couple (A/A′) remains chemically reversible [i.e. the ratio between the anodic (A′) and

Table 3. Selected bond lengths [Å] in $[\{Co_4(CO)_3(\mu_3\text{-}CO)_3(\mu_3\text{-}C_7H_7)\}_2\{\mu\text{-}\eta^4\text{:}\eta^4\text{-}(C_7H_9)_2\}]^{2-}$ **[4A]**$^{2-}$

Co1−Co2	2.447(2)	Co5−Co6	2.456(2)
Co1−Co3	2.447(2)	Co5−Co8	2.439(2)
Co1−Co_4	2.566(1)	Co5−Co7	2.545(2)
Co2−Co3	2.536(2)	Co6−Co8	2.536(2)
Co2−Co4	2.510(2)	Co6−Co7	2.501(2)
Co3−Co4	2.488(2)	Co7−Co8	2.505(2)
Co1−C15	1.912(5)	Co5−C36	1.915(6)
Co2−C15	2.015(5)	Co6−C36	2.009(6)
Co3−C15	2.047(5)	Co8−C36	2.022(6)
Co1−C16	2.190(5)	Co5−C35	2.122(6)
Co3−C16	1.935(6)	Co6−C35	1.946(6)
Co4−C16	1.927(6)	Co7−C35	1.927(6)
Co1−C17	2.147(5)	Co5−C37	2.149(6)
Co2−C17	1.950(6)	Co7−C37	1.911(6)
Co4−C17	1.913(5)	Co8−C37	1.944(7)
Co−C(CO)term	1.749(6)−1.752(5)	Co−C(CO)term	1.738(8)−1.759(6)
Co1−C2	2.091(5)	Co5−C22	2.082(5)
Co1−C3	2.009(5)	Co5−C23	2.012(5)
Co1−C4	2.010(5)	Co5−C24	2.022(5)
Co1−C5	2.089(5)	Co5−C25	2.096(6)
Co2−C8	2.236(6)	Co3−C12	2.155(6)
Co2−C9	2.032(6)	Co4−C13	2.129(6)
Co2−C10	2.399(7)	Co4−C14	2.089(6)
Co3−C11	2.055(6)	C−C(μ_3-C_7H_7)[a]	1.40(1)−1.43(1)
C1−C2	1.512(7)	C21−C22	1.515(7)
C1−C7	1.522(7)	C21−C27	1.529(7)
C2−C3	1.426(7)	C22−C23	1.432(7)
C3−C4	1.422(7)	C23−C24	1.427(7)
C4−C5	1.416(8)	C24−C25	1.416(8)
C5−C6	1.511(7)	C25−C26	1.501(8)
C6−C7	1.524(7)	C26−C27	1.518(7)
C1−C21	1.570(6)		

[a] The non-disordered ring bonded to Co2, Co3 and Co4.

Table 4. Half-wave potentials, $E_{1/2}$ [V], for $[\{Co_4(CO)_3(\mu_3\text{-}CO)_3(\mu_3\text{-}C_7H_7)\}_2\{\mu\text{-}(C_7H_9)_2\}]^{2-}$ **[4]**$^{2-}$ at a dropping mercury electrode in THF and CH_2Cl_2

	A/A′	B/B′	C/C′	D/D′	E/E′
THF	−0.57	−1.22	−0.12	−1.69	−2.22
CH_2Cl_2	−0.76	−1.34	−0.27	−1.75	[a]

[a] Hidden by solvent discharge.

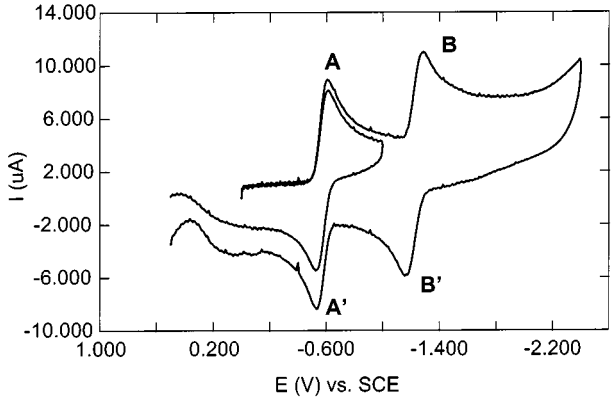


Figure 2. CV response of a THF solution of **3** at a GC electrode (scan rate 8 V s^{-1})

cathodic (A) peak currents, i_p^a/i_p^c, is unity] only at scan rates higher than 2 V/s. At lower scan rates, a new species is produced upon reoxidation at peak C′, giving rise to a reversible peak system C/C′ centred at $E_{1/2}$(C/C′) = −0.12 V. New peak systems are seen on scanning in the available cathodic window (up to −2.4 V) at $E_{1/2}$(D/D′) = −1.69 V and $E_{1/2}$(*E*/*E*′) = −2.22 V (Figure 3).

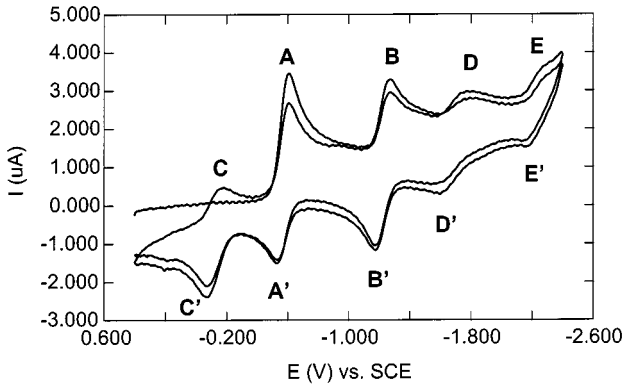


Figure 3. CV response of a THF solution of **3** at a GC electrode (scan rate 0.4 V s^{-1})

Surprisingly, the ratio $i_p^a(B')/i_p^c(B)$ is higher than unity at scan rates lower than 2 V/s. Furthermore, the heights of all the observed peaks are lower than $i_p^c(A)$. This is particularly evident at low scan rates (e.g. 100 mV/s, see Figure 4). It is interesting to note that even at very low scan rates, $i_p^a(B')$ does not disappear.

FT-IR spectroelectrochemistry (CO stretching region) performed in an OTTLE cell during the first reduction process shows a quantitative chemical conversion of **3** (νCO = 1980, 1730 cm^{-1}) to the "dimeric" dianion **[4]**$^{2-}$ (ν_{CO} = 1925, 1675 cm^{-1}), as verified by comparison with the IR spectrum of an authentic sample. Isosbestic points at 1957

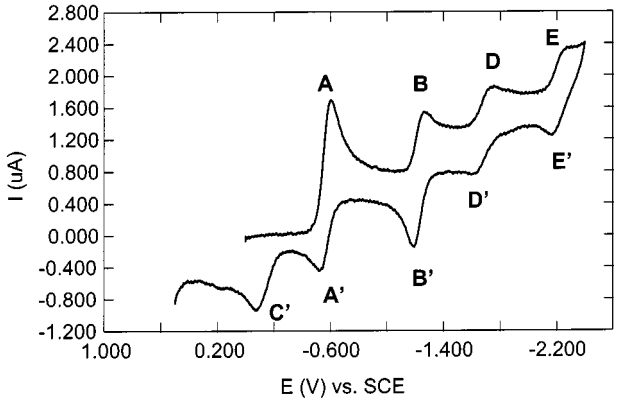


Figure 4. CV response of a THF solution of **3** at a GC electrode (scan rate 0.1 V s^{-1})

cm^{-1} and 1705 cm^{-1} are indicative of full conversion to the dimer in the course of the electrolysis (Figure 5). Reoxidation at the platinum electrode of the OTTLE cell completely restores the original spectrum of the parent compound **3**, suggesting complete chemical reversibility of the system over long-term electrolysis as well.

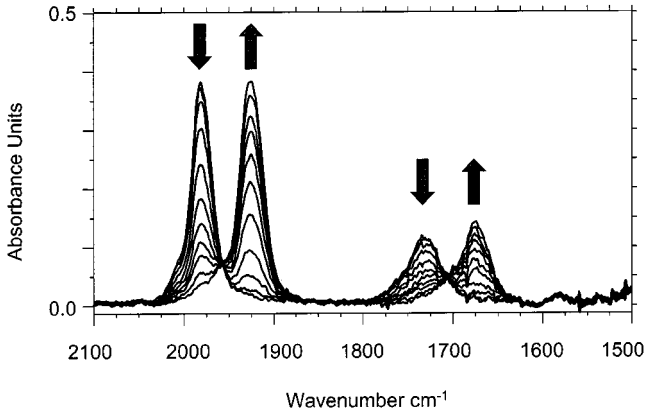


Figure 5. IR OTTLE spectra of a THF solution of **3** during the exhaustive reduction at $E_{app} \approx -0.8$ V

In analogy to CV, polarography of **3** (Figure 6, solid line) shows two reduction waves, A and B. At mercury, a further, very cathodic, reduction process is observed (wave F). Exhaustive electrolysis at a mercury-pool electrode ($E_{appl} = -0.8$ V) was followed by in situ polarography. As 1 F/mol was consumed, waves A and B completely disappeared and an apparent one-electron anodic oxidation wave C and two one-electron reduction waves D and E appeared (dotted line). Re-oxidation at potentials more positive than wave C did not fully restore the original cluster **3** as in OTTLE, probably due to interactions of the cobalt carbonyls with the mercury pool during re-oxidation. Such interactions of cobalt carbonyl derivatives with mercury have been observed several times,[14,15] and have been investigated in detail for the fragment $[Co(CO)_4]^-$.[16]

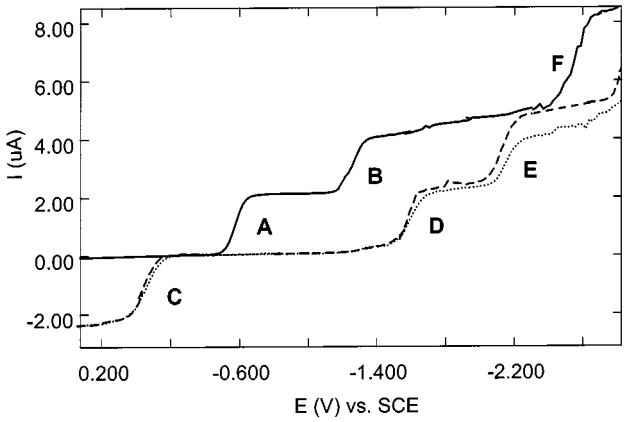


Figure 6. Polarographic responses of a THF solution of **3** recorded in situ during exhaustive electrolysis at a mercury-pool electrode; the solid line corresponds to the initial solution, while the dotted curve was recorded after 1 F/mol had been consumed at $E_{app} \approx -0.8$ V; the dashed curve is the polarographic response of a THF solution of an authentic sample of $[\mathbf{4}]^{2-}$

A pure sample of the dimer $[\mathbf{4}]^{2-}$ (the 86:14 mixture of isomers $[\mathbf{4A}]^{2-}$ and $[\mathbf{4B}]^{2-}$) (dashed line) was found to exhibit the same electrochemical behaviour. The redox waves of $[\mathbf{4}]^{2-}$ (i.e. D and E) are twice the height compared to that of an equimolar solution of Fc*, added as an internal standard. The electron stoichiometry (2 electrons) of both reduction processes was confirmed by coulometry. Furthermore, the polarographic slopes obtained from log-plot analyses and the ΔE_p values from the CV (both roughly 60 mV) are typical of a single-electron Nernstian process. Waves D and E assigned to $[\mathbf{4}]^{2-}$ (produced by exhaustive electrolysis of **3**) relate to two-electron processes, but correspond to half concentrations of the electroactive species, and therefore their heights are equal to those of waves A and B (assigned to the parent cluster **3**). Finally, $[\mathbf{4}]^{2-}$ exhibits the usual multi-electron chemical irreversible oxidation peak at +0.70 V at glassy carbon.

Discussion

A family of isoelectronic tetracobalt carbonyl cluster complexes exists where one face of the Co_4 tetrahedron is capped by a facial (μ_3) ligand. These include $[Co_4(CO)_6(\mu_2\text{-}CO)_3(\mu_3\text{-trithiane})]$ **(7)**,[17] $[Co_4(CO)_6(\mu_2\text{-}CO)_3\{\mu_3\text{-}HC(EPh_2)_3\}]$ **(8a)** (E = P), **(8b)** (E = As),[18] $[Co_4(CO)_3(\mu_3\text{-}CO)_3(\mu_3\text{-}C_8H_8)(L)]$ **(1)**,[5] and $[Co_4(CO)_3(\mu_3\text{-}CO)_3(\mu_3\text{-}C_7H_7)(L)]$ [L = η^5-C_7H_9 (**3**); η-C_5R_5, R = H, Me].[5] These derivatives of the parent binary carbonyl $[Co_4(CO)_{12}]$ are "electron precise" (60 valence electrons [VE]).[19] It has been demonstrated that the facial ligands tend to stabilize the tetrahedral Co_4 cluster core, resulting in a considerably reduced tendency to fragment during the course of chemical and electrochemical reactions. For example, $[Co_4(CO)_{12}]$ readily undergoes complete fragmentation when reduced in the absence of reactants.[6] The one-electron reduction product of **8a**, $[Co_4(CO)_9\{\mu_3\text{-}HC(PPh_2)_3\}]^-$ $[\mathbf{8a}]^-$, is more stable, but undergoes rapid ligand exchange at the apical

cobalt atom.[6b] The cyclooctatetraene-bridged clusters **1** have been shown to undergo pseudo-reversible electrochemical one-electron reductions, but are quantitatively converted to the stable trinuclear anion $[Co_3(CO)_3(\mu_2\text{-}CO)_3(\mu_3\text{-}C_8H_8)]^-$ $[\mathbf{2}]^-$ upon chemical reduction.[4]

A similar behaviour was expected of the cycloheptatrienyl-bridged cluster complexes **3**, from which we hoped to generate the trinuclear dianion $[Co_3(CO)_6(\mu_3\text{-}C_7H_7)]^{2-}$ $[\mathbf{9}]^{2-}$. However, our electrochemical studies have not produced any evidence for the formation of this species. The initial reduction product $[\mathbf{3}]^-$ is indeed transient, but further reaction occurs through intermolecular ligand−ligand coupling to give $[\mathbf{4}]^{2-}$, and not by degradation of the metal framework. With some caution,[20] this can be taken as evidence that the unpaired electron in $[\mathbf{3}]^-$ is essentially centred on the apical C_7H_9 ligand, and less so on the metal cluster. This view is also consistent with the formation of minor amounts of $[\mathbf{5}]^-$, which is the electron-precise product of hydrogen abstraction from the solvent or water by $[\mathbf{3}]^-$.

The formation of $[\mathbf{4}]^{2-}$ is regiospecific [carbon−carbon bond formation occurs exclusively at the carbon atom(s) in the enylic positions, adjacent to the unsaturated π-system of the C_7H_9 ligand], but not stereospecific. The absolute configuration (*R*,*R*) [and (*S*,*S*)] can be assigned to the bridgehead carbon atoms C1 and C21 in $[\mathbf{4A}]^{2-}$ on the basis of our structure determination. It seems likely that $[\mathbf{4B}]^{2-}$ is the achiral (*R*,*S*) isomer (*meso* form).

The formation of the Co_3Ru complex **6**, another electron-precise cluster, is more difficult to explain. It could be due to a stacking reaction of the ruthenium benzene reagent with the trinuclear dianion $[\mathbf{9}]^{2-}$, akin to the reaction of $[\mathbf{2}]^-$ with $[(\eta\text{-}C_5Me_5)Ru(NCMe)_3]^+$.[4] However, this would require that $[\mathbf{9}]^{2-}$ be present, at least in minor amounts, in the mixture of reduction products of **3**. The paramagnetism of the main product, $[\mathbf{3}]^-$, could prevent the detection of $[\mathbf{9}]^{2-}$ (expected to be diamagnetic) in the reaction mixture by NMR spectroscopy. This interpretation could explain the observation that formation of **6** is complete within a few minutes, whereas the subsequent dimerization of $[\mathbf{3}]^-$ is much slower.

Alternatively, a redox condensation of the tetranuclear $[\mathbf{3}]^-$ with $[(\eta\text{-}C_6H_6)Ru(NCMe)_3]^{2+}$ could take place, which would involve extrusion of a cobalt vertex. Here, the low yield of product **6** would be accounted for by the charge balance, which requires sacrifice of two molecules of $[\mathbf{3}]^-$ for the formation of one molecule of **6**.

A 60 VE count is attained by either of the two Co_4 cluster units in $[\mathbf{4A}]^{2-}$, as well as by $[\mathbf{5}]^-$. Hence, the uptake of an electron by **3**, followed by dimerization or hydrogen abstraction, is accompanied by a decrease of hapticity of the apical seven-membered ring ligand (from η^5 to η^4). The lengths of the endocyclic carbon−carbon bonds within the bridging $(C_7H_9)_2$ ring system conform to the pattern expected for η^4-cycloheptadiene ligands: they are shorter within the η^4-diene systems (mean value 1.42 Å) and longer in the remaining rings (mean value 1.52 Å). The bond C1−C21, which joins the two seven-membered rings, is slightly longer [1.570(6) Å] than would be expected for a single bond. This value compares well with the corresponding bond lengths in the dinuclear complexes $[\{(CO)_3Fe\}_2\{\mu\text{-}\eta^4\text{:}\eta^4\text{-}(C_7H_9)_2\}]$ [1.564(4) Å][21] and $[\{(\eta\text{-}C_5H_5)Co\}_2\{\mu\text{-}\eta^4\text{:}\eta^4\text{-}(C_7H_9)_2\}]$ **(10)** [1.564(5) Å].[22]

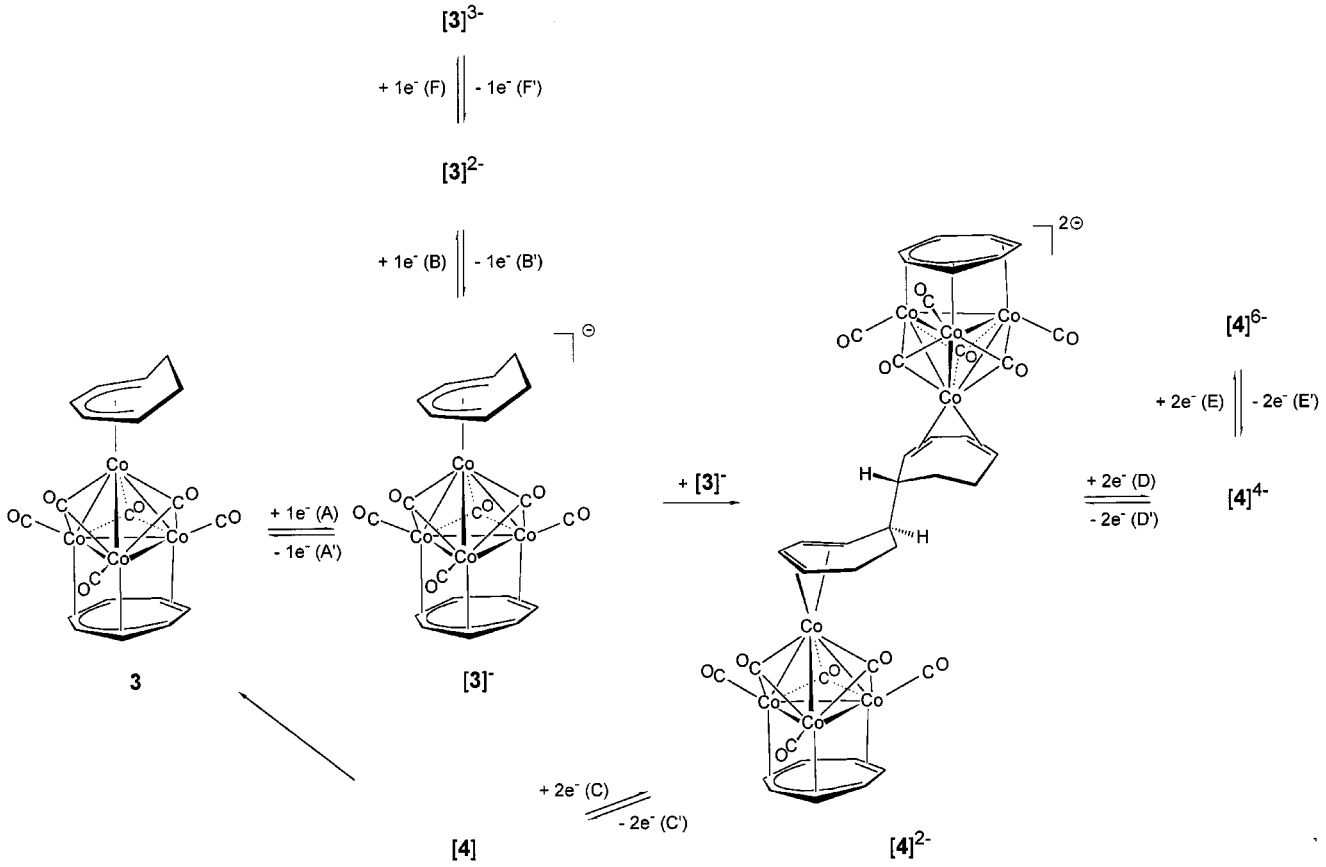
Within the limitations of the experimental accuracy, the geometry of the $Co_4(CO)_6$ cluster units in $[\mathbf{4A}]^{2-}$ is quite similar to that seen in other complexes containing the $Co_4(CO)_6(\mu_3\text{-}C_nH_n)$ moiety.[5] The coordination mode of the facial C_7H_7 rings approaches the $\mu_3\text{-}\eta^2\text{:}\eta^2\text{:}\eta^3$ fashion and is therefore slightly different from the $\mu_3\text{-}\eta^2\text{:}\eta^3\text{:}\eta^3$ coordination found in **3**.[5] However, owing to the small actual geometric differences between the various forms of the $\mu_3\text{-}\eta^7$ coordination mode, the experimental inaccuracies, and the low barrier to rotation, no great significance should be attached to this observation.

As expected, a high mobility of the facial C_7H_7 ligands in $[\mathbf{4}]^{2-}$, $[\mathbf{5}]^-$, and **6** is evident in solution, which can be explained in terms of rapid rotation of the seven-membered rings within their coordination planes. The ^1H and ^{13}C NMR chemical shifts of these ligands compare well with those observed in **3**.[5] It appears that a ^{13}C chemical shift of about $\delta = 60$ is typical for a C_7H_7 ligand facially coordinated to a Co_3 cluster face, with a minor high-field shift of about 5 ppm when the molecule bears a negative charge. This is in contrast to the much larger coordination shifts that have been reported for $Ru_3(\mu_3\text{-}C_7H_7)$ moieties [$\delta(^{13}C) \approx 39$].[23] The proton resonance of the η^6-benzene ligand in **6** appears at a chemical shift comparable to that found for apical benzene ligands in hexa- and pentanuclear ruthenium and mixed ruthenium osmium carbonyl cluster complexes.[24] Interestingly, resonances at higher field are observed when the $(\eta\text{-}C_6H_6)Ru$ moiety is part of a penta- or hexanuclear iron carbonyl cluster {e.g. $[Ru(\eta\text{-}C_6H_6)Fe_5C(CO)_{14}]$, $\delta(^1H) = 4.37$; $[Ru(\eta\text{-}C_6H_6)Fe_4C(CO)_{12}]$, $\delta(^1H) = 4.85$}.[25]

The electrochemical data can be accounted for by the mechanism depicted in Scheme 1.

The dimerization of the radical anion $[\mathbf{3}]^-$ to form $[\mathbf{4}]^{2-}$ explains the reversible re-oxidation C′. Interestingly, the oxidized form **4** is unstable in the long-term and decomposes back to **3** almost quantitatively. The dimerization reaction $[\mathbf{3}]^- + [\mathbf{3}]^- \rightarrow [\mathbf{4}]^{2-}$ is sufficiently fast to produce peaks D/D′ and E/E′ (Figure 3), attributable to further reduction of the dimer itself, but not so fast as to lead to complete loss of peaks B and A′ (Figure 4), assigned to further reduction and re-oxidation of the monomer $[\mathbf{3}]^-$, respectively. This justifies the differences in the peak heights discussed above. Contrasting behaviour, where the anomalous peak height was rationalized in terms of a catalytic mechanism, has been observed in a study of the electron-transfer chain reaction that follows the reduction of $[H_4Ru_4(CO)_{12}]$.[26] It is noteworthy that the dianion $[\mathbf{3}]^{2-}$ is much more stable than the monoanion $[\mathbf{3}]^-$ on the CV time scale. This accounts for the fact that $i_p^a(B')$ is higher than $i_p^c(B)$.

The redox behaviour of $[\mathbf{4}]^{2-}$, as outlined above, suggests that the two redox-active moieties, $Co_4(CO)_3(\mu_3\text{-}CO)_3(\mu_3\text{-}C_7H_7)(\eta^4\text{-}C_7H_9)$, directly bonded by a single



Scheme 1. Redox processes involving complexes **3** and **4**

carbon−carbon bond, act as two independent, non-interacting redox centres. For such a case, the two one-electron reduction processes are separated by 36 mV (statistical factor) and a single, double-height wave is expected.[27]

Digital simulation[28] (Figure 7) of the overall mechanism produced a shape similar to that observed experimentally (Figure 4). The homogeneous rate constant for the dimerization was evaluated as k_{DIM} (2 [**3**]$^-$ → [**4**]$^{2-}$) = 0.30 ± 0.05

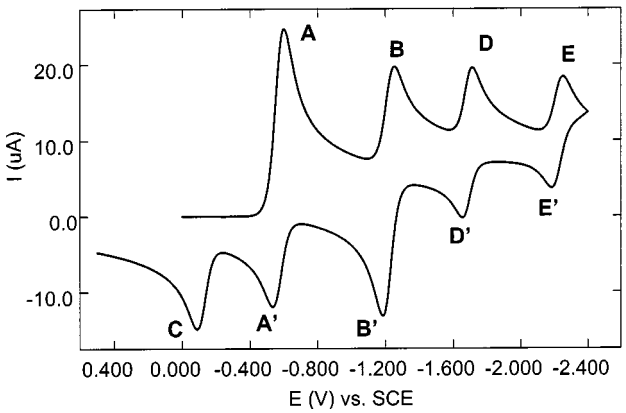
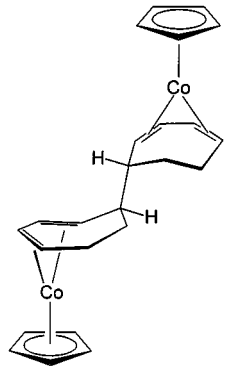


Figure 7. Digital simulation according to the mechanism in Scheme 1; scan rate 0.1 V s^{-1}; heterogeneous rate constant ($k°$) = 2 cm s^{-1}; α = 0.5; D(**3**) = 1 × 10^{-5} cm^2 s^{-1}; D(**4**) = 7 × 10^{-6} cm^2 s^{-1}; $E_{1/2}$(A/A′) = $E_{1/2}$(**3**/[**3**]$^-$) = −0.57 V; $E_{1/2}$(B/B′) = $E_{1/2}$([**3**]$^-$/[**3**]$^{2-}$) = −1.22 V; $E_{1/2}$(**4**/[**4**]$^-$) = −0.102 V; $E_{1/2}$([**4**]$^-$/[**4**]$^{2-}$) = −0.138 V; $E_{1/2}$([**4**]$^{2-}$/[**4**]$^{3-}$) = −1.672 V; $E_{1/2}$([**4**]$^{3-}$/[**4**]$^{4-}$) = −1.698 V; $E_{1/2}$([**4**]$^{4-}$/[**4**]$^{5-}$) = −2.202 V; $E_{1/2}$([**4**]$^{5-}$/[**4**]$^{6-}$) = −2.238 V; k_f (**4** → 2 **3**) = 0.2 s^{-1}; k_{DIM} (2 [**3**]$^-$ → [**4**]$^{2-}$) = 0.30 mM^{-1} s^{-1}



10

mM^{-1} s^{-1} (according to the DIM 1 mechanism proposed by Saveant et al.[29]), either by means of best-fitting of the experimental data[28] or by applying the method of Lasia[30] with different values for the scan rates (0.05−1 V/s) and concentrations of **3** (0.6−3 mM). The CV switching potential was 300 mV past the first cathodic peak potential.[30] Both methods gave a similar rate, but simulation produces an "*ad hoc*" working curve.

The redox-induced intermolecular coupling of the two cycloheptadienyl ligands has a precedent in mononuclear chemistry. Geiger et al.[22] observed that [(η-C_5H_5)Co(η^5-C_7H_9)]$^+$ undergoes two reductions, at −0.8 and −1.9 V, the latter process being irreversible. This complex generated the

"dimer" $[\{(\eta\text{-}C_5H_5)Co\}_2\{\mu\text{-}\eta^4\text{:}\eta^4\text{-}(C_7H_9)_2\}]$ **(10)** upon electrolysis at −1.0 V. The value found for the dimerization of the mononuclear cobalt complex (k_{DIM} = 1.35 mM^{-1} s^{-1})[31] is somewhat higher than that found in the present work; this is probably due to the presence of the bulkier tetracobalt unit in **3**. Whereas the dimer **10** is oxidized in two one-electron steps with limited electronic communication, the oxidation of $[\mathbf{4}]^{2-}$ occurs in a single two-electron step. Interestingly, dimer **10** is stable, whereas dimer **4** undergoes spontaneous fission of the newly formed C−C bond, thus constituting the basis of a very interesting redox cycle (see Conclusion).

For **10**, there was no indication that two stereoisomers had been formed. In the crystal used for the structure determination, the same (*R*,*R*) and (*S*,*S*) configurations of the bridgehead carbons as in $[\mathbf{4A}]^{2-}$ were found.

Conclusion

The propensity of cluster **3** to dimerize upon reduction to $[\mathbf{4}]^{2-}$ with the formation of an additional C−C bond and its reoxidation to **4**, which, in turn, is unstable and spontaneously reverts to **3** in a perfectly reversible manner by cleavage of this C−C bond, constitutes a very promising redox cycle. This system approaches the concept of a "molecular battery" proposed by Floriani,[32] i.e. a molecular device capable of storing and releasing pairs of electrons through the formation and cleavage of chemical bonds. This reservoir of electrons controlled by the reversible formation of C−C bonds may represent an interesting device for electrical energy storage.

Experimental Section

General Procedures: All operations were carried out under an atmosphere of purified nitrogen or argon (BASF R3−11 catalyst) using Schlenk techniques. Solvents were dried by conventional methods. Alumina used as a stationary phase for column chromatography was heated to 180−200 °C in vacuo for several days, deactivated with 5% water, and then stored under nitrogen. The cluster complex **3** was prepared as described previously.[5] NMR spectra were recorded on Bruker AC 200 and AVANCE DRX200 instruments (200.1 MHz for ^1H, 50.3 MHz for ^{13}C); ^1H and ^{13}C chemical shifts are reported *vs.* $SiMe_4$ and were determined by reference to internal $SiMe_4$ or residual solvent peaks. Infrared spectra were recorded from samples in CaF_2 cells on a Bruker IFS-28 Fourier-transform spectrometer (optical resolution 0.5 cm^{-1}). Elemental analyses were performed locally at the Microanalytical Laboratory of the Organisch-chemisches Institut der Universität Heidelberg and at the Mikroanalytisches Labor Beller, Göttingen.

$[PPh_4]_2[\{Co_4(CO)_3(\mu_3\text{-}CO)_3(\mu_3\text{-}C_7H_7)\}_2\{\mu_2\text{-}(C_7H_9)_2\}]$ ($[PPh_4]_2[\mathbf{4}]^{2-}$): A mixture of $[Co_4(CO)_3(\mu_3\text{-}CO)_3(\mu_3\text{-}C_7H_7)(\eta^5\text{-}C_7H_9)]$ **(3)** (1.1 g, 1.7 mmol) and $Na_2[Fe(CO)_4]\cdot 3/2$dioxane (0.64 g, 1.9 mmol) was dissolved in THF (50 mL) and the resulting solution was stirred for 30 min. at room temperature. All volatiles were then removed in vacuo, the residue was redissolved in THF (10 mL), and $[PPh_4]Br$ (3.0 g, 7.2 mmol) was added. After stirring for 1 h, the mixture was filtered and the filtrate was concentrated to a small volume. A tenfold excess of methanol was then added to precipitate the product as a mixture of diastereomers $[\mathbf{4A},\mathbf{B}]^{2-}[PPh_4]_2$ (860 mg, 54%). Partial separation of the isomers (about 86% purity for the less soluble $[\mathbf{4A}]^{2-}[PPh_4]_2$; about 80% purity for $[\mathbf{4B}]^{2-}[PPh_4]_2$) could be achieved by repeated recrystallization from THF/methanol or nitromethane. The mother liquor from the first precipitation with methanol was subsequently chromatographed on alumina (deactivated with 5% water, 2.5 × 20 cm). A red band was eluted from the column with CH_2Cl_2, from which 20 mg (1%) of $[Co_4(CO)_3(\mu_3\text{-}CO)_3(\mu_3\text{-}C_7H_7)(C_7H_{10})][PPh_4]$ ($[\mathbf{5}]^-[PPh_4]$) was isolated.

$[\mathbf{4}]^{2-}[PPh_4]_2$: IR ($CH_2Cl_2$): ν(CO) = 1955 (sh), 1926 (vs), 1702 (sh), 1675 (s) cm^{-1}. − $C_{88}H_{72}Co_8O_{12}P_2$ (1854.96): calcd. C 56.98, H 3.91; found C 56.43, H 4.10.

$[Co_4(CO)_3(\mu_3\text{-}CO)_3(\mu_3\text{-}C_7H_7)(C_7H_{10})][PPh_4]$ ($[\mathbf{5}]^-[PPh_4]$): A sample of **3** (270 mg, 0.46 mmol) in THF (30 mL) was treated with 0.5 mL of a 1 M solution of $Li[HBEt_3]$ in THF. After stirring for 30 min. at room temperature, all volatiles were removed in vacuo. The residue was redissolved in THF (5 mL) and to this solution, a solution of $[NnBu_4]Cl$ (2.4 g, 8.6 mmol) in water (40 mL) was added dropwise. After stirring for 30 min., the product was collected on a glass frit, washed with H_2O, toluene, and pentane, and dried in vacuo. Recrystallization from ethanol gave 100 mg (26%) of $[\mathbf{5}]^-[NnBu_4]$. − IR (CH_2Cl_2): ν(CO) = 1955 (sh), 1925 (vs), 1700 (sh), 1675 (s) cm^{-1}.

$[Ru(\eta\text{-}C_6H_6)Co_3(CO)_3(\mu_3\text{-}CO)_3(\mu_3\text{-}C_7H_7)]$ (6): A 1.6 mL aliquot of a 1 M solution of $Li[HBEt_3]$ in THF was added to a solution of **3** (0.92 g, 1.6 mmol) in THF (50 mL). After stirring for 1 h at room temperature, all volatiles were removed in vacuo. The residue was then treated with a solution of $[(\eta\text{-}C_6H_6)Ru(NCMe)_3][BF_4]_2$ (0.75 g, 1.6 mmol) in CH_2Cl_2 (50 mL). After 30 min., some insoluble material was removed by filtration. The filtrate was concentrated to dryness in vacuo, the black residue was washed with *n*-hexane, and then applied to the top of a column (2.5 × 20 cm) of alumina (deactivated with 5% water). Elution with toluene removed a light-brown band from the column. The product was then eluted with CH_2Cl_2 as a dark-brown band, from which 180 mg (18%) of black microcrystalline **6** was isolated. − ^1H NMR (CD_2Cl_2): δ = 3.20 (s, 7 H, C_7H_7), 5.35 (s, 6 H, C_6H_6). − $^{13}C\{^1H\}$ NMR (C_6D_6): δ = 59.8 (C_7H_7), 95.6 (C_6H_6). − IR (toluene): ν(CO) = 2000 (sh), 1973 (vs), 1715 (s) cm^{-1}. − $C_{19}H_{13}Co_3O_6Ru$ (615.18): calcd. C 37.10, H 2.13; found C 37.16, H 2.76.

Crystal Structure Determination: Single crystals of $[\mathbf{4A}][PPh_4]_2\cdot 1.5C_7H_8$ were grown from a solution of the 86:14 mixture of isomers $[\mathbf{4A}]^{2-}/[\mathbf{4B}]^{2-}$ in CH_2Cl_2 by layering with toluene at room temperature. Intensity data were collected on a Siemens-Stoe AED2 four-circle diffractometer at low temperature (Table 5). The structure was solved by direct methods and refined by full-matrix least-squares based on F^2 using all measured unique reflections. One of the $\mu_3\text{-}C_7H_7$ ligands, a phenyl ring in one of the $[PPh_4]^+$ cations, and a toluene solvate molecule were found to be disordered. Most non-hydrogen atoms were given anisotropic displacement parameters, except those of the disordered C_7H_7 and toluene rings. Some of the hydrogen atoms were localized in difference Fourier syntheses and were refined isotropically. The remaining hydrogen atoms were placed in calculated positions (except those of the disordered toluene).[33] The calculations were performed using the programs SHELXS-86 and SHELXL-97.[34] Graphical representations were produced using SCHAKAL-92.[35]

Table 5. Details of the crystal structure determination of $[\{Co_4(CO)_3(\mu_3\text{-}CO)_3(\mu_3\text{-}C_7H_7)\}_2\{\mu\text{-}\eta^4\text{:}\eta^4\text{-}(C_7H_9)_2\}][PPh_4]_2\cdot 1.5C_7H_8$ ($[4A]^{2-}$-$[PPh_4]_2$)

Formula	$C_{88}H_{72}Co_8O_{12}P_2\cdot 1.5C_7H_8$
Crystal system	triclinic
Space group	*P*-1
a [Å]	16.216(9)
b [Å]	16.321(9)
c [Å]	16.800(9)
α [°]	90.15(4)
β [°]	98.00(4)
γ [°]	104.37(4)
V [Å^3]	4262(4)
Z	2
M_r	1993.03
d_c [gcm^{-3}]	1.553
F_{000}	2034
μ(Mo-K_α) [mm^{-1}]	1.62
X-radiation, λ [Å]	Mo-K_α, graphite-monochromated, 0.71073
Data collect. temp. [°C]	−70
2θ range [°]	3−50
hkl ranges	$-19 \le h \le 18$ $-19 \le k \le 19$ $0 \le l \le 19$
Reflections measured	
Unique	15007
Observed [$I \ge 2\ \sigma(I)$]	10706
Parameters refined	1197
R values	
R (obsd. reflections only)	0.053
w*R*2 (all reflections)	0.143
($w = 1/[\sigma^2(F)+(A\cdot P)^2+B\cdot P]$,	
A, *B*	0.0655, 6.87
P	$\max[(F_o^2, 0) + 2\ F_c^2]/3$
GooF	1.023
Largest/smallest peak in Fourier [eÅ−3]	0.89/−0.59

Electrochemistry: THF was distilled from sodium benzophenone ketyl immediately prior to use. Tetrabutylammonium hexafluorophosphate (Aldrich) was recrystallized three times from 95% ethanol and dried in a vacuum oven at 110 °C overnight. Electrochemistry was performed with an EG&G PAR 273 electrochemical analyser connected to a PC, employing the software M270. A standard three-electrode cell was designed to allow the tip of the reference electrode to closely approach the working electrode. The reference used was the Standard Calomel Electrode (SCE). The working electrode for CV was composed of glassy carbon (GC); for polarography, a dropping mercury electrode (DME) with flow rate of 1.22 mg s^{-1} at a reservoir height of 0.5 m was employed. Drop time (typically 1 s) was controlled by an electromechanical hammer. A platinum wire served as the auxiliary electrode. Positive feedback *iR* compensation was applied routinely. All measurements were carried out under Ar in anhydrous deoxygenated THF or CH_2Cl_2. Solutions were 5×10^{-4} M in the compounds under study and 1×10^{-1} M in the supporting electrolyte, $[Bu_4N][PF_6]$. Since the oxidation process of ferrocene (Fc) overlaps with those of the compounds under study, we employed decamethylferrocene (Fc*) as an internal standard; the Fc*(0/1+) potential was evaluated as +0.11 V *vs.* SCE in THF.[36,37] The number of electrons transferred (n_{app}) in a particular redox process was determined by controlled potential coulometry at a mercury pool. Each experiment was carried out in duplicate. Spectroelectrochemistry was performed in an optically transparent thin-layer electrochemical (OTTLE) cell assembled as described previously;[38] the spectra were recorded on a Bruker Equinox 55 FT-IR spectrometer.

Acknowledgments

This work was supported by the Sonderforschungsbereich 247 der Universität Heidelberg, the Fonds der Chemischen Industrie, and MURST (Rome) (COFIN-98). The award of a Heisenberg Fellowship to H.W. is gratefully acknowledged. J.F. thanks the University of Torino for a visiting grant (scambi culturali).

[1] [1a] H. Vahrenkamp, *Adv. Organomet. Chem.* **1983**, *22*, 169. − [1b] W. E. Geiger, N. G. Connelly, *Adv. Organomet. Chem.* **1985**, *24*, 87. − [1c] W. E. Geiger, *Progr. Inorg. Chem.* **1985**, *33*, 275. − [1d] P. Lemoine, *Coord. Chem. Rev.* **1988**, *83*, 169. − [1e] S. R. Drake, *Polyhedron* **1990**, *9*, 455. − [1f] P. Zanello, *Struct. Bonding* **1992**, *79*, 101. − [1g] G. Longoni, C. Femoni, M. C. Iapalucci, P. Zanello, in *Metal Clusters in Chemistry* (Eds.: P. Braunstein, L. A. Oro, P. R. Raithby), Wiley-VCH, Weinheim, **1999**, vol. 2, ch. 3.9.

[2] [2a] N. J. Coville, M. O. Albers, *Coord. Chem. Rev.* **1984**, *53*, 227. − [2b] D. Astruc, *Angew. Chem.* **1988**, *100*, 662.

[3] For examples discussed recently in the literature, see: W. E. Geiger, M. J. Shaw, M. Wünsch, C. E. Barnes, F. H. Foersterling, *J. Am. Chem. Soc.* **1997**, *119*, 2804. M. P. Robben, P. H. Rieger, W. E. Geiger, *J. Am. Chem. Soc.* **1999**, *121*, 367.

[4] H. Wadepohl, S. Gebert, R. Merkel, H. Pritzkow, *Eur. J. Inorg. Chem.* **2000**, in print.

[5] [5a] H. Wadepohl, S. Gebert, H. Pritzkow, D. Braga, F. Grepioni, *Chem. Eur. J.* **1998**, *4*, 279. − [5b] H. Wadepohl, *Coord. Chem. Rev.* **1999**, *185−186*, 551.

[6] [6a]P. Chini, V. Albano, S. Martinengo, *J. Organomet. Chem.* **1969**, *16*, 471. − [6b] J. Rimmelin, P. Lemoine, M. Gross, D. de Montauzon, *Nouv. J. Chem.* **1983**, *7*, 453.

[7] [7a] G. Fachinetti, *J. Chem. Soc., Chem. Commun.* **1979**, 396. − [7b] H.-N. Adams, G. Fachinetti, J. Strähle, *Angew. Chem.* **1980**, *92*, 411.

[8] In this paper, the face of the M_4 cluster at which the μ_3-ligand is bound is referred to as the "basal M_3 plane". The fourth metal atom and the ligands attached to it are "apical".

[9] D. Osella, M. Ravera, C. Nervi, C. E. Housecroft, P. R. Raithby, P. Zanello, F. Laschi, *Organometallics* **1991**, *10*, 3253.

[10] G. F. Holland, D. E. Ellis, W. C. Trogler, *J. Am. Chem. Soc.* **1986**, *108*, 1884.

[11] Y. Mugnier, P. Reeo, C. Moise, E. Laviron, *J. Organomet. Chem.* **1983**, *254*, 111.

[12] [12a] J. C. Kotz, J. V. Petersen, R. C. Reed, *J. Organomet. Chem.* **1976**, *120*, 433. − [12b] A. M. Bond, B. M. Peake, B. H. Robinson, J. Simpson, D. J. Watson, *Inorg. Chem.* **1977**, *16*, 410.

[13] [13a] M. Arewgoda, P. H. Rieger, B. H. Robinson, J. Simpson, S. J. Visco, *J. Am. Chem. Soc.* **1982**, *104*, 5633. − [13b] D. Osella, E. Stein, G. Jaouen, P. Zanello, *J. Organomet. Chem.* **1991**, *401*, 37.

[14] [14a] D. Osella, L. Milone, C. Nervi, M. Ravera, *J. Organomet. Chem.* **1995**, *488*, 1. − [14b] N. Duffy, J. McAdam, C. Nervi, D. Osella, M. Ravera, B. Robinson, J. Simpson, *Inorg. Chim. Acta* **1996**, 99.

[15] S. W. Blach, A. M. Bond, R. Colton, *Inorg. Chem.* **1981**, *20*, 755.

[16] D. Osella, J. Fiedler, *Organometallics* **1992**, *11*, 3875.

[17] S. Rossi, J. Pursiainen, T. A. Pakkanen, *J. Organomet. Chem.* **1992**, *436*, 55.

[18] [18a] A. A. Bahsoun, J. A. Osborn, C. Voelker, J. J. Bonnet, G. Lavigne, *Organometallics* **1982**, *1*, 1114. − [18b] D. J. Darensbourg, D. J. Zalewski, T. Delord, *Organometallics* **1984**, *3*, 1210. − [18c] D. J. Darensbourg, D. J. Zalewski, A. L. Rheingold, R. L. Durney, *Inorg. Chem.* **1986**, *25*, 3281.

[19] D. M. P. Mingos, D. J. Wales, *Introduction to Cluster Chemistry*, Prentice-Hall, Englewood Cliffs, **1990**, ch. 2.

[20] D. Astruc, *Chem. Rev.* **1988**, *88*, 1189; *Acc. Chem. Res.* **1991**, *24*, 36.

[21] B. Niemar, J. Breimair, B. Wagner, K. Polborn, W. Beck, *Chem. Ber.* **1991**, *124*, 2227.

[22] W. E. Geiger, T. Gennett, G. A. Lane, A. Salzer, A. L. Rheingold, *Organometallics* **1986**, *5*, 1352.

[23] T. A. Cresswell, J. A. K. Howard, F. G. Kennedy, S. A. R. Knox, H. Wadepohl, *J. Chem. Soc., Dalton Trans.* **1981**, 2220.

[24] [24a] P. J. Dyson, B. F. G. Johnson, J. Lewis, M. Martinelli, D. Braga, F. Grepioni, *J. Am. Chem. Soc*. **1993**, *115*, 9062. – [24b] P. J. Dyson, B. F. G. Johnson, D. Reed, D. Braga, F. Grepioni, E. Parisini *J. Chem. Soc., Dalton Trans.* **1993**, 2817. – [24c] D. Braga, P. Sabatino, P. J. Dyson, A. J. Blake, B. F. G. Johnson, *J. Chem. Soc., Dalton Trans.* **1994**, 393. – [24d] J. Wing-Sze Hui, W.-T. Wong, *J. Organomet. Chem.* **1996**, *524*, 211. – [24e] T. Borchert, J. Lewis, P. R. Raithby, G. P. Shields, H. Wadepohl, *Inorg. Chim. Acta* **1998**, *274*, 201.

[25] S. Gebert, Ph.D. Thesis, Universität Heidelberg, **1997**; H. Wadepohl, S. Gebert, unpublished.

[26] D. Osella, C. Nervi, M. Ravera, J. Fiedler, V. Strelets, *Organometallics* **1995**, *14*, 2501.

[27] M. D. Ward, *Chem. Soc. Rev.* **1995**, *24*, 121 and references therein.

[28] The program, ESP (C. Nervi), is available at the URL: http://lem.ch.unito.it/chemistry/esp_manual.html.

[29] [29a] C. P. Andrieux, L. Nadjo, J. M. Saveant, *J. Electroanal. Chem.* **1970**, *26*, 147. – [29b] C. P. Andrieux, L. Nadjo, J. M. Saveant, *J. Electroanal. Chem.* **1973**, *42*, 223.

[30] A. Lasia, *J. Electroanal. Chem.* **1983**, *146*, 413.

[31] W. E. Geiger, personal communication.

[32] E. Gallo, E. Solari, N. Re, C. Floriani, A. Chiesi-Villa, C. Rizzoli, *J. Am. Chem. Soc.* **1997**, *119*, 5144, and references therein.

[33] Crystallographic data (excluding structure factors) for the structure reported in this paper have been deposited with the Cambridge Crystallographic Data Centre as supplementary publication no. CCDC-137254. Copies of the data can be obtained free of charge on application to The Director, CCDC, 12 Union Road, Cambridge CB2 1EZ, U.K. [Fax: (internat.) +44 (0)1223/336033; E-mail: teched@chemcrys.cam.ac.uk].

[34] *SHELXS-86*, G. M. Sheldrick, *Acta Crystallogr.* **1990**, *A46*, 467; *SHELXL-97*, G. M. Sheldrick, Universität Göttingen, **1997**.

[35] *SCHAKAL*-92, E. Keller, Universität Freiburg, **1992**.

[36] U. Kölle, F. Khouzami, *Angew. Chem. Int. Ed. Engl*. **1980**, *19*, 640.

[37] W. E. Geiger, in *Organometallic Radical Processes* (Ed.: W. C. Trogler), Elsevier, Amsterdam, **1990**, ch. 5.

[38] M. Krejcik, M. Danek, F. Hartl, *J. Electroanal.Chem.* **1991**, *317*, 179.

Received November 25, 1999
[I99435]

Self-Assembly of *meso*-Pyridylporphyrins and Zinc Phthalocyanines Through Axial Coordination

Xi-you Li[a] and Dennis K. P. Ng*[a]

Keywords: Porphyrins / Phthalocyanines / Self-assembly / Axial coordination / Zinc

Molecular assemblies of *meso*-pyridylporphyrins and zinc(II) 1,8,15,22-tetrakis(3-pentyloxy)phthalocyanine held through axial coordination are reported. Their formation has been revealed by ^{1}H NMR spectroscopy and photophysical measurements.

Introduction

Photo-induced electron- and energy-transfer in noncovalently bonded supramolecular assemblies has been studied extensively with the primary aim of harvesting solar energy and gaining a better understanding of photosynthesis, which is a marvellous but highly complex biological process.[1] Noncovalent assemblies containing porphyrins are of special importance because of their resemblance to nature, which also relies on supramolecular methods of assembly,[2] and the rich redox and photochemistry of this intriguing class of pigments.[3] Numerous porphyrin systems linked to a variety of electron acceptors, in particular quinone[4] and C_{60} derivatives,[5] have been examined. Supramolecular aggregates involving phthalocyanines, however, have received little attention despite the fact that these tetrapyrrole derivatives also exhibit fascinating physico-chemical properties.[6] Arrays of mixed porphyrin and phthalocyanine are mainly confined to the few examples of covalently linked systems,[7,8] sandwich-type complexes,[9] and face-to-face aggregates held by electrostatic interactions.[8] We describe herein the first edge-to-face arrays assembled through axial ligation of pyridyl substituents in porphyrins to zinc phthalocyanines. Although it is well-known that pyridine can relieve the extent of aggregation of zinc phthalocyanines (probably via axial coordination[10]) and that the formation of edge-to-face assemblies of the zinc(II) tribenzo(pyridino)porphyrazine has been inferred,[11] there has been a shortage of concrete experimental evidence supporting the axial coordination of zinc phthalocyanines which forms the basis of this work.[12]

Results and Discussion

The *meso*-tetra(4-pyridyl)porphyrin (**1**) and 1,8,15,22-tetrakis(3-pentyloxy)phthalocyaninatozinc(II) (**2**) were selected to construct multi(tetrapyrrole) arrays as the former is an excellent square-shaped building block[13] and the latter gives distinct and well-resolved ^{1}H NMR spectra, which facilitates the spectral analysis.[14] Figure 1 shows the ^{1}H NMR spectral changes of these macrocycles upon complexation. It can be seen that by adding one equiv. of **2** to **1** in $CDCl_3$, the three sets of aromatic signals for **2** experience a downfield shift ($\Delta\delta = 0.32$ for H_a, 0.11 for H_b, 0.10 for H_c), retaining the original multiplicity [Figure 1 (b) and (c)]. The multiplets for the 3-pentyloxy substituents (not shown) are also shifted downfield by ca. 0.1−0.2 ppm. The signals for the β-pyrrole, pyridyl and N−H protons of **1**, however, are shifted upfield and become broad [Figure 1 (a) and (c), the N−H band shifts from $\delta = -2.92$ to -3.03]. The broad signal at $\delta = 8.44$ is tentatively assigned to the β-pyrrole protons, while the broad band at $\delta = 7.70$ and the very weak tail around the solvent peak may be due to the pyridyl protons. These data are consistent with an edge-to-face dyad in which the phthalocyanine is deshielded by the ring current generated by the porphyrin macrocycle which falls into the shielding region of phthalocyanine. Similar spectral features have also been observed for related porphyrin aggregates.[13b,15] The broad nature of the porphyrin signals, in particular for the pyridyl protons, suggests that there is an extensive exchange between the coordinated and the free pyridyl groups. Due to the C_{4h} symmetry of the phthalocyanine, the resulting dyad does not possess an internal mirror plane, but a C_2 axis is present passing through two opposite pyridyl nitrogen atoms and the zinc(II) centre.[16] Therefore, some of the pyridyl protons become chemically equivalent and hence a restricted rotation of the pyridyl group along the C(*meso*)−C(pyridyl) bond may not contribute to the broadening of signals. Upon addition of four equiv. of **2** to **1** in $CDCl_3$, the NMR signals due to **2** are also shifted downfield to virtually the same extent, but the signals assigned to **1** are further broadened and shifted upfield [Figure 1 (d)]. This indicates that higher aggregates up to pentad [Figure 2 (a)] may be formed, which also exhibit relatively fast dynamic exchange processes.

The electronic absorption spectra of **1** (4×10^{-6} M), upon titration with **2** (from 4×10^{-6} to 2×10^{-5} M) in $CHCl_3$, and vice versa ([**2**] = 1×10^{-6} M, [**1**] from 1×10^{-6} to 1 ×

[a] Department of Chemistry, The Chinese University of Hong Kong,
Shatin, N.T., Hong Kong, China
Fax: (internat.) +852/2603−5057
E-mail: dkpn@cuhk.edu.hk

 © WILEY-VCH Verlag GmbH, D-69451 Weinheim, 2000 1434−1948/00/0808−1845 $ 17.50+.50/0

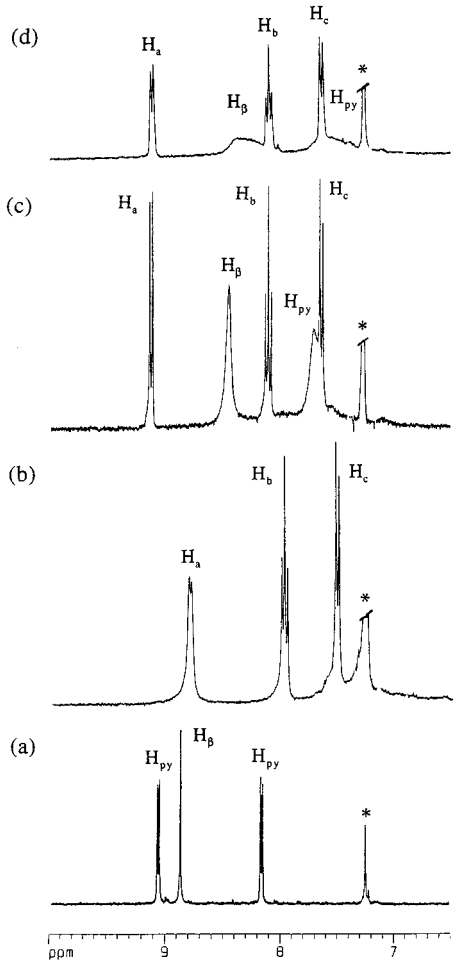


Figure 1. ^{1}H NMR spectra (aromatic region) of (a) **1**, (b) **2**, and mixtures of **1** and **2** in a (c) 1:1 and (d) 1:4 ratio in $CDCl_3$; * indicates residual solvent peak

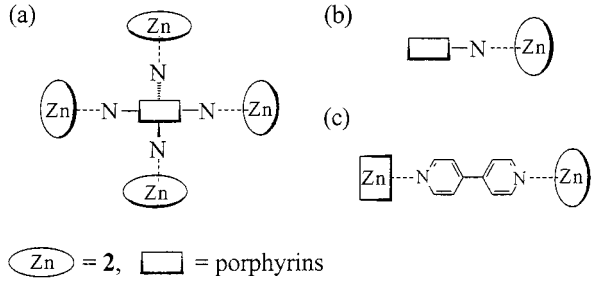
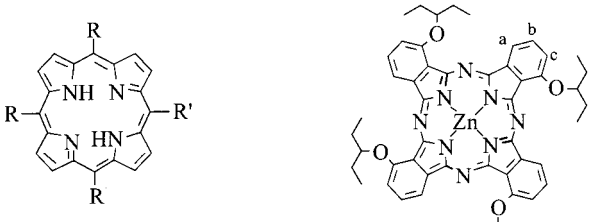


Figure 2. Schematic diagrams showing the structure of (a) **1**-(**2**)$_4$ pentad, (b) **4**−**2** dyad and (c) Zn(**5**)-bipy-**2**

10^{-5} M), remains essentially unchanged showing that the ground state π-π interactions between the perpendicularly disposed **1** and **2** are insignificant. The absence of interactions was also observed for oligoporphyrin systems linked in a similar fashion.[16] However, the fluorescence of **1** at 649 and 709 nm, upon excitation at 515 nm, diminishes gradually during titration with **2** in $CHCl_3$ (Figure 3). A similar fluorescence quenching is also observed by titrating a $CHCl_3$ solution of **2** (λ_{ex} = 615 nm, λ_{em} = 714 nm) with **1**. This mutual quenching phenomenon is likely to be due



Compound	R	R'
1	C_5H_4N	C_5H_4N
3	Ph	Ph
4	Ph	C_5H_4N
5	C_6H_4Me	C_6H_4Me

to a photo-induced electron transfer, as it is well-known that both porphyrins and phthalocyanines can act as electron donors or acceptors,[8,17] and no emission due to **2** is observed when **1** is excited which precludes an energy transfer pathway. In a control experiment, **1** was replaced with *meso*-tetraphenylporphyrin (**3**) of which the fluorescence spectra were recorded under identical conditions. There is no observable change in the fluorescence intensity of **3** upon titration with **2** which provides strong evidence for axial coordination of the pyridyl groups to the zinc(II) metal centre in **2**.

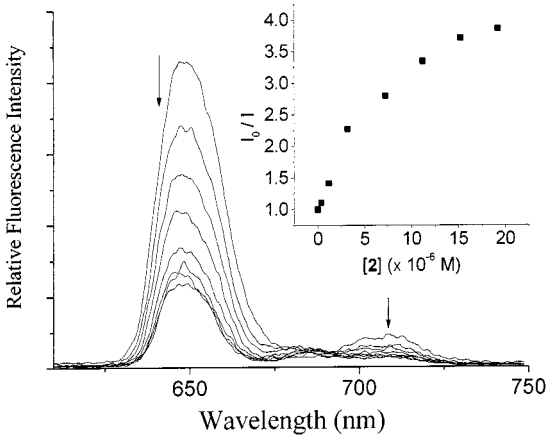


Figure 3. Fluorescence spectra of **1** (4×10^{-6} M) upon titration with **2** in $CHCl_3$. [**2**]: 0, 0.4, 1.2, 3.2, 7.2, 11.2, 15.2 and 19.2 × 10^{-6} M. The inset shows the Stern−Volmer plot for the fluorescence quenching at 649 nm

The association of *meso*-triphenyl(4-pyridyl)porphyrin (**4**) and **2** was also studied in which there is only one axial ligation [Figure 2 (b)]. Similarly, all the ^{1}H NMR signals due to **2** are shifted downfield while the signals assigned to **4** are slightly broadened and shifted upfield (see the Experimental Section). The fluorescence of **4** was also quenched by **2** and the association constant (K) for this edge-to-face dyad was determined by the Benesi−Hildebrand equation: $I_o/(I_o - I) = 1/A + 1/KA[\mathbf{2}]$, where I_o and I are the fluorescence intensity of **4** without and with the addition of **2**, respectively, and A is a constant related to the difference in the emission quantum yield of the complexed and uncomplexed **4**.[5b,18] By plotting $I_o/(I_o - I)$ vs. 1/[**2**] (Figure 4), a

perfect straight line was obtained from which the value of K was determined to be 4.2×10^4 M^{-1} which is comparable with the values reported for related porphyrin systems.[1c]

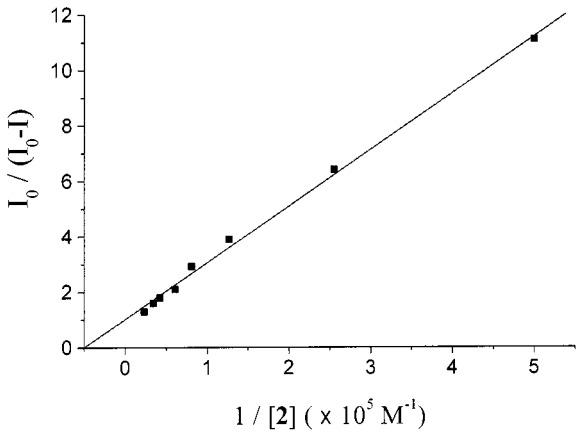


Figure 4. The Benesi−Hildebrand plot for determining the association constant between **2** and **4** (4×10^{-6} M) by fluorescence titration in $CHCl_3$

In an attempt to construct a face-to-face dyad of phthalocyanine and porphyrin linked through axial coordination, a mixture of zinc(II) *meso*-tetra(4-tolyl)porphyrin Zn(**5**), **2** and 4,4′-bipyridine (bipy) was examined. As zinc(II) tetrapyrroles normally bind to an additional ligand forming five coordinated species,[4b,13a] it was expected that apart from the hetero-dyad **2**-bipy-Zn(**5**) [Figure 2 (c)], the homo-dyads **2**-bipy-**2** and Zn(**5**)-bipy-Zn(**5**) should also be formed. Due to the presence of several dyads and the fact that some exhibit diastereomerism (those involving **2**), the ^{1}H NMR spectrum recorded in $CDCl_3$ is very complicated and cannot be unambiguously assigned. However, the formation of these face-to-face dimers is supported by the appearance of several broad bands at $\delta = 3.6-5.5$, which can be assigned to the coordinated bipy and the $OCHEt_2$ protons. The fluorescence quenching experiments provide more convincing evidence. The fluorescence intensity of Zn(**5**), when excited at 515 nm in the presence of bipy in $CHCl_3$ (both in 3.4×10^{-6} M), gradually decreases during titration with **2** (from 4.0×10^{-7} to 2.3×10^{-5} M). However, in the absence of bipy, the intensity remains relatively unchanged (Figure 5), showing that bipy plays a crucial role joining **2** and Zn(**5**) through coordination bonds.

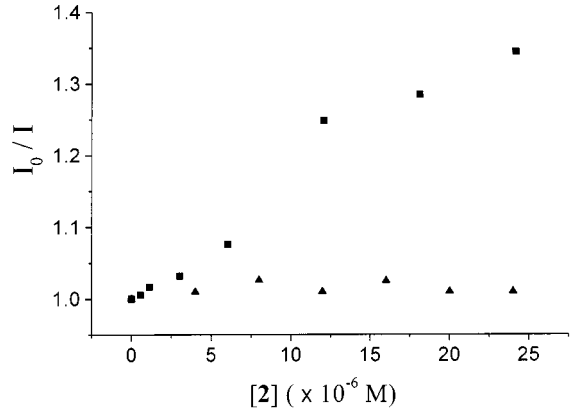


Figure 5. Stern−Volmer plots for the fluorescence quenching of Zn(**5**) by **2** with (■) or without (▲) the presence of bipy in $CHCl_3$; [Zn(**5**)] = [bipy] = 3.4×10^{-6} M

In summary, we have constructed, for the first time, assemblies of phthalocyanines and porphyrins through the relatively labile Zn(phthalocyanine)−N(pyridyl) axial ligation. Like many other supramolecules involving porphyrins, an efficient photo-induced electron transfer also occurs in these assemblies. By replacing the labile Zn^{II} ion with inert ions such as Ru^{II} and Os^{II}, it can be envisaged that more inert and diverse supramolecules based on phthalocyanines can be assembled.

Experimental Section

Compounds **2**,[14] **4**[16] and Zn(**5**)[19] were prepared by previously described methods. All other reagents and solvents were commercially available and used as received. Absorption and uncorrected fluorescence spectra were recorded on a Hitachi U-3300 spectrophotometer and a Hitachi F-4500 spectrofluorometer, respectively, both in $CHCl_3$ at ambient temperature. Phthalocyanine **2** was excited at 615 nm, while all the porphyrins were excited at 515 nm. The fluorescence intensities of porphyrins were based on the area under the fluorescence spectra in the region of 625−730 nm.

^{1}H NMR Studies: All ^{1}H NMR data were acquired on a Bruker DPX 300 (300 MHz) spectrometer at ambient temperature in $CDCl_3$, with Me_4Si as an internal standard. The concentration of **1** and **4** was kept at 0.5 mM. For a 1:1 mixture of **1** and **2**: $\delta = 9.12$ (d, $J = 7.5$ Hz, 4 H, H_a), 8.44 (br. s, 8 H, H_β), 8.09 (t, $J = 7.5$ Hz, 4 H, H_b), 7.70 (br. s, H_{py}), 7.64 (d, $J = 8.1$ Hz, 4 H, H_c), 4.88−4.94 (m, 4 H, OCH), 2.41−2.50 (m, 8 H, CH_2), 2.23−2.32 (m, 8 H, CH_2), 1.40 (t, $J = 7.5$ Hz, 24 H, CH_3), −3.03 (br. s, 2 H, NH). For a 1:4 mixture of **1** and **2**: $\delta = 9.11$ (d, $J = 7.5$ Hz, 16 H, H_a), 8.0−8.5 (br. s, H_β), 8.09 (t, $J = 7.5$ Hz, 16 H, H_b), 7.63 (d, $J = 7.8$ Hz, 16 H, H_c), 7.3−7.8 (br. s, H_{py}), 4.87−4.94 (m, 16 H, OCH), 2.40−2.47 (m, 32 H, CH_2), 2.22−2.31 (m, 32 H, CH_2), 1.40 (t, $J = 7.5$ Hz, 96 H, CH_3), −3.10 (br. s, 2 H, NH).[20] For a 1:1 mixture of **2** and **4**: δ 9.15 (d, $J = 9.0$ Hz, 4 H, H_a), 8.73−8.78 (m, 4 H, H_β), 8.60 (br. s, 2 H, H_β), 8.06−8.14 (m, 10 H, H_b & Ph), 7.63−7.74 (m, 15 H, H_c, H_β & Ph), 7.0−7.6 (br. s, 4 H, H_{py}), 4.93 (quintet, $J = 6.0$ Hz, 4 H, OCH), 2.22−2.40 (m, 8 H, CH_2), 2.42−2.56 (m, 8 H, CH_2), 1.41 (t, $J = 7.5$ Hz, 24 H, CH_3), −3.11 (br. s, 2 H, NH).

Determination of the Association Constant of the 4−2 Dyad by Fluorescence Titration: The concentration of **4** in $CHCl_3$ was kept at 4×10^{-6} M, while that for **2** was varied from 0 to 4×10^{-5} M. Upon excitation at 515 nm (where **2** has no absorption), fluorescence due to **4** was observed, and was monitored during the titration. The absorbance values at the excitation wavelength were first normalized before the fluorescence intensities were adjusted and taken. As all the absorbance values at this position were only ca. 0.1, it could be assumed that reabsorption was not significant.

Acknowledgments

This work was supported by the Research Grants Council of the Hong Kong Special Administrative Region, China (RGC ref. No. CUHK 4117/98P) and The Chinese University of Hong Kong (for partial support for a postdoctoral fellowship to XL).

[1] [1a] A. Harriman, J.-P. Sauvage, *Chem. Soc. Rev.* **1996**, 41−48. − [1b] T. Hayashi, H. Ogoshi, *Chem. Soc. Rev.* **1997**, *26*,

355−364. − [1c] M. D. Ward, *Chem. Soc. Rev.* **1997**, *26*, 365−375. [1d] M. Freemantle, *Chem. Eng. News* October 26, **1998**, 37−46. − [1e] P. Piotrowiak, *Chem. Soc. Rev.* **1999**, *28*, 143−150.

[2] K.-H. Rhee, Ed P. Morris, D. Zheleva, B. Hankamer, W. Kühlbrandt, J. Barber, *Nature*, **1997**, *389*, 522−526.

[3] K. Kalyanasundaram, *Photochemistry of Polypyridine and Porphyrin Complexes*, Academic Press, London, **1992**.

[4] See for example: [4a] H. Kurreck, M. Huber, *Angew. Chem. Int. Ed. Engl*. **1995**, *34*, 849−866 and references cited therein. − [4b] H. Imahori, K. Yamada, E. Yoshizawa, K. Hagiwara, T. Okada, Y. Sakata, *J. Porphyrins Phthalocyanines* **1997**, *1*, 55−66. − [4c] A. G. Hyslop, M. J. Therien, *Inorg. Chim. Acta*, **1998**, *275−276*, 427−434.

[5] See for example: [5a] T. Da Ros, M. Prato, D. Guldi, E. Alessio, M. Ruzzi, L. Pasimeni, *Chem. Commun*. **1999**, 635−636. − [5b] N. Armaroli, F. Diederich, L. Echegoyen, T. Habicher, L. Flamigni, G. Marconi, J.-F. Nierengarten, *New J. Chem*. **1999**, 77−83. − [5c] F. D'Souza, G. R. Deviprasad, M. S. Rahman and J.-p. Choi, *Inorg. Chem*. **1999**, *38*, 2157−2160.

[6] *Phthalocyanines − Properties and Applications* (Eds.: C. C. Leznoff, A. B. P. Lever), VCH, New York, **1989**, vol. 1; **1993**, vol. 2; **1993**, vol. 3; **1996**, vol. 4.

[7] [7a] N. Kobayashi, Y. Nishiyama, T. Ohya, M. Sato, *J. Chem. Soc., Chem. Commun*. **1987**, 390−392. − [7b] N. Kobayashi, T. Ohya, M. Sato, S.-i. Nakajima, *Inorg. Chem*. **1993**, *32*, 1803−1808. − [7c] X. Li, Q. Zhou, H. Tian, H. Xu, *Chin. J. Chem*., **1998**, *16*, 97−109. − [7d] J. Li, J. R. Diers, J. Seth, S. I. Yang, D. F. Bocian, D. Holten, J. S. Lindsey, *J. Org. Chem.* **1999**, *64*, 9090−9100. − [7e] J. Li, J. S. Lindsey, *J. Org. Chem.* **1999**, *64*, 9101−9108. − [7f] S. I. Yang, J. Li, H. S. Cho, D. Kim, D. F. Bocian, D. Holten, J. S. Lindsey, *J. Mater. Chem.* **2000**, *10*, 283−296.

[8] T.-H. Tran-Thi, *Coord. Chem. Rev.* **1997**, *160*, 53−91.

[9] [9a] D. K. P. Ng, J. Jiang, *Chem. Soc. Rev.* **1997**, *26*, 433−442. − [9b] J. W. Buchler, D. K. P. Ng, in *The Porphyrin Handbook* (Eds.: K. M. Kadish, K. M. Smith, R. Guilard), Academic Press, San Diego, **2000**, vol. 3, chapter 20.

[10] [10a] D. K. P. Ng, Y.-O. Yeung, W. K. Chan, S.-C. Yu, *Tetrahedron Lett*. **1997**, *38*, 6701−6704. − [10b] W.-F. Law, K. M. Lui, D. K. P. Ng, *J. Mater. Chem.* **1997**, *7*, 2063−2067.

[11] M. J. Cook, A. Jafari-Fini, *J. Mater. Chem*. **1997**, *7*, 2327−2329.

[12] It has recently been reported that azaferrocene quenches the fluorescence of sulfonated zinc(II) phthalocyanine in dimethyl sulfoxide in which a phthalocyanine-azaferrocene adduct linked through axial coordination may be involved (see J. Delaire, C. Giannotti, J. Zakrzewski, *J. Photochem. Photobiol. A: Chem*. **1998**, *112*, 205−207).

[13] [13a] R. K. Kumar, I. Goldberg, *Angew. Chem. Int. Ed. Engl*. **1998**, *37*, 3027−3030 and references cited therein. − [13b] A. Prodi, M. T. Indelli, C. J. Kleverlaan, F. Scandola, E. Alessio, T. Gianferrara, L. G. Marzilli, *Chem. Eur. J.* **1999**, *5*, 2668−2679.

[14] K. Kasuga, K. Asano, L. Lin, T. Sugimori, M. Handa, K. Abe, T. Kikkawa, T. Fujiwara, *Bull. Chem. Soc. Jpn*. **1997**, *70*, 1859−1865.

[15] [15a] K. Funatsu, A. Kimura, T. Imamura, A. Ichimura, Y. Sasaki, *Inorg. Chem.* **1997**, *36*, 1625−1635. − [15b] S. L. Darling, C. C. Mak, N. Bampos, N. Feeder, S. J. Teat, J. K. M. Sanders, *New J. Chem.* **1999**, *23*, 359−364.

[16] N−H exchange in free-base porphyrins is normally rapid on the NMR timescale at room temperature, see for example: N. Kariya, T. Imamura, Y. Sasaki, *Inorg. Chem*. **1997**, *36*, 833−839.

[17] No attempt was made to calculate the free energy change for both processes using the Rehm−Weller equation (D. Rehm, A. Weller, *Isr. J. Chem*. **1970**, *8*, 259) as electrochemical potentials of phthalocyanines are invariably erroneous due to the aggregation phenomena (see for example: H. Isago, C. C. Leznoff, M. F. Ryan, R. A. Metcalfe, R. Davids, A. B. P. Lever, *Bull. Chem. Soc. Jpn*. **1998**, *71*, 1039−1047).

[18] H. A. Benesi, J. H. Hildebrand, *J. Am. Chem. Soc*. **1949**, *71*, 2703−2707.

[19] G. H. Barnett, M. F. Hudson, K. M. Smith, *J. Chem. Soc., Perkin Trans. 1* **1975**, 1401−1403.

[20] Some of the pyridyl and β protons' signals of **1** were so broad that the integration could not be determined accurately.

Received December 2, 1999
[I99434]

1,2-Bis(trimethylsilyl)hydrazido Titanium Complexes

Brigitte Goetze,[a] Jörg Knizek,[a][+] Heinrich Nöth,[a][+] and Wolfgang Schnick*[a]

Keywords: Bis(trimethylsilyl)hydrazine / Hydrazido complexes / Nitrides / Titanium / Tris(trimethylsilyl)hydrazine

The silylhydrazido titanium complexes $[Cl_2Ti\{N_2H(SiMe_3)_2\}_2]$ (**1**), $[ClTi\{N_2H(SiMe_3)_2\}_3]$ (**2**), and $[(Cl_2Ti)_2\{N_2(SiMe_3)\}_2]$ (**3**) have been synthesized by reactions of the appropriate (trimethylsilyl)hydrazines with $TiCl_4$ in solution. The reactions are driven by the elimination of Me_3SiCl or LiCl after the dilithiation of bis(trimethylsilyl)hydrazine. According to NMR, mass spectrometry, and X-ray structure determination, products **1** and **2** are formed by the reaction of one equivalent of $TiCl_4$ with two or three equivalents of hydrazine, whereas compound **3** results from the reaction of two equivalents of $TiCl_4$ with two equivalents of hydrazine. According to the results of single-crystal X-ray diffraction investigations, complexes **1** and **3** feature an η^2-coordination of the hydrazido moiety to the titanium. In the crystals of **3**, both a chair and a twist form of the six-membered TiN_2TiN_2 rings are found, corresponding to different donor coordination modes of the hydrazido ligands to titanium. Temperature-dependent ^{29}Si NMR investigations indicate that both coordination modes co-exist in solution at low temperatures, but not at room temperature.

Introduction

In the context of the search for molecules with nitrido bridges between main group elements and transition metals, we have investigated the reactions of silazanes with various metal chlorides.[1−3] The obtained compounds have been studied with regard to their applicability as molecular precursors for the synthesis of solid-state materials of the M/Si/N system. A highly desirable property of these precursor compounds would be an ability to maintain either particular structural elements or a specific Si:M molar ratio during the transformation from the molecule to the solid-state compound. This approach has been elegantly applied for the synthesis of the nitride $SiPN_3$ starting from molecular $Cl_3SiNPCl_3$.[4]

Recently, we have extended our studies to titanium complexes of silylhydrazines. In this area, Leigh et al. have previously reported the crystal structures of the hydrazido titanium complexes $[(\eta^5\text{-}C_5H_5)(\eta^2\text{-}NHNMe_2)TiCl_2]$ and $[(\eta^5\text{-}C_5H_5)(\eta^2\text{-}NPhNH_2)TiCl_2]$ and have collected analytical data pertaining to some other titanium complexes with both cyclopentadienyl and hydrazido ligands.[5] Recently, Park et al. synthesized further cyclopentadienyl-substituted hydrazido titanium complexes with the aim of generating new Ziegler−Natta catalysts.[6]

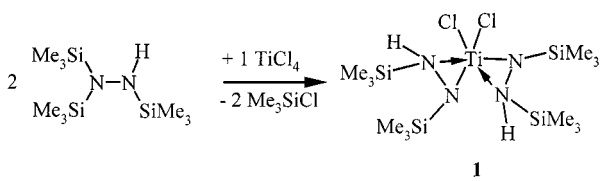
A further class of titanium complexes has been described by Winter et al. and by Mösch-Zanetti et al. Their complexes bear η^2-pyrazolato ligands rather than hydrazido ligands and no cyclopentadienyl ligands are used to stabilize them.[7,8]

We report herein on the synthesis and characterization of novel bis(trimethylsilyl)hydrazido titanium complexes without cyclopentadienyl ligands. The silylhydrazido titanium complexes $[Cl_2Ti\{N_2H(SiMe_3)_2\}_2]$ (**1**), $[ClTi\{N_2H(SiMe_3)_2\}_3]$ (**2**), and $[(Cl_2Ti)_2\{N_2(SiMe_3)\}_2]$ (**3**) have been synthesized by reaction of the appropriate silylhydrazines with $TiCl_4$. The products show η^2-coordination of the hydrazido moiety to titanium in the solid state. For **3**, both chair and twist forms of the six-membered TiN_2TiN_2 ring have been found in the solid state, corresponding to different donor coordination modes of the hydrazido ligands to titanium.

[a] Department Chemie, Ludwig-Maximilians-Universität München,
Butenandtstraße 5−13 (Haus D), D-81377 München, Germany
Fax: (internat.) +49-89/2180-7440
E-mail: wsc@cup.uni-muenchen.de
[+] Crystal structure analysis

Results and Discussion

The general synthetic approach for trimethylsilyl hydrazines is well established and some preparative methods for titanium complexes with alkyl-substituted hydrazido ligands have been described in the literature.[5,9] In order to avoid the formation of complexes with organic substituents at the metal center, we used $TiCl_4$ as the starting material. However, in several cases, we observed reduction of $TiCl_4$ by the trimethylsilylhydrazines as an unwanted side reaction. The undefined Ti^{III} species thus produced, which were deposited as green or brown precipitates, were not characterized further. Similar observations have been reported by Cotton et al., who recovered $[Ti_2Cl_9]^{3-}$ and $[Ti_3Cl_{12}]^{3-}$ from analogous precipitates.[10] In our investigations, the amorphous precipitates were carefully separated from the reaction mixtures in order to isolate the titanium hydrazido complexes without their decomposition.



1

Scheme 1. Synthesis of **1**

 © WILEY-VCH Verlag GmbH, D-69451 Weinheim, 2000 1434−1948/00/0808−1849 $ 17.50+.50/0

Reaction of $TiCl_4$ with two equivalents of 1,1,2-tris(trimethylsilyl)hydrazine, followed by elimination of two equivalents of Me_3SiCl, yielded the hydrazido titanium dichloride **1** (Scheme 1).

The elimination of Me_3SiCl could be qualitatively observed by ^{29}Si NMR spectroscopic monitoring of the reaction mixture. After the green Ti^{III} precipitate had been removed, **1** was isolated from the solution by crystallization at 0 °C. Once isolated, the crystals proved to be stable for several weeks, even at room temperature. It would seem that no intramolecular elimination of HCl or Me_3SiCl occurs, despite the fact that the relevant substituents are in close proximity in the molecule (Figure 1).

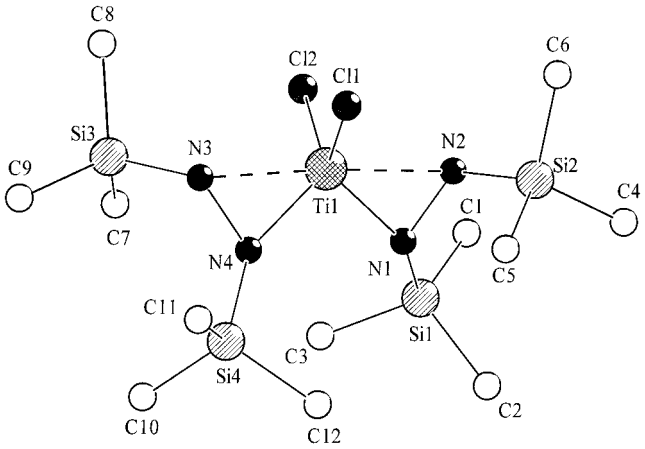


Figure 1. DIAMOND plot of the molecular structure of $Cl_2Ti[N_2H(SiMe_3)_2]_2$ (**1**)[11]

The X-ray crystal structure of **1** reveals the presence of two three-membered rings (Ti1−N1−N2 and Ti1−N4−N3) with N−N distances of 145 pm. In both cases, only one N atom (N1/N4) is actually bound to the titanium. Consequently, these N−Ti distances amount to just 189 pm, whereas the donor-coordinated N2/N3−Ti distances are about 215 pm. The corresponding bond angles are 60° at N2/N3 and 79° at N1/N4. The smallest angles are N1−Ti1−N2 and N3−Ti−N4, which measure 41° (Table 1).

The ^1H, ^{13}C, and ^{29}Si NMR spectra confirm the molecular structure of **1**. The ^{29}Si NMR spectrum shows two characteristic signals at δ = 10.15 and 23.03. The signal at δ = 10.15 can be attributed to the Si attached to the covalently bound N atom, whereas that Si bound to the NH group gives rise to a ^{29}Si NMR signal further downfield at δ = 23.03 (assigned by ^1H-coupled ^{29}Si NMR spectroscopy).

The mass spectrum clearly shows the molecular ion at m/z = 468. Mass spectrometry also revealed traces of a more volatile by-product, greater amounts of which could be generated from complex **1** and 1,1,2-tris(trimethylsilyl)hydrazine by Me_3SiCl elimination (Scheme 2). The reaction is very slow and its progress, including the elimination of Me_3SiCl, can be followed by NMR spectroscopy.

^1H, ^{13}C, and ^{29}Si NMR investigations unequivocally showed that **1** is completely transformed to **2** upon further reaction with the hydrazine. The ^{29}Si NMR spectrum of **2** features two signals at δ = 7.86 and 13.78. The signal at δ = 7.86 can be assigned to the silyl group attached to the covalently bound N atom by ^1H-coupled ^{29}Si NMR spectroscopy.

In the mass spectrum, the molecular ion of **2** (m/z = 608) could not be detected, but the fragmentation was nevertheless in accordance with the assumed composition. The calculated mass distributions of the ions at m/z = 463 and m/z = 389 correspond to the loss of two and three $SiMe_3$ groups, respectively. Unfortunately, **2** could not be obtained in crystalline form.

As known from the literature, the dilithiation of 1,1- and 1,2-substituted bis(trimethylsilyl)hydrazines invariably gives 1,2-substituted products.[12−14] Thus, after lithiation of a mixture of the bis(trimethylsilyl)hydrazines followed by treatment with $TiCl_4$, a titanium complex **3** with 1,2-substituted hydrazido ligands was obtained (Scheme 3).

In this reaction, a binuclear titanium complex is formed, in which the two N atoms of the hydrazido ligands are each bound to different Ti atoms. The X-ray crystal structure reveals that each covalently-bound N atom (e.g. N1) at one Ti atom (e.g. Ti2) is also involved in donor coordination to the other Ti atom (e.g. Ti1).

The X-ray crystal structure of **3** (Figure 2) also reveals that there are two different conformers **3a** and **3b** in the unit cell, which are present in a 1:2 molar ratio. Both of these are derived from the same six-membered ring system **3**, as shown in Scheme 3. The two conformers have the same composition and connectivity, but a different donor coordination of the N atoms to the Ti atoms (Scheme 4).

In the major conformer **3b**, both N atoms at Ti1 (N2 and N3) are involved in donor coordination to Ti2 on different sides of the ring, resulting in a twisted molecule with a twofold axis passing through Ti1 and Ti2. The second conformer **3a** has an inversion center and the N atoms coordinate on the same side of the six-membered ring with a parallel orientation of the hydrazido ligands, thereby leading to a chair conformation.

In both conformers, the Ti−Ti distances are very similar (271.7 and 271.8 pm). In both molecules, four TiN_2 three-membered rings with a covalent Ti−N bond measuring 194−198 pm and a weaker Ti−N donor bond measuring 214−228 pm are found.

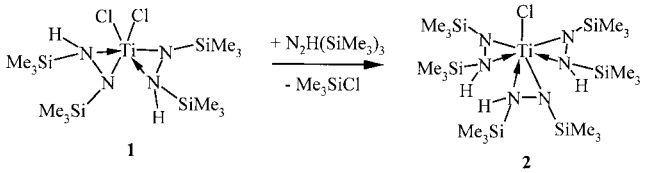
The N−N bond lengths are 136 pm in **3a** and 138 pm in **3b**. The corresponding bonding angles at titanium are about 38° in both conformers. The Ti−N−N bonding angles at the donor-coordinated N atom are about 58−63°, while the angles at the N atom closer to Ti are in the range 77−85°.

The two conformers have comparable angles and distances in their TiN_2 rings and can thus be expected to be very similar in energy. A comparison of the coordination modes of the silylhydrazines to the titanium atoms in **1**, **3a**, and **3b** likewise reveals no significant differences (Table 1).

A comparison of the structural parameters of the Ti−N−N three-membered rings in complexes **1**, **3a**, and **3b** with those of similar structural units in hydrazido titanium complexes reported in the literature[5,6] again reveals that the bond lengths and angles are all very similar, making this a characteristic structural feature.

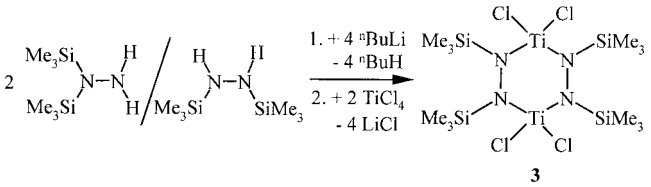
Table 1. Selected distances [pm] and angles [°] of **1**, **3a**, and **3b**; ESDs in parentheses

	1	**3a** (chair)	**3b** (twist form)
Ti−Ti	–	271.81(17), Ti3−Ti3A	271.72(11), Ti1−Ti2
N−N	146.1(5), N1−N2 145.7(6), N3−N4	136.3(5), N5−N6	138.2(5), N1−N2 137.7(5), N3−N4
N−Ti (covalent bond)	189.3(4), N1−Ti1 188.0(4), N4−Ti1	197.3(4), N5−Ti3 196.5(4), N6−Ti3A	193.6(4), N1−Ti2 194.8(4), N2−Ti1 197.9(4), N3−Ti1 198.2(4), N4−Ti2
N−Ti (donor bond)	214.0(4), N2−Ti1 215.9(5), N3−Ti1	222.0(4), N6−Ti3 219.4(5), N5−Ti3A	227.3(4), N1−Ti1 228.2(4), N2−Ti2 219.2(4), N3−Ti2 214.0(4), N4−Ti1
N−Ti−N	41.90(15), N1−Ti1−N2 41.26(16), N3−Ti1−N4	37.35(14), N5−Ti3−N6	37.25(13), N1−Ti1−N2 37.14(13), N1−Ti2−N2 38.81(13), N3−Ti1−N4 38.12(13), N3−Ti2−N4
Ti−N (covalent bond)−N	78.1, N2−N1−Ti1 79.8, N3−N4−Ti1	81.2(3), N6−N5−Ti3 80.3(3), N5−N6−Ti3A	85.1(2), N2−N1−Ti2 84.2(2), N1−N2−Ti1 76.9(2), N4−N3−Ti1 79.2(2), N3−N4−Ti2
Ti−N (donor bond)−N	60.0(2), N1−N2−Ti1 59.0(2), N4−N3−Ti1	62.0(2), N6−N5−Ti3A 61.4(2), N5−N6−Ti3	58.5(2), N2−N1−Ti1 57.7(2), N1−N2−Ti2 62.7(2), N4−N3−Ti2 64.3(2), N3−N4−Ti1



1 **2**

Scheme 2. Synthesis of **2**



3

Scheme 3. Synthesis of **3**

At room temperature, the ^{29}Si NMR spectrum of **3** features only one signal at $\delta = 24.87$. Low-temperature measurements in CD_2Cl_2 were then performed in order to ascertain whether the two conformations **3a** and **3b** co-exist in solution or only in the solid state (Figure 3).

The variable-temperature ^{29}Si NMR spectra confirm the existence of a six-membered ring without N donor coordination at room temperature. On lowering the temperature, increasing amounts of the two conformers **3a** and **3b** are formed in the solution. Two new signals appear in the spectra, downfield shifted by about 4 and 7 ppm. This downfield shift is due to the withdrawal of electron density from the N and Si atoms as a result of the donor coordination of the N atoms to the titanium. Spectral measurements in non-polar [D_8]toluene gave the same results, hence the formation of a donor complex with the solvent can be excluded. Low-temperature ^{1}H NMR spectra did not give useful results for further interpretation because the shift dif-

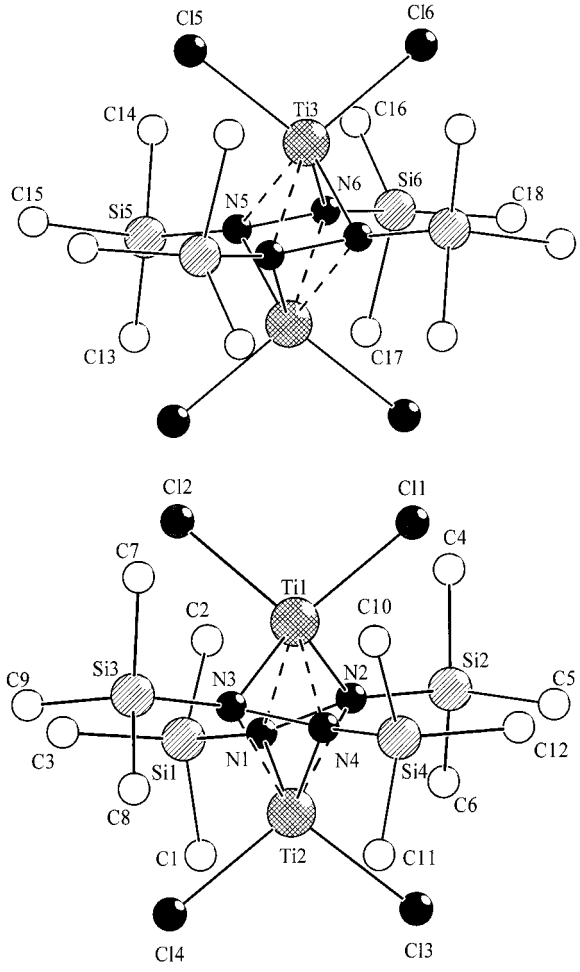
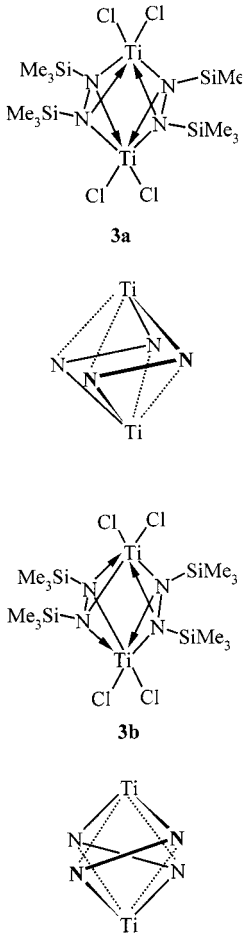


Figure 2. DIAMOND plot of the molecular structure of $(Cl_2Ti)_2[N_2(SiMe_3)]_2$ (**3a/3b**)[11]



Scheme 4. The two conformers **3a** and **3b** are found to be present in the solid

ferences of the trimethylsilyl protons in the spectra at different temperatures were too small.

Conclusion

As a common structural feature, all 1,2-bis(trimethylsilyl)hydrazido titanium complexes described in this paper have a Ti−N−Si bridge with an η^2-coordinated N−N moiety at titanium. The X-ray crystal structure of **1** reveals N atoms that are either covalently bound to Ti or coordinated to Ti through a weaker donor bond. For the two conformers of **3**, N atoms with both a covalent and a donor bond to Ti are found in the solid state. These examples show that the synthesis of a variety of related transition metal hydrazides should be possible.

Experimental Section

General Remarks: All reactions were performed under an atmosphere of dry argon. The solvents were dried by standard methods. All glassware was heated to 100 °C, evacuated, and filled with dry argon several times prior to use. NMR spectra were recorded on Jeol GSX-270 and EX-400 spectrometers at 20 °C. Chemical shifts

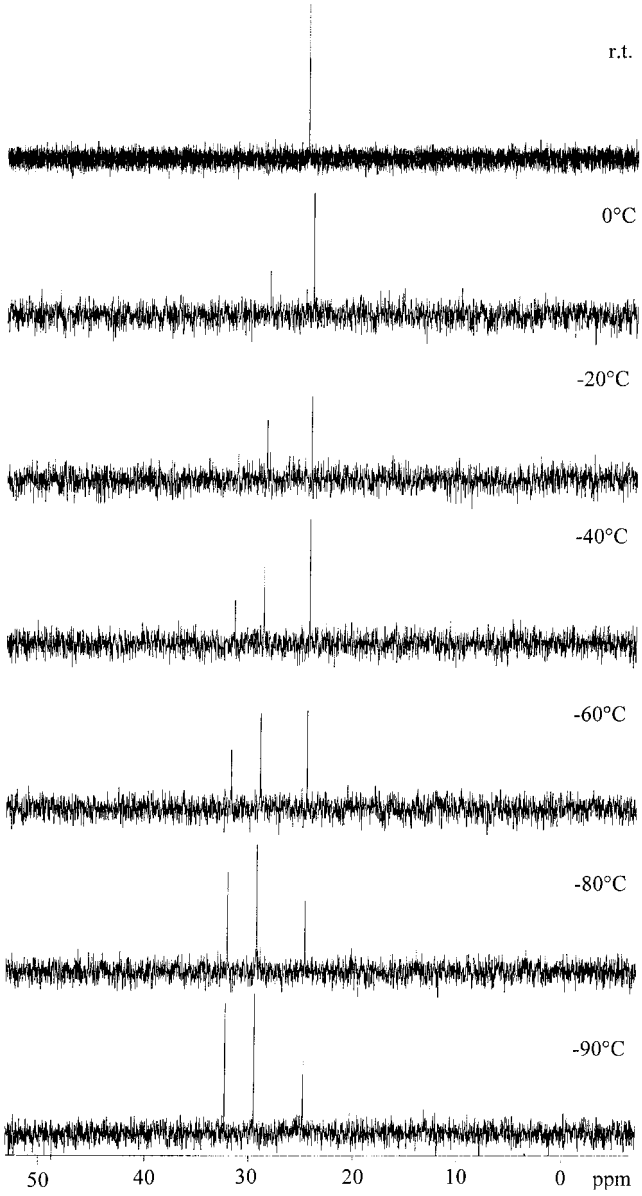


Figure 3. ^{29}Si NMR spectra of **3** at different temperatures

were determined by reference to the solvent resonances as internal standards. ^{29}Si NMR spectra were measured using the INEPT pulse sequence (TMS as external standard). Mass spectra (MS) were recorded on a Finnigan MAT spectrometer.

Elemental analysis was attempted, but due to the extreme sensitivity of the compounds the values obtained for **1** deviate from the expected composition. Likewise, it proved impossible to obtain reliable results for **2** and **3**.

Bis[*N*,*N*′-bis(trimethylsilyl)hydrazido]titanium Dichloride, $Cl_2Ti[N_2H(SiMe_3)_2]_2$ (1): 1,1,2-Tris(trimethylsilyl)hydrazine (0.70 g, 2.82 mmol) was dissolved in *n*-pentane (100 mL) at room temp. The resulting solution was cooled to −40 °C, whereupon $TiCl_4$ (0.84 mL, 0.77 mmol) was added dropwise. A green precipitate formed and the mixture was stirred at −10 °C for 2 h. The precipitate was then removed from the yellow solution by filtration and the filtrate was concentrated under reduced pressure at 0 °C. Yellowish crystals were obtained, which were recrystallized from *n*-pentane at 0 °C. The product proved to be stable under argon atmosphere at

room temp. for several weeks. Yield: 0.32 g (89%). – ^{1}H NMR ($CDCl_3$): δ = 0.23 [s, 18 H, $NSi(CH_3)_3$], 0.42 [s, 18 H, $NHSi(CH_3)_3$], 4.19 [s, 2 H, $NHSi(CH_3)_3$]. – ^{13}C NMR ($CDCl_3$): δ= –0.4 [$NSi(CH_3)_3$], 0.2 [$NHSi(CH_3)_3$]. – ^{29}Si NMR ($CDCl_3$): δ = 10.15 [$NSi(CH_3)_3$], 23.03 [$NHSi(CH_3)_3$] (assigned by ^{1}H-coupled ^{29}Si NMR spectroscopy). – MS (CI, *i*-butane): *m*/*z* (%) = 471 (9), 470 (23), 469 (12), 468 (27) [M^+], 455 (5), 453 (5) [M^+ – Me], 438 (3) [M^+ – 2 Me], 437 (8), 436 (17), 435 (47), 434 (48), 433 (91) [M^+ – Cl], 432 (32), 431 (9), 389 (6), 360 (3) [M^+ – Cl – $SiMe_3$], 228 (3), 227 (4), 192 (4), 178 (6), 177 (17), 176 (100) [$HN_2(SiMe_3)_2$ + 1], 175 (23) [$HN_2(SiMe_3)_2$], 174 (27) [$N_2(SiMe_3)_2$], 161 (5), 147 (10), 146 (60) [2$SiMe_3$], 132 (5), 130 (10). – $C_{12}H_{38}Cl_2N_4Si_4Ti$: calcd. C 30.69, H 8.16, N 11.93; found C 30.77, H 8.36, N 11.96.

Tris[*N*,*N*′-tris(trimethylsilyl)hydrazido]titanium Chloride, ClTi-[$N_2H(SiMe_3)_2$]$_3$ (2): Compound **1** (0.69 g, 1.47 mmol) and 1,1,2-tris(trimethylsilyl)hydrazine (0.75 g, 3.01 mmol) were dissolved in $CHCl_3$ (100 mL) and the mixture was refluxed for at least 16 h. The solvent and the excess tris(trimethylsilyl)hydrazine were then removed under reduced pressure to leave a brown solid. Yield: 0.77 g (86%). – ^{1}H NMR ($CDCl_3$): δ = 0.05 [s, 27 H, $NSi(CH_3)_3$], 0.11 [s, 27 H, $NHSi(CH_3)_3$], 1.24 [s, 3 H, $NHSi(CH_3)_3$]. – ^{13}C NMR ($CDCl_3$): δ = 1.8 [$NSi(CH_3)_3$], 1.9 [$NHSi(CH_3)_3$]. – ^{29}Si NMR ($CDCl_3$): δ = 7.86 [$NSi(CH_3)_3$], 13.78 [$NHSi(CH_3)_3$] (assigned by ^{1}H-coupled ^{29}Si NMR spectroscopy). – MS (CI, *i*-butane): *m*/*z* (%) = 464 (4), 463 (8) [M^+ + 1 – 2Si(Me)$_3$], 392 (9), 391 (30), 390 (40), 389 (100) [M^+ – 3$SiMe_3$], 388 (14), 387 (12), 375 (10), 374 (15), 373 (31), 358 (13), 357 (29), 341 (8), 249 (11), 248 (32) [$HN_2(SiMe_3)_3$], 233 (11), 160 (5), 147 (26), 146 (17) [2 $SiMe_3$], 145 (13), 132 (17), 130 (12).

Bis[*N*,*N*′-bis(trimethylsilyl)hydrazido]-*N*,*N*′-bis(titanium dichloride) ($Cl_2Ti)_2[N_2(SiMe_3)]_2$ (3): A mixture of 1,1-bis(trimethylsilyl)hydrazine and 1,2-bis(trimethylsilyl)hydrazine (1.39 g, 7.89 mmol) was dissolved in *n*-pentane (80 mL) at room temp. and *n*-butyllithium (9.86 mL, 15.78 mmol, 1.7 M in *n*-pentane) was added dropwise. The colorless solution rapidly became yellow and a white precipitate was deposited. After stirring for 1 h, a solution of $TiCl_4$ (0.87 mL, 7.89 mmol) in *n*-pentane (60 mL) was added dropwise at –40 °C. A green precipitate formed and the mixture was stirred at –20 °C for 2 h. The green solid was then removed from the red solution by filtration and the filtrate was concentrated under reduced pressure. Red crystals were obtained, which proved to be stable under argon atmosphere for several weeks at –20 °C. Yield: 1.64 g (71%). – ^{1}H NMR ($CDCl_3$): δ = 0.50. – ^{13}C NMR ($CDCl_3$): δ = 2.3. – ^{29}Si NMR ($CDCl_3$): δ = 24.87. – MS (CI, *i*-butane): *m*/*z* (%) = 588 (4), 586 (6) [M^+], 584 (5), 573 (3), 571 (5) [M^+ – Me], 569 (4), 551 (19) [M^+ – Cl], 549 (15), 478 (14) [M^+ – Cl – $SiMe_3$], 476 (14), 397 (13), 395 (10), 362 (13), 360 (12), 342 (76) [M^+ – 2Cl – $N_2(SiMe_3)_2$], 340 (100) [M^+ – 2 – 2Cl – $N_2(SiMe_3)_2$], 326 (14), 324 (16), 310 (9), 308 (11), 193 (5), 190 (7), 146 (16) [2 $SiMe_3$].

X-ray Crystallographic Study: All crystals had to be handled with due care under argon in a Schlenk system. The selected crystals

Table 2. Crystallographic data of **1** and **3**

Compound	**1**	**3**
Chem. formula	$C_{12}H_{38}Cl_2N_4Si_4Ti$	$C_{12}H_{36}Cl_4N_4Si_4Ti_2$
Formula weight	469.62	586.41
Cryst. size [mm^3]	0.6 × 0.15 × 0.1	0.20 × 0.20 × 0.10
Cryst. system	Monoclinic	Monoclinic
Space group	$P2_1/c$ (no. 14)	$P2_1/n$ (no. 14)
a [pm]	1186.04(4)	954.48(10)
b [pm]	1756.28(9)	4620.0(5)
c [pm]	1313.31(11)	988.20(11)
α [°]	90	90
β [°]	95.940(3)	94.194(2)
γ [°]	90	90
V [10^6 pm^3]	2721.2(3)	4346.0(8)
Z	4	6
d (calcd.) [Mg/m^3]	1.146	1.344
Radiation	Mo-K_α (graphite-monochromated) λ = 71.073 pm	Mo-K_α (graphite-monochromated) λ = 71.073 pm
μ [mm^{-1}]	0.690	1.092
F (000)	1000	1824
Index range	$-10 \le h \le 9$ $-21 \le k \le 21$ $-16 \le l \le 16$	$-12 \le h \le 12$ $-51 \le k \le 49$ $-12 \le l \le 12$
2θ [°]	3.88–55.40	3.52–55.84
T [K]	183	193
Structure solution program	SHELXL-97	SHELXL-97
No. refl. collected	13769	24498
No. refl. unique	4136	8362
No. refl. observed (4σ)	2154	4425
R (int.)	0.1018	0.0779
No. variables	213	391
Weighting scheme	$w^{-1} = \sigma^2F_0^2 + (0.0476P)^2$ $P = (F_0^2 + 2F_c^2)/3$	$w^{-1} = \sigma^2F_0^2 + (0.0491P)^2$ $P = (F_0^2 + 2F_c^2)/3$
GoF	0.776	0.963
Final *R* (4σ)	0.0510	0.0560
Final *wR*2	0.1146	0.1016
Larg. res. peak/hole [eÅ^{-3}]	0.380/–0.273	0.528/–0.659
Absorption correction	SADABS	SADABS
Max./min. transmission	1.000/0.8803	0.8986/0.8112

were covered with oxygen-free perfluoroether oil, mounted on a glass fiber, and transferred to the goniometer head of a Siemens SMART area detector. They were analyzed using graphite-monochromated Mo-K_α radiation (λ = 71.073 pm). The structures were solved by direct methods (SHELXL-97[15]; see Table 2).

Crystallographic data (excluding structure factors) for the structures reported in this paper have been deposited with the Cambridge Crystallographic Data Centre as supplementary publication nos. CCDC-140716 (**1**) and -140715 (**3**). Copies of the data can be obtained free of charge on application to the CCDC, 12 Union Road, Cambridge CB2 1EZ, U.K. [Fax: (internat.) +44-1223/336-033; E-mail: deposit@ccdc.cam.ac.uk].

Acknowledgments

Financial support by the Fonds der Chemischen Industrie and especially by the Deutsche Forschungsgemeinschaft (Schwerpunktprogramm "Nitridobrücken" and Gottfried Wilhelm Leibniz-Programm) is gratefully acknowledged. The authors would like to thank Rodica Dumitrescu and Prof. Dr. Fritz Kreißl of the Institute of Inorganic Chemistry, Technical University of Munich, for recording the mass spectra.

[1] B. Schwarze, W. Milius, W. Schnick, *Chem. Ber.* **1997**, *130*, 701−704.
[2] B. Schwarze, W. Milius, W. Schnick, *Z. Naturforsch.* **1997**, *52b*, 819−822.
[3] R. Bettenhausen, W. Milius, W. Schnick, *Chem. Eur. J.* **1997**, *3*, 1337−1341.
[4] H. P. Baldus, W. Schnick, J. Lücke, U. Wannagat, G. Bogedain, *Chem. Mater.* **1993**, *5*, 845−850.
[5] I. A. Latham, J. Leigh, *J. Chem. Soc., Dalton Trans.* **1986**, 385−391.
[6] S. B. Yoon, B.-J. Bae, I.-H. Suh, J. T. Park, *Organometallics* **1999**, *18*, 2049−2051.
[7] N. C. Mösch-Zanetti, R. Krätzer, C. Lehmann, T. R. Schneider, I. Usón, *Eur. J. Inorg. Chem.* **2000**, 13−16.
[8] C. Yélamos, M. J. Heeg, C. H. Winter, *Organometallics* **1999**, *18*, 1168−1176.
[9] K. Seppelt, W. Sundermeyer, *Chem. Ber.* **1969**, *102*, 1247−1252 and references cited therein.
[10] L. Cheng, F. A. Cotton, *Polyhedron* **1998**, *21*, 3727−3734.
[11] DIAMOND 2.1c, CRYSTAL IMPACT, K. Brandenburg & M. Berndt GbR, Postfach 1251, D-53002 Bonn, Germany, **1999**.
[12] N. Wiberg, E. Weinberg, W.-C. Joo, *Chem. Ber.* **1974,** *107*, 1764−1766 and references cited therein.
[13] C. Drost, C. Jäger, S. Freitag, U. Klingebiel, M. Noltemeyer, G. M. Sheldrick, *Chem. Ber.* **1994**, *127*, 845−847.
[14] H. Nöth, H. Sachedev, M. Schmidt, H. Schwenk, *Chem. Ber.* **1995**, *128*, 105−113.
[15] G. M. Sheldrick, *SHELXL-97*, University of Göttingen, **1997**.
Received February 29, 2000
[I00075]

Reversible Formation of a Cationic Palladium(II) Hydride $[HPd(PPh_3)_2]^+$ in the Oxidative Addition of Acetic or Formic Acid to Palladium(0) in DMF

Christian Amatore,*[a] Anny Jutand,*[a] Gilbert Meyer,[a] Italo Carelli,[b] and Isabella Chiarotto[b]

Keywords: Palladium / Formic acid / Acetic acid / Oxidative addition / Hydrido complex

The oxidative addition of acetic or formic acid to $Pd^0(PPh_3)_4$ in DMF affords a cationic palladium(II) hydride, [*trans*-$HPd(PPh_3)_2(DMF)]^+$, with acetate or formate as the counter anion. The two reactions are reversible. The equilibrium and kinetic constants of the oxidative additions have been determined.

Introduction

Many palladium-catalyzed reactions are initiated by the reaction of a palladium(0) complex with an acidic derivative.[1] Such reactions include: i) cycloisomerization of enynes,[1,2] ii) hydrocarbonylation and hydrocarboxylation of alkynes,[3] iii) isomerization of alkynes to 1,3-dienes,[1][2a] iv) hydrocarbonylation of aryl halides.[4] In all these reactions, the catalytic cycle is considered to be induced by a hydridopalladium complex formed by reaction of the palladium(0) complex and the acidic derivative.[1,5] This hydridopalladium complex undergoes *syn* addition to an alkyne (hydropalladation) which generates a vinylpalladium(II) complex, a key intermediate for further reactions. This reaction has been used for the synthesis of vinylpalladium(II) intermediates as an alternative to the oxidative addition of vinyl halides to palladium(0) complexes.[6] When the acidic derivatives are strong acids (e.g. HBF_4, HCl, CF_3CO_2H, HOTs), the hydridopalladium formation may be regarded as the protonation of basic Pd^0 to afford $HPdL_n^+$ complexes ($HPdL_3^+$ [7] or $HPdL_2S^+$,[8] S = solvent) [Equation (1)].

$$H^+ + Pd^0L_{n'} \rightarrow HPdL_n^+ + (n'-n)L \quad (1)$$

The palladium may then be considered as either Pd^0 ligated by a proton or as Pd^{II} ligated by a hydride,[5] albeit that the very negative shift of the ^1H NMR signal is more indicative of a hydride linked to a palladium(II) center. This is why this reaction is also considered as an oxidative addition.[5]

When weak carboxylic acids are involved (e.g. acetic acid,[1,2,3a,3d] formic acid[3b]), the reaction is regarded as an oxidative addition, i.e., insertion of palladium(0) into the H−X bond [Equation (2)].[1,5]

$$HX + Pd^0L_{n'} \rightarrow HPd^{II}XL_n + (n'-n)L \quad (2)$$

It is not clear whether the X anion remains ligated to the palladium(II) center or not. For example, for acetic acid, the palladium hydride was initially postulated as being $HPd(OAc)L_n$[2] but more recently as $HPdL_n^+$.[1] To date, none of these complexes have been characterized.[1]

$HPdXL_2$ intermediates are also formed in palladium-catalyzed Heck reactions involving aryl halides ArX,[9,10] as the product of a β-hydride elimination of the σ-organopalladium(II) halide complex, which also generates the arylated olefin. The base-promoted recycling of $HPdXL_2$ to Pd^0L_2, which completes the catalytic cycle, is considered as a reductive elimination, i.e., the reverse of the oxidative addition of HX to a Pd(0) complex. $HPdXL_2$ complexes are key intermediates in Heck reactions since re-addition of these complexes to the double bond after arylation is the origin of double bond isomerization.[9,10] In the presence of Ag^+ [11,12] or Tl^+ [13] cations able to capture the halide, a cationic complex $HPdL_2^+$ may also be formed when aryl triflates are used[14,15] due to the triflate anion's low affinity for palladium(II) complexes.[15,16] In such cases, re-addition of $HPdL_2^+$ to the olefin after arylation may not take place.[15] This is one explanation, among others, for the better regioselectivity generally observed when Heck reactions are performed under ionic conditions.[12,13]

In our attempts to define the mechanism of the palladium-catalyzed electro-hydrocarbonylation of aryl iodides to aryl aldehydes, performed in the presence of formic acid,[4] we established that the catalytic cycle was initiated by the reversible oxidative addition of formic acid to a palladium(0) complex to afford a cationic hydride complex $HPdL_2^+$ together with formate anions.[4] We now report some more details of this reaction and on its extension to acetic acid.

[a] Ecole Normale Supérieure, Département de Chimie, UMR CNRS 864024,
Rue Lhomond, F-75231 Paris Cedex 5, France
Fax: (internat.) + 33-14/432-3325
E-mail: amatore@ens.fr and Anny.Jutand@ens.fr
[b] Universita degli Studi "La Sapienza", Dipartimento di Ingegneria Chimica dei Materiali delle Materie Prime e Metallurgia 7,
via Castro Laurenziano, I-00185 Rome, Italy

 © WILEY-VCH Verlag GmbH, D-69451 Weinheim, 2000 1434−1948/00/0808−1855 $ 17.50+.50/0

Results and Discussion

Evidence for the Reversible Formation of a Cationic Palladium-Hydride $HPd(PPh_3)_2^+$ in the Oxidative Addition of Acetic or Formic Acid to $Pd^0(PPh_3)_4$ by Conductivity Measurements in DMF

The oxidative addition of acetic acid to $Pd^0(PPh_3)_4$ in DMF has been monitored at 25 °C by conductivity measurements. The conductivity κ of a solution of $Pd^0(PPh_3)_4$ (2 mM) increased after addition of n equivalents of acetic acid ($n > 1$) and reached a limit (Figure 1). This limiting value increased for values of n up to 100, but decreased in the presence of added PPh_3 (Figure 1).

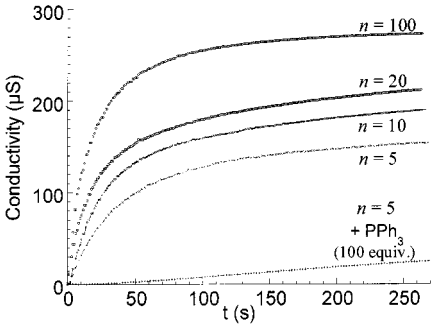


Figure 1. Conductivity measurements in DMF at 25 °C of a solution of $Pd^0(PPh_3)_4$ (2 mmol dm^{-3}) in the presence of n equivalents of acetic acid: n = 100, 20, 10, 5 in the absence of PPh_3 or in the presence of 100 equivalents of PPh_3 (when indicated)

Acetic acid is a weak acid in DMF (pK_a = 13.5).[17] Consequently, the concentration of the acetate anion and the proton is negligible compared to that of palladium(0) (2 mM). Their concentration was 8×10^{-5} mM when the acetic acid concentration reached 200 mM (n = 100). Nevertheless, the conductivity of acetic acid alone was first measured. It varied linearly with the square root of the acetic acid concentration, as expected for a weak acid. It varied from 1.7 to 6.9 μS when n was varied from 5 to 100 equivalents, respectively, so that the intrinsic conductivity of acetic acid was always negligible compared to that observed when acetic acid was added to $Pd^0(PPh_3)_4$ (Figure 1).

This series of experiments is evidence that the reaction of acetic acid and $Pd^0(PPh_3)_4$ affords ionic species which are involved in an equilibrium with the palladium(0) complex and acetic acid. PPh_3, whose overall effect is to decrease the concentration of the ionic species,[18] is then involved in the reverse reaction of this equilibrium. Since $Pd^0(PPh_3)_3$ is the major complex in solution [Equation (3)],[19] the observed overall equilibrium is described in [Equation (6)]. The inhibiting effect of PPh_3 strongly suggests that $Pd^0(PPh_3)_2$ participates in the reaction [Equations (4)−(5)], as in usual oxidative additions.[20] The mechanism of the oxidative addition of acetic acid to $Pd^0(PPh_3)_4$ may then be represented as in Equation (3) to (6) [reaction of $Pd^0(PPh_3)_4$ and acetic acid], in which the structure of the cationic complex has been established by spectroscopic techniques (vide infra).

$$Pd^0(PPh_3)_4 \rightleftharpoons Pd^0(PPh_3)_3 + PPh_3 \quad (3)$$

$$Pd^0(PPh_3)_3 \rightleftharpoons Pd^0(PPh_3)_2 + PPh_3 \quad (4)$$

$$Pd^0(PPh_3)_2 + CH_3CO_2H \rightleftharpoons HPd(PPh_3)_2^+ + CH_3CO_2^- \quad (5)$$

Overall equilibrium:

$$Pd^0(PPh_3)_3 + CH_3CO_2H \overset{K}{\rightleftharpoons} HPd(PPh_3)_2^+ + CH_3CO_2^- + PPh_3 \quad (6)$$

The reaction of $Pd^0(PPh_3)_4$ and formic acid was also monitored by conductivity measurements and led to similar results (Equation 7).[4]

However, the resulting solutions are less stable (the limiting value of the conductivity slightly increased with time) and the experiments have thus been performed at 0 °C. The equilibrium [Equation (7)] is fully displaced to the right-hand side in the presence of 70 equivalents of formic acid.

$$Pd^0(PPh_3)_3 + HCO_2H \overset{K}{\rightleftharpoons} HPd(PPh_3)_2^+ + HCO_2^- + PPh_3 \quad (7)$$

The molar conductances Λm have been calculated for the two complexes $[HPd(PPh_3)_2^+][CH_3CO_2^-]$ and $[HPd(PPh_3)_2^+][HCO_2^-]$ in DMF (Table 1). Their values are comparable to those reported for related complexes, e.g. $[HPd(PCy_3)_2(H_2O)^+][BF_4^-]$.[8]

Therefore, a cationic hydrido palladium(II) complex is formed by a reversible reaction starting from either acetic or formic acid.

Characterization of [*trans*-$HPd(PPh_3)_2(DMF)^+$][X^-] ($X^- = CH_3CO_2^-, HCO_2^-$)

Whereas neutral $HPdXL_2$ complexes have two coordinated phosphanes,[5] cationic palladium hydrides ligated by PPh_3 are usually characterized as three-coordinated complexes $HPdL_3^+$.[7e][7f] When cationic palladium hydrides are generated by the oxidative addition of acetic or formic acid to $Pd^0(PPh_3)_4$ in DMF, their ^{31}P NMR spectra exhibit a single signal for the ligated PPh_3 (Table 1) which is characteristic of a *trans* complex with two equivalent phosphorous, the fourth coordination site presumably being occupied by the solvent: *trans*-$HPd(PPh_3)_2(DMF)^+$. Despite the excess of PPh_3 from $Pd^0(PPh_3)_4$, the complex $HPd(PPh_3)_3^+$ is not formed in DMF. The solvent appears then to be a better ligand than a third PPh_3, presumably due to steric hindrance. This seems to be general since the oxidative addition of aryl triflates to $Pd^0(PPh_3)_4$ does not afford $ArPd(PPh_3)_3^+$, as is usually postulated, but *trans*-$ArPd(PPh_3)_2(DMF)^+$.[16]

The hydride has been characterized in both cases by its ^1H NMR signal, which has a negative chemical shift (Table 1).[21] The shifts of the ^1H and ^{31}P NMR signals for the two cationic complexes formed from either acetic acid or formic acid are very similar (Table 1) and do not depend significantly on the counter anion, acetate or formate, valid-

Table 1. Characterization of the cationic hydridopalladium(II) complex, $HPd(PPh_3)_2^+$ formed in the oxidative addition of $Pd^0(PPh_3)_4$ to acetic or formic acid in DMF (Equations 6 and 7)

L = PPh_3	Precursor	Molar conductivity (ohm^{-1} cm^2 mol^{-1})	H NMR (ppm)[a]	^{31}P NMR (ppm)[b]	E^p_{Red} (V)[c]	K/C_0[d]	k_f (M^{-1} s^{-1}) (k_b) (M^{-2} s^{-1})
$HPdL_2^+$	CH_3CO_2H	135[e] $[HPdL_2^+] + [CH_3CO_2^-]$	−7.48 (s)	20.77 (s)	−0.99[f] −0.85[g]	0.25 ± 0.01[e]	0.28[e] (560)[e]
$HPdL_2^+$	HCO_2H	110[h] $[HPdL_2^+] + [HCO_2^-]$	−7.28 (s)	20.97 (s)	−0.99[f]	0.5 ± 0.1[h]	0.012[h] (12)[h]

[a] 400 HMz; shifts are referred to TMS. Solvent: $CDCl_3$ containing 10% of DMF. − [b] 163 MHz, shifts are referred to H_3PO_4. Solvent: DMF containing 10% [D_6]acetone. − [c] Peak potentials in DMF are relative to SCE. Scan rate: 0.2 Vs^{-1} at 20 ° C. − [d] C_0 = $[Pd(PPh_3)_4]_0$ = 2 mM. − [e] 25 °C. − [f] At a carbon disk electrode. − [g] At a gold disk electrode. − [h] 0 °C. −

ating then the formulations used in Equation (6) and Equation (7).

Cyclic voltammetry, performed at a gold disk electrode, of a solution of $Pd^0(PPh_3)_4$, 2 mM in DMF (containing nBu_4NBF_4, 0.3 M) exhibits, at the gold electrode, the oxidation peak O_1 of $Pd^0(PPh_3)_3$ at + 0.057 V vs. SCE, whose peak current is proportional to the Pd^0 concentration (Figure 2a).[22]

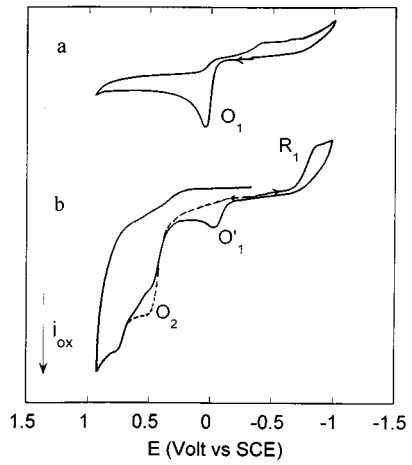


Figure 2. Cyclic voltammetry performed in DMF (containing nBu_4NBF_4, 0.3 mol dm^{-3}) at a steady gold disk electrode (0.5 mm diameter, scan rate: 0.2 V s^{-1}) at 20 °C: a) $Pd^0(PPh_3)_4$ (2 mmol dm^{-3}); b) $Pd^0(PPh_3)_4$ (2 mmol dm^{-3}) in the presence of 100 equivalents of acetic acid: (---) oxidation scan; (−) reduction scan performed first, followed by an oxidation scan

In the presence of 100 equivalents of acetic acid, the oxidation peak O_1 is no longer detected (Figure 2b, dashed voltammogram) indicating that the palladium(0) complex has undergone an oxidative addition reaction with acetic acid [Equation (6)]. The oxidation peak O_2 of the acetate anion is detected at +0.56 V. The voltammogram also exhibits a reduction peak R_1 at −0.85 V (Figure 2b, Table 1) which characterizes the reduction of the palladium(II) hydride complex formed in the oxidative addition. This reduction affords a palladium(0) complex, detected on the reverse scan by its oxidation peak O'_1 at −0.030 V (Figure 2b). Since acetate is the counter anion of the cationic palladium hydride, the reduction of $HPd(PPh_3)_2^+$ affords an anionic $Pd^0(PPh_3)_2(OAc)^-$ complex [Equation (8)].[23]

$$HPd(PPh_3)_2^+ + AcO^- + 1e \longrightarrow Pd^0(PPh_3)_2(OAc)^- + \tfrac{1}{2} H_2 \quad (8)$$

The voltammetric investigation of $Pd^0(PPh_3)_4$ in the presence of 100 equivalents of formic acid gives identical results[4] (Table 1). Whatever the precursor, acetic acid or formic acid, the same reduction peak R_1 is observed (Table 1), confirming that the same palladium hydride complex is formed in the oxidative addition of $Pd^0(PPh_3)_4$ to either acetic or formic acid [Equations (6) and (7)].

Determination of the Equilibrium and Kinetic Constants of the Oxidative Addition of $Pd^0(PPh_3)_4$ to Acetic or Formic Acid

The oxidative addition of acetic acid or formic acid to $Pd^0(PPh_3)_4$ obeys Equation (9). The equilibrium constant has been determined from the conductivity data (Figure 1).

$$Pd^0L_3 + HX \underset{}{\overset{K}{\rightleftharpoons}} HPdL_2^+ + X^- + L \quad (9)$$

L = PPh_3; HX = CH_3CO_2H, HCO_2H

Denoting x_{eq} as the equilibrium concentration ($t > 250$ s) of $HPdL_2^+$ and X^- relative to the initial concentration C_0 of $Pd^0(PPh_3)_3$, one gets [Equation (10)]:

$$K = \frac{[HPdL_2^+][X^-][L]}{[PdL_3][HX]} \qquad \frac{K}{C_0} = \frac{(x_{eq})^2(1+x_{eq})}{(1-x_{eq})(n-x_{eq})} \quad (10)$$

$x_{eq} = \kappa_{eq}/\kappa_{irrev}$; κ_{eq} = conductivity measured when the equilibrium in Equation (9) is fully established in the presence of n equivalents of HX ($t > 250$ s); κ_{irrev} = conductivity when the equilibrium in Equation (9) is totally displaced towards its right-hand side, ($n = 100$ for CH_3CO_2H and HCO_2H, $t > 250$ s). The values of K/C_0 were then calculated for acetic and formic acid from Equation (10) (Table 1).

The rate constant of the overall forward reaction [k_f in Equation (13)] has been determined in the presence of 100 equivalents of HX, so that the reverse reaction is negligible (irreversible reaction as in the uppermost curve in Figure 1).

$$Pd^0(PPh_3)_3 \underset{}{\overset{K_0}{\rightleftharpoons}} Pd^0(PPh_3)_2 + PPh_3 \quad (11)$$

$$Pd^0(PPh_3)_2 + HX \underset{k_-}{\overset{k_+}{\rightleftharpoons}} HPd(PPh_3)_2^+ + X^- \quad (12)$$

$$Pd^0(PPh_3)_3 + HX \underset{k_b}{\overset{k_f}{\rightleftharpoons}} HPd(PPh_3)_2^+ + X^- + PPh_3 \qquad K \quad (13)$$

Even under the conditions where the reaction in Equation (13) is irreversible, the PPh_3 released interferes in the mechanism through displacement of the equilibrium in Equation (11). If PPh_3 was in excess compared to $Pd^0(PPh_3)_4$, the kinetic law would simply be:

$\ln([Pd^0]_t/[Pd^0]_0) = -k_f[HX]t$

with $k_f = K_0k_+/[PPh_3]$. When starting from $Pd(PPh_3)_4$ alone, the concentration of PPh_3 is not constant [Equation (11)] and the kinetic law becomes:[22]

$2\ln([Pd^0]_t/[Pd^0]_0) - [Pd^0]_t/[Pd^0]_0 + 1 = -k_f[HX]t$

with $k_f = K_0k_+/C_0$. The value of k_f is then determined by plotting $2\ln(1 - x_t) + x_t$ *versus* time, up to 80% of conversion ($x_t = 1 - [Pd^0]_t/[Pd^0]_0$ with $x_t = \kappa_t/\kappa_\infty$; κ_t = conductivity at t; κ_∞ = final conductivity). k_f was calculated from the slope of the resulting regression line for acetic acid (Figure 3a) and formic acid (Figure 3b) (Table 1).

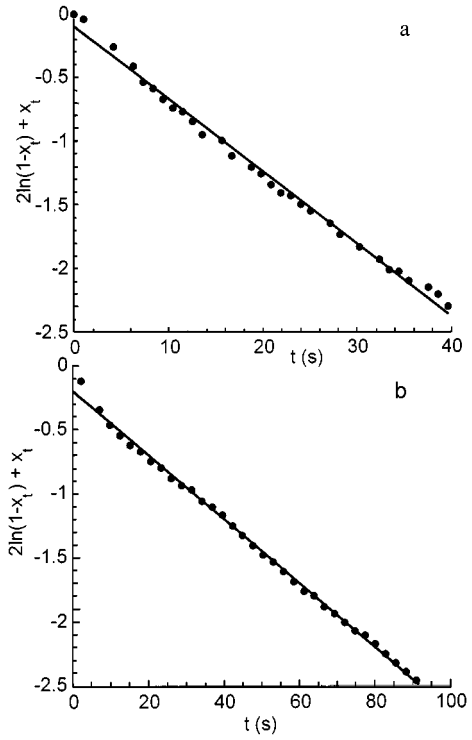


Figure 3. Kinetics of the oxidative addition of $Pd^0(PPh_3)_4$ (2 mmol dm^{-3} in DMF) under conditions where the reaction is irreversible, i.e.: a) acetic acid (0.2 mol dm^{-3}); b) formic acid (0.2 mol dm^{-3}); in both figures: plot of $2\ln(1 - x_t) + x_t$ *versus* time; $x_t = \kappa_t/\kappa_\infty$; κ_t = conductivity at t; κ_∞ = final conductivity

The value of the rate constant of the overall reverse reactions [k_b in Equation (13)] was then deduced from the equilibrium constant $K = k_f/k_b$ (Table 1).

Acetic acid is a weak acid in DMF. The concentration of the acetate anion and the proton are negligible (vide supra) compared to the palladium(0) concentration. However, this does not allow us to exclude direct protonation of $Pd^0(PPh_3)_2$. Discrimination between the two pathways: i) direct protonation of $Pd^0(PPh_3)_2$ by H^+ to form $HPdL_2^+$, or ii) oxidative addition of HX to $Pd^0(PPh_3)_2$ to form $H-Pd-XL_2$ followed by an ionization step, may be achieved by determination of the reaction order of HX under conditions where the equilibrium is totally shifted towards the cationic hydride complex (i.e. $n \geq 100$ equivalents for acetic acid, Figure 1). Indeed, a linear dependence of the observed rate constant on the acetic acid concentration would be in favor of an oxidative addition, whereas a linear dependence on the proton concentration, viz. with the square root of the acetic acid concentration, would be in favor of a protonation. The reaction of $Pd(PPh_3)_4$ with acetic acid is rather fast (Figure 1); consequently, only two concentrations of acetic acid could be tested (n = 100: k_{obs} = 0.057 s^{-1}; n = 200: k_{obs} = 0.104 s^{-1}). From these results, it ensues that the reaction order in acetic acid is close to unity, which is in favor of an oxidative addition of the H−OAc bond to palladium(0). The intermediate neutral complex, $HPdXL_2$ (X = acetate or formate) does not accumulate in the solution, thus its ionization is faster than its formation. Indeed, the kinetic curves in Figure 1, as well as those we have reported for formic acid,[4] do not exhibit any induction period which would result in a significant accumulation of such a neutral species. The degradation observed at 25 °C, when the formate anion is the counter anion, probably arises from a side reaction induced by this anion. Indeed, the intermediate neutral $HPd(OCHO)L_2$ complex is prone to undergo a well-known decarboxylation reaction[24] with formation of $HPdHL_2$, leading to H_2 and Pd^0L_2.

Conclusion

Oxidative addition of acetic acid or formic acid to a palladium(0) complex in DMF affords a cationic palladium hydride *trans*-$HPd(PPh_3)_2(DMF)^+$, with an acetate or a formate counter-anion. Both reactions are reversible and involve an unfavorable equilibrium so that a large excess of acid is required for the quantitative formation of the palladium hydride complex. This work therefore provides confirmation of the assumption made by Trost in the conclusion of one of his latest papers on this topic: "Such a species [the palladium hydride] undoubtedly is formed to some extent [from weak acids], albeit in an unfavorable equilibrium".[1]

This allows us to conclude that the catalytic reactions initiated by reaction of palladium(0) and acetic acid (or formic acid) proceed via a cationic palladium hydride *trans*-$HPd(PPh_3)_2(DMF)^+$, when they are performed in DMF.

The relative values of the kinetic constants k_f and k_b show that $HPdL_2^+$ is easily converted back to a Pd^0 complex. This reverse reaction is the step which completes the catalytic cycle of Heck reactions when they are performed under ionic conditions (from aryl triflates[14,15,25] or aryl halides in the presence of Ag^+ or Tl^+ salts[11−13,25]) with $Pd(OAc)_2$ as the palladium(0) precursor or when acetate ions are used as a base.

Experimental Section

General Remarks: ^{31}P (101 MHz) and ^{1}H (400 MHz) NMR spectra were recorded on a Bruker spectrometer. Cyclic voltammetry was performed with a home made potentiostat and wave form generator Tacussel GSTP4. The cyclic voltammograms were recorded on a Nicolet 301 oscilloscope. Conductivities were measured on a Tacussel CDM210 conductimeter (cell constant: 1 cm^{-1}).

Chemicals: DMF was distilled from calcium hydride under vacuum and kept under argon. Acetic and formic acids were obtained commercially and used as pure compounds. $Pd^0(PPh_3)_4$ was synthesized according to a reported procedure.[26]

Electrochemical Set-Up and Electrochemical Procedure for Voltammetry: Experiments were carried out in a three-electrode cell connected to a Schlenk line. The counter electrode was a platinum wire of ca. 1 cm^2 apparent surface area. The reference was a saturated calomel electrode (Tacussel) separated from the solution by a bridge filled with DMF (3 mL) containing nBu$_4$NBF$_4$ (0.3 M). DMF (12 mL) containing nBu$_4$NBF$_4$ (0.3 M) was introduced into the cell followed by $Pd(PPh_3)_4$ (28 mg, 0.024 mmol) and then 100 equivalents of acetic acid. Cyclic voltammetry was performed at a steady gold (0.5 mm diameter) or carbon (2 mm diameter) disk electrode at a scan rate of 0.2 V s^{-1}.

Acknowledgments

This work has been supported by the Centre National de la Recherche Scientifique (CNRS, UMR 8640), the Ministère de l'Education Nationale et de la Recherche et de la Technologie, and The Consiglio Nazionale delle Ricerche (CNR). Two undergraduate students T. Huy Lap and M. F. Perriot are thanked for their involvement in some of the experiments described in this work.

[1] For a recent review see: B. M. Trost, *Chem. Eur. J.* **1998**, *4*, 2405−2412.
[2] [2a] B. M. Trost, W. Pfrengle, H. Urabe, J. Dumas, *Acc. Chem. Res.* **1990**, *23*, 34−42. − [2b] B. M. Trost, D. L. Romero, F. Rise, *J. Am. Chem. Soc.* **1994**, *116*, 4268−4278.
[3] [3a] E. Drent, P. Arnoldy, P. H. M. Budzelaar, *J. Organomet. Chem.* **1993**, *455*, 247−253. − [3b] D. Zargarian, H. Alper, *Organometallics* **1993**, *12*, 712−724. − [3c] K. Huh, A. Orita, H. Alper, *J. Org. Chem.* **1993**, *58*, 6956−6957. − [3d] Y. Kushino, K. Itoh, M. Miura, M. Nomura, *J. Mol. Cat.* **1994**, *89*, 151−158.
[4] I. Carelli, I. Chiarotto, S. Cacchi, P. Pace, C. Amatore, A. Jutand, G. Meyer, *Eur. J. Org. Chem.* **1999**, 1471−1473.
[5] For a recent review on hydrido complexes of palladium, see: V. V. Grushin, *Chem. Rev.* **1996,** *96*, 2011−2033.
[6] [6a] B. M. Trost, W. Pfrengle, H. Urabe, J. Dumas, *J. Am. Chem. Soc.* **1992**, *114*, 1923−1924. − [6b] E. Negishi, L. S. Harring, Z. Owczarczyk, M. M. Mohamud, M. Ay, *Tetrahedron Lett.* **1992**, *33*, 3253−3256.
[7] [7a] M. L. H. Green, H. Munakata, *J. Chem. Soc., Chem. Commun.* **1971**, 549. − [7b] M. L. H. Green, H. Munakata, *J. Chem. Soc., Dalton. Trans.* **1974**, 269−272. − [7c] P. Meakin, R. A. Schunn, J. P. Jesson, *J. Am. Chem. Soc.* **1974,** *96*, 277−279. − [7d] R. A. Schunn, *Inorg. Chem.* **1976**, *15*, 208−212. − [7e] V. N. Zudin, V. D. Chinakov, V. M. Nekipelov, V. A. Likholobov, Y. I. Yermakov, *J. Organomet. Chem.* **1985**, *289*, 425−430. − [7f] A. R. Siedle, R. A. Newmark, W. B. Gleason, *Inorg. Chem.* **1991**, *30*, 2005−2009. − [7g] G. Verspui, I. I. Moiseev, R. A. Sheldon, *J. Organomet. Chem.* **1999,** *586*, 196−199.
[8] P. Leoni, M. Sommovigo, M. Pasquali, S. Midollini, D. Braga, P. Sabatino, *Organometallics* **1991**, *10*, 1038−1044.
[9] R. F. Heck, *Org. React.* **1982,** *27*, 345−390.
[10] W. Cabri, I. Candiani, *Acc. Chem. Res.* **1995**, *28*, 2−7.
[11] K. Karabelas, C. Westerlund, A. Hallberg, *J. Org. Chem.* **1985**, *50*, 3896−3900.
[12] M. M. Abelman, T. Oh, L. E. Overman, *J. Org. Chem.* **1987**, *52*, 4130−4133.
[13] R. Grigg, V. Loganathan, V. Santhakumar, V. Sridharan, A. Teasdale, *Tetrahedron Lett.* **1991**, *32*, 687−690.
[14] F. Ozawa, A. Kubo, Y. Matsumoto, T. Hayashi, E. Nishioka, K. Yanagi, K. Moriguchi, *Organometallics* **1993**, *12*, 4188−4196.
[15] J. M. Brown, K. K. Hii, *Angew. Chem. Int. Ed. Engl.* **1996**, *35*, 657−659.
[16] A. Jutand, A. Mosleh, *Organometallics* **1995**, *14*, 1810−1817.
[17] F. Maran, D. Celadon, M. G. Severin, E. Vianello, *J. Am. Chem. Soc.* **1991**, *113*, 9320−9329.
[18] It has been shown by ^{31}P NMR spectroscopy and conductivity measurements that the protonation of PPh_3 does not occur under our experimental conditions.
[19] B. E. Mann, A. Musco, *J. Chem. Soc., Dalton Trans.* **1968**, *14*, 5605−5614.
[20] J. F. Fauvarque, F. Pflüger, M. Troupel, *J. Organomet. Chem.* **1981**, *208*, 419−427.
[21] In $CDCl_3$, two broad ^{1}H NMR signals were observed for the hydride complex formed in the oxidative addition of formic acid to $Pd^0(PPh_3)_4$, at $\delta = -6.75$ and -7.17 (ratio: 1:1.3). This shows that some $HPd(PPh_3)_3^+$ complex was formed in $CDCl_3$. The high J(H-*trans*-P) coupling (168 Hz)[7e] results in a doublet for the hydride resonance at $\delta = -6.96$. Each signal should give a triplet due to the H-*cis*-P coupling but the two signals were too broad ($\Delta\nu_{1/2} = 81$ Hz) compared to the smaller J(H-*cis*-P) coupling constant, see ref.[7e]. After addition of DMF (10% in volume) a single broad signal ($\Delta\nu_{1/2} = 150$ Hz) is observed at $\delta = -7.28$ indicating the formation of *trans*-$HPd(PPh_3)_2(DMF)^+$.
[22] C. Amatore, A. Jutand, F. Khalil, M. A. M'Barki, L. Mottier, *Organometallics* **1993**, *12*, 3168−3178.
[23] A. Amatore, E. Carré, A. Jutand, M. A. M'Barki, G. Meyer, *Organometallics* **1995**, *14*, 5605−5614.
[24] T. Okano, N. Harada, J. Kiji, *Bull. Chem. Soc. Jpn.* **1994**, *67*, 2329−2332.
[25] A. de Mejeire, F. E. Meyer, *Angew. Chem. Int. Ed. Engl.* **1994**, *33*, 2379−2411.
[26] D. T. Rosevear, F. G. H. Stone, *J. Chem. Soc., A* **1968**, 164−167.

Received March 1, 2000
[I00078]

Si−NH−M Cage Compounds − Molecular Iminosilicates Containing Group 13 Metals and Their Functionalized Halogen Containing Derivatives

Carsten Rennekamp,[a] Peter Müller,[a] Jörg Prust,[a] Helge Wessel,[a] Herbert W. Roesky,*[a] and Isabel Usón[a]

Dedicated to Professor Jean-Marie Lehn on the occasion of his 60th birthday

Keywords: Aluminum / Gallium / Indium / Silicon / Cage compounds

The reaction of a kinetically stable triaminosilane $RSi(NH_2)_3$ (R = 2,6-*i*$Pr_2C_6H_3NSiMe_2$*i*Pr) (**1**) with trialkyl group 13 metal compounds MR_3 (R = Me, Et; M = Al, Ga, In) leads to Si–NH–M cage molecules, which increase in solubility from aluminum to indium in common weakly-coordinating organic solvents like toluene. These compounds may be regarded as model systems for group 13 metal containing iminosilicates. X-ray studies show a prismatic cage framework which is isostructural and isoelectronic with known heterosiloxanes. Further functionalization of these compounds without cleavage of the cage molecule was achieved by reaction with elemental bromine and iodine.

Introduction

The importance of nitrido silicates in materials science has been growing during the last years. New nitrido silicate structures with different compositions have been synthesized by Schnick et al. using silicondiimide $[Si(NH)_2]_x$ and various metals at high temperatures.[1] In these systems nitrogen has an important influence on the final properties of the materials, so that hardness and thermal stability are dramatically increased in comparison to the oxygen congeners.[2] Recently Jansen et al.[3] and Riedel et al.[4] reported on ternary and quaternary ceramics containing silicon, boron, nitrogen, and carbon. These systems may be regarded as nitridosilicates which are even more thermally stable than Si_3N_4.

The reaction of a stable triaminosilane $RSi(NH_2)_3$ with trialkyls of group 13 metals MR_3 (M = Al, Ga, In; R = Me, Et) leads to cage molecules which are isostructural and isoelectronic with the analogous heterosiloxanes. Consequently, triaminosilanes may be regarded as interesting precursors for developing nitrogen containing molecular silicate chemistry. The methyl groups of the aluminum compound are accessible for substitution reactions with elemental bromine and iodine. Compounds containing two and four halogen atoms were isolated without cleavage of the cage structure. The halogen containing compounds can serve as precursors for the synthesis of functionalized structures.

In this context we have prepared several ring and cage compounds using stable silanetriols as starting materials.[6] At present, little is known about soluble molecular nitrogen containing silicates. Therefore, we have focused on the synthesis of cage molecules starting from stable triaminosilanes which are easily prepared by ammonolysis of the corresponding trichlorosilanes[9−11] (Scheme 1).

$$RSiCl_3 + 6\,NH_3 \xrightarrow[-\,3\,NH_4Cl]{} RSi(NH_2)_3$$

R = 2,6-*i*$Pr_2C_6H_3NSiMe_2$*i*Pr

Scheme 1

The isoelectronic properties of the amino and hydroxy groups should lead to similar reactivities for silanetriols and triaminosilanes. This was first shown in the reaction using alumazene, where structurally similar products for both types of compounds were formed.[12]

Results and Discussion

Synthesis and Structural Properties of Triaminosilanes

Reaction of silanetriols with trialkyls of group 13 metals leads to different types of heterosiloxanes with alternating Si−O−M units e.g. ring, cubic or prismatic compounds, whereas the reaction of $AlMe_3$ with hitherto known triaminosilanes leads only to insoluble products.[13]

Replacing one methyl group of the $SiMe_3$ substituent in 2,6-*i*$Pr_2C_6H_3NSiMe_3Si(NH_2)_3$ by an isopropyl group increases the solubility of the triaminosilane and of the resulting products. The synthesis and the crystal structure of 2,6-*i*$Pr_2C_6H_3NSiMe_2$*i*$PrSi(NH_2)_3$ (**1**) has been reported.[11]

The X-ray structural analysis of **1** shows the interesting effect of this exchange on the degree of oligomerization in the crystal. Compound **1** is connected via hydrogen bonds as a tetramer, in contrast to 2,6-*i*$Pr_2C_6H_3NSiMe_3Si(NH_2)_3$ which is dimeric in the crystal structure.

Reaction of $AlMe_3$ with 1

Reaction of $AlMe_3$ with **1** in toluene at 0 °C leads to the formation of a white microcrystalline solid **2**, which has a

[a] Institut für Anorganische Chemie der Universität Göttingen
Tammannstraße 4, D-37077 Göttingen
Fax: (internat.) +49(0)−551/39−3373
E-mail: hroesky@gwdg.de

 © WILEY-VCH Verlag GmbH, D-69451 Weinheim, 2000 1434−1948/00/0808−1861 $ 17.50+.50/0

low solubility in common weakly coordinating solvents like pentane, hexane and toluene, but is soluble in coordinating solvents like tetrahydrofuran, dichloromethane or diethyl ether. Single crystals were obtained from a solution of [2,6-iPr$_2$C$_6$H$_3$NSiMe$_2$$i$PrSi(NH)$_3Al_2Me_3$]$_2$ (**2**) in a THF/hexane mixture (20:80) by evaporating the solvent over two weeks.[11]

The M_6N_6 core in the molecular structure of **2**, shown in Figure 1 can be described as a bitruncated square bipyramid. It is formed by four $SiAl_2N_3$ six-membered rings in a boat conformation, sharing the three *stern* atoms and the three *prow* atoms with each neighboring ring system. Thus, two planar four-membered $SiAlN_2$ rings are formed. In all of these rings the metal and nitrogen atoms occupy alternating sites.

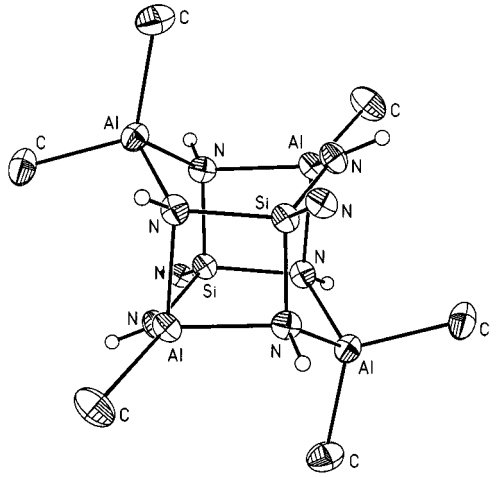
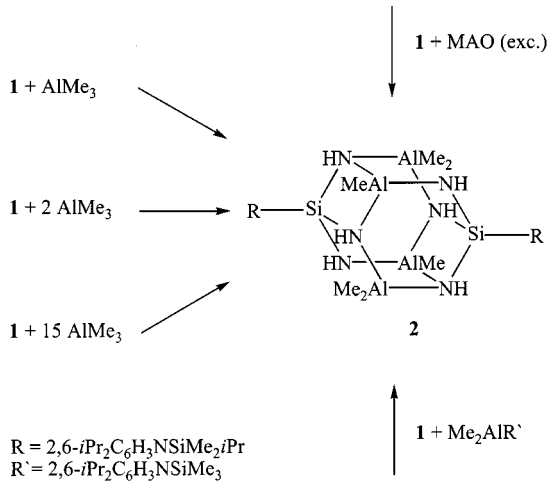


Figure 1. Central cage framework of the structure of **2** (organic substituents have been omitted for clarity)

The central framework of **2** is isostructural with the product of the reaction of diisobutyl aluminum hydride with the corresponding silanetriol.[6] In the mass spectrum the most intense peaks appear at *m*/*z* 433 (38%) and at 881 (100%) and are assigned to half of the molecular ion minus one methyl group and the molecular ion minus one methyl group respectively, which emphasizes the stability of **2** under these conditions.

Interestingly, this reaction is independent of the reaction temperature, time and the stoichiometry, but not of the solvent used. The reaction of **1** with $AlMe_3$ in different weakly coordinating solvents like hexane, pentane or toluene always gives **2**. In contrast to the corresponding silanetriol, the use of THF as solvent does not lead to a cubane but to a mixture of products, which could not be fully characterized.

The high selectivity in the formation of **2** is demonstrated in the reaction of MAO (methylaluminoxane), which contains some $AlMe_3$, and **1** to give single crystals of **2** and even the aminoalane $Me_2Al(iPr_2C_6H_3NSiMe_3)$ reacts with **1** to give **2** in high yield. The different reaction pathways are summarized in Scheme 2.



Scheme 2

Reaction of GaR_3 (R = Me, Et) and $InMe_3$ with 1

In general indiumtrialkyls show a remarkably different reaction behavior, which is due to the difference in their heats of formation and those of the corresponding aluminum and gallium compounds [$\Delta H°_f$ kJ/mol + 173 (In), −42 (Ga), −81 (Al)].[14] The comparable reaction pathways of the Al- and Ga-alkyls is indicted by the similar reaction products obtained on hydrolysis.[15]

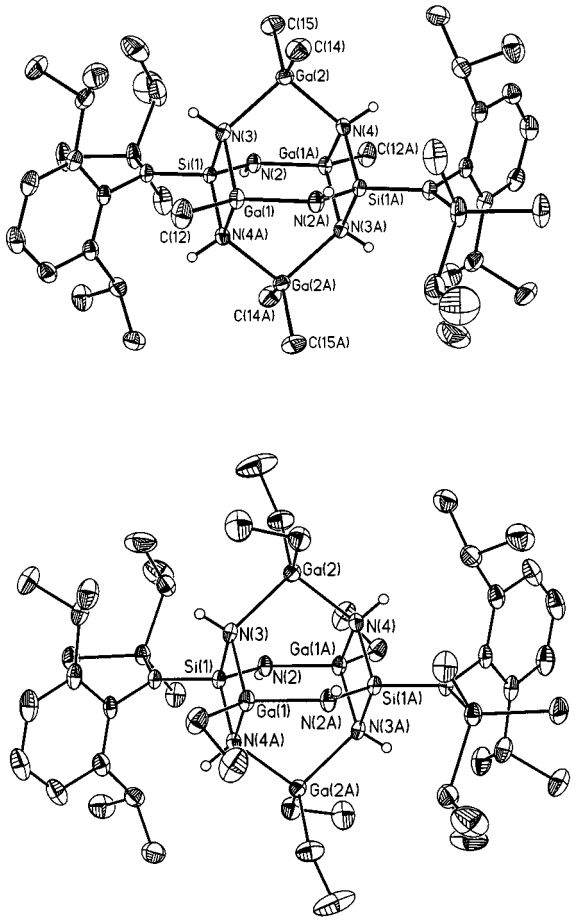


Figure 2. Crystal structures of **3** (top) and **4** (bottom) (hydrogen atoms are omitted for clarity). Selected bond lengths [pm] and angles [°] are given in Table 1. The ethyl groups in **4** are disordered

The reaction of MR_3 (M = Ga, In; R = Me, Et) with **1** in toluene at room temperature over 24 h yields a mixture of products, but heating the solutions at reflux for 1 h (in the case of the reaction of **1** with GaR_3) and 24 h (in the case of **1** with $InMe_3$) respectively leads to the formation of single crystals suitable for X-ray structural analysis. The molecular structures of $[RSi(NH)_3Ga_2Me_3]_2$ (**3**), $[RSi(NH)_3Ga_2Et_3]_2$ (**4**) and $[RSi(NH)_3In_2Me_3]_2$ (**5**) (R = 2,6-*i*$Pr_2C_6H_3$NSiMe_2*i*Pr) are shown in Figure 2 and Figure 3.

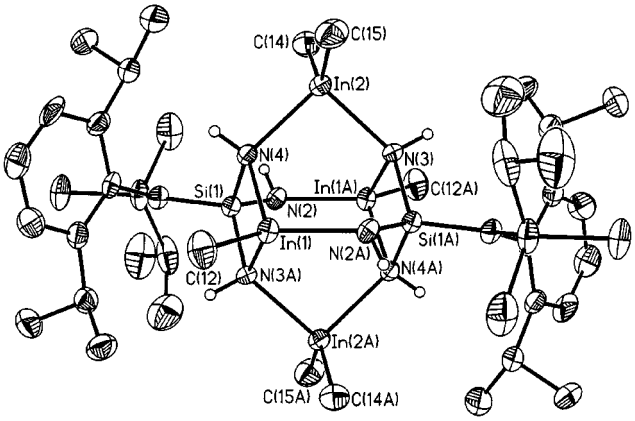


Figure 3. Crystal structure of **5** (hydrogen atoms are omitted for clarity). Selected bond lengths [pm] and angles [°] are given in Table 1

The similarity of the X-ray structures (**3**, **4**, **5**) to that of compound **2** is obvious. We preferentially describe the crystal structures of compounds **3** and **4** as representative examples for a detailed discussion of bond lengths and angles. Selected bond lengths and angles for **2**, **3, 4**, and **5** are given in Table 1. The planes described by Ga(1)Si(1)N(2)Ga(1A)-Si(1A)N(2A) and Ga(2)N(3)N(4)Ga(2A)N(3A)N(4A) form a dihedral angle of 90.7°. The N atoms can be divided into two types, having μ- and μ_3-bridging sites. The bond lengths of the μ_3-bridging N atoms are significantly longer than of the others (N(3)−Si(1) 177 pm, N(2)−Si(1) 168 pm, N(3)−Ga(1) 203 pm, N(2)−Ga(1) 189 pm). These differences and the cage constraints determine the angles in the polyhedron. Therefore the expected tetrahedral coordination spheres at N, Si and Ga are distorted. The angles within the four-membered rings vary from 80.4° to 94.6°, the angles in the six-membered rings are in the range 106.6° to 122.7°. The bond lengths and angles of **3** and **4** are equal within experimental error (Table 1). The crystallographic data of compounds **2**, **3**, **4**, and **5** are given in Table 2.

Interestingly, the mass spectral data of **3**, **4**, and **5** lead to results similar to those obtained for compound **2**, where cleavage of the cage into two monomeric species under EI-conditions is observed. However, the solution NMR spectra show a series of signals consistent with the solid state structures of **2**, **3**, **4**, and **5** respectively.

Comparison of 2, 3, 4, and 5

Trialkyls of group 13 metals react with **1** independent of stoichiometry to give the isostructural cage compounds **2**, **3, 4**, and **5**. A comparable reaction pathway for the corresponding silanetriols is not yet known, however heterosiloxanes which are isoelectronic and isostructural to **3** and **5** have been reported and underline the similar reaction behavior of **1**.

A few further observations should be briefly mentioned. All cage compounds have a remarkably high thermal stability and decompose at temperatures around 280 °C. Furthermore, their solubility increases from the aluminum to the indium compounds, which may be explained by the lower charge density at the indium centers as compared to the aluminum cage molecule. Although the reaction in coordinating solvents does not lead to the expected products, treatment of the isolated **2**, **3**, **4**, and **5** with THF, ether or dichloromethane does not result in the cleavage of the cage.

Table 1. Comparison of bond lengths [pm] and angles [°] of **2**, **3**, **4, 5**

	2 (M = Al)	**3** (M = Ga)	**4** (M = Ga)	**5** (M = In)
M(1)−N(2)	182.9(2)	189.1(2)	188.6(2)	208.8(5)
M(1)−N(3)	195.4(2)	204.4(2)	203.3(2)	223.3(6)
M(1)−N(4)	193.9(2)	200.9(2)	200.9(2)	219.9(5)
M(2)−N(4)	194.0(2)	201.1(2)	201.5(2)	220.4(5)
M(2)−N(3)	195.1(2)	202.8(2)	203.0(2)	221.2(5)
Si(1)−N(2)	168.4(2)	169.2(2)	167.9(2)	168.0(6)
Si(1)−N(3)	177.5(2)	177.4(2)	177.4(2)	175.5(5)
Si(1)−N(4)	178.0(2)	178.7(2)	177.7(2)	177.2(5)
N(2)−M(1)−N(4)	106.59(9)	106.51(8)	106.65(7)	103.1(2)
N(4)−M(1)−N(3)	82.52(8)	80.35(8)	80.44(7)	73.8(3)
N(2)−M(1)−Si(1)	114.39(7)	113.24(6)	113.20(6)	108.1(2)
N(4)−M(2)−N(3)	100.47(8)	98.43(8)	99.48(7)	95.5(2)
N(2)−Si(1)−N(3)	108.8(1)	109.1(1)	108.68(9)	109.8(3)
N(3)−Si(1)−N(4)	92.50(9)	94.48(9)	94.61(8)	97.9(3)
N(2)−Si(1)−M(1)	122.05(7)	123.91(7)	122.65(6)	126.4(2)
Si(1)−N(2)−M(1)	123.5(1)	122.8(1)	124.1(1)	125.5(3)
Si(1)−N(3)−M(2)	121.7(1)	123.2(1)	122.71(9)	128.1(3)
Si(1)−N(3)−M(1)	92.22(9)	92.12(9)	92.08(8)	93.8(2)
M(2)−N(3)−M(1)	114.16(9)	113.48(9)	112.84(8)	108.1(2)
Si(1)−N(4)−M(2)	118.5(1)	119.6(1)	119.72(9)	120.2(3)
M(1)−N(4)−M(2)	115.9(1)	114.95(9)	113.82(8)	114.9(2)

Table 2. Crystallographic data for **2**, **3**, **4, 5, 6a/6b** and **7a/7b**

	2	**3**	**4**
Formula	$C_{40}H_{84}Al_4N_8Si_4$	$C_{40}H_{84}Ga_4N_8Si_4$	$C_{46}H_{96}Ga_4N_8Si_4$
M	897.43	1068.39	1152.54
Crystal system	triclinic	triclinic	monoclinic
Space group	$P\bar{1}$	$P\bar{1}$	*C*2/*c*
Cell dimensions	*a* = 1029.6(2) pm; *b* = 1154.2(2) pm; *c* = 1206.8(2) pm; *α* = 94.86(3)°; *β* = 106.90(1)°; *γ* = 103.99(1)°	*a* = 1034.5(2) pm; *b* = 1163.1(2) pm; *c* = 1212.7(2) pm; *α* = 94.86(3)°; *β* = 106.90(1)°; *γ* = 103.99(1)°	*a* = 2368.1(6) pm; *b* = 1080.5(3) pm; *c* = 2326.6(5) pm; *β* = 102.56(2)°
Volume	1.3129(4) nm^3	1.3366(5) nm^3	5.810(3) nm^3
Z	1	1	4
δ_{calcd}	1.135 Mg/m^3	1.327 Mg/m^3	1.318 Mg/m^3
μ(Mo-K_α)	0.215 mm^{-1}	2.118 mm^{-1}	1.954 mm^{-1}
F(000)	488	560	
Crystal size [mm^3]	0.20 × 0.20 × 0.10	0.35 × 0.25 × 0.25	0.20 × 0.20 × 0.20
2θ-range	4.62 to 50.06°	3.56 to 52.86°	3.52 to 52.74°
Reflections coll	18464	13748	13287
Reflections obs.	4614 (R_{int} = 0.0397)	5437 (R_{int} = 0.0226)	5937 (R_{int} = 0.0342)
Data/restraints/parameter	4614/3/273	5437/3/273	5937/11/320
GoF on F^2	1.057	1.040	1.127
*R*1 (all data)	0.0599	0.0338	0.0360
*wR*2 (all data)	0.1072	0.0724	0.0685
Highest maximum and minimum	742 and −495 e·nm^{-3}	1889 and −993 e·nm^{-3}	370 and −555 e·nm^{-3}
	5	**6a/6b**	**7a/7b**
Formula	$C_{40}H_{84}In_4N_8Si_4$	0.78 $C_{38}H_{78}Al_4Br_2N_8Si_4$ 0.22 $C_{36}H_{72}Al_4Br_4N_8Si_4$ 0.50 C_7H_8	0.85 $C_{38}H_{78}Al_4I_2N_8Si_4$ 0.15 $C_{36}H_{72}Al_4I_4N_8Si_4$ 0.59 C_6H_6
M	1248.43	0.78 (1027.18) + 0.22 (1156.92) + 0.5 (92.14)	0.85 (1121.18) + 0.15 (1344.92) + 0.59 (78.11)
Crystal system	triclinic	monoclinic	monoclinic
Space group	$P\bar{1}$	$P2_1/n$	$P2_1/n$
Cell dimensions	*a* = 1011.6(2) pm; *b* = 1093.9(2) pm; *c* = 1335.0(2) pm; *α* = 99.08(1)°; *β* = 96.42(1)°; *γ* = 111.08(1)°	*a* = 1111.2(2) pm; *b* = 1511.3(3) pm; *c* = 1754.6(4) pm; *β* = 100.28(3)°	*a* = 1109.3(2) pm; *b* = 1508.4(3) pm; *c* = 1788.0(4) pm; *β* = 101.00(3)°
Volume	1.3352(4) nm^3	2.8993(10) nm^3	2.9369(10) nm^3
Z	1	4	2
δ_{calcd}	1.553 Mg/m^3	1.315 Mg/m^3	1.410 Mg/m^3
μ(Mo-K_α)	1.830 mm^{-1}	1.882 mm^{-1}	1.407 mm^{-1}
F(000)	632	1203	1278
Crystal size [mm^3]	0.20 × 0.20 × 0.10	0.40 × 0.40 × 0.30	0.20 × 0.10 × 0.10
2θ-range	4.38 to 46.50°	3.58 to 50.00°	4.62 to 54.00°
Reflections coll.	28307	34689	76585
Reflections obs.	(R_{int} = 0.0641)	5098 (R_{int} = 0.0445)	6399 (R_{int} = 0.0682)
Data/restraints/parameter	3842/3/273	6098/283/343	6399/167/308
GoF on F^2	1.166	1.036	1.044
*R*1 (all data)	0.0616	0.0421,	0.0619,
*wR*2 (all data)	0.1065	0.0872	0.1264
Highest maximum and minimum	2041 and −779 e·nm^{-3}	608 and −609 e·nm^{-3}	1374 and −942 e·nm^{-3}

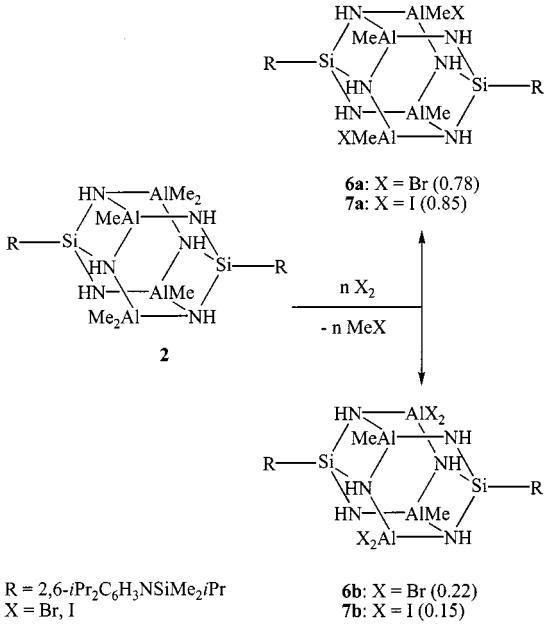
Treatment of 2 with Bromine and Iodine

A toluene solution of **2** was titrated at 0 °C with a small excess of bromine and iodine. Evaporation of the bromomethane and iodomethane, respectively, at room temperature, resulted in the formation of a mixture of products **6a/6b** and **7a/7b** (Scheme 3). Single crystals of **6a/6b** and **7a/7b** were obtained by recrystallization from warm toluene (60 °C). [16]

The solution and refinement of these structures show the presence of two different products, a mono- and a bis-halogen containing species at Al(1) and Al(1a). Molecular structures of **6a/6b** and **7a/7b** are shown in Figure 4 and Figure 5.

The halogenation has almost no influence on the prismatic core structure. Bond lengths and angles of the cages are equal within experimental error to those in **2** (see Table 1).

We observed that increasing the amount of halogen bound to the aluminum results in lower solubility, which in turn leads to preferred crystallization of the bis-halogen containing products (**6b,7b**) which have a high content in the crystal. ^{1}H NMR data and elemental analysis (of **6a/6b** and **7a/7b)** are consistent with the solid state structures,



Scheme 3

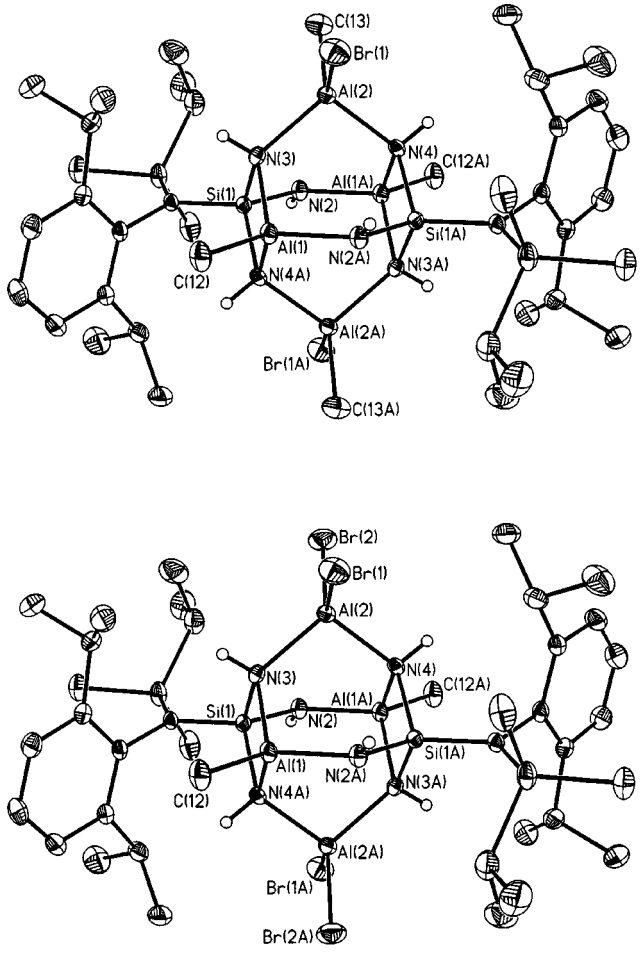


Figure 4. Crystal structures of **6a** (top) and **6b** (bottom) (hydrogen atoms are omitted for clarity). Selected bond lengths [pm] and angles [°] for **6a**: Al(2)−Br(1) 232.27(9), Al(2)−C(13) 197.1(13), C(13)−Al(2)−Br(1) 110.0(5); **6b**: Al(2)−Br(2) 220.6(5), Br(2)−Al(2)−Br(1) 113.4(2)

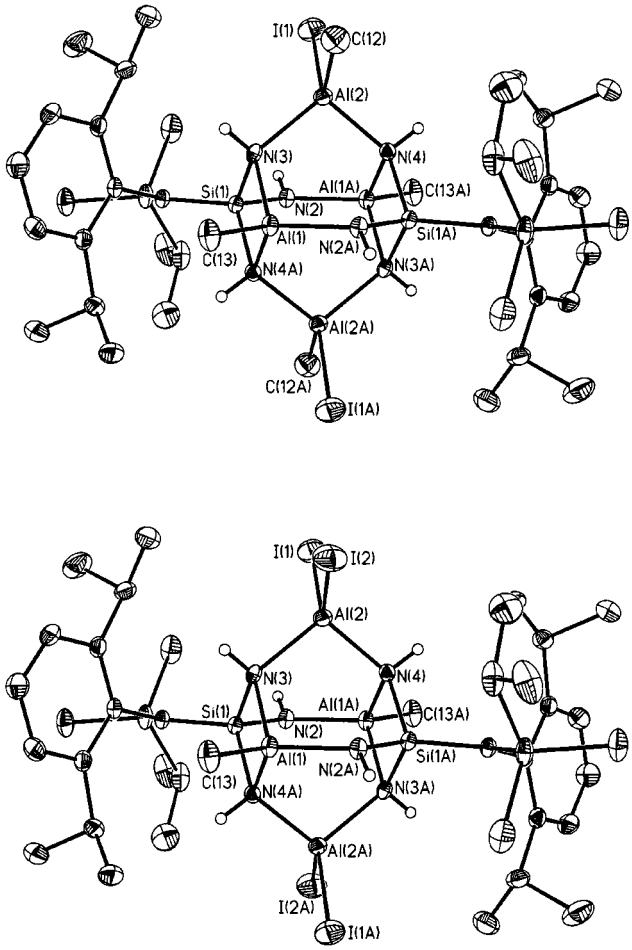


Figure 5. Crystal structures of **7a** (top) and **7b** (bottom) (hydrogen atoms are omitted for clarity). Selected bond lengths [pm] and angles [°] for **7a**: Al(2)−I(1) 257.0(1), Al(2)−C(12) 197.1(1), C(12)−Al(2)−I(1) 108.4(5); **7b:** Al(2)−I(2) 236.9(5), I(2)−Al(2)−I(1) 113.9(2)

whereas the mass spectra show several fragments which may be assigned to different halogen containing species.

The crystal structures of **6a/6b** and **7a/7b** are similar and interestingly the halogen atoms in **6a** and **7a** are located in a pseudo-trans position. At 0 °C a small excess (≈0.05 mmol) of the halogen gives the solution a characteristic color, which disappears at room temperature after 24 h. The bis-halogen containing products **6b** and **7b** are formed at higher temperatures. The second bromination step takes place at the same aluminum atom as the first, so both methyl groups at Al(1) and Al(1a) are substituted. Remarkably, only two compounds (**6a/6b**), containing two and four bromine atoms are observed, while an intermediate with three bromine atoms was not observed under these conditions.

By variation of the stoichiometry and the reaction time, we tried to synthesize the mono-, bis- and tris-bromine containing products and the related iodine compounds. X-ray structural analysis of the products showed that the crystals contain a variety of different molecules with the typical cage framework but they could not be refined, whereas under the reported reaction conditions **6a/6b** were formed several times in similar ratios.

Conclusion

By introducing a bulky substituent, we achieved to synthesize kinetically stable triaminosilanes which serve as starting materials to generate soluble iminosilicates. Based on our observations it should be possible to synthesize a variety of molecular iminosilicates and to extend this new area of chemistry. With the halogenation reaction, we present the first compounds in which there is further functionalization of the cage without cleavage of the framework. We are currently studying the use of these molecules as precursors for generating supramolecular systems under mild conditions by salt elimination reactions.

Experimental Section

General Techniques: All reactions were performed using Schlenk and dry box techniques. Solvents were appropriately dried and distilled under dinitrogen prior to use. − All NMR spectra were obtained in 5 mm tubes using dry degassed [D_8]THF as the solvent, referenced to $SiMe_4$ externally. The solubilities of the cage compounds are not sufficient for ^{13}C NMR spectroscopy. − Elemental analyses were performed by the Analytisches Chemisches Laboratorium des Instituts für Anorganische Chemie, Göttingen.

Compound **1**[11] and $GaEt_3$[17] were prepared according to literature methods. Other compounds are commercially available.

Preparation of 2 (Molar Ratio of 1 to $AlMe_3$ 1:2): A solution of $AlMe_3$ (2.3 mL, 2M in heptane) was added dropwise to a solution of **1** (0.8 g, 2.3 mmol) in toluene (20 mL) at −80 °C. As soon as gas evolution had ceased, the reaction mixture was warmed to room temperature and stirred for 12 h. The solvent was removed in vacuo and the remaining yellowish oil stirred in hexane. A white precipitate was filtered off. Compound **2** was obtained in 75% yield (0.77 g).

Preparation of 2 (Molar Ratio of 1 to $AlMe_3$ 1:1): Analogous preparation method. Yield 75%.

Preparation of 2 from 1 and $Me_2Al(iPr_2C_6H_3NSiMe_3)$: A solution of **1** (0.8 g, 2.2 mmol) in hexane (30 mL) was added dropwise to a solution of $Me_2Al(iPr_2C_6H_3NSiMe_3)$ (0.7 g, 2.2 mmol) in hexane (20 mL) at 0 °C. As soon as gas evolution had ceased, the reaction mixture was warmed to room temperature and stirred for 12 h. Finally the reaction mixture was heated to 30 °C for 1 h. The solvent was evaporated to 15 mL and the residue was filtered off. Yield 0.4 g **2** (82%).

Preparation of 2 from 1 and MAO: A solution of **1** (1.8 g, 5.1 mmol) in hexane (30 mL) was added dropwise to a solution of MAO in toluene (30.0 g, 10%, 517 mmol Al) at room temperature. The reaction mixture was stirred for 20 h. The flask was kept at room temperature for 21 d and single crystals suitable for X-ray structural analysis were formed. Yield 0.11 g **2** (5%), decomp. 280−285 °C. − ^1H NMR (200 MHz, [D_8]THF): δ = −1.37 (s, 6 H, $AlCH_3$), −0.83 [s, 12 H $Al(CH_3)_2$], 0.08 [s, 12 H, $Si(CH_3)_2iPr$], 0.89 [s, b, 6 H, $Si(NH)_3$], 1.15 [d, ^3J(H,H) = 7.1 Hz, 12 H, $CH(CH_3)_2$], 1.20 [d, ^3J(H,H) = 6.8 Hz, 12 H, $CH(CH_3)_2$], 1.32 [d, ^3J(H,H) = 6.8 Hz, 12 H, $CH(CH_3)_2$], 1.38 [sept, ^3J(H,H) = 7.1 Hz, 2 H, $CH(Me)_2$], 3.52 [sept, ^3J(H,H) = 6.8 Hz, 4 H, $CH(Me)_2$], 7.23 [s, 6 H, Ar−*H*). − IR ([cm^{-1}], KBr, Nujol): ṽ = 3407, 3345, 3328, 1383, 825, 753. − MS (EI); *m*/*z* (%): 433 (38) [1/2 M^+ − Me], 882 (100) [M^+ − Me]. − $C_{40}H_{84}Al_4N_8Si_4$ (897.43): calcd. C 52.54, H 9.44; found C 52.3, H 8.6.

Preparation of 3: A solution of $GaMe_3$ (0.53 g, 4.60 mmol) in toluene (10 mL) was added dropwise to a solution of **1** (0.80 g, 2.30 mmol) in toluene (15 mL) at room temperature. After stirring the solution for 12 h it was heated at reflux for 1 h. The reaction mixture was cooled (2 °C), and crystals suitable for X-ray structural analysis were obtained. The solvent was removed in vacuo, and the remaining solid was washed with pentane (5 mL). A colorless solid was filtered off. Yield 0.98 g (80%), decomp. 280 °C. − ^1H NMR (200 MHz, [D_8]THF): δ = −0.90 (s, 6 H, $GaCH_3$), −0.57 [s, 12 H $Ga(CH_3)_2$], 0.04 [s, 12 H, $Si(CH_3)_2iPr$], 0.82 [s, b, 2 H, Si(N*H*)GaMe], 1.05 [s, b, 4 H, $Si(NH)_2(Ga_2Me_3)_2$], 0.95 [d, ^3J(H,H) = 7.1 Hz, 12 H, $CH(CH_3)_2$], 1.05 [d, ^3J(H,H) = 6.8 Hz, 12 H, $CH(CH_3)_2$], 1.18 [d, ^3J(H,H) = 6.8 Hz, 12 H, $CH(CH_3)_2$], 1.42 [sept, ^3J(H,H) = 7.1 Hz, 2 H, $CH(Me)_2$], 3.48 [sept, ^3J(H,H) = 6.8 Hz, 4 H, $CH(Me)_2$], 7.09 (s, 6 H, Ar−*H*). − IR ([cm^{-1}], KBr, Nujol): ṽ = 3410, 3360, 3342, 1309, 827, 773. − MS (EI); *m*/*z* (%): 511 (48) [1/2 M^+ − Me], 1053 (100) [M^+ − Me]. − $C_{40}H_{84}Ga_4N_8Si_4$ (1068.39): calcd. C 44.97, H 7.92; found C 45.0, H 7.8.

Preparation of 4: A solution of $GaEt_3$ (1.07 g, 6.80 mmol) in toluene (10 mL) was added dropwise to a solution of **1** (1.20 g, 3.40 mmol) in toluene (10 mL) at room temperature, and stirred for 14 h followed by 1 h of heating at reflux. The reaction mixture was cooled to room temperature and after 24 h single crystals suitable for X-ray structural analysis were obtained. After the solvent was removed in vacuo the residue was stirred in pentane (5 mL), and a colorless solid was filtered off. Yield 1.47 g (75%), decomp. 285 °C. − ^1H NMR (200 MHz, [D_8]THF): δ = −0.05 [m, 4 H $Ga(CH_2Me)$], 0.52 [m, 8 H $Ga(CH_2Me)_2$], 0.15 [s, 12 H, $Si(CH_3)_2$-*i*Pr], 0.82 [s, b, 2 H, Si(N*H*)GaMe], 1.05 [s, b, 4 H, $Si(NH)_2(Ga_2Me_3)_2$], 1.17 [d, ^3J(H,H) = 7.1 Hz, 12 H, $CH(CH_3)_2$], 1.27 [d, ^3J(H,H) = 6.8 Hz, 12 H, $CH(CH_3)_2$], 1.41 [d, ^3J(H,H) = 6.8 Hz, 12 H, $CH(CH_3)_2$], 1.66 [sept, ^3J(H,H) = 7.1 Hz, 2 H, $CH(Me)_2$], 3.66 [sept, ^3J(H,H) = 6.8 Hz, 4 H, $CH(Me)_2$], 7.27 (s, 6 H, Ar−*H*). − IR ([cm^{-1}], KBr, Nujol): ṽ = 3411, 3360, 3342, 1363, 828, 751. − MS (EI); *m*/*z* (%): 547 (68) [1/2 M^+ − Et], 1123 (100) [M^+ − Et]. − $C_{46}H_{96}Ga_4N_8Si_4$ (1152.54): calcd. C 47.94, H 8.40; found C 48.2, H 8.20.

Preparation of 5: A solution of $InMe_3$ (0.53 g, 4.60 mmol) in toluene (10 mL) was added dropwise to a solution of **1** (0.80 g, 2.30 mmol) in toluene (15 mL) at room temperature. After stirring the solution for 1 h it was heated at reflux for 12 h. The solvent was removed in vacuo, and the remaining solid was washed with pentane (5 mL). A colorless solid was filtered off and dissolved in warm toluene (10 mL) at 60 °C. Formation of single crystals suitable for X-ray measurements was observed after 24 h. Yield 0.98 g (80%), decomp. 285 °C. − ^1H NMR (200 MHz, [D_8]THF): δ = −0.92 (s, 6 H, $InCH_3$), −0.42 [s, 12 H $In(CH_3)_2$], 0.14 [s, 12 H, $Si(CH_3)_2iPr$], 0.80 [s, b, 2 H, Si(N*H*)InMe], 1.15 [s, b, 4 H, $Si(NH)_2(In_2Me_3)_2$], 1.02 [d, ^3J(H,H) = 7.1 Hz, 12 H, $CH(CH_3)_2$], 1.05 [d, ^3J(H,H) = 6.8 Hz, 12 H, $CH(CH_3)_2$], 1.20 [d, ^3J(H,H) = 6.8 Hz, 12 H, $CH(CH_3)_2$], 1.40 [sept, ^3J(H,H) = 7.1 Hz, 2 H, $CH(Me)_2$], 3.46 [sept, ^3J(H,H) = 6.8 Hz, 4 H, $CH(Me)_2$], 7.09 (s, 6 H, Ar−*H*). − IR ([cm^{-1}], KBr, Nujol): ṽ = 3499, 3414, 3360, 1313, 802. − MS (EI); *m*/*z* (%): 609 (36) [1/2 M^+ − Me], 1233 (100) [M^+ − Me]. − $C_{40}H_{84}In_4N_8Si_4$ (1248.43): calcd. C 38.47, H 6.78; found C 38.8, H 6.8.

Preparation of 6a/6b: Bromine was added dropwise at 0 °C to a suspension of **2** (0.70 g, 0.78 mmol) in toluene (25 mL) until no color change was observed. One further drop of bromine was ad-

ded. The solution was stirred for 1 h at 0 °C. The MeBr was then removed in vacuo and the solution was allowed to warm to room temperature. Further solvent was removed (15 mL) and a white precipitate was formed, which was dissolved again by stirring the solution at 60 °C. Single crystals suitable for X-ray structural analysis were obtained after keeping the solution for 4 d at room temperature. Yield 0.39 g (43%), decomp. 295 °C. – ^{1}H NMR (200 MHz, [D$_8$]THF): (**6a**) δ = −1.07 (s, 6 H, AlCH_3), −0.83 [s, 6 H, Al(CH_3)Br], 0.10 [s, 12 H, Si(CH_3)$_2$*i*Pr], 0.76 [s, br, 6 H, Si(NH)$_3$], 1.13 [d, $^3J(H,H)$ = 7.1 Hz, 12 H, CH(CH_3)$_2$], 1.16 [d, $^3J(H,H)$ = 6.8 Hz, 12 H, CH(CH_3)$_2$], 1.32 [d, $^3J(H,H)$ = 6.8 Hz, 12 H, CH(CH_3)$_2$], 1.38 [sept, $^3J(H,H)$ = 7.1 Hz, 2 H, CH(Me)$_2$], 3.52 [sept, $^3J(H,H)$ = 6.8 Hz, 4 H, CH(Me)$_2$], 7.23 (m, 6 H, Ar−H); (**6b**) −1.17 (s, 6 H, AlCH_3), 0.08 [s, 12 H, Si(CH_3)$_2$*i*Pr], 0.89 [s, br, 6 H, Si(NH)$_3$], 1.15 [d, $^3J(H,H)$ = 7.1 Hz, 12 H, CH(CH_3)$_2$], 1.20 [d, $^3J(H,H)$ = 6.8 Hz, 12 H, CH(CH_3)$_2$], 1.40 [d, $^3J(H,H)$ = 6.8 Hz, 12 H, CH(CH_3)$_2$], 1.40 [sept, $^3J(H,H)$ = 7.1 Hz, 2 H, CH(CH$_3$)$_2$], 3.50 [sept, $^3J(H,H)$ = 6.8 Hz, 4 H, CH(CH$_3$)$_2$], 7.20 (m, 6 H, Ar−H). – IR ([cm^{-1}], KBr, Nujol): $\tilde{\nu}$ = 3408, 3348, 3330, 1381, 824, 752. – MS (EI); *m*/*z* (%): 1012 (100) [M$^+_{6a}$ − Me]; 1141 (12) [M$^+_{6b}$ − Me]. – $C_{44.56}H_{84.68}Al_4Br_{2.44}N_8Si_4$ (1101.80): calcd. C 46.58, H 9.41; found C 45.1, H 9.0.[16]

Preparation of 7a/7b: A solution of iodine in toluene (0.1 M) was added dropwise at 0 °C to a suspension of **2** (0.55 g, 0.61 mmol) in toluene (25 mL) until no color change was observed. One further drop of this solution was then added. The solution was stirred for 30 min at 0 °C and 1 h at room temperature. The MeI formed, as well as 15 mL of the solvent, were removed in vacuo and a white precipitate was formed. It was dissolved again by stirring the solution at 60 °C. Single crystals suitable for X-ray structural analysis were obtained from the solution after 4 d at room temperature. Yield 0.22 g (47%), decomp. 280−285 °C. – ^{1}H NMR (200 MHz, [D$_8$]THF): (**7a**) δ = −1.07 (s, 6 H, AlCH_3), −0.83 [s, 6 H, Al(CH_3)I], 0.10 [s, 12 H, Si(CH_3)$_2$*i*Pr], 0.76 [s, br, 6 H, Si(NH)$_3$], 1.13 [d, $^3J(H,H)$ = 7.1 Hz, 12 H, CH(CH_3)$_2$], 1.16 [d, $^3J(H,H)$ = 6.8 Hz, 12 H, CH(CH_3)$_2$], 1.32 [d, $^3J(H,H)$ = 6.8 Hz, 12 H, CH(CH_3)$_2$], 1.38 [sept, $^3J(H,H)$ = 7.1 Hz, 2 H, CH(Me)$_2$], 3.52 [sept, $^3J(H,H)$ = 6.8 Hz, 4 H, CH(Me)$_2$], 7.23 (m, 6 H, Ar−H); (**7b**): δ = −1.17 (s, 6 H, AlCH_3), 0.08 [s, 12 H, Si(CH_3)$_2$*i*Pr], 0.89 [s, b, 6 H, Si(NH)$_3$], 1.15 [d, $^3J(H,H)$ = 7.1 Hz, 12 H, CH(CH_3)$_2$], 1.20 [d, $^3J(H,H)$ = 6.8 Hz, 12 H, CH(CH_3)$_2$], 1.40 [d, $^3J(H,H)$ = 6.8 Hz, 12 H, CH(CH_3)$_2$], 1.40 [sept, $^3J(H,H)$ = 7.1 Hz, 2 H, CH(Me)$_2$], 3.50 [sept, $^3J(H,H)$ = 6.8 Hz, 4 H, CH(Me)$_2$], 7.20 (m, 6 H, Ar−H). – IR ([cm^{-1}], KBr, Nujol): $\tilde{\nu}$ = 3407, 3345, 3328, 1383, 825, 753. – MS (EI); *m*/*z* (%): 1106 (100) [M$^+_{7a}$ − Me], 1329 (6) [M$^+_{7b}$ − Me]. – $C_{41.24}H_{80.64}Al_4I_{2.30}N_8Si_4$ (1200.83): calcd. C 41.25, H 6.72; found C 40.1, H 6.3.[16]

X-ray Crystallography: Crystallographic data: Crystals were mounted on a glass fiber in a rapidly cooled perfluoropolyether.[18] Diffraction data were collected on a Stoe-Siemens-Huber four-circle-diffractometer coupled to a Siemens CCD area-detector at 133(2) K, with graphite-monochromated Mo-K_α radiation (λ = 71.073 pm).

The structures were solved by direct methods using SHELXS-97[19] and refined against F^2 on all data by full-matrix least squares with SHELXL-97.[20] All nonhydrogen atoms were refined anisotropically. In all structures the hydrogen atoms bound to N(2), N(3) and N(4) were found in the difference Fourier map and refined freely, all other hydrogen atoms were included in the model at geometrically calculated positions and refined using a riding model. The disordered ethyl groups in **4** were modeled with the help of similarity restraints for 1−2 and 1−3 distances and displacement parameters as well as rigid bond restraints for anisotropic displacement parameters. The cocrystallized products in the structures of **6a/b** and **7a/b** were treated as disorders and refined with the help of similarity and rigid bond restraints. The occupancies of **6a** and **6b** refined to a ratio of 80% to 20%, the ratio of **7a** and **7b** was found to be 85% to 15%.

Atomic coordinates, thermal parameters, bond lengths and angles have been deposited at the Cambridge Crystallographic Data Centre (CCDC). Any request to the CCDC for this material should quote the full literature citation and the reference number CCDC-140493 to CCDC-140498. Copies of the data can be obtained free of charge on application to CCDC, 12 Union Road, Cambridge CB2 1EZ, UK [Fax: (internat.) + 44-1223/336-033; E-mail: deposit@ccdc.cam.ac.uk].

Acknowledgments

We are grateful to the Deutsche Forschungsgemeinschaft, the Akademie der Wissenschaften in Göttingen, and the Witco GmbH for support of this work. C. R. is grateful to the Fonds der Chemischen Industrie for a fellowship.

[1] T. Schlieper, W. Schnick, *Z. Anorg. Allg. Chem.* **1995**, *621*, 1037−1041; T. Schlieper, W. Milius, W. Schnick, *Z. Anorg. Allg. Chem.* **1995**, *621*, 1380−1384; T. Schlieper, W. Schnick, *Z. Anorg. Allg. Chem* **1995**, *621*, 1535−1538.
[2] H. Huppertz, W. Schnick, *Angew. Chem.* **1996**, *108*, 2115−2116; *Angew. Chem. Int. Ed. Engl.* **1996**, *35*, 1983; H. Huppertz, W. Schnick, *Chem. Eur. J.* **1997**, *3*, 249−252.
[3] H.-P. Baldus, M. Jansen, *Angew. Chem.* **1997**, *109*, 338; *Angew. Chem. Int. Ed. Engl.* **1997**, *36*, 329−343.
[4] R. Riedel, A. Greiner, G. Miehe, W. Dreßler, H. Fuess, J. Bill, F. Aldinger, *Angew. Chem.* **1997**, *109*, 657−660; *Angew. Chem. Int. Ed. Engl.* **1997**, *36*, 603−606.
[5] F. J. Feher, K. J. Weller, *Organometallics* **1990**, *9*, 2638−2640; F. J. Feher, K. J. Weller, J. J. Schwab, *Organometallics* **1995**, *14*, 2009−2017.
[6] R. Murugavel, A. Voigt, M. G. Walawalkar, H. W. Roesky, *Chem. Rev.* **1996**, *96*, 2205−2236.
[7] M. Veith, M. Jarczyk, V. Huch, *Angew. Chem.* **1997**, *109*, 140−142; *Angew. Chem. Int. Ed. Engl.* **1997**, *36*, 117−119.
[8] M. R. Mason, M. S. Mashuta, J. F. Richardson, *Angew. Chem.* **1997**, *109*, 187−189; *Angew. Chem. Int. Ed. Engl.* **1997**, *36*, 239−241.
[9] K. Ruhlandt-Senge, R. A. Bartlett, M. M. Olmstead, P. P. Power, *Angew. Chem.* **1993**, *105*, 459−461; *Angew. Chem. Int. Ed. Engl.* **1993**, *32*, 425−427.
[10] K. Wraage, A. Künzel, M. Noltemeyer, H.-G. Schmidt, H. W. Roesky, *Angew. Chem.* **1995**, *107*, 2954−2956; *Angew. Chem. Int. Ed. Engl.* **1995**, *34*, 2645−2647.
[11] C. Rennekamp, A. Gouzyr, A. Klemp, H. W. Roesky, C. Brönneke, J. Kärcher, R. Herbst-Irmer, *Angew. Chem.* **1997**, *109*, 413−415; *Angew. Chem. Int. Ed. Engl.* **1997**, *36*, 404−406.
[12] H. Wessel, C. Rennekamp, D.-S. Waezsada, H. W. Roesky, M. L. Montero, I. Usón, *Organometallics* **1997**, *16*, 3243−3245.
[13] K. Wraage, unpublished results, **1995**.
[14] C. Elschenbroich, A. Salzer, *Organometallchemie*, 3. Aufl., Teubner Verlag, Stuttgart, **1993**.
[15] [15a] M. R. Mason, J. M. Smith, S. G. Bott, A. R. Barron, *J. Am. Chem. Soc.* **1993**, *115*, 4971−4984. – [15b] C. J. Harlan, M. R. Mason, A. R. Barron, *Organometallics* **1994**, *13*, 2957−2969. – [15c] C. C. Landry, C. J. Harlan, S. G. Bott, A. R. Barron, *Angew. Chem.* **1995**, *107*, 1315−1316; *Angew. Chem. Int. Ed. Engl.* **1995**, *34*, 1201−1202. – [15d] J. Storre, A. Klemp, H. W. Roesky, H.-G. Schmidt, M. Noltemeyer, R. Fleischer, D. Stalke, *J. Am. Chem. Soc.* **1996**, *118*, 1380−1386. – [15e] J. Storre, C. Schnitter, H. W. Roesky, H.-G. Schmidt, M. Noltemeyer, R. Fleischer, D. Stalke, *J. Am. Chem. Soc.* **1997**, *119*, 7505−7513. – [15f] C. J. Harlan, S. G. Bott, B. Wu, R. W. Lenz, A. R. Barron, *Chem. Commun.* **1997**, 2183−2184.

[16] The formula and the molecular mass respectively refers to the composition of the crystals analyzed by X-ray crystallography.
[17] R. A. Kovar, H. Derr, D. Brandau, J. O. Callaway, *Inorg. Chem.* **1975**, *14*, 2809−2814.
[18] T. Kottke, D. Stalke, *J. Appl. Crystallogr.* **1993**, *26*, 615−619.
[19] G. M. Sheldrick, *Acta Crystallogr. Sect. A* **1990**, *46*, 467−473.
[20] G. M. Sheldrick, *SHELXS 96*, University of Göttingen, **1996**.
Received February 17, 2000
[I00056]

Cyclooligomerization Reactions of Different Phosphaalkynes in the Presence of [W(CO)$_5$thf] − A Route to Tungsten-Stabilised Phosphorus Heterocycles

Peter Kramkowski[a] and Manfred Scheer*[a]

Dedicated to Professor Arndt Simon in occasion of his 60th birthday

Keywords: Phosphaalkynes / Tungsten / Cyclizations / 1,3-Diphosphete ligands / Reaction mechanisms

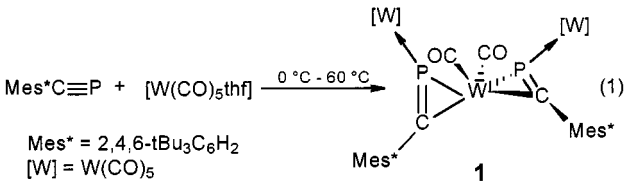
The reactivity of various phosphaalkynes versus [W(CO)$_5$thf] has been studied. The reaction with Mes*C≡P (Mes* = 2,4,6-tBu$_3$C$_6$H$_2$) exclusively leads to the low yield formation of [W(CO)$_2${(η^2-PCMes*)W(CO)$_5$}$_2$] (**1**). The reaction of the less bulky tBuC≡P with [W(CO)$_5$thf] results in high yields in [W(CO)$_2${η^4-(tBuC)$_2$P$_2$W(CO)$_5$}{η^2-(tBuCP)W(CO)$_5$}] (**2**) which possesses a 1,3-diphosphete ligand as well as a side-on coordinated tBuCP unit. Experiments employing MesC≡P (Mes = 2,4,6-Me$_3$C$_6$H$_2$) give the complexes [W(CO)$_4${η^4-(MesC)$_2$P$_2$}] (**3**), [W(CO)$_2${η^4-(MesC)$_2$P$_2$}{η^2-(MesCP)W(CO)$_5$}] (**4**) and [W(CO)$_2${η^4-(MesC)$_2$P$_2$W(CO)$_5$}⟨η^2-(MesCP)W(CO)$_5${μ-W(CO)$_4$}⟩] (**5**) which have a 1,3-diphosphete ligand in their coordination sphere and are partly substituted with an additional side-on coordinated MesC≡P unit. In **5**, two P atoms of the 1,3-diphosphete and the side-on coordinated MesC≡P are further bridged by a W(CO)$_4$ moiety. Additionally, the unusual product [{W(CO)$_3$}⟨η^6-1,2,4-(RC)$_3$P$_3${RCP→W(CO)$_5$}$_2$⟩] (R = Mes) (**6**) resulting from a pentamerization of MesC≡P initiated by [W(CO)$_5$thf], could be obtained in moderate yield. Comprehensive spectroscopical and structural investigations of all products are presented.

Introduction

Almost twenty years ago the first kinetically stabilised phosphaalkyne tBuC≡P was designed by G. Becker and coworkers.[1] The synthesis of this compound was further improved in the groups of M. Regitz and G. Becker and has therefore become accessible to all chemists.[2] The chemistry of tBuC≡P has undergone a rapid and exciting development. Co-oligomerization and complex-chemical stabilisation of such compounds have been intensively studied and reviewed in detail.[3,4] Investigations involving phosphaalkynes with a residue R different from tBu, however, are scarce. Only a few examples of complexes derived from AdC≡P[5] (Ad = C$_{10}$H$_{15}$) and Mes*C≡P[6,7] (Mes* = 2,4,6-tBu$_3$C$_6$H$_2$) are known in the literature. Our interest is focussed on the reactivity of RC≡P towards cluster frameworks such as e.g. *nido*-[Ru$_4$(CO)$_{13}$(μ$_3$-PPh)],[6] and especially on the use of phosphaalkynes in the metathesis reaction with alkoxides of the type [(RO)$_3$W≡W(OR)$_3$].[8,9] The goal of the latter chemistry has been the development of an efficient procedure for the synthesis of phosphido complexes of the type [(RO)$_3$W≡P]. Since these compounds possess a highly reactive metal-phosphorus triple bond, it is necessary to stabilise these complexes with Lewis-acidic M(CO)$_5$-fragments to form [(RO)$_3$W≡P→M(CO)$_5$] (M = Cr, W; R = tBu; 2,6-Me$_2$C$_6$H$_3$).[10] Before one is able to explore the three component system [(RO)$_3$W≡W(OR)$_3$]/RC≡P/[M(CO)$_5$thf], one must be aware of the reaction of phosphaalkynes with [M(CO)$_5$thf] alone. We established that [Cr(CO)$_5$thf] does not react at all with RC≡P, regardless of the reaction conditions employed. However, [W(CO)$_5$thf] reveals a broad reactivity towards Mes*C≡P, tBuC≡P and MesC≡P (Mes = 2,4,6-Me$_3$C$_6$H$_2$), which we have reported herein. Furthermore, for the first time metal complexes derived from MesC≡P have been synthesised. The molecular structures and spectroscopic properties of these novel compounds will be presented.

Results and Discussion

Mes*C≡P (Mes* = 2,4,6-tBu$_3$C$_6$H$_2$) reacts with [W(CO)$_5$thf] to give [W(CO)$_2${(η^2-PCMes*)W(CO)$_5$}$_2$] (**1**) in low yield (6%) and most of the phosphaalkyne remains unchanged regardless of the reaction conditions employed [Equation (1)].[7]

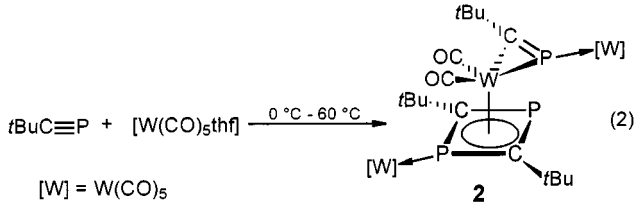


(1)

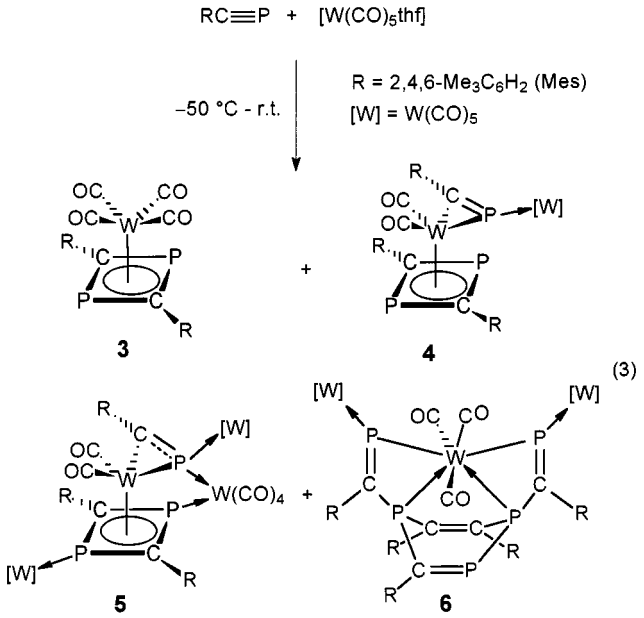
If the same reaction is performed with tBuC≡P, [W(CO)$_2${η^4-(tBuC)$_2$P$_2$W(CO)$_5$}{η^2-(tBuCP)W(CO)$_5$}] (**2**) is formed almost quantitatively as the only phosphorus-containing product [Equation (2)]. The same quantities of **2** are obtained independent of whether the reaction mixture is kept at ambient temperature for 48 h or refluxed for a period of 2 h.

[a] Institut für Anorganische Chemie der Universität Karlsruhe, D-76128 Karlsruhe, Germany
Fax: (internat.) + 49-721/661921
E-mail: mascheer@achibm6.chemie.uni-karlsruhe.de

 © WILEY-VCH Verlag GmbH, D-69451 Weinheim, 2000 1434−1948/00/0808−1869 $ 17.50+.50/0



The use of MesC≡P (Mes = 2,4,6-$Me_3C_6H_2$) in the reaction with [W(CO)$_5$thf], in the temperature range from −50 °C to ambient temperature, however, leads to a variety of different products [Equation (3)].



All products are purified and separated by column chromatography. The complexes **1**, **2**, **4** are red, **3** is a yellow, **5** is a dark-red, and **6** an orange-red crystalline compound. They are sufficiently stable in the solid state to allow brief handling in air. All compounds are readily soluble in all common organic solvents such as *n*-hexane, toluene, THF, or CH_2Cl_2, apart from **3** which reveals a poor solubility in *n*-hexane.

All products are spectroscopically characterised and their molecular structures are determined by single crystal X-ray structure analysis. The crystal structure and the spectroscopic data of **1**[7] and **6**[11] were published elsewhere. Although compound **2** has been published before,[9] the X-ray structure analysis of **2** reported herein is of much higher quality, and also the spectroscopic data are completed here as well.

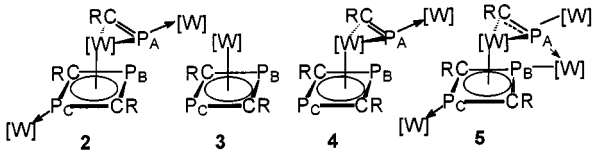
In **1** only side-on coordination of the large Mes*C≡P occurs which is probably due to steric reasons. The dominant feature of all other products is the occurrence of a cyclodimerization and in the case of **6** a pentamerization of RC≡P. Compounds **2**−**5** possess a 1,3-diphosphete moiety, which in **3** is the only ligand at tungsten besides 4 CO groups. In complexes **2**, **4**, and **5**, two of the CO ligands are replaced by a side-on coordinated phosphaalkyne which further coordinates to a W(CO)$_5$ group (c.f. Figures 1−4). A "head-to-tail" dimerization on 14-valence electron (VE) complexes of cobalt,[12] rhodium,[13] iron,[14] and molybdenum[15] and of 12VE fragments of zirconium and hafnium[16] have been observed in several compounds. However, additional side-on coordination of a phosphaalkyne at the capping metal fragment has not yet been found. While only a few examples exist for a trimerization,[17] and just one for a tetramerization[18] of phosphaalkyne, complex **6** is the first pentamerization product induced by a transition metal complex.[19]

Spectroscopic Properties of Compounds 2−6

The IR spectra of complexes **2**−**6** reveal bands for CO stretching frequencies in the range of 1900−2100 cm^{-1} as expected for terminal bound CO ligands. The mass spectra of **2**−**4** show the molecular ion peak and the expected fragmentation patterns.

The ^{31}P NMR data of **2**−**5** are summarised in Table 1. The signals of the ring phosphorus atoms (P_B and P_C) of the 1,3-diphosphete ligands appear in the region between δ = 13.0 (**2**) and 82.9 (**5**). These chemical shifts are in accordance with those observed for [{η^4−1,3-(*t*BuC)$_2$P$_2$}Fe(CO)$_3$] (δ = 38.1[14]) and [{η^4−1,3-(*t*BuC)$_2$P$_2$}CoCp*] (δ = 56.8[12a]) and seem to be fairly independent of whether coordination of the P atom to a W(CO)$_5$ group occurs or not. Zenneck et al. reported a chemical shift of +82.1 ppm for a 1,3-diphosphete complex of iron were both P atoms coordinate to a Cr(CO)$_5$ group.[20]

Table 1. ^{31}P NMR data for the compounds **2**−**5** in C_6D_6 at 298 K; *J* [Hz]



Compound	δ	*J*(P,P)	*J*(W,P)
2	P_A = 318.9 (d)	P_A,P_B = 38	231.5 & 61.0
	P_B = 13.1 (d)	P_B,P_A = 38	
	P_C = 14.0 (s)		235.0
3	$P_{B,C}$ = 58.1 (s)		62.2
4	P_A = 371.4 (t)	P_A,$P_{B,C}$ = 17	209.4 & 61.6
	$P_{B,C}$ = 64.9 (d)	$P_{B,C}$,P_A = 17	
5	P_A = 264.0 (s)		224.0 & 64.8
	P_B = 82.9 (s)		130.8
	P_C = 44.6 (s)		264.7

Coupling of the ring phosphorus to the tungsten carbonyl cap is only observed in the case of **3**. The signals of P_C in **2** and **5** bear one pair of tungsten satellites with coupling constants typical of an end-on coordination of a W(CO)$_5$ moiety.

The chemical shifts of the P_A atom of the side-on bound phosphaalkyne unit in **2**, **4**, and **5** are observed in the region

of δ = 264.0 (**5**) to 371.4 (**4**). The data are in good agreement with those of complex **1** (δ = 313[7]), which only possesses side-on coordinated phosphaalkynes. In **5** an unusual shift towards high field for the signal of P_A is observed which is because of the particular bonding situation in this complex due to the $W(CO)_4$ bridge between P_A and P_B. All P_A atoms in **2**, **4**, and **5** show the appropriate coupling pattern for a coordination to the end-on bound $W(CO)_5$ group and the side-on coordination to the $W(CO)_2$ cap, with coupling constants in the range of 209.0−224.0 Hz and 61.0−64.8 Hz, respectively. In the case of complexes **2** and **4**, a *J*(P,P) between the phosphorus of the side-on coordinated phosphaalkyne unit and the ring P atoms is observed. The coupling constants are within 38 and 17 Hz, a typical range for a coupling over two bonds.

Molecular Structures of 2−5

Compound **2** crystallises with two independent molecules in the unit cell. Both molecules possess essentially an identical structure. The following refers to molecule A.

The η^4-1,3-diphosphacyclobutadiene ring of **2** (Figure 1) reveals almost equidistant C−P distances and therefore is a square rather than a rectangle [*d*(P−C) = 1.768(14)−1.806(14) Å]. This is in good agreement with the bond lengths in the complexes [CpCo{η^4-(*t*BuC)$_2$P$_2$}] [*d*(P−C) = 1.79(1)−1.82(1) Å],[12b] [Cp*Co{η^4-(*t*BuC)$_2$P$_2$}] [*d*(P−C) = 1.797(3)−1.798(3) Å],[13] and [Mo{η^4-(*t*BuC)$_2$P$_2$}$_3$] [*d*(P−C) = 1.811(4)−1.860(5) Å][21]. In **2**, the ring is folded 169° along the C(13)−C(14) axis and is therefore essentially planar, since all atoms stand out of the idealised plane P(1)−P(2)−C(13)−C(14) by 0.06 Å only, on average. This 1,3-diphosphete unit coordinates to a $W(CO)_2$ cap, which is further coordinated side-on by a phosphaalkyne unit with *d*[W(1)−P(3)] = 2.369(4) and *d*[W(1)−C(23)] = 2.13(2) Å. The P−C bond length of this phosphaalkyne is elongated to 1.66(2) Å [c.f. in *t*BuC≡P: 1.54 Å[22]]. This distance is comparable to the observed bond lengths of the side-on coordinated *t*BuC≡P in [(Ph$_3$P)$_2$Pt{η^2-*t*BuCP}] [1.672(17) Å][23] or in [(Cp)$_2$Ti(PMe$_3$){η^2-*t*BuCP}] [1.634 Å].[24] This elongation is due to the back donation effects of the tungsten of the $W(CO)_2$ moiety into the π* orbitals of the C−P bond. The high degree of sp^2 hybridisation at C(23) is further reflected in the angle of 0.88° between the planes W(1)−C(23)−P(3) and P(3)−C(23)−C(24) (between the planes W(1)−C(23)−P(3) and W(3)−P(3)−C(23) the angle is 15.50°). The phosphorus atoms P(2) and P(3) further coordinate to $W(CO)_5$ fragments with bond lengths of 2.493(4) and 2.462(4) Å, respectively. This is in the range for coordinative bonds as observed e.g. in [$W(CO)_4$⟨(η^4-P_4){$W(CO)_5$}$_4$⟩] [average *d*(WP) = 2.445(7) Å].[25]

Complex **3** (Figure 2) is the first tungsten complex possessing only CO ligands, besides the 1,3-diphosphacyclobutadiene ring. The bond lengths inside the four-membered ring of **3** are slightly longer than those observed in **2** [*d*(P−C) = 1.818(3)−1.827(3) Å]. The ring system of **3** is almost planar (folding angle: 170.79°, measured along the C(3)−C(3A) axis, maximal deviation of the atoms from the idealised plane is ±0.05 Å, c.f. 0.06 Å in **2**). It is noteworthy that the mesityl ligands of the ring carbon atoms are almost in plane with the 1,3-diphosphete system. They are only twisted by 5.1°. Thus, it appears that a kind of delocalisation of three different π-systems is responsible for this effect.

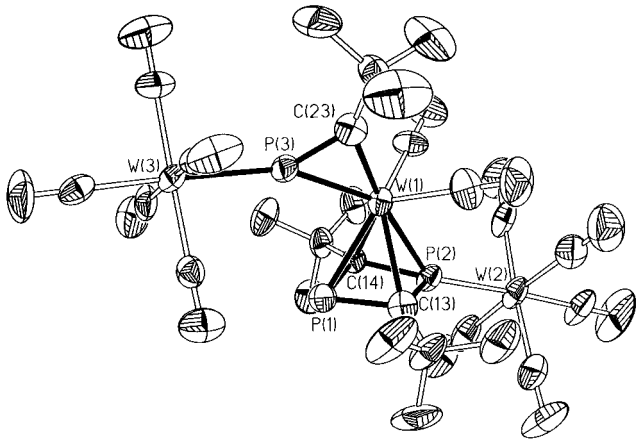


Figure 1. Molecular structure of [$W(CO)_2${η^4-(*t*BuC)$_2$P$_2$-$W(CO)_5$}{η^2-(*t*BuCP)$W(CO)_5$}] (**1**) (molecule A, ellipsoids drawn at 50% probability level). Selected bond lengths [Å] and angles [°]: P(1)−C(13) 1.806(14), P(1)−C(14) 1.791(14), P(2)−C(13) 1.768(14), P(2)−C(14) 1.778(13), P(1)−W(1) 2.495(4), P(2)−W(1) 2.551(4), C(13)−W(1) 2.33(2), C(14)−W(1) 2.368(2), P(3)−C(23) 1.66(2), P(3)−W(1) 2.369(4), C(23)−W(1) 2.13(2), P(2)−W(2) 2.493(4), P(3)−W(3) 2.462(4), C(14)−P(1)−C(13) 82.8(6), C(13)−P(2)−C(14) 84.5(6), P(1)−C(13)−P(2) 95.9(7), P(2)−C(14)−P(1) 95.7(7)

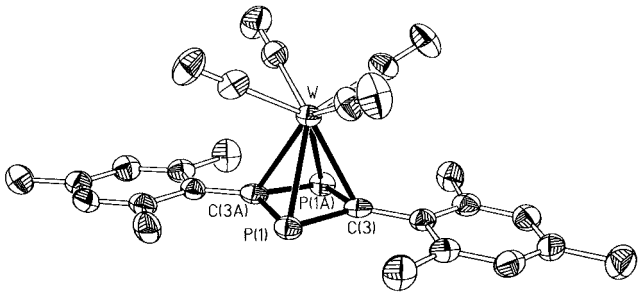


Figure 2. Molecular structure of [$W(CO)_4${η^4-(MesC)$_2$P$_2$}] (**3**) (ellipsoids drawn at 50% probability level). Selected bond lengths [Å] and angles [°]: P(1A)−C(3) 1.818(3), P(1)−C(3) 1.827(3), P(1)−W 2.5265(8), C(3)−W 2.364(3), C(3A)−P(1)−C(3) 83.92(13), P(1A)−C(3)−P(1) 95.67(13)

The molecular structure of **4** (Figure 3) is similar to the *t*Bu derivative **2**. The only difference is that in **4** none of the P atoms of the 1,3-diphosphete ligand bind to a $W(CO)_5$ group. However, the distances within the four-membered ring are slightly longer [*d*(P−C) = 1.793(4)−1.824(4) Å]. The ring system is folded along the C(18)−C(28) axis by 170.03° and is therefore in accordance with the observations for **2** and **3** (maximal deviation from the average plane in **4** is 0.06 Å). As in **2**, the side-on bound phosphaalkyne unit is coordinated to a further $W(CO)_5$ group. The bond length C(8)−P(1) of this moiety is 1.683(3) Å and is therefore only 0.023 Å longer than the corresponding bond in **2**. The degree of sp^2 hybridisation of C(8) is similar to **2** since the angles between the planes W(1)−C(8)−P(1) and P(1)−C(8)−C(9), and W(1)−C(8)−P(1) and

W(2)−P(1)−C(8) are in good agreement with **2** (**4**: 0.41 and 13.57°, respectively). In contrast to **3**, the mesityl moieties at the ring C atoms of the 1,3-diphosphete ligand are twisted by 10.7° in this complex, which is probably due to the steric influence of the side-on coordinated [MesC≡P→W(CO)$_5$] unit.

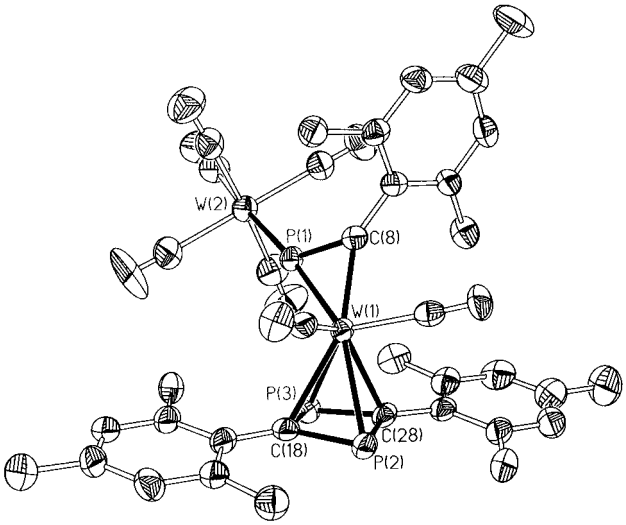


Figure 3. Molecular structure of [W(CO)$_2${η^4-(MesC)$_2$P$_2$}{η^2-(MesCP)W(CO)$_5$}] (**4**) (ellipsoids drawn at 50% probability level). Selected bond lengths [Å] and angles [°]: P(2)−C(18) 1.816(4), P(2)−C(28) 1.798(4), P(3)−C(18) 1.793(4), P(3)−C(28) 1.824(4), P(2)−W(1) 2.5518(12), P(3)−W(1) 2.5218(11), C(18)−W(1) 2.432(4), C(28)−W(1) 2.297(4), P(1)−C(8) 1.683(2), P(1)−W(1) 2.3644(11), C(8)−W(1) 2.072(3), P(1)−W(2) 2.4611(12), C(18)−P(2)−C(28) 83.7(2), C(28)−P(3)−C(18) 83.6(2), P(2)−C(18)−P(3) 96.1(2), P(2)−C(28)−P(3) 95.7(2)

The molecular structure of **5** (Figure 4) also features a capped 1,3-diphosphete ligand. In contrast to the complexes **2**−**4**, both of the P atoms of the diphosphete ligand in **5** coordinate to tungsten carbonyl fragments. One of the P atoms is coordinated to a W(CO)$_4$ moiety, which further bridges to the side-on coordinated phosphaalkyne. While the bond lengths and the grade of folding along the C(27)−C(37) axis of the ring are still in accordance with the data of **2**−**4** [d = 1.788(9)−1.817(9) Å; maximal deviation from the average plane is ±0.06 Å], the situation of the side-on coordinated MesC≡P unit has changed considerably due to the coordination of this phosphorus atom to the bridging W(CO)$_4$ group [W(2)] and a terminal W(CO)$_5$ moiety [W(3)]. The P(1)−C(17) bond length is 1.747(9) Å and is considerably elongated in comparison to **2** and **4** and can be considered as an elongated double bond. The low degree of sp^2 hybridisation of the atom C(17) in **5** becomes obvious when the angle between the planes W(1)−C(17)−P(1) and P(1)−C(17)−C(18) is 12.2° [between W(1)−C(17)−P(1) and W(3)−P(1)−C(17) the angle is 37.7°]. The considerable difference in the bonding situation of the side-on coordinated phosphaalkyne group is further reflected in the comparably short W(1)−C(17) distance, of only 2.032(8) Å [c.f. **2**: 2.13(2) Å and **4**: 2.072(3) Å] and the elongated W(1)−P(1) bond with 2.544(2) Å [c.f. **2**: 2.369(4) Å and **4**: 2.3644(11) Å]. The bond lengths of P(1)−W(2) and P(1)−W(3) [2.562(3) Å and 2.512(3) Å, respectively] are longer than the distances observed in **2** and **4**, but are still in the range for coordinative bonds as e.g. found in [Ph$_3$P→W(CO)$_5$] [d(W−P) = 2.544 Å].[26] The special situation of this P atom is also reflected in its ^{31}P NMR resonance signal as discussed above. Due to the coordination of P(2) to the W(CO)$_4$ bridge and P(3) to a W(CO)$_5$ group, the mesityl moieties of the ring carbon atoms are much more twisted as in **3** or **4**. In **5**, the angles between the planes of the mesityl groups at the atoms C(27) and C(37) and the idealised plane C(27), C(37), P(2), and P(3) are 77.1° and 78.9°, respectively.

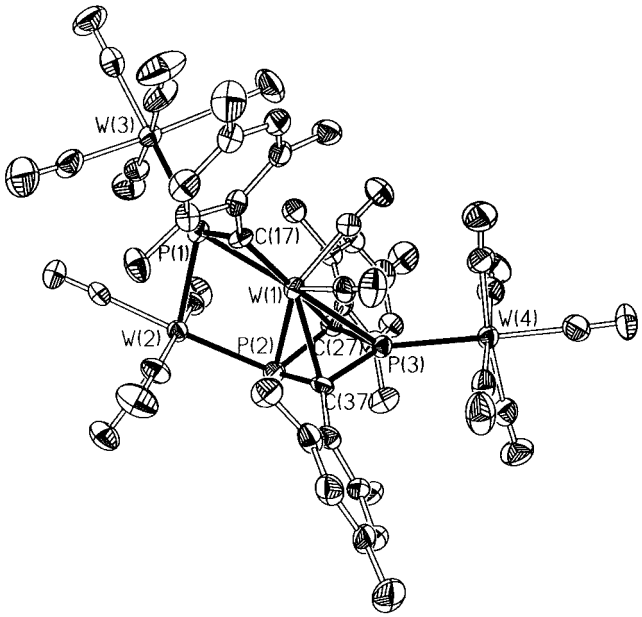
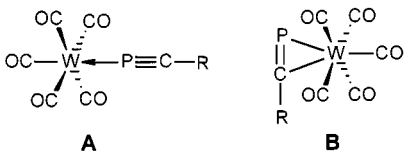


Figure 4. Molecular structure of **5** (ellipsoids drawn at 50% probability level). Selected bond lengths [Å] and angles [°]: P(2)−C(27) 1.817(9), P(2)−C(37) 1.803(9), P(3)−C(27) 1.788(9), P(3)−C(37) 1.800(9), P(2)−W(1) 2.466(3), P(3)−W(1) 2.550(3), C(27)−W(1) 2.424(8), C(37)−W(1) 2.287(9), P(1)−C(17) 1.747(9), P(1)−W(1) 2.544(2), C(17)−W(1) 2.032(8), P(1)−W(2) 2.562(3), P(1)−W(3) 2.512(3), P(2)−W(2) 2.446(3), P(3)−W(4) 2.446(2), C(27)−P(2)−C(37) 85.2(4), C(27)−P(3)−C(37) 86.2(4), P(2)−C(27)−P(3) 93.7(4), P(2)−C(37)−P(3) 93.8(4)

Proposal for a Reaction Pathway for the Formation of the Compounds 1−6

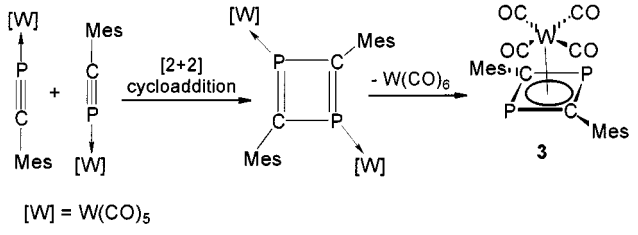
The nature of the products leads us to propose that the first step of these reactions must be the activation of the C≡P triple bond via the coordination of the phosphaalkyne to W(CO)$_5$. Two different coordination modes appear most likely, the end-on (**A**) or side-on (**B**) coordination.



To shed light onto this problem we followed the reaction of MesC≡P with [W(CO)$_5$thf] as a function of temperature by ^{31}P NMR spectroscopy. Indeed a singlet at δ = −74.3 ([D$_8$]toluene, 243 K; MesC≡P: δ = 2.1 (s), [D$_8$]toluene, 243 K) without any tungsten satellites is observed as an in-

termediate of this reaction. This singlet has a maximum intensity at 273 K and decreases after the signals of the products increase. For an end-on coordination of type **A** a singlet shifted into the highfield region bearing one pair of tungsten satellites is expected, revealing a coupling constant of approximately 150−280 Hz. Examples for complexes revealing an end-on coordinated phosphaalkyne are rare. In the complex $[(CO)_3W(PCy_3)_2(\eta^1\text{-}P{\equiv}CMes^*)]$, synthesised in our group, a highfield shift of 10 ppm is observed [δ = 24.4, J(W,P) = 280 Hz], in comparison to free Mes*C≡P.[27] In the group of Nixon, the compound $[FeH(\eta^1\text{-}P{\equiv}C\textit{t}Bu)(dppe)_2][BPh_4]$ could be isolated revealing a highfield shift of about 85 ppm after coordination of *t*BuC≡P (δ = −154; *t*BuC≡P: δ = −69.2).[28] A side-on coordination mode **B** requires a downfield shift as found for the P_A atoms of the side-on coordinated phosphaalkynes in **2**, **4**, and **5**. In this case only a small coupling between tungsten and phosphorus of less than 60 Hz would be expected due to the low s-character in the W−P bond. Recently Nixon et al. described a complex containing a η^2 coordinated phosphaalkyne in $[WF(C_6H_4CH_2NMeCH_2CH_2NMe_2)(CO)(\eta^2\text{-}P{\equiv}C\textit{t}Bu)]$ with a chemical shift at δ = 452.4 and a ^1J(W,P) of 82 Hz.[29] Although the high-field shift of our intermediate at δ = −74.3 seems to favour **A** as the first formed intermediate, without a resolved J(W,P) no unequivocal evidence for either of these activation modes could be achieved from the NMR spectroscopic experiment.

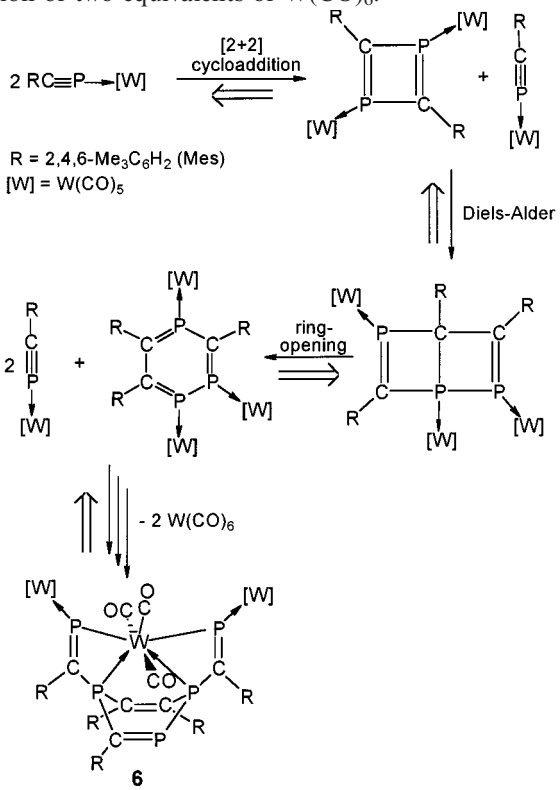
However, the nature of the reaction products also suggests a more end-on coordination as the first step. Firstly, this is supported by the fact that in reaction (1) Mes*C≡P does not form a 1,3-diphosphete ligand, which is likely starting from a complex of type **B**. In the case of the initially formed intermediate **A**, the bulky supermesityl group would interact sterically with the end-on coordinated $W(CO)_5$ group of the second phosphaalkyne and thus a [2+2] cycloaddition is inhibited. By contrast, for the sterically less encumbered MesC≡P the end-on intermediate **A** can undergo a cycloaddition and therefore the formation of **3** is best explained by the reaction shown in Scheme 1. Secondly, in the compounds **2**, **4**, **5**, and **6** all side-on coordinated phosphaalkynes further bear a $W(CO)_5$ group in end-on position.



Scheme 1. Proposed reaction pathway for the formation of **3**

Thus, we propose that in the first step two activated molecules of type **A** approach each other. Since a head-to-tail [2+2] cycloaddition is sterically hindered for the bulky supermesityl groups, the attack on a $W(CO)_5$ unit leads only to the spirocyclic product **1**. For *t*Bu as well as the mesityl substituents, cycloaddition is the predominant reaction pathway (Scheme 1). By elimination of $W(CO)_6$ as the driving force[30] a 1,3-diphosphete ring system capped by a $W(CO)_4$ group is generated to give compound **3**. After further elimination of CO, RC≡P→$W(CO)_5$ is coordinated side-on to give the complexes **2**, **4**, and **5**, respectively. Experiments conducted with complex **3** showed, that the phosphorus atoms of the 1,3-diphosphete ligand are still able to coordinate further $W(CO)_5$ units.

The proposed 1,3-diphosphete unit formed first can also serve as an intermediate for the formation of **6** (Scheme 2). A subsequent Diels−Alder reaction with further end-on activated phosphaalkyne leads then to a Dewar benzene like intermediate which reacts after ring opening with two more activated phosphaalkynes to give compound **6**, after elimination of two equivalents of $W(CO)_6$.



Scheme 2. Proposed reaction pathway for the formation of **6**

Conclusions

The comparison of the reactivity of different phosphaalkynes with $[W(CO)_5thf]$ reveals that MesC≡P possesses the highest potential for yielding novel complexes because its sterical and electronical properties are somewhat between those of the other phosphaalkynes used in former investigations. It is to be expected that further variations of these properties (e.g. in $R_2NC{\equiv}P$[31] and OC≡P,[32] respectively) influence the reaction behaviour dramatically and open up the approach to novel products.

Experimental Section

General Techniques: All reactions were performed under an atmosphere of dry argon using Schlenk and glove box techniques. Sol-

vents were purified and degassed by standard procedures and distilled prior to use. − NMR spectra were recorded on a Bruker AC 250 [^{1}H: 250.13 MHz; ^{31}P: 101.256 MHz; standard Me_4Si (^{1}H), 85% H_3PO_4 (^{31}P)]. − IR spectra were recorded in Nujol on a Bruker IFS 28 FT-IR-spectrometer. − MS: Finnigan MAT 711 at 70 eV. − Correct elemental analyses for the isolated products were performed by the analytical laboratory of the institute.

Reagents: Unless otherwise stated, commercial-grade chemicals were used without further purification. The silica gel was activated by removing all volatile substances at 180 °C in vacuo (10^{-3}Torr) for 48 h. [$W(CO)_5$thf] was prepared by irradiating a THF solution of $W(CO)_6$ in a UV apparatus for 2 h. *t*BuC≡P was synthesised as described in reference [2]. MesC≡P was obtained as published in ref.[33]

Crystal Structure Analysis of 2−5: Crystal structure analyses of **3** were performed on a STOE IPDS and of **2**, **4**, and **5** on a STOE STADI IV (ω-scan mode) diffractometer with Mo-K_α radiation (λ = 0.71073 Å) with empirical absorption corrections for **2**, **4**, and **5** (Psi-scans). Machine parameters, crystal data and data collection parameters are summarised in Table 2. The structures were solved by direct methods using SHELXS-86,[34a] full-matrix-least-squares refinement on F^2 in SHELXL-93[34b] with anisotropic displacement for non-H atoms. Hydrogen atoms were located in idealised positions and refined isotropically according to the riding model. Crystallographic data (excluding structure factors) for the structures reported in this paper have been deposited with the Cambridge Crystallographic Data Centre as supplementary publication no. CCDC-139093 to no. CCDC-139096. Copies of the data can be obtained free of charge on application to CCDC, 12 Union Road, Cambridge CB2 1EZ, UK (Fax: Int. code +(44)1223/336033; E-mail: deposit@ccdc.cam.ac.uk).

$[W(CO)_2\{\eta^4\text{-}(t\text{BuC})_2P_2\text{-}W(CO)_5\}\{\eta^2\text{-}(t\text{BuCP})W(CO)_5\}]$ (2): *t*BuC≡P (100 mg, 1 mmol) dissolved in *n*-hexane (10 mL) was added to [$W(CO)_5$thf] (25 mL of a 0.04 M THF solution, 1 mmol) at ambient temperature. Subsequently the solvent was reduced to 15 mL and the mixture allowed to stir for 48 h. All volatile substances were then removed in vacuo (10^{-3} Torr). The crude product was purified by column chromatography (silica gel, 30 × 2.5 cm, Merck 60) using a *n*-hexane/toluene mixture of 1:1. After reduction of the solvent to dryness the solid was recrystallised by toluene to afford 235 mg (60%) of red crystals of **2**. Crystals suitable for X-ray analysis were grown from concentrated toluene solutions. − $C_{27}H_{27}O_{12}P_3W_3$ (1187.98): calcd. C 27.30, H 2.29; found C 27.99, H 2.84. − IR [Nujol, $\tilde{\nu}$ (CO), cm^{-1}]: 2072(m), 2018(w), 1975(sh), 1954(vs). ^{1}H NMR (25 °C, C_6D_6): δ 1.66 (s, 9 H, CH_3), 0.87 (s, 18 H, CH_3). − $^{31}P\{^1H\}$ NMR (25 °C, C_6D_6): δ = 318.9 (P3, d), *J*(P,P) = 38 Hz, *J*(W,P) = 231.5 & 61 Hz, 14 (P2, s), *J*(W,P) = 235 Hz, 13.1 (P1, d) *J*(P,P) = 38 Hz. − EI MS: *m*/*z* (%) = 1187.8 (38) [M^+], 1103.9 (14) [M^+ − 3 CO], 1076.8 (2) [M^+ − 4 CO], 1019.9 (6) [M^+ − 6 CO], 991.9 (45) [M^+ − 7 CO].

Compounds 3−6: MesC≡P (162 mg, 1 mmol) was dissolved in *n*-hexane (10 mL) and cooled to −50 °C. At this temperature the solution was added to 10 mL of a THF solution of [$W(CO)_5$thf] (1 mmol). The mixture was allowed to warm up to room temperature and stirred for further 48 h. The reaction was monitored by ^{31}P NMR spectroscopy indicating a small grade of conversion. Then all volatile substances were removed in vacuo. This reaction was repeated twice, and the combined product mixtures were worked up by column chromatography (silica gel, 30 × 2.5 cm, Merck 60). The first fraction was eluted with a mixture of *n*-hexane/toluene (5:1) giving 100 mg of **3** (10.6%). The second fraction with *n*-hexane/toluene (2:1) yielding 200 mg of red **4** (19%). The third fraction was obtained from *n*-hexane/toluene (1:1) to give orange-

Table 2. Crystal data for the compounds **2−5**

	2	**3**	**4**	**5** · 1.5 C_7H_8
Empirical formula	$C_{27}H_{27}O_{12}P_3W_3$	$C_{24}H_{22}O_4P_2W$	$C_{37}H_{33}O_7P_3W_2$	$C_{56.5}H_{45}O_{16}P_3W_4$
Formula mass	1167.945	620.21	1050.24	1808.23
Crystal size [mm]	0.23 × 0.19 × 0.08	0.42 × 0.11 × 0.04	0.57 × 0.30 × 0.15	0.30 × 0.23 × 0.08
T [K]	200(2)	200(1)	200(2)	200(2)
Space group	$P\bar{1}$ (No. 2)	*Ccca* (No. 68)	$P\bar{1}$ (No. 2)	$P\bar{1}$ (No. 2)
Crystal system	triclinic	orthorhombic	triclinic	triclinic
a [Å]	15.103(3)	13.236(3)	10.908(2)	12.816(3)
b [Å]	15.829(3)	22.086(4)	10.927(2)	13.635(3)
c [Å]	17.441(4)	15.743(3)	16.455(3)	19.661(4)
α [°]	73.04(3)	90	86.53(3)	81.48(3)
β [°]	65.91(3)	90	76.52(3)	73.09(3)
γ [°]	83.77(3)	90	77.71(3)	63.27(3)
V [Å^3]	3640.7(13)	4602(2)	1863.4(6)	2935.3(10)
Z	4	8	2	2
d_c [g cm^{-3}]	2.167	1.790	1.872	2.046
μ_c [cm^{-1}]	96.41	51.87	63.44	79.60
Radiation [λ, Å]	Mo-*K*α (0.71073)			
Diffractometer	STOE STADI IV	STOE IPDS	STOE STADI IV	STOE STADI IV
2*Θ* range [°]	3.10 ≤ 2Θ ≤ 52.00	4.42 ≤ 2Θ ≤ 51.66	2.54 ≤ 2Θ ≤ 54.92	3.34 ≤ 2Θ ≤ 52
hkl range	−16 ≤ *h* ≤ 18, −18≤ *k* ≤ 19, 0 ≤ *l* ≤ 21	−15 ≤ *h* ≤ 14, −26 ≤ *k* ≤ 25, −19 ≤ *l* ≤ 18	−13 ≤ *h* ≤ 14, −14 ≤ *k* ≤ 14, 0 ≤ *l* ≤ 21	−14 ≤ *h* ≤ 15, −16 ≤ *k* ≤ 16, 0 ≤ *l* ≤ 24
Data / restraints / parameters	14186 / 0 / 829	2172 / 0 / 144	8273 / 0 / 460	11483 / 0 / 869
Independent reflections with $I > 2\sigma(I)$	8978 (R_{int} = 0.000)	1726 (R_{int} = 0.0431)	7571 (R_{int} = 0.0000)	9138 (R_{int} = 0.0000)
Goodness-of-fit on F^2	1.217	0.950	1.069	1.138
R_1[a]	0.0517, 0.0936	0.0219, 0.0542	0.0246, 0.0633	0.0397, 0.0932
wR_2 [b] [$I > 2\sigma(I)$]				
R_1 [a] wR_2 [b] (all data)	0.1164, 0.1377	0.0281, 0.0566	0.0289, 0.0683	0.0639, 0.1166
Largest diff peak, hole, [e Å^{-3}]	1.822, −1.278	0.829, −0.593	0.961, −1.826	2.819, −1.291

[a] $R = |F_0| - |F_c| / |F_0|$. − [b] $wR_2 = [\omega(F_0^2 - F_c^2)^2]/[(F_0^2)^2]^{1/2}$.

red **6** (100 mg, 10%). Dark red **5** could be eluted with pure toluene (130 mg, 7.6%). Crystals suitable for X-ray diffraction methods of all compounds were obtained by recrystallisation from toluene.

Properties of [W(CO)$_4${η^4-(MesC)$_2$P$_2$}] (3): $C_{24}H_{22}O_4P_2W$ (620.23): calcd. C 46.48, H 3.58; found C 46.32, H 3.21. − IR [Nujol, ṽ (CO), cm^{-1}]: 2052(s), 1977(vs). − ^{1}H NMR (25 °C, C_6D_6): δ 6.52 (s, 2 H, CH), 2.18 (s, 6H, CH_3), 1.99 (s, 3 H, CH_3). − ^{31}P{^{1}H} NMR (25 °C, [D$_8$]THF): δ = 58.1, J(W,P) = 62.2 Hz. − EI MS: m/z (%) = 620.1 (24) [M$^+$], 592.2 (7) [M$^+$ − CO], 564.1 (15) [M$^+$ − 2 CO], 536.1 (18) [M$^+$ − 3 CO], 506.1 (100) [M$^+$ − 4 CO].

Properties of [W(CO)$_2${η^4-(MesC)$_2$P$_2$}{η^2-(MesCP)W(CO)$_5$}] (4): $C_{37}H_{33}O_7P_3W_2$ (1050.3): calcd. C 42.31, H 3.17; found C 42.48, H 3.35. − IR [Nujol, ṽ (CO), cm^{-1}]: 2074(vs), 2027(vs), 1975(s), 1965(s), 1953(vs), 1932 (vs). − ^{1}H NMR (25 °C, C_6D_6): δ = 6.78 (s, 2 H, CH), 6.54 (s, 4 H, CH) 2.36 (s, 3 H, CH_3), 2.34 (s, 12 H, CH_3), 2.03 (s, 6 H, CH_3), 1.59 (s, 6 H, CH_3). − ^{31}P{^{1}H} NMR (25 °C, C_6D_6): δ = 371.4 (P1, t), J(P,P) = 17 Hz, J(W,P) = 209.4 & 61.6 Hz, 64.9 (P2,3, d), J(P,P) = 16 Hz. EI MS: m/z (%) = 1050.0 (48) [M$^+$], 938.0 (11) [M$^+$ − 4 CO], 910.0 (28) [M$^+$ − 5 CO], 881.9 (30) [M$^+$ − 6 CO], 852.0 (100) [M$^+$ − 7 CO]. − Properties of **5**: IR [Nujol, ṽ (CO), cm^{-1}]: 2084(w), 2072(s), 2046(m), 2038(m), 2004(m), 1995(s), 1970(vs), 1960(vs), 1950(vs), 1939(s). ^{1}H NMR (25 °C, C_6D_6): δ 7.1−6.49 aromatic protons, 2.889 (s, 6 H, CH_3), 2.806 (s, 3 H, CH_3), 2.199 (s, 6 H, CH_3), 2.1736 (s, 6 H, CH_3), 1.981 (s, 3 H, CH_3), 1.894 (s, 3 H, CH_3). − ^{31}P{^{1}H} NMR (25 °C, C_6D_6): δ = 264.0 (P1, s), J(W,P) = 224 & 64.8 Hz, 82.9 (P2, s), J(W,P) = 130.8 Hz, 44.6 (P3, s), J(W,P) = 264.7 Hz. Properties of **6**: $C_{63}H_{55}O_{13}P_5W_3$ (1726.54): calcd. C 43.83, H 3.21; found C 43.50, H 3.35 . − IR (Nujol, ṽ (CO), cm^{-1}): 2075(s), 2065(s), 2041(m), 1987(w), 1962(sh), 1950(vs), 1938(vs), 1931(vs), 1925(vs). − ^{1}H NMR (250.133 MHz, C_6D_6, 298 K, TMS): δ = 1.400, 1.422, 1.720, 1.819, 1.838, 1.900, 1.937, 1.979, 2.002, 2.061, 2.113, 2.163, 2.780, 2.864, 3.229 (CH_3, each s, 3 H, CH_3), 6.82−5.71 (10 singlets, each 1 H, aromatic protons). − ^{31}P{^{1}H} NMR [101.256 MHz, C_6D_6, 298 K, 85proz. H_3PO_4 ext., P_A = P(2), P_B = P(1), P_C = P(3), P_D = P(4), P_E = P(5)]: δ = 497.6 [P_A: d; $^2J(P_A,P_C)$ = 45 Hz, J(W,P_A) = 190 Hz], 456.1 [P_B: d; $^2J(P_B,P_D)$ = 42 Hz, J(W,P_B) = 190 Hz], 370.7 [P_E: dd; $^1J(P_E,P_D)$ = 280 Hz, $^2J(P_E,P_C)$ = 35 Hz], 50.8 [P_C: ddd; $^2J(P_C,P_A)$ = 45 Hz, $^2J(P_C,P_E)$ = 35 Hz, $^2J(P_C,P_D)$ = 15 Hz], 10.4 [P_D: ddd; $J(P_D,P_E)$ = 280 Hz, $^2J(P_D,P_B)$ = 42 Hz, $^2J(P_D,P_C)$ = 14 Hz, J(W,P_D) = 108 Hz].

Acknowledgments

The authors are grateful to the Deutsche Forschungsgemeinschaft and the Fonds der Chemischen Industrie for comprehensive financial support of this work. We appreciate the fruitful discussions with Prof. Dr. M. Regitz concerning the retrosynthesis of **6**.

[1] G. Becker, G. Gresser, W. Uhl, *Z. Naturforsch. B.* **1981**, *36*, 16−19.
[2] T. Allspach, M. Regitz, G. Becker, W. Becker, *Synthesis* **1986**, 31−36.
[3] [3a] A. Mack, M. Regitz, *Chem. Ber./Recueil* **1997**, *130*, 823−384. − [3b] M. Regitz, P. Binger, *Angew. Chem.* **1988**, *100*, 1541; *Angew. Chem. Int. Ed. Engl.* **1988**, *27*, 1484. − [3c] M. Regitz, *Chem. Rev.* **1990**, *90*, 191−213.
[4] [4a] J. F. Nixon, *Coord. Chem. Rev.* **1995**, *145*, 201−258. − [4b] J. F. Nixon, *Chem. Soc. Rev.* **1995**, 319. − [4c] J. F. Nixon, *Chem & Ind.* **1993**, 404. − [4d] J. F. Nixon, *Chem. Rev.* **1988**, *88*, 1327−1362.
[5] [5a] P. B. Hitchcock, M. J. Maah, J. F. Nixon, J. A. Zora, G. J. Leigh, M. A. Bakar, *Angew. Chem.* **1987**, *99*, 497; *Angew. Chem. Int. Ed. Engl.* **1987**, *26*, 474. − [5b] P. B. Hitchcock, M. J. Maah, J. F. Nixon, *Chem. Commun.* **1987**, 658−659.
[6] M. Scheer, J. Krug, P. Kramkowski, J. F. Corrigan, *Organometallics* **1997**, *16*, 5917−5922.
[7] P. Kramkowski, M. Scheer, G. Baum, *J. Organomet. Chem.* **1998**, *553*, 511−516.
[8] M. Scheer, P. Kramkowski, K. Schuster, *Organometallics* **1999**, *18*, 2874−2883.
[9] M. Scheer, K. Schuster, T. A. Budzichowski, M. H. Chisholm, W. E. Streib, *Chem. Commun.* **1995**, 1671−1672.
[10] [10a] P. Kramkowski, G. Baum, U. Radius, M. Kaupp, M. Scheer, *Chem. Eur. J* **1999**, *5*, 2890−2898. − [10b] M. Scheer, P. Kramkowski, K. Schuster, *Organometallics* **1999**, *18*, 2874−2883.
[11] P. Kramkowski, M. Scheer, *Angew. Chem.* **1999**, *111*, 3384−3387; *Angew. Chem. Int. Ed.* **1999**, *38*, 3183−3186.
[12] [12a] P. Binger, R. Milczarek, R. Mynott, M. Regitz, W. Rösch, *Angew. Chem.* **1986**, *98*, 645−546; *Angew. Chem. Int. Ed. Engl.* **1986**, *25*, 644−645. − [12b] P. Binger, R. Milczarek, R. Mynott, C. Krüger, H. Tsay, E. Raabe, M. Regitz, *Chem. Ber.* **1988**, *121*, 637−645.
[13] P. B. Hitchcock, M. J. Maah, J. F. Nixon, *Chem Commun.*, **1986**, 737−738.
[14] P. Binger, B. Biedenbach, R. Schneider, M. Regitz, *Synthesis* **1989**, 960−961.
[15] A. S. Weller, C. D. Andrews, A. D. Burrows, M. Green, J. M. Lynam, M. F. Mahon, C. Jones, *Chem. Commun*. **1999**, 2147−2148.
[16] P. Binger, S. Leininger, J. Stannek, B. Gabor, R. Mynott, J. Bruckmann, C. Krüger, *Angew. Chem.* **1995**, *107*, 2411−2414; *Angew. Chem. Int. Ed. Engl.* **1995**, *34*, 2227.
[17] [17a] P. Binger, S. Leininger, K. Günther, U. Bergsträßer, *Chem. Ber./Recueil* **1997**, *130*, 1491−1494. − [17b] R. Milczarek, W. Rüssler, P. Binger, K. Jonas, K. Angermund, C. Krüger, M. Regitz, *Angew. Chem.* **1987**, *99*, 957−905; *Angew. Chem. Int. Ed. Engl.* **1987**, *26*, 908−909. − [17c] P. Binger, S. Stutzmann, J. Stannek, K. Günther, P. Phillips, R. Mynott, J. Bruckmann, C. Krüger, *Eur. J. Inorg. Chem*. **1999**, 763−769.
[18] P. Binger, G. Glaser, B. Gabor, R. Mynott, *Angew. Chem.* **1995**, *107*, 114−116; *Angew. Chem. Int. Ed. Engl.* **1995**, *34*, 81.
[19] A metal-assisted pentamerisation of *t*BuC≡P to a metal-free pentamer starting from (η^4-1-methylnaphthalene)(η^6-toluene)iron was described by U. Zenneck et al.: D. H. Hu, H. Schäufele, H. Pritzkow, U. Zenneck, *Angew. Chem*. **1989**, *101*, 929; *Angew. Chem. Int. Ed. Engl.* **1989**, *28*, 900; D. Böhm, D. Hu. U. Zenneck, *Phorsphorus Sulfur Silicon* **1993**, *77*, 5.
[20] F. W. Heinemann, S. Kummer, U. Seiss-Brandl, U. Zenneck, *Organometallics* **1999**, *18*, 2021−2029.
[21] F. G. N. Cloke, K. R. Flower, P. B. Hitchcock, J. F. Nixon, *Chem Commun.* **1994**, 489−490.
[22] M. Y. Antipin, A. N. Chernega, K. A. Lysenko, Y. T. Struchkov, J. F. Nixon, *Chem Commun.* **1995**, 505−506.
[23] J. C. T. R. Burckett-St.Laurent, P. B. Hitchcock, H. W. Kroto, J. F. Nixon, *Chem. Commun.* **1981**, 1141−1142.
[24] P. Binger, in: *Multiple Bonds and Low Coordination in Phosphorus Chemistry* (Eds.: M. Regitz, O. J. Scherer), Thieme, Stuttgart **1990**, p. 91.
[25] M. Scheer, E. Hermann, J. Sieler, M. Oehme, *Angew. Chem*. **1991**, *103*, 1023−1024; *Angew. Chem. Int. Ed. Engl.* **1991**, *30*, 969.
[26] M. J. Aroney, I. E. Buys, M. S. Davies, T. W. Hambley, *J. Chem. Soc., Dalton Trans.* **1994**, 2827−2834.
[27] T. Gröer, G. Baum, M. Scheer, *Organometallics* **1998**, *17*, 5916−5919.
[28] M. F. Meidine, M. A. N. D. A. Lemos, A. J. L. Pombeiro, J. F. Nixon, P. B. Hichcock, *J. Chem. Soc., Dalton Trans.* **1998**, 3319−3323.
[29] M. H. A. Benvenutti, P. B. Hitchcock, J. L. Kiplinger, J. F. Nixon, T. G. Richmond, *Chem. Commun*. **1997**, 1539−1540.
[30] [M(CO)$_5$thf] (M = Cr, W) are known to be suitable CO acceptors. Comprehensive investigations in our group concerning the reaction of [Cp^{x}Co(CO)$_2$] or [Cp^{x}Rh(CO)$_2$] with P_4 in the presence of [M(CO)$_5$thf] revealed that the formation of [M(CO)$_6$] acts as the driving force in these conversions; compare: [30a] M. Scheer, C. Troitzsch, P. G. Jones, *Angew. Chem.* **1992**, *104*, 1395−1397; *Angew. Chem. Int. Ed. Engl.* **1992**, *31*, 1377−1379. − [30b] M. Scheer, U. Becker, J. C. Huffman, M. H. Chisholm, *J. Organomet. Chem.* **1993**, *461,* C1-C3. − [30c] M. Scheer, C. Troitzsch, L. Hilfert, M. Dargatz, E. Kleinpeter,

P. G. Jones, J. Sieler, *Chem. Ber.* **1995**, *128*, 251−257. – [30d] M. Scheer, U. Becker, *Chem. Ber.* **1996**, *129*, 1307−1310. – [30e] M. Scheer, U. Becker, *J. Organomet. Chem.* **1997**, *545*, 451−460.

[31] J. Grobe, D. L. Van, B. Lüth, M. Hegemann, *Chem. Ber.* **1990**, *123*, 2317−2320.

[32] G. Becker, W. Schwarz, N. Seidler, M. Westerhausen, *Z. Anorg. Allg. Chem.* **1992**, *612*, 72−82.

[33] A. Mack, E. Pierron, T. Allspach, U. Bergsträßer, M. Regitz, *Synthesis* **1998**, 1305.

[34] [34a] G. M. Sheldrick, *SHELXS-86*, University of Göttingen, **1986**. – [34b] G. M. Sheldrick, *SHELXL-93*, University of Göttingen, **1993**.

Received January 19, 2000
[I00018]

Syntheses of New Sulfur−Nitrogen Palladacycles − Crystal Structures of $[(AMTTO)PdBr_2]_2 \cdot 3.5THF$, $[(AMTTO)PdI_2]_2 \cdot 3MeOH$, $[(AMTTO)Pd(PPh_3)Br]Br \cdot MeOH$, and $[(AMTTO)Pd(PPh_3)I] \cdot 2MeOH$ (AMTTO = 4-Amino-6-methyl-1,2,4-triazine-3-thione-5-one)

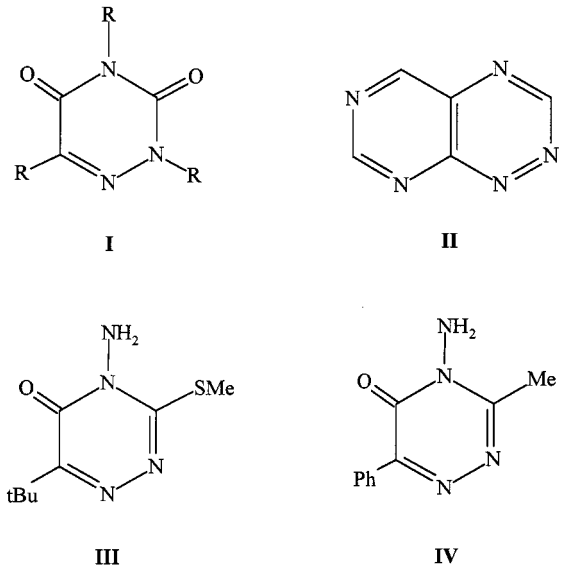
Mitra Ghassemzadeh,*[a] Mohammad Bolourtchian,[a] Soheila Chitsaz,[b] Bernhard Neumüller,[b] and Majid M. Heravi[c]

Keywords: Palladium / Triazines / Metallacycles / N ligands / S ligands

Reactions of $[(AMTTO)PdCl_2] \cdot MeOH$ (**1**) with sodium bromide and sodium iodide led to the palladacycles $[(AMTTO)PdBr_2]_2 \cdot 3.5THF$ (**2**) and $[(AMTTO)PdI_2]_2 \cdot 3MeOH$ (**3**) in excellent yields. Treatment of **2** and **3** with triphenylphosphane gave the complexes $[(AMTTO)Pd(PPh_3)Br]Br \cdot MeOH$ (**4**) and $[(AMTTO)Pd(PPh_3)I] \cdot 2MeOH$ (**5**), respectively. All the complexes have been characterized by IR spectroscopy, elemental analysis, as well as by X-ray diffraction studies. In addition, **4** and **5** have been characterized by ^{31}P NMR spectroscopy. Crystal data for **2** at −80 °C: triclinic, space group $P\bar{1}$, a = 1150.8(1), b = 1234.1(1), c = 1398.1(1) pm, α = 84.01(1)°, β = 86.84(1)°, γ = 66.40(1)°, Z = 2, R_1 = 0.0366; for **3** at −50 °C: orthorhombic, space group $Pbcn$, a = 1476.2(1), b = 1333.1(1), c = 1440.1(1) pm, Z = 4, R_1 = 0.0302; for **4** at −80 °C: monoclinic, space group $P2_1/c$, a = 993.0(1), b = 993.6(1), c = 2735.5(2) pm, β = 97.64(1)°, Z = 4, R_1 = 0.0464; for **5** at −70 °C: monoclinic, space group $P2_1/c$, a = 865.7(2), b = 3760.5(3), c = 861.1(1) pm, β = 97.56(1)°, Z = 4, R_1 = 0.0613.

Introduction

1,2,4-Triazines are well-known compounds and a variety of synthetic methods for the preparation of substituted derivatives are available. Compounds containing the 1,2,4-triazine moiety are found in natural materials and some of these exhibit biological activity. A large number of synthetic 1,2,4-triazines also show biological activity and have been used for various purposes. For example, 1,2,4-triazine-3,5-diones (**I**) represent aza analogues of pyrimidine nucleic acid bases. A number of neutral antibiotics are derivatives of pyrimido[5,4-*e*]-1,2,4-triazine (**II**). 4-Amino-6-*tert*-butyl-3-methylthio-1,2,4-triazine-5-one (**III**) and 4-amino-3-methyl-6-phenyl-1,2,4-triazine-5-one (**IV**) are used as herbicides (Scheme 1).[1a] Metal complexes of ligands such as S,N-heterocycles, amino acids, and proteins often exhibit enhanced biological activities compared to the uncomplexed ligand.[1b][1c]



Scheme 1. Four important classes of N-containing heterocycles

In our investigations, we have shown that AMTTO − a representative of 4-amino-6-alkyl-1,2,4-triazine-5-one − acts as a chelating ligand in a 1+1 fashion towards $AgNO_3$ in methanol {one strong Ag−S bond and a weak Ag−N contact leading to a distortion of a ideal linear [AMTTO-Ag-AMTTO]$^+$ ion} and as a bidentate chelating ligand towards $PdCl_2$ in methanol/acetonitrile to give the air-stable complexes $[(AMTTO)_2Ag]NO_3$ [2] and $[(AMTTO)PdCl_2] \cdot MeOH$ (**1**),[3] respectively. To the best of our knowledge, the latter constitutes the first palladacycle of AMTTO.

We have already studied the reactions of **1** with triphenylphosphane and sodium thiocyanate, which led to the air-stable complexes $[(AMTTO)Pd(PPh_3)Cl]Cl \cdot MeOH$ and $[(AMTTO)Pd(SCN)_2] \cdot MeOH$, respectively.[4]

In this paper, we wish to report the halide exchange reactions of **1** using sodium bromide and sodium iodide, as well

[a] Chemistry and Chemical Engineering Research Center of Iran, P.O. Box 18335-186, Tehran, Iran
[b] Fachbereich Chemie der Universität, Hans-Meerwein-Straße, D-35032 Marburg, Germany
[c] Department of Chemistry, School of Sciences, Azzahra University, Vanak, Tehran, Iran

 © WILEY-VCH Verlag GmbH, D-69451 Weinheim, 2000 1434−1948/00/0808−1877 $ 17.50+.50/0

as the reactions of the bromine and iodine palladacycles with triphenylphosphane.

Results and Discussion

Syntheses and Characterization of 2, 3, 4, and 5

Treatment of **1** with sodium bromide in THF at 20 °C gave **2**; similar treatment with sodium iodide in methanol/acetonitrile gave **3** [Equation (1) and (2)].

$$2\,[(AMTTO)PdCl_2] + 4\,NaBr \xrightarrow{THF;\ 20°C} \underset{\mathbf{2}}{[(AMTTO)PdBr_2]_2 \cdot 3.5THF} + 4\,NaCl \quad (1)$$

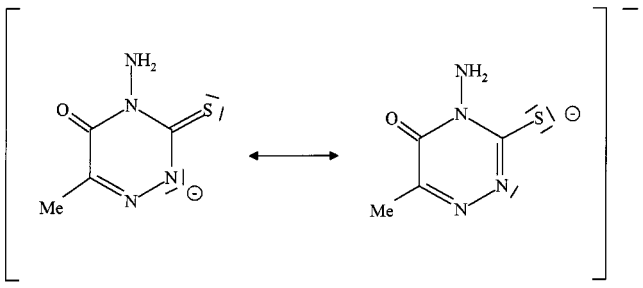
$$2\,[(AMTTO)PdCl_2] + 4\,NaI \xrightarrow{MeOH/MeCN;\ 20°C} \underset{\mathbf{3}}{[(AMTTO)PdI_2]_2 \cdot 3MeOH} + 4\,NaCl \quad (2)$$

Further treatment of **2** and **3** with PPh_3 in methanol at 20 °C led to **4** and **5**, respectively, according to Equation (3) and (4).

$$[(AMTTO)PdBr_2] + PPh_3 \xrightarrow{MeOH;\ 20°C} \underset{\mathbf{4}}{[(AMTTO)Pd(PPh_3)Br]Br \cdot MeOH} \quad (3)$$

$$[(AMTTO)PdI_2] + PPh_3 \xrightarrow{MeOH;\ 20°C} \underset{\mathbf{5}}{[(AMTTO)Pd(PPh_3)I] \cdot 2MeOH + HI} \quad (4)$$

In contrast to Equation (3), reaction according to Equation (4) gives the complex **5** incorporating the anionic ligand $[AMTTO]^-$ (**V**). This results from an abstraction of HI owing to the relatively high acidity of this particular NH group. The coordination of the sulfur atom leads to additional acidification of the amine function (see Scheme 2).



V

Scheme 2. Mesomeric forms of the anionic AMTTO ligand

Compounds **2–5** were found to be air-stable crystalline solids. The ^{13}C NMR spectrum of the ligand AMTTO has been published for the Ag complex $[Ag(AMTTO)_2]NO_3$ [2] and the data are almost unchanged in the spectra of **2–5**. The ^{31}P NMR spectra of **4** and **5** feature only one sharp singlet at $\delta = 30.3$ and $\delta = 26.2$, respectively, in accordance with the geometries of these compounds. In the IR spectra of **2–5**, three absorptions are seen at 452, 369, and 268 cm^{-1} for **2**, at 445, 373, and 173 cm^{-1} for **3**, at 450, 382, and 259 cm^{-1} for **4**, and at 449, 374, and 198 cm^{-1} for **5**, which can be assigned to ν(PdN), ν(PdS), and ν(PdX) absorptions.[5] C=O and C=N vibrations give rise to two bands at 1703 and 1604 cm^{-1} for **2**, at 1718 and 1612 cm^{-1} for **3**, at 1719 and 1595 cm^{-1} for **4**, and at 1725 and 1625 cm^{-1} for **5**. P–C vibrations of the PPh_3 moiety are seen in the range 749–711 cm^{-1} for **4** and in the range 745–691 cm^{-1} for **5**. The N–H valence vibrations give rise to broad bands at 3254 (**2**), 3230 (**3**), 3205 (**4**), and 3250 cm^{-1} (**5**). Broad O–H absorptions, attributable to hydrogen bonding, give rise to the bands at 3620, 3554, and 3472 cm^{-1} (**3**) and at 3446 cm^{-1} (**5**). The corresponding band for **4** could not localized accurately because of the measured line width.

Crystal Structures of 2–5

The structural data of the palladacycles show that **2** (Figure 1), **3** (Figure 2), and **5** (Figure 4) are neutral molecules incorporating [(AMTTO)Pd] complex fragments. **4** is a salt consisting of $[(AMTTO)Pd(PPh_3)Br]^+$ and Br^- ions, while **5** incorporates the anionic ligand $[AMTTO]^-$. The coordination geometry about the palladium center in each of these complexes is essentially square planar. In all the complexes, the bidentate AMTTO ligand is coordinated to palladium(II) forming a five-membered chelate ring. The coordination sphere of **2** is completed by two bromide anions, while that of **3** is completed by two iodide ions. The coordination sites in **4** and **5** are occupied by one halide ion (Br^- in **4**; I^- in **5**, Figure 3 and 4) and a triphenylphosphane ligand. The Pd–S bond lengths of 225.2(2)/225.9(2) and 227.4(2) pm found in **2** and **3**, respectively, do not differ significantly from the Pd–S distances of 227.5(2) and 226.6(2) pm in **4** and **5**. On comparing the data with the lowest literature values for thioether-palladium complexes, i.e. 228–229 pm, these distances are seen to be rather short.[6,7] The Pd–N atom distances are within the range observed for related compounds.[7] The Pd–N bond lengths [211.0(5) pm in **4**; 209.2(7) pm in **5**] are longer than those in **2** and **3** [204.2(6) and 207.9(5) pm, respectively]. This lengthening reflects the *trans* influence of the phosphane ligand. The Pd–X bonds *trans* to the sulfur atom [Pd1–Br1 and Pd2–Br4, 244.7(1) and 244.1(9) pm in **2**; Pd1–I2 259.73(6) pm in **3**] are somewhat longer than the Pd–X distances *cis* to S1 [Pd1–Br2 240.75(6) pm and Pd2–Br3 242.5(1) pm in **2**; Pd1–I1 257.50(6) pm in **3**], reflecting the greater *trans* influence of the sulfur atom as compared to the nitrogen atom. The presence of an $[AMTTO]^-$ ligand in **5** leads only to marginal differences in the bonding parameters due to the delocalization of the charge in **V** (Scheme 2).

The halide atoms in **4** and **5** are oriented *cis* to the nitrogen ligands of the heterocycle, indicating the strong influence of the π-acids C=S and PPh_3. The Pd–Br and Pd–I bond lengths (Pd–Br, mean 243 pm; Pd–I, mean 259.5 pm) are shorter than the sum of the single bond radii for palladium and the halides (Pd: 131 pm, Br: 114 pm, I: 133

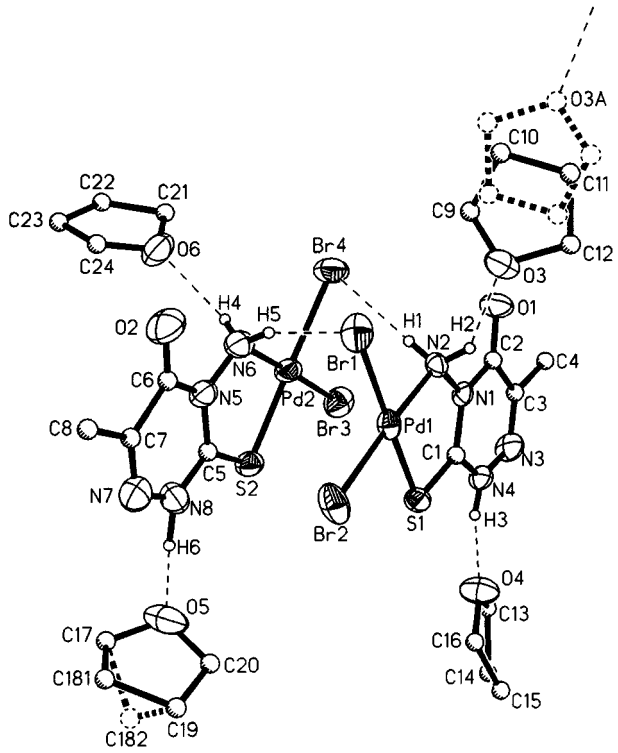


Figure 1. Molecular structure of **2** with showing disorder of the THF molecules (the C atoms are shown as spheres; most of the H atoms are omitted for the sake of clarity; 50% probability level)

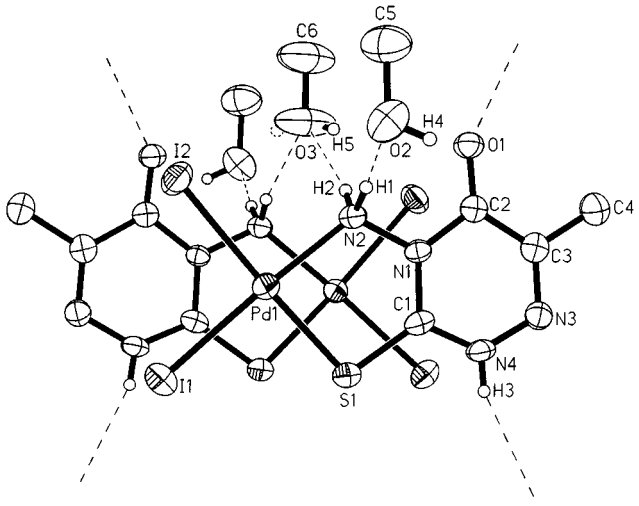


Figure 2. Molecular structure of **3** with showing disorder of the central methanol molecule (most of the H atoms are omitted for the sake of clarity)

pm),[8] but fall within the range observed for similar compounds.[9]

The Pd−P atom distances (average 225 pm) are shorter than the sum of the single bond radii for palladium and phosphorus, i.e. 241 pm,[10] are remarkably shorter than the $Pd^{II}-PPh_3$ bond reference value (230.2 pm) encountered in 248 entries,[11] and fall at the short end of a wide range (221−246 pm). The X−Pd−P angles, which measure 92.04(4)° in **4** and 92.64(7)° in **5**, are similar to values reported in the literature.[12]

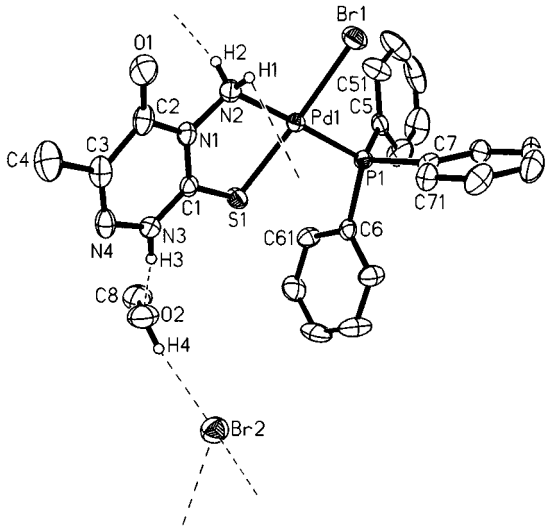


Figure 3. Molecular structure of **4** (most of the H atoms are omitted for the sake of clarity)

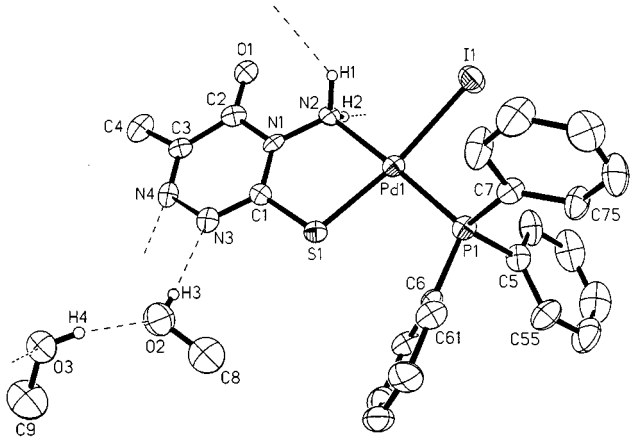


Figure 4. Molecular structure of **5** (most of the H atoms are omitted for the sake of clarity)

There are several medium to strong hydrogen bonds in the complexes. The two independent palladacycle units in **2** are held together by H···Br contacts [N2···Br4: 346.5(7); N6···Br1: 334.2(6) pm]. This leads to an angle of 7° between the "best" planes of the two complexes. THF molecules are hydrogen-bonded to H2 [N2···O3: 286.9(9) pm], H3 [N4···O4: 270.2(7) pm], H4 [N6···O6: 277.1(8) pm], and H6 [N8···O5: 265.3(9) pm]. The THF molecule O3→C12 is disordered about a center of symmetry (see Figure 1).

In **3**, two palladacycles are connected through a methanol molecule, which lies on a twofold axis. This means a disorder of the OH moiety O3−H5 over two positions [N2···O3: 287.9(8)°]. An additional methanol molecule is hydrogen-bonded to each NH_2 group [N2···O2: 282.6(7)° pm]. Each $[(AMTTO)PdI_2]_2 \cdot 3MeOH$ building block is part of a chain built up by N2−H1···O2 hydrogen bonds [N2···O2: 282.6(7)°; Figure 5] that extends along [010]. The palladacycles in **3** are slightly bent. The dihedral angle between the plane Pd1/I1/I2/N2/S2 and the ligand AMTTO amounts to 7°. In **4**, isotypical to the corresponding complex $[(AMTTO)PdCl(PPh_3)]Cl \cdot MeOH$,[4] N3 (NH function)

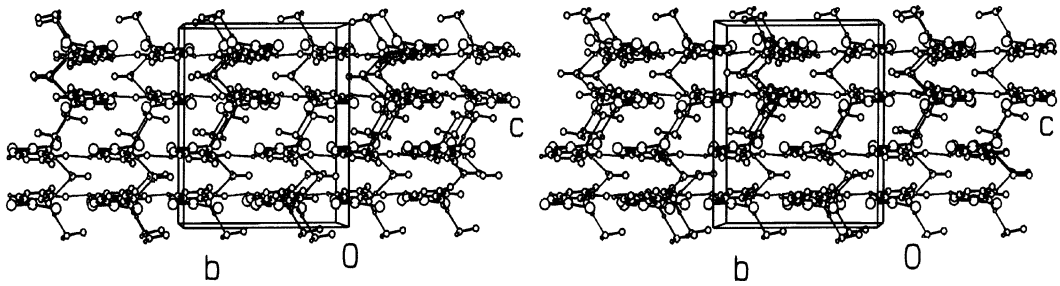


Figure 5. Stereoscopic view of the unit cell of **3**; the chains extending along [010] as a result of hydrogen bonding are also shown

is connected through the methanol molecule [N3···O2: 265.4(7) pm] to Br2 [counterion; O2···Br2: 322.3(5) pm] and then to two nitrogen atoms [N2a, N2b; NH_2 function; N2···Br2a: 338.1(5); N2···Br2b: 320.8(5) pm; Figure 3]. The packing of **4** has already been demonstrated for [(AMTTO)PdCl(PPh_3)]Cl·MeOH.[4] In **5**, medium to strong hydrogen bonds link the methanol molecules to N3 and to NH_2 groups of the adjacent AMTTO ligands, respectively (Figure 4). The contacts O3···O2 [266.7(9) pm], O2···N3 [286.9(9) pm], O3···N2a [278.7(9) pm], and N4···N2b [294.8(9) pm] give rise to a 2D-network of complex and solvate molecules that extends parallel to (010) (Figure 6).

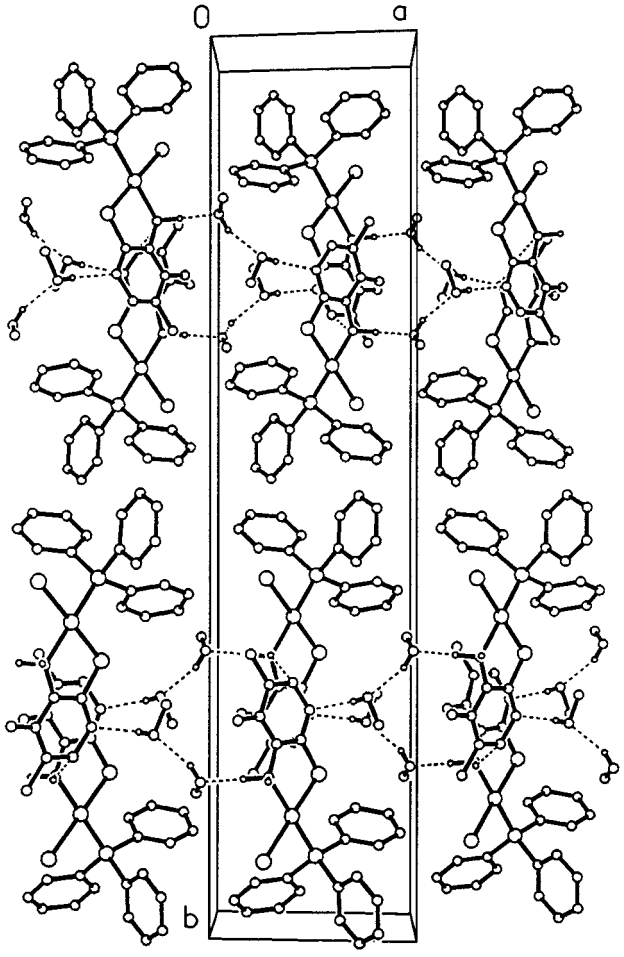


Figure 6. View of the unit cell of **5**; **5** forms layers built-up by hydrogen bonds parallel to (010)

Experimental Section

General Remarks: AMTTO[13] and **1**[3] were prepared according to literature procedures. − IR spectra were recorded on a Perkin−Elmer spectrometer 883 (KBr pellets, Nujol mulls, 4000−250 cm^{-1}) or on a Bruker IFS 88 instrument (CsBr discs, 4000−400 cm^{-1}; polyethylene discs, 500−100 cm^{-1}; Nujol mulls). − ^{31}P NMR spectra were recorded on a Bruker AC-200 spectrometer using 85% aqueous H_3PO_4 as an external standard. − Elemental analyses were performed by the following methods: C, H, N analyses: combustion method; halogen analyses: combustion and titration with $AgNO_3$; sulfur analyses: combustion and titration with $Ba(ClO_4)_2$; phosphorus: decomposition with $HClO_4$ and photometric analysis of the molybdophosphate; palladium analyses: decomposition with $HClO_4$ and analysis by atomic absorption spectroscopy. − The following chemicals were purchased from Merck and used without further purification: sodium bromide, sodium iodide, triphenylphosphane, methanol, and acetonitrile.

Synthesis of [(AMTTO)$PdBr_2$]$_2$·3.5THF (2): A solution of **1** (0.36 g, 0.98 mmol) in THF (20 mL) was treated with NaBr (0.20 g, 1.9 mmol) and the resulting mixture was stirred for 3 h at 20 °C. The white precipitate formed was filtered off and the filtrate was concentrated to a small volume (ca. 5 mL) until an orange solid separated. The crude product was filtered off and the clear solution was kept at 4 °C to give a second crop of orange crystals of **2**. − Yield: 0.96 g (95%). − $C_{22}H_{40}Br_4N_8O_{5.5}Pd_2S_2$ (1011.19): calcd. C 13.16, H 2.21, N 12.27, Br 35.01, Pd 23.31, S 7.02; found C 13.01, H 2.14, N 12.17, Br 34.90, Pd 23.35, S 6.97. − IR (Nujol): $\tilde{\nu}$ = 3254 [w, br, ν(NH)], 1703 [s, ν(C=O)], 1604 [m, ν(N=C)], 1588 (m), 1520 (m), 1321 (m), 1304 (s), 1233 (m), 1166 (m), 1036 (m), 974 (w), 930 (w), 875 (w), 802 (w), 749 (s), 675 (m), 646 (w), 606 (m), 528 (w), 506 (m), 452 [m, ν(PdN)], 409 (w), 369 [w, ν(PdS)], 310 (m), 268 [w, ν($PdBr_2$)], 246 (w), 198 (w), 165 (w).

Synthesis of [(AMTTO)PdI_2]$_2$·3MeOH (3): To a stirred solution of **1** (0.36 g, 0.98 mmol) in methanol/acetonitrile (1:1 *v*/*v*, 30 mL) at 20 °C was added NaI (0.29 g, 1.9 mmol). The reaction mixture was stirred for a further 5 h. The white solid formed was filtered off and the filtrate was concentrated to a volume of 10 mL and filtered once more. The filtrate was stored at 4 °C overnight to give orange crystals of **3**, which were collected by filtration and washed with cold methanol. − Yield: 1.05 g (93%). − $C_{11}H_{24}I_4N_8O_5Pd_2S_2$ (1133.0): calcd. C 11.66, H 2.14, N 9.89, I 44.81, Pd 18.79, S 5.66; found C 11.55, H 2.10, N 9.56, I 44.92, Pd 18.56, S 5.34. − IR (Nujol): $\tilde{\nu}$ = 3620 [vw, br, ν(OH)], 3554 [w, br, ν(OH)], 3472 [w, br, ν(OH)], 3230 [w, br, ν(NH)], 1719 [s, ν(C=O)], 1595 [m, ν(C=C)], 1538 (w), 1516 (w), 1492 (w), 1335 (m), 1301 (s), 1218 (w), 1150 (w), 1112 (w), 1048 (w), 973 (w), 926 (w), 602 (w), 512 (m), 445 [m, ν(PdN)], 409 (w), 373 [w, ν(PdS)], 325 (vw), 305 (w), 280 (vw), 253 (w), 228 (w), 201 (vw), 173 [w, ν(PdI_2)], 128 (vw) 112 (vw).

Reactions with PPh_3. − General Procedure: A solution of **2** (or **3**) (1.00 mmol) in methanol (30 mL) was treated with PPh_3 (0.26 g, 0.99 mmol) and the resulting mixture was stirred for 3 h at 20 °C. The solution was then concentrated to a small volume (ca. 10 mL) until a yellow solid separated. The crude product was filtered off and the clear filtrate was kept at 4 °C to give yellow crystals of **4** (or **5**).

Synthesis of [(AMTTO)Pd(PPh_3)Br]Br·MeOH (4): Yield: 0.64 g (90%). − $C_{23}H_{25}Br_2N_4O_2PPdS$ (718.73): calcd. C 38.44, H 3.51, N 7.80, Br 22.23, P 4.31, Pd 14.81, S 4.46; found C 38.26, H 3.46, N 7.72, Br 21.98, P 4.15, Pd 14.68, S 4.31. − IR (Nujol): $\tilde{\nu}$ = 3205 [w, br, ν(NH)], 1719 [vs, ν(C=O)], 1612 [m, ν(C=C)], 1573 (m), 1537 (m), 1435 (s), 1348 (m), 1301 (m), 1185 (w), 1146 (w), 1097 (s), 1045 (w), 1024 (w), 1000 (m), 966 (m), 936 (w), 750 (s), 712 (m), 692 (s), 655 (w), 619 (w), 601 (w), 536 (s), 507 (s), 450 [m, ν(NH)], 412 (w), 382 [m, ν(PdS)], 310 (vw), 259 [w, ν(PdBr)], 195 (m), 132 (vw). − ^{31}P NMR (CD_3OD): δ = 30.3 (s).

Synthesis of [(AMTTO)Pd(PPh_3)I]·2MeOH (5): Yield: 0.65 g (91%). − $C_{24}H_{28}IN_4O_3PPdS$ (716.87): calcd. C 40.21, H 3.94, N 7.82, I 17.78, P 4.32, Pd 14.85, S 4.47; found C 39.89, H 3.87, N 7.71, I 17.65, P 4.26, Pd 13.99, S 4.36. − IR (Nujol): $\tilde{\nu}$ = 3446 [vw, br, ν(OH)], 3250 [vw, br, ν(NH)], 1728 [vs, ν(C=O)], 1625 (m, C=

Table 1. Crystallographic data for **2**−**5**

Compound		**2**	**3**	**4**	**5**
Empirical formula		$C_{22}H_{40}Br_4N_8O_{5.5}Pd_2S_2$	$C_{11}H_{24}I_4N_8O_5Pd_2S_2$	$C_{23}H_{25}Br_2N_4O_2PPdS$	$C_{24}H_{28}IN_4O_3PPdS$
Formula mass		1101.19	1133.0	718.73	716.87
Crystal size (mm)		0.25 × 0.17 × 0.05	0.51 × 0.2 × 0.09	0.38 × 0.13 × 0.09	0.39 × 0.1 × 0.1
Crystal system		triclinic	orthorhombic	monoclinic	monoclinic
Space group		$P\bar{1}$ (no.2)[20]	*Pbcn* (no.60)	$P2_1/n$ (no.14)	$P2_1/c$ (no.14)
a [pm]		1150.8(1)	1476.2(1)	993.0(1)	865.7(2)
b [pm]		1234.1(1)	1333.1(1)	993.6(1)	3760.5(3)
c [pm]		1398.1(1)	1440.1(1)	2735.5(2)	861.1(1)
α [°]		84.01(1)	−	−	−
β [°]		86.84(1)	−	97.64(1)	97.56(1)
γ [°]		66.40(1)	−	−	−
Volume [$pm^3 \cdot 10^6$]		1809.4(3)	2834.0(3)	2675.0(4)	2778.9(8)
Z		2	4	4	4
$D_{calcd.}$ [$g \cdot cm^{-3}$]		2.021	2.655	1.785	1.713
Absorption correction		numerical	empirical	numerical	empirical
$\mu_{Mo\text{-}K\alpha}$ [cm^{-1}]		55.7	58.1	38.5	19.4
Temperature [K]		193	223	193	183
2θ range		4.0−52.06	2.0−50.0	4.22−51.9	5.76−50.0
Index range	*h*	−14→14	−1→17	−12→12	−10→10
	l	−15→15	−2→15	−12→12	−44→0
	k	−17→17	−1→17	−33→33	0→10
Reflections collected		14079	3896	20729	5346
Unique reflections (R_{int})		6530 (0.069)	2498 (0.0244)	5214 (0.0628)	4898 (0.0698)
Reflections with $F_o > 4\ \sigma(F_o)$		3262	1996	3502	3129
Parameters		443	170	407	331
R_1		0.0366	0.0302	0.0464	0.0611
wR_2 (all data)		0.0579[a]	0.0735[b]	0.106[c]	0.1352[d]
largest diff. peak and hole [$(e \cdot pm^{-3}) \cdot 10^{-6}$]		−0.72/0.59	−0.58/0.71	−0.82/0.8	−1.33/0.73

[a] $w = 1/[\sigma^2(F_o)^2]$. − [b] $w = 1/[\sigma^2(F_o) + (0.0375 \cdot P)^2]$; $P = [\max(F_o^2,0) + 2F_c^2]/3$. − [c] $w = 1/[\sigma^2(F_o) + (0.0555 \cdot P)^2]$. − [d] $w = 1/[\sigma^2(F_o) + (0.0375 \cdot P)^2 + 3.91 \cdot P]$.

Table 2. Selected bond lengths [pm] and bond angles [°] in **2**−**5**

2				**3**		**4**		**5**	
Pd1−Br1	244.7(1)	Pd2−Br3	242.5(1)	Pd1−I1	257.50(6)	Pd1−Br1	242.75(8)	Pd1−I1	261.58(9)
Pd1−Br2	240.75(9)	Pd2−Br4	244.10(9)	Pd1−I2	259.73(6)	Pd1−P1	225.0(1)	Pd1−P1	225.0(3)
Pd1−S1	225.2(2)	Pd2−S2	225.9(2)	Pd1−S1	227.4(2)	Pd1−S1	227.5(2)	Pd1−S1	226.6(2)
Pd1−N2	204.2(6)	Pd2−N6	205.3(8)	Pd1−N2	207.9(5)	Pd1−N2	211.0(5)	Pd1−N2	209.5(7)
S1−C1	169.4(7)	S2−C5	168.5(8)	S1−C1	169.2(6)	S1−C1	171.1(5)	S1−C1	173.1(9)
N1−N2	144.7(8)	N5−N6	144.3(8)	N1−N2	144.3(6)	N1−N2	141.3(7)	N1−N2	143(1)
C1−N1	136.8(7)	N5−C5	137.3(8)	N1−C1	135.3(7)	N1−C1	135.0(7)	N1−C1	137(1)
O1−C2	124.7(8)	O2−C6	121.2(8)	O1−C2	121.2(7)	O1−C2	119.8(8)	O1−C2	122(1)
N4−C1	131.3(8)	N8−C5	133.2(9)	N1−C2	138.7(7)	N1−C2	140.7(7)	N1−C1	140(1)
N3−N4	136.5(8)	N7−N8	137(1)	N3−N4	136.2(7)	N3−N4	137.4(6)	N3−N4	138(1)
Br1−Pd1−Br2	93.46(4)	Br3−Pd2−Br4	92.80(4)	I1−Pd1−I2	91.78(2)	Br1−Pd1−S1	172.90(4)	I1−Pd1−S1	171.38(7)
Br1−Pd1−S1	176.43(6)	Br3−Pd2−S2	91.21(6)	I1−Pd1−S1	91.04(4)	Br1−Pd1−P1	92.09(4)	I1−Pd1−P1	92.64(7)
Br2−Pd1−S1	89.82(6)	Br4−Pd2−S2	174.48(6)	I2−Pd1−S1	177.19(5)	S1−Pd1−P1	93.97(5)	S1−Pd1−P1	92.73(9)
Br1−Pd1−N2	89.5(2)	Br3−Pd2−N6	177.9(2)	I1−Pd1−N2	176.8(1)	Br1−Pd1−N3	88.8(1)	I1−Pd1−N2	89.6(2)
Br2−Pd1−N2	176.6(2)	Br4−Pd2−N6	89.2(2)	I2−Pd1−N2	91.2(1)	S1−Pd1−N2	84.8(1)	S1−Pd1−N2	85.3(2)
S1−Pd1−N2	87.3(2)	S2−Pd2−N6	86.9(2)	S1−Pd1−N2	86.0(1)	P1−Pd1−N2	174.5(1)	P1−Pd1−N2	176.7(2)
Pd1−N2−N1	114.3(4)	Pd2−N6−N5	114.3(5)	Pd1−N2−N1	114.1(3)	Pd1−S1−C1	97.3(2)	Pd1−S1−C1	99.7(3)
Pd1−S1−C1	97.6(3)	Pd2−S2−C5	97.9(3)	Pd1−S1−C1	97.9(2)	Pd1−N2−N1	114.0(3)	Pd1−N2−N1	114.8(5)

C), 1552 (m), 1500 (m), 1437 (m), 1322 (m), 1301 (m), 1228 (m), 1160 (vw), 1097 (m), 1008 (m), 968 (m), 928 (w), 847 (w), 746 (m), 691 (m), 639 (w), 602 (w), 534 (m), 506 (m), 449 [m, ν(PdN)], 409 (w), 374 [w, ν(PdS)], 308 (w), 285 (w), 227 (w), 198 [w, ν(PdI)], 139 (vw), 124 (vw). – ^{31}P NMR (CD_3OD): δ = 26.2 (s).

Crystal Structure Analyses of 2, 3, 4, and 5 (Table 1 and 2): The selected crystals of **2**–**5** were covered with a perfluorinated oil and mounted on the tip of a glass capillary under a flow of cold gaseous nitrogen. The orientation matrix and preliminary unit cell dimensions were determined from 2000 (**2**, Stoe IPDS), 2000 (**3**, Stoe IPDS), 15 (**4**, Siemens P4), and 15 (**5**, Enraf-Nonius CAD4) reflections (graphite-monochromated Mo-K_α radiation in all cases; λ = 71.073 pm). The final cell parameters were determined from 5000 reflections for **2** and **5**, and from 25 high-angle reflections for **3** and **4**. The intensities were corrected for Lorentz and polarization effects. In addition, absorption corrections were applied for **2** (numerical), **3** (empirical, 10 psi-scans), **4** (numerical), and **5** (empirical, 10 psi-scans). The structures were solved by the Patterson method for **2** and by direct methods for **3**–**5** (SHELXTL-Plus[14]) and refined against F^2 by full-matrix least-squares using the program SHELXL-97.[15] The hydrogen atoms (C–H) in **2** and **5** were calculated in ideal positions (refinement with a common displacement parameter). The hydrogen atoms of the NH groups were fixed at 85 pm (**2**) or freely refined (**5**). The positions of the H atoms in **3** were freely refined, except for the N2–H2, N3–H3, and O2–H4 distances, which were fixed at 85 pm. The hydrogen atoms in **4** were freely refined. Programs used were SHELXTL-Plus, SHELXL-97, SHELXTL,[16] ORTEP,[17] and PLATON.[18] Splitting models were applied to the following atoms: C181, C182 (and adjacent H atoms, occupancy factors: 0.7, 0.3; **2**); O3, C9, C10, C11, C12 (occupancy factor: 0.5; **2**), H5, H61, H62, H63 (occupancy factor: 0.5; **3**).[19]

Acknowledgments

Support of this work by the Deutsche Forschungsgemeinschaft and the Fonds der Chemischen Industrie is gratefully acknowledged.

[1] [1a] H. Neunhoeffer, in *Comprehensive Heterocyclic Chemistry*, vol. 3 (Eds.: A. R. Katritzky, C. W. Rees), Pergamon Press, Oxford, **1984**, p. 385–456. – [1b] M. Akbar Ali, S. E. Livingstone, *Coord. Chem. Rev.* **1974**, *13*, 101–132. – [1c] K. Severin, R. Bergs, W. Beck, *Angew. Chem. Int. Ed.* **1998**, *37*, 1722–1743.

[2] F. Adhami, M. Ghassemzadeh, M. M. Heravi, A. Taeb, B. Neumüller, *Z. Anorg. Allg. Chem.* **1999**, *625*, 1411–1412.

[3] M. Ghassemzadeh, K. Aghapoor, M. M. Heravi, B. Neumüller, *Z. Anorg. Allg. Chem.* **1998**, *624*, 1969–1972.

[4] B. Neumüller, M. M. Heravi, M. Ghassemzadeh, *Z. Anorg. Allg. Chem.* **1999**, *625*, 1908–1911.

[5] J. Weidlein, U. Müller, K. Dehnicke, *Schwingungsfrequenzen II*, Thieme Verlag, Stuttgart, **1986**.

[6] A. G. Orpen, L. Brammer, F. H. Allen, O. Kennard, D. G. Watson, R. Taylor, *J. Chem. Soc., Dalton Trans.* **1989**, S1–S83.

[7] [7a] T. Tuntulani, G. Musie, J. H. Reibenspies, M. Y. Darensbourg, *Inorg. Chem.* **1995**, *34*, 6279–6286. – [7b] J. Real, M. Pages, A. Polo, J. F. Piniella, A. Alvarez-Larena, *Chem. Commun.* **1999**, 277–278. – [7c] M. Gupta, R. E. Cramer, K. Ho, C. Pettersen, S. Mishina, J. Belli, C. M. Jensen, *Inorg. Chem.* **1995**, *34*, 60–65.

[8] J. E. Huheey, *Anorganische Chemie*, de Gruyter, Berlin, **1988**.

[9] [9a] R. Martin, H. J. Keller, B. Müller, *Z. Naturforsch*. **1985**, *40B*, 57–60. – [9b] T. N. Margulis, L. J. Zompa, *Inorg. Chim. Acta* **1992**, *201*, 61–67. – [9c] T. J. Giordano, W. M. Butler, P. G. Rasmussen, *Inorg. Chem.* **1978**, *17*, 1917–1922. – [9d] H. A. Ankersmit, P. T. Witte, M. Kooijman, M. T. Lakin, A. L. Spek, K. Goubitz, K. Vrieze, G. van Koten, *Inorg. Chem.* **1996**, *35*, 6053–6063. – [9e] P. F. Kelly, A. M. Z. Slawin, A. Soriano-Rama, *J. Chem. Soc., Dalton Trans.* **1996**, 53–59. – [9f] A. D. Ryabov, L. G. Kuz′mina, V. A. Polyakov, G. M. Kazankov, E. S. Ryabova, M. Pfeffer, R. van Eldik, *J. Chem. Soc., Dalton Trans.* **1995**, 999–1006. – [9g] A. Mayr, L.-F. Mao, *Inorg. Chem.* **1998**, *37*, 5776–5780. – [9h] A. S. Hirschon, W. K. Musker, M. M. Olmstead, J. L. Dallas, *Inorg. Chem.* **1981**, *20*, 1702–1706. – [9i] Z. Guo, U. Caselatto, G. Faraglia, R. Graziani, S. Sitran, *J. Chem. Soc., Dalton Trans.* **1993**, 2509–2513. – [9j] M. Kubota, S. Ohba, Y. Saito, *Acta Crystallogr.* **1991**, *C47*, 1727–1729.

[10] L. Pauling, *The Nature of the Chemical Bond*, 3rd ed., Cornell University Press, New York, **1960**.

[11] Established by a search of the Cambridge Structural Database: see F. H. Allen, O. Kennard, R. Taylor, *Acc. Chem. Res.* **1983**, *16*, 146–153.

[12] [12a] J. Vincente, I. Saura-Llames, M. G. Palin, P. G. Jones, M. C. R. de Arellano, *Organometallics* **1997**, *16*, 826–833. – [12b] J. Vicente, I. Saura-Llamas, P. G. Jones, *J. Chem. Soc., Dalton Trans.* **1993**, 3619–3624. – [12c] J. Albert, J. Granell, A. Luque, M. Font-Bardia, X. Solans, *J. Organomet. Chem.* **1997**, *545*, 131–137. – [12d] J. Albert, J. Granell, R. Moragas, M. Font-Bardia, X. Solans, *J. Organomet. Chem.* **1996**, *522*, 59–67. – [12e] J. Albert, J. Granell, A. Luque, J. Minguez, R. Moragas, M. Font-Bardia, X. Solans, *J. Organomet. Chem.* **1996**, *522*, 87–95. – [12f] J. Albert, J. Granell, J. Sales, M. Font-Bardia, X. Solans, *Organometallics* **1995**, *14*, 1393–1404. – [12g] T. Debaerdemaeker, A. Kutoglo, G. Schmid, L. Weber, *Acta Crystallogr.* **1973**, *B29*, 1283–1288. – [12h] E. van der Voort, P. van der Sluis, A. L. Spek, *Acta Crystallogr.* **1987**, *C43*, 461–463. – [12i] R. F. Wu, I. J. B. Lin, G. H. Lee, M. C. Cheng, Y. Wang, *Organometallics* **1990**, *9*, 126–130.

[13] A. Dornow, H. Menzel, P. Marx, *Chem. Ber.* **1964**, *97*, 2173–2178.

[14] G. M. Sheldrick, *SHELXTL-Plus*, Release 4.2 for Siemens R3 Crystallographic Systems, Siemens Analytical X-ray Instruments Inc., Madison (WI), **1990**.

[15] G. M. Sheldrick, *SHELXL-97*, Universität Göttingen, **1997**.

[16] G. M. Sheldrick, *SHELXTL*, Release 5.05/VMS for Siemens R3 Crystallographic Research Systems, Siemens Analytical X-ray Instruments Inc., Madison (WI), **1996**.

[17] C. K. Johnson, *ORTEP*, ORNL-3794, Oak Ridge National Laboratory, Tennessee, **1965**.

[18] A. L. Spek, *PLATON-98*, Universiteit Utrecht, **1998**.

[19] Further details can be obtained free of charge on application to the Cambridge Crystallographic Data Centre, 12 Union Road, Cambridge CB2 1EZ, U.K. [Fax: (internat.) +44 (0)1223 336033; E-mail: deposit@ccdc.cam.ac.uk] quoting the depository nos. CCDC-141168 (**2**), -141169 (**3**), -141170 (**4**), and -141171 (**5**).

[20] *International Tables for Crystallography*, 2nd ed., vol. A, Kluwer Academic Publishers, Dordrecht, **1989**.

Received March 2, 2000
[I00082]

Special Siloxamides: Metal Movements in a Crystalline Molecular Box

Michael Veith[a]

In memoriam Prof. Dr. H.-G. Unruh

Keywords: Lithium / Solid-state structures / Phase transitions / Si ligands / Dynamics in molecular solids

Metal salts of $[R–O–SiMe_2–N–SiMe_2–O–R]^-$ and $[R–N–SiR'_2–O–SiR'_2–N–R]^{2-}$ (R = *t*Bu, Me_3Si, *t*$BuMe_2Si$, Ph; R′ = Me, Et/Me, *i*Pr; Metal = Li, Na, K, Cu, Ag) have been synthesised and analysed in the crystalline state with respect to metal movements. Almost all compounds crystallize as dimers, for example $Li_2[t$BuO–$SiMe_2$–N–$SiMe_2$–O*t*$Bu]_2$ or $Li_4[t$BuN–$SiMe_2$–O–$SiMe_2$–N*t*$Bu]_2$, and form different solid-state phases. Whereas the Li atoms in the first example rotate at ambient temperature perpendicular to the NN axis of the molecule, they oscillate in the second example. The movements of the lithium atoms are coupled to ligand vibrations, and can be switched on and off by temperature changes. This switching is directly linked to phase transitions, that can be first order or second order. The other metallic atoms show no important dynamics, although phase transitions have also been found for these compounds.

Introduction

In the last ten years we have become aware of the fact that special amides of metallic elements (lithium amides being the most prominent representatives) show fluxional behaviour, mostly when dissolved in non-coordinating organic solvents.[1–3] The phenomenon is known for many amides of the main-group and transition-group metals, and the dynamics of these compounds can easily be followed by temperature-dependent NMR spectroscopy.[4] On analysing the molecules in more detail we found, compared to all other elements, the small lithium atoms in the amides have the largest amplitudes of movement, and that these amplitudes and the trajectories of the movements can be influenced by the composition of the amides. A spectacular example is the mixed metal amide $LiIn[(Me_3SiN)_2SiMe_2]_2$:[5] In this molecule the indium atom with a formal charge +3 is coordinated by the four nitrogen atoms, forming an indium-centred N_4 bisphenoid (elongated tetrahedron), pushing the lithium atom, with a formal charge +1, to the surface of the N_4 polyhedron. Because the lithium atom in this molecule is less tightly bound, it occupies several similar coordination sites, and in solution it rotates, over a certain time period, around the indium-centred N_4 core. The movement of the lithium atom can be determined experimentally, either by temperature-dependent ^{7}Li-, ^{13}C-, ^{1}H-, ^{29}Si-NMR spectroscopy, or by theoretical calculations.[6]

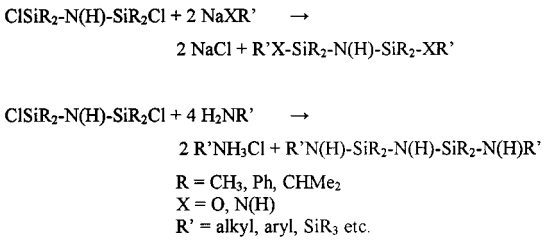
We were interested in finding out if similar lithium movements could be observed in crystalline solids. As the constraints of the crystal packing on the molecules and the intermolecular forces seemed to make such an attempt quite fruitless, we developed a concept which had two main ideas. The first idea was to use molecules which had a globular outer hydrogen shell to minimise the intermolecular van der Waals interactions. The second idea was to incorporate coordination holes in the molecular skeleton, so as to facilit-

[a] Institut für Anorganische Chemie, Universität des Saarlandes
Postfach 151150, 66041 Saarbrücken, Germany
Fax: (internat.) + 49-(0)681/302-3995
E-mail: veith@rz.uni-sb.de

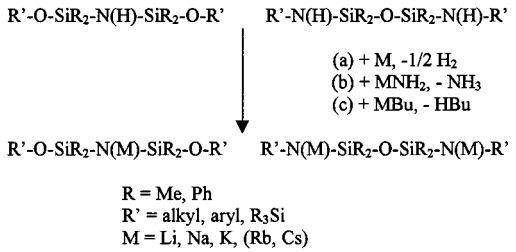


Michael Veith was born in 1944 in Goerlitz, Germany. He studied chemistry at the University of Munich, where he received his Diplom-Chemiker degree in 1969. Continuing work with Prof. N. Wiberg, he received his doctoral degree in 1971. He then moved to the University of Karlsruhe, where he started his postdoctoral work with Prof. H. Bärnighausen. In 1977 he completed his Habilitation in Inorganic Chemistry. Until the end of 1978 he was Privat-Dozent at the University of Karlsruhe. In 1979 he moved to the Technische Universität Braunschweig as a Professor of Inorganic Chemistry. In 1984 he moved to the University of Saarland (Saarbrücken) and became Full Professor. Since 1984 he has been in Saarbrücken despite several offers from other universities. He has received several awards, inter alia Leibniz-Preis, 1991. In 1981, he stayed as a visiting professor at the University of Bordeaux I (France) and in 1987 at the University of Utah (Salt Lake City, USA), in 1991 at the University Paul Sabatier (Toulouse, France), and in 1993 at the University Sophia Antipolis (Nice, France). His main interests are in the field of synthetic and structural chemistry, focusing on molecular compounds containing metal elements.

 © WILEY-VCH Verlag GmbH, D-69451 Weinheim, 2000 1434–1948/00/0909–1883 $ 17.50+.50/0



Scheme 1



Scheme 3

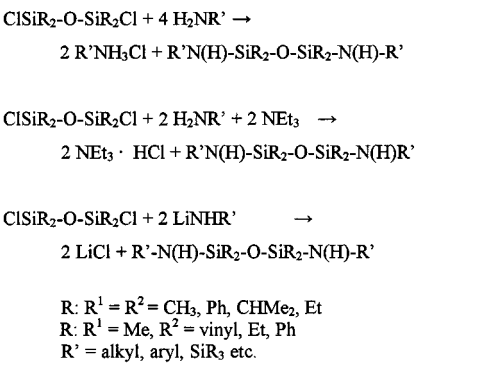
ate metal hops from an occupied non-metal coordination sphere to an unoccupied one.

The following compilation, which can be seen as an advanced report with a review-like character, is a summary of our actual knowledge on the motion of monovalent metal atoms in the molecular crystals of special metal amides. We would like to describe these dynamics as "lithium motion (or tunnelling) in a molecular box". The compounds we have investigated belong either to the series $[R'-O-SiR_2-N-SiR_2-O-R']_2M_2$ or to the series $[R'-N-SiR_2-O-SiR_2-N-R']_2M_4$ (R′ = substituent, M = monovalent metal, R = organic group). While these experiments were being conducted, several papers appeared on either lithium movements[7] or the use of the amido ligands specified above as assembling tools for different metallic elements.[8,9]

Syntheses

The most valuable precursor compounds for the siloxamines $R'-O-SiR_2-N(H)-SiR_2-O-R'$ and $R'-N(H)-SiR_2-O-SiR_2-N(H)-R'$ are either the bis(silyl)amine $ClSiR_2-N(H)-SiR_2Cl$[10] or the disiloxane $ClSiR_2-O-SiR_2Cl$.[11] As shown in Scheme 1 and Scheme 2, the chlorine atoms of chlorosilylamines and chlorosiloxanes can be easily substituted by amido or alkoxo groups in a straightforward way.[4]

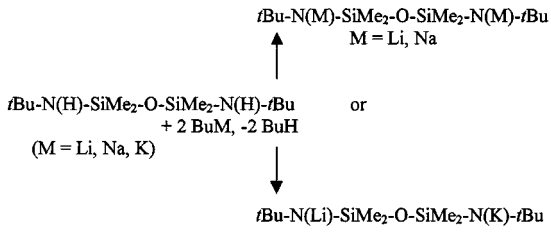
The transformation of these siloxamines into siloxamides can be achieved by a redox/metal route (a), a transamidation (b), or by organometallic compounds (c). All three possible reactions are shown in Scheme 3.[4]



Scheme 2

The reactions are very dependent on the alkali element and the substituent R′. The higher the electropositive character of the R′ group (e.g. CMe_3 vs. $SiMe_3$) the more preferable the replacement of the hydrogen atom by the alkali metal atom. Similarly, more electropositive alkali elements will normally more easily replace the hydrogen atom attached to the nitrogen atom. Finally, the organometallic route (3c) is more generally applicable, and gives the best yields for the metal amides.

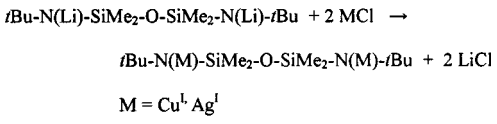
The solvents for these reactions should be completely dry and noncoordinating, such as pentane, hexane, and toluene, since adducts of the solvent with the alkali metals have to be avoided. The more electropositive alkali elements K, Rb, and Cs do not always give pure compounds, and are introduced into the amine $R'-N(H)-SiR_2-O-SiR_2-N(H)-R'$ less readily than lithium or sodium. This feature is exemplified by the reaction of tBu−N(H)−$SiMe_2$−O−$SiMe_2$−N(H)−tBu with butyllithium, -sodium,[12] and -potassium.[13] While the pure dilithium and disodium derivatives can be obtained in the first two cases, for potassium only a mixed metal derivative is obtained, which incorporates lithium as well as potassium (Scheme 4).



Scheme 4

The explanation for this unexpected reaction is the incomplete transformation of BuLi to BuK, when butyllithium is treated with potassium *tert*-butoxide prior to the reaction with the amine. Perhaps the "incomplete" BuK formation could be avoided by using potassium *tert*-pentoxide instead of potassium *tert*-butoxide.[14] Interestingly, the mixed metal derivative is isolated in high yields, which suggests that both metal atoms may be especially well accommodated in the molecule. As a matter of fact, tBu−N(Li)−$SiMe_2$−O−$SiMe_2$−N(K)−tBu is dimeric, as are most of the other derivatives, and the two alkali elements have very different coordination spheres (see below for more details of the structure). This structure cannot be achieved in a pure dilithium or dipotassium derivative.

The alkali metal derivatives shown in Scheme 3 can be transformed into other metal derivatives, using metal halides. Especially monovalent transition metals were of interest for our general study. The copper(I) and silver(I) derivatives of the $[t\text{Bu}-\text{N}-\text{SiMe}_2-\text{O}-\text{SiMe}_2-\text{N}-t\text{Bu}]^{2-}$ dianion have been obtained in high yields using this route (Scheme 5).



Scheme 5

The siloxamides of most alkali elements as well as the Cu^I and Ag^I derivatives that have been synthesised and characterised by our group are listed in Table 1.[15–19] Most of these compounds are dimeric in solution and in the crystalline state. So far there is only one exception to this rule: The compound $t\text{Bu}-\text{N(Li)}-\text{Si}(i\text{Pr})_2-\text{O}-\text{Si}(i\text{Pr})_2-\text{N(Li)}-t\text{Bu}$ is monomeric in solution as well as in the crystal (see also below).

The solution NMR spectra of the two families $[\text{R}'\text{OSiR}_2-\text{N(M)}-\text{SiR}_2\text{OR}']_2$ and $[\text{R}'\text{N(M)}-\text{SiR}_2-\text{O}-\text{SiR}_2-\text{N(M)R}']_2$ at room temperature are very simple, as all substituents R and R′ (^{1}H, ^{13}C NMR) and silicon atoms of the siloxamine backbone (^{29}Si) give resonances for only one species, the other groups being symmetry-related. This is in sharp contrast to the generally less symmetrical molecules in the crystalline solid. Consequently, many of these molecules show bond fluctuations in solution that are connected with metal movements or displacements. As we wanted to concentrate on such dynamics in the solid state, we will not discuss the solution phenomenon here in more detail.

Table 1. Siloxamides of the two different backbones O−Si−N−Si−O (**A**) and N−Si−O−Si−N (**B**)

	A
Z	$R_3C-O-SiMe_2-N-SiMe_2-O-CR_3$, R = CH_3 **Li_2Z_2, Na_2Z_2, K_2Z_2, Rb_2Z_2**
Z′	$Ph-O-SiMe_2-N-SiMe_2-O-Ph$ **$Li_2Z'_2$**
Z″	$Me_3Si-O-SiMe_2-N-SiMe_2-O-SiMe_3$ **$Li_2Z''_2$**
	B
X	$R_3C-N-SiR_2-O-SiR_2-N-CR_3$, R = CH_3 **Li_4X_2, Na_4X_2, $Li_2K_2X_2$, Cu_4X_2, Ag_4X_2**
X′	$R_3C-N-SiRR'-O-SiRR'-N-CR_3$, R = CH_3, R′ = $CH{=}CH_2$ **$Li_4X'_2$**
X^I	$R_3C-N-SiRR'-O-SiRR'-N-CR_3$, R = CH_3, R′ = CH_2-CH_3 **$Li_4X^I_2$, $Na_4X^I_2$**
X^{II}	$R_3C-N-SiR'_2-O-SiR'_2-N-CR_3$, R = CH_3, R′ = $CH(CH_3)_2$ **Li_2X^{II}**
L	$R_3Si-N-SiR_2-O-SiR_2-N-SiR_3$, R = CH_3 **Li_4L_2, Na_4L_2**
L′	$R_2R'Si-N-SiR_2-O-SiR_2-N-SiR'R_2$, R = CH_3, R′ = $C(CH_3)_3$ **$Li_4L'_2$**

Structural Characterisations of the Siloxamides

As the goal of our investigations was to study movements of atoms or molecular entities within a molecule, we have used different structural analysis techniques like X-ray diffraction on single crystals or powders, broad-line or MAS (magic angle spinning) NMR, differential thermal analysis (DTA), and Raman spectroscopy on single crystals. All these techniques have been used in the temperature-dependent mode, generally in the range between 120 and 350 K, using liquid nitrogen as a cooling agent or as a heated gas flow. Light microscopy on single crystals using polarised or cross-polarised light in the same temperature range was also employed. To verify our assumptions, which are based on our experimental results, we have tentatively used molecular dynamics calculations with mostly standard parameters.[20]

It became more and more evident from our experiments that phase transitions are connected with movements in the solid state. To avoid complications such as twinning, arising from symmetry reductions in single crystals, we have systematically also done X-ray diffraction experiments from phases, which have been grown as single crystals in the appropriate temperature range. Furthermore, we collected most of the X-ray diffraction data on a two-dimensional screen (IPDS system of Stoe, Darmstadt) in small angle steps, in order to obtain information about the whole reciprocal space.

High symmetries corresponding to unusual space groups for molecules can come either from dynamics or from severe static disorder of the constituent atoms. In this respect, the combination of X-ray diffraction techniques with solid-state NMR techniques is an excellent tool for deciding between these two possibilities.

Our findings are presented in several chapters which are linked in some logical sense (to follow and to verify our assumptions they have to be read together).

Rotation of Lithium Atoms within a Molecule: Siloxamides with the Skeleton O−Si−N−Si−O

The compound $\text{Li}_2[t\text{Bu}-\text{O}-\text{SiMe}_2-\text{N}-\text{SiMe}_2-\text{O}t\text{Bu}]_2$, designated in the following sections as **Li_2Z_2**, forms three different crystalline phases in the solid state.[15] At temperatures < 285 K a monoclinic phase is found, space group $P2_1/n$ with $Z = 4$. The space group with the number of molecules per cell is consistent with a close packing of organic molecules using the well-established principles of Kitaigorodskii.[21] A drawing of the molecule at 220 K is shown in Figure 1.

There are two main observations: The two "anionic" ligands within the molecule are opposite to each other in a cross-like manner, and are linked by two lithium "cations", which are bisphenoidally coordinated by two nitrogen and two oxygen atoms ("elongated" tetrahedron). The zigzag chain C−O−Si−N−Si−O−C is a little bit twisted, but the deviation from the plane is not intriguing, as the largest dihedral angle of two adjacent angles (O−Si−N−Si and Si−N−Si−O) is around 20°. As a consequence of these

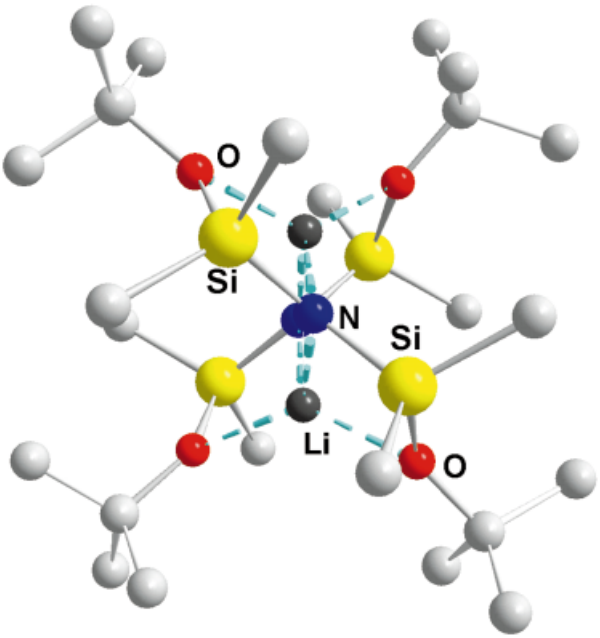


Figure 1. Spectroscopic view of $Li_2[t\text{Bu}-O-SiMe_2-N-SiMe_2-O t\text{Bu}]_2$, **$Li_2Z_2$**, in the monoclinic low-temperature phase (220 K), as obtained from X-ray diffraction analysis; view almost parallel to the NN axis of the molecule; for some distances and angles refer to Table 2

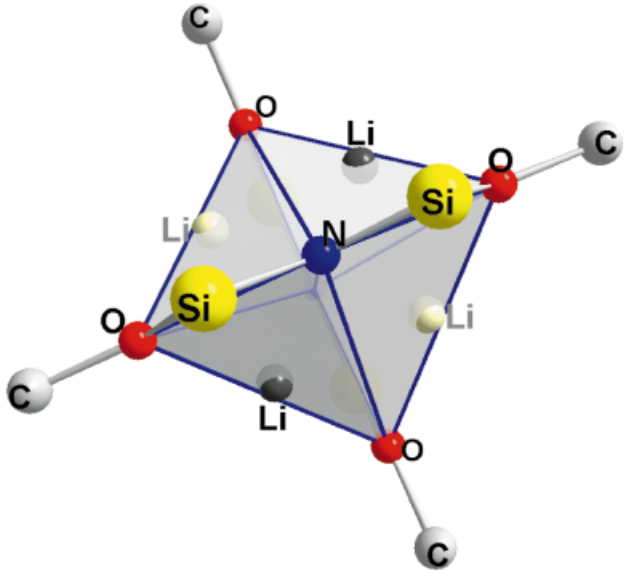


Figure 2. Inner part of the atomic skeleton of $Li_2[t\text{Bu}-O-SiMe_2-N-SiMe_2-O-t\text{Bu}]_2$ in the tetragonal phase (295 K), as obtained from X-ray diffraction analysis; the coordination polyhedra are drawn; each of the four N_2O_2 holes is occupied with Li/2 (see text)

mutual orientations of the ligands, two other bisphenoidal O_2N_2 coordination spheres are formed, that are unoccupied. In exact correspondence to the X-ray structure analysis of the monoclinic phase of **Li_2Z_2**, the ^{13}C-MAS NMR spectrum of the crystalline powder is quite complex, showing a multiplet of signals in the H_3C-Si region, that after deconvolution can be shown to be a superposition of eight equal signals due to eight different carbon atoms bonded to the four non-equivalent silicon atoms. Due to quadrupolar coupling of the coordinated nitrogen atoms, the ^{29}Si-MAS NMR resonances are broadened and structured, but it can again be shown that more than two resonances from silicon atoms are present in the spectrum (X-ray crystallography shows that four different silicon atoms are present in the unit cell).

When **Li_2Z_2** is allowed to warm up to room temperature (295 K), a new phase is found that is tetragonal (space group $P4_2/nmc$ with $Z = 2$). Whereas **Li_2Z_2**, in the monoclinic phase lacks symmetry [point symmetry $C_1(1)$], in the tetragonal phase the point symmetry is $D_{2d}(\bar{4}2m)$. The phase transition is reversible with a small hysteresis and an endothermic heat ($\Delta H = +0.45$ kJ/mol). The refinement of the X-ray structure of **Li_2Z_2** in $P4_2/nmc$ has only been possible with relatively high anisotropic displacement factors for Si, O, and N, and split atoms for most of the carbon atoms, the primary carbon atoms of the *tert*-butyl group being disordered around the O−C axis. The most striking feature is nevertheless the splitting of the two lithium atoms that occupy, with half of their electron count, the four coordination holes formed by the four oxygen and two nitrogen atoms (see Figure 2).

Again all the findings in the X-ray diffraction experiments are paralleled in the solid-state NMR spectra. The multiplet of the silyl carbon atoms of the monoclinic phase of **Li_2Z_2** after transition to the tetragonal phase degenerates to a single resonance line (^{13}C-MAS NMR). All carbon atoms of the dimethylsilyl groups become equivalent, consistent with the $D_{2d}(\bar{4}2m)$ point symmetry of the molecule. The silicon multiplet (^{29}Si-MAS NMR) also becomes a singlet after phase transition (not considering the quadrupolar splitting by N). These two experiments unambiguously show that the higher point symmetries found in the X-ray structure analysis are due to *dynamic* and not *static* disorder.

From the X-ray structure analysis of **Li_2Z_2** (considering temperature factors and split atom positions) we found that the lithium atoms (or in an ionic model: cations) clearly move to a larger extent than all other atoms of the molecule. The lithium movement can be followed directly by use of ^{6}Li- and ^{7}Li-NMR experiments applying the broad-line mode and the MAS mode. How can we describe this movement in the tetragonal phase? The most simple explanation would be that the lithium atoms (ions) are jumping from the occupied bisphenoidal O_2N_2 holes into the unoccupied ones. An approximate calculation (molecular mechanics in vacuo) of the barrier for this process using the parameters from the X-ray structure determinations of the monoclinic and tetragonal phase show that this jumping should be quite unfavourable, with activation energies around 60 kJ/mol (the lithium atoms are assumed to be positively charged).[20] Things become quite different, when the simultaneous movement of the ligands is included in the calculations: Now the barriers are drastically lowered and the activation energy is estimated to approximately 10 kJ/mol at 20°C.[20]

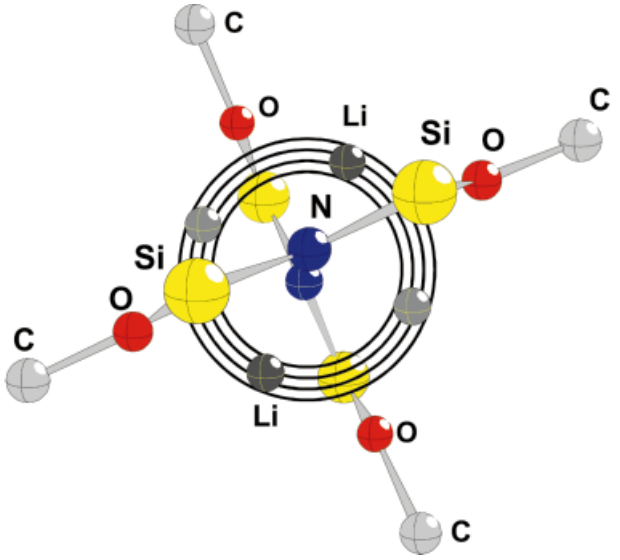


Figure 3. Sketch of the intramolecular lithium movements in the tetragonal phase of $Li_2[t\text{Bu}-O-SiMe_2-N-SiMe_2-O t\text{Bu}]_2$; the four split atom positions of lithium are shown; it should be noted that the lithium movements are accompanied by atom vibrations of the ligands (see also Figure 2)

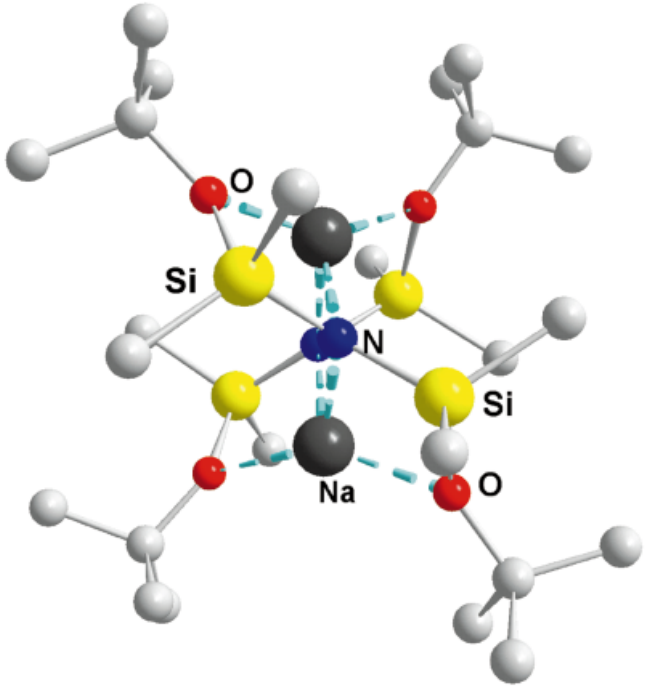


Figure 4. One of the two molecules [crystal point symmetry $C_2(2)$] present in the monoclinic phase of $Na_2[t\text{Bu}-O-SiMe_2-N-SiMe_2-O t\text{Bu}]_2$ (**Na_2Z_2**); for some distances and angles refer to Table 2; the view of the molecule is taken almost parallel to the NN axis of the molecule

In a crystalline solid, the amplitudes of movements of the atoms are nevertheless limited. On the other hand, the molecular shape and packing of **Li_2Z_2** is quite special; as can be deduced from two phenomena: The methyl groups of the *tert*-butyl moieties are turning around their O−C axes (as can be derived from X-ray structure analysis and ^{13}C-MAS NMR). The other phenomenon is found at temperatures > 400 K, where a second phase transition occurs and **Li_2Z_2** crystallises in a cubic face-centred lattice. This high-temperature phase is typical of a "plastic crystal phase", with molecules "tumbling" around their centres of gravity. Such "plastic crystal phases" are known for molecules that are either very globular in shape or possess weak intermolecular van der Waals interactions.[21]

Considering these two pieces of information, and the geometrical constraint of the O_2N_2 holes within the molecule, the movements of the lithium atoms can be described as follows: the lithium atoms, which to a first approximation can be assumed to be charged +1, are turning around the NN axis of the molecule, jumping from one O_2N_2 hole to the neighbouring hole. As the distances between two neighbouring N_2O_2 holes are small (the centres are 1.45 Å apart from one another in the tetragonal phase), the lithium atoms have to jump (or to turn) *simultaneously* to reduce the Li−Li repulsive forces. In Figure 3 the model of this rotation is sketched. Two models for the lowering of the activation energy can be discussed: One is using the tunnelling approach, assuming the lithium cations to be quite small. The other is considering, in addition to the jumping of the Li ions, a simultaneous high vibrational freedom of the ligands, which in the free molecule would lower the activation energy considerably (vide supra). Anyhow, the high displacements of vibration of the ligands have to be coupled to the lithium movements.

The two phase transitions in the solid **Li_2Z_2** are of first order, as can be deduced from the sharp changes of the cell parameters or of the spectroscopic properties (NMR) at the transition points. An elegant way to follow the phase transitions is Raman spectroscopy on single crystals: these methods show clearly that the two transitions occur instantaneously without softening of any vibrational mode.[22] Again this agrees with first-order phase transitions. Nevertheless, the hysteresis of the phase transition between the monoclinic and tetragonal phase is quite small, and the "lithium rotations" can be switched on and off, just by changing the temperature. Interestingly, this can even be made with a single crystal, which does not fall to pieces, as the volume of the cells is approximately unchanged (taking the double tetragonal cell). $P4_2/nmc$ and $P2_1/n$ are symmetry-related, but not in a direct super group/sub group relationship.[15]

We were very curious to know how an exchange of the lithium atom by sodium would influence the phase transitions, especially the movements in the molecules within the crystal lattice. Sodium has a larger radius compared to lithium [$r(Li^+) \approx 0.76$ Å; $r(Na^+) \approx 1.02$ Å], and its mass is approximately three times that of lithium.[23] Under these circumstances, a tunnelling of sodium cations seemed to be very improbable. The molecule $Na_2[t\text{BuO}-SiMe_2-N-SiMe_2-O t\text{Bu}]_2$, [**$Na_2Z_2$**], crystallises at temperatures below 250 K in an unknown lattice, and between 250 K and 350 K in the monoclinic space group $P2/n$ with $Z = 4$, very differently from **Li_2Z_2**. In the room-temperature phase there are two independent molecules in the unit cell, both situated on two-fold axes of the space group. In Figure 4 the

Table 2. Comparison of M−N, M−O, MM, NN, OO, and NO distances [Å] and O−M−O angles [°] in the two molecules $M_2[t\text{BuO}-\text{SiMe}_2-\text{N}-\text{SiMe}_2-\text{O}t\text{Bu}]_2$, $\mathbf{Li_2Z_2}$ (230 K) and $\mathbf{Na_2Z_2}$ (290 K); mean values, monoclinic phases

	M−N	M−O	NN	OO[a]	NO	OO[b]	O−M−O	MM
$\mathbf{Li_2Z_2}$	2.075(8)	1.990(8)	3.333(7)	3.711(7)	3.134(7)	4.504(7)	136.2(1)	2.473(9)
$\mathbf{Na_2Z_2}$	2.433(5)	2.282(5)	3.842(7)	4.456(7)	3.452(7)	5.001(7)	155.0(1)	2.972(4)
Δ [$\mathbf{Na_2Z_2}$ − $\mathbf{Li_2Z_2}$]	0.358	0.292	0.509	0.745	0.318	0.497	18.8	0.499

[a] N_2O_2 hole occupied by M. − [b] Unoccupied N_2O_2 hole.

molecular structure of one $\mathbf{Na_2Z_2}$ species is drawn; the two molecules differ from each other by the degree of disorder of the *tert*-butyl groups around the O−C axis. The molecules approach the D_2(222) point symmetry very closely, as may also be deduced from inspection of Figure 4.

Two major differences may be seen by comparing the monoclinic phases of $\mathbf{Na_2Z_2}$ with $\mathbf{Li_2Z_2}$. One discrepancy between the two compounds is easily recognised by closer inspection: The zigzag O−Si−N−Si−O chain in $\mathbf{Na_2Z_2}$ deviates more from an equiplanar arrangement (the mean O−SiSi−O dihedral angle is 73°) than in $\mathbf{Li_2Z_2}$ (45°). Consequently, looking down the NN axis of the molecule, the four silicon atoms with the nitrogen atoms are less perpendicularly oriented ($\mathbf{Na_2Z_2}$: Si−NN−Si = 116°) than in $\mathbf{Li_2Z_2}$ (Si−NN−Si = 100°). The second difference can be seen in the Na−O and Na−N distances in $\mathbf{Na_2Z_2}$. They are longer than the corresponding Li−O and Li−N distances in $\mathbf{Li_2Z_2}$ (monoclinic phases), and the sodium atoms (ions) are located far away of the centres of N_2O_2 holes (see also Δ values in Table 2). The lithium atoms are better accommodated in the O_2N_2 holes than the sodium atoms, which can for example be deduced from the O−Li−O angle (136°) and the corresponding angle in $\mathbf{Na_2Z_2}$ O−Na−O (155°). The large value of the latter shows that it tends towards linearity. The solid-state NMR spectra of $\mathbf{Na_2Z_2}$ agree with the structures found from X-ray diffraction. In the Si−C region of the ^{13}C-MAS NMR spectrum, at least four different peaks can be seen, that seem to come from the superposition of eight different resonances (four for each molecule, both of which have C_2 crystal symmetry). The four resonances are in accordance with the almost perfect D_2 symmetry of the molecules.

When crystals of $\mathbf{Na_2Z_2}$ are allowed to warm above 350 K, a phase transition can be observed by DTA with an endothermic $\Delta H \approx 5$ kJ/mol at 113°C. This phase transition can also be followed by temperature-dependent ^{13}C-MAS NMR (Figure 5). The crystal symmetry becomes orthorhombic, with a doubling of the volume of the monoclinic cell. An analysis of systematic absences in the X-ray powder diffraction experiment leads to a face-centred lattice (*Fd*2*d* or *Fddd*) with $Z = 8$, which has two consequences: All molecules in the unit cell are equal, and the point symmetry should be at least C_2, and is more likely D_2. In Figure 5 the two ^{13}C-MAS NMR spectra of the monoclinic and orthorhombic phase in the Me−Si region are shown for comparison.

As can be seen in the high temperature phase there are still *two* ^{13}C-NMR resonances for the CH_3−Si groups. This

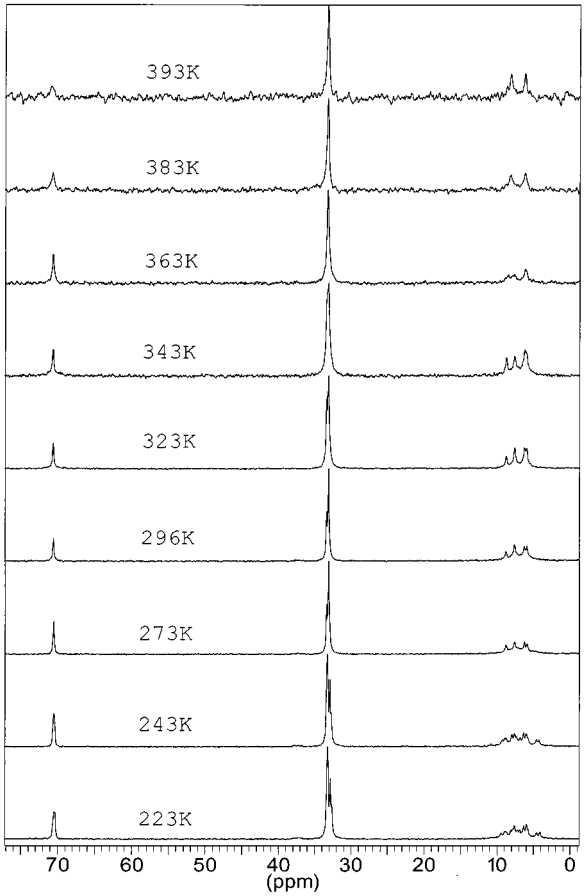


Figure 5. ^{13}C-MAS NMR spectra of $Na_2[t\text{Bu}-\text{O}-\text{SiMe}_2-\text{N}-\text{SiMe}_2-\text{O}t\text{Bu}]_2$ ($\mathbf{Na_2Z_2}$) between 190 and 380 K

agrees with either D_2 or C_2 point symmetry of the unique molecule present in the asymmetric unit. It also shows nicely, that *no sodium jumping* is occurring in this phase: If sodium jumping occurred then there should be a singlet for the 8 methyl groups attached to the silicon atoms. What might be the reason for the phase transition of $\mathbf{Na_2Z_2}$ at 400 K? The ^{13}C-NMR spectra indicate that most of the *tert*-butyl groups rotate in the high-temperature phase. At the same time, because of the new freedom of motion, the molecules can adopt higher point symmetries. This phase transition is another example of a temperature-dependent gain of motional freedom which we have already found for $Me_2Si(Nt\text{Bu})_2Sn(Nt\text{Bu})_2SiMe_2$ many years ago![24] The overall higher energy at 400 K cannot be used for sodium motions presumably because the trajectories for the heavy sodium atoms in $\mathbf{Na_2Z_2}$ are much longer than those of li-

thium atoms in **Li_2Z_2** and the sodium atom is larger and heavier than lithium (see before).

The high-temperature orthorhombic phase of **Na_2Z_2** can already be deduced from the monoclinic room-temperature phase as the cell dimensions may easily transformed to orthorhombic axes [a = 20.86(1), b = 10.303(8), c = 21.17(1) Å, β = 119.50(5)°]. The unusual presence of two different molecules of point symmetry C_2 in the $P2/n$ space group, on the other hand may be rationalised by a further low-temperature phase, the room-temperature structure being only a transient phase. Indeed, by cooling the polycrystalline sample, a further low-temperature phase was identified from ^{13}C-MAS NMR experiment (transition point: at 260 K). In this spectrum below 260 K, the C−Si region is split into many signals (at least 13−14 can be distinguished) which shows that in this low-temperature phase there are still two molecules in the asymmetric unit, but the point symmetry of these molecules is now reduced to C_1 (theoretically 16 signals should appear in the spectrum, Figure 5).

So far it seems that with the rise in temperature the **Na_2Z_2** compound is steadily gaining point symmetry showing two phase transitions: 260 K: 2 independent molecules with C_1 symmetries; > 260 → 400 K: 2 independent molecules with C_2 symmetries; > 400 K: 1 independent molecule with C_2 (or D_2) symmetry. The gain in point symmetry is paralleled by a gain in mobility of the ligand (for example rotations of *tert*-butyl groups around the O−C axes), but so far we have not found a clear hint from the temperature-dependent ^{13}C-MAS NMR spectra that the sodium atoms are moving like the Li in the **Li_2Z_2** compound.

The compounds $Li_2[Ph-O-SiMe_2NSiMe_2-O-Ph]_2$ [**Li_2Z_2'**] and $Li_2[Me_3Si-O-SiMe_2NSiMe_2-O-SiMe_3]_2$ [**Li_2Z_2"**] differ from **Li_2Z_2** in that the *tert*-butyl group of **Li_2Z_2** is replaced by phenyl and trimethylsilyl groups, respectively. **Li_2Z_2'** forms a normal van der Waals lattice at ambient temperature ($P-1$ with Z = 2), and there are no other low- or high-temperature phases within ±120°C.[16] The molecules (isostructural with **Li_2Z_2**) are dimeric with a central Li_2N_2 square, the Li−N distances being in the usual range of 2.061−2.097 Å.[25] The four Li−O distances are shorter than the Li−N distances, and have a mean value of 1.978(7) Å. In contrast with the phenyl derivative, the trimethylsilyl derivative **Li_2Z_2"** has long LiO distances [mean: 2.08(5) Å] and smaller Li−N distances [mean: 2.02(4) Å], but is similar to **Li_2Z_2** and **Li_2Z_2'** in its molecular structure. **Li_2Z_2"** crystalliszes in a monoclinic crystal system ($P2_1/c$ with Z = 4), and has a peculiar property when heated over 290 K. Its ^{13}C-MAS NMR spectrum becomes more simple, the multiple signals of the dimethylsilyl group of the room-temperature spectrum merging to two broad signals (δ = 5.0 and 7.1), and the four signals of the trimethylsilyl group changing into a singlet at δ = 2.7. This is a clear indication that ligand motions have to be considered, perhaps even accompanied by lithium hopping. At 355 K the spectrum becomes even simpler, with singlets for the dimethylsilyl and the trimethylsilyl groups. Unfortunately, until now, it has not been possible to obtain crystallographic proof for these assumptions.

We have also modified the O−Si−N−Si−O back bone by replacing O by other non-metallic elements such as nitrogen and carbon.[16] The following molecules have been prepared: $Li_2[Ph-SiMe_2NSiMe_2-Ph]_2$, $Li_2[(C_4H_3O)-SiMe_2-N-SiMe_2-(OC_4H_3)]_2$, $Li_2[Me_2N-SiMe_2-N-SiMe_2-NMe_2]_2$, $Li_2[Et_2N-SiMe_2-N-SiMe_2-NEt_2]_2$, $Li_2[i\text{Pr}(H)N-SiMe_2-N-SiMe_2-N(H)i\text{Pr}]_2$, and $Li_2[(C_4H_3S)-SiMe_2-N-SiMe_2-(SC_4H_3)]_2$. All these compounds show very similar structures to **Li_2Z_2**, **Li_2Z_2'**, or **Li_2Z_2"**, but none of these compounds has been found to give several solid crystalline phases. In summary, the lithium hopping or rotational movement found thus far has been restricted to the O−Si−N−Si−O back bone.

Siloxamides with the Skeleton N−Si−O−Si−N

The Lithium and Sodium Derivatives of $[Me_3E-N-SiMe_2-O-SiMe_2-N-EMe_3]^{2-}$, E = C, Si

As shown in the last chapter, the motion of the lithium atoms within the compound **Li_2Z_2** in the crystalline solid had a direct link to the empty holes within the molecules. Occupying these holes by further metal atoms should prevent the jumping of the metal atoms, and therefore the metal rotation should stop.

With this idea in mind we have exchanged the places of the oxygen and nitrogen atoms in the skeleton O−Si−N−Si−O. To maintain the number of electrons, the skeleton N−Si−O−Si−N has to adopt a further negative charge, raising the total charge to −2. Two of these ligands should therefore accommodate 4 positively charged metal atoms and consequently, assuming a similar general structure, should completely fill up the O_2N_2 coordination polyhedra.[17]

We have obtained crystalline solids of the compounds $Li_4[t\text{Bu}-N-SiMe_2-O-SiMe_2-Nt\text{Bu}]_2$; **$Li_4X_2$**, $Li_4[Me_3Si-N-SiMe_2-O-SiMe_2-N-SiMe_3]_2$; **$Li_4L_2$**, $Na_4[t\text{Bu}-N-SiMe_2-O-SiMe_2-Nt\text{Bu}]_2$; **$Na_4X_2$**, and $Na_4[Me_3Si-N-SiMe_2-O-SiMe_2-N-SiMe_3]_2$; **$Na_4L_2$**.[17] Between 190 and 380 K the compound **Li_4X_2** forms three crystalline phases, **Na_4X_2** two crystalline phases, and both **Li_4L_2** and **Na_4L_2** one unique crystalline phase. Except the low-temperature phase of **Li_4X_2** (powder diffraction) all phases have been analysed by single-crystal X-ray diffraction (see Table 3). Solid-state NMR spectra have been obtained for all compounds using ^{6}Li, ^{7}Li, ^{13}C, ^{29}Si in the temperature-dependent mode.

In Figure 6 and Figure 7 the results of the X-ray diffraction analyses on **Li_4L_2** and **Na_4L_2** at room temperature are depicted.[17] As may be deduced by comparison of **Li_4L_2** with **Li_2Z_2** (Figure 1 and 2) the overall structures are quite similar, with the metallic cations connecting the negatively charged ligands. As anticipated the four O_2N_2 coordination holes which originate like in **Li_2Z_2** from the mutual orientation of the ligands are filled. Surprisingly, the lithium atoms are not found at distinct places but occupy two sites in the polyhedra with 50% probability and which are 0.66 Å apart from one another. The crystal symmetry of the molecules in **Li_4L_2** is S_4, which means that all four coordination sites as well as the lithium atoms are symmetry-related.

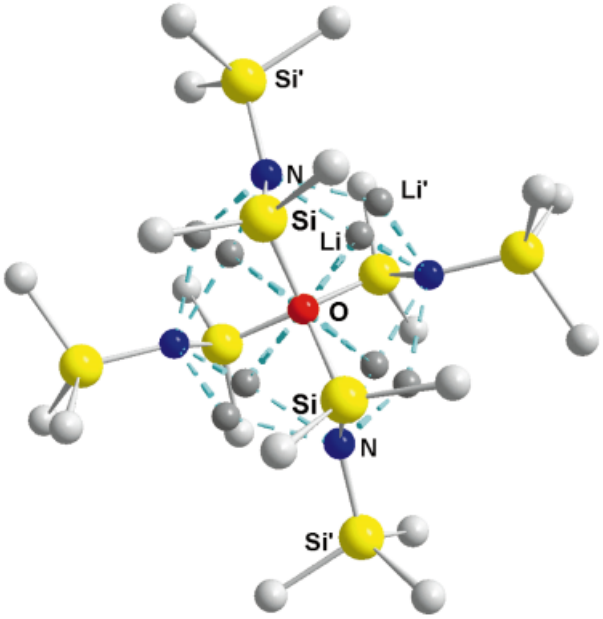


Figure 6. The molecular structure of $[Me_3Si-N-SiMe_2-O-SiMe_2-N-SiMe_3]_2Li_4$ (**Li_4L_2**) in the crystal at 290 K; the occupancy of the eight lithium positions is 50% (split atoms)

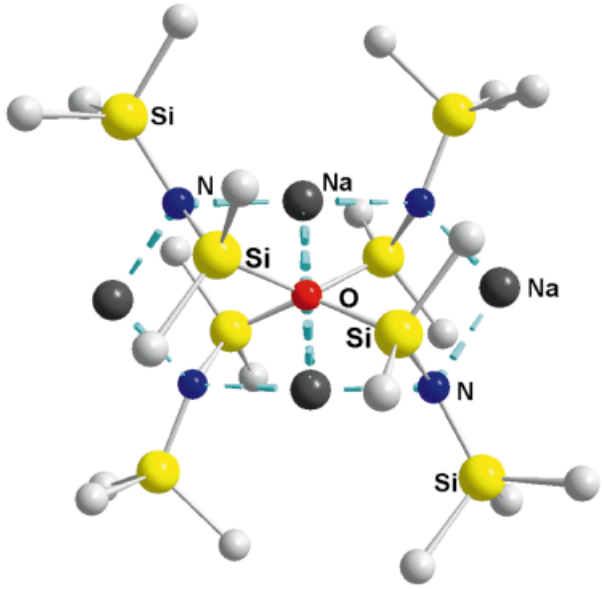


Figure 7. The molecular structure of $[Me_3Si-N-SiMe_2-O-SiMe_2-N-SiMe_3]_2Na_4$ (**Na_4L_2**) in the crystal at 290 K

What is the reason for equal distribution of four lithium atoms over eight sites in **Li_4L_2**? A closer look on the LiLi distances reveals that the inner sites, having the closest Li−O and Li−N distances [2.28(1) and 1.95(2) Å, respectively], are 2.37 Å apart. This distance should lead to a strong Li^+Li^+ repulsion, as may be deduced by a simple molecular mechanics calculation in the gas phase, or by comparison with other Li compounds (for the model calculation the lithium atoms have been assumed to have a charge of +1.0, and the N and O atoms −0.75 and −0.50, respectively).[20] Considering a combination of two inner and two outer sites of the lithium positions, the LiLi distances are increased to 2.91 Å and the Li^+Li^+ repulsions are consequently decreased. The outer sites of the lithium atoms show longer Li−N (2.037 Å) and Li−O distances (2.77 Å). Apparently there is a balance between the repulsion of the lithium atoms and the attraction from the O_2N_2 polyhedra. It seems likely that the splitting of the lithium positions is due to dynamical disorder with the two lithium sites representing the "return points" of lithium oscillations. This assumption can be verified as shown in the later sections.

The sodium derivative **Na_4L_2** is, to a crude approximation, similar to **Li_4L_2** and **Na_2Z_2**, as far as the general structure of the molecule is concerned. Closer inspection of Figure 7 nevertheless reveals that there are important differences. In contrast to the $S_4(\bar{4})$ symmetry of **Li_4L_2** the molecule **Na_4L_2** has no crystal symmetry but approaches $D_2(222)$ very closely. As a direct consequence of this different point symmetry, the four sodium atoms fall into two categories with two sodium atoms being coordinated by four basic atoms (two nitrogen and two oxygen atoms), and the other sodium atoms being coordinated only by two nitrogen atoms (not considering hydrogen interactions of CH_3 groups of the dimethylsilyl and trimethylsilyl entities). The dicoordinated sodium atoms have smaller Na−N distances when compared to the tetracoordinate (see Table 3) as expected. The N−SiSi−N dihedral angle in **Na_4L_2** is considerably larger than the corresponding angle in **Li_4L_2** (Table 3), and parallels our findings in the systems **Na_2Z_2** and **Li_2Z_2**. Another similarity to the former chapter is that in **Na_4L_2** there is no sodium movement, while in **Li_4L_2** lithium oscillations have to be considered.

Replacing the silicon atoms of the trimethylsilyl groups by the more electronegative carbon atoms should reduce the electron density at the nitrogen atoms. It should also reduce the ligating property of the nitrogen atoms to electropositive elements like Li or Na, and consequently should give more motional freedom to these atoms.

In Figure 8 the molecular structures of **Li_4X_2** and **Na_4X_2** are given either below 230 K or at ambient temperature as results of single-crystal X-ray diffraction analyses. It becomes evident, by comparison with Figure 6 and 7, that at lower temperatures, the structures of **Li_4X_2** and **Na_4X_2** compare almost perfectly with the structures of **Li_4L_2** and **Na_4L_2** (see also Table 3). The contrary is true for the structures determined at ambient temperature: Here the structural features are different, the crystal point symmetry of **Li_4X_2** being $D_{2d}(\bar{4}2m)$, and of **Na_4X_2** being $S_4(\bar{4})$. In the two cases the *tert*-butyl groups of the ligands are disordered around the C−O axes as result of rotational dynamics (which can be verified by solid-state ^{13}C NMR).

The LiLi separation of the two split positions is becoming longer by 0.13 Å in the room temperature phase [**Li_4X_2** (230 K): LiLi = 0.81 Å; **Li_4X_2** (290 K): LiLi = 0.94 Å] compared with that at 230 K. This is in accord with the model of Li oscillations becoming more important with raising temperature. A careful look at the electron-density map of the crystal-structure determination of **Li_4X_2** (290 K) reveals that other atoms of the compound besides lithium are

Table 3. Some selected bond lengths [Å], angles [°] and symmetry information for compounds with the backbone N−Si−O−Si−N

	Si−N	Si−O	N−Si···Si−N[a]	M−N[b] {N−M−N}	M−O	MM[c]	Symmetry[d] Space group [Z]
Li_4X_2 (296K)	1.669(4)	1.662(2)	0.0	1.917(3) 2.019(6)	2.37(1)	2.75(2) 2.03(2) min	***D_{2d}*** [D_{2d}] $P4_2/nmc$ [2]
Li_4X_2 (230K)	1.667(4)	1.655(2)	13.7(1)	1.93(1) 1.91(1)	2.49(2)	2.71(3) 2.09(2) min	***S_4*** [S_4] $P4_2/n$ [2]
Li_4L_2	1.685(2)	1.659(1)	27.5(1)	1.93(1) 1.97(1) 2.05(1) 2.03(1)	2.28(1)	2.91(2) 2.37(2) min	***S_4*** [S_4] $P4_2/n$ [2]
Na_4X_2 (296K)	1.655(5)	1.670(2)	44.9(1)	2.322(5) 2.311(5)	2.613(4)	3.240(5)	***S_4*** [S_4] $P4_2/n$ [2]
Na_4X_2 (200K)	1.652(6)	1.659(9)	36.6(1)	2.34(1) {178.1°} 2.36(1) {121.2°}	2.571(9)	3.172(5) 3.485(3)[×4]	**D_2** [C_1] $Pna2_1$ [4]
Na_4L_2	1.670(6)	1.675(8)	48.5(1)	2.416(9) {177.1°} 2.368(9) {116.1°}	2.507(9)	3.249(3) 3.689(3)[×4]	***D_2*** [C_1] $P2_1/n$ [4]
$Li_2K_2X_2$	1.659(5)	1.673(5)	10.5(1)	2.769[K] 1.959[Li]	2.395[Li]	2.95[Li−Li] 3.56[Li−K]	***D_2*** [C_2] $Aba2$ [4]
Cu_4X_2	1.721(5)	1.642(4)	11.2(1)	2.156(3) {165.0°}	3.08 [no bonding]	2.836(3)	***D_{2d}*** [C_2] $C2/c$ [4]
Ag_4X_2	1.729(5)	1.630(4)	11.7(1)	2.153(3) {165.2°}	3.11 [no bonding]	2.834(2)	***D_{2d}*** [C_2] $C2/c$ [4]

[a] Dihedral angle Si−N···N−Si in °. − [b] M−N distances and, in some compounds, corresponding N−M−N angles. − [c] Shortest distances between metal centres using inner and outer split atom positions; the values characterized by "min" show the shortest unrealistic distances. − [d] In the first line are point symmetries (bold: approximate; in brackets: crystal site symmetry). The second line gives the space groups with the number of molecules per unit cell in brackets.

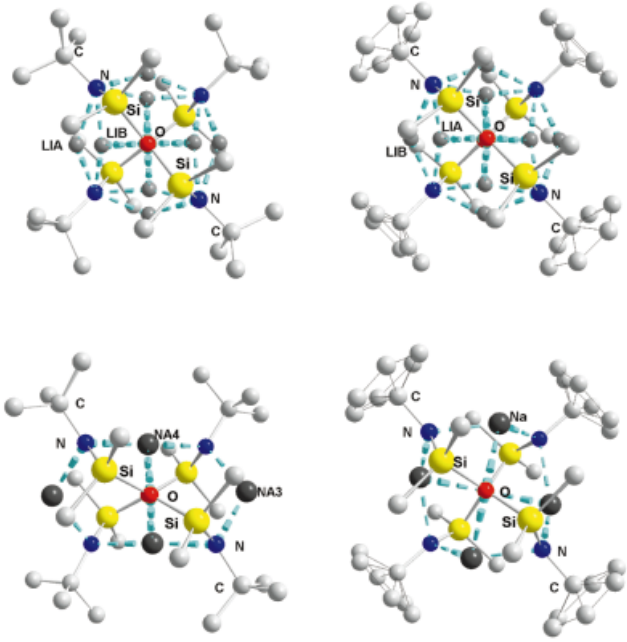


Figure 8. Comparison of the structures of [*t*Bu−N−$SiMe_2$−O−$SiMe_2$−N−*t*Bu]$_2M_4$, M = Li, Na (**Li_4X_2**, **Na_4X_2**) at different temperatures; on the left the low-temperature phases (200 K) are plotted, while on the right the same molecules are shown at ambient temperature

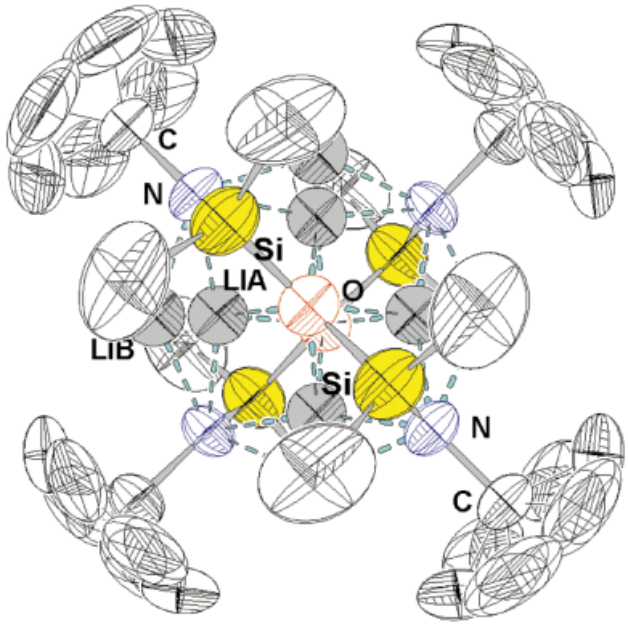


Figure 9. Molecular structure of Li_4[*t*Bu−N−$SiMe_2$−O−$SiMe_2$−N*t*Bu]$_2$ (**Li_4X_2**) at 290 K showing ellipsoids of thermal motion (50%)

"smeared out" (as may be seen from Figure 9 showing the anisotropic ellipsoids).

From Figure 9 it can also be concluded that apart from the rotations of the *tert*-butyl groups, the most important movement is that of the dimethylsilyl group that is perpen-

dicular to the mirror planes of the D_{2d} point symmetry. The phase transition of $\mathbf{Li_4X_2}$ (230 K) to $\mathbf{Li_4X_2}$ (290 K) has a direct group/subgroup relation ($P4_2/n \xrightarrow{t2} P4_2/nmc$): This is a serious hint for the presence of a second-order transition, which can be followed by spectroscopic techniques like NMR and Raman spectroscopy (see later).

The temperature-dependent structure change of $\mathbf{Li_4X_2}$ may be described as follows: At 230 K the molecules are highly librating in the crystal lattice, the movements becoming more important at higher temperatures. The most important amplitudes of movement are the lithium oscillations, followed by rotations of the *tert*-butyl groups and dimethylsilyl displacements perpendicular to the ON_2 plane of the ligand $[t\text{Bu}-\text{N}-\text{SiMe}_2-\text{O}-\text{SiMe}_2-\text{N}-t\text{Bu}]^{2-}$. A measurable quantity for the dimethylsilyl motion is the N−SiSi−N dihedral angle, which at 230 K has an equilibrium value of 13.7°. With raising temperature the dihedral value approaches 0°, corresponding with the equilibrium value of the high-temperature phase. The high molecular point symmetry D_{2d} is finally reached above 260 K (see NMR experiments) with free rotation of the *tert*-butyl groups. In the phase transition the N−SiSi−N angle can be defined, inter alia, as an ordering parameter.

The point symmetry of $\mathbf{Li_4X_2}$ (230 K) is $S_4(\bar{4})$, and from a packing point of view is not ideal for organic molecules.[21] It is not astonishing that at lower temperatures another crystalline phase for $\mathbf{Li_4X_2}$ is found which is stable below 170 K [$\mathbf{Li_4X_2}$ (160 K)]. We were not able to obtain single crystals from this phase, but have deduced from X-ray powder diffraction that the crystal system is lower than tetragonal, and could be orthorhombic or monoclinic.

The $\mathbf{Na_4X_2}$ compound shows two crystalline phases, the molecular structures of the compounds being quite different as may be concluded from Figure 8. At ambient temperature $\mathbf{Na_4X_2}$ crystallizes in the tetragonal lattice in space group $P4_2/n$ with $Z = 2$ as $\mathbf{Li_4X_2}$ at 230 K, and below 240 K $\mathbf{Na_4X_2}$ becomes orthorhombic (space group $Pna2_1$). While in the low-temperature phase the molecule has crystal point symmetry C_1 but deviates only a little from $D_2(222)$, in the high-temperature phase of $\mathbf{Na_4X_2}$ the crystal point symmetry is $S_4(\bar{4})$ (Table 3). In the low-temperature phase of $\mathbf{Na_4X_2}$ there are two types of sodium atoms, as in $\mathbf{Na_4L_2}$, and the structures of these two phases are very similar, omitting the *tert*-butyl/trimethylsilyl exchange. With respect to O and N in $\mathbf{Na_4X_2}$ (220 K) there are λ^2- and λ^4-Na atoms, while in $\mathbf{Na_4X_2}$ (290 K) all Na atoms are three-coordinate (see also Table 3). The phase transition in the Na_4X_2 system is of first order (vide NMR): The change in the molecular structure thus happens instantaneously.

The structural change in $\mathbf{Na_4X_2}$ associated with the phase transition from low to high temperature has three characteristics: (1) The sodium atoms become equivalent and change from $2 \times \lambda^2$-Na and $2 \times \lambda^4$-Na to $4 \times \lambda^3$-Na. The vibrations of the sodium atoms become stronger, but there is no evidence for a sodium oscillation as in the case of $\mathbf{Li_4X_2}$. (2) The different point symmetry of the molecule at higher temperature is accompanied by a substantial gain in volume [increase in volume/molecule = 34.6 Å^3 (3.6%); in the $\mathbf{Li_4X_2}$ system (230/290 K) the volume increase is 20.0 Å^3 (2.2%)]. This increase is used for rotational freedom of the *tert*-butyl groups. (3) The mutual orientation of the $[t\text{Bu}-\text{N}-\text{SiMe}_2-\text{O}-\text{SiMe}_2-\text{N}-t\text{Bu}]^{2-}$ ligands is changed, and the dihedral angles N−SiSi−N increase from 36.6° for $\mathbf{Na_4X_2}$ (220 K) to 44.9° for $\mathbf{Na_4X_2}$ (290 K). Whereas at 220 K the two ligands are symmetry-related by C_2 and have the same twisting direction (along the N−Si−O−Si−N skeleton), at 290 K the ligands have opposite twists. This is best seen by closer inspection of Figure 8.

In conclusion, the two phase transitions studied with $\mathbf{Li_4X_2}$ and $\mathbf{Na_4X_2}$ with X-ray diffraction techniques are similar with respect to obtaining motional freedom for the *tert*-butyl groups with increase in the temperature, but the effect on the metal atoms is different. While in the case of lithium the oscillations along two of the twofold axes of the D_{2d} symmetry become more important with increase in temperature, in the case of sodium there is one important displacement of these atoms at the transition point, without any further metal movements. The silicon derivatives $\mathbf{Li_4L_2}$ and $\mathbf{Na_4L_2}$ at ambient temperatures have molecular structures that can only be realised in $\mathbf{Li_4X_2}$ and $\mathbf{Na_4X_2}$ at lower temperatures. This is a direct consequence of the different charge distributions at nitrogen due to carbon/silicon exchange. The nitrogen atoms in $\mathbf{Li_4L_2}$ and $\mathbf{Na_4L_2}$ are more negatively charged than the same atoms in the $\mathbf{Li_4X_2}$ and $\mathbf{Na_4X_2}$ derivatives and therefore hinder the motional freedom of the metal atoms by a higher electrostatic component.

The models discussed so far have been checked by solid-state NMR. In Figure 10 and Figure 11 the ^{13}C-NMR spectra of $\mathbf{Li_4X_2}$ and $\mathbf{Na_4X_2}$ in the temperature range between 150 and 350 K are shown. In exact correspondence to the X-ray diffraction results the phase transitions in both systems are easily recognised, and temperatures of transition are paralleled. In the $\mathbf{Li_4X_2}$ system, starting with 150 K, the first transition occurs at 165 K. Below 165 K the ^{13}C-MAS NMR spectrum is highly structured especially in the dimethylsilyl region. Here at least six different signals can be recognised, which collapse at 165 K to two signals of equal intensity. From the number of signals it can be deduced that the point symmetry of the $\mathbf{Li_4X_2}$ below 165 K is less than C_2 and is most probably C_1 (8 signals are expected for this point symmetry). The broad peak of the primary carbon atoms in the *tert*-butyl groups hints at an ordered structure, ruling out any rotational movement. The spectral change at 165 K is sudden, in accord with a first order transition.

Above 168 K the spectrum of $\mathbf{Li_4X_2}$ is constantly changing with two major observations: (1) The intensity of the *tert*-butyl signal (methyl groups) with respect to the dimethylsilyl group is gradually increasing: This effect can be attributed to an initial rotation of the *tert*-butyl groups around the C−N axis becoming more and more important. (2) The space separation of the two methyl groups is almost constant between 165 K and 205 K. Between 205 K and 245 K the separation is constantly diminishing, the intensity of the signal growing and finally collapsing to a singlet at

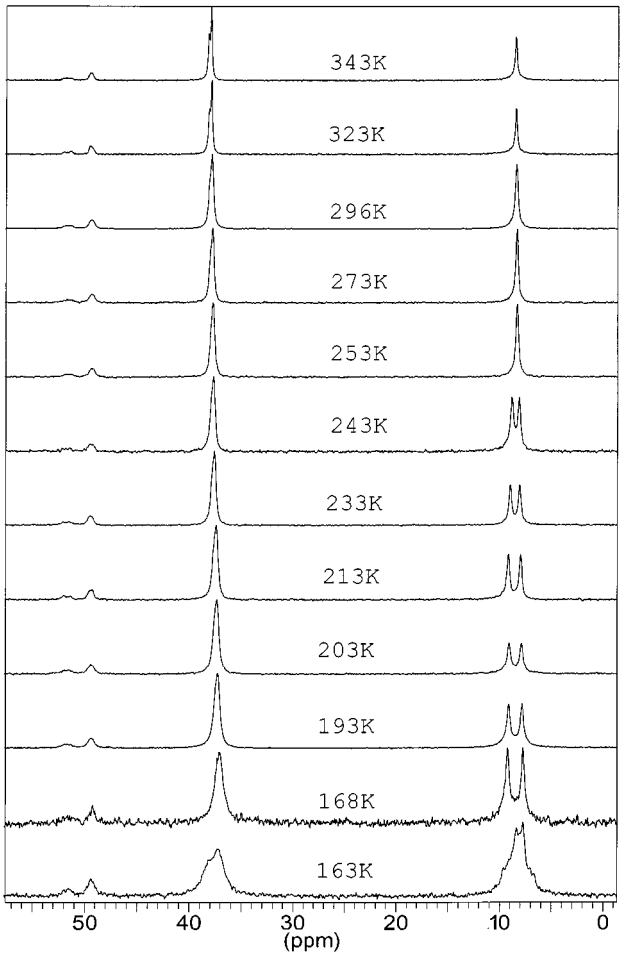


Figure 10. ^{13}C-MAS NMR spectrum of $\mathbf{Li_4X_2}$ between 150 and 350 K

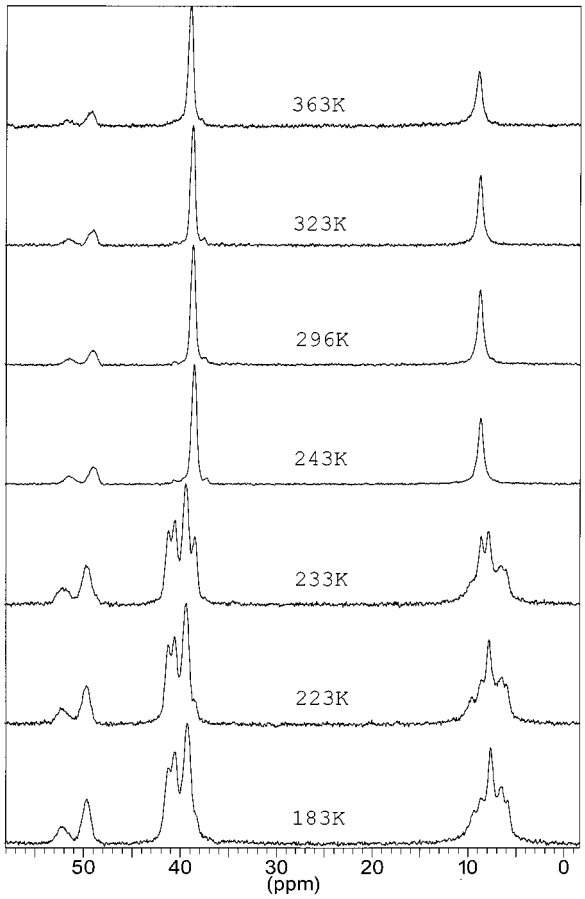


Figure 11. ^{13}C-MAS NMR spectrum of $\mathbf{Na_4X_2}$ between 150 and 350 K

245 K. The experiment seems to reflect the starting libration of the dimethylsilyl groups in the crystal, which become more and more intense with the N−SiSi−N dihedral angle approaching 0° (see before). It also confirms our assumption that the phase transition between $\mathbf{Li_4X_2}$ (230 K) and $\mathbf{Li_4X_2}$ (290 K) is of second order with a continuous change of parameters. It is interesting to note that the crystallographic S_4 symmetry is nicely reflected in the spectrum with one independent *tert*-butyl group and two independent methyl groups in the Me_2Si region.

Above 245 K the spectrum of $\mathbf{Li_4X_2}$ is in accordance with the crystallographic $D_{2d}(\bar{4}2m)$ symmetry, and two signals for all methyl groups within the molecule are measured. The tertiary carbon atom of the *tert*-butyl group is not affected during the phase transitions, as can be seen from Figure 10. This is due to the central position of the carbon atom which is shielded and suffers to a smaller extent from structural changes than a carbon atom situated on the outer sphere of the molecule. The two asymmetric resonances of the primary carbon atom are due to the quadrupole splitting of the nitrogen to which it is attached.

We have been lucky, to follow the phase transitions in $\mathbf{Li_4X_2}$ also by single-crystal Raman spectroscopy.[22] In Figure 12 a section of the spectrum (2600−3000 cm^{-1}) is shown, which has been obtained from a crystal oriented orthogonal to the [001] direction of the tetragonal phase.

The highest frequency of the C−H stretching modes is especially sensitive to the phase transition: At 150 K the signal at 2950 cm^{-1} is definitely different from the corresponding one at 160 K, which with increasing temperature is gradually changing. Very recently we have obtained a DSC curve of the phase transition around 245 K, which is shown in Figure 13.[26]

The λ curvature of the plot is reminiscent of the ideal second-order phase transition, the original model description being developed by P. Ehrenfest and L. D. Landau.[27] In conclusion, the Raman spectroscopy as well as the DSC experiment fully parallel our NMR and X-ray experiments and substantiate our earlier assumptions.

The solid-state ^{13}C-NMR experiments with $\mathbf{Na_4X_2}$ are not as straightforward as with $\mathbf{Li_4X_2}$ (Figure 11).

In accordance with the low crystal symmetry of the $\mathbf{Na_4X_2}$ molecule, in between 180 K and 220 K the Me_2Si group (at least 5 signals) and the *tert*-butyl groups (at least 3 signals) show up as multiplets. At 233 K the multiplets become more complex by addition of a further line to each of them. As can be deduced from the spectrum at 243 K, the additional peaks are from the high-temperature tetragonal phase. There is a coexistence of the two phases (orthorhombic and tetragonal) in accord with the first-order

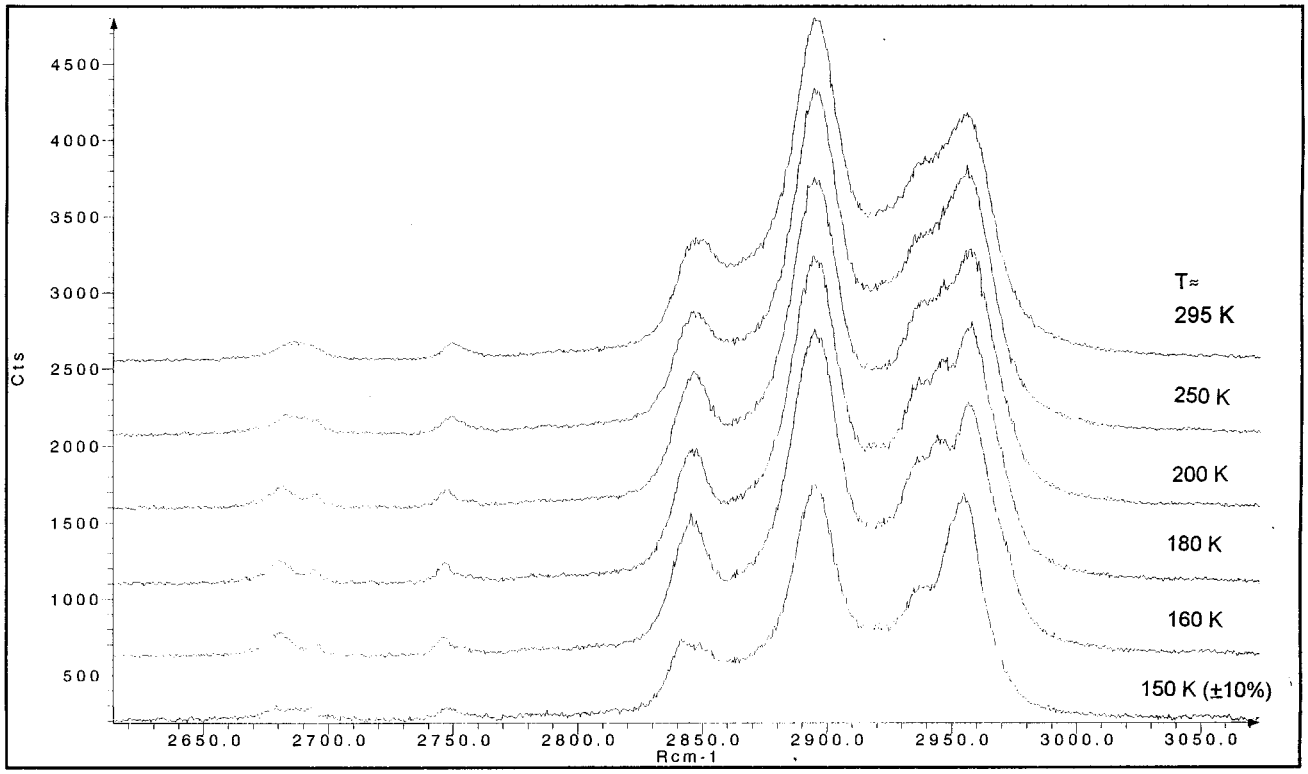


Figure 12. Section of Raman spectrum of $\mathbf{Li_4X_2}$ (2600−3100 cm^{-1}) at different temperatures (single crystal)

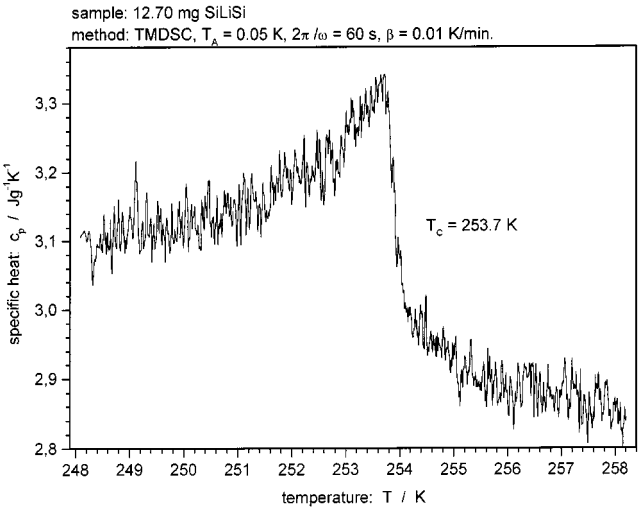


Figure 13. The "λ-transition" at 245 K found by micro-DSC for $\mathbf{Li_4X_2}$

phase transition. Above 233 K the spectrum of $\mathbf{Na_4X_2}$ is very simple, with two resonances for the *tert*-butyl and dimethylsilyl group and the quadrupolarly coupled tertiary carbon atom.

There is clearly a misfit between the X-ray results and the ^{13}C-NMR spectrum for the high-temperature phase of $\mathbf{Na_4X_2}$. As in the corresponding $\mathbf{Li_4X_2}$ (230 K) spectrum, the dimethylsilyl group should show up as two signals of equal intensity [in accordance with the $S_4(\bar{4})$ point symmetry]. What could be the reason for the observed singlet? There are several possibilities. As the signal of the high-temperature phase of $\mathbf{Na_4X_2}$ is very broad (the signal half-width broadness is double that of the corresponding $\mathbf{Li_4X_2}$ phase), the experiment could suffer from lack of resolution. Unfortunately, changing the experimental parameters (using a 500-MHz NMR equipment instead of a 200-MHz one) does not reveal any new insight, as the signal remains comparatively broad but is not structured. Another possible explanation could be that the X-ray structure solution of the tetragonal phase is wrong, due to undiscovered twinning. We are still in the process of proving or disproving these assumptions.

Besides ^{13}C-NMR techniques, ^{6}Li-, ^{7}Li-, and ^{29}Si NMR have also been used to follow the phase transitions (in $\mathbf{Li_4X_2}$ and $\mathbf{Na_4X_2}$). The most interesting is of course the Li NMR, as we could obtain direct information on the lithium mobility. To cut a long story short, two main observations have been made: (1) From the broad-line powder spectra the asymmetry parameter of the lithium position in $\mathbf{Li_4X_2}$ can be obtained. It changes from 0.11 at 150 K to 0.05 at 230 K and remains constant until 360 K, which is an accord with obtaining more axial symmetry (C_2). (2) Within the temperature range of 230 to 260 K the spinning side bands of the MAS spectra show a notable line broadening and consequently a reduced MAS sensitivity.[28] This dynamically induced line broadening seems to be a direct trace of the lithium movement. Above 270 K the spinning side bands sharpen again due to the increasing frequency of the molecular motion (see Figure 14).

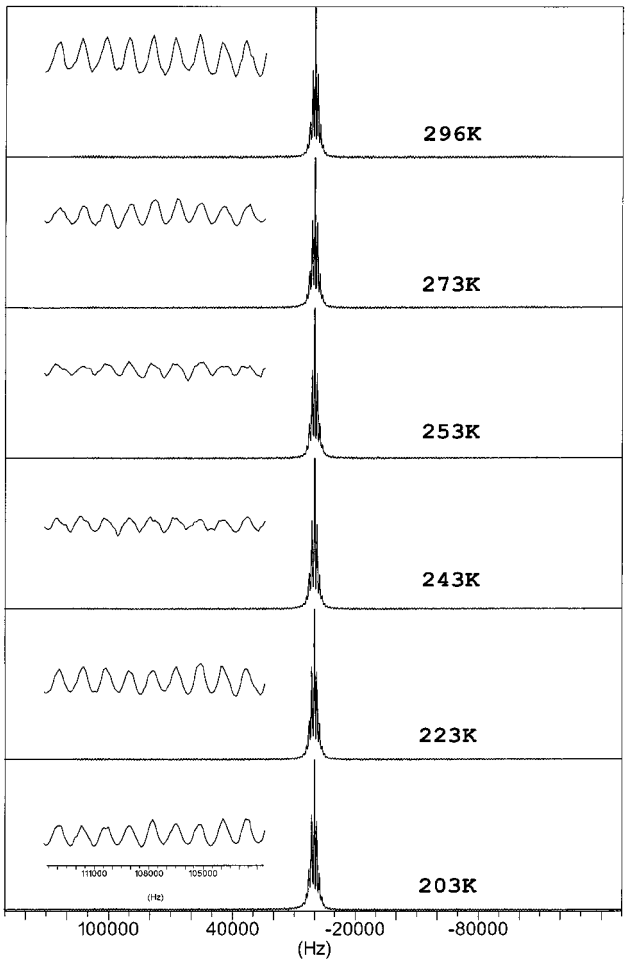


Figure 14. ^{7}Li-MAS spectra of $\mathbf{Li_4X_2}$; the expanded region of the spinning side bands shows the homogeneous line broadening with reduced efficiency of the MAS experiment at the phase transition

The N−Si−O−Si−N Skeleton with Different Substituents

Whereas in the last chapter the mobility of the lithium and sodium atoms has been shown to be influenced by a C/Si exchange at the nitrogen atoms of the N−Si−O−Si−N skeleton, in this chapter we present our results from more dramatically changing the substituents on the whole skeleton. Although we have followed these experiments by spectroscopic means, we only present the X-ray results.

The ligand $[t\text{Bu}-\text{SiMe}_2-\text{N}-\text{SiMe}_2-\text{O}-\text{SiMe}_2-\text{N}-\text{SiMe}_2-t\text{Bu}]^{2-}$ can be derived from $[\text{Me}_3\text{Si}-\text{N}-\text{SiMe}_2-\text{O}-\text{SiMe}_2-\text{N}-\text{SiMe}_3]^{2-}$ by exchange of a methyl group by the sterically demanding *tert*-butyl group at the outer silicon atoms. The compound $[t\text{Bu}-\text{SiMe}_2-\text{N}-\text{SiMe}_2-\text{O}-\text{SiMe}_2-\text{N}-\text{SiMe}_2-t\text{Bu}]_2\text{Li}_4$, $\mathbf{Li_4L'_2}$, has been analysed by X-ray diffraction, the result being shown in Figure 15.[17] Interestingly, even at room temperature, the lithium atoms are at rest and the structure obtained is quite different from $\mathbf{Li_4L_2}$. The molecule $\mathbf{Li_4L'_2}$ adopts almost $D_2(222)$ symmetry in the crystal (exact crystal symmetry C_1) with two pairs of different lithium atoms (λ^2-Li and λ^4-Li). The λ^2-Li atoms have further contacts with the methyl groups of the *tert*-butyl and the dimethylsilyl groups (LiC 3.0 Å), which explains nicely the stability of the structure.

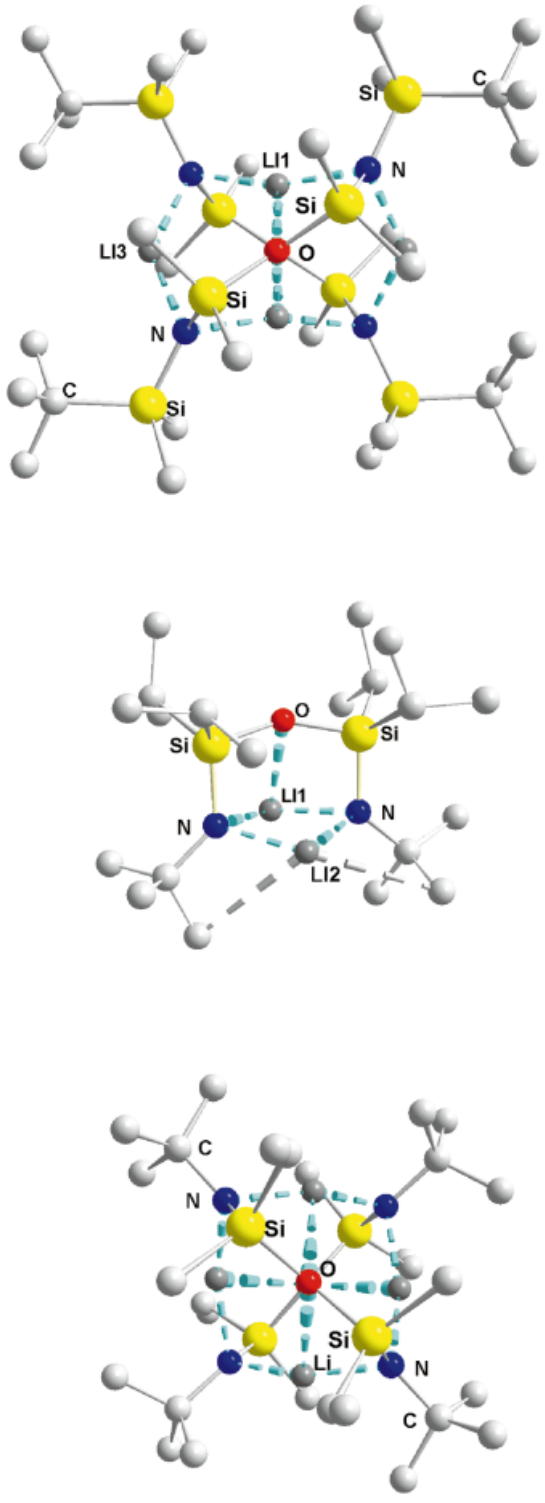


Figure 15. Molecular structures at 290 K of $\text{Li}_4[t\text{Bu}-\text{SiMe}_2-\text{N}-\text{SiMe}_2-\text{O}-\text{SiMe}_2-\text{N}-\text{SiMe}_2-t\text{Bu}]_2$ ($\mathbf{Li_4L_2}$), $\text{Li}_2[t\text{Bu}-\text{N}-\text{Si}(i\text{Pr})_2-\text{O}-\text{Si}(i\text{Pr})_2-\text{N}t\text{Bu}]$ ($\mathbf{Li_2X''}$), and $\text{Li}_4[t\text{Bu}-\text{N}-\text{Si}(\text{Me})(\text{CH}=\text{CH}_2)-\text{O}-\text{Si}(\text{Me})(\text{CH}=\text{CH}_2)-\text{N}-t\text{Bu}]_2$ ($\mathbf{Li_4X_2}$)

It seems likely that steric as well as electronic effects are responsible for the difference in the structure of $\mathbf{Li_4L_2'}$ compared with that of $\mathbf{Li_4L_2}$.

The steric influence can also be observed when the methyl groups at the silicon atoms of $[t\text{Bu}-\text{N}-$

$SiMe_2-O-SiMe_2-N-tBu]^{2-}$ are replaced by bulkier groups like isopropyl moieties. The corresponding lithium derivative of this ligand $[tBu-N-Si(iPr)_2-O-Si(iPr)_2-N-tBu]Li_2$, **$Li_2X$"**, is no longer dimeric, but monomeric. The isopropyl groups on the silicon atoms seem to prevent dimerisation, and **Li_2X"** can be obtained in its monomeric form even in the crystal (Figure 15). The two lithium atoms are very different in their coordination, the λ^3-Li possessing a small Li−O contact (2.34A) and longer Li−N bonds [1.99(1) Å], while the λ^2-Li has shorter Li−N bonds [1.978(2)Å]. Besides these bonds the λ^2-Li has two narrow distances to carbon (2.99 Å).

When the organic substituents on the silicon atoms in $[tBu-N-SiR_2-O-SiR_2-N-tBu]^{2-}$ are different, the silicon atoms become chiral, and the whole ligand can either belong to the *R*,*R* (*S*,*S*) or *R*,*S* (*S*,*R*) enantiomer (*R* and *S* designing the chirality of the two silicon centres). In the first case, assuming a planar ligand, the point symmetry of the anionic ligand is $C_2(2)$ while in the second case it is $C_s(m)$. We have prepared several examples of these ligands (see Table 1), and to our great surprise have found, that the ligands with the *R*,*R* (*S*,*S*) chirality exclusively crystallize as lithium salts, while in the mother liquor both enantiomers are present (^{1}H-NMR evidence). In Figure 15 the structure of $[tBu-N-Si\{(Me)(CH=CH_2)\}-O-Si\{(Me)(CH=CH_2)\}-NtBu]_2Li_4$, **$Li_4X_2$′**, is shown. The molecule crystallizes in the tetragonal space group $P\bar{4}2_1c$ with two molecules per unit cell, and has the crystal point symmetry S_4. As a consequence, each lithium atom is in the same atom environment, and is coordinated by two nitrogen, two oxygen, and two carbon atoms. Each molecule contains one ligand with (*R*,*R*) chirality at Si and a second one with (*S*,*S*) chirality. The lithium oscillation (not shown in the Figure) is less important than in the corresponding compound **Li_4X_2**, and the atoms can be refined without splitting positions (but with large anisotropic temperature factors). The N−SiSi−N dihedral angle is 12.4°, but as the substituents on silicon are different, there is no energetically equivalent position in the other twist form (dihedral angle −12.4°) and the system seems to avoid the passage to the other conformer. This explains the fact that **Li_4X_2** and **Li_4X_2′** are quite different at the same temperature (290 K), **Li_4X_2** showing large lithium oscillations while **Li_4X_2′** only has small amplitudes.

We can conclude from these substitution experiments that the structures of the molecules and the motion of the metal atoms can be easily manipulated. The results fit in nicely in our atomistic dynamic models.

The N−Si−O−Si−N Skeleton with Different Metallic Elements

So far we have compared the lithium and sodium derivatives of the same ligands. The compound $Li_2K_2[tBuN-SiMe_2-O-SiMe_2-NtBu]_2$, **$Li_2K_2X_2$**, belongs to the family **Li_4X_2** and **Na_4X_4** with the peculiarity of hosting two types of metallic atoms. Looking back to the structures we have known so far, it seemed unlikely that **$Li_2K_2X_2$** should adopt the S_4 symmetry of the tetragonal phase of **Na_4X_2** or the

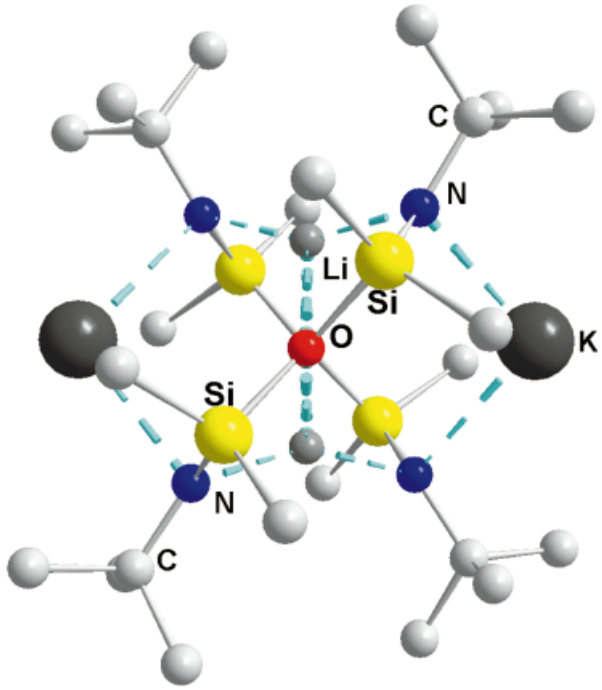


Figure 16. Molecular structure of $Li_2K_2[tBu-N-SiMe_2-O-SiMe_2-N-tBu]_2$ (**$Li_2K_2X_2$**) at 290 K in the solid; the smaller lithium atoms occupy the N_2O_2 holes while the bigger potassium atoms are situated on the outside

D_{2d} symmetry of the high-temperature phase of **Li_4X_2**. As a matter of fact, **$Li_2K_2X_2$** forms a structure very similar to the low-temperature phase of **Na_4X_2**, as can be seen from Figure 16.[17] Between 200 and 380 K we have found no hint for any phase transition as the ^{13}C-MAS NMR spectra remain unchanged.

While the smaller lithium atoms in **$Li_2K_2X_2$** occupy quasi-tetrahedral O_2N_2 holes, the two potassium atoms are too large to be accommodated in these coordination polyhedra and are only bonded by two nitrogen atoms. Furthermore, the potassium atoms have close contacts to carbon atoms of the *tert*-butyl ligands. The crystal symmetry of the whole molecule is C_2 (the two-fold axis passes through the lithium atoms), but the bond lengths and angles as well as the dispositions of the atoms reveal it to be close to D_2. As already discussed, **$Li_2K_2X_2$** is structurally similar to the orthorhombic phase of **Na_4X_2**. Contrary to this compound, no phase transition is observed as the two different elements are well accommodated in their respective coordination spheres. Comparing **$Li_2K_2X_2$** to **Li_4X_2** no lithium motion is observed in the former as there is no need to equilibrate between different lithium positions.

Other interesting cases to discuss are the monovalent transition metal derivatives $Cu_4[tBuN-SiMe_2-O-SiMe_2-NtBu]_2$, **$Cu_4X_2$**, and $Ag_4[tBuN-SiMe_2-O-SiMe_2-NtBu]_2$, **$Ag_4X_2$**. The two compounds have the same composition as **Li_4X_2** or **Na_4X_2** and are somewhat similar in their structures, but also show important differences to the alkali derivatives. In Figure 17, the structure of one of the two compounds, which are isotypic, is depicted as a result of an X-ray structure analysis.

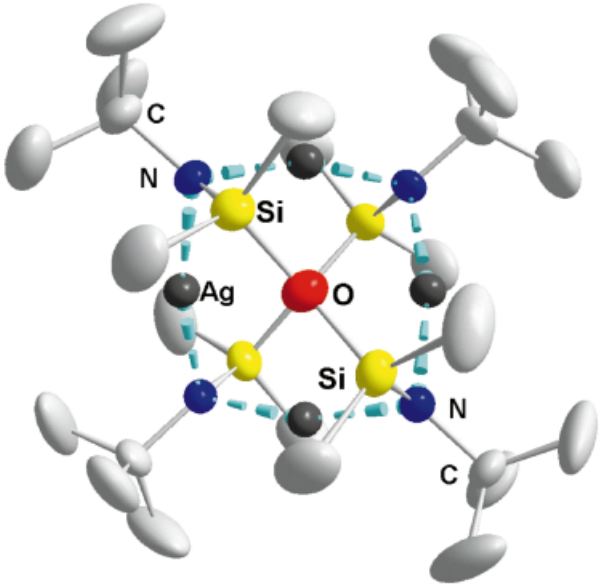


Figure 17. Molecular structure of $Ag_4[t\text{Bu}-N-SiMe_2-O-SiMe_2-N-t\text{Bu}]_2$ (**Ag_4X_2**) with ellipsoids of vibration (50%) at 290 K

The crystal point symmetry of the compounds is $C_2(2)$ but the deviation from $D_{2d}(\bar{4}2m)$ is almost negligible (the N−SiSi−N dihedral angles are 11.2° in **Cu_4X_2** and 11.7° in **Ag_4X_2**). Although belonging to the same molecular point symmetry, compared to the ambient-temperature phase of **Li_4X_2**, **Cu_4X_2**, or **Ag_4X_2** are distinctly different in their structures. The N−M−N bonds are almost linear (**Cu_4X_2**: N−Cu−N = 164.9°; **Ag_4X_2**: N−Ag−N = 165.2°) and there are no bonding interactions of the metal centres with the oxygen atoms. Furthermore, the anisotropic displacement factors of the metal atoms in the compounds are small and there is no evidence for metal oscillations as in compound **Li_4X_2**. The different behaviour of the copper and silver atoms compared to lithium is due to a well-known reason: The metal atoms are in a preferred s(d)p-bond configuration and there are numerous examples of this bonding type in the literature.[29]

Conclusions

We have been able to show that metal movements, especially of lithium (cations), are possible within a molecular skeleton in a crystalline solid. The motions of these metal atoms (ions) are linked to phase transitions and rotations or oscillations of atoms or groups within the molecular skeleton. The phase transitions are reflecting the change of overall symmetry of the molecular movements. The large vibrations within the ligands are necessary to minimize the activation energy of the metal motion.

In the systems **M_2Z_2** it can be clearly shown that only the lithium atoms (or in an ionic model: ions) are capable to jump from filled holes into empty ones. This jumping leads to a rotational motion that may proceed backwards or forwards (Figure 18). The rotational motion of the lithium atoms appears to be simultaneous, which means that the two metallic atoms within the molecule are jumping at the same time, because of electrostatic reasons. Although the sodium derivative also shows phase transitions to allow more motional freedom to the organic ligands, there is no evidence for a comparable sodium hopping or rotation. This leads to the conclusion that the lithium motion is perhaps better described as "lithium tunnelling". The trimethylsilyl derivative **Li_2Z_2**" has a structure very similar to **Li_2Z_2** in the monoclinic phase. Whereas the monoclinic phase of **Li_2Z_2** is stable up to 293 K, the monoclinic phase of **Li_2Z_2**" is stable up to 340 K. The higher charge transfer of the trimethylsilyl group to the oxygen atom compared to *tert*-butyl seems to be responsible for this effect.

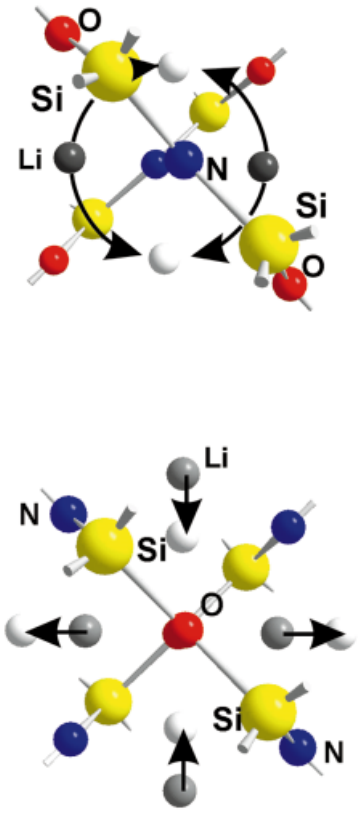


Figure 18. Comparison of the lithium movements within **Li_2Z_2** and **Li_4X_2** at ambient temperature. While in the case of **Li_2Z_2** there is a forward and backward rotation, in **Li_4X_2** there is a forward and backward oscillation; lithium positions are discriminated by white and grey colours; only one type of these coloured position is occupied at a time for electrostatic reasons

The complete fill-up of the N_2O_2 holes in siloxamides by metallic atoms has been realised by the use of the skeleton N−Si−O−Si−N in the place of O−Si−N−Si−O. Although the rotational lithium hopping is stopped by this transformation, the system is still highly fluctional in the crystal, with lithium oscillations occurring along two of the three twofold axes of the $D_{2d}(\bar{4}2m)$ point symmetry (Figure 18). As in the case of **Li_2Z_2**, temperature-dependent

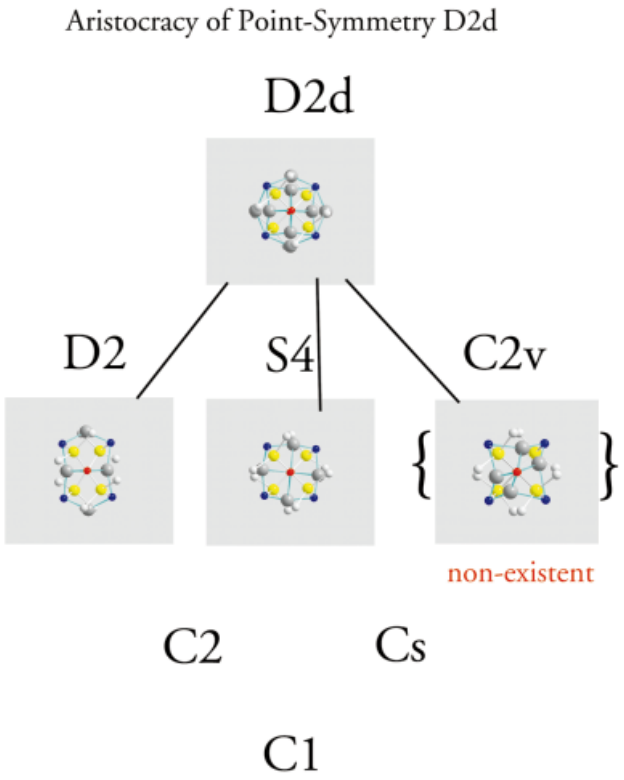


Figure 19. Symmetry tree of D_{2d}, S_4, and D_2; the sketch for C_{2v} is drawn for completeness but is not relevant

solid-state phase transitions have been found for $\mathbf{Li_4X_2}$. It is interesting to note that all structures determined within the $\mathbf{Li_4X_2}$ system or any other ligand derived from $[R-N-SiR'R''-O-SiR'R''-N-R]^{2-}$ can be classified within the $D_{2d}(\bar{4}2m)$ symmetry tree, as exemplified in Figure 19. From all point symmetries collected in Figure 19 only C_{2v} and C_s have not been realised in a crystalline compound, which is comprehensible because of the special arrangement of the two anionic ligands and the ionic repulsions of the four formal cations. As a matter of fact, all low-temperature structures can be classified to belong exactly or approximately to either D_2 or S_4 subgroup.

The second-order phase transition within $\mathbf{Li_4X_2}$ from space group $P4_2/n$ to $P4_2/nmc$ shows nicely that the amplitudes of the metal oscillations are temperature-dependent, and furthermore that ligand librations are involved in the whole process.

The replacement of lithium by sodium to form $\mathbf{Na_4X_2}$ parallels our findings within the O−Si−N−Si−O skeleton. Contrary to the lithium derivative $\mathbf{Li_4X_2}$ there are no important sodium oscillations. The phase transition from the orthorhombic to the tetragonal phase is again driven by entropy: In the high-temperature tetragonal phase all *tert*-butyl groups rotate around the N−C bonds, while in the low-temperature phase they are at rest. Only at the transition point do the sodium atoms show important displacements, but neither before nor after this transition point do the sodium atoms seem to be involved in important movements. The molecular point symmetry of $\mathbf{Na_4X_2}$ passes from approximately D_2 to S_4 at the transition, which means that in the transition state the D_{2d} symmetry has to be run through (Figure 19).

The *tert*-butyl/trimethylsilyl exchange on the nitrogen atoms in the lithium and sodium compounds enhances the ionic charge on nitrogen, and leads to a parallel effect with respect to the stability of structures. The structures found at room temperature with trimethylsilyl substituents and a N−Si−O−Si−N backbone can be only "copied" using *tert*-butyl in place of trimethylsilyl, if the temperature is maintained below ca. 250 K. Again, this corresponds with our findings in the O−Si−N−Si−O series.

The bulkiness of the ligands can influence the structure to such a point that no dimer can be formed any more (see $[t\mathrm{BuN-Si}(i\mathrm{Pr})_2-\mathrm{O-Si}(i\mathrm{Pr})_2-\mathrm{N}t\mathrm{Bu}]\mathrm{Li}_2$). The lithium/potassium derivative $\mathbf{Li_2K_2X_2}$ adopts the D_2 symmetry allowing different ligations to lithium and potassium atoms. The copper and silver derivatives $\mathbf{Cu_4X_2}$ and $\mathbf{Ag_4X_2}$ show almost linear N−M−N arrangements and no tendency to metal oscillations in accord with metal−nitrogen bonding different from that of lithium or sodium.

Metal motions in crystalline solids in distinct regions (metal movements in molecular boxes) merit increasing interest because they are anisotropic (in the cases discussed in this article the rotations or oscillations are perpendicular to the tetragonal [001] axis) and can be influenced. The simple switching on and off of these dynamics could lead to applications in solid-state physics. Instead of heat energy, a magnetic or electric field could also be used in principle.

Acknowledgments

I would like to thank S. Wieczorek, Dr. K. Fries, and Dr. J. Böhnlein-Maus for their synthetic work, Dr. V. Huch for the X-ray experiments, as well as Dr. M. Zimmer for solid-state NMR experiments. Prof. J. Krüger, Experimentalphysik, Saarbrücken, is acknowledged for the DSC curve of $\mathbf{Li_4X_2}$. With deep regret I have learnt of the sudden death of Prof. H. G. Unruh, Experimentalphysik, Saarbrücken, who conducted the single-crystal Raman experiments: I still remember well our fruitful discussions on phase transitions. This work has been financed partly by the Deutsche Forschungsgemeinschaft as well as the Fonds der Chemischen Industrie, which are acknowledged. I thank Dr. V. Subramanian for reading the manuscript.

[1] M. Veith, M. Zimmer, *Main Group Chem. News* **1994**, *2*, 12−16.
[2] M. Veith, M. Zimmer, P. Kosse, *Chem. Ber.***1994**, *127*, 2099−2102.
[3] M. Veith, M. Zimmer, *Z. Anorg. Allg. Chem.* **1996**, *622* 1471−1477.
[4] M. F. Lappert, P. P. Power, A. R. Sanger, R. C. Srivastava, *Metal and Metalloid Amides,* Ellis Horwood, New York − Chichester − Brisbane − Toronto, **1980**.
[5] M. Veith, M. Zimmer, S. Müller-Becker, *Angew. Chem.* **1993**, *105*, 1771−1773; *Angew. Chem. Int. Ed. Engl.* **1993**, *32*, 1731−1733.
[6] F. Maseras, A. Lledos, *J. Chem. Soc., Chem. Commun.* **1995**, 443−444.
[7] A. Sekiguchi, T. Matsuo, H. Sakurai, *Angew. Chem.* **1998**, *110*, 1752−1754; *Angew. Chem. Int. Ed.* **1998**, *37*, 1662−1664; Addition and Corrections: *Angew. Chem.* **1998**, *110*, 2569; *Angew. Chem. Int. Ed.* **1998**, *37*, 2292.
[8] A. J. Elias, H. W. Roesky, W. T. Robinson, G. M. Sheldrick, *J. Chem. Soc., Dalton Trans.* **1993**, 495−500.

[9] A. J. Elias, H. G. Schmidt, M. Noltemeyer, H. W. Roesky, *Eur. J. Solid State Inorg. Chem.* **1992**, *29 (Suppl.)*, 23−42.
[10] U. Wannagat, J. Herzig, P. Schmidt, M. Schulze, *Monatsh. Chem.* **1971**, *102*, 1817−1824.
[11] G. I. Harris, *J. Chem. Soc. B* **1970**, 488−500.
[12] L. Lochmann, J. Pospisil, D. Lim, *Tetrahedron Lett.* **1966**, *2*, 257−262.
[13] R. Pi, W. Bauer, B. Brix, C. Schade, P. von Ragué Scheyer, *J. Organomet. Chem.* **1986**, *306*, C1−C4.
[14] L. Lochmann, H. Jakubuv, L. Brandsma, *Collect. Czech. Chem. Commun.* **1993**, *58*, 1445−1451.
[15] M. Veith, M. Zimmer, K. Fries, J. Böhnlein-Maus, V. Huch, *Angew. Chem.* **1996**, *108*, 1647−1651; *Angew. Chem. Int. Ed. Engl.* **1996**, *35*, 1529−1533.
[16] M. Veith, A. Koban, K. Fries, P. Spaniol, R. Elsäßer, A. Rammo, V. Huch, U. Kleinsteuber, *Organometallics* **1998**, *17*, 2612−2618.
[17] M. Veith, S. Wieczorek, K. Fries, V. Huch, *Z. Anorg. Allg. Chem.* **2000**, *626*, 1237−1245.
[18] K. Fries, Dissertation, Saarbrücken, **1996**.
[19] M. Veith, S. Wieczorek, M. Zimmer, V. Huch, unpublished results.
[20] *HYPERCHEM 4.0*, Autodesk, Inc. USA **1996**. Parameters modified for Si and N by M. Veith.
[21] A. I. Kitaigorodskii, *Molecular Solids and Crystals*, Academic Press, New York, **1973**.
[22] H. G. Unruh, M. Veith, unpublished results.
[23] A. F. Hollemann, E. Wiberg, N. Wiberg, *Lehrbuch der anorganischen Chemie*, 101st ed., Walter de Gruyter, Berlin−New York, **1995**.
[24] M. Veith, *Z. Anorg. Allg. Chem.* **1978**, *446*, 227−236.
[25] R. E. Mulvey, *Chem. Soc. Rev.* **1991**, *20*, 167−209.
[26] J. Krüger, University of the Saarland, Physics Department, **1999**.
[27] N. G. Parsonage, L. A. K. Staveley, *Disorder in Crystals*, Clarendon Press, Oxford, **1978**, p. 1−45.
[28] J. H. Kristensen, H. Bildsoe, H. J. Jakobsen, N. C. Nielsen, *J. Magn. Reson*. **1992**, *100*, 437−443.
[29] L. E. Orgel, *J. Chem. Soc.* **1958**, 4186−4190.

Received November 15, 1999
[I99407]

Increased-Valence Structures for Qualitative Valence-Bond Representations of Electronic Structure for Electron-Rich Molecules

Richard D. Harcourt[a]

Keywords: Valence bonds / Increased-valence structures / Three-electron bonds / Singlet diradical structures / Bohr orbits

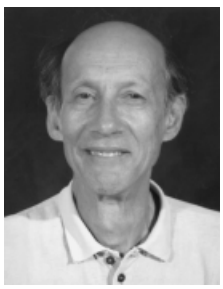
Whereas familiar Lewis-type valence-bond structures for singlet-spin systems involve electron-pair bonds and lone-pairs of electrons, increased-valence structures involve one-electron bonds and fractional electron-pair bonds. An increased-valence structure may be easily derived from a familiar Lewis structure via one-electron delocalizations of lone-pair electrons into two-centre bonding molecular orbitals. The increased-valence structure is equivalent to resonance between several Lewis structures, including the familiar Lewis structure from which it was derived, and therefore it is more stable than the latter structure. Some of the properties of increased-valence structures, and their associated Pauling three-electron bonds as diatomic components of these structures, are discussed, with specific reference to N_2O and the $Fe^{II}O_2$ linkages of oxyhaemoglobin. Applications to numerous other systems that involve 4-electron 3-centre, 6-electron 4-centre, and 6-electron 5-centre bonding units are presented. Brief consideration is also given to a speculative Bohr approach to electronic structure.

Introduction

Over the last two decades, there has been a resurgence of interest in valence-bond (VB) descriptions of the electronic structures of molecules.[1–5] My research has been concerned primarily with the qualitative development of the subject, particularly through the formulation of the *increased-valence* theory[4,5] for the large class of electron-rich molecules. For these molecules, the theory enables their familiar, traditional Lewis-type VB structures, with lone-pairs of electrons and electron-pair bonds, to be stabilized by means of one-electron delocalizations into bonding molecular orbitals (MOs). The resulting increased-valence structures are then able to provide new insights into the origins of bond properties, and how molecules react. Using an $Fe^{II}O_2$ linkage for oxyhaemoglobin, and N_2O, as examples, I shall redescribe some essential features of this theory, and give consideration to a number of the many applications that we have made to inorganic systems. Recent reviews that discuss a variety of examples include those of ref.[5,6] The reader who is more interested in the applications may omit those sections of this review that involve detailed formulations of VB wavefunctions. I shall also briefly redescribe aspects of a speculative approach to qualitative descriptions of electronic structure via Bohr circular orbit theory.[7] The essential purpose of both types of approach to electronic structure is to help provide "primitive patterns of understanding",[8] using mostly qualitative VB methods.

The simplest definition of an electron-rich bonding unit is that it involves N overlapping (hybrid or non-hybrid) atomic orbitals (AOs) centred on N atomic centres, with n electrons occupying these AOs, when $N < n < 2N$. Familiar examples involve 3-electron 2-centre, 4-electron 3-centre, and 6-electron 4-centre bonding, and we shall give primary attention to them here. Pauling designated the 3-electron 2-centre bonding unit as a "three-electron bond",[9] and this designation has continued to be used very widely. Although modifications to the term,[10] such as "three-electron two-orbital bond" and "three-electron hemi-bond" or "three-

[a] School of Chemistry, The University of Melbourne, Victoria 3010, Australia
E-mail: harcus@rubens.its.unimelb.edu.au



Richard Harcourt was born in Melbourne, Australia. In 1963, he received a Ph.D. degree in Chemistry from Monash University, under the supervision of Professor R. D. Brown. At the end of 1993, he took early retirement from his appointment as a Senior Lecturer in Physical Chemistry at the University of Melbourne, where he has continued to work as a Research Associate. His research has involved primarily valence-bond studies of the electronic structures of molecules, with particular emphasis given to the development and application of the increased-valence theory which he formulated three decades ago. Related research has involved energy transfer studies. A reformulation of Bohr orbit descriptions of electronic structure has also provided a fruitful (speculative) area of research.

MICROREVIEWS: This feature introduces the readers to the authors' research through a concise overview of the selected topic. Reference to important work from others in the field is included.

 © WILEY-VCH Verlag GmbH, D-69451 Weinheim, 2000 1434–1948/00/0909–1901 $ 17.50+.50/0

electron half-bond'' provide more accurate descriptions of its bonding properties, we shall use Pauling's designation here. Some of the properties of three-electron bonds will be discussed in the next Section. As will be discussed below, increased-valence structures for 4-electron 3-centre and 6-electron 4-centre bonding units involve three-electron bonds as diatomic components.

The Three-Electron Bond, or Three-Electron Half-Bond

In MO theory, the diatomic three-electron bond involves two bonding electrons and one antibonding electron. Thus if a and b are the overlapping AOs centred on the atomic nuclei A and B, the MO configuration is $(\psi_{ab})^2(\psi^*_{ab})^1$, in which $\psi_{ab} = a + kb$ and $\psi^*_{ab} = k^*a - b$ are orthogonal bonding and antibonding MOs. The k is a variationally controlled polarity parameter with $k^* = (k + <a|b>)/(1 + k<a|b>)$, and the maximum bond-order of 0.5 occurs when $k = 1$, thereby indicating that the designations "three-electron hemi-/half-bond[10]" provide a clearer description of the bonding properties.

$$(\psi_{ab})^2(\psi^*_{ab})^1 \propto (a)^1(\psi_{ab})^1(b)^1 \equiv (a)^2(b)^1 + k(a)^1(b)^2 \qquad (1)$$

It is easy to demonstrate[4,5,11] that the identities of Equation (1) obtain, or in terms of Slater determinants [cf. Equation (2)], in which α and β are the $m_s = +1/2$ and $m_s = -1/2$ electron-spin wavefunctions, and the antibonding ψ^*_{ab} electron is assumed to have an $m_s = +1/2$ spin quantum number. (The identity $|\psi_{ab}{}^{\alpha}\psi_{ab}{}^{\beta}\psi^*_{ab}{}^{\alpha}| \propto |a^{\alpha}\psi_{ab}{}^{\beta}b^{\alpha}|$ was deduced by Linnett.[12]) The $(a)^1(\psi_{ab})^1(b)^1$ configuration involves parallel spins for the a and b electrons, and therefore these two electrons are non-bonding (more accurately, net antibonding[13]); the responsibility for bonding belongs solely with the ψ_{ab} electron, whose spin is opposed to the spin for each of the a and b electrons. In Figure 1, the orbital diagrams that pertain to the identities of Equations (1) or (2) are displayed for $k = k^* = 1$ in the MOs. These identities form the basis for much of the discussion of the properties of increased-valence structures.

$$|\psi_{ab}{}^{\alpha}\psi_{ab}{}^{\beta}\psi^*_{ab}{}^{\alpha}| \propto |a^{\alpha}\psi_{ab}{}^{\beta}b^{\alpha}| \equiv |a^{\alpha}a^{\beta}b^{\alpha}| + k|a^{\alpha}b^{\beta}b^{\alpha}| \qquad (2)$$

Various VB symbolisms have been used to represent the three-electron bond,[4,5,11]. These include VB structures **1**−**6** and **7** ↔ **8**.

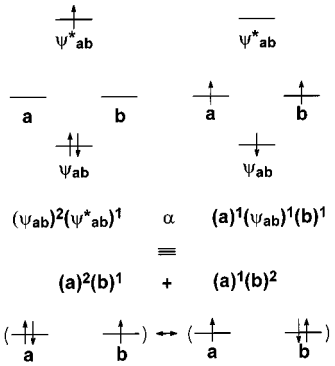
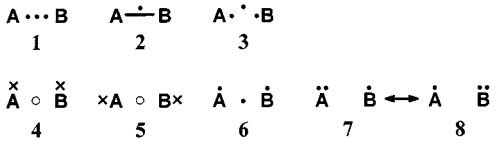


Figure 1. Orbital diagrams for the identities of Equation(1); ↑ ≡ $m_s = +1/2$, ↓ ≡ $m_s = -1/2$



(Atomic formal charges have been omitted from all generalized VB structures that use any of the symbols Y, A, B, C, and D to designate atomic centres.)

The symbolism of structure **1** was introduced by Pauling[9] in 1931, but since then, symbolisms such as **2** and **3** have sometimes been used.[3f,14] However because the equivalent MO theory indicates that the three-electron bond has a maximum bond order of 0.5, structure **2** is unsatisfactory and structures **1** and **3** do not make clear that two of the electrons are non-bonding (more-accurately, net antibonding) in character. Structures **4** and **5** (with spins, **x** for $m_s = +1/2$ and **o** for $m_s = -1/2$) and **6** (without spins) were introduced by Linnett,[12] and with only one bonding electron, they are more-clearly associated with the $|a^{\alpha}\psi_{ab}{}^{\beta}b^{\alpha}|$ configuration than are structures **1**−**3**. Therefore the Linnett symbolism is the preferred[4,5,11] VB symbolism for the three-electron bond. The second identity of Equation (1) shows that each of the three-electron bond VB structures **1**−**6** is equivalent to resonance between the canonical Lewis structures **7** and **8**.

When the odd-electron has $m_s = +1/2$ spin for example, each of the Lewis structures **7** and **8** may be used to generate the three-electron bond VB structure by delocalizing the $m_s = -1/2$ spin lone-pair electron into the ψ_{ab} bonding MO, as is indicated in **9** → **10** and **11** → **12**.



One-electron delocalizations of this type lead to stabilization of the Lewis structures **7** and **8**, and they will be used extensively throughout the paper to generate increased-valence structures from familiar Lewis-type VB structures for triatomic and polyatomic systems. When the extent of delocalization, via the value of the MO polarity parameter k, is determined variationally, a one-electron delocalization from an AO into a bonding MO, *always* generates a stabilization of the increased-valence structure relative to the Lewis structure from which it was derived.

Theory for the three-electron bond may be elaborated further by increasing the number of AOs which are used to accommodate the electrons.[11b] With three AOs (a′,a′′, and b) to accommodate the electrons of the Lewis structure **7**, and three additional AOs (a, b′, and b′′) to accommodate the electrons of the Lewis structure **8**, it has been deduced that a wavefunction of the form $\Psi = \Psi_1(VB) + \Psi_2(VB) = \Psi_1(MO) + \Psi_2(MO)$ may be constructed from each set of three AOs, for which the Ψ_1 and Ψ_2 are three-electron bond wavefunctions. The equivalence has been illustrated[11b] via the results of some ab initio calculations for the $^2\Sigma_u^-$ ground-states of H_2^- and He_2^+. The simplest example involves four AOs, (i.e. for $a' = a'' = a$, $b = b_0$, and $a = a_0$, $b' = b'' = b$) to give the $(a)^2(b_0)^1$ and $(a_0)^1(b)^2$ configurations for structures **7** and **8**, respectively. With H_2^- as the

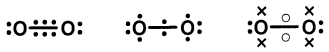
example, use of these AOs is sufficient to ensure that the dissociation products are $H^- + H$ or $H + H^-$, rather than the $H^{-0.5} + H^{-0.5}$ for a three-electron bond with two equivalent AOs. For H_2^-, the use of canonical double-zeta molecular orbitals constructed from 1s′ and 1s′′ atomic orbitals on each atomic centre must lead to ionization of this anion[11b] to form $H_2 + e^-$ when the exponents of the diffuse (1s′′) orbital components of these molecular orbitals are energy-optimized.

The relevance of three-electron bonds for VB descriptions of the electronic structures of high-spin transition metal complexes, F^+-type colour centres, *n*-type semiconductors and high T_c superconductors is described in ref.[5c], and references 26, 28, and 30 therein.

Linnett-type VB structures with electron-spins either indicated, or not indicated, as in structures **4** for example, and structure **6**, will be used in this Review to provide VB representations of the Pauling three-electron bond.

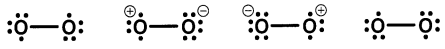
The Oxygen Molecule

The $^3\Sigma_g^-$ ground-state for the oxygen molecule O_2, has an electron-pair σ-bond and two three-electron π bonds, $(\pi_x)^2(\pi^*_x)^1$ and $(\pi_y)^2(\pi^*_y)^1$ with parallel spins for the antibonding π^*_x and π^*_y electrons. The Pauling and Linnett VB structures[9,12] for this molecule are **13**,[9] **14**[12] without spins, and **15**[12] with spins when it is assumed that the antibonding π^*_x and π^*_y electrons have $m_s = +1/2$ spin quantum numbers.



13 **14** **15**

Each of these structures is equivalent to resonance between the canonical Lewis structures **16**−**19**.



16 **17** **18** **19**

The results of ab initio VB calculations for O_2 from several laboratories[15,16] indicate that the uncharged VB structures **16** and **19** have larger weights than have the polar VB structures **17** and **18**. This result, which is not unexpected, reflects the operation of the electroneutrality principle.[9b]

Bonding of O_2 to Haemoglobin

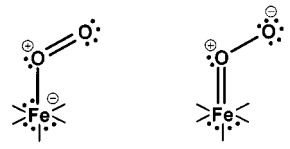
Theories of the bonding of O_2 to haemoglobin or myoglobin will be used here to introduce the concept of an increased-valence structure.

Haemoglobin (Hb) involves four iron atoms, each of which is formally high-spin ($S = 2$ spin) Fe^{II}, with four unpaired, parallel-spin electrons. When oxyhaemoglobin (HbO_2) is formed, four paramagnetic ($S = 1$ spin) O_2 molecules bind to the iron atoms, to give four $S = 0$ spin iron-O_2 linkages. Ever since this effect was first observed by Pauling and Coryell[17] in 1936, there has been debate with regard to how the electronic structure of each $S = 0$ spin iron-O_2 linkage should be (approximately) formulated.[18,19] The three primary models[17,20,21] that are usually considered are the following:

(a) Low-spin $Fe^{II}((t_{2g})^6, S = 0) + O_2^*((\pi^*_x)^2(\pi^*_y)^0, S = 0)$ (Pauling and Coryell);[17]

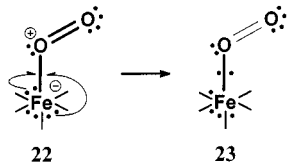
(b) Intermediate-spin $Fe^{II}((t_{2g})^5(e_g)^1, S = 1) + O_2((\pi^*_x)^1(\pi^*_y)^1, S = 1)$ (McClure, 1960),[20] with antiparallel spin-coupling of the unpaired antibonding π^*_x and π^*_y electrons of ground-state O_2 with those for the Fe^{II};

(c) Low-spin $Fe^{III}(S = 1/2) + O_2^-(S = 1/2)$ (Weiss, 1964),[21] with anti-parallel spin coupling for the unpaired electrons of Fe^{III} and O_2^-.

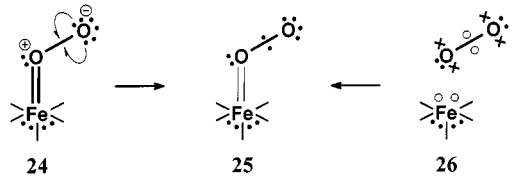


20 **21**

Attention will be given to models (a) and (b). The Pauling-Coryell model (a) involves[17] resonance between the familiar standard (or *Kekulé*-type) Lewis structures **20** and **21**, for which an $S = 0$ spin excited valence-state of O_2 :O::O: is coordinated with the low-spin Fe^{II} in structure **20**. From VB structures **20** and **21**, we can generate[18] VB structures **23** and **25** via the one-electron delocalizations indicated in **22** and **24** (cf. **9** → **10** and **11** → **12**).



22 **23**



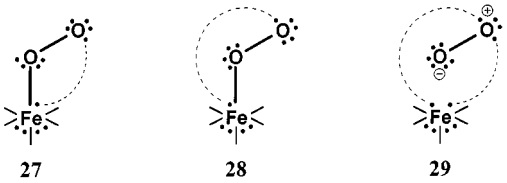
24 **25** **26**

VB structure **25** can also be constructed[18] by spin-pairing the two unpaired electrons of ground-state O_2 with the two unpaired electrons of intermediate-spin Fe^{II}, as in **26** → **25**.

The latter procedure involves e_g-π^*_x and t_{2g}-π^*_y spin-pairings for the appropriate pairs of overlapping orbitals, and it provides the VB representation for the McClure model of (b). We shall focus attention on VB structure **25**, but of course it will participate in resonance with the higher-energy structure **23**, (which involves the O_2 excited state). For reasons that will be discussed later when the general theory of 4-electron 3-centre bonding is outlined, VB structures **23**, **25**, and **31** below for N_2O, are examples of *increased-valence* structures.[4,5]

Because the three-electron bond structure for the O_2 ground-state is equivalent to resonance between four canonical Lewis structures, via the identity **14** ≡ **16**↔**17**↔**18**↔**19**, it follows[18] that the $Fe^{II}O_2$ VB structure **25** for model (b) is equivalent to resonance between the canonical Lewis structures **24** and **27**−**29** when it is assumed that the four electrons of the Fe^{II}=O_2 bond of structure **24**

occupy AOs, i.e. a Heitler-London type formulation of the wavefunction [a(1)b(2) + b(1)a(2) with a and b overlapping AOs] is used for each $Fe^{II}-O$ electron-pair bond. Because structures **27**−**29** do not involve Fe=O double bonds, the Fe=O bond-number or bond-order for increased-valence structure **25** is less than two. Thin bond lines are used to represent the fractional electron-pair bonds which are present in this structure, and in all increased-valence structures.[4−6] The extent to which structures **24** and **27**−**29** contribute to the equivalent Lewis structure VB resonance scheme determines the strength of the Fe=O bond.



27 **28** **29**

Each of the VB structures **27**−**29** is an example of a "*long-bond*" or "*formal-bond*", or *Dewar*-type canonical Lewis structure. A "long" or formal bond has negligible strength, and therefore the function of the pecked bond-line (----) which is sometimes used to represent this type of bond[22] is to indicate that the associated pair of electrons are spin-paired. Some workers do not show the presence of formal bonds, and the VB structure is then designated as a *singlet diradical* or *spin-paired diradical* structure. The formal bonding is not indicated in the increased-valence structure. The more-familiar Lewis structures of types **20** and **21**, are designated as *standard* or *Kekulé*-type canonical Lewis structures.

Increased-valence structures for electron-rich systems are equivalent to resonance between Kekulé- and Dewar-type Lewis structures. Therefore when the polarity parameters that are associated with the one-electron bonds of the increased-valence structures are chosen variationally, use of increased-valence structures *must provide a more stable VB representation of electronic structure* than does use of only the more familiar Kekulé-type Lewis structures alone.

Structure **27** is equivalent to the singlet-biradical structure which Goddard and Olafson have used[23] to represent the electronic structures of the $Fe^{II}O_2$ linkages of oxyhaemoglobin, via the McClure model (b). Because increased-valence structure **25** is equivalent to resonance between structures **24** and **27**−**29**, structure **25** must provide a lower-energy representation of the electronic structure than does either **24** or **27** alone.

The observed reduction[24] in the value of the O−O stretching frequency in HbO_2, namely from 1556 cm^{-1} (free O_2) to 1107 cm^{-1} (HbO_2), is sometimes cited as evidence for the Weiss model (c), but the results of MO calculations[25] indicate that little Fe → O_2 charge-transfer occurs.

O−O Bond Making and Breaking

Either an $Mn^{V}=O$ or an $Mn^{IV}=O$ species has been implicated in the formation of an O−O bond in the photosynthetic process.[26] We give consideration to the $Mn^{IV}=O$ here. An $S = 1/2$ spin VB structure for this species is usually represented as **I** of Figure 2.

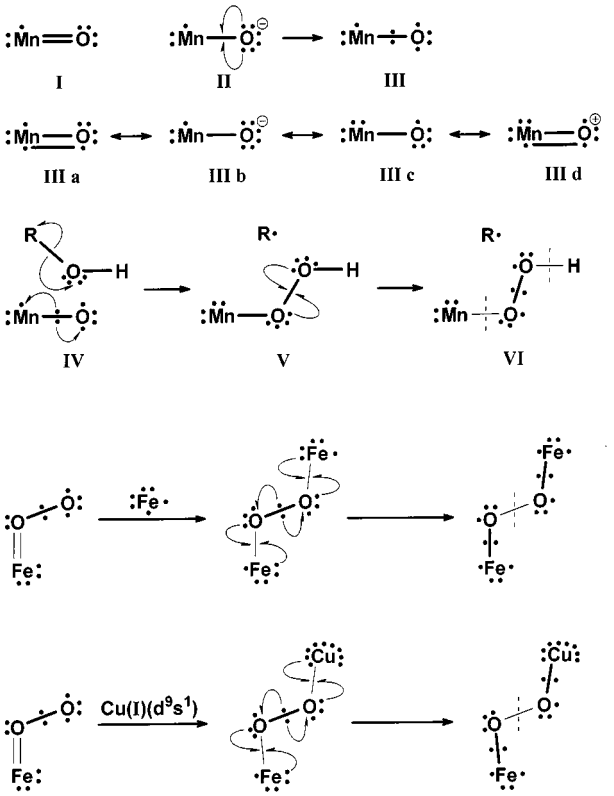


Figure 2. O−O bond-making via $Mn^{IV}O$ + ROH for photosyntheses, and O−O bond-breaking for $Fe^{II}O_2Fe^{II} \rightarrow 2\ Fe^{II}O$ and $Cu^{I}O_2Fe^{II} \rightarrow Cu^{I}O + Fe^{II}O$ decompositions; the $Fe^{II}O_2$ structure corresponds to the increased-valence structure **25**; formal charges are not indicated on the transition metal ions

However it may also be formulated as **II**, from which we may generate VB structure **III** with a three-electron bond. VB structure **III** has an Mn = O double bond whose electronic structure ($(\sigma)^2(\pi_x)^1(\pi_y)^1$) is similar to that of VB structure **15** for the O_2 ground-state. VB structure **III** is equivalent to resonance between the canonical Lewis structures **IIIa**−**IIId**, (with **IIIa** and **IIIb** corresponding to structures **I** and **II**), and therefore **III** is more stable than is either structure **I** or structure **II** alone. With a nitrogen atom replacing the Mn in these VB structures, a similar type of VB representation is relevant for the ground-state of NO.

Unlike structure **I**, the three-electron bond structure **III** locates unpaired electron spin-density on the oxygen atom. Therefore the $Mn^{IV}=O$ is able to react with ROH to generate $Mn^{III}OOH$ ($S = 1/2$) according to **IV** → **V**. The $Mn^{III}OOH$ has been postulated[26b] to be the precursor for O_2 formation. Further electronic reorganization, as indicated in **V** → **VI**, weakens the Mn-O and O-H bonds to generate O_2 + Mn^{II} + H. The **IV** → **V** → **VI** mechanism for the formation of the postulated $Mn^{III}OOH$ species provides an alternative to those provided in references 26b,c.

In Figure 2, increased-valence structures[4,6a] are also displayed for $Fe^{II}-O_2-Fe^{II}$ and $Cu^{I}-O_2-Fe^{II}$, in which the O_2 ground-state is bonded to Fe^{II}($S = 1$, $(t_{2g})^5(e_g)^1$) and Cu^{I}($S = 1$,$(t_{2g})^6(e_g)^3(4s)^1$). The electronic reorganization for

the $Fe^{II}-O_2-Fe^{II} \rightarrow 2\ Fe^{II}O$ and $Cu^{I}-O_2-Fe^{II} \rightarrow Cu^{I}O + Fe^{II}O$ decomposition processes, which have been associated with the oxidation of Fe^{II} porphyrin complexes[4,6a] and cytochrome c oxidase catalysis[4,6a] of $4\ H^+ + 4e + O_2 \rightarrow 2\ H_2O$, are indicated. Each of these decomposition processes involves the breaking of O−O three-electron bonds as well as the O−O σ-bond.

Increased-Valence Structures and N_2O

Ab initio VB calculations on the $Fe^{II}O_2$ linkage have yet to be performed in order to determine which of the canonical Lewis structures are of primary importance. However the results of both semi-empirical[27] and ab-initio[28,29] calculations have been reported for N_2O, whose Kekulé-type Lewis structure **30** is similar to **24** for $Fe^{II}O_2$. By delocalizing an oxygen $p\pi_x$ and an oxygen $p\pi_y$ electron into bonding π_x(ON) and π_y(ON) MOs respectively, we obtain increased-valence structure **31**, which is similar in type to VB structure **25** for the $Fe^{II}O_2$ linkage.

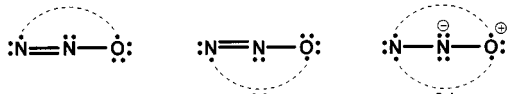


30 **31**

Using the three-electron bond identity,

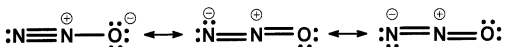


, it is easy to deduce that increased-valence structure **31** is equivalent to resonance between the Kekulé-type Lewis structure **30**, and the Dewar-type Lewis structures **32**−**34**, when the wavefunctions for the N−N π_x and π_y bonds are formulated using the Heitler−London type procedure (cf. discussion above for the $Fe=O_2$ bond of VB structure **25**).



32 **33** **34**

The results obtained from a variety of ab initio VB calculations for N_2O are reported in ref.[29] These results, which are in agreement with those obtained from our earlier semi-empirical VB studies,[27] show that the Dewar structures **32** and **33** in particular have an importance which is comparable with those for the familiar Kekulé-type structures **30**, **35**, and **36**.



30 **35** **36**

Resonance between the latter three structures is usually used to provide the primary qualitative VB representation of the electronic structure of N_2O, and of course increased-valence structures can also be generated[5,27,29] from the Lewis structures **35** and **36**, as well as from structure **30**.

The conclusion that N_2O has appreciable singlet diradical character has been exploited to develop VB mechanisms for a variety of reactions which involve this molecule. These reactions include: (a) thermal decomposition[29,30a] to generate either $N_2 + O^*$ or $2\ N_2 + O_2^*$, (b) $N_2O + X \rightarrow N_2 + OX$, for which X is a univalent radical,[29,30a,30b] (c) 1,3-dipolar cycloaddition reactions,[29,30a] (d) a unimolecular

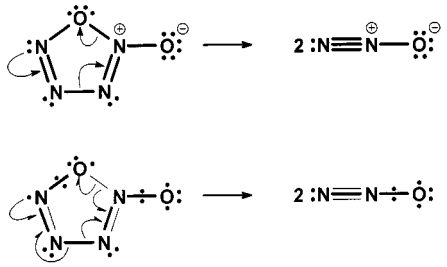


Figure 3. Standard Lewis VB and increased-valence representations for cyclic $N_4O_2 \rightarrow 2\ N_2O$ decomposition; the increased-valence representation involves lower energies for reactant and products

$C_{\infty v} \rightarrow C_{2v} \rightarrow D_{\infty h}$ isomerization process[31] and (e) NO + NCO → N_2O + CO.[5b] For each case, the primary "active space" involves four singly-occupied orbitals, and for them, the Rumer diagrams[30a,30b] allow for the existence of two $S = 0$ spin-pairing schemes − one for a reactant-like species and one for a product-like species. Therefore a crossing of potential energy curves is involved when proceeding from reactants to products[4,30a,30b,32]. The VB representation for the diradical mechanism for decomposition reactions of type (a) is contrasted[30b] with the usual type of polar mechanism that would be used to indicate how electronic reorganization might proceed, via the shifting of pairs of electrons. In Figure 3, these two types of VB representations[30b] are illustrated here for the decomposition of cyclic $N_4O_2 \rightarrow 2\ N_2O$, which has been calculated[33] to arise as an intermediate in the thermal decomposition of N_3-NO_2.

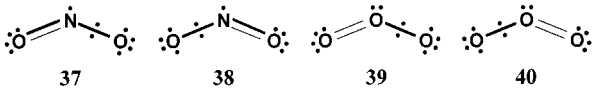
Some ab initio STO-6G VB calculations for N_2 have been performed,[34] in order to illustrate the effect of AO hybridization on the length of the N−N bond of N_2 relative to those of HN_3 and N_2O. For N_2, the electron-pair N−N σ-bond arises from the overlap of hybrid AOs of the form $h \approx 2p\sigma + 0.18(2s)$, whereas for N_2O, this bond involves the overlap of $2p\sigma + 0.18(2s)$ and $2p\sigma + 2s$ hybrid AOs. The results of calculations for N_2 with these two pairs of AOs give a bond shortening of 0.03 Å for the latter pair relative to the former pair. With this estimate, the N−N bond length of 1.13 Å for N_2O is ≈ 0.06 Å longer than is that for an N_2 with $2p\sigma + 0.18(2s)$ and $2p\sigma + 2s$ hybrid AOs. The fractionality of the N−N triple bond in increased-valence structure **31** is in agreement with the appreciable lengthening of the N−N bond of N_2O relative to that of an N_2 with the same AO hybridization.

Inspection of increased-valence structure **31** for N_2O reveals that more than eight electrons appear to be involved in bonding to the central nitrogen atom, i.e. an *apparent violation of the Lewis-Langmuir octet rule* occurs for this atom. In each of references 34 and 35, it is demonstrated that this effect is a consequence of the inclusion of the Dewar-type Lewis structures **32**−**34** as well as the Kekulé structure **30** in the canonical structure resonance scheme.

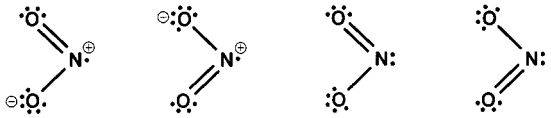
Increased-Valence Structures for NO_2, O_3, and SO_2

Increased-valence structures **37**−**40** for NO_2 and O_3 have now been derived − either from Lewis VB structures via one-electron delocalizations, or from three-electron bond

VB structures for the reactants O + NO and O + O_2 − and displayed on numerous occasions.[4,5,35,36] These increased-valence structures will be used in subsequent discussions.

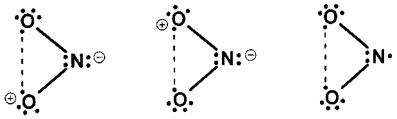


37 **38** **39** **40**



41 **42** **43** **44**

With $\sigma_v\Psi_{37} = \Psi_{38}$ and $\sigma_v\Psi_{38} = \Psi_{37}$, the $\Psi(^2A_1) = \Psi_{37} + \Psi_{38}$ resonance between increased-valence structures **37** and **38** for the ground-state of NO_2 is equivalent[35] to resonance between the canonical Lewis structures **41**−**47**.



45 **46** **47**

When the O−N−O bond-angle of NO_2 is near to the experimental value of 134°, a significant contribution from the Dewar-type Lewis structure **47** has been calculated to occur.[36] This structure is considered[35] to be primarily responsible for the retention of C_{2v} point-group symmetry for the experimentally-observed ground-state. For small bond-angles, the ground-state is calculated[37] to have $^2B_2$ symmetry in the C_{2v} point-group, and structure **47** then does not contribute[35] to the equivalent Lewis structure resonance scheme for $\Psi(^2B_2) = \Psi_{37} - \Psi_{38}$. Consequently for this state, one N−O bond can be stretched relative to the other, and $NO_2 \rightarrow NO + O$ dissociation then becomes possible.[35,36] Similar considerations may be used[35] to account for the $O_3 \rightarrow O_2 + O$ and $CO_2 \rightarrow CO + O$ thermal dissociations.

In Figure 4, increased-valence structures for NO_2 and O_3 are used to indicate how electronic reorganization can proceed for other reactions with these molecules as reactants.[4,5] The mechanisms displayed exploit the singlet diradical character which is present in the increased-valence structures. SO_2 and S_2O are homoelectronic with O_3, and with similar types of increased-valence structures, VB representations[38] for some reactions that involve these sulfur-containing molecules are displayed in Figure 4.

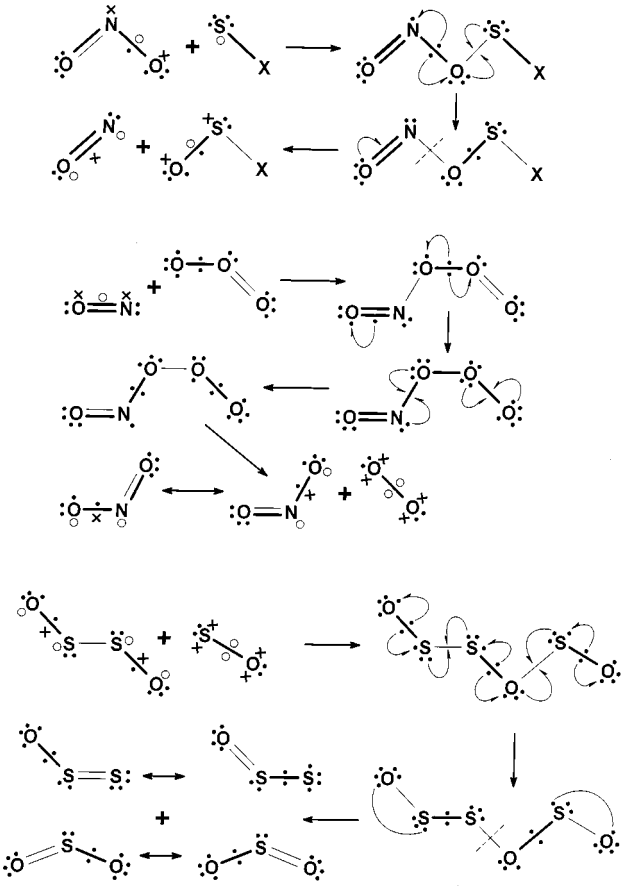
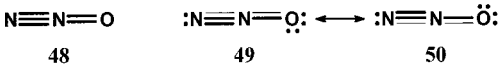


Figure 4. Increased-valence representations for $NO_2 + SX \rightarrow NO + OSX$ (X = halogen), $NO + O_3 \rightarrow NO_2 + O_2$, and $3\,SO \rightarrow SO_2 + S_2O$ via an $S = 1$ spin intermediate S_2O_2 (each of O_2, SO and S_2 has a $^3\Sigma_g^-$ ground-state; therefore an $S = 0 \leftarrow S = 1$ electronic excitation of one of the SO monomers must occur to obtain the $S = 1$ spin intermediate for S_2O_2; the reaction $2\,SO + S_2 \rightarrow 2\,S_2O$ may be similarly represented)

Spin-Coupled Valence-Bond Calculations

Other workers have used their *spin-coupled* VB techniques[3a,3b,39] to study the electronic structures of NO_2, N_2O, and other 1,3-dipolar (or zwitterionic-diradical hybrid)[32a] molecules, such as O_3, CH_2N_2, and HCNO. The calculations allocate a separate orbital for each active-space electron, and consider the different spin-pairing schemes that are available for these electrons. No orthogonality constraints are required for each pair of active-space orbitals in the spin-coupled calculations. These orbitals are designated as "distorted AOs" and may involve two or more atomic centres. Therefore they do not correspond to the one-centre AOs which are associated with the active-space electrons of the canonical Lewis structures.

The results of spin-coupled VB calculations have been interpreted to imply that 1,3-dipolar molecular species possess very little singlet diradical character.[3a,3b,39] For some of these molecules, such as N_2O, a similar conclusion was obtained from *biorthogonal* VB calculations.[40] In contrast, classical VB studies[27−29,36,41] indicate that singlet-diradical canonical Lewis structures can contribute appreciably to the ground-state resonance schemes. The difference in interpretation is associated[5a,28,35] with the use of the 2-centre or multicentre "distorted" AOs to accommodate at least some of the active-space electrons in the spin-coupled VB calculations. The use of these AOs conceals[5a,28,35] the presence of appreciable singlet-diradical character, which manifests itself in VB representations for reactions that involve 1,3-dipolar molecules[29−32] (for example, $NO + O_3 \rightarrow NO_2 + O_2$ in Figure 4).



48 **49** **50**

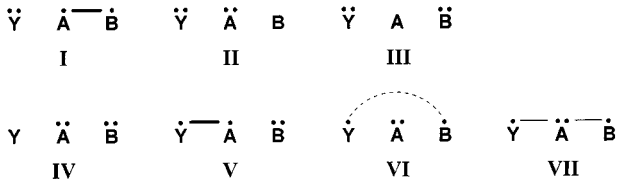


Figure 5. Canonical Lewis VB structures for $S = 0$ spin 4-electron 3-centre bonding unit, with three overlapping AOs; $\Psi_{\mathbf{I}} = |y^{\alpha}y^{\beta}a^{\alpha}b^{\beta}| + |y^{\alpha}y^{\beta}b^{\alpha}a^{\beta}|$, $\Psi_{\mathbf{II}} = |y^{\alpha}y^{\beta}a^{\alpha}a^{\beta}|$, $\Psi_{\mathbf{III}} = |y^{\alpha}y^{\beta}b^{\alpha}b^{\beta}|$, $\Psi_{\mathbf{IV}} = |a^{\alpha}a^{\beta}b^{\alpha}b^{\beta}|$, $\Psi_{\mathbf{V}} = |y^{\alpha}a^{\beta}b^{\alpha}b^{\beta}| + |a^{\alpha}y^{\beta}b^{\alpha}b^{\beta}|$, $\Psi_{\mathbf{VI}} = |y^{\alpha}a^{\beta}a^{\alpha}b^{\beta}| + |a^{\alpha}y^{\beta}b^{\alpha}a^{\beta}|$; with either a (non-orthogonal) double-zeta basis set, or an (orthogonal) expanded valence-shell AO basis set (a,d) for the two electrons on atom A in structure **VI**, canonical Lewis structure **VII** will also contribute to the VB resonance scheme; using the (a,d) basis, y-a and d-b spin-pairings give $\Psi_{\mathbf{VII}} = |y^{\alpha}a^{\beta}d^{\alpha}b^{\beta}| + |y^{\alpha}a^{\beta}b^{\alpha}d^{\beta}| + |a^{\alpha}y^{\beta}b^{\alpha}d^{\beta}| + |a^{\alpha}y^{\beta}d^{\alpha}b^{\beta}|$; a second $S = 0$ spin wavefunction, with a-d and y-b spin-pairings, may also be constructed

A 19th century-type of VB representation for N_2O is **48**, and a 20th century equivalent, **49** ↔ **50**, involve an apparent quinquevalence for the central nitrogen atom. VB structures of type **48** have been used frequently in discussions of the results of spin-coupled VB calculations. With a minimal basis set, it has been calculated that increased-valence structure **31** is more stable than the **49** ↔ **50** resonance.[42]

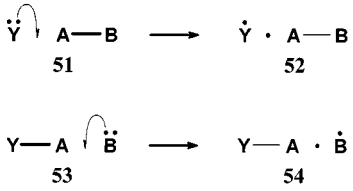
Increased-Valence Structures and 4-Electron 3-Centre Bonding

I shall now redescribe and develop further some of the general VB theory for 4-electron 3-centre bonding units, i.e. for four electrons distributed amongst three overlapping AOs located on three atomic centres.[4,5,30a,34,35,43]

For each of $Fe^{II}O_2$ and N_2O, there are two 4-electron 3-centre bonding units. For the purpose of the following discussion, it is easier to focus attention on those for N_2O. These bonding units arise from the presence of four π_x electrons and four π_y electrons, which are distributed between three overlapping $2p_x$ and three overlapping $2p_y$ AOs, respectively. For each $S = 0$ spin 4-electron 3-centre bonding unit, there are six[42,43] canonical Lewis VB structures, namely **I**−**VI** of Figure 5, in which Y, A, and B are the atomic centres, and y, a, and b are the associated (normalized) overlapping AOs. Each of the structures **I**, **V**, and **VI** has two singly occupied AOs, and their $S = 0$ spin wavefunctions are indicated in the caption for Figure 5.

Structures **I** and **V** are Kekulé-type structures, structure **VI** is a Dewar-type structure, and structures **II**−**IV** are of the polar type.

For any 4-electron 3-centre bonding unit, increased-valence structures[4,5,30a,34,35,43] may be constructed from Kekulé-type Lewis structures by delocalizing a non-bonding Y or B electron into a bonding Y−A or A−B MO, as is indicated in **51** → **52** and **53** → **54**.



The delocalized electron occupies the bonding localized MO (LMO) $\psi_{ay} = a + ly$ in structure **52** and the bonding LMO $\psi_{ab} = a + kb$ in structure **54**. When $\Psi_{\mathbf{I}}$ and $\Psi_{\mathbf{V}}$ are assumed to be the wavefunctions (cf. Figure 5) for structures **51** and **53** it follows that **52** ≡ **I** ↔ **VI** and **54** ≡ **V** ↔ **VI**, i.e. in each case, the increased-valence structure is equivalent to resonance between the Kekulé and Dewar canonical Lewis structures. Because of the absence of either an A−B or a Y−A electron-pair bond in the Dewar structure **VI**, the A−B bond in **52** and the Y−A bond of **54** are fractional electron-pair bonds.

The increased-valence structure **54** involves the $(y)^1(a)^1(\psi_{ab})^1(b)^1$ configuration. We have already demonstrated that the A-B three-electron bond configuration $(a)^1(\psi_{ab})^1(b)^1$ is proportional to the MO configuration $(\psi_{ab})^2(\psi^*_{ab})^1$, [cf. Equations (1) and (2), and Figure 1]. Therefore $(y)^1(a)^1(\psi_{ab})^1(b)^1$ is proportional to $(y)^1(\psi_{ab})^2(\psi^*_{ab})^1$, i.e. increased-valence structure **54** involves the spin-pairing of the y electron with the antibonding ψ^*_{ab} electron of the A-B three-electron bond. [In terms of Slater determinants, the $S = 0$ spin wavefunction is give by Equation (3).]

$$\Psi_{\mathbf{54}} = |y\beta a\alpha\psi_{ab}\beta b\alpha| + |y\alpha a\beta\psi_{ab}\alpha b\beta| \propto |y\beta\psi_{ab}\alpha\psi_{ab}\beta\psi^*_{ab}\alpha| + |y\alpha\psi_{ab}\beta\psi_{ab}\alpha\psi^*_{ab}\beta| \quad (3)$$

Consideration has been[34] given to the evaluation of atomic valencies for increased-valence structure **54**, with AO overlap integrals both excluded and included in the definition of valence. It has been demonstrated that the A-atom valence is able to exceed unity in this structure, whereas in each of the Kekulé-type Lewis structures, **I** and **V**, the A-atom valence is unity. Therefore with regard to its A-atom valence, VB structure **54** (and also **52**) may exhibit "increased-valence" relative to the Kekulé-type Lewis structures.

The results of experimental and theoretical studies of HXY-type rare-gas molecules (X = Kr or Xe; Y = Cl, Br, I, CN, ...) have been reviewed recently.[45] The H, X, and Y then correspond to the Y, A, and B of Figure 5. With X = Xe and Y = Cl, the origin of bonding is considered to be described[45,46] best as primarily an ion pair  , which is equivalent to structure **V** of Figure 5. However at non-dissociative interatomic distances, it will interact with , which corresponds to structure **VI** of Figure 5. Resonance between these canonical Lewis structures generates increased-valence structure **54** as  .

Increased-Valence Structures and Expansion of Valence-Shell

To stabilize further a 4-electron 3-centre bonding unit, additional AOs may be included on the atomic centres. We focus attention on the A-atom of increased-valence structure **54** by including a second orthogonal AO, which we designate as d. We now define a new A−B bonding MO as $\psi_{a'b} = a + kb + k'd = \psi_{ab} + k'd$. The resulting

$(y)^1(a)^1(\psi_{a'b})^1(b)^1$ configuration, (whose $S = 0$ spin wavefunction involves four Slater determinants, cf. $\Psi_{\mathbf{VII}}$ of Figure 5), may then be expressed according to Equation (4).

$$(y)^1(a)^1(\psi_{a'b})^1(b)^1 = (y)^1(a)^1(\psi_{ab})^1(b)^1 + k'(y)^1(a)^1(d)^1(b)^1 \quad (4)$$

$$\rightarrow \Psi_{\mathbf{54}}(k'=0) + k''\Psi_{\mathbf{VII}} \quad (5)$$

For $\Psi_{\mathbf{54}}(k' = 0)$, spin-pairing occurs between the y and ψ^*_{ab} electrons, whereas $\Psi_{\mathbf{VII}}$ involves y-a and d-b spin-pairings. Introduction of the d AO enables allowance for expansion of the A-atom valence-shell to occur via use of an increased-valence structure. To provide an example, we consider the axial F−Cl−F σ-bonding for ClF_3 of Figure 6.

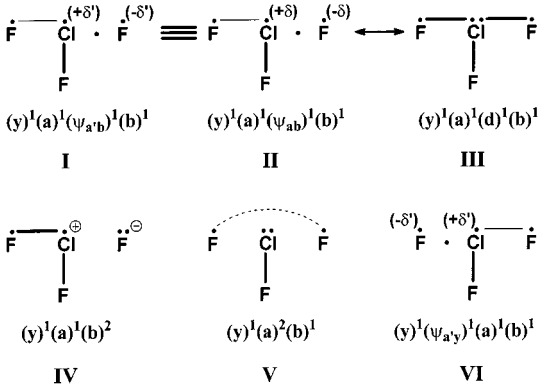


Figure 6. Increased-valence structures **I** and **VI** for ClF_3 with expanded valence-shell on the Cl atom; for the axial three-centre bonding, y, a, b and d are 2pσ(F), 3pσ(Cl), 2pσ(F) and $3d_{z^2}$(Cl) AOs; $\psi_{a'b} = a + kb + k'd = \psi_{ab} + k'd$, $\psi_{a'y} = a + ky + k'd = \psi_{ay} + k'd$, with y-a and $\psi_{a'b}$-b spin-pairings for structure **I** and b-a and $\psi_{a'y}$-y spin-pairings for structure **VI** (cf. $\Psi_{\mathbf{VII}}$ for structure **VII** in Figure 5)

If y = F($2p_z$), a = Cl($3p_z$), b = F($2p_z$), and d = Cl($3d_{z^2}$), then increased-valence structure **I** for ClF_3 is equivalent to resonance between the increased-valence structure **II** ($k' = 0$) and the expanded valence-shell structure **III**. In turn, increased-valence **II** ($k' = 0$) is equivalent to resonance between the canonical Lewis structures **IV** and **V** of Figure 6. A similar type of identity may be developed for the mirror-image increased-valence structure **VI** of Figure 6.

In ref.[35], analagous theory has also been developed for a double-zeta basis set (with a′ and a′′ AOs replacing the a and d AOs) on the A-atom. In subsequent discussions we shall not consider explicitly either double-zeta basis sets or expansion of the valence shell, but recognize that when appropriate, these types of basis sets may be introduced into the wavefunction for an increased-valence structure.

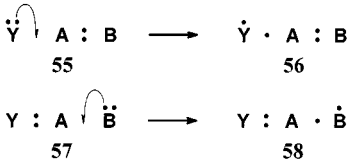
Numerous MO studies of the phenomenon of valence-shell expansion have been reported.[47] The difficulty for atoms of first-row elements to form many stable hypercoordinate compounds has been associated[34,43] with large values for the ionization energies of A-atoms in Lewis structures of type **VI** in Figure 5, when A is a first-row atom.

Localized MO Increased-Valence Structures

The identities **52** ≡ **I** ↔ **VI** and **54** ≡ **V** ↔ **VI** utilize the a and b AOs to accommodate the electrons of the fractional A-B electron-pair bond in increased-valence structure **52**, and the y and a AOs of the fractional Y−A electron-pair bond in increased-valence structure **54**. For a more general formulation of these bonds, these AOs are replaced by the Coulson−Fischer-type[48] LMOs of Equations (6) and (7) for the fractional A−B and Y−A bonds, respectively. The LMO VB structures that correspond to the canonical Kekulé structures **I** and **V** and the increased-valence structures **52** and **54**, are symbolized[5,30a,43] as **55** and **57**, and **56** and **58**, respectively, for which **55** ≡ **I**↔**II**↔**III**, **57** ≡ **V**↔**IV**↔**III**, and structures **I**−**V** here are those of Figure 5.

$$\psi''_{ab} = a + k''b,\ \psi'_{ba} = b + k'a \quad (6)$$

$$\psi''_{ay} = a + l''y,\ \psi'_{ya} = y + l'a \quad (7)$$



In the LMO Kekulé-type structures **55** and **57**, the one-electron delocalization that is needed to generate the LMO increased-valence structures **56** or **58** is indicated. As is the case for the (Heitler−London-type) increased-valence structures **52** and **54**, the delocalized electron occupies the Y−A bonding LMO $\psi_{ay} = a + ly$ in increased-valence structure **56**, and the A−B bonding LMO $\psi_{ab} = a + kb$ in increased-valence structure **58**. The A-atom valence in the LMO increased-valence structures **56** and **58** can exceed unity,[30a,43] and a demonstration of this result is provided again in the Appendix.

LMO Increased-Valence Structures and Donor-Acceptor Complexes

The simplest types of $S = 0$ spin wavefunctions for the LMO increased-valence structures **56** and **58** are those of Equations (8) and (11) respectively.[30a,43]

$$\Psi_{\mathbf{56}} = |\psi'_{ba}\alpha\psi''_{ab}\beta\psi_{ay}\alpha y\beta| + |\psi''_{ab}\alpha\psi'_{ba}\beta y\alpha\psi_{ay}\beta| \quad (8)$$

$$\Psi_{\mathbf{56}} = l\{(1 + k'k'')\Psi_{\mathbf{I}} + 2k'\Psi_{\mathbf{II}} + 2k''\Psi_{\mathbf{III}}\} + k''\Psi_{\mathbf{V}} + \Psi_{\mathbf{VI}} \quad (9)$$

$$\Psi_{\mathbf{56}} = l\Psi_{\mathbf{55}} + \Psi_{\mathbf{54}}'' \quad (10)$$

$$\Psi_{\mathbf{58}} = |\psi'_{ya}\alpha\psi''_{ay}\beta\psi_{ab}\alpha b\beta| + |\psi''_{ay}\alpha\psi'_{ya}\beta b\alpha\psi_{ab}\beta| \quad (11)$$

$$\Psi_{\mathbf{58}} = k\{(1 + l'l'')\Psi_{\mathbf{V}} + 2l'\Psi_{\mathbf{IV}} + 2l''\Psi_{\mathbf{III}}\} + l''\Psi_{\mathbf{I}} + \Psi_{\mathbf{VI}} \quad (12)$$

$$\Psi_{\mathbf{58}} = k\Psi_{\mathbf{57}} + \Psi_{\mathbf{52}}'' \quad (13)$$

When the AO expressions for ψ_{ay}, ψ_{ab} and the LMOs of Equations (6) and (7) are substituted into Equations (8) and (11), we obtain the linear combinations of Equations (9) and (12) respectively. These linear combinations show that the Dewar structure **VI** of Figure 5 is included in the equivalent canonical structure resonance schemes for the LMO increased-valence structures **56** and **58**. Equations (9)

and (12) are also equivalent to Equations (10) and (13) respectively, in which the the $\Psi_{54''}$ and $\Psi_{52''}$ correspond to Ψ_{54} and Ψ_{52} when k'' and l'' replace k and l in the latter configurations.

The lower-energy linear combination of Ψ_{56} and Ψ_{58}, via Equation (14), has seven variational parameters (k, l, k', k'', l', l'', and μ) whereas the lowest-energy linear combination of the $\Psi_{\mathbf{I}}-\Psi_{\mathbf{VI}}$ of Figure 5 involves five independent variational parameters. One type of correspondence between the two linear combinations is obtained when l' and l'' are set equal to k' and k'' respectively.

$$\Psi(\text{Increased-valence, LMO}) = \Psi_{56} + \mu\Psi_{58} \tag{14}$$

Each of Equations (10) and (13) represents a Mulliken-type wavefunction[30a,43] for either an intra- or an intermolecular complex when the complex involves an n-type donor (D), and a sacrificial acceptor (A). The simplest Mulliken-type representation for such a complex involves resonance between a "no bond" (D,A) and a dative (D^+-A^-) VB structure.[22] Thus when $\ddot{\mathbf{Y}}$ and **A : B** are identified as an electron-donor and an electron-acceptor, the VB structures **55** and **54** correspond to the (D,A) and (D^+-A^-) structures respectively, and according to Equation (10), increased-valence structure **56** is equivalent to resonance between these two structures. Similarly, increased-valence structure **58** is equivalent to resonance between (D,A) and (D^+-A^-) types of VB structures, with D = $\ddot{\mathbf{B}}$, A = **Y : A**, (D,A) = **57** and (D^+-A^-) = **52**. In each of the increased-valence structures, a one-electron bond links the donor to the acceptor.

One-Electron and Concerted Two-Electron Delocalizations into Bonding and Antibonding Molecular Orbitals

When $k'' = 1/k' = k$ in Equation (6), an approximate LMO wavefunction for VB structure **55** is given by Equation (15).

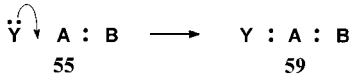
$$\psi_{\mathbf{55}} = |y^{\alpha}y^{\beta}\psi_{ab}{}^{\alpha}\psi_{ab}{}^{\beta}| \tag{15}$$

Some (concerted) delocalization of the y electrons into the antibonding MO $\psi^*_{ab} = k^*a - b$ generates the *approximate* MO wavefunction[49,50] of Equation (16), which provides the usual approximate MO formulation for the anomeric effect[51] and negative hyperconjugation.[52]

$$\Psi_1(\text{MO}) = |(y + \lambda\psi^*_{ab})^{\alpha}(y + \lambda\psi^*_{ab})^{\beta}\psi_{ab}{}^{\alpha}\psi_{ab}{}^{\beta}| \tag{16}$$

$$\Psi_1(\text{MO}) \equiv |y^{\alpha}y^{\beta}\psi_{ab}{}^{\alpha}\psi_{ab}{}^{\beta}| + \lambda(|y^{\alpha}\psi^*_{ab}{}^{\beta}\psi_{ab}{}^{\alpha}\psi_{ab}{}^{\beta}| + |\psi^*_{ab}{}^{\alpha}y^{\beta}\psi_{ab}{}^{\alpha}\psi_{ab}{}^{\beta}|) + \lambda^2|\psi^*_{ab}{}^{\alpha}\psi^*_{ab}{}^{\beta}\psi_{ab}{}^{\alpha}\psi_{ab}{}^{\beta}| \tag{17}$$

When the y electrons of structure **55** are delocalized into the Y−A bonding MO $\psi_{ya} = y + la$, according to **55** → **59**, the resulting wavefunction is given by Equation (18).



$$\psi_{\mathbf{59}} = |\psi_{ya}{}^{\alpha}\psi_{ya}{}^{\beta}\psi_{ab}{}^{\alpha}\psi_{ab}{}^{\beta}| \tag{18}$$

$$\psi_{\mathbf{59}} \equiv |y^{\alpha}y^{\beta}\psi_{ab}{}^{\alpha}\psi_{ab}{}^{\beta}| + l\{|y^{\alpha}a^{\beta}\psi_{ab}{}^{\alpha}\psi_{ab}{}^{\beta}| + |a^{\alpha}y^{\beta}\psi_{ab}{}^{\alpha}\psi_{ab}{}^{\beta}|\} + l2|a^{\alpha}a^{\beta}\psi_{ab}{}^{\alpha}\psi_{ab}{}^{\beta}| \tag{19}$$

Introduction of the identities $|\psi^*_{ab}{}^{\alpha}\psi_{ab}{}^{\alpha}| = (kk^* + 1)|a^{\alpha}b^{\alpha}|$ and $|\psi^*_{ab}{}^{\beta}\psi_{ab}{}^{\beta}| = (kk^* + 1)|a^{\beta}b^{\beta}|$ into Equation (17), and the identities $|a^{\alpha}\psi_{ab}{}^{\alpha}| = k|a^{\alpha}b^{\alpha}|$ and $|a^{\beta}\psi_{ab}{}^{\beta}| = k|a^{\beta}b^{\beta}|$ into Equation (19), we obtain[49] Equations (20) and (21), in which $\Psi_{\mathbf{IV}}$ is the wavefunction for VB structure **IV** of Figure 5. The $\Psi_1(\text{MO})$ and $\psi_{\mathbf{59}}$ are equivalent[49] when $\lambda = kl/(kk^* + 1)$. Therefore some concerted delocalization of the two lone-pair electrons of donor $\ddot{\mathbf{Y}}$ of VB structure **55** into the vacant *antibonding* MO of acceptor **A : B** is equivalent to the concerted delocalization of these electrons into the Y−A *bonding* MO, to give VB structure **59**.

$$\Psi_1(\text{MO}) \equiv \Psi_{\mathbf{55}} + \lambda(kk^* + 1)\Psi_{\mathbf{54}} + (kk^* + 1)^2\lambda^2\Psi_{\mathbf{IV}} \tag{20}$$

$$\psi_{\mathbf{59}} \equiv \Psi_{\mathbf{55}} + kl\Psi_{\mathbf{54}} + k^2l^2\Psi_{\mathbf{IV}} \tag{21}$$

VB Representations for Gas-Phase Nucleophilic Substitution Reactions

If Ÿ is a nucleophile and A:B is a substrate, then at each stage along the reaction coordinate, resonance between the LMO increased-valence structures **56** and **58** can be used to provide a "variationally-best" VB representation [cf. Equation (14)] for a gas-phase nucleophilic substitution reaction. In several publications,[5,30a,43,53] the generalized VB representation for this type of reaction has been presented. Here we consider a specific example, namely that of **I** → [**II** ↔ **III**] → **IV** of Figure 7 for the (Grotthuss) proton-transfer reaction $H_2O + H_3O^+ \rightarrow H_3O^+ + H_2O$. The LMO increased-valence structures **II** and **III** of Figure 7 are VB structures for reactant-like and product-like complexes respectively, and are formed via the one-electron delocaliz-

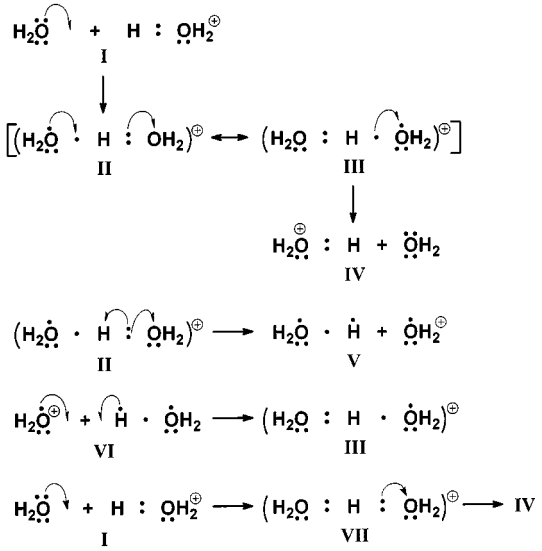


Figure 7. Valence-bond representations for the gas-phase proton-transfer reaction $H_2O + H_3O^+ \rightarrow H_3O^+ + H_2O$

ations that are indicated in this Scheme. At the conclusion of the reaction, the reactant-like complex **II** would dissociate according to **II** → **V** of Figure 7, whereas near the commencement of the reaction, the formation of the product-like complex **III** proceeds according to **VI** → **III** of Figure 7.

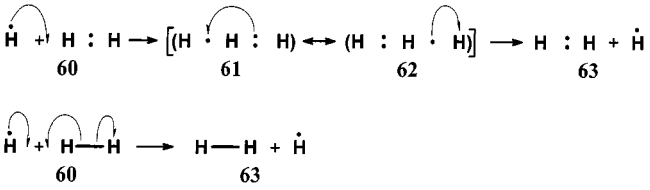
In ref.[5b,30a,53], the generalized forms of VB structures **I**−**VI** of Figure 7 have been used to construct state correlation diagrams for the conversion of reactants into products. These diagrams use a VB symbolism which differs from the symbolism used by Shaik and co-workers[3f] for this purpose. Shaik and co-workers[3f] use VB structures of type **2** to represent the three-electron bond structures − for example $HO_2 \therefore H$ and $H \therefore OH_2$ for the H_3O structures **V** and **VI**.

A qualitative MO description for nucleophilic substitution reactions is often formulated approximately according to the Ψ_1(MO) of Equation (16), i.e. electrons delocalize from the nucleophile orbital (y) into the antibonding MO (ψ^*_{ab}) of the substrate. As has been deduced above, this delocalization is equivalent to the concerted delocalization of the y electrons into the bonding MO (ψ_{ya}), according to **55** → **59**, or **I** → **VII** of Figure 7 here. According to Equation (20), the Ψ_1(MO) configuration of Equation (16) alone cannot generate the $H_3O^+ + H_2O$ products; the inclusion of the Ψ_{IV} (of Figure 5) of this Equation, to give an $H_2O^{2+}H_3O^-$ structure, prevents this from occurring. To obtain the correct dissociation products, it is then necessary to form[49] the linear combination $\Psi = C_1\Psi_1(MO) + C_2\Psi_2(MO)$, with Ψ_2(MO) given by Equation (22), in which $\psi_{ay} = a + \kappa y$ and $\psi^*_{ay} = \kappa^* a - y$. The LMO equivalent for this type of linear combination is examined in ref.[43], where it is demonstrated that the formation of the primary contributor to the VB representation of a reactant-like complex must proceed according to an initial *one-electron* delocalization, as in **I** → **II** of Figure 7, rather than by the *concerted electron-pair* delocalization which is associated with the Ψ_1(MO) of Equation (16).

$$\Psi_2(MO) = |(b + \lambda'\psi^*_{ay})^\alpha (b + \lambda'\psi^*_{ay})^\beta \psi_{ay}{}^\alpha \psi_{ay}{}^\beta| \qquad (22)$$

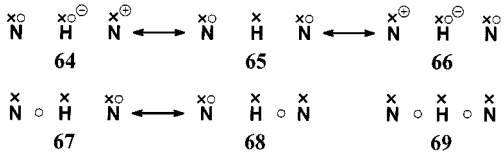
Three-Electron Three-Centre Bonding and VB Representations for Gas-Phase Radical Transfer Reactions

Although 3-electron 3-centre bonding units are not electron-rich, it is possible to construct increased-valence structures for them. The LMO VB structures **61** and **62** for H_3 in the formulation[54] **60** → [**61** ↔ **62**] → **63** for the radical transfer reaction H + H_2 → H_2 + H, provide examples. These structures represent reactant-like and product-like intermolecular species, respectively. The formulation **60** → [**61**↔**62**] → **63** indicates succinctly the nature of the electronic reorganization which may be involved in the conversion of reactants into products for a radical transfer reaction. This formulation is equivalent to the variationally best resonance between the eight (S = 1/2 spin) canonical Lewis structures that may be constructed from three overlapping AOs.[54] The electronic reorganization is also equivalent to the more familiar formulation of **60** → **63**.



Five-Electron Three-Centre Bonding

Each of NO_2, SO_2^-, and ClO_2 has a 5-electron 3-centre bonding unit;[5c,36,55] five electrons are distributed amongst three overlapping σ AOs (NO_2) or π-electron AOs (SO_2^- and ClO_2, when it is assumed that sulfur and chlorine 3d AOs do not participate in π-bonding as hybridization functions). For this type of bonding unit, three equivalent VB representations may be constructed,[5c,36,55] which we illustrate here for the NHN linkage[56] that arises when two nitrogen atoms are linked by a hydrogen atom in medium-ring bicyclic compounds.



(a) Resonance between the canonical Lewis structures **64**, **65**, and **66**.

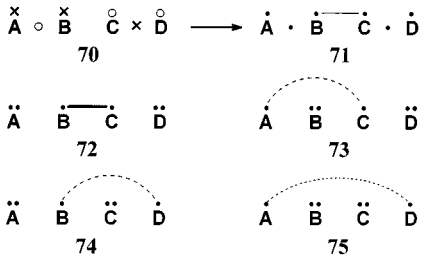
(b) Resonance between the three-electron bond structures **67** and **68**.

(c) The VB structure **69**, with two (non-independent) three-electron bonds.

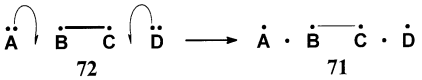
The wavefunction for each of these sets of VB structures is also equivalent[4,5c,36,55] to the 3-centre MO configuration $(\psi_1)^2(\psi_2)^2(\psi_3)^1$ for the five electrons.

Six-Electron Four-Centre Bonding: Theory

Six-electron 4-centre bonding units involve six electrons distributed amongst four overlapping AOs[4,5,57] located around four atomic centres. An increased-valence structure for an extended 6-electron 4-centre bonding unit is obtained[4,5,57a,57b] by spin-pairing in a Heitler−London manner the odd electrons of two three-electron bonds structures AB and CD, as is indicated in **70** → **71**.



Increased-valence structure **71** is equivalent to resonance between the canonical Kekulé structure **72** and the canonical Dewar structures **73**−**75**, and may also be derived[4,5,57] from the Kekulé structure **72** by delocalizing a non-bonding a and a non-bonding d electron into the A-B bonding MO and the C-D bonding MO, respectively.



72 **71**

For symmetrical 6-electron 4-centre bonding units it has been deduced[4,5c,57a] that Ψ_{71} is equivalent to the covalent component of the MO configuration $|\psi_1^{\alpha}\psi_1^{\beta}\psi_2^{\alpha}\psi_2^{\beta}\psi_3^{\alpha}\psi_3^{\beta}|$ with $\psi_1 = a + d + \lambda(b + c)$, $\psi_2 = a - d + k(b - c)$, $\psi_3 = \lambda^*(a + d) - (b + c)$, when the MO configuration is expressed as $\Psi_{covalent} + \Psi_{ionic}$. Configuration interaction increases the importance of $\Psi_{covalent}$ relative to Ψ_{ionic}. Theory for non-symmetrical 6-electron 4-centre bonding units is described in ref.[57d]

For a cyclic 6-electron 4-centre bonding unit, increased-valence structures **76** and **77** may be constructed.[4,5][57c] Resonance between these structures corresponds to the covalent component of a three-configuration MO-CI wavefunction.[5c,57c] It is also equivalent to resonance between four canonical Kekulé-type Lewis structures and two canonical Dewar-type Lewis structures.



76 **77**

Six-Electron Four-Centre Bonding: Some Applications

Over the last decade, we have studied the following systems, each of which involves one or more 6-electron 4-centre bonding units.

(a) $OClOClO_2$, to demonstrate that the existence of long intermolecular O−Cl bonds between the two ClO_2 moieties[58] is associated[55] with the presence of a Cl−O three-electron bond in each of these moieties.

(b) N_2O_4, N_2O_3, and N_2O_2 to account for variations in their N−N bond lengths (1.78 Å, 1.86 Å and 2.24 Å)[5b,59a,59b,60c] relative to the 1.45 Å for N_2H_4. The bond lengthenings are shown to be due primarily to (i) delocalization of oxygen lone-pair electrons into the AOs of the N−N σ-bond (N_2O_4), (ii) delocalization of NO_2-oxygen lone-pair electrons into the AOs of the N−N σ-bond and the orientations of the NO-nitrogen AOs, to give a (fractional) bent N−N σ-bond (N_2O_3), and (iii) orientations of the NO-nitrogen AOs to give a (fractional) bent N−N σ-bond, together with the consequent strong non-bonded repulsions between the nitrogen lone-pair electrons (N_2O_2).

(c) The D_{2h} and D_{2d} isomers of N_2O_4, in order to demonstrate[59c,60a] that *cis* O−O overlap in the planar conformer is primarily responsible for the barrier to rotation around the N−N bond of this species. The *cis* O−O overlap manifests itself in a stabilizing manner by appreciable delocalization of oxygen lone-pair electrons into the AOs of the N−N σ-bond, and covalent-ionic resonance (i.e. $O_2N-NO_2 \leftrightarrow O_2N^+NO_2^- \leftrightarrow O_2N^-NO_2^+$) is calculated to be needed to enhance this stabilizing effect.

(d) $S_2Cl_4^{2+}$,[57b] the linear cation $ICNI^+$,[57d] the N−N dimer of HNO,[60b] the D_{2h} dimer of O_2,[60d] and S_2N_2.[60e]

In Figure 8, increased-valence structures **I-III** are displayed for S_2O_2, $S_2O_4^{2-}$, and $S_2I_4^{2+}$, together with experimental estimates[4,38] for their bond lengths and those for S_2, SO, I_2^+, and "normal" S−S and S−I single bonds.The increased-valence structures are derived from either or both of the **70** → **71** or the **72** → **71** types processes for 6-electron 4-centre bonding units. Inspection of structures **I**−**III** reveals that the bond-orders implied by them are in qualitative accord with the experimental S−S, S−O, S−I, and I−I bond lengths for S_2O_2, $S_2O_4^{2-}$, and $S_2I_4^{2+}$. For example, the S−S bond order is less than two in **I**, less than unity in **II**, and equal to two in **III**, and the S-S lengths for S_2O_2, $S_2O_4^{2-}$, and $S_2I_4^{2+}$ are respectively longer than a double bond, longer than a single bond and somewhat shorter than a double bond.

In Figure 9, increased-valence structures for cyclic S_2N_2 are derived[60e] from the familiar zwitterionic Lewis structures via **72** → **71** type delocalizations. VB representations[38,61] for $S_2N_2 \rightarrow (SN)_x$ polymerization and electron conduction in the $(SN)_x$ polymer, are also displayed in Figure 9.

The Antiferromagnetism of the Copper Acetate Dimer

A 6-electron 4-centre bonding unit[5a,5c,62] is present in each $Cu^{II}(CH_3COO^-)Cu^{II}$ component of antiferromagnetic[63] $Cu_2(CH_3COO)_4 \cdot 2\,H_2O$, for which $J = (E_{singlet} - E_{triplet})/2 = -143\ cm^{-1}$.[63] It arises from the overlap of singly occupied $3d_{x^2-y^2}$ AOs on the Cu^{II} ions with a lone-pair AO on each oxygen atom of the CH_3COO^- ligand

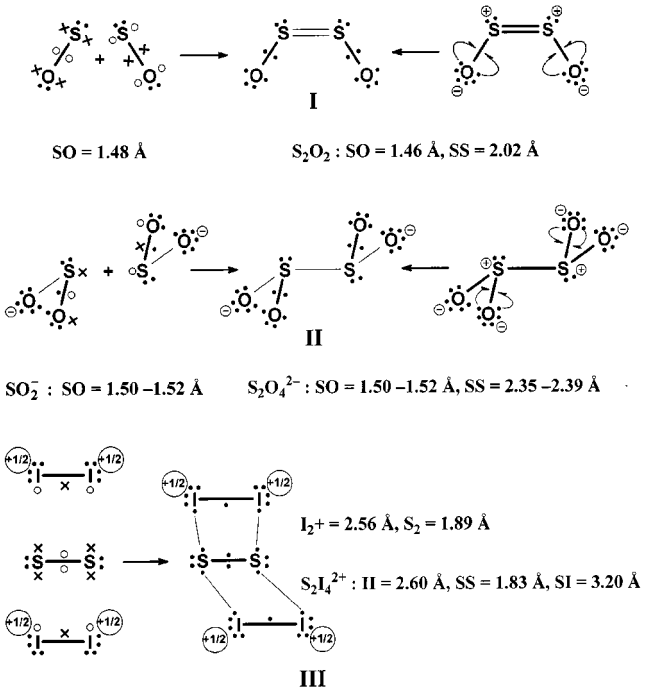


Figure 8. VB structures and bond-lengths for SO, S_2, SO_2^-, I_2^+, S_2O_2, $S_2O_4^{2-}$, and $S_2I_4^{2+}$ with 6-electron 4-centre bonding units; the increased-valence structure for SO_2^- is obtained by replacing the halogen X by O^- in the increased-valence structure displayed for XSO in Figure 4; estimates of the lengths of "normal" S−O, S−S, S−I, and I−I single bonds are 1.70, 2.06, 2.37, and 2.67 Å, respectively[4]

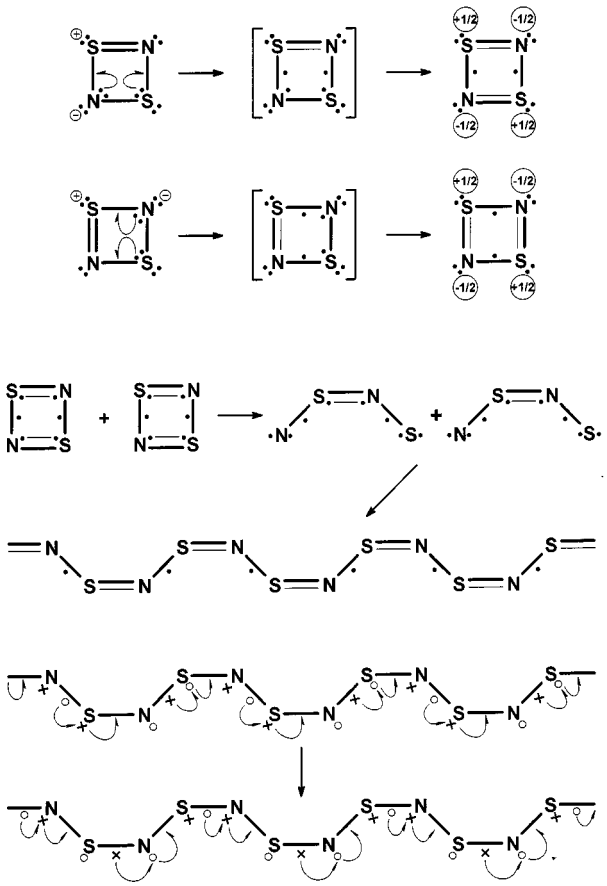


Figure 9. Derivation of increased-valence structures for S_2N_2, and VB representations for $S_2N_2 \rightarrow (SN)_x$ polymerization and electron conduction in $(SN)_x$

(Figure 10). The A and D atoms of VB structure **72** are the oxygen atoms, and B and C are the copper atoms. The oxygen lone-pair AOs overlap to a small extent, as do the $3d_{x^2-y^2}$ AOs. The origin of the antiferromagnetism has been associated primarily with superexchange, i.e. some delocalization of the oxygen lone-pair electrons into the singly-occupied $3d_{x^2-y^2}$ AOs, together with covalent-ionic resonance $[(CuO)(CuO) \leftrightarrow (CuO)^-(CuO)^+ \leftrightarrow (CuO)^+(CuO)^-]$.[5a,5c,62]

The primary type of covalent-ionic resonance involves[5a,5c,62] the $S = 0$ and $S = 1$ spin VB structures of Figure 10. These structures arise by the delocalization of one oxygen lone-pair electron into a singly-occupied copper AO. The $S = 0$ spin covalent and ionic structures correspond to the generalized Lewis structures of types **73** and **74** above, and **78** and **79**, respectively. (For the corresponding $S = 1$ structures, the two electrons that singly occupy AOs have parallel spins.) Because the AO overlap between the singly occupied non-adjacent AOs is small, the covalent VB structures are essentially degenerate, i.e. ${}^3E_{cov} \approx {}^1E_{cov} = E_{cov}$. It may be deduced[64] that the resulting expression for the magnetic exchange parameter that arises from these types of covalent-ionic resonance is approximately given by $J = (\beta_{bc} + \beta_{ad})^2 J_{CuO}/({}^1E_{ion} - E_{cov})^2$, in which β_{bc} and β_{ad} are O−O and Cu−Cu overlap-dependent resonance integrals, and J_{CuO} is the (negative) exchange integral for the

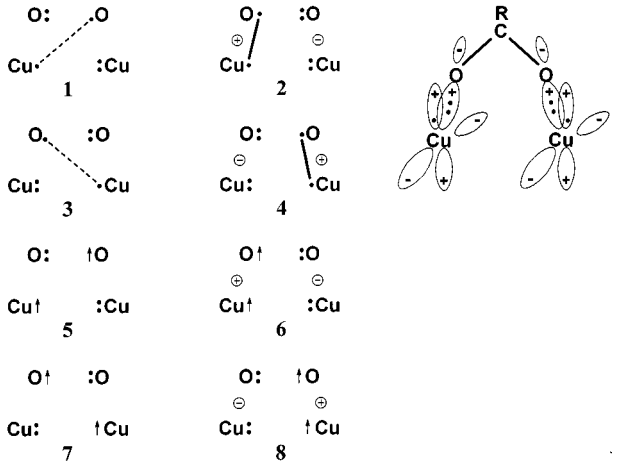


Figure 10. AOs for a 6-electron 4-centre bonding unit of $Cu^{II}(CH_3COO^-)Cu^{II}$,[5c] and the associated primary Lewis-type VB structures for a VB rationalization of the origin of the antiferromagnetism of Cu^{II} carboxylate dimers[5c]

Cu−O electron-pair bond of each $S = 0$ spin ionic structure.



78 **79**

Of course, covalent structures of types **72** and **75**, together with their ionic partners, also participate in resonance with the VB structures of types **73**, **74**, **78**, and **79**, and their contributions to the magnetic exchange parameter will modify the above expression for it. With $\psi_{ab} = a + kb$ and $\psi_{dc} = d + kc$, the *simplest* expression for J is then given by[64] Equation (23).

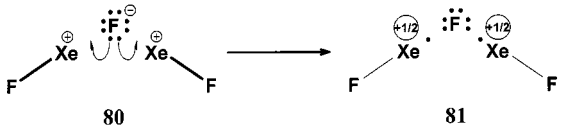
$$J = -2\{(\beta_{bc})^2/(\gamma_{bb} - \gamma_{bc}) - k^2 J_{CuO}(\beta_{bc} + \beta_{ad})^2/(\gamma_{ab} - \gamma_{ac})^2 + k^4(\beta_{ad})^2/(\gamma_{aa} - \gamma_{ad})\}/(k^2 + 1)^2 \quad (23)$$

In Equation (23), k is the "superexchange" parameter, which measures the extent of delocalization of electrons from the oxygen AOs (a and d) into the copper AOs (b and c) The $\gamma_{\upsilon\upsilon}$ are (two-electron) Coulomb integrals which involve a pair of AOs.

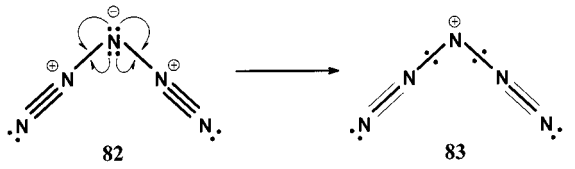
Six-Electron Five-Centre Bonding: $Xe_2F_3^+$ and N_5^+

The anion H_5^-, with five overlapping 1s AOs, provides a prototype example of a molecular system with a 6-electron 5-centre bonding unit.[65] For the $\mathbf{X}_a-\mathbf{Y}_b\ \mathbf{X}_c^-\ \mathbf{Y}_d-\mathbf{X}_e$ type Lewis structures of the non-linear ions $H_2F_3^-$, I_5^-, and $Xe_2F_3^+$, the AO on each **Y** atom which helps to form the terminal $\mathbf{Y}_b-\mathbf{X}_a$ or $\mathbf{Y}_d-\mathbf{X}_e$ bond also overlaps with the valence-shell doubly-occupied p_x and p_y AOs of the central halide anion, to generate two (non-orthogonal) 6-electron 5-centre bonding units. For either bonding unit, an increased-valence structure may be generated, as indicated in **80** → **81** for $Xe_2F_3^+$ when the p_x electrons of the F^- are delocalized. (For linear systems, only the p_x electrons form a 6-electron 5-centre bonding unit.) In increased-valence structure **81**, the terminal and central Xe−F bonds are respectively fractional electron-pair bonds, and one-electron

bonds. The lengths[66] of these bonds, 1.90 and 2.14 Å, are in agreement with these bond properties.



80 **81**



82 **83**

The recently prepared cation[67] N_5^+ involves two orthogonal 6-electron 5-centre bonding units, and the associated Lewis and increased-valence structures are[67b] **82** and **83**.

VB structure **83** indicates immediately that the terminal and central N−N bonds should be longer than N≡N bonds with the same AO hybridization (≈ 1.07 Å, cf. discussion for N_2O above), and substantially shorter than those for N−N bonds (≈ 1.45 Å). The calculated lengths (1.11 Å and 1.30 Å)[67] are in agreement with these deductions.

Valence Bond Alternatives to Triple Bonds

In this section and in the following two, increased-valence considerations are not needed for the primary discussion of the VB phenomena.

The results of ab initio VB calculations[68] for N_2 show that resonance between VB structures :N÷N: and :N÷N: with electron-pair σ bonds and one-electron π bonds, generates a lower energy than does the triple-bond structure :N≡N: with Coulson−Fischer-type[48] LMOs to accommodate the four electrons that form the two π bonds. When the wavefunctions for these two sets of structures are expressed as linear combinations of the wavefunctions for nine canonical Lewis structures, it is found that the triple-bond structure overestimates the importance of the polar canonical structures :N(-2)—N(+2): and :N(+2)—N(-2):, and this effect provides the explanation for the origin of the higher energy for the triple-bond structure.

In 1916, Lewis[69] was unable to accommodate the triple bond in his cubical atom model of electronic structure. In contrast cubical atom models, and Bohr orbit diagrams[7] for :N÷N: and :N÷N: may be constructed.

One-Electron and Two-Electron Transfer Processes

For the O_2 ground-state, two-electron transfer processes are required to convert structure **16** into structure **19**, and structure **17** into structure **18**, whereas one-electron transfers are needed to convert either structure **16** or **19** into each of structures **17** and **18**. Examples of phenomena whose origins may be rationalized in terms of either one-electron or two-electron transfer processes include:[70] (a) the mode of protonation[16] of symmetric anions such as HCO_2^- and NO_2^-, which occurs preferentially at one oxygen atom, i.e. asymmetric rather than symmetric geometries are obtained for HCOOH and HONO; (b) the asymmetry of xanthate and dithiocarbamate ligands in various complexes;[71] (c) energy transfer between donor and acceptor chromophores.[72]

Bohr Orbit Descriptions of Electronic Structure

Of course, the orbital theory forms the primary basis for modern descriptions of the electronic structure of matter. However as has been discussed on several occasions,[7,73] the Bohr orbit theory is also able to be used for this purpose. A Bohr orbit approach to electronic structure is based on a $2n \times n$ factorization of the atomic shell-structure formula $2n^2$, for which $n = 1, 2, 3, \ldots$ is the principal quantum number. This factorization is derived[7,73] by the application of a Heisenberg uncertainty relationship to the movement of electrons around Bohr orbits with principal quantum number n. It is deduced that there are n circular orbits (designated as $n_1, n_2, \ldots, n_n$) each of which can accommodate a maximum of $2n$ electrons. Two alternative derivations of the $2n^2$ formula are presented in ref.[7] The Bohr orbit theory falls outside the normal paradigm which is used to describe electronic structure, but it does provide qualitative models of electronic structure that accommodate the Lewis cubical atom model,[69] and arrangements of electrons in molecules which are appropriate for VB structures that arise in normal orbital theory. Aspects of previously published accounts of this subject have been reviewed in ref.[7], with new types of orbit diagrams provided for some of the systems considered previously.

In Figure 11, orbit diagrams are provided[7] for B_2H_6, and a variety of AF_N systems, when it is asssumed that there are N A−F electron-pair bonds in the associated VB structures. These orbit diagrams are based on the deduction that orbits with $n = 1, 2, 3, 4$, and 5 may accommodate a maximum of 2, 4, 6, 8, and 10 electrons, respectively, and these are the occupation numbers for the equatorial n_1 orbit for the H, B, P, S, Cl, Se, Br, and I atoms in Figure 11. Examples of new types of Bohr orbit calculations of the energies for H_2^+, H_2, and the helium isoelectronic sequence are provided in ref.[7,74]

Conclusions

As indicated in the Introduction, the primary purpose of this work is to help to provide "primitive patterns of understanding" of the electronic structures of molecules. In very different ways, the work provides examples of how orbital VB theory and the Bohr orbit theory are able to do this. It is to be hoped that the approaches which have been used to provide qualitative VB descriptions of electronic structure are not difficult to comprehend − the increased-valence theory provides a natural extension of familiar Lewis theory by one-electron delocalizations − and there-

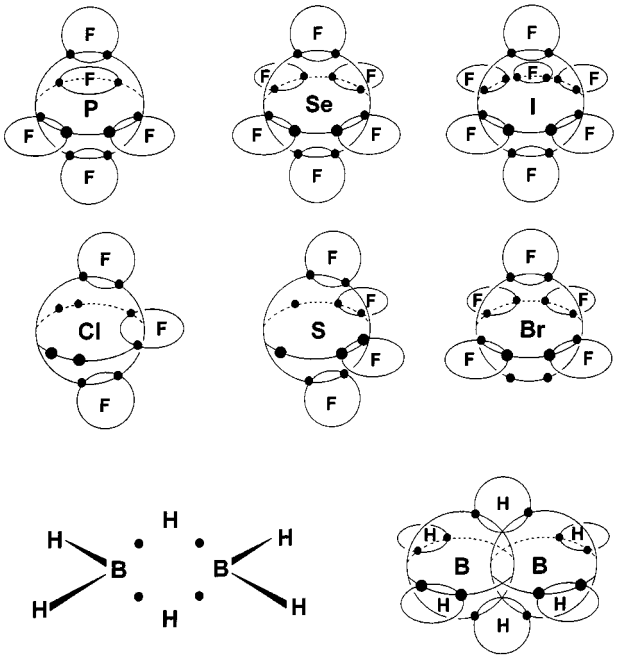


Figure 11. Bohr orbit diagrams for AF_N systems for (expanded valence-shell) Lewis VB structures with N A−F electron-pair bonds; six valence-shell electrons for each fluorine ligand are not indicated; a VB structure for B_2H_6 and the associated orbit diagram are also displayed

fore they may be useful to help bench chemists in their understanding of various aspects of chemical bonding.

Appendix: Valencies for LMO Increased-Valence Structures

For each of the LMO Kekulé structures **55** and **57**, the maximum valence for the A atom (V_a) is unity. In ref.[30a,43], expressions are deduced for the A-atom valencies for the LMO increased-valence structures **56** and **58**. The simplest definition of MO valence was used, namely that provided initally by Wiberg[75] for doubly occupied MOs, in which AO overlap integrals are omitted from the normalization constants. The derivation of the expression for V_a for increased-valence structure **56** is redescribed here.

If two electrons occupy the bonding MO $\psi_{ab} = (a + kb)/(k^2 + 1)^{05}$, the Wiberg valence[75] for the a-orbital is given by Equation (A1), in which P_{ab} is the Coulson bond order (with AO overlap integrals omitted). The maximum value for the valence is unity, which occurs when $k = 1$. However if ψ_{ab} is singly occupied, the bond-order is $k/(k^2 + 1)$, and the valence is then given by Equation (A2),[30a,43] with a maximum value of 0.5 when $k = 1$. When $k' = 1/k'' = k$ in Equation (9) for the LMO increased-valence structure **56**, we obtain Equation (A3) for the $(y)^1(\psi_{ay})^1(\psi_{ba})^2$ configuration, with $\psi_{ay} = a + ly$ and $\psi_{ba} = b + ka$. The A-atom valence is then given by Equation (A4) Pariser's procedure[76] is used to determine the P_{ay} and P_{ab} bond orders of Equations (A5) and (A6) from Equation (A3). An illustration of the use of this procedure is provided in ref.[77]

$$V_{ab} = (P_{ab})^2 = 4k^2/(k^2 + 1)^2 \quad \text{(A1)}$$

$$V_{ab} = 2(P_{ab})^2 = 2k^2/(k^2 + 1)^2 \quad \text{(A2)}$$

$$k\Psi_{31} = 2l(k\Psi_{I} + k^2\Psi_{II} + \Psi_{III}) + \Psi_{V} + k\Psi_{VI} \quad \text{(A3)}$$

$$V_a = V_{ay} + V_{ab} = 2(P_{ay})^2 + (P_{ab})^2 \quad \text{(A4)}$$

$$P_{ay} = 2l/\{2l^2(k^2 + 1) + 1\} \quad \text{(A5)}$$

$$P_{ab} = k\{4l^2(k^2 + 1) + 1\}/[\{2l^2(k^2 + 1) + 1\}(k^2 + 1)] \quad \text{(A6)}$$

When $k = l = 1$, $V_a = 1.13$. The maximum value for V_a is 1.212, which occurs when $k = 0.69$ and $l = 0.76$. In both cases, the A-atom valence exceeds the maximum value of unity that occurs in the Kekulé structures. Thus with regard to the valence of the A-atom, the designation "increased-valence" is appropriate for VB structure **56** (and also for VB structure **58**).

Acknowledgments

I thank (a) Professor T. M. Klapötke and Dr. A. Schulz at the Ludwig-Maximilians University, Munich, for their great enthusiasm and encouragement with regard to the use of VB methods, and (b) Mrs. Carmen Nowak, also at the Ludwig-Maximilians University, for her great help with the preparation and drawing of the VB structures and Figures.

As a consequence of the presence of four Slater determinants in the $S = 0$ spin wavefunction for Equation (4), the ψ_{ab} for the $\psi_{54}(k'=0)$ of Equation (5) is equal to $\psi_{ab} = a + 2kb$. It should also be stressed that the singlet diradical structure of type **VI** in Figure 5 contributes to the simplest canonical MO formulation of the wavefunction for a 4-electron 3-centre bonding unit (cf. C. A. Coulson, *J. Chem. Soc.* **1964**, 1442 for example). For a variety of MO and VB theorems that pertain to symmetrical 4-electron 3-centre bonding units, see R D. Harcourt, A. G. Harcourt, *J. Chem. Soc., Faraday Trans. 2* **1974**, *70*, 743.

[1] [1a] D. J. Klein, N. Trinajstić (Eds.), *Valence Bond Theory and Chemical Structure*, Elsevier, New York, **1990**. – [1b] D. J. Klein, N. Trinajstić, *J. Chem. Ed.* **1990**, *67*, 633. – [1c] J. Gerratt, W. J. Orville-Thomas (Eds.), *J. Mol. Struct. (Theochem)* **1991**, *229*. – [1d] *Pauling's Legacy − Modern Theory (Modelling) of Chemical Bonding* (Eds.: Z. B. Maksić, W. J. Orville-Thomas), Elsevier, New York, **1999**.

[2] [2a] N. Epiotis, *Unified Valence Bond Theory of Electronic Structure, Lecture Notes in Chemistry*, Springer-Verlag, Berlin, **1982**, vol. 29. – [2b] N. Epiotis, *Unified Valence Bond Theory of Electronic Structure − Applications. Lecture Notes in Chemistry* Springer-Verlag, Berlin, **1983**, vol. 33.

[3] [3a] D. L. Cooper, J. Gerratt, M. Raimondi, *Chem. Rev.* **1991**, *91*, 929. – [3b] J. Gerratt, D. L Cooper, P. B. Karadakov, M. Raimondi, *Chem. Soc. Rev.* **1997**, *26*, 87. – [3c] V. Bachler, *Theor. Chem. Acc.* **1997**, *92*, 223. – [3d] P. C. Hiberty, *J. Mol. Struct. (Theochem)* **1998**, *451*, 237. – [3e] P. B. Karadakov *Ann. Rep. Prog. Chem. C* **1998**, *94*, 3. – [3f] S. Shaik, A. Shurki, *Angew. Chem. Int. Ed.* **1999**, *38*, 586.

[4] R. D. Harcourt, *Qualitative Valence Bond Descriptions of Electron-Rich Molecules, Lecture Notes in Chemistry*, Springer-Verlag, Berlin, **1982**, vol. 30.

[5] [5a] R. D. Harcourt in *Valence Bond Theory and Chemical Structure* (Eds.: D. J. Klein, N. Trinajstić), Elsevier, New York, **1990**, p. 251. – [5b] R. D. Harcourt in *Quantum Mechanical Methods in Main-Group Chemistry* (Eds.: T. M. Klapötke, A. Schulz),

Wiley, Chichester, **1998**, p. 217. – [5c] R. D. Harcourt in *Pauling's Legacy – Modern Theory (Modelling) of Chemical Bonding* (Eds. Z. B. Maksić, W. J. Orville-Thomas), Elsevier, New York, **1999**, p. 443. For discussions of aspects of the theory by others, see ref.[6]

[6] [6a] A. van der Putten, A. Elzing, E. Visscher, E. Barendrecht, R. D. Harcourt, *J. Mol. Struct. (Theochem)* **1988**, *180*, 309. – [6b] S. J. Formosinho, in *Theoretical and Computational Models for Organic Chemistry* (Eds.: J. Formosinho et al.), Kluwer Academic Publishers, Dordrecht, The Netherlands, **1991**, p. 159. – [6c] T. M. Klapötke, *Chem. Ber./Recueil* **1997**, *130*, 443; – [6d] T. M. Klapötke, *Adv. Mol. Struct. Res.* **1997**, *3*, 288. – [6e] A. Schulz, *Rev. Inorg. Chem.* – [6f] P. C. Hiberty, *Israel J. Chem.*, **1983**, *23*, 10.

[7] R. D. Harcourt, *J. Mol. Struct. (Theochem)* **1995**, *338*, 197 and references 11–14 therein; **1996**, *369*, 216.

[8] C. A. Coulson, *Rev. Mod. Phys.* **1960**, *32*, 170.

[9] [9a] L. Pauling, *J. Am. Chem. Soc.* **1931**, *53*, 1367; L. Pauling, *J. Am. Chem. Soc.* **1931**, *53*, 3225. – [9b] L. Pauling, *The Nature of the Chemical Bond*, 3rd ed., Cornell University Press, Ithaca, New York, **1960**.

[10] [10a] A. R. Gregory, V. Malatesta, *J. Org. Chem.* **1980**, *45*, 122. – [10b] P. M. W. Gill, L. Radom, *J. Am. Chem. Soc.* **1988**, *110*, 4931. – [10c] B. D. Yeomans, D. G. Humphrey, G. A. Heath, *J. Chem. Soc., Dalton Trans.* **1997**, 4153.

[11] [11a] R. D. Harcourt, *J. Chem. Educ.* **1985**, *62*, 99. – [11b] R. D. Harcourt, *J. Phys. Chem. A* **1997**, *101*, 2496, 5962, and references therein for other recent studies of the three-electron bond.

[12] [12a] J. W. Linnett, *J. Am. Chem. Soc.* **1961**, *83*, 2643 – [12b] J. W. Linnett, *The Electronic Structures of Molecules*, Methuen, London, **1964**. – [12c] J. W. Linnett, *Sci. Prog. (Oxford)* **1972**, *60*, 1. – [12d] M. Green, J. W. Linnett, *J. Chem. Soc.* **1960**, 4959. For ab initio VB studies of Linnett C_6H_6 see: C. Amovilli, R. D. Harcourt, R. McWeeny, *Chem. Phys. Lett.* **1991**, *187*, 194.

[13] [13a] N. C. Baird, *J. Chem. Educ.* **1977**, 54, 291. – [13b] N. C. Baird, *Pure Appl. Chem.* **1977**, *49*, 293.

[14] [14a] M. L. McKee, *J. Phys. Chem.* **1996**, *100*, 3473; M. L. McKee, *J. Phys. Chem.* **1996**, *100*, 16444, and references therein. – [14b] B. Braieda, P. C. Hiberty, A. Savin, *J. Phys. Chem. A* **1998**, *102*, 7872. – [14c] F. M. Bickelhaupt, A. Diefenbach, S. P. de Visser, M. M. Nibbering, *J. Phys. Chem. A* **1998**, *102*, 9549. – [14d] L. S. Nichols, A. J. Illies, *J. Am. Chem. Soc.* **1999**, *121*, 9176.

[15] R. D. Harcourt, *Int. J. Quantum Chem.* **1997**, *61*, 547. For calculations with better basis sets, see also: [15a] R. McWeeny, *Int. J. Quantum Chem.* **1990**, 24, 773. – [15b] R. McWeeny, *J. Mol. Struct. (Theochem)* **1991**, *229*, 29. – [15c] C. P. Byrman, J. H. Lenthe, *Int. J. Quantum Chem.* **1996**, *58*, 351.

[16] R. D. Harcourt, *J. Phys. Chem.* **1992**, *96*, 7616,

[17] [17a] L. Pauling, C. D. Coryell, *Proc. Nat. Acad. Sci. U. S. A.* **1936**, *22*, 210. – [17b] L. Pauling, *Nature*, **1964**, *203*, 182.

[18] R. D. Harcourt, *Chem. Phys. Lett.* **1990**, *167*, 374 and references 4–9,12 therein. The relevant $S = 0$ spin theory is provided in several of these references.

[19] I. Bytheway, M. B. Hall, *Chem. Rev.* **1994**, *94*, 639.

[20] D. S. McClure, *Radiat. Res. Suppl.* **1960**, *2*, 218.

[21] J. J. Weiss, *Nature* **1964**, *202*, 83; J. J. Weiss, *Nature* **1964**, *203*, 183.

[22] R. S. Mulliken, *J. Chim. Phys.* **1964**, *61*, 20.

[23] [23a] W. A. Goddard III, B. D. Olafson, *Proc. Nat. Acad. Sci. U. S. A.* **1975**, *72*, 2335. – [23b] B. D. Olafson, W. A. Goddard III, *Proc. Nat. Acad. Sci. U. S. A.* **1977**, *74*, 1315.

[24] C. H. Barlow, J. C. Maxwell, W. J. Wallace, W. S. Caughey, *Biochem. Biophys. Res. Commun.* **1973**, *55*, 51.

[25] S. Yamamoto, H. Kashiwagi, *Chem. Phys. Lett.* **1993**, *205*, 306.

[26] [26a] M. Calvin in *Photochemical Conversion and Storage of Solar Energy* (Ed.: J. S. Connolly), Academic Press, New York, **1981**, p.1. – [26b] P. E. M. Siegbahn, R. H. Crabtree, *J. Am. Chem. Soc.* **1999**, *121*, 117. – [26c] J. Limburg, V. A. Szalai, G. W. Brudvig, *J. Chem. Soc., Dalton Trans.* **1999**, 1353. The bond-making and -breaking procedures displayed in Figure 2 here is also relevant for high-spin $Mn^{IV}O$.

[27] R. D. Harcourt, J. F. Sillitoe, *Aust. J. Chem.* **1974**, *27*, 691.

[28] P. C. Hiberty in *Valence Bond Theory and Chemical Structure* (Eds.: D. J. Klein, N. Trinajstić), Elsevier, New York, **1990**, p. 221.

[29] R. D. Harcourt, N. Hall, *J. Mol. Struct. (Theochem)* **1995**, *342*, 59 and references. therein; **1996**, *369*, 217. (Both single-zeta and double-zeta orbital basis sets for the eight π electrons were used in the calculations, and allowance was made for polarization of the N–N and N–O σ bonds.)

[30] [30a] R. D. Harcourt, *J. Mol. Struct. (Theochem)* **1997**, *398–399*, 93, and references therein. – [30b] R. D. Harcourt, *J. Mol. Struct. (Theochem)* **1995**,*342*, 51.

[31] F. Wang, R. D. Harcourt, *J. Phys. Chem. A* **2000**, *104*, 1304.

[32] [32a] R. D. Harcourt, *J. Mol. Struct.* **1972**, *12*, 351. – [32b] R. D. Harcourt, R. D. Little, *J. Am. Chem. Soc.* **1984**, *106*, 44.

[33] [33a] T. M. Klapötke, A. Schulz, I. C. Tornieporth-Oetting, *Chem. Ber.* **1994**, *127*, 2181. – [33b] S. Padmaja, Van Au, S. A. Madison,*J. Chem. Soc., Dalton Trans.* **1999**, 2933.

[34] R. D. Harcourt, *J. Mol. Struct*. **1993**, *300*, 243; see ref.[29] above for several corrections.

[35] R. D. Harcourt, *J. Mol. Struct. (Theochem)* **1992**, *259*, 155.

[36] R. D. Harcourt, *J. Chem. Soc., Faraday Trans.* **1991**, *87*, 1089.

[37] [37a] C. F. Jackels, E. R. Davidson, *J. Chem. Phys.* **1976**, *64*, 2908. – [37b] C. P. Blahous III, B. F. Yates, Y. Xie, H. F. Schaeffer III, *J. Chem. Phys.* **1990**, *93*, 8105.

[38] R. D. Harcourt, *J. Mol. Struct. (Theochem)* **1989**, *186*, 131.

[39] [39a] D. L. Cooper, J. Gerratt, M. Raimondi, *J. Chem. Soc., Perkin Trans. 2* **1989**, 1187.

[40] N. O. J. Malcolm, J. J. W. McDouall, *J. Comput. Chem.* **1994**, *15*, 1365.

[41] [41a] W. B. Floriano, S. R. Blaszkowski, M. A. C. Nascimento, *J. Mol. Struct. (Theochem)* **1995**, *335*, 51. – [41b] W. Wu, Y. Mo, Q. Zhang, *J. Mol. Struct. (Theochem)* **1993**, *283*, 227 – [41c] W. Wu, Y. Mo, Q. Zhang, *Chin. J. Chem.* **1993**, *11*, 490. – [41d] R. M. Parrondo, P. Karafiloglou, R. R. Papparlado, E. Sanchez, *J. Phys. Chem.* **1995**, *99*, 6461. See also: M. S. de Giambiagi, M. Giambiagi, J. Herrera, *Z. Naturforsch.* **1994**, *49a*, 754, via MO studies

[42] R. D. Harcourt, A. Schulz, *J. Phys. Chem. A*, in press.

[43] R. D. Harcourt, *Int. J. Quantum Chem.* **1996**, *60*, 553: 2 lines below Equation (32), replace Ψ_{12} with Ψ_{13}; p. 563, 9 lines down, replace (16) with (18).

[44] Some recent references that do not involve either Dewar-type Lewis structures or increased-valence structures in their VB descriptions of 4-electron 3-centre bonding units include: [44a] C. R. Landis, T. K. Firman, D. M. Root, T. Cleveland, *J. Am. Chem. Soc.* **1998**, *120*, 1842. – [44b] E. D. Glendening, F. Weinhold, *J. Comput. Chem.* **1998**, *19*, 593, 610, 628. – [44c] H. F. Bettinger, P. v. R. Schleyer, H. F. Schaefer III, *J. Am. Chem. Soc.* **1998**, *120*, 11439.

[45] M. Pettersson, J. Lundell, M. Räsänen, *Eur. J. Inorg. Chem.* **1999**, 729.

[46] I. Last, T. F. George, *J. Chem. Phys.* **1988**, *89*, 3071.

[47] [47a] R. Ponec, A. J. Duben, *J. Comput. Chem.* **1999**, *20*, 760 and references therein. – [47b] K.-Y. Akiba in *Chemistry of Hypervalent Compounds* (Ed. K.-Y. Akiba), Wiley-VCH, Inc., New York, **1999**, 1, and references therein.

[48] C. A. Coulson, I. Fischer, *Phil. Mag.* **1949**, *40,* 396.

[49] R. D. Harcourt, *J. Phys. Chem. A* **1999**, *103*, 4293.

[50] [50a] E. A. C. Lucken, *J. Chem. Soc.* **1959**, 2954. – [50b] J. F. A. Williams, *Trans. Faraday Soc.* **1961**, 57, 2089. – [50c] J. F. A. Williams, *Tetrahedron* **1962**, *18*, 1477. – [50d] References 1–10 for Section 14–2 of ref.[4] above. – [50e] F. Weinhold, *J. Mol. Struct. (Theochem)* **1997**, *398–399*, 181. It should be stressed that the MO formulation of Equation (16) here does not correspond to the canonical MO formulation; cf. ref.[18] above.

[51] J. M. White, C. I. Clark, *Top. Stereochem.* **1999**, *22*, 137, and references 5–7 therein.

[52] [52a] P. v. R. Schleyer, A. J. Kos, *Tetrahedron* **1983**, *39*, 1141. – [52b] A. E. Reed, P. v. R. Schleyer, *J. Am. Chem. Soc.* **1987**, *109*, 7362. – [52c] U. Salzner, P. v. R. Schleyer, *J. Am. Chem. Soc.* **1993**, *115*, 10231. Various types of designations and associated MO descriptions for intermolecular interactions have been summarized by: H. A. Bent, *Chem. Rev.* **1968**, *68*, 587.

[53] [53a] R. D. Harcourt, *J. Mol. Struct. (Theochem)* **1992**, *253*, 363. – [53b] R. D. Harcourt, *New. J. Chem.* **1992**, *16*, 667.

[54] [54a] R. D. Harcourt, *J. Mol. Struct. (Theochem)* **1991**, *229*, 39; for some corrections, see ref.[53a] above. – [54b] R. D. Harcourt, R. Ng, *J. Phys. Chem.* **1993**, 97, 12210; R. D. Harcourt, R. Ng, *J. Phys. Chem.* **1994**, *98*, 3226. For further studies of systems

with 3-electron 3-centre bonding units, see: [54c] R. D. Harcourt, *J. Organomet. Chem.* **1994**, *478*, 131. – [54d] G. D. Scholes, R. D. Harcourt, I. R. Gould, D. Phillips, *J. Phys. Chem. A* **1997**, *101*, 678.

[55] R. D. Harcourt, *J. Phys. Chem.* **1993**, *97*, 1351;

[56] R. Alder, *Tetrahedron* **1990**, *46*, 682.

[57] [57a] R. D. Harcourt, *J. Am. Chem. Soc.* **1980**, *102*, 5195; **1981**, *103*, 5625. – [57b] R. D. Harcourt, *J. Phys. Chem.* **1991**, *95*, 6916. – [57c] R. D. Harcourt, *J. Mol. Struct. (Theochem)* **1985**, *122*, 135. – [57d] R. D. Harcourt, T. M. Klapötke, P. S. White, *Inorg. Chem. Acta* **1998**, *269*, 1. The $S = 0$ spin wavefunction for increased-valence-structure **71** is given by the following expression:[4,5,57a,57b]

$$\Psi_{\mathbf{71}} = |\psi_{ab}{}^{\alpha}\psi_{ab}{}^{\beta}\psi_{cd}{}^{\alpha}\psi_{cd}{}^{\beta}\psi^{*}{}_{ab}{}^{\alpha}\psi^{*}{}_{cd}{}^{\beta}| + |\psi_{ab}{}^{\alpha}\psi_{ab}{}^{\beta}\psi_{cd}{}^{\alpha}\psi_{cd}{}^{\beta}\psi^{*}{}_{cd}{}^{\alpha}\psi^{*}{}_{ab}{}^{\beta}|$$
$$\propto |a^{\alpha}\psi_{ab}{}^{\beta}\psi_{cd}{}^{\alpha}d^{\beta}b^{\alpha}c^{\beta}| + |\psi_{ab}{}^{\alpha}a^{\beta}d^{\alpha}\psi_{cd}{}^{\beta}c^{\alpha}b^{\beta}|$$

[58] A. Rehr, M. Jansen, *Inorg. Chem.* **1992**, *31*, 4740.

[59] [59a] R. D. Harcourt, *J. Mol. Struct. (Theochem)* **1990**, *206*, 253. – [59b] R. D. Harcourt, *Croat. Chem. Acta* **1991**, *64*, 399. – [59c] R. D. Harcourt, *Chem. Phys. Lett.* **1994**, *218*, 175.

[60] [60a] R. D. Harcourt, F. L. Skrezenek, **1990**, *J. Phys. Chem. 96*, 1351. – [60b] R. D. Harcourt, F. L. Skrezenek, B. G. Gowenlock, *J. Mol. Struct. (Theochem)* **1993**, *284*, 87. – [60c] R. D. Harcourt, P. P. Wolynec, *J. Phys. Chem. A*, **2000**, *104*, 2138. – [60d] R. D. Harcourt, N. Pyper, *Int. J. Quantum Chem.* **1998**, *68*, 129. – [60e] R. D. Harcourt, T. M. Klapötke, A. Schulz, P. P. Wolynec, *J. Phys. Chem. A* **1998**, *102*, 1850.

[61] [61a] F. L. Skrezenek, R. D. Harcourt, *J. Am. Chem. Soc.* **1984**, *106*, 3934. – [61b] R. D. Harcourt, F. L. Skrezenek,. *J. Mol. Struct. (Theochem)* **1987**, *151*, 203.

[62] R. D. Harcourt, F. L. Skrezenek, R. G. A. R. Maclagan, *J. Am. Chem. Soc.* **1986**, *108*, 5403.

[63] B. N. Figgis, R. L. Martin, *J. Chem. Soc.* **1956**, 3837.

[64] R. D. Harcourt, unpublished.

[65] D. Cui, R. D. Harcourt, *J. Mol. Struct. (Theochem)* **1991**, *236*, 359.

[66] F. O. Sladky, P. A. Bulliner, N. Bartlett, B. G. de Boer, A. Zalkin, *Chem. Commun.* **1968**, 1048.

[67] [67a] K. O. Christie, W. W. Wilson, J. A. Sheehy, J. A. Boatz, *Angew. Chem. Int. Ed.* **1999**, *38*, 2004. – [67b] T. M. Klapötke, *Angew. Chem. Int. Ed.* **1999**, *38*, 2536.

[68] R. D. Harcourt, *J. Chem. Soc., Faraday Trans.* **1992**, *88*, 1119.

[69] G. N. Lewis, *J. Am. Chem. Soc.* **1916**, *38*, 762.

[70] One example involves the hypothesis[16] that the stability of the genetic code under normal conditions is associated with the extent of electronic reorganization that is needed to interconvert important VB structures for different isomers of the DNA bases.

[71] [71a] R. D. Harcourt, G. Winter, *J. Inorg. Nucl. Chem.* **1975**, *37*, 1039. – [71b] R. D. Harcourt, G. Winter, **1977**, *39*, 360. – [71c] R. D. Harcourt, E. R. T. Tiekink, *Aust. J. Chem.* **1987**, *40*, 611.

[72] [72a] R. D. Harcourt, G. D. Scholes, K. P. Ghiggino, *J. Chem. Phys.* **1994**, *101*, 10521. – [72b] R. D. Harcourt, K. P. Ghiggino, G. D. Scholes, S. Speiser, *J. Chem. Phys.* **1996**, *105*, 1897. – [72c] G. D. Scholes, R. D. Harcourt and G. Fleming, *J. Phys. Chem. B* **1997**, *101*, 7302. – [72d] R. D. Harcourt, K. P. Ghiggino, G. D. Scholes, R. P. Steer, *J. Chem. Phys.* **1998**,*109*, 1310 and references 8,9 therein. With $D = (d)^2$, $A = (a)^2$, $D^* = (d)^1(d^*)^1$, and $A^* = (a)^1(a^*)^1$, in which d, d*, a, and a* are chromophore donor and acceptor orbitals, the initial and final wavefunctions for equivalent chromophores are expressed as $\Psi_i = \Psi_1(D^*,A) + \lambda\Psi_2(D^+A^-) + \mu\Psi_3(D^-A^+)$ and $\Psi_f = \Psi_4(D,A^*) + \mu\Psi_2(D^+A^-) + \lambda\Psi_3(D^-A^+)$. Two-electron transfers convert Ψ_1 into Ψ_4 and Ψ_2 into Ψ_3, whereas one-electron transfers convert each of Ψ_1 and Ψ_4 into either Ψ_2 or Ψ_3. Second-order perturbation theory is used to evaluate the electronic excitation matrix element. Analysis of this matrix element reveals that the Coulomb integral and the Dexter exchange integral arise from two-electron transfers, whereas the overlap interactions are associated primarily with one-electron transfers, rather than the Dexter exchange integral.

[73] R. D. Harcourt, *Found. Chem.* **1999**, *1*, 293.

[74] R. D. Harcourt, *Phys. Lett. A* **1995**, *200*, 144.

[75] K. B. Wiberg, *Tetrahedron* **1968**, *24*, 1083.

[76] R. Pariser, *J. Chem. Phys.* **1956**, *24*, 250.

[77] R. D. Harcourt, *Aust. J. Chem.* **1969**, *22*, 279.

Received December 15, 1999
[I99459]

Contrasting Nonclassical Silicon−Hydrogen Interactions in Niobium and Tantalum Half-Sandwich Complexes: Si−H···M Agostic versus M−H···Si−Cl Interligand Hypervalent Interactions

Georgii I. Nikonov,*[a] Philip Mountford,*[b] Jennifer C. Green,[b] Paul A. Cooke,[c] Michael A. Leech,[d] Alexander J. Blake,[c] Judith A. K. Howard,[d] and Dmitry A. Lemenovskii[a]

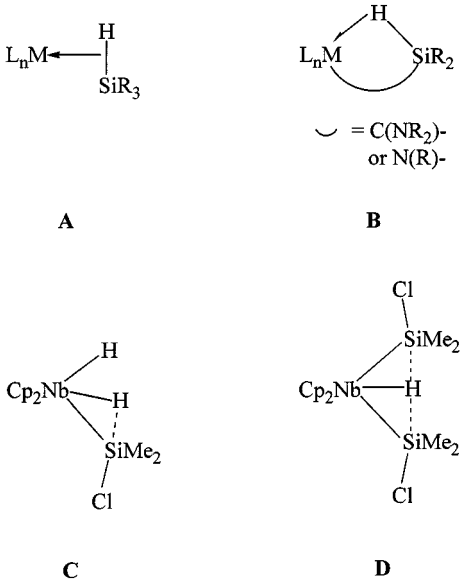
Keywords: Interligand interactions / Niobium / Tantalum / Silicon / Hydrides

Reaction of [CpM(NAr)(PMe_3)$_2$] (M = Nb, Ta; Ar = 2,6-C_6H_3*i*Pr$_2$) with $HSiClMe_2$ gives two remarkably different nonclassical Si···H···M products depending only on the identity of M; [CpTa(NAr)(H)($SiMe_2Cl$)(PMe_3)] possesses an unusual electron-rich M–H···Si interligand hypervalent interaction while [CpNb{η^3-N(Ar)$SiMe_2$–H}Cl(PMe_3)] is the first example of a β-agostic silylamine Si–H···M interaction showing a "stretched" Si–H bond.

Introduction

The study of complexes possessing interligand interactions is important for developing a better understanding of transition metal-mediated transformations. For example, nonclassical σ-complexes of the type $L_nM(\eta^2\text{-H}-X)$ (e.g. X = H, SiR_3, BR_2) serve as models for intermediates in oxidative addition/reductive elimination reactions,[1] while β-agostic $L_nM\cdots H-C$ systems lie on the reaction coordinate for the migratory insertion of alkenes into metal−hydride bonds.[2] Of particular relevance to this contribution are silicon-hydrogen bond complexes of the types **A** (η^2-silane species) and **B** (β-agostic M···H···Si) which are now well-established in the literature. Such metal−hydrogen−silicon interactions can best be described as three-centre, two-electron M···H···Si bonds formally arising from donation of Si−H σ-bond electron density to the metal (often with additional metal-to-Si−H σ* orbital back-donation); the interligand (i.e. Si···H) interactions in **A** and **B** may thus be classified as *electron deficient.*

We have recently reported a new type of M···H···Si interligand interaction found in certain niobocene silyl hydride complexes (**C** and **D**) which we classified as an *electron-rich*, interligand hypervalent interaction (IHI).[3] The IHI formally arises from donation of Nb−H bond electron density to the silicon−halogen antibonding orbital. this results in a three-centre, four-electron H···Si−Cl interaction, and in the case of **D** gives a five-centre, six-electron Cl−Si···H···Si−Cl bond. In both **C** and **D** silicon is five coordinate and hypervalent, with H and Cl occupying the apical sites of an approximate trigonal bipyramid. Experimental and theoretical studies by us[3] and others[4] have shown that the presence of a Si−Cl bond *trans* to hydride is crucial to developing shortened H···Si contacts and gives a concomitant lengthening of the Si−Cl bond. Analogous hypervalent interactions between a hydride ligand and a β-positioned silicon (β-IHI) have recently been found by Tilley and co-workers.[5]



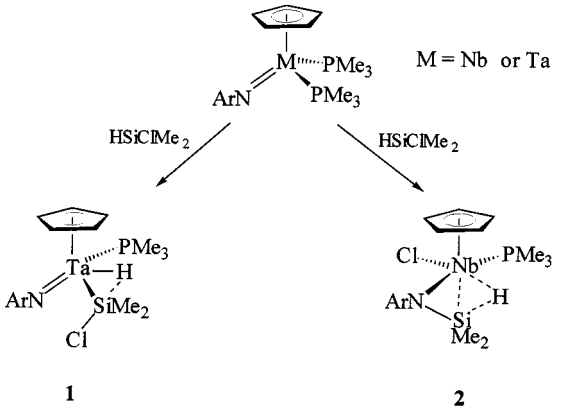
Given the current interest and importance of understanding the underlying factors controlling interligand interactions we were interested in finding new examples of complexes with unusual M···H···Si interactions. It is well-estab-

[a] Chemistry Department, Moscow State University, Vorob′evy Gory, 119899, Moscow, Russia
Fax: (internat.) + 7-(0)95/932-8846
E-mail: nikonov@org.chem.msu.su
[b] Inorganic Chemistry Laboratory, South Parks Road, Oxford OX1 3QR, UK
Fax: (internat.) + 44-(0)1865/272-690
E-mail: Philip.Mountford@chemistry.ox.ac.uk
[c] School of Chemistry, University of Nottingham, University Park, Nottingham NG7 2RD, UK
[d] Chemistry Department, University of Durham, South Road, Durham DH1 3LE, UK

 © WILEY-VCH Verlag GmbH, D-69451 Weinheim, 2000 1434−1948/00/0909−1917 $ 17.50+.50/0

lished that Cp^- and NR^{2-} (R is typically alkyl or aryl) are isolobal fragments,[6] and so complexes of the type $[Cp_2MX_3]$ and $[CpM(NR)(L)(X)_2]$ (M = group 5 metal; X, L = 1- and 2-electron donors) are also isolobal. Suitable group 5 precursor complexes $[CpM(NAr)(PMe_3)_2]$ (M = Nb or Ta; Ar = 2,6-$C_6H_3iPr_2$) were prepared from the corresponding $[CpM(NAr)Cl_2]$ complexes.[7]

The reactions of $[CpM(NAr)(PMe_3)_2]$ (M = Nb, Ta; Ar = 2,6-$C_6H_3iPr_2$) with $HSiClMe_2$ (see Scheme 1) give two dramatically different types of complex depending only on the identity of M. These are $[CpTa(NAr)(H)(SiMe_2Cl)(PMe_3)]$ (**1**, 60% isolated yield) and $[CpNb\{\eta^3\text{-}N(Ar)SiMe_2{-}H\}Cl(PMe_3)]$ (**2**, 84% isolated yield), each of which possesses a different type of nonclassical M···H···Si interaction.



1 **2**

Scheme 1. Reaction of $[CpM(NAr)(PMe_3)_2]$ (M = Nb or Ta; Ar = 2,6-$C_6H_3iPr_2$) with $HSiClMe_2$

The compound $[CpTa(NAr)(H)(SiMe_2Cl)(PMe_3)]$ (**1**) shows well-defined sets of signals for the Cp, NAr, $SiMe_2$ and PMe_3 ligands in its NMR spectra. The Ta−H resonance appears as a doublet [^2J(H−P) = 64.1 Hz] at δ = 5.13; the unusual low-field shift may be attributed to the anisotropy of the multiple bond to the imido ligand. Compound **1** is a rare example of a stable transition metal hydride complex supported by an imido group.[8] The solution NMR data are consistent with the solid state structure (Figure 1) which shows that the Ta-bound Si, hydride and P atoms all lie in the "bisecting plane" between the Cp and NAr ligands, consistent with the isolobal analogy between $[Cp_2MX_3]$ and $[CpM(NAr)(X)_2L]$. The silicon-bound chlorine atom is approximately *trans* to H(1) and also lies in this plane [maximum deviation from the calculated {Ta(1)−P(1)−H(1)−Si(1)−Cl(1)} least-squares plane = 0.13 Å].

The geometry at Ta in **1** closely resembles that of Nb in the nonclassical complexes $[Cp_2Nb(X)(H)(SiMe_2Cl)]$ (X = H **C** or $SiMe_2Cl$ **D**),[3] assuming that the arylimido group occupies the coordination site of one of the Cp rings. An analogous approximately *trans* position of apical Si−Cl and metal-bound H with the $\{MMe_2\}$ unit formally comprising an equatorial plane was previously observed in **C** and **D**. Recent experimental and theoretical studies have shown that comparatively short M−Si and long Si−Cl bonds are associated with interligand hypervalent interactions between the Si and H ligands.[3] The Si−Cl bond length of 2.177(2) Å in **1** is one of the longest reported for $[L_nM(SiR_2Cl)]$ (R = alkyl, aryl) complexes.[9] Furthermore, it is comparable to that found in the nonclassical complex **C** [Si−Cl = 2.170(2) Å], but significantly longer than that of **D** [Si−Cl = 2.163(1) Å]. The Ta−Si bond of 2.574(1) Å in **1** is the shortest reported to date [avg. 2.638, range 2.611−2.671 Å for six Ta^V nondisordered observations],[10] and is comparable to the Nb−Si bonds in **C** and **D** [Nb−Si = 2.579(2) and 2.597(1) Å, respectively]; these in turn are shorter than in other silyl derivatives of niobocene.[11]

Although the hydride ligand in **1** was crystallographically located and isotropically refined, the characteristically large estimated standard deviations (ca. 0.1 Å) associated with Ta−H and Si−H contacts do not allow for detailed discussion of the Si−H interaction. However, density functional theory (DFT) has conclusively been shown to provide valuable insight into transition metal complexes, including those with metal−hydrogen−ligand interactions.[12] A DFT partial geometry optimisation[13] of **1** allowing only the hydride position to change (starting with non-hydride atom coordinates taken from the X-ray study, and the hydride initially positioned *symmetrically* between Si and P) resulted in a structure with an Si−H contact of 2.158 Å, a P···H distance of 2.469 Å and a Ta−H distance of 1.888 Å. By way of comparison, Si···H contacts of 1.993−2.154 Å were previously calculated for the nonclassical model complexes $[Cp_2Nb(H)(SiH_2Cl)_2]$ and $[Cp_2Nb(H)_2(SiH_2Cl)]$.[3c,4]

Unambiguous experimental verification of the existence of the predicted *direct* Si−H bonding in compound **1** is the observed ^1J(Si−H) coupling constant of 33 ± 0.5 Hz. This ^1J(Si−H) is significantly larger then the postulated "nonbonding" value of 20 Hz,[1b] but is somewhat lower than the values (40−60 Hz) usually observed in silane σ-complexes. The observation of a "diminished" Si−H coupling constant in **1** is in complete agreement with our previous report that Si−H bonding through the IHI mechanism mainly involves silicon 3p orbitals.[3c]

In contrast to the formation of the tantalum derivative **1**, reaction of the niobium complex $[CpNb(NAr)(PMe_3)_2]$ with $HSiClMe_2$ gives exclusively $[CpNb\{\eta^3\text{-}N(Ar)SiMe_2{-}H\}Cl(PMe_3)]$ (**2**, see Scheme 1). The ^{1}H NMR spectrum of **2** shows, in addition to characteristic Cp, Ar, PMe_3 and $SiMe_2$ resonances, a high-field Nb−H resonance at δ = −5.67 indicative of substantial hydridic character.

The IR spectrum of **2** displays a band at 1620 cm^{-1} attributable to vibrations associated with the hydrogen bridging the silicon and niobium atoms. This band is closer to the typical region for ν(Nb−H) in niobocene hydrides (1750−1650 cm^{-1})[11,14] rather than to the typical ν(Si−H) region. For comparison, uncoordinated Si−H bonds exhibit ν(Si−H) bands at about 2100 cm^{-1}, whereas in d^0 Si−H···M β-agostic systems of type **B** this band is shifted to about 1800 cm^{-1}.[15] Therefore, the IR data also establish substantial hydridic character of the niobium-interacting hydrogen. However, the observed ^1J(Si−H) coupling con-

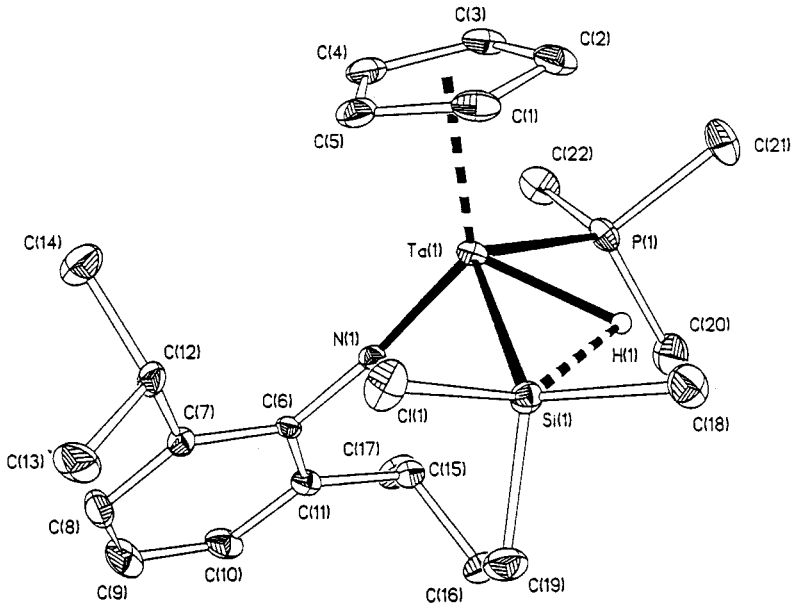
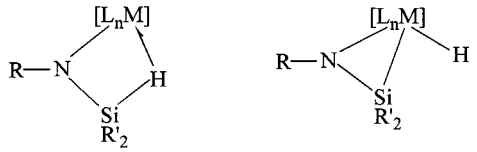


Figure 1. Molecular structure of [CpTa(NAr)(H)($SiMe_2Cl$)(PMe_3)] (**1**); displacement ellipsoids are drawn at the 25% probability level, except for H(1) which is shown as a sphere of arbitrary radius; H atoms except H(1) are excluded for clarity; selected bond lengths (Å) and angles (°) with estimated standard deviations in parentheses: Ta(1)−N(1) 1.821(4), Ta(1)−P(1) 2.550(1), Ta(1)−Si(1) 2.574(1), Cl(1)−Si(1) 2.177(2), Ta(1)−H(1) 1.6(1), Si(1)−H(1) 2.3(1), P(1)−H(1) 2.3(1); P(1)−Ta(1)−Si(1) 120.63(5), Cl(1)−Si(1)−Ta(1) 112.05(7)

stant of 96.6 Hz in **2** unambiguously reveals also direct bonding between this hydride and silicon (and comprehensively rules out the description of **2** as a classical η^2-silanimine hydride complex, **F**). It is noteworthy that this ^1J(Si−H) value is significantly diminished with respect to the values observed for d^0 Si−H···M β-agostic systems [^1J(Si−H) = 113−142 Hz] such as **E**.



β -agostic silylamine silanimine-hydride

E **F**

The X-ray structure of **2** (Figure 2) comprises of a Nb atom ligated by Cp, Cl and PMe_3 ligands, and the coordination sphere is completed by an η^3-N(Ar)$SiMe_2$−H ligand. The Nb···H···Si bridging hydrogen atom, H(1), was located from a Fourier difference map and refined isotropically. As for **1**, a DFT partial geometry optimisation[13] was carried out on **2** to assess the predicted position of H(1). All atomic positions were taken from the X-ray structure and the Nb···H···Si bridging hydrogen position was optimised while other atoms were kept fixed. The observed and calculated Nb−H distances are 1.91(5) and 1.931 Å; the corresponding Si−H distances are 1.52(5) and 1.771 Å, respectively. As for **1**, the experimental and theoretical values agree within the uncertainties and approximations associated with the two methods and are supported by the ^{1}H NMR spectroscopic data and ^1J(Si−H) values.

It is interesting to compare the Nb−H and Si−H distances for **2** with those of normal terminal Nb−H bonds (range ca. 1.60 −1.81 Å, depending on the experimental method[11b,14,16]), and with previously reported free or β-agostic Si−H bonds (range ca. 1.42−1.50 Å[15,17]). It is also instructive to consider the Nb(1)−N(1)−Si(1) angle of 89.1(2)° in **2**. This is comparable with M−N−Si angles found previously for silanimine compounds [86.1(1)° and 89.1(2)° for two examples[18]]; these are significantly smaller than the corresponding values for β-agostic (M···H−Si) silylamine (**E**) complexes [range 95.1(1) − 103.4(1)° for four examples[15]].

Therefore the elongated Nb−H and Si−H bonds, contracted Nb−Si−N angles, diminished ^1J(Si−H), along with other NMR and IR spectroscopic data suggest that the bonding in **2** is intermediate between a β-agostic d^2 silylamine (**E**) and a d^0 silanimine-hydride (**F**) structure. The electronic structure from the DFT calculations for **2** is in line with this interpretation and reveals a metal-based HOMO (corresponding formally to a d^2 complex) that is well set up for back-bonding into the Si−H σ* antibonding orbital. Compound **2** may be a useful model of the transition state for the as-yet-unknown migratory insertion of a silanimine into a metal−hydride bond.

In conclusion, the reaction of CpM(NAr)(PMe_3)$_2$ (M = Nb, Ta) with $HSiClMe_2$ gives remarkably different nonclassical Si···H···M products depending only on the identity of M. Compound **1** provides further evidence for the existence of electron-rich M−H···Si interligand hypervalent interactions, while compound **2** is the first example of a β-agostic

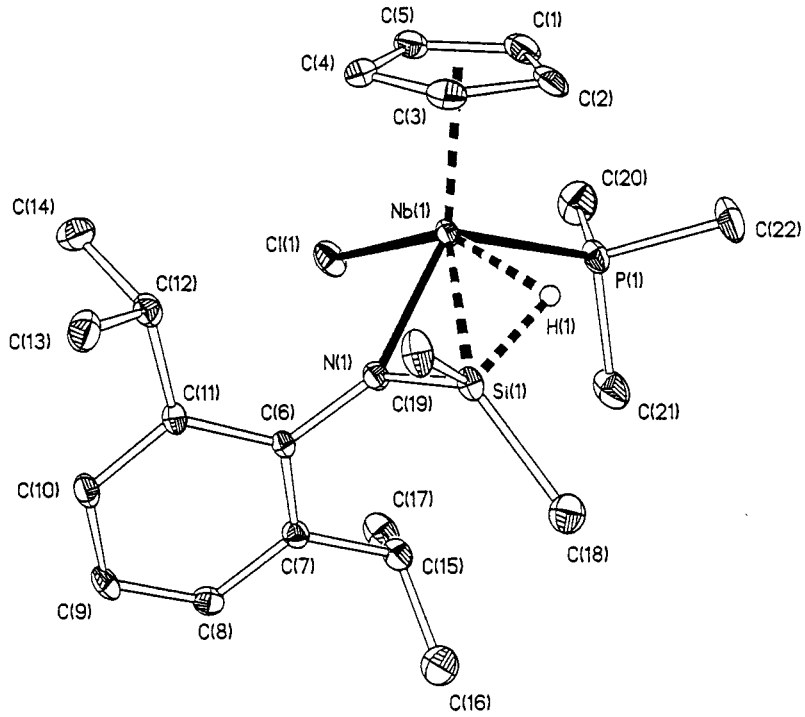


Figure 2. Molecular structure of [CpNb{η^3-N(Ar)SiMe$_2$−H}Cl(PMe$_3$)] (**2**); displacement ellipsoids are drawn at the 30% probability level, except for H(1) which is shown as a sphere of arbitrary radius; H atoms except H(1) are excluded for clarity; selected bond lengths (Å) and angles (°) with estimated standard deviations in parentheses: Nb(1)−N(1) 2.051(4), Nb(1)−P(1) 2.552(1), Nb(1)−Si(1) 2.646(1), Nb(1)−Cl(1) 2.497(1), Nb(1)−H(1) 1.91(5), Si(1)−H(1) 1.52(5), Si(1)−N(1) 1.704(4); Nb(1)−N(1)−Si(1) 89.09(16), Si(1)−Nb(1)−P(1) 109.37(5), Si(1)−Nb(1)−Cl(1) 123.42(5)

Si−H···M interaction showing such a "stretched" Si−H bond for a silylamine complex.

Experimental Section

Preparation of [CpTa(NAr)(H)(SiMe$_2$Cl)(PMe$_3$)] (1): To a solution of [CpTa(NAr)(PMe$_3$)$_2$] (1.03 g, 1.10 mmol) in pentane (30 mL) was added HClSiMe$_2$ (0.5 mL). After 14 h a light pink precipitate formed which was filtered off and dried in vacuo. Yield: 0.65 g (61%). − IR (Nujol): 1736 cm^{-1} ν(Ta−H). − ^{1}H NMR ([D$_6$]benzene): δ = 0.90 [d, J(H−P) = 8.5 Hz, 9 H, PMe$_3$], 0.95 (s, 3 H, SiMe$_2$), 1.23 (s, 3 H, SiMe$_2$), 1.23 [d, J(H−H) = 6.9 Hz, 6 H, CHMe_2], 1.27 [d, J(H−H) = 6.9 Hz, 6 H, CHMe_2], 4.04 [sept, J(H−H) = 6.9 Hz, 2 H, CHMe$_2$], 4.52 [d, J(H−P) = 1.5 Hz, 5 H, Cp], 5.13 [d, J(H−P) = 64.2 Hz, 1 H, Ta−H]. − ^{29}Si{^{1}H-selective} NMR ([D$_6$]benzene): δ = 91.7 [^1J(H−Si) = 33.3 Hz]. − ^{31}P{^{1}H} NMR ([D$_6$]benzene): δ = −4.3. − $C_{22}H_{38}ClNPSiTa$ (592.0): calcd. C 44.63, H 6.47, N 2.37; found C 44.72, H 6.46, N 2.30.

Preparation of [CpNb{η^3-N(Ar)SiMe$_2$−H}Cl(PMe$_3$)] (2): To a suspension of [CpNb(NAr)(PMe$_3$)$_2$] (1.46 g, 3.09 mmol) in pentane (15 mL) was added HSiClMe$_2$ (1.3 mL, excess). The mixture was kept 5 days to afford large dark-green crystals. These were filtered off, washed with cold pentane and dried in vacuo. Yield: 1.28 g (84%). The solution was reduced in volume to 5 mL and a second crop of **2** (0.20 g) crystallized after 3 days. − IR (Nujol): 1620 cm^{-1} ν(Nb−H). − ^{1}H NMR ([D$_6$]benzene): δ = −5.67 (s, 1 H, Nb−H), 0.22 (d, J = 0.9 Hz, 3 H, SiMe_2), 0.31 [d, J(H−P) = 2.0 Hz, 3 H, SiMe_2], 0.96 [d, J(H−P) = 7.8 Hz, 9 H, PMe$_3$], 1.14 (d, J = 6.8 Hz, 3 H, CHMe_2), 1.32 (overlapping 2 × d, J = 6.8 Hz, 6 H, 2 × CHMe_2), 1.50 (d, J = 6.7 Hz, 3 H, CHMe_2), 2.37 (sept, J = 6.8 Hz, 1 H, CHMe$_2$), 3.33 (sept, J = 6.7 Hz, 1 H, CHMe$_2$), 4.67 [d, J(H−P) 1.7 Hz, 5 H, Cp]. − ^{29}Si{^{1}H-selective} NMR ([D$_6$]benzene): δ = −52.1 [^1J(H−Si) = 96.6 Hz]. − ^{31}P{^{1}H} NMR ([D$_6$]benzene): δ = 11.5. − $C_{22}H_{38}ClNNbPSi$ (504.0): calcd. C 51.90, H 7.60, N 2.78; found C 51.9, H 7.71, N 2.60.

X-ray Crystallographic Study of 1 and 2: Crystals of **1** were grown from pentane, crystals of **2** from ether. For both structures the data were corrected for Lorentz and polarisation effects. Non-hydrogen atoms were refined anisotropically. All hydrogen atoms except hydride (which was located from Fourier difference synthesis and positionally refined isotropically), were placed in calculated positions and refined in a riding model.

Crystal data for 1: $C_{22}H_{38}ClNPSiTa$, 0.15 × 0.20 × 0.27 mm, monoclinic, space group $P2_1/c$, a = 15.893(1), b = 9.092(1), c = 19.136(2) Å, β = 112.568(3)°, V = 2553.47 Å^3, ρ = 1.54 g·cm^{-3}, μ(Mo-K_α) = 4.53 cm^{-1}, T = 150 K. Of 23837 data collected (0.96 ≤ θ ≤ 27.53°), 5838 [R(int) = 0.050] were independent and 4115 [$I > 3\sigma(I)$] reflections were used in the refinement of 249 parameters. An absorption correction based on multi-scans was applied (T_{min}, T_{max} = 0.368, 0.615). $R(F)$ = 0.030, $R(wF)$ = 0.035. Min./max. peaks in final difference map: 1.03/−0.63 e·Å^{-3}.

Crystal Data for 2: $C_{22}H_{38}ClNNbPSi$, 0.19 × 0.17 × 0.14 mm, monoclinic, space group $C2/c$, a = 31.391(6), b = 10.150(2), c = 16.945(3) Å, β = 111.30(3)°, V = 5030(2) Å^3, ρ = 1.331 g·cm^{-3}, μ(Mo-K_α) = 7.04 cm^{-1}, T = 150(2) K. Of 4813 data collected (1.0 ≤ θ < 25.5°), 4437 [R(int) = 0.0343] were independent [3557 reflections had $I > 2\sigma(I)$] and were used in the refinement of 313 parameters. An absorption correction (ψ-scans) was applied (T_{min}, T_{max} = 0.721, 0.913). $R(F)$ = 0.050, $R(wF^2)$ = 0.103. Min./max. peaks in final difference map: 1.427/−0.868 e·Å^{-3}.

Crystallographic data (excluding structure factors) for the two structures reported in this paper have been deposited with Cam-

bridge Crystallographic Data Centre as supplementary publication no. CCDC-33301 (**1**) and CCDC-33302 (**2**). Copies of the data can be obtained free of charge on application to The Director, CCDC, 12 Union Road, Cambridge CB2 1EZ, UK [Fax: (internat.) + 44-1223/336-033; E-mail: deposit@ccdc.cam.ac.uk.

DFT Studies: Calculations were performed using the density functional methods of the Amsterdam Density Functional (ADF) code Version 2.3.0.[13a] The basis set used triple-ζ accuracy sets of Slater orbitals with a single polarisation function added to main group atoms. The cores of the atoms were frozen. Vosko, Wilk and Nusair's local exchange correlation potential[13b] was employed with nonlocal exchange corrections by Becke[13c] and nonlocal correlation corrections by Perdew.[13d]

Whereas calculation on the whole "real" complex is unfeasible for us because of the time that it would take, attempted full DFT geometry optimisation of an oversimplified model of **2**, having hydrogen substituents on Si, P and N atoms, converged to a structure with quite different distances between Si and N. This shows (as we found in the chemistry) that substituents are important. Note that in the calculations, all of the distances and angles were chemically realistic, but obviously were more appropriate to a compound further along the reaction coordinate. It is well-known that in certain cases involving "weak" interactions the influence of steric/electronic substituent effects can be crucial.

Acknowledgments

We thank the Royal Society (London) for financial support through a joint research grant and Dr. N. H. Rees for recording the ^{29}Si NMR spectra. Part of this work has been carried out using the computational resources of a DEC 8400 multiprocessor cluster (Columbus/Magellan), provided by the U.K. Computational Chemistry Facility at Rutherford Appleton Laboratory.

[1] For reviews of σ-complexes see: [1a] R. H. Crabtree, *Angew. Chem. Int. Ed. Engl.* **1993**, *32*, 789−805. − [1b] U. Schubert, *Adv. Organomet. Chem.* **1990**, *30*, 151−187. − [1c] For a titanocene borane σ-complex see: C. N. Muhoro, X. He, J. F. Hartwig, *J. Am. Chem. Soc.* **1999**, *121*, 5033−5046.

[2] M. Brookhart, M. L. H. Green, L.-L. Wong, *Prog. Inorg. Chem.* **1988**, *36*, 1−124.

[3] [3a] G. I. Nikonov, L. G. Kuzmina, D. A. Lemenovskii, V. V. Kotov, *J. Am. Chem. Soc.* **1995**, *117*, 10133−10134. − [3b] G. I. Nikonov, L. G. Kuzmina, D. A. Lemenovskii, V. V. Kotov, *J. Am. Chem. Soc.* **1996**, *118*, 6333 [corr.]. − [3c] G. I. Nikonov, S. F. Vyboishchikov, L. G. Kuzmina, D. A. Lemenovskii, J. A. K Howard, *Chem. Eur. J.* **1999**, *5*, 2947−2963.

[4] M.-F. Fan, Z. Lin, *Organometallics* **1998**, *17,* 1092−1100.

[5] T. I. Gountchev, T. D. Tilley, *J. Am. Chem. Soc.* **1997**, *119*, 12831−12841.

[6] [6a] D. S. Williams, M. H. Schofield, R. R. Schrock, *Organometallics* **1993**, *12*, 4560−4571. − [6b] D. N. Williams, J. P. Mitchell, A. D. Pool, U. Siemeling, W. Clegg, D. C. R. Hockless, P. A. O'Neil, V. C. Gibson, *J. Chem. Soc, Dalton.Trans.* **1992**, 739−751. − [6c] J. Sundermayer, D. Runge, *Angew. Chem. Int. Ed. Engl.* **1994**, *33*, 1255−1257.

[7] These new compounds were prepared by adaptation of the literature method reported for [Cp*Nb(NAr)(PMe_3)$_2$]: M. C. W. Chan, J. M. Cole, V. C. Gibson, J. A. K. Howard, C. Lehnmamm, A. D. Poole, U. Siemeling, *J.Chem. Soc, Dalton.Trans.* **1998**, 103−111.

[8] For leading references see: D. E. Wigley, *Prog. Inorg. Chem.* **1994**, *42*, 239−481.

[9] [9a] K. E. Lee, A. M. Arif, J. A. Gladysz, *Chem. Ber.* **1991**, *124*, 309−320. − [9b] B. R. Jagirdar, R. Palmer, K. J. Klabunde, L. Radonovich, *Inorg. Chem.* **1995**, *34*, 278−283. − [9c] M. K. Hays, R. Eisenberg, *Inorg. Chem.* **1991**, *30*, 2623−2630. − [9d] T. S. Koloski, D. C. Pestana, P. J. Carroll, D. H. Berry, *Organometallics* **1994**, *13*, 489−499.

[10] "The United Kingdom Chemical Database Service", D. A. Fletcher, R. F. McMeeking and D. Parkin, *J. Chem. Inf. Comput. Sci.* **1996**, *36,* 746−749.

[11] [11a] M. D. Curtis, L. G. Bell, N. M. Buter, *Organometallics* **1985**, *4*, 701−707. − [11b] A. Antiñolo, F. Carrillo, M. Fajardo, A. Otero, M. Lanfranchi, M. A.Pellingheli, *Organometallics* **1995**, *14*, 1518−1521.

[12] See for example: [12a] P. Margl, L. Q. Deng and T. Ziegler, *J. Am. Chem. Soc.* **1999**, *121*, 154−162. − [12b] Y. Z. Han, L. Q. Deng and T. Ziegler, *J. Am. Chem. Soc.* **1997**, *119*, 5939−5945, and references therein.

[13] [13a] G. te Velde and E. J. Baerends, *J. Comput. Phys.* **1992**, *99*, 84−98. − [13b] S. H. Vosko, L. Wilk and M. Nusair, *Can. J. Phys.* **1980**, *58*, 1200−1211. − [13c] A. D. Becke, *Phys. Rev. A* **1988**, *38*, 2098−3100. − [13d] J. P. Perdew, *Phys. Rev. B* **1986**, *33*, 8822−8824. − [13e] J. P. Perdew, *Phys. Rev. B* **1986**, *34*, 7406.

[14] See, for example: G. I. Nikonov, L. G. Kuzmina, J. A. K. Howard, *Organometallics* **1997**, *16*, 3723−3725, and references therein.

[15] [15a] W. A. Herrmann, N. W. Huber, J. Behm, *Chem. Ber.* **1992**, *125*, 1405−1407. − [15b] L. J. Procopio, P. J. Carroll, D. H. Berry, *J. Am. Chem. Soc.* **1994**, *116*, 177−185. − [15c] W. A. Herrmann, J. Eppinger, M. Spiegler, O. Runte, R. Anwander, *Organometallics* **1997**, 16, 1813−1815.

[16] V. I. Bakhmutov, E. V. Vorontsov, G. I. Nikonov, D. A. Lemenovskii, *Inorg. Chem.* **1998**, *37*, 279−282.

[17] U. Schubert, M. Schwartz, F. Möller, *Organometallics* **1994**, *13*, 1554−1555.

[18] [18a] L. J. Procopio, P. J. Carroll, D. H. Berry, *J. Am. Chem. Soc.* **1991**, *113*, 1870−1872. − [18b] L. J. Procopio, P. J. Carroll, D. H. Berry, *Polyhedron* **1995**, *14*, 45−55.

Received January 29, 2000
[I00030]

Quinolylcyclopentadienylthallium: A Donor-Stabilized Thallium(I) Compound

Markus Enders,*[a] Jochen Fink,[a] and Hans Pritzkow[a]

Keywords: Thallium / Sandwich complexes / N ligands / Hemilabile ligands

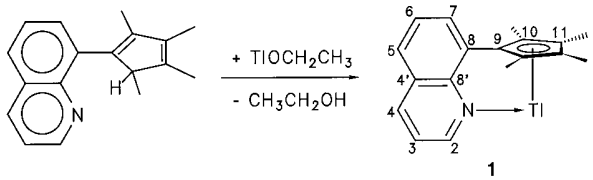
The synthesis and properties of 1-(8-quinolyl)-2,3,4,5-tetramethylcyclopentadienyl-thallium(I) (**1**) are described. The functionalised cyclopentadienyl ligand coordinates to the thallium through the five-membered ring and the nitrogen atom. Whereas the NMR investigation indicates a monomeric structure in solution, the crystal structure analysis shows the tendency to form an infinite zigzag polymeric chain in the solid state.

Introduction

Besides Cp thallium(I) compounds, most organothallium derivatives are Tl^{III} species.[1,2] Recently the synthesis of the first monomeric arylthallium(I) compound[2] has been reported. $CpTl^{I}$ compounds are mild reagents for the synthesis of cyclopentadienyl derivatives of main group elements, transition metals and lanthanoid metals.[3] Several solid-state structures of substituted CpTl compounds have been reported. For example C_5H_5Tl,[4] C_5Me_5Tl[5] and $(Me_3Si)C_5H_4Tl$[6] form infinite zigzag chain polymers. In contrast $(Me_3Si)_2C_5H_3Tl$[6] forms hexameric units. Our previous investigations on the complex chemistry of nitrogen-donor functionalised cyclopentadienyl ligands showed that rigid, bifunctional ligands prefer a chelating coordination with formation of half-sandwich compounds.[7] However for ligands in which a nitrogen-donor is connected with an alkyl chain to the cyclopentadienyl ring[8] many conformations are possible. Here we use a cyclopentadienyl system with a quinoline moiety directly attached. In this hemilabile chelate ligand, the two different functionalities are linked by a rigid C_2 spacer, which is itself embedded in the planar heterocycle. Only rotation about one bond is possible. In addition the nitrogen lone pair points towards the space below the plane of the Cp ring. As donor-stabilised thallium(I) compounds are very rare,[9,10] we tried to achieve an interaction between the thallium atom and the nitrogen donor with the help of the rigid 1-(8-quinolyl)-2,3,4,5-tetramethylcyclopentadienylligand (Cp^Q). Moreover the resulting Cp^Q-Tl should serve as a source of the Cp^Q ligand.

Results and Discussion

The reaction of 1-(8-quinolyl)-2,3,4,5-tetramethylcyclopentadiene with thallium(I) ethoxide in ethanol yields [1-(8-quinolyl)-2,3,4,5-tetramethylcyclopentadienyl]thallium(I) (**1**) (Cp^Q-Tl) as an orange precipitate in nearly quantitative yield (Scheme 1).



Scheme 1. Formation and numbering of **1**

Compound **1** is soluble in aromatic or polar aprotic solvents. Orange crystals are formed from toluene/pentane. They are air-stable for a few minutes and decompose at 142 °C. Compound **1** is less air- and light-sensitive than C_5Me_5Tl[5] or dimethylaminoethyl-Cp-thallium compounds, and the decomposition temperature is higher.[9] These properties indicate that the thallium atom is protected by an interaction with the quinolyl nitrogen. This assumption is supported by the ^1H and ^{13}C NMR spectra.

The ^1H NMR spectrum shows doublets due to coupling with thallium. Natural thallium consists of two isotopes ^{203}Tl (S = 1/2, 29.53%) and ^{205}Tl (S = 1/2, 70.47%). As the gyromagnetic ratios of the two isotopes differ only slightly ($\gamma(^{205}Tl)/\gamma(^{203}Tl) = 1.01$), the coupling constants $J(X,Tl^{205})$ and $J(X,Tl^{203})$ are nearly identical. The four methyl groups at the cyclopentadienyl ring form two doublets at $\delta = 2.27$ and $\delta = 2.38$ with a coupling constant $^3J(Tl,H) = 15.5$ Hz and 13.3 Hz, respectively. The $^3J(Tl,H)$ coupling constant for C_5Me_5Tl has been reported to be 18 Hz.[11] Only two methyl resonances are observed, because the molecule adopts C_S symmetry on the NMR time scale. Further structural information can be obtained by the analysis of the proton−thallium coupling constants in the quinoline substituent. The exact assignment of the proton resonances has been confirmed by double resonance techniques and by a H,H-COSY NMR spectrum. If the nitrogen atom is not coordinated to the thallium centre it must lie on the opposite side of the Cp ring. For this arrangement we would expect to observe a through-space $^1H,Tl$ coupling of the hydrogen atom H^7 [13] and no coupling to the protons H^2, H^3 and H^4. However, the opposite is true. All protons in the heterocyclic part of the quinoline couple with the thallium atom and no Tl,H coupling is observed in the homo-

[a] Anorganisch-Chemisches Institut der Universität,
Im Neuenheimer Feld 270, 69120 Heidelberg, Germany
Fax: (internat.) +49-(0)6221/545-609
E-mail: markus.enders@urz.uni-heidelberg.de

 © WILEY-VCH Verlag GmbH, D-69451 Weinheim, 2000 1434−1948/00/0909−1923 $ 17.50+.50/0

cyclic part. The coupling constant for the H^2 atom is 17.1 Hz, and for H^3 and H^4 it is 8.2 Hz. The Tl,H coupling behaviour clearly indicates that the nitrogen atom is bound to the thallium atom in solution. In addition, the absence of coupling to a second thallium atom shows that the complex is monomeric in solution.

These interpretations are supported by the ^{13}C NMR spectra. Except for three carbon atoms from the homocyclic part of the quinoline, all resonances are split into doublets because of coupling to a single thallium atom. The largest coupling constants are observed for the quaternary carbon atoms of the Cp ring with values of 124 Hz and 127 Hz. The four methyl groups show two doublets [J(Tl,H) = 69 Hz and 59 Hz].

The EI-MS spectrum of **1** gives the molecular ion at m/z = 453 with an intensity of 27% and a characteristic isotope distribution. The base peak at m/z = 248 originates from the free ligand. The C,H analysis confirms that no solvent molecules are coordinated to **1** in the solid state.

The constitution of **1** in solution, a monomeric molecule with C_s symmetry and nitrogen coordination to the metal atom, is deduced from the NMR spectra. In addition, we investigated the solid-state structure of **1** by X-ray diffraction (Figure 1).

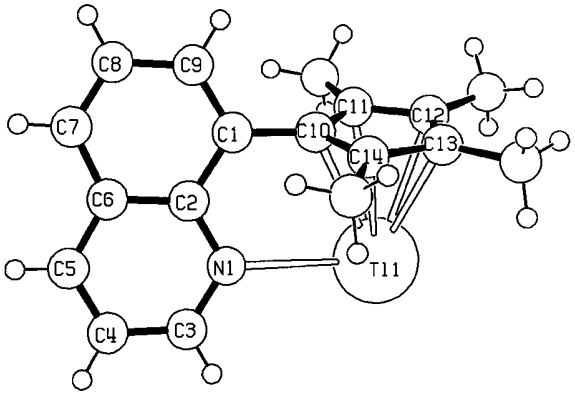


Figure 1. Solid state structure of **1**; selected bond lengths (Å) and angles (°):Tl1−N1 2.977(11), Tl1−C10 2.884(11), Tl1−C11 2.872(11), Tl1−C12 2.869(10), Tl1−C13 2.917(10), Tl1−C14 2.932(11), Tl1−C10′ 3.187(11), Tl1−C11′ 3.081(11), Tl1−C12′ 3.070(10), Tl1−C13′ 3.145(11), Tl1−C14′ 3.229(11), quinoline−Cp 110.2(8); C3−N1−Tl1 120.1(9), C2−N1−Tl1 120.2(8), C2−N1−C3 117.8(12)

In **1** the thallium atom is coordinated to the substituted Cp ring and the nitrogen atom. The distance between the metal and the centre of the Cp ring is 2.63 Å. A longer contact of 2.90 Å is observed to a neighbouring Cp ligand. Although this distance is quite long, **1** can be described as a zigzag chain polymer (Figure 2), an arrangement which is known for several CpTl compounds.[4−6,12] The Tl−Tl−Tl angle is 137.1°, a value similar to that in C_5H_5Tl (137°)[4] but smaller than in C_5Me_5Tl (145°).[5] However, in most reported structures of substituted CpTl complexes, the metal atom lies nearly equidistant between two Cp rings {e.g. C_5H_5Tl: d(Tl−Cp) = 2.75 Å,[4] C_5Me_5Tl: d(Tl−Cp) = 2.71 Å[5]}. In **1** the coordination of the nitrogen donor to the metal centre prevents a second Cp ring from binding strongly to the thallium atom. The Tl−N distance (2.97 Å) is quite long compared to reported Tl^I−N distances (2.52−2.95 Å).[14−18] Nevertheless there is a bonding interaction with formation of a chelating structure. This interpretation is supported by the sum of bonding angles around the nitrogen atom (C2−N−Tl, Tl−N−C3, C3−N−C2) which is 358.1°. Therefore the nitrogen atom lies in the plane of C2, C3 and Tl, so that the lone-pair of the nitrogen points directly at the thallium centre.

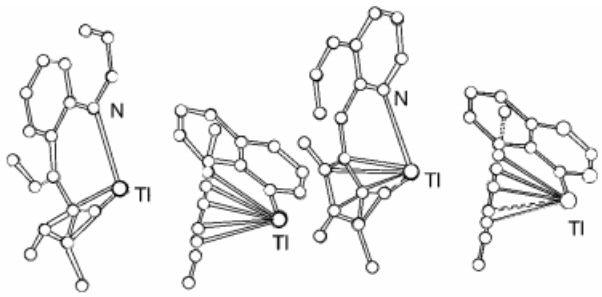


Figure 2. Solid state structure of **1** showing the arrangement as an infinite zigzag chain polymer; selected distances (Å) and angles (°): Tl−Cp 2.63 and 2.90, Tl−Tl 5.52(3); Tl−Tl−Tl 137.1(8)

Experimental Section

All reactions were carried out under nitrogen or argon atmosphere. 1-(8-quinolyl)-2,3,4,5,-tetramethylcyclopentadiene was prepared according to the reported procedure.[7]

1-(8-Quinolyl)-2,3,4,5-tetramethylcyclopentadienyl-thallium(I) (1): 1-(8-Quinolyl)-2,3,4,5-tetramethylcyclopentadiene (4.0 g, 16.0 mmol) was dissolved in 150 mL ethanol. At room temp. thallium ethoxide (4.0 g, 16.0 mmol) was added slowly to the pale yellow solution. Immediately the colour changed to deep orange. After 12 h magnetic stirring with the exclusion of light a bright orange precipitate was formed, which was then separated by filtration and washed with small portions of ethanol. After drying in vacuum, 7.0 g (96.8%) of **1** was obtained.

^1H NMR (C_6D_6): δ = 2.26 [d, ^3J(Tl,H) = 15.5 Hz, 6 H, 2 CH_3]; 2.38 [d, ^3J(Tl,H) = 13.3 Hz, 6 H, 2 CH_3], 6.78 [ddd, ^3J(H3,H4) = 4.0 Hz, ^3J(H3,H2) = 4.0 Hz, ^4J(Tl,H3) = 8.2 Hz, 1 H, H3], 7.31 [d, ^3J(H5,H6) = ^3J(H7,H6) = 4.0 Hz, 2 H, H5 and H7], 7.61 [ddd, ^3J(H4,H3) = 3.5 Hz, ^4J(H4,H2) = 1.9 Hz, ^5J(Tl,H4) = 8.2 Hz, 1 H, H4], 7.72 [t, ^3J(H6,H5) = ^3J(H6,H7) = 4 Hz, 1 H, H6], 8.21 [ddd, ^3J(H2,H3) = 4.2 Hz, ^4J(H2,H4) = 1.8 Hz, ^3J(Tl,H2) = 17.1 Hz, 1 H, H2]. − ^{13}C NMR: (C_6D_6) δ = 11.2 [d, J(Tl,C) = 59.2 Hz, CH_3], 11.7 [d, J(Tl,C) = 69.4 Hz, CH_3], 114.6 [d, J(Tl,C) = 145.2 Hz, C9], 115.1 [d, J(Tl,C) = 126.7 Hz, C10, C11], 117.3 [d, J(Tl,C) = 8.3 Hz, C8′], 120.4 [d, J(Tl,C) = 15.7 Hz, C3], 124.8 and 126.9 (s, C5, C7), 129.7 (s, C4′), 133.2 [d, J(Tl,C) = 29.6 Hz, C6], 136.9 [d, J(Tl,C) = 9.3 Hz, C4], 139.0 [d, J(Tl,C) = 26.8 Hz, C8], 147.2 [d, J(Tl,C) = 27.8 Hz, C2]. The assignment of all quinolyl atoms was confirmed from the H/H-COSY and C/H-COSY spectra. − EI-MS: m/z (%) = 453 (28) [M^+], 248 (100) [M^+ − Tl], 205 (38) [^{205}Tl], 203 (16) [^{203}Tl]. − $C_{18}H_{18}NTl$ (452.73l): calcd. C 47.67, H 4.00, N 3.09; found C 47.53, H 4.21, N 2.98.

Crystal Structure Determination of 1: Crystal data: $C_{18}H_{18}NTl$, M = 452.7, monoclinic, $P2_1/a$, a = 10.282(7), b = 15.162(11), c = 10.862(8) Å, β = 109.86(5)°, V = 1593(2) Å^3, Z = 4, d = 1.89 g cm^{-3}, μ = 10.1 mm^{-1}. Intensity data were collected at −70 °C with a Siemens-Stoe AED2 diffractometer [Mo-K_α radiation (λ = 0.71073 Å), ω-scans] up to θ = 25° (2805 unique reflections, 1866

observed with [$I > 2\sigma(I)$]. An empirical absorption correction (ψ-scans) was applied. The structure was solved by direct methods (SHELXS86[19]) and refined by full-matrix least-squares techniques (SHELXL93[19]) based on F^2 using all measured reflections and with anisotropic temperature factors for all non-hydrogen atoms. Hydrogen atoms were inserted in calculated positions. $R1 = 0.050$, $wR2 = 0.106$, 187 parameters, rest electron density 0.96, -1.24 e·Å^{-3}.

Crystallographic data (excluding structure factors) for the structure reported in this paper have been deposited with the Cambridge Crystallographic Data Centre as supplementary publication no CCDC-142406. Copies of the data can be obtained free of charge on application to CCDC, 12 Union Road, Cambridge CB2 1EZ, UK [Fax: (internat.) + 44-1223/336-033; E-mail: deposit@ccdc.cam.ac.uk].

[1] P. Jutzi, *Adv. Organomet. Chem.* **1986**, *26*, 217−295.

[2] M. Niemeyer, P. P. Power, *Angew. Chem.* **1998**, *111*, 1291−1294; *Angew. Chem. Int. Ed.* **1998**, *37*, 1277.

[3] G. B. Deacon, A. J. Koplick, T. D. Tuong, *Polyhedron* **1982**, *1*, 423−424; G. B. Deacon, P. I. Machinnon, T. W. Hambley, J. C. Taylor, *J. Organomet. Chem.* **1983**, *259*, 91−97; G. B. Deacon, A. J. Koplik, T. D. Tuong, *Aust. J. Chem.* **1984**, *37*, 517−525; M. D. Rausch, D. H. Edwards, R. D. Rogers, J. L. Atwood, *J. Am. Chem. Soc.* **1983**, *105*, 3882−3886; D. L. DuBois, C. W. Eigenbrot, J. A. Miedaner, J. C. Smart, R. I. Haltiwanger, *Organometallics* **1986**, *5*, 1405−1411; G. B. Deacon, C. M. Forsyth, W. C. Patalinghug, A. H. White, A. Dietrich, H. Schumann, *Aust. J. Chem.* **1992**, *45*, 567−582; B. Walther, A. Zschunke, B. Adler, A. Kolbe, S. Bauer, *Z. Anorg. Allg. Chem.* **1976**, *427*, 137−153; P. Jutzi, N. Burford, *Chem. Rev.* **1999**, *99*, 969−990.

[4] E. Frasson, F. Menegus, C. Panattoni, *Nature* **1963**, *199*, 1087−1089; J. F. Berar, G. Calvarin, C. Pommier, D. Weigel, *J. App. Crystallogr.* **1975**, *8*, 368−3XX; A. Dashti-Mommertz, B. Neumüller, S. Melle, D. Haase, W. Uhl, *Z. Anorg. Allg. Chem.* **1999**, *625*, 1828−1832.

[5] H. Werner, H. Otto, H. J. Kraus, *J. Organomet. Chem.* **1986**, *315*, C57−C60.

[6] S. Harvey, C. L. Raston, B. W. Skelton, A. H. White, M. F. Lappert, G. Srivastava, *J. Organomet. Chem.* **1978**, *328*, C1−C6.

[7] M. Enders, R. Rudolph, H. Pritzkow, *Chem. Ber.* **1996**, *129*, 459−463; M. Enders, R. Rudolph, H. Pritzkow, *J. Organomet. Chem.* **1997**, *549*, 251−256.

[8] J. Okuda, *Comm. Inorg. Chem.* **1994**, *16*, 185−205; P. Jutzi, T. Redeker, *Eur. J. Inorg. Chem.* **1998**, 663−674.

[9] J. Dalhaus, M. Bangel, P. Jutzi, *J. Organomet. Chem.* **1994**, *474,* 55−58.

[10] H. Schumann, A. Lentz, R. Weimann, *J. Organomet. Chem.* **1995**, *487*, 245−252.

[11] H. Schumann, C. Janiak, H. Khani, *J. Organomet. Chem.* **1987**, *330*, 347−355.

[12] M. B. Freeman, L. G. Sneddon, J. C. Huffmann, *J. Am. Chem. Soc.* **1977**, *99*, 5194−5196.

[13] O. W. Howarth, J. Nelson, V. McKee, *Chem. Commun.* **2000**, 21−22.

[14] K. Wieghardt, M. Kleine-Boymann, B. Nuber, J. Weiss, *Inorg. Chem.* **1986**, *25*, 1309−1313.

[15] J. Vicente, J. A. Abad, J. F. Gutierres-Jugo, *J. Chem. Soc., Dalton Trans.* **1989**, 2241−2245.

[16] K. Jacob, J. Scholz, K. Merzweiler, C. Pietzsch, *J. Organomet. Chem.* **1997**, *527*, 109−115.

[17] K. Jacob, J. Scholz, K. Merzweiler, C. Pietzsch, F. T. Edelmann, *J. Organomet. Chem.* **1995**, *501*, 71−77.

[18] D. Moras, R. Weiss, *Acta Cryst.* **1973**, *B29*, 1059−1063.

[19] G. M. Sheldrick, *SHELXS 86* **1986**, Universität Göttingen; G. M. Sheldrick, *SHELXL 97* **1997**, Universität Göttingen.

Received March 31, 2000
[I00129]

Borane-stabilized Boranediyls (Borylenes): Neutral *nido*-1-Borane-2,3,4,5,6-pentamethyl-2,3,4,5,6-pentacarbahexaboranes(6)

Peter Greiwe,[a] Alexandra Bethäuser,[a] Hans Pritzkow,[a] Thorsten Kühler,[b] Peter Jutzi,[b] and Walter Siebert*[a]

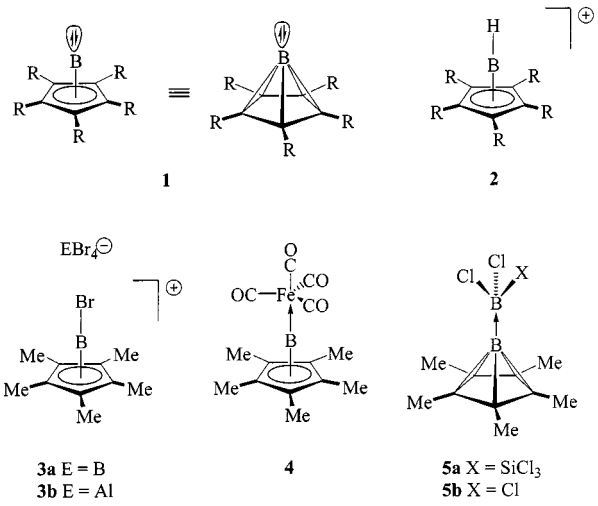
Dedicated to Professor Dr. Paul von Ragué Schleyer on the occasion of his 70th birthday

Keywords: Boranes / Borylene / Carboranes / Lewis acids

The reaction of $(C_5Me_5)_2Si$ or $(C_5Me_5)SiMe_3$ with B_2Cl_4 leads to the adducts $(C_5Me_5)B{\rightarrow}BCl_2SiCl_3$ (**5a**) or $(C_5Me_5)B{\rightarrow}BCl_3$ (**5b**), in which the Lewis acids stabilize the boranediyl fragments. Spectroscopic data and X-ray structure analyses confirm the adducts.

Introduction

In contrast to the heavier analogs of $[(\eta^5\text{-}C_5Me_5)E:]_n$, E = Al,[1] Ga,[2] In,[3] Tl[4] derivatives of (η^5-cyclopentadienyl)boranediyl **1** with a lone electron pair at boron are unknown. Protonation of hypothetical **1** could lead to the cation $[(\eta^5\text{-}C_5R_5)BH]^+$ (**2**) and formal addition of the bromonium ion Br^+ to the cation $[(\eta^5\text{-}C_5Me_5)B{-}Br]^+$, first obtained by Jutzi et al.[5] in the reaction of $Me_5C_5{-}GeMe_3$ with an excess of BBr_3 leading to **3a**. Schnöckel et al.[6] observed the formation of **3b** from the reaction of $[(C_5Me_5)Al]_4$ with BBr_3 and confirmed the proposed structure of the cation[5] as well as the calculated orientation of the substituents in **2** (R = H) towards the apical boron atom[7] by a crystal structure analysis. Very recently, Cowley et al.[8] prepared the tetracarbonyliron-pentamethylcyclopentadienylboranediyl complex **4** and reported a theoretical study on free and $Fe(CO)_4$-complexed borylenes.[9a] The related alanediyl compound $(C_5Me_5)Al{-}B(C_6F_5)_3$ has been synthesized.[9b] Compounds of the types **1**–**4** and the neutral polyhedron derivatives **5a,b** presented here are best described as *nido* clusters[10] with six skeletal atoms held together by $2n + 4 = 16$ skeletal electrons. We here present a new approach to stabilize the hypothetical boranediyl **1** (R = Me) as a Lewis base with the Lewis acids $Cl_3Si{-}BCl_2$ and BCl_3.



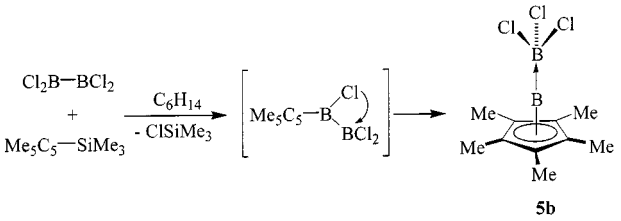
Results and Discussion

When $(\eta^5\text{-}C_5Me_5)_2Si$[11] is treated with B_2Cl_4 at −110 °C in pentane a red-brown suspension forms, which on warming to room temperature results in a yellow solution and a colorless solid, which turns violet on longer standing or on contact with air. The mass spectraof the crude product indicate the presence of two compounds (see Experimental Section), recrystallization from hot toluene yields **5a**.[12] Its EI and CI mass spectra do not show the M^+ peak; however, the $[M_2 - Cl]^+$ ion is seen in low intensity at *m/z* = 689. Besides the base peak in the CI spectrum at *m/z* = 327 $[M^+ - Cl]$ the only other fragment is found at *m/z* = 227 $[B_2SiCl_5]^+$ which is the base peak in the EI MS.

The ^1H NMR spectrum exhibits one signal at δ = 2.25 for the methyl groups indicative of a pentahapto structure, which is confirmed by two ^{13}C resonances at δ = 113.1 (C_5) and δ = 4.2 (CH_3). In the ^{11}B NMR spectrum two signals at δ = −6.2 (sp^3 boron) and δ = −51.7 (apical boron) are in agreement with a $C_5B{\rightarrow}B$ pyramidal arrangement. At room temperature, because of the partially relaxed scalar ^{11}B-^{11}B coupling, only the two inner lines of the 1:1:1:1 pattern are observed. At elevated temperatures (55 °C), due to the slower quadrupolar relaxation of the ^{11}B nuclei, the two outer lines appear as shoulders. The more precise value for

[a] Anorganisch-Chemisches Institut, Universität Heidelberg, Im Neuenheimer Feld 270, 69120 Heidelberg, Germany
Fax: (internat.) + 49-(0)6221/545-609
E-mail: ci5@ix.urz.uni-heidelberg.de
[b] Fakultät für Chemie der Universität, Universitätsstraße 25, 33615 Bielefeld, Germany
Fax: (internat.) + 49-(0)521/106-6026

 © WILEY-VCH Verlag GmbH, D-69451 Weinheim, 2000 1434–1948/00/0909–2927 $ 17.50+.50/0



Scheme 1. Formation of **5b**

the coupling constant $^1J(^{11}B,^{11}B)$ is measured for the resonance of the apical ^{11}B nucleus (125 ± 3 Hz).

These data support the formation of the borane-stabilized boranediyl adduct **5a**, which is confirmed by a crystal structure analysis.

A much simpler transfer of a C_5Me_5 group to a diborane(4) molecule occurs with $Me_5C_5-SiMe_3$ (Scheme 1). The reaction of equimolar amounts of $Me_5C_5-SiMe_3$ and B_2Cl_4 in hexane at low temperature leads to a colorless solid which is thermally stable up to 280 °C. Its NMR and mass spectra confirm the formation of **5b**: one signal at δ_H = 2.21 indicates pentahapto bonding of the C_5Me_5 group and two high-field signals prove the presence of one sp^3 hybridized (δ_B = 2.8) and one *apex* boron atom (δ_B = −53.0). The two different ^{11}B nuclei couple as described for **5a** [$^1J(^{11}B,^{11}B)$ = 121 ± 5 Hz]. The CI mass spectrum exhibits the base peak $[M - Cl]^+$ (*m/z* = 227) and the $[M_2 - Cl]^+$ peak (*m/z* = 491). The EI spectrum shows the base peak $[M - Cl]^+$ and the molecular-ion peak M^+ (*m/z* = 262) with the isotopic pattern expected for $C_{10}H_{15}B_2Cl_3$. Compound **5b** is only slightly sensitive to moisture but is decomposed in CH_2Cl_2 by gaseous HCl.

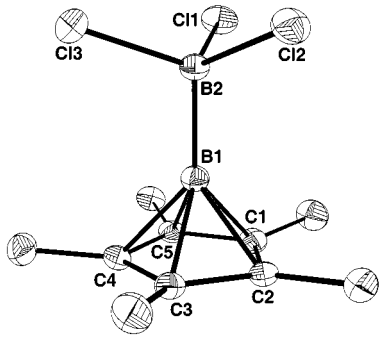


Figure 1. Molecular structure of **5b** in the crystal; selected bond lengths [Å] and angles [°] (values for **5a** given in brackets): B1−$C_{5\ plane}$ 1.260(3) [1.289(6)], B1−C_{ring} 1.747−1.756(3), av. 1.752 [1.752−1.773(8), av. 1.762], B1−B2 1.681(3) [1.686(7)]; X_{C5}−B1−B2 179.4 [176.7], B1−B2−Cl 110.0−110.5(1) [B1−B2−Si1 116.1(3); B1−B2−Cl1 110.1(4); B1−B2−Cl2 108.1(3)]; the methyl groups are bent out of the C_5 plane towards B1 by 5.6−7.2 (av. 6.4) in **5b** and by 3.3−5.2 (av. 4.5) in **5a**; hydrogens are omitted for clarity.

The ORTEP plot in Figure 1 shows the molecular structure of **5b**;[13] selected bond lengths and angles of **5a** and **5b** are listed in the legend. Both structures are very similar, the structure determination of **5b** being more accurate. Any small differences are caused by the presence of the $SiCl_3$ group. The average C−B bond length (1.75 Å) is identical to that in $[(\eta^5\text{-}Me_5C_5B-SiCl_2(\eta^1\text{-}C_5Me_5)]^+[Cl_3B(\eta^1\text{-}C_5Me_5)]^-$ [14] and lies between the values for **3b** (1.68 Å) and **4** (1.81 Å). The larger B−C distance in **4**[8] indicates a weaker bonding between boron and the C_5Me_5 ring, which is probably due to a less positive charge at the boranediyl moiety **1** (R = Me). In **5a,b** the $(C_5Me_5)B$ unit is attached to $XBCl_2$ with a B−B distance of 1.69 Å for **5a** and 1.68 Å for **5b**, which is in the range for a normal 2c-2e bond. The bulky $SiCl_3$ group causes a slight deviation of 3.3 ° from the expected linear B−B−X_{C5} arrangement (X_{C5} being the center of the C_5 ring) found for **5b**. The methyl groups of the C_5Me_5 ring are bent out of the C_5 plane towards the *apical* boron atom with an average angle of 4.6 (**5a**) and 6.4° (**5b**). Such a behavior was predicted theoretically[7] and has been verified experimentally in **3b** (3.9°) and in $[(\eta^5\text{-}Me_5C_5B-SiCl_2(\eta^1\text{-}C_5Me_5)]^+[Cl_3B(\eta^1\text{-}C_5Me_5)]^-$ (4.2°).[13]

The formation of **5a** may be rationalized by the assumption that the postulated oxidative addition product $(C_5Me_5)_2Si(Cl)-B(Cl)-BCl_2$ undergoes intra- and intermolecular substituent exchanges and a rearrangement occurs as proposed for **5b**.

Experimental Section

***nido*-1-(Trichlorosilyl)dichloroborane-2,3,4,5,6-pentamethyl-2,3,4,5,6-pentacarbahexaborane(6) 5a:** To a solution of decamethylsilicocene (1.19 g, 3.97 mmol) in 40 mL of pentane was condensed B_2Cl_4 (650 mg, 3.97 mmol) at −110 °C. A red-brown suspension immediately formed which, on warming to room temperature, became a yellow solution with a colorless precipitate (1.55 g). Its mass spectra indicated the presence of $(C_5Me_5)B-BCl_2-SiCl_2C_5Me_5$ (*m/z* = 462) and $(C_5Me_5)B-BCl_2-Si(C_5Me_5)_2Cl$ (*m/z* = 562) (or isomers). However, these products could not be isolated. The solid turned violet on contact with air or by storing under argon at room temperature for several weeks.[12] The crude product (80 mg) was recrystallized from hot toluene to give **5a** (25 mg).

^1H NMR ($CDCl_3$, 200 MHz): δ = 2.25 (s, 15 H). − ^{11}B NMR ($CDCl_3$, 64 MHz): δ = −51.7 (1 B, BC_5Me_5), −6.2 (1 B, sp^3B). − ^{13}C NMR ($CDCl_3$, 50 MHz): δ = 9.2 (CH_3), 113.1 (C_5). − CI-MS: *m/z* (%) = 689 (1.3) $[M_2^+ - Cl]$, 327 (100) $[M^+ - Cl]$, 227 (20) $[B_2SiCl_5^+]$. − EI-MS: *m/z* (%) = 327 (3) $[M^+ - Cl]$, 227 (100) $[B_2SiCl_5^+]$

***nido*-1-Trichloroborane-2,3,4,5,6-pentamethyl-2,3,4,5,6-pentacarbahexaborane(6) 5b:** A solution of B_2Cl_4 (600 mg, 3.57 mmol) in 60 mL of hexane was cooled to −100 °C and $Me_5C_5-SiMe_3$ (744 mg, 3.57 mmol) dissolved in 5 mL of hexane was added dropwise to give a red solution. The reaction mixture was allowed to warm to room temperature overnight yielding a yellow solution and a colorless precipitate (**5b**, 496 mg, 53%).

^1H NMR ($CDCl_3$, 200 MHz): δ = 2.21 (s, 15 H). − ^{11}B NMR ($CDCl_3$, 64 MHz): δ = −53.0 (1 B, BC_5Me_5), 2.8 (1 B, sp^3B). − ^{13}C NMR ($CDCl_3$, 50 MHz): δ = 8.9 (CH_3), 112.6 (C_5). − CI-MS: *m/z* (%) = 491 (63.0) $[M_2^+ - Cl]$, 227 (100) $[M^+ - Cl]$. − EI-MS: *m/z* (%) = 262 (0.7) $[M^+]$, 227 (100) $[M^+ - Cl]$

Crystal Structure Determinations: Data collection: Bruker AXS area detector (Mo-K_α λ = 0.71073 Å, −100 °C); structures solved by direct methods, full-matrix least-squares refinement on F^2.[14]

5a: Orthorhombic, $Pna2_1$, $C_{10}H_{15}B_2Cl_5Si{\cdot}C_7H_8$, *a* = 26.863(2), *b* = 9.0991(1), *c* = 9.0991(1) Å, *V* = 2224.1(5) Å^3, *Z* = 4; 3126 unique reflections, non-hydrogen atoms anisotropic, hydrogen atoms in

calculated positions (riding), 236 parameters $R_1 = 0.041$ (observed reflections), $wR_2 = 0.090$ (all reflections). The crystals were twinned showing tetragonal symmetry.

5b: Orthorhombic, $Pna2_1$, $C_{10}H_{15}B_2Cl_3$, $a = 11.9805(8)$, $b = 14.2209(10)$, $c = 7.5215(5)$ Å, $V = 1281.5(2)$ Å^3, $Z = 4$; 2713 unique reflections, non-hydrogen atoms anisotropic, hydrogen atoms isotropic, 209 parameters $R_1 = 0.030$ (observed reflections), $wR_2 = 0.070$ (all reflections).

Crystallographic data (excluding structure factors) have been deposited with the Cambridge Crystallographic Data Centre as supplementary publication nos. CCDC-140032 **(5a)** and CCDC-140427 **(5b)**. Copies of the data can be obtained free of charge on application to CCDC, 12 Union Road, Cambridge CB21EZ, UK [fax: (internat.) +44-1223/336−033; E-mail: deposit@ccdc.cam.ac.uk).

Acknowledgments

This work was supported by the Deutsche Forschungsgemeinschaft (Schwerpunkt Polyeder) and the Fonds der Chemischen Industrie.

[1] C. Dohmeier, Ch. Robl, M. Tacke, H. Schnöckel, *Angew. Chem.* **1991**, *103*, 594; *Angew. Chem. Int. Ed. Engl.* **1991**, *30*, 564.
[2] D. Loos, H. Schnöckel, J. Gauss, U. Schneider, *Angew. Chem.* **1992**, *104*, 1376; *Angew. Chem. Int. Ed. Engl.* **1992**, *31*, 1362.
[3] E. O. Fischer, H. P. Hofmann, *Angew. Chem.* **1957**, *69*, 639.
[4] H. Meister, *Angew. Chem.* **1957**, *69*, 533.
[5] P. Jutzi, A. Seufert, W. Buchner, *Chem. Ber.* **1979**, *112*, 2488−2493.
[6] C. Dohmeier, R. Köppe, Ch. Robl, H. Schnöckel *J. Organomet. Chem.* **1995**, *487*, 127−130.
[7] E. D. Jemmis, P. v. R. Schleyer, *J. Am. Chem. Soc.* **1982**, *104*, 4781−4788.
[8] A. H. Cowley, V. Lomeli, A. Voigt, *J. Am. Chem. Soc.* **1998**, *120*, 6401−6402.
[9] [9a] Ch. L. B. Macdonald, A. H. Cowley, *J. Am. Chem. Soc.* **1999**, *121*, 12113−12126. − [9b] J. D. Garden, A. Voigt, C. L. B. Macdonald, J. S. Silverman, A. H. Cowley, *J. Am. Chem. Soc.* **2000**, *122*, 950−951.
[10] K. Wade, *Adv. Inorg. Chem. Radiochem.* **1976**, *18*, 1; D. M. P. Mingos, *Adv. Organomet. Chem.* **1977**, *15*, 1.
[11] P. Jutzi, D. Kanne, C. Krüger, *Angew. Chem.* **1986**, *98*, 163; *Angew. Chem. Int. Ed. Engl.* **1986**, *25*, 164.
[12] The crude product is oxidized to violet unknown decomposition products by traces of oxygen. See also P. Jutzi, B. Krato, M. Hursthouse, A. J. Howes, *Chem. Ber.* **1987**, *120*, p. 566.
[13] U. Holtmann, P. Jutzi, Th. Kühler, B. Neumann, H.-G. Stammler, *Organometallics* **1999**, *18*, 5531−5538.
[14] G. M. Sheldrick, SHELXTL NT 5.1, Bruker AXS, Madison, Wisconsin **1999**.

Received April 3, 2000
[I00133]

Synthesis and Characterization of a Novel Calix[4]arene-Based Two-Coordinate Copper(I) Complex That Is Unusually Resistant to Dioxygen

Loïc Le Clainche,[a] Michel Giorgi,[b] and Olivia Reinaud*[a]

Keywords: Calixarenes / Copper / N Ligands / Bioinorganic chemistry / Coordination chemistry

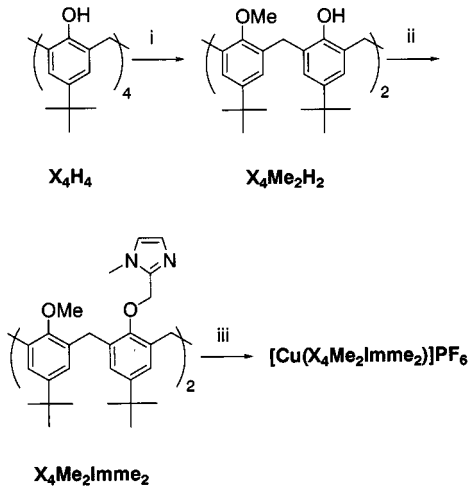
The ligand $X_4Me_2Imme_2$ was synthesized from *p-tert*-butylcalix[4]arene. Upon reaction with one equivalent of $Cu(NCMe)_4PF_6$, it led to the new two-coordinate copper(I) complex $[Cu(X_4Me_2Imme_2)]PF_6$ that was characterized by X-ray diffraction analysis. This complex revealed itself to be totally inert towards dioxygen in the solid state as well as in coordinating or protic solvents.

Introduction

Copper is a very important metal ion in biological systems, playing a very diverse role in living organisms.[1] It is involved in biochemical oxido-reduction processes, in electron transfers, as well as in the reversible binding of small gaseous molecules such as O_2 (Hemocyanin) or the plant hormone ethylene. Because the active form in these systems involves copper(I), the coordination chemistry of low-coordinate Cu^+ compounds is essential to the understanding of the metal reactivity. Due to the lack of useful spectroscopic probes for the Cu^I centers in native proteins, it is important to study its coordination chemistry with small artificial ligands.

Our main interest resides in the study of the chemical behavior of a metal ion in a biomimetic environment. For that purpose, we are trying to design supramolecular systems that allow the control of the metal nuclearity and reactivity. We recently showed that a calix[6]arene judiciously functionalized with three pyridine groups was particularly suited for stabilizing a cuprous ion in a tetrahedral mononuclear environment with a labile site included in a hydrophobic cavity. This was therefore a good model for type 2 centers in proteins.[2] We now describe the use of a calix[4]arene as a platform for the stabilization of a two-coordinate Cu^I complex with two biomimetic imidazolyl pendant arms. This complex appeared to be extremely resistant to O_2 oxidation and was stable in air for weeks, even in a potentially coordinating or protic solvent.

The new bidentate ligand $X_4Me_2Imme_2$ was prepared in two steps, as depicted in Scheme 1. *t*Bu-calix[4]arene (X_4H_4) was first converted into its 1,3-dimethyl ether ($X_4Me_2H_2$)[3] and then treated with 2-chloromethyl-1-methyl-1*H*-imidazole in the presence of NaH to produce $X_4Me_2Imme_2$ in 90% yield. Its ^1H NMR spectrum exhibited broad ill-defined resonances at room temperature. This indicated that the calixarene was mobile and not fixed in a cone conformation.



Scheme 1. Synthesis of the calixarene-based ditopic ligand $X_4Me_2Imme_2$ and complexation of copper(I); reagents and conditions: (i) K_2CO_3, MeOTs, MeCN, reflux 24 hours, 89%; (ii) NaH, 2-chloromethyl-1-methyl-1*H*-imidazole, THF/DMF, reflux 4 hours, 90%; (iii) $[Cu(MeCN)_4]PF_6$, $CHCl_3$, 90%

The reaction of $X_4Me_2Imme_2$ with one equivalent of $Cu(NCMe)_4PF_6$ in chloroform gave rise to a new cuprous complex, which spontaneously precipitated out of the solution (Scheme 1). Its elemental analysis was in good agreement with a compound of formula $[Cu(X_4Me_2Imme_2)]PF_6$. The corresponding ^1H NMR spectrum was well resolved and suggestive of a complex possessing a twofold symmetry. Suitable crystals for X-ray diffraction analysis were grown from a cold solution in $CHCl_3$/MeCN. The crystal structure of $[Cu(X_4Me_2Imme_2)]PF_6$ (Figure 1) showed a mononuclear complex where Cu^+ is coordinated to both imidazole

[a] Laboratoire de Chimie et Biochimie des Complexes Moléculaires, CNRS UMR 7576, E.N.S.C.P.,
11 rue Pierre et Marie Curie, 75231 Paris Cedex 05, France
Fax: (internat.) + 33-1/43260061
E-mail: reinaud@ext.jussieu.fr
[b] Laboratoire de Cristallochimie, CNRS UMR 6517, Centre scientifique Saint-Jérôme,
av. Escadrille Normandie-Niemen, 13397 Marseille Cedex 20, France

 © WILEY-VCH Verlag GmbH, D-69451 Weinheim, 2000 1434–1948/00/0909–1931 $ 17.50+.50/0

arms of the calix[4]arene-based ligand, which is in a cone conformation.

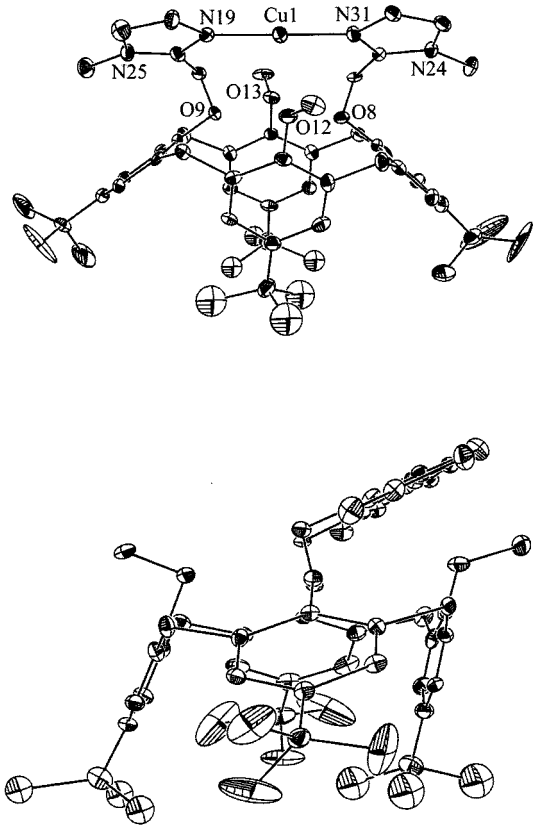


Figure 1. X-ray structure of $[Cu(X_4Me_2Imme_2)]PF_6$ (two different side views are displayed); selected atom distances (Å) and bond angles (°): Cu(1)−N(19) 1.87(1), Cu(1)−N(31) 1.867(9), N(19)−Cu(1)−N(31) 178.5(4); the counter ion and the solvent of crystallization have been omitted for clarity; for the same reason, only one occupancy site for each of the disordered *tert*-butyl groups is displayed

The Cu−N distances (1.87 Å) are similar to those previously reported for two-coordinate imidazole complexes.[4,5] The geometry at the metal center is almost linear (N−Cu−N = 178.5°) and the dihedral angle between the two imidazole rings is 3°, showing that they are almost coplanar. The plane of the imidazoles is bent on one side relative to the O13 oxygen, which is in close contact with the copper ion [Cu(1)···O(13) = 2.73 Å compared to Cu(1)···O(8) = 3.58 Å, Cu(1)···O(9) = 3.75 Å, Cu(1)···O(12) = 4.81 Å]. This may reflect a stabilizing electronic interaction between Cu^+ and one basic oxygen of the calixarene. In solution, however, the symmetrical ^1H NMR profile indicated that, if it exists at all, this interaction is averaged over both opposite phenoxyl groups and the coordination plane is probably flipping from one side to the other. $[Cu(X_4Me_2Imme_2)]PF_6$ exhibited an unusual stability towards dioxygen. In the solid state, it is indefinitely stable. In polar solvents such as DMSO or acetonitrile, or protic solvents like methanol, no oxidation of copper(I) has ever been observed, even if the solution is allowed to stand in an open flask for weeks.

This new copper(I) complex displays a geometry that is similar to previously reported two-coordinate copper(I) complexes with nitrogen donors.[4,5] Although the resulting linear geometry is known to disfavor O_2 and CO interaction,[4,5] our complex appeared to be unusually[4−6] resistant to oxidation with O_2 and did not coordinate CO. In contrast, the two-coordinate Cu^I complexes obtained with various unidentate imidazole ligands were reported to undergo rapid autoxidation in air, especially in a protic solvent. Curiously[6], we also found that the presence of two imidazole rings rather than two pyridine rings provided an enhanced stability of the copper(I) complex toward oxidation. Indeed, the copper(I) complex $[Cu(X_4Me_2Pic_2)]PF_6$ derived from the corresponding pyridine-based calix[4]arene ligand[7] was extremely sensitive to O_2 and underwent autoxidation in air within seconds.

The following points can rationalize these observations:
i) the exceptional inertness of the $[Cu(X_4Me_2Imme_2)]^+$ complex compared to the complexes derived from unidentate imidazole ligands is attributable to the highly favorable preorganization provided by the calix[4]arene platform rather than to steric hindrance;
ii) the enhanced stability of $[Cu(X_4Me_2Imme_2)]^+$ compared to the analogous pyridine-based complex is due to electronic factors and may be explained by an increased orbital overlap between the imidazole-nitrogen atom and copper(I) that stabilizes the two coordinate form for the imidazole-ligated species compared to the pyridine, as previously discussed by Sorrel.[4]

In conclusion, we have described a novel copper(I) complex that, although coordinatively unsaturated, revealed itself to be resistant to oxidation in a protic aerated environment. This emphasizes the importance of preorganization of the metal binding site as one of the key features that allows the control of the Cu^I reactivity. This may be reminiscent of biological systems, which either utilize copper(I) to bind or activate a small molecule[1] or stabilize it as in copper chaperones,[8] which transport and/or deliver Cu^I to other proteins in the cells.[9]

Experimental Section

$X_4Me_2Imme_2$: Under an argon atmosphere, a solution of $X_4Me_2H_2$ (500 mg, 0.74 mmol) in dry THF (10 mL) was introduced into a flask containing NaH (60% in oil washed twice with pentane; 0.9 g, 22 mmol) and the resulting mixture was stirred for 30 minutes. 2-Chloromethyl-1-methyl-1*H*-imidazole hydrochloride (0.74 g, 4.5 mmol) was added over a period of 5 minutes. After 4 hours at reflux, the solvents were removed under reduced pressure to a third volume and poured into water (110 mL). The crude precipitate was collected by filtration, washed with water (3 × 25 mL) and then chromatographed to give a white product which was dried under vacuum on KOH (580 mg, 90%). − M.p. 280 °C (dec.). − IR (KBr): $\tilde{\nu}$ = 1481, 1457, 1361, 1286, 1119, 1018, 978, 840 (PF_6) cm^{-1}. − ESI: *m/z* = 865.6 [M^+ + 1]. − $C_{56}H_{72}N_4O_4$ (864.6): calcd. C 77.78, H 8.33, N 6.48; found C 77.31, H 8.51, N 6.25.

$[Cu(X_4Me_2Imme_2)]PF_6$: To a solution of $X_4Me_2Imme_2$ (200 mg, 0.25 mmol) in $CHCl_3$ (1.4 mL) under an inert atmosphere was added dropwise $[Cu(NCMe)_4]PF_6$ (92 mg, 0.25 mmol). The mixture was stirred under argon. After 3 hours, the crude precipitate was

filtered, washed with heptane and dried under vacuum (KOH) to give a white solid (196 mg, 91%). M.p. 340 °C (dec.). − $C_{56}H_{72}N_4O_4CuPF_6{\cdot}2H_2O$ (1108): calcd. C 60.65, H 6.86, N 5.05; found C 60.90, H 6.62, N 4.95 − IR (KBr): $\tilde{\nu}$ = 1481, 1457, 1361, 1286, 1119, 1018, 978, 840 (PF_6) cm^{-1}. − ^1H NMR ([D$_6$]DMSO, 400 MHz, T = 298 K): δ = 0.72 (s, 18 H, *t*Bu), 1.29 (s, 18 H, *t*Bu), 2.98 (s, 6 H, OMe), 3.03 (s, 4 H, CH_{2eq}), 3.59 (s, 10 H, NMe and CH_{2ax}), 5.46 (s, 4 H, O−CH_2), 6.31 (s, 4 H, ArH), 7.19 (s, 4 H, ArH), 7.39 (s, 2 H, ImH), 7.48 (s, 2 H, ImH). The assignment of the signal corresponding to CH_{2ax} was achieved upon warming the sample to 50 °C: ^1H NMR ([D$_6$]DMSO, 400 MHz, T = 323 K): δ = 0.75 (s, 18 H, *t*Bu), 1.29 (s, 18 H, *t*Bu), 3.01 (s, 6 H, OMe), 3.03 (s, 4 H, CH_{2eq}), 3.59 (s, 6 H, NMe), 3.66 (s, 4 H, CH_{2ax}), 5.45 (s, 4 H, O−CH_2), 6.35 (s, 4 H, ArH), 7.18 (s, 4 H, ArH), 7.39 (s, 2 H, ImH), 7.50 (s, 2 H, ImH) − ^{13}C NMR ([D$_6$]DMSO, 100 MHz, T = 298 K): δ = 30.2 (Ar-α*C*H2), 30.8 (C*C*H$_3$), 31.5 (C*C*H$_3$), 33.3 (*C*CH$_3$ and N*C*H$_3$), 34.0 (*C*CH$_3$), 62.3 (O*C*H$_3$), 65.5 (Imme-α*C*H$_2$), 123.5 (C_{Imme}H), 124.6 (C_{Ar}H), 125.8 (C_{Ar}H), 127.4 (C_{Imme}H), 131.1 (C_{Ar}−CH_2), 135.6 (C_{Ar}−CH_2), 143.7 (C_{Ar}), 146.2 (C_{Ar}), 147.2 (C_{Imme}), 153.0 (C_{Ar}), 153.3 (C_{Ar}).

X-ray Crystallographic Study

[Cu ($X_4Me_2Imme_2$)]PF_6: [($C_{56}H_{72}N_4O_4$)Cu]PF_6: M = 1072, monoclinic, colorless crystals (0.3 × 0.2 × 0.2 mm) a = 17.552(1) Å, b = 16.955(1) Å, c = 21.860(1) Å, α = 90°, β = 100.44(1)°, γ = 90°, V = 6434.1(1) Å^3, space group $P2_1/c$, Z = 4, $\rho_{calcd.}$ = 1.54 g·cm^{-3}, μ(Mo-K_α) = 15.5 cm^{-1}, 9420 reflections collected at 298 K (Nonius KappaCCD diffractometer) in the 1−25° θ range, 9074 unique, 715 parameters refined on F using 5545 reflections [maXus][10] to final indices: $R1$ [$F > 3\sigma(F)$] = 0.087, $wR1$ ($w = 1/[\sigma^2(F) + 0.03F^2]$) = 0.099.

The complex and its counter ion co-crystallize with two molecules of chloroform in the asymmetric unit. During the refinement process, a disorder of position was observed for two *t*Bu groups. In each of them, the three terminal carbon atoms were split over two distinct sites with occupancy factors for the major and minor site, respectively, of 0.5−0.5 for one *t*Bu and 0.8−0.2 for the second *t*Bu. No hydrogen atoms were therefore introduced or refined on these disordered substituents.

Crystallographic data (excluding structure factors) for the structure reported in this paper have been deposited with the Cambridge Data Center as supplementary publication no. CCDC-138488. Copies of the data can be obtained free of charge on application to CCDC, 12 Union Road, Cambridge CB2 1 EZ, UK [Fax: (internat.) + 44-1223/336-033; E-mail: deposit@ccdc.cam.ac.uk].

[1] [1a] R. H. Holm, P. Kennepohl, E. I. Solomon, *Chem. Rev.* **1996**, *96*, 2239−2314. − [1b] W. Kaim, J. Rall, *Angew. Chem. Int. Ed. Engl.* **1996**, *35*, 43−60.

[2] [2a] S. Blanchard, L. Le Clainche, M-N. Rager, B. Chansou, J. P. Tuchagues, A. Duprat, Y. Le Mest, O. Reinaud, *Angew. Chem. Int. Ed.* **1998**, *37*, 2732−2735. − [2b] S. Blanchard, M.-N. Rager, A. Duprat, O. Reinaud, *New. J. Chem.* **1998**, 1143−1146.

[3] J. D. Van Loon, A. Arduini, L. Coppi, W. Verboom, A. Pochini, R. Ungaro, S. Harkema, D. N. Reinhoudt, *J. Org. Chem.* **1990**, *55*, 5639−5646.

[4] T. N. Sorell, D. L. Jameson, *J. Am. Chem. Soc.* **1983**, *105*, 6013−6018.

[5] I. Sanyal, K. D. Karlin, R. W. Strange, N. J. Blackburn, *J. Am. Chem. Soc.* **1993**, *115*, 11259−11270 and references cited therein.

[6] F. Khajenhouri, S. Motallebi, E. A. C. Lucken, *J. Mol. Struct.* **1995**, *345*, 277−281 and references cited therein.

[7] The ligand $X_4Me_2Pic_2$ (where Pic stands for Picolyl) was obtained according to the same synthetic scheme as for X_4Me_2-$Imme_2$ but replacing 2-chloromethyl-1-methyl-1*H*-imidazole with 2-chloromethyl-pyridine.

[8] In copper chaperones, the metal center is either trigonally or digonally coordinated to cysteines.

[9] M. D. Harrison, C. E. Jones, C. T. Dameron, *J. Biol. Inorg. Chem.* **1999**, *4*, 145−153.

[10] S. Mackay, C. J. Gilmore, C. Edwards, M. Tremayne, N. Stewart, K. Shackland, *maXus: a Computer Program for the Solution and Refinement of Crystal Structures from Diffraction Data*, University of Glasgow, Scotland, UK, Nonius BV, Delft, The Netherlands and MacScience Co. Ltd., Yokohama, Japan, **1998**.

Received January 31, 2000
[I00028]

Novel Urea Derivatives as Two-Step Redox Systems

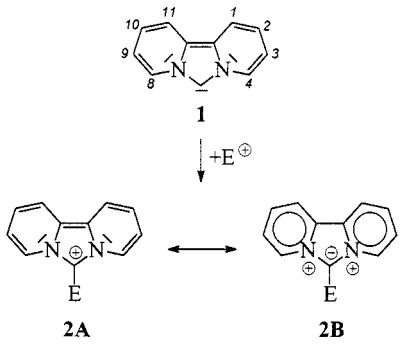
Robert Weiss,*[a] Sylvia Reichel[a]

Keywords: Carbenes / Cations / Radicals / Two-step redox systems / Semiempirical calculations

The structurally novel urea derivatives **4**–**6** have been synthesized by treating the nucleophilic dipyridoimidazol-2-ylidene **1** with elemental chalcogens Y (Y = S, Se, Te). The oxygen analogue **8** has been obtained indirectly by alkylation of the seleno urea **5**, followed by alkaline hydrolysis. All of these urea derivatives share two novel structural features: (i) their nitrogen centers represent the termini of the RED form of a two-step viologen-type redox system, and (ii) they can also be viewed as formally resulting from a cheletropic addition of CY to 2,2′-bipyridine. It has been demonstrated electrochemically that for Y = O, S, Se these ureas can be reversibly oxidized to the corresponding radical cations (SEM forms) at remarkably constant and negative potentials. This also applies to the heaviest congener of the series with Y = Te, except that in this case the oxidation process exhibits only quasi-reversibility. Electrochemical generation of the corresponding OX forms is observed quasi-reversibly at increasingly positive potentials with increasing mass of the chalcogen Y. However, the bis-oxidation of the telluro species **6** cannot be observed. These experimental results are discussed on the basis of semiempirical calculations for the RED, SEM, and OX forms under consideration. Semiempirical calculations also suggest that fragmentation of the novel urea derivatives into CY and 2,2′-bipyridine should be mildly endothermic for Y = O, but increasingly strongly endothermic with increasing mass of Y. This result is qualitatively in line with expectation considering the increasing reluctance of the heavier chalcogens to take part in multiple bonding to carbon. This phenomenon is also reflected in the mass spectrometric fragmentation patterns of the urea derivatives **4**–**6** and **8**.

Introduction

Recently, we reported on the generation of a novel type of nucleophilic carbene **1**, which alternatively can be considered as a 1:1 complex of singlet carbon and 2,2′-bipyridine.[1] In solution at −30 °C this species is stable for several hours and can be trapped by a multitude of electrophiles, both organic and inorganic, to give stable derivatives **2** (Scheme 1).



Scheme 1

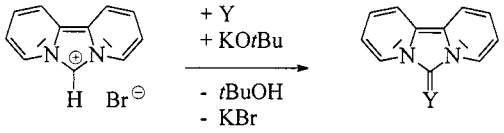
As can be inferred from inspection of the resonance structures **2A** and **2B**, the cationic substituent, which is introduced into a substrate through covalent bonding to **1**, is auto-adaptable to the electronic requirements of E. Thus, if the latter in **2** is a donor then resonance form **2A** is the major contributor, was **2B** more adequately describes the bonding situation when E is an acceptor. This unprecedented electronic flexibility intrinsic to **2** stems from the ability of the integrated two-step 2,2′-bipyridine redox system to act as an auto-umpolung device.[1]

In the present paper we report on the synthesis, structure, electrochemistry, and some reactions of adducts of **1** with S, Se, and Te as electrophiles, which represent novel redox-active urea derivatives. The synthesis of the corresponding oxygen analogue via an indirect route is also reported.

Results and Discussion

Synthesis and Characterization of Chalcogeno Ureas 4−6, 8[2]

Cyclic seleno and telluro ureas have previously been synthesized by treating Arduengo carbenes with Se and Te, respectively.[3] Similarly, dipyrido[1,2-*c*:2′,1′-*e*]imidazolylidene **1** can be transformed into the homologous chalcogeno ureas by treatment with elemental Te, Se, or even S. These orange-red to red compounds can be prepared most conveniently in yields > 80% in a one-pot reaction, where the carbene **1** is generated in situ from the imidazolium salt **3/Br⁻** with KO*t*Bu in the presence of the chalcogens. Compounds **4**−**6** are readily soluble in THF and are thus easily



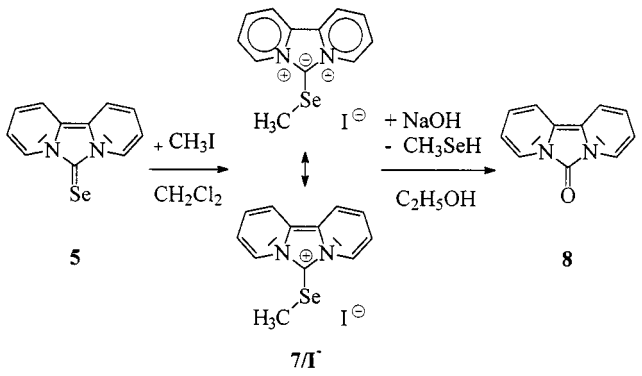
Scheme 2

[a] Institut für Organische Chemie der Universität Erlangen-Nürnberg,
Henkestrasse 42, D-91054 Erlangen, Germany
Fax: (internat.) +49-(0)9131/85-25876
E-mail: rweiss@organik.uni-erlangen.de

 © WILEY-VCH Verlag GmbH, D-69451 Weinheim, 2000 1434−1948/00/0909−1935 $ 17.50+.50/0

separated from salt-like components of the reaction mixture (Scheme 2).

Attempts to synthesize the parent compound of this series, i.e. the 6*H*-dipyrido[1,2-*c*:2′,1′-*e*]imidazolone **8**, by treating the carbene **1** with O_2 met with failure. However, **8** can be obtained indirectly by methylation of selenone **5** with CH_3I, followed by treatment of the resulting salt **7/I**$^-$ with NaOH in ethanol (Scheme 3).



Scheme 3

Two discrete sets of signals attributable to the 2,2′-bipyridine unit are observed in the ^{1}H NMR spectra of all of these urea derivatives. The set at lower field (**a** in Figure 1) can be plausibly attributed to the protons at C-1/C-11 and C-4/C-8, while that at higher field (**b** in Figure 1) can be attributed to the protons at C-2/C-10 and C-3/C-9. This is exemplified in Figure 1 in the case of the thio urea **4**.

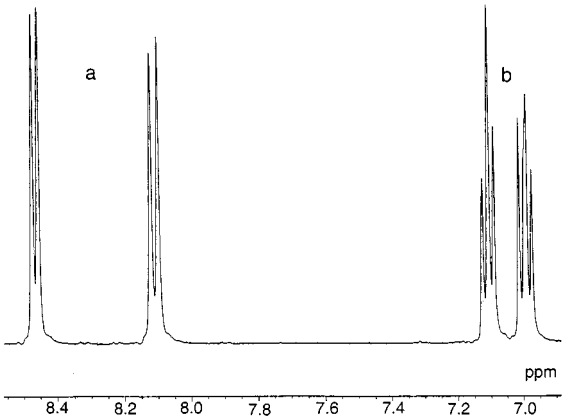


Figure 1. ^{1}H NMR spectrum of thio urea **4** (in $[D_6]$DMSO)

The ^{13}C NMR spectra of chalcogeno ureas **4**–**6**, **8** feature a set of five closely spaced signals due to the carbons of the bipyridine moiety, and one isolated signal due to the carbon atom adjacent to the chalcogen. The chemical shift of the latter varies with the nature of the chalcogen in a manner that does not lend itself to simple interpretation (see below). The complete set of data is collected in Table 1; Figure 2 shows the ^{13}C NMR spectrum of urea **8**.

Table 1. ^{13}C NMR shifts of the chalcogeno ureas **4**–**6** and **8**

	C=Y	C atoms of the 2,2′-bipyridine group
8 (Y = O)[a]	141.1	111.46, 112.29, 116.51, 117.24, 120.31
4 (Y = S)[b]	141.8	116.59, 118.26, 118.48, 118.92, 122.17
5 (Y = Se)[b]	133.4	117.53, 118.35, 119.69, 120.76, 123.45
6 (Y = Te)[b]	104.2	118.51, 118.64, 120.75, 123.47, 126.19

[a] in $CDCl_3$. – [b] in $[D_6]$DMSO.

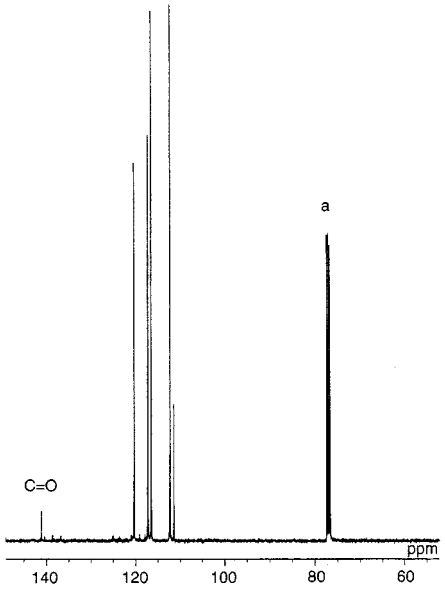
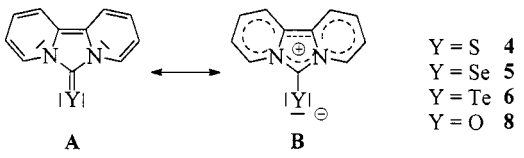


Figure 2. ^{13}C NMR spectrum of urea **8** (in $CDCl_3$ = **a**)

The heavy-atom effect of chalcogens Y in C=Y double bonds leads to increasingly low-field shifts of the signals of the corresponding C atoms with increasing atomic weight of Y, was the reverse is true for C–Y single bonds.[4] The data in Table 1 conform to the latter pattern, from which it can be concluded that the chalcogenones presented can best be characterized as having essentially single carbon–chalcogen bonds. This is particularly true for the heavier chalcogens Se and Te. Thus, resonance structure **B** (Scheme 4) will increasingly dominate the electron distribution in this set of chalcogenones on going from Y = O to Y = Te. This is in line with the increasingly low-field shifts observed for the ^{13}C NMR signals of the carbons of the bipyridine moiety within the same series of compounds (cf. Table 1).

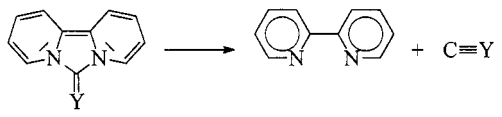


Scheme 4

The radical cations of chalcogenones **4**–**6**, **8** figure prominently in the mass spectra of these compounds. Their further decomposition depends dramatically on the specific

chalcogen present. Thus, while the radical cations of selenone **5** and tellurone **6** undergo loss of the chalcogen to yield the radical cation of carbene **1**, the corresponding radical cation of thione **4** would appear to be stable under the same mass spectrometric conditions. In contrast, the radical cation of 6*H*-dipyrido[1,2-*c*:2′,1′-*e*]imidazolone **8** decomposes into CO and the radical cation of 2,2′-bipyridine, a reaction that can be formally viewed as a C-transfer from carbene **1** to an oxygen atom.

Thermodynamic aspects of the thermal fragmentation of chalcogeno ureas **4**−**6** and **8** into 2,2′-bipyridine and the corresponding carbon monochalcogenides CY according to Scheme 5 have been assessed on the basis of semiempirical calculations (PM3).



Y	ΔH_R [kcal·mol^{-1}]
O	+10.19
S	+67.74
Se	+119.33
Te	+145.45

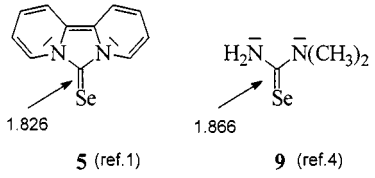
Scheme 5

For Y = O, this reaction is only moderately endothermic and would appear to be feasible either thermally or photochemically. Considering the more interesting fragmentations of **4**−**6**, for obvious reasons the endothermicity increases rapidly with increasing atomic weight of Y, such that these compounds do not appear to be useful precursors for the corresponding high-energy CY species (cf. Scheme 5). In any case, the reaction enthalpies given in Scheme 5 − although they are qualitatively reasonable − will have to be recalculated at higher levels of theory.

Two pieces of evidence indicate that the C−Y bonds in the novel chalcogenones presented in this paper are stronger than the corresponding bonds in known open-chain analogues:

(a) Imidazolone **8** exhibits a ν(CO) frequency of 1681 cm^{-1}, was the corresponding absorption in open-chain ureas is found at around 1660 cm^{-1}.

(b) The C−Se bond in selone **5**[1] is distinctly shorter than that in the open-chain seleno urea **9**[5] (Scheme 6).



Scheme 6

Theoretical calculations in conjunction with an NBO analysis[6] suggest that these effects are not due to an increase in π bond order relative to the open-chain urea analogues, but rather to an unusually high s content in the C(sp^x) orbital pointing towards the chalcogen Y. Bent's rules,[7] in agreement with the PM3 calculations, predict that the s content in this hybrid orbital should increase as the electronegativity of Y decreases. The results of calculations (PM3/NBO), as shown in Figure 3, point to an almost linear relationship between these two parameters.

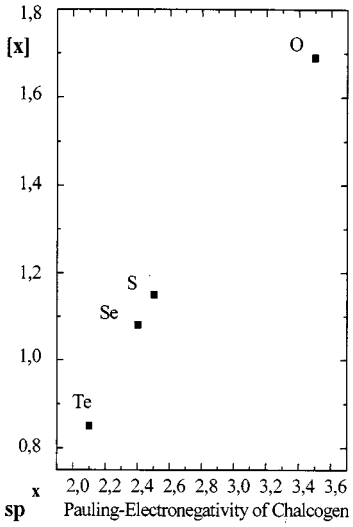


Figure 3. Hybridization C(sp^x) in the CY bond as a function of the electronegativity of the chalcogen

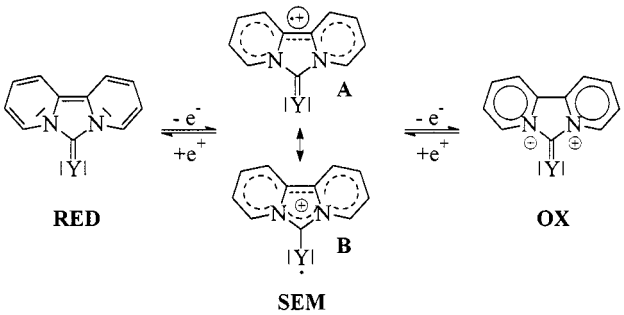
In this context, we refer to a recent communication[1] in which we presented NMR evidence showing that the carbon of the imidazolium C−H bond in **3** is virtually sp hybridized. This anomaly may be attributed to considerable angle strain in the five-membered ring, coupled with the pronounced electronegativity of the N centers. The same σ effect − albeit modulated by the nature of Y as indicated in Figure 3 − seems to be operative in the C−Y bonds of the chalcogenones considered in this paper.

Electrochemical Investigations

Chalcogenones **4**−**6** and **8** can be regarded as the RED[9] forms of a two-step redox system (cf. Scheme 7).

All members of the series of new chalcogenones presented show a first oxidation wave at around 0.3 V. The associated redox process is reversible for the three lighter chalcogens (see, for example, Figure 4) and quasi-reversible in the case of tellurium.

The measured $E_{1/2}$ values for the RED/SEM transition are seen to be remarkably insensitive to the nature of the chalcogen attached to the organic moiety. This is a consequence of resonance between the main contributors A and B in the SEM form (Scheme 7). The contribution of form A decreases as Y gets heavier as the bond energies of the corresponding CY double bonds rapidly increase. However, this is counterbalanced by a concomitant increase in the contribution of resonance structure B. In the latter, the high-energy structural element of a chalcogen radical center



According to cyclic voltammetric measurements, most of these redox processes can be realized electrochemically (Table 2).

Table 2. Oxidation potentials of the chalcogeno ureas **8** and **4**–**6** [V]

Compound	$E^{I}_{1/2}$ ($E^{ox}_{1/2}$ − $E^{red}_{1/2}$)[a]	$E^{II}_{1/2}$ [a]
8 (C=O)	+0.25 (rev, 0.059)	+0.74 (qrev)
4 (C=S)	+0.38 (rev, 0.056)	+1.27 (qrev)
5 (C=Se)	+0.25 (rev, 0.064)	+1.41 (qrev)
6 (C=Te)	+0.27 (qrev, 0.111)	–

[a] Supporting electrolyte: 0.1 N NEt_4BF_4/CH_3CN; reference electrode: Ag/AgCl; working and auxiliary electrode: platinum; standard: Ferrocene;[8] scan rate: 100 mVs^{-1}; rev = reversible; qrev = quasireversible

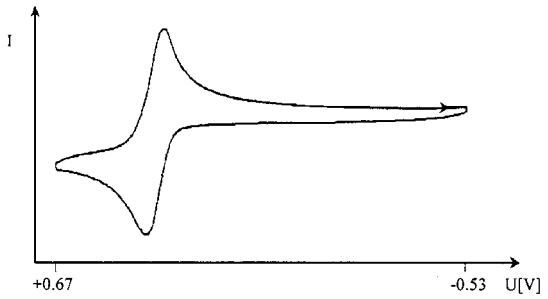


Figure 4. Cyclic voltammogram of thio urea **4**: first oxidation wave

is energetically compensated by the 14π aromatic dipyridoimidazolo substructure. As a consequence, the spin density on Y increases as Y gets heavier. This trend is corroborated by the results of calculations. An example is shown in Figure 5 and Figure 6, w the spin densities of SEM-**8** and SEM-**4** are compared.

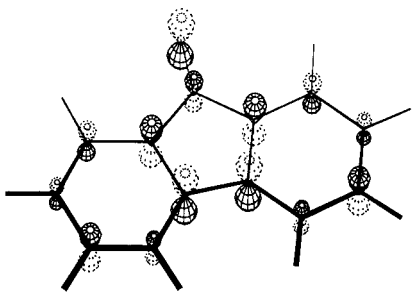


Figure 5. SOMO of the monooxidation product of **8** (Y = O, PM3)

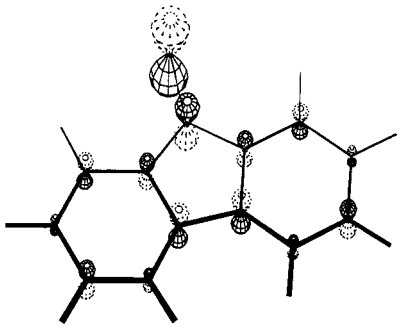


Figure 6. SOMO of the monooxidation product of **4** (Y = S, PM3)

Increasing concentration of spin density at the chalcogen center will increasingly favour dimerization of the corresponding SEM form to give a dichalcogenide. The observed loss of reversibility in the electrochemical oxidation of tellone **6** (Table 2) may be an indication of such a chemical process.

The second oxidation wave in the CV spectra corresponds in each case to the formation of the OX form. For this step, the $E_{1/2}$ values increase dramatically with increasing atomic weight of Y as a true CY double bond has to be formed – a distinct energetic disadvantage for the heavier chalcogens (see above).

Ongoing work in this area is focused on the chemical oxidation of chalcogenones **4**–**8**.

Experimental Section

General: All operations were performed under nitrogen atmosphere using standard Schlenk techniques. Solvents were dried by standard methods and distilled under N_2. – IR (KBr): Bruker IFS 25; abbreviations: w (weak), m (medium), s (strong), vs (very strong). – NMR: Jeol EX 400 and Jeol GX 400 (each 400 MHz and 100 MHz for ^1H and ^{13}C, respectively). For ^1H NMR: $CDCl_3$ as solvent, TMS as internal standard; [D_6]DMSO as solvent $\delta_H = 2.49$; for ^{13}C NMR: $CDCl_3$ as solvent $\delta_C = 77.0$; [D_6]DMSO as solvent $\delta_C = 39.5$. – EI-MS: Varian MAT 311A (70 eV). – Elemental analysis: Heraeus CHN-Rapid and Carlo Erba Elemental Analyser, Model 1106. Some of the compounds were found to absorb water during processing. – CV: PAR Model 170 Electrochemistry System.

6*H*-Dipyrido[1,2-*c*:2′,1′-*e*]imidazole-6-thione (4): To a suspension of dipyrido[1,2-*c*:2′,1′-*e*]imidazolium bromide **3/Br**$^-$ (0.41 g, 1.65 mmol) in THF (50 mL) was added sulfur (0.05 g, 1.65 mmol) followed, at −78 °C, by KO*t*Bu (0.19 g, 1.65 mmol). After 2 h, the mixture was filtered through Celite and the solid was washed with THF (20 mL). The combined filtrate and washings were concentrated to a volume of a few mL and petroleum ether (30 mL) was added. The resulting red suspension was filtered, and the collected solid was washed with petroleum ether (10 mL) and dried in vacuo for 2 h to give 0.28 g of **4** (85%); red solid; m.p. ≈ 200 °C. – IR (KBr): $\tilde{\nu}$ = 3078 (w), 1637 (s), 1615 (s), 1524 (s), 1413 (s), 1381 (vs), 1349 (w), 1336 (s), 1327 (s), 1302 (s), 1250 (s), 1212 (s), 1154 (s), 1131 (s), 1116 (s), 1001 (vs), 989 (s), 897 (w), 810 (w), 727 (vs), 689 (s), 671 cm^{-1} (w). – ^1H NMR ([D_6]DMSO): δ = 7.04 (m, 2 H), 7.14 (m, 2 H), 8.14 (m, 2 H), 8.47 (m, 2 H). – MS: *m*/*z* =

200 [M^+]. − $C_{11}H_8N_2S \cdot 0.25\ H_2O$ (with 0.25 H_2O: 204.7) (200.3): calcd. C 64.52, H 4.18, N 13.68; found C 64.72, H 3.89, N 13.90.

6*H*-Dipyrido[1,2-*c*:2′,1′-*e*]imidazole-6-selone (5): To a suspension of dipyrido[1,2-*c*:2′,1′-*e*]imidazolium bromide **3/Br**$^-$ (0.23 g, 0.93 mmol) in THF (50 mL) was added selenium (0.08 g, 1.03 mmol) followed, at −15 °C, by KO*t*Bu (0.13 g, 1.13 mmol). After 2 h, the mixture was filtered through Celite and the solid was washed with THF (10 mL). The combined filtrate and washings were concentrated to a volume of a few mL and pentane (30 mL) was added. The resulting red suspension was filtered, and the collected solid was washed with pentane (10 mL) and dried in vacuo for 2 h to give 0.20 g of **5** (87%); orange-red solid; m.p. ≈ 225 °C. − IR (KBr): $\tilde{\nu}$ = 3074 (w), 1644 (s), 1617 (w), 1558 (w), 1541 (w), 1524 (s), 1508 (w), 1415 (s), 1368 (vs), 1341 (w), 1325 (s), 1306 (w), 1252 (s), 1213 (s), 1154 (w), 1114 (w), 993 (s), 964 (w), 891 (w), 727 (vs), 689 cm^{-1} (w). − ^{1}H NMR ([D$_6$]DMSO): δ = 7.20 (m, 4 H), 8.28 (m, 2 H), 8.65 (m, 2 H). − MS: *m*/*z* = 248 [M^+], 168 [$C_{11}H_8N_2^+$ = carbene]. − $C_{11}H_8N_2Se$ (247.2): calcd. C 53.46, H 3.26, N 11.33; found C 52.97, H 3.38, N 11.47.

6*H*-Dipyrido[1,2-*c*:2′,1′-*e*]imidazole-6-tellone (6): To a suspension of dipyrido[1,2-*c*:2′,1′-*e*]imidazolium bromide **3/Br**$^-$ (0.22 g, 0.87 mmol) in THF (30 mL) was added tellurium (0.123 g, 0.96 mmol) followed, at −15 °C, by KO*t*Bu (0.12 g, 1.00 mmol). After 2 h, the mixture was filtered through Celite and the solid was washed with THF (10 mL). The combined filtrate and washings were concentrated to a volume of a few mL and petroleum ether (30 mL) was added. The red suspension was filtered, and the collected solid was washed with petroleum ether (10 mL) and dried in vacuo for 2 h to give 0.21 g of **6** (87%); orange-red solid, m.p. ≈ 160 °C (dec.). − IR (KBr): $\tilde{\nu}$ = 1645 (w), 1615 (w), 1525 (w), 1415 (s), 1350 (s), 1336 (w), 1311 (s), 1250 (s), 1214 (s), 1152 (w), 1123 (w), 1113 (w), 993 (w), 944 (w), 883 (w), 816 (w), 726 (vs), 689 cm^{-1} (w). − ^{1}H NMR ([D$_6$]DMSO): δ = 7.24 (m, 2 H), 7.35 (m, 2 H), 8.33 (m, 2 H), 8.78 (m, 2 H). − MS: *m*/*z* = 298 [M^+], 168 [$C_{11}H_8N_2^+$ = carbene]. − $C_{11}H_8N_2Te$ (295.8): calcd. C 44.67, H 2.73, N 9.47; found C 44.18, H 2.68, N 9.27.

6-(Methylseleno)dipyrido[1,2-*c*:2′,1′-*e*]imidazolium Iodide (7/I$^-$): To a solution of 6*H*-dipyrido[1,2-*c*:2′,1′-*e*]imidazoleselone **5** (0.14 g, 0.55 mmol) in CH_2Cl_2 (20 mL) at 0 °C, a solution of iodomethane (0.06 mL, 1.00 mmol) in CH_2Cl_2 (5 mL) was added over a period of 15 min. After 16 h, the yellow suspension was treated with Et_2O (30 mL), the mixture was filtered, and the collected solid was washed with Et_2O (10 mL) and dried in vacuo for 2 h to give 0.21 g of **7/I**$^-$ (99%); yellow solid. − IR (KBr): $\tilde{\nu}$ = 3007 (s), 2987 (m), 2914 (w), 1653 (w), 1618 (m), 1531 (w), 1427 (s), 1350 (m), 1312 (m), 1258 (vs), 1223 (m), 1159 (m), 1122 (m), 1003 (w), 904 (m), 769 (m), 741 (vs), 697 cm^{-1} (s). − ^{1}H NMR ([D$_6$]DMSO): δ = 2.41 (s, 3 H, CH_3), 7.69 (m, 4 H), 8.78 (m, 2 H), 8.99 (m, 2 H). − ^{13}C NMR ([D$_6$]DMSO): δ = 9.21 (CH_3), 112.36 (C−Se), 119.18, 121.33, 123.82, 123.85, 124.45. − MS: *m*/*z* = 247 [$C_{11}H_8N_2Se^+$ = selone], 168 [$C_{11}H_8N_2^+$ = carbene], 142 [CH_3I^+], 127 [I^+]. − $C_{12}H_{11}N_2ISe$ (389.1): calcd. C 37.04, H 2.85, N 7.20; found C 36.62, H 3.10, N 7.28.

6*H*-Dipyrido[1,2-*c*:2′,1′-*e*]imidazol-6-one (8): To a yellow suspension of 6-(methylseleno)dipyrido[1,2-*c*:2′,1′-*e*]imidazolium iodide **7/I**$^-$ (0.28 g, 0.72 mmol) in ethanol (20 mL) was added NaOH (1.5 g). After 18 h, the solvent was removed in vacuo, the orange solid was redissolved in CH_2Cl_2 (25 mL), and this solution was extracted with H_2O (3 × 30 mL). The organic layer was concentrated to dryness in vacuo and the red residue was suspended in petroleum ether (7 mL). The suspension was filtered at −30 °C, and the collected solid was washed with petroleum ether (3 mL) and dried in vacuo for 2 h to give 0.11 g of **8** (81%); red solid; m.p. ≈ 125 °C. − IR (KBr): $\tilde{\nu}$ = 3095 (m), 3079 (m), 3052 (m), 1768 (w), 1681 [vs, ν(C=O)], 1636 (s), 1613 (s), 1529 (m), 1470 (s), 1440 (m), 1415 (w), 1349 (s), 1299 (w), 1244 (m), 1186 (m), 1151 (m), 1139 (w), 1117 (m), 1089 (w), 978 (m), 757 (m), 731 (s), 710 (s), 644 cm^{-1} (w). − ^{1}H NMR ([D$_6$]DMSO): δ = 6.44 (m, 4 H), 7.32 (m, 2 H), 7.76 (m, 2 H). − MS: *m*/*z* = 184 [M^+], 156 [2,2′-bipyridine$^+$]. − $C_{11}H_8N_2O \cdot 0.125\ H_2O$ (184.2, 186.4 with crystal water): calcd. C 70.86, H 4.46, N 15.02; found C 70.99, H 4.10, N 14.79.

Acknowledgments

This work was supported by the Fonds der Chemischen Industrie and the Deutsche Forschungsgemeinschaft.

[1] R. Weiss, S. Reichel, M. Handke, F. Hampel, *Angew. Chem.* **1998**, *110*, 352−354; *Angew. Chem. Int. Ed.* **1998**, *37*, 344−347.
[2] B. L. Benac, E. M. Burgess, A. J. Arduengo III, *Org. Synth.* **1986**, *64*, 92−95.
[3] [3a] N. Kuhn, G. Henkel, T. Kratz, *Z. Naturforsch., Teil B* **1993**, *48*, 973−977. − [3b] N. Kuhn, G. Henkel, T. Kratz, *Chem. Ber.* **1993**, *126*, 2047−2049. − [3c] A. J. Arduengo III, F. Davison, H. V. R. Dias, J. R. Goerlich, D. Khasnis, W. J. Marshall, T. K. Prakasha, *J. Am. Chem. Soc.* **1997**, *119*, 12742−12749.
[4] H. O. Kalinowski, S. Berger, S. Braun, *^{13}C NMR-Spektroskopie*, Thieme, Stuttgart, **1984**, p. 170f.
[5] H. M. K. K. Pathirana, T. J. Weiss, J. H. Reibenspies, R. A. Zingaro, E. A. Meyers, *Z. Kristallogr.* **1994**, *209*, 697.
[6] S. Reichel, Dissertation, Universität Erlangen-Nürnberg, **1998**.
[7] H. A. Bent, *Chem. Rev.* **1961**, *61*, 275−311.
[8] T. Inagaki, H. S. Lee, T. A. Skotheim, Y. Okamoto, *J. Chem. Soc., Chem. Commun.* **1989**, 1181.
[9] The abbreviations RED, SEM, and OX indicate the reduced, mono-, and bis-oxidized forms of a two-step redox system, as introduced by K. Deuchert, S. Hünig, *Angew. Chem. Int. Ed. Engl.* **1978**, *17*, 875−886.

Received December 27, 1999
[I99471]

Regio- and Stereoselective Functionalization of *cyclo*-C_8 Compounds by Iterative Nucleophilic and Electrophilic Addition to Coordinated Cyclooctatetraene

Gerhard Lange,[a] Oliver Reimelt,[a] Lars Jessen,[a] and Jürgen Heck*[a]

Dedicated to Prof. Dr. Wolfgang Walter on the occasion of his 80th birthday

Keywords: Electrophilic additions / Hydrido complexes / Nucleophilic additions / Ruthenium / Cyclooctatetraene

The addition of various nucleophiles (Nu^1) to the cationic complex $[CpRu(\eta^6\text{-cot})]^+$ (**1**$^+$) has been performed and yielded the neutral complexes $CpRu(\eta^5\text{-}C_8H_8Nu^1)$ (**2**) [cot = cyclooctatetraene; Nu^1 = Me (**2a**), $CH(CO_2Me)_2$ (**2b**), CH=CH_2 (**2c**), C_6H_5 (**2d**), H (**2e**), D (**2f**), NMe_2 (**2g**), OMe, (**2h**), C≡C*t*Bu (**2i**)]. The nucleophiles Nu^1 add exclusively to the cot ring, and stereoselectively in the *exo* position with respect to the metal center. As evidenced by NMR spectroscopy the *cyclo*-C_8 ligand in **2c**, **2e**–**2i** is bound in a 1,2-η:5,6,7-η fashion in solution. The molecular structure analysis of **2c** [space group $P\bar{1}$, a = 757.9(1), b = 759.1(1), c = 1053.1(3) pm, α = 81.93(2), β = 80.22(1), γ = 88.73(1)°, V = 591.2(2) Å^3, Z = 2, R_{merge} = 0.0265] verifies the 1,2-η:5,6,7-η coordination mode of the *cyclo*-C_8 ligand in the solid state and shows the Nu^1 substituent to be in an *exo* position. For **2a** and **2b** a 1,2,3,4,5-η haptomer is also found, and this interconverts to the 1,2-η:5,6,7-η derivative in solution; in contrast, the *cyclo*-C_8 ligand of the phenyl derivative **2d** remains in the 1,2,3,4,5-η fashion. The protonation of the neutral complexes **2a**–**2d** by the addition of HBF_4 generates the new cationic products $[CpRu(\eta^6\text{-}C_8H_9Nu^1)]^+$ (**3**$^+$) [Nu^1 = Me (**3a**$^+$), $CH(CO_2Me)_2$ (**3b**$^+$), CH=CH_2 (**3c**$^+$), C_6H_5 (**3d**$^+$)]. When Nu^1 = $CH(CO_2Me)_2$ (**3b**$^+$) two different haptomers were isolated that exhibit 1,2-η:4,5,6,7-η and 1,2,3,4,5,6-η bonding modes, respectively. In solution the 1,2-η:4,5,6,7-η haptomer completely rearranges to the 1,2,3,4,5,6-η derivative. The crystal structure analysis of **3d**BF_4 [space group *Pbc*2(1), a = 1678.8(7), b = 1031.4(2), c = 981.8(2) pm, V = 1700.0(9) Å^3, Z = 4, R_{merge} = 0.032] confirms the 1,2-η:4,5,6,7-η bonding mode of the *cyclo*-C_8 ligand, which has also been indicated in solution. The second nucleophilic addition to the coordinated *cyclo*-C_8 ligand yields new neutral complexes that exist as two different haptomers depending on the steric demand of the two nucleophiles. The haptomer $CpRu(1,2,3,4,5\text{-}\eta\text{-}C_8H_9\text{-}6\text{-}Nu^1\text{-}8\text{-}Nu^2)$ (**4a**) is formed with Nu^1 = Nu^2 = $CH(CO_2Me)_2$ whereas with Nu^1 = Me, Nu^2 = $CH(CO_2Me)_2$ (**4b**) and Nu^1 = Nu^2 = Me (**4c**) the haptomer $CpRu(1,2\text{-}\eta\text{:}5,6,7\text{-}\eta\text{-}C_8H_9\text{-}4\text{-}Nu^1\text{-}8\text{-}Nu^2)$ is obtained. The protonation of **4a**–**4c** produces the cationic hydride species $[CpRu(H)(1,2,3,4,5\text{-}\eta\text{-}C_8H_9Nu^1Nu^2)]^+$ (**5**$^+$) [Nu^1 = Nu^2 = $CH(CO_2Me)_2$ (**5a**$^+$), Nu^1 = CH_3, Nu^2 = $CH(CO_2Me)_2$ (**5b**$^+$), Nu^1 = Nu^2 = Me (**5c**$^+$)] as indicated by the high-field shifted singlet for one proton below δ = −10 in the ^{1}H-NMR spectra. An X-ray structure analysis of a single crystal obtained from the protonation reaction of **4b** [space group $P2_1/c$, a = 1285.5(12), b = 1015.8(8), c = 1586.3(14) pm, β = 108.61(7)°, V = 1963(3) Å^3, Z = 4, R_{merge} = 0.0942] reveals a special disorder, the interpretation of which results in the structure determination of two independent complexes in a ratio of 59:41 differing by two hydrogen atoms in the formula. Both complexes are cations; one exhibits a disubstituted 1,2,3,4,5-η-bonded cyclooctadienyl ligand and an agostic interaction of the Ru center with a hydrogen atom at C5 of the *cyclo*-C_8 ligand (**5b**BF_4), whereas the second complex contains a cyclooctatriene ligand in a 1,2,3,4,5,6-η bonding mode without a metal hydride function (**6**BF_4). The coexistence of two different molecules in one single crystal that differ by two hydrogen atoms in addition to the agostic hydrogen atom in **5b**$^+$, points to an elimination of an H_2 molecule from **5b**$^+$ in the solid state to generate **6**$^+$. This suggestion is corroborated by the formation of a cationic complex **7**$^+$ as the main product in solution, which contains a *cyclo*-C_8 ligand without the malonate nucleophile [Nu^2 = $CH(CO_2Me)_2$], whereas a freshly prepared NMR sample only reveals **5b**$^+$ and **6**$^+$. In all of these products the Me nucleophile (Nu^1 = Me) is linked to a metal-coordinated carbon atom indicating an additional intramolecular hydrogen migration after the initial protonation.

Introduction

Nucleophilic addition to unsaturated organic ligands is very pertinent to synthetic organometallic chemistry.[1] Since this type of reaction displays pronounced stereo- and regioselectivity it is used in the synthesis of natural products.[2] More recent investigations demonstrate that this synthetic concept can be transferred to coordinated carbocycles like cyclooctatetraene,[3] which generates an access to multiple stereo- and regioselectively functionalized *cyclo*-C_8 ligands, and which may be of some importance in the synthesis of precursor compounds for *cyclo*-C_8 terpenoids.[4] In this paper we present results obtained from an iteratively applied reaction sequence of nucleophilic addition-protonation using different nucleophiles.

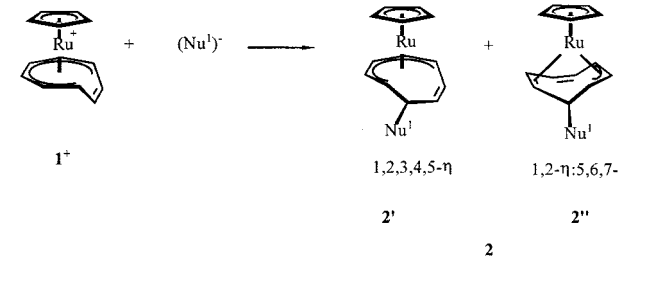
[a] Institut für Anorganische und Angewandte Chemie, Universität Hamburg,
Martin-Luther-King-Platz 6, 20146 Hamburg, Germany
Fax: (internat.) + 49-(0)40/42838-6945
E-mail: heck@chemie.uni-hamburg.de

 © WILEY-VCH Verlag GmbH, D-69451 Weinheim, 2000 1434−1948/00/0909−1941 $ 17.50+.50/0

Results and Discussion

Primary Nucleophilic Addition

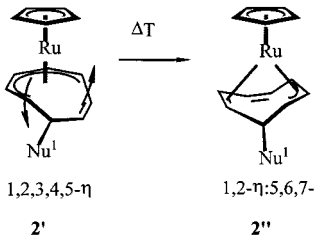
The initial nucleophilic addition to $[CpRu(\eta^6\text{-cot})]^+$ ($\mathbf{1}^+$) (Cp = cyclopentadienyl, cot = cyclooctatetraene) (Scheme 1) occurs exclusively at the cot ligand as predicted from the Davies−Green−Mingos rules.[5] In order to test the electrophilicity of the coordinated cot in $\mathbf{1}^+$, the charged heteronucleophiles OMe^- and NMe_2^- were also used; the nucleophilicity of neutral amines and phosphanes appeared to be too low to add to the cot ligand in $\mathbf{1}^+$.



Nu^1	Me	$CH(CO_2Me)_2$	$CH{=}CH_2$	C_6H_5	H	D	NMe_2	OMe	$C{\equiv}CtBu$
2	**a**	**b**	**c**	**d**	**e**	**f**	**g**	**h**	**i**

Scheme 1. Nucleophilic addition to $\mathbf{1}^+$

The assignment of the NMR signals can easily be performed by applying ^1H-^1H and ^1H-^{13}C correlation spectroscopy when the single proton signal of the nucleophile-bearing sp^3-carbon atom C8 is localized. When Nu^1 = Me or $CH(CO_2Me)_2$, two different isomers can be identified: in the isomer **2′** (e.g. **2a′** and **2b′**) the proton of the Nu^1-substituted carbon atom C8 couples with the vicinal protons of a coordinated and noncoordinated carbon−carbon double bond; in the second isomer **2′′** (e.g. **2a′′** and **2b′′**) the proton on C8 couples to protons of metal-bound carbon atoms only (Table 3). Since the number of metal-bound carbon atoms of the *cyclo*-C_8 ligands in both isomers are the same, and they only differ in the position of the coordinated carbon atoms in the *cyclo*-C_8 ring, we introduced the notation "hapticity isomers" or "haptomers".[6] Whereas haptomer **2a′** slowly rearranges in solution to **2a′′** at ambient temperature, the different haptomers of **2b** are sufficiently stable to be isolated separately.[6,7] ^1H-NMR experiments at T = 60 °C demonstrate a slow interconversion of **2b′** to **2b′′**. Apparently, the 1,2,3,4,5-η-haptomer **2′** is initially formed as the kinetically controlled product during the nucleophilic addition, and this gradually rearranges to the thermally more stable 1,2-η:5,6,7-η-haptomer **2′′** (Scheme 2).



Scheme 2. Proposed flip-flop mechanism for the 1,2,3,4,5-η/1,2-η:5,6,7-η haptomerism

For Nu^1 = $CH{=}CH_2$ (**2c**), H (**2e**), D (**2f**), NMe_2 (**2g**), OMe (**2h**), and $C{\equiv}CtBu$ (**2i**) the only isomer observed is the 1,2-η:5,6,7-η haptomer, a situation in contrast to **2d** (Nu^1 = C_6H_5), which has a 1,2,3,4,5-η structure as determined by NMR spectroscopy (see Table 3). No indications for a structural rearrangement in **2d** have been found. The reason for the interconversion of the haptomers **2a′** to **2a′′** and **2b′** to **2b′′** may be deduced from the steric demand of the nucleophile Nu^1. When sterically more crowded nucleophiles are used, such as a phenyl group or a substituted malonate $CR(CO_2Me)_2$ ($R \neq H$),[8] the 1,2,3,4,5-η haptomer is exclusively identified.

The influence of the steric demand of the nucleophile can also be rationalized by the crystal structure analysis of the vinyl derivative **2c**, which proves the 1,2-η:5,6,7-η coordination mode for **2c** in the solid state (Figure 1). The vinyl group is located in an *exo* position with respect to the metal center and opposite to the noncoordinating double bond. The carbon−carbon and ruthenium−carbon bonds are quite normal and are very similar to Ru−C bond lengths of pentadienyl−Ru moieties in open and semi-open ruthenocenes.[9] One exception is the Ru−C7 bond, which is elongated by more than 5 pm with respect to the other bond lengths between the Ru center and the metal-bound carbon atoms of the *cyclo*-C_8 ligand. Such a deviation of a Ru−C bond length in the vicinity to an sp^3-carbon atom from the mean value of other Ru−C bond lengths is found more often in (cyclooctatrienyl)ruthenium complexes.[10]

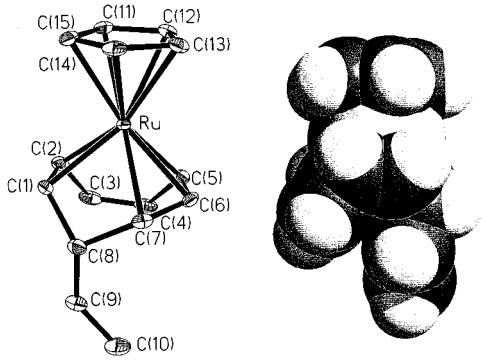


Figure 1. Molecular structure of **2c** (left: ORTEP plot, 30% thermal ellipsoids, the hydrogen atoms are omitted for clarity; right: space-filling model to illustrate the steric demand of the vinyl nucleophile and the noncoordinated double bond); selected bond lengths [pm]: Ru−C1 217.81(19), Ru−C2 219.0(2), Ru−C5 218.08(19), Ru−C6 215.74 (19), Ru−C7 224.3(2), C1−C2 142.3(3), C1−C8 154.2(3), C2−C3 149.1(4), C3−C4 132.2(4), C4−C5 149.5(3), C5−C6 143.2(3), C6−C7 138.9(3), C7−C8 153.1(3)

The most interesting structural features of **2c** concerning the formation of the different haptomers are the non-bond lengths between C8 and C9, and the carbon atom C3 of the non-coordinated double bond opposite to C8 and C9, which are 307.6(3) and 308.4(3) pm, respectively. The close proximity of these atoms to each other can be appreciated from the space-filling model shown in Figure 1. Larger nucleophiles would not allow the C3−C4 double bond to bend towards the nucleophile, and hence would favor the situation wherein C3 and C4 were kept in a metal-coordination mode.

To gain a deeper insight into the interconversion mechanism, hydride and deuteride addition from the borates $[BEt_3H]^-$ and $[BEt_3D]^-$ were performed and revealed the 1,2-η:5,6,7-η haptomers of **2e** (Nu = H) and **2f** (Nu = D). The NMR signals of the *endo* and *exo* protons of the sp^3-carbon atom (C8) in the *cyclo*-C_8 ligand of **2e** (Nu = H) are isochronic and show a triplet at δ = 2.87 due to the coupling with the two vicinal protons on C1 and C7, which are both quadruplets (Figure 2, A). The corresponding signal in the spectrum of **2f** (Nu = D, Figure 2, B) is now a doublet of doublets with similar coupling constants (J = 7.5 and 9.0 Hz). Each component is superimposed by a triplet caused by geminal coupling with the deuterium nucleus (J_{HD} = 1.7 Hz). Additionally, the integral of the signal at δ = 2.87 is only half that for **2e**. In agreement with this, the signals of the vicinal protons on C1 and C7 change their patterns to a triplet and a doublet of doublets, respectively, for **2f** (Table 3).

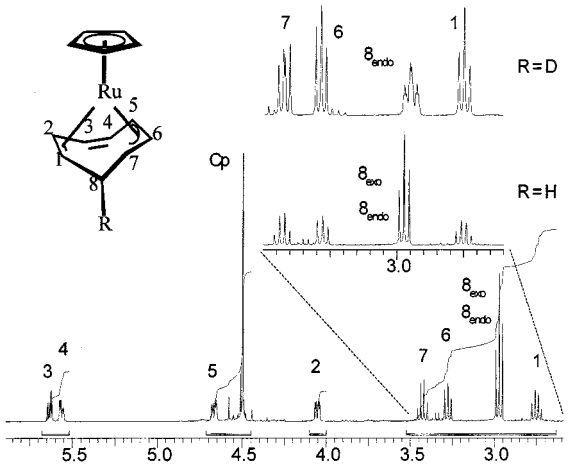
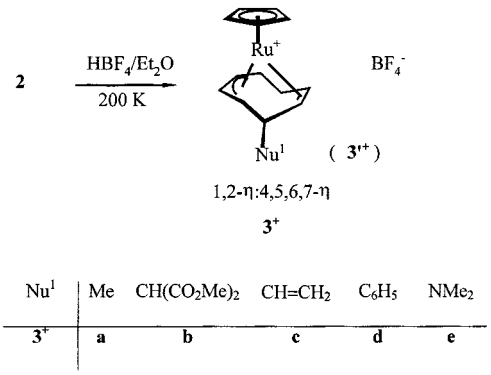


Figure 2. ^{1}H-NMR spectra of **2e** and **2f** illustrating the difference in the splitting pattern when the nucleophilic Nu^1 has changed from H^- to D^-

The ^{1}H-NMR spectra of **2e** and **2f** remain unchanged at temperatures up to 90 °C even after several days, which indicates that no hydrogen migration takes place. The thermal stability of the cyclooctatrienyl ligand in the Ru complexes **2f** is in sharp contrast to the corresponding iron complex, which demonstrates a complete scrambling of the deuterium atom under comparable conditions.[11] Therefore, assuming the *exo* addition of the hydride in strict analogy to the addition of any other nucleophile, the interconversion from the kinetically controlled 1,2,3,4,5-η product to the thermodynamically more stable 1,2-η:5,6,7-η haptomer is believed to be a flipping mechanism, as indicated in Scheme 2, rather than a hydrogen migration after the nucleophile has been added to the terminal carbon atom of the metal-coordinated part of the cot ligand.

First Protonation

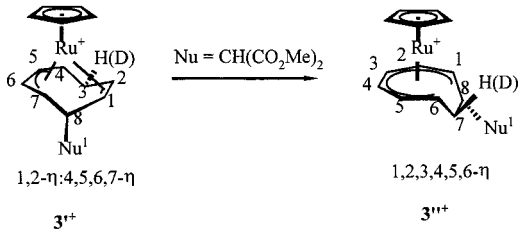
A second nucleophilic addition to the *cyclo*-C_8 ligand again requires a cationic complex. Therefore, some of the complexes of **2** were protonated with HBF_4 to yield the new cationic products $\mathbf{3}^+$ (Scheme 3) except for the cases where Nu^1 = NMe_2 (**2g**) and Nu^1= OMe (**2h**). The protonation of **2g** leads to a gradual cleavage of the NMe_2 group whereas for **2h** the methoxy group is completely split off. As evidenced by 1D- and 2D-NMR experiments the protonation of **2** occurs in position 3 of the *cyclo*-C_8 ligand to afford the cationic complex in a 1,2-η:4,5,6,7-η bonding mode ($\mathbf{3'}^+$, Scheme 3).



Scheme 3. Protonation of the cyclooctatrienyl complexes **2**

In order to ascertain the protonation site of the *cyclo*-C_8 ring (*exo* or *endo* with respect to the metal center) a protonation experiment was performed with **2b** [Nu^1 = $CH(CO_2Me)_2$] using a mixture of $DBF_4/HBF_4 \approx 4:1$. The comparison of the signal intensities in the ^{1}H-NMR spectra of the cationic product $\mathbf{3b}^+$ and its deuterated congener $\mathbf{3b}^+\mathbf{\text{-}D_1}$ clearly indicates position 3 as the site of the protonation (δ = 3.19) (Table 5). The resonance signal of the other proton of position 3 is found at δ = 1.99. Assuming that the anisotropy cone of diamagnetic sandwich compounds[12] also holds for the present Ru complexes, the signals of the protons in the *endo* position with respect to the metal center should be shifted downfield compared to the signal of the *exo* proton.[13] Conclusively, the protonation of **2** stereoselectively occurs in the *endo*-position with respect to the metal center, which is also in agreement with protonation experiments involving other sandwich compounds.[14] This stereoselectivity suggests a protonation of the metal center as a first step and a subsequent hydrogen migration to the *cyclo*-C_8 ligand.[14b]

The ^{1}H-NMR spectra of $\mathbf{3b}^+$ contain small signals due to a second isomer, which increase in intensity in the course of time. After 6 days at room temperature, the NMR signals of only one isomer are recorded and these correspond to the initial minor isomer, which was identified as the 1,2,3,4,5,6,-η haptomer. Apparently, the 1,2-η:4,5,6,7-η haptomer $\mathbf{3'}^+$ is converted into the 1,2,3,4,5,6,-η haptomer $\mathbf{3''}^+$ (Scheme 4). In addition to this haptotropic rearrangement it is evident from the ^{1}H-NMR spectra of $\mathbf{3b\text{-}D_1}^+$ that the *endo* proton on C3 of $\mathbf{3'}^+$ (δ = 3.19) has migrated to the *endo* position on C7 in $\mathbf{3''}^+$ (δ = 1.63) (Scheme 4). The position of this resonance still shows a distinct low-field shift compared to the signal of the other proton on C7 (δ =



Scheme 4. Proposed 1,5-hydrogen migration mechanism for the 1,2-η: 4,5,6,7-η/1,2,3,4,5,6-η haptomerism

−0.95, Table 5),[11,13] indicating the *endo* position of the deuterium atom.

It is interesting to note that the nature of the nucleophile does not consistently influence the hapticity of the eight-membered ligand. Whereas for $Nu^1 = CH(CO_2Me)_2$ the more stable isomer is the 1,2-η:5,6,7-η haptomer for the neutral complex **2b** and the 1,2,3,4,5,6-η haptomer for the cationic species **3b**$^+$, for $Nu^1 = C_6H_5$ the opposite is true: In **2d** the 1,2,3,4,5,-η bonding mode is favored, and upon protonation the coordination of the *cyclo*-C_8 ligand changes to the 1,2-η:4,5,6,7-η fashion in **3d**$^+$, a situation demonstrated by solution NMR studies and verified in the solid state structure (Figure 3).

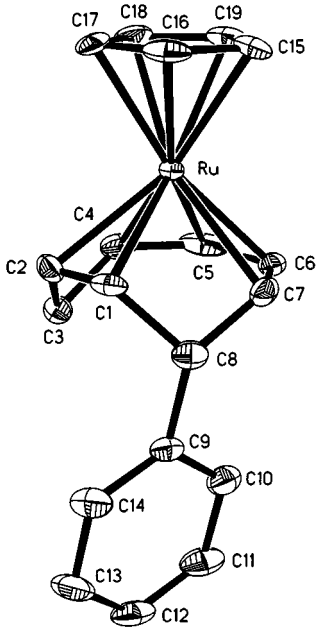
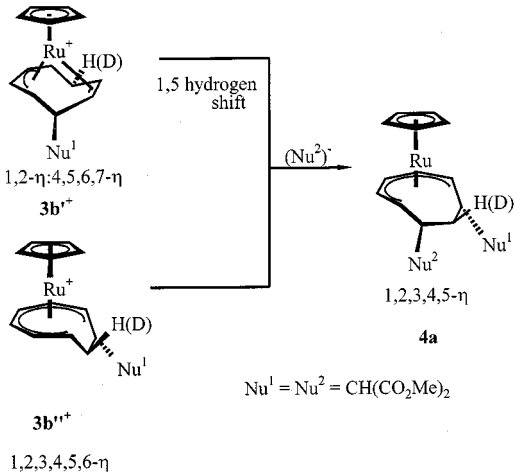


Figure 3. Molecular structure of **3d**BF_4 (ORTEP plot, 30% thermal ellipsoids, the hydrogen atoms and the counter ion are omitted for clarity); selected bond lengths [pm]: Ru−C1 228.1(4), Ru−C2 229.4(6), Ru−C4 226.5(6), Ru−C5 218.3(5), Ru−C6 220.7(5), C1−C2 135.8(8), C1−C8 150.7(7), C2−C3 150.7 (8), C3−C4 150.4(9), C4−C5 135.1(14), C5−C6 147.1(11), C6−C7 139.7 (10), C7−C8 153.7(8), C8−C9 154.9(6)

The crystal structure analysis of the phenyl derivative **3d**BF_4 reveals a η^6-coordination mode for the *cyclo*-C_8 ligand, wherein the noncoordinated carbon atoms of the eight-membered ring, C3 and C8, protrude from the plane of the metal-bound carbon atoms in an *exo* position with respect to the metal center. The non-bond lengths between C3 and C8, and C3 and C9 are 308.4(8) and 308.2(9) pm, respectively, which indicates a close proximity of the two sp^3-carbon atoms of the *cyclo*-C_8 ligand. A sterically more demanding nucleophile at C8 may push the C3 position to the metal center, thus inducing a metal−hydrogen interaction that could be a first step in the metal-assisted 1,5-hydrogen migration as found in **3b**$^+$ (see Scheme 4). The metal−carbon bond lengths in **3d**$^+$ are slightly elongated in comparison to the corresponding bond lengths of the neutral complex **2c** due to the positive charge in **3d**$^+$, which reduces the metal−ligand back donation. Accordingly, the C1−C2 bond length in **3d**$^+$ [135.5(8) pm] is distinctly shorter than the corresponding bond length in **2c** [142.3 (3) pm]. Also in agreement with the reduced metal−ligand back donation is the bond length alternation in the metal-bound butadiene part of the *cyclo*-C_8 ligand: C4−C5 135.1(14) pm, C5−C6 147.1(11) and C6−C7 139.7(10) pm.[15]

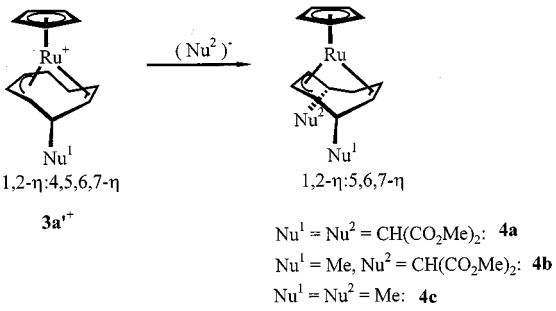
Second Nucleophilic Addition

The second nucleophilic addition can in principle give rise to two isomeric products depending on the type of haptomer used for this reaction. However, earlier attempts have already demonstrated that for $Nu^1 = CH(CO_2Me)_2$ the addition of the second nucleophile [$Nu^2 = CH(CO_2Me)_2$] only gives rise to the 6,8-bifunctionalized cyclooctadienyl complex **4a**[6] regardless of whether the starting haptomer is **3b**′$^+$ or **3b**′′$^+$. The nucleophilic addition to mixtures of partially deuterated **3b**′$^+$ and **3b**′′$^+$ yielded **4a** only with the deuterium atom exclusively in *endo* position at C7. Hence, **3b**′$^+$ has to rearrange to haptomer **3b**′′$^+$ by a 1,5-hydrogen migration before the second nucleophilic addition occurs (Scheme 5).[6]



Scheme 5. Nucleophilic addition to **3b**$^+$

This outcome contrasts the result of the second nucleophilic addition [Nu^2 = Me, $CH(CO_2Me)_2$] to complexes with Nu^1 = Me, which occurs exclusively in the 4-position of the cyclooctatriene ligand of **3a**$^+$ (Scheme 6).

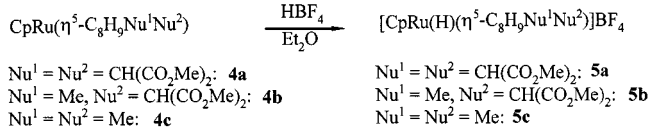


Scheme 6. Nucleophilic addition to **3a**$^+$

The ^{1}H- and ^{13}C-NMR spectra clearly demonstrate the low local symmetry (C_1) of the cyclooctadienyl ligand in **4b** [Nu^1 = Me, Nu^2 = $CH(CO_2Me)_2$] and **4c** (Nu^1 = Nu^2 = Me), in which the number of signals corresponds to the number of hydrogen and carbon atoms in the eight-membered ring in each case, whereas the NMR spectra of **4a** contain considerably fewer signals due to the C_s symmetry of the *cyclo*-C_8 ligand (Table 6). By means of ^{1}H-^{1}H and ^{1}H-^{13}C correlation spectra the different signals for **4b** and for **4c** can be assigned unequivocally and confirm the products **4b** and **4c** as 4,8-bifunctional cyclooctadienyl complexes.

Second Protonation

The bifunctionalized cyclooctadienyl complexes **4a**, **4b** and **4c** are easily protonated by the addition of HBF_4 to their ether solutions at low temperature. The products precipitate as light yellow solids and can be isolated by filtration (Scheme 7).

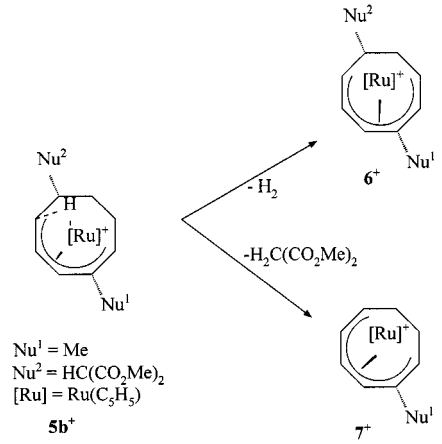


Scheme 7. Protonation of the cyclooctadienyl complexes **4a**−**4c**

In contrast to the first protonation, the second one gives rise to ruthenium complexes with a metal−hydride function as shown by the high-field shift of singlets from δ = −10.4 to −10.6 in the ^{1}H-NMR spectra.[16] No indication is found for the scrambling of proton positions that was observed in electronically related compounds like the protonated (cyclopentadienyl)(3-methylpentadienyl)ruthenium complex.[17,18] For **5a**$^+$ [Nu^1 = Nu^2 = $CH(CO_2Me)_2$] and **5c**$^+$ (Nu^1 = Nu^2 = Me) the ^{1}H-NMR spectra are similar to those of **4a** and **4c** apart from an overall distinct low-field shift of the signals for the metal-coordinated C−H units, which is due to the cationic nature of the complexes, and the hydrido signal at δ < −10 (Table 7). The coordination mode of the *cyclo*-C_8 ligand is therefore assumed to remain unchanged upon protonation of **4a** and **4c**. However, in solution the ^{1}H-NMR spectra provide evidence for a slow decomposition of the products, which form different Ru complexes that were not characterized further in the cases of **5a**$^+$ and **5c**$^+$.

The ^{1}H-NMR spectrum of a freshly prepared sample of the protonated product of **4b** [Nu^1 = Me, Nu^2 = $CH(CO_2Me)_2$] indicates the existence of two different species and displays remarkable differences to the spectrum of the precursor complex. The signal due to the Me substituent in the neutral complex **4b** appears as a doublet at δ = 0.96 in accordance with the Me signals of **4c** (δ = 1.02 and 1.20). The corresponding Me signals of the protonated species of the starting complex **4b** are observed as singlets, which are low-field shifted to δ = 2.32 for the major component (**5b**$^+$) and even to δ = 2.62 for the minor one (**6**$^+$). In contrast, the position of the corresponding Me signals in **5c**$^+$ does not differ significantly from that in the starting complex **4c**. The lack of a ^{1}H-^{1}H coupling for the Me substituent in **5b**$^+$ and **6**$^+$, as well as the distinct low-field shift of the Me signals, point to a metal coordination of the Me-substituted carbon atom in **5b**$^+$ and **6**$^+$. Therefore, in **5b**$^+$ and **6**$^+$ a hydrogen migration had to occur on the *cyclo*-C_8 ligand upon protonation.

The most striking difference between the ^{1}H-NMR spectra of **5b**$^+$ and **6**$^+$ is the lack of the hydrido signal at δ ≈ −10 for the minor product **6**$^+$. A careful analysis of the ^{1}H,^{1}H-COSY spectrum also proves that **6**$^+$ contains two hydrogen atoms less than **5b**$^+$. On keeping the solution of the NMR sample under an inert gas, a further product **7**$^+$ can be identified as a cationic cyclooctatriene complex without the malonate substituent (Table 7). The former malonate nucleophile can be identified in the ^{1}H-NMR spectrum as a free methyl malonate (δ = 3.36 and 3.70). The signals due to complexes **6**$^+$ and **7**$^+$ both grow in the course of time, whereas the signals due to **5b**$^+$ vanish. Hence, the hydride complex **5b**$^+$ decomposes in solution under cleavage of dihydrogen or methyl malonate (Scheme 8). Most interestingly, the formation of **5b**$^+$ and **6**$^+$ has been observed in a single crystal analysis.



Scheme 8. Elimination of H_2 and $H_2C(CO_2Me)_2$ from the cationic complex **5b**$^+$ in solution

Suitable crystals for an X-ray structure analysis of the protonation product of **4b** [Nu^1 = Me, Nu^2 = $CH(CO_2Me)_2$] were obtained from a dichloromethane/diethyl ether solution. The determination of the molecular structure was successful on the assumption of a disorder of the two cationic complexes in a ratio of 59:41, which differ

in the *cyclo*-C_8 ligands. Attempts were made to separate the carbon atoms C1, C5, C7, and C8 of the *cyclo*-C_8 ligands in different split positions. However, this procedure was only successful for C8. The positions of C1, C5, and C7 do not vary sufficiently in the two species to be calculated in different split positions. The best fit could be obtained by taking into account two cationic species, one bearing a 1,2,3,4,5-η-cyclooctadienyl ligand (**5b**$^+$, 59%) and the other a 1,2,3,4,5,6-η-cyclooctatriene ligand (**6**$^+$, 41%) (Figure 4).

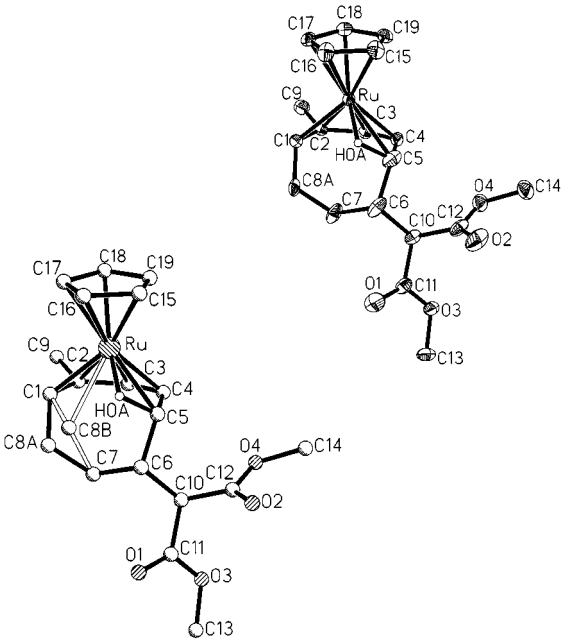
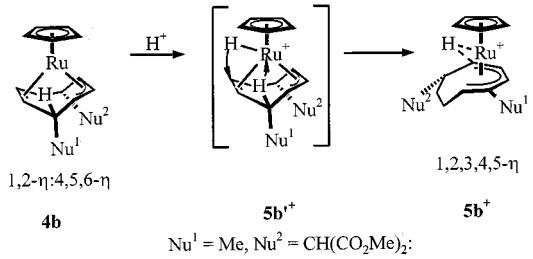


Figure 4. Molecular structures of **5b**BF_4 and **6**BF_4 as obtained from the X-ray crystal structure analysis of the protonation product of **4b**; top: **5b**BF_4 (ORTEP plot, 30% thermal ellipsoids, the anion and all H atoms except the H^- are omitted for clarity); bottom: superposition of **5b**BF_4 and **6**BF_4 (note the difference in the notation of C8A, C8B; C8A belongs to **5b**$^+$ and C8B to **6**$^+$); selected bond lengths [pm]: Ru−C1 217.7(7), Ru−C2 219.7(7), Ru−C3 220.8(7), Ru−C4 213.5(8), Ru−C5 227.3(8), Ru−C8A 246(2), Ru−H0A 173(13), C1−C2 140.8(10), C2−C3 144.0(10), C3−C4 143.8(10), C4−C5 147.6(13), C5−C6 151.0(12), C6−C7 151.8(11), C7−C8A 147.4(13), C7−C8B 152.0(10), C1−C8A 159.3(16), C1−C8B 143.6(9), C5−H0A 129(13)

The most prominent structural feature of **5b**$^+$ is the agostic hydrogen atom H0A between the Ru center and C5. The position of this hydrogen atom was found from the difference electron map. The Ru−H0A distance is 173(12) pm and the distance between C5 and H0A is calculated to be 129(13) pm. In accordance with the agostic hydrogen atom at C5, the Ru−C1−C4 bond lengths are distinctly shorter than the bond length between the Ru center and C5 [213.5(8)−220.8(7) pm vs. 227.3(8) pm]. The carbon−carbon bond length between C4 and C5, which is linked to the agostic hydrogen atom, seems to be elongated [147.6(13) pm] compared to the other carbon−carbon distances [140.8(10)−144.0(10) pm] of the metal-coordinated entity of the *cyclo*-C_8 ligand. Hence, the structural data of **5b**$^+$ much resemble those of the electronically related protonated (cyclopentadienyl)(3-methylpentadienyl)ruthenium.[18]

Another important result from the structure determination of **5b**$^+$ is the position of the first nucleophile (Nu^1 = Me) on the *cyclo*-C_8 ligand: the Me group is directly linked to the metal-bound carbon atom C2, as already indicated by the ^{1}H-NMR study. The carbon atoms C6, C7, and C8 are not metal-coordinated and are sp^3-hybridized with $Nu^2 = CH(CO_2Me)_2$ at C6.

Conclusively, the formation of **5b**$^+$ upon protonation of **4b** requires more than a simple protonation of the metal center, as evidenced for **5a**$^+$ and **5c**$^+$. Compound **4b** may first be protonated at the metal center to give the metal−hydride function (Scheme 9). Subsequently, the hydrogen atom could migrate to position 1 of the *cyclo*-C_8 ligand and, more or less simultaneously, the hydrogen atom at C3 migrates to the metal center leading to a 1,2,3,4,5-η coordination mode of the *cyclo*-C_8 ligand with the first nucleophile Me linked to a metal-coordinated carbon atom; the hydrogen atom at the metal center forms an agostic bond to C5. The formation of **6**$^+$ can be explained by the elimination of a hydrogen molecule from **5b**$^+$. It is worth mentioning that the dehydrogenated product **6**$^+$ is the only by-product when the crystalline material is freshly dissolved for an NMR sample, whereas the decomposition product **7**$^+$ is preferentially formed in solution (Scheme 8).



Scheme 9. Proposed mechanism for the formation **5b**$^+$

In a final step, the *cyclo*-C_8 ligand should be cleaved to yield stereo- and regioselectively functionalized cyclooctadiene compounds. This operation was successfully performed for **5a**$^+$ [$Nu^1 = Nu^2 = CH(CO_2Me)_2$][6] by the addition of a coordinating solvent (MeCN) to a suspension of **5a**$^+$ in diethyl ether, whereas for the methylated derivative **5b**$^+$ the cleavage of the corresponding cyclooctadiene failed. Alternatively, the cleavage of the *cyclo*-C_8 ligand was attempted by a protonation of the complexes **4b** and **4c** in the presence of a large excess of acetonitrile. As a result the cationic half-sandwich complex $[CpRu(MeCN)_3]^+$ could be recovered and this is the starting material for the synthesis of $[CpRucot]^+$ (**1**$^+$). However, the organic products of this reaction have not yet been characterized. The reaction conditions for a straight cleavage of the stereoselectively functionalized cyclooctadiene ligand are currently being investigated. Successful decomplexations of η^4-coordinated cyclooctatetraene and cyclooctadienes by photochemical and thermal methods have been reported previously.[19]

Conclusions

In this study we have shown that iterative nucleophilic and electrophilic additions to coordinated cyclooctatetraene

are useful tools for the synthesis of stereo- and regioselectively bifunctionalized *cyclo*-C_8 ligands. As demonstrated, the regioselectivity at the different stages of the nucleophilic additions and protonation reactions is controlled by the steric demand of the nucleophiles. Two different mechanisms for the rearrangements are proposed: (i) a flip-flop mechanism in which the product of the first nucleophilic addition changes from the kinetically controlled 1,2,3,4,5-η haptomer to the thermodynamically more stable 1,2-η:5,6,7-η haptomer (Scheme 2) in cases of small nucleophiles and (ii) a 1,5-hydrogen migration caused by the first protonation, which causes a rearrangement of the 1,2-η:4,5,6,7-η haptomer to the 1,2,3,4,5,6-η derivative [Nu^1 = $CH(CO_2Me)_2$] or vice versa when Nu^1 = Ph (see Scheme 5). A third rearrangement can be observed after the second protonation and leads to **5b**$^+$ [Nu^1 = Me, Nu^2 = $CH(CO_2Me)_2$], since the hydrogen atom of the carbon atom bearing Nu^1 is cleaved and a new sp^3-carbon atom is formed, as illustrated in Scheme 9 for **5b**$^+$. The cleavage of the desired *cyclo*-C_8 ligand was successful for the case where Nu^1 = Nu^2 = $CH(CO_2Me)_2$ but as yet has proved unsuccessful when Nu^1 = Nu^2 = Me and Nu^1 = Me, Nu^2 = $CH(CO_2Me)_2$. However, efforts to synthesize stereo- and regioselectively bifunctionalized cyclooctadienes through iterative nucleophilic and electrophilic additions will be continued due to the fact that it is a simple and hence attractive procedure to achieve more intricate organic reactions towards *cyclo*-C_8 terpenoids.

Experimental Section

All reactions were carried out under N_2 and all solvents were saturated with N_2. THF, Et_2O, hexane, and toluene were freshly distilled from the appropriate alkali metal or metal alloy. Dichloromethane was dried with CaH_2 and distilled under N_2. – NMR: Bruker AM 360 and Varian Gemini 200. – IR (Nujol mull, KBr cells): FT-IR 1720X (Perkin–Elmer). – EI-MS (70 eV): Finnigan MAT 311 A, Heraeus CHN-O-Rapid; Institut für Anorganische und Angewandte Chemie, Universität Hamburg. – [CpRu(η^6-cot)]PF_6 (**1**PF_6),[20] the sodium salts of the malonic ester[21] and lithium dimethylamide[22] were synthesized as described. Methyllithium as 5% solution in diethyl ether was purchased from Merck©, Li[BEt_3H] as a 1 M solution in THF from Aldrich and HBF_4 as a 54% solution in diethyl ether from Fluka.

X-ray Crystal Structure Analysis: Determination of the cell parameters and collection of the reflection intensities were performed with a Hilger & Watts [**2c**, **3d**BF_4] or Enraf–Nonius CAD4 [**5b**BF_4] four-circle diffractometer (see Table 1). SHELXS-86[23] was used for structure solving with direct methods and SHELXL-97[24] for structure refinement (refinement on F^2) (for crystallographic details see Table 1).

Crystal Structure Refinement of 2c: Hydrogen atoms on the Cp ring and on C8 were fixed in idealized positions. Positions of all other H atoms were refined free with equal C–H bond lengths in the sets of H1;H2;H5;H6;H7;H3;H4;H9 and H10a;H10b using the SADI operation. Thermal parameters of all protons were attached to the corresponding C atoms with a factor of 1.2.

Crystal Structure Refinement of 3d: Protons on the Cp and the phenyl ring, and on C3 and C8 were fixed in idealized positions. Positions of all other H atoms were refined free with equal C–H bond lengths using the SADI operation. Thermal parameters of all H atoms were attached to the corresponding C atoms with a factor of 1.2.

Crystal Structure Refinement of 5d: H atoms on the Cp ring and on C6, C8A, C9, C10, C13, and C14 were fixed in idealized positions. Positions of all other H atoms (except the agostic hydrogen atom) were refined free with C–H bond lengths fixed to 99 pm for H1, H3, H4, H5, H71, and H72, H71 and H72 were further fixed to equal distances to the vicinal C atoms C6 and C8A. Thermal parameters of all H atoms were attached to the corresponding C atoms with a factor of 1.5 for methyl and 1.2 for all others. The agostic hydrogen atom HOA was refined free in position and its thermal parameter set to 1.5 times the parameter of the Ru center. The site occupation factors for the disordered atoms were refined as a free variable.

Crystallographic data (excluding structure factors) for the structures reported in this paper have been deposited with the Cambridge Crystallographic Data Centre as supplementary publication no. CCDC-137491 (**2c**), -137492 (**3d**BF_4), and -137493 (**5b**BF_4 and **6**BF_4). Copies of the data can be obtained free of charge on application to CCDC, 12 Union Road, Cambridge CB2 1EZ, UK [Fax: (internat.) + 44-1223/336-033; E-mail: deposit@ccdc.cam.ac.uk].

General Procedure for the Synthesis of Compounds 2a–2i: A solution of the nucleophile in THF (or diethyl ether for Nu^1 = Me) was added dropwise to a suspension of **1** in 50 mL of THF or diethyl ether. The solvent was removed under reduced pressure, the residue was extracted with hexane or diethyl ether, and the extract filtered through Celite. After removal of the solvent, the product was normally obtained as a pale yellow oil. For more preparative details see Table 2, for ^{1}H- and ^{13}C-NMR data see Table 3.

(η^5-Cyclopentadienyl)(1,2,3,4,5-η-8-*exo*-methylcyclooctatrien-6-yl)ruthenium(II) (2a′): $C_{14}H_{16}Ru$ (285.37): calcd. C 58.93, H 5.65; found C 58.94, H 5.38.

(η^5-Cyclopentadienyl)(1,2-η:5,6,7-η-8-*exo*-methylcyclooctatrien-3-yl)ruthenium(II) (2a′′): IR (Nujol): $\tilde{\nu}$ = 1652 (C=C) cm^{-1}. – EI-MS (70 eV); *m/z* (%): 285 (91) [M^+], 270 (20) [$M^+ - CH_3$], 259 (100) [$CpRuC_7H_7^+$], 245 (58) [$CpRuC_6H_6^+$], 231 (1) [$CpRuC_5H_5^+$], 218 (2) [$CpRuC_4H_4^+$], 205 (2) [$CpRuC_3H_3^+$], 192 (2) [$CpRuC_2H_2^+$], 179 (1) [$CpRuCH^+$], 166 (23) [$CpRu^+$]. – $C_{14}H_{16}Ru$ (285.37): calcd. C 58.93, H 5.65; found C 58.62, H 5.69.

[1,2-η:5,6,7-η-8-*exo*-Bis(methoxycarbonyl)methylcyclooctatrien-3-yl](η^5-cyclopentadienyl)ruthenium(II) (2b′′): IR (Nujol): $\tilde{\nu}$ = 1733 (C=O), 1651 (C=C) cm^{-1}. – EI-MS (70 eV); *m/z* (%): 401 (91) [M^+], 375 (87) [$M - C_2H_2^+$], 283 (22) [$M - CO_2CH_3^+$], 270 (46) [$M - CH(CO_2CH_3)^+$], 258 (11) [$M - CH(CO_2CH_3)_2^+$], 245 (100) [$CpRuC_7H_7^+$], 232 (5) [$CpRuC_5H_5^+$], 167 (34) [$CpRu^+$], 104 (41) [$C_8H_8^+$], 101 (40) [Ru^+]. – $C_{18}H_{20}O_4Ru$ (401.45): calcd. C 53.86, H 5.02; found C 54.12, H, 5.18.

[1,2,3,4,5-η-8-*exo*-Bis(methoxycarbonyl)methylcyclooctatrien-6-yl]-(η^5-cyclopentadienyl)ruthenium(II) (2b′): The separation of **2b′** from the haptomer **2b′′** was performed by column chromatography (Al_2O_3/5% H_2O, toluene/diethyl ether = 1:1). Only **2b′** could be isolated.

(η^5-Cyclopentadienyl)(1,2-η:5,6,7-η-8-*exo*-vinylcyclooctatrien-3-yl)-ruthenium(II) (2c): Yellow crystalline product. – IR (Nujol): $\tilde{\nu}$ = 1656 (C=C_{free}), 1631 (C=C_{vinyl}) cm^{-1}. – EI-MS (70 eV); *m/z* (%): 297 (100) [M^+], 283 (18) [$M - CH_2^+$], 271 (98) [$M - C_2H_3^+$], 245

Table 1. Crystallographic details for **2c**, **3d**BF_4, and **5b**BF_4

Compound	**2c**	**3d**BF_4	**5b**BF_4
Empirical formula	$C_{15}H_{16}Ru$	$C_{19}H_{19}BF_4Ru$	$C_{19}H_{25}BF_4O_4Ru$
Molecular mass	297.35	435.22	505.27
T [K]	173(2)	173(2)	173(2)
Space group	$P\bar{1}$	$Pbc2(1)$	$P2(1)/c$
a [Å]	7.5790(10)	16.788(7)	12.855(12)
b [Å]	7.5910(10)	10.314(2)	10.158(8)
c [Å]	10.531(3)	9.818(2)	15.863(14)
α [°]	81.93(2)		
β [°]	80.220(10)		108.61(7)
γ [°]	88.730(10)		
V [Å^3]	591.2(2)	1700.0(9)	1963(3)
Z	2	4	4
$\rho_{calcd.}$[gcm^{-1}]	1.670	1.700	1.710
μ [mm^{-1}]	1.293	0.961	7.024
Crystal size [mm]	0.3 × 0.2 × 0.1	0.3 × 0.2 × 0.04	0.2 × 0.3 × 0.5
2θ range [°]	60.13	55.13	152.79
No. collected intensities	4181	4189	4319
No. observed intensities[a]	3239	1930	2895
No. of parameters	176	246	294
GooF (F^2, all data)	1.075	1.108	1.034
R_{merge} (all data)	0.0265	0.0322	0.0942
$R1$ (obs. data)	0.0234	0.0287	0.0562
$wR2$ (all data)	0.0588	0.0762	0.1577
max/min transmission	0.793/−0.934	1.382/−0.479	3.100/−3.277
Diffractometer	Hilger&Watts[b]	Hilger&Watts[b]	CAD4[c]

[a] Observation criterion $I > 4\sigma(I)$. − [b] Equipped with graphite-monochromized Mo-K_α radiation. − [c] Equipped with graphite-monochromized Cu-K_α radiation.

Table 2. Reacion conditions for the first nucleophilic addition

1 [mg /mmol]	MNu[1]	MNu[1] [mg/mmol]	T[a] [°C]	Solvent for reaction	Solvent for extraction	Product	Yield [mg (%)]
904.0/2.18	LiMe	53/2.41	r.t.	Et_2O	hexane	**2a**	495 (80)
748.0/1.8	$NaCH(CO_2Me)_2$	286/1.8	−78	THF	Et_2O	**2b**	410 (57)
582.0/1.4	$BrMgCH{=}CH_2$	131/1.4	r.t.	THF	hexane	**2c**	243 (58)
335.0/0.81	$BrMgC_6H_5$	2700/14	r.t.	Et_2O	hexane	**2d**	182 (65)
248.0/0.6	$LiB(C_2H_5)_3H$	64/0.6	−78	THF	hexane	**2e**	140 (87)
489.0/1.18	$LiB(C_2H_5)_3D$	125/1.2	−78	THF	hexane	**2f**	273 (85)
169.0/0.41	$LiN(Me)_2$	21/0.41	r.t.	THF	hexane	**2g**	100 (78)
295.0/0.7	NaOMe	38/0.7	−30	Et_2O	hexane	**2h**	143 (67)
181.0/0.44	LiC≡C*t*Bu	38/0.44	−78	THF	hexane	**2i**	90 (61)

[a] Reaction temperature, r.t.: room temperature.

(50) [$CpRuC_6H_6^+$], 167 (98) [$CpRu^+$], 102 (12) [Ru^+]. − $C_{15}H_{16}Ru$ (297.36): calcd. C 60.59, H 5.42; found C 60.21, H 5.59.

(η^5-Cyclopentadienyl)(1,2,3,4,5-η-8-*exo*-phenylcyclooctatrien-6-yl)ruthenium(II) (2d): Yellow powder. − IR (KBr): $\tilde{\nu}$ = 3078, 3051 (C−$H_{arom.}$), 3007, 2940 (C−$H_{aliph.}$), 1669 (C=C_{free}), 1595 (C=$C_{arom.}$) cm^{-1}. − EI-MS (70 eV); *m/z* (%): 347 (6) [M^+], 321 (7) [$CpRuC_{12}H_{11}^+$], 245 (3) [$CpRuC_6H_6^+$], 219 (100) [$CpRuC_4H_4^+$], 199 (22) [$CpRuC_2H_2^+$], 167 (9) [$CpRu^+$], 105 (7) [$C_8H_8^+$], 101 (3) [Ru^+]. − $C_{19}H_{18}Ru$ (347.44): calcd. C 65.69, H 5.22; found C 65.39, H 5.29.

(1,2-η:5,6,7-η-Cyclooctatrien-3-yl)(η^5-cyclopentadienyl)ruthenium(II) (2e): IR (Nujol): $\tilde{\nu}$ = 1645 (C=C) cm^{-1}. − EI-MS (70 eV); *m/z* (%): 271 (93) [M^+]. − $C_{13}H_{14}Ru$ (271.21): calcd. C 57.55, H 5.20; found C 57.57, H 5.30.

(η^5-Cyclopentadienyl)(1,2-η:5,6,7-η-8-*exo*-dimethylaminocyclooctatrien-3-yl)ruthenium (II) (2g): Yellow powder. − IR (Nujol): $\tilde{\nu}$ = 1657 (C=C), 1263 (C−N) cm^{-1}. − EI-MS (70 eV); *m/z* (%): 314 (100) [M^+], 300 (13) [M − CH_3^+], 285 (10) [M − $(CH_3)_2^+$], 271 (44) [M − $N(CH_3)_2^+$]. − $C_{15}H_{19}NRu$ (314.42): calcd. C 57.31, H 6.09, N 4.46; found C 57.53, H 6.06, N 4.24.

(Cyclopentadienyl)(1,2-η:5,6,7-η-8-*exo*-methoxycyclooctatrien-3-yl)ruthenium(II) (2h): Yellow powder. − IR (Nujol): $\tilde{\nu}$ = 1652 (C=C), 1225 (C−O) cm^{-1}. − EI-MS (70 eV); *m/z* (%): 301 (31) [M^+], 271 (16) [$CpRuC_8H_8^+$], 258 (8) [$CpRuC_7H_7^+$], 245 (18) [$CpRuC_6H_6^+$], 232 (5) [$CpRuC_5H_5^+$], 167 (27) [$CpRu^+$], 104 (54) [$C_8H_8^+$]. − $C_{14}H_{17}ORu$ (302.38): calcd. C 55.80, H 5.35; found C 55.83, H 5.55.

(Cyclopentadienyl)[1,2-η:5,6,7-η-8-*exo*-(3′,3′-dimethylbutyn-1′-yl)-cyclooctatrien-3-yl]ruthenium(II) (2i): IR (Nujol): $\tilde{\nu}$ = 1651 (C=C) cm^{-1}. − EI-MS (70 eV); *m/z* (%): 351 (71) [M^+], 336 (9) [M − CH_3^+], 322 (20) [M − $(CH_3)_2^+$], 306 (5) [M − $(CH_3)_3^+$], 292 (14) [M − $C(CH_3)_3^+$], 269 (5) [M − C≡$CC(CH_3)_3^+$]. − $C_{19}H_{20}Ru$ (349.46): calcd. C 64.93, H 6.31; found C 64.45, H 6.33.

General Procedure of the First Protonation: Compound **2** was dissolved in diethyl ether (50 mL) and allowed to react with HBF_4, which was dissolved in diethyl ether, at −78 °C. After warming to

Table 3. NMR data of the cyclooctatrienyl complexes **2a**−**2i**

2a′: ^{1}H NMR: δ = 4.50 (s, 5 H, Cp), 1.21 (d, $^3J_{8,Me}$ = 7.2 Hz, 3 H, Me), 3.96 (dd, $^3J_{1,8}$ = 5.5 Hz, $^3J_{1,2}$ = 9.0 Hz, 1 H, 1-H), 4.24 (dd, 1 H, 2-H), 5.56 (dd, $^3J_{2,3}$ = $^3J_{3,4}$ = 6.0 Hz, 1 H, 3-H), 4.51 (m, 1 H, 4-H), 3.70 (dd, $^3J_{4,5}$ = $^3J_{5,6}$ = 7.8 Hz, 1 H, 5-H), 5.78 (m, 1 H, 6-H), 5.29 (dd, $^3J_{6,7}$ = 12.5 Hz, $^3J_{7,8}$ = 2.7 Hz, 1 H, 7-H), 2.43 (m, 1 H, 8-H).
2a′′: ^{1}H NMR (C_6D_6): δ = 4.43 (s, 5 H, Cp), 0.89 (d, $^3J_{8,CH3}$ = 7.5 Hz, 3 H, Me), 2.93 (dd, $^3J_{1,8}$ = 8.0 Hz, 1 H, 1-H), 3.91 (dd, $^3J_{1,2}$ = 8.0 Hz, 1 H, 2-H), 5.65 (dd, $^3J_{2,3}$ = 2.4 Hz, 1 H, 3-H), 5.42 (dd, $^3J_{3,4}$ = 6.0 Hz, 1 H, 4-H), 4.63 (dd, $^3J_{5,6}$ = 8.0 Hz, $^3J_{4,5}$ = 3.4 Hz, 1 H, 5-H), 3.40 (m, 2 H, 6-H, 8-H), 3.78 (dd, $^3J_{7,8}$ = 9.3 Hz, $^3J_{6,7}$ = 7.4 Hz, 1 H, 7-H); [$CD_3C(O)CD_3$]: δ = 4.75 (s, 5 H, Cp), 0.64 (d, $^3J_{8,CH3}$ = 7.6 Hz, 3 H, Me), 2.99 (dd, $^3J_{1,8}$ = $^3J_{1,2}$ = 8.3 H, 1 H, 1-H), 3.83 (m, 2 H, 2-H, 7-H), 5.43 (dd, $^3J_{2,3}$ = 2.5 Hz, $^3J_{3,4}$ = 5.8 Hz, 1 H, 3-H), 5.22 (dd,$^3J_{4,5}$ = 3.2 Hz, 1 H, 4-H), 4.55 (dd, $^3J_{5,6}$ = 7.7 Hz, 1 H, 5-H), 3.50 (t, $^3J_{6,7}$ = 7.7 Hz, 1 H, 6-H), 3.40 (m, 1 H, 8-H). − ^{13}C{^{1}H} NMR (C_6D_6): δ = 79.5 (Cp), 24.1 (Me), 26.4 (C1), 68.2 (C2), 135.6 (C3), 134.2 (C4), 64.1 (C5), 77.3 (C6), 34.3 (C7), 34.0 (C8).
2b′: ^{1}H NMR (C_6D_6): δ = 4.43 (s, 5 H, Cp), 3.38 (s, 3 H, Me), 3.27 (s, 3 H, Me), 4.41 (m, 1 H, 1-H), 4.30 (dd, $^3J_{1,2}$ = 6.7 Hz, $^3J_{2,3}$ = 9.3 Hz, 1 H, 2-H), 5.51 (m, 2 H, 3-H, 6-H), 4.10 (dd, $^3J_{3,4}$ = 5.7 Hz, $^3J_{4,5}$ = 8.2 Hz, 1 H, 4-H), 3.66 (dd, $^3J_{5,6}$ = 8.2 Hz, 1 H, 5-H), 5.89 (m, 1 H, 7-H), 3.74 (m, 1 H, 8-H), 3.31 (d, $^3J_{8,9}$ = 11 Hz, 1 H, 9-H). − ^{13}C{^{1}H} NMR: δ = 79.6 (s, Cp), 169.3, 168.9 (C=O), 51.7, 51.6 (Me), 39.1 (C1), 75.5 (C2), 99.5 (C3), 76.4 (C4), 40.4 (C5), 129.3 (C6), 126.6 (C7), 43.2 (C8), 40.4 (C9).
2b′′: ^{1}H NMR (C_6D_6): δ = 4.34 (s, 5 H, Cp), 3.34 (s, 6 H, Me), 2.95 (dd, $^3J_{1,2}$ = $^3J_{1,8}$ = 8.0 Hz, 1 H, 1-H, H), 3.86 (dd, $^3J_{2,3}$ = 2.6 Hz, 1 H, 2-H), 5.73 (dd, $^3J_{3,4}$ = 6.0 Hz, 1 H, 3-H), 5.44 (dd, $^3J_{4,5}$ = 3.4 Hz, 1 H, 4-H), 4.57 (dd, $^3J_{5,6}$ = 8.1 Hz, 1 H, 5-H), 3.38 (dd, $^3J_{6,7}$ = 7.4 Hz, 1 H, 6-H), 3.90 (dd, $^3J_{7,8}$ = 9.2 Hz, 1 H, 7-H), 4.48 (m, 1 H, 8-H), 4.00 (d, $^3J_{1,9}$ = 12.1 Hz, 1 H, 9-H). − ^{13}C{^{1}H} NMR: δ = 80.5 (s, Cp), 169.3, 168.9, 167.3 (s, C=O), 58.3 (s, Me), 23.5 (C1), 68.5 (C2), 136.6 (C3), 134.7 (C4), 65.3 (C5), 78.4 (C6), 31.4 (C7), 40.3 (C8), 52.1 (C9).
2c: ^{1}H NMR (C_6D_6): δ = 4.45 (s, 5 H, Cp), 5.59 (m, 1 H, 9-H), 4.96 (dd, $^2J_{10,11}$ = 2.1 Hz, $^3J_{9,10}$ = 10.3 Hz, 1 H, 10-H), 4.77 (dd, $^3J_{9,11}$ = 17.4 Hz, 1 H, 11-H), 2.91 (dd, $^3J_{1,2}$ = $^3J_{1,8}$ = 7.8 Hz, 1 H, 1-H), 3.93 (dd, $^3J_{2,3}$ = 2.4 Hz, 1 H, 2-H), 5.54 (dd, $^3J_{3,4}$ = 5.9 Hz, 1 H, 3-H), 5.29 (dd, $^3J_{4,5}$ = 3.4 Hz, 1 H, 4-H), 4.63 (dd, $^3J_{5,6}$ = 7.5 Hz, 1 H, 5-H), 3.45 (dd, $^3J_{6,7}$ = 7.5 Hz, 1 H, 6-H), 3.75 (dd, $^3J_{7,8}$ = 7.5 Hz, 1 H, 7-H), 4.03 (m, 1 H, 8-H). − ^{13}C{^{1}H} NMR: δ = 79.8 (Cp), 144.6 (C9), 110.2 (C10), 24.2 (C1), 67.9 (C2), 135.3 (C3), 134.3 (C4), 64.7 (C5), 76.7 (C6), 30.1 (C7), 42.3 (C8).
2d: ^{1}H NMR (C_6D_6): δ = 7.70 (m, 1 H, *p*-Ph), 6.91 (m, 2 H, *m*-Ph), 7.08 (m, 2 H, *o*-Ph), 4.49 (s, 5 H, Cp), 4.13 (dd, $^3J_{1,8}$ = 5.6 Hz, $^3J_{1,2}$ = 8.8 Hz, 1 H, 1-H), 4.00 (dd, $^3J_{2,3}$ = 5.8 Hz, 1 H, 2-H), 5.57 (dd, $^3J_{3,4}$ = 5.8 Hz, 1 H, 3-H), 4.56 (dd, $^3J_{4,5}$ = 7.8 Hz, 1 H, 4-H), 3.69 (dd, $^3J_{5,6}$ = 7.8 Hz, 1 H, 5-H), 5.87 (dd, $^3J_{6,7}$ = 10.6 Hz, 1 H, 6-H), 5.43 (dd, $^3J_{7,8}$ = 2.7 Hz, 1 H, 7-H), 3.81 (m, 1 H, 8-H). − ^{13}C{^{1}H} NMR: δ = 79.5 (Cp), 149.0, 129.7, 126.1 (Phenyl-C), 39.8 (C1), 75.5 (C2), 99.5 (C3), 49.5 (C4), 30.2 (C5), 132.9 (C6), 131.6 (C7), 45.8 (C8).
2e: ^{1}H NMR (C_6D_6): δ = 4.40 (s, 5 H, Cp), 2.65 (m, 1 H, 1-H), 3.96 (dd, $^3J_{1,2}$ = 7.5 Hz, $^3J_{2,3}$ = 2.1 Hz, 1 H, 2-H), 5.46 (dd, $^3J_{3,4}$ = 6.1 Hz, 1 H, 3-H), 5.54 (dd, $^3J_{4,5}$ = 3.2 Hz, 1 H, 4-H), 4.57 (dd, $^3J_{5,6}$ = 7.5 Hz, 1 H, 5-H), 3.18 (dd, $^3J_{6,7}$ = 7.5 Hz, 1 H, 6-H), 3.33 (m, 1 H, 7-H), 2.87 (m, 2 H, 8_{endo}-H, 8_{exo}-H). − ^{13}C{^{1}H} NMR: δ = 79.6 (Cp), 12.4 (C1), 66.8 (C2), 135.0 (C3), 132.3 (C4), 63.4 (C5), 74.2 (C6), 21.7 (C7), 22.6 (C8).
2f: ^{13}C{H} NMR: δ = 22.6 (t, $^1J_{C,D}$ = 20.3 Hz, C7).
2g: ^{1}H NMR (C_6D_6): δ = 4.47 (s, 5 H, Cp), 1.99 (s, 6 H, Me), 2.86 (dd, $^3J_{1,2}$ = $^3J_{1,8}$ = 7.7 Hz, 1 H, 1-H), 3.52 (dd, $^3J_{2,3}$ = 2.3 Hz, 1 H, 2-H), 5.61 (dd, $^3J_{3,4}$ = 5.9 Hz, 1 H, 3-H), 5.43 (dd, $^3J_{4,5}$ = 3.3 Hz, 1 H, 4-H), 4.65 (dd, $^3J_{5,6}$ = 7.9 Hz, 1 H, 5-H), 3.19 (dd, $^3J_{6,7}$ = 7.8 Hz, 1 H, 6-H), 3.93 (dd, $^3J_{7,8}$ = 7.8 Hz, 1 H, 7-H), 3.63 (dd, 1 H, 8-H). − ^{13}C{^{1}H} NMR: δ = 79.9 (Cp), 39.8 (Me), 27.5 (C1), 67.4 (C2), 134.1 (C3), 132.9 (C4), 65.8 (C5), 78.5 (C6), 66.5 (C7), 34.1 (C8).
2h: ^{1}H NMR (C_6D_6): δ = 4.36 (s, 5 H, Cp), 3.02 (s, 3 H, Me), 2.99 (dd, $^3J_{1,2}$ = 7.9 Hz, $^3J_{1,8}$ = 7.3 Hz, 1 H, 1-H), 4.06 (dd, $^3J_{2,3}$ = 2.4 Hz, 1 H, 2-H), 5.68 (dd, $^3J_{3,4}$ = 6.0 Hz, 1 H, 3-H), 5.41 (dd, $^3J_{4,5}$ = 3.6 Hz, 1 H, 4-H), 4.68 (dd, $^3J_{5,6}$ = 7.8 Hz, 1 H, 5-H), 3.63 (dd, $^3J_{5,6}$ = $^3J_{6,7}$ = 7.8 Hz, 1 H, 6-H), 3.77 (dd, $^3J_{7,8}$ = 8.0 Hz, 1 H, 7-H), 4.56 (dd, $^3J_{1,8}$ = 7.3 Hz, 1 H, 8-H). − ^{13}C{^{1}H} NMR: δ = 79.8 (Cp), 50.8 (Me), 24.8 (C1), 67.8 (C2), 134.7 (C3), 132.6 (C4), 65.9 (C5), 76.0 (C6), 35.6 (C7), 30.1 (C8).
2i: [$CD_3C(O)CD_3$]: δ = 4.78 (s, 5 H, Cp), 1.18 (s, 9 H, Me), 2.97 (dd, $^3J_{1,2}$ = $^3J_{1,8}$ = 8.0 Hz, 1 H, 1-H), 3.91 (dd, $^3J_{2,3}$ = 2.4 Hz, 1 H, 2-H), 5.39 (dd, $^3J_{3,4}$ = 5.9 Hz, 1 H, 3-H), 5.15 (dd, $^3J_{4,5}$ = 3.2 Hz, 1 H, 4-H), 4.62 (dd, $^3J_{5,6}$ = 7.9 Hz, 1 H, 5-H), 3.45 (dd, $^3J_{6,7}$ = 6.9 Hz, 1 H, 6-H), 3.76 (dd, $^3J_{7,8}$ = 9.4 Hz, 1 H, 7-H), 4.08 (dd, $^3J_{7,8}$ = 9.4 Hz, 1 H, 8-H). − ^{13}C{^{1}H} NMR [$CD_3C(O)CD_3$]: δ = 80.4 (Cp), 30.0 (Me), 21.5 (C1), 69.0 (C2), 135.9 (C3), 133.5 (C4), 65.1 (C5), 75.9 (C6), 31.4 (C7), 66.9 (C8).

room temperature, the mixture was filtered and the residue washed several times with diethyl ether. The yellow residue was dissolved in dichloromethane, the product was precipitated with diethyl ether and dried under vacuum. For more preparative details see Table 4, for ^{1}H- and ^{13}C-NMR data see Table 5.

Table 4. Reaction conditions of the protonation reaction of **2a**−**2d**, **2g**, and **2h**

Starting material	Nu[1]	mg [mmol]	HBF_4 [ml]	Product BF_4 salts	Yield [mg (%)]
2a	Me	361.0 (1.27)	0.2	**3a**$^+$	433 (91)
2b	$CH(CO_2Me)_2$	652.0 (1.6)	0.23	**3b**$^+$	724 (91)
2c	$CH=CH_2$	162.0 (0.54)	0.07	**3c**$^+$	173 (72)
2d	C_6H_5	78.0 (0.23)	0.03	**3d**$^+$	76 (76)
2g	NMe_2	98.0 (0.31)	0.04	**1**$^+$ + **3e**$^+$	n.d.[a]
2h	OMe	63.0 (0.21)	0.03	**1**$^+$	75 (93)

[a] n.d. = not determined.

(η^5-Cyclopentadienyl)(1,2-η:4,5,6,7-η-8-*exo*-2-methylcycloocta-1,4,6-triene)ruthenium(II) Tetrafluoroborate (3aBF_4): IR (Nujol): $\tilde{\nu}$ = 1035 (BF_4) cm^{-1}. − EI-MS (70 eV); *m/z* (%): 286 (73) [M − BF_4^+], 271 (31) [M − BF_4 − CH_3^+], 259 (89) [$CpRuC_7H_8^+$], 245 (26) [$CpRuC_6H_6^+$], 232 (43) [$CpRuC_5H_5^+$], 217 (12) [$CpRuC_4H_4^+$], 205 (6) [$CpRuC_3H_3^+$], 191 (14) [$CpRuC_2H_2^+$], 179 (9) [$CpRuC_1H_1^+$], 167 (84) [$CpRu^+$], 143 (15) [$C_3H_3Ru^+$], 114 (11) [$C_1H_1Ru^+$], 105 (25) [$C_8H_9^+$], 104 (11) [$C_8H_8^+$], 102 (10) [Ru^+]. − $C_{14}H_{17}BF_4Ru$ (373.16): calcd. C 45.06, H 4.59; found C 44.35, H 5.40.

[1,2-η:4,5,6,7-η-8-*exo*-Bis(methoxycarbonyl)methylcycloocta-1,4,6-triene](η^5-cyclopentadienyl)ruthenium(II) Tetrafluoroborate (3b′BF_4): IR (Nujol): $\tilde{\nu}$ = 1733 (C=O), 1252−1156 (C−O), 1048 (BF_4) cm^{-1}. − EI-MS (70 eV); *m/z* (%): 401 (18) [M − BF_4^+], 343 (30) [M − BF_4 − $(CO_2CH_3)^+$], 282 (36) [M − BF_4-$(CO_2CH_3)_2^+$], 272 (12) [$CpRuC_8H_8^+$], 258 (16) [$CpRuC_7H_7^+$], 245 (18) [$CpRuC_6H_6^+$], 167 (76) [$CpRu^+$]. − $C_{18}H_{21}BF_4O_4Ru$ (489.27): calcd. C 44.19, H 4.33; found C 43.49, H 4.38.

(η^5-Cyclopentadienyl)(1,2-η:4,5,6,7-η-8-*exo*-vinylcycloocta-1,4,6-triene)ruthenium(II) Tetrafluoroborate (3cBF_4): IR (Nujol): $\tilde{\nu}$ = 1633 (C=C_{vinyl}), 1050 (BF_4) cm^{-1}. − EI-MS (70 eV); *m/z* (%): 297 (6) [M − BF_4^+], 271 (10) [$CpRuC_8H_8^+$], 196 (8) [$CpRuC_2H_2^+$], 178 (6) [$CpRuC_1H_1^+$], 167 (18) [$CpRu^+$]. − $C_{15}H_{17}BF_4Ru$ (385.20): calcd. C 46.78, H 4.45; found C 46.31, H 4.44.

(η^5-Cyclopentadienyl)(1,2-η:4,5,6,7-η-8-*exo*-phenylcycloocta-1,4,6-triene)ruthenium(II) Tetrafluoroborate (3dBF_4): IR (Nujol): $\tilde{\nu}$ = 1597, 1569 (C=C_{phenyl}), 1075 (BF_4) cm^{-1}. − EI-MS (70 eV); *m/z*

Table 5. NMR data of the protonated complexes **3a$^+$**−**3i$^+$**, obtained from [D$_6$]acetone solutions

3a$^+$: ^{1}H NMR: δ = 5.54 (s, 5 H, Cp), 0.70 (d, $^3J_{8,CH3}$ = 7.6 Hz, 3 H, Me), 3.79 (dd, $^3J_{1,2}$ = $^3J_{1,8}$ = 8.5 Hz, 1 H, 1-H), 3.67 (m, 1 H, 2-H), 3.13 (m, 1 H, 3$_{endo}$-H), 2.11 (m, 1 H, 3$_{exo}$-H), 4.49 (m, 1 H, 4-H), 5.66 (dd, $^3J_{4,5}$ = $^3J_{5,6}$ = 8.1 Hz, 1 H, 5-H), 5.57 (m, 1 H, 6-H), 4.84 (dd, $^3J_{7,8}$ = $^3J_{6,7}$ = 9.8 Hz, 1 H, 7-H), 3.56 (m, 1 H, 8-H). − ^{13}C{^{1}H} NMR: δ = 84.2 (Cp), 19.1 (Me), 32.7 (C-1), 39.6 (C-2), 21.5 (C-3), 33.2 (C-4), 91.6 (C-5), 90.6 (C-6), 45.1 (C-7), 27.8 (C-8).
3b′$^+$: ^{1}H NMR: δ = 5.59 (s, 5 H, Cp), 3.72 (s, 3 H, Me), 3.67 (s, 3 H, Me), 3.92 (dd, $^3J_{1,8}$ = $^3J_{7,8}$ = 8.1 Hz, 1 H, 1-H), 3.63 (m, 1 H, 2-H), 3.22 (m, 1 H, 3$_{endo}$-H), 1.81 (m, 1 H, 3$_{exo}$-H), 4.56 (m, 1 H, 4-H), 5.81 (dd, $^3J_{5,6}$ = $^3J_{4,5}$ = 8 Hz, 1 H, 5-H), 5.60 (m, 1 H, 6-H), 4.79 (dd, $^3J_{7,8}$ = $^3J_{6,7}$ = 9.8 Hz, 1 H, 7-H), 4.17 (m, 1 H, 8-H), 3.09 (d, $^3J_{8,9}$ = 12.4 Hz, 1 H, 9-H); (CD$_3$CN): δ = 5.35 (s, 5 H, Cp), 3.79 (s, 3 H, Me), 3.74 (s, 3 H, Me), 3.76 (dd, 1 H, 1-H), 3.27 (m, 1 H, 2-H), 3.17 (m, 3 H, 3$_{endo}$-H), 1.70 (m, 1 H, 3$_{exo}$-H), 4.35 (m, 1 H, 4-H), 5.51 (dd, 1 H, 5-H), 5.28 (m, 1 H, 6-H), 3.60 (dd, 1 H, 7-H), 4.10 (m, 1 H, 8-H), 2.95 (d, 1 H, 9-H). − ^{13}C{^{1}H} NMR: δ = 83.8 (Cp), 52.1 (Me), 167.7 (C=O), 35.6 (C1), 52.3 (C2), 18.0 (C3), 32.3 (C4), 90.6 (C5), 90.9 (C6), 41.4 (C7), 33.2 (C8), 55.2 (C9).
3b′$^+$-D$_1$: ^{13}C{^{1}H} NMR: δ = 17.6 (t, $^1J_{C,D}$ = 24.6 Hz, C3).
3b′′$^+$: ^{1}H NMR: δ = 5.67 (s, 5 H, Cp), 3.73 (s, 3 H, Me), 3.65 (s, 3 H, Me), 6.11 (dd, $^3J_{1,8}$ = 9.7 Hz, $^3J_{1,2}$ = 3.6 Hz, 1 H, 1-H), 5.43 (m, 2 H, 2-H, 6-H), 6.96 (dd, $^3J_{2,3}$ = $^3J_{3,4}$ = 8.4 Hz, 1 H, 3-H), 6.84 (dd, $^3J_{4,5}$ = 6.3 Hz, 1 H, 4-H), 6.26 (dd, $^3J_{5,6}$ = 6.3 Hz, 1 H, 5-H), 1.63 (m, 1 H, 7$_{endo}$-H), −0.95 (m, 1 H, 7$_{exo}$-H), 3.92 (m, 1 H, 8-H), 3.40 (d, $^3J_{8,9}$ = 8.3 Hz, 1 H, 9-H). − ^{13}C{^{1}H} NMR: δ = 87.2 (Cp), 52.3 (Me), 86.7 (C1), 85.7 (C2), 105.6 (C3), 95.5 (C4), 83.3 (C5), 78.01 (C6), 28.3 (C7), 32.3 (C8), 58.0 (C9).
3b′′-D$_1$: ^{13}C{^{1}H} NMR: δ = 27.1 (t, $^1J_{C,D}$ = 20.3 Hz, C7).
3c$^+$: ^{1}H NMR: δ = 5.57 (s, 5 H, Cp), 5.45 (m, 1 H, CH$_{vinyl}$), 4.91 (m, 1 H, CH$_{2,vinyl}$), 4.81 (m, 1 H, CH$_{2,vinyl}$), 3.95 (dd, $^3J_{1,2}$ = $^3J_{1,8}$ = 7.4 Hz, 1 H, 1-H), 3.62 (m, 1 H, 2-H), 2.95 (m, 1 H, 3$_{endo}$-H), 2.01 (m, 1 H, 3$_{exo}$-H), 4.41 (m, 1 H, 4-H), 5.50 (m, 1 H, 5-H), 5.75 (m, 1 H, 6-H), 4.67 (m, 1 H, 7-H), 4.20 (m, 1 H, 8-H). − ^{13}C{^{1}H} NMR: δ = 84.0 (Cp), 140.0 (CH$_{vinyl}$), 118.5 (CH$_{2,vinyl}$), 32.9 (C1), 33.1 (C2), 17.8 (C3), 36.8 (C4), 90.6 (C5), 92.6 (C6), 41.4 (C7), 37.2 (C8).
3d$^+$: ^{1}H NMR: δ = 5.62 (s, 5 H, Cp), 7.25 (m, 2 H, *m*-Ph), 7.14 (m, 1 H, *p*-Ph), 7.04 (m, 2 H, *o*-Ph), 4.37 (dd, $^3J_{1,2}$ = $^3J_{1,8}$ = 8.8 Hz, 1 H, 1-H), 3.64 (m, 1 H, 2-H), 2.63 (m, 1 H, 3$_{endo}$-H), 0.70 (m, 1 H, 3$_{exo}$-H), 4.32 (m, 1 H, 4-H), 5.77 (dd, $^3J_{4,5}$ = $^3J_{5,6}$ = 8.1 Hz, 1 H, 5-H), 5.91 (dd, $^3J_{6,7}$ = 9.3 Hz, 1 H, 6-H), 4.94 (dd, $^3J_{7,8}$ = 9.3 Hz, 1 H, 7-H), 4.84 (m, 1 H, 8-H). − ^{13}C{^{1}H} NMR: δ = 84.2 (Cp), 141.0, 129.1, 127.0, 124.8 (Phenyl-C), 31.9 (C1), 32.5 (C2), 38.5 (C2), 17.9 (C3), 37.6 (C4), 90.5 (C5), 93.0 (C6), 41.9 (C7), 38.5 (C8).
3e$^+$: ^{1}H NMR: δ = 5.76 (s, 5 H, Cp), 2.96 (s, 6 H, Me), 6.08 (m, 1 H, 1-H), 5.86 (dd, $^3J_{1,2}$ = $^3J_{2,3}$ = 8.9 Hz, 1 H, 2-H), 7.10 (dd, $^3J_{3,4}$ = 8.9 Hz, 1 H, 3-H), 6.94 (m, 1 H, 4-H), 6.42 (dd, $^3J_{4,5}$ = $^3J_{5,6}$ = 5.5 Hz, 1 H, 5-H), 5.13 (m, 1 H, 6-H), 2.17 (m, 1 H, 7$_{endo}$-H), −0.61 (m. 1 H, 7$_{exo}$-H), 4.90 (m, 1 H, 8-H).

(%): 347 (8) [M − BF_4^+], 321 (8) [M − (C_2H_2)-BF_4^+], 167 (10) [$CpRu^+$]. − $C_{19}H_{19}BF_4Ru$ (435.26): calcd. C 52.43, H 4.40; found C 51.82, H 4.58.

Second Nucleophilic Addition

[1,2,3,4,5-η-6,8-*exo*,*exo*-Bis{bis(methoxycarbonyl)methyl}-cyclooctadienyl](η^5-cyclopentadienyl)ruthenium(II) (4a): To a suspension of **3b**BF_4 (645 mg, 1.3 mmol) in THF (50 mL) was added a solution of $NaCH(CO_2CH_3)_2$ (223 mg, 1.45 mmol) in THF (20 mL) at room temperature. The solvent was removed under reduced pressure, the residue was extracted with toluene and the extract was filtered through Celite. After removal of the solvent, the product **4a** was obtained as a yellow powder. Yield: 558 mg (79%). For ^{1}H- and ^{13}C-NMR data see Table 6. − IR (KBr): $\tilde{\nu}$ = 2988 (C−H$_{arom.}$), 2947, 2923 (C−H$_{aliph.}$), 1729 (C=O), 1228 (C−O) 6cm^{-1}. − EI-MS (70 eV); *m*/*z* (%): 532 (11) [M$^+$], 402 (35) [M − $CH(CO_2CH_3)_2^+$], 343 (47) [M − $CH(CO_2CH_3)_2$ − (CO_2CH_3)], 283 (33) [$CpRuC_9H_{11}^+$], 272 (19) [$CpRuC_8H_8^+$], 258 (8) [$CpRuC_7H_7^+$], 245 (20) [$CpRuC_6H_6^+$], 167 (44) [$CpRu^+$], 101 (78) [Ru^+], 59 (100) [$C_2H_3O_2^+$]. − $C_{23}H_{28}O_8Ru$ (533.58): calcd. C 51.78, H 5.29; found C 51.63, H 5.60.

[1,2-η:5,6,7-η-4-*exo*-Bis(methoxycarbonyl)methyl-8-*exo*-methyl-cyclooctadienyl](η^5-cyclopentadienyl)ruthenium(II) (4b): To a suspension of **3a**BF_4 (298 mg, 0.8 mmol) in THF (30 mL) was added a solution of $NaCH(CO_2CH_3)_2$ (123 mg, 0.8 mmol) in THF (20 mL). The solvent was removed under reduced pressure, the residue was extracted with toluene and the extract filtered through Celite. After removal of the solvent, the product **4b** was obtained as a green oil. Yield: 200 mg (60%). For ^{1}H- and ^{13}C-NMR data see Table 6. − IR (Nujol): $\tilde{\nu}$ = 1754, 1732 (C=O), 1253, 1139 (C−O) cm^{-1}. − EI-MS (70 eV); *m*/*z* (%): 416 (19) [M$^+$], 357 (9) [M − $CO_2CH_3^+$], 297 (8) [M − $(CO_2CH_3)_2^+$], 285 (68) [M − $CH(CO_2CH_3)_2^+$], 270 (11) [$CpRuC_8H_8^+$], 259 (55) [$CpRuC_7H_7^+$], 245 (16) [$CpRuC_6H_6^+$], 232 (11) [$CpRuC_5H_5^+$], 217 (10) [$CpRuC_4H_4^+$], 204 (4) [$CpRuC_3H_3^+$], 191 (8) [$CpRuC_2H_2^+$], 178 (6) [$CpRuCH^+$], 167 (58) [$CpRu^+$], 105 (29) [$C_8H_8^+$], 101 (97) [Ru^+]. − $C_{19}H_{24}O_4Ru$ (417.50): calcd. C 54.67, H 5.79; found C 55.24, H 6.03.

Table 6. ^{1}H- and ^{13}C-NMR data of the products of the second nucleophilic addition (**4a**−**4c**)

4a: ^{1}H NMR (C_6D_6): δ = 4.45 (s, 5 H, Cp), 3.37, 3.35 (s, 12 H, Me), 3.84 (dm, $^3J_{1,2}$ = $^3J_{4,5}$ = 8.0 Hz, 2 H, 1-H, 5-H), 4.01 (dd, $^3J_{1,2}$ = $^3J_{4,5}$ = 8.0 Hz, $^3J_{2,3}$ = $^3J_{3,4}$ = 6.1 Hz, 2 H, 2-H, 4-H), 5.63 (t, $^3J_{2,3}$ = $^3J_{3,4}$ = 6.1 Hz, 1 H, 3-H), 2.83 (m, 2 H, 6-H, 8-H), 1.30 (m, 1 H, 7$_{endo}$-H), 0.19 (m, 1 H, 7$_{exo}$-H), 3.41 (d, $^3J_{6,9}$ = $^3J_{8,9'}$ = 7 Hz, 2 H, 9-H, 9′-H); [$CD_3C(O)CD_3$]: δ = 4.85 (s, 5 H, Cp), 3.68, 3.62 (s, 12 H, Me), 3.64 (m, 2 H, 1-H, 5-H), 4.15 (dd, 2 H, 2-H, 4-H), 6.01 (t, 1 H, 3-H), 2.36 (m, 2 H, 6-H, 8-H), 0.83 (d, 1 H, 7$_{endo}$-H), −0.18 (m, 1 H, 7$_{exo}$-H), 3.19 [d, 2 H, C*H*$(CO_2Me)_2$]. ^{13}C{^{1}H} NMR (C_6D_6): δ = 80.2 (Cp), 61.6 (Me), 169.1, 168.8 (C=O), 44.1 (C1, C5), 72.3 (C2, C4), 103.1 (C3), 42.9 (C6, C8), 27.8 (C7), 51.6 (C9).
4a-D$_1$: ^{13}C{^{1}H} NMR (C_6D_6): δ = 27.4 (t, $^1J_{C,D}$ = 17.4 Hz, C-7).
4b: ^{1}H NMR (C_6D_6): δ = 4.38 (s, 5 H, Cp), 0.96 (d, $^3J_{8,CH3}$ = 7.6 Hz, 3 H, Me), 3.43 (s, 3 H, OMe), 3.32 (s, 3 H, OMe), 2.95 (dd, $^3J_{1,8}$ = $^3J_{1,2}$ = 8.1 Hz, 1 H, 1-H), 3.51 (m, 1 H, 2-H), 1.38 (m, 1 H, 3$_{exo}$-H), 2.11 (m, 1 H, 3$_{endo}$-H), 4.14 (m, 1 H, 4-H), 4.78 (dd, $^3J_{4,5}$ = 5.3 Hz, 1 H, 5-H), 2.70 (dd, $^3J_{5,6}$ = 9.0 Hz, 1 H, 6-H), 3.70 (dd, $^3J_{7,8}$ = $^3J_{6,7}$ = 9.0 Hz, 1 H, 7-H), 3.38 (m, 1 H, 8-H), 3.55 (d, $^3J_{4,9}$ = 5.8 Hz, 1 H, 9-H). − ^{13}C{^{1}H} NMR (C_6D_6): δ = 79.4 (Cp), 168.8, 168.7 (C=O), 51.8 (OMe), 24.6 (Me), 26.6 (C1), 61.3 (C2), 29.1 (C3), 55.4 (C4), 66.6 (C5), 73.7 (C6), 42.8 (C7), 35.3 (C8), 60.0 (C9).
4c: ^{1}H NMR: δ = 4.44 (s, 5 H, Cp), 1.20 (d, $^3J_{8,CH3}$ = 6.8 Hz, Me), 1.02 (d, $^3J_{4,CH3}$ = 7.6 Hz, 3 H, Me), 2.99 (dd, $^3J_{1,8}$ = 8.0 Hz, 1 H, 1-H), 3.60 (dd, $^3J_{2,3}$ = 16 Hz, $^3J_{1,2}$ = 8.0 Hz, 1 H, 2-H), 1.23 (m, 1 H, 3$_{exo}$-H), 1.92 (m, 1 H, 3$_{endo}$-H), 3.43 (m, 1 H, 4-H), 4.56 (m, 1 H, 5-H), 2.66 (dd, $^3J_{5,6}$ = 9.5 Hz, 1 H, 6-H), 3.78 (dd, $^3J_{7,8}$ = $^3J_{6,7}$ = 9.0 Hz, 1 H, 7-H), 3.34 (m, 1 H, 8-H). − ^{13}C{^{1}H} NMR: δ = 79.0 (Cp), 33.3, 23.9 (Me), 24.4 (C1), 62.9 (C2), 26.0 (C3), 52.9 (C4), 72.9 (C5), 74.1 (C6), 41.3 (C7), 35.3 (C8).

Table 7. ^{1}H-NMR data of the protonated complexes **5a$^+$**−**5c$^+$**, **6$^+$**, and **7$^+$**

5a$^+$: ^{1}H NMR (CD_2Cl_2): δ = 5.52 (s, 5 H, Cp), 3.76 (s, 6 H, Me), 3.72 (s, 6 H, Me), −10.6 (s, 1 H, Ru-H), 3.85 (dd, $^3J_{1,8} = {}^3J_{1,2} = {}^3J_{4,5} = {}^3J_{5,6}$ = 4.0 Hz, 2 H, 1-H, 5-H), 5.58 (m, 2 H, 2-H, 4-H), 7.05 (t, $^3J_{2,3} = {}^3J_{3,4}$ = 6.9 Hz, 3-H), 2.66 (m, 2 H, 6-H, 8-H), 1.24 (m, 7_{endo}-H), 0.27 (m, 1 H, 7_{exo}-H), 3.36 (d, $^3J_{6,9} = {}^3J_{8,9'}$ = 6.7 Hz, 2 H, 9-H, 9′-H).
5b$^+$: ^{1}H NMR (CD_2Cl_2): δ = 5.41 (s, 5 H, Cp), 3.76, 3.66 (s, 6 H, OMe), 3.34 [d, $^3J_{6,CH}$ = 6.7 Hz, 1 H, C*H*(CO_2Me)$_2$], 2.27 (s, 3 H, Me), 4.01 (m 1 H, 1-H), 6.92 (d, $^3J_{3,4}$ = 6.7 Hz, 1 H, 3-H), 5.41 (m, 1 H, 4-H), 5.42 (m, 1 H, 5-H), 3.84 (m, 1 H, 6-H), 1.32 (m, 1 H, 7_{endo}-H), 0.34 (m, 1 H, 7_{exo}-H), 2.49 (m, 1 H, 8_{endo}-H), 1.84 (m, 1 H, 8_{exo}-H), −10.41 (s, 1 H, Ru-H).
5c$^+$: ^{1}H NMR (CD_2Cl_2): δ = 5.36 (s, 5 H, Cp), 0.69 (d, $^3J_{8,CH3}$ = 7.6 Hz, 3 H, Me), 1.07 (d, $^3J_{4,CH3}$ = 6.8 Hz, 3 H, Me), 4.34 (m, 1 H, 1-H), 3.59 (m, 1 H, 2-H), 3.06 (m, 1 H, 3_{endo}-H), 2.08 (m, 1 H, 3_{exo}-H), 2.23 (m 1 H, 4-H), 5.32 (m, 1 H, 5-H), 5.30 (m, 1 H, 6-H), 4.67 (m, 1 H, 7-H), 3.48 (m, 1 H, 8-H), −10.47 (s, 1 H, Ru-H).
6$^+$: ^{1}H NMR (CD_2Cl_2): δ = 5.43 (s, 5 H, Cp), 5.18 (m, 1 H, 1-H), 6.06 (d, $^3J_{1,2}$ = 7.9 Hz, 1 H, 2-H), 6.70 (d, $^3J_{4,5}$ = 8.8 Hz, 1 H, 4-H), 5.26 (dd, $^3J_{5,6}$ = 9.7 Hz, 1 H, 5-H), 5.85 (dm, $^3J_{5,6}$ = 9.7 Hz, 1 H, 6-H), 3.74 (m, 1 H, 7-H), 1.58 (m, 1 H, 8_{endo}-H), −0.85 (m, 1 H, 8_{exo}-H), 2.62 (s, 3 H, Me), 3.21 [d, $^3J_{7,CH(CO2Me)2}$ = 7.4 Hz, 1 H, C*H*(CO_2Me)$_2$], 3.75 [s, 6 H, CH(CO_2*Me*)$_2$].
7$^+$: ^{1}H NMR (CD_2Cl_2): δ = 5.30 (s, 5 H, Cp), 5.94 (m, 1 H, 1-H), 5.40 (m, 1 H, 3-H), 6.65 (m, 1 H, 4-H), 6.58 (m, 1 H, 5-H), 5.48 (m, 1 H, 6-H), 1.58 (m, 1 H, 7_{endo}-H), −0.45 (tdd, $^3J_{7exo,8endo}$ = 4.6 Hz, $^3J_{6,7exo}$ = 9.1 Hz, $^2J_{7exo,7endo}$ = 13.4 Hz, 7_{exo}-H), 2.70 (m, 1 H, 8_{endo}-H), 2.14 (m, 1 H, 8_{exo}-H), 2.63 (s, 3 H, *Me*)

(η^5-Cyclopentadienyl)(1,2-η:5,6,7-η-4,8-*exo*,*exo*-dimethylcyclooctadienyl)ruthenium(II) (4c): Methyllithium (1.29 mL, 2.1 mmol of a 5% solution in diethyl ether) was added to a suspension of **3a**BF_4 (770 mg, 2.06 mmol) in diethyl ether (40 mL). The solvent was removed under reduced pressure, the residue extracted with hexane and the extract filtered through Celite. After removal of the solvent, the product **4c** was obtained as a green oil. Yield: 593 mg (96%). For ^{1}H- and ^{13}C-NMR data see Table 6. − IR (Nujol): $\tilde{\nu}$ = 1620 (C=$C_{arom.}$) cm^{-1}. − EI-MS (70 eV); *m*/*z* (%): 300 (100) [M^+], 285 (64) [$M - CH_3^+$], 273 (43) [$CpRuC_8H_9^+$], 259 (57) [$CpRuC_7H_7^+$], 245 (13) [$CpRuC_6H_6^+$], 230 (9) [$CpRuC_5H_5^+$], 167 (57) [$CpRu^+$]. − $C_{15}H_{20}Ru$ (301.42): calcd. C 59.78, H 6.69; found C 59.68, H 6.52.

Protonation of the Cyclooctadienyl Complexes 4a−4c: The procedure for the protonation was performed as described for the protonation of **2** (vide supra). For ^{1}H-NMR data see Table 7.

{1,2,3,4,5-η-6,8-*exo,exo*-Bis[bis(methoxycarbonyl)methyl]-cyclooctadienyl}(η^5-cyclopentadienyl)hydridoruthenium(II) Tetrafluoroborate (5aBF_4): 613 mg of 4a, 0.22 mL of HBF_4 solution (54% solution in diethyl ether), 40 mL of diethyl ether, T = −65 °C. Yield: 581 mg (81%) of a yellow powder. − IR (KBr): $\tilde{\nu}$ = 3117 (C−$H_{arom.}$), 2956 (C−$H_{aliph.}$), 1732 (C=O), 1244 (C−O), 1058 (BF_4) cm^{-1}. − $C_{23}H_{29}BF_4O_4Ru$ (557.40): calcd. C 44.10, H 4.52; found C 44.13, H 4.69.

{1,2,3,4,5-η-6-*exo*-[Bis(methoxycarbonyl)methyl]-2-methylcyclooctadienyl}(η^5-cyclopentadienyl)hydridoruthenium(II) Tetrafluoroborate (5bBF_4): 137 mg (0.49 mmol) of 4b, 0.06 mL of HBF_4 solution (54% in diethyl ether), 60 mL diethyl ether, T = −70 °C. Yield: 168 mg (64%) of a yellow crystalline material. − IR (Nujol): $\tilde{\nu}$ = 1756 (C=O), 1232 (C−O), 1057 (BF_4) cm^{-1}. − EI-MS (70 eV); *m*/*z* (%): 418 (8) [$M - BF_4^+$], 357 (8) [$M - BF_4$-$(CO_2CH_3)_2^+$], 285 (18) [$M - BF_4$-$CH(CO_2CH_3)_2^+$], 259 (18) [$CpRuC_7H_7^+$], 232 (20) [$CpRuC_5H_5^+$], 167 (40) [$CpRu^+$]. − $C_{19}H_{25}BF_4O_4Ru$ (505.32): calcd. C 45.17, H 4.99; found C 44.72, H 4.96.

(η^5-Cyclopentadienyl)(1,2-η:5,6,7-η-4,8-*exo*,*exo*-dimethylcyclooctadienyl)hydridoruthenium(II) Tetrafluoroborate (5cBF_4): 214 mg (0.71 mmol) of **4c**, 0.1 mL of HBF_4 solution (54% in diethyl ether), 45 mL of diethyl ether, T = −78 °C. Yield: 190 mg (69%) of a yellow powder. − IR (Nujol): $\tilde{\nu}$ =1048 (BF_4) cm^{-1}. − $C_{15}H_{21}BF_4Ru$ (389.21): calcd. C 46.29, H 5.44; found C 45.14, H 5.30.

Acknowledgments

This work was supported by the Deutsche Forschungsgemeinschaft (DFG, HE 1309/2). We thank the BASF AG for a donation of cyclooctatetraene and the DEGUSSA AG for a donation of $RuCl_3$.

[1] [1a] A. J. Pearson, S. Mallik, R. Mortezali, M. W. D. Perry, R. J. Shively, Jr., W. J. Youngs, *J. Am. Chem. Soc.* **1990**, *112*, 8034−8041. − [1b] A. J. Pearson, *Acc. Chem. Res.* **1980**, *13*, 463. − [1c] A. J. Pearson, S. K. Kole, J. Yoon, *Organometallics* **1986**, *5*, 2075−2081. − [1d] A. J. Birch, B. M. R. Bandora, K. Chamberlain. B. Chauncey, P. Dahler, A. I. Day, I. D. Jenkins, L. F. Kelley, T. C. Knor, G. Kretschmer, A. J. Liepa, A. S. Narula, W. D. Raverty, E. Rizzardo, C. Sell, G. R. Stephenson, D. J. Thompson, D. H. Williamson, *Tetrahedron* **1981**, *37*, suppl. 1, 5289−5302. − [1e] L. A. P. Kane-Maguire, E. D. Honig, D. A. Sweigart, *Chem. Rev.* **1984**, *84*, 525−543. − [1f] P. S. Bratermann, in: *Reactions of Coordinated Ligands*, Plenum, New York, **1986**. − [1g] B. M. Trost, T. R. Verhoeven, in: *Comprehensive Organometallic Chemistry* (Eds.: G. Wilkinson, F. G. A. Stone, E. W. Abel), Pergamon, New York, **1982**, vol. 8, p. 799−938. − [1h] A. J. Pearson, *Comprehensive Organometallic Chemistry*, Pergamon, New York, **1982**, vol. 8, p. 939−1011. − [1i] J. W. Faller, K.-H. Chao, *Organometallics* **1984**, *3*, 927−932.

[2] [2a] G. R. Stephenson, in: *Organic Synthesis via Organometallics* (Eds.: K. H. Dötz and R. W. Hoffmann), Verlag Friedrich Vieweg and Sohn, Braunschweig, Germany, **1991**. − [2b] H. J. Knölker, R. Boese, K. Hartmann, *Angew. Chem.* **1989**, *101*, 1745−1747; *Angew. Chem. Int. Ed. Engl.* **1989**, *28*, 2. − [2c] H.-J. Knölker, M. Bauermeister, D. Bläser, R. Boese, J.-B. Pannek, *Angew. Chem.* **1989**, *101*, 225−227; *Angew. Chem. Int. Ed. Engl.* **1989**, *28*, 223. − [2d] A. J. Pearson, *Pure Appl. Chem.* **1983**, *55*, 1767. − [2e] M. Rosenblum, J. C. Watkins, *J. Am .Chem. Soc.* **1990**, *112*, 6316−6322. − [2f] I. M. Palotai, G. R. Stephenson, L. A. P. Kane-Maguire, *J. Organomet. Chem.* **1987**, *319*, C5-C10.

[3] P. T. Beurskens, W. P. Bosman, H. C. Brussaard, J. Heck, R. J. M. Klein Gebink, M. Maters, J. M. M. Smits, *J. Organomet. Chem.* **1994**, *469*, 197−203.

[4] M. A. Patane, N. A. Petasis, *Tetrahedron* **1992**, *48*, 5757−5821.

[5] S. G. Davies, M. L. H. Green, D. M. P. Mingos, *Tetrahedron* **1978**, *34*, 3047−3077.

[6] J. Heck, G. A. Lange, O. Reimelt, *Angew. Chem.* **1998**, *110*, 533−535; *Angew. Chem. Int. Ed.* **1998**, *37*, 520−522.

[7] O. Reimelt, Diploma Thesis, Universität Hamburg, **1998**.

[8] O. Reimelt, J. Heck, unpublished results.

[9] R. D. Ernst, R. Gleiter, J. C. Green, I. Hyla-Kryspin, G. Sergson, L. Stahl, M. L. Ziegler, *Organometallics* **1989**, *8*, 298−306; R. D. Ernst, *Acc. Chem. Res.* **1985**, *18*, 56−62.

[10] P. J. Harris, J. A. K. Howard, S. A. R. Knox, R. J. McKinney, R. P. Philipps, F. G. A. Stone, P. Woodward, *J. Chem. Soc., Dalton Trans.* **1978**, 403−416.

[11] M. Damen, E. T. K. Haupt, J. Heck, M. Maters, B. Voss, *Organometallics* **1995**, *14*, 44−48.

[12] C. Elschenbroich, J. Koch, J. Schneider, B. Spangenberg, P. Schiess, *J. Organomet. Chem.* **1986**, *317*, 41−54.

[13] M. Brookhart, Y. H. Hong, S. K. Noh, F. J. Timmers, *Organometallics* **1988**, *7*, 2458−2465.

[14] [14a] B. F. G. Johnson, J. Lewis, D. J. Yarrow, *J. Chem. Soc., Dalton Trans.* **1972**, 2084−2089. − [14b] B. Buchmann, U. Pian-

tini, W. von Philipsborn, A. Salzer, *Helv. Chem. Acta* **1987**, *70*, 1487−1506.
[15] A. C. Ontko, J. F. Houlis, R. C. Schnabel, D. M. Roddick, *Organometallics* **1998**, *17*, 5467−5476; B. E. Mann, G. A. Sun, *J. Organomet. Chem.* **1998**, *551*, 21−26.
[16] F. M. Conroy-Lewis, S. J. Simpson, *J. Chem. Soc., Chem. Commun.* **1987**, 1675−1676; E. Cesarotti, C. White, *J. Organomet. Chem.* **1985**, *287*, 123−125.
[17] D. N. Cox, R. Roulet, *J. Chem. Soc., Chem. Commun.* **1989**, 175−176.
[18] W. Trakarnpruk, I. Hyla-Kryspin, A. M. Arif, R. Gleiter, R. D. Ernst, *Inorg. Chim. Acta* **1997**, *259*, 197−202.
[19] [19a] J. L. Schrenk, K. R. Mann, *Inorg. Chem.* **1986**, *25*, 1906−1908. − [19b] K. Itoh, K. Masuda, T. Fukahori, K. Nakano, K. Aoki, H. Nagashima, *Organometallics* **1994**, *13*, 1020−1029. − [19c] M. E. Cucullu, L. Luo, S. P. Nolan, P. J. Fagan, N. L. Jones, J. C. Calabrese, *Organometallics* **1995**, *14*, 289−296.
[20] [20a] M. C. Baird, R. A. Zelonka, *Can. J. Chem.* **1972**, *50*, 3063−3072. − [20b] M. C. Baird, R. A. Zelonka, *J. Organomet. Chem.* **1972**, *44*, 383−389. − [20c] T. A. Stephenson, D. A. Tocher, *Org. Synth., Coll. Vol.* **1986**, *III*, 99−103. − [20d] T. P. Gill, K. R. Mann, *Organometallics* **1982**, *1*, 485−488.
[21] A. J. Pearson, *J. Chem. Soc., Perkin Trans. 1* **1977**, 2069−2077.
[22] L. Brandsma, H. D. Verkruijsse, *Preparative Polar Organometallic Chemistry*, vol. 1, Springer-Verlag, Berlin, Heidelberg, New York, **1987**.
[23] G. M. Sheldrick, *SHELXS-86*, Universität Göttingen, Deutschland, **1986**.
[24] G. M. Sheldrick, *SHELXL-97*, Universität Göttingen, Deutschland, **1997**.

Received February 10, 2000
[I00045]

Synthesis and π-Tweezer Properties of *tripod*Cobalt-Bisalkynyl Compounds $[CH_3C(CH_2PPh_2)_3Co(C{\equiv}CR)_2]$ − Application to the Oxidative Coupling of Alkynyl Groups

Rolf Rupp,[a] Gottfried Huttner,*[a] Heinrich Lang,[b] Katja Heinze,[a] Michael Büchner,[a] and Eric Robert Hovestreydt[c]

Dedicated to Prof. Peter Paetzold on the occasion of his 65th birthday

Keywords: Tripod ligands / Cobalt / π-Tweezers / Oxidative Coupling / Alkyne complexes

tripod$CoCl_2$ $[CH_3C(CH_2PPh_2)_3CoCl_2]$ (**1**) reacts with alkynyllithium reagents RC≡CLi to produce *tripod*$Co(C{\equiv}CR)_2$ (**2**). The neutral paramagnetic Co^{II} species **2** can be reduced to the anionic diamagnetic Co^{I} compounds $\mathbf{2}^-$, which can also be obtained by treating *tripod*CoCl (**3**) with two equivalents of LiC≡CR. Compounds **2** contain an $M(C{\equiv}CR)_2$ group with the alkynyl substituents in *cis*-positions to each other. The expectation that they might therefore act as π-tweezer ligands is born out by the characterisation of *tripod*$Co(C{\equiv}CR)_2$–NiCO (**4**). The *cis*-position of the alkynyl groups in **2** should also facilitate their oxidative coupling. This type of reaction is, in fact, observed when compounds **2** are treated with one-electron oxidants. Reaction of **2** with Cp_2Fe^+ leads to [*tripod*$Co(\eta^2$-R*C*≡*C*C≡CR)]$^+$ **(5)** in which one of the triple bonds of the diyne acts as a four-electron donor ligand while the other one remains uncoordinated. One-electron oxidation of **2** thus initiates a two-electron oxidative coupling of the alkynyl groups with concomitant one-electron reduction of Co^{II} (**2**) to Co^{I} (**5**). All compounds were characterised by the usual analytical and spectroscopic techniques including EPR spectroscopy. The structure of compounds **5** is exemplified by an X-ray analysis of [*tripod*$Co(\eta^2$-*t*Bu*C*≡*C*C≡C*t*Bu)](PF_6) (**5b**).

Introduction

The coordination chemistry of the [*tripod*cobalt] template $[CH_3C(CH_2PPh_2)_3Co]$ is characterised by the persistent pentacoordination in [*tripod*$CoL_2]^{n+}$ compounds, regardless of the oxidation state (Co^{III}: d^6, Co^{II}: d^7, Co^{I}: d^8).[1,2] While only pentacoordination is known for d^6- and d^7-electron configurations, lower oxidation states allow for pseudo-tetrahedral coordination.[2a,2b,3−8] With the geometric constraint imposed by the facial η^3-coordination of the *tripod* ligand, the co-ligands L in [*tripod*CoL_2] are necessarily *cis* to each other.

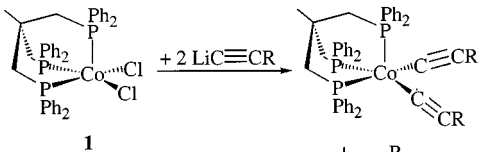
With this in mind, the synthesis of *cis*-bisalkynyl derivatives [*tripod*$Co(C{\equiv}CR)_2]^{n+}$ is a rewarding goal in view of the particular reactivity patterns documented for some specific *cis*-[$L_nM(C{\equiv}CR)_2$] *cis*-bisalkynyl compounds such as $[Cp_2M(C{\equiv}CR)_2]$ (M = Ti, Zr, Hf).[9] It is shown in this paper how the compounds [*tripod*$Co(C{\equiv}CR)_2]^{n+}$ (n = −1, 0) **2** are accessible, and how these bisalkynyl species may be used as π-tweezers in derivatives such as [*tripod*$Co(C{\equiv}CR)_2$−NiCO] (**4**). Compounds **2** may also serve as reagents for the oxidative coupling of the alkynyl ligands.

[a] Anorganisch-Chemisches Institut der Universität Heidelberg, Im Neuenheimer Feld 270, D-69120 Heidelberg, Germany
Fax: (internat.) +49(0)6221/545-707
E-mail: g.huttner@indi.aci.uni-heidelberg.de
[b] Technische Universität Chemnitz, Institut für Chemie, Lehrstuhl Anorganische Chemie, Straße der Nationen 62, D-09107 Chemnitz, Germany
Fax: (internat.) +49(0)371/531-1833
E-mail: heinrich.lang@chemie.tu-chemnitz.de
[c] Bruker-AXS GmbH, Product Support, D-76181 Karlsruhe, Germany
Fax: (internat.) +49(0)721/595-4506

Results and Discussion

Cobalt(II) Derivatives

[*tripod*$CoCl_2$] **(1)**[2b] reacts with two equivalents of the alkynyllithium compound LiC≡CR (R = Ph, *t*Bu, TMS) to give the corresponding bisalkynyl derivatives **2a**−**c**.[2a,2b]



1

	R
2a	Phenyl
2b	tert. Butyl
2c	Trimethylsilyl

In order to produce **2** in high yields, the reaction has to be performed at −80 °C in THF. Even at this low temper-

 © WILEY-VCH Verlag GmbH, D-69451 Weinheim, 2000 1434−1948/00/0909−1953 $ 17.50+.50/0

ature, the reactions are spontaneous and an immediate colour change from blue (**1** in THF[2b]) to brown (**2**) is observed. After changing the solvent from THF to toluene, with subsequent filtration, compounds **2** are obtained, by evaporation of the solvent, as microcrystalline black-brown powders. Derivatives of **1** that have only one alkynyl substituent and one remaining chloro substituent are not accessible by this procedure. If only one equivalent of LiC≡CR is used, a mixture of **1** and **2** results. This is in agreement with the observation that a 1:1 mixture of the clean compounds **1** and **2** does not result in alkynyl−chloro exchange.

While single crystals of **2** suitable for X-ray analysis could not be obtained, analytical data unequivocally established the structure as shown for **2**. Osmometric determination of the molecular mass of **2a** shows that compounds **2** are monomeric (see Experimental Section). Mass spectrometry shows the molecular ion in each case (Table 1). The C≡C bonds of **2** give rise to a characteristic ν(CC) absorption band in each case (Table 1). Compounds **2** are paramagnetic with an effective magnetic moment of 1.8 BM measured for **2a** at 25 °C (see Experimental Section).

Table 1. Analytical data for compounds **2**

Compound	**2a**	**2b**	**2c**
EPR (298 K, THF)[a]	$g_1 = 2.13, A_1 = 44$ G $g_2 = 2.04, A_2 = 45$ G	$g_1 = 2.13, A_1 = 45$ G $g_2 = 2.04, A_2 = 47$ G	$g_1 = 2.13, A_1 = 44$ G $g_2 = 2.04, A_2 = 45$ G
EPR (298 K, powder)	$g \approx 2.05$	$g \approx 2.05$	$g \approx 2.05$
EPR (100 K, powder)	$g \approx 2.05$	$g \approx 2.05$	$g \approx 2.05$
IR: $\tilde{\nu}$ CC [cm^{-1}]	2068 (w)	2068 (w)	2082 (w)
MS-EI: *m/z* [frag.]	885 [M$^+$]	845 [M$^+$]	877 [M$^+$]
CV: $E_{1/2}$ (ΔE) [mV][b]	−570 (90)	−670 (95)	−550 (80)
E_p^A [mV]	390	345	270
ΔE_{Fc} [mV]	130	155	125
elemental analysis	C: 80.17/*80.30*	C: 75.26/*74.27*	C: 69.77/*68.71*
calculated/*found*	H: 6.23/*5.82*[c]	H: 6.79/*7.03*	H: 6.54/*6.58*

[a] The *g* factors and hyperfine splitting constants were obtained by simulation of the experimental spectra. – [b] All measurements were performed in CH_2Cl_2 solutions; the potentials are given relative to the SCE electrode. – [c] Calculated for **2a** · 2.5 toluene.

All compounds show an EPR pattern characteristic of pentacoordinated [*tripod*Co^{II}L$_2$] species (Table 1).[2c] Solution EPR spectra at 25 °C (Figure 1, top) revealed the presence of two species with individual *g* factors and hyperfine splitting constants (Figure 1, middle spectra) which, by analogy to literature data, were interpreted as being due to idealised square pyramidal and idealised trigonal bipyramidal coordination modes.[2c] Powder EPR spectra (25 °C and −173 °C) show only one broad resonance with no resolved coupling to the ^{57}Co ($I = {}^7/_2$) nucleus (Table 1).

Cobalt(I) Derivatives

Cyclovoltammetric studies of **2a** in CH_2Cl_2 indicated that compounds **2** should undergo one-electron reduction to produce the corresponding anionic Co^I species [*tripod*Co(C≡CR)$_2$]$^-$ (Table 1). Reversible reduction of **2a** is observed at −574 mV with reference to a SCE (Table 1). Treating **2a** with an equimolar amount of Cp_2Co in toluene led to a brown powder similar to **2a** in colour. FAB-negative mass spectra of this powder show a signal for **2a**$^-$ (*m/z* = 885), while FAB-positive mass spectra demonstrate the presence of $CpCo^+$ (*m/z* = 189).

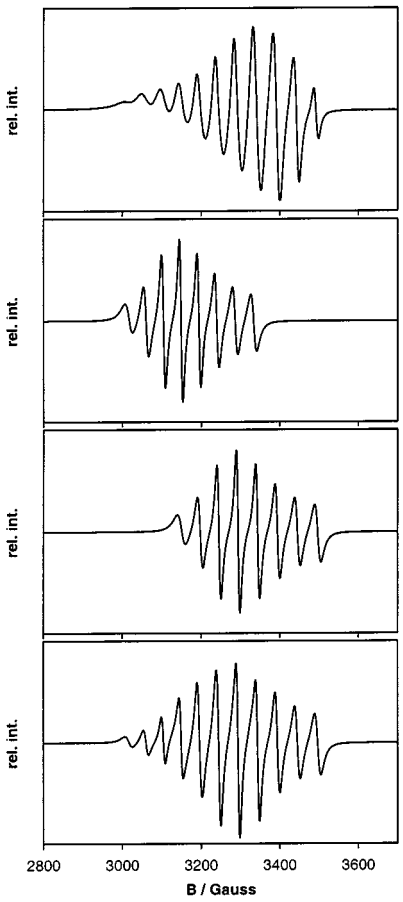
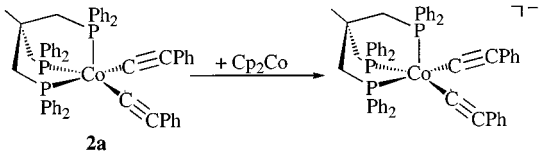
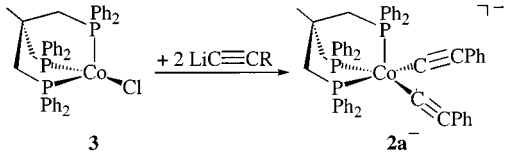


Figure 1. EPR spectrum of **2b** in THF at 298 K (top), simulations of the two individual components (middle) and composed simulated spectrum (bottom)



Due to difficulties in the purification of the [Cp_2Co][*tripod*Co(C≡CPh)$_2$] salt, a different preparative strategy to produce **2a**$^-$ was used. The cobalt(I) compound [*tripod*CoCl] (**3**)[2a,2b] was reacted with two equivalents of LiC≡CPh to produce the cobaltate(I) compound **2a**$^-$, which was isolated as its PPh_4^+ salt.

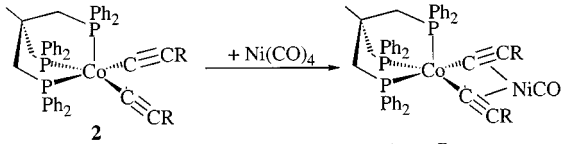


Elemental analysis and mass spectra are in agreement with the assigned structure (see Experimental Section). The ν(CC) vibration of **2a**$^-$ at 2049 cm^{-1} (see Experimental Section) is shifted to a lower wave number than that of **2a**

(2068 cm^{-1}) (Table 1), as would be expected if some charge is delocalised into the π-system of the ligand. Owing to the prolonged measuring time required, ^{13}C NMR spectra of the sensitive PPh_4^+**2a**$^-$ could not be obtained. A sharp ^{31}P NMR signal at δ = 32.1 and a well-resolved ^1H NMR spectrum clearly show that **2a**$^-$ is a diamagnetic Co^I compound. Anion **2a**$^-$ conforms to the 18-electron rule, and this may be one of the reasons for the observation that, regardless of the stoichiometry of LiC≡CPh and **3** (2:1 or 1:1), **2a**$^-$ is inevitably obtained and there is no indication of the formation of [*tripod*CoC≡CPh].

Reactions of the Bisalkynyl Compounds 2

The propensity of **2** to act as a π-tweezer compound is seen by the reaction of **2** with $Ni(CO)_4$ to give compounds **4**. A NiCO moiety is retained in the π-tweezer entity of **2**.



2

	R
4a	Phenyl
4b	tert. Butyl
4c	Trimethylsilyl

The structure of compounds **4** is in agreement with their analytical and spectroscopic data. Mass spectra of **4** show a prominent peak for [M^+ − CO] in each case (Table 2). The presence of the coordinated carbonyl group is evident from the corresponding ν(CO) IR bands for all compounds **4** (Table 2). This prominent band is observed at about 2000 cm^{-1}, which is in good agreement with the observation of the corresponding bands in π-tweezer compounds [$(RCp)_2M(C{\equiv}CR)_2{-}NiCO$] (M = Ti, Zr, Hf) at about the same wavenumbers.[9] This indicates that direct metal−nickel interactions are not really very important for the stability of this type of compound; if they were, the CO group would be sensitive to the presence of different types of L_nM entities to which the alkynyl groups are bound in [$L_nM(C{\equiv}CR)_2$].[9] In agreement with this interpretation is the observation that cyclovoltammetric reduction of **4b** (−605 mV vs. SCE, see Experimental Section) occurs at about the same potential as that of **2a** (−574 mV vs. SCE, Table 1). Compounds **4** are paramagnetic as are the parent compounds **2** from which they are derived. The EPR spectra of compounds **4** (Table 2) closely resemble those of **2** (Table 1) with only minor changes in *g* values and coupling constants. With **4c**, the hyperfine structure is not resolved and one broad resonance is observed at $g \approx 2.05$. The fact that two overlapping signals are observed for **4**, with the spectral pattern being similar to that observed for the parent compounds **2**, may be explained by the same type of reasoning as discussed for **2**. With **4**, it is of course necessary to assume that the bisalkynyl-Ni moiety changes place as a single unit such that the idealised trigonal bipyramidal and idealised square pyramidal coordination geometries may interchange.

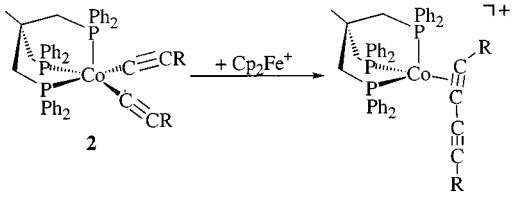
Table 2. Analytical data for compounds **4**

Compound	**4a**	**4b**	**4c**
EPR (298 K, THF))	$g_1 = 2.11$, $A_1 = 45$ G $g_2 = 2.02$, $A_2 = 48$ G	$g_1 = 2.11$, $A_1 = 48$ G $g_2 = 2.02$, $A_2 = 49$ G	$g \approx 2.005$
IR: $\tilde{\nu}$ CO [cm^{-1}]	1999 (s)	2001 (s)	2000 (s)
MS-FAB: *m/z* [frag.]	885 [M^+ − NiCO] 944 [M^+ − CO]	845 [M^+ − NiCO] 904 [M^+ − CO]	936 [M^+ − CO]
elemental analysis calculated/*found*	C: 71.63/*72.97* H: 5.08/*5.50*	C: 69.55/*67.49* H: 6.16/*6.31*	C: 60.14/*58.20* H: 5.70/*5.81*[a]

[a] Calculated for **4c** · 2 CH_2Cl_2.

In the chemistry of π-tweezer ligands, Cu^I and Ag^I have been found to be specifically prone to engage in bonding with π-tweezers.[9c] When solutions of **2** are treated with salts of these cations, however, the reaction is complicated by the propensity of **2** towards oxidation. Cyclovoltammetry of **2a** shows that the compound is irreversibly oxidised (Table 1) and this is what presumably happens when compounds **2** are treated with potentially oxidising metal ions.

Preparative oxidation of **2** with Cp_2Fe^+ results in a transformation of **2** into **5**.



2

	R
5a	Phenyl
5b	tert. Butyl
5c	Trimethylsilyl

The alkynyl groups of **2** undergo oxidative coupling to result in 1,3-diyne ligands with one of the two triple bonds being coordinated to the cobalt centre. The process is brought about by a single-electron transfer-step such that, while the alkyne groups are oxidised in a formal two-electron oxidation, the cobalt centre is reduced from Co^{II} in **2** to Co^I in **5**. The coupling of σ-bonded alkynyl compounds is not without precedent: with rhodium as the central atom in [$Rh^{III}(C{\equiv}C{-}Ph)_2(SnPh_3)(PiPr_3)_2$], oxidative coupling by I_2 to give *trans*-[$Rh^I(\eta^2$-Ph*C*≡*C*C≡CPh)($PiPr_3$)$_2$I] is formally similar to the transformation of **2** into **5**, since reduction of the central metal (in this case reduction of Rh^{III} to Rh^I) necessarily accompanies the oxidative coupling of the alkynyl ligands.[10,11]

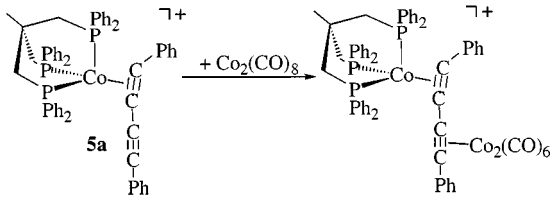
The salts **5**·PF_6 are obtained as analytically and spectroscopically pure green powders (Table 3) which show the peak for the molecular ion in their FAB mass spectra in each case. They are diamagnetic and show well-resolved NMR spectra. Their ^{31}P NMR resonances are observed in the range δ = 35 to 38 (Table 3). ^1H and ^{13}C NMR spectra reveal the signals of each constitutional group in the expected range (Table 3). The presence of one coordinated and one uncoordinated triple bond is evident from the corresponding ^{13}C NMR signals (Table 3). The presence of an

uncoordinated triple bond is also indicated by a weak ν(CC) IR band at 2100−2200 cm^{-1} (Table 3). Chemical proof for the existence of an uncoordinated reactive triple bond is found in the reaction of **5a** with $[Co_2(CO)_8]$.

Table 3. Analytical data for compounds **5**

Compound	5a	5b	5c
^{1}H NMR[a]			
tripod-CH_3	1.96 b, 3 H	1.83 b, 3H	1.95 b, 3 H
tripod-CH_2	2.68 b, 6 H	2.53 b, 6H	2.60 b, 6 H
aromat. H	7.07–7.54 m, 40 H	7.06–7.85 m, 30 H	7.01–7.30 m, 30 H
*t*Bu/$SiMe_3$[b]		1.36 br. s, 9 H	0.11 s, 18 H
		1.50 br. s, 9 H	
^{31}P NMR			
PPh_2	37.8 s	35.4 s	37.3 s
PF_6	−144.2 sept, $^1J_{PF}$ = 713 Hz	−144.2 sept, $^1J_{PF}$ = 713 Hz	−144.2 sept, $^1J_{PF}$ = 713 Hz
^{13}C{^{1}H} NMR			[c]
tripod-CH_3	36.6 m	36.6 m	
tripod-CH_2	32.6 m	33.3 m	
tripod-C_q	39.5 s	37.8	
aromat. C	123.8–133.6	128.8–133.9	
CH_3(*t*Bu)		30.5 s	
C_q(*t*Bu)		41.0 s	
C≡C	86.7 s; 100.8 s	77.3 s; 100.6 s	
Co-η^2-**C≡C**	163.3 s; 181.6 s	164.0 s; 200.9 s	
MS-FAB: *m/z* [frag.]	885 [M^+]	845 [M^+]	877 [M^+]
IR: $\tilde{\nu}$ PF [cm^{-1}]	846 (s)	843 (s)	840 (s)
IR: $\tilde{\nu}$ CC [cm^{-1}]	2155 (w)	2218 (w)	2121 (w)
elemental analysis:	C: 66.42/65.89	C: 64.24/*63.69*	C: 59.88/*60.13*
calculated/*found*	H: 4.79/5.01	H: 5.80/*6.21*	H: 5.62/*5.90*
HR-FAB: *m/z*		683.1597/*683.1547*	
calculated/*found*		845.3006/*845.2968*	

[a] All NMR measurements were performed in CD_2Cl_2. – [b] *t*Bu for **5b**, $SiMe_3$ for **5c**. – [c] No ^{13}C NMR data could be obtained owing to decomposition of the compound during the measurement.



This reaction, as performed under standard conditions, gives $[tripodCo(\eta^2\text{-}PhC{\equiv}CC{\equiv}CPh{-}Co_2(CO)_6)]^+$ as the main product.[12] This is apparent from the FAB mass spectra of its PF_6 salt which show the molecular ion (*m/z* = 1171, see Experimental Section) together with the peaks corresponding to the consecutive loss of up to five CO groups. The last CO group is lost together with the Co_2 entity, which was part of the coordinated $Co_2(CO)_6$ unit, apparently in one step leading to the mass peak of $[tripodCo(\eta^2\text{-}PhC{\equiv}CC{\equiv}CPh)]^+$ **5a**. The IR data of the $Co_2(CO)_6$ adduct of **5a** are also in agreement with its formulation as **5a**·$Co_2(CO)_6$ (see Experimental Section).[12] The ^{31}P NMR resonance of this compound is found at δ = 36.9 (see Experimental Section). Under carbonylating conditions, the carbonyl derivative $[tripodCo(CO)_2]^+$ is formed as a minor side-product, as indicated by its ^{31}P NMR resonance at δ = 24.1 (see Experimental Section) and by the FAB-MS signal of the molecular ion (*m/z* = 739, see Experimental Section).[2f] This observation also shows that the diyne, once it has been formed as a ligand at the [*tripod*Co] template, can be set free from the metal by extensive carbonylation.[13] The presence of the PF_6 counterion is corroborated by a strong ν(PF) vibration and by the corresponding ^{31}P NMR signal in each case (Table 3).

The structure of **5** is confirmed by an X-ray analysis of the PF_6 salt of **5b** (Table 4 and 5). A general view of **5b** is given in Figure 2 (left), as well as a projection of the structure onto the plane of the three phosphorus atoms (right).

Table 4. Bond lengths [pm], bond angles [°] and torsion angles [°] for **5b**

Co–P1	218.91 (15)
Co–P2	216.19 (14)
Co–P3	223.53 (17)
Co–C6	187.5 (5)
Co–C7	186.4 (5)
C6–C7	131.3 (8)
C7–C8	140.0 (8)
C8–C9	120.0 (8)
P1–Co–P2	84.57 (6)
P1–Co–P3	96.31 (6)
P2–Co–P3	92.48 (6)
C14–C6–C7	134.5 (5)
C6–C7–C8	140.1 (5)
C7–C8–C9	178.6 (6)
C8–C9–C10	177.8 (6)
C4–C1–P1–Co	12.5
C4–C2–P2–Co	34.9
C4–C3–P3–Co	31.0
Hz1–P1–C100–C101[a]	–18.6
Hz1–P1–C106–C107[a]	–6.1
Hz2–P2–C200–C201[a]	–2.4
Hz2–P2–C206–C207[a]	–2.9
Hz3–P3–C300–C301[a]	–34.1
Hz3–P3–C306–C307[a]	–74.0

[a] These torsion angles are defined with respect to auxiliary vectors Hz_x–P_x (x = 1–3) orthogonal to the plane spanned by the three P atoms and pointing towards the observer with respect to the orientation shown in Figure 2 (right): Hz_x–P_x–C_{ipso}–C_{ortho}.

Table 5. Crystal data for compound **5b**

Formula	$C_{53}H_{57}CoF_6P_4 \cdot 0.5$ THF
Molecular mass	1026.85
Crystal system	triclinic
Space group (no.)	*P*1bar (2)
a [pm]	1241.37 (2)
b [pm]	1469.37 (2)
c [pm]	1632.39 (1)
α [°]	84.1010 (0)
β [°]	77.268 (1)
γ [°]	69.723 (0)
Cell volume [10^6 pm^3]	2723.20(6)
Molecular units per cell	*Z* = 2
Density (calcd) [g cm^{-3}]	1.252
T [K]	296
Scan range	4.0° ≤ 2Θ ≤ 54.4°
Scan speed	10 sec/frame
Measured reflections	21864
Unique reflections	9137
Obs. reflections ($I \geq 2\sigma$)	4903
Parameters refined	614
Max. of residual electron density [10^{-6} e pm^{-3}]	0.69
Agreement factors	R_1 = 7.2%
(F^2 refinement)	R_w = 20.6%

From this second view in Figure 2, it becomes clear that there are at least two sets of chemically different phosphorus nuclei in **5b**. The fact that only one ^{31}P NMR signal

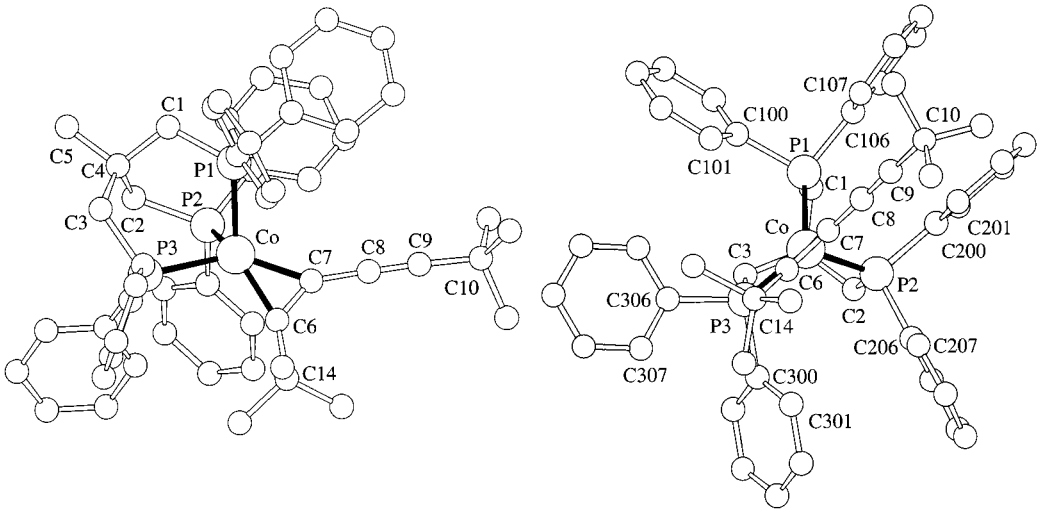


Figure 2. General view and projection of the structure of the cation of **5b**

is observed means that the coordinated alkyne group is free to adopt different rotational positions relative to the [*tripod*Co] scaffolding, with the vector radiating from the cobalt centre to the midpoint of the coordinated alkyne bond (C6−C7) interpreted as the axis of this rotation. With the coordinated alkyne bond seen as just one donor ligand, the coordination geometry around the cobalt may be described as idealised tetrahedral.

The *t*Bu substituent of the alkyne in **5b** makes the coordinated triple bond a rather bulky one. The rotational position of the alkyne ligand is such that the *t*Bu substituent (C14, Figure 2) of the coordinated alkyne ligand (C6−C7, Figure 2) is in an eclipsed position with respect to the Co−P3 bond. It follows that the *t*Bu−C≡C substituent (C8−C9−C10, Figure 2) at the other carbon centre of the coordinated alkyne (C7, Figure 2) is in a staggered position with respect to the Co−P1 and Co−P2 bonds (Figure 2). The steric strain imposed by the orientation of the alkyne ligand is mirrored by the geometric parameters of the $Co-P_3$ part of the compound. The distance Co−P3 (224 pm) is distinctly larger than the Co−P1 (220 pm) and Co−P2 (216 pm) distances. The P3−Co−P2 (92.5°) and P3−Co−P1 (96.3°) angles are definitely larger than the angle between the Co−P1 and Co−P2 bonds (84.6°). The rotational positions of the "phenyl-petals" also respond to this steric strain; the phenyl groups at P3 show distinctly larger rotation angles than those at P1 and P2 (Figure 2, Table 5).

The coordinated triple bond (C6−C7: 131.3 pm, Table 4 and 5) is approximately 11 pm longer than the uncoordinated one (C8−C9: 120.0 pm, Table 4 and 5). As expected, the coordination around the carbon atoms of the free triple bond is linear (C7−C8−C9: 176.6°; C8−C9−C10: 177.8°, Table 4 and 5), but the bond angles at the carbon atoms of the coordinated triple bond (C14−C6−C7: 134.5°; C6−C7−C8: 140.1°, Table 4 and 5) are distinctly different from 180°. The degree of this bending and the lengthening of the coordinated bond are indicative of a strong interaction between the alkyne and the metal.[15]

Based on the formalism of electron counting, the alkynes in **5** should act as four-electron donors since the compounds are diamagnetic and behave as 18-electron compounds,[14] while a 16-electron species [*tripod*CoL]$^+$ with L acting as a two-electron donor should be paramagnetic.[4−7] This follows from simple crystal-field-type arguments as well as from experience.[4−7,14] Assuming that the alkyne ligands in **5** act as four-electron donor moieties is in good agreement with the established rules correlating the ^{13}C NMR resonances of coordinated alkyne groups with the number of electrons which these groups donate to the metal.[15] The signals of the carbon atoms of the coordinated alkyne group in **5a** are observed at approximately δ = 160−180 and those of **5b** occur at δ = 164−200 (Table 3). The uncoordinated triple bonds give rise to signals between δ = 77 and δ = 101 in these compounds (Table 3). These latter shift values compare favourably with the ^{13}C NMR shifts reported for uncoordinated 1,3-diynes. In cobalt(I) compounds in which alkyne ligands can only act as two-electron donors (due to the electron count), ^{13}C NMR resonances of δ ≈ 100 are generally observed.[16] The C−C bond lengths in these compounds are found to be about 127 pm, which is definitely shorter than the C6−C7 distance (131 pm, Table 5) in **5b** where the alkyne acts as a four-electron donor.[16b]

The bonding of acetylenes at [*tripod*Co]$^+$ fragments has previously been reported, although no NMR spectroscopic data were given.[17]

Conclusion

*tripod*Co-bisalkyne compounds are easily prepared by the reaction of *tripod*Co-halides with LiC≡CR. Starting from [*tripod*$CoCl_2$] (**1**), neutral Co^{II} derivatives [*tripod*$Co(C{\equiv}CR)_2$] **(2)** are obtained. Anionic Co^{I} derivatives [*tripod*$Co(C{\equiv}CR)_2]^-$ **(2^-)** are found when [*tripod*CoCl] **(3)** is used as the starting material. The bisalkynyl compounds **2** are found to act as π-tweezer ligands with Ni(CO). It is

observed that they undergo one-electron oxidation which results in oxidative coupling of the alkynyl ligands to produce 1,3-diynes and concomitant reduction of Co^{II} to Co^{I} to produce $[tripodCo(\eta^2\text{-}RC{\equiv}CC{\equiv}CR)]^+$ **(5)**.

Experimental Section

General Remarks: Unless otherwise noted, all manipulations were carried out under argon by means of standard Schlenk techniques All solvents were dried by standard methods and distilled under argon.[18] The CD_2Cl_2 used for NMR spectroscopic measurements was degassed by three successive "freeze-pump-thaw" cycles and dried with 4 Å molecular sieves. − EPR: Bruker ESP 300 E, X-band, standard cavity ER 4102, temperature control unit Eurotherm B-VT 2000, external standard dipenylpicrylhydrazyl (DPPH); Simulation: XSophe Computer Simulation Software Suite, Version 1.0.4b, 1993−1999; XEPRView, Version 1.0, 1999; Bruker Analytik, Rheinstetten, Germany. − NMR: Bruker Avance DPX 200 at 200.12 MHz (^{1}H), 50.323 MHz (^{13}C{^{1}H}), 81.015 MHz (^{31}P{^{1}H}), T = 303 K; chemical shifts (δ) are given in ppm with respect to CD_2Cl_2 (^{1}H: δ = 5.32; ^{13}C: δ = 53.8) as internal standard. ^{31}P chemical shifts (δ) are given in ppm with respect to 85% H_3PO_4 (^{31}P: δ = 0) as external standard. − IR: Bruker IFS-66, KBr disks. − MS: Finnigan MAT 8230; Fast-atom bombardment (FAB) xenon, matrix: 4-nitrobenzyl alcohol. − HR-MS (FAB) JEOL JMS 700, matrix: 4-nitrobenzyl alcohol. − Magnetic measurements: Faraday balance with a Bruker electromagnet B-E 15 C8, Bruker Field Controller B-H 15, Sartorius vacuum-microbalance M25 D-S, Oxford Temperature Control Unit ITC-4; calibration with $K_3[Fe(CN)_6]$. − Molecular weight determinations: Knauer vapor-pressure osmometer No. 7311100000; calibration with dibenzil. − Elemental analyses: Microanalytical Laboratory of the Organisch-Chemisches Institut, Universität Heidelberg. − Melting points: Gallenkamp MFB-595 010, melting points are not corrected. − Cyclic voltammetry: Metrohm "Universal Meß- und Titriergefäß", Metrohm GC electrode RDE 628, platinum electrode, SCE electrode, Princeton Applied Research potentiostate Model 273, 10^{-3} M in 0.1 M nBu$_4$NPF$_6$/CH_2Cl_2.

General Procedure for the Synthesis of Compounds 2: Alkyne (2 mmol) was dissolved in Et_2O (5 mL) and deprotonated with nBuLi (0.8 mL, 2.5 M in n-hexane) at −80 °C. After 5 min, the reaction mixture was allowed to warm to room temperature. [$tripod$CoCl$_2$] (1 mmol, 753 mg) was dissolved in THF (25 mL) and cooled to −80 °C. The acetylide was added at −80 °C with a syringe, and a brown solution was immediately formed. After 10 min at −80 °C, the reaction mixture was allowed to warm to room temperature and the solvent was removed under reduced pressure. The resulting black-brown residue was dissolved in toluene and filtered to remove LiCl. After evaporation of the solvent, compounds **2** were obtained as microcrystalline black-brown powders. Attempts to obtain crystals suitable for X-ray crystallography were unsuccessful. Compounds **2** are highly soluble in organic solvents such as hexane, toluene, Et_2O, and methanol such that crystallisation by diffusion is unfeasible; slow evaporation of the solvent leaves them as microcrystalline powders only. Cooling the solutions down to −80 °C also did not result in single crystals.

μ_{eff} (**2a**, 25 °C) = 1.8 BM; osmometric determination of the molecular mass of compound **2a**: calcd./found: 885/887.

Preparation of PPh$_4$[$tripod$Co^{I}-(C≡CPh)$_2$], PPh$_4^+$2a$^-$: [$tripod$CoCl] **(3)** (1 mmol, 718 mg) was suspended in THF (20 mL). LiC≡CPh (2 mmol) in Et_2O (5 mL) was added at −80 °C. The reaction mixture was stirred for 10 min at this temperature and then allowed to warm to 25 °C resulting in a colour change from beige to red-brown. The solvent was evaporated and the residue dissolved in CH_2Cl_2. Ph_4PCl (1 mmol, 375 mg) was added and the reaction mixture stirred for 20 min. After removal of the solvent under reduced pressure, the residue was redissolved in toluene and filtered to remove LiCl. Evaporation of the solvent produced PPh_4^+**2a**$^-$ as a red-brown, air-sensitive powder. − ^{1}H NMR (CD_2Cl_2): δ = 1.28 (br. s, 3 H, CH_3), 2.46 (br. s, 6 H, CH_2), 7.07−7.48 (m, 60 H, H_{ar}). − ^{31}P NMR (CD_2Cl_2): δ = 26.8 (s, PPh$_4^+$), 32.1 (s, CH_2-P). − IR (KBr): ν(CC) = 2049 (w) cm^{-1}. − MS (FAB-negative): m/z = 885 [M$^-$]. − $C_{81}H_{69}CoP_4$ (1225.27): calcd. C 79.40, H 5.68; found C 78.21, H 5.82. − M.p. 145 °C (dec.).

General Procedure for the Synthesis of Compounds 4: Compound **2** (1 mmol) was dissolved in toluene and treated with a threefold excess of $Ni(CO)_4$. The reaction mixture was stirred for 2 h. No colour change took place, but a slow gas evolution was observed. The solvent was removed under reduced pressure and the residue recrystallised from CH_2Cl_2. After evaporation of the solvent, compounds **4** were obtained as black-brown microcrystalline powders.

CV (**4b**, CH_2Cl_2, vs. SCE): $E_{1/2}$ = 605 mV (rev.), ΔE = 90 mV.

General Procedure for the Synthesis of Compounds 5: Compound **2** (1 mmol) was dissolved in acetone (25 mL) and treated with $(Cp_2Fe)PF_6$ (1 mmol, 332 mg). The colour immediately changed from black-brown to green. The solvent was removed under reduced pressure and the resulting green residue was purified by chromatography on SiO_2 (ICN 32−63, 60 Å) with PE (boiling range 40−60 °C)/CH_2Cl_2 (5:1). After evaporation of the solvent, the PF_6 salts **5a**−**c** were obtained as fine black-green powders. Single crystals of compound **5b** suitable for X-ray diffraction were obtained after three months by diffusion of PE (boiling range 40−60 °C) into a solution of **5b** in THF.

Preparation of 5a·Co$_2$(CO)$_6$: Compound **5a** (0.1 mmol, 103 mg) was dissolved in acetone (10 mL). [$Co_2(CO)_8$] (0.15 mmol, 52 mg) was added and the reaction mixture was stirred for 1.5 h. A darkening of the solution was evident after a few minutes. The solvent was removed under reduced pressure and the residue was washed three times with Et_2O. After evaporation of the solvent, the $Co_2(CO)_6$ adduct of **5a** was obtained as a black microcrystalline powder.

^{31}P NMR (CD_2Cl_2): δ = 36.9 (s, CH_2-P). − IR (KBr): ν(CO) = 2100 (s), 2083 (s), 2054 (s), 2034 (s) cm^{-1}. − MS (FAB): m/z = 1171 [M$^+$], 1143 [M$^+$ − CO], 1115 [M$^+$ − 2CO], 1087 [M$^+$ − 3CO], 1059 [M$^+$ − 4CO], 1031 [M$^+$ − 5CO], 885 [M$^+$ − $Co_2(CO)_6$].

X-ray Crystallographic Study: The measurement was carried out on a Siemens AXS Smart CCD diffractometer using graphite-monochromated Mo-K_α radiation. All calculations were performed using the SHELXT PLUS software package. The structure was solved by direct methods with the SHELXS-97 program and refined with the SHELXL-97 program.[19] Graphical handling of the structural data during solution and refinement was performed with XPMA.[20] Atomic coordinates and anisotropic thermal parameters of the non-hydrogen atoms were refined by full-matrix least-squares calculations. Table 5 lists the data for the structure determination.

Crystallographic data (excluding structure factors) for the structure reported in this paper have been deposited with the Cambridge Crystallographic Data Centre as supplementary publication

no. CCDC-133001. Copies of data can be obtained free of charge on application to CCDC, 12 Union Road, Cambridge, Cambridge CB2 1EZ, UK [Fax: (internat.) +44-1223/336-033; E-mail: deposit@ccdc.cam.ac.uk].

Acknowledgments

We are indebted to the Deutsche Forschungsgemeinschaft (SFB 247) and the Fonds der Chemischen Industrie for financial support. One of us (R. R.) is indebted to the Graduiertenkolleg "Selektivität in der organischen und metallorganischen Synthese und Katalyse" for a scholarship. The unselfish cooperation of Dr. J. Groß and Mr. T. Jannack (MS); Mr. D. Günauer (CV) and Mrs. A. Dittes; Mrs. C. Vetter, Mrs. E. Weiß and Mr. F. Liebscher (elemental analysis) is gratefully acknowledged.

[1] L. Sacconi, F. Mani, *Trans. Met. Chem*. **1982**, *8*, 179−252.
[2] For further references see: [2a] L. Sacconi, S. Midollini, *J. Chem. Soc., Dalton Trans.* **1972**, 1213−1216. − [2b] K. Heinze, G. Huttner, L. Zsolnai, P. Schober, *Inorg. Chem*. **1997**, *36*, 5457−5469. − [2c] C. Bianchini, D. Masi, C. Mealli, *Inorg. Chem*. **1987**, *26*, 3683−3693. − [2d] S. Vogel, G. Huttner, L. Zsolnai, *Z. Naturforsch*. **1993**, *48b*, 641−652. − [2e] K. Heinze, G. Huttner, L. Zsolnai, A. Jacobi, P. Schober, *Chem. Eur. J.* **1997**, *3*, 732−743. − [2f] J. Ellerman, J. F. Schindler, *Z. Naturforsch*. **1975**, *30b*, 914−919. − [2g] A. Asam, B. Janssen, G. Huttner, L. Zsolnai, O. Walter, *Z. Naturforsch*. **1993**, *48b*, 1707−1714.
[3] [*tripod*CoCp]$^{2+}$ is a formal exception to the rule that [*tripod*CoL$_2$]$^{n+}$ compounds are five-coordinate in general.
[4] V. Sernau, G. Huttner, J. Scherer, O. Walter, *Chem. Ber*. **1996**, *129*, 243−245.
[5] P. Dapporto, S. Midollini, A. Orlandini, L. Sacconi, *Inorg. Chem*. **1976**, *11*, 2768−2770.
[6] S. Vogel, G. Huttner, L. Zsolnai, C. Emmerich, *Z. Naturforsch*. **1993**, *48b*, 353−363.
[7] J. Ellermann, J. F. Schindler, *Chem. Ber*. **1976**, *109*, 1095−1105.
[8] F. Cecconi, C. A. Ghilardi, S. Midollini, S. Moneti, A. Orlandini, M. Bacci, *J. Chem. Soc., Chem. Commun.* **1985**, 731.
[9] [9a] K. Yasufuku, H. Yamazaki, *Bull. Chem. Soc. Jpn*. **1972**, *45*, 2664. − [9b] H. Lang, M. Herres, L. Zsolnai, *Bull. Chem. Soc. Jpn.* **1993**, *66*, 429−431. − [9c] S. Back, G. Rheinwald, L. Zsolnai, G. Huttner, H. Lang, *J. Organomet. Chem*. **1998**, *563*, 73−79.
[10] [10a] E. H. Smith, J. Whittall, *Organometallics* **1994**, *13*, 5169−5172. − [10b] H. F. Klein, M. Heiden, M. He, T. Jung, C. Röhr, *Organometallics* **1997**, *16*, 2003−2004.
[11] H. Werner, O. Gevert, P. Haquette, *Organometallics* **1997**, *16*, 803−806.
[12] See for example: D. Osella, L. Milone, C. Nervi, M. Ravera, *Eur. J. Inorg. Chem*. **1998**, 1473−1477.
[13] V. Körner, Ph. D. Dissertation, Universität Heidelberg, **1996**.
[14] C. Elschenbroich, A. Salzer, *Organometallics* 2nd ed., VCH, Weinheim, **1992**.
[15] J. L. Templeton, B. C. Ward, *J. Am. Chem. Soc*. **1980**, *102*, 3288−3290.
[16] [16a] R. T. Kettenbach, W. Bonrath, H. Butenschön, *Chem. Ber.* **1993**, *126*, 1657−1669. − [16b] C. Benisch, J. Chavez, R. Gleiter, B. Nuber, H. Irngartinger, T. Oeser, H. Pritzkow, F. Rominger, *Eur. J. Inorg. Chem*. **1998**, 629−632.
[17] C. Bianchini, P. Dapporto, A. Meli, L. Sacconi, *J. Organomet. Chem*. **1980**, *193*, 117−126.
[18] *Organikum*, Deutscher Verlag der Wissenschaften, Berlin **1990**.
[19] [19a] G. M. Sheldrick, *SHELXS-97, Program for Crystal Structure Solution*, University of Göttingen, **1997**. − [19b] G. M. Sheldrick, *SHELXL-97, Program for Crystal Structure Refinement*, University of Göttingen, **1997**; http://shelx.uni-ac.gwdg.de/SHELX/index.html.
[20] L. Zsolnai, G. Huttner, *XPMA*, Universität Heidelberg **1994**, http://www.rzuser.uni-heidelberg.de/v54/xpm.html.

Received February 15, 2000
[I00058]

Ferric-Chloride-Promoted Oxidation of *p*-Anisidine to an *N*-Substituted Phenazine Derivative − Structural Elucidation, Protic Equilibria and Coordination Chemistry of the Phenazine

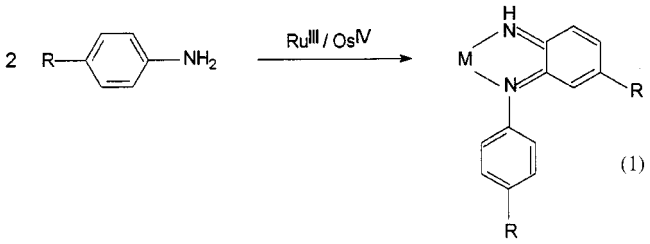
Amit K. Ghosh,[a] Kedar N. Mitra,[a] Golam Mostafa,[b] and Sreebrata Goswami*[a]

Keywords: C−N Bond formation / Oxidations / Polymerizations / Ruthenium / Osmium / Coordination chemistry / $FeCl_3$-promoted reactions

The reaction of hydrated ferric chloride and *p*-anisidine affords brown 6-*p*-anisyl-2-(*p*-anisylamino)-9-methoxy phenazine-3(4*H*)-*p*-anisylimine (LH) in moderate yield (35%). Plausible steps involved in this unusual fusion process are proposed. This phenazine spontaneously binds with H^+ to give a violet solution, p*K* for the reaction LH + $H^+ \rightleftarrows LH_2^+$ is 6.61 at 300 K. The protonated phenazine has been isolated as its chloride salt, $[LH_2Cl]$, the structure of which is described in authenticating the formation of LH directly from *p*-anisidine. The structural data reveal a planar dibenzo pyrazine moiety with an extensive delocalisation along the phenazine backbone. The protonation of LH occurs at the imine nitrogen. The spectral properties of both LH and $[LH_2]Cl$ are described. Both show well-resolved ^1H NMR spectra with four methyl resonances occurring in the range δ = 3.70 to 3.93. While $[LH_2]Cl$ shows two NH resonances at δ = 11.95 and 10.18, neutral LH displays only one such resonance at δ = 8.49. Aromatic proton resonances for these compounds appeared in the range δ = 5.79 to 8.04. The coordination abilities of the above phenazine were explored. It reacts spontaneously with $[M(aap)_2X_2]^{n+}$ (M = Ru^{II}, Os^{II}; aap = 2-(arylazo)pyridine; X = solvent, *n* = 2; X = Br^-, *n* = 0) to give cationic complexes of the general formula, $[M(aap)_2L]^+$ which were isolated as their perchlorate and bromide salts. These metal complexes were fully characterized. Their spectral properties indicate a bidentate anionic chelation of L^-, with deprotonation of the amine nitrogen. The complexes show multiple redox responses. The oxidised complexes are unstable and undergo chemical transformations. The reduction processes, on the other hand, are electrochemically reversible and presumably occur at the coordinated aap ligands.

Introduction

This work originated from our interest in metal-promoted oxidative dimerisation and polymerisation reactions of aromatic amines. In this respect, we have recently reported[1−3] the ruthenium(III)- and osmium(IV)-mediated *ortho* dimerisation of primary aromatic amines, $ArNH_2$, leading to *N*-aryl-1,2-diimino arenes [Equation (1)]. It may be relevant to add here that complexes of quinone-related 1,2-diimine ligands are of interest[4,5] in contemporary research and that *N*-substituted 1,2-diimino complexes of the above type were not possible to synthesise by conventional synthetic routes.



(1)

The above transformation is a combination of two major processes: oxidative *ortho* dimerisation of $ArNH_2$ and further oxidation of the resultant dimer would form the diimine ligand. Anodic oxidation of aromatic amines[6] associated with *para* coupling leading to *p*-benzidine or *p*-semidine are common. There are also examples of oxidation of $ArNH_2$ to diazo compounds, Ar−N=N−Ar. Oxidative dimerisation with C−N bond formation, as described in Equation (1), however, was not known in the literature. This transformation occurs only in the presence of O_2, which acts as an oxidising agent. It is proposed that the metal mediates this transformation by holding the amine residues in a suitable juxtaposition and also by taking part in the redox processes. The unusual observations in the above cases of ruthenium and osmium prompted us to seek parallel developments using iron as the mediator. Interestingly, a completely different set of reactions occur with hydrated $FeCl_3$. In this report we disclose our results of the $FeCl_3$-mediated polymerisation reaction of *p*-anisidine to an *N*-substituted phenazine derivative. A literature survey revealed that the formation of an intense violet colour on addition of $FeCl_3$ to a solution containing *p*-anisidine was noticed[7] long ago, but the nature of product of the reaction was not determined.

Successful isolation and characterisation of the above phenazine together with its coordination chemistry invol-

[a] Department of Inorganic Chemistry, Indian Association for the Cultivation of Science,
Calcutta 700 032, India
Fax: (internat.) + 91-33/473-2805
E-mail: icsg@mahendra.iacs.res.in
[b] Department of Physics, Krishnath College,
Berhampur, West Bengal, India

Supporting information for this article is available on the WWW under http://www.wiley-vch.de/home/eurjoc or from the author.

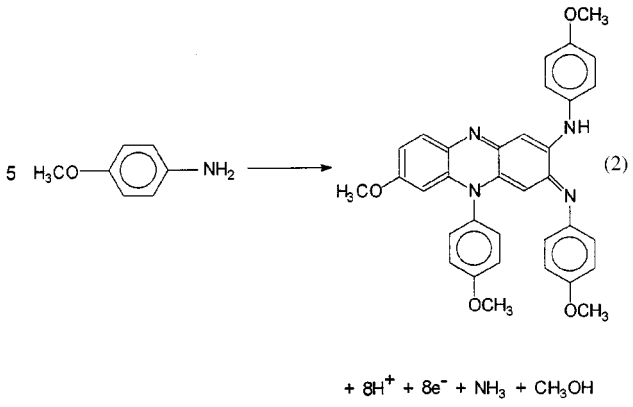
 © WILEY-VCH Verlag GmbH, D-69451 Weinheim, 2000 1434−1948/00/0909−1961 $ 17.50+.50/0

ving ruthenium and osmium constitute the major aspects of this report.

Results and Discussion

The Reaction

The reaction procedure consists of heating a mixture of hydrated $FeCl_3$ (100 mg) and a large excess of *p*-anisidine (2 g) at 120 °C in the air for one hour. The reaction occurs smoothly to produce an intense blue mixture. Usual work up (see Experimental Section) of the mixture followed by column chromatography (silica gel) afforded brown phenazine (LH) as the major product in 35% yield [(Equation (2)].



Beside the brown phenazine band, a mixture of blue and violet bands was also eluted with $CH_3CN/CHCl_3$ (1:4). We are as yet unable to obtain these in the pure state. This reaction only occurs neat and in the presence of O_2. It thus belongs to an example of the reaction class where catalytic activation[8] of dioxygen occurs by a transition metal ion.

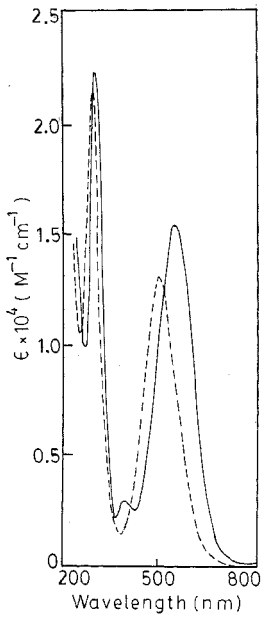


Figure 1. UV/Vis Spectra of LH (-------) and $[LH_2]Cl$ (− −) in acetonitrile

$$LH + H^+ \rightleftarrows LH_2^+ \cdots (3)$$

Characterisation of LH

The brown product isolated from the above reaction showed an intense FAB-MS peak at m/z = 558 confirming the formulation of the compound. The solution spectrum of LH in CH_3CN consists of a strong absorption at 505 nm

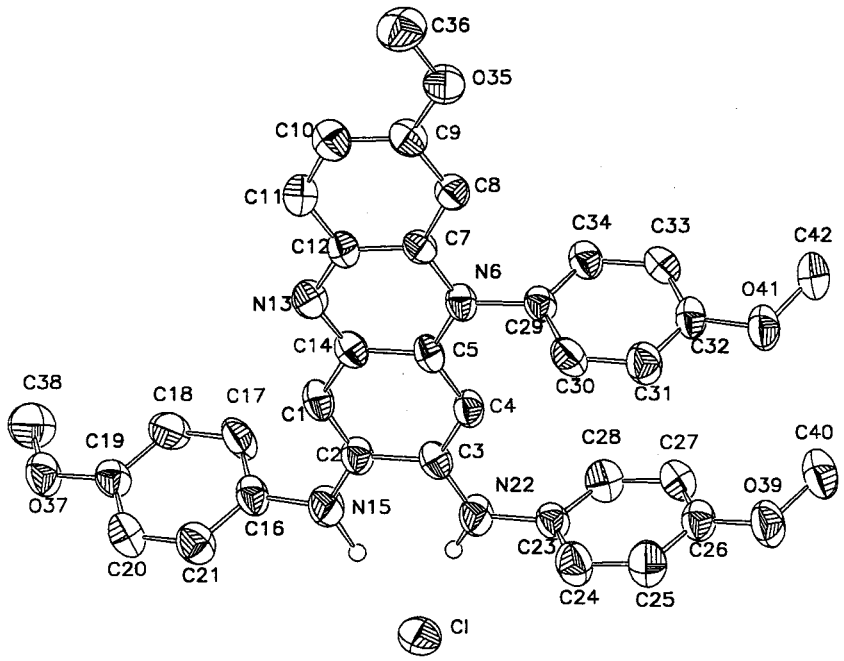
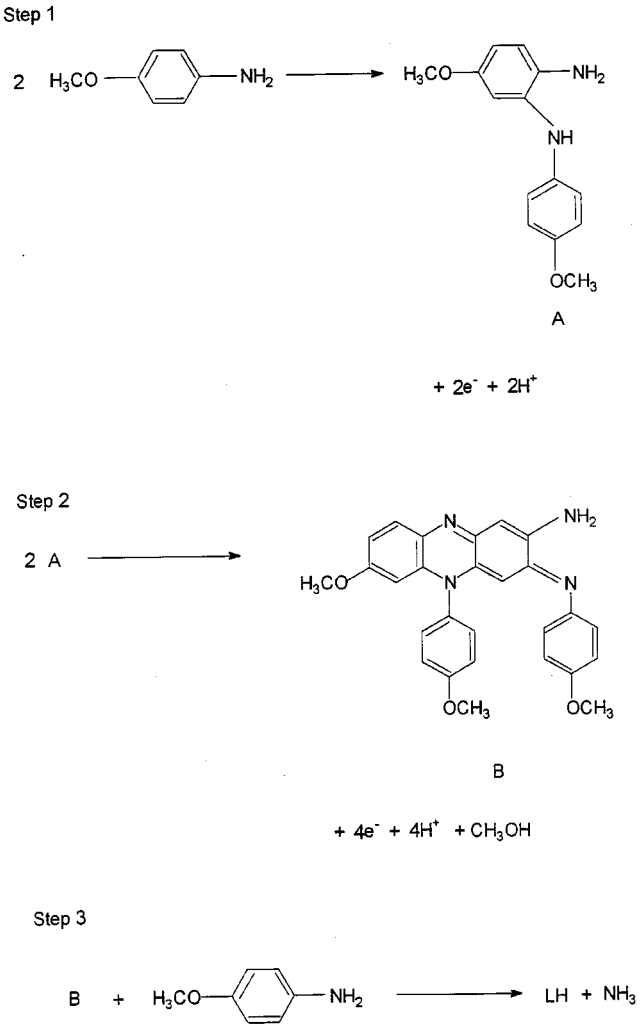


Figure 2. Molecular structure of $[LH_2]Cl$ showing the atom numbering scheme. Selected bond lengths [Å] : N(22)−C(3) 1.356(7), N(22)−C(23) 1.432(7), N(6)−C(5) 1.368(6), N(6)−C(7) 1.399(6), N(6)−C(29) 1.451(6), N(13)−C(14) 1.337(6), N(13)−C(12) 1.359(6), N(15)−C(2) 1.363(7), N(15)−C(16) 1.448(7), C(3)−C(4) 1.390(7), C(4)−C(5) 1.383(7), C(5)−C(14) 1.444(7), C(14)−C(1) 1.410(7), C(1)−C(2) 1.381(7), C(2)−C(3) 1.463(7)



Scheme 1. Plausible steps for the formation of phenazine

which may be attributed to extensive delocalisation (vide infra) along the phenazine backbone. Interestingly, the colour of the above solution became intense violet (λ_{max} 530 nm) on acidification. The spectra of these two are shown in Figure 1 and the spectral change as a function of $[H^+]$ is submitted as supplementary material (Figure S1). There is a sharp isosbestic point at 508 nm which indicates an acid-base equilibrium between LH and LH_2^+ [(Equation (3)]. The *pK* for this equilibrium reaction is 6.61±0.2 at 300 K. The chloride salt of the protonated phenazine, $[LH_2]Cl$ formed crystals suitable for X-ray structure determination. X-ray structure analysis[9] was used to authenticate the formation of $[LH_2]Cl$ and hence LH from a previously unknown reaction. A view of the molecule is shown in Figure 2, which indeed confirms the formation of a substituted phenazine with several C−N bond-formation processes.

The overall transformation is an 8 e^- + 8 H^+ transfer process and is accompanied by the elimination of one mol each of CH_3OH and NH_3. Oxidative dimerisation of *ortho* substituted aromatic amines, for example 1,2-diamino benzene or 2-amino phenol are documented in the literature.[8,10−11] These dehydrogenation processes proceed via radical intermediates[8,10b] which have been detected by EPR spectroscopy. It is proposed that the first and key step of *p*-anisidine → LH transformation is the dimerisation of the monoamine to produce *N*-aryl-1,2-diamino arene. This proposal is based on our results of the ruthenium- and osmium-promoted dimerisation reaction of *p*-anisidine. In those cases, however, the *N*-aryl diamine, once formed, undergoes dehydrogenation[2] to result in a coordinated 1,2-diimine [(Equation (1)]. In this case, once the *N*-aryl diamine is formed, it undergoes further dimerisation[11] and deamination processes to give LH. The plausible steps are shown in Scheme 1.

To the best of our knowledge, the formation of phenazine directly from a mono primary amine is not known. We wish to note here that identical reactions are also observed when neat *p*-anisidine is allowed to react with $CrCl_3$ or $RhCl_3$.

A close examination of the bond angles and distances of the salt $[LH_2]Cl$ reveals that the long chain, N15−C2−C1−C14−N13−C12−C11−C10−C9−C8−C7−N6−C5−C4−C3−N22 contains hybrid bonds. The ranges of bond lengths in this chain are C−C = 1.372 to 1.410Å and C−N = 1.337 to 1.399Å . Moreover, a least-square plane calculated through the 14 atoms of the dibenzo pyrazine fragment indicates that the skeleton is approximately planar; the largest deviation from the mean plane is 0.09Å. The planarity of the phenazine fragment, together with the bond length trends, indicates extensive delocalisation. This may be due to considerable contributions of the different resonance forms of the molecule. Furthermore, of the four substituents of the phenazine fragments, the two nitrogen atoms, *viz*. N15 and N22 deviate by 0.096 Å and 0.104 Å from the mean plane. The anisyl ring is almost perpendicular to the pyrazine ring. The torsion angle C5−N6−C29−C34 is 95.52°. This orientation minimises the steric interaction between *ortho* hydrogens *viz.* H30 and H34 and those on the phenazine, H4 and H8. Finally, it may be noted here that the crystal and molecular structure of $[LH_2]Cl$ is stabilised through[12] several hydrogen bonds.

Both LH and its conjugate acid $[LH_2]Cl$ show highly resolved ^1H NMR spectra (Figure 3). While there are two broad N−H resonances[13] at δ = 11.95 and 10.18 for $[LH_2]Cl$, the corresponding deprotonated compound LH showed only one broad resonance at δ = 8.49. The spectrum of the salt $[LH_2]Cl$ is better resolved and the resonances are shifted downfield from those for the corresponding neutral LH, as expected. The four methyl resonances appear in the range δ = 3.70 to 3.93, whereas the aromatic proton resonances are spread between δ = 5.79 and 8.04. Assignment of some of the resonances was not possible due to overlap of the resonances of unique protons. However, the H1 and H4 resonances in LH appear at δ = 6.18 and 5.79, respectively. The H1 signal appears as a doublet with *J* = 2.1 Hz. Irradiation of the signal at δ = 8.49 in LH results in the doublet at δ = 6.18 collapsing to a singlet, confirming that these two protons are magnetically coupled. These two resonances in the corresponding $[LH_2]Cl$ appear at δ = 6.38 and 6.24. Selected assignments

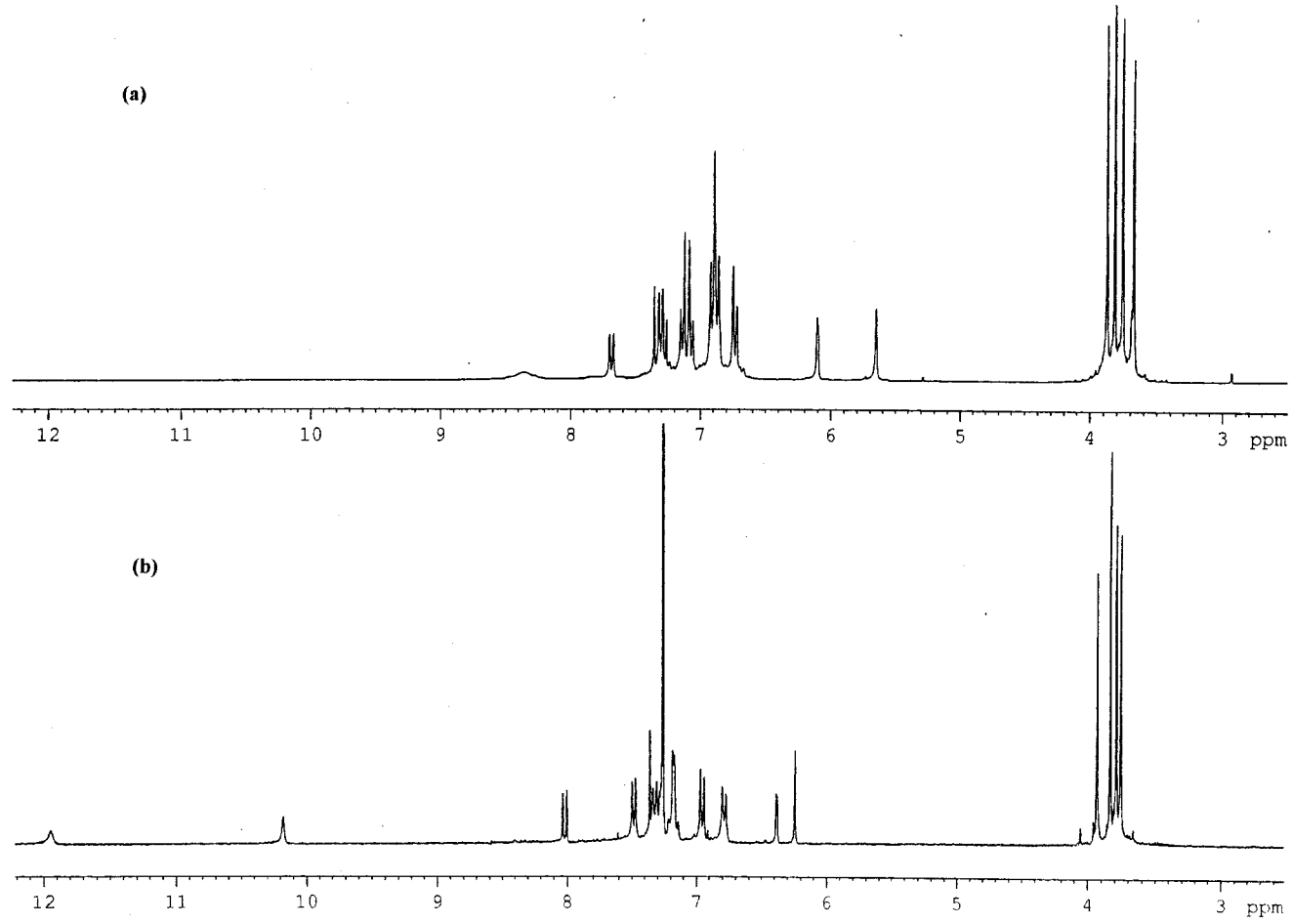


Figure 3. NMR spectra of (a) LH and (b) $[LH_2]Cl$ in $CDCl_3$

of the proton resonances are presented in the Experimental Section.

Binding of L to $M(aap)_2^{2+}$ moiety (M = Ru, Os)

The high affinity of the phenazine LH for H^+ led us to explore its coordination ability to transition metal ions. We chose $M(aap)_2^{2+}$ [M = Ru^{II} and Os^{II}, aap = 2-(arylazo)pyridine], as the possible binding sites. It may be relevant to note here that dipyrido phenazine complexes[14−16] of Ru^{II} and Os^{II} bind DNA and RNA by intercalation and represent an important class of molecular probes.

The compound LH reacts[17] smoothly with $[Ru(OH_2)_2(aap)_2]^{2+}$ in boiling methanol in the presence of a few drops of NEt_3 as base to yield a mixed *tris* chelate where L^- binds to Ru^{II} as a monoanionic bidentate ligand. Deprotonation of the amine nitrogen (N15), brought about by NEt_3, is essential for its chelation. The reaction of L^- with the dibromo analogue of osmium[18] under similar conditions proceeds at a much slower rate. The crude compounds were isolated as their perchlorate and bromide salts, respectively. Purification of the products was achieved by chromatography on silica gel column using different mixtures of $CHCl_3/CH_3CN$ as eluent. The mixed ligand complexes were obtained in high yields (75−80%). They are highly soluble in common organic solvents and their acetonitrile solutions behave as 1:1 electrolytes. The elemental analyses of these are consistent with the proposed composition $[M(aap)_2(L)]ClO_4$ (**1**).

Characterisation of $[M(aap)_2L]^+$

We employed several analytical methods to characterise the metal complexes, including ^1H NMR and UV/Vis spectroscopy, and cyclic voltammetry. The ^1H NMR spectrum of $[M(aap)_2(L)]^+$ contains several overlapping resonances in the aromatic region, owing to the presence of a large number of unique protons in these complexes. In this respect, the methyl resonances have been particularly useful for assessing the identity of the metal complexes. The $[M(pap)_2L]^+$ complexes display four −OMe signals in the range δ = 3.57−3.89 originating from the phenazine ligand; the corresponding *m*-tap complexes $[M(tap)_2L]^+$, on the other hand, display two extra methyl resonances at δ = 2.08 and 2.06, confirming the presence of two tap ligands in these compounds (Figure S2). Two methyl signals from the two tap ligands were expected due to the unsymmetric nature of the phenazine ligand. The disappearance of N−H

resonances in these complexes also indicates coordination of phenazine through N15 and N22. The number of ^{1}H NMR signals in these complexes is greater than those observed in LH and $[LH_2]^+$. The two pairs of doublets and one pair of triplets above $\delta = 7.5$ are assigned[19] to the pyridyl proton resonances, which further confirms the presence of two aap ligands in these compounds.

The phenazine ligand LH in the presence of 1 mM OH^- shows two intense transitions in the range 800−250 nm. One of these appears in the visible range at 490 nm while the other transition occurs at 280 nm. The solution colour of $[Ru(aap)_2L]^+$ is red-violet whereas that of the corresponding osmium analogue is blue-violet. The solution spectrum of the ruthenium complex consists of an intense transition at 545 nm. This transition is associated with at least two additional ill-defined shoulders occurring at longer wavelengths. The spectra of the corresponding osmium complexes showed multiple absorption peaks in the visible range. Each of them shows a transition at 790 nm and two more closely spaced transitions at 625 and 580 nm are also observed. The bivalent ruthenium and osmium complexes of aap, in general, display intense transitions in the visible range which are assigned to metal to ligand charge transfer (MLCT) transitions.[17−18] The number of absorption peaks in mixed ligand complexes varies depending on the presence of different acceptor orbitals. In the present complexes, the phenazine ligand itself has very intense visible range transition. Therefore, multiple transition possibilities,[20,21] originating from intra-ligand as well as MLCT transitions, exist in these complexes. The spectral data are collected in Table 1.

Table 1. Electronic spectral data

Compound	λ_{max}/nm(ε/M^{-1}cm^{-1})[a]			
LH	495(13110)	285(21230)		
LH_2Cl	540(15280)	390(2530)	290(22390)	
L^-[b]	575[c]	490	280	
$[Ru(pap)_2L]ClO_4$	555(18780)	340[c](21670)	295(28100)	
$[Ru(tap)_2L]ClO_4$	545(16900)	340[c](19400)	300(24520)	
$[Os(pap)_2L]Br$	790(5900)	625(12710)	580(12840)	310(21220)
$[Os(tap)_2L]Br$	785(5680)	620(12220)	570(11990)	315(22010)

[a] Solvent: acetonitrile. − [b] Qualitative spectrum generated by the addition of aqueous NaOH (in excess) to an acetonitrile solution of LH. − [c] Shoulder.

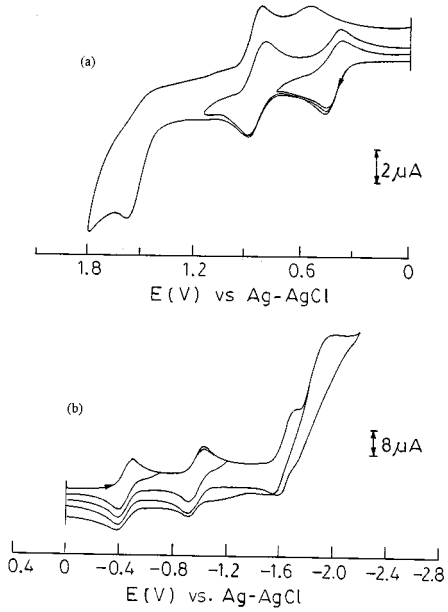


Figure 4. Cyclic voltammogram of $[Ru(m\text{-tap})_2L]ClO_4$; (a) anodic scan and (b) cathodic scan

Redox Properties

We employed cyclic voltammetry to determine the redox properties of the above ruthenium and osmium complexes. Figure 4 shows the multiple reduction waves of $[Ru(m\text{-tap})_2L]^+$ and the voltammetric data for all the complexes are collected in Table 2. The ruthenium complexes display three responses on the positive side of the Ag/AgCl reference. Of these, the couple with the lowest potential (0.45 *V*) is quasireversible with $i_{pa} > i_{pc}$, followed by a reversible couple at 0.97 *V*. Besides these, an irreversible anodic response of uncertain origin at 1.57 V was also observed. The first anodic response may be assigned to the oxidation of ruthenium(II) → ruthenium(III) in **1**. The next reversible response represents the ruthenium(II) → ruthenium(III) oxidation of a diimine analogue of **1** formed by the chemical transformation of electrogenerated $\mathbf{1}^+$. Ruthenium- and osmium-mediated electrochemical oxidation of the coordinated amine function are documented[17,22,23] in the literature. Keeping the above electrochemical transformations in mind, we examined whether the electrogenerated $\mathbf{1}^+$ would chemically be transformed to the diimine analogue of **1**. In practice, however, $\mathbf{1}^+$, produced by exhaustive electrolysis

Table 2. Electrochemical data[a]

	$E_{1/2}$/V(ΔE_p/mV)[b] Oxidation			Reduction			
$[Ru(pap)_2L]ClO_4$	0.47(70)	0.94(90)	1.56[c]	−0.38(90)	−0.89(100)	−1.63(150)	−2.07[d]
$[Ru(tap)_2L]ClO_4$	0.43(80)	0.85(90)	1.59[c]	−0.45(90)	−0.97(100)	−1.63(150)	−2.00[d]
$[Os(pap)_2L]Br$	0.68[e]			−0.39(80)	−0.88(60)	−1.57(60)	−2.27[d]
$[Os(tap)_2L]Br$	0.76[c]	0.91[c]	1.63[c]	−0.42(100)	−0.92(100)	−1.65(160)	−1.95[d]

[a] Conditions: solvent, acetonitrile; supporting electrolyte, NEt_4ClO_4 (0.1 M); working electrode, platinum for oxidation processes and glassy carbon for reduction processes; reference electrode, Ag/AgCl; solute concentration, 10^{-3} M. − [b] $E_{1/2}$ is calculated as the average of anodic (E_{pa}) and cathodic (E_{pc}) peak potentials; $\Delta E_p = E_{pa} - E_{pc}$. − [c] Irreversible E_{pa}. − [d] Irreversible E_{pc}. − [e] Irreversible E_{pa} with very large current.

of **1** at 0.70 V, yielded a mixture of compounds from which no pure product could be isolated. The responses in the case of osmium are more closely spaced and irreversible in nature.

The cathodic responses, on the other hand, are well defined. All the complexes showed three reversible couples along with a cathodic response of equal current (Figure 4) in the range −0.38 to −2.27 V. The coordinated ligand, pap, is known[17a] to undergo successive two-step one-electron transfer processes. Hence, these four responses may be attributed to the reductions of two aap ligands.

Conclusions

The direct formation of *N*-aryl phenazine (LH) from a mono aromatic primary amine, *viz*. *p*-anisidine, occurs through several oxidative carbon-nitrogen bond formation and cyclisation processes which otherwise do not occur with the free amine. This reaction is mediated by the ferric ion through the activation of O_2. This reaction is important in connection with the studies of chemical as well as electrochemical oxidations of primary aromatic amines. The coordination abilities of the anionic phenazine ligand $[L]^-$ have been explored. Our study of carbon-nitrogen bond formation processes using transition metal complexes as mediators is continuing.

Experimental Section

Materials: $RuCl_3 \cdot nH_2O$ was obtained from Arora Matthey and was digested three times with concentrated HCl before use. Solvents and chemicals used for syntheses were of analytical grade and used as received. The supporting electrolyte (TEAP) and solvents for electrochemical works were obtained as before.[17] $[Ru(aap)_2(OH_2)_2](ClO_4)_2 \cdot H_2O$ and $[Os(aap)_2Br_2]$ were prepared by literature methods.[17b,18b]

Physical Measurements: A Shimadzu UV 2100 UV/Vis spectrophotometer was used to record electronic spectra. The IR spectra were recorded with a Perkin−Elmer 783 spectrophotometer. ^1H NMR spectra in $CDCl_3$ were recorded on a Bruker Avance DPX 300 spectrophotometer, with $SiMe_4$ as internal standard. A Perkin−Elmer 240C elemental analyser was used to collect microanalytical data (C, H, N). Electrochemical measurements were performed under a dry nitrogen atmosphere on a PAR model 273-A electrochemistry system as described earlier.[20] All potentials reported in this work are referenced to Ag/AgCl and are uncorrected for junction contribution. The pH measurements were made with a μ-pH System 361 Systronics pH meter, standardised with buffers 7.0 and 9.2. A 70% CH_3CN/H_2O buffer mixture was employed. Electrical conductivities were measured by using a Systronics Direct Reading Conductivity meter 304. FAB-MS was obtained from JEOL AX 500/DA 5050 model mass spectrometer having a 70 eV ion source and direct inlet temperature of 180 °C.

Syntheses of Ligands

6-*p*-Anisyl-2-(*p*-anisylamino)-3(4*H*)-*p*-anisylimine-9-methoxyphenazine, (LH): A large excess of *p*-anisidine (2 g, 16.20 mmol) was added to hydrated $FeCl_3$ (100 mg, 0.60 mmol) and the mixture heated at 120 °C for 1 h. A violet melt resulted which was then extracted with dichloromethane, filtered and purified on a silica gel column (diameter:1 cm, height: 50 cm) After elution of the unchanged *p*-anisidine with pure chloroform, an intense red-violet band was eluted with chloroform/acetonitrile (19:1). On evaporation of the solvent and subsequent crystallisation from dichloromethane/hexane solutions dark red-brown crystals were obtained. Yield: 35%. − IR (KBr): $\tilde{\nu}$ = 1600 cm^{-1} (C=N), 3300 (N−H). − ^1H NMR ($CDCl_3$): δ = 8.50 (s, N−H, H_{15}), 7.77 (d, H_{10}, J = 9 Hz), 6.18 (d, H_1, J = 2.1 Hz), 5.79 (s, H_4), 3.89, 3.83, 3.77, 3.70 (s, 3 H, OCH_3). − $C_{34}H_{30}N_4O_4$ (558.6): calcd. C 73.11, H 5.37, N 10.03; found C 73.57, H 5.6, N 10.08.

Protonated Phenazine $[LH_2]^+$: A mixture of LH (56 mg, 0.10 mmol), dissolved in dichloromethane (20 mL) and very dilute aqueous HCl (10 mL, 1:20) was shaken vigorously in a separating funnel. The violet organic layer was then washed with water, collected and dried over anhydrous Na_2SO_4. Dark crystals of $[LH_2]Cl$ were obtained by slow diffusion of toluene into a dichloromethane solution of the compound. Yield: 98%. − IR (KBr): $\tilde{\nu}$ = 1615 cm^{-1} (C=N), 3300 (N−H). − ^1H NMR ($CDCl_3$): δ = 11.95 (s, N−H, H_{22}), 10.18 (s, N−H, H_{15}), 8.02 (d, H_{10}, J = 9.0 Hz), 7.36 (s, H_8), 6.95 and 6.79 (d, 2 H, *ortho* C−H of the anisyl rings, J = 8.4, 8.7 Hz, respectively), 6.38 (d, H_1, J = 2.4 Hz), 6.24 (s, H_4), 3.93, 3.83, 3.79, 3.76 (s, 3 H, OCH_3). $-C_{34}H_{31}ClN_4O_4$ (595.1): calcd. C 68.62, H 5.21, N 9.41; found C 68.70, H 5.18, N 9.40.

Syntheses of Complexes

6-*p*-Anisyl-2-(*p*-anisylamino)-3[(4*H*)-*p*-anisyliminobis(2-arylazo)-pyridine]-9-methoxyphenazineruthenium(II) Perchlorate, $[Ru(pap)_2L]ClO_4$: $[Ru(pap)_2(OH_2)_2](ClO_4)_2 \cdot H_2O$ (0.10 g, 0.13 mmol) and LH (0.08 g, 0.14 mmol) were dissolved in methanol (20 mL) and a few drops of NEt_3 added to the mixture. This reaction mixture was then heated at reflux for three hours. The colour of the solution became blue violet. The resulting solution was evaporated to dryness in a water bath and the crude product was purified on a silica gel column. Bands of different colours were first eluted with $CHCl_3$. Unreacted phenazine was then eluted with $CH_3CN/CHCl_3$ (1:12). Finally, an intense blue violet fraction was eluted with $CH_3CN/CHCl_3$ (1:6). After evaporation of solvent and subsequent recrystallisation from dichloromethane/hexane mixture, dark crystals of $[Ru(pap)_2L]ClO_4$ were obtained. Yield: 75%. − IR (KBr): $\tilde{\nu}$ = 1590 cm^{-1}(C=N), 1290 (N=N), 1100, 630 (ClO_4). − ^1H NMR ($CDCl_3$): δ = 3.84, 3.76, 3.72, 3.57 (OCH_3). − $C_{56}H_{47}ClN_{10}O_8Ru$ (1124.6): calcd. C 59.81, H 4.18, N 12.46; found C 59.76, H 4.20, N 12.42.

The corresponding ruthenium compound of 2-(*m*-tolylazo)pyridine was prepared using the same procedure except that $[Ru(mtap)_2(OH_2)_2](ClO_4)_2 \cdot H_2O$ was used instead of $[Ru(pap)_2(OH_2)_2](ClO_4)_2 \cdot H_2O$. Yield: 75%. − IR (KBr): $\tilde{\nu}$ = 1600 cm^{-1}(C=N), 1290 (N=N), 1100, 630 (ClO_4). − ^1H NMR ($CDCl_3$): δ = 3.89, 3.84, 3.80, 3.64 (OCH_3), 2.08, 2.06 (CH_3). − $C_{58}H_{51}ClN_{10}O_8Ru$ (1152.6): calcd. C 60.44, H 4.43, N 12.16; found C 60.68, H 4.56, N 12.15

6-*p*-Anisyl-2-(*p*-anisylamino)-3[(4*H*)-*p*-anisyliminobis(2-phenylazo)-pyridine]-9-methoxyphenazineosmium(II) Bromide, $[Os(pap)_2L]Br$: This compound was synthesized by allowing $[Os(pap)_2Br_2]$ (0.10 g,0.14 mmol) to react with phenazine (0.08 g,0.14 mmol) in boiling 2-methoxyethanol under N_2 atmosphere for five hours, using Na_2CO_3 as base. The solution was then evaporated to dryness and the solid residue dissolved in chloroform and subjected to column chromatography on a silica gel bed. After elution of the unchanged phenazine with $CH_3CN/CHCl_3$ (1:12), an intense blue-

violet fraction was eluted with $CH_3CN/CHCl_3$ (1:6). Solvent evaporation followed by recrystallisation from dichloromethane/hexane mixture afforded dark crystalline $[Os(pap)_2L]ClO_4$. Yield: 75%. – IR (KBr): $\tilde{\nu}$ = 1590 cm^{-1} (C=N), 1280 (N=N). – ^1H NMR ($CDCl_3$): δ = 3.86, 3.83, 3.81, 3.66 (OCH_3). – $C_{56}H_{47}BrN_{10}O_4Os$ (1194.2): calcd. C 56.32, H 3.93, N 11.73; found C 56.40, H 3.96, N 11.73.

The osmium compound of 2-(*m*-tolylazo)pyridine was prepared by the same procedure except that $[Os(m\text{-}tap)_2Br_2]$ was used instead of $[Os(pap)_2Br_2]$; yield 80% . – IR (KBr): $\tilde{\nu}$ = 1590 cm^{-1} (C=N), 1285 (N=N). – ^1H NMR ($CDCl_3$): δ = 3.84, 3.82, 3.79, 3.63 (OCH_3), 2.03, 2.01 (CH_3). – $C_{58}H_{51}BrN_{10}O_4Os$ (1222.2): calcd. C 57.05, H 4.18, N 11.47; found C 57.50, H 4.16, N 11.94

Crystallographic Data: X-ray quality crystals (0.4 × 0.3 × 0.3 mm) of $[LH_2^+]Cl$ were obtained by slow diffusion of a dichloromethane solution of the compound into toluene. Cell parameters were obtained by least squares fits of 25 machine-centred reflections. Data were collected (1.67 ≤ 2θ ≤ 22.52°) on a Nicolet R3m/V diffractometer (295) with graphite-monochromated Mo-K_α radiation (λ = 0.71073 Å). Two check-reflections measured after every 198 reflections showed no significant changes in intensity over 25 h. Data were corrected for Lorentz-polarisation effects. Of the 3948 reflections collected 3870 were unique (R_{int} = 0.0337) and 3867 reflections satisfying [$I > 2\sigma(I)$] were used for structure solution by direct methods and refined[9] by least-squares on F^2 using SHELXL93.The crystal data are collected in Table 3.

Table 3. Crystallographic data

Empirical formula	$C_{34}H_{31}ClN_4O_4$
M	595
Crystal system	Triclinic
Space group	*P*1(bar)
a/Å	8.651(6)
b/Å	12.768(6)
c/Å	14.106(7)
α/deg	80.71(4)
β/deg	83.96(5)
γ/deg	74.31(5)
U/$Å^{-3}$	1477.30(15)
Z	2
D_c/gm·cm^{-1}	1.338
R	0.0624
*wR*2	0.1406

Acknowledgments

Financial support received from the Council of Scientific and Industrial Research and the Department of Science and Technology, New-Delhi is gratefully acknowledged.

[1] K. N. Mitra, S. Goswami, *Inorg. Chem.* **1997,** *36,* 1322–1326.
[2] [2a] K. N. Mitra, S. Choudhury, A. Castiñeiras, S. Goswami, *J. Chem. Soc., Dalton Trans.* **1998,** 2901–2906. – [2b] K. N. Mitra, P. Majumdar, S.-M. Peng, A. Castiñeiras, S. Goswami, *Chem. Commun.* **1997,** 1267–1268.
[3] K. N. Mitra, S.-M. Peng, S. Goswami, *Chem. Commun.* **1998,** 1685–1686.
[4] [4a] R. A. Metcalfe, E. S. Dodsworth, S. S. Fielder, D. J. Stufkens, A. B. P. Lever, W. J. Pietro, *Inorg. Chem.* **1996,** *35,* 7741–7750. – [4b] R. A. Metcalfe, A. B. P. Lever, *Inorg. Chem.* **1997,** *36,* 4762–4771. – [4c] A. B. P. Lever, H. Masui, R. A. Metcalfe, D. J. Stufkens, E. S. Dodsworth, P. R. Auburn, *Coord. Chem. Rev.* **1993,** *125,* 317–331.
[5] [5a] A. M. Pyle, J. K. Barton, *Inorg. Chem.* **1987**, *26*, 3820–3823. – [5b] A. M. Pyle, Y.-M. Chiang, J. K. Barton, *Inorg. Chem.* **1990,** *29,* 4487–4495. – [5c] P. Belser, A. von Zelewsky, M. Zehnder, *Inorg. Chem.* **1981,** *20,* 3098–3103. – [5d] S. Joss, K. M. Hasselbach, H. B. Buergi, R. Wordel, F. E. Wagner, A. Ludi, *Inorg. Chem.* **1989,** *28,* 1815–1819.
[6] [6a] J. March, *Advanced Organic Chemistry*, 3rd ed., Wiley Interscience, New York, **1985,** p. 1034. – [6b] R. L. Hand, R. F. Nelson, *J. Am. Chem. Soc.* **1974,** *96,* 850–860. – [6c] W. S. Trahanovsky, *Oxidation in Organic Chemistry*, Academic Press, New York and London, **1973,** vol. 5, Part B, p. 73. – [6d] D.V. Banthorpe, E. D. Hughes, C. Ingold, *J. Chem. Soc.* **1964,** 2864–2901.
[7] S. D. Ross, M. Finkelstein, E. T. Rudd, *Anodic Oxidation,* Academic Press, New York, **1975**, p. 189.
[8] L. I. Simandi, T. Barna, S. Nemeth, *J. Chem. Soc., Dalton Trans.* **1996,** 473–478, and references therein.
[9] G. M Sheldrick, *SHELXL 93*, Program for the refinement of crystal structure, University of Göttingen, Germany.
[10] [10a] N. D. Rosso, B. Szpoganicz, A. E. Martell, *Inorg. Chim. Acta.* **1999,** *287,* 193–198. – [10b] L. I. Simandi, T. Barna, Z. Szevernenyi, S. Nemeth, *Pure Appl. Chem*. **1992,** *64,* 1511–1518. – [10c] S.-M. Peng, D. S. Liaw, *Inorg. Chim. Acta.* **1986,** *113,* L11–L12. – [10d] T. Nogami, T. Hishida, M. Yamada, H. Mikawa, Y. Shirota, *Bull. Chem. Soc. Jpn.* **1975,** *48,* 3709–3714.
[11] A. P. Kottenhahn, E. T. Seo, H. W. Stone, *J. Org. Chem.* **1963,** *28,* 3114–3120.
[12] V. R. Thalladi, T. Smolka, A. Gehrke, R. Boese, R. Sustmann, *New J. Chem.* **2000,** *24,* 143–147.
[13] P.-H. Cheng, H.-Y. Cheng, C.-C. Lin, S.-M. Peng, *Inorg. Chim. Acta*. **1990,** *169*, 19–21.
[14] R. B. Nair, E. S. Teng, S. L. Kirkland, C. J. Murphy, *Inorg. Chem.* **1998,** *37,* 139–141.
[15] [15a] A. H. Krotz, B. P. Hudson, J. K. Barton, *J. Am. Chem. Soc.* **1993,** *115,* 12577–12578. – [15b] D. B. Hall, R. E. Holmlin, J. K. Barton, *Nature* **1996,** *382,* 731–735. – [15c] P. J. Dandliker, R. E. Holmlin, J. K. Barton, *Science* **1997,** *275,* 1465–1468.
[16] [16a] R. E. Holmlin, J. K. Barton, *Inorg. Chem.* **1995,** *34,* 7–8. – [16b] R. E. Holmlin, E. D. Stemp, J. K. Barton, *J. Am. Chem. Soc.* **1996,** *118,* 5236–5244.
[17] [17a] S. Goswami, R. Mukherjee, A. Chakravorty, *Inorg. Chem.* **1983,** *22,* 2825–2832. – [17b] S. Goswami, A. R. Chakravarty, A. Chakravorty, *Inorg. Chem.* **1983,** *22,* 602–609.
[18] [18a] B. K. Ghosh, A. Mukhopadhyay, S. Goswami, S. Ray, A. Chakravorty, *Inorg. Chem.* **1984,** *23,* 4633–4639. – [18b] B. K. Ghosh, S. Goswami, A. Chakravorty, *Inorg. Chem.* **1983,** *22,* 3358–3360.
[19] A. K. Mahapatra, B. K. Ghosh, S. Goswami, A. Chakravorty, *J. Indian Chem. Soc.* **1986**, *63*, 101–104.
[20] [20a] S. Decurtins, F. Felix, J. Ferguson, H. U. Gudel, A. Ludi, *J. Am. Chem. Soc.* **1980,** *102*, 4102–4106. – [20b] E. M. Kober, T. J. Meyer, *Inorg. Chem.* **1982,** *21,* 3967–3977.
[21] S. Choudhury, A. K. Deb, S. Goswami, *J. Chem. Soc., Dalton Trans.* **1994,** 1305–1310.
[22] [22a] F. R. Keene, D. J. Salmon, T. J. Meyer, *J. Am. Chem. Soc.* **1976,** *98,* 1884–1889. – [22b] P. A. Adcock, F. R. Keene, *J. Am. Chem. Soc.* **1981,** *103,* 6494–6495.
[23] [23a] S. E. Diamond, G. M. Tom, H. Taube, *J. Am. Chem. Soc.* **1975**, *97,* 2661–2664. – [23b] P. A. Lay, A. M. Sergeson, B. W. Skelton, A. H. White, *J. Am. Chem. Soc.* **1982,** *104,* 6161–6164.

Received December 13, 1999
[I99457]

Syntheses and Carbonyliridium Complexes of Unsymmetrically Substituted Fluorous Trialkylphosphanes: Precision Tuning of Electronic Properties, Including Insulation of the Perfluoroalkyl Groups

Luke J. Alvey,[a] Ralf Meier,[a,b] Tibor Soós,[a,b] Paul Bernatis,[a] and John A. Gladysz*[a,b]

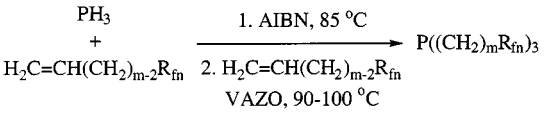
Keywords: Fluorine / Phosphanes / Donor−acceptor systems / Iridium / Carbonyl complexes

Reactions of iodides $I(CH_2)_mR_{f8}$ [m = 2–4; R_{f8} = $(CF_2)_7CF_3$] and $LiPH_2 \cdot DME$ (–45 °C, THF) give the primary phosphanes $PH_2(CH_2)_mR_{f8}$ (**7**–**9**; 48–76%). Radical-initiated reactions (100 °C) of **7** and $H_2C{=}CHCH_2R_{f8}$, **8** and $H_2C{=}CHR_{f8}$ or $H_2C{=}CHCH_2CH_2R_{f8}$, and **9** and $H_2C{=}CHCH_2R_{f8}$, give the title phosphanes $P[(CH_2)_mR_{f8}]_2[(CH_2)_{m'}R_{f8}]$ [m/m' = 2/3 (**10**), 3/2 (**11**), 3/4 (**12**), 4/3 (**13**); 70–76%]. The symmetrically substituted phosphane $P[(CH_2)_mR_{f8}]_3$ (m = 5, **6**) is similarly prepared from PH_3 and $H_2C{=}CHCH_2CH_2CH_2R_{f8}$, analogously to previously reported homologs [m = 2 (**2**), 3 (**4**), 4 (**5**)]. Reactions of **10**–**13** and **2**, **4**, **5**, and **6** with $[Ir(COD)Cl]_2$ and CO give *trans*-$Ir(CO)(Cl)(PR_2R')_2$ (70–83%). The IR ν_{CO} values show a monotonic decrease with increasing numbers of CH_2 groups. Phosphanes **13**, **5**, and **6** have the most CH_2 groups, and give ν_{CO} values 10, 7, and 4 cm^{-1} higher than the unfluorinated phosphane $P[(CH_2)_7CH_3]_3$. Hence, **6** provides nearly complete insulation of the iridium center from the electronegative perfluoroalkyl groups. Analogous rhodium derivatives of **4** and **5** are also described.

Introduction

The development of catalysts and reagents that have high affinities for "fluorous" phases has proceeded rapidly since Horváth described the concept and successful application of "fluorous biphase catalysis" in 1994.[1,2] This technique makes use of (1) the temperature-dependent miscibility of organic solvents with perfluorocarbons, perfluoroethers, or perfluoroamines,[3] and (2) "pony tails" of the formula $(CH_2)_m(CF_2)_{n-1}CF_3$ [abbreviated $(CH_2)_mR_{fn}$], which when added to catalysts and reagents in sufficient numbers, provide exceptional degrees of fluorous-phase immobilization. Reactions can be conducted in mixtures of organic and fluorous solvents under monophasic conditions at higher temperatures, and the products (which normally have much greater affinities for the organic solvent) separated from the fluorous catalyst or reagent under biphasic conditions at lower temperatures. The recovered catalyst can then be reused, or the transformed reagent can, in some manner, be recycled.

Most of the fluorous metal catalysts developed to date feature fluorous phosphanes.[1,4,5] This has in turn required syntheses of new phosphanes, as well as methodologies that are practical on larger scales. Earlier we reported convenient multigram syntheses of the symmetrically substituted fluorous trialkylphosphanes **1**−**5** listed in Scheme 1 by free-radical chain additions of PH_3 to the corresponding alkenes $H_2C{=}CH(CH_2)_{m-2}R_{fn}$.[6] The related phosphane **6** is new to this work and described further below. Note that **1**, **2**, and **3** define a series with progressively longer R_{fn} groups, and that **2**, **4**, **5**, and **6** define a series with progressively longer $(CH_2)_m$ segments between an R_{f8} group and the phosphorus atom.



Phosphane	$(CH_2)_mR_{fn}$	Partition coefficient $CF_3C_6F_{11}$/toluene (27 °C)
1	$(CH_2)_2R_{f6}$	98.8 : 1.2
2	$(CH_2)_2R_{f8}$	>99.7 : <0.3
3	$(CH_2)_2R_{f10}$	>99.7 : <0.3
4	$(CH_2)_3R_{f8}$	98.8 : 1.2
5	$(CH_2)_4R_{f8}$	98.9 : 1.1
6	$(CH_2)_5R_{f8}$	98.9 : 1.1

Scheme 1. Syntheses and partition coefficients of symmetrically substituted fluorous trialkylphosphanes **1**−**6**

The phosphanes **1**−**6** exhibit a number of interesting trends. For example, all fluorous-phase affinities − as measured by the partition coefficients in Scheme 1 − are high. However, they become higher as the R_{fn} group is lengthened in **1**−**3**. They also appear to decrease as the $(CH_2)_m$ segment is lengthened in **2**, **4**, **5**, and **6**. As would be intuitively expected, air oxidations become progressively faster in this

[a] Department of Chemistry, University of Utah, Salt Lake City, Utah 84112, USA
[b] Institut für Organische Chemie, Friedrich-Alexander Universität Erlangen-Nürnberg, Henkestrasse 42, D-91054 Erlangen, Germany

 © WILEY-VCH Verlag GmbH, D-69451 Weinheim, 2000 1434−1948/00/0909−1975 $ 17.50+.50/0

series. We sought to further fine tune these and other physical properties, and quantify the effect of the $(CH_2)_m$ segment length upon the phosphorus lone pair basicity.

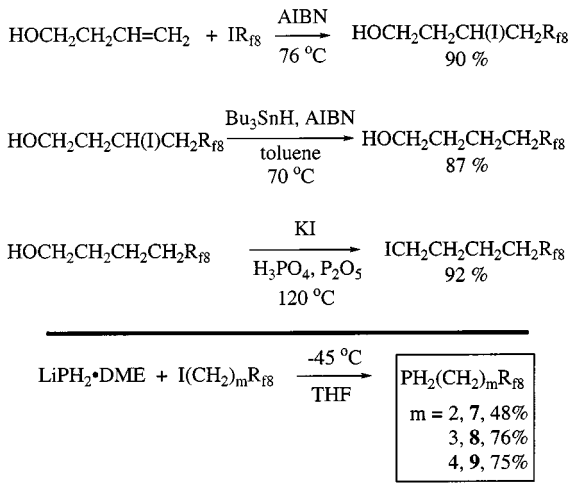
In this paper, we describe convenient syntheses of unsymmetrically substituted fluorous trialkylphosphanes of the formula $P[(CH_2)_mR_{f8}]_2[(CH_2)_{m'}R_{f8}]$. These feature mixtures of the types of pony tails in symmetrically substituted **2**, **4**, and **5**, and should thus have intermediate electronic characteristics. The unsymmetrical phosphanes are, together with **2**, **4**, **5**, and **6**, affixed to carbonylmetal fragments that provide IR assays of their donor/acceptor properties.[7] The most important results of this work are (1) a "toolkit" par excellence of nearly isosteric fluorous aliphatic phosphanes with precisely modulated electronic properties, and (2) the determination of the $(CH_2)_m$ segment lengths necessary to insulate the metal center from the electron-withdrawing R_{f8} groups.

Results

1. Phosphane Syntheses

We first sought convenient routes to the primary fluorous phosphanes $PH_2(CH_2)_mR_{f8}$ [m = 2 (**7**), 3 (**8**), 4 (**9**)]. These were anticipated to be versatile building blocks for many purposes, including free-radical additions to fluorous alkenes similar to those in Scheme 1. The strong nucleophile $LiPH_2 \cdot DME$ is easily prepared from PH_3 and *n*BuLi.[8] Hence, we set out to investigate alkylations, using the fluorous primary alkyl iodides $I(CH_2)_mR_{f8}$.

The iodide with two methylene groups, $I(CH_2)_2R_{f8}$, is commercially available. The next higher homolog, $I(CH_2)_3R_{f8}$, was prepared from the commercially available fluorous alcohol $HOCH_2CH_2CH_2R_{f8}$ and KI in an H_3PO_4/P_2O_5 slurry at 120 °C. A similar procedure has been communicated by another group.[9] The next higher homolog, $I(CH_2)_4R_{f8}$, has been reported only in patents.[10] It was synthesized on a 40-g scale in three steps as shown in Scheme 2 (top). First, the commercially available homoallylic alcohol $HOCH_2CH_2CH{=}CH_2$ and IR_{f8} were treated neat with a radical initiator to give $HOCH_2CH_2CH(I)CH_2R_{f8}$ in 90% yield after crystallization. Treatment with Bu_3SnH and a radical initiator gave the deiodinated alcohol $HOCH_2CH_2CH_2CH_2R_{f8}$ in 87% yield after crystallization. Related procedures for these two steps have been independently reported.[11] Subsequent reaction with KI in an H_3PO_4/P_2O_5 slurry at 120 °C gave analytically pure iodide in 92% yield after distillation.

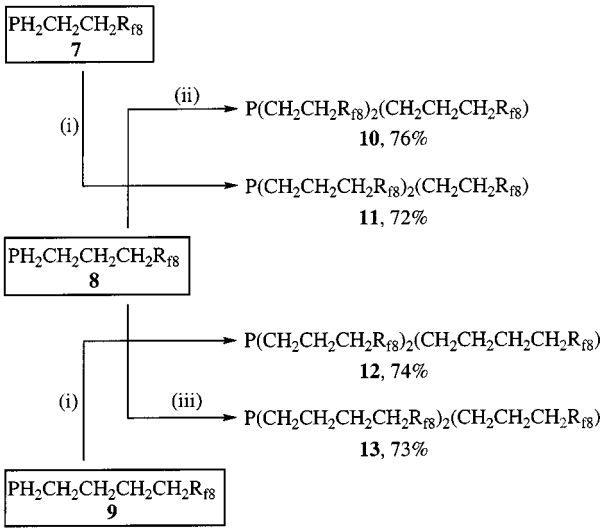


Scheme 2. Syntheses of building blocks for unsymmetrically substituted trialkylphosphanes

As depicted in Scheme 2 (bottom), $LiPH_2 \cdot DME$ and the fluorous iodides reacted in THF at −45 °C. Vacuum distillations gave the primary phosphanes **7** and **8** as clear liquids, and **9** as a low-melting white solid. The yield of **7** was slightly lower (49% vs. 75−76%), and some of the elimination product $H_2C{=}CHR_{f8}$ was detected in lower boiling fractions. A correct microanalysis was obtained for **9**, but not **7** and **8**. Accordingly, the ^1H NMR spectra of **7** and **8** (but not the ^{31}P NMR spectra) showed traces of impurities. The ^{31}P NMR spectra of **7**−**9** exhibited triplets diagnostic of two phosphorus-bound protons ($^1J_{PH}$ = 192−189 Hz; δ = −136.6 to −139.6, [D_8]THF), with much smaller longer-range couplings ($^2J_{PH}$ = 5−8 Hz) sometimes resolved. The ^1H NMR spectra showed PH_2 signals with the corresponding phosphorus coupling (dm, δ = 2.76−2.64, [D_8]THF).

The primary phosphanes **7**−**9** and slight excesses of the fluorous alkenes $H_2C{=}CH(CH_2)_{m-2}R_{f8}$ (m = 2−4;[6] 2.1−3.6 equiv.) reacted *neat* at 100 °C in the presence of a radical initiator (VAZO,[12] 5−6 mol-%). The combinations employed are illustrated in Scheme 3. The unsymmetrically substituted trialkylphosphanes $P[(CH_2)_mR_{f8}]_2[(CH_2)_{m'}R_{f8}]$ (**10**−**13**) were isolated as white powders in 76−72% yields (based upon **7**−**9**) after crystallization. They melted without decomposition between 49 and 69 °C, and were characterized by NMR spectroscopy and microanalysis, as described in the Experimental Section. The ^{31}P NMR signals of **10**−**13** (δ = −28.2, −31.3, −34.2, −33.6) were far downfield from those of **7**−**9**, as commonly seen for related tertiary and primary phosphanes. The $^1J_{CP}$, $^2J_{CP}$ and $^3J_{CP}$ values of **10**−**13** were of similar magnitude (17−15, 22−15 and 15−12 Hz), and always greater than those of **7**−**9** (e.g., $^1J_{CP}$ = 8−12 Hz). However, there were no obvious monotonic NMR-spectroscopic trends.

In the course of characterizing adducts of **12** and **13**, it became obvious that the inductive effect of the R_{f8} group was still being felt at the phosphorus atom. Hence, we sought the symmetrical phosphane with a five-methylene segment in every pony tail, $P[(CH_2)_5R_{f8}]_3$ (**6**). In order to apply the route in Scheme 1, the appropriate alkene was required. In previous work, we had shown that the iodides IR_{f8} and ICH_2R_{f8} were allylated by allyltri(*n*-butyl)stannane under free-radical chain conditions.[6] Thus, an analogous reaction was conducted with $I(CH_2)_2R_{f8}$, as shown in Equation (1). Workup gave the fluorous alkene $H_2C{=}CHCH_2CH_2CH_2R_{f8}$ in 52% yield after distillation (11-g scale). This compound has also been prepared by a related metal-catalyzed allylation.[13] Subsequent reaction with PH_3 (Scheme 1) gave **6** in 40% yield. Phosphane **6** was in general



Scheme 3. Syntheses of unsymmetrically substituted fluorous trialkylphosphanes **10**−**13** at 100 °C with VAZO (initiator) and i) $H_2C{=}CHCH_2R_{f8}$, ii) $H_2C{=}CHR_{f8}$, iii) $H_2C{=}CHCH_2CH_2R_{f8}$

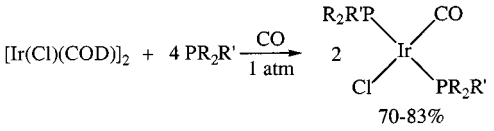
much less soluble than the lower homolog **5**. It dissolved in reasonable concentrations in the aromatic solvents toluene and $CF_3C_6H_5$, but was only sparingly soluble in perfluoro(methylcyclohexane), $CF_3C_6F_{11}$, the standard solvent for partition coefficients. Although **6** was always handled in a glove box, it would be expected to be more air-sensitive than **5**.[6]

$$\begin{matrix} Bu_3SnCH_2CH{=}CH_2 \\ + \\ ICH_2CH_2R_{f8} \end{matrix} \xrightarrow[\substack{CF_3C_6H_5 \\ \text{reflux}}]{\text{VAZO}} H_2C{=}CH(CH_2)_3R_{f8} \qquad (1)$$

2. Carbonylmetal Derivatives

We sought to probe the basicities of the preceding trialkylphosphanes. The IR ν_{CO} values of carbonylmetal complexes are sensitive measures of the donor/acceptor properties of the metal fragment and consequently the other ligands. As shown in Scheme 4, carbonyliridium compounds of the type *trans*-Ir(CO)(Cl)(PR_2R')$_2$ − analogs of Vaska's complex − are conveniently prepared by treating [Ir(COD)Cl]$_2$ with phosphanes and then carbon monoxide in appropriate stoichiometry.[14] We have previously synthesized such complexes of the R_{f6} phosphane **1** and tri-*n*-octylphosphane, $P[(CH_2)_7CH_3]_3$ (**14** and **23**, Scheme 4).[7] The latter phosphane contains the same number of carbon atoms as **1**, but no fluorine atoms. Hence, it is a good model for a fluorous trialkylphosphane where "complete insulation" of the phosphorus atom from the perfluoroalkyl groups has been achieved.

As summarized in Scheme 4, this procedure was repeated with the phosphanes **2** and **4**−**6** (Scheme 1), and **10**−**13** (Scheme 3). The corresponding iridium complexes **15**−**22** were isolated as analytically pure bright yellow powders in 70−83% yields. Adducts **15**−**21** were soluble in $CF_3C_6F_{11}$ and $CF_3C_6F_5$, but **22** was (like the free phosphane) only very slightly soluble in the former. All were sparingly soluble in THF, and insoluble in CH_2Cl_2. They were characterized by IR and ^{31}P NMR spectroscopy, as summarized in Scheme 4, as well as ^{1}H and/or ^{13}C NMR spectroscopy (Experimental Section). The IR measurements were made under identical conditions, at a resolution of ± 0.5 cm^{-1}. Analogous iridium complexes of some chiral, menthyl-substituted fluorous phosphanes are described elsewhere.[15]



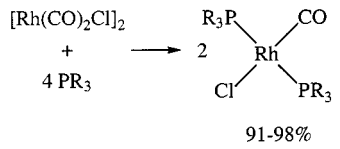
Complex	R	R'	IR $\tilde{\nu}_{CO}$ (cm^{-1})[a]	^{31}P NMR (δ)[b]
14	$(CH_2)_2R_{f6}$		1973.6[c]	18.2
15	$(CH_2)_2R_{f8}$		1973.9	17.5[d]
16	$(CH_2)_2R_{f8}$	$(CH_2)_3R_{f8}$	1965.2	15.5
17	$(CH_2)_3R_{f8}$	$(CH_2)_2R_{f8}$	1962.3	14.8
18	$(CH_2)_3R_{f8}$		1956.7	14.1
19	$(CH_2)_3R_{f8}$	$(CH_2)_4R_{f8}$	1954.8	13.5
20	$(CH_2)_4R_{f8}$	$(CH_2)_3R_{f8}$	1952.2	12.8
21	$(CH_2)_4R_{f8}$		1949.2	11.9
22	$(CH_2)_5R_{f8}$		1946.1	13.0[d]
23	$(CH_2)_7CH_3$		1942.3	14.0[e]

Scheme 4. Syntheses and key data for iridium complexes: [a] In $CF_3C_6H_5$, 10 mg/mL, spectrometer resolution ±0.5 cm^{-1}; [b] in $CF_3C_6F_{11}$ (unlocked; see Experimental Section); [c] this value was determined in $CF_3C_6H_5$ as part of this work (see also ref.[7]); [d] measured with a different spectrometer than the other compounds; [e] in C_6D_6 (insoluble in $CF_3C_6F_{11}$)

Complexes **15**−**22** exhibited several monotonic trends. The ^{31}P NMR signals moved steadily upfield, except for **22** which was prepared and characterized in our new laboratories in Germany. There was also a progressive increase in air sensitivities in solution. Vaska-type complexes readily form η^2-O_2 adducts,[7] and the trend is consistent with increasing electron density on the iridium atom. As solids, several complexes oxidized more rapidly than the nonfluorinated species **23**, although the reverse order has been quantified in solution.[7] Finally, the IR ν_{CO} values steadily shifted to lower wavenumbers, nearly reaching that of nonfluorinated **23**. This important trend is also in agreement with increasing electron density on the iridium atom, but further analysis is deferred to the Discussion section.

A rhodium analog of the preceding complexes, *trans*-Rh(CO)(Cl)[P[$(CH_2)_2R_{f6}$]$_3$]$_2$ (**24**),[7,16] has been previously synthesized as shown in Scheme 5. Similar reactions of [Rh(CO)$_2$Cl]$_2$ with phosphanes **4** and **5** gave the higher homologs **25** and **26** as yellow prisms in 93−91% yields after recrystallization. The IR ν_{CO} values and ^{31}P NMR

chemical shifts of **24**−**26** showed trends parallel to the iridium complexes (Scheme 5). The crystal structure of **24** was determined earlier.[7,16] X-ray data were also collected with **25**, using a CCD detector. However, the crystals were soft, the quality of the data set was poor, and refinement was thwarted by too much disorder near the ends of the pony tails. Extensive attempts were made to obtain crystals of other complexes in this study suitable for X-ray diffraction. Unfortunately, all efforts were unsuccessful.



Complex	R	IR $\tilde{\nu}_{CO}$ (cm^{-1})	^{31}P NMR (δ)
24	$(CH_2)_2R_{f6}$	1977[a]	23.5[b]
25	$(CH_2)_3R_{f8}$	1974[c]	19.2[d]
26	$(CH_2)_4R_{f8}$	1964[c]	17.5[d]

Scheme 5. Syntheses and key data for rhodium complexes: [a] In $CF_3C_6F_{11}$, from ref.[7]; [b] in [D_6]acetone (d, $^1J_{RhP}$ = 120 Hz), from ref.[7]; [c] in THF; [d] in [D_8]THF (d, $^1J_{RhP}$ = 117 Hz)

Discussion

The IR data for iridium complexes **14**−**23** in Scheme 4 and rhodium complexes **24**−**26** in Scheme 5 indicate a progressive increase in backbonding from the metal center to the carbonyl ligand. This in turn reflects the donor/acceptor properties of the phosphane ligands, and requires progressively increasing σ basicities, possibly augmented by very slightly diminishing π acidities. This conclusion is supported by collaborative photoelectron spectroscopy and calorimetric studies in progress,[17] as well as ongoing and earlier[1b] computational studies discussed below.

The IR data further show that the electronic properties of fluorous trialkylphosphanes can be precisely modulated by varying the lengths of the $(CH_2)_m$ segments. This can be done in concert, or by the new methodologies in Schemes 2 and 3, one pony tail at a time. Since the lengths of the $(CH_2)_m$ segments in a given phosphane do not differ by more than one (m/m' values), analyses can be cast in terms of the total number of methylene groups per phosphane − a quantity that varies from six (**1**, **2**) to fifteen (**6**). Complexes **14** and **15** also provide analytical reference points. Their nearly identical ν_{CO} values establish that the length of the perfluoroalkyl group can be neglected when it is six carbon atoms or longer.

Complexes **15**, **18**, **21**, and **22** feature symmetrically substituted phosphanes with six, nine, twelve, and fifteen methylene groups, respectively. The successive $\Delta\nu_{CO}$ increments (17.2, 7.5, 3.1 cm^{-1}) provide one basis for extrapolating to phosphanes with longer $(CH_2)_m$ segments. These represent 44−41% (7.5/17.2, 3.1/7.5) "transmission levels" per each increment of three methylene groups. As illustrated in Figure 1, this suggests ν_{CO} values of 1944.8, 1944.2, and 1943.9 cm^{-1} for the next three higher phosphanes $P[(CH_2)_mR_{f8}]_3$ (m = 6, 7, 8), and a limit of 1943.7 cm^{-1} for an infinite number of methylene groups. This is only slightly above the value for the nonfluorinated complex, **23** (1942.3 cm^{-1}). Thus, the phosphane **6** can be said to provide "nearly complete" insulation of the perfluoroalkyl groups from the iridium atom, the locus of the observed parameter. However, very slight improvements can be anticipated with additional methylene groups.

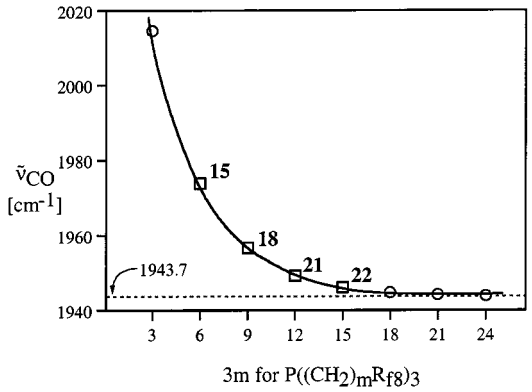


Figure 1. Relationship between IR ν_{CO} values of **15**, **18**, **21**, and **22**, and the total number of methylene groups in each phosphane ligand (□), and extrapolated values for homologous complexes (O)

Complexes **15**−**21** feature phosphanes in which the number of methylene groups increase from six to twelve. Here, the IR data illustrate the fine modulation of electronic properties. The largest $\Delta\nu_{CO}$ increments are 8.7 cm^{-1} (**15** vs. **16**) and 5.6 cm^{-1} (**17** vs. **18**). The others are in the range of 3.0−1.6 cm^{-1}. Although further arithmetic relationships can be noted, a particularly informative overview of all IR data is provided by Figure 2. In principle, any observable quantity that is a function of the number of repeat units x can be plotted versus $1/x$. Extrapolation to the y intercept ($1/x$ = 0) predicts a value for an infinite number of repeat units. The plot in Figure 2 is linear ($r^2 > 0.99$), and suggests a limit distinctly lower than that of the nonfluorinated complex **23**. However, we presently have greater confidence in the limiting value calculated from Figure 1.

There is the reciprocal question of the opposite limit − the ν_{CO} value of an analogous iridium complex of a tris(-perfluoroalkyl)phosphane, $P(R_{fn})_3$. We are not aware of any such compounds in the literature. However, tris(pentafluorophenyl)phosphane, $P(C_6F_5)_3$, gives a value of 1994 cm^{-1}.[18] Extrapolation of Figure 1, as described above, gives 2014.5 and 2109.7 cm^{-1} for the iridium complexes of $P(CH_2R_{f8})_3$ and $P(R_{f8})_3$. The former is in reasonable agreement with that expected from an extrapolation of Figure 2 [2019.2 cm^{-1}; $1/(2m + m')$ = 0.333], but such plots are not reliable for lower numbers of repeat units.

Returning to the most highly insulated complex **22**, note that the inductive effect of the perfluoroalkyl groups is transmitted through seven atoms − five methylene carbon atoms, a phosphorus, and an iridium atom. To be fair, three

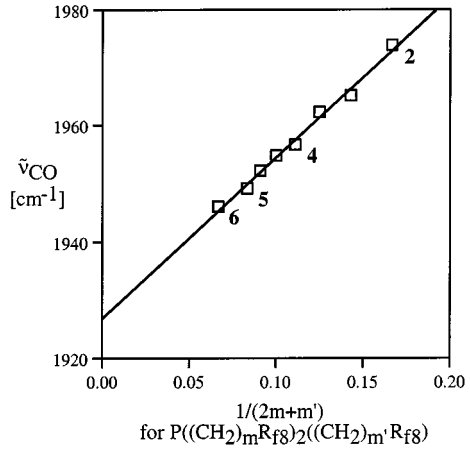


Figure 2. Relationship between IR ν_{CO} values of **15**−**22**, and the reciprocal of the total number of methylene groups in each phosphane ligand; selected ligands are designated by numbers for reference

pony tails converge at each phosphorus atom, and two phosphane ligands at the iridium atom. Normalization makes the data less dramatic. Nonetheless, to the best of our knowledge this represents the longest transmission of the inductive effect of a perfluoroalkyl group through a sequence of sp^3 atoms experimentally documented to date. Earlier, the pK_a values of amino acids $HO_2CCH(NH_2)(CH_2)_mCH_3$ and the ω-trifluoromethyl analogs $HO_2CCH(NH_2)(CH_2)_mCF_3$ were compared.[19] A measurable influence persisted through four sp^3 carbon atoms ($m = 3$).

We expect that the effect of the perfluoroalkyl groups in **1**−**6** and **10**−**13** will be more strongly felt when the locus of the observed parameter is the phosphorus atom (e.g., oxidation or ionization potential), and further studies are in progress.[17] We have characterized related fluorous trialkylamines $N[(CH_2)_mR_{f8}]_3$, and find a detectable influence upon basicities with five methylene groups.[20] At present, we have no evidence for "non-classical" transmission mechanisms (e.g., non-through-bond or non-field). However, in view of the tendency of fluorous groups to segregate − both intra- and intermolecularly − the possibility of a minor contribution remains an open question.

A computational study of the model fluorous trialkylphosphanes $P[(CH_2)_mCF_2CF_3]_3$ has been reported.[1b] The methylene chain lengths m were varied from zero to five. Both the phosphorus lone pair energies and the protonation energies reached asymptotic limits at five methylene groups (−9.2, −8.9 eV). However, they remained lower than those of the nonfluorinated reference compound $P[(CH_2)_3CH_3]_3$ (−8.7, −9.3 eV). Calorimetric data suggest that phosphane **1** is electronically similar to PMe_2Ph.[21] The latter gives an iridium complex with an IR ν_{CO} value of 1960 cm^{-1} (Nujol),[22] somewhat closer to those of phosphanes **4** and **11** (complexes **18**, **17**). However, in view of the different steric properties and measurement conditions, we regard this as a good agreement.

Phosphanes of the types **1**−**6** and **10**−**13** are very effective at immobilizing metal catalysts. For example, the tris(-phosphane)rhodium complexes $Rh(Cl)[P[(CH_2)_2R_{fn}]_3]$ give partition coefficients of 693:1 to 811:1 ($n = 6, 8$), and exhibit very low leaching levels when used for alkene hydroboration (e.g., 4.5−2.2 ppm rhodium/mol product).[4b] Related rhodium hydroformylation catalysts behave similarly.[1b] The bis(phosphane) iridium complexes **15**−**23** should have somewhat lower partition coefficients, but still at useful levels (**14**: ca. 333:1 or 99.7:0.3 by NMR spectroscopy).[7] Importantly, phosphanemetal catalysts are commonly optimized by extensive variation of the ligand. Thus, **1**−**6** and **10**−**13** provide an exceptional "tool kit" for the precise electronic tuning of tri-*n*-alkylphosphane based catalysts, irrespective of any recovery objective.

One of several obvious future directions for fluorous phosphane synthesis would involve extensions to secondary or tertiary alkyl-substituted systems. Bulky phosphorus substituents are a key design element in many catalysts of current interest,[23] and these would sterically complement the phosphanes described above. With regard to this objective and others, the primary phosphanes **7**−**9** constitute very attractive building blocks. Although the precursor $LiPH_2$ must be prepared from PH_3, one atmosphere is sufficient − in contrast to the autoclave conditions required for the symmetrical trialkylphosphanes **1**−**6** in Scheme 1.

In summary, this study has provided a series of nearly isosteric fluorous trialkylphosphanes with finely modulated electronic properties. The inductive effects of the perfluoroalkyl groups are almost completely insulated from the phosphorus atom in **6**, which features five methylene groups per pony tail. Future reports will describe additional characterization of the electronic properties of these ligands,[17] as well as related fluorous amines,[20] new types of fluorous phosphanes, and their applications in catalysis.

Experimental Section

General: All reactions and workups involving phosphanes were conducted under inert gases. Commercial chemicals were treated as follows: $CF_3C_6F_{11}$, $CF_3C_6H_5$, distilled from P_2O_5; THF, hexane, heptane, distilled from Na/benzophenone; CH_2Cl_2, distilled from CaH_2; C_6D_6, $CDCl_3$, [D$_8$]THF (Cambridge Isotope), IR_{f8}, $ICH_2CH_2R_{f8}$, $HOCH_2CH_2CH_2R_{f8}$, $H_2C{=}CHR_{f8}$ (Oakwood), $HOCH_2CH_2CH{=}CH_2$, $Bu_3SnCH_2CH{=}CH_2$, Bu_3SnH, AIBN, VAZO (Aldrich), $[Ir(COD)Cl]_2$, $[Rh(CO)_2Cl]_2$ (Strem), used as received; silica gel (Merck, grade 9385, 230−400 mesh), dried at 180 °C and $3{\cdot}10^{-3}$ Torr (24 h). − IR spectra were recorded with a Mattson Polaris spectrometer (0.5 cm^{-1} resolution). − NMR spectra were recorded with Varian or Jeol FT spectrometers at ambient probe temperature and referenced as follows: ^{1}H (300 MHz), external/residual C_6D_5H (δ = 7.16; external C_6D_6 lock for spectra in $CF_3C_6F_{11}$), residual [D$_7$]THF (δ = 3.58), residual [D$_5$]acetone (δ = 2.04), or residual $CHCl_3$ (δ = 7.27); ^{13}C (126 MHz), external C_6D_6 (δ = 128.39; lock for spectra in $CF_3C_6F_{11}$), internal [D$_8$]THF (δ = 67.57), or internal $CDCl_3$ (δ = 77.23); ^{31}P (121 MHz), external 85% H_3PO_4 (δ = 0.00); ^{19}F (282 MHz), external $CFCl_3$ (δ = 0.00). − Elemental analyses were conducted with a Carlo Erba EA1110 instrument (in-house, Erlangen), or by Atlantic Microlab (Norcross, Georgia).

$HOCH_2CH_2CH(I)CH_2R_{f8}$:[11a] A flask was charged with IR_{f8} (52.864 g, 96.826 mmol) and $HOCH_2CH_2CH{=}CH_2$ (8.456 g, 117.3 mmol). The solution was degassed (3 × freeze-pump-thaw) and AIBN (0.791 g, 4.82 mmol, 5 mol-%) was added. The mixture was heated at 76 °C. After 2 h, more AIBN (0.841 g, 5.12 mmol, 5 mol-%) was added. After 3 h, the solid mass was extracted with hot hexane (800 mL) and poured through filter paper. The filtrate was allowed to cool, and the resulting white crystals were collected on a frit. The filtrate was concentrated (100 mL), refluxed, and again cooled. A second crop of crystals was similarly collected. The filtrate was concentrated (20 mL), and a third crop similarly obtained. The crops were combined and dried by oil pump vacuum to give $HOCH_2CH_2CH(I)CH_2(CF_2)_7CF_3$ (53.578 g, 86.685 mmol, 90%), m.p. 82−83 °C (ref.[11a] 83 °C). − ^{1}H NMR ($CDCl_3$): δ = 4.56−4.47 (m, 1 H, C*H*I), 3.91−3.73 (m, 2 H), 3.07−2.75 (m, 2 H), 2.10−1.94 (m, 2 H), 1.46 (br s, 1 H, *H*O). − ^{19}F NMR ($CDCl_3$): δ = −81.3 (t, $^3J_{FF}$ = 9.2 Hz, 3 F, C*F*$_3$), −111.8 (dm, $^2J_{FF}$ = 272 Hz, 1 F), −114.6 (dm, $^2J_{FF}$ = 272 Hz, 1 F), −122.1 (m, 2 F), −123.2 (m, 4 F), −124.1 (m, 2 F), −126.6 (m, 2 F), −122.4 (m, 2 F). − MS (EI); *m*/*z* (%): 618 (3) [M^+], 491 (100) [M^+ − I], 473 (32) [M^+ − I, − H_2O], 441 (32), 395 (5), 219 (1) [$CF_3(CF_2)_3^+$], 169 (4) [$CF_3(CF_2)_2^+$], 119 (6) [$CF_3CF_2^+$], 69 (1) [CF_3^+]. − $C_{12}H_8F_{17}OI$ (618.06): calcd. C 23.32, H 1.30; found C 23.95, H 1.38.

$HOCH_2CH_2CH_2CH_2R_{f8}$:[11] A flask was charged with $HOCH_2CH_2$-$CH(I)CH_2R_{f8}$ (52.495 g, 84.933 mmol), Bu_3SnH (49.968 g, 171.68 mmol), AIBN (1.426 g, 8.684 mmol, 10 mol-%) and toluene (200 mL). The solution was stirred at 70 °C. After 4 h, the solvent was removed by rotary evaporation. The residue was dissolved in hexane (50 mL) and cooled to −20 °C. The resulting white crystals were collected on a frit. The filtrate was concentrated (10 mL) and cooled to −20 °C. A second crop of crystals was similarly collected. The crops were combined and dried by oil pump vacuum to give $HOCH_2CH_2CH_2CH_2R_{f8}$ (36.200 g, 73.551 mmol, 87%). − ^{1}H NMR ($CDCl_3$):[11] δ = 3.68 (t, $^3J_{HH}$ = 6.0 Hz, 2 H, HOC*H*$_2$), 2.19−2.01 (m, 2 H, C*H*$_2$CF$_2$), 1.75−1.61 (m, 4 H, C*H*$_2$C*H*$_2$CH$_2$CF$_2$), 1.36 (br s, 1 H, *H*O). − ^{19}F NMR ($CDCl_3$): δ = −81.3 (t, $^3J_{FF}$ = 9.2 Hz, 3 F, CF_3), −115.0 (m, 2 F), −122.2 (m, 2 F), −123.2 (m, 4 F), −124.0 (m, 2 F), −126.6 (m, 2 F), −122.4 (m, 2 F).

$ICH_2CH_2CH_2CH_2R_{f8}$:[10] A flask was charged with P_2O_5 (64.284 g, 452.88 mmol), H_3PO_4 (85%, 125 mL, 2.17 mol), KI (31.346 g, 188.83 mmol), and $HOCH_2CH_2CH_2CH_2R_{f8}$ (35.128 g, 71.372 mmol), and fitted with a condenser. The mixture was stirred at 120 °C for 4 h, allowed to cool, and diluted with water (100 mL). The solution was extracted with ether (3 × 100 mL). The combined ether extracts were washed with aqueous $Na_2S_2O_3$ (100 mL, 0.1 M) and dried ($MgSO_4$). The solvent was removed by rotary evaporation and the residue distilled (100−110 °C ca. $1{\cdot}10^{-3}$ Torr) to give $ICH_2CH_2CH_2CH_2R_{f8}$ as a white solid (39.575 g, 65.731 mmol, 92%), m.p. 50−51 °C. − ^{1}H NMR ($CDCl_3$): δ = 3.21 (t, $^3J_{HH}$ = 7 Hz, 2 H, IC*H*$_2$), 2.21−2.00 (m, 2 H), 1.99−1.87 (m, 2 H), 1.82−1.70 (m, 2 H). − ^{13}C{^{1}H} NMR ($CDCl_3$, partial): δ = 32.8 [s ($^1J_{CH}$ = 126 Hz),[25] one of *C*H$_2$*C*H$_2$CH$_2$CF$_2$], 30.1 [t, $^2J_{CF}$ = 22 Hz ($^1J_{CH}$ = 129 Hz),[25] *C*H$_2$CF$_2$], 21.6 [s ($^1J_{CH}$ = 129 Hz),[25] one of *C*H$_2$*C*H$_2$CH$_2$CF$_2$], 5.1 [s ($^1J_{CH}$ = 149 Hz),[25] I*C*H$_2$]. − ^{19}F NMR (δ, $CDCl_3$) −81.3 (t, $^3J_{FF}$ = 10 Hz, 3 F, C*F*$_3$), −114.8 (m, 2 F), −122.1 (m, 2 F), −122.3 (m, 4 F), −123.2 (m, 2 F), −123.9 (m, 2 F), −126.6 (m, 2 F). − MS (EI); *m*/*z* (%): 602 (10) [M^+], 475 (100) [M^+ − I], 455 (38) [M^+ − I, − HF]. − $C_{12}H_8F_{17}I$ (602.6): calcd. C 23.94, H 1.34; found C 23.87, H 1.28.

$PH_2CH_2CH_2R_{f8}$ (7): A Schlenk flask was charged with $ICH_2CH_2R_{f8}$ (8.958 g, 15.61 mmol) and THF (100 mL) and cooled to −45 °C (CH_3CN/N_2). Another Schlenk flask was charged with $LiPH_2 \cdot DME$ (2.020 g, 15.53 mmol)[8] and THF (50 mL). The second solution was added dropwise via cannula and with stirring to the first over a 30-min period. The cold bath was removed. After 2 h, the solvent was removed by oil pump vacuum, and $CF_3C_6H_5$ (20 mL) was added. The solution was filtered through a silica gel column (2 × 6 cm), which was rinsed with $CF_3C_6H_5$ (100 mL). The solvent was removed by oil pump vacuum, and the residue distilled (ca. 50−52 °C, 0.55 Torr) to give **7** as a colorless liquid (3.569 g, 7.434 mmol, 48%). − ^{1}H NMR ([D$_8$]THF): δ = 2.76 (dm, $^1J_{HP}$ = 192 Hz, 2 H, P*H*$_2$), 2.50−2.28 (m, 2 H, C*H*$_2$CF$_2$), 1.80−1.66 (m, 2 H, C*H*$_2$CH$_2$CF$_2$). − ^{13}C{^{1}H} NMR ([D$_8$]THF, partial): δ = 35.4 [dt, $^2J_{CP}$ = 2 Hz, $^2J_{CF}$ = 22 Hz ($^1J_{CH}$ = 130 Hz),[25] *C*H$_2$CF$_2$], 5.6 [dt, $^1J_{CP}$ = 12 Hz, $^3J_{CF}$ = 4 Hz ($^1J_{CH}$ = 130 Hz),[25] *C*H$_2$CH$_2$CF$_2$]. − ^{19}F NMR ([D$_8$]THF): δ = −82.0 (t, $^3J_{FF}$ = 11 Hz, 3 F, C*F*$_3$), −115.8 (pseudoquint, J_{FF} = 17 Hz, 2 F), −122.6 (m, 6 F), −123.5 (m, 2 F), −124.2 (m, 2 F), −127.0 (m, 2 F). − ^{31}P NMR ([D$_8$]THF): δ = −136.6 (t of pseudoquint, $^1J_{PH}$ = 192 Hz, $^2J_{PH}$ = 8 Hz). − Analytical data see text.

$PH_2CH_2CH_2CH_2R_{f8}$ (8): The reaction and workup given for **7** was repeated with $ICH_2CH_2CH_2R_{f8}$ (9.697 g, 16.49 mmol)[9] and $LiPH_2 \cdot DME$ (2.151 g, 16.54 mmol).[8] Distillation (56−58 °C, 0.55 Torr) gave **8** as a colorless liquid (6.188 g, 12.52 mmol, 76%). − ^{1}H NMR ([D$_8$]THF): δ = 2.67 (dm, $^1J_{HP}$ = 190 Hz, 2 H, P*H*$_2$), 2.22 (tm, $^3J_{HF}$ = 19 Hz, 2 H, C*H*$_2$CF$_2$), 1.89−1.75 (m, 2 H), 1.67−1.53 (m, 2 H). − ^{13}C{^{1}H} NMR ([D$_8$]THF, partial): δ = 32.4 [dt, $^3J_{CP}$ = 5 Hz, $^2J_{CF}$ = 22 Hz ($^1J_{CH}$ = 130 Hz),[25] *C*H$_2$CF$_2$], 25.1 [pseudoquadruplet, $^2J_{CP}$ = $^3J_{CF}$ = 4 Hz ($^1J_{CH}$ = 130 Hz),[25] *C*H$_2$CH$_2$CF$_2$], 14.2 [d, $^1J_{CP}$ = 10 Hz ($^1J_{CH}$ = 130 Hz),[25] P*C*H$_2$]. − ^{19}F NMR ([D$_8$]THF): δ = −82.0 (t, $^3J_{FF}$ = 9 Hz, 3 F, C*F*$_3$), −115.0 (pseudoquint, J_{FF} = 15 Hz, 2 F), −122.6 (m, 6 F), −123.5 (m, 2 F), −124.2 (m, 2 F), −127.0 (m, 2 F). − ^{31}P NMR ([D$_8$]THF): δ = −139.6 (t of pseudoquint, $^1J_{PH}$ = 190 Hz, $^2J_{PH}$ = 5 Hz). − Analytical data see text.

$PH_2CH_2CH_2CH_2CH_2R_{f8}$ (9): The reaction and workup given for **7** was repeated with $ICH_2CH_2CH_2CH_2R_{f8}$ (9.426 g, 15.66 mmol) and $LiPH_2 \cdot DME$ (2.036 g, 15.66 mmol).[8] Distillation (70−73 °C, 0.55 Torr) gave **9** as a white solid (5.967 g, 11.74 mmol, 75%), m.p. near room temperature. − ^{1}H NMR ([D$_8$]THF): δ = 2.64 (dm, $^1J_{HP}$ = 189 Hz, 2 H, P*H*$_2$), 2.28−2.08 (m, 2 H, C*H*$_2$CF$_2$), 1.75−1.47 (m, 6 H). − ^{13}C{^{1}H} NMR ([D$_8$]THF, partial) δ = 33.6 [d, $^2J_{CP}$ = 4 Hz ($^1J_{CH}$ = 130 Hz),[25] PCH$_2$*C*H$_2$], 31.2 [t, $^2J_{CF}$ = 22 Hz ($^1J_{CH}$ = 130 Hz),[25] *C*H$_2$CF$_2$], 22.2 [dt, $^3J_{CP}$ = 6 Hz, $^3J_{CF}$ = 4 Hz ($^1J_{CH}$ = 130 Hz),[25] *C*H$_2$CH$_2$CF$_2$], 14.2 [d, $^1J_{CP}$ = 9 Hz ($^1J_{CH}$ = 130 Hz),[25] P*C*H$_2$]. − ^{19}F NMR ([D$_8$]THF): δ = −82.1 (t, $^3J_{FF}$ = 10 Hz, 3 F, CF_3), −115.2 (pseudoquint, J_{FF} = 15 Hz, 2 F), −122.7 (m, 6 F), −123.5 (m, 2 F), −124.3 (m, 2 F), −127.1 (m, 2 F). − ^{31}P NMR ([D$_8$]THF): δ = −139.6 (br t, $^1J_{PH}$ = 189 Hz). − $C_{12}H_{10}F_{17}P$ (508.2): calcd. C 28.36, H 1.98; found C 28.18, H 1.93.

$P(CH_2CH_2R_{f8})_2(CH_2CH_2CH_2R_{f8})$ (10): A culture tube was charged with **7** (1.013 g, 2.050 mmol), $H_2C{=}CHR_{f8}$ (3.309 g, 7.417 mmol) and VAZO (0.029 g, 0.12 mmol, 6.0 mol-%). The mixture heated at 100 °C for 12 h and cooled. $CF_3C_6H_5$ (20 mL) was then added, and the mixture was filtered through a silica gel column (2 × 6 cm). The column was rinsed with $CF_3C_6H_5$ (100 mL). The filtrates were concentrated by oil pump vacuum (20 mL) and cooled to 10 °C. A white powder formed, which was collected on a frit. The filtrate was concentrated (10 mL) and cooled to 10 °C. A second crop of white powder formed. The combined crops were dried by oil pump vacuum to give **10** (2.160 g, 1.558 mmol, 76%), m.p. 59.5−60.0 °C.

– ^{1}H NMR ($CF_3C_6F_{11}$): δ = 2.27–2.04 (m, 6 H), 1.86–1.71 (m, 2 H), 1.70–1.59 (m, 4 H), 1.52–1.43 (m, 2 H). – $^{13}C\{^1H\}$ NMR ($CF_3C_6F_{11}$, partial):[26] δ = 32.2 [td, $^3J_{CP}$ = 13 Hz, $^2J_{CF}$ = 22 Hz ($^1J_{CH}$ = 130 Hz),[25] $CH_2CH_2CH_2CF_2$], 28.2 [pseudoquadruplet, $^2J_{CP}$ = $^2J_{CF}$ = 22 Hz ($^1J_{CH}$ = 130 Hz),[25] $PCH_2CH_2CF_2$], 26.9 [d, $^2J_{CP}$ = 15 Hz ($^1J_{CH}$ = 130 Hz),[25] $CH_2CH_2CH_2CF_2$], 17.1 [d, $^1J_{CP}$ = 17 Hz ($^1J_{CH}$ = 130 Hz),[25] $PCH_2CH_2CF_2$],[24] 16.9 [d, $^1J_{CP}$ = 17 Hz ($^1J_{CH}$ = 130 Hz),[25] $PCH_2CH_2CH_2CF_2$].[24] – ^{31}P NMR ($CF_3C_6F_{11}$): δ = –28.2 (s). – $C_{31}H_{14}F_{51}P$ (1386.3): calcd. C 26.86, H 1.02; found C 26.50, H 1.00.

$P(CH_2CH_2CH_2R_{f8})_2(CH_2CH_2R_{f8})$ (11): The reaction and workup given for **10** was repeated with **7** (1.027 g, 2.139 mmol), $H_2C{=}CHCH_2R_{f8}$ (2.832 g, 6.155 mmol)[6] and VAZO (0.027 g, 0.11 mmol, 5.0 mol-%). This gave **11** as a white powder (2.157 g, 1.540 mmol, 72%), m.p. 68.5–69.0 °C. – ^{1}H NMR ($CF_3C_6F_{11}$): δ = 2.26–2.00 (m, 6 H), 1.86–1.68 (m, 4 H), 1.68–1.55 (m, 2 H), 1.52–1.38 (m, 4 H). – $^{13}C\{^1H\}$ NMR ($CF_3C_6F_{11}$, partial):[26] δ = 32.3 [td, $^3J_{CP}$ = 13 Hz, $^2J_{CF}$ = 22 Hz ($^1J_{CH}$ = 130 Hz),[25] $CH_2CH_2CH_2CF_2$], 28.3 [pseudoquadruplet, $^2J_{CP}$ = $^2J_{CF}$ = 22 Hz ($^1J_{CH}$ = 130 Hz),[25] $PCH_2CH_2CF_2$], 27.1 [d, $^2J_{CP}$ = 15 Hz ($^1J_{CH}$ = 130 Hz),[25] $CH_2CH_2CH_2CF_2$], 17.2 [d, $^1J_{CP}$ = 16 Hz ($^1J_{CH}$ = 130 Hz),[25] $PCH_2CH_2CF_2$], 17.0 [d, $^1J_{CP}$ = 17 Hz ($^1J_{CH}$ = 130 Hz),[25] $PCH_2CH_2CH_2CF_2$]. – ^{31}P NMR ($CF_3C_6F_{11}$): δ = –31.3 (s). – $C_{32}H_{16}F_{51}P$ (1400.4): calcd. C 27.45, H 1.15; found C 27.35, H 1.11.

$P(CH_2CH_2CH_2R_{f8})_2(CH_2CH_2CH_2CH_2R_{f8})$ (12): The reaction and workup given for **10** was repeated with **8** (1.106 g, 2.176 mmol), $H_2C{=}CHCH_2R_{f8}$ (3.032 g, 6.589 mmol)[6] and VAZO (0.033 g, 0.14 mmol, 6.0 mol-%). This gave **12** as a white powder (2.309 g, 1.616 mmol, 74%), m.p. 59.0–59.5 °C. – ^{1}H NMR ($CF_3C_6F_{11}$): δ = 2.23–1.92 (m, 6 H), 1.83–1.63 (m, 6 H), 1.58–1.45 (m, 2 H) 1.45–1.34 (6 H). – $^{13}C\{^1H\}$ NMR ($CF_3C_6F_{11}$, partial):[26] δ = 32.4 [td, $^3J_{CP}$ = 12 Hz, $^2J_{CF}$ = 22 Hz ($^1J_{CH}$ = 130 Hz),[25] $CH_2CH_2CH_2CF_2$], 30.9 [t, $^2J_{CF}$ = 23 Hz ($^1J_{CH}$ = 130 Hz),[25] $CH_2CH_2CH_2CH_2CF_2$], 27.5 [d, $^2J_{CP}$ = 15 Hz ($^1J_{CH}$ = 130 Hz),[25] $PCH_2CH_2CH_2CF_2$],[24] 27.4, 25.8 [2 × d, J_{CP} = 15/15 Hz ($^1J_{CH}$ = 130/130 Hz),[25] $PCH_2CH_2CH_2CH_2$],[24] 21.9 [dm, $^3J_{CP}$ = 12 Hz ($^1J_{CH}$ = 130 Hz),[25] $CH_2CH_2CH_2CH_2CF_2$],[27] 17.1 [d, $^1J_{CP}$ = 17 Hz ($^1J_{CH}$ = 130 Hz),[25] $PCH_2CH_2CH_2CF_2$]. – ^{31}P NMR ($CF_3C_6F_{11}$): δ = –34.2 (s). – $C_{34}H_{20}F_{51}P$ (1428.4): calcd. C 28.59, H 1.41; found C 28.21, H 1.31.

$P(CH_2CH_2CH_2CH_2R_{f8})_2(CH_2CH_2CH_2R_{f8})$ (13): The reaction and workup given for **10** was repeated with **7** (0.555 g, 1.12 mmol), $H_2C{=}CHCH_2CH_2R_{f8}$ (1.105 g, 2.330 mmol)[6] and VAZO (0.016 g, 0.065 mmol, 6.0 mol-%). This gave **13** as a white powder (1.183 g, 0.8201 mmol, 73%), m.p. 49.0–49.5 °C. – ^{1}H NMR ($CF_3C_6F_{11}$): δ = 2.23–1.91 (m, 6 H), 1.83–1.62 (m, 6 H), 1.58–1.44 (m, 4 H), 1.44–1.32 (m, 6 H); $^{13}C\{^1H\}$ NMR ($CF_3C_6F_{11}$, partial):[26] δ = 32.4 [td, $^3J_{CP}$ = 12 Hz, $^2J_{CF}$ = 22 Hz ($^1J_{CH}$ = 130 Hz),[25] $CH_2CH_2CH_2CF_2$], 30.9 [t, $^2J_{CF}$ = 23 Hz ($^1J_{CH}$ = 130 Hz),[25] $CH_2CH_2CH_2CH_2CF_2$], 27.62 [d, $^2J_{CP}$ = 15 Hz ($^1J_{CH}$ = 130 Hz),[25] $PCH_2CH_2CH_2CF_2$], 27.58, 25.9 [2 × d, J_{CP} = 15/16 Hz ($^1J_{CH}$ = 130/130 Hz),[25] $PCH_2CH_2CH_2CH_2CF_2$], 21.9 [dm, $^3J_{CP}$ = 12 Hz ($^1J_{CH}$ = 130 Hz),[25] $CH_2CH_2CH_2CH_2CF_2$],[27] 17.2 [d, $^1J_{CP}$ = 17 Hz ($^1J_{CH}$ = 130 Hz),[25] $PCH_2CH_2CH_2CF_2$]. – ^{31}P NMR ($CF_3C_6F_{11}$): δ = –33.6 (s). – $C_{35}H_{22}F_{51}P$ (1442.4): calcd. C 29.14, H 1.54; found C 29.13, H 1.48.

$H_2C{=}CHCH_2CH_2CH_2R_{f8}$:[13] A Schlenk flask was charged with $ICH_2CH_2R_{f8}$ (25.000 g, 43.54 mmol), $Bu_3SnCH_2CH{=}CH_2$ (20.501 g, 61.91 mmol), VAZO (1.063 g, 4.35 mmol, 10 mol-%), and $CF_3C_6H_5$ (200 mL), and fitted with a condenser. The system was degassed (2 × freeze-pump-thaw) and refluxed. After 18 h, the solvent was removed by rotary evaporation (aerobic workup), and CH_2Cl_2 (200 mL) was added. The biphasic mixture was extracted with $CF_3C_6F_{11}$ (4 × 20 mL). The solvent was removed from the extracts by rotary evaporation. The residue was filtered through a silica gel column (2 × 10 cm), which was rinsed with $CF_3C_6F_{11}$ (100 mL). The solvent was removed from the filtrate by rotary evaporation and the residue distilled (62–64 °C, 3 mbar) to give $H_2C{=}CHCH_2CH_2CH_2R_{f8}$ as a colorless liquid (11.154 g, 22.85 mmol, 52%). – IR (neat or $CHCl_3$): $\nu_{C=C}$ = 1645 cm^{-1}. – ^{1}H NMR ($CDCl_3$): δ = 5.82–5.70 (ddt, $^3J_{HH}$ = 17, 11, 7 Hz, 1 H, $H_2C{=}CH$), 5.09–5.02 (m, 2 H, $H_2C{=}CH$), 2.18–1.99 (m, 4 H), 1.76–1.68 (m, 2 H). – $^{13}C\{^1H\}$ NMR ($CDCl_3$, partial): δ = 136.9 (s, $H_2C{=}CH$), 116.3 (s, $H_2C{=}CH$), 32.9 (s, $=CHCH_2$), 30.2 (t, $^2J_{CF}$ = 22 Hz, CH_2CF_2), 19.4 (s, $CH_2CH_2CF_2$). – ^{19}F NMR ($CDCl_3$): δ = –81.0 (t, $^3J_{FF}$ = 10 Hz, 3 F, CF_3), –114.5 (pseudoquint, 2 F), –121.9 (m, 2 F), –122.2 (m, 4 F), –122.9 (m, 2 F), –123.7 (m, 2 F), –126.3 (m, 2 F). – MS (FAB); *m/z* (%): 487 (100) [M^+ – 1]. – $C_{13}H_9F_{17}$ (488.2): calcd. C 31.98, H 1.86; found C 32.12, H 1.79.

$P(CH_2CH_2CH_2CH_2CH_2R_{f8})_3$ (6): A bomb was charged with $H_2C{=}CHCH_2CH_2CH_2R_{f8}$ (3.089 g, 6.33 mmol), AIBN (0.103 g, 0.63 mmol, 10 mol-%), and PH_3 (15 bar). The bomb was partially immersed in an oil bath (85 °C), and the contents stirred. After 24 h, the bomb was vented, purged and opened. The yellow solid was dissolved in $CF_3C_6H_5$ (10 mL), and a ^{31}P NMR spectrum showed a mixture of phosphanes $PH_{3-n}(CH_2CH_2CH_2CH_2CH_2R_{f8})_n$ (*n* = 1/2/3 9:36:55; δ = –140.7, –70.4, –32.8). VAZO (0.500 g, 2.04 mmol) and $H_2C{=}CHCH_2CH_2CH_2R_{f8}$ (2.000 g, 4.10 mmol) were added. The mixture was stirred at 100 °C. After 12 h, the mixture was cooled and filtered through a silica gel column (2 × 6 cm), which was rinsed with $CF_3C_6H_5$ (60 mL). The solvent was removed from the filtrates by oil pump vacuum. $CF_3C_6F_{11}$ (10 mL) was added, and a white powder [by-product; $^{31}P\{^1H\}$ NMR spectroscopy ($CF_3C_6H_5$): δ = –5.9] was removed by filtration. The solvent was removed from the filtrate by oil pump vacuum. The residue was dissolved in $CF_3C_6H_5$ and cooled to –32 °C. A white powder formed, which was collected on a frit and dried by oil pump vacuum to give **6** (1.281 g, 0.85 mmol, 40% based upon initial alkene charge), m.p. 44.0 °C. – ^{1}H NMR ($CF_3C_6F_{11}$): δ = 2.02–1.86 (m, 6 H), 1.62–1.22 (m, 24 H). – $^{13}C\{^1H\}$ NMR ($CDCl_3$, partial): δ = 30.58 (t, $^2J_{CF}$ = 22 Hz, CH_2CF_2), 30.59 (d, *J* = 13 Hz, $PCH_2CH_2CH_2$), 19.8 (s, $CH_2CH_2CF_2$). – $^{31}P\{^1H\}$ NMR ($CF_3C_6F_{11}$): δ = –33.7 (s). – MS (FAB); *m/z* (%): 1515 (100) [M^+ + O], 1499 (45) [M^+]. – $C_{39}H_{30}F_{51}P$ (1498.5): calcd. C 31.26, H 2.02; found C 31.50, H 2.36.

***trans*-Ir(CO)(Cl)[$P(CH_2CH_2R_{f8})_3$]$_2$ (15):** A Schlenk flask was charged with $[Ir(COD)Cl]_2$ (0.0170 g, 0.0253 mmol), $P(CH_2CH_2R_{f8})_3$ (**2**;[6] 0.140 g, 0.102 mmol) and $CF_3C_6H_5$ (7 mL). The solution was stirred for 20 min. The flask was momentarily evacuated and refilled with CO. After 1 h, the solution was concentrated by oil pump vacuum (ca. 2 mL), and hexane was added (10 mL). The yellow precipitate was collected on a frit and dried by oil pump vacuum to give **15** (0.110 g, 0.0366 mmol, 72%), m.p. 127.3–128.2 °C. – IR and ^{31}P NMR: Scheme 4. – ^{1}H NMR ($CF_3C_6F_{11}$): δ = 2.92–2.52 (m, 24 H). – $C_{61}H_{24}ClF_{102}IrOP_2$ (3000.3): calcd. C 24.42, H 0.81; found C 24.30, H 0.81.

***trans*-Ir(CO)(Cl)[$P(CH_2CH_2R_{f8})_2(CH_2CH_2CH_2R_{f8})$]$_2$ (16):** The reaction and workup given for **15** was repeated with $[Ir(COD)Cl]_2$ (0.0310 g, 0.0462 mmol), **10** (0.265 g, 0.191 mmol) and $CF_3C_6H_5$ (15 mL). This gave **16** as a yellow powder (0.195 g, 0.0644 mmol,

70%), m.p. 111.5−112.0 °C. − IR and ^{31}P NMR: Scheme 4. − ^{1}H NMR ($CF_3C_6F_{11}$): δ = 2.62−1.92 (m, 28 H). − $C_{63}H_{28}ClF_{102}IrOP_2$ (3028.3): calcd. C 24.99, H 0.93; found C 24.52, H 0.92.

***trans*-Ir(CO)(Cl)[P(CH$_2$CH$_2$CH$_2$R$_{f8}$)$_2$(CH$_2$CH$_2$R$_{f8}$)]$_2$ (17):** The reaction and workup given for **15** was repeated with $[Ir(COD)Cl]_2$ (0.013 g, 0.019 mmol), **11** (0.111 g, 0.0793 mmol) and $CF_3C_6H_5$ (10 mL). This gave **17** as a yellow powder (0.085 g, 0.028 mmol, 72%), m.p. 72.5−73.0 °C dec. − IR and ^{31}P NMR: Scheme 4. − ^{1}H NMR ($CF_3C_6F_{11}$): δ = 2.64−1.88 (m, 32 H). − $C_{65}H_{32}ClF_{102}IrOP_2$ (3056.4): calcd. C 25.54, H 1.06; found C 25.63, H 1.16.

***trans*-Ir(CO)(Cl)[P(CH$_2$CH$_2$CH$_2$R$_{f8}$)$_3$]$_2$ (18):** The reaction and workup given for **15** was repeated with $[Ir(COD)Cl]_2$ (0.0420 g, 0.0625 mmol), $P(CH_2CH_2CH_2R_{f8})_3$ (**4**;[6] 0.363 g, 0.257 mmol) and $CF_3C_6H_5$ (15 mL). This gave **18** as a yellow powder (0.290 g, 0.0940 mmol, 75%), m.p. 87.0−87.5 °C. − IR and ^{31}P NMR: Scheme 4. − ^{1}H NMR ($CF_3C_6F_{11}$): δ = 2.42−1.96 (m, 36 H). − ^{13}C{^{1}H} NMR ($CF_3C_6F_{11}$, partial): δ = 32.2 (tm, $^{2}J_{CF}$ = 22 Hz ($^{1}J_{CH}$ = 130 Hz),[25] *C*H$_2$CF$_2$), 24.6 (t, $^{3}J_{CF}$ = 16 Hz ($^{1}J_{CH}$ = 130 Hz),[25] *C*H$_2$CH$_2$CF$_2$), 16.2 (s ($^{1}J_{CH}$ = 130 Hz),[25] P*C*H$_2$). − $C_{67}H_{36}ClF_{102}IrOP_2$ (3084.4): calcd. C 26.09, H 1.18; found C 25.92, H 1.18.

***trans*-Ir(CO)(Cl)[P(CH$_2$CH$_2$CH$_2$R$_{f8}$)$_2$(CH$_2$CH$_2$CH$_2$CH$_2$R$_{f8}$)]$_2$ (19):** The reaction and workup given for **15** was repeated with $[Ir(COD)Cl]_2$ (0.0317 g, 0.0472 mmol), **12** (0.284 g, 0.199 mmol) and $CF_3C_6H_5$ (15 mL). This gave **19** as a yellow powder (0.227 g, 0.0729 mmol, 77%), m.p. 69.0−71.0 °C dec. − IR and ^{31}P NMR: Scheme 4. − ^{1}H NMR ($CF_3C_6F_{11}$): δ = 2.38−1.68 (m, 40 H). − $C_{69}H_{40}ClF_{102}IrOP_2$ (3112.5): calcd. C 26.63, H 1.30; found C 26.84, H 1.30.

***trans*-Ir(CO)(Cl)[P(CH$_2$CH$_2$CH$_2$CH$_2$R$_{f8}$)$_2$(CH$_2$CH$_2$CH$_2$CH$_2$R$_{f8}$)]$_2$ (20):** The reaction and workup given for **15** was repeated with $[Ir(COD)Cl]_2$ (0.0299 g, 0.0445 mmol), **13** (0.263 g, 0.182 mmol) and $CF_3C_6H_5$ (15 mL). This gave **20** as a yellow powder (0.2041 g, 0.06499 mmol, 73%), m.p. 82.5−83.5 °C dec. − IR and ^{31}P NMR: Scheme 4. − ^{1}H NMR ($CF_3C_6F_{11}$): δ = 2.38−1.68 (m, 44 H). − $C_{71}H_{44}ClF_{102}IrOP_2$ (3140.5): calcd. C 27.15, H 1.41; found C 27.15, H 1.42.

***trans*-Ir(CO)(Cl)[P(CH$_2$CH$_2$CH$_2$CH$_2$R$_{f8}$)$_3$]$_2$ (21):** The reaction and workup given for **15** was repeated with $[Ir(COD)Cl]_2$ (0.0304 g, 0.0452 mmol), $P(CH_2CH_2CH_2CH_2R_{f8})_3$ (**5**,[6] 0.295 g, 0.202 mmol) and $CF_3C_6H_5$ (15 mL). This gave **21** as a yellow powder (0.212 g, 0.0669 mmol, 74%), m.p. 72.0−72.5 °C dec. − IR and ^{31}P NMR: Scheme 4. − ^{1}H NMR ($CF_3C_6F_{11}$): δ = 2.20−1.98 (m, 24 H), 1.92−1.70 (m, 24 H). − ^{13}C{^{1}H} NMR ($CF_3C_6F_{11}$, partial): δ = 30.7 [t, $^{2}J_{CF}$ = 23 Hz ($^{1}J_{CH}$ = 130 Hz),[25] *C*H$_2$CF$_2$], 24.9 [t, $^{3}J_{CF}$ = 16 Hz ($^{1}J_{CH}$ = 130 Hz),[25] *C*H$_2$CH$_2$CF$_2$], 24.4, 21.8 [2 × s ($^{1}J_{CH}$ = 130/130 Hz), P*C*H$_2$*C*H$_2$]. − $C_{73}H_{48}ClF_{102}IrOP_2$ (3168.6): calcd. C 27.67, H 1.53; found C 27.56, H 1.37.

***trans*-Ir(CO)(Cl)[P(CH$_2$CH$_2$CH$_2$CH$_2$CH$_2$R$_{f8}$)$_3$]$_2$ (22):** A Schlenk flask was charged with $[Ir(COD)Cl]_2$ (0.0200 g, 0.030 mmol), **6** (0.1830 g, 0.122 mmol) and $CF_3C_6H_5$ (10 mL). The solution was stirred for 20 min. CO was bubbled through the orange solution for 10 min. After 1 h, the green solution was concentrated by oil pump vacuum (ca. 2 mL) and filtered through a silica gel column (2 × 2 cm), which was rinsed with $CF_3C_6H_5$ (10 mL). The filtrates were cooled to −32 °C. A yellow precipitate formed, which was collected on a frit and dried by oil pump vacuum to give **22** (0.1630 g, 0.050 mmol, 83%), m.p. 60.0−61.0 °C (capillary). − IR and ^{31}P NMR: Scheme 4. − ^{1}H NMR ($CF_3C_6F_{11}$): δ = 2.45−1.89 (m, 60 H). − ^{13}C{^{1}H} NMR ($CDCl_3$, partial): δ = 30.6 (t, $^{2}J_{CF}$ = 23 Hz, *C*H$_2$CF$_2$), 23.1 (m, *C*H$_2$CH$_2$CF$_2$), 20.3, 19.7, 19.4 (3 × s, P*C*H$_2$*C*H$_2$*C*H$_2$). − MS (FAB); *m*/*z* (%): 3253 (100) [M$^+$]. − $C_{79}H_{60}ClF_{102}IrOP_2$ (3252.8): calcd. C 29.17, H 1.86; found C 29.55, H 1.98.

***trans*-Rh(CO)(Cl)[P(CH$_2$CH$_2$CH$_2$R$_{f8}$)$_3$]$_2$ (25):** A Schlenk flask was charged with $[Rh(CO)_2Cl]_2$ (0.0071 g, 0.018 mmol), **4** (0.104 g, 0.0735 mmol) and $CF_3C_6H_5$ (10 mL). The solution was stirred for 1 h, and concentrated by oil pump vacuum (ca. 1 mL). CH_2Cl_2 was then added by vapor diffusion. After 48 h, the yellow prisms were collected by filtration and dried by oil pump vacuum to give **25** (0.100 g, 0.0334 mmol, 93%) m.p. 84.5−85.5 °C dec. − IR and ^{31}P NMR: Scheme 5. − ^{1}H NMR ([D$_8$]THF): δ = 2.50−2.20 (m, 12 H), 2.18−1.90 (m, 24 H). − $C_{67}H_{36}ClF_{102}OP_2Rh$ (2995.1): calcd. C 26.87, H 1.21; found C 26.59, H 1.25.

***trans*-Rh(CO)(Cl)(P(CH$_2$CH$_2$CH$_2$CH$_2$R$_{f8}$)$_3$)$_2$ (26):** The reaction and workup given for **25** was repeated with $[Rh(CO)_2Cl]_2$ (0.0080 g, 0.020 mmol), **5** (0.120 g, 0.0824 mmol) and $CF_3C_6H_5$ (10 mL). This gave **26** as yellow prisms (0.118 g, 0.0383 mmol, 96%) m.p. 86.0−87.0 °C dec. − IR and ^{31}P NMR: Scheme 5. − ^{1}H NMR ([D$_8$]THF): δ = 2.50−1.60 (m, 48 H). − $C_{73}H_{48}ClF_{102}OP_2Rh$ (3079.3): calcd. C 28.47, H 1.57; found C 28.22, H 1.63.

Acknowledgments

We thank the DOE, NSF, and DFG (GL 300/3−1) for support of this research, Dr. D. Rutherford for some preliminary observations, and Professor I. Horváth (Eötvös Loránd University) for helpful discussions.

[1] [1a] I. T. Horváth, J. Rábai, *Science* **1994**, *266*, 72−75. − [1b] I. T. Horváth, G. Kiss, R. A. Cook, J. E. Bond, P. A. Stevens, J. Rábai, E. J. Mozeleski, *J. Am. Chem. Soc.* **1998**, *120*, 3133−3143. − [1c] I. T. Horváth, *Acc. Chem. Res.* **1998**, *31*, 641−650.

[2] Additional review literature since 1999: [2a] E. de Wolf, G. van Koten, B.-J. Deelman, *Chem. Soc. Rev.* **1999**, *28*, 37−41. − [2b] R. H. Fish, *Chem. Eur. J.* **1999**, *5*, 1677−1680. − [2c] M. Cavazzini, F. Montanari, G. Pozzi, S. Quici, *J. Fluorine Chem.* **1999**, *94*, 183−193. − [2d] U. Diederichsen, *Nachr. Chem. Tech. Lab.* **1999**, *47*, 805−809.

[3] Survey of practical considerations and underlying physical principles: L. P. Barthel-Rosa, J. A. Gladysz, *Coord. Chem. Rev.* **1999**, *190*−*192*, 587−605.

[4] [4a] D. Rutherford, J. J. J. Juliette, C. Rocaboy, I. T. Horváth, J. A. Gladysz, *Catalysis Today* **1998**, *42*, 381−389. − [4b] J. J. J. Juliette, D. Rutherford, I. T. Horváth, J. A. Gladysz, *J. Am. Chem. Soc.* **1999**, *121*, 2696−2704. − [4c] L. V. Dinh, J. A. Gladysz, *Tetrahedron Lett.* **1999**, *40*, 8995−8998.

[5] [5a] B. Betzemeier, P. Knochel, *Angew. Chem. Int. Ed. Engl.* **1997**, *36*, 2623−2624; *Angew. Chem.* **1997**, *109*, 2736−2738. − [5b] R. Kling, D. Sinou, G. Pozzi, A. Choplin, F. Quignard, S. Busch, S. Kainz, D. Koch, W. Leitner, *Tetrahedron Lett.* **1998**, *39*, 9439−9442. − [5c] C. M. Haar, J. Huang, S. P. Nolan, J. L. Petersen, *Organometallics* **1998**, *17*, 5018−5024.

[6] L. J. Alvey, D. Rutherford, J. J. J. Juliette, J. A. Gladysz, *J. Org. Chem.* **1998**, *63*, 6302−6308.

[7] M.-A. Guillevic, C. Rocaboy, A. M. Arif, I. T. Horváth, J. A. Gladysz, *Organometallics* **1998**, *17*, 707−717.

[8] M. Baudler, K. Glinka, *Inorg. Synth.* **1990**, *27*, 227−235.

[9] J.-M. Vincent, A. Rabion, V. K. Yachandra, R. H. Fish, *Angew. Chem. Int. Ed. Engl.* **1997**, *36*, 2346−2349; *Angew. Chem.* **1997**, *109*, 2438−2440.

[10] Citations of patents that mention this compound: [10a] K. von Werner, *Chem. Abstr.* **1991**, *114*, 184774. − [10b] K. von Werner, *Chem. Abstr.* **1985**, *103*, 214859. − [10c] K. von Werner, *Chem. Abstr.* **1985**, *103*, 214859. − [10d] L. Foulletier, J. P. Lalu, *Chem. Abstr.* **1978**, *88*, 169572.

[11] [11a] J. O. Metzger, R. Mahler, A. Schmidt, *Liebigs Ann.* **1996**,

693−696. − [11b] See also: G. Johansson, V. Percec, G. Ungar, J. P. Zhou, *Macromolecules* **1996**, *29*, 646−660.
[12] A. Ravve, *Principles of Polymer Chemistry*; Plenum Press, New York, **1995**, p 38.
[13] R. Shimizu, T. Fuchikami, *Tetrahedron Lett.* **1996**, *37*, 8405−8408.
[14] M. Burk, R. H. Crabtree, *Inorg. Chem.* **1986**, *25*, 931−932.
[15] A. Klose, J. A. Gladysz, *Tetrahedron: Asymmetry* **1999**, *10*, 2665−2674.
[16] J. Fawcett, E. G. Hope, R. D. W. Kemmitt, D. R. Paige, D. R. Russell, A. M. Stuart, D. J. Cole-Hamilton, M. J. Payne, *Chem. Commun.* **1997**, 1127−1128.
[17] J. A. Gladysz, S. P. Nolan, P. R. Rademacher, and coworkers, work in progress.
[18] M. Selke, W. L. Karney, S. I. Khan, C. S. Foote, *Inorg. Chem.* **1995**, *34*, 5715−5720.
[19] M. Schlosser, *Angew. Chem. Int. Ed.* **1998**, *37*, 1496−1513; *Angew. Chem.* **1998**, *110*, 1538−1556.
[20] C. Rocaboy, W. Bauer, J. A. Gladysz, *Eur. J. Org. Chem*. **2000**, 2621−2628.
[21] C. Li, S. P. Nolan, I. T. Horváth, *Organometallics* **1998**, *17*, 452−456.
[22] A. J. Deeming, B. L. Shaw, *J. Chem. Soc. A* **1968**, 1887−1889.
[23] Recent lead references: [23a] A. Aranyos, D. W. Old, A. Kiyomori, J. P. Wolfe, J. P. Sadighi, S. L. Buchwald, *J. Am. Chem. Soc.* **1999**, *121*, 4369−4378. − [23b] G. Mann, C. Incarvito, A. L. Rheingold, J. F. Hartwig, *J. Am. Chem. Soc.* **1999**, *121*, 3224−3225.
[24] Splitting patterns are partially coincidental; chemical shift and coupling constants deduced from visible peaks.
[25] Determined from a separate ^{13}C NMR spectrum (without ^{1}H decoupling).
[26] Assignments of resonances to the two like or one unique $(CH_2)_xR_{f8}$ segments were made on the basis of intensities.
[27] The multiplet appears to be a triplet (ca. 2 Hz), which would logically be assigned as a $^{3}J_{CF}$ coupling. Hence, this signal is provisionally assigned to the $PCH_2CH_2CH_2CH_2R_{f8}$ carbon atom.

Received February 14, 2000
[I00053]

The Ligand 1,10-Phenanthroline-2,9-dicarbaldehyde Dioxime can Act Both as a Tridentate and as a Tetradentate Ligand − Synthesis, Characterization and Crystal Structures of its Transition Metal Complexes

Ariane Angeloff,[a] Jean-Claude Daran,*[a] Jean Bernadou,*[a] and Bernard Meunier[a]

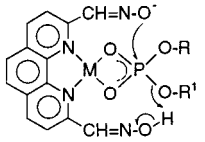
Keywords: Phenanthrolinedicarbaldehyde dioxime / N ligands / Cadmium / Cobalt / Zinc / Copper / Nickel

The polydentate ligand **L** has been prepared by treating 1,10-phenanthroline-2,9-dicarbaldehyde with hydroxylamine. This ligand and its complexes with Zn^{II}, Cu^{II}, Cd^{II}, Co^{II} and Ni^{II} were designed as potential agents for nucleic acid hydrolysis and have been characterized by elemental analysis, NMR spectroscopy, ES-MS and X-ray diffraction analysis. The ligand acts as a tridentate ligand in most cases, to form monomeric trigonal-bipyramidal, square-pyramidal or square-bipyramidal structures. In the case of metallation with cadmium nitrate it acts as a tetradentate ligand to give a pentagonal-bipyramidal structure. Dissociation of the oxime group to an oximate, which acts as an anionic bridging ligand, was observed in the case of metallation with zinc acetate thus giving rise to dimers and/or polymers.

Introduction

The metal-chelating properties of the 1,10-phenanthroline ligand and its derivatives have been utilized in a range of analytical reagents, as well as for the development of bioorganic probes.[1] In attempts to obtain hydrolytic chemical agents which are able to hydrolyze phosphodiester bonds in nucleic acids in the model of DNA or RNA nucleases,[2] we report here on the synthesis and the characterization of zinc, cadmium, copper, cobalt and nickel complexes of 1,10-phenanthroline-2,9-carbaldehyde dioxime. These complexes (metal cation) were designed to interact with the initial negatively charged phosphate, and to promote hydrolysis of the phosphodiester P−O bond through nucleophilic attack on the phosphorus atom by one oximate group, the other oxime group stabilizing the leaving oxygen atom (see hereafter for a possible schematic representation of the ternary system ligand/metal/phosphodiester: Scheme 1).[3−5] The oximate group has been chosen because it can effectively act as a nucleophile endowed with nucleolytic activity, as previously reported for free ligands such as pyridine-2-aldoxime[6] or simple inorganic complexes such as metallated complexes of 2-acetylpyridine oxime.[7] Although preliminary results on cleavage of nucleic acids models are rather deceiving, the interest for such structures lies also in the previously reported antitumor[8] and antimicrobial[9] activities of the phenanthrolinedicarbaldehyde derivative and/or of the corresponding dioxime ligand **L**. In the latter case, the activity might be related to the in vivo formation of metal chelates. In a related topic, the cytotoxic activity of tetradentate palladium complexes of phenanthroline-dimathanamines has been recently reported.[10]

The improved synthesis of the ligand 1,10-phenanthroline-2,9-dicarbaldehyde dioxime **L**, and the preparation and complete characterization of seven complexes of **L** are presented.



Scheme 1

[a] Laboratoire de Chimie de Coordination du CNRS,
205 route de Narbonne, 31077 Toulouse cedex 4, France
Fax: (internat.) + 33-5/61553003
E-mail: bernadou@lcc-toulouse.fr
daran@lcc-toulouse.fr

Synthesis and Characterization

The Ligand

The only reported method for the synthesis of 1,10-phenanthroline-2,9-dicarbaldehyde (Figure 1) involves the oxidation of the commercially available neocuproine by selenium dioxide in dioxane[11,12] or ethanol.[9] After completion of the reaction, the selenium separates as a yellow/red form which is difficult to filter, and some of it is retained in solution as a colloid. The elimination of selenium impurities is extremely difficult. This explains the fact that in the literature either the yield of the reaction is satisfactory (70%) but the product is analytically impure,[11] or the yields are not reported.[9,12] In addition, from an environmental viewpoint the replacement of SeO_2 by another oxidant is desir-

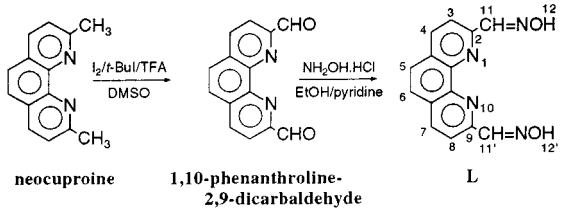


Figure 1. Synthesis of ligand **L**

 © WILEY-VCH Verlag GmbH, D-69451 Weinheim, 2000 1434−1948/00/0909−1985 $ 17.50+.50/0

able. Therefore, in order to prepare 1,10-phenanthroline-2,9-dicarbaldehyde, we used the procedure initially described for the oxidation of methyl to formyl groups in heteroaromatic derivatives with iodine in dimethyl sulfoxide,[13] a method which was improved later by using *tert*-butyl iodide.[14] This procedure, applied to neocuproine, gave pure 1,10-phenanthroline-2,9-dicrbaldehyde in 48% yield as a hemihydrate in crystalline form. This dialdehyde derivative was then converted into the dioxime **L** according to the method previously reported.[11] Compound **L** has been fully characterized, including a crystallographic study which allowed for the determination of the *E* configuration of the two oxime groups, and for the observation of the co-existence of two different conformations (*s-cis* and *s-trans*) around the $C_{Ar}-C(=N-)$ single bond between the oxime group and the phenanthroline unit in the crystal (see below). In solution, these two conformations are probably in fast equilibrium since the NMR spectrum for **L** in DMSO corresponds to a symmetrical molecule.

Metal Complexes (Figure 2)

The formation of nearly all complexes, besides one, was achieved at room temp. under approximately stoichiometric conditions (metal ion/ligand molar ratio was in the range 0.64 to 1.3), after 2−30 min of reaction in DMF ([Zn**L**Cl_2 and [Cu**L**Cl_2)], DMSO ([Zn**L**$(AcO)]_n$] or DMSO/H_2O ([Cd**L**Cl_2], [Co**L**Cl_2] and [Ni**L**(DMSO)Cl_2]). In all these cases, the reaction products were isolated as analytically pure species on spontaneous precipitation. Compound [Cd**L**(OH_2)(DMSO)$(NO_3)]^+$] was only prepared as crystals for X-ray diffraction analysis (see below). On the basis of elemental analyses, all complexes (whatever was the method of preparation), exhibited an unequivocal metal-to-ligand stoichiometry of 1:1. In some cases, one or two molecules of solvent were present (DMF, DMSO or water). Moreover, the CHN data showed that all complexes present existed as monomers, except [Zn**L**$(AcO)]_n$ which existed as dimer/polymer. The polymeric structure of this last compound was also confirmed by the NMR-spectroscopic data with

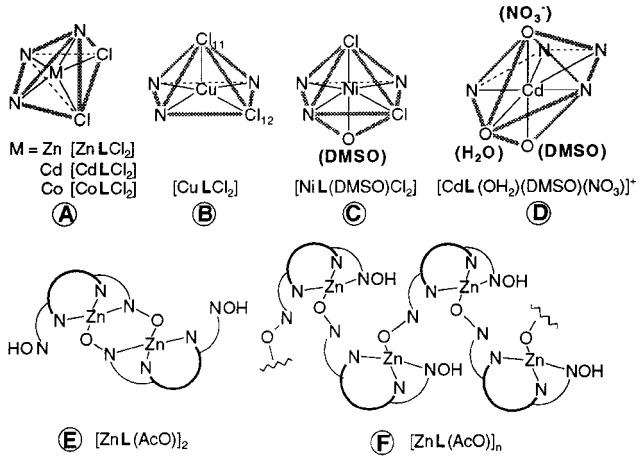


Figure 2. Proposed structures for complexes M−**L** (in structure **D**, one nitrate ion is outside the coordination sphere; in structure **E**/**F**, at least one acetate ion per metallated ligand is outside the coordination sphere)

the methyl resonance peak integrating for only one methyl group per metal unit and the other ligand in this case being an oximate bridging anion.

Data obtained by positive FAB-MS indicated that monocationic species corresponding to the complex having lost one proton $[\mathbf{L} + M - H^+]^+$ or retained one of the two anionic labile ligands $[\mathbf{L} + M + Cl^-]^+$, with an additional solvent molecule (water, DMSO), are usually observed. In addition, the redox-active copper complex gave some peaks corresponding to Cu^I monomeric $[\mathbf{L} + Cu^I]^+$ or dimeric species (dimer 2:1 $[2 \times \mathbf{L} + Cu^I]^+$). In ES-MS, only monocationic species were observed. They predominantly corresponded to the complex ligand/metal having lost one proton ($\mathbf{L} + M - H^+$) or retained one of the two anionic ligands ($\mathbf{L} + M + Cl^-$ or AcO^-). The presence of one or two solvent molecules could be observed, as well as in some cases, dehydration of the fragment (the aldoxime group giving possibly a nitrile function). In addition, we observed minor peaks, probably generated in the MS machine, corresponding to dimeric species of the type 2:1 (cases of $2 \times \mathbf{L} + Zn - H^+$, $2 \times \mathbf{L} + Cu^I$, $2 \times \mathbf{L} + Co^{III} - 2\,H^+$ and $2 \times \mathbf{L} + Ni^{II} - H^+$) or of the type 2:2 (cases of $2 \times \mathbf{L} + 2 \times Zn - 3\,H^+$, $2 \times \mathbf{L} + 2 \times Zn - 2\,H^+ + Cl^-$, $2 \times \mathbf{L} + 2 \times Zn - H^+ + 2\,Cl^-$, $2 \times \mathbf{L} + 2 \times Zn - 3\,H^+$, $2 \times \mathbf{L} + 2 \times Cu - 3\,H^+$ or $2 \times \mathbf{L} + 2 \times Cu - 2\,H^+ + Cl^-$, $2 \times \mathbf{L} + 2 \times Cd - H^+ + 2\,Cl^-$). The polymeric compound [Zn**L**$(AcO)]_n$ not only gave peaks for the monomeric species $\mathbf{L} + Zn - H^+$ (with addition or loss of one water molecule) but also for dimers of the type 2:2 ($2 \times \mathbf{L} + 2 \times Zn - 3\,H^+$ or $2 \times \mathbf{L} + 2 \times Zn - 2\,H^+ + AcO^-$) or trimers of the type 3:3 ($3 \times \mathbf{L} + 3 \times Zn - 5\,H^+$), these latter polymeric fragments being the most abundant.

On complexation of cadmium chloride with ligand **L** (giving [Cd**L**Cl_2]), we observed changes in the ^1H NMR spectrum with a broadening of the peaks corresponding to 4-H/7-H and 11-H/11′-H (pattern at $\delta = 8.92$), and to 12-H/12′-H (massif at $\delta = 12.73$). The other signals remained sharp and well resolved. Increasing the temperature up to 60° C allowed for the resolution of the broad signal at $\delta = 8.92$ into one doublet at $\delta = 8.90$ (4-H/7-H) and one singlet at $\delta = 8.89$ (11-H/11′-H) and for the significant reduction of the width of the 12-H/12′-H signal. A similar behaviour was observed for complex [Cd**L**(OH_2)(DMSO)$(NO_3)]^+$. Although the crystalline structures of [Cd**L**Cl_2] and [Cd**L**(OH_2)(DMSO)$(NO_3)]^+$ are different (see below), these NMR-spectroscopic data support a common symmetrical structure in solution, with the ligand acting as a tetradentate ligand. With regard to the two zinc derivatives [Zn**L**Cl_2] and [Zn**L**$(AcO)]_n$, the ^1H NMR spectra were too complex and did not give any structural information, except for [Zn**L**$(AcO)]_n$ where the aromatic/aliphatic proton ratio supports a structure with only one acetate group per molecule.

Description of the Crystal Structures of L, [ZnLCl_2], [CuLCl_2], [CdLCl_2], [CdL(OH_2)(DMSO)$(NO_3)]^+$, [CoLCl_2] and [NiL(DMSO)Cl_2]

The molecular structure of **L**, as determined by X-ray analysis, is shown with its atom labelling scheme in Fig-

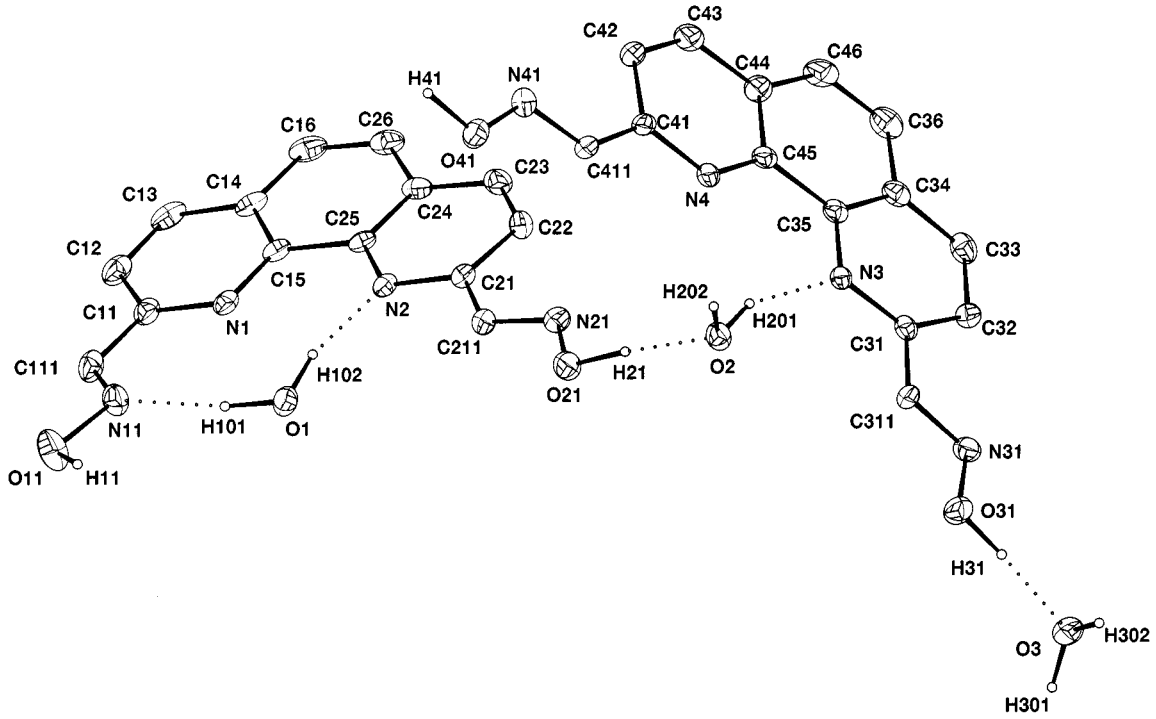


Figure 3. Molecular structure of **L** with atom labelling scheme illustrating the hydrogen bond between the two independent molecules (**La** and **Lb**) within the asymmetric unit; ellipsoids represent 30% probability; most of the hydrogen atoms have been omitted for clarity

ure 3. The asymmetric unit is composed of two independent molecules of the ligand and three water molecules. The two

Table 1. Bond lengths [Å] for ligand **L**; esd values in parentheses refer to the last significant digit

Molecule **a**		Molecule **b**	
O(11)−N(11)	1.407(4)	O(31)−N(31)	1.425(4)
O(21)−N(21)	1.403(4)	O(41)−N(41)	1.416(5)
N(2)−C(21)	1.350(5)	N(3)−C(31)	1.335(5)
N(2)−C(25)	1.362(5)	N(3)−C(35)	1.365(5)
N(1)−C(11)	1.351(5)	N(4)−C(41)	1.345(5)
N(1)−C(15)	1.355(5)	N(4)−C(45)	1.363(5)
N(11)−C(111)	1.282(5)	N(31)−C(311)	1.278(5)
N(21)−C(211)	1.272(5)	N(41)−C(411)	1.270(5)
C(11)−C(12)	1.395(6)	C(31)−C(32)	1.407(6)
C(11)−C(111)	1.457(6)	C(31)−C(311)	1.469(5)
C(12)−C(13)	1.368(6)	C(32)−C(33)	1.359(6)
C(13)−C(14)	1.407(6)	C(33)−C(34)	1.406(6)
C(14)−C(15)	1.413(6)	C(34)−C(35)	1.413(6)
C(14)−C(16)	1.428(6)	C(34)−C(36)	1.426(6)
C(15)−C(25)	1.457(5)	C(35)−C(45)	1.455(5)
C(16)−C(26)	1.351(6)	C(36)−C(46)	1.341(6)
C(21)−C(22)	1.398(6)	C(41)−C(42)	1.409(6)
C(21)−C(211)	1.463(6)	C(41)−C(411)	1.456(6)
C(22)−C(23)	1.360(6)	C(42)−C(43)	1.355(6)
C(23)−C(24)	1.403(6)	C(43)−C(44)	1.413(6)
C(24)−C(25)	1.406(6)	C(44)−C(45)	1.409(5)
C(24)−C(26)	1.434(6)	C(44)−C(46)	1.430(6)

molecules **La** and **Lb** (Table 1) are linked by hydrogen bonds through one of the water molecule (O2). Moreover, each of these water molecules is engaged in hydrogen bonding with symmetrically related molecules **La** and **Lb**, thus developing a three-dimensional hydrogen bond network (Table 2). The two molecules **La** and **Lb** have an essentially planar conformation with the largest deviation from the plane being 0.168(5)Å at O(11) for molecule **La** and −0.083(5) Å at O(41) for **Lb**. The largest deviation is observed for molecule **La** where there are hydrogen-bond interactions with the water molecule (O1) (Figure 3). The C−N and C−C distances in the phenanthroline fragment (Table 1) are within the range observed in related molecules.[15] In both molecules **La** and **Lb**, the oxime groups have an *E* configuration. However, if in molecule **Lb** the conformation of both oxime groups is *s-trans* with respect to the N atoms of the phenanthroline fragment, then in molecule **La** these two groups show two different conformations, *s-cis* and *s-trans*, around the C_{Ar}−C(=N) single bond. This difference in conformation is related to the occurrence of hydrogen bonds between the water molecule (O1) and the two N atoms, the N(11) of the oxime group and the N(2) of the phenanthroline fragment in molecule **La** (Table 2).

The crystallization of metal complexes, besides [Cd**L**Cl_2] (which was obtained by transmetallation of [Zn**L**Cl_2] in the presence of cadmium nitrate) and [Zn**L**(AcO)]$_n$ (unsuccessful crystallization attempts), was achieved at room temp. under approximately stoichiometric conditions (the metal/ligand ratio ranged from 1.3 to 1.9), after 2−7 days in DMSO or DMSO/H_2O. Since the three complexes [Zn**L**Cl_2], [Cd**L**Cl_2] and [Co**L**Cl_2] have closely related structures, only the molecular view of the cobalt complex [Co**L**Cl_2] with its atom labelling scheme is shown in Figure 4. The asymmetric unit also contains a DMSO solvent molecule which is hydrogen-bonded to the OH group of the

Table 2. Specified hydrogen bonds for ligand **L**

D−H [Å]	H···A [Å]	D···A [Å]	<(DHA) [°]	
1.04(3)	1.67(4)	2.664(5)	159(5)	O(11)−H(11)···O(1)[a]
1.03(3)	1.60(3)	2.620(4)	173(5)	O(21)−H(21)···O(2)
1.02(3)	1.66(3)	2.672(4)	173(5)	O(31)−H(31)···O(3)
1.02(3)	1.66(3)	2.670(4)	168(5)	O(41)−H(41)···O(1)[b]
1.00(3)	1.87(3)	2.860(5)	170(5)	O(1)−H(101)···N(11)
1.02(3)	1.82(3)	2.820(4)	166(5)	O(1)−H(102)···N(2)
0.99(3)	1.98(3)	2.915(4)	156(5)	O(2)−H(201)···N(3)
0.99(3)	2.39(5)	3.093(4)	127(4)	O(2)−H(201)···N(4)
1.00(3)	1.87(3)	2.870(4)	172(5)	O(2)−H(202)···O(31)[c]
1.01(3)	1.91(4)	2.842(4)	153(5)	O(3)−H(301)···O(21)[d]
1.01(3)	1.90(3)	2.845(4)	156(5)	O(3)−H(302)···O(41)[c]

[a] Symmetry transformations used to generate equivalent atoms: $-x-1, -y+2, -z+2$. − [b] $x+1, y, z$. − [c] $-x, -y+1, -z+2$. − [d] $-x-1, -y+1, -z+2$.

With regard to the complex [Cu**L**Cl_2 (Table 4), the asymmetric unit is composed of two molecules **a** and **b** of the complex and four DMSO solvent molecules which are each hydrogen-bonded to the OH groups. Although the metal atom is surrounded by the same ligands as in the previous complexes, the geometry around the metal center is best described as being a distorted square-pyramidal structure (Figure 2B and 5, Table 4); the N(1)−Cu(1)−Cl(12) angle increases to the mean value 151.8° (the corresponding N(1)−M−Cl(1) angles range from 121.2 to 127.7° for [Zn**L**Cl_2], [Cd**L**Cl_2] and [Co**L**Cl_2]), whereas the N(1)−Cu−Cl11) angle decreases to the mean value 99.7° (the corresponding angles range from 113.7 to 118.7° for [Zn**L**Cl_2], [Cd**L**Cl_2] and [Co**L**Cl_2]. Thus, in [Cu**L**Cl_2], the nitrogen atoms N(1), N(2), N(11) and the chrorine atom

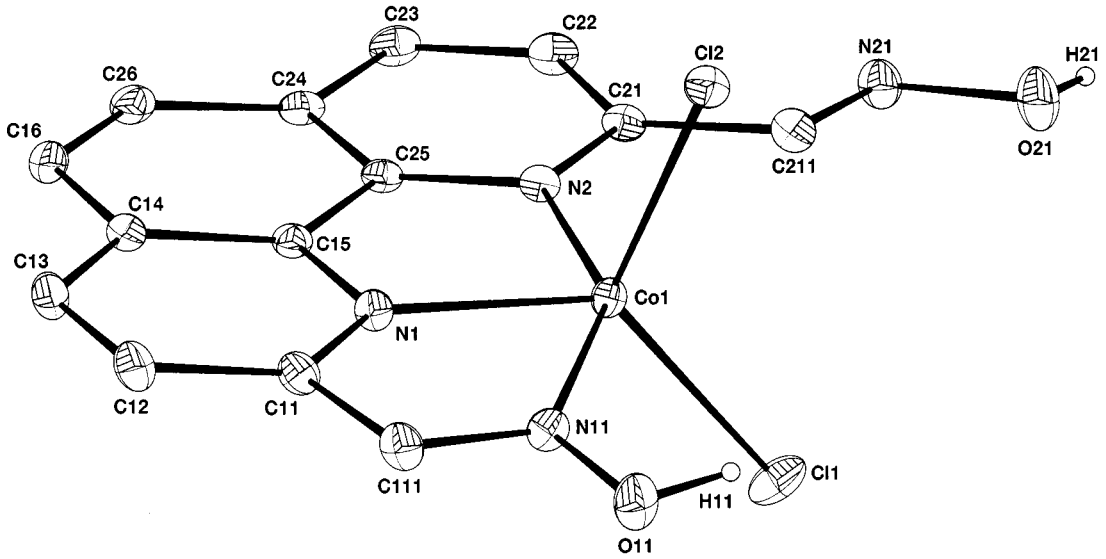


Figure 4. Molecular view of complex [Co**L**Cl_2 with atom labelling scheme; ellipsoids are drawn at 30% probability; hydrogen atoms have been omitted for clarity

coordinated oxime group. Such hydrogen bonding between the DMSO solvent and the complex occurs in all the related compounds. In these three complexes, the structure consists of a metal atom surrounded by one ligand **L** and two chlorine atoms in a distorted trigonal-bipyramidal geometry (Figure 2, **A** and Table 3). The axial positions are occupied by two nitrogen atoms N(2) and N(11) [N(2)−M−N(11) = 148.28(9)°, 138.03(15)° and 151.09(6)°, for the Zn, Cd and Co complexes, respectively]. The equatorial plane is made by the two chlorine atoms and the nitrogen atom N(1) of the phenanthroline fragment. The equatorial plane and the plane defined by the axial positions make a dihedral angle of 88.62(4)°. In the three complexes the metal center is coordinated to N(1), N(2) of the rigid 1,10-phenanthroline and to N(11) of the oxime group forming two fused five-membered rings with very acute N−M−N angles: N(1)−M−N(2) = 76.22(9)°, 69.58(15)° and 77.27(6)° and N(1)−M−N(11) = 72.07(9)°, 68.48(16)° and 73.94(6)°, for compounds [Zn**L**Cl_2], [Cd**L**Cl_2] and [Co**L**Cl_2], respectively.

Cl(12) form the basal plane, whereas Cl(11) occupies the apex position (Figure 2B). Applied to the five-coordinated structures [Cu**L**Cl_2), [Zn**L**Cl_2], [Cd**L**Cl_2] and [Co**L**Cl_2], the calculation of the geometric parameter $\tau = (\beta - \alpha)/60$ [α = N(1)−M−Cl (1 or 12), β = N(2)−M−N(11)] gives the values 0.03, 0.39, 0.28 and 0.42, respectively. Since τ is a parameter used as an index of the degree of trigonality,[16], these values support a tetragonal geometry for [Cu**L**Cl_2] (τ close to zero) and are in agreement with a structure intermediate between the perfectly tetragonal (τ = zero) and trigonal-bipyranidal (τ = 1) geometries for [Zn**L**Cl_2], [Cd**L**Cl_2] and [Co**L**Cl_2]. In [Cu**L**Cl_2], the Cu atom is 0.358 Å (mean value) above the best plane defined by the three N atoms and the Cl(12).. As in the previous three complexes, the metal center is coordinated to N(1) and N(2) of the rigid 1,10-phenanthroline and N(11) of one oxime group forming two fused five-membered rings with acute N−Cu−N angles: N(1)−Cu(1)−N(2) = 78.44(11)° for molecule **a** and 78.18(11)° for molecule **b**, N(1)−Cu(1)−

Table 3. Selected bond lengths [Å] and angles [°] for complexes [Zn**L**Cl_2], [Cd**L**Cl_2], and [Co**L**Cl_2]

	[Zn**L**Cl_2]	[Cd**L**Cl_2]	[Co**L**Cl_2]
Bond lengths			
M−N(1)	2.057(2)	2.292(4)	2.0193(16)
M−N(2)	2.275(3)	2.458(5)	2.2386(16)
M−Cl(2)	2.2553(9)	2.4367(14)	2.2529(8)
M−Cl(1)	2.2203(10)	2.4129(15)	2.2535(7)
M−N(11)	2.382(3)	2.470(5)	2.2726(17)
O(11)−N(11)	1.381(3)	1.380(6)	1.372(2)
O(21)−N(21)	1.388(3)	1.390(7)	1.387(2)
N(1)−C(11)	1.336(4)	1.331(7)	1.332(2)
N(1)−C(15)	1.355(4)	1.357(7)	1.349(2)
N(2)−C(21)	1.332(4)	1.328(7)	1.333(2)
N(2)−C(25)	1.358(4)	1.366(7)	1.358(2)
N(11)−C(111)	1.266(4)	1.281(7)	1.274(3)
N(21)−C(211)	1.272(4)	1.265(8)	1.268(3)
Angles [°]			
N(1)−M−N(2)	76.22(9)	69.58(15)	77.27/6)
N(1)−M−Cl(2)	118.70(7)	114.57(11)	113.70(5)
N(2)−M−Cl(2)	98.14(6)	97.33(10)	98.54(5)
N(1)−M−Cl(1)	123.20(7)	121.16(11)	127.72(5)
N(2)−M−Cl(1)	99.29(7)	95.27(11)	101.40(5)
Cl(2)−M−Cl(1)	117.99(4)	123.81(5)	118.06(3)
N(1)−M−N(11)	72.07(9)	68.48(16)	73.94(6)
N(2)−M−N(11)	148.28(9)	138.03(15)	151.09(6)
Cl(2)−M−N(11)	97.68(7)	101.21(10)	95.32(5)
Cl(1)−M−N(11)	97.25(7)	104.76(11)	94.16/5)

Table 4. Selected bond lengths [Å] and angles [°] for complex [Cu**L**Cl_2]

Molecule **a**		Molecule **b**	
Bond lengths			
Cu(1)−N(1)	1.949(3)	Cu(2)−N(3)	1.945(3)
Cu(1)−N(11)	2.132(3)	Cu(2)−N(31)	2.125(3)
Cu(1)−N(2)	2.193(3)	Cu(2)−N(4)	2.222(3)
Cu(1)−Cl(12)	2.2295(12)	Cu(2)−Cl(22)	2.2155(12)
Cu(1)−Cl(11)	2.4020(12)	Cu(2)−Cl(21)	2.4130(12)
O(11)−N(11)	1.361(3)	O(31)−N(31)	1.373(3)
O(21)−N(21)	1.385(4)	O(41)−N(41)	1.381(5)
N(1)−C(11)	1.336(4)	N(3)−C(31)	1.329(4)
N(1)−C(15)	1.346(4)	N(3)−C(35)	1.348(4)
N(2)−C(21)	1.334(4)	N(4)−C(41)	1.338(4)
N(2)−C(25)	1.359(4)	N(4)−C(45)	1.355(5)
N(11)−C(111)	1.277(4)	N(31)−C(311)	1.281(5)
N(21)−C(211)	1.279(5)	N(41)−C(411)	1.282(5)
Angles [°]			
N(1)−Cu(1)−N(11)	75.94(11)	N(3)−Cu(2)−N(31)	76.20(11)
N(1)−Cu(1)−N(2)	78.44(11)	N(3)−Cu(2)−N(4)	78.18(11)
N(11)−Cu(1)−N(2)	153.73(11)	N(31)−Cu(2)−N(4)	153.23(11)
N(1)−Cu(1)−Cl(12)	149.93(9)	N(3)−Cu(2)−Cl(22)	153.81(9)
N(11)−Cu(1)−Cl(12)	94.49(9)	N(31)−Cu(2)−Cl(22)	93.76(9)
N(2)−Cu(1)−Cl(12)	104.96(8)	N(4)−Cu(2)−Cl(22)	106.06(9)
N(1)−Cu(1)−Cl(11)	100.83(10)	N(3)−Cu(2)−Cl(21)	98.56(10)
N(11)−Cu(1)−Cl(11)	95.12(9)	N(31)−Cu(2)−Cl(21)	94.33(9)
N(2)−Cu(1)−Cl(11)	95.24(8))	N(4)−Cu(2)−Cl(21)	97.05(8)
Cl(12)−Cu(1)−Cl(11)	108.46(4)	Cl(22)−Cu(2)−Cl(21)	106.37(5)

N(11) = 75.94(11)° for molecule **a** and 76.20(11)° for molecule **b**.

A molecular view of complex [Ni**L**(DMSO)Cl_2] is shown in Figure 6 with its atom labelling scheme. The structure consists of a metal atom surrounded by one ligand **L**, two chlorine atoms and one DMSO linked by the O atom, in a distorted octahedral geometry. As in the previous complexes, the metal center is coordinated to N(1) and N(2) of the rigid 1,10-phenanthroline ligand and N(11) of one oxime group forming two fused five-membered rings (Table 3) with acute N−Ni(1)−N angles: N(1)−Ni(1)−N(2) = 77.53(17)° and N(1)−Ni(1)−N(11) = 74.68(17)°. These three nitrogen atoms occupy the equatorial plane which also contains the Cl(1) atom, whereas the axial positions are occupied by the second chlorine atom Cl(2) and the oxygen atom O(1) of the DMSO. All C, N and O atoms of the ligand, as well as the Cl(1) and Ni(1) atoms make an almost perfect plane, with the largest deviation from the plane being −0.13 Å at C(22). The hydrogen atom H(11) also belongs to this plane and there is a bonding interaction between it and Cl(1) [O(11)−H(11) = 1.015 Å; O(11)···Cl(1) = 3.097 Å; H(11)···Cl(1) = 2.256 Å; O(11)−H(11)···Cl(1) = 139.4°]. The atom H(21), which is out of the plane by 0.42 Å, is engaged in a bonding interaction with the atom O(1) of the [$-x + 3/2$, $y + 1/2$, z] symmetry-related molecule [O(21)−H(21) = 0.840 Å; O(21)···O(1) = 2.679 Å; H(21)···O(1) = 1.891 Å; O(21)−H(21)···O(1) = 155.5°], resulting in the formation of a two-dimensional hydrogen-bond network parallel to the *ab* plane.

A molecular view of complex [Cd**L**(OH_2)-$(DMSO)(NO_3)]^+$ is shown in Figure 6 with its atom labelling scheme. The cadmium atom presents a distorted pentagonal-bipyramidal geometry (Figure 2, **D**, Table 5); the equatorial plane is occupied by the four N atoms of ligand **L** and the oxygen atom of a water molecule, and the axial positions are occupied by two oxygen atoms belonging to a DMSO molecule and a nitrate anion. In this complex, the cadmium is coordinated to the four nitrogen atoms of the ligand resulting in the formation of three fused five-membered rings with very acute N−Cd−N angles, N(2)−Cd(1)−N(1) = 70.34(9)°, N(1)−Cd(1)−N(11) = 63.82(8)° and N(2)−Cd(1)−N(21) = 64.98(9)°. Of the four Cd−N distances, the two bonds connecting the metal center to the N atoms of the oxime groups are much longer, 2.720(3) and 2.780(3) Å, than the bonds involving the N atoms of the phenanthroline fragment, 2.341(3) and 2.369(2) Å. This lengthening may be a result of steric constraints. As a consequence of the coordination of the two nitrogen atoms N(11) and N(21), the two oximes have the same *s-cis* conformation around the C_{Ar}−C(=N) single bond. The unit also contains a free nitrate ion and a DMSO solvent molecule. The oxygen atom of DMSO and one of the oxygen atoms of the NO_3^- anion are connected, through hydrogen bonding, to the OH groups and also to the water molecule.

Since all these metal complexes have initially been designed as artificial nucleases with the potential ability to hydrolyze phosphomonoester and phosphodiester bonds, we performed some preliminary cleavage experiments using *p*-nitrophenyl phosphate as a substrate. As it is shown in Table 6, the hydrolytic activities of the zinc, copper, cobalt

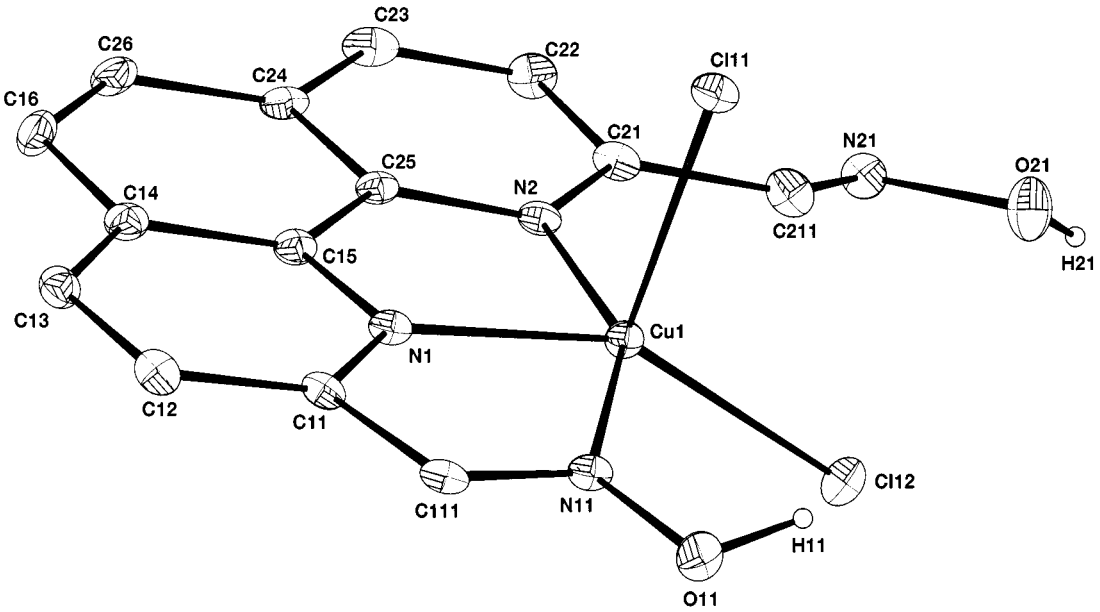


Figure 5. Molecular view of complex [Cu**L**Cl_2] with atom labelling scheme; ellipsoids are drawn at 30% probability; hydrogen atoms have been omitted for clarity

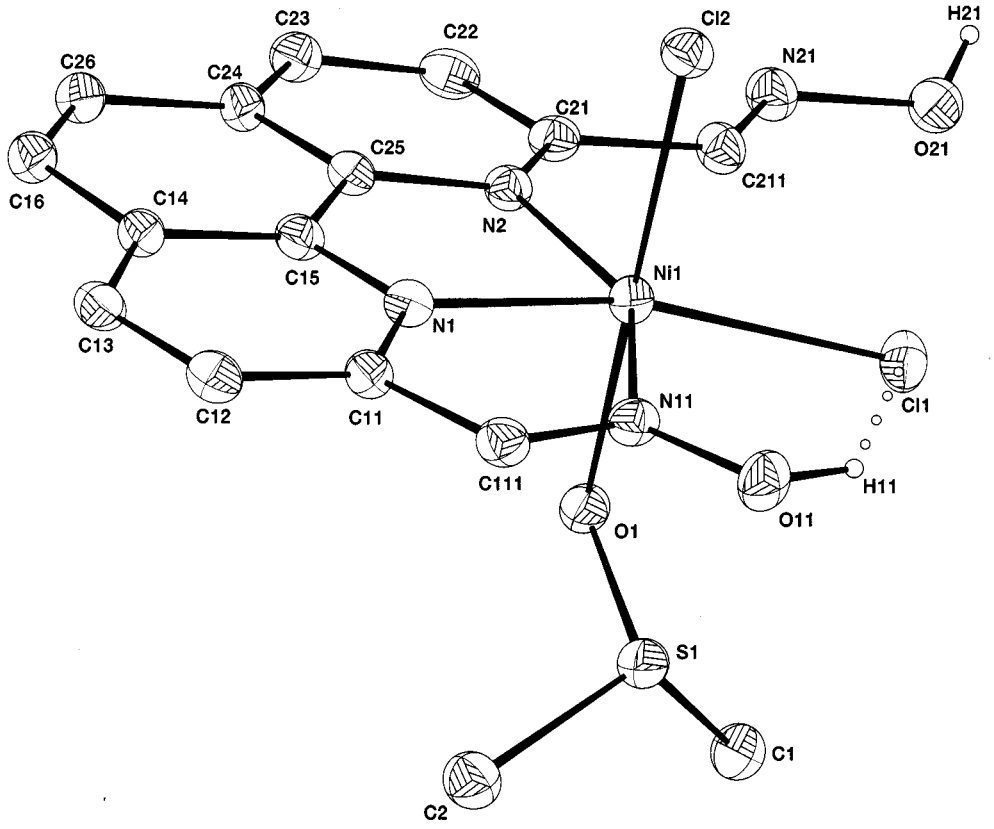


Figure 6. Molecular view of complex [Ni**L**(DMSO)Cl_2] with atom labelling scheme; ellipsoids are drawn at 30% probability; hydrogen atoms and non-coordinating lattice solvents molecules have been omitted

or nickel ions were not improved in the presence of ligand **L**. Moreover, the activity remained far below the activity of the lanthanide cerium salt alone, which is considered as one of the most reactive agents in the catalysis of DNA hydrolysis. It should be noted that in the case of cerium experiments, a slight but significant enhancement of its hydrolytic activity (+ 20 to + 80%) occurred in the presence of ligand **L**. This has also been observed during phosphodiester hy-

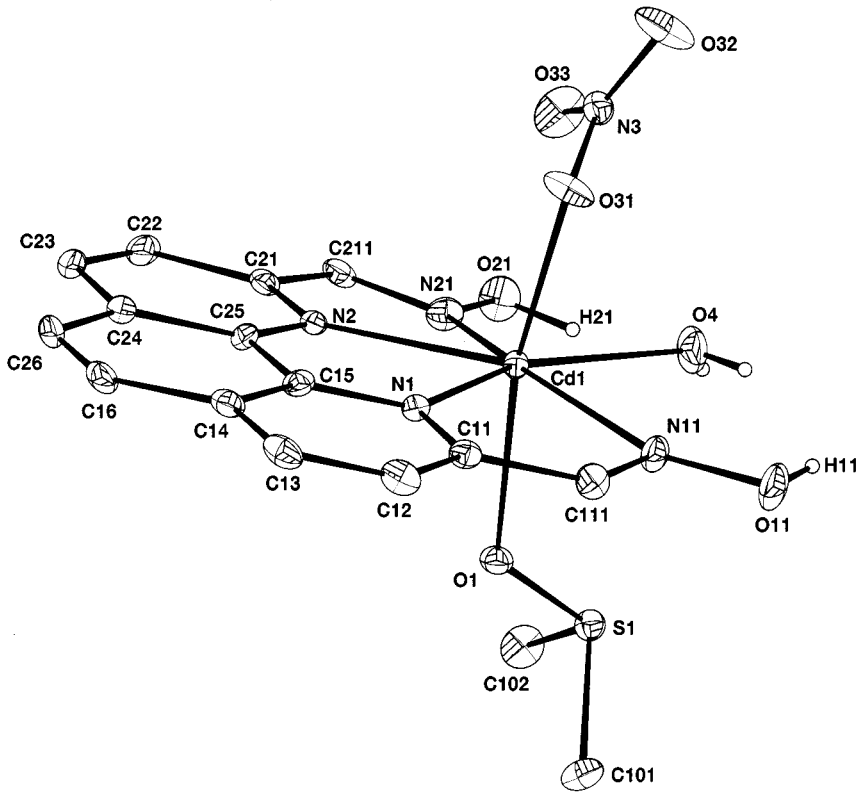


Figure 7. Molecular view of complex $[CdL(OH_2)(DMSO)(NO_3)]^+$ with atom labelling scheme; ellipsoids are drawn at 30% probability; hydrogen atoms and non coordinating anions have been omitted

Table 5. Selected bond lengths for complexes $[CdL(OH_2)(DMSO)(NO_3)]^+$ and $[NiL(DMSO)Cl_2]$

$[CdL(OH_2)(DMSO)(NO_3)]^+$		$[NiL(DMSO)Cl_2]$	
Cd(1)−O(4)	2.240(3)	Ni(1)−N(1)	2.008(4)
Cd(1)−O(1)	2.281(2)	Ni(1)−N(2)	2.216(4)
Cd(1)−O(31)	2.303(3)	Ni(1)−Cl(2)	2.351(2)
Cd(1)−N(2)	2.341(3)	Ni(1)−Cl(1)	2.394(2)
Cd(1)−N(1)	2.369(2)	Ni(1)−N(11)	2.131(4)
Cd(1)−N(21)	2.720(3)	Ni(1)−O(1)	2.131(4)
Cd(1)−N(11)	2.780(3)	O(11)−N(11)	1.373(6)
N(1)−C(11)	1.330(4)	O(21)−N(21)	1.402(6)
N(1)−C(15)	1.349(4)	N(1)−C(11)	1.337(7)
C(111)−N(11)	1.267(4)	N(1)−C(15)	1.337(8)
N(11)−O(11)	1.394(3)	N(2)−C(21)	1.320(7)
N(2)−C(21)	1.333(4)	N(2)−C(25)	1.384(7)
N(2)−C(25)	1.344(4)	N(11)−C(111)	1.289(7)
C(211)−N(21)	1.274(4)	N(21)−C(211)	1.282(7)
N(21)−O(21)	1.383(4)		
S(1)−O(1)	1.526(2)		
S(1)−C(101)	1.777(4)		
S(1)−C(102)	1.779(3)		
N(3)−O(32)	1.226(4)		
N(3)−O(33)	1.226(4)		
N(3)−O(31)	1.262(4)		

drolysis experiments using bis(*p*-nitrophenyl) phosphate as a substrate (data not shown).

Discussion

Previous studies[17] on complexes of the bidentate ligand 2,9-dimethyl-1,10-phenanthroline with Zn, Cu, Co and Ni have shown that these molecules possess a mirror plane which contains the metal and chlorine atoms and bisects the ligand molecule. The replacement of the two methyl groups by two oxime substituents introduces additional possibilities of chelation involving either the nitrogen or oxygen atoms of these groups. All the molecules presented here have provided unequivocal evidence for the structures of the 1:1 metal-ligand complexes. In all the complexes with chloro ligands, X-ray diffraction analyses showed a distorted trigonal-bipyramidal, a square-pyramidal or a square-bipyramidal structure involving the phenanthroline derivative as a tridentate ligand and coordination of the two chlorine atoms (Figure 2, **A**, **B** and **C**); the symmetry of the molecule was broken. However, as it was exemplified in two cases, the stereochemistry and the coordination number of the ligand may depend on the anion present.[18] Firstly, when ligand **L** was metallated with cadmium nitrate instead

Table 6. Hydrolysis of *p*-nitrophenyl phosphate (NPP) (expressed as mol-% conversion) by various metal ions and their complexes with and without ligand **L**

	Zn	Zn	Cu	Cu	Co	Ni	Ce	Ce
Run[a]	50 °C	80 °C	50 °C	80 °C	80 °C	80 °C	50 °C	80 °C
1 metal	−	20	−	25	18	−	85	100
2 metal + **L**	< 5	27	20	21	20	42	95	100

[a] Conditions: [NPP] = 500 μM; Zn^{2+}, Cu^{2+}, Co^{2+}, Ni^{2+} or Ce^{3+} cation 500 μM; metallated complex 500 μM (metal ion/**L**, 1:1); TRIS acetate buffer pH = 8 (50 mM) for 3 h at the indicated temperature.

of cadmium chloride, the crystal structure of $[Cd\mathbf{L}(OH_2)(DMSO)(NO_3)]^+$ appeared quite different from that of $[Cd\mathbf{L}Cl_2]$ (Figure 2, **D**). It showed a pentagonal-bipyramidal stereochemistry with the phenanthrolinedicarbaldehyde dioxime acting as a tetradentate ligand, whereas the three other ligands (H_2O, DMSO and one nitrato) contributed to the structure; the second nitrate ion was far away from the coordination sphere. In this molecule, the symmetry approaches C_{2v}, which is confirmed by the NMR-spectroscopic data. The second case is that of $([Zn\mathbf{L}(AcO)]_n$, obtained through metallation of **L** with zinc acetate. A polymer is probably formed, on the basis of elemental analysis, NMR and mass-spectrometric data. Figure 2 (**E** and **F**) shows two possible modes of connections for dimers or polymers. It is known that the oximate group can function as a bridge between two metal ions, through its deprotonated form, to afford bi- and trinuclear species[19] [in particular, see ref.[20] for an X-ray structure of a dimeric complex of 2,6-diacetylpyridine dioxime and Cu^{II} related to type **E** (Figure 2)]. It is probably the more acidic oximate group coordinated through the imine nitrogen atom on the metal center which is implicated in the coordination on the second metal ion through the deprotonated oxygen atom. This gives the proposed dimeric structure **E** that involves an almost planar six-membered ring (represented in Figure 2). Indeed, due to the linking effect involving the metal−ligand bond, the acid strength of the oxime group greatly increases, and depends on the nature of the metal ion.[21] As an example, the pK_a value of 2,6-diacetylpyridine dioxime is 10.2,[21] and that of the zinc complex is below 6[6b] and that of the copper(II) complex is 2.8.[22] So the oximate group can effectively compete with acetate as a ligand on the metal center (which is not the case when the anionic ligands are chloride ions), to give bridging coordination bonds resulting in the formation of dimeric or polymeric structures such as **E** and **F** in Figure 2. However, in the absence of an X-ray structure, we can neither exclude the "free" oxime ligand as a possible bridging group in the polymeric structure **F** (Figure 2), nor say if the acetate is within the coordination sphere (to give a five-coordinated structure as in $[Zn\mathbf{L}Cl_2]$ or outside (as a neutralizing charge).

All assignments of structures of complexes M−**L** were also confirmed by positive FAB-MS and ES-MS data. In addition, the ^1H NMR spectra of the diamagnetic zinc(II) and cadmium(II) complexes were recorded. The spectra of $[Zn\mathbf{L}Cl_2]$ (the broad peaks were not clearly resolved by an increase in temperature) and $[Zn\mathbf{L}(AcO)]_n$ (the complexity of NMR-spectroscopic patterns suggested a polymeric structure) did not afford further information on their structures in solution. The spectra of the cadmium complexes were more informative but rather atypical because of the coexistence of broad and sharp peaks for groups of protons of the same molecule. The exact nature of this unusual NMR spectrum (a similar case has been reported for cadmium complexes of 2,9-dihydrazino derivatives of 1,10-phenanthroline)[18] is debatable. A dynamic variation of coordination number of the cadmium(II) ions is a possible explanation. Equilibria between cadmium halide complexes are known,[23] and similar equilibria could be present here, ligand **L** acting either as a tridentate ligand (as in the crystal structure **A**, Figure 2) or a tetradentate ligand (as in crystal structure **D**, Figure 2), resulting in an asymmetrical or a symmetrical geometry of the complex, respectively. It was noteworthy that both complexes $[Cd\mathbf{L}Cl_2]$ and $[Cd\mathbf{L}(OH_2)(DMSO)(NO_3)]^+$ presented similar NMR profiles in solution (associating broad and sharp peaks), although the initial crystal structure was different. In both cases, the increase in temperature significantly reduced the width of the broad peaks to give signals corresponding to a symmetrical molecule (similar to that observed for the free ligand **L**). Therefore, in solution different species probably coexist.

We performed some preliminary experiments on the phosphomonoester bond cleavage with zinc, copper, cobalt and nickel acetate salts, both in the presence and absence of ligand **L**. No significant improvement of the catalytic activity of the metal cation in the presence of the ligand could be observed in these conditions. However, according to the present structural investigations on complexes M−**L**, the anions present in solution (introduced either as the counter ions of the metal cation or with the buffer) may play a crucial role in the structure of the various complexes in solution and, therefore, on their activity. Current investigations are focusing on defining the optimal conditions for use of these potential chemical nucleases as to expand the study to other metal complexes involving cerium or other lanthanides.

Conclusion

The attachment of an organic functional group to a metal-chelating ligand is an attractive way of developing the design of small metal complexes which are potentially able to hydrolyze the phosphodiester backbone of nucleic acids. In the present paper, we detailed the structure and the coordination geometry of an original series of metal complexes of a phenanthroline derivative bearing two aldoxime groups known for their highly nucleophilic properties. This series represents a range of complexes differing in the nature of the metal (Lewis acidity, size, etc.), the geometry of the crystal structure (trigonal-bipyramidal, square-pyramidal, square-bipyramidal and pentagonal-bipyramidal structures) or the conformational flexibility. These factors can affect the known in vivo biological interest of ligand **L** and its metal chelates and also their potential use as chemical nucleases in phosphodiester hydrolysis.[24]

Experimental Section

General: Commercially available reagents and all solvents were purchased from standard chemical suppliers and used without further purification. − ^1H NMR spectra were recorded with a Bruker AM 250 (250 MHz), [D_6]DMSO was used as a solvent δ_H = 2.62. − Elemental analyses were carried out by the "Service de Microana-

lyse du Laboratoire de Chimie de Coordination". − MS: Nermag R10−10, 70 eV (IE/DCI and FAB$^+$/*meta*-nitrobenzyl alcohol MNBA) or Perkin−Elmer SCIEX API 365 (electrospray) by the "Service de Spectrométrie de Masse de Chimie UPS−CNRS de Toulouse". For MS data, the indicated value for molecular or fragment peaks corresponded to the peak of higher intensity and are in agreement with calculated isotopic profiles. − UV/Vis: Hewlett−Packard 8452A diode array spectrophotometer, cuvettes of 1 cm pathlength. − IR: Perkin−Elmer 225 and 597. − Melting points were determined with a digital apparatus Electrothermal and are uncorrected.

1,10-Phenanthroline-2,9-dicarbaldehyde: Iodine was added (I_2, 7.02 g, 27.65 mmol, 2 equiv.) to a solution of neocuproine hemihydrate (2,9-dimethyl-1,10-phenanthroline, 3.0 g, 13.8 mmol, 1 equiv.) dissolved in DMSO (200 mL). The brown solution was stirred for 5 min at room temperature before 3.42 mL of 2-iodo-2-methylpropane (*t*BuI, 28.7 mmol, 2.07 equiv.) was added. Finally, trifluoroacetic acid (TFA, 3 mL, 38.94 mmol, 2.8 equiv.) was slowly added to the darkbrown solution by syringe and the mixture was stirred under reflux for 2 h (148 °C). After this, the solution was allowed to cool at room temperature. The excess of iodine was neutralized by slow addition of a solution of $Na_2S_2O_3$ (16 g/120 mL) and the dark precipitate formed was removed by filtration. 1,10-Phenanthroline-2,9-dicarbaldehyde was precipitated from the filtrate by addition of aqueous $NaHCO_3$ (10%) to pH = 4−5 and extracted with CH_2Cl_2. The organic phase was dried, concentrated and the residue was washed with ether to remove traces of DMSO. The crude product was recrystallized from acetone and dried under vacuum to give the pure compound (1.64 g, yield 48%). − M.p. 253 °C. − $C_{14}H_8N_2O_2 \cdot 1/2\ H_2O$ (245): calcd. C 68.57, H 3.70, N 11.42; found C 68.84, H 3.62, N 11.55. − ^{1}H NMR ([D$_6$]DMSO): δ = 10.48 (d, ^4J = 0.8 Hz, 2 H, CHO), 8.93 (dd, ^4J = 0.8 Hz, ^3J = 8.2 Hz, 2 H, 8-H and 3-H), 8.44 (d, ^3J = 8.2 Hz, 2 H, 4-H and 7-H), 8.42 (s, 2 H, 5-H and 6-H), 3.43 (s, 1 H, 0.5 H_2O). − MS (EI); *m*/*z* (%): 236 (30) [M$^+$], 208 (100) [M − CO]$^+$, 180 (3) [M − 2CO]$^+$. − MS (DCI/NH_3); *m*/*z* (%): 254 (100) [M + NH_4]$^+$, 237 (37) [MH]$^+$. − IR (KBr): $\tilde{\nu}$ = 1701 cm^{-1} (C=O) vs, 1617 (C=C) s. − UV/Vis (DMSO 0.2% in H_2O): λ_{max} (lg ε) = 236 nm (4.58), 278 (4.47), 314 (3.99), 332 (3.93), 348 (3.72).

1,10-Phenanthroline-2,9-dicarbaldehyde Dioxime (L): A suspension of 1,10-phenanthroline-2,9-dicarbaldehyde (400 mg, 1.69 mmol, 1 equiv.) in 10 mL of absolute ethanol was stirred at 60 °C for 10 min. $NH_2OH \cdot HCl$ was then progressively added (622 mg, 8.8 mmol, 5.2 equiv.). The addition of about 400 mg of hydroxylamine dissolved the dialdehyde within a few minutes to give a brown solution, after which a brown precipitate was obtained (after the complete addition of $NH_2OH \cdot HCl$). The reaction mixture, in 30 mL of absolute EtOH, was warmed to 80 °C and stirred for 20 min. The mixture was stirred at reflux (95 °C) for 2 h after the addition of pyridine (1.64 mL, 20.3 mmol, 12 equiv.). The reaction mixture was then allowed to cool at room temperature. After removal of the liquid phase, the precipitate was washed with 30 mL of water to eliminate the excess of $NH_2OH \cdot HCl$, recrystallized from water/DMSO (55:45, v/v) and dried under vacuum (352 mg, yield 78%). − $C_{14}H_{10}N_4O_2$ (266). − M.p. 267 °C. − $C_{14}H_{10}N_4O_2 \cdot 1/2\ H_2O$ 0.85 DMSO (341.3): calcd. C 55.20, H 4.71, N 16.40; found C 55.63, H 4.71, N 15.98. − ^{1}H NMR ([D$_6$]DMSO): δ = 12.07 (s, 2 H, NO*H*), 8.63 (d, ^3J = 8.2 Hz, 2 H, 3-H and 8-H), 8.53 (s, 2 H, C*H*(=NOH)), 8.29 (d, ^3J = 8.2 Hz, 2 H, 4-H and 7-H), 8.15 (s, 2 H, 5-H and 6-H). − MS (EI); *m*/*z* (%): 266 (30) [M$^+$], 248 (20) [M − H_2O]$^+$, 230 (18) [M − 2H_2O]$^+$. − IR (KBr): $\tilde{\nu}$ = 1615 cm^{-1} (C=N oxime) s. − UV/Vis (DMSO 0.2% in H_2O): λ_{max} (lgε) = 262 nm (4.33), 298 (4.35), 324 (4.00), 356 (3.40).

X-ray Diffraction Studies: Addition of a small amount of water in a concentrated solution of 1,10-phenanthroline-2,9-dicarbaldehyde dioxime in DMSO left at room temperature (25 °C), gave suitable yellow crystals for X-ray diffraction studies. Figure 3: ORTEP drawings of the ligand 1,10-phenanthroline-2,9-dicarbaldehyde dioxime hydrate. Selected bond lengths and angles are given in Table 1 and 2.

Dichloro(1,10-phenanthroline-2,9-dicarbaldehyde Dioxime)zinc [ZnLCl$_2$]: A solution of $ZnCl_2$ (12.8 mg, 94 μmol, final concentration 188 mM) in 100 μL of DMF was added to a brown solution of **L** (25 mg, 73 μmol, final concentration: 146 mM) in 400 μL of DMF. The expected complex, which precipitated immediately, was isolated by centrifugation and dried under vacuum to afford a brown powder (25 mg, 59.2 μmol, yield 81%). − $C_{14}H_{10}Cl_2N_4O_2Zn$ (402.5). − M.p > 360 °C. − $C_{14}H_{10}Cl_2N_4O_2Zn \cdot 1/3DMF$ (422.2): calcd. C 42.20, H 2.91, N 14.22; found C 42.28, H 2.89, N 14.29. − ^{1}H NMR ([D$_6$]DMSO): δ = 12.90 (br, N*O*H, N* = coordinated to Zn^{II}), 12.12 (br, NO*H*, N = free), 9.2−8.1 (8 H, 6 Ar−H + 2 H from C*H*=NOH), 8.07/3.0/2.85 (s, DMF). − MS (positive FAB, solution in DMSO); *m*/z (%): 329 (25) [**L** + Zn − H$^+$]$^+$, 365 (76) [**L** + Zn + Cl$^-$]$^+$, 443 (26) [**L** + Zn + Cl$^-$ + DMSO]$^+$. − MS (ES, solution in H_2O/DMSO); *m*/*z*: 310.9 [**L** + Zn − H$^+$ − H_2O]$^+$, 328.9 [**L** + Zn − H$^+$]$^+$, 346.9 [**L** + Zn − H$^+$ + H_2O]$^+$, 366.8 [**L** + Zn + Cl$^-$]$^+$, 595.1 (dimer 2:1 [2 × **L** + Zn − H$^+$]$^+$), 658.9 (dimer 2:2 [2 × **L** + 2 × Zn − 3H$^+$]$^+$), 695.0 (dimer 2:2 [2 × **L** + 2 × Zn − 2H$^+$ + Cl$^-$]$^+$, 733.0 (dimer 2:2 [2 × **L** + 2 × Zn − H$^+$ + 2Cl$^-$]$^+$, 737.0 (dimer 2:2 [2 × **L** + 2 × Zn − 3H$^+$ + DMSO]$^+$, 755.1 (dimer 2:2 [2 × **L** + 2 × Zn − 3H$^+$ + DMSO + H_2O]$^+$. − UV/Vis (DMSO 0.2% in H_2O): λ_{max} (lgε) = 262 nm (4.42), 298 (4.32), 320 (4.15), 356 (3.60), 382 (3.26).

X-ray Diffraction Studies: Crystals of [Zn**L**Cl$_2$] were obtained independently by addition of 500 μL of a DMSO solution of [$ZnCl_2$] (12.8 mg, 94 μmol, final concentration: 94 mM) to 1 mL of a brown DMSO solution of **L** (25 mg, 73 μmol, final concentration: 49 m^m). Under these conditions, the complex did not precipitate immediately and, by vapor diffusion of CH_2Cl_2, the solution afforded suitable yellow crystals after 2 d. Selected bond lengths and angles are given in Table 3.

(1,10-Phenanthroline-2,9-dicarbaldehyde Dioxime)zinc Bis(acetate) Monohydrate [ZnL(AcO)]$_n$: A solution of $Zn(OOCCH_3)_2 \cdot 2\ H_2O$ (20.5 mg, 93 μmol, 25 mM final) in 2 mL of DMSO was added to a brown solution of **L** (50 mg, 146 μmol, final concentration: 38.9 mM) in 1.75 mL of DMSO. The mixture was stirred for 30 min at room temperature, the precipitate was then isolated by centrifugation and dried under vacuum to afford a bright yellow powder (40 mg, 85.5 μmol, yield 97%). − M.p. > 360 °C. − $C_{16}H_{12}N_4O_4Zn \cdot H_2O$: calcd. C 47.14, H 3.46, N 13.74; found C 47.28, H 2.95, N 13.30. − ^{1}H NMR ([D$_6$]DMSO): δ = 12.50 (br, NOH), 9.2−8.1 (8 H, Ar−H + 2 H from C*H*=NOH), 1.85 (s, 3 H, CH_3COO), 8.07/3.0/2.85 (s, DMF). − MS (ES, solution in H_2O/MeOH); *m*/*z* (%): 310.9 [**L** + Zn − H$^+$ − H_2O]$^+$, 329.0 [**L** + Zn − H$^+$]$^+$, 347.0 [**L** + Zn − H$^+$ + H_2O]$^+$, 388.9 [**L** + Zn + AcO$^-$]$^+$, 595.1 (dimer 2:1 [2 × **L** + Zn − H$^+$]$^+$), 638.9 (dimer 2:2 [2 × **L** + 2 × Zn − 3H$^+$ − H_2O]$^+$), 656.7 (dimer 2:2 [2 × **L** + 2 × Zn − 3H$^+$]$^+$), 716.9 (dimer 2:2 [2 × **L** + 2 × Zn − 2H$^+$ + AcO$^-$]$^+$), 984.8 (trimer 3:3 [3 × **L** + 3×Zn − 5H$^+$]$^+$). − UV/Vis (DMSO 0.2% in H_2O): λ_{max} = 260 nm, 298, 324.

Dichloro(1,10-phenanthroline-2,9-dicarbaldehyde Dioxime)copper(II) [CuLCl$_2$]: A solution of $CuCl_2$ (12.6 mg, 94 μmol, final con-

centration 188 mM) in 100 μL of DMF was added to a brown solution of **L** (25 mg, 73 μmol, final concentration: 146 mM) in 400 μL of DMF. The expected complex, which precipitated immediately, was isolated by centrifugation and dried under vacuum to afford a greenish powder (26.5 mg, 66 μmol, yield 90%). − M.p. 300 °C (dec.). − $C_{14}H_{10}Cl_2CuN_4O_2$ (400.7): calcd. C 41.97, H 2.52, N 13.98; found C 42.22, H 2.02, N 13.88. − MS (positive FAB, solution in DMSO); *m/z* (%): 328 (46) [**L** + Cu^{II} − H^+]$^+$, 329 (100) [**L** + Cu^I]$^+$, 364 (35) [**L** + Cu^{II} + Cl^-]$^+$, 595 (20) [2 × **L** + Cu^I]$^+$. − MS (ES, solution in MeOH/H_2O); *m/z* (%): 267.1 [**L** + H^+], 285.0 [**L** + Cu^{II} − H^+ − (CH=NO)]$^+$, 309.8 [**L** + Cu^{II} − H^+ − H_2O]$^+$, 328.0 [**L** + Cu^{II} − H^+]$^+$, 594.1 (dimer 2:1 [2 × **L** + Cu^{II} − H^+]$^+$), 595.2 (dimer 2:1 [2 × **L** + Cu^I]$^+$), 654.9 (dimer 2:2 [2 × **L** + 2 × Cu^{II} − 3H^+]$^+$), 691.1 (dimer 2:2 [2 × **L** + 2 × Cu^{II} − 2H^+ + Cl^-]$^+$. − UV/Vis (DMSO 0.2% in H_2O): λ_{max} (lgε) = 272 nm (4.41), 324 (4.06), 370 (3.90).

X-ray Diffraction Studies: Crystals of [Cu**L**Cl_2] were obtained independently by addition of 40 μL of a DMSO solution of $CuCl_2$ (3.4 mg, 25 μmol, final concentration: 126 mM) to 160 μL of a brown DMSO solution of **L** (6.7 mg, 19.6 μmol, final concentration: 98 mM). In these conditions, the complex did not precipitate immediately, and by vapor diffusion of CH_2Cl_2, the solution afforded suitable orange red crystals after 5 d. Selected bond lengths and angles are given in Table 4.

Dichloro(1,10-phenanthroline-2,9-Dicarbaldehyde Dioxime)cadmium Bis(dimethylsulfoxide) [CdLCl_2]: 100 μL of an aqueous solution of $CdCl_2$ (17.2 mg, 94 μmol, final concentration 188 mM) was added to a brown solution of **L** (25 mg, 73 μmol, final concentration: 146 mM) in 400 μL of DMSO. The expected complex, which precipitated immediately, was isolated by centrifugation and dried under vacuum to afford a brown powder (24.5 mg, 40.5 μmol, yield 55%). − M.p. 300 °C − $C_{14}H_{10}CdCl_2N_4O_2$·2DMSO (605.3): calcd. C 35.68, H 3.63, N 9.25; found C 35.63, H 3.22, N 9.35. − ^{1}H NMR ([D_6]DMSO): δ = 12.73 (br. s, ca. 1.2 H, NO*H*), 8.92 (pattern, 4 H, 4-H, 7-H, 11-H and 11′-H), 8.42 (d, 2 H, ^3J = 8.3 Hz, 3-H and 8-H), 8.30 (s, 2 H, 5-H and 6-H), 2.66 (s, 12 H, 2DMSO) [recorded at 60° C, the broad signal at δ = 8.92 gave: δ = 8.90 (d, 2H, ^3J = 8.3 Hz, 4-H and 7-H), 8.89_5 (s, 2H, 11-H and 11′-H)]. − MS (positive FAB, solution in DMSO); *m/z* (%): 379 (23) [**L** + Cd^{II} − H^+]$^+$, 397 (18) [**L** + Cd^{II} − H^+ + H_2O]$^+$, 415 (100) [**L** + Cd^{II} + Cl^-]$^+$. − MS (ES, solution in H_2O + traces of DMSO); *m/z* (%): 267.0 [**L** + H^+], 378.9 [**L** + Cd^{II} − H^+], 397.0 [**L** + Cd^{II} − H^+ + H_2O]$^+$, 415.0 [**L** + Cd^{II} + Cl^-]$^+$, 475.0 [**L** + Cd^{II} − H^+ + H_2O + DMSO]$^+$, 790.9 (dimer 2:2 [2 × **L** + 2 × Cd^{II} − 2H^+ + Cl^-]$^+$), 924.9 (dimer 2:2 [2 × **L** + 2 × Cd^{II} − H^+ + 2Cl^- + DMSO + H_2O]$^+$), 984.9 (dimer 2:2 [2 × **L** + 2 × Cd^{II} − H^+ + 2Cl^- + 2DMSO]$^+$). − UV/Vis (DMSO 0.2% in H_2O): λ_{max} (lgε) = 236 nm (4.58), 260 (4.78), 264 (4.81), 322 (4.46), 350 (4.19).

X-ray Diffraction Studies: Crystals of compound [Cd**L**Cl_2] were obtained independently by adding 100 μL of an aqueous solution of $Cd(NO_3)_2$·$4H_2O$ (2.0 mg, 6.5 μmol, final concentration: 1.62 mM) to a solution of Zn**L**Cl_2 (2.0 mg, 4.9 μmol, final concentration: 1.2 mM) in 4 mL of a mixture of DMSO/H_2O (1:3), to induce the transmetallation. The solution was allowed to crystallize for 3 months (by slow solvent evaporation) at room temperature to afford yellow crystals suitable for X-ray analysis. Selected bond lengths and angles are given in Table 3.

Aqua(dimethylsulfoxide)(nitrato)(1,10-phenanthroline-2,9-dicarbaldehyde Dioxime)cadmium Nitrate [CdL(OH_2)(DMSO)(NO_3)]$^+$. − Analytical and X-ray Diffraction Studies: A solution of $Cd(NO_3)_2$·$4H_2O$ (29 mg, 94 μmol) in 100 μL of H_2O was added to a brown solution of **L** (25 mg, 73 μmol, final concentration: 146 mM) in 400 μL of DMSO. The expected complex did not precipitate immediately and, by vapor diffusion of CH_2Cl_2, the solution afforded suitable pale yellow crystals after 2 d. Figure 7: ORTEP drawing of the dinitrato(1,10-phenanthroline-2,9-dicarbaldehyde dioxime)cadmium complex. Selected bond lengths and angles are given in Table 5. − M.p. > 360 °C. − $C_{14}H_{10}CdN_6O_8$·DMSO·H_2O (598.8) − ^{1}H NMR ([D_6]DMSO): δ = 11.81 (br. s, ca. 1.5 H, NO*H*), 8.99 (pattern massif, 2 H, 4-H and 7-H), 8.67 (pattern massif, 2 H, 11-H and 11′-H), 8.37 (d, 2 H, ^3J = 8.0 Hz, 3-H and 8-H), 8.35 (s, 2 H, 5-H and 6-H), 2.60 (s, 6 H, DMSO) [recorded at 60° C, the broad signal at δ = 8.99 gave: δ = 8.96 (d, 2H, ^3J = 8.0 Hz, 4-H and 7-H), the broad signal at δ = 8.67 became a sharp singlet]. − MS (positive FAB, solution in DMSO/H_2O); *m/z* (%): 379 (61) [**L** + Cd − H^+]$^+$, 442 (100) [**L** + Cd + NO_3^-]$^+$, 457 (13) [**L** + Cd − H^+ + DMSO]$^+$, 520 (30) [**L** + Cd + NO_3^- + DMSO]$^+$, 598 (8) [**L** + Cd + NO_3^- + 2DMSO]$^+$, 818 (5) [2 × **L** + 2 × Cd + NO_3^- − 2H^+]$^+$. − MS (ES, solution in DMSO/H_2O); *m/z* (%): 379 [**L** + Cd − H^+]$^+$. − UV/Vis (DMSO 0.2% in H_2O): λ_{max} = 264 nm, 322, 348 (sh).

Dichloro(1,10-phenanthroline-2,9-dicarbaldehyde DioxDme)cobalt Mono(dimethyl sulfoxide) [CoLCl_2]: 100 μL of an aqueous solution of $CoCl_2$·$6H_2O$ (22.4 mg, 94 μmol, final concentration 188 mM) was added to a brown solution of **L** (25 mg, 73 μmol, final concentration: 146 mM) in 400 μL of DMSO. The expected complex, which precipitated after 30 min, was isolated by centrifugation and dried under vacuum to afford a brown powder (24.7 mg, 49.4 μmol, yield 68%). − M.p. > 360 °C. − $C_{14}H_{10}CoCl_2N_4O_2$·DMSO·0.2$CoCl_2$ (500.2): calcd. C 38.42, H 3.22, N 11.20; found C 38.31, H 2.74, N 11.27. − MS (ES, solution in DMSO/H_2O); *m/z* (%): 265.9 [**L**]$^+$, 305.9 [**L** + Co^{II} − H^+ − H_2O], 322.8 [**L** + Co^{III} − 2H^+], 323.8 [**L** + Co^{II} − H^+]$^+$, 589.0 (dimer 2:1 [2 × **L** + Co^{III} − 2H^+]$^+$). − UV/Vis (DMSO 0.2% in H_2O): λ_{max} (lgε) = 230 nm (4.51), 268 (4.67), 296 (4.44), 348 (4.16).

X-ray Diffraction Studies: Crystals of [Co**L**Cl_2] were obtained independently by addition of 40 μL of an aqueous solution of $CoCl_2$·$6H_2O$ (6 mg, 25 μmol, final concentration: 126 mM) to 160 μL of a brown DMSO solution of **L** (6.7 mg, 19.6 μmol, final concentration: 98 mM). Under these conditions, the complex did not precipitate immediately and, by vapour diffusion of CH_2Cl_2, the solution afforded suitable green/red dichroic crystals after 7 d. Figure 4: ORTEP drawing of the dichloro(1,10-phenanthroline-2,9-dicarbaldehyde dioxime)cobalt complex. Selected bond lengths and angles are collected in Table 3.

(Dichloro)(dimethylsulfoxide)(1,10-phenanthroline-2,9-dicarbaldehyde Dioxime)nickel Dihydrate Mono(dimethylsulfoxide) (NiL(DMSO)Cl_2): 100 μL of an aqueous solution of $NiCl_2$·$6H_2O$ (22.3 mg, 94 μmol, final concentration 188 mM) was added to a brown solution of **L** (25 mg, 73 μmol, final concentration: 146 mM) in 400 μL of DMSO. After concentrating the mixture to 350 μL, the expected complex precipitated and was isolated by centrifugation and dried under vacuum to afford a brown powder (37.2 mg, 63.3 μmol, yield 87%). − M.p. > 360 °C. − $C_{14}H_{10}Cl_2N_4NiO_2$·2DMSO·$2H_2O$ (588.1): calcd. C 36.76, H 4.46, N 9.53; found C 36.97, H 4.26, N 9.18. − MS (positive FAB, solution in DMSO/H_2O); *m/z* (%): 323 (100) [**L** + Ni − H^+]$^+$, 359 (8) [**L** + Ni + Cl^-]$^+$. − MS (ES, solution in DMSO/H_2O); *m/z* (%): 266.9 [**L** + H^+], 304.9 [**L** + Ni − H^+ − H_2O]$^+$, 322.9 [**L** + Ni − H^+]$^+$, 589.0 [2 × **L** + Ni − H^+]$^+$. − UV/Vis (DMSO 0.2% in H_2O): λ_{max} (lgε) = 260 nm (4.84), 316 (4.65), 364 (4.11).

Table 7. Crystal data for the ligand **L** and the complexes M-**L** (M-Zn, Ca, Cd, Cu and Ni)

Compound	**L**	[Zn**L**Cl_2]	[Cu**L**Cl_2]	[Cd**L**Cl_2]	[Co**L**Cl_2]	[Ni**L**(DMSO)Cl_2]	[Cd**L**(OH_2)(DMSO)(NO_3)]$^+$
Empirical formula	$C_{28}H_{26}N_8O_7$	$C_{36}H_{46}Cl_4N_8O_9S_4Zn$	$C_{36}H_{44}Cl_4Cu_2N_8O_8S_4$	$C_{18}H_{22}CdCl_2N_4O_4S_2$	$C_{16}H_{16}Cl_2CoN_4O_3S$	$C_{16}H_{16}Cl_2N_4NiO_2S$	$C_{18}H_{24}CdN_6O_{11}S_2$
Molecular mass	403.16	1135.59	1113.91	605.82	474.22	474.00	676.95
Crystal system	monoclinic	triclinic	triclinic	triclinic	monoclinic	orthorombic	triclinic
Space group	$P2_1/c$	$P\bar{1}$	$P\bar{1}$	$P\bar{1}$	$P2_1/c$	*Pbca*	$P\bar{1}$
a [Å]	7.5156(6)	11.4734(14)	9.100(2)	9.090(2)	15.872(3)	11.161(2)	9.274(5)
b [Å]	20.0795(15)	15.155(3)	16.396(3)	9.461(2)	7.517(2)	11.832(2)	9.951(5)
c [Å]	18.2339(14)	15.563(2)	16.890(3)	14.754(4)	15.563(2)	28.390(3)	14.769(5)
α [°]	90	99.268(16)	67.11(3)	103.06(3)	90	90	89.110(5)
β [°]	104.73(2)	97.949(14)	88.56(3)	92.37(3)	92.93(3)	90	78.440(5)
γ [°]	90	111.136(15)	80.77(3)	102.30(3)	90	90	75.520(5)
V [Å^3]	2751.5(4)	2433.8(6)	2289.6(8)	1202.4(5)	1942.6(7)	3749.0(8)	1292.0(10)
Z	4	2	2	2	4	8	2
F (000)	1224	1164	1140	608	964	1936	684
$\rho_{calcd.}$ [g cm^{-3}]	1.416	1.550	1.616	1.673	1.621	1.680	1.740
μ(Mo-K_α) [mm^{-1}]	0.105	1.434	1.403	1.336	1.291	1.457	1.074
No. of reflns. collected	17054	19251	20182	9592	17745	31110	12499
No. of unique reflns.	4297	7117	8339	3597	3715	3716	4655
Merging factor *R*(int)	0.1351	0.0326	0.0481	0.0662	0.0360	0.1282	0.0258
Data/restraints/parameters	4297/21/419	7117/188/619	8339/0/580	3597/85/296	3715/0/254	3716/0/251	4655/439/432
*R*1, *wR*2 [$I > 2\sigma(I)$]	0.0581, 0.1122	0.0323, 0.0802	0.0395, 0.0925	0.0481, 0.1297	0.0275, 0.0682	0.0551, 0.1343	0.0268, 0.0670
*R*1, *wR*2 (all data)	0.1381, 0.1370	0.0441, 0.0864	0.0658, 0.1047	0.0534, 0.1365	0.0350, 0.0716	0.0958, 0.1571	0.0307, 0.0765
$\Delta\rho_{min}/\Delta\rho_{max}$	−0.231/0.276	−0.442/0.488	−0.648/0.864	−1.286/0.834	−0.384/0.334	−0.903/0.491	−0.665/0.435
GOF	0.977	1.031	1.000	0.980	1.049	1.031	1.187

X-ray Diffraction Studies: Crystals of [Ni**L**(DMSO)Cl_2] were obtained independently by addition of 40 μL of a DMSO solution of $NiCl_2{\cdot}6H_2O$ (237.71) (6 mg, 25 μmol, final concentration: 126 mM) to 160 μL of a brown DMSO solution of **L** (6.7 mg, 19.6 μmol, final concentration: 98 mM). Under these conditions, the complex did not precipitate immediately and, by vapour diffusion of CH_2Cl_2, the solution afforded suitable green crystals after 5 d. Figure 6: ORTEP drawing of the dichloro(1,10-phenanthroline-2,9-dicarbaldehyde dioxime)nickel complex. Selected bond lengths and angles are collected in Table 3.

Crystal Structure Determination of the Ligand L and the Complexes [Zn$L$$Cl_2$], [Cu$L$$Cl_2$], [Cd$L$$Cl_2$], [Cd$L$$(OH_2)$(DMSO)$(NO_3)$]$^+$, [Co$L$$Cl_2$], and [Ni$L$(DMSO)$Cl_2$]: Data were collected with a Stoe IPDS (Imaging Plate Diffraction System) diffractometer equipped with an Oxford cryosystems Cooler Device. The final unit cell parameters were obtained by the least-squares refinement of 5000 reflections. Only statistical fluctuations were observed in the intensity monitors over the course of the data collections. All the structures were solved by direct methods (SIR92[25]) and refined by least-squares procedures on F^2. All H atoms attached to carbon atoms or to OH groups were introduced in calculations in idealised positions [d(CH) = 0.96 Å] and treated as riding models with isotropic thermal parameters, 20% higher than those of the carbon atoms to which they are attached. H atoms attached to water molecules were refined with an equivalent isotropic thermal parameter, the geometry of water molecules were restrained to have chemically reasonable dimensions. Some of the DMSO solvent molecules in [Zn$L$$Cl_2$], [Cd$L$$Cl_2$] and [Cd$L$$(OH_2)$(DMSO)$(NO_3)$]$^+$, and the free NO_3 in [Cd$L$$(OH_2)$(DMSO)$(NO_3)$]$^+$ are disordered. These disordered molecules were treated using the available tools in SHELXL-97. Least-squares refinements were carried out by minimising the function $\Sigma w(F_o^2 - F_c^2)^2$, where F_o and F_c are the observed and calculated structure factors. The weighting scheme used in the last refinement cycles was $w = 1/[\sigma^2(F_o^2) + (aP)^2 + bP]$ where $P = (F_o^2 + 2F_c^2)/3$. Models reached convergence with $R = \Sigma(||F_o| - |F_c||)/\Sigma(|F_o|)$ and $wR2 = \{\Sigma w(F_o^2 - F_c^2)^2/\Sigma w(F_o^2)^2\}^{1/2}$, having the values listed in Table 1. Crystal data and data collection parameters are summarized in Table 7. The calculations were carried out with the SHELXL-97 program[26] running on a PC. Molecular view was realised with the help of CAMERON[27] Fractional atomic coordinates, anisotropic thermal parameters for nonhydrogen atoms and atomic coordinates for H atoms have been deposited with the Cambridge Crystallographic Data Centre as supplementary publication no. CCDC-134158−134163 and -139259. The ligand **L** and the complexes [Zn$L$$Cl_2$], [Cu$L$$Cl_2$], [Cd$L$$Cl_2$], [Co$L$$Cl_2$], [Ni$L$(DMSO)$Cl_2$], and [Cd$L$$(OH_2)$(DMSO)$(NO_3)$]$^+$ are referenced under the following denominations, respectively: **2**, **3**·Cl_2, **4**·Cl_2, **5**·Cl_2, **6**·Cl_2, **7**·Cl_2 and **5**·$(NO_3)_3$. Copies of the data can be obtained free of charge on application to CCDC, 12 Union Road, Cambridge CB2 1EZ, UK [Fax: (internat.) + 44-1223/336-033; E-mail: deposit@ccdc.cam.ac.uk

Hydrolysis of *p*-Nitrophenyl Phosphate (NPP) with Various Metal Ions and Their Complexes with L: NPP was incubated with various metal ions in the absence (run 1) or the presence (run 2) of ligand **L** in 50 mM TRIS acetate buffer (pH = 8) at 50 or 80 °C, for 3.0 h. NPP and the metal salts were introduced as aqueous solutions and ligand **L** as a DMSO solution. The final volume (1 mL) contained 5% DMSO. Metal salts were introduced as acetates except for cerium (sulfate). The reactions were followed by reversed-phase HPLC (C18 Nucleosil, 10 μm, 250×4.6 mm; elution with methanol/5 mM ammonium acetate (45:55), adjusted to pH = 5 with acetic acid; detection at 320 nm).

Acknowledgments

We thank Anne Robert for her contribution to the recording and the interpretation of NMR spectra, Catherine Claparols for carrying out the mass analyses and Bruno Donnadieu for recording several X-ray data.

[1] P. G. Sammes, G. Yahioglu, *Chem. Soc. Rev.* **1994**, 327−336.
[2] *DNA cleavers and chemotherapy of cancer and viral diseases* (Ed. B. Meunier), Kluwer Academic Publishers, Dordrecht, **1996**, p. 211−223; G. Pratviel, J. Bernadou, B. Meunier, *Adv. Inorg. Chem.* **1998**, 251−312; E. L. Hegg, J. N. Burstyn, *Coord. Chem. Rev.* **1998**, *173*, 133−165; R. Krämer, *Coord. Chem. Rev.* **1999**, *182*, 243−261; N. H. Williams, B. Takasaki, M. Wall, J. Chin,

Acc. Chem. Res. **1999**, *32*, 485−493; M. Komiyama, N. Takeda, H. Shigekawa, *Chem. Commun.* **1999**, 1443−1451.

[3] [3a] D. S. Sigman, G. M. Wahl, D. J. Creighton, *Biochemistry* **1972**, *11*, 2236−2242. − [3b] R. Breslow, D-L. Huang, *Proc. Natl. Acad. Sci. USA* **1991**, *88*, 4080−4083. − [3c] J. G. J. Weijnen, A. Koudijs, G. A. Schellekens, J. F. J. Engbersen, *J. Chem. Soc., Perkin Trans. 2* **1992**, 829−834. − [3d] M. J. Young, D. Wahnon, R. C. Hynes, J. Chin, *J. Am. Chem. Soc*. **1995**, *117*, 9441−9447. − [3e] E. Kimura, Y. Kadama, T. Koike, M. Shiro, *J. Am. Chem. Soc.* **1995**, *117*, 8304−8311.

[4] S. Liu, A. D. Hamilton, *Tetrahedron Lett.* **1997**, *38*, 1107−1110.

[5] [5a] E. Kövari, R. Krämer, *J. Am. Chem. Soc.* **1996**, *118*, 12704−12709. − [5b] M. Wall, B. Linkletter, D. Williams, A-M. Lebuis, R. C. Hynes, J. Chin, *J. Am. Chem. Soc.* **1999**, *121*, 4710−4711.

[6] [6a] C. B. Reese, R. C. Titmas, L. Yau, *Tetrahedron Lett.* **1978**, *30*, 2727−2730. − [6b] A. K. Yatsimirsky, P. Gomez-Tagle, S. Escalante-Tovar, L. Ruiz-Ramirez, *Inorg. Chim. Acta* **1998**, *273*, 167−174.

[7] A. Kumbhar, S. Damle, P. Kulkarni, D. Srinivas, V. Chatur, *Indian J. Chem. A* **1996**, *35A*, 533−535.

[8] J. Mlochowski, J. Palus, *J. Prakt. Chem.* **1993**, *335*, 623−627.

[9] L. Garuti, A. Ferranti, S. Burnelli, L. Varoli, G. Giovanninetti, P. Brigidi, A. Casolari, *Boll. Chim. Farm.* **1989**, *128*, 136−140.

[10] G. Zhao, H. Sun, H. Lin, S. Zhu, X. Su, Y. Chen, *J. Inorg. Biochem.* **1998**, 173−177.

[11] C. J. Chandler, L. W. Deady, J. A. Reiss, *J. Heterocycl. Chem.* **1981**, *18*, 599−601.

[12] T. Wang, J. S. Bradshaw, P. Huszthy, X. Kou, N. K. Dalley, R. M. Izatt, *J. Heterocycl. Chem.* **1993**, *31*, 1−10.

[13] E. Vismara, F. Fontana, F. Minisci, *Gazz. Chim. Ital.* **1987**, *117*, 135−136.

[14] A. Markovac, C. L. Stevens, A. B. Ash, B. E. Hackley, Jr., *J. Org. Chem.* **1970**, *35*, 841−843.

[15] F. K. Klemens, C. E. A. Palmer, S. M. Rolland, P. E. Fanwick, D. R. McMillin, J. P. Sauvage, *New J. Chim.* **1990**, *14*, 129−133.

[16] A. W. Addisson, T. N. Rao, J. Reedijik, J. van Rijn, G. C. Verschoor, *J. Chem. Soc., Dalton Trans.* **1984**, 1349−1356.

[17] H. S. Preston, C. H. L. Kennard, *J. Chem. Soc. A* **1969**, 1956−1961.

[18] J. Lewis, T. D. O'Donoghue, *J. Chem. Soc., Dalton Trans.* **1980**, 736−742

[19] H. Okawa, M. Koikawa, S. Kida, *J. Chem. Soc., Dalton Trans.* **1990**, 469−475; J. A. Bertrand, J. H. Smith, P. G. Eller, *Inorg. Chem.* **1974**, *13*, 1649−1653.

[20] G. A. Nicholson, J. L. Petersen, B. J. McCormick, *Inorg. Chem.* **1980**, *19*, 195−200.

[21] G. I. H. Hanania, D. H. Irvine, *J. Chem. Soc.* **1962**, 2745−2749.

[22] G. A. Nicholson, C. R. Lazarus, B. J. McCormick, *Inorg. Chem.* **1980**, *19*, 192−195.

[23] F. A. Cotton, G. Wilkinson, *Advanced Inorganic Chemistry*, 3rd ed., Interscience, New York, **1972**, p. 513.

[24] E. L. Hegg, S. H. Mortimore, C. L. Cheung, J. E. Huyett, D. R. Powell, J. N. Burstyn, *Inorg. Chem.* **1999**, *38*, 2961−2968.

[25] SIR92, a program for automatic solution of crystal structures by direct methods: A. Altomare, G. Cascarano, G. Giacovazzo, A. Guagliardi, M. C. Burla, G. Polidori, M. Camalli, *J. Appl. Crystallogr.* **1994**, *27*, 435.

[26] G. M. Sheldrick, *SHELXL-97, Program for crystal structure refinement*, University of Göttingen, Germany, **1997**.

[27] D. J. Watkin, C. K. Prout, L. J. Pearce, *CAMERON*, Chemical Crystallography Laboratory, Oxford, UK, **1996**.

Received September 10, 1999
[I99322]

Novel Chiral Di-2-pyridyl Ketone Ligands: Crystal Structure of a Copper Complex and its Activity in the Copper-Catalyzed Enantioselective Cyclopropanation of Styrene

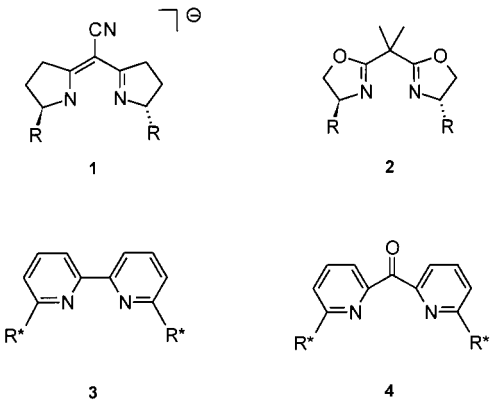
Hoi-Lun Kwong,*[a] Leung-Shi Cheng,[a] Wing-Sze Lee,[a] Wing-Leung Wong,[a] and Wing-Tak Wong[b]

Keywords: Chiral auxiliaries / Asymmetric catalysis / Pyridyl / Nitrogen heterocycles / Cyclopropanation / Copper

New C_2-symmetric chiral di-2-pyridyl ketones were prepared from readily available chiral bromopyridines. Their complexes with copper were synthesized and characterized by X-ray crystallography. The copper complexes were prepared in situ with the triflate anion and were found to be active in the catalysis of cyclopropanation with diazo esters and alkenes. Reaction yields were excellent and enantioselectivities of up to 61% were observed.

Introduction

The synthesis of chiral ligands has been of crucial importance in the development of transition metal-catalyzed enantioselective reactions.[1] Chiral *N*,*N*-bidentate ligands such as semicorrine **1** and bis-oxazoline **2** have been found to be highly effective chiral controllers in asymmetric reactions.[2−4] We are particularly interested in chiral 2,2′-bipyridines **3**, which are structurally similar to these ligands and have also been employed in asymmetric catalysis.[5−11] Our strategy has been to synthesize new chiral ligands based on chiral pyridine.[12] Although di-2-pyridyl ketone and its hydrated form are structurally similar to 2,2′-bipyridine and are known to form complexes with various metal ions,[13] to the best of our knowledge there have been no reports of the synthesis of chiral di-2-pyridyl ketone ligands or their use in asymmetric catalysis. Herein, we report the synthesis of the new chiral di-2-pyridyl ketone ligands **4** based on readily available chiral bromopyridines, and the preparation and crystal structure of a copper(II) complex. We also report the study of the catalytic activities of the copper complexes in asymmetric cyclopropanation.[14]



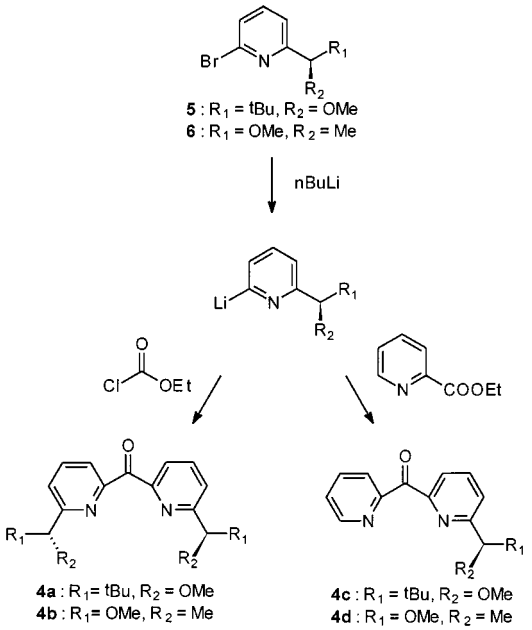
Results and Discussion

The synthesis of the chiral di-2-pyridyl ketone ligands **4a**−**d** is summarized in Scheme 1. The enantiomerically pure starting materials, the 2-bromopyridines **5** and **6**, could easily be prepared from commercially available 2,6-dibromopyridine.[6a][6b] Compounds **4a**−**b** were obtained by the reaction of lithiated **5** and **6** with ethyl chloroformate, while **4c**−**d** were prepared by using ethyl picolinate. The yields of **4a** and **4b** were both 65%, while those of **4c** and **4d** were 31 and 25%, respectively. The IR spectra of **4a**−**d** (KBr) show ν(C=O) in the range 1681−1687 cm^{-1}.

In order to investigate the coordination chemistry of these di-pyridyl ligands, the copper complex **7** was synthesized. It was obtained as a blue solid in good yield by mixing copper(II) perchlorate and **4a** in methanol and stirring overnight (Scheme 2). Crystals suitable for X-ray crystallography were obtained by recrystallization from acetonitrile/ether. The IR spectrum (KBr) shows ν(C=O) at 1687 cm^{-1}, which is identical to that of the free ligand. The X-ray crystal structure, shown in Figure 1, shows a 1:1 complex between Cu^{II} and the ligand. Table 1 summarizes the structural parameters of **7**. Ligand **4a** acts as a tetradentate ligand and the coordination geometry can be described as square pyramidal with the metal ion surrounded by two pyridine nitrogen atoms, two neutral oxygen atoms of the ether groups and one oxygen atom from one of the perchlorate anions. The perchlorate anion interacts with the copper(II) ion and occupies the apical position. Because of this interaction, the C_2 symmetry of the ligand is slightly distorted. The planar pyridine rings are twisted differently

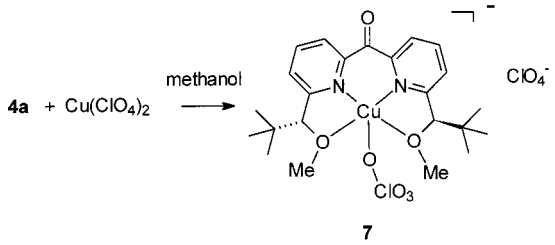
[a] Department of Biology and Chemistry, City University of Hong Kong,
Tat Chee Avenue, Kowloon, Hong Kong, China
Fax: (internat.) + 852-2788-7406
E-mail: bhhoik@cityu.edu.hk
[b] Department of Chemistry, The University of Hong Kong, Pokfulam Road, Hong Kong, China

 © WILEY-VCH Verlag GmbH, D-69451 Weinheim, 2000 1434−1948/00/0909−1997 $ 17.50+.50/0



Scheme 1. Synthesis of chiral di-2-pyridyl ketone ligands

around the planar ketone subunit C7−C(O)−C9 by torsional angles of 6.17° and 21.68°, and the planes of the two rings are twisted by 24.47° relative to each other. The copper−nitrogen bond lengths are 1.960 and 1.944 Å, which are slightly shorter than those of other achiral pyridyl ketone complexes.[13b][13f] They are also shorter than a related chiral dichloro(bipyridine)copper(II) complex reported previously,[11b] where the Cu−N bond lengths are both 2.017 Å. The bite angle of 96.3° made by the chiral dipyridyl ketone and copper is much larger than that observed for the chiral bipyridine complex (83°).[11b] The copper−oxygen bond lengths are 1.987 and 2.006 Å.



Scheme 2. Synthesis of complex **7**

Table 1. Structural parameters for **7**

Atoms	Bond Lengths (Å)
Cu(1)−O(1)	2.006(4)
Cu(1)−O(3)	1.987(5)
Cu(1)−O(9)	2.261(6)
Cu(1)−N(1)	1.960(7)
Cu(1)−N(2)	1.944(6)
O(2)−C(8)	1.196(9)
	Bond Angles (°)
O(1)−Cu(1)−O(3)	95.5(2)
O(1)−Cu(1)−O(9)	89.3(2)
O(1)−Cu(1)−N(1)	82.9(3)
O(3)−Cu(1)−O(9)	96.5(2)
O(3)−Cu(1)−N(2)	82.8(2)
O(9)−Cu(1)−N(1)	95.9(2)
O(9)−Cu(1)−N(2)	102.3(3)
N(1)−Cu(1)−N(2)	96.3(3)
O(2)−C(8)−C(7)	117.2(8)
O(2)−C(8)−C(9)	118.5(8)
C(7)−C(8)−C(9)	124.3(7)

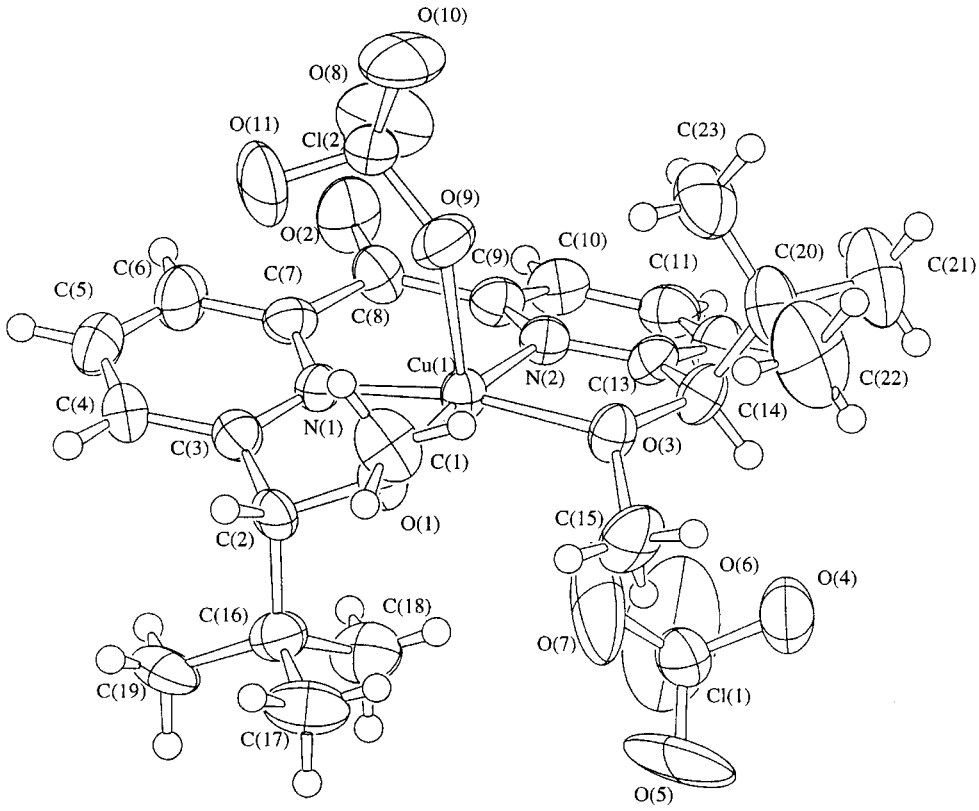
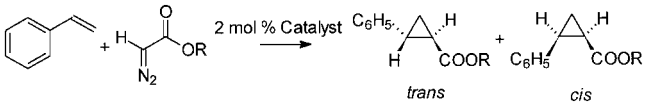


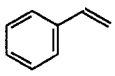
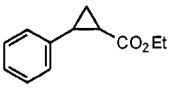
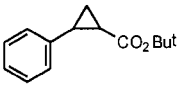
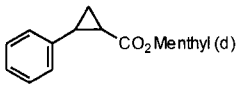
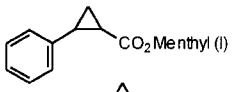
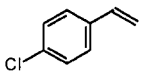
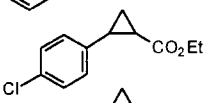
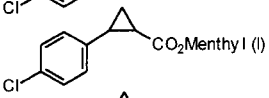
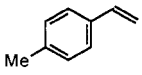
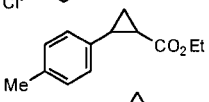
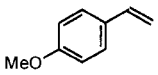
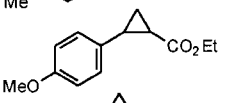
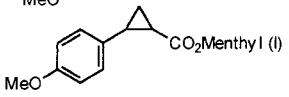
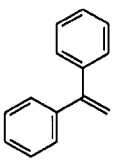
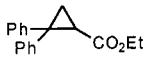
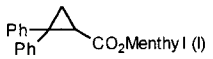
Figure 1. Molecular structure of complex **7**

The use of copper complexes prepared from CuOTf and bipyridines as catalysts in the cyclopropanation of alkenes have been reported by Katsuki et al. and our group.[9] To investigate if these dipyridyl ketone ligands had similar reactivity, we studied the cyclopropanation with complex **7** (Scheme 3). The perchlorate complex **7** was found to be an active catalyst in cyclopropanation with ethyl diazoacetate (EDA). A high *trans*/*cis* ratio (79:21) was obtained, but the complex showed very poor enantioselectivity (3% for both *trans* and *cis* isomers). On the other hand, the triflate complexes, which were prepared by reacting **4a**−**d** with copper(II) triflate, served as more selective catalysts. The results for asymmetric cyclopropanation of styrenes with different ligands are shown in Table 2. The reactions were carried out in the presence of 2 mol-% copper catalyst, 2.2 mol-% chiral ligand, 0.5 M alkyl diazoacetate and excess styrene (2.0 M). In all cases, the yields of the isolated cyclopropanes were excellent, but the enantioselectivities obtained were moderate. With EDA, the C_2-symmetric ligand **4a**, which contains the bulky *tert*-butyl group, gave the highest *ee* for both *trans* (50% *ee*) and *cis* (44% *ee*) isomers, whereas the C_2-symmetric ligand **4b** and the C_1-symmetric ligands **4c** and **4d** showed poor enantioselectivity. Compound **4a** was found to be the best ligand, although other styrene substrates were also tested. In all cases, the chemical yields of the cyclopropane ester were good. For substituted styrenes, the *trans*/*cis* ratios were about 60:40 (Table 2, entries 1, 8, 10 and 11) and the enantioselectivities were between 50 and 59% *ee* for the *trans* isomers and between 38 and 45% *ee* for the *cis* isomers. There is no strong dependence on en-



Scheme 3. Cyclopropanation of styrene

Table 2. Catalytic asymmetric cyclopropanation with chiral copper(II) dipyridyl ketone complexes

entry	ligand	substrate	product	*trans* : *cis*	% *ee*, *trans*	% *ee*, *cis*	yield %
1	**4a**			60 : 40	50 (1R,2R)	44 (1R,2S)	83
2	**4b**			60 : 40	21 (1S,2S)	21 (1S,2R)	95
3	**4c**			68 : 32	1 (1S,2S)	14 (1S,2R)	85
4	**4d**			62 : 38	10 (1R,2R)	28 (1R,2S)	68
5	**4a**			65 : 35	47 (1R,2R)	30 (1R,2S) ee	80
6	**4a**			64 : 36	34 (1R,2R)	26 (1R,2S)	76
7	**4a**			73 : 27	60 (1R,2R)	58 (1R,2S)	83
8	**4a**			61 : 39	54 (1R,2R)	38 (N.D.)[a]	92
9	**4a**			83 : 17	57 (1R,2R)	31 (N.D.)[a]	80
10	**4a**			61 : 39	59 (N.D)[a]	43 (N.D.)[a]	83
11	**4a**			61 : 39	56 (1R,2R)	45 (N.D.)[a]	88
12	**4a**			85 : 15	56 (1R,2R)	28 (N.D.)[a]	91
13	**4a**			–	49 (1R)		79
14	**4a**			–	61 (1R)		77

[a] Not determined.

antioselectivity and *trans*/*cis* selectivity with both electron-donating and withdrawing groups. A 49% *ee* was observed for 1,1-diphenylethene (entry 13).

The effect of the diazo ester structure on *trans*/*cis* diastereoselectivity and enantioselectivity was evaluated with *tert*-butyl-, L-menthyl- and D-menthyl diazoacetate. As can be seen from entries 1, 5, 6 and 7 in Table 2, the *trans*/*cis* ratios for styrene increase when the R group changes from an ethyl to a bulkier group. L-Menthyl shows the greatest improvement. This is consistent with the trend previously observed with other copper catalysts. However, the enantioselectivities for *trans* and *cis* isomers only show an improvement for the L-menthyl group (entry 7). Even higher *trans*/*cis* ratios are observed with chlorostyrene and methoxystyrene (entries 9 and 12). The enantioselectivities for chlorostyrene (entry 9), methoxystyrene (entry 12) and 1,1-diphenylethene (entry 14) all show an improvement with the use of L-menthyl diazoacetate. When the ligands **4a** and **4d** were used with copper (II) triflate, the absolute configurations of the cyclopropane ester products formed from styrene were determined to be (1*R*,2*R*) and (1*R*,2*S*) for the *trans* and *cis* isomers, respectively, while **4b** and **4c** induce the formation of the (1*S*,2*S*) and (1*S*,2*R*) enantiomers. It is interesting to note that although **4a** and **4c** were both synthesized from **5**, the C_2 ligand **4a** gives 1*R* products whereas the C_1 ligand **4c** leads to 1*S* products. A similar observation was also observed with **4b** and **4d**.

In order to know more about the active intermediate in the reaction, the relative rates of cyclopropanation for substituted styrenes using ligand **4a** with EDA were determined through competition experiments. The Hammett plot of $\log(k_x/k_H)$ versus $\sigma(+)$ is shown in Figure 2, and a good $\sigma(+)\rho$ correlation was obtained with $\rho = -0.74$. Although the ρ value is similar to that reported by Kodadek and Woo et al. (-0.85) and Pérez et al. (-0.68) for the cyclopropanation of substituted styrenes using an EDA/iron(II) phophyrin system[15] and EDA/copper(I) tris(pyrazolyl)borate,[16] respectively, correlations to σ instead of $\sigma(+)$ were found in the two latter systems. Nonetheless, the negative value for ρ supports the formation of an electrophilic metal−carbene complex intermediate and only a moderate positive-charge build-up at the benzylic carbon in the transition state. Although the mechanism is still elusive, it is believed that the metal carbene formed by the reaction between the Cu^I complex and the diazo compound is the active species. Based on the absolute configuration of the products obtained from the reaction with ligand **4a**, the sense of asymmetric induction observed here can be explained by the model shown in Scheme 4. This model is in agreement with that previously cited by Pfaltz for other *N*,*N*-bidentate ligands.[4a] In this model, ligand **4a** acts as a bidentate ligand and the metal carbenoid attacks the olefinic double bond according to pathway *a* and *b*. In case *a*, a repulsive steric interaction builds up between the ester group and the adjacent bulky *tert*-butyl group of the ligand. Therefore, pathway *b* is expected to be favored over pathway *a*. In case *b*, this will lead to the *cis*-(1*R*)- or *trans*-(1*R*)-cyclopropane esters, consistent with the experimental results.

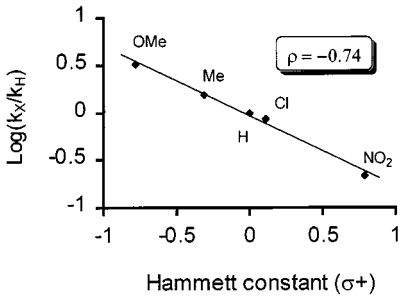
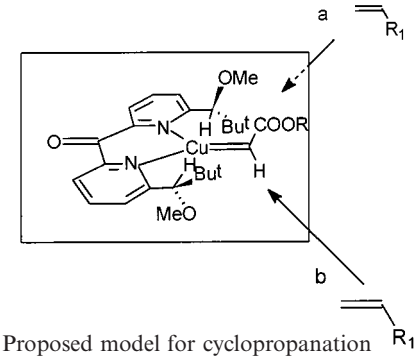


Figure 2. Hammett plot for the cyclopropanation of styrene with EDA using $Cu(OTf)_2$ and ligand **4a** as the catalyst



Scheme 4. Proposed model for cyclopropanation

Conclusion

In summary, we have successfully synthesized a novel chiral di-2-pyridyl ketone from the organometallic addition of a chiral pyridine derivative. The copper complexes of these ligands are active catalysts for cyclopropanation and *ee*s of up to 61% were observed. Comparison of the reactivity and enantioselectivity of ligand **4a** with other copper-catalyzed cyclopropanation reactions indicates that the active intermediates in these reactions are similar. We are continuing our efforts to study the use of these ligands in other catalytic asymmetric reactions.

Experimental Section

General Remarks: Toluene was distilled under N_2 from sodium. Dichloromethane and acetonitrile were distilled over calcium hydride. Diethyl ether and THF were distilled under N_2 over sodium/benzophenone. Chemicals were of reagent-grade quality and were obtained commercially. Infrared spectra were recorded in the range 500−4000 cm^{-1} as Nujol nulls or KBr plates on a Perkin−Elmer Model FTIR−1600 spectrometer. ^1H and ^{13}C NMR spectra were recorded on a Varian 300 MHz Mercury instrument. Positive ion FAB mass spectra were recorded as 3-nitrobenzyl alcohol matrices on a Finnagin MAT 95 spectrometer. Electron-ionization mass spectra were recorded on a Hewlett Packard 5890II GC instrument coupled with a 5970 mass-selective detector. Elemental analyses were performed on a Vario EL elemental analyser. Optical rotations were measured on a JASCO DIP−370 digital polarimeter.

Melting points were measured on an Electrothermal digital melting point apparatus.

General Procedure for the Synthesis of Ligands 4a and 4b: *n*-Butyllithium in hexane (2.5 M, 1.0 mL, 2.5 mmol) was added slowly to a solution of chiral bromopyridine (2.4 mmol) in THF (5.0 mL) at −78 °C. The resulting mixture was stirred at this temperature for 2 h. Ethyl chloroformate (1.2 mmol) in THF (5.0 mL) was cooled to −78 °C and added slowly to the yellowish brown solution. The solution was allowed to stir for 1 h. Methanol (5.0 mL) was then added and the mixture was warmed to room temperature. Water (5.0 mL) and HCl (10%, 5.0 mL) were then added. The layers were separated and the aqueous phase was extracted with CH_2Cl_2 (3 × 15 mL). The combined organic layers were washed with brine (50 mL) and dried with Na_2SO_4. The solvent was removed under reduced pressure and the crude product purified by column chromatography.

Ligand 4a: Following the above procedure with **5** and the usual workup, followed by chromatography with petroleum ether/EtOAc (7:1), gave **4a** (0.300 g, 65%). − $[\alpha]_D^{25}$ = +167.8 (*c* = 0.5, CH_2Cl_2). − IR (KBr): $\tilde{\nu}$ = 1687 cm^{-1}. − ^1H NMR ($CDCl_3$): δ = 0.92 (s, 18 H), 3.26 (s, 6 H), 4.06 (s, 2 H), 7.58 (d, *J* = 7.5 Hz, 2 H), 7.85 (t, *J* = 7.8 Hz, 2 H), 8.01 (d, *J* = 7.5 Hz, 2 H). − ^{13}C NMR ($CDCl_3$): δ = 26.1, 35.6, 57.8, 92.2, 123.9, 124.2, 135.8, 152.7, 160.2, 192.5. − Positive ion FAB mass spectra: *m*/*z* = 385 [M^+ + H]. − $C_{23}H_{32}N_2O_3$ (384.52): calcd. C 71.84, H 8.39, N 7.29; found C 72.49, H 8.29, N 6.78.

Ligand 4b: Following the above procedure with **6** and the usual workup, followed by chromatography with petroleum ether/EtOAc (5:1), gave **4b** (0.234 g, 65%). − $[\alpha]_D^{25}$ = −78.5 (*c* = 0.2, CH_2Cl_2). − IR (KBr): $\tilde{\nu}$ = 1681 cm^{-1}. − ^1H NMR ($CDCl_3$): δ = 1.48 (d, *J* = 6.0 Hz, 6 H), 3.34 (s, 6 H), 4.50 (q, *J* = 6.3 Hz, 2 H), 7.64−7.70 (m, 2 H), 7.89−8.10 (m, 4 H). − ^{13}C NMR ($CDCl_3$): δ = 22.1, 56.8, 80.4, 122.3, 123.9, 137.1, 153.2, 162.6, 192.5. − Positive ion FAB mass spectra: *m*/*z* = 301 [M^+ + H].

General Procedure for the Synthesis of Ligands 4c and 4d: *n*-Butyllithium in hexane (2.5 M, 1.0 mL, 2.5 mmol) was added slowly to a solution of chiral bromopyridine (1.2 mmol) in THF (5.0 mL) at −78 °C. The resulting mixture was stirred at this temperature for 2 h. Ethyl picolinate (1.2 mmol) in THF (5.0 mL) was cooled to −78 °C and added slowly to the yellowish brown solution and this mixture was then allowed to stir for 1 h. Methanol (5.0 mL) was then added and the mixture warmed to room temperature. Water (5.0 mL) and 10% HCl (5.0 mL) were then added. The layers were separated and the aqueous phase was extracted with CH_2Cl_2 (3 × 15 mL). The combined organic layers were washed with brine (50 mL) and dried with Na_2SO_4. The solvent was removed under reduced pressure and the crude product purified by column chromatography.

Ligand 4c: Following the above procedure with **5** and the usual workup, followed by chromatography with petroleum ether/EtOAc (5:1), gave **4c** (0.106 g, 31%). − $[\alpha]_D^{25}$ = +34.4 (*c* = 0.5, CH_2Cl_2). − IR (KBr): $\tilde{\nu}$ = 1686 cm^{-1}. − ^1H NMR ($CDCl_3$): δ = 0.94 (s, 9 H), 3.23 (s, 3 H), 4.02 (s, 1 H), 7.46−7.52 (m, 1 H), 7.60 (d, *J* = 8.1 Hz, 1 H), 7.84−7.92 (m, 2 H), 7.99 (d, *J* = 7.2 Hz, 1 H), 8.11 (d, *J* = 8.1 Hz, 1 H), 8.72 (d, *J* = 4.5 Hz, 1 H). − ^{13}C NMR ($CDCl_3$): δ = 26.1, 35.7, 57.7, 92.1, 123.4, 124.3, 125.2, 126.0, 136.1, 148.8, 152.7, 153.9, 160.1, 192.6. − Positive ion FAB mass spectra: *m*/*z* = 285 [M^+ + H].

Ligand 4d: Following the above procedure with **6** and the usual workup followed by chromatography with petroleum ether/EtOAc (1:1) gave **4d** (0.073 g, 25%). $[\alpha]_D^{25}$ = −78.4 (*c* = 1.0, CH_2Cl_2). − IR (KBr): $\tilde{\nu}$ = 1685 cm^{-1}. − ^1H NMR ($CDCl_3$): δ = 1.48 (d, *J* = 6.3 Hz, 3 H), 3.35 (s, 3 H), 4.52 (q, *J* = 6.0, 1 H), 7.44−7.56 (m, 1 H), 7.66 (d, *J* = 6.9 Hz, 1 H), 7.84−8.02 (m, 3 H), 8.13 (d, *J* = 7.2 Hz, 1 H), 8.68−8.82 (m, 1 H). − ^{13}C NMR ($CDCl_3$): δ = 22.1, 56.8, 80.3, 122.3, 123.9, 125.3, 126.2, 136.4, 137.1, 148.8, 153.0, 153.8, 162.9, 192.4. − Positive ion FAB mass spectra: *m*/*z* = 243 [M^+ + H].

Synthesis of Copper Complex 7: Complex **7** was synthesized by adding ligand **4a** (0.24 mmol) in methanol (5 mL) to a stirred solution of copper(II) perchlorate (0.1 mmol) in methanol (5.0 mL). The mixture was stirred overnight. The volume of the mixture was reduced to about 1 mL and ether was then added. The blue solid formed was collected (57 mg, 88% yield). − IR (KBr): $\tilde{\nu}$ = 1687 cm^{-1}. − $C_{23}H_{32}Cl_2CuN_2O_{11}$ (646.96): calcd. C 42.70, H 4.99, N 4.33; found C 43.08, H 4.78, N 3.93.

X-ray Crystallographic Study: Suitable crystals of complex **7** were grown by dissolving it in acetonitrile and allowing diethyl ether to diffuse into the solution. Diffraction data were obtained on a Rigaku AFC7R diffractometer at ambient temperature. Intensity data were corrected for Lorentz and polarization effects. Absorption corrections based on the χ-scan technique were also applied. The structure was solved by direct methods (SIR 92) and refined on *F* by least-squares analysis. The absolute structure of the molecule was determined by analysis of both configurations, including the anomalous scattering effect. Hydrogen atoms were placed in their ideal positions (C−H, 0.95 Å) and included in the structure factor calculations, but were not refined. All calculations were performed on a Silicon Graphics workstation using the TeXsan package. Crystal data and details of the measurements are collected in Table 3.

Table 3. Crystallographic data for **7**

Data	**7**
Formula	$C_{23}H_{32}Cl_2CuN_2O_{11}$
F_w	646.96
Crystal system	Monoclinic
Lattice type	Primitive
a/Å	10.177(5)
b/Å	8.662(4)
c/Å	15.841(5)
V/Å^3	1395.2(8)
Space group	$P2_1$(#4)
Z	2
μ(Mo-K_α)	10.34 cm^{-1}
Temperature	28.0°C
Reflections collected (unique)	2636
Obs. Reflections [$I > 1.5\sigma(I)$]	2119
No. of variables	351
$2\theta_{max}$ (deg)	50.0
R, R_w	0.048, 0.047

Crystallographic data (excluding structure factors) for the structure reported in this paper have been deposited with the Cambridge Crystallographic Data Centre as supplementary publication no. CCDC-140108. Copies of the data can be obtained free of charge on application to CCDC, 12 Union Road, Cambridge CB2 1EZ, UK [Fax: (internat.) + 44−1223/336−033; E-mail: deposit@ccdc.cam.ac.uk].

Procedure for Copper-Catalyzed Cyclopropanations: To a two-necked round bottom flask were added $Cu(OTf)_2$ (7.2 mg, 0.02 mmol), CH_2Cl_2 (2.0 mL) and the ligand (0.022 mmol) under

nitrogen. The solution was stirred at room temperature for 2 hours. The alkene (4.0 mmol) and diazoacetate (0.2 mmol) were then added and the mixture was warmed at an oil bath temperature of 40 °C for 0.5 h. A solution of diazoacetate (1.0 mmol) in CH_2Cl_2 (0.5 mL) was then added to the reaction mixture over a period of 4 hours using a syringe pump. After the addition of diazoacetate, the mixture was allowed to stir for 16 hours at room temperature. The mixture was then workedup by removing the solvent and purifying the crude product by column chromatography (hexane/EtOAc). All the cyclopropanes obtained are known compounds and were characterized by ^1H NMR, ^{13}C NMR and IR spectroscopy, and GC−MS. The enantiomeric excesses of the cyclopropanes were determined by capillary GC with Chiraldex β−PH column (30m × 0.25 mm) (entry 5) and HPLC with Daicel Chiralcel OJ column (entries 1−4, 8, 10, 13). For the substrates in entries 6, 7, 9, 11, 12 and 14, the *ee* values were determined by a previously reported procedure.[4a,17] Diastereoselectivities (*cis*/*trans* ratio) were measured by GC with an Ultra 2-crosslinked 5% PhMesilcone (25m × 0.2 mm × 0.33μm) column. Assignments of absolute configuration were by comparison with the elution order of authentic samples prepared by a literature procedure.[17]

General Procedure for Competition Reactions: To a two-necked round bottom flask were added $Cu(OTf)_2$ (3.6 mg, 0.01 mmol), CH_2Cl_2 (1.0 mL) and the ligand (0.011 mmol) under nitrogen. The solution was stirred at room temperature for 2 hours. Styrene (2.0 mmol), substituted styrene (2.0 mmol) and ethyl diazoacetate (0.1 mmol) were added and the mixture was warmed at an oil bath temperature of 40 °C for 0.5 h. A solution of diazoacetate (0.5 mmol) in CH_2Cl_2 (0.5 mL) was then added to the reaction mixture over a period of 4 hours using a syringe pump. After the addition of diazoacetate, the mixture was allowed to stir for 16 hours at room temperature. The ratios of the resulting cyclopropane esters were determined by GC.

Acknowledgments

Financial support for this research from the Hong Kong Research Grants Council and the City University of Hong Kong (grant no. 7/00039) is gratefully acknowledged.

[1] R. Noyori, *Asymmetric Catalysis in Organic Synthesis* Wiley, New York, **1994**; *Catalytic Asymmetric Synthesis* (Ed.: I. Ojima), VCH, New York, **1993**.
[2] A. Togni, L. M. Venanzi, *Angew. Chem. Int. Ed. Engl.* **1994**, *66*, 497.
[3] A. K. Ghosh, P. Mathivanan, J. Cappiello, *Tetrahedron: Asymmetry*, **1998**, *9*, 45; S.-G. Kim, C.-W. Cho, K. H. Ahn, *Tetrahedron: Asymmetry* **1997**, *8*, 1023; T. G. Gant, M. C. Noe, E. J. Corey, *Tetrahedron Lett*. **1995**, *36*, 8745; D. A. Evans, K. A. Woerpel, M. M. Hinman, M. F. Faul, *J. Am. Chem. Soc*. **1991**, *113*, 726; R. E. Lowenthal, A. Abiko, S. Masamune, *Tetrahedron Lett.* **1990**, *31*, 6005
[4] [4a] H. Fritschi, U. Leutenegger, A. Pfaltz, *Helv. Chim. Acta* **1988**, *71*, 1553. − [4b] H. Fritschi, U. Leutenegger, A. Pfaltz, *Angew. Chem. Int. Ed. Engl.* **1986**, *25*, 1005.
[5] J. Reedijk, in *Comprehensive Coordination Chemistry* (Ed.: G. Wilkinson), Pergamon Press, London, **1987**, Vol. 2, p 73; E. C. Constable, *Metals and Ligand Reactivity*, VCH, Weinheim, **1995**; E. C. Constable, *Adv. Inorg. Chem.* **1989**, *34*, 1.
[6] [6a] C. Bolm, M. Zender, D. Bur, *Angew. Chem. Int. Ed. Engl.* **1990**, *29*, 205. − [6b] C. Bolm, G. Schlingloff, K. Harms, *Chem. Ber.* **1992**, *125*, 1191. − [6c] C. Bolm, M. Ewald, M. Felder, *Chem. Ber.* **1992**, *125*, 1205. − [6d] C. Bolm, M. Ewald, *Tetrahedron Lett*. **1990**, *31*, 5011.
[7] P. Collomb, A. von Zelewsky, *Tetrahedron: Asymmetry* **1998**, *9*, 3911; P. Hayoz, A. von Zelewsky, *Tetrahedron Lett.* **1992**, *33*, 5165.
[8] G. Chelucci, G. A. Pinna, A. Saba, *Tetrahedron: Asymmetry* **1998**, *9*, 531; G. Chelucci, M. A. Cabras, C. Botteghi, C. Basoli, M. Marchetti, *Tetrahedron: Asymmetry* **1996**, *7*, 885.
[9] K. Ito, T. Katsuki, *Tetrahedron Lett.* **1993**. *34*, 2661; K. Ito, T. Katsuki, *Synlett*. **1993**, 638; K. Ito, S. Tabuchi, T. Katsuki, *Synlett*. **1992**, 575.
[10] H. Nishiyama, S. Yamaguchi, S.-B. Park, K. Itoh, *Tetrahedron: Asymmetry* **1993**, *4*, 143.
[11] [11a] H.-L. Kwong, K.-M. Lau, W.-S. Lee, W.-T. Wong, *New J. Chem.* **1999**, *23*, 629. − [11b] H.-L. Kwong, W.-S. Lee, H.-F. Ng, W.-H. Chiu, W.-T. Wong, *J. Chem. Soc., Dalton Trans.* **1998**, 1043.
[12] H.-L. Kwong, W.-S. Lee, *Tetrahedron: Asymmetry* **1999**, *10*, 3791.
[13] [13a] Z. E. Serna, M. G. Barandika, R. Cortés, M. K. Urtiaga, G. E. Barberis, T. Rojo, *J. Chem. Soc., Dalton Trans.* **2000**, 29. − [13b] Z. Serna, M. G. Barandika, R. Cortés, M. K. Urtiaga, M. I. Arriortua, *Polyhedron* **1998**, *18*, 249. − [13c] M. Bakkir, J. A. M. McKenzie, *J. Chem. Soc., Dalton Trans.* **1997**, 3571. − [13d] A. Basu, T. G. Kasar, N. Y. Sapre, *Inorg. Chem.* **1988**, *27*, 4539. − [13e] A. Basu, A. R. Saple, N. Y. Sapre, *J. Chem. Soc., Dalton Trans.* **1987**, 1797. − [13f] S.-L. Wang, J. W. Richardson Jr., S. J. Briggs, R. A. Jacobson, W. P. Jensen, *Inorg. Chim. Acta* **1986**, *111*, 67. − [13g] G. Annibale, L. Canovese, L. Cattalini, G. Natile, M. Biagini-Cingi, A.-M. Manotti-Lanfredi, A. Tiripicchio, *J. Chem. Soc., Dalton Trans.* **1981**, 2280. − [13h] M. C. Feller, R. Robson, *Aust. J. Chem.* **1968**, *21*, 2919.
[14] For a review of asymmetric cyclopropanation, see: M. P. Doyle, M. N. Protopopova, *Tetrahedron* **1998**, *54*, 7919.
[15] J. R. Wolf, C. G. Hanmaker, J.-P. Djukic, T. Kodadek, L. K. Woo, *J. Am. Chem. Soc.* **1995**, *117*, 9194.
[16] M. M. Díaz-Requejo, P. J. Pérez, M. Brookhart, J. L. Templeton, *Organometallics* **1997**, *16*, 4399.
[17] H. Nishiyama, Y Itoh, Y. Sugawara, H. Matsumoto, K. Aoki, K. Itoh, *Bull. Chem Soc. Jpn.* **1995**, *68*, 1247.

Received February 10, 2000
[I00052]

The Ferrocenyldiphenylpropargyl Cation − A Spectroscopic Comparison Among Stabilizing Substituents and Nucleophilic Additions

Markus Ansorge,[a] Kurt Polborn,[a] and Thomas J. J. Müller*[a]

Keywords: Ferrocene / Cations / Allenes / Pi interactions / NMR spectroscopy

The stable ferrocenyldiphenylpropargyl cation (**3**) is readily and quantitatively generated from the propargylic alcohol **2** with a slight excess of tetrafluoroboric acid in dichloromethane at −78 °C. The cationic species **3** was characterized by ^{1}H- and ^{13}C-NMR spectroscopy; nucleophilic trapping reactions gave rise to the formation of ferrocenyldiphenylallenes **9**.

Introduction

The discovery of transition metal stabilization of reactive intermediates[1] has not only initiated a remarkable theoretical interest but has also had a tremendous impact on the application of such species in synthetic chemistry, namely the synthesis of complex organic molecules.[2] Thus, carbenium ions can be stabilized by quite a number of organometallic substituents such as metallocene and half-sandwich complexes, particularly ferrocenyl, tricarbonylcyclobutadienyliron, cyclobutadienylcyclopentadienylcobalt, and benzenecarbonylchromium derivatives.[1,2] Electronically, this stabilization of cationic charges in the α-position of organometallic fragments can be rationalized by a strong d−p overlap from the transition metal centered occupied d orbitals to the vacant p_z orbital at the carbenium site, accompanied by a pronounced bending of the cationic side chain towards the metal center.[1a,1d,3] As a consequence, this strong electronic interaction manifests itself as a configurational and conformational fixation of the positively charged substituent and, ultimately, leads to highly stereoselective nucleophilic additions.

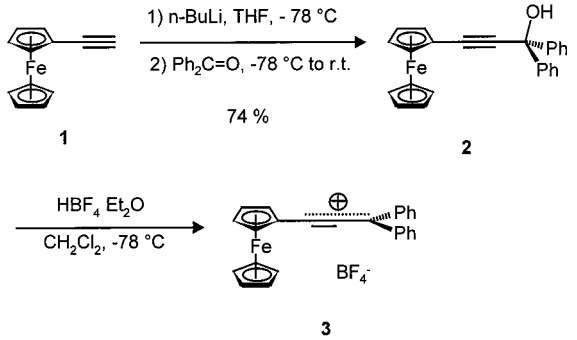
Although quite a number of substituted carbenium ions[4] have been known for some time, the investigation of the chemistry of transition metal stabilized cations with conjugated substituents, i.e. ambident electrophiles, is still in its infancy.[5] Recently, we showed that arenecarbonylchromium fragments efficiently stabilize α- and γ-propargyl cations and that α-propargyl cations can be trapped with nucleophiles to give arene complex substituted propargyl derivatives with excellent diastereoselectivity.[6] In particular, the peculiar ability to stabilize a cationic charge generated in the γ-position to the stabilizing substituent, as well as the ambident reactivity of propargyl cations giving rise either to allenes or alkynes,[7] prompted us to study the structure (UV/Vis and ^{13}C-NMR spectroscopy) and reactions of a related propargyl cation bearing the more powerful donor ferrocene as the stabilizing organometallic moiety in comparison to carbonylchromium-complexed arenes. Here, we wish to report our results on the spectroscopic characterization and nucleophilic trapping reactions of the stable ferrocenyldiphenylpropargyl cation[8] as well as on the spectroscopic comparison to the uncomplexed[9] and tricarbonylchromium-complexed[5b] phenyl analog.

[a] Department Chemie der Ludwig-Maximilians-Universität München
Butenandtstrasse 5−13 (Haus F), D-81377 München, Germany
E-mail: tom@cup.uni-muenchen.de

Results and Discussion

Generation of the Ferrocenyldiphenylpropargyl Cation (3)

Generally, propargyl cations can be generated from the corresponding propargyl derivatives with suitable leaving groups upon treatment with Lewis or Brønsted acids, in particular, this can be achieved in a fairly facile way upon acid-mediated ionization of propargyl alcohols. According to the synthesis of highly stable perferrocenylated propargyl cations by Bildstein,[10] our strategy towards ferrocenyl-substituted γ-propargyl cations commences with the addition of ferrocenyl acetylide [by deprotonation of ethynylferrocene (**1**) with butyllithium] to benzophenone to give the propargyl alcohol **2** in good yield (Scheme 1). Treatment of the propargylic alcohol **2** with a 1.5-fold excess of tetrafluoroboric acid−diethyl ether in dichloromethane solution at −78 °C[5b] led to the formation of a deep-green solution of the persistent allenyl/propargyl cation **3** in quantitative yield (according to NMR and UV/Vis spectroscopy, vide infra) within 5 min.



Scheme 1

 © WILEY-VCH Verlag GmbH, D-69451 Weinheim, 2000 1434−1948/00/0909−2003 $ 17.50+.50/0

Structure of the Propargyl Cation 3

As expected, and in agreement with cation generation studies of related propargyl cations,[5][9a] the ionization of the propargyl alcohol **2** to give the propargyl cation **3** results in a considerable downfield shift of almost all signals in the proton and carbon NMR spectra (Figure 1 and Figure 2, Table 1). Only the *ipso*-phenyl carbon resonance of **3** ($\delta = 141.52$, $\Delta_I = -3.35$) is shifted to high field, indicating an adjacent carbenium center. Thus, the positive charge is delocalized by resonance stabilization over the complete side chain including the substituted cyclopentadienyl ligand. Even the unsubstituted cyclopentadienyl ring of **3** (^{1}H: $\delta = 4.96$, $\Delta_I = +0.72$; ^{13}C: $\delta = 81.75$, $\Delta_I = +12.15$), and with it the ferrocenyl iron atom, experiences a significant downfield shift of the resonances, indicating their participation in the extensive charge stabilization. Most significantly, the downfield shifts of the carbon resonances of the quaternary signals of the propargyl/allenyl side chain reveal a dominant contribution of the allenylium canonical resonance structure **3B** to the stabilization of the cation generated at the γ-position as compared to the ferrocenyl moiety.

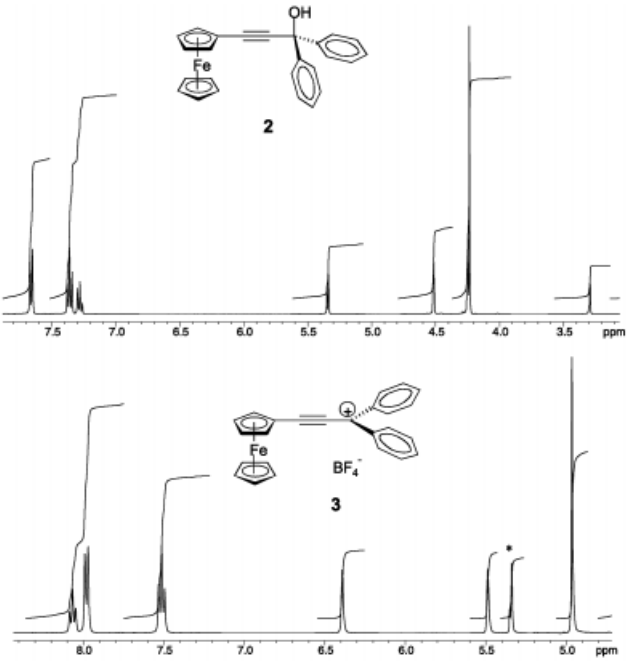
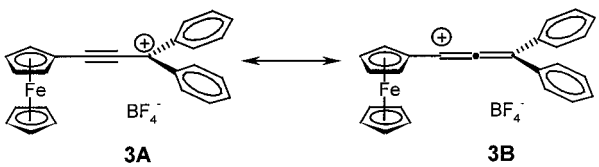


Figure 2. ^{1}H-NMR spectra (−70 °C, CD_2Cl_2, 400 MHz) of **2** (top) and **3** (bottom)



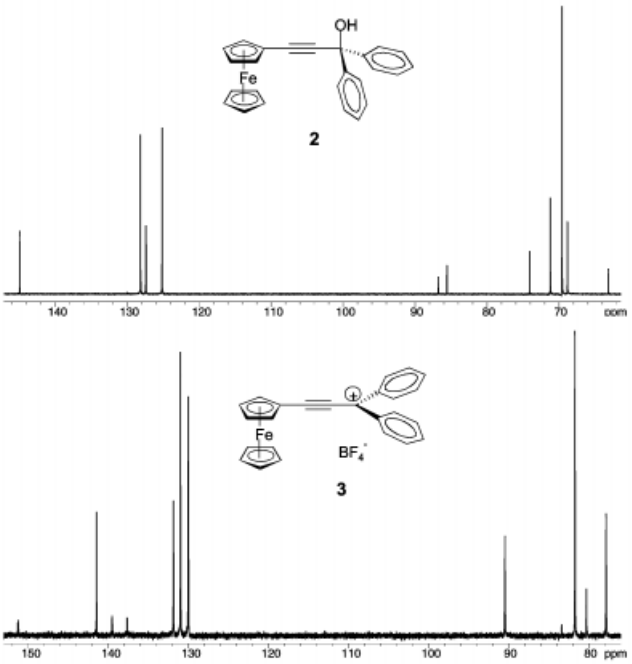
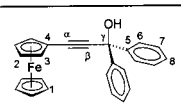
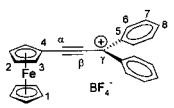


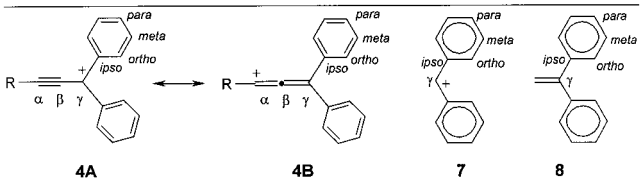
Figure 2. ^{13}C-NMR spectra of **2** (top) and **3** (bottom) (−70 °C, CD_2Cl_2, 100 MHz)

Table 1. Assignment and ionization shifts of ^{1}H- (400 MHz) and ^{13}C-NMR (100 MHz) signals (CD_2Cl_2, −70 °C) of **2** and **3**

	 2		 3		ionization shift Δ_I	
	^{1}H	^{13}C	^{1}H	^{13}C	Δ_I(^{1}H)	Δ_I(^{13}C)
C_1	4.24	69.90	4.96	81.75	+ 0.72	+12.15
C_2	4.25	68.85	5.49	77.85	+ 1.24	+9.00
C_3	4.52	71.24	6.39	90.50	+ 1.87	+19.26
C_4		74.09		80.30		+6.21
C_α		85.58		139.54		+53.96
C_β		86.81		137.68		+50.87
C_γ		63.21		151.30		+88.09
C_5		144.87		141.52		-3.35
C_6	7.68	128.10	7.98	131.01	+ 0.30	+2.91
C_7	7.36	125.13	7.51	130.02	+ 0.15	+4.89
C_8	7.28	127.37	8.07	131.89	+ 0.79	+4.52

A comparison of the carbon resonances of the propargyl cation bridge and the γ-terminal *p*-phenyl positions of the cations **4** (i.e., **5**,[9a] **6**,[5b] and **3**) reveals the increasing con-

Table 2. Selected carbon resonances of the propargylic cations **4** (i.e., **5**,[9a] **6**,[5b] and **3**) and the reference compounds **7**[11] and **8**[12]



R	C_α	C_β	C_γ	C_{para}	C_{meta}	Δ_π
phenyl[a] (**5**)	159.1	105.9	186.8	144.0	131.4	12.6
phenylCr(CO)$_3$[b] (**6**)	150.3	120.8	161.4	136.5	130.2	6.3
ferrocenyl[b] (**3**)	139.5	137.7	151.3	131.9	131.0	1.9
benzhydryl cation **7**	-	-	191.1	151.2	134.1	17.1
1,1-diphenyl ethene (**8**)	-	-	141.1	126.4	127.6	-0.7

[a] $FSO_3H-SbF_5-SO_2$, −60 °C. − [b] CD_2Cl_2 + HBF_4OEt_2, −70 °C.

tribution of the allenylium resonance structure **4B** upon varying the α-substituent from phenyl (**5**) to the organometallic donors $(OC)_3(Ph)Cr$ (**6**) and ferrocenyl (**3**) (Table 2). More specifically, the α-, γ- and terminal *p*-phenyl resonances decrease in this order, indicating a charge delocalization shift towards the α-substituent fragment. Simultaneously, the β-resonances increase towards an "allenic" direction. As reference systems for localized cations, the benzylhydryl cation (**7**)[11] represents a model for a carbenium ion only delocalized at the C_γ position and its phenyl substituents, as depicted in structure **4A**, whereas 1,1-diphenylethene (**8**)[12] serves as a model for an allenylium structure (**4B**) assuming the γ-carbon atom does not bear a positive charge and the charge is completely stabilized at the C_α position.

A linear correlation between the C_γ resonance (carbenium or quaternary benzyl center) and the Δ_π values ($\Delta_\pi = \delta_{para} - \delta_{meta}$) of the propargyl cations **4** and the reference compounds **7** and **8** establishes the dominant influence of the α-substituent on the π-delocalization of the positive

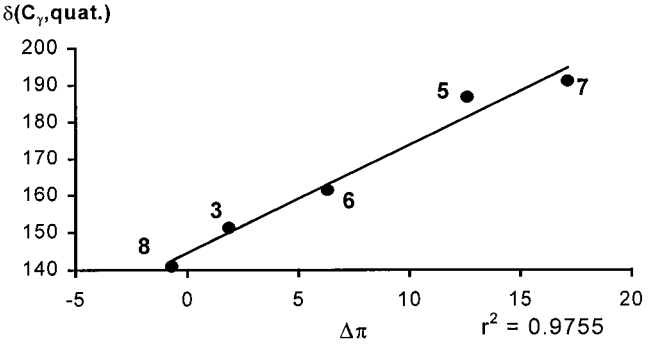


Figure 3. Correlation of the Δ_π values ($\Delta_\pi = \delta_{para} - \delta_{meta}$) and the C_γ resonance (carbenium or quaternary benzyl center) of the propargyl cations **3**, **5**, **6**, and the resonance compounds **7** and **8**

charge (Figure 3). According to a lever-rule model[5b,9a] the relative contributions of mesomeric forms to the stabilization of resonance-stabilized cations can be estimated by considering the C_γ-carbenium resonances or the *p*-phenyl carbon signal.[13] On applying the C_γ resonances the contribution of the α-substituent stabilization increases from 10 (**5**) to 59 (**6**) to 79% (**3**), whereas consideration of the *para* resonances gives rise to a 29 (**5**), 60 (**6**), and 78% (**3**) participation of the allenylium canonical structure **8B** in the electronic ground state.

Ionization with tetrafluoroboric acid−diethyl ether of a dichloromethane solution of **2** at −70 °C leads to a color change from yellow/orange to deep green. This change can be monitored by following the appearance of long-wavelength absorption bands with maxima at 310 (sh), 412, 483, and 856 nm (Figure 4) by UV/Vis spectroscopy. According to calculations on an MM2-optimized structure of **2** using the ZINDO/CI formalism with INDO/1 parameters[14] the absorptions at 856 nm (calcd. 688 nm; iron-centered $d_{x^2-y^2}$ orbital HOMO to the localized LUMO of the propargyl moiety), at 483 nm (calcd. 484 nm; d_{z^2} orbital HOMO-2 to the LUMO) and at 412 nm (calcd. 389 nm, d_{xz} orbital HOMO-3 to LUMO and calcd. 403 nm, d_{z^2} orbital HOMO-2 to LUMO) and at 310 nm (sh) [calcd. 326 nm, bound Cp ring (HOMO-8) to propargyl fragment (LUMO)

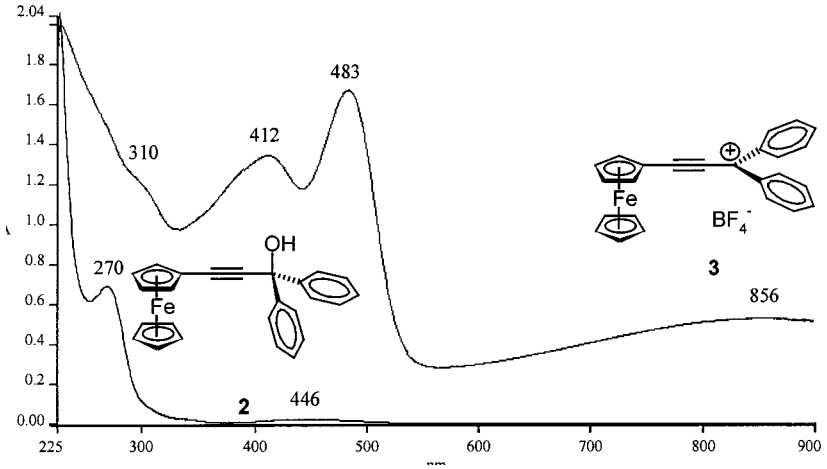
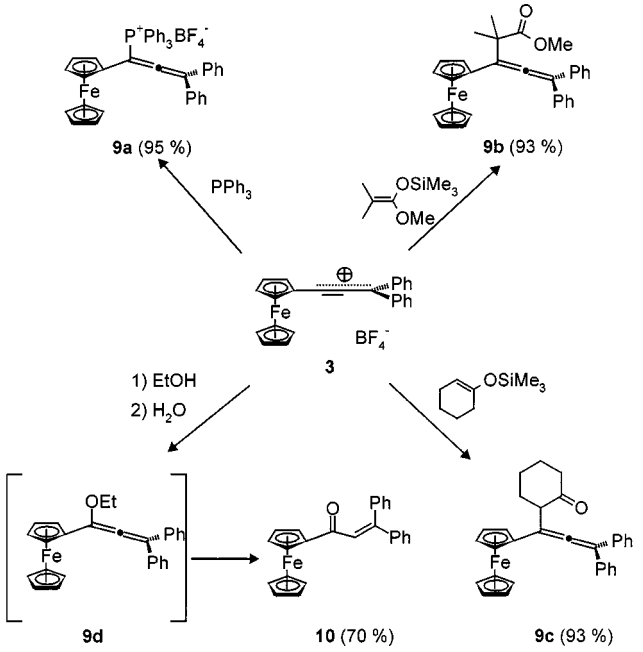


Figure 4. UV/Vis spectra of **2** (λ_{max} at 270 and 446 nm) and **3** (λ_{max} at 310sh, 412, 483, and 483 nm) at −70 °C (dichloromethane)

π-π* transition and calcd. 311 nm, from the phenyl rings to the propargyl fragment (HOMO-10 to LUMO)] are readily reproduced.

Nucleophilic Trapping Reactions of 3

The propargyl cation **3** can be trapped with different nucleophiles to furnish the allenes **9** in good to excellent yields (Scheme 2). Most interestingly, if ethanol is used as the nucleophile only the hydrolysis product, i.e. the enone **10**, can be isolated (70% yield). In significant contrast to the cations **5** and **6**, where the kinetically controlled ethanol attack gives rise to the formation of the corresponding propargyl ethers,[5b,15] the regioselectivity of the nucleophilic attack of ethanol on **3** is reversed to the α-position, which results in the generation of the allene intermediate **9d**. The increasing contribution of the allenylium canonical structure **4B** (vide supra) to the electronic ground state of **3** can be interpreted as an increase of the orbital coefficient at the α-position in the LUMO, the relevant orbital for kinetically controlled nucleophilic additions to the cations **4**.



Scheme 2

Due to the pronounced basicity the ferrocenyl-substituted allenes **9** tend to form ferrocenylallyl cations reversibly.[16] Only if the basicity is modulated by an electron-withdrawing group (**9a**), or if acid-sensitive nucleophiles, such as silyl enol ethers or silyl ketene acetals, successfully trap excess protons, by acting as proton sponges, can the formation of allyl cations be prevented.

The structural assignments of the allenes **9a**−**c** are fully supported by NMR, IR, elemental analysis and by an X-ray crystal structure analysis of **9b** (Figure 5, Table 3).[17] In the ^{1}H-NMR spectra the signals of the ferrocene protons appear between δ = 3.92 and 4.34. Most characteristically,

Table 3. Crystal data and structure refinements for **9b**

	9b
Empirical formula	$C_{30}H_{28}FeO_2$
Molecular mass	476.37
Temperature	298(2) K
Radiation	0.71073 Å; Mo-K_α
Crystal system	triclinic
Space group	$P\bar{1}$
Unit cell dimensions [Å]	a = 8.8576(17); α = 64.201(7), b = 11.7194(7); β = 75.284(12), c = 13.3764(15); γ = 84.435(9)
Volume [Å^3]	1209.0(3)
Z	2
Density (calculated)	1.309 g/cm^3
Absorption correction	ω2θ-scans
Absorption coefficient	0.648 mm^{-1}
Max. and min. transmission	0.9994 and 0.9556
F(000)	500
Crystal size [mm]	0.20 × 0.27 × 0.53
2θ range (min./max.)	2.38/23.97°
Index ranges	$-10 \le h \le 10$; $0 \le k \le 13$ $-13 \le l \le 15$
Reflections collected	3989
Independent reflections	3781 [R(int) = 0.0087]
Observed reflections	3270 [$I > 2\sigma$(I)]
Refinement method	SHELXL-93 on F^2
Data/restraints/parameters	3781/0/301
Goodness of fit on F^2	1.092
Final R indices [$I > 2\sigma(I)$]	
R_1	0.0322
wR_2	0.0793
R indices (all data)	
R_1	0.0391
wR_2	0.0841
Largest diff. peak and hole [e/Å^3]	0.194 and −0.252

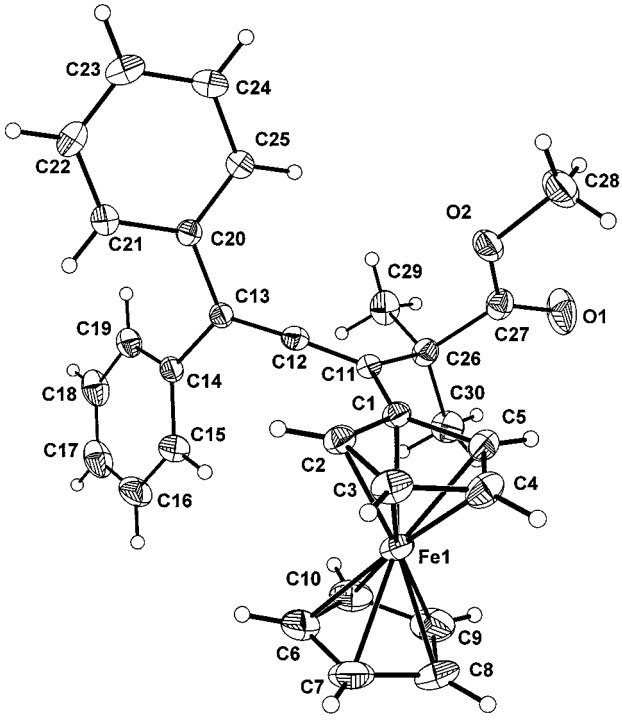


Figure 5. ORTEP plot of **9b**; selected bond lengths [Å], bond angles [°] and torsional angles [°]: C(1)−C(11) 1.482(3), C(11)−C(12) 1.312(3), C(12)−C(13) 1.316(3), C(1)−C(5) 1.431(3), C(4)−C(5) 1.412(3); C(12)−C(11)−C(1) 119.8(2), C(12)−C(11)−C(26) 119.9(2), C(11)−C(12)−C(13) 175.0(2); C(11)−C(1)−C(2)−C(3) 175.2(2), C(2)−C(1)−C(11)−C(12) 4.1(3), C(2)−C(1)−C(11)−C(26) 176.9(2)

the ^{13}C-NMR signals of the central allene carbon atoms are found between δ = 204.6 and 216.7 depending on the electronic nature of the substituent at the α-position. According to the X-ray crystal structure analysis (Figure 5) of the allene **9b**, the allene moiety is linear [C(11)−C(12)−C(13): 175°] and the allenic double bond lengths [C(11)−C(12): 1.31 Å and C(12)−C(13): 1.32 Å] lie within the expected range. Interestingly, the cyclopentadienyl ring and the allene fragment are arranged in an almost coplanar manner, although the ferrocenyl substituent is considered to be sterically bulky.

Conclusion

Ferrocene stabilizes propargyl cations generated at the γ-position to a large extent by delocalizing the positive charge evenly over the iron center and the unsubstituted cyclopentadienyl ring, as shown by NMR spectroscopy of the cation **3**. Therefore, the increasing contribution of the allenylium canonical structures in three different organic/organometallic propargyl cations **4** can be detected by carbon NMR spectroscopy and compared. For the ferrocenyl-substituted system a regioselectivity shift for the nucleophilic attack of ethanol from the propargyl to the allenyl position is the most significant difference between the phenyl and $(OC)_3(Ph)Cr$ analogs. Thus, organometallic substituents not only stabilize ambident electrophiles such as propargyl cations but also could allow a fine tuning of the regioselectivity of nucleophilic additions.

Experimental Section

All reactions involving ferrocene complexes were carried out in flame-dried Schlenk flasks under nitrogen by using septum and syringe techniques. Solvents were dried and distilled according to standard procedures.[18] − Column chromatography: Silica gel 60 (0.063−0.2 mm/70−230 mesh, Firma Merck Darmstadt). − TLC: Silica gel plates (60 F_{254} Merck, Darmstadt). − Melting points (uncorrected values): Reichert−Jung Thermovar. − Ethynylferrocene was synthesized according to a procedure of Rosenblum.[19] All other reagents were purchased from Merck, Aldrich, or Fluka, and used without further purification. − ^{1}H- and ^{13}C-NMR spectra: Bruker WM 300, Bruker AC 300, Bruker ARX 300 or Varian VXR 400S; [D_6]DMSO and [D_2]dichloromethane. − IR: Perkin−Elmer FT-IR spectrometer 1000 or Perkin−Elmer FT-IR Paragon 1000 PC. The samples were pressed into KBr pellets and the spectra recorded on NaCl plates. − UV/Vis: Beckman DK-2a, Beckman UV 5240, or Perkin−Elmer model Lambda 16; J&M TIDAS (transputer integrated diode array spectrometer) with a Hellma low-temperature quartz probe (UV/Vis cation characterization). − MS: Finnigan MAT 311-A/100MS, Finnigan MAT 90, and MAT 95Q. − Elemental analyses were carried out in the Microanalytical Laboratories of the Institut für Organische Chemie, Ludwig-Maximilians-Universität München.

3-Ferrocenyl-1,1-diphenylprop-2-yne-1-ol (2): To a cooled solution (−78 °C) of 1.00 g (4.90 mmol) of ethynylferrocene (**1**) in 40 mL of THF was added dropwise 3.20 mL (5.10 mmol) of a 1.6 M solution of butyllithium in hexanes over a period of 1 min. The reaction mixture was stirred for a further 60 min. To this reaction mixture was added dropwise a solution of 0.89 g (4.90 mmol) of benzophenone in 5 mL of THF and, after the addition, the mixture was allowed to warm up to room temperature over a period of 60 min. After the addition of 20 mL of water and extraction of the aqueous phase with diethyl ether (3 × 50 mL), the combined organic phases were dried with magnesium sulfate. After evaporation of the solvents, the residue was purified by chromatography on silica gel with a gradient of diethyl ether/pentane (1:10 → 1:1) to afford 1.42 g (74%) of the propargylic alcohol **2** as an orange crystalline product, m.p. 90−92 °C. − ^{1}H NMR ([D_6]DMSO, 300 MHz): δ = 4.25 (s, 5 H), 4.29 (d, *J* = 1.7 Hz, 2 H), 4.53 (dd, *J* = 1.7 Hz, 2 H), 6.74 (s, 1 H), 7.22 (m, 2 H), 7.33 (m, 4 H), 7.60 (m, 4 H); (CD_2Cl_2, 400 MHz): δ = 3.29 (s, 1 H), 4.24 (s, 5 H), 4.25 (m, 2 H), 4.52 (m, 2 H), 7.28 (t, *J* = 7.3 Hz, 2 H), 7.36 (dd, *J* = 7.3 Hz, 4 H), 7.68 (d, *J* = 7.8 Hz, 4 H). − ^{13}C NMR ([D_6]DMSO, 75 MHz): δ = 64.5 ($C_{quat.}$), 69.0 (CH), 69.8 (CH), 71.3 (CH), 73.4 ($C_{quat.}$), 84.6 ($C_{quat.}$), 89.5 ($C_{quat.}$), 125.9 (CH), 127.2 (CH), 128.2 (CH), 146.8 ($C_{quat.}$). − ^{13}C NMR (CD_2Cl_2, 100 MHz): δ = 63.2 ($C_{quat.}$), 68.9 (CH), 69.6 (CH), 71.2 (CH), 74.1 ($C_{quat.}$), 85.6 ($C_{quat.}$), 86.8 ($C_{quat.}$), 125.1 (CH), 127.4 (CH), 128.1 (CH), 144.9 ($C_{quat.}$). − MS (70 eV, EI); *m*/*z* (%): 392 [M^+] (61), 327 [$M^+ - C_5H_5$] (13), 254 [M^+ − CpFeOH] (31), 210 [$M^+ - Ph_2CO$] (100), 182 [Ph_2CO^+] (52), 152 [$Ph_2CO^+ - CH_2O$] (18), 105 [$PhCO^+$] (70), 77 [Ph^+] (27), 56 [Fe^+] (8). − IR (KBr): $\tilde{\nu}$ = 2230 cm^{-1}, 1627, 1599, 1489, 1449, 1408, 1339, 1264, 1194, 1178, 1165, 1156, 1101, 1061, 1028, 998, 922, 903, 885, 843, 818, 772, 753, 715, 701, 641, 630, 594, 542, 519, 498, 488, 451, 415. − UV/Vis (DMSO): λ_{max} (ε) = 271 nm (8900), 445 (3200). − $C_{25}H_{20}FeO$ (392.28): calcd. C 76.54, H 5.13; found C 76.51, H 5.22.

Preparation of the Propargyl Cation 3 for the NMR-Spectroscopic Characterization: To a solution of 20 μL of tetrafluoroboric acid−diethyl ether in 0.3 mL of CD_2Cl_2, placed in a nitrogen-flushed NMR tube capped with a rubber septum, was added a solution of 25 mg of **2** in 0.4 mL of CD_2Cl_2 at −78 °C. The NMR tube with the dark green solution was then quickly transferred to the NMR spectrometer (precooled to −70 °C).

Generation of the Propargyl Cation 3 and Nucleophilic Trapping Reaction (General Procedure): To a cooled solution (−78 °C) of 52 μL (0.32 mmol) of tetrafluoroboric acid (54% in diethyl ether) in 10 mL of dichloromethane was added dropwise a solution of 100 mg (0.25 mmol) of **2** in 5 mL of dichloromethane. After stirring for 60 min, a solution of 1.0 mmol of the corresponding nucleophile in 5 mL of dichloromethane was added. The mixture was then allowed to warm up to room temperature. After the addition of 10 mL of water, the solution was extracted with diethyl ether (**9a**: dichloromethane) (3 × 50 mL) and the combined organic phases were dried with magnesium sulfate. Evaporation of the solvents under reduced pressure furnished the products **9** (or **10**), which were recrystallized from diethyl ether/pentane or dichloromethane/diethyl ether to give good to excellent yields.

1-Ferrocenyl-3,3-diphenyl-1-(triphenylphosphonium)propa-1,2-diene Tetrafluoroborate (9a): According to the GP with 131 mg (0.50 mmol) of triphenylphosphane to give 170 mg (95%) of **9a**. Red crystals, m.p. 216−218 °C (dichloromethane/diethyl ether). − ^{1}H NMR (CD_2Cl_2, 300 MHz): δ = 3.98 (s, 5 H), 4.15 (m, 2 H), 4.34 (m, 2 H), 7.04−7.88 (m, 25 H). − ^{13}C NMR (CD_2Cl_2, 75 MHz): δ = 70.2 (CH), 70.2 (CH), 70.4 (CH, $J_{P,C}$ = 3.3 Hz), 86.7 ($C_{quat.}$), 93.7 ($C_{quat.}$, $J_{P,C}$ = 86.2 Hz), 116.9 ($C_{quat.}$), 118.1 ($C_{quat.}$, $J_{P,C}$ = 88.2 Hz), 128.4 (CH), 129.7 (CH), 129.9 (CH), 130.6 (CH, $J_{P,C}$ = 12.6 Hz), 132.7 ($C_{quat.}$), 134.5 (CH, $J_{P,C}$ = 9.9 Hz), 136.0 (CH, $J_{P,C}$ = 2.6 Hz), 216.8 ($C_{quat.}$, $J_{P,C}$ = 5.9 Hz). − MS (FAB), *m*/*z*: 637 [$M^+ - BF_4^-$], 375 [$M^+ - BF_4^- - PPh_3$]. − IR

(KBr): $\tilde{\nu}$ = 3435 cm^{-1}, 3083, 3057, 1914, 1818, 1627, 1596, 1586, 1490, 1484, 1439, 1411, 1342, 1315, 1283, 1226, 1189, 1160, 1108, 1083, 1056, 998, 945, 923, 901, 825, 772, 754, 728, 717, 695, 626, 607, 574, 551, 533, 521, 497, 439. − UV/Vis (DMSO): λ_{max} (ε) = 275 nm (18490), 374 (1260), 470 (790). − $[C_{43}H_{34}FeP^+BF_4^-]$ (724.36): calcd. C 71.30, H 4.73; found C 71.37, H 4.47.

Methyl 3-Ferrocenyl-2,2-dimethyl-5,5-diphenylpenta-3,4-dienecarboxylate (9b): According to the GP with 0.20 mL (1.0 mmol) of 1-methoxy-2,2-dimethyl-1-trimethylsiloxyethene to give 108 mg (93%) of **9b**. Orange crystals, m.p. 132−133 °C. Crystals suitable for X-ray structure analysis were obtained by slow crystallization from a concentrated DMSO solution of **9b**. − ^{1}H NMR ([D$_6$]DMSO, 300 MHz): δ = 1.42 (s, 6 H), 3.63 (s, 3 H), 3.92 (s, 5 H), 4.22 (m, 4 H), 7.42−7.44 (m, 10 H). − ^{13}C NMR ([D$_6$]DMSO, 75 MHz): δ = 26.1 (CH_3), 45.5 ($C_{quat.}$), 52.4 (CH_3), 67.4 (CH), 68.2 (CH), 69.3 (CH), 80.5 ($C_{quat.}$), 112.4 ($C_{quat.}$), 112.5 ($C_{quat.}$), 127.7 (CH), 128.0 (CH), 128.9 (CH), 136.2 ($C_{quat.}$), 176.3 ($C_{quat.}$), 204.7 ($C_{quat.}$). − MS (70 eV, EI); *m/z* (%): 476 [M^+] (100). − IR (KBr): $\tilde{\nu}$ = 3430 cm^{-1}, 3116, 3100, 3087, 3061, 2992, 2947, 1723, 1636, 1599, 1491, 1464, 1442, 1432, 1412, 1379, 1359, 1256, 1191, 1145, 1106, 1074, 1052, 1031, 1013, 1002, 973, 916, 867, 847, 823, 772, 762, 732, 695, 636, 624, 609, 601, 586, 505, 478. − UV/Vis (DMSO): λ_{max} (ε) = 283 nm (15100), 458 (2800). − $C_{30}H_{28}FeO_2$ (476.39): calcd. C 75.63, H 5.92; found C 75.84, H 6.07.

2-(1-Ferrocenyl-3,3-diphenylpropa-1,2-dienyl)cyclohexan-1-one (9c): According to the GP with 0.19 mL (1.0 mmol) of 1-trimethylsiloxycyclohexene to give 110 mg (93%) of **9c**. Orange crystals, m.p. 107−109 °C. − ^{1}H NMR ([D$_6$]DMSO, 300 MHz): δ = 1.64−2.33 (m, 9 H), 4.08 (m, 5 H), 4.20−4.34 (m, 4 H), 7.26−7.46 (m, 10 H). − ^{13}C NMR ([D$_6$]DMSO, 75 MHz): δ = 24.2 (CH_2), 27.6 (CH_2), 33.3 (CH_2), 41.6 (CH_2), 52.4 (CH), 66.1 (CH), 66.9 (CH), 68.6 (CH), 68.6 (CH), 69.1 (CH), 82.5 ($C_{quat.}$), 106.8 ($C_{quat.}$), 112.8 ($C_{quat.}$), 127.5 (CH), 127.6 (CH), 128.0 (CH), 128.0 (CH), 128.7 (CH), 128.8 (CH), 136.1 ($C_{quat.}$), 136.6 ($C_{quat.}$), 205.0 ($C_{quat.}$), 209.5 ($C_{quat.}$). − MS (70 eV, EI); *m/z* (%): 472 [M^+] (100). − IR (KBr): $\tilde{\nu}$ = 3435 cm^{-1}, 3080, 3054, 3022, 2934, 2860, 1706, 1630, 1597, 1491, 1447, 1411, 1380, 1349, 1336, 1310, 1296, 1246, 1197, 1156, 1126, 1105, 1072, 1060, 1028, 1001, 962, 920, 900, 874, 818, 769, 740, 696, 625, 608, 551, 505, 478, 452. − UV/Vis (DMSO): λ_{max} (ε) = 281 nm (18320), 446 (4530). − $C_{31}H_{28}FeO$ (472.40): calcd. C 78.81, H 5.97; found C 78.80, H 5.85.

1-Ferrocenyl-3,3-diphenylprop-2-en-1-one (10): According to the GP with 100 mg (2.1) of ethanol to give 70 mg (70%) of **10**. Red crystals, m.p. 75−78 °C. − ^{1}H NMR ([D$_6$]DMSO, 300 MHz): δ = 4.24 (s, 5 H), 4.56 (m, 2 H), 4.81 (m, 2 H), 7.08 (s, 1 H), 7.12−7.46 (m, 10 H). − ^{13}C NMR ([D$_6$]DMSO, 75 MHz): δ = 69.6 (CH), 69.8 (CH), 72.5 (CH), 81.1 ($C_{quat.}$), 124.1 (CH), 127.7 (CH), 127.9 (CH), 128.3 (CH), 128.7 (CH), 129.2 (CH), 129.4 (CH), 139.5 ($C_{quat.}$), 141.3 ($C_{quat.}$), 151.0 ($C_{quat.}$), 193.4 ($C_{quat.}$). − MS (70 eV, EI), *m/z* (%): 392 [M^+] (100). − IR (KBr): $\tilde{\nu}$ = 3435 cm^{-1}, 3082, 2927, 1647, 1570, 1490, 1443, 1411, 1376, 1278, 1232, 1156, 1106, 1076, 1029, 1000, 892, 823, 788, 769, 725, 698, 582, 527, 500, 485. − UV/Vis (DMSO): λ_{max} (ε) = 300 nm (12940), 377 (2400), 490 (14450). − $C_{25}H_{20}FeO$ (392.28): calcd. C 76.54, H 5.13; found C 76.67, H 5.21.

Acknowledgments

The financial support of the Fonds der Chemischen Industrie, Deutsche Forschungsgemeinschaft and the Dr.-Otto-Röhm-Gedächtnisstiftung is gratefully acknowledged. We wish to express our appreciation to Prof. H. Mayr for his generous support and the possibility of using his J&M UV/Vis spectrometer. We cordially thank Dr. David S. Stephenson for recording the low-temperature NMR spectra.

[1] For reviews see, e.g.: [1a] L. Haynes, R. Pettit, in: *Carbonium Ions* (Eds.: G. A. Olah, P. v. R. Schleyer), Wiley, New York, **1975**, vol. 5. − [1b] W. E. Watts, in: *Comprehensive Organometallic Chemistry* (Eds.: G. Wilkinson, F. G. A. Stone, E. W. Abel), Pergamon, Oxford, **1982**, vol. 8, chapter 59, pp. 1051. − [1c] A. Solladié-Cavallo, *Polyhedron* **1985**, *4*, 901−928. − [1d] G. Jaouen, *Pure Appl. Chem.* **1986**, *58*, 597−616. − [1e] K. M. Nicholas, *Acc. Chem. Res.* **1987**, *20*, 207−214. − [1f] A. J. M. Caffyn, K. M. Nicholas, in: *Comprehensive Organometallic Chemistry II* (Eds.: E. W. Abel, F. G. A. Stone, G. Wilkinson), Pergamon: Oxford, **1995**, vol. 12, pp. 685−702.

[2] For selected applications of transition metal stabilized carbenium ions for the synthesis of complex molecules see, e.g.: [2a] S. G. Davies, T. J. Donohoe, *Synlett* **1993**, 323−332. − [2b] M. Uemura, T. Kobayashi, Y. Hayashi, *Synthesis* **1986**, 386−388. − [2c] M. T. Reetz, M. Sauerwald, *Tetrahedron Lett.* **1983**, *24*, 2837−2840. − [2d] E. J. Corey, C. J. Helal, *Tetrahedron Lett.* **1996**, *37*, 4837−4840. [2e] G. G. Melikyan, K. M. Nicholas, in: *Modern Acetylene Chemistry* (Eds.: P. J. Stang, F. Diederich), VCH, Weinheim, **1995**, p. 118. − [2f] K. C. Nicolaou, W. M. Dai, *Angew. Chem.* **1991**, *103*, 1453−1481; *Angew. Chem. Int. Ed. Engl.* **1991**, *30*, 1387. − [2g] P. Magnus, T. Pitterna, *J. Chem. Soc., Chem. Commun.* **1991**, 541−543. − [2h] P. Magnus, *Tetrahedron* **1994**, *50*, 1397−1418. − [2i] G. Wagner, R. Herrmann, in: *Ferrocenes* (Eds.: A. Togni, T. Hayashi), VCH, Weinheim, **1995**, chapter 4. − [2j] A. J. Pearson, *Iron Compounds in Organic Synthesis*, Academic Press, London, **1994**.

[3] For semiempirical calculations see, e.g.: [3a] D. W. Clack, L. A. P. Kane-Maguire, *J. Organomet. Chem.* **1978**, *145*, 201−206. − [3b] P. A. Downton, B. G. Sayer, M. J. McGlinchey, *Organometallics* **1992**, *11*, 3281−3286; for recent computational studies on the DFT level of theory see, e.g.: [3c] A. Pfletschinger, T. K. Dargel, J. W. Bats, H.-G. Schmalz, W. Koch, *Chem. Eur. J.* **1999**, *5*, 537−545. − [3d] C. A. Merlic, J. C. Walsh, D. J. Tantillo, K. N. Houk, *J. Am. Chem. Soc.* **1999**, *121*, 3596−3606.

[4] For a recent monograph see, e.g.: *Stable Carbocation Chemistry* (Eds.: G. K. Surya Prakash, P. v. R. Schleyer), John Wiley and Sons, Inc., New York, **1997**.

[5] [5a] T. J. J. Müller, A. Netz, *Organometallics* **1998**, *17*, 3609−3614. − [5b] T. J. J. Müller, M. Ansorge, K. Polborn, *Organometallics* **1999**, *18*, 3690−3701.

[6] T. J. J. Müller, A. Netz, *Tetrahedron Lett.* **1999**, *40*, 3145−3148.

[7] [7a] M. Murray, *Methoden Org. Chem. (Houben-Weyl)* **1977**, vol. 5/2a, p. 991 ("Methoden zur Herstellung und Umwandlung von Allenen bzw. Kumulenen"). − [7b] H. Mayr, H. Klein, *J. Org. Chem.* **1981**, *46*, 4097−4100. − [7c] J.-P. Dau-Schmidt, H. Mayr, *Chem. Ber.* **1994**, *127*, 205−212. − [7d] S. M. Lukyanov, A. V. Koblik, L. A. Muradyan, *Russ. Chem. Rev.* **1998**, *67*, 817−856.

[8] [8a] T. S. Abram, W. E. Watts, *J. Chem. Soc., Perkin Trans. 1* **1977**, 1532−1536. − [8b] V. I. Boev, A. V. Dombrovskii, *J. Org. Chem. USSR (Engl. Transl.)* **1985**, *21*, 575−579. − [8c] E.-W. Koch, H.-U. Siehl, M. Hanack, *Tetrahedron Lett.* **1985**, *26*, 1493−1496.

[9] [9a] G. A. Olah, R. J. Spear, P. W. Westerman, J.-M. Denis, *J. Am. Chem. Soc.* **1974**, *96*, 5855−5859. − [9b] H. Mayr, E. Bäuml, *Tetrahedron Lett.* **1983**, *24*, 357−360. − [9c] E. Bäuml, H. Mayr, *Chem. Ber.* **1985**, *118*, 694−703.

[10] [10a] M. Buchmeiser, H. Schottenberger, *Organometallics* **1993**, *12*, 2472−2477. − [10b] J. Lukasser, H. Angleitner, H. Schottenberger, H. Kopacka, M. Schweiger, B. Bildstein, K. H. Ongania, K. Wurst, *Organometallics* **1995**, *14*, 5566−5578.

[11] H.-O. Kalinowski, S. Berger, S. Braun, *^{13}C NMR Spektroskopie, Georg Thieme Verlag, Stuttgart, New York,* **1984***, p. 371.*

[12] H.-O. Kalinowski, S. Berger, S. Braun, *^{13}C NMR Spektroskopie*, Georg Thieme Verlag, Stuttgart, New York, **1984**, p. 144.

[13] Relative contribution of **4B** = [δ(C_γ or C_{para} of **7**) − δ(C_γ or C_{para} of **4**)]/[δ(C_γ or C_{para} of **7**) − δ(C_γ or C_{para} of **8**)]×100%.

[14] *Quantum CAChe 3.0 Program*, Oxford Molecular Group, **1997**.

[15] T. Siegmund, Ph. D. Thesis, Universität München, **1999**.

[16] The adduct of diisopropylamine and **3** was identified by NMR spectroscopy to be the corresponding allyl cation. However, it was not possible either to deprotonate this allyl cation with an excess of amine base or to separate it from the ammonium salts by fractional recrystallization.

[17] Crystallographic data (excluding structure factors) for the structure reported in this paper have been deposited with the Cambridge Crystallographic Data Centre as supplementary publication no. CCDC-142337 (**9b**). Copies of the data can be obtained free of charge on application to CCDC, 12 Union Road, Cambridge CB2 1EZ, UK [Fax: (internat.) + 44-1223/336-033; E-mail: deposit@ccdc.cam.ac.uk].

[18] Various editors, *Organikum*, 14th edition, VEB Deutscher Verlag der Wissenschaften, Berlin, **1993**.

[19] M. Rosenblum, N. Brown, J. Papenmeyer, M. Applebaum, *J. Organomet. Chem.* **1966**, *6*, 173−180.

Received March 24, 2000
[I00115]

A New Diphosphane Derived from Carbohydrates as an Effective Ligand for Asymmetric Hydrogenation

Oscar Pàmies,[a] Gemma Net,[a] Aurora Ruiz,*[a] and Carmen Claver[a]

Keywords: Asymmetric hydrogenation / Phosphanes / Chiral ligands / Carbohydrates / Rhodium

A novel chiral diphosphane derived from D-(+)-xylose, 3,5-dideoxy-1,2-*O*-isopropylidene-3,5-bis(diphenylphosphanyl)-α-D-xylofuranose (Xylophos), and its cationic cyclooctadiene rhodium(I) complex have been synthesised and characterised. Excellent results were obtained with Xylophos in the asymmetric Rh-catalysed hydrogenation of acrylic acid derivatives (*ee*'s up to 98%). Hydrogenation results are explained in terms of the structure of the precatalyst $[Rh(cod)(Xylophos)]^+BF_4^-$.

Introduction

The use of chiral metal complexes as homogeneous molecular catalysts is one of the most powerful strategies in asymmetric synthesis.[1] A careful molecular design of the chiral ligands is particularly important for efficient asymmetric catalysis. Although much progress has been made in this area, and despite the large amount of relevant literature,[2] there is no straightforward way of predicting, a priori, the type of ligand required to achieve high levels of enantioselectivity.[3] The design of new ligands is still often the result of empirical methodology.

Since the work of Kagan with Diop[4] and Knowles with Dipamp,[5] many optically active chelating diphosphanes have been successfully used in transition-metal-based asymmetric catalysis.[1,2,6] In a chiral diphosphane, chirality can occur within the tethering carbon chain between the two phosphanes or at the phosphorus atoms. In spite of the early success achieved with Dipamp,[5] bisphosphanes containing stereogenic phosphorus atoms have been outnumbered by ligands based on PPh_2 groups attached to C-chiral backbones.[2] One advantage of these C-chiral diphosphanes is that their design makes use of the great abundance of naturally occurring chiral compounds. Surprisingly, although carbohydrates are easily available and results with bisphosphinites derived from glucose are excellent,[3,7] the number of diphosphanes derived from these kinds of natural compounds is rather low.[8]

Following our previous work on ligands derived from furanoses,[9] we report here the synthesis of a new diphosphane derived from xylofuranose, Xylophos (Figure 1), the solution structure of the precatalyst $[Rh(cod)(Xylophos)]^+BF_4^-$ and its use in the asymmetric Rh-catalysed hydrogenation of alkenes. An important feature of this new ligand is its lack of C_2 symmetry. It is commonly held that C_2-symmetric diphosphane ligands are endowed with superior properties in catalysis, principally because of the fewer competing diastereomeric intermediates.[1,10] Nevertheless, ligands without C_2 symmetry can eventually match the intermediates better and lead to very good enantioselective discriminations.[3,6i–6l,7,11]

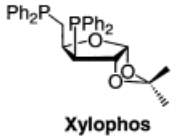


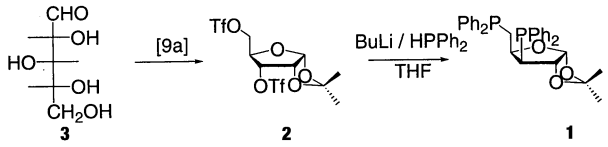
Figure 1. 3,5-Dideoxy-1,2-*O*-isopropylidene-3,5-bis(diphenylphosphanyl)-α-D-xylofuranose, Xylophos (**1**)

The related bisdiphenylphophinite,[12,13] 5-diphenylphosphane-3-diphenylphosphinite,[13] diphosphite,[9d,14] 5-diphenylphosphane[13] and 5-phosphane-3-methoxy[8a,15] molecules with the same protected xylofuranose backbone have already been described and applied to asymmetric catalysis with varying degrees of success.

Results and Discussion

Synthesis and Characterisation of Xylophos

The new diphosphane Xylophos (**1**) was obtained by adding a slight excess of lithium diphenylphosphide, in THF solvent at room temperature, to 1,2-*O*-isopropylidene-3,5-di-*O*-trifluoromethansulfonyl-D-ribofuranose (**2**), which had been prepared from commercially available D-(+)-xylose **3**[9a] (Scheme 1). It was isolated in high yield (75%) by flash chromatography under argon as a white crystalline solid, stable in the air in the solid state and slightly stable in solution.



Scheme 1. Synthesis of Xylophos **1**

[a] Universitat Rovira i Virgili,
Pl. Imperial Tàrraco 1, E-43005 Tarragona, Spain
Fax: (internat.) +34-977/559-563
E-mail: aruiz@quimica.urv.es

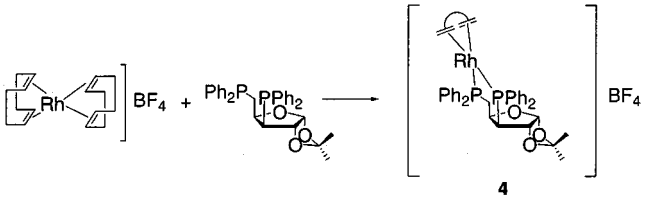
Supporting information for this article is available on the WWW under http://www.wiley-vch.de/home/eurjoc or from the author.

 © WILEY-VCH Verlag GmbH, D-69451 Weinheim, 2000 1434–1948/00/0909–2011 $ 17.50+.50/0

Xylophos (**1**) was characterised by elemental analysis, ^{1}H, ^{13}C and ^{31}P NMR spectroscopy and mass spectrometry. The signals of each of the phosphorus nuclei in the ^{31}P NMR spectrum are doublets, at $\delta = -27.4$ and -21.1, respectively, with $^{4}J(P,P) = 8.0$ Hz. Mass spectrometry shows the highest ion at $m/z = 526$, which corresponds to the molecular weight of Xylophos.

Synthesis and Characterisation of the Rh^{I} Complex

The reaction of Xylophos with $[Rh(cod)_2]^+BF_4^-$ in dichloromethane solution proceeded with the displacement of one cycloocta-1,5-diene ligand to afford the cationic complex $[Rh(cod)(Xylophos)]^+BF_4^-$ (**4**) (Scheme 2).



Scheme 2. Synthesis of the complex $[Rh(cod)(xylophos)]^+BF_4^-$ (**4**)

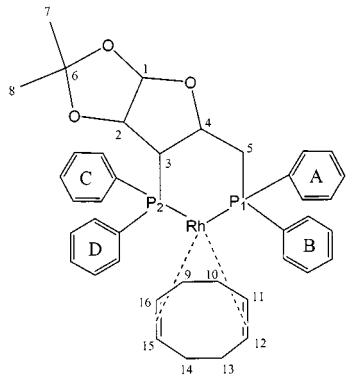
$[Rh(cod)(Xylophos)]^+BF_4^-$ was isolated as a yellow, moderately air-stable powder by adding diethyl ether. The elemental analysis of C and H matches the stoichiometry $[Rh(cod)(Xylophos)]_n^+(BF_4)_n^-$. The FAB mass spectrum shows the highest ion at $m/z = 737$, corresponding to the cationic mononuclear species. The IR spectrum shows a strong band between 1090 and 1050 cm^{-1} and a medium intensity band at 450 cm^{-1}, which are characteristic of the non-coordinated BF_4^- anion.[16]

Further details of the structure of the cation $[Rh(cod)(Xylophos)]^+$ were obtained by ^{1}H, ^{13}C and ^{31}P NMR spectroscopy. The spectral assignments (Table 1 and 2 and Experimental Section) were based on the information obtained by $^{1}H/^{1}H$ COSY, $^{13}C/^{1}H$ and $^{31}P/^{1}H$ correlation measurements in combination with the $^{1}H/^{1}H$ NOESY results. Special attention has been paid to conformational analysis of the six-membered chelate ring. This is directly related to the spatial orientation of the phenyl groups, which have been linked with the enantioselective efficiency of the catalysts.

Vicinal $^{1}H,^{1}H$ couplings in the sugar ring are in the typical range (0−7 Hz) of furanoside ring systems (Table 1)[17] and are similar to those found in other ligands derived from the same protected xylofuranose ring.[9] The coupling constant ^{3}J(1-H, 2-H) is larger than 3.5 Hz, which is consistent with the *cis* disposition of these protons in the 1,2-protected xylofuranose.[17]

In the ^{31}P NMR spectrum eight lines were obtained due to the ^{31}P, ^{31}P and ^{31}P, ^{103}Rh couplings (ABX system) (see Experimental Section). The signals of the phosphorus atoms P-1 and P-2 were assigned from the $^{31}P/^{1}H$ correlation spectrum, using the vicinal couplings between P-1/5-H and P-2/3-H, and the long range couplings between P-1/1-H and P-2/2-H (See supporting information).

Table 1. ^{1}H NMR assignments (500 MHz) of compound **4** in $CDCl_3$ solution (except aromatic protons)



Atom	δ (ppm)	Atom	δ (ppm)	Coupling constants (Hz)
1-H	5.27 (dd)	9-H	2.05 (m, 2 H)	^{3}J(1-H,2-H) = 4.0
2-H	4.71 (dd)	10-H	2.13 (m, 2 H)	^{x}J(1-H,P-1) = 1.8[a]
3-H	2.71 (dd)	11-H	4.12 (m)	^{3}J(2-H,P-2) = 6.0
4-H	4.22 (m)	12-H	4.83 (m)	^{3}J(3-H,4-H) = 6.5
5-H	2.54 (m)	13-H	2.58 (m, 2 H)	^{2}J(3-H,P-2) = 2.5
5′-H	2.81 (dddd)	14-H	2.69 (m, 2 H)	^{3}J(5′-H,5-H) = 13.5
7-H	1.14 (s, 3 H)	15-H	4.98 (m)	^{3}J(5′-H,4-H) = 7.5
8-H	1.18 (s, 3 H)	16-H	4.18 (m)	^{x}J(5′-H,P-2) = 14[a]
				^{x}J(5′-H,Rh) = 3.0[a]

[a] Probably through space.

Table 2. Selected ^{1}H NMR spectroscopic data (500 MHz) of the aromatic part of compound **4** in $CDCl_3$ solution

Phenyl	δ (ppm) *o*	*m*	*p*	*J* (Hz) *J*(P, H-*o*)	*J*(H-*o*,H-*m*)	*J*(H-*o*,H-*p*)
A (P_1)	8.05	7.73	7.73	6.2	4.5	2.7
B (P_1)	7.73	7.51	7.51	5.8	4.5	1.2
C (P_2)	8.11	7.75	7.75	6.2	4.5	2.7
D (P_2)	7.35	7.56	7.56	6.1	4.3	2.4

The ^{1}H NMR signals of the four phenyl groups were assigned in pairs to the phosphorus atoms, P-1 and P-2, according to the $^{31}P/^{1}H$ correlation spectrum (See supporting information).

The signals at $\delta = 8.05$ (2 H) and 7.24 (2 H) were therefore assigned to the *ortho* protons of the phenyl groups (A and B) attached to the phosphorus atom P-1, whereas the *ortho* protons of the phenyl groups attached to P-2 (C and D) were found at $\delta = 8.11$ (2 H) and 7.36 (2 H). By means of a $^{1}H/^{1}H$ COSY experiment (See supporting information), it was also possible to assign the *meta*- and *para* protons of the corresponding phenyl groups (Table 2). It is interesting to note that, in the ^{1}H NMR spectra, the proton signals of the phenyl groups A and C appear as a symmetric group at room temperature. This could indicate that all of these protons, plus the two phosphorus atoms and the rhodium atom, are in the same spin system, giving a second order spectrum.

A 2D-NOESY experiment was performed to obtain a spatial orientation of phenyl groups A−D. In the 2D-

NOESY spectrum of **4**, strong cross-peaks of the furanose protons with the *ortho*-protons were found for only two of the four phenyl groups, which are attached to different phosphorus atoms (P-1 and P-2). The other two phenyl groups have strong cross peaks with the olefinic protons of the cod. This means that only two phenyl moieties are spatially close to the furanoside ring: the phenyl with the *ortho* protons at δ = 8.05 (A), which correlate well with sugar proton 1-H, and the phenyl at δ = 8.11 (C), which correlates with sugar proton 2-H. The *ortho* protons at δ = 7.24 (B) correlate with proton 12-H and the *ortho* protons at δ = 7.36 (D) correlate with proton 15-H and even with 3-H.

The ^{13}C NMR data are given in the Experimental Section. The absolute assignment of these signals was made possible by the $^{13}C/^{1}H$ correlation spectrum. For the furanoside ligand, the signals of the carbons C-2 and C-4 appear as doublets due to coupling with one of the phosphorus atoms, while the carbon atoms C-3 and C-5 appear as doublets of doublets due to coupling with both phosphorus atoms. In the aromatic part of the ^{13}C NMR spectra, the phenyl carbon atoms give well-separated signals, except for the quaternary carbon atoms, which could not be assigned absolutely. The olefinic carbons appear as a doublet due to the ^{13}C, ^{31}P coupling with the respective phosphorus atoms. The geminal couplings ^{2}J(P,C-*o*) of the phenyl moieties A and C are greater than those of moieties B and D, which indicates an axial spatial arrangement of the phenyls A and C.[18]

Examination of models of the different theoretically possible conformations of the six-membered chelate ring showed that only in the chair (Figure 2) and the twist-chair conformations are two axial phenyl groups close to the furanoside protons H-1 and H-2, whereas in the boat conformation (Figure 2) the axial phenyl groups (A and C) are located *trans* to the furanoside ring. The twist conformations δ and λ (Figure 2) can definitely be excluded because only one phenyl group is spatially close to the furanoside ring. Moreover, the λ twist conformation is inaccessible because of the strong steric hindrance between the axial phenyl group (attached to P-1) and the furanoside ring. For the different conformations, molecular mechanics calculations (CERIUS 2) showed that the λ-twist-chair conformation is the most stable (Figure 3). This conformation, which is compatible with the NMR spectroscopic data, follows from the distortion in the chair conformation due to the steric hindrance between both axial phenyl groups.

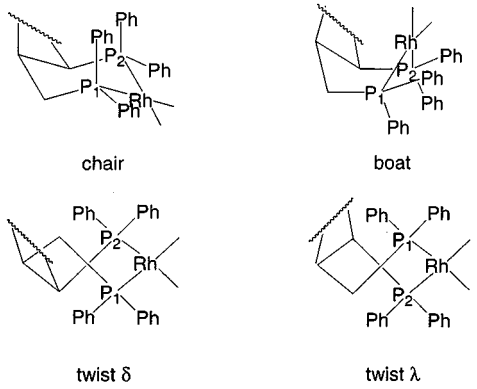


Figure 2. Schematic illustration of the usual possible conformations adopted by the six- membered chelate ring in **4**

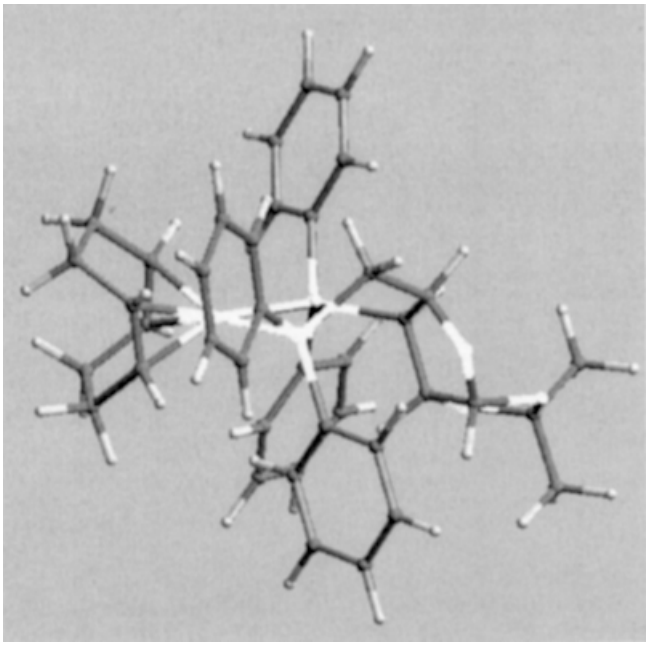
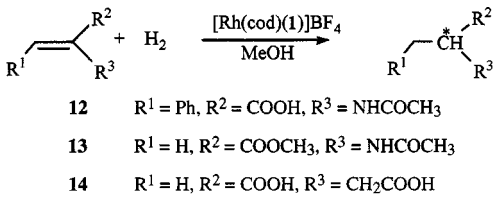


Figure 3. Minimised structure of $[Rh(cod)(xylophos)]^{+}BF_4^{-}$ (**4**) (CERIUS2)

The olefinic protons 11-H, 12-H, 15-H and 16-H of the cyclo-1,5-octadiene appear in the ^{1}H NMR spectrum as separate, broad signals, while the signals of the methylenic protons 9-H, 10-H, 13-H and 14-H are only partially resolved (Table 1). Only the signals of the two olefinic protons which are shifted downfield are well resolved, i.e. 12-H and 15-H. The relative assignment of the proton signals of the cod ring was made according to the $^{1}H/^{1}H$ COSY spectrum. The absolute assignment of these signals was possible from the NOESY spectrum. All carbon atoms of cyclo-1,5-octadiene are well resolved. The olefinic carbon atoms therefore appear as doublets of doublets due to the ^{13}C, ^{31}P and ^{13}C, ^{103}Rh couplings. The signals of only two methylenic carbons (C-13 and C-14) appear as doublets due to the ^{13}C, ^{31}P couplings, while the other two, which are significantly shifted downfield, appear as singlets.

Hydrogenation of Prochiral Olefins

The mononuclear cationic rhodium complex **4** with Xylophos was used in the asymmetric hydrogenation of prochiral olefins at 1 bar H_2 (Scheme 3). Conversion and enantioselectivities are shown in Table 3.



12 R^1 = Ph, R^2 = COOH, R^3 = $NHCOCH_3$

13 R^1 = H, R^2 = $COOCH_3$, R^3 = $NHCOCH_3$

14 R^1 = H, R^2 = COOH, R^3 = CH_2COOH

Scheme 3. Asymmetric hydrogenation of prochiral olefins

Table 3. Hydrogenation results using $[Rh(cod)(xylophos)]^+BF_4^-$ (**4**)[a]

Entry	Substrate	*t* (h)	% Conv.	% *ee*
1	**12**[b]	6	100	89 (*S*)
2	**13**[c]	6	100	91 (*S*)
3	**13**[c]	4	98	91 (*S*)
4	**13**[c]	1	50	92 (*S*)
5	**13**[c][d]	1	11	98 (*S*)
6	**14**[b]	6	100	62 (*R*)

[a] [Rh]/substrate = 1:100; substrate = 1 mmol; solvent = methanol (6 mL); T = 20 °C; P = 1 atm. − [b] Conversion measured by ^1H NMR and enantiomeric excesses determined by polarimetry. − [c] Conversions and enantiomeric excesses measured by GC. − [d] T = 0 °C.

Reaction of the prochiral olefin *Z*-α-acetamidocinnamic acid (**12**) afforded a quantitative yield of hydrogenation product with 89% *ee* at room temperature (entry 1). As with (*R*)-Prophos,[19] (*S*,*S*)-Diop[20] and (*R*,*R*)-Dipamp,[5b,21] the (*S*)-isomer of *N*-acetylphenylalanine was obtained. The sense of the asymmetric induction in this reaction has been widely studied and is correlated to the skewing of the ligand with respect to the P−Rh−P plane.[1e,3d,3e,11d] According to these studies, the formation of (*S*)-*N*-acetylphenylalanine indicates a λ-type array of the Rh-diphosphane chelate ring, which agrees with the structure determined by NMR spectroscopy (see NMR characterisation, above).

The related ester methyl 2-acetoamidoacrylate (**13**) gave similar results at room temperature (91% *ee*) (entries 2−4). Decreasing the temperature to 0 °C (entry 5) substantially improved the enantioselectivity (98% *ee*). These results are similar to those reported for such successful diphosphanes as Chiraphos, Dipamp, Diop, Binap, Bppfa, Duphos, Josiphos, Phanephos and Ferriphos.[22−25]

When itaconic acid (**14**) was used as the substrate, the enantioselectivity was significantly lower (62%) (entry 6). This agrees with the fact that diphosphanes which form five- or six-membered ring complexes are somewhat less tolerant in terms of substrate acceptability than the less-rigid seven-membered chelate rings e.g. 63% *ee* and 60% *ee* were obtained using the five-membered chelating ring Norphos[26] and the six-chelate ring Dioxop,[8a] respectively, while *ee*′s of up to 94% were obtained in the hydrogenation of **12**.[22]

Experimental Section

General Techniques: All syntheses were performed by standard Schlenk techniques under a nitrogen or argon atmosphere. The complex $[Rh(cod)_2]BF_4$ [16a] and 1,2-*O*-isopropylidene-3,5-di-*O*-trifluoromethan-sulfonyl-α-D-ribofuranose[9a] were prepared by previously described methods. Solvents were purified by standard procedures. All other reagents were used as purchased. Elemental analyses were performed on a Perkin−Elmer 240 B instrument. ^1H, $^{13}C\{^1H\}$ and $^{31}P\{^1H\}$ NMR spectra were recorded on a Variant Gemini 300 MHz or 500 MHz Spectrometer. Chemical shifts are relative to $SiMe_4$ (^1H and ^{13}C) as internal standard or H_3PO_4 (^{31}P) as external standard. All assignments of NMR spectra were determined by means of COSY, ^{31}P-^1H and ^{13}C-^1H correlation experiments. Standard pulse sequences were employed for the ^1H-2D-NOESY.[27] The phase-sensitive NOESY experiments used mixing times of 0.4 s. EI mass spectra were obtained on a HP 5989 A spectrometer. A VG-Autospec mass spectrometer was used for FAB mass spectral analyses. The matrix was *m*-nitrobenzyl alcohol. Gas chromatography analyses to obtain the enantiomeric excesses in the hydrogenation of methyl 2-acetoamidoacrylate were performed on a Hewlett−Packard 5890A instrument (fused silica capillary column 25 m × 0.25 mm Permabond L-Chirasil-Val) equipped with a Hewlett−Packard HP 3396 series II integrator. Optical rotations were measured at 25 °C on a Perkin−Elmer 241 MC polarimeter. Hydrogenation reactions were performed in a previously described hydrogen-vacuum line.[28] The molecular mechanics calculations were carried out with the program CERIUS[29] developed by Molecular Simulations (MSI) and the force field UFF developed by Rappe.[30] The electrostatic interactions were taken into account from the atomic changes generated by the Qeq method.[31]

Synthesis of 3,5-Dideoxy-1,2-*O*-isopropylidene-3,5-bis(diphenylphosphanyl)-α-D-xylofuranose (Xylophos, 1): *n*-Butyllithium (3.36 mL, 5.0 mmol) was slowly added to a solution of diphenylphosphane (0.7 g, 5.0 mmol) in THF (5 mL) at 0 °C. After 10 min at room temperature, a solution of 1,2-*O*-isopropylidene-3,5-di-*O*-trifluoromethanesulfonyl-α-D-ribofuranose (1.2 g, 2.64 mmol) in THF (3 mL) was added dropwise and the mixture was allowed to react for 1 hour after which the solvent was evaporated. The residue was purified by column chromatography (toluene) under argon to give the diphosphane as a white solid. Yield: 1.4 g (75%) (m.p. 171−172 °C). − ^1H NMR (300 MHz, $CDCl_3$, TMS): δ = 1.16 (s, 3 H, CH_3), 1.32 (s, 3 H, CH_3), 2.43 [ddd, ^2J(5′-H,5-H) = 13.2 Hz, ^3J(5′-H,4-H) = 6.6 Hz, ^2J(5′-H,P) = 1.9 Hz, 1 H, 5′-H′], 2.64 [ddd, ^2J(5-H,5′-H) = 13.2 Hz, ^3J(5-H,4-H) = 8.2 Hz, ^2J(5-H,P) = 2.2 Hz, 1 H, 5-H], 3.08 [d, ^3J(3-H,2-H) = 4.3 Hz, 1 H, 3-H], 4.41 (m, 1 H, 4-H), 4.49 [dd, ^3J(2-H,3-H)= 4.3 Hz, ^3J(2-H,1-H) = 4.0 Hz, 1 H, 2-H], 5.06 [d, ^3J(1-H,2-H) = 4.0 Hz, 1 H, H-1], 7.40−8.20 (m, 20 H, Ph). − ^{13}C NMR (75.432 MHz, $CDCl_3$, TMS): δ = 26.1 (CH_3), 26.3 (CH_3), 31.1 [dd, J(C-5,P) = 17.5 Hz, J(C-5,P) = 14.8 Hz, C-5], 46.2 [dd, J(C-3,P) = 20.9 Hz, J(C-3,P) = 5.5 Hz, C-3], 76.6 [dd, ^2J(C-4,P) = 16.9 Hz, ^2J(C-4,P) = 13.0 Hz, C-4], 83.9 [d, J(C-2,P) = 5.9 Hz, C-2], 104.2 (C-1), 110.7 (CMe_2), 128.4, 128.5, 128.6, 128.7, 128.8, 128.9, 129.0, 129.2, 132.6, 132.8, 133.0, 133.1, 133.2, 133.3, 133.9, 134.2 (CH=, Ph). − ^{31}P NMR (121.442 MHz, $CDCl_3$, H_3PO4): δ = −27.4 [d, ^4J(P,P) = 8 Hz, 1 P], −21.1 [d, ^4J(P,P) = 8 Hz, 1 P]. − MS (70 eV, EI): m/z = 526 [M^+]. − $C_{32}H_{32}O_3P_2$ (526.55): calcd. C 72.99, H 6.13; found C 72.61, H 6.25. − $[\alpha]_D^{20}$ = +16.1 (c = 1 in CH_2Cl_2)

Synthesis of $[Rh(cod)(Xylophos)]^+BF_4^-$ (4): Xylophos (**1**) (40.5 mg, 0.077 mmol) was added to a solution of $[Rh(cod)_2]^+BF_4^-$ (30 mg, 0.075 mmol) in dichloromethane (1 mL). After 10 minutes, the yellow product was obtained by precipitation with diethyl ether. Yield: 55 mg (88%). ^1H NMR (300 MHz, $CDCl_3$, TMS): see Table 1 and 2. − ^{13}C NMR (75.432 MHz, $CDCl_3$, TMS): δ = 26.2 (C-7 and C-8), 26.6 [dd, J(C-5,P) = 16.5 Hz, J(C-5,P) = 28.7 Hz, C-5], 27.6 (C-9), 27.7 (C-10), 32.6 [d, J(C-13,P) = 3.4 Hz, C-13], 32.9 [d, J(C-14,P) = 3.8 Hz, C-14], 43.4 [dd, J(C-3,P) = 12.9 Hz, J(C-3,P) = 25.8 Hz, C-3], 73.8 [d, J(C-4,P) = 7.6 Hz, C-4], 82.6 [d, J(C-2,P) = 4.78 Hz, C-2], 97.6 [dd, J = 8.1 Hz, J = 9.0 Hz, C-15], 100.15 [dd, J = 8.6 Hz, J = 10.0 Hz, C-16], 103.4 (C-1), 104.69 [dd, J = 9.8 Hz, J = 10.5 Hz, C-10], 105.8 [dd, J = 9.1 Hz, J = 10.8 Hz, C-9], 111.5 (C-6), 127.6 [dd, J(C,P) = 42.0 Hz, J = 1.9 Hz, C], 128.4 [d, J(C,P) = 43.8 Hz, C], 128.5 [d, J(C,P) = 40.5 Hz, C], 129.6 [d, J(C,P) = 10.3 Hz, C-*m* B], 129.8 [d, J(C,P) = 10.3 Hz, C-*m* D],

130.1 [d, J(C,P) = 12.2 Hz, C-*m* A], 130.2 [d, J(C,P) = 10.1 Hz, C-*o* B], 130.4 [d, J(C,P) = 13.7 Hz, C-*m* C], 130.6 [dd, J(C,P) = 43.9 Hz, J = 1.9 Hz, C], 130.9 [d, J(C,P) = 8.4 Hz, C-*o* D], 131.2 [d, J(C,P) = 2.3 Hz, C-*p* B], 131.4 [d, J(C,P) = 2.3 Hz, C-*p* D], 133.3 [d, J(C,P) = 2.3 Hz, C-*p* A], 133.6 [d, J(C,P) = 2.3 Hz, C-*p* C], 135.1 [d, J(C,P) = 12.2 Hz, C-*o* A], 135.5 [d, J(C,P) = 13.7 Hz, C-*o* C]. – ^{31}P NMR (121.442 MHz, $CDCl_3$, H_3PO_4): δ = 17 [dd, ^2J(P-1,P-2) = 43.7 Hz, ^1J(P-1,Rh) = 146.1 Hz, 1P, P-1], 17.4 [dd, ^2J(P-2,P-1) = 43.7 Hz, ^1J(P-2,Rh) = 145.4 Hz, 1P, P-2]. – MS (FAB): m/z = 737 [$M^{+\cdot}$]. – $C_{40}H_{44}BF_4O_3P_2Rh$ (824.44): calcd. C 58.27, H 5.38; found C 58.11, H 5.64.

Hydrogenation of Prochiral Olefins: In a typical run, a Schlenk flask was filled with a methanol solution (6 mL) of substrate (1 mmol) and catalyst precursor (8.24 mg, 0.01 mmol). It was then evacuated and purged three times with H_2. The reaction mixture was the shaken under H_2 (1 atm.) at 293 K. After the desired reaction time, the solvent was removed.

Work-Up of the Hydrogenation Products: The following procedures were used to isolate the hydrogenation products. For 2-methylsuccinic acid and *N*-acetylphenylalanine, the residue was dissolved in 0.5 M NaOH and separated from the insoluble catalyst by filtration. The filtrate was acidified with diluted HCl, extracted with ether and washed with water. The ether phase was dried over sodium sulfate and evaporated to dryness. The extent of the conversion was measured by ^{1}H NMR spectroscopy. The enantiomeric excesses were determined by polarimetry.[8a]

For *N*-acetylalanine methyl ester the residue was dissolved in CH_2Cl_2 and filtered through a plug of silica to remove the catalyst. Conversion and enantiomeric excesses were determined by gas chromatography.

Acknowledgments

We would like to thank the Spanish Ministerio de Educación y Cultura and the Generalitat de Catalunya (CIRIT) for their financial support (PB97−0407-CO5−01) and the Generalitat de Catalunya (CIRIT) for awarding a research grant (to O. P.). We thank Dr. P. Sandor (Varian, Darmstad) for recording the 500 MHz NMR experiments.

[1] [1a] H. Brunner, *Synthesis* **1988**, 645−654. – [1b] H. Brunner, *Top. Stereochem.* **1988**, *18*, 129−247. – [1c] W. A. Nugent, T. V. RajanBabu, M. J. Burk, *Science* **1993**, *259*, 479−483. – [1d] *Catalytic Asymmetric Synthesis* (Ed.: I. Ojima), VCH Publishers, New York, **1993**. – [1e] R. Noyori, *Asymmetric Catalysis in Organic Synthesis*, John Wiley, New York, **1994**. – [1f] *Applied Homogeneous Catalysis with Organometallic Compounds* (Eds.: B. Cornils, W. A. Herrmann), VCH, Weinheim, **1996**.

[2] H. Brunner, W. Zettlmeier, *Handbook of Enantioselective Catalysis*, VCH, Weinheim, **1993**.

[3] [3a] T. V. RajanBabu, T. A. Ayers, A. L. Casalnuovo, *J. Am. Chem. Soc.* **1994**, *116*, 4101−4102. – [3b] T. V. RajanBabu, T. A. Ayers, *Tetrahedron Lett.* **1994**, *35*, 4295−4298. – [3c] T. V. RajanBabu, A. L. Casalnuovo, *J. Am. Chem. Soc.* **1996**, *118*, 6325−6326. – [3d] T. V. RajanBabu, T. A. Ayers, G. A. Halliday, K. K. You, J. C. Calabrese, *J. Org. Chem.* **1997**, *62*, 6012−6028. – [3e] T. V. RajanBabu, B. Radetich, K. K. You, T. A. Ayers, A. L. Casalnuovo, J. C. Calabrese, *J. Org. Chem.* **1999**, *64*, 3429−3447 and references cited therein.

[4] H. B. Kagan, T. −P. Dang, *J. Am. Chem. Soc.* **1972**, *94*, 6429−6433.

[5] [5a] W. S. Knowles, M. J. Sabacky, B. D. Vineyard, *J. Chem. Soc., Chem. Commun.* **1972**, 10−11. – [5b] B. D. Vineyard, W. S. Knowles, M. J. Sabacky, G. L. Bachman, D. J. Weinkauff, *J. Am. Chem. Soc.* **1977**, *99*, 5946−5952.

[6] For recently reported representative chiral bisphosphanes see: [6a] P. J. Pye, K. Rossen, R. A. Reamer, N. N. Tsou, R. P. Volante, P. J. Reider, *J. Am. Chem. Soc.* **1997**, *119*, 6207−6208. – [6b] Y. Hamada, F. Matsuura, M. Oku, K. Hatano, T. Shioiri, *Tetrahedron Lett.* **1997**, *38*, 8961−8964. – [6c]S. Qiao, G. C. Fu, *J. Org. Chem.* **1998**, *63*, 4168−4169. – [6d] G. Zhu, X. Zhang, *J. Org. Chem.* **1998**, *63*, 9590−9593. – [6e] R. M. Stoop, A. Mezetti, F. Spindler, *Organometallics* **1998**, *17*, 668−679. – [6f] L. A. van der Veen, M. D. K. Boele, F. R. Bregman, P. C. J. Kamer, P. W. N. M. van Leeuwen, K. Goubitz, J. Fraanje, H. Schenk, C. Bo, *J. Am. Chem. Soc.* **1998**, *120*, 11616−11626. – [6g] Q. Jiang, Y. Jiang, D. Xiao, P. Cao, X. M. Zhang, *Angew. Chem. Int. Ed.* **1998**, *37*, 1100−1103. – [6h] R. Kuwano, S. Okuda, Y. Ito, *Tetrahedron: Asymmetry* **1998**, *9*, 2773−2775. – [6i] Y.-Y. Yan, M. Widhalm, *Tetrahedron: Asymmetry* **1998**, *9*, 3607−3610. – [6j] U. Nettekoven, P. C. Kamer, P. W. N. M. van Leeuwen, M. Widhalm, A. L. Speck, M. Lutz, *J. Org. Chem.* **1999**, *64*, 3996−4004. – [6k] F. Robert, G. Oehme, D. Sinou, *J. Mol. Cat.* **1999**, *139*, 105−108. – [6l] D. Carmichael, H. Doucet, J. M. Brown, *Chem. Commun.* **1999**, 261−262. – [6m] Yamanoi, T. Imamoto, *J. Org. Chem.* **1999**, *64*, 2988−2989. – [6n] J. J. Almena Perea, M. Lotz, P. Knochel, *Tetrahedron: Asymmetry* **1999**, *10*, 375−384. – [6o] Q. Jiang, D. Xiao, Z. Zhang, P. Cao, X. M. Zhang, *Angew. Chem. Int. Ed.* **1999**, *38*, 516−518. – [6p] F. Maienza, M. Wörle, P. Steffanut, A. Mezzetti, F. Spindler, *Organometallics* **1999**, *18*, 1041−1049. – [6q] A. Marinetti, J.-P. Genêt, S. Jus, D. Blanc, V. Ratevelomanana-Vidal, *Chem. Eur. J.* **1999**, *5*, 1160−1165.

[7] [7a] R. Selke, *React. Kinet. Catal. Lett.* **1979**, *10*, 135−138. – [7b] R. Selke, H. Pracejus, *J. Mol. Catal.* **1986**, *37*, 213. – [7c] R. Selke, *J. Organomet. Chem.* **1989**, *370*, 241−248. – [7d] R. Selke, *J. Organomet. Chem.* **1989**, *370,* 249−256. – [7e] R. Selke, C. Facklam, H. Foken, D. Heller, *Tetrahedron: Asymmetry* **1993**, *4*, 369−382. – [7f]R . Selke, M. Ohff, A. Riepe, *Tetrahedron* **1996**, *52*, 15079−15102.

[8] [8a] D. Lafont, D. Sinou, G. Descotes, *J. Organomet. Chem.* **1979**, *169*, 87−95. – [8b] T. H. Johnson, G. Rangarajan, *J. Org. Chem.* **1980**, *45*, 62−65. – [8c] I. Habus, Z. Raza, V. Sunjic, *Croat. Chem. Acta* **1988**, *61*, 857−866. – [8d] V. Sunjic, I. Habus, G. Snatzke, *J. Organomet. Chem.* **1989**, *370*, 295−304. – [8e] J. M. Brown, S. J. Cook, A. G. Kent, *Tetrahedron* **1986**, *42*, 5097−5104. – [8f] C. Li, B. Bernet, A. Vasella, E. A. Broger, A. Meili, *Carbohydr. Res.* **1991**, *216*, 149−169. – [8g] M. Sawamura, K. Kitayama, Y. Ito, *Tetrahedron: Asymmetry* **1993**, *4*, 1829−1832. – [8h] M. Reetz, S. R. Waldvogel, *Angew. Chem. Int. Ed. Engl.* **1997**, *36*, 865−867.

[9] [9a] O. Pàmies, G. Net, A. Ruiz, C. Bo, J. M. Poblet, C. Claver, *J. Organomet. Chem.* **1999**, *586*, 125−137. – [9b] O. Pàmies, G. Net, A. Ruiz, C. Claver, *Tetrahedron: Asymmetry* **1999**, *10*, 2007−2014. – [9c] O. Pàmies, M. Diéguez, G. Net, A. Ruiz, C. Claver, *J. Chem. Soc., Dalton Trans.* **1999**, 3439−3444. – [9d] O. Pàmies, G. Net, A. Ruiz, C. Claver, *Eur. J. Inorg. Chem.* **2000**, 1287−1294. – [9e] O. Pàmies, G. Net, A. Ruiz, C. Claver, S. Woodward, *Tetrahedron: Asymmetry* **2000**, *11*, 871−877. – [9f] O. Pàmies, M. Diéguez, G. Net, A. Ruiz, C. Claver, *Organometallics* **2000**, *19*, 1488−1496.

[10] [10a] J. K. Whitesell, *Acc. Chem. Res.* **1985**, *18*, 280−284. – [10b] J. K. Whitesell, *Chem. Rev.* **1989**, *89*, 1581−1590. – [10c] B. M. Trost, D. L. van Vranken, *Angew. Chem.* **1992**, *104*, 194−196.

[11] [11a] K. Inoguchi, S. Sakuraba, K. Achiwa, *Synlett* **1992**, 169−178. – [11b] T. Morimoto, M. Chiba, K. Achiwa, *Chem. Pharm. Bull.* **1993**, *41*, 1149−1156. – [11c] K. Nozaki, N. Sakai, T. Nanno, T. Higashijima, S. Mano, T. Horiuchi, H. Takaya, *J. Am. Chem. Soc.* **1997**, *119* 4413−4423. – [11d] J. Karas, G. Huttner, K. Heinze, P. Rutsch, L. Zsolnai, *Eur. J. Inorg. Chem.* **1999**, 405−420.

[12] R. Jackson, D. J. Thompson *J. Organomet. Chem.* **1978**, *159*, C29−C31.

[13] [13a] H. Brunner, W. Pieronczyk, *J. Chem. Res. (S)* **1980**, 74−75; *J. Chem. Res. (M)* **1980**, 1251−1274. – [13b] H. Brunner, W. Pieronczyk, *J. Chem. Res. (S)* **1980**, 76; *J. Chem. Res. (M)* **1980**, 1275−1288.

[14] G. J. H. Buisman, M. E. Martin, E. J. Vos, A. Klootwijk, P. C. Kamer, P. W. N. M. van Leeuwen, *Tetrahedron: Asymmetry* **1995**, *6*, 719−738.

[15] R. L. Whistler, C.-C. Wang, *J. Org. Chem.* **1968**, *33*, 4455−4458.

[16] [16a] M. Green, T. A. Kuc, S. H. Taylor, *J. Chem. Soc. A* **1971**, 2334−2337. − [16b] K. Nakamoto, *Infrared and Raman Spectra of Inorganic and Coordination Compounds*, 3rd ed., John Wiley & Sons, New York, **1978**, p. 136.
[17] B. Wright, L. Hughes, S. S. Qureshi, A. H. Davidson, *Magn. Reson. Chem.* **1988**, *26*, 1062−1067.
[18] [18a] W. J. Hälg, L. R. Öhrström, H. Rüegger, L. M. Venanzi, T. Gerfin, V. Gramlich, *Helv. Chim. Acta* **1993**, *76*, 788−803. − [18b] M. Michalik, T. Freier, M. Schwarz, R. Selke, *Magn. Reson. Chem.* **1995**, *33*, 835−840.
[19] M. D. Fryzuk, B. Bosnich, *J. Am. Chem. Soc.* **1978**, *100*, 5491−5494.
[20] C. Detellier, G. Gelbard, H. B. Kagan, *J. Am. Chem. Soc.* **1978**, *100*, 7556−7561.
[21] [21a] J. M. Brown, P. A. Chaloner, R. Glaser, S. Geresh, *Tetrahedron* **1980**, *36*, 815−825. − [21b] K. E. Koenig, W. S. Knowles, *J. Am. Chem. Soc.* **1978**, *100*, 7561−7564.
[22] P. A. Chaloner, M. A. Esteruelas, F. Joó, L. A. Oro, *Homogeneous Hydrogenation*, Kluwer Academic Publishers, Dordrecht, **1994**, p.143−146.
[23] A. Togni, C. Breutel, A. Schnyder, F. Spindler, H. Landert, A. Tijani, *J. Am. Chem. Soc.* **1994**, *116*, 4062−4066.
[24] P. J. Pye, K. Rossen, R. A. Reaner, N. N. Tsou, R. P. Volante, P. J. Reider, *J. Am. Chem. Soc.* **1997**, *119*, 6207−6208.
[25] J. J. Almena Perea, A. Börner, P. Knockel, *Tetrahedron Lett.* **1998**, *39*, 8073−8076.
[26] H. Brunner, W. Pieronczyk, B. Schönhammer, K. Streng, I. Bernal, J. Korp, *Chem. Ber.* **1981**, *114*, 1137−1149.
[27] D. J. States, R. A. Haberkorn, D. J. Ruben, *J. Magn. Reson.* **1982**, *48*, 286−292.
[28] C. Cativiela, J. Fernández, J. A. Mayoral, E. Meléndez, R. Usón, M. J. Fernández, *J. Mol. Catal.* **1982**, *16*, 19−25.
[29] CERIUS2, version 3.5, Molecular Simulations Inc., San Diego, USA **1997**.
[30] [30a] L. A. Castonguay, A. K. Rappé, *J. Am. Chem. Soc.* 1**992**, *114*, 5832−5842. − [30b] A. K. Rappé, C. J. Casewit, K. S. Colwell, W. A. Goddard, III, W. M. Skiff, *J. Am. Chem. Soc.* **1992**, *114*, 10024−10035. − [30c] A. K. Rappé, K. S. Colwell, C. J. Casewit, *Inorg. Chem.* **1993**, *32*, 3438−3450.
[31] A. K. Rappé, W. A. Goddard, III, *J. Phys. Chem.* **1991**, *95*, 3358−3363.

Received March 1, 2000
[I00079]

Gold(I) Complexes with Amine Ligands, 6[+]

Hydrogen Bonding Networks in Bis(amine)gold(I) Complexes with Disulfonylamide Anions

Birte Ahrens,[a,b] Steffi Friedrichs,[a,c] Regine Herbst-Irmer,[d] and Peter G. Jones*[a]

Keywords: Amines / Aurophilicity / Disulfonylamides / Gold / Hydrogen bonds

The use of disulfonylamines as counter-ions allows the synthesis of stable ionic gold(I) complexes with the amine ligands cyclohexylamine, benzylamine, 3-iodobenzylamine, morpholine, pyrrolidine, and piperidine. There is a considerable increase in stability for the morpholine complex compared to the previously synthesised chloro derivative; the benzylamine derivatives displayed better solubility and crystallinity than their chloro analogues. The use of silver disulfonylamine derivatives in the syntheses led in two cases to the incorporation of silver into the products, with concomitantly poor yields. Crystal structure determinations of eight complexes revealed, as expected, extensive systems of N–H···O hydrogen bonds. Amines with NH functions tend to form hydrogen-bonded chain motifs, those with NH_2 as donor group form layers of linked ring patterns. It thus seems that the packing can more easily be classified in terms of influence of the cation than of the anion. Some C–H···O hydrogen bonds were also observed, but play a less important role. Aurophilic contacts were not observed, although one mixed gold/silver complex displayed short Au···Ag contacts. Of the two compounds containing iodine, only one showed short I···I contacts.

Introduction

Our studies of gold(I) complexes with amine ligands have involved a detailed investigation of the role of secondary bonds in these compounds.[1] Two types of secondary contacts are most frequently observed: aurophilic interactions[2] and hydrogen bonds. Gold(I) complexes of aliphatic amines had previously been regarded as relatively unstable − a viewpoint easily rationalised in terms of incompatibility of the soft metal centre gold(I) and the hard nitrogen donor − in the absence of stabilising ligands, such as phosphanes. We believe that hydrogen bonds are particularly important in stabilising such complexes.

Until now we have generally used chloride as counter-ion or second ligand, because of the convenience of using chloro precursors such as chloro(tetrahydrothiophene)-gold(I). The use of more versatile hydrogen bond acceptors might be expected to increase the stability of gold(I)−amine complexes still further, at least in the solid state; we have therefore started to exchange the sterically and geometrically undemanding halogen anion for disulfonylamides, using as reagent the silver disulfonylamides in acetonitrile solution. For a similar recent example with the ligand (dppm)Se, see ref.[3]

Here we report the synthesis and structure of gold(I) compounds with cyclohexylamine (**1**, **6**, **8**), benzylamine (**2**), 3-iodobenzylamine (**3**), morpholine (**4**; this was not stable as a chloro complex), pyrrolidine (**5**), and piperidine (**9**) as the amine ligands and bis(methanesulfonyl)amide (**1**, **2**, **3**, **4**, **5**), bis(*p*-chlorobenzenesulfonyl)amide (**7**), bis(*p*-iodobenzenesulfonyl)amide (**8**), and *o*-benzenedisulfonylamide (= 1,1,3,3-tetraoxo-1,3,2-benzodithiazole; **6**) as the anions. The corresponding chloro derivatives of **2** and **3** were highly insoluble and at best microcrystalline, whereas that of **4** was unstable.[1]

Our previously studied chloride derivatives involved three chemically distinct types of complexes: LAuCl (e.g. L = 2-methylpyridine, piperidine),[4,5] $[L_2Au^+]Cl^-$ (e.g. L = piperidine, cyclohexylamine)[1] and $[L_2Au^+][AuCl_2^-]$ (e.g. L = pyridine,[6] 3-bromopyridine[7]). Some crystal structures showed more than one structural type in the same crystal. With L = pyrrolidine a by-product was obtained in which two molecules of LAuCl crystallised together with one ionic complex $[L_2Au^+]Cl^-$;[8] other workers have shown that with L = 2-aminopyridine, one molecule LAuCl crystallised together with one ionic complex $[L_2Au^+]$ $[AuCl_2]^-$.[9] However, none of the compounds we examined showed appreciable conductivity in acetone solution, hence an equilibrium favouring the molecular over the ionic form was proposed.[1] After exchanging the chloride for a disulfonyla-

[+] Part 5: Ref.[7]

[a] Institut für Anorganische und Analytische Chemie, Technische Universität Braunschweig, Postfach 3329, D-38023 Braunschweig, Germany
E-mail: jones@xray36.anchem.nat.tu-bs.de
[b] Present address: Chemistry Department, University of Cambridge, Lensfield Road, Cambridge CB2 1EW, UK
[c] Present address: Inorganic Chemistry Laboratory, University of Oxford, South Parks Road, Oxford OX1 3QR, UK
[d] Institut für Anorganische Chemie, Universität Göttingen, Tammannstr. 4, D-37077 Göttingen, Germany

 © WILEY-VCH Verlag GmbH, D-69451 Weinheim, 2000 1434−1948/00/0909−2017 $ 17.50+.50/0

mide, in the presence of additional amine ligand, only ionic structures are observed. These complexes do conduct in acetone solution, although not very strongly, e.g. Λ_c = 79 cm^2 Ω^{-1} mol^{-1} for [(cyNH$_2$)$_2^+$]NMs$_2^-$; cf. Λ_c = 140 cm^2 Ω^{-1} mol^{-1} in the case of 1:1 electrolytes such as PPN$^+$Cl$^-$. It is conceivable that some form of ionic association occurs in solution.

All crystallographically characterised complexes described here display hydrogen bonding. As would be expected, the resulting networks become more complex with increasing numbers of donor hydrogen atoms. Comparison of the resulting patterns shows a seemingly greater contribution to the packing from the cation than from the anion.

None of the complexes shows aurophilic interactions, although the unexpected complex **5** involves an Au···Ag contact (see below).

Within those complexes where iodine is present, either in the ligand or the anion, I···I ("soft-soft") interactions were expected. However, only in one case were I···I contacts observed [3.723(4) Å in **3**, cf. 4.3804(10) Å in **8**; sum of the van der Waals radii 3.96 Å].[10] This further supports the conclusion that the hydrogen bonds contribute most to the three-dimensional pattern in these complexes.

Results and Discussion

Complexes with Bis(methanesulfonyl)amide as Anion and Cyclohexylamine, Benzylamine, 3-Iodobenzylamine, Morpholine or Pyrrolidine as Ligand

[(CyNH$_2$)$_2$Au$^+$]NMs$_2^-$ [**1**, cyNH$_2$ = cyclohexylamine, NMs$_2$ = bis(methanesulfonyl)amide, Figure 1, Table 1] crystallised with two independent molecules in the asymmetric unit. [(Benzylamine)$_2$Au$^+$]NMs$_2^-$ (**2**, Figure 2, Table 2), [(3-iodobenzylamine)$_2$Au$^+$]NMs$_2^-$ (**3**, Figure 3, Table 3) and [(morpholine)$_2$Au$^+$]NMs$_2^-$ (**4**, Figure 4, Table 4) crystallised with one formula unit in the asymmetric unit. With pyrrolidine as the ligand, the "non-innocence" of the silver reagent was demonstrated by the formation of a different complex (**5**): instead of a single NMs$_2^-$ anion this complex contains the anion [Ag(NMs$_2$)$_2^-$], and involves a d^{10}–d^{10} interaction between Ag and the gold atom of the [(pyrrolidine)$_2$Au$^+$] cation (Figure 5, Table 5). Even under exact stoichiometric conditions for the expected reaction, only this complex was obtained. We assume that the d^{10}–d^{10} interaction, in addition to the hydrogen bonding, stabilises the complex. Its length [3.309(3) Å] lies in the typical range of purely aurophilic interactions,[11] but much shorter Au···Ag contacts have been observed in [Ag{[Au(μ-N^3,C^3-bzim)]$_3$}$_2$]$^+$BF$_4^-$ [2.731(2) to 2.922(2) Å, bzim = 1-benzylimidazolate][12] or in [Au$_4$Ag(CH$_2$SiMe$_3$)$_4$(μ-dppm)$_2$]SO$_3$CF$_3$ [2.7179(13) to 2.7822(13) Å, dppm = bis(diphenylphosphanyl)methane].[13]

Table 1. Selected bond lengths and angles for **1**

Au1–N2	205.0(10)	Au1–N1	205.3(10)
Au2–N4	202.9(12)	Au2–N3	203.3(11)
S1–O2	144.2(9)	S1–O1	144.6(9)
S1–N5	162.1(9)	S1–C1	175.7(11)
S2–O4	143.6(9)	S2–O3	144.6(9)
S2–N5	157.3(11)	S2–C2	176.8(12)
S3–O6	145.1(9)	S3–O5	146.4(9)
S3–N6	158.0(12)	S3–C3	177.7(12)
S4–O7	145.7(11)	S4–O8	145.7(9)
S4–N6	159.1(11)	S4–C4	174.8(11)
N2–Au1–N1	177.9(4)	N4–Au2–N3	178.9(5)
O2–S1–O1	115.9(6)	N5–S1–C1	107.8(5)
O4–S2–O3	115.9(6)	N5–S2–C2	106.3(6)
O6–S3–O5	117.1(6)	N6–S3–C3	107.0(6)
O7–S4–O8	116.5(6)	N6–S4–C4	107.7(6)
S2–N5–S1	119.8(6)	S3–N6–S4	120.3(6)

All gold atoms are linearly coordinated [N1–Au1–N2 177.9(4), N3–Au2–N4 178.9(5)° (**1**), N1–Au–N2 177.66(10)° (**2**), N1–Au–N2 177.4(5)° (**3**), N1–Au–N2 177.19(8)° (**4**), and N1–Au–N2 178.0(6)° (**5**)]. The Au–N bond lengths of 2.053(10), 2.050(10) (at Au1), 2.033(11), 2.029(12) Å (at Au2) (**1**), 2.047(2), 2.045(3) Å (**2**), 2.037(13), 2.031(12) Å (**3**), 2.051(2), 2.055(2) Å (**4**), and 2.029(10), 2.044(12) Å (**5**) are similar to those in (cyNH$_2$)$_2$Au$^+$Cl$^-$ [Au–N 2.036(9) to 2.051(8) Å],[1] (piperidine)$_2$Au$^+$Cl$^-$ [Au–N 2.050(6), 2.055(6) Å][1] or in (pyrrolidine)$_2$Au$^+$Cl$^-$

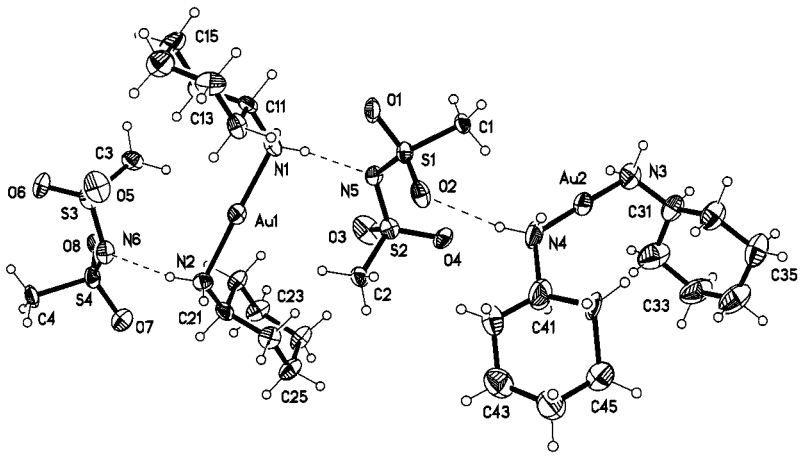


Figure 1. Bis(cyclohexylamine)gold(I) bis(methanesulfonyl)amide (**1**); asymmetric unit with numbering scheme; thermal ellipsoids are shown with 50% probability; hydrogen radii are arbitrary; dashed lines represent hydrogen bonds

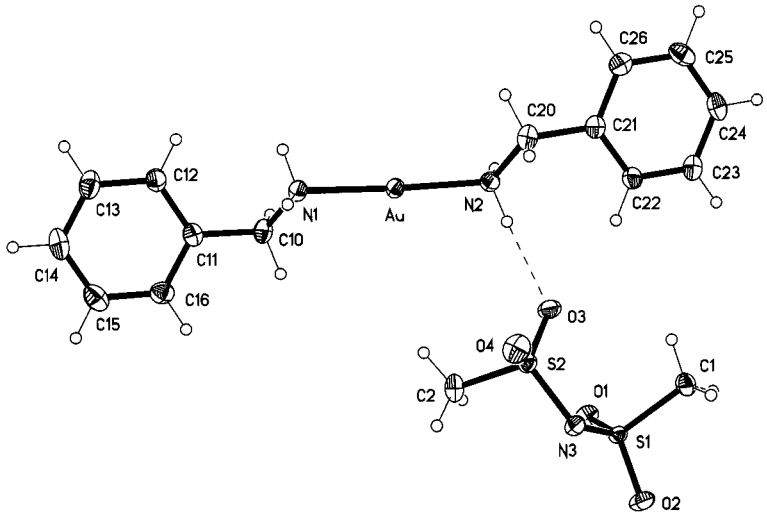


Figure 2. Bis(benzylamine)gold(I) di(methanesulfonyl)amide (**2**); asymmetric unit with numbering scheme; thermal ellipsoids are shown with 50% probability; hydrogen radii are arbitrary; dashed lines represent hydrogen bonds

Table 2. Selected bond lengths and angles for **2**

Au−N2	204.5(3)	Au−N1	204.7(2)
N1−C10	148.4(4)	C10−C11	151.1(4)
N2−C20	149.0(4)	C20−C21	151.2(4)
N3−S1	159.6(3)	N3−S2	159.8(3)
S1−O1	144.2(2)	S1−O2	145.1(2)
S1−C1	177.0(3)	S2−O4	144.5(2)
S2−O3	145.7(2)	S2−C2	175.0(3)
N2−Au−N1	177.66(10)	C10−N1−Au	117.36(19)
N1−C10−C11	113.1(3)	C20−N2−Au	115.15(19)
N2−C20−C21	113.4(2)	S1−N3−S2	120.96(15)
O1−S1−O2	115.54(14)	N3−S1−C1	106.34(15)
O4−S2−O3	116.30(15)	N3−S2−C2	105.88(15)

Table 3. Selected bond lengths and angles for **3**

Au−N2	203.1(12)	Au−N1	203.7(13)
I1−C13	215.0(17)	I2−C23	208.8(16)
N1−C10	150(2)	C10−C11	150(2)
N2−C20	150.8(19)	C20−C21	150(2)
N3−S2	156.9(14)	N3−S1	161.5(13)
C1−S1	178.3(17)	C2−S2	175.8(14)
S1−O2	144.3(11)	S1−O1	146.8(11)
S2−O3	144.1(11)	S2−O4	145.6(11)
N2−Au−N1	177.4(5)	C10−N1−Au	114.2(9)
C11−C10−N1	113.5(13)	C20−N2−Au	115.8(9)
C21−C20−N2	113.0(11)	S2−N3−S1	120.6(8)
O2−S1−O1	116.5(7)	N3−S1−C1	106.5(8)
O3−S2−O4	114.9(7)	N3−S2−C2	107.5(7)

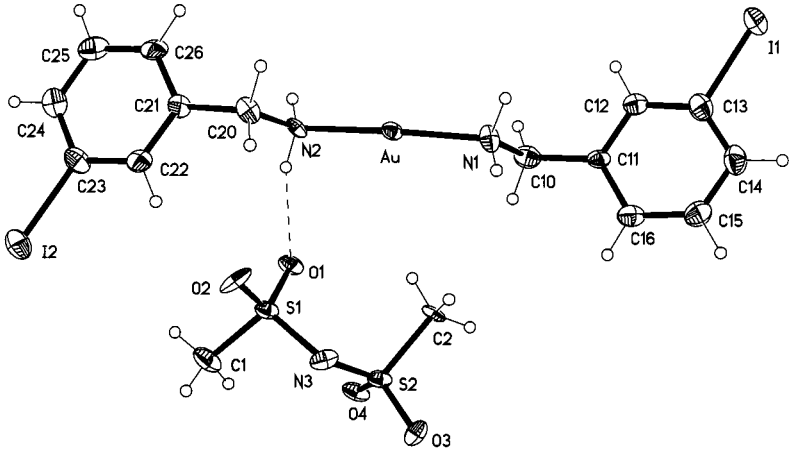


Figure 3. Bis(3-iodobenzylamine)gold(I) bis(methanesulfonyl)amide (**3**); asymmetric unit with numbering scheme; thermal ellipsoids are shown with 50% probability; hydrogen radii are arbitrary; dashed lines represent hydrogen bonds

[Au−N 2.052(5) to 2.055(7) Å].[1] The dimensions of **5** should however be interpreted with caution, because the cation is disordered over two positions (see Experimental Section; only the dimensions of the major component are discussed here) and because there is pseudosymmetry caused by the heavy atoms positioned approximately at 0.25,0.5,*z* in space group *Pna*2_1.[14]

The independent cations in **1** show different C−N···N−C torsion angles across the N−Au−N unit: The arrangement of the ligands at Au1 is antiperiplanar [C11−N1···N2−C21 169(1)°], and is eclipsed at Au2 [C31−N3···N4−C41 −18(1)°]. The former conformation is most common within this kind of cation, as in $[(cyNH_2)_2Au^+]Cl^-$ [C−N···N−C −174.2(9) and, because of inversion symmetry, 180°],[1] **2**

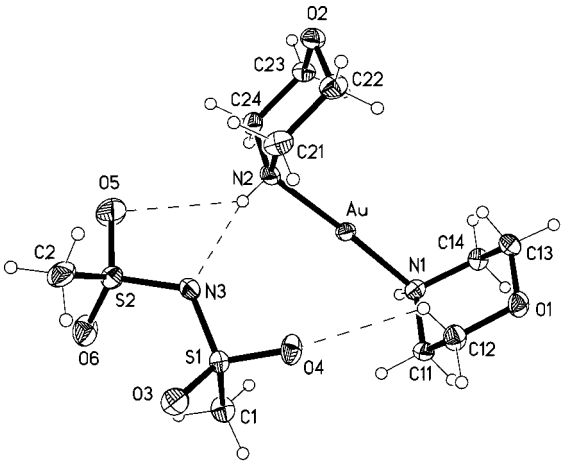


Figure 4. Bis(morpholine)gold(I) bis(methanesulfonyl)amide (**4**); asymmetric unit with numbering scheme; thermal ellipsoids are shown with 50% probability; hydrogen radii are arbitrary; dashed lines represent hydrogen bonds

Table 4. Selected bond lengths and angles for **4**

Au−N1	205.1(2)	Au−N2	205.5(2)
N3−S1	158.8(2)	N3−S2	159.9(2)
S1−O3	144.62(19)	S1−O4	145.66(19)
S1−C1	176.1(2)	S2−O5	144.5(2)
S2−O6	144.6(2)	S2−C2	176.5(3)
N1−Au−N2	177.19(8)	C11−N1−C14	108.0(2)
C11−N1−Au	112.24(16)	C14−N1−Au	114.52(16)
C21−N2−C24	108.3(2)	C21−N2−Au	114.35(18)
C24−N2−Au	114.55(17)	S1−N3−S2	122.47(14)
O3−S1−O4	115.56(12)	N3−S1−C1	108.29(13)
O5−S2−O6	117.06(15)	N3−S2−C2	107.08(14)

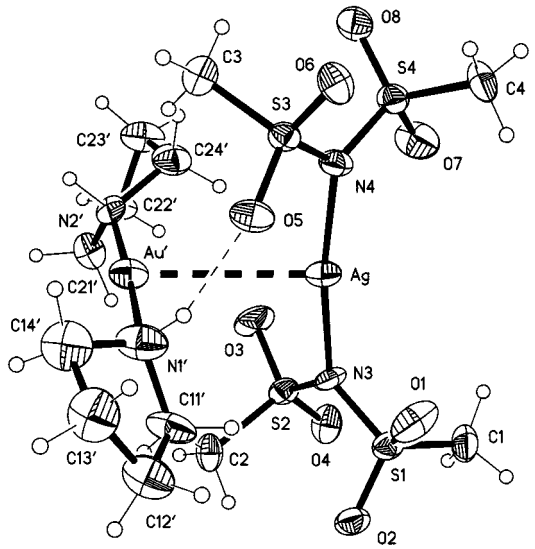


Figure 5. Bis(pyrrolidine)gold(I) bis[bis(methanesulfonyl)amide]argentate(I) (**5**); major disorder component with numbering scheme; thermal ellipsoids are shown with 50% probability; hydrogen radii are arbitrary; dashed lines represent hydrogen bonds; in the minor disorder component, the pyrrolidine ring involving N2 inverts to form an intramolecular hydrogen bond from N2 to O3; see also the corresponding packing diagrams in Figure 10

[C10−N1···N2−C20 179.5(2)°], and **3** [C10−N1···N2−C20 178.3(13)°].

The S−N bond lengths [1.569(14) to 1.627(8) Å, Table 6] in the NMs_2 anions of complexes **1** to **5** are similar to those in other metal complexes with bis(methanesulfonyl)amide {e.g. $[Ag_4(NMs_2)_4(H_2O)]$,[15] S−N 1.603(6) to 1.632(6) Å; S−N−S 118.0(4) to 120.6(4)°}. The corresponding S−N−S angles [119.8(6) to 122.47(14)°, Table 6] support the assumption of sp^2 hybridisation of the amide nitrogen atom.

Table 5. Selected bond lengths and angles for **5** (only the major disorder component of the cation is given)

Au′−N2′	202.9(10)	Au′−N1′	204.4(10)
Au′−Ag	330.9(3)	Ag−N3	212.3(7)
Ag−N4	212.2(7)	S1−O1	143.8(6)
S1−O2	144.2(8)	S1−N3	162.7(7)
S1−C1	174.7(11)	S2−O4	142.9(7)
S2−O3	144.0(7)	S2−N3	162.3(8)
S2−C2	176.9(9)	S3−O5	143.5(7)
S3−O6	143.4(7)	S3−N4	162.3(8)
S3−C3	176.0(9)	S4−O8	143.1(7)
S4−O7	145.8(7)	S4−N4	162.7(8)
S4−C4	176.9(11)		
N2′−Au′−N1′	176.5(8)	N2′−Au′−Ag	100.5(4)
N1′−Au′−Ag	82.6(8)	N3−Ag−N4	171.1(3)
N3−Ag−Au′	95.5(2)	N4−Ag−Au′	93.4(2)
O1−S1−O2	117.8(4)	N3−S1−C1	106.8(5)
O4−S2−O3	116.6(4)	N3−S2−C2	106.9(4)
O5−S3−O6	116.9(4)	N4−S3−C3	107.5(5)
O8−S4−O7	118.4(4)	N4−S4−C4	107.5(5)
S2−N3−S1	120.5(4)	S3−N4−S4	120.5(4)

The silver atom of the anion $[Ag(NMs_2)_2]^-$ in **5** is linearly coordinated [N3−Ag−N4 171.1(3)°]. The Ag−N bond lengths of 2.123(7) (Ag−N3) and 2.122(7) Å (Ag−N4) are similar to those in $[Ag(NCCH_3)_4][Ag(NMs_2)_2]$ of 2.129(2) Å.[16] The NMs_2 ligands at Ag in **5** are rotated with respect to each other across the N−Ag−N unit [S2−N3···N4−S3 101.4(6), S2−N3···N4−S4 −78.3(6)°], which may be in order to accommodate the hydrogen bonds. The N−Au−N and N−Ag−N bond axes in **5** are perpendicular to each other [N1′−Au′···Ag−N3 86.3(8), N1′−Au′···Ag−N4 −92.8(8)°].

One oxygen atom of every sulfonyl group of NMs_2 anions lies in or near the S−N−S bond plane. The resulting "W" shape is characteristic of the bis(methanesulfonyl)amide anion.[17] The two other oxygen atoms and the methyl groups lie above or below this plane and show a staggered conformation [absolute O−S−N−S torsion angles: 30.5(11) to 43.2(2), 159.1(9) to 171.5(7)°; Table 6]. Different signs are associated with the two different chirally frozen conformers of bis(methanesulfonyl)amide.

Within all bis(amine)gold(I) complexes with disulfonylamide as the anion, more hydrogen bond acceptors (A) are present than classical hydrogen bond donor groups (D) such as NH. Every disulfonylamide anion has five acceptor groups: the four oxygen atoms and the amide nitrogen atom. The cations of the complexes **1**, **2**, and **3** have four amine hydrogen atoms, the cations of **4** and **5** each have two amine hydrogen atoms. Logically, therefore, not all of the hydrogen bond acceptors can be involved in classical hydrogen bonding, whereas every amine hydrogen atom in the complexes **1** to **5** *is* involved in hydrogen bonding. Associated H bond dimensions H···A, D···A and D−H···A are shown in Table 7.

Table 6. Geometrical parameters of the bis(methanesulfonyl)amide anions

Compound		S−N [Å]	S−N−S [°]	O′−S−N−S [°]	O″−S−N−S [°]
1	S1−N5	1.621(9)	119.8(6)	−163.0(6)	−34.8(8)
	S2−N5	1.573(11)			
	S3−N6	1.580(12)	120.3(6)	168.0(6)	37.7(9)
	S4−N6	1.591(11)			
2	S1−N3	1.596(3)	120.96(15)	−166.8(2)	−38.5(2)
	S2−N3	1.598(3)			
3	S1−N3	1.615(13)	120.6(8)	−159.1(9)	−30.5(11)
	S2−N3	1.569(14)			
4	S1−N3	1.588(2)	122.47(14)	−170.7(2)	−43.2(2)
	S2−N3	1.599(2)			
5	S1−N3	1.627(7)	120.5(4)	−171.3(6)	−43.1(7)
	S2−N3	1.623(8)			
	S3−N4	1.623(8)	120.5(4)	−168.1(5)	−41.1(7)
	S4−N4	1.627(8)			

Table 7. N−H···X hydrogen bonds and unitary graph sets (N_1)

Comp.	Bond	H···A [Å][a]	H···A [Å][b]	D···A [Å][c]	D−HA [°]	N_1
1	N1−H1A···N5 *(a)*	2.05	1.95	2.962(14)	171.1	D
	N1−H1B···O3^{i} *(b)*	2.27	2.18	3.163(13)	163.3	D
	N2−H2A···O5^{ii} *(c)*	2.09	2.00	2.995(13)	166.2	D
	N2−H2B···N6 *(d)*	2.18	2.09	3.064(14)	160.1	D
	N3−H3A···O6^{i} *(e)*	2.27	2.18	3.161(13)	161.9	D
	N3−H3B···O1^{iii} *(f)*	2.12	2.02	3.030(14)	169.6	D
	N4−H4A···O7^{iv} *(g)*	2.13	2.03	3.040(19)	169.6	D
	N4−H4B···O2 *(h)*	2.18	2.09	3.008(14)	149.5	D
2	N1−H1A···N3^{v} *(j)*	2.06	1.96	2.974(3)	171.9	D
	N1−H1B···O2^{vi} *(k)*	2.03	1.96	2.827(3)	143.5	D
	N2−H2A···O3 *(l)*	2.08	1.98	2.990(3)	171.3	D
	N2−H2B···O1^{ii} *(m)*	2.35	2.30	2.974(3)	124.9	D
3	N1−H1A···O3^{vii} *(n)*	2.02	1.94	2.867(18)	151.9	D
	N1−H1B···N3^{viii} *(o)*	2.21	2.11	3.085(19)	159.9	D
	N2−H2A···O4^{ix} *(p)*	2.06	1.97	2.978(17)	172.2	D
	N2−H2B···O1 *(q)*	2.06	1.98	2.894(17)	149.4	D
4	N1−H1···O4^{x}	1.98(3)	1.88	2.857(3)	162(3)	D
	N2−H2···N3	2.18(4)	1.96	2.894(3)	154(4)	D
5	N1−H1···O5	2.08	2.00	2.94(5)	154	$R_2^2(12)$
	N2−H2···O3	1.79	1.71	2.68(3)	158	$R_2^2(12)$
	N1′−H1′···O5	1.99	1.71	2.86(3)	148	D
	N2′−H2′···O7^{xi}	2.23	2.15	3.12(2)	158	D
6	N1−H1A···O2	2.28	2.19	3.125(10)	154.5	$R_2^2(10)$
	N1−H1B···O2^{xii}	2.57	2.77	3.013(10)	110.3	$R_2^2(10)$
	N1−H1B···O1^{xiii}	2.49	2.43	3.141(9)	128.0	$C_2^2(10)$
8	N10−H10A···O2^{xi}	2.16(7)	1.89	2.896(10)	169(6)	D *or*[d]
	N10−H10A···O2′^{xi}	2.28(7)	2.06	2.948(11)	148(6)	$C_2^2(10)$
	N10−H10B···O1^{ix}	2.01(8)	1.89	2.883(9)	163(7)	D *or*[d]
	N10−H10B···O1′^{ix}	2.08(8)	1.97	2.964(10)	166(7)	$C_2^2(10)$
9	N1−H1···Cl1	2.39	2.32	3.245(10)	152.0	D
	N2−H2···Cl1^{xiv}	2.30	2.22	3.171(10)	155.3	D

[a] Hydrogen bonds without a standard deviation were based on a riding model. − [b] Distances with normalised N−H 1.02 Å.[30]. − [c] Cf. van der Waals radii: N 1.55, O 1.53, H 1.20, Cl 1.75 Å.[10] − [d] The assignment depends on whether the two hydrogen bonds to the two positions of the disordered oxygen atoms are considered as different [D] or identical [$C_2^2(10)$] for the graph theoretical analysis. − Operators: i: $-x, 1-y, -z$; ii: $1-x, 1-y, -z$; iii: $-x, 1-y, 1-z$; iv: $x, y, 1+z$; v: $2-x, 1-y, -z$; vi: $x, 1+y, z-1$; vii: $x-1, y, z$; viii: $1-x, 1-y, 1-z$; ix: $1-x, -y, 1-z$; x: $x+1, y, z$; xi: $x, y, z-1$; xii: $1-x, y, 1-z$; xiii: $0.5+x, 0.5-y, z$; xiv: $1-x, 3-y, 1-z$.

In complexes **1**, **2**, and **3**, with four amine hydrogen atoms per formula unit, layers are formed, containing rings of hydrogen bonds. In complex **4** and **5** (major component), with two amine hydrogen atoms per formula moiety, the molecules are arranged in chains.

Graph theoretical analysis[18] of the hydrogen bond patterns led to the following conclusions: Each individual hydrogen bond forms a distinct pattern. Rings were formed by combining two (binary level, N_2) or four hydrogen bonds (quaternary level, N_4). In **1,** the combination of four different rings forms the layers parallel to (1 0 1), see Figure 6. The rings are described by the graph sets $R_4^4(12)$, $R_4^4(16)$, $R_4^4(20)$ [all N_2] and $R_4^4(18)$ [N_4]. In **2** and **3**, the layers are formed parallel to (1 1 0) from rings on binary level [N_2] (Figure 7 and Figure 8). In **2**, these rings are described by the graph sets $R_4^4(12)$ and $R_4^4(16)$ and in **3** by $R_4^4(8)$, $R_4^4(12)$, $R_4^4(16)$. The different ring pattern in the layers of the two complexes with benzylamine ligands, **2** and **3,** is presumably influenced by the iodine substitution of the benzylamine in **3**. Apart from the obvious steric effects, the iodine atom shows, as mentioned above, a short contact of 3.723(4) Å to an iodine atom of the next layer.

The chains in **4** (parallel to the *x* axis) and **5** (parallel to the *z* axis) are formed by combination of the two independent hydrogen bonds present in these complexes (Figure 9 and Figure 10a). The chain in **4** is described by the graph set $C_2^2(8)$, in **5** by $C_2^2(10)$. The minor disorder component of **5**, in which the ring at N2 is inverted, involves solely intra-

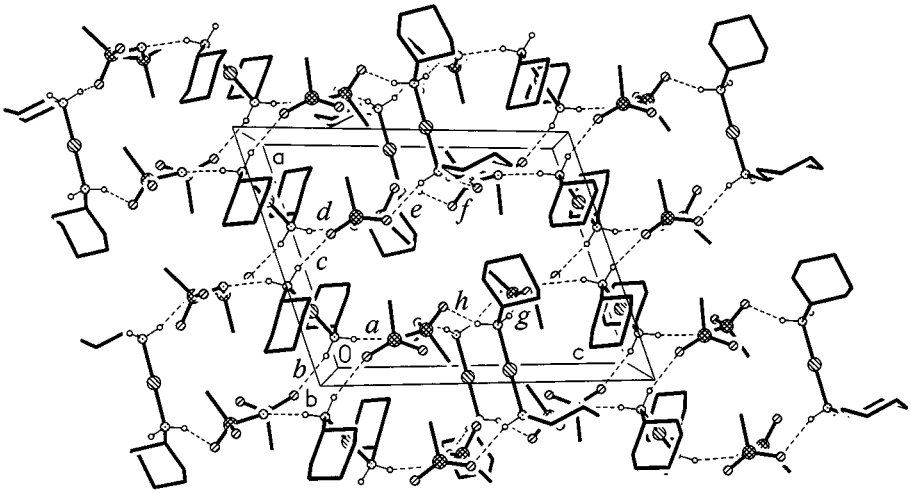


Figure 6. Bis(cyclohexylamine)gold(I) bis(methanesulfonyl)amide (**1**); layer structure; atom radii are arbitrary; dashed lines represent hydrogen bonds (Table 7); carbon-bonded hydrogen atoms are omitted for clarity

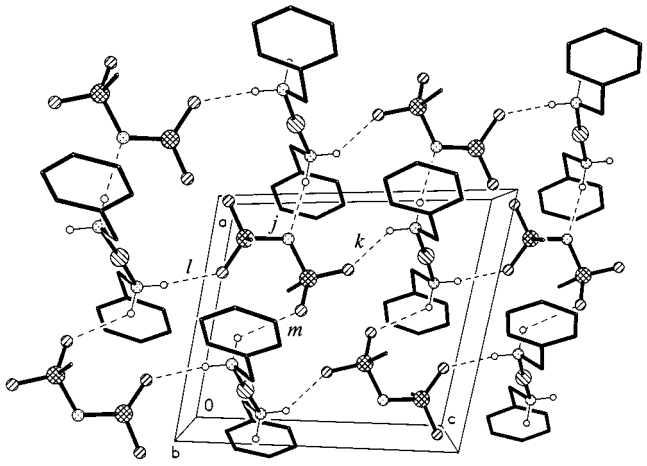


Figure 7. Bis(benzylamine)gold(I) bis(methanesulfonyl)amide (**2**); layer structure; atom radii are arbitrary; dashed lines represent hydrogen bonds (Table 7); carbon-bonded hydrogen atoms are omitted for clarity

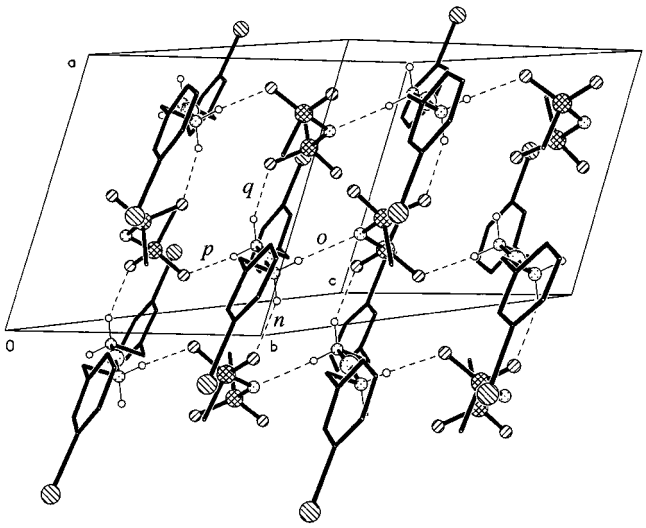


Figure 8. Bis(3-iodobenzylamine)gold(I) bis(methanesulfonyl)amide (**3**); layer structure; atom radii are arbitrary; dashed lines represent hydrogen bonds (Table 7); carbon-bonded hydrogen atoms are omitted for clarity; short I···I contacts are formed between layers and thus are not shown here

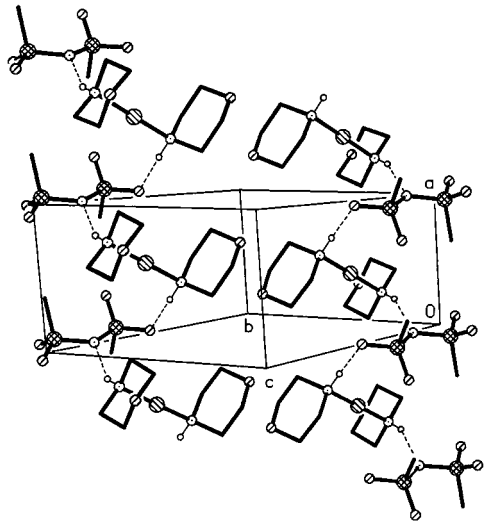


Figure 9. Bis(morpholine)gold(I) bis(methanesulfonyl)amide (**4**); chain structure; atom radii are arbitrary; dashed lines represent hydrogen bonds (Table 7); carbon-bonded hydrogen atoms are omitted for clarity

molecular hydrogen bonds; clearly the alternative direction of the N2−H2 vector presents a viable alternative hydrogen bonding system.

Complexes with Cyclohexylamine as Ligand and *o*-Benzenedisulfonylamide or Bis(*p*-halobenzenesulfonyl)amide as Anion

$[(CyNH_2)_2Au^+]-o$-benzodisulfonylamide (**6**, Figure 11) crystallised with half a formula unit in the asymmetric unit, together with dichloromethane (overall composition **6**/dichloromethane of 2:3). The gold and the amide nitrogen atom lie on a mirror plane; the gold atom is linearly coordinated [N1−Au−N1′ 177.1(4)°]. The Au−N bond length of 2.045(7) Å is similar to those in complex **1** [2.020(12) to 2.053(10) Å].

The *o*-benzenedisulfonylamide anion in **6** is conformationally more constrained than the other disulfonylamide anions, leading to a different arrangement of the acceptor groups. The S−N bond length of 1.554(5) Å is slightly shorter than in the NMs_2 anions in complexes **1** to **5** [1.569(14) to 1.638(9) Å] and also shorter than in the silver complexes of this anion {1.613(2) Å in $[Ag(H_2O)\{N(SO_2)_2C_6H_4\}]$,[19] 1.614(1) Å in $[Ag(NCCH_3)\{N(SO_2)_2C_6H_4\}]$}.[16] The S−N−S angle in **6** [119.7(7)°] is larger than in the silver complexes [111.6(2) and 116.7(1)°]. Hence, the shorter S−N bond length in **6** could be attributed to a greater sp^2 hybridisation of the amide nitrogen atom. This is in good agreement with the assumption of a greater degree of backbonding caused by the additional charge in the non-coordinating anion of **6**. The *o*-benzenedisulfonylamide anion is also present solely as a counter-ion in the structures of $[Ca(H_2O)_7][N(SO_2)_2C_6H_4]_2$[20] and $[Me_2Sn(H_2O)_4][N(SO_2)_2C_6H_4]_2$,[21] and here the situation is not so clear-cut; in both cases the S−N bond lengths [1.574(3) to 1.587(3) Å] are longer than in **6**, and the S−N−S bond angles [115.7(2), 114.9(2)°] are smaller than in **6**.

The five- and the six-membered ring of the anion are coplanar; the interplanar angle is 2.4(7)°. The oxygen atoms lie above or below the S−N−S′ plane. This conformation has an influence on the packing in the crystal, resulting in a cation showing the more unusual eclipsed conformation (C11−N1···N1′−C11′ 0°, by symmetry). Nevertheless, layers are also formed in **6** by combination of hydrogen-bonded rings (Figure 12, Table 8). The two crystallographically independent oxygen atoms of the anion are involved in hydrogen bonding (see Table 7). The amide nitrogen atom shows a long contact to the gold atom [Au···N2 3.382(10) Å; cf. sum of the van-der-Waals radii 3.21 Å][10] and is not involved in hydrogen bonding; a shorter Au···N contact of 3.009(7) Å was observed in the related complex bis(tetrahydrothiophene)gold(I) *o*-benzenedisulfonylamide.[22] Overall there are three independent hydrogen bonds present in **6**: N1−H1A···O2, N1−H1B···O2^{xii} and N1−H1B···O1^{xiii} (for symmetry operators see Table 7). H1B is the donor atom of a three-centre hydrogen bond, and O2 the acceptor atom of a bifurcated hydrogen bond.

The layers in **6** are in fact double layers, with the cations on the outside and the anions inside (Figure 12). The rings within the layers in **6** can be described with the graph sets $R_2^2(10)$ (combination of the two hydrogen bonds involving O2 with themselves), $R_4^2(8)$ and $R_2^4(8)$ (combination of two different hydrogen bonds).

Unfortunately, no crystals could be obtained from complex **7** with bis(*p*-chlorobenzenesulfonyl)amide as anion. $[(CyNH_2)_2Au^+]$−bis(*p*-iodobenzenesulfonyl)amide (**8**, Figure 13) crystallised with half a formula unit in the asymmetric unit. The gold atom lies on an inversion centre and the bis(sulfonyl)amide group of the anion is disordered over an inversion centre.

The gold atom in **8** is linearly coordinated by symmetry, with an N−Au bond length of 2.034(5) Å similar to those in $[(cyNH_2)Au^+]Cl^-$ [1] and complexes **1** to **3** [2.029(12) to 2.053(10) Å]. The ligands at Au are antiperiplanar (C−NN−C 180° by symmetry). The S−N bond lengths [1.569(9), 1.571(9) Å] are similar to those in the bis(methanesulfonyl)amide anions of complexes **1** to **5** [1.569(14) to 1.638(9) Å]. The S−N−S angle of 127.3(7)° in **8** is slightly larger [cf. 119.8(6) to 122.57(14)° in **1** to **5**], but this should be interpreted with caution because of the disorder of the anion.

Changing the anion from bis(methanesulfonyl)amide to bis(*p*-halobenzensulfonyl)amide should result in a greater influence of the anion on the crystal packing. With the latter anions, more secondary interactions, apart from hydrogen bonding, should be observable, e.g. halogen−halogen or even π···π interactions. However, none of these was observed in the crystal structure of **8**.

The disorder of the anion in **8** makes the bond lengths of the hydrogen bonds less precise, but the overall pattern, a layer parallel to (1 1 0), formed by combination of hydrogen-bonded rings, is similar to that in complexes **1** to **3** (Figure 14, Table 9). The rings in **8** can be described with the graph sets $R_4^4(12)$ and $R_4^4(20)$. Because of the disorder, assignment of a distinct level (N_2 or N_4) is not meaningful.

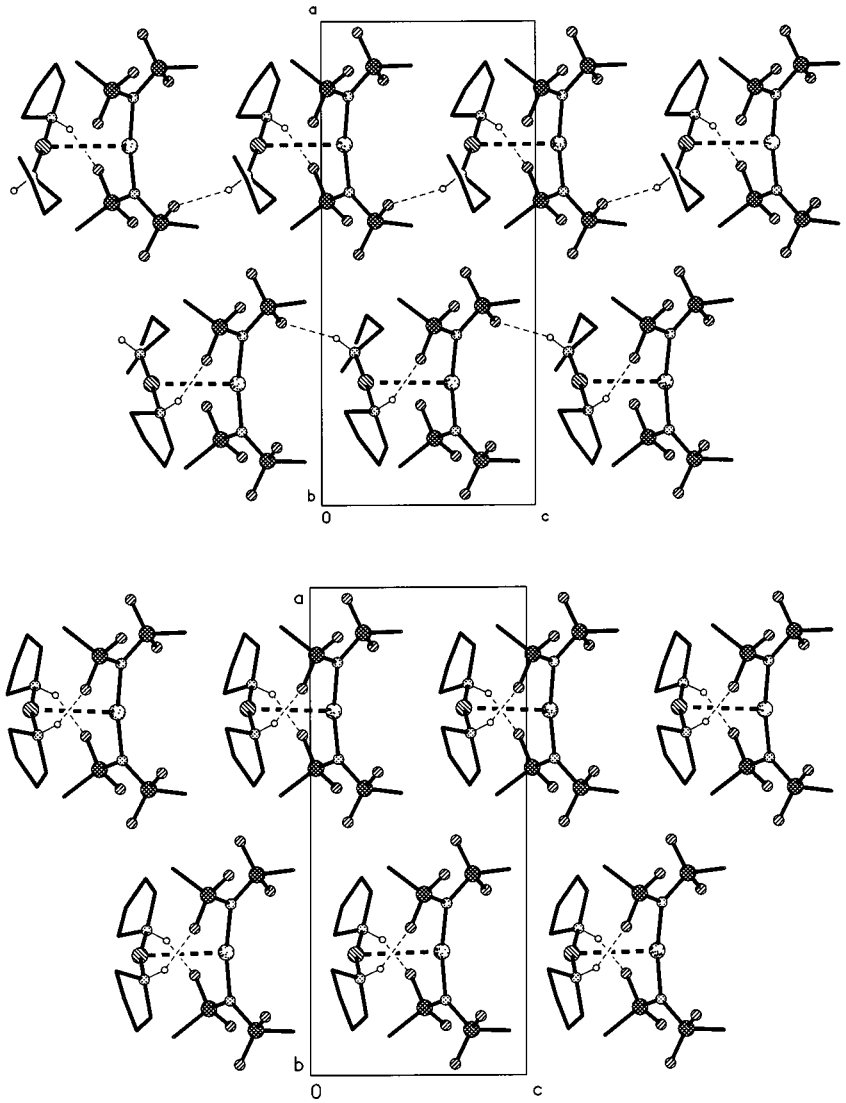


Figure 10. (a) Bis(pyrrolidine)gold(I) bis[bis(methanesulfonyl)amide]argentate(I) (**5**); projection of the chain structure involving the major disorder component; atom radii are arbitrary; dashed lines represent hydrogen bonds (Table 7); carbon-bonded hydrogen atoms are omitted for clarity; (b) an equivalent view of the minor disorder component showing the purely intramolecular hydrogen bonds

Non-Classical Hydrogen Bonding

Non-classical hydrogen bonds, i.e. hydrogen bonds with C−H as donor group, were previously the subject of controversial discussion, but are nowadays of accepted validity and the subject of great interest.[23] In complexes **1** to **4** the oxygen atoms not involved in classical hydrogen bonding showed hydrogen bonds of the type C−H···O, with uncorrected H···O in the range 2.35 to 2.73 Å (see Table 10). These hydrogen bonds can link neighbouring layers (complexes **1** to **3**) or chains (complex **4**); others connect molecules within the layer or chain. We do not discuss the disordered complexes, in which the alternative positions of the C−H functions render meaningful discussion impossible.

An Unexpected Complex with Piperidine as Ligand

Attempts to replace the chloride anion in $[(piperidine)_2Au^+]Cl^-$ [1] by NMs_2^-, as in the reactions described above, led not to the desired complex but to one with $AgCl_2^-$ as anion, again showing that silver can play an active (but undesired) role in such reactions. In the crystal structure of $[(piperidine)_2Au^+][AgCl_2^-]$ (**9**, Figure 15), the anion is not a discrete moiety, but forms polymeric chains, containing Ag_2Cl_2 squares [Ag−Cl 2.598(4) to 2.631(3) Å, Cl−Ag−Cl 96.96(9) to 113.78(12)°, see Table 11]. A search of the Cambridge structural database[24] revealed only two other complexes with this $[AgCl_2^-]_n$ chain, namely $[(CH_3)_4N^+][AgCl_2^-]$[25] and $[(CH_3C(O)CH_2C(O)CH_3)_3Si^+][AgCl_2^-]$.[26]

The cations in **9** lie above and below the Ag_2Cl_2 squares and form hydrogen bonds to the chlorine atoms (Figure 16). The conformation of the cation in **9** is slightly different from that of the $(piperidine)_2Au^+$ cation in the chloride complex.[1] The gold atom in **9** is, as usual, linearly coordinated [N1−Au−N2 179.3(4)°]. The N−Au bond lengths are slightly longer than in complexes **1** to **3** and in the chloride complex [N1−Au 2.104(10), N2−Au 2.098(11) Å, cf.

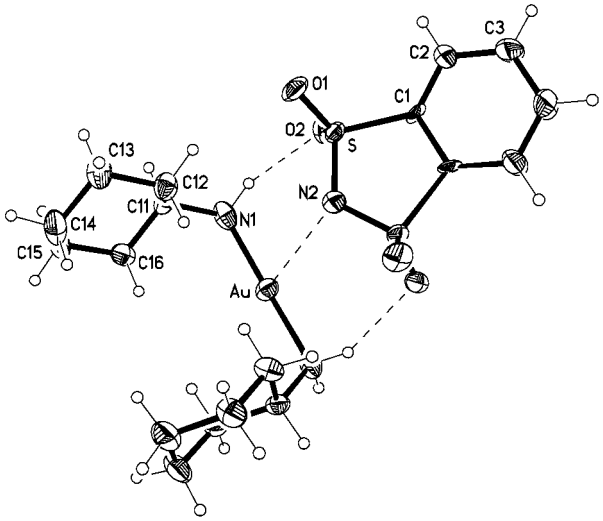


Figure 11. Bis(cyclohexylamine)gold(I) *o*-benzenedisulfonylamide dichloromethane solvate (2/3) (**6**); asymmetric unit with numbering scheme; solvent omitted; thermal ellipsoids are shown with 50% probability; hydrogen radii are arbitrary; dashed lines represent hydrogen bonds; one H atom at N1 is eclipsed

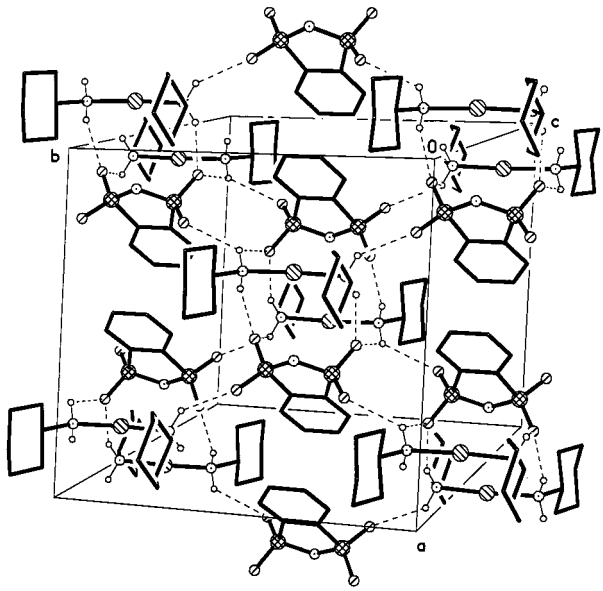


Figure 12. Bis(cyclohexylamine)gold(I) *o*-benzenedisulfonylamide dichloromethane solvate (2/3) (**6**); layer structure; atom radii are arbitrary; dashed lines represent hydrogen bonds (Table 7); carbon-bonded hydrogen atoms and dichloromethane molecules are omitted for clarity

Table 8. Selected bond lengths and angles for **6**

Au−N1	204.5(7)	S−O1	143.6(6)
S−O2	144.5(6)	S−N2	155.4(5)
S−C1	177.0(8)		
N1−Au−N1^{xxiii} [a]	177.1(4)	O1−S−O2	113.2(4)
N2−S−C1	99.0(4)	S−N2−S^{xxiii}	119.7(7)

[a] Symmetry transformations for equivalent atoms: xxiii: $x, -y + 1, z$.

N−Au 2.029(12) to 2.055(6) Å], but are similar to those in [(pyridine)$_2$Au$^+$][AuCl$_2^-$] [N−Au 2.08(3), 2.10(4) Å]. The main difference of the conformation of the cation, compared to the chloride complex, is the arrangement of the ligands at Au. In **9** it is a more eclipsed arrangement, in the chloride complex the arrangement is better described as staggered [C11−N1···N2−C21 1.1(12), C11−N1···N2−C25 127.1(11)°, cf. C11−N1···N2−C21 −68.6(7), C11−N1···N2−C25 164.0(6)° in the chloride]. This change in the conformation is probably due to the restricted conformation of the anion in **9**; in both complexes $R_4^2(12)$ rings are formed, but in **9** the chloride anions are fixed by the $AgCl_2$ chain.

Conclusion

Considerable similarities were found between all structures containing either N−H or NH_2 as hydrogen donor groups. The complexes with N−H as donor groups and NMs_2 as the anion (**4**, **5**) displayed a secondary structure consisting of chains. The gold complexes with pyrrolidine as ligand and chloride as anion had also been found to involve mainly chains as secondary pattern.[1,8]

Those complexes with piperidine as ligand and chloride as the anion behaved somewhat differently, showing either dimeric $(L_2Au^+Cl^-)_2$[1] or tetrameric $(LAuCl)_4$[5] structures. In both structures ring systems of hydrogen bonds could be recognised. The ring pattern of the dimeric structure is again found in **9**, but now with polymeric $AgCl_2^-$ as anion.

In all complexes with NH_2 as donor group (**1**, **2**, **3**, **6**, and **8**) layers containing ring patterns were formed; evidently the "extra" H donor facilitates the formation of two-dimensional hydrogen bond systems. These ring patterns are topologically closely related to those in [(cyNH$_2$)$_2$Au$^+$]Cl$^-$ [1] and even to those in the metal-free cyclohexylamine hemihydrochloride.[27]

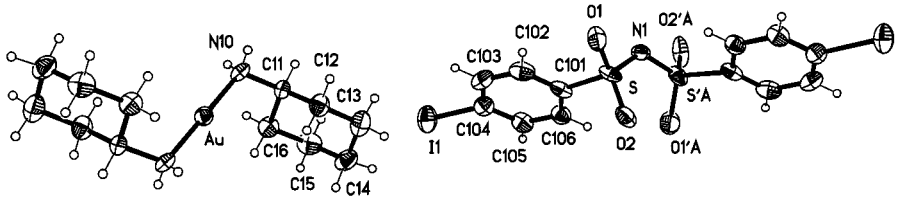


Figure 13. Bis(cyclohexylamine)gold(I) bis(*p*-iodobenzenesulfonyl)amide (**8**); asymmetric unit with numbering scheme; thermal ellipsoids are shown with 50% probability; hydrogen radii are arbitrary; dashed lines represent hydrogen bonds; only one position of the disordered anion is shown

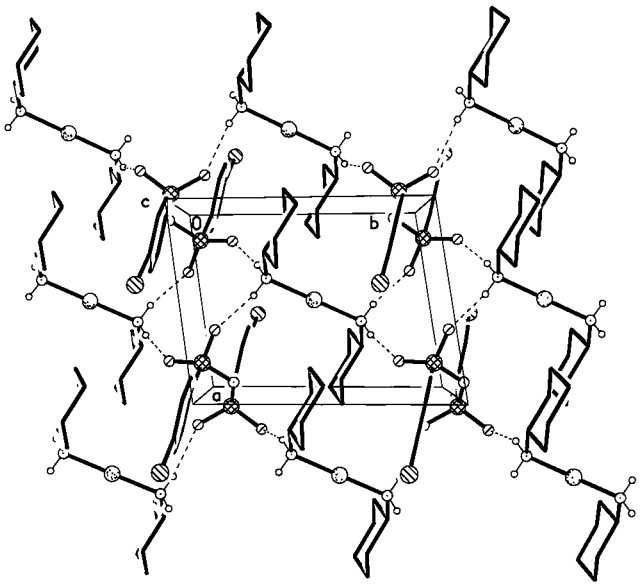


Figure 14. Bis(cyclohexylamine)gold(I) bis(*p*-iodobenzenesulfonyl)amide (**8**); layer structure; atom radii are arbitrary; dashed lines represent hydrogen bonds (Table 7); carbon-bonded hydrogen atoms are omitted for clarity; only one position of the disordered anion is shown

Table 9. Selected bond lengths and angles for **8**

Au−N10	203.4(5)	N1−S	156.9(9)
N1−S′[xxiv] [a]	157.1(9)	S−O2	143.9(9)
S−O1	144.1(10)	S−C101	177.4(11)
S′−O2′	145.6(10)	S′−O1′	146.0(9)
S′−C101	179.1(11)	C104−I1	210.2(6)
N10−Au−N10[ii]	180.0(3)	C11−N10−Au	119.3(3)
S−N1−S′[xxiv]	127.2(7)	O2−S−O1	117.2(8)
N1−S−C101	104.0(6)	O2′−S′−O1′	114.4(8)
N1[xxiv]−S′−C101	111.5(6)		

Symmetry transformations for equivalent atoms: xxiv: $-x, -y, -z + 2$; ii: $-x + 1, -y + 1, -z$.

Table 10. Selected C−H···O hydrogen bonds, with H···O < 2.7 Å, not normalised

Compound	Bond	H···O [Å]	C···O [Å]	C−H···O [°]
1	C1−H1C···O8[iv] [a]	2.41	3.295(14)	150
	C33−H33···O4[xv]	2.66	3.36(2)	128
2	C2−H2E···O4[v]	2.50	3.209(4)	129
	C15−H15···O4[xvi]	2.69	3.453(4)	138
3	C22−H22···O2	2.44	3.339(19)	158
4	C1−H1B···O3[x]	2.41	3.288(3)	149
	C1−H1C···O1[xvii]	2.64	3.453(2)	141
	C2−H2A···O2[xviii]	2.63	3.489(4)	146
	C12−H12A···O4	2.69	3.312(3)	121

[a] Operators: xv: $-x, 2 - y, 1 - z$; xvi: $x, y + 1, z$; xvii: $x, y - 1, z$; xviii: $-x, -y, -z$. For operators up to xiv, see Table 7.

We thus conclude that the packing influence of the cation, as exercised through the NH functions of the ligands, is greater than that of the anion.

Experimental Section

General: NMR spectra were measured with a Bruker AC 200 spectrometer in $CDCl_3$ solution with TMS as the internal standard (if not otherwise stated). Frequencies: 200.1 MHz (^{1}H), 50.3 MHz (^{13}C). − Mass spectra were recorded with a Finnigan MAT 8430. − All complexes were prepared as follows: 0.5 mmol of $L_2Au^+Cl^-$

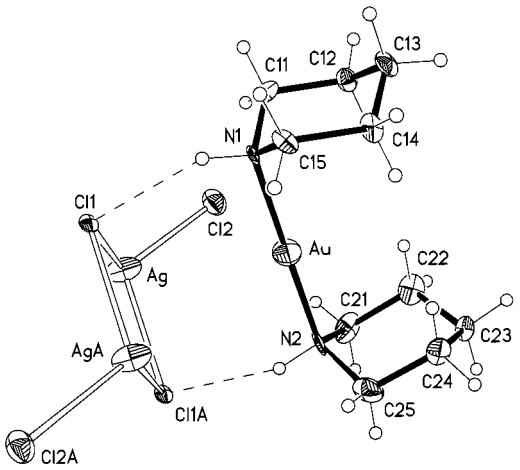


Figure 15. Bis(piperidine)gold(I) dichloroargentate(I), **9**, asymmetric unit with numbering scheme, extended by one $AgCl_2^-$ unit; thermal ellipsoids are shown with 50% probability; hydrogen radii are arbitrary; dashed lines represent hydrogen bonds

Table 11. Selected bond lengths and angles for **9**

Au−N2	209.8(11)	Au−N1	210.4(10)
Ag−Cl2	259.8(4)	Ag−Cl2[xxv]	260.2(4)
Ag−Cl1[xiv]	262.9(3)	Ag−Cl1	263.1(3)
Ag···Ag[xxv] [a]	313.1(2)		
N2−Au−N1	179.3(4)	C(11)−N(1)−C(15)	110.5(9)
C11−N1−Au	113.6(8)	C15−N1−Au	112.7(7)
C21−N2−C25	108.8(10)	C21−N2−Au	114.8(10)
C25−N2−Au	113.7(10)	Cl2−Ag−Cl2[xxv]	105.95(10)
Cl2−Ag−Cl1[xiv]	113.31(12)	Cl2[xxv]−Ag−Cl1[xiv]	113.73(12)
Cl2−Ag−Cl1	113.78(11)	Cl2[xxv]−Ag−Cl1	113.28(12)
Cl1[xiv]−Ag−Cl1	96.96(9)	Ag[xiv]−Cl1−Ag	83.04(9)
Ag−Cl2−Ag[xxv]	74.05(10)		

[a] Symmetry transformations for equivalent atoms: xxv: $-x + 2, -y + 3, -z + 1$; xiv: $-x + 1, -y + 3, -z + 1$.

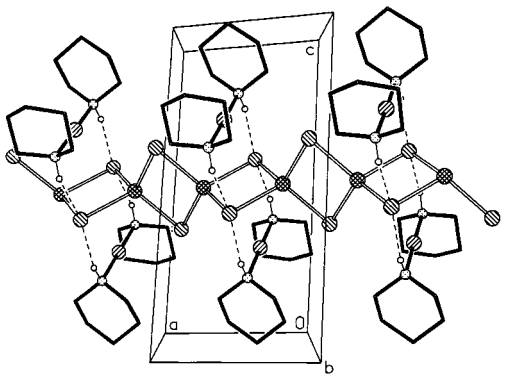


Figure 16. Bis(piperidine)gold(I) dichloroargentate (**9**); chain structure; atom radii are arbitrary; dashed lines represent hydrogen bonds (Table 7); carbon-bonded hydrogen atoms are omitted for clarity

(L = amine) was suspended in acetonitrile (10 mL). The silver salt of the disulfonylamide, kindly provided by Prof. A. Blaschette, TU Braunschweig, was added in 10% excess (0.55 mmol). The reaction mixture was stirred for 2 h at room temperature with exclusion of light. The precipitated AgCl was filtered off and washed with acetonitrile. The combined solutions were concentrated in vacuo and the white residue was recrystallised from CH_2Cl_2/petroleum ether (40:60) to obtain colourless crystals.

Bis(cyclohexylamine)gold(I) Bis(methanesulfonyl)amide (1): Yield 59%, dec. > 123 °C. − ^{1}H NMR ($CDCl_3$): δ = 1.29, m, 10 H, CH_2 (ax.); 1.66, m, 2 H, 4-CH_2 (eq.); 1.80, m, 4 H, 3-, 3′-CH_2 (eq.); 2.08, m, 4 H, 2-, 2′-CH_2 (eq.); 3.00, m, 2 H, CH; 3.08, s, 6 H, CH_3; 4.5, br., NH_2. − MS (FAB pos.): *m*/*z* = 395 (100% $[K]^+$); MS (FAB neg.): *m*/*z* = 172 (100% $[A]^-$). − Conductivity: Λ_c = 79 cm^2 Ω^{-1} mol^{-1}. − $C_{14}H_{32}AuN_3O_4S_2$ (567.52): calcd. C 29.63, H 5.68, N 7.40, S 11.30; found C 27.26, H 5.44, N 7.09, S 12.74.

Bis(benzylamine)gold(I) Bis(methanesulfonyl)amide (2): Yield 76%, dec. > 109°C. − ^{1}H NMR ($CDCl_3$): δ = 2.87, s, 6 H, CH_3; 3.96, br., 4 H, CH_2; 4.68, br., 4 H, NH_2; 7.32, m, 20 H, Ph. − $C_{16}H_{24}AuN_3O_4S_2$ (583.48): calcd. C 32.94, H 4.15, N 7.20, S 10.99; found C 33.03, H 4.21, N 7.29, S 11.03.

Bis(3-iodobenzylamine)gold(I) Bis(methanesulfonyl)amide (3): Dec. > 108°C. − ^{1}H NMR ($CDCl_3$): δ = 2.95, s, 6 H, CH_3; 4.11, s, 4 H, CH_2; 7.48, m, 8 H, Ph. − $C_{16}H_{22}AuI_2N_3O_4S_2$ (835.28): calcd. C 23.00, H 2.66, N 5.03, S 7.68; found C 22.94, H 2.61, N 4.82, S 7.61.

Bis(morpholine)gold(I) Bis(methanesulfonyl)amide (4): Yield 41%, dec. > 50°C. − ^{1}H NMR ($CDCl_3$): δ = 3.05, s, 6 H, CH_3; 3.27, m, 8 H, α-CH_2; 3.86, m, 12 H, β-CH_2. − $C_{10}H_{24}AuN_3O_6S_2$ (543.42): calcd. C 22.10, H 4.45, N 7.73, S 11.80; found C 21.39, H 4.33, N 7.43, S 10.86.

Bis(pyrrolidine)gold(I) Bis[bis(methanesulfonyl)amido-*N*]argentate(I) (5): Yield 81%, dec. > 104 °C. − ^{1}H NMR ($CDCl_3$): δ = 1.87, m, 8 H, β-CH_2; 2.99, m, 4 H, α-CH_2; 3.12, s, 12 H, CH_3; 3.54, m, 4 H, α-CH_2. − MS (FAB pos.): *m*/*z* = 72 (18% $[K\text{-}C_4H_8NAu]^+$); 339 (100% $[K]^+$); MS (FAB neg.): *m*/*z* (%) = 172 (100) $[A - C_2H_6AgO_4S_2]^-$; 450 (52) $[A - H]^-$; 452 (58) $[A + H]^-$. − $C_{12}H_{30}AgAuN_4O_8S_4$ (791.49): calcd. C 18.21, H 3.82, N 7.08 S, 16.21; found C 17.28, H 3.74, N 6.78, S 17.38.

Bis(cyclohexylamine)gold(I) *o*-Benzenedisulfonylamide (6): Yield 57%, dec. > 73°C. − ^{1}H NMR ($CDCl_3$): δ = 1.22, m, 10 H, CH_2 (ax.); 1.58, m, 2 H, 4-CH_2 (eq.); 1.73, m, 4 H, 3-, 3′-CH_2 (eq.); 2.02, m, 4 H, 2-, 2′-CH_2 (eq.); 3.08, m, 2 H, CH; 4.4, br., NH_2, 5.30, s, 2 H, CH_2Cl_2; 7.71, m, 2 H, β-Ph; 7.86, m, 2 H, α-Ph. − MS (FAB pos.): *m*/*z* (%) = 100 (100) $[K - C_6H_{12}NAu]^+$; 395 (71) $[K]^+$; MS (FAB neg.): *m*/*z* (%) = 218 (100) $[A]^-$. − $C_{18}H_{30}AuN_3O_4S_2$ (613.55) × 0.75 CH_2Cl_2: calcd. C 33.25, H 4.69, N 6.20, S 9.47; found C, 33.24 H, 4.65 N 6.25, S 10.90.

Bis(cyclohexylamine)gold(I) Bis(*p*-chlorobenzenesulfonyl)amide (7): Yield 57%, dec. > 88°C. ^{1}H NMR ([D$_6$]DMSO): δ = 1.17, m, 10 H, CH_2 (ax.); 1.58, m, 2 H, 4-CH_2 (eq.); 1.70, m, 4 H, 3-, 3′-CH_2 (eq.); 1.96, m, 4 H, 2-, 2′-CH_2 (eq.); 2.81, m, 2 H, CH; 5.4, br., NH_2; 7.42, m, 4 H, *m*-Ph; 7.63, m, 4 H, *o*-Ph. − MS (FAB pos.): *m*/*z* (%) = 100 (44) $[K - C_6H_{12}NAu]^+$; MS (FAB neg.): *m*/*z* (%) = 363 (100) $[A - H]^-$. − $C_{24}H_{34}AuCl_2N_3O_4S_2$ (760.56): calcd. C 37.90, H 4.51, N 5.52, Cl 9.32, S 8.43; found C 32.30, H 4.05, N 4.58, Cl 10.73, S 8.14.

Bis(cyclohexylamine)gold(I) Bis(*p*-iodobenzenesulfonyl)amide (8): Yield: very low (few crystals), dec. > 97°C. − $C_{24}H_{34}AuI_2N_3O_4S_2$ (943.49): calcd. C 30.55 H 3.63 N 4.45 S 6.80; found C 26.77 H 2.52 N 2.91 S 6.84.

Bis(piperidine)gold(I) Dichloroargentate(I) (9): Compound **9** was unexpectedly obtained following the general procedure using (piperidine)$_2$AuCl and $AgNMs_2$. − Yield: very low (few crystals), dec. > 87°C. − ^{1}H NMR ($CDCl_3$): δ = 1.76, br., 4 H, α-CH_2; 3.24, 6 H, β-, γ-CH_2. − $C_{10}H_{22}AgAuCl_2N_2$ (546.04): calcd. C 22.00, H 4.06, N 5.13; found C 22.58, H 4.24, N 5.11.

X-ray Structure Determinations: For crystal data, see Table 12 and Table 13. − *Data collection and reduction*: The crystals were mounted in inert oil on a glass fibre. Data were measured using Mo-K_α radiation (λ = 0.71073 Å) with a Siemens P4 diffractometer (**1**, **5**, **6**, **8**) or a Bruker Smart area detector (**2**, **3**, **4**, **9**), fitted with an LT-2 (P4) or LT-3 (Smart) low-temperature attachment. Semi-empirical absorption corrections were based on ψ-scans (XEMP) or on multiple scans (SADABS). *Structure solution and refinement*: Structures were solved by direct (**3**, **5**, **8**, **9**) or Patterson (**1**, **2**, **4**, **6**) methods and subjected to full-matrix least-squares refinement on F^2 (program SHELXL-97).[28] All non-hydrogen atoms were refined anisotropically. Hydrogen atoms were included using rigid methyl groups or a riding model, except that those bonded to a nitrogen atom were refined freely in **4** and with restrained bond lengths in **8**. For several structures (see Table 12 and 13), particularly the disordered **5** and **8**, an extensive system of restraints to displacement parameters was employed to improve refinement stability of light atoms in the presence of gold. The Flack *x* parameter for the non-centrosymmetric structure **5** refined to −0.001(7).[29] The complete cation of **5** is disordered over two positions with occupation factors 0.37 (unprimed atoms) and 0.63 (primed atoms). The gold and silver atom positions correspond closely to space group *Aba*2, in which a doubly disordered model can also be refined, but too many reflections are observed that should be systematically absent. By lowering the symmetry, it was hoped to find an ordered model, but this proved impossible even in *P*1. It is unlikely that X-ray methods alone can resolve the space group ambiguity. The central $N(SO_2)_2$ moiety of the anion of **8** is disordered over two positions with occupation factors 0.5. Clearly the dimensions of both disordered structures should be interpreted with caution. The high *R* values and high residual electron densities of structures **3** and **9** may be attributed to poor crystal quality, and unsatisfactory absorption correction with SADABS, associated with extreme crystal forms (thin plate, needle).

Crystallographic data (excluding structure factors) have been deposited with the Cambridge Crystallographic Data Centre

Table 13. Crystallographic data

Compound	**1**	**2**	**3**	**4**
Formula	$C_{14}H_{32}AuN_3O_4S_2$	$C_{16}H_{24}AuN_3O_4S_2$	$C_{16}H_{22}AuI_2N_3O_4S_2$	$C_{10}H_{24}AuN_3O_6S_2$
M_r	567.51	583.47	835.25	543.41
Crystal habit	Colourless plate	Colourless prism	Colourless plate	Colourless prism
Crystal size [mm]	0.24×0.20×0.04	0.19×0.07×0.05	0.20×0.08×0.01	0.29×0.12×0.09
Crystal system	Triclinic	Triclinic	Triclinic	Triclinic
Space group	$P-1$	$P-1$	$P-1$	$P-1$
Cell dimensions				
a [Å]	11.227(3)	9.6578(10)	8.978(14)	5.8123(6)
b [Å]	13.649(4)	10.5065(12)	9.084(15)	9.5145(10)
c [Å]	14.550(4)	11.3968(12)	15.556(18)	15.5486(16)
α [°]	105.62(2)	65.651(2)	74.49(7)	88.212(2)
β [°]	107.30(2)	73.539(2)	73.95(7)	82.518(2)
γ [°]	93.915(19)	74.447(2)	76.53(8)	89.669(2)
V [Å^3]	2023.2(10)	995.12(19)	1157(3)	852.12(15)
Z	4	2	2	2
D_x [Mg m^{-3}]	1.863	1.947	2.397	2.118
μ [mm^{-1}]	7.500	7.628	9.229	8.907
F(000)	1120	568	776	528
T [°C]	−100	−130	−130	−130
$2\theta_{max}$ [°]	50	61	57	61
Transmission	0.30−0.86	0.58−0.96	0.66−0.96	0.41−0.70
No. of reflections				
Measured	6958	12254	12367	10503
Independent	6919	6004	5839	5140
R_{Int}	0.023	0.049	0.099	0.038
Parameters	458	237	255	209
Restraints	550	16	142	0
$wR2(F^2$, all refl.)	0.135	0.055	0.196	0.049
$R1[F>2\sigma(F)]$	0.053	0.027	0.077	0.021
S	0.91	0.98	1.02	1.02
Max. Δ/σ	< 0.001	0.002	< 0.001	0.001
Max. Δρ [eÅ^{-3}]	1.41	1.89	4.36	1.21

Table 13. *(Continued)*

Compound	**5**	**6**	**8**	**9**
Formula	$C_{12}H_{30}AgAuN_4O_8S_4$	$C_{19.5}H_{33}AuCl_3N_3O_4S_2$	$C_{24}H_{34}AuI_2N_3O_4S_2$	$C_{10}H_{22}AgAuCl_2N_2$
M_r	457.33	740.93	943.43	546.03
Crystal habit	Colourless tablet	Colourless plate	Colourless plate	Colourless needle
Crystal size [mm]	0.60×0.30×0.10	0.24×0.14×0.04	0.40×0.40×0.03	0.30×0.03×0.02
Crystal system	Orthorhombic	Monoclinic	Triclinic	Triclinic
Space group	$Pna2_1$	$C2/m$	$P-1$	$P-1$
Cell dimensions				
a [Å]	18.545(2)	12.572(2)	6.6744(6)	6.618(3)
b [Å]	15.970(2)	13.593(3)	8.6880(8)	9.394(4)
c [Å]	8.221(2)	15.988(3)	13.2291(12)	13.250(6)
α [°]	90	90	81.622(8)	104.488(10)
β [°]	90	98.301(16)	80.386(8)	90.033(10)
γ [°]	90	90	80.471(8)	110.571(8)
V [Å^3]	2434.9(7)	2703.7(10)	740.39(12)	743.1(5)
Z	4	4	1	2
D_x [Mg m^{-3}]	2.159	1.820	2.166	2.440
μ [mm^{-1}]	7.209	5.923	7.227	11.515
F(000)	1536	1460	448	512
T [°C]	−100	−74	−100	−130
$2\theta_{max}$ [°]	50	50	50	57
Transmission	0.37−0.95	0.58−0.89	0.24−0.86	0.74−0.96
No. of reflections				
Measured	7094	2521	5179	8050
Independent	4132	2406	2589	3753
R_{Int}	0.028	0.058	0.019	0.076
Parameters	373	156	204	145
Restraints	548	96	208	0
$wR2(F^2$, all refl.)	0.106	0.087	0.076	0.219
$R1[F>2\sigma(F)]$	0.043	0.047	0.029	0.074
S	1.07	0.83	0.98	1.05
Max. Δ/σ	0.001	0.001	< 0.001	< 0.001
Max. Δρ [eÅ^{-3}]	0.97	1.39	1.05	5.6

under the numbers CCDC-138802−138809. Copies may be obtained without charge from: CCDC, Union Road, Cambridge CB2 1EZ, UK [Fax: internat. + 44-1223/336-033; E-mail: deposit@ccdc.cam.ac.uk].

Acknowledgments

We thank the Fonds der Chemischen Industrie (Frankfurt) for financial support and Mr. A. Weinkauf for technical assistance.

[1] B. Ahrens, P. G. Jones, A. K. Fischer, *Eur. J. Inorg. Chem.* **1999**, 1103−1110.
[2] [2a] H. Schmidbaur, *Gold Bull.* **1990**, *23*, 11−21. − [2b]H. Schmidbaur, *Chem. Soc. Rev.* **1995**, 391−400.
[3] B. Ahrens, P. G. Jones, *Z. Naturforsch., Sect. B* **1999**, *54*, 1474−1477.
[4] P. G. Jones, B. Ahrens, *Z. Naturforsch., Sect. B* **1998**, *53*, 653−662.
[5] J. J. Guy, P. G. Jones, M. J. Mays, G. M. Sheldrick, *J. Chem. Soc., Dalton Trans.* **1977**, 8−10.
[6] H. N. Adams, W. Hiller, J. Strähle, *Z. Anorg. Allg. Chem.* **1982**, 485, 81−91.
[7] P. G. Jones, M. Freytag, *Chem. Commun.* **2000**, 277−278.
[8] P. G. Jones, B. Ahrens, *Chem. Ber.* **1997**, *130*, 1813−1814.
[9] J. H. K. Yip, R. Feng, J. J. Vittal, *Inorg. Chem.* **1999**, *38*, 3586−3589.
[10] A. Bondi, *J. Phys. Chem.* **1964**, *68*, 441−451.
[11] S. S. Panthaneni, G. R. Desiraju, *J. Chem. Soc., Dalton Trans.* **1993**, 319−322.
[12] A. Burini, J. P. Fackler, Jr., R. Galassi, B. R. Pietroni, R. J. Stapler, *Chem. Commun.* **1998**, 95−96.
[13] M. Contel, J. Garrido, M. C. Gimeno, M. Laguna, *J. Chem. Soc., Dalton Trans.* **1998**, 1083−1084.
[14] R. E. Marsh, V. Schomaker, F. H. Herbstein, *Acta Crystallogr., Sect. B* **1998**, *54*, 921−924.
[15] M. Näveke, P. G. Jones, A. Blaschette, D. Schomburg, H. K. Cammenga, M. Epple, *Z. Anorg. Allg. Chem.* **1993**, *619*, 1027−1036.
[16] A. Blaschette, P. G. Jones, T. Hamann, M. Näveke, D. Schomburg, H. K. Cammenga, M. Epple, I. Steppuhn, *Z. Anorg. Allg. Chem.* **1993**, *619*, 912−922.
[17] A long series of dimesylamide structures has been published by Prof. A. Blaschette and co-workers; for a recent example, see: K. Wijaya, O. Moers, A. Blaschette, P. G. Jones, *Z. Naturforsch., Sect. B* **1999**, *54*, 1441−1449.
[18] J. Bernstein, R. E. Davis, L. Shimoni, N.-L. Chang, *Angew. Chem.* **1995**, *107*, 1689−1708; *Angew. Chem. Int. Ed. Engl.* **1995**, *34*, 1545−1554.
[19] P. G. Jones, T. Hamann, A. Blaschette, H. K. Cammenga, M. Epple, *Z. Anorg. Allg. Chem.* **1993**, *619*, 1441−1445.
[20] O. Moers, A. Blaschette, P. G. Jones, *Acta Crystallogr., Sect. C* **1997**, *53*, 845−848.
[21] I. Hippel, P. G. Jones, A. Blaschette, *J. Organotmet. Chem.* **1993**, *448*, 63−67.
[22] S. Friedrichs, P. G. Jones, *Acta Crystallogr., Sect. C*, in press.
[23] [23a] G. A. Jeffrey, *J. Mol. Struct.* **1999**, *485−486*, 293−298. − [23b] T. Steiner, *New J. Chem.* **1998**, 1099−1103. − [23c] G. R. Desiraju, T. Steiner, *The Weak Hydrogen Bond*, Oxford University Press, Oxford, **1999**.
[24] F. H. Allen, O. Kennard, *Chem. Des. Autom. News* **1993**, *8*, 31−37.
[25] G. Helgesson, M. Josefsson, S. Jagner, *Acta Crystallogr., Sect. C* **1988**, *44*, 1729−1731.
[26] D. Hogerle, V. Link, U. Thewalt, *Z. Naturforsch., Sect. B* **1993**, *48,* 691−693.
[27] P. G. Jones, B. Ahrens, *Eur. J. Org. Chem.* **1998**, 1687−1688.
[28] G. M. Sheldrick, *SHELXL-97, Program for crystal structure refinement*, University of Göttingen, **1997**.
[29] H. D. Flack, *Acta Crystallogr., Sect. A* **1983**, *39*, 876−881.
[30] T. Steiner, *Acta Crystallogr. Sect. B* **1998**, *54*, 456−463.

Received March 14, 2000
[I00096]

Reactions of Sodium-Potassium Alloys with Inert Gas Impurities − Potential Hazards after Oxidation

Jacqueline Desreumaux,*[a] Marielle Calais,[a] René Adriano,[a] Serge Trambaud,[a] Charles Kappenstein,[b] and Marcel Nguefack[b]

Keywords: FBR Chemistry / Oxidations / Sodium / Potassium / Alloys

A bibliographical study of the reactions of NaK alloys with their oxides did not explain the related accidents that have occurred in the past, particularly those involving the handling of bubblers installed to remove traces of oxygen and water vapor from blanket gases of LMFR (liquid metal fast reactors). Moreover, it revealed a controversy with respect to the explosive hazard of the NaK alloys + KO_2 reaction. A thermodynamic study of the reaction of a NaK alloy with oxygen as well as experimental work on mixtures containing NaK and different oxides (KO_2, Na_2O, Na_2O_2) led to the conclusion that violent reactions occurring at ambient temperature, were always linked to the presence of hydrated superoxides or hydroxides. On contact with NaK alloys, these hydrated compounds lead to the formation of hydrogen with a release of heat causing the decomposition of potassium superoxide KO_2 and the simultaneous release of oxygen. The oxidation of liquid NaK alloy, by bubbling a mixture of argon and air containing traces of water vapor ($H_2O < 5$ vpm), leads to the formation of mainly KO_2, besides the hydrated compounds $Na_2O_2{\cdot}2H_2O$, $NaOH{\cdot}H_2O$ and $KOH{\cdot}H_2O$. The gas follows preferential paths and the product obtained is highly heterogeneous in both composition and hardness (porous parts and dense parts). Hydrated superoxide and hydroxides treated under vacuum result in nearly quantitative dehydration after heating at 100 °C. For storage elements or safety valves, containing NaK that has been submitted to slow surface oxidation and hydration, the oxidized layer contains KO_2, $Na_2O_2{\cdot}nH_2O$ and hydrated hydroxides of sodium and potassium. In order to avoid any hazard due to the contact of the oxides with the residual NaK alloy during transport or under impact, it is necessary to freeze the alloy and to reheat it very slowly. Operations such as draining should also be performed slowly, after having calibrated the tanks (temperature and pressure). Therefore the use of NaK liquid alloy to purify gases is questionable; as preferential paths are established, it remains impossible to predict the period of efficiency of a bubbler. Moreover, the NaK alloy does not chemically transform all traces of water vapor; because some remains present in the form of hydrated products, leading to the formation of wastes with a potential hazard during storage or destruction. In our opinion, this method of purification should be abandoned.

Introduction

NaK alloys are liquids at room temperature and this peculiarity explains their common use in the nuclear industry:[1] coolants for fast neutron reactors, fluids in heat transfer systems, gas purifiers, moving barriers of pressure in safety valves, filling liquids of acoustic wave-guides in sonar systems. Nevertheless several accidents due to explosions have been described concerning the use or during storage of NaK alloys or even potassium alone. These accidents have been reviewed,[2] but no clear explanations were given concerning the possible chemical reactions leading to these explosions, although the influence of some of the oxidized products of the alloy seems to be a key factor.

A bibliographical study of the reactions of NaK alloys with their oxides remained scarce and did not allow for the explanation of all related accidents, particularly those linked to the handling of bubblers. Moreover, they revealed a controversy with respect to the NaK + KO_2 reaction, considered explosive by Sloan and Whitby[3] and harmless by Commander.[4] More recent laboratory tests[5,6] did not confirm the explosion hazard linked to the NaK + KO_2 reaction.

In order to have a better understanding of the reaction leading to the potential explosion due to the storage and destruction of NaK wastes, the present study was undertaken with the following objectives:

(i) to review the structural data of the different oxides of sodium and potassium;

(ii) to perform a thermodynamic analysis to obtain further knowledge on the formation of various sodium and potassium oxides and their identification and reactivity;

(iii) to carry out experimental work on different mixtures to confirm literature data concerning the melting and decomposition temperatures of various sodium and potassium oxides and to characterize these products using differential scanning calorimetry, mass spectrometry and X-ray diffraction;

(iv) to study the stability of a mixture of NaK liquid alloy with sodium oxide Na_2O, sodium peroxide Na_2O_2 or potassium superoxide KO_2, using differential calorimetry, mass spectrometry and tests in glove box; and finally

[a] CEA/DRN/DER/STPI/LPCP, CE Cadarache,
13108 Saint-Paul-lez-Durance, France
E-mail: desreumaux@drncad.cea.fr
[b] UMR CNRS 6503, Equipe de Catalyse par les Métaux; Faculté des Sciences,
40 Avenue du Recteur Pineau; 86022 - Poitiers, France
E-mail: Charles.Kappenstein@campus.univ-poitiers.fr

 © WILEY-VCH Verlag GmbH, D-69451 Weinheim, 2000 1434−1948/00/0909−2031 $ 17.50+.50/0

(v) to define as precisely as possible the conditions for a potential hazard.

The NaK alloy used for the tests was NaK-56 (56 wt-% K) which corresponds to the composition of the NaK alloy used for the cold traps of the Superphenix Reactor.

Finally, NaK oxidation tests have been performed through sweeping or bubbling of argon and dry air containing H_2O or CO_2 as impurities, in order to simulate realistic conditions of oxide formation and to characterize the products thus formed. The results will permit the proposal of new explanations concerning the accidents or incidents linked to the use of bubblers.

Results and Discussion

1. Structural Data

Structural data, density, molar volume and PDF references are gathered in Table 1 for the compounds: Na, K, KNa_2, K_2O, K_2O_2, KO_2, Na_2O, Na_2O_2, NaO_2, $Na_2O_2{\cdot}2H_2O$, $Na_2O_2{\cdot}8H_2O$. From this table the following conclusions can be obtained:

(i) The molar volume of the oxides is smaller than the molar volume of the metals or alloys, therefore the oxides cannot afford a protection against further oxidation.

(ii) Sodium peroxide presents hydrated phases.

(iii) The structure of Na_2O and K_2O are identical.

(iv) The other oxides display different structural data which means that there is no possibility of extended solid solutions.

2. Phase Diagram

The Na-K phase diagram is given in Figure 1.[7] Despite the identical structures of Na and K metals, the solubility in the solid state remains low (< 5% in atoms) which is in agreement with the rather high difference in metallic radii (1.86 Å for Na and 2.30 Å for K); the solubility curves are represented by dotted lines because the solubility limits are not precisely known. Only one stoichiometric compound Na_2K is present on this diagram, with a non-congruent melting point. Recent theoretical analyses of the liquid curves[8] and of the sodium-potassium eutectic,[9] agree with the experimental diagram. The vertical line corresponding to the NaK-56 alloy cuts the liquid curve and the eutectic segment at 5 and −12.5 °C, respectively. It can be noted that the real alloy composition is not constant and is dependent on the lot and storage conditions. It may vary from 56 to 52 weight% in K, corresponding to 43 to 39 atom%.

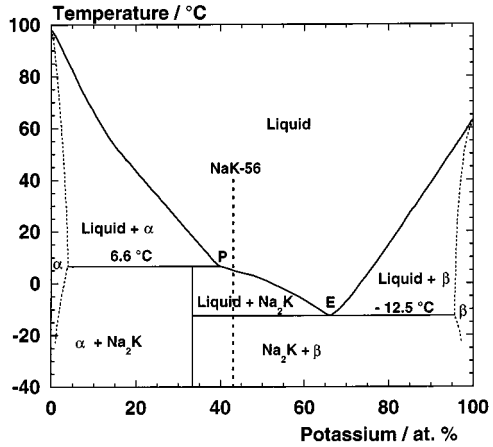


Figure 1. Sodium-potassium liquid solid phase diagram. The diagram was numerized from the figures given in ref.[7]

3. Thermodynamic Analysis

3.1. Formation of Liquid Alloy

The formation of the liquid NaK-56 alloy corresponds to the reaction:

$$0.57\ \mathrm{Na(s\ or\ l)} + 0.43\ \mathrm{K(s\ or\ l)} = \mathrm{Na_{0.57}K_{0.43}(l)} \quad (1)$$

Table 1. Crystallographic data and molar volumes

Phase	PDF file number	Molar wt g mol^{-1}	Crystal system and lattice	Formula unit number	Volume Å^3	Density g cm^{-3}	Molar vol. cm^3 mol^{-1}
METALS AND ALLOYS							
K	01−500	39.1	Cubic, I	$Z = 2$	140.6	0.86	45.5
Na	22−948	23.0	Cubic, I	$Z = 2$	79.0	0.97	23.7
KNa_2	10−244	85.1	Hexagonal, P	$Z = 4$	594.5	0.95[a]	29.9
POTASSIUM COMPOUNDS							
K_2O	23−493	94.2	Cubic, F	$Z = 4$	268.2	2.33[a]	20.2
K_2O_2	32−827	110.2	Orthorhombic, C	$Z = 4$[b]	305.0	2.40[a]	23.0
KO_2	43−1020	71.1	Tetragonal, I	$Z = 2$	109.0	2.16	32.9
KOH	21−645	56.1	Monoclinic, P	$Z = 2$	87.2	2.14[a]	26.2
$KOH{\cdot}H_2O$	36−791	74.1	Monoclinic, P	$Z = 4$	254.9	1.92	38.6
SODIUM COMPOUNDS							
Na_2O	23−528	62.0	Cubic, F	$Z = 4$	171.9	2.27	13.7
Na_2O_2	09−075	78.0	Hexagonal, P	$Z = 3$	149.8	2.50	15.6
NaO_2	6−500	55.0	Orthorhombic, P	$Z = 2$	81.2	2.25[a]	24.4
$Na_2O_2{\cdot}2H_2O$	15−064	114.0					
$Na_2O_2{\cdot}8H_2O$	15−032	222.1	Monoclinic, C	$Z = 4$[b]	929.1		
NaOH	35−1009	40.0	Orthorhombic, C	$Z = 4$	131.7	2.02[a]	19.8
$NaOH{\cdot}H_2O$	30−1194	58.0	Orthorhombic, P	$Z = 8$	447.9	1.72[a]	33.7

[a] Calculated. − [b] Assumption.

The use of a liquid NaK alloy requires the knowledge of the values of the standard thermodynamic functions H, S and G for this alloy. The enthalpies of mixing versus the composition have been determined at 111 ± 2 °C from liquid sodium and potassium, by Yokokawa and Kleppa.[10] From these data, the authors concluded that the behavior is close to ideality for alloys with a sodium mol fraction x_{Na} higher than 0.5. The work of Cafasso et al.[11] on the determination of the excess Gibbs energies of mixing was performed at the same temperature in order to obtain the activities and activity coefficients of sodium and potassium for such alloys. Their results agree well with the previous conclusion on the range of ideality. From these data and the thermodynamic data of Na and K at 111 °C, it was possible to obtain the thermodynamic values for the formation of $Na_{0.57}K_{0.43}$(l), as well as the data for the reactants and product at the same temperature (reference temperature 25 °C):

$\Delta_r H° = 0.748$ kJ mol^{-1} $\Delta_r S° = 5.604$ J K^{-1} mol^{-1}
$\Delta_r G° = -1.404$ kJ mol^{-1}
for 0.57 Na(l) + 0.43 K(l):
$H°_{384} = 5.085$ kJ mol^{-1} $S°_{384} = 71.77$ J K^{-1} mol^{-1}
for $Na_{0.57}K_{0.43}$(l):
$H°_{384} = 5.833$ kJ mol^{-1} $S°_{384} = 77.37$ J K^{-1} mol^{-1}

The standard data at 25 °C were calculated from the melting enthalpies, melting entropies and constant pressure heat capacities for Na and K. The heat capacity of the liquid alloy was estimated from the heat capacities of liquid sodium (31.83 J K^{-1} mol^{-1} at 98 °C) and liquid potassium (32.14 J K^{-1} mol^{-1} at 63 °C) which change very slowly with temperature. The data for the formation of $Na_{0.57}K_{0.43}$(l) at 25 °C are:

$\Delta_r H° = 3.113$ kJ mol^{-1} $\Delta_r S° = 12.20$ J K^{-1} mol^{-1}
$\Delta_r G° = -0.514$ kJ mol^{-1}
for 0.57 Na(s) + 0.43 K(s):
$H°_{298} = 0$ kJ mol^{-1} $S°_{298} = 57.14$ J K^{-1} mol^{-1}
for $Na_{0.57}K_{0.43}$(l):
$H°_{298} = 3.113$ kJ mol^{-1} $S°_{298} = 69.34$ J K^{-1} mol^{-1}

The formation of the alloy is endothermic and the driving force is the entropy factor. These values are in agreement with different theoretical calculations using the pseudo-potential model applied to hard sphere mixtures.[12–15]

In comparison with the values calculated for the different oxidation reactions (vide infra), the data given above are lower by two to three orders of magnitude, therefore the corrections needed for the substitution of the pure metals by the liquid alloy can reasonably be neglected.

3.2. Sodium-Oxygen System

Figure 2 represents the Ellingham diagram (Gibbs energy versus temperature) for the formation of the oxygenated compounds of sodium according to the equations:

$$4\ Na(s\ ou\ l) + O_2(g) = 2\ Na_2O(s)\quad \Delta_r G°_{298} = -758\ kJ\ mol^{-1} \quad (2)$$

$$2\ Na_2O(s) + O_2(g) = 2\ Na_2O_2(s)\quad \Delta_r G°_{298} = -141\ kJ\ mol^{-1} \quad (3)$$

$$Na_2O_2(s) + O_2(g) = 2\ NaO_2(s)\quad \Delta_r G°_{298} = +12\ kJ\ mol^{-1} \quad (4)$$

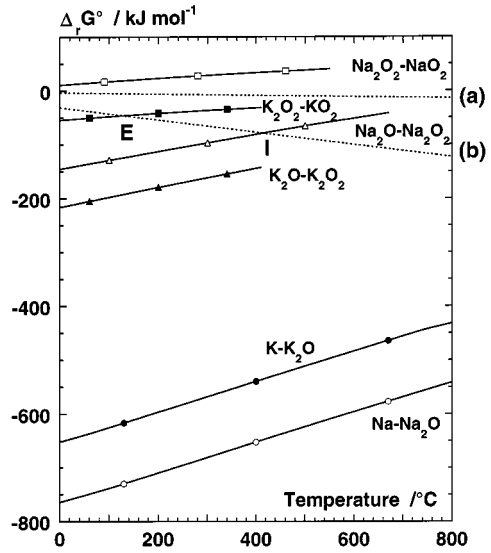


Figure 2. Ellingham diagram for the successive formation of oxygenated compounds of sodium (white points) and potassium (black points). The dotted lines represent the free enthalpy of dioxygen for a partial pressure of (a) 0.2 bar and (b) 10^{-6} bar. E and I are the crossing points between line (b) and the formation curves of KO_2 and Na_2O_2

This diagram shows that in the presence of excess sodium, the stable product is Na_2O, therefore, metallic sodium will reduce the higher oxides. The presence of an excess of oxygen leads to the formation of a stable peroxide, Na_2O_2, at atmospheric pressure. For the sodium superoxide NaO_2, the corresponding values are positive, implying that this compound is only stable under high oxygen pressure.

Figure 2 also represents the variations of the Gibbs energy of gaseous oxygen for the partial pressure of O_2 in air (0.2 bar, dotted line a), and also for a partial pressure of 10^{-6} bar (dotted line b) which corresponds to a dioxygen concentration of only 1 ppmv (part per million in volume). The latter is in line with the magnitude of the impurity level in the gases. The stability of the peroxide Na_2O_2, with regard to the decomposition at atmospheric pressure, can be deduced from the respective positions of the corresponding curve and line b; this peroxide is stable up to a temperature of about 420 °C which corresponds to the crossing point I. Sodium superoxide is not stable in the considered temperature range and decomposes according to the reverse of Equation (4). Therefore, in the presence of an excess of oxygen , there is a predominant formation of sodium peroxide Na_2O_2 on the oxide crust, while Na_2O is stable only in direct contact with sodium. From a kinetic point of view, Na_2O_2 represents the primary product of the reaction which maintains the O–O bond, while the formation of Na_2O requires the full breaking of this bond.

3.3. Reactions with Water Vapor

In the presence of water vapor, the oxide Na_2O can transform into sodium hydroxide NaOH and can then form the successive hydrates $NaOH{\cdot}nH_2O$ (n = 1, 2, ...). Sodium peroxide can also form hydrates $Na_2O_2{\cdot}nH_2O$ (n = 1, 2, 8) which should remain stable provided they are not in direct

contact with metallic sodium. Data are available for the octa-hydrate $Na_2O_2 \cdot 8H_2O(s)$ that allows for the checking of its stability according to the equation:

$$Na_2O_2(s) + 8\ H_2O(g) = Na_2O_2 \cdot 8H_2O(s) \qquad \Delta_r G^\circ_{298} = -193\ kJ\ mol^{-1} \quad (5)$$

The equilibrium at room temperature corresponds to a partial pressure $p(H_2O)$ of about 6×10^{-5} bar.[16] These data show that the hydrates can be formed in the presence of traces of water, in agreement with the highly hygroscopic nature of sodium peroxide.

3.4. Potassium-Oxygen System

The successive formation of oxygenated compounds of potassium are also displayed in Figure 2, according to the balanced equations:

$$4\ K(s\ or\ l) + O_2(g) = 2\ K_2O(s) \qquad \Delta_r G^\circ_{298} = -646\ kJ\ mol^{-1} \quad (6)$$

$$2\ K_2O(s) + O_2(g) = 2\ K_2O_2(s) \qquad \Delta_r G^\circ_{298} = -211\ kJ\ mol^{-1} \quad (7)$$

$$K_2O_2(s) + O_2(g) = 2\ KO_2(s) \qquad \Delta_r G^\circ_{298} = -53\ kJ\ mol^{-1} \quad (8)$$

All the species are stable at 20 °C with regard to decomposition. K_2O_2 is also stable with regard to disproportionation into KO_2 and K_2O. At ambient temperature, the superoxide KO_2 is in equilibrium with a very low partial pressure of oxygen $p(O_2)$ of about 10^{-9} bar at 20 °C. According to the diagram, KO_2 begins to decompose at 130 °C at a pressure of 10^{-6} bar (crossing point E on Figure 2). It will thus form and remain stable at ambient temperature, even if gaseous oxygen is present in trace amounts only.

As the superoxide is the first product to be formed (kinetic product), the stable product on the outer layer of the oxide crust will be $KO_2(s)$, which should constitute the predominant species in accordance with the results of Gardener.[6] Therefore, the conditions favorable to the formation of the superoxide are those in which oxygen is in the presence of a small proportion of metal, mainly on the walls and on the outer surface of the crusts that form above the NaK alloy. According to Gardener,[6] KO_2 begins to decompose at around 130 °C under 8×10^{-6} bar, a value of the same order of magnitude that can be deduced from the thermodynamic data (10^{-6} bar).

3.5. Sodium-Potassium Comparison: The Case of NaK Alloys

Figure 2 clearly shows differences in stability with respect to the decomposition of higher oxides into lower oxides: Na_2O is more stable than K_2O, whereas K_2O_2 and KO_2 are more stable than Na_2O_2 and NaO_2 ,respectively. At 25 °C and above 10^{-6} bar (dotted line b), KO_2 is stable and will be formed, whereas even with an oxygen pressure of 1 bar, NaO_2 cannot be formed from Na_2O_2 ($\Delta_r G > 0$).

The oxides Na_2O or K_2O can react with KO_2 according to the equations:

$$KO_2(s) + K_2O(s) = 1.5\ K_2O_2(s) \quad {}_{\Delta r}G^\circ_{298} = -80\ kJ\ mol^{-1} \quad (9)$$

$$2\ KO_2(s) + 2\ Na_2O(s) = K_2O_2(s) + 2\ Na_2O_2(s) \qquad \Delta_r G^\circ_{298} = -89\ kJ\ mol^{-1} \quad (10)$$

For both reactions, $\Delta_r G^\circ$ is negative in the temperature range 0−100 °C. On the other hand, KOH, NaOH and $NaOH \cdot H_2O$ cannot react with KO_2:

$$KO_2(s) + 2\ KOH(s) = 1.5\ K_2O_2(s) + H_2O(l) \qquad \Delta_r G^\circ_{298} = +119\ kJ\ mol^{-1} \quad (11)$$

$$2\ KO_2(s) + 4\ NaOH(s) = K_2O_2(s) + 2\ Na_2O_2(s) + 2\ H_2O(l) \qquad \Delta_r G^\circ_{298} = +198\ kJ\ mol^{-1} \quad (12)$$

For all these reactions, $\Delta_r G^\circ$ is positive in the same temperature range.

4. Model for Oxidation of Na-K Alloys

According to the above results, the most likely predominant phases in the presence of oxygen are: sodium peroxide Na_2O_2 and potassium superoxide KO_2. On direct contact with the alloy, a $Na_2O + K_2O$ mixture may occur since Na_2O and K_2O are the only thermodynamically stable oxides in the presence of an excess of NaK alloy.

All the oxygenated compounds display a higher density than the NaK alloy, and should therefore fall to the bottom of the containers, thus being protected against any further reactions. This behavior is not observed as the oxide layers remain on the surface of the alloy. This experimental result could be explained by the formation of a porous oxide layer that cannot be wetted by the metallic alloy. As the liquid alloy cannot penetrate this layer, the apparent density of the oxide layer (i.e. including the pore volume) has to be taken into account. This apparent density is therefore less than the bulk density of the alloy and leads to an apparent molar volume greater than that of the alloy.

Moreover, some oxygenated compounds are very hygroscopic and in the presence of traces of water vapor, the formation of hydrates such as $Na_2O_2 \cdot 8H_2O$, $Na_2O_2 \cdot 2H_2O$, $NaOH \cdot H_2O$ or $KOH \cdot H_2O$ is likely to occur.

Under these conditions, the layer of oxides can come off from the surface of the alloy, making any subsequent reduction of sodium peroxide or potassium superoxide by the alloy impossible. The layer or crust of oxides can be schematized as presented in Figure 3. In the areas that are in contact with the alloy, a thin layer of a $K_2O + Na_2O$ mixture can play the role of buffer between the alloy and the external part of the crust.

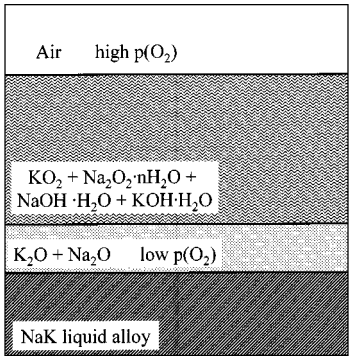


Figure 3. Model for the oxide layers on the surface of Na-K alloys

The accidents and explosions that occurred during handling or upon impact may be explained by the contact of the external part of the oxide crust with the liquid alloy. This contact is likely to cause an exothermic reduction of the potassium superoxide KO_2 by the NaK alloy if, the kinetics is not too slow. The heat released could then favor the decomposition or further reaction of KO_2 according to the strongly exothermic equations:

$$2\ KO_2(s) + 2\ K(l) = 2\ K_2O(s) + O_2(g) \qquad \Delta_rG°_{298} = -164\ kJ\ mol^{-1} \quad (13)$$

$$2\ KO_2(s) + 2\ Na(l) = K_2O(s) + Na_2O(s) + O_2(g) \qquad \Delta_rG°_{298} = -220\ kJ\ mol^{-1} \quad (14)$$

In the case of hydrated oxides, other possible reactions can lead to the release of hydrogen:

$$Na_2O_2{\cdot}8H_2O(s) + 8\ Na(l) = Na_2O_2(s) + 8\ NaOH(s) + 4\ H_2(g) \qquad \Delta_rG°_{298} \approx -1000\ kJ\ mol^{-1} \quad (15)$$

$$NaOH{\cdot}H_2O(s) + Na(l) = 2\ NaOH(s) + 1/2\ H_2(g) \qquad \Delta_rG°_{298} = -132\ kJ\ mol^{-1} \quad (16)$$

$$KOH{\cdot}H_2O(s) + K(l) = 2\ KOH(s) + 1/2\ H_2(g) \qquad \Delta_rG°_{298} \approx -130\ kJ\ mol^{-1} \quad (17)$$

The heat released by these reaction is likely to cause the endothermic decomposition of KO_2 and the simultaneous release of oxygen, which could lead to an explosion of the $H_2(g) + O_2(g)$ mixture.

On the basis of these assumptions, an experimental program was initiated, including the following tests:

(i) Reactions of pure KO_2, Na_2O_2 and Na_2O with the alloy NaK-56;

(ii) Reaction of hydrated peroxide or hydroxide with the alloy;

(iii) Reaction of a $Na_2O_2{\cdot}nH_2O + KO_2$ mixture placed in contact with the alloy;

(iv) Oxidation tests on NaK-56 and characterization of the products obtained.

5. Reactions of NaK-52 Alloy with Oxides, Peroxides, and Superoxides

5.1. Thermal Stability of Pure Compounds

The differential scanning calorimetry (DSC) measurements performed on pure NaK alloy show the eutectic point at −12.7 °C and that the liquid form exists at 8.3 °C in accordance with the phase diagram (Figure 1). The melting enthalpy of the alloy is 2.17 kJ mol^{-1} a value in good agreement with the calculated data for Na (2.21 kJ mol^{-1}) and K (2.11 kJ mol^{-1}).[22]

The stability of pure and hydrated oxides was studied using DSC and mass spectrometry. The reactants have been characterized by X-ray diffraction. The results are gathered in Table 2 and they give rise to the following observations:
Na_2O is stable up to 1000 °C (not given in Table 2);
For Na_2O_2, the endothermic phenomenon at 490 °C seems to be the melting of the peroxide. This value is slightly higher than that given in the literature i.e. 460 °C;[17]

KO_2 decomposes slowly under our operating conditions above 130 °C. From the literature, the melting point lies between 380 and 500 °C.

Hydrated Na_2O_2 releases water and oxygen above 50 °C with a maximum at 100 °C for H_2O and at 200 °C for oxygen.

The diffractograms show that pure sodium and potassium oxides are hygroscopic, as the hydrated compounds $NaOH{\cdot}H_2O$, $KOH{\cdot}H_2O$ and $Na_2O_2{\cdot}nH_2O$ were also observed. The hydration of Na_2O_2, performed in an exsiccator with water vapor under a water-pump vacuum, results in the formation of $Na_2O_2{\cdot}2H_2O$; when the hydration reaction is performed in air, there is the predominant formation of Na_2CO_3, $Na_2O_2{\cdot}2H_2O$ and $Na_2O_2{\cdot}8H_2O$.

For the superoxide KO_2, the mass spectrometry analysis revealed a release of oxygen at the beginning of heating (estimated between 50 and 100 °C), whereas the thermodynamic calculation predicted decomposition from 130 °C for an oxygen pressure of 10^{-6} bar. These values are not in

Table 2. Stability and characterization of pure and hydrated oxides.

Compounds	Na_2O_2	KO_2	Hydrated Na_2O_2
Supplier (purity)	Osi (95%)	Merck (96.5%)	Prepared
Phase identification	Na_2O_2 major	KO_2 major	$Na_2O_2{\cdot}2H_2O$
byX-ray diffraction	$Na_2O_2{\cdot}2H_2O$	$KOH{\cdot}H_2O$	Na_2O_2 and $NaOH{\cdot}H_2O$
Calorimetry:			
Reactant mass	0.538 g	0.520 g	
Temperature range	20−600 °C	20−600 °C	
Main thermal events under heating	Slight exotherm, 444 °C (−2.4 J g^{-1}) Endotherm, 490 °C (53 J g^{-1}) (melting)	Endotherm, 130 °C (50.3 J g^{-1}) Slight exotherm, 153 °C (−14 J g^{-1}) From 430 °C, reaction leading to loss of tightness at 500 °C	
Conclusion	Melting at 480−490 °C	Decomposition above 130 °C	
Mass spectrometry	1.49 g	0.996 g	3.72 g
Temperature range	20−500 °C	20−500 °C	20−300 °C
Gas release	Main but slight release of H_2O above 100 °C. Slight release of O_2; max. at 200 °C	Release of oxygen from 50−100 °C. Max. at 200 °C.	Release of water (predominant) and oxygen above 50 °C O_2 max. at 200 °C

disagreement as the vacuum needed for the MS measurements is much lower than this value. The maximum for oxygen release is situated at 200 °C and corresponds to a partial pressure of 10^{-6} bar (Figure 4).

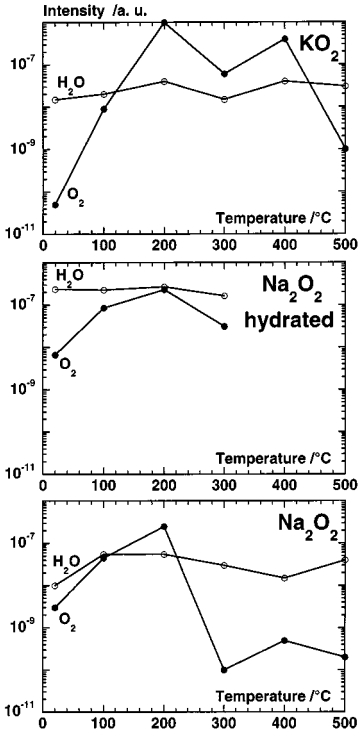


Figure 4. Mass spectra results for the release of water vapor and oxygen, versus temperature for the compounds KO_2, Na_2O_2 and hydrated Na_2O_2

Sodium peroxide displays a mass loss of 8.7 wt-% at the end of the test. This loss indicates the likely and partial formation of Na_2O, the whole decomposition corresponding to a loss of mass of 20.5%. In addition, Na_2O_2 contains impurities (H_2O, CO_2, etc.) evidenced by mass spectrometry in agreement with the very hygroscopic and basic character of Na_2O_2 (higher than that of KO_2). Its decomposition rate is lower than that of KO_2 by more than one order of magnitude.

The decomposition of hydrated sodium peroxide $Na_2O_2{\cdot}nH_2O$ shows a constant predominant loss of H_2O from the very beginning of heating (Figure 4), and a minor loss of oxygen with a maximum at 200 °C.

5.2. Reactions of NaK Alloy with Na_2O_2

Using the DSC 111 calorimeter, two tests were performed, with the aim to vary the temperature around 0 °C (cycles between − 20 and + 20 °C) in order to simulate natural thermal cycling, then followed by high temperature cycles. The results are given in Table 3.

1st test: 18 cycles −20 to 20 °C; 4 cycles 20 to 390 °C; 4 cycles −20 to 20 °C.

2nd test: 10 cycles −20 to 20 °C; 2 cycles 20 to 420 °C; 4 cycles −20 to 20 °C.

A significant part of the results of the second test are presented in Figure 5. Before the temperature rise, the thermograms of the thermal cycling around ambient temperature show the characteristic NaK melting and solidification peaks corresponding to the liquid and eutectic lines and we can see only minor changes between the first cycle and the tenth cycle. The heating leads to slightly endothermic reactions between 33 and 53 °C, followed by an exothermic reaction above 170 °C; after the first temperature rise, we observe the formation of metallic potassium which is revealed by the appearance of a peak at about 60 °C (Figure 5). For test 2 the weight of potassium is estimated to be about 10 mg.

From the thermodynamic data, an exothermic reaction is expected between the alloy and Na_2O_2 which would lead to the formation of the more stable oxide Na_2O:

$$2\ NaK(l) + Na_2O_2(s) \rightarrow 2\ Na_2O(s) + 2\ K(l)$$
$$\Delta r H^\circ_{298} = -327\ kJ\ mol^{-1} \quad (18)$$

This reaction consumes sodium and therefore leads to a change in the composition of the alloy, up to the formation of metallic potassium. The weight balance is given in Table 4 and takes into account the excess peroxide Na_2O_2 which can react with potassium in a second step giving, as final products, a mixture of Na_2O, K_2O and K. The calculated weight of remaining potassium (7.8 mg) is in agreement with the value deduced from DSC measurements (10 mg).

Table 3. Reaction of NaK-56 alloy with Na and K oxides. Results of differential scanning calorimetry

	NaK + Na_2O_2 Test 1	Test 2	NaK + KO_2 Test 1	Test 2	Test 3
Mass of NaK-56	0.037 g	0.024 g	0.024 g	0.0082 g	0.049 g
Mass of Na_2O_2 or KO_2	0.041 g	0.024 g	0.027 g	0.0057 g	0.050 g
Main thermal phenomena under heating	Endotherm at 45 °C Endotherm at 60 °C (melting of K) Exotherm at 166 °C Large exotherm at 240 °C	Endotherm 33 to 53 °C Large exotherm above 172 °C	Exotherm > 167 °C Large exotherm above 195 °C	Exotherm > 167 °C	Exotherm > 167 °C Large exotherm at 190 °C
NaK consumed	Yes	Yes	Yes, partially	Yes	
Potassium formation	Yes	Yes (0.010 g)	No	Yes (≈ 0.001 g)	Yes
Apparatus	DSC 111	DSC 111	DSC 111	DSC 111	HTC

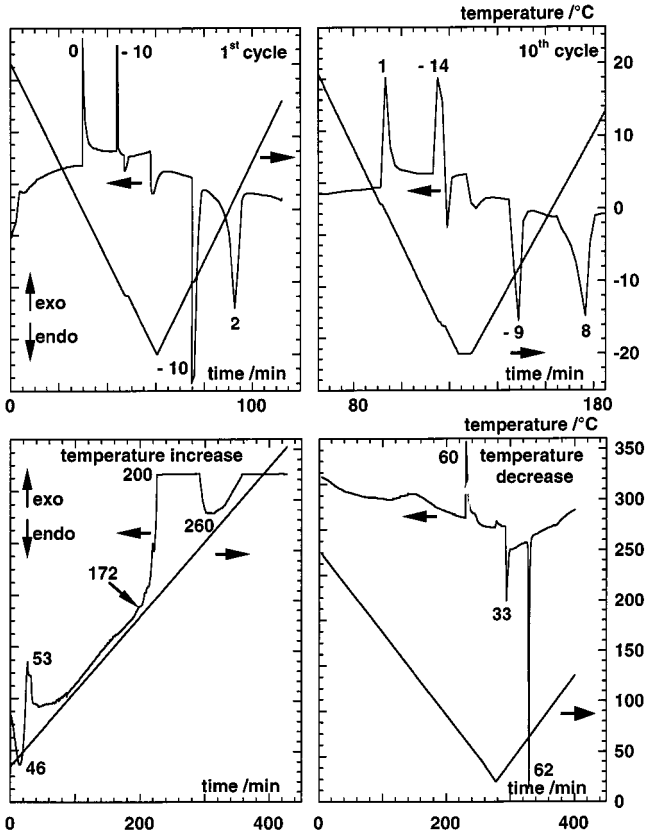


Figure 5. DSC curves for the reaction between NaK alloy and Na_2O_2:1st cycle between 20 and −20 °C; 10th cycle between 20 and −20 °C; increase from 20 to 420 °C and cooling from 420 to 20 °C. See test 2 in Table 3

Table 4. Example of mass and mol balance for the reaction NaK + Na_2O_2 (Test 2)

	NaK (24.3 mg)		Na_2O_2 (24.4 mg)			
	Na	K	Na	O	Na_2O	K_2O
Initial mass/48.7 mg	10.7	13.6	14.4	10.0	0	0
Initial amount/mmol	0.47	0.35	0.62	0.62	0	0
Intermediate amount/mmol	0	0.35	0.15	0.15	0.47	0
Final amount /mmol	0	0.2	0	0	0.545	0.075
Final mass/48.7 mg	0	7.8	0	0	33.8	7.1

Intermediate reaction: $Na_2O_2(s)$ (excess) + 2 Na(l) → 2 $Na_2O(s)$; Final reaction: $Na_2O_2(s)$ + 2 K(l) (excess) → $Na_2O(s)$ + $K_2O(s)$.

After the temperature rise, the low temperature cycles (−20 to +20 °C) do not show the previous NaK peaks, which is in agreement with the proposed reactions. Therefore, these results are consistent with the thermodynamic calculations which suggested the enrichment of the alloy in potassium due to the formation of the more stable Na_2O.

Another mixture of the NaK alloy (0.41 g) and Na_2O_2 (1.00 g) was analyzed by mass spectrometry, but no significant gas release was observed, in agreement with the explanations given in Table 4.

5.3. Reactions of the NaK Alloy with KO_2

Two tests were performed using the DSC 111 calorimeter and one test using the HTC calorimeter. The test conditions and results are gathered in Table 3. For test 1 and test 2 the same cycling as with Na_2O_2, i.e. between 20 and −20 °C, displays the characteristic peaks of the NaK alloy, even after heating at 150 °C. During heating (up to 300 °C), exothermic peaks appear above 167 °C (Figure 6 for test 3). For test 1, the expected reaction would lead, after completion, to the disappearance of the alloy and to the formation of a mixture of Na_2O, K_2O and K_2O_2; experimentally, the alloy is only partially consumed and no potassium can be evidenced, showing an incomplete reaction. Test 2, performed with more NaK alloy, displays the same exothermic peaks above 167 °C, but leads to a complete disappearance of the alloy and to the formation of potassium (about 1.0 mg). This is in agreement with a complete reaction leading to the formation of Na_2O, K_2O and K (calculated weight 1.1 mg).

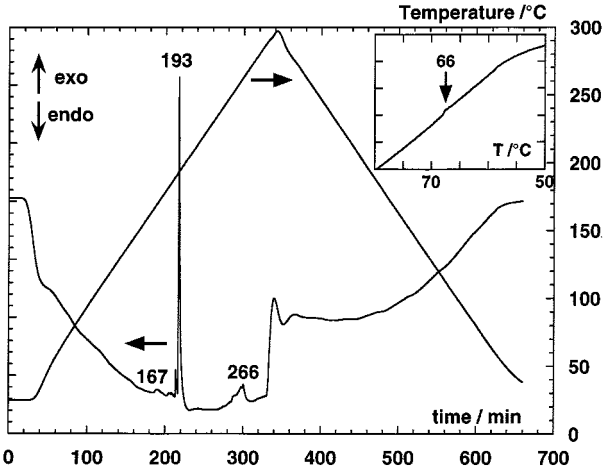


Figure 6. HTC curves for the reaction between NaK alloy and KO_2 (Table 3, test 3). The window represents an enlargement of the last part of the curve versus temperature

The exothermic reactions that appear at 167 °C (Figure 6) are reproducible since this temperature is strictly identical on both instruments, with different reactant masses and different proportions. Below this temperature, there is no violent reaction, even after an induction period. This is in agreement with Sloan.[1] Moreover, the low temperature thermal cycling has little effect on the reaction between the NaK alloy and KO_2 superoxide. For test 3, the reaction is incomplete and leads to a heterogeneous mixture of the products; the formation of potassium is seen by a very tiny exothermic peak at 66 °C (see window in Figure 6).

The influence of these exothermic events on the endothermic decomposition of potassium superoxide was examined by means of mass spectrometry. A mixture of NaK alloy (0.46 g) and KO_2 (0.49 g) was placed under inert atmosphere (glove box) into the sample container equipped with a tight connection. The temperature was increased in steps from ambient temperature up to 300 °C. The measurements performed in the 150−160 °C range showed a considerable increase in oxygen corresponding to the decomposition of KO_2. The same reaction performed in the presence of Na_2O from 20 to 200 °C displayed similar results,

showing that sodium oxide is very stable and plays no role in the reaction between the NaK alloy and KO_2.

5.4. Reaction of NaK + KO_2 + Na_2O_2

One test was performed using the DSC 111 calorimeter and one using the HTC calorimeter. The results are given in Table 5. Figure 7, obtained with the HTC apparatus (test 2), shows a rapid and significant exothermic reaction from 170 °C, greater than that observed during the NaK + KO_2 reaction. The formation of potassium is evidenced during the cooling (see window in Figure 7).

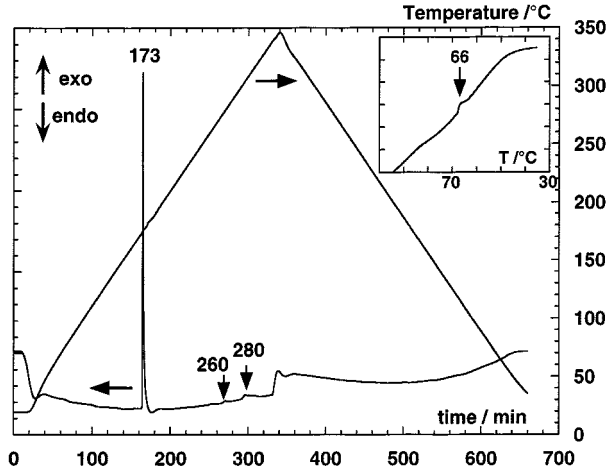


Figure 7. HTC curves for the reaction between NaK alloy and KO_2 + Na_2O_2 (Table 4, test 2). The window represents an enlargement of the last part of the curve versus temperature

5.5 Discussion About the Role of Potassium Superoxide

The tests carried out between the NaK alloy and sodium peroxide and/or potassium superoxide, revealed significant exothermic reactions above 170−180 °C. Therefore, KO_2 is effectively responsible for a significant heat release, but only above a temperature of about 170 °C, with subsequent consumption of the sodium of the NaK alloy. Na_2O_2 is also responsible for significant exothermic reactions above 200 °C, but only slight reactions with the alloy occur as soon as ambient temperature is reached. Therefore, the explosive behavior of such mixtures at ambient temperature imply another kind of reactions; KO_2 alone cannot be responsible for the triggering of this phenomenon.

The formation of metallic potassium during several tests was confirmed, displaying the selective consumption of the sodium of the NaK alloy, in accordance with the formation of the more stable Na_2O oxide. The completed reactions deduced from the thermodynamic data can be experimentally evidenced, but some tests leads to incomplete reactions and the products are more relevant to the kinetics of the processes (heterogeneous mixtures) than to the reaction thermodynamics.

6. Reactions of NaK-52 Alloy with Hydrated Oxides and Peroxides

These tests were performed in a glove box under argon in a 20 mL glass flask equipped with a thermocouple. The oxides were added separately or simultaneously to about two grams of NaK alloy. The mixture was then manually agitated so as to ensure good contact between the alloy and the oxides. The operating conditions and the results of all the tests are given in Table 6. Preliminary tests were carried out with KO_2 and non hydrated Na_2O_2 for comparison purposes. The reaction was slightly exothermic, but neither the addition of Na_2O_2, nor that of KO_2 caused a violent reaction, in agreement with the results of Gardener.[6] These results confirm, on larger scale (than that used in the calorimetric experiments), that there is no significant reaction at ambient temperature between NaK alloy and sodium peroxide or potassium superoxide, whether they are added successively or simultaneously (Table 6, tests 1 and 2). The results described by Commander,[4] i.e. ignition after an induction period of 18 minutes under inert gas, were therefore not confirmed.

6.1. Reaction of NaK with $Na_2O_2 \cdot nH_2O$

Test on NaK + Na_2O_2 Hydrated in Air

The sodium peroxide was hydrated in ambient air before the test and corresponds to a mixture of dihydrate $Na_2O_2 \cdot 2H_2O$ (minor) and octahydrate $Na_2O_2 \cdot 8H_2O$ (major), aside from sodium carbonate Na_2CO_3. Three tests were performed and the operating conditions and results are given in Table 6. The NaK + hydrated peroxide reaction, performed in a glove box, is violent (Photo 1) and occurs at ambient temperature when the two reagents come into contact (Tests 3a and 3b, Table 6). These tests are the

Table 5. Differential calorimetric analysis of the reactions of NaK-56 alloy with sodium peroxide and potassium superoxide

	NaK + KO_2 + Na_2O_2 Test 1	Test 2
Temperature range	+20 to −20 to +20 °C 20 to 250 to 44 °C 44 to 250 to 20 °C	20 to 350 °C to 20 °C 5 cycles
Mass of NaK	0.0411 g	0.0752 g
Mass of Na_2O_2	0.0206 g	0.0366 g
Mass of KO_2	0.008 g	0.0376 g
Main thermal events during heating	Large exothermic reaction above 180 °C	Large exothermic reaction at 170 °C
NaK consumed	About 1/3 of the initial alloy	Not measured
Formation of potassium	Yes	Yes
Apparatus	DSC	HTC

Table 6. Evolution of the reaction temperature of NaK-56 alloy in the presence of pure or hydrated oxides and hydroxides

Test N°	Initial conditions					Temperature evolution
1	NaK 2.035 g	+	Na_2O_2 0.604 g	+	KO_2 0.320 g	Slightly exothermic reaction 22 to 28 °C in 4 min
	Reactants added successively					
2	NaK 2.030 g	+	Na_2O_2 0.250 g	+	KO_2 0.321 g	Slight exothermic reaction 24 to 27 °C NaK brilliant under the film
	Reactants added simultaneously					
3a	NaK 2.04 g	+	Na_2O_2 hydrated in air 0.577 g			Violent reaction: 21 to 146 °C in 3 min, explosion, grey smoke. Glass flask broken
3b	NaK 2.05 g	+	Na_2O_2 hydrated in air 0.212 g			Violent reaction: smoke, sparks 23 to 78 °C in 3 min.
4	NaK 2.2 g	+	Na_2O_2 hydrated in air 0.632 g			Slightly exothermic reaction: 21 to 27 °C. Brilliant NaK alloy mixed with parts of oxide
	Na_2O_2 stored in glove box for one week					
5	NaK 2.74 g	+	hydrated Na_2O_2 0.326 g			Violent reaction: 25 to 306 °C in 2 min; flames, smoke
	Hydration in water vapor under vacuum					
6	NaK 2.45 g	+	KO_2 0.250 g	+	hydrated Na_2O_2 0.578 g	Violent reaction: 23 to 380 °C in 30 s; flames, smoke
	Hydration in water vapor under vacuum; oxides added simultaneously					
7	NaK 2.14 g	+	NaOH slightly hydrated 1.01 g + 0.519 + 0.52 g + 0.69 g			NaOH as received; slight reaction: 22 to 34 °C in 5 min 34 to 38 °C in 3 min 38 to 51 °C in 3 min
8	NaK 2.14 g	+	KOH slightly hydrated 0.63 g + 1.19 g			KOH as received Slight reaction: 25 to 31 °C in 1 min 31 to 33 °C in 3 min; dull grey mixture

first ones showing that the occurrence of an explosion is linked to the presence of water in the hydrated peroxide; moreover, the final temperature depends on the amount of hydrated peroxide (compare 3a and 3b). A possible explanation of these results is as follow: in a first step, a surface reaction between the water molecules and the liquid alloy alters the wetting ability of the oxide crust by the alloy; then the alloy penetrates rapidly into the porosity of the peroxide and the reaction becomes violent, resulting in the exothermic formation of hydrogen which first reacts with the peroxide, then with the oxygen released by the temperature increase. The explosion is therefore due to the simultaneous formation of hydrogen and oxygen from the following strongly exothermic reactions ($\Delta rH°$ in kJ mol^{-1}):

$$NaK(l) + Na_2O_2{\cdot}2H_2O(s) \rightarrow NaOH(s) + KOH(s) + Na_2O_2(s) + H_2(g) \quad -242 \quad (19)$$

$$Na_2O_2(s) + H_2(g) \rightarrow 2\ NaOH(s) \quad -339 \quad (20)$$

$$2\ Na_2O_2{\cdot}2H_2O(s) \rightarrow 4\ NaOH(s) + 2\ H_2O(g) + O_2(g) \quad -33 \quad (21)$$

$$2\ H_2(g) + O_2(g) \rightarrow 2\ H_2O(g) \quad -483 \quad (22)$$

The values for equations (19) and (21) are based on a value of about -1121 kJ mol^{-1} for the formation enthalpy of $Na_2O_2{\cdot}2H_2O$; this value was estimated from the corresponding value given for $Na_2O_2{\cdot}8H_2O$ (-2943 kJ mol^{-1}).[18]



Photo 1. Results of the reaction between NaK alloy and sodium peroxide hydrated in air (Table 6, test 3b)

The storage of hydrated Na_2O_2 for one week in glove box, apparently dried the compound with a loss of its reactivity (Test 4, Table 6). This test confirms that the water molecules of the hydrate are responsible for the highly exothermic reaction or explosion.

Test on NaK + Na_2O_2 Hydrated Under Water Pump Vacuum

The diffractogram (Figure 8) of the hydrated product protected by a layer of polyethylene film, displays the presence of the phases Na_2O_2, $Na_2O_2{\cdot}2H_2O$ and the hydrated hydroxide $NaOH{\cdot}H_2O$, showing that the peroxide was only partially hydrated. Although the hydrates formed are not the same as those observed in the previous tests ($Na_2O_2{\cdot}8H_2O$ in one case and $Na_2O_2{\cdot}2H_2O$ plus $NaOH{\cdot}H_2O$ in another case), the reaction is violent in both cases (Table 6, Test 5). These very violent exothermic reactions are due to the presence of hydration water in the solid mixtures. The release of hydrogen exhibits a limited risk as these operations were performed in a glove box, but in air, actual explosions could occur.

Test on NaK + KO_2 + Hydrated Na_2O_2

The previous hydrated peroxide was mixed with KO_2 inside the glove box and then inserted together into the NaK alloy (Table 6, Test 6). In comparison with Test 1, the very violent resulting reaction is clearly due to the hydrated peroxide.

Test on NaK + NaOH

Slightly hydrated sodium hydroxide pellets (97%) were ground in air, and analyzed using X-ray diffraction: NaOH is found to be the predominant species besides the hydrates $NaOH{\cdot}H_2O$ and $Na_2CO_3{\cdot}7H_2O$ (Table 6, Test 7). The alloy reacts only slightly in the presence of sodium hydroxide, with a release of hydrogen. Repeated additions of hydroxide does not produce significant reactions.

Test on NaK + KOH

Potassium hydroxide pellets (87%) were ground and analyzed. KOH is the predominant phase besides $KOH{\cdot}H_2O$ and K_2CO_3 (Table 6, Test 8). The reaction is less exothermic than that with the sodium hydroxide due to the the lower hygroscopic behavior of KOH.

In conclusion, the violence of the reaction between NaK alloys and hydrated sodium peroxide, sodium hydroxide or potassium hydroxide, depends on the degree of hydration of the reagents and therefore on their history. The reaction remains difficult to predict and therefore portrays a random character. The simultaneous presence of hydrated sodium peroxide and potassium superoxide leads to a faster and more exothermic reaction.

7. Oxidation of NaK Alloy by Oxygen in Presence of H_2O Impurities

7.1. Preparation of Oxidized NaK Alloy by Sweeping Argon and Air

Two tests were performed in glass crucibles and the operating conditions and results are given in Table 7. The first test was carried out in one day and shows that sweeping with argon and air containing H_2O impurities (<5 vpm) results in the formation of a yellow mixture containing hydrated peroxide and hydroxides, in addition to the predominant species KO_2 (Photo 2). The phases observed are in agreement with the thermodynamic data: the oxides Na_2O and K_2O can react with KO_2 and are therefore absent, whereas the hydrates $KOH{\cdot}H_2O$ and $NaOH{\cdot}H_2O$ do not react with KO_2 and can coexist.

The second test was performed over one week and the behavior of the NaK alloy differs from the one observed in the previous test. A few hours after the beginning of the oxidation, the ball of NaK shows numerous excrescences; after a few days, the swellings took on a cauliflower-like appearance (Photo 3) with two predominant phases: KO_2 and $Na_2O_2{\cdot}2H_2O$ (Table 7, test 2). In this case, the water impurities in the argon during the first step seem to play an important role.

In conclusion, sweeping with a gas containing water impurities leads to a concentration of the water molecules through the formation of hydrated hydroxides and peroxides and not to the reduction of water into hydrogen. The traces of water vapor are only partially eliminated and therefore the role assigned to the NaK alloy is not fulfilled

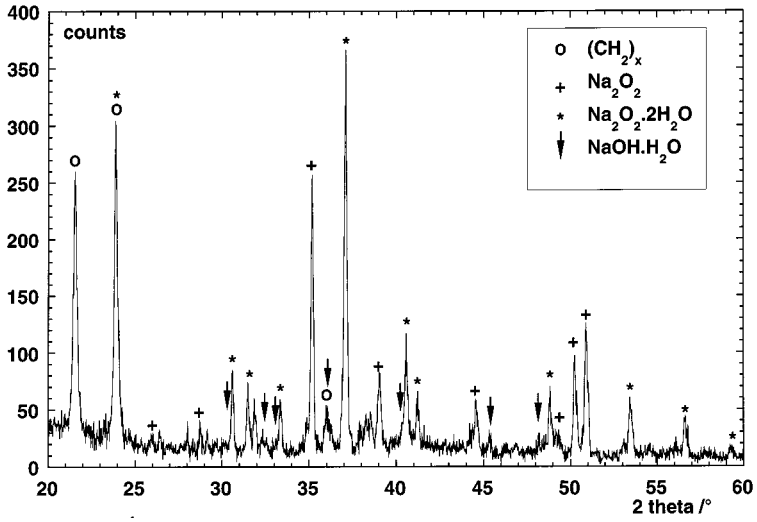


Figure 8. Raw diffractogram of sodium peroxide after hydration under water pump vacuum. The polyethylene peaks are due to the protecting layer. Dwell time 1 s; step 0.02 °

Table 7. Oxidation of the NaK alloy by argon and air sweeping

	Conditions	Aspect	Composition
Test 1 1.03 g	Sweeping 23 h with argon (3 L min^{-1}) and air (3 to 5 L min^{-1}), then storage in a closed flask	Intense yellow product	KO_2 predominant + $Na_2O_2{\cdot}2H_2O$ + $NaOH{\cdot}H_2O$ + $KOH{\cdot}H_2O$
Test 2 2.28 g	Sweeping 13 h with argon (6 L min^{-1}) then 8 h with argon and air (5 L min^{-1}) followed by 150 h with air (3 L min^{-1})	Cauliflower-like aspect, yellow at end of test	KO_2, major + $Na_2O_2{\cdot}2H_2O$, major + $NaOH{\cdot}H_2O$



Photo 2. Yellow product obtained during the oxidation of NaK alloy by argon and air sweeping (Table 7, test 1)

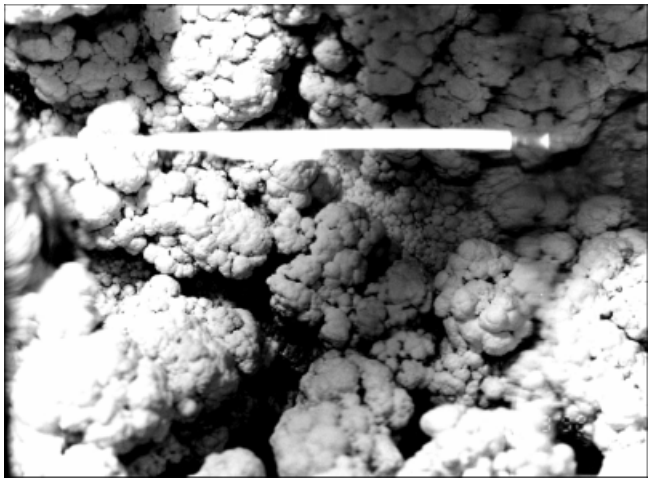


Photo 3. Product obtained during the oxidation of NaK alloy by argon and air sweeping (Table 7, test 2)

because it leads predominantly to an accumulation of the H_2O impurities. The products thus obtained confirm the reactions expected from a thermodynamic basis (NaK-56 is represented by the approximate formula NaK):

$$2\ NaK(l) + 3\ O_2(g) \rightarrow Na_2O_2(s) + 2\ KO_2(s) \quad (23)$$

$$NaK(l) + 2\ H_2O(g) \rightarrow NaOH(s) + KOH(s) + H_2(g) \quad (24)$$

$$Na_2O_2(s) + n\ H_2O(g) \rightarrow Na_2O_2{\cdot}nH_2O(s) \text{ with } n = 2 \text{ or } 8 \quad (25)$$

$$NaOH(s) + H_2O(g) \rightarrow NaOH{\cdot}H_2O(s) \quad (26)$$

$$KOH(s) + H_2O(g) \rightarrow KOH{\cdot}H_2O(s) \quad (27)$$

7.2. Preparation of Oxidized NaK Using Argon and Air Bubbling

The purpose of this test was to represent a real bubble chamber at a laboratory scale, with a continuous circulation of gas containing water impurities ($\leq$ 5 vpm) in the NaK liquid alloy. Air was added to the argon flow in order to accelerate the oxidation of the NaK alloy. The oxidation was performed in a glove box.

The test lasted three months (including 500 h of bubbling) during which a total of 30 m^3 of argon and 60 m^3 of azoxy (reconstituted dry air) were alternatively or simultaneously bubbled into the liquid alloy (9.95 g). The mass of water impurities passing through the alloy totals 0.36 g and it serves either to hydrolyze the NaK alloy into NaOH and KOH, or to hydrate Na_2O_2, NaOH and KOH.

During the argon bubbling, the previously very brilliant NaK alloy first becomes dull gray, then starts to whiten in selected areas due to the water and oxygen impurities. The bottom of the reactor is coated with very fine gray beads that are ejected. Bubbling with air results in the formation of yellowish areas, which then become clear yellow. This always occurs along the preferential paths. The start of the azoxy gas flow sometimes causes orange flames and grayish smoke which are then extinguished by argon sweeping. Throughout the test, the ejection of small gray beads is observed. At the end of the test, the mixture is very heterogeneous: orange crusts adhering closely to the walls, grayish parts and metallic NaK. After the test, four samples were taken from these various parts and the results of the X ray diffraction analyses are given in Table 8. Figure 9 represents the diffractogram of the sample BAG 2 and five species could be identified. After 30 min in air, we observe a swelling of the sample and the disappearance of the peaks corresponding to sodium hydroxide due the very hygroscopic behavior of these compounds.

These series of tests show that when the NaK alloy is exposed to the sweeping or bubbling of argon and dry air containing water impurities, the products KO_2, $KOH{\cdot}H_2O$, $NaOH{\cdot}H_2O$ and $Na_2O_2{\cdot}2H_2O$ are always formed The mixture is heterogeneous, certain areas are very hard, whereas others are flaky. Differences in color can be observed. It is also observed that the gas follows preferential paths due to the heterogeneous nature of the crust. Therefore certain areas are oxidized and hydrated whereas other parts of the alloy remain in the metallic state. The argon is likely to circulate without being really purified.

Table 8. Products obtained after oxidation of the NaK alloy by argon and air bubbling for three months

	Aspect	Identified products (XRD)
BAG 1	Yellow crust taken from the surface of the NaK during the test	KO_2 predominant + $KOH{\cdot}H_2O$ + $Na_2O_2{\cdot}2H_2O$
BAG 2	Grey ashes and yellow crusts taken during the test	KO_2 + $KOH{\cdot}H_2O$ + $Na_2O_2{\cdot}2H_2O$ + $NaOH{\cdot}H_2O$ + NaOH + amorphous phase
BAG 3	Grey area (end of test)	KO_2 + $Na_2O_2{\cdot}H_2O$ + $KOH{\cdot}H_2O$ + $NaOH{\cdot}H_2O$ + NaOH
BAG 4	Yellow area (end of the test)	KO_2 + $KOH{\cdot}H_2O$ + $Na_2O_2{\cdot}2H_2O$ + $NaOH{\cdot}H_2O$

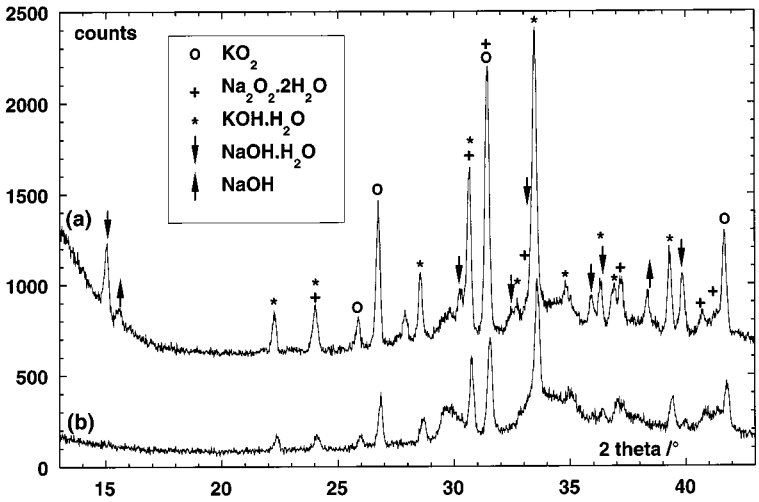


Figure 9. Raw diffractogram of NaK alloy after oxidation by argon and air bubbling during 3 months (Table 8, sample BAG 2).(a) Initial; (b) after 30 min in air. Dwell time 0.5 s; step 0.02 °



Photo 4. Product obtained during the oxidation of NaK alloy by argon and air bubbling for three months (Table 8)

These observations are very important as they explain the hazards of oxidized NaK alloy. Porous crusts containing superoxides, hydrated peroxides and hydroxides, can form on the surface or along the walls and can violently come into contact with the remaining alloy following impact. A slow surface reaction then occurs that can result in the modification of the wetting ability of the oxide crust. The NaK penetrates the pores, which then leads to a violent reaction.

8. Hydration and Dehydration of Sodium and Potassium Oxides and Hydroxides

The aim of these experiments was to examine the possibility to reduce or eliminate the hydration water of the oxidation crust through treatment in vacuum. Hydration was performed using water vapor under water pump vacuum for 12 h. The product was then placed under vacuum (10^{-2} to 10^{-3} bar) for 24 to 60 h at ambient temperature. Dehydration was completed by heating for 24 to 48 h at 110 °C under primary vacuum, followed by cooling. All the results are given in Table 9.

During the dehydration treatment, hydrated peroxide $Na_2O_2{\cdot}2H_2O$ disappears and is partially transformed into NaOH. The hydrated products $NaOH{\cdot}H_2O$ and $Na_2CO_3{\cdot}10H_2O$ are present only in minute amounts, and therefore less likely to react further. After being placed under vacuum, the sample of sodium peroxide becomes harder, but its apparent volume does not change. After

Table 9. Oxide and hydroxide hydration and dehydration tests. (tr = traces)

	Na_2O_2	KO_2	NaOH	KOH
Hydration				
Mass	8.274 g	1.301 g	23.076 g	6.091 g
Increase in mass	1.235 g	Change into liquid KOH	2.963 g	1.308 g
Hydrate obtained	$Na_2O_2{\cdot}2H_2O$ + Na_2O_2	No hydrate formation	$NaOH{\cdot}H_2O$ + NaOH	$KOH{\cdot}H_2O$ + KOH
Dehydration				
Mass	4.086 g		6.406 g	2.673 g
Weight loss after vacuum and heating	0.442 g		0.616 g	0.414 g
% initial water eliminated	83%		85%	86%
Products after dehydration	Na_2O_2 + NaOH + $NaOH{\cdot}H_2O$ (tr) + $Na_2CO_3{\cdot}10H_2O$		NaOH + $NaOH{\cdot}H_2O$ (tr)	KOH + $KOH{\cdot}H_2O$ (tr)

heating under vacuum, the sample expands considerably and migrats up to the upper level of the recipient.

Potassium superoxide KO_2 does not form hydrated products but is decomposed, giving KOH. For NaOH, the hydration leads to the formation of $NaOH{\cdot}H_2O$ and the vacuum treatment eliminates at least 85% of the water previously fixed. The product is practically dry. The same results are obtained for potassium hydroxide (Table 9).

The products rehydrate very rapidly, as soon as they are no longer under vacuum. Dehydration had to be completed by heating at 100 to 110 °C in order to reach irreversible dehydration levels of about 85%. It is observed during the tests that the hydrated products become partially dehydrated in the glove box (water content < 1 vpm). Therefore, it may be possible to dehydrate a product by circulating hot argon, provided the latter is completely dried. Before performing this type of dehydration on a larger scale in a bubbler containing liquid NaK, laboratory tests are essential to check whether the crust layers that detach and expand, could fall into the liquid NaK and cause exothermic reactions. Laboratory tests have to be developed in order to study the complex geometry, similar to that in real bubblers.

General Conclusion

To the best of our knowledge this is the first laboratory demonstration of an explosion due to gas contaminants (oxygen and water vapor). The previous results were obtained by addition of water or hydrocarbon to the alloy.[4]

The main results of the structural and thermodynamic analysis are as follows:

(i) All the oxygenated compounds of sodium and potassium are denser than the NaK alloy and should therefore fall to the bottom of recipients, which is not observed. The molar volumes of the different oxides are lower than the molar volumes of the metals or alloys.

(ii) The oxide layer that is formed must contain predominantly Na_2O_2 and KO_2. This crust is porous and cannot be wetted by the alloy.

(iii) There is a possible formation of hydrated compounds such as $Na_2O_2{\cdot}8H_2O$; $Na_2O_2{\cdot}2H_2O$; $NaOH{\cdot}H_2O$ and $KOH{\cdot}H_2O$.

(iv) If the oxide crust comes in contact with the NaK alloy, the hydration water can react, leading to a release of hydrogen. As the thermal decomposition of KO_2 results in a release of oxygen, a violent reaction could occur, resulting in an explosion.

The experimental study leads to the following conclusions:

(i) Sodium peroxide Na_2O_2 is stable up to 490 °C and potassium superoxide KO_2 decomposes above 130 °C, resulting in oxygen release.

(ii) The NaK + Na_2O_2 reaction shows great instability which results in the formation of several non-identified compounds. The exothermic reactions begin above 166 °C and increases considerably at 204 °C, but does not release any significant amount of gas.

(iii) The NaK + KO_2 reaction starts at 167 °C and is easily reproducible, with the formation of potassium metal and the release of oxygen due to the thermal decomposition of KO_2. Thermal cycling between −20 and +20 °C has little effect.

(iv) The NaK + KO_2 + Na_2O_2 reaction is highly exothermic above 170 °C; the presence of Na_2O_2 contributes significantly to an increase in released heat.

Tests performed in a glove box on greater quantities display the same results, in disagreement with the high exothermicity mentioned by several authors. On the other hand, the use of hydrated sodium peroxide leads to violent or even explosive reactions. The hydration of Na_2O_2 results in the formation of $Na_2O_2{\cdot}2H_2O$ and/or $Na_2O_2{\cdot}8H_2O$ and $NaOH{\cdot}H_2O$ and the quantity of water absorbed and the degree of hydration determine the random explosive character of the reaction.

The laboratory preparation of oxidized NaK alloy by the sweeping or bubbling of argon and air mixture, containing less than 5 vpm of H_2O, leads to the formation of potassium superoxide KO_2 and hydrated peroxide and oxides: $Na_2O_2{\cdot}2H_2O$, $KOH{\cdot}H_2O$ and $NaOH{\cdot}H_2O$. The water impurities are therefore not eliminated, but they are concentrated into the oxide product crust. In the presence of initial alloy, these products can produce exothermic or explosive reactions, depending on the degree of hydration of the peroxide and hydroxides.

The product mixture is very heterogeneous containing gray parts, orange crusts adhering closely to the walls together with metallic NaK alloy. The gas flow follows preferential paths, certain parts of the alloy are oxidized and hydrated, while other parts remain in the metallic state. These important observations explain the danger of oxidized NaK crusts formed at the surface or along the walls of the bubblers containing hydrated oxides; if they can rapidly come in contact with the remaining metallic alloy following impact, explosions can occur.

The bubblers in service on fast reactors are generally largely oversized. When argon follows preferential paths through the crust forming hydrates, and when saturation is reached, the argon is likely to circulate without being purified. It is therefore impossible to assess the duration of the efficiency of these bubblers. Therefore, in our opinion, this method of purification should be abandoned.

The dehydration tests performed on hydrated peroxide and hydroxide show that the products can be dried under primary vacuum at 100 °C. Drying of the products placed in glove boxes under purified argon ($\leq$ 1 vpm H_2O) is also observed. However, as these hydrated products expand when heated, the crusts could detach and come into contact with the remaining alloy. Therefore, to achieve dehydration on complex geometry, such as those of real bubblers, it is indispensable to perform laboratory tests in order to check whether exothermic reactions can occur, resulting in the accidental contact of these reagents.

Experimental Section

Structural Data: The structural data needed for this work (space group, cell parameters, density) were extracted from Powder Diffraction Files (PDF).[19] They are related to the sodium-potassium alloy phases and the different oxides of sodium and potassium. The main data are given in Table 1.

Thermodynamic Data: The purpose of this analysis was to establish the thermodynamic values concerning the various possible reactions: reaction enthalpy $\Delta_r H°$, entropy $\Delta_r S°$ and Gibbs energy $\Delta_r G°$. These values were calculated and tabulated according to the temperature in the 25−500 °C range and involve all the possible Na-K-O combinations available in the literature. The primary thermodynamic data concern the values tabulated for the following species:

K(s and l), KO_2(s), K_2O(s), K_2O_2(s); Na(s and l), NaO_2(s), Na_2O(s), Na_2O_2(s); O_2(g), H_2O(g), CO_2(g)

They were extracted from two recent data bases[20,21] or from the NIST files.[18] The HSC program was used for part of the calculations.[22] The effect of water vapor and carbon dioxide was taken into account. As standard thermodynamic data concerning NaK alloys were not found, all the diagrams, therefore, refer to sodium and potassium.

Chemicals: The commercially available potassium and sodium oxides are: sodium oxide Na_2O (Osi, France, 98%), sodium peroxide Na_2O_2 (Osi, France, 95%, aggregate size $\approx$ 1.5 mm) and potassium superoxide KO_2 (Merck, Germany, 96.5%, aggregate size $\approx$ 0.2 mm). They were ground before use. The NaK-56 liquid alloy was purchased from Callery Company, PA, USA. It corresponds to 56 wt-% K or 43 at-% K and will be denoted $Na_{0.57}K_{0.43}$. Data for $Na_{0.57}K_{0.43}$ alloy are: molar mass 29.8 g mol^{-1}; molar volume 33.5 cm^3 mol^{-1}; density 0.89 g cm^{-3}. The purity of the gases are: argon quality U, $O_2 < 5$ vpm, $H_2O < 5$ vpm; Azoxy N_2/O_2: 80%/20%, $H_2O < 5$ vpm. They were used without any further purification.

Apparatus and Measurements

***Differential Scanning Calorimetry*:** The tests involving pure oxides were performed between ambient temperature and 1300 °C by means of a Multi HTC SETARAM calorimeter with alumina as a reference. Inconel crucible (Ni-Cr-Fe alloy), volume 6.5 cm^3. The samples were studied under argon. Most of the calorimetric tests were performed using a DSC 111 SETARAM type calorimeter (temperature range −120 °C to 800 °C) in order to observe the melting point of NaK, (solid at −12.6 °C) and to calculate the amount of remaining NaK alloy. Volume of the stainless steel crucible: 0.170 cm^3. The samples were placed under argon. The results from the DSC 111 apparatus were numerized afterwards. For both apparatus, the calibration in temperature and enthalpy was performed with pure metals and the Joule effect. The heating rate was 1 K min^{-1}. The reported temperatures corresponded to the onset of the peaks.

***Mass Spectrometer*:** The laboratory mass spectrometer used was a quadripole-type residual gas analyzer, model Anagaz 200, marketed by the Quad/Service company. The samples were placed in a container equipped with a tight stainless steel connection, or in a crucible inserted into the container. They were first placed under primary vacuum, then swept with argon (N55 quality, $H_2O < 2$ vpm; $N_2 < 0.5$ vpm; $O_2 < 0.5$ vpm). The temperature of the sample was raised from ambient temperature up to 500 °C in a 100 °C step at a heating rate of 5 K min^{-1} between each 1 h plateau. The calibration was performed with the pure corresponding gases (H_2O, O_2).

***X-ray Diffraction*:** The diffractograms were obtained at room temperature with a Siemens D500 (Poitiers) or D5000 diffractometer (Cadarache) equipped with a copper anode [$\lambda(K_\alpha)$ = 1.54188 Å] and a back graphite monochromator, under the following conditions: dwell time 1 or 0.5 s; step 0.02 °; 2 theta range 5 to 80 °; divergence slit 1°. As most of the samples are air and particularly moisture sensitive, the samples were placed on the sample holder under argon and protected with polymer film for the D5000 diffractometer (Parafilm M, American National Can; XRD profile corresponding to polyethylene) or measured twice under air without protection for the D500 apparatus. The identified phases were the same but no quantitative analysis could be undertaken. The identification of the peaks was obtained by comparison with the PDF file (program Search of the Diffract-AT package, Socabim, France). Examples of raw diffractograms are given in Figure 8 and 9.

Reactivity Apparatus

***Measurement of the Reaction Temperature*:** In a glove-box filled with argon, about 2 g of liquid NaK alloy were introduced into a 20 mL glass flask equipped with a thermocouple. The oxide(s) were added separately or simultaneously and the mixture was manually stirred in order to ensure good contact between the alloy and the oxides.

***Preparation of Oxidized NaK by Sweeping*:** The apparatus (Figure 10) was made of a glass tube containing the boat (1 to 2 g of NaK alloy) and supplied by two inlets equipped with a flowmeter, one for argon and the other for the Azoxy mixture. The two gases were introduced independently or together. A coil was used to homogenize the mixture of argon and azoxy gases.

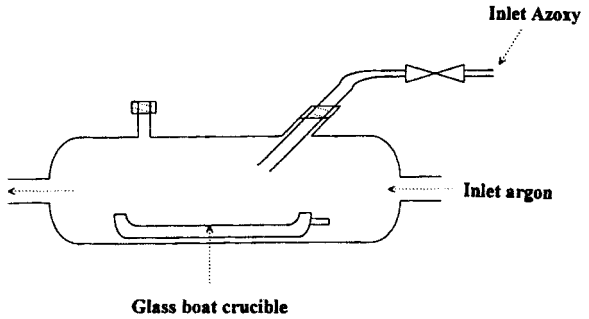


Figure 10. Device used for the preparation of oxidized NaK by sweeping

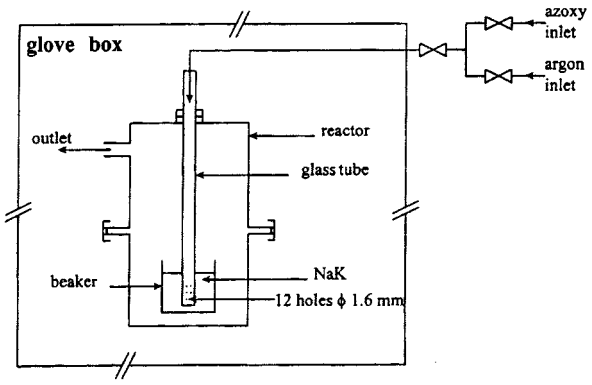


Figure 11. Device used for the preparation of oxidized NaK by bubbling

***Preparation of Oxidized NaK by Bubbling*:** Figure 11 shows the apparatus placed in a glove box. The NaK alloy (9.95 g) was placed in a beaker, which was itself enclosed in a reactor, with two gas inlet tubes (argon and Azoxy), permitting to bubble directly in the liquid alloy.

Acknowledgments

M. N. and C. K. thank the CEA (Commissariat à l'Energie Atomique) for financial support. CEA/DER/STPI/LPCP thanks LACCO laboratory for their great interest and collebration during this work.

[1] S. A. Sloan, *Proc. Int. Conf. Liq. Met. Technol. Energy Prod.* **1977**, Meeting **1976,** *2*, 675−80. (Eds: M. H. Cooper), NTIS, Springfield, VA.
[2] Safeguards Bulletin Issue **2/66**. *Authority Health and Safety Branch* Risley, UKAEA.
[3] S. A. Sloan, S. R. Whitby, *Microscope* **1977**, *25*, 237−43.
[4] J. C. Commander, Report (1975), *ANCR-1217*, 43 pp. Avail.: NTIS. From: *Nucl. Sci. Abstr.* **1975**, 32(9), Abstr. No. 21922.
[5] V. M. Sinclair, *UK Atomic Energy Authority, Reactor Group, Technical Memorandum* Jan. **1972**, TRG 6501 DERE UK AEA.
[6] N. J. L. Gardener, T. H. Green, DFR/DSWP/ **1984**, *84*, 127. OETD/SWP/ **1984,** *84*, 12.
[7] [7a] M. Hansen, K. Anderko, *Constitution of binary alloys*, McGraw-Hill: New York, 1958. − [7b] *Kirk Othmer Encyclopedia of Chemical Technology*, **1996**, *18,* 202−206.
[8] L. J. Gallego, J. M. Lopez, J. A. Alonso, *Z. Naturforsch. A* **1984**, *39A,* 842−5.
[9] D. R. Anderson, **1969**, 168 pp. Avail.: 70−1432: *Diss. Abstr. Int. B* **1970**, *30,* 3581.
[10] T. Yokokawa, O. J. Kleppa, *J. Chem. Phys.* **1964**, *40*, 46−54.
[11] F. A. Cafasso, M. Khanna and H. M. Feder, *Advanced Physics* **1967,** *16*, 535−43.
[12] I. H. Umar, A. Meyer, M. Watabe, W. H. Young, *J. Phys. F* **1974**, *4*, 1691−706.
[13] R. N. Singh, S. Singh, *Physica B+C (Amsterdam)* **1985**, *128,* 304−8.
[14] M. J. Zhu, D. M. Bylander, L. Kleinman, *Phys. Rev. B: Condens. Matter* **1996**, *53*, 14058−62.
[15] T. Khajil, *Turk. J. Phys.,* **1996**, *20*, 199−209.
[16] G. Hill, D. Holan, S. Kinrade, *Can. J. Chem.* **1997**, *75,* 46−50.
[17] P. Pascal, *Nouveau Traité de Chimie minérale, Tome II, Lithium, Sodium,* Masson: Paris, **1966.**
[18] *NIST Chemical Thermodynamic Database*, (NIST Standard Reference Database 2), *NIST JANAF Thermochemical Tables* (NIST Standard Reference Database 13), National Institute of Standards and Technology: Gaithersburg, MD, USA. FILE program.
[19] *Powder Diffraction File* (PDF-2), International Centre for Diffraction Data: Newtown Square, PA 19073−3273, USA.
[20] I. Barin, *Thermochemical Data of Pure Substances*, VCH Weinheim, Third Edition, **1995**.
[21] O. Knacke, O. Kubaschewski, K. Hesselmann, *Thermochemical Properties of Inorganic Substances,* Springer Verlag, Berlin **1991**, Second Edition.
[22] *HSC Chemistry, Chemical Reaction and Equilibrium Software with Extensive Thermochemical Database,* Version 3.0, Outokumpu Research Oy, Pori, Finland, **1997**.

Received November 26, 1999
[I99431]

Insertion of Isocyanide into Metal−Carbon Bonds of Alkylchloro(pentamethylcyclopentadienyl)niobium- and -tantalum Complexes − X-ray Structure of [TaCp*Cl_2(CH_2CMe_2Ph){η^2-C(CH_2CMe_2Ph)=N(2,6-$Me_2C_6H_3$)}] and Unexpected Decomposition of Alkyldichloro(η^2-iminoacyl) Complexes of Tantalum

Aurora Castro,[a] Mikhail V. Galakhov,[a] Manuel Gómez,*[a] Pilar Gómez-Sal,[a] Avelino Martín,[a] Fernando Sánchez,[a] and Patricia Velasco[a]

Keywords: Niobium / Tantalum / Metallacycles / η^2-Iminoacyl complexes / Insertions

Methylation of NbCp*Cl_2Me_2 using excess $ZnMe_2$ gives NbCp*$ClMe_3$ (**1**) which has been found to exhibit a Berry pseudorotation process on the NMR time scale (log A = 12.2 ± 0.3, E_a = 12.2 ± 0.4 kcal·mol^{-1}, $\Delta H^{\neq}$ = 11.6 ± 0.4 kcal·mol^{-1}, $\Delta S^{\neq}$ = −4.4 ± 1.3 e.u., $\Delta G^{\neq 298K}$ = 12.9 kcal·mol^{-1}). Alternatively, lithium dimethylamide reacts with NbCp*Cl_2Me_2 to form NbCp*$Me_2(NMe_2)_2$ (**2**) which decomposes in solution under the elimination of methane to give the (dimethylamido)methylazaniobacyclopropane derivative NbCp*Me(NMe_2)(η^2-CH_2NMe) (**3**). Reaction of NbCp*Cl_2Me_2 with 1 equiv. of 2,6-$Me_2C_6H_3NC$ results in a double methyl group migration to give the dichloroazaniobacyclopropane complex [NbCp*Cl_2\{η^2-CMe_2N(2,6-$Me_2C_6H_3$)\}] (**4**). Dialkyldichloro complexes TaCp*Cl_2R_2 [Cp* = η^5-C_5Me_5; R = CH_2SiMe_3 (**5**), CH_2CMe_2Ph (**6**), CH_2CMe_3 (**7**), $CH_2C_6H_5$ (**8**)] were obtained by treating TaCp*Cl_4 with the requisite amounts of the appropriate alkylating agents. Reactions of the dialkyldichloro complexes TaCp*Cl_2R_2 (**5**–**8**) with 1 equiv. of 2,6-$Me_2C_6H_3NC$ resulted in migration of only one of the two alkyl groups to give (alkyl)dichloro(η^2-iminoacyl) complexes [TaCp*Cl_2R\{η^2-C(R)=NAr\}] [Ar = 2,6-$Me_2C_6H_3$; R = CH_2SiMe_3 (**9**), CH_2CMe_2Ph (**10**), CH_2CMe_3 (**11**), $CH_2C_6H_5$ (**12**)]. The molecular structure of complex **10** has been determined by X-ray diffraction analysis. The η^2-iminoacyl complexes **9**–**12** decompose in [D_6]benzene or *n*-hexane solutions to give [TaCp*Cl_2\{N(2,6-$Me_2C_6H_3$)\}] and the corresponding *trans* or *cis* olefins R′–CH=CH–CH_2–R′ [R′ = $SiMe_3$ (**9o**), CMe_2Ph (**10o**), CMe_3 (**11o**), C_6H_5 (**12o**)]. A mechanism for this reaction is proposed. All the new compounds have been characterized by IR spectrophotometry, ^{1}H- and ^{13}C{^{1}H}-NMR spectroscopy, and elemental analysis.

Introduction

Migratory insertion of coordinated unsaturated molecules, such as carbon monoxide[1] or isocyanides,[2] into metal−alkyl bonds and the reactivity[3] of the resulting metal−acyl and metal−iminoacyl functions is one of the most important organometallic reactions, with many synthetic applications stemming from the C−C bond formation under mild reaction conditions. Several years ago, we reported the results of a systematic study[4] concerning the insertion of isocyanides into the tantalum−methyl bonds of various chloro(methyl)(pentamethylcyclopentadienyl) derivatives TaCp*$Cl_{4-x}Me_x$, which led to the synthesis of η^2-iminoacyl (x = 1), azatantalacyclopropane (x = 2), and (alkenylamido)imido (x = 3, 4) complexes.

In this context, the last years have witnessed a rapid development of early transition metal chemistry associated with imine ligands.[3,5] In these complexes, the imine linkage is typically found to bind strongly to the metal centre in an η^2-CN fashion and therefore they can be described as azametallacyclopropane derivatives. Although iminetantalum complexes have been postulated as intermediates in several organometallic transformations,[3a,3g,3i,6] only a few have been isolated and fully characterized.[4a,7] The formation of η^2-imino ligands at early transition metal centres can be achieved by the cyclometallation of dialkylamido ligands,[3g,3h] by alkyl or hydride reduction of η^2-iminoacyl ligands,[3b,3d,3e,3m,7e] by transfer of a hydrogen atom from an aminemetal complex,[7d] or in a few cases by addition of imines to low-valent metal derivatives.[3j,3k,5a,5j] Such an η^2 geometry has been identified in the crystal structures of some iminetantalum[4a] and -tungsten[3d,3e] complexes, and similar structures have been proposed for imine complexes of tantalum,[3a,8] zirconium,[3b] titanium,[9] and Group 8 metals.[10] Moreover, novel azazirconacyclopropane derivatives have been isolated[11] by orthometallation of 2,6-diethylpyridine with the cationic complex [$ZrCp_2Me(THF)$]$^+$. The analogous acetonetantalum or oxotantalacyclopropane complexes TaCp*X_2(η^2-$OCMe_2$), (X = Cl,[6] Me[1b]) are also thought to involve bonding through both the carbon and oxygen atoms.

In view of the high reactivities[3b,4,5a,5d,12] exhibited by these species, we decided to extend the study to bulky alkyltantalum derivatives. Thus, we report herein on the synthesis, insertion reactions, and intramolecular rearrange-

[a] Departamento de Química Inorgánica, Universidad de Alcalá de Henares, Campus Universitario,
E-28871 Alcalá de Henares, Spain
Fax: (internat.) + 34-91/885-4683
E-mail: manuel.gomez@uah.es

 © WILEY-VCH Verlag GmbH, D-69451 Weinheim, 2000 1434−1948/00/0909−2047 $ 17.50+.50/0

ment processes of the complexes obtained by treating dialkyldichloro(pentamethylcyclopentadienyl)niobium- and -tantalum(V) complexes with 2,6-$Me_2C_6H_3NC$.

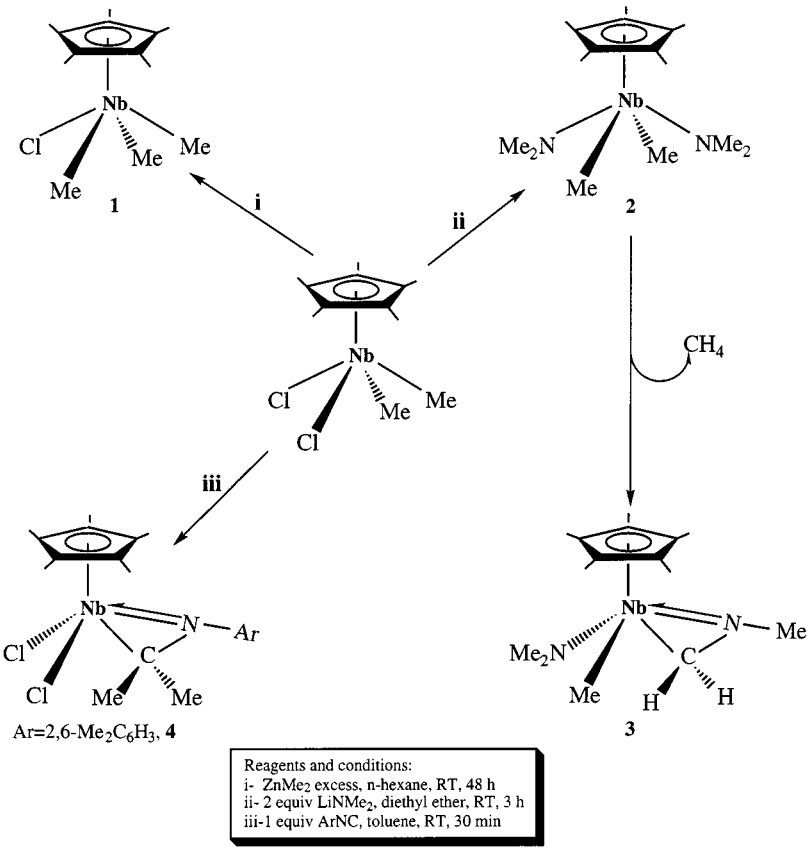
Results and Discussion

Alkylation and Insertion Reactions of $NbCp^*Cl_2Me_2$

The (chloro)trimethyl complex $NbCp^*ClMe_3$, **1**, was obtained by treatment of the dichlorodimethyl derivative[13] with an excess of $ZnMe_2$ (see Scheme 1). The ^{1}H- and $^{13}C\{^1H\}$-NMR spectra of **1** in [D_6]benzene solution at room temperature show only one signal for the three methyl groups, whereas the ^{1}H-NMR spectrum in [D_8]toluene solution at 223 K shows two narrow resonances in a 1:2 ratio. This NMR behaviour corresponds to a Berry pseudorotation process,[3g,14] akin to that reported for other tantalum complexes,[15] and is consistent with a four-legged pianostool geometry in the ground state. The kinetic parameters (log A = 12.2 ± 0.3, E_a = 12.2 ± 0.4 kcal·mol^{-1}, $\Delta H^{\neq}$ = 11.6 ± 0.4 kcal·mol^{-1}, $\Delta S^{\neq}$ = −4.4 ± 1.3 e.u., $\Delta G^{\neq 298K}$ = 12.9 kcal·mol^{-1}), calculated on the basis of the ^{1}H-DNMR data,[16] are consistent with such an intramolecular process with only a small variation in the entropy and thus support our proposed interpretation.

$NbCp^*Cl_2Me_2$ also reacts with 2 equiv. of lithium dimethylamide at room temperature in diethyl ether to give the expected product $NbCp^*Me_2(NMe_2)_2$ (**2**), which rapidly decomposes in solution under elimination of methane to give the η^2-imine complex $NbCp^*Me(NMe_2)(\eta^2$-$CH_2NMe)$ (**3**). Several attempts to separate **2** and **3** as microcrystalline materials proved unsuccessful and their structures have been proposed solely on the basis of ^{1}H-NMR data (see Experimental Section). The ^{1}H-NMR spectrum of **3** features one singlet due to the Cp* ring, one signal due to the NMe_2 moiety, two signals due to the methyl resonances of Nb−Me and N−Me, respectively, and two doublets due to the methylene protons. This NMR behaviour is in accordance with the chiral character of the metal centre. In view of the observation of the resonances of the CH_2 unit at δ_{av} = 1.25 with a typical geminal proton-proton coupling constant value ($^2J_{H-H}$ = 4.88 Hz) for a cyclopropane ring,[17] **3** must be described as an azaniobacyclopropane complex (see Scheme 1).

On addition of 1 equiv. of 2,6-$Me_2C_6H_3NC$ to toluene solutions of $NbCp^*Cl_2Me_2$ under rigorously anhydrous conditions, brown-red solutions were obtained, from which [$NbCp^*Cl_2\{\eta^2$-$CMe_2N(2,6$-$Me_2C_6H_3)\}$] (**4**) was recovered as a brown solid on removal of the solvent (Scheme 1). The equivalence of the methyl groups in the NMR spectra is consistent with a C_s-symmetry complex possessing a plane of symmetry defined by the niobium, the nitrogen, and the carbon atoms that is perpendicular to the plane of the pentamethylcyclopentadienyl ring. Previously, we have reported[4a] the synthesis, the mechanism of formation, and the crystal structure of a similar azatantalacyclopropane com-



Scheme 1

plex. In the present case, we were unable to obtain adequate single crystals for X-ray diffraction analysis, but like the tantalum analogue the structure must be a distorted trigonal bipyramid with the chlorine and nitrogen atoms occupying the equatorial plane positions and the centroid of the Cp* ring and the azaniobacyclopropane C atom occupying the apical sites.

When the same reaction was repeated at room temperature using 2 equiv. of isocyanide, a different sequence of reactions occurred leading to the diamagnetic pseudooctahedral niobium(III) complex $NbCp^*Cl_2(CN\text{-}2,6\text{-}Me_2C_6H_3)_3$. We have isolated this complex previously[18] by reducing $NbCp^*Cl_4$ with 2 equiv. of Na/Hg in the presence of a stoichiometric amount of isocyanide. This behaviour is in contrast to that observed in the case of $TaCp^*Cl_2Me_2$,[4b] which, in the presence of 2 equiv. of an isocyanide, gives the corresponding dichloro imido complex $TaCp^*Cl_2(NAr)$ (Ar = 2,6-$Me_2C_6H_3$, 2,4,6-$Me_3C_6H_2$) under elimination of the arylimine ketene Ar−N=C=CMe_2. The same dichloro tris(isocyanide) complex is obtained when 1 equiv. of the appropriate isocyanide is added to a toluene solution of the azaniobacyclopropane complex **4** at room temperature.

Synthesis and Reactivity of Dialkyldichloro(pentamethylcyclopentadienyl)tantalum(V) Complexes

On treating *n*-hexane suspensions of the complex $TaCp^*Cl_4$ with stoichiometric amounts of the alkylating reagents MgClR (R = CH_2SiMe_3, CH_2CMe_2Ph, CH_2Ph) or $Mg(CH_2CMe_3)_2(THF)_2$ under rigorously anhydrous conditions at room temperature, suspensions were obtained from which the dialkyldichloro complexes $TaCp^*Cl_2R_2$ [R = CH_2SiMe_3 (**5**), CH_2CMe_2Ph (**6**), CH_2CMe_3 (**7**), CH_2Ph (**8**)] could be isolated in good yields (see Scheme 2). The dineopentyl and dibenzyl derivatives **7** and **8** have been described previously by Schrock et al.[19] Several attempts to prepare **5**−**8** using stoichiometric amounts of lithium reagents proved unsuccessful and in all cases only unidentified reduction products were obtained. Complexes **5**−**8** were found to be air- and moisture-sensitive, and soluble in both *n*-hexane and aromatic solvents.

When 1 equiv. of the isocyanide 2,6-$Me_2C_6H_3NC$ was added to *n*-hexane solutions of the dialkyldichlorotantalum complexes **5**−**8** under a rigorously dry inert gas or in a sealed NMR tube, reddish solutions were obtained. After work-up, the alkyldichloro(η^2-iminoacyl)tantalum complexes [$TaCp^*Cl_2R\{\eta^2\text{-}C(R)=NAr\}$] [Ar = 2,6-$Me_2C_6H_3$; R = CH_2SiMe_3 (**9**), CH_2CMe_2Ph (**10**), CH_2CMe_3 (**11**), CH_2Ph (**12**)] could be recovered (Scheme 2). This behaviour is in contrast to that observed for the dichlorodimethyl derivative,[4] which, in the presence of 1 equiv. of isocyanide, gives a dichloroazatantalacyclopropane complex as a result of a migration of the second methyl group to the electrophilic iminoacyl carbon atom of the dichloro(η^2-iminoacyl)(methyl) intermediate. In the present case, the remaining bulkier alkyl substituent does not migrate. On the other hand, the same η^2-iminoacyl complexes **9**−**12** are obtained upon reaction of 2 equiv. of the isocyanide with the starting dialkyldichloro compounds in [D_6]benzene at room temperature and no bis(η^2-iminoacyl) species are detected.

All of the complexes **9**−**12** were found to be soluble in most organic solvents, including saturated hydrocarbons. They are extremely air- and moisture-sensitive, and rigorously dried solvents and handling under dry inert gases were found to be imperative for successful preparations.

The molecular structure of compound **10** is shown in Figure 1 and selected bond lengths and angles are given in Table 1. Complex **10** crystallizes in the space group $P2_1/c$ with the two possible enantiomers of the molecule present in the unit cell.

As can be seen, complex **10** is a monomer with the tantalum atom in a pseudooctahedral environment, where the centroid of the pentamethylcyclopentadienyl ring and the carbon atom of the iminoacyl group occupy the axial positions. The tantalum atom is located 0.61(1) Å above the plane formed by the C21, Cl1, Cl2, and N1 atoms.[20] The C=N bond of the iminoacyl group is almost perpendicular [75.0(2)°] to the plane formed by the two chlorine atoms, N1, and C21 of the neopentyl group. The difference between this angle and that for ideal perpendicularity accounts for the fact that two enantiomers are present in the unit cell.

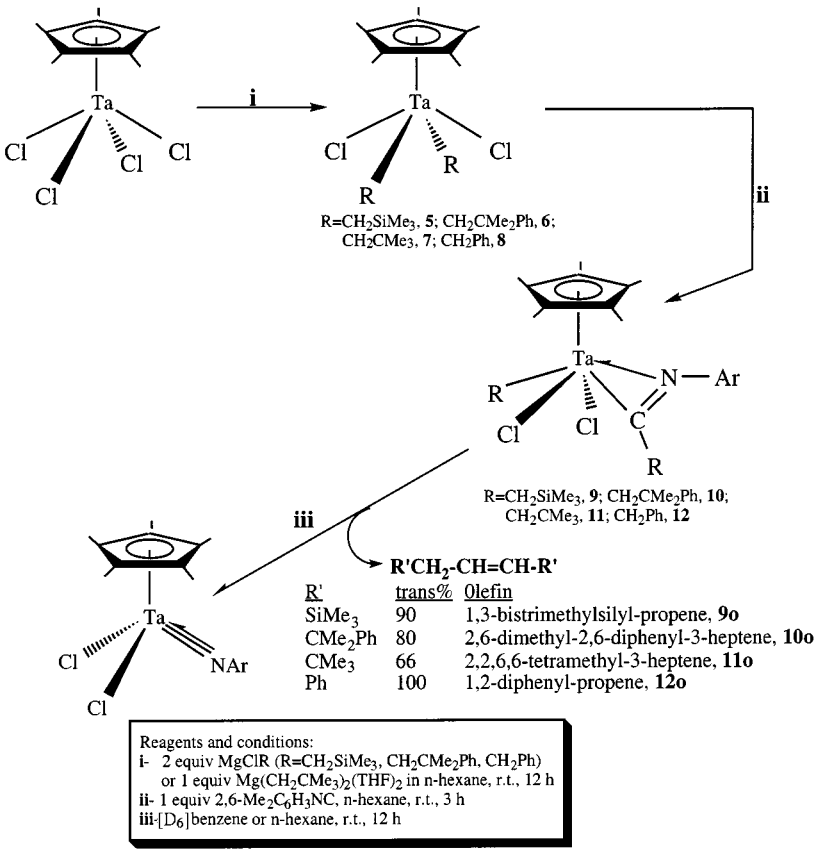
On the other hand, the *trans* effect of the iminoacyl group makes the distances between Ta1 and C11 [2.523(7) Å], C14 [2.528(7) Å], and C15 [2.591(7) Å] longer than the other two Ta−Cl distances [Ta1−C12 2.415(6) Å, Ta1−C13 2.437(6) Å].

Bond lengths in the η^2-iminoacyl group [N1−C41 1.262(7), N1−C42 1.482(7), and C41−C31 1.500(8) Å] are within the range found for other compounds[21] for which a C=N double bond and an η^2 coordination has been proposed. The plane formed by the aromatic ring C42−C47 is rotated by 70.6(2)° with respect to that formed by N1, C41, C42, and C31, partially preventing electronic delocalization over the iminoacyl and aromatic groups.

The IR, ^{1}H- and $^{13}C\{^1H\}$-NMR spectroscopic data (see Experimental Section) are consistent with the expected pseudooctahedral geometries of these η^2-iminoacyl complexes. The NMR spectra of **9**−**12** in [D_6]benzene solution at room temperature show the expected equivalence of the α-CH_2 protons of the inserted and non-inserted alkyl groups, in accordance with the *trans* disposition of the chlorine atoms and due to fast exchange between the two enantiomeric structures found in the solid state, the transition state of this process having C_s symmetry. Moreover, the 2,6-$Me_2C_6H_3$ ring of the η^2-iminoacyl ligand is characterized by C_{2v} local symmetry (Scheme 3).

The IR spectra of all the complexes show the characteristic absorptions for the pentamethylcyclopentadienyl ring ($\tilde{\nu}_{C-C}$ = 1027 cm^{-1})[22] and the trimethylsilyl substituent {$\tilde{\nu}$ = 1250 cm^{-1} [$\delta_{as}(CH_3)$]}.[23] Absorptions due to the C(R)=N, Ta−C, and Ta−Cl stretching vibrations are observed at $\tilde{\nu}$ = 1559,[23d,24] 525,[23d,25] and 278 cm^{-1},[23c,26] respectively.

In [D_6]benzene or *n*-hexane solution, **9**−**12** were found to spontaneously, albeit slowly, decompose at room temperature (see Scheme 4) to give a mixture of two components,



Scheme 2

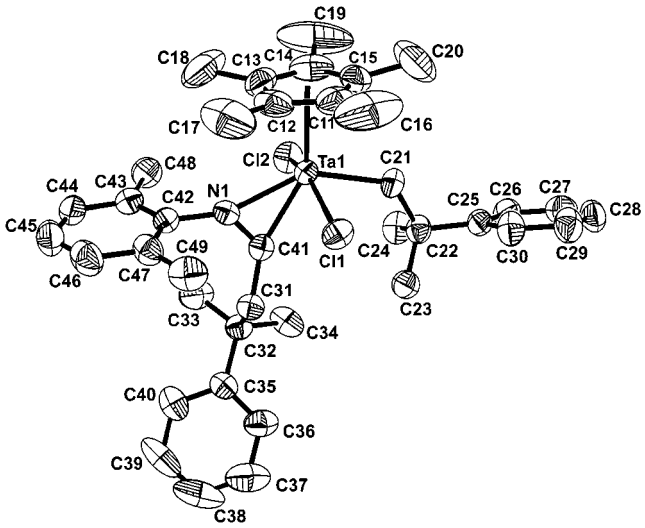


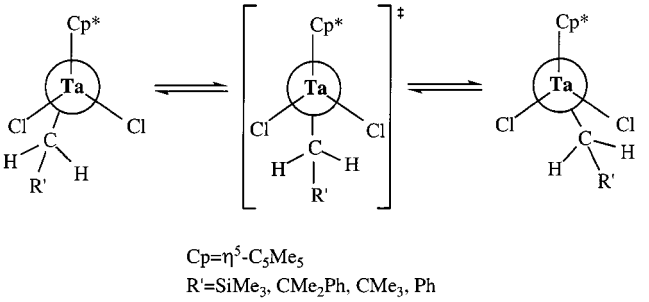
Figure 1. ORTEP view of the molecular structure of complex **10** with ellipsoids drawn at a 50% level

Table 1. Selected bond lengths [Å] and angles [°] for compound **10**

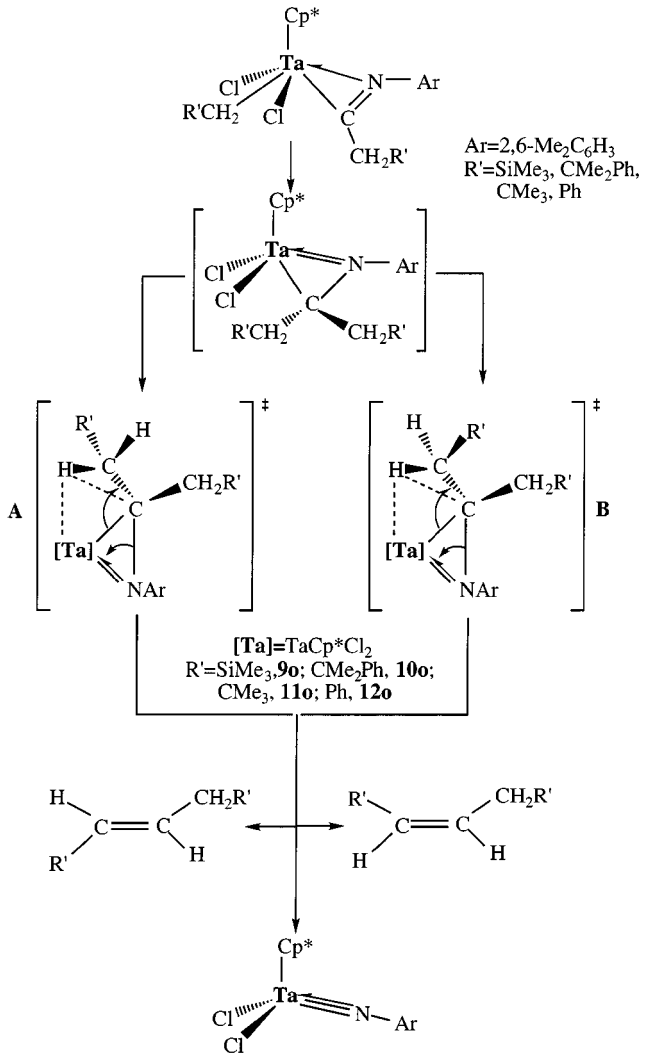
Ta(1)−N(1)	2.154(5)	Ta(1)−C(41)	2.175(6)
Ta(1)−C(21)	2.257(6)	Ta(1)−C(12)	2.415(6)
Ta(1)−Cl(2)	2.418(2)	Ta(1)−C(13)	2.437(6)
Ta(1)−Cl(1)	2.438(2)	Ta(1)−C(11)	2.523(7)
Ta(1)−C(14)	2.528(7)	Ta(1)−C(15)	2.591(7)
N(1)−C(41)	1.262(7)	N(1)−C(42)	1.481(7)
C(31)−C(41)	1.500(8)	C(42)−C(47)	1.396(8)
C(42)−C(43)	1.396(9)		
N(1)−Ta(1)−C(41)	33.89(18)	N(1)−Ta(1)−C(21)	142.4(2)
C(41)−Ta(1)−C(21)	108.8(2)	N(1)−Ta(1)−Cl(2)	85.10(12)
C(41)−Ta(1)−Cl(2)	82.55(14)	C(21)−Ta(1)−Cl(2)	84.04(16)
N(1)−Ta(1)−Cl(1)	89.55(13)	C(41)−Ta(1)−Cl(1)	77.49(14)
C(21)−Ta(1)−Cl(1)	83.17(16)	Cl(2)−Ta(1)−Cl(1)	151.32(6)
C(41)−N(1)−C(42)	128.8(5)	C(41)−N(1)−Ta(1)	73.9(3)
C(42)−N(1)−Ta(1)	156.3(4)	C(22)−C(21)−Ta(1)	131.2(4)
C(41)−C(31)−C(32)	118.6(5)	N(1)−C(41)−C(31)	125.0(5)
N(1)−C(41)−Ta(1)	72.2(3)	C(31)−C(41)−Ta(1)	158.5(4)

a dichloro(imido)tantalum compound [TaCp*Cl_2{N(2,6-$Me_2C_6H_3$)}][4a] together with *cis* and *trans* olefins R′−CH_2−CH=CH−R′ [R′ = $SiMe_3$ (**9o**), CMe_2Ph (**10o**), CMe_3 (**11o**), Ph (**12o**)],[27] which were fully characterized by NMR spectroscopy (see Experimental Section).

This transformation can be rationalized in terms of migration of the metal-bonded alkyl group to the iminoacyl carbon centre in the first step to give the intermediate dialkylazatantalacyclopropane complexes (see Scheme 4),



Scheme 3



Scheme 4

which cannot be detected during monitoring of the entire reaction by ^{1}H-NMR spectroscopy. However, the cyclopropane structure favours agostic interactions between the β-hydrogen atoms of the alkyl groups and the tantalum atom, leading to concerted four-centre transition states **A** and **B**.

Subsequent 2,1-migration of the hydrogen atom, probably through formation of a Ta hydride, and back-rearrangement gives the imido complex[4a] with elimination of the corresponding olefins **9o**−**12o**. The relative disposition of R′ and CH_2R' groups in **A** and **B** is dependent on the β-hydrogen atom that participates in an agostic interaction with the metal centre and thus determines the stereochemistry of the final olefins.

The data reported here are in contrast to our previous results concerning the insertion of isocyanides into Ta−C bonds of dimethyltantalum derivatives[4a] and show that these are more stable compared to the complexes **9**−**12**, probably due to steric factors.

Experimental Section

General: All reactions and manipulations were carried out under argon using standard Schlenk-tube and cannula techniques or in a conventional argon-filled MBraun glove-box.[28] Solvents were refluxed over appropriate drying agents and distilled and degassed prior to use: diethyl ether (sodium/benzophenone), *n*-hexane and [D_6]benzene (Na/K alloy). Literature methods were employed for the syntheses of the starting materials NbCp*Cl_2Me_2,[13] TaCp*Cl_2R_2 [19] [R = CH_2CMe_3 (**3**), CH_2Ph (**4**)], TaCp*Cl_4,[29] and $Mg(CH_2CMe_3)_2(THF)_2$.[30] 2 M $ZnMe_2$ in toluene (Aldrich), $LiNMe_2$ (Aldrich), 2,6-$Me_2C_6H_3NC$ (Aldrich), and MgClR (R = CH_2SiMe_3, 1 M in diethyl ether; CH_2CMe_2Ph, 0.5 M in diethyl ether; CH_2Ph 2 M in THF) (Aldrich) were purchased as reagent-grade materials and were used without further purification.

Infrared spectra were recorded with a Perkin−Elmer 583 spectrophotometer (4000−200 cm^{-1}) with samples as Nujol mulls between CsI plates or in polyethylene pellets. − ^{1}H- and $^{13}C\{^1H\}$-NMR spectra were recorded with Varian Unity 300 and Varian Unity 500 Plus spectrometers; chemical shifts were referenced to the ^{13}C (δ = 128) and residual ^{1}H (δ = 7.15) resonances of the [D_6]benzene solvent. − C, H, N analyses were carried out with a Perkin−Elmer 240C microanalyzer.

Synthesis of NbCp*$ClMe_3$ (1): A 2 M solution of $ZnMe_2$ in toluene (6.00 mmol, 3 mL) was added dropwise to NbCp*Cl_2Me_2 (1.00 g, 3.06 mmol) in *n*-hexane (100 mL) at room temperature to give an orange suspension. After stirring for 48 h, all volatiles were removed under reduced pressure and the residual red-orange solid was extracted with *n*-hexane (3 × 10 mL). The combined extracts were filtered and the filtrate was concentrated to a volume of 10 mL; on cooling overnight at −40 °C, **1** was deposited as a red-orange microcrystalline solid. Yield 0.37 g (40%). − IR (Nujol): $\tilde{\nu}$ = 1024 cm^{-1} s, 803 w, 723 w, 467 s, 326 s. − ^{1}H NMR (C_6D_6, 20 °C): δ = 1.54 (s, 15 H, C_5Me_5), 1.25 (s, 9 H, Nb−Me). − ^{1}H NMR (C_7D_8, −50 °C): δ = 1.44 (s, 15 H, C_5Me_5), 1.22 (s, 6 H, Nb−Me), 1.12 (s, 3 H, Nb−Me). − $^{13}C\{^1H\}$ NMR (C_6D_6, 20 °C): δ = 119.6 (C_5Me_5), 64.9 (br., Nb−Me), 11.6 (C_5Me_5). − $C_{13}H_{24}ClNb$ (308.694): calcd. C 50.58, H 7.84; found C 50.68, H 7.79.

Reaction of NbCp*Cl_2Me_2 with $LiNMe_2$: NbCp*Cl_2Me_2 (0.50 g, 1.53 mmol) and $LiNMe_2$ (0.16 g, 3.14 mmol) were stirred in diethyl ether (50 mL) at room temperature for 3 h. The resulting suspension was filtered and the solvent was removed from the filtrate to leave an oily residue. ^{1}H-NMR analysis showed this to consist of a mixture of [NbCp*$Me_2(NMe_2)_2$] (**2**) and [NbCp*$Me(NMe_2)(\eta^2$-$CH_2NMe)$] (**3**) in a 1:2 molar ratio. All attempts to separate the compounds by recrystallization were unsuccessful. − ^{1}H NMR (C_6D_6, 20 °C): **2**: δ = 3.00 (s, 12 H, Me_2N−Nb), 1.65 (s, 15 H, C_5Me_5), 0.38 (s, 6 H, Me−Nb); **3**: δ = 3.63 (s, 3 H, CH_2NMe), 2.72 (s, 6 H, Me_2N−Nb), 1.73 (s, 15 H, C_5Me_5), 1.51 (d, 1 H), 1.01 (d, $^2J_{H-H}$ = 4.88 Hz, 1 H, CH_2NMe), 0.53 (s, 3 H, Me−Nb).

Synthesis of [NbCp*$Cl_2\{\eta^2$-CMe_2−N(2,6-$Me_2C_6H_3$)}] (4): A solution of NbCp*Cl_2Me_2 (0.50 g, 1.53 mmol) in toluene (20 mL) was treated with (2,6-$Me_2C_6H_3$)NC (0.20 g, 1.53 mmol) under rigorously anhydrous conditions. The mixture was stirred for 30 min and then filtered. The filtrate was concentrated to dryness and the residue was washed with cold *n*-hexane (2 × 10 mL) to leave **4** as a brown microcrystalline solid. Yield 0.53 g (76%). − IR (Nujol): $\tilde{\nu}$ = 1259 cm^{-1} m, 1023 m, 768 m, 723 m, 371 m. − ^{1}H NMR (C_6D_6, 20 °C): δ = 6.94 (br., 3 H, $H_3C_6Me_2N$), 2.10 (s, 6 H, $Me_2C_6H_3N$), 2.00 (s, 6 H, Me_2C), 1.63 (s, 15 H, C_5Me_5). − $^{13}C\{^1H\}$ NMR

(C_6D_6, 20 °C): δ = 150.0, 132.2, 128.8, 124.0 (C_i, C_o, C_m, C_p, $C_6H_3Me_2N$), 122.8 (C_5Me_5), not observed (CMe_2), 28.7 (Me_2C), 20.4 ($Me_2C_6H_3N$), 11.1 (C_5Me_5). − $C_{21}H_{30}Cl_2NNb$ (460.29): calcd. C 54.80, H 6.57, N 3.04; found C 54.94, H 6.62, N 3.17.

Synthesis of TaCp*Cl$_2$R$_2$ [R = CH$_2$SiMe$_3$ (5), CH$_2$CMe$_2$Ph (6)]: A 1.0 M (**5**) or 0.5 M (**6**) solution of MgClR in diethyl ether (4.36 mmol; R = CH_2SiMe_3, 4.36 mL; CH_2CMe_2Ph, 8.73 mL) was added to a suspension of TaCp*Cl_4 (1.00 g, 2.18 mmol) in *n*-hexane (40 mL) at room temperature and the mixture was stirred for 12 h. The $MgCl_2$ formed was removed by filtration and the resulting filtrate was concentrated to a volume of ca. 10 mL. On cooling to −40 °C, orange (**5**) or red (**6**) microcrystalline solids were deposited.

Data for 5: Yield: 0.73 g (60%). − IR (Nujol): $\tilde{\nu}$ = 1327 cm^{-1} s, 1241 vs, 1024 m, 952 vs, 835 vs, 749 vs, 716 vs, 681 vs, 615 w, 567 m, 453 m, 365 m, 332 s, 269 vs. − ^{1}H NMR (C_6D_6, 20 °C): δ = 1.89 (s, 15 H, C_5Me_5), 0.79 (s, 4 H, H_2CSiMe_3), 0.42 (s, 18 H, Me_3SiCH_2). − ^{13}C{^{1}H} NMR (C_6D_6, 20 °C): δ = 124.78 (C_5Me_5), 94.57 (CH_2SiMe_3), 12.83 (C_5Me_5), 3.36 (Me_3SiCH_2). − $C_{18}H_{37}Cl_2Si_2Ta$ (561.52): calcd. C 38.50, H 6.64; found C 38.46, H 6.54.

Data for 6: Yield: 0.85 g (60%). − IR (Nujol): $\tilde{\nu}$ = 1597 cm^{-1} w, 1260 w, 1176 m, 1078 s, 1026 s, 804 w, 767 vs, 699 vs, 359 m, 301 vs. − ^{1}H NMR (C_6D_6, 20 °C): δ = 7.46 (d, $^3J_{H-H}$ = 7.5 Hz, 2 H), 7.25 (t, $^3J_{H-H}$ = 7.5 Hz, 2 H), 7.06 (t, $^3J_{H-H}$ = 7.5 Hz, 1 H, $H_5C_6CMe_2CH_2$), 1.83 (s, 6 H, CH_2CMe_2Ph), 1.73 (s, 15 H, C_5Me_5), 1.35 (s, 2 H, H_2CCMe_2Ph). − ^{13}C{^{1}H} NMR (C_6D_6, 20 °C): δ = 158.0, 125.75, 125.2, 116.05 (C_i, C_o, C_m, C_p, $C_6H_5Me_2CCH_2$), 124.34 (C_5Me_5), 44.05 (CH_2CMe_2Ph), 32.76 (CH_2CMe_2Ph), 31.4 (CH_2CMe_2Ph), 12.63 (C_5Me_5). − $C_{30}H_{41}Cl_2Ta$ (653.512): calcd. C 55.14, H 6.32; found C 54.96, H 6.18.

Synthesis of [TaCp*Cl$_2$R{η^2-C(R)=NAr}] [Ar = 2,6-Me$_2$C$_6$H$_3$; R = CH$_2$SiMe$_3$ (9), CH$_2$CMe$_2$Ph (10), CH$_2$CMe$_3$ (11), CH$_2$Ph (12)]

9−11: Under rigorously anhydrous conditions, *n*-hexane (20 mL) was added to a mixture of the complex TaCp*Cl_2R_2 (0.50 g; R = CH_2SiMe_3, 0.89 mmol; CH_2CMe_2Ph, 0.76 mmol; CH_2CMe_3, 0.94 mmol) and CN(2,6-$Me_2C_6H_3$) (R = CH_2SiMe_3, 0.116 g, 0.89 mmol; CH_2CMe_2Ph, 0.10 g, 0.76 mmol; CH_2CMe_3, 0.123 g, 0.94 mmol) in a Schlenk tube. The color quickly changed to dark red and after stirring for 3 h at room temperature, the resulting solution was filtered and the filtrate was concentrated to a volume of ca. 10 mL. Cooling at −40 °C overnight led to the deposition of microcrystalline solids identified as **9**, **10** (red), and **11** (red-orange).

Data for 9: Yield: 0.26 g (43%). − IR (Nujol): $\tilde{\nu}$ = 1553 cm^{-1} m, 1250 s, 1175 s, 1094 m, 1024 m, 980 s, 852 vs, 726 s, 672 m, 602 w, 573 w, 518 w, 449 w, 342 m, 268 s. − ^{1}H NMR (C_6D_6, 20 °C): δ = 6.90 (t, $^3J_{H-H}$ = 7.5 Hz, 1 H), 6.81 [d, $^3J_{H-H}$ = 7.5 Hz, 2 H, $H_3C_6Me_2N{=}C(CH_2SiMe_3)$], 3.44 [s, 2 H, $H_3C_6Me_2N{=}C(CH_2SiMe_3)$], 2.05 [s, 6 H, $H_3C_6Me_2N{=}C(CH_2SiMe_3)$], 1.93 (s, 15 H, C_5Me_5), 0.60 (s, 2 H, Ta−CH_2SiMe_3), 0.52 (s, 9 H, Ta−CH_2SiMe_3), 0.10 [s, 9 H, $H_3C_6Me_2N{=}C(CH_2SiMe_3)$]. − ^{13}C{^{1}H} NMR ($C_6D_6$, 20 °C): δ = 256.73 [$H_3C_6Me_2N{=}C(CH_2SiMe_3)$], 141.32, 132.92, 127.02, 125.41 [C_i, C_o, C_m, C_p, $H_3C_6Me_2N{=}C(CH_2SiMe_3)$], 129.45 ($C_5Me_5$), 51.76 [$H_3C_6Me_2N{=}C(CH_2SiMe_3)$], 31.32 (Ta−$CH_2SiMe_3$), 20.13 [$H_3C_6Me_2N{=}C(CH_2SiMe_3)$], 11.64 ($C_5Me_5$), 4.05 (Ta−$CH_2SiMe_3$), 0.66 [$H_3C_6Me_2N{=}C(CH_2SiMe_3)$]. − $C_{27}H_{46}Cl_2NSi_2Ta$ (692.698): calcd. C 46.82, H 6.69, N 2.02; found C 47.00, H 6.80, N 2.11.

Data for 10: Yield: 0.24 g (40%). − IR (Nujol): $\tilde{\nu}$ = 1536 cm^{-1} m, 1493 m, 1324 s, 1187 m, 1096 m, 1028 m, 982 m, 764 vs, 701 vs, 577 w, 548 w, 394 w, 350 s, 315 m, 285 m. − ^{1}H NMR (C_6D_6, 20 °C): δ = 7.70 (m, 2 H), 7.32 (m, 2 H), 7.11 (m, 2 H), 6.97 [m, 4 H, $H_3C_6Me_2N{=}C(CH_2CMe_2C_6H_5)$ and Ta−$CH_2CMe_2C_6H_5$], 6.80 (t, $^3J_{H-H}$ = 7.69 Hz, 1 H), 6.65 [d, $^3J_{H-H}$ = 7.69 Hz, 2 H, $H_3C_6Me_2N{=}C(CH_2CMe_2Ph)$], 4.19 [s, 2 H, $H_3C_6Me_2N{=}C(CH_2CMe_2Ph)$], 2.07 [s, 6 H, $H_3C_6Me_2N{=}C(CH_2CMe_2Ph)$], 1.82 (s, 15 H, C_5Me_5), 1.80 (s, 6 H, Ta−CH_2CMe_2Ph), 1.75 (s, 2 H, Ta−CH_2CMe_2Ph), 1.49 [s, 6 H, $H_3C_6Me_2N{=}C(CH_2CMe_2Ph)$]. − ^{13}C{^{1}H} NMR ($C_6D_6$, 20 °C): δ = 259.26 [$H_3C_6Me_2N{=}C(CH_2CMe_2Ph)$], 181.96−124.86 [several phenyl, $H_3C_6Me_2N{=}C(CH_2CMe_2C_6H_5)$ and Ta−$CH_2CMe_2C_6H_5$], 159.15−119.26 [several phenyl, $H_3C_6Me_2N{=}C(CH_2CMe_2C_6H_5)$], 125.57 ($C_5Me_5$), 88.56 [$H_3C_6Me_2N{=}C(CH_2CMe_2Ph)$], 51.10 (Ta−$CH_2CMe_2Ph$), 43.80 (Ta−$CH_2CMe_2Ph$), 40.18 [$H_3C_6Me_2N{=}C(CH_2CMe_2Ph)$], 32.81 (Ta−$CH_2CMe_2Ph$), 30.95 [$H_3C_6Me_2N{=}C(CH_2CMe_2Ph)$], 11.14 ($C_5Me_5$). − $C_{39}H_{50}Cl_2NTa$ (784.685): calcd. C 59.69, H, 6.42, N 1.78; found C 59.83, H 6.40, N 1.76.

Data for 11: Yield: 0.25 g (40%). − IR (Nujol): $\tilde{\nu}$ = 1556 cm^{-1} s, 1233 s, 1166 s, 1096 m, 1019 m, 830 m, 769 vs, 724 w, 649 m, 603 w, 510 w, 340 s, 279 vs, 231 m. − ^{1}H NMR (C_6D_6, 20 °C): δ = 6.83 (m, 1 H), 6.77 [m, 2 H, $H_3C_6Me_2N{=}C(CH_2CMe_3)$], 3.64 [s, 2 H, $H_3C_6Me_2N{=}C(CH_2CMe_3)$], 2.02 [s, 6 H, $H_3C_6Me_2N{=}C(CH_2CMe_3)$], 1.90 (s, 15 H, C_5Me_5), 1.59 [s, 9 H, $H_3C_6Me_2N{=}C(CH_2CMe_3)$], 1.54 (s, 2 H, Ta−$CH_2CMe_3$), 1.07 (s, 9 H, Ta−$CH_2CMe_3$). − ^{13}C{^{1}H} NMR ($C_6D_6$, 20 °C): δ = 260.94 [$H_3C_6Me_2N{=}C(CH_2CMe_3)$], 141.70, 132.63, 129.50, 127.00 [C_i, C_o, C_m, C_p, $H_3C_6Me_2N{=}C(CH_2CMe_3)$], 125.74 ($C_5Me_5$), 88.10 [$H_3C_6Me_2N{=}C(CH_2CMe_3)$], 50.36 (Ta−$CH_2CMe_3$), 37.41 [$H_3C_6Me_2N{=}C(CH_2CMe_3)$], 36.10 [$H_3C_6Me_2N{=}C(CH_2CMe_3)$], 34.22 (Ta−$CH_2CMe_3$), 31.70 (Ta−$CH_2CMe_3$), 20.19 [$H_3C_6Me_2N{=}C(CH_2CMe_3)$], 11.66 ($C_5Me_5$). − $C_{29}H_{46}Cl_2NTa$ (660.548): calcd. C 52.73, H 7.02, N 2.12; found C 52.93, H 7.04, N 2.28.

12: A solution of TaCp*$Cl_2(CH_2Ph)_2$ (0.50 g, 0.88 mmol) in *n*-hexane (15 mL) was treated with the isocyanide (2,6-$Me_2C_6H_3$)NC (0.115 g, 0.88 mmol) under rigorously anhydrous conditions. The color of the solution rapidly changed from brown-green to purple and after 2 h, a red microcrystalline precipitate had separated. This was collected by filtration, washed with a small volume of cold *n*-hexane, and dried in vacuo.

Data for 12: Yield: 0.31 g (50%). − IR (Nujol): $\tilde{\nu}$ = 1614 cm^{-1} m, 1590 m, 1290 m, 1262 s, 1162 s, 1100 s, 1064 s, 1024 s, 804 s, 724 vs, 690 s, 352 m, 280 m. − ^{1}H NMR (C_6D_6, 20 °C): δ = 7.84 (m, 3 H), 7.52 [m, 2 H, $H_3C_6Me_2N{=}C(CH_2C_6H_5)$], 6.96 (m, 2 H), 6.50 [m, 1 H, $H_3C_6Me_2N{=}C(CH_2Ph)$], 6.70 (m, 5 H, Ta−$CH_2C_6H_5$), 3.86 [s, 2 H, $H_3C_6Me_2N{=}C(CH_2Ph)$], 2.11 (s, 2 H, Ta−$CH_2C_6H_5$), 1.89 (s, 15 H, C_5Me_5), 1.61 [s, 6 H, $H_3C_6Me_2N{=}C(CH_2Ph)$]. − ^{13}C{^{1}H} NMR (C_6D_6, 20 °C): δ = 258 [$H_3C_6Me_2N{=}C(CH_2Ph)$], 152.58−122.31 [several phenyl, $H_3C_6Me_2N{=}C(CH_2C_6H_5)$ and Ta−$CH_2C_6H_5$], 124.94 (C_5Me_5), 70.53 [$H_3C_6Me_2N{=}C(CH_2Ph)$], 37.74 (Ta−$CH_2C_6H_5$), 20.45 [$H_3C_6Me_2N{=}C(CH_2Ph)$], 11.39 (C_5Me_5). − $C_{33}H_{38}Cl_2NTa$ (700.528): calcd. C 56.58, H 5.47, N 2.00; found C 56.48, H 5.63, N 2.28.

Decomposition Reaction of [TaCp*Cl$_2$R{η^2-C(R)=NAr}] [Ar = 2,6-Me$_2$C$_6$H$_3$; R = CH$_2$SiMe$_3$ (9), CH$_2$CMe$_2$Ph (10), CH$_2$CMe$_3$ (11), CH$_2$Ph (12)]: A solution of **9−12** (0.50 mmol) in [D_6]benzene was placed in a valved NMR tube under rigorously anhydrous conditions. The reaction was monitored by ^{1}H- and ^{13}C-NMR spectroscopy until no further change was observed (ca. 12 h). The final spectrum was indicative of complete transformation of the starting material to a mixture of the two components, i.e. a dichloro(imido)

complex $TaCp^*Cl_2(NAr)$ and an olefin **9o**−**12o** (*cis*/*trans* isomers).[27]

X-ray Structure Determination of 10: A red, block-shaped crystal of compound **10**, crystallized from *n*-hexane at −40°C, was mounted in a glass capillary in a random orientation on an Enraf−Nonius CAD-4 four-circle automatic diffractometer and examined with graphite-monochromated Mo-K_α radiation (λ = 0.71073 Å). Crystallographic and experimental details for **10** are summarized in Table 2. Intensities were corrected for Lorentz and polarization effects in the usual manner. Intensity measurements were performed by ω-θ scans in the range $6° < 2\theta < 50°$.

Table 2. Crystal and X-ray structural analysis data for the compound $[TaCp^*Cl_2(CH_2CMe_2Ph)\{\eta^2\text{-}C(CH_2CMe_2Ph)=N(2,6\text{-}Me_2\text{-}C_6H_3)\}]$ (**10**)

Empirical formula	$C_{39}H_{50}Cl_2NTa$
Molecular mass	784.65
Temperature [K]	293(2)
Crystal system	monoclinic
Space group	$P2_1/c$
a, *b*, *c* [Å]	16.602(4), 11.411(5), 20.522(4)
β [°]	112.66(4)
Volume; *Z*	3587(2) Å^3; 4
Density (calculated)	1.453 g/cm^3
μ (Mo-K_α)	3.240 mm^{-1}
F(000)	1592
Crystal size	0.40 × 0.35 × 0.32 mm
Index ranges	$0 < h < 19$, $0 < k < 13$, $-24 < l < 22$
Reflections collected	6507
Independent reflections	6276 (R_{int} = 0.0454)
Observed reflections [$I > 2\sigma(I)$]	5251
Data/restraints/parameters	6276/0/399
Goodness-of-fit on F^2	0.903
Final R indices [$I > 2\sigma(I)$]	$R1$ = 0.040, $wR2$ = 0.101
R indices (all data)	$R1$ = 0.054, $wR2$ = 0.110
Largest diff. peak and hole	1.828 and −1.793 eÅ^{-3}

The structure was solved by direct methods (SHELXS-97)[31] using the WINGX package and refined by least-squares against F^2 (SHELXL-97). Of the 6507 measured reflections, 6276 were independent; $R1$ = 0.040 and $wR2$ = 0.101 [for 5251 reflections with $F > 4\sigma(F)$]. The values of $R1$ and $wR2$ are defined as $R1 = \Sigma||F_o| - |F_c||/[\Sigma|F_o|]$; $wR2 = \{[\Sigma w(F_o^2 - F_c^2)^2]/[\Sigma w(F_o^2)^2]\}^{1/2}$, where $w = 1/[\sigma^2(F_o^2) + (0.081)^2 + 9.023P]$, $P = (F_o^2 + 2F_c^2)/3$, and σ was obtained from the counting statistics. All non-hydrogen atoms were refined anisotropically, while the hydrogen atoms were introduced in calculated positions in the final cycle of the refinement and refined using a riding model with thermal parameters fixed at U = 0.08 Å^2.

Crystallographic data (excluding structure factors) for the structure reported in this paper have been deposited with the Cambridge Crystallographic Data Centre as supplementary publication no. CCDC-139661. Copies of the data can be obtained free of charge on application to the CCDC, 12 Union Road, Cambridge CB2 1EZ, U.K. [Fax: (internat.) + 44-1223/336-033; E-mail: deposit@ccdc.cam.ac.uk].

Acknowledgments

We are grateful to the DGICYT (Project PB-97−0761) for financial support of this research.

[1] [1a] F. Calderazzo, *Angew. Chem.* **1977**, *89*, 305−317. − [1b] C. D. Wood, R. R. Schrock, *J. Am. Chem. Soc.* **1979**, *101*, 5421−5422. − [1c] E. J. Kuhlmann, J. J. Alexander, *Coord. Chem. Rev.* **1980**, *33*, 195−225.

[2] [2a] P. M. Treichel, *Adv. Organomet. Chem.* **1973**, *11*, 21−86. − [2b] R. A. Andersen, *Inorg. Chem.* **1979**, *18*, 2928−2932.

[3] [3a] Y. Takahashi, N. Onoyama, Y. Ishikawa, S. Motojima, K. Sugiyama, *Chem. Lett.* **1978**, 525−528. − [3b] P. T. Wolczanski, J. E. Bercaw, *J. Am. Chem. Soc*. **1979**, *101*, 6450−6452. − [3c] P. T. Wolczanski, J. E. Bercaw, *Acc. Chem. Res.* **1980**, *13*, 121−127. − [3d] K. W. Chiu, R. A. Jones, G. Wilkinson, A. M. R. Galas, M. B. Hursthouse, *J. Am. Chem. Soc.* **1980**, *102*, 7979−7980. − [3e] K. W. Chiu, R. A. Jones, G. Wilkinson, A. M. R. Galas, M. B. Hursthouse, *J. Chem. Soc., Dalton Trans.* **1981**, 2088−2097. − [3f] E. Singleton, H. E. Oosthuizen, *Adv. Organomet. Chem.* **1983**, *22*, 209−310. − [3g] J. M. Mayer, C. J. Curtis, J. E. Bercaw, *J. Am. Chem. Soc.* **1983**, *105*, 2651−2660. −[3h] W. A. Nugent, D. W. Overall, S. J. Holmes, *Organometallics* **1983**, *2*, 161−162. − [3i] L. R. Chamberlain, I. P. Rothwell, J. C. Huffman, *J. Chem. Soc., Chem. Commun.* **1986**, 1203−1205. −[3j] T. Sielisch, U. Behrens, *J. Organomet. Chem.* **1986**, *310*, 179−187. − [3k] H. Brunner, J. Wachter, J. Schmidbauer, *Organometallics* **1986**, *5*, 2212−2219. −[3l] L. D. Durfee, P. E. Fanwick, I. P. Rothwell, K. Folting, J. C. Huffman, *J. Am. Chem. Soc.* **1987**, *109*, 4720−4722. − [3m] L. R. Chamberlain, B. D. Steffey, I. P. Rothwell, J. C. Huffman, *Polyhedron* **1989**, *8*, 341−349. − [3n] L. D. Durfee, J. E. Hill, P. E. Fanwick, I. P. Rothwell, *Organometallics* **1990**, *9*, 75−80.

[4] [4a] M. V. Galakhov, M. Gómez, G. Jimenez, P. Royo, M. A. Pellinghelli, A. Tiripicchio, *Organometallics* **1995**, *14*, 1901−1910. − [4b] M. V. Galakhov, M. Gómez, G. Jimenez, P. Royo, M. A. Pellinghelli, A. Tiripicchio, *Organometallics* **1995**, *14*, 2843−2854.

[5] [5a] E. J. Roskamp, S. F. Pedersen, *J. Am. Chem. Soc.* **1978**, *109*, 6551. − [5b] S. L. Buchwald, B. T. Watson, M. W. Wannamaker, J. C. Dewan, *J. Am. Chem. Soc.* **1989**, *111*, 4486−4494. − [5c] J. R. Strickler, D. E. Wigley, *Organometallics* **1990**, *9*, 1665−1669. − [5d] N. Coles, M. C. J. Harris, R. J. Whitby, J. Blagg, *Organometallics* **1994**, *13*, 190−199. − [5e] B. Richter, J. Scholz, J. Sieler, K.-H. Thiele, *Angew. Chem. Int. Ed. Engl.* **1995**, *34*, 2649−2651. − [5f] D. A. Gately, J. R. Norton, P. A. Goodson, *J. Am. Chem. Soc.* **1995**, *117*, 986−996. − [5g] P. Legzdins, P. J. Lundmark, S. J. Rettig, *Organometallics* **1996**, *15*, 2988−2993. − [5h] Y. Makioka, Y. Taniguchi, Y. Fujiwara, K. Takaki, Z. Hou, Y. Wakatsuki, *Organometallics* **1996**, *15*, 5476−5478. − [5i] M. J. Scott, S. J. Lippard, *Organometallics* **1997**, *16*, 5857−5868. − [5j] K. Takai, T. Ishiyama, H. Yasue, T. Nobunaka, M. Itoh, T. Oshiki, K. Mashima, K. Tani, *Organometallics* **1998**, *17*, 5128−5132.

[6] M. Gómez, P. Gómez-Sal, G. Jimenez, A. Martín, P. Royo, J. Sánchez-Nieves, *Organometallics* **1996**, *15*, 3579−3587.

[7] [7a] D. R. Neithamer, L. Párkányi, J. F. Mitchell, P. T. Wolczanski, *J. Am. Chem. Soc.* **1988**, *110*, 4421−4423. − [7b] J. R. Strickler, M. A. Bruck, D. E. Wigley, *J. Am. Chem. Soc.* **1990**, *112*, 2814−2816. − [7c] D. P. Smith, J. R. Strickler, S. D. Gray, M. A. Bruck, R. S. Holmes, D. E. Wigley, *Organometallics* **1992**, *11*, 1275−1288. − [7d] J. M. Boncella, M. L. Cajigal, K. A. Abboud, *Organometallics* **1996**, *15*, 1905−1912. − [7e] J. R. Clark, P. E. Fanwick, I. P. Rothwell, *Organometallics* **1996**, *15*, 3232−3237.

[8] C. Airoldi, D. C. Bradley, G. Vuru, *Transition Met. Chem.* **1979**, *4*, 64.

[9] E. Klei, Thesis, Rijksuniversiteit Groningen, The Netherlands, **1981**.

[10] [10a] J. Browning, H. D. Empsall, M. Green, F. G. A. Stone, *J .Chem. Soc., Dalton Trans.* **1973**, 381−387. − [10b] D. Walther, *Z. Anorg. Allg. Chem.* **1977**, *431*, 17−30.

[11] A. S. Guram, D. C. Swenson, R. F. Jordan, *J. Am. Chem. Soc*. **1992**, *114*, 8991−8996.

[12] [12a] M. Jensen, T. Livinghouse, *J. Am. Chem. Soc.* **1989**, *111*, 4495−4496. − [12b] E. J. Roskamp, P. S. Dragovich, J. B. Hartung, Jr., S. F. Pedersen, *J. Org. Chem.* **1989**, *54*, 4736−4737. − [12c] T. Imamoto, S. Nishimura, *Chem. Lett.* **1990**, 1141−1142. − [12d] H. Ito, T. Taguchi, Y. Hanzawa, *Tetrahedron Lett.* **1992**, *33*, 4469−4472. − [12e] T. Honda, S.-I. Satoh, M. Mori, *Organometallics* **1995**, *14*, 1548−1550. −[12f] Y. Gao, Y. Yoshida, F. Sato, *Synlett* **1997**, 1353−1354.

[13] P. A. Belmonte, F. G. N. Cloke, K. H. Theopold, R. R. Schrock, *Inorg. Chem.* **1984**, *23*, 2365−2367.

[14] [14a] S. J. McLain, C. Wood, R. R. Schrock, *J. Am. Chem. Soc*. **1979**, *101*, 4558−4570. − [14b] P. Kubàcek, R. Hoffman, Z. Havlas, *Organometallics* **1982**, *1*, 180−188.

[15] I. de Castro, M. V. Galakhov, M. Gómez, P. Gómez-Sal, A. Martín, P. Royo, *J. Organomet. Chem.* **1996**, *514*, 51−58.
[16] [16a] S. Abragam, *The Principles of Nuclear Magnetism*, Clarendon Press, Oxford, **1961**.[16b] K. M. Jackman, F. A. Cotton, *DNMR Spectroscopy*, Academic Press, New York, **1975**.
[17] E. Pretsch, T. Clerc, J. Seibl, W. Simon, *Tablas para la Elucidación Estructural de Compuestos Orgánicos*, Ed. Alhambra, **1980**.
[18] M. I. Alcalde, J. de la Mata, M. Gómez, P. Royo, M. A. Pellinghelli, A. Tiripicchio, *Organometallics* **1994**, *13*, 462−467.
[19] [19a] S. J. McLain, R. R. Schrock, P. R. Sharp, M. R. Churchill, W. Youngs, *J. Am. Chem. Soc.* **1979**, *101*, 263−265. − [19b] L. W. Messerle, P. Jennische, R. R. Schrock, G. Stucky, *J. Am. Chem. Soc.* **1980**, *102*, 6744−6752.
[20] PARST: [20a] M. Nardelli, *Comput. Chem.* **1983**, *7*, 95−98. − [20b] M. Nardelli, *J. Appl. Crystallogr.* **1995**, *28*, 659.
[21] L. D. Durfee, I. P. Rothwell, *Chem. Rev.* **1988**, *88*, 1059−1079.
[22] R. B. King, M. B. Bisnette, *J. Organomet. Chem.* **1967**, *8*, 287−297.
[23] [23a] M. Gómez, G. Jimenez, P. Royo, J. M. Selas, P. R. Raithby, *J. Organomet. Chem.* **1992**, *439*, 147−154. − [23b] I. de Castro, J. de la Mata, M. Gómez, P. Gómez-Sal, P. Royo, J. M. Selas, *Polyhedron* **1992**, *11*, 1023−1027. − [23c] A. Castro, M. Gómez, P. Gómez-Sal, A. Manzanero, P. Royo, *J. Organomet. Chem.* **1996**, *518*, 37−46. − [23d] A. Castro, M. V. Galakhov, M. Gómez, P. Gómez-Sal, A. Martín, F. Sánchez, *J. Organomet. Chem.* **2000**, *595*, 36−53.
[24] [24a] E. Klei, J. H. Telgen, J. H. Teuben, *J. Organomet. Chem.* **1981**, *209*, 297−307. − [24b] L. R. Chamberlain, L. D. Durfee, P. E. Fanwick, L. Kobriger, S. L. Latesky, A. K. McMullen, I. P. Rothwell, K. Folting, J. C. Huffman, W. E. Streib, R. Wang, *J. Am. Chem. Soc.* **1987**, *109*, 390−402.
[25] [25a] G. W. A. Fowles, D. A. Rice, D. Wilkins, *J. Chem. Soc., Dalton Trans.* **1972**, 2313−2318; G. W. A. Fowles, D. A. Rice, D. Wilkins, *J. Chem. Soc., Dalton Trans.* **1974**, 1080−1084. − [25b] R. R. Schrock, P. Meakin, *J. Am. Chem. Soc.* **1974**, *96*, 5288−5290. − [25c] C. Santini-Scampucci, J. D. Riess, *J. Chem. Soc., Dalton Trans.* **1973**, 2436−2440.
[26] [26a] K. Nakamoto, *Characterization of Organometallic Compounds*, 4th ed. (Ed.: M. Tsutsui), Interscience, New York, **1986**. − [26b] R. J. H. Clark, M. A. Coles, *J. Chem. Soc., Dalton Trans.* **1974**, 1462−1467. − [26c] A. Antiñolo, M. Fajardo, A. Otero, P. Royo, *J. Organomet. Chem.* **1982**, *234*, 309−314; A. Antiñolo, M. Fajardo, A. Otero, P. Royo, *J. Organomet. Chem.* **1983**, *246*, 269−278; A. Antiñolo, M. Fajardo, A. Otero, P. Royo, *J. Organomet. Chem* **1984**, *265*, 35−43.
[27] NMR data for olefins R′−C^1H_2−C^2H=C^3H−R′ (**9o**−**12o**). − ^{1}H NMR (C_6D_6, 20 °C): **9o** (R′ = $SiMe_3$), *trans* isomer: δ = 6.38 (dt, $^3J_{H2-H1}$ = 6.8 Hz, $^3J_{H2-H3}$ = 14.1 Hz, 1 H, R′−CH_2−C*H*=CH−R′), 5.48 (dt, $^3J_{H2-H3}$ = 14.1 Hz, 1 H, R′−CH_2−CH=C*H*−R′), 2.20 (d, 2 H, R′−CH_2−CH=CH−R′), 0.19 (s, 9 H, R′−CH_2−CH=CH−SiMe_3), −0.01 (s, 9 H, Me_3Si−CH_2−CH=CH−R′). − **10o** (R′ = CMe_2Ph), *trans* isomer: δ = 5.51 (dt, $^3J_{H3-H1}$ = 2 Hz, $^3J_{H2-H3}$ = 15.5 Hz, 1 H, R′−CH_2−CH=C*H*−R′), 5.27 (dt, $^3J_{H2-H1}$ = 15.5 Hz, 1 H, R′−CH_2−C*H*=CH−R′), 2.26 (dd, 2 H, R′−CH_2−CH=CH−R′), 1.22 (s, 12 H, PhMe_2C−CH_2−CH=CH−CMe_2Ph); *cis* isomer: δ = 5.59 (dt, $^3J_{H2-H3}$ = 11.7 Hz, $^4J_{H3-H1}$ = 2 Hz, 1 H, R′−CH_2−CH=C*H*−R′), 5.16 (dt, $^3J_{H2-H3}$ = 11.7 Hz, $^3J_{H2-H1}$ = 7 Hz, 1 H, R′−CH_2−C*H*=CH−R′), 2.01 (dd, 2 H, R′−CH_2−CH=CH−R′), 1.32 (s, 6 H), 1.03 (s, 6 H, PhMe_2C−CH_2−CH=CH−CMe_2Ph). − **11o** (R′ = CMe_3), *trans* isomer: δ = 5.46 (dt, $^3J_{H2-H3}$ = 12.2 Hz, $^4J_{H1-H3}$ = 1.8 Hz, 1 H, R′−CH_2−CH=C*H*−R′), 5.31 (dt, $^3J_{H2-H3}$ = 12.2 Hz, $^3J_{H1-H2}$ = 6.5 Hz, 1 H, R′−CH_2−C*H*=CH−R′), 2.12 (dd, 2 H, R′−CH_2−CH=CH−R′), 1.12 (s, 9 H, R′−CH_2−CH=CH−CMe_3), 0.90 (s, 9 H, Me_3C−CH_2−CH=CH−R′) [^{13}C{^{1}H} DEPT NMR data: **11o**, *trans* isomer: δ = 141.23 (C^3), 126.14 (C^2), 42.13 (C^1); *cis* isomer: δ = 144.58 (C^3), 122.25 (C^2), 47.4 (C^1)]; *cis* isomer: δ = 5.47 (dt, $^3J_{H2-H3}$ = 12 Hz, $^4J_{H1-H3}$ = 1.8 Hz, 1 H, R′−CH_2−CH=C*H*−R′), 5.42 (dt, J_{H2-H3} = 12 Hz, $^3J_{H1-H2}$ = 6.5 Hz, 1 H, R′−CH_2−C*H*=CH−R′), 1.88 (dd, 2 H, R′−CH_2−CH=CH−R′), 1.01 (s, 9 H, R′−CH_2−CH=CH−CMe_3), 0.88 (s, 9 H, Me_3C−CH_2−CH=CH−R′). − **12o** (R′ = Ph), *trans* isomer: δ = 6.30 (dt, $^3J_{H2-H3}$ = 16 Hz, $^4J_{H1-H3}$ = 1 Hz, 1 H, R′−CH_2−CH=C*H*−R′), 6.18 (dt, $^3J_{H2-H3}$ = 16 Hz, $^3J_{H1-H2}$ = 6.9 Hz, 1 H, R′−CH_2−C*H*=CH−R′), 3.30 (dd, 2 H, R′−CH_2−CH=CH−R′). (For **10o** and **12o**: The spectral region corresponding to the phenyl protons cannot be analyzed, but the integral is 10 H for each isomer of **10o** and for the *trans* isomer of **12o**.)
[28] R. J. Errington, *Advanced Practical Inorganic and Metalorganic Chemistry*, Blackie A & Pan Imprint of Chapman & Hall, London, UK, **1997**.
[29] [29a] W. A. Herrmann, W. Kalcher, H. Biersack, J. Bernal, M. Creswick, *Chem. Ber.* **1981**, *114*, 3558−3571. −[29b] R. D. Sanner, S. T. Carter, W. J. Bruton, *J. Organomet. Chem.* **1982**, *240*, 157−162.
[30] R. R. Schrock, *J. Organomet. Chem.* **1976**, *122*, 209−225.
[31] G. M. Sheldrick, *SHELX-97: Programs for Crystal Structure Analysis (Release 97−2)*, Universität Göttingen, Germany, **1998**.

Received February 2, 2000
[I00033]

Synthesis and Single-Crystal X-ray Diffraction Studies of New Cyclometallated Phenylimidazole Palladium(II) Compounds

Mariela Lousame,[b] Alberto Fernández,[b] Margarita López-Torres,[b] Digna Vázquez-García,[b] José M. Vila,*[a] Antonio Suárez,[b] Juan M. Ortigueira,[a] and Jesús J. Fernández*[b]

Keywords: C−H activation / Nitrogen heterocycles / P ligands / Palladium

Cyclometallation of 1,4,5-trimethyl-2-phenylimidazole, **L**, with $Pd(OAc)_2$ gave exclusively the dinuclear *anti* isomer with bridging acetate ligands, **1**. Subsequent treatment of **1** with sodium chloride gave the corresponding dinuclear compound with bridging chloride ligands, **2**. Treatment of **2** with mono or diphosphanes led to partial or total bridge-splitting reactions, yielding mono or polynuclear compounds, **3**–**9**, depending on the palladium/phosphane ratio and the nature of the phosphane. The structure of **7** has been determined by X-ray diffraction analysis. Compounds **1** and **2** react with triphos to give the mononuclear compound, **10**, in which the phosphane acts as a terdentate ligand. The crystal structure of **10** confirms the pentacoordination of the palladium(II) centre, involving a long Pd–N interaction.

Introduction

Intramolecular activation of aromatic C−H bonds of coordinated ligands by transition metals, i.e. the cyclometallation reaction, has been widely investigated.[1−7] It has proved useful in numerous applications, such as the synthesis of new organometallic and organic compounds, many of which are obtained through insertions of unsaturated species into the metal−carbon bond,[8,9] the isolation of enantiomerically pure planar chiral compounds,[10] the design of complexes with interesting photochemical and electrochemical properties,[11] and their use as efficient catalytic materials[12−14] or liquid crystals.[15,16] The most abundant examples of cyclometallated compounds are those in which the metallated carbon atom is part of a phenyl ring.[4,5,17]

Cyclometallation reactions of heterocyclic derivatives have, in contrast, been less extensively studied, although such compounds can be expected to exhibit unique properties, not shown by their phenyl analogues, in applied fields of chemistry, biology, and pharmacy.[18] In recent years, the characterization of luminescent transition metal ions coordinated to heterocyclic organic ligands has attracted great interest; these systems exhibit new properties not seen for the pure organic molecules or transition metal compounds, which show only dd* transitions.[19] Other important aspects are the design of new liquid crystals,[20,21] as well as studies on cyclometallated palladium and platinum complexes that show remarkable and specific antitumor activity toward some forms of cancer[22,23] or other interesting biological properties.[24,25]

We have been interested in cyclometallation reactions of Schiff-base ligands derived from amines, diamines, and dialdehydes[26] and we have also reported five-membered metallacycles derived from substituted imidazoles with palladium(II)[27,28] and manganese(I).[29] In the present paper, we report the synthesis and characterization of a new series of mono- and polynuclear cyclometallated compounds of palladium(II) derived from a substituted imidazole ligand in conjunction with mono- and polyphosphanes

Results and Discussion

For the convenience of the reader, the compounds and reactions are shown in Schemes 1 and 2. The compounds described in this paper were characterized by elemental analysis (C, H, N), IR spectroscopy, and mass spectrometry (data in the Experimental Section), as well as by ^1H and $^{31}P\{^1H\}$ NMR spectroscopy (see Table 1).

The ligand was synthesized according to the method described by Lettau,[30] through reduction of the imidazole *N*-oxide derivative (see Scheme 1). Treatment of 1,4,5-trimethyl-2-phenylimidazole (**L**) with $Pd(OAc)_2$ in glacial acetic acid under argon at 50 °C gave the dimeric acetate-bridged *ortho*-palladated complex $[\{Pd[o\text{-}C_6H_4C{=}NC(Me){=}C(Me)NMe]\}(\mu\text{-}O_2CMe)]_2$, **1**. The FAB mass spectrum of **1** shows peaks at m/z = 701, 642, and 583 attributable to $[M^+]$, $[M^+ - OAc]$, and $[M^+ - 2OAc]$, respectively, taking into account the distribution of palladium isotopes.[31] The IR spectrum of **1** features two strong bands at 1580 cm^{-1} and 1420 cm^{-1}, attributable to the $\nu_{as}(COO)$ and $\nu_s(COO)$ stretching vibrations of the acetate ligand, respectively.[32] The methyl groups of the acetate ligands give rise to just one singlet in the ^1H NMR spectrum at δ = 2.13 (Table 1), indicating that they are equivalent. This is consistent with

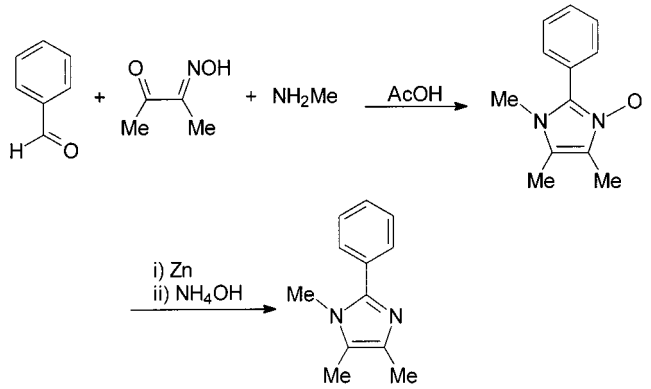
[a] Departamento de Química Inorgánica, Universidad de Santiago de Compostela,
E-15706 Santiago de Compostela, Spain
Fax: (internat.) +34/81-595012
E-mail: qideport@usc.es
[b] Departamento de Química Fundamental,
Universidad de La Coruña,
E-15071 La Coruña, Spain

 © WILEY-VCH Verlag GmbH, D-69451 Weinheim, 2000 1434−1948/00/0909−2055 $ 17.50+.50/0

Table 1. ^{1}H and ^{31}P{^{1}H} NMR data

	δ(H2)[a]	δ(H3)	δ(H4)	δ(H5)	δ(NMe)	δ(Me)	δ(P)[b]	Others
L	7.58 dd[c]	7.42 m	7.42 m	7.42 m	3.55 s	2.23 s		$\delta(H_6)$ = 7.58 dd
	^3J(H2H3) = 8.0[d]					2.20 s		^3J(H6H5) = 8.0
	^4J(H2H4) = 1.7							^4J(H6H4) = 1.7
1	6.96 d	6.68 m	6.68 m	6.68 m	3.34 s	1.73 s		$\delta(O_2CMe)$ = 2.13 s
	^3J(H2H3) = 7.6					1.71 s		
2	7.74 d	7.08 m	7.08 m	7.08 m	3.76 s	2.13 s		
	^3J(H2H3) = 7.8					2.12 s		
3[e]		6.87 td	6.73 td	6.65 m	3.83 s	2.54 s	43.00 s	
		^3J(H2H3) = 7.4	^3J(H4H5) = 7.4	^4J(PH5) = 6.5		2.18 s		
		^3J(H3H4) = 7.4	^4J(H4H2) = 1.2					
		^4J(H3H5) = 1.2						
4[e]		6.84 t	6.25 m	6.25 m	3.86 s	2.39 s	29.44 s	δ(C=CH_2) = 4.40 m
		^3J(H2H3) = 7.3				2.25 s		
		^3J(H3H4) = 7.3						
5[e]		6.84 t	6.45 m	6.45 m	3.80 s	2.55 s	32.64 s	
		^3J(H2H3) = 7.2				2.20 s		
		^3J(H3H4) = 7.2						
6[e]		6.75 t	6.40 m	6.40 m	3.80 s	2.54 s	31.64 s	δ(C_5H_5) =
		^3J(H2H3) = 7.3				2.18 s		4.97 b, 4.50 b
		^3J(H3H4) = 7.3						
7[e]		7.12 t	6.75 t	6.90 m	3.98 s	2.18 s	12.72 d	δ(C=CH_2) = 6.16 m
		^3J(H2H3) = 7.5	^3J(H4H5) = 7.5	^4J(PH5) = 9.4, 7.1		1.69 s	−8.57 d	
		^3J(H3H4) = 7.5					J(PP) = 12.7	
8[e]		7.05 t	6.51 t	6.71 m	3.83 s	2.09 s	25.98 d	
		^3J(H2H3) = 7.3	^3J(H4H5) = 7.3	^4J(PH5) = 9.3, 7.2		1.65 s	−4.82 d	
		^3J(H3H4) = 7.3					J(PP) = 59.4	
9[e]		6.96 t	6.45 t	6.71 m	3.94 s	2.08 s	35.70 d	δ(C_5H_5) =
		^3J(H2H3) = 7.4	^3J(H4H5) = 7.4	^4J(PH5) = 9.5, 7.0		1.62 s	8.58 d	4.69 m, 4.43 m
		^3J(H3H4) = 7.4					J(PP) = 42.3	
10[e]		6.78 t	5.93 t	6.26 t	3.27 s	2.02 s	82.56 t	
		^3J(H2H3) = 7.3	^3J(H4H5) = 7.3	^4J(PH5) = 7.3		1.56 s	41.48 d	
		^3J(H3H4) = 7.3					J(PP) = 28.0	

[a] ^{1}H NMR in $CDCl_3$, except for compound **2**, which was studied in [D_6]DMSO; measured at 200 MHz (ca. 20 °C), chemical shifts (δ) in ppm (±0.01) downfield from $SiMe_4$. – [b] ^{31}P{^{1}H} NMR in $CDCl_3$; measured at 81 MHz (ca. 20 °C), chemical shifts (δ) in ppm (±0.01) downfield from 85% H_3PO_4; *trans*-^4J(PH5) > *cis*-^4J(PH5); $\delta(P_{trans\text{-}N}) > \delta(P_{trans\text{-}C})$. – [c] s, singlet; d, doublet, dd, doublet of doublets, m, multiplet, b, broad. – [d] Coupling constants in Hz. – [e] Not assigned; obscured by the phosphane resonance.



Scheme 1

a *trans* geometry of the cyclometallated moieties in the *anti* isomer.[33–35] Some cyclopalladation reactions of substituted imidazoles lead to a mixture of the two possible geometrical isomers, *anti* and *syn*, but the reasons for this difference in behaviour are not clear.[28,36,37]

A doublet at δ = 6.96 can be assigned to the H2 proton, whilst the H3, H4, and H5 resonances appear as a multiplet centred at δ = 6.68. The shift towards lower frequency of these signals, as well as of those of the imidazole ring methyl groups, as compared with the signals of the free ligand, may be attributed to a shielding effect that arises as a result of the "open-book" configuration of the complex. The cyclometallated ligands are nearly face-to-face, similar to the situation observed in the related dimers.[38,39]

A metathesis reaction of **1** with aqueous sodium chloride afforded the chloride-bridged complex [{Pd[*o*-C_6H_4C=NC(Me)=C(Me)NMe]}(μ-Cl)]$_2$, **2**. The IR spectrum of the product shows two ν(Pd–Cl) bands at 321 and 289 cm^{-1}, consistent with an asymmetric Pd_2Cl_2 bridging unit.[40] Complex **2** was found to be poorly soluble in the common organic solvents, but its full characterization by ^{1}H NMR was possible in [D_6]DMSO. The phenyl proton signals were seen to be shifted to higher frequencies as compared with the corresponding signals for compound **1**. This can be rationalized in terms of the planar arrangement in **2**, as opposed to the "open-book" geometry of **1**, in agreement with previously reported structural data.[41,42] Whereas in the free ligand the resonance of the NMe group of the imidazole ring is close to the value found in 1-methylimidazole,[43] suggesting that the imidazole and phenyl rings are mutually tilted by ca. 45°, in compound **2** the N–Me resonance is seen to be shifted to higher frequency by 0.21 ppm. This shift may be caused by the deshielding effect of the metallated phenyl ring and shows that the two rings have an almost coplanar disposition.

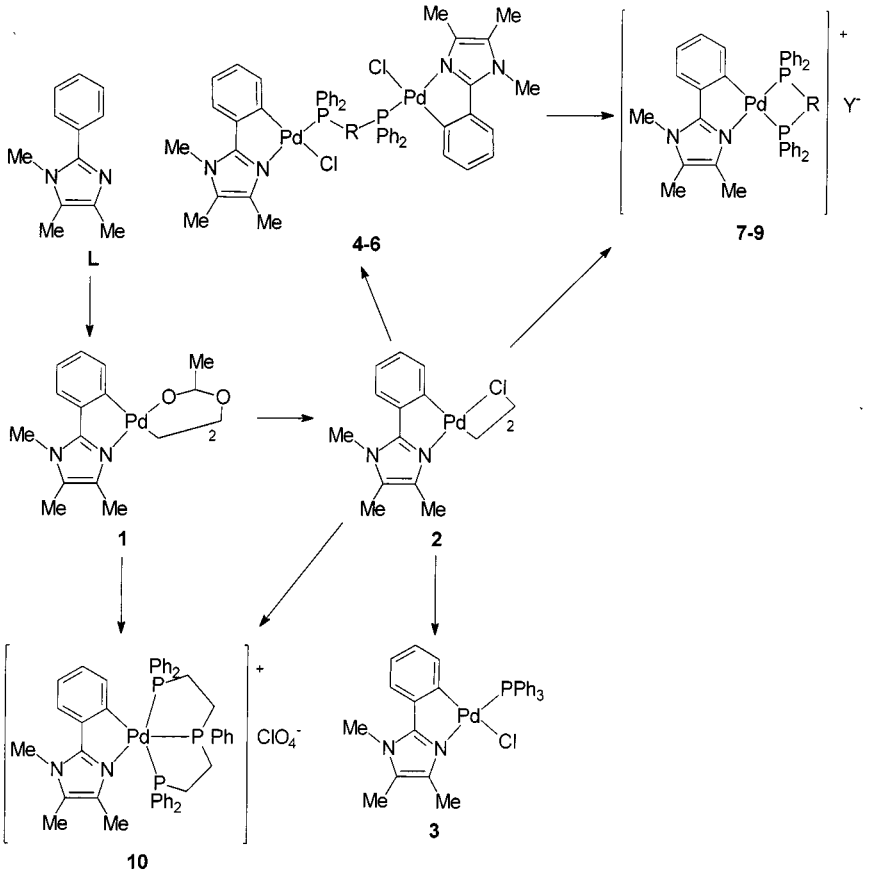
In view of the importance of palladium-assisted synthesis of heterocycles, some reactions of compounds **1** and **2** with

unsaturated molecules were examined. Thus, **1** and **2** were treated with, e.g. phenylacetylenes, in order to ascertain the ability of the complexes to undergo insertion of organic molecules into the Pd−C bond. Unfortunately, our attempts did not meet with success and only intractable mixtures were obtained. Nevertheless, more recent results from our laboratory show that when these reactions are carried out with cyclomanganated phenylimidazole ligands, successful insertion of unsaturated organic molecules, e.g. 1-phenyl-1-propyne, into the Mn−C bond is observed with formation of a stable seven-membered ring containing the metal atom. We are currently engaged in developing this work further.

Chloride-bridge cleavage reactions were observed when [{Pd[*o*-C_6H_4C=NC(Me)=C(Me)NMe]}(μ-Cl)]$_2$ (**2**) was treated with triphenylphosphane in a 1:2 molar ratio, giving the mononuclear cyclometallated complex **3**. Likewise, treatment of **2** with the diphosphanes 1,1-bis(diphenylphosphanyl)ethene (vdpp), 1,3-bis(diphenylphosphanyl)propane (dppp), or 1,1′-bis(diphenylphosphanyl)ferrocene (dppf) in a 1:1 molar ratio was found to give the dinuclear cyclometallated complexes **4**, **5**, and **6**, respectively (see Scheme 2). The $^{31}P\{^1H\}$ NMR spectra feature a singlet in all cases, shifted to higher frequency compared with the free phosphane, consistent with phosphorus coordination to the metal centre.[44] The δP values suggest that the phosphane is *trans* to the nitrogen atom and, in the case of the dinuclear compounds with the diphosphane acting as a bridging ligand, indicate that the two phosphorus nuclei are equivalent. The ^1H NMR spectra show the H4 and H5 proton signals shifted to lower frequencies by 0.3−0.8 ppm, as a result of the shielding effect of the phosphane phenyl rings. These signals are overlapped for compounds **4**−**6**, but can be clearly distinguished in the case of compound **3**. The H5 resonance shows coupling to the phosphorus atom [^4J(PH5) = 6.5 Hz], confirming the *cis* geometry of the phosphane and the metallated phenyl group.

For complexes **3**−**6**, the IR spectra show a band at ca. 275 cm^{-1} attributable to the ν_{as}(Pd−Cl) *trans* to the C_{phenyl} atom,[45] confirming that only a single isomer is present in each case. The FAB mass spectra show, among others, peaks attributable to [M^+] (**3**, **5**), [$M^+ - CH_2$] (**4**), and [$M^+ - Cl$] (**6**) ions, thereby confirming the dinuclear nature of these complexes (see Experimental Section). We have recently reported that complexes similar to **4** are subject to an interconversion between two conformations in solution, leading either to electrolyte species or to molecular compounds.[46,47]

Treatment of the chloride-bridged complex (**2**) with vdpp, dppp, or dppf in a 1:2 molar ratio in the presence of silver trifluoromethanesulfonate, ammonium hexafluorophosphate, or sodium perchlorate in acetone at room temperature yielded the mononuclear cyclometallated compounds **7**, **8**, and **9**, respectively. The products no longer contain Pd−Cl bonds and the diphosphane is chelated to the metal



Scheme 2

centre through the two phosphorus atoms. These compounds could also be prepared by reaction of the corresponding dinuclear species with the diphosphane in a 1:1 molar ratio in the presence of the ionic salt. The FAB mass spectra show similar fragmentation patterns, featuring peaks attributable to [M^+] and [M^+ − diphosphane] ions (see data in the Experimental Section). The conductivity data for complexes **7−9** (125−150 $\Omega^{-1}cm^2mol^{-1}$ in 10^{-3} mol·dm^{-3} solutions in dry acetonitrile) show that they are 1:1 electrolytes.[48]

The $^{31}P\{^1H\}$ NMR spectra feature two doublets, suggesting that the two phosphorus atoms are non-equivalent. The assignment of the doublets was made on the assumption that a ligand of greater *trans* influence shifts the resonances of the phosphorus nuclei *trans* to it to lower frequency.[44] This was confirmed by means of selective decoupling experiments (see Table 1).

The H4 and H5 resonances are shifted to lower frequency in the ^1H NMR spectra (*cf.* compounds **3−6**), although the signal order is reversed in this case, with the H4 signal showing the largest shift. We suggest that this is due to the different spatial shielding of the phenyl rings on the phosphorus atom *trans* to nitrogen, i.e. whether the phosphane ligand is in a bridging or a chelating mode. The H5 resonance is seen to be coupled to both phosphorus nuclei [$^4J(P_{trans\text{-}C}H)$ ca. 11 Hz, $^4J(P_{trans\text{-}N}H)$ ca. 8 Hz]. The 4-Me signal is shifted downfield by ca. 0.5 ppm due to the shielding effect of the PPh_2 groups *trans* to carbon. This is most noticeable in compounds **8** and **9** due to the larger chelate ring size. These findings were confirmed by an X-ray crystal structure determination of compound **7** (see Experimental Section).

Reaction of **1** with bis(2-diphenylphosphanylethyl)phenylphosphane (triphos) and sodium perchlorate in a 1:2 molar ratio in acetone at room temperature yielded the mononuclear complex **10** (see Scheme 2). The compound could also be obtained by treatment of **2** with triphos under similar conditions. The IR spectrum revealed an absence of bands in the range 1600−1400 cm^{-1} characteristic of COO stretching vibrations of acetate groups. The microanalytical data were consistent with the empirical formula [(L−H)Pd(triphos)][ClO_4], while the FAB mass spectrum showed the appropriate peak attributable to the [M^+] ion.

The $^{31}P\{^1H\}$ NMR spectrum shows a triplet [δ = 82.56 ppm, 1 P, $^3J(PP)$ = 28.0 Hz] and a doublet (δ = 41.48, 2 P), shifted to higher frequencies with respect to the signals of the free phosphane, in agreement with phosphorus coordination to the metal centre. The ^1H NMR spectrum shows that the ligand proton signals appear at lower frequencies compared to the corresponding signals in compounds **7−9**, especially those attributable to H4, H5, N−Me, and 4-Me, which are shifted by ca. 0.4−0.6 ppm. This may be rationalized in terms of the remarkable shielding effect of the phenyl rings of the phosphane. The signal attributable to H5 only shows coupling to one phosphorus nucleus [$^4J(PH5)$ = 7.3 Hz]. The crystal structure of **10** has been determined by X-ray diffraction analysis (vide infra).

Crystal and Molecular Structures of 7 and 10

Suitable crystals were grown by slowly evaporating the solvent from chloroform solutions of complexes **7** and **10**. The labelling schemes for the complexes are shown in Figures 1 and 2. Both crystals consist of discrete molecules, separated by normal van der Waals distances. Crystallographic data and selected interatomic distances and angles are listed in Table 2 and 3.

Table 2. Crystal data and structure refinement for complexes **7** and **10**

	7	**10**
Formula	$C_{40}H_{36}N_2O_3F_3P_2SCl_3Pd$	$C_{47}H_{47}N_2O_4Cl_4P_3Pd$
M_r	956.46	1044.98
Temperature (°K)	293(2)	293(2)
Wavelength (Å)	0.71073	0.71073
Crystal syst.	Triclinic	Triclinic
Space group	$P\bar{1}$	$P\bar{1}$
Cell dimensions		
a (Å)	12.248(1)	11.195(1)
b (Å)	14.203(1)	15.433(1)
c (Å)	22.287(1)	15.783(1)
α	114.870(1)	74.916(1)
β (°)	107.226(1)	72.017(1)
γ	90.586(1)	72.438(1)
V (Å^3)	2135.0(2)(8)	2430.5(2)
Z	2	2
μ (mm^{-1})	0.798	0.744
Crystal size (mm)	0.80 × 0.60 × 0.50	0.80 × 0.75 × 0.30
$2\theta_{max}$ (°)	52	52
Reflections:		
collected	12349	13933
unique	7938 (R_{int} = 0.060)	9054 (R_{int} = 0.087)
Transmissions	1.00, 0.57	1.00, 0.74
no. of parameters	496	561
S	1.079	1.001
R [F, $I > 2\sigma(I)$]	0.0699	0.0597
wR [F^2, all data]	0.2000	0.1981
max. Δ/σ	0.001	0.001
max. ρ (e Å^3)	1.456	0.901

Table 3. Selected bond distances (Å) and angles (°) in complexes **7** and **10**

7		**10**	
Pd(1)−C(1)	2.033(5)	Pd(1)−C(1)	2.087(4)
Pd(1)−N(1)	2.068(4)	Pd(1)−P(2)	2.2889(12)
Pd(1)−P(2)	2.2575(14)	Pd(1)−P(3)	2.3036(12)
Pd(1)−P(1)	2.3843(13)	Pd(1)−P(1)	2.3164(11)
P(1)−C(11)	1.816(6)	Pd(1)−N(2)	2.488(4)
P(2)−C(11)	1.830(5)	N(2)−C(7)	1.332(6)
C(11)−C(12)	1.308(9)	C(1)−C(6)	1.430(6)
N(1)−C(7)	1.352(7)	C(6)−C(7)	1.457(7)
C(1)−C(6)	1.383(8)		
C(6)−C(7)	1.462(9)		
C(1)−Pd(1)−N(1)	80.7(2)	P(3)−Pd(1)−P(1)	153.91(4)
C(1)−Pd(1)−P(2)	98.59(18)	P(3)−Pd(1)−N(2)	117.98(10)
P(2)−Pd(1)−P(1)	72.75(5)	P(1)−Pd(1)−N(2)	88.06(9)
N(1)−Pd(1)−P(1)	107.95(13)	C(1)−Pd(1)−P(1)	92.90(12)
C(11)−P(1)−Pd(1)	89.54(17)	C(1)−Pd(1)−P(3)	94.56(12)
C(11)−P(2)−Pd(1)	93.23(19)	C(1)−Pd(1)−N(2)	76.88(15)
P(1)−C(11)−P(2)	98.1(3)	P(2)−Pd(1)−P(1)	84.88(4)
C(6)−C(1)−Pd(1)	115.3(4)	P(2)−Pd(1)−P(3)	84.13(5)
C(7)−N(1)−Pd(1)	112.1(4)	P(2)−Pd(1)−N(2)	111.05(10)
N(1)−C(7)−C(6)	118.8(5)	C(6)−C(1)−Pd(1)	116.5(3)
C(1)−C(6)−C(7)	113.0(5)	C(7)−N(2)−Pd(1)	104.5(3)
		C(1)−C(6)−C(7)	118.0(4)
		N(2)−C(7)−C(6)	122.4(4)

In compound **7**, the palladium(II) centre is bonded to four atoms: one adjacent *ortho*-carbon and one nitrogen of the 1,4,5-trimethyl-2-phenylimidazole ligand, and two phosphorus atoms of a chelating 1,1-bis(diphenylphosphanyl)ethene in a slightly distorted square-planar coordination environment (see Figure 1). The sum of the angles about palladium is 360.03°, with the distortions more noticeable in the somewhat reduced "bite" angles enforced by the chelation. The requirements of the five- and four-membered chelate rings dictate C(1)−Pd(1)−N(1) and P(1)−Pd(1)−P(2) bond angles of 80.7(2)° and 72.75(5)°, respectively. The latter value is considerably smaller value than that of the corresponding angle in free vdpp, i.e. 118.4°.[49] The geometry about the palladium atom is almost planar; displacements from the least-squares plane formed by the metal centre and the atoms bonded to it [Pd(1), C(1), N(1), P(1), and P(2)] are as follows: Pd(1): 0.0157 Å, C(1): −0.0231 Å, N(1): 0.0127 Å, P(1): −0.0202 Å, and P(2): 0.0149 Å.

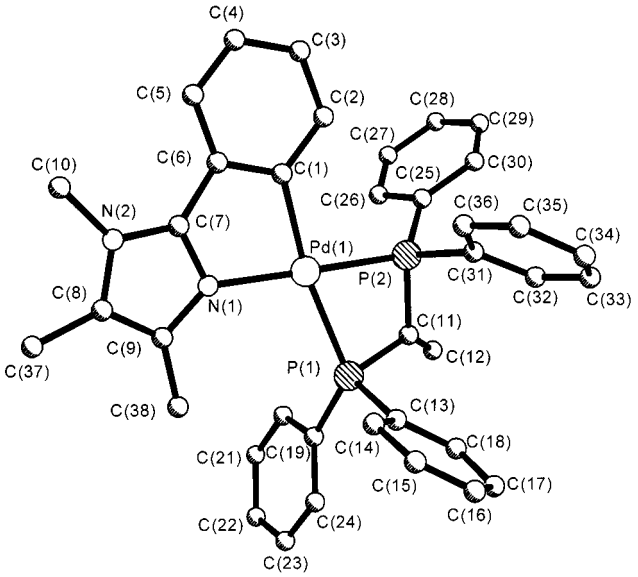


Figure 1. ORTEP projection of the $[\{Pd[o\text{-}C_6H_4C{=}NC(Me){=}C(Me)NMe]\}\{Ph_2PC(=CH_2)PPh_2\text{-}P,P'\}]^+$ cation, corresponding to complex **7**

The palladium−nitrogen bond length, 2.068(4) Å, is longer than the predicted single-bond value of 2.011 Å, based on the sum of the covalent radii for sp^2 nitrogen and palladium, i.e. 0.701 and 1.31 Å, respectively,[50] reflecting the *trans* influence of the phosphorus atom.[51] The palladium−carbon bond length, 2.033(5) Å, is slightly shorter than the expected value of 2.081 Å (based on the sum of covalent radii for sp^2 carbon and palladium, i.e. 0.771 and 1.31 Å, respectively), but is longer than in related complexes for which partial multiple-bond character of the Pd−C bond has been proposed.[27,52,53] This suggests some degree of multiple-bond character in the Pd−C(aryl) linkage, and also reflects the *trans* influence of the phosphorus atom responsible for the observed lengthening. The palladium−phosphorus bond lengths are shorter than the sum of the single bond radii for the relevant atoms, 2.41 Å, suggesting some partial double-bond character, as has also been observed in some related examples.[27,54] The differing *trans* influence is clearly illustrated by the palladium−phosphorus distances *trans* to carbon, Pd(1)−P(1), and *trans* to nitrogen, Pd(1)−P(2), i.e. Pd(1)−P(1) = 2.3843(13) Å vs. Pd(1)−P(2) = 2.2575(14) Å. In complex **7**, the C(11)−C(12) bond length is 1.308(9) Å, which is within the range expected for a carbon−carbon double bond and is shorter than the value of 1.34 Å found in free vdpp.

Apart from the phenyl phosphane rings and the methyl groups, the compound is approximately planar. The mean deviations from the least-squares planes determined for the metallated phenyl ring (C1, C2, C3, C4, C5, C6; plane 1), the imidazole ring (N1, C7, N2, C8, C9; plane 2), and the metallacycle (Pd1, C1, C6, C7, N1; plane 3) are 0.0025, 0.0022, and 0.0150 Å, respectively. The angles between the planes are as follows: plane 1/plane 2: 4.2°, plane 1/plane 3: 2.0°, and plane 2/plane 3: 3.1°. The chelate phosphane ring is not planar, showing a mean deviation from the ideal plane of 0.1619 Å. The vinylidene carbon atoms, C(11) and C(12), are displaced from the plane formed by the metal centre and the phosphorus atoms [Pd(1), P(1), P(2), plane 4] by 0.5323 and 1.3178 Å, respectively. The angles between plane 4 and the other planes are: plane 1/plane 4: 1.3°, plane 2/plane 4: 5.3°, and plane 3/plane 4: 2.5°.

In compound **10**, the palladium(II) centre is bonded to four atoms: the adjacent *ortho*-carbon and three phosphorus atoms of the bis(diphenylphosphanylethyl)phenylphosphane. An additional fifth linkage results from a weak interaction between the palladium and one nitrogen of the imidazole ligand, giving an overall distorted bipyramidal-trigonal coordination (see Figure 2). The equatorial plane is formed by the palladium, the nitrogen, and the terminal phosphorus atoms of the phosphane ligand. The metallated carbon and the central phosphorus complete the coordination sphere at the apical positions. The geometry about the palladium centre is almost planar; displacements from the least-squares plane formed by Pd(1), N(2), P(1), and P(3) are as follows: Pd(1): −0.186 Å, N(2): 0.0033 Å, P(1): 0.0071 Å, and P(3): 0.0081 Å. The main distortions in this plane are seen in the widened P(3)−Pd(1)−P(1) bond angle, 153.91(4)°, and the reduced P(1)−Pd(1)−N(2) bond angle, 88.06(9)°, although the sum of the angles at the palladium in the equatorial plane is 359.95°. On coordination, the donor atoms of the chelating imidazole occupy *cis* sites with a reduced bond angle [C(1)−Pd(1)−N(2)] of 76.88(15)°.

The palladium−nitrogen bond length, 2.488(4) Å, is longer than the predicted single bond value of 2.011 Å, and is slightly longer than the Pd−N bond length of 2.23(2) Å characteristic of an authentic trigonal-bipyramidal Pd^{II} complex.[55] Nevertheless, it is much shorter than the range of values, i.e. 2.71−2.80 Å and 2.576(4) Å,[55] hitherto reported for cyclopalladated compounds in which a weak Pd···N interaction has been assumed to be present.[56−59] More recently, we have found very short Pd−N bond lengths in palladium(II) cyclometallated compounds incorporating the triphos ligand.[60] We have reasoned that this is due to a change from the more common square-

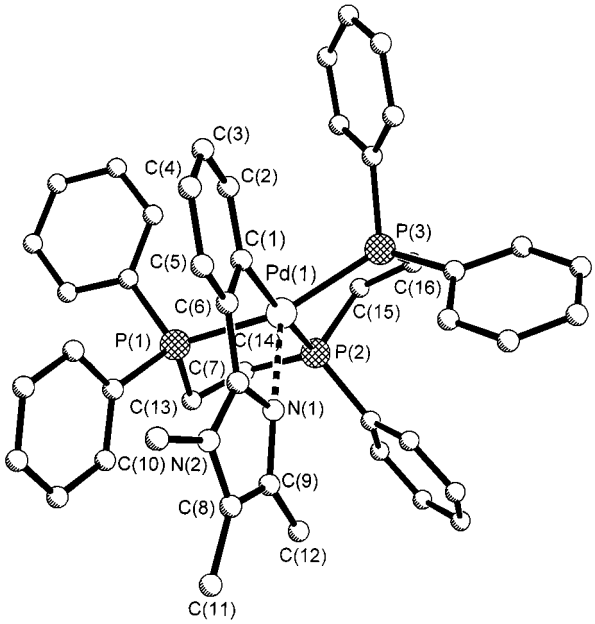


Figure 2. ORTEP projection of the $[\{Pd[o\text{-}C_6H_4C{=}NC(Me){=}C(Me)NMe]\}(Ph_2PCH_2CH_2)_2PPh\text{-}P,P'\text{-}P''\}]^+$ cation, corresponding to complex **10**

planar geometry of Pd^{II} towards a trigonal-bipyramidal arrangement, which brings the nitrogen atom sufficiently close to the palladium such that a true bonding interaction may be postulated. In the light of this result, we changed the organic metallated moiety in order to verify that it was indeed mainly the triphos ligand that was responsible for this new situation in the palladium coordination sphere. Thus, bidentate Schiff-bases, azobenzenes,[61] and phenylimidazoles were used. Compound **10** represents an example of the latter type of ligand, the results for which we describe in the present paper. Thus, the data presented here seem to confirm that with triphos as a terdentate chelating ligand, unusually short Pd−N distances may be obtained, allowing a new insight into the chemistry of cyclopalladated compounds.

The Pd(1)−C(1) bond length, 2.087(4) Å, is longer than is usually found in related complexes bearing a phosphane ligand in the *trans* position. The Pd−P bond lengths, Pd(1)−P(1): 2.3164(11), Pd(1)−P(2): 2.2889(12), and Pd(1)−P(3): 2.3036(12) Å, are suggestive of slight double-bond character of the palladium−phosphorus linkages.

The cyclometallated moiety is somewhat distorted from planarity, mainly due to the imidazole ring. The mean deviations from the least-squares planes determined for the metallated phenyl ring (C1, C2, C3, C4, C5, C6; plane 1), the imidazole ring (N1, C7, N2, C11, C12; plane 2), and the metallacycle (Pd1, C1, C6, C7, N2; plane 3) amount to 0.0099, 0.0035, and 0.0471 Å, respectively. The angles between planes are as follows: plane 1/plane 2: 17.6°, plane 1/plane 3: 4.7°, and plane 2/plane 3: 15.1°. The angles between the equatorial plane formed by Pd(1), P(1), P(3), and N(2) (plane 4) are as follows: plane 1/plane 4: 83.4°, plane 2/plane 4: 90.8°, and plane 3/plane 4: 87.9°. Thus, the compound is clearly pentacoordinated, even though the imidazole ring is slightly tilted with respect to the phenyl and cyclometallated rings, and the Pd−N distance is rather long. These distortions can be rationalized taking into account the low tendency of palladium(II) to generate pentacoordinated complexes.

Experimental Section

General Remarks: All solvents were dried according to standard methods.[62] The following compounds were used as received from commercial sources: palladium(II) acetate from Strem Chemicals, diacetylmonooxime from Carlo Erba, zinc, aqueous methylamine, PPh_3, and $Ph_2PCH_2CH_2CH_2PPh_2$ (dppp) from Acros, and silver trifluoromethanesulfonate, benzaldehyde, and $Ph_2PC_5H_4FeC_5H_4PPh_2$ (dppf) from Aldrich. $Ph_2PC(=CH_2)PPh_2$ (vdpp) was prepared according to procedures described elsewhere.[63] − Elemental analyses were carried out by the Servicios Generales de la Universidad de La Coruña using a Carlo Erba Model 1108 elemental analyzer. − IR spectra were recorded from samples in Nujol mulls or polythene discs on a Perkin−Elmer 1330 spectrophotometer. − NMR spectra were recorded from samples in $CDCl_3$ or [D$_6$]DMSO solutions on a Bruker AC 200F spectrometer and were referenced to internal $SiMe_4$ (^1H) or external 85% H_3PO_4 ($^{31}P\{^1H\}$). − Mass spectra were measured on a QUATRO mass spectrometer with a Cs ion-gun and NOBA or 3-NBA as the matrix.

Synthesis of 1,4,5-Trimethyl-2-phenylimidazole, $C_6H_5C{=}NC(Me){=}C(Me)NMe$ (L): Benzaldehyde (5.3 g, 0.049 mol), 40% aq. methylamine (3.87 g, 0.049 mol), and diacetylmonooxime (4.95 g, 0.049 mol) were added to glacial acetic acid (60 mL). After refluxing for 2 h, the solution was cooled, zinc (10 g, 0.152 mol) was added, and the resulting mixture was refluxed for a further 1 h and then kept overnight at room temperature. The zinc acetate formed was filtered off. Treatment of the filtrate with ammonium hydroxide resulted in the separation of a yellow oil, which was extracted with toluene (3 × 30 mL). The combined organic extracts were dried with anhydrous sodium sulfate, filtered, and then concentrated in vacuo to give a yellow solid, which was recrystallized from toluene. Yield: 55.9%. − $C_{12}H_{14}N_2$ (186.2): calcd. C 77.4, H 7.6, N 15.0; found C 77.0, H 7.4, N 15.2. − FAB-MS: *m*/*z* = 186 [M^+], 171 [M^+ − Me].

Synthesis of $[\{Pd[o\text{-}C_6H_4C{=}NC(Me){=}C(Me)NMe]\}(\mu\text{-}O_2CMe)]_2$ (1): 1,4,5-Trimethyl-2-phenylimidazole (0.432 g, 2.322 mmol) and palladium(II) acetate (0.500 g, 2.228 mmol) were added to glacial acetic acid (50 mL) to give a yellow solution. After heating at 50 °C for 10 min. under argon, the solution was cooled and filtered. The collected solid was washed with glacial acetic acid and cold ethanol, and dried in vacuo. Yield: 75.1%. − $C_{28}H_{32}N_4O_4Pd_2$ (701.4): calcd. C 48.0, H 4.6, N 8.0; found C 48.3, H 4.7, N 8.0. − IR: $\tilde{\nu}$ = 1580 [s, ν_{as}(COO)], 1420 [s, ν_s(COO)]. − FAB-MS: *m*/*z* = 701 [M^+], 642 [M^+ − OAc], 583 [M^+ − 2AcO], 476 [$(L-H)_2Pd^+$], 291 [$(L-H)Pd^+$].

Synthesis of $[\{Pd[o\text{-}C_6H_4C{=}NC(Me){=}C(Me)NMe]\}(\mu\text{-}Cl)]_2$ (2): An aqueous solution of NaCl (ca. 10^{-2} M) was added dropwise to a solution of **1** (0.252 g, 0.360 mmol) in acetone (ca. 20 mL). The resulting mixture was stirred for 4 days, after which a yellow solid had precipitated. This was filtered off, washed with water and cold acetone, and dried in vacuo. Yield: >95%. − $C_{24}H_{26}Cl_2N_4Pd_2$ (654.2): calcd. C 44.1, H 4.0, N 8.6; found C 44.2, H 3.9, N 8.5. − IR: $\tilde{\nu}$ = 321 [m, $\nu(Pd-Cl_{trans\text{-}N})$], 289 [m, $\nu(Pd-Cl_{trans\text{-}C})$].

Synthesis of [Pd{*o*-$C_6H_4C{=}NC(Me){=}C(Me)NMe$}($PPh_3$)(Cl)] (3): To a solution of **2** (32 mg, 0.049 mmol) in acetone (ca. 15 mL) was added PPh_3 (26 mg, 0.098 mmol). The resulting mixture was stirred for 3 h at room temperature, after which a precipitate had formed. This was filtered off, washed with cold acetone, and dried in vacuo. Yield: 74.5%. − $C_{30}H_{28}ClN_2PPd$ (589.4): calcd. C 61.1, H 4.8, N 4.7; found C 61.4, H 4.7, N 4.8. − IR: $\tilde{\nu}$ = 277 [m, ν(Pd−Cl)]. − FAB-MS: *m*/*z* = 589 [M^+], 553 [M^+ − Cl], 291 [(L−H)Pd^+].

Synthesis of [{Pd[*o*-$C_6H_4C{=}NC(Me){=}C(Me)NMe$]}$_2$[μ-$Ph_2PC(=CH_2)PPh_2$](μ-Cl)]Cl (4): To a solution of **2** (34 mg, 0.052 mmol) in acetone (ca. 15 mL) was added vdpp (20 mg, 0.052 mmol). The resulting mixture was stirred for 12 h at room temperature, after which a precipitate had formed. This was filtered off, washed with cold acetone, dried in vacuo, and recrystallized from dichloromethane/*n*-hexane. Yield: 90.9%. − $C_{50}H_{48}Cl_2N_4P_2Pd_2$ (1050.6): calcd. C 57.1, H 4.6, N 5.3; found C 57.1, H 4.6, N 5.2. − IR: $\tilde{\nu}$ = 282 [m, ν(Pd−Cl)]. − FAB-MS: *m*/*z* = 1001 [M^+ − Cl − CH_2].

Compounds **5** and **6** were similarly prepared and were isolated as solids.

[{Pd[*o*-$C_6H_4C{=}NC(Me){=}C(Me)NMe$](Cl)}$_2$(μ-$Ph_2PCH_2CH_2CH_2PPh_2$)] (5): Yield: 62.5%. − $C_{51}H_{52}Cl_2N_4P_2Pd_2$ (1066.6): calcd. C 57.4, H 4.9, N 5.2; found C 57.6, H 5.1, N 5.0. − IR: $\tilde{\nu}$ = 275 [m, ν(Pd−Cl)]. − FAB-MS: *m*/*z* = 1067 [M^+], 1031 [M^+ − Cl], 739 [(L−H)PdCl(PP)$^+$], 704 [(L−H)Pd(PP)$^+$], 291 [(L−H)Pd^+].

[{Pd[*o*-$C_6H_4C{=}NC(Me){=}C(Me)NMe$](Cl)}$_2$(μ-$Ph_2PC_5H_4FeC_5H_4PPh_2$)] (6): Yield: 78.1%. − $C_{58}H_{54}Cl_2FeN_4P_2Pd_2$ (1208.5): calcd. C 57.6, H 4.5, N 4.6; found C 57.6, H 4.3, N 4.7. − IR: $\tilde{\nu}$ = 285 [m, ν(Pd−Cl)]. − FAB-MS: *m*/*z* = 1173 [M^+ − Cl], 846 [(L−H)Pd(PP)$^+$], 291 [(L−H)Pd^+].

Synthesis of [{Pd[*o*-$C_6H_4C{=}NC(Me){=}C(Me)NMe$]}{$Ph_2PC(=CH_2)PPh_2$-*P,P′*}]($CF_3SO_3$) (7): To a solution of **2** (32 mg, 0.049 mmol) in acetone (ca. 15 mL) was added silver trifluoromethanesulfonate (25 mg, 0.098 mmol). The resulting mixture was stirred for 30 min. at room temperature, and then filtered through Celite to eliminate the silver chloride precipitate. To the filtrate was added vdpp (38 mg, 0.098 mmol) and the resulting solution was stirred for 2 days. The precipitate formed was filtered off, washed with cold acetone, dried in vacuo, and recrystallized from chloroform/*n*-hexane. Yield: 74.6%. − $C_{39}H_{35}F_3N_2O_3P_2PdS$ (837.1): calcd. C 55.9, H 4.2, N 3.3; found C 55.9, H 4.0, N 3.3.

Synthesis of [{Pd[*o*-$C_6H_4C{=}NC(Me){=}C(Me)NMe$]}($Ph_2PCH_2CH_2CH_2PPh_2$-*P,P′*)]($PF_6$) (8): To a solution of **2** (32 mg, 0.049 mmol) in acetone (ca. 15 mL) was added dppp (40 mg, 0.098 mmol). The mixture was stirred for 2 h at room temperature, and then an excess of ammonium hexafluorophosphate was added. The resulting mixture was stirred for 1 h, and then water was added dropwise until a precipitate formed. This was filtered off, washed with water, cold acetone, and ethanol, and dried in vacuo. Yield: 87.5%. − $C_{39}H_{41}F_6N_2P_3Pd$ (851.0): calcd. C 55.2, H 4.6, N 3.3; found C 55.5, H 4.4, N 3.2. − FAB-MS: *m*/*z* = 704 [M^+], 518 [Pd(PP)$^+$], 291 [(L−H)Pd^+].

Compound **9** was similarly prepared using dppf and sodium perchlorate as appropriate and was isolated as a solid.

[{Pd[*o*-$C_6H_4C{=}NC(Me){=}C(Me)NMe$]}($Ph_2PC_5H_4FeC_5H_4PPh_2$-*P,P′*)]($ClO_4$) (9): Yield: 94.8%. − $C_{46}H_{41}ClFeN_2O_4P_2Pd$ (945.5): calcd. C 58.4, H 4.4, N 3.0; found C 58.1, H 4.2, N 3.0. − FAB-MS: *m*/*z* = 846 [M^+], 660 [Pd(PP)$^+$], 291 [(L−H)Pd^+].

Synthesis of [{Pd[*o*-$C_6H_4C{=}NC(Me){=}C(Me)NMe$]}{($Ph_2PCH_2CH_2$)$_2$PPh-*P,P′-P″*}]($ClO_4$) (10): To a solution of **1** (27 mg, 0.038 mmol) in acetone (ca. 10 mL) was added triphos (41 mg, 0.077 mmol). The mixture was stirred for 2 h at room temperature, and then excess sodium perchlorate was added. The resulting mixture was stirred for a further 1 h and then water was added dropwise until a precipitate formed. This was filtered off, washed with water and ethanol, dried in vacuo, and recrystallized from chloroform/*n*-hexane. Yield: 84.0%. − $C_{46}H_{46}ClN_2O_4P_3Pd$ (925.6): calcd. C 60.0, H 5.0, N 3.0; found C 59.9, H 5.1, N 3.1. − FAB-MS: *m*/*z* = 826 [M^+], 640 [Pd(PP)$^+$], 291 [(L−H)Pd^+].

X-ray Crystallographic Study:[64] Three-dimensional X-ray data were collected for **7** and **10** at room temperature in the θ range 2.67 to 26.00° on a Siemens Smart CCD diffractometer by the ω-scan method. Reflections were measured from a hemisphere of data made up of frames each covering 0.3° in ω. Of the 12349 (**7**) and 13933 (**10**) reflections measured, all of which were corrected for Lorentz and polarization effects and for absorption by semiempirical methods based on symmetry-equivalent and repeated reflections [minimum and maximum transmission coefficients 0.57 (**7**), 0.74 (**10**), and 1.00 (**7**, **10**)]; 7081 (**7**) and 8028 (**10**) independent reflections exceeded the significance level $|F| > 4.0\,\sigma|F|$. The structure was solved by direct methods and refined by full-matrix least-squares on F^2. Hydrogen atoms were included in calculated positions and refined in riding mode. Refinement converged at a final R_1 = 0.0699 (**7**) 0.0597 (**10**) [wR_2 = 0.2000 (**7**), 0.1981 (**10**) for all data] with allowance for thermal anisotropy of all non-hydrogen atoms. Geometrical constrains were used in the trifluoromethanesulfonate (**7**) and perchlorate (**10**) ions. The structure solution and refinement were carried out using the program package SHELX-97.[65]

Acknowledgments

We thank the Xunta de Galicia (Proyecto XUGA20913B96) and the Universidad de La Coruña for financial support.

[1] M. I. Bruce, *Angew. Chem. Int. Ed. Engl.* **1977**, *16*, 73−86.
[2] V. V. Dunina, O. A. Zalevskaya, V. M. Potapov, *Russ. Chem. Rev.* **1988**, *57*, 250−269.
[3] J. Dehand, M. Pfeffer, *Coord. Chem. Rev.* **1976**, *18*, 327−352.
[4] I. Omae, *Chem. Rev.* **1979**, *79*, 287−321.
[5] I. Omae, *Coord. Chem. Rev.* **1988**, *83*, 137−167.
[6] E. C. Constable, *Polyhedron* **1984**, *3*, 1037−1057.
[7] A. D. Ryabov, *Chem. Rev.* **1990**, *90*, 403−424.
[8] A. D. Ryabov, *Synthesis* **1985**, *3*, 233−252.
[9] J. Spencer, M. Pfeffer, *Adv. Met.-Org. Chem.* **1998**, *6*, 103−144.
[10] G. Zhao, Q. G. Wang, T. C. W. Wak, *Organometallics* **1998**, *17*, 3437−3441, and references therein.
[11] A. von Zelewski, P. Belser, P. Hayos, R. Dux, X. Hua, A. Suckling, H. Stoeckli-Evans, *Coord. Chem. Rev.* **1994**, *132*, 75−137.
[12] A. Bose, C. H. Saha, *J. Mol. Catal.* **1989**, *49*, 271−275.
[13] B. L. Shaw, S. D. Perera, E. A. Staley, *Chem. Commun.* **1998**, 1361−1362.
[14] M. Ohff, A. Ohff, D. Milstein, *Chem. Commun.* **1999**, 357−358.
[15] P. Espinet, M. A. Esteruelas, L. A. Oro, J. L. Serrano, E. Sola, *Coord. Chem. Rev.* **1992**, *117*, 215−274.
[16] J. L. Serrano (Ed.), *Metallomesogens: Synthesis, Properties and Applications*, VCH, Weinheim, **1996**, see, in particular, chapter 6, by M. Marcos.
[17] G. R. Newkome, W. E. Puckett, V. K. Gupta, G. E. Kiefer, *Chem. Rev.* **1986**, *86*, 451−489.
[18] A. R. Katritzky, C. W. Rees, E. F. V. Scriven, *Comprehensive Heterocyclic Chemistry II*, vol. 3, Elsevier, Oxford, **1996**.
[19] M. Glasbeek, R. Sitters, E. van Veldhoven, A. von Zelewski, W. Humbs, H. Yersin, *Inorg. Chem.* **1998**, *37*, 5159−5163.
[20] A. El-Ghayoury, L. Douce, A. Skoulios, R. Ziessel, *Angew. Chem. Int. Ed.* **1998**, *37*, 1255−1258.

[21] I. Yilmaz, O. Bekàroglu, *J. Chem. Res. (S)*, **1998**, 374−375.
[22] C. Navarro-Ranninger, I. Lopez-Solera, V. M. Gonzalez, J. M. Perez, J. H. Rodriguez, J. L. Garcia-Ruano, P. Raithby, J. R. Masaguer, C. Alonso, *J. Med. Chem*. **1993**, *36*, 3795−3801.
[23] C. Navarro-Ranninger, I. Lopez-Solera, V. M. Gonzalez, J. M. Perez, A. Alvarez-Valdes, A. Martin, P. Raithby, J. R. Masaguer, C. Alonso, *Inorg. Chem.* **1996**, *35*, 5181−5187.
[24] J. W. Suggs, M. L. Dube, M. Nichols, *J. Chem. Soc., Chem. Commun.* **1993**, 307−309.
[25] F. Zamora, S. Rico, P. Amo-Ochoa, *J. Inorg. Biochem*. **1997**, *68*, 257−263.
[26] J. M. Vila, M. Gayoso, M. T. Pereira, A. Suárez, J. J. Fernández, J. M. Ortigueira, A. Fernández, M. López-Torres, *Trends in Organomet. Chem.* **1997**, *2*, 21−37, and references therein.
[27] A. Suarez, J. M. Vila, E. Gayoso, M. Gayoso, W. Hiller, A. Castiñeiras, J. Strähle, *Z. Inorg. Allg. Chem.* **1986**, *535*, 213−218.
[28] A. Suarez, J. M. Vila, M. T. Pereira, E. Gayoso, M. Gayoso, *Synth. React. Inorg. Met.-Org. Chem.* **1990**, *20*, 1425−1440.
[29] A. Suarez, J. M. Vila, M. T. Pereira, E. Gayoso, M. Gayoso, *J. Organomet. Chem.* **1987**, *335*, 359−363.
[30] H. Lettau, *Z. Chem*. **1970**, *10*, 338−339 and 431−432.
[31] L. Tusek-Bozic, M. Curic, P. Traldi, *Inorg. Chim. Acta* **1997**, *254*, 49−55.
[32] K. Nakamoto, "*Infrared and Raman Spectra of Inorganic and Coordination Compounds*", 5th ed., J. Wiley & Sons, New York, **1997**.
[33] F. Zamora, V. M. González, J. M. Pérez, J. R. Masaguer, C. Alonso, C. Navarro-Ranninger, *Appl. Organomet. Chem.* **1997**, *11*, 491−497.
[34] J. M. Vila, M. Gayoso, M. T. Pereira, M. López, G. Alonso, J. J. Fernández, *J. Organomet. Chem.* **1993**, *445*, 287−294.
[35] B. Teijido, A. Fernández, M. López-Torres, S. Castro-Juiz, J. M. Ortigueira, J. M. Vila, J. J. Fernández, *J. Organomet. Chem.* **2000**, *598*, 71−79.
[36] F. Zamora, S. Luna, P. Amo-Ochoa, L. A. Martínez-Cruz, A. Vegas, *J. Organomet. Chem.* **1996**, *522*, 97−103.
[37] C. Navarro-Ranninger, F. Zamora, L. A. Martínez-Cruz, R. Isea, J. R. Masaguer, *J. Organomet. Chem.* **1996**, *518*, 29−36.
[38] M. T. Pereira, J. M. Vila, E. Gayoso, M. Gayoso, W. Hiller, J. Strähle, *J. Coord. Chem.* **1988**, *18*, 245−252.
[39] C. Navarro-Ranninger, F. Zamora, I. López-Solera, A. Monge, J. R. Masaguer, *J. Organomet. Chem.* **1996**, *506*, 149−154.
[40] J. M. Vila, M. Gayoso, A. Fernández, N. A. Bailey, H. Adams, *J. Organomet. Chem.* **1993**, *448*, 233−239.
[41] J. M. Vila, M. Gayoso, M. T. Pereira, J. M. Ortigueira, A. Fernández, N. A. Bailey, H. Adams, *Polyhedron* **1993**, *12*, 171−180.
[42] G. Zhao, Q. G. Wang, T. C. W. Mak, *J. Chem. Soc., Dalton Trans.* **1998**, 1241−1247.
[43] G. S. Reddy, R. T. Hogbood Jr., J. H. Goldstein, *J. Am. Chem. Soc.* **1962**, *84*, 336−340.
[44] P. S. Pregosin, R. W. Kuntz, *^{31}P and ^{13}C NMR of Transition Metal Phosphane Complexes*, in NMR 16 (Eds.: P. Diehl, E. Fluck, R. Kosfeld), Springer, Berlin, **1979**.
[45] B. Crociani, T. Boshi, R. Pietropaolo, U. Belluco, *J. Chem. Soc. A* **1970**, 531−535.
[46] J. M. Vila, J. M. Ortigueira, E. Gayoso, M. Gayoso, A. Castiñeiras, W. Hiller, J. Strähle, *Inorg. Chim. Acta* **1991**, *179*, 171−178.
[47] J. M. Vila, M. Gayoso, J. J. Fernández, J. M. Ortigueira, A. Fernández, N. A. Bailey, H. Adams, *J. Organomet. Chem.* **1994**, *471*, 259−263.
[48] W. J. Geary, *Coord. Chem. Rev.* **1971**, *7*, 81−122.
[49] H. Schmidbaur, R. Herr, J. Riede, *Chem. Ber.* **1984**, *117*, 2322−2327.
[50] L. Pauling, "*The Nature of the Chemical Bond*", 3rd ed., Cornell University Press, Ithaca, New York, **1960**, pp. 224.
[51] J. M. Vila, M. Gayoso, M. López-Torres, J. J. Fernández, A. Fernández, J. M. Ortigueira, N. A. Bailey, H. Adams, *J. Organomet. Chem.* **1996**, *511*, 129−138.
[52] J. M. Vila, M. T. Pereira, J. M. Ortigueira, M. López-Torres, A. Castiñeiras, D. Lata, J. J. Fernández, A. Fernández, *J. Organomet. Chem.* **1998**, *556*, 31−39, and references therein.
[53] B. Teijido, A. Fernández, M. López-Torres, J. M. Vila, J. J. Fernández, unpublished results.
[54] R. Bosque, C. López, X. Solans, M. Font-Bardiá, *Organometallics* **1999**, *18*, 1267−1274.
[55] J. Vicente, A. Arcas, D. Bautista, P. G. Jones, *Organometallics* **1997**, *16*, 2127−2138.
[56] F. Cecconi, C. A. Ghilardi, S. Midollini, S. Moneti, A. Orlandini, G. Scapacci, *J. Chem. Soc., Chem. Commun.* **1989**, 211−216.
[57] J. Granell, J. Sales, J. Vilarrasa, J. P. Declerq, G. Germain, C. Miravitlles, X. Solans, *J. Chem. Soc., Dalton Trans.* **1983**, 2441−2446.
[58] J. Granell, D. Sainz, J. Sales, X. Solans, M. Font-Altaba, *J. Chem. Soc., Dalton Trans.* **1986**, 1785−1790.
[59] I. R. Butler, M. Kalaji, L. Nehrlich, M. Hurthouse, I. Karaulov, K. M. A. Malik, *J. Chem. Soc., Chem. Commun.* **1995**, 459−460.
[60] J. M. Vila, M. T. Pereira, J. M. Ortigueira, J. J. Fernández, A. Fernández, M. López-Torres, H. Adams, *Organometallics* **1999**, *18*, 5484−5487.
[61] M. López-Torres, A. Fernández, J. M. Vila, J. J. Fernández, unpublished results.
[62] D. D. Perrin, W. L. F. Armarego, D. L. Perrin, "*Purification of Laboratory Chemicals*", 3rd ed., Pergamon, London, **1988**.
[63] I. J. Colquhoun, W. McFarlane, *J. Chem. Soc., Dalton Trans.* **1982**, 1915−1921.
[64] Crystallographic data (excluding structure factors) for the structures reported in this paper have been deposited with the Cambridge Crystallographic Data Centre as supplementary publication nos. CCDC-132677 and -132678. Copies of the data can be obtained free of charge on application to the CCDC, 12 Union Road, Cambridge CB2 1EZ, U.K. [Fax: (internat.) +44 (0)1223/336033; E-mail: deposit@ccdc.cam.ac.uk].
[65] G. M. Sheldrick, *SHELX-97, An Integrated System for Solving and Refining Crystal Structures from Diffraction Data*, University of Göttingen, Germany, **1997**.

Received September 8, 1999
[I99321]

Electron-Poor Olefin Polymerization Catalysts Based on Semi-Fluorinated Bis(phosphane)s

Roland Wursche,[a] Tony Debaerdemaeker,[b] Martti Klinga,[c] and Bernhard Rieger*[a]

Keywords: Fluorine / Phosphanes / Palladium / Platinum / Polymerizations

Two semi-fluorinated bis(phosphane)s, *P,P′*-(1,2-ethanediyl)-bis[bis(2,4,5-trifluorophenyl)phosphane] (**3a**), *P,P′*-(1,2-ethanediyl)bis[bis(2,4-difluorophenyl)phosphane] (**3b**), and their corresponding Pd^{II}- and Pt^{II}-dichloro complexes (**4a**,**b** and **6a**,**b**) have been synthesized. Complexation of *P,P′*-(1,2-ethanediyl)bis{bis[3,5-di(trifluoromethyl)phenyl]phosphane} (**3c**) and *P,P′*-(1,2-ethanediyl)bis[bis(pentafluorophenyl)phosphane] (**3d**) afforded the related compounds **4c**,**d** and **6c**. The Pd^{II}-diiodo complexes **5c**,**d** have been obtained from **4c**,**d** by halide exchange with NaI. The solid-state structures of compounds **4b** and **5c**,**d** have been determined by single-crystal X-ray diffraction analysis. Activation of **4b**–**d** with MAO produced efficient catalysts for the polymerization of 2-norbornene, which have proved to be superior to the Pd^{II}-dichlorides derived from the more electron-rich, structurally related *P,P′*-(1,2-ethanediyl)bis(diphenylphosphane) (DPPE) or *P,P′*-(1,3-propanediyl)bis(diphenylphosphane) (DPPP).

Introduction

Bidentate phosphanes $R_2PCH_2CH_2PR_2$ (R = alkyl, aryl) play an important role in the synthesis of tailored organometallic complexes for catalytic purposes. Potential applications range from the field of asymmetric hydrogenation, as carried out with chiral rhodium(I) compounds, for example, to C−C bond-forming processes in the case of the Grignard cross-coupling reaction.[1−3] Apart from examples specific to isolated molecules, late transition metal complexes of bis(phosphane)s are also versatile catalysts for the construction of polymeric materials. With an appropriate choice of the ligand sphere, Ni^{II} compounds can be used to synthesize either high molecular weight poly(olefin)s or oligomeric products.[4,5]

Recently, bis(phosphane)s $(R^f)_2P(CH_2)_2P(R^f)_2$ (R^f may be, for instance, pentafluorophenyl- or perfluoroalkyl-) have attracted attention as a new class of chelating ligands.[6,7] The electron-withdrawing character of the fluorine substituents strongly alters the electronic behaviour of the phosphorus atoms, leading to ligands that show weak σ-donor characteristics, but a high level of π-acceptor capacity. Consequently, bis(phosphane)s of this type form electron-poor transition metal complexes, e.g. Cr, Mo, Fe, Pt, Ru, Rh, and Ir compounds.[8−15] For catalytic applications, it may be advantageous that, unlike most typical strong π-acceptor ligands such as CO, NO and PF_3, bis(phosphane)s can easily be modified in a steric or electronic way by changing their substitution pattern.

We report herein on the synthesis and structural characterization of new electron-poor Pd^{II} and Pt^{II} complexes based on ethylene-bridged ligands $(Ar^f)_2P(CH_2)_2P(Ar^f)_2$, which differ in the substitution patterns at their arene moieties. To explore the potential of this class of compounds as catalysts for the polymerization of olefinic substrates, polymerization experiments have been conducted with 2-norbornene as the monomer.

Results and Discussion

Ligands

Ethylene-bridged bis(phosphane)s are most conveniently prepared by reaction of *P,P′*-(1,2-ethanediyl)bis(dichlorophosphane) **(1)** with an organometallic reagent, usually a lithiated or Grignard compound.[16,17] This method not only circumvents the time-consuming and laborious synthesis of secondary phosphanes, it also proceeds smoothly to afford the desired bidentate phosphanes in a one-pot procedure.

For the syntheses of *P,P′*-(1,2-ethanediyl)bis[bis(2,4,5-trifluorophenyl)phosphane] **(3a)** and *P,P′*-(1,2-ethanediyl)-bis[bis(2,4-difluorophenyl)phosphane] **(3b)**, we employed fluorinated phenyllithiums as the metallated components, which were prepared from the corresponding bromo derivatives through halogen−metal exchange using *n*-butyllithium at −78 °C in diethyl ether (Figure 1). *P,P′*-(1,2-ethanediyl)bis{bis[3,5-di(trifluoromethyl)phenyl]phosphane} **(3c)** was prepared from the Grignard compound 3,5-bis(trifluoromethyl)benzenemagnesium bromide **(2c)**, generated according to a literature procedure from 1-bromo-3,5-bis(trifluoromethyl)benzene and magnesium tur-

[a] University of Ulm, Department of Inorganic Chemistry II, Materials & Catalysis,
Albert-Einstein-Allee 11, D-89069 Ulm, Germany
Fax: (internat.) +49-(0)731/502-3039
E-mail: bernhard.rieger@chemie.uni-ulm.de
[b] Universität Ulm, Sektion Röntgen- und Elektronenbeugung, Albert-Einstein-Allee 11, D-89069 Ulm, Germany
[c] Department of Chemistry, University of Helsinki, P. O. Box 55, FIN-00014 Helsinki, Finland

 © WILEY-VCH Verlag GmbH, D-69451 Weinheim, 2000 1434−1948/00/0909−2063 $ 17.50+.50/0

nings.[18] A multi-step synthesis of **3c** has been reported previously, but is less favourable from an economic viewpoint.[19] Compounds **3a** and **3b** exhibit ^{31}P absorptions at $\delta = -30.2$ and -31.9, respectively. These signals are situated upfield from the resonance reported for the unsubstituted *P,P'*-(1,2-ethanediyl)bis(diphenylphosphane) ($\delta = -12.5$),[20] whereas in the case of **3d** a ^{31}P chemical shift of $\delta = -44.5$ is observed.[7] This reflects the partial fluorination of the phenyl substituents in compounds **3a**,**b** and further suggests that they may also form electron-poor complexes, although this effect should be less pronounced than in the case of **3d**.

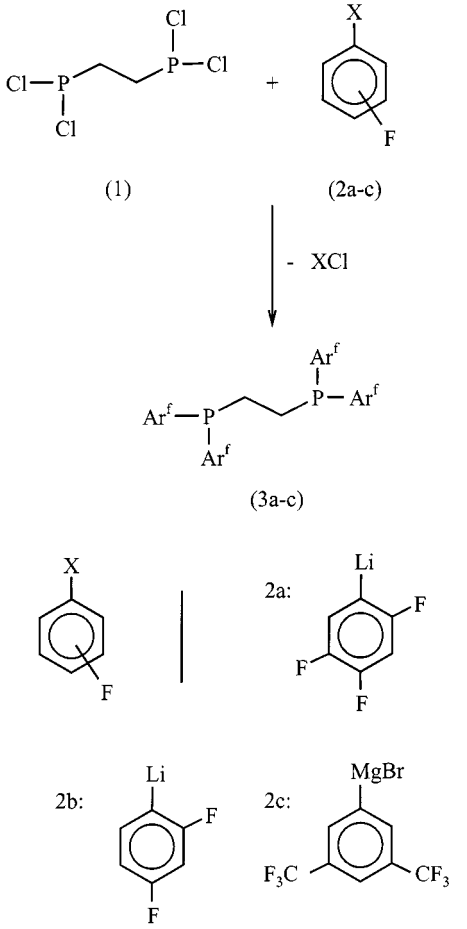


Figure 1. Synthesis of the semi-fluorinated bis(phosphane)s **3a**, **3b**, and **3c**

Complexes

For the synthesis of the Pd^{II}- and Pt^{II}-dichloro complexes of **3a**–**c** (denoted in Figure 2 as **4a**–**c** and **6a**–**c**, respectively) we used suitable organometallic precursors, which were reacted with the ligands at ambient temperature. Compound **4d** was prepared according to a modified literature procedure.[14] All the complexes were obtained as ivory-coloured, microcrystalline solids, except **4d**, which exhibited a distinct yellow aspect. Single crystals of **4b** were obtained from a tetrachloroethane solution.

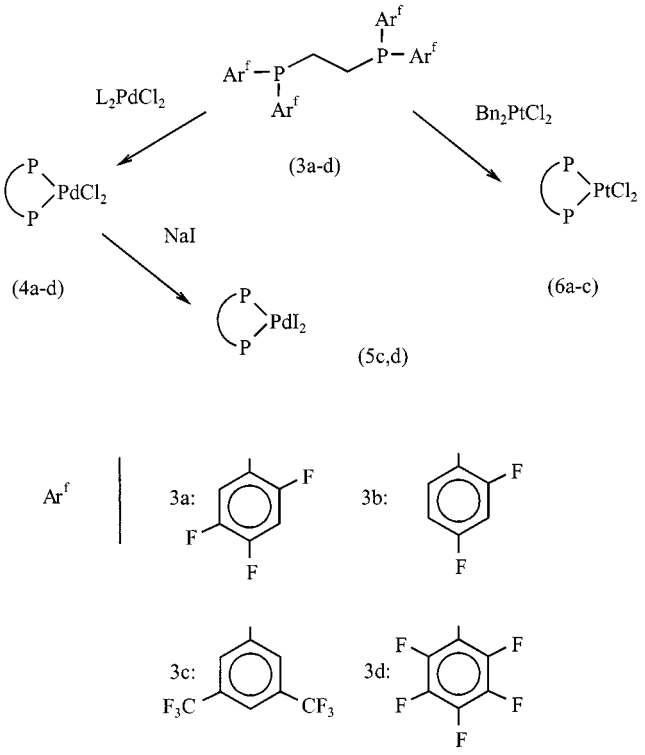


Figure 2. Preparation of the Pd^{II} and Pt^{II} complexes of the semi-fluorinated bis(phosphane)s **3a**, **3b**, **3c**, and **3d**; $\mathbf{L_2}$ = COD (1,5-cyclooctadiene) in the synthesis of **4b** and **4d**; Bn = benzonitrile

Replacement of the chloride substituents of **4d** by treatment with sodium iodide yielded **5d** as a dark-red complex. Slow evaporation of the solvent from an acetone solution produced crystals suitable for an X-ray structure analysis. Halide exchange was also performed on **4c**, leading to a red product that was identified as **5c** (Figure 3, Table 1). Single crystals of this compound suitable for structure investigation could be grown from an acetone solution; their analysis allowed a direct comparison with **5d**, any influence of the different halide ligands being excluded.

In the case of compound **5c** (space group: *C*2/*c*), 3.5 molecules of acetone were found to be included within the unit cell, which are omitted from the ORTEP plot for the sake of clarity. One of the crystallographically determined acetone molecules was found to have a site occupancy factor of 0.75, both showing a slight disordering. The anisotropic displacement factors were also rather large for the CF_3 groups, but dividing the fluorine atoms into two positions could not be satisfactorily accomplished. Similar effects have been observed in an X-ray structure analysis of [{BISBI-(3,5-CF_3)}(PPh_3)Ir(CO)H].[21] Here, three out of four CF_3 moieties were found to be disordered at 133 K. These observations may serve to illustrate the fluxional behaviour of trifluoromethyl substituents in the solid state. The average C–F bond lengths in **5c** (1.301 Å) are in agreement with the literature data (1.338 Å).[19]

Only a few crystal structures of complexes of **3d** have hitherto been reported, specifically those of [(**3d**)$_2$$Pt^0$],[12] *trans*-[$\eta^5$-($C_5H_5$)Mo(**3d**)(CO)Cl],[14] [(**3d**)Rh(PPh_3)Cl],[22]

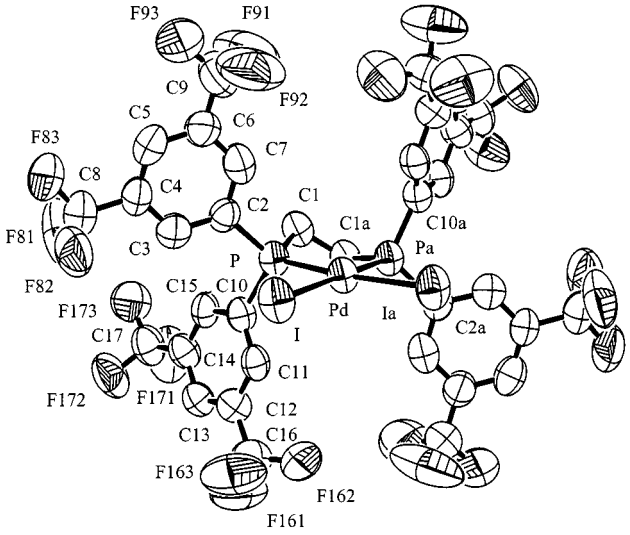


Figure 3. ORTEP plot of complex (**3c**)PdI_2, **5c**, showing the atom labelling scheme; atoms labelled *a* were generated by symmetry operations; thermal ellipsoids are depicted at a 50% probability level

Table 1. Selected bond lengths [Å] and angles [°] in **5c**

Distances		Angles	
Pd−I	2.6349(15)	P−Pd−Pa[a]	85.81(14)
Pd−P	2.244(3)	P−Pd−Ia[a]	88.83(8)
P−C10	1.807(11)	I−Pd−Ia[a]	96.70(7)
P−C2	1.811(10)	C10−P−C2	106.9(5)
P−C1	1.813(10)	C10−P−C1	103.6(5)
		C2−P−C1	106.3(5)

[a] Generated by symmetry operations: $-x + 1$, y, $-z + 1/2$.

and [M(Cp*)(**3d**)Cl]BF_4 (M = Rh, Ir).[23] The crystal structure of **3d** itself is also known.[23] As regards the bond distances between the phosphorus atoms and the metal, comparable results have been obtained for **5d** (space group: $P2_1/n$) and the Pt^0 complex (average Pt−P distance 2.288 Å), the values being somewhat lower for Pd^{II} (Figure 4,

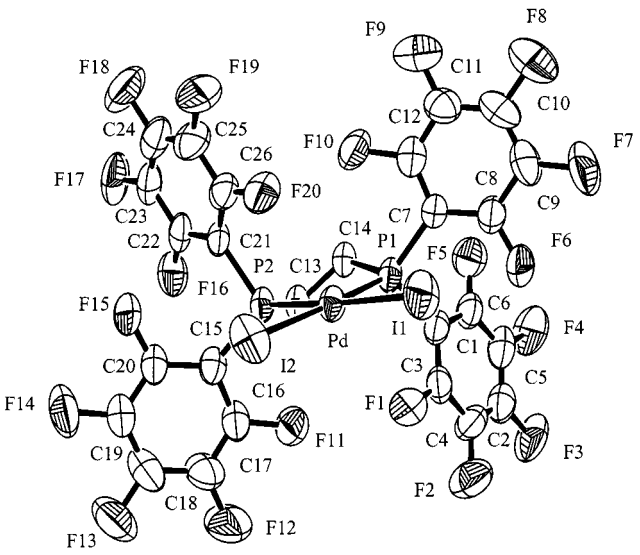


Figure 4. ORTEP plot of complex (**3d**)PdI_2, **5d**, showing the atom labelling scheme; thermal ellipsoids are depicted at a 50% probability level

Table 2. Selected bond lengths [Å] and angles [°] in **5d**

Distances		Angles	
Pd−P1	2.265(3)	P1−Pd−P2	85.48(12)
Pd−P2	2.247(3)	P1−Pd−I1	92.23(11)
Pd−I1	2.630(2)	P2−Pd−I2	88.09(11)
Pd−I2	2.645(2)	I1−Pd−I2	94.18(9)
P1−C7	1.814(10)	C15−P2−C13	108.2(5)
P1−C1	1.830(10)	C15−P2−C21	107.2(4)
P1−C14	1.850(9)	C13−P2−C21	102.5(5)
P2−C15	1.812(10)	C7−P1−C1	105.8(4)
P2−C13	1.831(10)	C7−P1−C14	107.5(5)
P2−C21	1.835(9)	C1−P1−C14	99.8(5)
C13−C14	1.531(13)		

Table 2). The P−C bond lengths are in the same range as observed previously, but in the present study the shortest distances have been seen in [(**3d**)PdI_2] **(5d)**.[12,14] The average C−F bond length calculated for **5d** (1.340 Å) matches the value determined for the Mo complex (1.344 Å).[16] The non-fluorinated complex diiodo-[*P*,*P*′-(1,2-ethanediyl)bis-(diphenylphosphane)]palladium(II) has Pd−I bond lengths of 2.6649(8)/2.6446(10) Å and Pd−P bond lengths of 2.2608(14)/2.2756 Å, which resemble the corresponding values found for **5c**,**d** (Table 1 and 2).[24] Moreover, the P−Pd−P bond angle of 85.59(5)° and the I−Pd−I bond angle of 92.73(3)° are similar to the results observed for the fluorinated species **5c**,**d**.

Complex **4b** (space group: *I*2/*a*) was found to crystallize with two molecules of tetrachloroethane (Figure 5, Table 3).

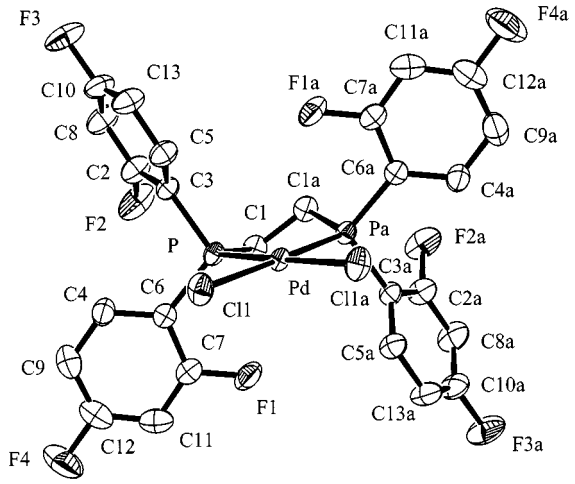


Figure 5. ORTEP plot of complex (**3b**)$PdCl_2$, **4b**, showing the atom labelling scheme; atoms labelled *a* were generated by symmetry operations; thermal ellipsoids are depicted at a 50% probability level

Table 3. Selected bond lengths [Å] and angles [°] in **4b**

Distances		Angles	
Pd−P	2.233(7)	P−Pd−Pa[a]	85.94(4)
Pd−Cl1	2.342(7)	Cl1−Pd−Cl1a[a]	92.11(4)
P−C6	1.804(3)	C6−P−C3	106.73(12)
P−C1	1.835(3)	C6−P−C1	106.79(13)
P−C3	1.812(3)	C3−P−C1	106.97(13)

[a] Generated by symmetry operations: $-x + 3/2$, y, $-z + 1$.

Its P−C bonds are generally shorter than those in the structures of **5c**,**d**, whereas the C−P−C bond angles are seemingly widened. The C−F bond lengths to the *o*- and *p*-fluorines are on average 1.351 Å, slightly longer than in the pentafluorinated aromatics. Two crystal structures of the non-fluorinated parent compound, dichloro-{*P,P′*-(1,2-ethanediyl)bis[diphenylphosphane]}palladium(II) can be found in the literature.[25,26] These show significant deviations as regards, for example, the P−Pd−P bond angle [88.3(1)° vs. 85.82(7)°] and the Pd−P bond lengths [2.284(3) and 2.264(3) Å vs. 2.233(2) and 2.226(2) Å]. This has been attributed to a packing effect arising from the incorporation of one molecule of dichloromethane in the second case. The latter values are nevertheless in good agreement with the Pd−P bond length in **4b** [2.233(7) Å] and the associated P−Pd−P bond angle [85.94(4)°]. The Pd−Cl bond length in **4b** (2.342 Å) is also close to the values observed in the non-fluorinated complex [2.361(2) and 2.357(2) Å].

Polymerization

In contrast to early transition metal systems, complexes of the late transition metals are most often found to dimerize or oligomerize olefins as a result of a competition between chain propagation and β-hydride elimination.[27,28] This is illustrated by the fact that, until recently, just a few examples of late transition metal catalyzed formation of high molecular weight poly(ethylene) were known.[29−31] However, it has since been demonstrated that Pd^{II}- and Ni^{II}-based systems with bulky diimine ligands are not only capable of producing high molecular weight poly(ethylene), but even poly(α-olefin)s.[32,33] This finding was attributed to a blocking of β-hydride elimination by the sterically demanding ligand system. Since the ligands discussed in this work were not designed to meet this requirement, 2-norbornene was used as the monomer as, in this case, a chain termination process based on β-hydride elimination is thermodynamically unfavourable.[34,35] In the case of the semi-fluorinated complexes **4b−d**, addition of 2-norbornene to a solution of the MAO-activated[36] species led to the immediate precipitation of poly(norbornene). Due to the heat of reaction evolved in the polymerization process, this was accompanied by a warming of the reaction vessel. Under analogous experimental conditions, the structurally related complexes DPPE-$PdCl_2$, DPPP-$PdCl_2$,[37] and DPPP-$NiCl_2$[38] were found to give lower conversions, whereas the Pt^{II} complex **6c**[39] failed to produce any poly(norbornene) (Table 4).

Table 4. Polymerization results for semi-fluorinated complexes in comparison with the performances of structurally similar non-fluorinated compounds

	Catalyst	Reaction time (min.)	Monomer conversion (%)
1	DPPE-$PdCl_2$	15	51.4
2	DPPP-$PdCl_2$	15	49.7
3	4b	10	94.7
4	4c	15	100
5	4c	10	94.1
6	4d	15	85.7
7	6c	15	0
8	DPPP-$NiCl_2$	15	6.3

Polymer Characterization

The poly(norbornene)s synthesized in the course of this study were found to be completely insoluble in common organic solvents. In the case of the palladium-catalyzed norbornene polymerization, this lack of solubility has been proposed to originate from an *diisotactic* microstructure of the polymer, whereas Ni and Co complexes have been reported to produce *erythro-syndiotactic* material that shows satisfactory solubility up to molecular weights of one million and beyond.[35,40,41] In this regard, it is noteworthy that the polymer formed by DPPP-$NiCl_2$ was also found to be insoluble. As a consequence, polymer characterization could only be carried out by means of solid-state methods. The solid-state ^{13}C NMR spectrum features broad resonances in the range $\delta = 25-60$. Major absorptions are seen at $\delta = 52.5$, 48.6, 40.9, and 35.3 that are not fully baseline-resolved. This finding is due to the bicyclic nature of the monomer and can also be taken as evidence pointing to a complex polymer microstructure. As far as we can conclude from the spectral data, polymerization with the late transition metal catalysts examined here proceeds according to an insertion-type mechanism, since vinylic resonances resulting from a hypothetical ring-opening propagation step are not observed.[42−44] In the FT-IR (KBr) spectrum, strong bands are observed at 2946 cm^{-1} (CH_2 units) and 2867 cm^{-1} (CH units), resembling the typical C,H valence absorptions, whereas bands at 1478 cm^{-1} and 1454 cm^{-1} can be attributed to C,H bond deformation. A weak absorption at 707 cm^{-1} is assigned to CH_2 rocking. In accordance with the literature data, no glass transition below the onset of thermal decomposition could be detected for the prepared poly(norbornene)s by DSC methods.[34]

Conclusion

The treatment of novel electron-poor Pd^{II} complexes based on semi-fluorinated bis(phosphane)s with methylaluminoxane (MAO) affords active catalysts for the insertion polymerization of 2-norbornene, which display increased monomer conversions compared to catalysts derived from non-fluorinated, more electron-rich compounds. Comparisons of the crystallographic data of **4a** with those of the parent compound dichloro-[*P,P′*-(1,2-ethanediyl)bis(diphenylphosphane)]palladium(II), and those of **5c**,**d** with the data for diiodo-[*P,P′*-(1,2-ethanediyl)bis(diphenylphosphane)]palladium(II) revealed no significant structural differences. Therefore, despite the fact that there seems to be no clear relationship between the degree of fluorination and the monomer conversion, the improved polymerization results obtained with the fluorinated species may be ascribed to their altered electronic properties.

Owing to the comparatively low steric demand in the apical positions, the investigated catalysts are not suitable for the polymerization of α-olefins to high molecular weight poly(olefin)s since the competing displacement of β-H elimination products by incoming olefin molecules cannot be sufficiently suppressed.[27,28,32,33] Consequently, these complexes can be expected to act as oligomerization catalysts for α-olefins. In terms of activity towards the polymerization of 2-norbornene, ligand-free systems[35,40,41] based on simple metal salts, for instance Pd^{II}, Ni^{II}, or Co^{II} compounds, are presumably superior to the investigated catalysts, but lack the structural versatility of bis(phosphane) complexes, which potentially may be helpful in controlling olefin insertion processes. Thus, it should be interesting to combine a bulky ligand geometry, which meets the requirements outlined up above, with partial fluorination to obtain new late transition metal catalysts for the synthesis of poly(olefin)s.

Experimental Section

Materials: *P,P′*-(1,2-ethanediyl)bis[bis(pentafluorophenyl)phosphane] (99%), *P,P′*-(1,2-ethanediyl)bis(dichlorophosphane) (min. purity 97%; received in a sealed glass ampoule, which was opened immediately prior to use), and dichlorobis(benzonitrile)platinum(II) (Bn_2PtCl_2) (99%) were purchased from Strem Chemicals; 1-bromo-2,4-difluorobenzene (98%+), 1-bromo-2,4,5-trifluorobenzene (98%+), and 1-bromo-3,5-bis(trifluoromethyl)benzene (98%+) were from Lancaster. Mg turnings and 2-norbornene were obtained from Merck. Dichloro[*P,P′*-(1,3-propanediyl)bis(diphenylphosphane)]nickel(II), dichloro[*P,P′*-(1,2-ethanediyl)bis(diphenylphosphane)]palladium(II), dichloro[*P,P′*-(1,3-propanediyl)bis(diphenylphosphane)]palladium(II), and *n*-butyllithium (0.1 M in *n*-hexane) were purchased from Fluka. MAO was supplied by WITCO (10% *w*/*w* in toluene). Dichlorobis(benzonitrile)palladium(II) (Bn_2PdCl_2) and dichloro(1,5-cyclooctadiene)palladium(II) ($CODPdCl_2$) were prepared according to literature procedures.[45,46] Tetrahydrofuran was distilled from sodium benzophenone ketyl, toluene from potassium benzophenone ketyl. Dichloromethane was refluxed with calcium hydride and distilled. Ethanol was dried with sodium/diethyl phthalate. Dry acetone (max. 0.01% H_2O) was purchased from Merck. All operations relating to the preparation and complexation of the bis(phosphane) ligands were carried out under an argon atmosphere employing standard Schlenk techniques. The synthesized complexes were found to be stable towards air and moisture and do not require any special conditions for storage.

Methods: ^1H, ^{13}C, and ^{31}P NMR spectra were recorded on a Bruker AMX 500 spectrometer. Chemical shifts (δ) are given in ppm and were referenced to residual ^1H NMR signals and to the ^{13}C NMR signals of the deuterated solvents, respectively. ^{31}P chemical shifts were referenced to external 85% H_3PO_4. ^{19}F NMR spectra were recorded on a Bruker AC 200 spectrometer employing an external $CFCl_3$ standard for calibration. Solid-state ^{13}C NMR spectra (CP-MAS) were recorded on a Bruker DSX 400 spectrometer and referenced using glycine. − IR spectra were recorded on a Bruker IFS 113V spectrophotometer using samples in KBr pellets. − FAB mass spectra were measured on a Finnigan SSQ 7000 spectrometer using a matrix of 2-nitrophenyl octyl ether. − Elemental analyses were performed in the Microanalytical Section of the University of Ulm. − X-ray structure determinations of compounds **4b** and **5d** were carried out on a STOE IPDS diffractometer (Universität Ulm); **5c** was analyzed on a Rigaku AFC-7S diffractometer (University of Helsinki). All measurements were made using graphite-monochromated Mo-K_α radiation (wavelength 0.71073 Å; fine-focus sealed tube).

Synthesis of the Ligands L_2 (3a−c)

***P,P′*-(1,2-Ethanediyl)bis[bis(2,4,5-trifluorophenyl)phosphane] (3a):** In a 500-mL Schlenk flask equipped with a dropping funnel 1-bromo-2,4,5-trifluorobenzene (6.1 mL, 51.8 mmol) was dissolved in dry diethyl ether (50 mL) and the solution was cooled to −78 °C by employing a dry ice/2-propanol bath. Over a period of 30 min., a solution of *n*-butyllithium in *n*-hexane (32.4 mL, 1.6 M) was added by means of the dropping funnel. Following this addition, stirring was continued for 15 min. The funnel was then rinsed with dry diethyl ether (5 mL) and charged with a solution of *P,P′*-(1,2-ethanediyl)bis(dichlorophosphane) (2.0 g, 8.9 mmol) in diethyl ether (25 mL), which was added maintaining a temperature of −78 °C. The solution was then allowed to warm to room temperature. After hydrolysis with degassed water, the ethereal phase was separated and dried with anhydrous magnesium sulfate. The solvent was evaporated in vacuo to yield a yellowish product. Recrystallization from ethanol/acetone afforded **3a** as a white crystalline solid. Yield: 4.4 g (80.5%). − ^1H NMR ($CDCl_3$): δ = 7.03 (m, 4 H, Ar), 6.91 (m, 4 H, Ar), 2.17 (m, 4 H, CH_2). − ^{13}C NMR ($CDCl_3$): δ = 159.6 [d, $^1J(^{19}F,^{13}C)$ = 246.5 Hz], 151.4 [ddd, $^1J(^{19}F,^{13}C)$ = 242.7 Hz, $^2J(^{19}F,^{13}C)$ = 15.1 Hz, $^2J(^{19}F,^{13}C)$ = 12.6 Hz], 147.9 [dd, $^1J(^{19}F,^{13}C)$, = 249.0 Hz, $^2J(^{19}F,^{13}C)$ = 12.6 Hz], 121.1, 118.6, 106.3 [dd, $^2J(^{19}F,^{13}C)$ = 30.2 Hz, $^2J(^{19}F,^{13}C)$ = 8.8 Hz], 20.9. − ^{19}F NMR ($CDCl_3$): δ = −105.9 (m, *o*-F), −130.3 (m, *p*-F), −141.8 (m, *m*-F). − ^{31}P NMR ($CDCl_3$): δ = −30.2. − $C_{26}H_{12}F_{12}P_2$ (614.3): calcd. C 50.8, H 2.0; found C 50.6, H 2.1.

***P,P′*-(1,2-Ethanediyl)bis[bis(2,4-difluorophenyl)phosphane] (3b):** Compound **3b** was synthesized according to the procedure described for **3a** starting from 1-bromo-2,4-difluorobenzene (10 g, 51.8 mmol) and 1,2-bis(dichlorophosphanyl)ethane (2.0 g, 8.9 mmol). Yield: 3.6 g (74.5%). − ^1H NMR ($CDCl_3$): δ = 7.22 (m, 4 H, Ar), 6.84 (m, 4 H, Ar), 6.76 (m, 4 H, Ar), 2.19 (m, 4 H, CH_2). − ^{13}C NMR ($CDCl_3$): δ = 165.5 [dd, $^1J(^{19}F,^{13}C)$, = 56.6 Hz, $^2J(^{19}F,^{13}C)$ = 11.3 Hz], 163.4 [dd, $^1J(^{19}F,^{13}C)$ = 60.4 Hz, $^2J(^{19}F,^{13}C)$ = 12.6 Hz], 134.8 [dd, $^2J(^{19}F,^{13}C)$ = 15.1 Hz, $^2J(^{19}F,^{13}C)$ = 8.8 Hz], 118.6 (pseudo-triplet due to coupling with ^{19}F and ^{31}P; coupling constants are 20.1 Hz and 16.4 Hz but unequivocal assignment is not possible), 111.9 [d, $^2J(^{19}F,^{13}C)$ = 20.1 Hz], 104.3 [dd, $^2J(^{19}F,^{13}C)$ = 27.7 Hz, $^2J(^{19}F,^{13}C)$ = 25.2 Hz], 21.0. − ^{19}F NMR ($CDCl_3$): δ = −100.4 (m, *o*-F), −108.9 (m, *p*-F). − ^{31}P NMR ($CDCl_3$): δ = −31.9. − $C_{26}H_{16}F_8P_2$ (542.4): calcd. C 57.5, H 2.9; found C 57.3, H 2.8.

***P,P′*-(1,2-Ethanediyl)bis{bis[3,5-di(trifluoromethyl)phenyl]phosphane} (3c):** At 0 °C, a solution of bis(3,5-trifluoromethyl)phenylmagnesium bromide, prepared from magnesium turnings (1.75 g, 72.0 mmol) and 1-bromo-3,5-bis(trifluoromethyl)benzene (17.1 g, 58.4 mmol) in dry diethyl ether (130 mL) was added to a solution of *P,P′*-(1,2-ethanediyl)bis(dichlorophosphane) (2.0 g, 8.9 mmol) in dry diethyl ether (40 mL). Stirring was continued for 24 h at room temperature. The reaction mixture was then hydrolyzed with degassed water (100 mL) and the resulting precipitate was collected by filtration and extracted with warm acetone. Evaporation of the solvent left a slightly brownish solid, which was recrystallized from dichloromethane/acetone. Yield: 6.9 g (82.3%). − ^1H NMR ([D_6]acetone): δ = 8.10 (s, 8 H, Ar), 8.03 (s, 4 H, Ar), 2.73 (m, 4 H, CH_2). − ^{13}C NMR ([D_6]acetone): δ = 142.1, 134.2, 132.4 [q,

$^2J(^{19}F,^{13}C)$ = 34.0 Hz], 124.7 [q, $^1J(^{19}F,^{13}C)$ = 271.6 Hz, CF_3], 124.1, 23.5 [d, $^1J(^{31}P, ^{13}C)$ = 3.8 Hz]. − ^{19}F NMR ([D$_6$]acetone): δ = −62.6. − ^{31}P NMR ([D$_6$]acetone): δ = −3.4. − $C_{34}H_{16}F_{24}P_2$ (942.4): calcd. C 43.3, H 1.7; found C 43.3, H 2.1.

Preparation of the Complexes L_2PdCl_2 (4a−d)

Dichloro{*P,P′*-(1,2ethanediyl)bis[bis(2,4,5-trifluorophenyl)-phosphane]}palladium(II) (4a): Bn_2PdCl_2 (0.345 g, 0.9 mmol) was added to a solution of **3a** (0.61 g, 1.0 mmol) in dry CH_2Cl_2 (25 mL). After stirring for 16 h at room temperature, the yellowish white precipitate was collected by filtration, thoroughly washed with diethyl ether, and dried under high vacuum. Yield: 0.32 g (45.1%). − ^1H NMR ([D$_6$]DMSO): δ = 7.90 (m, 8 H, Ar), 2.85 (m, 4 H, CH_2). − ^{19}F NMR ([D$_6$]DMSO): δ = −99.1 (m, *o*-F), −124.1 (m, *p*-F), −140.3 (m, *m*-F). − ^{31}P NMR ([D$_6$]DMSO): δ = 64.4. − $C_{26}H_{12}Cl_2F_{12}P_2Pd$ (791.6): calcd. C 39.5, H 1.5; found C 39.1, H 1.5.

Dichloro{*P,P′*-(1,2-ethanediyl)bis[bis(2,4-difluorophenyl)-phosphane]}palladium(II) (4b): Compound **3b** (2.9 g, 53.5 mmol) was added to a solution of $CODPdCl_2$ (1.14 g, 40.0 mmol) in dry CH_2Cl_2 (75 mL). After stirring at room temperature for 16 h, the product was precipitated by pouring the reaction mixture into *n*-pentane (500 mL), collected by filtration, washed with *n*-pentane, and dried under high vacuum. Yield: 2.39 g (83.0%). − ^1H NMR ([D$_6$]DMSO): δ = 7.86 (m, 4 H, Ar), 7.58 (m, 4 H, Ar), 7.38 (m, 4 H, Ar), 2.74 (m, 4 H, CH_2). − ^{19}F NMR ([D$_6$]DMSO): δ = −94.4 (m, *o*-F), −100.7 (m, *p*-F). − ^{31}P NMR ([D$_6$]DMSO): δ = 64.3. − $C_{26}H_{16}Cl_2F_8P_2Pd$ (719.7): calcd. C 43.4, H 2.2; found C 43.6, H 2.7.

Dichloro[*P,P′*-(1,2-ethanediyl)bis{bis[3,5-di(trifluoromethyl)phenyl]-phosphane}]palladium(II) (4c): Compound **3c** (0.85 g, 0.9 mmol) was added to a solution of Bn_2PdCl_2 (0.345 g, 0.9 mmol) in dry acetone (20 mL). After stirring at room temperature for 16 h, the product was precipitated by pouring the reaction mixture into diethyl ether (50 mL). The yellowish-white solid was collected by filtration, washed with diethyl ether, and dried under high vacuum. Yield: 0.95 g (94.0%). − ^1H NMR ([D$_6$]acetone): δ = 8.76 (s, 4 H, Ar), 8.73 (s, 4 H, Ar), 8.34 (s, 4 H, Ar), 3.64 (m, 4 H, CH_2). − ^{19}F NMR ($CDCl_3$): δ = −62.5. − ^{31}P NMR ([D$_6$]acetone): δ = 67.7. − $C_{34}H_{16}Cl_2F_{24}P_2Pd$ (1119.7): calcd. C 36.5, H 1.4; found C 36.2, H 1.7.

Dichloro{*P,P′*-(1,2-ethanediyl)bis[bis(pentafluorophenyl)phosphane]}palladium(II) (4d): In a 250-mL Schlenk flask, $CODPdCl_2$ (0.358 g, 1.25 mmol) and **3d** (0.95 g, 1.25 mmol) were suspended in dry toluene (35 mL) and the mixture was heated to 110 °C for 5 h. After cooling to room temperature, the product was collected by filtration and washed with diethyl ether (2 × 25 mL). Drying under high vacuum yielded 1.1 g (94%) of a yellow powder. − ^1H NMR ([D$_6$]DMSO at 80 °C): δ = 3.21 (m, 4 H, CH_2). − ^{31}P NMR ([D$_6$]DMSO at 80 °C): δ = 37.8. − MS (FAB): *m/z* = 900.6 [M^+ − Cl], 863.8 [M^+ − 2Cl]. − $C_{26}H_4Cl_2F_{20}P_2Pd$ (935.6): calcd. C 33.4, H 0.4; found C 33.4, H 0.8.

Preparation of the Complexes L_2PdI_2 (5c,d)

[*P,P′*-(1,2-Ethanediyl)bis{bis[3,5-di(trifluoromethyl)phenyl]phosphane}]diiodopalladium(II) (5c): Compound **4c** (0.3 g, 0.27 mmol) was treated with NaI (0.12 g, 0.8 mmol) in dry acetone (30 mL). After evaporation of the solvent, the residue was extracted with CH_2Cl_2. The orange-red product was then precipitated from the concentrated CH_2Cl_2 solution by adding diethyl ether (50 mL). Yield: 0.23 g (65.9%). − ^1H NMR ([D$_6$]acetone): δ = 8.63 (d, 8 H, Ar), 8.35 (s, 4 H, Ar), 3.46 (m, 4 H, CH_2). − ^{19}F NMR ([D$_6$]acetone): δ = −62.5. − ^{31}P NMR ([D$_6$]acetone): δ = 69.3. − $C_{34}H_{16}F_{24}I_2P_2Pd$ (1302.6): calcd. C 31.4, H 1.2; found C 31.1, H 1.0.

{*P,P′*-(1,2-Ethanediyl)bis[bis(pentafluorophenyl)phosphane]}diiodo-palladium(II) (5d): With gentle heating, **4d** (0.3 g, 0.32 mmol) was dissolved in dry acetone (60 mL). NaI (0.144 g, 0.96 mmol) was added, the mixture was stirred for 30 min, and then the solvent was removed in vacuo. The red residue was redissolved in the minimum volume of acetone and purified by column chromatography (SiO_2, particle size 0.063−0.200 mm, Merck) using acetone as the eluent. Evaporation of the solvent from the appropriate fraction left a red microcrystalline product. Yield: 0.27 g (73.7%). − ^1H NMR ([D$_6$]acetone): δ = 3.21 (m, 4 H, CH_2). − ^{31}P NMR ([D$_6$]acetone): δ = 33.6. − $C_{26}H_4F_{20}I_2P_2Pd$ (1118.5): calcd. C 27.9, H 0.4; found C 27.4, H 0.8.

Preparation of the Complexes L_2PtCl_2 (6a−c)

Dichloro{*P,P′*-(1,2-ethanediyl)bis[bis(2,4,5-trifluorophenyl)-phosphane]}platinum(II) (6a): Prepared analogously to **6c** from Bn_2PtCl_2 (0.33 g, 0.7 mmol) and **3a** (0.47 g, 0.77 mmol). Yield: 0.32 g (52.0%). − ^1H NMR ([D$_6$]DMSO): δ = 7.91 (m, 4 H, Ar), 7.86 (m, 4 H, Ar), 2.76 (m, 4 H, CH_2). − ^{31}P NMR ([D$_6$]DMSO): δ = 43.0 [^1J (^{195}Pt, ^{31}P) = 3677.1 Hz]. − $C_{26}H_{12}Cl_2F_{12}P_2Pt$ (880.3): calcd. C 35.5, H 1.4; found C 35.7, H 1.2.

Dichloro{*P,P′*-(1,2-ethanediyl)bis[bis(2,4-difluorophenyl)-phosphane]}platinum(II) (6b): Prepared analogously to **6c** from Bn_2PtCl_2 (0.25 g, 0.53 mmol) and **3b** (0.30 g, 0.56 mmol). Yield: 0.35 g (81.7%). − ^1H NMR ([D$_6$]acetone): δ = 7.98 (m, 4 H, Ar), 7.26 (m, 8 H, Ar), 2.85 (m, 4 H, CH_2). − ^{19}F NMR ([D$_6$]acetone): δ = −95.4 (m, *o*-F), −102.4 (m, *p*-F). − ^{31}P NMR ([D$_6$]acetone):

Table 5. Crystal data and structure refinement for **4b**

Empirical formula[a]	$C_{30}H_{20}Cl_{10}F_8P_2Pd$
Formula weight	1055.30
Crystal size [mm]	0.38 × 0.29 × 0.23
Temperature [K]	293(2)
Wavelength [Å]	0.71073
Crystal system	monoclinic
Space group	*I*2/*a*
Unit cell dimensions [Å, °]	*a* = 20.855(2) *b* = 8.528(6), *c* = 23.200(2) β = 104.291(12)
Volume [Å^3]	3998.2(6)
Z	4
Calculated density [g/cm^3]	1.753
Absorption coefficient [mm^{-1}]	1.274
F (000)	2072
Θ range [°]	2.02 to 25.93
Index ranges	25 ≥ *h* ≥ −25, 10 ≥ *k* ≥ −10, 28 ≥ *l* ≥ −28
Reflections collected/unique	27301/3810 [*R*(int) = 0.0329]
Refinement method	Full-matrix least-squares on F^2
Data/restraints/parameters	3810/0/231
Goodness-of-fit on F^2	1.059
Final *R* indices, [$I > 2\sigma(I)$]	*R*1 = 0.032, *wR*2 = 0.0848
R indices (all data)	*R*1 = 0.0372, *wR*2 = 0.0888
Largest diff. peak and hole [e/Å^{-3}]	0.860 and −0.684

[a] Data collection, cell refinement and data reduction were performed with STOE IPDS. For structure solution SHELXS-97 and structure refinement SHELXL-97 (both Sheldrick, 1997) were used. Molecular Graphics: ORTEP III. Non hydrogen-atom sites were obtained with direct methods and are anisotropically refined. Hydrogen atoms are refined by riding model on calculated positions.

Table 6. Crystal data and structure refinement for **5c**

Empirical formula[a]	$C_{44.5}H_{37}F_{24}I_2O_{3.5}P_2Pd$
Formula weight	1505.88
Crystal size [mm]	0.45 × 0.35 × 0.25
Temperature [K]	193(2)
Wavelength [Å]	0.71073
Crystal system	monoclinic
Space group	*C*2/*c*
Unit cell dimensions [Å, °]	a = 24.969(9), b = 8.705(7), c = 27.843(8), β = 107.09(3)
Volume [Å^3]	5785(5)
Z	4
Calculated density [g/cm^3]	1.729
Absorption coefficient [mm^{-1}]	1.558
F (000)	2920
Θ range [°]	2.61 to 23.99
Index ranges	$28 \geq h \geq 0$, $9 \geq k \geq 0$, $30 \geq l \geq -31$
Reflections collected/unique	4163/4065, [*R*(int) = 0.0503]
Completeness to Θ = 23.99 (%)	89.8
Refinement method	Full-matrix least-squares on F^2
Data/restraints/parameters	4065/108/361
Goodness-of-fit on F^2	1.114
Final *R* indices [$I > 2\sigma(I)$]	*R*1 = 0.0786, *wR*2 = 0.1980
R indices (all data)	*R*1 = 0.0951, *wR*2 = 0.2101
Largest diff. peak and hole [e/Å^{-3}]	0.474 and −0.260

[a] Data collection, cell refinement and data reduction were performed with TEXSAN (Molecular Structure Corporation, 1993). For structure solution SHELXS-97 and structure refinement SHELXL-97 (both Sheldrick, 1997) were used. Molecular Graphics: ORTEP III. Non-hydrogen atom positions were obtained with direct methods and are anisotropically refined. Hydrogen atoms are refined by riding model on calculated positions. One solvent acetone molecule is partly disordered, namely C(21)−C(22)-[O(1)]−C(23), and has a site occupation factor of 0.75. A SWAT parameter was introduced for diffuse solvent modelling

Table 7. Crystal data and structure refinement for **5d**

Empirical formula[a]	$C_{26}H_4F_{20}I_2P_2Pd$
Formula weight	1118.43
Crystal size [mm]	0.15 × 0.23 × 0.38
Temperature [K]	293(2)
Wavelength [Å]	0.71073
Crystal system	monoclinic
Space group	$P2_1/n$
Unit cell dimensions [Å, °]	a = 11.617(10), b = 14.958(8), c = 19.931(19), β = 95.05(11)
Volume [Å^3]	3450(5)
Z	4
Calculated density [g/cm^3]	2.153
Absorption coefficient [mm^{-1}]	2.548
F (000)	2088
Θ range [°]	2.05 to 24.01
Index ranges	$13 \geq h \geq -13$, $17 \geq k \geq -17$, $22 \geq l \geq -22$
Reflections collected/unique	31481/5290 [*R*(int) = 0.1043]
Completeness to Θ = 24.01 (%)	93.3
Refinement method	Full-matrix least-squares on F^2
Data/restraints/parameters	5290/0/460
Goodness-of-fit on F^2	1.026
Final *R* indices [$I > 2\sigma(I)$]	*R*1 = 0.0637, *wR*2 = 0.1691
R indices (all data)	*R*1 = 0.0900, *wR*2 = 0.1870
Largest diff. peak and hole [e/Å^{-3}]	1.181 and −1.702

[a] A relatively suitable crystal for diffraction was cut out of a soft crystalline bulk. This "crystal" diffracted only up to 24 degrees. Since the faces of the crystal were arbitrary they could not be used for conducting an absorption correction. The measured intensities were corrected for Lorentz and polarization effects. Data collection, cell refinement and data reduction were performed with STOE IPDS. The structure determination was done by direct methods using XMY (Debaerdemaeker, 1993),[47] for structure refinement SHELXL-97 (Sheldrick, 1997) was utilized. The positions of the hydrogen atoms were calculated (riding model) and refined isotropically. Molecular Graphics: ORTEP III.

δ = 42.5 [^1J (^{195}Pt, ^{31}P) = 3663.2 Hz]. − $C_{26}H_{16}Cl_2F_8P_2Pt$ (808.3): calcd. C 38.6, H 2.0; found C 38.9, H 2.3.

Dichloro[*P,P'*-(1,2-ethanediyl)bis{bis[3,5-di(trifluoromethyl)phenyl]-phosphane}]platinum(II) (6c): Compound **3c** (0.35 g, 0.37 mmol) was added to a solution of Bn_2PtCl_2 (0.159 g, 0.33 mmol) in dry CH_2Cl_2 (20 mL). The yellow colour of the starting material faded within a few minutes as a white precipitate formed. After stirring for 16 h at room temperature, the precipitate was collected by filtration, washed with diethyl ether and *n*-pentane, and dried under high vacuum. Yield: 0.31 g (78.5%). − ^{1}H NMR ([D$_6$]acetone): δ = 8.72 (d, 8 H, Ar), 8.34 (s, 4 H, Ar), 3.49 (m, 4 H, CH_2). − ^{31}P NMR ([D$_6$]acetone): δ = 50.9 [^1J(^{195}Pt, ^{31}P) = 3582.5 Hz]. − $C_{34}H_{16}Cl_2F_{24}P_2Pt$ (1208.4): calcd. C 33.8, H 1.3; found C 33.6, H 1.1.

General Procedure for the Polymerization of 2-Norbornene: A 250-mL Schlenk flask was evacuated and purged with argon three times. The vessel was then charged with the appropriate pre-catalyst (usually 3.74 × 10^{-5} mol) suspended in the requisite volume of dry toluene such that, together with the MAO solution, a final total volume of 100 mL was obtained. Addition of the MAO solution (10% *w*/*w* in toluene) led to an immediate conversion of the pre-catalyst, as was evident from the dissolution of the suspended material and the formation of a clear red-brown solution. Following the introduction of 2-norbornene (4.75 g, 50.5 mmol), the reaction was usually allowed to proceed for 10−15 min. and then the polymerization was quenched by pouring the mixture into a glass beaker containing MeOH (500 mL)/conc. hydrochloric acid (5 mL). The product was collected by filtration and dried under high vacuum at 80 °C for 24 h to yield a fine white powder. − ^{13}C NMR (CP-MAS): Resonances not baseline-resolved; peaks at δ = 57.4, 55.8, 52.5, 48.6, 40.9, 35.3, 30.1. − FT-IR (KBr): $\tilde{\nu}$ = 2946, 2867, 1478, 1454, 1300, 707 cm^{-1}.

Crystallographic Data: Crystallographic data for the structures reported in this paper have been deposited with the Cambridge Crystallographic Data Centre as supplementary publications nos. CCDC-136063 (**4b**, Table 5), -135995 (**5c**, Table 6), and -136062 (**5d**, Table 7). Copies of the data can be obtained free of charge on application to CCDC, 12 Union Road, Cambridge CB2 1EZ, U.K. [Fax: (internat.) +44-1223/336-033; E-mail: deposit@ccdc.cam.ac.uk].

Acknowledgments

The authors would like to thank the Bundesministerium für Bildung und Forschung (BMBF) as well as BASF AG for generous financial support. The X-ray structure determination of **5c** was carried out by Martti Klinga (University of Helsinki, Finland), whose cooperation is gratefully acknowledged. Compounds **4b**, **5d** were kindly analyzed at the University of Ulm, Germany, by Dr. A. Debaerdemaeker.

[1] Recent review: H.-U. Blaser, *Tetrahedron: Asymmetry* **1991**, *2*, 843 and references cited therein.
[2] K. Tamo, K. Sumitami, M. Kumada, *J. Am Chem. Soc.* **1972**, *94*, 4374.
[3] M. Kumada, *Pure Appl. Chem.* **1980**, *52*, 669.
[4] G. Wilke, *Angew. Chem. Int. Ed. Engl.* **1988**, *27*, 185.
[5] V. M. Möhring, G. Fink, *Angew. Chem. Int. Ed. Engl.* **1985**, *24*, 1001.

[6] M. F. Ernst, D. M. Roddick, *Inorg. Chem.* **1989**, *28*, 1624.
[7] R. L. Cook, J. G. Morse, *Inorg. Chem.* **1982**, *21*, 4103.
[8] R. C. Schnabel, D. M. Roddick, *ACS Symp. Ser.* **1994**, *55*, 421 and references cited therein.
[9] R. C. Schnabel, R. S. Carroll, D. M. Roddick, *Organometallics* **1996**, *15*, 655.
[10] B. L. Bennett, J. Birnbaum, D. M. Roddick, *Polyhedron* **1995**, *14*, 187.
[11] M. F. Ernst, D. M. Roddick, *Organometallics* **1990**, *9*, 1586.
[12] M. F. Ernst, D. M. Roddick, *Inorg. Chem.* **1990**, *29*, 3627.
[13] M. Brookhart, W. A. Chandler, A. C. Pfister, C. C. Santini, P. S. White, *Organometallics* **1992**, *11*, 1263.
[14] R. K. Merwin, R. C. Schnabel, J. D. Koola, D. M. Roddick, *Organometallics* **1992**, *11*, 2972.
[15] L. D. Field, M. P. Wilkinson, *Organometallics* **1997**, *16*, 1841.
[16] R. B. King, W. M. Rhee, *Inorg. Chem.* **1978**, *17*, 2961.
[17] R. J. Burt, J. Chatt, W. Hussain, G. J. Leigh, *J. Organomet. Chem.* **1979**, *182*, 203.
[18] H. Nishida, N. Takada, M. Yoshimura, T. Sonoda, H. Kobayashi, *Bull. Chem. Soc. Jpn.* **1984**, *57*, 2600.
[19] C. P. Casey, E. L. Paulsen, E. W. Beuttenmueller, B. R. Proft, L. M. Petrovich, B. A. Matter, D. R. Powell, *J. Am. Chem. Soc.* **1997**, *119*, 11817 and related supplementary material.
[20] P. E. Garrou, *Inorg. Chem.* **1975**, *14*, 1435.
[21] BISBI = 2,2′-bis[(diphenylphosphanyl)methyl]-1,1′-biphenyl.
[22] M. J. Atherton, K. S. Coleman, J. Fawcett, J. H. Holloway, E. G. Hope, A. Karacar, L. A. Peck, G. C. Saunders, *J. Chem. Soc., Dalton Trans.* **1995**, 4029.
[23] M. J. Atherton, K. S. Coleman, J. Fawcett, J. H. Holloway, E. G. Hope, A. Karacar, D. R. Russell, G. C. Saunders, *J. Chem. Soc., Dalton Trans.* **1996**, 3215.
[24] W. Oberhauser, C. Bachmann, T. Stampfl, R. Haid, P. Brügeller, *Polyhedron* **1997**, *16*, 2827.
[25] S. Singh, N. K. Jha, P. Narula, T. P. Singh, *Acta Crystallogr. C* **1995**, *51*, 593.
[26] W. L. Steffen, G. J. Palenik, *Inorg. Chem.* **1976**, *15*, 2432.
[27] F. Rix, M. Brookhart, *J. Am. Chem. Soc.* **1995**, *117*, 1137.
[28] M. Peuckert, W. Keim, *Organometallics* **1983**, *2*, 594.
[29] G. F. Schmidt, M. Brookhart, *J. Am. Chem. Soc.* **1985**, *107*, 1443.
[30] M. Brookhart, A. F. Volpe, Jr., D. M. Lincoln, I. T. Horvath, J. M. Millar, *J. Am. Chem. Soc.* **1990**, *112*, 5643.
[31] U. Klabunde, S. D. Ittel, *J. Mol. Catal.* **1987**, *41*, 123.
[32] L. K. Johnson, C. M. Killian, M. Brookhart, *J. Am. Chem. Soc.* **1995**, *117*, 6414.
[33] MAO-activated complexes of Fe^{II} or Co^{II} ligated by tripodal imine-containing ligands with sterically demanding substituents have been shown to produce high molecular weight linear poly(ethylene)s: B. L. Small, M. Brookhart, A. M. A. Bennett, *J. Am. Chem. Soc.* **1998**, *120*, 4049. For the synthesis of oligomers (M_w 260−470) using an iron catalyst, see: G. J. P. Britovsek, V. C. Gibson, B. S. Kimberley, P. J. Maddox, S. J. McTavish, G. A. Solan, A. J. P. White, D. J. Williams, *Chem. Commun.* **1998**, 849.
[34] J. Melia, E. Connor, S. Rush, S. Breunig, C. Mehler, W. Risse, *Macromol. Symp.* **1995**, *89*, 433.
[35] B. L. Goodall, G. M. Benedikt, L. H. McIntosh III, D. A. Barnes (B. F. Goodrich Co.), World Patent WO 95 14048 A1; *Chem. Abstr.* **1995**, *123*, 341322p.
[36] The dichloro complexes are presumably dimethylated by MAO and then one methyl group is abstracted to produce the active monomethyl species. Such an activation process has previously been proposed for an Ni^{II}-based system: D. Pappalardo, M. Mazzeo, C. Pellechia, *Makromol. Chem. Rapid. Commun.* **1997**, *18*, 1017.
[37] DPPP = *P,P′*-(1,3-propanediyl)bis(diphenylphosphane), DPPE = *P,P′*-(1,2-ethanediyl)bis(diphenylphosphane).
[38] Steric factors must be taken into account in understanding the polymerization behaviour of DPPP-$NiCl_2$. Due to the lower ionic radius of Ni^{II} and, as a consequence, enhanced steric interactions between the ligand, the growing polymer chain, and the coordinated monomer, this complex is less active in the polymerization of norbornene.
[39] In the case of Pt−alkyl complexes, the insertion process of a C=C bond is energetically less favourable than for Pd or Ni complexes due to the high stability of the Pt−C bond.
[40] F. P. Alt, W. Heitz, *Macromol. Chem. Phys.* **1998**, *199*, 1951.
[41] B. L. Goodall, L. H. McIntosh III, L. F. Rhodes, *Macromol. Symp.* **1995**, *89*, 421.
[42] R. R. Schrock, *Acc. Chem. Res.* **1990**, *23*, 158.
[43] B. M. Novak, W. Risse, R. H. Grubbs, *Adv. Polym. Sci.* **1992**, *102*, 47.
[44] A. S. Abu-Surrah, B. Rieger, *J. Mol. Catal. A: Chemical* **1998**, *128*, 239.
[45] D. Drew, J. R. Doyle, *Inorg. Synth.* **1972**, *13*, 52.
[46] J. R. Doyle, P. E. Slade, H. B. Jonassen, *Inorg. Synth.* **1960**, *6*, 218.
[47] T. Debaerdemaeker, *Z. Kristallogr.* **1993**, *206*, 173.

Received November 3, 1999
[I99389]

Stereochemical Equivalence of P^{III}-Bonded Hydrogen Atoms and $|Se^{IV}$ Lone Electron Pairs in $Sr(H_2PO_3)_2$ and $Sr(HSeO_3)_2$

Kai Boldt,[a] Bernward Engelen,*[a] Martin Panthöfer,[a] and Klaus Unterderweide[a]

Keywords: Hydrogen bonds / IR spectroscopy / Stereochemical equivalence / Strontium / Phosphates / Selenates

$Sr(H_2PO_3)_2$ and $Sr(HSeO_3)_2$ have been characterized by means of single crystal X-ray diffraction and FT-IR absorption spectroscopy. The IR spectra exhibit split AB band systems in the OH stretching mode region due to Fermi resonance interactions of the ν(OH) with the in-plane bending modes of the hydroxyl groups. The compounds crystallize in a new structure type and are isotypic, if the P-bonded hydrogen atoms of $Sr(H_2PO_3)_2$ and the lone electron pairs of $Sr(HSeO_3)_2$ are considered to be equivalent. The coordination of Sr is that of a distorted square antiprism. The SrO_8 polyhedra share three common edges and are additionally connected via O–X–O bonds of the isolobal XO_2OH^- ions (X = HP^{III}, $|Se^{IV}$) of tetrahedral and trigonal (ψ-tetrahedral) configuration, respectively. The resulting layers $^2_\infty[Sr(XO_2OH)_2]$ are connected via circular hydrogen bond systems of tetrameric $[XO_2OH^-]_4$ groups of a cyclooctane like chair topology. Both the P-bonded hydrogen atoms and the lone electron pairs of the $HP^{III}O_2OH^-$ and the $|Se^{IV}O_2OH^-$ ions, respectively, form channels along [001] and induce the same crystal structure. This is new for acid salts of the type $M^{II}(XO_2OH)_2{\cdot}nH_2O$ with X = HP^{III} and $|Se^{IV}$.

Introduction

Strontium hydrogen phosphate(III), $Sr(H_2PO_3)_2$, and strontium hydrogen selenate(IV), $Sr(HSeO_3)_2$, have been isolated by Ebert et al.[1−4] as part of their studies of the solubility diagrams of the quasiternary systems SrO-P_2O_3-H_2O and SrO-SeO_2-H_2O, respectively. The selenium compound has been characterized by means of thermal analysis as well as IR absorption spectroscopy and some X-ray data.[4−6] Since the corresponding phosphates(III) tend to form supersaturated solutions, they are difficult to obtain, especially in the form of single crystals. The knowledge about this class of compounds is thus poor.[1−3] Such acid salts are of special interest because of: i) the strong and medium-strong hydrogen bonds, and hence the formation and transformation of AB and ABC band systems in the OH stretching mode region of the existing hydroxyl groups,[6,7] ii) the possible stereochemical equivalence of the P-bonded hydrogen atom of the phosphate(III) and the lone electron pair of the selenate(IV), which one can find for some corresponding neutral salts, e.g., for $CuHPO_3{\cdot}2H_2O$[8]/$CuSeO_3{\cdot}2H_2O$[9] and $MgHPO_3{\cdot}6H_2O$[10]/$MgSeO_3{\cdot}6H_2O$[11−12], but not for acid compounds of the type $M^{II}(HXO_3)_2{\cdot}nH_2O$ (X = HP^{III} and $|Se^{IV}$), and iii) their possible nonlinear optical and dielectrical properties. In this context we report on the crystal structures and FT-IR absorption spectra of $Sr(H_2PO_3)_2$ and $Sr(HSeO_3)_2$.

[a] Anorganische Chemie II, Universität Siegen,
D-57068 Siegen, Germany
Fax: (internat.) +49-271/740-2555
E-mail: engelen@chemie.uni-siegen.de

Results and Discussion

Crystal Structures

$Sr(H_2PO_3)_2$ (*a*P26) and $Sr(HSeO_3)_2$ (*a*P22) both crystallize in a triclinic unit cell in the space group $P\bar{1}$ with Z = 2 (see Table 1). Except for the P-bonded hydrogen atoms of $Sr(H_2PO_3)_2$ they are isotypic. All atoms occupy general positions 2*i* with Sr^{2+} and two crystallographically different XO_2OH^- ions with X = HP^{III} and $|Se^{IV}$, P1, P2, Se1 and Se2, in the asymmetric unit.

In both structures, Sr is square antiprismatically surrounded by eight oxygen atoms of seven different XO_2OH^- ions (see Figure 1). The isolobal XO_2OH^- ions have tetrahedral (HPO_2OH^-) and trigonal pyramidal (ψ-tetrahedral, SeO_2OH^-) configuration and act as both bidentate and bridging ligands (Figure 1). Due to the mono- and bidentate coordination of Sr through XO_2OH^- (see Figure 1) the SrO_8 square antiprisms are strongly distorted. The Sr−O distances range from 251 to 276 pm and 254 to 285 pm for the acid phosphate(III) and selenate(IV) compound, respectively (see Table 2). Nevertheless, the respective mean values, 263(10) and 262(10) pm, are nearly equal. They are in the range of the Sr−O distances of other oxosalts of eight-coordinate Sr.[13−15]

Due to the different coordinations through Sr and H (see Figure 1) the non-hydrogen atoms of the two XO_2OH^- ions of the asymmetric unit are differently, but only slightly, distorted from the possible *m* symmetry (see Table 2). The mean X−O and X−OH distances (150 and 159 pm for X = HP^{III} and 166 and 178 pm for $|Se^{IV}$) and O−X−O angles (111 and 101° for X = HP^{III} and $|Se^{IV}$, respectively) are in good agreement with those found for other acid phosphates(III)[16] and selenates(IV).[7,17−19] Although O23 is not coordinated to Sr, the corresponding X−O distance is

 © WILEY-VCH Verlag GmbH, D-69451 Weinheim, 2000 1434−1948/00/0909−2071 $ 17.50+.50/0

Table 1. Data collection and refinement parameters of $Sr(H_2PO_3)_2$ and $Sr(HSeO_3)_2$[a]

	$Sr(H_2PO_3)_2$	$Sr(HSeO_3)_2$
Formula weight /g·mol^{-1}	249.59	343.56
Temperature /K	293(2)	293(2)
Wavelength /pm	71.073	71.069
Crystal system, space group	triclinic, $P\bar{1}$	triclinic, $P\bar{1}$
Lattice constants /pm, /°	a = 581.3(1), α = 97.69(3)	a = 586.8(1), α = 97.23(1)
	b = 722.5(1), β= 104.51(3)	b = 727.7(1), β= 104.06(1)
	c = 806.0(2) pm, γ = 106.47(3)	c = 779.1(1), γ = 106.20(1)
Volume /nm^3	0.3065(1)	0.30314(8)
Z, $\rho_{calc.}$ /Mg·m^3	2, 2.704	2, 3.764
Absorption coefficient /mm^{-1}	9.277	20.859
F(000)	240	312
Crystal size /mm^3	0.20 × 0.19 ×· 0.15	0.14 × 0.10 × 0.10
Θ_{min}, Θ_{max} /°	3.56, 28.05	2.76, 39.97
Index ranges	$-7 \le h \le 7$	$-10 \le h \le 9$
	$-9 \le k \le 9$	$-12 \le k \le 13$
	$-10 \le l \le 10$	$-1 \le l \le 14$
total reflections	3468	3736
unique reflections, R_{int}	1393, 0.034	2994, 0.052
Completeness to Θ = 28.05°	92.8%	79.9%
Absorption correction	Numerical	Empirical
T_{min}, T_{max}	0.23, 0.31	0.24, 0.28
Refinement method	Full-matrix least-squares on F^2	
Data/restraints/parameters	1393/2/95	2994/2/89
S	1.035	1.072
$R1$, $wR2$ [$I>2\sigma$ (I)]	0.026, 0.055	0.026, 0.048
$R1$, $wR2$ (all)	0.036, 0.058	0.047, 0.052
Extinction coefficient	0.023(3)	0.0127(8)
δ_{min}, δ_{max} /10^{-6} e·pm^3	−0.6(2), 0.7(2)	−0.9(2), 0.8(2)

[a] Further details of the crystal structure investigations, the atomic coordinates and the displacement parameters can be obtained from the Fachinformationszentrum Karlsruhe, D-76344 Eggenstein-Leopoldshafen (Germany) [Fax: (internat.) +49-7247/808-666; E-mail: crysdata@fiz.karlsruhe.de) on quoting the depository numbers CSD-410936 [$Sr(H_2PO_3)_2$] and CSD-410935 [$Sr(HSeO_3)_2$].

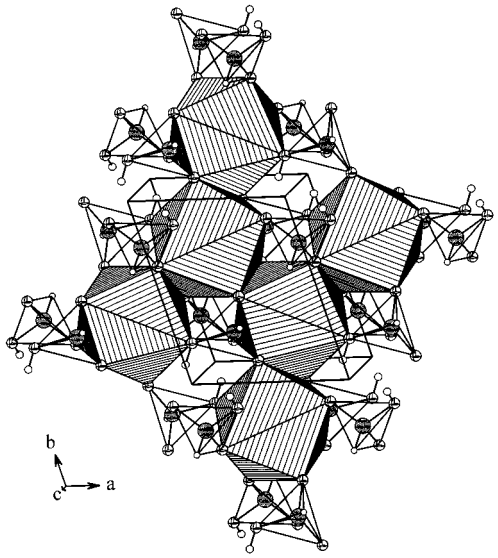


Figure 1. Crystal structure of $Sr(H_2PO_3)_2$ approximately (5°) along [001] representing the SrO_8 polyhedra and their linkage; except for hydrogen atoms H1 and H2, the crystal structure of $Sr(HSeO_3)_2$ is identical; the displacement ellipsoids are drawn at a level of 50% probability

only slightly shorter than that of the other hydroxyl group (O13, see Table 2). The dihedral angles H−P−O−H of the HPO_2OH^- ions (−70 and 64°) point to a *syn*-clinal conformation of the PH and OH groups. This means that the orientation of the HP and OH groups of $Sr(H_2PO_3)_2$ corresponds much better to that found in phosphorous acid, H_3PO_3, (76° for the mean value[20]) than to that found in other acid salts (e.g. 46° in LiH_2PO_3[21]).

The SrO_8 antiprisms share three edges and are additionally connected via O−X−O bonds with the result that layers $^2_\infty[Sr(XO_2OH)_2]$ are formed parallel to (001) (see Figure 1 and 2). The layers are interconnected via medium-strong hydrogen bonds, O23−H23···O22, with O−H···O distances of 277 and 280 pm for $Sr(H_2PO_3)_2$ and $Sr(HSeO_3)_2$, respectively, (see Figure 2 and Table 2). Thus the resulting structures are of type b1[22] with respect to the inter-layer forces. A second hydrogen bond, O13−H13···O22, appears in the layers with O−H···O distances of 272 and 274 pm, respectively. Thus O22 acts as a hydrogen-bond acceptor for both hydrogen bonds. As a result, a zero-dimensional hydrogen-bond system is formed, in which two XO_2OH^- ions (P2, Se2) form a cyclooctane-like ring system between the layers (see Figure 2 and Figure 3). The XO_2OH^- ions belonging to P1 and Se1, respectively, are connected biaxially to this ring system in the 1,5 position by the intra-layer hydrogen bond (see Figure 2 and 3). Because of the synergetic effect,[23] i.e., the coordination of O13 through Sr, the intra-layer H-bond (O13−H13···O22) is shorter than to the inter-layer H-bond (O23−H23···O22) although both hydrogen bonds have the same H-bond acceptor (O22, see Table 2 and Figure 2, 3).

The P-bonded H-atoms (H1 and H2) of $Sr(H_2PO_3)_2$ are not hydrogen-bonded. They are arranged around the centers of symmetry at the 1*e* (P1) and 1*c* (P2) positions of the space group $P\bar{1}$, respectively, to form channels along [100]

Table 2. Selected interatomic distances (pm) and angles (°) for $Sr(H_2PO_3)_2$ and $Sr(HSeO_3)_2$

$Sr(H_2PO_3)_2$		$Sr(HSeO_3)_2$	
Sr−O_8 square antiprism			
Sr−O11	273.0(3)	Sr−O11	263.4(2)
Sr−O11[a]	252.1(2)	Sr−O11[a]	253.6(2)
Sr−O12	269.9(3)	Sr−O12	282.7(2)
Sr−O12[b]	251.2(2)	Sr−O12[b]	253.6(2)
Sr−O13[c]	275.5(3)	Sr−O13[c]	269.7(2)
Sr−O21[b]	261.8(3)	Sr−O21[b]	258.1(2)
Sr−O21[c]	254.1(3)	Sr−O21[c]	253.7(2)
Sr−O22	268.5(3)	Sr−O22	262.6(2)
XO_2OH^-			
P1−O11	150.3(2)	Se1−O11	165.6(2)
P1−O12	149.7(2)	Se1−O12	165.7(2)
P1−O13	159.4(3)	Se1−O13	178.9(2)
P1−H1	124(4)		
O11−P1−O12	112.6(2)	O11−Se1−O12	101.0(1)
O11−P1−O13	112.1(1)	O11−Se1−O13	102.4(1)
O12−P1−O13	108.2(1)	O12−Se1−O13	99.7(1)
P2−O21	149.1(3)	Se2−O21	164.8(2)
P2−O22	152.3(2)	Se2−O22	167.4(2)
P2−O23	157.6(3)	Se2−O23	177.6(2)
P2−H22	128(4)		
O21−P2−O22	116.3(2)	O21−Se2−O22	106.3(1)
O21−P2−O23	106.3(2)	O21−Se2−O23	94.78(9)
O22−P2−O23	109.9(1)	O22−Se2−O23	99.9(1)
H-bonds			
O13−H11	88(2)	O13−H1	88.(2)
O13···O22[d]	271.7(3)	O13···O22[b]	274.3(3)
O13−H11···O22[d]	171(5)	O13−H1−O22	163(4)
O23−H21	91(2)	O23−H2	89(2)
O23···O22[e]	276.5(4)	O23···O22[d]	280.3(3)
O23−H21···O22[e]	164(4)	O23−H2···O22[d]	167(4)

[a] Symmetry operator: −x+1, −y, −z+1. − [b] Symmetry operator: −x+1, −y+1, −z+1. − [c] Symmetry operator: x+1, y, z. − [d] Symmetry operator: −x, −y, −z+1. − [e] Symmetry operator: −x, −y, −z.

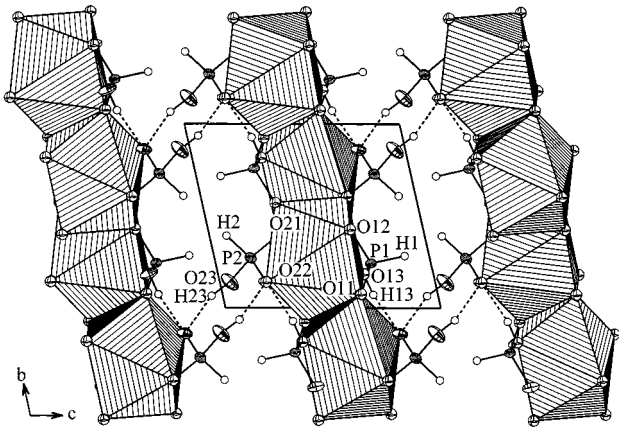


Figure 2. Crystal structure of $Sr(H_2PO_3)_2$ along [100] representing the $^2_\infty[Sr(HPO_2OH)_2]$ layers and the hydrogen bonds (dotted lines); see also Figure 1

(see Figure 2). In $Sr(HSeO_3)_2$, the free electron pairs of $|Se^{IV}$ are oriented in the same directions as the P−H bonds of $Sr(H_2PO_3)_2$. Because of the P···H and H···H repulsion of the nonbonded P and H atoms around the channels along [100], the mean values of the accompanying smallest P···P and Se···Se distances, are 12% larger in $Sr(H_2PO_3)_2$ (479pm) than in $Sr(HSeO_3)_2$ (427 pm). This gives an explanation for the finding that, despite the much longer Se−O distances, the cell volume is smaller in the selenate(IV) compound (see

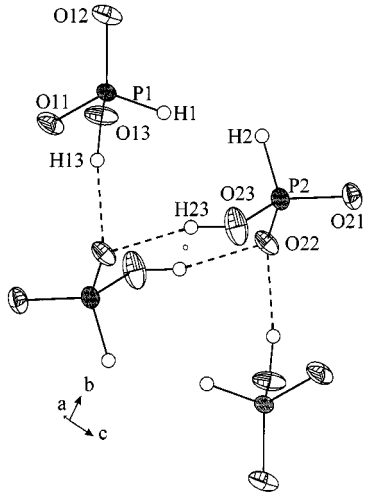


Figure 3. Zero-dimensional hydrogen bond system of $Sr(H_2PO_3)_2$; see also Figure 1

Table 1 and 2). Nevertheless, the interlayer hydrogen bond (O23−H23···O22) is shorter for $Sr(H_2PO_3)_2$, i.e., the oxygen atoms of HPO_2OH^- are stronger H-bond acceptors than those of SeO_2OH^- (see also[23,24]).

Vibrational Spectroscopy

The IR absorption spectra of $Sr(H_2PO_3)_2$ and $Sr(HSeO_3)_2$ at low (100 K) and room temperature are shown in Figure 4. The band assignment is given in Table 3. The IR spectra of acid salts are well-known for the splitting of the OH stretching modes, ν(OH), of hydroxyl groups into AB or ABC band systems (see ref.[6] and the literature cited therein). The broad bands around 3000 and 2350 cm^{-1} in the spectra of $Sr(HSeO_3)_2$ can be assigned to such an AB band system. Due to the two different hydroxyl groups of the asymmetric unit, both the A and B bands are split into at least two bands. The IR spectra of $Sr(H_2PO_3)_2$ also exhibit broad absorptions around 3000 cm^{-1} belonging to an A band, but the B band region is dominated by the PH stretching modes of the phosphate(III) groups.

In the region of the in-plane bending mode bands, δ(OH), of the hydroxyl groups for both compounds, band doublets appear between 1150 and 1250 cm^{-1}. Like the splitting of the PH stretching modes (see Figure 4 and Table 3), the appearance of these doublets confirms the presence of two crystallographically different hydroxyl groups and XO_2OH^- ions. The frequencies of the B bands of $Sr(HSeO_3)_2$ are slightly lower than the first overtones of the δ(OH) frequencies, pointing to a Fermi resonance interaction of the in-plane bending modes with the ν(OH) of the hydroxyl groups (see also ref.[6]).

Between 680 and 750 cm^{-1} a similar doublet is observed in the IR spectra of $Sr(H_2PO_3)_2$, which has to be assigned to the out-of-plane bending modes, γ(OH), of the hydroxyl groups. The band at 689 cm^{-1} in the LT spectrum of $Sr(HSeO_3)_2$ can also be assigned to one of the γ(OH) modes. The corresponding high frequency γ(OH) band is covered by the SeO stretching modes of the SeO_2OH^- ions.

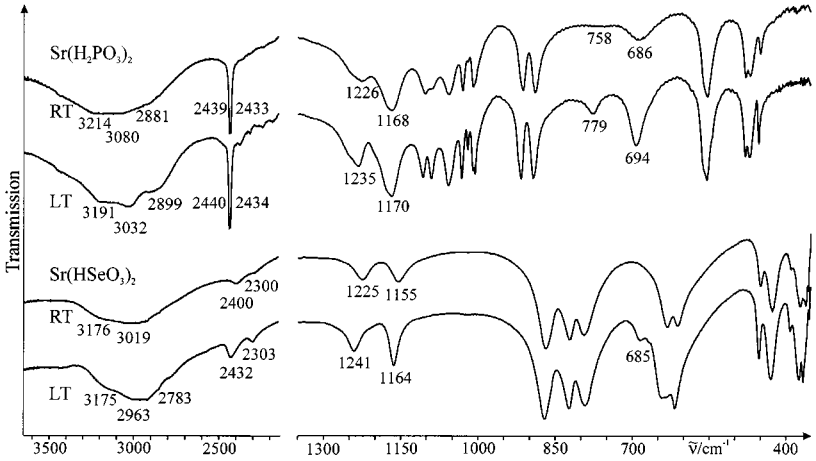


Figure 4. FT-IR absorption spectra at 100 K (LT) and room temperature (RT) of $Sr(H_2PO_3)_2$ and $Sr(HSeO_3)_2$

Table 3. Position and assignment of the IR absorption bands of $Sr(H_2PO_3)_2$ and $Sr(HSeO_3)_2$

$Sr(H_2PO_3)_2$		$Sr(HSeO_3)_2$		Assignment
LT	RT	LT	RT	
3191	3214	3175	3176	$\nu(OH)_A$
3032	3080	2963	3019	
2899	2881	2783		
2440	2439			$\nu(PH)$
2434	2433			
		2432	2400	$\nu(OH)_B/2\delta(OH)$
		2303	2300	
1235	1226	1241	1225	$\delta(OH)$
1170	1168	1164	1155	
1107	1103			$\nu(PO) + \delta(HPO)$
1091	1090			
1058	1058			
1033	1031			
1021	1020			
1008	1010			
917	914			$\nu(PO)_{OH}$
894	890			
		871	869	$\nu_s(SeO)$
		823	822	$\nu_{as}(SeO)$
		792	794	
779	758			$\gamma(OH)$
694	686	685		
		643	632	$\nu(SeO)_{SeOH}$
		618	612	
556	554			$\delta(OPO)$
480	479			
472	471			
		454	450	$\delta(OSeO)$
		430	427	
		392	390	
		375	372	
		367	360	

Taking into account that both the δ(OH) and the γ(OH) are shifted to higher frequencies, if the respective hydrogen bond is strengthened and shortened, (see refs.[6,25]), the high frequency δ(OH) and γ(OH) bands can be assigned to the stronger intra-layer hydrogen bond O13−H13···O22, whereas the respective low frequency bands belong to the weaker inter-layer hydrogen bond O23−H23···O22. For both compounds, the respective pairs δ(OH)/d(O···O) and γ(OH)/d(O···O) fulfil the corresponding frequency vs. O−H···O distance correlations (see refs.[6,25] and the literature cited therein).

Experimental Section

Single crystals of $Sr(H_2PO_3)_2$ and $Sr(HSeO_3)_2$ were obtained from concentrated aqueous solutions of $Sr(H_2PO_3)_2$ and $Sr(HSeO_3)_2$ at 80 and 22 °C after 3 and 22 days, respectively (see also refs.[1,6]).

X-ray powder diffraction data for the lattice parameter refinement have been determined from X-ray powder diffractograms (Cu-$K\alpha_1$ radiation) using a Siemens D5000 X-ray powder diffractometer. For the profile fitting and the refinement of the lattice parameters the program package WinXPow[26] was used.

The X-ray intensities for the structure determination of $Sr(H_2PO_3)_2$ were collected on a STOE-IPDS image-plate diffractometer (Mo-$K\alpha$, graphite monochromator) in the oscillation mode. After data reduction a numerical absorption correction based on an experimental crystal description was applied.[27] The X-ray intensities for the structure determination of $Sr(HSeO_3)_2$ were collected on an Enraf−Nonius CAD4 diffractometer (Mo-$K\alpha$, graphite monochromator). After data reduction, an empirical absorption correction[28] was applied.

The structures were solved by direct methods and subsequent Fourier syntheses, and refined by full-matrix least-squares techniques with anisotropic displacement parameters for the non-hydrogen atoms using the programs SHELXS97[29] and SHELXL97.[30] All hydrogen atoms were located from difference Fourier maps. The coordinates of the hydrogen atoms bonded to phosphorous were refined with isotropic displacement parameters fixed at 1.2 times the equivalent isotropic displacement parameter of the bonded phosphorous atom. All hydrogen atoms bonded to oxygen were refined to an O−H distance of 92 pm (DFIX restraint) and isotropic displacement parameters were fixed at 1.5 times the equivalent isotropic displacement parameter of the bonded oxygen atom. Scattering factors for neutral atoms were used.[31] An empirical extinction correction had to be applied.[30] Graphics were obtained with DIAMOND 2.1.[32] Further details of data collection and refinement are given in Table 1.

FT-IR absorption spectra were recorded on a Bruker IFS 113v Fourier-Transform spectrometer equipped with a Graseby-Specac P/N 21.500 cryostat using the KBr-disc method.

Acknowledgments

The authors wish to thank the Deutsche Forschungsgemeinschaft and the Fonds der Chemischen Industrie for financial support.

[1] Z. Dlouhý, M. Ebert, V. Veselý, *Coll. Czech. Chem. Commun.* **1959**, *24*, 2801−2802.
[2] M. Ebert, J. Eysseltová, A. Rottová, *Coll. Czech. Chem. Commun.* **1970**, *35*, 1824−1831.
[3] I. Lukes, M. Ebert, *Coll. Czech. Chem. Commun.* **1980**, *45*, 2283−2289.
[4] M. Ebert, D. Havlicek, *Coll. Czech. Chem. Commun.* **1982**, *47*, 1923−1930.
[5] T. Losoi, J. Valkonen, *Finn. Chem. Lett.* **1985**, *1*, 1−8.
[6] K. Unterderweide, B. Engelen, K. Boldt, *J. Mol. Struct.* **1994**, *322*, 233−239.
[7] B. Engelen, K. Boldt, H. Müller, K. Unterderweide, *J. Mol. Struct.* **1997**, *436−437*, 247−256.
[8] M. Handlovic, *Acta Crystallogr. B* **1969**, *25*, 227−231.
[9] G. Gattow, *Acta Crystallogr.* **1958**, *11*, 377−383.
[10] D. E. C. Corbridge, *Acta Crystallogr.* **1956**, *9*, 991−994.
[11] R. Weiss, J.-P. Wendling, D. Grandjean, *Acta Crystallogr.* **1966**, *20*, 563−566.
[12] L. Andersen, O. Lindqvist, J. Moret, *Acta Crystallogr. C* **1984**, *40*, 586−589.
[13] A. Boudjada, R. Masse, J. C. Guitel, *Acta Crystallogr. B* **1978**, *34*, 2692−2695.
[14] M. A. Simonov, S. I. Troyanov, E. Kemnitz, D. Hass, M. Kammler, *Kristallografiya* **1988**, *33*, 145−146.
[15] H. Effenberger, *Acta Crystallogr. C* **1987**, *43*, 182−184.
[16] J. Loub, *Acta Crystallogr. B* **1991**, *47*, 468−473.
[17] K. Boldt, B. Engelen, K. Unterderweide, *Acta Crystallogr. C* **1997**, *53*, 666−668.
[18] K. Boldt, B. Engelen, H. Müller, M. Panthöfer, K. Unterderweide, *J. Mol. Struct.* **1999**, *475*, 35−41.
[19] B. Engelen, K. Boldt, K. Unterderweide, U. Bäumer, *Z. Anorg. Allg. Chem.* **1995**, *621*, 331−339.
[20] G. Becker, H. D. Hausen, O. Mundt, W. Schwarz, C. T. Wagner, *Z. Anorg. Allg. Chem.* **1990**, *591*, 17−31.
[21] G. B. Johansson, O. Lindqvist, *Acta Crystallogr. B* **1976**, *32*, 412−414.
[22] A. F. Wells, *Structural Inorganic Chemistry*, 4th ed., Clarendon Press, Oxford, **1975**, pp. 30−33.
[23] H. D. Lutz, *Struct. Bonding* **1988**, *69*, 97−125.
[24] H. D. Lutz, K. Beckenkamp, H. Möller, *J. Mol. Struct.* **1994**, *322*, 263−266.
[25] H. Ratajczak, W. J. Orville-Thomas, *J. Mol. Struct.* **1967−68**, *1*, 449−461.
[26] STOE & CIE, WinXPow, Darmstadt, **1999**.
[27] STOE & CIE, XSHAPE 1.02, Darmstadt, **1997**.
[28] A. C. T. North, D. C. Philips, F. S. Matthews, *Acta Crystallogr. A* **1968**, *24*, 351−359.
[29] G. M. Sheldrick, SHELXS-97, *Program for the solution of Crystal Structures*, University of Göttingen, Germany, **1997**.
[30] G. M. Sheldrick, SHELXL-97, *Program for Structures Refinement*, University of Göttingen, Germany, **1997**.
[31] *International Tables for X-ray Crystallography, Vol. C*, (Ed.: A. J. C. Wilson), Kluwer Academic Publishers, Dordrecht, **1995**.
[32] Crystal Impact, DIAMOND 2.1, Bonn, **1999**.

Received February 17, 2000
[O00057]

The Hemilabile [2-(Dimethylamino)ethyl]cyclopentadienyl Ligand and Nickel: Preparation and Structural Analysis of New Cationic and Neutral Complexes

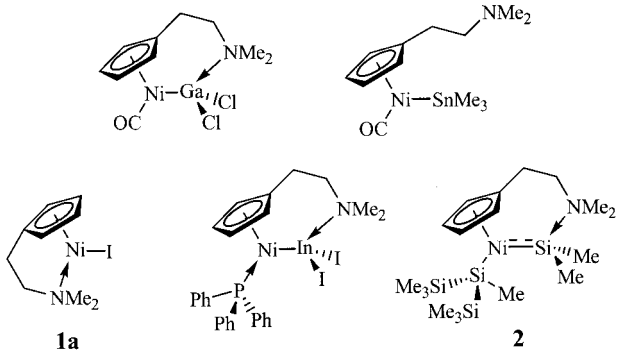
Oliver Segnitz,[a] Manuela Winter,[a] Klaus Merz,[b] and Roland Fischer*[a]

Keywords: Coordination chemistry / Nickel / Cyclopentadienes / Cations / Density functional calculations

Various new compounds containing the [2-(dimethylamino)-ethyl]cyclopentadienyl (Cp^N) moiety coordinated to a nickel centre have been synthesized. A new derivative Me_3SiCp^NNiI (**1b**) was obtained by a previously described pathway, while the reaction of its older analogue Cp^NNiI (**1a**) with $Tl[PF_6]$ and the subsequent interception of the intermediate cation in THF with two equivalents of PPh_3 or dmpe ($Me_2PCH_2CH_2PMe_2$) yielded the two ionic species $[Cp^NNi(PPh_3)]^+PF_6^-$ (**4**) and $[Cp^NNi(dmpe)]^+PF_6^-$ (**5**), respectively. The direct substitution of the halide functionality in **1a** with MesMgBr (Mes = 2,4,6-trimethylphenyl) in THF gave the pentane-soluble neutral complex Cp^NNiMes (**6**). Compounds **1b**, **4**, **5**, and **6** were characterized by ^1H, ^{13}C, and ^{31}P (if phosphorous is present) NMR spectroscopy, elementary analyis, mass spectrometry, and single crystal X-ray diffractometry. The model compounds $[Cp^NNi(PH_3)]^+$, Cp^NNiMe, Cp^NNiPh, and $[Cp^NNi(OH_2)]^+$ were further studied by DFT calculations at the B3LYP level of theory.

Introduction

Donor-functionalized cyclopentadienyl ligands in general, and their *N*-functionalized derivatives (carrying a side-chain containing an amino function) in particular, have been well renowned for their ability to either stabilize adjacent electron-deficient centres and unusual coordination states of the respective metal centre, or to promote hitherto unseen reactions when the donor is bound in a hemilabile way. The introduction of a donor-substituted alkyl side-chain has also provided additional room for other functionalities to further alter the steric demands, stability, solubility, catalytic activity and thus the electronic structure and chemical properties of the respective parent compound in general.[1] Our work on [2-(dimethylamino)ethyl]cyclopentadienyl complexes of group-10 metals (see Scheme 1) eventually led to the discovery of the rearrangement of a tris(trimethylsilyl)silyl group at the $[Cp^NNi]$ fragment to yield the first structurally characterized silanediyl(silyl)metal complex **2**.[2,3] The obvious importance of the $[Cp^NNi]^+$ fragment, and the fact that related indenyl derivatives like $[(1\text{-MeInd})Ni(PPh_3)]^+BF_4^-$ were reported to catalyze the dehydropolymerization of $PhSiH_3$ to linear chains[4] and the dimerization of ethylene at a very high rate,[5] as well as other similar systems containing cyclopentadienyl-substituted cationic nickel species as potential reactive intermediates [e.g. $(\pi\text{-}C_3H_5)Ni(PCy_3)Br/EtAlCl_2$[6]], led us to further investigate the chemistry of potential $[Cp^NNi]^+$ precursors and their behaviour towards various donors and nucleophiles.



Scheme 1

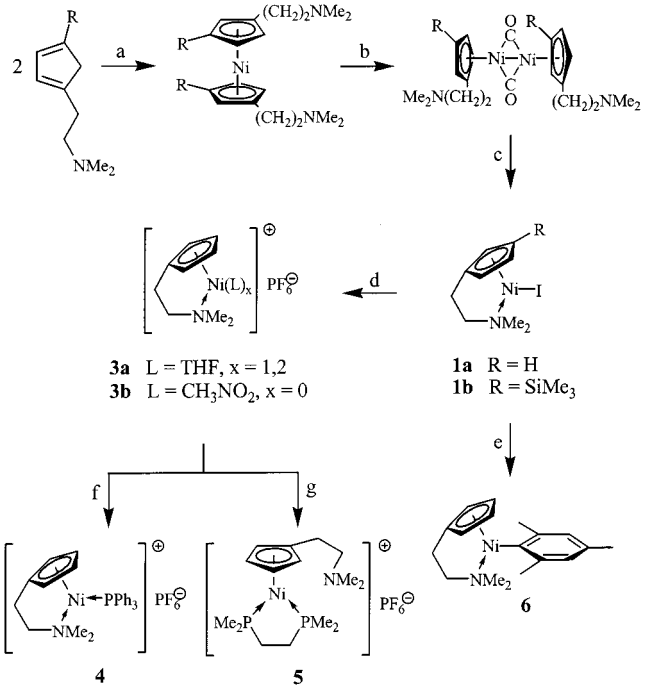
Results and Discussion

Synthesis

An overview of the work presented here is depicted in Scheme 2. The preparation and characterization of the complex Cp^NNiI (**1**) has already been reported earlier.[2] However, the synthesis outlined there suffered from rather low yields and was therefore slightly modified. The Cp^NH ligand was prepared according to a procedure described by Wang et al.[7] The deprotonation of Cp^NH was performed using Et_2NH instead of *n*BuLi in THF.[8] The use of the milder base allowed a much cleaner conversion of $NiBr_2$ to give the corresponding nickelocene derivative and therefore a high vacuum sublimation to obtain the pure product was no longer necessary.

[a] Lehrstuhl für Anorganische Chemie II, Ruhr-Universität Bochum,
Universitätsstrasse 150, D-44780 Bochum, Germany
Fax: (internat.) + 49-(0)234/321-4174
E-mail: rfischer@aci.ruhr-uni-bochum.de
[b] Lehrstuhl für Anorganische Chemie I, Ruhr-Universität Bochum,
Universitätsstrasse 150, D-44780 Bochum, Germany
Fax: (internat.) + 49-(0)234/321-4378
E-mail: Klaus.Merz@ruhr-uni-bochum.de

 © WILEY-VCH Verlag GmbH, D-69451 Weinheim, 2000 1434–1948/00/0909–2077 $ 17.50+.50/0



Scheme 2. General overview (R = H, $SiMe_3$); a: 1. 2 *n*BuLi/THF, 2. $NiBr_2$/THF, 3. sublimation at 180 °C or 1. $NiBr_2/Et_2NH$, 2. extraction with pentane; b: 1. $Ni(CO)_4$/toluene, 2. extraction with pentane; c: 1. I_2/THF, 2. crystallization from toluene; d: 1. $Tl[PF_6]$/THF or CH_3NO_2; e: 1. MesMgBr/THF, 2. crystallization from pentane; f: 1. PPh_3/THF, 2. crystallization from acetone; g: 1,2-bis(dimethylphosphanyl)ethan (dmpe)/THF, 2. crystallization from acetone

Thus, the enhanced overall yield of **1a** made its use for more thorough investigations feasible. This new approach further enabled us to produce less readily available derivatives such as Me_3SiCp^NNiI (**1b**) {Me_3SiCp^N = [2-(dimethylamino)ethyl]-3-(trimethylsilyl)cyclopentadienyl}[9] with an additional substituent attached to the cylopentadienyl ring. We treated **1a** with several halide-abstracting reagents ($Na[BPh_4]$, silver and thallium salts), to introduce a more weakly bonded anion. This was done with the aim of preparing a "naked" cation $[Cp^NNi]^+$ and exploring its role in the synthesis of **2**. The use of $Tl[PF_6]$ proved to be the best choice in this case. It is not quite clear from the integral ratios derived from the ^1H NMR spectra of **3a** how many thf molecules are bound to the metal centre (see Figure 3). Compound **3b**, however, loses all its coordinated nitromethane molecules upon evaporation of the solvent and the red colour of its solution gives way to the green colour of the microcrystalline powder of compounds **3a** and **3b**. Both substances underwent decomposition at room temperature or upon redissolution. Additionally, compound **3b** could only be observed when the solvent was condensed into the reaction vessel and the mixture was allowed to slowly warm to room temperature. If the synthesis was performed at room temperature without any cooling or if a solution of **3b** was heated above 70 °C, the cation readily reacted with the nitromethane to produce a light-yellow substance. The nature of the new species has not yet been fully clarified and more investigations are currently underway. In order to obtain a derivative that can be better characterized and to prove the existence of the cationic species we introduced various phosphorus-containing ligands into the system to enhance the stability. The triphenylphosphane adduct **4** could be isolated as a dark red powder, while intercepting the cations **3a** and **3b** with 1,2-(dimethylphosphanyl)ethane (dmpe) produced the light-red coloured compound **5**. Both compounds were much more stable than **3a** and **3b** and were analyzed by ^1H, ^{13}C, and ^{31}P NMR spectroscopy, elementary analysis, and mass spectrometry. Suitable crystals for X-ray diffraction could be grown in both cases. It is also possible to substitute the iodine atom in **1a** by a more direct means. Various nucleophiles react in the expected way by replacing the halide on the nickel centre. There are, however, only a few known examples that do not suffer from decomposition even at relatively low temperatures. The compound $Cp^NNi(Mes)$ (Mes = 2,4,6-trimethylphenyl) was one derivative that was stable up to ambient temperatures and could be subjected to X-ray single crystal diffraction. Other analytical data for the intensely red substance was also found to be in excellent agreement with the proposed structure.

Analytical Data for Me_3SiCp^NNiI (1b)

As in the case of **1a**, the ^1H NMR spectrum indicates the presence of a coordinated (dimethylamino)ethyl moiety. The proton resonances for the ethylene bridge in the free ligand (both at δ = 2.47) shift upfield to δ = 0.15 for the H atom β to the amino group and to δ = 2.29 for the H atom in the α position. It is striking that the α-methylene group in **1a** undergoes a downfield shift upon coordination of the side-chain.[2] Another major difference is presented when comparing the δ values of the protons attached to the Cp ring; they differ by 1 ppm (δ ≈ 5.3 for **1a** and 4.3 for **1b**). The broad and not very well-resolved proton signals and the complete absence of any resonances even at low temperatures in the ^{13}C NMR measurement, hint at the presence of a paramagnetic species. It is still unclear whether this is caused by **1b** in its form given in Scheme 2, or whether it originates from an equilibrium in solution.

The trimethylsilyl derivative **1b** of **1a** was obtained by the same route[2] and crystals were grown from a pentane solution at 5 °C (Figure 1, Table 1). The monomeric species crystallizes in the space group *Pbca*.

At a first glance both molecules **1a** and **1b** seem to be closely related, but a more thorough look reveals the impact the additional trimethylsilyl group has on the overall symmetry of complex **1b**. Most of the crucial bond lengths for **1b** given in Table 1 are longer than those for **1a**, giving **1b** a "blown-up" appearance when compared with its parent compound. The now asymmetric substitution of the cyclopentadienyl ring and the size of the new substituent also effect a distortion that can be explained by various facts. The Ni−C(1···5) distances vary over an untypically long range from 2.03 to 2.22 Å, with the Ni−C3 bond of 2.223 Å being unusually long. The displacement of the nickel atom

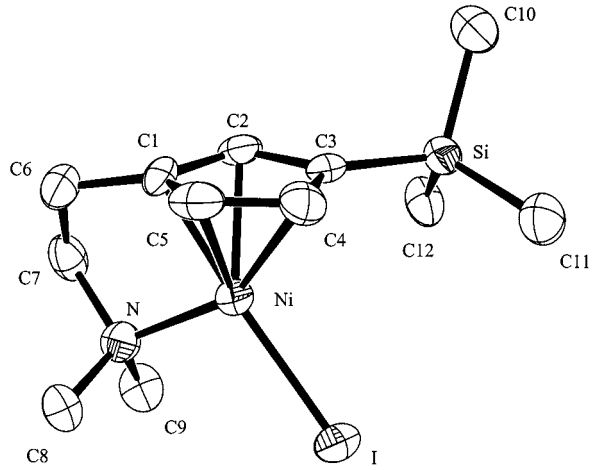


Figure 1. ORTEP drawing of Me_3SiCp^NNiI in the solid state, using 50% probability ellipsoids; hydrogen atoms are omitted for clarity

Table 1. Selected bond lengths [Å] and angles [°] for compound **1b**

Ni−I	2.527(2)	N−C8	1.504(10)
Ni−N	2.023(7)	N−C9	1.513(11)
Ni−Cp[a]	1.77	C1−C2	1.453(8)
Ni−C1	2.033(8)	C2−C3	1.433(8)
Ni−C2	2.152(8)	C3−C4	1.455(8)
Ni−C3	2.223(7)	C4−C5	1.431(8)
Ni−C4	2.179(8)	C5−C1	1.430(8)
Ni−C5	2.152(7)	C3−Si	1.886(8)
N−C7	1.509(11)		
Cp[a]−Ni−I	134.7	Cp[a]−C3−Si	178.6
I−Ni−N	102.1(2)	C1−C6−C7	107.4(7)
N−Ni−Cp[a]	123.0	C6−C7−N	110.6(6)
Cp[a]−C1−C6	170.0		

[a] The abbreviation Cp denotes the center of the cyclopentadienyl ring.

away from the central Cp axis and the resulting disturbed coordination is also mirrored in the ring itself: a weak eneallyl distortion (the C2−C3 bond length of 1.433 Å, as opposed to the C4−C5 and C5−C1 bonds of length 1.431 Å and 1.430 Å, respectively), and a slightly higher RMS deviation of 0.028 Å from the plane than that in **4** and **5**. The Ni−I and Ni−N bonds are within the expected range, although the Ni−N bond with a length of 2.023 Å shorter.[10] Unlike in **1a** the deviations of e.g. C6−C7−N from the tetrahedral angle are not as remarkable, but this cannot be interpreted as a sign for a system under less stress. This will be discussed in more detail later on. The angles around the metal centre in **1b** compare well with those in **1a** and are within well-known limits.[11]

Analytical Data for $[Cp^NNi(PPh_3)]^+PF_6^-$ (4)

The ^{13}C NMR resonances of **4** (the first cation of its type) show nothing out of the ordinary even in comparison with those of non-charged Cp^NNiX complexes, but the ^1H NMR spectrum somewhat differs from those of other compounds with a coordinated side-chain.[2] Although the signals of the Cp protons appear in the same region as in **1b**, the signals of the H atoms in the amino moiety are both shifted downfield compared with those of free Cp^NH. Moreover, the resonances for the two methylene groups in **4** are very close to each other which is typical for a free, uncoordinated side-chain as was reported for $[Cp^{*N}Ni(CO)]_2$,[12] and $[Cp^NNi(CO)]_2$,[2] and confirmed with the preparation of **5**. In fact, this data and the fact that two equivalents of PPh_3 were used in the reaction and that species like $[Cp^NNi(PPh_3)_2]^+$ were detected in the FAB mass spectra of **4**, led us to the initial conclusion that the new compound was of the formula $[Cp^NNi(PPh_3)_2]^+PF_6^-$, with a dangling amino side-chain very similar to that in **5**. In the ^{31}P NMR spectra the phosphorus signal of the PPh_3 ligand shifts from $\delta = -6$ to $\delta \approx +30$ upon coordination. A related effect is observed for **5** where another downfield shift for the signals of the coordinated P donors occurs.

A crystal of the cationic product **4** grown from an acetone solution at −30 °C, revealed the true structure of $[Cp^NNi(PPh_3)]^+PF_6^-$ (Figure 2, Table 2). It was solved in the space group *P*2(1) and consists of monomeric cations with the formula indicated, with noninteracting hexafluorophosphate anions.

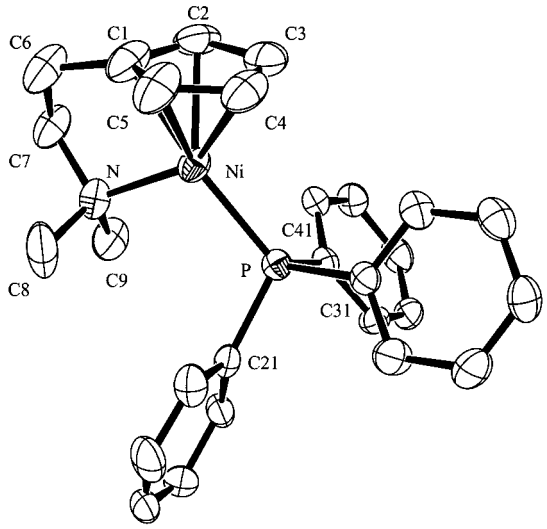


Figure 2. ORTEP drawing of the cation $[Cp^NNi(PPh_3)]^+$ in the solid state, using 50% probability ellipsoids; hydrogen atoms are omitted for clarity

Table 2. Selected bond lengths [Å] and angles [°] for compound **4**

Ni−P1	2.2001(14)	N−C7	1.499(6)
Ni−N	2.012(5)	N−C8	1.477(7)
Ni−Cp[a]	1.740	N−C9	1.475(7)
Ni−C1	2.055(6)	C1−C2	1.435(8)
Ni−C2	2.130(6)	C2−C3	1.384(9)
Ni−C3	2.137(7)	C3−C4	1.427(10)
Ni−C4	2.110(5)	C4−C5	1.395(9)
Ni−C5	2.130(6)	C5−C1	1.406(9)
Cp[a]−Ni−P1	134.7	C6−C7−N	110.5(5)
P1−Ni−N	105.9(13)	C21−P1−C31	102.4(2)
N−Ni−Cp[a]	119.4	C31−P1−C41	99.7(2)
Cp[a]−C1−C6	168.6	C41−P1−C21	107.0(2)
C1−C6−C7	107.2(5)		

[a] The abbreviation Cp denotes the center of the cyclopentadienyl ring.

Although a twofold excess of PPh_3 was employed in the reaction only one molecule of the phosphane is found in the final product. This completes the distorted trigonal coordination sphere around the nickel centre that is otherwise

composed of the cyclopentadienyl ring and the amino function from its side-chain. The distortion is caused by the higher spatial demand of the 5-membered ring and the phenyl groups of the phosphane ligand, causing the N−Ni−P1 angle of 105.9° to be significantly smaller than 120°. Despite the link that exists between the ring and the N donor, the angle N−Ni−Cp (119.4°) corresponds quite well to the ideal value. Alternatively, the nickel(II) cation could also be described as a distorted trigonal bipyramid when the Cp group is viewed as a 6-electron ligand occupying three coordination sites. The ring itself is nearly planar with a deviation of 0.025 Å from the least-squares plane, although the bond lengths suggest some contribution from an ene-allyl form (two short adjacent bonds, C4−C5 and C5−C1, opposite an even shorter bond, C2−C3).[13] The Ni−C(1···5) bond lengths of 2.06−2.14 Å, and thus the Ni−Cp distance of 1.74 Å are within the range expected from similar unsubstituted derivatives.[13,14] The deviation of the C1−C6−C7 angle (107.5° in **1a** and 112.1° in **4**) and the C6−C7−N angle (116.2° in **1a** and 110.5° in **4**) from the ideal tetrahedral angle had already been attributed to the overall strain imposed on the molecule by the coordination of the donor-functionalized side-chain to the nickel atom.[2] The same angles in **5** with an uncoordinated side-chain, however, are equally large (C1−C6−C7 is 115.7° and C6−C7−N is 115.6°) which puts the former conclusion in question. In spite of the cationic nature of **4** the Ni−N and Ni−P1 bonds are not shorter when compared with related neutral complexes as one might instinctively expect. Other Ni−P bonds usually lie in the range from 2.14 to 2.20 Å (the Ni−P bond in **4** has a length of 2.20 Å which lies in the upper region of this range), regardless of the charge on the nickel centre. Steric and more subtle electronic reasons seem to prevail here. The same is true for the length of the Ni−N bond: 2.01 Å in **4** and 1.96 Å in **1a** (a closely related neutral species). It falls well within the usual range of dative amine−nickel bonds of 2.00−2.20 Å.[10] The bond lengths and angles in the phenyl ligands at the phosphorus atom are within normal limits. The idealized propeller-like arrangement of free PPh_3 is disturbed by steric interactions between one of the methyl groups of the N donor and the phenyl substituents.

DFT Calculations

Since it was not possible to structurally characterize a donor-free compound containing a $[Cp^NNi]^+$ cation we began to look for other means to describe this reactive species. Complex **4** was the first to be discovered of the complexes described herein, therefore it served as a starting point for our theoretical investigations. A modified model compound, $[Cp^NNi(PH_3)]^+$ (**4a**), was subjected to geometry optimizations using the Gaussian98 package.[15] A good agreement with the experimentally derived structure (while at the same time being computationally not too demanding for our systems) was obtained at the DFT level using Becke's three-parameter fit of the exchange-correlation potential (B3LYP)[16] in conjunction with the McLean-Chandler (12s, 9p) → (631111, 52111) basis set[17] for phosphorus, the Wachters-Hay all-electron basis set[18] for nickel (3d and 1f polarization functions were added for P and Ni) and the 6-31G(d) basis set[19] for C, H, and N atoms (Figure 3, Table 3).

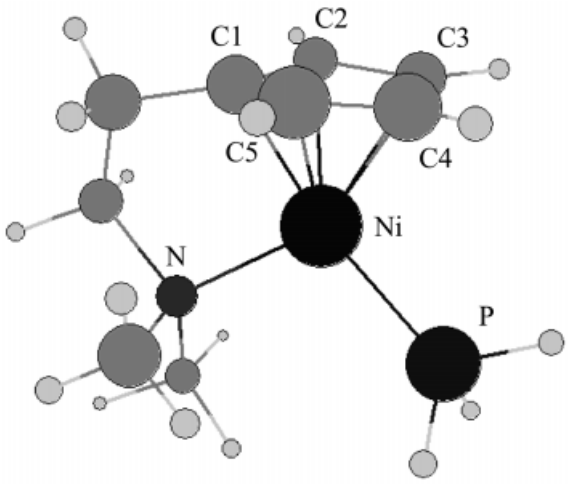


Figure 3. Structure obtained from a DFT calculation on $[Cp^NNi(PH_3)]^+$ (**4a**)

Table 3. Selected bond lengths [Å] and angles [°] for compound **4a**

Ni−P	2.209	N−C7	1.516
Ni−N	1.997	N−C8	1.491
Ni−Cp[a]	1.740	N−C9	1.489
Ni−C1	2.019	C1−C2	1.452
Ni−C2	2.149	C2−C3	1.394
Ni−C3	2.162	C3−C4	1.459
Ni−C4	2.130	C4−C5	1.404
Ni−C5	2.147	C5−C1	1.436
Cp[a]−Ni−P	132.6	Cp[a]−C1−C6	170.3
P−Ni−N	104.6	C1−C6−C7	107.3
N−Ni−Cp[a]	122.7	C6−C7−N	111.2

[a] The abbreviation Cp denotes the center of the cyclopentadienyl ring.

The computed bond lengths and angles in **4a** compare very well with those in **4** which justifies the use of PH_3 instead of PPh_3 in the model complex. The experimentally derived Ni−N and Ni−P distances are in excellent agreement with those in **4a**. The Ni−C bond lengths in **4a** vary over a slightly wider range from 2.02 to 2.16 Å making the Cp ring more puckered. However, the distance between the metal centre and the centre of the 5-membered ring are identical in **4** and **4a**. In both complexes the C1 atom is tilted towards the nickel centre which is a result of the coordination of the side-chain. A similar ene-allyl distortion can be found in **4a** as well, with all C−C distances in the Cp ring being slightly larger than those in **4**. Both the HOMO and LUMO are dominated by two π-interactions between the metal centre and the Cp ligand which shows the closeness of **4** to other 18-electron $CpML_2$ fragments[13]: two molecular orbitals with distinct d character (d_{xz} for the HOMO and d_{yz} for the LUMO, respectively) at the nickel centre interact with the ring via two MOs that correspond to the energetically degenerate e_1 orbitals of a free Cp^- fragment of D_{5h} symmetry. The LUMO also shows some strong involvement with sp^3-like MOs located on the N and

P donor. According to an NBO analysis, the metal centre bears a charge of +0.97 while the nitrogen with the highest electronegativity in the system carries the lowest charge with −0.55. The phosphorus atom appears in a nearly neutral state (−0.12).

Encouraged by these initial results we extended our theoretical investigations to include the non-phosphorus systems Cp^NNiMes (**6**) and $[Cp^NNi(OH_2)]^+$. The latter one was introduced as a model complex for the intermediate $[Cp^NNi(thf)]^+$ and should bring us closer to the naked cation $[Cp^NNi]^+$, the focus of interest. The same method and basis sets that were employed for **4a** were used to calculate the optimized structures of Cp^NNiMe (**7**), Cp^NNiPh (**8**) and $[Cp^NNi(OH_2)]^+$ (**9**). Table 4 displays crucial bond lengths and angles for **4a**, **7**, **8**, and **9**.

The replacement of the mesityl moiety in **6** with a methyl group to give the simplified model compound **7** caused the Ni−C bond to increase from 1.908 Å in **6** to 1.936 Å in **7**. To remedy this, we returned to the computationally more demanding phenyl ligand (i.e. moving from an sp^3 to an sp^2 centre) to be closer to the actual complex Cp^NNiMes (**6**). This resulted in the desired contraction of the Ni−C bond that was now in very good agreement with the experimentally observed distance in **6**, while all other bonds and angles remained much the same. In both cases the three bond angles around the nickel centre are similar to those determined by X-ray diffraction. It has to be pointed out here that the computed Ni−C bond length in Cp^NNiMe (**7**) corresponds quite well to that in known complexes such as $CpNi(PPh_3)CF_3$[20] and $CpNi(PPh_3)(CH_2SO_2Ph)$[21] that also contain nickel-bonded sp^3 carbon centres, while those in $CpNi(PPh_3)C_6F_5$[22,23] and $CpNi(PPh_3)C_6H_5$[23] correspond to that in Cp^NNiPh (**8**). The substitution of the amine donor by an isolobal phosphorus ligand does not influence the Ni−C bond to a large extent, and the chosen theoretical method generally reproduces the experimental Ni−C bond lengths in those compounds.

With these facts in mind we subjected model compound **9** to geometry optimizations at the aforementioned level of theory. By replacing the PPh_3 ligand with a water molecule, most bond lengths in the complex core undergo a contraction while the hydrogen atoms of the water molecule are tilted away from the dimethylamino group. The Cp ligand is 1.738 Å from the nickel centre, with a very short Ni−C1 distance of 1.980 Å, while the amine donor lies 1.977 Å away from the metal atom. This trend is also mirrored in the charge distributions taken from an NBO analysis: The nickel atom carries a higher positive charge of +1.06 while the oxygen and nitrogen atoms bear negative charges of −0.97 and −0.55, respectively. Thus, both the Ni−N and Ni−O bond are much more polar than the corresponding bonds in complex **4a**, attributing to the comparatively short bonds in **9**. Not surprisingly, the frontier molecular orbitals of **9** are very similar to those of compound **4a** (Figure 4).

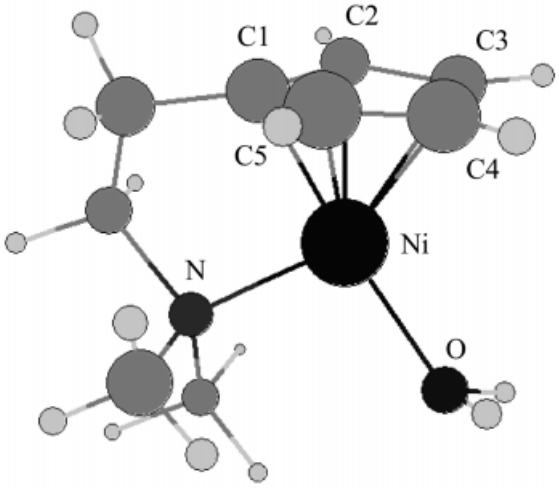


Figure 4. Structure obtained from a DFT calculation on $[Cp^NNi(OH_2)]^+$ (**9**)

One consequence of such a shortening of bond lengths could be the overall instability of this proposed intermediate. This would explain the experimental observations or cause the nitrogen donor to detach from the metal centre to possibly make room for the coordination of other thf molecules. Further research is currently in progress to elucidate this feature which would strongly influence the overall reactivity of the complex $[Cp^NNi]^+$ in terms of its possible catalytic behaviour.

Analytical Data for $[Cp^NNi(dmpe)]^+PF_6^-$ (5)

The spectroscopic behaviour of the aminoalkyl side-chain of **5** in the ^1H NMR spectra indicates the absence of a co-

Table 4. Selected bond lengths [Å] and angles [°] for compounds **4a**, **7**, **8**, and **9**

Compound	$[Cp^NNi(PH_3)]^+$ **4a**	Cp^NNiMe **7**	Cp^NNiPh **8**	$[Cp^NNi(OH_2)]^+$ **9**
Ni−X (X = C, O, P)	2.209	1.936	1.908	1.995
Ni−N	1.997	1.998	2.004	1.977
Ni−C(1···5)	2.019−2.162	2.088−2.179	2.084−2.179	1.980−2.185
Ni−Cp[a]	1.740	1.766	1.760	1.738
Cp−Ni−X (X = C, O, P)	132.6	137.4	137.2	137.6
Cp−Ni−N	122.7	122.3	122.2	124.5
N−Ni−X (X = C, O, P)	104.6	100.3	100.5	97.9

[a] The abbreviation Cp denotes the center of the cyclopentadienyl ring.

ordinated side-chain to the nickel centre.[2,12] All proton signals of the ethylene bridge appear in the same region at δ ≈ 2.48 (almost identical to the values for free Cp^NH of δ ≈ 2.47) due to a coincidentally small difference in their chemical shifts. This results in a badly resolved muliplet. This feature has already been observed with several other related compounds [see discussion for $[Cp^NNi(PPh_3)]^+PF_6^-$ (**4**)]. The resonances for the Cp ring range from δ = 5.43 to 5.53 and are comparable with those of **1a** (δ = 5.26−5.31). A general downfield shift is observed for the δ values of the dmpe ligand signal. A comparison with the free donor shows that all proton signals move from δ = 1.41 and 1.00, respectively, to δ ≈ 1.78 in **5**. This shift is much smaller for the ^{13}C nuclei, but again more obvious for the signals of the two phosphorus atoms that move from δ = −47 to +57.

The second cationic species with a free donor-functionalized side-chain could be isolated by treating a thf solution of $[Cp^NNi(thf)_x]^+PF_6^-$ (x = 1,2) with one equivalent of dmpe and recrystallizing the product **5** from acetone at −30 °C (Figure 5, Table 5). Like compound **4** the solid-state structure shows monomeric cations $[Cp^NNi(dmpe)]^+$ with an Ni−P3 distance to the counter anion greater than 6 Å. It was solved in the space group *Pna*2(1).

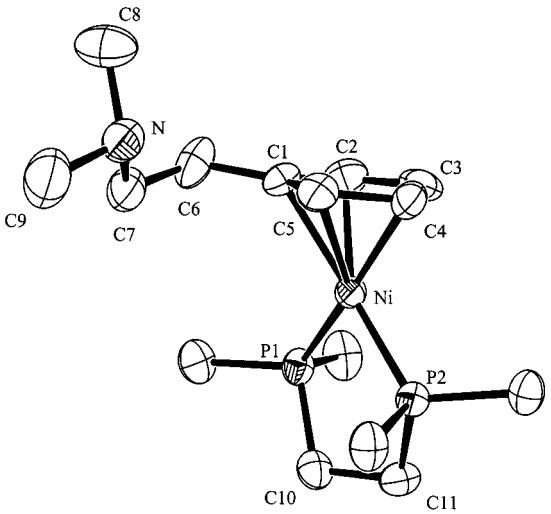


Figure 5. ORTEP drawing of the cation $[Cp^NNi(dmpe)]^+$ in the solid state, using 50% probability ellipsoids; hydrogen atoms are omitted for clarity

Table 5. Selected bond lengths [Å] and angles [°] for compound **5**

Ni−P1	2.121(2)	P1−C10	1.815(6)
Ni−P2	2.128(2)	C10−C11	1.529(10)
Ni−Cp[a]	1.720	P2−C11	1.805(7)
Ni−C1	2.144(7)	C1−C2	1.453(10)
Ni−C2	2.068(9)	C2−C3	1.397(11)
Ni−C3	2.090(7)	C3−C4	1.393(11)
Ni−C4	2.049(8)	C4−C5	1.446(10)
Ni−C5	2.139(7)	C5−C1	1.376(10)
Cp[a]−Ni−P1	133.2	C6−C7−N	115.6(7)
Cp[a]−Ni−P2	137.2	Ni−P1−C10	107.8(2)
P1−Ni−P2	89.37(7)	Ni−P2−C11	107.0(2)
Cp[a]−C1−C6	173.7	P1−C10−C11	106.7(5)
C1−C6−C7	115.7(7)	P2−C11−C10	108.7(5)

[a] The abbreviation Cp denotes the center of the cyclopentadienyl ring.

The use of the bidentate ligand dmpe as a donor had the expected result. Due to the stronger Ni−P bond and the chelate effect, the amine donor is now detached from the nickel atom and replaced by the second phosphorus atom of the ligand. The dmpe ligand and the cyclopentadienyl ring again form a distorted trigonal coordination sphere around the centre. The P1−Ni−P2 angle of 89.4° is a consequence of the ethylene bridge linking the two phosphorus centres resulting in the Cp−Ni−P1 and Cp−Ni−P2 angles larger than 120°. Ranging from 2.07 to 2.14 Å, the Ni−C(1···5) distances compare well with those in **4** and thus the Ni−Cp distances are 1.72 and 1.74 Å, respectively. The shape of the cyclopentadienyl rings with a deviation of 0.026 Å from the least-squares plane and a similar, yet more distinct, ene-allyl distortion in **5**, stress the analogy. However, the C1 carbon atom in **4** is part of the "allyl" group, while in **5** it belongs to the "ene" double bond. Other cations of the general formula $[CpNi(PR_3)_2]^+$ [R = Me, Et, Ph, or $(PR_3)_2$ = bis(diphenylphosphanyl)ethane] have been described previously.[13,14] While the Ni−C(1···5) bond lengths in **5** correspond to literature values (2.06−2.15 Å), the two Ni−P distances of 2.12 and 2.13 Å are shorter than those reported (2.14−2.20 Å). This could be because of the restrictions that the ethylene bridge forces upon the phosphorus ligands and the relatively small methyl groups that are less prone to steric encumbrance when compared with e.g. phenyl. As mentioned earlier, the magnitudes of the angles C1−C6−C7 (115.7°) and C6−C7−N (115.6°) in the free side-chain are similar to the corresponding ones in **4**, with a coordinated N donor and are thus also larger than 109.5°. Since the alkyl chain in **5** is not subject to any obvious strain the difference cannot be explained in this way.

Analytical Data for Cp^NNiMes (6) (Mes = 2,4,6-Trimethylphenyl)

With respect to the ^1H NMR spectrum complex **6** is the most well-behaved substance of those reported herein. All peaks are very clearly resolved and show no broadening. The protons of the Cp ring exhibit two resonances (δ = 4.69 and 6.22, respectively) expected from the simple substitution pattern. The δ values for the mesityl moiety in the

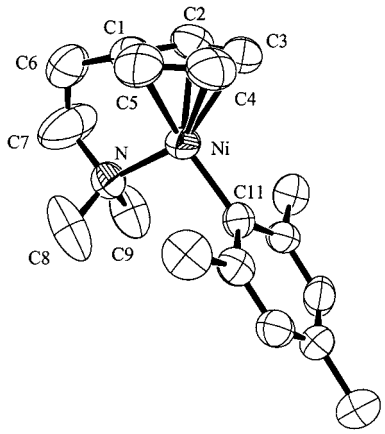


Figure 6. ORTEP drawing of the cation Cp^NNiMes in the solid state, using 50% probability ellipsoids; hydrogen atoms are omitted for clarity

Table 6. Selected bond lengths [Å] and angles [°] for compound **6**

Ni−C11	1.912(6)	N−C7	1.465(10)
Ni−N	1.974(6)	N−C8	1.452(9)
Ni−Cp[a]	1.745	N−C9	1.491(9)
Ni−C1	2.055(7)	C1−C2	1.389(10)
Ni−C2	2.133(7)	C2−C3	1.367(11)
Ni−C3	2.104(7)	C3−C4	1.404(11)
Ni−C4	2.102(8)	C4−C5	1.382(11)
Ni−C5	2.159(8)	C5−C1	1.438(10)
Cp[a]−Ni−C11	137.2	C1−C6−C7	111.8(7)
C11−Ni−N	101.9(2)	C6−C7−N	122.9(9)
N−Ni−Cp[a]	120.9	Ni−C11−C12	122.1(5)
Cp[a]−C1−C6	167.1	Ni−C11−C16	122.1(5)

[a] The abbreviation Cp denotes the center of the cyclopentadienyl ring.

^{1}H and ^{13}C NMR spectra are all shifted to lower field in comparison with the free mesitylene, with the protons and carbon atoms closest to the metal centre experiencing the largest displacement.

Suitable crystals for X-ray crystallography of **6** were grown from a pentane solution. The deep-red solid contains the complex in monomeric form and was solved in the space group *Pbca* (Figure 6, Table 6).

Previously described complexes that bear a close relationship to **6** like $CpNi(PPh_3)C_6F_5$,[22,23] $CpNi(PPh_3)C_6H_5$,[23] or compounds that also contain an Ni−C bond such as $CpNi(PPh_3)CF_3$[24] and $CpNi(PPh_3)(CH_2SO_2Ph)$,[25] cover a range from 1.90 to 1.96 Å for the Ni−C distance. The corresponding bond length in **6** of 1.912 Å thus compares well with those of the above-mentioned aryl compounds (1.904 and 1.914 Å, respectively). All other bond lengths and angles resemble those found in compounds **1a** and **4**. The amine donor bond of 1.974 Å is a shorter example of its kind and is similar to that in **1a**. A range of 2.06 to 2.16 Å for the Ni−C(1···5) lengths and a look at the C−C distances within the 5-membered ring (1.39−1.44 Å) further emphasize the resemblance. However, the angle C6−C7−N of 122.9° in the donor-functionalized sidechain is somewhat larger than in any of the other complexes.

Conclusion

By employing the halide abstracting reagent $Tl[PF_6]$, it is possible to produce an unstable cation $[Cp^NNi]^+$ from the precursor Cp^NNiI (**1a**). The subsequent trapping with the two phosphorus ligands PPh_3 and dmpe leads to the isolabile complexes $[Cp^NNi(PPh_3)]^+PF_6^-$ (**4**) and $[Cp^NNi(dmpe)]^+PF_6^-$ (**5**) that can easily be characterized. The obvious cationic character of **1a** is further demonstrated by replacing the iodine functionality in a direct nucleophilic substitution with the Grignard reagent MesMgBr to give Cp^NNiMes (**6**). The preparation of the $[Cp^NNi]^+$ species and ongoing theoretical calculations making use of appropriate models will serve as a starting point for further exploration of other bond-activating reactions or catalytic applications besides the one that leads to complex **2**. Thus, reactions of $[Cp^NNi]^+$ created in situ, the study of other derivatives Cp^NNiX, and the behavior of **1a** towards other anions and neutral substrates will be the focus of our oncoming research.

Experimental Section

General Remarks: All reactions and manipulations were carried out under argon utilizing standard Schlenk and glovebox techniques. Solvents were dried with a sodium/paraffin suspension or sodium/potassium, distilled and stored over molecular sieves (Merck, 4 Å) under inert conditions. − NMR spectra were recorded with Bruker DPX 250 and Bruker DRX 400 spectrometers. ^{1}H and ^{13}C NMR chemical shifts are referred to the remaining proton signals of the deuterated solvents and referenced to TMS. ^{31}P NMR chemical shifts are referred to the external standard H_3PO_4. The NMR solvents were dried with sodium/potassium alloy as mentioned above and degassed prior to use. − The mass spectra were performed with a Varian MAT CH5 by FAB ionization unless otherwise indicated. − Elemental analysis was provided by the Microanalytical Laboratory of the Ruhr-Universität Bochum employing a C-,H-,N-Analysenautomat of the type CHN-O-Rapid with heat conductivity detection (Heraeus). The abbreviations used in this section are $Cp^N = \eta^5\text{-}C_5H_4(CH_2CH_2NMe_2)$, Me = CH_3, Ph = C_6H_5, dmpe = $Me_2PCH_2CH_2PMe_2$, and Mes = 2,4,6-trimethylphenyl (mesityl). [2-(Dimethylamino)ethyl]cyclopentadiene (Cp^NH)[7] and 1-[2-(dimethylamino)ethyl]-3-(trimethylsilyl)cyclopentadiene (Me_3SiCp^NH)[9] were prepared according to literature procedures. A modified procedure for the synthesis of $Cp^N{}_2Ni$ and $Me_3SiCp^N{}_2Ni$ was used to produce the two nickelocene derivatives,[8] all follow-up products through to **1a** and **1b** were synthesized as previously described.[2] It included the use of diethylamine as a milder base instead of *n*-butyllithium, and the extraction of the dark green oils with *n*-pentane without following sublimation. All other chemicals were commercially available and used without further purification.

Synthesis of Me_3SiCp^NNiI (1b): I_2 (0.64 g, 2.50 mmol) in THF (10 mL) was added slowly at −78 °C to a stirred solution of $Me_3SiCp^N{}_2Ni_2(CO)_2$ (1.50 g, 2.50 mmol) in 20 mL of THF. The resulting black suspension was warmed to room temperature and stirred for another hour. After evaporation of the solvent, the residue was extracted three times with 25 mL of *n*-pentane. The dark blue solution was concentrated to about 20 mL and the product crystallized at 5 °C. Complex **1b** was obtained as dark violet needles in 45% yield (0.89 g). − ^{1}H NMR (250.13 MHz, [D$_6$]acetone, 25 °C): δ = 0.03 [s, 9 H, Si(CH_3)$_3$], 0.15 (t, 2 H, $CH_2CH_2NMe_2$), 2.29 (t, 2 H, $CH_2CH_2NMe_2$), 2,47 [s, 6 H, N(CH_3)$_2$], 4.32−4.37 (m, br., 4 H, Cp*H*). − ^{13}C{^{1}H} NMR (62.90 MHz, [D$_6$]acetone, 25 °C): no signals detected. − MS(FAB); *m*/*z* (%): 393 (28) [M$^+$], 266 (50) [$Me_3SiCp^NNi^+$], 136 (24) [Cp^{N+}], 73 (50) [$SiMe_3^+$], 58 (100) [$CH_2NMe_2^+$]. − $C_{12}H_{22}INNiSi$ (394.0) ***((AUTHOR: Please check all molecular masses!))***: calcd. C 36.58, H 5.63, N 3.56; found C 34.78, H 5.24, N 3.25.

Synthesis of $[Cp^NNi(PPh_3)]^+PF_6^-$ (4) and $[Cp^NNi(dmpe)]^+PF_6^-$ (5): Compound **1a** (100 mg, 0.32 mmol) was dissolved in 10 mL of THF, cooled to −78 °C and $Tl[PF_6]$ (109 mg, 0.31 mmol) was added to the solution. The suspension was allowed to warm to −40 °C and stirred for 1 h until the violet colour of **1a** had disappeared and was replaced by the yellow color of the precipitated TlI.

Reaction with PPh_3: Addition of PPh_3 (170 mg, 0.65 mmol) immediately produced a deep red mixture. After stirring at room temper-

Table 7. Crystallographic data for compounds **1b**, **4**, **5** and **6**

	1b	**4**	**5**	**6**
Empirical formula	$C_{12}H_{22}INNiSi$	$C_{27}H_{29}F_6NNiP_2$	$C_{15}H_{30}F_6NNiP_3$	$C_{18}H_{25}NNi$
Molecular mass	394.0	602.2	490.0	314.1
Temperature [K]	293(2)	203(2)	203(2)	293(2)
Wavelength [Å]	0.71073	0.71073	0.71073	0.71073
Crystal system	orthorhombic	monoclinic	orthorhombic	orthorhombic
Space group	*Pbca*	*P*2(1)	*Pna*2(1)	*Pbca*
a [Å]	13.744(14)	8.796(4)	16.719(6)	12.020(2)
b [Å]	12.982(14)	15.435(2)	12.704(4)	15.202(2)
c [Å]	36.51(4)	10.277(1)	10.003(6)	17.823(3)
α [°]	90	90	90	90
β [°]	90	108.26(2)	90	90
γ [°]	90	90	90	90
Volume [Å^3]	6515(12)	1325.0(6)	2125(2)	3256.6(9)
Z	8	2	4	8
Density (calculated) [g/cm^3]	1.605	1.509	1.532	1.281
Absorption coefficient [mm^{-1}]	3.139	0.913	1.190	1.182
F(000)	3128	620	1016	1344
Crystal size [mm^3]	0.1 × 0.1 × 0.2	0.6 × 0.3 × 0.2	0.5 × 0.5 × 0.4	0.5 × 0.3 × 0.3
θ range [°]	1.85−24.85	2.09−25.00	2.01−27.50	2.29−25.00
Index ranges	$-14 \le h \le 11$ $-14 \le k \le 15$ $-42 \le l \le 15$	$0 \le h \le 10$ $0 \le k \le 18$ $-12 \le l \le 11$	$0 \le h \le 21$ $-16 \le k \le 0$ $0 \le l \le 12$	$-10 \le h \le 10$ $-18 \le k \le 5$ $-10 \le l \le 20$
Reflections collected	14175	2594	2580	4867
Independent reflections	14175	2594	2580	4867
Observed relfections [$I > 2\sigma(I)$]	5358	2431	2580	2362
Refinement method	Full-matrix least-squares on F^2	Full-matrix least-squares on F^2	Full-matrix least-squares on F^2	Full-matrix least-squares on F^2
Data/restr./param.	5358/0/289	2428/1/336	2580/1/241	2350/0/186
Goodness-of-fit on F^2	0.893	0.821	0.810	0.950
Final *R* indices [$I > 2\sigma(I)$]	*R1* = 0.0520 *wR2* = 0.1250	*R1* = 0.0330 *wR2* = 0.0614	*R1* = 0.0445 *wR2* = 0.0979	*R1* = 0.0565 *wR2* = 0.1228
R indices (all data)	*R1* = 0.0978 *wR2* = 0.1476	*R1* = 0.0456 *wR2* = 0.0635	*R1* = 0.0724 *wR2* = 0.1043	*R1* = 0.1248 *wR2* = 0.1854
Largest diff. Peak and hole [eÅ^{-3}]	1.318 and −1.473	0.267 and −0.355	1.093 and −0.554	0.333 and −0.459

ature for 30 min, the solvent was removed in vacuo and the residue washed twice with 10 mL toluene. Extraction with acetone and storage at −30 °C gave **4** as deep red plate-like crystals in 44% yield (84 mg). − ^{1}H NMR (250.13 MHz, [D$_6$]acetone, 25 °C): δ = 2.13 [s, 9 H, N(CH$_3$)$_2$], 3.22−3.27 (t, 4 H, C*H*$_2$C*H*$_2$NMe$_2$), 4.32 (m, br., 4 H, Cp*H*), 7.65−7.97 [m, 15 H, P(C$_6$*H*$_5$)$_3$]. − ^{13}C{^{1}H} NMR (62.90 MHz, [D$_6$]acetone, 25 °C): δ = 25.6 (*C*H$_2$CH$_2$NMe$_2$), 53.2 [N(*C*H$_3$)$_2$], 78.0 (CH$_2$*C*H$_2$NMe$_2$), 87.4 (*o*-*C*$_5$H$_4$), 103.9 (*m*-*C*$_5$H$_4$), 118.7 (*i*-*C*$_5$H$_4$), 129.6−134.5 [P(*C*$_6$H$_5$)$_3$]. − ^{31}P{^{1}H} NMR (101.25 MHz, [D$_6$]acetone, 25 °C): δ = −143.0 (sept, *P*F$_6$), 29.9 [*P*(C$_6$H$_5$)$_3$]. − MS(FAB); *m*/*z* (%): 456.1 (37) [Cp^{N}Ni(PPh$_3$)$^+$], 194 (11) [Cp^{N}Ni$^+$], 154 (100), 136 (83) [Cp^{N+}]. − $C_{27}H_{29}F_6NNiP_2$ (602.2): calcd. C 53.85, H 4.85, N 2.33; found C 53.14, H 4.84, N 2.31.

Reaction with dmpe: Addition of dmpe (48 mg, 0.32 mmol) gave the mixture a light pink colour. After warming to room temperature and stirring for 30 min, the solvent was evaporated. The residue was washed twice with 10 mL of toluene and extracted with acetone. Crystallization at −30 °C gave product **5** as red crystals in 60% yield (94 mg). − ^{1}H NMR (250.13 MHz, [D$_6$]acetone, 25 °C): δ = 1.78 (m, 4 H, C*H*$_2$PMe$_2$), 1.79 [d, 6 H, P(C*H*$_3$)$_2$], 2.47 (m, 4 H, C*H*$_2$C*H*$_2$NMe$_2$), 5.49 (m, 4 H, Cp*H*). − ^{13}C{^{1}H} NMR (62.90 MHz, [D$_6$]acetone, 25 °C): δ = 16.5 [P(*C*H$_3$)$_2$], 26.5 (*C*H$_2$CH$_2$NMe$_2$), 28.2 (*C*H$_2$PMe$_2$), 45.1 [N(*C*H$_3$)$_2$], 61.0 (CH$_2$*C*H$_2$NMe$_2$), 91.1 (*o*-*C*$_5$H$_4$), 91.8 (*m*-*C*$_5$H$_4$), no signal for *i*-*C*$_5$H$_4$ detected. − ^{31}P{^{1}H} NMR (101.25 MHz, [D$_6$]acetone, 25 °C): δ = −143.0 (*P*F$_6$), 57.0 (CH$_2$*P*Me$_2$). − MS(FAB); *m*/*z* (%): 344 (100) [Cp^{N}Ni(dmpe)$^+$], 329 (5) [Cp^{N}Ni(dmpe)$^+$ − CH$_3$], 208 (10) [Ni(dmpe)$^+$], 154 (32), 136 (27) [Cp^{N+}], 120 (6) [dmpe − 2 CH$_3$], 89 (7) [Me$_2$PCH$_2$CH$_2$]. − $C_{15}H_{30}F_6NNiP_3$ (490.0): calcd. C 36.77, H 6.17, N 2.86; found C 37.01, H 5.36, N 2.98.

Synthesis of Cp^{N}NiMes (6): At −78 °C, 0.95 mL of a 0.65 M solution of MesMgBr (0.62 mmol) in THF was added to **1a** (200 mg, 0.62 mmol), dissolved in 20 mL THF. The mixture was allowed to warm to room temperature. The colour turned from dark violet to dark red at about −40 °C and MgBrI started to precipitate. After stirring for 30 min at ambient temperature, the solvent was removed in vacuo and the residue was extracted with 20 mL of *n*-pentane. Concentration of the solution to a volume of about 5 mL and storing it at 5 °C yielded **6** as dark red prism-shaped single crystals in 75% yield (146 mg). − ^{1}H NMR (250.13 MHz, C$_6$D$_6$, 25 °C): δ = 1.37 (t, 2 H, C*H*$_2$CH$_2$NMe$_2$), 1.85 [s, 6 H, N(C*H*$_3$)$_2$], 2.02 (t, 2 H, CH$_2$C*H*$_2$NMe$_2$), 2.52 (s, 3 H, *p*-C*H*$_3$), 3.51 (s, 6 H, *o*-C*H*$_3$), 4.69 (s, 2 H, Cp*H*), 6.22 (s, 2 H, Cp*H*), 7.07 (s, 2 H, C$_6$*H*$_2$). − ^{13}C{^{1}H} NMR (62.90 MHz, C$_6$D$_6$, 25 °C): δ = 21.2 (*p*-*C*H$_3$), 25.7 (*C*H$_2$CH$_2$NMe), 29.3 (*o*-*C*H$_3$), 52.1 [N(*C*H$_3$)$_2$], 76.7 (CH$_2$*C*H$_2$NMe), 82.2 (*o*-*C*$_5$H$_4$), 99.1 (*m*-*C*$_5$H$_4$), 102.3 (*i*-*C*$_5$H$_4$), 125.4 (*i*-*C*$_6$H$_2$), 128.6 (*m*-*C*$_6$H$_2$), 138.3 (*p*-*C*$_6$H$_2$), 146.9 (*o*-*C*$_6$H$_2$). − MS(FAB); *m*/*z* (%): 313 (100) [M$^+$], 194 (21) [Cp^{N}Ni$^+$], 154 (83), 136 (61) [Cp^{N+}], 120 (10) [Mes$^+$]. − $C_{18}H_{25}NNi$ (314.1): calcd. C 68.83, H 8.02, N 4.46; found C 68.49, H 8.71, N 4.34.

Crystal Structure Determination: Additional crystallographic data on the structural determination of compounds **1b**, **4**, **5** and **6** are listed in Table 7. Intensity data for **4** and **5** were collected with a Siemens P4 diffractometer (Mo-K_α radiation, λ = 0.71073 Å, graphite monochromator, ω-scan). Empirical absorption corrections were applied. The structures were solved by direct methods[26]

and refined by least-squares methods based on F^2 with all observed reflections.[27] The thermal reliability index $wR2$ is defined as $[\Sigma w(F_o^2 - F_c^2)^2/\Sigma w(F_o^2)^2]^{1/2}$. All non-hydrogen atoms were refined anisotropically.

Crystals of **1b** and **6** were mounted on a goniometer using the perfluoro ether technique with cooling (T = 203 K). Data collections were performed with a Bruker-axs-SMART diffractometer (Mo-K_α radiation λ = 0.71073 Å, graphite monochromator, ω-scan). Empirical absorption corrections (ψ-scans) were applied. The structure solutions were done with direct methods[26] and the structure refinement (full-matrix least-squares against F^2) was undertaken with anisotropic structural parameters for all non-hydrogen atoms.[28]

Crystallographic data (excluding structure factors) for the structures reported in this paper have been deposited with the Cambridge Crystallographic Data Centre: CCDC-138909 (**1b**), -138904 (**4**), -138903 (**5**), and -138905 (**6**). Copies of the data can be obtained free of charge by application to CCDC, 12 Union Road, Cambridge CB2, 1EZ, UK [Fax: (int. code) + 44-1223/336-001; E-mail: deposit@ccdc.cam.ac.uk].

Acknowledgments

We thank the Fonds der Chemischen Industrie for generous financial support of this project.

[1] [1a] J. Okuda, *Comments Inorg. Chem.* **1994**, *16*, 185−205. − [1b] P. Jutzi, T. Redeker, *Eur. J. Inorg. Chem.* **1998**, 663−674 and references therein.
[2] R. A. Fischer, S. Nlate, H. Hoffmann, E. Herdtweck, J. Blümel, *Organometallics* **1996**, *15*, 5746−5752.
[3] S. Nlate, E. Herdtweck, R. A. Fischer, *Angew. Chem.* **1996**, *108*, 1957−1959.
[4] F.-G. Fontaine, T. Kadkhodazadeh, D. Zargarian, *J. Chem. Soc. Chem. Commun.* **1998**, 1253−1254.
[5] R. Vollmerhaus, F. Bélanger-Gariépy, D. Zargarian, *Organometallics* **1997**, *16*, 4762−4764.
[6] B. Bogdanovic, B. Spliethoff, G. Wilke, *Angew. Chem. Int. Ed. Engl.* **1980**, *19*, 622.
[7] T.-F. Wang, T.-Y. Lee, J.-W. Chou, C.-W. Ong, *J. Organomet. Chem.* **1992**, *423*, 31−38.
[8] G. Brauer, *Handbuch der Präparativen Anorganischen Chemie*, vol. 3, 3rd ed., Ferdinand Enke Verlag, Stuttgart, **1981**, p. 1849.
[9] J. Dahlhaus, M. Bangel, P. Jutzi, *J. Organomet. Chem.* **1994**, *474*, 55−58.
[10] [10a] W.-P. Leung, H.-K. Lee, Z.-Y. Zhou, T. C. W. Mak, *J. Organomet. Chem.* **1993**, *462*, 7. − [10b] N. A. Bell, F. Glockling, A. McGregor, M. L. Schneider, H. M. M. Shearer, *Acta Crystallogr., Sect. C* **1984**, *40*, 623.
[11] [11a] R. A. Fischer, E. Herdtweck, T. Priermeier, *Inorg. Chem.* **1994**, *33*, 934−943. − [11b] J. Weiss, T. Priermeier, R. A. Fischer, *Inorg. Chem.* **1996**, *35*, 71.
[12] P. Jutzi, T. Redeker, H.-G. Stammler, B. Neumann, *J. Organomet. Chem.* **1995**, *498*, 127−137.
[13] P. L. Holland, M. E. Smith, R. A. Andersen, R. G. Bergman, *J. Am Chem. Soc.* **1997**, *119*, 12815−12823.
[14] [14a] M. I. Bruce, J. R. Rodgers, M. R. Snow, F. S. Wong, *J. Organomet. Chem.* **1982**, *240*, 299−309. − [14b] C. Liqing, P. Kezhen, C. Xirian, Z. Lun, *J. Struct. Chem.* **1984**, *3*, 125. − [14c] J. J. Schneider, U. Denninger, J. Hagen, C. Krüger, D. Bläser, R. Boese, *Chem. Ber./Recueil* **1997**, *130*, 1433−1440.
[15] M. J. Frisch, G. W. Trucks, H. B. Schlegel, G. E. Scuseria, M. A. Robb, J. R. Cheeseman, V. G. Zakrzewski, J. A. Montgomery, Jr., R. E. Stratmann, J. C. Burant, S. Dapprich, J. M. Millam, A. D. Daniels, K. N. Kudin, M. C. Strain, O. Farkas, J. Tomasi, V. Barone, M. Cossi, R. Cammi, B. Mennucci, C. Pomelli, C. Adamo, S. Clifford, J. Ochterski, G. A. Petersson, P. Y. Ayala, Q. Cui, K. Morokuma, D. K. Malick, A. D. Rabuck, K. Raghavachari, J. B. Foresman, J. Cioslowski, J. V. Ortiz, A. G. Baboul, B. B. Stefanov, G. Liu, A. Liashenko, P. Piskorz, I. Komaromi, R. Gomperts, R. L. Martin, D. J. Fox, T. Keith, M. A. Al-Laham, C. Y. Peng, A. Nanayakkara, C. Gonzalez, M. Challacombe, P. M. W. Gill, B. Johnson, W. Chen, M. W. Wong, J. L. Andres, C. Gonzalez, M. Head-Gordon, E. S. Replogle, J. A. Pople, *Gaussian 98, Revision A.7*, Gaussian, Inc., Pittsburgh PA, **1998**.
[16] A. D. Becke, *J. Chem. Phys.* **1993**, *98*, 299.
[17] [17a] A. D. McLean, G. S. Chandler, *J. Chem. Phys.* **1980**, *72*, 5639. − [17b] R. Krishnan, J. S. Binkley, R. Seeger, J. A. Pople, *J. Chem. Phys.* **1980**, *72*, 650.
[18] [18a] A. J. H. Wachters, *J. Chem. Phys.* **1970**, *52*, 1033. − [18b] P. J. Hay, *J. Chem. Phys.* **1977**, *66*, 4377.
[19] [19a] R. Ditchfield, W. J. Hehre, J. A. Pople, *J. Chem. Phys.* **1971**, *54*, 724. − [19b] W. J. Hehre, R. Ditchfield, J. A. Pople, *J. Chem. Phys.* **1972**, *56*, 2257. − [19c] P. C. Hariharan, J. A. Pople, *Mol. Phys.* **1974**, *27*, 209. − [19d] P. C. Hariharan, J. A. Pople, *Theor. Chim. Acta* **1973**, *28*, 213. − [19e] M. S. Gordon, *Chem. Phys. Lett.* **1980**, *76*, 163.
[20] M. R. Churchill, T. A. O'Brien, *J. Chem. Soc. A* **1970**, 161−167.
[21] M. Julia, H. Lauron, J. N. Verpeaux, Y. Jeannin, C. Bois, *J. Organomet. Chem.* **1988**, *358*, C11−C16.
[22] M. R. Churchill, T. A. O'Brien, *J. Chem. Soc. A* **1968**, 2970−2976.
[23] M. R. Churchill, T. A. O'Brien, *J. Chem. Soc. A* **1969**, 266−272.
[24] M. R. Churchill, T. A. O'Brien, *J. Chem. Soc. A* **1970**, 161−167.
[25] M. Julia, H. Lauron, J. N. Verpeaux, Y. Jeannin, C. Bois, *J. Organomet. Chem.* **1988**, *358*, C11−C16.
[26] G. M. Sheldrick, *SHELX86*, Univ. Göttingen, **1986**.
[27] G. M. Sheldrick, *SHELXL97*, Univ. Göttingen, **1997**.
[28] G. M. Sheldrick, *SHELXL93*, Univ. Göttingen, **1993**.

Received January 17, 2000
[I00014]

Fe_4S_4 Clusters Functionalized with Molecular Receptor Ligands

Robertus J. M. Klein Gebbink,[a] Stephen I. Klink,[a] Martinus C. Feiters,*[a] and Roeland J. M. Nolte*[a]

Keywords: Iron−sulfur clusters / Electrochemistry / High-potential iron−sulfur proteins / Host−guest chemistry

Cubane-type Fe_4S_4 clusters have been functionalized with the concave dithiol ligands $\mathbf{L^{Xyl}}2H$ and $\mathbf{L^{Ac}}2H$, derived from a diphenylglucoluril-based receptor molecule. In the monomeric cluster compounds $[Fe_4S_4(\mathbf{L^{Xyl}})_2](PPh_4)_2$ (cluster **A**) and $[Fe_4S_4(\mathbf{L^{Ac}})_2](PPh_4)_2$ (cluster **B**), an Fe_4S_4 core is combined with receptor sites for alkali metal ions and aromatic guest molecules. Molecular modelling studies show that the Fe_4S_4 core in compound **B** is tightly encapsulated by its two dithiol ligands, whereas this is not the case for compound **A**. However, unlike the clusters in High-Potential Iron–sulfur Proteins (HiPIP′s), the Fe_4S_4 core in **B** is still accessible to solvent molecules, as has been established by solution electrochemical studies. Both cluster compounds bind alkali metal ions and undergo anodic shifts in their $2^-/3^-$ reduction potentials upon binding of these ions. Electrochemical titrations indicate the complexation of four alkali metal ions per cluster compound. Binding by cluster **B** takes place preferentially at the exterior of the receptor ligands, whereas in the case of cluster **A** the ions also bind to the interior of the receptor. The more open structure of **A** allows the binding of dimethylparaquat **5** [$K_{ass} = (5.6 \pm 0.6) \times 10^3\ m^{-1}$] to this cluster compound. On complexation, the first reduction potential of the guest molecule shifts in the cathodic direction, whereas the reduction potential of the cluster remains unaffected. This observation can be rationalized by assuming that the twofold positively charged guest molecule binds between the aromatic side-walls of the receptor ligands, whereas the one-electron reduced, singly charged positive species is not bound.

Introduction

The properties of prosthetic groups in enzymes are often governed by the protein matrix. Well-known examples are the iron−porphyrin complexes in proteins and enzymes, which can have various properties and functions depending on, e.g., the axial ligation of the central metal ion.[1] Such effects have been studied in great detail in model systems.[2] Another well-studied example is the group of proteins that incorporate an Fe_4S_4 cluster in their active sites. The factors that determine the properties of the cluster are reasonably well understood, largely due to the pioneering model studies by the group of Holm.[3] Fe_4S_4-containing electron-transfer proteins can be divided into two classes, viz. ferredoxins and high-potential iron−sulfur proteins (HiPIP′s), which have low and high reduction potentials, respectively, compared to most physiological redox partners. Of the various oxidation states possible for Fe_4S_4 clusters, ferredoxins cycle between the $[Fe_4S_4(SR)_4]^{2-}$ and $[Fe_4S_4(SR)_4]^{3-}$ states, and HiPIP′s between the $[Fe_4S_4(SR)_4]^{1-}$ and $[Fe_4S_4(SR)_4]^{2-}$ states.[4a] Apart from this, the differences between these two classes are assumed to arise from (i) the number of hydrogen bonds between the peptide backbone and the cluster or its ligands,[4b] (ii) the hydrophobicity of the protein environment of the cluster,[4c] and (iii) the accessibility of the cluster to solvents. The first two aspects have been rather well mimicked with the help of model systems, but model studies on the latter aspect have been much more limited. Okuno and co-workers have described an Fe_4S_4 cluster ligated by a macrocyclic tetradentate thiol ligand.[5] In DMSO solution, the 1^- oxidized state of this cluster, which can be considered as a model of the oxidized form of a HiPIP, was found to be stabilized by the lipophilic macrocyclic ligand. Tabushi et al. have prepared a cluster sandwiched between two cyclodextrin rings.[6] Although this compound showed a remarkable stability in water, no effect of the cyclodextrin moiety on the redox potentials of the Fe_4S_4 cluster was observed. Gorman et al.[7] have shown that increasing the generation of ligands of Fe_4S_4 clusters encapsulated by dendrimers makes the cluster both kinetically and thermodynamically more difficult to reduce. Several half-encapsulated clusters have been reported in the literature, e.g. the 3:1 subsite-differentiated clusters prepared by Holm et al.,[4a−4c] Evans et al.,[8a] and Nolte et al.,[8b−8d] and a tetrathiol-derived cluster based on diphenylglycoluril.[8e][8f] For these clusters, only a slight influence of the ligands on the redox potentials of the Fe_4S_4 core was observed. Apparently, a snug and spherical ligand arrangement is needed to provide a synthetic Fe_4S_4 cluster with a solvophobic environment that stabilizes a higher oxidation state.

In this paper, we describe the synthesis of two bowl-shaped dithiol ligands $\mathbf{L^{Xyl}}2H$ and $\mathbf{L^{Ac}}2H$ (see Chart 1), together with the synthesis and characterization of their Fe_4S_4 cluster compounds **A** and **B**. These ligands were designed with the idea that binding to an Fe_4S_4 cluster would lead to a "closed shell" structure showing interesting redox properties. Figure 1 shows the energy-minimized structure

[a] Department of Organic Chemistry, NSR Center, University of Nijmegen,
1 Toernooiveld, NL-6525 ED Nijmegen, The Netherlands
Fax: (internat.) +31-24/365-2676
E-mail: mcf@sci.kun.nl

 © WILEY-VCH Verlag GmbH, D-69451 Weinheim, 2000 1434−1948/00/0909−2087 $ 17.50+.50/0

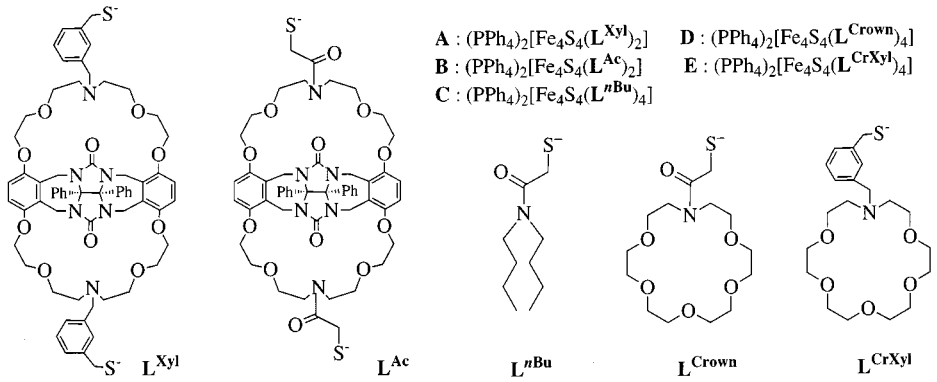


Chart 1

of cluster compound **B**. The space-filling representation (left) suggests that the cluster core (shown in light) is fully encapsulated within the two receptor ligands. Another reason for choosing $L^{Xyl}2H$ and $L^{Ac}2H$ is that these ligands contain receptor sites for binding metal ions and organic guest molecules.[9,10] This opens the possibility of investigating how the electrochemical properties of compounds **A** and **B** change under the influence of such ions and guests.

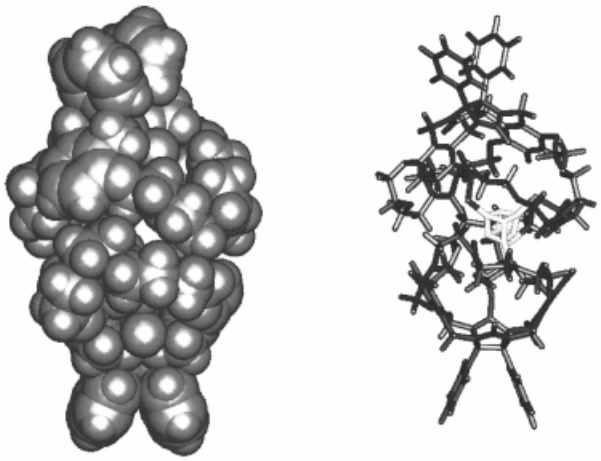


Figure 1. Energy-minimized structure of compound **B**; the ligands are shown in dark, the cluster atoms in light

Results and Discussion

Ligand Synthesis

The ligands $L^{Xyl}2H$ and $L^{Ac}2H$ were synthesized by routes analogous to those that we have used previously for the synthesis of the corresponding crown ether thiols.[9] Starting from the diaza receptor molecule **1a**, alkylation with two equivalents of α-bromo-α′-thioacetyl-*m*-xylene yielded the protected dithiol **2** (see Scheme 1). Removal of the acetate protecting groups was effected by treatment with 3% HCl in methanol. As it was not desirable to subject dithiol $L^{Xyl}2H$ to any purification procedure due to its air sensitivity, the deprotection time was extended to 7 days. TLC analysis indicated that this period was required to ensure complete deprotection of **2**. The overall yield of $L^{Xyl}2H$ was 46%.

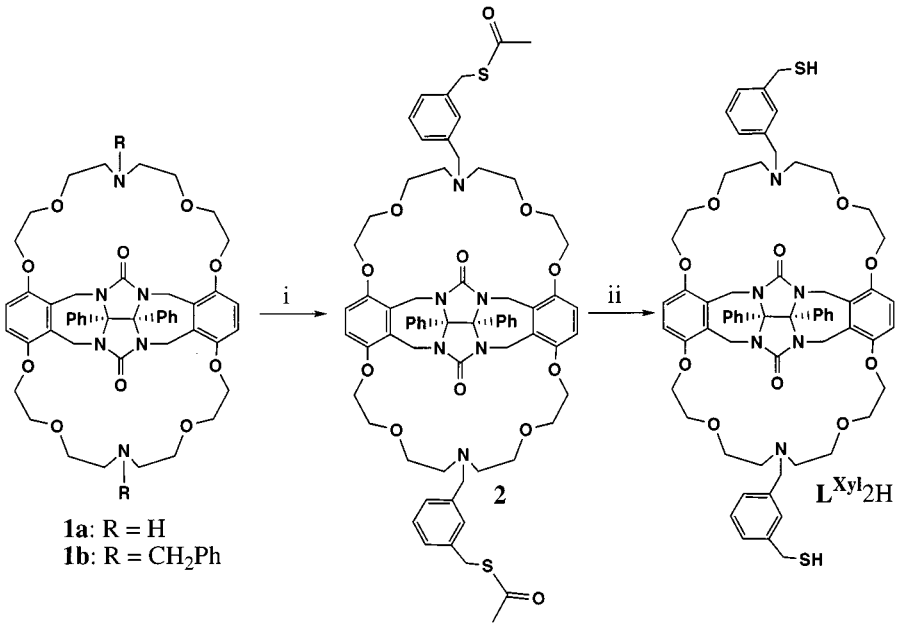
Scheme 2 depicts the synthetic route for the preparation of the dithiol ligand $L^{Ac}2H$. Amidation of receptor **1a** with 2 equivalents of α-chloroacetyl chloride gave compound **3** in reasonable yield (60%). Treatment of this compound with an excess of potassium thiocarboxylate resulted in the formation of the dithioacetate **4**, which was deprotected over a period of 5 days by treatment with 3% HCl in methanol. This procedure gave dithiol $L^{Ac}2H$ in 54% overall yield.

Conformational and Binding Properties of Amidated Receptors 3 and 4

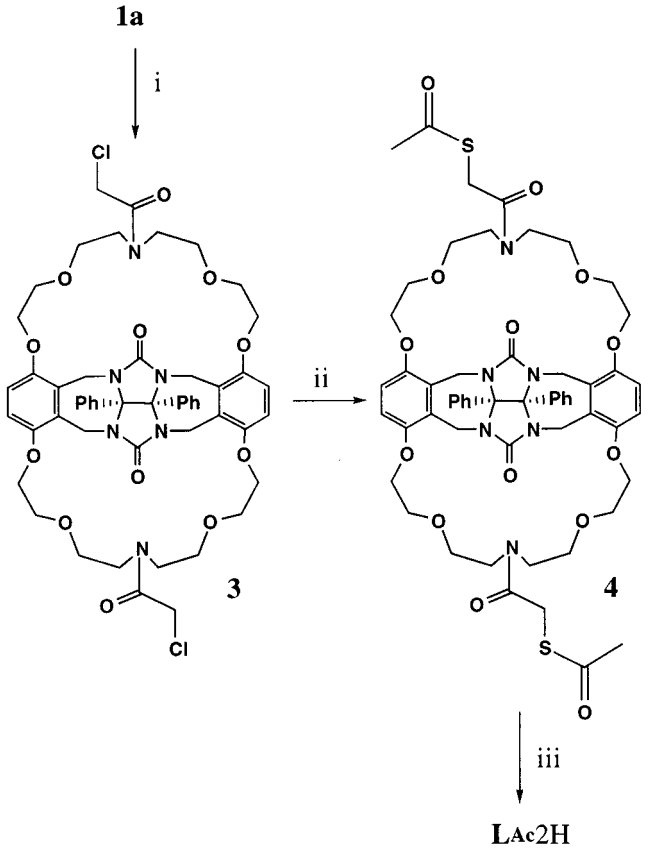
Although chromatographic analysis indicated that the receptor compounds **3** and **4** were pure, ^{1}H NMR analysis was initially considered to be indicative of the additional presence of other receptor species. Due to conformational restrictions, the protons of the methylene groups connecting the aromatic side-walls to the diphenylglycoluril backbone in **3**, **4**, and $L^{Ac}2H$ behave as AX spin systems.[11] Figure 2 depicts the resonances of the two methylene protons (H_a) in **3** that point upwards in relation to the receptor backbone. The other half of the AX system is obscured by the signals of the crown ether rings. Three doublets for receptors **3** and $L^{Ac}2H$ and two for receptor **4** are observed at around $\delta = 5.7$, instead of just one doublet as anticipated beforehand. Additionally, a multiplet is found for the aromatic wall protons, which normally give a singlet. This splitting is also evident in the ^{13}C NMR spectra of these compounds, where multiple signals are seen for the carbon atoms to which the aforementioned protons are attached.

^{1}H NMR experiments in which the temperature dependence of the multiple signals was monitored showed that these features can be ascribed to the presence of slowly interconverting conformers of one and the same compound. Increasing the temperature results in coalescence of the multi-doublet signals into one doublet and of the multiplet into one singlet (not shown). The coalescence temperatures were determined as 340 K for receptor **3** and 325 K for receptor **4** (90 MHz).

Apparently, amidation of the nitrogen atoms in the aza-crown ether rings of the basket-shaped receptor molecules



Scheme 1



Scheme 2. Synthesis of dithiol receptor ligand $L^{Xyl}2H$; (i) **1a**, 2 equiv. α-bromo-α′-thioacetyl-*m*-xylene, K_2CO_3, DMF, 40 °C; (ii) 3% HCl/MeOH, N_2

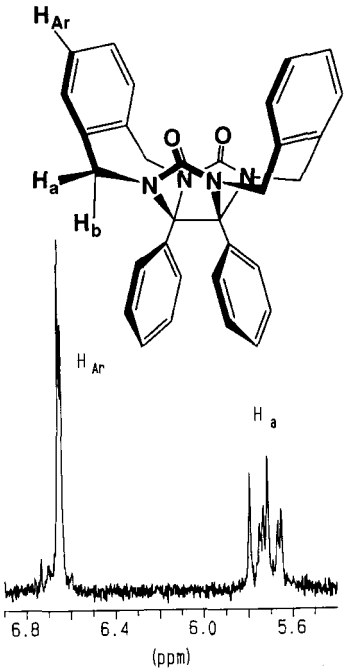


Figure 2. ^1H NMR spectrum of compound **3** in $CDCl_3$ (298 K)

introduces considerable rigidity into these systems. As a result, several conformations can be observed by NMR. Figure 3 shows the different orientations that the amide functions can adopt with respect to the rest of the receptor molecule; the corresponding conformers are proposed to be slowly interconverting on the NMR time scale. The amide functions can point either up or down with respect to the crown ether plane (Figure 3a) and in either position they can again occupy two orientations by rotation about the C(O)−N bond (Figure 3b). The latter two orientations are expected to interconvert more easily than the "up/down" conformers. In the "down" position, the amide groups can be expected to exert a significant influence on the methylene AX spin system, resulting in different signals due to the difference in local environment enforced by these groups. In the "up" position, the amide groups do not have such an influence on this spin system. This explanation accounts for

the observation of three AX doublets with approximate intensity ratios of 1:1:2 in the case of **3**. In a similar way, the amide groups in the "up" positions create a different environment for the aromatic wall protons, whereas in the "down" position no such modification of the environment is induced. This accounts for the observation of multiple resonances for the protons and carbon nuclei of the aromatic side walls. The ease of interconversion of the conformers and, therefore, the spectral characteristics, will depend on the functionalization of the amide group. For this reason, three doublets are observed for the methylene H_a protons of receptors **3** and $\mathbf{L^{Ac}}2H$, as opposed to just two doublets for receptor **4**.

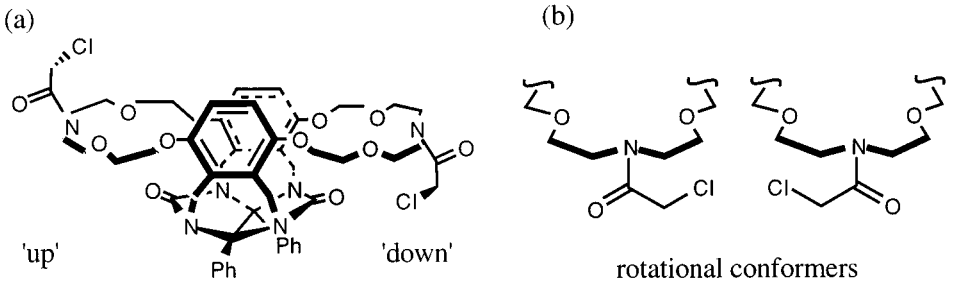


Figure 3. Different conformers of compound **3**

A liquid/liquid (chloroform/water) extraction experiment with potassium picrate revealed that potassium ions are weakly bound by receptor **3** (the association constant K_{ass} was not determined). NMR analysis showed that the presence of these ions did not influence the ratio of the conformers. Addition of resorcinol (1,3-dihydroxybenzene) to solutions of **3** in the presence or absence of K^+ ions resulted in one single AX pattern due to the H_a protons and a singlet due to the aromatic wall protons in the ^1H NMR spectrum. Apparently, the aromatic guest molecule is bound by just one of the conformers of **3**. On the basis of CPK models, we tentatively propose this to be the "up/up" conformer. The K_{ass} was determined as 640 ± 10 M^{-1}. This value is significantly lower than the association constants determined for resorcinol and the related receptors **1a** and **1b** (see Scheme 1, K_{ass} = 2000 and 2900 M^{-1}, respectively).[12] This low binding affinity is probably due to the extra energy that is needed to bring the receptor into the conformation for resorcinol binding.

Cluster Synthesis and Characterization

Procedures similar to those described previously[9] for the synthesis of crown ether-derived clusters were used to prepare the clusters $[Fe_4S_4(\mathbf{L^{Xyl}})_2](PPh_4)_2$ (cluster **A**) and $[Fe_4S_4(\mathbf{L^{Ac}})_2](PPh_4)_2$ (cluster **B**) from the two bidentate receptor ligands $\mathbf{L^{Xyl}}2H$ and $\mathbf{L^{Ac}}2H$, respectively. Initially, $[Fe_4S_4Cl_4](PPh_4)_2$ was used as the starting material for the synthesis of cluster **A**. A DMF solution of this compound was slowly added to a dilute DMF solution (< 1 mM) containing two equivalents of the ligand $\mathbf{L^{Xyl}}2H$ and four equivalents of $(NBu_4)OH$ as a base. The progress of the reaction was monitored by DPV analysis of aliquots withdrawn from the mixture. Besides the formation of the desired product, characterized by a reductive peak at −1.74 V, an unknown by-product was also observed ($E_{p,c}$ = −1.36 V). At the point where DPV analysis indicated no further change in the composition of the reaction mixture, the products were isolated by means of precipitation followed by filtration. The by-product was removed by washing with CH_2Cl_2. NMR analysis showed that the desired Fe_4S_4 product was isolated as the tetrabutylammonium salt, probably because this salt is less soluble than the tetraphenylphosphonium salt. After isolation and washing with CH_2Cl_2, the product obtained was indeed found to be poorly soluble; it did not dissolve in DMF and only very poorly in DMSO.

Attempts to prepare cluster **A** through in situ synthesis in an electrochemical cell failed. An unidentified precipitate was formed, which might have originated from the excess tetrabutylammonium salt present as the supporting electrolyte. These procedures either failed to yield the desired product or produced it in a form unsuitable for further analysis. $[Fe_4S_4(S\mathit{t}Bu_4)](PPh_4)_2$ was therefore used as the starting material in all subsequent experiments. The fact that no base is needed with this starting material was thought to be favourable for the syntheses of the clusters **A** and **B**. Ligand-exchange reactions were performed by applying a dynamic vacuum after rapid mixing of dilute DMF solutions of the *tert*-butyl thiolate cluster with two equivalents of the appropriate ligand. After six hours, DPV analysis was indicative of complete conversion into a single product in each case. Both cluster compounds were isolated as black, shiny solids. We were unable to grow crystals from the isolated materials; the use of counterions known to favour crystallization of related compounds, i.e. $(NBu_3Bzl)^+$,[13] was not successful in the present case.

The newly synthesized cluster compounds were first characterized by electrochemical means. Our earlier experience with crowned cluster compounds showed this to be an excellent method for examining the formation of the clusters as well as their redox chemistry.[9] Due to the sensitivity of the CV and DPV techniques, it was also anticipated that any formation of soluble oligomeric or polymeric materials would be detectable in this way.

Table 1 lists the electrochemical characteristics of the $2^-/3^-$ reduction of cluster compounds **A** and **B** in DMF solution. The half-wave potentials ($E_{1/2}$) for reduction of these compounds resemble the values determined for related crown ether-functionalized clusters, e.g. **D**.[9] On CV ana-

lysis, a chemically reversible reduction process was observed for cluster **A**, whereas this process was found to be electrochemically quasi-reversible due to a relatively slow electron-transfer rate. For cluster **B**, the opposite behaviour was found, viz. an electrochemically reversible but chemically quasi-reversible reduction (see Figure 4). These results are indicative of significantly better defined redox processes for clusters **A** and **B** than for the previously studied crowned cluster compounds. Apparently, the fact that the cluster cores in **A** and **B** are ligated by bidentate rather than monodentate ligands prevents the occurrence of irreversible redox chemistry involving thiolate ligands not coordinated to the cluster core. The peak separations suggested that no oligomeric or polymeric materials had been formed, as much larger separations would have been expected if this had been the case. For neither of the two cluster compounds was a reversible $2^-/1^-$ oxidation process observed.

Table 1. Electrochemical characteristics of the $2^-/3^-$ reduction of cluster compounds **A** and **B** in DMF

[a]	Electrode	**A** Pt	PGE	**B** Pt	PGE
CV	$E_{1/2}$ (V)	−1.78	−1.75	−1.60	−1.64
	ΔE_p (mV)	100	90	70	60
	i_b/i_f	1.0	−[b]	0.59	−[b]
DPV	E_p (V)	−1.74	−1.74	−1.62	−1.61
	$W_{1/2}$ (mV)	107	160	140	108

[a] Potentials are given against the Fc/Fc^+ couple in the same solvent. PGE = Pyrolytic graphite edge. − [b] Due to the large capacitative current these values could not be determined.

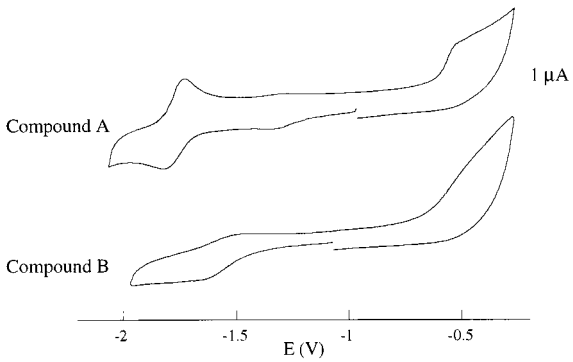


Figure 4. Cyclic voltammograms of compounds **A** and **B** in DMF (reductive scans, Pt working electrode)

Earlier studies by our group on semi-encapsulated cluster compounds showed that the use of graphite electrodes was advantageous in their electrochemical analysis.[7,8] In the present case, however, a graphite working electrode instead of a platinum one was not found to be beneficial. Instead, lower current responses were found, which complicated the analysis. No significant changes in peak potentials were observed. Moreover, compounds **A** and **B** could be electrochemically analyzed without the need for Ba^{2+} ions as promoting or modulating species. This clearly sets these compounds apart from their semi-encapsulated analogues[8b−8f] and suggests that the cluster cores in **A** and **B** are surrounded by the ligands in such a way that no effective dipole moment exists in these complexes. These results also confirmed that complexes **A** and **B** were isolated as monomeric materials.

It was hoped that by surrounding the Fe_4S_4 cluster with a large spherical ligand a solvophobic environment around the cluster core might be created and that the redox centre would be shielded from the electrode. However, the electrochemical properties of **A** and **B**, as outlined above, do not suggest that this shielding is effective for either of the two compounds. This is not unexpected for **A** because the xylylene spacers between the cluster and the receptor sites in this compound are relatively long, exposing the redox site to the solvent and to the electrode surface. On the other hand, modelling studies suggested that compound **B** should be able to adopt a compact and closed structure (see also Figure 1). As such a structure was seemingly not present in DMF, we decided to use DMSO as the solvent for the electrochemical measurements. The choice of DMSO was based on NMR studies (vide infra), which indicated that the Fe_4S_4 core of **B** is tightly embraced by its ligands in this solvent. For comparison purposes, the electrochemical properties of two structurally related cluster compounds were also studied in this solvent. These compounds bear dibutylamine (compound **C**) and monoaza-18-crown-6 acetyl thiolate ligands (compound **D**), respectively (see Chart 1).[9]

For the dibutylamine thiolate functionalized compound **C**, a reversible reduction process was observed under normal conditions (not shown). A small pre-wave was visible for the $2^-/3^-$ reduction process ($E_{1/2}$ = −1.52 V), which arises either because of coordination of solvent molecules to the cluster core or due to absorption of the reduced species onto the electrode. For the crown ether functionalized compound (cluster **D**), the current response was rather low and again a pre-wave associated with the reduction of the cluster was observed. The addition of $Ba(ClO_4)_2$ considerably improved the current response and also induced an anodic shift in the reduction potential ($E_{p,red}$ = −1.58 V). The origins of these effects have been discussed previously[9] and originate from metal ion binding by the crown ether ligands. For compound **B**, a poorly defined voltammogram was obtained, showing a very faint reductive feature at a similar potential as found for compound **D** in this solvent. Addition of $Ba(ClO_4)_2$ again led to an increased current response and an anodic shift in $E_{p,red}$. In this case, an irreversible reduction was observed at around −1.42 V, a potential similar to that measured for the pre-wave of compound **D**. For neither of the three cluster compounds was a clear, reversible oxidation process observed under any of the investigated conditions.

The results of the aforementioned experiments show that the increasing ligand size on going from cluster compound **C**, to **D**, and then **B** leads to increasingly hampered electron-transfer from the cluster compound to the electrode in DMSO. Furthermore, shielding of the cluster core by the large receptor ligand does not in this case lead to stabilization of higher oxidation states of the cluster. In previous studies, Okuno et al.[5] showed that their cluster compound, in which the cluster is coordinated by a sterically encum-

bered macrocyclic tetrathiolate ligand, undergoes a reversible $2^-/1^-$ transition in DMSO at a potential significantly more positive than that of several model compounds.[5] Data in DMF were not reported for this particular compound. Normally, higher oxidation states of iron–sulfur clusters would be expected to be stabilized in apolar solvents and destabilized in polar solvents such as DMF or DMSO.[14] Okuno and co-workers concluded that the compact structure of their compound in DMSO leads to stabilization of the 1^- oxidation state through the creation of a solvophobic environment. Although a similar behaviour might be expected in our system, the stabilization of a higher oxidation state is apparently not possible. This may be due to the rather polar nature of the crown ether fragments in our receptor ligands or due to the fact that the cluster core is still accessible to solvent molecules in spite of the tight ligand encapsulation.

The absorption spectra of compounds **A** and **B** were found to correlate very well with the spectra of the structurally related crown ether compounds (see Table 2).[9] This confirms that the Fe_4S_4 cubane core is retained in the new compounds. It also indicates that the local environment of the thiolate sulfur atoms[4c] in **A** and **B** is similar to that in the crown ether analogues. The ligand-to-metal charge-transfer (LMCT) absorption bands at ca. 400 nm in Fe_4S_4 clusters are known to undergo a blue shift in solvents of high ε.[15] Similar blue shifts have been observed for cluster compounds bearing sterically encumbered thiolate ligands, which were additionally shown to display reversible $2^-/1^-$ transitions in CV and were therefore presented as HiPIP

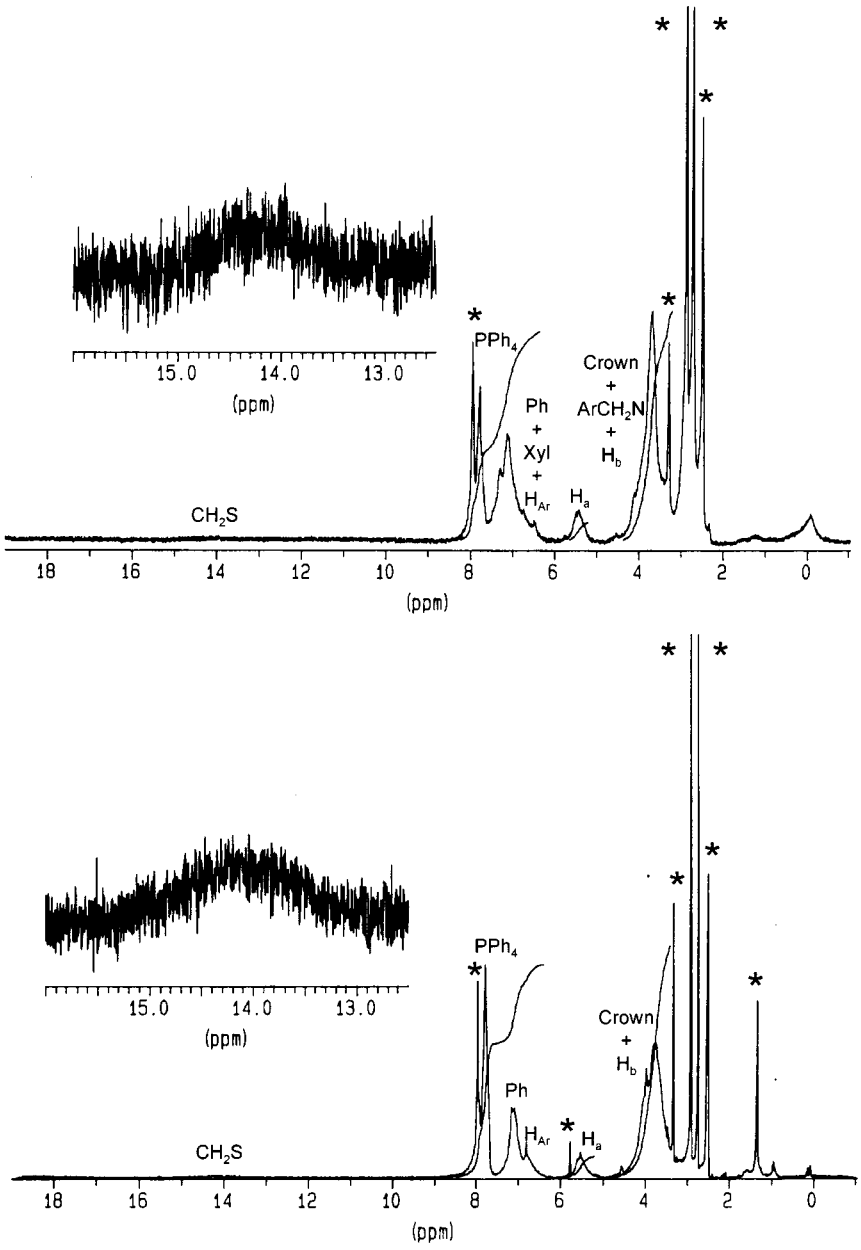


Figure 5. ^1H NMR spectra of cluster compounds **A** (top) and **B** (bottom) in $[D_6]$DMSO

models.[16] The fact that no such blue shifts are observed for compounds **A** and **B** is in line with their electrochemical behaviour (no reversible $2^-/1^-$ transitions).

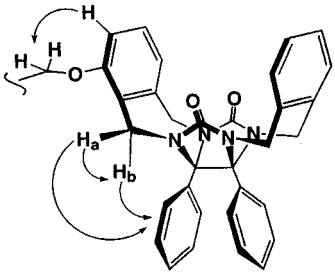
Table 2. UV/Vis data of cluster compounds in DMF

Compound	λ_{max}
A	290, 420, 620 (sh)
$[NBu_4]_2[Fe_4S_4(SBzl)_4]$	300 (sh), 420
B	295, 340 (sh), 415, 622 (sh)
C	301, 415, 620 (sh)
D	300, 410, 660 (sh)

The ^1H NMR spectra of compounds **A** and **B** exhibit the typical features of Fe_4S_4 thiolate clusters,[9] i.e. large chemical shifts and broadened peaks (see Figure 5). The resonances of the methylene protons adjacent to the thiolate sulfur atoms are observed as broad signals at around $\delta = 14$ (see Table 3 for details). The chemical shifts of these signals were found to increase linearly with temperature in the region 298−348 K (not shown). The other proton signals of **A** and **B** are also somewhat broadened, suggesting either that these protons lie in the proximity of a paramagnetic centre or that the complexes adopt different conformations that are in rapid exchange on the NMR time scale. A complete assignment of the peaks was performed in the case of compound **B** by means of a 2D-COSY experiment, the coupling constant of the $ArCH_2N$ protons of the diphenylglycoluril unit being determined by 2D-DQF-COSY experiments (see Experimental Section).

In cluster compound **D**, which, like compound **B**, also bears α-mercaptoacetyl ligands, the crown ether ligands have a somewhat restricted conformational freedom, as was concluded from the appearance of two discrete and relatively sharp signals due to the CH_2S protons.[9] Such an inequivalence in chemical shift is not observed for the CH_2S protons in **B**. Instead, the signals are broad, the width at half peak height being 1.4 ppm as compared to 0.4 ppm in the case of compound **D**. This broadening might be indicative of the superposition of several peaks, implying that two or more CH_2S groups in **B** have somewhat different orientations with respect to the cluster core, and hence that the ligation of the cluster core in **B** is not symmetrical. Moreover, some flexibility of the ligands with respect to the cluster core leading to slowly exchanging conformers might be possible. Similar considerations probably apply to compound **A**, the structure of which can be expected to be much more flexible than that of **B**.

Due to the broadening of the signals in the one-dimensional ^1H spectrum, it was not possible to establish whether the ligands of compound **B** existed in more than one conformation. The solution structure of compound **B** was therefore studied in more detail by means of a 2D-NOESY experiment. Part of the 2D-NOESY spectrum of compound **B** is shown in Figure 6. Several contact cross-peaks are apparent, first and foremost between the two $ArCH_2N$ protons of the diphenylglycoluril backbone themselves and between one of these protons (H_a) and the protons (PhH′s) of the phenyl rings at the bottom of the receptor ligand. In addition, an interaction is in evidence between the aromatic wall protons and the methylene protons in the crown ether part of the ligand. Most of these through-space interactions were expected on the basis of earlier NMR studies on diphenylglycoluril-based receptor molecules,[11] but the H_a−PhH interaction is new. 2D-NOESY experiments on compound **3** and cluster compound **A** showed no spatial proximity of these protons.



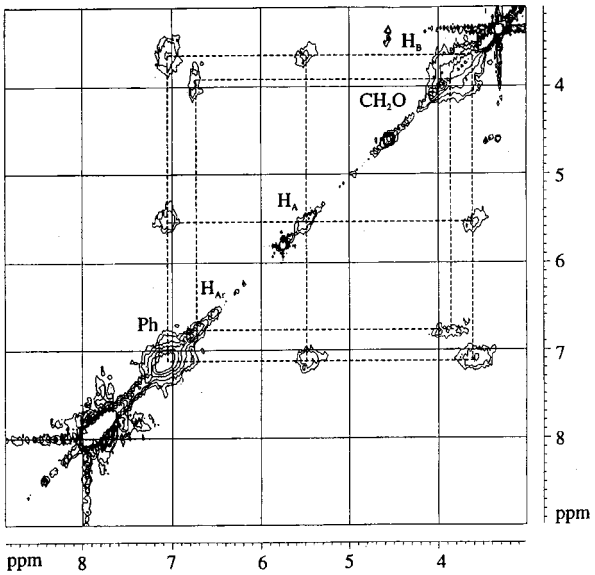


Figure 6. 2D-NOESY spectrum of cluster compound **B** in $[D_6]DMSO$

All the protons for which cross-peaks are observed (except the aforementioned H_a and PhH′s) can be assumed to lie in close proximity to one another on the basis of crystallographic analyses of two related receptor molecules[17] and of several other clip molecules.[18] Conformational isomers

Table 3. ^1H NMR temperature-dependence of isotropically shifted ligand signals in cluster compounds **A** and **B** in $[D_6]DMSO$

		Free ligand (δ/ppm)	Cluster (δ/ppm)	ΔH^{iso} (ppm)	$\Delta H^{iso}/T$ (Hz/K)
A	CH_2S	4.0	14.3	−10.3	−5.96
B	CH_2S	4.1	14.1	−10.0	−5.18

can be obtained by "flipping" the aromatic walls, as has been observed previously for receptor molecules bearing naphthalene walls.[19] Such a "flipping" process might explain the close proximity of H_a and the PhH′s, but it has never been observed for clip molecules with benzene walls. Examination of CPK models of compound **B** suggests that a different type of conformational rearrangement may occur in the backbone of ligand $\mathbf{L^{Ac}}$ upon coordination to an Fe_4S_4 cluster. In order to allow the two thiol groups of $\mathbf{L^{Ac}}$ to reach the cubane cluster, the receptor ligands have to adopt a bent conformation (see Figure 7). This leads to conformational stress in the two crown ether rings, which can be overcome by pushing the aromatic walls somewhat closer together; the latter process can be accomplished through rotation of the $ArCH_2N$ methylene groups. This, in turn, places these methylene groups in closer proximity to the phenyl rings at the rear side of the diphenylglycoluril framework. Overall, this would result in a more snug fit of the bidentate ligands around the cluster core.

pounds **A** and **B** in DPV upon the addition of various metal ions are listed in Table 4. These changes are all in the anodic direction, showing that reduction of the cluster cores is facilitated by the addition of metal ions. This also indicates a higher affinity of the reduced clusters for these metal ions as compared to the oxidized clusters. The addition of metal ions was found to have little if any influence on the chemical and electrochemical reversibility of the $2^-/3^-$ reductions of **A** and **B**, which was already satisfactory in the absence of any additive (vide supra).

The promoting effects of the various alkali metal ions, as evaluated from the increase in peak current (i_p) in DPV, are distinctly different for compounds **A** and **B** (not shown). For all the metal ions tested, a distinct promoting effect was seen in the case of **A**, but for **B** these effects were only observed with metal ions that also showed a significant modulating effect.[20] Except in the case of Li^+, addition of the first equivalents of a metal ion to compound **A** resulted in an increased current response in both DPV and CV, which

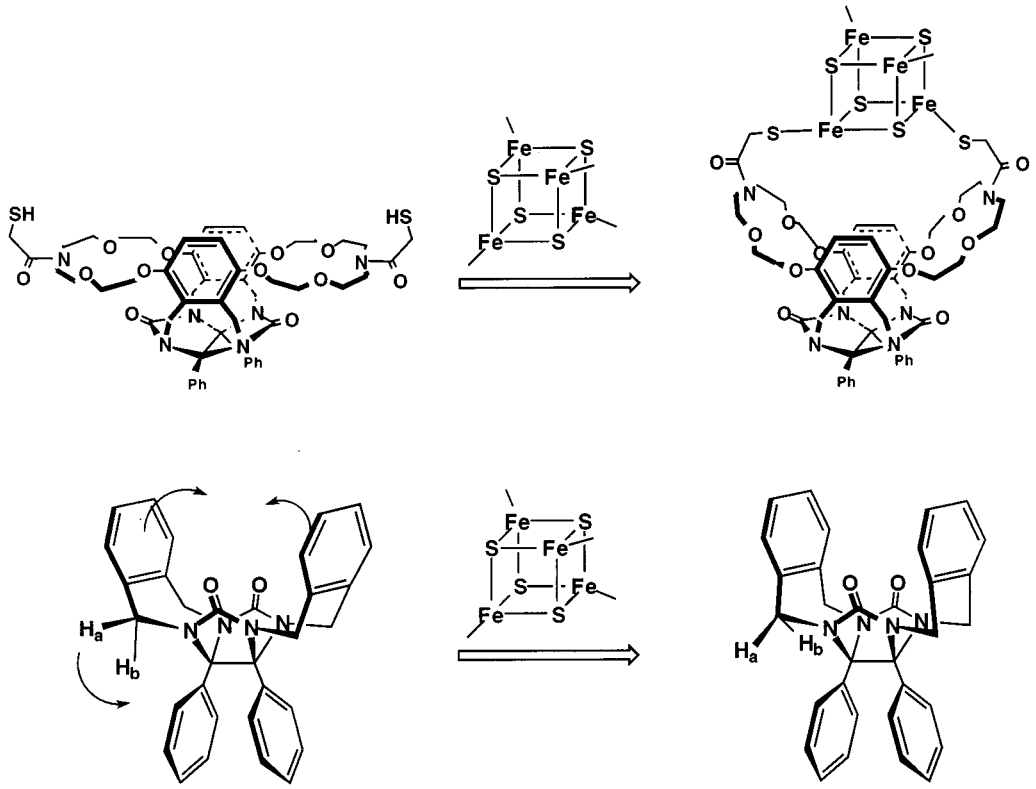


Figure 7. Proposed conformational rearrangement of the crown ether rings (top) and the aromatic walls (bottom) of the receptor ligands upon coordination to the cubane core in **B**

Electrochemical Response Towards Metal Ions

Compounds **A** and **B** each contain a redox-active site that lies in close proximity to two receptor sites for charged guests. It was therefore of interest to study the electrochemical behaviour of **A** and **B** towards alkali and alkaline earth metal ions. Figure 8 shows the titration curves of compound **A** with Na^+ and Ba^{2+} ions as followed by DPV and CV. The changes in the peak potentials (E_p′s) for compsuggests binding of the metal ions to this cluster compound (see Figure 8a and 8b, respectively, for Na^+). Figure 9 shows the titration curves, where E_p and i_p are plotted against the amount of metal ion added to compound **A**. For **B**, an increased current response was only observed with Ba^{2+} ions (titration curves not shown). We propose that the increased current responses seen in CV and DPV are not the result of electrode modifications (metal ion absorption), but are due to the fact that the overall negative

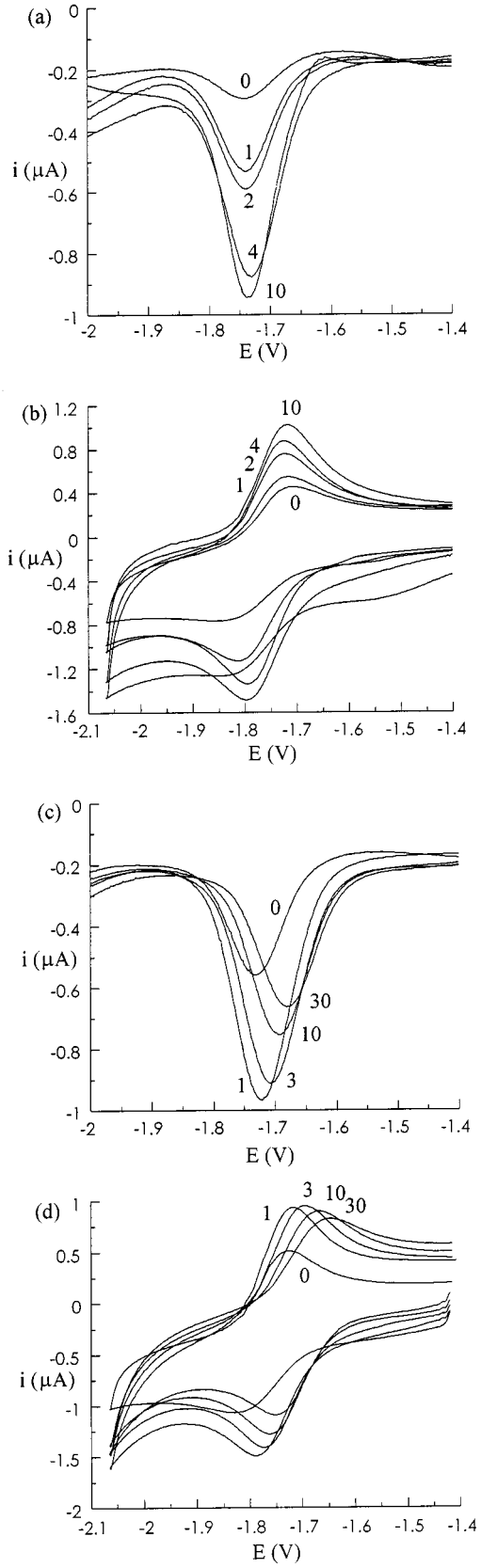


Figure 8. (a) DPV and (b) CV titrations of compound **A** with Na^+ ions; (c) DPV and (d) CV titrations of compound **A** with Ba^{2+} ions; numbers refer to the equivalents of metal ions per cluster

Table 4. Changes in DPV peak potentials (mV) of compounds **A** and **B** upon addition of 10 equivalents of various metal ions in DMF

	A[a]	**B**[a]
Li^+	(0)	(10)
Na^+	10 (30)	(0)
K^+	10 (20)	(20)
Mg^{2+}	0 (20)	(40)
Ba^{2+}	40 (50)	110 (140)

[a] The value for an excess of metal ions is given in brackets.

charge of the cluster is reduced or even becomes positive upon the binding of metal ions. The fact that no increase in current response is observed when Li^+, Na^+, or K^+ ions are added to compound **B** suggests that this receptor compound has a much lower affinity for these metal ions than compound **A**.

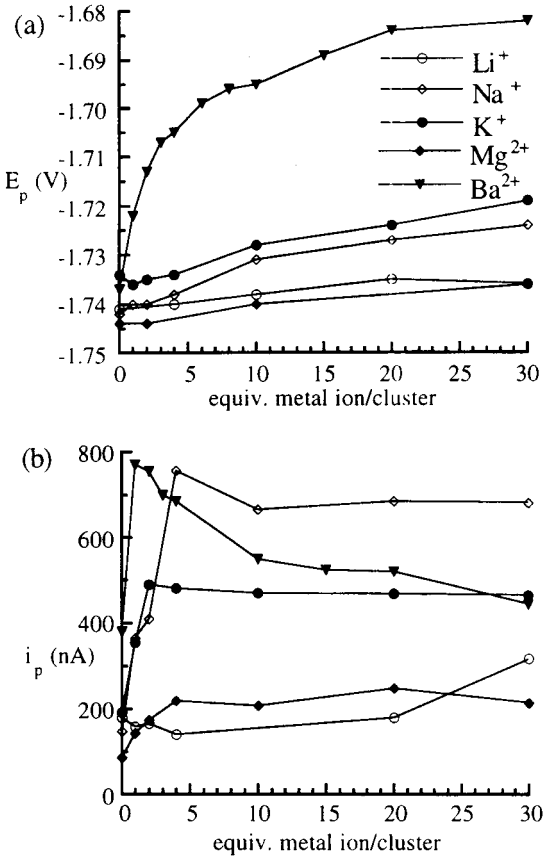


Figure 9. Titration of compound **A** with various alkali and alkaline earth metal ions as followed by DPV; (a) changes in E_p, (b) changes in i_p

The changes in E_p for compound **A** are much smaller than those observed for the related crown ether cluster compound **E**.[9] Nevertheless, the trend in metal ion dependence is the same. In the case of the crown ether compound, the selective response was shown to stem from electrostatic forces, mediated in a "through-bond" manner by a putative "lariat-type" interaction. In the case of compound **A**, the response appears to be mainly determined by the affinities of the metal ions for the crown ether units of the ligands.

The metal ion binding properties in chloroform solution of the central framework of **A**, viz. the diphenylglycoluril-based basket compound **1a**, have been determined previously.[21] It was shown that Li^+, Na^+, and K^+ are bound to **1a** with K_{ass}'s of 0.38×10^6 M^{-1}, 0.83×10^6 M^{-1}, and 1.9×10^6 M^{-1}, respectively. The binding of these metal ions takes place in a 1:1 clamshell fashion.[21] The binding constants for Mg^{2+} and Ba^{2+} can be expected to be somewhat higher than those for Li^+ and K^+, respectively, taking into account the sizes and charge densities of these ions. Given the high binding affinities of the basket molecule **1a** for alkali metal ions, larger changes in E_p than those listed in Table 4 might have been expected for compound **A**. Apparently, the metal ions are not bound in close proximity to the redox centre in **A**. This is confirmed by the fact that in DPV and CV compound **A** displays continuous wave rather than multi-wave behaviour. The clamshell binding mode proposed for **1a** seems to be unlikely for **A** because the E_p titration curve with Ba^{2+} suggests that this cluster compound binds four metal ions rather than two. Each crown ether fragment in **A** seemingly takes up one metal ion. The metal ions can either "nestle" in the cavity of the receptor ligand ("top" binding) or bind at its exterior ("bottom" binding, see Figure 10). Examination of CPK models showed that the four oxygen atoms and nitrogen atom in each of the aza crown ether rings, together with one of the carbonyl groups from the ligand backbone, form a circular array of donor atoms with an internal diameter comparable to that of 18-crown-6. Analysis of the i_p titration curves suggests that compound **A** has a similar metal ion binding profile as 18-crown-6, *viz.* $Li^+ < Mg^{2+} < Na^+ < K^+ < Ba^{2+}$, which also explains the modulating effects observed for compound **A**.

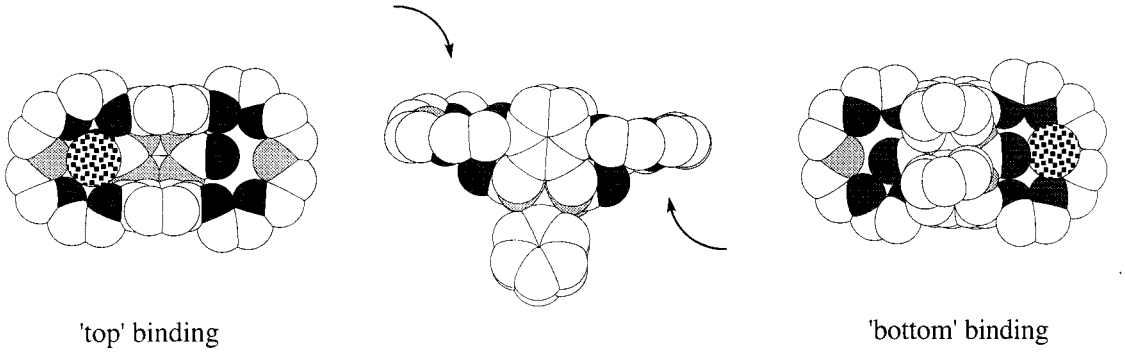


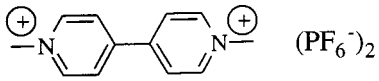
Figure 10. Proposed binding modes of metal ions by compound **A**

The modulation characteristics of compound **B** appear to be determined by similar, crown ether dependent binding factors. Due to the fact that the nitrogens in its crown ether rings are amidated, the binding characteristics of **B** are different from those of compound **A**. Furthermore, as there is less free space between the cluster core and the ligands in **B** than in **A**, the binding of metal ions can be expected to take place preferentially at the exterior (bottom side) of the cavities, as shown in Figure 10 (right). The absence of any increase in current response with Li^+, Na^+, and K^+ ions suggests that the affinity of compound **B** for these cations is low, probably due to the aforementioned amidation of the nitrogens of the crown ether rings. However, as a result of the smaller spacer groups, any bound metal ion will be closer to the cluster core in **B**. Electrostatic forces will therefore be more dominant in compound **B** than in **A**. This may explain the large electrochemical effect of Ba^{2+} ions compared to, e.g., Li^+ and Mg^{2+} ions in the case of the former compound.

Binding of Aromatic Guests by Cluster Compound A

The results presented in the previous sections suggest an open and relatively flexible structure for cluster compound **A**, with binding sites that are accessible to guests. In order to probe this accessibility, the binding of aromatic molecules by compound **A** was also investigated. Diphenylglycoluril receptors are known to bind various aromatic guest molecules in nonpolar solvents such as chloroform and dichloromethane.[12] For solubility reasons, the binding properties of compound **A** were evaluated in DMF. DPV titrations of **A** with 1,2-dinitrobenzene, 2,3-dicyanohydroquinone, and 2,3-dibromohydroquinone showed that the redox potential of the cluster was not affected by these additives. Separate UV/Vis titrations using compound **A** and receptor molecule **1a** revealed that in DMF neither of these host compounds binds the aforementioned guest molecules, in accordance with the outcome of the DPV experiments. Addition of *o*-phenylenediammonium dipicrate to the DMF solutions of **A** was found to result in degradation of the complex, probably due to protonation of the cluster core.

More recently, it has been shown that paraquats (1,1′-disubstituted 4,4′-bipyridinium salts) are very strongly bound by basket-shaped receptors based on diphenylglycoluril, even in polar solvents such as acetonitrile and methanol.[17b] Titration of model compound **1b** (Scheme 1) with dimethylparaquat **5** (Chart 2) in DMF resulted in the development of a band at 402 nm in the UV/Vis spectrum, indicating the formation of a charge-transfer (CT) complex between these two components.[22] The binding constant was determined to be $K_{ass} = 155 \pm 3$ M^{-1}. This value is considerably lower than the binding constant measured for this host–guest combination in 1:1 (*v*/*v*) chloroform/methanol, *viz.* $K_{ass} = 6000$ M^{-1}.[17b]



5

Chart 2

The binding of paraquat **5** by compound **A** was proven by electrochemical titration experiments. Figure 11a depicts the CV titration of **5** with **A**; it shows the two reversible reduction steps for **5** at −0.89 and −1.29 V, and the reduction of **A** at −1.78 V. Clearly, the first reduction of **5** is influenced by the host compound **A**, as was also indicated by DPV (see Figure 11b, where the change in $E_{p,red}$ is plotted against twice the host concentration). The second reduction potential of **5** and the reduction potential of **A** are not affected.

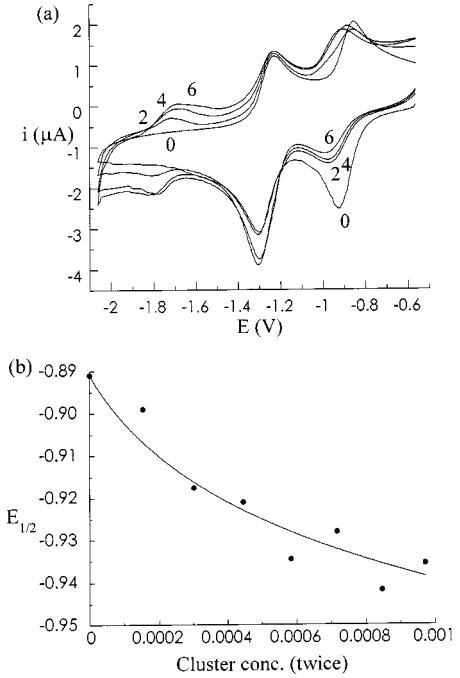


Figure 11. (a) CV titration of compound **5** with **A**, and (b) the change in E_p for the first reduction of **5** as function of twice the cluster concentration; for an explanation, see text; numbers in (a) refer to the number of molar equivalents of clusters relative to **5**

From these observations, it was concluded that only the twofold positively charged paraquat species is bound by **A**. The single positively charged and neutral species apparently have no affinity for this compound. This also explains why the reduction potential of **A** is unaffected by **5**; only a small increase in ΔE_p is observed. Binding stabilizes the dicationic form of **5** and makes it more difficult to reduce this compound, resulting in the observed anodic changes in $E_{1/2}$. We analyzed these changes, assuming the formation of a 2:1 paraquat−host complex, with the help of Equation (1), where $E_{1/2}$ is the observed half-wave potential, $E_{1/2}^{free}$ the half-wave potential of **5** without any additive, and [H] the concentration of the host compound.

$$E_{1/2} = E_{1/2}^{free} - 0.059 \log (1 + K_{ass}[H]) \quad (1)$$

Assuming that the two binding sites in **A** behave completely independently, the actual host concentration was taken as twice the concentration of cluster compound **A**. With the help of Equation (1), the curve in Figure 11b was obtained, from which a binding constant of $K_{ass} = (5.6 \pm 0.6) \times 10^3$ M^{-1} was calculated.

In separate experiments, we also added $[Fe_4S_4(SCH_2Ph)_4]^{2-}$ to paraquat **5**. This was shown to have no effect on the electrochemical behaviour of **5**. It is therefore concluded that the combination of a concave binding site and a negatively charged cluster fragment significantly enhances binding of paraquat **5** to basket-shaped receptors derived from diphenylglycoluril, viz. its binding constant increased from $K_{ass} = 155$ M^{-1} in **1b** to $K_{ass} = 5.6 \times 10^3$ M^{-1} in cluster compound **A**.

Conclusions

The electrochemical and spectral properties of the compounds **A** and **B** strongly suggest that these compounds, as isolated, are monomeric and contain an intact Fe_4S_4 cubane core. The formulation of **A** and **B** as $[Fe_4S_4(\mathbf{L^{Xyl}})_2](PPh_4)_2$ and $[Fe_4S_4(\mathbf{L^{Ac}})_2](PPh_4)_2$ therefore seems to be justified. NMR studies have shown compound **B** to have a relatively compact structure, in which the cluster is encapsulated by the concave receptor ligands. The extent of encapsulation is not such that it creates a solvophobic environment similar to that in Fe_4S_4 cluster containing proteins of the HiPIP class.

The structure of compound **A** was found to be less compact than that of compound **B**, implying that the binding sites of the receptor ligands in **A** are more accessible to guest molecules than those in **B**. The electrochemical responses of the two compounds towards alkali and alkaline earth metal ions indeed indicated that compound **A** has an "open" structure while compound **B** has a more or less "closed" structure. The cavity-forming ligands of **A** are also capable of binding a dicationic paraquat guest, but not its reduced forms. This binding interaction was found to influence the redox properties of the guest molecule.

Experimental Section

For a detailed description of the materials and methods used, the reader is referred to the related paper.[9]

Additional methods: 2D NMR spectra (COSY and NOESY) were recorded on a Bruker WM-200 instrument. In the NMR titration experiments, the changes in the chemical shifts of the host and guest molecules were monitored at varying host and at constant guest concentrations. − For electrochemical experiments, an Ag/AgCl reference electrode and 0.2 M tetrabutylammonium perchlorate supporting electrolyte solution were used, with DMSO as the solvent. − Calculations were performed on Silicon Graphics Challenge and Silicon Graphics Indigo II workstations using the QUANTA molecular modelling package with the CHARMm 3.3 force field. The Fe_4S_4 core was fixed and only the attached basket ligand structure was minimized.

2a,8,9,12,13,14,15,17,18,25,26,29,30,31,32,34,35,38b-Octadecahydro-2a,38b-diphenyl-13,30-1*H*,4*H*-6,37:20,23-dietheno-2,22:3,21-dimethano-5*H*,11*H*,28*H*,38*H*-7,10,16,19,24,27,33,36-octaoxa-2,3,4a,13,30,38a-hexaazacyclopenta[*cd*]cyclotetratriacont[*g*]azulene-1,4-dione (1a): This compound and derivative **1b** were synthesized according to a previously published procedure.[23]

2a,8,9,12,13,14,15,17,18,25,26,29,30,31,32,34,35,38b-Octadecahydro-2a,38b-diphenyl-13,30-bis(α-thioacetyl-*m*-xylyl)-1*H*,4*H*-6,37:20,23-dietheno-2,22:3,21-dimethano-5*H*,11*H*,28*H*,38*H*-7,10,16,19,24,27,33,36-octaoxa-2,3,4a,13,30,38a-hexaazacyclopenta[*cd*]cyclotetratriacont[*g*]azulene-1,4-dione (2): To a solution of **1a** (328 mg, 0.380 mmol) in DMF (15 mL) containing a small amount of K_2CO_3, a solution of α-bromo-α′-thioacetyl-*m*-xylene (195 mg, 0.75 mmol) in DMF (5 mL) was added dropwise. The resulting mixture was stirred overnight at 40 °C under an N_2 atmosphere. After removal of the solvent in vacuo, the residue was taken up in CH_2Cl_2 (40 mL) and the resulting solution was washed twice with brine and dried over $MgSO_4$. Purification by flash chromatography (silica, $CHCl_3$/MeOH/TEA, 96:3:1, *v*/*v*) yielded 425 mg (91%) of **2** as a white powder; m.p. 186 °C. − ^{1}H NMR (200 MHz, $CDCl_3$): δ = 2.31 [s, 6 H, C(O)CH_3], 2.88 (t, *J* = 5.7 Hz, 8 H, NC$H_2$$CH_2$O), 3.69−4.15 (m, 36 H, CH_2O, NC*H*HAr, NCH_2ArCH_2S), 5.67 (d, *J* = 16.1 Hz, 4 H, NCH*H*Ar), 6.73 (s, 4 H, ArH), 7.11 (s, 10 H, PhH), 7.31 (m, 8 H, ArH). − FT-IR (KBr, cm^{-1}): $\tilde{\nu}$ = 3057, 3029 (ArH), 2922, 2869 (CH_2), 1711 (C=O, urea), 1690 (C=O, thio ester), 1459, 1426 (CH_2), 1131, 1017 (COC), 770, 603 (Ar). − FAB-MS; *m*/*z*: 1233 [M + 1]$^+$. − No satisfactory elemental analysis could be obtained for this compound.

2a,8,9,12,13,14,15,17,18,25,26,29,30,31,32,34,35,38b-Octadecahydro-2a,38b-diphenyl-13,30-bis(α-thio-*m*-xylyl)-1*H*,4*H*-6,37:20,23-dietheno-2,22:3,21-dimethano-5*H*,11*H*,28*H*,38*H*-7,10,16,19,24,27,33,36-octaoxa-2,3,4a,13,30,38a-hexaazacyclopenta[*cd*]cyclotetratriacont[*g*]azulene-1,4-dione (L^{Xyl}2H): A solution of **2** (195 mg, 0.158 mmol) in methanol (10 mL) containing 3% HCl was stirred under N_2 atmosphere for 7 days at ambient temperature. Thereafter, TLC analysis showed one single, nitroprusside-positive spot. The reaction mixture was then partitioned between CH_2Cl_2 (20 mL) and water (10 mL). After neutralization with saturated aqueous $NaHCO_3$ solution, the organic layer was separated, washed with further water, and dried over $MgSO_4$. After removal of the solvent in vacuo, the desired product (90 mg, 50%) was obtained as a white powder. − ^{1}H NMR (200 MHz, $CDCl_3$): δ = 1.75 (t, *J* = 7.54 Hz, 2 H, SH), 2.89 (br. s, 4 H, NC$H_2$$CH_2$O), 3.62−4.08 (m, 36 H, CH_2O, NC*H*HAr, NCH_2ArCH_2, ArCH_2S), 5.60 (d, *J* = 16.1 Hz, 4 H, NCH*H*Ar), 6.63 (s, 4 H, ArH), 7.04 (s, 10 H, PhH), 7.19−7.32 (m, 8 H, ArH). − FAB-MS; *m*/*z*: 1149 [M + 1]$^+$. − No satisfactory elemental analysis could be obtained for this compound.

2a,8,9,12,13,14,15,17,18,25,26,29,30,31,32,34,35,38b-Octadecahydro-2a,38b-diphenyl-13,30-bis(α-chloroacetyl)-1*H*,4*H*-6,37:20,23-dietheno-2,22:3,21-dimethano-5*H*,11*H*,28*H*,38*H*-7,10,16,19,24,27,33,36-octaoxa-2,3,4a,13,30,38a-hexaazacyclopenta[*cd*]cyclotetratriacont[*g*]azulene-1,4-dione (3): A solution of α-chloroacetyl chloride (100 mg, 0.90 mmol) in CH_2Cl_2 (5 mL) was added dropwise to a solution of **1a** (180 mg, 0.210 mmol) and TEA (40 μL) in CH_2Cl_2 (15 mL). The reaction mixture was stirred overnight at ambient temperature. After the addition of further CH_2Cl_2 (50 mL), the mixture was washed twice with saturated aqueous $NaHCO_3$ solution and once with water, and dried over $MgSO_4$. Purification by column chromatography (silica, $CHCl_3$/MeOH, 99:1, *v*/*v*) yielded 128 mg (60%) of **3** as a white powder; m.p. 271 °C (dec.). − ^{1}H NMR (400 MHz, $CDCl_3$): δ = 3.59−4.41 (m, 32 H, CH_2O, CH_2N, NC*H*HAr, CH_2Cl), 5.68, 5.70, 5.74 (3 d, *J* = 16.35, 17.22, 16.47 Hz, 4 H, NCH*H*Ar), 6.66 (m, 4 H, ArH), 7.09 (m, 10 H, PhH). − ^{13}C NMR (75 MHz, $CDCl_3$): δ = 37.07 (NCH_2Ar), 45.73, 45.79, 49.71, 49.82 (CH_2Cl), 68.39, 68.62, 68.97, 69.36, 69.44, 69.73, 70.05 (CH_2O, N$CH_2$$CH_2$O), 85.08 (NCN), 110.37, 110.49, 111.18, 111.28 (ArC), 127.78, 128.08, 128.27, 128.41, 128.53, 128.62 (PhC, ArC), 133.64 (PhC), 149.43, 149.61, 150.23, 150.59 (ArC), 157.94 [NC(O)N], 167.59 [*C*(O)CH_2]. − FT-IR (KBr, cm^{-1}): $\tilde{\nu}$ = 3068, 3041 (ArH), 2923, 2865 (CH_2), 1711 (C=O, urea), 1653 (C=O, amide), 1459, 1426 (CH_2), 1088, 1075 (COC), 768, 695 (Ar). − FAB-MS; *m*/*z*: 1029 [M + 1]$^+$. − $C_{52}H_{58}Cl_2N_6O_{12}$·$CH_3OH$ (1062.0): calcd. C 59.94, H 5.88, N 7.91; found C 59.80, H 5.99, N 7.90.

2a,8,9,12,13,14,15,17,18,25,26,29,30,31,32,34,35,38b-Octadecahydro-2a,38b-diphenyl-13,30-bis(α-thioacetyl-acetyl)-1*H*,4*H*-6,37:20,23-dietheno-2,22:3,21-dimethano-5*H*,11*H*,28*H*,38*H*-7,10,16,19,24,27,33,36-octaoxa-2,3,4a,13,30,38a-hexaazacyclopenta[*cd*]cyclotetratriacont[*g*]azulene-1,4-dione (4): Under N_2 atmosphere, a solution of potassium thiocarboxylate (114 mg, 2.50 mmol) in DMF (5 mL) was added dropwise to a solution of **3** (100 mg, 0.094 mmol) in DMF (10 mL) and the resulting mixture was stirred overnight under the exclusion of light. It was subsequently filtered and the filtrate was concentrated in vacuo. The residue was dissolved in CH_2Cl_2 (50 mL) and this solution was washed twice with saturated aqueous $NaHCO_3$ solution and dried over $MgSO_4$. Purification by column chromatography (silica, $CHCl_3$/MeOH, 99:1, *v*/*v*) yielded 100 mg (96%) of **4** as a white powder; m.p. 259 °C. − ^{1}H NMR (300 MHz, $CDCl_3$): δ = 2.38 [s, 6 H, C(O)CH_3], 3.69−4.16 (m, 32 H, CH_2O, CH_2N, NC*H*HAr, CH_2S), 5.71, 5.74 (2 d, *J* = 16.23, 16.29 Hz, 4 H, NCH*H*Ar), 6.67 (m, 4 H, ArH), 7.11 (m, 10 H, PhH). − ^{13}C NMR (75 MHz, $CDCl_3$): δ = 30.90 (CH_3), 37.62 (NCH_2Ar), 46.69, 50.57 (CH_2S), 69.19, 69.34, 69.79, 70.01, 70.12, 70.31, 70.45, 70.66 (CH_2O, N$CH_2$$CH_2$O), 85.72 (NCN), 110.43, 112.22 (ArC), 128.62, 128.87, 128.97, 129.03, 129.18, 129.31 (PhC, ArC), 133.64 (PhC), 150.35, 150.41, 150.96, 151.05 (ArC), 158.08 [NC(O)N], 168.85 [*C*(O)CH_2], 195.87 [SC(O)]. − FT-IR (KBr, cm^{-1}): $\tilde{\nu}$ = 3062 (ArH), 2924, 2866 (CH_2), 1724 (C=O, thio ester), 1711 (C=O, urea), 1689 (C=O, amide), 1458 (CH_2), 1129, 1092 (COC), 770 (CCl). − FAB-MS; *m*/*z*: 1109 [M + 1]$^+$. − $C_{56}H_{64}N_6O_{14}S_2$ (1109.2): calcd. C 60.64, H 5.82, N 7.58, S 5.78; found C 60.27, H 5.70, N 7.41, S 5.80.

2a,8,9,12,13,14,15,17,18,25,26,29,30,31,32,34,35,38b-Octadecahydro-2a,38b-diphenyl-13,30-bis(α-thioacetyl)-1*H*,4*H*-6,37:20,23-dietheno-2,22:3,21-dimethano-5*H*,11*H*,28*H*,38*H*-7,10,16,19,24,27,33,36-octaoxa-2,3,4a,13,30,38a-hexaazacyclopenta[*cd*]cyclotetratriacont[*g*]azulene-1,4-dione (L^{Ac}2H): This compound was synthesized as described for L^{Xyl}2H. As starting material, **4** (100 mg, 0.090 mmol) was used. This was suspended in MeOH (5 mL) containing 3% HCl. CH_2Cl_2 was added to this suspension until a clear solution was obtained. After workup, 92 mg (100%) of L^{Ac}2H was obtained as a white powder; m.p. 275 °C (dec.). − ^{1}H NMR (200 MHz, $CDCl_3$): δ = 2.20 (dt, *J* = 2, 6 Hz, 2 H, SH), 3.51−4.25 (m, 32 H, CH_2O, CH_2N, NC*H*HAr, CH_2S), 5.69, 5.70, 5.75 (3 d, *J* = 16.24, 16.16, 16.21 Hz, 4 H, NCH*H*Ar), 6.66 (m, 4 H, ArH), 7.10 (m, 10 H, PhH). − FT-IR (KBr, cm^{-1}): $\tilde{\nu}$ = 3064, 3025 (ArH), 2920, 2847 (CH_2), 2536 (SH), 1711 (C=O, urea), 1642 (C=O, amide), 1460, 1426 (CH_2), 1129, 1087 (COC), 770, 703 (Ar). − FAB-MS; *m*/*z*: 1025 [M + 1]$^+$. − $C_{52}H_{60}O_{12}N_6S_2$ (1025.2): calcd. C 60.92, H 5.90, N 8.20, S 6.26; found C 61.05, H 5.87, N 8.13, S 6.23.

$(PPh_4)_2[Fe_4S_4(L^{Xyl})_2]$ (Cluster A): A suspension of $(PPh_4)_2[Fe_4S_4(StBu)_4]$ (55.2 mg, 0.040 mmol) in DMF (5−10 mL)

was added dropwise to a stirred solution of dithiol $\mathbf{L^{Xyl}}2H$ (93 mg, 0.081 mmol) in DMF (30 mL). The resulting mixture was stirred in vacuo for ca. 30 min. and then under N_2 atmosphere overnight. It was then filtered through a glass sinter disc and concentrated in vacuo. A large volume of Et_2O was carefully added to precipitate the product. After storage overnight at −20 °C, the product, a black solid, was isolated by decantation of the supernatant and drying in vacuo. The yield was not determined. − ^{1}H NMR (200 MHz, [D$_6$]DMSO): δ = 2.77 (br. m, 16 H, NCH_2CH$_2$O), 3.42−4.12 (m, 64 H, CH$_2$O, NC*H*HAr, NCH_2ArCH$_2$), 5.50 (br. m, 8 H, NCH*H*Ar), 6.50 (br. s, 8 H, ArH), 7.14 (br. s, 20 H, PhH), 7.80 (m, 40 H, PPh_4), 14.30 (br. s, 8 H, CH_2S). − UV/Vis (DMF): λ_{max} (ε/ M^{-1}·cm^{-1}) = 295 (33,600), 423 (11,100), 620 nm (sh, 1800). For further characterization, see text.

$(PPh_4)_2[Fe_4S_4(L^{Ac})_2]$ (Cluster B): To a suspension of dithiol $\mathbf{L^{Ac}}2H$ (100 mg, 0.097 mmol) in DMF (25 mL) was added dropwise a suspension of $(PPh_4)_2[Fe_4S_4(S\mathit{t}Bu)_4]$ (51 mg, 0.037 mmol) in DMF (10 mL). The resulting mixture was stirred under dynamic vacuum for 30 min. and then overnight under N_2 atmosphere. After filtration, the filtrate was concentrated in vacuo to a volume of a few mL. A large volume of Et_2O was then carefully added and the reaction flask was placed in a refrigerator at −20 °C overnight. This resulted in the precipitation of a black powder. After a second precipitation with Et_2O, the product was dried in vacuo. The yield was not determined. − ^{1}H NMR (200 MHz, [D$_6$]DMSO): δ = 3.42−3.96 (m, 60 H, CH$_2$O, CH$_2$N), 3.66 (8 H, NC*H*HAr), 5.51 (br. m, *J* = 13.3 Hz, 8 H, NCH*H*Ar), 6.80 (br. m, 8 H, ArH), 7.08 (m, 20 H, PhH), 7.78 (m, 40 H, PPh_4), 14.09 (br. s, 8 H, CH_2S). − UV/Vis (DMF): λ_{max} (ε/ M^{-1}·cm^{-1}) = 295 (40,200), 340 (sh, 17,400), 415 (13,400), 622 nm (sh, 3400). For further characterization, see text.

Acknowledgments

This work was supported by the Dutch Foundation for Chemical Research (SON, now CW) with financial aid from the Dutch Foundation for Scientific Research (NWO). The authors thank Dr. A. E. Rowan for help in the molecular modelling study.

[1] S. J. Lippard, J. M. Berg, *Principles of Bioinorganic Chemistry*, University Science Books, Mill Valley, CA, **1994**.

[2] [2a] M. Momenteau, in *Supramolecular Control of Structure and Reactivity* (Ed.: A. D. Hamilton), John Wiley & Sons, **1996**, pp. 155−223. − [2b] P. J. Dandliker, F. Diederich, J.-P. Gisselbrecht, A. Louatti, M. Gross, *Angew. Chem.* **1995**, *107*, 2906−2909; *Angew. Chem. Int. Ed. Engl.* **1995**, *34*, 2725−2728, and references therein.

[3] For selected reviews, see: [3a] R. H. Holm, *Acc. Chem. Res.* **1977**, *10*, 427−434. − [3b] R. H. Holm, S. Ciurli, J. A. Weigel, *Prog. Inorg. Chem.* **1990**, *38*, 1−74. − [3c] A. Nakamura, N. Ueyama, *Adv. Inorg. Chem.* **1989**, *33*, 39−67. − [3d] H. Beinert, R. H. Holm, E. Münck, *Science* **1997**, *277*, 653−659. − [3e] H. Beinert, *J. Biol. Inorg. Chem.* **2000**, *5*, 2−15.

[4] [4a] C. W. Carter Jr., J. Kraut, S. T. Freer, R. A. Alden, L. C. Sieker, E. Adman, L. H. Jensen, *Proc. Natl. Acad. Sci. USA* **1972**, *69*, 3526−3529. − [4b] E. Adman, K. D. Watenpaugh, L. H. Jensen, *Proc. Natl. Acad. Sci. USA* **1975**, *72*, 4854−4858. − [4c] I. Rayment, G. Wesenberg, T. E. Meyer, M. A. Cusanovich, H. M. Holden, *J. Mol. Biol.* **1992**, 672−686.

[5] Y. Okuno, K. Uoto, O. Yonemitsu, T. Tomohiro, *J. Chem. Soc., Chem. Commun.* **1987**, 1018−1020.

[6] Y. Kuroda, Y. Sasaki, Y. Shiroiwa, I. Tabushi, *J. Am. Chem. Soc.* **1988**, *110*, 4049−4050.

[7] C. B. Gorman, B. L. Parkhurst, W. Y. Su, K.-Y. Chen, *J. Am. Chem. Soc.* **1997**, *119*, 1141−1142.

[8] [8a] D. J. Evans, G. Garcia, G. J. Leigh, M. S. Newton, M. D. Santana, *J. Chem. Soc., Dalton Trans.* **1992**, 3229−3234. − [8b] G. P. F. van Strijdonck, J. A. E. H. van Haare, P. J. M. Hönen, R. C. G. M. van der Schoor, M. C. Feiters, J. G. M. van der Linden, J. J. Steggerda, R. J. M. Nolte, *J. Chem. Soc., Dalton Trans.* **1997**, 449−461. − [8c] G. P. F. van Strijdonck, J. A. E. H. van Haare, J. G. M. van der Linden, J. J. Steggerda, R. J. M. Nolte, *Inorg. Chem.* **1994**, *33*, 999−1000. − [8d] G. P. F. van Strijdonck, P. T. J. H. ten Have, M. C. Feiters, J. G. M. van der Linden, J. J. Steggerda, R. J. M. Nolte, *Chem. Ber./Recueil* **1997**, *130*, 1151−1157. − [8e] C. F. Martens, M. M. G. Bongers, P. J. A. Kenis, R. Czajka, M. C. Feiters, J. G. M. van der Linden, R. J. M. Nolte, *Chem. Ber./Recueil* **1997**, *130*, 23−33. − [8f] C. F. Martens, H. H. L. Blonk, T. Bongers, J. G. M. van der Linden, G. Beurskens, P. T. Beurskens, J. M. M. Smits, R. J. M. Nolte, *J. Chem. Soc., Chem. Commun.* **1991**, 1623−1625.

[9] For a discussion on related crown ether-functionalized iron−sulfur clusters and their electrochemical properties, see: R. J. M. Klein Gebbink, S. I. Klink, M. C. Feiters, R. J. M. Nolte, *Eur. J. Inorg. Chem.* **2000**, 253−264.

[10] Molecular receptors of the diphenylglycoluril-type have also been functionalized with ferrocenyl groups for similar purposes, see: G. C. Dol, P. C. J. Kamer, F. Hartl, P. W. N. M. van Leeuwen, R. J. M. Nolte, *J. Chem. Soc., Dalton Trans.* **1998**, 2083−2089.

[11] See for example: R. P. Sijbesma, Ph.D. Dissertation, Univ. of Nijmegen, **1992**.

[12] R. P. Sijbesma, R. J. M. Nolte, *J. Org. Chem.* **1991**, *56*, 3122−3124.

[13] P. K. Mascharak, K. S. Hagen, J. T. Spence, R. H. Holm, *Inorg. Chim. Acta* **1988**, *80*, 157−170.

[14] H. L. Blonk, O. Kievit, E. K.-H. Roth, J. Jordanov, J. G. M. van der Linden, J. J. Steggerda, *Inorg. Chem.* **1991**, *30*, 3231−3234.

[15] [15a] J. Neiman, A. J. Naaktgeboren, J. Reedijk, *Inorg. Chim. Acta* **1984**, *93*, L9−L11. − [15b] R. J. Kassner, W. J. Yang, *J. Am. Chem. Soc.* **1977**, *99*, 4351−4355.

[16] N. Ueyama, T. Terakawa, T. Sugawara, M. Fuji, A. Nakamura, *Chem. Lett.* **1984**, 1287−1290.

[17] [17a] C. F. Martens, R. P. Sijbesma, R. J. M. Klein Gebbink, A. L. Spek, R. J. M. Nolte, *Recl. Trav. Chim. Pays-Bas* **1993**, *112*, 400−403. − [17b] A. P. H. J. Schenning, B. de Bruin, H. Kooijman, A. L. Spek, A. E. Rowan, R. J. M. Nolte, *Angew. Chem.* **1995**, *107*, 2288−2289; *Angew. Chem. Int. Ed. Engl.* **1995**, *34*, 2132−2134.

[18] See, for example: J. N. H. Reek, Ph.D. Dissertation, Univ. of Nijmegen, **1996**.

[19] R. P. Sijbesma, R. J. M. Nolte, *J. Am. Chem. Soc.* **1991**, *113*, 6695−6696.

[20] For a more elaborate discussion on the origin of these effects, see ref.[9]

[21] J. W. H. Smeets, L. van Dalen, V. E. M. Kaats-Richter, R. J. M. Nolte, *J. Org. Chem.* **1990**, *55*, 454−461.

[22] Dissolution of paraquat **5** in DMF yields a slightly blue-colored solution. This blue color suggests the formation of paraquat mono radical cations. It should be noted that side reactions involving this radical species might have complicated the experiments discussed here. As a consequence, the reported K_{ass} values should be treated with caution.

[23] J. W. H. Smeets, R. P. Sijbesma, L. van Dalen, A. L. Spek, W. J. J. Smeets, R. J. M. Nolte, *J. Org. Chem.* **1989**, *54*, 3710−3717.

Received November 24, 1999
[I99428]

Crystal Structure and Magnetic Behavior of the Decamethylferrocenium and Decamethylchromocenium Salts of Bis(ethylenedithiolato)nickel, $[M(Cp^*)_2][Ni(edt)_2]$ − Magnetic Anisotropy and Metamagnetic Behavior of $[Fe(Cp^*)_2][Ni(edt)_2]$

Vasco da Gama,*[a] Dulce Belo,[a] Sandra Rabaça,[a] Isabel C. Santos,[a] Helena Alves,[a] João C. Waerenborgh,[a] M. Teresa Duarte,[b] and Rui T. Henriques[b]

Keywords: Molecule-based magnets / Solid-state structures / Metamagnetism / Magnetic properties / Mössbauer spectroscopy

New electron-transfer salts, $[M(Cp^*)_2][Ni(edt)_2]$, with M = Fe and Cr, were prepared and shown to be isostructural by X-ray crystallographic studies. The molecular structure of $[Ni(edt)_2]^-$ is reported here for the first time. The solid-state structure consists of an array of parallel alternating donors, $[Fe(Cp^*)_2]^{\bullet+}$, and acceptors, $[Ni(edt)_2]^{\bullet-}$, ··DADADA·· stacks along [101]. At high temperatures ($T > 50$–100 K), the magnetic susceptibility obeys the Curie–Weiss expression, with the θ values of –5 and –6.7 K for the Ni and Cr compounds respectively, revealing dominant AFM interactions. At low temperatures metamagnetic behavior was observed in case of $[Fe(Cp^*)_2][Ni(edt)_2]$, with $T_N = 4.2$ K and $H_C = 14$ kG at 2 K, resulting from high magnetic anisotropy, due to the coexistence of strong FM DA intrachain interactions and strong AFM (DA and AA) interchain interactions. Single-crystal magnetization measurements with $[Fe(Cp^*)_2][Ni(edt)_2]$ showed that the transition from the AFM state to the FM high-field state was induced by the application of a magnetic field parallel to the stacking axis. In these compounds the AFM interchain (DA and AA) interactions play a dominant role, due to the large spin density on the periphery of the acceptor and the close AA and DA interchain contacts. Above 4.2 K the ^{57}Fe Mössbauer spectra of $[Fe(Cp^*][Ni(edt)_2]$ exhibit the classical low spin Fe^{III} ferrocenium singlet. Below this temperature a poorly resolved hyperfine pattern is observed (estimated hyperfine field ca. 350 kG at 3.5 K). The analysis of the spectra obtained in applied fields of 20 kG and 50 kG is consistent with a strongly anisotropic **g** tensor. A pronounced temperature dependence of the spectra in a field of 50 kG suggests the presence of spin-lattice relaxation effects.

Introduction

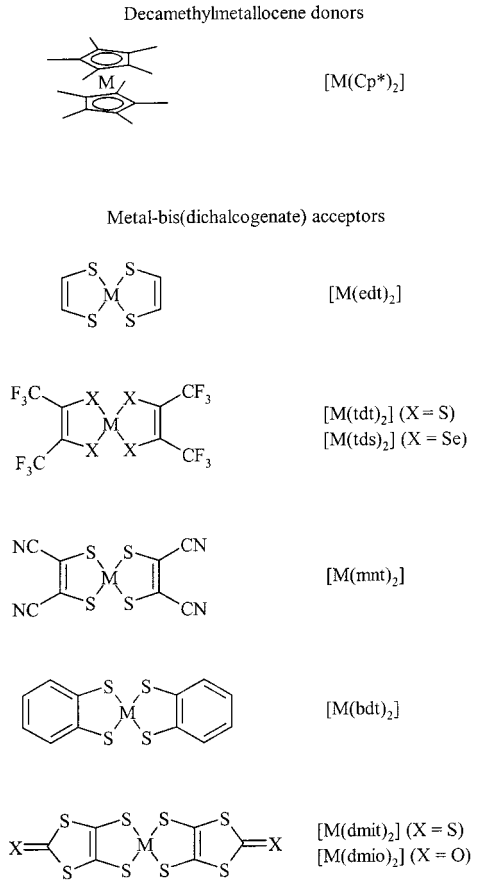
Since the observation of bulk ferromagnetism in $[Fe(Cp^*)_2](TCNE)$,[1,2] substantial efforts have been devoted to the study of molecule-based magnets, in particular to electron-transfer salts based on decamethylmetallocenium donors and planar acceptors.[3,4] Bulk ferromagnetism was observed in several other similar metallocenium-based electron-transfer salts,[4] and a study of the structure-magnetic property relationship revealed the need for a 1D $D^+A^-D^+A^-D^+A^-$ chain structure to achieve ferromagnetic coupling and bulk ferromagnetism.[4]

Following the extensive use of conjugated polynitriles like TCNE and TCNQ as acceptors, planar monoanionic $S = 1/2$ metal−bis(dichalcogenate) complexes, $[M(X_2C_2R_2)_2]^-$ (M = Ni, Pd and Pt; X = S, Se), have also been used in the preparation of molecule-based magnets. These acceptors seem particularly promising due to the presence of the peripheral heteroatoms, which are expected to favor the existence of extended magnetic interactions, thus giving rise to stronger magnetic interactions and higher magnetic ordering temperatures. However, up to now, in most cases the structural motifs obtained differ from the simple alternating form mentioned above, and were observed only in the decamethylmetallocenium $[M(tdt)_2]^-$,[5,6] and $[M(tds)_2]^-$ [7] salts. We believe this is due to the dimensions of the complexes, as in this case, in spite the bulky CF_3 group, the acceptors and the Me_5C_5 ligand of the donor have comparable dimensions and are quite suitable for the simple alternating chain motif. In the salts with other dithiolate complexes, the larger R groups lead to larger axial dimensions, as with $[M(mnt)_2]^-$,[5] $[M(bdt)_2]^-$,[8] $[M(dmit)_2]^-$,[9,10] and $[M(dmio)_2]^-$,[10,11] which show structural motifs where the acceptors, or face to face pairs of acceptors, alternate with side by side pairs of donors (Scheme 1).

As the structural aspect seems to be rather significant in determining the magnetic properties of these types of molecular materials, in order to obtain the desired 1D $D^+A^-D^+A^-D^+A^-$ chain structure motif, we decided to study the electron-transfer salts based on decamethylmetallocenium cations and the anionic complex $[Ni(edt)_2]^-$, for which some preliminary results were reported.[8] This is the smaller dithiolene complex and in this case the S and C

[a] Dep. de Química, Instituto Tecnológico e Nuclear, Est. Nacional 10, 2686-953 Sacavém, Portugal
Fax: (internat.) + 351-21/994-1455
E-mail: vascog@itn1.itn.pt
[b] Dep. Eng. Química, Instituto Superior Técnico, Av. Rovisco Pais, 1049-001 Lisboa, Portugal
Fax: (internat.) + 351-21/846-4455
E-mail: teresa.duarte@ist.utl.pt

 © WILEY-VCH Verlag GmbH, D-69451 Weinheim, 2000 1434−1948/00/0909−2101 $ 17.50+.50/0



Scheme 1

atoms from the ligand are quite to interact with the atoms from neighboring molecules, and particularly strong intra- and interchain magnetic interactions are predicted for these salts.

The first model to achieve some consensus in the interpretation of the magnetic properties of this type of molecular materials was an extended version of McConnell's configuration interaction (CI) mechanism,[12] often designated as the McConnell II mechanism. However, the theoretical criticism and observation of FM in $[Cr(Cp^*)_2]^+$-based compounds,[13,14] in contradiction with the predictions of the McConnell II mechanism (AFM coupling) led to the appearance of alternative mechanisms, such as a more complex version of the McConnell II mechanism[15] and a model based on the molecular spin polarization effect,[3] designated as the McConnell I mechanism, which agreed quite well with the experimental observations. However, the recent report of a new series of compounds, $[M(Cp^*)_2][Ni(tds)_2]$ (M = Fe, Mn, Cr),[7] where the magnetic coupling is compatible with the predictions of the simple version of the McConnell II mechanism, and in contradiction with the McConnell I mechanism, which has been by far the most widely used tool for dealing with magnetic coupling and ordering in molecular magnetic materials, clearly indicates the need to reexamine the model. The study of the series of electron-transfer salts $[M(Cp^*)_2][Ni(edt)_2]$ (M = Fe, Mn, Cr) and, in particular, the nature of the magnetic coupling in the different compounds of the series is also expected to contribute to the debate regarding the mechanism of the intra- and intermolecular magnetic interactions in the decamethylmetallocenium-based salts.

Results and Discussion

Synthesis

The compounds $[M(Cp^*)_2][Ni(edt)_2]$, M = Fe (**1**) and Cr (**2**), were prepared by the same procedure: saturated equimolar solutions of $[Fe(Cp^*)_2]BF_4$ [12] or $[Cr(Cp^*)_2]PF_6$ [16] and $(Et_4N)[Ni(edt)_2]$[17] in acetonitrile were combined and the resulting compounds precipitated on standing. Dark brownish, needle-shaped crystals were collected by filtration. The preparation of $[Mn(Cp^*)_2][Ni(edt)_2]$ was also attempted by a similar method, but in this case a dark powder was obtained with an elemental analysis indicative of probable decomposition during the synthesis.

Crystal Structure

It was possible to determine the X-ray crystal structure of **1**, while in the case of compound **2**, it was only possible to determine the cell parameters due to the poor quality of the crystals, showing that **1** and **2** are isostructural. Crystal and experimental data are summarized in Table 1.

Table 1. Crystallographic data for compounds **1** and **2**

	1	**2**[a]
Empirical formula	$C_{24}H_{34}FeNiS_4$	$C_{24}H_{34}CrNiS_4$
Molecular mass	565.32	561.47
Crystal system	monoclinic	monoclinic
Space group	*C*2/*m*	*C*2/*m*
Lattice constants [Å, °]	*a* = 13.319(2)	*a* = 13.44(2)
	b =13.698(8)	*b* =13.66(2)
	c =8.719(1)	*c* =8.96(2)
	β =125.06(1)	β =124.2(2)
Volume [Å^3]	1302.1(8)	1320(3)
Z	2	2
Density (calcd.) [Mg/m^3]	1.442	1.413
Abs. coefficient [mm^{-1}]	1.611	
F(000)	592	
θ range [°]	2.39−27.99	
Index range (*h*,*k*,*l*)	−17/0, −18/1, −9/11	
Scan type	ω-2θ	
Program data collection	CAD4	
Data reduction	Molen	
No. of collected refl.	1847	
No. of unique refl.	1649 (R_{int}=0.052)	
No.of used refl./param.	1647/77	
Absorption correction	ψ scans	
Transm.: max., min.	0.9994, 0.8655	
Structure refinement	Full-matrix least squares on F^2	
S on F^2	1.124	
R, wR_2 [$I > 2\sigma(I)$]	0.0536, 0.1028	
Δρ: max., min. [e/Å^3]	0.325, −0.31	

[a] Only the unit cell parameters were determined.

The monoclinic unit cell of **1** comprises unique cation and anion molecules. For $[Ni(edt)_2]^{\bullet-}$, whose structure is reported here for the first time, the atom labeling, selected

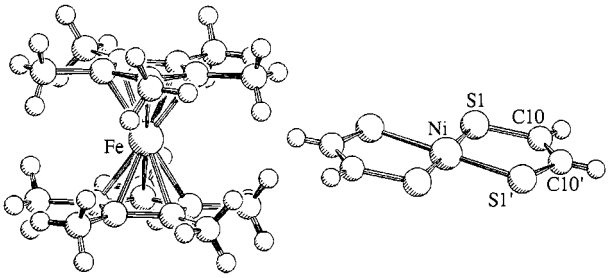


Figure 1. Perspective view of the molecular structure of **1** showing the numbering scheme for $[Ni(edt)_2]^-$; the primed and unprimed atoms are related by a mirror plane; selected bond lengths [Å] and angles [°]: Ni−S(1) 2.140(2), S(1)−C(10) 1.707(8), C(10)−C(10′) 1.32(2); S(1)−Ni−S(1′) 91.40(13), Ni−S(1)−C(10) 103.6(3), S(1)−C(10)−C(10′) 120.7(3)

bond lengths and angles are given in Figure 1. This radical anion shows a D_{2h} local symmetry, is planar and the Ni−S, S−C, and C−C distances, 2.140(2), 1.707(8), and 1.32(2) Å, 2are in good agreement with values found in other square-planar Ni^{III} dithiolate complexes.[18] The C−C distance in $[Ni(edt)_2]^-$ is relatively short when compared with the observed values in other complexes, such as $[Ni(tdt)_2]^-$, $[Ni(mnt)_2]^-$, and $[Ni(bdt)_2]^-$, 1.40(2), 1.352(8), and 1.404(2) Å, respectively.[18] This suggests the existence of a larger charge density on the C atoms for $[Ni(edt)_2]^-$. Preliminary data for the crystal structure of the neutral Ni^{IV} complex, $[Ni(edt)_2]^0$,[19] revealed shorter M−S and S−C distances, 2.100 and 1.687(5) Å, along with a larger C−C distance, 1.358(7) Å, which is consistent with the antibonding nature of the Ni−S and S−C interactions and the bonding nature of the C−C interaction.[20] The $[Fe(Cp^*)_2]^{\bullet+}$ radical cation has a C_5 local symmetry and the two C_5 rings show a staggered conformation, which is similar to those observed for a large number of salts with other acceptors.[5,12] The average Fe−C, C−C, and C−Me distances, 2.091(6), 1.416(8), and 1.502(9) Å, are in good agreement with the values observed for those salts.[5,12]

Similarly to the structures of the isostructural salts $[M(Cp^*)_2][M'(tdt)_2]$ (with M = Fe, M′ = Ni[5] and M = Mn, M′ = Ni, Pd, Pt[6]), in the case of **1** the crystal structure consists of a parallel arrangement of 1D chains of alternate radical donors (D), $[Fe(Cp^*)_2]^{\bullet+}$, and acceptors (A), $[Ni(edt)_2]^{\bullet-}$, DADADA, where the stacking axis corresponds to [101]. The intrachain Fe−Ni distance is 5.477 Å, as shown in Figure 2(a). Unlike the series $[M(Cp^*)_2]$-$[M'(tdt)_2]$, where no interionic short contacts were found, in the structure of **1** intrachain short contacts between the nickel and one of the carbon atoms from the cyclopentadienyl ring were observed, with a Ni−C distance of 3.678 Å, as illustrated in Figure 2 (a). The angle between the stacking axis and the C_5 ring from $[Fe(Cp^*)_2]^{\bullet+}$ is 79.69°. The angle between the NiS_4 plane of the radical anions and the stacking axis is 78.63°. The dihedral angle between the C_5 ring and the NiS_4 plane is 1.07° with a distance between the two planes of 2.984 Å. The existence of the short intrachain D-A contacts in this compound is expected to lead to a significantly stronger intrachain FM coupling than is observed in the case of the $[M(Cp^*)_2]$-$[M'(tdt)_2]$ series.

In the unit cell there are four distinct chains, shown in Figure 2 (b), displaying three unique interchain arrangements, I−II and II−IV, which are out-of-registry,[4] and I−III that has an in-registry[4] arrangement. The intrachain separations are 8.017, 8.678, and 13.698 Å, for the I−II, II−IV, and I−III pairs, respectively. Figure 3 shows these arrangements, along with the shortest distances between the metal centers from different chains and the closest interchain, interionic contacts (in italics). For the out-of-registry pair I−II, the shortest interchain MM distances are 8.119 (FeNi), 9.553 and 10.029 Å (FeFe or NiNi). In the case of the out-of-registry pair II−IV the shortest interchain MM separations are 8.720 (FeFe or NiNi), 9.835 and 10.740 Å (Fe Ni). For the in-registry pair I−III the

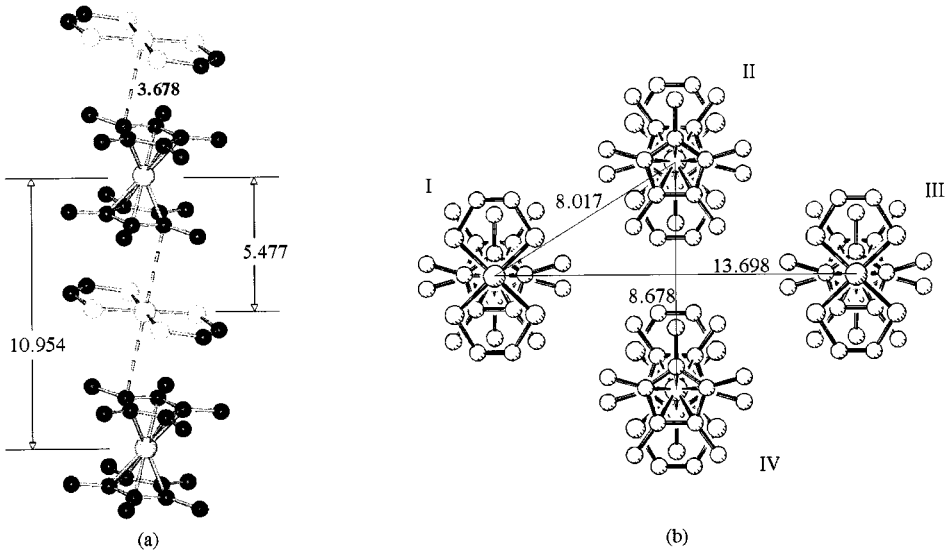


Figure 2. (a) 1D DADADA chain in **1**, the thick dotted lines represent the intraion Ni−C short contacts, 3.678 Å; (b) view normal to the chains (along [101]), showing the four unique chains, I, II, III, IV for **1** (hydrogen atoms were omitted for clarity)

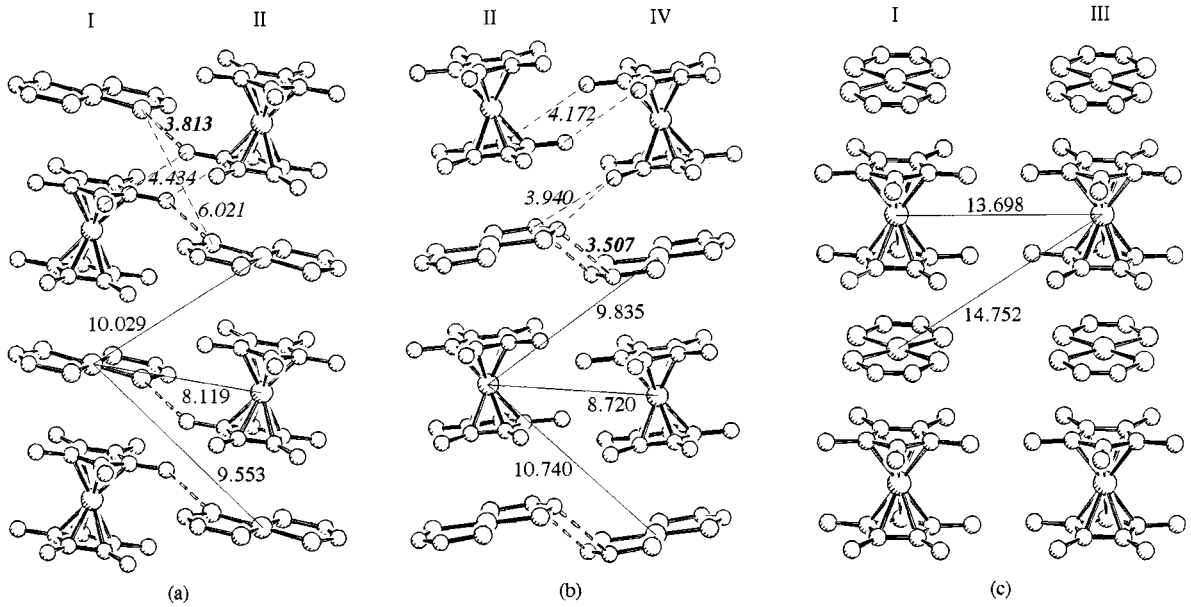


Figure 3. (a), (b) Out-of-registry arrangement of chains I−II and II−IV, respectively; (c) in-registry arrangement of chains I−III; the solid lines show the closest interchain M−M distances and the dashed lines the closest interchain interionic distances (hydrogen atoms were omitted for clarity)

shorter interchain FeFe (or NiNi) distance is 13.698 Å and the shorter FeNi distance is 14.752 Å.

Since the magnetic ordering is a bulk property, the interchain interactions are as important as the intrachain interactions and this information is essential in order to understand the spin-spin interactions that dominate the magnetic behavior. For compound **1**, although no interchain contacts shorter than the sum of the van der Waals radii were detected, relatively short DA and AA interionic interchain distances were observed in the cases of the arrangements I−II and II−IV, respectively. In the I−II pair the shortest distance (3.813 Å) corresponds to SC contacts, from a sulfur atom of the acceptor and a C from one of the methyl groups of the Me_5C_5 fragment, as shown in Figure 3 (a). In the II−IV pair, the shortest interionic interchain distance (3.507 Å) corresponds to CC contacts from the acceptors, as shown in Figure 3 (b).

As in the case of the intrachain interactions, the interchain coupling must also be considerably stronger in **1** than in the $[M(Cp^*)_2][M'(tdt)_2]$ compounds, as in these compounds the presence of the relatively bulky CF_3 groups isolate the S−C=C−S portion of the ligand, where most (50−70%) of the spin density must reside,[21] from the ions in the neighboring chains. In compound **1** the atoms of the S−C=C−S fragment are free to interact with the ions in the neighboring chains, and as shown in Figure 3, the S and C atoms are relatively close to atoms from different chains. The interchain spin interactions, due to the CC contacts from the acceptors, are expected to be of particular importance, since a considerable spin density must reside on those atoms. Additionally, in this case the interactions are predicted to be AFM in nature since the spin density on both atoms must have the same parity.

Magnetic Properties

Magnetization measurements with polycrystalline samples of **1** were obtained between 2 and 300 K using the Faraday method. The magnetic susceptibility, χ, follows the Curie−Weiss expression, $\chi_M = C/(T - \theta)$, between 100 and 300 K, with $\theta = -5 \pm 4$ K. From measurements made with three different samples considerable scatter was observed in the room-temperature effective moment, μ_{eff}, and values ranging from 3.15 to 3.95 μ_B were obtained. This can be attributed to orientation effects due to the applied field, together with the large anisotropy of the g value of $[Fe(Cp^*)_2]^{\bullet+}$, where $g_{\parallel} = 4.4$, $g_{\perp} = 1.3$ and $<g> = 2.8$.[12] In this case, assuming independent spins and a random orientation and a g value of 2.06 for the acceptor,[22] a value of 3.0 μ_B for μ_{eff} is predicted, but orientation effects could give rise to values as large as 4.2 μ_B. At low temperatures, the magnetic susceptibility was observed to show a considerable field dependence. The temperature dependence of the product, χ_T, for two measurements with the same sample of **1** is shown in Figure 4. The solid circles correspond to a ZFC measurement with an applied field of 10 kG, and fit (dotted line) Curie−Weiss behavior, with $\theta = -7.8$ K. The open circles refer to data obtained at 5 kG, where the alignment of the sample was induced through the application of a 50-kG magnetic field, the fit of the results with the Curie−Weiss expression (solid line) gave a θ value of −1.6 K. The different θ values observed for the random and field-oriented measurements suggest the existence of strong anisotropy in the magnetic coupling in the case of **1**.

In the case of compound **2**, the magnetic susceptibility data were obtained using a Faraday magnetometer, with a freshly prepared polycrystalline sample. The magnetic sus-

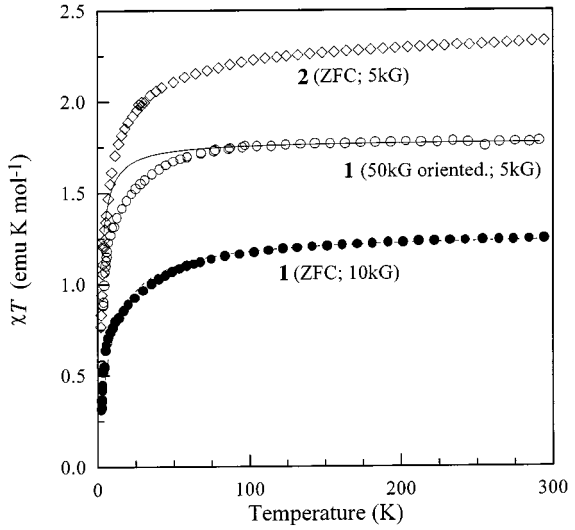


Figure 4. χ_T temperature dependence for compounds **1** (circles) and **2** (diamonds); in the case of **1**, the closed circles refer to a ZFC measurement at 10 kG and the open circles refer to a measurement at 5 kG, where the sample was previously subjected to a 50-kG applied field, at 2 K

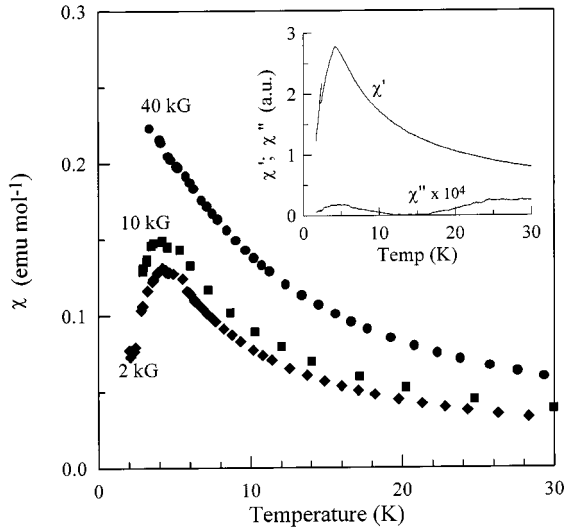


Figure 5. χ temperature dependence for **1**, with applied fields of 2 kG (diamonds), 10 kG (squares) and 40 kG (circles); the inset shows the χ' and χ'' temperature dependence

ceptibility, χ, relative to a ZFC measurement with an applied field of 5 kG, between 50 and 300 K follows the Curie−Weiss law, with $\theta = -6.7$ K. The χ_T temperature dependence for **2** is shown in Figure 4 (diamonds). The observed room-temperature effective moment ($\mu_{eff} = 4.31\ \mu_B$) is in good agreement with the expected value, 4.24 μ_B, calculated for two non-interacting spins, with $S = 1/2$ and $S = 3/2$, assuming that the g values of the donor and the acceptor are 2.0[16] and 2.06,[22] respectively. Previous measurements showed unexpectedly low values for the Curie constant, which can be attributed to partial decomposition of the sample. The observed values for the magnetization field dependence at 2 K in the case of this compound are considerably lower to those calculated from the Brillouin function, indicating a strong AFM coupling. Unexpectedly, this compound was observed to be EPR-silent, which may be due to the existence of a different phase of this compound, possibly neutral. This would also explain the lower values of the magnetic susceptibility observed in previous measurements.

In order to investigate the field-dependent behavior of **1** observed at low temperatures, a series of measurements of the field cooled magnetization temperature dependence at different values of the applied field were made, as shown in Figure 5. From these experiments it was possible to observe the existence of a field-induced transition. As the sample is cooled below 30 K, in a field of 2 kG (Figure 5 − diamonds) χ increases, reaches a maximum at 4.1 K and decreases significantly at lower temperatures, indicating that an AFM phase transition occurs. With an applied field of 10 kG (Figure 5 − circles), the behavior is similar, but there is small shift in the maximum to lower temperatures (3.9 K), at higher applied fields the maximum broadens and shifts to lower temperatures. At fields higher than 20 kG this maximum is no longer observed, suggesting that a field-induced transition occurs. Dynamic susceptibility measurements enabled the determination of the Néel temperature, $T_N = 4.2$ K, which corresponds to a peak observed on both the in-phase, χ' and the out-of-phase, χ'', components, as shown in the inset of Figure 5.

The field dependence of the magnetization at 2, 3, and 6 K for compound **1** is shown in Figure 6 for a polycrystal-

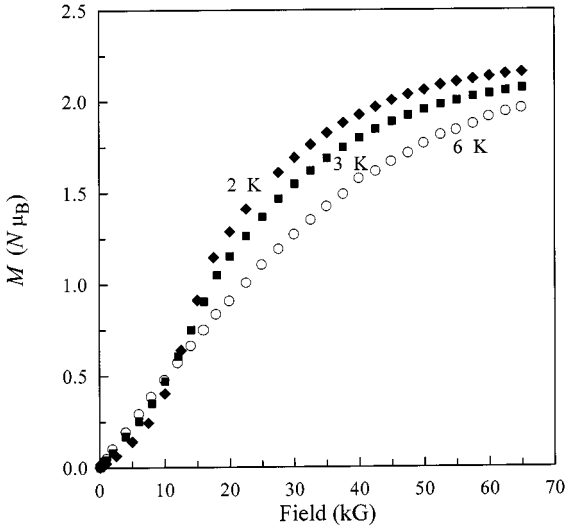


Figure 6. Magnetization field dependence for **1**, at 2, 3, and 6 K

line, pre-aligned sample. Below T_N, the curves exhibit sigmoidal behavior, typical of metamagnetism. At low fields, the magnetization increases slowly with the field and, at fields on the order of 5 kG, the increase is accentuated, showing an upward curvature. At fields in the order of 12−15 kG, the magnetization is nearly linearly dependent on the field and for higher fields a downward curvature is observed. This sigmoidal behavior is more pronounced at lower temperatures and, at fixed temperatures, it was observed to be more pronounced for previously aligned samples than nearly fixed, randomly oriented samples. For

this field-induced transition, at 2 K, the critical field, defined as the value of the field were dM/dH shows a maximum, is H_C = 14 kG. No hysteresis was observed in the isothermals, as expected for a metamagnetic transition. This behavior is very similar to that observed in other highly anisotropic compounds, such as the electron-transfer salts $[Mn(Cp^*)_2][M(tdt)_2]$ (M = Ni, Pd, Pt)[6] or compounds with extended covalent networks such as $M(pyr)_2Cl_2$ (M = Co, Fe, Ni).[23]

In order to study the magnetic anisotropy of compound **1**, single-crystal measurements were performed on a SQUID magnetometer. Due to the needle-shaped form of the crystals two configurations were used for these measurements, one (L) with the applied field parallel to the axis of the crystals, which correspondes to a^* and is relatively close to the stacking direction [101], making an angle of 5.65°. In a second configuration (T), the field was applied along a random direction in the plane perpendicular to a^*.

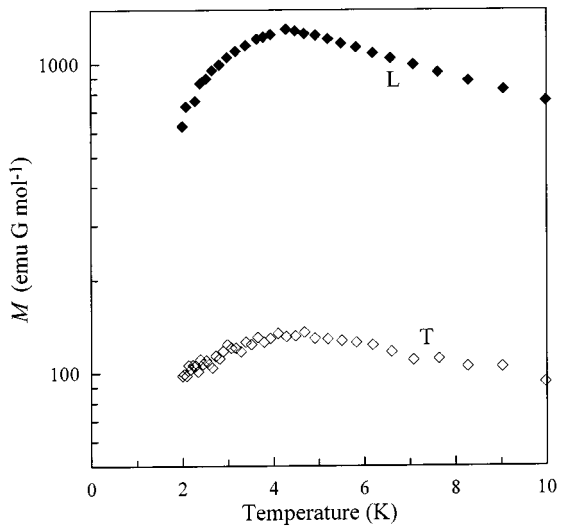


Figure 7. Single-crystal magnetization temperature dependence for **1** with an applied field of 5 kG, parallel (solid symbols) and perpendicular (open symbols) to the crystal axis

Figure 7 shows the magnetization temperature dependence for the two configurations, with an applied field of 5 kG. Crystals of 70 and 75 μg were used in L and T configurations, respectively, the results for configuration L are represented by the closed symbols and for T by the open symbols. The magnetization temperature dependence observed for both configurations is qualitatively similar, with a maximum at ca. 4.5 K, indicating the existence of AFM transitions in both configurations. The values relative to the L configuration are almost one order of magnitude higher than the ones from the T configuration, which is attributed essentially to the anisotropy in the g value of the donor.

In the case of the L configuration, at 2 K, the single-crystal magnetization field dependence is consistent with

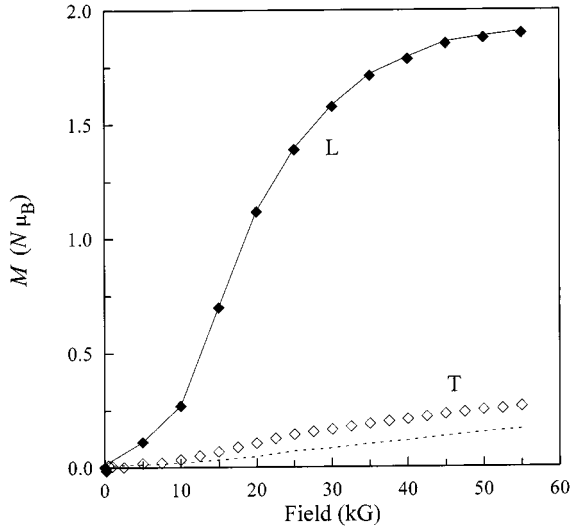


Figure 8. Single-crystal magnetization field dependence for **1**, at 2 K, with the applied field parallel (solid symbols) and perpendicular (open symbols) to the crystal axis; the estimated values of $M_{\parallel}$ and $M_{\perp}$ are represented by the solid and dashed lines, respectively

the existence of a field-induced phase transition, with a critical field of 14 kG, as indicated by the isothermal sigmoidal behavior, shown in Figure 8 (closed symbols). At 55 kG the magnetization reaches a value of 1.95 $N\mu_B$, and is not yet saturated, which is usual in metamagnetic materials if the temperature is not much lower than T_N.[6,23] The high-field state is consistent with an FM state, where the saturation magnetization, $M_S = g_D S_D + g_A S_A \approx 3\ N\mu_B$, with $S_D = S_A = 1/2$, $g_D = 3.95$ (a tilting of 10° of the axis of the donor relative to the field was considered) and $g_A = 2.06$. For a ferrimagnetic state the expected value for the saturation magnetization $M_S = g_D S_D - g_A S_A \approx 0.91\ N\mu_B$, is much smaller than the values obtained for the high-field state. For the T configuration, the magnetization is much lower than in L, and, as shown by the open symbols in Figure 8, the magnetization field dependence is almost linear, as expected for an AFM.

In order to estimate the field dependence of $M_{\parallel}$ and $M_{\perp}$, a mathematical treatment of the values measured along a^* ($M^{a*}{}_{\parallel}$), L configuration, and in the plane perpendicular to a^* ($M^{a*}{}_{\perp}$), T configuration, where made. For $M_{\parallel}$ a very good agreement with $M^{a*}{}_{\parallel}$ was obtained, with a negligible deviation (< 2%) in comparison to the experimental error, which is in the order of 5%. The field dependence of $M_{\parallel}$ is represented by the solid line in Figure 8. A linear field dependence was obtained for $M_{\perp}$ (dotted line in Figure 8). Unlike the values observed for the L configuration, in this case the values of $M^{a*}{}_{\perp}$ are clearly larger than the ones obtained for $M_{\perp}$ due to the contribution of $M_{\parallel}$.

The single-crystal magnetization measurements confirmed the high magnetic anisotropy of **1**. The transition from the AFM low-field state to a FM high-field state was observed to occur only with the applied field parallel to the stacking axis, which confirms the FM nature of the intrachain DA coupling and the AFM nature of the interchain interactions. The small dimensions of the crystals and air

sensitivity of **2** prevented determination of the single-crystal measurements on this compound.

The magnetic properties of **1** reveal features that are somewhat unusual among the class of highly anisotropic compounds displaying metamagnetism. The magnetic behavior of compound **1** seems to be dominated by AFM interactions, whereas in most compounds of this class the FM interactions are dominant. One other aspect is related to the magnitude of the critical field, which is particularly high in the case of compound **1**.

In order to achieve a better understanding of the magnetic behavior of compound **1,** its crystal structure and magnetic properties can be compared with those of the isostructural series $[M(Cp^*)_2][M'(tdt)_2]$.[6] The magnetic behavior of those compounds is dominated by strong intrachain FM interactions coexisting with weak interchain AFM interactions, which in the case of the Mn compounds leads to metamagnetism. In these highly anisotropic compounds $T_N \propto |E_{intra}E_{inter}|^{1/2}$,[14] where the intrachain DA interaction, $E_{intra} \propto S_D S_A J_{DA}$, and E_{inter} is the weaker effective interchain interaction. The absence of magnetic ordering in the case of $[Fe(Cp^*)_2][Ni(tdt)_2]$ is attributed to a lower value of E_{intra}, as the donor in this case has a smaller spin $S = 1/2$, while in the Mn compounds $S = 1$. As mentioned above, in the case of compound **1** stronger intrachain and interchain magnetic coupling are expected, which is consistent with the larger value of $T_N = 4.2$ K as compared with the observed values for the $[Mn(Cp^*)_2][M(tdt)_2]$ compounds, 2.4, 2.8, and 2.3 K for M = Ni, Pd, and Pt, respectively.[6] The interchain coupling in compound **1** is expected to be exceptionally strong, and the interchain AFM coupling must be comparable to the intrachain FM coupling, considering the apparent domination of AFM interactions observed from the magnetic susceptibility temperature dependence (Figure 4).

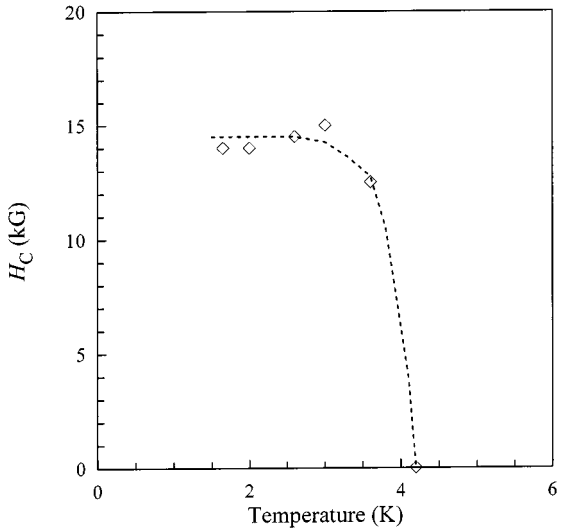


Figure 9. Critical field temperature dependence for **1**; the line represents a fit to the experimental results

A simple Ising model was used in the study of the metamagnetic transitions in the compounds $FeCl_2 \cdot 2\,H_2O$ and $CoCl_2 \cdot 2\,H_2O$,[24] with an intrachain and two interchain constants, and for those compounds the metamagnetic transition fields are proportional to the interchain exchange constants. In the case of compound **1**, the high value of the observed critical field of ca. 14 kG, one order of magnitude larger than in the case of the $[Mn(Cp^*)_2][M(tdt)_2]$ compounds, can be attributed to a considerably larger interchain coupling for **1**.

As compound **2** is isostructural with **1**, it is reasonable to expect that, as observed for **1**, the magnetic behavior must be dominated by the DA intrachain and by the AA and DA interchain interactions. The magnetic susceptibility temperature dependence and the magnetization field dependence indicate that in **2** the magnetic behavior is clearly dominated by strong AFM interactions. In this compound quite strong AFM interchain interaction are expected, as in **1**, and the DA intrachain interactions must be considerable weaker, as indicated by the magnetic behavior of the $[M(Cp^*)_2](TCNE)$, with M = Fe ($S = 1/2$), Mn ($S = 1$), and Cr ($S = 3/2$) salts.[15] These compounds show FM ordering, with $T_C = 4.8$, 8.8, and 3.1 K for the Fe, Mn, and Cr compounds, respectively, and as in a simple mean-field model T_C is proportional to J and $S(S+1)$.[15] The lower value of T_C in the $[Cr(Cp^*)_2]^+$ salt suggests that, in this case, J_{DA} is considerably weaker in relation to the other compounds, as this is the case with the higher S value. Therefore, in compound **2**, the strong AFM interchain interactions could dominate the magnetic behavior and thus it would not be possible to determine the (FM or AFM) nature of the DA intrachain interactions. Unlike the AFM DA intrachain coupling observed for $[Cr(Cp^*)_2][Ni(tds)_2]$,[7] in case of compound **2** the dominant interchain interactions enable discussion of the validity of the several spin-spin coupling mechanisms.

Mössbauer Spectroscopy

Mössbauer spectra of compound **1** from 78 to 4.4 K exhibit a single line (Figure 10). The ionic form of the compound, $[Fe(Cp^*)_2]^+[Ni(edt)_2]^-$, can be confirmed by the non-observation of quadrupole splitting along with the fact that the estimated values for the isomer shift, $\delta = 0.48$ mm/s (relative to metallic Fe at room temperature) are typical of low-spin, $S = 1/2$, Fe^{III} decamethyl ferrocenium.[25] This singlet is slightly larger at 4.4 K (half width, $\Gamma = 0.47$ mm/s) than at 78 K ($\Gamma = 0.38$ mm/s), but below 4.4 K the spectrum suddenly broadens and gives rise to a partially resolved hyperfine split spectrum in agreement with the magnetic ordering observed at 4.2 K in the magnetization measurements. At 3.5 K the broad sextuplet fitted to the observed spectrum (Figure 10) corresponds to a hyperfine field of ca. 350 kG.

The spectra obtained at 4.4 K with applied fields of 20 and 50 kG and at 20 K with a 50 kG applied field, shown in Figure 11, can be interpreted by the spin Hamiltonian for the $S = 1/2$ electronic ground state [Equation (1)]

$$\mathbf{H}_{NE} = \mu_B(\mathbf{H}_{ext} \cdot \mathbf{g} \cdot \mathbf{S}_{eff}) + \mathbf{I} \cdot \mathbf{A} \cdot \mathbf{S}_{eff} + \mathbf{I} \cdot \mathbf{P} \cdot \mathbf{I} - g_N \cdot \mu_N \cdot \mathbf{H}_{ext} \cdot \mathbf{I}, \quad (1)$$

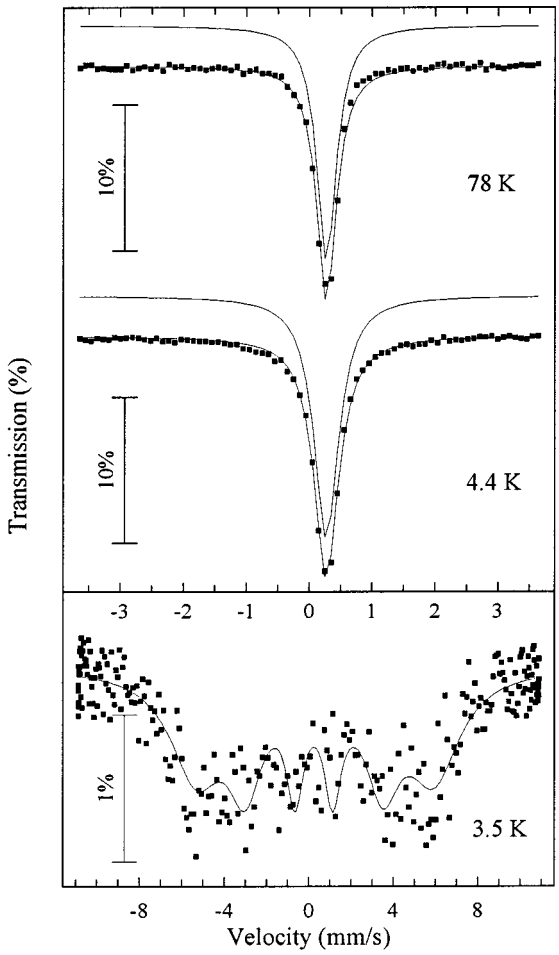


Figure 10. Mössbauer spectra of **1** obtained at 78, 4.4, and 3.5 K; the calculated functions are plotted on the experimental points; note the different velocity scale for the spectrum at 3.5 K

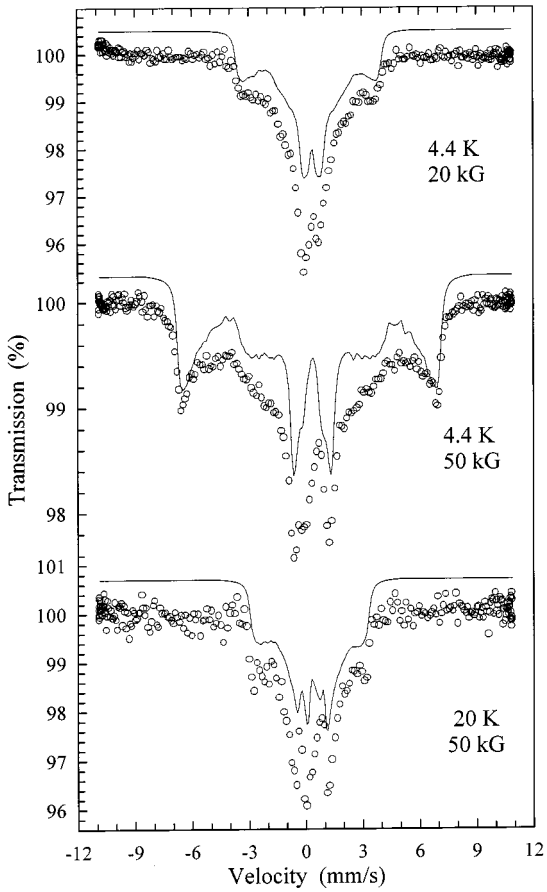


Figure 11. Mössbauer spectra of **1** with applied magnetic fields of 20 and 50 kG obtained at 4.4 K and of 50 kG at 20 K; the simulated spectra calculated using the spin Hamiltonian are also plotted slightly shifted

where **g**, **A** and **P** are tensors describing the electronic Zeeman interaction, the magnetic hyperfine interaction and the electricinteraction respectively. The principal axes of **g** and **A** are assumed to be the same but **P** is allowed to have different axes (ξ, ψ, ζ), which are obtained from those of **g** or **A** through a rotation with Euler angles α, β, γ. **I P I** may be rewritten as [Equation (2)]

$$\mathbf{I}\cdot\mathbf{P}\cdot\mathbf{I}=\frac{1}{4}eQV_{\zeta\zeta}\left\{\left[I_\zeta^2-\frac{1}{3}I(I+1)+\frac{\eta}{3}\left(I_\xi^2-I_\psi^2\right)\right]\right\}, \quad (2)$$

and we may define [Equation (3)]

$$\mathbf{H}_{\mathrm{int}}=-\frac{\mathbf{A}\cdot\langle\mathbf{S}_{\mathrm{eff}}\rangle}{g_{\mathrm{N}}\mu_{\mathrm{N}}}. \quad (3)$$

Theoretical simulations employing the above spin Hamiltonian were calculated by a modified version of the program by Münck et. al.[26] Assuming fast relaxation and using g_{xx} = 1.3, g_{yy} = 1.3, and g_{zz} = 4.4,[12] $\Delta E_{\mathrm{Q}} = eQV_{\zeta\zeta}$ = −0.17 mm/s, η = 0, $A_{xx}/(g_{\mathrm{N}}\mu_{\mathrm{N}})$ = −110 kG, $A_{yy}/(g_{\mathrm{N}}\mu_{\mathrm{N}})$ = −110 kG, and $A_{zz}/(g_{\mathrm{N}}\mu_{\mathrm{N}})$ = +820 kG, the calculated simulations are plotted on the experimental spectra (Figure 11). Non-zero values of α, β, and γ were considered but did not improve the fit of the simulation to the experimental spectra. The estimated ΔE_{Q}, as well as the **g** and **A** values, are similar to those reported for decamethylferrocenium hexafluorophosphate.[27]

Since electronic relaxation is fast, the ^{57}Fe nucleus is unable to follow the rapid fluctuations of the magnetic field $\mathbf{H}_{\mathrm{int}}$ due to the unpaired electrons and senses only the thermal average spin corresponding to the m_{S} = +1/2 and m_{S} = −1/2 levels. The magnetically split Mössbauer spectra reveal that the average $\mathbf{H}_{\mathrm{int}}$ is not zero. Furthermore a strong temperature and field dependence of the effective magnetic fields at the ^{57}Fe nuclei is shown by the smaller splitting between the outer peaks in the spectra at 20 K with $\mathbf{H}_{\mathrm{ext}}$ = 50 kG or at 4.4 K with $\mathbf{H}_{\mathrm{ext}}$ = 20 kG. These observations are consistent with an appreciable difference in the Boltzmann population of spin-up and spin-down molecules and reflect the decrease in the thermal population of the excited m_{S} sublevel with increasing temperature and decreasing applied external magnetic field.

The spectra obtained with an applied field of 50 kG (either at 4.4 or at 20 K) bear a close resemblance to those obtained under the same experimental conditions for other decamethylferrocenium compounds characterized by a fast relaxation rate.[27] Several factors (such as relaxation rates slower than the ideal fast relaxation limit, admixtures of

electronic excited states into the ground electronic state in high magnetic fields, etc.) already mentioned by Cohn et al.[27] can influence the appearance of the Mössbauer spectra of magnetically perturbed ferrocenium cations and may explain the lack of fit between the experimental data and the simulated spectra at the Doppler velocity range around 0 mm/s. In this case significant texture effects caused by the needle shape of the crystals used in the preparation of the Mössbauer absorber should also be considered. While calculating simulated spectra, 500 different applied field directions distributed uniformly over an octant of the unit sphere associated with the **g** and **A** axes were summed, assuming a randomly oriented sample. The needle shape of the crystals is expected to cause a significant increase in the relative number of particles with the needle axis approximately perpendicular to the external field. Since the angle of the g_{zz} axis relative to the stacking direction is of the order of 10°, the weight of the contribution to the spectra of the cations with g_{zz} perpendicular to the applied field is larger than in the case of a randomly oriented sample.

As observed for other decamethylferrocenium salts, $[Fe(Cp^*)_2]^+[Ni(edt)_2]^-$ also shows an appreciable **g** and **A** tensor anisotropy. Furthermore, the A_z value is positive, suggesting a large orbital contribution to the hyperfine field, which along the z axis is larger in absolute value than the negative isotropic contact term. This is explained by the appreciable orbital angular momentum in the electronic ground state of this complex.[27]

Conclusion

As predicted, the small dimensions of the acceptor, $[Ni(edt)_2]^-$, lead to a linear chain structural motif in the electron-transfer salts, $[M(Cp^*)_2][Ni(edt)_2]$, with M = Ni and Cr. The large spin density on the peripheral S−C= C−S fragment of the acceptor ligands and its accessibility were expected to lead to the existence of particularly strong inter- and intrachain magnetic interactions. In fact, for $[Fe(Cp^*)_2][Ni(edt)_2]$ there are strong FM intrachain interactions, due to DA intrachain short contacts coexisting with strong AFM interchain interactions, resulting from the AD and AA interchain contacts. In this compound magnetization measurements revealed the existence of a metamagnetic behavior (T_N = 4.2 K and H_C = 14 kG) in agreement with the high anisotropy of the magnetic coupling. Single-crystal measurements revealed that, below 4.2 K, the transition from the AFM low-field to the FM high-field state can be induced by the application of a magnetic field parallel to the stacking axis. The magnetic behavior of $[Cr(Cp^*)_2][Ni(edt)_2]$ is dominated by the strong interchain AFM interactions and in this case it was not possible to determine the exact (FM/AFM) nature of the intrachain DA interactions, which prevented a discussion of the validity of the spin-spin coupling models for these compounds.

Experimental Section

General Remarks: Decamethylferrocenium tetrafluoroborate and decamethylchromocenium hexafluorophosphate were obtained from decamethylferrocene (Aldrich) and decamethylchromocene (Strem), respectively, by literature procedures.[12,16] The $(Et_4N)[Ni(edt)_2]$ salt was prepared as described in the literature.[17] Acetonitrile was distilled from P_2O_5 under nitrogen, and deaereated either by successive alternate freezing and evacuation cycles or by bubbling argon through the solvent for ca. half an hour. All the syntheses were carried out under nitrogen or argon, in gloveboxes or using Schlenk techniques. − Elemental analyses were carried out with a Carlo Erba (EA 1110-CHNS-O).

$[Fe(Cp^*)_2][Ni(edt)_2]$ (1): Dark green needle-shaped crystals of this compound were obtained by mixing $[Fe(Cp^*)_2]BF_4$ (124 mg, 0.30 mmol) in acetonitrile (2 mL) with $(Et_4N)[Ni(edt)_2]$ (111 mg, 0.30 mmol) in acetronitrile (7 mL). After standing at room temperature overnight, the crystalline product was collected by vacuum filtration in 63% yield (107 mg, 0.19 mmol). − $C_{24}H_{34}FeNiS_4$ (565.3): calcd. C 50.99, H 6.06, S 22.68; found C 50.58, H 5.76, S 21.75. − Crystallization by slow solvent evaporation from concentrated acetonitrile or dichloromethane solutions of $[Fe(Cp^*)_2][Ni(edt)_2]$ afforded large needle-shaped crystals suitable for X-ray diffraction and single-crystal magnetic studies.

$[Cr(Cp^*)_2][Ni(edt)_2]$ (2): The compound was prepared by the addition of $[Cr(Cp^*)_2]PF_6$ (80 mg, 0.17 mmol) in acetonitrile (1.5 mL) to $(Et_4N)[Ni(edt)_2]$ (62.6 mg, 0.17 mmol) in acetonitrile (5 mL). After standing for 2 h, brown needle-shaped crystals were collected by vacuum filtration in 49% yield (47.1 mg, 0.84 mmol). − $C_{24}H_{34}CrNiS_4$ (561.5): calcd. C 51.34, H 6.10; found C 51.11, H 6.49. − Crystallization attempts, following the procedure described for **1**, gave small needle-shaped crystals. Partial decomposition during the crystallization was observed to occur.

Magnetic Characterization: Static magnetic susceptibility data of $[M(Cp^*)_2][Ni(edt)_2]$ (M = Fe and Cr) polycrystalline samples, using Teflon sample holders, were obtained between 1.8 and 300 K using an Oxford Instruments Faraday system having a 70-kG superconducting magnet. For $[Fe(Cp^*)_2][Ni(edt)_2]$ magnetization data, between 1.5 and 300 K, were also obtained using the extraction method with an Oxford Instruments Magnetometer (MagLab System 2000), with a 120-kG superconducting magnet. Dynamic susceptibility measurements, in a zero applied static magneticfield and an alternating field of 1 G at 1 kHz, were also obtained with the MagLab system. The single-crystal magnetization measurements were obtained with a Quantum Design SQUID (MPS) magnetometer, between 2 and 10 K, with a 55-kG superconducting magnet. Magnetization measurements, in case of $[Cr(Cp^*)_2][Ni(edt)_2]$, were also obtained with the SQUID magnetometer for polycrystalline samples, using a quartz sample holder. Susceptibility and magnetization data were corrected for contributions due to sample holder and core diamagnetism, estimated from tabulated Pascal constants. Electronic paramagnetic resonance spectra were obtained with an X-band spectrometer (Bruker ESP 300) equipped with a helium flow cryostat (Oxford ESR 300).

Mössbauer Spectroscopy: ^{57}Fe-Mössbauer spectra were collected at 78, 4.4, and 3.5 K using a conventional spectrometer with a 50-mCi ^{57}Co source in an Rh matrix and a sinusoidal velocity-vs.-time wave form. The spectrometer was calibrated with an α-Fe foil. Needle-shaped crystals of **1** were mixed with perspex powder and the resulting material was pressed into a perspex sample holder in order to obtain a disk-shaped Mössbauer absorber, containing ca. 5 mg of natural Fe/cm^2. Spectra with the sample in an applied external magnetic field, $\mathbf{H}_{ext}$ (20 and 50 kG), parallel to the γ-ray beam, were obtained at 4.4 and 20 K using a superconducting coil. The spectra obtained at zero applied field were fitted to Lorentzian

lines using a modified version of the non-linear least-squares computer method of Stone.[28]

X-ray Crystallographic Study: A single crystal of **1** with approximate dimensions of $1.4 \times 0.35 \times 0.25$ mm was used for X-ray data collection with an Enraf Nonius Cad4 diffractometer, with graphite-monochromated Mo-K_α radiation ($\lambda = 0.71069$ Å), at room temperature. The structure was solved by direct methods using SHELXS-86[29] and refined with SHELXL-93.[30] All non-hydrogen atoms were refined anisotropically and hydrogen atoms were placed at calculated positions with isotropic temperature factors $U(H) = 1.2U_{eq}(C)$. All crystal and molecular representations were prepared with SCHAKAL-97.[31] The unit cell of compound **2** was determined using a single crystal with approximate dimensions of $0.8 \times 0.15 \times 0.1$ mm with an Enraf Nonius Cad4 diffractometer (Mo-K_α radiation). However, in this case the poor quality of the crystal prevented the X-ray structure determination. A summary of the crystal data and refinement procedures is given in Table 1. Crystallographic data (excluding structure factors) for the structure(s) reported in this paper have been deposited with the Cambridge Crystallographic Data Centre as supplementary publication no. CCDC-137238. Copies of the data can be obtained free of charge on application to CCDC, 12 Union Road, Cambridge CB2 1EZ, UK [Fax: (internat.) + 44-1223/336-033; E-mail: deposit@ccdc.cam.ac.uk].

Acknowledgments

This work was partially supported by "Fundação para a Ciência e Tecnologia" under contracts 2/2.1/QUI/203/94 and PBIC/C/2204/95 from PRAXIS XXI program.

[1] J. S. Miller, J. C. Calabrese, A. J. Epstein, W. Bigelow, J. H. Zhang, W. M. Reiff, *J. Chem. Soc., Chem. Commun.* **1986**, 1026−1028.
[2] S. Chittipeddi, K. R. Cromack, J. S. Miller, A. J. Epstein, *Phys. Rev. Lett.* **1987**, *58*, 2695−2698.
[3] O. Kahn, *Molecular Magnetism*, VCH Publ., New York, **1993**, chapter 11 and references therein.
[4] J. S. Miller, A. J. Epstein, in: *Research Frontiers in Magnetochemistry* (Ed.: C. J. O'Connor), World Scientific, Singapore, **1993**, p. 283−302, and references therein.
[5] J. S. Miller, J. C. Calabrese, A. J. Epstein, *Inorg. Chem.* **1989**, *28*, 4230−4238.
[6] W. E. Broderick, J. A. Thompson, B. M. Hoffman, *Inorg. Chem.* **1991**, *30*, 2958−2960.
[7] V. Gama, S. Rabaça, C. Ramos, D. Belo, I. C. Santos, M. T. Duarte, *Mol. Cryst. Liq. Cryst.* **1999**, *335*, 81−90.
[8] V. Gama, D. Belo, I. C. Santos, R. T. Henriques, *Mol. Cryst. Liq. Cryst.* **1997**, *306*, 17−24.
[9] W. E. Broderick, J. A. Thompson, M. R. Godfrey, M. Sabat, B. M. Hoffman, *J. Am. Chem. Soc.* **1989**, *111*, 7656−7657.
[10] S. Rabaça, V. Gama, D. Belo, I. C. Santos, M. T. Duarte, *Synth. Met.* **1999**, *103*, 2302−2303.
[11] M. Fettouhi, L. Ouahab, E. Codjovi, O. Kahan, *Mol. Cryst. Liq. Cryst.* **1995**, *273*, 29−33.
[12] J. S. Miller, J. C. Calabrese, H. Rommelmann, S. R. Chittipeddi, J. H. Zhang, W. M. Reiff, A. J. Epstein; *J. Am. Chem. Soc.* **1987**, *109*, 769−781.
[13] D. M. Eichhorn, D. C. Skee, W. E. Broderick, B. M. Hoffman, *Inorg. Chem.* **1993**, *32*, 491−492.
[14] W. E. Broderick, B. M. Hoffman, *J. Am. Chem. Soc.* **1991**, *113*, 6334−6335.
[15] J. S. Miller, A. J. Epstein, *Angew. Chem. Int. Ed. Engl.* **1994**, *33*, 385−415, and references therein.
[16] J. L. Robbins, N. Edelstein, B. Spencer, J. C. Smart, *J. Am. Chem. Soc.* **1982**, *104*, 1882−1893.
[17] W. Schroth, J. Peschel, *Chimia* **1964**, *18*, 171−173.
[18] C. Mahadevan, M. Seshasayee, P. Kuppusamy, P. T. Manoharan, *J. Cryst. Spectrosc. Res.* **1985**, *15*, 305−316.
[19] [19a] K. W. Browall, T. Bursh, L. V. Interrante, J. S. Kasper, *Inorg. Chem.* **1972**, *11*, 1800−1806. − [19b] Z. S. Herman, R. F. Kirchner, G. H. Loew, U. T. Mueller-Westerhoff, A. Nazzal, M. C. Zerner, *Inorg. Chem.* **1982**, *21*, 46−56.
[20] M. Sano, H. Adachi, H. Yamatera, *Bull. Chem. Soc. Jpn.* **1981**, *54*, 2639−2641.
[21] W. B. Heuer, A. E. True, P. N. Swepston, B. M. Hoffman, *Inorg. Chem.* **1988**, *27*, 1474−1482.
[22] J. A. MacLeaverty, in: *Progress in Inorganic Chemistry*, vol. 10 (Ed.: F. A. Cotton), Intersc. Publ., **1968**, p. 49−221.
[23] S. Foner, R. B. Frankel, W. M. Reiff, B. F. Little, G. J. Long, *Solid State Commun.* **1975**, *16*, 159−161.
[24] A. Narath, *Phys. Rev.* **1965**, *139*, A1221-A1227.
[25] J. S. Miller, J. C. Calabrese, R. L. Harlow, D. A. Dixon, J. H. Zhang, W. M. Reiff, S. R. Chittipeddi, M. A. Selover, A. J. Epstein, *J. Am. Chem. Soc.* **1990**, *112*, 5496−5506.
[26] E. Münck, J. L. Groves, T. A. Tumolillo, P. G. Debrunner, *Comput. Phys. Chem.* **1973**, *5*, 225−238.
[27] M. Cohn, M. Timken, D. N. Hendrickson, *J. Am. Chem. Soc.* **1984**, *106*, 6683−6689.
[28] J. C. Waerenborgh, F. Teixeira de Queiroz, *Research Report*, Laboratório Nacional de Engenharia e Tecnologia Industrial, Instituto de Ciências e Engenharia Nucleares, **1984**.
[29] G. M. Sheldrick, *SHELXS-86, A Program for Crystal Structure Determination*, University of Göttingen, Germany, **1990**.
[30] G. M. Sheldrick, *SHELXL-93, A Program for Crystal Structure Refinement*, University of Göttingen, Germany, **1993**.
[31] E. Keller, *SCHAKAL-97, A Computer Program for the Representation of Molecular and Crystallographic Models*, Kristallographisches Institut der Universität Freiburg i. Br., Germany, **1997**.

Received December 3, 1999
[I99422]

Complexation Properties of Heteroditopic Cryptands towards Cu^{2+}, Zn^{2+}, Cd^{2+}, and Pb^{2+} in Aqueous Solution: Crystal Structures of $[(H_5L1)(ClO_4)_5]\cdot 4\,H_2O$ and $[(NiL2Cl)Cl]\cdot 5.5\,H_2O\cdot CH_3OH$

Carla Bazzicalupi,[a] Prasun Bandyopadhyay,[b] Andrea Bencini,[a] Antonio Bianchi,*[a] Claudia Giorgi,[a] Barbara Valtancoli,[a] Dulali Bharadwaj,[b] Parimal K. Bharadwaj,*[b] and Ray J. Butcher[c]

Keywords: Macrocycles / Cryptands / Thermodynamics / Coordination chemistry

The protonation and metal ion (Cu^{2+}, Zn^{2+}, Cd^{2+}, Pb^{2+}) complexation abilities of three heteroditopic cryptands in solution are described and the relevant equilibrium constants are reported. The two distinct binding subunits of the ligands act cooperatively in the coordination of $M(H_2O)^{2+}$ (M = metal ion) species. The cryptand **L1** binds five protons in very acidic solution and crystallizes as $[(H_5\mathbf{L1})(ClO_4)_5]\cdot 4\,H_2O$ in the monoclinic space group $P2_1/n$ with a = 14.281(4), b = 14.313(7), c = 24.082(8) Å, β = 92.00(2)°, Z = 4, R = 0.079, and $wR2$ = 0.2010. The molecule shows an *endo-endo* conformation with a pseudo-threefold symmetry axis passing through the two bridgehead nitrogen atoms. All the cryptands (**L1**–**L3**) readily form inclusion complexes with Cu^{2+}, Ni^{2+}, Zn^{2+}, Cd^{2+}, and Pb^{2+} ions at the tren end of the cavity. The crystal structure of $[(Ni\mathbf{L2}Cl)Cl]\cdot 5.5\,H_2O\cdot CH_3OH$ is also reported [$C2/c$, a = 26.671(6), b = 16.784(4), c = 18.591(8) Å, β = 101.006(14)°, Z = 8, R = 0.091, and $wR2$ = 0.1424]. The Ni^{II} ion resides in a trigonal-bipyramidal coordination environment with the equatorial sites occupied by the three secondary nitrogen atoms of the cryptand and the axial sites occupied by a bridgehead nitrogen atom and a Cl^- ion.

Introduction

Macrocyclic ligands containing various binding functionalities are a topic of considerable current interest due to their ability to show highly selective recognition of different substrates, including both charged (cations, anions) and neutral molecules.[1−9] Among such ligands, macrobicyclic cryptands have attracted great interest since they are characterized by a three-dimensional arrangement of donor atoms and are capable of replacing the first solvation shell of the target species, thereby shielding the complexed species from the external environment.[8−19] However, when the number of cryptand donor atoms is insufficient to complete the coordination environment of the enclosed substrate, the inclusion of partially solvated species is observed. This is the case, for instance, with several transition metal complexes of the macrobicyclic cryptands **L1**−**L3** (Figure 1), where coordinated solvent molecules or anions are drawn into the cavity along with the metal ion.[20−23] Ligands such as **L1**−**L3** display interesting molecular structures composed of two different tripodal binding sites separated by three aromatic rings, which form a highly hydrophobic region. Such ligand structures have proved to be particularly effective in hosting metal ions since they stabilize metal−ligand bonds that are otherwise unstable.[24] The tripodal N_4 moiety represents a well-suited binding site for transition metal ions, although there are insufficient enough donor atoms to saturate the coordination spheres of many metal ions. As a result, the binding properties of the metal ions are directed towards the coordination of further species from the medium, which are constrained to occupy coordination sites located in, or in the proximity of, the hydrophobic region defined by the aromatic rings. Metal ions in such coordination environments, in conjunction with the remaining empty space in the ligand cavity, can be utilized in homogeneous catalytic reactions.[22] As a matter of fact, the secondary species linked to the metal ions display peculiar coordination features in that they are able to interact with both the donor atoms of the empty ligand moiety[21] and the π electron clouds of the benzene rings.[23] Moreover, derivatives of these cryptands have been shown to be well-suited for studying chelation-enhancement of fluorescence[25] and for the construction of ordered structures such as vesicles[26] and Langmuir−Blodgett films.[27] In spite of the large amount of information acquired about these ligands and their complexes, nothing is known regarding the thermodynamics of ligand protonation and metal ion complexation in solution. In order to fill in this gap, we performed the study described herein.

[a] Department of Chemistry, University of Florence,
Via Maragliano 75/77, 50144 Florence, Italy
Fax: (internat.) + 39-055/354845
E-mail: bianchi@chim1.unifi.it
[b] Indian Institute of Technology Kanpur,
Kanpur 208016, India
Fax: (internat.) + 91-512/590007
E-mail: pkb@iitk.ernet.in
[c] Department of Chemistry, Howard University,
Washington, DC 20059, USA
E-mail: rbutcher@fac.howard.edu

 © WILEY-VCH Verlag GmbH, D-69451 Weinheim, 2000 1434−1948/00/0909−2111 $ 17.50+.50/0

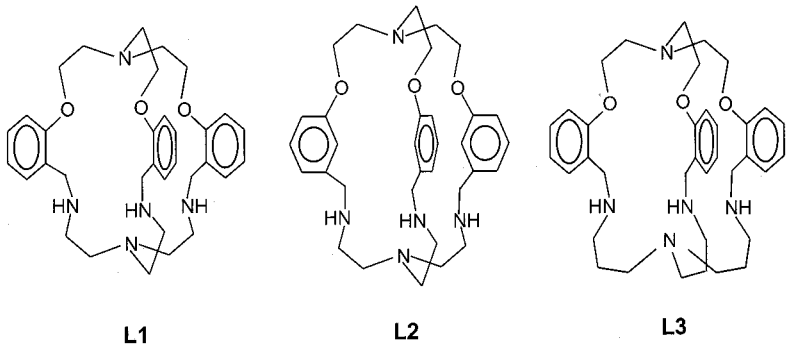


Figure 1. Ligand drawings

Results and Discussion

Ligand Protonation

The protonation constants of cryptands **L1**−**L3**, determined in 0.10 mol dm^{-3} Me_4NNO_3 at 298.1 K, are listed in Table 1. In the case of **L3**, it was not possible to determine the first protonation constant due to precipitation occurring in the pH region where the $HL3^{3+}$ species should be formed.

Table 1. Logarithms of ligand protonation constants determined in 0.10 mol dm^{-3} Me_4NNO_3 at 298.1 K

	L1 log K[a]	**L2**	**L3**
$L + H^+ = LH^+$	10.45(7)	9.74(6)	
$HL^+ + H^+ = LH_2^{2+}$	10.44(2)	8.68(6)	8.9(1)
$H_2L^{2+} + H^+ = LH_3^{3+}$	5.56(6)	7.47(8)	8.8(1)
$H_3L^{3+} + H^+ = LH_4^{4+}$	3.46(6)	5.6(1)	4.6(1)
$H_4L^{4+} + H^+ = LH_5^{5+}$		2.4(1)	2.9(1)

[a] Values in parentheses are standard deviations in the last significant figure.

The three molecules display rather different protonation properties. Firstly, it can be noted that while in very acidic solutions **L1** is able to form the fully protonated species, as demonstrated by the crystal structure of $[(H_5\mathbf{L1})(ClO_4)_5]\cdot 4\,H_2O$, in the pH range 2.5−10.5 used to determine the protonation constants it behaves, at most, as a tetraprotic base ($H_4\mathbf{L1}^{4+}$). In the same pH range, **L2** and **L3** are able to form the fully protonated species ($H_5\mathbf{L2}^{5+}$, $H_5\mathbf{L3}^{5+}$), indicating higher overall basicities. The first two protonation constants of **L1**, however, are considerably higher than the corresponding values for **L2** and **L3**, while the third and fourth values are significantly lower. Furthermore, the first two protonation constants of **L1** are surprisingly similar within experimental error. It is a common characteristic of cryptand polyamines to display peculiar protonation behavior. This can often be attributed to the presence of solvent molecules in the cavity, which contribute to the stabilities of the protonated species through hydrogen bonding.[23,28,30] As a matter of fact, as shown by recent crystal structures, $H_2\mathbf{L1}^{2+}$ and $H_2\mathbf{L2}^{2+}$ are able to bind one[30] and two[23] water molecules, respectively, forming significant hydrogen-bond networks within the cavity involving the ammonium groups. In $[(H_2\mathbf{L1})\subset H_2O]^{2+}$, the water molecule seems to be bound more strongly than in the $H_2\mathbf{L2}^{2+}$ cryptate due to the direct participation of both the binding moieties in the former. This is, in turn, a consequence of the different connectivity of the tripodal binding moieties to the benzene rings, the *ortho*-substituted cryptand allowing closer approach of the bridgehead nitrogen atoms than the *meta*-substituted one. Hence, it seems likely that efficient cooperativity of the two opposite binding subunits, as mediated by a cryptate water molecule, is responsible for the higher basicity of **L1** in the first two protonation steps. In **L3**, the benzene rings are *ortho*-substituted but, unlike **L1**, it is more flexible as the tren [tris(2-aminoethyl)amine] unit is replaced by trpn [tris(3-aminopropyl)amine] (Figure 1).

An alternative explanation of such behavior may be found in the abilities of similar cryptand molecules to promote the coordination of anionic species.[19] Inclusion of a negatively charged substrate would lead to stabilization of the positively charged receptor through charge neutralization and, depending on the nature of the anion, through the formation of intramolecular hydrogen bonds. Accordingly, the marked loss of basicity observed in the third and fourth protonation steps of **L1** might stem from disruption of the internal structure as a result of the guest species interacting with the final protonation sites. Indeed, the crystal structure of the compound $[(H_5\mathbf{L1})(ClO_4)_5]\cdot 4\,H_2O$ shows an empty $H_5\mathbf{L1}^{5+}$ cation (Figure 2) that displays evident stress stemming from the electrostatic repulsion between positive charges.

The crystal structure of $[(H_5\mathbf{L1})(ClO_4)_5]\cdot 4\,H_2O$ reveals the presence of discrete $H_5\mathbf{L1}^{5+}$ cations, perchlorate anions, and solvating water molecules. The $H_5\mathbf{L1}^{5+}$ cation interacts with three external perchlorate anions and a water molecule through strong hydrogen bonds (Figure 2, Table 2). The N···N and O···O interatomic distances (Table 2) are consistent with the presence of a pseudo-threefold symmetry axis passing through the two bridgehead nitrogen atoms of $H_5\mathbf{L1}^{5+}$. As a result of electrostatic repulsion, the cavity of $H_5\mathbf{L1}^{5+}$ is expanded, albeit only slightly, with respect to that of the free **L1** cryptand.[21] This expansion is mainly manifested in a lengthening of the distances between the secondary nitrogen atoms of the tetraamine moiety, the O···O distances within the opposite tripodal subunit being less affected by protonation (Table 2). The distance between the bridgehead nitrogen atoms in **L1** [6.249(5) Å][21] is maintained in $H_5\mathbf{L1}^{5+}$ [6.25(2) Å]. As a consequence of the aforementioned expansion, $H_5\mathbf{L1}^{5+}$ displays some molecular strain. This is evident from the bond angles in the ligand

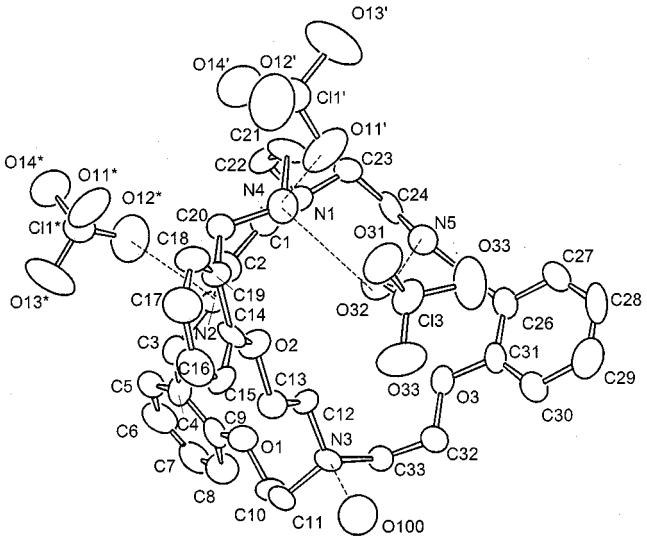


Figure 2. A perspective view of **1** showing the atom numbering scheme

Table 2. Selected intramolecular distances [Å], bond angles [°], and hydrogen-bond lengths [Å] for **1** and **2**

1		**2**	
N1···N3	6.25(2)[a]	Ni···N(2)	2.243(6)
N5···N4	5.54(2)	Ni···N(12)	2.017(6)
N4···N2	4.59(2)	Ni···N(3)	2.055(6)
O1···O2	4.77(2)	Ni···N(1)	2.151(6)
O1···O3	5.28(1)	Ni···Cl(1)	2.303(2)
O2···O3	5.04(1)		
		N(12)−Ni−N(3)	85.9(2)
		N(12)−Ni−N(1)	85.8(2)
		N(3)−Ni−N(1)	94.5(2)
		N(12)−Ni−N(2)	82.6(2)
		N(3)−Ni−N(2)	97.2(2)
		N(1)−Ni−N(2)	162.7(2)
		N(12)−Ni−Cl(1)	110.86(18)
		N(3)−Ni−Cl(1)	163.15(17)
		N(1)−Ni−Cl(1)	88.88(18)
		N(2)−Ni−Cl(1)	83.42(18)

H*y*drogen bond distances for **1**

N5···O32		2.82(2)
N4···O32		2.86(2)
N2···O12	$-x + 1.5, y - 0.5, -z + 1.5$	2.94(2)
N4···O11	$x-1, y, z$	3.01(2)
N3···O100		2.82(2)
O100···O14	$-x + 1.5, y + 0.5, -z + 1.5$	2.99(2)
O200···O11	$x - 1, y, z$	2.88(3)
O200···O500	$x - 1, y, z$	2.38(5)
O400···O500	$-x + 1, -y + 1, -z + 1$	2.15(6)
O500···O33	$x + 1, y, z$	2.77(4)

[a] Values in parentheses are standard deviations in the last significant figure.

chains, which are, on average, significantly larger (mean value 112.4°) than the value expected for sp^3 carbon atoms. The protonated nitrogen atoms N(2), N(4), and N(5) interact with three external perchlorate anions (Figure 2), two of which are symmetry-related (Table 2). The other ClO_4^- anion (Cl3) bridges two ammonium groups (Figure 2). All the anions are strongly bound to the protonated cryptand, as evidenced by the short hydrogen-bond lengths (Table 2). While in the unprotonated **L1** and the diprotonated $[(H_2\mathbf{L1})\subset H_2O]^{2+}$ cryptate the bridgehead nitrogen atoms adopt an *endo-endo* conformation, in $H_5\mathbf{L1}^{5+}$ the acidic proton bound to the bridgehead N(3) points towards the exterior of the molecular cavity, interacting with an external water molecule [N(3)···O(100) distance 2.82(2) Å]. No such hydrogen bonding involving the other bridgehead nitrogen atom can be detected. Consequently, the bridgehead nitrogen atoms assume an *endo-exo* conformation (Figure 2). It thus seems reasonable that the formation of very stable cryptate species is responsible for the high stability of **L1** in the early stages of protonation, while conformational changes, disruption of the cryptate structure, and strong electrostatic repulsions between positive charges combine to produce a rapid loss of stability in the later protonation stages.

Further investigations are in progress aimed at ascertaining the nature of the cryptate species. As a matter of fact, in a recent communication the inclusion, both in solution and in the solid state, of two nitrate anions in the cavity of a similar cryptand has been reported.[19]

Complex Formation

The macrobicyclic ligands **L1**−**L3** are potential heteroditopic receptors for metal ions, being composed of two dissimilar tripodal binding subunits. While the tetraamine moiety has proved to be suitable for the coordination of transition metal ions,[20−23,31] the ethereal moiety can be expected to be effective in the binding of "harder" cations. In order to determine the coordination properties of these ligands in aqueous solution, we have studied the complexation of various metal ions such as Ni^{2+}, Cu^{2+}, Zn^{2+}, Cd^{2+}, and Pb^{2+}, as well as of alkali and alkaline earth cations. From the results of this study, it is clear that the three ligands do not show any tendency to form complexes with alkali or alkaline earth cations, while they are capable of forming stable complexes with the remaining metal ions. Nevertheless, the ethereal moieties of these ligands display a poor propensity to remain vacant; indeed, as shown by crystal structure determinations,[21,23] they are well suited for strong hydrogen-bonding interactions with water molecules inside the ligand cavity, in particular with water molecules linked to metal ions coordinated to the opposite tetraamine site, as is observed in the crystal structures of the Ni^{2+} complex[21] with **L1** and the Cu^{2+} complex[23] with **L2**. Similar features have been observed previously for other cryptand ligands.[28,32]

The cryptand **L2** readily forms a mononuclear complex with Ni^{2+}, which has been isolated as $[(Ni\mathbf{L2}Cl)Cl]\cdot 5.5\,H_2O\cdot CH_3OH$. The crystal structure of this complex reveals the presence of $[\mathbf{L2}\subset NiCl]^+$ cations (Figure 3), chloride anions, and methanol and water molecules of crystallization. The Ni^{2+} cation achieves pentacoordination through ligation by the N_4 ligand moiety and a chloride ion, Cl(1), in a trigonal-bipyramidal fashion (Table 2), where the secondary amino nitrogen atoms N(1) and N(2) occupy the axial positions (Figure 3). This coor-

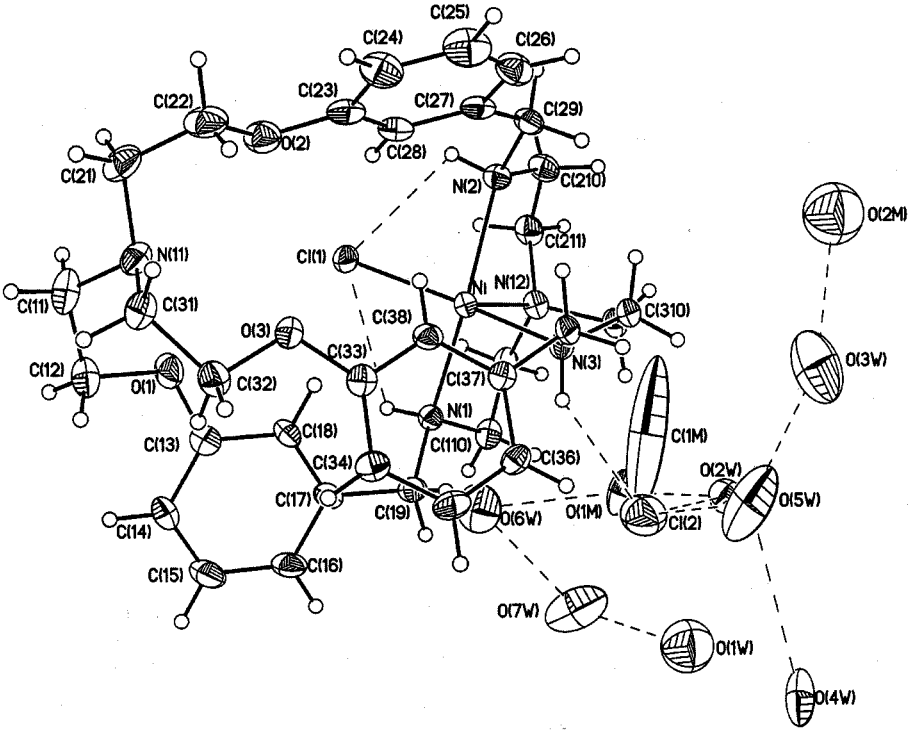


Figure 3. A perspective view of **2** showing the atom numbering scheme

dination geometry is quite similar to that in the pentagonal-bipyramidal cascade complex[20] of the Cu^{2+} ion with the same ligand. Cl(1) also shows hydrogen-bonding interactions with the amine nitrogen atoms N(1) and N(2) [Cl(1)···N(1) 3.121(5) Å; Cl(1)···N(2) 3.025(6) Å]. Seven water and two methanol molecules are also present in the crystal lattice. Both the methanol molecules and three of the water molecules show large thermal displacements and are assigned half-occupancy. All bond lengths and bond angles in the cryptand moiety have typical values within statistical error limits.

It is noteworthy that, although chloride anions and water molecules are similarly drawn into the cryptand cavity by coordinated metal ions, the water cryptate is stabilized by hydrogen bonding to the ethereal oxygen atoms, whereas the chloride ions form hydrogen bonds with the metal-coordinated amine groups.

Stability Constants

The stability constants for the Cu^{2+}, Zn^{2+}, Cd^{2+}, and Pb^{2+} complexes with **L1** and **L2**, as well as for the Cu^{2+} and Zn^{2+} complexes with **L3**, are reported in Table 3. As mentioned in the Experimental Section, it was not possible to study the complexation of Cd^{2+} and Pb^{2+} with **L3** due to solubility problems. Stability constants for the Ni^{2+} complexes of the three ligands could not be determined, again due to solubility problems.

L1 forms both $ML1^{2+}$ and hydroxylated $ML1(OH)^{+}$ species with all the metal ions except for Cu^{2+}, while **L2** and **L3** are also able to form the monoprotonated species. In the case of the Zn^{2+} and Cd^{2+} complexes with **L2**, however, formation of a hydroxylated species was not observed due to precipitation occurring in alkaline solution. Although the set of stability constants is incomplete, some interesting conclusions regarding the coordination properties of these ligands can be drawn. Firstly, it can be noted that some dimensional recognition is exhibited by these cryptands. As a matter of fact, considering the metal ions (Zn^{2+}, Cd^{2+},

Table 3. Logarithms of complexation constants determined in 0.10 mol dm^{-3} Me_4NNO_3 at 298.1 K

Reaction	**L1**	**L2** log K[a]	**L3**
$Cu^{2+} + L = CuL^{2+}$	15.22(3)	14.36(3)	
$Cu^{2+} + HL^{+} = CuLH^{3+}$		11.2(1)	7.44(3)
$CuL^{2+} + H^{+} = CuLH^{3+}$		6.6(1)	8.70(8)
$CuL^{2+} + OH^{-} = CuLOH^{+}$		5.6(1)	4.38(8)
$Zn^{2+} + L = ZnL^{2+}$	8.83(5)	7.06(6)	
$Zn^{2+} + HL^{+} = ZnLH^{3+}$		5.07(6)	4.8(1)
$ZnL^{2+} + H^{+} = ZnLH^{3+}$		7.76(6)	7.45(2)
$ZnL^{2+} + OH^{-} = ZnLOH^{+}$	3.78(7)		3.66(6)
$Cd^{2+} + L = CdL^{2+}$	11.14(2)	7.35(8)	
$Cd^{2+} + HL^{+} = CdLH^{3+}$		6.94(8)	
$CdL^{2+} + H^{+} = CdLH^{3+}$		7.94(9)	
$CdL^{2+} + OH^{-} = CdLOH^{+}$	3.83(3)		
$Pb^{2+} + L = PbL^{2+}$	13.09(2)	9.52(9)	
$Pb^{2+} + HL^{+} = PbLH^{3+}$	6.95(9)		
$PbL^{2+} + H^{+} = PbLH^{3+}$	7.16(9)		
$PbL^{2+} + OH^{-} = PbLOH^{+}$	3.25(5)	3.8(1)	

[a] Values in parentheses are standard deviations in the last significant figure.

Pb^{2+}) for which ligand-field stabilization is not possible, complex stability is seen to increase with increasing metal ion size. Such a trend in the coordination ability is evidently connected with the macrobicyclic nature of these ligands, since an opposite trend in stabilities is observed for the Zn^{2+} and Cd^{2+} complexes with the ligand tris(2-aminoethyl)amine, tren {log K = 14.5 for $Zn(tren)^{2+}$, log K = 11.7 for $Cd(tren)^{2+}$,[33a] log K = 10.21(1) for $[Pb(tren)]^{2+}$ [33b]}, which can be considered as an acyclic analogue of the tetraamine moieties of **L1** and **L2**. Due to their bicyclic structures, cryptands are more rigid than acyclic molecules. Consequently, they show a reduced tendency to modify their arrangements so as to satisfy the coordination requirements of metal ions. The present cryptands are apparently too large to give a good fitting with all the studied metal ions, which accounts for the observed stability increase with increasing cation dimensions.

The complexation ability has been found to be highly dependent on the ligand structure. While the lower tendency of **L3** to form complexes with the present metal ions was expected, due to the formation of six-membered chelate rings rather than the more stable five-membered ones formed by **L1** and **L2**, the difference in stability between the complexes of **L1** and **L2** is rather surprising. All complexes formed by **L1** are considerably more stable than those with **L2**, this difference in stability amounting to more than three orders of magnitude in the case of the Cd^{2+} and Pb^{2+} complexes. It is worth noting that, on the basis of X-ray crystallographic studies[20,22] on free **L1** and **L2** and their metal complexes, the cavity in **L2** has been shown to be much more rigid compared to that in **L1**. Consequently, the entering metal ion cannot adjust the coordination geometry to its liking in the former.

Conclusion

Cryptand ligands are characterized by rigid structures and consequently simple ligand modifications can lead to significant changes in their binding properties. This has clearly been shown to occur with **L1**−**L3**. In particular, the presence of *ortho*-substituted aromatic spacers in **L1** gives rise to an evident enhancement in basicity and metal ion coordination properties with respect to **L2**, which contains *meta*-substituted spacers. These cryptands show a particular tendency to form inclusion complexes in which multiple species are enclosed in the ligand cavity. In spite of this tendency and of the presence of two separate binding subunits in the ligands, **L1**−**L3** are not able to form binuclear metal complexes in aqueous solution. Nevertheless, in accordance with their structures, these ligands display heteroditopic properties in metal ion coordination since the two distinct binding subunits act cooperatively in the binding of $M(H_2O)^{2+}$ (M = metal ion) species. Furthermore, the abilities of these cryptands to promote inclusive coordination make these compounds promising candidates for the binding and recognition of anionic substrates, both in the presence and absence of coordinated metal ions.

Experimental Section

General Procedures and Materials: Cryptands **L1**−**L3** were synthesized as described previously[20,23,34] and were used in the form of free amines. − Crystals of $[(H_5\mathbf{L1})(ClO_4)_5] \cdot 4\,H_2O$ (**1**) suitable for single-crystal X-ray analysis were obtained by slow evaporation of the solvents at room temperature from a solution containing **L1** and an excess of $HClO_4$ in ethanol/H_2O (80:20, v/v). − $C_{33}H_{58}Cl_5N_5O_{27}$ (1134.1): calcd. C 34.95, H 5.16, N 6.18; found C 35.0, H 5.2, N 6.2. − ***Caution!*** *Care must be taken when treating organic compounds with perchloric acid as potentially explosive mixtures may be formed.* − $[(Ni\mathbf{L2}Cl)Cl] \cdot 5.5\,H_2O \cdot CH_3OH$ (**2**) was prepared by adding a solution of $NiCl_2 \cdot 6\,H_2O$ (0.24 g, 0.1 mmol) in MeOH (5 mL) to **L2** (0.056 g, 0.1 mmol) in MeOH (5 mL). A bluish-green solid separated immediately, which was collected by filtration, washed with MeOH, and dried in air. Recrystallization from MeCN afforded X-ray quality single crystals as green rectangular parallelepipeds. − $C_{34}H_{60}Cl_2N_5NiO_{9.5}$ (820.5): calcd. C 49.77, H 7.37, N 8.54; found C 49.7, H 7.4, N 8.5.

Crystal Structure Determination: A summary of X-ray data collection, structure solution, and refinement for both **1** and **2** is presented in Table 4. In each case, the cell parameters were determined by least-squares refinement of diffractometer setting angles for 25 carefully centered reflections. The intensities of two standard reflections were monitored every hour during data collection to check the stability of the diffractometer and of the crystal. Intensity data were corrected for Lorentz and polarization effects and, in the case of **1**, an absorption correction was applied once the structure had been solved by the DIFABS method.[35] In the case of **2**, an analytical absorption correction was applied. Both structures were solved by direct methods[36] and refined by full-matrix least-squares techniques on F^2 using SHELXL-97[37a] and SHELX-93[37b] for **1** and **2**, respectively, which use the analytical approximation for atomic scattering factors and anomalous dispersion corrections for all atoms taken from ref.[38] Anisotropic displacement parameters were used for all non-hydrogen atoms. In each case, hydrogen atoms were introduced in calculated positions. For **1**, an overall unrefined temperature factor was assigned for the hydrogen atoms, while for **2** overall refined thermal parameters were used for aliphatic, amino, and aromatic hydrogen atoms. Crystallographic data

Table 4. Crystal data and structure refinement for $[H_5\mathbf{L1}](ClO_4)_5 \cdot 4\,H_2O$ and $[(Ni\mathbf{L2}Cl)Cl] \cdot 5.5\,H_2O \cdot CH_3OH$

Empirical formula	$C_{33}H_{58}Cl_5N_5O_{27}$	$C_{34}H_{60}Cl_2N_5NiO_{9.5}$
Formula mass	1134.09	820.48
Temperature	298 K	293 K
Wavelength	0.71069 Å	0.71069 Å
Crystal system	monoclinic	monoclinic
Space group	$P2_1/n$	$C2/c$
Unit cell dimensions	a = 14.281(4) Å	a = 26.671(6) Å
	b = 14.313(7) Å	b = 16.784(4) Å
	c = 24.082(8) Å	c = 18.591(4) Å
	β = 92.00(2)°	β = 101.006(14)°
Volume	4920(3) Å^3	8169(3) Å^3
Z	4	8
Density (calculated)	1.531 Mg/m^3	1.333 Mg/m^3
Absorption coefficient	0.389 mm^{-1}	0.662 mm^{-1}
Crystal size	0.3 × 0.2 × 0.15 mm	0.35 × 0.34 × 0.27 mm
Final R indices $[I > 2\sigma(I)]$	$R1$ = 0.0790	$R1$ = 0.0912
	$wR2$ = 0.2010[a]	$wR2$ = 0.1424
R indices (all data)	$R1$ = 0.1860	$R1$ = 0.2077
	$wR2$ = 0.2906[a]	$wR2$ = 0.3122

[a] $R = \Sigma||F_o| - |F_c||/\Sigma|F_o|$; $wR^2 = [\Sigma w(F_o^2 - F_c^2)^2/\Sigma wF_o^4]^{1/2}$.

(excluding structure factors) for the structures reported in this paper have been deposited with the Cambridge Crystallographic Data Centre as supplementary publication nos. CCDC-140417 and CCDC-140418 for **1** and **2**, respectively. Copies of the data can be obtained free of charge on application to the CCDC, 12 Union Road, Cambridge CB2 1EZ, U.K. [Fax: (internat.) + 44-1223/336-033; E-mail: deposit@ccdc.cam.ac.uk].

Potentiometric Measurements: All pH-metric measurements (pH = $-\log [H^+]$) used for the determination of protonation and complex formation constants were performed in 0.10 mol dm^{-3} Me_4NNO_3 solutions at 298.1 ± 0.1 K using equipment and methodologies described in a previous report.[39] The combined Ingold 405 S7/120 electrode was calibrated as a hydrogen concentration probe by titrating known amounts of HCl with CO_2-free Me_4NOH solutions and determining the equivalent point by Gran's method.[40] This allows determination of the standard potential E^o and the ionic product of water [pK_w = 13.83(1) at 298.1 ± 0.1 K in 0.1 mol dm^{-3} Me_4NNO_3]. At least three measurements were performed for each system. In all experiments, the ligand concentration [L] was $5 \cdot 10^{-4}$ mol dm^{-3}, while in the complexation experiments the metal ion concentration was about 0.8 [L]. Test measurements were performed in presence of higher metal ion concentrations in order to confirm that no polynuclear complexes were formed. The pH range investigated was 2.5−10.5 for all measurements, although in some cases the formation of precipitates curtailed the useful range for the determination of equilibrium constants. This was the case at pH > 8 in the titrations performed to determine the protonation constants of **L3** and the stability constants of the Zn^{2+} and Cd^{2+} complexes with **L2**. In the case of **L3**, only the complexes with Cu^{2+} and Zn^{2+} were sufficiently soluble for adequate study. Complexation reactions with these ligands were found to be rather slow. For this reason, equilibration times of 5−15 min were necessary after each addition of titrant. Conventional potentiometric titrations were performed to determine the stability constants in the system Pb^{2+}/tren ([tren] = $1 \cdot 10^{-3}$ mol dm^{-3}, [Pb^{2+}] = 0.8 [tren]) under the same experimental conditions (0.1 mol dm^{-3} Me_4NNO_3, 298.1 ± 0.1 K). The computer program HYPERQUAD[41] was used to calculate both protonation and complexation constants from the e.m.f. data.

Acknowledgments

Financial support from the Department of Science and Technology, New Delhi, India (to P. K. B.) and from the Italian Ministero dell'Università e della Ricerca Scientifica e Tecnologica (MURST) is gratefully acknowledged.

[1] *Synthesis of Macrocycles: The Design of Selective Complexing Agents* (Eds.: J. J. Christensen, R. M. Izatt), Wiley, New York, **1987**.
[2] K. B. Mertes, J.-M. Lehn, *Multidentate Macrocyclic and Macropolycyclic Ligands*, in: *Comprehensive Coordination Chemistry* (Ed.: G. Wilkinson), Pergamon Press, Oxford, **1987**, p. 915.
[3] J.-M. Lehn, *Angew. Chem. Int. Ed. Eng.* **1988**, *27*, 89.
[4] L. F. Lindoy, *The Chemistry of Macrocyclic Ligand Complexes*, Cambridge University Press, Cambridge, **1989**.
[5] *Cation Binding by Macrocycles* (Eds.: Y. Inoue, G. W. Gokel), Marcel Dekker, New York, **1991**.
[6] F. Diederich, *Cyclophanes*, The Royal Society of Chemistry, Cambridge, **1991**.
[7] D. J. Cram, J. M. Cram, *Container Molecules and Their Guests*, The Royal Society of Chemistry, Cambridge, **1994**.
[8] J.-M. Lehn, *Supramolecular Chemistry: Concepts and Perspectives*, VCH, Weinheim, **1995**.
[9] *Supramolecular Chemistry of Anions* (Eds.: A. Bianchi, K. Bowman-James, E. Garcia-España), Wiley-VCH, New York, **1997**.
[10] M. E. Barr, P. H. Smith, W. E. Anthoine, B. Spencer, *J. Chem. Soc., Chem Commun.* **1993**, 1649.
[11] C. Harding, J. Nelson, M. C. R. Symons, J. Wyatt, *J. Chem. Soc., Chem.Commun.* **1994**, 2499.
[12] C. Bazzicalupi, A. Bencini, A. Bianchi, V. Fusi, L. Mazzanti, P. Paoletti, B. Valtancoli, *Inorg. Chem.* **1995**, *34*, 3003.
[13] A. Bencini, A. Bianchi, S. Brazzini, V. Fusi, C. Giorgi, P. Paoletti, B. Valtancoli, *Inorg. Chim. Acta* **1998**, *273*, 326.
[14] J.-L. Pierre, P. Chautemps, S. Refaif, C. Beguin, A. El Marzouki, G. Serratrice, E. Saint-Aman, P. Rey, *J. Am. Chem. Soc.* **1995**, *117*, 1965.
[15] S.-G. Kang, K. Ryu, M. P. Suh, J. H. Jeong, *Inorg. Chem.* **1997**, *36*, 2478.
[16] J. Nelson, V. McKee, G. Morgan, in *Progress in Inorganic Chemistry* (Ed.: K. D. Karlin), Wiley, New York, **1998**, p. 167.
[17] G. Morgan, V. McKee, J. Nelson, *J. Chem. Soc., Chem. Commun.* **1995**, 1649.
[18] R. J. A. Jansen, L. F. Lindoy, O. A. Mathews, G. B. V. Mehan, A. N. Sobeleb, A. H. White, *J. Chem. Soc., Chem. Commun.* **1995**, 735.
[19] S. Mason, T. Clifford, L. Seib, K. Kuczera, K. Bowman-James, *J. Am. Chem. Soc.* **1998**, *120*, 8899.
[20] D. K. Chand, P. K. Bharadwaj, *Inorg. Chem.* **1996**, *35*, 3380.
[21] P. Ghosh, S. S. Gupta, P. K. Bharadwaj, *J. Chem. Soc., Dalton Trans.* **1997**, 935.
[22] D. K. Chand, P. K. Bharadwaj, *Inorg. Chem.* **1997**, *36*, 5658.
[23] D. K. Chand, P. K. Bharadwaj, *Inorg. Chem.* **1998**, *37*, 5050.
[24] K. G. Ragunathan, P. K. Bharadwaj, *Proc. Indian Acad. Sci. (Chem. Sci.)* **1995**, *107*, 519.
[25] P. Ghosh, P. K. Bharadwaj, S. Mandal, S. J. Ghosh, *J. Am. Chem. Soc.* **1996**, *118*, 1553.
[26] P. Bandyopadhyay, P. K. Bharadwaj, *Langmuir* **1998**, *14*, 7537.
[27] G. Das, P. Ghosh, P. K. Bharadwaj, *Langmuir* **1997**, *13*, 3582.
[28] J.-M. Lehn, *Acc. Chem. Res.* **1978**, *11*, 49.
[29] C. Bazzicalupi, A. Bencini, A. Bianchi, V. Fusi, P. Paoletti, B. Valtancoli, *J. Chem Soc. Perkin Trans. 2* **1994**, 815.
[30] D. K. Chand, K. G. Ragunathan, T. C. W. Mak, P. K. Bharadwaj, *J. Org. Chem.* **1996**, *61*, 1169.
[31] P. Ghosh, P. K. Bharadwaj, *J. Chem. Soc., Dalton Trans.* **1997**, 2673.
[32] C. Bazzicalupi, A. Bencini, A. Bianchi, V. Fusi, C. Giorgi, P. Paoletti, B. Valtancoli, *J. Chem. Soc., Dalton Trans.* **1994**, 3581.
[33] [33a] R. M. Smith, A. E. Martell, *NIST Critical Stability Constants Database*, version 4.0, **1997**. − [33b] Values determined in the present work: log K = 10.21(1) for Pb^{2+} + tren = $[Pb(tren)OH]^+$; log K = 2.71(6) for $Pb(tren)^{2+}$ + OH^- = $[Pb(tren)OH]^+$ (0.1 mol dm^{-3} Me_4NNO_3, 298.1 ± 0.1 K).
[34] K. G. Ragunathan, P. K. Bharadwaj, *Tetrahedron Lett.* **1992**, 7581.
[35] N. Walker, D. D. Stuart, *Acta Crystallogr. Sect. A* **1983**, *39*, 158.
[36] A. Altomare, G. Cascarano, C. Giacovazzo, A. Guagliardi, *J. Appl. Crystallogr.* **1993**, *26*, 343.
[37] [37a] G. M. Sheldrick, *SHELXL-97*, University of Göttingen, Germany, **1997**. − [37b] G. M. Sheldrick, *SHELXL-93. Program for the Refinement of Crystal Structures*, University of Göttingen, Germany, **1993**.
[38] *International Tables for X-ray Crystallography*, Kynoch Press, Birmingham, England, **1974**, vol. IV.
[39] A. Bianchi, L. Bologni, P. Dapporto, M. Micheloni, P. Paoletti, *Inorg. Chem.* **1984**, *23*, 1201.
[40] G. Gran, *Analyst (London)* **1952**, *77*, 661.
[41] P. Gans, A. Sabatini, A. Vacca, *Talanta* **1996**, *43*, 1739.

Received February 16, 2000
[I00050]

Rhodium and Iridium Complexes Derived from *trans*-[MCl(CO)(PPh_3)$_2$] (M = Rh, Ir) and Pyridine-2-thiolate or 4,6-Dimethylpyrimidine-2-thiolate Ligands: *S*-Monodentate Coordination versus *S,N*-Chelation and *S,N*-Bridging; Reactivity of *trans*-[Ir('Spy')(CO)(PPh_3)$_2$] and *trans*-[Ir('SpymMe$_2$')(CO)(PPh_3)$_2$] towards Acid

Lutz Dahlenburg*[a] and Michael Kühnlein[a]

Keywords: Iridium / Rhodium / S ligands / Chelates / Bridging ligands

Treatment of *trans*-[IrCl(CO)(PPh_3)$_2$] with the sodium salts of the *S,N*-hybrid ligands, pyridine-2-thiol ('pySH') and 4,6-dimethylpyrimidine-2-thiol ('Me$_2$pymSH'), produced *trans*-[Ir('Spy')(CO)(PPh_3)$_2$] (**1**) and *trans*-[Ir('SpymMe$_2$')(CO)(PPh_3)$_2$] (**2**), containing *S*-monodentate thiolato ligands. In contrast, the reactions between *trans*-[RhCl(CO)(PPh_3)$_2$] and the two bifunctional thiolate ligands yielded the PPh_3-loss products [{Rh(μ-'Spy'-κ*N*,κ*S*)(CO)(PPh_3)}$_2$] (**3**) and [Rh('SpymMe$_2$'-κ*N*,κ*S*)(CO)(PPh_3)] (**4**), whose structures in the solid state were determined by single-crystal X-ray diffraction. In binuclear complex **3**, the bridging pyridine-2-thiolate ligands are bound to the adjacent metal centers through their N and S atoms in a head-to-tail manner. The crystal structure of **4** consists of mononuclear molecules possessing four-membered Rh–S–C–N chelate rings with the sulfur atom *trans* to the CO ligand. In solution, both **3** and **4** display temperature-dependent dynamic behavior. Reaction of **2** with trifluoroacetic acid resulted in protonation of the iridium atom and ring closure to form the monopositive chelate complex [IrH('SpymMe$_2$'-κ*N*,κ*S*)(CO)(PPh_3)$_2$]$^+$, which was isolated and characterized by X-ray crystallography as the hydrogen bis(trifluoroacetate) salt [IrH('SpymMe$_2$'-κ*N*,κ*S*)(CO)(PPh_3)$_2$][H(O_2CCF_3)$_2$] (**5a**). Protonation of both the iridium and one pyrimidine nitrogen atom was observed in the analogous reaction of **2** with HBF_4, which afforded the 4,6-dimethylpyrimidinium-2-thiolato chelate complex [IrH(2-$SC_4HNN(H)Me_2$-4,6-κ*N*,κ*S*)(CO)(PPh_3)$_2$](BF_4)$_2$ as a mixture of two isomers, having the hydride ligand either *trans* to S (**5c**) or *trans* to N (**5d**). The complex [IrH('Spy')$_2$(CO)(PPh_3)$_2$] (**6**) resulted from oxidative addition of pyridine-2-thiol to **1** or reaction of *trans*-[IrCl(CO)(PPh_3)$_2$] with an excess of the 'pySH' ligand. Complex **6** reacted with HBF_4 in $CHCl_3$ with cleavage of one Ir–S bond and protonation at the metal center to produce the ionic chelate complex [IrH('Spy'-κ*N*,κ*S*)(CO)(PPh_3)$_2$]BF_4 (**7**) which was also fully characterized by X-ray analysis.

Introduction

Our recent interest has focused on the chelation of bidentate *P,N* and *P,O* ligands, in particular with respect to the reactivity of their transition metal complexes towards Brønsted acids.[1,2,3] In this context, two ring-opened iridium(III) compounds, [$IrHCl_2$(CO)(PPh_3)($PPh_2C_6H_4N$(-Me)H-2)][2] and [$IrHCl_2$(CO)(PPh_3)($PPh_2C_6H_4OH$-2)],[3] resulting from reaction of their parent iridium(I) chelate complexes *trans*-[Ir(CO)(PPh_3)($PPh_2C_6H_4$E-2)] (E = NMe, O) with hydrogen chloride, have been shown to exist as mixtures of Ir−$PPh_2C_6H_4$EH-2 rotamers which are stabilized by intramolecular −N(Me)H···Cl(Ir) and −OH···H(Ir)···Cl hydrogen bonding. Following these studies, we have turned our attention to iridium and rhodium complexes derived from the requisite Vaska-type precursors *trans*-[MCl(CO)(PPh_3)$_2$] and bifunctional ligands having soft *S* and hard *N* ends, such as pyridine-2-thiol, NC_5H_4SH-2 ('pySH'), and 4,6-dimethylpyrimidine-2-thiol, 4,6-$Me_2C_4HN_2$-SH-2 ('Me$_2$pymSH'), respectively.

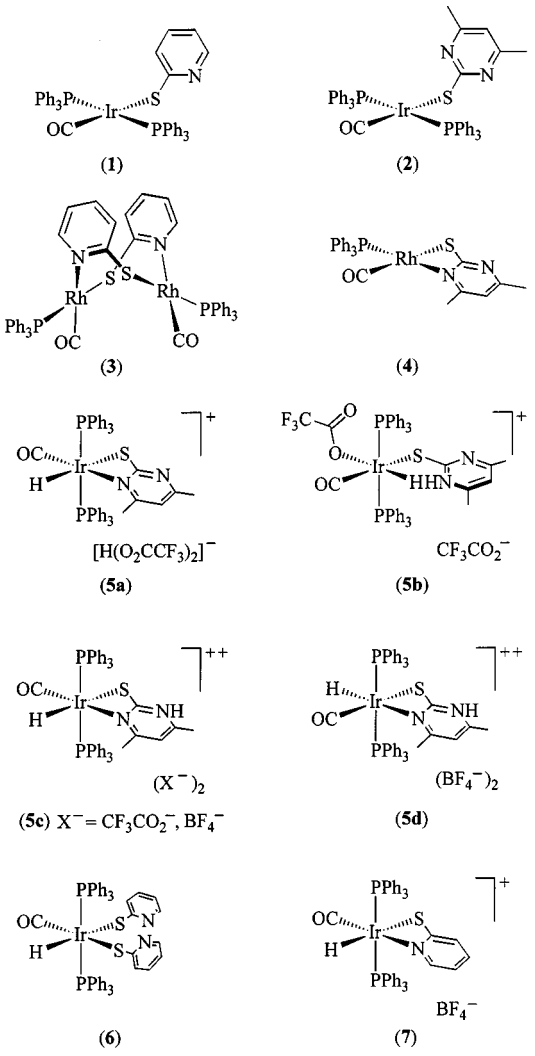
Both the ligands and their conjugate bases are ubiquitous *S,N* donors that form a wide variety of complexes with p-, d-, and also f-block metals.[4−8] The published work concerning the chemistry of relevant coordination compounds of the platinum group metals rhodium and iridium in their lower oxidation states is dominated by di- and trinuclear complexes with *S,N*-bridging thiolates, derived from bimetallic olefin and carbonyl precursors, such as [M_2(μ-Cl)$_2$(diolefin)$_2$] (M = Rh,[9a−9c,10a] Ir[9d,10a]) or [Rh_2(μ-Cl)$_2$(CO)$_4$].[11]

The compounds reported in this paper (Scheme 1) were synthesized with the principal objectives of (i) investigating the coordination properties of the two *S,N* donors in Vaska-type environments and (ii) elucidating the reactivity of the resulting complexes towards Brønsted acids. Because of the basicity of the pyridine and pyrimidine heterocycles, and owing to the pronounced basic character of the metal ion in coordinatively unsaturated d^8 complexes, protonation of four-coordinate Rh^I and, specifically, Ir^I compounds [MX(CO)L$_2$] bearing *S*-monodentate 'Spy' or 'SpymMe$_2$' ligands by strong acids was expected to occur both at the

[a] Institut für Anorganische Chemie der Universität Erlangen-Nürnberg
Egerlandstrasse 1, D-91058 Erlangen, Germany
Fax: (internat.) + 49-(0)9131/85-27387
E-mail: dahlenburg@chemie.uni-erlangen.de

 © WILEY-VCH Verlag GmbH, D-69451 Weinheim, 2000 1434−1948/00/0909−2117 $ 17.50+.50/0

metal center and the nitrogen atom. The resulting products could exhibit intramolecular N−H···H−M hydrogen bonding, as it has been previously demonstrated that pyridine-2-thiol, if coordinated as a monodentate $HN^+C_5H_4S^-$ zwitterion, has a distinct propensity to behave as a weakly acidic N−H donor toward weakly basic Ir^{III}−H acceptor functions.[12] In this connection, the behavior towards protic acids of two related Rh^I and Ir^I complexes $[M(S_2NC_7H_4)(CO)(PPh_3)]$ with *S*-monodentate benzothiazole-2-thiolate ligands is worth mentioning: Protonation of the rhodium derivative with HBF_4 takes place at the noncoordinated nitrogen atom giving $[Rh(S_2N(H)C_7H_4)(CO)(PPh_3)_2]BF_4$,[9e,9f] in contrast to the iridium homologue where protonation occurs at the metal center with production of the hydridoiridium(III) complex $[IrH(S_2NC_7H_4)(CO)(PPh_3)_2]BF_4$.[9f]



Scheme 1

Results and Discussion

Syntheses and Solid-State Structures of Rh^I and Ir^I Thiolates

The *S*-monodentate pyridine-2- and 4,6-dimethylpyrimidine-2-thiolato derivatives *trans*-[Ir('Spy')(CO)$(PPh_3)_2$] (**1**) and *trans*-[Ir('SpymMe_2')(CO)$(PPh_3)_2$] (**2**) were formed smoothly by combining the sodium salts of the respective thiols and Vaska's complex, *trans*-[IrCl(CO)$(PPh_3)_2$], in a 1:1 stoichiometry in THF at room temperature. The $^{31}P\{^1H\}$ NMR spectra of the two compounds consist of singlets (δ = 23.1 for **1** and 19.4 for **2**), indicating the expected pairs of equivalent phosphane ligands (Scheme 1).

Under the conditions chosen for the preparation of **1**, the rhodium(I) complex *trans*-[RhCl(CO)$(PPh_3)_2$] and sodium pyridine-2-thiolate underwent Cl^-/'pyS^-' exchange accompanied by elimination of a phosphane ligand to give the binuclear PPh_3-loss product $[\{Rh(\mu\text{-'Spy'})(CO)(PPh_3)\}_2]$ (**3**). Prior to this work, a highly fluxional complex of identical composition was reported to result from solution equilibration of $[Rh_2(\mu\text{-'Spy'})_2(CO)_3(PPh_3)]$, affording $[\{Rh(\mu\text{-'Spy'})(CO)_2\}_2]$ together with $[\{Rh(\mu\text{-'Spy'})(CO)(PPh_3)\}_2]$.[9b] From the $^{31}P\{^1H\}$ NMR data observed at the slow exchange limit, an unspecified ground-state structure with equivalent PPh_3 ligands *trans* to the sulfur atoms was tentatively inferred for this dirhodium compound.[9b] Complex **3** is also fluxional in solution (see below) and adopts a solid-state structure consisting of bimetallic molecules in which both pyridine-2-thiolate ligands bridge two *cis* coordination sites of the metal centers through their S and N atoms, the pairs of Rh−N and Rh−S bonds being *trans* to the CO and PPh_3 ligands, respectively (Figure 1). The coordination planes of the two metal centers are inclined to each other at an angle of 34.9°. In addition, the donor atoms coordinated to Rh(1) and Rh(2) are staggered, the torsion angles being −46.4 and −51.3° for the N(1)−Rh(1)···Rh(2)−N(2) and C(1)−Rh(1)···Rh(2)−C(2) fragments, and 134.7 and 137.7° for S(1)−Rh(1)···Rh(2)−S(2) and P(1)−Rh(1)···Rh(2)−P(2), respectively. The molecular structure of **3** thus closely resembles those of the related tetracarbonyl and thiazoline-2-thiolato-bridged species $[\{Rh(\mu\text{-'Spy'-}\kappa N,\kappa S)(CO)_2\}_2]$[9b] and $[\{Rh(\mu\text{-}S_2NC_3H_4\text{-}\kappa N,\kappa S)(L)(L')\}_2]$ (L, L′ = COD;[10a] CO, PMe_3;[10b] CO, PPh_3[10b]), similarly containing twisted nonparallel metal coordination planes, linked in a head-to-tail fashion by the nitrogen and mercapto sulfur atoms of two *N*-heterocyclic thiolate bridges. The Rh(1)···Rh(2) separation, 3.1952(5) Å, is shorter than that of 3.2435(3) Å in $[\{Rh(\mu\text{-}S_2NC_3H_4\text{-}\kappa N,\kappa S)(CO)(PPh_3)\}_2]$[10b] and presumably reflects the observation that the tilt of the coordination planes in **3**, 34.9°, is somewhat closer to parallel than the 38.5° observed in the latter compound. All metal-to-ligand bond lengths (Figure 1) are as expected as compared to those of structurally analogous dirhodium derivatives.[9b,10a,10b]

Surprisingly, treatment of *trans*-[RhCl(CO)$(PPh_3)_2$] with 4,6-dimethylpyrimidine-2-thiolate did not afford any *S*,*N*-linked or *S*-bridged binuclear product, but resulted in formation of the unusual four-membered Rh−S−C−N metallaheterocycle [Rh('SpymMe_2'-$\kappa N,\kappa S$)(CO)(PPh_3)] (**4**). The X-ray structure analysis of this complex showed the presence of molecules with a slightly distorted planar coordination geometry (Figure 2), as evidenced (i) from the sum

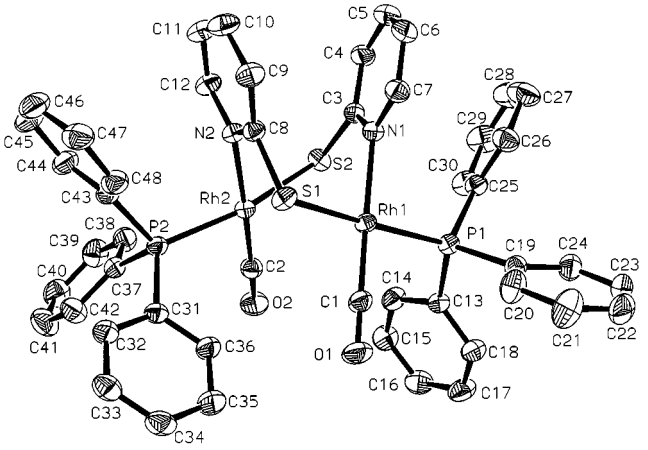


Figure 1. Molecular structure of [{Rh(μ-'Spy'-κ*N*,κ*S*)(CO)(PPh_3)}$_2$] (**3**); selected interatomic distances [Å] and angles [°]: Rh(1)···Rh(2) 3.1952(5), Rh(1)−S(1) 2.3929(8), Rh(1)−P(1) 2.2871(7), Rh(1)−N(1) 2.122(2), Rh(1)−C(1) 1.807(3), Rh(2)−S(2) 2.4053(7), Rh(2)−P(2) 2.2768(7), Rh(2)−N(2) 2.118(2), Rh(2)−C(2) 1.828(3), S(1)−C(8) 1.749(3), S(2)−C(3) 1.749(3), N(1)−C(3) 1.353(3), N(2)−C(8) 1.359(3); S(1)−Rh(1)−P(1) 169.98(3), N(1)−Rh(1)−C(1) 176.9(1), S(1)−Rh(1)−N(1) 88.35(6), S(1)−Rh(1)−C(1) 90.22(9), P(1)−Rh(1)−N(1) 92.53(6), P(1)−Rh(1)−C(1) 88.40(9), S(2)−Rh(2)−P(2) 165.96(3), N(2)−Rh(2)−C(2) 175.4(1), S(2)−Rh(2)−N(2) 87.93(6), S(2)−Rh(2)−C(2) 91.01(9), P(2)−Rh(2)−N(2) 91.36(6), P(2)−Rh(2)−C(2) 88.58(9), Rh(1)−S(1)−C(8) 105.62(9), Rh(2)−N(2)−C(8) 119.6(2), S(1)−C(8)−N(2) 117.6(2), Rh(2)−S(2)−C(3) 107.90(9), Rh(1)−N(1)−C(3) 120.0(2), S(2)−C(3)−N(1) 119.6(2)

of the of the four interligand *cis* angles, 354.08°, and (ii) from the angles between the normals to the planes defined by the P−Rh−C(1) and N(1)−Rh−S, or the C(1)−Rh−N(1) and P−Rh−S fragments, which are 3.94° and 4.06°, respectively. The four-membered chelate ring exhibits a bend along the N(1)···S vector of 4.31°, i.e., it adopts a very flat folded conformation. Considerable ring strain is evident from the small chelate bite angle of only 69.03(7)°. The metal-to-nitrogen bond in **4**, 2.128(2) Å, is somewhat longer than the two Rh−N distances observed for **3**, 2.118(2) and 2.122(2) Å, in spite of being *trans* to the PPh_3 ligand which has a weaker *trans* influence than the carbonyl ligand *trans* to the nitrogen atoms in **3**. By contrast, the length of the Rh−S bond opposite to the CO ligand with its strong *trans* influence in **4**, 2.371(1) Å, is slightly shorter than the Rh−S distances in **3**, 2.3929(8) and 2.4053(7) Å, where the mercapto groups are coordinated *trans* to the PPh_3 ligand. The small N(1)−Rh−S bite angle (see above) and the acute valence angle at the sulfur atom in **4**, 80.89(9)°, emphasize the strain within the small chelate ring, since an increase of the Rh−S bond length, accompanied by a shortening of the Rh−N linkage, would result in further unfavorable compression of the Rh−S−C angle.

Structures of Rhodium Complexes 3 and 4 in Solution

The structures adopted by two rhodium(I) thiolates in solution diverge considerably from those in the solid state, scrambling of the phosphane ligands and rearrangement processes arising from facile interconversion of the coordination modes of the two *S*,*N*-bonded thiolates being common phenomena.

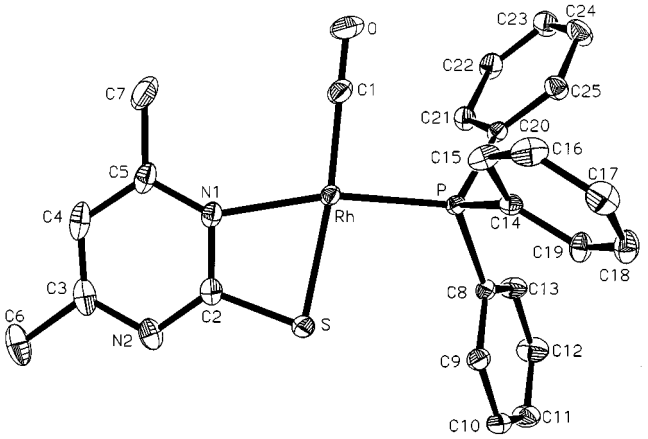


Figure 2. Molecular structure of [Rh('SpymMe$_2$'-κ*N*,κ*S*)(CO)(PPh_3)] (**4**); selected bond lengths [Å] and angles [°]: Rh−S 2.3715(14), Rh−P 2.2475(6), Rh−N(1) 2.128(2), Rh−C(1) 1.843(3), S−C(2) 1.743(3), N(1)−C(2) 1.362(3), N(2)−C(2) 1.326(3); S−Rh−C(1) 173.39(8), P−Rh−N(1) 165.88(6), S−Rh−P 97.15(3), S−Rh−N(1) 69.03(7), P−Rh−C(1) 89.27(9), N(1)−Rh−C(1) 104.6(1), Rh−S−C(2) 80.89(9), Rh−N(1)−C(2) 99.6(1), S−C(2)−N(1) 110.3(2)

At 35 °C, the $^{31}P\{^1H\}$ NMR spectrum of chelate complex **4** consists of a time-averaged singlet (δ = 39.4 in CD_2Cl_2) rather than the expected ^{103}Rh-coupled doublet, thereby indicating rapid phosphane exchange at ambient temperature. On cooling to −80 °C, this signal broadens, shifts slightly upfield, and eventually becomes a sharp doublet centered at δ = 37.7 [^1J(Rh,P) = 126 Hz] which reversibly collapses into a single line as the temperature is raised (Figure 3). The corresponding proton spectra of **4**, recorded as a function of temperature in CD_2Cl_2, contain a sharp singlet (δ = 1.89) of relative intensity 6 at 25 °C, which broadens and finally collapses as the solution is cooled to −80 °C. At even lower temperatures (about −90 °C), two separate resonances of equal intensity begin to emerge at δ = 1.58 and 1.86. At the slow exchange limit, these data are in accordance with a ground-state structure showing two different environments for the methyl groups, as observed for the solid state. Obviously, at higher temperatures, the CH_3 residues undergo rapid site exchange, accompanied by reversible PPh_3 dissociation. Time-averaging of the methyl environments may occur by fast interconversion of species having either the pyrimidine nitrogen atom N-1 or its counterpart N-3 bound to the metal center; Scheme 2, Equation (1). Previously, such nitrogen scrambling between the coordinated and noncoordinated sites of pyrimidine chelates has been established for the monomeric (4-methylpyrimidine-2-thiolato)palladium complex [PdCl('SpymMe-4'-κ*N*,κ*S*)(PMe_3)], resulting from cleavage of the parent dimer [{PdCl(μ-'SpymMe-4'-κ*N*,κ*S*)(PMe_3)}$_2$] in solution.[6b] Alternatively, chelate complex **4**, with its Rh−P bond *trans* to the N atom could rapidly interconvert at room temperature with an isomer having the phosphorus and sulfur atoms in mutually *trans* positions; Scheme 2, Equation (2). On the basis of the available data, we cannot determine whether the dynamic behavior of **4** is caused by nitrogen scrambling or by interconversion of species with Rh−N or Rh−S bonds *trans* to Rh−P, nor can we rule out

the possibility that both mechanisms are operative. Note, however, that the exchange of PPh_3 ligands observed at higher temperatures, i.e., the intermediacy of the formally three-coordinate {Rh('SpymMe$_2$'-κ*N*,κ*S*)(CO)}, is more readily reconciled with the interconversion of species having either the sulfur or the nitrogen atom *trans* to the phosphorus atom than with ligand scrambling according to Equation (1), for which loss of chelation with intermediate formation of *S*-monodentate {Rh('SpymMe$_2$'-κ*S*)(CO)(PPh_3)} is the sole prerequisite.

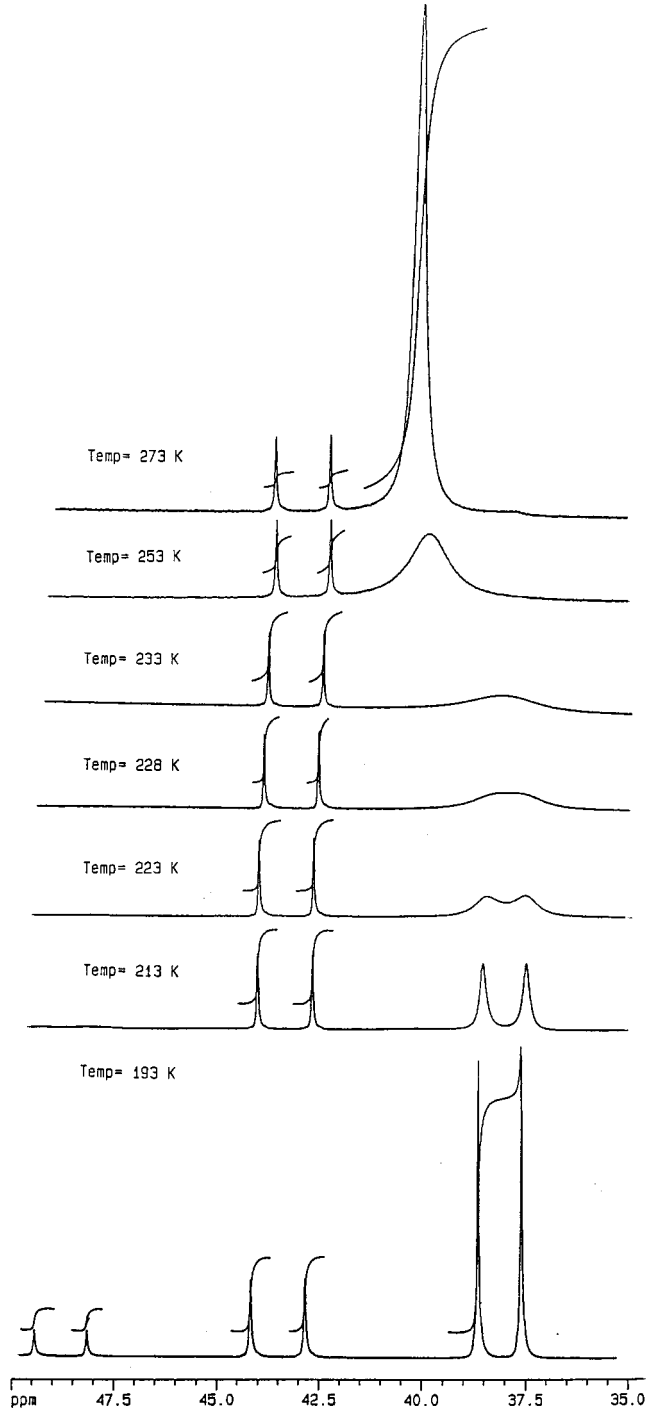
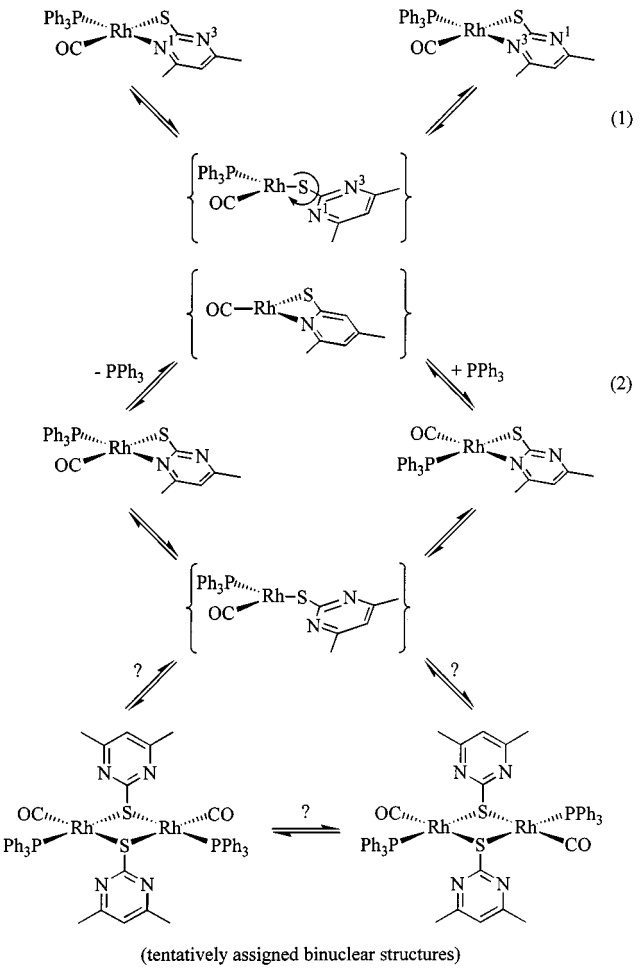


Figure 3. Temperature-dependent $^{31}P\{^1H\}$ NMR spectra of [Rh('SpymMe$_2$'-κ*N*,κ*S*)(CO)(PPh_3)] (**4**); CD_2Cl_2 solutions



Scheme 2. Structures believed to account for the dynamic behavior of [Rh('SpymMe$_2$'-κ*N*,κ*S*)(CO)(PPh_3)] (**4**) in solution

Complex **4** is not the only species present in solution at lower temperatures, since the temperature-dependent emergence of the ^{31}P doublet arising from **4** is accompanied by the appearance of additional Rh-coupled resonances which are *not* observed for freshly prepared samples at ambient temperature, but show up as sharp doublets centered at δ = 43.1 (J = 161 Hz) and 48.4 (J = 157 Hz) when the solution is first cooled to 0 °C and then to −80 °C (Figure 3). These shift values and coupling constants closely resemble those of the *cis*-(*P*,*P*) and *trans*-(*P*,*P*) forms of a number of thiolato-*S*-bridged dirhodium complexes [{Rh(μ-SAr)(CO)(PPh_3)}$_2$]: $\delta \approx 43$ (*cis*), 45 (*trans*); ^1J(Rh,P) ≈ 160 Hz.[13] For this reason, the low-field resonance at δ = 48.4 emerging below −60 °C is tentatively attributed to a thiolato-*S*-bridged binuclear isomer of **4** with the two phosphane ligands in *trans* positions, the signal located at δ = 43.1 correspondingly being assigned to the isomeric *cis* form. Both species can arise from **4** by loss of chelation (vide supra) followed by dimerization and, vice versa, may be cleaved to reform the monomer either with the Rh−N or the Rh−S bond *trans* to the PPh_3 ligand. Once formed, the resonance centered at δ = 43.1 persists as a sharp doublet on raising the temperature, which shows that the associ-

ated molecules are nonfluxional on the NMR time scale and interconvert with those of **4** only very slowly, if at all.

The $^{31}P\{^1H\}$ NMR spectrum of the dirhodium complex **3**, recorded in CD_2Cl_2 at −80 °C, displays two sharp doublets at δ = 37.0 [^1J(Rh,P) = 132 Hz] and 41.7 [^1J(Rh,P) = 162 Hz] with relative intensities 9 and 1, respectively. The latter signal obviously corresponds to the low-temperature resonance {δ = 42.1, ^1J(Rh,P) = 162 Hz; [D_6]acetone, −60 °C} previously assigned to the structurally uncharacterized PPh_3-disubstituted complex [{Rh(μ-'Spy')(CO)(PPh_3)}$_2$] which Oro and co-workers observed in acetone solution as a rearrangement product of [Rh_2(μ-'Spy')$_2$(CO)$_3$(PPh_3)].[9b] In line with the tentative spectral assignments made above, we attribute the less intense doublet exhibited by **3** in dichloromethane at δ = 41.7 to a thiolato-*S*-bridged *cis*-(*P*,*P*)-isomeric form of **3**, viz. [{Rh(μ-'Spy'-κ*S*)(CO)(PPh_3)}$_2$]. The more intense doublet at δ = 37.0 is then thought to arise from the *S*,*N*-bridged dirhodium complex **3** itself. It should be emphasized that in the structurally similar, albeit nonfluxional, thiazoline-2-thiolato-bridged complex [{Rh(μ-$S_2NC_3H_4$-κ*N*,κ*S*)(CO)(PPh_3)}$_2$], the ^{31}P nuclei resonate at δ = 39.8 although their coupling to the rhodium nucleus (164 Hz) is larger.[10b] On raising the temperature to −40 °C, the slow exchange limit signal attributed to **3** collapses reversibly into a time-averaged signal which remains broad and shifts upfield to δ ≈ 25 if the solution is warmed to ca. 35 °C, thereby indicating a chemical exchange process but providing no further information. Reversible broadening of the doublet assigned to the *S*-bridged dimer [{Rh(μ-'Spy'-κ*S*)(CO)(PPh_3)}$_2$] on warming and cooling the solution likewise points to some unknown dynamic behavior of the associated molecules, which in this respect are clearly different from the rigid species giving rise to the sharp doublet at δ = 41.3 in the temperature-dependent $^{31}P\{^1H\}$ spectra of **4** (Figure 3). Facile interconversion of binuclear structures bridged by pyridine-2-thiolato ligands in different bonding modes is well documented[9b,9c] but seems to be less feasible for structures involving the sterically more demanding 4,6-dimethylpyrimidine-2-thiolate system.

Protonation of Iridium Complexes 1 and 2

Treatment of **1** or **2** with hydrogen chloride in CH_2Cl_2 results in protolytic cleavage of the Ir−S bond and oxidative addition of HCl to give the long-known complex [$IrHCl_2$(CO)(PPh_3)$_2$].[14] While only uncharacterized mixtures of products were isolated from reactions between **1** and HBF_4 or CF_3CO_2H, clean protonation of the iridium atom was observed to occur if **2** was combined with excess trifluoroacetic acid in dichloromethane. The resulting product, formally a 1:2 adduct between **1** and CF_3CO_2H, was characterized by X-ray diffraction as the hydrogen bis(trifluoroacetate) salt of a monopositive hydridoiridium(III) complex, [IrH('SpymMe$_2$'-κ*N*,κ*S*)(CO)(PPh_3)$_2$][H(O_2CCF_3)$_2$], containing the pyrimidine-2-thiolate ligand in a chelating coordination mode (Scheme 1, **5a**; Figure 4), rather than the hoped-for trifluoroacetate-coordinated [IrH{OC(O)CF_3}(2-$SC_4HNN(H)Me_2$-4,6)(CO)(PPh_3)$_2$]-

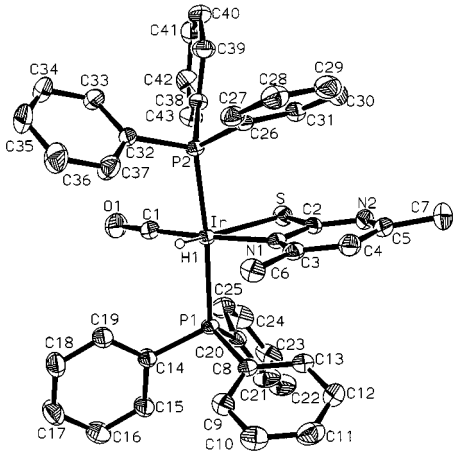


Figure 4. Molecular structure of [IrH('SpymMe$_2$'-κ*N*,κ*S*)(CO)(PPh_3)$_2$]$^+$ (cation of **5a**); selected bond lengths [Å] and angles [°]: Ir−S 2.481(2), Ir−P(1) 2.367(1), Ir−P(2) 2.367(1), Ir−N(1) 2.080(5), Ir−C(1) 1.858(8), Ir−H(1) 1.31(6), S−C(2) 1.727(7), N(1)−C(2) 1.360(8), N(2)−C(2) 1.320(8); P(1)−Ir−P(2) 173.02(6), N(1)−Ir−C(1) 174.5(3), S−Ir−P(1) 94.57(6), S−Ir−P(2) 92.31(6), S−Ir−N(1) 66.7(1), S−Ir−C(1) 108.0(2), P(1)−Ir−N(1) 91.5(1), P(1)−Ir−C(1) 90.5(2), P(2)−Ir−N(1) 90.1(1), P(2)−Ir−C(1) 88.5(2), S−Ir−H(1) 154(3), P(1)−Ir−H(1) 94(3), P(2)−Ir−H(1) 79(3), N(1)−Ir−H(1) 89(3), C(1)−Ir−H(1) 96(3), Ir−S−C(2) 79.5(2), Ir−N(1)−C(2) 104.3(4), S−C(2)−N(1) 109.5(5)

O_2CCF_3 (Scheme 1, **5b**), featuring intramolecular hydrogen bonding[12] between the Ir−H fragment and the N−H bond of a monodentate zwitterionic pyrimidinium-2-thiolate ligand. The sulfur atom of the four-membered Ir−S−C−N heterocycle is *trans* with respect to Ir−H, the metal-bound pyrimidine nitrogen atom being *trans* to the carbonyl group. The highly strained chelate ring [bite angle S−Ir−N(1), 66.7(1)°] exhibits a bend along the N(1)···S vector of 3.41°. As a consequence of the pronounced weakening of the *trans* influence of the hydride ligand, the Ir−S distance, 2.481(2) Å, is much longer than the metal−sulfur bond in chelate complex **4** [2.371(1) Å], resulting in the valence angle at the sulfur atom shrinking from 80.89(9)° in molecule **4** to 79.5(2)° in cation **5a**$^+$. The [H(O_2CCF_3)$_2$]$^-$ ion encountered in structure **5a** is precedented, typical examples are the alkali metal salts M[H(O_2CCF_3)$_2$)], where M = K, Rb, or Cs,[15] and the trifluoroacetic acid tetrahydrate which adopts the ionic structure [H_5O_2][H(O_2CCF_3)$_2$]·$6H_2O$.[16] The geometry, optimized for the "best"[17] hydrogen bond in the [H(O_2CCF_3)$_2$]$^-$ anion of **5a** (O−H, 0.82 Å; H···O, 1.71 Å; O···O, 2.53 Å, OHO, 170.7°), is quite normal and compares well with those of earlier determinations. The planes defined by the two carboxylate fragments are twisted about the O−H···O bond, such that the angle between them is 71.9°.

Although the hydrogen bis(trifluoroacetate) anion is known to be stabilized by short and strong hydrogen bonds,[16b] it is somewhat surprising that in the crystal structure analysis, the second molecule of CF_3CO_2H (pK_a = 0.18) consumed in the protonation of **2** binds to the $CF_3CO_2^-$ counterion rather than the basic pyrimidine nitrogen atom of the [IrH('SpymMe$_2$'-κ*N*,κ*S*)(CO)(PPh_3)$_2$]$^+$ cation formed in the first step.[18] It

is difficult to ascertain whether this bonding situation is restricted to the solid state or whether and to what extent the $[H(O_2CCF_3)_2]^-$ ion persists in solution. Proton NMR spectra of CD_2Cl_2 solutions of **5a** did contain a sharp singlet at $\delta = 15.0$, indicative of hydroxy protons involved in hydrogen-bonding, but otherwise remained inconclusive as the complex could not be isolated completely free from lattice water (see Experimental Section) which rapidly exchanges with the acid. Using HBF_4 to protonate compound **2** led to formation of the tetrafluoroborate [IrH('S-pymMe$_2$'-κ*N*,κ*S*)(CO)$(PPh_3)_2$]BF_4·HBF_4 as a formal analogue of the trifluoroacetate **5a**. In contrast with the latter, the cation of the BF_4^- salt exists as two isomers which differ in the bonding of the hydride ligand, which may be *trans* to the S atom, δ(IrH) = −14.46 (t), or *trans* to the N atom, δ(IrH) = −16.57 (t).[19] Based on the relative peak areas of these hydride signals and the associated methyl singlets at $\delta = 1.88$ and 2.45 (IrH *trans* to S) and $\delta = 2.17$ and 2.40 (IrH *trans* to N), the isomer ratio *trans*-(*H*,*S*)/*trans*-(*H*,*N*) can be estimated as 67:33, in good agreement with the ^{31}P spectra containing singlets at δ = 8.2 and 9.0 with relative intensities 60:40. Dichloromethane solutions of the tetrafluoroborate also displayed a concentration-dependent, broadened proton resonance in the range $8 < \delta < 13$, attributable to a nitrogen-bonded proton engaged in further hydrogen bonding, presumably to BF_4^-. Hence, the two isomeric tetrafluoroborates are tentatively assigned structures **5c** and **5d** with *N*-protonated 4,6-dimethylpyrimidinium-2-thiolato chelate ligands.

Pyridine-2-thiol oxidatively adds to *trans*-[Ir('Spy')(CO)$(PPh_3)_2$] (**1**), forming [IrH('Spy')$_2$(CO)$(PPh_3)_2$] (**6**). This complex is more directly prepared by reaction of *trans*-[IrCl(CO)$(PPh_3)_2$] with an excess of the 'pySH' ligand in the presence of triphenylphosphane to prevent PPh_3 dissociation. The *trans*-(*P*,*P*)-*cis*-(*S*,*S*) coordination geometry shown for **6** in Scheme 1 is suggested by spectral data. In particular, the $^{31}P\{^1H\}$ NMR spectrum displays a singlet ($\delta = 7.61$), and the proton NMR spectrum contains an IrH triplet which shows equal *cis* coupling (10.8 Hz) to the two equivalent ^{31}P nuclei and is shifted to much lower frequencies ($\delta = -13.54$) than appear to be diagnostic of the presence of *trans*-H−Ir−CO units ($\delta \approx -9$) in carbonylhydrido complexes of the general type [IrH(X)(Y)(CO)$(PR_3)_2$].[21−23] Iridium complex **6** reacts with HBF_4 in $CHCl_3$ solution by cleavage of one Ir−S bond and protonation at the metal center to form the ionic chelate complex [IrH('Spy'-κ*N*,κ*S*)(CO)$(PPh_3)_2$]BF_4 (**7**). The cation of this compound is isoelectronic with [OsH('Spy'-κ*N*,κ*S*)(CO)$(PPh_3)_2$] which was previously isolated as a mixture of two *trans*-(*P*,*P*) isomers having the hydrido ligand *trans* to the N atom or *trans* to the S atom.[5a][20a] The X-ray structure analysis of **7** showed that [IrH('Spy'-κ*N*,κ*S*)(CO)$(PPh_3)_2]^+$ exists in the *trans*-(*P*,*P*)-*trans*-(*H*,*S*) form (Figure 5). Bond lengths and angles within the near-planar four-membered ring (bend along N···S vector, 2.20°) are similar to those found for pyrimidine-2-thiolato derivative **5**: Ir−S 2.507(2) Å; Ir−N 2.069(5) Å; S−Ir−N 66.3(1)°; Ir−S−C(2) 78.7(2)°.

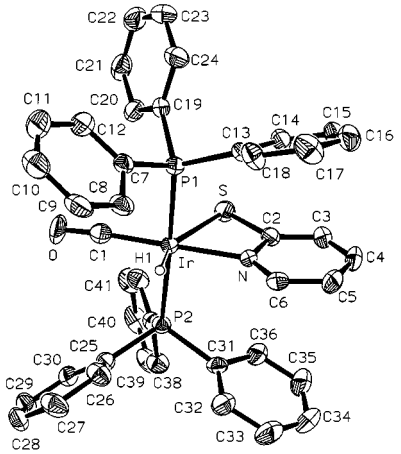


Figure 5. Molecular structure of [IrH('Spy'-κ*N*,κ*S*)(CO)$(PPh_3)_2]^+$ (cation of **7**); selected bond lengths [Å] and angles [°]: Ir−S 2.508(2), Ir−P(1) 2.371(1), Ir−P(2) 2.357(1) Ir−N 2.069(5), Ir−C(1) 1.853(8), Ir−H(1) 1.49(7), S−C(2) 1.725(6), N−C(2) 1.351(8); P(1)−Ir−P(2) 174.16(6), N−Ir−C(1) 177.9(3), S−Ir−P(1) 92.56(6), S−Ir−P(2) 93.14(6), S−Ir−N 66.3(1), S−Ir−C(1) 111.7(3), P(1)−Ir−N 90.3(1), P(1)−Ir−C(1) 90.4(2), P(2)−Ir−N 90.9(1), P(2)−Ir−C(1) 88.6(2), S−Ir−H(1) 154(2), P(1)−Ir−H(1) 84(2), P(2)−Ir−H(1) 91(2), N−Ir−H(1) 88(2), C(1)−Ir−H(1) 94(3), Ir−S−C(2) 78.7(2), Ir−N−C(2) 105.1(4), S−C(2)−N 110.0(5)

While treatment of the osmium(II) complex [OsH('Spy'-κ*N*,κ*S*)(CO)$(PPh_3)_2$] with HBF_4 resulted in the formation the highly acidic, yet stable, dihydrogen derivative [Os(H_2)('-Spy'-κ*N*,κ*S*)(CO)$(PPh_3)_2$]BF_4,[20] no similar transformation was observed on attempted protonation of **7**. Previously, a model for predicting the properties of dihydrogen complexes $[M(H_2)L_5]$ was described,[24] based on estimated electrochemical potentials $E_{1/2}(d^5/d^6)$ calculated by use of Lever's ligand additivity approach[25] for six-coordinate complexes. It was concluded that dihydrogen complexes $[M(H_2)L_5]$ that are stable with respect to loss of H_2 at ambient temperature will correspond to hypothetical dinitrogen complexes $[M(N_2)L_5]$ with potentials $E_{1/2}(d^5/d^6)$ of about 2 V versus NHE if the H_2 ligand is *trans* to a σ donor on a Group 7, 8, or 9 metal ion; on the other hand, dinitrogen complexes with potentials above 2 V will have corresponding $[M(H_2)L_5]$ species that lose dihydrogen irreversibly at 20−25 °C, possibly with the exception of $[Ir^{III}(H_2)L_5]^{n+}$ where stable metal−H_2 bonding appears feasible up to potentials $E_{1/2}([Ir^{IV}(H_2)L_5]^{n+}/[Ir^{III}(H_2)L_5]^{(n-1)+})$ of ca. 2.2 V.[24] By use of the sum of additive electrochemical ligand parameters, ΣE_L, as proposed by Lever (E_L = 0.99 V for CO, 0.68 V for N_2, and 0.39 V for PPh_3)[25a] and Morris ($E_L = -0.28$ V for chelating 'Spy$^-$'),[20b] and the linear correlation $E_{1/2} = 0.7\Sigma E_L + 1.3$, suggested by Morris for the Ir^{IV}/Ir^{III} redox couple,[24] the $E_{1/2}(d^5/d^6)$ value for a hypothetical dinitrogen-containing dication [Ir(N_2)('Spy'-κ*N*,κ*S*)(CO)$(PPh_3)_2]^{2+}$ is estimated at ca. 2.8 V, far beyond the limit where stable bonding of H_2 could be expected for a dipositive dihydrogen species [Ir(H_2)('Spy'-κ*N*,κ*S*)(CO)$(PPh_3)_2]^{2+}$!

Conclusion

This work has shown that the Vaska-type complexes *trans*-[MCl(CO)(PPh_3)$_2$] (M = Rh, Ir) react with bifunctional anionic pyridine- and 4,6-dimethylpyrimidine-2-thiolates to yield products whose nature is sensitive to the metal center and the steric requirements of the ligands. With iridium(I), both 'Spy$^-$' and 'SpymMe$_2^-$' act as *S*-monodentates to give the complexes, *trans*-[Ir('Spy')(CO)(PPh_3)$_2$] (**1**) and *trans*-[Ir('SpymMe$_2$')(CO)(PPh_3)$_2$] (**2**), which result from simple anion exchange. In similar reactions, *trans*-[RhCl(CO)(PPh_3)$_2$] undergoes loss of both the chloride ion and one PPh_3 ligand, affording derivatives in which the two anionic *S*,*N* donors act as bidentate bridging or chelate ligands. With 'Spy$^-$' as an entering ligand we see the formation of bimetallic [{Rh(μ-'Spy'-κ*N*,*S*)(CO)(PPh_3)}$_2$] (**3**) where the two pyridine-2-thiolate moieties act as *S*,*N* bridges in the head-to-tail arrangement frequently encountered[9b,10] for heterocyclic ligands with *N*−C−*S* donor sets. The sterically more demanding 4,6-dimethylpyrimidine-2-thiolate system, on the other hand, does not give any related doubly *S*,*N*-bridged binuclear product with nearly parallel heterocyclic rings but rather acts as a chelate ligand towards Rh^I, producing the unusual four-membered ring complex [Rh('SpymMe$_2$'-κ*N*,κ*S*)(CO)(PPh)$_3$] (**4**). Because of facile interconversion of the bonding modes of the *S*,*N*-coordinated ligands, the structures adopted by **3** and **4** in the solid state are not maintained in solution but show temperature-dependent dynamic behavior.

Reaction of iridium complexes bearing *S*-bonded 'Spy' and 'SpymMe$_2$' ligands with strong acids (CF_3CO_2H, HBF_4) results in protonation of only the metal center, except for the *trans*-(*H*,*S*) and *trans*-(*H*,*N*) isomers of [IrH(2-$SC_4HNN(H)Me_2$-4,6-κ*N*,κ*S*)(CO)(PPh_3)$_2$](BF_4)$_2$ where NMR spectroscopy suggests that protonation at the noncoordinated nitrogen atom of the pyrimidine heterocycle also occurs. There was no indication of reactions leading to products displaying "nonclassical" intramolecular IrH···HN hydrogen bonding. The failure to isolate such derivatives within the family of complexes studied here is accounted for by the ease of the 'Spy' and 'SpymMe$_2$' ligands to act as *S*,*N* donor chelates in spite of their small bite angles. This prevents the formation of hydridoiridium derivatives containing *S*-monodentate thiolate ligands with "dangling" pyridyl or pyrimidinyl substituents, which would allow a sufficiently close approach of the ring nitrogen atoms to the Ir−H bond.

Experimental Section

General Remarks: All manipulations were performed under nitrogen using standard Schlenk techniques. Solvents were distilled from the appropriate drying agents prior to use. − IR: Mattson Polaris. − NMR: Bruker DPX 300 (300.1 MHz for ^{1}H, 121.5 MHz for ^{31}P) at 20 ± 2 °C (if not stated otherwise) with TMS as internal or with H_3PO_4 as external standard (downfield positive). − The starting complexes *trans*-[RhCl(CO)(PPh_3)$_2$][26] and *trans*-[IrCl(CO)(PPh_3)$_2$][27] were prepared by literature methods; the ligands pyridine-2-thiol and 4,6-dimethylpyrimidine-2-thiol were used as obtained commercially.

***trans*-[Ir('Spy')(CO)(PPh_3)$_2$] (1):** A solution of pyridine-2-thiol (170.1 mg, 1.53 mmol) in THF (10 mL) was treated with sodium hydride (36.8 mg, 1.54 mmol) at room temperature for 1 h and then added to a suspension of *trans*-[IrCl(CO)(PPh_3)$_2$] (1.002 g, 1.28 mmol) in THF (25 mL). The dark red mixture was stirred for 1 h at ambient conditions and then concentrated to dryness. The residue was taken up in toluene (60 mL) and the solution was filtered through a layer of sea sand/Celite. Concentration of the filtrate to 5 mL and careful addition of pentane (60 mL) caused the precipitation of a yellow-orange powder which was recrystallized from dichloromethane to give the product complex as orange crystals; yield 880 mg (80%). − IR (KBr): $\tilde{\nu}$ = 1924 (CO) cm^{-1}. − ^{1}H NMR ($CDCl_3$): δ = 6.08 (d, *J* = 8.1 Hz, 1 H, C_5H_4N), 6.28 (d, *J* = 8.4 Hz, 1 H, C_5H_4N), 6.42 ("t", *J* = 13.2 Hz, 1 H, C_5H_4N), 6.62 ("t", *J* = 13.2 Hz, 1 H, C_5H_4N), 7.3−7.4 (m, 18 H, C_6H_5), ca. 7.6 (m, 12 H, C_6H_5). − ^{31}P{^{1}H} NMR ($CDCl_3$): δ = 21.3. − $C_{42}H_{34}IrNOP_2S$ (855.0): calcd. C 59.00, H 4.01, N 1.64, S 3.75; found C 59.15, H 4.00, N, 1.53, S 3.93.

***trans*-[Ir('SpymMe$_2$')(CO)(PPh_3)$_2$] (2):** 4,6-Dimethylpyrimidine-2-thiol (85.4 mg, 0.61 mmol) was deprotonated by treatment with an equimolar amount of sodium methoxide in methanol (5 mL). The resulting solution was added dropwise to a stirred suspension of *trans*-[IrCl(CO)(PPh_3)$_2$] (44.2 mg, 0.56 mmol) in THF. After stirring for 3 h at ambient conditions, the solvent was removed in vacuo to leave a semisolid residue which was re-dissolved in benzene (25 mL). Filtration through sea sand/Celite followed by concentration of the filtrate to ca. 3 mL gave a clear solution from which the product was isolated by slow addition of pentane (50 mL); yield 420 mg (85%) as orange microcrystals. − IR (KBr): $\tilde{\nu}$ = 1928 (CO) cm^{-1}. − ^{1}H NMR ($CDCl_3$): δ = 1.73 (s, 6 H, CH_3), 5.55 (s, 1 H, C_4H), ca. 7.3 (m, 18 H, C_6H_5), ca. 7.5 (m, 12 H, C_6H_5). − ^{31}P{^{1}H} NMR ($CDCl_3$): δ = 19.4. − $C_{43}H_{37}IrN_2OP_2S$ (884.2): calcd. C 58.36, H 4.22, N 3.17, S 3.62; found C 58.50, H 4.25, N 3.08, S 3.39.

[{Rh(μ-'Spy'-κ*N*,κ*S*)(CO)(PPh_3)}$_2$] (3): A procedure analogous to that for **1** was employed, using *trans*-[RhCl(CO)(PPh_3)$_2$] (549.7 mg, 0.80 mmol) and sodium pyridine-2-thiolate (117.2 mg, 0.88 mmol) in THF (30 mL) at room temperature for 3 h. Crystallization of the product from dichloromethane/pentane furnished the orange complex as the compound [{Rh(μ-'Spy'-κN,κS)(CO)(PPh_3)}$_2$·CH_2Cl_2 (**3**·CH_2Cl_2); yield 360 mg (82%). − IR (KBr): $\tilde{\nu}$ = 1937 (CO) cm^{-1}. − ^{1}H NMR (CD_2Cl_2, −40 °C): δ = 5.65 ("t", *J* = 12.4 Hz, 2 H, C_5H_4N), 6.19 (d, *J* = 8.2 Hz, 2 H, C_5H_4N), 6.37 ("t", *J* = 10.2 Hz, 2 H, C_5H_4N), 6.55 (d, *J* = 5.1 Hz, 2 H, C_5H_4N), 7.1−7.3 (m, 18 H, C_6H_5), ca. 7.5 (m, 12 H, C_6H_5). − ^{31}P{^{1}H} NMR (CD_2Cl_2, −80 °C): δ = 37.0 [d, ^1J(Rh,P) = 132 Hz]. − $C_{48}H_{38}N_2O_2P_2Rh_2S_2$·$CH_2Cl_2$ (1092): calcd. C 53.91, H 3.69, N 2.57; found C 54.26, H, 3.34, N, 2.25.

[Rh('SpymMe$_2$'-κ*N*,κ*S*)(CO)(PPh_3)] (4): The yellow-orange complex was prepared as for **2** by allowing *trans*-[RhCl(CO)(PPh_3)$_2$] (590.4 mg, 0.85 mmol) to react with a 10% excess of methanolic sodium 4,6-dimethylpyrimidine-2-thiolate in THF (20 mL); yield 410 mg (91%). − IR (KBr): $\tilde{\nu}$ = 1968 (CO) cm^{-1}. − ^{1}H NMR (CD_2Cl_2): δ = 1.89 (s, 6 H, CH_3), 5.72 (s, 1 H, C_4H), ca. 7.4 (m, 9 H, C_6H_5), ca. 7.7 (m, 6 H, C_6H_5). − ^{31}P{^{1}H} NMR (CD_2Cl_2, −80

°C): δ = 37.7 [d, ^1J(Rh,P) = 126 Hz]. − $C_{25}H_{22}N_2OPRhS$ (532.4): calcd. C 56.40, H 4.17, N 5.26, S 6.02; found C 56.84, H 4.22, N 5.28, S 5.92.

[IrH('SpymMe$_2$'-κ*N*,κ*S*)(CO)(PPh$_3$)$_2$][H(O$_2$CCF$_3$)$_2$] (5a): Complex **2** (144.6 mg, 0.16 mmol) was allowed to react with an excess of neat trifluoroacetic acid (40 μL, ca. 0.5 mmol) in dichloromethane (20 mL) at room temperature for 30 min. Slow concentration of the mixture caused the product to precipitate as bright yellow crystals containing 1 molecule of lattice water per formula unit (**5a**·H_2O); yield 160 mg (88%). − IR (KBr): ṽ = 1792 (C=O), 2053 (CO), 2170 (IrH) cm^{-1}. − ^{1}H NMR (CD_2Cl_2): δ = −13.01 [t, *cis*-^2J(P,H) = 10.5 Hz, 1 H, IrH], 1.47, 2.20 (both s, 3 H each, both CH_3), 6.28 (s, 1 H, C_4H), ca. 7.4 (m, 18 H, C_6H_5), ca. 7.7 (m, 12 H, C_6H_5), 15.0 (s, OH). − ^{31}P{^{1}H} NMR (CD_2Cl_2): δ = 8.2 (s). − $C_{47}H_{39}F_6IrN_2O_5P_2S$·$H_2O$ (1130): calcd. C 49.95, H 3.66, N 2.48; found C 49.54, H 3.24, N 2.16.

[IrH(2-SC$_4$HNN(H)Me$_2$-4,6-κ*N*,κ*S*)(CO)(PPh$_3$)$_2$](BF$_4$)$_2$ (Mixture of Isomers 5c and 5d): A solution of **2** (189.5 mg, 0.21 mmol) in dichloromethane (20 mL) was treated with HBF_4 (30 μL, 54% in Et_2O). The mixture was stirred for 2.5 h at ambient conditions and then concentrated to dryness. The residue was re-dissolved in CH_2Cl_2 (8 mL) and the resulting solution was filtered and diluted with pentane (40 mL) to furnish the product as a light yellow microcrystalline precipitate containing solvent of crystallization; yield 190 mg (79%). − **5c:** ^{1}H NMR (CD_2Cl_2): δ = −14.46 [t, *cis*-^2J(P,H) = 9.9 Hz, 1 H, IrH], 1.88, 2.45 (both s, 3 H each, both CH_3), 7.05 (s, 1 H, C_4H), ca. 7.6 (m, C_6H_5). − ^{31}P{^{1}H} NMR (CD_2Cl_2): δ = 8.2 (s). − **5d:** ^{1}H NMR (CD_2Cl_2): δ = −16.57 [t, *cis*-^2J(P,H) = 10.8 Hz, 1 H, IrH], 2.17, 2.40 (both s, 3 H each, both CH_3), 7.03 (s, 1 H, C_4H), ca. 7.6 (m, C_6H_5). − ^{31}P{^{1}H} NMR (CD_2Cl_2): δ = 9.0 (s). − Isomeric distribution (from ^{1}H NMR): **5**c, 67%; **5d**, 33%. − $C_{43}H_{39}B_2F_8IrN_2OP_2S$·$CH_2Cl_2$ (1145): calcd. C 46.17, H 3.61, N 2.45, S 2.79; found C 46.15, H 3.76, N 2.61, S 2.45.

[IrH('Spy')$_2$(CO)(PPh$_3$)$_2$] (6): A 1:2 mixture of *trans*-[IrCl(CO)(PPh$_3$)$_2$] (480.4 mg, 0.62 mmol) and pyridine-2-thiol (140.2 mg, 1.26 mmol) was combined with excess triphenylphosphane (880 mg, 3.35 mmol) in benzene (80 mL). Stirring at room temperature for 24 h caused the product complex to separate from solution as a light yellow precipitate; yield 350 mg (58%). − IR (KBr): ṽ = 2036 (CO), 2177 (IrH) cm^{-1}. − ^{1}H NMR ($CDCl_3$): δ = −13.54 (t, *cis*-^2J(P,H) = 10.8 Hz, 1 H, IrH), 5.87 (d, *J* = 7.2 Hz, 2 H, C_5H_4N), 6.48 ("t", *J* = 14.4 Hz, 1 H, C_5H_4N), 6.66 ("t", *J* = 14.3 Hz, 1 H, C_5H_4N), 6.94 ("t", *J* = 16.2 Hz, 2 H, C_5H_4N), 7.07 (d, *J* = 6.8 Hz, 2 H, C_5H_4N), 7.2−7.6 (m, 30 H, C_6H_5). − ^{31}P{^{1}H} NMR ($CDCl_3$): δ = 7.6 (s). − $C_{47}H_{39}IrN_2OP_2S_2$ (966.1): calcd. C 58.43, H 4.07, N 2.90; found C 58.60, H 4.20, N 2.68.

[IrH('Spy'-κ*N*,κ*S*)(CO)(PPh$_3$)$_2$]BF$_4$ (7): A solution of **6** (170.1 mg, 0.18 mmol) in chloroform (10 mL) was stirred with HBF_4 (0.3 mL, 54% in E_2O) at ambient conditions for 1 h. Dilution of the mixture with diethyl ether (70 mL) resulted in the precipitation of **7** (150 mg, 88%) as bright yellow crystals. − IR (KBr): ṽ = 2047 (CO), 2162 (IrH) cm^{-1}. − ^{1}H NMR ($CDCl_3$): δ = −13.52 (t, *cis*-^2J(P,H) = 11.0 Hz, 1 H, IrH), 5.94 (d, *J* = 8.3 Hz, 1 H, C_5H_4N), 6.34 ("t", *J* = 14.9 Hz, 1H, C_5H_4N), 6.93 ("t", *J* = 15.5 Hz, 1 H, C_5H_4N), 7.02 (d, *J* = 6.2 Hz, 1 H, C_5H_4N), 7.4−7.6 (m, 30 H, C_6H_5). − ^{31}P{^{1}H} NMR ($CDCl_3$): δ = 7.5 (s). − $C_{42}H_{35}BF_4IrNOP_2S$ (942.7): calcd. C 53.51, H 3.74, N 1.49, S, 3.40; found C 53.17, H 3.73, N 1.59, S 3.40.

X-ray Structure Determinations: Single crystals of **3**·CH_2Cl_2 (size 0.55 × 0.43 × 0.26 mm), **4** (size 0.45 × 0.40 × 0.24 mm), **5a** (size 0.38 × 0.30 × 0.13 mm), and **7** (approximate size 0.4 × 0.2 × 0.2 mm) were grown from dichloromethane/pentane (**3**·CH_2Cl_2, **4**), chloroform/diethyl ether (**7**), and by crystallizing the hydrate **5a**·H_2O from dichloromethane. Diffraction measurements were made at −70 ± 2 °C (**4**) and 20 ± 2 °C (**3**·CH_2Cl_2, **5a**, **7**) on an Enraf−Nonius CAD-4 diffractometer using graphite-monochromated Mo-K_α radiation (λ = 0.71073 Å): orientation matrices and unit cell parameters from the setting angles of 25 centered medium-angle reflections; collection of the diffraction intensities by ω scans (data corrected for absorption by ψ scans; **3**·CH_2Cl_2: T_{min} = 0.61, T_{max} = 0.78; **4**: T_{min} = 0.69, T_{max} = 0.81; **5a**: T_{min} = 0.40, T_{max} = 0.70; **7**: T_{min} = 0.33, T_{max} = 0.54;). The structures were solved by direct methods employing the SIR-92[28] program system and subsequently refined by full-matrix least-squares procedures on F^2 (SHELX-97[29]) with allowance for anisotropic thermal motion of all non-hydrogen atoms. The residual electron density remaining after refinement of the structural model resulting for **3**·CH_2Cl_2 suggested threefold rotational disorder of the solvate molecule about the Cl−C−Cl bisector, which was accounted for by assigning the particular chlorine positions split occupancies of 0.333 each. The CF_3 groups of the hydrogen-bridged trifluoroacetate ions in structure **5** were found to be disordered over two sites with refined occupancies of 0.25:0.75 and 0.33:0.67, respectively. H atoms were included in the molecular models assuming ideal geometry and using appropriate riding models (Ir*H* of **5a** and **7** located from final Δ*F* maps). Some diffuse residual electron density near the inversion center of the triclinic unit cell of **5a** was modeled by assuming the presence of 1 molecule of lattice water originating from the synthesis and remaining after crystallization. − **3·CH$_2$Cl$_2$:** $C_{49}H_{40}Cl_2N_2O_2P_2Rh_2S_2$ (1092); triclinic, $P\bar{1}$, *a* = 11.260(1), *b* = 13.436(1), *c* = 16.881(3) Å, α = 78.87(1), β = 74.57(1), γ = 76.848(7)°, *V* = 2373.3(5) Å^3, *Z* = 2, $d_{calcd.}$ = 1.528 g cm^{-3}, μ(Mo-K_α) = 1.004 mm^{-1}; 2.52° ≤ Θ ≤ 29.97°, 14439 reflections (0 ≤ *h* ≤ +15, −18 ≤ *k* ≤ +18, −22 ≤ *l* ≤ +23) collected, 13789 unique; *wR* = 0.096 for all data and 586 parameters, *R* = 0.039 for 10393 structure factors $F_o > 4\sigma(F_o)$. − **4:** $C_{25}H_{22}N_2OPRhS$ (532.4); triclinic, $P\bar{1}$, *a* = 9.254(7), *b* = 10.035(2), *c* = 13.0940(8) Å, α = 93.05(1), β = 93.71(2), γ = 101.33(2)°, *V* = 1187.1(9) Å^3, *Z* = 2, $d_{calcd.}$ = 1.489 g cm^{-3}, μ(Mo-K_α) = 0.894 mm^{-1}; 2.51° ≤ Θ ≤ 30.08°, 7187 reflections (−13 ≤ *h* ≤ +13, −14 ≤ *k* ≤ +14, 0 ≤ *l* ≤ +18) collected, 6908 unique; *wR* = 0.120 for all data and 283 parameters, *R* = 0.029 for 6215 structure factors $F_o > 4\sigma(F_o)$. − **5a·H$_2$O:** $C_{47}H_{41}F_6IrN_2O_6P_2S$ (1130); triclinic, $P\bar{1}$, *a* = 11.771(1), *b* = 14.100(1), *c* = 15.573(1) Å, α = 85.418(8), β = 83.124(9), γ = 69.235(9)°, *V* = 2397.4(3) Å^3, *Z* = 2, $d_{calcd.}$ = 1.565 g cm^{-3}, μ(Mo-K_α) = 2.967 mm^{-1}; 2.64° ≤ Θ ≤ 25.97°, 10526 reflections (−14 ≤ *h* ≤ +14, −17 ≤ *k* ≤ +17, −1 ≤ *l* ≤ +19) collected, 9397 unique; *wR* = 0.115 for all data and 612 parameters, *R* = 0.046 for 7494 structure factors $F_o > 4\sigma(F_o)$. − **7:** $C_{42}H_{35}BF_4IrNOP_2S$ (942.7); orthorhombic, *Pbca*, *a* = 18.766(3), *b* = 18.104(1), *c* = 23.404(2) Å, *V* = 7951(1) Å^3, *Z* = 8, $d_{calcd.}$ = 1.575 g cm^{-3}, μ(Mo-K_α) = 3.544 mm^{-1}; 2.60° ≤ Θ ≤ 23.97°, 7863 reflections (−1 ≤ *h* ≤ +21, −1 ≤ *k* ≤ +20, −26 ≤ *l* ≤ +2) collected, 6215 unique; *wR* = 0.074 for all data and 482 parameters, *R* = 0.033 for 3830 structure factors $F_o > 4\sigma(F_o)$. − Crystallographic data (excluding structure factors) for the structures reported in this paper have been deposited at the Cambridge Crystallographic Data Centre and allocated the deposition numbers CCDC-136220 (**7**), -136221 (**5a**·H_2O), -136222 (**4**), and -136223 (**3**·CH_2Cl_2). Copies of the data can be obtained free of charge on application to CCDC, 12 Union Road, Cambridge CB2 IEZ, UK [Fax: (internat.) + 44-1223/336-033; E-mail: deposit@ccdc.cam.ac.uk].

Acknowledgments

Support of this work by the Fonds der Chemischen Industrie (Frankfurt/Main) and by Degussa AG is gratefully acknowledged. We are also indebted to Dr. M. Moll and Dr. A. Zahl for recording the NMR spectra.

[1] L. Dahlenburg, K. Herbst, H. Berke, *J. Organomet. Chem*. **1999**, *585*, 225−233.
[2] L. Dahlenburg, K. Herbst, *Chem. Ber./Recueil* **1997**, *130*, 1693−1698.
[3] L. Dahlenburg, K. Herbst, M. Kühnlein, *Z. Anorg. Allg. Chem.* **1997**, *623*, 250−258.
[4] [4a] E. S. Raper, *Coord. Chem. Rev.* **1985**, *61*, 115−184. − [4b] E. S. Raper, *Coord. Chem. Rev.* **1996**, *153*, 199−255. − [4c] E. S. Raper, *Coord. Chem. Rev.* **1997**, *165*, 475−576.
[5] [5a] P. Mura, B. G. Olby, S. D. Robinson, *J. Chem. Soc., Dalton Trans.* **1985**, 2101−2112. − [5b] B. G. Olby, S. D. Robinson, *Inorg. Chim. Acta* **1989**, *165*, 153−162, and references cited therein.
[6] [6a] J. H. Yamamoto, W. Yoshida, C. M. Jensen, *Inorg. Chem.* **1991**, *30*, 1353−1357. − [6b] G. P. A. Yap, C. M. Jensen, *Inorg. Chem*. **1992**, *31*, 4823−4828.
[7] Y. Nakatsu, Y. Nakamura, K. Matsumoto, S. Ooi, *Inorg. Chim. Acta* **1992**, *196*, 81−88, and references cited therein.
[8] D. J. Rose, K. P. Maresca, P. B. Kettler, Y. D. Chang, V. Soghomomian, Q. Chen, M. J. Abrams, S. K. Larsen, J. Zubieta, *Inorg. Chem.* **1996**, *35*, 3548−3558, and references cited therein.
[9] [9a] L. A. Oro, M. A. Ciriano, F. Viguri, A. Tiripicchio, M. Tiripicchio-Camellini, F. J. Lahoz, *Nouv. J. Chim*. **1986**, *10*, 75−77. − [9b] M. A. Ciriano, F. Viguri, J. J. Pérez-Torrente, F. J. Lahoz, L. A. Oro, A. Tiripicchio, M. Tiripicchio-Camellini, *J. Chem. Soc., Dalton Trans.* **1989**, 25−32. − [9c] M. A. Ciriano, J. J. Pérez-Torrente, F. Viguri, F. J. Lahoz, L. A. Oro, A. Tiripicchio, M. Tiripicchio-Camellini, *J. Chem. Soc., Dalton Trans.* **1990**, 1493−1502. − [9d] M. A. Ciriano, F. Viguri, L. A. Oro, A. Tiripicchio, M. Tiripicchio-Camellini, *Angew. Chem.* **1987**, *99*, 452−453; *Angew. Chem. Int. Ed. Engl.* **1987**, *26*, 444−445. − [9e] M. A. Ciriano, J. J. Pérez-Torrente, F. J. Lahoz, L. A. Oro, *J. Organomet. Chem*. **1993**, *455*, 225−233. − [9f] M. A. Ciriano, J. A. López, L. A. Oro, J. J. Pérez-Torrente, M. Lanfranchi, A. Tiripicchio, M. Tiripicchio-Camellini, *Organometallics* **1995**, *14*, 4764−4775.
[10] [10a] T. Sielisch, M. Cowie, *Organometallics* **1988**, *7*, 707−714. − [10b] M. Cowie, T. Sielisch, *J Organomet. Chem.* **1988**, *348*, 241−254.
[11] A. J. Deeming, M. N. N. Meah, H. A. Dawes, M. B. Hursthouse, *J. Organomet. Chem*. **1986**, *299*, C25−C28.
[12] [12a] A. J. Lough, S. Park, R. Ramachandran, R. H. Morris, *J. Am. Chem. Soc*. **1994**, *116*, 8356−8357. − [12b] S. Park, R. Ramachandran, A. J. Lough, R. H. Morris, *J. Chem. Soc., Chem. Commun*. **1994**, 2201−2202. − [12c] S. Park, A. J. Lough, R. H. Morris, *Inorg. Chem.* **1996**, *35*, 3001−3006.
[13] K. Osakada, K. Matsumoto, T. Yamamoto, A. Yamamoto, *Organometallics* **1985**, *4*, 857−862.
[14] L. Vaska, J. W. DiLuzio, *J. Am. Chem. Soc.* **1961** *83*, 2784−2785.
[15] L. Goli[1], J. C. Speakman, *J. Chem. Soc.* **1965**, 2530−2542.
[16] [16a] D. Mootz, D. Boenigk, *Z. Naturforsch., Teil B* **1984**, *39*, 298−304. − [16b] D. Mootz, M. Schilling. *J. Am. Chem. Soc.* **1992**, *114*, 7435−7439.
[17] H atom position generated by the HFIX 83 option of SHELX-97, see ref.[29]
[18] Structure **5a** was initially refined as the 1:2 complex salt [IrH(2-$SC_4HNN(H)Me_2$-4,6-κ*N*,κ*S*)(CO)(PPh_3)$_2$](O_2CCF_3)$_2$ (Scheme 1; **5c**; $X^- = CF_3CO_2^-$) containing a dipositive cation with a pyridinium-2-thiolato ligand protonated at N(2). A subsequent validation check with the PLATON-99 program package (see ref.[30]), however, revealed an unusual short nonbonded contact distance of 2.53 Å between two carboxylate oxygen atoms of the two trifluoroacetate counterions located at general positions x_1, y_1, z_1 and $-x_2 - 1$, $-y_2$, $-z_2 + 1$. Furthermore, checking of the derived structural model showed that the polar N(2)−H bond had no acceptor acting as a weak base towards the acidic pyrimidinium proton. To account for these problems, the 1:1 complex salt [IrH('$SpymMe_2$'-κ*N*,κ*S*)(CO)(PPh_3)$_2$][H(O_2CCF_3}$_2$] with an O−H···O-bridged hydrogen bis(trifluoroacetate) anion was taken as the basis for the final stages of refinement.
[19] These isomer assignments are in accordance with trends in the ^{1}H NMR data reported by others (ref.[20b,21−23]) according to which the hydride resonance of the isomeric form having the hydride ligands *trans* to the more electronegative atom, e.g. N, appears at lower frequencies than that in which the M−H bond is *trans* to a less electronegative donor atom such as sulfur.
[20] [20a] M. Schlaf, A. J. Lough, R. H. Morris, *Organometallics* **1993**, *12*, 3808−3809. − [20b] M. Schlaf, A. J. Lough, R. H. Morris, *Organometallics* **1996**, *15*, 4423−4436.
[21] A. J. Deeming, B. L. Shaw, *J. Chem. Soc. A* **1969**, 1128−1134.
[22] B. L. Shaw, R. E. Stainbank, *J. Chem. Soc., Dalton Trans.* **1972**, 223−228.
[23] J. A. van Doorn, C. Masters, C. van der Woude, *J. Chem. Soc., Dalton Trans.* **1978**, 1213−1220.
[24] R. H. Morris, *Inorg. Chem.* **1992**, *31*, 1471−1478.
[25] [25a] A. B. P. Lever, *Inorg. Chem*. **1990**, *29*, 1271−1285. − [25b] A. B. P. Lever, *Inorg. Chem*. **1991**, *30*, 1980−1985.
[26] D. Evans, J. A. Osborn, G. Wilkinson, *Inorg. Synth.* **1968**, *11*, 99−101.
[27] J. P. Collman, C. T. Sears, Jr., M. Kubota, *Inorg. Synth.* **1990**, *28*, 92−94.
[28] A. Altomare, G. Cascarona, C. Giacovazzo, A. Guagliardi, M. C. Burla, G. Polidori, M. Camalli, *SIR-92 − Program Package for Solving Crystal Structures by Direct Methods*, Bari, Perugia and Rome, **1992**; *J. Appl. Crystallogr.* **1994**, *27*, 435−436.
[29] G. M. Sheldrick, *SHELX-97 − Programs for Crystal Structure Analysis (Release 97−2)*, Göttingen, **1997**.
[30] A. L. Spek, *PLATON-99*, Utrecht, **1999**.

Received November 23, 1999
[I99423]

Ag^{I} Cryptates of *N,N′*-Bridged 1,10-Diazacyclooctadeca-5,14-diynes − A Comparison Between the Complexes and the Free Ligands

Rolf Gleiter,*[a] Thomas von Hirschheydt,[a] and Frank Rominger[a]

Dedicated to Professor Günter Helmchen on the occasion of his 60th birthday

Keywords: Silver / Alkyne Complexes / Cryptands / N Ligands

The bicyclic diaza alkynes **1**–**3** react quantitatively with silver triflate to give the corresponding cryptates **4**–**6**. The solid-state structures of the silver(I) complexes **4** and **6** were determined by means of X-ray diffraction studies. A comparison of the molecular structures of **4** and **6** with those of the uncomplexed ligands **1** and **3** reveals drastic changes in the conformations of the ligands. Evidence for an interaction of the silver ions with alkyne units in **4** and **6** was found from a high-field shift of the ^{13}C signal for the sp carbons in the ^{13}C NMR spectrum.

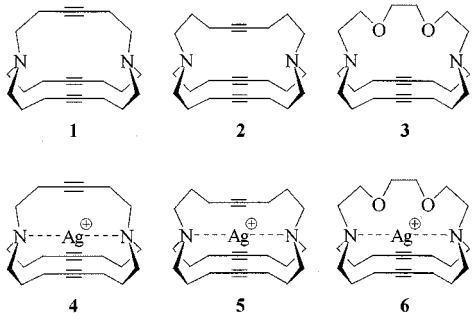
Introduction

Silver complexes of olefins are legion and have been reviewed on several occasions.[1] Less extensive are reports on silver complexes with benzene derivatives and alkynes even though several silver complexes with benzene derivatives[2] and alkynes[3] have been characterized by X-ray investigations. The formation of weak complexes between π-systems and silver ions has also been demonstrated by spectroscopic means[4] and solubility measurements,[5a] and has been used for analytical purposes.[5b]

We have recently synthesized a series of (1,*k*+2)diazabicyclo[*k,l,m*]alkanes[6] in which the bridges contain either alkyne or benzene units. The larger systems incorporate silver(I) and copper(I) ions[6c,6e] and thus provide further examples in which an alkyne or benzene unit is situated in close proximity to a metal ion. The examples shown so far reveal no evidence for an interaction of the metal ion with the π-system; instead, bonding to the amine center(s) is preferred. To contribute further to the question of silver−alkyne interactions we have investigated the silver complexes of the *N,N′*-bridged 1,10-diazacyclooctadeca-5,14-diynes **1**−**3**.[6d] These systems provide a rather flexible cage and thus might respond to a central silver ion with a considerable change of geometry, in such a way that a silver−alkyne interaction might result.

Results and Discussion

The reaction of the bicyclic compounds **1**−**3** with a small excess of silver(I) triflate in dichloromethane leads, in all three cases, to the corresponding cryptates **4**−**6** in quantitative yields (Scheme 1). The colorless crystals are sensitive to light in solution but proved to be stable in the solid state.



Scheme 1

X-ray Analysis

In the cases of **4** and **6**, we were able to grow single crystals by recrystallization from methanol. In Figure 1 and 2 we compare the molecular structures of **1** and **3** with those of **4** and **6**. Table 1 lists the most relevant bond distances in **1**, **3**, **4** and **6**.

A comparison between the congeners **1** and **4**, **3** and **6** reveals considerable conformational changes caused by the silver ion. This shows up in the torsional angle between the triple bonds of the 1,10-diazacyclooctadeca-5,14-diyne units and the N−N distances (Table 1). In compound **1** the bridgeheads adopt the *out/out* conformation with an N−N distance of 5.57 Å. In **4** this distance is reduced to 4.92 Å, while the torsional angle[7] between the triple bonds is enlarged from 23° in **1** to 82° in **4**. In compound **3** the *in/in* conformation is adopted with an N−N distance of 6.12 Å. In **6** the N−N distance is reduced to 4.57 Å. This reduction goes along with a considerable change of the torsional angle between the triple bonds from 20° in **3** to 81° in **6**.

In both silver complexes the metal ion is situated approximately in the center of the cage. The triflate anion no longer participates in the coordination sphere of the metal. Figure 1 and 2 also reveal that, in **4** and **6**, the N−Ag−N

[a] Organisch-Chemisches Institut der Universität Heidelberg, Im Neuenheimer Feld 270, D-69120 Heidelberg, Germany
E-mail: rolf.gleiter@urz.uni-heidelberg.de

 © WILEY-VCH Verlag GmbH, D-69451 Weinheim, 2000 1434−1948/00/0909−2127 $ 17.50+.50/0

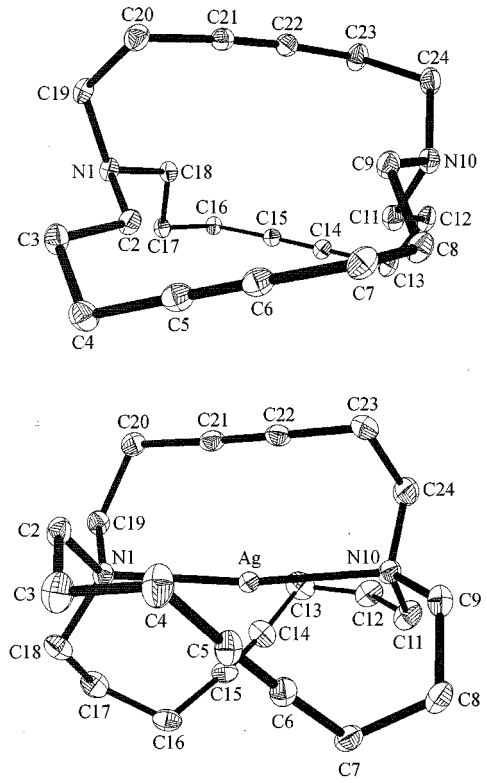


Figure 1. ORTEP plots (25% ellipsoid probability) of the molecular structures of **1** (top) and **4** (bottom)

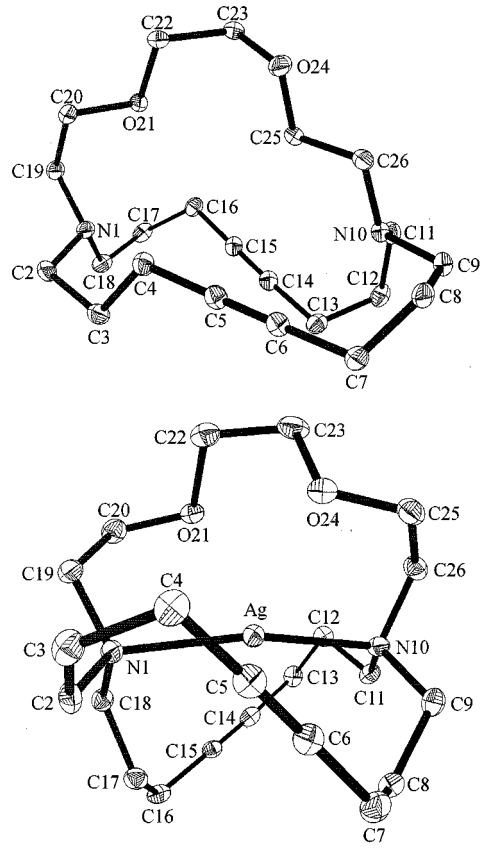


Figure 2. ORTEP plots (25% ellipsoid probability) of the molecular structures of **3** (top) and **6** (bottom)

Table 1. Selected bond lengths [Å] in **1**, **3**, **4** and **6**

	1	**3**	**4**	**6**
N1−N10	5.567(2)	6.122(1)	4.921(3)	4.566(6)/4.566(6)
Ag−N1			2.452(2)	2.323(4)/2.326(4)
Ag−N10			2.479(2)	2.283(4)/2.284(4)
Ag−C5			2.667(3)	2.777(6)/2.774(6)
Ag−C6			2.580(3)	2.921(6)/2.927(6)
C5−C6	1.189(2)	1.193(2)	1.203(4)	1.187(8)/1.207(8)
Ag−C14			2.624(3)	3.951(6)/3.995(6)
Ag−C15			2.588(3)	3.960(5)/3.995(6)
C14−C15	1.186(2)	1.192(2)	1.193(5)	1.190(8)/1.167 (8)
Ag−C21			2.572(3)	
Ag−C22			2.550(3)	
C21−C22	1.185(2)		1.199(4)	
Ag−O21				2.625(4)/2.656(4)
Ag−O24				2.678(4)/2.607 (4)

bonds are not linear but slightly bent: 173° in **4** and 164° in **6**. The Ag−N distances vary between 2.45 Å and 2.48 Å for **4** and 2.32 Å and 2.28 Å for **6**. In both cases they are 0.1 to 0.3 Å longer than those Ag−N distances reported for several $Ag(NH_3)_2^+$ complexes.[8] The values obtained for the Ag−N distances in the cases of **4** and **6** are close to the Ag−N distances reported for the silver complex of 1,8-diazabicyclo[6.6.6]eicosa-4,11,17-triyne.[6c]

To judge the possibility of a metal−alkyne interaction we considered the distances between the triple bonds and the silver ions in **4** and **6** (Table 1). In compound **4** these distances vary between 2.55 Å and 2.67 Å. In compound **6** the variation of the Ag−C(sp) distances is larger and ranges from 2.77 Å to 4.00 Å. A comparison with the Ag−C(sp) distances of other silver alkyne complexes[3,6c] reveals values that are spread between 2.225 Å for a highly strained alkyne[3e] and from 2.85 Å to 3.05 Å in unstrained species.[3d] Based on this comparison we can describe the interaction between the silver ion and the triple bonds in **4** as a bonding one. The same arguments applied to **6** lead to the conclusion that only one triple bond (C5−C6) interacts with the metal. We ascribe this preference to a coordination of the silver ion in **6** with the oxygen atoms. The distances found in the case of **6** [Ag−O21 = 2.656(4) Å and Ag−O24 = 2.607(4) Å] are very similar to those reported for silver complexes of oligo(ethylenoxy)-bridged stilbenes.[9]

^{13}C NMR Investigations

In Figure 3 we have compared the ^{13}C NMR spectra of **1** and **4** (Figure 3a) as well as **3** and **6** (Figure 3b). The comparison between **1** and **4** shows a significant change in the area between δ = 75 and 80 where the sp-hybridized carbon signals are anticipated.

We find for **1** a small signal at δ = 81.8 for the two carbons of the hexyne bridge and at δ = 80.8 a signal of almost double intensity for the four sp carbon atoms of the two octyne bridges. After complexation with Ag^+, the latter signal remains almost unchanged, whereas the smaller signal is shifted upfield by 2.9 ppm.

In the case of the ^{13}C NMR spectrum of **6** at −60 °C we find two signals at δ = 81.1 and δ = 79.2. A comparison with the ^{13}C NMR spectrum of **3** (Figure 3b) suggests the

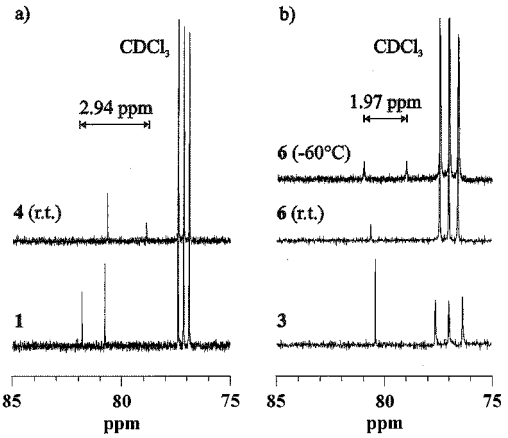


Figure 3. a) Section of the ^{13}C NMR spectrum ($CDCl_3$, 125.76 MHz) of **1** and **4** at room temperature; b) Section of the ^{13}C NMR spectrum ($CDCl_3$, 75.47 MHz) of **3** at room temperature and −60 °C

assignment of the low-field peak to the uncomplexed alkyne unit of **6** while the peak at δ = 79.2 should be assigned to the alkyne unit close to the silver ion.

The observed upfield shift due to complexation with the silver ion is unusual and has so far only been reported for the silver(I) complexes of highly strained thiacycloheptynes[3e] and some alkyne silver(I) hexafluoroacetylacetonato complexes.[3f] In the other silver complexes investigated so far[3] a low-field shift has been encountered. We ascribe the upfield shifts in **4** and **6** due to a close proximity of the metal ion and the triple bond, which is forced by the ligand. The observed upfield shift of the ^{13}C signal upon complexation with Ag^+ implies a better shielding of the sp carbon nuclei and, accordingly, a higher electron density at the coordinated triple bond than at the uncomplexed alkyne group. A possible explanation of this observation is due to the Dewar−Chatt−Duncanson model.[10] It suggests a back donation of electron density from the nitrogen lone pairs through the d orbitals of the silver ion into the antibonding π* orbital of the triple bond.

Conclusions

The incorporation of a silver ion into the cages of **1** and **3** results in drastic changes of the conformations of the ligands. The driving force for this change is a close interaction between the nitrogen centers and the metal. This has been achieved by torsion of both 4-octyne bridges around the N−N axis. As a side effect of these conformational changes we observe close contacts between the silver ion and the triple bonds in the solid state and in solution.

Experimental Section

General Remarks: All reactions were carried out under argon atmosphere with magnetic stirring in dry, degassed CH_2Cl_2. The ^1H and ^{13}C NMR spectra were recorded in $CDCl_3$ with Bruker WH 300 and Avance 500 instruments, respectively. Mass spectra were obtained with a JEOL JMS 700 spectrometer.

General Procedure for the Complexation: One equivalent of the cryptand (**1**−**3**) was added to 1.1 equivalents of silver(I) triflate in dry degassed CH_2Cl_2 under argon and stirred for one hour with the exclusion of light. The solvent was removed in vacuo and the

Table 2. Crystallographic data for **4** and **6**

	4	**6**
Formula	$C_{23}H_{32}AgF_3N_2O_3S$	$C_{24}H_{36}AgF_3N_2O_6S$
M [g mol^{-1}]	581.44	645.48
Temperature [K]	200(2)	293(2)
Crystal system	Monoclinic	Monoclinic
Space group	$P2_1/c$	$P2_1/c$
Z	4	8
a [Å]	12.9234(3)	25.7617(1)
b [Å]	8.9937(2)	8.5768(4)
c [Å]	21.4056(4)	26.0432(1)
α [°]	90	90
β [°]	102.631(1)	105.106(1)
γ [°]	90	90
Volume [Å^3]	2427.74(9)	5555.5(5)
ρ [g cm^{-3}]	1.591	1.54
μ (Mo-K_α) [mm^{-1}]	0.967	0.861
Scan range (θ) [°]	1.6−25.5	1.3−25.6
hkl range	−15/14, −10/10, −22/24	−30/30, −10/10, −30/30
Reflections collected	17586	41817
Independent reflections	4190	9740
	R(int) = 0.0226	R(int) = 0.0517
Observed reflections	3660 [$I > 2\sigma(I)$]	6437 [$I > 2\sigma(I)$]
Absorption correction	Semi-empirical from equivalents	Semi-empirical from equivalents
max./min. transmission	0.86/0.70	0.96/0.77
data/restraints/parameters	4190 /12/326	9740/0/669
GoF on F^2	1.07	1.06
largest diff. peak and	0.95	1.18
hole [e Å^{-3}]	−0.73	−0.88
final R indices	R_1 = 0.030	R_1 = 0.051
[$I > 2\sigma(I)$]	wR_2 = 0.072	wR_2 = 0.111

remaining white solid recrystallized from methanol yielding colorless crystals in the case of **4** and **6**. For **5** only polymorphic material was obtained.

Ag^I ⊂{1,10-Diazabicyclo[8.8.6]tetracosa-5,14-diyne}trifluoromethanesulfonate (4): FAB-MS: *m/z* (%) = 431.1 [**4** − CF_3SO_3]$^+$ ($^{12}C_{22}{}^1H_{32}{}^{107}Ag^{14}N_2$: 431.2).[11] − ^{1}H NMR ($CDCl_3$, 500 MHz): δ = 1.79−1.99 (m, 8 H), 2.55 (t, *J* = 6.4 Hz, 8 H), 2.61−2.70 (m, 12 H), 2.72−2.79 (m, 4 H). − $^{13}C\{^1H\}$ NMR ($CDCl_3$, 125.76 MHz) δ = 17.9, 18.5, 25.6, 55.8, 56.2 (CH_2), 78.9, 80.7 (C≡C).

Ag^I⊂{1,10-Diazabicyclo[8.8.8]hexacosa-5,14-diyne}trifluoromethanesulfonate (5): FAB-MS: *m/z* (%) = 459.2 [**5** − CF_3SO_3]$^+$ ($^{12}C_{24}{}^1H_{36}{}^{107}Ag^{14}N_2$: 459.2).[11] − ^{1}H NMR ($CDCl_3$, 500 MHz): δ = 1.94 (br. s, 12 H), 2.44 (br. s, 12 H), 2.70 (br. s, 12 H). − $^{13}C\{^1H\}$ NMR ($CDCl_3$, 25.8 MHz) δ = 17.9, 27.4, 55.7 (CH_2), 81.5 (C≡C).

Ag^I⊂{4,7-Dioxa-1,10-diazabicyclo[8.8.8]hexacosa-14,22-diyne}-trifluoromethanesulfonate (6): FAB-MS: *m/z* (%) = 467.1 ($^{12}C_{22}{}^1H_{32}{}^{107}Ag^{14}N_2O_2$: 467.2).[11] − ^{1}H NMR ($CDCl_3$, 300 MHz): δ = 1.81−2.04 (m, 8 H), 2.28−2.42 (m, 8 H), 2.59−2.84 (m, 8 H), 3.69 (s, 4 H), 3.76−3.88 (m, 4 H). − $^{13}C\{^1H\}$ NMR ($CDCl_3$, 75.47 MHz, 25 °C) δ = 17.4, 28.1, 53.0, 55.2, 64.6, 67.4 (CH_2), 80.8 (C≡C); ($CDCl_3$, 75.47 MHz, −60 °C) δ = 15.9, 17.9, 26.8, 29.3, 51.6, 53.5, 55.1, 63.6, 66.6 (CH_2), 79.2, 81.1 (C≡C).

X-ray Crystallographic Study: The measurements on crystals of **4** and **6** were performed on a Bruker SMART CCD X-ray diffractometer using graphite-monochromated Mo-K_a radiation (λ = 0.71073 Å). The SMART software package[12] was used for data collection as well as frame integration. Structure solution was carried out using the SHELXTL V5.10 software package.[13] Intensities were corrected for Lorentz and polarization effects. All structures were solved by direct methods. Full-matrix least-squares refinement was carried out against F^2. The non-hydrogen atoms were refined anisotropically. The hydrogen atoms were taken into account at calculated positions. Further details are listed in Table 2. The crystal of **6** contained two independent molecules in the asymmetric unit (see Table 1 and 2).

Crystallographic data (excluding structure factors) for the structures reported in this paper have been deposited with the Cambridge Crystallographic Data Centre as supplementary publication no. CCDC-138336 (**4**) and 138337 (**6**). Copies of the data can be obtained free of charge on application to CCDC, 12 Union Road, Cambridge CB2 1EZ, UK [Fax: (internat.) + 44-1223/336-033; E-mail: deposit@ccdc.cam.ac.uk].

Acknowledgments

This work was supplied by the Deutsche Forschungsgemeinschaft (SFB 247), the Fonds der Chemischen Industrie and the BASF Aktiengesellschaft, Ludwigshafen.

[1] [1a] M. A. Bennett, *Chem. Rev.* **1962**, *62*, 611−652. − [1b] H. W. Quinn, J. H. Tsai, *Advan. Inorg. Radiochem.* **1969**, *12*, 217−373. − [1c] C. D. M. Beverwijk, G. J. M. Van der Kerk, A. J. Leusink, J. G. Noltes, *Organomet. Chem. Rev.* **1970**, *75*, 215−280. − [1d] M. Herberhold, Metal-π Complexes Vol. 2, Elsevier, Amsterdam **1972**, 232−256.

[2] [2a] H. C. Kang, A. W. Hanson, B. Eaton, V. Boekelheide, *J. Am. Chem. Soc.* **1985**, *107*, 1979−1985. − [2b] T. Seppälä, E. Wegelius, K. Rissanen, *New J. Chem.* **1998**, 789−791.

[3] [3a] J. D. Ferrara, A. Djebli, C. Tessier-Youngs, W. J. Youngs, *J. Am. Chem. Soc.* **1988**, *110*, 647−649. − [3b] R. Gleiter, M. Karcher, D. Kratz, M. L. Ziegler, B. Nuber, *Chem. Ber.* **1990**, *123*, 1461−1468. − [3c] H. Meier, Y. Dai, *Tetrahedron Lett.* **1993**, *34*, 5277−5280. − [3d] T. Nishinaga, T. Kawamura, K. Komatsu, *Chem. Commun.* **1998**, 2263−2264. − [3e] P. Schulte, U. Behrens, *J. Organomet. Chem.* **1998**, *563*, 235−249. − [3f] K.-M. Chi, C.-T. Lin, S.-M. Peng, G.-H. Lee, *Organomet.* **1996**, *15*, 2660−2663.

[4] G. S. Lewandos, D. K. Gregston, F. R. Nelson, *J. Organomet. Chem.* **1976**, *118*, 363−374.

[5] [5a] J. L. Pierre, P. Baret, P. Chautemps, M. Armand, *J. Am. Chem. Soc.* **1981**, *103*, 2986−2988. − [5b] J. Gross, G. Harder, F. Vögtle, H. Stephan, K. Gloe, *Angew. Chem.* **1995**, *107*, 523−526; *Angew. Chem. Int. Ed. Engl.* **1995**, *34*, 481−484.

[6] [6a] R. Gleiter, K. Hövermann, J. Ritter, B. Nuber, *Angew. Chem.* **1995**, *107*, 867−869; *Angew. Chem. Int. Ed. Engl.* **1995**, *34*, 789−791. − [6b] V. Wolfart, R. Gleiter, H. Irngartinger, T. Oeser, C. Krieger, *Eur. J. Org. Chem.* **1998**, 2803−2809. − [6c] A. Kunze, R. Gleiter, F. Rominger, *Chem. Commun.* **1999**, 171−172. − [6d] T. v. Hirschheydt, V. Wolfart, R. Gleiter, H. Irngartinger, T. Oeser, F. Rominger, F. Eisenträger, *J. Chem. Soc., Perkin Trans. 2,* **2000**, 175−183. − [6e] A. Kunze, S. Bethke, R. Gleiter, F. Rominger, *Org. Lett.* **2000**, *2*, 609−612.

[7] The torsional angle between opposite triple bonds is defined as follows: C(sp)−center-of-triple-bond−center-of-opposite-triple-bond−C(sp).

[8] U. Zachwieja, H. Jacobs, *Z. Krist.* **1992**, *201*, 207−212.

[9] T. Futterer, A. Merz, J. Lex, *Angew. Chem.* **1997**, *109*, 619−622; *Angew. Chem. Int. Ed. Engl.* **1997**, *36*, 611−613.

[10] M. J. S. Dewar, *Bull. Soc. Chim. France* **1951**, C71−C79; J. Chatt, L. A. Duncanson, *J. Chem. Soc.* **1953**, 2939−2947.

[11] Observed isotopic pattern fits the calculated one.

[12] Bruker Analytical X-ray Division, Madison, WI, **1996**.

[13] G. M. Sheldrick, Bruker Analytical X-ray System, Madison, WI, **1997**.

Received January 10, 2000
[I00026]

Highly Lewis Acidic Bifunctional Organoboranes

Warren E. Piers,*[a] Geoffrey J. Irvine,[a] and V. Clifford Williams[b]

Keywords: Boranes / Lewis acids / Anions / Metallocenes

Chelating Lewis acids have not been developed to the same degree as multidentate Lewis bases. Nonetheless, such compounds have attracted interest due to their potential for the enhanced activation of basic substrates and the selective binding of anions. Organodiboryl compounds form a class of bidentate Lewis acids which have a long, but relatively underdeveloped history. Many examples exist where donor groups on boron serve to stabilize the Lewis acid centers. More recently, advances in the chemistry of diboryls with highly Lewis acidic boron centers substituted with perfluoroaryl groups have been made. In particular, compounds of general formula $(F_5C_6)_2B$–linker–$B(C_6F_5)_2$ have been prepared and their chemistry examined. In this Microreview, we survey the classes of bifunctional boron Lewis acids known, including their synthesis, properties and anion binding chemistry. Particular emphasis is placed on the role these Lewis acids play in olefin polymerization catalyst generation from simple metallocene precursors.

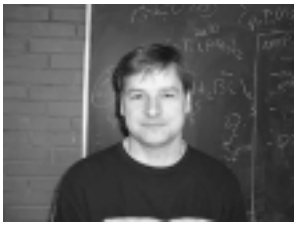
Introduction

Despite the early recognition of the potential utility of multidentate Lewis acids, development in this area has lagged far behind the extensive chemistry associated with chelating Lewis bases.[1] The reasons for this stem partly from the synthetic difficulties associated with the preparation of molecules with multiple Lewis acid sites, which in turn is related to the high reactivity of these species. These factors can be partially ameliorated by the incorporation of groups capable of stabilizing the Lewis acid centers through either strong σ-donation or π-bonding. In fact, most of the examples of group 13 element based bidentate Lewis acids in the literature make use of this strategy, at least to some degree.[2] Since one of the primary reasons for investigating these molecules is to achieve a greater degree of substrate activation, reducing the Lewis acid strength of each center to some extent defeats the purpose of their preparation.

[a] Department of Chemistry, University of Calgary,
2500 University Drive N. W., Calgary, Alberta,
Canada T2N 1N4
Fax: (internat.) + 1-403/289-9488
E-mail: wpiers@ucalgary.ca
[b] Inorganic Chemistry Laboratory, University of Oxford,
South Parks Road, Oxford OX1 3QR, UK



Warren Piers was born in Edmonton, Alberta in 1962 before moving to the Vancouver area where he grew up. He obtained his B. Sc. degree at the University of British Columbia in 1984 and continued there as a NSERC Postgraduate Scholar under the tutelage of Prof. Michael Fryzuk, graduating with a Ph. D. in 1988. He then spent two years at the California Institute of Technology as an NSERC and Killam Postdoctoral Fellow with Prof. John Bercaw, gaining expertise in early transition metal organometallic chemistry. In 1990, he joined the Chemistry and Biochemistry Department at the University of Guelph as an Assistant Professor. In 1995, he joined the Chemistry Department at the University of Calgary as an Associate Professor; he was recently promoted to Full Professor. Honors awarded include the Province of Ontario's John C. Polanyi Prize in Chemistry (1991) and an Alfred P. Sloan Foundation Research Fellowship (1996–2000).



Geoffrey J. Irvine, a native New Zealander, received his Ph. D. in 1996 from the University of Auckland under the supervision of Professor Warren Roper and Dr. James Wright. He then carried out Postdoctoral Research with Associate Professor Scott Bohle at the University of Wyoming, followed by a year of Postdoctoral work with Professor Warren Piers at the University of Calgary. His current interests are in the fields of homogeneous catalysis, materials chemistry and transition metal mediated organic transformations.



V. Clifford Williams studied chemistry at St Catherine's College Oxford, where he worked in the group of Prof. Malcolm L. H. Green. He received his D. Phil in 1998 having worked on high oxidation state imido and low coordination number amido complexes of uranium. Upon completion, he worked with Professor Warren Piers for a year on the synthesis of chelating boranes and noncoordinating anions. Currently, he is back at the Inorganic Chemistry Laboratory, Oxford with Malcolm Green as part of the team who are working on the synthesis and chemistry of single walled carbon nanotubes.

MICROREVIEWS: This feature introduces the readers to the authors' research through a concise overview of the selected topic. Reference to important work from others in the field is included.

 © WILEY-VCH Verlag GmbH, D-69451 Weinheim, 2000 1434–1948/00/1010–2131 $ 17.50+.50/0

Nonetheless, impressive advances have been made in the synthesis and use of aluminum,[3] mercury,[4] tin[5] and titanium[6] based bifunctional Lewis acids, which show that two Lewis acid centers can act in concert to effect increased substrate activation or greater reaction selectivity.

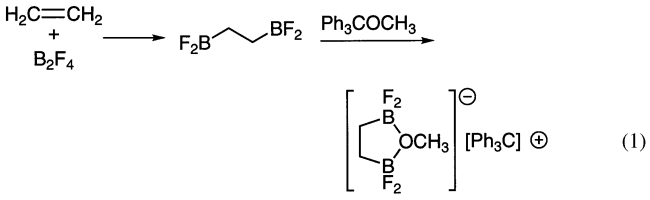
It has been recognized for many years that the pentafluorophenyl group is an excellent replacement for a halogen ligand in boron Lewis acids.[7] For example, the C_6F_5 group has similar σ-electron-withdrawing powers to those of Cl and F but the B−C_{aryl} bonds in $B(C_6F_5)_3$ are more kinetically inert in the presence of protic agents.[8] Therefore, although $B(C_6F_5)_3$ loses some Lewis acidity due to the front strain associated with the bulkier C_6F_5 substituents,[9] it is more easily handled and generally as effective as BX_3 Lewis acids in terms of strength,[9,10] without the problems inherent with reactive B−X bonds.

A natural extension of the rise to prominence of this monodentate Lewis acid[11] is a recent surge of activity in the preparation of multifunctional boranes (and other group 13 elements) in which the boron centers are of comparable Lewis acid strength to the highly Lewis acidic monofunctional boranes $RB(C_6F_5)_2$ (R = alkyl, alkenyl, aryl, C_6F_5). Although interest in these compounds arises primarily because of their role in the activation of neutral organometallic complexes for olefin polymerization processes, such diboryl targets are also of interest in the arenas of organic synthesis,[12] anion recognition[13] and the formation of new polymeric materials.[14] Furthermore, two strong, proximal Lewis acid centers have the potential to act as "superelectrophiles".[15]

After setting the stage with a brief history of strongly Lewis acidic bifunctional boranes, we will discuss recent developments in this area, along with specific related examples. The bidentate Lewis acids will be grouped by the number of atoms in the bridge connecting them; diboranes with no atom in the bridge, i.e. diborane(4) compounds R_2B-BR_2, will not be considered here. Although it has been shown that such compounds can bind two Lewis bases,[16] their potential as chelating acids is negligible. These compounds do, however, have potential as reagents for the preparation of chelating organodiboryl Lewis acids, and this chemistry has to some extent been reviewed elsewhere.[2b]

History of Highly Lewis Acidic Organodiboryl Compounds

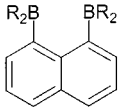
The first important study aimed at investigating the chelating properties of a bidentate Lewis acid was conducted by Shriver and Biallas in the late 1960's.[17] The reactions of a bidentate version of the quintessential boron-based Lewis acid (BF_3) with simple Lewis bases and anions were investigated. They found that $F_2BCH_2CH_2BF_2$, prepared by mixing ethylene and B_2F_4 at low temperature,[18] did not readily chelate neutral bases, but that anions such as OMe^- were bound by both borane centers. Given the high reactivity of the B−F bonds in this bidentate Lewis acid, incorporation of the anions required weakly basic reagents such as Ph_3COMe [Equation (1)] to avoid metathetical replacement of the boron fluorides. Amido bridging groups were also incorporated as their tropylium salts.



(1)

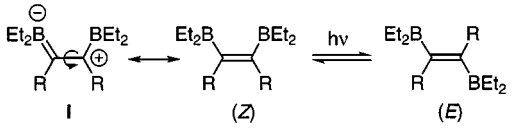
This compound was the first diboryl derivative with strongly Lewis acidic boron centers, but despite these early and very promising successes, research in bifunctional borane Lewis acid chemistry appears to have been sporadic for close to two decades subsequent to these publications. Although $F_2BCH_2CH_2BF_2$ is a relatively simple looking compound on paper, looks can be deceiving; undoubtedly the difficulties in preparing and handling this compound, in particular the synthesis of the precursor B_2F_4, have something to do with its disappearance from the literature since the seminal studies of Shriver and Biallas. Perhaps the disappointing performance of this acid in binding neutral Lewis bases, of most interest to organic chemists, also contributed to its demise.

A series of papers by Katz in the mid 1980's describing the use of a 1,8-bis(dimethylboryl)naphthalene (**1a**) as a "hydride sponge" was the next major study on the applications of a chelating diboryl.[19] Other anions, such as F^- and OH^- were also bound effectively by this compound. Katz showed quantitatively, through competitive binding studies involving monodentate analogs, that two boron centers are better than one for binding these anions. To bind chloride, however, the more Lewis acidic chloro derivative **1b** was required.[20] This compound was prepared via a transmetallation reaction between an organomercury precursor and BCl_3 in refluxing toluene in 86% yield. Although sensitive B−Cl functions tended to limit the usefulness of this species, the other side of the coin is that these bonds may be readily functionalized. To this end, Reilly and Oh have recently used the Katz compound to prepare chiral bidentate Lewis acids in situ via derivatization of the chloro boranes with chiral ligands such as (*R*)-BINOL, for use in Diels−Alder couplings.[21] However, it is unclear whether the two borane centers cooperate in activating the substrates in this system.



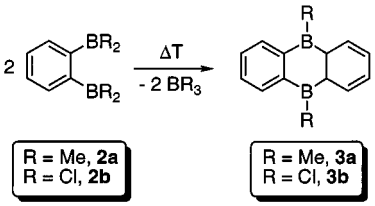
R = Me, **1a**
R = Cl, **1b**

Two final types of organodiboryls we wish to mention highlight some of the chemistry which might be expected to feature prominently in more strongly Lewis acidic organodiboryls. The groups of Köster and Wrackmeyer[22] and Siebert[23] have both published widely on 1,2-diboryls bridged by alkenyl fragments. A variety of methods for the synthesis of these compounds has been developed, including addition of X_2B-BX_2 or BI_3 across the C≡C bond of internal alkynes. Like the Katz compounds discussed above, the *cis*-alkenyl diboryls are capable of binding various first row halogen equivalents when the BR_2 fragments are *cis* disposed about the C=C double bond. In Köster's work, the R substituent was for the most part the relatively electron rich, but metathetically inert, ethyl group, and incorporation of the anions X^- can be accomplished by treatment of the diboryls with various potassium salts.[22a] The free *cis*-1,2-diboryls, however, were found to be susceptible to photoisomerization about the double bond, producing equilibrium mixtures of the (*Z*) and (*E*) isomers [Equation (2)].[22b] The barrier to double bond isomerization is decreased because the empty p orbital on the boryl centers can overlap with the C=C π-bond and lower the bond order of the double bond through resonance structures akin to **I**, allowing for more facile isomerization. This phenomenon might be expected to be more prevalent in diboryls with stronger Lewis acidic boron centers, such as the pentafluorphenyl-substituted family considered here. However, it should be noted that only the (*Z*) isomer is capable of chelating anions and the foundational work of Katz[19] has shown that these anions are thermodynamically favored over their monodentate analogs.



(2)

One way to avoid this problem is to incorporate backbones which cannot isomerize. Kaufmann et al. were the first to prepare the 1,2 phenylene bridged tetrachlorodiboryl species via metathesis from aryl silane[24] or stannane[25] precursors. This work brought to light the thermal instability of some of these compounds towards condensation reactions which eliminate BR_3. For example, heating 1,2-$C_6H_4(BR_2)_2$ (**2a**, R = Me; **2b**, R = Cl) leads to loss of BR_3 and production of the 9,10-diboraanthracene compounds **3** [Equation (3)]. As will be seen, these 9,10-diboraanthracene derivatives are interesting Lewis acids in their own right, but in terms of the synthetic targets **2**, their generation is an undesirable side reaction which must be overcome. Eisch and his group have extended the scope of boron−tin exchange reactions substantially in an effort to produce organodiboryls with a variety of backbones, including −C≡C−, RC=CR and 1,2-C_6H_4,[26] and note that this thermally induced condensation reaction is a feature of the chemistry of diboryls with backbones other than 1,2-C_6H_4.

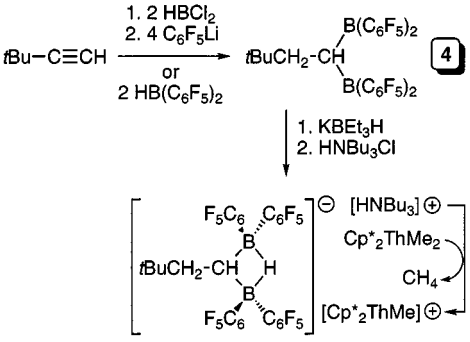


(3)

Development of the chemistry of chelating organoboranes, while not extensive, does have a rich history, as the above discussion briefly illustrates. Nevertheless, until very recently diboryl Lewis acids incorporating perfluoroaryl groups have not been explored. Given the considerable advantages of the C_6F_5 group, such compounds have great potential as anion receptors, olefin polymerization initiators and as synthons for the preparation of new weakly coordinating anions. The performance of a given diboryl in each of these areas will be influenced strongly by the nature of the bridge employed to link the two Lewis acid centers. In addition to its effects on the Lewis acid strength of the borane centers, the backbone will dictate the bite angle of the chelate and the separation of the two borane centers and hence the nature of the anions which will be most strongly bound. We now consider the recent progress in perfluoraryl-substituted diboryl Lewis acids, grouped by the number of atoms in the bridge connecting the two boron centers.

$B(Ar_F)_2$ Units Bridged by One Atom

The first report of a bidentate borane incorporating C_6F_5 groups came from the Marks group in 1994.[27] The borane $tBuCH_2CH[B(C_6F_5)_2]_2$ **(4)** was prepared by the metathetical route shown in Scheme 1.



Scheme 1

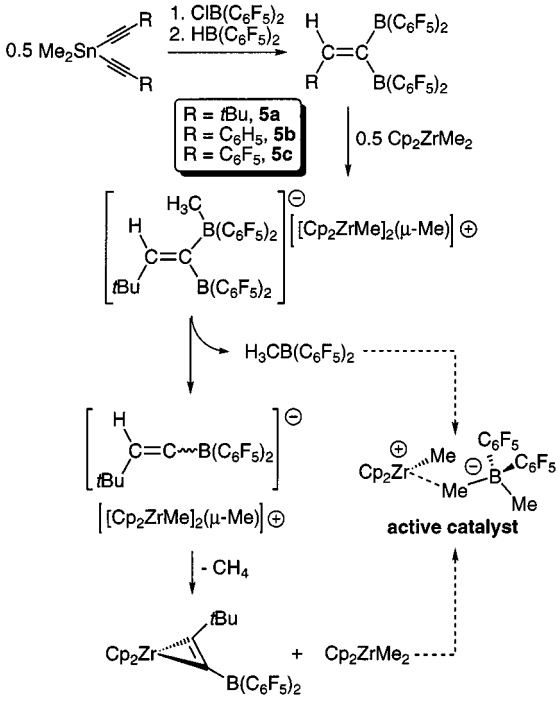
We have also shown that this borane, along with other examples, can be prepared via dihydroboration of terminal alkynes using the hydroboration reagent $HB(C_6F_5)_2$.[28] The motivation for this work was to employ these boranes as precursors to weakly coordinating anions in homogeneous olefin polymerization catalysts. To this end, Marks developed a route for converting the free 1,1-diboryl to the $[HNBu_3]^+$ salt of the μ-hydridodiborate which, in combination with the thoracene catalyst precursor $Cp_2*Th(CH_3)_2$ formed stable ion pairs capable of polymerizing ethylene, or

hydrogenating 1-hexene in the presence of dihydrogen. It was envisioned that diborate anions from this family of boranes would more effectively delocalize the negative charge, and thus reduce the coulombic interaction between cation and anion, leading to more active catalysts. This expectation was borne out in slightly increased activities for ethylene polymerization and 1-hexene hydrogenation compared to cationic permethylthoracene catalysts incorporating more conventional $[H_3CB(C_6F_5)_3]^-$ or $[B(C_6F_5)_4]^-$ counteranions.[27] The lack of H^- transfer back to the thorium center also suggested that the hydride is effectively chelated by the two borane centers, another potential advantage of bidentate Lewis acids for this particular application.

Although reactions of the free bifunctional borane tBuCH$_2$CH[B(C$_6$F$_5$)$_2$]$_2$ with dialkyl metallocenes were not reported in detail, the need to convert into an anionic hydridodiborate prior to use suggests that the free borane is not very effective as an activator by itself. In our brief exploration of the chemistry of these diboryl alkanes, we found evidence that facile retrohydroboration, yielding (*E*)-tBuCH=CHB(C$_6$F$_5$)$_2$ and HB(C$_6$F$_5$)$_2$, has a dominating influence on the reactivity of these species towards Lewis bases. As an example, when **4** was treated with one equivalent of acetone, the small amounts of HB(C$_6$F$_5$)$_2$ present in solutions of tBuCH$_2$CH[B(C$_6$F$_5$)$_2$]$_2$ reacted rapidly with the acetone to yield iPrOB(C$_6$F$_5$)$_2$, leaving (*E*)-tBuCH=CHB(C$_6$F$_5$)$_2$;[29] the reaction is pulled in this direction by the facile retrohydroboration equilibrium present in the system. Given the high reactivity of metallocenes toward HB(C$_6$F$_5$)$_2$,[30] this represents a potential problem for the use of this type of diboryl for direct activation of neutral organometallic alkyls which must be circumvented by prior formation of a diborate. Even if methide abstraction was favored, our study of a closely related system suggests that other problems can arise.

As an alternative to diborate formation, retrohydroboration can be precluded by incorporating unsaturation in the backbone; hence, we prepared the 1,1-diboryl alkenes[31] RCH=CH[B(C$_6$F$_5$)$_2$]$_2$ (R = tBu, **5a**; C$_6$H$_5$, **5b**; C$_6$F$_5$, **5c**) using tin−boron exchange/hydroboration procedures as shown in Scheme 2.[32]

In combination with Cp$_2$ZrMe$_2$, these 1,1-diboryls form reasonably active ethylene polymerization catalysts, although ion-pair stability was only moderate given the propensity of the methide anions formed to eject H$_3$CB(C$_6$F$_5$)$_2$[30a] (Scheme 2). Spectroscopic studies on the ion-pairs formed from **5a** and Cp$_2$ZrMe$_2$, in the absence of ethylene, show that the abstracted methide ligand is associated with the boron center *trans* to the tBu group, the most sterically accessible Lewis acid in this crowded system. Sterically undemanding Lewis bases also coordinate exclusively to this boron center in reactions with **5a**.[29] Loss of H$_3$CB(C$_6$F$_5$)$_2$ from this anion is presumably facilitated by the stability of the boryl-substituted vinyl anion,[33] which rapidly couples with the cationic zirconocene center. Separate experiments showed that the boryl alkyne zirconocene derivative is not capable of polymerizing ethylene under the reaction conditions and thus represents a catalytic dead-



Scheme 2

end. The methyl borane, however, is itself a strong Lewis acid capable of partial abstraction of methide from Cp$_2$ZrMe$_2$ and, indeed, careful analysis of the data from ethylene polymerization experiments led us to conclude that the active catalyst in these systems is in fact the ion pair derived from H$_3$CB(C$_6$F$_5$)$_2$ and Cp$_2$ZrMe$_2$! Clearly, Marks' strategy of preparing stable anions from groups which are readily chelated[27] (i.e. H^- and not CH_3^-) prior to incorporation into a catalyst system was appropriate for these systems.

Two other one-atom bridged diboryl Lewis acids have been prepared and characterized. Green and co-workers incorporated an HN bridge,[34] while the μ-oxo species [(C$_6$F$_5$)$_2$B]$_2$(μ-O) (affectionately known as "BOB") has been prepared by both our lab and that of Collins[35] by controlled hydrolysis of either HB(C$_6$F$_5$)$_2$ or ClB(C$_6$F$_5$)$_2$. A priori, a reduction in the Lewis acid strength of the boron centers in both of these molecules may be expected due to π-donation from the bridging atom; geometrical parameters from the X-ray structures of (Me$_3$Si)$_2$NB(C$_6$F$_5$)$_2$[34] and "BOB" indicate that B−N and B−O π-bonding is significant. Interestingly, however, the B−O−B moiety in BOB is not linear; bending occurs so that one boron center is able to accept donation of a lone pair from one of the *ortho* fluorine groups of the other borane.[35] The binding of anions or Lewis bases to these compounds has not been explored as yet.

Selectivities for binding various anions X^- by bidentate Lewis acids will obviously be profoundly influenced by the bite angle provided by the backbone linker. In these one-atom bridged diboryls, the bite angle can be parameterized

Table 1. Selected geometrical parameters for 1,1-diboryl Lewis Acids

Compound	B···B (Å)	B−atom−B (°)
$[(C_6F_5)_2B]_2(O)$		154.05(12)
$[(C_6F_5)_2B]_2(NH)$	2.53[a]	134.0[a]
tBuCH$_2$CH[B$(C_6F_5)_2]_2$	2.63[a]	116.1[a]
$\{t$BuCH$_2$CH[B$(C_6F_5)_2]_2\}(\mu$-H)$^-$	1.94	75.0[b]
tBuCH=CH[B$(C_6F_5)_2]_2$	2.673(8)	118.7(4)
PhCH=CH[B$(C_6F_5)_2]_2$	2.731(2)	123.22(13)
(C_6F_5)CH=CH[B$(C_6F_5)_2]_2$	2.721(6)	121.7(4)

[a] Estimated values based on semi-empirical AM1 geometry optimization calculation. − [b] B−C−B.

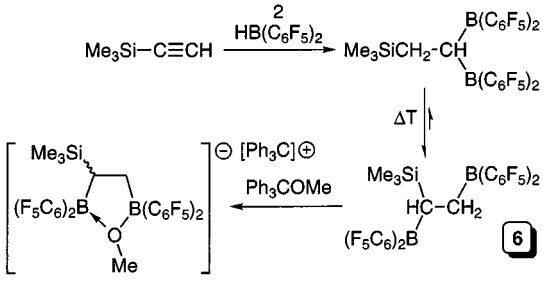
by the B−atom−B angle and the B···B distance; Table 1 collates these data for the compounds discussed in this section.

The values for the B−atom−B angles and interboron distances in $[(C_6F_5)_2B]_2$(NH) and tBuCH$_2$CH[B$(C_6F_5)_2]_2$ were obtained from a semi-empirical AM1 geometry optimization.[36] These calculated geometries around the central bridging atom are somewhat larger than the ideals of 120°and 109.5°, probably a consequence of the steric bulk of the bis-pentafluorophenylboryl substituents. Nonetheless, there is a high degree of flexibility in the saturated carbon backbone as demonstrated by the experimentally determined geometrical parameters found for the hydridodiborate anion. Although the chelation of halide anions by tBuCH$_2$CH[B$(C_6F_5)_2]_2$ is covered in the patent pertaining to Marks' work,[37] not much has been reported so far concerning the anion binding selectivities of this type of diboryl Lewis acid. The flexibility inherent in the system suggests it should bind larger anions than hydride.

In modifying the backbone to an alkenyl fragment, the bite angle of the chelate is necessarily affected since the bridging carbon is now sp^2 hybridized. Although the experimental values for B−C−B in the 1,1-diboryl alkenes **5a−c** are not much larger than the calculated value for the free, saturated analog, there should be markedly less flexibility than that associated with the unsaturated system. In particular, the variation possible in the B···B separation might be expected to be smaller for these diboryls. Indeed, treatment of **5a** with KEt$_3$BH indicated that hydride addition occurred, although pure material was not isolated and it was unclear if the hydride moiety was bound by both boron centers. Bromide, on the other hand, was not complexed at all when **5a** was treated with PPNBr, indicating perhaps that Br$^-$ (ionic radius = 1.82Å) is too large to fit into the chelate region of this type of diboryl. These preliminary results suggest that one-carbon bridged diboryls will not strongly bind larger anions and thus may be moderately hydride specific. However, more extensive investigations will be necessary to delineate the binding characteristics of this family of diboryls in more detail.

B(Ar$_F$)$_2$ Units Bridged by Two Atoms

The pioneering work of Shriver,[17] Köster,[22] Siebert,[23] and Kaufmann[24,25] described above provides obvious choices for a two-carbon linker for highly Lewis acidic, chelating organodiboryls: saturated alkyl, *cis*-alkenyl, and 1,2-phenylene. As the foregoing discussion has highlighted, saturated alkyl backbones are generally problematic due to the facility of retrohydroboration reactions. We have found one exception, however, and that is the 1,2-diboryl alkane formed upon double hydroboration of Me$_3$SiC≡CH (Scheme 3).[28a]



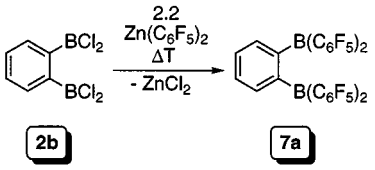
Scheme 3

Initially, a mixture of the 1,1 and 1,2 substituted isomers is observed, but upon heating gently for a couple of hours, complete conversion into the thermodynamic 1,2 species **6** is observed. This isomer is favored due to a ground state β-silicon effect which is energetically appreciable in these highly electrophilic boranes.[38] Perhaps this effect also contributes to the observation that this particular saturated diboryl derivative is less prone to the retrohydroboration complication found for **4**.

Compound **6** is not a particularly effective olefin polymerization co-catalyst on its own: stoichiometric reactions with [Cp$_2$ZrMe$_2$] show that rapid C$_6$F$_5$ transfer back to the zirconium center from the putative [**6**·Me]$^-$ anion occurs in solution. We have found this to be a common decomposition pathway for anions of this general form, i.e. [RR′B$(C_6F_5)_2]^-$, perhaps a reflection of the greater nucleophilicity of this more electron-rich borate anion. Deployment of Marks' strategy, i.e., converting **6** into an anion with an activating countercation, yields more encouraging results. For example, **6** reacts smoothly with trityl methyl ether (Ph$_3$COMe) to give an OMe anion (Scheme 3) as an orange solid.[39] The precise details of its structure are unknown, but two signals at δ = 41.4 and 5.7 in the ^{11}B NMR spectrum and a complex (but clean) ^{19}F NMR spectrum containing signals for four chemically different C$_6$F$_5$ groups point to an unsymmetrical structure as depicted in the scheme. The metallocene activating properties of **6** and its derivatives are currently under investigation.

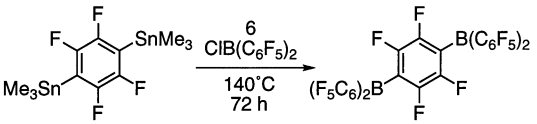
Of more interest as target diboryls are those with unsaturated *cis*-alkenyl- or 1,2-phenylene-type backbones, since these are more rigid and the effectiveness of electron-withdrawing backbones would be heightened due to the conjugation possible. Our efforts towards the 1,2 alkenyl objectives, in addition to inherent synthetic challenges, have to some extent been beset by the photoisomerization problem identified in Köster′s studies.[22b] We have, however, recently made significant progress towards the 1,2-phenylene-bridged systems, preparing both the unsubstituted and perfluorinated members of this family of compounds.[40]

The proteo substituted 1,2-phenylene bridged derivative **7a** was straightforwardly prepared from Kaufmann's tetrachlorodiborane 1,2-$C_6H_4(BCl_2)_2$ (**2b**)[24,25,41] and $[Zn(C_6F_5)_2]$[42] as a C_6F_5 transfer agent[43] [Equation (4)]. The intraboron region of this molecule is quite sterically hindered and the Lewis acidity of the two boron centers is dampened by virtue of the nonfluorinated backbone substituent;[44] consequently the anion binding chemistry of this species is somewhat limited. Nevertheless, the B···B separation in this molecule is 3.263(3)Å and the anions SCN^-, Cl^-, Br^-, OMe^- were found to interact with both boron centers in a bridging binding mode. ^{19}F NMR spectroscopic studies on the interaction of **7a** with these anions revealed only weak coordination and, in some cases, an equilibrating mixture of reactants and products could be observed. In all cases examined, the weak binding of these anions precluded isolation of the products from solution. Neutral donor molecules such as THF did not appear to bind appreciably in solution, attesting to the steric demands of this Lewis acid.



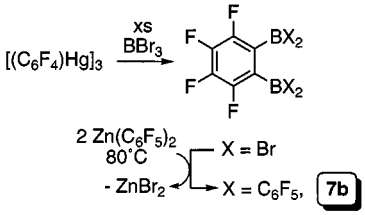
(4)

Of course, a system with a fully fluorinated phenylene backbone would be of more interest due to the increased Lewis acidity of the boron centers and the incorporation of more robust $B-C_{backbone}$ bonds. As is common, the more desirable target molecule is considerably more difficult to prepare! Our first attempts involved boron−tin exchanges between the trimethyltin-substituted perfluoroaryl precursor 1,2-$C_6F_4(SnMe_3)_2$[45] and $ClB(C_6F_5)_2$.[46] With two equivalents of the chloroborane, we found the major products to be 1,2-$C_6F_4(SnClMe_2)_2$ and $H_3CB(C_6F_5)_2$,[30a] the products of chloro−methyl exchange. We did not push this route any further, not wanting to sacrifice too much $ClB(C_6F_5)_2$, but Marks et al. have shown in a recently published patent[47] that the closely related 1,4-substituted diboryl Lewis acid can be prepared by this method [Equation (5)] using six equivalents of $ClB(C_6F_5)_2$.



(5)

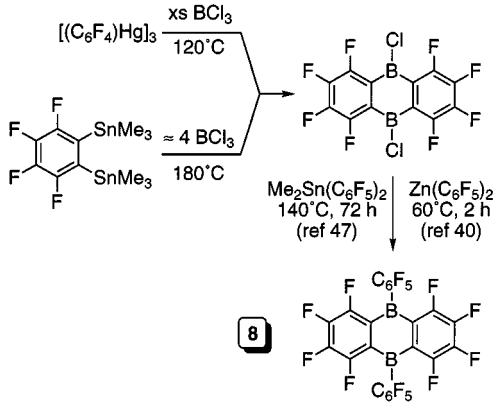
Eventually, we settled on the mercury trimer $[(C_6F_4)Hg]_3$[48] as a "C_6F_4" synthon for the preparation of **7b**. Reaction of $[(C_6F_4)Hg]_3$ with BBr_3 gives 1,2-$C_6F_4(BBr_2)_2$ which must be converted relatively quickly to the fully perfluoroaryl-substituted system using $[Zn(C_6F_5)_2]$ due to its thermal instability [Equation (6)]. The first two C_6F_5 groups are incorporated at ambient temperatures, but the third and fourth require heating to install successfully. The solid state structure of **7b** reveals a B···B separation of 3.138(2)Å, large enough to incorporate at least first row element anions comfortably; indeed, this compound has a rich anion binding chemistry associated with it (vide infra).



(6)

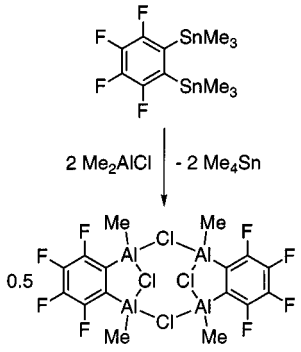
While **7b** is quite thermally stable, the tetrahalides are susceptible to the condensation reaction observed by Kaufmann and Eisch, producing 9,10-diboraanthracene derivatives. Both our group[40] and the Marks group[47] have made this observation independently (Scheme 4). In our laboratory, we noted that reaction of the mercury trimer with BCl_3 instead of BBr_3 leads directly to $[1,2\text{-}C_6F_4B(Cl)]_2$, which in turn could be converted into the pentafluorophenyl-substituted derivative **8** by treatment with $[Zn(C_6F_5)_2]$. Similarly, Marks' patent discloses a preparation of **8** which involves treatment of the organotin precursor 1,2-$C_6F_4(SnMe_3)_2$ with excess BCl_3 at high temperatures. In both procedures the high temperatures necessary to effect the transmetallations preclude isolation of 1,2-$C_6F_4(BCl_2)_2$, which condenses rapidly under these conditions. It is also possible that condensation occurs from the product of one transmetallation step, i.e. 1,2-$[C_6F_4(BCl_2)(SnMe_3)]$.[47b] To convert into **8**, Marks uses the organotin C_6F_5 transfer agent $[(C_6F_5)_2SnMe_2,]$,[49] which serves as well as the zinc reagent.

The entropically favorable condensation reaction is driven by the high temperatures used in the transmetallation reactions involving BCl_3 and the organomercury or -tin precursors. The greater facility of the transmetallation reaction between $[(C_6F_4)Hg]_3$ and BBr_3 (allowing for lower reaction temperatures) is part of the reason this reaction leads to the desired tetrabromide 1,2-$C_6F_4(BBr_2)_2$. Qualitatively, the condensation of 1,2-$C_6F_4(BCl_2)_2$ appears to occur under milder conditions. In



Scheme 4

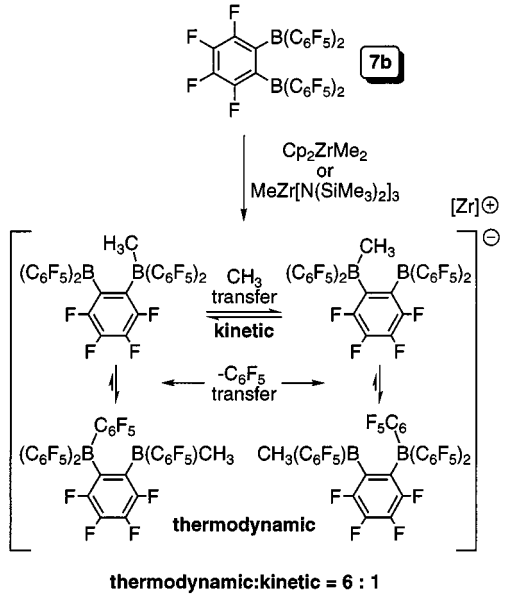
a closely related study recently reported by Gabbaï et al.,[50] the reaction of 1,2-$C_6F_4(SnMe_3)_2$ with Me_2AlCl at room temperature produces the dimer shown in Equation (7).[51] Possibly, this intriguing dimer provides a model for how the elimination of BCl_3 from 1,2-$C_6F_4(BCl_2)_2$ occurs. The Gabbaï group has also reported related derivatives of indium.[52]



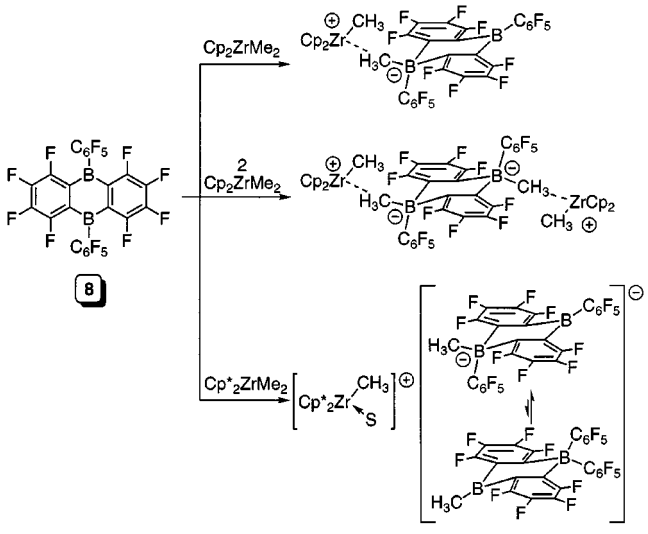
(7)

Both perfluorinated diboryl- **(7b)**[53] and diboraanthracene **(8)**[47,53] activate $[Cp_2ZrMe_2]$ to form active ethylene polymerization catalysts. In the case of the former activator, the anion formed upon methide abstraction from the metallocene is an equilibrating mixture of two species (Scheme 5). In other words, the poorly bridging methide anion is not chelated by the two Lewis acid sites. Nonetheless, detailed dynamic ^{19}F NMR spectroscopy experiments indicate that exchange of both CH_3 and C_6F_5 between the boron centers is occurring. In particular, the pattern of cross-peaks observed in the resonances for the backbone fluorine atoms can only be accounted for by invoking transfer of both groups, although, qualitatively, transfer of CH_3 is slower than transfer of the aryl group. In this system, the major anion is the one containing the tetraaryl borate moiety; this is apparent from the integrals observed for key resonances in the ^{19}F NMR spectrum of the mixture, and from an X-ray analysis of this major species using the tris-amido cation $\{Zr[N(SiMe_3)_2]_3\}^+$ to engender crystallinity. Thus, the other boron center consists of a neutral borane containing a $B-CH_3$ moiety. We postulate that this species is able to complex $[Cp_2ZrMe]^+$ in much the same way as $AlMe_3$,[54] accounting at least in part for the slightly lower activities observed for catalysts derived from **7b** and $[Cp_2ZrMe_2]$ in comparison to the parent $B(C_6F_5)_3$/$[Cp_2ZrMe_2]$ system.[53]

The bifunctional borane **7b** does not appear to abstract two methyl groups when treated with excess $[Cp_2ZrMe_2]$. In contrast, diboraanthracene **(8)** will react with one or two equivalents of $[Cp_2ZrMe_2]$ to form the ion pairs shown in Scheme 6. Marks has shown that the borane centers in **8** are strongly Lewis acidic,[47b][47c] relative to $B(C_6F_5)_3$, and they appear to act essentially independently to activate two equivalents of metallocene. It is likely that the ion pair formed from **8** and one equivalent of $[Cp_2ZrMe_2]$ is stabilized by close contact between the ions via the abstracted methide bridging group.[55] We have shown in unpublished work that when a more separated ion pair is formed by employing a bulkier metallocene such as $[Cp^*_2ZrMe_2]$, the anion formed from **8** and CH_3^- is susceptible to C_6F_5 migration as shown in the reaction scheme. As was observed for the related compound **7b**, the anion formed following methide abstraction from the metallocene is a mixture of two species. The major species in solution is the anticipated kinetic product containing the aryl−methyl−borate moiety and a neutral arylborane center. This species is readily identified in the ^{19}F NMR spectrum by comparison with the ion pair formed from $[Cp_2ZrMe_2]$. The minor species possesses a trigonal $B-CH_3$ center and a diarylborate functionality. This anion is C_{2v} symmetric, giving rise to a simplified ^{19}F NMR spectrum and comprises ca. 16% of the product mixture. The facility with which C_6F_5 migration occurs in this system is probably related to the magnitude of ion pair association. Our experiments show that **8** is comparable to $B(C_6F_5)_3$ as a co-catalyst for ethylene polymerization using $[Cp_2ZrMe_2]$,[53] and the Dow/North-



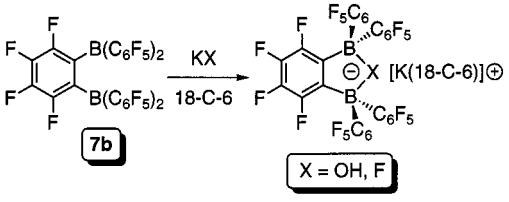
Scheme 5



Scheme 6

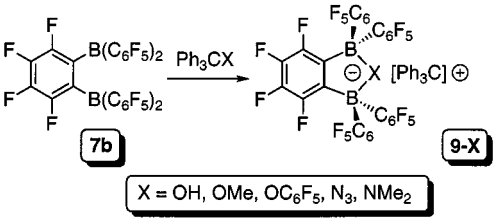
western Patent claims significantly higher performance (an order of magnitude) using **8** vs. $B(C_6F_5)_3$ in conjunction with a titanium based CGC catalyst.[47]

Since the methide anion of **7b** exhibits the behavior described above, we have sought to convert it into a weakly coordinating anion with countercations capable of activating neutral organometallic precursors. The B···B separation of 3.138(2)Å suggests that small first row anions may be incorporated. Indeed, solutions of **7b** in dichloromethane soak up one equivalent of KF or KOH rapidly; addition of 18-C-6 allows for isolation of these potassium salts [Equation (8)].[40] Spectroscopic data indicate that both F^- and OH^- are held between the two boron centers in a symmetrical fashion, although a crystal structure of the former does reveal that the fluoride is tilted out of the B−C−C−B plane.[56] A dynamic process in which this μ-F wags in and out of this plane could account for the observed temperature dependence of the chemical shift for this fluorine atom in the ^{19}F NMR spectrum.[40]

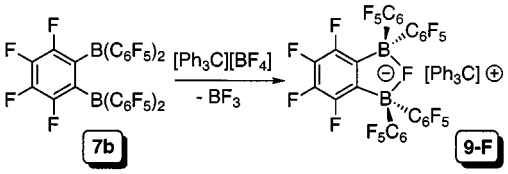


(8)

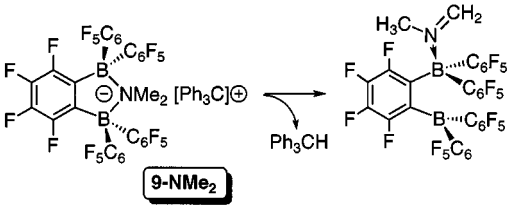
Anions with cations more amenable to olefin polymerization applications can be straightforwardly prepared by reacting **7b** with various trityl derivatives Ph_3C-X (X = OH, OMe,[57] OC_6F_5,[57] N_3, NMe_2); the fluoride derivative is generated upon treatment of **7b** with $[Ph_3C]^+[BF_4]^-$ [Equations (9) and (10)]. These reactions are generally rapid and quantitative by NMR spectroscopy and, with the exception of X = NMe_2, the resulting trityl salts, **9−X**, are stable in solution and the solid state. In **9−NMe$_2$**, the trityl cation abstracts H^- from a methyl group of the bridging amido to form an imine adduct of **7b** in which only one of the borane Lewis acids interacts with $H_2C{=}NMe$ [Equation (11)]. Interestingly, this type of behavior is not in evidence for **9−OMe**; even heating at moderate temperatures for several hours did not lead to formation of any Ph_3CH, although other decomposition processes did occur. Preparation of compounds **9−NR$_2$** without abstractable β-hydrogens using trityl amine reagents failed due to the greater steric bulk of these species. However, we are optimistic that NR_2 groups can be employed in conjunction with ammonium salts as cations allowing for study of this family of anions.



(9)

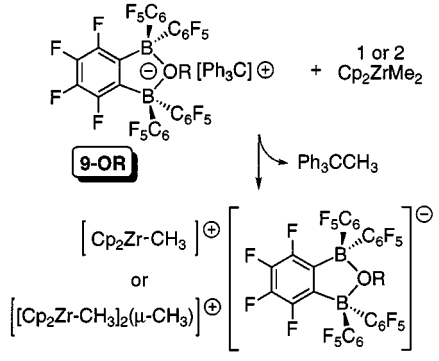


(10)



(11)

The bite angles (B−O−B) found for **9−OMe** [117.72(12)°] and **9−OC$_6$F$_5$** [115.4(5)°], which are close to ideal for sp^2 hybridized oxygen, suggest that the alkoxides are bound quite tightly by **7b**. Of the stable trityl salts **9**, the μ-alkoxides are highly effective as weakly coordinating anions in metallocenium chemistry, particularly **9−OC$_6$F$_5$**.[57] Thus, the monomeric and dimeric metallocenium cations derived from $[Cp_2ZrMe_2]$ and one or one half equivalents of **9−OR**, respectively, were found to be stable in bromobenzene solution for several hours (Scheme 7).[57] Little is known about the details of the ion−ion contact in these compounds as efforts to crystallize these species have thus far failed, and solution studies in more noncoordinating solvents such as toluene are plagued by the formation of liquid clathrates. Clearly, the OC_6F_5-derived anion is less coordinating towards $[Cp_2ZrMe]^+$ than the OMe species, as evidenced by the lower stability of the monomeric ion pair derived from **9−OC$_6$F$_5$** in the absence of monomer, and its greater polymerization activity in the presence of monomer.[57] It should be noted, however, that both anions are remarkably robust. Decomposition processes at room temperature appear to involve only the cation, since the ^{19}F NMR spectra of the anions remain unchanged over time. Upon heating, some C_6F_5 transfer to zirconium is observed, but no evidence of OR transfer is discernable. Furthermore, **7b** rapidly abstracts OCH_3^- from $[Cp_2Zr(OCH_3)_2]$; although the cation in the resulting species is not very stable, the ^{19}F and ^{11}B NMR spectra show clean formation of the μ-OCH_3 anion. Taken together, these observations suggest that these μ-OR anions of **7b** are ther-



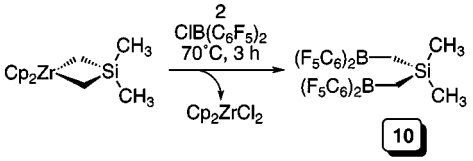
Scheme 7

modynamically stable in the presence of metallocenium cations.

This contrasts with the anions **9−F** and **9−N_3**, which rapidly transfer the X^- anion to zirconium when the cationic center is formed upon removal of a methide by the trityl abstractor.[58] In these systems, clean reactions are observed when the trityl salts are treated with two equivalents of $[Cp_2ZrMe_2]$, and the chemistry which ensues is depicted in Scheme 8 for the case of **9−F**. The first equivalent of metallocene undergoes alkide abstraction but the ion pair formed forthwith is not observed. Rather, a new ion pair in which the anion is the methide anion of **7b** described above, is the only product seen. The cation is a μ-F dimer (^{19}F NMR resonance at δ = −90.4[59]) formed from $[Cp_2ZrMe]^+$ and the neutral methyl fluoride $[Cp_2Zr(Me)F]$ produced in the first step. Similar species appear to be formed in the reaction involving **9−N_3**, as evidenced by the signature ^{19}F NMR spectrum for **[7b·Me]**$^-$;[53] the cationic portion of this ion pair has not been rigorously characterized, although the ^1H NMR spectra are consistent with a dimeric μ-N_3 metallocenium ion.

$B(Ar_F)_2$ Units Bridged by Three or More Atoms

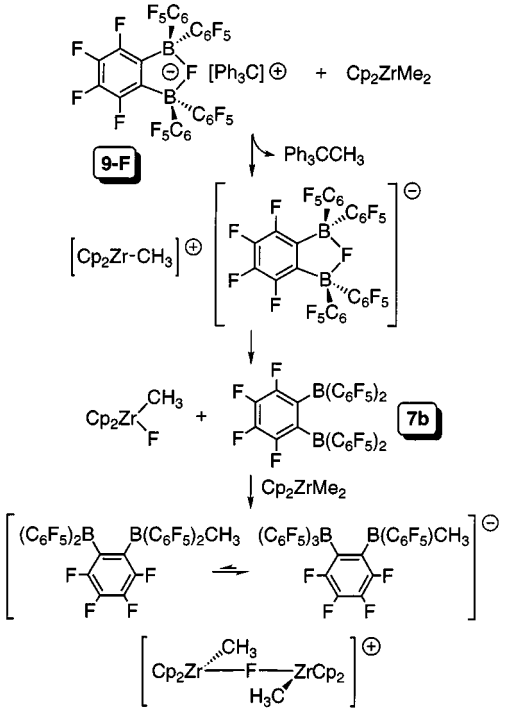
In theory, longer bridges should provide diboryl derivatives capable of binding larger anions. To this end, we prepared the three-atom bridged system **10**[60] shown in Equation (12). We felt the lack of β-hydrogens would make this an effective backbone and, furthermore, the compound is trivially synthesized using Petersen's zirconasilacyclobutane[61] and $ClB(C_6F_5)_2$. The 1,3-diboryl compound **10** is a relatively weak Lewis acid, binding acetophenone only at low temperature and failing to react with trityl methyl ether at room temperature. It is possible that the Lewis acidity of the borane centers is tempered somewhat by the β-silicon atom in the backbone (see above[38]), but other factors must be involved since **6** reacts smoothly with Ph_3COMe (see Scheme 3 above). The reactions of **10** with $[Cp_2ZrMe_2]$ are complex, characterized by the rapid production of $[Cp_2Zr(C_6F_5)Me]$. The ultimate fate of the anion is unknown and, given the compound's properties, we have not pursued its chemistry further.



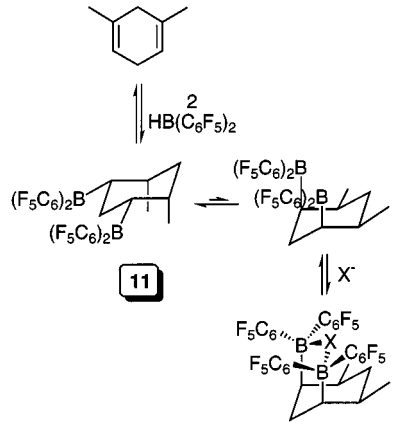
(12)

Green and co-workers have synthesised a 1,3 diborylcyclohexyl compound **11**, by hydroborating 1,3-dimethylcyclohexa-1,4-diene with two equivalents of $HB(C_6F_5)_2$ as shown in Scheme 9.[62] Addition of the borane is highly regiospecific, and the favored conformation places the two boryl groups in the equatorial sites. Binding studies with suitable anions suggest that the molecule can change conformation such that the two borane centers occupy axial sites, tethered via chelation. However, because of reversible anion binding, there are sufficient quantities of the unbound diboryl Lewis acid present. Due to the reversibility of the initial hydroboration, reactions involving reagents which react with $HB(C_6F_5)_2$ deplete the system of **11**.

Green and co-workers have also reported the preparation and reactivity of difunctional boronous esters with either tetrahydro or tetrafluorocatecholate bridges [Equation (13)].[62] Reaction of the catechols with $ClB(C_6F_5)_2$ produces **12a** and **12b** in good yield. Both compounds are weaker Lewis acids than most of the preceding C_6F_5-substituted diboryls discussed by virtue of the π donating oxygen on the boron centers. In the presence of neutral Lewis bases, both borons of **12b** act independently. Thus, with one equivalent of a Lewis base (such as acetone or THF) one boron center binds whilst the other remains three coordinate, but if the base is present in excess, both coordinate

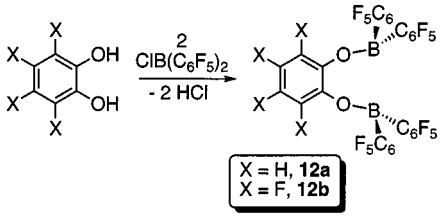


Scheme 8



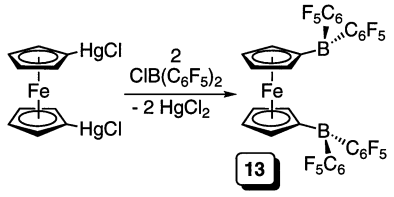
Scheme 9

weakly. In the presence of dimethyl zirconocene, compound **12b** rapidly transfers catecholate to zirconium, leaving two equivalents of $MeB(C_6F_5)_2$, suggesting that the thermodynamic stability of this type of ion pair relative to neutral products is poor.



(13)

A final example from our group utilizes a ferrocenyl backbone to connect two $B(C_6F_5)_2$ moieties. Although we have not explored the anion binding capabilities of this system to a great degree, others have found that 1,1′-substituted diboryl metallocenes bind hydroxide anion effectively.[63] The diborylferrocene compound **13** is straightforwardly prepared from a transmetallation reaction using the well-known 1,1′-bis(chloromercuri)ferrocene[64] [Equation (14)].[65] Direct borylation with $HB(C_6F_5)_2$ is possible but does not proceed selectively to the 1,1′ substituted system and requires harsh conditions. Competitive binding studies using ketones indicates that **13** is a poorer Lewis acid than a comparative species, namely $C_6H_5B(C_6F_5)_2$.



(14)

Conclusions and Future Prospects

Marks′ initial report in 1994[27] was the beginning of an intense period of research into diboryl compounds of general formula $(F_5C_6)_2B-linker-B(C_6F_5)_2$. Our work in this area has taught us some lessons regarding what the "linker" should be in order to be an effective bidentate Lewis acid. Specifically, the best performing compounds contain backbones which are both unsaturated (no β-hydrogens) and electron-withdrawing (preferably perfluorinated). The former feature prevents the facile retrohydroboration of $HB(C_6F_5)_2$, while the latter engenders more inert $B-C_{backbone}$ bonds (i.e., more stable backbones) and more Lewis acidic boron centers. This is an important point, since the greater steric bulk of these diboryls tends to dampen the Lewis acidity of the individual boron centers. Furthermore, a perfluorinated backbone prevents rapid back transfer of C_6F_5 groups to metallocenium cations in olefin polymerization applications by lowering the nucleophilicity of the borate formed upon methide abstraction.

With these features in mind, there is much opportunity for further development in this area. New backbones, different aryl groups on boron and more extensive and imaginative anion binding chemistry are areas we continue to explore. The development of chiral versions of these diboryls[66] is also of interest, both for stereospecific olefin polymerization and applications to organic synthesis.[67] While several of the compounds described are relatively poor activators themselves, their power lies in their use as synthons for the preparation of very weakly coordinating anions with other, stronger countercation activators (Ph_3C^+, HNR_3^+).[27,57] The effectiveness of these anions lies in the diboryl′s ability to sequester small anions through strong chelation and steric protection in the bidentate pocket of the bifunctional borane binding site.

Acknowledgments

WEP wishes to express his gratitude to all the talented co-workers cited for the work described herein, in particular Dr. Katrin Köhler, whose work laid the foundation for our efforts in this area. Also, the important contributions of collaborators Scott Collins (Waterloo) for polymerization studies, William Clegg (Newcastle) for X-ray crystallography and Todd Marder (Durham) are acknowledged. The authors also thank Prof. Malcolm Green (Oxford) for allowing inclusion of unpublished work from his group and Prof. Tobin Marks for sharing results prior to publication. Financial support for our work was provided by the Natural Sciences and Engineering Council of Canada's Strategic Projects program (STR192869) and the EPSRC (UK) . WEP thanks the Alfred P. Sloan Foundation for a Research Fellowship (1996−00).

[1] [1a] J. Vaugeois, M. Simard, J. D. Wuest, *Coord. Chem. Rev.* **1995**, *145*, 55−73. − [1b] J. D. Wuest, *Acc. Chem. Res.* **1999**, *32*, 81−89.

[2] Multifunctional boranes with donating substituents are not part of the scope of this review. For leading references see: [2a] G. J. Irvine, M. J. G. Lesley, T. B. Marder, N. C. Norman, C. R. Rice, E. G. Robins, W. R. Roper, G. R. Whittell, L. J. Wright, *Chem. Rev.* **1998**, *98*, 2685−2723. − [2b] G. Lesley, T. B. Marder, N. C. Norman, C. R. Rice, *Main Group Chem. News* **1998**, *5*, 4−11. − [2c] K. Nozaki, M. Yoshida, H. Takaya, *Bull Chem. Soc. Jpn.* **1996**, *69*, 2043−2052. − [2d] A. Maderna, H. Pritzkow, W. Siebert, *Angew. Chem. Int. Ed. Engl.* **1996**, *35*, 1501−1503. − [2e] M. Bluhm, A. Maderna, H. Pritzkow, S. Bethke, R. Gleiter, W. Siebert, *Eur. J. Inorg. Chem.* **1999**, 1693−1700. − [2f] T. Ishiyama, S. Momota, N. Miyaura, *Synlett* **1999**, 1790−1792. − [2g] C. N. Iverson, M. R. Smith, III, *Organometallics* **1997**, *16*, 2757−2759.

[3] [3a] T. Ooi, M. Takahashi, K. Maruoka, *Angew. Chem. Int. Ed.* **1998**, *37*, 835−837. − [3b] T. Ooi, T. Miura, K. Maruoka, *Angew. Chem. Int. Ed.* **1998**, *37*, 2347−2349.

[4] [4a] J. Vaugeois, J. D. Wuest, *J. Am. Chem. Soc.* **1998**, *120*, 13016−13022. − [4b] M. Tschinkl, A. Schier, J. Riede, F. P. Gabbaï, *Organometallics* **1999**, *18*, 1747−1753. − [4c] M. Tschinkl, A. Schier, J. Riede, F. P. Gabbaï, *Angew. Chem. Int. Ed.* **1999**, *38*, 3547−3549.

[5] N. Asao, P. Liu, K. Maruoka, *Angew. Chem. Int. Ed. Engl.* **1997**, *36*, 2507−2509.

[6] N. Asao, S. Kii, H. Hanawa, K. Maruoka, *Tetrahedron Lett.* **1998**, *39*, 3729−3732.

[7] A. G. Massey, A. J. Park, *J. Organomet. Chem.* **1964**, *2*, 245−250.

[8] [8a] A. G. Massey, A. J. Park, *J. Organomet. Chem.* **1966**, *5*, 218−225. − [8b] L. Doerrer, M. L. H. Green, *J. Chem. Soc., Dalton Trans.* **1999**, 4325−4329.

[9] L. Luo, T. J. Marks, *Topics in Catalysis* **1999**, *7*, 97−106.

[10] H. Jacobsen, H. Berke, S. Döring, G. Kehr, G. Erker, R. Fröhlich, O. Meyer, *Organometallics* **1999**, *18*, 1724−1735.

[11] W. E. Piers, T. Chivers, *Chem. Soc. Rev.* **1997**, 345−354.

[12] H. Yamamoto, K. Ishihara, *Eur. J. Org. Chem.* **1999**, 527−538.

[13] [13a] P. D. Beer, *Chem. Commun.* **1996**, 689−696. − [13b] M. F. Hawthorne, Z. Zheng, *Acc. Chem. Res.* **1997**, *30*, 267−276.

[14] M. Fontani, F. Peters, W. Scherer, W. Wachter, M. Wagner, P. Zanello, *Eur. J. Inorg. Chem.* **1998**, 1453−1465.

[15] [15a] G. A. Olah, *Angew. Chem. Int. Ed. Engl.* **1993**, *32*, 761−788. − [15b] E. Negishi, *Chem. Eur. J.* **1999**, *5*, 411−423.

[16] W. Clegg, C. Dai, F. J. Lawlor, T. B. Marder, P. Nguyen, N. C. Norman, N. L. Pickett, W. P. Power, A. J. Scott, *J. Chem. Soc., Dalton Trans.* **1997**, 839−846.

[17] [17a] D. F. Shriver, M. J. Biallas, *J. Am. Chem. Soc.* **1967**, *89*, 1078−1081. − [17b] M. J. Biallas, *J. Am. Chem. Soc.* **1969**, *91*, 7290−7292. − [17c] M. J. Biallas, *Inorg. Chem.* **1971**, *10*, 1320−1322.

[18] P. Ceron, A. Finch, J. Frey, J. Kerrigan, T. Parsons, G. Urry, H. I. Schlesinger, *J. Am. Chem. Soc.* **1959**, *81*, 6368−6371.

[19] H. E. Katz, *J. Org. Chem.* **1985**, *50*, 5027−5032.

[20] H. E. Katz, *Organometallics* **1987**, *6*, 1136−1138.

[21] M. Reilly, T. Oh, *Tetrahedron Lett.* **1994**, *35*, 7209−7212.

[22] [22a] R. Köster, G. Seidel, K. Wagner, B. Wrackmeyer, *Chem. Ber.* **1993**, *126*, 305−317, and references therein. − [22b] R. Köster, G. Seidel, B. Wrackmeyer, *Chem. Ber.* **1993**, *126*, 319−330, and references therein.

[23] [23a] W. Siebert, M. Hildenbrand, P. Hornbach, G. Karger, H. Pritzkow, *Z. Naturforsch., B: Chem. Sci.* **1989**, *44*, 1179−1186. − [23b] H. Schultz, G. Gabbert, H. Pritzkow, W. Siebert, *Chem. Ber.* **1993**, *126*, 1593−1595.

[24] W. Schacht, D. E. Kaufmann, *J. Organomet. Chem.* **1987**, *331*, 139−152.

[25] D. E. Kaufmann, *Chem. Ber.* **1987**, *120*, 901−905.

[26] J. J. Eisch, B. W. Kotowicz, *Eur. J. Inorg. Chem.* **1998**, 761−769.

[27] L. Jia, X. Yang, C. L. Stern, T. J. Marks, *Organometallics* **1994**, *13*, 3755−3757.

[28] [28a] D. J. Parks, R. E. v H. Spence, W. E. Piers, *Angew. Chem. Int. Ed. Engl.* **1995**, *34*, 809−811. − [28b] D. J. Parks, W. E. Piers, G. P. A. Yap, *Organometallics* **1998**, *17*, 5492−5503.

[29] K. Köhler, W. E. Piers, *Can. J. Chem.* **1998**, *76*, 1249−1255.

[30] [30a] R. E. v H. Spence, W. E. Piers, Y. Sun, M. Parvez, L. R. MacGillivray, M. J. Zaworotko, *Organometallics* **1998**, *17*, 2459−2469. − [30b] K. S. Cook, W. E. Piers, S. J. Rettig, *Organometallics* **1999**, *18*, 1575−1577.

[31] For examples of 1,1′-diboryl alkenes incorporating halogen substituents, see ref.[23a] and: H. Schultz, H. Pritzkow, W. Siebert, *Z. Naturforsch.* **1993**, *48b*, 719−722.

[32] K. Köhler, W. E. Piers, A. P. Jarvis, S. Xin, Y. Feng, A. M. Bravakis, S. Collins, W. Clegg, G. P. A. Yap, T. B. Marder, *Organometallics* **1998**, *17*, 3557−3566.

[33] [33a] S. Krishnamurthy, H. C. Brown, *J. Org. Chem.* **1980**, *45*, 849−856. − [33b] T. Yoshida, E. Negishi, *J. Chem. Soc., Chem. Commun.* **1974**, 762−763. − [33c] A. Pelter, K. Smith, H. C. Brown, *Borane Reagents*, Academic Press, New York, **1988**, 22−23.

[34] J. R. Galsworthy, M. L. H. Green, V. C. Williams, A. N. Chernega, *Polyhedron* **1998**, *17*, 119−124.

[35] S. Collins, J. Tian, N. J. Taylor, unpublished results.

[36] Spartan Version 3.1, Wavefunction Inc., Irvine, California.

[37] T. J. Marks, L. Jia, X. Yang, U. S. Patent 5,447,895, **1995** (Northwestern University).

[38] D. J. Parks, W. E. Piers, *Tetrahedron* **1998**, *54*, 15469−15488.

[39] ^{1}H NMR (CD_2Cl_2, 300 K, 300.138 MHz): δ = 8.28 (t, $^3J_{H-H}$ = 8 Hz, 3 H, *p*-C_6H_5), 7.87 (m, 6 H, *m*-C_6H_5), 7.68(d, $^3J_{H-H}$ = 8 Hz, 6 H, *o*-C_6H_5), 3.39 (s, 3 H, OCH_3), 1.41 (dd, $^2J_{H-H}$ = 14 Hz, $^3J_{H-H}$ = 13 Hz, 1 H, $CH_2B(C_6F_5)_2$), 0.98 (d, $^3J_{H-H}$ = 13 Hz, 1 H, $(Me_3Si)CH$), 0.89 (d, $^2J_{H-H}$ = 13 Hz, 1 H, $CH_2B(C_6F_5)_2$), −0.39 (s, 9 H, $SiMe_3$). − ^{19}F NMR (CD_2Cl_2, 300 K, 282.371 MHz): δ = −128.1 (d, 2F, *o*-C_6F_5), −129.1 (d, 2F, *o*-C_6F_5), −133.2 (s, br, 2F, *o*-C_6F_5), −136.5 (d, 2F, *o*-C_6F_5), −160.5 (t, 1F, *p*-C_6F_5), −160.7 (t, 1F, *p*-C_6F_5), −163.3 (t, 1F, *p*-C_6F_5), −163.8 (t, 1F, *p*-C_6F_5), −166.1 (m, 2F, *m*-C_6F_5) −166.5 (m, 2F, *m*-C_6F_5), −166.8 (m, 2F, *m*-C_6F_5), −167.4 (m, 2F, *m*-C_6F_5). − ^{11}B NMR: (CD_2Cl_2, 300 K): δ = 41.4, 5.7. G. J. Irvine, L. Somlai, W. E. Piers, unpublished results.

[40] V. C. Williams, W. E. Piers, W. Clegg, S. Collins, T. B. Marder, *J. Am. Chem. Soc.* **1999**, *121*, 3244−3245.

[41] Eisch has noted some problems with the published preparation of **2b** starting from 1,2-$(Me_3Sn)_2C_6H_4$.[26] To avoid Me transfer to boron we therefore prepared it from the arylsilane precursor, and to suppress condensation of the product to the 9,10-diboraanthracene, we minimized the heating of the chloroborane during purification and workup.

[42] P. Sartori, M. Weidenbruch, *Chem. Ber.* **1967**, *100*, 3016−3023.

[43] Y. Sun, W. E. Piers, M. Parvez, *Can. J. Chem*. **1998**, *76*, 513−517.

[44] P. A. Deck, C. L. Beswick, T. J. Marks, *J. Am. Chem. Soc.* **1998**, *120*, 1772−1784.

[45] T. Chivers, *J. Organomet. Chem.* **1969**, *19*, 75−80.

[46] R. D. Chambers, T. Chivers, *J. Chem. Soc.* **1965**, 3933−3939.

[47] [47a] M. H. Mcadon, P. N. Nickias, T. J. Marks, D. J. Schwartz, WO 99/06413, **1999** (Dow Chemical Co. and Northwestern University). − [47b] M. V. Metz, D. J. Schwartz, C. L. Stern, P. N. Nickias, T. J. Marks, *Angew. Chem. Int. Ed.* **2000**, *39*, 1312. − [47c] T. J. Marks, *Abstracts of the 217th National ACS Meeting*, **1999**, Anaheim, CA, #0015.

[48] P. Sartori, A. Golloch, *Chem. Ber.* **1968**, *101*, 2004−2009.

[49] R. D. Chambers, T. Chivers, *J. Chem. Soc.* **1964**, 4782−4790.

[50] M. Tschinkl, R. E. Bachman, F. P. Gabbäi, *Chem. Commun.* **1999**, 1367−1368.

[51] For a related study see: J. J. Eisch, K. Mackenzie, H. Windsich, C. Krüger, *Eur. J. Inorg. Chem.* **1999**, 153−162, and references therein.

[52] [52a] F. P. Gabbaï, A. Schier, J. Riede, D. Schichl, *Organometallics* **1996**, *15*, 4119−4121. − [52b] F. P. Gabbaï, A. Schier, J. Riede, *Angew. Chem. Int. Ed.* **1998**, *37*, 622−624.

[53] V. C. Williams, C. Dai, Z. Li, S. Collins, W. E. Piers, W. Clegg, M. R. J. Elsegood, T. B. Marder, *Angew. Chem. Int. Ed.* **1999**, *38*, 3695−3698.

[54] M. Bochmann, S. L. Lancaster, *Angew. Chem. Int. Ed. Engl.* **1994**, *33*, 1634−1637.

[55] X. Yang, C. L. Stern, T. J. Marks, *J. Am. Chem. Soc.* **1994**, *116*, 10015−10031.

[56] This structure determination was obtained subsequent to publication of our initial report. V. C. Williams, W. E. Piers, W. Clegg, M. R. J. Elsegood, unpublished results.

[57] V. C. Williams, G. J. Irvine, W. E. Piers, Z. Li, S. Collins, W. Clegg, M. R. J. Elsegood, T. B. Marder, *Organometallics* **2000**, *19*, 1619.

[58] W. E. Piers, V. C. Williams, G. J. Irvine, S. Collins, C. Dai, Z. Li, W. Clegg, M. R. J. Elsegood, *Abstracts of the 218th National ACS Meeting*, **1999**, New Orleans, LA, #295.

[59] A shift of δ = −88.3 was observed for the μ-F group in this cation with a different counteranion: L. Li, T. J. Marks, *Organometallics* **1998**, *17*, 3996−4003.

[60] Synthesis of **10**: $Cp_2Zr(CH_2Si(CH_3)_2CH_2)$ (0.56 g, 1.8 mmol) and $ClB(C_6F_5)_2$ (1.38 g, 3.6 mmol) were dissolved in hexanes (30 mL) and heated for three hours at 70°C. Upon cooling the solution was decanted from the Cp_2ZrCl_2 precipitate and the hexanes removed in vacuo, leaving a white solid. This was redissolved in 20 mL of hexanes, filtered and crystallized at −30°C. Yield: 0.98 g, 70%. ^{1}H NMR (C_6D_6): δ = 2.02 (s, 4 H, CH_2), −0.07 (s, 6 H, CH_3). − ^{11}B NMR: δ = 68 (br). − $^{13}C\{^1H\}$ NMR: δ = 30.8 (s, CH_2), 1.8 (CH_3). − ^{19}F: δ = −130.0 (m, 8F, *o*-C_6F_5), −146.7 (t, 4F, *p*-C_6F_5), 161.0 (m, 8F, *m*-C_6F_5). − EI-MS 610 (M − C_6F_5), 417 [M − $CH_2B(C_6F_5)_2$]. − $C_{28}H_{10}B_2F_{20}Si$ (776.07): calcd. C 43.2, H 1.3; found C 43.0, H 1.0.

[61] [61a] W. R. Tikkanen, J. Z. Liu, J. W. Egan, Jr., J. L. Petersen, *Organometallics* **1984**, *3*, 825−830. − [61b] W. R. Tikkanen, J. W. Egan, Jr., J. L. Petersen, *Organometallics* **1984**, *3*, 1646−1650.

[62] D. Haussinger, M. Muller, M. L. H. Green, *XVIIIth Interna-*

tional Conference on Organometallic Chemistry, **1998**, Munich, Germany.
[63] G. E. Herberich, U. Englert, A. Fischer, D. Wiebelhaus, *Organometallics* **1998**, *17*, 4769−4775.
[64] M. D. Rausch, L.P. Klemann, A. Siegel, R. F. Kovar, T. H. Gund, *Synth. Reactiv. Inorg. Metal-Org. Chem.* **1973**, *3*, 193−198.
[65] B. E. Carpenter, M. Sc. Thesis, University of Calgary, **1999**.
[66] B. Schilling, V. Kaiser, D. E. Kaufmann, *Chem. Ber./Recueil* **1997**, *130*, 923−932.
[67] [67a] D. J. Parks, W. E. Piers, *J. Am. Chem. Soc.* **1996**, *118*, 9440−9441. − [67b] J. M. Blackwell, K. L. Foster, V. H. Beck, W. E. Piers, *J. Org. Chem.* **1999**, *64*, 4887−4892. − [67c] J. M. Blackwell, W. E. Piers, M. Parvez, *Org. Lett.* **2000**, *2*, 695−698.
Received February 11, 2000
[I00047]

Fluorescent Chemosensors Containing Polyamine Receptors

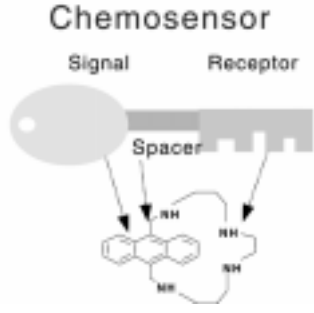
Fernando Pina,*[a] M. Alexandra Bernardo,[a] and Enrique García-España[b]

Keywords: Sensors / Fluorescence / Polyamines / Receptors / Cation and anion coordination

Chemosensors have attracted interest in many different scientific fields, such as environmental chemistry, medicine, and the processing and storage of information. These molecular-scale devices have the advantage of working on the same spatial scale as the chemical structures that are responsible for macroscopic behaviour observed in the environment or those associated with health problems. Moreover, they allow the construction of molecular-scale devices for information storage. In this review, we describe a family of chemosensors based on a polyamine receptor and a fluorescent signalling unit. Polyamine receptors are water-soluble ambidentate receptors; they are able to coordinate either metal ions, when sufficient deprotonated amino groups are available, or anionic species, when there are sufficient protonated amino groups. On the other hand, the use of fluorescent signalling units confers the advantage of an immediate visual response/signal.

Introduction

A standard chemosensor can be defined as a molecule containing three basic units, each one performing a precise function: (i) a receptor unit, (ii) a signalling unit, and (iii) a spacer (Scheme 1).[1,2] The first of these, the receptor unit, plays the role of recognizing and reversibly binding a given target substrate. The signalling unit, in turn, must be capable of either producing a signal or significantly altering its signal intensity in response to the binding of the substrate,



Scheme 1. Schematic representation of a chemosensor

[a] Departamento de Química, Centro de Química Fina e Biotecnologia, Universidade Nova de Lisboa,
Quinta da Torre, 2825 Monte de Caparica, Portugal
E-mail: fjp@dq.fct.unl.pt
[b] Departament de Química Inorgànica, Facultat de Química, Universitat de València,
c/Dr. Moliner 50, 46100 Burjassot (València), Spain
E-mail: enrique.garcia-es@uv.es



Fernando Pina was born in Lisbon, Portugal. He has been Professor of Chemistry at the Faculdade de Ciências e Tecnologia, Universidade Nova de Lisboa, since 1985, and is coordinator of the Photochemistry Research Unit. His research interests are focused on the areas of supramolecular chemistry, chemosensors, and molecular-level devices.



M. Alexandra Bernardo was born in 1968 in Portugal. She graduated in Chemistry at the Faculdade de Ciências e Tecnologia, Universidade Nova de Lisboa, in 1992. She is currently completing her Ph.D. thesis on supramolecular photochemistry and fluorescent chemosensors.



Enrique García-España was born in Valencia, Spain, and has been Professor at the Inorganic Chemistry Department of the University of Valencia since 1985. His main research interests lie in the supramolecular chemistry of metal ions and anions.

MICROREVIEWS: This feature introduces the readers to the authors' research through a concise overview of the selected topic. Reference to important work from others in the field is included.

 © WILEY-VCH Verlag GmbH, D-69451 Weinheim, 2000 1434–1948/00/1010–2143 $ 17.50+.50/0

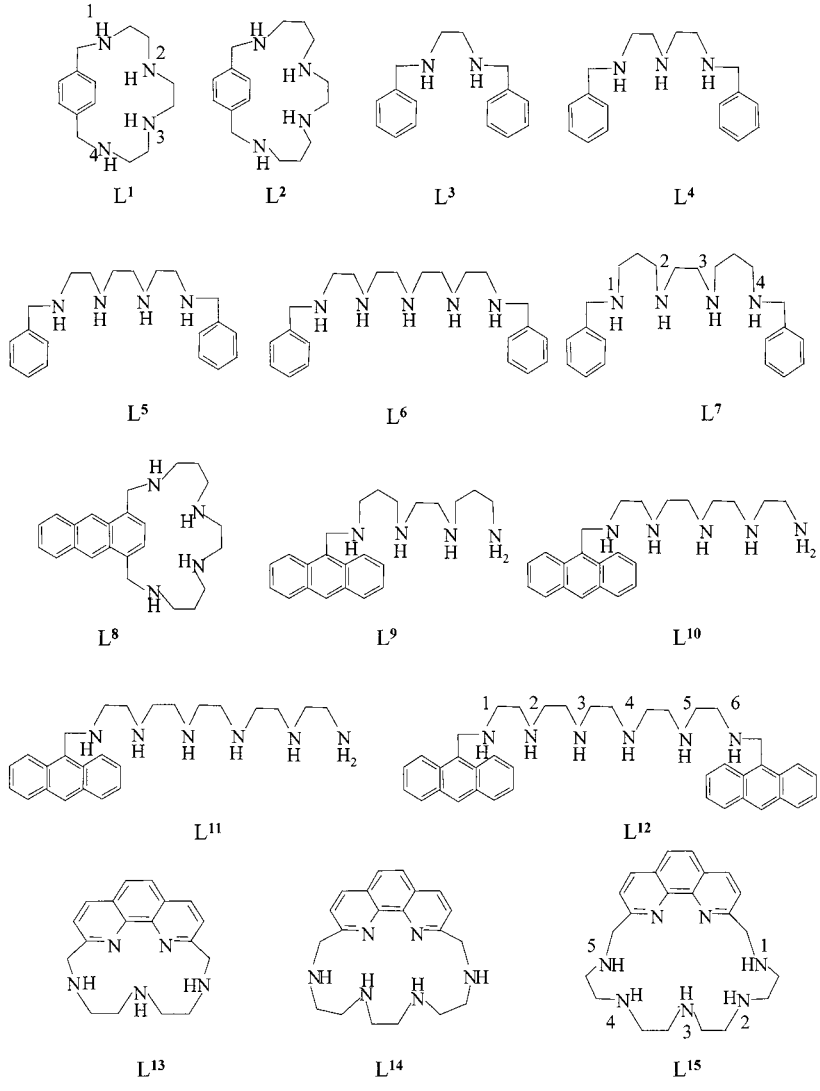
preferably without changing the other photochemical properties. With fluorescent chemosensors, chelation enhancement of the fluorescence (CHEF) or chelation enhancement of the quenching (CHEQ) are commonly encountered responses. Finally, the third unit, the spacer, links the binding and signalling units and controls their mutual separation and geometrical arrangement. These parameters play a crucial role in determining the performance of the device.

A particularly interesting goal is the development of chemosensors capable of functioning in aqueous solution, as highlighted by Czarnick.[2c] Many chemosensors that function efficiently in less polar solvents do not give adequate responses in water either due to low solubility limits or owing to weak complexation of the target species.[1,2] This is a severe drawback because water is the solvent in which most chemical processes occur. In order to achieve sufficiently strong complexation of anions or metal ions in water, a rational approach is the use of polyamine fragments as receptor units. Polyamine compounds are well known as ambidentate receptors capable of coordinating metal ions when sufficient deprotonated amino groups are available, or anionic species when there are sufficient protonated amino groups. Therefore, their binding capacities can be readily tuned by adjusting the pH value.[3] This is a further reason why these compounds have been synthesized and their properties explored.

In this paper, we have attempted to review the effects of the binding of protons, cations, and anions on families of fluorescent chemosensors containing receptor units based on open-chain or cyclic polyamine fragments (Scheme 2). Excellent reviews dealing with earlier work in the field of fluorescent sensors have been published by Czarnick[2c] and by de Silva et al.[1b]

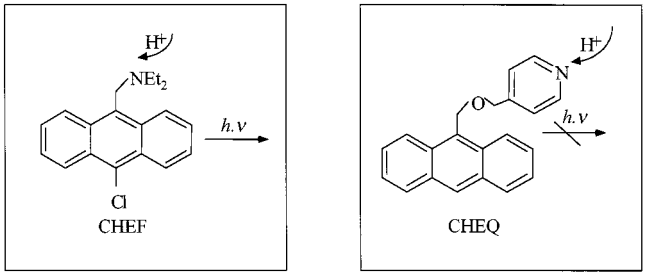
Sensing Protons

CHEQ or CHEF effects on the fluorescence emission resulting from the binding of protons are rather common. Systems of this type have been used to construct ON/OFF switches, which is a very important goal in the growing field of semiochemistry.[4,5] The two effects can be illustrated by



Scheme 2. Chemical structures of the fluorescent chemosensors studied

the following examples based on the anthracene chromophore (Scheme 3).[6,7]



Scheme 3. Examples of systems that function as ON/OFF switches

In the first case, a quenching process involving photoinduced electron transfer (PET) from the free lone pair of the amine pendant arm to the excited fluorophore occurs. This process can be inhibited when the amine is protonated (pK_a = 7.7), resulting in the appearance of a fluorescence emission.[6,7] In the second case, the species containing the pyridinium fragment quenches fluorescence, while this is not the case with unprotonated pyridine. Therefore, protonation has the opposite effect and thus the intensity of the fluorescence emission decreases on increasing the mole fraction of the protonated form (pK_a = 5.0). In this case, the quenching effect has been ascribed to an electron-transfer process from the photo-excited fluorophore to the pyridinium fragment.[7]

Benzene Fluorophore

Polyazacyclophane Macrocyclic Receptors

The azacyclophanes 2,5,8,11-tetraaza[12]paracyclophane (L^1) and 2,6,9,13-tetraaza[14]paracyclophane (L^2) are cyclic chemosensors constructed by linking a polyamine chain and a 1,4-dimethylbenzene fragment (Scheme 2).

According to crystallographic, NMR, and molecular mechanics studies, in solution these compounds preferentially adopt conformations in which the polyamine chain is arched above the aromatic ring. Indeed, this feature could also be observed in a structure reported by Altava et al.[8] for the analogous compound 13,14,16,17-tetramethyl-2,6,10-triaza[11]paracyclophane, which contains a triamine chain as the receptor unit and a durene moiety as the fluorophore. On the other hand, the structure shows that the three acidic protons located on the aliphatic nitrogen atoms are in an *exo* disposition and that the macrocycle assumes an overall open conformation. This arrangement minimizes the electrostatic repulsion between the charged polyammonium groups. It is important to note that the benzylic nitrogen atoms are located ca. 1.45 Å above the plane defined by the aromatic ring. On the other hand, the distance between the benzylic nitrogen atoms is remarkably large, amounting to 6.85 Å.

In spite of the low fluorescence emission quantum yield of the benzene fluorophore, which precludes any practical application, the properties shown by chemosensors of this type are very much representative of the general behaviour exhibited by chemosensors based on a polyamine receptor. Owing to the presence of the spacer between the signalling and the receptor units, these compounds show absorption and fluorescence emission spectra that largely resemble those of the benzene chromophore. This behaviour is more or less general, also being observed when the benzene ring is substituted by other signalling units (vide infra).

The protonation sequence of this family of receptors has been studied in detail by ^{13}C and ^{1}H NMR.[9,10] According to these studies, the protons on the two central nitrogen atoms are the most easily removed. In Figure 1, the fluorescence emission titration curves of L^1 and L^2 are presented, showing the mole fraction distributions of the various protonated species as determined by potentiometry.

The deprotonation sequence of the chemosensors is also included for discussion purposes. By inspection of the figure it can clearly be seen that the fully protonated species gives rise to the highest emission intensity and that removal of the first proton leads to a large decrease in the fluorescence emission intensity. However, total extinction of the emission is only observed following loss of the second proton from the other central nitrogen atom.

The quenching effect of the fluorescence emission can easily be explained in terms of an exergonic intramolecular electron-transfer process from the lone pair of the amines to the excited fluorophore.[9] However, protonation of the amines increases their oxidation potential by ca. 2.1 eV,[11] changing the process from an exoergonic to an endergonic one. Therefore, the fully protonated forms of these chemosensors exhibit the highest fluorescence emission intensities. Another aspect to take into account is the relative position of the lone pairs with respect to the π system. The probability of electron transfer depends on the distance between the two partners, as well as on the overlap between the donor and the acceptor orbitals. Removal of the central protons leads to a decrease in the overall electrostatic repulsion and hence the nitrogen atoms labelled N2 and N3 can become closer to the π system favouring the quenching process (Figure 1).

Finally, the weak fluorescence emission observed for the triprotonated species $[H_3L^1]^{3+}$ can be ascribed to the fact that the two central nitrogen atoms are equivalent and hence share the proton; this would still provide a certain degree of protection for the lone pairs.

The fluorescence emission titration curve of L^2 is similar to that of L^1 (Figure 1), suggesting that it may be similarly interpreted. However, the triprotonated form of L^2 exhibits a less efficient quenching effect than in the case of L^1. The two compounds differ in the dimensions of their chains, i.e. 12 atoms in L^1 compared with 14 atoms in L^2. For this reason, the central nitrogen atoms in L^2 are further away from the π system than in L^1, and consequently the electron-transfer process is less efficient.

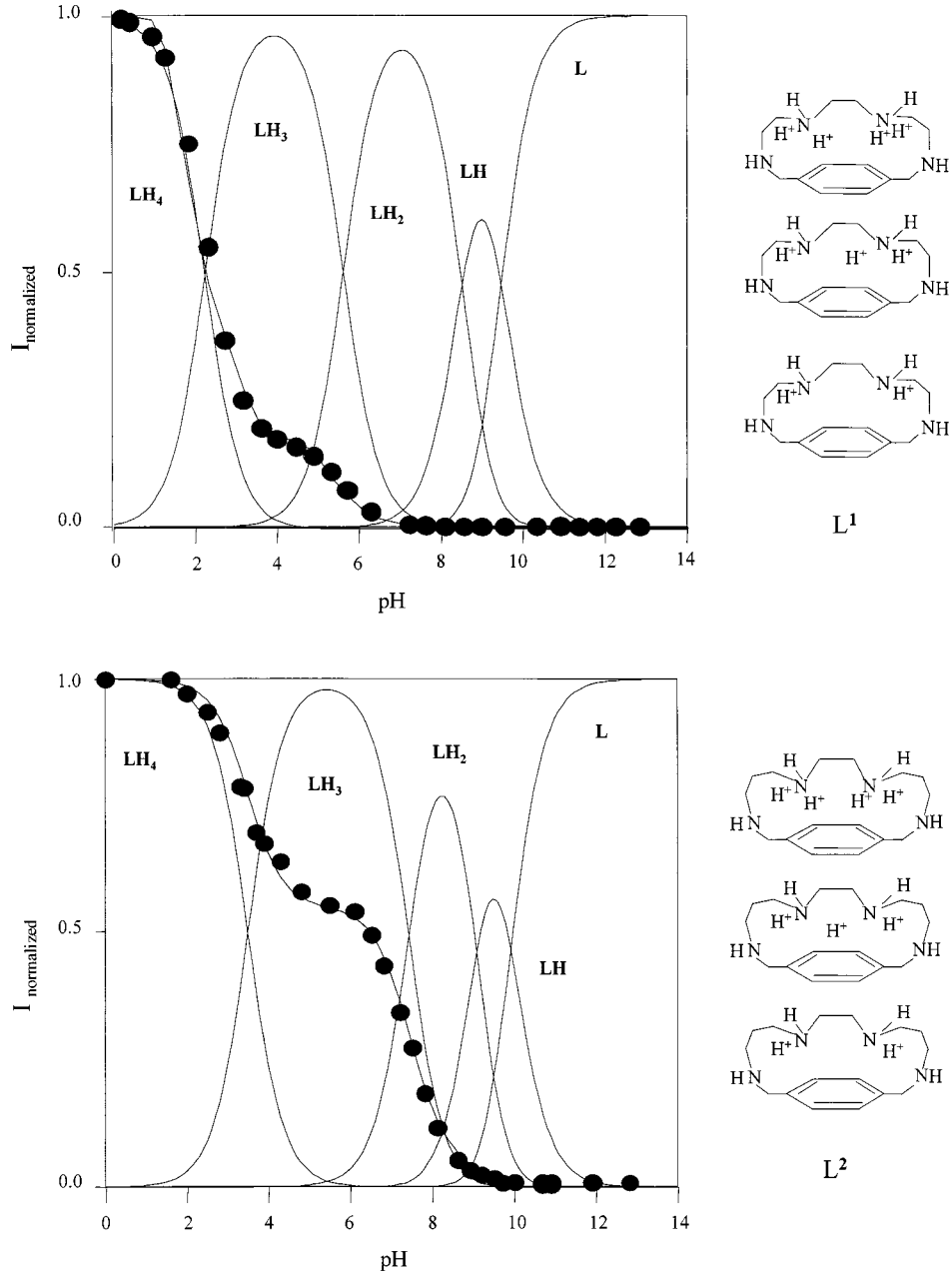


Figure 1. Fluorescence emission titration curves, along with the mole fraction distribution and deprotonation sequence of the chemosensors L^1 and L^2

N,N′-Dibenzylated Polyamine Receptors

In this class of compounds the signalling unit is made up of two terminal benzene rings, separated by a spacer from a polyamine open-chain receptor of variable length, L^3 to L^7 (Scheme 2).

The fluorescence emission titration curves (Figure 2) were obtained using the same methodology as mentioned above. The intensity of the fluorescence emission spectrum of the smallest member of this family, L^3, is practically unaffected by the loss of the first proton. This result suggests that, in contrast to the findings of Thomas and Davidson[12,13] regarding the naphthalene fluorophore, the benzylic nitrogen atoms in these compounds are not very efficient in inducing the quenching process. This becomes apparent when compound L^4 is used, for which a significant quenching effect is observed upon removal of the first proton from a nitrogen atom in the centre of the chain.

The fluorescence emission titration curve of L^5 raises another interesting question. In this case, a moderate quenching effect is seen following the first deprotonation. By comparing L^4 with L^5, it can be concluded that while in the former receptor electron transfer from the lone pair of the central deprotonated nitrogen atom to either benzene ring should be equally probable, in L^5 only one of the benzene rings is suitably orientated. The other ring is too distant from the free lone pair to permit an efficient electron trans-

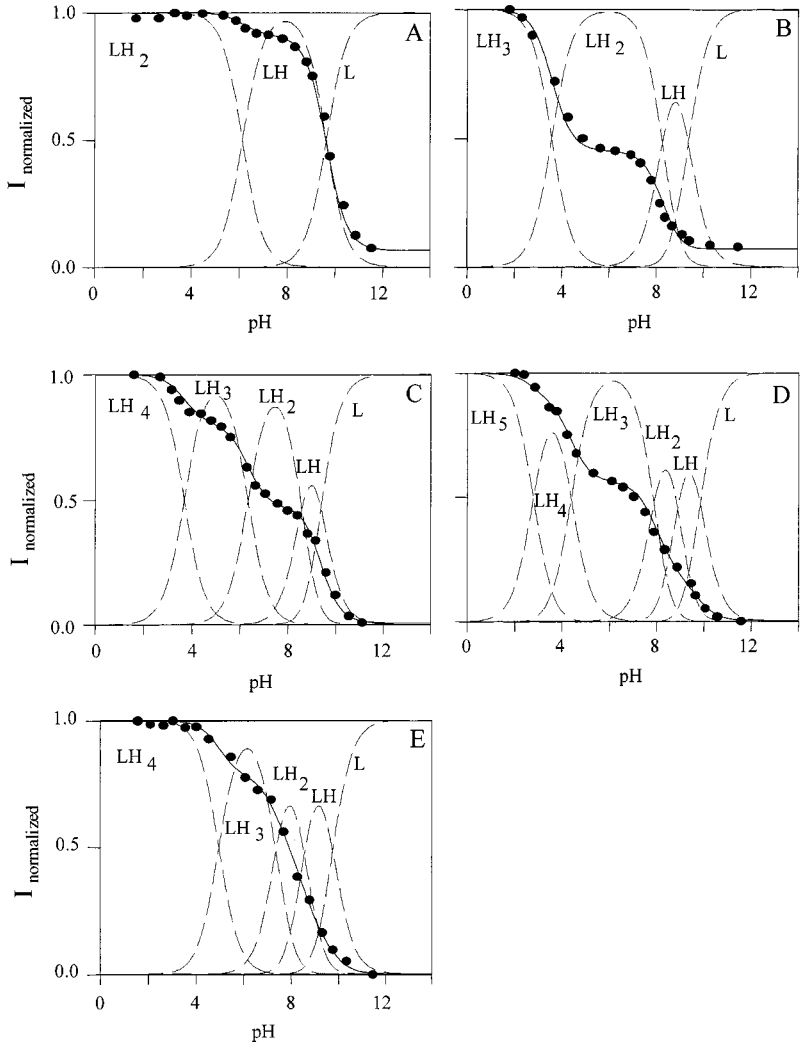


Figure 2. Fluorescence emission titration curves of A-L[3], B-L[4], C-L[5], D-L[6], and E-L[7], along with the respective mole fraction distribution curves

fer. On this basis, L[5] can be predicted to show ca. one-half of the efficiency of L[4], which is indeed borne out by experiment (see Figure 2). Removal of a second proton from L[5] (which is known to occur from the central atoms as well) should double the electron-transfer probability, as is also observed experimentally.

The largest member of this family, L[6], has a chain bearing five nitrogen atoms. The first two deprotonation steps occur at the nitrogen atoms labelled N2 and N4. At this stage, the situation can be compared with that resulting from the first deprotonation of L[3] or with that following the second deprotonation of L[5].

The fluorescence emission titration curves of compound L[7] were also determined. In this compound, nitrogen atoms N1 and N2 as well as N3 and N4 are separated from the benzene fragments by three carbon atoms, rather than two in the case of L[5]. This structural feature is reflected in the titration curve of L[7] in that the quenching observed upon removing two protons is less efficient than in the case of L[5].

Anthracene Fluorophore

A great improvement in the efficiency of polyamine-based chemosensors can be achieved by substituting benzene, which has a low fluorescence quantum yield, φ_f = 0.06, by a more intrinsically luminescent unit, such as naphthalene, φ_f = 0.21, or anthracene, φ_f = 0.3. In this section, we report a family of chemosensors incorporating anthracene fluorophore.[14,15] In Figure 3, the titration curves of the chemosensors L[8] and L[9] are presented. As for the benzene analogues, the fluorescence emission is almost totally quenched when the two central nitrogen atoms are deprotonated.

An identical pattern is apparent in the fluorescence emission titration curves of the linear analogues L[10] and L[11], also shown in Figure 3. The quenching effect is seen when nitrogen atoms N2 and N3 are completely deprotonated. In effect, according to CPK models, these two nitrogen atoms are the only ones that can overlap efficiently with the π system of the anthracene.

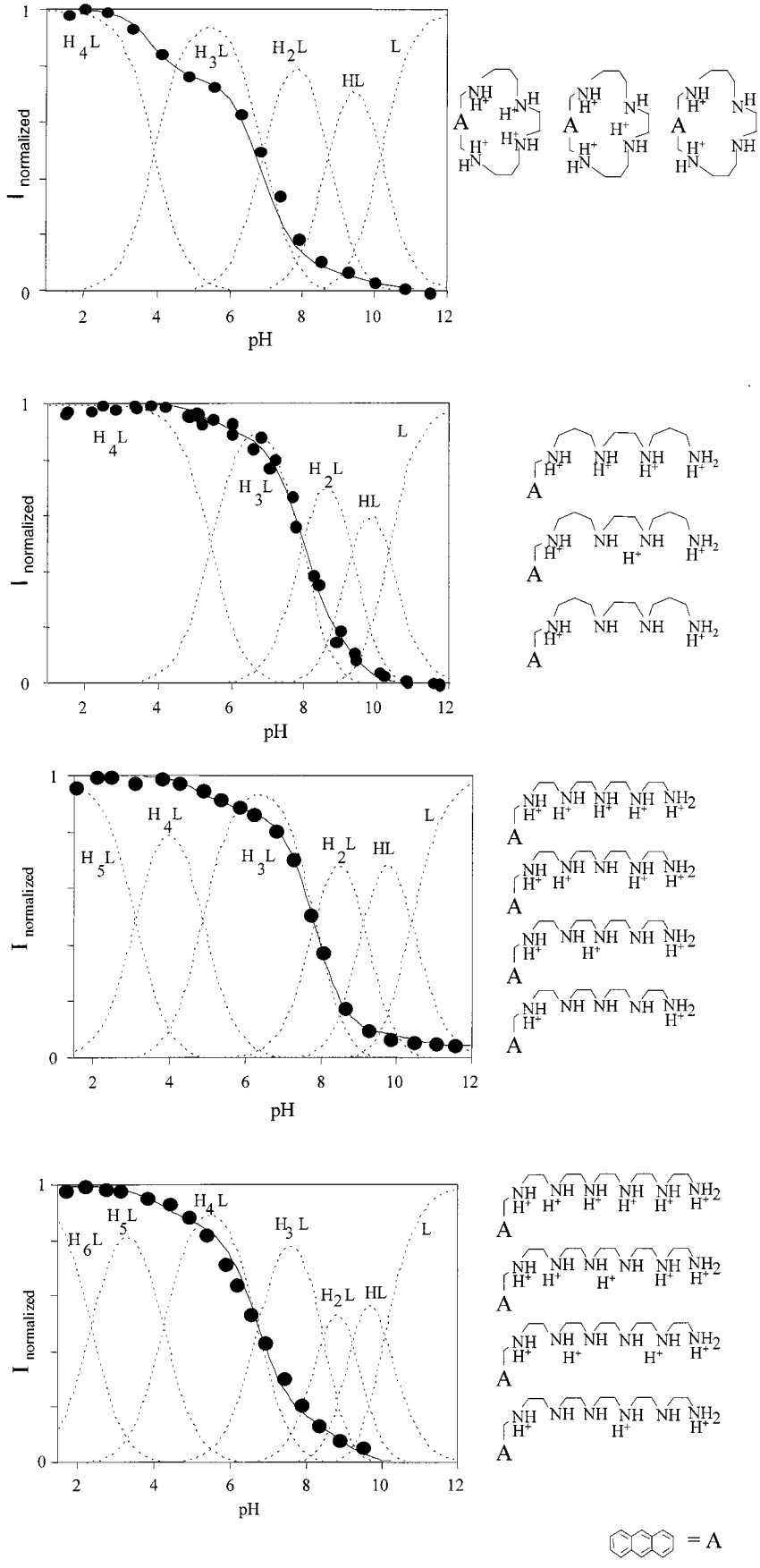


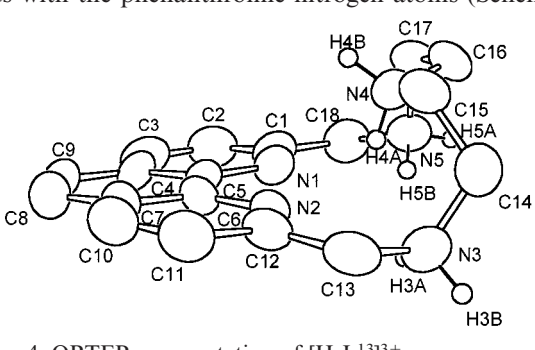
Figure 3. Fluorescence emission titration curves for L^8, L^9, L^{10}, and L^{11}, along with the respective mole fraction distribution curves and deprotonation sequence of the chemosensors

Phenanthroline Fluorophore

The first generation of chemosensors were based on aromatic heterocycles, e.g. those containing nitrogen or oxygen atoms, and their functions (binding and signalling) stemmed from the same part of the molecule. For this reason, they were called *intrinsic chemosensors*. Among these, phenanthroline derivatives have received much attention in recent years by virtue of their intense fluorescence and due to the presence of two aromatic nitrogen atoms that can act cooperatively in binding cations.[16] In the second generation of chemosensors, known as *conjugate chemosensors*, the binding and signalling moieties of the molecule are separated by a spacer and the two functions can be ascribed to different parts of the molecule, as shown in Scheme 2.[1]

In this context, a new series of polyamine macrocycles containing a phenanthroline unit as an integral part of the cyclic framework has recently been reported.[17,18] The simplest member of the series, 2,5,8-triaza[9]-10,23-phenanthrolinophane, L^{13}, contains a triamine chain linking the 2,9-phenanthroline positions. Therefore, this system can be considered as being both an intrinsic and a conjugate chemosensor: While the polyamine unit is used exclusively for the function of binding, the phenanthroline unit can be used not only for signalling but for binding as well.

In the crystal structure of the fully protonated form of L^{13}, containing three bromide anions as counterions, the macrocycle is seen to adopt a bent configuration. The phenanthroline unit and the benzylic nitrogen atoms N3 and N5 are almost coplanar, and this plane makes a dihedral angle of 104.10°, with the plane formed by the N3, N4, and N5 amino groups. The aliphatic amino groups (N4, N5, and N6) are in an *endo* conformation, enabling H-bond interactions inside the macrocyclic cavity. Specifically, the hydrogen atom linked to the central amine group points inside the macrocyclic cavity, giving rise to intramolecular H bonds with the phenanthroline nitrogen atoms. The nitrogen atoms N3 and N5 are also partially enclosed in the ligand cavity, and thus they can also form intramolecular H bonds with the phenanthroline nitrogen atoms (Scheme 4).



Scheme 4. ORTEP representation of $[H_3L^{13}]^{3+}$

As for the benzene and anthracene analogues, the absorption spectra of the whole molecules resemble that of the phenanthroline chromophore and protonation of the chain has only a small influence on their shape and intensity. However, the fluorescence emission spectra are completely quenched at basic pH values. When considering a fluorophore such as phenanthroline, containing lone pairs, the possibility of inversion between the strongly emissive π-π* state and the poorly emissive n-π* state has to be taken into account. In particular, protonation can stabilize the n-π* state relative to the π-π* state, leading to inversion of the states and thus to a decrease in the fluorescence emission intensity. This is the most probable explanation for the quenching effect observed for the fully protonated form. As discussed above, in this form, the nitrogen atoms of the phenanthroline unit are involved in H bonds with the protons of the chain. On removing the first proton, which is known to occur from the central nitrogen atom, the chemosensor becomes more emissive. At this point, two opposite effects come into operation. On the one hand, the intramolecular hydrogen bond becomes weaker and thus the fluorescence emission tends to increase. On the other hand, deprotonation of the central atom leaves the respective nitrogen lone-pair free to participate in the quenching process by electron transfer, which is thermodynamically favourable. However, a general feature of this class of compounds is that only when a benzylic nitrogen atom is deprotonated is the emission extinguished, and hence the diprotonated form is still emissive. This behaviour is exactly opposite to that seen with polyazacyclophane and *N,N′*-dibenzylated polyamine chemosensors (vide infra). This difference can be attributed to the fact that in the latter compounds the benzylic amino groups are in an *exo* conformation, whereas in the phenanthroline derivatives an *endo* conformation is adopted.

By increasing the length of the polyamine moiety, i.e. by replacing the diethylenetriamine chain by a triethylenetetraamine unit, L^{14}, or a tetraethylenepentaamine unit, L^{15}, larger macrocycles are obtained. The fluorescence emission titration curves show essentially the same features, i.e. a total quenching at basic pH and a partial quenching at very acidic pH values (Figure 4).

As a matter of fact, the marked decrease in the fluorescence emission intensity in very acidic media corresponds to the formation of the fully protonated forms of these compounds. This quenching effect increases in the order $L^{13} < L^{14} < L^{15}$, exactly mirroring the increasing involvement of the nitrogen atoms in stabilizing the protonated forms through hydrogen bonding. The observed decrease in the fluorescence emission can thus be rationalized in terms of possible inversion of the energy between the n-π* state and the π-π* state upon protonation (even partial) of the phenanthroline nitrogen atoms.

As observed for L^{13}, the larger macrocycles show a dramatic quenching effect at more basic pH values. In the case of L^{14}, the emission disappears with the loss of the second proton, while for L^{15} this is only seen on removing the third proton. In both cases, the resulting forms correspond to deprotonation at the benzylic nitrogen atoms. Once again, this behaviour seems to indicate a quenching process involving electron transfer from the lone pairs of the deprotonated amines to the excited phenanthroline. Because

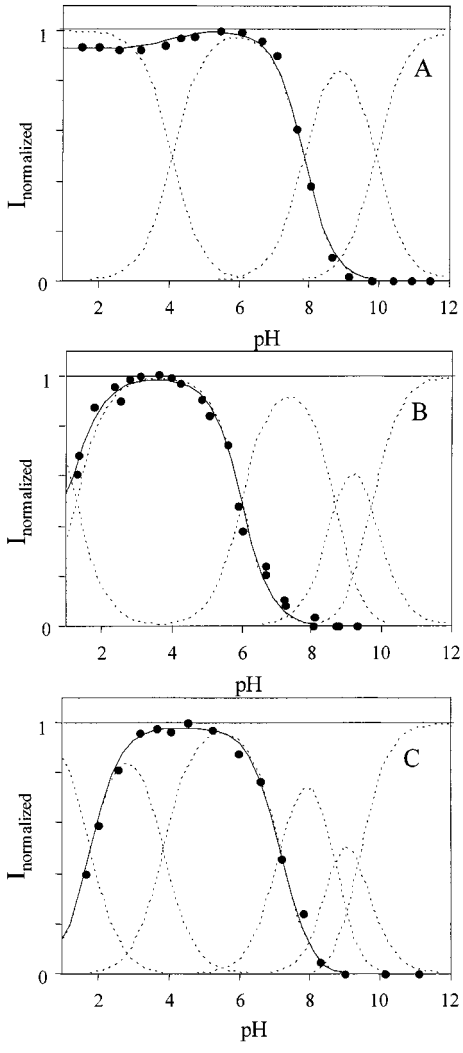


Figure 4. Fluorescence emission titration curves of A-L[13], B-L[14], and C-L[15], along with the respective mole fraction distribution curves

phenanthroline is only ca. 0.1 eV more difficult to reduce than anthracene, the process is also thermodynamically favourable.

Sensing Metal Cations

Photoelectron transfer from the amines to the excited fluorophore can also be suppressed by the binding of a cation at the receptor unit because, like the proton, the positively charged metal ion can increase the oxidation potential of the amine. However, coordination to metals such as copper(II) or nickel(II) can give rise to an enhancement of the quenching as the presence of such metal ions can offer alternative, non-radiative pathways, e.g. through the formation of non-radiative charge-transfer states. This situation can generally be detected through the appearance of new, intense absorption bands in the UV/Vis spectrum. The metal ion can also participate in the quenching by energy transfer or electron transfer, or quench through the heavy-atom effect. Some of these quenching processes are, however, precluded when the electronic configuration of the metal ion is d^{10}. This is the case with the zinc(II) and cadmium(II) cations, complexes of which can exhibit CHEF effects.

Sensing Zinc(II)

Complexes involving zinc(II) have attracted much attention, not only because of the large CHEF effect exhibited by this metal ion upon coordination, but also in view of the key roles played by such complexes in the active sites of zinc-containing enzymes such as carbonic anhydrase.[19−21]

The zinc(II) complexes of polyazacyclophanes and *N,N′*-dibenzylated polyamine receptors have been studied in detail. The absorption spectra of the chemosensors are not substantially altered in the presence of this metal ion, as reported by Czarnik in the case of a series of anthrylazamacrocycles.[2]

As for proton binding, plotting the fluorescence emission titration curves in conjunction with the mol fraction distributions of the various species present in solution, as determined by potentiometry, proved very helpful in understanding the emissive behaviour of these systems. This procedure led to good fitting and allowed us to dissect the relative contribution of each species present to the overall emission.

Zinc(II) Complexes with Polyazacyclophane Macrocyclic Receptors

In the case of polyazacyclophane macrocyclic receptors, the presence of a *p*-phenylene spacer prevents the simultaneous coordination of both benzylic nitrogen atoms to the same metal ion. This feature leads to unsaturated coordination sites, often of low symmetry, that are of interest with regard to the promotion of particular reactivities such as the stabilization of low-valent metal complexes or the activation of hydrolytic pathways.[22−25]

The structural characteristics of these compounds are reflected in the fluorescence emission properties of their various forms. In all the $[ML]^{2+}$ complexes, one of the benzylic nitrogen atoms is neither protonated nor coordinated and can thus take part in a PET quenching process, thereby accounting for the lack of an emission (Figure 5).

Curiously, in these cases, the two titration curves (in the presence and absence of the metal) are identical; only H_4L^{4+} and H_3L^{3+} are emissive and these species do not interact appreciably with zinc(II), hence their mol fraction distributions as a function of the pH value are not significantly affected.

At this point, the question arises as to why the benzylic nitrogen atoms should become efficient at quenching when involved in the metal complex, even though they are seemingly poor quenchers in the free chemosensor. A likely explanation for this behaviour is that these benzylic nitrogen atoms would be transformed from an *exo* conformation in the uncoordinated macrocycle to an essentially *endo* conformation in the coordinated complex.

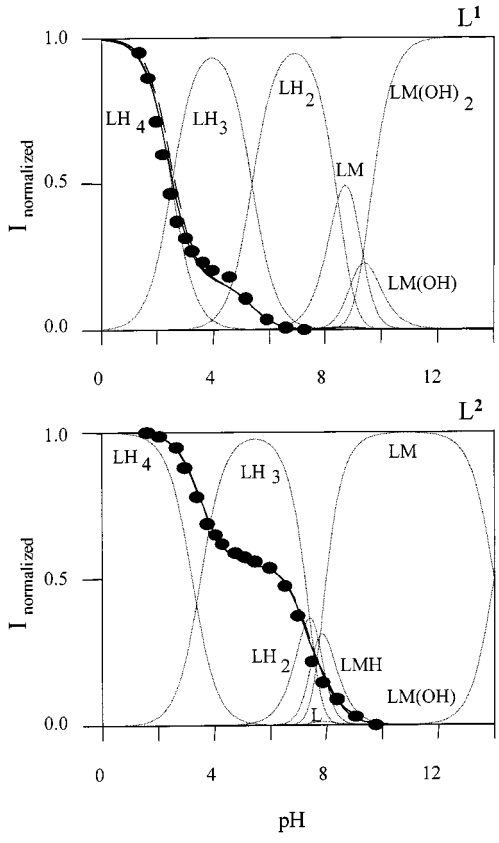


Figure 5. Steady-state fluorescence emission titration curves of (a) L^1, (b) L^2, in the absence of zinc(II) (traced line) and in the presence of an equimolar amount of zinc(II) (full line); mole fraction distributions in the presence of zinc(II) are also represented (full line)

Zinc(II) Complexes with *N*,*N*′-Dibenzylated Receptors

The fluorescence emission titration curves for the zinc(II) complexes with ligands L^3 to L^7 are presented in Figure 6.[26]

On comparing the fluorescence emission properties of these complexes with those of the polyazacyclophane analogues, it can be seen that for these ligands the $[ZnL]^{2+}$ complexes and the protonated analogues are emissive, except in the case of the largest member of this family.

In the case of the ligands L^4 and L^5, three complexes $[ZnL]^{2+}$, $[ZnL(OH)]^{+}$, and $[ZnL(OH)_2]$, could be detected by potentiometry, showing significant, weak, and no emission, respectively. In all the complexes, the nitrogen atoms can be expected to be fully involved in the coordination to the metal center, except in the case of the dihydroxy complexes, where the lack of an emission may be rationalized in terms of partial decomplexation. The zinc(II) complexes display emissions with quantum yields ca. half of that of the emissions detected for the fully protonated forms of the free ligands. This implies that coordination to the zinc(II) ion, like protonation, prevents the PET between the amines and the fluorophore, albeit less efficiently. When the water coordinated to the zinc(II) cation loses a proton, the protective effect of the metal ion decreases and is lost completely following removal of a second proton from another water ligand. In the case of L^6, potentiometric titrations

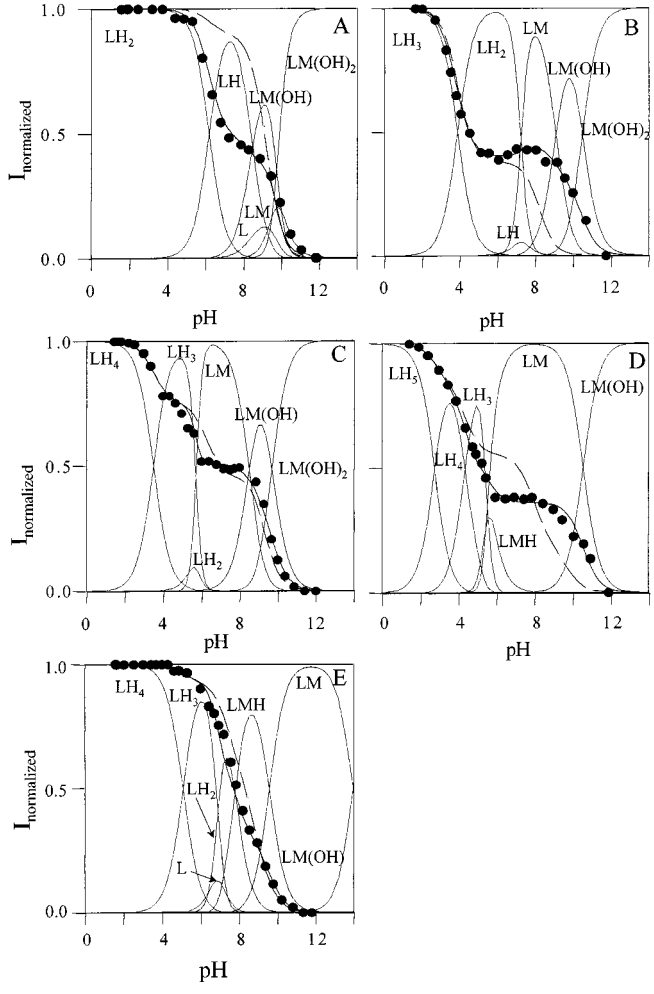


Figure 6. Steady-state fluorescence emission titration curves of A-L^3, B-L^4, C-L^5, D-L^6, and E-L^7 in the absence of zinc(II) (traced line) and in the presence of an equimolar amount of zinc(II) (full line); mole fraction distributions in the presence of zinc(II) are also represented (full line)

predict the existence of the species $[ZnHL]^{3+}$, $[ZnL]^{2+}$, and $[ZnL(OH)]^{+}$. The lack of fluorescence emission for the form $[ZnL]^{2+}$ can be explained by the fact that in this species only four of the five nitrogen atoms are involved in the binding, allowing the free nitrogen atom to carry out the quenching process.

Zinc(II) Complexes with Anthracene Fluorophores

The fluorescence emission titration curves for the zinc(II) complexes of the chemosensors L^9 to L^{11} are presented in Figure 7.[14]

This class of compounds shows some remarkable advantages in comparison with the chemosensors incorporating a benzene unit: (i) substantially higher fluorescence quantum yields, (ii) much greater differences in emission between the free and the complexed forms.

Inspection of Figure 7 shows that the metal complexes however $[ZnL]^{2+}$ as well as their protonated forms are strongly emissive, with the sole exception of the $[ZnL^{11}]^{2+}$ species. In contrast, the hydroxo complexes are not emissive. A puzzling matter that needs to be addressed is the contrast

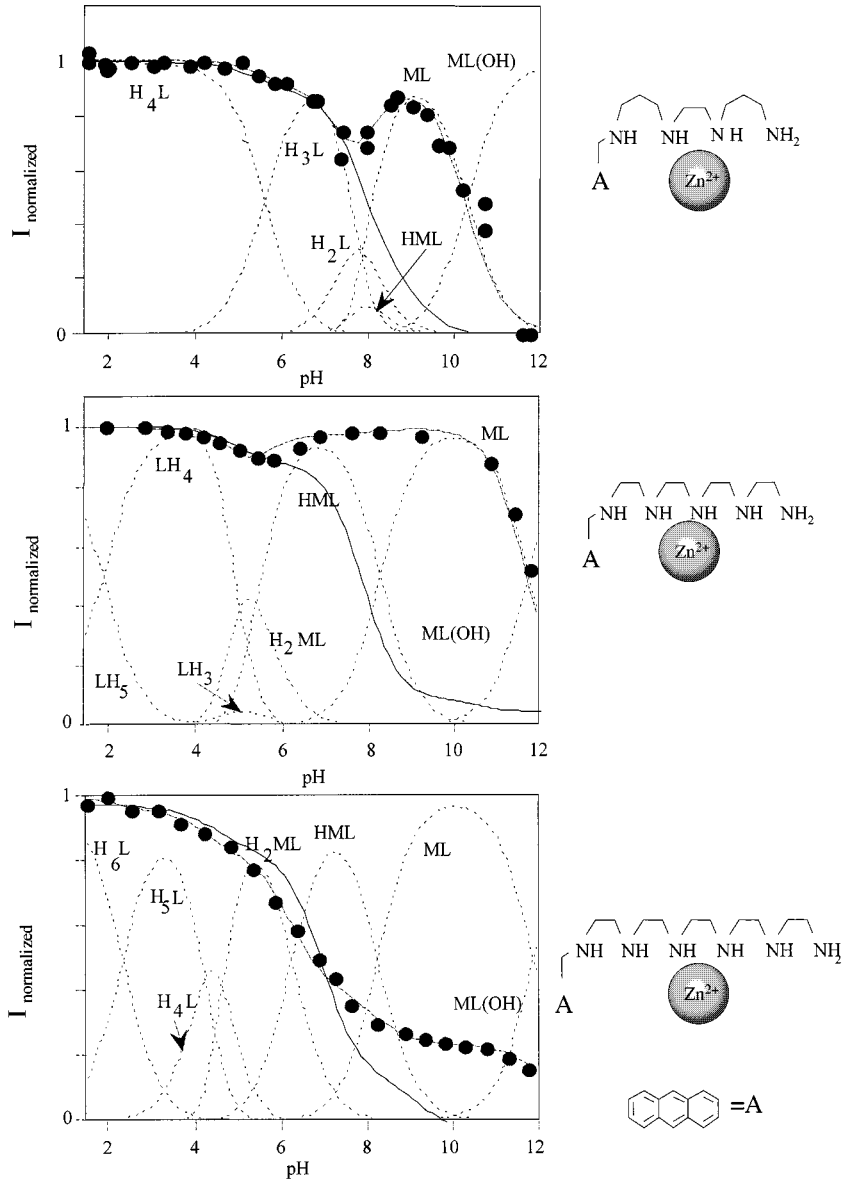


Figure 7. Steady-state fluorescence emission titration curves of L^9 to L^{11} in the absence of zinc(II) (full line) and in the presence of an equimolar amount of zinc(II) (traced dotted line); mole fraction distributions in the presence of zinc(II) are also represented (dotted line)

between the intense fluorescence emission of the species $[ZnL^{10}]^{2+}$ and the weak emission of the complex $[ZnL^{11}]^{2+}$.

Assuming that in these compounds the best coordination is achieved when four nitrogen atoms are simultaneously bound to the metal center, the $[ZnL^{11}]^{2+}$ species would possess a free or only weakly coordinated nitrogen atom, which could thus be responsible for quenching.

An interesting feature that emerges from Figure 7 is the crucial importance of the receptor length. The best performance was observed with the chemosensor of intermediate length.

In general, zinc(II) complexation by the conjugate chemosensors gives rise to two different effects: (i) the mol fraction distributions of the highly protonated and emissive forms of the free ligand are decreased and shifted to lower pH values, and these are replaced by less emissive metal complexes, thereby explaining the CHEQ effect; and (ii) it allows the existence of emissive metal complexes under conditions of moderately basic pH values where, in the absence of the metal ion, no emissive species of the free ligand are present, thereby leading to a CHEF effect. These two effects are thus the result of the existence of differentiated domains for each type of emissive species.

Zinc(II) Complexes with Phenanthroline Chromophores[17,18]

The crystal structure of the complex $[ZnL^{13}(H_2O)](ClO_4)_2$ indicates that the coordination geometry around the metal atom can be described as a distorted tetrahedron, the vertices of which are occupied by the phenanthroline nitrogen atoms N1 and N2, the central aliphatic nitrogen atom N4, and a water molecule. The zinc(II) cation forms two long bonds to the benzylic nitrogen atoms (N3−Zn 2.460 Å, N5−Zn 2.512 Å) so as to achieve a pseudo-prismatic geometry, the bases of the prism being defined by N2,

N3, N4 and N1, O1, N5, respectively (Figure 8A). According to this structure, both benzylic nitrogen atoms are weakly involved in metal coordination. A similar effect has been described for polyazamacrocyclic receptors containing a benzene unit as an integral part of the ring.[26] Furthermore, the phenanthroline unit displays electron-withdrawing properties, which reduce the basicity and the donor ability of the benzylic amino groups adjacent to the heteroaromatic moiety. These characteristics disfavour coordination of the metal center by the benzylic amino groups, leading to an unsaturated coordination environment for the zinc(II) ion. As a consequence, water molecules can be bound at the free binding sites of the metal center, as has indeed been shown by a crystal-structure analysis of the complex. Facile deprotonation of the coordinated water gives the hydroxo complex in aqueous solution at slightly alkaline pH values, as well as a dihydroxo species in strongly alkaline solutions. The aforementioned structural characteristics strongly affect the fluorescence emission features of this zinc(II) complex. Figure 8B shows the fluorescence emission titration curve of L^{13} in the presence of equimolar amounts of zinc(II) ions, from which an efficient quenching effect is apparent.

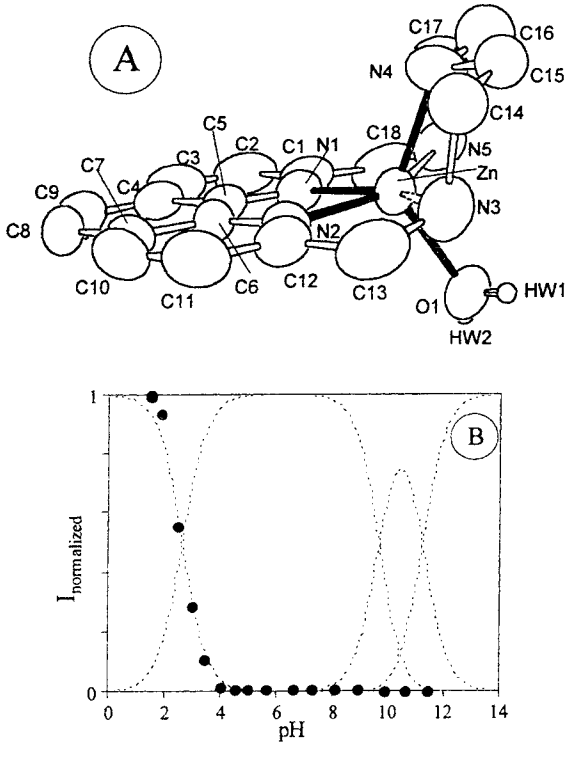


Figure 8. **A**: ORTEP representation of the $[ZnL^{13}(H_2O)]^{2+}$ cation; **B**: fluorescence emission titration curve of L^{13} in the presence of an equimolar amount of zinc(II)

This unexpected behaviour can be rationalized by considering the particular characteristics of the ligand L^{13} and of its zinc(II) complexes. According to the structure of the complex cation $[ZnL^{13}(H_2O)]^{2+}$, both benzylic amino groups are weakly involved in the metal coordination. These nitrogen atoms are close to the fluorophore and, as shown previously, they are able to efficiently quench the fluorescence. Moreover, no protonated forms of the zinc(II) complex could be detected by potentiometry. Therefore, in this complex the lone pairs on the benzylic nitrogen atoms are available for the electron-transfer process, accounting for the lack of fluorescence emission.

Sensing Cadmium(II)

Figure 9 shows the fluorescence emission titration curves obtained for the chemosensors L^9 to L^{11} in the presence of equimolar quantities of cadmium(II). The basic trend is similar to that observed for the complexes with zinc(II). However, due to the lower propensity of the cadmium(II) complexes to form hydroxo species when compared with zinc(II), the fluorescence emission extends to more basic pH values. For example, strong fluorescence emissions can still be detected at pH = 12.

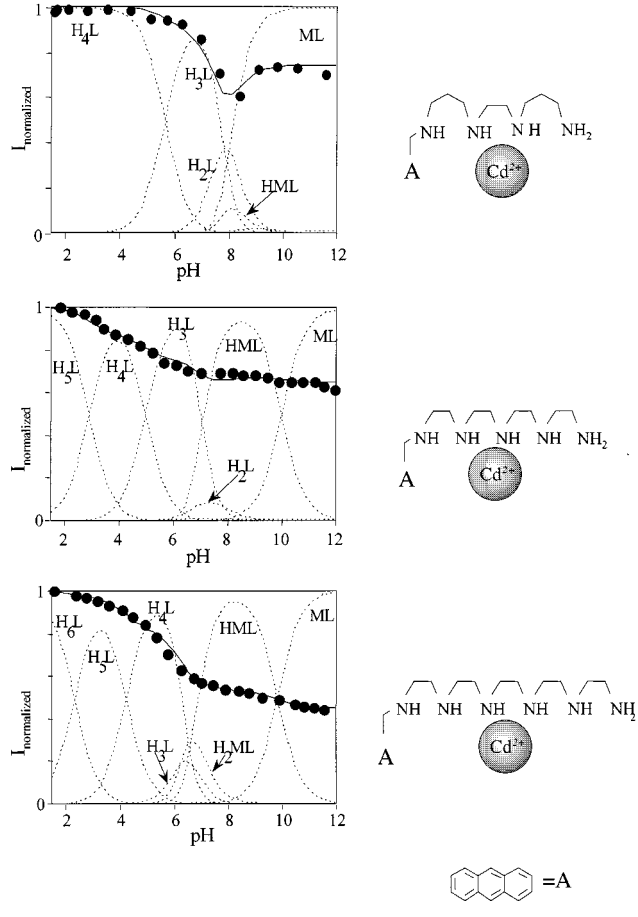


Figure 9. Fluorescence emission titration curves obtained for the chemosensors L^9 to L^{11} in the presence of equimolar quantities of cadmium(II)

Sensing Copper(II)

In contrast to the situation with zinc(II) ions, complexation of copper(II) ions by L^1 to L^7 leads to large increases in the molar absorption coefficients as well as to blue shifts in the UV/Vis absorption maxima. These new

and very intense bands are characteristic of charge-transfer processes and are indicative of significant interactions between the molecular orbitals of the ligand and those of the metal center (Figure 10A). As a consequence, the excited states are no longer centred on the ligand but display metal character. No fluorescence emission was observed for these complexes, the recorded fluorescence being purely due to protonated forms of the free ligands (Figure 10B). According to potentiometric studies, several species with all the nitrogen atoms involved in coordination to the metal ion and/or protonated are present in solution. In spite of this, no emission was observed. A possible explanation for the absence of fluorescence emission in the copper(II) complexes can be found in the charge-transfer characteristics of the excited state, which can offer a channel for the deactivation of the excited state involving the metal center.

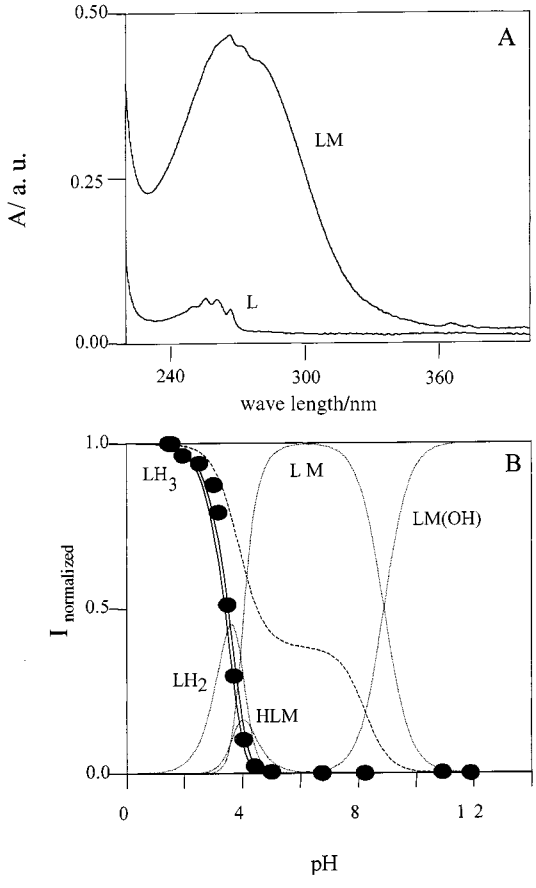


Figure 10. **A**: Absorption spectra of L^4 at pH = 6, in the absence and in the presence of an equimolar amount of copper(II); **B**: fluorescence emission titration curves obtained for L^4 in the presence of an equimolar amount of copper(II)

Sensing Anions

The chemosensors described throughout this work can also be used to bind anions. One of the obvious strategies for achieving this goal is to work at pH values at which the polyamine receptor is fully or partially protonated, thereby using electrostatic attraction as a driving force for anion binding. In another strategy, complexes of the polyamine ligands with strong Lewis acids such as divalent metal ions, in particular zinc(II), are used as receptors. Adducts of this type show strong affinities for anions as the metal center offers a coordination site at which the substrate can be bound. This latter strategy has been brilliantly developed by Kimura and co-workers. These authors have designed molecules based on the well-known [12]aneN_4 and [12]aneN_3 macrocyclic receptors. Coordination of substrates such as benzoic acid,[27] phthalic acid,[27] sulfonamides,[28] or carboxamides[29] is favoured by strong interactions between the zinc(II) ion and the respective anions. In this regard, macrocyclic receptors bearing pendant arms incorporating additional donor atoms are particularly interesting. This is exemplified by the receptor cyclen, which has pendant aromatic sulfonamide moieties that can bind to the metal center through their sulfonamide *N*-anions.[31] Pendant arms containing phenolate,[30] dimethylaminopropyl,[31] pyridine,[31] uracil,[32] and alcohol[33] moieties have also been described.

Sensing Nucleotides

Nucleotide sensing and quantification by means of luminescent probes represents an important target in supramolecular chemistry due to their many biological and biomedical implications. Lehn and co-workers have prepared two very interesting multi-site binding receptors based on the well-known macrocyclic structure of 1,13-dioxa-4,7,10,16,19,22-hexaazatetracosane (bisdien); to which one or two acridine luminescent groups, respectively, have been covalently bonded to the central nitrogen atoms of these polyamine fragments through aminopropyl side-arms. The second of these receptors seems to be particularly well suited for nucleotide recognition since, apart from displaying large variations in its emission properties upon coordination to nucleotides, it does not induce hydrolytic ATP cleavage.[34] Other types of receptors developed by Lehn and Zinic were based on bis(phenanthridinium) fragments; their emissions were subject to large quenching effects as a result of π-stacking interactions with the adenine moieties of nucleotides.[35] These interactions gave constants as high as ca. 5.8 logarithmic units and were independent of the polyphosphate chains of the nucleotides.

Recently, it was shown that, in spite of their apparent simplicity, the chemosensors L^9, L^{10}, and L^{11}, but not L^8, strongly interact with nucleotides exhibiting high degrees of selectivity for ATP. The presence of the anthracene unit allows the chemical inputs to be readily transformed into light signals.[36]

pH-Metric titrations of aqueous solutions of L^9 and ATP in a 1:1 molar ratio over the pH range 2.5−11 show the formation of ATP−L^9 adducts with degrees of protonation varying from 6 to 1.7. The distribution diagram is depicted in Figure 11. The conditional stability constants vary from 6.5 to 2 in the pH range explored. Fluorimetric titrations on the ATP−L^9 system show a bell-shaped curve; thus, light emission is strongly quenched at pH values lower than 4,

the emission reappears at pH ≈ 7, and then decreases once more, eventually disappearing at pH > 10. A similar result has been obtained by Czarnick et al.[37] in a study of the complexation of various anions, such as ATP, by two anthrylpolyamines.

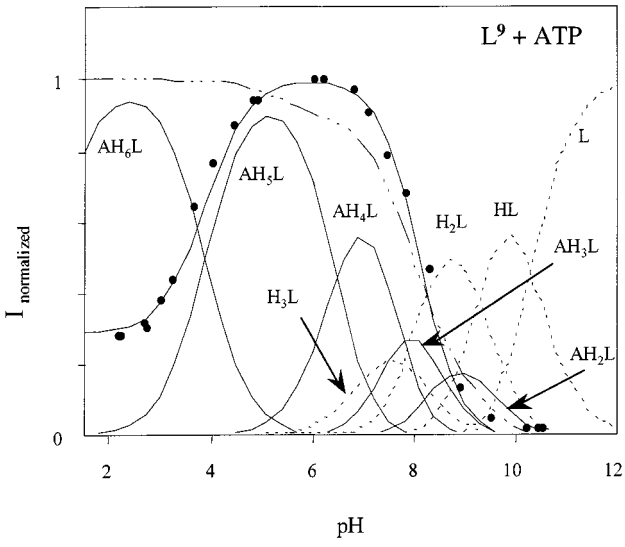


Figure 11. Fluorescence emission titration curves of L^9 in presence of equimolar amounts of ATP (•); fitting (——) was achieved as a linear combination of the mole fraction distribution of the various adducts as determined by potentiometry; the titration curve in the absence of ATP (—···—) is also included for comparison purposes

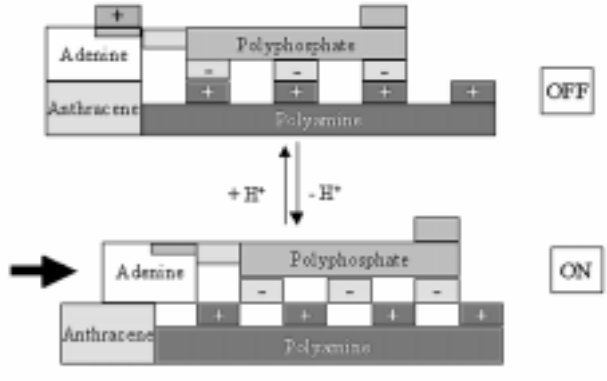
We suggest that this behaviour may be interpreted on the basis of the various species formed in solution, and considering the luminescent behaviour of the free receptor.

As mentioned above, from spectrofluorimetric titrations of the free receptor it could be inferred that H_4L^{4+} and H_3L^{3+} were the only emissive species, with a relative fluorescence emission quantum yield of $\Phi(H_4L^{4+})/\Phi(H_3L^{3+}) = 0.85$. In the presence of ATP, these species continue to emit, irrespective of whether they are complexed to ATP or free, except for the H_6LA^{6+} species formed by the association of the fully protonated receptor L^9 and the diprotonated form of ATP, which gives rise to a quenching effect. Comparing the fluorescence emission titration curves of the free and complexed receptor (Figure 11), the small increase in the fluorescence emission (CHEF) observed for the ATP−L^9 system at a neutral pH value can be attributed to the increase in apparent basicity of the receptor that occurs upon coordination to ATP. Perhaps the most striking feature of this system is the dramatic CHEQ effect (almost 60%) observed at pH < 4 (see Figure 11). A plausible interpretation of such quenching could be a π-stacking interaction between the anthracene unit of the receptor and the adenine fragment of the guest species, resulting by the charge state of both of them at these pH values. Evaluation of the stability constants at pH = 2.0 provides a value of 5.8 logarithmic units. Interestingly, the monoprotonated form of ATP does not give rise to such a quenching effect. It seems likely that the matching between the triphosphate chain of $HATP^{3-}$ and the polyammonium fragment of L^9 alters the relative disposition of the aromatic moieties in the two molecules, thereby preventing efficient π-stacking. On examining the behaviour of ADP, AMP, adenine, and tripolyphosphate, it was observed that only the first of these produced a CHEQ effect, however with a much lower constant (log K = 3.7 at pH = 2.2) than that found for ATP.

Therefore, it seems that the molecular topology of the receptor is a key factor in facilitating the π-stacking pattern. Indeed, experiments carried out with the anthracenophane 2,6,9,13-tetraaza[14](9,10)-anthracenophane (L^8) did not reveal any significant effect. On the other hand, analogous ligands containing the same fluorophore but with different polyamine chains (L^{10} and L^{11}) give rise to similar CHEQ effects with very similar association constants (L^{10}: log K = 5.6; L^{11}: log K = 5.4; both at pH = 2.2). It is noteworthy that the constants obtained are not affected by the chain length or the number of nitrogen atoms in the chain, but only by the molecular arrangement of the receptor. The values of these stability constants are, on the other hand, rather similar to those obtained by Lehn and Zinic for the interaction of ATP and other nucleotides with their bis-(phenanthridinium)-based receptors.[35]

A related receptor can be constructed by appending two methylanthracene fragments at both ends of a linear pentamethylenehexaamine chain, L^{12}. Interaction of L^{12} with ATP also leads to a very significant quenching of the emission at low pH values, from which an association constant of log K = 5.7 at pH = 2.2 can be calculated.

The similar values of the constants obtained for ATP binding with all the receptors at acidic pH values, together with the lack of notable effects for AMP and adenine, suggest that the requirements for observing significant CHEQ effects are: (i) a certain degree of anchorage of the polyphosphate chain of ATP by the polyammonium fragments of the receptor, and (ii) topological complementarity of the partners (see Scheme 5).



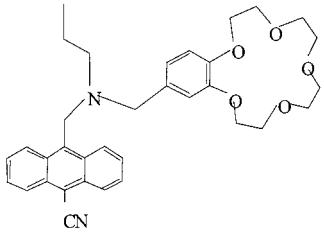
Scheme 5. Schematic representation of ATP "anchorage"

These results highlight the potential use of these simple receptors as efficient luminescent ATP chemosensors. Further work is currently in progress with the aim of obtaining related receptors with improved binding characteristics.[37]

Molecular Devices and Machines

Logic Gates at a Molecular-Level

Chemosensors can be regarded as devices that behave essentially as logic gates since in these systems chemical binding (the "input") results in a change in fluorescence intensity (the "output") of the receptor, which can be translated as a simple logic operation. Among other authors,[37,39,40] de Silva and co-workers were the first to contribute to this growing field of chemistry.[3] For example, an AND logic gate operating with two input channels was described.[41] In this system, the fluorescence signal depends on whether hydrogen ions, sodium ions, or both are bound to the receptor molecule (Scheme 6).



Scheme 6. Chemical structure of de Silva's ligand that operates as a logic device[41]

Recently, we described a NAND logic gate based on the system ATP−L^9 (Figure 11).[36] The initial state is that of the free chemosensor in the pH range 5−8. The inputs are obtained by: (i) addition of protons in order to reach a final pH of ca. 2, and (ii) addition of a slight excess of ATP at pH = 6. We consider there to be a final output of 1 when the intensity of the fluorescence emission exceeds 0.8 relative units, and of 0 when the intensity of the emission is below 0.4 relative units. In the absence of any input, the system exhibits fluorescence emission and thus the output signal is 1. The same output is obtained if only ATP or protons are added to the solution. When both inputs are present, a quenching effect occurs and the output becomes 0 (see Table 1).

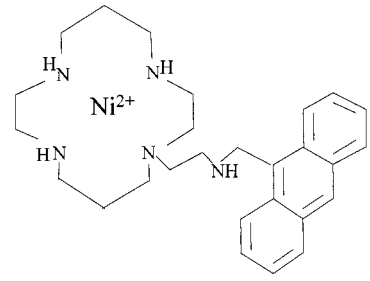
Table 1. Truth table of the logic operation NAND

$[H^+]$	[ATP]	Em
0	0	1
0	1	1
1	0	1
1	1	0

Molecular Machines

Metal Scorpionate Complexes

One interesting system, based on the presence of a pendant arm, has been reported by Fabbrizzi and coworkers.[42] This system uses the Ni^{II} complex of a cyclam ring separated from an anthracene chromophore by a methylene spacer (Scheme 7).



Scheme 7. Chemical structure of Fabbrizzi's molecular machine[42]

The fully protonated form, corresponding to a structure where the protonated alkylamine side chain is forced away from the ring through electrostatic repulsion, exhibits the most intense emission. A fluorimetric titration in acetonitrile/water (4:1) showed that on removing the first proton (from the alkylamine side chain) the emission was reduced to 60% of the original. In this last species the metal center is hexacoordinated by the cyclam nitrogen donors at the equatorial positions and by the alkylamine group and water molecule at the axial positions. Complete quenching occurs upon removal of a second proton from the water molecule linked to the metal center. All these processes are reversible and thus the system can be considered as an elementary molecular machine driven by the pH value. The pendant arm is forced to oscillate between the metal center and a more distant point by modulation of an external parameter, i.e. the pH value.

Conclusions

The study of supramolecular species capable of existing in different states that may be interconverted by external stimuli is a topic of great interest and has led to predictable applications in the field of nanotechnology. Fluorescent chemosensors containing polyamine receptors are versatile systems capable of detecting cations or anions and, depending on their incorporated units, function as molecular devices or machines. The systems reported in this review are capable of detecting substrates at low concentrations and exhibit high sensitivity in water. However, their selectivities still need to be improved if they are to find application in real situations.

Acknowledgments

We are indebted to the Fundação para a Ciência e Tecnologia (Portugal) and DGICYT Project no. PB96−0796-CO2 (Spain) for financial support. M. A. B. wishes to thank the Portuguese Junta Nacional de Investigação Cientifica e Tecnologica (Praxis XXI/BD/4504/94) for financial support.

[1] [1a] R. A. Bissel, A. P. de Silva, H. Q. N. Gunaratne, P. L. M. Lynch, G. E. M. Maguire, K. R. A. S. Sandanayake, *Chem. Soc. Rev.* **1992**, 187. − [1b] A. P. de Silva, H. Q. Gunaratne, T. Gunnlaugsson, A. J. M. Huxley, C. P. McCoy, J. T. Rademacher, T. E. Rice, *Chem. Rev.* **1997**, *97*, 1515.

[2] [2a] A. W. Czarnik, *Fluorescent Chemosensors for Ion and Molecule Recognition*, American Chemical Society, Washington DC, **1992**. − [2b] J.-P. Desvergne, A. W. Czarnick, *Chemosensors for Ion and Molecular Recognition*, NATO ASI Series, Series C,

vol. 492, Kluwer Academic Press, Dordrecht, **1997**. – [2c] A. W. Czarnik, *Acc. Chem. Res.* **1994**, *27*, 302.
[3] A. P. de Silva, S. A. de Silva, K. R. A. S. Sandanayake, *J. Chem. Soc., Chem. Commun.* **1989**, 1056.
[4] J.-M. Lehn, *Supramolecular Chemistry: Concepts and Perspectives*, VCH, Weinheim, **1995**.
[5] V. Balzani, F. Scandola, *Supramolecular Photochemistry*, Ellis Horwood, Chichester, England, **1991**.
[6] A. P. de Silva, R. A. D. D. Rupashing, *J. Chem. Soc., Chem. Commun.* **1985**, 1669.
[7] A. P. de Silva, H. Q. N. Gunaratne, C. P. M. Coy, *Chem. Commun.* **1996**, 2399.
[8] B. Altava, A. Bianchi, C. Bazzicalupi, M. I. Burgete, E. Garcia-España, S. V. Luis, J. F. Miravet, *Supramol. Chem.* **1997**, *8*, 287.
[9] M. A. Bernardo, A. J. Parola, F. Pina, E. Garcia-España, V. Marcelino, S. V. Luis, J. F. Miravet, *J. Chem. Soc., Dalton Trans.* **1995**, 993.
[10] A. Andrés, C. Bazzicalupi, A. Bianchi, E. Garcia-España, S. V. Luis, J. F. Miravet, J. A. Ramirez, *J. Chem. Soc., Dalton Trans.* **1994**, 1995.
[11] A. Gilbert, J. Baggott, *Essentials of Molecular Photochemistry*, Blackwell Scientific Publications, Oxford, **1991**.
[12] E. A. Chandross, H. T. Thomas, *Chem. Phys. Lett.* **1971**, *9*, 393.
[13] D. R. G. Brimage, R. S. Davidson, *J. Chem. Soc., Chem. Commun.* **1971**, 1385.
[14] M. A. Bernardo, F. Pina, B. Escuder, E. Garcia-España, M. L. Godino-Salido, J. Latorre, S. V. Luis, J. A. Ramirez, C. Soriano, *J. Chem. Soc., Dalton Trans.* **1999**, 915.
[15] F. Pina, M. A. Bernardo, S. Alves, E. Garcia-España, work in progress.
[16] P. G. Sammes, G. Yahioglu, *Chem. Soc. Rev.* **1994**, *23*, 327.
[17] C. Bazzicalupi, A. Bencini, A. Bianchi, C. Giorgi, V. Fusi, B. Valtancoli, M. A. Bernardo, F. Pina, *Inorg. Chem.* **1999**, *38*, 3806.
[18] A. Bencini, M. A. Bernardo, A. Bianchi, V. Fusi, C. Giorgi, F. Pina, B. Valtancoli, *Eur. J. Inorg. Chem.* **1999**, 1911.
[19] E. Kimura, T. Koike, *Chem. Commun.* **1998**, 1495.
[20] B. König, M. Pelka, H. Zieg, T. Ritter, H. Bouas-Laurent, R. Bonneau, J.-P. Desvergne, *J. Am. Chem. Soc.* **1999**, *121*, 1681.
[21] M. Shionoya, E. Kimura, M. Shiro, *J. Am. Chem. Soc.* **1993**, *115*, 6730.
[22] A. Doménech, J. V. Folgado, E. Garcia-España, S. V. Luis, J. M. Llinares, J. F. Miravet, J. A. Ramirez, *J. Chem. Soc., Dalton Trans.* **1995**, 541.
[23] A. Doménech, E. Garcia-España, V. Marcelino, B. Altava, S. V. Luis, J. F. Miravet, A. Bianch, L. Ferrini, *Inorg. Chim. Acta* **1996**, 123.
[24] M. I. Burguete, B. Escuder, E. Garcia-España, S. V. Luis, J. F. Miravet, *Tetrahedron Lett.* **1994**, 9075.
[25] B. Altava, M. I. Burguete, S. V. Luis, J. F. Miravet, E. Garcia-España, V. Marcelino, C. Soriano, *Tetrahedron* **1997**, *53*, 4571.
[26] M. A. Bernardo, F. Pina, E. Garcia-España, J. Latorre, S. V. Luis, J. M. Llinares, J. A. Ramirez, C. Soriano, *Inorg. Chem.* **1998**, *37*, 3935.
[27] E. Kimura, T. Ikeda, M. Shionoya, M. Shiro, *Angew Chem. Int. Ed. Engl.* **1995**, *34*, 663.
[28] E. Kimura, T. Shiota, T. Koike, M. Shiro, M. Kodama, *J. Am. Chem. Soc.* **1990**, *112*, 5805.
[29] E. Kimura, T. Koike, M. Shiota, Y. Iitaka, *Inorg. Chem.* **1990**, *29*, 4621.
[30] E. Kimura, T. Koike, K. Toriumi, *Inorg. Chem.* **1988**, *27*, 3687.
[31] N. W. Alcock, A. C. Benniston, P. Moore, G. A. Pike, S. C. Rawle, *J. Chem. Soc., Chem. Commun.* **1991**, 706.
[32] E. Kimura, H. Kitamura, T. Koike, M. Shiro, *J. Am. Chem. Soc.* **1997**, *119*, 10909.
[33] E. Kimura, I. Nakamura, T. Koike, M. Shionoya, Y. Kodama, T. Ikeda, M. Shiro, *J. Am. Chem. Soc.* **1994**, *116*, 4764.
[34] H. Fenniri, M. W. Hosseini, J.-M. Lehn, *Helv. Chim. Acta* **1997**, *80*, 786.
[35] P. Cudic, M. Zinic, V. Tomisic, V. Simeon, J.-P. Vigneron, J.-M. Lehn, *J. Chem. Soc., Chem. Commun.* **1995**, 1073.
[36] M. T. Albelda, M. A. Bernardo, E. Garcia-España, M. L. Godino-Salido, S. V. Luis, M. J. Melo, F. Pina, C. Soriano, *J. Chem. Soc., Perkin Trans. 2* **1999**, 2545.
[37] M. E. Huston, E. U. Akkaya, A. W. Czarnik, *J. Am. Chem. Soc.* **1989**, *111*, 8735.
[38] F. Pina, E. Garcia-España, M. J. Melo, M. A. Bernardo, work in progress.
[39] M. W. Hosseini, A. J. Blacker, J.-M. Lehn, *J. Am. Chem. Soc.* **1990**, *112*, 3896.
[40] S. A. V. Arman, A. W. Czarnik, *Supramolecular Chem.* **1993**, *1*, 99.
[41] A. P. de Silva, H. Q. N. Gunaratne, C. P. McCoy, *Nature* **1993**, *364*, 42.
[42] L. Fabbrizzi, M. Licchelli, P. Pallavicini, L. Parodi, *Angew. Chem. Int. Ed.* **1998**, *37*, 800.

Received December 31, 1999
[I99480]

Synthesis and Crystal Structures of Monomeric Diamidonickel(II) Complexes

Hung Kay Lee,*[a] Yu Peng,[a] Steven C. F. Kui,[a] Ze-Ying Zhang,[a] Zhong-Yuan Zhou,[a] and Thomas C. W. Mak[a]

Keywords: Nickel / Amides / Chelates / Magnetic properties / N ligands

The thermally stable nickel(II) diamides [NiL_2] [L = $^-N(SiMe_3)(8\text{-}C_9H_6N)$ (**1**), $^-N(SitBuMe_2)(8\text{-}C_9H_6N)$ (**2**)] have been synthesized from the reaction of $NiCl_2$ with the appropriate lithium amide. X-ray crystallography revealed that the amido ligands bind in a chelating manner, forming a distorted tetrahedral environment around the nickel center. Complexes **1** and **2** have magnetic moments of 3.05 and 2.74 μ_B, respectively, which indicate a d^8 electronic configuration with two unpaired electrons.

Introduction

The study of late transition metal amides has elicited considerable interest due to their involvement in a number of important reactions, ranging from industrial processes[1] to biological phenomena.[2] Among these reactions, the formation of C−N bonds by insertion of unsaturated compounds into the highly reactive M−N bonds has attracted much attention in the past decade.[3] Although an enormous amount of effort has gone into the synthesis of late transition metal amides, structural data for these complexes are still scarce due to the lability of the M−N bonds. It is generally believed that M−N bonds are relatively weak due to an incompatibility that exists between the "hard" anionic amido ligand and the "soft" low-valent late transition metal center.[4−5] Alternatively, on the basis of orbital arguments, the "reluctance" of the electronically saturated late transition metal center to function as a π-acceptor for the amido nitrogen lone-pair electrons through M−N (*d*←*p*) π-interactions also imposes a destabilizing effect on these complexes.[6]

Examples of fully characterized nickel amide complexes containing $Ni-NR_2$ bonds are rare, in contrast to those of nickel complexes containing Ni−X bonds (X = alkyl, halide, hydrido). An early attempt to prepare nickel(II) diamides by reacting $NiCl_2(PPh_3)_2$ with $LiN(SiMe_3)_2$ was unsuccessful and only the three-coordinate nickel(I) complex $[Ni\{N(SiMe_3)_2\}(PPh_3)_2]$ was obtained.[7] By using a "hybrid" ligand consisting of both a hard amido ligand and soft phosphane donors, Fryzuk et al. have successfully synthesized the nickel(II) amide $[Ni(Cl)\{N(SiMe_2CH_2PPh_2)_2\}]$.[8] Recently, a series of monomeric nickel(II) amides $[Ni(Mes)(L)(PMe_3)_2]$ [Mes = mesityl; L = ^-NHPh, $^-N(Ph)C(O)CHPh_2$, $^-N(Ph)\{C(O)NHtBu\}$] that contain supporting phosphane ligands have been prepared and structurally characterized by Abboud, Boncella, and coworkers.[3d,9] Delocalization of the lone pair of electrons on the amido nitrogens to the π molecular orbitals of the ligands and/or π-interactions between the lone pair electrons with the nickel center in these complexes have been observed.

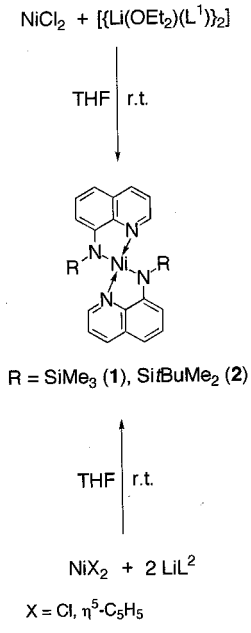
In recent years, a number of novel metal amides containing the bulky *N*-functionalized amido ligands [$^-N(Ph)(2\text{-}C_5H_4N)$],[10,11] [$^-N(SiMe_3)(2\text{-}C_5H_3N\text{-}6\text{-}Me)$],[12] [$^-N(SiMe_3)(2\text{-}C_5H_3N\text{-}4\text{-}Me)$],[13] and [$^-N(SiMe_3)(8\text{-}C_9H_6N)$],[12a,12b,12d,14] have been synthesized and structurally characterized. Interestingly, these amido ligands can bind to the metal centers in a number of bonding modes, for example as monodentate amido ligands, bidentate *N*,*N*-chelating ligands or bidentate *N*,*N*-bridging ligands. However, late transition metal amides derived from these ligands are still rare.[13a] Currently, we are interested in the structure and reactivities of metal amides. One of our synthetic strategies involves the use of bulky chelate ligands in order to stabilize those otherwise kinetically labile transition metal amido complexes. Several sterically more demanding *N*-functionalized amido ligands, namely [$^-N(SitBuMe_2)(2\text{-}C_5H_3N\text{-}6\text{-}Me)$], [$^-N(SitBuPh_2)(2\text{-}C_5H_3N\text{-}6\text{-}Me)$], and [$^-N(SitBuMe_2)(8\text{-}C_9H_6N)$] have been prepared in our laboratory and shown to be capable of stabilizing a number of novel main group and transition metal amides with unusual coordination geometries.[15] In this communication, we report the synthesis and crystal structures of two novel monomeric nickel(II) amido complexes, namely $[Ni\{N(SiMe_3)(8\text{-}C_9H_6N)\}_2]$ (**1**) and $[Ni\{N(SitBuMe_2)(8\text{-}C_9H_6N)\}_2]$ (**2**).

Addition of $[\{Li(OEt_2)(L^1)\}_2]$ [L^1 = $^-N(SiMe_3)(8\text{-}C_9H_6N)$][12a] to a slurry of anhydrous $NiCl_2$ in THF at ambient temperature gave the homoleptic nickel(II) amide **1** in satisfactory yield (Scheme 1). Complex **2** was prepared analogously by the reaction of $NiCl_2$ with two molar equivalents of the lithium reagent LiL^2 [L^2 = $^-N(SitBuMe_2)(8\text{-}C_9H_6N)$]. The latter was prepared by lithiation of HL^2 [15] with a solution of *n*BuLi in hexane. Compound **2** could also be obtained by the reaction of nickelocene with two molar equivalents of LiL^2 in THF at

[a] Department of Chemistry, The Chinese University of Hong Kong,
Shatin, New Territories, Hong Kong SAR, P. R. China
Fax: (internat.) +852/2603-5057
E-mail: hklee@cuhk.edu.hk

 © WILEY-VCH Verlag GmbH, D-69451 Weinheim, 2000 1434−1948/00/1010−2159 $ 17.50+.50/0

room temperature. Both **1** and **2** were isolated as very air-sensitive, reddish brown crystals. They are thermally stable at room temperature and can be stored indefinitely under an inert atmosphere. They have been characterized by ^{1}H NMR spectroscopy, mass spectrometry and elemental analysis,[16] in addition to single-crystal X-ray diffraction studies. In the solid state, complex **1** consists of two independent molecules of nearly the same structure (Figure 1), which are also analogous to that of **2** (Figure 2). Both complexes are mononuclear and exhibit a distorted tetrahedral coordination geometry around the nickel center, with each pair of amido ligands binding in an *N*,*N*-chelating manner. The Ni−$N_{quinolyl}$ bond lengths in **1** [1.92−2.06(1) Å] and **2** [2.00−2.03(1) Å], are slightly shorter than the Ni−$N_{pyridyl}$ bond lengths of 2.093 Å (av.) in the trinickel(II) complex of dipyridylamide $[Ni_3(L^3)_4Cl_2]$ [L^3 = $^-$N(2-$C_5H_4N)_2$], in which the amido ligands bind in a *N*,*N*-bridging manner.[17]



Scheme 1

The nearly trigonal planar geometry around the amido nitrogen centers [sum of bond angles (av.): 359.7° and 360.0° in **1** and 359.3 in **2**] are consistent with sp^2-hybridized nitrogen atoms. The average Si−N bond lengths of 1.710 and 1.716 Å in **1** and 1.739 Å in **2**, are not significantly different from those typical for aminosilanes (ca. 1.73 Å).[4] This suggests the presence of a significant Si−N ($d\leftarrow p$) π-bonding interaction. Delocalization of the lone-pair electrons of the amido nitrogen onto the quinolyl ring is also evidenced by the relatively short N_{amido}−$C_{quinolyl}$ distances of 1.361 and 1.365 Å (av.) in **1**, which are similar to the N_{amido}−C_{phenyl} distance of 1.354(5) Å in *trans*-[Ni(Mes)(NHPh)(PMe_3)$_2$] (**3**).[3d,9a] The observed Ni−N_{amido} distances of 1.92−1.94(1) Å in **1** are relatively short and are similar to the observed Ni−N distances of 1.924(2) Å in [Ni(Cl){N($SiMe_2CH_2PPh_2$)$_2$}][8] (**4**) and 1.932(3) Å in

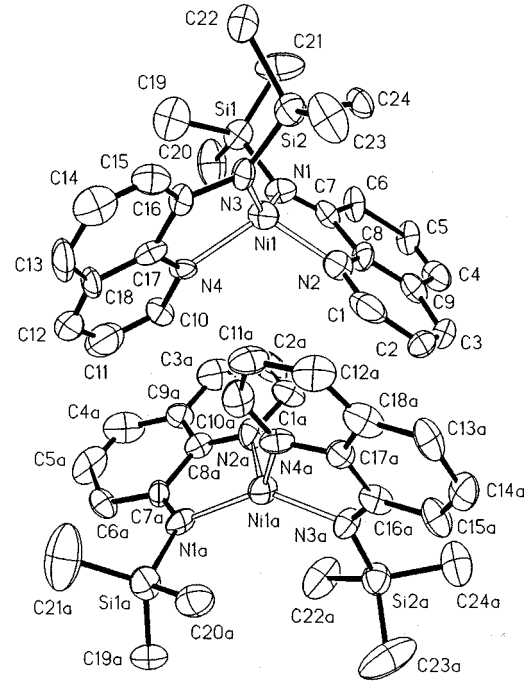


Figure 1. Perspective view of the two independent molecules (30% thermal ellipsoids) in the crystal structure of [Ni{N($SiMe_3$)(8-C_9H_6N)}$_2$] (**1**) with the atomic labeling scheme; selected bond lengths [Å] and bond angles [°]: Ni(1)−N(1) 1.94(1), 1.93(1), Ni(1)−N(2) 1.92(1), 2.00(1), Ni(1)−N(3) 1.92(1), 1.93(1), Ni(1)−N(4) 2.06(1), 2.00(1), Si(1)−N(1) 1.73(1), 1.67(1), Si(2)−N(3) 1.69(1), 1.76(1), N(1)−C(7) 1.26(2), 1.34(2), N(3)−C(16) 1.46(1), 1.39(1); N(1)−Ni(1)−N(2) 82.2(7), 84.5(6), N(3)−Ni(1)−N(4) 85.0(6), 82.4 (6), N(1)−Ni(1)−N(3) 138.2(2), 138.9(2), C(7)−N(1)−Si(1), 126(1), 127(1), C(7)−N(1)−Ni(1) 114(1), 113(1), Si(1)−N(1)−Ni(1) 119.6(8), 120.7(7), C(16)−N(3)−Si(2) 127(1), 128(1), C(16)−N(3)−Ni(1) 112(1), 114(1), Si(2)−N(3)−Ni(1) 121.6(7), 117.9(8)

3,[3d,9a] suggesting that weak π-bonding interactions between the amido nitrogens and the nickel center may be present in **1**. Apparently, ligand L^1 behaves as a weak π-acceptor in this case. The average Ni−N_{amido} distance in **2** [1.94(1) Å] is similar to those in **3** and **4**, but slightly shorter than that of 1.974(3) Å in *trans*-[Ni(Mes)-{N(Ph)C(O)$CHPh_2$}(PMe_3)$_2$] (**5**),[3d,9b] where an Ni−N π-interaction was suggested to be absent in the latter complex. Since the structures of ligands L^1 and L^2 are similar, we surmise that Ni−N π-bonding interaction may also be present in complex **2**.

The N_{amido}−Ni−$N_{pyridyl}$ bite angles in **1** and **2** are similar, falling within the range 79.6(7)° to 89.1(6)°. The interligand angles N_{amido}−Ni−N_{amido} of 158.1(4)° in **2** are much larger than the corresponding angles of 138.2(2)° and 138.9(2)° in **1**. This may be due to the presence of the sterically more demanding Si*t*BuMe_2 groups in **2**.

The ^{1}H NMR spectra of **1** and **2** show broad signals with significant isotropic shifts. The resonance signals have been assigned on the basis of their relative intensities and are summarized in Table 1. Both complexes show one set of resonance signals, indicating that each pair of amido ligands in each complex molecule are chemically equivalent. Complex **1** shows one signal due to the $SiMe_3$ groups, whereas two signals are observed for the $SiMe_2$ moiety of

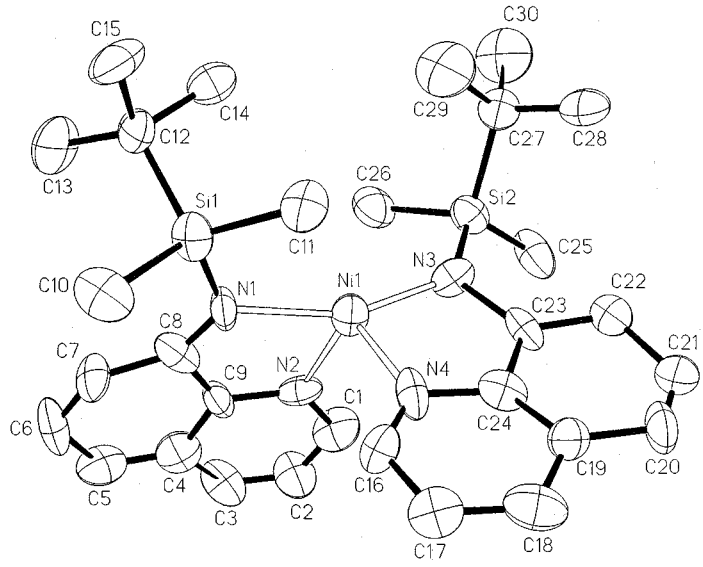


Figure 2. Moleçular structure of [Ni{N(Si*t*BuMe$_2$)(8-C$_9$H$_6$N)}$_2$] (**2**) (30% thermal ellipsoids) with the atomic labeling scheme; selected bond lengths [Å] and bond angles [°]: Ni(1)−N(1) 2.03(1), Ni(1)−N(2) 2.00(1), Ni(1)−N(3) 1.85(1), Ni(1)−N(4) 2.03(1), Si(1)−N(1) 1.76(1), Si(2)−N(3) 1.72(1), N(1)−C(8) 1.32(3), N(3)−C(23) 1.49(3); N(1)−Ni(1)−N(2) 79.6(7), N(3)−Ni(1)−N(4) 89.1(6), N(1)−Ni(1)−N(3) 158.1(4), C(8)−N(1)−Si(1) 131(1), C(8)−N(1)−Ni(1) 112(1), Si(1)−N(1)−Ni(1) 116.3(8), C(23)−N(3)−Si(2) 119(1), C(23)−N(3)−Ni(1) 111(1), Si(2)−N(3)−Ni(1) 128.7(9).

Table 1. ^{1}H NMR spectroscopic data of **1** and **2**

Compound	Aryl	*t*Bu	$SiMe_2$	$SiMe_3$
1	−52.8 (br, 1 H), −27.9 (br, 1 H), −18.0 (br, 1 H), 25.8 (br, 1 H), 74.9 (br, 1 H), 179.0 (br, 1 H)	−	−	19.8 (br, 6 H)
2	−46.3 (br, 1 H), −21.6 (br, 1 H), −14.6 (br, 1 H), 23.7 (br, 1 H), 74.1 (br, 1 H), 185.2 (br, 1 H)	6.7 (br, 9 H)	22.6 (br, 3 H), 35.2 (br, 3 H)	−

complex **2**. It is noteworthy that the two Me substituents on the Si*t*BuMe$_2$ group of ligand L^2 are prochiral. The two prochiral Me substituents on the Si*t*BuMe$_2$ groups in complex **2** are nonequivalent due to the presence of the chiral nickel center. A similar case has been observed for the *cis*-dioxo-Mo^{VI} and -W^{VI} amido compounds, [MoO$_2$(L^2)$_2$] and [WO$_2$(L^2)$_2$].[18] Mass spectra of both complexes show the presence of the respective parent ion [M]$^+$. This suggests that both complexes are monomeric in the gas phase, as they are in the solid state. The respective magnetic moments of 3.05 and 2.74 μ_B for **1** and **2**, as measured by the Evans NMR method,[19] are close to the spin-only value of 2.83 μ_B for two unpaired electrons but slightly lower than the expected values for tetrahedral nickel(II) species.[20] One plausible reason for these values may be the presence of a tetrahedral-to-square-planar-type equilibrium for both complexes in solution.[21]

In conclusion, the two homoleptic mononuclear nickel(II) amide complexes [Ni(L^n)$_2$] [L^n = L^1 (**1**), L^2 (**2**)] have been successfully synthesized and structurally characterized. To the best of our knowledge, they are the first example of *homoleptic* mononuclear nickel(II) diamides containing *N*-functionalized amido ligands to be reported. We are currently investigating the reactivities of these two complexes towards carbon−nitrogen bond formation by their reactions with unsaturated electrophilic compounds such as PhNCO and PhCN.

Experimental Section

Synthesis of [Ni(L^1)$_2$] (1): To a stirred suspension of anhydrous NiCl$_2$ (0.09 g, 0.66 mmol) in THF (20 mL) at 0 °C was slowly added a solution of [{Li(OEt$_2$)(L^1)}$_2$] (0.39 g, 0.66 mmol) in THF (20 mL). The resulting solution was stirred at room temperature for 12 h, whereupon a reddish brown solution with a white precipitate was obtained. All volatiles were removed in vacuo and the residue was extracted with hexane. The extract was filtered and concentrated to ca. 10 mL. Upon cooling of the solution to −30 °C, complex **1** was obtained as reddish brown crystals. They were washed with cold pentane and dried under vacuum. Yield: 0.23 g (71%), m.p. 192−194 °C (dec.). − MS (70 eV, EI): *m*/*z* (%) = 489 (93) [M]$^+$, 474 (91) [M − CH$_3$]$^+$, 459 (23) [M − 2CH$_3$]$^+$. − ^{1}H NMR (300 MHz, C$_6$D$_6$): δ = −52.8 (br, 2 H, qui), −27.9 (br, 2 H, qui), −18.0 (br, 2 H, qui), 19.8 (br, 18 H, SiMe$_3$), 25.8 (br, 2 H, qui), 74.9 (br, 2 H, qui), 179.0 (br, 2 H, qui). − Magnetic moment μ_{eff} = 3.05 BM. − C$_{24}$H$_{30}$N$_4$NiSi$_2$ (489.40): calcd. C 58.90, H 6.18, N 11.44; found C 58.63, H 6.06, N 11.65.

Synthesis of [Ni(L^2)$_2$] (2): This complex was prepared in 66% yield by an analogous procedure as described for **1**, starting from NiCl$_2$ and LiL^2. M.p. 218−219 °C (dec.). − MS (70 eV, EI): *m*/*z* (%) =

573 (34) $[M]^+$, 558 (4) $[M - CH_3]^+$, 516 (100) $[M - t\text{Bu}]^+$. – ^{1}H NMR (300 MHz, C_6D_6): δ = −46.3 (br, 2 H, qui), −21.6 (br, 2 H, qui), −14.6 (br, 2 H, qui), 6.7 (br, 18 H, Si*t*Bu), 22.6 (br, 6 H, $SiMe_2$), 23.7 (br, 2H qui), 35.2 (br, 6 H, $SiMe_2$), 74.1 (br, 2 H, qui), 185.2 (br, 2 H, qui). – Magnetic moment μ_{eff} = 2.74 BM. – $C_{30}H_{42}N_4NiSi_2$ (573.56): calcd. C 62.82; H,7.38, N 9.76; found C 61.22, H 7.17, N 9.39.

X-ray Crystallography:[22] The crystallographic data for complexes **1** and **2** are shown in Table 2. All crystals were grown from toluene solutions. Single crystals suitable for X-ray diffraction studies were sealed in capillaries under dinitrogen. X-Ray data were collected on a Rigaku RAXIS-IIC diffractometer at 294 K using graphite-monochromatized Mo-K_α radiation (λ = 0.71073 Å) by taking oscillation photos. The structures were solved by direct-phase determination using the computer program SHELX-97 on a PC 486 computer and refined by full-matrix least-squares with anisotropic thermal parameters for the non-hydrogen atoms. Hydrogen atoms were introduced in their idealized positions and included in structure-factor calculations with assigned isotropic temperature factors.

Table 2. Selected X-ray data collection and structure analysis parameters for **1** and **2**

	1	**2**
Molecular formula	$C_{24}H_{30}N_4NiSi_2$	$C_{30}H_{44}N_4NiSi_2$
Molecular weight	489.41	575.58
Crystal size/mm	0.5 × 0.4 × 0.4	0.38 × 0.20 × 0.18
Crystal system	Monoclinic	Monoclinic
Space group	*Cc*	*Cc*
a/Å	18.536(4)	18.928(4)
b/Å	15.225(3)	8.3706(17)
c/Å	18.433(4)	20.174(4)
β/°	91.35(3)	104.00(3)
Z	8	4
V/Å^3	5200.5(18)	3101.4(11)
Density/g cm^{-3}	1.250	1.233
μ/mm^{-1}	0.856	0.728
Reflections collected	4726	3243
Unique data measured	4726	2095
Observed data with $I \leq 2\sigma(I)$	2642	1732
No. of variables	560	335
Final *R* indices $[I \leq 2\sigma(I)]$[a]	*R*1 = 0.0410, *w*R2 = 0.0961	*R*1 = 0.0666, *w*R2 = 0.1751
R indices (all data)[a]	*R*1 = 0.1179, *w*R2 = 0.1223	*R*1 = 0.0777, *w*R2 = 0.1896

[a] $R1 = \Sigma||F_o| - |F_c||/\Sigma|F_o|$; $wR2 = \{\Sigma[w(F_o^2 - F_c^2)^2]/\Sigma[w(F_o^2)^2]\}^{1/2}$.

Acknowledgments

This research work was supported by a Direct Grant (A/C 2060157) of The Chinese University of Hong Kong.

[1] D. M. Roundhill, *Chem. Rev.* **1992**, *92*, 1−27.
[2] R. H. Holm, P. Kennepohl, E. I. Solomon, *Chem. Rev.* **1996**, *96*, 2239−2314.
[3] [3a] A. L. Casalnuovo, J. C. Calabrese, D. Milstein, *J. Am. Chem. Soc.* **1988**, *110*, 6738−6744. – [3b] R. A. Widenhoefer, S. L. Buchwald, *Organometallics* **1996**, *15*, 2755−2763. – [3c] J. P. Wolfe, S. L. Buchwald, *J. Am. Chem. Soc.* **1997**, *119*, 6054−6058. – [3d] D. D. VanderLende, K. A. Abboud, J. M. Boncella, *Inorg. Chem.* **1995**, *34*, 5319−5326. – [3e] M. S. Driver, J. F. Hartwig, *J. Am. Chem. Soc.* **1996**, *118*, 7217−7218. – [3f] R. Dorta, P. Egli, F. Zürcher, A. Togni, *J. Am. Chem. Soc.* **1997**, *119*, 10857−10858.
[4] M. F. Lappert, P. P. Power, A. R. Sanger, R. C. Srivastava, *Metal and Metalloid Amides*, Ellis Horwood, Chichester, **1980**, and references cited therein.
[5] [5a] H. E. Bryndza, W. Tam, *Chem. Rev.* **1988**, *88*, 1163−1188. – [5b] M. D. Fryzuk, C. D. Montgomery, *Coord. Chem. Rev.* **1989**, *95*, 1−40.
[6] J. M. Mayer, *Comments Inorg. Chem*. **1988**, *8*, 125−135.
[7] D. C. Bradley, M. B. Hursthouse, R. J. Smallwood, A. J. Welch, *J. Chem. Soc., Chem. Commun*. **1972**, 872−873.
[8] M. D. Fryzuk, P. A. MacNeil, S. J. Rettig, A. S. Secco, J. Trotter, *Organometallics* **1982**, *1*, 918−930.
[9] [9a] D. D. VanderLende, J. M. Boncella, K. A. Abboud, *Acta Crystallogr., Sect. C* **1995**, *C51*, 591−593. – [9b] J. Penney, D. D. VanderLende, J. M. Boncella, K. A. Abboud, *Acta Crystallogr., Sect. C* **1995**, *C51*, 2269−2271.
[10] [10a] D. Barr, W. Clegg, R. E. Mulvey, R. Snaith, *J. Chem. Soc., Chem. Commun*. **1984**, 700−701. – [10b] D. Barr, W. Clegg, R. E. Mulvey, R. Snaith, *J. Chem. Soc., Chem. Commun*. **1984**, 469−470.
[11] [11a] M. Polamo, M. Leskelä, *J. Chem. Soc., Dalton Trans.* **1996**, 4345−4349. – [11b] M. Polamo, M. Leskelä, *Acta Chem. Scand.* **1997**, *51*, 449−454.
[12] [12a] L. M. Engelhardt, G. E. Jacobsen, P. C. Junk, C. L. Raston, B. W. Skelton, A. H. White, *J. Chem. Soc., Dalton Trans.* **1988**, 1011−1020. – [12b] L. M. Engelhardt, G. E. Jacobsen, P. C. Junk, C. L. Raston, A. H. White, *J. Chem. Soc., Chem. Commun*. **1990**, 89−91. – [12c] L. M. Engelhardt, G. E. Jacobsen, W. C. Patalinghug, B. W. Skelton, C. L. Raston, A. H. White, *J. Chem. Soc., Dalton Trans.* **1991**, 2859−2868. – [12d] L. M. Engelhardt, M. G. Gardiner, C. Jones, P. C. Junk, C. L. Raston, A. H. White, *J. Chem. Soc., Dalton Trans.* **1996**, 3053−3057. – [12e] C. L. Raston, B. W. Skelton, V.-A. Tolhurst, A. H. White, *Polyhedron* **1998**, *17*, 935−942.
[13] [13a] A. Spannenberg, P. Arndt, R. Kempe, *Angew. Chem. Int. Ed.* **1998**, *37*, 832−835. – [13b] A. Spannenberg, H. Fuhrmann, P. Arndt, W. Baumann, R. Kempe, *Angew. Chem. Int. Ed.* **1998**, *37*, 3363−3365, and references cited therein.
[14] L. M. Engelhardt, P. C. Junk, W. C. Patalinghug, R. E. Sue, C. L. Raston, B. W. Skelton, A. H. White, *J. Chem. Soc., Chem. Commun*. **1991**, 930−932.
[15] [15a] H. K. Lee, Y. Peng, Y.-L. Wong, Z.-Y. Zhou, T. C. W. Mak, unpublished results. – [15b] Y. Peng, *M. Phil. Thesis*, The Chinese University of Hong Kong, **1999**.
[16] Reproducible elemental analysis data for complex **2** could not be obtained due to the high sensitivity of the complex towards air and moisture.
[17] [17a] T. J. Hurley, M. A. Robinson, *Inorg. Chem*. **1968**, *7*, 33−38. – [17b] R. Clérac, F. A. Cotton, K. R. Dunbar, C. A. Murillo, I. Pascual, X. Wang, *Inorg. Chem*. **1999**, *38*, 2655−2657.
[18] H. K. Lee, Y.-L. Wong, Z.-Y. Zhou, Z.-Y. Zhang, Dennis K. P. Ng, Thomas, C. W. Mak, *J. Chem. Soc., Dalton Trans.* **2000**, 539−544.
[19] D. F. Evans, *J. Chem. Soc*. **1959**, 2003−2005.
[20] L. Sacconi, F. Mani, A. Bencini in: *Comprehensive Coordination Chemistry*, (Eds.: G. Wilkinson), Pergamon Press, Oxford, **1987**, *Vol. 5*, p. 45−68.
[21] R. H. Holm, in: *Dynamic Nuclear Magnetic Resonance Spectroscopy*, (Eds.: L. M. Jackman, F. A. Cotton), Academic Press, New York, **1975**, p.317−376.
[22] Crystallographic data (excluding structure factors) for the structures reported in this paper have been deposited with the Cambridge Crystallographic Data Centre as supplementary publication nos. CCDC-138623 (**1**) and CCDC-138624 (**2**). Copies of the data can be obtained free of charge on application to CCDC, 12 Union Road, Cambridge CB2 1EZ, UK [Fax: (internat.) + 44-1223/336-033; E-mail: deposit@ccdc.cam.ac.uk].

Received January 18, 2000
[I00017]

The Energy Profile of Proton Transfer from Brønsted Acids to Terminal Hydrides in Transition Metal Complexes Can Be Estimated by Combining in situ IR and NMR Spectroscopy

Natalia V. Belkova[a], Ekaterina V. Bakhmutova,[a,c] Elena S. Shubina,[a] Claudio Bianchini,*[b] Maurizio Peruzzini,*[b] Vladimir I. Bakhmutov,*[a,c] Lina M. Epstein*[a]

Keywords: Hydrides / Hydrogen bonding / Rhenium / IR spectroscopy / NMR spectroscopy

The enthalpy and entropy changes relative to the stepwise reaction of [(triphos)Re(CO)$_2$H] with perfluoro-*tert*-butyl alcohol in CH_2Cl_2 to give first the hydrogen-bonded adduct [(triphos)Re(CO)$_2$H···HOC(CF$_3$)$_3$] and then the stable non-classical dihydrogen complex [(triphos)Re(CO)$_2$(η^2-H$_2$)]$^+$ have been estimated by a combination of in situ IR and NMR experiments in the temperature range from 200 to 260 K [triphos = MeC(CH$_2$PPh$_2$)$_3$].

Introduction

The reactions of hydrido metal complexes with Brønsted acids yielding cationic nonclassical η^2-H$_2$ derivatives have been interpreted for a long time as proceeding straightforwardly by proton attack at terminal hydride ligands.[1] Experimental evidence for an alternative, stepwise, mechanistic picture has recently been provided, however. This involves the intermediacy of H-bonded species prior to H_2 ligand formation, as shown in Equation (1). In particular, the use of protic acids of different strength has allowed the interception and unambiguous characterisation of several H-bonded [MH]···HX species.[2,3]

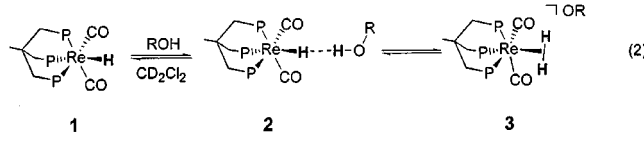
$$\text{M-H} \rightleftharpoons \text{M-H}\cdots\text{HO-R} \rightleftharpoons \text{M-(H}_2\text{)} \qquad (1)$$

The enthalpy values associated with the formation of the H-bonded adducts have been determined for some systems in nonpolar or low-polarity solvents.[2a–2c,3b,3c] In contrast, the thermodynamic parameters relative to the M−H···H−OR → M−(η^2-H$_2$) step have only been reported for the reaction of the dihydride *trans*-[RuH$_2$(dppm)$_2$] (dppm = diphenylphosphanylmethane) with phenol in toluene.[3a] Unexpectedly large enthalpy (17 kcal mol^{-1}) and entropy (75.8 e.u.) values were obtained.[3a]

[a] A. N. Nesmeyanov Institute of Organoelement Compounds, Vavilovstr. 28, V-334, Moscow, Russia, 117813
Fax (internat.) +7-095/135-5085
E-mail: epst@ineos.ac.ru
[b] ISSECC CNR,
Via Jacopo Nardi, 39, 50132 Firenze, Italy
Fax (internat.) +39-055/247-8366
E-mail: bianchin@fi.cnr.it, peruz@fi.cnr.it
[c] Chemistry Department, Centro de Investigacion y de Estudios Avanzados del I.P.N.,
A.P. 14−740, C. P. 07000, Mexico D. F., Mexico
E-mail: vladimir@mail.cinvestav.mx

Results and Discussion

In this communication, we show that the energy associated with each stage of the proton transfer process in Equation (1), as well as the overall energy involved, can be calculated using a combined IR and NMR approach. To this purpose, the interaction of the Re^{III} hydride [(triphos)Re(CO)$_2$H] (**1**) [triphos = MeC(CH$_2$PPh$_2$)$_3$][4] with perfluoro-*tert*-butyl alcohol (PFTB) was studied in dichloromethane. We chose **1** for the simple reason that some data relative to the equilibrium shown in Equation (2) were already available.[3b,3c]



(2)

It may be useful to recall here that the η^2-H$_2$ complex [(triphos)Re(CO)$_2$(η^2-H$_2$)]$^+$ (**3**) is completely stable from 200 to 260 K in CH_2Cl_2.[3c,4] In this temperature range, the occurrence of a dynamic equilibrium involving the three species shown in Equation 2 was unambiguously demonstrated; moreover, the enthalpy values relative to the formation of several H-bonded adducts of the formula [(triphos)Re(CO)$_2$H···HOR] were calculated from IR spectroscopy using the Iogansen equation $-\Delta H = 18\Delta\nu/(720 + \Delta\nu)$.[2a,3b] For ROH = PFTB, a medium strength H-bonded adduct **2** was obtained with an enthalpy value of 6.0 kcal mol^{-1}.[3c]

The overall energy gain involved in the proton transfer reaction **1** → **3** has now been calculated from the temperature dependence of the protonation constant K_{1-3} for the equilibrium illustrated in Equation 2 [c(**1**) = 5 × 10^{-3} M, c(PFTB) = 5 × 10^{-2} M]. The values of K_{1-3} = [**3**]/[**2**+**1**] were determined from significant intensity changes of the ν_{sym}(CO) band at 2005 cm^{-1} of **3**. Figure 1 shows that this

 © WILEY-VCH Verlag GmbH, D-69451 Weinheim, 2000 1434−1948/00/1010−2163 $ 17.50+.50/0

band is well separated from any other band in the region, while the ν(CO) bands of **2** (1930 and 1984 cm^{-1}) overlap with those of **1**, and the first band of **2** is partially masked by ν_{asym}(CO) of **3** at 1940 cm^{-1}. The values $-\Delta H°_{1-3}$ = 8.3 ± 0.4 kcal mol^{-1}, $-\Delta S°_{1-3}$ = 31.6 ± 1.8 e.u. were determined from a plot of $\ln K_{1-3}$ vs. $1/T$ (Table 1) in the temperature range from 200 to 260 K.

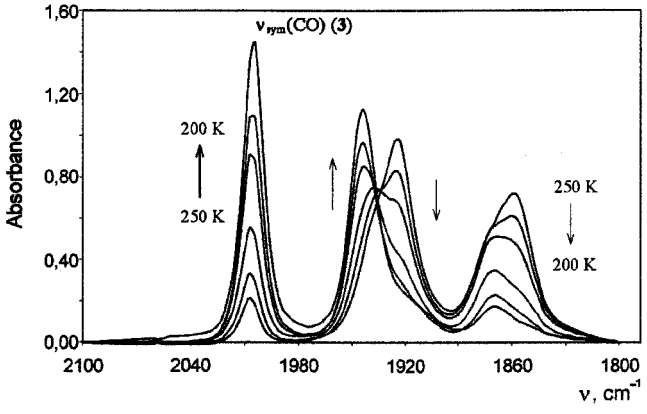


Figure 1. Variable-temperature IR spectra (ν_{CO} range) of complex **1** (0.005 M) in the presence of a 10-fold excess of PFTB in the temperature range between 250 and 200 K (interval 10 K)

Table 1. Values of formation constants K_{1-3} and K_{2-3} obtained from IR and NMR spectroscopic data, respectively

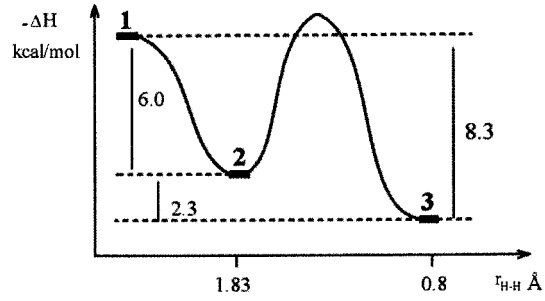
T, K	K_{1-3}	*T*, K	K_{2-3}
200	176.6	200	5.2
210	43.4	230	2.8
220	24.8	240	1.7
230	9.5	260	1.4
240	4.5		
250	2.5		

A ^{1}H NMR analysis in CD_2Cl_2 for the system **1**/PFTB has allowed us to calculate the energy associated with the formation of **3** from **2**. The equilibrium constants K_{2-3} for this reaction were determined at several temperatures in the 200−260 K range from the integral intensities of the hydride signals of **3** (−4.8 ppm) and **2** (−6.28 ppm). For a large excess of alcohol (e.g. 10 equivalents of PFTB), there is no free **1** at 200 K and therefore the equilibrium constant K_{2-3} between **2** and **3** can easily be calculated. The molar fractions of the H-bonded species **2** at higher temperatures were calculated from the observed average chemical shifts using a standard procedure.[3c] From this study, the enthalpy ($-\Delta H°_{2-3}$ = 2.3 kcal mol^{-1}) and entropy ($-\Delta S°_{2-3}$ = 8.4 e.u.) associated with the transformation of **2** into **3** were thus estimated.

As reported above, the enthalpy relative to the formation of **2**, determined independently by IR spectroscopy,[3c] is 6.0 kcal mol^{-1}. Adding this value to the value of 2.3 kcal mol^{-1}, obtained for the **2** → **3** conversion by NMR spectroscopy, gives a total $-\Delta H°$ of 8.3 kcal mol^{-1} for the **1** + PFTB → **3** reaction, which is identical to the enthalpy calculated by IR methods for the same process.

In conclusion, we have shown here that the energy profile of a proton-transfer reaction involving an H-bonded intermediate can reliably be evaluated by a combination of independent IR and NMR experiments.

Scheme 1 illustrates the energy profile for the transformation of **1** into **3** *via* **2**. The potential energy curve shows two minima: the first is due to the formation of the H-bonded species with r = 1.83 Å[3c] while the lower energy one is due to the thermodynamically favoured η^2-H_2 complex **3**, for which an H−H distance of 0.81 Å was previously reported assuming fast rotation of the H_2 ligand.[4]



Scheme 1. Energy profile for the transformation of **1** into **3** via **2**.

The energetic level of the transition state for the **2** → **3** conversion is shown only qualitatively in Scheme 1, while that for the formation of **2** is not even shown as the formation of H-bonded adducts is a diffusion-controlled process.[5] Indeed, the transformation of **2** into **3** is too slow on the NMR timescale (10^1−10^{-6} s) and separated hydride signals for the two compounds were observed with no broadening of the resonances over the range of temperature investigated. Accordingly, the reaction has a lifetime longer than 10 s, which in turn provides an upper limit of 10^{-1} s^{-1} for the rate constant. The lower limit of the rate constant may be estimated roughly considering that our IR technique does not allow one to monitor the band intensity changes for processes faster than 10^{-2} s^{-1} (it takes one minute for mixing the reagents and loading the sample into the cryostat). Since no intensity change with time was observed, it could be assumed that the lifetime of the proton transfer is shorter than 1−2 min, which provides a lower limit of 10^{-2} s^{-1} for the rate constant.[6] It may be thus concluded that the transformation of **2** into **3** presumably proceeds with a rate constant between 10^{-2} and 10^{-1} s^{-1} with an activation barrier $\Delta G^{‡}$(200 K) from 12 to 13 kcal mol^{-1}. This estimate falls within the ranges reported in the literature (10^{-4}−10^{-1} dm^3 mol^{-1} s^{-1}; 1−40 kcal mol^{-1}).[7,8]

Experimental Section

All manipulations were carried out under a dry argon atmosphere using standard Schlenk techniques. Dichloromethane was distilled from CaH_2 prior to use. All IR and NMR measurements were carried out as previously described.[3c] Complex **1** was prepared as reported in the literature.[4]

Acknowledgments

Thanks are due to NATO (contract *"^{2}H-Relaxation as a tool to study hydrogen transfer reactions"*, grant HTECH-CRG 972135), CNR/RAS agreement and RFBR (project No 99−03−33270) for financial support.

[1] P. G. Jessop, R. H. Morris, *Coord. Chem. Rev.* **1992**, *121*, 155.

[2] [2a] E. S. Shubina, N. V. Belkova, A. N. Krylov, E. V. Vorontsov, L. M. Epstein, D. G. Gusev, M. Niedermann, H. Berke, *J. Am. Chem. Soc.* **1996**, *118*, 1105. − [2b] N. V. Belkova, E. S. Shubina, A. V. Ionidis, L. M. Epstein, H. Jacobsen, A. Messmer, H. Berke, *Inorg. Chem.* **1997**, *36*, 1522. − [2c] E. S. Shubina, N. V. Belkova, A. V. Ionidis, N. S. Golubev, S. N. Smirnov, P. Schah-Mohammedi, L. M. Epstein, *Izv. Akad. Nauk., Ser. Khim*., **1997**, 1405 (*Russ. Chem. Bull.* **1997**, *44*, 1349). − [2d] J. Wessel, J. C. Lee, E. Peris, C. P. Yap, J. B. Fortin, J. C. Ricci, G. Sini, A. Albinati, T. F. Koetzle, O. Eisenstein, A. L. Rheingold, R. H.Crabtree, *Angew. Chem. Int. Ed. Engl.* **1995,** *34,* 2507. − [2e] E. Peris, J. Wessel, B. P. Pattel, R. H. Crabtree. *J. Chem. Soc., Chem. Commun.* **1995**, 2175. − [2f] B. P. Pattel, J. Wessel, W. Yao, J. C. Lee, E. Peris, T. F. Koetzle, C. P. Yap, J. B. Fortin, J. C. Ricci, G. Sini, A. Albinati, O. Eisenstein, A. L. Rheingold, R. H. Crabtree, *New J. Chem.* **1997**, *21*, 413.

[3] [3a] J. A. Ayllon, C. Gervaux, S. Sabo-Etienne, B. Chaudret, *Organometallics* **1997**, *16*, 2000. − [3b] L. M. Epstein, E. S. Shubina, *Ber. Bunsenges. Phys. Chem.* **1998**, *102*, 359. − [3c] E. S. Shubina, N. V. Belkova, E. V. Bakhmutova, E. V. Vorontsov, V. I. Bakhmutov, A. V. Ionidis, C. Bianchini, L. Marvelli, M. Peruzzini, L. M. Epstein, *Inorg. Chim. Acta* **1998**, *280*, 302. − [3d] S. Gruendemann, S. Ulrich, H.-H. Limbach, N. S. Golubev, G. S. Denisov, L. M. Epstein, S. Sabo-Etienne, B. Chaudret, *Inorg. Chem*. **1999**, *38*, 2550.

[4] C. Bianchini, A. Marchi, L. Marvelli, M. Peruzzini, A. Romerosa, R. Rossi, A. Vacca, *Organometallics* **1995**, *14*, 3203.

[5] S. Scheiner, *Hydrogen Bonding*, Oxford University Press, Oxford, UK, 1997.

[6] Unpublished results from the INEOS laboratory (Moscow, Russia) show that the proton transfer from PFTB to [CpRu(CO)(PCy_3)H], proceeding with a rate constant of 2×10^{-3} s^{-1}, can be studied by IR spectroscopy following the intensity changes of ν(CO) bands with time.

[7] [7a] G. Orlova, S. Scheiner, *J. Phys. Chem. A* **1998**, *102*, 4813. − [7b] G. Orlova, S. Scheiner, T.Kar, *J. Phys. Chem. A* **1999**, *103*, 514.

[8] [8a] M. G. Basallote, J. Duran, M. J. Fernandez-Trujillo, M. A. Manez, J. R. Torre, *J. Chem. Soc., Dalton Trans.* **1998**, 745. − [8b] M. G. Basallote, J. Duran, M.J. Fernandez-Trujillo, M. A. Manez, *J. Chem. Soc., Dalton Trans.* **1998**, 2205.

Received April 7, 2000
[I00136]

P−H-Functionalized Phosphanyl Alcohols: $RHPCH_2CHMeOH$ and 2-PHR-1-OH-cyclo-C_6H_{10} (R = Ph, 2,4,6-$Me_3C_6H_2$, 2,4,6-iPr$_3C_6H_2$) and Molecular Structures of (C_R,C_R,P_R/C_S,C_S,P_S)-2-PH(2,4,6-iPr$_3C_6H_2$)-1-OH-cyclo-C_6H_{10} and its Dilithio Salt $[Li_2(THF)_{0.5}\{(C_R,C_R/C_S,C_S)$-2-P(2,4,6-$iPr_3C_6H_2$)-1-O-cyclo-$C_6H_{10}\}]_4$

Thomas Koch,[a] Steffen Blaurock,[a] Fernando Somoza, Jr.,[a] Evamarie Hey-Hawkins*[a]

Keywords: P−H-Functionalized phosphanyl alcohols / Dilithium derivatives / Molecular structures

The P–H-functionalized phosphanyl alcohols $RHPCH_2CHMeOH$ [R = Ph (**1**), 2,4,6-$Me_3C_6H_2$ (Mes) (**2**), 2,4,6-iPr$_3C_6H_2$ (Tipp) (**3**)] and 2-PHR-1-OH-cyclo-C_6H_{10} [(R = Ph (**4**), Mes (**5**), Tipp (**6**)] have been prepared by ring-opening of propene oxide or cyclohexene oxide, respectively, with the appropriate LiPHR species, followed by hydrolytic workup and distillation (**1**–**4**) or recrystallization (**5**, **6**). **1**–**6**, which were obtained as diastereomeric mixtures, have been characterized spectroscopically (^{1}H, ^{13}C, ^{31}P NMR, IR, MS). Only in the case of **6** could separation of the diastereomers be achieved by fractional crystallization and the molecular structure of the racemic isomer (C_R,C_R,P_R/C_S,C_S,P_S) has been determined. In situ double deprotonation of **1**–**6** with BuLi gave the corresponding dianions **1a**–**6a**. The molecular structure of the dilithio salt $[Li_2(THF)_{0.5}\{(C_R,C_R/C_S,C_S)$-2-P(2,4,6-$iPr_3C_6H_2$)-1-O-cyclo-$C_6H_{10}\}]_4$ (**6a**) has been determined and shows that it is tetrameric in the solid state with a central Li_8 cluster.

Introduction

While tertiary phosphanyl alcohols are employed as ligands in catalytically active transition metal complexes,[1] the corresponding secondary P−H-functionalized phosphanyl alcohols have received only little attention. As early as 1965, Issleib et al. reported the ring-opening of oxiranes by alkali metal phosphanides, which, after hydrolytic workup, gave tertiary or secondary phosphanyl alcohols. The products were, however, only characterized by elemental analysis and IR spectroscopy.[2] In 1991, Heinicke et al. reported the formation of the primary phosphanyl alcohols $H_2PCH_2CHR'OH$ (R′ = H, Me, Ph) by ring-opening of ethene, propene, or styrene oxides with sodium phosphanide, $NaPH_2$.[3] In 1997, Thiel et al. used the stereoselective ring-opening of cyclohexene oxide by lithium diphenylphosphanide to prepare chiral phosphanyl alcohols.[4]

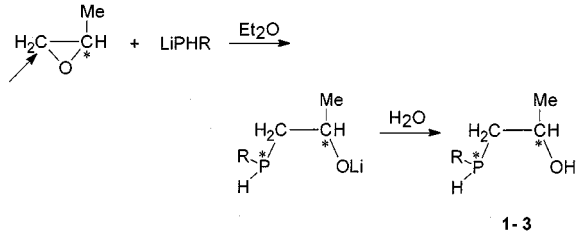
Primary[3,5] and secondary[6,7] phosphanyl alcohols have hitherto been used for the preparation of organic P heterocycles. Their ligation properties are, however, largely unstudied.

We now report the synthesis and spectroscopic characterization of the P−H-functionalized phosphanyl alcohols $RHPCH_2CHMeOH$ [R = Ph (**1**), 2,4,6-$Me_3C_6H_2$ (Mes) (**2**), 2,4,6-iPr$_3C_6H_2$ (Tipp) (**3**)] and 2-PHR-1-OH-cyclo-C_6H_{10} [(R = Ph (**4**), Mes (**5**), Tipp (**6**)], as well as the molecular structures of the diastereoisomerically pure phosphanyl alcohol (C_S,C_S,P_S/C_R,C_R,P_R)-2-PH(2,4,6-iPr$_3C_6H_2$)-1-OH-cyclo-C_6H_{10} (**6**) and its dilithio salt $[Li_2(THF)_{0.5}(C_S,C_S/C_R,C_R)$-2-P(2,4,6-$iPr_3C_6H_2$)-1-O-cyclo-$C_6H_{10}]_4$ (**6a**). Syntheses of **1**[2,7] and **4**[2] have been reported previously, but both compounds were only characterized by elemental analysis and IR spectroscopy.[2] Although a ^{1}H NMR spectrum has been reported for **1**, no diastereomers were observed.[7]

Results and Discussion

Synthesis of $RHPCH_2CHMeOH$ [R = Ph (1), 2,4,6-$Me_3C_6H_2$ (Mes) (2), 2,4,6-iPr$_3C_6H_2$ (Tipp) (3)] and 2-PHR-1-OH-cyclo-C_6H_{10} [(R = Ph (4), Mes (5), Tipp (6)] and their Dilithio Salts

The P−H-functionalized phosphanyl alcohols $RHPCH_2CHMeOH$ [R = Ph (**1**),[2,7] Mes (**2**), Tipp (**3**)] were obtained by ring-opening of propene oxide with LiPHR, followed by hydrolytic workup and distillation [Equation (1)].



(1)

[a] Institut für Anorganische Chemie der Universität Leipzig, Johannisallee 29, D-04103 Leipzig, Germany
E-mail: hey@server1.rz.uni-leipzig.de

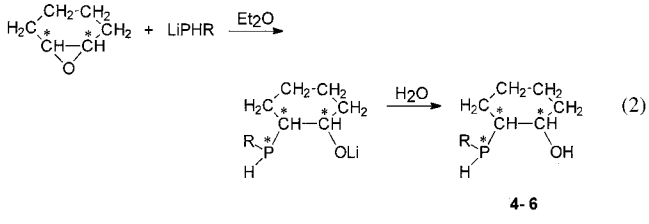
 © WILEY-VCH Verlag GmbH, D-69451 Weinheim, 2000 1434−1948/00/1010−2167 $ 17.50+.50/0

As in base-catalyzed ring-opening reactions, one C−O bond of the oxirane ring is selectively cleaved by the nucleophilic phosphanide anion, which attacks the sterically less hindered C atom.

As **1**−**3** have two chiral centres, two pairs of diastereomers are formed [*meso* (C_S,P_R/C_R,P_S) and *rac* (C_S,P_S/C_R,P_R)], which are obtained in a 1:1 ratio. Subsequent distillation furnished **1**−**3** as colourless, viscous oils. **3** was found to solidify at room temperature (m.p. 35 °C). The diastereomers could not be separated either by distillation or by fractional crystallization.

In their proton-coupled ^{31}P NMR spectra, **1**−**3** give rise to two doublets due to the two diastereomers. The spectrum of the Ph derivative **1** features a signal at low field compared to those of **2** and **3** [**1**: δ = −63.4 ($^1J_{P-H}$ = 210.6 Hz), −64.1 ($^1J_{P-H}$ = 210.6 Hz); **2**: δ = −97.7 (d, $^1J_{P-H}$ = 217.0 Hz), −98.9 (d, $^1J_{P-H}$ = 218.7 Hz); **3**: δ = −105.2 ($^1J_{P-H}$ = 215.5 Hz), −105.9 ($^1J_{P-H}$ = 217.1 Hz)].

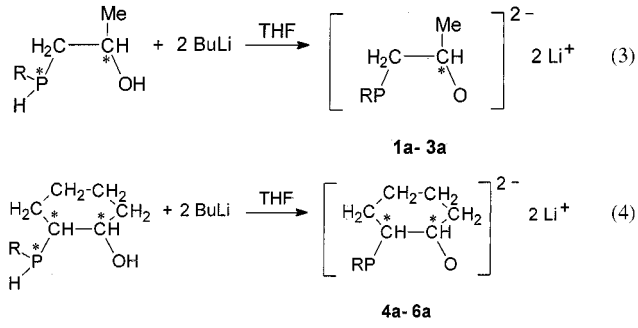
Analogously to **1**−**3**, the phosphanyl alcohols 2-PHR-1-OH-cyclo-C_6H_{10} [(R = Ph (**4**),[2] Mes (**5**), Tipp (**6**)], which contain three chiral centres (C, C, P), could be prepared by selective ring opening of cyclohexene oxide with LiPHR, followed by hydrolytic workup [Equation (2)]. **4** was obtained as a colourless oil, whereas **5** and **6** were recovered as colourless solids. The diastereoselective ring-opening of the oxirane by the nucleophilic phosphanide anion yielded only two pairs of diastereomers (ratio 2:3 for **4** and **6**, 1:1 for **5**), which could not be separated by distillation. However, in the case of **6**, it was found that the diastereomers could be separated by fractional crystallization.



4-6 (2)

Compounds **4**−**6** give rise to two doublets in their proton-coupled ^{31}P NMR spectra due to the two pairs of diastereomers with C_S,C_S,P_R/C_R,C_R,P_S and C_S,C_S,P_S/C_R,C_R,P_R configurations. The signals of **5** (δ = −105.3 and −106.0) are shifted to high field relative to those of **4** (δ = −40.9 and −45.5) and **6** (δ = −77.6 and −89.9).

The bifunctionalized phosphanyl alcohols **1**−**6** could be doubly deprotonated with BuLi in THF to give the dianions Li_2[RPCH$_2$CHMeO] [R = Ph (**1a**), Mes (**2a**), Tipp (**3a**)] [Equation (3)] and Li_2[2-RP-1-O-cyclo-C_6H_{10}] [R = Ph (**4a**), Mes (**5a**), Tipp (**6a**)] [Equation (4)], which were characterized by ^{31}P NMR spectroscopy. The spectra of the dianions **2a**, **4a**, **5a**, and **6a** in THF feature two broad signals, indicating dynamic processes involving ligand exchange in solution. In the case of **6a**, this was further verified by a crystal structure determination.



(3)

(4)

Molecular Structures of (C_R,C_R,P_R/C_S,C_S,P_S)- 2-PH(2,4,6-*i*Pr$_3$C$_6$H$_2$)-1-OH-cyclo-C_6H_{10} (6) and Its Dilithio Salt [Li_2(THF)$_{0.5}${(C_R,C_R/C_S,C_S)-2-P(2,4,6-*i*Pr$_3$C$_6$H$_2$)-1-O-cyclo-C_6H_{10}}]$_4$ (6a)

Colourless crystals of **6** were obtained by repeated recrystallization from pentane. **6** crystallizes in the centrosymmetric monoclinic space group $P2_1/c$. Only the diastereomer with C_R,C_R,P_R/C_S,C_S,P_S configuration (OH and PHR in equatorial positions) was found to be present in the unit cell (Figure 1). A section of the three-dimensional structure shows that molecules of one enantiomer are stacked along the *b*-axis. Two such stacks are related by a 2_1 axis, and the molecules of these two stacks of the two enantiomers are connected through hydrogen (OH) bonds (Figure 2) resulting in a helical arrangement. The inversion centre generates the other enantiomer.

The excellent ligation properties of the 2-P(2,4,6-*i*Pr$_3$C$_6$H$_2$)-1-O-cyclo-C_6H_{10} dianion are exemplified by the solid-state structure of **6a**. This salt could be obtained from pentane in the form of small, pale-yellow, very air-sensitive crystals of rather poor quality (monoclinic centrosymmetric space group $P2_1/c$). In the solid state, the compound forms tetrameric molecules composed of eight lithium atoms and four phosphanidoalkoxides. Two independent molecules are present in the asymmetric unit. In both of these, the eight lithium atoms form a polyhedron in which two trigonal

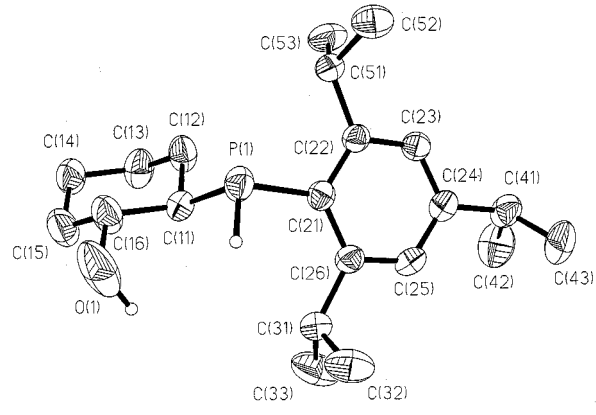


Figure 1. Molecular structure of **6**; only one enantiomer (C_R,C_R,P_R configuration) is shown; selected bond lengths [Å] and angles [°]: P(1)−C(21) 1.845(2), P(1)−C(11) 1.869(2), O(1)−C(16) 1.429(3), O(1)−HO(1) 1.19(4), P(1)−H(1) 1.27(2); C(21)−P(1)−C(11) 102.70(9), C(12)−C(11)−P(1) 110.9(2), C(16)−C(11)−P(1) 110.0(2), C(22)−C(21)−P(1) 118.3(1), C(26)−C(21)−P(1) 122.8(1), O(1)−C(16)−C(15) 111.0(2), O(1)−C(16)−C(11) 111.5(2)

prisms share one square face and are twisted by 90° (Figure 3). The Li−Li distances range from 2.47(2) to 2.83(2) Å. This polyhedron has four triangular faces and four square faces. The four phosphorus atoms of the phosphanidoalkoxide cover the triangular faces, while the four oxygen atoms of the ligand are located above the square faces in such a way that the oxygen and phosphorus atoms belonging to one phosphanidoalkoxide ligand are located on adjacent faces of the Li_8 polyhedron [P(1) and O(1), P(2) and O(2), P(3) and O(3), and P(4) and O(4) are located next to each other (Figure 4 and Figure 5); Li−O 1.962(16)−2.096(14) Å, Li−P 2.490(15)−2.699(16) Å for both molecules]. Thus, the four oxygen atoms and the four phosphorus atoms form distorted tetrahedra. In addition, four THF molecules are coordinated to four of the eight Li

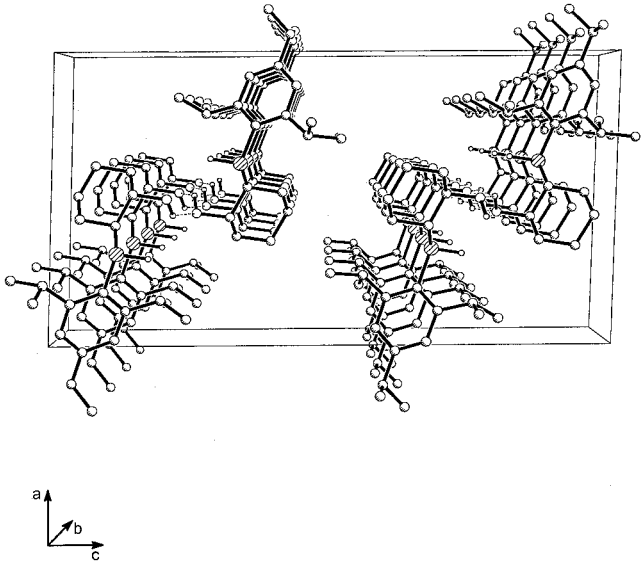


Figure 2. Molecular structure of **6**; section of the three-dimensional arrangement

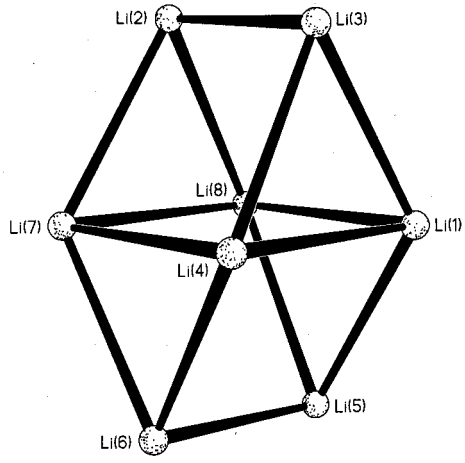


Figure 3. Central Li_8 cluster in **6a** (only one of the two independent molecules is shown); Li(1)−Li(5) 2.66(2), Li(1)−Li(3) 2.67(2), Li(1)−Li(8) 2.79(2), Li(1)−Li(4) 2.80(2), Li(2)−Li(3) 2.47(2), Li(2)−Li(8) 2.67(2), Li(2)−Li(7) 2.72(2), Li(3)−Li(4) 2.654(19), Li(4)−Li(6) 2.66(2), Li(4)−Li(7) 2.83(2), Li(5)−Li(6) 2.47(2), Li(5)−Li(8) 2.67(2), Li(6)−Li(7) 2.63(2), Li(7)−Li(8) 2.80(2)

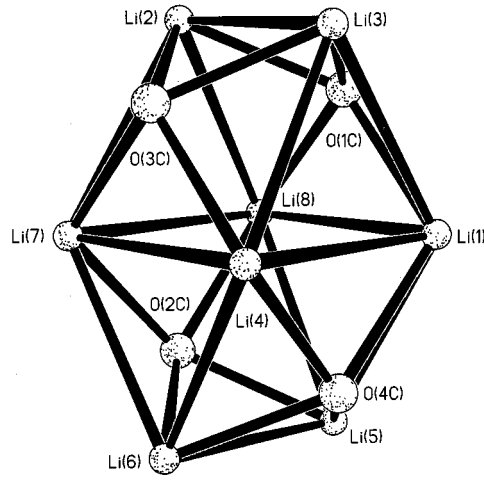


Figure 4. Central Li_8O_4 cluster in **6a** (only one of the two independent molecules is shown); O(1C)−Li(3) 1.980(15), O(1C)−Li(2) 1.997(16), O(1C)−Li(1) 2.037(15), O(1C)−Li(8) 2.085(16), O(2C)−Li(5) 1.962(16), O(2C)−Li(8) 1.986(15), O(2C)−Li(6) 1.997(17), O(2C)−Li(7) 2.072(15), O(3C)−Li(3) 1.998(15), O(3C)−Li(2) 2.008(15), O(3C)−Li(7) 2.020(16), O(3C)−Li(4) 2.083(15), O(4C)−Li(6) 1.965(16), O(4C)−Li(5) 2.011(17), O(4C)−Li(4) 2.012(15), O(4C)−Li(1) 2.096(14)

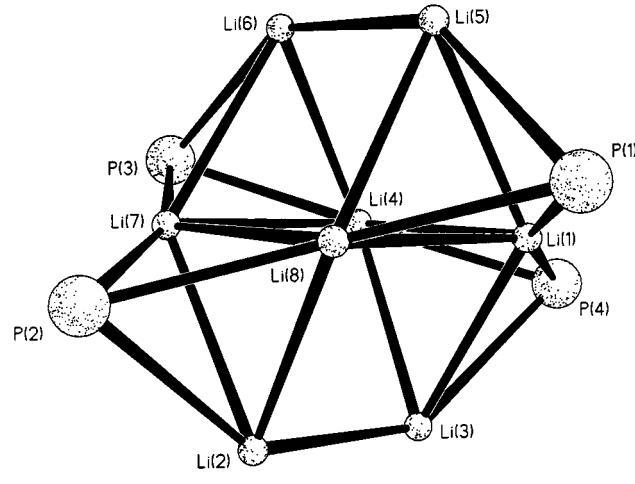


Figure 5. Central Li_8P_4 cluster in **6a** (only one of the two independent molecules is shown); P(1)−Li(8) 2.514(13), P(1)−Li(1) 2.563(15), P(1)−Li(5) 2.685(15), P(2)−Li(7) 2.523(15), P(2)−Li(8) 2.558(13), P(2)−Li(2) 2.699(16), P(3)−Li(4) 2.524(14), P(3)−Li(7) 2.589(15), P(3)−Li(6) 2.686(15), P(4)−Li(1) 2.490(15), P(4)−Li(4) 2.549(14), P(4)−Li(3) 2.680(14)

atoms, Li(2), Li(3), Li(5), and Li(6). A view of the whole molecule is given in Figure 6. The molecule has C_2 symmetry [the noncrystallographic C_2 axis bisects Li(2)−Li(3) and Li(5)−Li(6)], and the four phosphanidoalkoxide ligands have alternatingly *R*/*R*, *S*/*S*, *R*/*R*, and *S*/*S* configuration at the chiral C atoms. Thus, the formation of this cluster can be regarded as a self-assembly of chiral molecules.

Although Li_8 clusters are known,[9] the topology of the Li_8 core in **6a** is very unusual. While lithium clusters have been observed in electron-deficient alkyl or aryllithium compounds,[10] polyhedral arrangements of lithium phosphanides have been observed only recently. In 1995, Drieß et al. reported the formation of clusters of the di- and trimetallated compounds $R^1R^2Si(PR^3Li)_2$ (R^1 = *t*Bu, R^2 = Tipp,

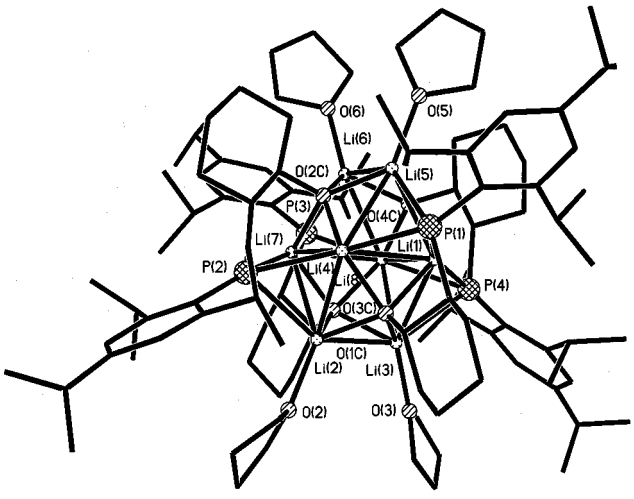


Figure 6. Molecular structure of $[Li_2(THF)_{0.5}\{(C_R,C_R/C_S,C_S)$-2-P(2,4,6-*i*Pr$_3C_6H_2$)-1-O-cyclo-C$_6H_{10}\}]_4$ (**6a**) (only one of the two independent molecules is shown)

R^3 = $SiPh_3$) and $EtSi(PR^3Li)_3$ (R^3 = Si*i*Pr$_3$).[11] In the former, two dimeric molecules $[R^1R^2Si(PR^3Li)_2]_2$ are connected through an Li_2Cl_2 square. In the latter, a dimer of $EtSi(PR^3Li)_3$ is observed, in which the $Li_6P_6Si_2$ fragment forms a distorted rhombododecahedron. The Li−P distances range from 2.55(3) to 2.67(3) Å in the dimetallated compound and from 2.449(5) to 2.562(5) Å in the trimetallated compound and are thus comparable with those in **6a**.

We have already shown that the phosphanylalkoxides reported here can be employed as ligands in mono- and dinuclear complexes.[12] Further studies of the ligation properties of **1**−**6** and their dianions **1a**−**6a** in transition metal complexes are currently in progress.

Experimental Section

General Remarks: All experiments were carried out under purified dry argon. Solvents were dried and freshly distilled under argon. The NMR spectra were recorded with a Bruker AVANCE DRX 400 spectrometer. ^{1}H NMR: internal standard solvent, external standard TMS; ^{13}C NMR (100.6 MHz): internal standard solvent, external standard TMS; ^{31}P NMR (162 MHz): external standard 85% H_3PO_4; ^{7}Li NMR (155.5 MHz): external standard 1 M LiCl in D_2O. The ^{13}C NMR spectra were assigned with the aid of 2D $^{13}C\{^1H\}$ NMR spectra and $^{13}C\{^{31}P,^1H\}$ NMR spectra. − IR spectra were recorded on a Perkin−Elmer System 2000 FT-IR spectrometer in the range 350−4000 cm^{-1}. − Melting points were determined in sealed capillaries under argon and are uncorrected. − Propene oxide and cyclohexene oxide are commercially available. RPH_2 (R = Ph,[13] Mes,[14] Tipp[14]) were prepared according to literature procedures.

General Procedure for the Synthesis of the Phosphanyl Alcohols 1−6: The primary phosphane RPH_2 was dissolved in Et_2O (200 mL) and an equimolar amount of a BuLi solution in hexane was added at −50 °C. The mixture was allowed to warm to room temp. and stirred for a further 2 h. The pale-yellow solution was then cooled to −50 °C once more, whereupon an equimolar amount of propene oxide or cyclohexene oxide was slowly added. The resulting mixture was allowed to warm to room temp. once more, stirred for 2 h, and then hydrolyzed with 50 mL of a 4 M NH_4Cl solution. After stirring for 12 h, the ethereal phase was separated, the aqueous phase was washed with Et_2O (3 × 20 mL), and the combined ethereal phases were dried over Na_2SO_4. The solution was filtered and the solvent was removed in vacuo. The resulting oil was distilled under reduced pressure.

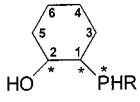
1-(Phenylphosphanyl)-2-propanol (1): Prepared from $PhPH_2$ (12.7 g, 115 mmol), 1.5 M BuLi solution in hexane (80 mL, 120 mmol), and propene oxide (6.8 mL, 140 mmol). Yield: 9.8 g (51%); colourless oil (b.p. 91 °C, 1 × 10^{-1} Torr). − ^{1}H NMR (C_6D_6): δ = 7.40 (m, 4 H, 2 isomers, Ph), 7.07 (m, 6 H, 2 isomers, Ph), 4.24 (d of t, $^1J_{P-H}$ = 210.5 Hz, $^3J_{H-H}$ = 1.7 Hz, 1 H, 1 isomer, PH), 4.18 (d of t, $^1J_{P-H}$ = 210.5 Hz, $^3J_{H-H}$ = 1.7 Hz, 1 H, 1 isomer, PH), 3.75 (sext., $^3J_{H-H}$ = 6.5 Hz, 1 H, 1 isomer, C*H*Me), 3.69 (sext., $^3J_{H-H}$ = 6.4 Hz, 1 H, 1 isomer, C*H*Me), 2.22 (br. s, 2 H, 2 isomers, OH), 2.1−1.73 (m, 4 H, 2 isomers, P−CH_2), 1.25−1.12 (m, 6 H, 2 isomers, CH_3). − $^{13}C\{^1H\}$ NMR (C_6D_6): δ = 136.7 (d, $^3J_{P-C}$ = 10.5 Hz, 4 C, 2 isomers, *m*-CH of Ph), 134.6 (d, $^2J_{P-C}$ = 15.9 Hz, 4 C, 2 isomers, *o*-CH of Ph), 130.9 (2 C, 2 isomers, *p*-CH of Ph), 67.4 (d, $^2J_{P-C}$ = 9.5 Hz, 1 C, 1 isomer, O−CH), 66.9 (d, $^2J_{P-C}$ = 10.1 Hz, 1 C, 1 isomer, O−CH), 35.0 (d, $^1J_{P-C}$ = 25.5 Hz, 1 C, 1 isomer, P−CH_2), 34.8 (d, $^1J_{P-C}$ = 27.5 Hz, 1 C, 1 isomer, P−CH_2), 25.3 (d, $^3J_{P-C}$ = 9.8 Hz, 1 C, 1 isomer, CH_3), 25.2 (d, $^3J_{P-C}$ = 10.6 Hz, 1 C, 1 isomer, CH_3); *ipso*-C of Ph not observed. − ^{31}P NMR (C_6D_6): δ = −63.4 (d, $^1J_{P-H}$ = 210.6 Hz), −64.1 (d, $^1J_{P-H}$ = 210.6 Hz). − $C_9H_{13}OP$ (168.17): calcd. C 64.3, H 7.8, P 18.4; found C 64.0, H 8.1, P 18.0.

1-Mesitylphosphanyl-2-propanol (2): Prepared from $MesPH_2$ (8.0 g, 53.0 mmol), 1.5 M BuLi solution in hexane (35 mL, 53.0 mmol), and propene oxide (3.7 mL, 53.0 mmol). Yield: 6.2 g (56%); colourless oil (b.p. 100−115 °C, 8 × 10^{-3} Torr). − ^{1}H NMR (C_6D_6): δ = 6.75 (s, 4 H, 2 isomers, *m*-CH of Mes), 4.39 (d of t, $^1J_{P-H}$ = 218.5 Hz, $^3J_{H-H}$ = 7.3 Hz, 1 H, 1 isomer, PH), 4.33 (d of t, $^1J_{P-H}$ = 218.0 Hz, $^3J_{H-H}$ = 7.5 Hz, 1 H, 1 isomer, PH), 3.76 (sext., $^3J_{H-H}$ = 6.2 Hz, 1 H, 1 isomer, C*H*Me), 3.69 (sext., $^3J_{H-H}$ = 6.3 Hz, 1 H, 1 isomer, C*H*Me), 2.51 (br. s, 2 H, 2 isomers, OH), 2.43 (s, 12 H, 2 isomers, *o*-CH_3), 2.10 (s, 6 H, 2 isomers, *p*-CH_3), 2.05−1.85 (m, 2 H, 1 isomer, P−CH_2), 1.65−1.50 (m, 2 H, 1 isomer, P−CH_2), 1.11 (d, $^3J_{H-H}$ = 6.2 Hz, 3 H, 1 isomer, CH_3), 1.09 (d, $^3J_{H-H}$ = 6.1 Hz, 3 H, 1 isomer, CH_3). − $^{13}C\{^1H\}$ NMR (C_6D_6): δ = 142.7 (d, $^2J_{P-C}$ = 12.0 Hz, 2 C, 1 isomer, *o*-C of Mes), 142.7 (d, $^2J_{P-C}$ = 12.0 Hz, 2 C, 1 isomer, *o*-C of Mes), 138.6 (d, $^4J_{P-C}$ = 11.0 Hz, 2 C, 2 isomers, *p*-C of Mes), 131.0 (d, $^1J_{P-C}$ = 14.2 Hz, 1 C, 1 isomer, *ipso*-C of Mes), 131.0 (d, $^1J_{P-C}$ = 14.2 Hz, 1 C, 1 isomer, *ipso*-C of Mes), 130.0 (4 C, 2 isomers, *m*-C of Mes), 68.2 (d, $^2J_{P-C}$ = 9.6 Hz, 1 C, 1 isomer, O−CH), 67.6 (d, $^2J_{P-C}$ = 10.7 Hz, 1 C, 1 isomer, O−CH), 32.9 (d, $^1J_{P-C}$ = 14.4 Hz, 1 C, 1 isomer, P−CH_2), 32.9 (d, $^1J_{P-C}$ = 14.9 Hz, 1 C, 1 isomer, P−CH_2), 25.3 (1 C, 1 isomer, CH_3), 25.2 (1 C, 1 isomer, CH_3), 23.9 (2 C, 1 isomer, *o*-CH_3 of Mes), 23.8 (2 C, 1 isomer, *o*-CH_3 of Mes), 21.7 (2 C, 2 isomers, *p*-CH_3 of Mes). − ^{31}P NMR (C_6D_6): δ = −97.7 (d, $^1J_{P-H}$ = 217.0 Hz), −98.9 (d, $^1J_{P-H}$ = 218.7 Hz). − EI MS: *m*/*z* (%) = 210 (78) [M^+], 150 (100) [$PHMes^+$], 119 (88) [Mes^+], and fragmentation products thereof. − IR (KBr): $\tilde{\nu}$ = 3356 cm^{-1} [br, s, ν(OH)], 2335 [s, ν(PH)]. − $C_{12}H_{19}OP$ (210.25): calcd. C 68.6, H 9.1, P 14.7; found C 68.1, H 9.3, P 13.9.

1-(Triisopropylphenylphosphanyl)-2-propanol (3): Prepared from $TippPH_2$ (9.0 g, 38.6 mmol), 1.5 M BuLi solution in hexane (26 mL, 39.0 mmol), and propene oxide (3 mL, 43.0 mmol). Yield: 7.0 g (62%); colourless oil (b.p. 110−140 °C, 2 × 10^{-2} Torr), which was found to solidify at room temp. (m.p. 35 °C). − ^{1}H NMR (C_6D_6): δ = 7.16 (s, 4 H, 2 isomers, *m*-H of Tipp), 4.50 (d of t, $^1J_{P-H}$ =

216.1 Hz, $^3J_{H-H}$ = 7.3 Hz, 2 H, 2 isomers, PH), 3.84 (sept., $^3J_{H-H}$ = 7.0 Hz, 4 H, 2 isomers, *o*-C*H*Me$_2$ of Tipp), 3.74 (m, $^3J_{H-H}$ = 5.8 Hz, 2 H, 2 isomers, C*H*Me), 2.78 (sept., $^3J_{H-H}$ = 7.0 Hz, 2 H, 2 isomers, *p*-C*H*Me$_2$ of Tipp), 2.03 and 1.65 (m, 4 H, 2 isomers, P−CH$_2$), 1.34 [d, $^3J_{H-H}$ = 6.7 Hz, 12 H, 2 isomers, *o*-CH(CH_3)$_2$ of Tipp], 1.26 [d, $^3J_{H-H}$ = 6.8 Hz, 12 H, 2 isomers, *p*-CH(CH_3)$_2$ of Tipp], 1.20 [d, $^3J_{H-H}$ = 6.7 Hz, 12 H, 2 isomers, *o*-CH(CH_3)$_2$ of Tipp], 1.07 (d, $^3J_{H-H}$ = 6.1 Hz, 6 H, 2 isomers, CHCH_3); OH not observed. − ^{13}C{H} NMR (C_6D_6): δ = 154.0 (d, $^2J_{P-C}$ = 10.4 Hz, 4 C, 2 isomers, *o*-C of Tipp), 150.6 (d, $^4J_{P-C}$ = 10.1 Hz, 2 C, 2 isomers, *p*-C of Tipp), 122.4 (s, 4 C, 2 isomers, *m*-C of Tipp), 67.9 (d, $^2J_{P-C}$ = 12.1 Hz, 1 C, 1 isomer, O−CH), 67.6 (d, $^2J_{P-C}$ = 12.9 Hz, 1 C, 1 isomer, O−CH), 35.6 (d, $^1J_{P-C}$ = 13.7 Hz, 1 C, P−CH$_2$), 35.6 (d, $^1J_{P-C}$ = 13.9 Hz, 1 C, P−CH$_2$), 35.4 (s, 2 C, 2 isomers, *p*-C*H*Me$_2$ of Tipp), 33.7 (s, 2 C, 1 isomer, *o*-C*H*Me$_2$ of Tipp), 33.6 (s, 2 C, 1 isomer, *o*-C*H*Me$_2$ of Tipp), 25.8 [s, 4 C, 2 isomers, *p*-CH(CH_3)$_2$ of Tipp], 25.6 (s, 2 C, 2 isomers, CHCH_3), 25.2 [d, $^4J_{P-C}$ = 3.1 Hz, 4 C, 1 isomer, *o*-CH(CH_3)$_2$ of Tipp], 24.8 [d, $^4J_{P-C}$ = 3.6 Hz, 4 C, 1 isomer, *o*-CH(CH_3)$_2$ of Tipp]; *ipso*-C of Tipp not observed. − ^{31}P NMR (C_6D_6): δ = −105.2 (d, 1 isomer, $^1J_{P-H}$ = 215.5 Hz), −105.9 (d, 1 isomer, $^1J_{P-H}$ = 217.1 Hz). − EI MS: *m*/*z* (%) = 294 (79) [M$^+$], 235 (50) [PHTipp$^+$], 203 (100) [Tipp$^+$], and fragmentation products thereof. − IR (KBr): $\tilde{\nu}$ = 3377 cm^{-1} [br, s, ν(OH)], 2330 [m, ν(PH)]. − $C_{18}H_{31}OP$ (294.41): calcd. C 73.4, H 10.6, P 10.5; found C 73.0, H 10.5, P 10.3.

Numbering scheme for the cyclohexyl ring:



2-(Phenylphosphanyl)cyclohexan-1-ol (4): Prepared from $PhPH_2$ (5.0 g, 46.0 mmol), 1.5 M BuLi solution in hexane (30 mL, 46.0 mmol), and cyclohexene oxide (4.6 mL, 46.0 mmol). Yield: 4.8 g (51%); colourless oil (b.p. 70−75 °C, 3×10^{-2} Torr). − ^{1}H NMR (C_6D_6): δ = 7.52 (m, 4 H, 2 isomers, Ph), 7.11 (m, 6 H, 2 isomers, Ph), 4.57 (d of d, $^1J_{P-H}$ = 216.6 Hz, $^3J_{H-H}$ = 3.8 Hz, 1 H, 1 isomer, PH), 4.21 (d of d, $^1J_{P-H}$ = 213.1 Hz, $^3J_{H-H}$ = 5.0 Hz, 1 H, 1 isomer, PH), 3.40 (m, $^3J_{H-H}$ = 4.1 Hz, 1 H, 1 isomer, O−CH), 3.23 (m, $^3J_{H-H}$ = 4.2 Hz, 1 H, 1 isomer, O−CH), 2.40 (br. s, 2 H, 2 isomers, OH), 1.96−0.85 (m, 18 H, 2 isomers, Cy). − ^{13}C{H} NMR (C_6D_6): δ = 136.4 (d, $^2J_{P-C}$ = 15.9 Hz, 2 C, 1 isomer, *o*-C of Ph), 135.5 (d, $^2J_{P-C}$ = 15.1 Hz, 2 C, 1 isomer, *o*-C of Ph), 135.2 (d, $^4J_{P-C}$ = 12.4 Hz, 1 C, 1 isomer, *p*-C of Ph), 134.8 (d, $^4J_{P-C}$ = 12.1 Hz, 1 C, 1 isomer, *p*-C of Ph), 129.6 (d, 2 C, 2 isomers, *ipso*-C, partially obscured by solvent signal), 129.2 (d, $^3J_{P-C}$ = 6.2 Hz, 2 C, 1 isomer, *m*-C of Ph), 129.2 (d, $^3J_{P-C}$ = 5.4 Hz, 2 C, 1 isomer, *m*-C of Ph), 73.7 (d, $^2J_{P-C}$ = 9.1 Hz, 1 C, 1 isomer, O−CH), 73.1 (d, $^2J_{P-C}$ = 8.8 Hz, 1 C, 1 isomer, O−CH), 44.4 (d, $^1J_{P-C}$ = 12.7 Hz, 1 C, 1 isomer, P−CH), 43.2 (d, $^1J_{P-C}$ = 10.3 Hz, 1 C, 1 isomer, P−CH), 37.1 (d, $^3J_{P-C}$ = 6.3 Hz, 1 C, 1 isomer, C3 of Cy), 36.9 (d, $^3J_{P-C}$ = 5.1 Hz, 1 C, 1 isomer, C3 of Cy), 32.0 (d, $^2J_{P-C}$ = 3.8 Hz, 1 C, 1 isomer, C6 of Cy), 30.7 (d, $^2J_{P-C}$ = 10.0 Hz, 1 C, 1 isomer, C6 of Cy), 27.1 (d, $^3J_{P-C}$ = 6.4 Hz, 1 C, 1 isomer, C5 of Cy), 26.6 (d, $^3J_{P-C}$ = 7.9 Hz, 1 C, 1 isomer, C5 of Cy), 25.6 (1 C, 1 isomer, C4 of Cy), 25.5 (1 C, 1 isomer, C4 of Cy). − ^{31}P NMR (C_6D_6): δ = −40.9 (d, $^1J_{P-H}$ = 213.8 Hz), −45.5 (d, $^1J_{P-H}$ = 217.1 Hz). − EI MS: *m*/*z* (%) = 208 (47) [M$^+$], 190 (83) [M$^+$ − H_2O], 109 (58) [PHPh$^+$], and fragmentation products thereof. − IR (KBr): $\tilde{\nu}$ = 3385 cm^{-1} [br, s, ν(OH)], 2286 [s, ν(PH)]. − $C_{12}H_{17}OP$ (208.24): calcd. C 69.2, H 8.2, P 14.9; found C 68.7, H 8.0, P 14.5.

2-(Mesitylphosphanyl)cyclohexan-1-ol (5): Prepared from $MesPH_2$ (10.0 g, 66.0 mmol), 1.5 M BuLi solution in hexane (47 mL, 70.0 mmol), and cyclohexene oxide (7.4 mL, 77.0 mmol). Yield: 7.1 g (43%); white solid (m.p. 110−115 °C). − ^{1}H NMR (C_6D_6): δ = 6.79 (s, 4 H, 2 isomers, *m*-C*H* of Mes), 4.79 (d of d, $^1J_{P-H}$ = 222.3 Hz, $^3J_{H-H}$ = 4.8 Hz, 1 H, 1 isomer, PH), 4.08 (d of d, $^1J_{P-H}$ = 216.6 Hz, $^3J_{H-H}$ = 6.8 Hz, 1 H, 1 isomer, PH), 3.48 (m, 1 H, 1 isomer, O−CH), 3.38 (m, 1 H, 1 isomer, O−CH), 2.55 (s, 6 H, 2 isomers, *o*-CH_3 of Mes), 2.45 (s, 6 H, 2 isomers, *o*-CH_3 of Mes), 2.09 (s, 6 H, 2 isomers, *p*-CH_3 of Mes), 2.0−0.87 (m, 18 H, 2 isomers, Cy); OH not observed. − ^{13}C{^{1}H} NMR (C_6D_6): δ = 144.1 (d, $^2J_{P-C}$ = 12.0 Hz, 2 C, 1 isomer, *o*-C of Mes), 142.9 (d, $^2J_{P-C}$ = 11.8 Hz, 2 C, 1 isomer, *o*-C of Mes), 139.0 (1 C, 1 isomer, *p*-C of Mes), 138.4 (1 C, 1 isomer, *p*-C of Mes), 130.1 (4 C, 2 isomers, *m*-C of Mes), 130.0 (d, $^1J_{P-C}$ = 20.4 Hz, 2 C, 2 isomers, *ipso*-C of Mes), 75.6 (d, $^2J_{P-C}$ = 9.5 Hz, 1 C, 1 isomer, O−CH), 75.1 (d, $^2J_{P-C}$ = 13.2 Hz, 1 C, 1 isomer, O−CH), 43.9 (d, $^1J_{P-C}$ = 12.0 Hz, 1 C, 1 isomer, P−CH), 42.2 (d, $^1J_{P-C}$ = 12.3 Hz, 1 C, 1 isomer, P−CH), 37.1 (d, $^3J_{P-C}$ = 10.0 Hz, 2 C, 2 isomers, C3 of Cy), 30.3 (d, $^2J_{P-C}$ = 15.6 Hz, 2 C, 2 isomers, C6 of Cy), 27.0 (d, $^3J_{P-C}$ = 10.7 Hz, 2 C, 2 isomers, C5 of Cy), 25.7 (d, $^4J_{P-C}$ = 3.9 Hz, 2 C, 2 isomers, C4 of Cy), 24.4 (d, $^3J_{P-C}$ = 12.0 Hz, 2 C, 2 isomers, *o*-CH_3 of Mes), 24.4 (d, $^3J_{P-C}$ = 10.9 Hz, 2 C, 2 isomers, *o*-CH_3 of Mes), 21.7 (d, $^5J_{P-C}$ = 2.5 Hz, 2 C, 2 isomers, *p*-CH_3 of Mes). − ^{31}P NMR (C_6D_6): δ = −105.3 (d, $^1J_{P-H}$ = 215.5 Hz), −106.0 (d, $^1J_{P-H}$ = 215.5 Hz). − EI MS: *m*/*z* (%) = 250 (50) [M$^+$], 151 (67) [PHMes$^+$], and fragmentation products thereof. − IR (KBr): $\tilde{\nu}$ = 3335 cm^{-1} [br, s, ν(OH)], 2339 [s, ν(PH)]. − $C_{15}H_{23}OP$ (250.32): calcd. C 72.0, H 9.3, P 12.4; found C 71.5, H 8.9, P 13.0.

2-(Triisopropylphenylphosphanyl)cyclohexan-1-ol (6): Prepared from $TippPH_2$ (12.3 g, 53.0 mmol), 1.5 M BuLi solution in hexane (38 mL, 57.0 mmol), and cyclohexene oxide (5.4 mL, 53.0 mmol). Yield: 12.7 g (72%); colourless oil (b.p. 170 °C, 5×10^{-3} Torr), which was found to solidify at room temp. Recrystallization from pentane yielded single crystals (m.p. 156 °C). − ^{1}H NMR (C_6D_6): δ = 7.18 (s, 4 H, 2 isomers, *m*-CH of Tipp), 5.04 (d of d, $^1J_{P-H}$ = 220.0 Hz, $^3J_{H-H}$ = 5.7 Hz, 1 H, 1 isomer, PH), 4.38 (d of d, $^1J_{P-H}$ = 216.0 Hz, $^3J_{H-H}$ = 6.2 Hz, 1 H, 1 isomer, PH), 4.09 (sept., $^3J_{H-H}$ = 4.5 Hz, 2 H, 1 isomer, *o*-C*H*Me$_2$ of Tipp), 3.85 (sept., $^3J_{H-H}$ = 3.5 Hz, 2 H, 1 isomer, *o*-C*H*Me$_2$ of Tipp), 3.46 (m, 2 H, 2 isomers, O−CH), 2.76 (sept., $^3J_{H-H}$ = 5.0 Hz, 2 H, 2 isomers, *p*-C*H*Me$_2$ of Tipp), 2.15−1.08 (m, 18 H, 2 isomers, Cy), 1.35 [d, $^3J_{H-H}$ = 6.7 Hz, 12 H, 1 isomer, *o*-CH(CH_3)$_2$ of Tipp], 1.30 [d, $^3J_{H-H}$ = 6.8 Hz, 6 H, 1 isomer, *p*-CH(CH_3)$_2$ of Tipp], 1.27 [d, $^3J_{H-H}$ = 6.9 Hz, 6 H, 1 isomer, *p*-CH(CH_3)$_2$ of Tipp], 1.21 [d, $^3J_{H-H}$ = 6.8 Hz, 12 H, 1 isomer, *o*-CH(CH_3)$_2$ of Tipp]; OH not observed. − ^{13}C{^{1}H} NMR (C_6D_6): δ = 155.0 (d, $^2J_{P-C}$ = 11.1 Hz, 2 C, 1 isomer, *o*-C of Tipp), 153.9 (d, $^2J_{P-C}$ = 11.0 Hz, 2 C, 1 isomer, *o*-C of Tipp), 150.6 (1 C, 1 isomer, *p*-C of Tipp), 150.2 (1 C, 1 isomer, *p*-C of Tipp), 127.4 (d, $^1J_{P-C}$ = 15.9 Hz, 2 C, 2 isomers, *ipso*-C of Tipp), 122.3 (t, 4 C, 2 isomers, *m*-C of Tipp), 75.6 (d, $^2J_{P-C}$ = 10.6 Hz, 1 C, 1 isomer, O−CH), 75.1 (d, $^2J_{P-C}$ = 13.9 Hz, 1 C, 1 isomer, O−CH), 45.7 (d, $^1J_{P-C}$ = 12.0 Hz, 1 C, 1 isomer, P−CH), 43.3 (d, $^1J_{P-C}$ = 12.9 Hz, 1 C, 1 isomer, P−CH), 37.3 (d, $^3J_{P-C}$ = 6.2 Hz, 1 C, 1 isomer, C3 of Cy), 36.9 (d, $^3J_{P-C}$ = 6.6 Hz, 1 C, 1 isomer, C3 of Cy), 35.3 (s, 4 C, 2 isomers, *o*-C*H*Me$_2$ of Tipp), 33.7 (d, $^2J_{P-C}$ = 14.6 Hz, 1 C, 1 isomer, C6 of Cy), 33.6 (d, $^2J_{P-C}$ = 14.9 Hz, 1 C, 1 isomer, C6 of Cy), 32.7 (s, 2 C, 2 isomers, *p*-C*H*Me$_2$ of Tipp), 29.3 (d, $^3J_{P-C}$ = 15.2 Hz, 1 C, 1 isomer, C5 of Cy), 27.5 (d, $^4J_{P-C}$ = 2.8 Hz, 1 C, 1 isomer, C4 of Cy), 27.0 (d, $^3J_{P-C}$ = 10.4 Hz, 1 C, 1 isomer, C5 of Cy), 25.7, 25.6, 25.5, 25.3, 25.2, 25.1 [12 C, 2 isomers, CH(CH_3)$_2$ of Tipp], 24.6 (d, $^4J_{P-C}$ = 4.8 Hz, 1 C, 1 isomer, C4 of Cy). − ^{31}P NMR (C_6D_6): δ = −77.6 (d, $^1J_{P-H}$ = 216.0 Hz), −89.9 (d,

$^1J_{P-H}$ = 220.0 Hz). − EI MS: *m/z* (%)= 334 (63) [M^+], 235 (52) [$PHTipp^+$], 203 (100) [$Tipp^+$], and fragmentation products thereof. − IR (KBr): $\tilde{\nu}$ = 3452 cm^{-1} [br, s, ν(OH)], 2359 [s, ν(PH)]. − $C_{21}H_{35}OP$ (334.48): calcd. C 75.4, H 10.5, P 9.3; found C 73.2, H 10.6, P 9.0.

Dianions 1a−6a: 1−6 were treated with two equivalents of BuLi in THF at −50 °C. Subsequent warming to room temp. gave the dilithio salts Li_2[$RPCH_2CHMeO$] [R = Ph (**1a**), Mes (**2a**), Tipp (**3a**)] [Equation (3)] and Li_2[2-RP-1-O-cyclo-C_6H_{10}] [R = Ph (**4a**), Mes (**5a**), Tipp (**6a**)] [Equation (4)], of which only **6a** was isolated. The deprotonation could be monitored by ^{31}P NMR and ^7Li NMR spectroscopy (solvent THF/C_6D_6). − **1a**: ^{31}P NMR: δ = −76.9 (br. s). − ^7Li NMR: δ = 1.5 (s), 1.3 (s), 1.2 (s), 0.9 (s). − **2a**: ^{31}P NMR: δ = −82.0 (br. s), −87.2 (br. s). − ^7Li NMR: δ = 1.4 (s), 1.3 (s), 1.0 (s). − **3a**: ^{31}P NMR: δ = −42.9 (br. s). − ^7Li NMR: δ = 4.6 (br. s), 3.9 (br. s). − **4a**: ^{31}P NMR: δ = −18.3 (br. s), −45.9 (br. s). − ^7Li NMR: δ = 5.6 (br. s), 5.0 (br. s), 4.5 (br. s). − **5a**: ^{31}P NMR: δ = −81.5 (br. s), −96.0 (br. s). − ^7Li NMR: δ = 4.3 (br. s), 3.9 (br. s). − **6a**: ^{31}P NMR: δ = −81.4 (br. s), −95.6 (br. s). − ^7Li NMR: δ = 4.3 (br. s), 3.9 (br. s), 3.7 (br. s). Crystals of **6a** were obtained from pentane.

Data Collection and Structure Refinement of 6 and 6a:

6: Experimental data (a total of 13072 reflections) were collected at *T* = 220(2) K on a Siemens CCD (SMART) diffractometer in the range 1.5 < Θ < 26.2° using monochromated Mo-K_α radiation (λ = 0.71073 Å). Of these, a total of 3740 reflections were considered as unique (R_{int} = 0.0637). All observed reflections were used in the determination of the unit cell parameters. The studied specimen was a white single crystal of dimensions 0.4 × 0.2 × 0.1 mm. Crystal data for **6** are as follows: $C_{21}H_{35}OP$, M_r = 334.46, space group $P2_1/c$ (no. 14), *a* = 13.755(1), *b* = 5.955(1), *c* = 25.444(1) Å, β = 91.529(1)°, *V* = 2083.3(2) $Å^3$ at *T* = 220(2) K, *Z* = 4, $D_{calcd.}$ = 1.066 Mg m^{-3}, μ(Mo-K_α) = 0.136 mm^{-1}; absorption correction with SADABS.[15]

The positions of the P, O, and C atoms were located using direct methods (SHELXTL-PLUS).[16] Subsequent least-squares refinement and difference electron density map calculations revealed the positions of the H atoms. Final full-matrix least-squares refinement of 348 parameters with a unit weighting scheme (P, O, and C atoms anisotropic approximation; H atoms isotropic approximation) converged to *R*1 = 0.0497, *wR*2 = 0.1282 [for reflections with $I > 2\sigma(I)$], *R*1 = 0.0606, *wR*2 = 0.1363 (all data).

6a: Experimental data (a total of 160515 reflections) were collected at *T* = 210(2) K on a Siemens CCD (SMART) diffractometer in the range 1.0 < Θ < 25.6° using monochromated Mo-K_α (λ = 0.71073 Å) radiation. Of these, a total of 40798 reflections were considered unique (R_{int} = 0.1687). All observed reflections were used in the determination of the unit cell parameters. The studied specimen was a white single crystal of dimensions 0.4 × 0.3 × 0.1 mm. Crystal data for **6a** are as follows: $C_{100}H_{164}Li_8O_8P_4$, M_r = 1673.71, space group $P2_1/c$ (no. 14), monoclinic, *a* = 27.929(1), *b* = 36.492(1), *c* = 24.992(1) Å, β = 110.668(1)°, *V* = 23833(2) $Å^3$ at *T* = 210(2) K, *Z* = 8, $D_{calcd.}$ = 0.933 Mg m^{-3}, μ(Mo-K_α) = 0.106 mm^{-1}; absorption correction with SADABS.[15]

The positions of the Li, P, O, and C atoms were located using direct methods (SHELXTL-PLUS);[16] H atoms were placed in calculated positions. Final full-matrix least-squares refinement of 2161 parameters with a unit weighting scheme (Li, P, O, and C atoms anisotropic approximation; H atoms isotropic approximation) converged to *R*1 = 0.1559, *wR*2 = 0.3746 [for reflections with $I > 2\sigma(I)$], *R*1 = 0.3221, *wR*2 = 0.4570 (all data).

Crystallographic data (excluding structure factors) for the structures reported in this paper have been deposited with the Cambridge Crystallographic Data Centre (**6:** CCDC-141876, **6a:** CCDC-141875). Copies of the data can be obtained free of charge on application to The Director, CCDC, 12 Union Road, Cambridge, CB2 1EZ, U.K. [Fax: (internat.) +44 (0)1223 336033; E-mail: deposit@ccdc.cam.ac.uk].

Acknowledgments

We gratefully acknowledge support by the Fonds der Chemischen Industrie, the Sächsische Landesgraduiertenförderung (S. B.), the Alexander von Humboldt Foundation (F.S.), and the German−Israeli Foundation (Grant no. I-142/95).

[1] [1a] These results have been presented in part at the *XVIII International Conference on Organometallic Chemistry*, Munich, 16−22 August, **1998**. − [1b] W. Keim, *Angew. Chem*. **1990**, *102*, 251; *Angew. Chem. Int. Ed. Engl.* **1990** *29*, 235. − [1c] C. A. Willoughby, R. R. Duff, W. M. Davis, S. L. Buchwald, *Organometallics* **1996**, *15*, 472.
[2] K. Issleib, H.-R. Roloff, *Chem. Ber*. **1965**, *98*, 2091.
[3] J. Heinicke, I. Kovacs, L. Nyulaszi, *Chem. Ber*. **1991**, *124*, 493.
[4] C. L. Thurner, M. Barz, M. Spiegler, W. R. Thiel, *J. Organomet. Chem*. **1997**, *541*, 39.
[5] J. Heinicke, *Trends in Organomet. Chem.* **1994**, *1*, 307.
[6] J. Heinicke, U. Jux, R. Kadyrov, M. He, *Heteroatom Chem.* **1997**, *8*, 383; J. Heinicke, M. He, R. Kadyrov, P. G. Jones, *Heteroatom Chem.* **1998**, *9*, 183.
[7] K. L. Marsi, M. E. Co-Sarno, *J. Org. Chem*. **1977**, *42*, 778.
[8] F. A. Carey, R. J. Sundberg, *Organische Chemie*, VCH Verlagsgesellschaft, Weinheim, **1995**.
[9] M. G. Davidson, J. A. K. Howard, S. Lamb, C. W. Lehmann, *Chem. Commun*. **1997**, 1607.
[10] A.-M. Sapse, P. von Ragué Schleyer (Eds.), *Lithium Chemistry − A Theoretical and Experimental Overview*, Wiley, Chichester, **1995**.
[11] M. Drieß, G. Huttner, N. Knopf, H. Pritzkow, L. Zsolnai, *Angew. Chem*. **1995**, *107*, 354; *Angew. Chem. Int. Ed. Engl.* **1995**, *34*, 316.
[12] T. Koch, S. Blaurock, E. Hey-Hawkins, M. Galan-Fereres, D. Plat, M. S. Eisen, *J. Organomet. Chem*. **2000**, *595*, 126.
[13] W. Kuchen, H. Buchwald, *Chem. Ber*. **1958**, *91*, 2296.
[14] S. Kurz, Ph. D. thesis, University of Leipzig, **1995**.
[15] G. M. Sheldrick, *SADABS: A Program for Empirical Absorption Correction*, Göttingen, **1998**.
[16] *SHELXTL-PLUS*, Siemens Analytical X-ray Instruments, Inc., **1990**, *XS: Program for Crystal Structure Solution, XL: Program for Crystal Structure Determination, XP: Interactive Molecular Graphics.*

Received February 23, 2000
[I00070]

Synthesis of 2,2′,5,5′-Tetraphenyl-1,1′-diarsacalcocene and -strontocene

Matthias Westerhausen,*[a] Christin Birg,[a] and Holger Piotrowski[a]

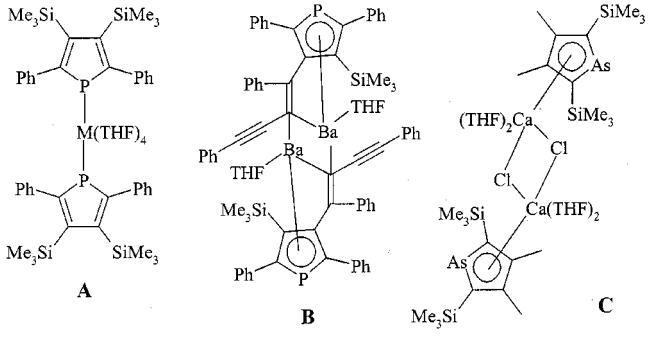
Keywords: Arsenic / As ligands / Calcium / Strontium / Heterocycles / Reaction mechanisms

The metalation of $H_2As–Si\mathit{i}Pr_3$ with bis(tetrahydrofuran-*O*)calcium- and -strontium bis[bis(trimethylsilyl)amide] yields tetrakis(tetrahydrofuran-*O*)calcium- (**1a**) and -strontium bis(triisopropylsilylarsanide) (**2a**). These compounds are in equilibrium with their dimers **1b** (Ca) and **2b** (Sr) by elimination of THF. The addition of diphenylbutadiyne to a THF/toluene solution of **1** and **2** gives bis(tetrahydrofuran-*O*)calcium- (**3**) and -strontium bis(2,5-diphenylarsolide) (**4**). The proposed reaction mechanism explains the formation of the $(\mathit{i}Pr_3Si)_2As^-$ and 2,5-diphenyl-3,4-bis(phenylethynyl)arsolide anions based on an intermolecular $H/Si\mathit{i}Pr_3$ exchange reaction. The latter anion was characterized by X-ray crystallography with the binuclear cation $[(THF)_3Ca\{\mu\text{-}As(H)Si\mathit{i}Pr_3\}_3Ca(THF)_3]^+$ (**5**). The arsolide ligands of **3** and **4** are η^5-bonded to the metal centers, whereas **5** crystallizes as a solvent-separated ion pair.

Introduction

The reaction of calcium and strontium bis[bis(trimethylsilyl)phosphanide] with diphenylbutadiyne yields the corresponding alkaline earth metal bis[2,5-diphenyl-3,4-bis(trimethylsilyl)-1-phosphacyclopentadienides] **A** (Scheme 1).[1] The reaction mechanism includes addition as well as 1,3-trimethylsilyl migration steps. The molecular structures of the calcium and strontium derivatives show metal−phosphorus σ-bonds. In contrast to this reaction, the homologous barium bis(phosphanide) $(THF)_4Ba[P(SiMe_3)_2]_2$ reacts differently with diphenylbutadiyne.[2] The main feature besides the central Ba_2C_2 cycle of the formed molecule **B** (Scheme 1) is a η^5-bonded phospholide moiety.

The reduction of 1-chloro-3,4-dimethyl-2,5-bis(trimethylsilyl)arsole yields the corresponding η^5-bonded arsolide **C**.[3] However, only heteroleptic compounds were prepared and no dismutation reactions of 1,1′-dipentelametallocenes have been observed thus far.



Scheme 1. Schematic representation of the phospholides **A** and **B**, and the arsolide **C**

In contrast to these recent examples of pentela-substituted alkaline earth metallocenes, the compounds calcocene[4] and decamethylcalcocene,[5] as well as their strontium analogues,[6,7] are well-known. This topic has been reviewed lately by Hanusa.[8]

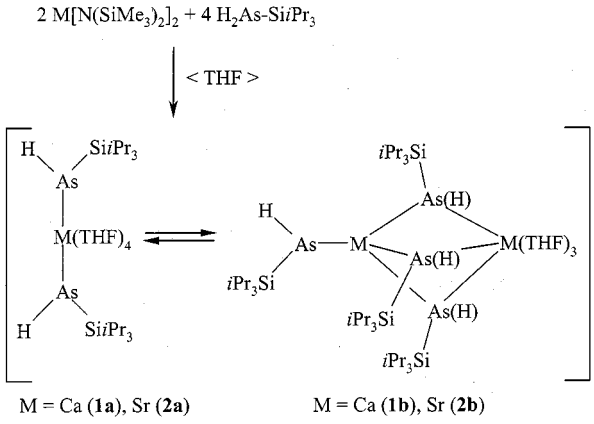
We are interested in these 1,1′-dipentelametallocenes in order to investigate the coordination behavior of the anions, as well as the use of these compounds as transfer reagents for phospholide and arsolide ligands. In transition metal phospholides the anions are known to vary between η^1- and η^5- coordination depending on the transition metal fragment, and to obey the 18-electron rule.[9] Recently, a potassium phospholide with a chain structure and η^5-bonded bridging anions was published.[10] The most widely used phospholide transfer reagents are the lithium derivatives prepared by the reduction of 1-phenylphospholes with lithium metal.[9] Here we propose a reaction mechanism for the reaction of calcium- and strontium bis(triisopropylsilylarsanide) with diphenylbutadiyne. The drastically reduced tendency of the $Si\mathit{i}Pr_3$ substituent to show a 1,3-shift leads to a different mechanism than that suggested for the formation of **A** and **B**. This route offers the possibility of preparing trialkylsilyl-free 1,1′-diarsacalcocenes and -strontocenes.

Results and Discussion

The metalation of triisopropylsilylarsane[11] with calcium- and strontium bis[bis(trimethylsilyl)amide][12] yields the corresponding alkaline earth metal bis(arsanides) **1a** and **2a** according to Scheme 2. These monomeric derivatives are expected to be in equilibrium with their dimers **1b** and **2b**, as shown in Scheme 2. This fact leads to broadened resonances (**1a** and **1b**) or a doubling of the signals (**2a** and **2b**). Similar monomer−dimer equilibria are well-known in the chemistry of alkaline earth metal bis(phosphanides)[13] − strontium-[14] and barium bis(triisopropylsilylphosphanide)[15] show this equilibrium even in donor solvents such as THF.

[a] Department Chemie, Ludwig-Maximilians-Universität München,
Butenandtstrasse 9 (Haus D), 81377 München, Germany
Fax: (internat.) +49-(0)89/2180-7867
E-mail: maw@cup.uni-muenchen.de

 © WILEY-VCH Verlag GmbH, D-69451 Weinheim, 2000 1434−1948/00/1010−2173 $ 17.50+.50/0



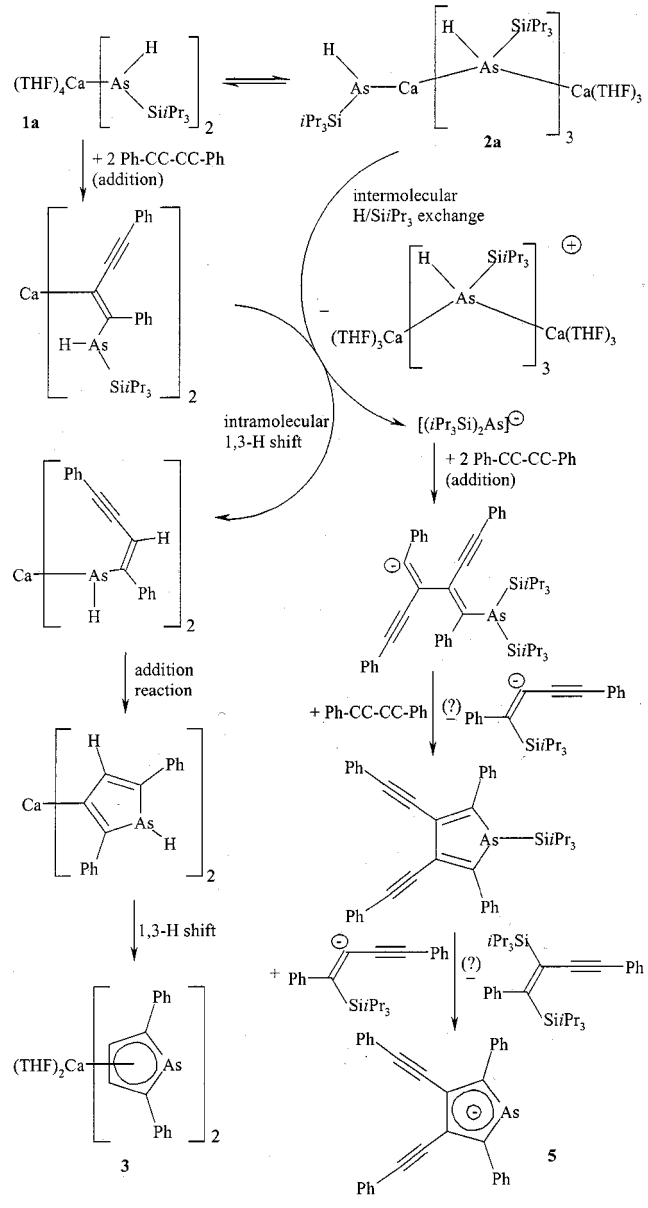
Scheme 2. Synthesis of tetrakis(tetrahydrofuran-*O*)calcium- and -strontium bis(triisopropylsilylarsanide) as well as their monomer-dimer equilibria

Dismutation reactions of alkaline earth metal bis(triisopropylsilylphosphanides) as well as -arsanides) have not been observed thus far. Even after prolonged heating of these compounds in THF or toluene neither bis(triisopropylsilyl)phosphanide and -arsanide anions, nor H_2P^- and H_2As^- ligands were detected.

The reaction of the above described triisopropylsilylarsanides of calcium (**1**) and strontium (**2**) with diphenylbutadiyne in a solvent mixture of toluene and THF gives the poorly soluble bis(tetrahydrofuran-*O*)calcium- (**3**) and -strontium bis(2,5-diphenylarsolide) (**4**). After precipitation of **3** the remaining solution was reduced to a few milliliters. Cooling to 5 °C gave crystalline **5** which was characterized by X-ray crystallography. Methanolysis of the reaction solution and mass spectrometric investigations allowed the identification of $HAs(SiiPr_3)_2$ and $C_{25}H_{31}Si$, a triisopropyl-substituted 1,4-diphenylbutenyne. The proposed mechanism based on these findings is represented in Scheme 3.

The first reaction step is the addition of **1a** and **2a** to a C≡C triple bond, followed by a 1,3-H migration. An intramolecular shift of a triisopropylsilyl substituent seems to be impossible in contrast to the mobility of the trimethylsilyl group.[16] However, an intermolecular H/Si*i*Pr$_3$ exchange reaction allows a second similar reaction sequence, namely the addition of the alkaline earth metal−arsenic bond to the remaining C≡C bond with a subsequent intramolecular 1,3-H migration. Thus, the 2,5-diphenylarsolide anion is formed (left column of Scheme 3).

This intermolecular H/Si*i*Pr$_3$ exchange yields a bis(triisopropylsilyl)arsanide ligand. The addition of this anion to a diphenylbutadiyne gives a carbanion which attacks another molecule of Ph−C≡C−C≡C−Ph. The elimination of a triisopropylsilanide leaves a 1-triisopropylsilyl-2,5-diphenyl-3,4-bis(phenylethynyl)-1-arsacyclopenta-2,4-diene. The silanide adds to another diphenylbutadiyne; the resulting carbanion abstracts the iPr_3Si^+ cation from the arsenic atom and leaves the 2,5-diphenyl-3,4-bis(phenylethynyl)arsolide anion. This would lead to the formation of 1,4-diphenyl-1,2-bis(triisopropylsilyl)but-1-ene-3-yne. The constitution of the anion was confirmed by crystallization as the solvent-separated ion pair **5** with the cation $\{(THF)_3Ca[\mu\text{-}As(H)SiiPr_3]_3Ca(THF)_3\}^+$, and X-ray structure determination, whereas the mass spectrometric investigation of the reaction solution gave fragments which could arise from the triisopropylsilyl-substituted but-1-ene-3-yne. Furthermore, methanolysis of the reaction mixture gave $HAs(SiiPr_3)_2$ which proves the intermolecular H/Si*i*Pr$_3$ exchange reaction. In the course of our investigations, elimination of the already well-known hexakis(triisopropyl)disilane, as well as $HSiiPr_3$, was not observed. However, despite not being able to isolate analytically pure **5**, the formation of this compound supports the reaction mechanism proposed in Scheme 3. Furthermore, Becker and co-workers[17] have investigated the reaction of lithium bis(trimethylsilyl)phosphanide with diphenylethyne in THF. Tetrakis(tetrahydrofuran-*O*)lithium tetraphenylphospholide has been isolated as a solvent-separated ion pair in approximately 60% yield.



Scheme 3. Proposed reaction mechanism for the synthesis of bis(tetrahydrofuran-*O*)calcium- and -strontium bis(2,5-diphenylarsolide)

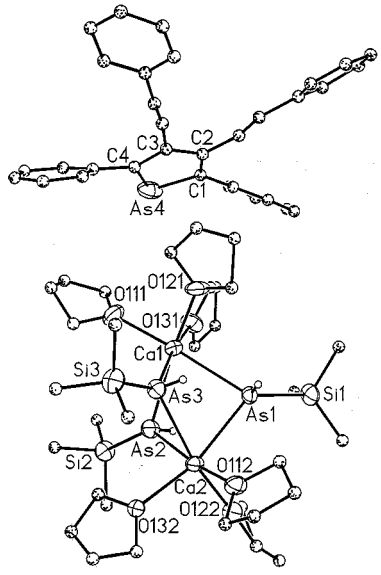


Figure 1. Molecular structure of the ion pair $[(THF)_3Ca[\mu\text{-}As(H)Si\mathit{i}Pr_3]_3Ca(THF)_3]^+$ $[2,5\text{-}Ph_2\text{-}3,4\text{-}(Ph{-}C{\equiv}C)_2AsC_4]^-$ (**5**); the carbon atoms are shown with arbitrary radii, the methyl groups and hydrogen atoms, with the exception of the As−H moieties, are omitted for clarity; all other atoms are drawn with 40% ellipsoids; neither of the THF molecules intercalated between the ions are shown for reasons of clarity; selected bond lengths (pm): Ca1−As1 304.5(2), Ca1−As2 307.9(3), Ca1−As3 307.1(2), Ca2−As1 305.3(2), Ca2−As2 306.7(2), Ca2−As3 305.7(3), As1−Si1 232.1(3), As2−Si2 231.3(3), As3−Si3 231.2(3), As4−C1 187.9(14), As4−C4 183.1(15), C1−C2 141(2), C2−C3 141(2), C3−C4 139(2)

However, in this reaction the fate of the trimethylsilyl groups remains unknown.[17]

Figure 1 shows the molecular structure of the solvent-separated ion pair **5**. The rather poor quality of the structure determination results from the disordering within the cation, which is not shown. Furthermore, two THF molecules with high thermal motion of the atoms are incorporated between the ions. The structural data are therefore not discussed in detail. The solvent-separated ion pair **5** consists of a binuclear cation with three bridging triisopropylsilylarsanide substituents; the central fragment is a trigonal Ca_2As_3 bipyramid. The Ca−As bond lengths vary in a very narrow range from 304.4(2) to 307.9(2) pm and are slightly longer than in $(THF)_4Ca[As(SiMe_3)_2]_2$.[18] The coordination spheres of the arsenic atoms As1, As2, and As3 are flattened with the Ca−As−Si and Ca1−As(n)−Ca2 angles ranging from 132.2(1)° to 139.6(1)° and from 84.99(6)° to 85.82(6)°, respectively, and neglecting the hydrogen atoms.

The arsolide cycle shows a delocalization of the anionic charge as expected for an isolated anion. The As−C bond lengths, taking into account the e.s.d. values, are of the same order of magnitude, and are comparable to those found in arsinine (arsabenzene)[19] and 2,3,6-triphenylarsinine.[20] The C−As−C angle in **5** has a value of 87.7(7)°.

NMR Spectroscopy

The NMR spectroscopic data of bis(tetrahydrofuran-*O*)calcium- (**3**) and -strontium bis(2,5-diphenylarsolide) (**4**) is summarized in Table 1. Their similarity and hence the lack of influence of the alkaline earth metal on the chemical shifts implies the mainly ionic character of the metal−arsolide interaction. The α-carbon atoms (C2,5) at the arsenic atom show a strong downfield shift. However, similar values are also found for tetrakis(tetrahydrofuran-*O*)calcium bis[2,5-diphenyl-3,4-bis(trimethylsilyl)phospholide] **A**[1] with η^1-bonded phospholide ligands. The chemical shifts of the ^{13}C atoms of the aromatic five-membered cycles are not dependent on either the binding mode, or on the pentele or alkaline earth metal atoms. This observation supports the interpretation of these compounds as mainly ionic.

Table 1. NMR data of bis(tetrahydrofuran-*O*)calcium- (**3**) and −strontium (**4**) bis(2,5-diphenylarsolide)

Compound	**3**[a]	**4**[a]
^{1}H		
δ(3,4-H)	7.57	7.53
δ(Ph, *o*)	7.21	7.21
δ(Ph, *m*)[b]	7.62	7.59
δ(Ph, *p*)	7.07	7.06
δ(THF)	1.72	1.76
δ(THF)	3.57	3.61
$^{13}C\{^1H\}$		
δ(C-3,4)	125.1	125.1
δ(C-2,5)	163.4	164.5
δ(Ph, *i*)	141.9	141.9
δ(Ph, *o*)[b]	125.1	124.9
δ(Ph, *m*)[b]	128.3	128.4
δ(Ph, *p*)	121.4	121.7
δ(THF)	24.4	24.4
δ(THF)	66.5	66.5

[a] Solvent: [D_8]THF, 30 °C. − [b] Assignment to *meta* and *ortho* positions uncertain and probably reversed.

Molecular Structure of 3

Bis(tetrahydrofuran-*O*)calcium bis(2,5-diphenylarsolide) **3** crystallizes with two crystallographically independent molecules in the asymmetric unit. Figure 2 shows one of the essentially equal molecules and its numbering scheme. The arsolide ligands are η^5-bonded to the calcium centers. The distances between the calcium atoms and the centers of the arsolide cycles lie between 254.1 and 257.5 pm. The Ca−O bond lengths vary in the very narrow and characteristic[13] region of 235.7 and 238.9 pm.

The arsolide ligands show a delocalization of the anionic charge within the five-membered cycle, the C(1*n*)−As(*n*)−C(4*n*) angles are approximately 87 °. The mean As−C bond of 190.5 pm is longer than that in the isolated arsolide anion of **5**. On the other hand, the Ca−As distances are only slightly larger than in the polycyclic cation of **5**. However, these structural parameters are in agreement with those of a calcium-bonded 3,4-dimethyl-2,5-bis-(trimethylsilyl)arsolide ligand.[1]

An interaction between the arsolide anion and the phenyl substituents in the 2,5-positions can be excluded. The bond lengths C(1*n*)−C(11*n*) and C(4*n*)−C(14*n*) (n = 1, 2, 3, 4) with a mean value of 146.9 pm is characteristic of a C−C single bond between two sp^2 hybridized carbon atoms.[21]

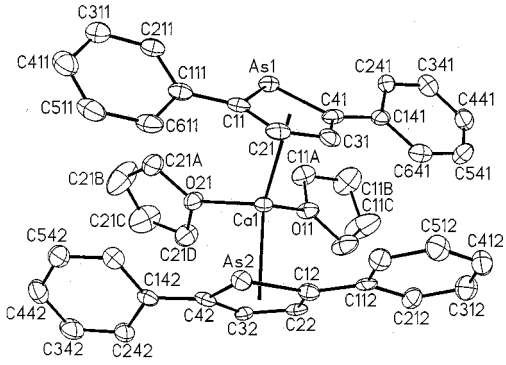


Figure 2. Molecular structure and numbering scheme of bis(tetrahydrofuran-*O*)calcium bis(2,5-diphenylarsolide) **(3)**; only one molecule is shown; hydrogen atoms are omitted for clarity, the ellipsoids represent a probability of 40%; selected bond lengths (pm): Ca1−As1 309.04(9), Ca1−C11 292.2(4), Ca1−C21 285.1(4), Ca1−C31 282.2(4), Ca1−C41 284.7(4), As1−C11 190.9(4), C11−C21 137.2(6), C21−C31 137.8(6), C31−C41 140.1(6), C41−As1 190.6(5), Ca1−As2 307.50(9), Ca1−C12 283.1(5), Ca1−C22 278.9(4), Ca1−C32 282.6(4), Ca1−C42 287.9(3), As2−C12 189.8(4), C12−C22 139.1(5), C22−C32 139.1(6), C32−C42 140.4(5), C42-As2 190.6(4), Ca1−O11 237.8(3), Ca1−O21 235.7(3); selected angles (°): C11-As1−C41 86.1(2), C12-As2−C42 87.1(2), O11−Ca1−O21 82.9(1)

The small angles between the normals of the phenyl planes on the one side and the arsolide plane on the other are rather small (25.2° and 20.4°); however, this orientation is a consequence of the intramolecular steric repulsion between the substituents and the packing of the molecules in the crystal.

Conclusion

The substitution pattern of the alkaline earth metal bis(arsanides) influence the mechanism of their reactions with diphenylbutadiyne. The migration of the sterically demanding triisopropylsilyl groups is avoided, instead an intermolecular H/Si*i*Pr$_3$ exchange reaction is observed. As a consequence of this reaction two different arsolide substituents have been characterized by X-ray crystallography: the 2,5-diphenylarsolide and the 2,5-diphenyl-3,4-diphenylethynylarsolide anion. The latter was not isolated as a diarsacalcocene, as the bulky binuclear cation $[(THF)_3Ca[\mu\text{-}As(H)Si\textit{i}Pr_3]_3Ca(THF)_3]^+$ was necessary for stabilization and crystallization.

The 1,1′-diarsacalcocene **3** and -strontocene **4** are available in high purity due to their poor solubility in toluene. However, these compounds have a limited use as synthons for arsolide transfer reactions because of a rather poor yield with regard to the alkaline earth metal or the arsenic atoms.

Experimental Section

General Remarks: All experiments and manipulations were carried out under argon purified by passage through a BTS catalyst and P_4O_{10}. Reactions were performed by using standard Schlenk techniques and using dried, thoroughly deoxygenated solvents. The starting materials $(THF)_2Ca[N(SiMe_3)_2]_2$,[12,22,23] $(THF)_2Sr[N(SiMe_3)_2]_2$,[12,22,23] and $H_2AsSi\textit{i}Pr_3$[11] were prepared according to literature procedures. NMR spectra were recorded on Jeol GSX270 and EX400 spectrometers. A Perkin−Elmer Paragon 1000 PC spectrophotometer was used to record the IR spectra; solid substances were examined as Nujol mulls between KBr plates (vs: very strong, s strong, m: medium, w: weak, vw: very weak, sh: shoulder). The frequencies in the region of the Nujol vibrations were not listed.

Tetrakis(tetrahydrofuran-*O*)calcium Bis(triisopropylsilylarsanide) (1): Triisopropylsilylarsane (1.17 g, 4.98 mmol) was added at room temp. to a solution of of bis(tetrahydrofuran-*O*)calcium bis[bis(trimethylsilyl)amide] (0.96 g, 1.90 mmol) in 20 mL of THF. The volume of the reaction mixture was reduced to approximately a quarter of the original volume. At 4 °C a precipitate of **1** was obtained as air- and moisture-sensitive colorless crystals, yield: 1.03 g (1.30 mmol), 68%. − Dec. above 140 °C without melting. − ^{1}H NMR ([D$_8$]toluene, 30 °C): δ = 1.03 (d, ^3J = 6.0 Hz, 18 H, CH$_3$), 0.97 (sept, ^3J = 6.0 Hz, 3 H, CH), 1.55 and 3.50 (THF). − ^{13}C{^{1}H} NMR ([D$_8$]toluene, 30 °C): δ = 15.1 (CH), 18.7 (CH$_3$), 25.4 and 67.4 (THF). − ^{29}Si{^{1}H} NMR ([D$_8$]toluene, 30 °C): δ = 31.1. − IR: $\tilde{\nu}$ = 2091 vs [ν(AsH)], 1293 w, 1260 w, 1249 w, 1232 sh, 1178 vw, 1159 vw, 1093 sh, 1071 s, 1036 s, 1016 s, 992 s, 967 w, 954 m, 918 s, 882 vs, 833 m, 803 w, 743 w, 672 s, 653 s, 609 s, 573 s, 560 s, 502 s, 464 s, 445 m, 420 m, 385 m, 363 sh cm^{-1}. − MS (70 eV); *m*/*z* (%): 59 (89) [SiC$_2$H$_7$], 61 (7), 73 (83) [SiC$_3$H$_9$], 75 (15) [As], 87 (54) [SiC$_4$H$_{11}$], 103 (11), 115 (100) [SiC$_6$H$_{15}$], 131 (16), 157 (24) [SiC$_9$H$_{21}$], 158 (21) [HSiC$_9$H$_{21}$], 207 (30), 300 (19) [Si$_2$C$_{17}$H$_{40}$], 390 (7) [CaAs$_2$Si$_2$C$_{10}$H$_{24}$]. − $C_{18}H_{44}As_2CaSi_2$ (506.6, THF-free): calcd. C 42.67, H 8.75; found C 43.16, H 8.84.

Tetrakis(tetrahydrofuran-*O*)strontium Bis(triisopropylsilylarsanide) (2): Triisopropylsilylarsane (1.17 g, 4.98 mmol) was added to a solution of bis(tetrahydrofuran-*O*)strontium bis[bis(trimethylsilyl)amide] (1.05 g, 1.90 mmol) in 10 mL of THF. All volatile materials were removed under vacuum and the remaining yellowish powder dried until a pressure of 0.01 Torr was reached. Yield: 1.43 g (1.70 mmol), 89%. − Dec. above 140 °C without melting. − ^{1}H NMR ([D$_8$]toluene, 30 °C):δ = 1.28 (d, ^3J = 6.4 Hz, 18 H, CH$_3$), 1.27 (sept, ^3J = 6.4 Hz, 3 H, CH), 1.48 and 3.56 (THF). − ^{13}C{^{1}H} NMR ([D$_8$]toluene, 30 °C): δ = 15.4 (CH), 20.3 (Me), 25.5 and 67.6 (THF). − ^{29}Si{^{1}H} NMR ([D$_8$]toluene, 30 °C): δ = 31.2. − IR: $\tilde{\nu}$ = 2052 s [ν(AsH)]; 1295 vw, 1249 sh, 1225 w, 1179 vw, 1071 s, 1036 vs, 1015 s, 968 w, 953 w, 917 s, 882 vs, 663 s, 646 vs, 593 s, 575 vs, 558 s, 503 s, 462 m, 424 vw, 386 w, 360 vw cm^{-1}. − $C_{18}H_{44}As_2Si_2Sr$ (554.2, THF-free): calcd. C 44.71, H 8.66; found C 42.18, H 8.30.

Bis(tetrahydrofuran-*O*)calcium Bis(2,5-diphenylarsolide) (3): 1 (1.12 g, 1.41 mmol) in 3 mL of THF, and diphenylbutadiyne (0.30 g, 1.41 mmol) were combined in 20 mL of unstirred toluene. After 7 days the NMR spectroscopic control measurements showed the complete consumption of diphenylbutadiyne. The brown reaction mixture was reduced to two thirds of the original volume. At 4 °C crystals of **3** precipitated. Washing of the solid with small portions of toluene left analytically pure **3** (0.31 g, 0.42 mmol, 30% with regard to calcium). The mother liquor and the toluene washing were combined. After reduction of the volume and cooling to 4 °C crystals of **3** and bis[tris(tetrahydrofuran-*O*)calcium] tris(μ-triisopropylsilylarsanide) 2,5-diphenyl-3,4-bis(phenylethynyl)arsolide (**5**) [m. p. 115 °C (dec.); ^{1}H NMR: δ = 1.16 (CH$_3$ and CH), 6.78−7.66 (phenyl), 1.77 and 3.64 (THF)], precipitated, however, analytically pure **5** was not obtained from this reaction. − Physical data of **3**: dec. above 250 °C without melting. − NMR data see Table 1. − IR: $\tilde{\nu}$ = 1315 vw, 1295 vw, 1267 s, 1249 w, 1202 vw, 1277 w, 1156 w, 1137 vw, 1105 vw, 1073 s, 1026 vs, 1019 vs, 999 w, 984 vw, 968

vw, 953 vw, 903 m, 875 s, 841 sh, 802 vs, 756 vs, 693 vs, 672 w, 666 w, 653 w, 620 vw, 590 vw, 554 w, 525 w, 514 vw, 452 w, 430 s, 299 vw, 291 vw cm^{-1}. – $C_{40}H_{40}As_2CaO_2$ (742.7): calcd. C 64.69, H 5.43; found C 63.09, H 5.78.

Bis(tetrahydrofuran-*O*)strontium Bis(2,5-diphenylarsolide) (4): Tetrakis(tetrahydrofuran-*O*)strontium bis(triisopropylsilylarsanide) (**2**) (1.60 g, 1.90 mmol) was dissolved in a mixture of 5 mL of THF and 15 mL of toluene. Diphenylbutadiyne (0.39 g, 1.9 mmol) was added to this yellowish solution which turned brown within a few hours. After two days stirring at room temp., the reaction mixture was concentrated to half its volume and **4** precipitated. Washing with toluene left an almost colorless powder of **4** (0.55 g, 0.7 mmol, 37% with regard to strontium). - Dec. above 250 °C without melting. – NMR data see Table 1. – IR: $\tilde{\nu}$ = 1316 vw, 1293 vw, 1265 s, 1185 vw, 1175 vw, 1157 w, 1099 m, 1073 s, 1029 s, 1023 s, 999 w, 982 vw, 970 vw, 902 m, 878 m, 847 w, 840 w, 800 s, 756 vs, 693 s, 666 vw, 620 vw, 589 vw, 554 w, 524 vw, 510 vw, 497 vw, 453 vw, 431 m, 422 vw, 405 vw, 396 vw cm^{-1}. – $C_{40}H_{40}As_2O_2Sr$ (790.2): calcd. C 60.80, H 5.10; found C 59.03, H 5.39.

Structure Determinations: Single crystals of **3** and **5** were covered with oil[24] and mounted on a STOE IPDS diffractometer with graphite monochromated Mo-K_α radiation (λ = 71.073 pm). Crystallographic parameters and details of data collection are summarized in Table 2. The structures were solved by direct methods and refined with the software packages SHELXL-93 and SHELXL-97.[26] Neutral scattering factors were taken from Cromer and Mann[27] and for the hydrogen atoms from Stewart et al.[28] For **3** neither absorption nor extinction corrections were applied.

Table 2. Crystallographic data of **3** and **5,** as well as details of the structure solution and refinement procedures

Compound	**3**	**5**
Formula	$C_{40}H_{40}As_2CaO_2$	$C_{91}H_{150}As_4Ca_2O_8Si_3$
Formula mass [$gmol^{-1}$]	742.67	1836.26
T [K]	200(2)	200(2)
Space group[25]	$P2_1/n$	$P\bar{1}$
a [pm]	1637.19(8)	1403.5(1)
b [pm]	1739.82(8)	1675.8(1)
c [pm]	2417.54(13)	2434.5(2)
α [°]	90	108.166(9)
β [°]	94.354(6)	96.771(9)
γ [°]	90	90.934(9)
V [nm^3]	6866.3(6)	5394.2(7)
Z	8	2
$d_{calcd.}$ [gcm^3]	1.4369	1.1306(2)
μ [mm^{-1}]	2.130	1.401
F(000)	3056	1948
Scan range [°]	$3.6 < 2\theta < 48.1$	$3.3 < 2\theta < 47.9$
Collected data	23605	31005
Unique data	10103	15766
Data with $I > 2\sigma(I)$	5965	5868
Parameters	811	803
Restraints	0	312
wR_2[a] (all data, on F^2)	0.0580	0.2398
wR_2[a] [$I > 2\sigma(I)$]	0.0517	0.2062
R_1[a] [$I > 2\sigma(I)$]	0.0338	0.0805
GOF[b] on F^2	0.779	0.897
Residual density [$eÅ^{-3}$]	0.348/-0.280	1.017/-0.439

[a] Definition of the R values: $R_1 = (\Sigma|\,|F_o| - |F_c|\,|)/\Sigma\,|F_o|$; $wR_2 = \{\Sigma[w(F_o^2 - F_c^2)^2]/\Sigma[w(F_o^2)^2]\}^{1/2}$ with $w^{-1} = \sigma^2(F_o^2) + (aP)^2$. – [b] $s = \{\Sigma[w(F_o^2 - F_c^2)^2]/(N_o - N_p)\}^{1/2}$.

The non-hydrogen atoms of **3** were refined anisotropically. The H-atoms were considered with a riding model under restriction of ideal symmetry at the corresponding atom. The asymmetric unit contains two molecules.[29] The structure of **5** consists of a solvent-separated ion pair with two additional THF molecules in the cavities. Whereas the non-hydrogen atoms of the anion were refined anisotropically, all other C atoms were considered isotropically. The isopropylsilyl groups and part of the THF ligands show a two-site disorder. All hydrogen atoms were refined using a riding model with ideal geometry at the corresponding carbon and arsenic atoms.

Acknowledgments

This work was financially supported by the Deutsche Forschungsgemeinschaft and the Fonds der Chemischen Industrie. We thank Prof. Dr. P. Klüfers for his kind support. Furthermore, C. Birg wishes to express her gratitude to the State of Bavaria, Germany for a Ph. D. scholarship granted.

[1] M. Westerhausen, M. H. Digeser, H. Nöth, W. Ponikwar, T. Seifert, K. Polborn, *Inorg. Chem.* **1999**, *38*, 3207–3214.
[2] M. Westerhausen, M. H. Digeser, H. Nöth, T. Seifert, A. Pfitzner, *J. Am. Chem. Soc.* **1998**, *120*, 6722–6725.
[3] M. Westerhausen, M. H. Digeser, C. Gückel, H. Nöth, J. Knizek, W. Ponikwar, *Organometallics* **1999**, *18*, 2491–2496.
[4] R. Zerger, G. Stucky, *J. Organomet. Chem.* **1974**, *80*, 7–17.
[5] R. A. Anderson, J. M. Boncella, C. J. Burns, R. Blom, A. Haaland, H. V. Volden, *J. Organomet. Chem.* **1986**, *312*, C49–C52.
[6] [6a] E. O. Fischer, G. Stölzle, *Chem. Ber.* **1961**, *94*, 2187–2193. – [6b] B. G. Gowenlock, W. E. Lindsell, B. Singh, *J. Chem. Soc., Dalton Trans.* **1978**, 657–664.
[7] R. Blom, K. Faegri, H. V. Volden, *Organometallics* **1990**, *9*, 372–379.
[8] [8a] T. P. Hanusa, *Chem. Rev.* **1993**, *93*, 1023–1036. – [8b] See also: P. Jutzi, N. Burford, *Chem. Rev.* **1999**, *99*, 969–990 and literature cited therein.
[9] [9a] D. L. Kershner, F. Basolo, *Coord. Chem. Rev.* **1987**, *79*, 279–292. – [9b] F. Mathey, *Chem. Rev.* **1988**, *88*, 429–453. – [9c] F. Mathey, *Coord. Chem. Rev.* **1994**, *137*, 1–52. – [9d] J. F. Nixon, *Coord. Chem. Rev.* **1995**, *145*, 201–258.
[10] F. G. N. Cloke, P. B. Hitchcock, J. F. Nixon, D. J. Wilson, *Organometallics* **2000**, *19*, 219–220.
[11] M. Westerhausen, M. Wieneke, W. Schwarz, *J. Organomet. Chem.* **1999**, *572*, 249–257.
[12] [12a] M. Westerhausen, *Inorg. Chem.* **1991**, *30*, 96–101. – [12b] see also: M. Westerhausen, *Trends Organomet. Chem.* **1997**, *2*, 89–105.
[13] M. Westerhausen, *Coord. Chem. Rev.* **1998**, *176*, 157–210.
[14] M. Westerhausen, C. Birg, M. Krofta, P. Mayer, T. Seifert, H. Nöth, A. Pfitzner, T. Nilges, H.-J. Deiseroth, *Z. Anorg. Allg. Chem.* **2000**, *626*, in press.
[15] M. Westerhausen, M. H. Digeser, M. Krofta, N. Wiberg, H. Nöth, J. Knizek, W. Ponikwar, T. Seifert, *Eur. J. Inorg. Chem.* **1999**, 743–750.
[16] See for example: [16a] M. Westerhausen, M. H. Digeser, W. Schwarz, *Inorg. Chem.* **1997**, *36*, 521–527. – [16b] M. Westerhausen, M. H. Digeser, W. Schwarz, *Z. Anorg. Allg. Chem.* **1997**, *623*, 1237–1242.
[17] G. Becker, G. Ditten, K. Hübler, U. Hübler, K. Merz, M. Niemeyer, N. Seidler, M. Westerhausen, Z. Zheng, *Organosilicon Chemistry II: From Molecules to Materials*, (Eds.: N. Auner, J. Weis), VCH, Weinheim, **1996**, p. 161–186.
[18] M. Westerhausen, W. Schwarz, *Z. Naturforsch.* **1995**, *50b*, 106–114.
[19] T. C. Wong, L. S. Bartell, *J. Mol. Struct.* **1978**, *44*, 169–175.
[20] P. Jutzi, *Angew. Chem.* **1975**, *87*, 269–283; *Angew. Chem. Int. Ed. Engl.* **1975**, *14*, 232–246.
[21] J. March, *Advanced Organic Chemistry: Reactions, Mechanisms, and Structure*, 3rd Ed., J. Wiley, New York, **1985**, p. 18–20.
[22] M. Westerhausen, M. Hartmann, N. Makropoulos, B. Wieneke, M. Wieneke, W. Schwarz, D. Stalke, *Z. Naturforsch.* **1998**, *53b*, 117–125.
[23] D. C. Bradley, M. B. Hursthouse, A. A. Ibrahim, K. M. Abdul Malik, M. Motevalli, R. Möseler, H. Powell, J. D. Runnacles, A. C. Sullivan, *Polyhedron* **1990**, *9*, 2959–2964.

[24] [24a] T. Kottke, D. Stalke, *J. Appl. Crystallogr.* **1993**, *26*, 615−619. − [24b] D. Stalke, *Chem. Soc. Rev.* **1998**, *27*, 171−178.

[25] *International Tables for Crystallography*, Vol. A, *Space Group Symmetry*, 2nd Ed., (Ed.: T. Hahn), D. Reidel, Dordrecht, **1984**.

[26] G. M. Sheldrick *SHELXL-93*, Universität Göttingen, **1993**; *SHELXL-97*, Universität Göttingen, **1997**.

[27] D. T. Cromer, J. B. Mann *Acta Crystallogr.* **1968**, *A24*, 321−324.

[28] R. F. Stewart, E. R. Davidson, W. T. Simpson, *J. Chem. Phys.* **1965**, *42*, 3175−3187.

[29] Crystallographic data (excluding structure factors) for the structure of **3** has been deposited with the Cambridge Crystallographic Data Centre as supplementary publication no. CCDC-141345. Copies of the data can be obtained on application to CCDC, 12 Union Road, Cambridge CB2 1EZ, UK [E-mail: deposit@ccdc.cam.ac.uk].

Received March 7, 2000
[I00088]

A Novel Triangular Trinuclear μ_3-CO_3 Ferromagnetic Cu^{II} Compound Prepared in situ from CO_2 Uptake in Air. X-ray Structure, Spectroscopy and Magnetism

Gerard A. van Albada,[a] Ilpo Mutikainen,[b] Olivier S. Roubeau,[a] Urho Turpeinen,[b] and Jan Reedijk*[a]

Keywords: X-ray structure / Copper / N ligands / Magnetic properties / Carbon dioxide fixation

The new trinuclear compound $[Cu_3(bpy)_6(\mu_3\text{-}CO_3)](BF_4)_4(H_2O)_2(C_2H_6O)$ (in which bpy = 2,2′-bipyridine) has been synthesized from $Cu(BF_4)_2$ and bpy in aqueous ethanol by rapid uptake of atmospheric CO_2. The structure of the compound has been determined by X-ray crystallography; it was found to crystallise in the triclinic space group $P\bar{1}$ with a = 13.405(7), b = 13.691(7), c = 21.446(8) Å, α = 82.87(4), β = 73.57(4), γ = 64.32(4)°, Z = 2. The three copper atoms are connected to each other through the oxygen atoms from the bridging carbonato group, giving a triangular array of copper atoms. Each copper has a distorted square-pyramidal environment with a basal plane formed by three nitrogen atoms of the two chelating bipyridine groups and the oxygen atom of the bridging carbonato group (Cu–N/O distances about 2.0 Å). The apical position is formed at each copper by the fourth nitrogen atom of the bipyridines with distances varying from 2.120(5) to 2.188(5) Å. A weak ferromagnetic interaction is observed between the copper(II) ions. All data were fitted using the Hamiltonian $H = -J_{12}(\mathbf{S_1}\cdot\mathbf{S_2}) - J_{13}(\mathbf{S_1}\cdot\mathbf{S_3}) - J_{23}(\mathbf{S_2}\cdot\mathbf{S_3})$. Observed parameters are J = 10.6 cm^{-1} and a very weak antiferromagnetic intercluster interaction with zj' = −1.2 cm^{-1}.

Introduction

Over the years many efforts have been made in the search for compounds that can act as a CO_2 catcher, i.e. insertion of CO_2 from the atmosphere into coordination compounds. Insertion reactions of CO_2, such as into metal−ligand bonds, are not uncommon and in recent years many review papers have been published on this subject.[1] Several dinuclear copper(II) compounds have been synthesized by means of fixation of CO_2 from air.[2] The carbonate anion itself is a versatile bridging ligand, which can bind in different modes to generate dinuclear, trinuclear, tetranuclear, and even one- or two-dimensional systems,[3] and the study of this subject is also important in relation to the zinc(II) compounds in carbonic anhydrases (CA).[4]

Absorption of CO_2 into a trinuclear copper(II) compound was suggested in 1968 on the basis of IR spectra,[10] but to the best of our knowledge only five crystal structures of this type of trinuclear copper(II) carbonato compound have been solved and published together with their magnetic properties.[4−9]

With the ligand 2,2-bipyridine (abbreviated as bpy), X-ray structures of dinuclear μ-hydroxo-bridged copper(II) coordination compounds with the general formula $[Cu(OH)(bpy)]_2(A)_x$ (x = 1,2 and A = ClO_4^-,[11] $CF_3SO_3^-$,[12] SO_4^{2-},[13] NO_3^-,[14a,14b] $C_4O_4^{2-}$ [14c] are known.

With perchlorate or nitrate as an anion, the X-ray structures of the mononuclear compounds with the general formula $Cu(bpy)_x(A)_2$ (x = 1−3) have been published.[14b,15] However, with tetrafluoroborate as an anion, only a mononuclear compound, $Cu(bpy)_2(BF_4)_2$, has been reported so far.[16] Following earlier research on dinuclear hydroxo and alkoxo-bridged copper(II) coordination compounds,[17] we attempted to synthesize the dinuclear hydroxo-bridged compound with the anion BF_4^- in the same way as for the other hydroxo-bridged compounds with bpy. However, in this case it was not the dinuclear hydroxo-bridged that was obtained, but surprisingly the trinuclear carbonato-bridged compound $[Cu_3(bpy)_6(\mu\text{-}CO_3)](BF_4)_4(H_2O)_2(C_2H_6O)$. It is remarkable that this compound has not been found earlier, considering the thorough research undertaken with the ligand bpy over many years. The title compound was subsequently easily synthesized in an artificial CO_2 atmosphere. With Zn^{II} and bpy as a ligand, the carbonato-bridged trinuclear compound $[Zn_3(bpy)_6(CO_3)(H_2O)](ClO_4)_4(bpy)\cdot 2H_2O$ is also known.[18] In this study we report the synthesis, spectroscopic and magnetic properties as well as the X-ray structure of the title compound.

[a] Leiden Institute of Chemistry, Gorlaeus Laboratories, Leiden University,
P.O. Box 9502, 2300 RA Leiden, Netherlands
E-mail: mailto:reedijk@chem.leidenuniv.nl
[b] Laboratory of Inorganic Chemistry, Department of Chemistry, University of Helsinki,
P.O. Box 55 (A.I.Virtasen aukio 1), 00014, Helsinki, Finland

 © WILEY-VCH Verlag GmbH, D-69451 Weinheim, 2000 1434−1948/00/1010−2179 $ 17.50+.50/0

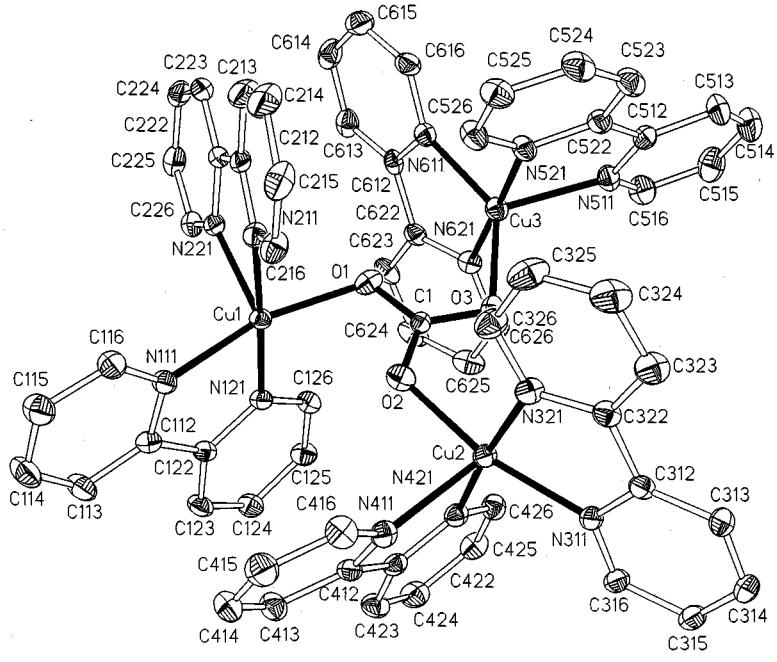


Figure 1. ORTEP plot showing the structure of $[Cu_3(bpy)_6(\mu\text{-}CO_3)](BF_4)_4(H_2O)_2(C_2H_6O)$ with atom-labeling scheme; hydrogen atoms, noncoordinating tetrafluoroborate anions, ethanol and water molecules are omitted for clarity

Results and Discussion

Description of the Crystal Structure of $[Cu_3(bpy)_6(\mu_3\text{-}CO_3)](BF_4)_4(H_2O)_2(C_2H_6O)$

The structure contains the unit $[Cu_3(bpy)_6(\mu_3\text{-}CO_3)]$, which is depicted in Figure 1, and the relevant bond length and bond angle information is given in Table 1. The unit cell also contains four noncoordinating tetrafluoroborate anions, one ethanol and two water molecules.

The three copper(II) atoms are connected to each other through the oxygen atoms from the bridging carbonato group, giving a triangular array of copper atoms. Each copper has a distorted square pyramidal environment with a basal plane formed by three nitrogen atoms of the two bichelating bipyridine groups and the oxygen atom of the bridging carbonato group (Cu−N/O distances about 2.0 Å). The apical position is formed at each copper by the fourth nitrogen atom of the bipyridines with distances that vary from 2.120(5) to 2.188(5) Å. The distortion from square pyramidal is different for each copper atom and this can be seen from the angles of each basal plane [Cu1 (basal plane O1−N211−N111−N121), angles 176.92(18) and 164.41(17)°; Cu2 (basal plane O2−N321−N311−N421), angles 172.8(2) and 166.76(17)°; Cu3 (basal plane O3−N521−N611−N621), angles 178.4(2) and 138.91(17)°]. This difference can be best expressed with the parameter τ (for 5 coordinated coordination compounds τ describes the relative amount of trigonality; τ = 0 for a square pyramid and τ = 1 for a trigonal bipyramid),[19] which has values of 0.21, 0.10 and 0.66 for Cu1, Cu2 and Cu3, respectively. The distances between the copper(II) atoms are also different and are large (Cu1−Cu2 4.64, Cu1−Cu3 4.72, Cu2−Cu3 5.00 Å).

The structures of compounds **1**−**4** in Table 2, in which the three coppers are almost equivalent, are quite different from that of compound **5**, in which all three copper atoms have a trigonal bipyrimidal geometry (τ values of 0.78, 0.81, and 0.83 for Cu1, Cu2, and Cu3, respectively).

The geometry in the related Zn compound, $[Zn_3(bpy)_6(\mu_3\text{-}CO_3)(H_2O)](ClO_4)_4(bpy)\cdot 2H_2O$,[18] is quite different; two of the Zn^{II} atoms have a distorted octahedral $N_4O(O_{water})$ geometry and the third Zn^{II} atom has a distorted trigonal-bipyramidal geometry with an N_4O environment.

Spectroscopy

The ligand field spectrum of the title compound shows a broad asymmetric band with a maximum at about $13.7\cdot 10^3$ cm^{-1} and a shoulder at about $10.1\cdot 10^3$ cm^{-1}; these absorptions are in agreement with a distorted square pyramidal $Cu(N)_x(O)_y$ geometry.[20]

In the infrared spectrum the most significant bands are those of the carbonato anion, which are reported in the literature at 1475, 1425, 837, 782, and 672 cm^{-1} for the compound $Cu_3(dpt)_3(\mu_3\text{-}CO_3)(ClO_4)_2\cdot 2H_2O$ (in which dpt = dipropylenetriamine)[10] and at 1476, 1423, 841, 694 cm^{-1} for the compound $[Zn_3(bpy)_6(\mu_3\text{-}CO_3)(H_2O)](ClO_4)_4(bpy)\cdot 2H_2O$.[18]

In the title compound the out-of-plane vibration at 839 cm^{-1} (medium intensity) is the best indication of the presence of CO_3 in the compound, as this spectral range is completely transparent in the monomeric compound $Cu(bpy)_3(BF_4)_2$.

EPR

The EPR spectrum of the title compound at room temperature shows a broad absorption centered around g =

Table 1. Bond lengths [Å] and angles [°]

Cu(1)−N(121)	1.983(4)
Cu(1)−N(211)	2.001(4)
Cu(1)−O(1)	2.022(4)
Cu(1)−N(111)	2.028(5)
Cu(1)−N(221)	2.156(5)
Cu(2)−O(2)	1.969(4)
Cu(2)−N(321)	1.987(5)
Cu(2)−N(421)	2.007(4)
Cu(2)−N(311)	2.040(4)
Cu(2)−N(411)	2.188(5)
Cu(3)−N(621)	1.974(5)
Cu(3)−N(521)	1.992(5)
Cu(3)−N(611)	2.055(5)
Cu(3)−O(3)	2.078(5)
Cu(3)−N(511)	2.120(5)
N(121)−Cu(1)−N(211)	176.92(18)
N(121)−Cu(1)−O(1)	94.76(17)
N(211)−Cu(1)−O(1)	88.03(18)
N(121)−Cu(1)−N(111)	80.64(18)
N(211)−Cu(1)−N(111)	96.34(19)
O(1)−Cu(1)−N(111)	164.41(17)
N(121)−Cu(1)−N(221)	102.30(17)
N(211)−Cu(1)−N(221)	78.95(18)
O(1)−Cu(1)−N(221)	90.35(16)
N(111)−Cu(1)−N(221)	105.16(18)
O(2)−Cu(2)−N(321)	94.46(18)
O(2)−Cu(2)−N(421)	89.20(17)
N(321)−Cu(2)−N(421)	172.8(2)
O(2)−Cu(2)−N(311)	166.76(17)
N(321)−Cu(2)−N(311)	80.53(19)
N(421)−Cu(2)−N(311)	94.55(18)
O(2)−Cu(2)−N(411)	85.92(18)
N(321)−Cu(2)−N(411)	107.28(19)
N(421)−Cu(2)−N(411)	79.16(19)
N(311)−Cu(2)−N(411)	107.24(18)
N(621)−Cu(3)−N(521)	178.4(2)
N(621)−Cu(3)−N(611)	80.0(2)
N(521)−Cu(3)−N(611)	98.3(2)
N(621)−Cu(3)−O(3)	91.28(18)
N(521)−Cu(3)−O(3)	89.90(18)
N(611)−Cu(3)−O(3)	138.91(17)
N(621)−Cu(3)−N(511)	101.3(2)
N(521)−Cu(3)−N(511)	79.3(2)
N(611)−Cu(3)−N(511)	109.90(18)
O(3)−Cu(3)−N(511)	111.19(17)

2.13 with a very weak shoulder at about $g = 2.42$. For the five other known trinuclear carbonato-bridged compounds the g values also lie at around $g = 2.12$ (see Table 2).

In frozen solution (DMF/methanol mixture) at 77 K a resolved $d_{x^2-y^2}$ spectrum is obtained with a $g_\perp$ value of 2.06, a $g_{//}$ of 2.26, with an $A_{//}$ value of 15.9 mT. A poorly resolved nitrogen hyperfine splitting is observed with 5 lines, indicating 2 nitrogens around the copper atom. This observation indicates that the compound is dissociated in this solution.

Magnetic Properties

To better understand the magnetic interaction, mediated through the CO_3^{2-} bridge, the magnetic susceptibilities of powdered samples were measured from 4 to 250 K and the results are shown in Figure 2 in the form of χ_m vs. T and μ_{eff} vs. T plots. The effective magnetic moment, μ_{eff}, measured from 250 to about 100 K has an almost constant value of about 3.3−3.4 μ_B. This value compares well with that expected for three uncoupled spins $S = {}^1/_2$ ($\mu_{eff} = 3.0\ \mu_B$, spin only value) and is also observed in other trinuclear triangular compounds.[4,21] Below 100 K the magnetic moment increases gradually until a maximum is reached at 5 K. The increase can be ascribed to a ferromagnetic interaction between the Cu^{II} ions.[4,7] The magnetic data were fitted to the theoretical expression for the magnetic susceptibility for a trinuclear triangular system, which is based on the general Hamiltonian[22,23] for the description of the interaction: $H = -J_{12}\ (\mathbf{S}_1 \cdot \mathbf{S}_2) - J_{13}\ (\mathbf{S}_1 \cdot \mathbf{S}_3) - J_{23}\ (\mathbf{S}_2 \cdot \mathbf{S}_3)$

in which the exchange integrals, J_{ij}, are negative for antiferromagnetic and positive for ferromagnetic interactions.

Although the three Cu^{II} ions are not completely identical (not related by a C_3 axis), we have assumed the Cu^{II} triangle to be equilateral. Considering three different Cu^{II} ions would only yield more ambiguous J_{ij} parameters, since they are strongly related to each other,[23a] and in our case without a better quality of fit. The g tensors and the J_{ij} parameters were therefore considered to be identical for the three Cu^{II} ions, and only one J value was considered.

The expression for the molar susceptibility then becomes:[22,23] $\chi_m = [Ng^2\mu_B{}^2/(4\ k_B\ (T + \Theta))] \times F$, where $\Theta = -(zJ'/k_B) \times F$

In this formula $F = [1 + 5\ \exp(3J/2kT)]/[1 + \exp(3J/2kT)]$ and the parameters N, g, μ_B, k_B, and T have their usual meanings.[22,23] The exchange parameter is denoted as J and the parameter zJ' empirically takes into account the intercluster interactions of z nearest neighbors.

Using the g value given by the EPR spectra and free variation of J did not give satisfactory results; therefore both J and g were left free in the least-squares fitting procedure, first considering $zJ' = 0$. Once the best fit was reached, the intercluster interaction was also introduced into the fitting procedure.

So, with variation of the three parameters J, zj', and g, and by minimizing the function $R = (\chi_m T_{calc} - \chi_m T_{obs})^2/(\chi_m T_{obs})^2$, the best fit was obtained for $J = 10.6\ cm^{-1}$, $zj' = -1.2\ cm^{-1}$, $g = 2.22$, and $R = 2.4 \cdot 10^{-4}$.

This low J value and rather weak interaction is not surprising since the distances between the copper(II) atoms are quite large (Cu−Cu separation of about 4.78 Å). As can be seen from Table 2, the present parameters agree well with the first four carbonato-bridged trinuclear compounds (compounds 1−4 in Table 2) reported in the literature. In fact, only compound **5** shows a very weak antiferromagnetic interaction,[9] the reasons for which are currently not understood.

Conclusion

In this paper a compound is described that is readily formed by absorption of CO_2 from the atmosphere, yielding a trinuclear carbonato-bridged compound having a $[Cu_3(bpy)_6(\mu_3\text{-}CO_3)]$ chromophore. The Cu^{II} ions are weakly coupled in a ferromagnetic manner, as also observed

Table 2. X-ray structure parameters and magnetism for Cu^{II} trinuclear μ_3-CO_3 compounds

Compound[a]	Coordination (chromophore)	Cu−X dist.(Å)	EPR (solid, RT)	Mag. susc. (cm^{-1})	ref.
1 $[Cu_3(pip)_3(H_2O)_3(\mu_3\text{-}CO_3)](NO_3)_4$	$CuN_3O(O_w)$	Cu−N,$O_{(av)}$ 2.00 Cu−O_w 2.25[b]	2.13	J = 9.64 zJ' = −0.079[c]	[5]
2 $[Cu_3(L)_3(\mu_3\text{-}CO_3)](ClO_4)_4$	$CuN_3O(O)$	Cu−N,$O_{(av)}$ 2.00 Cu−O 2.53	2.10 (br)	J = 8.2[d]	[4,6]
3 $[Cu_3(Medpt)_3(\mu_3\text{-}CO_3)](ClO_4)_4$	$CuN_3O(O_{ClO4})$	Cu−N,$O_{(av)}$ 2.00 Cu−$O_{(av)}$ 2.45	2.11	J = 12.6 zJ' = −0.68[e]	[7]
4 $[Cu_3(L2)_3(\mu_3\text{-}CO_3)](ClO_4)_4\cdot 2H_2O$	$CuN_3O(N)$	Cu−N,$O_{(av)}$ 2.00 Cu−N 2.10	[f]	J = 17.2[d]	[8]
5 $[Cu_3(TPA)_3(\mu_3\text{-}CO_3)](ClO_4)_4$	$CuN_3O(N)$	Cu−N,$O_{(av)}$ 2.04 Cu−$N_{(av)}$ 2.20	[f]	J = −1.19[d]	[9]
6 $[Cu_3(bpy)_6(\mu_3\text{-}CO_3)](BF_4)_4(H_2O)_2(C_2H_6O)$	$CuN_3O(N)$	Cu−N,$O_{(av)}$ 2.01 Cu−$N_{(av)}$ 2.15	$g_\perp$ 2.13 $g_{//}$ 2.42 (br,vw)	J = 10.6 zJ' = −1.2	this work

[a] Abbreviations: (v)w = (very)weak, br = broad, av = average value, O_w = O of water, RT = room temperature, av = average. − pip = 2-[2-(2-pyridyl)ethyliminomethyl]pyridine; L= macrocycle [15]aneN_3O_2; Medpt = bis(3-aminopropyl)methylamine; L2 = 1,4,7,10-tetraazabicyclo[5.5.3]pentadecane; TPA = tris(pyridylmethyl)amine; bpy = 2,2′-bipyridine. − [b] Each copper also has a distance of 2.69 Å to another carbonate oxygen. − [c] The magnetic susceptibility was also measured for the isostructural compound $[Cu_3(pip)_3(H_2O)_3(\mu_3\text{-}CO_3)](ClO_4)_4$, and is J = 8.94, zJ' = −0.075 cm^{-1} (ref.[5]). − [d] No intercluster interaction was considered in the fitting procedure. − [e] The magnetic susceptibility was also measured for the related compound $[Cu_3(dpt)_3(\mu_3\text{-}CO_3)](ClO_4)_4$ [dpt = bis(3-aminopropyl)amine] and is J = 15.8, zJ' = −0.015 cm^{-1} (ref.[7]). − [f] Not given.

in a few analogous compounds (see Table 2). In addition, a very weak antiferromagnetic coupling is observed between trinuclear moieties.

As yet only a few compounds of this type have been reported and characterized structurally and magnetically (Table 2). Further research aimed at the synthesis of more examples of this type of compound, using the synthetic methods described in this paper, is currently in progress.

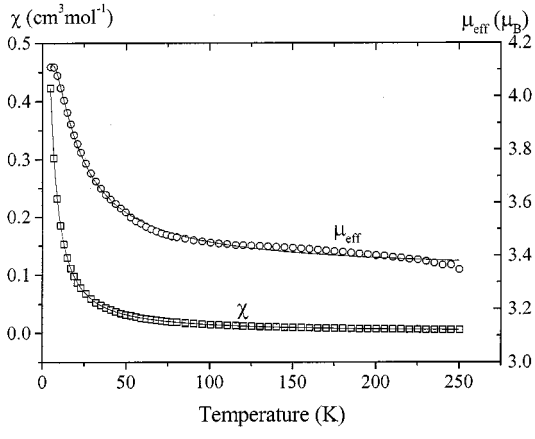


Figure 2. A plot of temperature dependence of χ_m vs. T (□) and μ_{eff} vs. T (○) is shown; the solid line represents the calculated curve for the parameters J = 10.6 cm^{-1}, zj' = −1.2 cm^{-1} and g = 2.22, see text

Experimental Section

General: All chemicals were used as received. The ligand 2,2′-bipyridine was obtained from Acros Organics, Belgium, and used without further purification.

C, H, N, and Cu determinations were performed by the Microanalytical Laboratory of University College, Dublin, Ireland. − Ligand field spectra were obtained on a Perkin−Elmer Lambda 900 spectrophotometer using the diffuse reflectance technique, with MgO as a reference. − X-band EPR spectra were obtained on a Jeol RE2x electron spin resonance spectrometer using DPPH (g = 2.0036) as a standard. − FTIR spectra were obtained on a Perkin−Elmer Paragon 1000 FTIR spectrophotometer equipped with a Golden Gate ATR device, using the reflectance technique (4000−300 cm^{-1}).

Magnetic susceptibility measurements (4−300 K) were carried out using a Quantum Design MPMS-5S SQUID magnetometer (measurements carried out at 1 T). Data were corrected for magnetization of the sample holder, for TIP of copper(II) and for diamagnetic contributions, which were estimated from the Pascal constants.

Synthesis of the Title Compound: 0.3 g (1.3 mmol) of copper(II) tetrafluoroborate and 0.4 g (2.6 mmol) of bpy were each dissolved in 10 mL of ethanol/water (1:1) and the solutions mixed carefully together. A few drops of 2 M sodium hydroxide solution was added in such a way that no precipitation was observed. The mixture was filtered and, after several weeks to a month standing in the open, air blue crystals separated. The crystals were filtered off and washed with ethanol.

When the same procedure was followed in an excicator under a CO_2 atmosphere (dry ice) the crystals were formed within a few days.

Attempts to synthesize the compounds by the addition of sodium or potassium carbonate yielded only the monomeric $Cu(bpy)_2(BF_4)_2$ compound.

Elemental analysis: $C_{63}H_{60}B_4Cu_3F_{16}N_{12}O_7$ (1635.1): calcd. C 46.3, H 3.7, N 10.3, Cu 11.7; found C 46.5, H 3.4, N 10.8, Cu 11.4.

X-ray Data Collection and Structure Determination: A blue prismatic crystal was selected and mounted on a glass fiber using the oil drop method.[24a] Data were collected on a Rigaku AFC-7S diffractometer (graphite-monochromated Mo-$K\alpha$ radiation, ω-2θ scans). The intensity data were corrected for Lorentz and polarization effects, for absorption (psi-scan absorption correction) and extinction. Two tetrafluoroborate groups and an ethanol solvent molecule were disordered. Two positions were assigned to F31, F32, and F33 atoms with a population parameter of 0.5. The other disordered tetrafluoroborate group was refined as two rigid groups with a population parameter of 0.5. The ethanol molecule was refined isotropically. All other non-hydrogen atoms were refined an-

isotropically. H atoms except those belonging to the water molecules were introduced in calculated positions and refined with fixed geometry with respect to their carrier atoms. The structure was solved by direct methods. The programs TEXSAN,[24b] SHELXS-97,[24c] SHELXL-97[24d] were used for data reduction, structure solution, and structure refinement, respectively. Refinement of F^2 was performed against all reflections. The weighted R-factor wR and goodness of fit S are based on F^2, while conventional R-factors are based on F, with F set to zero for negative F^2. Crystal data and numerical details of the structure determination are given in Table 3. Crystallographic data (excluding structure factors) for the structure in this paper have been deposited with the Cambridge Crystallographic Data Centre as supplementary publication no. CCDC-139540. Copies of the data can be obtained free of charge on application to CCDC, 12 Union Road, Cambridge CB2 1EZ, UK [Fax: (internat.) +44(1223)336-033, E-mail: deposit@ccdc.cam.ac.uk].

Table 3. Crystal data and details of the structure determination

Crystal data	
Compound	$Cu_3B_4C_{63}F_{16}H_{60}N_{12}O_7$
Mol. wt.	1635
Crystal system	triclinic
Space group	$P\bar{1}$
a (Å)	13.405(7)
b (Å)	13.691(7)
c (Å)	21.446(8)
α (°)	82.87(4)
β (°)	73.57(4)
γ (°)	64.32(4)
V (Å^3)	3402(3)
Z	2
D_{calc} (g cm^{-3})	1.596
$F(000)$	1658
μ (cm^{-1})	1.035
Crystal size (mm)	0.42 × 0.30 × 0.22
Data collection and refinement	
Radiation	Mo-K_α, 0.71073 Å
Total data coll.	12867
Independent refl. (R_{int})	12383 (0.0221)
Observed refl. [$I > 2\sigma(I)$]	9589
No.of refined params.	979
Final $R1$, $wR2$[a]	0.0677, 0.1836
Min. and max. resd. dens. e·Å^{-3}	1.192, −0.779

[a] Weighting scheme: $w = 1.0/[\sigma^2(F_o^2) + (0.1614 \cdot P)^2 + 16.3151 \cdot P]$.

Acknowledgments

The work described in the present paper has been supported by the Leiden University Study group WFMO (Werkgroep Fundamenteel Materialen Onderzoek).

[1] [1a] D. A. Palmer, R. van Eldik, *Chem. Rev.* **1983**, *83*, 651−731. − [1b] D. H. Gibson, *Coord. Chem. Rev.* **1999**, *185−186*, 335−355. − [1c] D. Walther, M. Ruben, S. Rau, *Coord. Chem. Rev.* **1999**, *182*, 67−100. − [1d] X. Yin, J. R. Moss, *Coord. Chem. Rev.* **1999**, *181*, 27−59.

[2] [2a] Y. Nishida, A. Yatani, Y. Nakao, J.-I. Taka, S. Kashino, W. Mori, S. Suzuki, *Chem. Lett.* **1999**, 135−136 and references cited therein. − [2b] N. Kitajima, S. Hikichi, M. Tanaka, Y. Moro-oka, *J. Am. Chem. Soc.* **1993**, *115*, 5496−5508 and references cited therein. − [2c] P. E. Kruger, G. D. Fallon, B. Moubaraki, K. J. Berry, K. S. Murray, *Inorg. Chem.* **1995**, *34*, 4808−4814.

[3] [3a] F. W. B. Einstein, A. C. Willis, *Inorg. Chem.* **1981**, *20*, 609−614. − [3b] A. Escuer, E. Peñalba, R. Vicente, X. Solans, M. Font-Bardía, *J. Chem. Soc., Dalton Trans.* **1997**, 2315−2319.

[4] C. Bazzicalupi, A. Bencini, A. Bencini, A. Bianchi, F. Corana, V. Fusi, C. Giorgi, P. Paoli, P. Paoletti, B. Valtancoli, C. Zanchini, *Inorg. Chem.* **1996**, *35*, 5540−5548.

[5] G. Kolks, S. J. Lippard, J. V. Waszczak, *J. Am. Chem. Soc.* **1980**, *102*, 4833−4835.

[6] C. Bazzicalupi, A. Bencini, A. Bianchi, V. Fusi, P. Paoletti, B. Valtancoli, *J. Chem. Soc., Chem. Commun.* **1995**, 1555−1556.

[7] A. Escuer, R. Vicente, E. Peñalba, X. Solans, M. Font-Bardía, *Inorg. Chem.* **1996**, *35*, 248−251.

[8] J. Springborg, J. Glerup, I. Søtofte, *Acta Chem. Scand.* **1997**, *51*, 832−838.

[9] S. Yan, J. Cui, X. Liu, P. Cheng, D. Liao, Z. Jiang, G. Wang, H. Wang, X. Yao, *Science in China (Series B)* **1999**, *42*, 535−542.

[10] N. F. Curtis, R. W. Hay, Y. M. Curtis, *J. Chem. Soc. (A)* **1968**, 182−187

[11] M. Toofan, A. Boushehri, M. Ul-Haque, *J. Chem. Soc., Dalton Trans.* **1976**, 217−219.

[12] I. Castro, J. Faus, M. Julve, C. Bois, J. A. Real, F. Lloret, *J. Chem. Soc., Dalton Trans.* **1992**, 47−52.

[13] [13a] A. T. Casey, B. F. Hoskins, F. D. Whillans, *Chem. Commun.* **1970**, 904−905. − [13b] B. F. Hoskins, F. D. Whillans, *J. Chem. Soc., Dalton Trans.* **1975**, 1267−1272. − [13c] B. N. Figgis, R. Mason, A. R. P. Smith, J. N. Verghese, G. A. Williams, *J. Chem. Soc., Dalton Trans.* **1983**, 703−711.

[14] [14a] R. J. Majeste, E. A. Meyers, *J. Phys. Chem.* **1970**, *74*, 3497−3500. − [14b] A. Tadsanaprasittipol, H.-B. Kraatz, G. D. Enright, *Inorg. Chim. Acta* **1998**, *278*, 143−149. − [14c] I. Castro, J. Faus, M. Julve, M. Verdaguer, A. Monge, E. Gutierrez-Puebla, *Inorg. Chim. Acta* **1990**, *170*, 251−257.

[15] [15a] O. P. Anderson, *J. Chem. Soc., Dalton Trans.* **1972**, 2597−2601. − [15b] H. Nakai, *Bull. Chem. Soc. Jpn.* **1971**, *44*, 2412−2415. − [15c] H. Nakai, S. Ooi, H. Kuroya, *Bull. Chem. Soc. Jpn.* **1970**, *43*, 577. − [15d] R. J. Fereday, P. Hodgson, S. Tyagi, B. J. Hathaway, *J. Chem. Soc., Dalton Trans.* **1981**, 2070−2077. − [15e] K. J. Catalan, S. Jackson, J. D. Zubkowski, D. L. Perry, E. J. Valente, L. A. Feliu, A. Polanco, *Polyhedron* **1995**, *14*, 2165−2171. − [15f] C. Simmons, A. Clearfield, W. Fitzgerald, S. Tyagi, B. Hathaway, *J. Chem. Soc., Chem. Commun.* **1983**, 189−190. − [15g] C. J. Simmons, A. Clearfield, W. Fitzgerald, S. Tyagi, B. J. Hathaway, *Inorg. Chem.* **1983**, *22*, 2463−2466. − [15h] C. J. Simmons, B. J. Hathaway, K. Amornjarusiri, B. D. Santarsiero, A. Clearfield, *J. Am. Chem. Soc.* **1987**, *109*, 1947−1958. − [15i] H. Nakai, *Bull. Chem. Soc. Jpn.* **1977**, *50*, 531−532. − [15j] I. I. Mathews, H. Manohar, *Acta Cryst.* **1991**, *C47*, 2213−2214.

[16] J. Foley, D. Kennefick, D. Phelan, S. Tyagi, G. Hathaway, *J. Chem. Soc., Dalton Trans.* **1983**, 2333−2338.

[17] [17a] G. A. van Albada, M. T. Lakin, N. Veldman, A. L. Spek, J. Reedijk, *Inorg. Chem.* **1995**, *34*, 4910−4917. − [17b] G. A. van Albada, W. J. J. Smeets, A. L. Spek, J. Reedijk, *Inorg. Chim. Acta* **1997**, *260*, 151−161. − [17c] S. Amani Komaei, G. A. van Albada, I. Mutikainen, U. Turpeinen, J. Reedijk, *Eur. J. Inorg. Chem.* **1998**, 1577−1579. − [17d] S. Amani Komaei, G. A. van Albada, J. G. Haasnoot, H. Kooijman, A. L. Spek, J. Reedijk, *Inorg. Chim. Acta* **1999**, *286*, 24−29. − [17e] S. Amani Komaei, G. A. van Albada, I. Mutikainen, U. Turpeinen, J. Reedijk, *Polyhedron* **1999**, *18*, 1991−1997.

[18] X.-M. Chen, Q.-Y. Deng, G. Wang, Y.-J. Xu, *Polyhedron* **1994**, *13*, 3085−3089.

[19] A. W. Addison, T. N. Rao, J. Reedijk, J. van Rijn, G. C. Verschoor, *J. Chem. Soc., Dalton Trans.* **1984**, 1349−1356.

[20] [20a] B. J. Hathaway, in: *Comprehensive Coordination Chemistry* (Eds.: G. Wilkinson, R. D. Gill and J. A. McCleverty), Pergamon Press, Oxford, **1987**, Vol. 5. − [20b] G. A. van Albada, I. Mutikainen, U. Turpeinen, J. Reedijk, *Eur. J. Inorg. Chem.* **1998**, 547−549. − [20c] G. A. van Albada, P. J. van Koningsbruggen, I. Mutikainen, U. Turpeinen, J. Reedijk, *Eur. J. Inorg. Chem.* **1999**, 2269−2275.

[21] J. Shi, P. Cheng, M. Miao, Y. Liu, D. Liao, Z. Jiang, G. Wang, *Trans. Metal Chem.* **1996**, *21*, 512−514.

[22] O. Kahn, *Molecular Magnetism*, VCH, New York, **1993** and references cited therein.

[23] [23a] A. Bencini, C. Benelli, A. Dei, D. Gatteschi, *Inorg. Chem.* **1985**, *24*, 695−699. − [23b] M. Angaroni, G. A. Ardizzoia, T. Beringhelli, G. La Monica, D. Gatteschi, N. Masciocchi, M. Moret, *J. Chem. Soc., Dalton Trans.* **1990**, 3305−3309.

[24] [24a] T. Kottke, D. Stalke, *J. Appl. Crystallogr.* **1993**, *26*, 615−619. − [24b] TEXSAN. *Single Crystal Structure Analysis Software*, Version 1.6, Molecular Structure Corporation, The Woodlands, TX.77381, USA, **1993**. − [24c] G. M. Sheldrick, SHELXS97, *Program for crystal structure determination*, University of Göttingen, Germany, **1997**. − [24d] G. M. Sheldrick, SHELXL97, *Program for crystal structure refinement*, University of Göttingen, Germany, **1997**.

Received February 8, 2000
[I00041]

Organometallic Nickel(II) Complexes Containing Thiolate and Dithiocarbamate Ligands

Gregorio Sánchez,[a] Francisco Ruiz,[a] José L. Serrano,[b] M. Carmen Ramírez de Arellano,[c] and Gregorio López*[a]

Keywords: Phosphanes / Nickel / S ligands / Dithiocarbamate complexes / Bioinorganic chemistry

The mono(pentafluorophenyl)nickel(II) complexes $[Ni(C_6F_5)ClL_2]$ (L = $PPhMe_2$, PPh_2Me; L_2 = dppe) react with KSR (R = Ph, C_6H_4Me-*p*, C_6H_4OMe-*p*, C_6H_4Cl-*p*, $C_6H_3Cl_2$-2,6, $C_6H_4NO_2$-*p*) at room temperature in acetone/dichloromethane to give the mononuclear thiolate complexes $[Ni(C_6F_5)(SR)L_2]$. The binuclear μ-thiolate complex $[\{Ni(C_6F_5)(PPhMe_2)\}_2(\mu\text{-}SC_6H_4NO_2\text{-}p)_2]$ is obtained by reaction of $KSC_6H_4NO_2$-*p* with the same chloro complex in refluxing dichloromethane. A single-crystal X-ray diffraction study of $[Ni(C_6F_5)(SC_6H_4NO_2\text{-}p)(PPhMe_2)_2]$ and $[\{Ni_2(C_6F_5)_2(PPhMe_2)_2(\mu\text{-}SC_6H_4NO_2\text{-}p)_2]$ has established the mononuclear and binuclear nature of the complexes. The dithiocarbamatenickel complexes $[Ni(C_6F_5)(S_2CNR_2)L]$ (L = $PPhMe_2$, PPh_2Me, PEt_3; R = Et, *i*Pr; R_2 = C_5H_{10}, C_4H_8O) have been prepared by reaction of $[Ni(C_6F_5)ClL_2]$ (L = $PPhMe_2$, PPh_2Me, PEt_3) with the alkali metal salt of the corresponding dithioacid. A single-crystal X-ray diffraction study of $[Ni(C_6F_5)(S_2CNiPr_2)(PPhMe_2)]$ has established the mononuclear nature of the complex, and the geometry around each Ni atom as that of a tetrahedrally distorted square-planar geometry. Analytical (C, H, N), spectroscopic (IR, ^1H, and ^{19}F NMR), and mass spectrometry (FAB) data have been used for structural assignments.

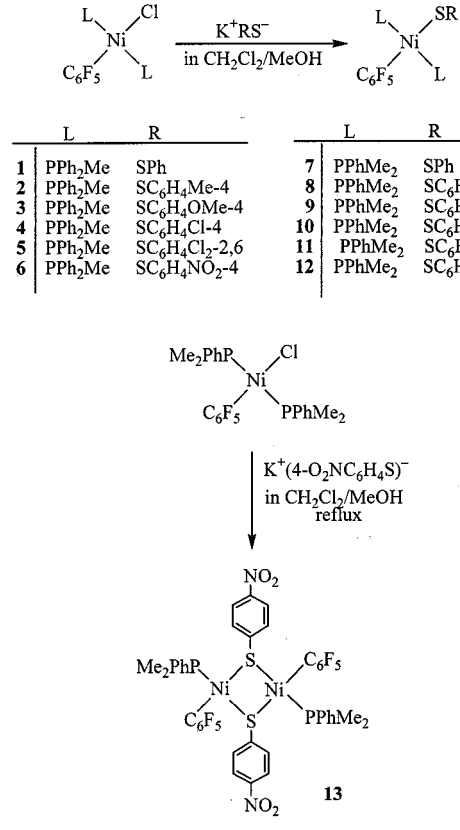
Introduction

Monomeric late transition-metal thiolate complexes have been receiving increasing attention,[1−3] in part because of their relevance as models of biologically redox-active metalloproteins.[4] Nickel complexes with S-donor ligands are present in many hydrogenases.[5] Nickel(II) thiolates are generally square-planar species with a strong tendency to form dimers and oligomers.[6−9] Despite the great amount of work devoted to the study of metal−thiolate complexes,[1] fundamental knowledge of the structures of mononuclear species is relatively sparse.[10,11] Di- and trinuclear pentafluorophenylnickel complexes have been prepared by treating the di-μ-hydroxo-complex $[NBu_4]_2[\{Ni(C_6F_5)_2(\mu\text{-}OH)\}_2]$ with thiols.[12] Considering related complexes with S-donor ligands, mononuclear derivatives such as $[Ni(C_6F_5)_2(S_2CNR_2)]^-$,[13] $[Ni(S_2CNEt_2)(PPh_3)_2]^+$,[14] and $[Ni(S_2COEt)_2(PPh_3)]$[15] have also been studied.

Results and Discussion

Mononuclear Thiolate Complexes

The addition of a methanolic solution of the corresponding alkali metal arylthiolate to a solution of $[Ni(C_6F_5)ClL_2]$ (L = $PPhMe_2$, PPh_2Me) in dichloromethane results in the rapid formation of the mononuclear arylthiolate complexes $[Ni(C_6F_5)(SR)L_2]$ (**1**−**12**) shown in Scheme 1. The forma-



	L	R
1	PPh_2Me	SPh
2	PPh_2Me	SC_6H_4Me-4
3	PPh_2Me	SC_6H_4OMe-4
4	PPh_2Me	SC_6H_4Cl-4
5	PPh_2Me	$SC_6H_4Cl_2$-2,6
6	PPh_2Me	$SC_6H_4NO_2$-4

	L	R
7	$PPhMe_2$	SPh
8	$PPhMe_2$	SC_6H_4Me-4
9	$PPhMe_2$	SC_6H_4OMe-4
10	$PPhMe_2$	SC_6H_4Cl-4
11	$PPhMe_2$	$SC_6H_4Cl_2$-2,6
12	$PPhMe_2$	$SC_6H_4NO_2$-4

Scheme 1

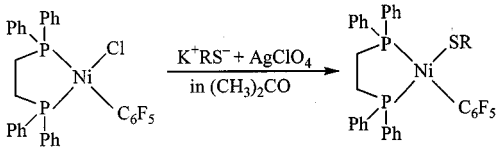
[a] Departamento de Química Inorgánica, Universidad de Murcia, E-30071 Murcia, Spain
E-mail: gll@fcu.um.es
[b] Departamento de Ingeniería Minera, Geológica y Cartográfica. Universidad Politécnica de Cartagena, E-30203 Cartagena, Spain
[c] Departamento de Química Orgánica, Facultad de Farmacia, Universidad de Valencia, E-46100 Valencia, Spain

 © WILEY-VCH Verlag GmbH, D-69451 Weinheim, 2000 1434−1948/00/1010−2185 $ 17.50+.50/0

tion of these mononuclear complexes takes place at ambient temperature; on increasing the temperature, loss of a phosphane ligand may occur, and the binuclear μ-arylthiolate would be the reaction product. In fact, when the solution containing $[Ni(C_6F_5)Cl(PPhMe_2)_2]$ and $KSC_6H_4NO_2$-4 was boiled under reflux, the binuclear complex $[\{Ni(C_6F_5)(PPhMe_2)\}_2(\mu\text{-}SC_6H_4NO_2\text{-}4)_2]$ (**13** in Scheme 1) was obtained. The *trans* influence of the pentafluorophenyl ligand should favour the dissociation of one phosphane molecule, and the resulting vacant coordination site is occupied by a μ-arylthiolate group.

The ^{19}F NMR spectra of complexes **1**−**13** show the expected three-resonance signals for a pentafluorophenyl ring freely rotating around the carbon−nickel bond (2 F_o:1 F_p:2 F_m). The experimental NMR pattern consists of a doublet for the *o*-fluorine atoms, a triplet for the *p*-fluorine atom and multiplet for the *m*-fluorine atoms. The observation of a single signal in the ^{31}P NMR spectra indicates that complexes **1**−**12** all have the *trans* geometry shown in Scheme 1. The same *trans* geometry should also be assigned to complex **13** because only one set of ^1H resonances for the 4-$O_2NC_6H_4S$ group is found in the ^1H NMR spectrum (two doublets for 2,6-H and 3,5-H, respectively, although one doublet is overlapped with the multiplet of the phenyl group.

In acetone, $[Ni(C_6F_5)Cl(dppe)]$ reacts with $AgClO_4$ with elimination of AgCl; on removing the precipitated AgCl, the addition of an alkali metal thiolate (in methanol) to the resulting solution gives the corresponding mononuclear thiolates **14**−**19** shown in Scheme 2. The ^{19}F NMR spectra of these complexes are qualitatively similar to those of **1**−**12**, but the ^{31}P NMR spectroscopic data indicate the presence of two nonequivalent phosphorus atoms, one *trans* to S and one *trans* to C, and two ^{31}P resonances are found in the range δ = 50−56; the multiplet structure of the low-field signal is due to coupling to the *o*-fluorine atoms of the pentafluorophenyl group and this signal is consequently assigned to the phosphorus atom *trans* to C_6F_5.



14: R = Ph
15: R = SC_6H_4Me-4
16: R = SC_6H_4OMe-4
17: R = SC_6H_4Cl-4
18: R = $SC_6H_4Cl_2$-2,6
19: R = $SC_6H_4NO_2$-4

Scheme 2

The neutral compounds **1**−**19** show the characteristic infrared absorptions of the pentafluorophenyl group[16] at ca. 1630m, 1495vs, 1050s, 950vs, and 780s cm^{-1}.

Crystal Structures of Complexes 12 and 13

The X-ray crystal structure determinations carried out for complexes $[Ni(C_6F_5)(SC_6H_4NO_2\text{-}4)(PPhMe_2)_2]$ **(12)** and $[\{Ni(C_6F_5)(PPhMe_2)\}_2(\mu\text{-}SC_6H_4NO_2\text{-}4)_2]$ **(13)** show the mono- and di-nuclearity of these complexes. A view of complex **12** is depicted in Figure 1, and relevant bond lengths and bond angles are shown in Table 1. The Ni atom and the four atoms coordinated to it deviate slightly from the plane defined by them. The Ni−C distance is similar to values found in other pentafluorophenylnickel compounds;[17,18] the strong *trans* influence of the C_6F_5 group is manifested by a lengthening of the Ni−S bond, giving a distance of 2.233 Å, which is significantly longer than those found in homoleptic nickel-thiolate complexes.[19]

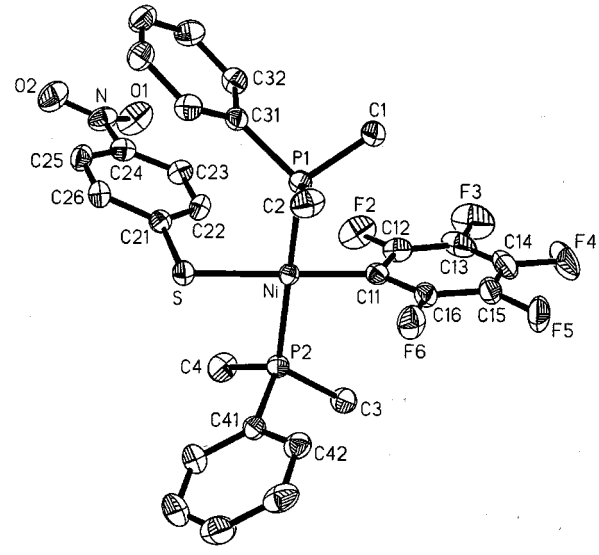


Figure 1. Molecular structure of compound **12**

The structure of complex **13** consists of centrosymmetric binuclear molecules with two Ni atoms bridged by arylthiolate groups (Figure 2). Bond lengths and bond angles are given in Table 1. The nickel atoms have approximately square-planar coordination, the deviation from the ideal geometry being revealed by the S−Ni−S angles. The Ni−S distances, 2.2140(11) and 2.2490(11), are quite similar to those found in the asymmetric binuclear complex $[(C_6F_5)_2Ni(\mu\text{-}SPh)_2Pd(dppe)]$ [2.214(2) and 2.2509(14)].[20] In the trinuclear complex $[Ni_3(C_6F_5)_4(\mu\text{-}SEt)_4]$ a weighted mean Ni−S distance of 2.203(5) was observed.[12]

Dithiocarbamate Complexes

The addition of a methanolic solution of the alkali metal dithiocarbamate (diethyldithiocarbamate, diisopropyldithiocarbamate, piperidinecarbodithioate, and morpholinecarbodithioate) to a solution of $[Ni(C_6F_5)ClL_2]$ (L = $PPhMe_2$, PPh_2Me, PEt_3) in dichloromethane results in the formation of the dithiocarbamate complexes $[Ni(C_6F_5)(S_2CNR_2)L]$ (**20**−**31**) with loss of one phosphane molecule (Scheme 3).

The ^{19}F NMR spectra of the dithiocarbamatenickel complexes exhibit the three signals (2 F_o:1 F_p:2 F_m) corresponding to a freely rotating C_6F_5 ring, and the ^{31}P NMR spectra show the single resonance expected for the phosphane ligand. The most relevant IR absorptions of coordinated dithiocarbamate are those originating from the thioureide group. In complexes **20**−**31**, the C−N and C−S stretching vibrations[21,22,23] are found at 1550−1450 cm^{-1} and 995−970 cm^{-1}, respectively, and the presence of only one

Table 1. Selected bond lengths [Å] and angles [°] for complexes **12**, **13**, and **24**

12		**13**		**24**	
Bond lengths					
Ni−C(11)	1.911(2)	Ni−C(1)	1.899(4)	Ni−C(1)	1.923(2)
Ni−P(1)	2.2087(7)	Ni−S	2.2140(11)	Ni−S(1)	2.2029(5)
Ni−P(2)	2.1905(7)	Ni−P	2.1807(12)	Ni−S(2)	2.2144(5)
Ni−S	2.2335(7)	Ni−S#1	2.2490(11)	Ni−P	2.1683(5)
Bond angles					
C(11)−Ni−P(1)	89.98(7)	C(1)−Ni−P	88.17(14)	C(1)−Ni−P	91.80(5)
C(11)−Ni−P(2)	91.63(7)	P−Ni−S	97.73(4)	C(1)−Ni−S(1)	91.40(5)
P(1)−Ni−S	89.01(2)	C(1)−Ni−S#1	90.53(14)	P−Ni−S(2)	98.11(2)
P(2)−Ni−S	89.42(3)	S−Ni−S#1	83.72(4)	S(1)−Ni−S(2)	78.77(2)

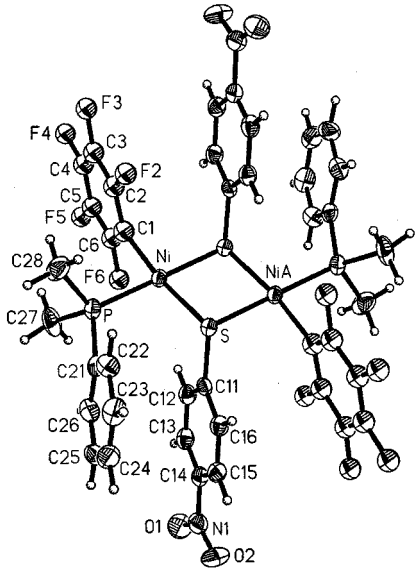


Figure 2. Molecular structure of compound **13**

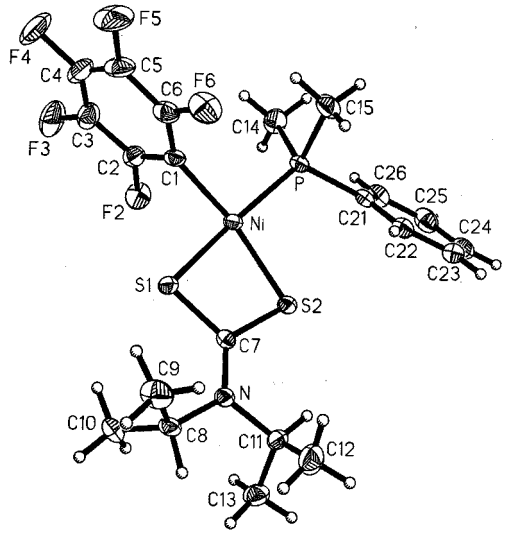
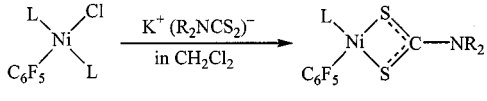


Figure 3. Molecular structure of compound **24**



	L	R		L	R
20	PPh_2Me	Et	**26**	PPh_2Me	C_5H_{10}
21	$PPhMe_2$	Et	**27**	$PPhMe_2$	C_5H_{10}
22	PEt_3	Et	**28**	PEt_3	C_5H_{10}
23	PPh_2Me	*i*Pr	**29**	PPh_2Me	C_4H_8
24	$PPhMe_2$	*i*Pr	**30**	$PPhMe_2$	C_4H_8
25	PEt_3	*i*Pr	**31**	PEt_3	C_4H_8

Scheme 3

band for ν(CS) is consistent with bidentate coordination of the dithiocarbamate.[24,25] Since the C=N and C−N stretching vibrations are usually found at 1690−1640 and 1350−1250 cm^{-1},[25] the thioureide band at 1550−1450 cm^{-1} indicates that the C−N bond in the coordinated $(S_2CNR_2)^-$ has considerable double bond character. However, the ^1H NMR spectra of complexes **20**−**31** indicate that rotation of the NR_2 group around the C−N bond is not hindered.

Crystal Structure of Complex 24

The structure of $[Ni(C_6F_5)(S_2CN\textit{i}Pr_2)(PPhMe_2)]$ (**24**) has been determined by X-ray crystallography. An ORTEP diagram is provided in Figure 3, and relevant bond lengths and angles are reported in Table 1. The overall coordination geometry about the nickel atom is essentially square planar. The S1−Ni−S2 angle is restricted by the chelate ring to 78.77(2)°. The P−Ni−S2 bond angle compensates to a great extent for the low angle by opening to 98.11(2)° with the C1−Ni−S1 angle at 91.40(5)°. The strong Ni−C_6F_5 bonding is evident in the nonequivalent Ni−S1 and Ni−S2 bond lengths and the *trans* influence exerted by the pentafluorophenyl ring is higher than that of the phosphane ligand lengthening the bond Ni−S2 giving a distance of 2.2144(5) Å, longer than the distance Ni−S1, 2.2029(5).

Conclusion

This work shows that mononuclear Ni-thiolate complexes $[Ni(C_6F_5)(SR)L_2]$ can be conveniently prepared by metathetical reactions carried out with the corresponding chloro complexes $[Ni(C_6F_5)ClL_2]$. The reaction temperature is a decisive factor in the formation of the mononuclear thiolate complex. At room temperature the mononuclear thiolato complex is the outcome of the metathetical reaction, but if the reaction is carried out in refluxing dichloromethane the binuclear thiolate complex is obtained with the concomitant release of one L molecule. The dithiocarba-

mate complexes are similarly obtained when $[Ni(C_6F_5)ClL_2]$ is treated with KS_2CNR_2.

Experimental Section

General Methods: C, H, and N analyses were carried out with a Carlo Erba instrument. − Infrared spectra were recorded with a Perkin−Elmer 16F-PC-FT spectrophotometer using Nujol mulls between polyethylene sheets. − ^1H, ^{31}P, and ^{19}F NMR spectra were recorded with a Bruker AC 200E or a Varian 300 spectrometer. − Conductance measurements were performed with a Crison 525 conductimeter (in acetone solution, $c \approx 5 \times 10^{-4}$ mol·dm^{-3}). − Decomposition temperatures were determined with a Reichert microscope. − All solvents were dried by conventional methods. − The compounds $[Ni(C_6F_5)Cl(PPhMe_2)_2]$,[18] $[Ni(C_6F_5)Cl(PPh_2Me)_2]$,[19] $[Ni(C_6F_5)Cl(dppe)]$,[26] and $[Ni(C_6F_5)Cl(PEt_2)_2]$[19] were prepared as described elsewhere.

$[Ni(C_6F_5)(SR)L_2]$; L = PPh_2Me and R = Ph (1), C_6H_4Me-*p* (2), C_6H_4OMe-*p* (3), C_6H_4Cl-*p* (4), $C_6H_4Cl_2$-2,6 (5), $C_6H_4NO_2$-*p* (6); L = $PPhMe_2$ and R = Ph (7), C_6H_4Me-*p* (8), C_6H_4OMe-*p* (9), C_6H_4Cl-*p* (10), $C_6H_4Cl_2$-2,6 (11), $C_6H_4NO_2$-*p* (12): A solution of $[Ni(C_6F_5)ClL_2]$ (0.164 mmol) in dichloromethane (10 mL) was added to a solution of KSR (0.164 mmol) in methanol (10 mL), and the solution was stirred at room temperature for 30 min. It was concentrated under reduced pressure to ca. 5 mL. The addition of water (ca. 1 mL) caused precipitation of a red solid, which was filtered off, washed with hexane and air-dried. The complexes were recrystallized from dichloromethane/hexane.

1: Yield: 72%. − $C_{38}H_{31}F_5NiP_2S$ (735.4): calcd. C 62.1, H 4.2, S 4.4; found C 62.0, H 4.4, S 4.2. − M.p. 156 °C (dec.). − ^1H NMR ([D$_6$]acetone): δ = 1.7 (t, 6 H, PPh_2*Me*), 7.0 (m, 3 H, SPh), 7.2 (m, 12 H, P*Ph* $_2$Me), 7.5 (m, 8 H, P*Ph*$_2$Me), 7.7 (d, 2 H, SPh). − ^{19}F NMR ([D$_6$]acetone): δ = −116.7 (d, J_{om} = 25.0 Hz, 2 F_o), −162.3 (t, J_{mp} = 19.8 Hz, 1 F_p), −163.7 (m, 2 F_m). − $^{31}P\{^1H\}$ NMR ([D$_6$]acetone): δ = 8.4 (s).

2: Yield: 70%. − $C_{39}H_{33}F_5NiP_2S$ (749.4): calcd. C 62.5, H 4.4, S 4.3; found C 62.2, H 4.5, S 4.6. − M.p. 160 °C (dec.). − ^1H NMR ([D$_6$]acetone): δ = 1.7 (t, 6 H, PPh_2*Me*), 2.2 (s, 3 H, SC_6H_4*Me*-*p*), 6.8 (d, 2 H, SC_6H_4Me-*p*), 7.2 (m, 12 H, PPh_2Me), 7.5 (m, 8 H, PPh_2Me), 7.7 (d, 2 H, SC_6H_4Me-*p*). − ^{19}F NMR ([D$_6$]acetone): δ = −116.6 (d, J_{om} = 24.6 Hz, 2 F_o), −162.5 (t, J_{mp} = 20.0 Hz, 1 F_p), −163.8 (m, 2 F_m). − $^{31}P\{^1H\}$ NMR ([D$_6$]acetone): δ = 8.3 (s).

3: Yield 76%. − $C_{39}H_{33}F_5NiOP_2S$ (765.4): calcd. C 61.2, H 4.3, S 4.2; found C 61.0, H 4.6, S 4.5. − M.p. 155 °C (dec.). − ^1H NMR ([D$_6$]acetone): δ = 1.7 (t, 6 H, PPh_2*Me*), 3.7 (s, 3 H, SC_6H_4*MeO*-*p*), 6.5 (d, 2 H, SC_6H_4MeO-*p*), 7.4 (m, 14 H, PPh_2Me), 7.5 (m, 6 H, PPh_2Me), 7.6 (d, 2 H, SC_6H_4MeO-*p*). − ^{19}F NMR ([D$_6$]acetone): δ = −116.6 (d, J_{om} = 22.9 Hz, 2 F_o), −162.5 (t, J_{mp} = 21.4 Hz, 1 F_p), −163.8 (m, 2 F_m). − $^{31}P\{^1H\}$ NMR ([D$_6$]acetone): δ = 8.3 (s).

4: Yield 77%. − $C_{38}H_{30}ClF_5NiP_2S$ (769.8): calcd. C 59.3, H 3.9, S 4.2; found C 59.5, H 4.2, S 4.4. − M.p. 150 °C (dec.). − ^1H NMR ([D$_6$]acetone): δ = 1.7 (t, 6 H, PPh_2*Me*), 6.8 (d, 2 H, SC_6H_4Cl-*p*), 7.2 (m, 14 H, PPh_2Me), 7.4 (m, 6 H, PPh_2Me), 7.6 (d, 2 H, SC_6H_4Cl-*p*). − ^{19}F NMR ([D$_6$]acetone): δ = −116.6 (d, J_{om} = 24.8 Hz, 2 F_o), −161.8 (t, J_{mp} = 19.8 Hz, 1 F_p), −163.4 (m, 2 F_m). − $^{31}P\{^1H\}$ NMR ([D$_6$]acetone): δ = 8.0 (s).

5: Yield 74%. − $C_{38}H_{29}Cl_2F_5NiP_2S$ (804.3): calcd. C 56.7, H 3.6, S 4.0; found C 56.5, H 3.8, S 4.1. − M.p. 160 °C (dec.). − ^1H NMR ([D$_6$]acetone): δ = 1.7 (t, 6 H, PPh_2*Me*), 6.5 (t, 1 H, $SC_6H_4Cl_2$-2,6), 6.9 (d, 2 H, $SC_6H_4Cl_2$-2,6), 7.4 (m, 12 H, PPh_2Me), 8.0 (m, 8 H, PPh_2Me). − ^{19}F NMR ([D$_6$]acetone): δ = −113.6 (d, J_{om} = 26.9 Hz, 2 F_o), −162.3 (t, J_{mp} = 20.8 Hz, 1 F_p), −163.8 (m, 2 F_m). − $^{31}P\{^1H\}$ NMR ([D$_6$]acetone): δ = 4.0 (s).

6: Yield 76%. − $C_{38}H_{30}F_5NNiO_2P_2S$ (780.4): calcd. C 58.5, H 3.9, N 1.8, S 4.1; found C 58.7, H 4.1, N 1.9, S 4.3. − M.p. 170 °C (dec.). − ^1H NMR ([D$_6$]acetone): δ = 1.6 (t, 6 H, PPh_2*Me*), 7.3 (m, 12 H, PPh_2Me), 7.5 (m, 8 H, PPh_2Me, $SC_6H_4NO_2$-*p*), 7.6 (d, 2 H, SC_6H_4Cl-*p*). − ^{19}F NMR ([D$_6$]acetone): δ = −117.2 (d, J_{om} = 23.5 Hz, 2 F_o), −160.9 (t, J_{mp} = 19.7 Hz, 1 F_p), −162.6 (m, 2 F_m). − $^{31}P\{^1H\}$ NMR ([D$_6$]acetone): δ = 7.6(s).

7: Yield 79%. − $C_{28}H_{27}F_5NiP_2S$ (611.2): calcd. C 55.0, H 4.5, S 5.2; found C 55.2, H 4.8, S 5.3. − M.p. 120 °C (dec.). − ^1H NMR ([D$_6$]acetone)]: δ = 1.3 (t, 12 H, PPh*Me*$_2$), 7.0 (m, 3 H, SPh), 7.3 (m, 10 H, $PPhMe_2$), 7.8 (d, 2 H, SPh). − ^{19}F NMR ([D$_6$]acetone): δ = −117.6 (d, J_{om} = 27.0 Hz, 2 F_o), −161.1 (t, J_{mp} = 19.7 Hz, 1 F_p), −163.3 (m, 2 F_m). − $^{31}P\{^1H\}$ NMR ([D$_6$]acetone): δ = −3.7.

8: Yield 71%. − $C_{29}H_{29}F_5NiP_2S$ (625.3): calcd. C 55.7, H 4.7, S 5.1; found C 55.5, H 4.8, S 5.4. − M.p. 130 °C (dec.). − ^1H NMR ([D$_6$]acetone): δ = 1.3 (t, 12 H, PPh*Me*$_2$), 2.2 (s, 3 H, Me), 6.8 (d, 2 H, SC_6H_4Me-*p*), 7.2 (m, 10 H, $PPhMe_2$), 7.7 (d, 2 H, SC_6H_4Me-*p*). − ^{19}F NMR ([D$_6$]acetone): δ = −116.6 (d, J_{om} = 26.6 Hz, 2 F_o), −162.5 (t, J_{mp} = 20.0 Hz, 1 F_p), −163.8 (m, 2 F_m). − $^{31}P\{^1H\}$ NMR ([D$_6$]acetone): δ = −3.6 (s).

9: Yield 75%. − $C_{29}H_{29}F_5NiOP_2S$ (641.2): calcd. C 54.3, H 4.6, S 5.0; found C 54.6, H 4.9, S 4.9. − M.p. 135 °C (dec.). − ^1H NMR ([D$_6$]acetone): δ = 1.3 (t, 12 H, PPh*Me*$_2$), 3,7 (s, 3 H, MeO), 6.6 (d, 2 H, SC_6H_4MeO-*p*), 7.2 (m, 10 H, $PPhMe_2$), 7.7 (d, 2 H, SC_6H_4MeO-*p*). − ^{19}F NMR ([D$_6$]acetone): δ = −117.5 (d, J_{om} = 27.9 Hz, 2 F_o), −161.1 (t, J_{mp} = 20.0 Hz, 1 F_p), −163.3 (m, 2 F_m). − $^{31}P\{^1H\}$ NMR ([D$_6$]acetone): δ = −3.7 (s).

10: Yield 81%. − $C_{28}H_{26}ClF_5NiP_2S$ (645.7): calcd. C 52.1, H 4.1, S 5.0; found C 52.4, H 4.0, S 4.8. − M.p. 130 °C (dec.). − ^1H NMR ([D$_6$]acetone): δ = 1.3 (t, 12 H, PPh*Me*$_2$), 6.9 (d, 2 H, SC_6H_4Cl-*p*), 7.2 (m, 10 H, $PPhMe_2$), 7.7 (d, 2 H, SC_6H_4Cl-*p*). − ^{19}F NMR ([D$_6$]acetone): δ = −117.7 (d, J_{om} = 24.8 Hz, 2 F_o), −160.7 (t, J_{mp} = 19.8 Hz, 1 F_p), −163.0 (m, 2 F_m). − $^{31}P\{^1H\}$ NMR ([D$_6$]acetone): δ = −3.8.

11: Yield 80%. − $C_{28}H_{25}Cl_2F_5NiP_2S$ (680.1): calcd. C 49.4, H 3.7, S 4.7; found C 49.6, H 3.9, S 4.9. − M.p. 155 °C (dec.). − ^1H NMR ([D$_6$]acetone): δ = 1.3 (t, 12 H, PPh*Me*$_2$), 6.7 (t, 1 H, $SC_6H_4Cl_2$-2,6), 7.1 (d, 2 H, $SC_6H_4Cl_2$-2,6), 7.2 (m, 10 H, $PPhMe_2$). − ^{19}F NMR ([D$_6$]acetone): δ = −115.9 (d, J_{om} = 26.9 Hz, 2 F_o), −161.5 (t, J_{mp} = 20.8 Hz, 1 F_p), −163.5 (m, 2 F_m). − $^{31}P\{^1H\}$ NMR ([D$_6$]acetone): δ = −5.8.

12: Yield 83%. − $C_{28}H_{26}F_5NNiO_2P_2S$ (656.2): calcd. C 51.2, H 4.0, N 2.1, S 4.9; found C 51.0, H 4.1, N 2.0, S 4.7. − M.p. 160 °C (dec.). − ^1H NMR ([D$_6$]acetone): δ = 1.3 (t, 12 H, PPh*Me*$_2$), 7.2 (m, 12 H, $PPhMe_2$ + $SC_6H_4NO_2$-*p*), 7.7 (d, 2 H, $SC_6H_4NO_2$-*p*). − ^{19}F NMR ([D$_6$]acetone): δ = −117.2 (d, J $_{om}$ = 23.5 Hz, 2 F_o), −160.9 (t, J_{mp} = 19.7 Hz, 1 F_p), −162.6 (m, 2 F_m). − $^{31}P\{^1H\}$ NMR ([D$_6$]acetone): δ = −3.8.

$[\{Ni(C_6F_5)(PPhMe_2)\}_2(\mu\text{-}SC_6H_4NO_2\text{-}p)_2]$ (13): A solution of $[Ni(C_6F_5)Cl(PPhMe_2)_2]$ (0.164 mmol) in dichloromethane (10 mL) was added to a solution of $KSC_6H_4NO_2$-*p* (0.164 mmol) in methanol (10 mL), and the solution was heated under reflux for 5 h.

The solvent was then partly evaporated under reduced pressure to half the original volume, and the addition of diethyl ether caused the precipitation of a red-brown solid, which was filtered off, washed with hexane and air-dried. The complex was recrystallized from dichloromethane/diethyl ether. − Yield: 83%. − $C_{40}H_{30}F_{10}N_2Ni_2O_4P_2S_2$ (1036): calcd. C 46.4, H 2.9, N 2.7, S 6.2; found C 46.1, H 3.1, N 2.6, S 6.5. − M.p. 165 °C (dec.). − ^{1}H NMR ([D$_6$]acetone): δ = 1.3 (t, 12 H, PPh*Me*$_2$), 7.3 (m, 14 H, PPh*Me*$_2$ + $SC_6H_4NO_2$-*p*), 7.8 (d, 4 H, $SC_6H_4NO_2$-*p*). − ^{19}F NMR ([D$_6$]acetone): δ = −116.2 (d, J_{om} = 30.2, 2 F$_o$), −160.2 (t, J_{mp} = 19.7, 1 F$_p$), −162.4 (m, 2 F$_m$). − ^{31}P{^{1}H} NMR ([D$_6$]acetone): δ = − 5.0.

[Ni(C_6F_5)(SR)(dppe)]; R = Ph (14), C_6H_4Me-*p* (15), C_6H_4OMe-*p* (16), C_6H_4Cl-*p* (17), $C_6H_4Cl_2$–2,6 (18), $C_6H_4NO_2$-*p* (19): $AgClO_4$ (0.157 mmol) was added to a solution of [Ni(C_6F_5)Cl(dppe)] (100 mg, 0.157 mmol) in acetone (20 mL). After stirring at room temperature for 1 h, the precipitated AgCl was filtered off and the resulting solution was added to a solution of KSR (0.157 mmol) in methanol (10 mL). The solution was then stirred at room temperature for 30 min. It was concentrated under reduced pressure to ca. 5 mL. The addition of water (ca. 1 mL) caused precipitation of a brown solid, which was filtered off, washed with hexane and air-dried. The complexes were recrystallized from dichloromethane/hexane.

14: Yield 77%. − M.p. 215 °C (dec.). − $C_{38}H_{29}F_5NiP_2S$ (733.3): C 62.2, H 4.0, S 4.4; found C 62.0, H 4.2, S 4.6. − ^{1}H NMR ([D$_6$]acetone): δ = 2.1 (m, 4 H, dppe), 6.6 (m, 3 H, SPh), 7.1 (d, 2 H, SPh), 7.4 (m, 16 H, dppe), 8.0 (m, 4 H, dppe). − ^{19}F NMR ([D$_6$]acetone): δ = −116.9 (m, 2 F$_o$), −164.1 (t, J_{mp} = 21.4, 1 F$_p$), −165.2 (m, 2 F$_m$). ^{31}P{^{1}H} NMR ([D$_6$]acetone): δ = 50.4 (m, P$_A$), 54.8 (d, ^2J = 40.4, P$_B$).

15: Yield 81%. − $C_{39}H_{31}F_5NiP_2S$ (747.4): calcd. C 62.7, H 4.2, S 4.3; found C 62.4, H 4.3, S 4.5. − M.p. 195 °C (dec.). − ^{1}H NMR ([D$_6$]acetone): δ = 2.1 (s, 3 H, SC_6H_4*Me*-*p*), 2.5 (m, 4 H, dppe), 6.3 (d, 2 H, SC_6H_4Me-*p*), 6.8 (d, 2 H, SC_6H_4Me-*p*), 7.4 (m, 20 H, dppe). − ^{19}F NMR ([D$_6$]acetone): δ = −116.9 (m, 2 F$_o$), −164.7 (t, J_{mp} = 21.4 Hz, 1 F$_p$), −165.4 (m, 2 F$_m$). − ^{31}P{^{1}H} NMR ([D$_6$]acetone): δ = 50.5 (m, P$_A$), 54.5 (d, ^2J = 40.4 Hz, P$_B$).

16: Yield 82%. − $C_{39}H_{31}F_5NiOP_2S$ (763.4): calcd. C 61.4, H 4.1, S 4.2; found C 61.5, H 4.4, S 4.3. − M.p. 198 °C (dec.). − ^{1}H NMR ([D$_6$]acetone): δ = 2.1 (m, 4 H, dppe), 3.6 (s, 3 H, SC_6H_4*MeO*-*p*), 6.3 (d, 2 H, SC_6H_4MeO-*p*), 7.0 (d, 2 H, SC_6H_4MeO-*p*), 7.4 (m, 16 H, dppe), 8.0 (m, 4 H, dppe). − ^{19}F NMR ([D$_6$]acetone): δ = −116.9 (m, 2 F$_o$), −164.3 (t, J_{mp} = 21.4 Hz, 1 F$_p$), −165.0 (m, 2 F$_m$). − ^{31}P{^{1}H} NMR ([D$_6$]acetone): δ = 50.4 (m, P$_A$), 54.3 (d, ^2J = 40.4 Hz, P$_B$).

17: Yield 84%. − $C_{38}H_{28}ClF_5NiP_2S$ (767.8): calcd. C 59.5, H 3.7, S 4.2; found C 59.8, H 4.0, S 4.3. − M.p. 190 °C (dec.). − ^{1}H NMR ([D$_6$]acetone): δ = 2.1 (m, 4 H, dppe), 6.7 (d, 2 H, SC_6H_4Cl-*p*), 7.0 (d, 2 H, SC_6H_4Cl-*p*), 7.5 (m, 16 H, dppe), 8.0 (m, 4 H, dppe). − ^{19}F NMR ([D$_6$]acetone): δ = −116.8 (m, 2 F$_o$), −163.2 (t, J_{mp} = 21.4 Hz, 1 F$_p$), −164.8 (m, 2 F$_m$). − ^{31}P{^{1}H} NMR ([D$_6$]acetone): δ = 52.1 (m, P$_A$), 56.1 (d, ^2J = 41.4 Hz, P$_B$).

18: Yield 80%. − $C_{38}H_{27}Cl_2F_5NiP_2S$ (802.2): calcd. C 56.9, H 3.4, S 4.0; found C 57.0, H 3.2, S 4.2. − M.p. 205 °C (dec.). − ^{1}H NMR ([D$_6$]acetone): δ = 2.2 (m, 4 H, dppe), 6.6 (t, 1 H, $SC_6H_3Cl_2$-2,6), 6.9 (d, 2 H, $SC_6H_3Cl_2$-2,6), 7.4 (m, 16 H, dppe), 8.0 (m, 4 H, dppe). − ^{19}F NMR ([D$_6$]acetone): δ = −114.2 (m, 2 F$_o$), −163.8 (t, J_{mp} = 19.8 Hz, 1 F$_p$), −164.5 (m, 2 F$_m$). − ^{31}P{^{1}H} NMR ([D$_6$]acetone): δ = 52.0 (m, P$_A$), 54.6 (m, P$_B$).

19: Yield 86%. − $C_{38}H_{28}F_5NNiO_2P_2S$ (778.3): calcd. C 58.6, H 3.6, N 1.8, S, 4.1; found C 58.8, H 3.5, N 2.0, S 4.2. − M.p. 200 °C (dec.). − ^{1}H NMR ([D$_6$]acetone): δ = 2.2 (m, 4 H, dppe), 7.2 (d, 2 H, $SC_6H_4NO_2$-*p*), 7.4 (m, 4 H, dppe), 7.6 (m, 12 H, dppe), 7.9 (m, 4 H, dppe), 8.2 (d, 2 H, $SC_6H_4NO_2$-*p*). − ^{19}F NMR ([D$_6$]acetone): δ = −116.7 (m, 2 F$_o$), −162.1 (t, J_{mp} = 21.4 Hz, 1 F$_p$), −164.2 (m, 2 F$_m$). − ^{31}P{^{1}H} NMR ([D$_6$]acetone): δ = 51.2 (d, ^2J = 42.7 Hz, P$_A$), 56.0 (d, P$_B$).

[Ni(C_6F_5)(S_2CNR_2)L]; R = Et and L = PPh_2Me (20), $PPhMe_2$ (21), PEt_3 (22); R = *i*Pr and L = PPh_2Me (23), $PPhMe_2$ (24), PEt_3 (25); R = C_5H_{10} and L = PPh_2Me (26), $PPhMe_2$ (27), PEt_3 (28); R = C_4H_8 and L = PPh_2Me (29), $PPhMe_2$ (30), PEt_3 (31): Potassium dialkyldithiocarbamate (0.164 mmol) was added to a solution of [Ni(C_6F_5)ClL_2] (0.164 mmol) in acetone (20 mL) and the solution was stirred at room temperature for 15 min. It was concentrated under reduced pressure to ca. 5 mL. The addition of water (1 mL) caused precipitation of an orange solid, which was filtered off, washed with hexane and air-dried. The complexes were recrystallized from dichloromethane/hexane.

20: Yield 82%. − $C_{24}H_{23}F_5NNiPS_2$ (574.2): calcd. C 50.2, H 4.0, N 2.4, S 11.2; found C 50.3, H 3.8, N 2.5, S 11.5. − M.p. 124 °C (dec.). − ^{1}H NMR ([D$_6$]acetone): δ = 1.2 (t, 6 H, Et), 1.4 (t, 3 H, PPh_2Me), 3.6 (m, 4 H, Et), 7.4 (m, 6 H, PPh_2Me), 7.6 (m, 4 H, PPh_2Me). − ^{19}F NMR ([D$_6$]acetone): δ = −116.7 (d, 2 F$_o$, J_{om} = 23.7), −161.8 (t, $J_{m,p}$ = 19.7 Hz, 1 F$_p$), −164.3 (m, 2 F$_m$). − ^{31}P{^{1}H} NMR ([D$_6$]acetone): δ = 15.4 (s).

21: Yield 79%. − $C_{19}H_{21}F_5NNiPS_2$ (512.7): calcd. C 44.6, H 4.1, N 2.7, S 12.5; found C 44.3, H 3.9, N 2.6, S 12.4. − M.p. 119 °C (dec.). − ^{1}H NMR ([D$_6$]acetone): δ = 1.2 (t, 6 H, Et), 1.4 (m, 6 H, $PPhMe_2$), 3.6 (m, 4 H, Et), 7.4 (m, 3 H, PPh_2Me), 7.6 (m, 2 H, PPh_2Me). − ^{19}F NMR ([D$_6$]acetone): δ = −117.1 (d, J_{om} = 25.8 Hz, 2 F$_o$), −161.5 (t, J_{mp} = 19.2 Hz, 1 F$_p$), −164.3 (m, 2 F$_m$). − ^{31}P{^{1}H} NMR ([D$_6$]acetone): δ = 1.4 (s).

22: Yield 72%. − $C_{17}H_{25}F_5NNiPS_2$ (492.2): calcd. C 41.5, H 5.1, N 2.8, S 13.0; found C 41.2, H 5.0, N 2.8, S 13.1. − M.p. 112 °C (dec.). − ^{1}H NMR ([D$_6$]acetone): δ = 1.2 (m, 15 H, Et + PEt_3), 1.3 (m, 6 H, PEt_3), 3.6 (q, 4 H, Et). − ^{19}F NMR ([D$_6$]acetone): δ = −116.3 (d, J_{om} = 25.0, 2 F$_o$), −161.7 (t, J_{mp} = 19.7 Hz, 1 F$_p$), −164.2 (m, 2 F$_m$). − ^{31}P{^{1}H} NMR ([D$_6$]acetone): δ = 21.0 (s).

23: Yield 71%. − $C_{26}H_{27}F_5NNiPS_2$ (602.3): calcd. C 51.9, H 4.5, N 2.3, S 10.6; found C 51.6, H 4.4, N 2.4, S 10.4. − M.p. 151 °C (dec.). − ^{1}H NMR ([D$_6$]acetone): δ = 1.4 (m, 15 H, *i*Pr + PPh_2Me), 4.5 (m, 2 H, *i*Pr), 7.4 (m, 6 H, PPh_2Me), 7.6 (m, 4 H, PPh_2Me). − ^{19}F NMR ([D$_6$]acetone): δ = −116.4 (d, J_{om} = 23.4 Hz, 2 F$_o$), −162.1 (t, J_{mp} = 19.7 Hz, 1 F$_p$), −164.4 (m, 2 F$_m$). − ^{31}P{^{1}H} NMR ([D$_6$]acetone): δ = 15.3 (s).

24: Yield 78%. − $C_{21}H_{25}F_5NNiPS_2$ (540.2): calcd. C 46.7, H 4.6, N 2.6, S 11.9; found C 46.6, H 4.5, N 2.5, S 11.7. − M.p. 136 °C (dec.). − ^{1}H NMR ([D$_6$]acetone): δ = 1.4 (m, 18 H, *i*Pr + $PPhMe_2$), 4.5 (m, 2 H, *i*Pr), 7.4 (m, 3 H, $PPhMe_2$), 7.6 (m, 2 H, PPh_2Me). − ^{19}F NMR ([D$_6$]acetone): δ = −116.7 (d, J_{om} = 24.0, 2 F$_o$), −161.6 (t, J_{mp} = 19.5 Hz, 1 F$_p$), −164.2 (m, 2 F$_m$). − ^{31}P{^{1}H} NMR ([D$_6$]acetone): δ = 1.3 (s).

25: Yield 75%. − $C_{19}H_{29}F_5NNiPS_2$ (520.4): calcd. C 43.9, H 5.6, N 2.7, S 12.3; found C 44.0, H 5.6, N 2.6, S 12.2. − M.p. 115 °C (dec.). − ^{1}H NMR ([D$_6$]acetone): δ = 1.4 (m, 27 H, *i*Pr + PEt_3), 4.5 (m, 2 H, *i*Pr). − ^{19}F NMR ([D$_6$]acetone): δ = −116.2 (d, J_{om} = 25.0 Hz, 2 F$_o$), −161.9 (t, J_{mp} = 19.8 Hz, 1 F$_p$), −164.3 (m, 2 F$_m$). − ^{31}P{^{1}H} NMR ([D$_6$]acetone): δ = 20.3 (s).

Table 2. Crystal data and parameter of data collection for complexes **12**, **13**, and **24**

	12	**13**	**24**
Empirical formula	$C_{28}H_{26}F_5NNiO_2P_2S$	$C_{40}H_{30}F_{10}N_2Ni_2O_4P_2S_2$	$C_{21}H_{25}F_5NNiPS_2$
Formula mass	656.21	1036.14	540.22
Temperature	293(2) K	173(2) K	173(2) K
Absorption coefficient	9.30 cm^{-1}	12.18 cm^{-1}	11.08 cm^{-1}
Crystal system	monoclinic	monoclinic	monoclinic
Space group	$P2_1/c$	$P2_1/c$	$P2_1/c$
Unit cell dimensions	a = 15.647(4) Å	a = 10.2451(14) Å	a = 14.6464(12)
	b = 10.4481(14) Å	b = 8.38.01(10) Å	b = 11.9076(10)
	c = 19.035(3) Å	c = 23.523(3) Å	c = 13.8742(12)
	β = 114.21(2)°	β = 97.681(10)°	β = 101.086(6) °
Z; V Å^3	4; 2838.3(9) Å^3	2; 2001.5(5) Å^3	4; 2374.6(3) Å^3
Density (calculated)	1.361 g·cm^{-3}	1.719 g·cm^{-3}	1.511 g·cm^{-3}
Wavelength (Mo-K_α)	0.71073 Å	0.71073 Å	0.71073 Å
F (000)	1344	1048	1112
Independent reflections	4937	3514	4183
Parameters	365	248	286
$R1$	0.0429	0.0653	0.0283
$wR2$	0.1011	0.1162	0.0591

26: Yield 77%. − $C_{25}H_{23}F_5NNiPS_2$ (586.26): calcd. C 51.2, H 3.9, N 2.4, S 10.9; found C 51.1, H 4.0, N 2.4, S 10.6. − M.p. 170 °C (dec.). − ^{1}H NMR ([D$_6$]acetone): δ = 1.6 (m, 9 H, C_5H_{10} + PPh_2Me), 3.7 (m, 4 H, C_5H_{10}), 7.4 (m, 6 H, PPh_2Me), 7.6 (m, 4 H, PPh_2Me). − ^{19}F NMR ([D$_6$]acetone): δ = −116.7 (d, J_{om} = 24.0, 2 F_o), −161.8 (t, J_{mp} = 19.8 Hz, 1 F_p), −164.3 (m, 2 F_m). − ^{31}P{^{1}H} NMR ([D$_6$]acetone): δ = 15.6 (s).

27: Yield 76%. − $C_{20}H_{21}F_5NNiPS_2$ (524.2): calcd. C 45.8, H 4.0, N 2.7, S 11.2; found C 45.6, H 4.1, N 2.7, S 12.0. − M.p. 180 °C (dec.). − ^{1}H NMR ([D$_6$]acetone): δ = 1.2 (t, 6 H, $PPhMe_2$), 1.4 (m, 6 H, $C_5H_{10}N$), 3.7 (m, 4 H, $C_5H_{10}N$), 7.4 (m, 3 H, $PPhMe_2$), 7.6 (m, 2 H, PPh_2Me). − ^{19}F NMR ([D$_6$]acetone): δ = 117.0 (d, J_{om} = 23.5 Hz, 2 F_o), −161.3 (t, J_{mp} = 19.2 Hz, 1 F_p), −164.1 (m, 2 F_m). − ^{31}P{^{1}H} NMR ([D$_6$]acetone): δ = 1.8 (s).

28: Yield 74%. − $C_{18}H_{25}F_5NNiPS_2$ (504.2): calcd. C 42.9, H 5.0, N 2.8, S 12.7; found C 42.7, H 4.9, N 2.7, S 12.6. − M.p. 160 °C (dec.). − ^{1}H NMR ([D$_6$]acetone): δ = 1.2 (m, 15 H, PEt_3), 1.7 (m, 6 H, C_5H_{10}), 3.7 (m, 4 H, C_5H_{10}). − ^{19}F NMR ([D$_6$]acetone): δ = −116.4 (d, J_{om} = 24.2 Hz, 2 F_o), −161.6 (t, J_{mp} = 19.6 Hz, 1 F_p), −164.2 (m, 2 F_m). − ^{31}P{^{1}H} NMR ([D$_6$]acetone): δ = 21.3 (s).

29: Yield 75%. − $C_{24}H_{21}F_5NNiOPS_2$ (588.2): calcd. C 49.0, H 3.6, N 2.4, S 10.9; found C 48.9, H 3.7, N 2.3, S 10.7. − M.p. 147 °C (dec.). − ^{1}H NMR ([D$_6$]acetone): δ = 1.6 (m, 3 H, PPh_2Me), 3.7 (m, 8 H, C_4H_8O), 7.4 (m, 6 H, PPh_2Me), 7.6 (m, 4 H, PPh_2Me). − ^{19}F NMR ([D$_6$]acetone): δ = −116.9 (d, J_{om} = 23.5 Hz, 2 F_o), −161.4 (t, J_{mp} = 19.8 Hz, 1 F_p), −164.1 (m, 2 F_m). − ^{31}P{^{1}H} NMR ([D$_6$]acetone): δ = 15.3 (s).

30: Yield 79%. − $C_{19}H_{19}F_5NNiOPS_2$ (526.16): calcd. C 43.4, H 3.6, N 2.7, S 12.2; found C 43.3, H 3.5, N 2.6, S 12.3. − M.p. 142 °C (dec.). − ^{1}H NMR ([D$_6$]acetone): δ = 1.4 (m, 6 H, $PPhMe_2$), 3.7 (m, 8 H, C_4H_8O), 7.4 (m, 3 H, $PPhMe_2$), 7.6 (m, 2 H, PPh_2Me). − ^{19}F NMR ([D$_6$]acetone): δ = −117.3 (d, J_{om} = 23.8 Hz, 2 F_o), −160.9 (t, J_{mp} = 19.5 Hz, 1 F_p), −163.9 (m, 2 F_m). − ^{31}P{^{1}H} NMR ([D$_6$]acetone): δ = 1.8 (s).

31: Yield 74%. − $C_{17}H_{23}F_5NNiOPS_2$ (506.2): calcd. C 40.3, H 4.6, N 2.8, S 12.7; found C 40.5, H 4.4, N 2.9, S 12.7. − M.p. 128 °C (dec.). − ^{1}H NMR ([D$_6$]acetone): δ = 1.6 (m, 15 H, PEt_3), 3.7 (d, 4 H, C_4H_8O), 3.8 (d, 4 H, C_4H_8O). − ^{19}F NMR ([D$_6$]acetone): δ = −116.6 (d, J_{om} = 24.0 Hz, 2 F_o), −161.3 (t, J_{mp} = 19.8 Hz, 1 F_p), −164.0 (m, 2 F_m). − ^{31}P{^{1}H} NMR ([D$_6$]acetone): δ = 21.4 (s).

Determination of the X-ray Crystal Structures of 12, 13, and 24: Single crystals of complexes **12** (approximate dimensions 0.75 × 0.50 × 0.40 mm), **13** (0.50 × 0.30 × 0.20 mm), and **24** (0.60 × 0.50 × 0.30 mm) were mounted on a Siemens P4 diffractometer with LT2 temperature attachment. The crystallographic data are shown in Table 2. The scan method was ω with $2\Theta_{max}$ = 50° for the three cases, empirical Ψ-scan mode absorption was made. The structures were solved by direct methods and refined anisotropically on F^2.[26] The final R factors were 0.0367, 0.0451 and 0.0233 in **12**, **13**, and **24**, respectively {R_w = 0.0986, 0.1091, and 0.058, $w = 1/[\sigma^2 (F^2) + (aP)^2 + bP]$ where $P = (F_o^2 + 2F_c^2)/3$ and a and b are constants set by the program} over the observed reflections [$I > 2\sigma(I)$]. Crystallographic data (excluding structure factors) for the structures reported in this paper have been deposited with the Cambridge Crystallographic Data Centre as supplementary publications no. CCDC-139088 to CCDC-139090. Copies of the data can be obtained free of charge on application to The Director, CCDC, 12 Union Road, Cambridge CB2 1EZ, UK [Fax: (internat.) +44−1223/336-033, E-mail: deposit@chemcrys.cam.ac.uk].

Acknowledgments

The support of this work by the Dirección General de Enseñanza Superior e Investigación Científica (project PB97−1036), Spain, is gratefully acknowledged. J.L.S. thanks CAJAMURCIA, Spain, for a grant.

[1] P. J. Blower, J. R. Dilworth, *Coord. Chem. Rev.* **1987**, *76*, 121−185.
[2] R. J. Angelici, *Acc. Chem. Rev.* **1988**, *21*, 387−394.
[3] T. Yamamoto, K. Hataya, K. Osakada, *Inorg. Chem.* **1993**, *32*, 2360−2365.
[4] P. P. Power, S. C. Shoner, *Angew. Chem. Int. Ed. Eng.* **1991**, *30*, 330−332.
[5] R. Cammack, in *The Bioinorganic Chemistry of Nickel* (Ed.: J. R. Lancaster), VCH, New York, **1989**, ch. 8.
[6] A. D. Watson, Ch. P. Rao, J. R. Dorfman, R. H. Holm, *Inorg. Chem.* **1985**, *24*, 2820−2826.
[7] W. Tremel, M. Kriege, B. Krebs, G. Henkel, *Inorg. Chem.* **1988**, *27*, 3886−3895.
[8] G. S. White, D. W. Stephan, *Organometallics* **1988**, *7*, 903−910.
[9] T. A. Wark, D. W. Stephan, *Organometallics* **1989**, *8*, 2836−2843.
[10] M. J. Jiménez, M. C. Puerta, P. Valerga, *J. Chem. Soc., Dalton Trans.* **1996**, 1935−1939.

[11] J. Darkwa, F. Bothata, L. M. Koczon, *J. Organomet. Chem.* **1993**, *455*, 235−240.
[12] G. Sánchez, F. Ruiz, M. D. Santana, G. García, G. López, J. A. Hermoso, M. Martínez- Ripoll, *J. Chem. Soc., Dalton Trans.* **1994**, 19−23.
[13] G. López, G. Sánchez, G. García, J. García, A. Sanmartín, M. D. Santana, *Polyhedron* **1991**, *10*, 2821−2825.
[14] K. Ramalingan, G. Aravamundan, M. Seshasayee, *Inorg. Chim. Acta* **1987**, *128*, 231−235.
[15] E. R. T. Tiekink, G. Winter, *Aust. J. Chem.* **1986**, *39*, 813−817.
[16] E. Maslowsky, *Vibrational Spectra of Organometallic Compounds*, Wiley, New York, **1977**, p.437.
[17] G. López, G. García, G. Sánchez, J. García, J. A. Hermoso, A. Vegas, M. Martínez-Ripoll, *Inorg. Chem.* **1992**, *31*, 1518−1523.
[18] G. Sánchez, F. Ruiz, J. García, M. C. Ramírez de Arellano, G. López, *Helv. Chim. Acta* **1997**, *80*, 2477−2485.
[19] D. Swenson, N. C. Baenziger, D. Coucouvanis, *J. Am. Chem. Soc.* **1978**, *100*, 1932−1934.
[20] G. Sánchez, F. Momblona, M. Sánchez, J. Pérez, G. López, J. Casabó, E. Molins, C. Miravitlles, *Eur. J. Inorg. Chem.* **1998**, 1119−1204.
[21] D. Catheline, E. Román, D. Astruc, *Inorg. Chem.* **1984**, *23*, 4508−4514.
[22] M. B. Hursthouse, M. A. Malik, M. Motevalli, P. O′Brian, *Organometallics* **1991**, *10*, 730−732.
[23] R. Vicente, A. Escuer, J. Ribas, A. Dei, X. Solans, T. Calvet, *Polyhedron* **1990**, *9*, 1729−1735.
[24] F. Bonati, R. Ugo, *J. Organomet. Chem.* **1967**, *10*, 257−261.
[25] R. Kellner, G. St. Nikolov, N. Trendafilova, *Inorg. Chim. Acta* **1984**, *84*, 233−239.
[26] SHELXTL-5.0, Siemens Analytical X-Ray Instruments, Madison, WI.

Received February 14, 2000
[I00061]

Reactivity of The P_4 Molecule with Cobalt(I) and Rhodium(I) Polyphosphane Fragments

Massimo Di Vaira,[a] Markus P. Ehses,[a] Maurizio Peruzzini,[b] and Piero Stoppioni*[a]

Keywords: Phosphorus / Cobalt / Rhodium / NMR spectroscopy / Phosphanes

The reaction of white phosphorus with the electronically and coordinatively unsaturated systems $[(PP_3)M]^+$ [PP_3 = tris(2-diphenylphosphanylethyl)phosphane; M = Co, Rh] and $[(NP_3)Rh]^+$ [NP_3 = tris(2-diphenylphosphanylethyl)amine] in tetrahydrofuran affords new tetraphosphorus complexes. The PP_3 metal fragments yield the trigonal bipyramidal $[(PP_3)M(\eta^1\text{-}P_4)]^+$ complex cations [M = Co^I **(1)**, Rh^I **(2)**] containing the intact P_4 molecule bonded end-on to the metal. In contrast, the $[(NP_3)Rh]^+$ system yields an octahedral rhodium(III) complex of formula $[(NP_3)Rh(\eta^2\text{-}P_4)]BPh_4$ **(3)** which contains a bicyclotetraphosphane ligand (P_4^{2-}) coordinated to the metal through the wing-tip P atoms. Compound **3** forms through the oxidative addition of the P_4 molecule to the metal fragment. These new tetraphosphorus derivatives, which are very reactive, have been characterized in solution at low temperature by ^{31}P NMR spectroscopy.

Introduction

White phosphorus, P_4, is highly reactive towards a variety of organometallic and transition metal fragments. Very often the reactions proceed through complicated multistep thermal or photochemical degradation and aggregation to form metal complexes containing P_n groups for which the original tetrahedral tetraphosphorus topology is no longer evident.[1] Although specific steps of the progressive disruption of the tetrahedral molecule have been documented only in some instances,[2] among the numerous compounds described there are many complexes containing P_n units which may be formally considered as resulting from the initial interaction of the metal fragment with the intact P_4 molecule, followed by stepwise disruption of P−P bonds. The P_n units which have been found to form through the metal-mediated degradation of P_4 are shown in Scheme 1 according to the number of bond(s) which have been cleaved. Coordination of the intact P_4 molecule has been achieved through the end-on[3] and side-on[4] coordination modes, the formally possible face coordination mode having only been postulated on spectroscopic grounds.[4a] The insertion of a metal fragment into a P−P bond to form a bicyclotetraphosphane (**A** in Scheme 1) is generally considered to be the first step in the degradation of the tetrahedral molecule.[5] A second bond of the original P_4 may be cleaved either next to the first one or opposite to it, yielding three-, **C**,[5a,6] or four-membered, **B**, cyclic P_4 ligands; planar and bent topologies of the latter are known.[5d,7] Starting from **C**, the cleavage of another bond may furnish tetraphosphorus ligands, with either tripodal, **D**,[8] or chain arrangements, **E**,[5f,9] or it may produce two separated units, **F**, i.e. one *cyclo*-P_3 ring and a single P atom.[10] Open P_3 structures are less common,[11] whereas numerous examples exist where P_4 is cleaved into two P_2 units, **G**.[12]

Up to now the course of the reaction of P_4 with a metal fragment has been difficult to predict. This is due in part to the small number of stable complexes containing the intact P_4 molecule. Furthermore, these complexes are either poorly soluble or too reactive to be isolated and characterized by standard techniques. Hence, systematic studies on the factors favouring specific activation modes and on the reactivity of such complexes are sparse.

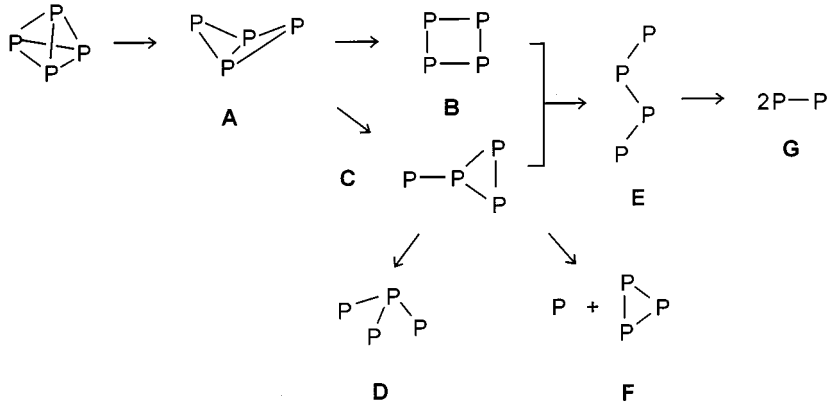
We have investigated the reactivity of white phosphorus toward group 9 coordinatively and electronically unsaturated fragments stabilized by tripodal tetradentate ligands, which are known to be excellent precursors for the activation of H−H and C−H bonds.[13] The $[(PP_3)M]^+$ species [PP_3 = tris(2-diphenylphosphanylethyl)phosphane; M = Co, Rh] react with white phosphorus yielding adducts of formula $[(PP_3)M(\eta^1\text{-}P_4)]^+$ in which the intact P_4 molecule is η^1 bound to the metal. In contrast, the related $[(NP_3)Rh]^+$ [NP_3 = tris(2-diphenylphosphanylethyl)amine] fragment yields a compound of formula $[(NP_3)Rh(\eta^2\text{-}P_4)]BPh_4$, which contains a bicyclotetraphosphane ligand (P_4^{2-}) coordinated to the metal through the wing-tip P atoms. The complex forms through the oxidative addition of the P_4 molecule to the metal fragment. The compounds are extremely reactive and have been characterized in solution at low temperature.

Results and Discussion

The reaction at room temperature of $[(PP_3)CoH]$, dissolved in THF under argon, with CF_3SO_3Me, under nitrogen, yields the dinitrogen complex cation $[(PP_3)CoN_2]^+$ [14]

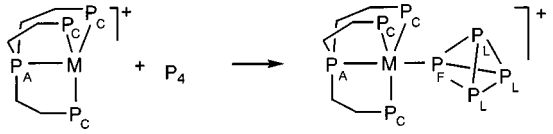
[a] Dipartimento di Chimica, Università di Firenze,
via Maragliano 77, 50144, Firenze, Italy
E-mail: stopmora@chim1.unifi.it
[b] I.S.S.E.C.C., C.N.R.,
via J. Nardi 39, 50132 Firenze, Italy
E-mail: peruz@fi.cnr.it

 © WILEY-VCH Verlag GmbH, D-69451 Weinheim, 2000 1434−1948/00/1010−2193 $ 17.50+.50/0



Scheme 1. Phosphorus units from formal stepwise cleavage of P−P bonds in the P_4 tetrahedron

and two species, denoted *a* and *b* in ref.[15], where their NMR spectroscopic data are reported. They exhibit an AC_3 $^{31}P\{^1H\}$ spin system suggestive of a trigonal geometry. Such species are likely to consist of the $[(PP_3)Co]^+$ cation and/or the complexes resulting from the interaction of the unsaturated 16e$^-$ fragment with the solvent or with the weakly coordinating $CF_3SO_3^-$ anion. These species react immediately with P_4 at temperatures as low as −70 °C to form a P_4 complex **(1)** (Scheme 2) which is stable up to −40 °C and decomposes unspecifically at higher temperature. Interestingly, the dinitrogen complex cation does not react with P_4 in the range of temperatures within which the P_4 adduct is stable.



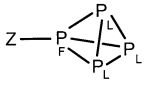
Scheme 2. Reaction of $[(PP_3)M]^+$ species with white phosphorus

Monitoring the electrophilic attack on the rhodium complex $[(PP_3)RhH]$ at −20 °C with CF_3SO_3Me by ^{31}P NMR spectroscopy provides evidence for three species (*a′*, *b′* and *c′*; NMR in ref.[16]) each exhibiting an AC_3X spin system, characteristic of rhodium(I) complex cations with trigonal geometry; such species are likely to consist of the $[(PP_3)Rh]^+$ cation and of the complexes resulting from its interaction with the solvent or with the weakly coordinating $CF_3SO_3^-$ anion. Interestingly, such electrophilic attack, carried out at low temperature, does not yield the square pyramidal cations which have been observed by performing the reaction at room temperature.[13] The three $[(PP_3)Rh]^+$ synthons react at −50 °C with an equimolar amount of P_4 yielding the complex cation $[(PP_3)Rh(\eta^1\text{-}P_4)]^+$ **(2)**, Scheme 2, which is stable up to −20 °C and decomposes unspecifically at higher temperature. The high reactivity of the cations **1** and **2** prevented their isolation as pure solids, and accordingly they have been characterized in solution by $^{31}P\{^1H\}$ NMR spectroscopy.

The $^{31}P\{^1H\}$ NMR spectra of the complexes **1** and **2** do not change in the temperature ranges investigated (from −70 to −40 °C for **1** and from −50 to −20 °C for **2**), which allows us to exclude dynamic behaviour. They exhibit four resonances (see the Experimental Section) with intensity ratios 1:3:1:3, the most significant difference between the spectra of the cobalt and of the rhodium derivative being due to the coupling with ^{103}Rh in compound **2**. Thus the cobalt derivative exhibits an AC_3FL_3 spin system and the rhodium derivative gives an AC_3FL_3X spin system, which are both consistent with a trigonal bipyramidal geometry around the metal. The metal should therefore be bound to the four donors of the tripodal PP_3 ligand and to one phosphorus atom of the intact P_4 molecule. The shifts and the coupling constants of the polyphosphane P atoms are typical for cobalt(I)[14] and rhodium(I)[13] complexes with trigonal bipyramidal geometry. The phosphorus atom (P_F) of the P_4 molecule which is bound to the metal is deshielded with respect to those of the "distal" P_3 face; the latter are only slightly affected by the nature of the metal fragment and have chemical shifts close to that of free P_4. These data are in accordance with those found for the few other complexes containing an intact P_4 molecule end-on bound to a metal fragment (Table 1). The values of the direct coupling constants $^1J_{P_FP_L}$ for all compounds, ranging from 185 to 235 Hz, are relatively close to each other. The bridgehead phosphorus of the PP_3 ligand in the two compounds is highly deshielded with respect to the value found for PP_3 in cobalt(I)[17] and rhodium(I)[13] complexes with coligands such as CO, PPh_3, CH_3, Ph, Cl^- and H^- in the fifth position.

In an attempt to rationalize some aspects of the bonding in these compounds both extended-Hückel[18] (EH) and ab initio[19] Hartree−Fock (HF) calculations were undertaken on model systems where the presence of the polyphosphane ligand was simulated by four properly arranged PH_3 groups and the coligand was the η^1-coordinated P_4 cage or, for comparison, the CO or Cl^- moiety. The HF calculations were of the single-point energy type, except for a preliminary set in which the metal−phosphorus distances were optimized: the ratios between distances at the energy minimum (individual values being unreliable at the level of the

Table 1. $^{31}P\{^1H\}$ NMR spectroscopic data of the P_4 molecule bound end-on to a metal fragment (Z)

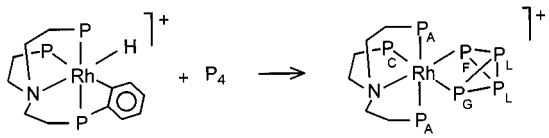


Z	δP_F	δP_L	$^1J(P_F\text{-}P_L)$	$\Delta\delta(P_L\text{-}P_L)$	Ref.
$[(PP_3)Co]^+$	-333.5	-472.3	219.0	138.8	[a]
$[(PP_3)Rh]^+$	-372.5	-493.8	226.5	121.3	[a]
$[(triphos)Re(CO)_2]^+$	-390.5	-488.9	235.7	98.4	[3a]
$[(CO)_3(PPh_3)MoP_4]$	-400.2	-480.0	185.0	79.8	[3b]
$[(CO)_3(PPh_3)WP_4]$	-422.0	-473.0	204.0	51.0	[3b]

[a] Data of the present work.

model) showed that the P_4 cage is competitive with the PH_3 groups as a ligand. The basis set in the HF calculations was either the LANL2DZ,[20] or it ranged from the 6−31G(d)[21] to the 6−311+G(d,p)[22] if the Rh metal was replaced by Co in the model. The pattern of atomic charges yielded by the EH calculations run with standard parameters[18] agrees with the trend expected in view of the NMR results, with the phosphorus atom in the bridgehead position of the phosphane ligand bearing a higher positive charge than the peripheral P atoms and with positive/negative charges for the coordinating/distal P_4 atoms. The HF calculations yield a similar pattern if polarization functions are included in the basis set. Although with differences in detail, both types of calculations give the same picture for bonding of the cage molecule to the metal, through an analysis of the changes in the atomic-orbital occupancies as the P_4 molecule is allowed to approach the metal centre from a distance. A synergic mechanism is in action, with σ-donation from the apical P_4 atom to the metal and back-donation from metal π orbitals. The latter shift of electron density reaches the distal P atoms of the cage through its peripheral MO′s. As expected, there are substantial analogies with the picture obtained for the model with the CO coligand and notable differences with respect to the Cl^- model. The values of the isotropic shielding tensor for atoms of the P_4 model compound agree with the expected trend, but the calculations do not provide a clue to the significantly higher deshielding of the bridgehead polyphosphane P atom in a P_4 than in a (for example) CO derivative.

The *ortho*-metallated product[13] which forms by electrophilic attack of CF_3SO_3Me on $[(NP_3)RhH]$ reacts in a short time at −20 °C (see Scheme 3) with a stoichiometric amount of P_4 in THF yielding, after addition of $NaBPh_4$, a pale-red compound of formula $[(NP_3)Rh(\eta^2\text{-}P_4)]BPh_4$ **(3)**. The solid, which has been isolated at low temperature, may be stored under inert atmosphere at room temperature but it decomposes in solution above 10 °C. Compound **3** exhibits at 0 °C a $^{31}P\{^1H\}$ NMR spectrum (see the Experimental Section) which presents five resonances with intensity ratios 2:1:1:1:2; it has been successfully simulated as an A_2CFGL_2X spin system. The two low-field resonances at $\delta = 29.8$ and -12.5 are due to the phosphorus atoms of the NP_3 ligand and are consistent with an octahedral rhodium(III)[13] complex having two chemically and magnetically equivalent phosphorus atoms (P_A) *trans* to each other and the third one (P_C) in the *cis* position (Scheme 3). The three high-field resonances are due to the four phosphorus atoms of the P_4 unit. Those at comparatively low field are assigned to atoms, P_F ($\delta = -224.3$) and P_G ($\delta = -194.5$) occupying the coordination sites, hereafter "equatorial", lying opposite the P_C and the NP_3 nitrogen positions. Finally, the resonance ($\delta = -237.8$) occurring at higher field is attributed to the two phosphorus atoms of the bicyclotetraphosphane (P_L) which are not bound to the metal. The P_F and P_G signals, in view of their different multiplicities, have been assigned considering that the one with higher multiplicity should be due to the phosphorus atom (P_G) lying *trans* to the P_C phosphorus atom of NP_3. The equivalence of the P_L sites suggests that the bond joining them should be normal to the equatorial plane and parallel to the line connecting the P_A positions. The weak coupling (40 Hz; see Experimental Section) between the inequivalent wing-tip atoms (P_F and P_G) in compound **3**, points to an open P_4 frame, which accounts for the presence of "through-metal" geminal coupling of the coordinating P atoms.

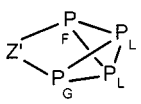


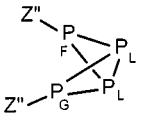
Scheme 3. Reaction of $[(NP_3)Rh]^+$ species with white phosphorus

On lowering the temperature below −40 °C the P_L and P_A signals become more complex and the positions of the sites are no longer equivalent. On the other hand, the chemical shifts of all absorptions, and the shapes of the remaining three signals, are substantially unchanged. The reversibility of this diversification points to the presence of a dynamic behaviour. The low activation barrier and the small deviations in the NMR parameters for the P_A and P_L sets suggest limited changes in stereochemistry for the two pairs of phosphorus atoms on the NMR time-scale at low temperature.

The NMR spectroscopic data for coordinating bicyclotetraphosphane in complexes of this type reported up to now appear in Table 2; they refer to compounds which contain insertion products of one metal fragment into a P−P bond (*endo-endo*) or two metal fragments bound to the wing-tip P atoms of the butterfly skeleton (*exo-exo*). As might be expected, the chemical shift of the wing-tip atoms depends heavily on the electronic and steric properties of the metal fragment. These resonances are shifted to lower field with respect to the P_2 backbone phosphorus atoms, which exhibit absorptions between $\delta = -377$ and -214, in the high-field region typical for phosphorus atoms participating in small cycles.[23] Interestingly, the chemical shift difference ($\Delta\delta = \delta P_F - \delta P_L$) within the P_4 ligand is smaller for the heavier group-9 complexes.

Table 2. $^{31}P\{^{1}H\}$ NMR spectroscopic data of the bicyclotetraphosphane unit bound to metal fragment(s) (Z′, Z")





Z′	δP_F	δP_G	δP_L	$^{1}J(P_F\text{-}P_L)$	$^{1}J(P_G\text{-}P_L)$	$\Delta\delta(P_L\text{-}P_L)$	Ref.
$[(NP_3)Rh]^+$	-224.3	-194.5	-237.8	160.0	166.0	13.5	[a]
$[Cp''_2Hf]$	117.5	117.5	-219.3	193.9	193.9	336.8	[5f]
$[Cp^*_2Zr]$	93.3	93.3	-214.0	201.1	201.1	307.3	[5f]
[Cp*CoCO]	-258.2	-258.2	-335.9, -376.9	156	156	77.7	[5d]
[Cp"RhCO]	-310.0	-310.0	-325.6, -341.9	160	160	15.6	[5g]
[(triphos)IrH]	-235.0	-251.3	-272.7	133.0	141.3	37.7	[5a]
Z"							
[Cp'''Fe(CO) 2]	-81.4	-81.4	-237.8	183.0	183.0	156.4	[5e]

[a] Data of the present work.

The remarkable difference in reactivity between $[(PP_3)Rh]^+$ and $[(NP_3)Rh]^+$ toward white phosphorus is in line with other results reported for the organometallic chemistry of the two systems.[13,14] The attainment of a pseudo-octahedral coordination geometry, as proposed for **3**, involves a considerable increase for one of the P−Rh−P angles formed by the peripheral P atoms of the ligand. It was pointed out on the basis of EH calculations on model systems for the tripod ligand and the four-coordinate metal[24] that such deformation should be easier for $[(NP_3)Rh]^+$ than for $[(PP_3)Rh]^+$ as a consequence of the early occurrence of a HOMO−LUMO avoided crossing in the former case. By similar (EH) calculational procedures we expect the $[(NP_3)Rh]^+$ system to be more prone to distortion than the $[(NP_3)Co]^+$ one because of a smaller HOMO−LUMO gap for the former, in the undistorted geometry over a range of reasonable metal−donor atom distances. These conclusions (easier angle opening in presence of the NP_3 ligand and of the Rh metal) are supported by trends in single-point energy values calculated by the HF method with LANL2DZ basis functions at various points of the deformation path and for various sets of metal−donor atom distances (one NH_3 group being used in addition to the PH_3 groups to mimic the NP_3 donors). However, the angle opening is definitely disfavoured in all cases if a fifth ligand, such as η^1-P_4, is allowed to approach the metal from the direction opposite the bridgehead atom position, since this has a dramatic effect on the HOMO−LUMO gap, reducing the extent of the intended crossing and the effects on the rehybridization at the metal, which are essential for a process of oxidative addition. On the other hand, it appears that suitable conditions for the oxidative addition may consist of a concerted P−Rh−P angle opening and side-on P_4 approach to the two prospective pseudo-octahedral sites. As shown in Figure 1, produced by the EH calculations, even in the early stages of such a path the metal atom develops a suitable hybrid HOMO to interact with the LUMO of the P_4 fragment. As a consequence of this, even at a distance of ca. 2.8 Å between the metal centre and each of the two P_4 atoms, set at 2.4 Å from each other, a 70% decrease in the value of the overlap population of the approaching P−P bond has already occurred, while the values for the incipient Rh−$P(P_4)$ bonds are already half as large as those for the bonds formed by rhodium with the phosphane P atoms.

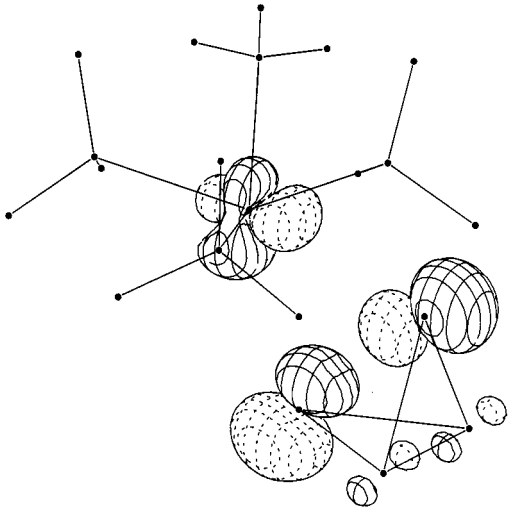


Figure 1. Drawing, from EH calculations, of significant parts of the HOMO for the model of $[(NP_3)Rh]^+$ interacting with partially cleaved P_4; according to a fragment orbital analysis, the main contributions are from the fragment cation HOMO and the P_4 LUMO; the bonding Rh···$P(P_4)$ and antibonding P···P interactions may be appreciated

Experimental Section

General: All reactions and manipulations were performed under an atmosphere of dry oxygen-free argon, unless otherwise stated. THF was freshly distilled from potassium; toluene and diethyl ether were freshly distilled from sodium. – $^{31}P\{^1H\}$ NMR spectra were measured in [D_8]THF on a Bruker AC 200 spectrometer at 81.02 MHz. Chemical shifts are relative to 85% H_3PO_4 as external standard at 0.00 ppm. – Analytical data for carbon, hydrogen, nitrogen and phosphorus were obtained from the Microanalytical Laboratory of the Department of Chemistry of the University of Florence. – The hydride complexes [(PP_3)CoH],[14] [(PP_3)RhH] and [(NP_3)RhH][13] were prepared according to the literature methods; CF_3SO_3Me (Aldrich) was used as purchased and stored at 0 °C.

Synthesis of [(PP_3)Co(P_4)]CF_3SO_3 (1): Neat CF_3SO_3Me (0.05 mmol) stored under nitrogen was added at room temperature to [(PP_3)CoH] (36 mg, 0.05 mmol) dissolved in [D_8]THF (0.8 mL). The resulting solution was stirred for 10 min and then cooled to −70 °C. P_4 (0.055 mmol) dissolved in THF (0.7 mL) was added and the resulting solution was immediately investigated at this temperature by NMR spectroscopy. – $^{31}P\{^1H\}$ ([D_8]THF, 233 K, 81.02 MHz): δ = 194.8 (dm, $^2J_{P_AP_C}$ = 35.0 Hz, $^2J_{P_AP_F}$ = 178.0 Hz, $^3J_{P_AP_L}$ = 5.0 Hz, 1 P, P_A), 73.6 (ddm, $^2J_{P_CP_F}$ = 71.0 Hz, $^3J_{P_CP_L}$ = 1.7 Hz, 3 P, P_C), −333.5 (m, $^1J_{P_FP_L}$ = 219.0 Hz, 1 P, P_F), −472.3 (dm, 3 P, P_L).

Synthesis of [(PP_3)Rh(P_4)]CF_3SO_3 (2): The rhodium derivative was prepared following the same procedure as described for **1** by adding P_4 (0.05 mmol) dissolved in THF (0.5 mL) to the clear solution obtained by adding CF_3SO_3Me (0.04 mmol) to [(PP_3)RhH] (31 mg, 0.04 mmol) in [D_8]THF (0.5 mL). – $^{31}P\{^1H\}$ ([D_8]THF, 223 K, 81.02 MHz): δ = 175.3 (ddm, $^1J_{P_ARh}$ = 111.9 Hz, $^2J_{P_AP_C}$ = 15.3 Hz, $^2J_{P_AP_F}$ = 399.3 Hz, $^3J_{P_AP_L}$ = 12.7 Hz, 1 P, P_A), 59.8 (ddd, $^1J_{P_FRh}$ = 134.8 Hz, $^2J_{P_CP_F}$ = 61.0 Hz, 3 P, P_C), −372.5 (m, $^1J_{P_FRh}$ = 111.0 Hz, $^1J_{P_FP_L}$ = 226.5 Hz, 1 P, P_F), −493.8 (dd, 3 P, P_L).

Synthesis of [(NP_3)Rh(P_4)]BPh_4 (3): CF_3SO_3Me (0.16 mmol) was added to a suspension of [(NP_3)RhH] (114 mg, 0.15 mmol) in THF (20 mL) at room temperature in a Schlenk tube and stirred for 30 min. The resulting clear yellow solution was cooled to −10 °C and P_4 (20 mg, 0.16 mmol) dissolved in THF (5 mL) was added. The solution turned dark red within 3 h. Solid $NaBPh_4$ (103 mg, 0.3 mmol) was then added. Concentration of the resulting solution at −30 °C yielded orange red microcrystals within 7 days, which were separated from the solvent, washed with toluene, diethyl ether and dried (120 mg, yield *ca* 67%). – $^{31}P\{^1H\}$ ([D_8]THF, 253 K, 81.02 MHz): δ = 29.8 (dd, $^1J_{P_ARh}$ = 110.6 Hz, $^2J_{P_AP_C}$ = 24.8 Hz, 2 P, P_A), −12.5 (ddt, $^1J_{P_CRh}$ = 86.0 Hz, $^2J_{P_CP_G}$ = 40.0 Hz, 1 P, P_C), −194.5 (tq, $^1J_{P_GRh}$ = 40 Hz, $^2J_{P_GP_L}$ = 166.0, $^2J_{P_GP_F}$ = 40 Hz, 1 P, P_G), −224.3 (tt, $^1J_{P_FRh}{}^1J_{PFRh}$ = 40 Hz, $^1J_{P_FP_L}$ = 160 Hz, 1 P, P_F), −237.8 (tm, 2 P, P_L). – $C_{66}H_{62}BNP_7Rh$ (1199.7): calcd. C 66.07, H 5.21, N 1.17, P 18.07; found C 66.02, H 5.26, N 1.09, P 17.85.

Acknowledgments

We acknowledge financial support by the Italian Ministero dell′Università e della Ricerca Scientifica e Tecnologica. The work has been possible by support for a post-doctoral grant (M. P. E.) from the "Gemeinsamen Hochschulsonderprogramm III von Bund und Ländern" of the DAAD (German Academic Exchange Service). This work was supported by the European Commission (INCO ERB-IC15CT960746). We thank Prof. Alessandro Bencini for help with the use of the Gaussian package.

[1] [1a] O. J. Scherer, *Acc. Chem. Res.* **1999**, *32*, 751. – [1b] J. Wachter, *Angew. Chem. Int. Ed.* **1998**, *37*, 750. – [1c] K. H. Whitmire, *Adv. Organomet. Chem.* **1998**, *42*, 2. – [1d] O. J. Scherer, *Angew. Chem. Int. Ed. Engl.* **1990**, *29*, 1104. – [1e] W. A. Herrmann, *Angew. Chem. Int. Ed. Engl.* **1986**, *25*, 56.

[2] [2a] M. Scheer, U. Becker, *J. Organomet. Chem.* **1997**, *545–6*, 451. – [2b] O. J. Scherer, G. Schwarz, G. Wolmershäuser, *Z. Anorg. Allg. Chem.* **1996**, *622*, 951. – [2c] M. Scheer, U. Becker, *Chem. Ber.* **1996**, *129*, 1307. –[2d] M. Scheer, E. Herrmann, J. Sieler, M. Oehme, *Angew. Chem. Int. Ed. Engl.* **1991**, *30*, 969.

[3] [3a] M. Peruzzini, L. Marvelli, A. Romerosa, R. Rossi, F. Vizza, F. Zanobini, *Eur. J. Inorg. Chem.* **1999**, 931. – [3b] T. Gröer, G. Baum, M. Scheer, *Organometallics* **1998**, *17*, 5916. – [3c] P. Dapporto, L. Sacconi, P. Stoppioni, F. Zanobini, *Inorg. Chem.* **1981**, *20*, 3834. – [3d] P. Dapporto, S. Midollini, L. Sacconi, *Angew. Chem. Int. Ed. Engl.* **1979**, *12*, 469.

[4] [4a] A. P. Ginsberg, W. E. Lindsell, K. J. McCullough, C. R. Sprinkle, A. J. Welch, *J. Am. Chem. Soc.* **1986**, *108*, 403. –[4b] W. E. Lindsell, K. J. McCullough, *J. Am. Chem. Soc.* **1983**, *105*, 4487.

[5] [5a] M. Peruzzini, J. A. Ramirez, F. Vizza, *Angew. Chem. Int. Ed. Engl.* **1998**, *37*, 2257. – [5b] M. Scheer, U. Becker, E. Matern, *Chem. Ber.* **1996**, *129*, 721. – [5c] M. Scheer, M. Dargatz, A. Rufinska, *J. Organomet. Chem.* **1992**, *440*, 327. – [5d] O. J. Scherer, M. Swarowsky, G. Wolmershäuser, *Organometallics* **1989**, *8*, 841. – [5e] O. J. Scherer, T. Hilt, G. Wolmershäuser, *Organometallics* **1998**, *17*, 4110. – [5f] O. J. Scherer, M. Swarowsky, H. Swarowsky, G. Wolmershäuser, *Angew. Chem. Int. Ed. Engl.* **1988**, *27*, 694. –[5g] R. Alsfasser, *Diploma thesis*, Kaiserslautern, **1988**.

[6] F. Hey, M. F. Lappert, J. L. Atwood, S. G. Bott, *J. Chem. Soc., Chem. Commun.* **1987**, 597.

[7] [7a] O. J. Scherer, J. Vondung, G. Wolmershäuser, *Angew. Chem. Int. Ed. Engl.* **1989**, *28*, 1355. – [7b] O. J. Scherer, J. Vondung, G. Wolmershäuser, *J. Organomet. Chem.* **1989**, *376*, C35.

[8] [8a] O. J. Scherer, J. Braun, G. Wolmershäuser, *Chem. Ber.* **1990**, *123*, 471. – [8b] O. J. Scherer, T. Dave, J. Braun, G. Wolmershäuser, *J. Organomet. Chem.* **1988**, *350*, C20.

[9] F. Cecconi, C. A. Ghilardi, S. Midollini, A. Orlandini, *Inorg. Chem.* **1986**, *25*, 1766.

[10] [10a] M. H. Chisholm, K. Folting, J. W. Pasterczyk, *Inorg. Chem.* **1988**, *27*, 3057. – [10b] M. Scheer, U. Becker, J. Magull, *Polyhedron* **1998**, *17*, 1983.

[11] [11a] A. Barth, G. Huttner, M. Fritz, L. Zsolnai, *Angew. Chem. Int. Ed. Engl.* **1990**, *29*, 929. – [11b] H. Brunner, U. Klement, W. Meier, J. Wachter, O. Serhadle, M. L. Ziegler, *J. Organomet. Chem.* **1987**, *335*, 339.

[12] [12a] O. J. Scherer, M. P. Ehses, G. Wolmershäuser, *Angew. Chem. Int. Ed Engl.* **1998**, *37*, 507. – [12b] L. Y. Goh, C. K. Chu, R. C. S. Wong, T. W. Hamley, *J. Chem. Soc., Dalton Trans.* **1989**, 1951. – [12c] C. F. Campana, A. Vizi-Orosz, G. Pàlyi, L. Markò, L. F. Dahl, *Inorg. Chem.* **1979**, *18*, 3054. – [12d] H. Schäfer, D. Binder, D. Fenske, *Angew. Chem. Int. Ed. Engl.* **1985**, *24*, 522.

[13] C. Bianchini, D. Masi, A. Meli, M. Peruzzini, F. Zanobini, *J. Am. Chem. Soc.* **1988**, *110*, 6411.

[14] C. Bianchini, C. Mealli, A. Meli, M. Peruzzini, F. Zanobini, *J. Am. Chem. Soc.* **1988**, *110*, 8725.

[15] $^{31}P\{^1H\}$ {[D_8]THF, δ (ppm); *J* (Hz)]}: 253 K. *a*: 147.5 (q, $^2J_{P_AP_C}$ = 23.0 Hz, 1 P, P_A), 50.0 (d, 3 P, P_C); *b*: 143.5 ($^2J_{P_AP_C}$ = 32.0 Hz, 1 P, q, P_A), 48.5 (d, 3 P, P_C).

[16] $^{31}P\{^1H\}$ {[D_8]THF, δ (ppm); *J* (Hz)]}: 253 K. *a′*: 141.2 (dq, $^1J_{P_ARh}$ = 141.7 Hz, $^2J_{P_AP_C}$ = 15.4 Hz, 1 P, P_A), 45.0 (dd, $^1J_{P_CRh}$ = 128.7 Hz, 3 P, P_C); *b′*: 137.8 (dq, $^1J_{P_ARh}$ = 132.2 Hz, $^2J_{P_AP_C}{}^2J_{P_AP_C}$ = 15.3 Hz, 1 P, P_A), 46.9 (dd, $^1J_{P_CRh}$ = 128.6 Hz, 3 P, P_C); *c′*: 136.0 (dq, $^1J_{P_ARh}$ = 130.8 Hz, $^2J_{P_AP_C}$ = 13.1 Hz, 1 P, P_A), 47.9 (dd, $^1J_{P_CRh}$ = 130.8 Hz, 3 P, P_C).

[17] W. H. Hohman, D. J. Kountz, D. W. Meek, *Inorg. Chem.* **1986**, *25*, 616.

[18] C. Mealli, D. M. Proserpio, *J. Chem. Educ.* **1990**, *67*, 399.

[19] *Gaussian 98*, *Revision A.7*, M. J. Frisch, G. W. Trucks, H. B. Schlegel, G. E. Scuseria, M. A. Robb, J. R. Cheeseman, V. G. Zakrzewski, J. A. Montgomery, Jr., R. E. Stratmann, J. C. Burant, S. Dapprich, J. M. Millam, A. D. Daniels, K. N. Kudin, M. C. Strain, O. Farkas, J. Tomasi, V. Barone, M. Cossi, R. Cammi, B. Mennucci, C. Pomelli, C. Adamo, S. Clifford, J.

Ochterski, G. A. Petersson, P. Y. Ayala, Q. Cui, K. Morokuma, D. K. Malick, A. D. Rabuck, K. Raghavachari, J. B. Foresman, J. Cioslowski, J. V. Ortiz, A. G. Baboul, B. B. Stefanov, G. Liu, A. Liashenko, P. Piskorz, I. Komaromi, R. Gomperts, R. L. Martin, D. J. Fox, T. Keith, M. A. Al-Laham, C. Y. Peng, A. Nanayakkara, C. Gonzalez, M. Challacombe, P. M. W. Gill, B. Johnson, W. Chen, M. W. Wong, J. L. Andres, C. Gonzalez, M. Head-Gordon, E. S. Replogle, J. A. Pople, Gaussian, Inc., Pittsburgh PA, **1998**.

[20] P. J. Hay, W. R. Wadt, *J. Chem. Phys.* **1985**, *82*, 270.

[21] R. Ditchfield, W. J. Hehre, J. A. Pople, *J. Chem. Phys.* **1971**, *54*, 724.

[22] P. J. Hay, *J. Chem. Phys.* **1977**, *66*, 4377

[23] M. Di Vaira, L. Sacconi, P. Stoppioni, *J. Organomet. Chem.* **1983**, *250*, 183.

[24] C. Mealli, C. A. Ghilardi, A Orlandini, *Coord. Chem. Rev.* **1992**, *129*, 399.

Received March 31, 2000
[I00125]

Synthesis, Structures, and Crystalline Packing Features of [Co(tren)(amino acidato-*N*,*O*)]$X_2 \cdot nH_2O$ (X = ClO_4^-, I^-)

Jiwen Cai,*[a] Xiaopeng Hu,[b] Xiaolong Feng,[a] Weiyan Shao,[a] Liangnian Ji,*[b] and Ivan Bernal*[c]

Keywords: Cobalt / Tripodal ligands / N ligands / Amino acids

The crystal structures of several novel compounds, *trans*(*N*,*t*-*N*) isomers of [Co(tren)(DL-phenylalaninato)]$(ClO_4)_2$ (**1**), [Co(tren)(L-phenylalaninato)]$I_2 \cdot H_2O$ (**2**), [Co(tren)(L-prolinato)]$I_2 \cdot H_2O$ (**3**), [Co(tren)(L-tryptophanato)]$(ClO_4)_2 \cdot {}^1/_2H_2O$ (**4**), [Co(tren)(L-valinato)]$I_2 \cdot {}^1/_3H_2O$ (**5**), [Co(tren)(L-isoleucinato)]I_2 (**6**), and [Co(tren)(L-leucinato)]I_2 (**7**), have been determined. Their packing arrangements indicate that the complex cations in all of the compounds form helical strings running along their crystallographic axes, for both chiral and racemic amino acidato species. Intermolecular double and single hydrogen bonds are formed by the carbonyl oxygens and amino hydrogens of the tren ligand or of the amino acidato moiety, either directly or by the assistance of water molecules of hydration. In this fashion, [Co(tren)(amino acidato-*N*,*O*)]$^{2+}$ is strung together into helical arrays. In the racemic compounds, the complex cations of different strings have opposite chirality. Phenylalanine is racemized during the coordination process, under mild pH (7.5–8.0) and temperature (60 °C). This is quite unusual. Finally, 1D and 2D (COSY) ^{1}H NMR spectra were recorded, in which compound **4** shows interesting cross-peak correlations between the phenyl protons and amino protons.

Introduction

Recently, it was reported[1] that the monooxamide anion is hydrolyzed by dihalo-Co^{III} complexes containing various types of polyamine tetradentate ligands, such as $(en)_2$, 3,2,3-tet (1,5,8,12-tetraaminododecane), trien, or tren, to give their corresponding oxalato compounds. Thus, we decided to systematically investigate the mechanism of this hydrolytic process of amide and peptide cleavage catalyzed by *cis*-$[CoN_4Cl_2]^+$, in comparison with that of *cis*-$[CoN_4(H_2O)(OH)]^{2+}$ reported by Buckingham, et al.[2–9] Of particular interest are the chiral and stereochemical problems associated with this process.

Our first efforts were directed towards the synthesis and characterization of the structures of $[Co(N_4)(\text{amino acidato})]^{2+}$ (N_4 = trien and tren) complexes with different types of amino acids. This data could then be used to help identify the steric nature of the hydrolysis products, which is not available crystallographically. Here, we report the crystal structures, including packing features, of seven novel *trans*(*N*,*t*-*N*) isomers of [Co(tren)(DL-phenylalaninato)]$(ClO_4)_2$ (**1**), [Co(tren) (L-phenylalaninato)]$I_2 \cdot H_2O$ (**2**), [Co(tren)(L-prolinato)]$I_2 \cdot H_2O$ (**3**), [Co(tren)(L-tryptophanato)]$(ClO_4)_2 \cdot {}^1/_2H_2O$ (**4**), [Co(tren)(L-valinato)]$I_2 \cdot {}^1/_3H_2O$ (**5**), [Co(tren)(L-isoleucinato)]I_2 (**6**), [Co(tren)(L-leucinato)]I_2 (**7**), where *trans*(*N*,*t*-*N*) refers to one of the two possible geometric isomers in which the tertiary nitrogen atom of tren is in the position *trans* to the amide nitrogen of the amino acidato cation.[10]

The starting amino acids used for the preparation are all of the natural L form. The DL-phenylalaninato was obtained as a result of racemization during the synthesis in mild pH (7.5−8.0) and temperature (60 °C). Finally, of particular interest is the observation that chiral helical arrays are observed in all of the crystals examined, both in the optically active and the racemic forms of amino acidato complexes.

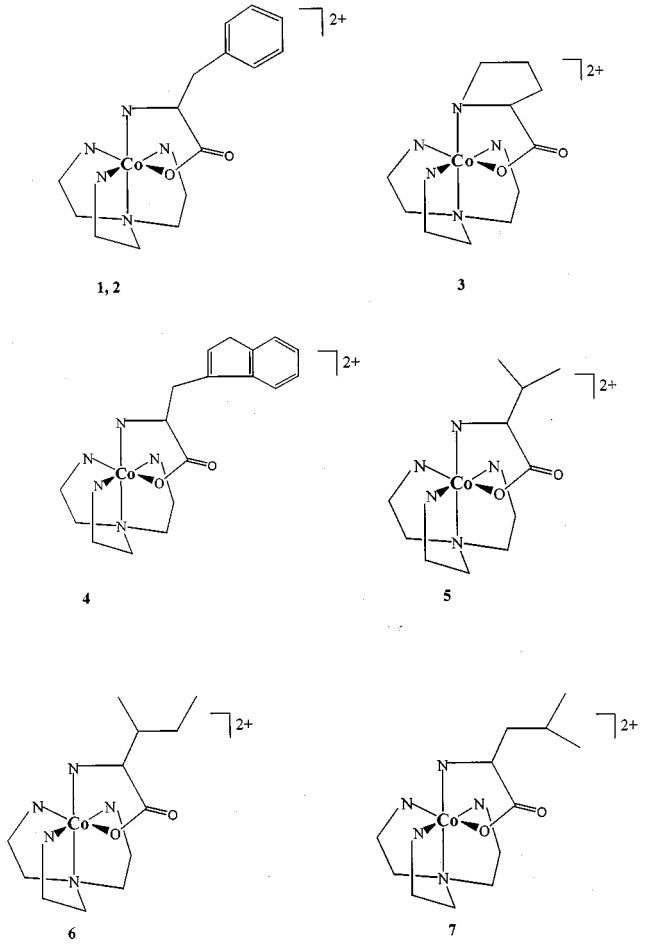
Results and Discussion

Racemization of Phenylalanine

The starting materials used in this study were all of the natural L form of the amino acids. Interestingly, we found that one of the amino acids, phenylalanine, racemized during the process of preparation under very mild conditions of pH (7.5−8.0) and temperature (60 °C); while no crystallographic evidence of racemization was observed for the other amino acids involved in this study. The mechanism of amino acid racemization reactions involves the removal of the α-hydrogen and the stabilization of the resulting planar carbanion. It has been reported that racemization of phenylalanine takes place in vitamin B_6-amino acid Schiff base copper complexes in mildly acidic solutions,[11] in which the activation of the αC−H group is due to the π-π intermolecular interaction which is claimed to be the reason

[a] Instrumentation Analysis & Research Center Zhongshan University,
Guangzhou, 510275 P. R. China,
Fax: (internat.) +86 20/84038784,
E-mail: puscjw@zsu.edu.cn
[b] Department of Chemistry Zhongshan University,
Guangzhou, 510275 P. R. China,
[c] Department of Chemistry University of Houston,
Houston, TX 77024-5641 U. S. A.
Fax: (internat.) +1 713/7432709
E-mail: ibernal@uh.edu

 © WILEY-VCH Verlag GmbH, D-69451 Weinheim, 2000 1434−1948/00/1010−2199 $ 17.50+.50/0



for the unusual racemization. Racemization of phenylalanine has also been observed in bis(2,2′-bipyridine) ruthenium(II) complexes in basic solution.[12] The asymmetric transformation of α-amino acids promoted by optically active Co^{III} complexes at pH 10−12 carbonate buffer has been examined by Yamaguchi.[13] However, the influence of substituents of the amino acid on the isomerization process was not elucidated, and further efforts are required to explain the unusual phenylalanine racemization observed in this study, for the following reasons: (1) It takes place under rather mild condition; (2) No crystallographic evidence of racemization is observed for other chelated amino acids, such as proline, tryptophan, valine, isoleucine, and leucine, under the same solution conditions.

Finally, we are aware that the fact that some of these complexes crystallize in enantiomorphic space groups does not necessarily mean that they are pure optically active compounds to begin with. It could be the result of conglomerate crystallization of the racemates.[14] Therefore, other experimental measurements, such as CD spectra, were required to exclude the possibility that other amino acids were racemized under the same conditions, and then proceeded to undergo conglomerate crystallization. Such a process has been documented in the case of Schiff base.[15]

Description of the Structures and Packing

Compounds **1** and **2**: With regard to the conformation of the coordination sphere, the most obvious difference between these two complexes is the orientation of the phenyl rings, as indicated in Figure 1 and Figure 2. The ^1H NMR spectra of these two compounds are identical implying that packing effects could be the driving force for this difference. In compound **1**, a single hydrogen bond between the carbonyl oxygen of one complex and the amino hydrogen of the amino acidato ligand from an adjacent complex leads to a head-to-tail linking of complexes of the same chirality to form cation strings running along the *c* axis. Looking down the *c* axis, one can see a column-like structure of the complexes, with the phenyl rings stacked on top of one another. The counter anions fill the gaps between the columns.

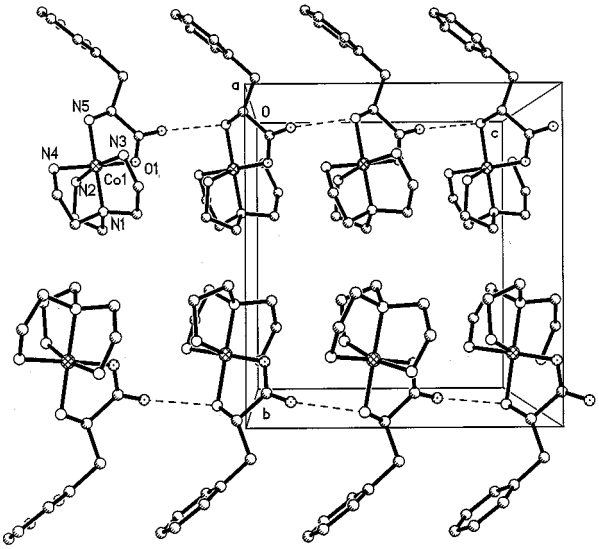


Figure 1. Spiral strings formed by the cations in the racemic compound **1**. The chirality of phenylanine shown is D. Cation strings run along *c* axis. When looking down along the *c* axis, phenyl rings and cations pack on top of each other, forming a column-like structure. Selected bond lengths: Co1−O1 1.903(3), Co1−N1 1.945(4), Co1−N2 1.955(4), Co1−N3 1.979(4), Co1−N4 1.954(4), Co1−N5 1.948(4) Å

The optically active form of compound **2** has a similar hydrogen-bonding motif, except that the chain runs along the *a* axis, and the phenyl rings are positioned around the chain axis.

Compounds **3**−**5**: Figure 3 shows that in compound **3** the cations are 'stitched' together in zigzag chains by an intermediary water molecule. In compound **4**, there are two independent molecules in the asymmetric unit. Figure 4 shows that the hydrogen-bonding motif is slightly different from that observed in compounds **1**−**3**. There are two cations in the repeating unit of the helical strings. Two intermolecular hydrogen-bonding interactions are observed in compound **5**, in which the cations interact in a head-to-tail fashion, see Figure 5. In this case, the carbonyl oxygen interacts with both the amino hydrogens of tren and with those of the amino acidato ligand.

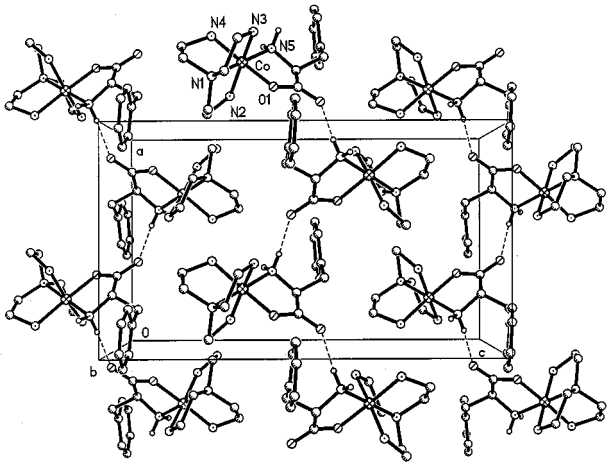


Figure 2. Spiral strings formed in compound **2**. Zigzag chains run along the *a* axis. When looking down along the *a* axis, phenyl rings wrap around the axis, instead of packing on top of each other as observed in compound **1**. Spiral strings run in space in ↑ ↓ fashion. Selected bond lengths: Co−O1 1.900(3), Co−N1 1.948(4), Co−N2 1.968(4), Co−N3 1.960(4), Co−N4 1.955(4), Co−N5 1.948(4) Å

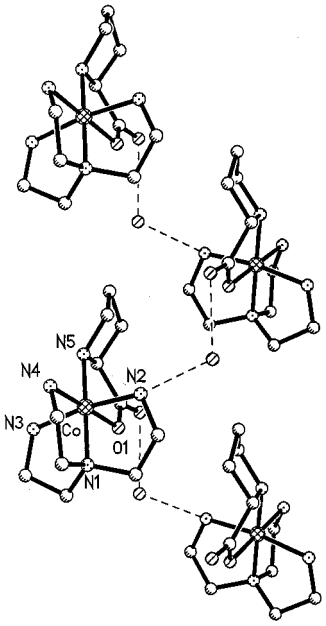


Figure 3. Spiral strings formed in compound **3**. The cations are "stitched" together by a water molecule, instead of direct cation-cation interaction. Selected bond lengths: Co−O1 1.900(3), Co−N1 1.960(5), Co−N2 1.965(5), Co−N3 1.974(5), Co−N4 1.956(5), Co−N5 1.959(5) Å

Compound **6**: Compound **6** contains helical strings running along the *b* axis with the typical head-to-tail hydrogen bonding observed in compound **5**, see Figure 6. In the reported racemic structure, a pair of head-to-head hydrogen bonds is formed between two complexes when the counter anions are iodides,[10b] whereas the perchlorate crystallizes in conglomerate solid solution, in the space group $P3_1$.[10c] A similar hydrogen-bonding motif is observed in the perchlorate complex as that in compound **6**, except that the

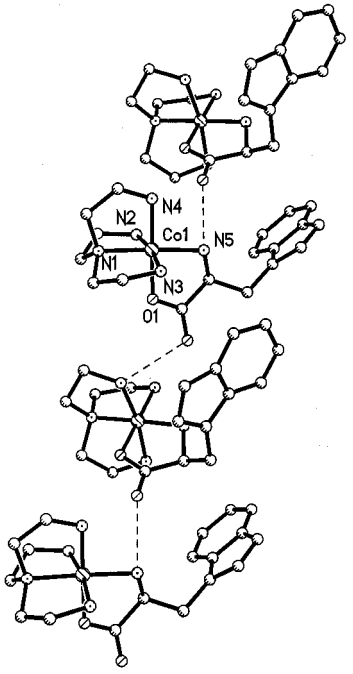


Figure 4. Spiral strings formed in compound **4**. There are two independent cations in the asymmetric unit and the conformation of the aromatic rings are slightly different. Selected bond lengths of Co1: Co1−O1 1.899(3), Co1−N1 1.949(5), Co1−N2 1.942(5), Co1−N3 1.957(5), Co1−N4 1.929(4), Co1−N5 1.952(4) Å

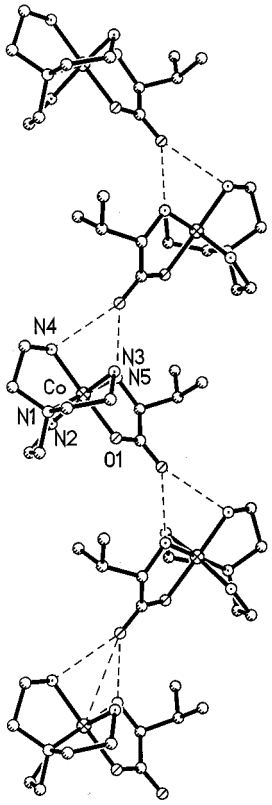


Figure 5. Spiral strings formed in compound **5**. Note that the hydrogen-bonding motif has been changed from single for the aromatic-substituted side chain to double for the aliphatic side chain. Selected bond lengths: Co−O1 1.921(3), Co−N1 1.949(4), Co−N2 1.953(4), Co−N3 1.968(4), Co−N4 1.940(4), Co−N5 1.948(4) Å

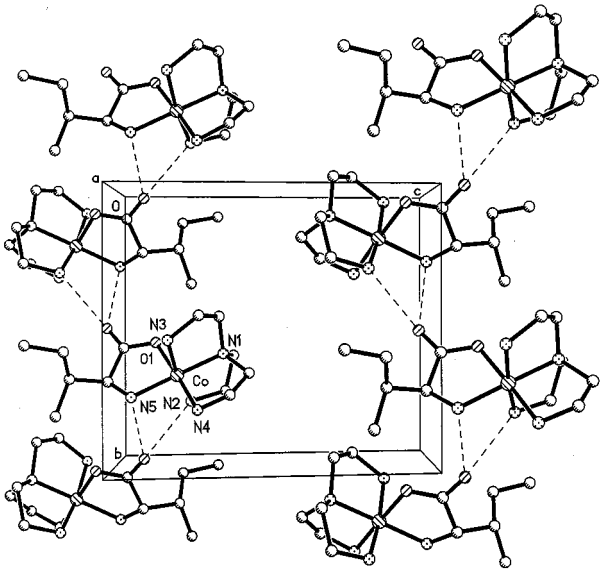


Figure 6. Spiral strings formed in compound **6**. Strings run in space in ↑ ↑ fashion. Selected bond lengths: Co−O1 1.906(4), Co−N1 1.943(5), Co−N2 1.974(5), Co−N3 1.984(6), Co−N4 1.935(5), Co−N5 1.940(5) Å

amino acidato groups in the different strings have different chirality.

Compound **7**: This compound crystallizes in the same unit cell, space group, and packing mode as the racemate reported previously.[10c] They make an interesting pair of optically active and racemic compounds that crystallize in the same space group with very similar packing properties. The racemic mixture is actually a conglomerate solid solution, in which the D and L form of the amino acidato group occupy alternative positions in the lattice. Interested readers are referred to the original copy for more detail.

Fundamental aspects of the packing modes adopted by the optically active and racemic species of [Co(tren)(amino acidato)]$^{2+}$ are the chiral helical strings observed in these systems:

(1) All helical strings are formed by intermolecular hydrogen bonds. In less bulky substituted amino acids such as valine, leucine, isoleucine, there are double hydrogen bonds; while with bulkier substituted amino acids such as phenylalanine, tryptophan, and proline, there are single hydrogen bonds. In both situations, the carbonyl oxygen atoms interact with the amino hydrogens of tren and/or with those of the amino acidato fragment.

(2) Hydrogen-bonding interactions can be very strong, as indicated by the favorable angles and distances. For instance, in compound **2**, the angle of N−H···O is 172° and N···O = 3.0 Å for the intermolecular hydrogen bond; while for **1**, the angle is 153° and the distance is 2.8 Å;

(3) Strings run in space either in a head-to-head ↑ ↑ fashion, as observed in compound **6**; or in a head-to-tail ↑ ↓ fashion, as observed in compound **2**;

(4) In the racemic form, helical strings have a similar packing mode as that observed in the optically active one, and intermolecular hydrogen-bonding interactions bring complexes of the same chirality together in those strings.

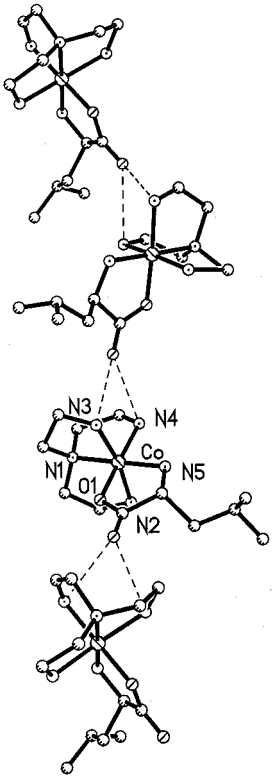


Figure 7. Spiral strings formed in compound **7**. The intermilecular hydroge-bonding interactions are the same as those observed in the racemic complex, except that the amino acidato ligands in different strings have different chirality in the racemic structure. Selected bond lengths: Co−O1 1.884(3), Co−N1 1.948(4), Co−N2 1.965(4), Co−N3 1.980(4), Co−N4 1.960(4), Co−N5 1.938(4) Å

However, the complexes of adjacent strings have opposite chirality. Since the hydrogen-bonding fashion observed in the racemic crystal is the same as that observed in the optically active form, we refer to it as the "chiral recognition motif" of these systems;

(5) Based upon our observations and understanding of conglomerate crystallization,[16] we can predict that [Co(tren)(amino acidato-*N*,*O*)]$^{2+}$ is a system that tends to favor conglomerate crystallization, if the "right stitching agents", (i.e. the counter anions and solvent), are chosen. This is consistent with the reported crystal structures of *trans*(*N*,*t*,*N*)-[Co(tren)(DL-leu)]I_2, *trans*(*N*,*t*,*N*)-[Co(tren)(DL-Ilu)]$(ClO_4)_2$, and *trans*(*N*,*t*,*N*)-[Co(tren) (DL-Val)]$(ClO_4)_2$.[10c]

1D and 2D ^{1}H NMR Spectra

In order to identify the individual protons, COSY spectra of compounds **1** to **4** were recorded. Individual peaks are resolved. Chemical shifts for the amino protons of tren range from δ = 3.92 to 5.09. It is difficult to assign chemical shifts for individual alkyl protons from the three different $N-CH_2-CH_2-NH_2$ arms. The spectra show that, for all four compounds, shifts from two arms are close, δ ≈ 2.9 and 3.3, while the others shift more upfield, δ ≈ 2.6 and 3.1. The upfield shifts are assigned to the arm that is *trans* to the carbonyl oxygen (referring to the coordinated position to Co^{III}). Interestingly, we observe that in the COSY

spectra of compound **4**, there are three cross peaks between three pairs of protons from the aromatic ring and the amino groups of tren; they are δ = 7.41 and 3.92, 7.13 and 4.18, 7.04 and 4.26, respectively. Based on the molecular structure shown in Figure 4, these protons are far away from each other and are not in parallel planes, therefore, there should not be any correlation. At present, we have no explanation for this long-range correlation.

Conclusion

It is interesting to note that chiral helical strings are formed among the cations $[Co(tren)(amino\ acidato)]^{2+}$, irrespective of the chirality and the nature of the substituted side chain of the amino acids. We hope that this observation will provide some information to further understand the chiral recognition processes that so readily occur in biological processes.

Experimental Section

All reagents were commercially available and used as received. − Elemental analyses were carried out with a Perkin−Elmer 240 elemental analyzer. − ^{1}H NMR spectra were recorded on a Varian UNITY/NOVA 500 NMR spectrometer using [D_6]DMSO as the solvent and TMS as the internal standard. A small amount of D_2O was added to the solution in order to assign the exchangeable protons after the spectra was recorded in [D_6]DMSO.

Safety Notes: Perchlorate salts of metal complexes with organic ligands are potentially explosive. Only a small amount of material should be prepared and handled with great care.

Syntheses: Compounds were prepared according to the synthetic procedure originally described by Collman.[4] The pH of an aqueous solution of *cis*-α-[Co(tren)Cl_2]Cl (1.0 g, 0.003mol), was adjusted to 7.5−8.0 using freshly prepared 10% NaOH solution, whereupon the color of the solution changed to pink. An equimolar amount of amino acid was added while the pH was kept at 7.5−8.0. After heating at 60 °C for several hours in a water bath, the resulting solution was cooled to room temperature and filtered. Calculated amounts of KI or $NaClO_4$ were added to the resulting solution, and crystals suitable for X-ray diffraction were obtained after several days.

Elemental Analyses and ^{1}H NMR Spectroscopic Data

[Co(tren)(DL-phenylalaninato)]$(ClO_4)_2$ (1): $C_{15}H_{28}Cl_2CoN_5O_{10}$ (568.25): calcd. C 31.70, N 12.33, H 4.97; found C 30.20, N 12.60, H 4.81. Yield: 0.54 g, 30%.

[Co(tren)(L-phenylalaninato)]$I_2 \cdot H_2O$ (2): $C_{15}H_{30}CoI_2N_5O_3$ (641.17): calcd. C 28.01, N 10.93, H 4.72; found C 27.92, N 10.82, H 4.80. Yield: 0.74 g, 36%.

Compounds **1** and **2** have identical ^{1}H NMR: δ = 7.41 (d, ^3J = 8.0 Hz, 2 H, CH), 7.32 (d, ^3J = 7.5 Hz, 2 H, CH), 7.31 (t, ^3J = 9.0 Hz, 1 H, CH), 5.70 (t, ^3J = 8.0 Hz, 1 H, NH), 5.01 (m, 1 H, NH), 4.99 (m, 1 H, CH_2), 4.54 (t, ^3J = 10.0 Hz, 1 H, NH), 4.42 (m, 1 H, CH_2), 4.18 (m, 1 H, CH_2), 4.04 (m, 1 H, NH_2), 3.93 (m, 1 H, NH_2), 3.54 (m, 1 H, CH), 3.26−3.42 (m, 5 H, CH_2), 3.11 (t, ^3J = 7.5 Hz, 2 H, CH_2), 2.98 (m, 4 H, CH_2), 2.88 (dd, ^2J = 15 Hz, ^3J = 11.5 Hz, 1 H, CH_2), 2.66 (t, ^3J = 7.5 Hz, 2 H, CH_2).

[Co(tren)(L-prolinato)]$I_2 \cdot H_2O$ (3): $C_{11}H_{28}CoI_2N_5O_3$ (591.11): calcd. C 22.35, N 11.85, H 4.77, found C 22.51, N 10.79, H 4.70. − ^{1}H NMR: δ = 6.75 (m, 1 H, NH), 5.09 (m, 1 H, NH_2), 5.04 (m, 1 H, NH_2), 4.74 (m, 1 H, NH_2), 4.55 (m, 2 H, NH_2), 4.09 (m, 1 H, CH_2), 3.87 (d, ^3J = 9.0 Hz, 1 H, CH), 3.41 (m, 2 H, CH_2), 3.21 (m, 4 H, CH_2), 3.01 (dd, ^2J = 10 Hz, ^3J = 5.0 Hz, 1 H, CH_2), 2.93 (m, 3 H, CH_2), 2.72 (m, 2 H, CH_2), 2.43 (m, 1 H, CH_2), 2.14 (m, 1 H, CH_2), 1.96 (m, 1 H, CH_2), 1.89 (m, 1 H, CH_2), 1.74 (m, 1 H, CH_2). − Yield: 0.65 g, 34%.

[Co(tren)(L-tryptophanato)]$(ClO_4)_2 \cdot {}^1/_2H_2O$ (4): $C_{17}H_{31}Cl_2CoN_6O_{10.50}$ (617.30): calcd. C 33.04, N 13.60, H 5.02; found C, 35.91, N 11.42, H 5.97. − Yield: 0.72 g, 39%. − ^{1}H NMR: δ = 10.99 (s, 1 H, NH), 7.52 (d, ^3J = 8.0 Hz, 1 H, CH), 7.41 (d, ^3J = 7.5 Hz, 1 H, CH), 7.31 (d, ^3J = 2.0 Hz, 1 H, CH), 7.13 (td, ^3J = 8.0 Hz, ^4J = 1.0 Hz, 1 H, CH), 7.04 (td, ^3J = 8.0 Hz, ^4J = 1.0 Hz, 1 H, CH), 5.8 (m, 1 H, NH_2), 5.04 (m, 2 H, NH_2), 4.56 (m, 2 H, NH_2), 4.28 (m, 1 H, NH_2), 4.18 (m, 1 H, NH_2), 3.92 (m, 1 H, NH_2), 3.61 (m, 1 H, CH), 3.39 (m, 1 H, CH_2), 3.31 (m, 4 H, CH_2), 3.11 (t, ^3J = 6.0 Hz, 2 H, CH_2), 2.98 (m, 4 H, CH_2), 2.91 (m, 1 H, CH_2), 2.63 (t, ^3J = 6.0 Hz, 2 H, CH_2).

[Co(tren)(L-valinato)]$I_2 \cdot {}^1/_3H_2O$ (5): $C_{11}H_{28.67}CoI_2N_5O_{2.33}$ (581.06): calcd. C 22.71, N 12.04; H 4.93; found C, 23.89, N 12.58, H 5.32. − Yield: 0.71 g, 39%. − ^{1}H NMR: δ = 5.96 (t, J = 9.5 Hz, 1 H, NH_2), 5.03 (m, 1 H, NH_2), 4.73 (t, ^3J = 10.0 Hz, 1 H, NH_2), 4.50−4.40 (m, 3 H, NH_2), 4.18 (t, ^3J = 9.5 Hz, 1 H, NH_2), 3.98 (t, ^3J = 9.0 Hz, 1 H, NH_2), 3.42−3.30 (m, 4 H, CH_2), 3.24 (m, 3 H, CH_2, CH), 3.16−2.99 (m, 4 H, CH_2), 2.75 (brt, ^3J = 5.5 Hz, 2 H, CH_2), 2.21 (m, 1 H, CH_2), 1.09 (d, ^3J = 6.5 Hz, 3 H, CH_3), 0.93 (d, ^3J = 7.0 Hz, 3 H, CH_3).

[Co(tren)(L-isoleucinato)]I_2 (6): $C_{12}H_{30}CoI_2N_5O_2$ (589.14): calcd. C 24.46, N 11.19, H 5.13; found C 25.01, N 11.30, H 4.92. − Yield: 0.78 g, 41%. − ^{1}H NMR: δ = 6.01 (t, ^3J = 9.0 Hz, 1 H, NH_2), 5.05 (m, 1 H, NH_2), 4.74 (t, ^3J = 10.5 Hz, 1 H, NH_2), 4.49 (m, 2 H, NH_2), 4.38 (m, 1 H, NH_2), 4.21 (m, 1 H, NH_2), 3.98 (m, 1 H, NH_2), 3.43−3.27 (m, 5 H, CH_2, CH), 3.20 (m, 2 H, CH_2), 3.03−2.92 (m, 4 H, CH_2), 2.73 (m, 2 H, CH_2), 1.89 (m, 1 H, CH), 1.49 (m, 1 H, CH_2), 1.17 (m, 1 H, CH_2), 1.06 (d, ^3J = 7.0 Hz, 3 H, CH_3), 0.90 (t, ^3J = 7.5 Hz, 3 H, CH_3).

[Co(tren)(L-leucinato)]I_2 (7): $C_{12}H_{30}CoI_2N_5O_2$ (589.13): calcd. C 24.46, N 11.19, H 5.13, found C 25.21, N 11.53, H 4.98. − Yield: 0.66 g, 35%. − ^{1}H NMR: δ = 5.95 (t, ^3J = 9.5 Hz, 1 H, NH_2), 5.00 (m, 2 H, NH_2), 4.77 (t, ^3J = 10.0 Hz, 1 H, NH_2), 4.50 (m, 1 H, NH_2), 4.35 (m, 1 H, NH_2), 4.04 (m, 2 H, NH_2), 3.34 (m, 5 H, CH_2, CH), 3.15 (m, 2 H, CH_2), 3.01−2.94 (m, 4 H, CH_2), 2.72 (m, 2 H, CH_2), 1.85 (m, 2 H, CH), 1.61 (m, 2 H, CH_2), 0.99 (d, ^3J = 7.0 Hz, 3 H, CH_3), 0.94 (d, ^3J = 6.5 Hz, 3 H, CH_3).

X-ray Crystallography

Experimental details of the X-ray analyses are provided in Table 1 and Table 2. All diffraction data were collected on a Bruker Smart 1000 CCD diffractometer with graphite monochromated Mo-K_α radiation (λ= 0.71073 Å) at room temperature using the program SMART[17] and processed by SAINT+.[18] Absorption correction was applied by SADABS.[19]

Space groups of these compounds were determined from systematic absences and further justified by the results of refinement. In compound **1**, it was noted that the $|E^*E - 1| = 0.831$ and that systematic absences indicate that it crystallizes in the polar (non-centro-

Table 1. Crystallographic and experimental data for **1**−**4**

	1	**2**	**3**	**4**
Empirical formula	$C_{15}H_{28}Cl_2CoN_5O_{10}$	$C_{15}H_{30}CoI_2N_5O_3$	$C_{11}H_{28}CoI_2N_5O_3$	$C_{17}H_{31}Cl_2CoN_6O_{10.5}$
Formula weight	568.25	641.17	591.11	617.31
Crystal system	Orthorhombic	Orthorhombic	Orthorhombic	Monoclinic
Space group	$Pca2_1$	$P2_12_12_1$	$P2_12_12_1$	$P2_1$
a [Å]	17.797(2)	10.1712(5)	9.0236(7)	11.1393(16)
b [Å]	11.7763(14)	12.6054(7)	10.9085(9)	18.459(3)
c [Å]	10.9053(14)	17.6765(10)	19.4365(15)	11.8131(16)
β [°]				94.003(3)
Volume [Å^3]	2285.6(5)	2266.3(2)	1913.2(3)	2423.2(6)
Z	4	4	4	4
Density (calc.) [g/m^3]	1.651	1.879	2.052	1.692
Absorption coefficient [mm^{-1}]	1.046	3.505	4.144	0.997
F(000)	1176	1248	1144	1280
Crystal size [mm]	0.5×0.2×0.2	0.3×0.15×0.13	0.4×0.2×0.2	0.25×0.15×0.15
Θ Range of data collection	2.07 to 27.03	2.14 to 27.00	1.98 to 27.07	1.73 to 27.08
reflections collected	7722	13806	6821	14836
Independent/observed refls [$I>2\sigma(I)$]	3340/2802	4960/4095	3701/3175	10062/5924
Transmission	0.8180−0.6227	0.6785−0.4195	0.4913−0.2881	0.8648−0.6912
Data/restraints/parameters	3340/1/316	4960/0/235	3701/0/199	10062/1/658
Goodness-of-fit on F^2	0.983	0.971	0.952	0.879
Final *R* indices [$I>2\sigma(I)$]	$R1 = 0.0415$	$R1 = 0.0303$	$R1 = 0.0367$	$R1 = 0.0496$
$wR2 = 0.1139$	$wR2 = 0.1139$	$wR2 = 0.0772$	$wR2 = 0.0795$	$wR2 = 0.0987$
R indices (all data)	$R1 = 0.0505$	$R1 = 0.0397$	$R1 = 0.0444$	$R1 = 0.0966$
$wR2 = 0.1094$	wR2 = 0.1094	$wR2 = 0.0801$	$wR2 = 0.0808$	$wR2 = 0.1101$

Table 2. Crystallographic and experimental data for **5**−**7**

Compound	**5**	**6**	**7**
Empirical formula	$C_{11}H_{28.7}CoI_2N_5O_{2.3}$	$C_{12}H_{30}CoI_2N_5O_2$	$C_{12}H_{30}CoI_2N_5O_2$
Formula weight	581.12	589.14	589.14
Crystal system	Orthorhombic	Monoclinic	Trigonal
Space group	$P2_12_12_1$	$P2_1$	$P3_2$
a [Å]	11.5598(6)	8.6576(7)	9.1653(5)
b [Å]	18.5803(10)	10.0933(8)	9.1653(5)
c [Å]	27.7747(16)	11.8068(9)	20.9419(16)
β [°]		98.1810(10)	
Volume [Å^3]	5965.6(6)	1021.22(14)	1523.49(17)
Z	12	2	3
Density(calc.) [g/m^3]	1.941	1.916	1.926
Absorption coefficient [mm^{-1}]	3.980	3.873	3.897
Crystal size mm	0.3×0.2×0.2	0.4×0.2×0.15	0.4×0.3×0.3
F(000)	3376	572	858
Θ Range of data collection	1.32 to 27.05	1.74 to 27.02	2.57 to 27.02
Reflections collected	21406	6115	5421
Independent/observed refls [$I>2\sigma(I)$]	12800/10282	3721/3485	3266/3046
Transmission	0.5032−0.3814	0.5940−0.3062	0.5095−0.3877
Data/restraints/parameters	12800/0/577	3721/1/194	3266/1/199
Goodness-of-fit on F^2	0.934	1.028	1.057
Final *R* indices [$I>2\sigma(I)$]	$R1 = 0.0316$	$R1 = 0.0406$	$R1 = 0.0263$
	$wR2 = 0.0591$	$wR2 = 0.1045$	$wR2 = 0.0658$
R indices (all data)	$R1 = 0.0456$	$R1 = 0.0433$	$R1 = 0.0291$
	$wR2 = 0.0620$	$wR2 = 0.1060$	$wR2 = 0.0666$

symmetric) space group $Pca2_1$, suggesting that phenylalanine racemizes during the synthetic procedure. In all cases, the structures were solved by direct methods and refined using full-matrix least-squares/difference Fourier techniques using SHELXTL.[20−22] All non-hydrogen atoms were refined with anisotropic displacement parameters. All hydrogen atoms of the ligands were then placed at idealized positions and refined as riding atoms with the relative isotropic parameters of the heavy atoms to which they are attached. Figure 1 through 7 show the cation conformations and packing feature of these complexes. Crystallographic data (excluding structure factors) for the structures reported in this paper have been deposited with the Cambridge Crystallographic Data Center as supplementary publication number CCDC 141454 − CCDC 141460. Copies of the data can be obtained free of charge on application to CCDC, 12 Union Road, Cambridge CB2 1EZ, UK. Fax: (internat.) + 44−1233/336-033; E-mail: deposit@ccdc.cam.ac.uk.

Acknowledgments

This work is supported by the National Nature Science Foundation of China (No. 29801006), whom we thank for their generosity.

[1] H. Chun, B. J. Salinas, I. Bernal, *Eur. J. Inorg. Chem.* **1999**, 723−728.
[2] [2a]J . P. Collman, D. A. Buckingham, *J. Am. Chem. Soc*. **1963**,

85, 3039−3040. − [2b] D. A. Buckingham, J. P. Collman, D. A. Happer, L. J. Marzilli, *J. Am. Chem. Soc.* **1967**, *89*, 1082−1087.
[3] J. P. Collman, D. A. Buckingham, *Inorg. Chem.* **1967**, *6*, 1803−1087.
[4] E. Kimure, S. Young, J. P. Collman, *Inorg. Chem*. **1970**, 9, 1183−1191.
[5] R. Gillard, D. A. Phipps, *J Chem. Soc., Chem. Commun*. **1970**, 800−801.
[6] D. A. Buckingham, P. J. Cresswell, R. J. Dellaca, M. Dwyer, G. J. Gainford, L. G. Marzilli, I. E. Maxwell, W. T. Robinson, A. M. Sergrson, K. R. Turnbull, *J. Am. Chem. Soc.* **1974**, *96*, 1713−1725.
[7] A. Y. Girgis, J. I. Legg, *J. Am. Chem. Soc.* **1972**, *94*, 8420−8425.
[8] K. W. Bentley, E. H. Creaser, *Inorg. Chem.* **1974**, *13,* 1115−1121.
[9] P. A. Sutton, D. A. Buckingham, *Acc. Chem. Res.* **1987**, 357−364.
[10] [10a] K.Yamanari, A. Fuyuhiro, *Chemistry Letter* **1991**, 1551−1554. − [10b] K.Yamanari, A. Fuyuhiro, *Bull. Chem. Soc. Jpn.* **1995**, *68*, 2543−2550. − [10c] K.Yamanari, A. Fuyuhiro, *Bull. Chem. Soc. Jpn.* **1996**, *69*, 1289−1296.
[11] I. I. Mathews, H. Manohar, *Polyhedron* **1991**, *10*, 2163−2169.
[12] T. Nagai, *Bull. Chem. Soc. Jpn.* **1989**, *62*, 2897−2901.
[13] M. Yamaguchi, S. Yamamatsu, T. Furusawa, S. Yano, M. Saburi, S. Yoshikawa, *Inorg. Chem.* **1980**, *19*, 2010−2016.
[14] J. Jacques, A. Collet, S. H. Wilen, Enantiomers, Racemates, and Resolutions, Krieger Publication, Florida, **1991**, p. 4.
[15] I. Bernal, W. H. Ries, H. Brunner, D. K. Rastogi, *J. Organometal. Chem.* **1985**, *290*, 353−361.
[16] [16a] J. Cai, J. Myrczek, I. Bernal, *J. Chem. Soc. Dalton Trans.* **1995**, 611−619. − [16b] I. Bernal, J. Cetrullo, J. Cai, *Trans. Metal Chem.* **1994**, *19*, 221−229. − [16c] I. Bernal, J. Cetrullo, J. Cai, R. A. Geanangel, J. H. Worrell, *J. Chem. Soc., Dalton Trans.* **1995**, 99−104. − [16d] I. Bernal, J. Myrczek, J. Cai, *Polyhedron* **1993**, *12*, 1149−1155. − [16e] I. Bernal, J. Cai, F. Somoza, *J. Coord. Chem.* **1997**, *42*, 33−44. − [16f] I. Bernal, J. Cetrullo, J. Myrczek, J. Cai, W. T. Jordan, *J. Chem. Soc., Dalton Trans.* **1993**, 1771−1776.
[17] Bruker AXS, SMART, Version 5.0, Bruker AXS, Madison, WI, USA, **1998**.
[18] Bruker AXS, SAINT+, Version 6.0, Bruker AXS, Madison, WI, USA, **1999**.
[19] R. Blessing, *Acta Cryst*. **1995**, *A51*, 33−38.
[20] Bruker AXS, SHELXTL, Version 5.1, Bruker AXS, Madison, WI, USA, **1998**.
[21] G. M. Sheldrick, SHELXS-97, Program for X-ray Crystal Structure Solution. Göttingen University, Germany, **1997**.
[22] G. M. Sheldrick, SHELXL-97, Program for X-ray Crystal Structure Refinement. Göttingen University, Germany, **1997**.

Received March 8, 2000
[I00098]

Orientation and Restricted Rotation of Lopsided N-Donor Heterocyclic Bioligands in Octahedral Ruthenium Complexes

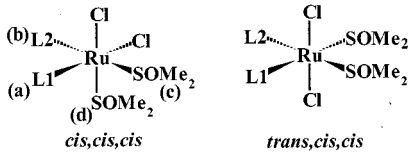
Enzo Alessio,*[a] Elisabetta Iengo,[a] Ennio Zangrando,[a] Silvano Geremia,[a] Patricia A. Marzilli,[b] and Mario Calligaris[a]

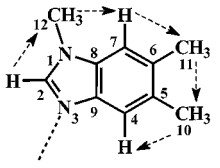
Keywords: Ruthenium / Dimethyl sulfoxide / N ligands / Molecular dynamics / Atropisomerism / Bioinorganic chemistry

In order to analyze the roles of steric and electrostatic factors in determining the orientation and dynamic behavior of benzimidazole-type ligands in Ru^{II}(dimethyl sulfoxide) complexes, compounds of the general formula $RuX_2(dmso\text{-}S)_{2-n}(CO)_n(L)_2$ [X = Cl, Br; L = 1,5,6-trimethylbenzimidazole (Me_3Bzm), benzimidazole (Bzm); n = 0–2] with *cis* and *trans* arrangements of the X ligands, have been prepared and structurally characterized both in solution and in the solid state, by NMR and X-ray techniques, respectively. New descriptors, based on the torsion angles about the Ru–N bonds, are introduced for a more efficient definition of the head-to-head (HH) and head-to-tail (HT) orientations of the heterocyclic nitrogen bases. Similar descriptors, based on the torsion angles about the Ru–S bonds, are used to define the orientation of the dimethyl sulfoxide ligands. The experimental molecular conformations are discussed on the basis of molecular mechanics (MM) calculations. The electrostatic interaction between the halide ligands and the positively charged N_2CH proton on the imidazole ring has been found to be the essential factor in determining the specific orientation of one Me_3Bzm base, both in the solid state and in solution. The different stabilities of the HH and HT base conformations observed in solution, in the solid state, and in the isolated molecules are rationalized in terms of solvation and packing effects. The larger solvent-accessible surface area in the HH conformation as compared with that in the HT form leads to more effective intermolecular interactions, which are responsible for stabilizing the former geometry in the condensed phase.

Introduction

The *cis*-M(L1)(L2) unit, where L1 and L2 are either the same or different planar aromatic N-donor ligands, is a common motif in biological systems, in particular in cross-links formed by DNA with metal anticancer drugs and in metalloenzymes.[1] These units are usually highly dynamic and difficult to evaluate in solution. Consequently, there have been relatively few cases where rotation of the L1 and L2 ligands about the M−N bond has proved to be sufficiently slow for structural and dynamic features to be assessed.[2−8] We have found that improved insight into the features of such units can be gained by studying complexes of the bioligand 1,5,6-trimethylbenzimidazole (Me_3Bzm) (Scheme 1) and comparing the results of studies on analogs with the non-biological pyridine ligands. Various types of information can be gained since bioligands are typically non-C_2-symmetric (i.e. lopsided), whereas the selected non-biological ligands are C_2-symmetric. When both ligands in the *cis*-M(L1)(L2) unit are lopsided, there are four possible major rotamers: two with head-to-head (HH) orientation and two with head-to-tail (HT) orientation (Scheme 2). When only one ligand is lopsided, there are two rotamers. When neither ligand is lopsided, there is only one possible rotamer. If the lopsided ligands L1 and L2 are identical, and the metal center and "spectator" (also called carrier) ligands form a highly symmetric carrier ligand−metal center moiety, only one HH rotamer is possible. One further feature is that some of the HT rotamers may be enantiomers.



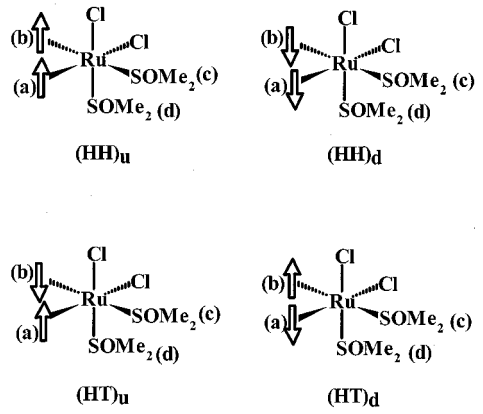


Scheme 1. Schematic representation of the generic octahedral *c*,*c*,*c*-$RuCl_2(dmso\text{-}S)_2(L1)(L2)$[9] (left, with labeling scheme of ligand positions) and *t*,*c*,*c*-$RuCl_2(dmso\text{-}S)_2(L1)(L2)$[9] (right) isomers; in this work L1 = L2 = Me_3Bzm (bottom, showing numbering scheme and intraligand NOE connectivity path), while either one or both dmso-S ligands may be replaced by CO

We recently reported that restricted rotation about Ru−N bonds in octahedral complexes of the type *cis*,*cis*,*cis*-$RuCl_2(dmso\text{-}S)_2(L1)(L2)$[9] (L1 *trans* to Cl, L2 *trans* to dmso-S; Scheme 1) allows assessment of the relative ori-

[a] Dipartimento di Scienze Chimiche, Università di Trieste, Via Giorgieri 1, 34127 Trieste, Italy
E-mail: alessi@univ.trieste.it
[b] Department of Chemistry, Emory University, Atlanta, GA 30322, USA
Supporting information for this article is available on the WWW under http://www.wiley-vch.de/home/eurjic or from the author.

 © WILEY-VCH Verlag GmbH, D-69451 Weinheim, 2000 1434−1948/00/1010−2207 $ 17.50+.50/0



Scheme 2. Schematic representation of the four possible major rotamers of *c*,*c*,*c*-$RuCl_2$(dmso-S)$_2$(Me_3Bzm)$_2$ (**1**); Me_3Bzm is indicated with an arrow, with the head corresponding to B2H

entation and dynamic motion of two *cis*-coordinated N-donor aromatic ligands. The use of C_2-symmetric ligands, such as pyridine (py) and 3,5-lutidine (3,5-lut), in combination with non-C_2-symmetric ligands such as Me_3Bzm and 1,2-dimethylimidazole (1,2-Me_2Im) provides more insight than the use of either type alone.[1−5,8] NMR investigations of the dynamic behavior of such compounds in solution showed that, at ambient temperature, they exist in a definite number of conformers that are in an essentially slow-exchange equilibrium, the position of which depends on the nature of the nitrogen bases.

The results obtained with Me_3Bzm were particularly significant as they indicated that its dynamic behavior was strongly influenced not only by steric factors, but also by electrostatic interactions.[1] In Me_3Bzm, which is a nucleopurine analog, the N_2CH proton on the imidazole ring (B2H) is relatively acidic and hence bears a partial positive charge (δ+), which is increased upon coordination to metal centers. We found that in ruthenium(II)[1−5] and rhenium(V)[8] Me_3Bzm complexes, the electrostatic attraction between the $N_2CH^{\delta+}$ proton(s) and the negative ligands (e.g. oxo, Cl) is important in determining the observed conformations. In particular, the solid-state structures of *c*,*c*,*c*-$RuCl_2$(dmso-S)$_2$(Me_3Bzm)$_2$, *c*,*c*,*c*-$RuCl_2$(dmso-S)$_2$(1,2-Me_2Im)(Me_3Bzm), and *c*,*c*,*c*-$RuCl_2$(dmso-S)$_2$(py)(Me_3Bzm) showed that the Me_3Bzm *trans* to dmso-S has the same orientation in the three complexes, with the mean plane of the ligand almost bisecting the Cl−Ru−Cl angle and B2H almost equidistant from the two Cl atoms. Moreover, for *c*,*c*,*c*-$RuCl_2$(dmso-S)$_2$(1,2-Me_2Im)(Me_3Bzm) and *c*,*c*,*c*-$RuCl_2$(dmso-S)$_2$(py)(Me_3Bzm) we found no evidence of the other possible geometrical isomer, i.e. that with Me_3Bzm *trans* to Cl. In solution, extensive NMR investigations provided strong evidence that, at ambient temperature, the Me_3Bzm *trans* to dmso-S remains relatively fixed, maintaining an orientation very similar to that found in the solid state; the dynamic behavior of the other N-donor ligand depends on its nature.[2−4] In *c*,*c*,*c*-$RuCl_2$(dmso-S)$_2$(Me_3Bzm)$_2$, the Me_3Bzm *trans* to Cl slowly (on the NMR time scale) flips between two orientations at ca. 180°, thus generating one HH and one HT rotamer of almost equal stability. Only the rare (at the time) HH atropisomer was found in the solid state.[2,3]

The imidazole ring is a common feature of many biological ligands. The electrostatic interaction between the $N_2CH^{\delta+}$ proton and the other ligands is likely to be of general relevance for all those biological systems in which metal sites are bound to imidazole rings (e.g. B_{12} systems, Pt drug adducts of DNA, metalloenzymes, and metalloproteins).[1]

In order to analyze in greater detail the roles of steric and electrostatic factors in determining the orientation and dynamic behavior of the Me_3Bzm ligand, we have prepared and studied some new Me_3Bzm (and Bzm) Ru^{II} compounds closely related to those mentioned above. As compared to the thoroughly investigated complex *c*,*c*,*c*-$RuCl_2$(dmso-S)$_2$(Me_3Bzm)$_2$ (**1**), we have changed the nature of the halogen (Br vs. Cl), the geometry of the complex (*trans*,*cis*,*cis* vs. *cis*,*cis*,*cis*),[9] and the number of dmso-S ligands (replaced by CO molecules). Thus, we have prepared and investigated on the basis of NMR and X-ray structural data in conjunction with molecular mechanics (MM) calculations, the two series of geometrical isomers of the formula *cis*,*cis*,*cis*- and *trans*,*cis*,*cis*-RuX_2(dmso-S)$_{2-n}$(CO)$_n$(L)$_2$ [X = Cl, Br; L = 1,5,6-trimethylbenzimidazole (Me_3Bzm), benzimidazole (Bzm); n = 0−2]. In particular, the compounds reported here are: *c*,*c*,*c*-$RuBr_2$(dmso-S)$_2$(Me_3Bzm)$_2$ (**2**), *t*,*c*,*c*-$RuCl_2$(dmso-S)$_2$(Me_3Bzm)$_2$ (**3**), *t*,*c*,*c*-$RuCl_2$(dmso-S)$_2$(Bzm)$_2$ (**4**), *c*,*c*,*c*-$RuCl_2$(dmso-S)(CO)(Me_3Bzm)$_2$ (**5**), *t*,*c*,*c*-$RuCl_2$(dmso-S)(CO)(Me_3Bzm)$_2$ (**6**), and *c*,*c*,*c*-$RuCl_2$(CO)$_2$(Me_3Bzm)$_2$ (**7**). Finally, with the aim of establishing whether the polarity of the medium of crystallization and/or packing interactions might affect the solid-state molecular conformation, we recrystallized **1** from hot benzene rather than from dmso/acetone mixtures,[3] which furnished crystals of *c*,*c*,*c*-$RuCl_2$(dmso-S)$_2$(Me_3Bzm)$_2$·2C_6H_6 (**8**). The crystal structure of **8** has been determined, as have those of **2**−**6**.

Results

Crystal and Molecular Structures

Coordination distances and sulfoxide bond lengths and angles for complexes **2**−**6** and **8** (Table 1 and 2) fall well within the ranges of values found in Ru^{II} compounds.[10] Merging the present data with those reported previously, mean values of 2.139(6) and 2.440(4) Å are obtained, respectively, for the Ru−N and Ru−Cl distances *trans* to sulfur, while those not *trans* to sulfur amount to 2.110(4) and 2.417(4) Å, respectively. The observed lengthenings of 0.029 Å (Ru−N) and 0.023 Å (Ru−Cl) confirm the *trans* influence of *S*-bonded dmso on the relevant Ru−N and Ru−Cl bonds.[10a] The Ru−C and Ru−S bond lengths in the carbonyl derivatives [1.832(6) and 2.284(1) Å, respectively, in **5**; 1.843(4) and 2.284(1) Å in **6**] are close to those reported for Ru^{II}(monocarbonyl)(dmso-S) complexes.[11] Interestingly, the Ru−S distances in **5** and **6** [2.284(1) Å] are significantly longer than those in **1**−**4** and **8** [av. 2.248(3) Å], as would be expected following the introduc-

tion of a strong π acceptor ligand into the coordination sphere.[11] Furthermore, the previously observed deformation of the Ru−N−C bond angles in benzimidazole complexes is also fully confirmed here. In fact, the average Ru−N(1)−C(5), Ru−N(1)−C(14), Ru−N(2)−C(15), and Ru−N(2)−C(24) bond angles measure 123.6(8)°, 130.8(6)°, 120.5(3)°, and 134.3(5)°, respectively, in agreement with previous data.[2,3,5]

Table 1. Selected bond lengths [Å] and angles [°] for compounds *c*,*c*,*c*-$RuBr_2$(dmso-S)$_2$(Me_3Bzm)$_2$ (**2**), *c*,*c*,*c*-$RuCl_2$(dmso-S)(CO)(Me_3Bzm)$_2$ (**5**), and *c*,*c*,*c*-$RuCl_2$(dmso-S)$_2$(Me_3Bzm)$_2$·$2C_6H_6$ (**8**)

	2	**5**	**8**
Distances	L = S(2), X = Br	L = C(3), X = Cl	L = S(2), X = Cl
Ru−N(1)	2.118(5)	2.109(4)	2.103(2)
Ru−N(2)	2.145(6)	2.115(4)	2.135(2)
Ru−S(1)	2.249(2)	2.284(1)	2.2484(9)
Ru−L	2.256(2)	1.832(6)	2.2415(8)
Ru−X(1)	2.5635(9)	2.393(1)	2.4326(9)
Ru−X(2)	2.589(1)	2.448(2)	2.4419(9)
S(1)−O(1)	1.473(6)	1.465(5)	1.479(3)
L−O(2)	1.478(5)	1.147(8)	1.472(2)
Angles			
X(1)−Ru−X(2)	89.17(4)	88.17(6)	88.40(3)
X(1)−Ru−S(1)	91.79(5)	89.27(5)	93.88(4)
X(1)−Ru−L	87.53(5)	88.9(2)	87.62(3)
X(1)−Ru−N(1)	175.8(2)	175.6(1)	175.02(7)
X(1)−Ru−N(2)	89.0(2)	89.3(1)	88.02(7)
S(1)−Ru−L	96.54(7)	93.3(2)	96.80(3)
S(1)−Ru−N(1)	91.1(2)	92.2(1)	89.29(7)
S(1)−Ru−N(2)	174.3(2)	178.6(1)	172.95(7)
L−Ru−N(1)	95.2(2)	95.1(2)	95.82(7)
L−Ru−N(2)	89.1(2)	86.4(2)	90.05(7)
N(1)−Ru−N(2)	87.9(2)	89.2(2)	88.4(1)
Ru−N(1)−C(5)	120.1(5)	123.5(4)	120.3(2)
Ru−N(1)−C(11)	134.2(4)	130.7(4)	134.6(2)
Ru−N(2)−C(12)	122.0(5)	124.8(4)	121.4(2)
Ru−N(2)−C(18)	131.7(5)	129.5(3)	132.4(2)
Ru−S(1)−O(1)	120.1(2)	118.8(2)	121.2(1)
Ru−S(1)−C(1)	112.6(3)	111.3(3)	110.7(1)
Ru−S(1)−C(2)	114.1(3)	12.3(3)	111.9(1)
C(1)−S(1)−C(2)	98.2(4)	96.9(5)	99.0(2)
Ru−L−O(2)	119.4(2)	173.2(6)	119.3(1)
Ru−L−C(3)	114.7(3)	−	113.6(1)
Ru−L−C(4)	110.7(3)	−	111.2(1)
C(3)−L−C(4)	98.0(4)	−	97.5(2)

A summary of the solid-state conformational parameters for the RuX_2(dmso-S)$_2$(L1)(L2) (X = Cl, Br; L1, L2 = Me_3Bzm, Bzm, or 1,2-Me_2Im) and $RuCl_2$(dmso-S)(CO)(Me_3Bzm)$_2$ complexes is given in Table 3 (see Discussion for conformation descriptors). These data show that, in spite of the presence of benzene molecules of crystallization, the molecular structure of the complex *c*,*c*,*c*-$RuCl_2$(dmso-S)$_2$(Me_3Bzm)$_2$ in **8** is comparable to that in **1**. Analogously, the molecular conformation of the bromo derivative *c*,*c*,*c*-$RuBr_2$(dmso-S)$_2$(Me_3Bzm)$_2$ (**2**) is very similar to that of **1**, and is practically unaffected by the presence of ethanol molecules in the lattice. The same labeling scheme has been used for the RuX_2(dmso-S)$_{2-n}$(CO)$_n$(Me_3Bzm)$_2$ moiety in all the complexes (X = Cl or Br, n = 0−2), as illustrated in Figures 1, 2 and 3, which show the molecular structures of **2**, **3**, **5**, and **6**.

Table 2. Selected bond lengths [Å] and angles [°] for compounds *t*,*c*,*c*-$RuCl_2$(dmso-S)$_2$(Me_3Bzm)$_2$ (**3**), *t*,*c*,*c*-$RuCl_2$(dmso-S)$_2$(Bzm)$_2$ (**4**), and *t*,*c*,*c*-$RuCl_2$(dmso-S)(CO)(Me_3Bzm)$_2$ (**6**)

	3	**4**	**6**
Distances	L = S(2)	L = S(2)	L = C(3)
Ru−N(1)	2.177(2)	2.155(3)	2.168(3)
Ru−N(2)	2.134(2)	2.128(3)	2.112(3)
Ru−S(1)	2.2402(9)	2.2349(9)	2.284(1)
Ru−L	2.2604(8)	2.2673(9)	1.843(4)
Ru−Cl(1)	2.4128(9)	2.4054(9)	2.388(1)
Ru−Cl(2)	2.4117(9)	2.4309(9)	2.404(1)
S(1)−O(1)	1.478(3)	1.482(3)	1.474(3)
L−O(2)	1.475(3)	1.482(2)	1.132(5)
Angles			
Cl(1)−Ru−Cl(2)	177.57(3)	177.19(3)	177.81(4)
Cl(1)−Ru−S(1)	93.85(3)	94.93(3)	91.36(4)
Cl(1)−Ru−L	86.05(3)	84.24(3)	90.0(2)
Cl(1)−Ru−N(1)	94.02(7)	94.58(7)	87.11(9)
Cl(1)−Ru−N(2)	90.73(7)	89.73(7)	87.71(9)
S(1)−Ru−L	93.50(3)	93.80(3)	93.5(2)
S(1)−Ru−N(1)	91.32(7)	93.14(8)	87.90(9)
S(1)−Ru−N(2)	174.38(7)	174.89(7)	173.62(9)
L−Ru−N(1)	175.16(7)	173.04(7)	176.8(2)
L−Ru−N(2)	90.07(7)	88.74(7)	92.8(2)
N(1)−Ru−N(2)	85.09(9)	84.4(1)	85.8(1)
Ru−N(1)−C(5)	119.2(2)	121.1(2)	123.3(3)
Ru−N(1)−C(11)	135.9(2)	133.7(2)	130.5(2)
Ru−N(2)−C(12)	124.7(2)	123.7(2)	121.6(3)
Ru−N(2)−C(18)	130.2(2)	129.9(2)	132.3(3)
Ru−S(1)−O(1)	119.3(1)	117.2(1)	117.1(1)
Ru−S(1)−C(1)	110.5(1)	111.2(2)	111.3(2)
Ru−S(1)−C(2)	114.4(1)	116.5(2)	113.3(2)
C(1)−S(1)−C(2)	98.4(2)	98.9(2)	100.6(3)
Ru−L−O(2)	115.8(1)	114.4(1)	178.8(5)
Ru−L−C(3)	113.8(2)	115.5(2)	−
Ru−L−C(4)	114.7(1)	115.6(1)	−
C(3)−L−C(4)	98.6(2)	98.2(2)	−

Solution Studies

For the sake of clarity, the labeling schemes for the coordination positions of the ligands[9] and for the Me_3Bzm protons (Scheme 1) used in this work are the same as those used in our previous reports.[1−5] In particular, we label the base *trans* to Cl as "a", the base *trans* to S as "b", and the dmso ligands *trans* to "b" and Cl as "c" and "d", respectively.

cis,cis,cis Compounds

cis,cis,cis-$RuCl_2$(dmso-S)(CO)(Me_3Bzm)$_2$ (**5**)

This complex can be thought of as being formally derived from **1** through the replacement of dmso-S "d" by CO (Scheme 3). The ^{1}H NMR spectrum of **5** shows only one set of peaks for each non-equivalent Me_3Bzm ligand and one resonance for each diastereotopic dmso-S methyl group (Figure 4), as expected for an unsymmetrical *cis,cis,cis* complex. All resonances are sharp and no evidence for conformational equilibria due to hindered rotation of the nitrogen ligands is apparent at room temperature.

Table 3. Base and dmso solid-state conformational parameters, Ψ and Φ [°], with their diastereotopomer descriptors of some *c*,*c*,*c*- and *t*,*c*,*c*-$RuX_2(dmso\text{-}S)_{2-n}(CO)_n(L1)(L2)$ complexes, with X = Cl, Br; *n* = 0, 1; L1, L2 = Me_3Bzm, Bzm, 1,2-Me_2Im

Complex		Ψ_a	Ψ_b	base		Φ	Ψ_c	Ψ_d	dmso	
Δ *c*,*c*,*c*-$RuCl_2(dmso\text{-}S)_2(Me_3Bzm)_2$ [a]	**1**	−45.8	131.5	$(HH)_u$	H_4H_2	47.7	−13.7	83.6	$(HH)_d$	$H_0H_{\pi/2}$
Δ *c*,*c*,*c*-$RuCl_2(dmso\text{-}S)_2(Me_3Bzm)_2{\cdot}2C_6H_6$ [b]	**8**	−48.2	136.1	$(HH)_u$	H_4H_2	48.5	−11.5	90.4	$(HH)_d$	$H_0H_{\pi/2}$
Δ *c*,*c*,*c*-$RuBr_2(dmso\text{-}S)_2(Me_3Bzm)_2$ [a]	**2**	−44.9	138.1	$(HH)_u$	H_4H_2	45.8	−2.5	91.3	$(HH)_d$	$H_0H_{\pi/2}$
Δ *c*,*c*,*c*-$RuCl_2(dmso\text{-}S)_2(1,2\text{-}Me_2Im)(Me_3Bzm)$ [c]		129.1	136.5	$(HT)_d$	H_2H_2	43.8	−26.0	80.2	$(HH)_d$	H_4H_1
Δ *c*,*c*,*c*-$RuCl_2(dmso\text{-}S)(CO)(Me_3Bzm)_2{\cdot}0.5MeOH$ [b]	**5**	−57.2	144.2	$(HH)_u$	H_4H_2	68.3[d]	−92.0[e]			
t,*c*,*c*-$RuCl_2(dmso\text{-}S)_2(Me_3Bzm)_2$ [b]	**3**	−74.5[f]	126.2	HH	H_4H_2	78.6	29.1	161.7	HT	H_2H_1
t,*c*,*c*-$RuCl_2(dmso\text{-}S)_2(Bzm)_2$ [b]	**4**	−58.0[f]	127.3	HH	H_4H_2	54.4	32.4	159.9	HT	H_2H_1
t,*c*,*c*-$RuCl_2(dmso\text{-}S)(CO)(Me_3Bzm)_2$ [b]	**6**	123.0	−36.9	HH	H_2H_4	61.3	−108.6[e]			

[a] Ref.[3] – [b] Present work. – [c] Ref.[4] – [d] Mean value between the two locations of the Me_3Bzm ligand. – [e] Torsion angle C(3)−Ru−S(1)−O(1), C(3) substituting S(2). – [f] Bases "a" and "b" are exchangeable, and consequently so are dmso "c" and "d".

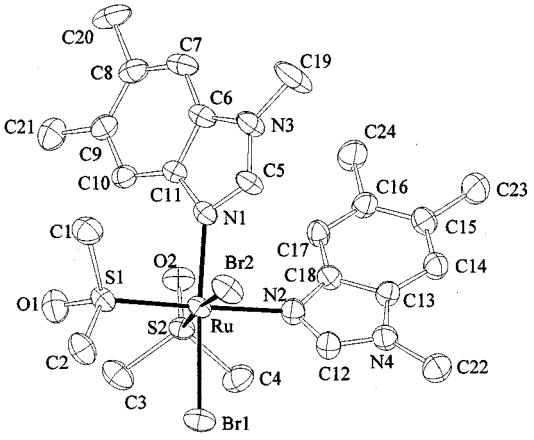


Figure 1. Molecular structure of the compound *c*,*c*,*c*-$RuBr_2(dmso\text{-}S)_2(Me_3Bzm)_2$ (**2**) (thermal ellipsoids drawn at a 40% probability level); the same scheme also applies to **8**, substituting the bromine atoms with chlorine atoms

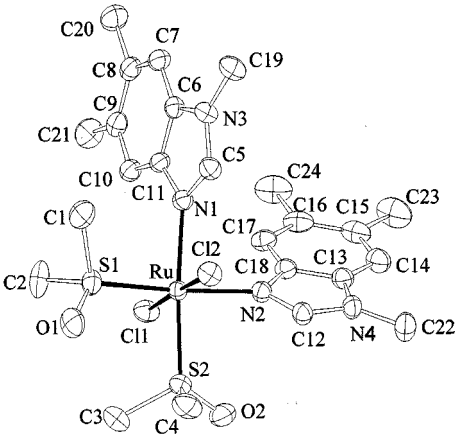


Figure 2. Molecular structure of the compound *t*,*c*,*c*-$RuCl_2(dmso\text{-}S)_2(Me_3Bzm)_2$ (**3**) (thermal ellipsoids drawn at a 40% probability level); the same scheme also applies to **4** with the exclusion of methyl groups C(19)−C(24)

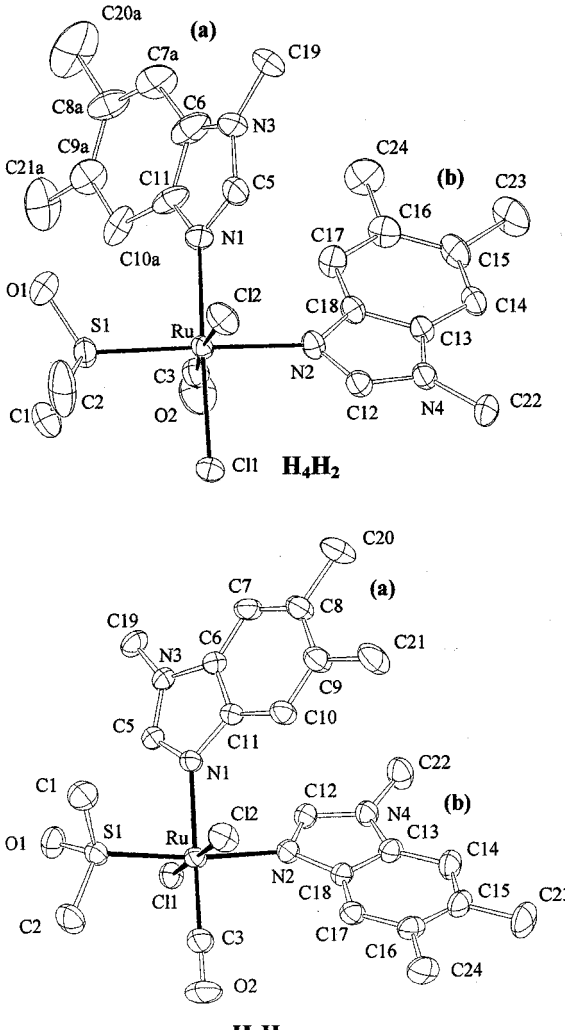
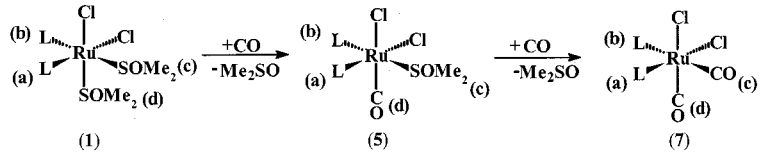


Figure 3. Molecular structures of the compounds *c*,*c*,*c*-$RuCl_2(dmso\text{-}S)(CO)(Me_3Bzm)_2$ (**5**) (top) and *t*,*c*,*c*-$RuCl_2(dmso\text{-}S)(CO)(Me_3Bzm)_2$ (**6**) (bottom, thermal ellipsoids drawn at a 40% probability level) with the relative conformational descriptors

Even though two isomers with a *cis*,*cis*,*cis* geometry are possible, depending on whether CO is *trans* to Cl or to Me_3Bzm, we isolated exclusively the compound in which CO is *trans* to Cl (as confirmed by the X-ray structure, see below) and found no evidence to suggest the existence of the other isomer. The resonances were assigned with the aid of a NOESY spectrum (Table 4); the intra-ligand NOE connectivity path ($B2H-B12H_3-B7H-B10H_3-B11H_3-B4H$; Scheme 1) allowed designation of the signals arising from each Me_3Bzm moiety, while the final assignment of the Me_3Bzm position as either "a" (i.e. *cis* to the dmso-S) or "b" (i.e. *trans* to dmso-S) was accomplished through the inter-ligand NOE contacts. In particular, from



Scheme 3

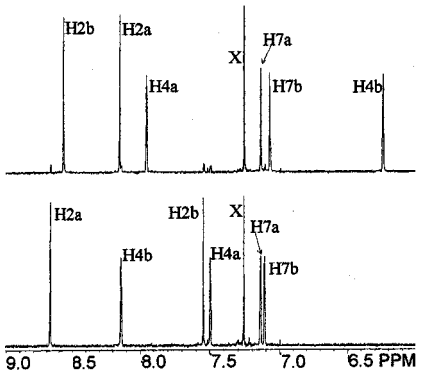


Figure 4. Downfield region of the ^{1}H NMR spectrum ($CDCl_3$, 400 MHz) of *c*,*c*,*c*-$RuCl_2$(dmso-S)(CO)(Me_3Bzm)$_2$ (**5**) (top) and *t*,*c*,*c*-$RuCl_2$(dmso-S)(CO)(Me_3Bzm)$_2$ (**6**) (bottom); resonances of Me_3Bzm "a" and "b" are labeled with a and b, respectively

a clear NOE cross-peak between the B4H resonance at δ = 7.96 and the dmso peak at δ = 3.11, it could be established that the two ligands are *cis* to one another. The overall chemical shift patterns of the Me_3Bzm "a" and "b" ligands in **5** closely resemble those found in the HH rotamer of *c*,*c*,*c*-$RuCl_2$(dmso-S)$_2$(Me_3Bzm)$_2$ (**1**-HH, Table 4); in particular, the (B4H)b and ($B10H_3$)b signals are upfield shifted, suggesting that these protons might reside within the shielding cone of Me_3Bzm "a". Similarly, the upfield shift of the (B2H)a signal and, to a lesser extent, that due to ($B12H_3$)a, can be attributed to their positions within the shielding cone of Me_3Bzm "b". According to such arguments, an HH conformation similar to that found in the crystal structure of **5** (see below and Table 3) is most likely maintained in solution.

of B4H, is maintained. It might be argued that such differences are caused by the presence of CO instead of dmso-S in the coordination sphere of the ruthenium center. However, the Me_3Bzm chemical shifts are very similar in the corresponding mono-Me_3Bzm derivatives, *c*,*c*,*c*-$RuCl_2$(dmso-S)$_2$(CO)(Me_3Bzm) and *cis*,*fac*-$RuCl_2$(dmso-S)$_3$(Me_3Bzm), which differ only in the presence of a CO molecule in place of a dmso-S ligand in position "a".[12] This finding suggests that the differences in Me_3Bzm chemical shifts found between **1**-HH and **5** are not due to the different ligand environments (CO vs. dmso-S), but rather to a slightly different average mutual tilt between the two HH ligands in solution.[1]

The ambient-temperature NMR spectrum of **5**, which shows only one set of resonances, is consistent with two hypotheses: either both the Me_3Bzm ligands are in rapid motion about the Ru−N bonds, averaging the HH conformation, or they both remain in relatively fixed positions. Variable-temperature NMR spectra of **5** in CD_2Cl_2 showed a partial broadening of the peaks only at $T < -90$ °C, which is still compatible with both hypotheses (the very low temperature broadening might also be due to restricted motion of the sulfoxides).

cis,*cis*,*cis*-$RuCl_2(CO)_2(Me_3Bzm)_2$ (**7**)

Further formal replacement of the remaining dmso-S ligand in **5** by CO led to compound **7**, in which both positions "c" and "d" are occupied by CO ligands (Scheme 3). Overall, the Me_3Bzm resonances of **7** give rise to a pattern similar to that seen for **5** and typical of the HH orientation

Table 4. Chemical shifts (δ values) of *c*,*c*,*c*-$RuCl_2$(dmso-S)(CO)(Me_3Bzm)$_2$ (**5**), *t*,*c*,*c*-$RuCl_2$(dmso-S)(CO)(Me_3Bzm)$_2$ (**6**), and *c*,*c*,*c*-$RuCl_2(CO)_2(Me_3Bzm)_2$ (**7**) in $CDCl_3$ compared to those of the corresponding ligands in the HH conformer of *c*,*c*,*c*-$RuCl_2$(dmso-S)$_2$(Me_3Bzm)$_2$ (**1**)

	5		**6**		**7**		**1**[a]	
	Me_3Bzm "a"	Me_3Bzm "b"	Me_3Bzm "a"	Me_3Bzm "b"	Me_3Bzm "a"	Me_3Bzm "b"	Me_3Bzm "a"	Me_3Bzm "b"
B2H	8.15	8.56	8.67	7.55	7.82	8.83	7.43	8.90
B4H	7.96	6.24	7.50	8.14	7.63	6.16	8.25	6.11
B7H	7.14	7.07	7.14	7.11	7.19	7.17	7.06	7.17
$B10H_3$	2.44	1.86	2.05	2.39	2.52	1.90	2.48	1.85
$B11H_3$	2.43	2.26	2.31	2.40	2.46	2.30	2.41	2.31
$B12H_3$	3.56	3.78	3.82	3.55	3.57	3.88	3.36	3.92
	dmso-S "c"		dmso-S "c"				dmso-S "c"	
	3.55	3.11	3.41				3.55	2.86

[a] Conformer HH.

Despite the general similarity between the Me_3Bzm chemical shift patterns of **5** and **1**-HH, there are, nevertheless, some notable differences, particularly in the signal shifts of Me_3Bzm "a". Thus, while in **1**-HH the B4H signal appears further downfield than that of B2H, in **5** the "normal" order, i.e. the B2H signal further downfield than that (Table 4); the presence of CO in place of the residual dmso-S apparently has no significant effect on the resonances of the *trans*-coordinated Me_3Bzm. In this case, a NOESY spectrum did not allow us to distinguish between positions "a" and "b" and thus we assumed the HH orientation of the two Me_3Bzm ligands to be very similar to that in **5**.

However, a "reciprocal" HH orientation cannot be excluded (see below for **6**). From the point of view of the dynamics of the Me_3Bzm ligands, the ^1H NMR spectrum of **7** (which remained essentially unchanged in the temperature range +20 to −90 °C) is consistent with both the hypotheses advanced for **5**.

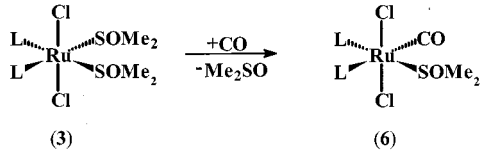
trans,cis,cis Compounds

trans,cis,cis-$RuCl_2$(dmso-S)$_2$(Me_3Bzm)$_2$ (**3**)

The room-temperature reaction of *trans*-$RuCl_2$(dmso-S)$_4$ with an excess of Me_3Bzm selectively yielded the bis-substituted adduct **3**, which is a geometrical isomer of *c,c,c*-$RuCl_2$(dmso-S)$_2$(Me_3Bzm)$_2$ (**1**) (Scheme 1). The NMR spectrum of **3** is very simple (one set of peaks due to the two equivalent Me_3Bzm ligands and one sharp resonance due to the four equivalent dmso-S methyl groups) and consistent with the C_{2v} symmetry of the complex (considering the ligands as point groups). This NMR spectral pattern indicates that at room temperature the two Me_3Bzm ligands are in rapid motion about the Ru−N bonds, most probably going from one HT conformation to the other, through the HH conformation. The variable-temperature behavior of the NMR spectrum of **3** (CD_2Cl_2) is rather complicated and scarcely informative; all resonances broaden as the temperature is lowered to below −20 °C, and at −60 °C two sets of peaks in an almost 1:2 ratio begin to appear. However, on decreasing the temperature further, some of the signals broaden once more. These findings suggest that on lowering the temperature the rate of more than one molecular motion in **3** is sequentially decreased.

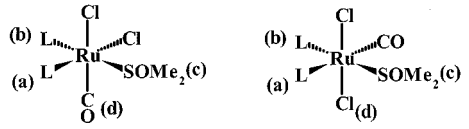
trans,cis,cis-$RuCl_2$(dmso-S)(CO)(Me_3Bzm)$_2$ (**6**)

The formal replacement of a dmso-S ligand in **3** by a CO ligand (Scheme 4) led to *trans,cis,cis*-$RuCl_2$(dmso-S)(CO)(Me_3Bzm)$_2$ (**6**), which is a geometrical isomer of **5** (Scheme 5). Compound **6**, while maintaining the overall geometry of **3**, nevertheless, has lower symmetry and thus provided useful spectroscopic information.



(3) (6)

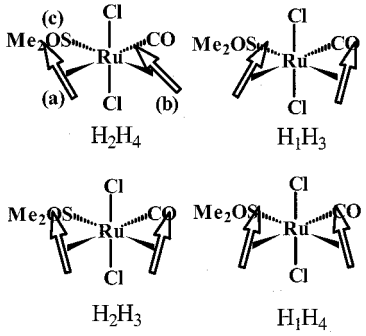
Scheme 4



Scheme 5 (5) (6)

The NMR spectrum of **6** (Figure 4), in agreement with the geometry of the complex (confirmed by X-ray structure analysis, see below), consists of a set of resonances due to each non-equivalent Me_3Bzm ligand and a singlet due to the two enantiotopic methyl groups of the dmso-S ligand (δ = 3.41). This means that the N,N,S,C plane is a plane of symmetry for the complex and, as in **3**, the two Me_3Bzm ligands have averaged "side" (S) orientations. The signals were assigned with the aid of an NOESY spectrum (Table 4); an NOE cross-peak between the dmso-S and the B4H signal at δ = 8.14 allowed us to establish which of the Me_3Bzm ligands was *cis* to dmso-S. In **6**, the two *cis*-Me_3Bzm ligands and the dmso-S ligand have the same *mer* arrangement as in the geometrical isomer **5**, so that the same labeling scheme can be used (Scheme 5). Indeed, the NMR spectra of **6** and **5** are quite similar and both are in agreement with an HH orientation of the two bases. However, in **6** the chemical shift patterns of Me_3Bzm "a" and "b" are inverted with respect to those in **5** (Figure 4).

It might be argued that the different Me_3Bzm chemical shift patterns in **5** and **6** are due to the strong *trans* effect of the CO ligand. However, on the basis of results obtained for similar compounds,[13] substitution of dmso-S by CO is expected to affect the resonance of the proton closest to the N−Ru, i.e. B2H of Me_3Bzm "a", only marginally (ca. 0.3 ppm). The large chemical shift variations for the protons of Me_3Bzm "a" quite distant from the coordination site (e.g. $B10H_3$) and, above all, for the protons of Me_3Bzm "b" can thus safely be ascribed to a different mutual tilt of the two HH bases in **6** as compared to the situation in **5**. Indeed, in **6**, due to the lower symmetry compared to **3**, the two HH bases may either be leaning toward the dmso-S in position "c" or toward the CO (conformers H_2H_4 and H_1H_3 in Scheme 6, respectively; see Discussion). The NMR spectrum suggests that in solution the HH orientation of the two bases in **6** is such that (B4H)a and ($B10H_3$)a reside within the shielding cone of Me_3Bzm "b"; models show that this is accomplished when the two HH bases are inclined toward the dmso-S (conformer H_2H_4). This orientation, which is the opposite to that found in **1** and **5**, is also evident in the solid-state structure (Figure 3, Table 3).



Scheme 6

Variable-temperature NMR experiments in CD_2Cl_2 showed that the resonances of the two bases in **6** begin to broaden only at temperatures below −80 °C, while at such temperatures the dmso-S resonance splits into two equally intense peaks (δ = 3.35 and 3.31). This behavior suggests that at room temperature the two HH bases are most probably in rapid motion between two equivalent HH orientations, one above and the other below the N,N,S,C plane, thus averaging out as an "S" orientation. These motions

might be accompanied by that of dmso-S [so that the electrostatic interaction between (B2H)a and the oxygen atom of dmso is maintained]. At very low temperature (−80 °C), these motions (or those of the dmso-S ligand) become slow on the NMR time scale, the N,N,S,C pseudo-symmetry plane is lost, and the two methyl groups of the dmso-S become diastereotopic.

Discussion

Conformational Definitions

In unsymmetrical octahedral complexes of the type *c*,*c*,*c*-$RuCl_2(X)(Y)(Me_3Bzm)_2$, where X, Y = dmso-S or CO, two HH and two HT diastereotopomers are possible. Thus, it is necessary to designate the possible HH and HT geometries. In fact, taking the chlorine atom *cis* to both N ligands as a reference, quite different environments are achieved if the head of the Me_3Bzm ligand (B2H) is directed toward this chlorine atom or points in the opposite direction. We will indicate these positions as "up" (u) and "down" (d), respectively, so that the two HH geometries will be labeled as $(HH)_u$ and $(HH)_d$ (Scheme 2). For a more precise description of the HT conformations, the orientation of one of the two bases must be selected; we shall assume that the "u" and "d" descriptors in $(HT)_u$ and $(HT)_d$ always refer to the head of ligand "a". Furthermore, for a complete stereochemical description of such complexes, we reiterate that they can exist as enantiomeric pairs, the chirality of which can be described as Δ and Λ, taking the N···N and Cl···Cl vectors as skew lines.[14] The schemes and Figures 1−3 depict Δ enantiomers.

In order to study hindered rotation about the Ru−N bonds, torsion angles must be introduced, such as $\Psi_a = N_b-Ru-N_a-C_{\alpha a}$ and $\Psi_b = N_a-Ru-N_b-C_{\alpha b}$, where the subscripts a and b refer to the two nitrogen bases and C_α is the carbon atom in position 2 (Scheme 1). These parameters provide a precise description of all the possible HH and HT conformations, and also allow a distinction to be made between the different "head" orientations (see below). In the case of the enantiomorph Δ, $-180° < \Psi_a < 0°$ and $0° < \Psi_b < 180°$ for $(HH)_u$, and $0° < \Psi_a < 180°$, $-180° < \Psi_b < 0°$ for $(HH)_d$. The angular relationships between $(HH)_u$ and $(HH)_d$ are interchanged for the enantiomorph Λ. For the isomers $(HT)_u$ and $(HT)_d$, the ranges for the torsion angles are $-180° < \Psi_{a,b} < 0°$ and $0° < \Psi_{a,b} < 180°$, respectively. The Ψ angles also provide a quantitative measure of the mutual tilt of the two bases, which vanishes only when $\Psi_a = \Psi_b = \pm 90°$. If $\Psi = 0°$ or 180°, the hypothetical side (S) orientation occurs.

However, the (u) and (d) descriptors alone cannot adequately describe all the possible HH and HT conformations. For example, in the case of *t*,*c*,*c*-$RuCl_2(X)(Y)(Me_3Bzm)_2$ complexes there are no enantiomorphs, and the distinction between the "up" and "down" conformers is meaningless. Obviously, when X = Y, positions "a" and "b" are interchangeable; however, when X = CO and Y = dmso-S, as in *t*,*c*,*c*-$RuCl_2$(dmso-S)(CO)$(Me_3Bzm)_2$ (**6**), the two Me_3Bzm ligands are no longer equivalent, and substantially different HH and HT geometries are possible (see Scheme 6 with four HH conformers in **6**). The same concept also applies to *cis*,*cis*,*cis* complexes in which, for each $(HH)_{u/d}$ and $(HT)_{u/d}$ conformation, the two lopsided bases can have a range of different reciprocal orientations.

On the basis of the Ψ values, it is possible to formulate a new descriptor, such as $H_{\Psi a}H_{\Psi b}$ (head Ψ_a−head Ψ_b), to represent the mutual orientation of two *cis* lopsided ligands. For a simpler representation, we can use the notation H_iH_j (head *i*−head *j*), where *i* and *j* refer to the quadrants of Ψ_a and Ψ_b, respectively (*i*, *j* = 1: $0° < \Psi < 90°$; *i*, *j* = 2: $90° < \Psi < 180°$; *i*, *j* = 3: $180° < \Psi < 270°$; *i*, *j* = 4: $270° < \Psi < 360°$). This provides a simple means of describing in detail each HH and HT conformation; for example, the four HH conformers depicted in Scheme 6 can be described as H_2H_4, H_1H_3, H_2H_3, and H_1H_4, respectively. The system is particularly convenient when the torsion angles are around ±45° (or supplementary values), as found for lopsided aromatic bases.

The inter-base dihedral angle (Φ) has often been used to describe the conformations of metal complexes containing *cis* nitrogen bases.[15−17] This parameter, however, is of limited scope since, as is clear from the data in Table 3, different orientations (HH and HT) may have almost identical Φ values.

In *cis*,*cis*,*cis* complexes, when X = Y = dmso-S, the same conformational descriptors defined above for Me_3Bzm can be used for the two *cis*-dmso ligands, considering the position of the sulfoxide oxygen atom (taken as the head of the ligand) with respect to the RuS_2 plane and of the chlorine atom *cis* to both dmso ligands. If the oxygen atom lies in the RuS_2 plane, it is in a "planar" (P) orientation. Rotation about the Ru−S bonds is described by the torsion angles $\Psi_c = O_c-S_c-Ru-S_d$ and $\Psi_d = O_d-S_d-Ru-S_c$. In the case of the Δ enantiomorph, $0° < \Psi_c < 180°$, $-180° < \Psi_d < 0°$ and $-180° < \Psi_c < 0°$, $0° < \Psi_d < 180°$, for $(HH)_u$ and $(HH)_d$, respectively. For the $(HT)_u$ and $(HT)_d$ isomers (descriptors u and d being referred to the head of ligand "c"), the ranges of both the torsion angles, Ψ (= Ψ_c, Ψ_d), are: $0° < \Psi < 180°$ for $(HT)_u$ and $-180° < \Psi < 0°$ for $(HT)_d$. However, when the torsion angles are close (±15°) to the limiting values of 0°, 90°, 180°, and 270°, as for Ψ_c and Ψ_d in *cis*-sulfoxides, the more general descriptor $H_{\Psi c}H_{\Psi d}$ would seem to be more appropriate, e.g. $H_0H_{\pi/2}$ and H_0H_π, when $\Psi_c = 0°$ and $\Psi_d = 90°$ and 180°, respectively (see Table 3).

Molecular Conformations

It is interesting (cf. Table 3) that all the Δ *c*,*c*,*c*-RuX_2(dmso-S)$_2(Me_3Bzm)_2$ derivatives display HH geometries (more precisely, H_4H_2) for the Me_3Bzm ligands in the solid state, irrespective of the nature of X (Cl or Br) or of their different packing and van der Waals interactions with polar (ethanol, **2**; methanol, **5**) or apolar (benzene, **8**) solvent molecules of crystallization. However, in solution they all undergo equilibration with HT isomers of comparable stability (Table 5). It is thus clear that intermolecular pack-

Table 5. Rotamer distribution in solution and calculated relative strain energy ratios for *c*,*c*,*c*-$RuX_2(dmso\text{-}S)_{2-n}(CO)_n(L1)(L2)$ complexes, with X = Cl, Br; n = 0, 1; L1, L2 = Me_3Bzm, Me_2Im

Complex	Rotamers	Population ratios	Relative strain energy ratios
c,*c*,*c*-$RuCl_2(dmso\text{-}S)_2(Me_3Bzm)_2$	HH, HT[a]	1:0.8[a]	2.1:0[b]
c,*c*,*c*-$RuBr_2(dmso\text{-}S)_2(Me_3Bzm)_2$	HH, HT[a]	1:0.8[a]	
c,*c*,*c*-$RuCl_2(dmso\text{-}S)_2(1,2\text{-}Me_2Im)(Me_3Bzm)$	HH, HT[c]	1:5.0[c]	1.1:0[b]
c,*c*,*c*-$RuCl_2(dmso\text{-}S)_2(1,2\text{-}Me_2Im)_2$	HT, HH, HT, HH[c]	1.5:3.4:1.5:1[c]	0.6:0:0.9:1.3[d]
c,*c*,*c*-$RuCl_2(dmso\text{-}S)(CO)(Me_3Bzm)_2$	HH, HT[b]	1.0:0[b]	0:0.2[b]

[a] Ref.[3] – [b] Present work. – [c] Ref.[4] – [d] Ref.[18a]

ing forces are responsible for the exclusive crystallization of one form. From Table 3, it is evident that the formal substitution of a Me_3Bzm ligand by 1,2-Me_2Im (which occurs only at position "a") causes a stabilization of the HT geometry in the solid state, which is partially maintained in solution (Table 5).[4] Interestingly, in the case of *c*,*c*,*c*-$RuCl_2(dmso\text{-}S)_2(1,2\text{-}Me_2Im)(3,5\text{-lut})$, two rotamers (R1, R2) with opposite orientations of the 1,2-Me_2Im ligand were found to be present in the same crystal (ratio 0.63:0.37) as well as in solution (ratio 0.7:0.3).[5] Overall, the results indicate that the nature and relative abundance of the rotamers in solution depends markedly on the nature of the nitrogen bases; in the solid state, the equilibrium position can easily be shifted from the solution position by crystal packing effects that stabilize only one of the conformers. Generally, as shown by MM calculations,[18] the solid-state geometry corresponds to the lowest strain energy structure.

As already mentioned, it has been postulated that the hindered rotation of Me_3Bzm "b" in *c*,*c*,*c*-$RuCl_2(dmso\text{-}S)_2(Me_3Bzm)_2$ (**1**) arises from the electrostatic attraction between its acidic B2H proton and the negatively charged Cl ligands.[1] This hypothesis is supported by the present MM calculations. In fact, in the two lowest-energy conformers of Δ **1**, $(HT)_d$ and $(HH)_u$, (Table 6), Ψ_b is always about 135.6°, well within the range of 131.5−138.1° found in the solid state (Table 3). In both cases, rotation of 180° about the Ru−N_b bond ($\Psi_b \approx -44°$) causes a significant increase in the molecular strain energy [4.4 kcal mol^{-1} $(HT)_d \rightarrow (HH)_d$; 4.0 kcal mol^{-1} $(HH)_u \rightarrow (HT)_u$]; about 3 kcal mol^{-1} of this increase can be attributed to a decrease in the attractive electrostatic term (Table 6).

The favorable features of this orientation for Me_3Bzm "b" are further shown by the results relating to *c*,*c*,*c*-$RuCl_2(dmso\text{-}S)_2(1,2\text{-}Me_2Im)(Me_3Bzm)$, for which only the $(HT)_d$ (namely H_2H_2) conformer is present in the solid state and also predominates in solution (Table 5). MM calculations are in agreement with this observation, the energy of the $(HT)_d$ conformer being 1.1 kcal mol^{-1} lower than that of the $(HH)_u$ form (Table 7).

Another important result of this work is the observation that in all the Δ *c*,*c*,*c*-$RuCl_2(dmso\text{-}S)_2(L1)(L2)$ compounds in Table 3, the dmso conformation is invariably $(HH)_d$, with average values for Ψ_c and Ψ_d of $-14 \pm 12°$ and $86 \pm 6°$, respectively. This conformation corresponds to structures in which the O atom of each dmso lies approximately in the coordination plane perpendicular to the Ru−S bond of the other dmso, with the methyl groups of each dmso straddling a Ru−Cl bond. Similar conformations are found in all the minimum-energy structures calculated for the $(Me_3Bzm)_2$ and $(1,2\text{-}Me_2Im)(Me_3Bzm)$ derivatives (Tables 6 and 7). When this conformation is changed, there is a marked increase in the strain energy (Table 7). Interestingly, NMR data suggest that this geometry of the *cis*,*cis*-$RuCl_2(dmso\text{-}S)_2$ fragment is also predominant in solution.[5] In **5**, the presence of a CO group in "d" induces a rotation of ca. 80° about the Ru−S bond for dmso-S "c" (dmso O atom in the coordination plane and methyl groups again straddling a Ru−Cl bond), showing that the interligand steric interactions play a crucial role in determining the dmso orientation. Furthermore, density functional calculations on Ru^{II}(dmso-S) model molecules have shown that, even in the case of significant π bonding, steric factors far outweigh electronic effects.[19]

For *t*,*c*,*c*-$RuCl_2(dmso\text{-}S)_2(Me_3Bzm)_2$ (**3**), in agreement with the solution NMR data, MM results show (Table 8) that molecules with HT and HH base conformations have almost the same energy (max. difference 0.32 kcal mol^{-1}). Each conformer can adopt two structures with very similar minimum energies, differing only in the dmso orientation. Similar results have been obtained for *t*,*c*,*c*-$RuCl_2(dmso\text{-}S)_2(Bzm)_2$ (**4**) (Table 9). In both cases, crystallization stabilizes the HH geometry (Table 3). In solution, in agreement with NMR results, quick flipping between the isoenergetic

Table 6. Total strain energy E [kcal mol^{-1}] with the stretching (E_s), bending (E_b), torsional (E_t), van der Waals (E_v), and electrostatic (E_e) contributions [kcal mol^{-1}] for the four lowest-energy diastereotopomers of Δ *c*,*c*,*c*-$RuCl_2(dmso\text{-}S)_2(Me_3Bzm)_2$; torsion angles Ψ [°] with the base and dmso conformation descriptors are also given

E	Ψ_a	Ψ_b	base		Ψ_c	Ψ_d	dmso		E_s	E_b	E_t	E_v	E_e
3.87	135.5	135.9	$(HT)_d$	H_2H_2	−30.5	88.1	$(HH)_d$	H_4H_1	2.47	45.6	0.28	−3.09	−41.4
6.03	−45.9	135.4	$(HH)_u$	H_4H_2	−16.2	95.5	$(HH)_d$	H_4H_2	2.48	47.0	0.06	−1.87	−41.6
8.31	132.3	−42.6	$(HH)_d$	H_2H_4	−30.4	105.4	$(HH)_d$	H_4H_2	2.55	45.6	0.07	−1.45	−38.4
10.0	−53.0	−46.6	$(HT)_u$	H_4H_4	−22.2	109.1	$(HH)_d$	H_4H_2	2.60	46.8	0.02	−0.72	−38.7

Table 7. Total strain energy E [kcal mol^{-1}] with the stretching (E_s), bending (E_b), torsional (E_t), van der Waals (E_v), and electrostatic (E_e) contributions [kcal mol^{-1}] for the four lowest-energy diastereotopomers of Δ *c*,*c*,*c*-$RuCl_2$(dmso-S)$_2$(1,2-Me_2Im)(Me_3Bzm); torsion angles Ψ [°] with the base and dmso conformation descriptors are also given

E	Ψ_a	Ψ_b	base		Ψ_c	Ψ_d	dmso		E_s	E_b	E_t	E_v	E_e
6.18	132.1	136.9	$(HT)_d$	H_2H_2	−26.9	91.7	$(HH)_d$	H_4H_2	2.12	44.0	3.56	−2.90	−40.6
7.28	−40.7	135.3	$(HH)_u$	H_4H_2	−20.9	99.1	$(HH)_d$	H_4H_2	2.15	45.2	3.59	−2.31	−41.4
9.93	127.2	−43.4	$(HH)_d$	H_2H_4	−29.9	109.7	$(HH)_d$	H_4H_2	2.18	43.9	3.50	−1.75	−37.9
11.1	135.1	140.1	$(HT)_d$	H_2H_2	−28.7	−169.4	$(HT)_d$	H_4H_3	2.45	45.6	3.77	−2.45	−38.3

HH and HT geometries may be envisaged, to give an average side orientation.

Table 8. Total strain energy E [kcal mol^{-1}] with the stretching (E_s), bending (E_b), torsional (E_t), van der Waals (E_v), and electrostatic (E_e) contributions [kcal mol^{-1}] for the four lowest-energy diastereotopomers of *t*,*c*,*c*-$RuCl_2$(dmso-S)$_2$(Me_3Bzm)$_2$; torsion angles Ψ [°] with the base and dmso conformation descriptors are also given

E	Ψ_a	Ψ_b	base	Ψ_c	Ψ_d	dmso	E_s	E_b	E_t	E_v	E_e
11.34	130.5	125.2	HT	24.3	168.8	HT	2.57	46.1	0.55	−2.35	−35.5
11.45	129.4	124.8	HT	8.7	−178.1	PP[a]	2.66	46.3	0.61	−0.94	−37.2
11.48	−57.2	130.0	HH	22.7	168.7	HT	2.63	46.8	0.15	−0.83	−37.2
11.66	−57.2	129.0	HH	20.0	178.0	HT	2.71	46.9	0.18	0.01	−38.1

[a] Both oxygen atoms in the Ru−S_2 plane.

Table 9. Total strain energy E [kcal mol^{-1}] with the stretching (E_s), bending (E_b), torsional (E_t), van der Waals (E_v), and electrostatic (E_e) contributions [kcal mol^{-1}] for the four lowest-energy diastereotopomers of *t*,*c*,*c*-$RuCl_2$(dmso-S)$_2$(Bzm)$_2$; torsion angles Ψ [°] with the base and dmso conformation descriptors are also given

E	Ψ_a	Ψ_b	base	Ψ_c	Ψ_d	dmso	E_s	E_b	E_t	E_v	E_e
8.24	130.4	125.3	HT	24.2	168.8	HT	1.98	44.9	0.26	−0.93	−38.0
8.36	129.5	125.0	HT	9.3	−178.4	PP	2.07	45.3	0.29	0.45	−39.7
8.43	129.5	−58.0	HH	22.9	168.7	HT	2.05	45.6	0.06	0.21	−39.5
8.60	128.7	−57.5	HH	21.5	177.3	HT	2.13	45.8	0.08	0.99	−40.4

Unlike in the *cis*,*cis*,*cis* compounds, the solid-state conformation of the dmso groups in the *trans*,*cis*,*cis* compounds (**3** and **4**) is HT, with Ψ values of about 31° and 161° (Table 3). These values are close to the minimum energy structure values of about 24° and 169° (Tables 8 and 9). In this conformation, the two oxygen atoms are significantly displaced from the Ru−S_2 plane (ca. ±0.45 Å). However, MM calculations indicate that the energy difference between these HT arrangements and the PP arrangement (both oxygen atoms in the Ru−S_2 plane) is very small (ca. 0.1 kcal mol^{-1}) (Tables 8 and 9). In fact, a strictly symmetry-determined PP geometry of pairs of *cis*-sulfoxide ligands has been observed in *trans*-RuX_2(dmso-S)$_4$ complexes (X = Cl, Br).[20]

As in the case of **5**, substitution of one dmso group in **6** by CO causes a significant rotation about the Ru−S bond of the remaining dmso (Ψ_c approximately from 32° to −109°, Table 3). Most interestingly, the HH base mutual orientation in **6** is opposite to that found in **3** (as well as **1** and **5**), as shown by the Ψ_a and Ψ_b values (Table 3 and Figure 3). In fact, the base orientation in **3** is H_4H_2, while in **6** it is H_2H_4, as also found in solution. Such an arrangement of the neutral ligands brings the positively charged B2H of base "a" close to the negatively charged oxygen atom of dmso (H···O 3.0 Å) and to one chloride ligand (H···Cl 2.9 Å).

Limitations and Prospects for the MM Force Field

As discussed above, the force field used in the present MM calculations can describe the lowest strain energy structures in good agreement with those found in the solid state. The force field has also been found to be adequate for studying the possible rotamer distributions in solution for Ru^{II}(dimethyl sulfoxide) complexes containing lopsided nitrogen ligands such as 3,5-lutidine and 1,2-dimethylimidazole.[18a] However, inspection of the data in Table 5 shows that, unlike for the other derivatives, for *c*,*c*,*c*-$RuCl_2$(dmso-S)$_2$(Me_3Bzm)$_2$ (**1**) the strain energy ratio is not in agreement with the solution NMR data, which show that the HH and HT diastereotopomers are present in an approximately equimolar ratio. In fact, according to the MM results (Table 6), the diastereotopomer $(HT)_d$ should be predominant with a strain energy 2.1 kcal mol^{-1} lower than that of $(HH)_u$ due to a more negative contribution of the van der Waals term. It seems likely that this "anomalous" solution behavior observed in the case of *cis*-Me_3Bzm ligands is related to the larger surface area of Me_3Bzm compared to smaller ligands such as 1,2-Me_2Im and the consequently stronger interactions with solvent molecules. In fact, in solution, the two isomers of **1** are present in an almost 1:1 ratio, but only one form is present in the solid state, showing the importance of the packing intermolecular interactions. The "failure" of the MM calculations to give the lowest energy topomer in solution for **1** should be mainly due to the neglection of the effects of solvent interactions. The solvent-accessible surface area (SA) for *c*,*c*,*c*-$RuCl_2$(dmso-S)$_2$(Me_3Bzm)$_2$ is 738.7 Å^2 for the HH diastereoisomer and 718.2 Å^2 for the HT form, while it amounts to 720.7 and 705.6 Å^2, respectively, for the HH and HT isomers of *c*,*c*,*c*-$RuCl_2$(dmso-S)(CO)(Me_3Bzm)$_2$ (**5**). The greater SA values for the HH geometries could allow for more effective interactions with the solvent molecules, thereby stabilizing these forms in solution.

In any case, it must be kept in mind that the force field constants used in this work have been optimized only on the basis of crystal structure data.[18a] No thermodynamically observable parameter has been introduced, hence the calculated energy differences must be considered with caution. Another limitation of the present MM method re-

lates to the evaluation of energy barriers for rotation about the Ru−N bonds. These barriers are probably overestimated owing to the inability of the force field to describe non-minimum-energy structures. For this, non-harmonic functions and correlation terms would need to be introduced. Thus, the energy barrier of about 17 kcal mol^{-1} calculated for rotation about the Ru−N bonds in **1** must be considered merely as an indication of hindered rotation. On the other hand, a similar energy barrier of about 16 kcal mol^{-1} has been calculated for the *trans* compound **3**, for which fast rotation about the Ru−N bonds has been found in solution, showing the limited meaning of these values.

Conclusions

We have investigated the factors that influence the relative orientation and dynamic motion of the *cis*-Ru$(Me_3Bzm)_2$ unit in Ru^{II}(dimethyl sulfoxide) compounds of the general formula $RuCl_2(dmso\text{-}S)_{2-n}(CO)_n(Me_3Bzm)_2$ ($n = 0-2$). Complexes with *cis* and *trans* arrangements of the Cl ligands have been prepared and structurally characterized both in solution and in the solid state by NMR and X-ray techniques, respectively. The results have been compared with those obtained previously with the thoroughly studied *c*,*c*,*c*-$RuCl_2(dmso\text{-}S)_2(Me_3Bzm)_2$ (**1**). The influences of the nature of the halide ligands (Br vs. Cl) and of the medium of crystallization on the solid-state conformation of **1** have been also investigated. The experimental molecular conformations have been discussed on the basis of molecular mechanics (MM) calculations.

While for **1** two almost equally populated ligand orientations (HH and HT) are found in solution, replacement of one or both dmso-S molecules by CO ligands leads to the complexes *c*,*c*,*c*-$RuCl_2(dmso\text{-}S)(CO)(Me_3Bzm)_2$ (**5**) and *c*,*c*,*c*-$RuCl_2(CO)_2(Me_3Bzm)_2$ (**7**), respectively, for which only one HH orientation is preferentially populated in solution. It remains unclear as to whether in such conformers rotation of the bases about the Ru−N bonds is slow or very fast on the NMR time scale; in other words, the torsional barriers have not been estimated. Only the HH orientation was found in the solid-state structure of **5**.

We have found that the two *cis*-Me_3Bzm bases also maintain a preferential HH orientation when the geometry of the Cl ligands is changed from *cis* to *trans*; the preference for such an orientation has been demonstrated in solution for *t*,*c*,*c*-$RuCl_2(dmso\text{-}S)(CO)(Me_3Bzm)_2$ (**6**) and in the solid state for both **6** and *t*,*c*,*c*-$RuCl_2(dmso\text{-}S)_2(Me_3Bzm)_2$ (**3**). In the corresponding benzimidazole (Bzm) compound, *t*,*c*,*c*-$RuCl_2(dmso\text{-}S)_2(Bzm)_2$ (**4**), the two bases are also HH disposed in the solid state. In solution at ambient temperature, NMR evidence indicates that the two *t*,*c*,*c* complexes **3** and **6** behave differently. Thus, while the two *cis*-Me_3Bzm ligands are in rapid motion about the Ru−N bonds in **3**, most probably going from one HT conformation to the other through the HH conformation, in **6** the two bases are seemingly in rapid motion between two equivalent HH orientations, one above and the other below the N,N,S,C plane, thus averaging out as an "S" orientation. Moreover, both in solution and in the solid state, the mutual tilt of the HH bases in **6** is the opposite to that found in **1** and **5**.

Electrostatic interaction between the halide ligands and the positively charged N_2CH proton on the imidazole ring has been found to be the essential factor in determining the specific orientation of one Me_3Bzm base, both in the solid state and in solution. Comparison of the solid-state and solution structures with those predicted by MM calculations has revealed that intermolecular interactions can play a significant role in determining the orientation of the second Me_3Bzm ligand.

Experimental Section

Reagents: Analytical-grade solvents were used without further purification. All reagents, including CD_2Cl_2 and $CDCl_3$, were purchased from Aldrich.

Starting Materials: *cis*-$RuCl_2(dmso)_4$,[20] *trans*-$RuCl_2(dmso\text{-}S)_4$,[20] *cis*,*fac*-$RuCl_2(dmso)_3(CO)$,[11] *trans*-$RuCl_2(dmso)_3(CO)$,[11] *c*,*c*,*c*-$RuCl_2(dmso)_2(CO)_2$,[11] *c*,*c*,*c*-$RuCl_2(dmso\text{-}S)_2(Me_3Bzm)_2$ (**1**),[3] *c*,*c*,*c*-$RuBr_2(dmso\text{-}S)_2(Me_3Bzm)_2$ (**2**),[3] and *t*,*c*,*c*-$RuCl_2(dmso\text{-}S)_2(Bzm)_2$ (**4**)[21] were prepared by known methods.

***trans*,*cis*,*cis*-$RuCl_2(dmso\text{-}S)_2(Me_3Bzm)_2$ (3):** The complex was synthesized using as starting material either *cis*-$RuCl_2(dmso)_4$ (path a) or, preferably, *trans*-$RuCl_2(dmso\text{-}S)_4$ (path b): (a) Me_3Bzm (0.36 g, 2.25 mmol) was added to a solution of *cis*-$RuCl_2(dmso)_4$ (0.5 g, 1 mmol) in chloroform (20 mL) and the reaction was allowed to proceed overnight at room temperature. The mixture was then concentrated in vacuo to a volume of ca. 5 mL, diethyl ether (5 mL) was added dropwise, and the resulting solution was stored at 4 °C. Deep-yellow microcrystals of the product formed within 24 h, which were collected by filtration, washed with diethyl ether, and dried in vacuo. Yield 0.3 g (40%). The product was found to crystallize with one molecule of chloroform and is therefore better formulated as *t*,*c*,*c*-$RuCl_2(dmso\text{-}S)_2(Me_3Bzm)_2 \cdot CHCl_3$. Further concentration of the mother liquor yielded a second crop of precipitate. However, ^1H NMR analysis showed this to be a mixture of **3** and the *c*,*c*,*c* isomer **1**. − (b) *trans*-$RuCl_2(dmso\text{-}S)_4$ was treated with Me_3Bzm under the same conditions as used for the *cis* isomer in procedure (a). In this case, the yield was higher (70%) and no evidence for formation of the corresponding *c*,*c*,*c* isomer **1** was found. − Recrystallization from CH_2Cl_2/dmso mixtures (50:1) and subsequent addition of diethyl ether yielded crystals suitable for X-ray analysis (yield 70%). − $C_{24}H_{36}Cl_2N_4O_2RuS_2$ (648.6): calcd. C 44.4, H 5.59, N 8.63, S 9.88; found C 44.4, H 5.54, N 8.58, S 9.98. − ^1H NMR ($CDCl_3$): δ = 2.19 (s, 6 H, $B11H_3$), 2.32 (s, 6 H, $B10H_3$), 3.33 (s, 12 H, dmso-S), 3.63 (s, 6 H, $B12H_3$), 7.06 (s, 2 H, B7H), 8.18 (s, 2 H, B4H), 8.34 (s, 2 H, B2H).

***cis*,*cis*,*cis*-$RuCl_2(dmso\text{-}S)(CO)(Me_3Bzm)_2$ (5):** *cis*,*fac*-$RuCl_2(dmso)_3(CO)$ (0.19 g, 0.44 mmol) was partially dissolved in toluene (12 mL). Me_3Bzm (0.21 g, 1.31 mmol) was added and the resulting mixture was heated to reflux. A clear, pale-yellow solution was obtained within 30 min and then a precipitate of the same color formed. After 1.5 h, the hot mixture was filtered, and the collected

solid was washed with cold toluene and diethyl ether and dried in vacuo at room temperature (yield 50%). ^{1}H NMR analysis showed the crude product to contain up to 20% *t*,*c*,*c*-$RuCl_2$(dmso-S)(CO)$(Me_3Bzm)_2$ (**6**). Pure **5** (according to NMR) was obtained by recrystallization of this crude product from acetone/dmso mixtures (0.25 g in 5 mL of acetone and 0.1 mL of dmso) and subsequent careful addition of diethyl ether at room temperature (yield 75%). − $C_{23}H_{30}Cl_2N_4O_2RuS$ (598.5): calcd. C 46.1, H 5.05, N 9.36; found C 46.2, H 5.06, N 9.46. − Crystals of **5** suitable for X-ray analysis were obtained by recrystallization from methanol.

***trans*,*cis*,*cis*-$RuCl_2$(dmso-S)(CO)$(Me_3Bzm)_2$ (6):** *trans*-$RuCl_2$-$(dmso)_3$(CO) (0.20 g, 0.46 mmol) was dissolved in methanol (16 mL) and Me_3Bzm (0.18 g, 1.15 mmol) was added. The reaction was allowed to proceed for 24 h at room temperature and then the mixture was concentrated to half of its original volume. A yellow, microcrystalline product precipitated within 24 h, which was collected by filtration, washed with cold methanol and diethyl ether, and dried in vacuo at room temperature (yield 80%). Crystals suitable for X-ray analysis were obtained upon slow diffusion of *n*-hexane into a chloroform solution of the complex. −

Table 10. Crystallographic data and refinement details for compounds **2**−**6** and **8**

	2·0.5 C_2H_5OH	**3**	**4**
Empirical formula	$C_{25}H_{39}Br_2N_4O_{2.5}RuS_2$	$C_{24}H_{36}Cl_2N_4O_2RuS_2$	$C_{18}H_{24}Cl_2N_4O_2RuS_2$
M_r	760.61	648.66	564.50
Crystal system	triclinic	monoclinic	orthorhombic
Space group	$P\bar{1}$	$P2_1/c$	*Pbca*
a [Å]	11.574(1)	15.290(3)	27.332(6)
b [Å]	11.730(2)	10.625(2)	11.599(1)
c [Å]	12.395(4)	17.933(2)	14.517(3)
α [°]	99.55(2)		
β [°]	89.87(2)	94.51(1)	
γ [°]	103.62(2)		
V [Å^3]	1611.6(6)	2904.3(9)	4602.2(14)
Z	2	4	8
$D_{calcd.}$ [mg m^{-3}]	1.567	1.483	1.629
μ(Mo-K_α) [mm^{-1}]	3.124	0.895	1.117
F(000)	766	1336	2288
θ limits [°]	2.24−27.97	2.23−27.96	2.30−29.96
Index ranges	$-15 \le h \le 15$	$-20 \le h \le 20$	$0 \le h \le 38$
	$-15 \le k \le 15$	$0 \le k \le 14$	$0 \le k \le 16$
	$0 \le l \le 16$	$0 \le l \le 23$	$0 \le l \le 20$
Data collected	8132	7581	7397
Unique data (R_{int})	7777 (0.025)	6951 (0.019)	7397
Observed reflections [$I > 2\sigma(I)$]	4831	4686	4391[a]
Parameters	353	326	266
Goodness-of-fit, *S*	1.174	1.144	1.067
*R*1, *wR*2 [$I > 2\sigma(I)$][b]	0.0480, 0.1112	0.0302, 0.0671	0.0349, 0.0896
*R*1, *wR*2 (all data)[b]	0.1278, 0.1688	0.0810, 0.0914	[a]
Residuals [e·Å^{-3}]	1.018, −0.790	0.498. −0.670	0.679, −0.689

	5·0.5 CH_3OH	**6**·0.5 CH_3OH	**8**·2 C_6H_6
Empirical formula	$C_{23.5}H_{32}Cl_2N_4O_{2.5}RuS$	$C_{23}H_{30}Cl_2N_4O_2RuS$	$C_{36}H_{48}Cl_2N_4O_2RuS_2$
M_r	614.56	598.5	804.87
Crystal system	triclinic	triclinic	monoclinic
Space group	$P\bar{1}$	$P\bar{1}$	$P2_1/c$
a [Å]	8.2245(7)	9.019(1)	13.790(2)
b [Å]	10.984(1)	10.879(1)	13.505(3)
c [Å]	16.036(2)	15.801(2)	21.410(5)
α [°]	106.81(1)	74.52(1)	
β [°]	98.37(1)	76.07(1)	97.36(2)
γ [°]	94.96(1)	75.08(1)	
V [Å^3]	1359.2(3)	1418.9(3)	3954.4(14)
Z	2	2	4
D_{calcd} [mg m^{-3}]	1.502	1.438	1.352
μ(Mo-K_α) [mm^{-1}]	0.880	0.843	0.672
F(000)	630	630	1672
θ limits [°]	2.01−27.97	2.15−26.99	2.12−27.98
Index ranges	$-10 \le h \le 10$	$-11 \le h \le 11$	$-18 \le h \le 18$
	$-14 \le k \le 14$	$-13 \le k \le 13$	$0 \le k \le 17$
	$0 \le l \le 21$	$0 \le l \le 20$	$0 \le l \le 28$
Data collected	6772	6464	10186
Unique data (R_{int})	6542 (0.027)	6179 (0.019)	9528 (0.095)
Observed reflections [$I > 2\sigma(I)$]	5390	4922	6612
Parameters	377	324	434
Goodness-of-fit, *S*	1.050	1.088	1.142
*R*1, *wR*2 [$I > 2\sigma(I)$][b]	0.0488, 0.1497	0.0420, 0.1234	0.0369, 0.0741
*R*1, *wR*2 (all data)[b]	0.0764, 0.2345	0.0566, 0.1303	0.0795, 0.0951
Residuals [e Å^{-3}]	1.281, −1.268	0.987, −0.551	0.498, −0.430

[a] Only reflections with $I > 3\sigma(I)$ were used in the refinement. − [b] $R1 = \Sigma||F_o| - |F_c||/\Sigma|F_o|$, $wR2 = [\Sigma w(F_o^2 - F_c^2)^2/\Sigma w(F_o^2)^2]^{1/2}$.

$C_{23}H_{30}Cl_2N_4O_2RuS$ (598.5): calcd. C 46.1, H 5.05, N 9.36; found C 45.9, H 5.16, N 9.30.

***cis*,*cis*,*cis*-$RuCl_2(CO)_2(Me_3Bzm)_2$ (7):** *c*,*c*,*c*-$RuCl_2(CO)_2(dmso)_2$ (0.11 g, 0.28 mmol) was partially dissolved in ethanol (20 mL). Me_3Bzm (0.10 g, 0.62 mmol) was added and the resulting mixture was heated to reflux for 1.5 h. A clear, colorless solution was obtained within 10 min. On cooling, a white precipitate formed, which was collected by filtration, washed with cold ethanol and diethyl ether, and dried in vacuo at room temperature (yield 52 mg, 40%). ^1H NMR analysis showed this precipitate to consist of *c*,*c*,*t*-$RuCl_2(CO)_2(Me_3Bzm)$(dmso-S). − $C_{14}H_{18}Cl_2N_2O_3RuS$ (466.3): calcd. C 36.0, H 3.89, N 6.01; found C 36.0, H 3.77, N 6.00. − ^1H NMR ($CDCl_3$): δ = 2.44 and 2.42 (s, 3 H each, $B10H_3$ and $B11H_3$), 3.53 (s, 6 H, dmso-S), 3.86 (s, 3 H, $B12H_3$), 7.23 (s, 1 H, B7H), 7.37 (s, 1 H, B4H), 8.45 (s, 1 H, B2H). − Concentration of the mother liquor to a volume of 3 mL and addition of diethyl ether induced the precipitation of a second crop of white solid, which was likewise collected by filtration, washed with cold ethanol and diethyl ether, and dried in vacuo at room temperature (yield 60 mg, 40%). ^1H NMR analysis showed this second precipitate to consist of *c*,*c*,*c*-$RuCl_2(CO)_2(Me_3Bzm)_2$ slightly contaminated by the first product. Pure **7** was obtained by slow diffusion of methanol into a chloroform solution of the complex. − $C_{22}H_{24}Cl_2N_4O_2Ru$ (548.4): calcd. C 48.2, H 4.41, N 10.21; found C 48.0, H 4.40, N 10.18.

X-ray Diffraction: X-ray data were collected at room temperature [273(2) K] with an Enraf−Nonius CAD4 diffractometer using graphite-monochromated Mo-K_α radiation (λ = 0.71073 Å). The data were corrected for Lorentz and polarization effects by using a local program for data reduction. All the structures were solved by Patterson and Fourier methods,[22] and refined on F^2 by full-matrix least-squares methods.[23] Difference Fourier syntheses revealed the presence of a molecule of ethanol in **2** and of methanol in **5**, which were assigned occupancy factors of 0.5 on the basis of the Fourier peaks. Hydrogen atoms were placed in calculated positions (excluding those of the alcohol molecules in **2** and **5**) and were refined as riding, setting the U_{iso} to 1.2 × U_{eq} values of the parent carbon atoms. The crystal structure of the carbonyl derivative **5** is characterized by a disordered arrangement of the six-membered ring of the Me_3Bzm ligand [namely C(7)−C(10), C(20), C(21)] over two positions with statistical occupancy factors of 50%. Unit cell data and experimental conditions are summarized in Table 10. Crystallographic data (excluding structure factors) for the structures reported in this paper have been deposited with the Cambridge Crystallographic Data Centre and allocated the deposition numbers CCDC-139103−139108. Copies of the data can be obtained free of charge on application to the CCDC, 12 Union Road, Cambridge CB2 1EZ, U.K. [Fax: (internat.) + 44-1223/336-033; E-mail: deposit@ccdc.cam.ac.uk].

Molecular Mechanics: Calculations were performed with a Pentium 130 PC with the HyperChem 4.5 molecular modeling package[24] using the force field and procedures previously described for other Ru^{II}(sulfoxide complexes).[18] In calculating the electrostatic contributions, a distance-dependent relative permittivity was used. For the carbonyl derivatives, C and O charges were calculated by the semi-empirical method ZINDO/1 (C 0.33, O −0.10).[24] Stretching and bending force field constants involving the Ru−CO group, not included in the previous force field,[18] were calculated by Badger's rule, using the parameters given by Herschbach and Laurie,[25] and by Halgren's equation,[26] respectively. The following *d* and θ values were assumed: Ru−C 1.85 Å, C−O 1.14 Å, Ru−C−O 180°, X−Ru−C 90° and 180° for *cis* and *trans* X donors, respectively. Solvent-accessible surface areas were calculated by means of a HyperChem routine using a radius of 1.4 Å for the probe molecule.

Acknowledgments

This work was supported by the Italian MURST in the framework of the Project "Pharmacological and Diagnostic Properties of Metal Complexes" (coordinator Professor G. Natile). We thank Johnson Matthey for a loan of hydrated $RuCl_3$. P. A. M. acknowledges NIH grant GM 29222 for support.

[1] L. G. Marzilli, P. A. Marzilli, E. Alessio, *Pure Appl. Chem.* **1998**, *70*, 961−968.
[2] L. G. Marzilli, M. Iwamoto, E. Alessio, L. Hansen, M. Calligaris, *J. Am. Chem. Soc.* **1994** *116*, 815−816.
[3] E. Alessio, M. Calligaris, M. Iwamoto, L. G. Marzilli, *Inorg. Chem*. **1996**, *35*, 2538−2545.
[4] M. Iwamoto, E. Alessio, L. G. Marzilli, *Inorg. Chem*. **1996**, *35*, 2384−2389.
[5] E. Alessio, E. Zangrando, R. Roppa, L. G. Marzilli, *Inorg. Chem*. **1998**, *37*, 2458−2463.
[6] L. G. Marzilli, S. O. Ano, F. P. Intini, G. Natile, *J. Am. Chem. Soc.* **1999**, *121*, 9133−9142.
[7] A. H. Velders, A. C. G. Hotze, J. G. Haasnoot, J. Reedijk, *Inorg. Chem*. **1999**, *38*, 2762−2763.
[8] [8a]E. Alessio, L. Hansen, M. Iwamoto, L. G. Marzilli, *J. Am. Chem. Soc.* **1996**, *118*, 7593−7600. − [8b]E. Alessio, E. Zangrando, E. Iengo, M. Macchi, P. A. Marzilli, L. G. Marzilli, *Inorg. Chem.* **2000**, *39*, 294−303.
[9] The geometrical descriptors *cis*,*cis*,*cis*- (abbreviated *c*,*c*,*c*-) and *trans*,*cis*,*cis*- (abbreviated *t*,*c*,*c*-) refer to the relative geometries of pairs of ligands, either similar or dissimilar, in the order in which they appear in the chemical formula of the complex. See also Scheme 1.
[10] [10a] M. Calligaris, O. Carugo, *Coord. Chem. Rev.* **1996**, *153*, 83−154. − [10b] M. Calligaris, *Croat. Chem. Acta* **1999**, *72*, 147−169.
[11] E. Alessio, B. Milani, M. Bolle, G. Mestroni, P. Faleschini, F. Todone, S. Geremia, M. Calligaris, *Inorg. Chem.* **1995**, *34*, 4722−4734.
[12] The ^1H chemical shifts of Me_3Bzm ($CDCl_3$) in *c*,*c*,*c*-$RuCl_2$(dmso-S)$_2$(CO)(Me_3Bzm) and *cis*,*fac*-$RuCl_2$(dmso-S)$_3$(Me_3Bzm) are reported for the sake of comparison: *c*,*c*,*c*-$RuCl_2$(dmso-S)$_2$(CO)(Me_3Bzm): δ = 2.41 ($B11H_3$), 2.44 ($B10H_3$), 3.85 ($B12H_3$), 7.21 (B7H), 7.92 (B4H), 8.62 (B2H); *cis*,*fac*-$RuCl_2$(dmso-S)$_3$(Me_3Bzm): δ = 2.39 ($B10H_3$ and $B11H_3$), 3.87 ($B12H_3$), 7.21 (B7H), 7.87 (B4H), 8.82 (B2H). Peaks were assigned with the aid of NOESY spectra.
[13] E. Alessio, M. Macchi, S. L. Heath, L. G. Marzilli, *Inorg. Chem.* **1997**, *36*, 5614−5623.
[14] *Nomenclature of Inorganic Chemistry* (Ed.: G. L. Leigh), Blackwell, Oxford, U.K., **1990**; A. von Zelewsky, in *Stereochemistry of Coordination Compounds*, J. Wiley, Chichester, U.K., **1995**.
[15] J. D. Orbell, L. G. Marzilli, T. J. Kistenmacher, *J. Am. Chem. Soc*. **1981**, *103*, 5126−5133.
[16] S. Geremia, E. Alessio, F. Todone, *Inorg. Chim. Acta* **1996**, *253*, 87−90.
[17] E. Zangrando, F. Pichierri, L. Randaccio, B. Lippert, *Coord. Chem. Rev.* **1996**, *156*, 275−332.
[18] [18a] S. Geremia, M. Calligaris, *J. Chem. Soc., Dalton Trans.* **1997**, 1541−1547. − [18b] S. Geremia, L. Vicentini, M. Calligaris, *Inorg. Chem*. **1998**, *37*, 4094−4103. − [18c] S. Geremia, M. Calligaris, Yu. N. Kukushkin, A. V. Zinchenko, V. Yu. Kukushkin, *J. Mol. Struct.* **2000**, *516*, 49−56.
[19] M. Stener, M. Calligaris, *J. Mol. Struct. (Theochem)* **2000**, *497*, 91−104.
[20] E. Alessio, G. Mestroni, G. Nardin, W. M. Attia, M. Calligaris, G. Sava, S. Zorzet, *Inorg. Chem*. **1988**, *27*, 4099−4106.
[21] M. Henn, E. Alessio, G. Mestroni, M. Calligaris, W. M. Attia, *Inorg. Chim. Acta* **1991**, *187*, 39−50.

[22] G. M. Sheldrick, "SHELXS-86: Program for structure solution", *Acta Crystallogr.* **1990**, *A46*, 467−473.
[23] G. M. Sheldrick, *SHELXL-97: Program for crystal structure refinement*, University of Göttingen, Germany, **1997**.
[24] *HYPERCHEM*, Hypercube, Inc., Waterloo, Ont., Canada, **1994**.
[25] D. R. Herschbach, V. W. Laurie, *J. Chem. Phys.* **1961**, *35*, 458−463.
[26] T. A. Halgren, *J. Am. Chem. Soc.* **1990**, *112*, 4710−4723.
Received January 19, 2000
[I00019]

Rhodium(III) Aqua Ion Salts of Ambivalent Self Assembled Superanion Capsules

Alexander Drljaca,[a] Michaele J. Hardie,[a] Timothy J. Ness,[a] and Colin L. Raston*[a]

Keywords: Calixarenes / Capsules / Crown compounds / Rhodium / Supramolecular chemistry

The self assembled superanionic capsule [{Na^+⊂(18-crown-6)$(OH_2)_2$}⊂{(*p*-sulfonatocalix[4]arene^{4-})$_2$}]$^{7-}$ (X^{7-}) forms a 1:1 crystalline complex with dinuclear $[Rh_2(\mu\text{-}OH)_2(H_2O)_8]^{4+}$ when the cation is treated with sodium *p*-sulfonatocalix[4]arene and 18-crown-6 at pH 2. The overall composition of the crystalline solid is $[Rh_2(\mu\text{-}OH)_2(H_2O)_8][X + 3\ H^+]\cdot 11.5H_2O$. Treatment of a complex mixture of polynuclear rhodium(III) aqua ions in perchloric acid with excess sodium *p*-sulfonatocalix[4]arene and 18-crown-6 at pH 2, results in selective retrieval of the tri- and tetranuclear rhodium(III) species in a single 1:1 co-crystallised phase, isolated as the hydrate salt with overall composition $[Rh_3(\mu\text{-}OH)_4(H_2O)_{10}][Rh_4(\mu\text{-}OH)_6(H_2O)_{12}][2\ X + 3\ H^+][Na(H_2O)(ClO_4)]_2\cdot 27H_2O$. The tri- and tetranuclear Rh cations both have a cyclic structure with μ-hydroxide and terminal water ligands. Despite the differences in cation charge and size both complexes show the same arrangement of polynuclear cations and superanions although the trimer/tetramer complex shows additional coordination of a second Na centre by the calixarenes. At pH 0.35 the reaction leads to the selective retrieval of the tetranuclear cation in the complex $[Rh_4(\mu\text{-}OH)_6(H_2O)_{12}][X + \{X - 2\ H_2O\} + 8\ H^+]\cdot 33H_2O$, where a second type of dehydrated superanion is found, where the two sodium bound water molecules have been replaced by O-centres of calixarene sulfonate groups, illustrating the versatile nature of the superanion chemistry.

Introduction

Selective crystallisation of polynuclear metal aqua cations from solutions containing a range of complex polynuclear aqua species has recently been established for a self-assembled superanion capable of taking on different charge to accommodate the surrounding cations.[1,2] The superanion [{Na^+⊂(18-crown-6)$(OH_2)_2$}⊂{(*p*-sulfonatocalix[4]arene^{4-})$_2$}]$^{7-}$, abbreviated hereafter as X^{7-}, is composed of a central sodium ion bound by two *trans* water molecules and an 18-crown-6, and this complex is shrouded by two *p*-sulfonatocalix[4]arenes which hydrogen bond to the inner-sphere water molecules creating a Russian doll-like assembly (Figure 1). Cohesion in the solid state comes from interplay of different supramolecular interactions, notably hydrogen bonding, which includes those for water molecules of crystallisation, electrostatics, π-stacking, and van der Waals. Thus far $[Cr_4(OH)_6(H_2O)_{12}]^{6+}$ and $[Al_{13}O_4(OH)_{24}(H_2O)_{12}]^{7+}$ have been selectively retrieved from complex mixtures using this approach.[1,2] Electrostatic repulsion between the calixarenes in the superanions is overcome by the large cations being situated close to the sulfonate groups of adjacent calixarenes. Purified solutions of $[Cr_2(OH)_2(H_2O)_8]^{4+}$ and $[Cr_3(OH)_4(H_2O)_{10}]^{5+}$ can form crystalline complexes with protonated X^{7-}, however the cations are partially occupied with a high degree of dynamic disorder, and cohesion in the solid state is derived instead from extensive π stacking and hydrogen bonding interactions between the superanions.[1] The related though smaller anionic capsule [H_4(cyclam)⊂{(*p*-sulfonatocalix[4]arene)$_2$}]$^{4-}$ also forms a crystalline complex with $[Cr_2(OH)_2(H_2O)_8]^{4+}$ where the cation is once more ordered and forms close interactions with the sulfonate groups of the superanion.[3] The ionic capsules in this work relate to a recent surge of studies on the self assembly of molecular capsules constructed mainly using hydrogen bonding,[4,5] although hydrophobic interactions and metal coordination mechanisms are also known.[4] Examples of second sphere supramolecular complexation are rare, limited to a metal−cryptate−cavitand assembly[6] as well as second sphere cyclodextrin complexes.[7]

In further exploring this approach we have investigated superanion complexation of polynuclear rhodium(III) aqua cations. Solutions of pure dinuclear rhodium(III) cation $[Rh_2(\mu\text{-}OH)_2(H_2O)_8]^{4+}$ with crown ether and sulfonated calixarene at low pH give a crystalline complex of the superanion in a 1:1 ratio with the dinuclear rhodium(III) cation, with composition $[Rh_2(\mu\text{-}OH)_2(H_2O)_8][X + 3\ H^+]\cdot 11.5H_2O$, **1**. Remarkably, we find that with a mixture of Rh^{III} oligomers treated under the same conditions, the tri- and tetranuclear cations, $[Rh_3(\mu\text{-}OH)_4(H_2O)_{10}]^{5+}$ and $[Rh_4(\mu\text{-}OH)_6(H_2O)_{12}]^{6+}$, Figure 1, are retrieved from solution in a single 1:1 co-crystallised phase, as a hydrate salt of the self assembled ionic capsule and Na perchlorate with overall composition $[Rh_3(\mu\text{-}OH)_4(H_2O)_{10}][Rh_4(\mu\text{-}OH)_6(H_2O)_{12}][2\ X + 3\ H^+][Na(H_2O)(ClO_4)]_2\cdot 27H_2O$, **2**. The ability to co-crystallise two large polynuclear aqua cations in the same solid is without precedent. Moreover, of the two cations, only the trinuclear one has been studied with its existence in solution postulated on the basis of NMR experiments,[8] and there is considerable uncertainty on the nature of higher nuclearity species. Previous work

[a] Department of Chemistry, Monash University, Clayton, Melbourne, Victoria 3800 Australia
Fax: (internat.) +6-13/9905-4597
E-mail: c.raston@sci.monash.edu.au

 © WILEY-VCH Verlag GmbH, D-69451 Weinheim, 2000 1434−1948/00/1010−2221 $ 17.50+.50/0

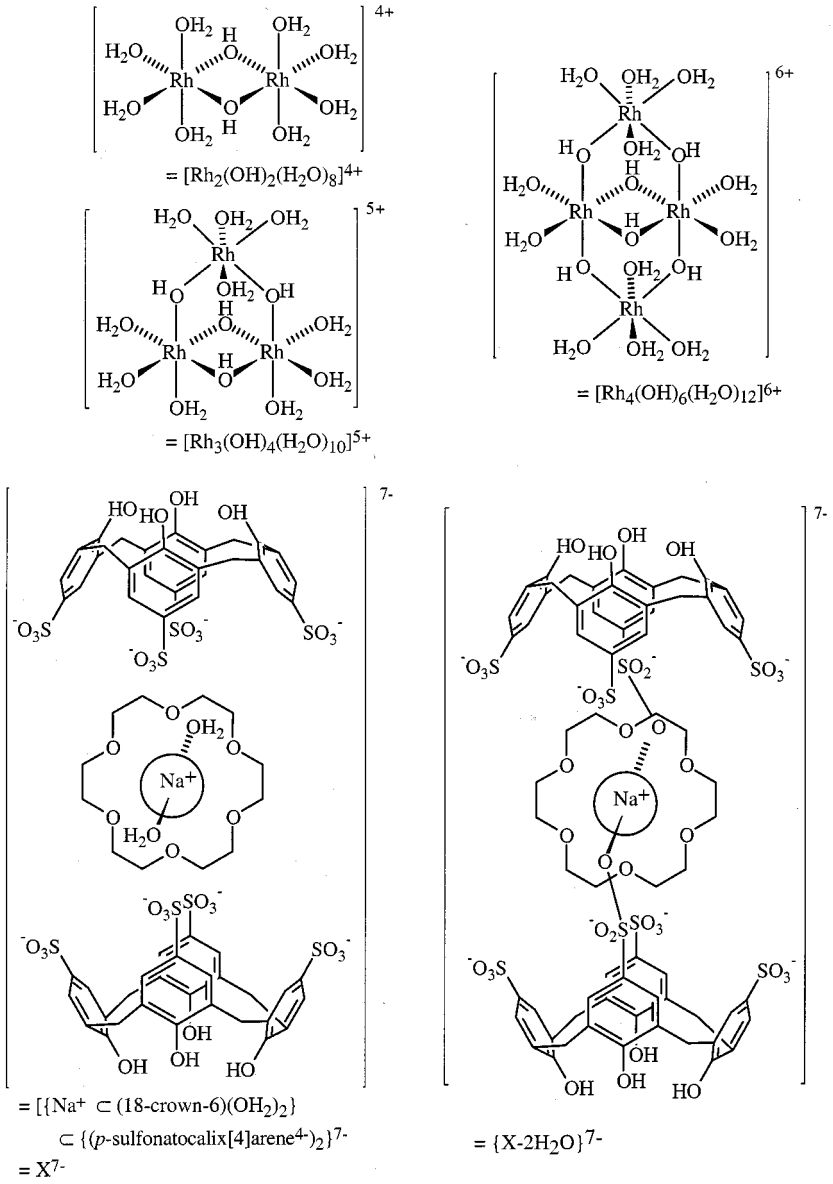


Figure 1. Polynuclear rhodium(III) aqua ions identified as salts of the protonated superanion X^{7-}, and the dehydrated superanion $\{X - 2\,H_2O\}^{7-}$ formed on treating mixtures of the polynuclear species with excess sodium *p*-sulfonatocalix[4]arene and 18-crown-6 at low pH, isolated as hydrates of $[Rh_2(OH)_2(H_2O)_8][X + 3\,H^+]$, $[Rh_3(OH)_4(H_2O)_{10}][Rh_4(OH)_6(H_2O)_{12}][2\,X + 3\,H^+][Na(H_2O)ClO_4]_2$, and $[Rh_4(\mu\text{-}OH)_6(H_2O)_{12}][X + \{X - 2\,H_2O\} + 8\,H^+]$; X = $[\{Na^+(18\text{-crown-}6)(OH_2)_2\}\{(p\text{-sulfonatocalix[4]arene}^{4-})_2\}]^{7-}$

authenticating polynuclear rhodium(III) cations in the solid state is restricted to studies on the dinuclear cations,[9,10] with the related mixed Rh^{III}/Cr^{III} dimer also characterised.[11] Oligomeric chromium(III) solutions under the same conditions result in retrieval of the tetranuclear species rather than both the tri- and tetranuclear in the present system. Changes in pH can, however, lead to the selective retrieval of the tetranuclear Rh^{III} species in the complex $[Rh_4(\mu\text{-}OH)_6(H_2O)_{12}][X + \{X - 2\,H_2O\} + 8\,H^+]\cdot 33H_2O$, **3**. Here $[Rh_4(\mu\text{-}OH)_6(H_2O)_{12}]^{6+}$ crystallises with the superanion X^{7-} and a radically altered superanion $\{X - 2\,H_2O\}^{7-}$ which is devoid of the two *trans* water molecules with the two calixarenes coordinating directly to the central Na^+ via sulfonate groups, Figure 1, and demonstrates the hitherto unknown ability of the capsule to accommodate large cations by forming different structures, which adds to the previously established versatility inherent in being able to alter its degree of protonation.

Results and Discussion

Yellow crystals of complex **1** formed on the evaporation over several days of an aqueous solution containing $[Rh_2(\mu\text{-}OH)_2(H_2O)_8](ClO_4)_4$, and an excess of sodium *p*-sulfonatocalix[4]arene and 18-crown-6, acidified to pH 2 with aqueous perchloric acid. The solid-state structure was determined from X-ray diffraction data collected at 123(1) K. The complex $Rh_2(\mu\text{-}OH)_2(H_2O)_8][X + 3\,H^+]\cdot 11.5H_2O$, **1** crystallises in a triclinic cell [a = 13.5248(3), b = 16.7318(4), c = 25.1930(5) Å, α = 105.583(5), β = 97.061(4), γ = 108.522(5)°] and the structure was solved in $P\bar{1}$. The struc-

ture consists of three major structural components − the superanion capsule and the dinuclear cation in two orientations, as well as water molecules at hydrogen bond distances to these moieties. Three of the total of eight sulfonate groups of the superanion capsule are required to be protonated to achieve overall charge balance. These protons were not located crystallographically and could reside on any of the eight crystallographically distinct sulfonate groups. Surprisingly, the structure of **1** is not isostructural with, or extensively disordered, as in the chromium(III) analogue,[1] where the cations are disordered over several sites within the unit cell. These differences may relate to the larger size of the cation in the present case and/or different polarisation effects.

The $[Rh_2(\mu\text{-}OH)_2(H_2O)_8]^{4+}$ cation in **1** is unexceptional relative to that established for a less-versatile supramolecular approach.[9] The structure of the superanion X^{7-} is similar to those found in the analogous anions in the structures containing the di-, tri-, and tetranuclear chromium(III) cations,[1] and the Keggin ion aluminium(III) cluster, where there is also a calixarene in the crystal lattice that is not part of a capsule.[2] The crown ether within the superanion shows severe dynamic disorder, which is not unusual for crown ether structures.[12]

The extended structure of **1** features a complicated array of hydrogen bonds complemented by additional supramolecular interactions such as electrostatics. There are two types of cation behaviour with both positioned at the periphery of the hydrophilic sulfonate equator of the globular superanion. Numerous hydrogen bonds from the coordinated hydroxides and waters of the cations to the sulfonate groups of the superanion overcome electrostatic repulsion associated with the two sulfonated calixarene molecules, Figure 2. One cation, with the Rh−μ-$(OH)_2$−Rh plane roughly perpendicular to the approximate plane of the crown ether, is located very close to the hydrophilic periphery of two superanions in **1** with O···O hydrogen bond lengths 2.53 to 2.71 Å. The other type of cation sits at the outer edges of four superanions, bridging between them through hydrogen bonding interactions at O···O distances 2.63 to 2.70 Å. The array of hydrogen bonding interactions between the cations and superanions form an infinite two dimensional network, a section of which is shown in Figure 3. In the overall crystal lattice these 2D networks stack in layers through RSO···HOR′ hydrogen bonds (O···O distance 2.71 Å) between calixarenes of different networks. This is quite distinct from the inter-superanion stacking observed in the su-

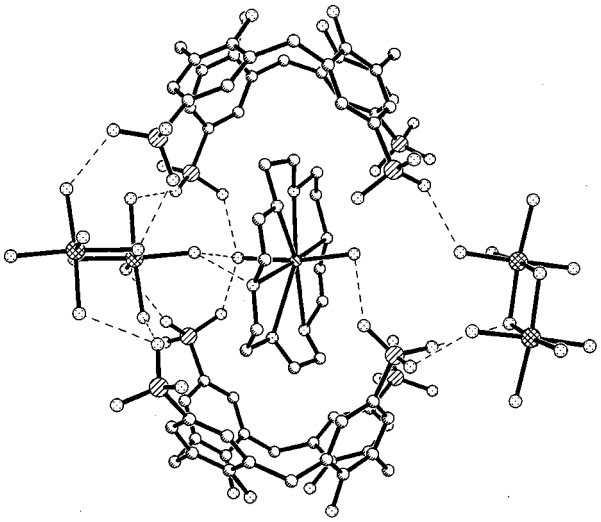


Figure 2. Close contacts between superanion and Rh dinuclear cations in $[Rh_2(\mu\text{-}OH)_2(H_2O)_8][X + 3\,H^+]\cdot 11.5H_2O$ (**1**); dashed lines indicate hydrogen bonds; only one disordered sulfonate group is shown for clarity

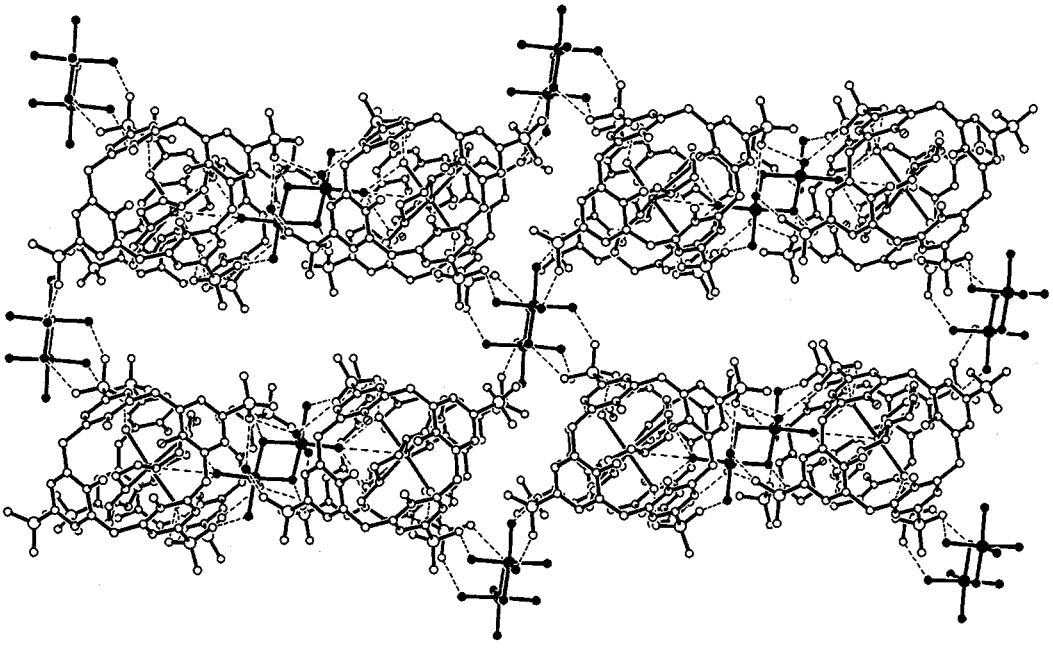


Figure 3. Section of the infinite two dimensional hydrogen bonded network of superanions and dinuclear cations (highlighted in black) of **1**

peranion complexes of $[Cr_2(OH)_2(H_2O)_8]^{4+}$ and $[Cr_3(OH)_4(H_2O)_{10}]^{5+}$ with X^{7-}, where RSO···HOR′ hydrogen bonding was more extensive and complemented by π stacking.

Pale yellow crystals of complex **2** were obtained in a similar manner to **1**, however with a mixture of polynuclear rhodium(III) aqua ions at pH 2 formed by treating aqueous rhodium(III) perchlorate (0.1 M) with sodium hydroxide (1 M) to give a pH 13, then acidifying the resulting solution after 2 hours with perchloric acid. Under such conditions, mononuclear, dinuclear, trinuclear, and higher oligomers are known to exist.[8,9] The solid-state structure was determined from X-ray diffraction data collected at 123(1) K. The complex $[Rh_3(\mu\text{-}OH)_4(H_2O)_{10}][Rh_4(\mu\text{-}OH)_6(H_2O)_{12}][2\,X + 3\,H^+][Na(H_2O)(ClO_4)]_2 \cdot 27H_2O$, **2** crystallises in a triclinic cell [a = 13.8992(2), b = 17.0191(5), c = 26.6441(7) Å, α = 75.268(3), β = 88.328(5), γ = 68.768(5)°] and the structure was solved in $P\bar{1}$. As for **1** the structure consists of three major structural components − the superanion capsule, trinuclear, and tetranuclear cations as well as sodium perchlorate with the sodium coordinated to the calixarenes, and numerous water molecules. Three of the sixteen sulfonate groups are required to be protonated for charge balance and could reside on any of the eight crystallographically independent sulfonates.

The trinuclear $[Rh_3(\mu\text{-}OH)_4(H_2O)_{10}]^{5+}$ of **2** is located close to a crystallographic inversion centre leading to a static disorder of the cation over two positions with some shared oxygen sites having both water and hydroxide character, Figure 4. Such a disorder makes the Rh−O distances

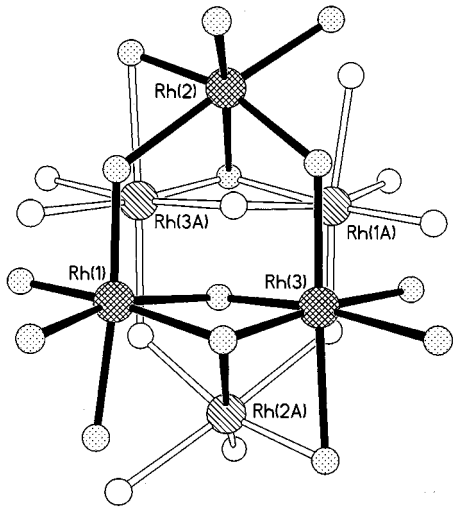


Figure 4. The disordered trinuclear cation $[Rh_3(\mu\text{-}OH)_4(H_2O)_{10}]^{5+}$ from the crystal structure of $[Rh_3(\mu\text{-}OH)_4(H_2O)_{10}][Rh_4(\mu\text{-}OH)_6(H_2O)_{12}][2\,X + 3\,H^+][Na(H_2O)ClO_4]_2 \cdot 27\,H_2O$ (**2**)

somewhat unreliable, however general structural features are unequivocal. The μ-OH bridged cyclic structure of the trinuclear cation is isostructural with that of the chromium(III) analogue,[1] but this is at odds with the assigned linear structure based on ^{103}Rh NMR studies. However, the NMR data showing two resonances in a 1:2 ratio is consistent with the triangular structure.[8] The structure of the tetranuclear $[Rh_4(\mu\text{-}OH)_6(H_2O)_{12}]^{6+}$ cation is likewise the same as that for the chromium(III) analogue,[1] and is cyclic with two Rh centres coordinated by two terminal water mo-

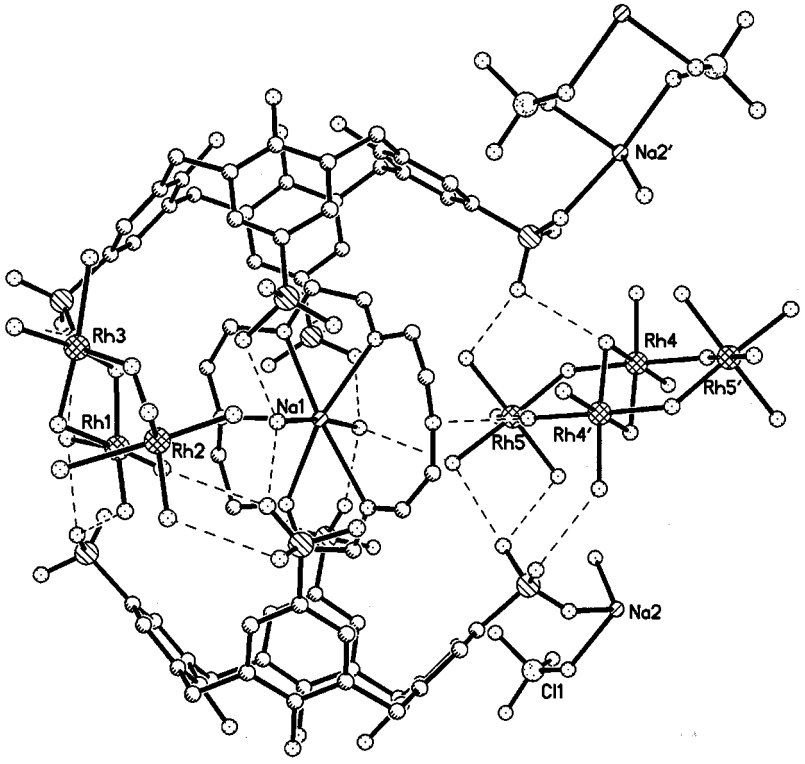


Figure 5. Interactions between the superanion and polynuclear cations in **2** and coordination of Na perchlorate moiety; for the sake of clarity only one position for the disordered sulfonate and trinuclear cation groups are shown

lecules and four bridging hydroxides, the other metal centres coordinated by four terminal water molecules and two bridging hydroxides. Rh−OH_2 distances ranges from 2.024(5) to 2.053(6) Å, and Rh−OH distances were from 1.991(5) to 2.007(5) Å.

The structure of the superanion X^{7-} is slightly different to that of **1** and analogous systems,[1,2] with the central Na^+ in **2** coordinating to only five of the six crown ether oxygen atoms at Na−O distances from 2.55(1) to 2.740(9) Å as well as two *trans* water molecules [Na−O distances 2.294(9) and 2.376(7) Å] in a distorted pentagonal bipyramidal geometry, Figure 5. The sixth oxygen is pulled out of the Na^+ coordination sphere by a weak hydrogen bond to a hydroxide of the Rh tetramer at an O···O separation 2.91 Å. The superanion is somewhat tilted when compared with analogous superanions, which appears to be caused by sulfonate groups coordinating to Na^+ centres, Figure 5.

Complexes **1** and **2** both have an overall polynuclear cation to superanion ratio of 1:1, and the packing of these components in their respective crystal lattices is similar, evident in their comparable unit cell parameters. The extended structure of **2**, however, combines two-dimensional hydrogen-bonded networks of polynuclear cations and superanions with metal-coordinated chains running parallel to the *a* axis formed by calixarenes coordinating to Na^+ metal centres. The hydrogen bonded networks are topologically identical to those found in **2**, with the disordered trinuclear $[Rh_3(\mu\text{-}OH)_4(H_2O)_{10}]^{5+}$ positioned close to the hydrophilic equator of two superanions forming hydrogen bonds at O···O separations 2.46 to 2.88 Å, and the tetranuclear $[Rh_4(\mu\text{-}OH)_6(H_2O)_{12}]^{6+}$ forming hydrogen bonding interactions (O···O separations 2.64 to 2.91 Å) at the outer edges of four superanions. The Na^+ centres within the coordinate chain are six-coordinate, bonding to a terminal water, two bridging perchlorates in a *cis* arrangement, two bridging calixarenes and a terminal calixarene, Figure 6. The bridging calixarenes coordinate to one Na^+ centre through a sulfonate group [Na−O 2.293(7) Å] and to a second Na^+ centre through a hydroxy group [Na−O 2.524(7) Å] of an arene ring adjacent to that of the coordinated sulfonate. Each Na^+ centre has a bridging calixarene coordinating through a sulfonate group and a calixarene bound through a hydroxy group, and these two calixarenes have their cavities oriented in opposite directions and belong to superanions of different 2D hydrogen bonded networks. The terminal calixarene coordinates through a dynamically disordered sulfonate group at distances 2.24(1) and 2.56(2) Å and is in the same orientation as the sulfonate-bound calixarene. Coordination of Na^+ by the sulfonate groups of sulfonated calixarenes has been previously reported;[13] however, this is the first structurally authenticated example of hydroxy coordination, which has been observed for other types of calixarenes.[14] The coordinated Na−perchlorate−calixarene chain is complemented by π-π stacking between arenes of calixarenes in opposite orientations with aromatic centroid−centroid separations ca. 3.9 Å.

Yellow crystals of $[Rh_4(\mu\text{-}OH)_6(H_2O)_{12}][X + \{X - 2\,H_2O\} + 8\,H^+]\cdot 33H_2O$ (**3**) were grown in a similar manner to **2** at pH 0.35, and the solid-state structure was determined from X-ray diffraction data collected at 123(1) K. The complex **3** crystallises in a triclinic cell [a = 17.2141(3), b = 18.1947(3), c = 20.7066(3) Å, α = 88.218(1), β = 77.304(1), γ = 62.429(1) °] and the structure was solved in $P\bar{1}$. The complex **3** has a 1:1:1 ratio of tetranuclear cation, superanion X^{7-}, and dehydrated superanion

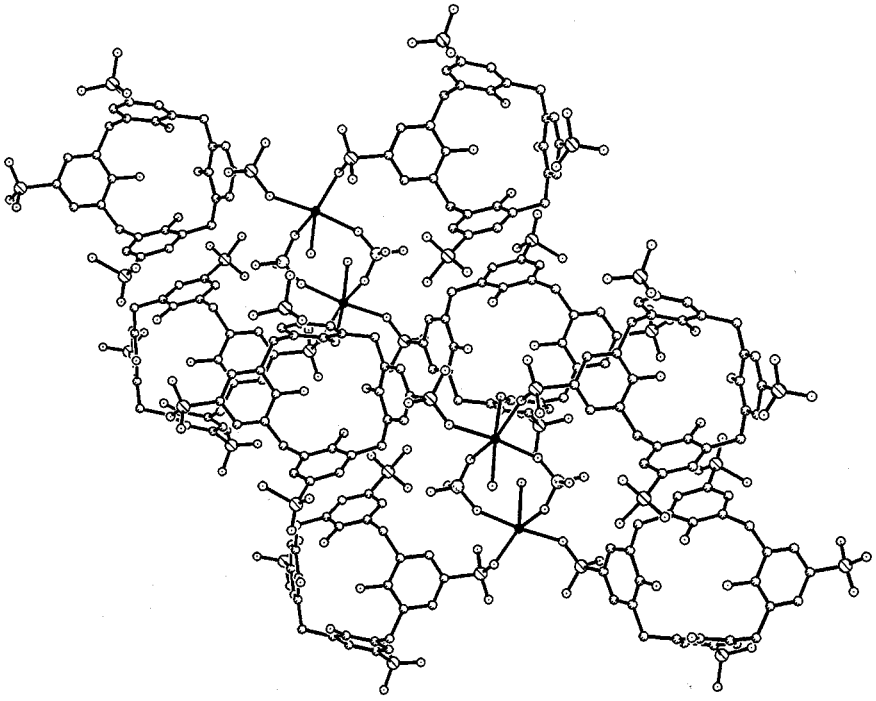


Figure 6. Chain structure of **2** formed by coordination of Na (highlighted in black) by two bridging perchlorates; two bridging calixarenes with sulfonate and hydroxy binding, with terminal water and calixarene ligands also shown

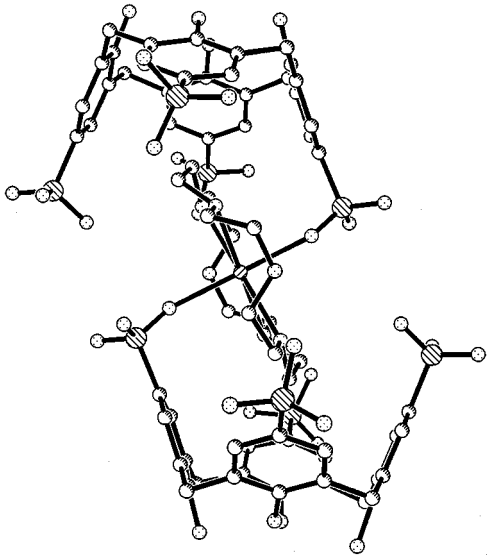


Figure 7. Dehydrated superanion $\{X - 2\,H_2O\}^{7-}$ from the crystal structure of $[Rh_4(\mu\text{-}OH)_6(H_2O)_{12}][X + \{X - 2\,H_2O\} + 8\,H^+]\cdot 33H_2O$ (**3**); displacement of the two calixarene bowls from their usual head-to-head arrangement is clearly visible

$\{X - 2\,H_2O\}^{7-}$ as well as 31 solvent water molecules, and requires a total of eight sulfonate groups to be protonated for charge balance. Not surprisingly given the size of the crystal structure determination, protons were not located crystallographically. The higher ratio of capsules to cations in this structure relative to that of **1** and **2** is consistent with complex formation from a more acidic solution.

The tetranuclear cation is identical to that of **2** and the superanion X^{7-} is similar to those previously reported.[1,2] The structure of the superanion $\{X - 2\,H_2O\}^{7-}$ is skewed considerably from the capsule structure of X^{7-}. The two axial water molecules coordinated to the Na^+ centre in X^{7-} are not present in the dehydrated superanion. Instead the axial coordination positions are occupied by oxygens of sulfonate groups from each of the two calixarene moieties that form the shell of the superanion. The Na−OS distance of 2.319(9) Å requires that one sulfonate group from each of the calixarene subunits is pulled in towards the Na perturbing the usual head-to-head arrangement of calixarenes, leaving the superanion open at each side, Figure 7. The central Na^+ is octahedral and coordinates to four of the six crown ether oxygens [Na−O distances 2.580(8)−2.539(8) Å], with the other two crown oxygens forming hydrogen bonds to solvent water at O···O separation 2.34 Å.

Hydrogen bonding is the dominant interaction present between the different components in complex **3**. Each tetranuclear cation forms hydrogen-bonding interactions to the sulfonate groups of four superanions; two X^{7-} capsules positioned opposite each other across the cation, and two $\{X - 2\,H_2O\}^{7-}$ superanions, at O···O separations of 2.61 to 2.79 Å. Each superanion, whether X^{7-} or $\{X - 2\,H_2O\}^{7-}$, hydrogens bonds to two tetranuclear cations, extending into a two dimensional rectangular grid array shown in Figure 8. Within the crystal lattice the two dimensional grids stack offset to one another and show hydroxy to sulfonate hydrogen bonding and π stacking between calixarenes of adjacent grids, Figure 9. Each superanion forms such interactions to other superanions of both the X^{7-} and $\{X - 2\,H_2O\}^{7-}$ persuasion, at π-π centroid separations 3.53 to 3.78 Å and O···O distances 2.81−3.01 Å. Interestingly, unlike in other examples of π stacking complemented by

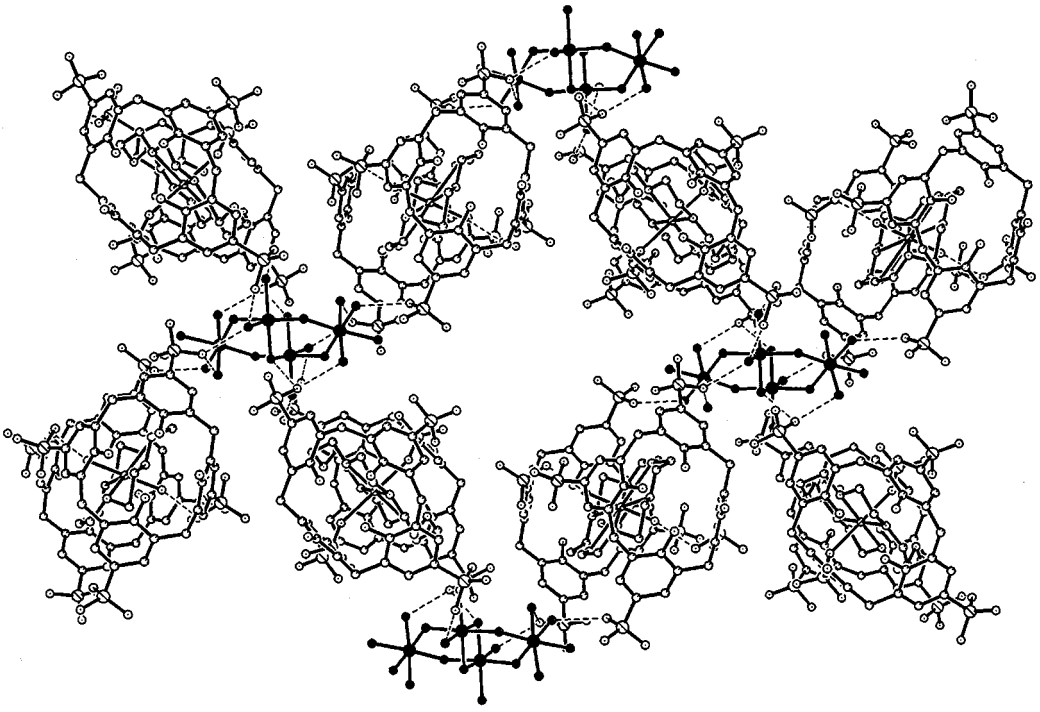


Figure 8. Section of the infinite hydrogen bonded grid structure formed by tetranuclear cations $[Rh_4(\mu\text{-}OH)_6(H_2O)_{12}]^{6+}$ and superanions X^{7-} and $\{X - 2\,H_2O\}^{7-}$ in **3**; for the sake of clarity only one position for the disordered sulfonate in the X^{7-} superanion is shown

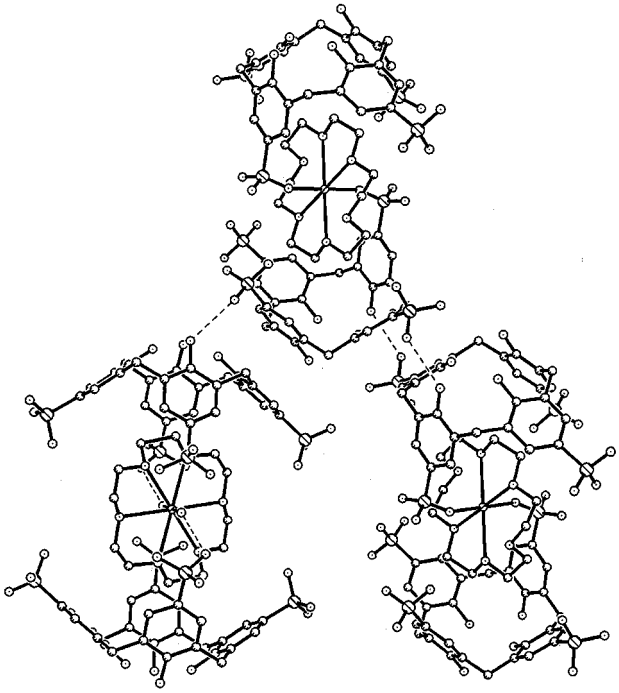


Figure 9. Hydrogen bonding and π-π stacking interactions between superanions of **3**; for the sake of clarity only one position for the disordered sulfonate in the X^{7-} superanion is shown

RSO···HOR′ hydrogen bonding where both interactions occur in the one pair of HO−aryl−SO_3 moieties, the sulfonate groups are oriented such that they accept a hydrogen bond from a hydroxy group adjacent to the aromatic ring involved in the π stack. Spaces within the lattice are occupied by disordered solvent water molecules.

Previously established types of superanions have demonstrated an ability to exist in various states of negative charge, and to either include or exclude Na^+ from the inner core of the capsule depending on reaction conditions. Now it is also seen that the nature of the coordination sphere of the capsule can be altered by a slight variation in reaction conditions. The ambivalent nature of the superanion assembly, either X^{7-} or $\{X - 2\,H_2O\}^{7-}$ in their various protonated forms, is noteworthy, and may be a consequence of crystal packing. The nature of the compounds present in solution is yet to be realised, and has proved a difficult task for all such systems to date.

Conclusions

The ability of the superanion to take on different charges via protonation of the terminal sulfonate is evident in the current structures, and the work further highlights its versatility in complexing two disparate polynuclear species both in charge, size, and shape, in the same lattice, which is without precedent in polynuclear aqua cation chemistry. The complexation of mixed Rh^{III} and Cr^{III} clusters is also likely to lead to some selectivity and for this system only the dinuclear species has been authenticated.[11] The ambivalent nature of the capsule X^{7-} versus $\{X - 2\,H_2O\}^{7-}$ is surprising and highlights the complexity in studying these systems introducing another structural assembly parameter. Overall, our approach to crystallising large cations is indeed more general than initially realised, and the concept of forming capsules by using large cations to overcome the electrostatic repulsion between the two calixarenes has implications in forming capsules with a large array of different organic and inorganic substrates in the core.

Experimental Section

Preparation of 1−3: A mixture of monomeric and oligomeric Rh^{III} cations was produced by treating aqueous rhodium(III) perchlorate (0.1 M) with sodium hydroxide (1 M) to pH 13, standing for 2 hours then acidifying with 60% perchloric acid to approximate pH 2. Solutions containing pure $[Rh_2(\mu\text{-}OH)_2(H_2O)_8](ClO_4)_4$ in aqueous acid were obtained by chromatographic techniques.[8] Crystals of $[Rh_2(\mu\text{-}OH)_2(H_2O)_8][X + 3\,H^+] \cdot 11.5\,H_2O$ (**1**) were obtained by adding an excess of sodium *p*-sulfonatocalix[4]arene and 18-crown-6 to such a solution, adjusting the pH to 2 with aqueous perchloric acid and standing the solution uncapped in ambient conditions for several days. Crystals of $[Rh_3(\mu\text{-}OH)_4(H_2O)_{10}][Rh_4(\mu\text{-}OH)_6(H_2O)_{12}][2\,X + 3\,H^+][Na(H_2O)(ClO_4)]_2 \cdot 27\,H_2O$ **2** were obtained in a similar fashion using the unpurified mixture of Rh^{III} cations in acid. Conditions for the formation and crystallisation of $[Rh_4(\mu\text{-}OH)_6(H_2O)_{12}][X + \{X - 2\,H_2O\} + 8\,H^+] \cdot 33\,H_2O$ **3** were identical to those of **2** except with the initial pH less than 1. Reliable elemental analytical data could not be obtained due to the large proportion of solvent water present in the crystalline complexes.

Crystal Structure Determination: All crystals were sensitive to loss of solvent and were mounted on a glass capillary under oil. Data for **1**−**3** were collected at 123(1) K on an Enraf−Nonius KappaCCD diffractometer with Mo-K_α radiation (λ = 0.71073 Å). Data were corrected for Lorentzian and polarisation effects but not absorption. The structures were solved by direct methods (SHELXS-97) and refined with either a full matrix or blocked-matrix least-squares refinement on F^2 (SHELXL-97). Unless otherwise indicated all non-hydrogen atoms were refined anisotropically. Results of the structure refinements are summarised in Table 1, while details of the treatment of disorder and hydrogens are given below.

$[Rh_2(\mu\text{-}OH)_2(H_2O)_8][X + 3\,H^+] \cdot 11.5H_2O$ (1): One sulfonate group and the crown ether showed dynamic disorder. The sulfonate group was modelled as having O sites disordered over two positions with occupancies 0.7 and 0.3. The behaviour of the crown ether moiety suggested a severe dynamic disorder, probably rotation about the $H_2O-Na-OH_2$ axis, that could not be adequately modelled. The eventual model used has all carbon positions refined with a common set of displacement parameters and all oxygen positions refined with a common set of displacement parameters, although it is recognised that some positions may have mixed C/O character. The higher than usual displacement parameters and some nonsensical bond lengths and angles are a consequence of this disorder. There were a number of disordered water molecules with low occupancy some of which were refined isotropically and C−H hydrogen atoms on the calixarenes were included at calculated positions with a riding refinement.

Table 1. Crystal structure data and details of structure refinement for **1** to **3**

Formula	**1** $C_{68}H_{112}NaO_{61.5}Rh_2S_8$	**2** $C_{136}H_{251}Cl_2Na_4O_{149}Rh_7S_{16}$	**3** $C_{136}H_{236}Na_2O_{129}Rh_4S_{16}$
M_r [g mol^{-1}]	2398.87	5666.56	4905.85
Crystal system	triclinic	triclinic	triclinic
Space group	$P\bar{1}$	$P\bar{1}$	$P\bar{1}$
a [Å]	13.5248(3)	13.8992(2)	17.2141(3)
b [Å]	16.7318(4)	17.0191(5)	18.1947(3)
c [Å]	25.1930(5)	26.6441(7)	20.7066(3)
α [°]	105.583(5)	75.268(3)	88.218(1)
β [°]	97.061(4)	88.328(5)	77.304(1)
γ [°]	108.522(5)	68.768	62.429(1)
V [Å^3]	5069.8(2)	5667.9(2)	5547.4(2)
Z	2	1	1
$\rho_{calcd.}$ [g cm^{-1}]	1.571	1.660	1.457
μ [mm^{-1}]	0.600	0.791	0.55
Refinement type	Full matrix	Block matrix	Full matrix
2θ max [°]	56.6	56.6	55.0
Reflns collected	32085	61992	54268
Unique reflns	22105	26802	25421
R_{int}	0.038	0.061	0.059
Obs. refln $I > 2\sigma(I)$	15966	14320	13875
Restraints	0	0	18
Parameters	1257	1546	1204
R_1 (obs data)	0.0894	0.1151	0.1299
wR_2 (all data)	0.2622	0.3092	0.2149
S	1.036	1.718	1.340

$[Rh_3(\mu\text{-}OH)_4(H_2O)_{10}][Rh_4(\mu\text{-}OH)_6(H_2O)_{12}][2\,X + 3\,H^+][Na(H_2O)(ClO_4)]_2\cdot 27H_2O$ (2): The trinuclear $[Rh_3(\mu\text{-}OH)_4(H_2O)_{10}]$ was located over an inversion centre resulting in a static disorder over two positions each at 0.5 occupancy with some shared oxygen sites at full occupancy. A disordered sulfonate was modelled with O sites over two positions at 0.5 occupancies. There were a number of disordered water molecules with low occupancy some of which were refined isotropically and C−H hydrogen atoms on the calixarenes and crown ether were included at calculated positions with a riding refinement.

$[Rh_4(\mu\text{-}OH)_6(H_2O)_{12}][X + \{X - 2\,H_2O\} + 8\,H^+]\cdot 33H_2O$ (3): The behaviour of the crown ether in the X^{7-} capsule suggested dynamic disorder, and was modelled in a similar manner to the disordered crown in **1**. Two of the sulfonate groups on the X^{7-} capsule also displayed dynamic disorder. The oxygen atoms of these sulfonates were refined isotropically, with the oxygen positions split over two sites at 0.7:0.3 occupancies for one of the disordered sulfonate groups, and S−O bond lengths, and O···O non-bond lengths restrained to maintain a chemically reasonable model. Disordered water molecules were also refined isotropically and C−H hydrogen atoms on the calixarenes and crown ethers were included at calculated positions with a riding refinement.

Crystallographic data (excluding structure factors) for the structures reported in this paper have been deposited with the Cambridge Crystallographic Data Centre as supplementary publication no. CCDC-138364, (**1**), CCDC-138365, (**2**) and CCDC-138366, (**3**). Copies of the data can be obtained free of charge on application to CCDC, 12 Union Road, Cambridge CB2 1EZ, UK [fax: (internat) +44-1223/336-033; E-mail: deposit@ccdc.cam.ac.uk].

Acknowledgments

This work is supported by the Australian Research Council.

[1] A. Drljaca, M. J. Hardie, C. L. Raston, L. Spiccia, *Chem. Eur. J.* **1999**, *5*, 2295.
[2] A. Drljaca, M. J. Hardie, C. L. Raston, *Dalton Trans.* **1999**, 3639.
[3] A. Drljaca, M. J. Hardie, S. Airey, C. L. Raston, *Chem. Commun.* **1999**, 1137.
[4] [4a] M. M. Conn, J. Rebek Jr., *Chem. Rev.* **1997**, *97*, 1647 and references therein. – [4b] B. Olenyuk, M. D. Levin, J. A. Whiteford, J. E. Shield, P. J. Stang, *J. Am. Chem. Soc.* **1999**, *121*, 10434.
[5] [5a] J. Kang, J. Rebek Jr., *Nature* **1997**, *385*, 50. – [5b] T. Heinz, D. M. Rudkevich, J. Rebek Jr., *Nature* **1998**, *394*, 764. – [5c] J. M. Rivera, T. Martin, J. Rebek Jr., *Science* **1998**, *279*, 1021. – [5d] K. R. Castellano, D. M. Rudkevich, J. Rebek Jr., *J. Am. Chem. Soc.* **1996**, *118*, 10002. – [5e] L. R. MacGillivray, J. L. Atwood, *Nature* **1997**, *389*, 469. – [5f] O. Mogek, M. Pons, V. Bohmer, W. Vogt, *J. Am. Chem. Soc.* **1997**, *119*, 5706. – [5g] K. N. Rose, L. J. Barbour, G. W. Orr, J. L. Atwood, *Chem. Commun.* **1998**, 407. – [5h] R. G. Chapman, J. C. Sherman, *J. Am. Chem. Soc.* **1995**, *117*, 9081. – [5i] K. Nakamura, C. Sheu, A. E. Keating, K. N. Houk, J. C. Sherman, R. G. Chapman, W. L. Jorgensen, *J. Am. Chem. Soc.* **1997**, *119*, 4321. – [5j] K. Murayama, K. Aoki, *Chem. Commun.* **1998**, 607.
[6] A. Lützey, A. R. Renslo, C. A. Schalley, B. M. O'Leary, J. Rebek Jr., *J. Am. Chem. Soc.* **1999**, *121*, 7455.
[7] [7a] S. Kamitori, K. Hirotsu, T. Higuchi, *J. Am. Chem. Soc.* **1987**, *109*, 2409. – [7b] F. Vögtle, W. M. Müller, *Angew. Chem. Int. Ed. Engl.* **1979**, *18*, 623.
[8] M. C. Read, J. Glaser, M. Sandstrom, I. Toth, *Inorg. Chem.* **1992**, *31*, 4155.
[9] R. Cervini, G. D. Fallon, L. Spiccia, *Inorg. Chem.* **1991**, *30*, 831.
[10] A. Drljaca, A. Zahl, R. van Eldik, *Inorg. Chem.* **1998**, *37*, 3948.
[11] S. J. Crimp, G. D. Fallon, L. Spiccia, *J. Chem. Soc., Chem. Commun.* **1992**, 197.
[12] Recent examples of structures with disordered crown ethers include: [12a] S. Chadwick, K. Ruhlandt-Senge, *Chem. Eur. J.* **1998**, *4*, 1768. – [12b] D. L. Clark, D. W. Keogh, P. D. Palmer, B. L. Scott, C. D. Tait, *Angew. Chem. Int. Ed.* **1997**, *37*, 164. – [12c] R. B. Dyer, D. H. Metcalf, R. G. Ghirardelli, R. A. Palmer, E. M. Holt, *J. Am. Chem. Soc.* **1986**, *108*, 3621.
[13] [13a] J. L. Atwood, G. W. Orr, N. C. Means, F. Hamada, H.

Zhang, S. G. Bott, K. D. Robinson, *Inorg. Chem.* **1992**, *31*, 603. – [13b] J. L. Atwood, D. L. Clark, R. K. Juneja, G. W. Orr. K. D. Robinson, R. L. Vincent, *J. Am. Chem. Soc.* **1992**, *114*, 7558.

[14] For example: [14a] A. Zanotti-Gerosa, E. Solari, L. Giannini, C. Floriani, A. Chiesi-Villa, C. Rizzoli, *J. Am. Chem. Soc.* **1998**, *120*, 437. – [14b] S. R. Dubberley, A. J. Blake, P. Mountford, *Chem. Commun.* **1997**, 1603.

Received March 27, 2000
[I00114]

Synthesis, Structure, and Magnetic Properties of a Tris[3-(2-pyridyl)-1,2,4-triazole]iron(II) Spin-Crossover Complex

Arno F. Stassen,[a] Matthijs de Vos,[a] Petra J. van Koningsbruggen,[b] Franz Renz,[b] Jürgen Ensling,[b] Huub Kooijman,[c] Anthony L. Spek,[d][+] Jaap G. Haasnoot,*[a] Philipp Gütlich,[b] and Jan Reedijk[a]

Dedicated to Professor Heinrich Vahrenkamp on the occasion of his 60th birthday

Keywords: Spin crossover / Iron / Magnetic properties / Moessbauer spectroscopy / N ligands

The synthesis and characterization of tris[3-(pyridin-2-yl)-1,2,4-triazole]iron(II) bis(tetrafluoroborate), obtained from the reaction of 3-(pyridin-2-yl)-1,2,4-triazole (Hpt) and hexaaquairon(II) tetrafluoroborate, $[Fe(H_2O)_6](BF_4)_2$, is described, together with its crystal structures at two temperatures. X-ray crystallographic parameters are as follows: $[Fe(Hpt)_3](BF_4)_2 \cdot nH_2O$ ($n \approx 2$) at 250 K: orthorhombic space group *Pbam*, a = 15.8068(18) Å, b = 17.2800(14) Å, c = 21.215(2) Å, V = 5794.7(10) Å^3, and Z = 8. $[Fe(Hpt)_3](BF_4)_2 \cdot nH_2O$ ($n \approx 2$) at 95 K: orthorhombic space group *Pbam*, a = 15.7080(12) Å, b = 17.1023(16) Å, c = 21.006(2) Å, V = 5643.1(9) Å^3, and Z = 8. The Fe^{II} ions are (at both temperatures) octahedrally surrounded in a *mer*-configuration. The complex has been subjected to both ^{57}Fe Mössbauer spectroscopy and magnetic susceptibility measurements. The ^{57}Fe Mössbauer spectrum shows the presence of two different iron(II) sites. The high-spin fraction vs. T curve of the crossover, obtained by SQUID measurements, is gradual and without hysteresis, with $T_{1/2}$ = 135 K.

Introduction

Nowadays there is increasing interest in new bistable iron(II) spin-crossover compounds.[1,2] A variety of iron(II) compounds are known to show a transition from the high-spin state [HS, $S = 2$, $^5T_{2g}$ (O_h)] to the low-spin state [LS, $S = 0$, $^1A_{1g}$ (O_h)] on cooling.[2−4]

Iron(II) compounds incorporating substituted 1,2,4-triazole ligands have been found to undergo spin transition. In several cases, hysteresis effects and rather high transition temperatures have been found.[5−23] Generally speaking, when dealing with linear polynuclear Fe^{II} compounds of 1,2,4-triazole ligands, the spin-crossover behaviour is abrupt and may show hysteresis,[5,7,11−16,19,21,22,24,25] but this is not the case for shorter oligomers.[26−28] For mononuclear 1,2,4-triazole-containing iron(II) spin-crossover systems, the spin crossover has always been found to be gradual and without any hysteresis.[9,10,18,29,30]

^{57}Fe Mössbauer spectroscopy studies on $[Fe(Hpt)_3](Anion)_2(Solvent)_x$ [Hpt = 3-(pyridin-2-yl)-1,2,4-triazole (see Figure 1); Anion = Cl^-, ClO_4^-, PF_6^-, BF_4^-; Solvent = ethanol, water] and $[Fe(H3mpt)_3](Anion)_2(Solvent)_x$ [H3Mpt = 3-methyl-5-(pyridin-2-yl)-1,2,4-triazole; Anion = ClO_4^-, PF_6^-; Solvent = water] have been reported by Stupik et al.[9,10] and by Sugiyarto et al.[31] Clearly, these mononuclear compounds exhibit continuous Fe^{II} spin-crossover behaviour. The Fe^{II} ion resides in a six-nitrogen environment made up of three bidentate chelating 3-(pyridin-2-yl)-1,2,4-triazole ligands coordinating through N4 of the 1,2,4-triazole and the pyridine N. The asymmetric nature of the bidentate ligand may lead to the formation of FeL_3 units having *facial* or *meridional* geometry. Both Stupik and Sugiyarto observed[9,10,31] that the spin transition was affected by the presence of different solvent molecules. This contributes to the complicated spin-crossover behaviour evident from the ^{57}Fe Mössbauer spectra. They also observed two different iron(II) high-spin sites in the hydrated BF_4^- complex, but did not mention the ratio between the two sites. In addition, Sugiyarto et al.[31] reported comparable observations for the hydrated BF_4^- and ClO_4^- iron(II) tris[3-(pyridin-2-yl)-1,2,4-triazole] compounds.

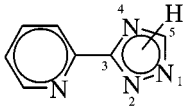


Figure 1. Structure of 3-(pyridin-2-yl)-1,2,4-triazole (Hpt)

[a] Leiden Institute of Chemistry, Gorlaeus Laboratories, Leiden University,
P.O. Box 9502, NL-2300 RA Leiden, The Netherlands
Fax: (internat.) +31−715274671
E-mail: haasnoot@chem.leidenuniv.nl
[b] Institut für Anorganische Chemie und Analytische Chemie, Universität Mainz,
Staudingerweg 9, D-55099 Mainz, Germany
[c] Bijvoet Center for Biomolecular Research, Utrecht University,
Padualaan 8, NL-3584 CH Utrecht, The Netherlands
E-mail: a.l.spek@chem.uu.nl
[+] Address correspondence pertaining to crystallographic studies to this author.

 © WILEY-VCH Verlag GmbH, D-69451 Weinheim, 2000 1434−1948/00/1010−2231 $ 17.50+.50/0

However, these results have not yet been satisfactorily explained, and hence a further study on this interesting class of compounds was undertaken.

In this paper, the synthesis, crystal structures at 250 K and 95 K, and physical properties of the iron(II) Hpt coordination complex of the anion BF_4^- are described in detail.

Results and Discussion

Structure of the Complex

X-ray crystal structure analyses have been carried out at two temperatures, i.e. at 250 K, where the complex is almost completely high spin, and at 95 K, which is below the transition temperature and hence most of the iron(II) ions participating in the spin-crossover behaviour are in the low-spin state. The molecular structure showing the atomic numbering scheme is depicted in Figure 2, while relevant bond length and bond angle information is given in Table 1 and Table 2. At both temperatures, the space group is *Pbam* with $Z = 8$. The asymmetric unit contains one $Fe(Hpt)_3$ moiety. Structural analysis of the complex shows that at both temperatures the iron(II) is octahedrally surrounded by three Hpt ligands, which bind through N2 of the pyridine ring and N4 of the triazole ring in a *mer* configuration.

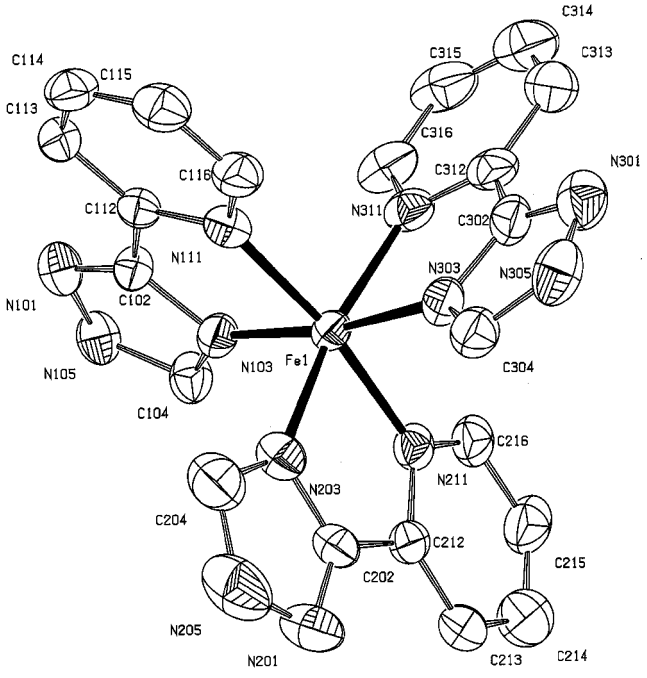


Figure 2. Displacement ellipsoid plot drawn at a 50% probability level of the complex cation $[Fe(Hpt)_3](BF_4)_2 \cdot nH_2O$ at 95 K

Table 1. Relevant bond lengths in $[Fe(Hpt)_3](BF_4)_2 \cdot nH_2O$ at 95 K and 250 K

Bond	Length at 95 K [Å]	Length at 250 K [Å]
Fe−N(103)	2.003(3)	2.127(4)
Fe−N(203)	2.011(3)	2.160(4)
Fe−N(303)	2.009(3)	2.154(4)
Fe−N(111)	2.051(3)	2.202(3)
Fe−N(211)	2.041(3)	2.199(4)
Fe−N(311)	2.047(3)	2.229(4)

Table 2. Important angles in $[Fe(Hpt)_3](BF_4)_2 \cdot nH_2O$ at 95 K and 250 K

Bond angle	Angle at 95 K	Angle at 250 K
N(103)−Fe−N(303)	171.19(13)	164.82(14)
N(111)−Fe−N(211)	171.04(12)	166.71(12)
N(203)−Fe−N(311)	169.33(12)	163.95(17)
N(103)−Fe−N(111)	80.68(12)	77.13(13)
N(203)−Fe−N(211)	80.17(13)	77.00(15)
N(303)−Fe−N(311)	80.33(13)	75.53(15)
N(103)−Fe−N(203)	96.25(13)	100.75(16)
N(103)−Fe−N(211)	92.05(12)	92.43(13)
N(103)−Fe−N(311)	93.20(12)	93.62(15)
N(111)−Fe−N(203)	95.08(12)	96.67(15)
N(111)−Fe−N(303)	93.24(12)	92.74(13)
N(111)−Fe−N(311)	91.31(12)	93.45(14)
N(203)−Fe−N(303)	90.77(13)	91.53(15)
N(211)−Fe−N(303)	94.41(12)	99.04(13)
N(211)−Fe−N(311)	94.57(12)	95.42(14)

Because of rotational and positional disorder of the tetrafluoroborate and water molecules, it was not possible to determine any positional parameters for these molecules. This disorder suggests the absence of hydrogen bonding. This is surprising, because both N1 and N2 of the triazole ring can form hydrogen bonds, either in amino or imino form.[32]

Comparison of the bond angles of the N−Fe−N axes at the two temperatures shows that at low temperature the angles are closer to 180°, as would be expected for a $^1A_{1g}$ octahedral structure. The N−Fe−N angles involving the nitrogen atoms on different axes are also closer to those of a regular octahedron at 95 K than at 250 K. The ligand bite angles increase from 75.53−77.13° at 250 K to 80.17−80.86° at 95 K. The other nonlinear N−Fe−N angles decrease from 91.53−100.75° (average 95.1°) at 250 K to 90.77−96.25° (average 93.4°) at 95 K. Considering that at this temperature 35% of the complexes are still in the high-spin state, the actual angles in the low-spin complex will be even closer to 90°.

The Fe−N bond length contracts by approximately 0.15 Å on cooling to 95 K. These observations can be rationalized as follows. For iron(II) complexes surrounded by neutral ligands, Equation (1) holds, where μ is the dipole moment of the ligand and r the average metal−ligand distance.[1]

$$10Dq \approx \frac{\mu}{r^6} \quad (1)$$

From this equation, Equation (2) can be derived.

$$\frac{10Dq^{LS}}{10Dq^{HS}} = \left(\frac{r_{HS}}{r_{LS}}\right)^6 \approx 1.74 \quad (2)$$

The value for an iron(II) spin-crossover complex is normally ca. 1.74. The value obtained by applying Equation (2) in the case of $[Fe(Hpt)_3](BF_4)_2 \cdot n\,H_2O$ is lower than 1.74, specifically 1.57. The difference between the calculated and measured values arises from the fact that at both temper-

atures not all the iron(II) ions are in the same spin state. From magnetic and Mössbauer measurements, it has been concluded that at 95 K a residue of 36.1% high-spin and at 250 K a residue of 2.5% of low-spin iron(II) ions is present. The actual Fe−N bond length for a pure low-spin state will be closer to 2.00 Å, and using this value in Equation 2 would generate the expected dipole moment.

Because the contribution to the structure factors associated with the counter ions and solvent was taken into account using the SQUEEZE procedure as incorporated in PLATON,[33] no exact molecular formula could be determined from the crystal structure. However, considering the number of electrons associated with the counterions and solvent in conjunction with the elemental analysis, the molecular formula could be calculated. Assuming that only cations of the formula $[Fe(Hpt)_3]^{2+}$, anions BF_4^-, and water were present, the molecular formula $[Fe(Hpt)_3](BF_4)_2 \cdot nH_2O$, $n = 2$, was derived.

The stability of the complex was tested by heating it for several hours at 50 °C and by storing it in vacuo for one day. Under neither conditions were the elemental analysis or magnetic susceptibility affected. Thus, despite the fact that the water molecules are seemingly not involved in strong hydrogen bonding, they are not readily removed from the complex.

^{57}Fe Mössbauer Spectroscopic Measurements

^{57}Fe Mössbauer spectra were recorded at temperatures of 300 K, 205 K, 150 K, 80 K, 32 K, 10 K, and 4.2 K. A representative selection of the spectra is shown in Figure 3. Least-squares-fitted parameters are listed in Table 3. In all the spectra, three doublets have been assigned. Of these, one is characteristic of Fe^{II} in the low-spin state, while the other two are characteristic of Fe^{II} in the high-spin state.[34] We shall refer to the high-spin doublet with the larger quadrupole splitting as HSa, and to the other as HSb. Stupik[9,10] and Sugiyarto[31] also detected a second high-spin site, but it is not clear as to whether the site they detected was identical to HSb (these authors did not analyse the spectra in more detail). Schreiner[29] also detected a second high-spin site in $[Fe(Hpt)_3](BF_4)_2 \cdot H_2O/EtOH$, to the extent of 7% at 100 K (31% at 300 K), which was reported to behave similarly as that found in the present work. The area fraction of the HSb site is only 6% at 205 K and decreases to 3% at 4.2 K, which is close to the experimental limit. Its corresponding Fe^{II} low-spin state doublet probably coincides with the aforementioned major low-spin doublet. The molar ratios of the molecules in the spin states can be derived from the area fractions by taking equal Mössbauer−Lamb factors for the low-spin and high-spin states.[35,36]

At 300 K, a pure high-spin state doublet is present (unresolved HSa and HSb). At 205 K, a low-spin doublet of weak intensity is visible, associated with 8% of the ions. This low-spin doublet clearly increases in intensity on going from 205 to 80 K (from 8% to 67%), while the doublet associated with the HSa site gradually diminishes from 86% at 205 K to 30% at 80 K. At the latter temperature, the spin

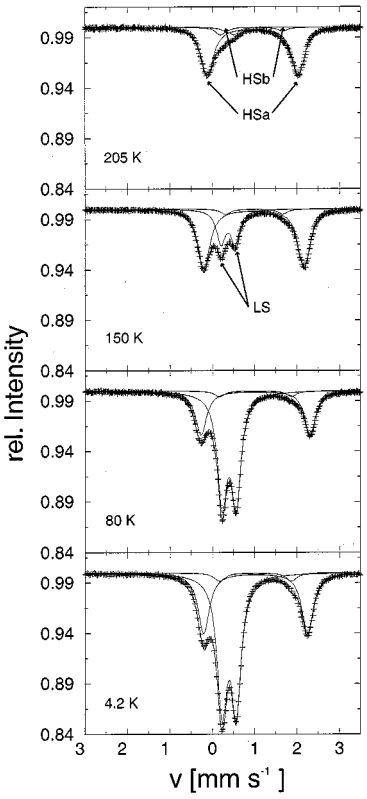


Figure 3. ^{57}Fe Mössbauer spectral measurements at 205, 150, 80, and 4.2 K

crossover is almost complete. Further cooling to 4.2 K results only in an additional 2% increase in the intensity of the low-spin doublet to 69%. The distribution of high-spin and low-spin species found at the measured temperatures is in agreement with the magnetic measurements.

When a spin-crossover compound is cooled very rapidly, i.e. quenched, it is possible that high-spin ions are unable to relax to the low-spin state, but remain thermally spin trapped in the metastable high-spin state.[37−39] This phenomenon is called thermal spin trapping. Mössbauer spectra measured after rapid cooling, i.e. by taking a sample at 300 K and placing it in a cryostat at 4.2 K, revealed that a fraction of the iron(II) ions, approximately 6%, is trapped in the high-spin state (see Table 3). It is mainly the HSb site that exhibits the spin state trapping.

The presence of a second high-spin site (HSb) indicates a different local surrounding from the majority (HSa), arising from the distribution of the solvent and anions.

Magnetic Susceptibility Measurements

Figure 4 shows the product of χT and T for $[Fe(Hpt)_3](BF_4)_2 \cdot 2\,H_2O$, where χT is the molar magnetic susceptibility, recorded in the temperature range 4−325 K as a function of temperature T. The curve provides evidence for $S = 2$ (HS) ⇄ $S = 0$ (LS) spin-crossover behaviour. At room temperature, all iron(II) ions are in the high-spin state ($\chi T = 3.52$ cm^{3}Kmol^{-1}). Below 75 K, the value of χT falls to 0.72 cm^{3}Kmol^{-1}. This indicates the presence of a signi-

Table 3. Least-squares fitted Mössbauer parameters for $[Fe(Hpt)_3](BF_4)_2 \cdot 2\,H_2O$

T (K)	δ(LS)[a] (mm s^{-1})	ΔE_Q(LS) (mm s^{-1})	Γ(LS) (mm s^{-1})	A_{LS} (%)	δ(HS) (mm s^{-1})	ΔE_Q(HS) (mm s^{-1})	Γ(HS) (mm s^{-1})	A_{HS} (%)	δ(HS) (mm s^{-1})	ΔE_Q(HS) (mm s^{-1})	Γ(HS) (mm s^{-1})	A_{HS} (%)
205	0.34(1)	0.32(1)	0.15(1)	8	0.95(0)	2.14(1)	0.25(1)	86	1.10(1)	1.35(1)	0.19(1)	6
150	0.37(1)	0.33(1)	0.15(1)	27	0.98(1)	2.36(1)	0.25(1)	68	1.10(1)	1.35(1)	0.19(1)	5
80	0.39(1)	0.33(1)	0.16(1)	67	1.02(1)	2.57(1)	0.23(1)	30	1.13(1)	1.70(1)	0.20(1)	3
32	0.40(1)	0.33(1)	0.16(1)	69	1.03(1)	2.54(1)	0.22(1)	28	1.13(1)	1.70(1)	0.20(1)	3
10	0.40(1)	0.33(1)	0.16(1)	69	1.03(1)	2.45(1)	0.20(1)	28	1.13(1)	1.70(1)	0.20(1)	3
4.2	0.40(1)	0.33(1)	0.16(1)	69	1.03(1)	2.47(1)	0.20(1)	28	1.13(1)	1.75(1)	0.20(1)	3
After quenching from 300 K (approx. 100 K s^{-1})												
4.2	0.40(1)	0.33(1)	0.16(1)	63	1.04(1)	2.45(1)	0.20(1)	29	1.13(1)	1.80(1)	0.20(1)	7

[a] δ = isomer shift, ΔE_Q = quadrupole splitting, Γ = line width, A_{HS} = area fraction of the HS doublets. Statistical standard deviations are given in parentheses.

ficant residue of high-spin iron(II) ions, as is also evident from the low-temperature Mössbauer spectrum. The spin transition is very gradual, with $T_{1/2}$ = 135 K. The parameter $T_{1/2}$ is defined as the temperature in a thermally driven spin equilibrium at which, for the iron(II) ions involved in spin transition, the amounts of high-spin and low-spin molecules are equal. The entire measurement required 5 h 45 min, corresponding to a heating rate of approximately 1.1 $Kmin^{-1}$ in steps of 2.5 K.

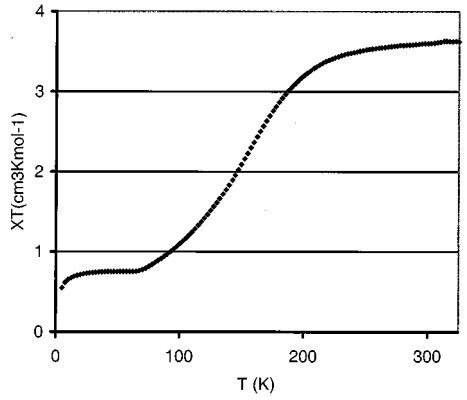


Figure 4. Plot of χT vs. T for $[Fe(Hpt)_3](BF_4)_2 \cdot 2\,H_2O$

The spin transition takes place without hysteresis. Furthermore, the spin-crossover behaviour is easily detected, since the compound is highly thermochromic. On cooling to 77 K, its colour changes from yellow to deep purple.

Figure 5 shows the γ_{HS} vs. T curve plotted over the temperature range 4−320 K. The high-spin molar fraction γ_{HS} was deduced from the ^{57}Fe Mössbauer data area fractions by taking equal Mössbauer−Lamb factors for low-spin state and high-spin state doublets.[35,36] It may be assumed from the Mössbauer measurements that below 80 K 30% of the high-spin sites are not involved in the spin-crossover process. This makes it possible to simulate the spin-crossover curve using Equation (3), which is derived from the regular solution model.[40]

$$\ln\left[\frac{1-\gamma_{HS}}{\gamma_{HS}}\right] = \frac{\Delta H + \Gamma(1-2\gamma_{HS})}{RT} - \frac{\Delta S}{R} \qquad (3)$$

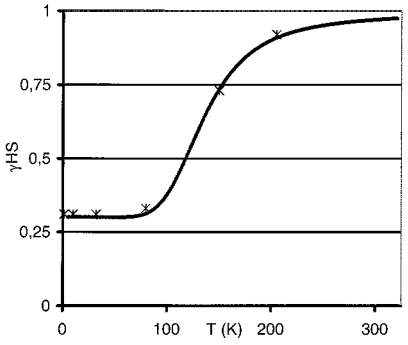


Figure 5. Fitted high-spin molar fraction, based on Mössbauer data, vs. T for $[Fe(Hpt)_3](BF_4)_2 \cdot 2\,H_2O$ (* = actual Mössbauer measurements)

In Equation (3), R is the molar gas constant, ΔH is the enthalpy change, and ΔS is the entropy change associated with the spin crossover. Least-squares fitting leads to ΔH = 6.4 kJ mol^{-1}, ΔS = 47 J K^{-1} mol^{-1}, and a mean-field interaction parameter Γ smaller than 0.1 kJ mol^{-1}. The spin crossover may be considered as being almost non-cooperative.[1,41]

Complexes of hexaaquairon(II) tetrafluoroborate with 3-(pyridin-2-yl)-1,2,4-triazole have been prepared in aqueous solutions at pH 7 to 14. The resulting complexes all exhibit identical spin-crossover behaviour and also give identical elemental analysis results. This excludes the presence of the deprotonated ligand (pt^-).

Ligand-Field Spectroscopy

The ligand-field spectrum of the present complex was measured in the diffuse reflection mode at room temperature and at liquid-nitrogen temperature. The $^5T_2 \rightarrow {}^5E$ transition is seen at 850 nm (11.765 cm^{-1}), while the $^1A_1 \rightarrow {}^1T_1$ transition appears at 530 nm (18.868 cm^{-1}). These values are in the regions normally observed for the corresponding d−d transitions in spin-crossover behaviour materials.[1]

Conclusion

In this paper, the spin-crossover complex tris(Hpt)Fe^{II} with tetrafluoroborate as anion has been reported. This complex is formed as the *meridional* isomer, just as the previously[9,10] studied $[Fe(Hpt)_3](ClO_4)_2 \cdot (Solvent)_x$. Bidentate coordination by the Hpt ligand takes place through N4 of the 1,2,4-triazole and the pyridine N. Details of the X-ray structure determination concerning the location of the tetrafluoroborate and water cannot be reported owing to high positional and rotational disorder of the counterion and solvent. The transition temperature $T_{1/2}$ has been determined as 135 K.

During the spin transition, the geometry of the complex does not change significantly. The average $Fe^{II}-N$ bond length decreases by approximately 0.15 Å. The average N−Fe−N bond angles become closer to those of an ideal octahedron on going from the high-spin to the low-spin state.

In the Mössbauer spectrum, two high-spin iron(II) sites with different populations are observed, with the HSa site clearly showing spin-crossover behaviour. Although a suitably intense doublet associated with the low-spin state is observed, it is not possible to determine whether only one low-spin site is present or whether the signals of two different sites are overlapping. The weak intensity HSb site is at the experimental limit of detection, hence no further conclusions can be made concerning the spin-crossover behaviour at this site. On rapid cooling, a small fraction of the high-spin ions can be thermally trapped in a metastable high-spin state.

It is difficult to compare these results with previously published observations on the $[Fe(Hpt)](BF_4)_2 \cdot 2H_2O$ complex.[9,10,31] These authors also noticed two types of high-spin site, but the data were not analysed further.

The disorder of the solvent molecules and counterions found in the crystal structure gives an indication that neither are involved in hydrogen bonding to the triazole rings of the Hpt ligands. Moreover, the distance between the nitrogens of the triazole ring and the electron density of the counterions and water molecules is too great for hydrogen bonding. The water molecules are nevertheless strongly bound to the complex and cannot be easily removed.

Approximately 30% of the Fe^{II} ions do not participate in the thermal spin transition. It is possible that the distribution of water molecules in the crystal lattice is responsible for this. In the almost identical system $[Fe(Hpt)_3](BF_4)_{1.2}(SO_4)_{0.4} \cdot 3H_2O$,[42] the spin transition does not have an associated high-spin residue at low temperature. It is known that in a few systems the solvent molecules are essential for the spin transition.[43,44] It seems likely that in the present system, due to a non-uniform distribution of water molecules in the lattice, some Fe^{II} ions remain in the high-spin state.

A small proportion (6%) of the iron(II) ions (HSb) experience a different coordination than that described in this article. There are several possibilities for the different coordination of HSb. One explanation is that the ligand is coordinated to the iron(II) through N2 of the triazole ring instead of N4. This would lead to a difference in the coordination sphere and hence in the Mössbauer spectrum; unfortunately, the difference that such a coordination would cause in the structural analysis is smaller than the experimental error. A further possibility is that the deprotonated ligand (pt^-) is present. In this case, 6% of the iron(II) ions would be surrounded by a deprotonated pt^- ligand and have only one tetrafluoroborate counterion in their coordination spheres. However, crystallization experiments at high pH (from 7 to 14) produced materials giving identical results in elemental analysis and susceptibility measurements. Therefore, this possibility can be excluded. A third possibility is that 6% of the crystals have the *facial* orientation. This different coordination could lead to a difference in both the ligand field and quadrupole splitting. In the *mer*-isomer, the three ligands are magnetically non-equivalent, whereas in the *fac*-isomer, the three ligands are magnetically equivalent as this isomer possesses a C_3-axis of symmetry.[45]

Both the first and third options are feasible. Triazole is known to be able to coordinate through N2 as well as through N4,[7,21,26] while both *fac*- and *mer*-isomers of (pydridin-2-yl)-1,2,4-triazole complexes are known.[31,45] Both the linkage and geometrical isomerism will cause a change in ligand field. Whether this variation is sufficiently large to be observed by Mössbauer spectroscopy remains uncertain.

Experimental Section

General Remarks: Ligand-field spectra of the solid were obtained on a Perkin−Elmer Lambda 900 spectrophotometer in the 2000−200 nm range using the diffuse reflectance technique, with MgO as a reference.

Magnetic susceptibilities were measured in the temperature range 5−325 K on a Quantum Design MPMS-5S SQUID operating at 0.1 Tesla. Data were corrected for magnetization of the sample holder and diamagnetic contributions, which were estimated using Pascal constants ($\chi_D = -2.85 \cdot 10^{-4}$ cm^3mol^{-1}).[46]

^{57}Fe Mössbauer spectra of the polycrystalline compound $[Fe(Hpt)_3](BF_4)_2 \cdot 2H_2O$ were recorded using a conventional spectrometer with the sample placed in a helium cryostat allowing variation of the temperature between 4 K and 300 K. As the source, ^{57}Co in rhodium at 293 K was used. The data were evaluated using the programs MOSFUN[35] and EFFI.[36] The high-spin molar fraction was estimated from the area fractions by taking equal Mössbauer−Lamb factors for low-spin and high-spin states.

Preparation of the Compounds: All chemicals were obtained commercially in adequately pure states. The ligand Hpt was synthesized from 2-cyanopyridine, hydrazine monohydrate, and formic acid according to the method described in literature.[32,47] Hpt: $C_7H_6N_4$ (146.2): calcd. C 57.53, H 4.14, N 38.33; found C 56.68, H 4.65, N 38.63.

$[Fe(Hpt)_3](BF_4)_2 \cdot 2H_2O$ was prepared under argon atmosphere by dissolving $[Fe(H_2O)_6](BF_4)_2$ (0.34 g, 1 mmol) and Hpt (0.44 g, 3 mmol) in hot, deoxygenated water (20 mL), to yield a clear brown solution. On standing in a closed flask at room temperature for

Table 4. Crystallographic data for $[Fe(Hpt)_3](BF_4)_2 \cdot nH_2O$ at 95 K and 250 K

Compound	T = 95 K	T = 250 K
	Crystal data	
Formula[a]	$C_{21}H_{18}FeN_{12} \cdot 2BF_4 \cdot 2H_2O$	$C_{21}H_{18}FeN_{12} \cdot 2BF_4 \cdot 2H_2O$
Molecular weight[a]	703.94	703.94
Crystal system	Orthorhombic	Orthorhombic
Space group	*Pbam* (no. 55)	*Pbam* (no. 55)
a [Å]	15.7080(12)	15.8068(18)
b [Å]	17.1023(16)	17.2800(14)
c [Å]	21.006(2)	21.215(2)
V [Å^3]	5643.1(9)	5794.7(10)
D_{calcd} [g cm^{-3}][a]	1.6572(2)*	1.6138(2)*
D_{obsd} [g cm^{-3}]		1.68
Z (mononuclear units)	8	8
$F(000)$ [a]	2848	2848
μ [mm^{-1} [Mo-K_α][a]	0.66	0.64
Crystal colour	red-brown	yellow-brown
	Data collection	
θ_{min}, θ_{max} [deg.]	1.6, 25.25	1.6, 25.25
X-ray exposure [h]	4	2
Data set	−18:18, −20:20, −25:25	−18:14, −20:16, −25:17
Total data	44707	22091
Total unique data	5273	5337
R_{int}	0.0907	0.0541
R_σ	0.0395	0.0552
	Refinement	
No. of refined params.	307	307
Final $R1$[b]	0.0681 [4433 $I > 2\sigma(I)$]	0.0740 [3766 $I > 2\sigma(I)$]
Final $wR2$[c]	0.1587	0.2039
Goodness of Fit	1.140	1.041
w^{-1}[d]	$\sigma^2(F^2) + (0.462P)^2 + 11.59P$	$\sigma^2(F^2) + (0.00755P)^2 + 13.51P$
$(\Delta/\sigma)_{av}$, $(\Delta/\sigma)_{max}$	<0.001, <0.001	<0.001, <0.001
Min. and max. residual density [e Å^{-3}]	−0.36, 0.36	−0.35, 0.33

[a] Including disordered anion and solvent contributions. − [b] $R1 = \Sigma \mid |F_o| - |F_c| \mid / \Sigma |F_o|$. − [c] $wR2 = \{\Sigma[w(F_o^2 - F_c^2)^2] / \Sigma[w(F_o^2)^2]\}^{1/2}$. − [d] $P = [\mathrm{Max}(F_o^2, 0) + 2F_c^2]/3$.

a few days, clear yellow block-shaped crystals were deposited. − $[Fe(Hpt)_3](BF_4)_2 \cdot 2\,H_2O$ (703.9): calcd. C 35.83, H 3.15, N 23.88, F 21.59; found C 35.93, H 3.32, N 23.9, F 19.6.

Crystal Structure Determination of $[Fe(Hpt)_3](BF_4)_2$: A single crystal of dimensions 0.10 × 0.15 × 0.30 mm was mounted on a Lindemann glass capillary and placed in the cold nitrogen stream of the diffractometer. Data were collected on an Enraf−Nonius KappaCCD diffractometer on a rotating anode (Mo-K_α radiation, graphite monochromator, λ = 0.71073 Å, Lp correction, no absorption correction). Two data sets were recorded from this crystal, one at T = 95 K and one at T = 250 K. Structure determination revealed that the only geometrical differences between these structures were those related to the spin transition. Since the data for the 250 K structure were rather poor due to crystal deterioration, an additional data set was collected on a second crystal of dimensions 0.20 × 0.35 × 0.35 mm. Geometric data pertaining to the two structures measured at 250 K proved to be equal within experimental error. The data for the 250 K structure reported here refer to the second data set. Pertinent data relating to the structure determinations are collected in Table 4. The structures were solved by direct methods using SHELXS-86.[48] Refinement on F^2 was performed with SHELXL-97.[49] The hydrogen atoms were included in the refinement in calculated positions riding on their carrier atoms. The non-hydrogen atoms were refined with anisotropic thermal parameters. The hydrogen atoms were refined with a fixed isotropic displacement parameter related to the value of the equivalent isotropic displacement parameter of their carrier atoms. The BF_4 counterions were found to be disordered and located in a region also containing disordered solvent molecules, probably water. The contribution to the structure factors associated with counterions and solvent was taken into account using the SQUEEZE procedure as incorporated in PLATON.[33] A total of 840 e were found in a volume of 1800 Å^3, equally distributed between two symmetry-related cavities. Neutral atom scattering factors and anomalous dispersion corrections were taken from the International Tables for Crystallography.[50] Geometrical calculations and the generation of illustrations were performed with PLATON.[33]

Crystallographic data (excluding structure factors) for the structures reported in this paper have been deposited with the Cambridge Crystallographic Data Centre as supplementary publication nos. CCDC-140484/140485. Copies of the data can be obtained free of charge on application to the CCDC, 12 Union Road, Cambridge CB2 1EZ, U.K. [Fax: (internat.) +44 (0)1223/336033; E-mail: deposit@ccdc.cam.ac.uk].

Acknowledgments

Financial support by the European Union, allowing regular exchange of preliminary results with several European colleagues within the TOSS network under contract ERB-FMRX-CT980199, is gratefully acknowledged. Additional support by the ESF program Molecular Magnets is also kindly acknowledged. The work described in this paper has been supported by the Leiden University Study Group, WFMO, and has been performed under the aus-

pices of the Graduate Research School, HRSMC, a joint activity of Leiden University and the two Universities in Amsterdam. This work was also partly financially supported (A.L.S.) by the Council for the Chemical Sciences of the Netherlands Organization for Scientific Research (CW-NWO). Finally, financial support from the Materialwissenschaftliches Forschungszentrum der Universität Mainz and the Fonds der Chemischen Industrie is also gratefully acknowledged.

[1] P. Gütlich, A. Hauser, H. Spiering, *Angew. Chem. Int. Ed. Engl.* **1994**, 2024−2054.
[2] E. König, G. Ritter, S. K. Kulshreshtha, *Chem. Rev.* **1985**, 219−234.
[3] O. Kahn, C. J. Martinez, *Science* **1998**, *5347*, 44−48.
[4] P. Gütlich, in *Structure and Bonding* (Eds.: M. J. Clarke, P. Hemmerich, J. B. Goodenough, J. A. Ibers, C. K. Jørgensen, J. B. Neilands, D. Reiden, R. Weiss, R. J. P. Williams), Springer, Berlin, **1981**, p. 83−196.
[5] W. Vreugdenhil, J. H. van Diemen, R. A. G. de Graaff, J. G. Haasnoot, J. Reedijk, *Polyhedron* **1990**, *24*, 2971−2979.
[6] J. G. Vos, R. A. G. de Graaff, J. G. Haasnoot, A. M. van der Kraan, P. de Vaal, J. Reedijk, *Inorg. Chem.* **1994**, 2905−2910.
[7] W. Vreugdenhil, J. G. Haasnoot, O. Kahn, P. Thuéry, J. Reedijk, *J. Am. Chem. Soc.* **1987**, 5272−5273.
[8] G. Vos, R. A. le Fêbre, R. A. G. de Graaff, J. G. Haasnoot, J. Reedijk, *J. Am. Chem. Soc.* **1983**, 1682−1693.
[9] P. Stupik, J. H. Zhang, M. Kwiecien, W. M. Reiff, J. G. Haasnoot, R. Hage, J. Reedijk, *Hyperfine Interactions* **1986**, 725−727.
[10] P. Stupik, W. M. Reiff, R. Hage, J. Jacobs, J. G. Haasnoot, J. Reedijk, *Hyperfine Interactions* **1988**, 343−346.
[11] A. Ozarowski, Y. Shunzhong, B. R. McGarvey, A. Mislankar, J. E. Drake, *Inorg. Chem.* **1991**, 3167−3174.
[12] W. Vreugdenhil, S. Gorter, J. G. Haasnoot, J. Reedijk, *Polyhedron* **1985**, *10*, 1769−1775.
[13] O. Kahn, J. Krober, C. Jay, *Adv. Mater.* **1992**, *11*, 718−728.
[14] C. Jay, F. Grolière, O. Kahn, J. Kröber, *Mol. Cryst. Liq. Cryst.* **1993**, 255−262.
[15] J. Kröber, J. Audière, R. Claude, E. Codjovi, O. Kahn, J. G. Haasnoot, F. Grolière, C. Jay, A. Bousseksou, J. Linarès, F. Varret, A. Gonthier-Vassal, *Chem. Mater.* **1994**, 1404−1412.
[16] J. Kröber, E. Codjovi, O. Kahn, F. Grolière, C. Jay, *J. Am. Chem. Soc.* **1993**, 9810−9811.
[17] K. H. Sugiyarto, H. A. Goodwin, *Aust. J. Chem.* **1994**, 263−277.
[18] K. H. Sugiyarto, D. C. Craig, A. D. Rae, H. A. Goodwin, *Aust. J. Chem.* **1993**, 1269−1290.
[19] P. J. van Koningsbruggen, Y. Garcia, E. Codjovi, R. Lapouyade, O. Kahn, L. Fournès, L. Rabardel, *J. Mater. Chem.* **1997**, *10*, 2069−2075.
[20] Y. Garcia, P. J. van Koningsbruggen, G. Bravic, P. Guionneau, A. Chasseau, G. L. Cascarano, J. Moscovici, K. Lambert, A. Michalowicz, O. Kahn, *Inorg. Chem.* **1997**, 6357−6365.
[21] Y. Garcia, P. J. van Koningsbruggen, E. Codjovi, R. Lapouyade, O. Kahn, L. Rabardel, *J. Mater. Chem.* **1997**, *6*, 857−858.
[22] C. Cantin, H. Daubric, J. Kliava, Y. Servant, L. Sommier, O. Kahn, *J. Phys. Condens. Matt.* **1998**, *31*, 7057−7064.
[23] C. Janiak, T. G. Scharmann, J. C. Green, R. P. G. Parkin, M. J. Kolm, E. Riedel, W. Mickler, J. Elguero, R. M. Claramunt, D. Sanz, *Chem. Eur. J.* **1996**, *8*, 992−1000.
[24] K. H. Sugiyarto, D. C. Graig, A. D. Rae, H. A. Goodwin, *Aust. J. Chem.* **1994**, 869−890.
[25] E. Codjovi, L. Sommier, O. Kahn, C. Jay, *New J. Chem.* **1996**, *5*, 503−505.
[26] J. J. A. Kolnaar, G. van Dijk, H. Kooijman, A. L. Spek, V. G. Ksenofontov, P. Gütlich, J. G. Haasnoot, J. Reedijk, *Inorg. Chem.* **1997**, *11*, 2433−2440.
[27] J. J. A. Kolnaar, Ph.D. Thesis, Leiden University, **1998**.
[28] C. Janiak, T. G. Scharmann, T. Brauniger, J. Holubova, M. Nadvornik, *Z. Anorg. Allg. Chem.* **1998**, *5*, 769−774.
[29] A. Schreiner, Ph.D. thesis, University of Mainz **1995**.
[30] P. J. Kunkeler, P. J. van Koningsbruggen, J. P. Cornelissen, A. N. van der Horst, A. M. van der Kraan, A. L. Spek, J. G. Haasnoot, J. Reedijk, *J. Am. Chem. Soc.* **1996**, *9*, 2190−2197.
[31] K. H. Sugiyarto, D. C. Craig, A. D. Rae, H. A. Goodwin, *Aust. J. Chem.* **1995**, 35−54.
[32] R. Hage, Ph.D. Thesis, Leiden University, **1991**.
[33] A. L. Spek, *Acta Crystallogr.* **1990**, C34.
[34] P. Gütlich, R. Link, A. Trautwein, *Mössbauer Spectroscopy and Transition Metal Chemistry*, Springer, Berlin, **1978**.
[35] E. W. Müller, Ph.D. Thesis, University of Mainz, Germany, **1982**.
[36] H. Spiering, *EFFI Program for Mössbauer Spectra Fitting*, University of Mainz, Germany, **1999**.
[37] H. A. Goodwin, K. H. Sugiyarto, *Chem. Phys. Lett.* **1987**, *5*, 470−474.
[38] A. Hauser, *Chem. Phys. Lett.* **1986**, *6*, 543−548.
[39] G. Ritter, E. Konig, W. Irler, H. A. Goodwin, *Inorg. Chem.* **1978**, *2*, 225.
[40] C. P. Schlichter, H. G. Drickamer, *J. Chem. Phys.* **1972**, 2142.
[41] P. Gütlich, A. Hauser, H. Spiering, *Angew. Chem.* **1994**, 2109.
[42] O. Roubeau, A. F. Stassen, M. d. Vos, J. G. Haasnoot, J. Reedijk, to be published.
[43] R. Claude, J. Zarembowitch, M. Philoche-Levisalles, F. d'Yvoire, *New J. Chem.* **1991**, 625−641.
[44] R. Hernandez-Molina, A. Mederos, S. Dominguez, P. Gili, C. Ruiz-Perez, A. Castineiras, X. Solans, F. Lloret, J. A. Real, *Inorg. Chem.* **1998**, *20*, 5102−5108.
[45] R. Hage, J. G. Haasnoot, J. Reedijk, J. G. Vos, *Inorg. Chim. Acta* **1986**, 73−76.
[46] I. M. Kolthoff, P. J. Elving, *Treatise on Analytical Chemistry, Vol. 4*, New York, **1963**.
[47] M. Uda, Y. Hisazumi, K. Sato, S. Kubota, *Chem Pharm. Bull.* **1976**, *12*, 3103−3108.
[48] G. M. Sheldrick, *SHELXS-86: Program for crystal structure determination*, University of Göttingen, Germany, **1986**.
[49] G. M. Sheldrick, *SHELXL-97−2: Program for crystal structure refinement*, University of Göttingen, Germany, **1996**.
[50] A. J. C. Wilson, *International Tables for Crystallography, Volume C*, Kluwer Academic Publishers, Dordrecht, The Netherlands, **1992**.

Received February 18, 2000
[I00060]

Ring-Opening of Lawesson's Reagent: New Syntheses of Phosphono- and Amidophosphono-Dithioato Complexes − Structural and CP-MAS ^{31}P-NMR Characterization of [*p*-$CH_3OPh(X)PS_2]_2M$ (X = MeO, *i*PrNH; M = Ni^{II}, Pd^{II}, and Pt^{II})

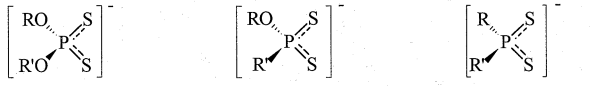
M. Carla Aragoni,[a] Massimiliano Arca,[a] Francesco Demartin,[b] Francesco A. Devillanova,[a] Claudia Graiff,[c] Francesco Isaia,[a] Vito Lippolis,[a] Antonio Tiripicchio,[c] and Gaetano Verani*[a]

Keywords: Nickel / Palladium / Platinum / S ligands / NMR spectroscopy / Phosphonodithioates / Lawesson's reagent

The opening of the P_2S_2 tetraatomic ring of Lawesson's reagent (**4**) has proved versatile in synthesizing phosphono- and amidophosphono-dithioato mononuclear complexes [*p*-$CH_3OPh(X)PS_2]_2M$ [X = CH_3O, *i*PrNH; M = Ni^{II}, Pd^{II}, Pt^{II}]. A one-step reaction of **4** with the appropriate metal salt in CH_3OH, or in the presence of a stoichiometric amount of *i*$PrNH_2$ in $CHCl_3$, is used in the direct synthesis of the Ni^{II} and Pd^{II} complexes, but does not work in the Pt^{II} complexes. Alternatively, these syntheses can be carried out: i) by preparation and isolation of *O*-methyl(4-methoxyphenyl)phosphonodithioate (**6**) salts or isopropylamido(4-methoxyphenyl)-phosphonodithioate (**7**) salts by treating **4** with CH_3O^- in CH_3OH or with *i*$PrNH_2$, respectively; ii) by reaction of **6** or **7** with MCl_2 or K_2MCl_4 [M = Ni^{II}, Pd^{II}, Pt^{II}] to give *trans*-bis[*O*-methyl(4-methoxyphenyl)phosphonodithioato]M and *trans*-bis[isopropylamido(4-methoxyphenyl)phosphono-dithioato]M complexes. Following these routes, *trans*-bis[*O*-methyl(4-methoxyphenyl)phosphonodithioato]M [M = Ni (**8a**), Pd (**8b**), and Pt (**8c**)] and *trans*-bis[isopropylamido(4-methoxyphenyl)phosphonodithioato]M [M = Ni (**9a**), Pd (**9b**), and Pt (**9c**)] complexes have been synthesized and fully characterized by FAB mass, FT-IR, FT-Raman, UV/Vis, and CP-MAS ^{31}P-NMR spectroscopy; the crystal structures of **7**, **8b**, **8c**, and **9a** are also reported.

Introduction

Organophosphodithio compounds, such as phospho-ro-,[1] phosphono-, and phosphanyl-dithioates[2] **1**, **2**, and **3** and corresponding metal complexes, play important roles in industrial and agricultural fields,[3] e.g. additives to lubricant oils,[4] extraction reagents for metal ions,[3,5] flotation agents for mineral ores,[3] insecticides,[3,6] rodenticides,[3,6] and pesticides.[3,6] Furthermore, phosphonate derivatives have assumed a great importance as a replacement of the phosphate moiety in biologically active molecules[7] in the past decades. Many papers have been published on the synthesis and coordination chemistry of **1** and **3**,[1,2,5,8] but, because of synthetic difficulties,[9] only a few have dealt with **2**.



In fact, phosphonodithioate syntheses from organophosphanyl chlorides[9a] or P_4S_{10},[10] involve several laborious reaction steps. A synthesis of phosphonodithioic acid derivatives developed by Martin et al. involves the use of the appropriate Grignard reagent and 2-chloro-1,3,2-dithiaphospholane,[11] but several reaction steps are also required. Under the appropriate conditions, compounds such as 1,3-dithia-2,4-diphosphetane 2,4-disulfide derivatives can give a ring opening, as shown for the well-known Lawesson's reagent (**4**).[12] Although a large amount of information describing the reactivity of **4** can be found in the literature, very little can be found about the reactions of these substrates with transition metal ions[13] or main group elements.[14] We report two novel and facile synthetic routes for preparing complexes with type **2** ligands, i.e. phosphono- and amidophosphono-dithioate, *p*-$CH_3OPh(X)PS_2^-$, X = CH_3O, *i*PrNH, with Ni^{II}, Pd^{II}, and Pt^{II}.

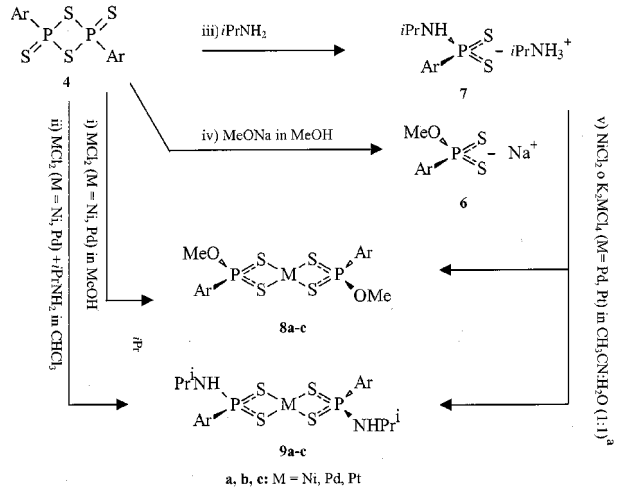
[a] Dipartimento di Chimica Inorganica ed Analitica, Cittadella Universitaria,
S. P. per Sestu Km 0.700, 09042 Monserrato, Cagliari, Italy
[b] Dipartimento di Chimica Strutturale e Stereochimica Inorganica e Centro CNR,
Via G. Venezian 21, 20133 Milano, Italy
[c] Dipartimento di Chimica Generale ed Inorganica, Chimica Analitica, Chimica Fisica
Centro di Studi's per la Strutturistica Diffrattometrica del CNR
Pareo Area delle Scienze 17 A
43100 Parma, Italy

 © WILEY-VCH Verlag GmbH, D-69451 Weinheim, 2000 1434−1948/00/1010−2239 $ 17.50+.50/0

Results and Discussion

Reactivity

In an attempt to optimize the synthesis of a new class of nickel dithiolenes[15] using **4** as a sulfuring agent, we incidentally obtained Ni^{II} complexes of **2**, from which *trans*-bis[*O*-ethyl(4-methoxyphenyl)phosphonodithioate]Ni complex **5**, was structurally characterized;[21] this one-step reaction is shown in the pathway i) of Scheme 1. The ring opening of **4**, required in the formation of the complexes, requires a nucleophilic agent that is the same solvent, for example MeOH in i). Another way of inducing the ring opening of **4** to yield complexes is to use an amine in a stoichiometric amount relative to **4**, in an inert solvent in order to avoid competition reactions. Isopropylamine, $iPrNH_2$, has been chosen as a model compound and was used in $CHCl_3$ as shown in pathway ii). However, in both i) and ii) only phosphono- and amidophosphono-dithioate complexes of Ni^{II} (**8a**, **9a**) and Pd^{II} (**8b**, **9b**) were obtained, the former in higher yields than the latter. In contrast, in spite of several attempts, Pt^{II} complexes (**8c**, **9c**) were never obtained. To prepare Pt^{II} complexes, a different route was successfully attempted through the dithioato ligands **6** and **7**, see pathways iii), iv), and v). Here the two bases, sodium methoxide in MeOH and the amine working both as reagent and solvent, induce the ring opening of **4** to give phosphono- and amidophosphono-dithioate ligands **6** and **7**. As shown in pathway v), these ligands yielded phosphono- and amidophosphono-dithioato complexes **8a**−**8c** and **9a**−**9c**, respectively, almost quantitatively, when treated with $NiCl_2$ and K_2MCl_4 [M = Pd^{II}, Pt^{II}] in $MeCN/H_2O$. However, these experiments show that the difficulty in obtaining platinum complexes according to i) and ii) does not depend on their stabilities.



Ar = 4-methoxyphenyl. – [a] The reaction with K_2NiCl_4 has not been attempted.

Scheme 1

Crystal Structures

The crystal structures of **7**, **8b**, **8c**, and **9a** have been determined by single-crystal X-ray diffraction; ORTEP views of the structures together with atom-numbering schemes are shown for **7** (Figure 1), **8c** (Figure 2), and **9a** (Figure 3); some selected bond lengths and angles of **7**, **8b**, and **8c** are given in Table 1; those of compound **9c** in Table 2. The structures of the isostructural phosphonodithioates **8b** and **8c** consist of centrosymmetric square-planar complexes with the metal atom coordinated by the four S atoms of the two *S*,*S*-bidentate ligands. The two M−S bond lengths are comparable [Pd−S(1) and Pd−S(2) are 2.354(1) and

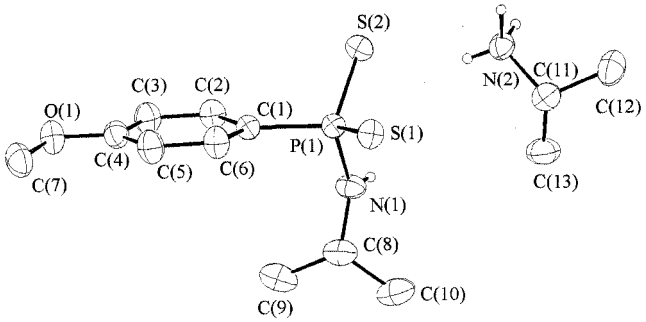


Figure 1. ORTEP drawing and atom-labeling scheme for the isopropylammonium salt of **7**; hydrogen atoms are partially omitted for clarity

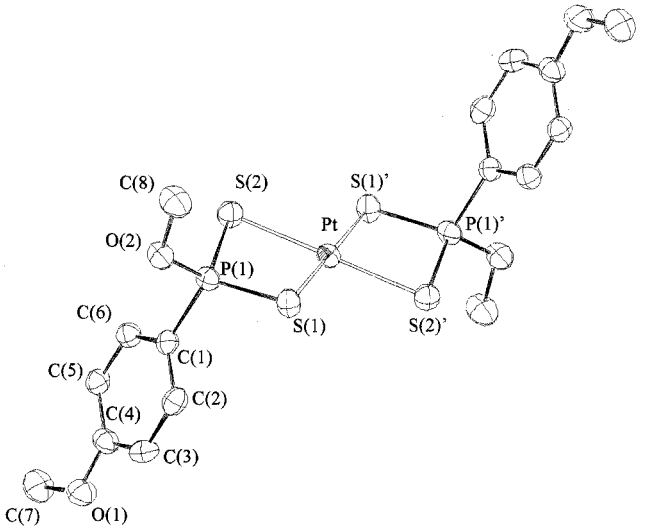


Figure 2. ORTEP drawing and atom-labeling scheme for compound **8c**; hydrogen atoms are omitted for clarity

2.353(1) Å, Pt−S(1) and Pt−S(2) are 2.336(2) and 2.349(2) Å] as previously found for the similar (phosphonodithioato)nickel(II) complex **5** [2.220(1) and 2.222(1) Å].[21] The P atoms are in a pseudo-tetrahedral environment involving the carbon atom of the 4-methoxyphenyl group, the oxygen atom of the methoxy group, and the two S atoms. The P−S bond lengths [2.010(1) and 2.009 (1) Å for **8b**, and 2.011(3) and 2.010 (1) Å for **8c**] are also equal, suggesting a symmetrically delocalized P−S π bond. The P−S bond lengths are comparable with those found in **5**, in the *trans*-bis(*O*-ethylphenyl)phosphonodithioate of Ni,[9d] Pd,[9e] and

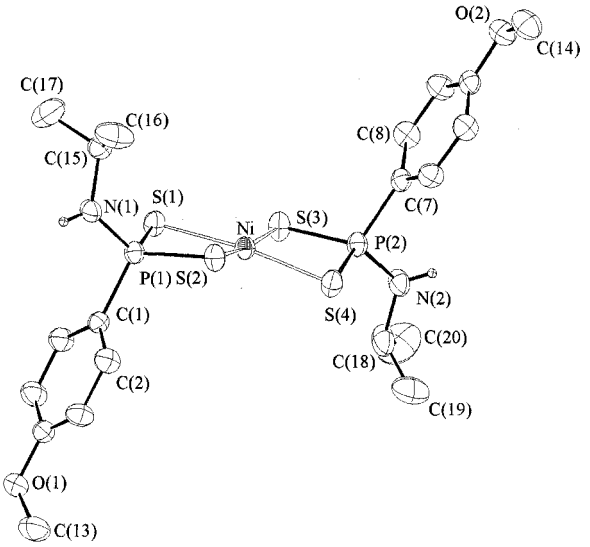


Figure 3. ORTEP drawing and atom-labeling scheme for compound **9a**; hydrogen atoms are partially omitted for clarity

Pt,[9e] and in analogous complexes with type **1** and **3** ligands,[8] and only differ from those found in *trans*-bis[(*O*-isopropyl)ethylphosphonodithioato]Ni[16] in which P−S single bonds, 2.031 Å, and P=S double bonds, 1.900 Å, are present.

The crystal structure of the *trans*-bis[isopropylamido(4-methoxyphenyl)phosphonodithioato]Ni complex **9a**, shows that the metal atom is coordinated by the four S atoms of two *S*,*S*-bidentate ligands. Also in this case, the four Ni−S bond lengths are comparable [2.225(2), 2.227(2), 2.228(2), and 2.216(2) Å], and the four P−S bond lengths [2.012(3), 2.016(3), 2.014(2), and 2.017(2) Å] are nearly identical, suggesting a delocalized P−S π bond, as for **8b** and **8c**. The structure of **9a** closely resembles that of **5**, where P−N bonds replace P−O bonds. The structure of **7**, which contains a unique example of an amidophosphonodithioate anion reported in the literature, displays structural features similar to those reported for type **1**[17] and **3**[18] salts, with similar P−S bond lengths [1.989(1) and 2.000(1) Å] according to a delocalization of the negative charge over the S−P−S fragment. A significant difference between the values of the two P−S bonds [1.945(2) and 1.969(2) Å] has only been found in the case of $K[S_2P(OCH_2Ph)_2]$.[17a] The P−N bond length [1.655(3) Å] in **7** is appreciably longer than those found in **9a** [1.619(4) and 1.622(4) Å].

Table 1. Selected bond lengths [Å] and angles [°] for the isopropylammonium salt of **7**

	7 salt[a]	**8b**[b]	**8c**[c]
M−S(1)	−	2.340(1)	2.336(2)
M−S(2)	−	2.354(1)	2.349(2)
C(4)−O(1)	1.369(4)	1.362(4)	1.355(9)
P(1)−X	1.655(3)	1.583(3)	1.583(5)
S(1)−P(1)	1.989(1)	2.010(1)	2.011(3)
S(2)−P(1)	2.000(1)	2.009(1)	2.010(3)
C(1)−P(1)	1.816(3)	1.784(4)	1.792(8)
C(8)−X	1.466(4)	1.467(7)	1.456(9)
S(1)−M−S(1)′	−	180.0	180.0
S(1)−M−S(2)	−	85.23(4)	84.47(8)
S(1)−M−S(2)′	−	94.77(4)	95.53(8)
P(1)−S(1)−M	−	83.58(5)	84.3(1)
P(1)−S(2)−M	−	83.26(5)	83.9(1)
X−P(1)−C(1)	104.5(1)	101.2(2)	101.5(3)
X−P(1)−S(1)	112.5(1)	112.9(1)	113.6(3)
X−P(1)−S(2)	107.0(1)	113.4(1)	113.7(3)
S(2)−P(1)−S(1)	114.29(5)	104.54(6)	103.1(1)
C(1)−P(1)−S(1)	109.6(1)	113.0(1)	113.7(3)
C(2)−C(1)−P(1)	119.2(2)	119.6(3)	120.0(6)
C(6)−C(1)−P(1)	122.7(2)	121.3(3)	122.0(7)
C(1)−C(2)−C(3)	120.9(3)	119.5(4)	120.6(8)
C(8)−X−P(1)	123.5(2)	119.0(3)	119.8(5)

[a] X = N(1); ′ = $-x$, $-y$, $-z$. − [b] M = Pd; X = O(2). − [c] M = Pt; X = O(2).

Table 2. Selected bond lengths [Å] and angles [°] for compound **9a**

Ni(1)−S(4)	2.216(2)	S(4)−Ni(1)−S(2)	92.37(6)
Ni(1)−S(1)	2.225(2)	S(1)−Ni(1)−S(2)	87.65(6)
Ni(1)−S(2)	2.227(2)	S(4)−Ni(1)−S(3)	87.62(6)
Ni(1)−S(3)	2.228(2)	S(1)−Ni(1)−S(3)	93.25(5)
S(1)−P(1)	2.012(2)	P(1)−S(1)−Ni(1)	84.93(6)
S(2)−P(1)	2.016(2)	P(1)−S(2)−Ni(1)	84.79(6)
S(3)−P(2)	2.014(2)	P(2)−S(3)−Ni(1)	84.94(6)
S(4)−P(2)	2.017(2)	P(2)−S(4)−Ni(1)	85.19(6)
P(1)−N(1)	1.619(4)	N(1)−P(1)−C(1)	103.0(2)
P(2)−N(2)	1.622(4)	N(1)−P(1)−S(1)	114.9(2)
N(1)−H(1N)	0.76(4)	N(1)−P(1)−S(2)	114.2(2)
N(2)−H(2N)	0.85(5)	S(1)−P(1)−S(2)	99.84(7)
		N(2)−P(2)−C(7)	102.6(2)
		N(2)−P(2)−S(3)	114.0(2)
		N(2)−P(2)−S(4)	116.0(2)
		S(3)−P(2)−S(4)	99.49(7)
		C(15)−N(1)−P(1)	124.5(4)
		C(18)−N(2)−P(2)	124.2(4)
		P(2)−N(2)−C(18)	124.2(4)

CP-MAS ^{31}P NMR

Sodium *O*-methyl(4-methoxyphenyl)phosphonodithioate shows a signal at δ = 110.4, which is expectedly different from the value observed for the isopropylammonium isopropylamido(4-methoxyphenyl)phosphonodithioate (δ = 72.7). This value is comparable with the previously reported value for methylammonium methylamido(4-methoxyphenyl)phosphonodithioate (δ = 82.3), which was measured in methylamine solution.[19] Analogous differences are also observed for the corresponding Ni, Pd, and Pt complexes of the two classes of ligands; the ^{31}P-NMR chemical shift for **8a−c** (δ = 97.3, 110.2, 105.7, respectively) was always found downfield relative to those measured for **9a−c** (δ = 71.7, 84.1, 81.7, respectively). The observation that the variation of the S−P−S bond angle affects the ^{31}P chemical shifts[20] seems to be confirmed by these measurements. In fact, within the same series (e.g. **5**, **8b**, **8c**, and **7**, **9a**), a bigger value of the ^{31}P-NMR chemical shift corresponds to an increase in the bond angle.

Conclusions

The easy one-step reaction between Lawesson's reagent (**4**) and alcohols ROH or amines $R'NH_2$ leads to phosphono- and amido-phosphonodithioato ligands (**6** and **7** for R = Me and R′ = *i*Pr, respectively). From these ligands,

the corresponding Ni^{II}, Pd^{II}, and Pt^{II} complexes (**8a−c**, **9a−c**) have been synthesized and fully characterized by means of spectroscopic and diffractometric techniques. The mild reaction conditions and high yields allow the introduction of the desired groups in the phosphono- and amidophosphono-dithioato ligands. This opens interesting perspectives in obtaining novel materials starting from alcohols and amines having intrinsic peculiarities.

Experimental Section

General: All reagents and solvents were purchased from Aldrich or Merck and used without further purification. − Elemental analyses were performed with an EA1108 CHNS-O Fisons instrument. − Infrared spectra were recorded with a Bruker IFS55 spectrometer at room temperature using a flow of dried air. Far-IR (500−50 cm^{-1}) spectra (resolution 2 cm^{-1}) were recorded as polythene pellets with a Mylar beam-splitter and polythene windows. Middle IR spectra (resolution 2 cm^{-1}) were recorded as KBr pellets, with a KBr beam-splitter and KBr windows. − FT-Raman spectra were recorded with a resolution of 2 cm^{-1} using a Bruker RFS100 FT-Raman spectrometer, fitted with an In−Ga−As detector (room temperature) operating with an Nd-YAG laser (excitation wavelength 1064 nm) with a 180° scattering geometry. The excitation power was modulated between 100 and 250 mW. − CP-MAS solid-state ^{31}P-NMR spectra were recorded with a Varian Unity Inova 400-MHz instrument operating at 161.9 MHz with samples packed into a zirconium oxide rotor. The ^{31}P-NMR chemical shifts were calibrated indirectly through the 85% H_3PO_4 peak ($\delta = 0.0$).

(4-Methoxyphenyl)-*O*-methylphosphonodithioate (6), Sodium Salt: A mixture of MeONa (0.76 g, 15 mmol) and **4** (3.00 g, 7.42 mmol) in methanol was heated at reflux for 1 h, and the solvent was then removed under reduced pressure to give a white solid (3.41 g, 90%). − M.p. > 290 °C with decomposition. − $C_8H_{10}NaO_2PS_2$ (256.2): calcd. C 37.5, H 3.9, S 25.0; found C 36.7, H 4.2, S 24.2. − FAB mass spectrum (gly/MeOH/H_2O matrix); *m*/*z*: 233; calcd. for $C_8H_{10}O_2PS_2$ 233 with correct isotopic distribution. − FT-IR (3500−100 cm^{-1}): 3060vw, 3006vw, 2936w, 2833w, 2091w, 1601vs, 1570s, 1501vs, 1466m, 1441m, 1403m, 1383w, 1298s, 1261vs, 1179s, 1152w, 1131w, 1113s, 1106s, 1150w, 1025m, 996vs, 831s, 802m, 748vs, 671vs, 629m, 559s, 511m, 474m, 466w, 437w, 382m, 227w cm^{-1}. − FT-Raman (3500−50 cm^{-1}; relative intensities in parentheses related to the highest peak taken equal to 10.0): 3065 (4.0), 3014 (1.8), 2933 (1.9), 2833 (1.9), 1592 (5.4), 1450 (1.3), 1185 (1.8), 1107 (6.7), 1006 (1.3), 801 (4.9), 654 (2.2), 627 (2.7), 559 (6.9), 523 (1.9), 414 (2.8), 388 (5.4), 364 (2.3), 255 (2.7), 194 (2.7), 92 (10) cm^{-1}. − CP-MAS ^{31}P NMR: $\delta = 110.4$ (s), 111.1 (s), 113.8 (s).

Isopropylamido(4-methoxyphenyl)phosphonodithioate (7), Isopropylammonium Salt: A weighed amount of **4** (1.60 g, 3.96 mmol) was stirred in isopropylamine (50 mL). After a few minutes, the solvent was removed under reduced pressure to give the salt as a white solid (1.28 g, quantitative). Crystals suitable for X-ray analysis were grown from an isopropylamine solution. − M.p. 175 °C. − $C_{13}H_{25}N_2OPS_2$ (320.4): calcd. C 48.7, H 7.9, N 8.7, S 20.0; found C 49.4, H 8.2, N 9.0, S 20.3. − FAB mass spectrum (3-NOBA matrix); *m*/*z*: 321; calcd. for $C_{13}H_{25}N_2OPS_2$ 320 with correct isotopic distribution. − FT-IR (3500−100 cm^{-1}): 3328m, 3000mbr, 1597vs, 1571s, 1497vs, 1466s, 1392m, 1303s, 1294s, 1250vs, 1175s, 1161m, 1135m, 1101s, 1032s, 1004s, 831s, 815m, 798m, 647vs, 622vs, 562vs, 460w cm^{-1}. − FT-Raman (3500−50 cm^{-1}; relative intensities in parentheses related to the highest peak taken equal to 10.0): 3329 (0.9), 3062 (3.3), 2978 (4.2), 2941 (3.5), 2880 (1.7), 2839 (1.4), 1593 (3.8), 1465 (1.5), 1302 (1.4), 1183 (1.8), 1101 (5.4), 798 (4.0), 624 (1.7), 623 (1.9), 566 (5.9), 522 (2.2), 114 (5.9), 69 (10.0) cm^{-1}. − CP-MAS ^{31}P NMR: $\delta = 72.7$ (s).

***trans*-Bis[(4-methoxyphenyl)-*O*-methylphosphonodithioato]Ni (8a):** The synthesis, melting point, and elemental analysis of **8a** have already been reported.[20] − FAB mass spectrum (3-NOBA matrix); *m*/*z*: 524; calcd. for ^{58}Ni 524 with correct isotopic distribution. − Electronic spectrum in CH_2Cl_2: 248 (30820), 328 (22890), 388 (1660), 536 (110), 694 nm (100 M^{-1} cm^{-1}). − FT-IR (3500−100 cm^{-1}): 2997vw, 2941vw, 2837vw, 1597vs, 1567w, 1500s, 1440w, 1307m, 1294s, 1269vs, 1177s, 1165vw, 1118vs, 1029m, 1011s, 1003vs, 836m, 789vs, 667s, 640s, 622m, 550s, 524m, 435m, 375m, 351m, 297w, 277vw, 202vw, 165vw cm^{-1}. − FT-Raman (3500−50 cm^{-1}; relative intensities in parentheses related to the highest peak taken equal to 10.0): 3074 (3.8), 2998 (2.1), 2943 (3.8), 2838 (1.4), 1590 (6.3), 1566 (1.2), 1259 (1.2), 1118 (7.2), 1002 (1.2), 801 (2.8), 667 (2.6), 639 (3.3), 553 (9.1), 491 (1.2), 440 (1.3), 314 (6.1), 296 (1.7), 278 (1.7), 238 (2.6), 102 (9.7), 84 (10.0) cm^{-1}. − CP-MAS ^{31}P NMR: $\delta = 97.3$ (s).

***trans*-Bis[(4-methoxyphenyl)-*O*-methylphosphonodithioato]Pd (8b):** The complex has been synthesized according to reaction (iii) (a) or reaction (v) (b) in Scheme 1. − (a): A mixture of $PdCl_2$ (0.30 g, 1.7 mmol) and **4** (0.70 g, 1.7 mmol) in methanol (60 mL) was heated at reflux for 2 h, and the solvent was then removed under reduced pressure. The resulting orange solid was washed with CH_3CN and dried under vacuum (0.84 g, yield 86%). − (b): A CH_3CN/H_2O solution (1:1, v/v, 10 mL) of K_2PdCl_4 (0.2 g, 0.6 mmol) was added dropwise to a sodium salt solution of **6** (0.56 g, 2.2 mmol) in the same mixture of solvents. After heating at reflux for 2 h, the resulting orange solid was filtered off, washed with the same mixture of solvents, and vacuum-dried (0.21 g, 60%). Crystals suitable for X-ray diffraction analysis were grown by slow evaporation of a 1:1 $CHCl_3/CH_3OH$ solution. − M.p. 203 °C. − $C_{16}H_{20}O_4P_2PdS_4$ (572.9): calcd. C 33.5, H 3.5, S 22.4; found C 33.7, H 3.7, S 22.2. − FAB mass spectrum (3-NOBA matrix); *m*/*z*: 572; calcd. for ^{106}Pd 572 with correct isotopic distribution. − Electronic spectrum in $CHCl_3$: 248 (22530), 302 (31480), 352 (4310), 474 nm (380 M^{-1} cm^{-1}). − FT-IR (3500−100 cm^{-1}): 3002vw, 2965vw, 2943w, 2837vw, 1595vs, 1566m, 1502s, 1442m, 1407w, 1309m, 1296s, 1263vs, 1181s, 1117vs, 1027s, 1012vs, 1002vs, 829m, 792vs, 664s, 636m, 611s, 545vs, 525m, 430m, 372w, 348w, 313s, 200vw, 168vw cm^{-1}. − FT-Raman (3500−50 cm^{-1}; relative intensities in parentheses related to the highest peak taken equal to 10.0): 3071 (1.5), 3004 (1.2), 2943 (2.5), 2839 (2.0), 1591 (5.4), 1116 (6.9), 800 (3.5), 668 (2.5), 637 (3.0), 611 (1.6), 548 (10.0), 523 (1.7), 484 (1.9), 432 (2.5), 374 (1.2), 326 (9.4), 275 (2.1), 186 (1.6), 114 (8.0), 84 (3.1) cm^{-1}. − CP-MAS ^{31}P NMR: $\delta = 110.2$ (s).

***trans*-Bis[(4-methoxyphenyl)-*O*-methylphosphonodithioato]Pt (8c):** A solution of K_2PtCl_4 (0.2 g, 0.6 mmol) in CH_3CN/H_2O (1:1, v/v, 10 mL) was added dropwise to a solution of the sodium salt of **6** (0.56 g, 2.2 mmol) in the same mixture of solvents (40 mL). After heating at reflux for 1.5 h, the resulting yellow solid was filtered off, washed with the same mixture of solvents, and vacuum-dried (0.29 g, 73%). Crystals of **8c** were prepared by slow evaporation of a CH_2Cl_2/CH_3OH (1:1) mixture. − M.p. 189 °C. − $C_{16}H_{20}O_4P_2PtS_4$ (661.6): calcd. C 29.0, H 3.0, S 19.4; found C 29.4, H 3.0, S 19.7. − FAB mass spectrum (3-NOBA matrix); *m*/*z*: 661; calcd. for ^{195}Pt 661 with correct isotopic distribution. − Electronic spectrum in CH_2Cl_2: 258 (33700), 294 (9260), 418 nm (170 M^{-1} cm^{-1}). − FT-IR (3500−100 cm^{-1}): 3007vw, 2965w, 2940m, 2837w,

1595s, 1566m, 1502s, 1458w, 1309m, 1297m, 1264s, 1183m, 1118vs, 1026m, 1011vs, 1003vs, 829m, 795vs, 665s, 636m, 612s, 545s, 526w, 429m, 374w, 303m cm^{-1}. − FT-Raman (3500−50 cm^{-1}; relative intensities in parentheses related to the highest peak taken equal to 10.0): 3074 (2.1), 2943 (2.6), 1590 (5.1), 1566 (1.1), 1308 (1.3), 1257 (0.9), 1185 (1.3), 1117 (8.7), 802 (4.8), 667 (2.6), 637 (1.7), 612 (1.6), 547 (10.0), 523 (1.7), 482 (2.2), 432 (3.0), 342 (4.2), 316 (3.5), 282 (2.1), 188 (3.1), 127 (10.0), 82 (8.6) cm^{-1}. − CP-MAS ^{31}P NMR: δ = 104.4 (s), 105.7 (s).

***trans*-Bis[*N*-isopropyl(4-methoxyphenyl)amidophosphono-dithioato]Ni (9a):** A mixture of **4** (1.7 g, 4.2 mmol) and $NiCl_2 \cdot 6\,H_2O$ (1.0 g, 4.2 mmol) in isopropylamine was heat at reflux for 48 h, and the solvent removed under reduced pressure. The residue was dissolved in $CHCl_3$, and the resulting solution was cooled to −18 °C after filtration. The obtained purple solid was filtered off, dried under vacuum, and recrystallized from CH_2Cl_2. The yield was quantitative (2.4 g). Crystals of **9a** were obtained by diffusion of Et_2O vapors into a CH_2Cl_2 solution. − M.p. 175 °C with decomposition. − $C_{20}H_{30}N_2NiO_2P_2S_4$ (579.4): calcd. C 41.5, H 5.2, N 4.8, S 22.1; found C 41.4, H, 5.5 N 4.9, S 22.1. − FAB mass spectrum (3-NOBA matrix); *m*/*z*: 578; calcd. for ^{58}Ni 578 with correct isotopic distribution. − Electronic spectrum in CH_2Cl_2: 246 (29900), 328 (21600), 388 (1410), 528 (120), 686 nm (100 M^{-1} cm^{-1}). − FT-IR (3500−100 cm^{-1}): 3334m, 3024w, 2967w, 1595vs, 1572m, 1499s, 1453m, 1405m, 1383m, 1292w, 1250vs, 1181m, 1130wsh, 1115vs, 1020s, 893m, 814wsh, 806m, 608m, 547s, 528m, 386w, 353m, 281w, 202w, 153w, 121vw cm^{-1}. − FT-Raman (3500−50 cm^{-1}; relative intensities in parentheses related to the highest peak taken as equal to 10.0): 3057 (1.3), 2969 (1.3), 1595 (2.7), 1179 (1.4), 1114 (4.2), 800 (1.5), 661 (1.0), 634 (1.6), 600 (1.0), 550 (6.0), 313 (3.5), 164 (5.5), 103 (10.0) cm^{-1}. − CP-MAS ^{31}P NMR: δ = 71.7 (s).

***trans*-Bis[*N*-isopropyl(4-methoxyphenyl)amidophosphono-dithioato]Pd (9b):** A solution of K_2PdCl_4 (0.2 g, 0.6 mmol) in CH_3CN/H_2O (1:1, v/v, 10 mL) was added dropwise to a solution of the isopropylammonium salt of **7** (0.7 g, 2 mmol) in the same mixture of solvents (40 mL). The product was obtained quantitatively (0.4 g) as an orange solid, which was filtered off, washed with the same mixture of solvents, vacuum-dried, and recrystallized from a $CHCl_3/CH_3OH$ mixture (1:1, v/v). − M.p. 205 °C. − $C_{20}H_{30}N_2O_2P_2PdS_4$ (627.1): calcd. C 38.3, H 4.8, N 4.5, S 20.4; found C 38.6, H 5.0, N 4.5, S 19.9. − FAB mass spectrum (3-NOBA matrix); *m*/*z*: 626; calcd. for ^{106}Pd 626 with correct isotopic distributions. − Electronic spectrum in $CHCl_3$: 248 (27400), 304 (34500), 352 (4500), 470 nm (320 M^{-1} cm^{-1}). − FT-IR (3500−100 cm^{-1}): 3337m, 3024vw, 2959w, 2868vw, 2836vw, 1595s, 1571w, 1495s, 1455w, 1405m, 1293w, 1250vs, 1181m, 1164w, 1130wsh, 1113vs, 1019s, 895m, 828w, 815m, 807m, 659m, 599m, 542s, 529w, 470w, 462vw, 393w, 384w, 314m, 278vw, 150vw cm^{-1}. − FT-Raman (3500−50 cm^{-1}; relative intensities in parentheses related to the highest peak taken equal to 10.0): 3339 (0.5), 3091 (0.8), 3056 (2.4), 3027 (2.4), 2959 (2.0), 2928 (1.4), 1585 (4.1), 1458 (0.8), 1303 (0.8), 1248 (1.1), 1178 (2.0), 1113 (5.7), 1026 (0.6), 897 (0.5), 800 (1.9), 660 (1.1), 623 (1.9), 596 (1.6), 544 (6.3), 436 (1.0), 397 (1.3), 384 (1.4), 327 (6.4), 292 (2.1), 231 (1.7), 164 (7.9), 126 (4.6), 105 (10.0) cm^{-1}. − CP-MAS ^{31}P NMR: δ = 84.1 (s).

***trans*-Bis[*N*-isopropyl(4-methoxyphenyl)amidophosphono-dithioato]Pt, (9c):** A solution of K_2PtCl_4 (0.25 g, 0.60 mmol) in CH_3CN/H_2O (1:1, v/v, 10 mL) was added dropwise to a solution of the isopropylammonium salt of **7** (0.37 g, 1.2 mmol) in the same mixture of solvents (40 mL). After heating at reflux for 2 h, the resulting yellow solid was filtered off, washed with the same mixture of solvents, and vacuum-dried (0.33 g, yield 76%). Crystals of **9c** were grown by slow evaporation of a 1:1 CH_2Cl_2/CH_3OH mixture. − M.p. 205 °C. − $C_{20}H_{30}N_2O_2P_2PtS_4$ (715.7): calcd. C 33.6, H 4.2, N 3.9; S 17.9; found C 33.8, H 4.2, N 4.0, S 17.8. − FAB mass spectrum (3-NOBA matrix); *m*/*z*: 715; calcd. for ^{195}Pt 715 with correct isotopic distribution. − Electronic spectrum in $CHCl_3$: 258 (32300), 298 (8980), 422 nm (230 M^{-1} cm^{-1}). − FT-IR (3500−100 cm^{-1}): 2960w, 2920vw, 2867vw, 2835vw, 1594s, 1570w, 1497s, 1455w, 1440vw, 1404m, 1383w, 1293m, 1249vs, 1181m, 1164w, 1112vs, 1019vs, 895m, 827vw, 814s, 807s, 658m, 598m, 540s,

Table 3. Summary of X-ray single-crystal data and structure refinement parameters for the isopropylammonium salt of **7**, **8b**, **8c**, and **9a**

	7 (salt)	**8b**	**8c**	**9a**[a]
Empirical formula	$C_{13}H_{25}N_2OPS_2$	$C_{16}H_{20}O_4P_2PdS_4$	$C_{16}H_{20}O_4P_2PtS_4$	$C_{20}H_{30}N_2NiO_2P_2S_4$
Molecular mass	320.44	572.94	661.59	579.35
Temperature [K]	293(2)	293(2)	293(2)	293(2)
Crystal system	triclinic	monoclinic	monoclinic	triclinic
Space group	$P\bar{1}$	$P2_1/c$	$P2_1/c$	$P\bar{1}$
a [Å]	9.134(3)	11.934(4)	11.912(4)	11.196(4)
b [Å]	15.923(5)	6.580(3)	6.554(3)	12.557(5)
c [Å]	6.302(3)	14.609(4)	14.664(4)	11.095(4)
α [°]	95.84(4)	90	90	92.04(4)
β [°]	97.47(4)	108.59(2)	108.73(2)	104.75(5)
γ [°]	101.11(5)	90	90	114.92(5)
Volume [$Å^3$]	884.1(6)	1087.3(8)	1084.2(8)	1349.7(10)
Z	2	2	2	2
D_c [g cm^{-3}]	1.204	1.75	2.027	1.43
Wavelength [Å]	1.54184 (Cu-K_α)	0.71073 (Mo-K_α)	0.71073 (Mo-K_α)	1.54184 (Cu-K_α)
F (000)	344	576	640	604
θ range [°]	3−70	3−25	3.44−28.12	3−70
Unique refl. with $I > 2\sigma(I)$	3356	1654	2633	5121
Final *R*1, *wR*2 indices[b]	0.053, 0.151	0.029, 0.036	0.036, 0.071	0.048, 0.120
No. of variables	272	124	127	289
GOF	1.021	0.877	0.757	0.742
Min/max height in final Δρ map [$eÅ^{-3}$]	−0.48/0.53	−0.22/0.38	−1.58/1.06	−0.39/0.48

[a] The cell parameters of **9c** have also been measured: triclinic, space group $P\bar{1}$, a = 11.173(2), b = 12.640(4), c = 11.266(3) Å, α = 91.06 (3), β = 104.67(2), γ = 115.72(1)°. The reflections have not been collected, since **9c** is isostructural with **9a**. − [b] $R1 = \Sigma|F_o - F_c|/|\Sigma(F_o)|$; $wR2 = [\Sigma[w(F_o^2 - F_c^2)^2]/\Sigma[w(F_o^2)^2]]^{1/2}$.

494vw, 393vw, 382vw, 308m cm^{-1}. – FT-Raman (3500–50 cm^{-1}; relative intensities in parentheses related to the highest peak taken equal to 10.0): 3057 (3.2), 2959 (2.8), 2927 (1.9), 1594 (5.3), 1459 (1.2), 1247 (1.5), 1179 (2.7), 1121 (7.2), 800 (2.4), 659 (1.4), 631 (1.8), 542 (8.2), 463 (1.3), 399 (1.8), 383 (1.7), 349 (2.1), 316 (3.3), 234 (1.5), 169 (5.0), 103 (10.0) cm^{-1}. – CP-MAS ^{31}P NMR: δ = 81.7 (s).

X-ray Structure Determination of 7 (Isopropylammonium Salt), 8b, 8c, and 9a: Crystallographic and experimental details of the data collection and refinement of the structures of **7** (isopropylammonium salt), **8b**, **8c**, and **9a** are reported in Table 3, while the molecular structures are depicted in Figures 1–3. The intensity data of the salt of **7** and **9a** were collected with an Enraf–Nonius CAD-4 single-crystal diffractometer, using the graphite-monochromated Cu-K_α radiation and the $\theta/2\theta$ scan technique. The intensity data of **8c** were collected with a Siemens AED single-crystal diffractometer, using graphite-monochromated Mo-K_α radiation and the $\theta/2\theta$ scan technique. The intensity data of **8b** were collected with a CAD-4 single-crystal diffractometer, using graphite-monochromated Mo-K_α radiation and the ω scan technique. Data were corrected in the usual manner for Lorentz and polarization effects, as well as for absorption.[22,23] – The structures were solved by Patterson and Fourier methods, and refined by full-matrix least-squares procedures based on F_o^2, first with isotropic displacement parameters, and then with anisotropic displacement parameters in the last cycles of refinement for all non-hydrogen atoms. The hydrogen atoms were introduced into the geometrically calculated positions, and refined "riding" on the corresponding carbon atoms for **8b**, **8c**, and **9a**; in the case of **7** (isopropylammonium salt), the hydrogen atoms were clearly found in the ΔF map and refined isotropically. – All calculations were performed using the SHELXS[24] and SHELXL[25] systems of crystallographic computer programs. – Lists of atomic coordinates for the non-H atoms, coordinates for the hydrogen atoms, and anisotropic displacement parameters, crystallographic data (excluding structure factors) for the structures reported in this paper have been deposited with the Cambridge Crystallographic Data Center as supplementary publications nos. CCDC-140139 (**7** isopropylammonium salt), -140140 (**8b**), -140141 (**8c**), and -140142 (**9a**). Copies of the data can be obtained free of charge on application to CCDC, 12 Union Road, Cambridge CB2 1EZ, UK [Fax: (internat.) + 44-1223/336-033; E-mail: deposit@ccdc.cam.ac.uk].

Acknowledgments

We thank the University of Nottingham, School of Chemistry, Mass Spectroscopy Service for the FAB-mass determinations. We thank the Regione Autonoma della Sardegna and MURST (Ministero per l'Università e la Ricerca Scientifica e Tecnologica) for support.

[1] J. R. Wasson, G. M. Woltermann, H. J. Stoklosa, *Fortschr. Chem. Forsch. (Top. Curr. Chem.)* **1973**, *35*, 65.
[2] W. Kuchen, H. Hertel, *Angew. Chem. Int. Ed. Engl.* **1969**, *8*, 89.
[3] [3a] H. So, Y. C. Lin, G. S. Huang Gibbs, S. T. Chang Terny, *Wear* **1993**, *166*, 17. – [3b] V. V. Mikhailov, Yu V. Kokhanov, K. Kazaryan, E. N. Matreeva, A. Kozodoi, *Plast. Massy* **1970**, *9*, 23. – [3c] M. Fuller, M. Kasrai, J. S. Sheasby, G. M. Bancroft, K. Fyfe, K. H. Tan, *Tribology Lett.* **1995**, 367.
[4] [4a] P. G. Harrison, M. J. Begley, T. Kikabhai, F. Killer, *J. Chem. Soc., Dalton Trans.* **1986**, 925. – [4b] Y. Lin, *Lubr. Eng.* **1995**, *51*(10), 855. – [4c] A. J. Burn, I. Gosney, C. P. Warrens, J. P. Wastle, *J. Chem. Soc., Perkin Trans. 2* **1995**, 265. – [4d] E. S. Yamaguchi, P. R. Ryason, *Tribo Test* **1996**, *3*(2), 123. – [4e] S. Contarini, G. Tripaldi, G. Ponti, S. Lizzit, A. Baraldi, G. Paolucci, *Appl. Surf. Sci.* **1997**, *108*(3), 359. – [4f] B. Chen, J. Song, Y. Ye, J. Dong, *Tribologia* **1998**, *29*(2), 207.
[5] R. C. Mehrotra, G. Srivastava, B. P. S. Chauhan, *Coord. Chem. Rev.* **1984**, *55*, 207, refs. 2–6 therein.
[6] [6a] R. B. Fearing, E. N. Walsh, J. J. Menn, A. H. Freiberg, *J. Agr. Food Chem.* **1969**, *17*(6), 1261. – [6b] D. A. Wustner, J. Desmarchelier, T. R. Fukuto, *Life Sci.* **1972**, *11*(11), 583. – [6c] Y. Miyata, Y. Takahashi, H. Ando, *Kag. Keis. Kenkyusho Hok., Hokagaku-hen* **1988**, *41*(2), 159; *Chem. Abstr.* **1988**, *109*, 144077. – [6d] N. K. Roy, *Pesticides A* **1990**, *1989–90*, 13.
[7] [7a] R. Engel, *Chem. Rev.* **1976**, *77*, 349. – [7b] K. H. Scheidt, in: *Nucleotide Analogues*; Wiley & Sons, New York, **1980**, p. 96–141. – [7c] R. Engel, in: *The Role of Phosphonates in Living Systems* (Ed.: R. L. Hildebrand), CRC Press, Boca Raton, FL, **1983**, p. 93–138. – [7d] G. M. Blackburn, D. E. Kent, *J. Chem. Soc., Perkin Trans. 1* **1986**, 913. – [7e] G. R. J. Thatcher, A. S. Campbell, *J. Org. Chem.* **1993**, *58*, 2272. – [7f] M. de F. Fernandez, C. P. Vlaar, H. Fan, Y.-H. Liu, F. R. Fronczek, R. P. Hammer, *J. Org. Chem.* **1995**, *60*, 7390.
[8] For some reviews on these compounds see: [8a] I. Haiduc, *Revs. Inorg. Chem.* **1981**, *3*, 353. – [8b] I. Haiduc, D. B. Sowerby, S.-F. Lu, *Polyhedron* **1995**, *14*, 3389. – [8c] I. Haiduc, D. B. Sowerby, *Polyhedron* **1996**, *15*, 2469.
[9] [9a] L. Malatesta, R. Pizzotti, *Chim. Ind.* **1945**, *27*, 6. – [9b] L. Malatesta, R. Pizzotti, *Chim. Ind.* **1946**, *76*, 167. – [9c] P. S. Shetty, P. Jose, Q. Fernando, *J. Chem. Soc., Commun.* **1968**, 788. – [9d] H. Hartung, *Z. Chem.* **1967**, *7*, 241. – [9e] J. P. Fackler, Jr., L. D. Thompson, Jr., *Inorg. Chim. Acta* **1981**, *48*, 45.
[10] I. Kennosuke, N. Shukichi, O. Itaru, (Nippon Chemical Industrial Co., Ltd. Japan) 7417, 245, **1974**.
[11] S. F. Martin, A. S. Wagman, G. G. Zipp, M. K. Gratchev, *J. Org. Chem.* **1994**, *59*, 7957.
[12] [12a] B. Yde, N. M. Yuosif, U. Pedersen, I. Thomsen, S.-O. Lawesson, *Tetrahedron* **1984**, *40*, 2047. – [12b] S. Scheibye, R. Shabana, S.-O. Lawesson, *Tetrahedron* **1982**, *38*, 993. – [12c] R. Shabana, S. Scheibye, K. Clausen, S. O. Olesen, S.-O. Lawesson, *Nouv. J. Chim.* **1980**, *4*, 47. – [12d] S. Sheibye, B. S. Pedersen, S.-O. Lawesson, *Bull. Soc. Chim. Belg.* **1978**, *87*, 229. – [12e] B. S. Pedersen, S. Scheibye, N. H. Nilsson, S.-O. Lawesson, *Bull. Soc. Chim. Belg.* **1978**, *87*, 223. – [12f] S. Scheibye, B. S. Pedersen, S.-O. Lawesson, *Bull. Soc. Chim. Belg.* **1978**, *87*, 299.
[13] [13a] R. Jones, D. J. Williams, P. T. Wood, J. D. Woollins, *Polyhedron* **1987**, *6*, 539. –[13b] G. A. Zank, T. B. Rauchfuss, *Organometallics* **1984**, *3*, 1191.
[14] C. J. Carmalt, J. A. C. Clyburne, A. H. Cowley, V. Lomeli, B. G. McBurnett, *Chem. Commun.* **1998**, 243.
[15] [15a] M. C. Aragoni, M. Arca, F. Demartin, F. A. Devillanova, A. Garau, F. Isaia, F. Lelj, V. Lippolis, G. Verani, *J. Am. Chem. Soc.* **1999**, *121*, 7098. – [15b] M. Arca, F. Demartin, F. A. Devillanova, A. Garau, F. Isaia, F. Lelj, V. Lippolis, S. Pedraglio, G. Verani, *J. Chem. Soc., Dalton Trans.* **1998**, 3731.
[16] S. P. Bone, D. B. Sowerby, R. Constantinescu, L. Haiduc, *J. Chem. Research (S)* **1979**, 69.
[17] [17a] P. Coppens, C. H. MacGillavry, S. G. Hovenkamp, H. Douwes, *Acta Crystallogr.* **1962**, *15*, 765. – [17b] J. P. Hazel, R. L. Collin, *Acta Crystallogr.* **1972**, *B28*, 2279. – [17c] A. A. Pinkerton, N. J. Terrill, *Acta Crystallogr.* **1988**, *C44*, 567. – [17d] A. E. Kalinin, V. G. Andrianov, Yu T. Struchov, *Izv. Akad. Nauk SSSR, Ser. Khim.* **1979**, 783; *Engl. Transl.* 727.
[18] [18a] G. Svenson, J. Albertson, *Acta Chem. Scand.* **1989**, *C45*, 395. – [18b] A. A. Pinkerton, *Acta Crystallogr.* **1990**, *46*, 2255.
[19] E. Von Fluk, H. Binder, *Zeit. Anorg. Allg. Chem.* **1970**, *377*, 298.
[20] P. G. Harrison, T. Kikabhai, *J. Chem. Soc., Dalton Trans.* **1987**, 807, and refs. therein.
[21] M. Arca, A. Cornia, F. A. Devillanova, A. C. Fabretti, F. Isaia, V. Lippolis, G. Verani, *Inorg. Chim. Acta* **1997**, 262, 81.
[22] F. Ugozzoli, *Comput. Chem.* **1987**, *11*, 109.
[23] A. C. T. North, D. C. Phillips, F. S. Mathews, *Acta Crystallogr., Sect. A* **1968**, *24*, 351.
[24] G. M. Sheldrick, *SHELXS Program for the solution of crystal structures*, University of Göttingen, Göttingen, Germany, **1986–97**.
[25] G. M. Sheldrick, *SHELXL Program for the refinement of crystal structures*, University of Göttingen, Göttingen, Germany, **1992–97**.

Received February 16, 2000
[I00063]

Synthesis and Characterization of the Phosphorus Halide–Boron Halide Complexes X_3PBY_3 (X = Cl, Br, I; Y = Br, I) by ^{31}P MAS NMR, IR, and Raman Spectroscopy and the Crystal Structure of Br_3PBBr_3

Christoph Aubauer,[a] Günter Engelhardt,[b] Thomas M. Klapötke,*[a] Heinrich Nöth,[a][+] Axel Schulz,[a] and Marcus Warchhold[a][+]

Keywords: Density functional calculations / Phosphorus / Boron / Halides / NMR spectroscopy / Raman spectroscopy

The phosphorus halide–boron halide complexes X_3PBY_3 (X = Cl, Br, I; Y = Br, I) were prepared and characterized by Raman and IR spectroscopy. Density functional theory (B3LYP) was applied to calculate structural and vibrational data. Assignments of the vibrational normal modes for these Lewis acid–base adducts were made on the basis of their Raman and IR spectra in comparison with computational results. The compounds Cl_3PBBr_3, Br_3PBBr_3, I_3PBBr_3, and I_3PBI_3 were also studied by solid-state ^{31}P MAS NMR spectroscopy. Second-order ^{31}P–$^{79,81}Br$ dipolar coupling effects were observed in the ^{31}P MAS NMR spectrum of Br_3PBBr_3. The molecular structure of Br_3PBBr_3 was determined by X-ray diffraction.

Introduction

As early as 1893 Tarible synthesized the first phosphorus halide–boron halide complex Br_3PBBr_3 from the reaction of PBr_3 and BBr_3 in CS_2.[1] Subsequently, papers have appeared regarding the syntheses of the phosphorus halide–boron halide complexes Cl_3PBBr_3,[2,3] Cl_3PBI_3,[3,4] Br_3PBI_3,[3] I_3PBBr_3,[3,5] I_3PBI_3,[3,5–7] and the di-adduct of P_2I_4 with BBr_3 $P_2I_4{\cdot}2BBr_3$[7] although only elemental analyses, melting points, and the infrared spectra of the adducts I_3PBBr_3, I_3PBI_3, $P_2I_4{\cdot}2BBr_3$.[5,7] were published for the characterization of these species.

In 1978 Terao and co-workers reported nuclear quadrupole resonance (NQR) experiments (^{79}Br and ^{127}I) for the Lewis acid–base complexes X_3PBY_3 (X = Br, I; Y = Br, I).[8] In 1983 the same authors also published Br–P–Br and Br–B–Br bond angles for Br_3PBBr_3, which were derived from an ^{81}Br NQR study.[9] Nevertheless, X-ray structural data for these phosphorus halide–boron halide donor–acceptor complexes were not available in the literature except for the related phosphane–haloboranes Me_3PBY_3 (Y = Cl, Br, I),[10] $(SiMe_3)_3PBY_3$ (Y = Cl, Br)[11] and Ph_3PBBr_3.[12]

Previous work has shown that the donor behavior of phosphorus trihalides depends on the electronegativity of the halogen substituents.[13,14] For the phosphorus trihalides, the order of stability for the 1:1 donor–acceptor complexes with boron trihalides is $PCl_3 < PBr_3 < PI_3$.[3] PF_3 appears to have no donor properties if only σ bonding is considered.[15] The order of stability of the adducts formed from boron trihalides with phosphorus trihalides is $BF_3 < BCl_3 < BBr_3 < BI_3$.[16]

Prior to the study described here these complexes had only been poorly investigated and so we repeated the syntheses and characterized the complexes by Raman and IR spectroscopy. In comparison with the results of density functional theory calculations, the vibrational spectra of these species were studied and a systematic order for assigning the vibrational normal modes was found. The compounds Cl_3PBBr_3, Br_3PBBr_3, I_3PBBr_3, and I_3PBI_3 were studied by ^{31}P MAS NMR. The structure of Br_3PBBr_3 was determined by X-ray diffraction.

Results and Discussion

All the compounds reported here were prepared from the reaction of one equivalent of phosphorus trihalide with one equivalent of the boron trihalide.

We attempted to dissolve the iodine-containing adducts I_3PBBr_3 (**5**) and I_3PBI_3 (**6**) in solvents such as CS_2, CH_2Cl_2, CH_3CN, $CFCl_3$, and SO_2 but found the solubility of these complexes to be very limited. The saturated solution in CS_2 contains essentially only very small amounts of the phosphorus trihalide PI_3 and the corresponding boron trihalide BY_3 (Y = Br, I), as indicated by ^{31}P- and ^{11}B-NMR studies.

In contrast to **5** and **6**, the complexes Cl_3PBBr_3 (**1**), Cl_3PBI_3 (**2**), Br_3PBBr_3 (**3**), and Br_3PBI_3 (**4**) dissolve in CH_2Cl_2 and CS_2. ^{31}P- and ^{11}B-NMR studies showed, besides signals for PX_3 (X = Cl, Br, I) and BY_3 (Y = Cl, Br,

[a] Department of Chemistry, Ludwig-Maximilians-Universität München,
Butenandtstraße 5–13 (Haus D), 81377 Munich, Germany
Fax: (internat.) + 49-(0)89/2180-7492
E-mail: tmk@cup.uni-muenchen.de
[b] Institut für Technische Chemie I, Universität Stuttgart, 70550 Stuttgart, Germany
[+] X-ray structure investigations.

 © WILEY-VCH Verlag GmbH, D-69451 Weinheim, 2000 1434–1948/00/1010–2245 $ 17.50+.50/0

I), resonances for several of the mixed species PX_aY_b and BX_aY_b (a, b = 1, 2; $a \neq b$).

Sublimation of these adducts leads to decomposition into PX_3 (X = Cl, Br, I) and BY_3 (Y = Br, I) and we therefore concluded that all phosphorus halide−boron halide complexes **1**−**6** exist only in the solid state.

In the cases of Br_3PBBr_3 (**3**), I_3PBBr_3 (**5**), and I_3PBI_3 (**6**), sublimation could be used to purify these adducts. For Cl_3PBBr_3 (**1**), Cl_3PBI_3 (**2**), and Br_3PBI_3 (**4**) only decomposition products such as mixed species, halogen and uncharacterized products were observed.

Experimental data for the mixed halogen substituted species (X_3PBY_3, X ≠ Y) showed that halogen exchange only occurs in X_3PBY_3, where Y represents the heavier halogen [temperature for the halogen exchange; Cl_3PBBr_3 (**1**) 35−42 °C, Cl_3PBI_3 (**2**) 0 °C, and Br_3PBI_3 (**4**) room temp.].

Another aim of our investigation was the preparation of $P_2I_4{\cdot}2BBr_3$, a compound that was claimed as being isolated in 1901 by Tarible in the reaction of P_2I_4 with two equivalents of BBr_3.[17] Baudler and Fricke did not succeed in repeating Tarible's work,[18] whereas Cowley et al. claimed to have isolated the compound on the basis of IR data.[5]

The Raman spectrum of the yellow solid, obtained from the reaction of P_2I_4 and BBr_3 in CS_2 according to the literature,[5] displayed unequivocally the Raman lines of I_3PBBr_3 (**5**). The vibrational data are very similar to those obtained by Cowley and Cohen[5] and so it can be assumed that P_2I_4 disproportionates into PI_3 (which forms the observed adduct with BBr_3) and a polymeric iodide $(PI)_n$. The same disproportionation was suggested for the reaction of P_2I_4 with BI_3 resulting in the formation of I_3PBI_3.[5]

Vibrational Spectroscopy

Raman and IR Spectra of X_3PBY_3 (X = Cl, Br, I; Y = Br, I) (1−6)

Table 1 and Table 2 summarize the computed and experimentally observed vibrational frequencies of the compounds **1**−**6** synthesized in this study. Figure 1 shows the Raman spectra of the adducts X_3PBY_3 (**3**: X, Y = Br; **6**: X, Y = I) and Figure 2 the Raman spectra of Cl_3PBBr_3 (**1**), Cl_3PBI_3 (**2**), and I_3PBBr_3 (**5**). The vibrational spectra are in good agreement with our calculations (B3LYP) and allow structural assignments to be made. It should be noted that the computation was carried out for a single, isolated (gas-phase) molecule. There may well be significant differences between gas-phase and solid-state spectra.

The two broad peaks in the Raman spectra of **1**, **3**, and **5** in the range of ca. 700−590 cm^{-1} represent the asymmetric stretching vibration of the BBr_3 unit (ω_1) in the complex. The asymmetric B−I stretching mode (ω_1) can be observed in the Raman spectra of **2**, **4**, and **6** in the range of ca. 650−570 cm^{-1} (broad and weak peaks). In contrast to the Raman spectra, two very intense peaks can be assigned to this vibration in the IR spectrum of **6**. (The adducts **2** and **4** decompose rapidly at room temperature and, for this reason, IR data are not available. Compound **4** was contaminated with disproportionation products and therefore its spectrum is not included in Figure 2.) The asymmetric P−X stretching frequency, ω_3, can be found for X = Cl at 590 cm^{-1} (**1**) and for X = Br at 421 cm^{-1} (**3**). Similarly, the values for the asymmetric stretching mode [ν_4 (E), PX_3] for $OPCl_3$ and $OPBr_3$ are reported to be at 581 and 488 cm^{-1},

Table 1. Calculated and observed vibrational frequencies for Br_3PBBr_3 (**3**) and I_3PBI_3 (**6**)

Br_3PBBr_3 (**3**) Calculation[a]	Raman	IR	I_3PBI_3 (**6**) Calculation[a]	Raman	IR	Assignment
657 (128)	650 (0.5)/ 627 (0.5)	687s/ 652vs/ 626s	565 (64)	592 (0.5)/ 572 (0.5)	591m/ 565s	ω_1, ν_{as} (BX_3)
452 (27)	484 (1)/ 475 (0.5)	472vs	440 (38)	n.o.	422w	ω_2, ν (P−B)
436 (102)	n.o.	421m	359 (77)	389 (3)	384vs	ω_3, ν_{as} (PX_3)
359 (198)	374 (3)	380vs	298 (101)	303 (3)/ 288 (0.5)	329w/ 306s/ 288w	ω_4, ν_s (PX_3), ν (P−B), ν_s (BX_3)
229 (9)	235 (10)	234w	157 (1)	163 (10)		ω_{5a}, ν_s (PX_3), ν (P−B), δ_s (BX_3)
175 (1)	186 (2)		122 (0)	126 (6)		ω_{6a}, δ_s (PX_3), ν (P−B), δ_s (BX_3)
161 (0)	169 (4)		113 (0)	120 (6)		ω_7, δ_{as} (PX_3), δ_{as} (BX_3) (bend)
125 (0)	131 (1)		87 (0)	93 (2)		ω_8, δ_{as} (PX_3), δ_{as} (BX_3) (wag)
92 (0)	102 (4)		70 (0)	75 (1)		ω_9, δ_{as} (PX_3), δ_{as} (BX_3) (wag)
75 (0)	73 (0.5)		64 (0)			ω_{10a}, ν (P−B)
56 (0)			50 (0)			ω_{11}, δ_{as} (PX_3), δ_{as} (BX_3) (wag)
28 (0)			26 (0)			ω_{12} (torsion)

[a] In parentheses: IR intensity [km mol^{-1}].

Table 2. Calculated and observed vibrational frequencies for Cl_3PBBr_3 (**1**), Cl_3PBI_3 (**2**), Br_3PBI_3 (**4**) and I_3PBBr_3 (**5**)

Cl_3P-BBr_3 (**1**) Calculation[a]	Raman	IR	Cl_3P-BI_3 (**2**) Calculation[a]	Raman	Br_3P-BI_3 (**4**) Calculation[a]	Raman	I_3P-BBr_3 (**5**) Calculation[a]	Raman	IR	Assignment
669 (156)	693 (0.5, br) 671 (0.5, br)	689s	566 (135)	576 (3)	567 (83)	616 (0.5, br) 575 (0.5, br)	673 (101)	656 (0.5, br) 589 (0.5, br)	647sh 597sh	ω_1, ν_{as} (BY_3)
562 (6)	602 (2)	600br	575 (33)	588 (3)	487 (1)	471 (2)	404 (154)	402 (2)	399s	ω_2, ν_s (P–B)
550 (123)	590 (0.5)	588vs	545(100)	n.o.	431 (100)	n.o.	365 (79)	n.o.	361m	ω_3, ν_{as} (PX_3)
410 (232)	463 (4)	465sh	408 (157)	451 (7)	337 (155)	351 (3)	326 (77)	332 (3)	333vs	ω_4, ν_s (PX_3), ν (P–B), ν_s (BY_3)
							224 (9)	221 (7)	219m	ω_{5a}, ν_s (PX_3), ν (P–B), δ_s (BY_3)
288 (4)	301 (10)	302m	281 (18)	281 (8)	182 (0)	195 (10)				ω_{5b}, δ_s (PX_3), ν (P–B), ν_s (BY_3)
225 (4)	231 (6)	231m	161 (0)	168 (10)	151 (0)	147 (6)				ω_{6a}, δ_s (PX_3), ν (P–B), δ_s (BY_3)
							125 (2)	141 (10)		ω_{6b}, δ_s (PX_3), ν (P–B)
217 (2)	224 (5)		215 (2)	224 (6)	139 (0)	127 (3)	153 (2)	157 (3)		ω_7, δ_{as} (PX_3), δ_{as} (BY_3) (bend)
158 (0)	168 (1)/ 164 (1)		141 (0)	150 (5)	104 (0)		99 (0)	109 (3)		ω_8, δ_{as} (PX_3), δ_{as} (BY_3) (wag)
123 (0)	131 (6)		97 (0)	101 (5)	83(0)	88 (4)	73 (0)	83 (3)		ω_9, δ_{as} (PX_3), δ_{as} (BY_3) (wag)
106 (0)	128 (5)		103 (0)	114 (3)	77 (0)					ω_{10a}, ν (P–B) ω_{10b}, ν (P–B), δ_{as} (BY_3)
							64 (1)	64 (0.5)		ω_{10c}, δ_s (PX_3), ν (P–B)
69 (0)			62 (0)	71 (1)	53 (0)		47 (0)			ω_{11}, δ_{as} (PX_3), δ_{as} (BY_3) (wag)
38 (0)			44 (0)		30 (0)		26 (0)			ω_{12} (torsion)

[a] In parentheses: IR intensity [km mol^{-1}].

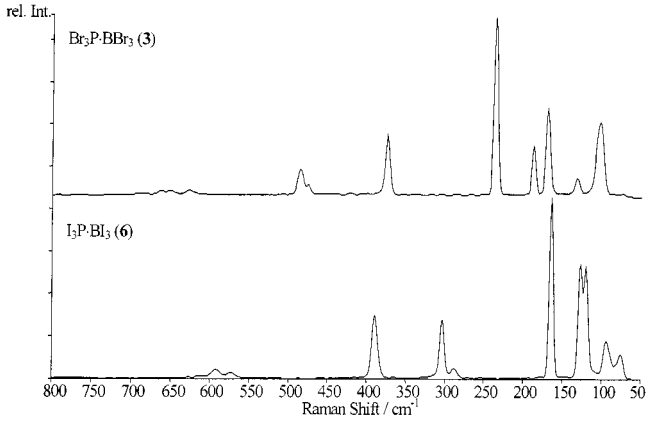


Figure 1. Raman spectra of Br_3PBBr_3 (**3**) and I_3PBI_3 (**6**)

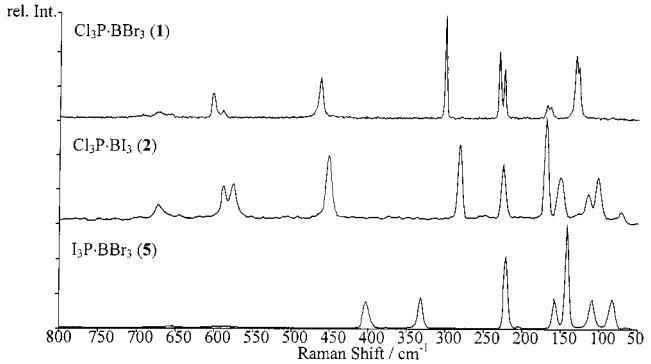


Figure 2. Raman spectra of Cl_3PBBr_3 (**1**), Cl_3PBBr_3 (**2**), and I_3PBBr_3 (**5**)

respectively.[19] The experimental values in the vibrational spectra (IR, Raman) of I_3PBI_3 (**6**) at 387 cm^{-1} and in the IR spectrum of I_3PBBr_3 (**5**) at 361 cm^{-1} can be assigned to the asymmetric stretching vibration of the PI_3 unit (ω_3). Similar vibrational frequencies were reported for the asymmetric stretching modes in the PI_4^+ salts $PI_4^+EI_4^-$ (E = Al, Ga, In)[20,21] at 380 cm^{-1} [ν_3 (T_2), PI_4^+] and in the $P_2I_5^+$ salts $P_2I_5^+EI_4^-$ (E = Al, Ga, In) at 382 cm^{-1}.[22]

Almost purely symmetric P–B stretching vibrations (ω_2) can be observed at 602 (**1**), 588 (**2**), 475 (**3**), 471 (**4**), 402 (**5**), and 422 cm^{-1} (**6**). With heavier halogen substituents the P–B stretching modes are shifted to lower frequencies. The experimental values for the corresponding modes of the related complexes H_3PBY_3 (Y = Cl, Br, I) are found in the range of 679 to 699 cm^{-1}.[23,24]

The assignments of ω_4 to ω_{12} are not as straightforward as those for ω_1 to ω_3. These motions can be described as mixtures of stretches and deformations.

The vibrational mode ω_4, which can be interpreted as a mixture of a P–B stretching mode and symmetric stretching vibrations of the phosphorus trihalide and the boron trihalide units, can be observed and has a similar trend to ω_2: 463 (**1**), 451 (**2**), 377 (**3**), 351 (**4**), 333 cm^{-1} (**5**), and 300 cm^{-1} (**6**).

The mode ω_{5a}, observed as intense peaks in the Raman spectra of **3** (235), **5** (220), and **6** (163), can be described as mixtures of P–B, symmetric PX_3 (X = Cl, Br, I) stretching and symmetric BY_3 (Y = Br, I) deformation modes. A sim-

ilar combination mode, assigned as ω_{5b}, can be observed at 301 (**1**), 281 (**2**), and 195 cm^{-1} (**4**).

The intense Raman frequencies (ω_{6a}), assigned as a combination mode of symmetric deformation modes of the phosphorus halide and boron halide units and a P−B stretching vibration ("umbrella" vibration, $PX_3 + BY_3$ out-of-phase), at 231(**1**), 168 (**2**), 186 (**3**), 147 (**4**), and 126 cm^{-1} (**6**) are reduced to lower wave numbers with heavier halogen substituents.

The bending modes of the PX_3 (X = Cl, Br, I) and BY_3 (Y = Br, I) units, ω_7, can be assigned to peaks with medium intensity in the Raman spectra at 224 (**1**, **2**), 169 (**3**), 127 (**4**), 157 (**5**), and 120 cm^{-1} (**6**).

The normal modes ω_8 to ω_{12} represent fairly complex mixtures of different deformation modes with the exception of the low-lying frequency ω_{10a}, which represents the stretching mode of the entire PX_3 unit towards the BY_3 unit.

Temperature-Dependent Raman Spectra

Br_3PBBr_3 (**3**) decomposes at 61 °C to give a colorless liquid that essentially contains PBr_3 and BBr_3. We recorded the Raman spectra of compound **3** in the temperature region between 20 and 80 °C in steps of 5 °C. Above 60 °C the Raman spectra showed five intense peaks at 383 [ν_1 (A_1), PBr_3], 279 [ν_1 (A_1'), BBr_3], 162 [ν_2 (A_1), PBr_3], 152 [ν_4 (E'), BBr_3], and 115 cm^{-1} [ν_4 (E), PBr_3], which can be assigned to the normal modes of PBr_3 and BBr_3 in the liquid phase.[25,26] The decomposition is reversible. The white Br_3PBBr_3 can be reformed by cooling the liquid to room temperature.

On recording the Raman spectrum of I_3PBBr_3 (**5**) in the temperature range between 20 and 170 °C, we observed that I_3PBBr_3 decomposes into liquid PI_3 {320 [ν_3 (E)], 298 [ν_1 (A_1)], 112 [ν_2 (A_1)], and 82 [ν_4 (E)] cm^{-1}}[27] and BBr_3. Slow cooling of the sample to room temperature led to a yellow solid, which was identified as I_3PBBr_3 with small amounts of I_2 as an impurity. This experiment indicates that halogen exchange does not occur as long as X is heavier than Y (X_3PBY_3).

The melting range of the complex Cl_3PBBr_3 (**1**) is 35−42 °C. The Raman spectrum of the colorless liquid, obtained by heating freshly synthesized Cl_3PBBr_3, shows that at 45 °C the complex decomposes into PCl_3 {514 [ν_3 (E)], 505 [ν_1 (A_1)], 259 [ν_2 (A_1)], and 190 [ν_4 (E)] cm^{-1}},[25] PBr_3 (see above), BCl_3 {472 [ν_1 (A')], 255 [ν_4 (E')] cm^{-1}}[26] and BBr_3 (see above) by halogen exchange. Heating of a sample for 2 d at 70 °C led to a colorless liquid that contained only PBr_3 and BCl_3. It appears that the complex undergoes total halogen exchange. An adduct of Br_3PBCl_3 was not formed after the halogen exchange had occurred, even at temperatures below −130 °C. This result is in agreement with the reports of Holmes,[4] who found that there is no reaction between PBr_3 with BCl_3. Moreover, our density functional calculations show that none of the phosphorus trihalides form 1:1 Lewis acid−base complexes with boron trichloride.

Solid-State ^{31}P-NMR Spectroscopy

The ^{31}P MAS NMR spectra of the compounds I_3PBI_3 (**6**), I_3PBBr_3 (**5**), Br_3PBBr_3 (**3**), and Cl_3PBBr_3 (**1**) are displayed in Figure 3 and the shift data derived from the spectra are summarized in Table 3. The two I_3PBY_3 (Y = Br, I) adducts **5** and **6** show typical spinning side band patterns due to chemical shift anisotropy as observed previously for $PI_4^+EF_6^-$ (E = As, Sb)[20] and $P_2I_5^+EI_4^-$ (E = Al, Ga, In).[22] The central lines of the anisotropy patterns were identified by variation of the spinning frequency and the magnitude of the shift anisotropy δ_{CSA} was estimated by simulation of the side band intensities using the PC program Bruker WINFIT. The spectrum of I_3PBBr_3 (**5**) shows a second weak pattern at δ_{iso} = 237, which originates from PI_3 impurities in the sample.[22]

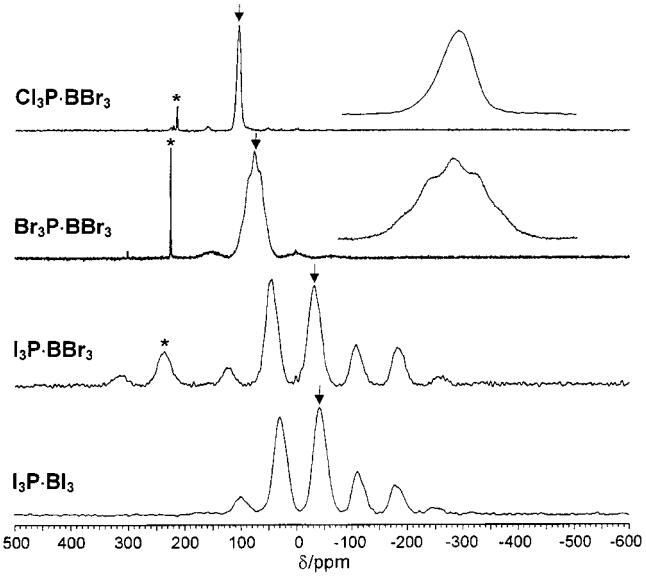


Figure 3. ^{31}P MAS NMR spectra (161.96 MHz) of X_3PBY_3 adducts; the isotropic resonance positions are indicated by arrows, asterisks denote PX_3 impurities (PI_3 in I_3PBBr_3, Br_3P in Br_3PBBr_3, and PCl_3 in Cl_3PBBr_3), all the other lines are spinning side bands; the inserts in the Br_3PBBr_3 and Cl_3PBBr_3 spectra are expanded plots of the resonances centered at δ = 76.9 and 105.3, respectively

Table 3. ^{31}P-NMR isotropic chemical shifts, δ_{iso}, shift anisotropies, δ_{CSA}, and coordination shifts, $\Delta\delta_{coord}$, of X_3PBY_3 compounds (in ppm)

	δ_{iso}	$\Delta\delta_{coord}$[a]	δ_{CSA}[b]
I_3PBI_3 (**6**)	−41.5	−278	−190
I_3PBBr_3 (**5**)	−31.0	−268	−210
Br_3PBBr_3 (**3**)	+76.9	−149	–
Cl_3PBBr_3 (**1**)	+105.3	−110	–

[a] $\Delta\delta_{coord} = \delta_{iso}(X_3P{\cdot}BY_3) - \delta_{iso}(PX_3)$. − [b] $\delta_{CSA} = \delta_{33} - \delta_{iso}$.

The spectra of Br_3PBBr_3 (**3**) and Cl_3PBBr_3 (**1**) exhibit only very weak spinning side bands, indicating small chemical shift anisotropies of the phosphorous atoms in these compounds. Besides the main signals of the adducts (indic-

ated by arrows in Figure 3), narrow lines appear at low field that are attributed to small amounts of PX_3 impurities with X = Br (δ = 226) in Br_3PBBr_3 (**3**) and X = Cl (δ = 214) in Cl_3PBBr_3 (**1**).

Surprisingly, the resonance of Br_3PBBr_3 (**3**) shows an apparent "multiplet" structure (see insert in Figure 3) that is independent of the spinning speed and may formally be simulated by seven overlapping component lines with an equidistant separation of about 1780 Hz. Both the line separation and the intensity distribution rule out a simple explanation in terms of scalar spin-spin coupling between the ^{31}P and the directly bonded $^{79,81}Br$ nuclei [both Br isotopes have a nuclear spin of 3/2, $^1J(^{31}P-^{79,81}Br)$ of 300−380 Hz is reported[28] for PBr_3]. Most probably, the observed "splittings" are caused by second-order effects resulting from dipolar couplings of the ^{31}P with the adjacent $^{79,81}Br$ nuclei, which are not averaged out by magic-angle spinning because of the large quadrupole interaction of the bromine nuclei. Similar effects arising from interactions of ^{31}P with neighboring spin-3/2 quadrupolar nuclei have been observed before for the spin pair $^{31}P-^{63,65}Cu$ in bis(trimethylphosphane) copper(I) nitrate[29] and, more relevant in the context of this study, for $^{31}P-^{35,37}Cl$ in the PCl_4^+ and PCl_6^- ions of solid phosphorus pentachloride.[29] In the latter case, "multiplet" resonances are observed in the ^{31}P MAS NMR spectra that are very similar to the one obtained for Br_3PBBr_3 (**3**). A detailed analysis of this type of second order effect[29] has shown that complex MAS NMR spectra of the spin-1/2 nucleus may arise if the Zeeman interaction of the spin-3/2 nucleus is comparable to, or smaller than, its quadrupole interaction. Under such circumstances the spin states of the quadrupolar nucleus are no longer quantized along the external magnetic field and new terms are introduced in the combined Zeeman-quadrupole Hamiltonian with a different angular dependence than the usual $(3\cos^2\theta - 1)$ term, which is averaged by MAS. The dipolar interaction between the spin-1/2 and the spin-3/2 nucleus may then be reintroduced and gives rise to complex spectral patterns. The quadrupole coupling constant $C_Q = e^2qQ/\mathrm{hbar}$ of the bromine nuclei in the PBr_3 group of Br_3PBBr_3 (**3**) is 426 MHz for ^{81}Br[9] and 518 MHz for ^{79}Br.[8] On comparing these values with the Larmor frequencies of $\nu_L(^{81}Br) = 108$ MHz and $\nu_L(^{79}Br) = 100$ MHz (at 9.4 T), it becomes clear that the quadrupole interaction far exceeds the Zeeman interaction and dipolar coupling may be effective in the ^{31}P MAS NMR spectrum of Br_3PBBr_3 (**3**). To estimate the magnitude of the effect on the spectrum, we calculated the line positions of the ^{31}P multiplets arising from the dipolar coupling with a single Br nucleus for both isotopes following the principles derived in ref.[29] To this end, the parameter $K = -3C_Q/[4S(2S-1)\gamma_S B_o]$ and the dipolar constant $D = (\mu_o/4\pi)\gamma_I\gamma_S\mathrm{hbar}r_{IS}^{-3}$ were calculated, where $C_Q = e^2qQ/\mathrm{hbar}$ is the quadrupole coupling constant; $S = 3/2$, the nuclear spins of $^{79,81}Br$; γ_I and γ_S the magnetogyric ratios of ^{31}P and $^{79,81}Br$, respectively; $B_o = 9.4$ T, the magnetic field used in this study; $r_{IS} = 2.152$ Å, the P−Br distance from Table 4. Values of $K = 1.291$ and 0.986 and $D = 1416$ and 1527 Hz are obtained for the ^{79}Br and ^{81}Br isotopes, respectively. Using these values, the expected spectra were taken from Figure 3 of ref.[29] and are schematically depicted in Figure 4. Theoretically the shape of each resonance is a powder pattern with characteristic divergences and shoulders, but in practice these will be smeared out resulting in broad lines that are approximated by Gaussian lines of equal peak height in Figure 4. It is apparent from this figure that the dipole interaction even with a *single* ^{79}Br or ^{81}Br nucleus already results in splitting of the ^{31}P MAS NMR spectrum into four resonances extending over a spectral range of about 6 kHz, in contrast to the single narrow line to be expected for the unperturbed ^{31}P MAS NMR spectrum. The theoretical spectra of Figure 4 are, of course, not very similar to that observed experimentally for Br_3PBBr_3 (**3**). However, in this molecule the ^{31}P nucleus is coupled to three ^{79}Br and three ^{81}Br nuclei (natural isotopic abundance about 50% each), and further complications by interactions with the ^{11}B nucleus cannot be ruled out. Theoretical calculations of MAS line shapes of spin-1/2 nuclei which interact with three or more spin-3/2 nuclei are difficult and, at present, not feasible. However, such calculations should result in very complex spectral patterns that are not simple superpositions of spectra characterized by interaction with a single quadrupolar nucleus. This conclusion is in full agreement with the experimental findings. It should be noted that, to the best of our knowledge, Br_3PBBr_3 (**3**) is the first example for the observation of second order $^{31}P-^{79,81}Br$ dipolar coupling effects in a ^{31}P MAS NMR spectrum.

Similar dipolar splittings are not observed in the ^{31}P MAS NMR spectra of the I_3PBY_3 (Y = Br, I) and the

Table 4. Theoretical and experimental bond lengths [Å] and angles [°]

		d(PB)	*d*(BY)	*d*(PX)	≤(YBY)	≤(XPX)
BI_3	(calcd.)	–	2.142	–	120.0	–
	(exp.)[a]	–	2.100(1)	–	120.00(2)	–
BBr_3	(calcd.)	–	1.912	–	120.0	–
BCl_3	(calcd.)	–	1.759	–	120.0	–
	(exp.)	–	1.75(2)	–	120.0	–
PI_3	(calcd.)	–	–	2.511	–	103.6
	(exp.)[c]	–	–	2.463(5)	–	102.0(3)
PBr_3	(calcd.)	–	–	2.264	–	101.9
	(exp.)[d]	–	–	2.212(3), 2.216(4)	–	99.0(2), 101.3(2)
PCl_3	(calcd.)	–	–	2.097	–	100.8
	(exp.)[e]	–	–	2.0343(12), 2.0186(23)	–	100.04(7), 100.19(7)
I_3PBI_3	(calcd.)	2.090	2.231	2.481	114.4	105.1
Br_3PBI_3	(calcd.)	2.065	2.232	2.222	114.5	104.3
Cl_3PBI_3	(calcd.)	2.035	2.235	2.049	114.8	103.8
I_3PBBr_3	(calcd.)	2.155	1.984	2.474	115.2	105.8
Br_3PBBr_3	(calcd.)[f]	2.135	1.985	2.200	115.3	104.8
Cl_3PBBr_3	(calcd.)	2.103	1.987	2.048	115.1	102.9

[a] X-ray diffraction: M. A. Ring, J. D. H. Donnay, W. S. Koski, *Inorg. Chem.* **1962**, *1*, 109. – [b] X-ray diffraction: M. Atoji, W. N. Lipscomb, *J. Chem. Phys.* **1957**, *27*, 195. – [c] X-ray diffraction: E. T. Lance, J. M. Haschke, D. R. Peacor, *Inorg. Chem.* **1976**, *15*, 780. – [d] X-ray diffraction: P. R. Enjalbert, J. Galy, *Acta Crystallogr.* **1979**, *B35*, 546. – [e] X-ray diffraction: H. Hartl, M. Rama, *Z. Naturforsch.* **1979**, *34B*, 1035. – [f] See Table 5 for experimental data.

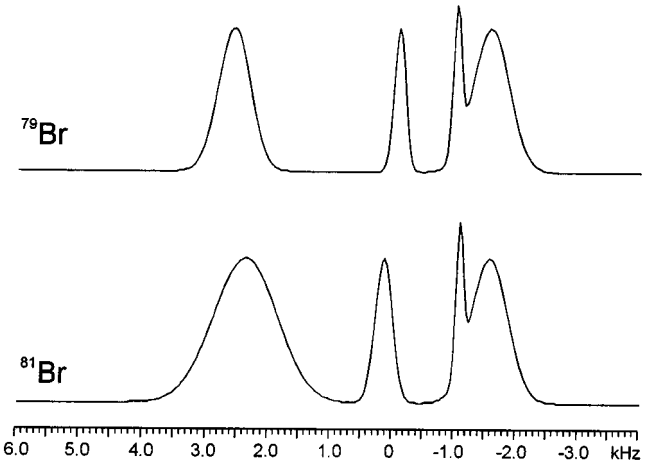


Figure 4. Schematic presentation of theoretical ^{31}P MAS NMR spectra resulting from second-order dipolar splittings with a single ^{81}Br and ^{79}Br nucleus (see text); the frequency scale is relative to the unperturbed ^{31}P resonance at 0 kHz

Cl_3PBBr_3 (**1**) compounds. ^{127}I has a nuclear spin of $S = 5/2$ and a very large C_Q [1931 MHz in I_3PBBr_3 (**5**)[8]] but no theoretical treatment of the dipolar interaction between spin-1/2 and spin-5/2 nuclei has been available so far. Since ^{35}Cl also has $S = 3/2$, the same calculations as considered above for Br_3PBBr_3 (**3**) were carried out for Cl_3PBBr_3 (**1**). The use of $C_Q = 60$ MHz[31] and $\nu_L = 39.2$ MHz for the ^{35}Cl nucleus and $r_{P-Cl} = 1.9$ Å results in the values $K = 0.383$ and $D = 668$ Hz. The theoretical spectrum derived from the data in Figure 3 of ref.[29] consists of two resonance lines that are 380 and 250 Hz wide and are separated by about 750 Hz. Considering the experimental line width of about 1400 Hz, these splittings cannot be resolved, which explains the observation of a single but slightly asymmetric resonance in the ^{31}P MAS NMR spectrum of Cl_3PBBr_3 (**1**) (Figure 3).

On complexing the phosphorus halide molecules with the boron halide the ^{31}P resonance is shifted significantly to higher field, the related "coordination shifts" $\Delta\delta_{coord} = \delta(X_3PBY_3) - \delta(PX_3)$ are summarized in Table 3. The upfield shift is largest for I_3PBI_3 (**6**) and decreases for the X_3PBBr_3 complexes in the order X = I > Br > Cl. However, the coordination shifts do not reflect the increasing charge transfer from the PX_3 donor to the BBr_3 acceptor groups (X = Cl > Br > I) and the concomitant increase of the ionicity of the P−X bonds in these compounds. The coordination shifts, on the other hand, have to be attributed to an increase of the heavy-atom effect at the four-coordinated phosphorus atom in the X_3PBY_3 complexes due to the increased s-character in the P−X bond.[20] Moreover, theoretical studies of NMR chemical shifts revealed that the chemical shift is largely determined by the topology of the electron density distribution at the atom rather than by its partial charge.[32]

Structure

Selected structural data for all X_3PBY_3 adducts (X = Cl, Br, I; Y = Br, I) and monomers are summarized in Table 4. The molecular structures of all species were fully optimized at the B3LYP level. Most of the P−B adducts were shown to possess stable minima at the B3LYP level (no imaginary frequencies), whereas a stable minimum could not be found for any of the X_3PBCl_3 adducts. All adducts possess C_{3v} symmetry with a staggered orientation of the BX_3 and PY_3 fragments. All structural parameters are in good agreement with those of other covalent P−B adducts.[10,11,12]

It should be noted, that the structures of such weakly bound systems may differ considerably between gas phase and the solid state.[33]

Br_3PBBr_3 (**3**, Figure 5) crystallizes in the orthorhombic space group *Pnma* with $Z = 4$. Single-crystal X-ray structure determination showed that the skeletal atoms of this molecule possess a slightly distorted C_{3v} symmetry with a staggered conformation. The P−B bond length was found to be 2.01(2) Å, which is significantly longer than in the corresponding phosphane−haloborane adducts R_3PBBr_3 (R = Me,[10] Ph,[12] $SiMe_3$[11]) and corresponds to a bond order of less than 1. This situation can be explained by the greater electron transfer within Me_3PBI_3 due to the positive inductive effect of the methyl groups, whereas in case of Br_3PBBr_3 and all the other X_3PBY_3 adducts the halogen Y decreases the donor strength of the P atom. In addition, the LP(Y) → σ*(BP) donor-acceptor interactions account for longer B−P distances and introduce a small amount of B−Y π bonding, which results in shorter B−Y distances.

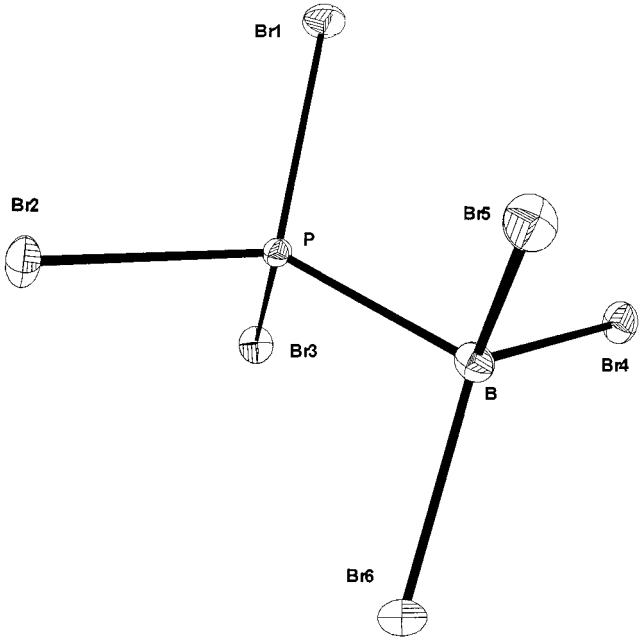


Figure 5. ORTEP plot of Br_3PBBr_3 (**3**)

Table 5 shows the comparison of bond lengths and bond angles of Br_3PBBr_3 (**3**) and the related phosphorus−boron adducts. The X-ray crystal data of **3** confirm that the Br−P−Br and Br−B−Br bond angles are significantly different from the experimental bond angles reported for Br_3PBBr_3 in a ^{81}Br NQR study.[9] The angles and B−Y and P−X distances in all adducts do not change much in the

different X_3PBY_3 species. However, there are more pronounced differences in the B−P distances.

Table 5. Selected bond lengths [Å] and angles [°] for Br_3PBBr_3 (**3**)

P−B[a]	2.01(2)	B−Br(4)[b]	1.96(2)
P−Br(1)	2.151(4)	B−Br(5)	1.99(1)
P−Br(2)	2.152(3)	B−Br(6)	1.99(1)
P−Br(3)	2.152(3)		
Br(1)−P−Br(2)[c]	106.6(1)	B−P−Br(1)	114.0(6)
Br(1)−P−Br(3)	106.6(1)	B−P−Br(2)	110.9(3)
Br(2)−P−Br(3)	107.5(2)	B−P−Br(3)	110.9(3)
Br(4)−B−Br(5)[d]	114.7(6)	Br(4)−B−P	104.1(8)
Br(4)−B−Br(6)	114.7(6)	Br(5)−B−P	104.2(6)
Br(5)−B−Br(6)	113.2(9)	Br(6)−B−P	104.2(6)

[a] Cf.: *d*(P−B) = 1.998(21) [$(SiMe_3)_3P{\cdot}BBr_3$];[11] 1.924(12) [$Me_3P{\cdot}BBr_3$];[10] 1.988(10) [$Ph_3P{\cdot}BBr_3$].[12] − [b] Cf.: *d*(B−Br) = 1.995(20) to 2.035(20) [$(SiMe_3)_3P{\cdot}BBr_3$];[11] 2.016(10) to 2.025(6) [$Me_3P{\cdot}BBr_3$];[10] 1.978(10) to 2.013(9) [$Ph_3P{\cdot}BBr_3$].[12] − [c] Cf.: ^{81}Br NQR study, <(Br−P−Br) = 107.0 (±0.1) to 109.1 (±0.3);[9] 108.3(9) to 109.7(10) [$(SiMe_3)_3P{\cdot}BBr_3$];[11] 110.0(5) to 110.6(4) [$Me_3P{\cdot}BBr_3$].[10] − [d] Cf.: ^{81}Br NQR study, <Br−B−Br = 111.2 (±0.1) to 111.5 (±0.1).[9]

The calculated B−Y bond lengths in all adducts are much longer than in the isolated BY_3 moieties. Upon complexation, the lengthening of the B−Y bonds increases from BBr_3 to BI_3 adducts. This can be attributed to the greater π bonding character of the B−Y bonds in the isolated BY_3 molecules than in the adducts which increases from I to Cl.

Upon coordination, the lone pair electrons on the P atom are partially donated, resulting in a shrinking of the P−X bonds (compared to the PX_3 fragment) and opening of the X−P−X angles. This shortening is related to the dramatically increasing "s" character in the P−X bond of the complex [e.g. $h_P(PI_3) \approx sp^{17.20}$ vs. $h_P(I_3PBI_3) \approx sp^{2.71}$].

Additionally, the more electronegative Cl ligands in PCl_3 lead to better orbital overlap due to orbital contraction and, therefore, to a better electron transfer and a shorter B−P bond length. This feature is in agreement with Durig and Shen's finding for the H_3PBH_3 (1.943 Å) and F_3PBH_3 (1.836 Å) complexes.[34]

Conclusion

The structure and the vibrational normal modes of phosphorus halide−boron halide complexes Cl_3PBBr_3 (**1**), Cl_3PBI_3 (**2**), Br_3PBBr_3 (**3**), Br_3PBI_3 (**4**), I_3PBBr_3 (**5**), and I_3PBI_3 (**6**) have been calculated, discussed and compared with the experimental values. Vibrational assignments have been made on the basis of the Raman and IR spectra in comparison with computational results. Our calculations agree reasonably with the experimental data.

Temperature-dependent Raman experiments indicate that halogen exchange cannot be observed as long as X is heavier than Y in X_3PBY_3 (e.g. in I_3PBBr_3). In contrast, halogen exchange occurs when Y is heavier (e.g. within Cl_3PBBr_3).

The adducts Cl_3PBBr_3 (**1**), Br_3PBBr_3 (**3**), I_3PBBr_3 (**5**), and I_3PBI_3 (**6**) have been characterized by solid-state ^{31}P MAS NMR spectroscopy. The solid-state ^{31}P MAS NMR spectra reveal an increasing upfield shift for the X_3PBY_3 complexes in the order X = Br < I and Y = Cl < Br < I due to heavy-atom effects. The ^{31}P MAS NMR of Br_3PBBr_3 (**3**) represents the first example of second order $^{31}P-^{79,81}Br$ dipolar coupling effects.

All P−B bond lengths are rather long due to destabilizing donor−acceptor interactions. The increasing s character of the P−X bond in the complexes results in a opening of the X−P−X angles.

Adduct structures that represent true minima were found for all X_3PBY_3 species except for the cases where BCl_3 was the Lewis acid.

Experimental Section

General Remarks: All compounds reported here are moisture-sensitive, some extremely so, and decompose within a few seconds if exposed to the atmosphere. Consequently, strictly anaerobic and anhydrous conditions were employed for their synthesis. Any subsequent manipulations were carried out inside a dry-box under dry nitrogen. PBr_3, PCl_3, PI_3, BBr_3, and BI_3 (all Aldrich) were used as received. CS_2 was refluxed with P_4O_{10} and distilled before used. − ^{31}P-NMR spectra were measured at 161.96 MHz with a BRUKER MSL-400 NMR spectrometer under magic-angle-spinning (MAS) conditions. A standard double-bearing MAS probe for 4-mm rotors was used with spinning frequencies up to 12 kHz. Single-pulse acquisition with 1-μs pulse width (corresponding to 25° flip angle) and 5-s pulse repetition was applied. The samples were filled in 4-mm zirconia rotors under nitrogen in a glove box. The spectra were referenced to 85% aqueous phosphoric acid. Simulations of spectra were carried out with the PC program WINFIT from the BRUKER WINNMR software package. − Raman spectra of powdered solid samples contained in glass capillary tubes were obtained with with a Perkin−Elmer 2000 NIR spectrometer in the range 800−50 cm^{-1}. The low-temperature spectra were recorded using a Ventacon low-temperature cell and the high-temperature spectra were obtained using a Ventacon high-temperature cell. − IR spectra of Nujol mulls between CsI plates were taken in the range 800−200 cm^{-1} with a Nicolet 520 FT IR spectrometer. − For the determination of decomposition points, samples were heated in sealed glass capillaries in a Büchi B450 instrument.

Cl_3PBBr_3 (1): Cl_3PBBr_3 was prepared by addition of BBr_3 (1.56 g, 6.23 mmol) to PCl_3 (1.57 g, 11.40 mmol) with stirring at −40 °C. A colorless solid formed immediately. After warming the mixture to −30 °C, the remaining PCl_3 was removed under dynamic vacuum. − Yield: 1.50 g (44%) of a colorless solid, m.p. 35−42 °C (decomp.).

Cl_3PBI_3 (2): Cl_3PBI_3 was prepared by addition of PCl_3 (1.57 g, 11.40 mmol) to BI_3 (0.92 g, 2.35 mmol) with stirring at −40 °C. A colorless solid formed immediately. After warming the mixture to −30 °C, the remaining PCl_3 was removed under dynamic vacuum. − Yield: 1.30 g (95%) of a colorless solid, m.p. 0 °C (decomp.). − *Note:* Compound **2** undergoes halogen exchange above 0 °C, as indicated by a change in color from colorless to yellow. The impurity at 673 cm^{-1} in the Raman spectrum of **2** is due to this halogen exchange.

Br_3PBBr_3 (3): Br_3PBBr_3 was prepared by addition of PBr_3 (1.66 g, 6.13 mmol) in CS_2 to CS_2 solutions of BBr_3 (1.76 g, 7.03 mmol) with stirring at −40 °C. A colorless solid formed immediately. After

stirring for 15 min, the solid was filtered off. Traces of the solvent were removed under dynamic vacuum at room temperature. − Yield: 2.64 g (83%) of a colorless solid, m.p. 61 °C (decomp.).

Br_3PBI_3 (4): Br_3PBI_3 was prepared by addition of PBr_3 (0.42 g, 1.55 mmol) in CS_2 to CS_2 solutions of BI_3 (0.61 g, 1.55 mmol) with stirring at −40 °C. A yellow solid formed immediately. After stirring for 15 min, the solid was filtered off. Traces of the solvent were removed under dynamic vacuum at room temperature. − Yield: 0.92 g (90%) of a yellow solid, m.p. 150 °C (decomp., halogen exchange).

I_3PBBr_3 (5): I_3PBBr_3 was prepared by addition of PI_3 (1.63 g, 3.95 mmol) in CS_2 to CS_2 solutions of BBr_3 (0.99 g, 3.95 mmol) with stirring at −40 °C. A yellow precipitate formed immediately. After stirring for 15 min, the precipitate was isolated by filtering twice and washing with CS_2. Traces of CS_2 were removed under dynamic vacuum at room temperature. − Yield: 2.90 g (51%) of a yellow solid, m.p. 158−160 °C (decomp.).

I_3PBI_3 (6): I_3PBI_3 was prepared by addition of PI_3 (1.24 g, 3.01 mmol) in CS_2 to CS_2 solutions of BI_3 (1.17 g, 3.01 mmol) with stirring at room temperature. An orange precipitate formed immediately. After stirring for 15 min, the precipitate was isolated by filtration and washed with CS_2 until the filtrate was colorless. Traces of CS_2 were removed under dynamic vacuum at room temperature. − Yield: 1.88 g (78%) of an orange solid, m.p. > 250 °C (decomp.).

Computational Methods: The structure and vibrational data for the phosphorus halide−boron halide complexes **1**−**6** were calculated using the density functional theory with the program package Gaussian 94.[35] For P and B a standard 6-31G(d) basis set was used and for I, Br, and Cl a quasi-relativistic pseudopotential (I: ECP46MWB; Br: ECP28MWB; Cl: ECP10MWB)[36] and a (5s5p1d)/[3s3p1d]-DZ+P basis set.[37] The computations were carried out at the DFT level using the hybrid method B3LYP, which includes a mixture of Hartree−Fock exchange with DFT exchange-correlation. Becke's 3 parameter functional, where the non-local correlation is provided by the LYP expression (Lee, Yang, Parr correlation functional), was used as implemented in Gaussian 94. For a concise definition of the B3LYP functional see ref.[38]

Crystal Structure Analysis of 3: BBr_6P, M = 521.24, crystal size: 0.40 × 0.10 × 0.10 mm, colorless prism, orthorhombic, space group *Pnma*, a = 12.195(3), b = 11.054(2), c = 7.053(1) Å, V = 850.8(4) Å^3, Z = 4, $d_{calcd.}$ = 3.641 Mg m^{-3}, μ = 25.418 mm^{-1}, $F(000)$ = 920. Siemens P4 diffractometer with CCD area detector, scan type: hemisphere, Mo-K_α, (λ = 0.71073 Å), T = 185 K, 2θ range = 6.68−55.20° in $-15 \le h \le 15$, $-11 \le k \le 11$, $-9 \le l \le 9$, reflections collected: 5006, independent reflections: 962 (R_{int} = 0.0634), observed reflections: 733 [$F > 4\sigma(F)$], T_{max}/T_{min} = 0.1854/0.0350. Structure solution and refinement program: SHELXL-97,[39] direct methods, data-to-parameter ratio: 22.4:1 (17.0:1 [$F > 4\sigma(F)$]), final R indices [$F > 4\sigma(F)$]: $R1$ = 0.0842, $wR2$ = 0.2131, $R1$ = 0.0976, $wR2$ = 0.2204 (all data), GOF on F^2 = 1.123, largest and mean Δ/σ: 0.000, 0.000, largest difference peak/hole: 2.666, −3.458 e Å^{-3}. − Further details of the crystal structure investigation may be obtained from the Fachinformationszentrum Karlsruhe, D-76344 Eggenstein-Leopoldshafen, Germany, on quoting the depository number CSD-41194.

Acknowledgments

We gratefully acknowledge the support of the Fonds der Chemischen Industrie and the University of Munich. We also wish to thank Mr. G. Spieß for his help with the Raman experiments and the Leibniz Rechenzentrum for a generous allocation of CPU time. In addition we would like to thank Prof. Martin Kaupp for valuable discussions. We would also like to thank both referees for helpful comments.

[1] J. Tarible, *C. R. Acad. Sci.* **1893**, *116*, 1521.
[2] E. Wiberg, K. Schuster, *Z. Anorg. Allg. Chem.* **1933**, *213*, 94.
[3] A. F. Armington, J. R. Weiner, G. H. Moates, *Inorg. Chem.* **1966**, *5*, 483.
[4] R. R. Holmes, *J. Inorg. Nucl. Chem.* **1960**, *12*, 266.
[5] A. H. Cowley, S. T. Cohen, *Inorg. Chem.* **1965**, *4*, 1200.
[6] R. F. Mitchell, J. A. Bruce, A. F. Armington, *Inorg. Chem.* **1964**, *3*, 915.
[7] G. W. Chantry, A. Finch, P. N. Gates, D. Steele, *J. Chem. Soc. A* **1966**, 896.
[8] H. Terao, T. Okuda, H. Negita, *Bull. Chem. Soc. Jpn.* **1978**, *51*, 710.
[9] H. Terao, M. Fukura, T. Okuda, H. Negita, *Bull. Chem. Soc. Jpn.* **1983**, *56*, 1728.
[10] D. L. Black, R. C. Taylor, *Acta Crystallogr.* **1975**, *B31*, 1116.
[11] M. S. Lube, R. L. Wells, P. White, *Inorg. Chem.* **1996**, *35*, 5007.
[12] F. Weller, M. Möhlen, K. Dehnicke, *New Cryst. Struct.* **1997**, *212*, 159.
[13] D. S. Payne, *Quart. Rev.* **1961**, *15*, 173.
[14] R. R. Holmes, *J. Chem. Educ.* **1963**, *40*, 125.
[15] cf. R. W. Parry, T. C. Bissot, *J. Am. Chem. Soc.* **1956**, *78*, 1524.
[16] D. Cook, *Can. J. Chem.* **1963**, *41*, 522.
[17] J. Tarible, *C. R. Acad. Sci.* **1901**, *132*, 204.
[18] M. Baudler, G. Fricke, *Z. Anorg. Allg. Chem.* **1963**, *319*, 212.
[19] M. L. Dewaulle, F. Francois, *C. R. Acad. Sci.* **1945**, *220*, 817.
[20] M. Kaupp, Ch. Aubauer, G. Engelhardt, T. M. Klapötke, O. L. Malkina, *J. Chem. Phys.* **1999**, *110*, 1729.
[21] Ch. Aubauer, T. M. Klapötke, A. Schulz, *Int. J. Vibr. Spectrosc.* **1999**, *3*, 4; (http://www.ijvs.com/volume3/edition2/section4.htm).
[22] Ch. Aubauer, G. Engelhardt, T. M. Klapötke, A. Schulz, *J. Chem. Soc., Dalton Trans.* **1999**, 1729.
[23] J. R. Durig, S. Riethmiller, V. F. Kalasinsky, J. D. Odom, *Inorg. Chem.* **1974**, *13*, 2729.
[24] J. D. Odom, S. Riethmiller, J. D. Witt, J. R. Durig, *Inorg. Chem.* **1973**, *12*, 1123.
[25] R. J. H. Clark, D. M. Rippon, *J. Mol. Spectrosc.* **1974**, *72*, 58.
[26] R. J. H. Clark, P. D. Mitchell, *J. Chem. Phys.* **1972**, *56*, 2225.
[27] H. Stammreich, R. Forneris, Y. Tavares, *J. Chem. Phys.* **1956**, *25*, 580.
[28] *Multinuclear NMR* (Ed.: J. Mason), Plenum Press, New York, **1989**, p. 454.
[29] E. M. Menger, W. S. Veeman, *J. Magn. Reson.* **1982**, *46*, 257.
[30] R. K. Harris, A. Root, *Mol. Phys.* **1989**, *66*, 993.
[31] *Nuclear Quadrupole Resonance in Chemistry* (Eds.: G. K. Semin, T. A. Babushkina, G. G. Yakobsen), Wiley, **1975**, p. 473.
[32] [32a] U. Pidun, M. Stahl, G. Frenking, *Chem. Eur. J.* **1996**, *2*, 869. − [32b] W. Kutzelnigg, U. Fleischer, M. Schindler, *NMR* **1990**, *23*, 165.
[33] [33a] R. Jürgens, J. Almlöf, *Chem. Phys. Lett.* **1991**, *276*, 263. − [33b] R. Ahlrichs, M. R. Bär, M. Häser, E. Sattler, *Chem. Phys. Lett.* **1991**, *184*, 353.
[34] J. R. Durig, Z. Shen, *J. Mol. Struct. (Theochem)* **1997**, *397*, 179.
[35] M. J. Frisch, G. W. Trucks, H. B. Schlegel, P. M. W. Gill, B. G. Johnson, M. A. Robb, J. R. Cheeseman, T. Keith, G. A. Peterson, J. A. Montgomery, K. Raghavachari, M. A. Al-Laham, V. G. Zakrzewski, J. A. Ortiz, J. B. Foresman, C. Y. Peng, P. Y. Ayala, W. Chen, M. W. Wong, J. L. Andres, E. S. Replogle, R. Gomperts, R. L. Martin, D. J. Fox, J. S. Binkley, D. J. Defrees, J. Baker, J. P. Stewart, M. Head-Gordon, C. Gonzales, J. A. Pople, *Gaussian 94*, Revision B.2, Gaussian, Inc., Pittsburgh, **1995**.
[36] [36a] P. Schwerdtfeger, M. Dolg, W. H. E. Schwarz, G. A. Bowmaker, P. D. W. Boyd, *J. Chem. Phys.* **1989**, *91*, 1762. − [36b] A.

Bergner, M. Dolg, W. Kuechle, H. Stoll, H. Preuss, *Mol. Phys.* **1993**, *80*, 1431.
[37] M. Kaupp, P. v. R. Schleyer, H. Stoll, H. Preuss, *J. Am. Chem. Soc.* **1991**, *113*, 1602.
[38] [38a] C. W. Bauschlicher, H. Partridge, *Chem. Phys. Lett.* **1994**, *231*, 277. − [38b] A. D. Becke, *J. Chem. Phys.* **1993**, *98*, 5648. − [38c] A. D. Becke, *Phys. Rev. A* **1988**, *38*, 3098. − [38d] C. Lee, W. Yang, R. G. Parr, *Phys. Rev. B* **1988**, *37*, 785. − [38e] S. H. Vosko, L. Wilk, M. Nusair, *Can. J. Phys.* **1980**, *58*, 1200. −
[39] G. M. Sheldrick, *SHELXL-97*, Program for Crystal Structure Determination, University of Göttingen, Germany, **1997**.

Received March 17, 2000
[I00099]

Aluminium Hydrazides: Dimeric Bis(*tert*-butyl)aluminium Hydrazides with Six-Membered Al_2N_4 and Five-Membered Al_2N_3 Heterocycles

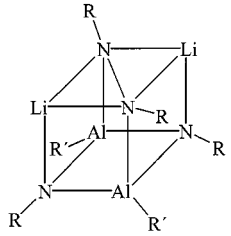
Werner Uhl,*[a] Jens Molter,[a] and Rainer Koch[b]

Keywords: Aluminium / Hydrazides / Heterocycles / Rearrangements / Ab initio calculations

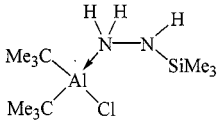
Treatment of the hydrazine adduct $(Me_3C)_2AlCl\cdot NH_2NHSiMe_3$ (**2**) with *n*-butyllithium afforded the colorless dialkylaluminium hydrazide $(Me_3C)_2AlN(SiMe_3)NH_2$ (**3**) by the release of butane and the precipitation of LiCl. Hydrazide **3** gave a dimer in solution and in the solid state. As shown by a crystal structure determination, a six-membered Al_2N_4 heterocycle with two intact endocyclic N–N bonds was formed by a head-to-tail dimerization. Upon sublimation of **3** in vacuum, a rearrangement was observed which gave an isomeric compound **4** after the migration of a hydrogen atom of a hydrazido ligand. The molecular core of **4** comprises a five-membered Al_2N_3 heterocycle, in which the Al atoms are bridged by one hydrazido ligand similar to **3**. The second ligand, however, has only one nitrogen atom in a bridging position with an exocyclic N–N bond. A similar compound (**5**) was obtained by the reaction of bis(*tert*-butyl)aluminium chloride with phenylhydrazine and *n*-butyllithium.

Introduction

Aluminium and gallium hydrazides found considerable interest in recent literature, because they are potentially useful as starting materials for the formation of the corresponding nitrides by chemical vapor deposition or by thermolysis of macroscopic samples. Several methods for the synthesis of those compounds were published, such as the treatment of hydrazines with trialkylelement compounds by the release of alkane,[1−3] the formation of hydrogen in a similar reaction by employing dialkylaluminium hydride[4] or $LiAlH_4$,[5] the reaction of lithium hydrazides with dialkylelement chlorides,[5,6] and the hydroalumination of azobenzene.[7] We tried to synthesize aluminium hydrazides by the reaction of dilithium bis(trimethylsilyl)hydrazide with dialkylaluminium chlorides. However, by partial cleavage of the N−N bonds, mixtures of products were formed from which cage compounds such as **1** were isolated in low yields (Scheme 1).[8] These cages contain a dimeric iminoalane, in which the Al_2N_2 heterocycle is bridged by a hydrazido ligand with an intact N−N bond. A heterocubane-type structure is formed by the addition of two lithium atoms. Boron hydrazides were obtained by the reaction of trimethylsilylhydrazine derivatives with boron halides[9] and the release of chlorotrimethylsilane. As was recently shown by our group, this method could not be applied to the synthesis of aluminium hydrazides.[10] Instead, bis(trimethylsilyl)hydrazine reacted with dialkylaluminium chlorides by dismutation to yield tris(trimethylsilyl)hydrazine and trimethylsilylhydrazine, which is thermally unstable[11] and was stabilized here by the formation of adducts **2** with the coordinatively unsaturated Al atoms (Scheme 1).[10] As is reported here, these adducts are excellent starting materials for the synthesis of aluminium hydrazides under mild conditions.



1 (R = $SiMe_3$; R′ = CMe_3)



2

Scheme 1

Results and Discussion

Reaction of the Adduct $(Me_3C)_2AlCl\cdot NH_2NHSiMe_3$ with *n*-Butyllithium

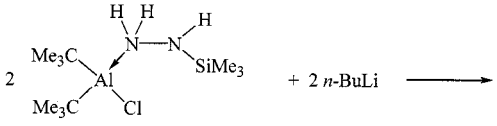
A suspension of the adduct $(Me_3C)_2AlCl\cdot NH_2NHSiMe_3$ (**2**) in *n*-hexane was treated with an equimolar quantity of *n*-butyllithium at −30 °C. A clear solution was formed upon heating the mixture to room temperature, and LiCl precipitated slowly by stirring the solution over a period of 12h. As shown by NMR spectroscopy, adduct **2** was completely consumed, and two products were formed in the ratio of 10 (**3**) to 1. This ratio remained unchanged despite many attempts at recrystallization from different solvents and at different temperatures. We assumed that compound **3** may exist in equilibrium with another species and may for instance dissociate in solution. Indeed, the concentration of the by-product increased with temperature, and at 80 °C we observed a ratio of about 3 (**3**) to 1. The similar reactions of adduct **2** with methyl- or *tert*-butyllithium gave the product **3** only in very poor yields, but in all cases the by-product was detected in almost the same ratio by NMR spectro-

[a] Fachbereich Chemie der Philipps Universität, Hans-Meerwein-Straße, 35032 Marburg, Germany
Fax: (internat.) + 49-6421/282-8917
[b] Fachbereich Chemie der Carl von Ossietzky Universität, Postfach 2503, 26111 Oldenburg, Germany

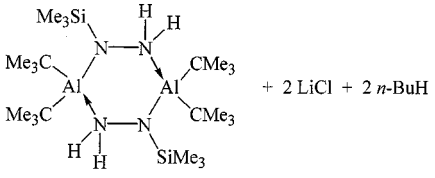
 © WILEY-VCH Verlag GmbH, D-69451 Weinheim, 2000 1434−1948/00/1010−2255 $ 17.50+.50/0

scopy. Some characteristics of this product are discussed below.

The mixture containing **3** as the main component was isolated in a yield of 69%. Compound **3** gave two singlets in the ^{1}H NMR spectrum, with an intensity ratio of 2:1 for the *tert*-butyl and trimethylsilyl hydrogen atoms. A single, broad resonance at $\delta = 4.32$ was assigned to the N−H protons. The integration gave one NH_2 group for each trimethylsilyl substituent, and thus one N−H proton had been removed from the adduct **2**. The composition of **3** as a dimeric dialkylaluminium hydrazide possessing a six-membered Al_2N_4 heterocycle was ascertained by a crystal structure determination (see below) and is depicted in Equation (1). As expected, the strong base *n*-butyllithium did not deprotonate the NH_2 moiety of adduct **2**, but the more acidic N−H proton of the $NH(SiMe_3)$ group, because an anion in this position is strongly stabilized by hyperconjugation[12] with the $SiMe_3$ substituent. The precipitation of lithium chloride led to the formation of an aluminium hydrazide, which gave a dimer owing to the presence of the NH_2 groups. The dimeric formula unit was also detected in benzene solution.

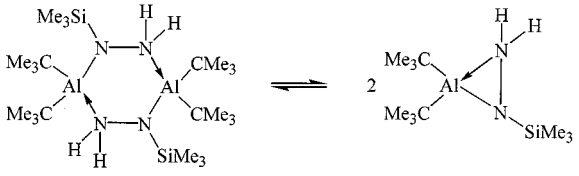


2



3

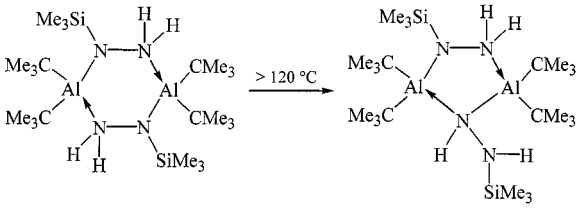
The by-product discussed above had two resonances for the $SiMe_3$ and CMe_3 hydrogen atoms in the intensity ratio of 1:2 ($\delta = 0.06$ and 1.29, respectively) similar to **3**, but two different resonances were now observed for two N−H protons at $\delta = 3.11$ and 2.68. In contrast to **3**, a strong dependence of the spectrum on temperature was observed. While the $SiMe_3$ singlet remained unchanged upon cooling of a solution in toluene to −80 °C, the resonance of the *tert*-butyl groups was split into two singlets ($\delta = 1.49$ and 1.24). The N−H protons gave a very broad resonance at +80 °C, which split into two resonances at about 50 °C. At 0 °C, two doublets were observed with chemical shifts of $\delta = 3.11$ and 2.68 and a coupling constant of $J = 4.6$Hz. We assume that this by-product results from partial dissociation of dimeric **3** into a monomeric species, which is favored in hot solutions [Equation (2)]. Its particular NMR data are in agreement with a three-membered AlN_2 heterocycle containing a dative $AlNH_2$ bond and a nonplanar environment of the negatively charged N atom, which is attached to the exocyclic trimethylsilyl group. A similar and still unpublished structure was recently observed by our group. The $SiMe_3$ substituent is thus neighbored by one hydrogen atom and one *tert*-butyl group, which causes the splitting of the corresponding resonances in the ^{1}H NMR spectrum. At higher temperature a rapid inversion of the configuration at that nitrogen atom occurs, which results in the equilibration of the hydrogen and the *tert*-butyl substituents in accordance with the observations in the temperature-dependent NMR spectra. The inversion barrier was estimated from these NMR data[13] to be about 65 kJ/mol. The low value of the molar mass of **3,** which was detected in benzene solution, may be caused by its partial dissociation. Other compounds are consistent with the NMR data. For instance, the dimeric aluminium hydrazide $[(Me_3C)_2Al-NH-NHSiMe_3]_2$ may be formed by a hydrogen shift in both hydrazido ligands. A similar shift was observed with compound **3** as discussed below, but in all cases the rearrangement was observed with only one hydrazido ligand of the dimer, even at an elevated temperature, and a prolonged reaction time in solution was required. That hydrogen shift is irreversible, and it seems quite implausible that the completely rearranged product may exist in a temperature-dependent equilibrium in our NMR experiment. Besides the resonances discussed so far, other signals with a very low intensity are observed in the NMR spectra. These are either characteristic of compound **4** (next section) or could not be assigned to a particular species (two resonances of equal intensity at $\delta = 3.78$).



3

Rearrangement of 3

Owing to the unknown structure of the by-product in all isolated samples of **3**, we tried to purify this product by sublimation under vacuum. Sublimation occurred at a temperature of 120−140 °C at 10^{-3} Torr. However, NMR spectroscopy showed that a new product (**4**) was formed in a yield of 97% [Equation (3)]. Compound **4** was also obtained by heating solutions of **3** in benzene at 70 °C for 12 h. According to the NMR spectroscopic characterization and crystal structure determination, a hydrogen shift occurred with one of the hydrazido ligands so that each of its nitrogen atoms was attached to one hydrogen atom. The size of the central heterocycle changed. A five-membered ring was now observed with one bridging hydrazido ligand similar to compound **3** and one rearranged hydrazido group, only one nitrogen atom of which is in a bridging position. The latter hydrazido group has an intact N−N bond with an exocyclic $NH(SiMe_3)$ group.



3 4

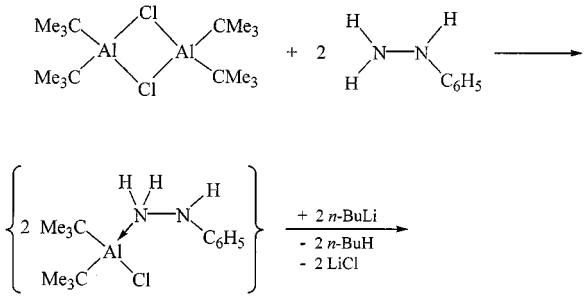
Owing to this particular molecular symmetry, which is retained in solution, we obtained a more complicated ^{1}H NMR spectrum. The $SiMe_3$ substituents, one attached to an endocyclic and the other bonded to an exocyclic nitrogen atom, gave rise to two resonances. Four different *tert*-butyl groups resulted owing to the chiral environment of the bridging nitrogen atom. Similarly, all N−H protons are chemically different and give rise to two AX spin systems by vicinal or geminal H−H coupling. The downfield resonances were assigned to the NH_2 group, because of their larger coupling constants and smaller differences in their chemical shifts. To the best of our knowledge, a similar rearrangement of a hydrazido ligand in oligomeric aluminium or gallium compounds has never been observed before. However, the shift of hydrogen atoms and silyl groups was observed in disilylhydrazine derivatives, where this process seems to be catalyzed by bases and leads to an equilibration of the 1,1- and 1,2-substituted species.[14]

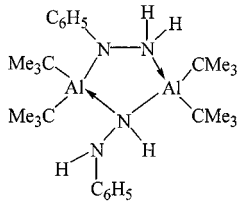
Reactions with Phenylhydrazine

Phenylhydrazine is insoluble in hexane, and all reactions were carried out in toluene as solvent. Treatment of bis(*tert*-butyl)aluminium chloride with phenylhydrazine yielded a colorless precipitate, which was soluble in warm toluene and which probably contained an adduct similar to compound **2** described above. It was not isolated here, but directly treated with *n*-butyllithium at room temperature. The ^{1}H NMR spectrum of the crude reaction product, which was obtained after filtration and evaporation of the solvent, showed that in contrast to the reaction of the trimethylsilyl derivative described above, a six-membered heterocycle was not formed. Instead, a rearranged compound analogous to **4** containing a five-membered heterocycle in its molecular center was obtained under mild conditions [**5**, Equation (4)]. After recrystallization from a mixture of toluene and *n*-hexane, colorless crystals of **5** were isolated. The NMR spectra of **5** were similar to those of compound **4** with four different *tert*-butyl resonances and two AX spin-systems of the N−H protons. Although we changed the reaction conditions such as temperature and solvents systematically, we never found any evidence for the formation of an intermediate analogous to **3** with a six-membered Al_2N_4 heterocycle.

Crystal Structures of Compounds 3, 4 and 5

Compound **3** crystallizes with two independent molecules in the unit cell, each of which is localized on a crystallographic center of symmetry. Both molecules are similar, and therefore only one of the molecular structures is depicted in Figure1. They possess centrosymmetric six-membered





5

Al_2N_4 heterocycles in their molecular centers, in which two hydrazido ligands bridge both aluminium atoms. Each Al atom has an Al−N bond to a N−$SiMe_3$ group and is further attached to one NH_2 group by a dative Al−N interaction. The heterocycles adopt a chair conformation. Similar structures with an endocyclic N−N bond are rare. One derivative was recently published by the group of Nöth with the compound $[Me_2AlN(SiMe_3)NH(CMe_3)]_2$.[5] Two six-membered Ga_2N_4 heterocycles were observed in the compound $[MeGa(\mu\text{-}NHNC_6H_5)_2GaMe]_2$, which adopts an overall hexagonal prismatic structure.[1] In most cases, however, only one nitrogen atom of the hydrazido group bridges two Al or Ga atoms with the N−N bond in an exocyclic position and the formation of E_2N_2 (E = Al, Ga) and Ga_3N_3 heterocycles.[1,3,4]

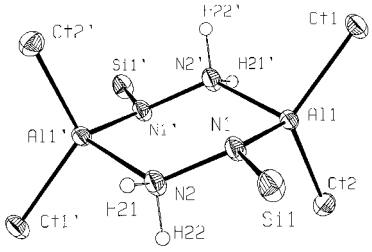


Figure 1. Molecular structure and numbering scheme of compound **3**; the thermal ellipsoids are drawn at the 40% probability level; methyl groups are omitted for clarity; hydrogen atoms with arbitrary radius; selected bond lengths [pm] and angles [°]: Al1−N1 186.7(1), Al1−N2 200.4(1), N1−N2 148.2(1), N1−Si1 174.4(1), Al2−N3 187.8(1), Al2−N4 199.8(1), N3−N4 148.3(2), N3−Si2 175.1(1); N2−Al1−N1 102.96(5), Al1−N1−N2 114.39(8), Al1−N1−Si1 131.14(6), N2−N1−Si1 109.23(8), N1−N2−Al1 126.69(8), N4−Al2−N3 102.84(5), Al2−N3−N4 111.80(8), Al2−N3−Si2 129.74(6), N4−N3−Si2 114.27(9), N3−N4−Al2 120.02(9)

The N−N bond lengths (148.2 pm on average) are similar to those usually observed in hydrazine derivatives,[15] in aluminium hydrazides[2−5,8,10] or in dilithium bis(trimethylsilyl)hydrazide.[16] The Al−N distances (187.2 and 200.1 pm) differ strongly. As expected, longer ones were observed

for the dative[17] bonds Al1−N2′ and Al2−N4′. The N atoms N2 and N4 of the NH_2 groups have a distorted tetrahedral coordination sphere, while the tricoordinated nitrogen atoms N1 and N3 attached to the Al and Si atoms deviate only slightly from planarity, with sums of the bond angles of 354.8° and 355.8°. As can be expected with a hyperconjugative interaction, the N−Si bond lengths are short (174.7 pm).

The compounds **4** (Figure 2), an isomer of **3**, and **5** (Figure 3) have five-membered Al_2N_3 heterocycles in their molecular centers. One hydrazido ligand bridges both Al atoms in a similar manner as in compound **3** with an intact NH_2 group, but only one nitrogen atom of the second ligand is in a bridging position, while the second nitrogen atom is part of an exocyclic $NH(SiMe_3)$ group. Thus, one hydrogen atom of the NH_2 group moved, and each N atom is attached to one H atom. To the best of our knowledge, a similar structure has not yet been observed. The heterocycles adopt a twisted conformation, as can be derived from the torsion angles in the ring[18] (clockwise starting with N1−N2: 34.9°, −25.3°, 7.5°, 6.8°, −25.0° of **4**; 45.4°, −34.1°, 8.4°, 9.3°, −32.1° of **5**).

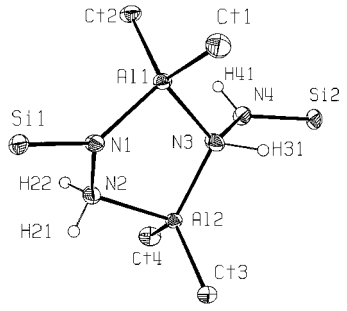


Figure 2. Molecular structure and numbering scheme of compound **4**; the thermal ellipsoids are drawn at the 40% probability level; methyl groups are omitted for clarity; hydrogen atoms with arbitrary radius; selected bond lengths [pm] and angles [°]: Al1−N1 188.5(2), Al1−N3 201.1(2), Al2−N2 200.3(2), Al2−N3 193.2(2), N1−N2 148.7(2), N3−N4 143.4(2), N1−Si1 174.4(2), N4−Si2 173.09(8); N1−Al1−N3 95.88(7), Al1−N3−Al2 112.64(7), N3−Al2−N2 93.34(7), Al2−N2−N1 115.2(1), N2−N1−Al1 114.0(1), Al1−N3−N4 116.2(1), Al2−N3−N4 115.2(1), Al1−N1−Si1 134.67(8), N2−N1−Si1 109.5(1)

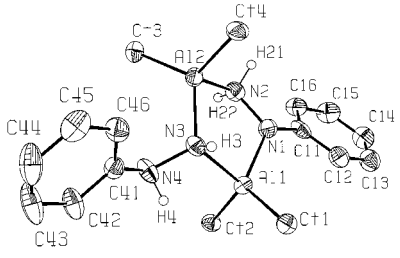


Figure 3. Molecular structure and numbering scheme of compound **5**; the thermal ellipsoids are drawn at the 40% probability level; methyl groups are omitted for clarity; hydrogen atoms with arbitrary radius; selected bond lengths [pm] and angles [°]: Al1−N1 193.9(3), Al1−N3 201.5(3), Al2−N2 205.9(2), Al2−N3 192.2(3), N1−N2 142.5(4), N3−N4 144.8(4), N1−C11 140.8(4), N4−C41 143.7(4); N1−Al1−N3 92.3(1), Al1−N3−Al2 113.3(1), N3−Al2−N2 93.3(1), Al2−N2−N1 109.7(2), N2−N1−Al1 115.7(2), Al1−N3−N4 108.5(2), Al2−N3−N4 114.5(2), Al1−N1−C11 124.5(2), N2−N1−C11 111.9(3)

The exocyclic N−N bond of compound **4** is shorter (N3−N4 143.4 pm) than the endocyclic one (N1−N2 148.7 pm), which resembles that of the hydrazido bridges in **3**. The reverse situation was observed for the phenylhydrazine derivative **5**, which had the shortest N−N bond in the ring (N1−N2 142.5 pm; N3−N4 144.8 pm). This observation may reflect the different charge separation in the molecules with a more effective charge-transfer to the phenyl group than to the trimethylsilyl group. Indeed, the phenyl groups are almost ideally in plane with the N−N bonds to allow mesomeric stabilization (torsion angles N1−N2−C11−C12 167.2°, N1−N2−C11−C16 −15.0°; −162.8° and 20.7° for the second phenyl group). The C−N bond to the anionic nitrogen atom [140.8(4) pm] is slightly shorter than that to the exocyclic nitrogen atom [143.7(4) pm]. The N−Si bonds of **4** are similar (N1−Si1 174.4 pm and N4−Si2 173.1 pm) and comparable with those observed for **3**. Each Al atom of both compounds is coordinated by two N atoms with alternating short and long bond lengths. The distances to the bridging nitrogen atom N3 are very similar [201.3 (Al1) and 192.7 pm (Al2) on average for both compounds **4** and **5**], but the distances to the hydrazido bridges differ with larger separations to the phenyl hydrazido group (**4**: Al1−N1 188.5 pm; Al2−N2 200.3 pm; **5**: Al1−N1 193.9 pm; Al2−N2 205.9 pm).

Quantum Mechanical Calculations

Two of the main issues of the preceding experimental findings are the rearrangement of compound **3** to give the five-membered ring **4** and the appearance of a by-product with an AlN_2 ring core. Previous studies on aluminium-containing molecules have shown that the application of the HF/6−31G* method/basis set combination gives good agreement with experimental structural data.[8,19,20] Larger basis sets led only to a slight improvement of the description of geometries and their use is not essential for our investigation.[19,20] We extended our current study to including density functional theory methods (in particular the hybrid functional approach Becke3LYP) and, where applicable, also to second-order perturbation theory (MP2) in order to assess the performance of the above methods for the calculation of relative energies. These studies were restricted to those compounds which had methyl instead of *tert*-butyl groups and *N*-silyl (SiH_3) instead of *N*-trimethylsilyl substituents (**3a**, **4a**).

The rearrangement of compound **3** which may exist in both a chair or a twist-boat conformation leads to the five-membered ring **4**. When considering a second migration, a four-membered ring, **6**, is formed with two rearranged hydrazido groups and only one nitrogen atom of each ligand bridging both Al atoms. The results of the Hartree−Fock and B3LYP calculations are summarized in Figure 4 and Table 1. It can be seen clearly that once again the Hartree−Fock-predicted geometrical data of **3a** and **4a** agree well with the experimental structures. The same is true for the DFT-calculated geometry which is slightly better for contacts not involving Al. As for the relative energies of the four isomeric structures, both methods give the

same energetic ordering with almost identical differences separating the compounds: The five-membered ring **4a** is found to be the most stable isomer, followed by the chair conformation of **3a**. The least likely structures are the twist-boat conformation of **3a** and the Al_2N_2 heterocycle **6**. These data suggest that the rearrangement of **3** will indeed lead to **4**, which is thermodynamically favored over the former and over the completely rearranged compound **6**.

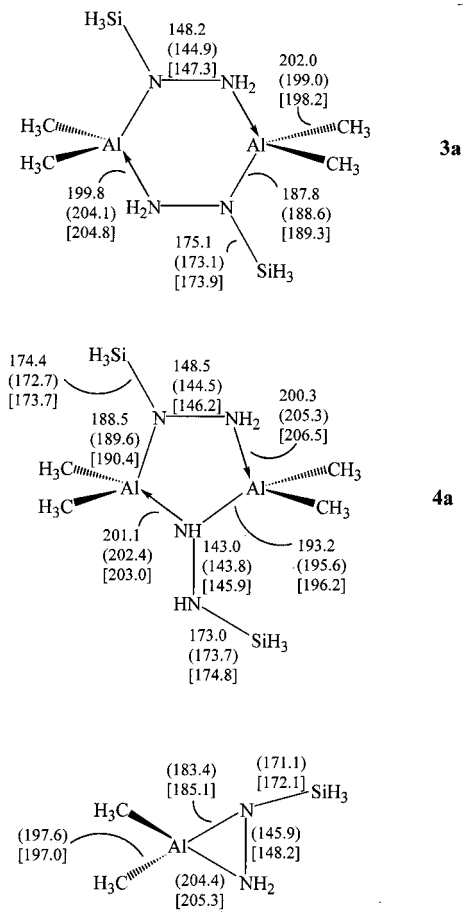
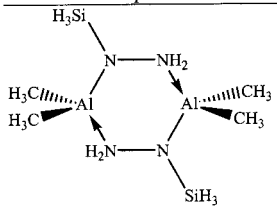
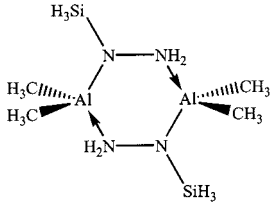
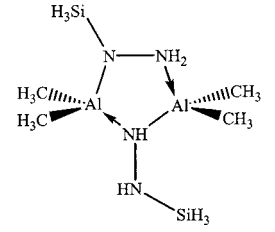
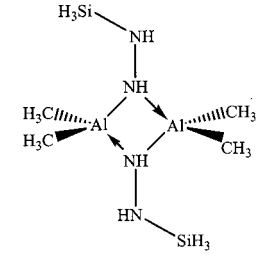


Figure 4. Selected bond lengths [pm] of compounds **3a**, **4a** and of the monomer of **3a** (experimental data without brackets, HF/6−31G* data in round brackets, B3LYP/6−31G* data in square brackets)

The existence of the second molecule which is in equilibrium with **3** [Equation (2)] and which is probably a monomer was also examined by means of quantum chemical methods. Five isomeric structures of this monomeric compound were calculated at the HF, the B3LYP and the MP2 level of theory (Table 2, structural parameters Figure 4). The most stable isomer is indeed the three-membered ring structure which has been previously assumed. It is favored over the next stable molecules by almost 20 kJ/mol. These results clearly show that if dissociation of **3** occurs, it will form the above-mentioned AlN_2 heterocycle. However, this process is calculated to be endothermic by almost 150 kJ/mol at 0 K. The entropy advantage reduces this difference to a surmountable barrier of 72 kJ/mol at 298 °C (laboratory conditions).

Table 1. Calculated relative energies [kJ/mol] with HF/6−31G* ZPVE corrections of compounds **3a**, **4a**, and **6**

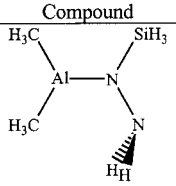
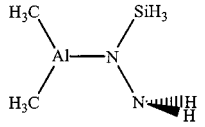
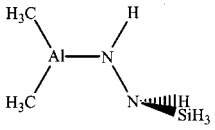
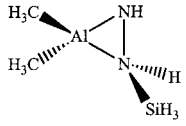
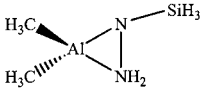
Compound	HF/6-31G*	B3LYP/6-31G*
 **3a** chair conformation	0.0	0.0
 **3a** twistboat conformation	7.4	8.4
 **4a**	-2.4	-2.0
 **6**	7.8	9.0

It is interesting to note that the HF and the DFT approach are both suitable for the examination of the compounds reported here. Not only are the calculated geometries of comparable quality, but the relative HF and B3LYP energies of both series of monomeric and dimeric structures are also very close. This finding confirms previous observations with similar calculations.[19]

Experimental Section

General: All procedures were carried out under purified argon in dried solvents (toluene with Na/benzophenone; *n*-hexane with $LiAlH_4$). The adduct **2**, bis(trimethylsilyl)hydrazine and $(Me_3C)_2AlCl$ were synthesized as described in refs.[10,11,21]. Phenylhydrazine (Aldrich) was distilled prior to use, and the solution of *n*-butyllithium in *n*-hexane (Aldrich) was used without further purification.

Table 2. Calculated relative energies [kJ/mol] with HF/6−31G* ZPVE corrections of the monomeric isomers

Compound	HF/6-31G*	B3LYP/6-31G*	MP2/6-31G*
	0.0	0.0	0.0
	0.6	-0.6	0.6
	6.5	7.0	13.1
	17.6	18.5	10.2
	-17.4	-17.1	-20.0

Synthesis of (μ-2,2-Dihydro-1-trimethylsilylhydrazido-1κN¹:2κN²)-(μ-2,2-dihydro-1-trimethylsilylhydrazido-2κN¹:1κN²)bis[di(*tert*-butyl)aluminium] (3): A cooled (−30 °C) suspension of the adduct **2** (1.52g, 5.43mmol) in *n*-hexane (40mL) was treated with a solution of *n*-butyllithium in hexane (1.6 M, 3.4mL, 5.43mmol). The mixture was slowly warmed to room temperature, stirred for 12 h, filtered and concentrated. The residue was dissolved in a small volume of *n*-hexane. Colorless crystals of **4** (0.91g, 69%) were obtained on cooling the solution to −50 °C. − M.p. (argon, sealed capillary): 192 °C (dec.). − ^{1}H NMR (C_6D_6, 300MHz, 298K): δ = 0.15 (s, 18 H, $SiMe_3$), 1.11 (s, 36 H, CMe_3), 4.32 (s, 4 H, NH_2). − ^{13}C NMR (C_6D_6, 100.6MHz): δ = 0.25 ($SiMe_3$), 16.2 (AlC), 31.9 (C*Me*$_3$). − IR (CsBr, paraffin): ν = 3272 (w) cm^{-1}, 3243 (w), 3215 (w), 3201 (vw, νNH), 2925 (vs), 2855 (vs), 2726 (w), 2700 (w, paraffin, νCH_3), 1564 (m, δNH), 1462 (vs), 1378 (s, paraffin) 1285 (m), 1255 (s), 1231 (s, δCH_3), 1177 (w), 1000 (m), 972 (m), 955 (m), 901 (s, νC_3C), 868 (s), 836 (vs), 810 (s), 747 (s, ρCH_3) 677 (w, ν_{as}SiC) 626 (m, ν_sSiC), 579 (m), 547 (m), 511 (w), 493 (w, νAlC, νAlN), 403 (w), 357 (w, δSiC). − MS (EI); *m/z* (%): 431.3 (41) [$M^+ - C_4H_9$], 244.0 (58) [1/2 M^+]. − $C_{22}H_{58}Al_2N_4Si_2$ (488.86): calcd. Al 11.0; found Al 10.8. − Mol. mass: 450 (cryoscopically in benzene). − NMR characterization of the by-product: ^{1}H NMR ([D$_8$]toluene, 300MHz, 353K): δ = 0.08 (s, 18 H, $SiMe_3$), 1.23 (s, 36 H, CMe_3), 2.86 (br., 2 H, NH_2). − ^{1}H NMR ([D$_8$]toluene, 300MHz, 273K): δ = 0.06 (s, 9 H, $SiMe_3$), 1.29 (s, 18 H, CMe_3), 2.68 and 3.11 (each d, $^2J_{HH}$ = 4.6Hz, 1 H, NH). − ^{1}H NMR ([D$_8$]toluene, 300MHz, 193K): δ = 0.04 (s, 9 H, $SiMe_3$), 1.24 and 1.49 (each s, 9 H, CMe_3), 2.73 and 3.05 (each s, br., 1 H, NH).

Synthesis of (μ-2,2-Dihydro-1-trimethylsilylhydrazido-1κN¹:2κN²)-(μ-1,2-dihydro-2-trimethylsilylhydrazido-1κN¹:2κN¹)bis[di(*tert*-butyl)aluminium] (4): Compound **5** (1.12g, 2.29mmol) was sublimed in vacuo (10^{-3} Torr) at a bath temperature of 120−140 °C to yield the pure product **6**. In a similar procedure, **6** was obtained directly from the crude product of the synthesis of **5** (1.09g, 97%). − M.p. (argon, sealed capillary): 56 °C. − ^{1}H NMR (C_6D_6, 300MHz): δ = 0.11 and 0.13 (each s, 9 H, $SiMe_3$), 1.10, 1.15, 1.20 and 1.26 (each s, 9 H, CMe_3), 2.78 and 3.15 (each d, $^3J_{HH}$ = 5.3Hz, 1 H, NH of the 1,1-bridging hydrazido ligand), 3.94 and 4.13 (each d, $^2J_{HH}$ = 11Hz, 1 H, NH of the 1,2-bridging hydrazido ligand). − ^{13}C NMR (C_6D_6, 75.5MHz): δ = 0.1 and −0.1 ($SiMe_3$), 14.3 and 18.3 (AlC), 31.94, 32.68 and 32.73 (C*Me*$_3$, the first resonance has double the intensity of the last two signals). − IR (CsBr, paraffin): ν = 3397 (w) cm^{-1}, 3277 (vw), 3248 (w), 3206 (vw, νNH), 2953 (vs), 2924 (vs), 2853 (vs), 2834 (vs), 2764 (w), 2729 (w), 2704 (w), 2625 (vw) paraffin, νCH; 1568 (m, δNH) 1466 (vs), 1377 (s, paraffin), 1358 (s), 1296 (w), 1254 (vs, δCH_3), 1209 (m), 1179 (w), 1113 (sh), 1045 (s), 1003 (m), 953 (m), 937 (m, νC_3C), 895 (vs), 839 (vs), 810 (vs), 748 (s, ρCH_3), 719 (m), 675 (m), 652 (s, ν_{as}SiC), 627 (m), 615 (m), 604 (m, ν_sSiC, νSiN), 575 (m), 550 (m), 517 (m), 476 (m), 467 (sh), 421 (m), 401 (m, νAlC, νAlN), 347 (w, δSiC). − MS (EI); *m/z* (%): 431.7 (18) [$M^+ - C_4H_9$], 244.2 (33) [1/2 M^+]. − $C_{22}H_{58}Al_2N_4Si_2$ (488.86): calcd. Al 11.0; found Al 10.9. − Mol. mass: 478 (cryoscopically in benzene).

Synthesis of (μ-2,2-Dihydro-1-phenylhydrazido-1κN¹:2κN²)(μ-1,2-dihydro-2-phenylhydrazido-1κN¹:2κN¹)bis[di(*tert*-butyl)aluminium] (5): A solution of of bis(*tert*-butyl)aluminium chloride (3.27g, 18.5mmol) in toluene (20mL) was added to a cooled (0 °C) solution of phenylhydrazine (2.00g, 18.5mmol) in toluene (40mL). The mixture was warmed to room temperature and stirred until the precipitate was completely dissolved. A mixture of a solution of *n*-butyllithium in *n*-hexane (1.6 M, 11.6mL, mmol) and toluene (20mL) was added. After stirring at room temperature for 5 h, LiCl was filtered off, and the solvent was removed under vacuum. The residue was treated with a mixture of toluene and *n*-hexane (50mL, 1:1) and filtered. The filtrate was concentrated and gave the colorless product **5** (2.77g, 60%) upon cooling to 0 °C. − M.p. (argon, sealed capillary): 146 °C. − ^{1}H NMR (C_6D_6, 300MHz): δ = 0.99, 1.16, 1.23 and 1.32 (each s, 9 H, CMe_3), 3.96 (d, $^3J_{HH}$ = 3.1Hz, 1 H, NH of the 1,2-bridging hydrazido ligand), 4.44 and 4.64 (each d, $^2J_{HH}$ = 10.7Hz, 1 H, NH of the 1,2-bridging hydrazido ligand), 5.48 (d, $^3J_{HH}$ = 3.1Hz, 1 H, NH of the 1,1-bridging hydrazido ligand), 6.64, 6.68, 6.70, 6.74, 6.80, 6.82 and 6.86 (all phenyl, not able to to assign further owing to the overlap of resonances), 7.28 and 7.13 (pseudo-t, line distance 7.7Hz). − ^{13}C NMR (C_6D_6, 75.5MHz): δ = 33.1, 33.5, 33.8 and 34.4 (C*Me*$_3$), 113.5, 114.5, 120.9, 123.4, 131.9, 132.0, 151.0 and 155.0 (all phenyl), AlC not detected. − IR (CsBr, paraffin): ν = 3394 cm^{-1} (w), 3349 (w), 3218 (w), 3183 (w), 3132 (vw, νNH), 2956 (vs), 2924 (vs), 2854 (vs), 2730 (w), 2701 (w, paraffin, νCH), 1600 (m, phenyl), 1578 (m, δNH), 1463 (vs), 1378 (s, paraffin), 1308 (m), 1259 (s, δCH_3), 1220 (m), 1180 (w), 1155 (w), 1091 (vw), 1082 (w), 1040 (w), 986 (m), 930 (w), 870 (m), 809 (m), 749 (s), 723 (w, νCN, νC_3C, ρCH_3), 686 (s), 675 (m), 601 (w, δphenyl), 564 (w), 539 (m), 523 (w), 464 (w), 435 (w, νAlC, νAlN), 412 (w), 371 (vw), 338 (w, δC_3C). − MS (EI); *m/z* (%): 439.3 (1) [$M^+ - C_4H_9$], 325.1 (100) [$M^+ - 3\ C_4H_9$], 248.0 (5) [1/2 M^+]. − $C_{28}H_{50}Al_2N_4$ (496.69): calcd. Al 10.9; found Al 10.6.

Crystal Structure Determinations: Single crystals of the compounds **3** and **4** were obtained by recrystallization from *n*-hexane. Compound **5** was recrystallized from a mixture of toluene and *n*-hexane. Crystal data and structure refinement parameters are given in Table3.[24] Compound **4** showed a disorder of the exocyclic N4−$SiMe_3$ group. Its atoms were refined in split positions with occupancy factors of 0.70 and 0.30. The atoms of the minor com-

Table 3. Crystal data, data collection parameters and structure refinement of compounds **3**, **4** and **5**

	3	**4**	**5**
Formula	$C_{22}H_{58}Al_2N_4Si_2$	$C_{22}H_{58}Al_2N_4Si_2$	$C_{28}H_{50}Al_2N_4$
Crystal system	triclinic	monoclinic	monoclinic
Space group	$P\bar{1}$; No. 2[22]	$P2_1/c$; No. 14[22]	$I2/a$; No. 15[22]
Z	2	4	16
Temperature [°C]	−80	−80	−80
$d_{calcd.}$ [g/cm^3]	1.012	1.023	1.069
a [pm]	1097.4(1)	903.5(2)	3196.4(1)
b [pm]	1235.5(1)	1764.6(4)	1175.18(4)
c [pm]	1248.4(1)	2013.5(4)	3375.01(8)
α [°]	102.38(1)	90	90
β [°]	92.83(1)	98.76(3)	103.092(3)
γ [°]	102.69(1)	90	90
V [10^{-30} m^3]	1604.7(3)	3173(1)	12348.0(7)
μ [mm^{-1}]	0.146	0.182	0.115
Crystal size [mm]	0.90 × 0.68 × 0.44	0.55 × 0.50 × 0.50	0.35 × 0.30 × 0.24
Diffractometer		Stoe-IPDS	
Radiation		Mo-K_α, graphite monochromator	
2Θ range [°]	5.38 ≤ 2Θ ≤ 52.2	4.1 ≤ 2Θ ≤ 52.0	4.0 ≤ 2Θ ≤ 52.0
Index ranges	−13 ≤ h ≤ 13	−11 ≤ h ≤ 11	−39 ≤ h ≤ 38
	−15 ≤ k ≤ 15	−21 ≤ k ≤ 21	−14 ≤ k ≤ 14
	−15 ≤ l ≤ 15	−24 ≤ l ≤ 24	−38 ≤ l ≤ 38
Independent reflections	5820	6159	11331
Reflections $F > 4\sigma(F)$	4911	4677	6137
Parameters	305	320	707
$R = \Sigma\|\|F_o\| - \|F_c\|\|/\Sigma\|F_o\|$ $[F > 4\sigma(F)]$	0.0340	0.0395	0.0596
$wR^2 = [\Sigma w(F_o^2 - F_c^2)^2/\Sigma w(F_o^2)^2]^{1/2}$ (all data)	0.0982	0.1176	0.1687
Max./min. residual [10^{30} e/m^3]	0.34/−0.21	0.35/−0.28	0.72/−0.42

ponent were refined isotropically with restrictions of bond lengths and angles. Two *tert*-butyl groups of compound **5** (CT4 and CT7) were rotationally disordered, the methyl groups were refined with restrictions of bond lengths and angles and occupancy factors of 0.64 and 0.36. Program: SHELXTL-Plus, SHELXL-93[23] solutions by direct methods; full-matrix refinement with all independent structure factors.

Quantum Chemical Calculations: The Hartree−Fock[25] method (including electron correlation at the MP2(fc) level of theory) and the Becke3LYP[26] approach in combination with the 6−31G* basis set were used to optimize the ground-state structure and to characterize the bonding situation. The located structures were confirmed as minima through calculation and analysis of the vibrational frequencies (HF/6−31G*). The energies given in Tables1 and 2 include the scaled zero-point vibrational energy corrections. All calculations were carried out with the GAUSSIAN 98 system of programs.[27]

Acknowledgments

We are grateful to the Deutsche Forschungsgemeinschaft and the Fonds der Chemischen Industrie for generous financial support.

[1] D. W. Peters, E. D. Bourret, M. P. Power, J. Arnold, *J. Organomet. Chem*. **1999**, *582*, 108−115; D. W. Peters, M. P. Power, E.D. Bourret, J. Arnold, *Chem. Commun*. **1998**, 753−754.

[2] V. C. Gibson, C. Redshaw, A. J. P. White, D. J. Williams, *Angew. Chem*. **1999**, *111*, 1014−1016; *Angew. Chem. Int. Ed*. **1999**, *38*, 961−964.

[3] Y. Kim, J. H. Kim, J. E. Park, H. Song, J. T. Park, *J. Organomet. Chem*. **1997**, *545−546*, 99−103; D. Cho, J. E. Park, B.-J. Bae, K. Lee, B. Kim, J. T. Park, *J. Organomet. Chem.* **1999**, *592*, 162−167.

[4] J. S. Silverman, C. D. Abernethy, R. A. Jones, A. H. Cowley, *Chem. Commun.* **1999**, 1645−1646.

[5] H. Nöth, T. Seifert, *Eur. J. Inorg. Chem*. **1998**, 1931−1938.

[6] D. A. Neumayer, A. H. Cowley, A. Decken, R. A. Jones, V. Lakhotia, J. G. Ekerdt, *Inorg. Chem*. **1995**, *34*, 4698−4700.

[7] R. J. Wehmschulte, P. P. Power, *Inorg. Chem.* **1996**, *35*, 2717−2718.

[8] W. Uhl, J. Molter, R. Koch, *Eur. J. Inorg. Chem.* **1999**, 2021−2027.

[9] K. Niedenzu, P. Fritz, W. Weber, *Z. Naturforsch., B* **1967**, *22*, 225−226.

[10] W. Uhl, J. Molter, W. Saak, *Z. Anorg. Allg. Chem.* **1999**, *625*, 321−328.

[11] U. Wannagat, W. Liehr, *Z. Anorg. Allg. Chem*. **1958**, *297*, 129−136; U. Wannagat, *Adv. Inorg. Chem. Radiochem*. **1964**, *6*, 225−278; U. Wannagat, W. Liehr, *Angew. Chem*. **1957**, *69*, 783.

[12] R. Steudel, *Chemie der Nichtmetalle*, Walter de Gruyter, Berlin, **1998**; T. M. Klapötke, I. C. Tornieporth-Oetting, *Nichtmetallchemie*, VCH, Weinheim, **1994**.

[13] H. Günther, *NMR-Spektroskopie*, Georg Thieme Verlag, Stuttgart, **1983**, p. 229.

[14] R. E. Bailey, R. West, *J. Am. Chem. Soc*. **1964**, *86*, 5369−5370; R. West, M. Ishikawa, R. E. Bailey, *J. Am. Chem. Soc*. **1966**, *88*, 4648−4652; R. West, M. Ishikawa, R. E. Bailey, *J. Am. Chem. Soc*. **1967**, *89*, 4068−4072; R. West, *Pure Appl. Chem*. **1969**, *19*, 291−307.

[15] K. Bode, U. Klingebiel, *Adv. Organomet. Chem*. **1996**, *40*, 1−43; S. Dielkus, C. Drost, R. Herbst-Irmer, U. Klingebiel, *Angew. Chem*. **1993**, *105*, 1689−1690; *Angew. Chem. Int. Ed. Engl.* **1993**, *32*, 1625−1626; C. Glidewell, D. W. H. Rankin, A. G. Robiette, G. M. Sheldrick, *J. Chem. Soc., A* **1970**, 318−320; Y. Morino, T. Iijima, Y. Murata, *Bull. Chem. Soc. Jpn.* **1960**, *33*, 46−48.

[16] K. Bode, C. Drost, C. Jäger, U. Klingebiel, M. Noltemeyer, Z. Zak, *J. Organomet. Chem*. **1994**, *482*, 285−292; C. Drost, C. Jäger, S. Freitag, U. Klingebiel, M. Noltemeyer, G. M. Sheldrick, *Chem. Ber*. **1994**, *127*, 845−847; N. Metzler, H. Nöth, H. Sachdev, *Angew. Chem*. **1994**, *106*, 1837−1839; *Angew. Chem. Int. Ed. Engl*. **1994**, *33*, 1746−1748; E. Gellermann, U. Klingebiel, M. Schäfer, *Z. Anorg. Allg. Chem.* **2000**, *626*, 1131−1136.

[17] A. Haaland, in *Coordination Chemistry of Aluminum* (Ed.: G. H. Robinson), VCH, Weinheim, **1993**. Further recent examples for dative versus covalent ionic Al−N interactions: K. Kincaid, C. P. Gerlach, G. R. Giesbrecht, J. R. Hagadorn, G. D. Whitener, A. Shafir, J. Arnold, *Organometallics* **1999**, *18*, 5360−5366; N. Emig, F. P. Gabbaï, H. Krautscheid, R. Réau, G. Bertrand, *Angew. Chem.* **1998**, *110*, 1037−1040; *Angew. Chem. Int. Ed. Engl*. **1998**, *37*, 989−992; W. Uhl, F. Hanne-

mann, W. Saak, R. Wartchow, *Eur. J. Inorg. Chem.* **1999**, 771−776; N. Emig, H. Nguyen, H. Krautscheid, R. Réau, J.-B. Cazaux, G. Bertrand, *Organometallics* **1998**, *17*, 3599−3608; D. A. Atwood, J. A. Jegier, M. P. Remington, D. Rutherford, *Austr. J. Chem*. **1996**, *49*, 1333−1338; I. Krossing, H. Nöth, H. Schwenk-Kircher, *Eur. J. Inorg. Chem*. **1998**, 927−939.

[18] R. Allmann, in: A. L. Rheingold, *Homoatomic Rings, Chains and Macromolecules of Main-Group Elements*, Elsevier, Amsterdam, **1977**.

[19] W. Uhl, T. Spies, R. Koch, W. Saak, *Organometallics* **1999**, *18*, 4598−4602.

[20] J. Müller, U. Ruschewitz, O. Indris, H. Hartwig, W. Stahl, *J. Am. Chem. Soc*. **1999**, *121*, 4647−4652.

[21] W. Uhl, J. Wagner, D. Fenske, G. Baum, *Z. Anorg. Allg. Chem*. **1992**, *612*, 25−34; H. Lehmkuhl, O. Olbrysch, H. Nehl, *Liebigs Ann. Chem*. **1973**, 708−714.

[22] *International Tables for Crystallography, Space Group Symmetry* (Ed.: T. Hahn), Kluwer Academic Publishers, Dordrecht-Boston-London, **1989**, vol. A.

[23] *SHELXTL-Plus, Release 4.2* for Siemens R3 Crystallographic Research Systems, Siemens Analytical X-ray Instruments Inc., Madison, USA, **1990**; G. M. Sheldrick, *SHELXL-93*, *Program for the Refinement of Structures*, Universität Göttingen, **1993**.

[24] The crystallographic data of **3**, **4** and **5** (excluding structure factors) were deposited with the Cambridge Crystallographic Data Centre as supplementary publication no. CCDC-139526 (**3**), -139527 (**4**) and -139528 (**5**). Copies of the data can be obtained free of charge on application to CCDC, 12 Union Road, Cambridge CB2 1EZ, UK (Fax: internat. + 44-1223/336-033; E-mail: deposit@ccdc.cam.ac.uk).

[25] W. J. Hehre, L. Radom, P. v. R. Schleyer, J. A. Pople, Ab initio *Molecular Orbital Theory*; Wiley, New York, **1986**.

[26] [26a] C. Lee, W. Yang, R.G. Parr, *Phys. Rev.* **1988**, *B37*, 785−789. − [26b] A. D. Becke, *J. Chem. Phys.* **1993**, *98*, 5648−5652.

[27] M. J. Frisch, G. W. Trucks, H. B. Schlegel, G. E. Scuseria, M. A. Robb, J. R. Cheeseman, V. G. Zakrzewski, J. A. Montgomery, R. E. Stratmann, J. C. Burant, S. Dapprich, J. M. Millam, A. D. Daniels, K. N. Kudin, M. C. Strain, O. Farkas, J. Tomasi, V. Barone, M. Cossi, R. Cammi, B. Mennucci, C. Pomelli, C. Adamo, S. Clifford, J. Ochterski, G. A. Petersson, P. Y. Ayala, Q. Cui, K. Morokuma, D. K. Malick, A. D. Rabuck, K. Raghavachari, J. B. Foresman, J. Cioslowski, J. V. Ortiz, B. B. Stefanov, G. Liu, A. Liashenko, P. Piskorz, I. Komaromi, R. Gomperts, R. L. Martin, D. J. Fox, T. Keith, M. A. Al-Laham, C. Y. Peng, A. Nanayakkara, C. Gonzalez, M. Challacombe, P. M. W. Gill, B. G. Johnson, W. Chen, M. W. Wong, J. L. Andres, M. Head-Gordon, E. S. Replogle, J. A. Pople, Gaussian 98 (Revision A.7), Gaussian, Inc., Pittsburgh, PA, **1998**.

Received March 3, 2000
[I00084]

Mesoporous Silicas Modified with Dioxomolybdenum(VI) Complexes: Synthesis and Catalysis

Paula Ferreira,[a] Isabel S. Gonçalves,[a] Fritz E. Kühn,[b] André D. Lopes,[a] Manuel A. Martins,[a] Martyn Pillinger,[a] Anabela Pina,[a] João Rocha,*[a] Carlos C. Romão,[c] Ana M. Santos,[b] Teresa M. Santos,[a] and Anabela A. Valente[a]

Keywords: Mesoporosity / MCM materials / Oxo complexes / Molybdenum / Supported catalysts / Epoxidations

The dioxomolybdenum(VI) fragment MoO_2X_2 has been confined within the ordered mesopores of pure siliceous hexagonal MCM-41 and cubic MCM-48 molecular sieves either by direct grafting (solvent impregnation) with $MoO_2X_2(THF)_2$ or by using a spacer ligand [L = $NC(CH_2)_2Si(OEt)_3$]. The materials have been characterised by elemental analysis, powder X-ray diffraction, N_2 adsorption, IR spectroscopy, and magic-angle spinning NMR spectroscopy (^{13}C, ^{29}Si). All catalysts, homogeneous and heterogenised, are active in the epoxidation of cyclooctene with *tert*-butyl hydroperoxide.

Introduction

Homogeneous molybdenum(VI) (Halcon[1]) and heterogeneous titanium(IV)/SiO_2 (Shell[2]) catalysts are the basis of important industrial processes for the epoxidation of propylene, with alkyl hydroperoxides as the oxygen source. The high selectivities and (for a heterogeneous catalyst) high activities of the Ti^{IV}/SiO_2 catalyst prompted the design of novel shape-selective catalysts based on the concept of confinement of redox active metal centres in microporous and mesoporous oxides.[3] This strategy has been particularly successful in the case of titanium silicate materials.[4] Effective catalysts were obtained by incorporating titanium atoms into the framework sites of medium-pore silicalite I and II (TS-1 and TS-2, 5.5 Å pore size),[5] large-pore zeolite β (7 Å),[6] and mesoporous MCM-41 (typically 25−30 Å).[7] In a different approach, isolated tetrahedral Ti^{IV} species were grafted onto the surface of MCM-41 and MCM-48 by reaction of the pendant silanol (Si−OH) groups with titanocene dichloride precursors, followed by calcination.[8] Ti-MCM materials are important as catalysts as they are capable of oxidising relatively bulky reactants.

MCM-41 and MCM-48 are members of the M41S family of ordered mesoporous siliceous materials, formed by surfactant templating methods.[9] They both have very high surface areas (1000 $m^2\ g^{-1}$), high pore volumes (1 $cm^3\ g^{-1}$) and very narrow pore size distributions, tuneable in the range 16−100 Å. Despite the fact that MCM-48 and MCM-41 possess very different surfaces, it is evident that both materials behave similarly in grafting reactions with organometallics and coordination complexes, as observed for example in the case of derivatisation with the *ansa*-bridged ferrocene (1,1′-ferrocenediyl)dimethylsilane.[10] The structure of MCM-41 can be described as a hexagonal arrangement of cylindrical pores embedded in a matrix of amorphous silica. MCM-48 possesses a three-dimensional pore structure, with a silica interface that can be modelled by a minimal surface of the gyroid type.[11] MCM-48 therefore has some advantages over MCM-41 as a catalyst support material.

Early Mo^{VI}/SiO_2 catalysts were not as successful as Ti^{IV}/SiO_2 catalysts due to the rapid leaching of the metal ion. Recently, the synthesis of MoS-1 and MoS-2 has been described.[12] These would be expected to consist of the $Mo^{VI}O_2$ species attached to the framework defect sites. MoS-1 was reported to be an active catalyst for the chemoselective oxidation of thioethers to the corresponding sulfoxides, and MoS-2 was reported to be active in the oxidative dehydrogenation of ethanol to acetaldehyde. Isolated Mo^{VI} active sites have also been grafted onto the inner surfaces of MCM-41, via a molybdenocene dichloride precursor in a manner analogous to that mentioned above for titanium, to generate a catalyst which was tested for the oxidative dehydrogenation of methanol.[13] Another useful strategy for the confinement of metal centres in molecular sieves is the covalent attachment of coordination complexes via a spacer ligand (tethering). The tethering of chiral dioxomolybdenum(VI) complexes to the internal surface of a mesoporous USY-zeolite afforded a catalyst for the asymmetric epoxidation of allylic alcohols.[14]

We recently reported on the synthesis of *cis*-MoO_2^{2+} complexes of the type $MoO_2X_2L_n$ (X = Cl, Br) by reaction of solvent substituted $MoO_2X_2(Solv)_n$ complexes (Solv =

[a] Department of Chemistry, University of Aveiro
3810-193 Aveiro, Portugal
Fax: (internat) + 351-234/370084
E-mail: rocha@dq.ua.pt
[b] Anorganisch-chemisches Institut der Technischen Universität München,
Lichtenbergstraße 4, 85747 Garching bei München, Germany
[c] Instituto de Tecnologia Química e Biológica
Quinta do Marquês, EAN, Apt 127, 2781-901 Oeiras, Portugal

 © WILEY-VCH Verlag GmbH, D-69451 Weinheim, 2000 1434−1948/00/1010−2263 $ 17.50+.50/0

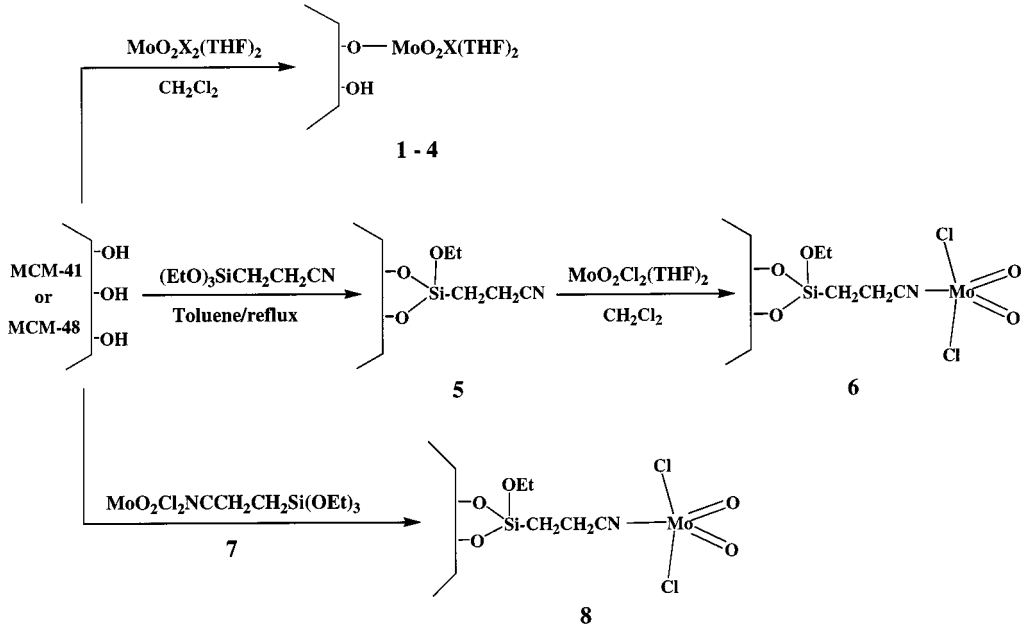
THF, CH_3CN, other nitrile molecules) with mono- and bidentate nitrogen and oxygen ligands.[15] The activity of the dissolved complexes as catalysts in olefin epoxidation with *tert*-butyl hydroperoxide (TBHP) was tested. In this article we report on the heterogenisation of the MoO_2X_2 fragment in MCM-41 and MCM-48 by either direct grafting with $MoO_2X_2(THF)_2$ or by using a spacer ligand [L = $NC(CH_2)_2Si(OEt)_3$]. The materials have been characterised by elemental analysis, powder X-ray diffraction (XRD), N_2 adsorption, IR spectroscopy, and magic-angle spinning (MAS) NMR spectroscopy (^{13}C, ^{29}Si). Preliminary experiments have been carried out to test the behaviour of the materials as catalysts for the epoxidation of cyclooctene with TBHP.

Results and Discussion

The supported materials MCM-41-MoO_2X_2 [X = Cl (**1**); X = Br (**2**)] and MCM-48-MoO_2X_2 [X = Cl (**3**); X = Br (**4**)] were prepared by diffusion of an excess of $MoO_2X_2(THF)_2$ (X = Cl, Br) into calcined and dehydrated MCM-41/MCM-48, in dry dichloromethane. The powders were washed repeatedly with dichloromethane to remove the unchanged oxides, and dried in vacuum at room temperature for several hours. Convenient and improved preparations of MCM-41-(spacer ligand)-MoO_2Cl_2 (**6**)/(**8**) were also developed by reacting MCM-41 with an excess of the nitrile with a triethoxysilyl group [$NC(CH_2)_2Si(OEt)_3$] in toluene, producing MCM-41-$Si(OEt)_nCH_2CH_2CN$ (**5**). This was followed by the addition of $MoO_2Cl_2(THF)_2$, or by the reaction of a solution of $MoO_2Cl_2NC(CH_2)_2Si(OEt)_3$ (**7**) with MCM-41. The products were isolated by filtration and washed thoroughly with ether to remove the unchanged oxide before drying in vacuum at room temperature. The molybdenum complex $MoO_2Cl_2NC(CH_2)_2Si(OEt)_3$ (**7**) was prepared by using a ligand exchange procedure,[15] in which the ligand was reacted with $MoO_2Cl_2(THF)_2$ in CH_2Cl_2 at room temperature. The resulting complex was isolated in excellent yield. The IR spectrum contained two bands assigned to Mo=O stretching modes (947, 916 cm^{-1}) as well as a band belonging to the nitrile ligand [ν(N≡C) = 2258 cm^{-1}]. This C≡N stretching mode is shifted to higher wavenumbers with respect to the free nitrile [ν(N≡C) = 2248 cm^{-1}] due to the coordination to the metal centre, and supports the presence of only one coordinating nitrile ligand.[15a] This unexpected result is not due to the steric bulk of the nitrile ligand but rather due to the fact that one of the ethoxide groups is directed towards the free coordinating position, *cis* to the position occupied by the nitrile group. A general summary of the reactions of these materials with the oxides is presented in Scheme 1.

The successful synthesis of the supported catalysts is confirmed by elemental analysis. The four initial materials **1**−**4** and **6** contained between 0.5 and 1.0 mass-% Mo, which is more than adequate for catalytic applications.[14] In compounds **1**−**4** the IR spectra do not clearly show bands for the two *cis*-Mo=O stretching modes, due to the small percentage of Mo. The products were pale blue powders and not visibly air-sensitive after exposure to air for several hours. Material **8** contained approximately 3.5 mass-% Mo. This is consistent with a coverage of molybdenum atoms of 4.6×10^{-25} mol/nm^2 (0.27 Mo atoms per nm^2). The IR spectra for the supported catalysts **6** and **8** provided evidence for the retention of the nitrile ligand [ν(N≡C) ≈ 2260 cm^{-1}].

The powder XRD patterns of the parent calcined (pristine) MCM-41 and MCM-48 can be indexed on a hexagonal unit cell (using the strongest reflection, d_{100}, a = 40.37 Å) and a cubic unit cell (using the strongest reflection, d_{211}, a = 82.38 Å), respectively,. The pattern for MCM-41 also displays a broad secondary feature at $2\theta \approx 4.6°$ where



Scheme 1

(110) and (200) reflections would be expected for a hexagonally ordered material such as MCM-41 (Figure 1). The absence of resolved peaks indicates that any structural order of the material did not extend over a long range. A very similar result was obtained by Schmidt et al. for a purely siliceous MCM-41 prepared as in this work using the surfactant $[(C_{14}H_{29})NMe_3]Br$.[16] The data for the Mo-modified MCM materials are consistent with the retention of the hexagonal and cubic mesoporous structures throughout the grafting process (Figure 1).

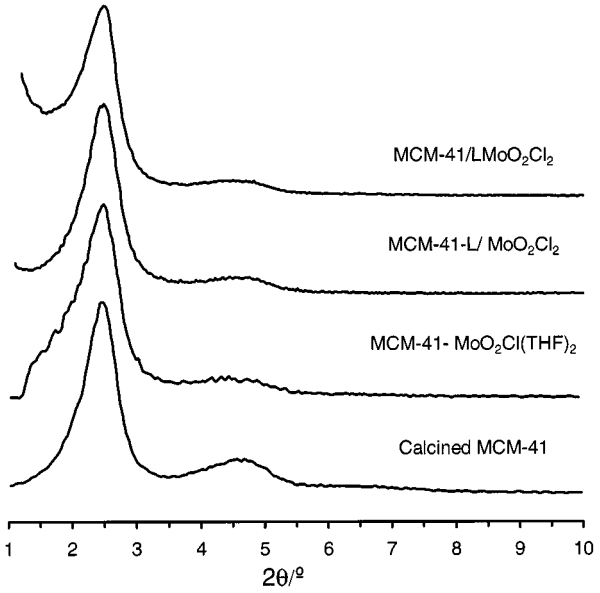


Figure 1. Powder XRD patterns of calcined (pristine) MCM-41 and functionalised samples

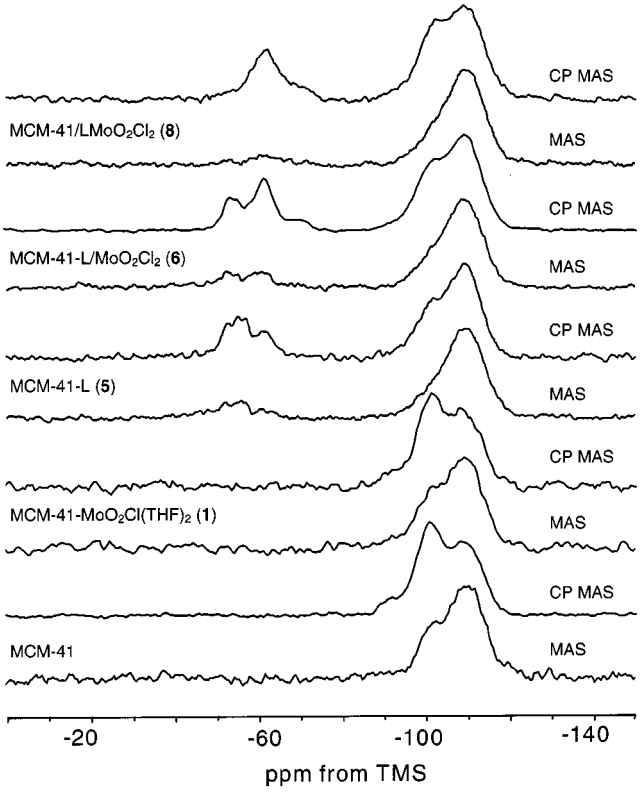


Figure 2. ^{29}Si MAS and CP MAS NMR spectra of calcined (pristine) MCM-41 and functionalised samples

The ^{29}Si CP MAS NMR spectra of MCM-41/MCM-48 functionalised with $MoO_2X_2(THF)_2$ (X = Cl, Br, **1**−**4**) exhibit two broad overlapping peaks at δ = −108 and −101 assigned to the Q^4 and Q^3 units of the silica framework, respectively, where $Q^n = Si(OSi)_n(OH)_{4-n}$, $n = 2-4$ (Figure 2, for material **1**). A small amount of Q^2 environments is also present (faint peak at δ = −91). The ^{29}Si CP MAS and MAS NMR spectra both show that the relative intensity of the Q^3 (and Q^2) peak changes only slightly upon functionalisation. This is consistent with the low metal loading (≤ 1% Mo) and perhaps also with a weak interaction (monopodal anchoring) of the molybdenum complexes with the surface.

For materials **5**, **6** and **8** the incorporation of the covalently linked organic group is confirmed by ^{29}Si CP MAS and MAS NMR spectroscopy, which shows distinct resonances for the organosilica species [$T^m = RSi(OSi)_m(OEt)_{3-m}$, $m = 1-3$] and for the silica network (Figure 2). For material MCM-41-Si(OEt)$_n$CH$_2$CH$_2$CN (**5**), grafting of the surface with the triethoxysilyl group [$NC(CH_2)_2Si(OEt)_3$] gives additional peaks between δ = −60.8 and −52.8, assigned to the T^1 and T^2 centres. The liquid-state ^{29}Si NMR spectrum for neat $NC(CH_2)_2Si(OEt)_3$ exhibits one resonance at δ = −49.8. As expected, the grafting process also shows a decrease in the relative intensity of the Q^3 resonance and a concomitant increase in the intensity of the Q^4 resonance. This is consistent with the IR spectrum which shows characteristic absorption bands for the covalently linked organic groups [ν(N≡C) = 2257 cm^{-1}].

After addition of the fragment MoO_2Cl_2 to material **5** to give material **6**, significant changes are observed in the region of the ^{29}Si CP MAS NMR spectrum corresponding to the organosilica centres. Three broad overlapping signals are observed at δ = −52.7, −60.7 and −70, assigned to the T^1, T^2 and T^3 environments, respectively. The relative intensities of the T^2 and T^3 resonances are noticeably enhanced in the spectrum of **6** relative to that of **5**, which suggests that the nitrile ligand underwent further condensation on the silica surface during the reaction. MCM-41/Si(OEt)$_n$CH$_2$CH$_2$CNMoO$_2$Cl$_2$ (**8**) presents a broad resonance at δ = −61.9 assigned mainly to the T^2 centres, $RSi(OSi)_2(OEt)$, and also a faint broad resonance at −70.1, assigned to the T^3 centres, $RSi(OSi)_3$. In comparison, the complex **7** exhibits only one well-defined resonance at δ = −62.5 in the ^{29}Si MAS NMR spectrum.

The ^{13}C CP MAS NMR spectrum of MCM-41-Si(OEt)$_n$CH$_2$CH$_2$CN (**5**) exhibits one faint peak at δ = 120 assigned to N*C*R, two peaks at δ = 58.6 and 10.4 assigned to the ethoxide group, and two well-defined peaks at δ = 16.6 and 7.7 assigned to NC−*C*H$_2$− and −*C*H$_2$−Si, respectively. The ^{13}C CP MAS NMR spectrum of MCM-41−Si(OEt)$_n$CH$_2$CH$_2$CN/MoO$_2$Cl$_2$ (**6**) is similar, except that the peaks corresponding to the ethoxide group (δ = 57.7 and 10.4) are not as intense as the peaks corresponding to the NC−CH$_2$−CH$_2$−Si fragment. Also, the resonance

at δ = 128 assigned to N≡*C* is shifted downfield slightly compared with **5** as a result of coordination to the MoO_2Cl_2 fragment. Material **8** presents a similar spectrum with δ = 128.6, 120.2 (*C*≡N), 59.0 (O−*C*H_2−), 15.9 (NC−*C*H_2−), 9.4 (−*C*H_3, −*C*H_2−Si) (Figure 3).

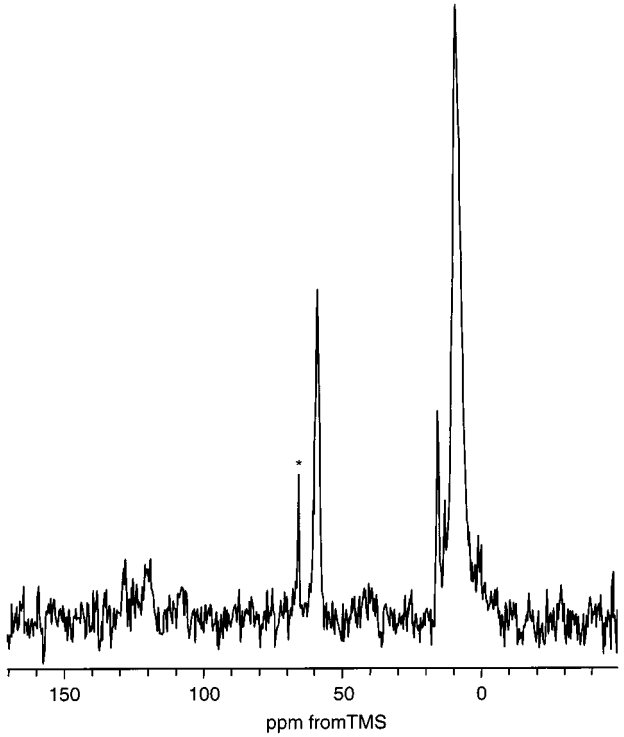


Figure 3. ^{13}C CP MAS NMR spectrum of MCM-41/LMoO_2Cl_2 (**8**), L = $NCCH_2CH_2Si(OEt)_n$; * denotes solvent

The N_2 adsorption-desorption isotherms of the solids recorded at 77 K are shown in Figure 4. The isotherms of the MCM-41 and MCM-48 materials are of Type IV according to the IUPAC, characteristic of mesoporous solids (intermediate pore size).[17] The physisorption process consists of monolayer-multilayer adsorption followed by capillary condensation of N_2 in the mesopores, below the expected condensation pressure of N_2. With the exception of MCM-41 and MCM-41/ LMoO_2Cl_2 (**8**), which show small hysteresis of adsorption and desorption (Figure 4), all samples have reversible N_2 adsorption isotherms.

The textural parameters determined from the isotherms are given in Table 1. The results for the parent MCM-41 and MCM-48 materials are in agreement with published values.[18,19] With direct grafting of $MoO_2X_2(THF)_2$ on MCM-41 (**1** and **2**), the N_2 adsorption isotherms of the modified and parent samples are very similar. The values of the BET specific surface areas (S_{BET}) and the specific total pore volumes (V_P) of the parent MCM-41 solid decrease between 4 and 7%. By changing the support to cubic mesoporous MCM-48, with the exception of the S_{BET} value for MCM-48-$MoO_2Br(THF)_2$ (**4**), no significant changes of the textural parameters are observed, and are negligible for MCM-48-$MoO_2Cl(THF)_2$ (**3**).

The N_2 adsorption isotherms of the functionalised MCM-41 materials **6** and **8** are different from that of the parent calcined MCM-41, demonstrating a lower uptake (Figure 4). On reaction of $MoO_2Cl_2(THF)_2$ with MCM-41-L (**5**) to give **6**, or on direct grafting of MoO_2Cl_2L (**7**) to give **8**, the values of S_{BET} decrease by 10.6 and 21.2%, respectively, and the values of V_P decrease by 45.1 and 39.0%, respectively (Table 1). These changes in adsorption properties can be attributed to successful grafting of the MoO_2Cl_2 fragment and/or to the tethering ligand $NCCH_2CH_2Si(OEt)_3$. The lower P/P_0 coordinates of the inflection points and the less sharp step of the isotherms in the region of capillary condensation of N_2 in the mesopores of the functionalised materials relative to that of the parent MCM-41 solid, may be assigned to changes in pore size distribution due to derivatisation of the internal silica surface of the mesoporous host. Brunel et al. observed similar changes in the features of the isotherms of MCM-41 upon grafting of functional molecules.[20]

The homogeneous and heterogenised Mo-complexes were tested for the epoxidation of cyclooctene with TBHP as the oxygen source at 55 °C. Typical catalytic runs are shown in Figure 5 and 6, and selectivities and total activities are given in Table 2 (calculated after 120 min reaction time). Reactions were also performed with pure calcined MCM-41/48 and, as expected, no significant epoxide formation was observed under these conditions. Pure calcined MCM-41 was previously found to be inactive in cyclohexene epoxidation with TBHP.[21]

For MCM-41-$MoO_2Cl(THF)_2$ (**1**), 31% conversion was observed after 2 h reaction with 100% selectivity to the epoxide (Figure 5, Table 2). Similar results were obtained for MCM-48-$MoO_2Cl(THF)_2$ (**3**). By contrast, the reaction with MCM-41-$MoO_2Br(THF)_2$ (**2**) was slow and the selectivity to cyclooctene oxide was very low (17% conversion of cyclooctene after 2 h with 56% selectivity to the oxide). This difference in activity between chlorodioxomolybdenum complexes and their bromo analogues has been noted recently by Kühn et al. for the homogeneous catalytic epoxidation of cyclooctene with complexes of the type $MoO_2X_2L_n$ (L = mono- and bidentate nitrogen and oxygen ligand).[15b] The time-dependent curves for MCM-41-$MoO_2X(THF)_2$ are of the same type as that reported recently for the catalytic activity of dissolved $MoO_2Br_2(CH_3CN)_2$ in cyclooctene epoxidation.[15a] This indicates that both reactions take place through the same mechanism, without any significant change in the reaction pathway. The appearance of these curves does not indicate the transformation of the original catalyst to another species during the reaction time and does not show an observable induction period. Similar results were obtained for the material prepared by reacting $MoO_2Cl_2(THF)_2$ with the ligand-grafted MCM-41-L. Indeed, the total activity, calculated after 2 h reaction and expressed as mols of cyclooctene produced per mol of molybdenum atoms per hour, is very similar for MCM-41-$MoO_2Cl(THF)_2$ (**1**) and MCM-41-L/MoO_2Cl_2 (**6**) (Table 2).

The kinetic profiles for the epoxidation of cyclooctene catalysed by homogeneous and heterogenised $MoO_2Cl_2NC(CH_2)_2Si(OEt)_3$ (**7**) are similar (Figure 6).

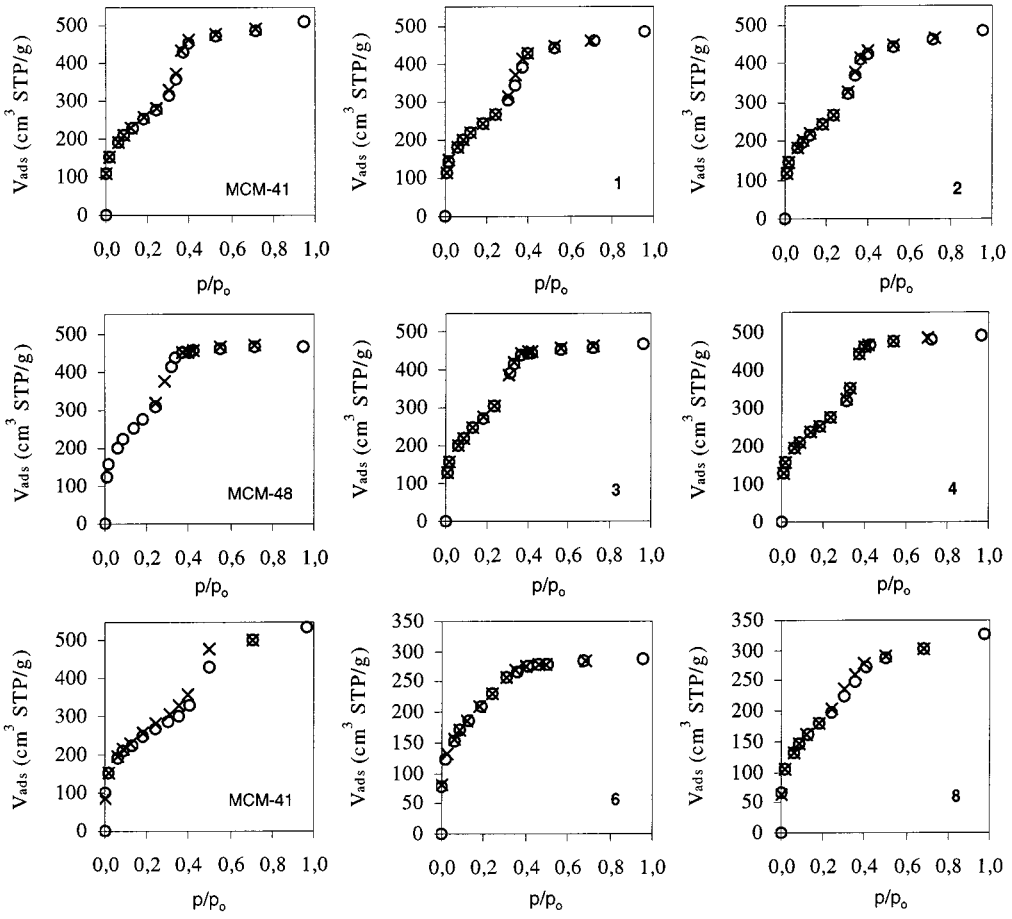


Figure 4. Nitrogen adsorption isotherms measured at 77 K of MCM solid materials before and after grafting/tethering of MoO_2X_2 complexes; open circle: adsorption; ×: desorption

Table 1. Textural parameters of MCM samples from N_2 isotherms at 77 K

	S_{BET} [m^2g^{-1}]	ΔS_{BET}[a] (%)	V_P [cm^3g^{-1}]	ΔV_P[b] (%)
MCM-41[c]	970.2	–	0.79	–
MCM-41-$MoO_2Cl(THF)_2$ (**1**)	916.0	−5.6	0.74	−6.6
MCM-41-$MoO_2Br(THF)_2$ (**2**)	926.2	− 4.5	0.75	−6.6
MCM-48	1095.4	–	0.75	–
MCM-48-$MoO_2Cl(THF)_2$ (**3**)	1083.9	−1.0	0.72	−4.0
MCM-48-$MoO_2Br(THF)_2$ (**4**)	982.1	−10.3	0.75	–
MCM-41[d]	893.4	–	0.82	–
MCM-41-L/MoO_2Cl_2 (**6**)	798.5	−10.6	0.45	−45.1
MCM-41/LMoO_2Cl_2 (**8**)	704.0	−21.2	0.50	−39.0

[a] Variation of surface area in relation to parent MCM material. – [b] Variation of total pore volume in relation to parent MCM material. – [c] MCM-41 sample used to prepare **1** and **2**. – [d] MCM-41 sample used to prepare **6** and **8**.

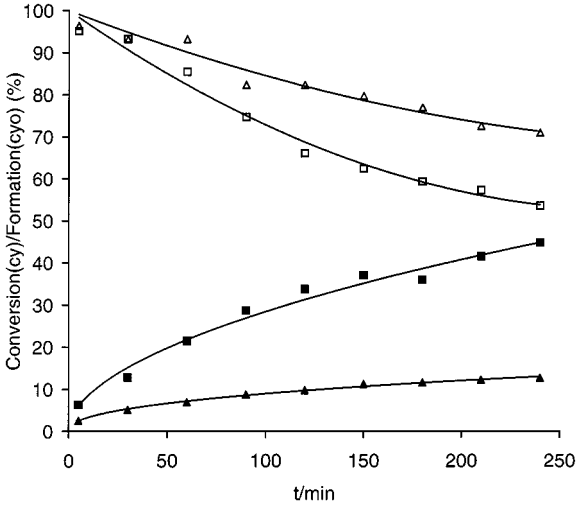


Figure 5. Kinetic profile for the epoxidation of cyclooctene with MCM-41-$MoO_2Cl(THF)_2$ (**1**) (solid square, open square) and MCM-41-$MoO_2Br(THF)_2$ (**2**) (solid triangle, open triangle) at 55 °C (solid symbols represent cyclooctene oxide formation and open symbols represent cyclooctene conversion); see text and Experimental Section for reaction details

After a very quick increase in the yield within the first 5 min the reaction velocities slow down. Thus, for the complex in solution, the yield of cyclooctene oxide formed was about 70% after 30 min, increasing by only a further 3% up to 4 h. A possible explanation for this sudden decrease in activity is the reaction of the active Mo complex in solution with *tert*-butyl alcohol. It has previously been reported that the epoxidation of 1-octene by a TiO_2-on-SiO_2 catalyst and TBHP in benzene at 80 °C exhibits marked autoretardation, attributed to the formation of *tert*-butyl alcohol during the epoxidation process.[22] For the MCM-41-supported complex, the yield of cyclooctene oxide formed was about 28% after 5 min, increasing to about 50% after 4 h. The total

Table 2. Selectivities and total activity (of cyclooctene oxide formed after 120 min reaction) of homogeneous and MCM-41/48-heterogenised dioxomolybdenum catalysts, with or without spacer ligand L = $NCCH_2CH_2Si(OEt)_n$

	Total activity (of cyo formed) [mols mol_{Mo}^{-1} h^{-1}]	Selectivity (%)
MCM-41-$MoO_2Cl(THF)_2$ (**1**)	128	100
MCM-41-$MoO_2Br(THF)_2$ (**2**)	57.0	56
MCM-48-$MoO_2Cl(THF)_2$ (**3**)	83.2	99
MCM-48-$MoO_2Br(THF)_2$ (**4**)	47.1	52
MCM-41-L/MoO_2Cl_2 (**6**)	122	100
MoO_2Cl_2L (**7**)	38.1	90
MCM-41/LMoO_2Cl_2 (**8**)	38.9	93

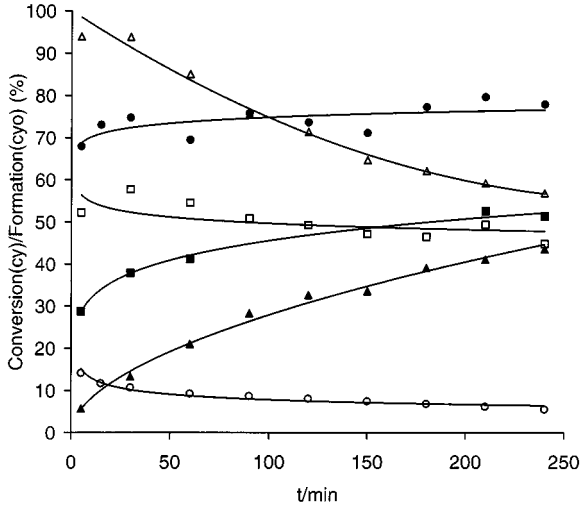


Figure 6. Kinetic profile for the epoxidation of cyclooctene with MCM-41-L/MoO_2Cl_2 (**6**) (solid triangle, open triangle), MCM-41/LMoO_2Cl_2 (**8**) (solid square, open square) and MoO_2Cl_2L (**7**) (solid circle, open circle) at 55 °C (solid symbols represent cyclooctene oxide formation and open symbols represent cyclooctene conversion); see text and Experimental Section for reaction details

activity achieved after 2 h reaction was very similar to that for the complex in solution, when the conversion per Mo is considered (Table 2). An initial turnover frequency of 3.5 mmol cyclooctene oxide per g of catalyst per min could be achieved, or 9.5 mol cyclooctene oxide per mol molybdenum atoms per min. These values are of a similar magnitude to those reported for the catalytic oxidation of cyclohexene with surface-grafted Ti-MCM-41[8a] and Ti-ITQ-2[23] catalysts (ITQ-2 is a crystalline layered silica). In a duplicate reaction with MCM-41/LMoO_2Cl_2 (**8**), the reaction mixture was filtered at the reaction temperature after 60 min, and then the filtrate was continued to be tested for activity at the reaction temperature. It was found that cyclooctene continued to be converted at a low rate, similar to that observed for the unfiltered reaction. This indicates that leaching may have occurred during the reaction, and that after 60 min at least part of the observed activity was due to the molybdenum in solution. More detailed studies are required to ascertain if the initial catalytic activity (up to 1 h) was mainly heterogeneous in nature.

Experimental Section

General: All preparations and manipulations were performed using standard Schlenk techniques under oxygen-free and water-free nitrogen. Commercial grade solvents were dried and deoxygenated by refluxing at least 24 h over appropriate drying agents under nitrogen, and were freshly distilled prior to use. − Powder XRD data were collected with a Phillips X'pert diffractometer using Cu-K_α radiation filtered by Ni. − Microanalyses were performed at the TU Munich. − Infrared spectra were recorded with a BIORAD FTS 575 C spectrometer with 1000 scans, and KBr and PE windows for mid and far infrared, respectively. − ^{29}Si and ^{13}C NMR spectra were recorded at 79.49 and 100.62 MHz, respectively, with a (9.4 T) Bruker MSL 400P spectrometer. ^{29}Si magic-angle-spinning (MAS) NMR spectra were recorded with 40° pulses, spinning rates 5.0−5.5 kHz and 60 s recycle delays. ^{29}Si CP MAS NMR spectra were recorded with 5.5 ms ^1H 90° pulses, 8 ms contact time, a spinning rate of 4.5 kHz and 4 s recycle delays. Chemical shifts are quoted in parts per million with respect to TMS. ^{13}C CP MAS NMR spectra were recorded with a 4.5 μs ^1H 90° pulse, 2 ms contact time, a spinning rate of 8 kHz and 4 s recycle delays. Chemical shifts are quoted in parts per million with respect to TMS. − Nitrogen adsorption data were recorded gravimetrically using a CI electronic MK2-M5 microbalance. Equilibrium at each data point was monitored using CI electronics Labweigh software and the pressure was monitored with an Edwards Barocel pressure sensor. The parent calcined MCM-41 and MCM-48 solids were degassed at 723 K whereas the modified samples were degassed at a lower temperature of 413 K to further minimise the destruction of their functionalities. All samples were kept constant at the degassing temperature, overnight (> 14 h), to give a residual pressure of ca. 10^{-2} Pa, and then cooled to room temperature prior to the adsorption measurements. The BET specific surface areas (S_{BET}) were calculated using the BET equation for relative pressures, in the range P/P_0 = 0.05−0.3, taking the cross-sectional area of a nitrogen molecule as 16.2 $Å^2$. The specific total pore volumes (micropore plus mesopore, V_P) were estimated from the nitrogen uptake at $P/P_0 \approx 0.95$, using the density of N_2 in its normal liquid state ($\rho = 0.8081$ g cm^{-3}). − The hexagonal channel host MCM-41 was synthesised using $[(C_{14}H_{29})NMe_3]Br$ according to published procedures.[9] After calcination (540 °C/6 h), the material was characterised by powder XRD, N_2 adsorption and FTIR spectroscopy. − The cubic channel host MCM-48 was synthesised using $[(C_{16}H_{33})NMe_3]Cl$ according to published procedures.[24] After calcination (540 °C/6 h), the material was characterised by powder XRD, N_2 adsorption and FTIR spectroscopy. − The precursors MoO_2Br_2,[25] MoO_2Cl_2,[25] and $MoO_2X_2(THF)_2$ (X = Cl, Br)[26] were prepared as described previously. − ^{13}C MAS NMR spectroscopy of $MoO_2X_2(THF)_2$ (25 °C): δ = 74.3 (THF), 25.9 (THF).

Preparation of Materials of General Formula MCM-41/48-$MoO_2X(THF)_2$ (X = Cl, Br): Calcined MCM-41/48 (0.5 g) was activated at 180 °C in vacuum (10^{-2} Pa) for 3 h and treated with excess of $MoO_2X_2(THF)_2$ (X = Cl, Br) in CH_2Cl_2 (20 mL). The mixture was stirred at room temperature for 2 d. The solution was filtered and the pale blue solid washed three times with 15-mL portions of CH_2Cl_2, before drying in vacuum at room temperature for several hours.

MCM-41-$MoO_2Cl(THF)_2$ (1): Anal. found Mo 1.10. − ^{29}Si MAS NMR spectrum exhibits one broad resonance at δ = −109.4 and a shoulder at δ = −101.3. ^{29}Si CP MAS NMR spectrum exhibits two broad resonances at δ = −101.1 (Q^3) and δ = −108.2 (Q^4), and a faint peak at δ = −91.8 (Q^2).

MCM-41-$MoO_2Br(THF)_2$ (2): Anal. found Mo 0.7. – ^{29}Si MAS NMR spectrum exhibits one broad resonance at δ = −108.5 and a shoulder at δ = −100.8. ^{29}Si CP MAS NMR spectrum exhibits two broad resonances at δ = −100.6 (Q^3) and δ = −108.7 (Q^4), and a faint peak at δ = −91.2 (Q^2).

MCM-48-$MoO_2Cl(THF)_2$ (3): Anal. found Mo 0.7. – ^{29}Si MAS NMR spectrum exhibits one broad resonance at δ = −108.5 and a shoulder at δ = −101.7. ^{29}Si CP MAS NMR spectrum exhibits two broad resonances at δ = −101.7 (Q^3) and δ = −108.8 (Q^4), and a faint peak at δ = −91.2 (Q^2).

MCM-48-$MoO_2Br(THF)_2$ (4): Anal. found Mo 0.5. – ^{29}Si MAS NMR spectrum exhibits one broad resonance at δ = −108.8 and a shoulder at δ = −101.4. ^{29}Si CP MAS NMR spectrum exhibits two broad resonances at δ = −101.1 (Q^3) and δ = −108.8 (Q^4), and a faint peak at δ = −91.2 (Q^2).

Preparation of MCM-41-Si$(OEt)_n$$CH_2CH_2CN$ (5): Calcined MCM-41 (0.5 g) was activated at 180 °C under vacuum for 2 h and treated with excess of $NCCH_2CH_2Si(OEt)_3$ in toluene (30 mL). The mixture was stirred under reflux for 66 h. The solution was filtered and the white solid washed several times with 20-mL portions of ether, before drying under vacuum at 100 °C for several hours. – Anal. found C 7.90, H 1.86, N 2.14. – IR (KBr): $\tilde{\nu}$ = 3441 cm^{-1} (vs), 3038 (w), 2981 (m), 2932 (m), 2257 (m), 1706 (w), 1638 (s), 1397 (m), 1232 (vs), 1083 (vs), 955 (m), 795 (s), 700 (w), 592 (w), 455 (s). – ^{29}Si MAS NMR spectrum exhibits broad resonances at δ = −109.5, −60.8 and −52.8. – ^{29}Si CP MAS NMR spectrum exhibits two broad resonances at δ = −109.0 (Q^4) and δ = −101.6 (Q^3), a faint peak at δ = −92.3 (Q^2), and two broad overlapping signals at δ = −60.3 and −51.9. – ^{13}C CP MAS NMR spectrum (25 °C): δ = 120.2 (*C*≡N), 58.6 (O−*C*H_2−), 16.6 (NC−*C*H_2−), 10.2 (−*C*H_3), 7.7 (−*C*H_2−Si).

Preparation of MCM-41-Si$(OEt)_n$$CH_2CH_2CN$/$MoO_2Cl_2$ (6): A suspension of activated MCM-41-Si$(OEt)_n$$CH_2CH_2CN$ (0.46 g) was treated with excess of $MoO_2Cl_2(THF)_2$ in CH_2Cl_2 (30 mL). The mixture was stirred at room temperature for 8 h. The solution was filtered and the pale blue solid washed twice with 15-mL portions of CH_2Cl_2, and one portion of ether (20 mL), before drying under vacuum at room temperature for several hours. – Anal. found C 12.63, H 2.15, Mo 1.0, N 1.86. – IR (KBr): $\tilde{\nu}$ = 3432 cm^{-1} (vs), 2987 (m), 2259 (m), 1637 (s), 1429 (m), 1234 (vs), 1082 (vs), 946 (m), 887 (w), 796 (s), 566 (w), 455 (s), 299 (m). – ^{29}Si MAS NMR spectrum exhibits one broad resonance at δ = −108.3, and three broad overlapping signals at δ = −52.7, −60.7 and −70.0. – ^{29}Si CP MAS NMR spectrum exhibits two broad resonances at δ = −109.0 (Q^4) and δ = −102.0 (Q^3), a faint peak at δ = −90.8 (Q^2), and three broad overlapping signals at δ = −52.7, −60.7 and −70.0. – ^{13}C CP MAS NMR spectrum (25 °C): δ = 128 (*C*≡N), 57.7 (O−*C*H_2−), 16.8 (NC−*C*H_2−), 10.4 (−*C*H_3), 7.8 (−*C*H_2−Si).

Preparation of $MoO_2Cl_2NCCH_2CH_2Si(OEt)_3$ (7): A solution of $MoO_2Cl_2(THF)_2$ (0.83 g, 2.42 mmol) in CH_2Cl_2 (20 mL) was treated with $NCCH_2CH_2Si(OEt)_3$ (1.05 g, 4.84 mmol), and the mixture was vigorously stirred for 30 min. The resulting solution was filtered and concentrated to dryness to give a yellow-brown oil. The very air-sensitive product was washed with hexane and dried in vacuum. Yield: 0.97 g (96%). – $C_9H_{19}Cl_2MoNO_5Si$ (416.18): calcd. C 25.97, H 4.60, N 3.37; found C 26.18, H 4.83, N 3.61. – Selected IR (KBr): $\tilde{\nu}$ = 2258 cm^{-1} (s, N≡C), 947 (vs, Mo=O), 916 (vs, Mo=O). – ^{13}C NMR spectrum($CDCl_3$, 400 MHz, 20 °C): δ = 121.1 (*C*≡N), 59.3 (O−*C*H_2−), 18.7 (NC−*C*H_2−), 11.9 (−*C*H_3), 8.8 (−*C*H_2−Si). – ^{29}Si MAS NMR spectrum (25 °C): δ = −62.5.

Preparation of MCM-41/Si$(OEt)_n$$CH_2CH_2CNMoO_2Cl_2$ (8): Calcined MCM-41 (0.75 g) was activated at 180 °C under vacuum for 2 h and treated with excess of $MoO_2Cl_2NCCH_2CH_2Si(OEt)_3$ (**7**) (0.70 g) in toluene (30 mL). The mixture was stirred at room temperature for 2 h. The solution was filtered and the pale blue solid washed three times with 20-mL portions of ether, before drying under vacuum for several hours. – Anal. found C 9.04, H 1.81, Mo 3.5, N 1.27. – IR (KBr): $\tilde{\nu}$ = 3441 cm^{-1} (vs), 2982 (m), 2937 (m), 2912 (w), 2260 (m), 1706 (w), 1638 (s), 1495 (w), 1448 (w), 1429 (m), 1394 (m), 1373 (w), 1322 (w), 1232 (vs), 1083 (vs), 955 (m), 734 (w), 696 (w) 549 (m), 334 (w). – ^{29}Si MAS NMR spectrum exhibits one broad resonance at δ = −108.2. – ^{29}Si CP MAS NMR spectrum exhibits two broad resonances at δ = −108.9 (Q^4) and δ = −101.7 (Q^3), a faint peak at δ = −91.2 (Q^2), one broad resonance at δ = −61.9 and a faint broad resonance at −70.1. – ^{13}C MAS NMR spectrum (25 °C): δ = 128.6, 120.2 (*C*≡N), 65.8, 59.0 (O−*C*H_2−), 15.9 (NC−*C*H_2−), 9.4 (−*C*H_3, −*C*H_2−Si).

Catalytic Reactions with Modified Mesoporous Materials/Dioxomolybdenum(VI) Complexes as Catalysts: *cis*-Cyclooctene (800 mg, 7.3 mmol), di-*n*-butyl ether (800 mg,) internal standard), **1**–**8** (175 mg, as catalyst) and 2 mL of 5.5 M *tert*-butyl hydroperoxide in decane were added to a thermostated reaction vessel and stirred for 24 h at 50 °C. – The course of the reaction was monitored by quantitative GC analysis. Samples were taken every 30 min, diluted with dichloromethane, and chilled in an ice bath. For the destruction of hydroperoxide and removal of water, a catalytic amount of manganese dioxide and magnesium sulfate was added. After the gas evolution had ceased, the resulting slurry was filtered through a filter-equipped Pasteur pipette and the filtrate injected into the GC column. – The conversion of cyclooctene and the formation of cyclooctene oxide was calculated from a calibration curve (r^2 = 0.999) recorded prior to the reaction course.

Acknowledgments

We thank PRAXIS XXI for partial funding. P. F. (Ph.D. student) thanks PRAXIS XXI for a grant and I. S. G. is grateful to the CRUP (Acções Integradas Programme) for their generous support. A. M. S. is grateful to the Bayerische Forschungsstiftung for a fellowship and F. E. K. thanks Prof. Dr. W. A. Herrmann for his continuous support.

[1] [1a] Halcon (J. Kollar), U.S. Pat. 3,351,635, **1967**; *Chem. Abstr.* **1968**, *68*, 2094. – [1b] Halcon (J. Kollar), U.S. Pat. 3,350,422, **1967**; *Chem. Abstr.* **1968**, *68*, 278.

[2] [2a] R. A. Sheldon, *Aspects of Homogeneous Catalysis* (Ed.: R. Ugo), vol. 4, Reidel, Dordrecht, The Netherlands, **1981**, p. 1. – [2b] R. A. Sheldon, *J. Mol. Catal.* **1980**, *7*, 107–126.

[3] [3a] R. A. Sheldon, I. W. C. E. Arends, H. E. B. Lempers, *Catalysis Today* **1998**, *41*, 387–407. – [3b] R. A. Sheldon, M. Wallau, I. W. C. E. Arends, U. Schuchardt, *Acc. Chem. Res.* **1998**, *31*, 485–493.

[4] R. Murugavel, H. W. Roesky, *Angew. Chem. Int. Ed. Engl.* **1997**, *36*, 477–479.

[5] [5a] M. Taramasso, G. Perego, B. Notari (Enichem), US Pat. 4 410 501, **1981**; *Chem. Abstr.* **1981**, *95*, 137. – [5b] B. Notari, *Stud. Surf. Sci. Catal.* **1987**, *37*, 413.

[6] [6a] T. Blasco, M. A. Camblor, A. Corma, J. Pérez-Pariente, *J. Am. Chem. Soc.* **1993**, *115*, 11806–11813. – [6b] M. A. Camblor, M. Constantini, A. Corma, L. Gilbert, P. Esteve, A. Martinez, S. Valencia, *Chem. Commun*. **1996**, 1339–1340.

[7] A. Corma, M. T. Navarro, J. Pérez-Pariente, *J. Chem. Soc., Chem. Commun*. **1994**, 147–148.

[8] [8a] T. Maschmeyer, F. Rey, G. Sankar, J. M. Thomas, *Nature* **1995**, *378*, 159−162. − [8b] L. Marchese, E. Gianotti, V. Dellarocca, T. Maschmeyer, F. Rey, S. Coluccia, J. M. Thomas, *Phys. Chem. Chem. Phys.* **1999**, *1*, 585−592. − [8c] P. Ferreira, I. S. Gonçalves, F. E. Kühn, M. Pillinger, J. Rocha, A. M. Santos, A. Thursfield, *Eur. J. Inorg. Chem.*, **2000**, 551−557.

[9] [9a] C. T. Kresge, M. E. Leonowicz, W. J. Roth, J. C. Vartuli, J. S. Beck, *Nature* **1992**, *359*, 710−712. − [9b] J. S. Beck, J. C. Vartuli, W. J. Roth, M. E. Leonowicz, C. T. Kresge, K. D. Schmitt, C. T.-W. Chu, D. H. Olson, E. W. Sheppard, S. B. McCullen, J. B. Higgins, J. L. Schlenker, *J. Am. Chem. Soc.* **1992**, *114*, 10834−10843.

[10] [10a] S. O'Brien, J. Tudor, S. Barlow, M. J. Drewit, S. J. Heyes, D. O'Hare, *Chem. Commun.* **1997**, 641−642. − [10b] P. Ferreira, I. S. Gonçalves, F. Mosselmans, M. Pillinger, J. Rocha, A. Thursfield, *Eur. J. Inorg. Chem*. **2000**, 97−102.

[11] V. Alfredsson, M. Anderson, *Chem. Mater.* **1996**, *8*, 1141.

[12] [12a] P. S. Raghavan, V. Ramaswamy, T. T. Upadhya, A. Sudalai, A. V. Ramaswamy, S. Sivasanker, *J. Mol. Catal. A: Chem*. **1997**, *122*, 75−80. − [12b] P. S. Raghavan, M. P. Vinod, *J. Mol. Catal. A: Chem*. **1998**, *135*, 47−53.

[13] I. J. Shannon, T. Maschmeyer, R. D. Oldroyd, G. Sankar, J. M. Thomas, H. Pernot, J. −P. Balikdjian, M. Che, *J. Chem. Soc., Faraday Trans.* **1998**, *94*, 1495−1499.

[14] A. Corma, A. Fuerte, M. Iglesias, F. Sánchez, *J. Mol. Catal. A: Chem*. **1996**, *107*, 225−234.

[15] [15a] F. E. Kühn, E. Herdtweck, J. J. Haider, W. A. Herrmann, I. S. Gonçalves, A. D. Lopes, C. C. Romão, *J. Organomet. Chem*. **1999**, *583*, 3−10. − [15b] F. E. Kühn, A. D. Lopes, A. M. Santos, E. Herdtweck, J. J. Haider, C. C. Romão, A. G. Santos, *J. Mol. Catal. A: Chem.*, **2000**, *151*, 147−160.

[16] R. Schmidt, M. Stöcker, E. Hansen, D. Akporiaye, O. H. Ellestad, *Microporous Mater.* **1995**, *3*, 443.

[17] S. J. Gregg, K. S. W. Sing, *Adsorption, Surface Area and Porosity*, 2nd ed., Academic Press, London, **1982**.

[18] M. D. Alba, A. Becerro, J. Klinowski, *J. Chem. Soc., Faraday Trans.* **1996**, *92*, 849.

[19] A. A. Romero, M. D. Alba, W. Zhou, J. Klinowski, *J. Phys. Chem. B* **1997**, *101*, 5294.

[20] D. Brunel, A. Cauvel, F. Fajula, F. DiRenzo, *Stud. Surf. Sci. Catal.* **1995**, *97*, 173.

[21] R. D. Oldroyd, J. M. Thomas, T. Maschmeyer, P. A. MacFaul, D. W. Snelgrove, K. U. Ingold, D. D. M. Wayner, *Angew. Chem. Int. Ed. Engl.* **1996**, *35*, 2787−2790.

[22] R. A. Sheldon, J. A. Van Doorn, *J. Catal*. **1973**, *31*, 427.

[23] A. Corma, U. Díaz, V. Fornés, J. L. Jordá, M. Domine, F. Rey, *Chem. Commun.* **1999**, 779−780.

[24] [24a] A. Monnier, F. Schüth, Q. Huo, D. Kumar, D. Margolese, R. S. Maxwell, G. D. Stucky, M. Krishnamurty, P. Petroff, A. Firouz, M. Janicke, B. F. Chmelka, *Science* **1993**, *261*, 1299. − [24b] J. Xu, Z. Luan, H. He, W. Zhou, L. Kevan, *Chem. Mater.* **1998**, *10*, 3690.

[25] R. Colton, I. B. Tomkins, *Aust. J. Chem.* **1965**, *18*, 447.

[26] [26a] M. Minelli, J. H. Enemark, R. T. C. Brownlee, M. J. O′Connor, A. G. Wedd, *Coord. Chem. Rev.* **1985**, *68*, 169. − [26b] F. E. Kühn, A. M. Santos, A. D. Lopes, I. S. Gonçalves, E. Herdtweck, C. C. Romão, *J. Mol. Catal. A: Chem.*, in press.

Received February 25, 2000
[I00074]

Transition Metal Ion Complexes of 2,2′-Bipyridyl-3,3′-diol and 2,2′-Bipyridyl-3-ol: Spectroscopic Properties and Solvent-Dependent Binding Modes

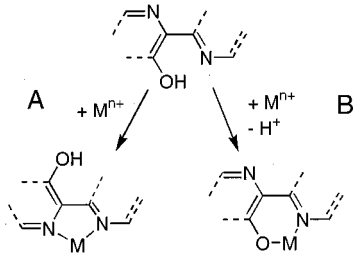
Knut Rurack*[a] and Reiner Radeglia[a]

Keywords: Chelates / Hydroxy bipyridyls / Fluorescence / Cadmium / Zinc / N ligands

The complexation behaviour of 2,2′-bipyridyl-3,3′-diol and 2,2′-bipyridyl-3-ol, $BP(OH)_2$ and BPOH, with various heavy and transition metal ions has been investigated in aqueous, alcoholic, and acetonitrile solutions. Whereas the complexes with paramagnetic ions and Hg^{II} are non-fluorescent, Zn^{II} and Cd^{II} form highly fluorescent complexes, their coordination geometries depending on the solvent proticity and hydrogen-bond donating ability. Through a comparative study with the corresponding chelates of 2,2′-bipyridyl (bipy), *N*,*O*-coordination in a six-membered ring chelate has been found to be the dominant binding mode in both the Zn^{II} and Cd^{II} complexes in the protic solvents water and ethanol. Only for Zn^{II} and BPOH is exclusive *N*,*N*′-chelation found in acetonitrile. NMR measurements on $BP(OH)_2$, BPOH, and bipy in the presence of Zn^{II} and Cd^{II} in acetonitrile confirmed these findings.

Introduction

Controlling the binding modes of metal ion complexes is of particular interest in many fields of bioorganic and bioinorganic chemistry.[1] In many biochemical processes, metal ion complexes with specific or unusual coordination geometries are involved, e.g. in enzymes or metalloproteins.[2] Accordingly, metal ion complexes play an important role in medicinal chemistry and drug design.[3] Here, single conformers of chemically and stoichiometrically identical complexes often show drastically different biological activities.[4] Since many organic ligands possess various heteroatoms and functional groups, competing coordination reactions can interfere. For instance, many aminophilic transition metal ions strongly prefer a five-membered *N*,*N*′-chelate (route A, Scheme 1) over a six-membered *N*,*O*-chelate (route B).[5] However, when both binding sites are present in a single molecule as, e.g., in some hydroxy-substituted heterocyclic biaryls or Schiff-base derivatives,[6] the question arises as to how a certain ion coordinates in a particular environment (these features are not only restricted to open-chain ligands but are also found, e.g., in cavity-forming crown compounds).[7] Although important, the chemical nature and structure of the (bi- or multidentate organic) ligand, for instance the geometrical arrangement or flexibility of the molecule, or possible mechanisms of intramolecular stabilization, are not the only decisive factors governing the formation of a specific structure in a certain complex. In liquid media the (counter)ions present and/or the solvent molecules also play a role, depending on the number of free coordination sites at the central ion in the complex (as defined by the geometry of the coordination sphere and the number of chelating ligands present) as well as on the affinity between the metal ion and these other potential (usually monodentate) ligands. Moreover, interactions between the chelating ligand and the solvent can also have an effect on the structural features of a complex, i.e. the proticity or polarity of a particular (solvent) environment can favour certain intra- or intermolecular stabilization modes and can thus either promote or hamper specific central ion−ligand interactions. Especially for chelating ligands that are able to form stabilizing intramolecular hydrogen bonds, e.g. some derivatives of hydroxy-substituted bipyridyls, the proton affinity or protic character of the solvent should play a major role in directing complex formation along, for instance, route A or B (Scheme 1).



Scheme 1. Generalized scheme of possible chelation mechanisms operative in metal ion complexation by hydroxy-substituted *N*-containing heterocyclic biaryls (the structures do not indicate actual complex stoichiometries)

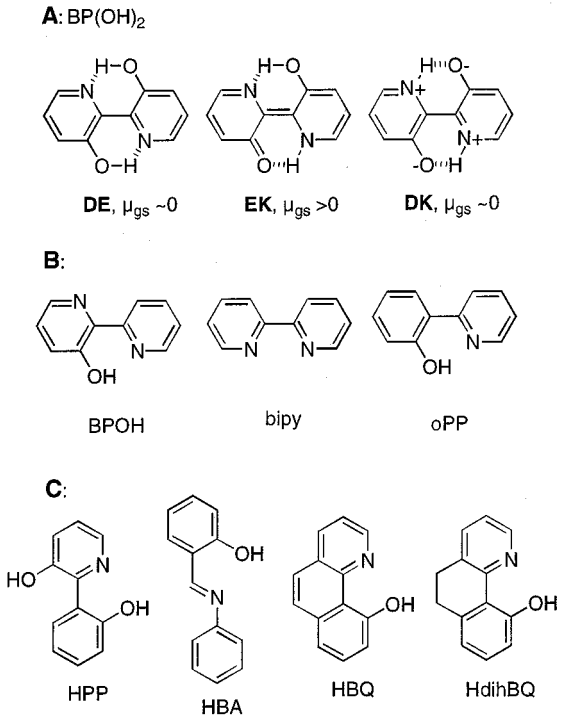
As an extension of our work on the metal ion binding and sensing abilities of 2,2′-bipyridyl-3,3′-diol [$BP(OH)_2$, Scheme 2, A] as well as the spectroscopic properties of its complexes in water,[8−11] we directed our studies towards the characterization of the actual binding modes in these coordination compounds as well as in the corresponding complexes of the reference compound 2,2′-bipyridyl-3-ol (BPOH, Scheme 2, B) in highly polar solvents. Considering the crucial role of the nature of the solvent and counterion, we aimed to elucidate the structures of the complexes dir-

[a] Dept. I.3902, Bundesanstalt für Materialforschung und -prüfung,
Richard-Willstätter-Straße 11, 12489 Berlin, Germany
Fax: (internat.) +49 (0)30/8104 5817
E-mail: knut.rurack@bam.de

Supporting information for this article is available on the WWW under http://www.wiley-vch.de/home/eurjic or from the author.

 © WILEY-VCH Verlag GmbH, D-69451 Weinheim, 2000 1434−1948/00/1010−2271 $ 17.50+.50/0

ectly in solution by employing metal ion perchlorates (as weakly donating counterions with a low coordinating ability) and neat, highly polar, protic (water, ethanol) as well as aprotic (acetonitrile) solvents. Moreover, we included the chemically closely related ligand *o*-(2-pyridino)phenol (oPP) and the parent compound 2,2′-bipyridyl (bipy) in our studies (Scheme 2, B). Since in pure water at ambient pH, $BP(OH)_2$ and BPOH only bind to heavy and transition metal ions such as Zn^{II}, Cd^{II}, Cu^{II}, or Ni^{II} and since only the complexes of the first two ions are fluorescent,[8,10,11] the present work focuses on the investigation of the Zn^{II} and Cd^{II} complexes of the (bi)pyridyl ligands by means of absorption, steady-state as well as time-resolved fluorescence, and NMR spectroscopy.



Scheme 2. **A**: Chemical structure and enol-keto tautomerism of $BP(OH)_2$ (DE, EK, DK, and μ_{gs} denote the dienol, enol-keto, and "diketo" tautomers, and the ground state dipole moment, respectively); **B**: chemical structures of the investigated BPOH, bipy, and oPP; **C**: chemical structures of related HPP, HBA, HBQ, and HdihBQ

Results and Discussion

Uncomplexed Ligands

The photophysical properties of uncomplexed $BP(OH)_2$ and BPOH in water, ethanol, and acetonitrile are included in Table 1.

In accordance with results published by other research groups,[12−16] $BP(OH)_2$, with its two strong internal hydrogen bonds (Scheme 2, A), shows the characteristic features of ESIPT (*e*xcited *s*tate *i*ntramolecular *p*roton *t*ransfer) fluorescence in polar organic solvents. Thus, the absorption and emission bands are broad, structureless, and largely Stokes-shifted (absorption and fluorescence excitation spectra match) and are centred at the same energies as in apolar or medium polarity organic solvents (Table 1). Consequently, the photophysical mechanism involves excitation of the only stable ground-state dienol (DE) tautomer, an ultrafast double ESIPT process,[17] and emission from a zwitterionic "diketo" (^{1}DK*) tautomer. Besides unchanged spectral features, with increasing solvent polarity and proticity radiationless deactivation of the excited singlet state(s) is enhanced, resulting in larger rate constants for non-radiative decay on going from *n*-hexane [$k_{nr} = (1 - \varphi_f)/\tau_f = 2.2 \cdot 10^8$ s^{-1}] to acetonitrile ($9.0 \cdot 10^8$ s^{-1}). As possible mechanisms accounting for the non-radiative loss of energy of ^{1}DK*, solute−solvent interactions (especially in protic solvents), torsional motions of the two pyridyl rings or the occurrence of *t*wisted *i*ntramolecular *c*harge *t*ransfer (TICT), the proximity effect (due to close-lying nπ* states), and triplet population are discussed.[13,16,18,19]

In water, the intramolecular hydrogen bonds are partially broken up and stabilization of the planar conformation is reduced resulting in a spectroscopically very different ground-state behaviour and reduced fluorescence quantum yields.[8,10,11,15,20] For the doubly-distilled water employed here (pH = 6.4, see Experimental Section), the positions of the global and second absorption band maxima are included in Table 1. In contrast, the fluorescence spectrum consists of the characteristic strongly Stokes-shifted band suggesting that upon excitation all the various conformers or tautomers undergo rapid transformation to emissive ^{1}DK*. Accordingly, k_{nr} (= $21.3 \cdot 10^8$ s^{-1}) is also increased in water. In pure doubly-distilled water, time-resolved fluorescence measurements revealed bi-exponential decays with a relative amplitude of ≥ 0.98 for the main emitting species (Table 1), but since this behaviour is not critical with regard to the results and interpretations of the present complexation experiments, we will not go into further detail here (the same holds true for BPOH, see below.).

In the case of BPOH, the position of the absorption band in aprotic solvents is also independent of the solvent polarity. The emission band of very weak intensity is largely Stokes-shifted and, due to a non-zero dipole moment of the emitting monoketo tautomer, its spectral position is more strongly solvent polarity-dependent than that of ^{1}DK* of $BP(OH)_2$ {$\Delta\tilde{\nu}$(abs−em) [MeCN−3-MP] = 1000 cm^{-1} for BPOH cf. $\Delta\tilde{\nu}$(abs−em) [MeCN−Hex] = 300 cm^{-1} for $BP(OH)_2$; Table 1}.[13,16,21,22] The weaker fluorescence of BPOH as compared to $BP(OH)_2$ is mainly due to enhanced flexibility (with possible TICT-state formation), based on the lack of a second stabilizing hydrogen bond, and low-lying nπ* transitions.[13,16]

In protic solvents, solute−solvent interactions change the fluorescence behaviour of BPOH, i.e. the emission spectrum is blue-shifted and the fluorescence quantum yield increases (ethanol cf. acetonitrile in Table 1), but in alcohols the absorption spectrum remains unchanged. Only water induces stronger effects and a red-shifted shoulder appears in the absorption spectrum while emission occurs at 23000 cm^{-1}. Although the fluorescence quantum yield increases further on going from ethanol to water, it is still much lower than that of $BP(OH)_2$ and thus hampered fluorescence lifetime

Table 1. Spectroscopic data for $BP(OH)_2$ and BPOH in various solvents at 298 K

	Solvent[a]	ε_r[b]	$\tilde{\nu}$(abs) [10^3 cm^{-1}]	$\tilde{\nu}$(em) [10^3 cm^{-1}]	$\Delta\tilde{\nu}$(abs−em) [cm^{-1}]	φ_f	τ_f [ns]
$BP(OH)_2$	Hex	1.9	29.2	19.8	9400	0.30	3.1
	Et_2O	4.3	29.4	19.6	9800	0.21	2.6
	MeCN	35.9	29.4	19.7	9700	0.09	1.0
	EtOH	24.6	29.4	20.7	8700	0.18	2.1
	MeOH	32.7	29.2	20.8	8400	0.10	1.2
	H_2O	80.2	28.8,[c] 24.8 (23.2)	21.3 (23.6)	7500	0.04[d]	0.45, 4.8[e]
BPOH	3-MP	1.9	30.8[f]	17.8[f]	13000[f]	$5.5\cdot10^{-3}$[g]	[h]
	Et_2O	4.3	30.8[i]	17.1[i]	13700[i]	n.r.[j]	n.r.
	MeCN	35.9	30.9	16.9	14000	$1.3\cdot10^{-4}$	n.d.[k]
	EtOH	24.6	30.9	17.2	13700	$1.2\cdot10^{-3}$	n.d.
	H_2O	80.2	31.3[l] (27.0)	23.0	8300	$5.0\cdot10^{-3}$ [d]	n.d.

[a] Hex = *n*-hexane, Et_2O = diethyl ether, MeCN = acetonitrile, EtOH = ethanol, MeOH = methanol, 3-MP = 3-methylpentane. – [b] Ref.[65]. – [c] Global maximum (see Figure 1, B), ratio of 28.8:24.8:23.2 = 2.4:1.4:1. – [d] With excitation at the absorption maximum. – [e] Relative amplitudes vary with excitation and emission wavelength and are always > 0.98 for the fast component. – [f] Ref.[22]. – [g] Ref.[24]. – [h] The room temperature fluorescence lifetime data published to date are controversial: whereas Tokumura et al. reported bi-exponential decay kinetics with lifetimes of 80 and 410 ps,[22] Kaczmarek et al. reported a value of 3.02 ns.[24] – [i] Ref.[16]. – [j] Not reported. – [k] Not determined due to limited time resolution of the instrumental set-up employed. – [l] Global maximum, ratio of 31.3:27.0 = 7.9:1.

measurements with the instrumental set-up employed (temporal resolution >100 ps).

The importance of the two internal hydrogen bonds in $BP(OH)_2$ is additionally stressed by the fact that similar observations as for BPOH were made for all the "flexible" related compounds, oPP (investigated here and in refs.[23,24]), HPP,[24] and HBA[25] (Scheme 2, C) in organic solvents, in which they are at best only weakly fluorescent (in aqueous solutions of $0.5 < pH < 13.5$, oPP is non-fluorescent[26,27]). On the other hand, all those compounds that are effectively "forced" to be planar are at least moderately fluorescent, e.g. HBQ[23,28,29] and HdihBQ[23] (Scheme 2, C), supporting the generally accepted reaction scheme outlined above. Most probably, besides close-lying nπ* states, rapid torsional motions break up the tight intramolecular hydrogen bond detected for some of these compounds in the ground state through the appearance of a characteristic signal at low field in the ^{1}H NMR spectra, i.e. at $\delta = 14.14$ for BPOH, at $\delta = 14.51$ for $BP(OH)_2$ (see below), and at $\delta = 14.3$ for oPP.[30]

The parent compound bipy is very weakly or non-fluorescent in pure water at room temperature. However, the origin of the weak fluorescence reported in some publications is still a matter of debate.[31]

Complexes

Before going into detail on the different binding modes of the fluorescent complexes of $BP(OH)_2$ and BPOH, the general implications concerning the effects of para- and diamagnetic cations, ion selectivities, complex stoichiometries, as well as the main absorption and emission features will be discussed, as exemplified by the complexes of $BP(OH)_2$ in water.

Complexes of $BP(OH)_2$ in Water

Steady-State Absorption and Fluorescence

In pure water, only complexation to the metal ions Zn^{II}, Cd^{II}, Hg^{II}, Cu^{II}, Ni^{II}, and Co^{II} leads to a change in both the absorption (Figure 1, A) and emission spectra (shown for the d^{10} metal ions in Figure 1, B); no effects are observed for Fe^{II}, Mn^{II}, or Pb^{II}, nor for Ca^{II}, Mg^{II}, or Na^{I}. Whereas the complexes $BP(OH)_2$ forms with paramagnetic transition metal ions, i.e. Cu^{II} or Ni^{II}, are non-fluorescent, in the case of the diamagnetic heavy metal ions of the d^{10} group, only Hg^{II} forms a non-fluorescent complex (Figure 1, B). The Zn^{II} and Cd^{II} complexes are highly fluorescent (Figure 1, B).[8,10,11] The spectroscopic data are collected in Table 2; the full overlap of the absorption bands of the complexes and the free ligand follows from Figure 1.

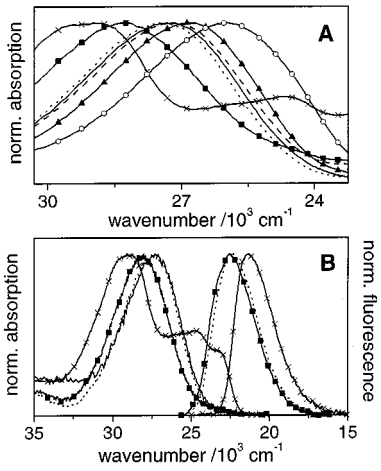


Figure 1. Normalized steady-state absorption spectra of [$M^{II}\subset$BP(OH)$_2$] in pure water: **A**: free $BP(OH)_2$ (×) and complexes with Cd^{II} (■), Zn^{II} (· · ·), Hg^{II} (−), Co^{II} (− − −), Ni^{II} (▲), and Cu^{II} (○); **B**: Spectra of the d^{10} metal ion complexes [excitation at 370 nm, $Hg^{II}\subset BP(OH)_2$ is non-fluorescent]; for both plots, $c_L = 3\cdot10^{-6}$ M and $c_M = 5\cdot10^{-5}$ (Cu^{II}), $1\cdot10^{-4}$ (Ni^{II}), $1\cdot10^{-3}$ (Co^{II}, Hg^{II}), $3\cdot10^{-3}$ (Zn^{II}), $7\cdot10^{-3}$ (Cd^{II}), i.e. full complexation is achieved

For all the complexes, the absorption bands of lowest energy remain ligand-centred electronic transitions of ππ* nature showing typical features of absorption bands of organic chromophores, i.e. broad, structureless bands with relatively high extinction coefficients ($\varepsilon > 10^3$ M$^{-1}\cdot$cm^{-1}). Metal-centred d-d transitions were not observed at the concentrations used and, in the case of the paramagnetic ions,

Table 2. Spectroscopic properties and apparent complex stability constants (see text) of the complexes of $BP(OH)_2$ in water at 298 K

M^{II}	$\tilde{\nu}$(abs) [10^3 cm^{-1}]	$\tilde{\nu}$(em) [10^3 cm^{-1}]	φ_f	τ_f [ns]	log K^{app}
Cu^{II}	26.0	–	–	–	5.9
Ni^{II}	26.9	–	–	–	5.0
Co^{II}	27.1	–	–	–	4.7
Zn^{II}	27.5	22.5	0.62	6.17	4.2
Cd^{II}	28.2	22.6	0.53	5.24	3.6
Hg^{II}	27.3	–	–	–	4.4

no metal-to-ligand (MLCT) or ligand-to-metal (LMCT) charge-transfer bands were found. However, due to its exceptional features (internal hydrogen bonds, enol-keto tautomerism), the characteristic shifts often observed upon complexation are obscured by the very broad absorption spectrum of $BP(OH)_2$ in neat aqueous solution. For example, with 8-hydroxyquinoline (8-HQ), the absorption bands of the metal ion complexes are well-separated and red-shifted by ca. 4500 cm^{-1}, most probably due to a more covalent nature of the transition metal−quinoline nitrogen bond.[32] Similar shifts as for 8-HQ are observed for the complexes of bipy (4460 cm^{-1} for the Zn^{II} complex, see below), but in the case of $BP(OH)_2$ the bands are strongly overlapped and only the maximum of the main band is slightly red-shifted (Figure 1).

Opposite tendencies can be derived from the emission measurements, i.e. different effects of para- and diamagnetic cations with strong similarities within each group, the only exception being Hg^{II}. All the paramagnetic ions and Hg^{II} quench the fluorescence without any spectral shifts, suggesting static quenching to be the main force. The emission spectra of the Zn^{II} and Cd^{II} complexes are very similar and largely overlap with the emission band of the free ligand [blue-shifted by ca. 20 nm (≈1000 cm^{-1}), Figure 1, B].[10,11] Fluorescence excitation spectra recorded at full complexation resemble the absorption spectra of both the Zn^{II} and Cd^{II} cation complexes.

Spectroscopic Titrations and Complex Stoichiometry

For all the cations studied, isosbestic points are observed in their UV/vis spectrophotometric titrations [as an example, see the titration of $BP(OH)_2$ with Cu^{II} in ref.[9]; for fluorometric titrations and the opposite effects of para- and diamagnetic cations, see Figure S2, Supplementary Material]. Analysis of the titration data according to the method of continuous variations[33] yielded a complex stoichiometry of 1:2, i.e. ML_2 (see ref.[9]; an example of an analysis according to this method is given in the Supporting Information). In all the UV/vis spectrophotometric and fluorometric titrations performed with $BP(OH)_2$ and various metal ions, no divergent spectral features were found, making a discrimination between the 1:1 and 1:2 complexes impossible in this way. However, fitting the titration curves was only found to yield acceptable results for a sum of a 1:1 and a 2:1 complexation model[34] in some cases (Zn^{II}, Cd^{II}), both complexes showing similar spectroscopic behaviour. For the other, more strongly coordinating ions, the complex stability constants are too high to be reliably determined by this method and the relatively poor solubility of $BP(OH)_2$ in terms of a c_{L0} titration (see Experimental Section) made such a reverse titration (titration of M with L) impossible. Thus, in order to compare the binding strengths of all the cations, the apparent complex stability constants log K^{app} were determined spectroscopically and are included in Table 2 (for a description of the procedure, see Experimental Section). As can be deduced from Table 2, the order of log K^{app} can be described by the Irving−Williams order[35] and the ion selectivity is comparable to that shown by other so-called "general" ligands with bidentate *N*,*O*-chelating sites such as 8-HQ, pyridine-2-carboxylic acid, or aryl-azomethine ligands.[6,36−39] Provided they are not significantly conformationally restricted, these ligands do not show any enhanced selectivity for particular ions.[6,36]

On analysis of the fluorescence excitation spectra recorded for solutions containing different amounts of free ligand and complex, the spectra could always be described by a linear combination of the fluorescence excitation spectra of the free ligand and the 1:1 complex. Thus, the 1:1 and 1:2 complexes show identical fluorometric behaviour and cannot be distinguished by steady-state fluorescence spectroscopy either.

Time-Resolved Fluorescence

The effect of complexation on the fluorescence decay kinetics of $BP(OH)_2$ reflects the observations made by means of the steady-state fluorescence experiments. Addition of quenching ions such as Cu^{II} and Hg^{II} to a solution of $BP(OH)_2$ in water leads only to a slight variation in fluorescence lifetime but to a strong decrease in the amplitude, when comparing the photons emitted over a certain time interval, i.e. static quenching occurs (this is observed at any combination of excitation and emission wavelengths).

In contrast, for Zn^{II} and Cd^{II}, in agreement with an increase in fluorescence quantum yield, a chelation-induced increase in fluorescence lifetime is observed, leading to the appearance of a new long-lived fluorescence decay component, its lifetime being cation specific (Table 2).[8,10,11] A time-resolved fluorometric titration reveals that with increasing metal ion concentration the relative amplitude of the short-lived decay component decreases and, correspondingly, the relative amplitude of the long-lived decay component increases. No ion concentration-dependent variations in the lifetime of the long-lived decay component are evident, thus supporting the observations made by steady-state spectroscopy, i.e. identical spectroscopic behaviour of the 1:1 and 1:2 complexes. This is also confirmed by fluorescence decay measurements at different emission wavelengths and global analysis of the data. Thus, ground-state heterogeneity[11] can be assumed and suggests that fluorescence deactivation is fast as compared to excited-state decomplexation, i.e. the complexes are stable in both the ground and excited states.

The faster decay of the fluorescence of the Cd^{II} complex can be rationalized in terms of the heavy atom effect.[40] Assuming that in the tightly bound complexes the main route of non-radiative deactivation is intersystem crossing ($k_{nr} \approx k_{isc}$), the heavy atom effect can be quantified by using a central field single-electron approximation for the relationship between k_{isc} and the spin−orbit coupling constant.[41] Accordingly, $\log k_{nr} + \log n^6$ (n = quantum number) gives a measure of the heavy atom effect and the values calculated for the Zn^{II} and Cd^{II} complex amount to 11.4 and 12.1, in good agreement with published values for the related 8-HQ complexes of these ions.[41]

Binding Modes of the Zn^{II} and Cd^{II} Complexes of the (Substituted) Bipyridyls (and oPP) in Water, Ethanol, and Acetonitrile

Although the spectroscopic behaviour of the complexes of $BP(OH)_2$ reveals certain tendencies, the real nature of the complexes in terms of Scheme 1 and the background given in the Introduction is still unclear. A theoretically possible route C (not shown in Scheme 1), the formation of a sterically unfavoured seven-membered ring due to coordination to both hydroxyl groups, can be ruled out on the basis of thermodynamic considerations.[42,43] The necessary deprotonation of two hydroxyl groups at pH ≈ 7, the order of complex stability constants (the highest K is observed for the aminophilic cation Cu^{II}), the general preferences of the "soft" metal ions (in terms of Pearson's concept of hard and soft acids and bases)[44] for "soft" donor heteroatoms, and the unfavoured geometry of the resulting chelate render this mechanism very unlikely. However, chelate formation according to routes A and B in Scheme 1 has to be considered, as has been shown by Cargill Thompson et al.[45]

Before going into detail on the various complexes, it is noteworthy that whereas $BP(OH)_2$, BPOH, and bipy show complexation-induced spectroscopic effects upon addition of Zn^{II} and Cd^{II} in all three solvents investigated, very weakly fluorescent oPP ($\varphi_f < 10^{-5}$) does not show any pronounced changes in its photophysical properties upon addition of cations. Even in organic solvents, only small effects are observed at a high excess of metal ion (e.g. >500-fold excess of Zn^{II}). Thus, the behaviour of oPP will be discussed separately below. The spectroscopic data for the Zn^{II} and Cd^{II} complexes of BPOH and bipy are reported in Table 3, along with the data for the corresponding $BP(OH)_2$ complexes.

Absorption and Fluorescence Spectroscopy in Water

In pure water, the Zn^{II} and Cd^{II} complexes of both BPOH and $BP(OH)_2$ show very similar absorption and emission behaviour (Figure 2, Table 3). The spectral band

Table 3. Spectroscopic properties of the Zn^{II} and Cd^{II} complexes of $BP(OH)_2$, BPOH, and bipy in water (W), ethanol (E), and acetonitrile (A; So. = solvent)

Ion /So.	Ligand	$\tilde{\nu}$ (abs) [10^3 cm^{-1}]	$\tilde{\nu}$(em) [10^3 cm^{-1}]	$\Delta\tilde{\nu}$ (abs–em) [cm^{-1}]	ϕ_f	τ_f [ns]	k_f [10^8 s^{-1}]	k_{nr} [10^8 s^{-1}]
Zn^{II} / W	$BP(OH)_2$	27.5	22.5	5000	0.62	6.17	1.00	0.61
	BPOH	27.0	21.8	5200	0.59	6.71	0.88	0.61
	bipy	33.9	30.8	3100	0.34	1.43	2.38	4.61
Zn^{II} / E	$BP(OH)_2$	25.6	21.5	4100	0.55	6.07	0.91	0.74
	BPOH[a]	25.2	20.8	4400	(0.26)		-	-
	BPOH[b]	30.0[c]	20.6 (26.6)[d]	9400	0.47	6.21	0.76	0.85
	bipy	33.9	30.8	3100	0.10	0.72	1.39	12.5
Zn^{II} / A	$BP(OH)_2$[a]	24.7	21.8	2900	-	6.01	-	-
	$BP(OH)_2$[c]	30.5[f]	25.5, 20.6	5000, 9900	n.d.[g]	1.37[h]	-	-
	$BP(OH)_2$[c]	24.7	21.8	2900	0.47	5.87	(0.80)	(0.90)
	BPOH	30.4[c]	27.5	2900	0.36	1.31	2.75	4.88
	bipy	33.9	30.6	3300	0.27	1.48	1.82	4.93
Cd^{II} / W	$BP(OH)_2$	28.2	22.6	5600	0.53	5.24	1.01	0.90
	BPOH	27.2	22.0	5200	0.48	5,79	0.92	0.99
	bipy	33.9	30.8	3100	0.05	0.29	1.72	32.7
Cd^{II} / E	$BP(OH)_2$	26.7	22.0	4700	0.54	5.30	1.02	0.87
	BPOH[a]	26.0	21.0	5000	(0.26)		-	-
	BPOH[b]	30.2[c]	21.1	9100	0.45	5.50	0.82	1.00
	bipy	33.9	30.8	3100	0.05	0.29	1.92	30.5
Cd^{II} / A	$BP(OH)_2$	27.6	22.2	5400	0.46	5.18	0.89	1.04
	BPOH	30.7[c]	27.4 (21.1)	3300	0.10[i]	0.26[j]	3.85	34.6
	bipy	33.9	30.8	3100	0.07	0.23	3.04	40.4

[a] Intermediate complex observed in the titration experiments at $x_{M/L} \leq 0.5$. − [b] Data obtained at highest ion excess (ML complex). − [c] Center of the band displaying a double maximum. − [d] Intensity of the band at 26600 cm^{-1} ca. one-hundredth of the total fluorescence intensity. − [e] Data obtained at highest Zn^{II} excess possible: two different absorption and emission bands. − [f] From fluorescence excitation spectrum. − [g] Not determined because full complexation could not be reached. − [h] Observed at 25500 cm^{-1}; τ_1 = 0.61 ns and τ_2 = 5.30 ns when recorded at 21800 cm^{-1}. − [i] φ_f^{rel} (band at 21100 cm^{-1}) = 0.02. − [j] τ_2 = 5.44 ns (a_{rel} = 0.27) when observed at 21100 cm^{-1}.

positions for both absorption and emission differ by ≤ 1000 cm^{-1} and the fluorescence quantum yields and lifetimes are very similar as well. Consequently, this leads to similar rate constants for radiative and non-radiative deactivation.

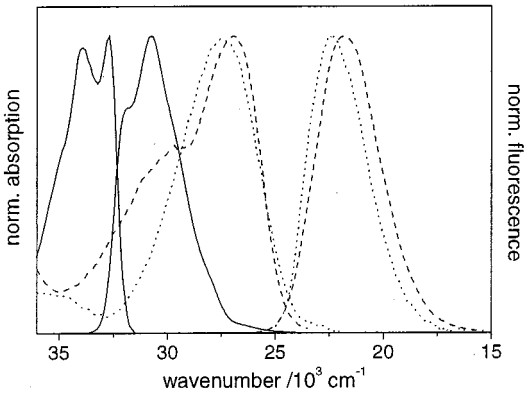


Figure 2. Steady-state spectra of the Zn^{II} complexes of $BP(OH)_2$ (· · · ·), BPOH (− − −), and bipy (−) in pure water [full complexation; excitation at absorption maximum; $c_L = 3 \cdot 10^{-6}$ M, $c_M = 7.5 \cdot 10^{-5}$ M in the case of bipy, $1 \cdot 10^{-3}$ in the case of BPOH, and for $BP(OH)_2$ see caption of Figure 1]

On the other hand, the behaviour of the corresponding complexes of bipy is clearly different. The Stokes shifts observed are only two-thirds the size of those observed for the hydroxy bipyridyls, the fluorescence quantum yields are considerably lower, and, in particular, the fluorescence decays more rapidly by a factor of ca. 4.5.

Accordingly, this effect should be predominantly reflected in different k_{nr} values. Indeed, the value found for Zn^{II}⊂bipy, for example, is almost an order of magnitude greater than those obtained for Zn^{II}⊂BPOH and Zn^{II}⊂B-$P(OH)_2$. This effect is even more pronounced in the case of Cd^{II}. Thus, the "activity" of nπ* state interaction is higher in the bipy complexes than in the other two complexes and the influence of the heavy atom (or ion) Cd^{II} is more pronounced in the case of these smaller chelates with a five-membered ring structure [note that because of the higher stability of the bipy complexes (see below), enhanced torsional motions about the central bipyridyl bond seem to play only a minor role]. Furthermore, besides the shift in absorption (electrostatic polarization induced by M^{II}), M^{II}-⊂bipy complexes show the characteristically structured absorption bands, with the vibrational structure being better resolved.[46] On the other hand, on comparing k_f and k_{nr} of M^{II}⊂$BP(OH)_2$ with those of free $BP(OH)_2$, it is obvious that the rate constant for fluorescence deactivation remains constant (within experimental error, Table 1), but that the contributions of competing non-radiative deactivation channels of the first excited singlet state are markedly reduced [it is interesting to note that tight binding of $BP(OH)_2$ in the complexes further reduces k_{nr} by a factor of 3.5 as compared to k_{nr} in apolar solvents such as *n*-hexane ($k_{nr} = 2.2 \cdot 10^8 s^{-1}$)].

Absorption and Fluorescence Spectroscopy in Ethanol

Ethanol, being less polar than water but still capable of hydrogen-bond formation, induces similar effects as water, but some noticeable differences in complex formation are observed, especially in the case of BPOH. For M^{II}⊂B-$P(OH)_2$ and M^{II}⊂bipy, a behaviour similar to that in water is observed. The only deviations are slightly blue-shifted spectra in the case of M^{II}⊂$BP(OH)_2$ and a marked drop in fluorescence quantum yield and lifetime for the Zn^{II} complex of bipy. The exceptional behaviour of this complex in ethanol is unclear and will not be discussed further. However, the data obtained for Zn^{II}⊂bipy are still different from those measured for the corresponding complexes of its hydroxy derivatives. Cd^{II}⊂bipy shows the expected features and, in acetonitrile (see below), the behaviour of Zn^{II}⊂bipy is again comparable to that in water.

For M^{II}/BPOH, complex formation is very remarkable. At low metal ion concentrations up to a metal-to-ligand ratio $x_{M/L} = 0.5$, the complex formed resembles that of $BP(OH)_2$. In Figure 3, A, the UV/vis spectrophotometric titration spectra for BPOH with Zn^{II} up to $x_{M/L} = 0.5$ are displayed, clearly showing the characteristic features (see Table 3 for the corresponding data). On addition of more Zn^{II} to the solution, the band at 25200 cm^{-1} diminishes and a new band appears at 30000 cm^{-1} (Figure 3, B). This band displays the typical characteristics of the Zn^{II}⊂bipy complex (blue-shifted and structured, cf. A and B, Figure 4). However, the emission spectra measured up to a 1000-fold excess of Zn^{II} (e.g. "− − −" in Figure 4, A) resemble that of Zn^{II}⊂$BP(OH)_2$ (Figure 4, B, " · · · · ") and the fluorescence decay has almost the same lifetime (Table 3).

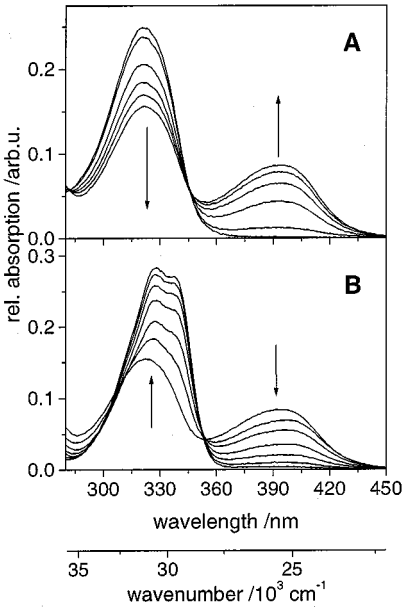


Figure 3. UV/vis spectrophotometric titration of BPOH with Zn^{II} in ethanol; **A**: steps for $x_{M/L} = 0.1-0.5$; **B**: steps for $x_{M/L} = 0.5-50$ (arrows indicate changes upon Zn^{II} addition); measurements were performed in 100 mm absorption cells with $c_L = 3.7 \cdot 10^{-6}$ M; the second *x* axis (wavenumber scale) is included for better comparison with data presented in the text and tables

Only on the high energy side (enlarged emission spectrum marked "—" in Figure 4, A) is a weak band centred at 26600 cm^{-1} visible. In view of the emission properties of Zn^{II}⊂bipy, i.e. low φ_f and fast decay kinetics, emission from

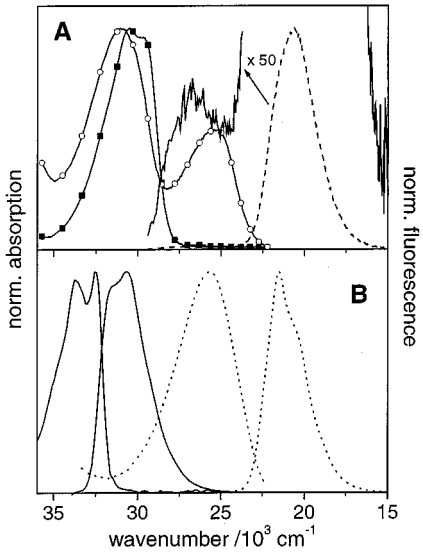


Figure 4. Steady-state spectra of the Zn^{II} complexes of the (substituted) bipyridyls in ethanol; **A**: absorption spectra of $Zn^{II}\subset(BPOH)_2$ (○), $Zn^{II}\subset BPOH$ (■), and emission spectrum of $Zn^{II}\subset BPOH$ (− − − −); the enlarged high-energy side (−) of the emission spectrum is also included ($c_L = 3\cdot10^{-6}$ M, $c_M = 1.5\cdot10^{-3}$ M); **B**: spectra of the Zn^{II} complexes of $BP(OH)_2$ (· · · · ·) and bipy (−) in ethanol (full complexation; excitation at absorption maximum; $c_L = 3\cdot10^{-6}$ M, $c_M = 7.5\cdot10^{-5}$ M)

an *N*,*N*′-chelated $Zn^{II}\subset BPOH$ complex might be expected to be weak in ethanol as well. However, the fluorescence excitation spectra recorded at 27000 cm^{-1} and 20800 cm^{-1} are similar and resemble the absorption spectrum of the 1:1 complex centred at 30000 cm^{-1}. Furthermore, closer inspection of Figure 4 provides a possible explanation for the fluorometric results. Assuming that in an equilibrium situation involving intermediately formed "$Zn^{II}\subset BP(OH)_2$-like" complexes still in the solution, light emitted from the "$Zn^{II}\subset$bipy-like" complex is absorbed by this species and is then re-emitted with its characteristic stronger fluorescence, the blue-shifted emission of the "$Zn^{II}\subset$bipy-like" complex should be quenched.

Absorption and Fluorescence Spectroscopy in Acetonitrile

In acetonitrile, a solvent of comparable polarity lacking H-bond donating ability, the tendencies observed in ethanol are even more pronounced. Only the Cd^{II} complex of $BP(OH)_2$ shows almost identical spectroscopic features in all three solvents employed. For $Zn^{II}/BP(OH)_2$, the metal ion concentration-dependent spectroscopic behaviour resembles that of Zn^{II}/BPOH in ethanol. At low concentrations, the features seen for $Zn^{II}\subset BP(OH)_2$ in aqueous solution are observed, but with a large excess of Zn^{II}, a blue-shifted band centred at 25500 cm^{-1} appears in the emission spectrum (Figure 5). The changes in absorption are negligible but in Figure 5 the differences between the fluorescence excitation spectra recorded in both emission bands can be seen. Observation at 19200 cm^{-1} yields a band corresponding to the absorption band of the 1:2 complex (cf. the close similarity of the spectra marked "−" and " ○" in Figure 5). Furthermore, emission wavelength-dependent

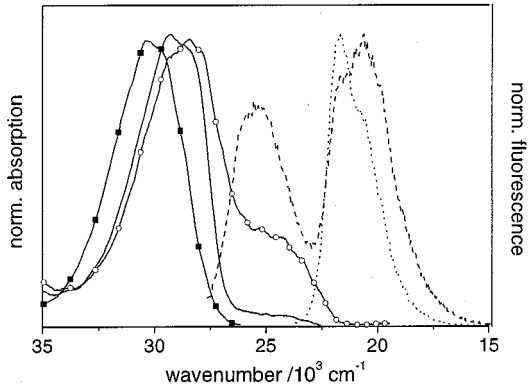


Figure 5. Steady-state spectra of $Zn^{II}/BP(OH)_2$ in acetonitrile; absorption (−) and emission (· · · ·, excitation at 24500 cm^{-1}) spectra of the ML_2 complex; emission spectrum at high Zn^{II} excess (both complexes present, − − −, excitation at 29500 cm^{-1}), and fluorescence excitation spectra at high Zn^{II} excess (observation at 25600 cm^{-1} = ■; observation at 19200 cm^{-1} = ○)

fluorescence decay data support the results (1.37 ns at 25500 cm^{-1} cf. ca. 6 ns at 21800 cm^{-1}, see Table 3).

For $Zn^{II}\subset BPOH$, only the absorption band at 30400 cm^{-1} and an emission band at 27500 cm^{-1} are seen, irrespective of the Zn^{II} concentration (Table 3). The similarity between the photophysical properties of $Zn^{II}\subset$bipy and $Zn^{II}\subset BPOH$, including typical characteristics (vibrational structure) of the $M^{II}\subset$bipy absorption bands, is remarkable (Table 3 and Figure S3, Supplementary Material). The higher-energy emission band, absent in ethanol, indicates the formation of a "$Zn^{II}\subset$bipy-like" chelate in acetonitrile. In accordance with the different behaviour of the Zn^{II} and Cd^{II} complexes of $BP(OH)_2$, for Cd^{II}/BPOH some "$Cd^{II}\subset BP(OH)_2$-like" chelate is still observed at low Cd^{II} concentrations.

The data presented thus far lead to the conclusion that the complexes investigated can be divided into two groups according to their spectroscopic behaviour in the different solvents [these "spectroscopic reference structures" are termed "$Zn^{II}\subset$bipy-like" and "$Cd^{II}\subset BP(OH)_2$-like"].

$Zn^{II}/BP(OH)_2$: "$Cd^{II}\subset BP(OH)_2$-like" in all the solvents except in acetonitrile at high excess of Zn^{II};

Zn^{II}/BPOH: "$Cd^{II}\subset BP(OH)_2$-like" in water and at low metal ion concentrations in ethanol, "$Zn^{II}\subset$bipy-like" in acetonitrile and at high metal ion concentrations in ethanol;

Cd^{II}/BPOH: "$Cd^{II}\subset BP(OH)_2$-like" in water and at low metal ion concentrations in ethanol and acetonitrile, "$Zn^{II}\subset$bipy-like" at high metal ion concentrations in ethanol and acetonitrile;

Cd^{II}/bipy: "$Zn^{II}\subset$bipy-like".

The fact that the bipy complexes display their characteristic behaviour in all the solvents and that the only other chelate structure that may conceivably be formed in the complexes of the hydroxy derivatives is that arising from *N*,*O*-chelation indicates that this structure is most probably the favourable one for the chelates of the *o*-hydroxy bipyridyls in protic solvents. Unfortunately, due to the different behaviour of oPP (see below), *N*,*O*-chelates could not be directly detected by means of optical spectroscopy and thus ^{1}H NMR experiments were additionally performed. [Note

that complexation of $BP(OH)_2$ to Cu^{II} in acetonitrile does not lead to the formation of an *N,N′*-chelate. The main absorption band remains centred at ca. 29000 cm^{-1}, but the shape of the spectrum very much resembles that of $BP(OH)_2$ in pure water, i.e. the Cu^{II} complex displays a second maximum at 23800 cm^{-1} ($\varepsilon \approx {}^1/_2\ \varepsilon_{max}$) and a shoulder at ca. 22600 cm^{-1} ($\varepsilon \approx {}^1/_3\ \varepsilon_{max}$). Thus, it seems possible that with the aid of complex formation, even the study of different enol(ate) and keto tautomers in solvents of different polarities and proticities is possible. As might have been expected, the Cu^{II} complex is non-fluorescent in acetonitrile (and also in ethanol).]

Stabilities of the Complexes

Analyzing titrations of $BP(OH)_2$, BPOH, and bipy with Zn^{II} in the three solvents studied, the apparent complex stability constants determined support the conclusions drawn on the basis of the photophysical properties.

In water, BPOH and $BP(OH)_2$ yield comparable log K^{app} values of 4.1 and 4.2 and the value for Zn^{II}/bipy amounts to 4.9. The particular behaviour of BPOH in ethanol is well-reflected by the shape of the titration curve monitored at 360 nm (Figure 6, middle section), while in acetonitrile the similarity of the Zn^{II}/bipy and Zn^{II}/BPOH complexes is evident. Furthermore, whenever *N,O*-chelation occurs, it is not only the work necessary for desolvation of the cation and ligand and the enthalpic and entropic contributions gained by complex formation that have to be considered, but the work necessary for deprotonation also becomes important. Since we determined the apparent (spectroscopic) complex stabilities here, further investigations are necessary to study the effect of the different solvents on the true log K_1 for the reaction $M + L \rightleftharpoons ML$ (see, e.g., ref.[47]).

oPP

As mentioned above, only very small cation-induced effects on the photophysical properties of oPP were found in the course of these investigations. This is consistent with results reported previously in the literature, where oPP was described as being non-fluorescent at room temperature[24] and the only complexation reaction in water to yield spectroscopic effects was found to be that involving Be^{II} ions.[27] Besides Kábrt and Holzbecher, Johnston and Freiser reported on the complexation of oPP with Cu^{II} in water/dioxane (50:50), but for all the *o*-(2-heterocycle)phenol derivatives (with heterocycle = pyridyl, imidazolinyl, benzimidazolyl, isoquinolinyl) investigated by these researchers, the stability constant obtained for oPP was the smallest.[26] In the crystalline state, the strong internal hydrogen bond (oPP shows the shortest N−O distance in X-ray structures of the *o*-hydroxy bipyridyls)[24] represents a counterforce to the conformation oPP has to adopt in all the complexes synthesized to date (e.g. a twist of ca. 25° between the aryl rings in a Co^{III} complex,[48] and of 34° in a $[Ru^{II}bipy_2oPP]$ complex[30]). Furthermore, for the Co^{III} complex of oPP, Ganis et al. observed a broad distribution of twist angles (22−29°) for the ligand in the crystalline state, suggesting that in the complex oPP has a low rotational energy barrier.[48] In accordance with our observations, this could point to the formation of a (loose) complex in solution, which is spectroscopically inaccessible.

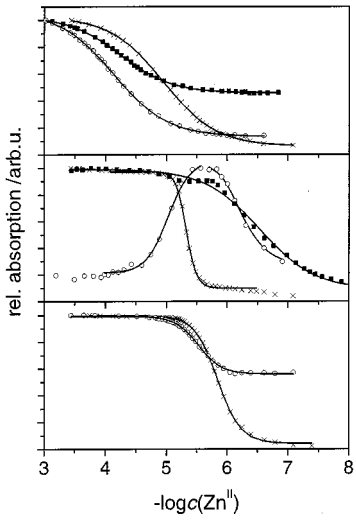


Figure 6. Titration curves $[A(\lambda)_{norm}$ vs. $-\log c_{Zn}]$ for $BP(OH)_2$, BPOH, and bipy with Zn^{II} in water (top), ethanol (middle), and acetonitrile (bottom); $BP(OH)_2$ = ■, monitored at 365 nm (H_2O) and 370 nm (EtOH); BPOH = ○, monitored at 371 nm (H_2O), 360 nm (EtOH), and 335 nm (MeCN); bipy = ×, monitored at 307 nm (H_2O), 307 nm (EtOH), and 305 nm (MeCN); solid lines represent fits according to the procedure described in the Experimental Section; because of the strong overlap of the bands of the two complexes involved in a titration of $BP(OH)_2$ with Zn^{II} in MeCN, the comparatively low complex stability of these complexes, and the limited solubility of $Zn(ClO_4)_2$ in MeCN, these data are omitted in the bottom graph for better clarity

NMR Spectroscopy in Acetonitrile

In order to verify the chelate structures anticipated for $M^{II}/BP(OH)_2$ in polar solvents, the ^1H NMR spectra of $BP(OH)_2$, BPOH, and bipy, as well as their Zn^{II} and Cd^{II} complexes were recorded in deuterated acetonitrile (CD_3CN). The data are collected in Table 4.

Table 4. ^1H NMR chemical shifts (ppm from TMS) of the heteroaromatic protons of $BP(OH)_2$, BPOH, and bipy (solvent = CD_3CN, counterion = perchlorate, $c_L = 1{\cdot}10^{-4}$ M, $c_{Zn} = 2{\cdot}10^{-3}$ M, c_{Cd} = 0.185 M)

	Position 3	4	5	6	3′	4′	5′	6′
bipy	8.410	8.875	7.371	8.647	–	–	–	–
+ Zn^{II}	8.492	8.314	7.828	8.793	–	–	–	–
+ Cd^{II}	8.491	8.262	7.800	8.721	–	–	–	–
BPOH	–	7.304	7.292	8.184	8.564	8.014	7.451	8.575
+ Zn^{II}	–	7.819	7.669	8.386	9.072	8.259	7.746	8.794
+ Cd^{II}	–	7.769[a]	7.624[a]	8.266[a]	9.1[b]	8.188	7.702	8.691
$BP(OH)_2$	–	7.441	7.385	8.116	–	–	–	–
+ Zn^{II}	–	7.472	7.409	8.131	–	–	–	–
+ Cd^{II}	–	7.54	7.540	8.140	–	–	–	–

[a] Broad. – [b] Very broad.

An important feature with regard to the determination of the nature of the complexes is the presence and position of the signal due to the OH group involved in internal hydrogen-bond formation (Scheme 2). For the free ligands,

this signal was found at the expected low field position, i.e. at $\delta = 14.14$ for BPOH and at $\delta = 14.51$ for $BP(OH)_2$. In the case of BPOH, addition of Zn^{II} ions led to a drastic shift in the position of this signal such that it appeared at $\delta = 9.22$. In contrast to this observation, the signal remains at $\delta = 14.5$ in $Zn^{II}/BP(OH)_2$, although it is broadened. Thus, the "proton chelate" in BPOH is "cracked" upon Zn^{II} complexation, but remains at least partially intact in $Zn^{II}/BP(OH)_2$ (case A in Scheme 1; see ref.[45] and, concerning the effects of internal hydrogen bonding, cf. the ^{15}N and ^{17}O NMR studies by Sitkowski et al.[49]).

The same conclusion could be drawn from the changes in the chemical shifts of the signals of the heteroaromatic protons. It is well-known that upon complexation the conformation of bipy changes from its favoured *trans* form in inert solvents to the corresponding *cis* form in the complex (bidentate chelate).[50,51] Although complex formation with bipy is accompanied by only minor changes in chemical shifts,[51,52] the downfield shifts of the 4-H and 5-H signals are especially characteristic.

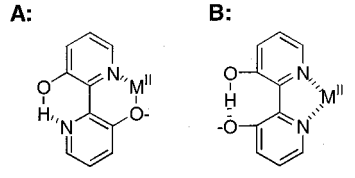
For BPOH, these shifts are of the same magnitude as for bipy (Table 4 and Figure S4, Supplementary Material). This result further supports the explanation that Zn^{II} is bound by BPOH in acetonitrile through *N*,*N*′-coordination with accompanying loss of the intramolecular hydrogen bond of the ligand. On the other hand, for $BP(OH)_2$, virtually no changes in the positions of the resonances of the aromatic protons are observed upon complexation. The signals are merely broadened due to the dynamics of exchange effects. This broadening is even more pronounced in the Cd^{II} complex, although the effects induced by both ions are similar (Table 4).

Unfortunately, due to the relatively high concentrations required for the NMR measurements and the rather poor solubility of Zn^{II} salts in acetonitrile, it was not possible to identify the proposed *N*,*N*′-chelate at high excess of Zn^{II} over $BP(OH)_2$ (see above). In the case of Cd^{II}, no such complex was observed in any experiment.

Five- vs. Six-Membered Chelates and the Influence of "Proton Chelates"

For some combinations of solvent, ion, and ligand [notably for protic solvents, Cd^{II}, and $BP(OH)_2$], the chelation behaviour found for the *o*-hydroxy bipyridyls is characterized by two unusual complexation features: (i) the formation of a six-membered ring in spite of the fact that the five-membered ring is usually more stable, and (ii) a preference for *N*,*O*-chelation over *N*,*N*′-chelation of "soft" or "borderline"[5,44] metal ions. These ions usually prefer coordination by π-donating (heterocyclic) nitrogen atoms to that by σ-donating oxygen atoms.[5]

In the case of $BP(OH)_2$, the chelate with a five-membered ring, which represents the only possible structure for $M^{II}\subset$bipy, is only favoured to some extent in solvents possessing no H-bond donating ability, e.g. acetonitrile. Only in such solvents does the possibility of forming the relatively unstable seven-membered "proton chelate" (case B in Scheme 3) with an intramolecular O−H−O bridge exist. Its formation or otherwise could not be clarified in this work. All attempts to grow crystals of this complex species were unsuccessful and the observation of a characteristic signal at $\delta \approx 18$ (O−H−O bridge)[45] in the ^1H NMR spectra was not possible due to the limited solubility of Zn^{II} salts in acetonitrile. Thus, the fact that the stability of hydrogen bond bridges ("proton chelate") is greatly enhanced for six-membered rings as compared to five- or seven-membered rings seems to be the main driving force here.[37,42,43] The strong seven-membered "proton chelate" reported by Cargill Thompson et al. for a mononuclear $Ru^{II}bipy_2-BP(OH)_2$ complex[45] seems to be the weaker structure in the present complexes. It is mainly the increase in mesomeric stabilization and resonance in the six-membered ring (higher degree of aromaticity) that renders the hydrogen bond stable in six-membered rings and accounts for this structural preference. The stabilizing mesomeric effect in the *N*,*O*-chelate can be rationalized as a "tautomeric electron-pair shift" leading to enhanced electron delocalization. Stabilization of six-membered metal ion chelates by six-membered "proton chelates" has been observed previously.[53] Furthermore, for six-membered chelates in azomethine derivatives, only minor differences between the "proton chelate" and the metal ion chelate have been observed, i.e. it is mainly the lone electron pair on the nitrogen atom that takes part in coordination and the aromatic ring π-electrons are little involved in the binding of the metal ion.[54] Here again, six-membered "proton chelates" are the most stable.[37,38] Moreover, all the observations of enhanced stability of six-membered chelates listed above have been made for systems in aqueous solutions. In the case of the *N*,*N*′-chelated $Ru^{II}bipy_2-BP(OH)_2$ complex described by Cargill Thompson et al., the limited possibilities in an $Ru^{II}bipy_2$-prearranged coordination sphere seem to favour deprotonation and *cis* chelation of $BP(OH)_2$ as the third ligand. Unfortunately, the low solubility of Zn^{II} in acetonitrile prevented the estimation of both the fluorescence quantum yield and lifetime of the 1:1 $Zn^{II}\subset BP(OH)_2$ complex, thus making a further verification of the conformation of the ligands impossible here. [Note that, as compared to the planarity of the type of chelate reported by Cargill Thompson et al., *N*,*N*′-chelation of $BP(OH)_2$ without deprotonation of a hydroxy group would lead to steric crowding of the OH groups and distortion of ligand planarity, resulting in blue-shifted spectra and a change in the rate constant, as has been observed for complexes of 3,3′-dimethyl-2,2′-bipyridyl.[55]]



Scheme 3. Chelation mechanisms for $M^{II}\subset BP(OH)_2$ formation, including possible stabilization modes by intramolecular hydrogen bonding (the structures do not indicate actual complex stoichiometries)

The results obtained for BPOH support the findings for $BP(OH)_2$. Even this ligand, for which *N*,*N*′-chelation should be more easily achievable owing to reduced steric hindrance (due to the lack of one *o*-hydroxyl group), favours *N*,*O*-chelation in aqueous solutions and for the primarily formed ML_2 complexes in ethanol. The formation of an additional "proton chelate" is not possible, but (a) solvent molecule(s) can saturate the second pyridyl nitrogen atom by hydrogen bonding [in the hydroxy bipyridyls where negative charge can be transferred from the oxygen to a nitrogen atom (Scheme 2), the pyridyl nitrogen atoms are more strongly π-basic]. In agreement with the solvent-dependent spectroscopic results, the only slightly smaller log-K^{app} value for $Zn^{II}\subset BPOH$ as compared to $Zn^{II}\subset BP(OH)_2$ in water suggests that in the latter the stabilization by the remaining intramolecular hydrogen bond is of a very delicate nature.

For the fluorescent complexes, a comparison of k_f and k_{nr} for $M^{II}/BP(OH)_2$ with those for the free ligand reveals that the stability of the planar ligand is increased in the complex, resulting in comparable rate constants for fluorescence deactivation (Table 1 cf. Table 3) but reduced rate constants for non-radiative deactivation. Thus, k_{nr} of the complexes is even smaller than that of the free ligand in apolar solvents such as *n*-hexane. The similarity of the photophysical properties of the "mono-enolate complex" $M^{II}\subset BPOH$ to those of $M^{II}\subset BP(OH)_2$ in water (and to some extent in ethanol) and the completely different behaviour of most M^{II}/oPP complexes suggests that the second pyridyl nitrogen atom (and not necessarily the whole PT site) may be important with regard to stabilization in both the ground and excited states in this medium. As for $BP(OH)_2$, upon charge-transfer in the excited state, the charge density on both nitrogen atoms was found to increase for BPOH and oPP.[12,13,24]

The stronger tendency of Cd^{II} to form six-membered *N*,*O*-chelates is in agreement with results obtained by other researchers on Cd^{II} and Zn^{II} complexes of mixed *N*,*O*-containing macrocyclic ligands.[56] Here, the tendency for exclusive *N*-coordination is generally higher for Zn^{II} than for Cd^{II}.[56]

Correspondingly, the observed drastic decrease in fluorescence intensity in the complexes with paramagnetic ions is due to the formation of a stable non-fluorescent complex, i.e. static quenching occurs.[57] Complexation of Hg^{II} results in the same static quenching effect, only in this case the heavy atom effect accounts for a higher intersystem crossing rate. For none of the quenching cations could complex-specific decay components with a fluorescence lifetime >100 ps be detected with the experimental set-up employed.

Conclusion

Investigations of the complexation behaviour of $BP(OH)_2$ and BPOH in aqueous, alcoholic, and acetonitrile solutions have revealed that the heavy and transition metal ion binding properties of $BP(OH)_2$ are rather non-selective and that chelation-induced fluorescence enhancement is only observed for the d^{10} metal ions Zn^{II} and Cd^{II}. Upon complexation to Hg^{II} or paramagnetic ions, static quenching occurs. Two different chelates of the Zn^{II} and Cd^{II} complexes of the *o*-hydroxy bipyridyls have been characterized by means of solvent-dependent optical spectroscopic and NMR studies. Here, the preference for *N*,*N*′-coordination over *N*,*O*-coordination increases with decreasing proticity of the solvent in the order water < ethanol < acetonitrile and is more pronounced for Zn^{II} than for Cd^{II} as well as for the complexes of BPOH compared to those of $BP(OH)_2$. The photophysical data of the *N*,*N*′-chelates of both hydroxy-substituted ligands are very similar to those of the *N*,*N*′-chelated reference complexes $M^{II}\subset$bipy. Thus, by controlling the proticity or hydrogen-bond donating ability of the environment in particular, it is possible to direct metal ion binding along a certain path to yield specifically coordinated complexes with multifunctional ligands.

Experimental Section

Materials: $BP(OH)_2$ (98%+, purchased from Aldrich and showing essentially the same features as a freshly prepared sample[58] kindly provided by Prof. H. Langhals, Ludwig-Maximilians-Universität München), bipy (99%+, Aldrich), as well as BPOH and oPP (both gifts from Dr. F. Vollmer, Technische Universität Berlin, synthesized according to ref.[24]) were checked by TLC (Kieselgel F_{254}, Merck) and used as received. Stock substrate solutions, typically $1\cdot10^{-3}$ M (in acetonitrile and ethanol) or $5\cdot10^{-5}$ M (in water), were kept under nitrogen and stored in the dark at 4 °C. Metal perchlorates purchased from Merck, Acros, or Aldrich were of the highest available purity and were dried (vacuum oven) to a definite water content employing various procedures adapted from ref.[59] For example, Hg^{II} perchlorate was dried at 75 °C for 12 h yielding $Hg^{II}(ClO_4)_2\cdot 3\,H_2O$, while $Zn^{II}(ClO_4)_2\cdot 2\,H_2O$ was obtained by drying the commercial product at 100 °C in vacuo for 12 h. Stock solutions, typically $1\cdot10^{-3}$ to 0.1 M (depending on the solubility of the metal salt in the relevant solvent), were stored under nitrogen in the dark at 4 °C (**Caution**: Perchlorate salts present a potential explosion hazard and should be handled with care and possibly only in small quantities!). Ethanol and acetonitrile (Aldrich) were of UV-spectroscopic grade. Doubly-distilled water (pH 6.39) was provided by the Laboratory for Trace Elemental Analysis, BAM, Berlin.

Steady-State Absorption and Fluorescence Spectroscopy: UV/vis spectra were recorded on a Carl Zeiss Specord M400/M500 absorption spectrometer, while steady-state emission spectra were measured with a Perkin−Elmer LS50B and a Spectronics Instruments 8100 spectrofluorometer. To determine the relative fluorescence quantum yields (φ_f), the optical densities (OD) of the solutions at the excitation wavelengths were adjusted to 0.1 ± 0.001 in 100 mm absorption cells. These solutions were then transferred to a 10 mm quartz cell and the fluorescence measurements were performed with a standard 90° geometry and with excitation and emission polarizers set at 0° and 54.7°. Quinine sulfate dihydrate (NIST standard reference material SRM 936) in 0.1 N H_2SO_4 (φ_f = 0.51 ± 0.03)[60] and $BP(OH)_2$ in cyclohexane (φ_f = 0.31 ± 0.02)[12b] were used as fluorescence standards. All fluorescence spectra presented here have been corrected for the spectral response of the detection system (calibrated quartz halogen lamp placed inside an integrating

sphere; Gigahertz-Optik) and for the spectral irradiance of the excitation channel (calibrated silicon diode mounted at a sphere port; Gigahertz-Optik). The fluorescence quantum yields were calculated from 4 independent measurements; the uncertainties in the measurements were estimated to be ±5% (for $\varphi_f > 0.2$), ±10% (for $0.2 > \varphi_f > 0.02$), ±20% (for $0.02 > \varphi_f > 5\cdot10^{-3}$), and ±30% (for $5\cdot10^{-3} > \varphi_f$), respectively.

Time-Resolved Fluorescence Spectroscopy: Fluorescence lifetimes (τ_f) were measured with synchrotron radiation from the Berlin Storage Ring for Synchrotron Radiation (BESSY).[61] The fluorescence was collected at right angles (monochromators with a spectral bandwidth of 8 nm) and the excitation wavelength of the synchrotron radiation was selected with a monochromator of 2 nm spectral bandwidth. The pulsed excitation source BESSY allowed for a temporal resolution of 100 ps (single-bunch mode; 4.8 MHz). The fluorescence decay curves were recorded with a time-correlated single-photon counting set-up and a time division of 55.5 ps channel^{-1}; typical count rates were of the order of $1\cdot10^3$ counts s^{-1}. For the fluorescence decay measurements, data were accumulated up to 5000 counts in the peak channel for a single decay. The temporal calibration of the experimental set-up for the time-resolved measurements was checked with Rose Bengal in methanol ($\tau_f = 0.50 \pm 0.02$ ns),[62] 1,4-bis(5-phenyloxazol-2-yl)benzene (POPOP) in ethanol ($\tau_f = 1.35 \pm 0.20$ ns),[63] and fluorescein 27 in 0.1 N NaOH ($\tau_f = 4.50 \pm 0.03$ ns).[63] For all the decay measurements, emission polarizers were set at 54.7°.

NMR Spectroscopy: One- and two-dimensional NMR spectra [COSY (90°) and $^{13}C/^{1}H$ HECTOR] were recorded on a Bruker DMX 400 spectrometer (5 mm tube, CD_3CN, deuterium lock). The ^1H NMR spectra of the free ligands were assigned on the basis of the typical coupling patterns for such compounds. In particular, the signals due to 6-H (α to the pyridyl nitrogen atom), showing a decreased vicinal coupling constant ^3J(5-H, 6-H),[64] were easily identified. Application of the method of incremental schemes,[64] well-established for pyridyl systems, revealed a good agreement between the measured and tabulated data and the coupling constants obtained correspond well with data reported for pyridyl systems in the literature.[64] In the case of BPOH, additional measurements were necessary to fully assign all the seven ^1H signals. A two dimensional ^1H-^1H correlation spectrum (COSY) allowed the separation of the three-spin system of the hydroxypyridyl moiety and the four-spin system of the pyridyl ring. The close similarity of the 4-H and 5-H signals (AB part of an ABX spectrum) and of the 3′-H and 6′-H signals could be resolved by means of hetero-correlated ^{13}C-^1H spectra (partly including ^1H-^1H homo-coupling).

Complex Stability Constants: The complex stability constants K reported herein were determined from absorption measurements (in 50 or 100 mm absorption cells) by adding aliquots of the appropriate metal ion solution to a solution of the ligand (c_{M0} titration). Besides large errors encountered in absorption (or fluorescence) measurements at (very) low ligand concentrations (very dilute solutions), the solubility of the ligands (especially in water and when a high excess toward the end of the titration is required) proved to be the limiting factor for performing c_{L0} titrations in order to determine K values of high order (1:2, 1:3 complexes) or successive K_n values. The latter was also hampered by the spectral similarities of the individual complexes. In the case of high complex stability constants [e.g. for complexes of $BP(OH)_2$ with paramagnetic ions] as well as mixed stoichiometries, fitting of the c_{M0} titration data to 1:1 and 1:2 complexes yielded no K_n values of acceptable accuracy. Thus, in order to obtain a measure for all the cations investigated, the apparent complex stability constant K^{app} was obtained by carrying out c_{M0} titrations with similar c_{L0} and fitting the sigmoidal curve of a $\Delta A(\lambda)$ vs. $-\log c_M$ plot. When no diverse spectral features occur in such a c_{M0} titration, K^{app} corresponds best to the process $M + ML_2 \rightarrow 2\,ML$.

Acknowledgments

Financial support from the Deutsche Forschungsgemeinschaft (K. R.) and the Fonds der Chemischen Industrie (R. R.) is gratefully acknowledged.

[1] [1a] *Bioinorganic Chemistry* (Ed.: A. X. Trautwein), Wiley-VCH, Weinheim, **1997**. – [1b] *Bioinorganic Chemistry* (Ed.: D. P. Kessissoglou), NATO ASI Series: Ser. C, Vol. 459, Kluwer, Dordrecht, **1995**. – [1c] I. Bertini, *Bioinorganic Chemistry*, Univ. Science Books, Mill Valley, CA, **1994**. – [1d] *Metals and Their Compounds in the Environment* (Ed.: E. Merian), VCH, Weinheim, **1991**.

[2] [2a] R. H. Holm, P. Kennepohl, E. I. Solomon, *Chem. Rev.* **1996**, *96*, 2239–2314. – [2b] H. Sigel, *Coord. Chem. Rev.* **1995**, *144*, 287–319. – [2c] C. P. Rao, K. Geetha, M. S. S. Raghavan, A. Sreedhara, K. Tokunaga, T. Yamaguchi, V. Jadhav, K. N. Ganesh, T. Krishnamoorthy, K. V. A. Ramaiah, R. K. Bhattacharyya, *Inorg. Chim. Acta* **2000**, *297*, 373–382.

[3] [3a] S. J. Berners-Price, P. J. Sadler, *Coord. Chem. Rev.* **1996**, *151*, 1–40. – [3b] V. Sharma, D. Piwnica-Worms, *Chem. Rev.* **1999**, *99*, 2545–2560. – [3c] A. Y. Louie, T. J. Maede, *Chem. Rev.* **1999**, *99*, 2711–2734. – [3d] R. Bakhtiar, E.-I. Ochiai, *General Pharmacology* **1999**, *32*, 525–540. – [3e] Z. Guo, P. J. Sadler, *Angew. Chem. Int. Ed.* **1999**, *38*, 1512–1531.

[4] [4a] A. Berkessel, J. W. Bats, M. Bolte, T. Neumann, L. Seidel, *Chem. Ber.* **1997**, *130*, 891–897. – [4b] G. Parkin, *Inorg. Chem.* **1996**, *35*, 2415–2420.

[5] [5a] F. Umland, *Theorie und Praktische Anwendung von Komplexbildnern*, Akademische Verlagsgesellschaft, Frankfurt/M., **1971**, pp. 80–129. – [5b] R. D. Hancock, A. E. Martell, *Chem. Rev.* **1989**, *89*, 1875–1914.

[6] [6a] U. Casellato, P. A. Vigato, M. Vidali, *Coord. Chem. Rev.* **1977**, *23*, 31–117. – [6b] J. Császár, *Acta Phys. Chem., Szeged* **1982**, *28*, 35–43. – [6c] J. Császár, *Acta Phys. Chem., Szeged* **1982**, *28*, 45–58. – [6d] J. Császár, *Acta Phys. Chem., Szeged* **1982**, *28*, 59–75.

[7] [7a] G. Reid, M. Schröder, *Chem. Soc. Rev.* **1990**, *19*, 239–269. – [7b] *Cation Binding by Macrocycles* (Eds.: Y. Inoue, G. W. Gokel), Marcel Dekker, New York, **1990**. – [7c] M. M. Bernardo, M. J. Heeg, R. R. Schroeder, L. A. Ochrymowycz, D. B. Rorabacher, *Inorg. Chem.* **1992**, *31*, 191–198. – [7d] E. A. Ambundo, M.-V. Deydier, A. J. Grall, N. Aguera-Vega, L. T. Dressel, T. H. Cooper, M. J. Heeg, L. A. Ochrymowycz, D. B. Rorabacher, *Inorg. Chem.* **1999**, *38*, 4233–4242.

[8] K. Rurack, U. Resch, M. Senoner, S. Dähne, *J. Fluoresc.* **1993**, *3*, 141–143.

[9] K. Rurack, M. Senoner, U. Resch, S. Dähne, *J. Inf. Rec. Mater.* **1994**, *21*, 683–684.

[10] U. Resch, K. Rurack, *Proc. SPIE-Int. Soc. Opt. Eng.* **1997**, *3105*, 96–103.

[11] K. Rurack, U. Resch-Genger, W. Rettig, *J. Photochem. Photobiol., A: Chem.* **1998**, *118*, 143–149.

[12] [12a] H. Bulska, *Chem. Phys. Lett.* **1983**, *98*, 398–402. – [12b] H. Bulska, *J. Lumin.* **1988**, *39*, 293–299.

[13] H. Bulska, A. Grabowska, Z. R. Grabowski, *J. Lumin.* **1986**, *35*, 189–197.

[14] A. Grabowska, L. Kaczmarek, *Pol. J. Chem.* **1992**, *66*, 715–731.

[15] P. Borowicz, A. Grabowska, L. Kaczmarek, A. Lés, L. Adamowicz, *Chem. Phys. Lett.* **1995**, *239*, 282–289.

[16] F. Vollmer, W. Rettig, *J. Photochem. Photobiol., A: Chem.* **1996**, *95*, 143–155.

[17] [17a] H. Zhang, P. van der Meulen, M. Glasbeek, *Chem. Phys. Lett.* **1996**, *253*, 97–102. – [17b] D. Marks, H. Zhang, M. Glasbeek, P. Borowicz, A. Grabowska, *Chem. Phys. Lett.* **1997**, *275*, 370–376. – [17c] D. Marks, P. Prosposito, H. Zhang, M. Glasbeek, *Chem. Phys. Lett.* **1998**, *289*, 535–540. – [17d] D. Marks, H. Zhang, P. Borowicz, A. Grabowska, M. Glasbeek, *Chem.*

Phys. Lett. **1999**, *309*, 19−28. − [17e] P. Borowicz, A. Grabowska, A. Les, L. Kaczmarek, B. Zagrodzki, *Chem. Phys. Lett.* **1998**, *291*, 351−359.
[18] J. Sepiol, A. Grabowska, H. Bulska, A. Mordzinski, F. Perez Salgado, R. P. H. Rettschnick, *Chem. Phys. Lett.* **1989**, *163*, 443−448.
[19] A. L. Sobolewski, L. Adamowicz, *Chem. Phys. Lett.* **1996**, *252*, 33−41.
[20] L. B.-Å. Johansson, L. Persson, H. Langhals, *J. Chem. Soc., Faraday Trans.* **1996**, *92*, 4909−4911.
[21] P. Borowicz, A. Grabowska, R. Wortmann, W. Liptay, *J. Lumin.* **1992**, *52*, 265−273.
[22] K. Tokumura, O. Oyama, H. Mukaihata, M. Itoh, *J. Phys. Chem. A* **1997**, *101*, 1419−1421.
[23] D. LeGourrierec, S. M. Ormson, R. G. Brown, W. Rettig, *BESSY Annual Rep.* **1995**, 473−475.
[24] L. Kaczmarek, R. Balicki, J. Lipkowski, P. Borowicz, A. Grabowska, *J. Chem. Soc., Perkin Trans. 2* **1994**, 1603−1610.
[25] M. I. Knyazhansky, N. I. Makarova, A. V. Metelitsa, V. A. Kharlanov, V. A. Pichko, E. P. Olehnovich, *Book of Abstracts*, XVI IUPAC Symposium on Photochemistry, Helsinki, IUPAC, **1996**, 328−329.
[26] W. D. Johnston, H. Freiser, *Anal. Chim. Acta* **1954**, *11*, 301−308.
[27] L. Kábrt, Z. Holzbecher, *Collect. Czech. Chem. Commun.* **1976**, *41*, 540−547.
[28] T. Fujii, T. Murakami, T. Mabuchi, T. Tsuchida, Y. Yokoya, N. Nakamura, S. Wakabayashi, T. Yamazaki, I. Yamazaki, *J. Fac. Eng. Shinshu Univ.* **1993**, *73*, 39−47.
[29] [29a] M. L. Martinez, W. C. Cooper, P.-T. Chou, *Chem. Phys. Lett.* **1992**, *193*, 151−154. − [29b] P.-T. Chou, C.-Y. Wei, *J. Phys. Chem.* **1996**, *100*, 17059−17066. − [29c] A. Sytnik, M. Kasha, *Proc. Natl. Acad. Sci. USA* **1994**, *91*, 8627−8630. − [29d] A. Sytnik, J. C. Del Valle, *J. Phys. Chem.* **1995**, *99*, 13028−13032.
[30] B. M. Holligan, J. C. Jeffery, M. K. Norgett, E. Schatz, M. D. Ward, *J. Chem. Soc., Dalton Trans.* **1992**, 3345−3351.
[31] [31a] J. Kotlicka, Z. R. Grabowski, *J. Photochem.* **1979**, *11*, 413−418. − [31b] M. S. Henry, M. Z. Hoffman, *J. Am. Chem. Soc.* **1977**, *99*, 5201−5203. − [31c] M. S. Henry, M. Z. Hoffman, *J. Phys. Chem.* **1979**, *83*, 618−625. − [31d] S. Dhanya, P. K. Bhattacharyya, *J. Photochem. Photobiol., A: Chem.* **1992**, *63*, 179−185.
[32] F. Umland, *Theorie und Praktische Anwendung von Komplexbildnern*, Akademische Verlagsgesellschaft, Frankfurt/M., **1971**, pp. 174−193.
[33] W. C. Vosburgh, G. R. Cooper, *J. Am. Chem. Soc.* **1941**, *63*, 437−442.
[34] M. V. Alfimov, A. V. Churakov, Y. V. Fedorov, O. A. Fedorova, S. P. Gromov, R. E. Hester, J. A. K. Howard, L. G. Kuz'mina, I. K. Lednev, J. N. Moore, *J. Chem. Soc., Perkin Trans. 2* **1997**, 2249−2256.
[35] H. Irving, R. J. P. Williams, *Nature (London)* **1948**, *162*, 746−747.
[36] F. Umland, *Theorie und Praktische Anwendung von Komplexbildnern*, Akademische Verlagsgesellschaft, Frankfurt/M., **1971**, pp. 45−149.
[37] E. Bayer, *Chem. Ber.* **1957**, *90*, 2325−2338.
[38] E. Jungreis, S. Thabet, in: *Chelates in Analytical Chemistry* (Eds.: H. A. Flaschka, A. J. Barnard, Jr.), Marcel Dekker, New York, **1969**, pp. 149−177.
[39] [39a] A. C. Braithwaite, N. T. Waters, *J. Inorg. Nucl. Chem.* **1973**, *35*, 3223−3229. − [39b] A. C. Braithwaite, P. E. Wrigth, N. T. Waters, *J. Inorg. Nucl. Chem.* **1975**, *37*, 1669−1674.
[40] D. S. McClure, *J. Chem. Phys.* **1952**, *20*, 682−686.
[41] F. E. Lytle, D. R. Storey, M. E. Juricich, *Spectrochim. Acta* **1973**, *29A*, 1357−1369.
[42] G. Schwarzenbach, *Adv. Inorg. Radiochem.* **1961**, *3*, 257−285.
[43] R. W. Parry, in *The Chemistry of the Coordination Compounds* (Eds.: J. C. Bailar, Jr., D. H. Busch), Reinhold, New York, **1956**, pp. 221−252.
[44] [44a] R. G. Pearson, *J. Am. Chem. Soc.* **1963**, *85*, 3533−3539. − [44b] R. G. Pearson, *Inorg. Chem.* **1988**, *27*, 734−740.
[45] A. M. W. Cargill Thompson, J. C. Jeffery, D. J. Liard, M. D. Ward, *J. Chem. Soc., Dalton Trans.* **1996**, 879−884.
[46] H. L. Schläfer, *Z. Phys. Chem., Neue Folge* **1956**, *8*, 373−386.
[47] [47a] T. Burchard, B. G. Cox, P. Firman, H. Schneider, *Ber. Bunsenges. Phys. Chem.* **1994**, *98*, 1526−1533. − [47b] T. Burchard, P. Firman, H. Schneider, B. G. Cox, *Ber. Bunsenges. Phys. Chem.* **1994**, *98*, 1534−1540. − [47c] B. G. Cox, J. Garcia-Rosas, H. Schneider, *J. Am. Chem. Soc.* **1981**, *103*, 1384−1389.
[48] P. Ganis, A. Saporito, A. Vitagliano, G. Valle, *Inorg. Chim. Acta* **1988**, *142*, 75−79.
[49] J. Sitkowski, L. Stefaniak, L. Kaczmarek, G. A. Webb, *J. Mol. Struct.* **1996**, *385*, 65−67.
[50] E. Castellucci, L. Angeloni, G. Marconi, E. Venuti, I. Baraldi, *J. Phys. Chem.* **1990**, *94*, 1740−1745.
[51] F. Vögtle, *Supramolekulare Chemie*, B. G. Teubner, Stuttgart, 2nd ed., **1992**, p. 36.
[52] S. Castellano, H. Günther, S. Ebersole, *J. Phys. Chem.* **1965**, *69*, 4166−4176.
[53] F. Umland, *Theorie und Praktische Anwendung von Komplexbildnern*, Akademische Verlagsgesellschaft, Frankfurt/M., **1971**, pp. 109, 124.
[54] F. Umland, B. K. Poddar, H. Stegemeyer, *Z. Analyt. Chem.* **1966**, *216*, 125−150.
[55] K. Nakamaru, *Bull. Chem. Soc. Jpn.* **1982**, *55*, 2697−2705.
[56] K. R. Adam, K. P. Dancey, A. J. Leong, L. F. Lindoy, B. J. McCool, M. McPartlin, P. A. Tasker, *J. Am. Chem. Soc.* **1988**, *110*, 8471−8477.
[57] [57a] T. L. Banfield, D. Husain, *Trans. Faraday Soc.* **1969**, *65*, 1985−1991. − [57b] A. W. Varnes, R. B. Dodson, E. L. Wehry, *J. Am. Chem. Soc.* **1972**, *94*, 946−950.
[58] C. Naumann, H. Langhals, *Synthesis* **1990**, 279−281.
[59] *Gmelins Handbuch der Anorganischen Chemie. Chlor*, 8th ed., VCH, Berlin, **1927**.
[60] R. A. Velapoldi, in: *Advances in Standards and Methodology in Spectrophotometry* (Eds.: C. Burgess, K. D. Mielenz), Elsevier Science, Amsterdam, **1987**, pp. 175−193.
[61] M. Vogel, W. Rettig, *Ber. Bunsenges. Phys. Chem.* **1987**, *91*, 1241−1247.
[62] D. F. Eaton, *J. Photochem. Photobiol., B: Biol.* **1988**, *2*, 523−530.
[63] R. A. Velapoldi, M. S. Epstein, in *Luminescence Applications in Biological, Chemical, Environmental, and Hydrological Sciences* (Ed.: M. C. Goldberg), Vol. 383, ACS Symposium Series, American Chemical Society, Washington DC, **1989**, pp. 98−126.
[64] E. Pretsch, T. Clerc, J. Seibl, W. Simon, *Tables of Spectral Data for Structure Determination of Organic Compounds*, Springer, Berlin, **1989**, pp. H275, H315.
[65] *Handbook of Photochemistry* (Eds.: S. L. Murov, I. Carmichael, G. L. Hug), 2nd ed., Marcel Dekker, New York, **1993**.

Received April 4, 2000
[I00131]

Protonated *O,S*-Dimethyl Dithiocarbonate − Synthesis, Spectroscopic Characterization and the Crystal Structure of $(CH_3O)(CH_3S)CSH^+SbF_6^-$

Rolf Minkwitz*[a] and Frank Neikes[a]

Keywords: Carbocations / IR spectroscopy / Raman spectroscopy / NMR spectroscopy / Protonations

Dithiocarbonic acid *O,S*-dimethyl ester reacts with the super acidic system HF/MF_5 (M = As, Sb) to form $(MeO)(MeS)CSX^+MF_6^-$ (M = As, Sb; X = H, D). $(MeO)(MeS)CSH^+SbF_6^-$ crystallizes in the monoclinic space group $P2_1/n$ (No. 14) with a = 8.634(2) Å, b = 9.521(3)Å, c = 12.509(4) Å, β = 97.39 (2)° and 4 formula units per cell. The reaction of *O,S*-dimethyl dithiocarbonate with the super acidic systems XF/MF_5 (X = H, D; M = As, Sb) is discussed with regard to the formation of the salts, and Raman, IR, ^1H NMR, and ^{13}C NMR spectra of $(MeO)(MeS)CSX^+MF_6^-$ (M = As, Sb; X = H, D) are reported.

Introduction

In our investigations of mono-, di-, and trihydroxy carbenium ions and mercapto carbenium ions, we wanted to know how *O,S*-carbonic acids behave in super acidic media.[1−5] We had to fall back on derivatives of the acids, since the free monothio- and dithiocarbonic acids have not yet been isolated. Dialkylxanthogenic acids are well known in the literature, where the work of Gattow and co-workers in the area of the chalcogenocarbonic acids and sulfur chemistry should be mentioned.[6,7]

Nevertheless, until now, single-crystal X-ray investigations have only been conducted on metal xanthogenates, for example $Sn[S_2COMe]_2$ or $Cd[S_2COC_2H_5]_2$.[8,9] X-ray investigations of a positively charged OCS_2 skeleton are not known. Alkyl xanthogenates decompose in the presence of aqueous acids, since the alkyl xanthogenic acid intermediate is formed, which is not stable under normal conditions. To avoid decomposition in super acidic systems the use of dialkyl xanthogenates, which can be handled easily at ambient temperature, is recommended. As the crystal structures of the hydroxy dimethoxy carbenium cation and mercapto dimethylthio carbenium cation and Olah's NMR studies show, all methyl groups are located in *trans* positions.[4,5] The same configuration is expected for the cation formed by protonation of dimethyl xanthogenates. However, it remains to be determined whether a 1,3-methyl shift to form the $(MeS)_2COH^+$ cation (**I**), protonation to form an oxonium cation (**II**) or protonation to form a sulfonium cation (**III**) takes place (Figure 1). The X-ray structure and further investigations are of interest for this reason.

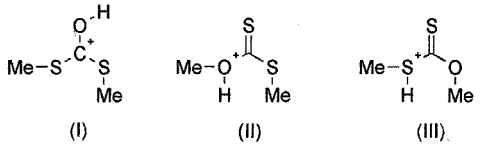


Figure 1. Potential reaction products

[a] Anorganische Chemie, Fachbereich Chemie der Universität Dortmund,
44221 Dortmund, Germany

Results and Discussion

Formation of $(MeO)(MeS)CSH^+$ Salts

The best way to form the precursor (MeO)(MeS)CS for reaction in the super acidic system XF/MF_5 (M = As, Sb; X = H, D) is by the known reaction of NaOMe and CS_2 (Equation 1) followed by reaction with MeI[10] (Equation 2). Other reactions using alkali salts of dithiocarbonic acids such as $Na_2OC(S)S$ and methyl halides do not lead to uniform products (Equation 3).

$$NaOMe + CS_2 \rightarrow MeOC(S)SNa \quad (1)$$

$$NaS(S)COMe + MeI \rightarrow (MeO)(SMe)C{=}S \quad (2)$$

$$Na_2OC(S)S + 2MeI \rightarrow (MeO)(MeS)C{=}S + (MeS)_2C{=}O \quad (3)$$

Mercapto methoxy methylthio carbenium hexafluorometallate can be isolated from the protonation of (MeO)-(MeS)CS in the super acidic systems HF, $(DF)/MF_5$ (M = As, Sb) (Equation 4).

$$(MeO)(MeS)C{=}S + HF/MF_5 \rightarrow (MeO)(MeS)CSH^+MF_6^- \text{ (M= As, Sb)} \quad (4)$$

The resulting yellow salts, sensitive towards moisture and soluble in SO_2, decompose above −25 °C in the case of the arsenate and above −29 °C in the case of the antimonate into substances which were not further investigated. The salts can be stored without decomposition under inert conditions at −70 °C. Crystals of $(MeO)(MeS)CSH^+$-SbF_6^-suitable for X-ray diffraction studies could be isolated.

^1H and ^{13}C NMR Spectra of $(MeO)(MeS)CSH^+MF_6^-$ (M = As, Sb)

The ^1H NMR spectra at −60 °C of freshly prepared $(MeO)(MeS)CSH^+AsF_6^-$ and $(MeO)(MeS)CSH^+SbF_6^-$ in

 © WILEY-VCH Verlag GmbH, D-69451 Weinheim, 2000 1434−1948/00/1010−2283 $ 17.50+.50/0

SO_2, with TMS as external standard, show singlets at δ = 4.98 and 4.90, respectively, for the protons of the methoxy groups and singlets at δ = 3.09 and 3.04, respectively, for the methylthio groups. The signals for the remaining mercapto groups are observed at δ = 6.99 and 7.2. In the ^{13}C NMR spectra, the signals at δ = 17.79 and 69.36 for the AsF_6^- species, and at δ = 17.68 and 68.79 for the SbF_6^- species, are assigned to the CH_3-S and CH_3-O groups and the singlets at δ = 221.9 and 221.4 are assigned to the carbon of the OCS_2 group. These results are comparable to the ^1H-NMR spectra of the $(HS)_3C^+$ and $(HO)(HS)_2C^+$ cations observed by G. A. Olah, as well as investigations of Barany et al. and our previous NMR investigations.[4,5,10,11]

Raman and IR Spectra of $(MeO)(MeS)CSX^+MF_6^-$ (M = As, Sb; X = H, D)

The infrared and Raman spectra of $(MeO)(MeS)CSD^+$ AsF_6^- are depicted in Figure 2. The observed frequencies of the $(MeO)(MeS)CSX^+$ salts of AsF_6^- and SbF_6^- (X = H, D) are summarized in Table 1. The assignments for the $(MeO)(MeS)CSX^+$ cation were made by comparison to the frequencies of $(MeS)_2CS$ and the $[MeOCS_2]^-$ anion.[4,5,12–14] On the assumption that the $(MeO)(MeS)CSX^+$ cation (X = H, D) has a C_1 point symmetry, 33 Raman- and IR-active fundamental vibrations are expected. The antisymmetric and symmetric stretching modes of the methyl groups are observed in the region 2933–3035 cm^{-1}.

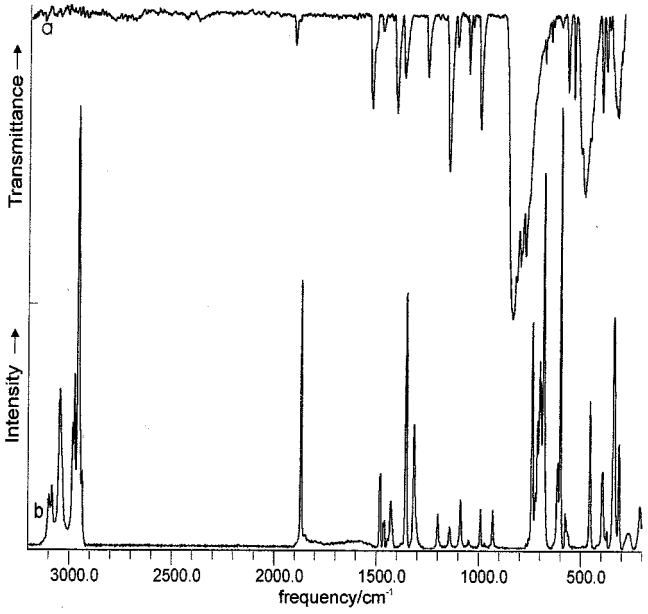


Figure 2. Infrared spectrum (trace A) and Raman spectrum (trace B) of $(MeO)(MeS)CSD^+AsF_6^-$

As with the precursor, different conformations arise in the solid, whereby the large number of valence modes can be explained.[15] The ν(SH) mode is observed at 2570 cm^{-1}, and the H/D shift to ca. 1860 cm^{-1} is almost in accordance with the expected shift.[16] The ν(SH) vibration mode in the AsF_6^- salt is shifted ca. 20 cm^{-1} to higher frequencies because the interaction between the anion and cation is weaker than in the SbF_6^- compound. This results in the loss of anion symmetry, which can be seen in the many anion vibration modes of the AsF_6^- salt. The deformation and rocking modes of the methyl groups are observed in their normal ranges of 1480–1300 cm^{-1} and 1000–880 cm^{-1}. A sharp Raman line and IR band is detected at 570 cm^{-1} and is assigned to the OCS_2 skeleton out of plane deformation mode.

The symmetric degradation is responsible for the additional As–F stretching modes. A complete assignment of the vibrational frequencies would require force field calculations.

Crystal Structure of $(CH_3O)(CH_3S)CSH^+SbF_6^-$

Mercapto methoxy methylthio carbenium hexafluoroantimonate crystallizes in the monoclinic space group $P2_1/n$ (No. 14) with four formula units per unit cell (Table 3).[17] The bond lengths and angles are listed in Table 2. Figure 3 shows the salt with atom labels, and the arrangement of $(MeO)(MeS)CSH^+SbF_6^-$ in the unit cell is depicted in Figure 4. For the data reduction, a semiempirical correction determined from ψ-scan data, and structure solution and refinement programs in the SHELXTL package and PARST were used.[18–21] The antimony and sulfur atoms were located by the Patterson method. All other atoms were determined by difference Fourier synthesis. A final refinement with anisotropic (except H atoms) thermal parameters gave a value of $R = 0.071$.

Both C(3)–S bond lengths of 1.702(7) Å and 1.692(7) Å and the C(3)–O(1) bond length of 1.293(9) Å lie in the range between typical single and double bonds.[22] If one takes the measured lengths as a basis, one comes to the conclusion that the positive charge is equally distributed over the central sp^2-hybridized C(3) carbon atom. The C(3)–O(1) bond length can be compared to the lengths of the CO bonds in the dihydroxy methyl carbenium cation and the $C(OH)_3^+$ cation. The C(3)–S(1) length, as well as the C(3)–S(2) bond length, is comparable with the corresponding lengths in the $(MeS)_2CSH^+$ cation.[1,2,4,5] The sum of angles around C(3) amounts to 360°, which indicates planar sp^2 hybridization. The torsion angles of the methyl groups, with a maximum deviation of 2.5°, indicate that they are not located in the OCS_2 plane.

The S(1)···F(4) distance of 2.903 Å indicates an S(1)–H(1)···F(4) hydrogen bond with an angle of 155°. A further donor–acceptor reciprocal effect exists between S(1) and F(2a) with a length of 2.903 Å, forming an eight-membered ring in a chair conformation (Figure 5). There are additional contacts but because of their longer interatomic distances, they are not considered. The ideal octahedron structure of the anion is not distorted, with almost ideal angles of 90° and lengths in the range of 1.863(5)–1.879(5) Å.

Table 1. Raman, IR frequencies, and possible assignment of $(CH_3O)(CH_3S)CSX^+MF_6^-$ (X = H, D; M = As, Sb)

$(CH_3O)(CH_3S)CSX^+AsF_6^-$				$(CH_3O)(CH_3S)CSX^+SbF_6^-$			
X = H		X = D		X = H	X = D		Possible
IR	Raman	IR	Raman	Raman	IR	Raman	Assignment
	3097(9)		3097(12)				ν CH_3
	3082(10)		3082(13)	3068(9)		3069(16)	ν CH_3
	3044(32)		3045(35)	3039(13)		3029(32)	ν CH_3
						3007(10)	ν CH_3
	2982(24)		2982(28)			2993(24)	ν CH_3
	2974(34)		2973(39)			2976(27)	ν CH_3
	2956(95)		2957(100)	2961(22)		2961(40)	ν CH_3
			2937(17)	2939(15)		2943(53)	ν CH_3
						2922(54)	ν CH_3
2566m	2569(59)	1864w	1869(60)	2538(63)	1846m	1850(53)	ν SX
1481m	1483(16)	1479sh	1483(16)	1480(9)		1481(23)	δ CH_3
1475m	1480(16)	1474m	1479(17)		1478s		δ CH_3
1461m	1465(7)		1464(6)	1460(10		1460(8)	δ CH_3
1454m	1458(7)	1458sh	1458(6)		1459m	1452(9)	δ CH_3
				1434(10)	1438m	1437(10)	δ CH_3
1426m	1428(12)	1426w	1429(11)		1428m		δ CH_3
				1419(8)	1420m	1420(8)	δ CH_3
1352m	1356(54)	1348m	1354(57)	1350(35)	1349s	1349(65)	δ CH_3
1313m	1317(26)	1312m	1316(28)	1310(20)	1305s	1312(33)	δ CH_3
					1227s	1222(5)	ν O−CS
1200m	1201(13)	1193m	1198(8)	1196(10)		1195(10)	ν CH_3−O
					1191m	1190(10)	ν CH_3−O
					1160m	1165(24)	ν CH_3−O
	1148(5)		1141(5)	1142(3)	1142sh		ν CH_3−O
1095m	1096(18)	1083s	1087(11)	1087(6)			ν C−S
					1069vs		ν C−S
1054m	1055(4)	1044w	1048(2)		1040m		ν C−S
996m	998(15)	988s	991(9)	996(8)	986m	989(7)	ρ CH_3
				972(3)	973m	974(7)	ρ CH_3
957m	959(7)			958(3)		940(22)	ρ CH_3
		926s	930(9)		929s		ρ CH_3
882w	885(7)			887(7)			ρ CH_3
						732(20)	ν S−CH_3
				702(18)	696m	708(31)	ν S−CH_3
610m		613sh	613(19)				ν S−COS
	605(100)	600m	602(99)	601(53)	599w	601(65)	ν S−COS
	575(7)	570w	575(8)	572(10)	568m	572(9)	γ OCS_2 out of plane
517w		516w					δ OCS
482m		482m			482w		δ OCS
453m	455(37)	452m	455(33)	450(15)	449m	452(43)	γ OCS_2 in plane
417s		414sh					δ SCS
				400(7)			δ SCS
						361(11)	δ SCS
	342(54)		339(52)	346(38)		345(29)	δ SCS
274s	268(5)	275m	263(4)				δ SCS
244s		240sh					δ SCS
		229m		229(4)		221(13)	τ CH_3
	208(11)		209(10)				τ CH_3
753vs		758vs		648(100)	662vs		ν MF_6
	737(45)	739vs	738(51)		654vs	650(100)	ν MF_6
719vs	720(11)	719vs	722(12)		646sh	640(77)	ν MF_6
	713(25)		713(29)				ν MF_6
			702(42)				ν MF_6
694vs	698(39)	693vs	697(37)	278(35)		282(31)	ν MF_6
680s	683(78)	678sh	684(85)				ν MF_6
	590(11)						ν MF_6
396m	394(18)	394s	393(17)				ν MF_6
370m	370(6)	367sh	371(4)				ν MF_6
309s	311(22)	309m	312(23)				ν MF_6

Conclusion

The protonation of (MeO)(MeS)CS succeeds in super acidic systems, forming the expected carbenium ion. A clear statement about the structure of the cation can be made due to X-ray structure analysis. The Raman spectra of the salts show that in the solid state several conformations are present, which makes assignment of the spectra more difficult. The NMR spectra in SO_2 were assigned, and only one conformation was observed. If the solvent is carefully removed, crystals with a single conformation, in the all-*trans* position, are formed, as was shown by the X-ray diffraction study.

Table 2. Bond lengths [Å] and angles [°] for (MeO)(MeS)-$CSH^+SbF_6^-$

Bond	Length [Å]	Angle	[°]
Sb(1)−F(1)	1.863(5)	F(1)−Sb(1)−F(2)	88.7(2)
Sb(1)−F(5)	1.868(5)	F(1)−Sb(1)−F(3)	178.6(2)
Sb(1)−F(3)	1.870(5)	F(1)−Sb(1)−F(4)	90.2(2)
Sb(1)−F(2)	1.871(5)	F(1)−Sb(1)−F(5)	90.5(3)
Sb(1)−F(4)	1.873(5)	F(1)−Sb(1)−F(6)	89.6(2)
Sb(1)−F(6)	1.879(5)	F(3)−Sb(1)−F(6)	89.9(2)
S(1)−C(3)	1.702(7)		
S(1)−H(1)	1.39(9)	C(3)−S(1)−H(1)	98(4)
S(2)−C(3)	1.692(7)	C(3)−S(2)−C(2)	101.3(4)
S(2)−C(2)	1.783(10)	C(3)−O(1)−C(1)	120.2(7)
O(1)−C(3)	1.293(9)	O(1)−C(3)−S(1)	120.5(5)
O(1)−C(1)	1.469(11)	O(1)−C(3)−S(2)	118.3(5)
		S(2)−C(3)−S(1)	121.2(4)

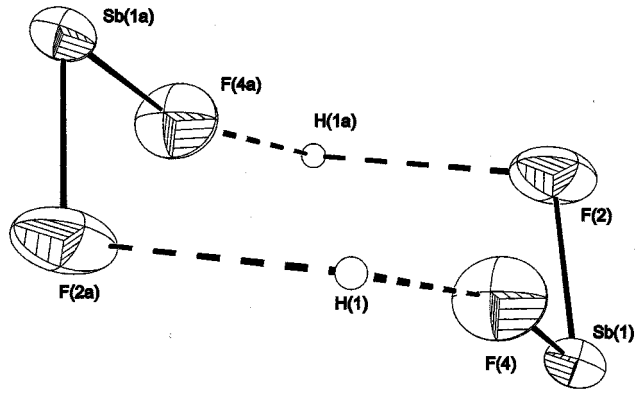


Figure 5. Structure of the chair-conformation 8-membered ring

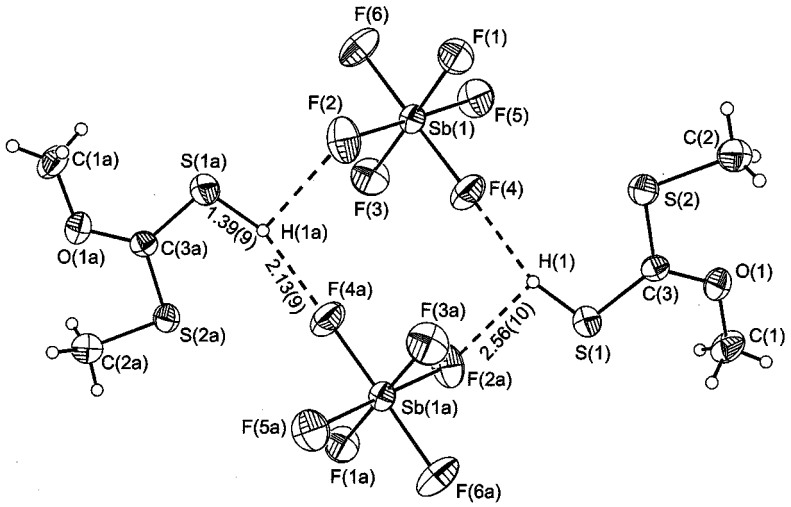


Figure 3. ORTEP of (MeO)(MeS)$CSH^+SbF_6^-$ with contacts; thermal ellipsoids are drawn at the 50% probability level

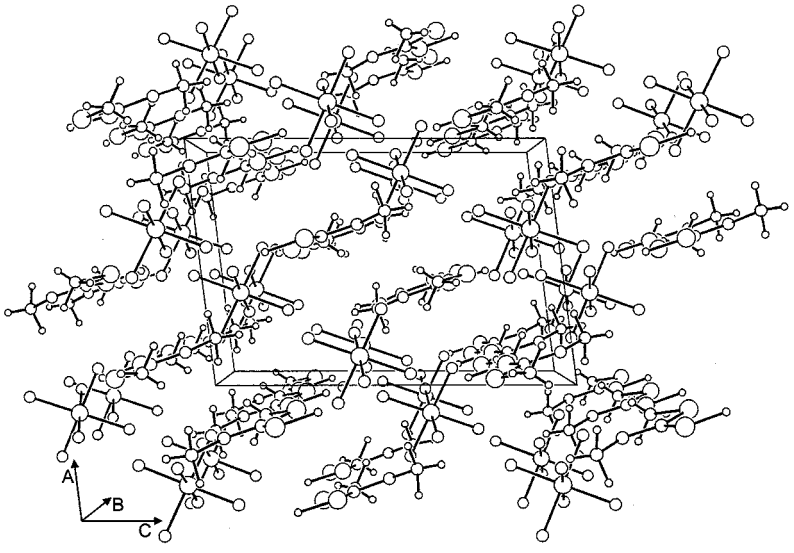


Figure 4. Structure of (MeO)(MeS)$CSH^+SbF_6^-$, showing the arrangement in the crystal lattice

Experimental Section

All synthetic work and sample handling was conducted by standard Schlenk techniques and a standard vacuum line (stainless steel or glass). SbF_5 (Merck) was fractionally distilled. Drying of HF and SO_2 were carried out by literature methods. Reactions in HF/DF were carried out in a KEL-F reactor with a KEL-F valve. − Infrared spectra were recorded with a Bruker IFS 113V spectrophotometer. Spectra of dry powders were obtained on a CsI plate in a cooled IR cell. − The Raman spectra were recorded with a Yobin von T64000 (ISA) using a CCD detector (EEV CCD15-11) and an Ar^+ laser tube (514.5 nm) from Spectra Physics. The spectra were recorded in a glass cell cooled with liquid nitrogen. − The NMR spectra were recorded with a Bruker DPX 300 spectrometer with TMS as external standard. − Single crystals were placed in Lindemann capillaries in a cooled stream of dry nitrogen, and an X-ray diffraction study was carried out at −100 °C using an Enraf-Nonius Mach3 automated diffractometer.

Preparation of (MeO)(MeS)CS: *O*,*S*-Dimethyl dithiocarbonate was prepared by reaction of NaOMe (20 g, 0.37 mol) with excess dry CS_2 (35 g, 0.46 mol) in dry diethyl ether solvent. After filtration and drying under dynamic vacuum at room temperature the residue was treated with excess MeI (55 g, 0.38 mol) at 25 °C.[10] After 2 h, the excess MeI was removed under reduced pressure at −10 °C and the remaining yellow liquid distilled at 10 °C under dynamic vacuum in 89% yield based on NaOMe.

Preparation of (MeO)(MeS)CSX$^+$MF$_6^-$ (X = H, D; M = As, Sb): ***Caution! Avoid contact with these compounds and note that hydrolysis of AsF$_6^-$ salts and SbF$_6^-$ salts forms HF, which burns the skin and causes irreparable damage. Safety precautions should be taken when using and handling these materials!*** In a typical experiment, *O*,*S*-dimethyl dithiocarbonate (0.24 g, 2 mmol) and anhydrous XF (X= H, D) (4 g, 0.2 mol) were combined at −196° C and placed in a KEL-F reactor. Arsenic pentafluoride (0.34 g, 2 mmol) or antimony pentafluoride (0.44 g, 2 mmol) was added to this mixture at −196 °C and the contents of the reactor were warmed to −78 °C. After 10 min, slow removal of all volatile material under vacuum at −78 °C gave a slightly yellow solid residue that was identified as (MeO)(MeS)CSX$^+$MF$_6^-$ (X= H, D; M= As, Sb). The remaining (MeO)(MeS)CSH$^+$SbF$_6^-$ contained crystals suitable for X-ray diffraction studies. The salts can be stored under inert conditions at −70 °C without decomposition.

Table 3. Crystal data and structure refinement for (MeO)(MeS)CSH$^+$SbF$_6^-$

Empirical formulae	$C_3H_7F_6OS_2Sb$
Molecular mass	358.96
Temperature	173(2) K
Wavelength	0.71069 Å
Crystal system	Monoclinic
Space group	$P2_1/n$
Unit cell dimensions	a = 8.634(2) Å b = 9.521(3) Å, β = 97.39(2)° c = 12.509(4) Å
Volume	1019.8(5) Å^3
Z	4
Density (calculated)	2.338 Mg/m^3
Absorption coefficient	3.163 mm^{-1}
F(000)	680
Crystal size	0.3 × 0.2 × 0.3 mm
Theta range for data collection	3.06° to 25.97°
Index ranges	$-10 \le h \le 10$, $0 \le k \le 11$, $0 \le l \le 15$
Reflections collected	2085
Independent reflections	1994 [R_{int} = 0.0246]
Absorption correction	ψ scans
Max. and min. transmission	0.9982 and 0.8569
Refinement method	Full-matrix least squares on F^2
Data/restraints/parameters	1994/0/140
Goodness-of-fit on F^2	1.113
Final R indices [$I > 2\sigma(I)$]	$R1$ = 0.047, $wR2$ = 0.106
R indices (all data)	$R1$ = 0.071, $wR2$ = 0.113
Largest diff. peak and hole	1.463 and −0.874 eÅ^{-3}

Acknowledgments

This work was supported by the Deutsche Forschungsgemeinschaft and the Fonds der Chemischen Industrie.

[1] R. Minkwitz, S. Schneider, M. Seifert, H. Hartl, *Z. Anorg. Allg. Chem.* **1996**, *622*, 1404.
[2] R. Minkwitz, S. Schneider, *Angew. Chem. Int. Ed.* **1999**, *38*, 714.
[3] R. Minkwitz, S. Schneider, H. Preut, *Angew. Chem. Int. Ed.* **1998**, *37*, 494.
[4] R. Minkwitz, F. Neikes, *Eur. J. Inorg. Chem.* **2000**, 1261−1265.
[5] R. Minkwitz, F. Neikes, *Inorg. Chem.* **1999**, *38*, 5960−5963.
[6] G. Gattow, W. Behrendt, in: *Topic in Sulfur Chemistry* (Ed.: A. Senning), vol. 2, Thieme, Stuttgart **1977**.
[7] M. Dräger, G. Gattow, *Angew. Chem. Intern. Ed. Engl.* **1968**, *7*, 868−879.
[8] P. F. R. Ewings, P. G. Harrison, T. J. King, *J. Chem. Soc. Dalton Trans.* **1976**, 1399−1403.
[9] Y. Iimura, T. Ito, H. Hagihara, *Acta Crystallogr.* **1972**, *B28*, 2271−2279.
[10] G. Barany, A. L. Schroll, A. W. Mott, D. A. Halsrud, *J. Org. Chem.* **1983**, *48*, 4750−4761.
[11] G. A. Olah, A. T. Ku, A. M. White, *J. Org. Chem.* **1969**, *34*, 1827.
[12] K. Herzog, E. Steger, P. Rosmus, S. Scheithauer, R. Mayer, *J. Mol. Struct.* **1969**, *3*, 339.
[13] M. Dräger, G. Gattow, *Chem. Ber.* **1971**, *104*, 1429.
[14] R. Mattes, G. Pauleickhoff, *Spectrochim. Acta* **1973**, *29A*, 1339.
[15] W. Knoth, G. Gattow, *Z. Anorg. Allg. Chem.* **1987**, *550*, 109−115.
[16] J. Weidlein, U. Müller, K. Dehnicke, *Schwingungsspektroskopie*, G. Thieme, Stuttgart, **1982**.
[17] Crystallographic Data (excluding structure factors) for the structure of (MeO)(MeS)CSH$^+$SbF$_6^-$ included in this paper have been deposited with the Cambridge Crystallographic Data Centre as supplementary publication no. CCDC-145117. Copies of the data can be obtained free charge on application to CCDC, 12 Union Road, Cambridge CB2 1 EZ, UK [Fax: (internat.) + 44-1223/336-033; E-mail: deposit@cccdc.cam.ac.uk].
[18] M. Nardelli, *Comput. Chem.* **1983**, *7*, 95.
[19] G. Sheldrick, *SHELXS 86*, University of Göttingen, Germany, **1986**.
[20] G. Sheldrick, *SHELXL 93*, University of Göttingen, Germany, **1993**.
[21] E. Keller, *SCHAKAL, Program for the Graphic Representation of Molecular and Crystallographic Models*, Albert-Ludwig-University of Freiburg, **1988**.
[22] F. H. Allen, O. Kennard, D. G. Watson, L. Brammer, A. G. Orpen, R. Taylor, *J. Chem. Soc., Perkin Trans. 2* **1987**, S1−S19.

Received March 3, 2000
[I00124]

Structural Investigations of Tetra- and Octasubstituted (Phthalocyanine)ruthenium Complexes by EXAFS Spectroscopy

Achim Weber,[a] Teja S. Ertel,[a] Ulrich Reinöhl,[a] Helmut Bertagnolli,*[a] Meret Leuze,[b] Michael Hees,[b] and Michael Hanack*[b]

Keywords: EXAFS spectroscopy / Ruthenium / Phthalocyanines / Structure elucidation

To obtain more structural information of (phthalocyaninato)-ruthenium compounds, an EXAFS investigation was carried out on amorphous tBu$_4$PcRu (**1**), tBu$_4$PcRu(3-Clpy)$_2$ (**2**), PcRu(3-Fpy)$_2$ (**3**) and (C$_5$H$_{11}$O)$_8$PcRu(3-Clpy)$_2$ (**4**). Structural models for the four compounds are deduced from the atomic distances determined around the metal centre. A dimeric structure was found for **1**, while bisaxial arrangement of the ligands was shown for **2, 3** and **4**, and the structural parameters were also determined.

Introduction

In recent years (phthalocyanine)ruthenium complexes have been investigated with particular regard to their preparation, chemistry, and structure.[1−3] Some years ago, we reported the first synthesis of pure (phthalocyananinato)ruthenium(II) (PcRu) by thermal decomposition of PcRu(DMSO)$_2$·2DMSO.[4] Later, we developed a convenient method for obtaining PcRu from the corresponding bis-(isoquinoline) complex PcRu(iqnl)$_2$, which decomposes at 250 °C with formation of pure PcRu.[5]

Due to the insolubility of PcRu − like most other (phthalocyanine)metal complexes − in common organic solvents, bulky (e.g. *tert*-butyl) or long-chain (e.g. alkyl or alkyloxy) groups are introduced onto the periphery of the Pc macrocycles to improve their solubility. The *tert*-butyl group is particularly suitable for increasing the solubility of phthalocyanines in organic solvents. Tetrasubstituted phthalocyanines usually exhibit higher solubilities than the octasubstituted analogues. The two principal reasons are that the isomeric mixture of four tetrasubstituted phthalocyanines leads to a lower degree of order in the solid state compared to the symmetrically octasubstituted phthalocyanines, and the higher dipole moment of the tetrasubstituted Pcs caused by the unsymmetrical arrangement of the substituents on the periphery of the macrocycle.[2] [Tetrakis(*tert*-butyl)phthalocyaninato]ruthenium(II) tBu$_4$PcRu (**1**),[6a] bis(3-chloropyridine)[tetrakis(*tert*-butyl)-phthalocyaninato]ruthenium(II) tBu$_4$PcRu(3-Clpy)$_2$ (**2**)[6a] (all mixtures of structural isomers), and several (octaalkyloxyphthalocyaninato)ruthenium compounds[5,6b,6c] are examples of soluble (phthalocyanine)ruthenium complexes. The thermal decomposition of the peripherally substituted R$_m$PcRu(3-Clpy)$_2$ provided the basis for the preparation of novel bridged [R$_m$PcRu(L)]$_n$ oligomers with L = pyz (pyrazine), dib (1,4-diisocyanobenzene), tz (*s*-tetrazine), and others as a new class of intrinsic semiconductors.[2,6b]

The crucial problem in the exact structural determination of (phthalocyanine)ruthenium compounds (PcRu) is that most of the compounds can only be prepared as amorphous or microcrystalline samples. In a previous paper we reported EXAFS studies on dimeric PcRu.[7] Our results are consistent with a dimeric structure having a short Ru−Ru contact of 2.41 Å. This agrees with LAXS investigations on the same system.[3] The existence of a Ru−Ru double bond is also confirmed by measurement of the magnetic moment, which amounts to 2.54 μ_B at room temperature.[7]

Now the question arises as to whether the formation of dimers is restricted to PcRu or whether it is a common phenomenon of (phthalocyanine)ruthenium compounds. There are some indications for the latter assumption, for example the magnetic moment of tBu$_4$PcRu has a value which is similar to PcRu.[6a] Temperature-dependent measurements of the magnetic susceptibility show **1** to exhibit paramagnetic behaviour with strong coupling. The magnetic moment increases from 0.63 μ_B (T = 20 K) to 1.68 μ_B (T = 300 K), i.e. it approximates asymptotically the spin-only value of one unpaired electron (1.73 μ_B). Compound **1** therefore has only one spin per ruthenium(II) ion, although for a d^6 transition metal ion in a square-planar ligand field two unpaired electrons are expected. This implies that **1** exists as a dimeric structure with a ruthenium−ruthenium double bond. For homometallic (porphyrin)metal dimers a molecular orbital diagram was developed[8] which proposes that only d electrons participate in metal−metal bonding. In addition, the reasonable assumption that the dimers have D_{4h} (eclipsed) or D_{4d} (staggered) symmetry was made. The σ bonds to the porphyrin nitrogen atoms involve the metal $d_{x^2-y^2}$ levels, and the high-energy σ* orbitals may be ig-

[a] Institut für Physikalische Chemie, Universität Stuttgart
Pfaffenwaldring 55, 70569 Stuttgart, Germany
Fax: (internat.) + 49-(0)711/685-4443
E-mail: h.bertagnolli@ipc.uni-stuttgart.de
[b] Institut für Organische Chemie, Universität Tübingen
Auf der Morgenstelle 18, 72076 Tübingen, Germany
Fax: (internat.) + 49-(0)7071/295244
E-mail: hanack@uni-tuebingen.de

 © WILEY-VCH Verlag GmbH, D-69451 Weinheim, 2000 1434−1948/00/1010−2289 $ 17.50+.50/0

nored for a metal-metal bonding.[8] The remaining d orbitals (d_{xz}, d_{yz}, d_{z^2}, and d_{xy}) are available for the metal−metal bonding along the *z* axis. Dimeric (porphyrin)- as well as (phthalocyanine)ruthenium(II) complexes possess 12 d-electrons and consequently the resulting electronic configuration, $\sigma^2\pi^4\delta^{nb4}\pi^{*2}$, produces a formal Ru−Ru double bond with two unpaired electrons (one per macrocycle). On the other hand one has to take into consideration that the four *tert*-butyl groups in **1** could cause steric hindrance if a dimeric structure is formed as in PcRu.

In order to answer these questions we performed EXAFS measurements on *t*Bu$_4$PcRu (**1**). In addition we carried out EXAFS measurements on *t*Bu$_4$PcRu(3-Clpy)$_2$ (**2**), PcRu(3-Fpy)$_2$ (**3**) and $(C_5H_{11}O)_8$PcRu(3-Clpy)$_2$ (**4**), for which crystal structures are not yet available, to obtain some structural data of these bissubstituted PcRu complexes. Furthermore, we intended to prove whether the different ligands are arranged in a strictly bisaxial disposition, and whether the different ligands (3-chloropyridine in **2** and **4**, 3-fluoropyridine in **3**) or the different phthalocyanine macrocycles [unsubstituted (**3**), 2,3-tetra- (**2**) and 1,4-octa-substituted (**4**) (see Figure 4)] have any structural effects on the local environment around the ruthenium centre.

Results and Discussion

[Tetrakis(*tert*-butyl)phthalocyaninato]ruthenium(II) (1)

As can be seen in the Fourier transform (see Figure 1b), there are several visible shells. In fitting the EXAFS function, we must describe it by at least six shells. Fitting the data by six shells seems to be many, but is not for two reasons. First, the coordination numbers were fixed to the known values of the phthalocyanine molecule. Second, the four shells of the phthalocyanine macrocycle marked with A in Table 1 (see Figure 2) can only be independently fitted such that the determined distances lead to meaningful interatomic distances in the macrocycle itself. Taking these considerations into account, the number of parameters decreases from 12 to 9 and are clearly less than the number of independent data points (22).[9] We successfully applied this data evaluation in previous work on (phthalocyaninato)ruthenium.[7]

Without any knowledge of the structure, one would expect that the ruthenium atom is located in the plane of the phthalocyanine ring. A planar arrangement of the atoms should give rise to a considerable contribution of multiple scattering to the EXAFS spectrum. Defining the multiple scattering unit as shown in Figure 3, we found in several calculations that for this geometrical arrangement the relevant maximum order of multiple scattering is three. But in all fits we could not describe the experimental spectrum satisfactorily. In particular, the characteristic features of the experimental $k^3\cdot\chi(k)$ function between 4.0 and 9.0 Å^{-1} could not be reproduced (see Figure 1c).

Since only single scattering contributes to the EXAFS function, we are forced to assume that either the ruthenium atom is not positioned in the plane of the ring, or the ring

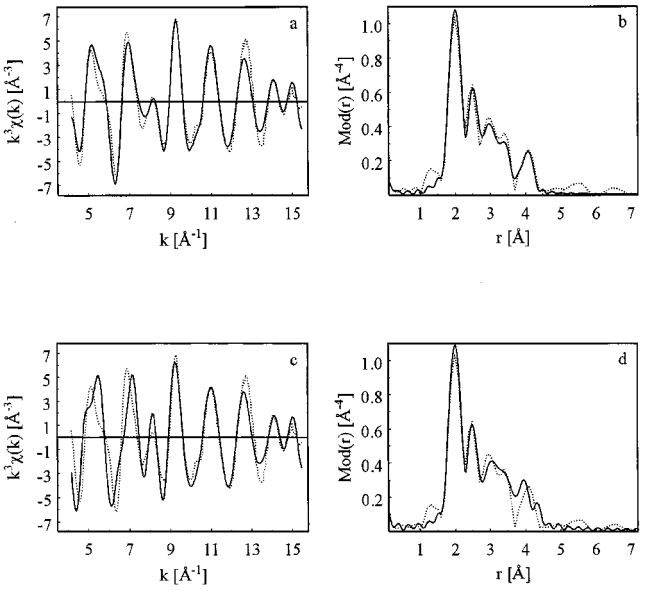


Figure 1. Experimental (dotted line) and calculated (solid line) $k^3\cdot\chi(k)$ function (a,c) (k range: 3.50−15.30 Å^{-1}) and their Fourier transforms (b,d) of *t*Bu$_4$PcRu (**1**) [see Table 1 for fitting parameters, considering single scattering only (a,b), including triple scattering paths (c,d)]

Table 1. EXAFS-determined structural data of **1**

[a]		R [Å]	N	σ [Å]	ΔE_0 [eV]	Fit index
Ru−N	(A)	2.01±0.02	4.0	0.055±0.009	19.96	25.91
Ru−C	(A)	3.05±0.03	8.0	0.067±0.011		
Ru−N	(A)	3.23±0.03	4.0	0.039±0.009		
Ru−C	(A)	4.04±0.04	8.0	0.071±0.009		
Ru−Ru	(B)	2.42±0.03	1.0	0.077±0.011		
Ru−N	(B)	3.38±0.03	4.0	0.040±0.009		

[a] Absorber−backscatterer distance r, coordination number N and Debye-Waller factor σ with their calculated standard deviation. The letters in parentheses refer to the model in Figure 2 and indicate the molecule where the backscattering atom is located.

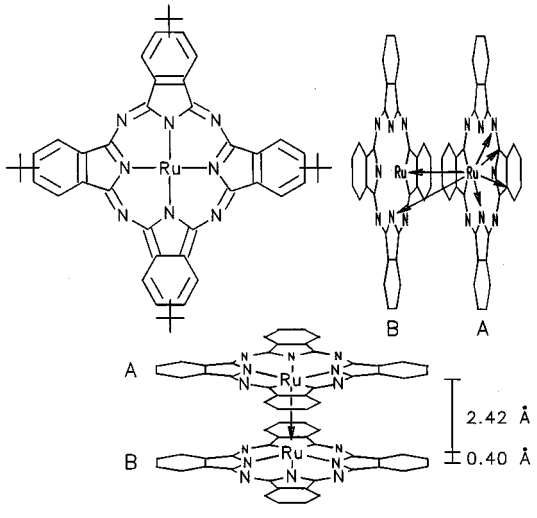


Figure 2. Structural model of *t*Bu$_4$PcRu (**1**) including the assignment of the determined distances to the corresponding atoms (see Table 1); for reasons of clarity, not all nitrogen atoms and *tert*-butyl groups are shown

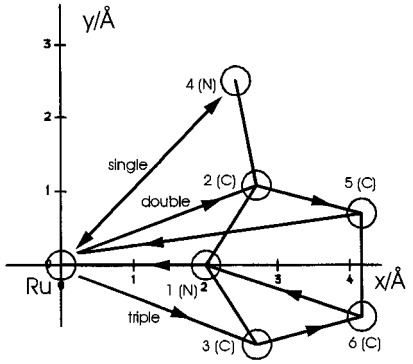


Figure 3. Defined multiple scattering unit for tBu$_4$PcRu (**1**) illustrating single, double and triple scattering paths

itself is not planar, or both. In order to check the dependence of the amount of multiple scattering from the out-of-plane displacement of the ruthenium atom in an idealized planar macrocycle we performed systematic calculations. We found the rather astonishing result that the amount of multiple scattering does not depend very strongly on the out-of-plane position of the ruthenium atom. Only if the displacement amounts to 1.75 Å does the contribution of the multiple scattering almost vanish. Since such a large displacement of the ruthenium atom is quite unlikely, we have to conclude that the nonplanarity of the macrocycle is the main cause of the absence of any multiple scattering and the possible displacement of the ruthenium atom − if existing − plays only a minor role. From the determined distances it is not possible to make any structural statements concerning the nonplanarity of the macrocycle.

Besides the four shells of the phthalocyanine macrocycle already discussed, a significant improvement in the fit index can be obtained if we assume a Ru−Ru distance of 2.42 Å in the simulation of the spectrum. Additionally, we found four nitrogen backscatterers at 3.38 Å. These distances can be assigned to the corresponding atoms in the macrocycle B (see Figure 2 and Table 1). In the context of the above discussion regarding the absence of any multiple scattering and the possible explanation for this, the presence of a Ru−Ru interaction at a distance of 2.42 Å is surely an indication that besides the nonplanarity of the macrocycle, an out-of-plane displacement of the ruthenium atom is also to a small degree responsible for the absence of any multiple scattering. Without the displacement, it is probably impossible to get the two ruthenium atoms this close. If we make the simplified assumption that the four nitrogen atoms of the phthalocyanine macrocycle forming the first coordination shell lie in a plane, the displacement of the ruthenium atom can be appraised in the following way. From crystallographic data[10,11] we know that the metal−nitrogen distance of planar systems, e.g. in phthalocyaninatomanganese tetracyanoethenide, is typically 1.97±0.3 Å. As an N−N diagonal distance of 3.94±0.6 Å follows from this value, we can calculate that the ruthenium atom is located 0.4±0.2 Å out of the plane of the macrocycle (see Figure 2). We note that this triangulation depends critically on both the measured Ru−N distance and the assumed N−center distance. It is given here only as a rough estimation of the amount of the possible displacement. Our data are also compatible with an in-plane geometry for **1**.

[Bis(3-chloropyridine)[tetrakis(*tert*-butyl)phthalocyaninato]-ruthenium(II) (2)

For a similar quality simulation of the EXAFS function of compound **2** (see Figure 4), at least six shells are necessary (see Table 2 and Figure 5a and 5b). These are the four shells of the phthalocyanine macrocycle and two nitrogen backscatterers at 2.53 Å, which can only be assigned to the ligand 3-chloropyridine, because no ring atoms are located within this distance. Furthermore, there are four carbon backscatterers at a distance of 3.43 Å, which also belong to 3-chloropyridine. As can be seen in Figure 5c and 5d, the four carbon backscatterers at 3.43 Å are necessary for a complete description of the experimental EXAFS function.

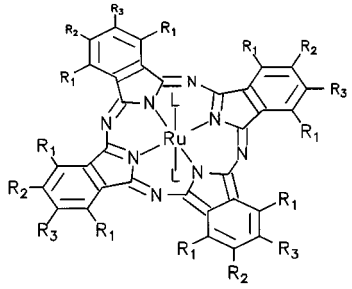


Figure 4. Schematic structural model of R$_n$PcRu(L)$_2$ (**2** for R$_2$ or R$_3$ = tBu, R$_1$ = H and L = 3-chloropyridine, **3** for R$_1$ = R$_2$ = R$_3$ = H and L = 3-fluoropyridine, **4** for R$_2$ = R$_3$ = H, R$_1$ = R$_4$ = C$_5$H$_{11}$O and L = 3-chloropyridine)

Table 2. EXAFS-determined structural data of **2**

[a]		R [Å]	N	σ [Å]	ΔE_0 [eV]	Fit index
Ru−N	(A)	2.03±0.02	4.0	0.060±0.009	19.13	21.74
Ru−C	(A)	3.07±0.03	8.0	0.056±0.009		
Ru−N	(A)	3.31±0.03	4.0	0.053±0.009		
Ru−C	(A)	4.00±0.04	8.0	0.075±0.010		
Ru−N	(L)	2.53±0.03	2.0	0.086±0.011		
Ru−C	(L)	3.43±0.03	4.0	0.048±0.009		

[a] Absorber−backscatterer distance r, coordination number N and Debye-Waller factor σ with their calculated standard deviation. The letters in parentheses refer to the model in Figure 4 and indicate the molecule where the backscattering atom is located.

With the distances to the ligand determined as Ru−N (2.53 Å) and Ru−C (3.43 Å), an N−C distance in 3-chloropyridine of 1.38 Å can be calculated (see Figure 6), in good agreement with the expected value of 1.34 Å for the intramolecular C−N distance in pyridine.[12] In one of our previous works[7] we found an Ru−Ru distance at 4.14 Å in PcRu(nBuNH$_2$)$_2$. No Ru−Ru distance in this range could be found in **2**. These results led us to the conclusion that the 3-chloropyridine molecule is vertically located below and above the phthalocyanine macrocycle and forms an octahedral arrangement around the ruthenium centre (see Figure 4 and Figure 6) together with the four nitrogen

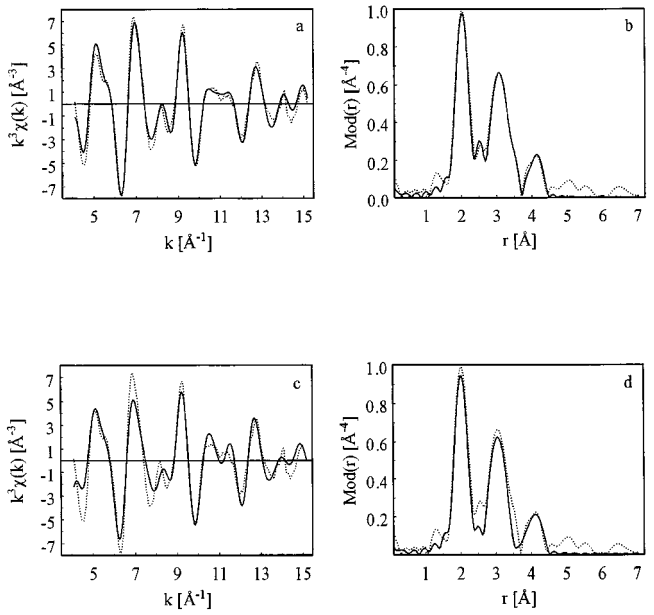


Figure 5. Experimental (dotted line) and calculated (solid line) $k^3 \cdot \chi(k)$ function (a,c) (k range: 3.45−15.15 Å^{-1}) and their Fourier transforms (b,d) of tBu$_4$PcRu(3-Clpy)$_2$ (**2**) [see Table 2 for fitting parameters, six shells model (a,b) and five shells model (c,d), respectively]

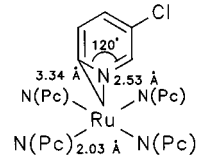


Figure 6. A detailed view from Figure 4; the ligand, the ruthenium centre and the first nitrogen backscatterers are shown

atoms of the phthalocyanine macrocycle. The axial coordination of the 3-chloropyridine ligand prevents the formation of a dimeric phthalocyanine unit coupled over an Ru−Ru double bond. The absence of any multiple scattering in **2** is surely only a result of the nonplanarity of the macrocycle and an out-of-plane displacement is very unlikely. This is because this displacement would lead to a distorted octahedral geometry, and the fact that in **2** no short Ru−Ru interaction is detectable as in compound **1** and PcRu.[7]

[Bis(3-fluoropyridine)phthalocyaninato]ruthenium(II) (3)

As in **2**, six shells are required to describe the EXAFS function (see Table 3 and Figure 7). Again, these are the four shells of the phthalocyanine macrocycle and, additionally, two nitrogen backscatterers at 2.57 Å, which only can be assigned to the ligand 3-fluoropyridine, because no ring atoms are located within this range. Furthermore, there are four carbon backscatterers at a distance of 3.41 Å, also from 3-fluoropyridine. In comparison to **2**, the distance of the ruthenium absorber and the nitrogen backscatterers of the ligand are not significantly different from each other.

Table 3. EXAFS-determined structural data of **3**

[a]		R [Å]	N	σ [Å]	ΔE_0 [eV]	Fit index
Ru−N	(A)	2.02±0.02	4.0	0.063±0.009	20.40	30.77
Ru−C	(A)	3.03±0.03	8.0	0.050±0.009		
Ru−N	(A)	3.23±0.03	4.0	0.080±0.009		
Ru−C	(A)	4.03±0.04	8.0	0.078±0.010		
Ru−N	(L)	2.57±0.03	2.0	0.098±0.011		
Ru−C	(L)	3.41±0.03	4.0	0.053±0.009		

[a] Absorber−backscatterer distance r, coordination number N and Debye-Waller factor σ with their calculated standard deviation. The letters in parentheses refer to the model in Figure 4 and indicate the molecule where the backscattering atom is located.

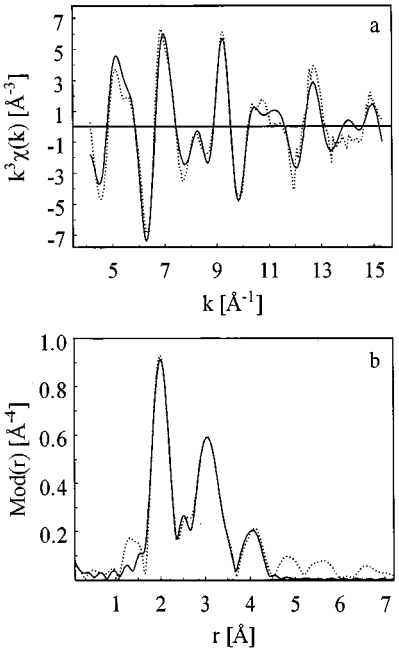


Figure 7. Experimental (dotted line) and calculated (solid line) $k^3 \cdot \chi(k)$ function (a) (k range: 4.15−15.35 Å^{-1}) and their Fourier transforms (b) of PcRu(3-Fpy)$_2$ (**3**) (see Table 3 for fitting parameters)

Table 4. EXAFS-determined structural data of **4**

[a]		R [Å]	N	σ [Å]	ΔE_0 [eV]	Fit index
Ru−N	(A)	2.03±0.02	4.0	0.062±0.009	20.70	25.46
Ru−C	(A)	3.04±0.03	8.0	0.051±0.009		
Ru−N	(A)	3.26±0.03	4.0	0.073±0.009		
Ru−C	(A)	4.03±0.04	8.0	0.073±0.010		
Ru−N	(L)	2.55±0.03	2.0	0.088±0.011		
Ru−C	(L)	3.42±0.02	4.0	0.049±0.009		

[a] Absorber−backscatterer distance r, coordination number N and Debye-Waller factor σ with their calculated standard deviation. The letters in parentheses refer to the model in Figure 4 and indicate the molecule where the backscattering atom is located.

[Bis(3-chloropyridine)octakis(pentyloxy)phthalocyaninato]-ruthenium(II) (4)

As with compounds **2** and **3**, at least six shells are necessary to describe the EXAFS function (see Table 4 and Figure 8). As the structure and the determined structural para-

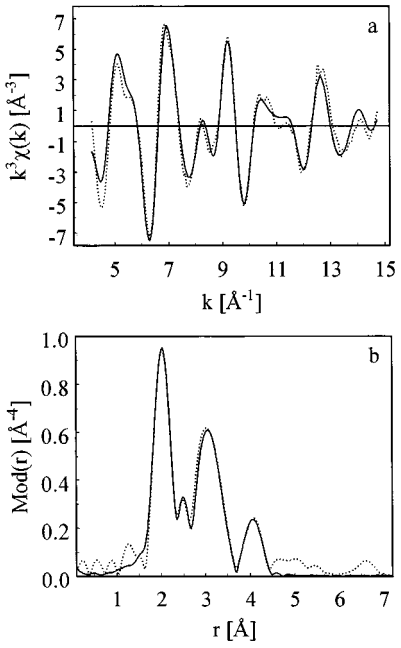


Figure 8. Experimental (dotted line) and calculated (solid line) $k^3 \cdot \chi(k)$ function (a) (k range: 3.50−14.80 Å^{-1}) and their Fourier transforms (b) of $(C_5H_{11}O)_8$PcRu(3-Clpy)$_2$ (**4**) (see Table 4 for fitting parameters)

meters of the PcRu complexes **2**, **3** and **4** are very similar, we refrain from further discussion of the structure of compound **4**.

Conclusion

It was possible to deduce structural models for tBu$_4$PcRu (**1**), tBu$_4$PcRu(3-Clpy)$_2$ (**2**), PcRu(3-Fpy)$_2$ (**3**) and $(C_5H_{11}O)_8$PcRu(3-Clpy)$_2$ (**4**) by EXAFS spectroscopy. The structure of tBu$_4$PcRu (**1**) is very similar to that of PcRu,[7] which forms a dimer. However, one has to take into consideration the four *tert*-butyl groups on both of the Pc rings, which could lead to severe steric hindrance in a dimeric structure of **1**. According to model considerations, the interaction between two *tert*-butyl groups, even in an eclipsed conformation, is not very high, e.g. if both rings adopt the C_{4h} structure, because the distance of the two coplanar Pc rings in **1** is 3.2 Å. This is also the case for the three additional structural isomers of tBu$_4$PcRu (**1**), namely the D_{2h}, C_{2v}, and the C_s isomers.[13] Less steric interaction of the *tert*-butyl groups will occur if the dimer (tBu$_4$PcRu)$_2$ is formed from two different structural isomers of tBu$_4$PcRu, e.g. if it is a mixture of the C_{4h} and the D_{2h} isomer. The Ru−Ru-distance in **1** and in the unsubstituted PcRu are quite similar.[7] This also points to a low steric interaction between the *tert*-butyl groups on both Pc rings in **1**. A dimeric structure for **1** is therefore quite feasible. Attempts to calculate the interactions between the *tert*-butyl groups by using the standard HyperChem program was not successful due to the large number of atoms in the dimer **1**.

Sixfold coordination of the ruthenium atom occurs in compounds in **2**, **3** and **4**. The ligands are axially located in an octahedral arrangement on both sides of the phthalocyanine macrocycle. The differences in the environment around the ruthenium centre between the PcRu with the 3-chloropyridine ligands and the 3-fluoropyridine ligands and the unsubstituted, tetra- and octa-substituted macrocycles are not very large, but it should be noted that the distances of the ruthenium atom to the nitrogen backscatterers of the pyridine ligands become smaller, and the distances of the ruthenium atom to the second nitrogen backscatterers of the phthalocyanine macrocycle increase in the sequence **3** > **4** > **2**. This could be interpreted as being due to non-planar Pc rings in these compounds.

Experimental Section

General Remarks: ^{1}H, ^{13}C NMR: Bruker AC 250 (^{1}H: 250.133 MHz, ^{13}C: 62.902 MHz). − UV/Vis: Shimadzu UV−365. − FT IR: Bruker IFS 48. − Elemental analyses: Carlo Erba Elemental Analyser 1104, 1106. − MS: Varian Mat 711.

[Tetrakis(*tert*-butyl)phthalocyaninato]ruthenium(II) (tBu$_4$PcRu, 1): [Tetrakis(*tert*-butyl)phthalocyaninato]ruthenium(II) was prepared by thermal decomposition of bis(3-chloropyridine)[tetrakis(*tert*-butyl)phthalocyaninato]ruthenium(II) (**2**).[6a] − $C_{48}H_{48}N_8Ru$ (838.03): calcd. C 68.71, H 5.77, N 13.36; found C 68.00, H 5.99, N 13.01.

Bis(3-chloropyridine)[tetrakis(*tert*-butyl)phthalocyaninato]-ruthenium(II) (tBu$_4$PcRu(3-Clpy)$_2$, 2): Bis(3-chloropyridine)[tetrakis(*tert*-butyl)phthalocyaninato]ruthenium(II) (**2**) was prepared from 4-*tert*-butylphthalonitrile, $RuCl_3 \cdot 3H_2O$ and 3-chloropyridine according to the method described.[6a] − $C_{58}H_{56}Cl_2N_{10}Ru$ (1065.13): calcd. C 65.39, H 5.30, Cl 6.57, N 13.16; found C 65.39, H 6.06, Cl 6.57, N 13.19.

Phthalocyaninatoruthenium PcRu (**5**) was prepared according to the method described earlier.[4,5]

Bis(3-fluoropyridine)phthalocyaninatoruthenium (PcRu(3-Fpy)$_2$, 3): A mixture of (phthalocyaninato)ruthenium (**5**) (100 mg, 0.16 mmol), 3-fluoropyridine (31.5 mg, 0.32 mmol) and chloroform (10 mL) was heated at reflux for 6 h. The solution was poured into methanol/water (3:1) and the precipitate was centrifuged and dried. Purification was carried out by column chromatography (silica gel, chloroform, R_f = 0.65). After drying (50 °C, 0.01 Torr), pure **3** was obtained; yield 79 mg (61%). − $C_{42}H_{24}F_2N_{10}Ru$ (808.12): calcd. C 62.37, H 2.99, N 17.33; found C 62.51, H 3.02, N 16.97. − ^{1}H NMR (250 MHz, $CDCl_3$): δ = 2.21 (m, 2 H, 3-Clpy), 2.36 (m, 2 H, 3-Clpy), 5.24 (m, 2 H, 3-Clpy), 5.83 (m, 2 H, 3-Clpy), 7.97 (m, 8 H, Pc), 9.22 (m, 8 H, Pc). − IR (KBr): $\tilde{\nu}$ = 3111 cm^{-1} (vw), 3057 (vw), 2924 (vw), 1607 (w), 1582 (m), 1489 (vs), 1433 (m), 1414 (m), 1325 (m), 1288 (m), 1242 (m), 1238 (m), 1169 (vs), 1124 (vs), 1065 (m), 845 (m), 804 (m), 773 (m), 690 (w). − UV/Vis ($CHCl_3$): λ_{max} = 627 nm (Q), 573 sh, 402 sh, 369 sh, 312 (B).

Bis(3-chloropyridine)[1,4,8,11,15,18,22,25-octakis(pentyloxy)phthalocyaninato]ruthenium(II) (4): A mixture of 3,6-dipentyloxyphthalonitrile (3.0 g, 10 mmol), $RuCl_3 \cdot 3H_2O$ (650 mg, 2.5 mmol), 3-chloropyridine (570 mg, 5 mmol) and DBU (1 mL) in 2-ethoxyethanol (30 mL) was heated at reflux for 7 d under nitrogen, while monitoring the reaction by TLC (SiO_2/$CHCl_3$, R_f = 0.8). The solution was poured into methanol/water (3:1) and the precipitate was centrifuged and dried. The dry precipitate was subsequently subjected to Soxhlet extraction with methanol for 10 h.

Purification was carried out by column chromatography (silica gel, chloroform). After drying (60 °C, 0.01 Torr, 6 h) pure **4** was obtained; yield 485 mg (12.7%), green powder. − $C_{82}H_{104}Cl_2N_{10}O_8Ru$ (1529.77): calcd. C 64.37, H 6.86, Cl 4.58, N 9.16; found C 64.04, H 6.88, Cl 4.60, N 9.13. − ^{1}H NMR (250 MHz, $CDCl_3$): δ = 1.02 (t, J = 6.8 Hz, 24 H, CH_3), 1.56 (m, 32 H, 2 CH_2), 2.30 (m, 16 H, CH_2), 2.50 (m, 2 H, 3-Clpy), 2.51 (m, 2 H, 3-Clpy), 4.84 (t, J = 6.4 Hz 16 H, CH_2), 5.22 (m, 2 H, 3-Clpy), 6.10 (m, 2 H, 3-Clpy), 7.29 (s, 8 H, Pc). − ^{13}C NMR (250 MHz, $CDCl_3$): δ = 13.9 (CH_3), 22.7 (CH_2), 28.3 (CH_2), 29.3 (CH_2), 71.5 (−O−CH_2), 115.7 (Pc), 122.5 (3-Clpy), 129.6 (Pc), 130.5 (3-Clpy), 133.0 (3-Clpy), 143.3 (Pc), 148.5 (3-Clpy), 148.9 (3-Clpy), 150.4 (Pc). − IR (KBr): $\tilde{\nu}$ = 3097 cm^{-1} (vw), 3033 (vw), 2954 (s), 2927 (s), 1597 (m), 1498 (vs), 1465 (m), 1308 (m), 1283 (s), 1261 (s), 1219 (vs), 1111 (s), 1062 (s), 972 (w). − UV/Vis ($CHCl_3$): λ_{max} = 699 nm (Q), 630, 405, 312 (B). − MS (FAB, NBA); *m/z*: 1529.9 [M^+], 1303.8 [$M^+ - 2 \times$ 3-Clpy].

The EXAFS measurements of tBu$_4$PcRu (**1**), tBu$_4$PcRu(3-Clpy)$_2$ (**2**), PcRu(3-Fpy)$_2$ (**3**) and ($C_5H_{11}O)_8$PcRu(3-Clpy)$_2$ (**4**) were performed at the ruthenium K edge at 22118.0 eV at the beamline A1 at the *Hamburger Synchrotronstrahlungslabor* (HASYLAB) at DESY, Hamburg, at 25 °C, with an Si<311> double crystal monochromator under ambient conditions (5.4 GeV, beam current 100 mA). The tilt of the second monochromator crystal was set to 30% harmonic rejection. Energy resolution was estimated to be about 10 eV at the ruthenium K edge. Data were collected in transmission mode with ion chambers, which were continuously flushed with argon. Energy calibration was monitored with a 20-μm thick ruthenium metal foil. All measurements were performed under an inert gas. The samples were embedded in a polyethylene matrix, of which the thickness was adjusted to an absorption jump of Δμ = 1.5. Data were analysed with a program package specially developed for the analysis of amorphous samples.[14] The program AUTOBK of the University of Washington[15] was used for background removal and the program EXCURV92[16] for the evaluation of the XAFS functions. First, background absorption was removed from the experimental absorption spectrum by subtraction of a Victoreen-type polynomial. Then the background-subtracted spectrum was convoluted with a series of increasingly broader Gauss functions and the common intersection point of the convoluted spectra was taken as energy E_0.[14] To determine the smooth part of the spectrum, corrected for pre-edge absorption, a piecewise polynomial was used. It was adjusted in such a way that the low-R components of the resulting Fourier transform were minimal. After division of the background-subtracted spectrum by its smooth part, the photon energy was converted into a photoelectron wave number scale. The resulting EXAFS function was weighted with k^3. Data analysis in k space was performed according to the curved wave multiple scattering formalism of the program EXCURV92.[16] The mean free path of the scattered electrons was calculated from the imaginary part of the potential (VPI was set to −4.00), the amplitude reduction factor AFAC was fixed at 0.8 and an overall energy shift ΔE_0 was assumed.

Acknowledgments

We wish to thank HASYLAB (Hamburg) for kind support of synchrotron radiation and the Fonds der Chemischen Industrie for generous financial support. This work has been supported by the DFG.

[1] *Phthalocyanines, Properties and Applications* (Eds. C. C. Leznoff, A. B. P. Lever), vol. 1−4, VCH, New York, **1989−1994**.
[2] [2a] M. Hanack, M. Lang, *Adv. Mater.* **1994**, *6*, 819−833. − [2b] H. Schultz, H. Lehmann, M. Rein, M. Hanack, *Struct. Bonding* **1991**, *74*, 41−146. − [2c] M. Hanack, M. Lang, *Chemtracts: Org. Chem.* **1995**, *8*, 131−165.
[3] A. Capobianchi, A. M. Paoletti, G. Pennesi, G. Rossi, R. Caminiti, C. Ercolani, *Inorg. Chem.* **1994**, *33*, 4635−4640.
[4] W. Kobel, M. Hanack, *Inorg. Chem.* **1986**, *25*, 103−107.
[5] [5a] M. Hanack, J. Osío-Barcina, E. Witke, J. Pohmer, *Synthesis* **1992**, 211−214. − [5b] M. Hanack, R. Polley, *Synthesis* **1997**, 295−296.
[6] [6a] M. Hanack, S. Knecht, R. Polley, *Chem. Ber.* **1995**, *128*, 929−933. − [6b] M. Hanack, M. Hees, E. Witke, *New J. Chem.* **1998**, 169−172. − [6c] B. D. Rihter, M. E. Kenney, W. E. Ford, M. A. Rodgers, *J. Am. Chem. Soc.* **1990**, *112*, 8064−8070.
[7] H. Bertagnolli, A. Weber, W. Hörner, T. S. Ertel, U. Reinöhl; M. Hanack, M. Hees, R. Polley, *Inorg. Chem.* **1997**, *36*, 6397−6400.
[8] [8a] F. A. Cotton, N. F. Curtis, C. B. Harris, B. F. G. Johnson, S. J. Lippard, J. T. Mague, W. R. Robinson, J. S. Wood, *Science* **1964**, *145*, 1305−1307. − [8b] F. A. Cotton, *Inorg. Chem.* **1965**, *4*, 334−336.
[9] G. Bunker, S. S. Hasnain, D. E. Sawyers, in *X-ray Absorption Fine Structure: International Workshop on Standards and Criteria in XAFS* (Ed.: S. S. Hasnain), Ellis Horwood, Chichester, **1991**, pp. 751−770.
[10] L. H. Vogt, Jr., A. Zalkin, D. H. Templeton, *Inorg. Chem.* **1967**, *6*, 1725−1730.
[11] J. S. Miller, C. Vazquez, J. C. Calabrese, R. S. McLean, A. Epstein, *Adv. Mater.* **1994**, *6*, 217−221.
[12] C. D. Johnson, "Pyridines and their Benzo Derivates: (i) Structure" in *Comprehensive Heterocyclic Chemistry II*, vol. 2 (Vol. Eds.: A. J. Boulton, A. McKillop), Pergamon, Oxford, **1994**, pp. 99−164.
[13] M. Sommerauer, C. Rager, M. Hanack, *J. Am. Chem. Soc.* **1996**, *118*, 10085−10093.
[14] T. S. Ertel, H. Bertagnolli, S. Hückmann, U. Kolb, D. Peter, *Appl. Spectrosc*. **1992**, *46*, 690−698.
[15] M. Newville, P. Livins, Y. Yakoby, J. J. Rehr, E. A Stern, *Phys. Rev. B* **1993**, *47*, 14126−14131.
[16] S. J. Gurman, N. Binsted, I. Ross, *J. Phys. C* **1986**, *19*, 1845−1861.

Received February 22, 2000
[I00067]

ortho-Metalation of Triarylphosphane at Cobalt and Template Synthesis of Chelating 2-(Diarylphosphanyl)aroyl Ligands

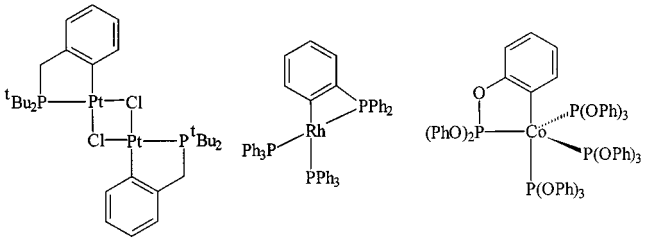
Hans-Friedrich Klein,*[a] Sven Schneider,[a] Mengzhen He,[a] Ulrich Floerke,[b] and Hans-Juergen Haupt[b]

Keywords: Metalations / Insertion reactions / Hydrogenations / Cobalt / Structure elucidation

Elimination of methane from thermally labile $CoMe(PPh_3)(PMe_3)_3$ generates *ortho*-metalated $Co(2\text{-}Ph_2PC_6H_4)(PMe_3)_3$ (**1**). Addition of dihydrogen causes ring-opening which is followed by a ligand dismutation reaction giving $CoH(PMe_3)_4$ and $CoH(PMe_3)_2(PPh_3)_2$. The system does not catalytically hydrogenate olefins. CO insertion into the Co–C bond of **1** results in ring expansion and constitutes a template synthesis of the anionic 2-phosphanylbenzoyl chelate ligand as shown in the molecular structure of $Co(2\text{-}Ph_2PC_6H_4CO)(CO)(PMe_3)_2$ (**3**). Oxidative addition of iodomethane transforms **1** into diamagnetic $CoMeI(2\text{-}Ph_2PC_6H_4)(PMe_3)_2$ (**7**), while benzoyl chloride oxidizes **1** to paramagnetic $CoCl(2\text{-}Ph_2PC_6H_4)(PMe_3)_2$ (**8**). The preservation of the four-membered metallacycle in three successive oxidation states is supported by single-crystal X-ray analyses of **1**, **7**, and **8**.

Introduction

C−H activation of hydrocarbons,[1] particularly that involving aromatic compounds, and cyclometalation[2] of arylphosphanes are important areas of research with respect to homogeneous catalysis. *ortho*-Metalations of triarylphosphanes, e.g. the metalation of benzylphosphanes (**A**) or phenyl phosphites (**C**), represent some early examples.



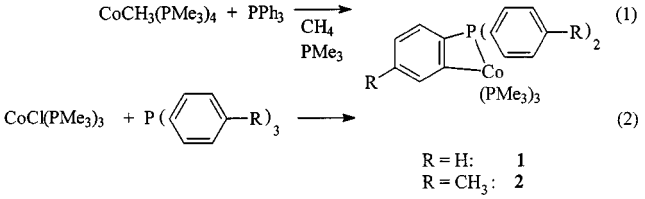
A B C

When coordinated to platinum metals, e.g. as in Keim's rhodium complex **B**,[3a] triphenylphosphane has in many cases been shown to form four-membered metallacycles.[3] With iron, cobalt, or nickel, only a few examples have been reported. While $Fe(C_2H_4)(Ph_2PCH_2CH_2PPh_2)_2$ is *ortho*-metalated only under irradiation,[4] $CoH(N_2)(PPh_3)_3$ has been shown by several groups to undergo H/D exchange in all *ortho* positions.[5] In solution, $CoCH_3(PPh_3)_3$ spontaneously eliminates methane. No *ortho*-metalated species have been isolated from these systems. Only in the presence of styrene was an *ortho*-metalated species generated, which has still to be fully characterized.[6] Although no *ortho*-metalation through C−H activation has been described for alkyl- or hydridonickel(II) or -nickel(0) complexes with phenylphosphanes, the reaction of (pentachlorophenyl)diphenylphosphane with nickel(0) affords a metallacyclic complex,[7] which undergoes ring-opening through substitution of its P-donor function with triphenylphosphane. Although H_2 smoothly hydrogenates the rhodium(I) complex **B** under ring-opening, retention of the four-membered metallacycle was observed in both oxidative addition reactions and ring-expansion reactions with CO[8] and diphenylacetylene.[9]

With trimethylphosphanes as supporting ligands, we have observed quite similar properties and reactivities in the cobalt(I) system and report here on the syntheses, reactions, and structural investigations of such complexes.

Results and Discussion

When combined with triphenylphosphane in tetrahydrofuran, $CoCH_3(PMe_3)_4$ eliminates methane to form the metallacyclic complex **1** according to Equation (1). Addition of triphenylphosphane to $CoCl(PMe_3)_3$, followed by methyllithium (Equation 2), affords **1** in essentially quantitative yield.



Using tris(4-methylphenyl)phosphane in place of triphenylphosphane in a synthesis according to Equation 2, the analogous complex **2** is obtained in 95% yield. Both complexes form large quadrangular crystals with black faces,

[a] Institut für Anorganische Chemie der Technischen Universität Darmstadt,
Petersenstraße 18, 64285 Darmstadt, Germany
[b] Anorganische und Analytische Chemie der Universität Paderborn,
Warburger Straße 100, 33095 Paderborn, Germany

 © WILEY-VCH Verlag GmbH, D-69451 Weinheim, 2000 1434−1948/00/1010−2295 $ 17.50+.50/0

which appear dark red when illuminated. In dry air, solid **1** and **2** remain unchanged for ca. two hours, although their solutions are decomposed within a few minutes if air is admitted.

Their infrared spectra display the characteristic *ortho*-metalation bands at $\tilde{\nu}$ = 722 cm^{-1} (**1**) and 726 cm^{-1} (**2**), which correspond to out-of-plane CH vibrations.[3c] The ^{31}P NMR spectra (−40 °C) feature an AM_2X pattern of three signals with J(AM) = 49 Hz (**1**) and 48 Hz (**2**), which is consistent with a trigonal-bipyramidal arrangement of donor atoms with one axial (A) and two equatorial (M) trimethylphosphanes. The equatorial chelate P nucleus X displays a high-field signal characteristic of four-membered metallacycles[10] with J(AX) = 70 Hz and J(MX) = 87 Hz.

The trigonal-bipyramidal configuration of **1** has been confirmed in the crystal. Figure 1 shows the first molecular structure of an *ortho*-metalated arylcobalt complex. The bond lengths are as expected for Co^{I} centered in a trigonal bipyramid of CP_4 donor atoms.[11] The bond angles at cobalt deviate from ideal symmetry because of steric repulsions. Those of the axial P4 atom appear to be augmented by 5°, and the small chelate bite angle [C16−Co−P1 = 71.48(10)°] causes a bending of the main axis towards the chelate ring [C16−Co−P4 = 168.00(11)°]. Thus, the properties and the molecular structure prove **1** (18 metal-valence electrons) to be a true homologue of its 16-electron rhodium congener **B**.

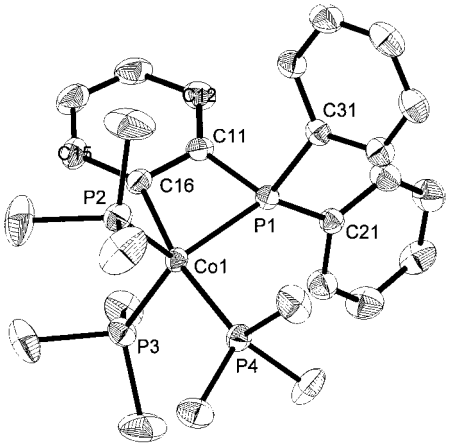
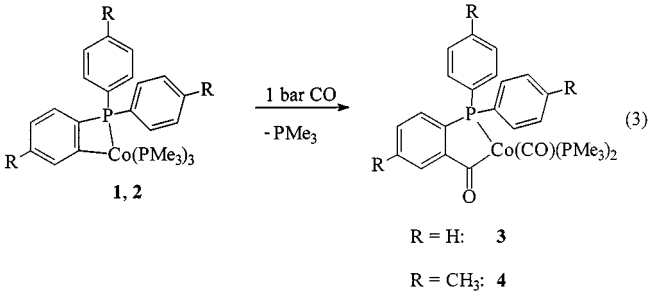


Figure 1. Molecular structure of **1** (ORTEP plot with hydrogen atoms omitted); selected bond lengths [Å] and angles [°]: Co−C16 1.990(3), Co−P1 2.2170(10), Co−P2 2.1744(11), Co−P3 2.1710(12), Co−P4 2.1826(11), P1−C11 1.795(3), P1−C31 1.842(3), P1−C21 1.843(3), C11−C16 1.399(5), C11−C12 1.377(5), C12−C13 1.392(5), C13−C14 1.357(6), C14−C15 1.387(5), C15−C16 1.400(5); C16−Co−P3 86.89(10), C16−Co−P2 88.80(11), P3−Co−P2 118.64(5), C16−Co−P4 168.00(11), P3−Co−P4 98.91(4), P2−Co−P4 97.48(4), C16−Co−P1 71.48(10), P3−Co−P1 118.22(4), P2−Co−P1 117.92(4), P4−Co−P1 96.53(4), C11−P1−C31 106.13(16), C11−P1−C21 104.57(16), C31−P1−C21 101.64(15), C11−P1−Co 83.81(12), C31−P1−Co 124.66(11), C21−P1−Co 128.92(11), C11−C16−C15 114.8(3), C11−C16−Co 104.1(2), C16−C11−P1 100.3(2)

Reaction with Carbon Monoxide

At ambient temperature under 1 bar CO, THF solutions of complexes **1** and **2** react with two molar equivalents of CO according to Equation 3. An in situ transformation also occurs after *ortho*-metallation, as described by Equations 1 or 2.



Compound **3** has previously been obtained by C,H activation of 2-diphenylphosphanylbenzaldehyde.[11] Compounds **3** and **4** show analogous infrared absorptions of their carbonyl ligands at $\tilde{\nu}$ = 1953 and 1946 cm^{-1} (C≡O) and benzoyl groups $\tilde{\nu}$ = 1916 and 1909 cm^{-1} (C=O), respectively. When compared with the ^{31}P NMR spectroscopic data for **1** and **2**, the largest difference is seen in the shift of the chelate P atom. On going from a four-membered to a five-membered metallacycle, a low-field shift of 115 ppm is found, which is of the expected order.[10] The two trimethylphosphane ligands give rise to a broad singlet at δ = 9, which splits into a doublet at −40 °C. The coupling constant [J(PP) = 81 Hz] is indicative of a P−Co−P angle of about 120°, which is in perfect agreement with the molecular structure of **3**[12] (Figure 2). The cobalt atom is centered in a trigonal bipyramid comprising three equatorial P-donor functions. The chelate bite angle [P1−Co−C1 = 85.03(9)°] is similar to that in **1**, and the metallacycle shows a normal Co−C bond length only slightly longer than in **1** [Co−C1 = 1.960(3) Å]. Surprisingly, the groups with the largest *trans* influence are almost perfectly aligned along an axis [C1−Co−C20 = 176.3(2)°].

In the observed configuration, the carbonyl ligand can be expected to dissociate freely from **3**. A further carbonyl ligand may be mobilized through a decarbonylation reaction of the acyl function, restoring the four-membered metallacycle. In an attempted ligand equilibration reaction, regarding **3** as a source and **1** as an acceptor of carbonyl groups, no exchange of ligands was observed.

In further attempts to prepare the desired compound from either $CoMe(CO)(PMe_3)_3$ [13] and triphenylphosphane or from $CoCl(CO)(PMe_3)_3$ [14] and MeLi in the presence of triphenylphosphane, no *ortho*-metalation was observed.

Hydrogenation of Metallacycles

Under ambient conditions (20 °C, 1 bar H_2) in pentane or diethyl ether, **1** undergoes a ring-opening reaction to form mixed-ligand cobalt hydrides according to Equations 4 and 5. While **5** can be crystallized from pentane, **6** may be obtained through a ligand dismutation reaction and precipitated as an orange solid as it is insoluble in diethyl ether.

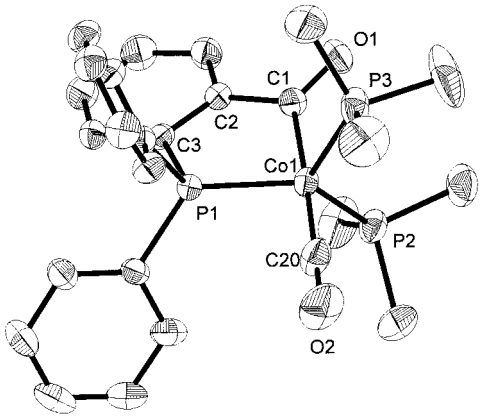
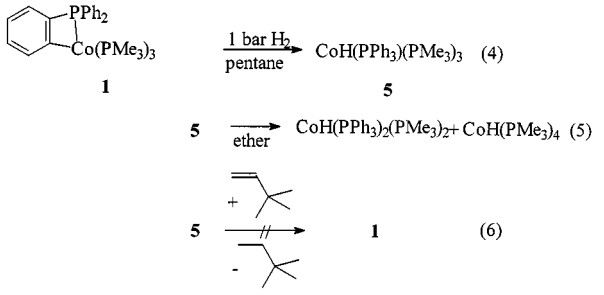


Figure 2. Molecular structure of **3** (ORTEP plot with hydrogen atoms omitted); selected bond lengths [Å] and angles [°]: Co−C1 196.0(3), Co−P1 215.02(10), Co−P2 217.38(9), Co−C3 181.7(3), Co−C20 174.3(4), C20−O2 115.3(4), C1−O1 122.1(3), C1−C2 154.0(4), C2−C3 138.2(4), P1−C3 181.7(3); C1−Co−P1 85.03(9), C1−Co−P2 83.70(9), C1−Co−P3 89.56(9), C1−Co−C20 176.3(2), P1−Co−P2 123.91(3), P1−Co−P3 115.42(4), P1−Co−C20 93.47(12), P2−Co−P3 119.23(4), P2−Co−C20 94.35(13), C20−Co−P3 94.18(13), Co−C1−C2 117.2(2), C1−C2−C3 117.9(2), C2−C3−P1 111.2(2), C3−P1−Co 104.65(9), Co−C1−O1 126.9(2), O1−C1−C2 115.9(3)



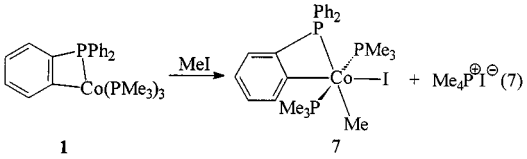
The hydrogenation reaction cannot be reversed by adding an olefin. Cyclohexene, 1-octene, and even 3,3-dimethylbut-1-ene, with its large heat of hydrogenation, remain unreactive. Such equilibria would, in principle, make the pair of compounds **1** and **5** a homogeneous hydrogenation catalyst involving *ortho*-metalated intermediates as are supposedly involved in Parshall's ruthenium system.[15] However, with (trimethylphosphane)cobalt compounds, hydrogenation reactions appear to be generally rather slow.

The catalytic activity of **1** and **5** in the hydrogenation of 1-octene was tested under 70 bar H_2 at 80 °C, but none was found. Hydrogen uptake was only observed with **1**, which was found to correspond to a stoichiometric reaction according to Equation 4.

Oxidative Addition and Oxidation

The ease with which it is hydrogenated under ambient conditions makes complex **1** a candidate for oxidative addition reactions. Using iodomethane as a substrate, the interesting question arises as to whether attack by the metal would proceed as a regioselective addition or promote ring-opening through a subsequent reductive C−C coupling reaction.

Within 15 h, the appearance of a light-brown coloration and a white precipitate of tetramethylphosphonium iodide indicated reaction according to Equation 7. However, trimethylphosphane was only partly quaternated in a side reaction, and addition of a second molar equivalent of iodomethane did not improve the yield of dark-brown crystals of **7** obtained from either diethyl ether or pentane. The use of a tenfold excess of iodomethane completely suppressed the formation of **7** and led to some $CoMe_2(I)(PMe_3)_3$ [16] as a product of a subsequent ring-opening reaction, as well as a cobalt-containing dark-green solid, which proved insoluble and was not identified.



In the ^{1}H NMR spectrum of **7**, the $CoCH_3$ protons resonate at δ = 0.51, which is close to the chemical shift seen for $CoMe_2(I)(PMe_3)_3$,[16] and are coupled to two *cis*-trimethylphosphane ligands [^3J(PH) = 9.5 Hz] and a *trans*-chelating phosphorus atom [^3J(PH) = 1.8 Hz], which gives rise to a high-field signal (δ(P) = −40) in the ^{31}P NMR spectrum, indicative of a four-membered metallacycle. All spec-

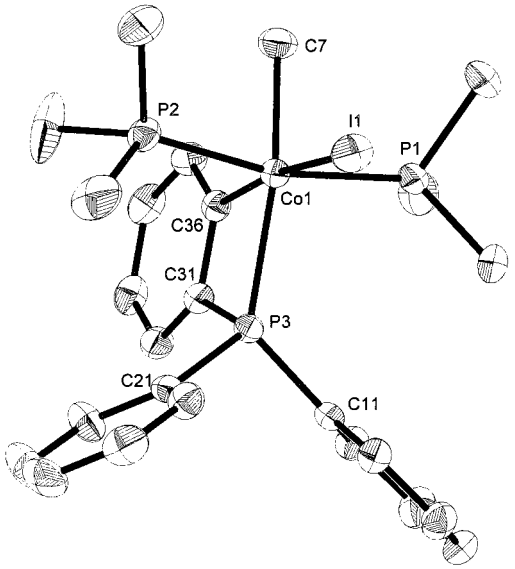
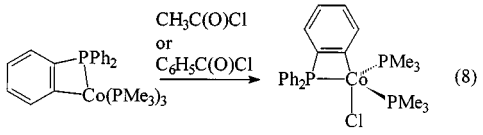


Figure 3. Molecular structure of **7** (ORTEP plot with hydrogen atoms omitted); selected bond lengths [Å] and angles [°]: I−Co 2.7099(6), Co−C36 1.942(3), Co−C7 2.039(3), Co−P1 2.2381(11), Co−P2 2.2425(11), Co−P3 2.3467(10), P3−C31 1.799(3), P3−C11 1.829(3), P3−C21 1.830(3), C31−C36 1.395(4), C31−C32 1.389(4), C32−C33 1.374(5), C33−C34 1.375 (5), C34−C35 1.384(5), C35−C36 1.398(4); C36−Co−C7 89.60(15), C36−Co−P1 94.06(10), C7−Co−P1 84.50(11), C36−Co−P2 91.88(10), C7−Co−P2 83.90(12), P1−Co−P2 166.92(4), C36−Co−P3 69.98(10), C7−Co−P3 159.57(11), P1−Co−P3 96.01(4), P2−Co−P3 96.97(4), C36−Co−I 171.33(10), C7−Co−I 98.96(11), C31−P3−C21 110.33(16), C31−P3−Co 80.77(11), C21−P3−Co 125.96(11), C11−P3−Co 127.73(11), P1−Co−I 88.17(3), P2−Co−I 87.69(3), P3−Co−I 101.46(3), C31−P3−C11 107.12(15), C31−P3−C21 110.32(16), C11−P3−C21 100.23(15), C31−P3−Co 80.77(11), C36−C31−P3 101.2(2), C31−C36−Co 108.0(2), C35−C36−Co 134.5(3)

troscopic data are thus compatible with an octahedral configuration of **7** in solution.

Crystals of **7** proved to be stable in air for more than two days and could thus be mounted on an X-ray diffractometer without inert gas protection. The molecular structure (Figure 3) confirms the configuration of **7** as derived from the spectroscopic data. The iodo and methyl ligands lie in the plane of the chelate ring, and the two carbon−cobalt bonds are mutually orthogonal [C7−Co−C36 = 89.60(15)°]. The trimethylphosphane ligands are positioned in an axis perpendicular to the chelate ring and appear slightly bent [P1−Co−P2 = 116.92(4)°] towards the $CoCH_3$ group. This bending and the small bite angle of the chelating ligand [C36−Co−P3 = 69.98(10)°] reflect the spatial requirements of the iodo ligand. The strong *trans* influence of the $CoCH_3$ group and the weak effect of the iodo ligand cause an elongation of Co−P3 by 0.1 Å compared with Co−P1 and Co−P2 and a contraction of Co−C36 by 0.045 Å compared with the corresponding Co−C16 distance in **1**. Therefore, the molecular structure of **7** appears to be the result of a regioselective *cis* addition of iodomethane.

With benzoyl chloride or acetyl chloride, oxidation is observed rather than oxidative addition, as in the rhodium system.[8]



(8)

1 **8**

The cobalt(II) complex **8** (17 valence electrons) was obtained as the only cobalt-containing species in 50−60% yield, while the remaining hydrocarbon moieties have yet to be characterized.

Dark-brown quadrangular crystals could be grown from pentane or diethyl ether and proved to be stable in moist air for more than two hours. The thermal stability, color, and multitude of infrared bands in the fingerprint region are very similar to those observed for **7**, although the crystal habit is different.

The molecular structure of **8** (Figure 4) can be related to a trigonal bipyramid similar to that of **1**. The chelate bite angle [C36−Co−P1 = 71.28(12)°] has a value intermediate between those of **1** and **7**. Distances from the cobalt atoms to the trimethylphosphanes are 0.04 Å longer than those not subject to a strong *trans* influence in **1**. The chelate P atom is almost 0.15 Å farther away from the metal center, although in the opposite direction there is a methyl group in **1** and a void in **8**, which is defined by bond angles P2−Co−P3 = 157.70(5)° and Cl−Co−C36 = 170.49(12)°. This space is large enough for, although not occupied by, a hydride ligand, as indicated by the fact that there no bands in the Co−H region of the infrared spectrum (1980−1880 cm^{-1}), and solid **8** has paramagnetic properties as would be expected for a total of 17 metal-valence electrons.

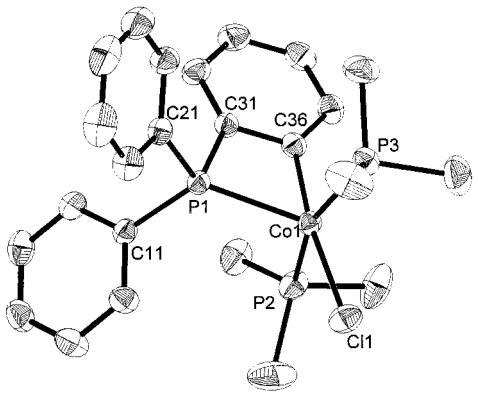
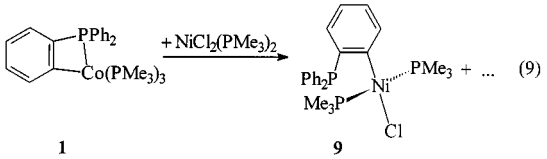


Figure 4. Molecular structure of **8** (ORTEP plot with hydrogen atoms omitted); selected bond lengths [Å] and angles [°]: Co−C36 1.926(4), Co−P1 2.3631(11), Co−P2 2.2179(12), Co−P3 2.2096(12), Co−Cl 2.3014(13), P1−C11 1.831(4), P1−C31 1.811(4), P1−C21 1.840(4), C31−C36 1.397(6), C31−C32 1.390(6), C32−C33 1.388(6), C33−C34 1.377(7), C34−C35 1.386(7), C35−C36 1.402(6); C36−Co−P1 71.28(12), C36−Co−P2 86.85(12), P3−Co−P2 157.70(5), C36−Co−Cl 170.49(12), P3−Co−Cl 88.48(5), P2−Co−Cl 89.79(5), C36−Co−P1 71.28(12), P3−Co−P1 98.53(5), P2−Co−P1 101.87(4), Cl−Co−P1 118.15(4), C31−P1−C11 109.17(19), C31−P1−C21 107.08(19), C11−P1−C21 102.53(19), C31−P1−Co 78.85(14), C11−P1−Co 118.65(13), C21−P1−Co 134.16(14), C36−C31−P1 103.1(3), C31−C36−C35 117.2(4), C31−C36−Co 106.7(3), C35−C36−Co 136.0(3)

Although the actual molecular symmetries of **1**, **7**, and **8** are lower than those of idealized coordination polyhedra, the angles around the cobalt atom change in a way as to suggest a smooth transition from a trigonal bipyramid in **1** through an intermediate geometry in **8** to an approximate octahedron in **7**.

Transmetalation Reaction

In reactions of $NiCl_2(PMe_3)_2$ with one or two molar equivalents of methyllithium in the presence of triphenylphosphane, no evidence of *ortho*-metalation has been observed. Besides elemental nickel, the mixture of soluble species produced was invariably found to contain $Ni(PMe_3)_4$, $Ni(PPh_3)(PMe_3)_3$, and $Ni(PPh_3)_2(PMe_3)_2$. However, the *ortho*-metalated chelate ligand might be transferred to nickel according to Equation 9.

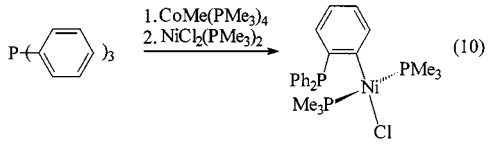


(9)

1 **9**

A light-green powder was obtained as a cobalt-containing residue, from which no soluble compound could be extracted. From a diethyl ether solution containing a considerable quantity of $Ni(PMe_3)_4$, honey-colored cubes of **9** were crystallized in 55% yield, which proved to be stable in air for more than two hours. The infrared spectrum features all the bands typical of *ortho*-metalated triphenylphos-

phane, while the NMR spectra show singlets indicating fast exchange of the ligands as in *trans*-NiCl(Me)(PMe_3)$_2$. At −40 °C, the ^{31}P NMR spectrum shows an A_2B pattern of resonances at δ = −5.4 (2 P) and δ = −7.0 (1 P) with a coupling constant [^2J(PP) = 21 Hz] falling in the range reported for related square-planar nickel(II) compounds.[7] These data are consistent with the presumption that the configuration of **9** is *trans*-square planar and the arylphosphane donor is uncoordinated.



(10)

The transmetalation reaction (Equation 9) provides access to an *ortho*-metalated triphenylphosphane without the need for halogenated arylphosphane precursors through a two-step synthetic procedure (Equation 10).

Conclusion

Methylcobalt(I) complexes incorporating triphenylphosphane ligands spontaneously eliminate methane forming four-membered metallacycles, which remain unchanged in oxidation or oxidative addition reactions. Ring-opening by dihydrogen occurs in a slow reaction and cannot be easily reversed. Under the conditions employed, the system is not an active hydrogenation catalyst. Insertion of carbon monoxide into the metallacycle constitutes a template synthesis of the C,P-chelating (2-diphenylphosphanyl)benzoyl ligand.

Experimental Section

General Procedures and Materials: All air-sensitive and volatile materials were handled using standard vacuum techniques and were stored under argon. − Microanalyses: Kolbe Microanalytical Laboratory, Mülheim/Ruhr, FRG. − Melting points/decomposition temperatures: Sealed capillaries, uncorrected values. − Chemicals (Merck/Schuchardt) were used as purchased, although liquids were degassed in vacuo by a freeze-pump-thaw procedure. Literature methods were followed for the preparation of CoMe(PMe_3)$_4$,[13] CoCl(PMe_3)$_3$,[14] and $NiCl_2(PMe_3)_2$.[17] − IR: Nujol mulls between KBr discs, Bruker spectrophotometer type FRA 106. − NMR: ^{1}H and ^{13}C NMR spectra (300 and 75 MHz, respectively) were recorded with a Bruker ARX-300 spectrometer, ^{31}P NMR spectra (81 MHz) with a Bruker AM-200 instrument. ^{13}C and ^{31}P resonances were obtained with broad-band proton decoupling.

[(2-Diphenylphosphanyl)phenyl-*C*^{1},*P*]tris(trimethylphosphane)cobalt (1). − Method a: CoCl(PMe_3)$_3$ (3.38 g, 11.0 mmol) in THF (60 mL) was combined with triphenylphosphane (2.75 g, 10.5 mmol) in THF (10 mL) at −70 °C to give a green solution. After 5 min, 0.9 M MeLi solution in diethyl ether (6.6 mL, 10.5 mmol) was added to afford an orange solution, which turned deep red on warming to 20 °C. After 4 h, the volatiles were removed in vacuo and the residue was extracted with toluene (50 mL) through a glass sinter disc (G3). Evaporation of the solvent from the extract and drying of the residue in vacuo afforded a black microcrystalline solid. Crude yield 5.70 g (99%) of **1**; yield after recrystallization from 30 mL of pentane 4.5 g (79%). − **Method b:** CoMe(PMe_3)$_4$ (880 mg, 2.30 mmol) in THF (50 mL) and triphenylphosphane (630 mg, 2.40 mmol) in THF (10 mL) were combined at −70 °C. On warming to 20 °C, the mixture took on a deep-red color. After 60 h, the volatiles were removed in vacuo and the residue was extracted with pentane (30 mL). Crystallization at 4 °C afforded dark-red quadrangular rods. Yield 690 mg (55%) of **1**; decomp. > 115 °C. − ^{1}H NMR ([D$_8$]THF): δ = 1.13 (br. s, 9 H, PCH_3), 1.26 (br. s, 18 H, PCH_3), 6.29 (m, 1 H, CH), 6.45 (m, 1 H, CH), 6.65 (m, 1 H, CH), 6.85 (m, 1 H, CH), 7.22 (m, 6 H, CH), 7.69 (m, 4 H, CH). − ^{13}C NMR (300 MHz, [D$_8$]THF): δ = 22.1 (m, PCH_3), 22.9 (m, PCH_3), 118.4 (m, 4-C/6-C), 119.6 (m, 6-C/4-C), 126.2 (s, 5-C), 126.4 (s, *p*-C), 126.6 (s, *m*-C), 131.8 [d, ^2J(PC) = 9 Hz, *o*-C], 140.1 [d, ^2J(PC) = 9 Hz, 2-C], 154.2 (m, *i*-C), 170.0 (m, 1-C). − ^{31}P NMR ([D$_8$]THF, 233 K): δ = −32 [dt, $^2J(P_{eq}P_{eq})$ = 87 Hz, $^2J(P_{ax}P_{eq})$ = 70 Hz, 1 P, PPh_2], −4 [dd, $^2J(P_{eq}P_{eq})$ = 87 Hz, $^2J(P_{ax}P_{eq})$ = 49 Hz, 2 P, PMe_3], 23 [dt, $^2J(P_{eq}P_{ax})$ = 70 Hz, $^2J(P_{eq}P_{ax})$ = 49 Hz, 1 P, PMe_3]. − $C_{27}H_{41}CoP_4$ (548.2): calcd. C 59.13, H 7.53, P 22.59; found C 59.21, H 7.40, P 22.68.

{2-[Bis(4-methylphenyl)phosphanyl]-5-methylphenyl-*C*^{1},*P*}-tris(trimethylphosphane)cobalt (2). − Method a: CoCl(PMe_3)$_3$ (840 mg, 2.60 mmol) in THF (50 mL) was combined with tris(4-methylphenyl)phosphane (790 mg, 2.60 mmol) in THF (10 mL) at −70 °C to give a green solution. After 5 min, 2.6 M MeLi solution in diethyl ether (1.6 mL, 2.60 mmol) was added to afford an orange solution, which turned deep red on warming to 20 °C. After 15 h, the volatiles were removed in vacuo and the residue was extracted with pentane (30 mL). Crystallization at 4 °C afforded dark-red quadrangular rods. Yield 580 mg (38%) of **2**; m.p. 142−144 °C. − ^{1}H NMR (200 MHz, [D$_8$]THF): δ = 1.10 [d, ^2J(PH) = 9 Hz, 9 H, PCH_3], 1.25 (br. s, 18 H, PCH_3), 2.01 (s, 3 H, CCH_3), 2.29 (s, 6 H, CCH_3), 6.18 (m, 2 H, CH), 6.71 (br. s, 1 H, CH), 7.04 [d, ^3J(HH) = 7 Hz, 4 H, CH], 7.56 [dd, ^3J(HH) = 8 Hz, ^3J(PH) = 8 Hz, 4 H, CH]. − ^{13}C NMR (75.4 MHz, [D$_8$]THF): δ = 19.4 (s, CH_3), 20.7 (s, CH_3), 22.1 (m, PCH_3), 22.9 (m, PCH_3), 119.2−171.6 (C). − ^{31}P NMR ([D$_8$]THF, 233 K): δ = −34 [dt, $^2J(P_{eq}P_{eq})$ = 87 Hz, $^2J(P_{ax}P_{eq})$ = 70 Hz, 1 P, PPh_2], −5 [dd, $^2J(P_{eq}P_{eq})$ = 87 Hz, $^2J(P_{ax}P_{eq})$ = 49 Hz, 2 P, PMe_3], 22 [dt, $^2J(P_{eq}P_{ax})$ = 70 Hz, $^2J(P_{eq}P_{ax})$ = 49 Hz, 1 P, PMe_3]. − $C_{30}H_{47}CoP_4$ (548.2): calcd. C 61.02, H 8.02, P 20.98; found C 60.69, H 7.80, P 21.39.

Carbonyl[2-(diphenylphosphanyl)benzoyl-*C*^{1},*P*]bis-(trimethylphosphane)cobalt (3): CoMe(PMe_3)$_4$ (880 mg, 2.30 mmol) in THF (50 mL) and triphenylphosphane (610 mg, 2.30 mmol) in THF (10 mL) were combined at −70 °C and then the resulting solution was allowed to warm to 20 °C in vacuo. After 3 h, CO was admitted, and the mixture was stirred under 1 bar CO for 15 h. The volatiles were then removed in vacuo and the residue was extracted with pentane (30 mL). Crystallization at 4 °C afforded dark-red crystals. Yield 300 mg (24%) of **3**; m.p. 141−143 °C. − IR (Nujol): $\tilde{\nu}$ = 1917 cm^{-1} (C≡O), 1582 (C=C), 1551 (C=O). − ^{1}H NMR (300 MHz, [D$_8$]THF): δ = 1.13 [t′, $|^2J(PH) + {}^4J(PH)|$ = 7.1 Hz, 18 H, PCH_3], 7.33 (m, 8 H, CH), 7.47 (m, 1 H, CH), 7.56 (m, 4 H, CH), 7.66 (m, 1 H, CH). − ^{13}C NMR (75.4 MHz, [D$_8$]THF): δ = 18.3 (m, PCH_3), 119.4−156.0 (C), 222.4 (m, C≡O), 261.1 (m, C=O). − ^{31}P NMR ([D$_8$]THF): δ = 8.7 [d, $^2J(P_{eq}P_{eq})$ = 69 Hz, 2 P, PMe_3], 83.0 (br. s, 1 P, PPh_2).

{2-[Bis(4-methylphenyl)phosphanyl]-5-methylbenzoyl-*C*^{1},*P*}carbonyl-bis(trimethylphosphane)cobalt (4): CoMe(PMe_3)$_4$ (760 mg, 2.00 mmol) in THF (50 mL) and tri-*p*-tolylphosphane (610 mg, 2.30 mmol) in THF (10 mL) were combined at −70 °C and then

the resulting mixture was allowed to warm to 20 °C in vacuo. After 3 h, CO was admitted, and the mixture was stirred under 1 bar CO for 15 h. Workup as in the case of **3** afforded dark-red crystals. Yield 300 mg (26%); m.p. 162−164 °C. − IR (Nujol): $\tilde{\nu}$ = 1909, 1863 cm^{-1} (C≡O), 1598 (C=C), 1572, 1546 (C=O). − ^1H NMR (300 MHz, [D_8]THF): δ = 1.11 [t′, $|^2J(PH) + {}^4J(PH)|$ = 7.2 Hz, 18 H, PCH_3], 2.31 (s, 6 H, CCH_3), 2.35 (s, 3 H, CCH_3), 7.12 [d, $^3J(HH)$ = 7.9 Hz, 4 H, CH], 7.16 [d, $^3J(HH)$ = 7.6 Hz, 1 H, CH], 7.26 (s, 1 H, C^6-H), 7.42 [dd, $^3J(PH)$ = 10.0 Hz, $^3J(HH)$ = 8.1 Hz, 4 H, C^2−H], 7.51 [dd, $^4J(PH)$ = 5.8 Hz, $^3J(HH)$ = 7.5 Hz, 4 H, C^3−H]. − ^{13}C NMR (75.4 MHz, [D_8]THF): δ = 15.7 (s, CH_3), 20.2 [t′, $|^1J(PC) + {}^3J(PC)|$ = 26 Hz, PCH_3], 21.3 (s, CH_3), 121.6 [d, $^2J(PC)$ = 20 Hz, 3-C], 129.5 [d, $^3J(PC)$ = 9 Hz, *m*-C], 130.6 (s, 4-C/6-C), 131.1 (s, 6-C/4-C), 132.8 [d, $^2J(PC)$ = 13 Hz, *o*-C], 137.8 [d, $^1J(PC)$ = 35 Hz, *ipso*-C], 139.3 (s, *p*-C), 140.6 [d, $^2J(PC)$ = 32 Hz, 2-C], 140.8 (s, 5-C), 158.7 [d, $^1J(PC)$ = 62 Hz, 1-C], 222.7 (m, C≡O), 263.1 (m, C=O). − ^{31}P NMR ([D_8]THF, 233 K): δ = 9.0 [d, $^2J(P_{eq}P_{eq})$ = 81 Hz, 2 P, PMe_3], 80.5 [t, $^2J(P_{eq}P_{ax})$ = 81 Hz, 1 P, PPh_2]. − $C_{29}H_{38}CoO_2P_3$ (570.1): calcd. C 61.06, H 6.71, P 16.29; found C 60.88, H 6.95, P 15.71.

Hydrogenation of 1: Hydrogenation of **1** (250 mg, 0.50 mmol) in diethyl ether (30 mL) by stirring for 15 h under 1 bar of H_2 furnished a red solid, which was isolated by decantation and washing. Yield 50 mg of **5** (27% based on PPh_3); decomp. > 158 °C. − IR (Nujol): $\tilde{\nu}$ = 1941 cm^{-1} (Co−H), 1582 (C=C). − ^1H NMR (200 MHz, [D_8]THF): δ = −17.30 (br. s, 1 H, CoH), 1.11 (br. s, 27 H, PCH_3), 7.18−7.41 (m, 15 H, CH). − ^{31}P NMR ([D_8]THF): δ = 4.8 (br. s, 3 P, PCH_3), 58.5 (br. s, 1 P, PPh_3). − $C_{27}H_{43}CoP_4$ (550.5): calcd. C 58.91, H 7.87, P 22.51; found C 57.92, H 7.34, P 21.73. − All volatiles were removed in vacuo from the light-red solution, and the solid residue was taken up in pentane (30 mL). At −25 °C, red plates crystallized. Yield 180 mg of **6** (60% based on PPh_3); decomp. > 171 °C. − IR (Nujol): $\tilde{\nu}$ = 1967 cm^{-1} (Co−H), 1582 (C=C). − ^1H NMR (300 MHz, [D_8]THF): δ = −17.70 (m, 1 H, CoH), 0.93 (br. s, 18 H, PCH_3), 7.11 (m, 18 H, CH), 7.36 (m, 12 H, CH). − ^{31}P NMR ([D_8]THF): δ = 5.5 (br. s, 2 P, PCH_3), 56.3 (br. s, 2 P, PPh_3).

[2-(Diphenylphosphanyl)phenyl-*C*^{1},*P*]iodo(methyl)bis(trimethylphosphane)cobalt (7): 1 (840 mg, 1.50 mmol) in THF (30 mL) was combined with iodomethane (0.10 mL, 210 mg, 1.50 mmol) in THF (30 mL) at −70 °C. The solution was allowed to warm to ambient temperature and within 30 min took on a light-brown color and became turbid. After 15 h at 20 °C, the volatiles were removed in vacuo and the brown solid was extracted with diethyl ether. On storage of the extract at 4 °C, dark-brown crystals were obtained. Yield 390 mg (42%); m.p. 123−124 °C. − ^1H NMR (300 MHz, [D_8]THF): δ = 0.51 [dt, $^3_{cis}J(PH)$ = 9.5 Hz, $^3_{trans}J(PH)$ = 1.8 Hz, 3 H, $CoCH_3$], 0.98 [t′, $|^2J(PH) + {}^4J(PH)|$ = 3.7 Hz, 18 H, PCH_3], 6.73 (br. s, 1 H, CH), 7.05 (m, 2 H, CH), 7.22 [d, $^3J(HH)$ = 8 Hz, 1 H, CH], 7.33 (m, 6 H, CH), 7.77 (m, 4 H, CH). − ^{13}C NMR (75.4 MHz, [D_8]THF): δ = 14.2 [t′, $|^1J(PC) + {}^3J(PC)|$ = 27 Hz, PCH_3], 121.6 [d, $^3J(PC)$ = 6 Hz, 4-C], 126.6 (s, 5-C/6-C), 127.6 [d, *J*(PC) = 8 Hz, *o*-C/*m*-C], 128.0 (s, *p*-C), 130.9 [d, *J*(PC) = 9 Hz, *m*-C/*o*-C], 134.4 [d, $^2J(PC)$ = 20 Hz, 3-C], 137.5 [d, $^1J(PC)$ = 14 Hz, *ipso*-C]. − ^{31}P NMR ([D_8]THF, 233 K): δ = 9.6 (s, 2 P, PMe_3), −40.2 (s, 1 P, PPh_2). − $C_{25}H_{35}CoIP_3$ (614.0): calcd. C 48.88, H 5.74, P 15.13; found C 48.78, H 5.62, P 15.88.

Chloro[2-(diphenylphosphanyl)phenyl-*C*^{1},*P*]bis(trimethylphosphane)cobalt (8). − Method a: 1 (310 mg, 0.6 mmol) in THF (40 mL) was combined with benzoyl chloride (80 mg) in THF (1 mL) at −70 °C. Warming to 20 °C afforded a dark-brown solution which, after stirring for 16 h, was concentrated to dryness in vacuo. The residue was extracted with pentane to remove traces of $CoCl(PMe_3)_3$ (IR control) and then with diethyl ether, from which dark-brown quadrangular rods were crystallized. Yield 150 mg (50%) of **8**. − **Method b:** At −70 °C in vacuo, acetyl chloride (210 mg, 1.50 mmol) in THF (30 mL) was condensed into a vessel containing **1** (740 mg, 1.40 mmol) in THF (30 mL). The resulting mixture was allowed to warm to ambient temperature; within 5 min a light-green solid separated, which slowly redissolved. After 15 h at 20 °C, a red-brown solution was obtained, which was concentrated to dryness in vacuo. The residue was extracted with pentane, and on storage of the extract at 4 °C dark-brown crystals were obtained. Yield 660 mg (59%) of **8**; m.p. 123−124 °C. − IR (Nujol): $\tilde{\nu}$ = 1582 cm^{-1}, 1552 (C=C). − $C_{24}H_{32}ClCoP_3$ (507.1): calcd. C 56.76, H 6.35, P 18.30; found C 56.68, H 6.35, P 18.22.

Chloro[2-(diphenylphosphanyl)phenyl]bis(trimethylphosphane)nickel (9): 1 (830 mg, 1.5 mmol) and $NiCl_2(PMe_3)_2$ (420 mg) were combined in diethyl ether (60 mL) at −70 °C. Warming to 20 °C afforded a dark-brown solution which, after 16 h, had taken on a greenish-brown appearance. It was then concentrated to dryness in vacuo. Extraction of the residue with diethyl ether afforded a greenish-brown solution, storage of which at 4 °C led to the deposition of honey-colored quadrangular rods. Yield 420 mg (55%) of **9**; m.p. 165−168 °C. − IR (Nujol): $\tilde{\nu}$ = 1581 cm^{-1}, 1554 (C=C). − ^1H NMR (300 MHz, [D_8]THF): δ = 0.89 (br. s, 1 H, 18 H, PCH_3), 6.70 [t, $^3J(PH)$ = 7.2 Hz, 1 H, CH], 6.85 [t, $^3J(PH)$ = 7.1 Hz, 1 H, CH], 6.93 [d, $^2J(PH)$ = 5 Hz, 1 H, CH], 7.31 (m, 7 H, CH), 7.44 (m, 4 H, CH). − ^{13}C NMR (75.4 MHz, [D_8]THF): δ = 13.2 [t′, $|^1J(PC) + {}^3J(PC)|$ = 30 Hz, PCH_3], 121.4, 127.3, 132.3 (s, 4-C, 5-C, 5-C), 129.0 (s, *p*-C), 129.1 [d, $^3J(PC)$ = 6 Hz, *m*-C], 134.9 [d, $^2J(PC)$ = 17 Hz, *o*-C], 136.6 [dt, $^2J(PC)$ = 25 Hz, $^4J(PC)$ = 6 Hz, 3-C], 140.4 [d, $^1J(PC)$ = 15 Hz, *ipso*-C], 137.5 (m, 2-C), 169.4 (m, 1-C). − ^{31}P NMR ([D_8]THF, 233 K): δ = −5.4 (B_2, PMe_3), −7.0 (A, PPh_2); AB_2 spin system, *J*/δ = 0.16 with $^2J(PP)$ = 21 Hz. − $C_{24}H_{32}ClNiP_3$ (506.1): calcd. C 56.79, H 6.35, P 18.31; found C 56.64, H 6.60, P 18.22.

Table 1. Crystal data for compounds **1** and **3**

	1	**3**
Empirical formula	$C_{27}H_{41}CoP_4$	$C_{26}H_{32}CoO_2P_3$
Molecular mass	548.4	528.4
Crystal size [mm]	0.32 × 0.52 × 0.38	0.52 × 0.38 × 0.47
Crystal system	orthorhombic	monoclinic
Space group	*Pbca*	$P2_1/n$
a [Å]	16.366(3)	13.2532(14)
b [Å]	18.919(6)	16.618(2)
c [Å]	19.049(3)	13.887(2)
α [°]	90	90
β [°]	90	96.304(8)
γ [°]	90	90
V [Å^3]	5898(2)	3039.9(5)
Z	8	4
$D_{calcd.}$ [g/cm^3]	1.235	1.142
μ(Mo-K_α) [mm^{-1}]	0.812	−
Temperature [K]	293(2)	293(2)
Data coll. range [°]	4.3 ≤ 2Θ ≤ 55	−
h	0 ≤ *h* ≤ 21	−1 ≤ *h* ≤ 5
k	−24 ≤ *k* ≤ 1	−19 ≤ *k* ≤ 19
l	−1 ≤ *l* ≤ 24	−16 ≤ *l* ≤ 16
No. reflect. measured	7594	2411
No. unique data	6775 (R_{int} = 0.0421)	−
Parameters	298	271
GoF on F^2	0.996	1.029
*R*1 [$I \geq 2\sigma(I)$]	0.0446	0.0526
*wR*2 (all data)	0.1076	0.1617

Hydrogenation Tests: A 1-L stainless steel autoclave was charged with 1-octene (15.4 g) in pentane (130 mL) under argon. A solution of either **5** or **1** (430 mg) in pentane (10 mL) was added under hydrogen pressure, which was maintained at 70 bar by continuous feeding. The system was kept at 30 °C for 8 h until no further uptake of hydrogen was observed. The volatiles were then collected in a cold trap in vacuo and were shown to contain 1-octene and less than 1% octane (GC).

Crystal Structure Analyses: Crystal data are presented in Table 1 and Table 2. Data collection: Complex **1**: A dark-red specimen was sealed under argon in a glass capillary and mounted on a Siemens P4 diffractometer. Intensities were collected (ω scans) using graphite-monochromated Mo-K_α radiation; Lp corrections and absorption corrections based on ψ-scans were applied. The structure was solved by direct and conventional Fourier methods. All non-hydrogen atoms were treated anisotropically; hydrogen atoms were treated with a riding model in idealized positions. − Complex **3**: A dark-brown specimen was sealed and mounted as described for **1**. Data collection as for **1**. The structure was solved using Patterson and Fourier methods. Refinement as for **1**. − Complex **7**: A dark-brown specimen was sealed and mounted as described for **1**. Data collection, structure solution, and refinement as for **1**. − Complex **8**: A dark-brown specimen was sealed and mounted as described for **1**. Data collection, structure solution, and refinement as for **1**. − Crystallographic data (excluding structure factors) for the structures reported in this paper have been deposited with the Cambridge Crystallographic Data Centre as supplementary publication nos. CCDC-116690 for **1**, CCDC-136410 for **3**, CCDC-116691 for **7**, and CCDC-116692 for **8**. Copies of the data can be obtained free of charge on application to the CCDC, 12 Union Road, Cambridge CB2 1EZ, U.K. [Fax: (internat.) + 44-1223/336-033; E-mail: deposit@ccdc.cam.ac.uk].

Table 2. Crystal data for compounds **7** and **8**

	7	**8**
Empirical formula	$C_{25}H_{35}CoIP_3$	$C_{24}H_{32}ClCoIP_3$
Molecular mass	614.3	507.8
Crystal size [mm]	0.28 × 0.38 × 0.30	0.28 × 0.58 × 0.48
Crystal system	monoclinic	monoclinic
space group	$P2_1/n$	Cc
a [Å]	10.529(2)	10.065(1)
b [Å]	17.364(2)	17.617(2)
c [Å]	14.877(2)	14.838(2)
α [°]	90	90
β [°]	92.41(1)	96.96(1)
γ [°]	90	90
V [Å^3]	2717.5(7)	2611.6(5)
Z	4	4
$D_{calcd.}$ [g/cm^3]	1.501	1.291
μ(Mo-K_α) [mm^{-1}]	1.955	0.952
Temperature [K]	293(2)	293(2)
Data coll. range [°]	$4.5 \le 2\Theta \le 55$	$4.6 \le 2\Theta \le 55$
h	$-13 \le h \le 1$	$-1 \le h \le 13$
k	$-1 \le k \le 22$	$-1 \le k \le 22$
l	$-19 \le l \le 19$	$-19 \le l \le 19$
No. reflect. measured	7725	3731
No. unique data	6241 (R_{int} = 0.0239)	3503 (R_{int} = 0.0205)
Parameters	272	262
GoF on F^2	0.973	1.013
$R1$ [$I \ge 2\sigma(I)$]	0.0378	0.0345
$wR2$ (all data)	0.0776	0.0839

Acknowledgments

Support of this work by the Deutsche Forschungsgemeinschaft and the Fonds der Chemischen Industrie is gratefully acknowledged. We thank Prof. G. Luft and Dipl.-Ing. H. P. Dornik, Institute of Chemical Technology, TU Darmstadt, for running the catalytic tests of **1** and **5** in the hydrogenation of 1-octene.

[1] A. E. Shilov, G. B. Shul'pin, *Chem. Rev.* **1997**, *97*, 2879−2932.
[2] S. Trofimenko, *Inorg. Chem.* **1973**, *12*, 1215−1221.
[3] [3a] W. Keim, *J. Organomet. Chem.* **1968**, *14*, 179−184. − [3b] B. Longato, F. Morandini, S. Bresadola, *J. Organomet. Chem.* **1975**, *88*, C7−C8. − [3c] M. A. Bennett, D. L. Milner, *J. Chem. Soc., Chem. Commun.* **1967**, 581−582. − [3d] B. R. James, L. D. Markham, D. K. W. Wang, *J. Chem. Soc., Chem. Commun.* **1974**, 439−440. − [3e] D. J. Cole-Hamilton, G. Wilkinson, *J. Chem. Soc., Dalton Trans.* **1977**, 797−804. − [3f] A. J. Cheney, B. E. Mann, B. L. Shaw, R. M. Slade, *J. Chem. Soc., Chem. Commun.* **1970**, 1176−1177. − [3g] M. A. Bennett, T. Dirnberger, D. C. R. Hockless, E. Wenger, A. C. Willis, *J. Chem. Soc., Dalton Trans.* **1998**, 271−277.
[4] G. Hata, H. Kondo, *J. Am. Chem. Soc.* **1968**, *90*, 2278−2281. A. Misono, Y. Uchida, T. Saito, K. M. Song, *J. Chem. Soc., Chem. Commun.* **1967**, 419−420. − [5b] A. Sacco, M. Rossi, *Inorg. Chim. Acta* **1968**, *2*, 127−132. − [5c] J. H. Enemark, B. R. Davis, J. A. McGinnety, J. A. Ibers, *J. Chem. Soc., Chem. Commun.* **1968**, 96−97. − [5d] A. Yamamoto, S. Kitazume, L. S. Pu, S. Ikeda, *J. Am. Chem. Soc.* **1971**, *93*, 371−380. − [5a]
[6] Y. Kubo, A. Yamamoto, S. Ikeda, *J. Organomet. Chem.* **1973**, *59*, 353−364.
[7] M. Font-Bardia, J. González-Platas, G. Muller, D. Panyella, M. Rocamora, X. Solans, *J. Chem. Soc., Dalton Trans.* **1994**, 3075−3084.
[8] W. Keim, *J. Organomet. Chem.* **1969**, *19*, 161−168.
[9] J. S. Ricci, J. A. Ibers, *J. Organomet. Chem.* **1971**, *27*, 261−271.
[10] P. E. Garrou, *Chem. Rev.* **1981**, *81*, 229−266.
[11] H.-F. Klein, U. Lemke, M. Lemke, A. Brand, *Organometallics* **1998**, *17*, 4196−4201.
[12] U. Lemke, Dissertation, TU Darmstadt, **1998**.
[13] H.-F. Klein, H. H. Karsch, *Chem. Ber.* **1975**, *108*, 944−955.
[14] H.-F. Klein, H. H. Karsch, *Inorg. Chem.* **1975**, *14*, 473−477.
[15] G. W. Parshall, *Acc. Chem. Res.* **1970**, *3*, 139−144.
[16] H.-F. Klein, H. H. Karsch, *Chem. Ber.* **1975**, *108*, 956−966.
[17] K. A. Jensen, O. Dahl, *Acta Chem. Scand.* **1968**, *22*, 1044−1045.

Received March 29, 2000
[I00122]

Heteroatom-Bridged Calixarenes

Burkhard König*[a] and Maria Hechavarria Fonseca[a]

Dedicated to Prof. Dr. Martin A. Bennett on the occasion of his 65th birthday

Keywords: Macrocycles / Calixarenes / Supramolecular chemistry / Host−guest chemistry / Crown compounds

Macrocycles have always played an important role in supramolecular chemistry. Macrocycles with rigid subunits, known as calixarenes, are an important subclass of these compounds. While carbon-bridged calixarenes have been studied intensively and are used for practical applications, heteroatom-bridged calixarenes have entered the stage more recently. This review summarizes the current knowledge of synthesis and properties of heteroatom-bridged calixarenes in the year 2000.

Introduction

Macrocyclic compounds are of great importance in supramolecular chemistry whenever selective molecular recognition is desired.[1] The reason for this is obvious; selective recognition requires intermolecular forces that are strong enough to stabilize the assembly, but at the same time allow the dynamic formation and breaking of intermolecular bonds to reach the aggregate that represents the thermodynamic minimum. Weak bonds, such as hydrogen bonds, electrostatic interactions, or kinetically labile coordination to metal ions, fulfill this requirement. However, compared to covalent or metallic bonds, these interactions are usually weak and contribute only a small enthalpic stabilization energy to the aggregate. Therefore, the loss of entropy in the assembly process becomes a significant factor in determining the stability of the supramolecular structure.[2] Macrocyclic preorganization reduces the loss of entropy in aggregate formation by achieving a more restricted conformation as compared to acyclic compounds. This makes macrocycles good host compounds in recognition and self-assembly processes; indeed, this phenomenon has long been known as the macrocyclic effect.[3]

From the large number of macrocycles with potential binding abilities, compounds with rigid, aromatic or heteroaromatic subunits have received special attention. Fully or partially conjugated macrocycles of this kind, such as porphyrins **1**, are widely found in nature, with hemoglobin and chlorophyll the most common. A nonconjugated macrocycle possessing sub-heterocyclic pyrrol rings **2** was synthesized more than 100 years ago by Baeyer from pyrrol and acetone.[4] Somewhat later the formation of cyclic condensation products from *para-tert*-butylphenol and formaldehyde was discovered, but it took another 50 years before the structures of the different calixarenes were determined and protocols for their selective synthesis were developed.[5]

[a] Institut für Organische Chemie, Universität Regensburg
93040 Regensburg, Germany
Fax: (internat.) + 49-941/943-1717
E-mail: burkhard.koenig@chemie.uni-regensburg.de



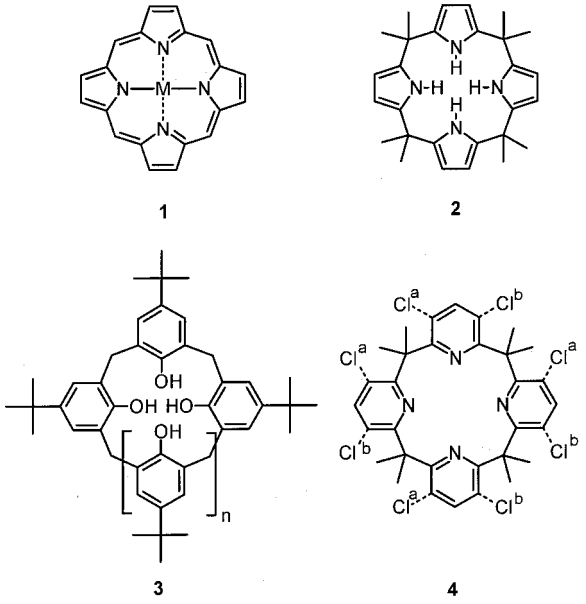
María Hechavarria Fonseca was born in 1974 in Cuba. She studied chemistry at the Universities of Santiago de Cuba and Havana from 1991 until 1996. In 1998 she obtained her Master's degree in the group of Prof. F. Coll at the University of Havana. Last year she received a DAAD Scholarship for her PhD studies in the group of Prof. Burkhard König. Her research interests are the synthesis of artificial receptors and the molecular recognition of natural products.

Burkhard König received his doctorate in 1991 from the University of Hamburg under the direction of Prof. de Meijere. He continued his scientific education as a postdoctoral fellow with Prof. M. A. Bennett, Canberra, Australia, and Prof. B. M. Trost, Stanford, U. S. A. In 1996 he obtained his "Habilitation" at the Technical University of Braunschweig and since 1999 he has been Professor at the University of Regensburg. His current research interests focus on intermolecular interactions, which naturally includes the chemistry of macrocycles.

MICROREVIEWS: This feature introduces the readers to the authors' research through a concise overview of the selected topic. Reference to important work from others in the field is included.

 © WILEY-VCH Verlag GmbH, D-69451 Weinheim, 2000 1434−1948/00/1111−2303 $ 17.50+.50/0

The chemistry of mainly calix[4]- (**3**, $n = 1$), calix[6]- (**3**, $n = 3$) and calix[8]arenes (**3**, $n = 5$) has been thoroughly studied, and the search for new calixarenes is still ongoing, as illustrated by the recent synthesis of calix[4]pyridines **4**.[6] The reasons for the very successful application of heteroaromatic and aromatic calixarenes as artificial receptor molecules are apparent: Depending on their conformation they provide an inner cavity for inclusion of guests, functional groups can be selectively introduced to build binding sites in three dimensions, and the parent calixarene macrocycles are in many cases available in large quantities from simple starting materials (Scheme 1).



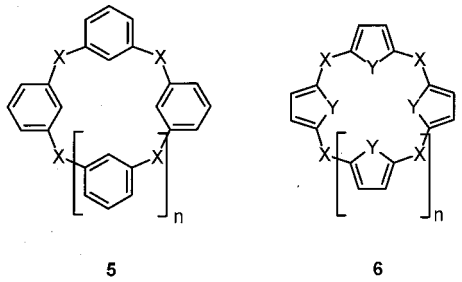
Scheme 1. Conjugated and nonconjugated macrocycles with rigid subunits: porphyrin (**1**), *meso*-octamethylcalix[4]pyrrole (**2**), *para-tert*-butylcalix[3+*n*]arene (**3**), and chlorocalix[4]pyridine (**4**)

Calixarenes in which the carbon methylene bridge between the arene or heteroarene units is replaced by a heteroatom are much less studied. For such compounds the name hetero-calixarenes will be used in this article. The introduction of a heteroatom as the bridge provides an additional opportunity to tune the ring size, conformation, and binding properties of the macrocycle. Synthetic approaches to both classes of compounds are rather different. While the main synthetic routes to carbon-bridged calixarenes are condensation reactions of arenes or heteroarenes and carbonyl compounds, this reaction is in most cases not suitable for the introduction of heteroatom bridges.

In this account we will summarize recent reports of the synthesis and the binding properties of heteroatom-bridged calixarenes that have appeared in the literature. We include our own investigations on silicon-, sulfur-, and germanium-bridged macrocycles.

Results and Discussion

Most heteroatom-bridged calixarenes discussed in this paper are described by the two general formulae **5** and **6** shown in Scheme 2. The substitution pattern of the arene rings in **5** is not restricted to *meta*-, *ortho*- and *para*-substituted rings as part of the macrocycle and mixtures of substitution patterns are included. The arene ring may contain additional heteroatoms. As a classification scheme, we will use the bridging heteroatoms X in the order of the main groups of the periodic table. As five-membered heterocyclic rigid subunits of the calixarene, furans (Y = O), thiophenes (Y = S) and *N*-methylpyrrols (Y = Me−*N*) are considered. Macrocycles with three ($n = 0$) to six ($n = 3$) rigid arene or heteroarene units are covered in this review.

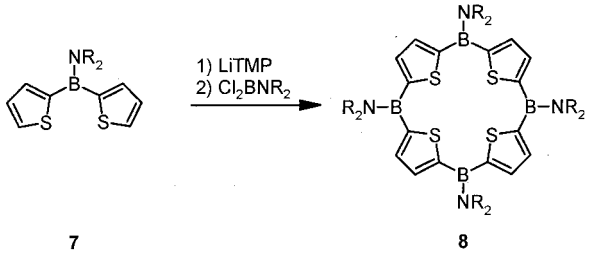


Scheme 2. General formulae of heterocalixarenes covered in this review

1. Group IIIA Elements

1.1 Boron

The first boron-bridged tetrathiaporphyrinogen **8** has been reported only recently.[7] The macrocycle was synthesized in remarkable 62% yield from *N*,*N*-dimethylbis(2-thienyl)borylamine **7** via the dilithio compound. No polymer formation was observed in the reaction although this was the initial objective of the experiment. The X-ray structure analysis shows that all four bridging boron atoms do not lie in a single plane, as it is the case for the analogous carbon-[8] and silicon-bridged compounds (Scheme 3).



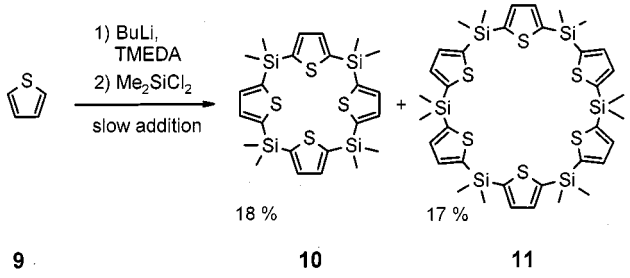
Scheme 3. Synthesis of a boron-bridged tetrathiaporphyrinogen; LiTMP = lithium-2,2,6,6,-tetramethylpiperidid; R = *i*Pr

2. Group IVA Elements

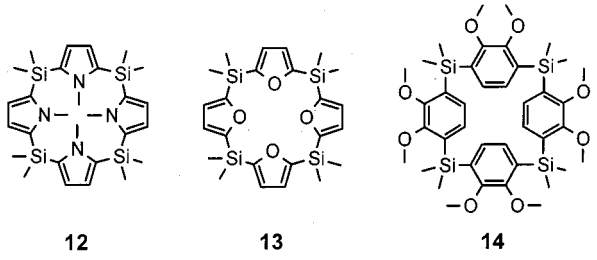
2.1 Silicon

The element closely related to carbon, silicon, has been widely used for the synthesis of macrocycles with rigid aromatic or heteroaromatic subunits. The first report appeared in 1973 by Kauffmann et al.[9] who obtained a macrocycle **10** consisting of four thiophene rings bridged by dimethylsilyl groups from the reaction of a lithiated dimethylsilyl-

bridged bis(thiophene) in 16% yield. Later silicon-bridged macrocycles, such as **10** and **11**, were reported by Corriu and Moreau as by-products in polymerization reactions (Scheme 4).[10] We have further developed protocols for silicon-bridged macrocycles, which now allow the synthesis of a wide variety of lipophilic macrocycles with weak coordination sites. In this strategy carbo- or heterocyclic dianions react with bis(electrophiles), such as Me_2SiCl_2.[11] The low solubility of the dianions in petroleum ether solvent and the very fast reaction of the slowly added bis(electrophile) generate *pseudo*-dilute conditions. The synthesis of macrocycles therefore proceeds under high substrate concentrations. Variation of the heterocyclic dianion yields the macrocyclic structures **12** and **13** (Scheme 5).



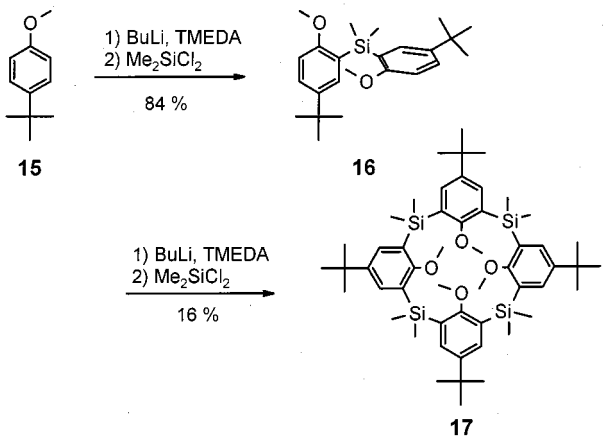
Scheme 4



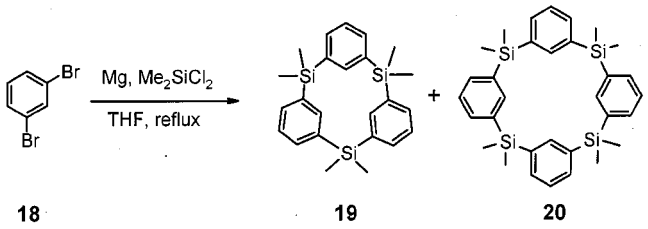
Scheme 5

An extension of the synthesis to sila[1_4]paracyclophanes **14** or silicon-bridged calix[4]arenes **17** is possible by a two-step route: Aromatic anions, generated by *ortho*-lithiation, react with Me_2SiCl_2 to give silicon-bridged dimers **16** (Scheme 6). Double deprotonation of **16** generates the dianion for cyclization. Metal salt extraction experiments from aqueous solutions revealed a much smaller affinity towards the silicon-bridged macrocycles as compared to crown ethers. In some cases high selectivities were observed, but it was not possible to establish a rational structure-selectivity relationship.

Yoshida et al.[12] have obtained the unsubstituted parent trisilacalix[3]arene (trisila[1.1.1]*meta*-cyclophane) **19** and tetrasilacalix[4]arene **20** (tetrasila[1.1.1.1]*meta*-cyclophane) from 1,3-dibromobenzene (**18**), Me_2SiCl_2, and magnesium in 12 and 2% yield, respectively (Scheme 7). The X-ray structure analysis revealed that **19** adopts a saddle structure and **20** a 1,2-alternate structure in the solid state. An isomer of **19**, trisila[1.1.1]*ortho*-cyclophane, has been previously prepared by Sakurai et al.[13] Mass spectrometry showed that **19** and **20** do form complexes with silver cations. Association constants have not been reported.[12]



Scheme 6

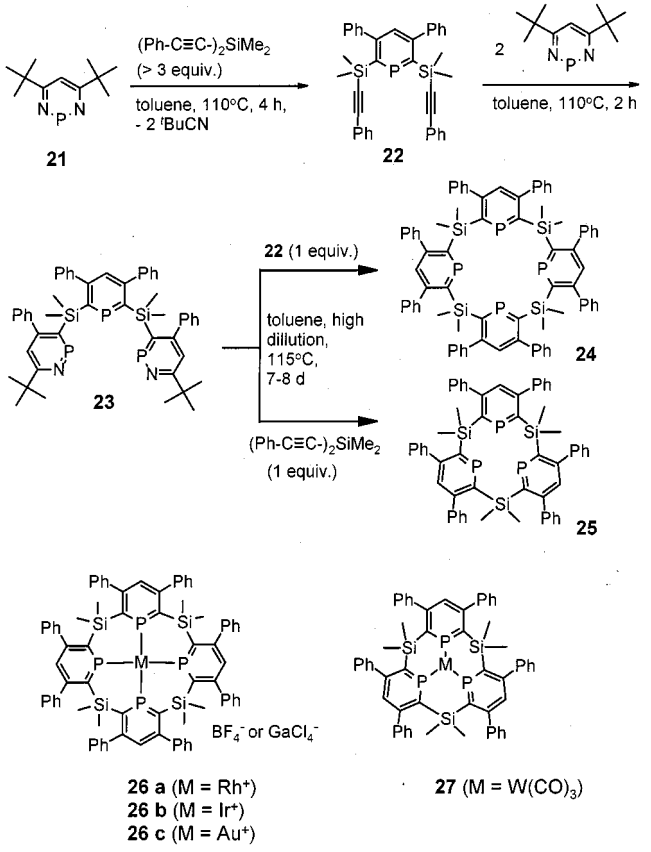


Scheme 7

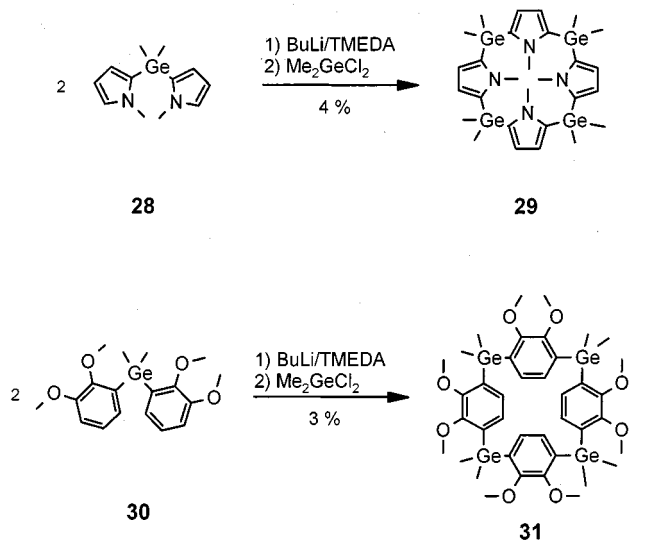
A successful synthesis of silicon-bridged dicoordinate phosphorous macrocycles was reported by Mathey, Le Floch, and co-workers.[14] They used a previously established, versatile route to phosphinines[15] based on the [4+2] cycloaddition of alkynes with 1,3,2-diazaphosphanes for the synthesis. The 1,3,2-diazaphosphinine **21** was first allowed to react with a threefold excess of dialkynylsilane to give **22** in 60 to 70% yield (Scheme 8). Next, compound **22** was allowed to react with two equivalents of diazaphosphinine **21** to give **23**. Under high dilution conditions **23** reacted with one equivalent of **22** to give the calix[4] derivative **24** or the calix[3] derivative **25** under similar conditions, both in 20% yield. The macrocycles act as ligands with strong π-acceptor properties. From compound **24** the rhodium and iridium complexes **26a** and **b** have been prepared and from macrocycle **25** the $W(CO)_3$ complex **27**. Reaction of **24** with AuI gave the first macrocyclic gold(I) complex **26c**, which can be reduced with sodium or potassium to a paramagnetic gold(0) complex.[14c]

2.2 Germanium

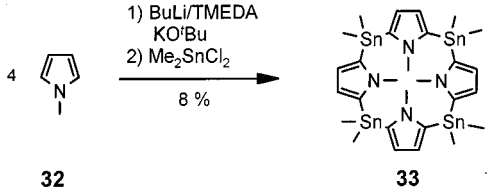
Extension of the reaction of the bis(carbanions) with Me_2SiCl_2 to Me_2GeCl_2 revealed significant differences: While the reaction of monolithiated heterocycles, such as furan, thiophene or *N*-methylpyrrole with Me_2GeCl_2 gave Me_2Ge-bridged dimers in good yield, the reaction of 2,5-dianions with Me_2GeCl_2 mostly yielded a mixture of linear oligomers instead of macrocycles. However, reaction of stoichiometric amounts of Me_2GeCl_2 with the 5,5′-dianion of **28** and **30** gave macrocycles **29** and **31**, respectively (Scheme 9), both in low yield.[16] The reaction of other dianions of Me_2Ge-bridged aromatic and heteroaromatic



Scheme 8



Scheme 9



Scheme 10

dimers yielded mixtures of linear oligomers exclusively. The size and distribution of the oligomers was investigated by gel permeation chromatography. The monomodal distribution in all cases indicates a regular, unbranched structure for the oligomers, with an average size being from 4 to 17 repeating units. The UV spectra of Me_2Ge- and Me_2Si-bridged arenes and heteroarenes show a small, but distinct bathochromic shift of λ_{max} with increasing molecule size. The extent of this shift differs only slightly for Me_2Si- and Me_2Ge-bridged molecules, which shows the similar abilities of these elements to electronically link the π-systems by σ-conjugation.[17]

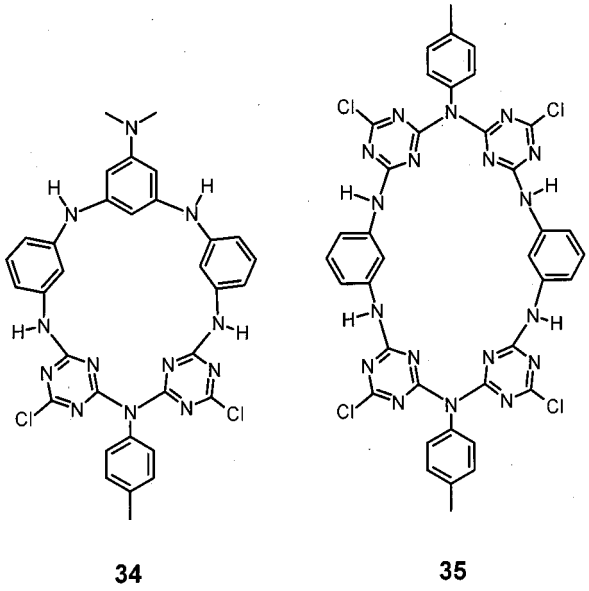
2.3 Tin

Tin can substitute for silicon or germanium in the macrocycles. Compound **33** was synthesized from the *N*-methylpyrrol dianion and Me_2SnCl_2 as described before (Scheme 10).[11b] The nearly identical NMR spectra of **33** and **12** indicate similar structures for both compounds. However, macrocycle **33** is rather unstable and decomposes rapidly if stored in air.

3. Group VA Elements

3.1 Nitrogen

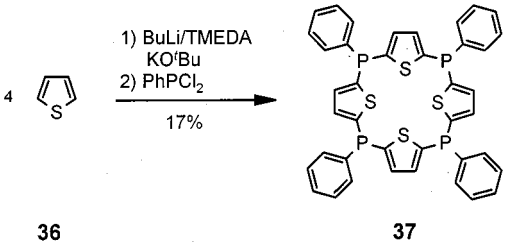
The nitrogen-bridged macrocycles **34** and **35** with aromatic subunits have been obtained from the reaction of trichlorotriazene with primary amines and diamines in stepwise procedures (Scheme 11).[18,19] The synthetic strategy allows for the incorporation of a wide variety of substituents. A first example of nitrogen-bridged calixarenes of structure **5** with X = NCH_3 (n = 1) has been reported in the literature very recently,[20] but so far no information about the binding properties is available. The advances in methods for the formation of nitrogen−carbon bonds to arenes[21] makes it likely that many more such compounds will soon be available.



Scheme 11

3.2 Phosphorus

The reaction of $PhPCl_2$ with the 2,5-dianion of thiophene gave macrocycle **37** in 17% yield (Scheme 12).[11b] The ^{31}P resonance shows the formal oxidation level to be +3 for the phosphorus bridge. However, the sensitivity of the compound towards oxidation did not allow for metal extraction studies.



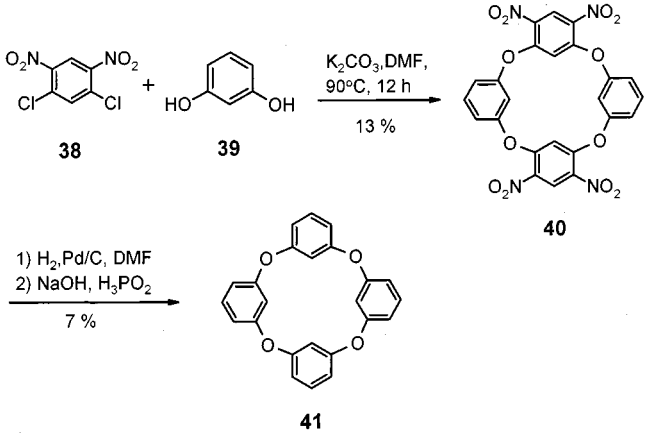
36 **37**

Scheme 12

4. Group VIA Elements

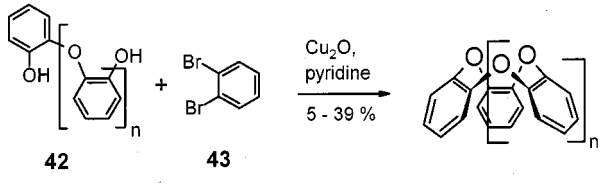
4.1 Oxygen

Several oxygen-bridged calixarenes have been prepared. Such compounds, which can be described as fully aromatic crown ethers, have been prepared to investigate the influence of a more rigid structure and less basic binding sites on the binding selectivity of crown ethers towards metal cations. The synthesis uses either nucleophilic aromatic substitution of activated arenes[22] (Scheme 13) or Ullmann-type reactions of bis(hydroxyaryl) ethers **42** with 1,2-dibromobenzene (**43**) in the presence of copper salts and pyridine (Scheme 14).[23] The structure of **44** with $n = 1$ has been determined in the solid state and was found to have a C_2-symmetric saddle form. Crown compounds **44** (n = 4,5) were tested by extraction methods for their extraction abilities, but no complexes were formed with lithium, sodium, potassium, calcium, or ammonium cations.



38 **39** **40** **41**

Scheme 13

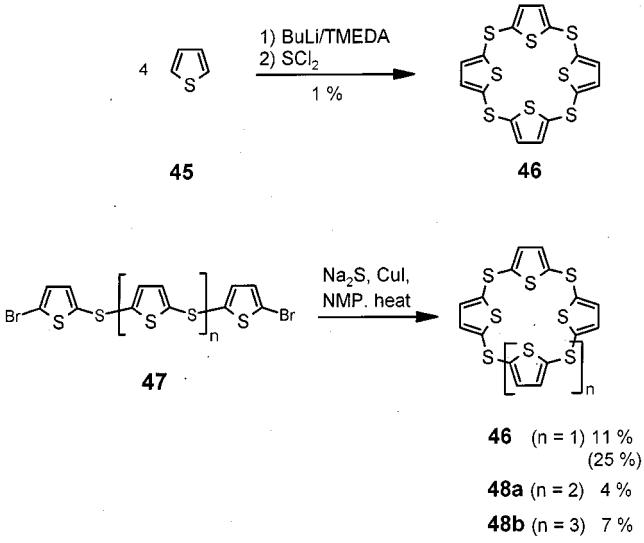


42 **43** **44**

Scheme 14

4.2 Sulfur

A large variety of sulfur-bridged calixarenes and heterocalixarenes have appeared in the literature. A simple extension of the previously described synthesis via 2,5-dilithiothiophenes to bis(electrophiles), such as SCl_2 yields thiacalix[4]arene **46**, although in very low yield (Scheme 15).[24] The reaction of dibromo derivatives of linear sulfur-bridged thiophenes with Na_2S and copper salts in NMP as reported by Nakayama et al. gave access to **46** in higher yield and gave larger thiacalixarenes **48**.[25]



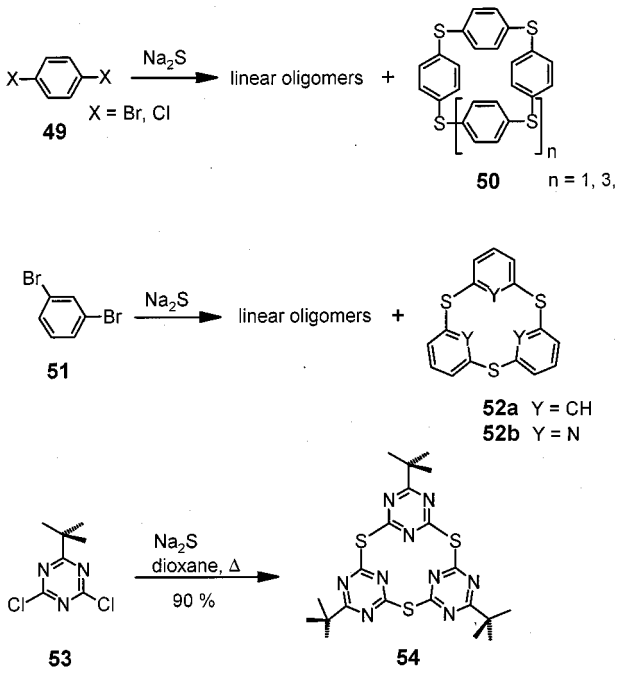
45 **46** **47**

46 (n = 1) 11 % (25 %)
48a (n = 2) 4 %
48b (n = 3) 7 %

Scheme 15. Synthesis of sulfur-bridged thiacalixarenes; the yield of compound **46** increases to 25% if CuI is replaced by Cs_2CO_3

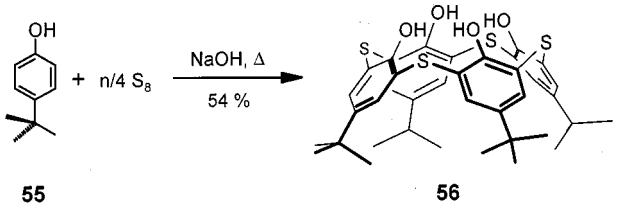
The reaction of *para*- or *meta*-dichlorobenzene or -dibromobenzene and sodium sulfide results in the formation of linear polyphenylene sulfides that contain small amounts (ca. 3%) of sulfur-bridged macrocycles of various ring sizes. From the low molecular weight fractions, several macrocycles, such as **50** or **52a**, with 3−6 benzene units have been isolated by extraction, chromatography and recrystallization, and characterized spectroscopically (Scheme 16).[26] An X-ray structure analysis has been reported for compound **52a**. The analogous thiacalix[3]pyridine **52b** was obtained from intermolecular condensation of 6-chloropyridine-2-thione in the presence of P_2S_5, but no yield was reported.[27] In 90% yield a sulfur-bridged calix[3]azine **54** was synthesized from 6-*tert*-butyl-2,4-dichloro-1,3,5-triazine (**53**) and Na_2S in dioxane. The X-ray analysis of the molecule revealed a surprisingly flat structure with each triazine

ring participating in π-stacking interactions with neighboring molecules.[28]



Scheme 16

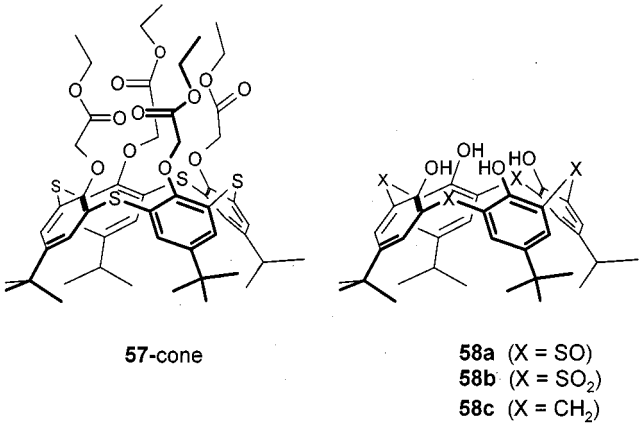
Most reports have appeared on the synthesis and properties of tetrahydroxytetrathiacalix[4]arenes. The synthesis of tetrahydroxy-*para-tert*-butyltetrathiacalix[4]arene (**56**) starts from *para-tert*-butylphenol (**55**), as in the parent methylene-bridged system. Heating of **55** with elemental sulfur and NaOH in tetraethylene glycol dimethyl ether results in the



Scheme 17

formation of **56** in 54% yield (Scheme 17). Small amounts of the corresponding thiacalix[5]- and thiacalix[6]arenes were isolated by HPLC.[29] The synthesis of all possible isomers of *para-tert*-butylcalix[4]arenes in which methylene bridges were partly replaced by sulfur linkages has also been reported.[30] The X-ray structure analysis of **56** shows the inclusion of dichloromethane in the cavity under the conditions of crystallization. The molecule has a cone conformation in the solid state.[31] The compound is an interesting ligand for metal ion coordination. An antiferromagnetic copper complex with copper acetate is obtained in DMF. The X-ray structure analysis shows a square cluster of four copper(II) ions with phenoxy and sulfur bridges sandwiched between two fully deprotonated calixarenes, thus forming a ditopic, divergent receptor.[32] Zinc(II) ions are coordinated by the bridging sulfur atom and the phenolic oxygen atom to form a complex coordination structure.[33] The high affinity of **56** for transition metal ions was also demonstrated by quantitative extraction of Co^{2+}, Cu^{2+}, and Zn^{2+} salts from the aqueous phase into chloroform.[34] Alkylation of the hydroxy groups of tetrahydroxythiacalixarenes has been used to lock the macrocycle conformation and thereby tune complexation properties. Depending on the counterion of the base used in the alkylation reaction, the conformer distribution is altered from the cone as the major product with sodium ions to the 1,3-alternate conformation with cesium ions present. The results suggest that a template effect is the main controlling factor. X-ray structure analysis of the 1,3-alternate conformer showed the formation of channels in the solid state.[35] NMR investigations showed a higher conformational flexibility for the tetraethyl ether of thiacalix[4]arene in comparison with the methylene-bridged calixarene. The larger cavity of the sulfur-bridged macrocycle is a likely rationale for this observation.[36] Extraction studies with the different conformers of tetrakis[(ethoxycarbonyl)methoxy]-thiacalix[4]arene **57** (Scheme 18) showed a higher affinity of the cone conformer for sodium ions, whereas the 1,3-alternate conformer extracts preferentially potassium and rubidium ions. The extraction ability of the partial cone conformer was found to be lower for all metal ions.[37] The stoichiometry of the complex of cone-**57** with sodium ion was determined to be 1:1 with the stability constant of $10^{2.85}$ L mol^{-1} in 50% (v/v) $CDCl_3/CD_3OD$. For details of percentage cation extracted and experimental conditions, see ref.[37]

Water-soluble sulfonated tetrathiacalix[4]arenes have been used for the removal of small halogenated organic substances, such as CH_2Cl_2 or $CHCl_3$, from water. By formation of a ternary complex of the negatively charged thiacalixarene, an anion-exchange resin and the halogenated organic compound, almost perfect removal of organic pollutants, with removal rates of more than 99.9% from water, was achieved.[38] Thiacalix[4]arene derivatives, which are modified with di- and tridansyl moieties, have been prepared to investigate their metal-sensing abilities in aqueous solution. Such molecules with two dansyl groups are able to detect metal cations in aqueous solution by variation of the fluorescence intensity, but observed selectivities are low.[39]



Scheme 18

Oxidation of **56** with H_2O_2 in glacial AcOH yielded sulfonylcalixarene **58b** in 59% yield (Scheme 18). The X-ray analysis revealed the formation of a three-dimensional network of hydrogen bonds between the OH and SO_2 groups, whereby the calixarenes adopt a 1,3-alternate conformation.[40] Stepwise oxidation of **55** to sulfinyl- and sulfonylcalix[4]arenes was achieved with stoichiometric amounts of $NaBO_3$ in chloroform.[41] Extraction experiments (see Table 1) showed that sulfonylcalix[4]arene **58b** completely lost the ability of thiacalixa[4]arenes, such as **56**, to extract transition metal ions. With **58b**, alkaline earth metal ions, in particular Ca^{2+}, are extracted. Interestingly, sulfinylcalixarene **58a** shows affinity for both transition and alkaline earth metal ions in extraction experiments.[41]

Table 1. Percentage of extracted transition metal and alkaline earth metal cations by calixarenes from the aqueous phase into chloroform; for detailed experimental conditions, see ref.[41]

Compound	Transition metal (pH = 8.0)			Alkaline earth metal (pH = 10)			
	Co^{2+}	Ni^{2+}	Cu^{2+}	Zn^{2+}	Mg^{2+}	Ca^{2+}	Ba^{2+}
58c	5	1	1	6	0	0	3
56	99	97	99	99	1	0	7
58a	99	99	17	99	99	91	99
58b	9	2	4	10	60	100	80

Conclusion

The introduction of heteroatoms as bridging atoms in calixarene macrocycles offers additional opportunities to modify their properties, affinity and selectivity for binding ions or molecules. So far, the number of known heteroatom-bridged calixarenes is still rather limited compared with carbocyclic calixarenes, and the relation of macrocyclic structure to selectivity of binding is obvious in only very few cases. However, if ongoing research in this field will provide the knowledge to better predict binding properties, as it is the case for crown ethers and cryptands, designed heteroatom-bridged calixarenes will have the potential to serve as selective ionophores and host molecules for many applications.

Acknowledgments

Support of our own work on heteroatom-bridged macrocycles from the Fonds der Chemischen Industrie is acknowledged. M. H. F. thanks the Deutscher Akademischer Austauschdienst (DAAD) for a scholarship.

[1] [1a] A. B. Smith, B. C. Miller, *Chem. Ber.* **1996**, *129*, 222−233; *Comprehensive Supramolecular Chemistry* (Eds.: J. L. Atwood, J. E. D. Davies, D. D. Macnicol, F. Vögtle, J.-M. Lehn, G. W. Gokel), vol 1, Elsevier, Oxford, UK, **1996**. − [1b] J.-M. Lehn, *Supramolecular Chemistry*, VCH, Weinheim **1995**. − [1c] F. Vögtle, *Supramolekulare Chemie*, Teubner, Stuttgart **1991**. − [1d] F. Cramer (Ed.), *Erkennen als geistiger und molekularer Prozeß*, VCH, Weinheim **1991**. − [1e] S. H. Gellmann (Ed.), *Chem. Rev. (Molecular Recognition)* **1997**, *97*, 1231−1734.

[2] G. M. Whitesides, J. P. Mathias, C. T. Seto, *Science* **1991**, *254*, 1312−1319.

[3] B. Dietrich, P. Viout, J.-M. Lehn, *Macrocyclic Chemistry*, VCH, Weinheim, **1993**.

[4] [4a] A. Baeyer, *Ber. Dtsch. Chem. Ges.* **1886**, *19*, 2184−2185. − [4b] P. A. Gale, J. L. Sessler, V. Kral, *Chem. Commun.* **1998**, 1−8.

[5] C. D. Gutsche, *Calixarenes*, in: *Monographs in Supramolecular Chemistry* (Ed.: J. F. Stoddart), The Royal Society of Chemistry, Cambridge, UK, **1989**.

[6] V. Kral, P. A. Gale, P. Anzenbacher, K. Jursikova, V. Lynch, J. L. Sessler, *Chem. Commun.* **1998**, 9−10.

[7] F. H. Carré, R. J.-P. Corriu, T. Deforth, W. E. Douglas, W. S. Siebert, W. Weinmann, *Angew. Chem.* **1998**, *110*, 654−655; *Angew. Chem. Int. Ed.* **1998**, *37*, 652−654.

[8] E. Vogel, P. Röhrig, M. Sicken, B. Knipp, A. Herrmann, M. Pohl, H. Schmickler, J. Lex, *Angew. Chem.* **1989**, *101*, 1683−1687; *Angew. Chem. Int. Ed. Engl.* **1989**, *28*, 1651−1655.

[9] T. Kauffmann, H. H. Kniese, *Tetrahedron Lett.* **1973**, *41*, 4043−4046.

[10] P. Chicart, R. J. P. Corriu, J. E. Moreau, F. Garnier, A. Yassar, in: *Inorganic and Organometallic Polymers with Special Properties* (Ed.: R. M. Laine), NATO ASI Series, **1992**, vol. 206, p. 179−190.

[11] [11a] B. König, M. Rödel, P. Bubenitschek, P. G. Jones, *Angew. Chem.* **1995**, *107*, 752−754; *Angew. Chem. Int. Ed. Engl.* **1995**, *34*, 661−662. − [11b] B. König, M. Rödel, P. Bubenitschek, P. G. Jones, I. Thondorf, *J. Org. Chem.* **1995**, *60*, 7406−7410.

[12] M. Yoshida, M. Goto, F. Nakanishi, *Organometallics* **1999**, *18*, 1465−1470.

[13] H. Sakurai, Y. Eriyama, A. Hosomi, Y. Nakadaira, C. Kabuto, *Chem. Lett.* **1984**, 595−596.

[14] [14a] N. Avarvari, N. Mézailles, L. Ricard, P. Le Floch, F. Mathey, *Science* **1998**, *280*, 1587−1589. − [14b] N. Avarvari, N. Maigrot, L. Ricard, P. Le Floch, F. Mathey, *Chem. Eur. J.* **1999**, *5*, 2109−2118. − [14c] N. Mézailles, N. Avarvari, N. Maigrot, L. Ricard, F. Mathey, P. Le Floch, L. Cataldo, T. Berclaz, M. Geoffroy, *Angew. Chem.* **1999**, *111*, 3390−3393; *Angew. Chem. Int. Ed.* **1999**, *38*, 3194−3197.

[15] [15a] N. Avarvari, P. Le Floch, F. Mathey, *J. Am. Chem. Soc.* **1996**, *118*, 11978−11979. − [15b] N. Avarvari, P. Le Floch, L. Ricard, F. Mathey, *Organometallics* **1997**, *16*, 4089−4098.

[16] B. König, M. Rödel, *Chem. Ber.* **1997**, *130*, 412−423.

[17] U. Weidner, A. Schweig, *Angew. Chem.* **1972**, *84*, 550; *Angew. Chem. Int. Ed. Engl.* **1972**, *11*, 536.

[18] [18a] H. Graubaum, G. Lutze, B. Costisella, *J. Prakt. Chem./Chem.-Ztg.* **1997**, *339*, 266−271. − [18b] H. Graubaum, G. Lutze, F. Tittelbach, M. Bartoszek, *J. Prakt. Chem./Chem.-Ztg.* **1995**, *337*, 401−404.

[19] H. Graubaum, G. Lutze, B. Costisella, B. Linden, *J. Prakt. Chem./Chem.-Ztg.* **1997**, *339*, 672−674

[20] [20a] A. Ito, Y. Ono, K. Tanaka, *J. Org. Chem.* **1999**, *64*, 8236−8241. − [20b] A. Ito, Y. Ono, K. Tanaka, *Angew. Chem.* **2000**, *112*, 1114−1117; *Angew. Chem. Int. Ed.* **2000**, *39*, 1072−1075.

[21] [21a] J. P. Wolfe, S. Wagaw, J.-F. Marcroux, S. L. Buchwald, *Acc. Chem. Res.* **1998**, *31*, 805−818. − [21b] R. A. Singer, J. P. Sadighi, S. L. Buchwald, *J. Am. Chem. Soc.* **1998**, *12*, 213−214. − [21c] J. F. Hartwig, *Acc. Chem. Res.* **1998**, *31*, 852−860.

[22] [22a] N. Sommer, H. A. Staab, *Tetrahedron Lett.* **1966**, 2837−2841. − [22b] F. Lehmann, *Tetrahedron* **1974**, *30*, 727−733. − [22c] E. E. Boros, C. W. Andrews, A. O. Davis, *J. Org. Chem.* **1996**, *61*, 2553−2555. − [22d] F. Bottino, S. Foti, S. Pappalardo, *Tetrahedron* **1976**, *32*, 2567−2570.

[23] [23a] C. W. Bird, M. Singh, *Chem. Ind.* **1974**, 749−750. − [23b] T. Weiss, P. Schulz, G. Klar, *Z. Naturforsch.* **1974**, *29b*, 156−158. − [23c] D. E. Kime, J. K. Norymberski, *J. Chem. Soc., Perkin Trans. 1* **1977**, 1048−1052. − [23d] K. Deuten, G. Klar, *Z. Naturforsch.* **1981**, *36b*, 1526−1531.

[24] B. König, M. Rödel, I. Dix, P. G. Jones, *J. Chem. Res. (S)* **1997**, 69.

[25] J. Nakayama, N. Katano, Y. Sugihara, A. Ishii, *Chem. Lett.* **1997**, 897−898.

[26] [26a] M. L. Kaplan, W. D. Reents, *Tetrahedron Lett.* **1982**, *23*, 373−374. − [26b] V. A. Sergeev, V. I. Nedel'kin, A. V. Astankov, *Izv. Akad. Nauk SSSR, Ser. Khim., Engl. Transl.* **1988**, 1770. − [26c] V. A. Sergeev, V. I. Nedel'kin, A. V. Astankov, A. V.

Nikiforov, E. M. Alov, Y. A. Moskvichev, *Izv. Akad. Nauk SSSR, Ser. Khim., Engl. Transl.* **1990**, 763−766. − [26d] V. A. Sergeev, Y. E. Ovchinnikov, V. I. Nedel'kin, A. V. Astankov, O. B. Andrianova, V. E. Shklover, I. A. Zamaev, Y. T. Struchkov, *Izv. Akad. Nauk SSSR, Ser. Khim., Engl. Transl.* **1989**, 1440−1444.

[27] K. R. Reistad, P. Groth, R. Lie, K. Undheim, *J. Chem. Soc., Chem. Commun.* **1972**, 1059−1060.

[28] [28a] M. Mascal, J. L. Richardson, A. J. Blake, W.-S. Li, *Tetrahedron Lett.* **1997**, 38, 7639−7640. − [28b] In an earlier report the reaction of 2,4-dichloro-6-phenyl-1,3,5-triazine with Na_2S was described to give a mixture of oligomeric materials: G. A. Loughran, G. F. Ehlers, J. L. Burkett, *J. Heterocycl. Chem.* **1966**, *3*, 143−148.

[29] K. Kumagai, M. Hasegawa, S. Miyanari, Y. Sugawa, Y. Sato, T. Hori, S. Ueda, H. Kamiyama, S. Miyano, *Tetrahedron Lett.* **1997**, *38*, 3971−3972.

[30] T. Sone, Y. Ohba, K. Moriya, H. Kumada, K. Ito, *Tetrahedron* **1997**, *53*, 10689−10698.

[31] H. Akdas, L. Bringel, E. Graf, M. W. Hosseini, G. Mislin, J. Pansanel, A. De Cian, J. Fischer, *Tetrahedron Lett.* **1998**, *39*, 2311−2314.

[32] G. Mislin, E. Graf, M. W. Hosseini, A. Bilyk, A. K. Hall, J. M. Harrowfield, B. W. Skelton, A. H. White, *Chem. Commun.* **1999**, 373−374.

[33] N. Iki, N. Morohashi, C. Kabuto, S. Miyano, *Chem. Lett.* **1999**, 219−220.

[34] N. Iki, N. Morohashi, F. Narumi, S. Miyano, *Bull. Chem. Soc. Jpn.* **1998**, *71*, 1597−1603.

[35] [35a] P. Lhoták, M. Himl, S. Pakhomova, I. Stibor, *Tetrahedron Lett.* **1998**, *39*, 8915−8918. − [35b] H. Akdas, G. Mislin, E. Graf, M. W. Hosseini, A. De Cian, J. Fischer, *Tetrahedron Lett.* **1999**, *40*, 2113−2116.

[36] J. Lang, H. Dvorakova, I. Bartosova, P. Lhotak, I. Stibor, R. Hrabal, *Tetrahedron Lett.* **1999**, *40*, 373−376.

[37] N. Iki, F. Narumi, T. Fujimoto, N. Morohashi, S. Miyano, *J. Chem. Soc., Perkin Trans. 2* **1998**, 2745−2750.

[38] N. Iki, T. Fujimoto, T. Shindo, K. Koyama, S. Miyano, *Chem. Lett.* **1999**, 777−778.

[39] [39a] M. Narita, Y. Higuchi, F. Hamada, H. Kumagai, *Tetrahedron Lett.* **1998**, *39*, 8687−8690. − [39b] Only the binding constants for Al^{3+} cations are reported in the paper, with a value of 3500 (+/−600) L/mol (two dansyl moieties) and 1200 (+/−170) L/mol (three dansyl moieties).

[40] [40a] G. Mislin, E. Graf, M. W. Hosseini, A. De Cian, J. Fischer, *Chem. Commun.* **1998**, 1345−1346. − [40b] G. Mislin, E. Graf, M. W. Hosseini, A. De Cian, J. Fischer, *Tetrahedron Lett.* **1999**, *40*, 1129−1132.

[41] N. Iki, H. Kumagai, N. Morohashi, K. Ejima, M. Hasegawa, S. Miyanari, S. Miyano, *Tetrahedron Lett.* **1998**, *39*, 7559−7562.

Received March 17, 2000
[I00100]

Reactivity of Copper(I) Complexes Towards Dioxygen

Siegfried Schindler*[a]

Keywords: Copper / Oxygen / Bioinorganic chemistry / Tripodal ligands / Peroxo complexes

Efforts to model the reactions of copper enzymes with dioxygen with low molecular weight complexes have been quite successful during recent years. Guided by Nature, intriguing model systems for the active sites of such proteins have been developed. In the course of these investigations, it has been discovered that a whole variety of copper–dioxygen adducts form when simple copper(I) complexes are oxidized with dioxygen. The course of these reactions depends on the temperature, the ligands present, and the solvent. The effects of these parameters (especially the effect of ligand modification) on the reactivity of copper(I) complexes towards dioxygen are discussed in detail in this review.

Introduction

Oxidations play important roles in biochemistry, industrial processes, and organic syntheses.[1] For example, controlled partial oxidation of hydrocarbons is necessary to convert petrochemical feedstock into industrial organic chemicals. For economic reasons, there is much interest in the chemical industry in the use of dioxygen as the primary oxidant. However, these processes depend greatly on metal catalysts to promote the rates and enhance the selectivities of the reactions.

Copper ions are found in the active sites of many redox-active metalloproteins that transport (hemocyanin) or transfer molecular oxygen [e.g. tyrosinase (an oxygenase), dopamine β-hydroxylase, or ascorbate oxidase].[2–9] A key step in these redox reactions is the activation of dioxygen upon binding at the active site prior to the reaction with a substrate (Equation (1)).

[a] Institute of Inorganic Chemistry,
University of Erlangen-Nürnberg,
Egerlandstraße 1, D-91058 Erlangen, Germany
Fax: (internat.) + 49(0)-9131/852-7387
E-mail: schindls@anorganik.chemie.uni-erlangen.de

$$\text{Metalloenzyme or Metal Complex} \xrightleftharpoons{O_2} \text{Oxy-Form} \xrightarrow{\text{Substrate}} \text{Product} \qquad (1)$$

The interest in preparing low molecular weight model complexes for such copper enzymes is twofold. First, the models provide a better understanding of the biological molecules.[3,8] Second, they assist in the development of new catalysts for selective oxidations under mild conditions.[1,10] Therefore, it is of great interest to elucidate the factors that govern the (reversible) binding and activation of dioxygen in various natural oxygen transport systems, i.e. mono- and dioxygenases. Guided by Nature, intriguing model systems for the active sites of copper-containing dioxygen-binding enzymes have been synthesized. These systems are discussed here in detail.

Considerable effort has been directed towards the development of useful catalytic systems for mild and selective oxidations with dioxygen. The feasibility of this has recently been demonstrated with different model compounds for galactose oxidase. In the presence of these complexes, alcohols were catalytically oxidized to aldehydes.[11,12]

This review article gives an overview of the structurally characterized compounds that have been obtained by re-

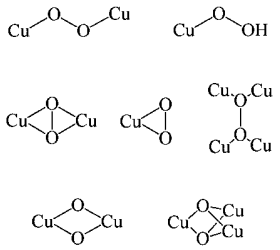


Siegfried Schindler studied chemistry at the Technical University of Darmstadt where he received his Ph. D. with Prof. Horst Elias. He then worked as a postdoctoral fellow with Dr. Carol Creutz at Brookhaven National Laboratory, New York, USA. He began his Habilitation in the group of Prof. Rudi van Eldik supported by a DFG scholarship at the Private University of Witten/Herdecke in 1993, focussing on the activation of small molecules. In 1994, he moved to the University of Erlangen-Nürnberg where he completed his Habilitation in 1997. He was a visiting professor at the University of Odense, Denmark, in 1997 and at the University of Vienna, Austria, in 1999. His research interests are centred on synthetic and kinetic studies of the reactions of transition metal complexes with dioxygen, carbon dioxide, carbon monoxide, and nitrogen oxide.

MICROREVIEWS: This feature introduces the readers to the authors' research through a concise overview of the selected topic. Reference to important work from others in the field is included.

 © WILEY-VCH Verlag GmbH, D-69451 Weinheim, 2000 1434–1948/00/1111–2311 $ 17.50+.50/0

acting copper(I) complexes with dioxygen [or in some cases copper(II) complexes with hydrogen peroxide]. Coordination modes of "dioxygen" adopted in copper complexes that have been structurally characterized are shown in Scheme 1. More detailed information on these compounds can be found in the original references as well as in a series of review articles on various aspects of copper(I)/dioxygen chemistry.[3,8,10,13–15] Furthermore, this article deals with binding and activation of dioxygen in copper(I) complexes according to the first part of Equation (1). It details how this reaction can be optimized, mainly through ligand modification ("ligand tuning"), but also by varying reaction conditions such as concentration, solvent, and temperature.

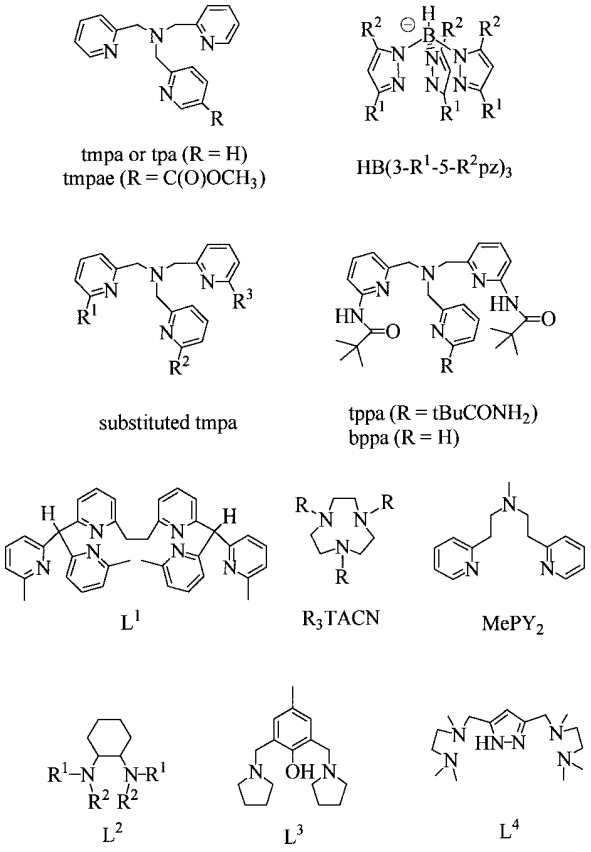


Scheme 1. Dioxygen binding modes in structurally characterized copper complexes

Structurally Characterized Copper Peroxo, Superoxo, and Oxo Complexes

For a long time, copper–peroxo complexes were postulated as intermediates in the reaction of copper(I) complexes with dioxygen.[16,17] However, a structural characterization of such a complex was not available until 1988.[18] At that time, Karlin and co-workers synthesized and characterized a complex incorporating a *trans*-μ-1,2-peroxo-bridged dicopper(II) moiety.[18,19] It was obtained from the reaction of $[(tmpa)Cu(CH_3CN)]^+$ {tmpa = tris[(2-pyridyl)-methyl]amine, sometimes abbreviated as tpa; Scheme 2} with dioxygen. Shortly thereafter, a copper complex with a μ-η^2:η^2-peroxo bridge, prepared by the reaction of $[Cu\{HB(3,5\text{-}i\mathrm{Pr}_2pz)_3\}]$ [$HB(3,5\text{-}i\mathrm{Pr}_2pz)_3$ = hydrido-tris(3,5-isopropyl)pyrazolylborate anion, Scheme 2; $HB(3\text{-}R^1\text{-}5\text{-}R^2pz)_3$, $R^1 = R^2 = i\mathrm{Pr}$] with O_2 (or by careful addition of aqueous hydrogen peroxide to the μ-dihydroxo dimer complex $[Cu_2\{HB(3,5\text{-}i\mathrm{Pr}_2pz)_3\}_2(OH)_2]$) was described by Kitajima and co-workers.[3,20] Its spectroscopic features closely resembled those observed for oxy-hemocyanin, the oxygen-transport protein of arthropods and molluscs, which has a dinuclear copper center in its active site. The similarity of the model complex and the protein was confirmed soon afterwards when the crystal structure of the *oxy*-hemocyanin of *Limulus polyphemus* subunit II was solved.[2]

When $HB(3\text{-}t\mathrm{Bu}\text{-}5\text{-}i\mathrm{Pr}_2pz)_3$ [Scheme 2; $HB(3\text{-}R^1\text{-}5\text{-}R^2pz)_3$, $R^1 = t\mathrm{Bu}$, $R^2 = i\mathrm{Pr}$] was used instead of $HB(3,5\text{-}i\mathrm{Pr}_2pz)_3$ it was possible to isolate and structurally characterize a side-on bound superoxo copper complex.[21] To date, only one other X-ray crystal structure of a copper–superoxo complex has been reported by Jitsukawa, Masuda, and co-workers with a η^1 "end-on" superoxide



Scheme 2. Ligands used in structurally characterized copper–dioxygen adducts

stabilized by hydrogen-bonding interactions with the surrounding tppa ligand (tppa = tris{[6-(pivaloylamido)-2-pyridyl]methyl}amine; Scheme 2).[22] This finding was questioned by Tolman and co-workers, who showed that the published X-ray data had probably been misinterpreted.[13] It now seems more likely that a monocopper hydroxide was obtained rather than a superoxo complex.

When Jitsukawa, Masuda, and co-workers reacted $[Cu^{II}(bppa^-)]ClO_4$ or $[Cu^{II}(bppa)(CH_3COO)]ClO_4$ (bppa = bis[(6-pivaloylamido)-2-pyridylmethyl](2-pyridylmethyl)amine; Scheme 2) with hydrogen peroxide in acetonitrile, they obtained a mononuclear copper hydroperoxo complex, which was characterized by X-ray crystallography and resonance Raman spectroscopy.[23]

Recently, Kodera et al. succeeded in synthesizing and structurally characterizing a new dinuclear copper complex with a μ-η^2:η^2-peroxo bridge that proved to be unusually stable at room temperature (the half-life at 25 °C was reported to be 25.5 h).[24] This compound was obtained when the dinuclear complex $[Cu_2L^1](PF_6)_2$ (L^1 = 1,2-bis{2-[bis(6-methyl-2-pyridyl)methyl]-6-pyridyl}ethane; Scheme 2) was reacted with O_2 in dichloromethane.

An important finding with regard to understanding the reactions of copper(I) with dioxygen was reported by Tolman and co-workers.[13,14,25–29] Using substituted triazacyclononane (Scheme 2; R_3TACN), these authors showed for the first time that copper μ-η^2:η^2-peroxo-bridged complexes can undergo interconversion with bis(μ-oxo)dicopper(III)

complexes. These new species were characterized spectroscopically, and the crystal structures were solved for $[(BN_3TACN)_2Cu_2(\mu\text{-}O)_2]^{2+}$ (BN_3TACN = 1,4,7-tribenzyl-1,4,7-triazacyclononane) and $[(i\text{Pr}_4\text{-dtne})Cu_2(\mu\text{-}O)_2]^{2+}$ [$i\text{Pr}_4$-dtne = 1,2-bis(4,7-diisopropyl-1,4,7-triaza-1-cyclononyl)ethane, Scheme 4; L^7: X = *m*-xylyl].[13,14]

When copper(I)−MePY2 {MePY2 = *N,N*-bis[2-(2-pyridyl)ethyl]methylamine; Scheme 2} was reacted with dioxygen at low temperatures, $[(MePY2)Cu-(O_2)-Cu(MePY2)]^{2+}$ was obtained.[30] Its crystal structure reveals a geometry halfway between that of a side-on peroxide and that of a bis(μ-oxo) core. However, X-ray absorption and resonance Raman spectroscopy provided clear evidence that this does not describe the true structure. Thus, the crystalline material was in fact found to be a solid solution composed of approximately 20% of the bis(μ-oxo) core and 80% of the side-on peroxide isomer. A mixture of these two species was also observed in solution.[31]

Very recently, it has been shown that introduction of two 6-methylpyridyl groups into the tmpa ligand (substituted tmpa, R^1 = H, R^2, R^3 = Me; Scheme 2) prevents the formation of *trans*-μ-1,2-peroxo-bridged dicopper(II) species in a trigonal-bipyramidal structure, probably due to the steric requirements of the two 6-methylpyridyl groups. Instead, formation of a brown bis(μ-oxo)dicopper(III) complex, $[Cu_2(O)_2(Me_2\text{-tmpa})_2](PF_6)_2\cdot(CH_3)_2CO$, is observed, the crystal structure of which has been reported.[32]

Two further examples of oxo-bridged copper complexes with peralkylated 1,2-cyclohexanediamine ligands (L^2, Scheme 2; R^1 and R^2 = Me and/or Et) have been structurally characterized by Stack and co-workers.[33,34] With R^1 = Me and R^2 = Et, a $Cu_2(\mu\text{-}O)_2$ core almost isostructural with that of $[(BN_3TACN)_2Cu_2(\mu\text{-}O)_2]^{2+}$ was obtained, although the Cu···Cu distance was shorter by 0.05 Å.[34] Interestingly, with R^1 = R^2 = Me, a unique trinuclear cluster compound with two μ_3-oxide ligands and three copper ions was obtained.[33] The structure was formally described as a mixed-valence cluster of two copper(II) ions and a single copper(III) ion bridged by two μ_3-oxo ligands.

An example of an exceptionally stable copper−peroxo complex has been reported by Krebs and co-workers.[15,35,36] By reacting a mixture of 2,6-bis(pyrrolidinomethyl)-4-methylphenol (L^3, Scheme 2), copper(II) perchlorate, and triethylamine with hydrogen peroxide (or 3,5-di-*tert*-butylcatechol), these authors obtained a tetranuclear copper complex with the peroxo ligand bound end-on in a μ_4-$(\eta^1)_4$ mode. When the same reaction was performed in the absence of hydrogen peroxide (or 3,5-di-*tert*-butylcatechol), a tetranuclear copper−oxo complex with a μ_4-O^{2-} unit was formed. The crystal structures of the two complexes are closely related; there is also evidence to suggest that the two species are interconvertible.

A further new example of a tetranuclear copper complex with a slightly different μ_4-peroxo coordination has recently

Table 1. Crystallographic and spectroscopic properties of copper−dioxygen adducts

Complex	Binding Mode	X-ray O---O/Cu---Cu (Å)	Resonance Raman cm^{-1}	UV-vis λ (nm) (ε ($cm^{-1}M^{-1}$))	Reference
$[(HB(3\text{-}tBu\text{-}5\text{-}iPr_2pz)_3)Cu(O_2)]$	side-on bound superoxo	1.22(3)/–	1111 ($^{16}O_2$) 1062 ($^{18}O_2$)	352 (2330) 510 (230) 660 (shoulder)	21
$[(tmpa)_2Cu_2(O_2)]^{2+}$	*trans*-μ-1,2-peroxo	1.432(6)/4.359(1)	832 ($^{16}O_2$)	440 (2000) 525 (11500) 590 (shoulder)	18, 19
$[\{HB(3,5\text{-}iPr_2pz)_3\}_2Cu_2(O)_2]$	μ-η^2:η^2-peroxo	1.412/3.560	741 ($^{16}O_2$) 698 ($^{18}O_2$)	349 (21000) 551 (800)	3, 20
$[Cu(bppa)(OOH)]^+$	end-on bound hydroperoxo	1.460(6)/–	856 ($^{16}O_2$) 810 ($^{18}O_2$)	380 (890) 660 (150) 830 (250)	23
$[L^1Cu_2(O_2)]^{2+}$	μ-η^2:η^2-peroxo	1.485(8)/3.477(7)	760 ($^{16}O_2$) 719 ($^{18}O_2$)	360 (24700) 532 (1530)	24
$[(BN_3TACN)_2Cu_2(\mu\text{-}O)_2]^{2+}$	bis(μ-oxo)	2.287(5)/2.794(2)	602, 612 ($^{16}O_2$) 583 ($^{18}O_2$)	318 (12000) 430 (14000)	14, 27
$[(iPr_4\text{-dtne})Cu_2(\mu\text{-}O)_2]^{2+}$	bis(μ-oxo)	2.35/2.783(1)	585 ($^{16}O_2$) 564 ($^{18}O_2$)	316 (13000) 414 (14000)	14, 29
$[(MePY2)_2Cu_2(O_2)]^{2+}$	μ-η^2:η^2-peroxo and bis(μ-oxo)	1.67/3.45	577 ($^{16}O_2$) 551 ($^{18}O_2$)	355 (14700) 410 (2500) 530 (400)	30
$[Cu_2(O)_2(Me_2\text{-tmpa})_2](PF_6)_2$	bis(μ-oxo)	2.32(1)/2.758(4)	590 ($^{16}O_2$) 564 ($^{18}O_2$)	378 (~22000) 494 (330)	32
$[(L^2)_2Cu_2(\mu\text{-}O)_2]^{2+}$ R^1 = Me and R^2 = Et	bis(μ-oxo)	2.344(1)/2.743(1)	610 ($^{16}O_2$) 587 ($^{18}O_2$)	306 (21000) 401 (28000)	34
$[(L^2)_3Cu_3O_2]^{3+}$ R^1 and R^2 = Me	μ_3-oxide	2.37/2.641(3) and 2.704(3)	607 ($^{16}O_2$) 583 ($^{18}O_2$)	355 (15000) 480 (1400) 620 (800)	33
$[Cu_4(L^3)_2(O_2)(OMe)_2(ClO_4)]^+$	μ_4-peroxo	1.453(4)/2.994(2) and 3.030(2)	878 ($^{16}O_2$) 841 ($^{18}O_2$)	384 (9700) 587 (610)	35, 36
$[Cu_4(L^4)_2(O_2)(OH)_2]^{2+}$	μ_4-peroxo	1.497(5)/2.986 and 3.902	not reported	360 (3100) 631 (260)	37

been reported by Meyer and Pritzkow using a multidentate pyrazolate ligand (L^4, Scheme 2).[37]

Crystallographic and spectroscopic properties of the aforementioned copper−dioxygen adducts are summarized in Table 1.

Kinetics and Thermodynamics of Copper(I)/Dioxygen Interaction

As described above, copper superoxo, peroxo, and bis(μ-oxo) complexes are rather unstable and are therefore difficult to crystallize. Consequently, other methods have to be used to identify and characterize these species, especially when they are only short-lived oxidation intermediates. Oxidations with dioxygen can be followed by UV/Vis spectrophotometry (see below). However, this technique should not be used exclusively to characterize the complexes that are formed in these reactions. Instead, resonance Raman spectra should also be recorded. This method allows detailed insight into the binding mode of the dioxygen.[30,33,34,38]

Among the most powerful tools for detailed investigations of bioinorganic transformations are kinetic studies.[10,39] Among the first researchers to investigate the oxidation of copper(I) complexes with dioxygen in water were Zuberbühler and co-workers.[16] Although dioxygen complexes could not be detected spectroscopically at first, unstable copper−dioxygen intermediates were postulated.[16,17] In a number of cases, kinetic evidence clearly implied the intermediacy of CuO_2^+ and $Cu_2O_2^{2+}$ species.[16] However, no information concerning their stabilities, spectroscopic properties, or structures was available. This situation improved dramatically when it was discovered that $[(tmpa)Cu(CH_3CN)]^+$ reacts with dioxygen to form a copper−peroxo complex that is stable at low temperatures (see above). After detailed kinetic investigations, a mechanism for the reaction of $[(tmpa)Cu(CH_3CN)]^+$ with dioxygen was postulated (Equations (2)−(4); L = tmpa).[40] Most importantly, for the first time it was possible to spectroscopically detect the formation of a superoxo complex (Equation (2)) prior to the formation of a peroxo compound.

$$[(L)Cu(RCN)]^+ + O_2 \rightleftharpoons [(L)Cu(O_2)]^+ + RCN \quad (2)$$

$$[(L)Cu(RCN)]^+ + [(L)Cu(O_2)]^+ \rightleftharpoons [(L)Cu(O_2)Cu(L)]^{2+} + RCN \quad (3)$$

$$[(L)Cu(O_2)Cu(L)]^{2+} \longrightarrow \text{irreversible decay} \quad (4)$$

Since most of these reactions are very fast, their kinetic investigation requires special low-temperature stopped-flow instruments operating with diode-array techniques. Furthermore, data fitting of the obtained time-resolved UV/Vis spectra is only possible with modern global fitting routines (including all data sets and spectra of intermediates).[17] These methods allow the determination of multi-step kinetic mechanisms, including kinetic and equilibrium constants, and the elucidation of complete UV/Vis spectra of intermediates.

A recent review article describes the kinetics and thermodynamics of the copper(I)/dioxygen interaction.[17] Therefore, only selected aspects concerning this particular interaction are mentioned in the present article, together with some new findings.

As mentioned above, copper μ-η^2:η^2-peroxo-bridged complexes are capable of interconversion with bis(μ-oxo)-dicopper(III) compounds. A kinetic study has shown that there is a rapid equilibrium between these two species (ligand R_3TACN, R = *i*Pr; Scheme 2).[28,41] Furthermore, it has been proposed that the oxygenation involves rate-determining formation of a mononuclear superoxo complex followed by a faster reaction with a second molecule of the monomeric copper(I) complex.

Dinuclear copper(I) complexes have been synthesized by linking mononuclear units as described below, in the hope that these "pre-organized" systems would stabilize the copper−peroxo unit. Kinetic measurements showed that this could indeed be achieved, but that this approach only works when the linked mononuclear units are not under any strain.[13,14,17,29,42−45] A linker that introduces steric strain leads to intermolecular rather than intramolecular formation of copper−peroxo complexes. Consequently, the dinuclear peroxo complexes should not be more stable than those obtained from the mononuclear compounds. This was confirmed in principle, but it was also observed that intermolecular oxidation can lead to quite stable polynuclear copper−peroxo complexes.[43]

Recently, the author's group succeeded in carrying out kinetic investigations on the reaction of a dinuclear copper(I) complex, $[Cu_2-H-XYL-H]^{2+}$ (ligand H−XYL−H is shown in Scheme 8), with dioxygen under high-pressure conditions.[46] This study turned out to be quite a challenge because the reaction of the oxygen-sensitive compound could only be investigated in organic solvents at low temperatures by means of stopped-flow techniques *and* under high pressure (this was accomplished using a high-pressure stopped-flow unit assembled in-house). For the first time, activation volumes for the formation $\Delta V^{\#} = -15.0 \pm 2.5$ cm^3/mol (as well as for the back reaction, $\Delta V^{\#} = +4.4 \pm 0.5$ cm^3/mol) and the decomposition ($\Delta V^{\#} = -4.1 \pm 0.7$ cm^3/mol) of a dinuclear copper−peroxo complex were obtained. Furthermore, solvent effects on this reaction were investigated. The reaction mechanism in acetone was shown to be more complicated than that in dichloromethane owing to an additional equilibrium between the dinuclear copper(I) complex and a less reactive isomer.

It should be pointed out that while there are clearly many similarities between dinuclear copper(I) complexes and hemocyanin, there are also many differences. For example, the reaction of the dinuclear copper(I) complex $[Cu_2-H-XYL-H]^{2+}$ (Scheme 8) with dioxygen is pressure dependent while that of deoxy-Hc is not.[46,47] More importantly, the oxidation of the protein proceeds very rapidly in water, while the model complexes investigated to date could only be studied in organic solvents.[48] Moreover,

when the protein is reacted with carbon monoxide it only binds one molecule, clearly indicating that the two copper(I) sites are differently shielded towards the reaction with substrates. The model complexes studied thus far bind one carbon monoxide molecule per copper(I) ion.[49]

General Approach

To optimize the reactions of copper(I) complexes with dioxygen in order to obtain stable copper−dioxygen adducts, most research groups follow a similar general strategy.

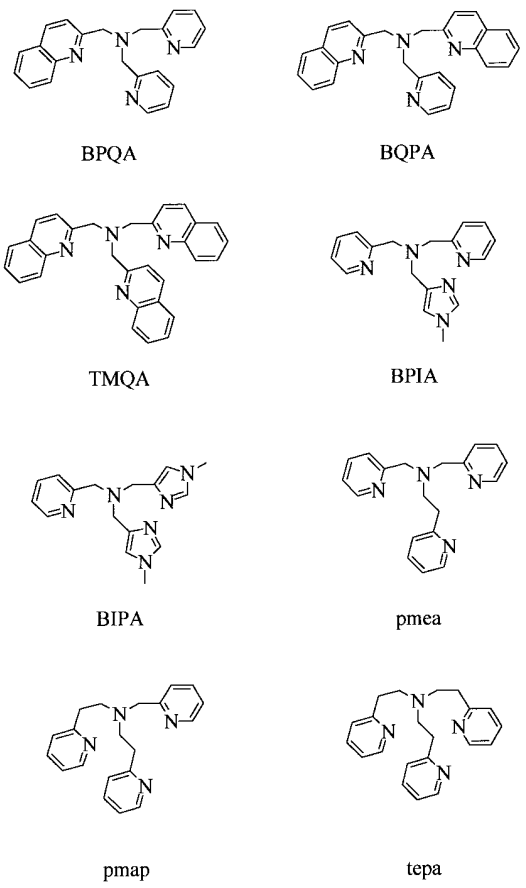
Temperature variation offers an important means of stabilizing copper superoxo, peroxo, or bis(μ-oxo) complexes. Thus, while many of these compounds are unstable at room temperature, they can be stored at low temperatures for months and can be isolated under these conditions. For example, by working at −80 °C, Karlin and co-workers were able to isolate and structurally characterize the first copper−peroxo complex.[18] For this reason, many studies on the behavior of copper(I) complexes towards dioxygen are performed using low-temperature techniques.[14,17,28,46,50] In principle, it should also be possible to bring about some of the temperature effects through pressure changes. However, for the relevant systems it is quite difficult and often impossible to accomplish pressure changes with the given experimental set-ups.

The most important method for modulating the reaction behavior of copper(I) complexes is modification of their ligands, either by introducing different donor atoms, changing chelate ring sizes, or using substituents that can influence the ligand sterically or electronically. Moreover, mononuclear units can be linked to form larger pre-organized ligand systems. This review is mainly focussed on how these chemical modifications affect the reactivity of copper complexes towards dioxygen. Quite recently, theoretical calculations have been used to predict the structures and/or reactivities of promising copper complexes (see below). Furthermore, the solvent can play an important role in the reaction of copper(I) complexes with dioxygen.

In general, a detailed study starts with a copper(I) complex that shows an interesting reaction behavior towards dioxygen. A detailed kinetic investigation is then undertaken and, in some cases, theoretical calculations are performed. The results are used to chemically modify the ligand in order to optimize the desired transformation.

Copper(I) Complexes with Tripodal Ligands Derived from tmpa

As discussed above, the tripodal complex $[Cu(tmpa)(CH_3CN)]^+$ has proved to be very useful for studying the reactions of copper(I) complexes with dioxygen. In order to gain further insight into these transformations, tmpa has been chemically modified and the resulting effects have been investigated.



Scheme 3. tmpa and derivatives

Karlin and co-workers replaced the pyridine moieties with sterically more demanding quinolyl groups in a stepwise manner. This yielded the ligands BPQA [bis(2-pyridylmethyl)(2-quinolylmethyl)amine], BQPA [bis(2-quinolylmethyl)(2-pyridylmethyl)amine], and TMQA [tris(2-quinolylmethyl)amine] shown in Scheme 3.[40,51] On going from tmpa to TMQA, dramatic differences in the reactivities of the corresponding copper(I) complexes towards dioxygen were observed. A detailed kinetic study showed that when $[Cu(BPQA)]^+$ was reacted with dioxygen at low temperatures, only the peroxo complex $[(BPQA)Cu(O_2)Cu(BPQA)]^{2+}$ could be detected; the formation of a superoxo complex was not observed under these conditions. In contrast, although reaction of $[Cu(BQPA)]^+$ with dioxygen led initially to the peroxo complex, this then immediately formed the 1:1 adduct, i.e. the superoxo complex $[(BQPA)Cu(O_2)]^+$. In the case of $[Cu(TMQA)]^+$, no interaction with dioxygen was observed.[40] According to the authors, steric effects are the most important factors in rationalizing these variations in reactivity.

Similar effects have been observed upon the successive introduction of three methyl groups at the 6-positions of the three pyridine moieties of tmpa (Scheme 2; substituted tmpa: R^1, R^2, R^3 = CH_3 or H).[52,53] As discussed above, with Me_2tmpa as ligand a bis(μ-oxo)dicopper(III) complex was obtained.[32] However, no detailed kinetic study has yet been performed.

Furthermore, the introduction of three phenyl groups at the 6-positions of the three pyridine moieties of tmpa renders the resulting copper(I) complex (Scheme 2; substituted tmpa: R^1, R^2, R^3 = phenyl) inert towards dioxygen.[54]

The introduction of steric hindrance in the tris(pyrazolyl)borate ligand [$HB(3\text{-}R^1\text{-}5\text{-}R^2pz)_3$, Scheme 2] allowed the synthesis and structural characterization of a copper−superoxo complex (see above).[21] Using the same approach, Jitsukawa, Masuda, and co-workers introduced three pivalolylamino groups at the 6-positions of the pyridine moieties of tmpa (Scheme 2; tppa). They hoped that the increased steric hindrance would lead to the formation of a copper−superoxo (1:1 adduct) instead of a peroxo complex.[22,55,56] Although these authors claimed to have structurally characterized a superoxo complex $[(tppa)Cu(O_2)]^+$, there is strong evidence that the described compound was actually $[(tppa)Cu(OH)]^+$ (see above).[57] Using bppa (Scheme 2), the same researchers were able to isolate and structurally characterize a copper−hydroperoxo complex (see above). Here, the hydroperoxo ligand is stabilized by hydrogen bonding.[23]

Karlin and co-workers also synthesized copper(I) complexes with tripodal ligands incorporating imidazolyl donor groups rather than pyridine (BPIA = {bis[(2-pyridyl)methyl(1-methylimidazol-2-yl)methyl]amine}; BIPA = {bis[(1-methylimidazol-2-yl)methyl]-(2-pyridyl)methylamine}, Scheme 3).[58] Interestingly, these complexes are dinuclear as solids, but dissociate into mononuclear species in solution. When $[Cu(BPIA)]^+$ was reacted with dioxygen at low temperatures, it exhibited very similar UV/Vis spectroscopic features to those of the parent $[(TMPA)Cu(RCN)]^+$, as well as of the quinolyl-containing $[Cu(BPQA)]^+$. For this reason, the formation of the peroxo complex $[(BPIA)CuO_2(BPIA)]^{2+}$ with a *trans*-(μ-1,2 peroxo) dicopper(II) moiety was postulated. This indicates that when one of the three pyridyl rings is substituted by some other donor group, the steric and electronic environment around the copper(I) center remains the same. However, when two pyridine groups are substituted by two imidazole donors, the copper−dioxygen chemistry becomes greatly altered. When $[Cu(BIPA)]^+$ was exposed to dioxygen at low temperatures in propionitrile, a red species was formed. It could not be fully characterized as it proved to be unstable under these conditions. Its UV/Vis spectrum was similar to that of the μ-η^2:η^2-peroxo compound $[\{HB(3,5\text{-}i\text{Pr}_2pz)_3\}Cu(O_2)Cu\{HB(3,5\text{-}i\text{Pr}_2pz)_3\}]$ described above. However, the molar extinction coefficients were much lower, probably owing to rapid decomposition of the red compound. In view of the lack of further evidence, these results that are based on UV/Vis measurements alone must be treated with caution.

Clearly, all these studies on Cu^I and Cu^{II} species with similar ligands show that small changes in ligand architecture can have a strong influence on the reactivity. In the active sites of enzymes, the nature of the ligand donors plays an important role in forcing the metal ions to participate in the desired biochemical transformations. Thus, further studies of ligand variations should provide valuable insights into fundamental aspects of biologically relevant coordination chemistry. With this in mind, it was decided to compare the reactivity of copper(I), copper(I)/O_2, and copper(II) complexes of other tripodal ligands derived from tmpa.[59]

On coordination of tmpa to copper ions, five-membered chelate rings are formed. If the carbon chain lengths in tmpa are increased by the introduction of pyridineethyl instead of pyridinemethyl groups, the ligands pmea {*N*,*N*-bis[(2-pyridyl)methyl]-2-(2-pyridyl)ethylamine}, pmap {*N*,*N*-bis[2-(2-pyridyl)ethyl]-(2-pyridyl)methylamine}, and tepa {tris[2-(2-pyridyl)ethyl]amine} are obtained (Scheme 3). Recently, the copper(I) and copper(II) complexes of pmea and pmap have been structurally characterized in this laboratory;[59] the copper(I) and copper(II) complexes of tmpa and tepa have been described previously.[19,60−62] In the case of tmpa and tmpae (Scheme 2), the copper(I) complex normally crystallizes in a trigonal-bipyramidal geometry with an additional acetonitrile molecule in the axial position.[19,60] This is not the case when the sterically demanding triphenylphosphane is used as an additional ligand.[19] The trigonal-bipyramidal geometry of $[(tmpa)Cu(CH_3CN)]^+$ is retained when this compound is oxidized with dioxygen to give a copper(II)−peroxo complex.[19] Furthermore, the copper(II) complex $[(tmpa)CuCl]^+$ is structurally very similar to the peroxo complex.[19,61] That the trigonal-bipyramidal geometries of the copper(II) complexes are retained in solution was confirmed by UV/Vis and EPR measurements.[19] In contrast, neither Cu^I nor Cu^{II} complexes of pmea, pmap, or tepa are trigonal bipyramidal.[59,61,62] The copper(I) complexes are best described as distorted tetrahedra without any additional ligands. The copper(II) complexes show distorted square-pyramidal geometries.

These differences are reflected in the reaction behavior towards dioxygen. While $[(tmpa)Cu(CH_3CN)]^+$ is oxidized at low temperatures to give a stable peroxo complex, this is not the case for any other compound of this series.[59] When $[(pmea)Cu]^+$ is reacted with dioxygen at low temperatures, only a very unstable peroxo complex is produced. With $[(pmap)Cu]^+$, no such intermediate is detected during oxidation; $[(tepa)Cu]^+$ does not react with dioxygen.[59] From these findings, it is clear that in this series of complexes an increase in chelate ring size leads to a dramatic destabilization of the copper−dioxygen adducts.

A similar effect has been observed on increasing the carbon chain lengths in tren [tren = tris(2-aminoethyl)amine; Scheme 5]. As discussed below, it proved impossible to isolate crystals of a copper(I) complex with tren, because at higher concentrations this compound undergoes disproportionation to copper(II) and copper metal.[50] However, using $N[(CH_2CH_2CH_2NH_2)_2CH_2CH_2NH_2]$ or $N(CH_2CH_2CH_2NH_2)_3$, the copper(I) complexes could be isolated and structurally characterized.[63] Again, it was found that in contrast to the other complexes of this series, the copper(I) complex with $N(CH_2CH_2CH_2NH_2)_3$ as ligand is stable towards dioxygen, similar to $[(tepa)Cu]^+$ de-

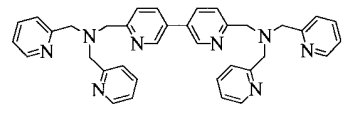
scribed above. Crystal structures of the copper(II) complexes of these ligands have been reported.[64]

Linking Mononuclear Units and Theoretical Calculations

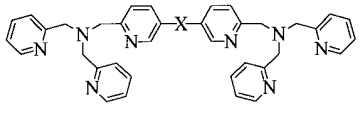
The studies on the oxidation of copper(I) complexes with tmpa-like ligands clearly demonstrate that the copper−peroxo complex with tmpa is most stable. Therefore, it should be possible to optimize this reaction by chemically connecting two tmpa units to a pre-organized dinuclear copper(I) site.

An interesting approach in this regard was the use of bipyridine as the "bridging" unit. The resulting ligand btmpa (6,6′-bis{[bis(2-pyridylmethyl)amino]methyl}-2,2′-bipyridine, also abbreviated as btpa) is shown in Scheme 4. Crystal structures of its dinuclear copper(II) complexes have been published.[65,66] When the dinuclear copper(I) complex was reacted with dioxygen, only a very slow oxidation was observed; dioxygen intermediates could not be detected.[66,67] Karlin and co-workers rationalized this finding in terms of a steric hindrance created by the chelate sites, which influences the molecular geometry around the copper ions.[66] This causes the dinuclear copper complexes to exhibit spectroscopic and electrochemical properties dissimilar to those of their parent tmpa analogues.

In the light of these findings, it became clear that the two mononuclear units had to be separated by a real spacer.

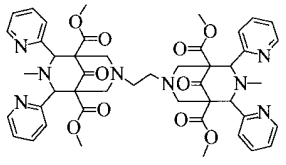


btmpa (btpa)

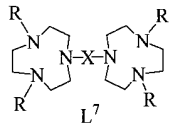


$D^1 = -CH_2-CH_2-$

$L^5 = -CH_2-O-CH_2-$



L^6



L^7

Scheme 4. Ligands for the synthesis of dinuclear copper complexes

This was accomplished by linking two tmpae units (Scheme 2), giving rise to the ligand D^1 shown in Scheme 4 ($X = -CH_2CH_2-$).[42,43] The crystal structure of the dinuclear copper(I) complex shows that the bond lengths and angles at each copper(I) ion are very similar to those in the mononuclear units of the copper(I) complexes of tmpa and tmpae. A detailed kinetic study on the reaction of dioxygen with these complexes showed that there was a big difference between the behavior of the copper(I) complexes of tmpa and tmpae and that of the dinuclear complex, so that different reaction pathways must exist.[42,43]

While the formation of a copper−superoxo (dinuclear complex:O_2 = 1:1) and a copper−peroxo complex (1:1) could still be observed, the formation of a 1:2 superoxo complex and intermolecular copper−peroxo complexes was also detected. The intramolecular formation of $[(D^1)Cu_2(O_2)]^{2+}$ was found to be significantly faster than the generation of the corresponding 2:1 complexes $[(tmpa)Cu(O_2)(tmpa)]^{2+}$ and $[(tmpae)Cu(O_2)(tmpae)]^{2+}$, the latter being formed in an intermolecular fashion from mononuclear precursors. However, its structure seems to be strained. Therefore, the intermolecular arrangement of oligomeric peroxo complexes is preferred; in particular, a stable cyclic trimer is observed. As the authors point out, the Cu_2-O_2 μ-peroxo complex (or complexes) containing D^1 is (or are) in fact more stable than those of the mononucleating ligands tmpa or tmpea. However, it was not the naively expected intramolecular species $[(D^1)Cu_2(O_2)]^{2+}$, but rather highly associated Cu_2-O_2 compounds that formed in an intermolecular fashion (species that cannot possibly form with ligands such as tmpa and tmpae).

A combination of synthetic work and molecular mechanics modelling on these intramolecular copper−peroxo complexes with different spacer groups X (Scheme 4) led to the preparation of the ligand L^5 ($X = CH_2-O-CH_2$).[44][68] When the corresponding dinuclear copper complex was reacted with dioxygen, a relatively stable peroxo complex was formed, indicating that the longer linker arm in L^5 relieves the strain observed for $[(D^1)Cu_2(O_2)]^{2+}$ and significantly enhances adduct formation at room temperature.

The same approach of combining theoretical calculations with synthetic work for linking mononuclear units has been used by Comba and co-workers.[69] This group investigated the reaction of dioxygen with a mononuclear copper(I) complex {with the ligand methyl 2,4-bis(2-pyridinyl)-3,7-diazabicyclo[3.3.1]nonane-9-diol-1,5-dicarboxylate} and detected a quite stable peroxo compound. In order to further increase the stability of the oxygenation product, a linker for two of the mononuclear units had to be designed. Molecular mechanics modelling studies showed that an ethyl spacer would be most appropriate. The calculations were confirmed when a much more stable copper−peroxo complex was obtained after the dinuclear copper(I) complex of this ligand (L^6, Scheme 4) was reacted with dioxygen. In collaboration with this group, investigations of the oxidation of these complexes using low-temperature stopped-flow instrumentation have been started in this laboratory. A complex kinetic behavior has been observed, with several

dioxygen adducts being detected spectrophotometrically. As yet, these have not been unequivocally identified.[70]

Furthermore, theoretical calculations have been used to design a macrocyclic ligand (MEPY22PZ, Scheme 6) for a dinuclear copper(I) complex, which has again been shown to form a quite stable peroxo complex on reaction with dioxygen (see below).[71]

As discussed above, Kodera et al. successfully increased the stability of copper−peroxo complexes by linking mononuclear structures.[24] Indeed, they synthesized and structurally characterized the most stable dinuclear copper μ-η^2:η^2-peroxo complex (ligand L^1, Scheme 2) yet published.

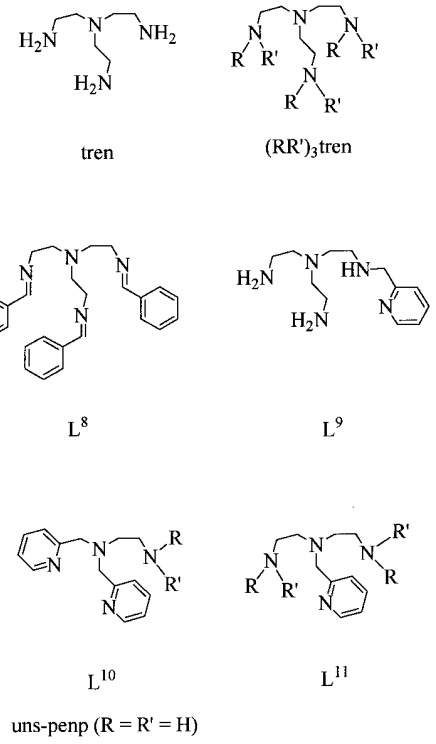
The choice of the linker X in L^7 (Scheme 4) also influences the reaction pathways of the corresponding copper(I) complexes.[14] With X = $-CH_2-CH_2-$, only the bis(μ-oxo) core is obtained and there are no spectroscopic indications of the presence of a peroxo isomer. With the more expanded *m*-xylyl linker, complications occur because here again both intra- and intermolecular complex formation is observed.

Ligands Derived from tren

Because small changes in the ligand environment can have a dramatic effect on the reactivity of copper(I) complexes towards dioxygen, it is important to chemically vary the ligands in a systematic manner and to study the effects. One of the disadvantages of using tmpa and derivatives, as well as many other ligands described above, is the fact that chemical modification of these compounds can be difficult and time consuming. Therefore, a series of tripodal ligands that could be easily modified and then studied kinetically was sought.

As a starting material, tren (Scheme 5), an amine produced in industrial quantities, was chosen. It is a versatile tetradentate ligand, known to form trigonal-bipyramidal complexes with copper(II) ions in the solid state as well as in solution [similar to the copper(II) tmpa complexes discussed above]. One of the axial positions is occupied by the tertiary amine nitrogen, the other by water or some other monodentate ligand.[72−77] This geometry is important with regard to ligand substitution reactions because copper(II) complexes with tetragonal distorted geometry react very rapidly (approaching the diffusion limit), whereas copper(II) complexes with trigonal-bipyramidal geometry react much more slowly [this may be one of the reasons for the different reaction behavior of the copper(I) complexes with tmpa, pmea, and pmap discussed above].[76,78−82] Furthermore, tren can easily be modified to yield a whole family of tripodal ligands.

As yet, it has proved impossible to isolate crystals of a copper(I) complex with tren, because at higher concentrations this compound undergoes disproportionation to copper(II) and copper metal.[50] Nevertheless, dilute solutions of $[Cu(tren)]PF_6$ {or more likely $[Cu(tren)(RCN)]PF_6$} could be obtained by mixing stoichiometric amounts of $[Cu(CH_3CN)_4]PF_6$ and tren in propionitrile or acetone under inert conditions. Using low-temperature stopped-flow equipment, it was possible to detect spectrophotometrically the fast formation (faster than the mixing time of the instrument) of an unstable dioxygen adduct at −90 °C in propionitrile.[77] Its UV/Vis spectrum is very similar to that of the superoxo complex $[(tmpa)CuO_2]^+$ (characteristic absorbance at λ_{max} = 410 nm). Therefore, it is proposed that the complex $[(tren)CuO_2]^+$ had been formed. Owing to its instability, resonance Raman data that might have provided further evidence for the formation of a superoxo complex could not be obtained. The decomposition of this compound became faster on increasing the temperature; time-resolved spectra of this reaction at −70 °C are shown in Figure 1.



Scheme 5. tren and derivatives

In contrast to $[(tmpa)Cu(O_2)]^+$, which reacts with $[(tmpa)Cu(CH_3CN)]^+$ to yield $[(tmpa)Cu(O_2)Cu(tmpa)]^{2+}$ (Equation (3)), no copper tren peroxo complex could be detected under these conditions. Most probably, the superoxo complex reacts with protons provided by tren and a copper(II) complex and hydrogen peroxide are formed as final products. In tmpa copper(I) complexes, protons are not provided by the ligand and this reaction is not observed in propionitrile. In contrast, the formation of $[(tmpa)Cu(O_2)Cu(tmpa)]^{2+}$ is also dramatically disfavored when the reaction of $[(tmpa)Cu(CH_3CN)]^+$ with dioxygen is performed in methanol, a protic solvent. Furthermore, it was found that when acid was added to $[(tmpa)Cu(O_2)Cu(tmpa)]^{2+}$, a copper(II) complex and hydrogen peroxide were produced as the final products.[83] The structural characterization of a hydroperoxo complex discussed above lends further support to this alternative reaction pathway.

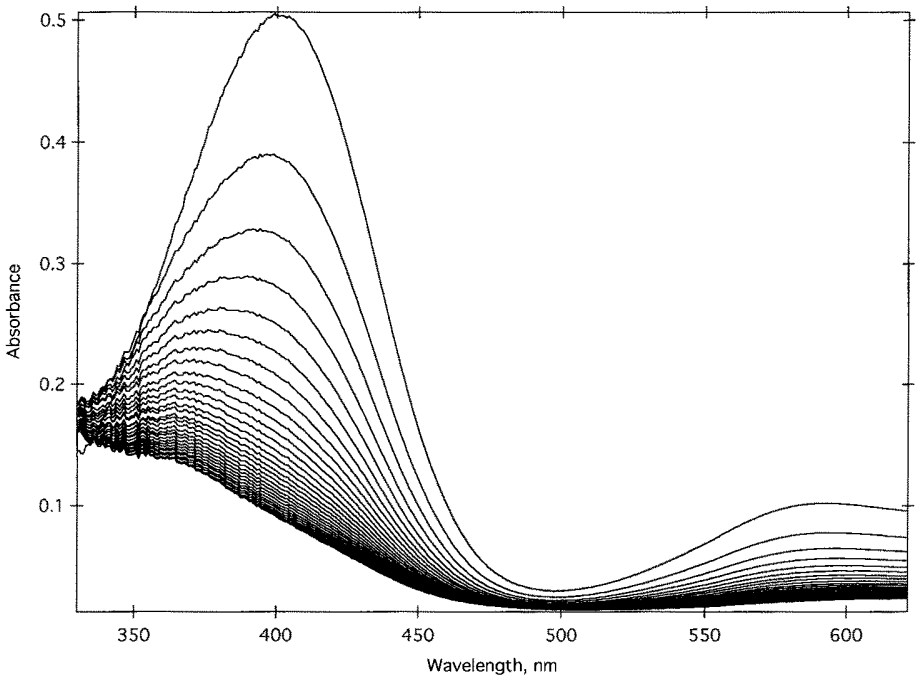


Figure 1. Reaction of $[(tren)Cu(RCN)]PF_6$ with dioxygen at −70 °C in dry propionitrile ([complex] = 0.26 mM, $[O_2]$ = 0.8 mM, Δt = 1.1 s)

To gain further insight into the reaction mechanism, Me_3tren [2,2′,2′′-tris(2-monomethylamino)triethylamine, Scheme 5; R = H, R′= Me] was synthesized. Once again, however, it proved impossible to isolate a solid copper(I) complex.[77] However, copper(II) complexes with Me_3tren could easily be synthesized and characterized.[76,77] First, the dinuclear species $[(Me_3tren)Cu-CN-Cu(Me_3tren)](ClO_4)_3$ was obtained, which is a further example of the few known $Cu^{II}-CN$ complexes.[76] Additionally, the trigonal-bipyramidal complex $[(Me_3tren)CuCl]ClO_4$ could be crystallized, which is structurally very similar to $[(tren)CuCl]ClO_4$.[77]

The reaction of a stoichiometric mixture of $[Cu(CH_3CN)_4]PF_6$ and Me_3tren in propionitrile with dioxygen at −90 °C also provided spectroscopic evidence for the superoxo complex $[(Me_3tren)Cu(O_2)]^+$. As in the oxidation of the copper(I) tren complex described above, a copper−peroxo complex was not observed under these conditions. However, there is one clear difference between the two systems. For reasons not yet understood, $[(Me_3tren)CuO_2]^+$ is much more stable than $[(tren)CuO_2]^+$. Work is currently in progress aimed at clarifying this.

As shown above, an increase in steric hindrance can facilitate the synthesis of a copper−superoxo complex. To test this approach further, the ligand Bz_3tren [tris(2-benzylaminoethyl)amine, Scheme 5; $(RR')_3tren$: R = H, R′ = benzyl] was used instead of Me_3tren.[77] As expected, it proved impossible to isolate a solid copper(I) complex because of disproportionation. Crystal structures of the copper(II) complexes $[(Bz_3tren)Cu(H_2O)](ClO_4)_2$ and $[(Bz_3tren)CuCl]ClO_4$ have been determined.[77] Both show trigonal-bipyramidal geometry, with the latter being very similar to $[(Me_3tren)CuCl]ClO_4$ and $[(tren)CuCl]ClO_4$. An ORTEP plot of $[(Bz_3tren)Cu(H_2O)]^{2+}$ is shown in Figure 2. Evidently, there

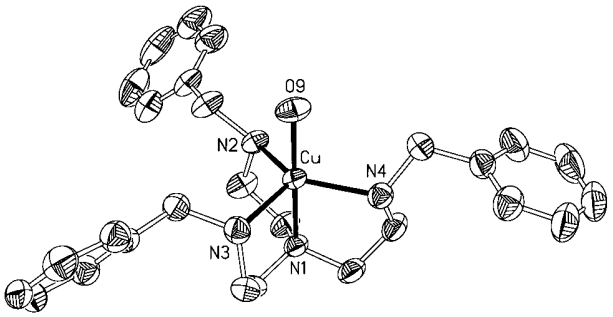


Figure 2. ORTEP view of $[(Bz_3tren)Cu(H_2O)]^{2+}$; thermal ellipsoids are drawn at a 50% probability level; hydrogen atoms are omitted for the sake of clarity

is no significant steric hindrance when only three hydrogen atoms in tren are replaced by bulky groups; the three benzyl groups are turned away sideways.

Most surprisingly, a stoichiometric mixture of $[Cu(CH_3CN)_4]PF_6$ and Bz_3tren in propionitrile showed a reaction behavior towards dioxygen different from that of Me_3tren.[77] Time-resolved spectra recorded at −70 °C are shown in Figure 3. Even though a detailed kinetic study has not yet been performed, the spectra provide evidence for the formation of $[(Bz_3tren)CuO_2]^+$ and $[(Bz_3tren)CuO_2Cu(Bz_3tren)]^{2+}$ as the spectral features are similar to the known UV/Vis spectra of copper−superoxo and −peroxo complexes.[40,51] The absorbance maxima of the superoxo $[(Bz_3tren)CuO_2]^+$ (λ_{max} = 406 nm) and peroxo $[(Bz_3tren)CuO_2Cu(Bz_3tren)]^{2+}$ (λ_{max} = 506 nm) complexes were assigned accordingly. However, resonance Raman spectra are still needed to confirm this assignment. According to these results, the reaction pathway is similar to that described for $[(tmpa)Cu(CH_3CN)]^+$ by Equations (2)−(4). The considerable differences in the behavior of the three

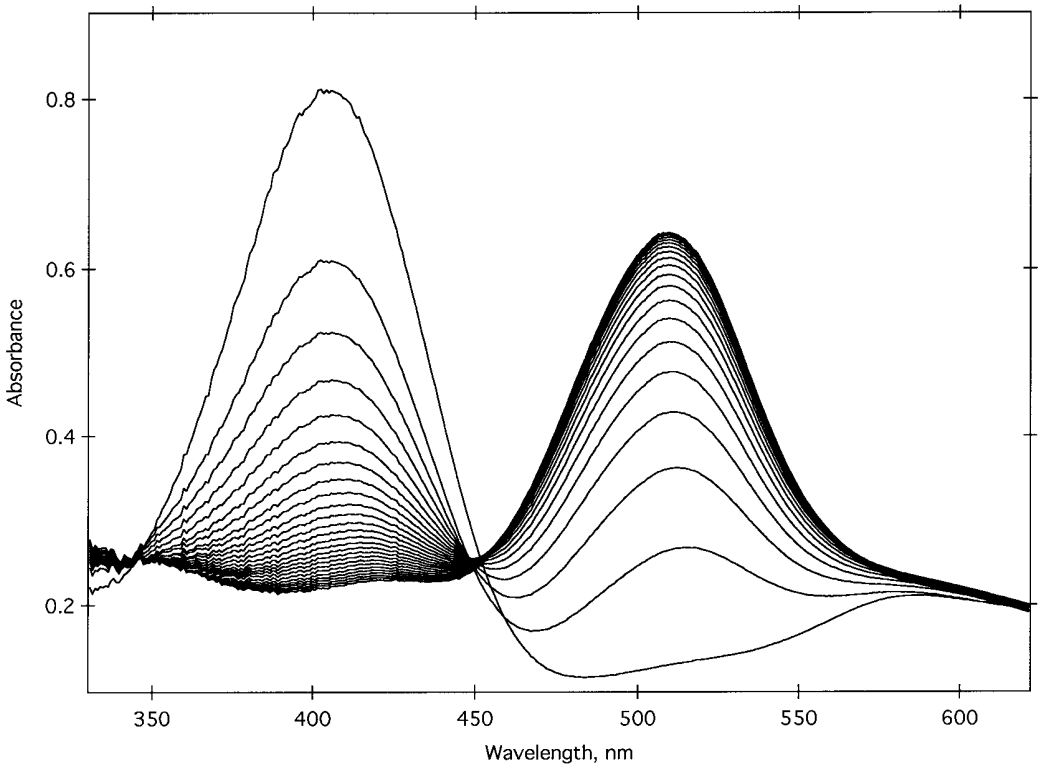


Figure 3. Reaction of $[(Bz_3tren)Cu(RCN)]PF_6$ with dioxygen at −80 °C in dry propionitrile ([complex] = 0.25 mM, $[O_2]$ = 4.4 mM, Δt = 35.2 s)

complexes $[Cu(tren)]^+$, $[Cu(Me_3tren)]^+$, and $[Cu(Bz_3tren)]^+$ towards dioxygen have yet to be explained; further investigations are necessary.

At the beginning of these investigations, the now commercially available amine Bz_3tren was synthesized by reacting benzaldehyde with tren followed by a reduction with sodium borohydride.[84] This prompted investigations of the reaction behavior of the copper(I) complex with the initially formed imine ligand (L^8, Scheme 5).[77,85,86] In contrast to tren and its derivatives, the soft imine donor groups in L^8 have a large stabilizing effect on the soft copper(I) ion. Therefore, the corresponding copper(I) complex can easily be synthesized and structurally characterized.[85,86] However, when this complex was reacted with dioxygen in a variety of solvents at different temperatures, dioxygen intermediates were not detected.[77,85] This finding is well in line with earlier results on the reaction of dioxygen with various copper imine complexes.[87−89] All kinetic investigations suggest the formation of a copper peroxo (or superoxo) complex, but it has proved impossible to detect these compounds spectroscopically. Most probably, the dioxygen intermediate immediately reacts further to yield a decomposition product (steady-state concentration of dioxygen intermediates). As yet, no explanation has been offered as to why this especially seems to be the case for copper(I) imine complexes.

To avoid effects caused by ligand protons, Me_6tren [tris(2-dimethylaminoethyl)amine, Scheme 5; R = R′ = Me], i.e. fully methylated tren, was used.[50,90] The solutions of Me_6tren and Cu^I salts proved to be extremely sensitive towards traces of dioxygen or moisture; oxidation or disproportionation of the complex was frequently observed before the pure, crystalline copper(I) complex $[Cu(Me_6tren)]ClO_4$ could be isolated.[50]

The geometry of $[Cu(Me_6tren)]ClO_4$ is best described as trigonal pyramidal, but a weak interaction with the perchlorate anion cannot be neglected. This anion occupies the axial position of a trigonal-bipyramidal arrangement constituted by three of the four oxygen atoms and the copper(I) ion. This structure is unusual because of the weak interaction between the perchlorate anion and the copper(I) cation. After crystallizing $[Cu(Me_6tren)]ClO_4$ from acetonitrile, one would expect to find an additional acetonitrile molecule coordinated to the copper ion in the axial position (instead of perchlorate); this was found for the copper(I) complex with tmpa as discussed above. A comparison of this complex with $[Cu(Me_6tren)]ClO_4$ reveals that the bond lengths and bond angles are quite different.[50]

When $[Cu(Me_6tren)]ClO_4$ was reacted with dioxygen at low temperatures in a stopped-flow instrument, spectral changes indicative of the formation of the superoxo $[Cu(Me_6tren)O_2]^+$ and peroxo $[(Me_6tren)Cu(O_2)Cu(Me_6tren)]^{2+}$ complexes were observed; the latter was further characterized by resonance Raman measurements, $\nu(O-O) = 880\ cm^{-1}$.[50] A detailed kinetic study of this reaction is currently in progress. From the data obtained to

date, it is clear that the reaction pathway is similar to that described for $[(tmpa)Cu(CH_3CN)]^+$ by Equations (2)−(4). However, there is one major difference: $[Cu(tmpa)O_2]^+$ immediately undergoes further reaction to give the peroxo complex (Equation (3)), whereas $[Cu(Me_6tren)O_2]^+$ reacts much more slowly.[50]

The aforementioned findings show that copper(I) complexes with tren or its derivatives form dioxygen adducts during oxidation. Consequently, this represents an excellent approach for systematically synthesizing a series of tripodal ligands that can be used to test the differences in behavior of the corresponding copper(I) complexes towards dioxygen. In principle, combinatorial chemistry could now be used to synthesize and investigate copper(I) complexes with a large variety of tripodal ligands.

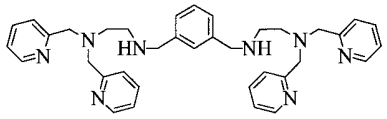
By reacting tren with aldehydes followed by reduction, a series of R_3tren ligands (Scheme 5; R′ = H) can be synthesized. Further reaction with organic chlorides or the use of aldehydes and sodium cyanoborohydride allows the preparation of a wide variety of $R_3R'_3$tren ligands (Scheme 5). When these R groups provide additional donor atoms, several copper ions can be bound by the ligand; for example, reaction of tren with picolyl chloride or 2-vinylpyridine allowed the isolation of trinuclear copper complexes.[91,92] It is also possible to chemically alter tren without modifying all three arms. An example where only one amine arm was altered has been described by Spiccia and co-workers (L^9, Scheme 5).[93]

In order to avoid ligand mixtures when only one or two additional groups were introduced into tren, the amines L^{10} and L^{11} were used (Scheme 5; R = R′ = H; ligand L^{10} is abbreviated as uns-penp[94]). Both of these amines have been known for a long time[94,95] (uns-penp was actually "rediscovered" after 10 years as a "new" ligand![96]) but surprisingly they have been little used in the synthesis of novel transition metal complexes.[94−98] The reaction of uns-penp with an aldehyde (pyridinealdehyde or salicylaldehyde, for example), followed by a reduction, allows the selective introduction of one additional donor group. Recent work has shown the modified uns-penp ligand to be extremely useful in the synthesis of iron and manganese complexes.[99−102] Ligand L^{11} permits the selective introduction of two further donor groups. Further work in this area using these new ligands for the synthesis and investigation of copper(I)/(II) complexes is ongoing in the author's laboratory.[103]

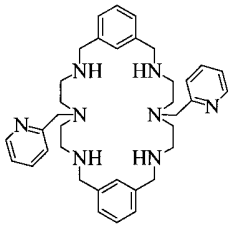
There is a further advantage in using these ligands. As discussed above, pyridine donors stabilize copper(I) complexes and facilitate their investigation. Preliminary experiments have indicated that the copper(I) uns-penp complex does not form a peroxo compound when it is reacted with dioxygen,[104] although this needs to be confirmed. In contrast, when the protons in L^{10} and L^{11} (Scheme 5; R = R′ = Me) were replaced by methyl groups, quite stable peroxo complexes could be detected as intermediates during oxidation.[103] These new ligands can be regarded as the two "missing links" between Me_6tren and tmpa.

Bridging Ligands Derived from tren and Derivatives

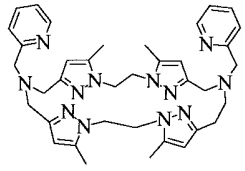
The use of uns-penp is also advantageous in that this ligand can be easily linked together, much more easily than tmpa itself. By reacting uns-penp with dialdehydes and reducing the imines to amines (organic chlorides can also be used), it was found that different bridging groups (or spacer molecules) could be introduced between the two units. This allowed a "tuning" of the distances between the two uns-penp units. It has been found that different xylyl linkers dramatically affect the stabilities of the corresponding copper−peroxo complexes. A peroxo complex with a *m*-xylyl spacer bridging the two uns-penp units (L^{12}, Scheme 6) proved to be the most stable.



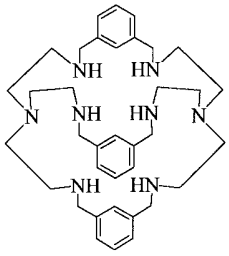
L^{12}



L^{13}



MEPY22PZ



L^{14}

Scheme 6. Ligands for the synthesis of dinuclear copper complexes

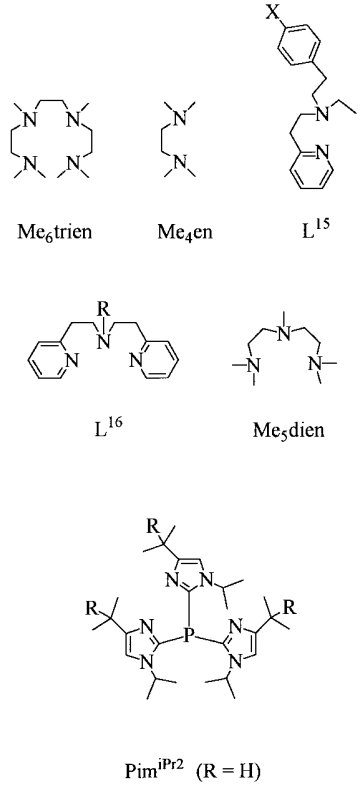
The above results suggest that the mononuclear units should be connected through more than one linker molecule. Connecting the tripodal amines with two linkers leads to macrocyclic ligands; an example currently being synthesized in the author's laboratory is shown in Scheme 6 (L^{13}). The potential of this approach has been highlighted by Bol et al., who synthesized the macrocyclic ligand MEPY22PZ (Scheme 6).[71,105] In this example, the tripodal units are connected through pyrazolyl/ethyl linkers. When the dinuclear copper(I) complex of this ligand was reacted with dioxygen, an extremely stable peroxo complex was formed. Theoretical calculations were also employed in the design of this ligand.[71]

When three linkers are used to connect two tren units, cryptands are obtained. A typical example is L^{14}, shown in

Scheme 6. However, when dinuclear copper(I) complexes of this and other cryptands with different linker molecules were reacted with dioxygen, only slow oxidation was observed and dioxygen intermediates could not be detected spectroscopically [this is similar to the reaction described above with btmpa (btpa); Scheme 4].[106]

Other Amines Related to tren

Once it had been established that aliphatic amines derived from tren are useful tools for studying copper(I)/dioxygen reactions, it was decided to investigate an additional series of amines.[48] The copper(I) complex of Me_6trien {*N*,*N*′-bis[2′-(dimethylamino)ethyl]-*N*,*N*′-dimethylethane-1,2-diamine; Scheme 7}, an isomer of Me_6tren, can be synthesized by a comproportionation reaction in water.[107] With this in mind, attempts were made to characterize a copper−dioxygen adduct in aqueous solution. However, although the copper(I) and copper(II) complexes of Me_6trien could be synthesized and characterized, no copper−dioxygen adduct could be detected when the copper(I) complex was treated with dioxygen (neither in aqueous nor organic media).[48]



Scheme 7. Various amine ligands

Me_4en (tetramethylethylenediamine; Scheme 7) can be viewed as being a part of Me_6trien or Me_6tren. The behavior of its copper(I) complex with a ratio of ligand to copper of 2:1 resembles that of the copper(I) complex of Me_6trien.[48] Crystal structures show the two compounds to be isostructural. The situation changes when Me_4en and copper(I) are used in a stoichiometric ratio of 1:1. Under these circumstances, complexes with Me_4en or other alkylated ethylenediamines become quite reactive towards dioxygen; on the basis of kinetic data, a variety of peroxo and oxo complexes have been postulated to form during oxidation.[108−112] This was proven by the fact that ligand L^2 (Scheme 2), which is very similar to the alkylated ethylenediamines, could be used to obtain the structurally characterized bis(μ-oxo) copper complexes described above.[33,34]

Furthermore, it has been shown that such bidentate ligands can be used for intramolecular aromatic and aliphatic hydroxylations.[113][114] In a recent study, copper(I) complexes of *N*-ethyl-*N*-[2-(2-pyridyl)ethyl]-2-phenylethylamine (L^{15}, Scheme 7; X = OMe, Me, H, Cl, NO_2) were investigated.[114] Time-resolved UV/Vis spectra as well as resonance Raman spectra provided strong evidence that bis(μ-oxo) complexes were formed during the oxidations.

Copper complexes with bidentate and tridentate ligands have been successfully employed in investigating the oxidation of intramolecular ligands or substrates.[25,31,115−121] Copper complexes incorporating L^{16} (Scheme 7; R = Me, phenyl) provide important insight into these reactions.[31,118,119]

The above results are corroborated by investigations on tridentate ligands carried out in this laboratory. Copper(I) and copper(II) complexes of Me_5dien (1,1,4,7,7-pentamethyldiethylethylenetriamine; Scheme 7) have previously been structurally characterized.[122,123] Me_5dien can be regarded as Me_6trien or Me_6tren with one arm missing.[48,50] Time-resolved spectra of the reaction of copper(I) Me_5dien with dioxygen at −90 °C are shown in Figure 4.[104] These spectra strongly suggest that a bis(μ-oxo) complex is formed. However, as yet it has not been possible to obtain resonance Raman data to prove this. Since Me_5dien can also be regarded as an open-chain analogue of a substituted triazacyclononane (Scheme 2), it will be interesting to investigate whether increased steric hindrance in this amine will allow the observation of similar peroxo/bis(μ-oxo) equilibria as seen for the copper complexes of R_3TACN.

These results suggest that in future researchers should turn from complicated ligand systems to simple amines that can be easily modified. Combinatorial chemistry might also be considered as being potentially helpful. It should be mentioned at this point that Karlin and co-workers have already succeeded in producing peroxo complexes by reacting copper(I) complexes of the simple ligand imidazole with dioxygen.[124,125]

Many of the hitherto characterized dinuclear copper complexes have not been mentioned in this article. Most of these have been described in detail in several monographs or review articles; some more recent work is described in refs.[8,10,49,126−132] It should be pointed out that these dinuclear complexes can be described as linked mononuclear units (Scheme 8).

Ligand type (a) represents a general example of the linked tripodal units discussed above (e.g. L^{12}, Scheme 6). Reducing the number of donor atoms leads to ligands of types (b) and (c). Here, bidentate or tridentate ligands (sim-

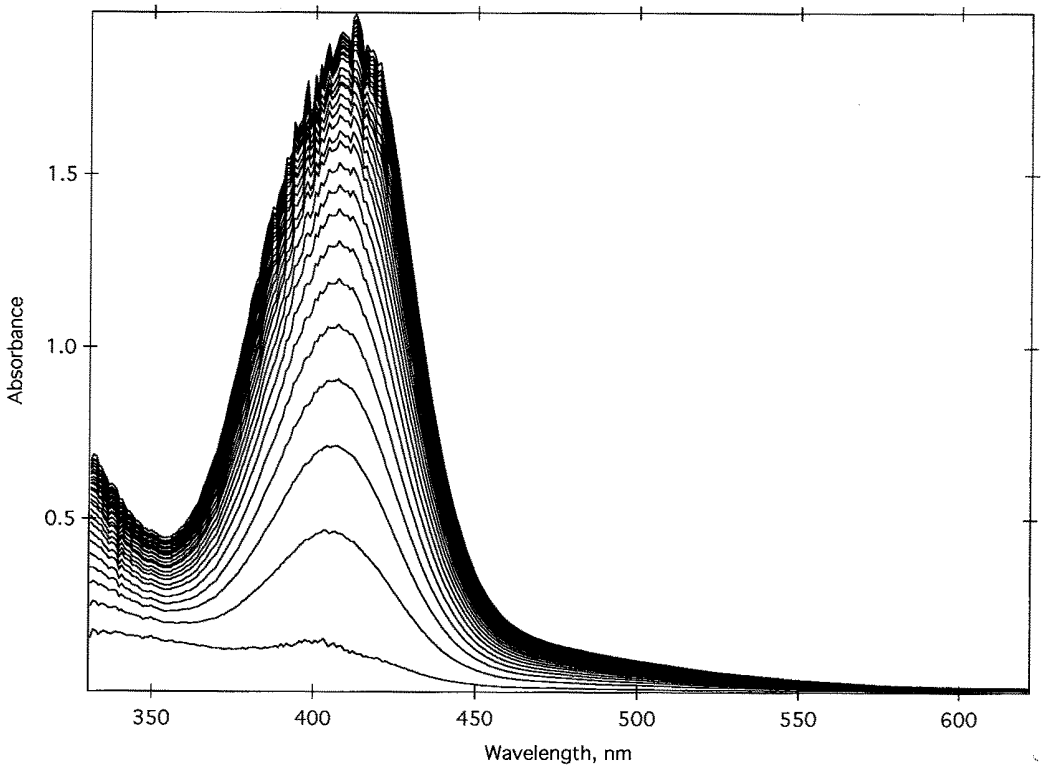
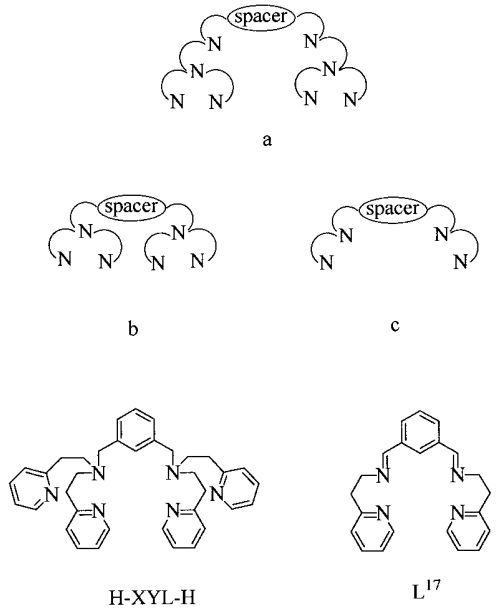


Figure 4. Reaction of $[(Me_5dien)Cu(RCN)]PF_6$ with dioxygen at −90 °C in dry propionitrile ([complex] = 0.36 mM, $[O_2]$ = 4.4 mM, Δt = 0.15 s)



Scheme 8. Ligands for the synthesis of dinuclear copper complexes

ilar to en, dien, or derivatives thereof) are connected through spacer molecules. An example of ligand type (b) is provided by H−XYL−H shown in Scheme 8 (another example would be ligand L^7 in Scheme 4, where the N donor units constitute a tridentate macrocycle).[46] The dinuclear copper complex of this ligand was discussed above. The ligand itself can be described as two L^{16} units (Scheme 7) bridged by a *m*-xylyl spacer. An example of ligand type (c) is the imine ligand L^{17} shown in Scheme 8.[8] Recently, amine ligands similar to L^{17} have been used in investigations of dinuclear copper complexes.[130,131,133]

The dinuclear copper(I) complexes of ligands of types (b) and (c) have been used to study the intramolecular benzene hydroxylation that occurs when some of these are reacted with dioxygen.[8,10,46,49,87,126−131,133] As yet, the mechanisms of such intramolecular aromatic or aliphatic hydroxylations are not well understood.[113]

Effect of Solvent

In the course of the investigations described above, it was found that the solvent played an important role in many reactions of copper(I) complexes with dioxygen. Propionitrile proved to be useful for studying the oxidations of copper(I) complexes with tripodal ligands such as tmpa or Me_6tren.[17,50] However, according to Equations (2) and (3), propionitrile is not only a solvent but a competing ligand as well, shifting the equilibria to the left. Acetone only shows weak ligating properties towards copper(I), so a dramatic effect was observed when this solvent was used instead of propionitrile.[44,50] In acetone, it proved possible to observe the copper−peroxo complexes of tmpa and Me_6tren even at room temperature. It was not possible to use dichloromethane as the copper(I) complexes of the tripodal ligands reacted with this solvent.[134] Methanol was not suitable either as it was found to have a dramatic destabilizing effect on the peroxo complexes.[50] This can probably be attributed to the protons of this solvent, similar to

the effect observed when tren was used as a ligand (see above).

Such solvent effects are not observed with other copper(I) complexes. For example, the copper(I) complex of Pim*i*Pr$_2$ (Scheme 7) produced a dioxygen adduct (evidence was found for the formation of a copper−peroxo complex) in both methanol and acetone.[135,136] Here, the protons of the solvent do not seem to have a destabilizing effect.

Dichloromethane has been used for investigating the reactions of dinuclear copper(I) complexes with dioxygen at low temperatures. For example, the oxidation of $[Cu_2-H-XYL-H]^{2+}$ (H−XYL−H; Scheme 8) has been studied in both dichloromethane and acetone.[46] While differences in the reaction behavior were observed, no dramatic stabilization of the peroxo complex was evident in either of these solvents. In contrast, nitrile solvents suppress the intramolecular hydroxylation observed in the former two solvents. Again, this may be explained in terms of the strong binding of nitrile molecules.

Furthermore, depending on the solvent, the formation of either μ-η^2:η^2-peroxo-bridged or bis(μ-oxo)dicopper(III) compounds can be favored.[28]

Decomposition Reactions

While the binding of dioxygen is not yet perfectly understood, much insight into this reaction has been gained. This is much less true for decomposition reactions. In some instances, hydrogen peroxide is probably formed while the ligand of the complex remains intact. However, oxidation of the ligand is also a possibility. Only in a few cases has selective intramolecular hydroxylation been observed, leading to products that could be characterized (examples are given above). The detailed mechanisms of these reactions are still not understood.

A very interesting reaction ensues following the oxidation of [(tmpa)Cu(CH$_3$CN)]PF$_6$, which involves a fluoride abstraction. The product, a fluoride-bridged copper(II) complex, has been isolated and structurally characterized.[137]

Conclusions

In this article, an overview of the progress that has been made concerning the activation of dioxygen with copper(I) complexes has been presented. While it is still not possible to predict the reaction pathway for a copper(I) complex and dioxygen, the studies performed in recent years allow a much better understanding of these reactions than in the past. As indicated above, a more systematic investigation on this type of oxidation is still necessary. The contribution of the author's group to this task has been the development of a ligand building block system starting from simple amines. This system (similar to Lego or Tinker Toys) allows the synthesis of a large number of new ligands for copper(I) complexes. In principle, it should also permit a combinatorial approach. Even though selective substrate oxidation with copper(I) complexes and dioxygen has not been discussed in detail here, it seems most likely that in the near future many more oxidation catalysts will be based on these systems.

Acknowledgments

I thank my co-workers Michael Becker, Markus Schatz, Florian Thaler, and Gemma Romualdo Torres, as well as my collaborators, whose names are listed in the references. They have contributed superbly to this research and their efforts are greatly appreciated. Financial support was provided by Prof. Rudi van Eldik (University of Erlangen-Nürnberg), the Deutsche Forschungsgemeinschaft, and the Volkswagen-Stiftung.

Note Added in Proof (June 20, 2000): While this microreview was accepted for publication, a summary on copper−dioxygen species and copper−oxo species was published: A. G. Blackman, W. B. Tolman, "Copper−Dioxygen and Copper−Oxo Species Relevant to Copper Oxygenases and Oxidases", in *Structure & Bonding* (Ed.: B. Meunier), Springer-Verlag, Berlin, Heidelberg, **2000**, vol. 97, p. 179−211.

[1] R. A. Sheldon, *J. Mol. Cat., A*: Chemical, Special Edition, **1997**, 117.
[2] K. A. Magnus, H. Ton-That, J. E. Carpenter, *Chem. Rev.* **1994**, *94*, 727−735.
[3] N. Kitajima, Y. Moro-oka, *Chem. Rev.* **1994**, *94*, 737−757.
[4] K. Lerch, *A.C.S. Symp. Ser.*, **1995**, *600*, 64−80.
[5] Á. Sánchez-Ferrer, J. N. Rodríguez-López, F. García-Cánovas, F. García-Carmona, *Biochim. Biophys. Acta* **1995**, *1247*, 1−11.
[6] J. P. Klinman, *Chem. Rev.* **1996**, *96*, 2541−2561.
[7] E. I. Solomon, U. M. Sundaram, T. E. Machonkin, *Chem. Rev.* **1996**, *96*, 2563−2605.
[8] K. D. Karlin, Z. Tyeklár (Eds.), *Bioinorganic Chemistry of Copper*, Chapman & Hall, New York, **1993**.
[9] M. Pascaly, I. Jolk, B. Krebs, *Chemie in unserer Zeit* **1999**, *33*, 334−341.
[10] J. Reedijk (Ed.), *Bioinorganic Catalysis*, Second Edition, Marcel Dekker, New York, **1999**.
[11] Y. Wang, J. DuBois, B. Hedman, K. Hodgson, T. Stack, *Science* **1998**, *279*, 537−540.
[12] P. Chaudhuri, M. Hess, T. Weyhermüller, K. Wieghardt, *Angew. Chem. Int. Ed.* **1999**, *38*, 1095−1098.
[13] W. B. Tolman, *Acc. Chem. Res.* **1997**, *30*, 227−237.
[14] P. L. Holland, W. B. Tolman, *Coord. Chem. Rev.* **1999**, *190−192*, 855−869.
[15] R. Than, A. Feldmann, B. Krebs, *Coord. Chem. Rev.* **1999**, *182*, 211−241.
[16] A. D. Zuberbühler in *Metal Ions in Biological Systems* (Ed.: H. Sigel), Marcel Dekker, New York, **1976**, *5*, 325−368.
[17] K. D. Karlin, S. Kaderli, A. D. Zuberbühler, *Acc. Chem. Res.* **1997**, *30*, 139−147.
[18] R. R. Jacobson, Z. Tyeklár, A. Farooq, K. D. Karlin, S. Liu, J. Zubieta, *J. Am. Chem. Soc.* **1988**, *110*, 3690−3692.
[19] Z. Tyeklár, R. R. Jacobson, N. Wei, N. N. Murthy, J. Zubieta, K. D. Karlin, *J. Am. Chem. Soc.* **1993**, *115*, 2677−2689.
[20] N. Kitajima, K. Fujisawa, Y. Mor-oka, K. Toriumi, *J. Am. Chem. Soc.* **1989**, *111*, 8975−8976.
[21] K. Fujisawa, M. Tanaka, Y. Moro-oka, N. Kitajima, *J. Am. Chem. Soc.* **1994**, *116*, 12079−12080.
[22] M. Harata, K. Jitsukawa, H. Masuda, H. Einaga, *J. Am. Chem. Soc.* **1996**, *116*, 10817−10818.
[23] A. Wada, M. Harata, K. Hasegawa, K. Jitsukawa, H. Masuda, M. Mukai, T. Kitagawa, H. Einaga, *Angew. Chem. Int. Ed.* **1998**, *37*, 798−799.
[24] M. Kodera, K. Katayama, Y. Tachi, K. Kano, S. Hirota, S. Fujinami, M. Suzuki, *J. Am. Chem. Soc.* **1999**, *121*, 11006−11007.

[25] S. Mahapatra, J. A. Halfen, E. C. Wilkinson, L. J. Que, W. B. Tolman, *J. Am. Chem. Soc.* **1994**, *116*, 9785−9786.

[26] S. Mahapatra, J. A. Halfen, E. C. Wilkinson, G. F. Pan, C. J. Cramer, L. Que, W. B. Tolman, *J. Am. Chem. Soc.* **1995**, *117*, 8865−8866.

[27] S. Mahapatra, J. A. Halfen, E. C. Wilkinson, G. F. Pan, X. D. Wang, V. G. Young, C. J. Cramer, L. Que, W. B. Tolman, *J. Am. Chem. Soc.* **1996**, *118*, 11555−11574.

[28] J. A. Halfen, S. Mahapatra, E. C. Wilkinson, S. Kaderli, V. G. Young, L. Que, A. D. Zuberbühler, W. B. Tolman, *Science* **1996**, *271*, 1397−1400.

[29] S. Mahapatra, V. Young, S. Kaderli, A. D. Zuberbühler, W. Tolman, *Angew. Chem. Int. Ed. Engl.* **1997**, *36*, 130−133.

[30] E. Pidcock, S. DeBeer, H. V. Obias, B. Hedman, K. O. Hodgson, K. D. Karlin, E. I. Solomon, *J. Am. Chem. Soc.* **1999**, *121*, 1870−1878.

[31] H. V. Obias, Y. Lin, N. N. Murthy, E. Pidcock, E. I. Solomon, M. Ralle, N. J. Blackburn, Y.-M. Neubold, A. D. Zuberbühler, K. D. Karlin, *J. Am. Chem. Soc.* **1998**, *120*, 12960−12961.

[32] H. Hayashi, S. Fujinami, S. Nagatomo, S. Ogo, M. Suzuki, A. Uehara, Y. Watanabe, T. Kitagawa, *J. Am. Chem. Soc.* **2000**, *122*, 2124−2125.

[33] A. P. Cole, D. E. Root, P. Mukherjee, E. I. Solomon, T. D. P. Stack, *Science* **1996**, *273*, 1848−1850.

[34] V. Mahadevan, Z. Hou, A. P. Cole, D. E. Root, T. K. Lal, E. I. Solomon, T. D. P. Stack, *J. Am. Chem. Soc.* **1997**, *119*, 11996−11997.

[35] J. Reim, B. Krebs, *Angew. Chem. Int. Ed. Engl.* **1994**, *33*, 2040.

[36] J. R. Reim, R. Werner, W. Haase, B. Krebs, *Chem. Eur. J.* **1998**, *4*, 289−298.

[37] F. Meyer, H. Pritzkow, *Angew. Chem*. **2000**, in press.

[38] E. I. Solomon, F. Tuczek, D. E. Root, C. A. Brown, *Chem. Rev.* **1994**, *94*, 827−856.

[39] H. H. Thorp, V. L. Pecoraro (Eds.), *Mechanistic Bioinorganic Chemistry*, A.C.S., Washington DC, **1995**.

[40] K. D. Karlin, N. Wei, B. Jung, S. Kaderli, P. Niklaus, A. Zuberbühler, *J. Am. Chem. Soc.* **1993**, *115*, 9506−9514.

[41] J. Cahoy, P. L. Holland, W. B. Tolman, *Inorg. Chem.* **1999**, *38*, 2161−2168.

[42] N. Wei, D.-H. Lee, N. N. Murthy, Z. Tyeklár, K. D. Karlin, S. Kaderli, B. Jung, A. D. Zuberbühler, *Inorg. Chem.* **1994**, *33*, 4625−4626.

[43] D. H. Lee, N. Wei, N. N. Murthy, Z. Tyeklár, K. D. Karlin, S. Kaderli, B. Jung, A. D. Zuberbühler, *J. Am. Chem. Soc.* **1995**, *117*, 12498−12513.

[44] K. D. Karlin, D.-H. Lee, S. Kaderli, A. D. Zuberbühler, *Chem. Commun.* **1997**, 475−476.

[45] S. Mahapatra, S. Kaderli, A. Llobet, Y. Neuhold, T. Palanché, J. Halfen, V. Young, T. Kaden, L. Que, A. D. Zuberbühler, W. Tolman, *Inorg. Chem*. **1997**, *36*, 6343−6356.

[46] M. Becker, S. Schindler, K. D. Karlin, T. K. Kaden, S. Kaderli, T. Palanché, A. D. Zuberbühler, *Inorg. Chem.* **1999**, 1989−1995.

[47] H. D. Projahn, S. Schindler, R. van Eldik, D. G. Fortier, C. R. Andrew, A. G. Sykes, *Inorg. Chem.* **1995**, *34*, 5935−5941.

[48] M. Becker, F. Heinemann, F. Knoch, W. Donaubauer, G. Liehr, S. Schindler, G. Golub, H. Cohen, D. Meyerstein, *Eur. J. Inorg. Chem.* **2000**, 719−726.

[49] T. N. Sorrell, *Tetrahedron* **1989**, *45*, 3−68.

[50] M. Becker, F. Heinemann, S. Schindler, *Chem. Eur. J.* **1999**, *5*, 3124−3129.

[51] N. Wei, N. N. Murthy, Q. Chen, J. Zubieta, K. D. Karlin, *Inorg. Chem.* **1994**, *33*, 1953−1965.

[52] K. Uozumi, Y. Hyashi, M. Suzuki, A. Uehara, *Chem. Lett.* **1993**, 963−966.

[53] H. Nagao, N. Komeda, M. Mukaida, M. Suzuki, K. Tanaka, *Inorg. Chem.* **1996**, *35*, 6809−6815.

[54] C.-l. Chuang, K. Lim, Q. Chen, J. Zubieta, J. W. Canary, *Inorg. Chem.* **1995**, *34*, 2562−2568.

[55] M. Harata, K. Jitsukawa, H. Masuda, H. Einaga, *Chem. Lett.* **1996**, 813−814.

[56] M. Harata, K. Jitsukawa, H. Masuda, H. Einaga, *Bull. Chem. Soc. Jpn*. **1998**, *71*, 637−645.

[57] L. M. Berreau, S. Mahapatra, J. A. Halfen, V. G. Young, W. B. Tolman, *Inorg. Chem.* **1996**, *35*, 6339−6342.

[58] N. Wei, N. N. Murthy, Z. Tyeklár, K. D. Karlin, *Inorg. Chem.* **1994**, *33*, 1177−1183.

[59] M. Schatz, M. Becker, F. Thaler, F. Hampel, S. Schindler, M. Schatz, R. R. Jacobson, Z. Tyeklár, N. N. Murthy, Q. Chen, J. Zubieta, K. D. Karlin, submitted to *Inorg. Chem.*

[60] B. S. Lim, R. H. Holm, *Inorg. Chem.* **1998**, *37*, 4898−4908.

[61] K. Karlin, J. Hayes, S. Juen, J. Hutchinson, J. Zubieta, *Inorg. Chem.* **1982**, *21*, 4106−4108.

[62] K. Karlin, J. Hayes, J. Hutchinson, J. Hyde, J. Zubieta, *Inorg. Chim. Acta* **1982**, *64*, L219−L220.

[63] A. M. Dittler-Klingemann, F. E. Hahn, unpublished results

[64] A. M. Dittler-Klingemann, F. E. Hahn, *Inorg. Chem.* **1996**, *35*, 1996−1999.

[65] A. Dossing, A. Hazell, H. Toftlund, *Acta Chem. Scand.* **1996**, *50*, 95−101.

[66] D. Lee, N. N. Murthy, K. D. Karlin, *Inorg. Chem.* **1997**, *36*, 5785−5792.

[67] S. Schindler, H. Toftlund, unpublished results.

[68] P. Comba, P. Hilfenhaus, K. Karlin, *Inorg. Chem.* **1997**, *36*, 2309−2313.

[69] H. Börzel, P. Comba, C. Katsichis, W. Kiefer, A. Lienke, V. Nagel, H. Pritzkow, *Chem. Eur. J.* **1998**, *5*, 1716−1721.

[70] H. Börzel, P. Comba, M. Schatz, S. Schindler, manuscript in preparation

[71] J. E. Bol, W. L. Driessen, A. Y. N. Ho, B. Maase, L. Que, J. Reedijk, *Angew. Chem. Int. Ed. Engl.* **1997**, *36*, 998−1000.

[72] P. C. Jain, E. C. Lingafelter, *J. Am. Chem. Soc.* **1967**, *89*, 6131−6136.

[73] M. Duggan, N. Ray, B. Hathaway, G. Tomlinson, P. Brint, K. Pelin, *J. Chem. Soc., Dalton Trans.* **1980**, 1342−1348.

[74] A. Marzotto, A. Ciccarese, D. A. Clemente, G. Valle, *J. Chem. Soc., Dalton Trans.* **1995**, 1461−1468.

[75] Z.-L. Lu, C.-y. Duan, Y.-P. Tian, X.-z. You, H.-K. Fun, B.-C. Yip, *Polyhedron* **1996**, *15*, 1769−1774.

[76] F. Thaler, C. D. Hubbard, F. W. Heinemann, R. van Eldik, S. Schindler, I. Fábián, A. M. Dittler-Klingemann, F. E. Hahn, C. Orvig, *Inorg. Chem.* **1998**, *37*, 4022−4029.

[77] M. Schatz, G. Rommualdo Torres, M. Becker, G. Liehr, O. Walter, S. Schindler, manuscript in preparation.

[78] G. Cayley, D. Cross, P. Knowles, *J. Chem. Soc., Chem. Commun.* **1976**, 837−838.

[79] G. R. Cayley, I. D. Kelly, P. F. Knowles, K. D. S. Yadav, *J. Chem. Soc., Dalton Trans.* **1981**, 2370−2372.

[80] D. H. Powell, P. Furrer, P. Pittet, A. E. Merbach, *J. Phys. Chem*. **1995**, *99*, 16622−16629.

[81] D. H. Powell, A. E. Merbach, I. Fábián, S. Schindler, R. van Eldik, *Inorg. Chem.* **1994**, *33*, 4468−4473.

[82] A. M. Dittler-Klingemann, C. Orvig, F. E. Hahn, F. Thaler, C. Hubbard, R. van Eldik, S. Schindler, I. Fábián, *Inorg. Chem.* **1996**, *35*, 7798−7803.

[83] P. P. Paul, Z. Tyeklár, R. R. Jacobson, K. D. Karlin, *J. Am. Chem. Soc.* **1991**, *113*, 5322−5332.

[84] A. A. Naiini, W. M. P. B. Menge, J. G. Verkade, *Inorg. Chem.* **1991**, *30*, 5009−5012.

[85] D. Walther, K. Hamza, H. Görls, W. Imhof, *Z. Anorg. Allg. Chem*. **1997**, *623*, 1135−1143.

[86] E. C. Alyea, G. Ferguson, M. Jennings, Z. Xu, *Polyhedron* **1990**, *9*, 739−741.

[87] M. Becker, S. Schindler, R. van Eldik, *Inorg. Chem.* **1994**, *33*, 5370−5371.

[88] S. Ryan, H. Adams, D. Fenton, M. Becker, S. Schindler, *Inorg. Chem.* **1998**, *37*, 2134−2140.

[89] A. Feldmann, B. Krebs, S. Schindler, unpublished results

[90] S. Schindler, C. D. Hubbard, R. van Eldik, *Chem. Soc. Rev.* **1998**, *27*, 387−393.

[91] K. Karlin, Q. Gan, A. Farooq, S. Liu, J. Zubieta, *Inorg. Chim. Acta* **1989**, *165*, 37−39.

[92] S. T. Frey, H. H. J. Sun, N. N. Murthy, K. D. Karlin, *Inorg. Chim. Acta* **1996**, *242*, 329−338.

[93] G. A. McLachlan, G. D. Fallon, R. L. Martin, L. Spiccia, *Inorg. Chem.* **1995**, *34*, 254−261.

[94] J. Mandel, C. Maricondi, B. Douglas, *Inorg. Chem.* **1988**, *27*, 2990−2996.

[95] H. Adams, N. A. Bailey, W. D. Carlisle, D. E. Fenton, G. Rossi, *J. Chem. Soc., Dalton Trans.* **1990**, 1271−1283.

[96] G. S. Matouzenko, A. Bousseksou, S. Lecocq, P. J. van Koningsbruggen, M. Perrin, O. Kahn, A. Collet, *Inorg. Chem.* **1997**, *36*, 2975−2981.
[97] J. Mandel, B. Douglas, *Inorg. Chim. Acta* **1989**, *155*, 55−69.
[98] O. Horner, M.-F. Charlot, A. Boussac, E. Anxolabéhère-Mallart, L. Tchertanov, J. Guilhem, J.-J. Girerd, *Eur. J. Inorg. Chem.* **1998**, 721−727.
[99] I. Bernal, I. M. Jensen, K. M. Jensen, C. J. McKenzie, H. Toftlund, J. P. Tuchagues, *J. Chem. Soc., Dalton Trans.* **1995**, 3667−3675.
[100] K. B. Jensen, C. J. McKenzie, L. P. Nielsen, J. Z. Pedersen, H. M. Svendson, *Chem. Commun.* **1999**, 1313−1314.
[101] A. J. Simaan, F. Banse, P. Mialane, A. Boussac, S. Un, T. Kargar-Grisel, G. Bouchoux, J.-J. Girerd, *Eur. J. Inorg. Chem.* **1999**, 993−996.
[102] O. Horner, E. Anxolabéhère-Mallart, M.-F. Charlot, L. Tchertanov, J. Guilhem, T. A. Mattioli, A. Boussac, J.-J. Girerd, *Inorg. Chem.* **1999**, *38*, 1222−1232.
[103] M. Schatz, M. Leibold, O. Walther, F. Heinemann, S. Schindler, manuscript in preparation
[104] M. Schatz, S. Schindler, unpublished results
[105] R. H. Bode, J. E. Bol, W. L. Driessen, F. B. Hulsbergen, J. Reedijk, A. L. Spek, *Inorg. Chem.* **1999**, *38*, 1239−1243.
[106] M. Becker, J. Nelson, S. Schindler, unpublished results
[107] G. Golub, H. Cohen, D. Meyerstein, *J. Chem. Soc., Chem. Commun.* **1992**, 397−398.
[108] M. A. El-Sayed, *Inorg. Chim. Acta* **1992**, *197*, 197−201.
[109] M. A. El-Sayed, K. Z. Ismail, T. A. El-Zayat, G. Davies, *Inorg. Chim. Acta* **1994**, *217*, 109−119.
[110] M. A. El-Sayed, G. Davies, T. S. Kasem, *Inorg. Chem.* **1990**, *29*, 4730−4735.
[111] G. Davies, M. A. El-Sayed, M. Henary, *Inorg. Chem.* **1987**, *26*, 3266−3273.
[112] G. Davies, M. A. El-Sayed, *Comments Inorg. Chem.* **1985**, *4*, 151−162.
[113] P. L. Holland, K. R. Rodgers, W. B. Tolman, *Angew. Chem. Int. Ed.* **1999**, *38*, 1139−1142.
[114] S. Itoh, M. Taki, H. Nakao, P. L. Holland, W. B. Tolman, L. J. Que, S. Fukuzumi, *Angew. Chem. Int. Ed.* **2000**, *39*, 398−400.
[115] M. Réglier, C. Jorand, B. Waegell, *J. Chem. Soc., Chem. Commun.* **1990**, 1752−1755.
[116] J. A. Halfen, V. G. Young, W. B. Tolman, *J. Am. Chem. Soc.* **1996**, *118*, 10920−10921.
[117] D. H. Lee, N. N. Murthy, K. D. Karlin, *Inorg. Chem.* **1996**, *35*, 804−805.
[118] S. Itoh, T. Kondo, M. Komatsu, Y. Ohshiro, C. Li, N. Kanehisa, Y. Kai, S. Fukuzumi, *J. Am. Chem. Soc.* **1995**, *117*, 4714−4715.
[119] S. Itoh, H. Nakao, L. M. Berreau, T. Kondo, M. Komatsu, S. Fukuzumi, *J. Am. Chem. Soc.* **1998**, *120*, 2890−2899.
[120] V. Mahadevan, J. L. DuBois, B. Hedman, K. O. Hodgson, T. D. P. Stack, *J. Am. Chem. Soc.* **1999**, *121*, 5583−5584.
[121] I. Blain, M. Giorgi, I. De Riggi, M. Réglier, *Eur. J. Inorg. Chem.* **2000**, 393−398.
[122] M. J. Scott, R. H. Holm, *J. Am. Chem. Soc.* **1994**, *116*, 11357−11367.
[123] M. J. Scott, S. C. Lee, R. H. Holm, *Inorg. Chem.* **1994**, *33*, 4651−4662.
[124] I. Sanyal, K. D. Karlin, R. W. Strange, N. J. Blackburn, *J. Am. Chem. Soc.* **1993**, *115*, 11259−11270.
[125] I. Sanyal, R. W. Strange, N. J. Blackburn, K. D. Karlin, *J. Am. Chem. Soc.* **1991**, *113*, 4692−4693.
[126] E. Spodine, J. Manzur, *Coord. Chem. Rev.* **1992**, *119*, 171−198.
[127] T. N. Sorrell, V. A. Vankai, M. L. Garrity, *Inorg. Chem.* **1991**, *30*, 207−210.
[128] E. Monzani, L. Quinti, A. Perotti, L. Casella, M. Gullotti, L. Randaccio, S. Geremia, G. Nardin, P. Faleschini, G. Tabbi, *Inorg. Chem.* **1998**, *37*, 553−562.
[129] G. Alzuet, L. Casella, M. L. Villa, O. Carugo, M. Gullotti, *J. Chem. Soc., Dalton Trans.* **1997**, 4789−4794.
[130] D. Ghosh, R. Mukherjee, *Inorg. Chem.* **1998**, *37*, 6597−6605.
[131] D. Ghosh, T. K. Lal, S. Ghosh, R. Mukherjee, *Chem. Commun.* **1996**, 13.
[132] L. Santagostini, M. Gullotti, E. Monzani, L. Casella, R. Dillinger, F. Tuczek, *Chem. Eur. J.* **2000**, *6*, 519−522.
[133] F. Thaler, G. Liehr, S. Schindler, manuscript in preparation.
[134] R. R. Jacobson, Z. Tyeklár, K. D. Karlin, *Inorg. Chim. Acta* **1991**, *181*, 111−118.
[135] W. E. Lynch, D. M. J. Kurtz, S. Wang, R. A. Scott, *J. Am. Chem. Soc.* **1994**, *116*, 11030−11038.
[136] T. N. Sorrell, W. E. Allen, P. S. White, *Inorg. Chem.* **1995**, *34*, 952−960.
[137] R. R. Jacobson, Z. Tyeklár, K. D. Karlin, J. Zubieta, *Inorg. Chem.* **1991**, *30*, 2035−2040.

Received February 9, 2000
[I00038]

Reactivity of Triosmium Carbonyl Clusters with 1,8-Diaminonaphthalene − Synthesis and Structural Characterization of Amido, Diamido, and *C*-Metalated Trinuclear Derivatives

Javier A. Cabeza,*[a] Heinrich Nöth,[b] María de Jesús Rosales-Hoz,[c] and Gloria Sánchez-Cabrera[c]

Keywords: Osmium / Amido complexes / Cluster compounds / Metalation reactions / N ligands

The compounds $[Os_3(CO)_{12}]$ and $[Os_3(\mu\text{-}H)_2(CO)_{10}]$ do not react with 1,8-diaminonaphthalene (H_2dan) under thermal conditions (110 °C, 30 min). However, $[Os_3(CO)_{10}(MeCN)_2]$ reacts with H_2dan (THF, reflux temperature) to give two isomers of $[Os_3(\mu\text{-}H)(\mu\text{-}Hdan)(CO)_9]$ (**1** and **2**). In toluene at reflux temperature, these reagents afford $[Os_3(\mu\text{-}dan)(CO)_{10}]$ (**3**). Compound **2** can be converted into **3** under thermal conditions, but no interconversion between **1** and **2** has been observed. The three compounds have been characterized by X-ray diffraction methods. Compound **1** arises from the *C*-metalation of H_2dan in a position adjacent to an NH_2 group; this generates a hydride and a ligand that interacts with the three metal atoms through one of the NH_2 groups, through the metalated carbon atom (which spans an Os–Os edge), and through one of the C=C bonds of the metalated ring. In compound **2**, the hydride arises from the oxidative addition of an N–H bond of H_2dan; the resulting ligand interacts with two of the three metal atoms through the amido NH fragment (bridging position) and through the remaining NH_2 group. Compound **3** is derived from the transformation of both NH_2 groups of H_2dan into amido NH groups and consists of a 50-electron trinuclear cluster with the longest edge doubly-bridged by both amido groups.

Introduction

The last fifteen years have witnessed the renaissance of amido-metal chemistry, particularly that of the early transition metals.[1] The inert nature of the R_2N-M bond in these complexes has allowed the design of reactive metal centers specifically tailored to allow reactions in areas such as the activation of poorly reactive molecules, homogeneous catalysis, and organic synthesis.[1] The amido-metal chemistry of the late transition metals has received much less attention[2−11] as a consequence of the thermodynamically less favorable combination of "soft" metals with "hard" ligands. However, the relative lability of the R_2N-M bonds in these complexes has recently been shown to be useful in facilitating reactions such as the formation of C−N bonds through the insertion of unsaturated organic molecules into the R_2N-M bonds.[11]

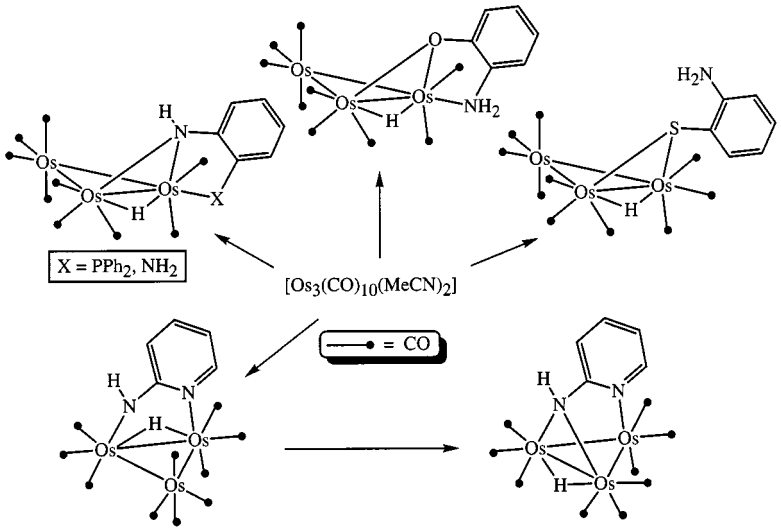
The chemistry of ruthenium carbonyl amido complexes is rather well documented in the literature,[2−4] whereas in the case of osmium only a few carbonyl amido derivatives have been reported. Pentafluoroaniline reacts with $[Os_3(CO)_{12}]$ to give $[Os_3(\mu\text{-}H)(\mu\text{-}NHC_6F_5)(CO)_{10}]$.[5] *ortho*-Functionalized anilines, such as 2-diphenylphosphanylaniline,[3d,6] 1,2-diaminobenzene,[7] and 2-aminophenol[7] react with $[Os_3(CO)_{10}(MeCN)_2]$ to give $[Os_3(\mu\text{-}H)(\mu\text{-}ZC_6H_4X)(CO)_9]$ (Scheme 1). However, the reaction of $[Os_3(CO)_{10}(MeCN)_2]$ with 2-aminothiophenol gives $[Os_3(\mu\text{-}H)(\mu\text{-}SC_6H_4NH_2)(CO)_{10}]$ (Scheme 1) as a consequence of the "softer" character of the sulfur atom.[7] Some 2-amino heterocycles, such as 2-aminopyridine, give amido derivatives when treated with osmium clusters (Scheme 1).[8,9a] The reactivities of other primary and secondary amines towards trinuclear osmium clusters have also been studied.[9]

As far as amido complexes of the late transition metals derived from 1,8-diaminonaphthalene (H_2dan) are concerned, a rich derivative chemistry has been reported for binuclear compounds of ruthenium,[4] rhodium, and iridium[10] incorporating the diamido ligand dan (which is formed by the loss of two NH protons from H_2dan). In these complexes, the basicity of the diamido ligand increases the nucleophilic character of the metal atoms, enhancing their reactivity towards electrophiles (protons, metal fragments, etc.).[4c,4d,4e,10e] In addition, the *cis*-labilizing effect of the "hard" amido fragment promotes regioselective carbonyl substitution processes in positions *cis* to the amido ligand.[4a]

The hitherto obtained results summarized above prompted us to study the reactivity of osmium carbonyl clusters towards 1,8-diaminonaphthalene. We now report that this study has led to the synthesis of amido, diamido, and *C*-metalated triosmium derivatives.

[a] Departamento de Química Orgánica e Inorgánica, Instituto de Química Organometálica "Enrique Moles", Universidad de Oviedo-CSIC,
E-33071 Oviedo, Spain
Fax: (internat.) +34-98/510-3446
E-mail: jac@sauron.quimica.uniovi.es
[b] Institut für Anorganische Chemie, Universität München, Butenandtstraße 5−13, Haus D, D-81377 München, Germany
[c] Departamento de Química, CINVESTAV-IPN, Apartado Postal 14−740, 07000 México D.F., México

 © WILEY-VCH Verlag GmbH, D-69451 Weinheim, 2000 1434−1948/00/1111−2327 $ 17.50+.50/0



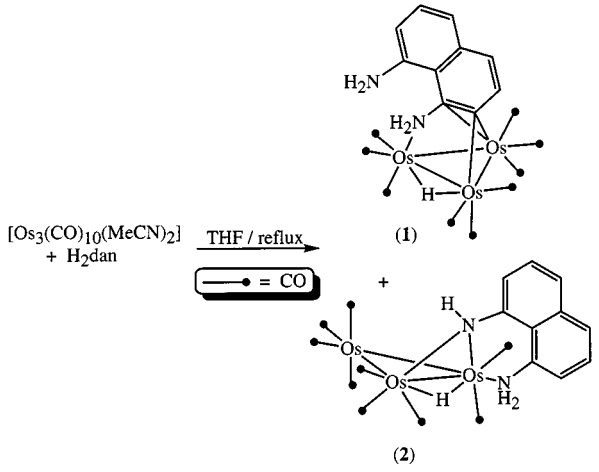
Scheme 1

Results

Synthesis of Compounds 1−3

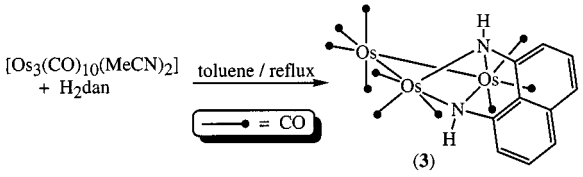
The compounds $[Os_3(CO)_{12}]$ and $[Os_3(\mu\text{-}H)_2(CO)_{10}]$ do not react with 1,8-diaminonaphthalene (H_2dan) under thermal conditions (toluene, reflux temperature, 30 min).

However, the activated[12a] cluster $[Os_3(CO)_{10}(MeCN)_2]$ reacts with H_2dan in THF (reflux temperature, 30 min) to give two isomers of $[Os_3(\mu\text{-}H)(\mu\text{-}Hdan)(CO)_9]$ (compounds **1** and **2** in Scheme 2), in a 1:4 mol ratio, which may be separated by chromatographic methods. The product ratio remains unchanged after longer reaction times.



Scheme 2

In an attempt to induce the reaction of two H_2dan molecules with $[Os_3(CO)_{10}(MeCN)_2]$, the latter was treated with an excess of H_2dan in refluxing toluene. A new compound, subsequently identified as $[Os_3(\mu\text{-dan})(CO)_{10}]$ (**3**) was isolated in 58% yield (Scheme 3). We later found that the excess of H_2dan is unnecessary and that the reaction temperature is the crucial factor for the formation of **3**. In fact, this compound could also be prepared, albeit in lower yield (42%), by thermolysis of **2** in refluxing toluene.



Scheme 3

Structural Characterization of Compounds 1−3

The trinuclear nature of **1**−**3** and the isomeric character of **1** and **2** were indicated by their microanalyses and mass spectra, but the information obtained from their IR and NMR spectroscopic data was insufficient to assign their molecular structures, which were determined by X-ray diffraction methods.

The structure of complex **1** is depicted in Figure 1. Selected structural parameters are listed in Table 1. The compound is formed by *C*-metalation of H_2dan in a position adjacent to an NH_2 group. This generates a hydride ligand, which spans the Os(1)−Os(2) edge, and a ligand that interacts with the three metal atoms through one of the NH_2 groups [Os(1)−N(1) = 2.12(1) Å], through the metalated carbon atom C(2), which spans an Os−Os edge, and through the carbon atom C(1). Analysis of the Os−C distances indicates a σ-type interaction with Os(2) [Os(2)−C(2) = 2.13(2) Å] and a π-type interaction with Os(3) [Os(3)−C(1) = 2.35(1); Os(3)−C(2) = 2.30(1) Å]. The ligand shell is completed by nine carbonyl ligands, three on each metal atom.

Figure 2 shows the molecular structure of complex **2**. Selected bond lengths and angles are listed in Table 1. In this compound, an Os−Os edge is doubly-bridged by a hydride ligand and by the amido fragment of an *N*-monodeprotonated H_2dan ligand [Os(1)−N(1) = 2.176(9); Os(2)−N(1) = 2.119(8) Å], of which the NH_2 group is also attached to one

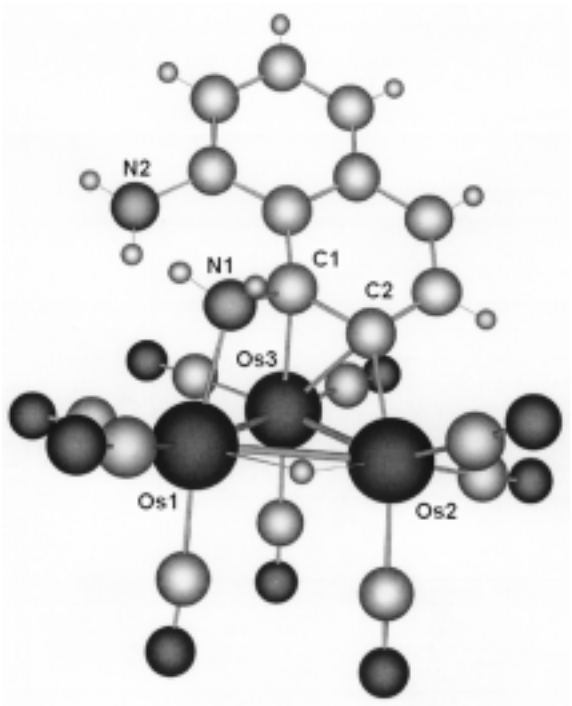


Figure 1. Molecular structure of compound **1**

Table 1. Selected distances [Å] and angles [°] in compounds **1**−**3**

	1	**2**	**3**
Os(1)−Os(2)	2.957(2)	2.7846(9)	3.088(1)
Os(1)−Os(3)	2.816(1)	2.8510(8)	2.878(1)
Os(2)−Os(3)	2.776(1)	2.7974(8)	2.869(1)
Os(1)−N(1)	2.12(1)	2.176(9)	2.18(1)
Os(1)−N(2)			2.16(1)
Os(2)−N(1)		2.119(8)	2.16(1)
Os(2)−N(2)		2.18(1)	2.17(1)
Os(2)−C(2)	2.13(2)		
Os(3)−C(1)	2.35(2)		
Os(3)−C(2)	2.30(1)		
Os(1)−Os(2)−Os(3)	58.74(3)	61.43(2)	57.63(3)
Os(1)−Os(3)−Os(2)	63.83(3)	59.07(2)	65.02(3)
Os(2)−Os(1)−Os(3)	57.42(3)	59.51(2)	75.35(2)
Os(1)−N(1)−Os(2)		80.8(3)	90.6(4)
Os(1)−N(2)−Os(2)			90.9(4)
Os(2)−C(2)−Os(3)	77.5(7)		

of the metal atoms of the same edge [Os(2)−N(2) = 2.18(1) Å] in a position approximately *trans* to the Os(2)−Os(3) edge. The ligand shell is completed by nine carbonyl ligands, of which four are attached to Os(3), three to Os(1), and two to Os(2).

Figure 3 shows the molecular structure of complex **3**. Selected bond lengths and angles are collected in Table 1. This compound is formed by the transformation of both NH_2 groups of H_2dan into NH groups and consists of a 50-electron trinuclear cluster in which the longest (open?) edge [Os(1)−Os(2) = 3.088(1) Å] is doubly-bridged by both NH groups [av. Os−N = 2.17(1) Å]. The ligand shell of the cluster is completed by ten carbonyl ligands, of which four are attached to Os(3), three to Os(1), and three to Os(2). The naphthalene plane lies perpendicular to the Os(1)−Os(2) edge, resulting in an overall (not crystallographic) C_{2v} symmetry. This symmetry is maintained in solution, as indicated by the ^{1}H NMR spectrum, which shows only four resonances for the naphthalene and NH protons.

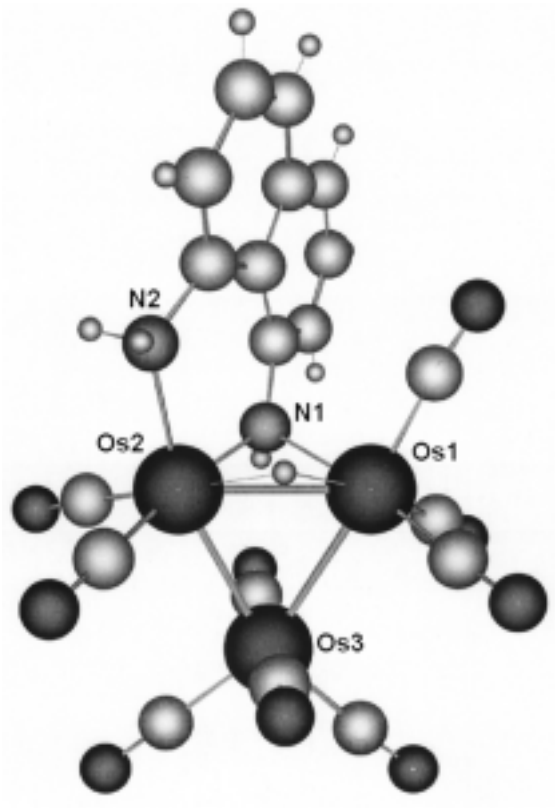


Figure 2. Molecular structure of compound **2**

Discussion

The compound $[Os_3(CO)_{12}]$ is kinetically very stable and generally requires very high temperatures to initiate its reactions, particularly those involving CO substitution.[12b] However, the fact that $[Os_3(\mu\text{-}H)_2(CO)_{10}]$ does not react with H_2dan under thermal conditions seems somewhat surprising as this unsaturated cluster is very reactive.[12c] Indeed, it has been reported that the saturated adducts $[Os_3H(\mu\text{-}H)(CO)_{10}(L)]$ (L = NH_3, NH_2R, NHR_2) can be prepared at room temperature by treating $[Os_3(\mu\text{-}H)_2(CO)_{10}]$ with ammonia gas either in the solid state[13] or in solution,[14] or with primary and secondary amines in solution.[15] In the case of H_2dan, the existence of intramolecular hydrogen bonding involving both NH_2 groups may account for its lower reactivity as compared with that of other amines.

The fact that the isomeric compounds **1** and **2** do not mutually interconvert under thermal conditions indicates that neither is an intermediate in the synthesis of the other, although they may be formed from a common intermediate {probably the product of substitution of the acetonitrile ligands in $[Os_3(CO)_{10}(MeCN)_2]$ by H_2dan}. The fact that compound **3** can be prepared by thermolysis of **2** does not necessarily imply that **2** is an intermediate in the synthesis

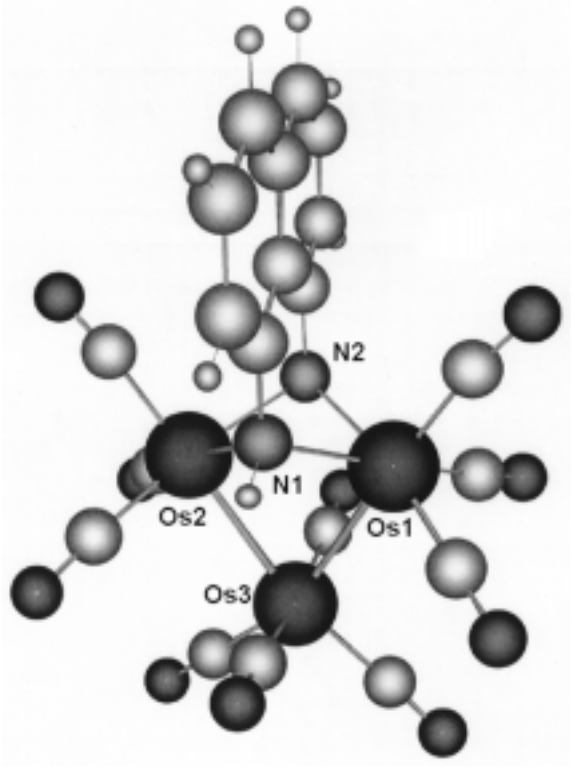


Figure 3. Molecular structure of compound **3**

of **3** from $[Os_3(CO)_{10}(MeCN)_2]$ and H_2dan. It should be noted that **3** has ten CO ligands, whereas **2** has only nine, and that some cluster decomposition occurs in refluxing toluene, since some minor products, including $[Os_4(\mu\text{-}H)_2(CO)_{13}]$, are also formed.

As far as we are aware, the *C*-metalation (as in complex **1**) and the mono *N*-metalation (as in complex **2**) of H_2dan have no precedents in the coordination chemistry of this diamine, although the structure of **2** is reminiscent of those of the ruthenium and osmium cluster complexes $[M_3(\mu\text{-}H)(\mu\text{-}HNC_6H_4X)(CO)_{10}]$ derived from 1,2-diaminobenzene (X = NH_2; M = Ru,[16] Os[7]) and 2-diphenylphosphanylaniline (X = PPh_2; M = Ru,[3d] Os[6]) (Scheme 1). The coordination mode of the dan ligand in complex **3** (symmetric, doubly-bridging six-electron donor) has previously been observed in binuclear complexes of ruthenium,[3c,4a,4b] rhodium, and iridium,[10] and in some trinuclear derivatives resulting from the addition of metallic electrophiles to these binuclear compounds;[4c,4d,10e] however, no homometallic trinuclear complexes incorporating the dan ligand as a doubly-bridging six-electron donor (as in complex **3**) have previously been reported.

It is also interesting to remark that in ruthenium carbonyl cluster chemistry, the binuclear complex $[Ru_2(\mu\text{-dan})(CO)_6]$ is the sole product of the reaction of $[Ru_3(CO)_{12}]$ with H_2dan.[4a,16] Thus, the osmium chemistry described in this article has no parallel in ruthenium chemistry. This can be rationalized by considering the low reactivity of H_2dan (as mentioned above) and the stronger metal−metal bonds of osmium as compared with those of ruthenium.[12b] Thus, H_2dan requires a high temperature for reaction with $[Ru_3(CO)_{12}]$ (toluene under reflux) and Os−Os bonds withstand this temperature whereas Ru−Ru bonds are more easily cleaved.

Experimental Section

General Remarks: Solvents were dried over sodium diphenyl ketyl (THF, hydrocarbons) or calcium hydride (dichloromethane) and distilled under nitrogen prior to use. The reactions were carried out under nitrogen using Schlenk vacuum line techniques and were routinely monitored by solution IR spectroscopy (carbonyl stretching region) and by spot TLC (silica gel). − All reagents were purchased as analytically pure samples, except for anhydrous Me_3NO, which was obtained by azeotropic distillation of $Me_3NO{\cdot}2H_2O$ in toluene. − IR: Perkin−Elmer FT 1720-X. − ^{1}H NMR: Bruker AC-200 and AC-300 spectrometers, room temperature, $SiMe_4$ as internal standard. − Microanalyses: Perkin−Elmer 2400. − MS: VG Autospec double-focusing mass spectrometer operating in the FAB+ mode; ions were produced with a standard Cs^+ gun at ca. 30 kV; 3-nitrobenzyl alcohol (NBA) was used as matrix; data quoted refer to the most abundant molecular ion isotopomer.

$[Os_3(\mu\text{-}H)(\mu\text{-}Hdan)(CO)_9]$ (Isomers 1 and 2): A solution of Me_3NO (9.5 mg, 0.127 mmol) in acetonitrile (2 mL) was added dropwise to a solution of $[Os_3(CO)_{12}]$ (50 mg, 0.055 mmol) in dichloromethane (15 mL) over a period of 15 min. After stirring for 1 h, complete conversion of $[Os_3(CO)_{12}]$ into $[Os_3(CO)_{10}(MeCN)_2]$ had occurred (IR control). The excess Me_3NO was removed by passing the solution through a short column (1 × 5 cm) of neutral alumina (activity I). The solvent was removed under reduced pressure and the solid residue was redissolved in THF (20 mL). Freshly sublimed 1,8-diaminonaphthalene (13 mg, 0.082 mmol) was added and the resulting solution was stirred at reflux temperature for 30 min. The solvent was then removed under reduced pressure and the residue was separated by preparative TLC on silica gel. Elution with hexane/dichloromethane (1:1) afforded three bands. The first band (pale yellow) was found to contain a small amount of an unidentified compound and was discarded. Workup of the second (yellow-orange) and third (yellow) bands afforded compounds **1** (6 mg, 11%) and **2** (25 mg, 46%), respectively.

Analytical and Spectroscopic Data for Compound 1: $C_{19}H_{10}N_2O_9Os_3$ (980.89): calcd. C 23.27, H 1.03, N 2.86; found C 23.52, H 1.28, N 2.75. − FAB-MS: *m*/*z* = 982 [M^+]. − IR (CH_2Cl_2): ν(CO) = 2085 (m), 2056 (s), 2024 (vs), 2002 (m), 1985 (m), 1966 (w) cm^{-1}. − ^{1}H NMR ($CDCl_3$): δ = 8.86 (br. d, *J* = 9.4 Hz, 1 H), 7.86 (d, *J* = 8.8 Hz, 1 H), 7.4−7.0 (m, 2 H), 6.69 (d, *J* = 8.8 Hz, 1 H), 4.03 (br. s, 2 H, NH_2), 3.75 (br. s, 2 H, NH_2), −14.60 (s, 1 H, μ-H).

Analytical and Spectroscopic Data for Compound 2: $C_{19}H_{10}N_2O_9Os_3$ (980.89): calcd. C 23.27, H 1.03, N 2.86; found C 23.38, H 1.27, N 2.71. − FAB-MS: *m*/*z* = 982 [M^+]. − IR (CH_2Cl_2): ν(CO) = 2089 (m), 2049 (vs), 2007 (m), 1995 (s), 1990 (s), 1978 (sh), 1965 (sh), 1918 (m) cm^{-1}. − ^{1}H NMR ($CDCl_3$): δ = 7.8−7.0 (m, 6 H), 6.48 (br. s, 1 H, NH), 5.94 (d, *J* = 12.7 Hz, 1 H of NH_2), 5.48 (d, *J* = 12.7 Hz, 1 H of NH_2), −12.31 (s, 1 H, μ-H).

$[Os_3(\mu\text{-dan})(CO)_{10}]$ (3): A solution of 1,8-diaminonaphthalene (13 mg, 0.082 mmol) and $[Os_3(CO)_{10}(MeCN)_2]$ (0.055 mmol, prepared in situ as described above) in toluene (15 mL) was stirred at reflux temperature for 30 min. The solvent was then removed under reduced pressure and the residue was separated by preparative TLC on silica gel. Multiple elution with hexane/dichloromethane (2:1)

Table 2. Summary of crystal and refinement data for compounds **1**−**3**

	1	**2**	**3**
Formula	$C_{19}H_{10}N_2O_9Os_3$	$C_{19}H_{10}N_2O_9Os_3$	$C_{20}H_8N_2O_{10}Os_3$
Formula weight	980.89	980.89	1006.88
Crystal system	monoclinic	triclinic	triclinic
Space group	$P2_1/n$	$P\bar{1}$	$P\bar{1}$
a [Å]	10.521(1)	8.585(2)	8.786(2)
b [Å]	15.165(1)	11.572(2)	10.105(2)
c [Å]	14.043(1)	12.122(2)	14.089(3)
α [°]	90	69.70(1)	82.22(3)
β [°]	94.077(2)	77.09(1)	72.45(3)
γ [°]	90	87.74(1)	82.22(3)
V [Å^3]	2235.1(4)	1100.0(4)	1160.9(4)
Z	4	2	2
F(000)	1752	876	900
D(calcd.) [g cm^{-3}]	2.915	2.961	2.881
Crystal size [mm]	0.22 × 0.11 × 0.05	0.34 × 0.10 × 0.02	0.56 × 0.56 × 0.34
T [K]	193(2)	293(2)	293(2)
Radiation (λ [Å])	Mo-K_α (0.71073)	Mo-K_α (0.71073)	Mo-K_α (0.71073)
μ [mm^{-1}]	17.065	17.337	16.436
θ range [°]	1.98 to 28.35	2.44 to 25.05	2.47 to 25.07
Min./max. h, k, l	−12/12, −11/12, −17/17	−9/10, −12/13, 0/14	−9/10, −11/12, 0/16
Reflns. collected	12872	3870	4079
Unique reflns. (R_{int})	4033 (0.0606)	3870 (0.0000)	4079 (0.0000)
Reflns. $F > 4\sigma(F)$	2884	3035	3565
Absorption correction	ψ scans	ψ scans	ψ scans
Max./min. trans. factors	0.483/0.095	1.000/0.259	1.000/0.361
Parameters, restraints	298, 0	298, 0	317, 0
GoF (on F^2)	0.991	1.023	1.074
$R1$, $wR2$ [$F > 4\sigma(F)$]	0.0791, 0.1875	0.0403, 0.1001	0.0445, 0.1219
$R1$, $wR2$ (all data)	0.1033, 0.2026	0.0635, 0.1073	0.0536, 0.1261
Max./min. Δρ [e Å^{-3}]	4.563/−7.756	1.594/−3.394	2.396/−2.262

afforded four bands. The first band (yellow) was found to contain a small amount of $[Os_4(\mu\text{-}H)_2(CO)_{13}]$ (IR identification).[17] The third and fourth bands contained very small amounts of unidentified products. Workup of the second band (yellow) afforded compound **3** (32 mg, 58%). − $C_{20}H_8N_2O_{10}Os_3$ (1006.88): calcd. C 23.86, H 0.80, N 2.78; found C 24.01, H 1.02, N 2.73. − FAB-MS: m/z = 1008 [M$^+$]. − IR (CH_2Cl_2): ν(CO) = 2095 (w), 2066 (vs), 2038 (m), 2002 (s), 1982 (m), 1969 (sh) cm^{-1}. − ^{1}H NMR ($CDCl_3$): δ = 7.55 (d, J = 8.1 Hz, 1 H), 7.26 (d, J = 8.1 Hz, 1 H), 7.18 (d, J = 8.1 Hz, 1 H), 3.89 (br. s, 1 H, NH).

X-ray Crystallographic Studies: Crystal data and details of the structures of compounds **1**−**3** are listed in Table 2. The selected crystal of compound **1** was covered with perfluoropolyether oil, attached to the tip of a glass fibre, and then mounted on the Euler cradle of a Siemens P4 four-circle diffractometer equipped with a CCD area detector and an LT2 low-temperature device. Unit cell dimensions were calculated from four sets of data collected at 193 K with different crystal orientations over 15 frames, each with Δψ = 0.3°. Data collection was carried out in the hemisphere mode at 193 K, at two different χ settings with Δψ = 0.3° for each series, over a total of 100 frames. Structure solution was performed by the Patterson method, followed by successive difference Fourier cycles.[18] Non-hydrogen atoms were refined anisotropically, while hydrogen positions were calculated with the exception of those bonded to the nitrogen atoms. An absorption correction was applied by empirical methods.

Crystals of complexes **2** and **3** were mounted on glass fibres and their unit cell dimensions were determined from the angular settings of 25 reflections with 10 < θ < 12° on a Nonius CAD4 diffractometer. Both structures were solved by direct methods followed by successive difference Fourier cycles using SHELXL.[19] In both cases, an empirical absorption correction was applied. Non-hydrogen atoms were refined anisotropically, while hydrogen atoms were geometrically positioned and included in the refinement with fixed isotropic values.

Crystallographic data (excluding structure factors) for the structures reported in this paper have been deposited with the Cambridge Crystallographic Data Centre as supplementary publication nos. CCDC-142357 (**1**), CCDC-142356 (**2**), and CCDC-142355 (**3**). Copies of the data can be obtained free of charge on application to the CCDC, 12 Union Road, Cambridge CB2 1EZ, U.K. [Fax: (internat.) +44-1223/336-033; E-mail: deposit@ccdc.cam.ac.uk].

Acknowledgments

This work has been supported by the Spanish DGESIC (grants PB95−1042 and PB98−1555 to J.A.C.), the Mexican CONACYT (M.J.R.H.), and the Agencia Española de Cooperación Internacional (Programa de Cooperación Científica con Iberoamérica).

[1] R. Kempe, *Angew. Chem. Int. Ed.* **2000**, *39*, 468−493 and references therein.

[2] For reviews on late transition metal amido complexes, see: [2a] M. D. Fryzuk, D. D. Montgomery, *Coord. Chem. Rev.* **1989**, *95*, 1−40. − [2b] H. E. Bryndza, W. Tam, *Chem. Rev.* **1988**, *88*, 1163−1188.

[3] For reviews and articles on bi- and trinuclear ruthenium carbonyl amido complexes, see: [3a] J. A. Cabeza, J. M. Fernández-Colinas, *Coord. Chem. Rev.* **1993**, *126*, 319−336. − [3b] M. I. Bruce, M. P. Cifuentes, M. G. Humphrey, *Polyhedron* **1991**, *10*, 277−322. − [3c] K. B. Shiu, C. H. Li, T. J. Chan, S. M. Peng, M. C. Cheng, S. L. Wang, F. L. Liao, M. Y. Chiang, *Organometallics* **1995**, *14*, 524−529. − [3d] C. J. Adams, M. I. Bruce, P. A. Duckworth, P. A. Humphrey, O. Kühl, E. R. T. Tiekink, W. R. Cullen, P. Braunstein, S. Coco-Cea, B. W. Skelton, A. H. White, *J. Organomet. Chem.* **1994**, *467*, 251−281. − [3e] J. A. Cabeza, M. A. Martínez-García, V. Riera, S. García-Granda, J. F. van der Maelen, *J. Organomet. Chem.* **1996**, *514*, 197−202.

[4] [4a] J. A. Cabeza, J. M. Fernández-Colinas, V. Riera, M. A. Pellinghelli, A. Tiripicchio, *J. Chem. Soc., Dalton Trans.* **1991**, 371−377. − [4b] P. L. Andreu, J. A. Cabeza, V. Riera, F. Robert, Y. Jeannin, *J. Organomet. Chem.* **1989**, *372*, C15−C18. − [4c] J. A. Cabeza, J. M. Fernández-Colinas, V. Riera, S. García-Granda, J. F. van der Maelen, *Inorg. Chim. Acta* **1991**, *185*, 187−192. − [4d] J. A. Cabeza, J. M. Fernández-Colinas, V. Riera, S. García-Granda, J. F. van der Maelen, *Inorg. Chem.* **1992**, *31*, 1233−1238. − [4e] J. A. Cabeza, J. García-Díez, V. Riera, *Eur. J. Inorg. Chem.* **1998**, 1792−1732.

[5] N. V. Podberezskaya, V. A. Maksakov, I. V. Bragina, E. D. Korniets, E. N. Ipatov, P. D. Semyannikov, S. P. Gubin, *Koord. Khim.* **1988**, *14*, 978; *Chem. Abstr.* **1989**, *111*, 39546t.

[6] E. W. Ainscough, A. M. Brodie, S. L. Ingham, J. M. Waters, *J. Organomet. Chem.* **1994**, *468*, 229−234.

[7] J. A. Cabeza, M. A. Martínez-García, V. Riera, S. García-Granda, D. Ardura, *J. Organomet. Chem.* **1996**, *525*, 133−138.

[8] A. J. Deeming, R. Peters, M. B. Hursthouse, J. D. J. Backer-Dirks, *J. Chem. Soc., Dalton Trans.* **1982**, 1205−1211.

[9] [9a] A. J. Deeming, in *Comprehensive Organometallic Chemistry II* (Eds.: E. W. Abel, F. G. A. Stone, G. Wilkinson, D. F. Shriver, M. I. Bruce), vol. 7, Pergamon, Oxford, U.K., **1995**, p. 731 and references therein.[9b] H. D. Kaesz, *J. Organomet. Chem.* **1990**, *383*, 413−420 and references therein.

[10] [10a] M. V. Jiménez, E. Sola, J. A. López, F. J. Lahoz, L. A. Oro, *Chem. Eur. J.* **1998**, 1398−1410. − [10b] M. J. Fernández, J. Modrego, F. J. Lahoz, J. A. López, L. A. Oro, *J. Chem. Soc., Dalton Trans.* **1990**, 2587−2591. − [10c] L. A. Oro, M. J. Fernández, J. Modrego, J. A. López, *J. Organomet. Chem.* **1985**, *287*, 409−417. − [10d] M. J. Fernández, J. Modrego, L. A. Oro, M. C. Apreda, F. H. Cano, C. Foces-Foces, *Inorg. Chim. Acta* **1989**, *157*, 61−64. − [10e] M. J. Fernández, J. Modrego, L. A. Oro, M. C. Apreda, F. H. Cano, C. Foces-Foces, *J. Chem. Soc., Dalton Trans.* **1989**, 1249−1252. − [10f] H. Matsuzaka, K. Ariga, H. Kase, T. Kamura, M. Kondo, S. Kitagawa, M. Yamasaki, *Organometallics* **1997**, *16*, 4514−4516.

[11] See, for example: [11a] R. L. Cowan, W. C. Trogler, *J. Am. Chem. Soc.* **1989**, *111*, 4750−4761. − [11b] H. E. Bryndza, W. C. Fultz, W. Tam, *Organometallics* **1985**, *4*, 939−940. − [11c] D. D. van der Lende, K. A. Abboud, J. M. Boncella, *Inorg. Chem.* **1995**, *34*, 5319−5326. − [11d] J. A. Cabeza, I. del Río, M. Moreno, V. Riera, F. Grepioni, *Organometallics* **1998**, *17*, 3027−3033.

[12] [12a] ref.[9a] p. 686. − [12b] ref.[9a] p. 684. − [12c] ref.[9a] p. 687.

[13] S. Aime, W. Dastrú, R. Gobetto, A. J. Arce, *Organometallics* **1994**, *13*, 4232−4236.

[14] S. Aime, M. Férriz, R. Gobetto, E. Valls, *Organometallics* **1999**, *18*, 2030−2032.

[15] S. Aime, R. Gobetto, E. Valls, *Organometallics* **1997**, *16*, 5140−5142.

[16] J. A. Cabeza, V. Riera, M. A. Pellinghelli, A. Tiripicchio, *J. Organomet. Chem.* **1989**, *376*, C23−C25.

[17] J. A. Krause, U. Siriwardane, T. A. Salupo, J. R. Wermer, D. W. Knoeppel, S. G. Shore, *J. Organomet. Chem.* **1993**, *454*, 263−271.

[18] G. M. Sheldrick, *SHELX-93*, University of Göttingen, Germany, **1993**.

[19] G. M. Sheldrick, *SHELXL-97, Version 97−2*, University of Göttingen, Germany, **1997**.

Received April 14, 2000
[I00145]

Synthesis and X-ray Crystal Structures of $(C_5HiPr_4)Ln(BH_4)_2(THF)$ (Ln = Nd and Sm), Versatile Precursors for Polymerization Catalysts

Denise Barbier-Baudry,*[a] Olivier Blacque,[a] Abderrafia Hafid,[b] Abdelaziz Nyassi,[b] Helmuth Sitzmann,[c] and Marc Visseaux[a]

Keywords: Lanthanides / Uranium / Metallocenes / Bulky ligands / Boron / Hydrides / Polymerization

The new half metallocenes $[(C_5HiPr_4)Ln(BH_4)_2(THF)]$ [Ln = Sm (**1**) and Nd (**2**)], and $[(C_5HiPr_4)U(BH_4)_3]$ (**3**) have been synthesized. The crystal structures of **1** and **2** and of the metallocenes $[(C_5HiPr_4)_2Ln(BH_4)]$ [Ln = Sm (**4**) and Nd (**5**)] have been determined. The substitution of the BH_4 groups of **1** and **2** by a nitrogen-based ligand is possible. In the presence of butyllithium, these complexes show an activity in isoprene and styrene polymerization.

Introduction

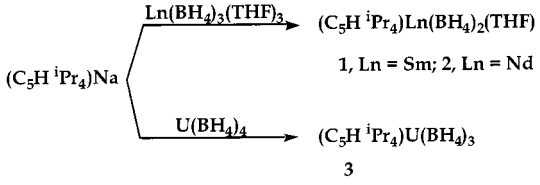
A large number of metallocene catalysts for olefin polymerization have been reported during the last decade. Nowadays, much interest has been placed in the synthesis of half metallocenes, such as, for example, amidocyclopentadienyl compounds for the stereospecific polymerization of α-olefins or styrene.[1] Lanthanide organometallic complexes are analogous to cationic zirconium derivatives and the synthesis of monocyclopentadienyl complexes of the early lanthanides could offer the opportunity to access a great variety of new catalysts. The organometallic chemistry of these elements is actually largely based on biscyclopentadienyl (or related) complexes.[2] We considered that the use of the sterically demanding ligand C_5HiPr_4 [3] could allow an easy synthesis of monocyclopentadienyl derivatives. In order to avoid the incorporation of alkali metal salts leading to the formation of undesirable anionic complexes,[4] borohydrides were used, the pseudohalide BH_4 anion being more electron donating than the chloride ion. In this preliminary communication we present the synthesis and some aspects of the reactivity of $[(C_5HiPr_4)Ln(BH_4)_2(THF)]$ [Ln = Sm (**1**) and Nd (**2**)] and $[(C_5HiPr_4)U(BH_4)_3]$ (**3**). The latter uranium complex, which is tetracoordinate, could be considered as a model of both zirconium and anionic lanthanide $[(C_5HiPr_4)Ln(BH_4)_3]^-$ moieties. Until now, no example of a lanthanide monocyclopentadienylbisborohydride has been reported.

[a] Laboratoire de Synthèse et d'Electrosynthèse Organométalliques (L.S.E.O., UMR 5632 CNRS), Faculté des Sciences Mirande, Université de Bourgogne,
21000 Dijon, France
Fax: (internat.) +33-3/80696084
E-mail: baudryd@u-bourgogne.fr.
[b] Laboratoire de Chimie Physique, Faculté des sciences d'El Jadida
BP 20, El Jadida, Morocco
[c] FB Chemie der Universität,
Erwin-Schrödinger Straße, 67663 Kaiserslautern, Germany

Results and Discussion

Synthesis

Reaction of the tetraisopropylcyclopentadienyl sodium salt C_5HiPr_4Na with $[Sm(BH_4)_3(THF)_3]$, $[Nd(BH_4)_3(THF)_3]$ or unsolvated $[U(BH_4)_4]$ in toluene (or THF) at room temperature, affords the analytically pure monocyclopentadienyl complexes $[(C_5HiPr_4)Sm(BH_4)_2(THF)]$ (**1**), $[(C_5HiPr_4)Nd(BH_4)_2(THF)]$ (**2**) and $[(C_5HiPr_4)U(BH_4)_3]$ (**3**), isolated in ca. 50−60% yield (Scheme 1). These complexes are stable and melt without decomposition around 170 °C. The monomeric structure of **1** and **2** was established by an X-ray structural analysis. The easy sublimation of **3** also indicates a monomeric structure, as is usually observed for analogous uranium compounds.[5]



Scheme 1. Synthesis of complexes **1**−**3**

Monopermethylated cyclopentadienyl lanthanide complexes are less numerous than the disubstituted ones, and most of the complexes obtained from the halide compounds are hexacoordinated complexes of general formula $[Cp^*LnX_2(THF)_3]$ or $[Cp^*LnX_3M(THF)_2]$ ($Cp^* = C_5Me_5$, X = Cl or I, M = Li or Na).[6] The simultaneous use of the very bulky tetraisopropylcyclopentadienyl ligand and of the borohydrides as starting materials allows the formation of monomeric, four-coordinate complexes.

Characterisation

The IR spectra of complexes **1**, **2**, and **3** show the characteristic pattern of a tridentate BH_4 group.[7]

 © WILEY-VCH Verlag GmbH, D-69451 Weinheim, 2000 1434−1948/00/1111−2333 $ 17.50+.50/0

Table 1. ^{1}H NMR spectra of compounds **1**−**6** (C_6D_6, 300 K)

Product[metal]	HCp	H*i*Pr	Me*i*Pr	BH_4
1[a] [Sm]	8	4.2; 3.0	2.2; 1.1 −0.5; −0.7	−10.5
4 [Sm]	17.1	6.8; −0.1	1.8; −0.5 −0.9; −5.1	−7.5
2[a] [Nd]	−15.2	8.4; 1.1	9.8; −3.5 −7.6; −11.0	114.0
5 [Nd]	−9.8	29.0; 0.8	6.8; 5.1 −3.7; −33.7	74.4
3 [U]	24.9	−0.3; −1.1	20.8; 2.00 −12.3; −27.1	53.6
6 [U]	−41.0	43.1; −6.0	23.3; 11.4 2.1; −31.9	−57.8

[a] THF: δ = −0.01 and −0.51* (**1**), −3.5* and −9.16 (**2**). * Confused with a methyl signal, separated at higher temperature.

The NMR spectra of these paramagnetic complexes were recorded in C_6D_6, at variable temperature, to differentiate overlapping signals. The large signal of the BH_4 group, the coordinated THF and the seven signals of the substituted cyclopentadienyl ligand are observed (Table 1). In the spectrum of **2,** the borohydride signal is observed at very low field, as expected in consequence of the strong contact contribution in a neodymium complex. As generally observed for analogous neodymium and samarium complexes, the signals of the H atoms with the highest contact influence (CpH and BH_4) are observed at opposite ends of the spectrum: [Sm]CpH: δ = 10.7; [Nd]CpH: δ = −15.2 (see Table 1). The line widths are similar to those usually observed for paramagnetic uranium, samarium and neodymium complexes,[8] except for two very large signals, which are shifted to much higher field, for the methyl groups of **1** and **2**. At higher temperature (70 °C), these signals are significantly sharpened and exhibit a normal line width. The broadening of these signals cannot be explained only on the basis of the paramagnetic nature of the complexes, but is more likely to be related to a dynamic process: at ambient temperature the rotation of the four methyl groups located close to the metal would be restricted.

For **3,** no significant broadening of the methyl signals was observed; the rotation appears to be free, probably because of the decreased steric hindrance when a THF molecule is replaced by a BH_4 group.

The X-ray crystallographic analyses of **1** and **2** (Figure 1, Ln = Nd) reveal the same monomeric pseudo-tetrahedral structure, with one THF molecule coordinated.[9]

Reactivity

On an NMR scale, we looked at the substitution of the borohydride groups by other ligands. We tried to obtain first the hindered biscyclopentadienyl complexes. In the presence of an excess of $C_5H_iPr_4Na$, with gentle heating (50 °C), the monocyclopentadienyl complexes **1**,**2** and **3** can be slowly (48 h) converted into the corresponding biscyclopentadienyl complexes **4**, **5** and **6**, respectively. Bulk syntheses of **4** and **5** afforded crude material which could not be obtained analytically pure, even after crystallisation. Nevertheless, crops of X-ray quality crystals of **4** and **5** were obtained, and the two compounds were found to be isostructural (Figure 2, Ln = Sm). These monomeric borohydrides are the first examples of tetracoordinated complexes of the early lanthanides; all the other early lanthanide borohydrides described are pentacoordinate,[10] dimeric,[11] or dinuclear complexes.[12]

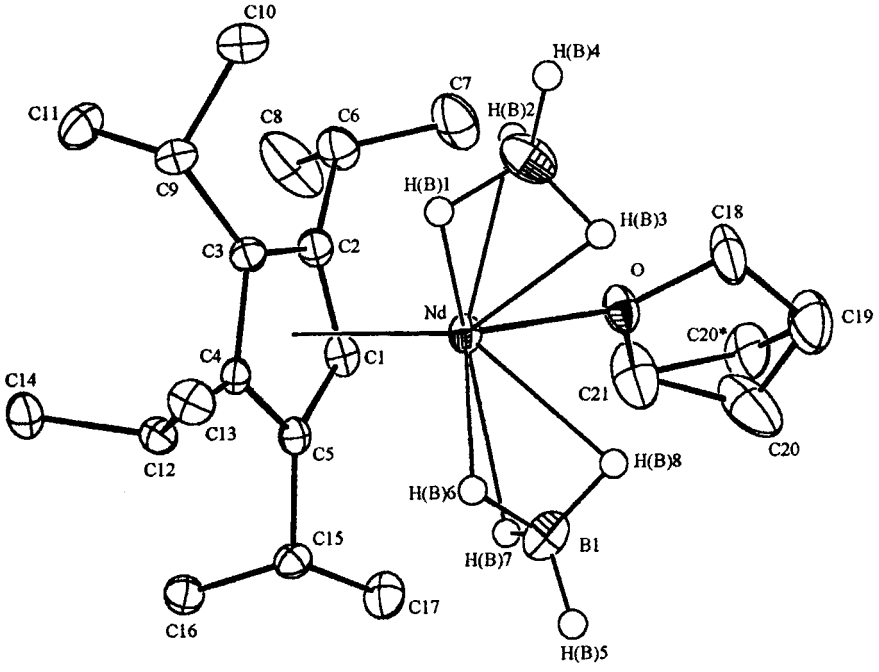


Figure 1. Molecular structure of **2**; selected interatomic distances (Å): Nd−Cp1 2.446, Nd−B1 2.605(3), Nd−B2 2.595(3), Nd−H(B)1 2.32(3), Nd−H(B)2 2.33(3), Nd−H(B)3 2.41(4), Nd−H(B)6 2.28(6), Nd−H(B)7 2.33(4), Nd−H(B)8 2.38(5); Cp1 is the geometric center of the C1−C5 ring

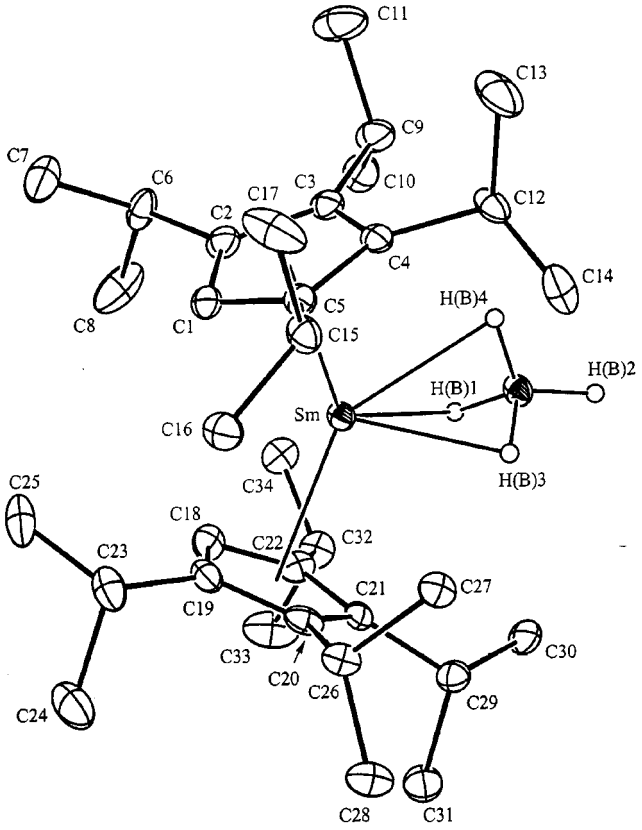
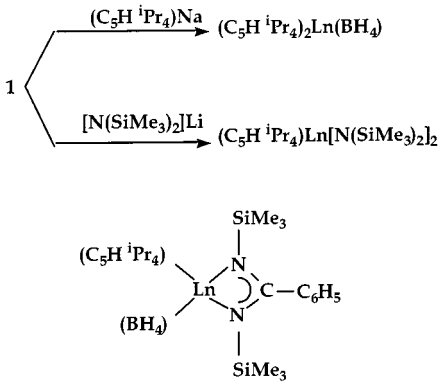


Figure 2. Molecular structure of **4**; selected interatomic distances (Å) and angles (°): Sm−Cp1 2.475, Sm−Cp2 2.436, Sm−B 2.579(3), Sm−H(B)1 2.30(4), Sm−H(B)3 2.28(4), Sm−H(B)4 2.45(4), Cp1−Sm−Cp2 138.7; Cp1 and Cp2 are the geometric centers of the C1−C5 and C18−C22 rings

Ligand exchanges are commonly observed for uranium and lanthanide complexes, but here the bulkiness of the tetraisopropylcyclopentadienyl ligand markedly slows down the exchange process: the complete equilibrium shift of a mixture of $[(C_5HiPr_4)_2Sm(BH_4)]$ **(4)** and $[Sm(BH_4)_3(THF)_3]$ to form **1** requires one week, whereas the metathesis of C_5H_4tBu derivatives requires only one day.[13]

By mixing a stoichiometric amount of **1** and $LiN(SiMe_3)_2$, a new set of signals reveals the presence of the diamido complex $[(C_5HiPr_4)Sm\{N(SiMe_3)_2\}_2]$ mixed with ca 50% of unreacted **1**. By using the more bulky chelating benzamidinate ligand $C_6H_5C(NSiMe_3)_2$, it was possible to substitute one BH_4 ligand of **1** or **3** (Scheme 2).



Scheme 2. Reactivity of compound **1**

Polymerization Experiments

The above-described experiments clearly showed that a new series of organolanthanide complexes could be synthesized from tetraisopropylcyclopentadienyllanthanide borohydrides. We are currently investigating the access to catalytic systems: After addition of one equivalent of BuLi, a benzene solution of **1** or **2** was found to be active towards the polymerization of isoprene, affording 95% of 1,4-*trans*-poly(isoprene) (5 h, 50 °C, M_n = 90 000, I_p = 1.5). These results are in good agreement with the formation of an active organolanthanide species; anionic polymerization with BuLi gives a high percentage of 1,4-*cis*-poly(isoprene).

Under the same conditions, styrene is polymerized to give syndiotactic rich (ca 75% by ^{13}C NMR) polystyrene (16 h, 50 °C, yield 90%, M_n = 300 000, I_p = 1.6).

Conclusion

We have reported the first structures of half-metallocene bisborohydrides of lanthanides. The simultaneous use of the very bulky tetraisopropylcyclopentadienyl and borohydride ligands allows the easy production of monocyclopentadienyl complexes of neodymium and samarium, with an unusually low coordination number. The stable hemimetallocene complexes **1** and **2** are convenient precursors of new catalysts for styrene and isoprene polymerization. From these complexes, one expect the development of a rich new organolanthanide chemistry.

Experimental Section

General Procedures: All reactions were performed under an argon atmosphere in a Jacomex glove box or on a vacuum line. The solvents were dried, deoxygenated and distilled from benzophenone ketyl just before use. NMR spectra were recorded on AC 80, AC 200 or DRX 500 Bruker spectrometers at 300 K. IR spectra were recorded in nujol mulls with a Bruker IFS/66V spectrometer. The syntheses of C_5HiPr_4Na,[3] $U(BH_4)_4$,[14] $Ln(BH_4)_3(THF)_n$ (Ln = Nd,[15] Sm[16]), and the benzamidinate ligand[17] were made as previously described. Polymerization experiments were performed by classical procedures,[18] and GPC analyses were carried out on a Gynkotek P580 apparatus. Elemental analyses were performed with a Fisons EA 1108 CHON apparatus. X ray Data collection: Nonius Kappa CCD diffractometer, Mo-K_α radiation (λ = 0.71073 Å), graphite monochromator.

$[(C_5HiPr_4)Sm(BH_4)_2(THF)]$ (1): $[Sm(BH_4)_3(THF)_3]$ (600 mg, 1.45 mmol) and C_5HiPr_4Na (370 mg, 1.45 mmol) were placed in a flask connected to a vacuum line, and toluene (25 mL) was added by condensation. After stirring for one hour at ambient temperature, the resulting orange solution was separated by filtration and the solvent was removed in vacuo. The crude solid was extracted with pentane and, after a slow crystallization, crystals suitable for X-ray analysis were obtained. After concentration of the mother liquor, a second crop of analytically pure crystals of **1** was obtained (yield 60%). M.p. 165 °C. − IR: $\tilde{\nu}$ = 2461 cm^{-1}, 2200, 2130 (BH_4). − $C_{21}H_{45}B_2OSm$ (486): calcd. C 51.94, H 9.34; found C 52.24, H 9.21.

[($C_5H_iPr_4$)Nd(BH_4)$_2$(THF)] (2): As described for **1**, but with THF as solvent, the dichroic blue-pink **2** was obtained in 55% yield from $Nd(BH_4)_3(THF)_3$ (104 mg, 0.26 mmol) and C_5HiPr_4Na (65.7 mg, 0.26 mmol). M.p. 170 °C. − IR: $\tilde{\nu}$ = 2457 cm^{-1}, 2193, 2127 (BH_4). − $C_{21}H_{45}B_2ONd$ (479): calcd. C 52.60, H 9.46; found C 53.36, H 10.09.

[($C_5H_iPr_4$)U(BH_4)$_4$] (3): From $U(BH_4)_4$ (260 mg, 0.872 mmol) and C_5HiPr_4Na (223 mg, 0.872 mmol), the synthesis of **3** was performed as for **1**, except that the pure compound was obtained as pale orange crystals by sublimation (100 °C, 2 Torr) of the crude material. By crystallization from cold pentane, very thin needles, unsuitable for X-ray structural determination, were obtained. M.p. 160 °C. − IR: $\tilde{\nu}$ = 2516 cm^{-1}, 2178, 2100 (BH_4). − $C_{17}H_{41}B_3U$ (516): calcd. C 39.57, H 8.01; found C 39.77, H 8.36.

[($C_5H_iPr_4$)$_2$Sm(BH_4)] (4), [($C_5H_iPr_4$)$_2$Nd(BH_4)] (5), and [($C_5H_iPr_4$)$_2$U(BH_4)$_2$] (6): Preliminary experiments on an NMR scale allowed the determination of the reaction time and the nature of the obtained products before the attempts at bulk synthesis. Typical experiment for **4**: Compound **1** (8 mg, 0.016 mmol) and C_5HiPr_4Na (4.2 mg, 0.016 mmol) were weighed in an NMR tube, 0.5 mL of C_6D_6 was added and the mixture was stirred by sonication until the two solids dissolved. After 48 h at 50° C, an orange red solution and a colorless precipitate were obtained. The volatiles were then removed in vacuo and a new aliquot of C_6D_6 was added. The spectrum of **4** (mixed with diamagnetic impurities) was observed.
Bulk synthesis allowed the production of crude **4**, **5** and **6** as pasty colored solids mixed with pale, oily, impurities. Slow crystallization from cold pentane afforded some crystals of **4** (red) and **5** (green) suitable for X ray analyses. These crystals were collected for analysis and analytically pure samples of **4** and **5** were obtained after repeating the crystallization. $C_{34}H_{62}BSm$ (631): calcd. C 64.61, H 9.88; found C 64.85, H 10.23. − $C_{34}H_{62}BNd$ (625): calcd. C 65.24, H 10.99; found C 65.49, H 10.44.

X-ray Analysis: Needles of **1** (orange), **2** (blue), **4** (red), and **5** (green) obtained from the bulk synthesis were cut and mounted on a goniometer head.[9] Compounds **1** and **2**, and compounds **4** and **5,** were found to be isostructural.

Crystallographic data (excluding structure factors) for compounds **2** and **4** have been deposited with the Cambridge Crystallographic Data Centre as supplementary publication no. CCDC-143895 (**2**) and CCDC-143896 (**4**). Copies of the data can be obtained free of charge on application to CCDC, 12 Union Road, Cambridge CB2 1EZ, UK [Fax: (internat.) + 44-1223/336-033; E-mail: deposit@ccdc.cam.ac.uk; www: http://www.ccdc.cam.ac.uk].

Reactivity: [(C_5HiPr_4)Sm(BH_4)$_2$(THF)] (11 mg, 0.023 mmol) and Na($NSiMe_3$)$_2$ (4.2 mg, 0.023 mmol) were weighed in an NMR tube, 0.5 mL of C_6D_6 was added and the mixture was stirred by sonication until the two solids dissolved. After 3 h, a yellow-orange solution and a colorless precipitate were obtained. The volatiles were then removed in vacuo and a new aliquot of C_6D_6 was added. A mixture of **1,** Sm[$(N(SiMe_3)_2]_3$ (ca 5%) and [(C_5HiPr_4)$_2$Sm{$(N(SiMe_3)_2$}$_2$] was observed. Silylamido compound: ^{1}H NMR (C_6D_6): δ = 13.97 (HCp), 3.35 and 2.00 (H*i*Pr), 2.51, 1.86, 0.87, −0.19(Me), −4.05 ($SiMe_3$). The mixture was heated for four days at 50 °C, beside the previously observed signals, only a small set of new signals, ca 10% intensity, was observed. Similar experiments were conducted with Li[$C_6H_5C(NSiMe_3)_2$], and a new benzamidinate complex was formed: ^{1}H NMR (C_6D_6): δ = 12.50 (HCp), 10.89, 8.18, 7.99 (C_6H_5), 4.94, 3.85, 3.30, and 2.95 (H*i*Pr), 2.23, 2.06, 1.05, 1.00, 0.87, 0.10 (6 H) and −0.68 (Me), 0.28, 0.14 and −1.26 (MeSi), −2.62 ($SiMe_3$), −10.88 (BH_4).

Polymerizations: Polymerizations were performed as previously described:[18] In a glove box, the lanthanide precursor (5 mg) was introduced into the polymerization flask, a stoichiometric amount of BuLi (1 M hexane solution) was added with a syringe and the monomer (1 mL) was immediately added. The reaction mixture was kept in a thermostatic bath at 50 °C for a given time. After the polymerization was finished, the flask was opened and the solution was poured into 200 mL of ethanol. The crude polymer was washed twice with ethanol and dried under vacuum. The polymers were analyzed by ^{1}H and ^{13}C NMR spectroscopy, the molecular weights were determined by GPC with a polystyrene standard.

[1] [1a] A. Döhring, J. Göhre, P. W. Jolly, B. Kryger, J. Rust, G. P. Verhovnik, *Organometallics* **2000**, *19*, 388. − [1b] M. Galan-Fereres, T. Koch, E. Hey-Hawkins, M. S. Eisen, *J. Organomet. Chem*. **1999**, *580*, 145. − [1c] K. C. Hultzsch, P. Voth, K. Beckerle, T. P. Saniol, J. Okuda, *Organometallics* **2000**, *19,* 5836.

[2] [2a] M. Ephritikhine, *Chem. Rev.* **1997**, *97*, 2193. − [2b] H. Schumann, J. A. Meese-Marktscheffel, L. Esser, *Chem. Rev.* **1995**, *95,* 865.

[3] H. Sitzmann, *J. Organomet. Chem*. **1988**, *354*, 203.

[4] [4a] W. J. Evans, R. A. Keyer, J. W. Ziller, *Organometallics* **1993**, *12*, 2618. − [4b] G. L. Soloveichik, *New J. Chem*. **1995**, *19*, 597.

[5] D. Baudry, E. Bulot, P. Charpin, M. Ephritikhine, M. Lance, M. Nierlich, J. Vigner, *J. Organomet. Chem*. **1989**, *371*, 163.

[6] See X-ray structures reported in reference [2b] p. 942.

[7] T. J. Marks, J. R. Kolb, *Chem. Rev.* **1977**, *77*, 263.

[8] G. N. Lamar, W. de W. Horrocks, R. H. Holm, Jr, *NMR of Paramagnetic Molecules*, Academic Press, New York, **1973**, 529.

[9] Crystal data: Complex **2**: $C_{21}H_{45}B_2NdO$, *FW* = 479.43, blue crystal, 0.5 × 0.3 × 0.2 mm, monoclinic, space group $P2_1/c$ (No. 14), a = 11.9660(4) Å, b = 8.7190(3) Å, c = 23.7070(7) Å, β = 94.710(1), V = 2465.0(1) Å^3, Z = 4, $\rho_{calcd.}$ = 1.292 g·cm^{-3}, F(000) = 996, μ = 2.112 mm^{-1}, T = 110(2) K, 21799 reflections collected, 5402 independent and 5014 observed reflections [$I \geq 2\sigma(I)$], 268 refined parameters, R = 0.028, wR^2 = 0.071, max. residual electron density 0.89 (−1.13) e·Å^{-3}; complex **4**: $C_{34}H_{62}BSm$, *FW* = 632.0, red crystal, 0.25 × 0.15 × 0.10 mm, monoclinic, space group $P2_1/n$ (No. 14), a = 9.8440(2) Å, b = 15.2450(3) Å, c = 23.1310(3) Å, β = 101.9730(9), V = 3395.8(1) Å^3, Z = 4, $\rho_{calcd.}$ = 1.236 g·cm^{-3}, F(000) = 1332, μ = 1.748 mm^{-1}, T = 110(2) K, 179884 reflections collected, 7732 independent and 6709 observed reflections [$I \geq 2\sigma(I)$], 357 refined parameters, R = 0.032, wR^2 = 0.077, max. residual electron density 1.26 (−1.37) e·Å^{-3}.

[10] D. Deng, X. Zheng, C. Qian, J. Sun, L. Zhang, *J. Organomet. Chem*. **1994**, *466*, 95.

[11] [11a] E. B. Lobkovsky, Y. K. Gun′ko, B. M. Bulychev, G. L. Soloveichik, M. Y. Antipin, *J. Organomet. Chem*. **1991**, *406*, 343. − [11b] Y. K. Gun′ko, B. M. Bulychev, G. L. Soloveichik, V. K. Belsky, *J. Organomet. Chem*. **1992**, *424*, 289. − [11c] S. Cendrowski-Guillaume, M. Nierlich, M. Lance, M. Ephritikhine, *Organometallics* **1998**, *17*, 786.

[12] T. Arliguie, M. Lance, M. Nierlich, M. Ephritikhine, *J. Chem. Soc., Dalton Trans.* **1997**, 2501.

[13] D. Baudry, A. Dormond, B. Lachot, M. Visseaux, G. Zucchi, *J. Organomet. Chem*. **1997**, *547*, 157.

[14] V. V. Volkov, K. G. Myakishev, *Radiokhim*. **1980**, *22*, 745.

[15] U. Mirsaidov, T. G. Rotenberg, T. N. Ymova, *Dokl. Akad. Nauk. SSSR* **1976**, *19*, 30.

[16] U. Mirsaidov, I. B. Shaimuradov, M. Khikmatov, *Russ. J. Inorg. Chem*. **1986**, *5*, 753.

[17] M. Wedler, F. Knosel, M. Noltemeyer, F. T. Edelmann, U. Berhens, *J. Organomet. Chem*. **1990**, *388*, 21.

[18] D. Barbier-Baudry, P. Desmurs, A. Dormond, *C. R. Acad. Sci*. **1999**, *IIc*, 375.

Received May 9, 2000
[I00184]

Organophosphorus Compounds, 155[‡]

1,2-Additions of Organomagnesium Halides to Phosphaalkynes: Synthesis of 2-Phospha-1-vinylmagnesium Halides and a Novel Type of Magnesium-Phosphorus Cage Compound

Jens Renner,[a] Uwe Bergsträßer,[a] Paul Binger,*[a] and Manfred Regitz*[a]

Dedicated to Professor Marianne Baudler on the occasion of her 80th birthday

Keywords: Additions / Phosphaalkynes / Grignard reagents / Phosphavinylmagnesium halides / Cage compounds

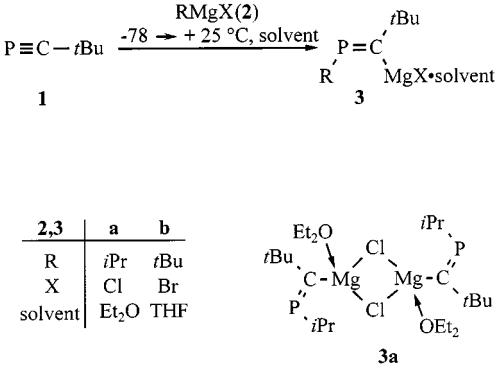
Grignard reagents such as isopropyl- and *tert*-butylmagnesium halide (**2a:** X = Cl**; 2b:** X = Br) react with *tert*-butylphosphaacetylene **(1)** in a regio- and stereoselective 1,2-addition process at –78 °C to give the 2-phospha-1-vinylmagnesium halides **3a,b** in high yields. At elevated temperatures, the phosphavinylmagnesium chloride **3a** reacts with two more equivalents of **1** to afford the previously unknown magnesium-phosphorus cage compound **4**, the structure of which has been confirmed by X-ray-analysis.

Introduction

The recent report on the synthesis of phosphavinyl-Grignard compounds by way of a regio- and stereospecific 1,2-addition of Grignard reagents to *tert*-butylphosphaacetylene **(1)**[2] prompted us to report our results in this field.

Results and Discussion

In the course of our investigations on the use of metallocene[3] and η^8-cyclooctatetraene trunk complexes[4] of zirconium and hafnium in the synthesis of new heterocyclic organophosphorus compounds, we attempted to use the di(isopropoxy)(η^2-propene)titanium complex[5] – readily accessible from titanium tetraisopropoxide and isopropylmagnesium chloride **(2a)** – as a starting material in an appropriate cyclooligomerization protocol of, for example, *tert*-butylphosphaacetylene **(1)**. In these experiments we found that the Grignard reagent reacts with **1** at least as rapidly as with titanium tetraisopropoxide with the result that an inseparable mixture was obtained from the reaction. As a logical consequence, we then performed the reaction of **1** with isopropylmagnesium chloride **(2a)** in the absence of the titanium complex in diethyl ether at −78 °C and found that the metal−carbon bond in **2a** underwent stereo- and regioselective addition to the triple bond of **1** (Scheme 1). As described by Jones et al. for other organomagnesium halides,[2] the 2-phospha-1-vinylmagnesium chloride monoetherate **(3a)** (colorless) was obtained in this case in 100% yield. In the crystalline form the compound exists as the dimer. The phosphaalkyne **1** reacted analogously with one equivalent of *tert*-butylmagnesium bromide **(2b)** to furnish orange crystals of the THF adduct **3b** in 74% yield.



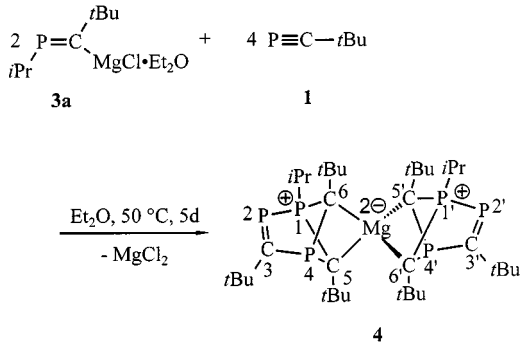
Scheme 1. Synthesis of some phosphavinyl Grignard reagents

The NMR spectroscopic data of the novel phospha-1-vinylmagnesium halides are in good agreement with the values previously reported.[2] Thus, the ^{31}P NMR spectra show signals at δ = 339.4 **(3a)** and 355.1 **(3b)**. These signals, considered together with the low-field ^{13}C NMR signals of the olefinic carbon atoms at δ = 262.1 (d, $^1J_{C,P}$ = 72.1 Hz, **3a**) and 258.9 (d, $^1J_{C,P}$ = 69.6 Hz, **3b**), unambiguously illustrate the presence of the phosphaalkene moiety. An X-ray crystallographic analysis of **3a** demonstrates in this case also the regio- and stereochemistry of the 1,2-addition of isopropylmagnesium chloride, as well as the dimeric structure in the solid state.[6] As already shown by Jones and coworkers, the preparation of phosphavinylmagnesium halides is a general method with regard to the originally em-

[‡] Part 154: Ref.[1]

[a] Fachbereich Chemie der Universität Kaiserslautern, Erwin-Schrödinger-Straße, 67663 Kaiserslautern, Germany
Fax: (internat.) + 49-(0)631/205-3921
Email: regitz@rhrk.uni-kl.de

 © WILEY-VCH Verlag GmbH, D-69451 Weinheim, 2000 1434−1948/00/1111−2337 $ 17.50+.50/0



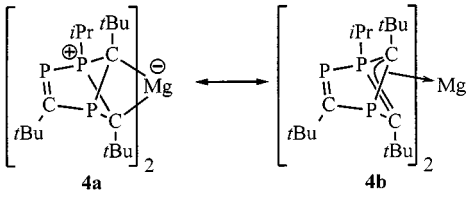
Scheme 2. Synthesis of the new magnesium phosphorus cage compound **4**

ployed Grignard reagent.[2] Preliminary experiments in our laboratory have confirmed this aspect and have also revealed that other kinetically stabilized phosphaalkynes are also amenable to this reaction.

Some phosphavinyl Grignard reagents of the type *trans*-Mes*P=C(R)MgBr (Mes* = C_6H_2-*t*Bu_3-2,4,6; R = halogen, $SiMe_3$) have previously been prepared, albeit only in situ, by other routes and used in synthesis.[7]

Compounds **3a** and **3b** are not only stable at room temperature in the solid state but also in solution. In the presence of at least two equivalents of **1**, however, **3a** undergoes further reaction even at room temperature (Scheme 2, as can be seen from the change from colorless to red. At 50 °C the reaction is complete after five days. The novel magnesium complex **4** formed by the incorporation of two equivalents of **1** is obtained as dark red crystals in 72% yield.

The structure of the complex **4** was unequivocally demonstrated by X-ray crystallography (Figure 1). This shows that the magnesium is in a tetrahedral environment linked by two Mg−C-σ bonds to each of the two 1,2,4-triphosphabicyclo[2.1.1]hexenediyl units. Compound **4** crystallizes without incorporation of solvent molecules and no longer contains chlorine atoms. Both of the bicyclic units contain a four-coordinated phosphorus atom, and accordingly the complex must have a betaine structure in which the bicyclic units each bear a formal positive charge, leaving the magnesium atom with two formal negative charges. To the best of our knowledge, organomagnesium compounds of this type have not been described before.[8] The individual atomic separations found are mostly in agreement with previously reported values. Thus, the bond lengths of between 2.247 and 2.284 Å found for the four Mg−C bonds are in agreement with the reported characteristic values for known organomagnesium compounds.[9] The two bicyclic ligands exhibit P−C, P=C, and P−P bond lengths of 1.878−1.943, 1.663−1.682, and 2.2637−2.2702 Å, respectively, which can be considered as normal.[10,11] The only exceptions are the P1−C6 and P1−C5 (as well as the P1′−C6′ and P1′−C5′) bond lengths of 1.778−1.793 Å, which are considerably shortened in comparison with the values for normal P−C single bonds. From these findings, we can deduce that the structure of the complex **4** must involve not only the betaine structure **4a** but also the η^3-structure **4b** (Scheme 3).



Scheme 3. Mesomeric structures of compound **4**

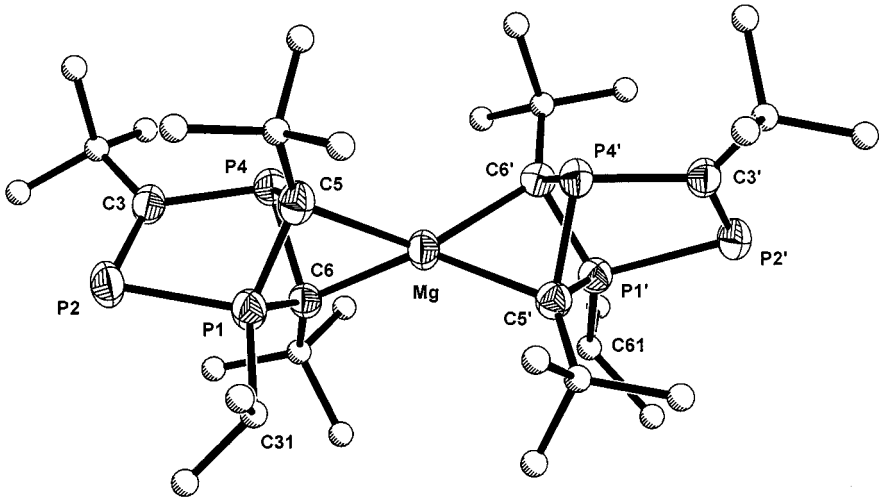
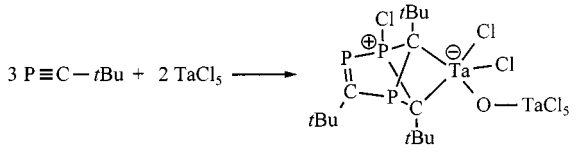


Figure 1. Molecular structure of **4**; selected bond lengths [Å] and angles [°]; H omitted for clarity, displacement ellipsoids at 50% probability: Mg−C5 2.284(3), Mg−C5′ 2.252(3), Mg−C6 2.247(3), Mg−C6′ 2.271(3), C5−P4 1.885(3), C5−P1 1.793(4), C6−P4 1.889(3), C6−P1 1.788(3), P1−P2 2.2637(14), P1−C31 1.850(3), P2−C3 1.682(3), C3−P4 1.932(3), C5′−P4′ 1.888(3), C5′−P1′ 1.778(3), C6′−P4′ 1.877(3), C6′−P1′ 1.779(3), P1′−P2′ 2.2702(12), P1′−C61 1.836(4), P2′−C3′ 1.664(4), C3′−P4′ 1.943(3); C5−Mg−C6 65.18(12), C5−Mg−C6′ 132.52(13), C5−Mg−C5′ 134.90(12), C6−Mg−C5′ 138.80(13), C6−Mg−C6′ 135.06(12), C5′−Mg−C6′ 64.71(11), Mg−C5−P4 82.08(13), Mg−C5−P1 89.3(2), Mg−C6−P4 83.01(13), Mg−C6−P1 90.60(14), Mg−C5′−P4′ 82.24(12), Mg−C5′−P1′ 91.08(13), Mg−C6′−P4′ 81.95(12), Mg−C6′−P1′ 90.42(13), P1−C5−P4 82.45(14), C5−P4−C6 80.6(2), C5−P4−C3 101.0(2), C6−P4−C3 99.10(14), P4−C6−P1 82.46(14), C6−P1−C5 85.9(2), C6−P1−P2 105.14(10), C5−P1−P2 105.50(11), P1−P2−C3 86.05(11), P2−C3−P4 115.8(2), P1′−C5′−P4′ 82.72(14), C5′−P4′−C6′ 79.99(14), C5′−P4′−C3′ 99.17(14), C6′−P4′−C3′ 100.96(14), P4′−C6′−P1′ 82.99(13), C6′−P1′−C5′ 85.7(2), C6′−P1′−P2′ 105.35(11), C5′−P1′−P2′ 104.72(11), P1′−P2′−C3′ 86.65(11), P2′−C3′−P4′ 115.5(2)

On the basis of the crystal structure analysis we were also able to assign the NMR spectroscopic data of complex **4**. As a result of the C_2-symmetry of **4**, only three signals are observed in the ^{31}P NMR spectrum for the six phosphorus atoms. The two olefinic P-atoms give a double doublet signal at δ = 174.1 with $^1J_{P,P}$ = 284.8 and $^2J_{P,P}$ = 14.2 Hz. The neighboring, four-coordinated P-atoms give a signal at δ = 67.2 with a $^2J_{P,P}$ coupling constant of 38.7 Hz. Finally, the two $\sigma^3\lambda^3$ P-atoms produce a signal (also a double doublet) at δ = 27.0 (see Experimental Section). The ^{13}C NMR spectrum reveals a signal for the vinylic C-atoms at δ = 262.0. This signal appears as a doublet of doublets of doublets and confirms the magnetic equivalence of the respective atoms in the two ligands. The carbon atoms bonded to magnesium give rise to two doubled, pseudo-triplet signals at δ = 110.1 and 109.9 with $^1J_{C,P}$ couplings of 57.1 Hz (56.2 Hz) and small $^2J_{C,P}$ couplings of 4.0 Hz each. Similarly, the ^1H NMR spectrum of **4** contains three signals for the six *tert*-butyl groups at δ = 1.57, 1.12 and 1.10, while the two isopropyl groups produce a complicated multiplet at δ = 2.76−2.58 for the two CH groups and two signals at δ = 1.71 and 1.63 for the four methyl groups.

The skeleton of the two ligands at magnesium is already known: it was first observed in the monomeric tantalum complex **5** obtained from the reaction of tantalum pentachloride with three equivalents of **1** (Scheme 4).[12] The mechanism of formation of **4** is still unknown as it has not yet been possible to isolate or identify any intermediates. It is possible that the mechanism proposed by Becker and coworkers [12] for the formation of **5** is also applicable to **4** even though other routes are feasible.



1 **5**

Scheme 4. Synthesis of the tantalum phosphorus compound **5**[12]

We are currently investigating the synthetic potential of these phosphavinylmagnesium compounds as well as the reactivity of complexes of the type **4**.

Experimental Section

All experiments were carried out under argon in anhydrous solvents. − MS: Finnigan MAT 90. − ^1H and ^{13}C NMR: Bruker AC 200 and Bruker AMX 400; chemical shifts were determined relative to solvent signals and converted into the TMS scale. − ^{31}P NMR: Bruker AC 200 (80.8 MHz); external standard H_3PO_4. − Chemicals: 2,2-dimethylpropylidynephosphane [*tert*-butylphosphaacetylene, **(1)**] was prepared according to a published procedure;[13] the Grignard reagents are commercially available.

(*Z*)-1-*tert*-Butyl-2-isopropyl-2-phosphavinylmagnesium Chloride (3a): To a solution of **1** (0.1 mL, 90% solution in hexamethyldisiloxane, 0.72 mmol) in Et_2O (2 mL) cooled to −78 °C was added dropwise a 2 M solution of isopropylmagnesium chloride **(2a)** in Et_2O (0.36 mL, 0.72 mmol). The color of the reaction solution changed spontaneously from colorless to yellow and **3a** precipitated. After stirring for 2.5 h at this temperature and a further 12 h at room temperature, a yellow solution was obtained from which **3a** crystallized out at +4 °C. − Yield 200 mg (100%) **3a** as monoetherate. − m.p. > 295 °C (dec.). − ^1H NMR (400.1 MHz, CD_2Cl_2): δ = 3.94 (q, $^3J_{H,H}$ = 7.0 Hz, 4 H, OCH_2−CH_3), 1.91 [sept, $^3J_{H,H}$ = 6.9 Hz, 1 H, CH(CH$_3$)$_2$], 1.29 (t, $^3J_{H,H}$ = 7.0 Hz, 6 H, OCH$_2$−CH_3), 1.21 [d, $^4J_{H,P}$ = 2.2 Hz, 9 H, C(CH_3)$_3$], 1.14 [dd, $^3J_{H,P}$ = 11.8 Hz, $^3J_{H,H}$ = 6.9 Hz, 6 H, CH(CH_3)$_2$]. − $^{13}C\{^1H\}$ NMR (100.6 MHz, CD_2Cl_2): δ = 262.1 (d, $^1J_{C,P}$ = 72.1 Hz, P=*C*), 65.7 (s, O*C*H$_2$CH$_3$), 43.4 [d, $^2J_{C,P}$ = 13.4 Hz, *C*(CH$_3$)$_3$], 36.5 [d, $^1J_{C,P}$ = 34.8 Hz, *C*H(CH$_3$)$_2$], 33.8 [d, $^3J_{C,P}$ = 19.1 Hz, C(*C*H$_3$)$_3$], 22.9 [d, $^2J_{C,P}$ = 15.3 Hz, CH(*C*H$_3$)$_2$], 14.2 (s, OCH$_2$−*C*H$_3$). − $^{31}P\{^1H\}$ NMR (80.8 MHz, C_6D_6): δ = 339.4 (s). − MS (EI, 35 eV); *m/z* (%): 277 (5) [M^+], 144 (39) [M^+ − MgCl − Et_2O], 101 (19) [PC*t*BuH$^+$], 87 (18) [*i*PrPCH$^+$], 74 (30) [Et_2O], 70 (30) [CH*t*Bu$^+$], 69 (55), 59 (34), 57 (71) [*t*Bu$^+$], 43 (96), 41 (100), 31 (96).

(*Z*)-1,2-Di-*tert*-butyl-2-phosphavinylmagnesium Bromide (3b): In analogy to the preparation of **3a** a solution of **1** (0.1 mL, 90% solution in hexamethyldisiloxane, 0.72 mmol) in THF (2 mL) was treated dropwise with a 1.57 M solution of **2b** in THF (0.46 mL, 0.72 mmol) to obtain 154 mg (74%) of **3b** as a solvate complex in the form of orange crystals. − m.p. > 295 °C (dec.). − ^1H NMR (400.1 MHz, CD_2Cl_2): δ = 3.95 (m, 4 H, THF), 1.90 (m, 4 H, THF), 1.26 [d, $^4J_{H,P}$ = 2.5 Hz, 9 H, C(CH_3)$_3$], 1.18 [d, $^3J_{H,P}$ = 9.3 Hz, 9 H, C(CH_3)$_3$]. − $^{13}C\{^1H\}$ NMR (100.6 MHz, CD_2Cl_2): δ = 258.9 (d, $^1J_{C,P}$ = 69.6 Hz, P=*C*), 69.6 (s, THF), 44.1 [d, $^2J_{C,P}$ = 16.7 Hz, *C*(CH$_3$)$_3$], 34.1 [d, $^1J_{C,P}$ = 20.5 Hz, P*C*(CH$_3$)$_3$], 32.2 [d, $^3J_{C,P}$ = 15.7 Hz, C(*C*H$_3$)$_3$], 31.2 [d, $^2J_{C,P}$ = 12.4 Hz, C(*C*H$_3$)$_3$], 25.6 (s, THF). − $^{31}P\{^1H\}$ NMR (80.8 MHz, C_6D_6): δ = 355.1 (s).

Bis[3,5,6-tri-*tert*-butyl-1-isopropyl-1,2,4-triphosphabicyclo[2.1.1]hex-2-ene-5,6-diyl]-magnesium (4): To a solution of **1** (0.2 mL, 90% solution in hexamethyldisiloxane, 1.44 mmol) in Et_2O (2 mL) cooled to −78 °C was added a 2 M solution of isopropylmagnesium chloride **(2a)** in Et_2O (0.72 mL, 1.44 mmol). After the mixture had been stirred for 1 h at −78 °C and a further hour at room temperature, the ^{31}P NMR spectrum of the mixture showed the presence of **3a** as the sole product. The reaction mixture was transferred to a pressure Schlenk tube, a further 2 equivalents of **1** (0.4 mL, 2.88 mmol) were added, and the mixture heated at 50 °C for 5 days. During this time a white precipitate formed and the color of the reaction solution changed to red. The solution was separated by decantation and the precipitate washed with several 1-mL portions of ether. The volume of the collected solutions was reduced under vacuum to ca. 4 mL. Cooling to +4 °C resulted in the precipitation of **4** in the form of red crystals suitable for X-ray crystallography. − Yield 740 mg (72%). − m.p. 238 °C (dec.). − ^1H NMR (200.1 MHz, CD_2Cl_2): δ = 2.76 − 2.58 [m, 1 H, CH(CH$_3$)$_2$], 1.71 [dd, $^3J_{H,P}$ = 6.9 Hz, $^3J_{H,H}$ = 5.2 Hz, 3 H, CH(CH_3)$_2$] and 1.63 [dd, $^3J_{H,P}$ = 7.1 Hz, $^3J_{H,H}$ = 5.3 Hz, 3 H, CH(CH_3)$_2$], 1.57 [d, $^4J_{H,P}$ = 1.5 Hz, 9 H, C(CH_3)$_3$], 1.12 [s, 9 H, C(CH_3)$_3$], 1.10 [s, 9H, C(CH_3)$_3$]. − ^{13}C NMR (100.6 MHz, C_6D_6, 55 °C): δ = 262.0 (ddd, $^1J_{C,P}$ = 94.8 Hz, $^1J_{C,P}$ = 47.4 Hz, $^2J_{C,P}$ = 40.5 Hz, P=*C*), 110.1 (dpt, $^1J_{C,P}$ = $^1J_{C,P}$ = 57.1 Hz, $^2J_{C,P}$ = 4.0 Hz, Mg−*C*) and 109.9 (dpt, $^1J_{C,P}$ = $^1J_{C,P}$ = 56.2 Hz, $^2J_{C,P}$ = 4.0 Hz, Mg−*C*), 44.3 [pt, $^2J_{C,P}$ = $^2J_{C,P}$ = 13.8 Hz, Mg−C−*C*(CH$_3$)$_3$] and 44.1 [pt, $^2J_{C,P}$ = $^2J_{C,P}$ = 13.8 Hz, Mg−C−*C*(CH$_3$)$_3$], 40.5 [dd, $^2J_{C,P}$ = 7.8 Hz, $^2J_{C,P}$ = 6.0 Hz, P=C−*C*(CH$_3$)$_3$], 39.1 [ddd, $^1J_{C,P}$ = 21.6 Hz, $^2J_{C,P}$ = 8.6 Hz, $^3J_{C,P}$ = 5.2 Hz, *C*H(CH$_3$)$_2$], 36.0−35.7 [m, Mg−C−C(*C*H$_3$)$_3$], 32.7 [dd, $^3J_{C,P}$ = 10.4 Hz, $^3J_{C,P}$ = 6.9 Hz, P=C−C(*C*H$_3$)$_3$], 20.2 [d, $^3J_{C,P}$ = 9.5 Hz, CH(*C*H$_3$)$_2$]. − $^{31}P\{^1H\}$ NMR (80.8 MHz, CD_2Cl_2): δ = 174.1 (dd, $^1J_{P,P}$ = 284.8 Hz, $^2J_{P,P}$ = 14.2 Hz, P2 and P2′), 67.2 (dd,

$^1J_{P,P}$ = 284.8 Hz, $^2J_{P,P}$ = 38.7 Hz, P1 and P1′), 27.0 (dd, $^1J_{P,P}$ = 38.7 Hz, $^2J_{P,P}$ = 14.2 Hz, P4 and P4′). − MS (EI, 35 eV), *m*/*z* (%): [M^+] not observed; 345 (42) [$C_{18}H_{36}P_3^+$], 245 (14) [$C_{13}H_{27}P_2^+$], 231 (18) [$C_{10}H_{18}P_3^+$], 169 (49) [$C_{10}H_{18}P^+$], 131 (60) [$C_5H_9P_2^+$], 101 (18), 99 (14), 69 (47) [$C_5H_9^+$], 57 (100) [tBu$^+$], 43 (38) [iPr$^+$], 41 (49).

Crystal Structure Analysis of 4: STOE Imaging Plate Diffraction System, graphite monochromator, Mo-K_α radiation (λ = 0.71073 Å), cell determination and refinement by STOE programs Ver. 2.75, structure solution by direct methods (SHELXS-86[14]) and structure refinement by SHELXL-93,[15] hydrogen atoms were included in the refinement using riding models. $C_{36}H_{68}MgP_6$; M = 711.0 g·mol^{-1}; monoclinic; space group $P2_1/c$ (No. 14), lattice constants a = 11.276(2), b = 17.599(4), c = 21.888(4) Å, β = 102.47(3)°, V = 4241(2) Å^3; Z = 4; $D_{calcd.}$ = 1.114 Mg/m^3; μ = 2.91 cm^{-1}; T = 293(2) K; crystal size 0.35 × 0.20 × 0.15 mm^3; 1.85 ≤ Θ ≤ 24.16°. 29644 reflections collected, 6344 independent reflections ($R_{int.}$ = 0.1222); 388 parameters; w^{-1}= [$\sigma^2(F_o^2)$ + (0.0253P)^2], P = [(F_o^2) + 2F_c^2]/3; R^1 = 0.0485, wR^2 = 0.0933 for 3999 reflections with I > 2σ(I) and R^2 = 0.0844, wR^2 = 0.1037 for all data; residual electron density 428 e·nm^{-3} and −271 e·nm^{-3}, S = *GOF* (on F^2)= 1.017.

Crystallographic data (excluding structure factors) for the structure(s) included in this paper have been deposited with the Cambridge Crystallographic Data Centre as supplementary publication no. CCDC-148262. Copies of the data can be obtained free of charge on application to CCDC, 12 Union Road, Cambridge CB2 1EZ, UK [Fax: (internat.) + 44-1223/336-033; Email: deposit@ccdc.cam.ac.uk].

Acknowledgments

We thank the Fonds der Chemischen Industrie for generous financial support. We are grateful to the Deutsche Forschungsgemeinschaft (Graduate College Phosphorus Chemistry as a Connecting Link between Various Chemical Disciplines) for financial support and a post-graduate grant (to J. R.).

[1] J. Simon, G. J. Reiß, U. Bergsträßer, H. Heydt, M. Regitz, *Eur. J. Inorg. Chem.* **2000**, submitted for publication.
[2] D. E. Hibbs, C. Jones, A. F. Richards, *J. Chem. Soc., Dalton Trans.* **1999**, 3531−3532.
[3] [3a] P. Binger, B. Biedenbach, C. Krüger, M. Regitz, *Angew. Chem.* **1987**, *99*, 798−799; *Angew. Chem. Int. Ed. Engl.* **1987**, *26*, 764−765. − [3b] P. Binger, T. Wettling, R. Schneider, F. Zurmühlen, U. Bergsträßer, J. Hofmann, G. Maas, M. Regitz, *Angew. Chem.* **1991**, *103,* 208−211; *Angew. Chem. Int. Ed. Engl*. **1991**, *30*, 207−210. − [3c] T. Wettling, B. Geißler, R. Schneider, S. Barth, P. Binger, M. Regitz, *Angew. Chem.* **1992**, *104*,761−762; *Angew. Chem. Int. Ed. Engl.* **1992**, *31*, 758−759. − [3d] B. Geißler, S. Barth, U. Bergsträßer, M. Slany, J. Durkin, P. B. Hitchcock, M. Hofmann, P. Binger, J. F. Nixon, P. von Ragué Schleyer, M. Regitz, *Angew. Chem.* **1995**, *107*, 485−488; *Angew. Chem Int. Ed. Engl.* **1995**, *34*, 484−487.
[4] [4a] P. Binger, G. Glaser, B. Gabor, R. Mynott, *Angew. Chem.* **1995**, *107*, 114−116; *Angew. Chem. Int. Ed. Engl.* **1995**, *34*, 81−83. − [4b] P. Binger, S. Leininger, J. Stannek, B. Gabor, R. Mynott, J. Bruckmann, U. Krüger, *Angew. Chem.* **1995**, *107*, 2411−2414; *Angew. Chem. Int. Ed. Engl.* **1995**, *34*, 2227−2230. − [4c] P. Binger, S. Leininger, K. Günther, U. Bergsträßer, *Chem. Ber./Recueil* **1997**, *130*, 1491−1494.
[5] K. Harada, H. Urabe, F. Sato, *Tetrahedron Lett.* **1995**, *36*, 3203−3206.
[6] We have not presented a detailed discussion of the molecular structure with numerical data because the crystal structure analysis of an analogue of **3a** (cyclopentyl in place of isopropyl) has already been published, see. ref.[2]
[7] [7a] M. van der Sluis, V. Beverwijk, A. Termaten, E. Gavrilova, F. Bickelhaupt, H. Kooijman, N. Veldman, A. L. Spek, *Organometallics* **1997**, *16*, 1144−1152. − [7b] M. van der Sluis, J. B. M. Wit, F. Bickelhaupt, *Organometallics* **1996**, *15*, 174−180.
[8] *Handbook of Grignard Reagents* (Eds.: G. S. Silverman, P. E. Rakita), Marcel Dekker Inc., New York, **1996**.
[9] H. Uhm in ref.[8] p. 117−144.
[10] R. Appel, in *Multiple Bonds and Low Coordination in Phosphorus Chemistry* (Eds.: M. Regitz, O. J. Scherer), Thieme, Stuttgart, **1990**, pp. 157.
[11] *CRC Handbook of Chemistry and Physics, 73rd Ed.* (Ed.: D. R. Lide), CRC Press, Boca Raton, **1992**, p. 1124.
[12] [12a] G. Becker, W. Becker, R. Knebel, H. Schmidt, M. Mildenbrand, M. Westerhausen, *Phosphorus Sulfur* **1987**, *30*, 349−352. − [12b] G. Becker, W. Becker, R. Knebel, H. Schmidt, U. Weber, M. Westerhausen, *Nova Acta Leopold. (Neue Folge)* **1985**, *59*, 55−67.
[13] [13a] W. Rösch, T. Allspach, U. Bergsträßer, M. Regitz in *Synthetic Methods of Organometallic and Inorganic Chemistry* (Ed: W. A. Herrmann), Vol. 3, Thieme, Stuttgart, **1996**, pp. 11. − [13b] W. Rösch, U. Hees, M. Regitz, *Chem. Ber.* **1987**, *120*, 1645−1652.
[14] G. M. Sheldrick, *SHELXS-86*, *Programm for Crystal Structure Solution*, University of Göttingen, **1990**.
[15] G. M. Sheldrick, *SHELXL-93*, *Program for Crystal Structure Refinement*, University of Göttingen, **1993**.

Received May 12, 2000
[I00197]

A Three-Dimensional, Cyano-Bridged Cluster−Metal Coordination Compound with Large Cavities

Vladimir P. Fedin,*[a] Alexander V. Virovets,[a] Irina V. Kalinina,[a] Vladimir N. Ikorskii,[a] Mark R. J. Elsegood,[b] and William Clegg[b]

Keywords: Tungsten / Tellurium / Cobalt / Cyanides / Crystal engineering

By very slow diffusion of aqueous solutions of $CoCl_2 \cdot 6H_2O$ and $K_6[W_4Te_4(CN)_{12}] \cdot 5H_2O$ through silica gel, single crystals of $[Co(H_2O)_4]_3[W_4Te_4(CN)_{12}] \cdot 15.38H_2O$ were obtained. A complete X-ray structure determination reveals an extremely porous, three-dimensional neutral cluster-expanded framework structure with large water-filled cuboidal cavities.

Introduction

Reactions of mononuclear aquo- and cyano-transition metal complexes lead to the formation of an extensive family of cyanide-bridged metal−metal coordination polymers.[1,2] This class of compounds has the potential for use in molecular separation because large cavities are formed in some cases.[3,4] Recently, octahedral $[Re_6E_8(CN)_6]^{4-}$ (E = S, Se, Te) cluster complexes with an outer ligand topologically equivalent to hexacyanometallates have been shown to react with transition metal ions to precipitate a range of framework solids with unprecedented structures.[5] Cluster-expanded Prussian blue analogues of the composition $M_4[Re_6E_8(CN)_6] \cdot nH_2O$ (M = Ga, Fe)[6] and $[Cd_2(H_2O)_4][Re_6S_8(CN)_6] \cdot 14H_2O$[7] with large, water-filled cavities have been obtained. In the Cd compound the volume of each water-filled cavity is 345 Å^3, and the cavities represent 62% of the total volume of the structure. Another example of a porous compound based on a cyanide cluster is $(H_5O_2)_2Zn_3[Re_6Se_8(CN)_6] \cdot 18H_2O$[8] with a hexagonal cavity of ca. 11 × 11 × 5 Å filled by hydroxonium cations and water molecules.

The synthesis and crystallization of cyanide-bridged coordination polymers with structural and functional similarity to inorganic zeolites continues to be a challenging problem. Recently we have described the syntheses, X-ray structure determination and properties of cubane-type M_4E_4 (M = Mo, W; E = S, Se, Te) water-soluble cyano complexes.[9] Here we report for the first time that cuboidal cluster complexes of T_d symmetry can be used for the preparation of framework solids with voluminous cavities.[10]

[a] Institute of Inorganic Chemistry, Russian Academy of Sciences, pr. Lavrentjeva 3, Novosibirsk 630090, Russia
E-mail: cluster@che.nsk.su
[b] Department of Chemistry, The University of Newcastle upon Tyne,
Newcastle upon Tyne NE1 7RU, UK

Results and Discussion

An aqueous solution of $CoCl_2 \cdot 6H_2O$ was added slowly to an aqueous solution of mixed-valence (3.5) $K_6[W_4Te_4(CN)_{12}] \cdot 5H_2O$ to give, in quantitative yield, well-formed cuboidal dark red-brown crystals of composition $[Co(H_2O)_4]_3[W_4Te_4(CN)_{12}] \cdot 8H_2O$ (**1**). The compound is X-ray amorphous after drying in air (XRD, Philips APD 1700). The compound was characterized by elemental analysis, IR spectroscopy, thermogravimetry and magnetochemical measurements. The FT-IR spectrum of **1** clearly shows the presence of H_2O and two types of cyanide ligands: the terminal W−CN fragments exhibit a sharp, intense band at 2100 cm^{-1} {compared with ν(CN) = 2097 cm^{-1} for $K_6[W_4Te_4(CN)_{12}] \cdot 5H_2O$},[9] whereas the W−CN−Co bridges exhibit a broader line shifted to higher frequency (2127 cm^{-1}). The effective magnetic moment of 4.72 μB calculated per Co atom is reasonable for three isolated high-spin Co^{2+} ions per formula unit. The N end of the cyanide ligand is a weak field ligand and thus stabilizes a high-spin state. Thermogravimetric analysis in Ar revealed complete dehydration of **1** by 150 °C, with no further significant weight loss below 450 °C. The FT-IR spectra of **1** and a dehydrated sample (150 °C, vacuum, 1 h) confirm that only minor perturbation occurs in the arrangement of the framework upon complete dehydration. The structure of X-ray amorphous compound **1** is still unknown.

Further attempts were made to prepare single crystals from the system $Co^{2+}/[W_4Te_4(CN)_{12}]^{6-}$. Very slow diffusion of aqueous solutions of $[W_4Te_4(CN)_{12}]^{6-}$ and $[Co(H_2O)_6]^{2+}$ through silica gel for eight weeks resulted in cuboidal dark red-brown crystals (**2**) suitable for an X-ray single-crystal analysis. The composition of compound **2**, according to diffraction data, is $[Co(H_2O)_4]_3[W_4Te_4(CN)_{12}] \cdot 15.38H_2O$, the calculated density being approximately half of that measured for **1**.

The local coordination environment of the Co atom and the structure of the $[W_4Te_4(CN)_{12}]^{6-}$ cluster complex are shown in Figure 1. Each Co^{2+} ion exhibits pseudo-octahedral coordination, with four water ligands and two nitrogen atoms of the cyanide ligands bound in a *trans* arrangement.

 © WILEY-VCH Verlag GmbH, D-69451 Weinheim, 2000 1434−1948/00/1111−2341 $ 17.50+.50/0

The arrangement of water around Co^{2+} is disordered over two symmetrically equivalent positions. A structure determination revealed a cubic three-dimensional neutral framework of cuboidal $[W_4Te_4]^{6+}$ and $[Co(H_2O)_4]^{2+}$ fragments linked through bridging cyanide ligands (Figure 2). There are 12 cobalt atom positions around each W_4Te_4 cluster. These positions are statistically half-occupied, and therefore each cluster is linked to six cobalt atoms to give a primitive cubic lattice of ReO_3 type with clusters and cobalt atoms in the Re and O positions, respectively. The centres of the cluster anions follow a primitive cubic motif, although not face-centred as in Prussian blue. The large cavities are filled by highly disordered water molecules. Our attempts to resolve the disorder by assuming lower symmetry space groups were unsuccessful.

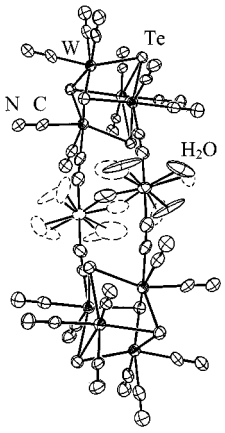


Figure 1. Fragment of structure of **2** showing the $[Co(H_2O)_4]^{2+}$ bridges between $[W_4Te_4(CN)_{12}]^{6-}$ anions, 30% probability ellipsoids; the W−W bonds are omitted for clarity; the disordered positions of Co atoms and water molecules are shown by dashed lines; main bond lengths (Å): W−W, 2.952(2), W−Te, 2.6889(17), W−C, 2.078(19), C−N, 1.20(2), Co−N, 2.096(17), Co−O, 2.15(4)−2.19(5).

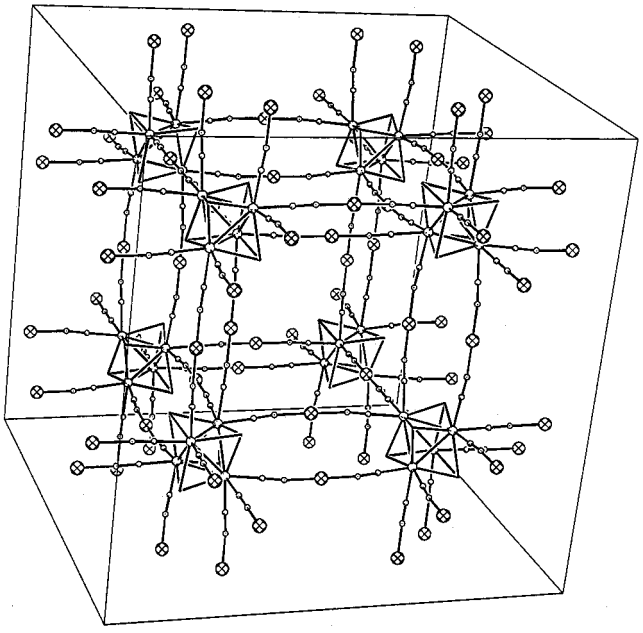


Figure 2. Crystal packing of **2**; all water molecules are omitted for clarity; all disordered positions of Co^{2+} ions are shown, but only one half of them are occupied.

The cavity in **2** of O_h symmetry has the centre at the point with coordinates (1/2, 1/2, 1/2). The O(3) atoms coordinated to the cobalt atoms form a cubic cubeoctahedron (the coordination polyhedron in the *ccp* structure) around the centre of the cavity. The diameter of the cubeoctahedron is 10.05 Å and the edges are of 5.05 Å. The calculated packing coefficient of **2** is unusually low at 0.354. The framework occupies only 27.3% of the unit cell, which means that the total Van der Waals volume of cavities and portals is 1520.1 $Å^3$ per formula unit of **2**. For comparison, the calculated void volumes per formula unit of $Na_{12}[Al_{12}Si_{12}O_{48}]$ (zeolite A) and $H_2[Al_2Si_{94}O_{192}]\cdot 24H_2O$ (zeolite ZSM-5) are 557 $Å^3$ and 2365 $Å^3$, respectively.

Our experiments show that crystals of compound **2** are very unstable. Water loss happens within a few minutes at room temperature resulting in an amorphous product which is identical to **1** according to the chemical analysis and physical measurement data. Crystals of **2** can be kept in native silica gel for a long time.

Investigations probing the electrochemistry and inclusion properties of this and related cyano-bridged cuboidal M_4E_4 (M = Mo, W; E = S, Se, Te) cluster-metal framework solids are in progress.

Experimental Section

Preparation of $[Co(H_2O)_4]_3[W_4Te_4(CN)_{12}]\cdot 8H_2O$ (1): Diffusion of 3 mL of an aqueous solution of $CoCl_2\cdot 6H_2O$ (0.076 g, 0.319 mmol) through silica gel in a narrow-diameter tube into 15 mL of an aqueous solution of $K_6[W_4Te_4(CN)_{12}]\cdot 5H_2O$ (0.100 g, 0.053 mmol) for two weeks resulted in a dark red-brown compound which was isolated by filtration, washed with water, and dried in air. Yield 0.108 g of $[Co(H_2O)_4]_3[W_4Te_4(CN)_{12}]\cdot 8H_2O$ (97%). Satisfactory elemental analyses (C, H, N, W, Te, Co) were obtained. − IR (KBr pellet): $\tilde{\nu}$ = 2127 s, ν(CN), 2100 s, ν(CN), 1600 s, br, δ(HOH), 450 m, ν(WC)/δ(WCN) cm^{-1}. − The magnetic susceptibility was measured at 300 K: $2.78\cdot 10^{-2}$ $cm^{-3}\cdot mol^{-1}$. The density of **1** was measured by microburette method: 3.34 gcm^{-3}.

Preparation of 2: Diffusion of aqueous solutions of $K_6[W_4Te_4(CN)_{12}]\cdot 5H_2O$ (0.05 $mol\cdot L^{-1}$) and $CoCl_2\cdot 6H_2O$ (0.1 $mol\cdot L^{-1}$) through silica gel in a U-tube for eight weeks resulted in cuboidal single crystals of **2** suitable for X-ray single crystal analysis.

X-ray Crystal Structure Determination of 2: The X-ray structural analysis was carried out at 160 K on a Bruker SMART CCD diffractometer (Mo-K_α, λ = 0.71073 Å, graphite monochromator, standard techniques, narrow frames of 0.3°, 40 s/frame). The crystal was covered by a frozen drop of oil to prevent decomposition. *Crystal data*: $C_{12}H_{54.76}Co_3N_{12}O_{27.38}Te_4W_4$, mol. Wt. 2228.0, cubic, space group $Fm\bar{3}m$, a = 25.577(6) $Å^3$, U = 16732(7) $Å^3$, Z = 8, D_c = 1.769 gcm^{-3}. A total of 25728 reflections were collected up to θ_{max} = 28.6°, of which 1103 were unique (R_{int} = 0.0768). Absorption corrections (μ = 7.476 mm^{-1}) were applied by the SADABS program with transmission factors ranging from 0.417 to 0.604. The structure was solved by direct methods and refined by full-matrix least-squares methods on F^2 in an anisotropic approximation using the SHELX-97 set of programs.[11] Hydrogen atoms were not located. It was found that the Co atom position has half occupancy, along with the water molecules attached to it. Some of

the uncoordinated water molecules are also disordered, and their occupancy factors and displacement parameters were refined to reasonable values. Final *R* values: *R1* = 0.0418 for 422, $F_o \geq 4\sigma(F)$, *wR2* = 0.1438, GOF = 0.931 for all unique data. The packing coefficient and the volume of the framework were calculated by the KPACK program[12] using 600 test points per 1 Å^3 and the following atomic radii (Å): C, 1.71, O, 1.40, N, 1.55, Te, 2.15, W, 1.37 (metallic).

Crystallographic data for the structure reported in this paper have been deposited with the Cambridge Crystallographic Data Centre as supplementary publication no. CCDC-144302. Copies of the data can be obtained free of charge on application to the CCDC, 12 Union Road, Cambridge CB2 1EZ, U.K. [Fax: (internat.) +44-1223/336-033; E-mail: deposit@ccdc.cam.ac.uk].

Acknowledgments

This work was supported by RFBR (99−03−32788) and INTAS (96−1256). AVV thanks the Royal Society for financial support. The authors thanks S. V. Belaya for density measurements, and the EPSRC (UK) for equipment funding.

[1] K. R. Dunbar, R. A. Heintz, *Prog. Inorg. Chem*. **1997**, *45*, 283 and references therein.

[2] T. Iwamoto, in *Comprehensive Supramolecular Chemistry, Solid-state Supramolecular Chemistry: Crystal Engineering*, Vol. 6 (Eds.: D. D. MacNicol, F. Toida, R. Bishop), Pergamon, Oxford, **1996**, p. 643 and references therein.

[3] O. M. Yaghi, G. Li, H. Li, *Nature* **1995**, *378*, 703.

[4] T. Niu, X. Wang, A. J. Jacobson, *Angew. Chem. Int. Ed.* **1999**, *38*, 1934; P. Schwarz, E. Siebel, R. D. Fischer, N. A. Davies, D. C. Apperley, R. K. Harris, *Chem. Eur. J.* **1998**, *4*, 919; A. M. A. Ibrahim, E. Siebel, R. D. Fischer, *Inorg. Chem*. **1998**, *37*, 3521; T. Niu, J. Lu, X. Wang, J. D. Korp, A. J. Jacobson, *Inorg. Chem*. **1998**, *37*, 5324; J. Lu, W. T. A. Harrison, A. J. Jacobson, *Angew. Chem. Int. Ed. Engl*. **1995**, *34*, 2557; J. Lu, W. T. A. Harrison, A. J. Jacobson, *Inorg. Chem*. **1996**, *35*, 4271.

[5] N. G. Naumov, A. V. Virovets, M. N. Sokolov, S. B. Artemkina, V. E. Fedorov, *Angew. Chem. Int. Ed.* **1998**, *37*, 1943; L. G. Beauvais, M. P. Shores, J. R. Long, *Chem. Mater*. **1998**, *10*, 3783.

[6] M. P. Shores, L. G. Beauvais, J. R. Long, *J. Am. Chem. Soc*. **1999**, *121*, 775.

[7] M. P. Shores, L. G. Beauvais, J. R. Long, *Inorg. Chem*. **1999**, *38*, 1648.

[8] N. G. Naumov, A. V. Virovets, V. E. Fedorov, *Inorg. Chem. Commun.* **2000**, *3*, 71.

[9] V. P. Fedin, I. V. Kalinina, A. V. Virovets, N. V. Podberezskaya, A. G. Sykes, *Chem. Commun.* **1998**, 237; V. P. Fedin, I. V. Kalinina, D. G. Samsonenko, Y. V. Mironov, M. M. Sokolov, S. V. Tkachev, A. V. Virovets, N. V. Podberezskaya, M. R. J. Elsegood, W. Clegg, A. G. Sykes, *Inorg. Chem*. **1999**, *38*, 1956; A. Müller, R. Jostes, W. Eltzner, C.-S. Nie, E. Diemann, H. Bögge, M. Zimmermann, M. Dartmann, U. Reinsch-Vogell, S. Che, S. J. Cyvin, B. N. Cyvin, *Inorg. Chem*. **1985**, *24*, 2872.

[10] Tetrahedral $[Ge_4S_{10}]^{4-}$ clusters have been used to construct porous three-dimensional frameworks: O. M. Yaghi, Z. Sun, D. A. Richardson, T. L. Groy, *J. Am. Chem. Soc*. **1994**, *116*, 807; C. L. Bowes, W. U. Huynh, S. J. Kirkby, A. Malek, G. A. Ozin, S. Petrov, M. Twardowski, D. Young, R. L. Bedard, R. Broach, *Chem. Mater*. **1996**, *8*, 2147; C. L. Cahill, J. B. Parise, *Chem. Mater*. **1997**, *9*, 807.

[11] G. M. Sheldrick,. SADABS, absorption corrections for area-detector data, Univ. of Göttingen, Germany, 1997; G. M. Sheldrick, SHELXTL for Windows NT, Bruker AXS Inc., Madison, Wi., USA, 1998.

[12] A. V. Virovets, N. V. Podberezskaya, *Kristallografia* **1992**, *37*, 1017 (in Russian).

Received May 15, 2000
[I00201]

Chromophores Encapsulated in Gold Complexes: DPP Dyes with Novel Properties

Heinz Langhals,*[a] Michael Limmert,[b] Ingo-Peter Lorenz,*[b] Peter Mayer,[b] Holger Piotrowski,[b] and Kurt Polborn[a]

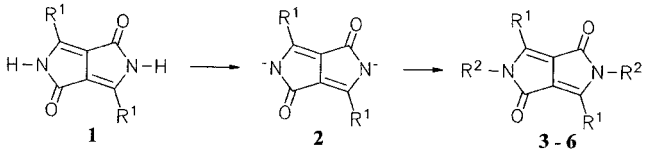
Dedicated to Prof. Dr. R. Huisgen on the occasion of his 80th birthday

Keywords: Gold / Copper / Dyes / Fluorescence spectroscopy / UV/Vis spectroscopy

Colour pigments of the DPP type (R^2 = H) were deprotonated and coordinated to transition metals [$R^2 = M(PPh_3)_2$ (M = Cu, Ag) and $AuPPh_3$]. Dyes were obtained with novel properties such as high solubilities, high fluorescence quantum yields and bathochromic absorptions. The crystal structures indicate a torsion of the planes of the rings of the substituents R^1 with respect to the plane of the chromophore depending on the complex fragment.

Introduction

The diaryl DPP dyes **1**[1] (DPP = **d**iketo**p**yrrolo**p**yrrol) belong to the most recently developed classes of technical pigments. Their good properties as pigments are supported by the formation of intermolecular hydrogen bond structures. However, these hydrogen bonds are also a disadvantage for the use of **1** for fluorescence applications because they diminish fluorescence quantum yields in many cases. For example, the fluorescence quantum yield[2] of **1a** was found to be only 50%. The formation of hydrogen bonds can be inhibited by an alkylation[3] or an arylation[4] at the nitrogen atoms. The coordination of the nitrogen atoms to metal ions would be a further possibility for the blocking these positions. The elements of the first subgroup would be suitable for this purpose and the formation of polymeric networks should be prevented by the coordination of at least one further coordination site by bulky substituents such as in compounds **4**–**6** (Scheme 1). The entire chromophore would be thus shielded against external influences.



R^1	C_6H_5	4-Cl-C_6H_4	3,5-di-*t*-bu.-C_6H_3
1 - 6	a	b	c

R^2	CH_3	$((C_6H_5)_3P)_2Cu$	$(C_6H_5)_3PAg$	$(C_6H_5)_3PAu$
	3	4	5	6

Scheme 1. Derivatives of DPP dyes

Results and Discussion

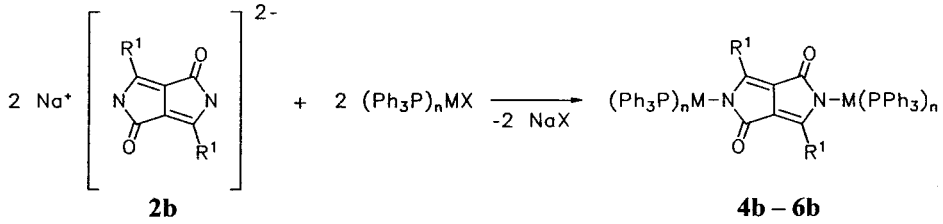
One mol DPP **(1a)** was allowed to react according to this concept with two mol hexamethyldisilazane sodium salt to give the dianion of DPP **(2a)**, and then with a mixture of two mol copper(I) chloride and two mol triphenylphosphane to obtain a violet, rather persistent, but absolutely insoluble material. A polymeric structure is probably responsible for the low solubility. An increase of the amount of triphenylphosphane to six mol or more results in partially soluble components in the reaction product. The filling of two coordination sites initially gave appreciably better results: bis(triphenylphosphane)copper(I) nitrate reacts with **2a** to give the complex **4a**. A substitution at the *p*-position of the phenyl groups in **1** with chloride **(1b)** results, after initial formation of **2b**, in the appreciably more-stable complex **4b**. Suitable single crystals of **4b** could be obtained for an X-ray single crystal structure analysis. Compound **1b** however, was preferred for the following synthesis because a higher stability was generally found for metal complexes with the chlorine derivative, see Scheme 2.

With silver(I) tetrafluoroborate and triphenylphosphane, compound **2a** forms the homogeneously soluble and brilliant violet complex **5b** with two triphenylphosphane ligands at each silver ion. However, no suitable single crystals could be obtained for a crystal structure analysis.

Even better results were obtained from the reaction of **2b** with triphenylphosphanegold(I) chloride: compound **6b** was obtained as a bright-red crystalline powder and well-

[a] Department Chemie, Universität München,
Butenandtstr. 5–13 (Haus F), 81377 München, Germany
Fax: (internat.) +49-89/2180-7640
E-mail Langhals@lrz.uni-muenchen.de
[b] Department Chemie, Universität München,
Butenandtstr. 5–13 (Haus D), 81377 München, Germany
Fax: (internat.) +49-89/2180-7867
E-Mail: ipl@cup.uni-muenchen.de

 © WILEY-VCH Verlag GmbH, D-69451 Weinheim, 2000 1434–1948/00/1111–2345 $ 17.50+.50/0



	4b	5b	6b
M	Cu^+	Ag^+	Au^+
l	2	2	1
X	NO_3^-	BF_4^-	Cl^-

Scheme 2

formed single crystals suitable for an X-ray crystal structure analysis were isolated. The X-ray structure shows a bond of one triphenylphosphane group with one gold(I) ion and a linear N1−Au1−P1 arrangement. Complex **6b** is completely stable under argon at room temperature and can even be stored in air for several days.

The single crystal structure analysis of **4b** (Figure 1) and **6b** (Figure 2) indicates the different composition and structures of the inversion symmetrical copper(I) and gold(I) compounds. The copper atoms in **4b** are trigonal planar, and are surrounded by the phosphorus atoms of the phosphane ligands and the N atom of the DPP dianion **2b**. The P_2CuN skeletons are planar and the Cu atoms pressed out-of-plane by 18°. The two P_2Cu planes and the planes of the rings R^1 are twisted by 70° and 25°, respectively, with respect to the central planes of the molecules. This indicates the enormous steric demand of the 12 covering phenyl groups.

The gold atoms in **6b** are linearly coordinated[5] to one N and one P atom so that a linear arrangement of all N, Au and P atoms results. The two phosphane ligands are staggered with their phenyl groups so that there is enough room

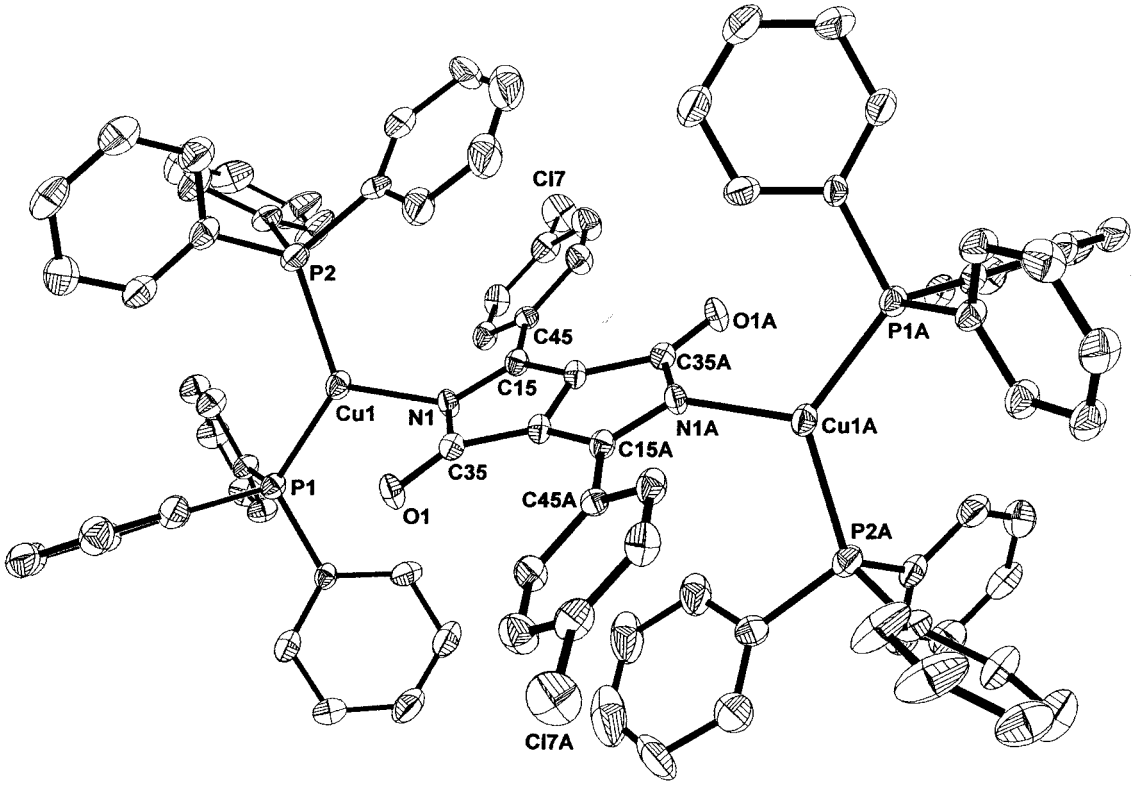


Figure 1. Crystal structure of **4b**; selected bond lengths [Å] and angles [°]: Cu1−N1 1.984(5), Cu1−P1 2.229(2), Cu1−P2 2.253(2), C15−C45 1.478(9), N1−Cu1−P1 118.7(2), N1−Cu1−P2 113.7(2), P1−Cu1−P2 127.48(7); sum of angles at N = 355.52°, sum of angles at Cu = 360°

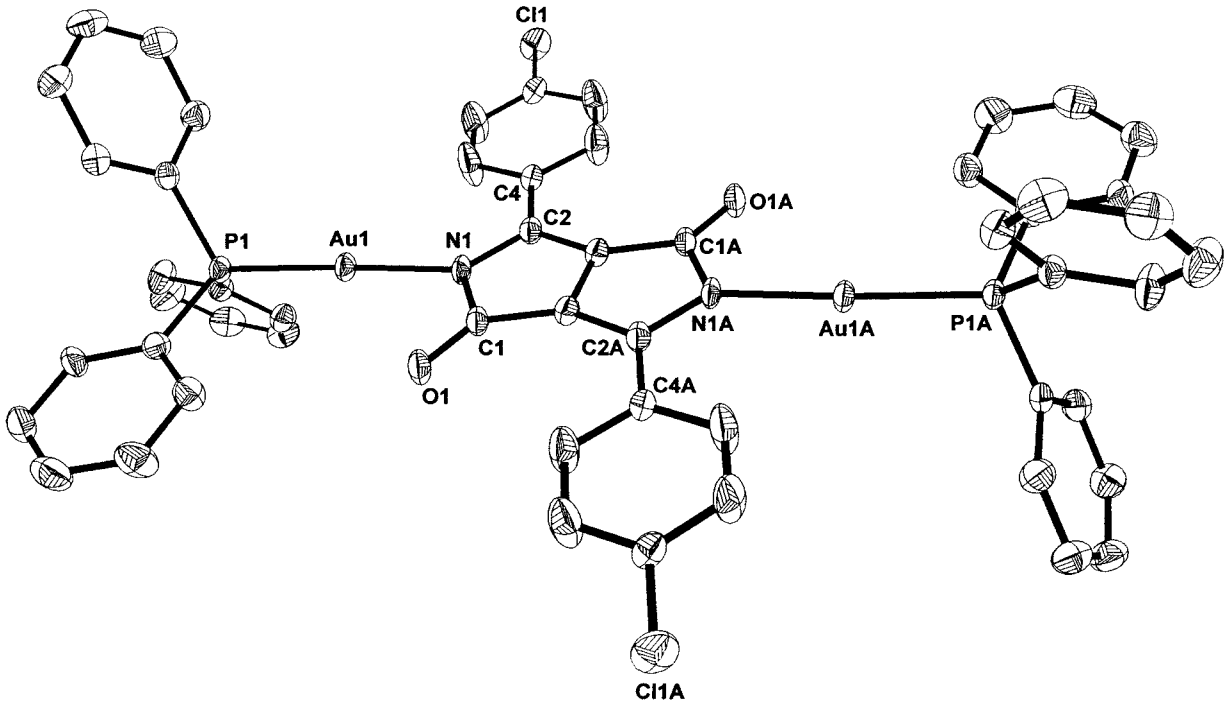


Figure 2. Crystal structure of **6b**; selected bond lengths [Å] and angles [°]: Au1−N1 2.047(5), Au1−P1 2.230(2), C2−C4 1.467(10), N1−Au1−P1 175.3(2); sum of angles at N1 = 360°

for the planarization of R^1 into the plane of the chromophore; this geometry is also preferred for electronic reasons.

Dye **1c** was used as a reference for the UV/Vis spectra of **4b−6b**, because of its sufficiently high solubility caused by the four solubilising *tert*-butyl groups in the *m*-positions of the phenyl groups.[6,7] Compound **1c** exhibits a structured UV/Vis absorption spectrum in chloroform solution (λ_{max} = 507 nm) and a mirror-type fluorescence spectrum (λ_{max} = 513 nm), see Figure 3.

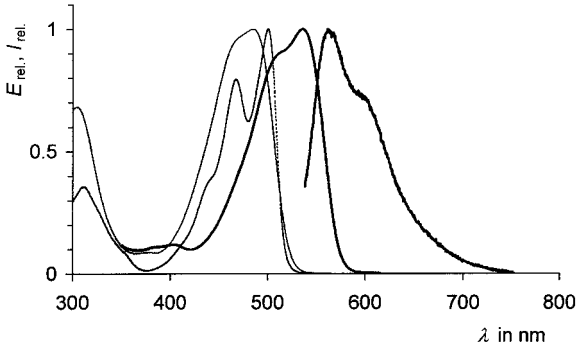


Figure 3. UV/Vis absorption and fluorescence spectrum of **6b** (—) and the absorption spectra of **1c** (···) and **3c** (—) in chloroform

A methylation of the nitrogen atoms **(3c)** will block the formation of hydrogen bonds and thus increase the fluorescence quantum yields by several percent and induce a hypsochromic shift of the UV/Vis absorption with a substantial loss of spectral structure (see Figure 3). A blocking of the nitrogen atoms by complexation with $AuP(C_6H_5)_3$ also increases the fluorescence quantum yield; however, in contrast to the former, a bathochromic shift is obtained (absorption: λ_{max} = 535.4 nm; fluorescence: λ_{max} = 561 nm; **6a** absorbs at 530 nm, see Figure 3). The changes in the UV/Vis spectra can be explained in terms of changes in the torsion angles of the aryl substituents. A torsion angle of 15° was calculated (AM1) for the phenyl groups in **1a**. This angle is probably representative of the dissolved dye. An *N*-methylation increases the torsion angle to 30° in **3c** and induces a hypsochromic shift because of the decoupling of the two π-systems. In contrast to this, the phenyl groups in the more bathochromically absorbing gold complex **6b** are completely turned into the plane of the chromophore. This corresponds to the bathochromic absorption of the planar blue dianion **2a**; a planar structure was also calculated for **2a** (AM1).

The fluorescence quantum yield of **1a** was found to be 50%. A complexation with copper **(4b)** decreases the quantum yield to 20%; this corresponds to the well-known fluorescence quenching effect of copper ions. The fluorescence quantum yield is further diminished in the silver complex **5b** to 17%. Surprisingly, the fluorescence quantum yield is strongly increased by coordination with gold ions so that 99% was obtained for **6b**. Solutions of **6b** in chloroform are bright yellow in daylight and purple in transmitted light. All complexes **4b**, **5b** and **6b** exhibit a red, solid-state fluorescence.

The high fluorescence quantum yield of **6b** indicates the efficient supporting effect of the bulky gold substituents for fluorescence. Interestingly, in contrast to alkyl groups the gold substituents allow the complete planarization of the chromophore, including the phenyl substituents (R^1 = **b**). This is a further indicator for the efficient shielding of the chromophore against aggregation because such a large planar π-system would otherwise exhibit a very high tend-

ency for aggregation. Furthermore, the fluorescence quantum yield of **6b** of nearly 100% excludes a notable intersystem crossing rate to triplet states. This is remarkable because one might expect a pronounced heavy-atom effect on the I.S.C.-rate by gold because of its high atomic weight. This will be the subject of further investigations.

Experimental Section

2b: Addition of $NaN(SiMe_3)_2$ (0.30 mL, 1.00 M solution in THF) to a well-stirred suspension of **1b** (50 mg, 0.14 mmol) in 10 mL of DMF (cf. ref [8]) yielded a blue solution of **2b**, which was used in all further reactions.

4b: Compound **2b** was added dropwise to $(PPh_3)_2CuNO_3$ (195 mg, 0.30 mmol) in 5 mL of DMF at ambient temperature and left stirring for two hours. The solvent was removed under vacuum at 60 °C, the residue dissolved in 10−15 mL $CHCl_3$ and filtered (P3). The solution was carefully diluted with *n*-hexane and stored at −20 °C for some days, after which time **4b** had precipitated as violet crystals. To improve the yield the solution can be layered with some more *n*-hexane. Yield: 111 mg (42%) of **4b** as violet crystals, m.p. 165 °C. − IR (KBr): $\tilde{\nu}$ = 3075 cm^{-1}, 3035, 1607, 1598, 1579, 1556, 1521, 1481, 1435, 1408, 1342, 1300, 1277, 1262, 1214, 1182, 1157, 1121, 1093, 1070, 1027, 1011, 998, 837, 828, 820, 773, 741, 694, 642, 628, 618, 527, 516, 507, 490, 442, 431. − ^1H NMR (270 MHz, $CDCl_3$): δ = 7.15−7.37 (m, 68 H, Ph, 4-Cl−C_6H_4). − $^{31}P\{^1H\}$ NMR (109.37 MHz, $CDCl_3$): δ = −2.4 (s, PPh_3). − UV ($CDCl_3$): λ_{max} (ε) = 547.7 nm (1), 572 sh (0.91). − Solid-state fluorescence: λ_{max} (I_{rel}) = 642. − FAB-MS: *m/z* = 1007 [M^+ − 2PPh_3], 587 [$Cu(PPh_3)_2$], 325 [$CuPPh_3$], 262 [PPh_3]. − $C_{90}H_{68}Cu_2Cl_2N_2O_2P_4$·4$CHCl_3$ (1890): calcd. C 54.93, H 3.52, N 1.33; found C 55.49, H 3.66, N 1.46.

5b: Compound **2b** was added to a stirred solution of $AgBF_4$ (58 mg, 0.30 mmol) and PPh_3 (236 mg, 0.90 mmol) in 5 mL of DMF. After 1 hour **5b** was formed as a violet solid. The solvent was removed and the residue washed with acetone (25 mL, three times) and diethyl ether (25 mL) and dried in vacuum. Soxhlet extraction of the crude product with 200 mL CH_2Cl_2 in the dark and covering the solution with a layer of *n*-hexane gave **5b** as a violet powder. Yield: 134 mg (59%), m.p. 223 °C. − IR (KBr) $\tilde{\nu}$ = 3082 cm^{-1}, 3053, 1597, 1577, 1553, 1522, 1480, 1435, 1408, 1337, 1300, 1278, 1213, 1180, 1158, 1122, 1092, 1027, 1011, 998, 839, 818, 772, 743, 715, 694, 644, 630, 618, 513, 504, 490, 437. − ^1H NMR (270 MHz, $CDCl_3$): δ = 7.15−7.45 (m, 68 H, Ph, 4-ClC_6H_4). − $^{31}P\{^1H\}$ NMR (109.37 MHz, $CDCl_3$): δ = 8.56 (s, PPh_3) . − UV ($CDCl_3$): λ_{max} (ε) = 525.8 nm (0.81), 560.1 (1.00). − Solid-state fluorescence: λ_{max} (I_{rel}) = 662. − FAB-MS: *m/z* = 1096 [M^+ − 2 PPh_3], 631 [$Ag(PPh_3)_2$], 369 [$AgPPh_3$]. − $C_{90}H_{68}Ag_2Cl_2N_2O_2P_4$ (1620): calcd. C 66.73, H 4.20, N 1.73; found C 65.09, H 4.27, N 1.93.

6b: Addition of **2b** to a stirred solution of Ph_3PAuCl (148 mg, 0.30 mmol) in 5 mL of DMF gave **6b** as a red solid. The product was purified analogously to **5b**; it was dissolved in 50 mL of warm $CHCl_3$, filtered (P3) and layered with *n*-hexane to give red crystals of **6b**. Yield: 135 mg (64%) of **6b** as a red powder, m.p. > 300 °C. − IR (KBr) $\tilde{\nu}$ = 3082 cm^{-1}, 3053, 1699, 1673, 1615, 1574, 1484, 1436, 1405, 1330, 1302, 1277, 1200, 1183, 1119 1102, 1092, 1027, 1011, 996, 836, 743, 711, 694, 545, 509, 484, 451, 440. − ^1H NMR (270 MHz, $CDCl_3$): δ = 8.71 [d, ^3J (H,H) = 8.62 Hz, 4H, 4-Cl−C_6H_4], 7.45−7.60 (m, 30 H, Ph_3P), 7.26 [d, ^3J (H,H) = 8.88 Hz, 4H, 4-Cl−C_6H_4]. − $^{31}P\{^1H\}$ NMR (109.37 MHz, $CDCl_3$): δ = 33.01 (s, PPh_3). − $^{13}C\{^1H\}$ NMR (67.5 MHz, $CDCl_3$): δ = 170, 134.99, 134.39, 134.19, 131.91, 131.86, 131.45, 129.78, 129.62, 129.39, 129.25, 128.71, 128.27. − FAB-MS: *m/z* = 1274 [M^+], 814 [M^+ − $AuPPh_3$], 721 [$Au(PPh_3)_2$], 459 [$AuPPh_3$]. − UV ($CDCl_3$): λ_{max} (ε) = 512.5 nm sh (23400), 535.4 (26000). − Fluorescence ($CHCl_3$): λ_{max} (I_{rel}) = 561 nm (1.0), 597 (0.72); solid-state fluorescence: λ_{max} (I_{rel}) = 633 nm (1.0), 690 sh (0.4). − $C_{54}H_{38}Au_2Cl_2N_2O_2P_2$·2$CHCl_3$ (1512): calcd. C 44.72, H 2.66, N 1.86; found C 43.91, H 2.67, N 1.93.

X-ray Crystal Structure Analysis: 4b: $C_{96}H_{74}Cl_{14}Cu_2N_2O_6P_4$, M_r = 2098.94, single crystal 0.30 × 0.10 × 0.10 mm^3, space group *P*1(bar), *a* = 12.683 (2), *b* = 13.247 (3), *c* = 16.676 (3) Å, *α* = 112.67 (2), *β* = 106.301 (19), *γ* = 86.86 (2), *V* = 2477.0 (8) $Å^3$, *Z* = 1, $\rho_{ber.}$ = 1.407 g·cm^{-3}. − Technical data: 2*Θ*-range 3−48°, radiation: Mo-K_α (*λ* = 0.71073 Å), area-detection at 200 K. − Data collection: a total of 13688 reflections, 7050 unique and 2752 observed [$I \geq 2\sigma(I)$]. Absorption correction: numerical, *μ* = 0.924 mm^{-1}, min./max. transmission 0.7943/0.9353. − Structure solution and refinement: SHELXS-97 (Sheldrick, 1997) and SHELXL-97 (Sheldrick, 1997), the structure was solved by direct methods and refined by full-matrix least-squares on F^2, H-atoms and inserted formic acid molecules were refined isotropically, all others were refined anisotropically. 542 Parameters, *R* = 0.0524, *wR*2 = 0.0921 for [$I \geq 2\sigma(I)$], largest peak and hole *ρ* = −0.313/0.663 e·$Å^{-3}$.
6b: $C_{56}H_{40}Au_2Cl_8N_2O_2P_2$, M_r = 1512.37, single crystal 0.47 × 0.40 × 0.1 mm^3, space group *P*1(bar), *a* = 10.285(2), *b* = 11.8523 (13), *c* = 12.835 (2) Å, *α* = 90.569 (10), *β* = 106.128 (14), *γ* = 113.774 (13)°, *V* = 1362.2 (4) $Å^3$, *Z* = 1, $\rho_{calcd.}$ = 1.844 g·cm^{-3}. − Technical data: 2*Θ*-range: 5−48°, radiation: Mo-K_α (*λ* = 0.71073 Å), *ω*-2*θ*-scan at 293 (2) K. − Data collection: a total of 4529 reflections, 4259 unique and 3764 observed [$I \geq 2\sigma(I)$]. Absorption correction: semiempirical *μ* = 5.874 mm^{-1}, min./max. transmission 0.4598/0.9980. − Structure solution and refinement: SHELXS-86 (Sheldrick, 1990) and SHELXL-93 (Sheldrick, 1993), the structure was solved by direct methods and refined by full-matrix least-squares on F^2, H-atoms were refined isotropically, all others were refined anisotropically. 325 Parameters, *R* = 0.0359, R_w = 0.0887 for [$I \geq 2\sigma(I)$], largest peak and hole *ρ* = −1.015/2.035 e·$Å^{-3}$.
Crystallographic data (excluding structure factors) for the structure(s) included in this paper have been deposited with the Cambridge Crystallographic Data Centre as supplementary publication nos. CCDC-137742 (**6b**) and -137784 (**4b**). Copies of the data can be obtained free of charge on application to CCDC, 12 Union Road, Cambridge CB2 1EZ, UK [Fax: (internat.) + 44-1223/336-033; Email: deposit@ccdc.cam.ac.uk].

Acknowledgments

We thank the Deutsche Forschungsgemeinschaft and the Fonds der Chemischen Industrie for financial support. The doctoral scholarship for M. L. of the Freistaat Bayern is appreciated.

[1] Review: A. Iqbal, M. Jost, R. Kirchmayr, J. Pfenninger, A. Rochat, O. Wallquist, *Bull. Soc. Chim Belg.* **1988**, *97*, 615−634.
[2] Determined according to: H. Langhals, J. Karolin, L. B.-Å. Johansson, *J. Chem. Soc., Faraday Trans.* **1998**, *94*, 2919−2922.
[3] T. Potrawa, H. Langhals, *Chem. Ber.* **1987**, *120*, 1075−1078.
[4] H. Langhals, T. Grundei, T. Potrawa, K. Polborn, *Liebigs Ann.* **1996**, 679−682.
[5] See similar metal complexes with biologically active ligands: D. Koch, K. Sünkel, W. Beck, *Z. Naturforsch. B* **1999**, *546*, 92−102, and references therein.

[6] H. Langhals, *Ger. patent* 3016764 (April 30, **1980**); *Chem. Abstr.* **1982**, *96*, P70417x.
[7] H. Langhals, *Nachr. Chem. Tech. Lab.* **1980**, *28*, 716−718; *Chem. Abstr.* **1981**, *95*, R9816q.
[8] M. Poppe, Dissertation München, **1998**; M. Limmert, planned dissertation München, **2000**.

Received May 18, 2000
[I00206]

Synthesis and Crystal Structure of a Palladium Metallacyclic Complex: A Key Intermediate in the Carbonylation of Azobenzene to *N*-Phenyl Urethane

Andrea Sessanta o Santi,[a] Barbara Milani,*[a] Ennio Zangrando,[a] and Giovanni Mestroni[a]

Keywords: Carbonylations / Crystal structure / Metallacycles / N ligands / Palladium

The reductive carbonylation of azoxybenzene to *N*-phenyl urethane via azobenzene is promoted by the catalytic system based on palladium, bidentate nitrogen-donor chelating ligands N-N [N-N = 1,10-phenanthroline (phen) and its substituted derivatives] and the acid cocatalyst [(N-N)H][PF_6], the same catalyst as for the reductive carbonylation of nitroaromatic compounds to the corresponding carbamates. The possible key intermediate of the azobenzene → *N*-phenyl urethane transformation has been synthesised and fully characterised.

Introduction

Since 1962 the reductive carbonylation of nitroaromatic compounds has been an interesting field of research, both from the academic and industrial point of view, due to the demand for a new, phosgene-free method for the synthesis of carbamates.[1]

The industrial development of a powerful catalytic system is dependent both on its catalytic activity and on the selectivity towards the carbamate. In this system the main by-products are: aniline, *N*,*N*′-diphenylurea, azobenzene and azoxybenzene. Therefore, the comprehension of the factors which control both the formation and the transformation of these side-products are of great interest.

This reaction is homogeneously catalysed by systems based on different metals, such as ruthenium, rhodium and palladium.[1] The palladium-based system with nitrogen-donor chelating ligands, in the presence of a weak Brønsted acid as cocatalyst, is the most promising up to now.[2,3]

Mechanistic studies have been carried out based mainly on either the isolation or the spectroscopic detection of several metallacyclic derivatives, which should be directly involved in the catalytic cycle.[4−6] In particular, the structural characterization of two metallacyclic intermediates of general formula [(N-N)Pd*C*(O)N(Ar)O*C*(O)] **(1)** (**1a:** N-N = phen, Ar = Ph; **1b:** N-N = 4,4′-di(*tert*-butyl)-2,2′-bipyridyl, Ar = *p*-*tert*-butylphenyl; the italic letters indicate the atoms of the metallacyclic fragment bound to the palladium centre), which differ in the N-N ligand and the aryl group, has been reported by Osborn[4c] and by us.[5]

In this paper we report the isolation and the complete characterization, both in the solid state and in solution, of the symmetric metallacycle [(N-N)Pd*C*(O)N(Ph)N(Ph)*C*(O)] **(2)** [**2a:** N-N = phen; **2b:** N-N = 3,4,7,8-tetramethyl-1,10-phenanthroline (tm-phen)]. This complex is proposed as a "key-intermediate" for the carbonylation of azobenzene to *N*-phenyl urethane. Some preliminary catalytic results are also presented.

Results and Discussion

During the investigation of the catalytic cycle involved in the reductive carbonylation of nitroaromatic compounds to urethanes, we isolated, in high yield, the metallacyclic derivative [(phen)Pd*C*(O)N(Ph)O*C*(O)] **(1a)**, starting from [Pd(phen)($CH_3COO)_2$] in a nitrobenzene/alcohol mixture, under mild reaction conditions.[5] When the same precursor was treated with azobenzene, instead of nitrobenzene, at room temperature, in the presence of free phen and under a CO pressure of 40 atm., a pale yellow solid, formulated as [(phen)Pd*C*(O)N(Ph)N(Ph)*C*(O)], was obtained. After 24 h the yield was about 20% and this increased to 50% on prolonging the reaction time to 60 h. The addition of an excess of chelating ligand was necessary to prevent the formation of palladium metal, which occurs on increasing the reaction temperature. Moreover, no solid was isolated when the reaction was carried out under atmospheric CO pressure. The yield of the reaction is also affected by the nature of the nitrogen ligand. Actually, it further decreases when the tm-phen is used instead of phen (from 20% to 5%). All these data indicate that the formation of the metallacycle **2a** occurs with more difficulty than that of the corresponding derivative **1a**.

Yellow crystals of **2a** suitable for an X-ray analysis were obtained by slow diffusion of diethyl ether into a chloroform solution of the compound. Its molecular structure is shown in Figure 1.

The Pd centre exhibits the expected square-planar coordination geometry with Pd−N and Pd−C distances of 2.148(6) and 2.173(5) Å, and 1.947(7) and 1.963(7) Å, respectively, which are comparable to those observed in the closely related Pd metallacyclic complexes [(N-N)Pd*C*(O)N(Ar)O*C*(O)].[4c,5] The phenyl rings are structurally disor-

[a] Dipartimento di Scienze Chimiche, Università degli Studi di Trieste
Via Licio Giorgieri 1, 34127 Trieste, Italy
Fax: (internat.) + 39-040/676-3903
E-mail: milani@dsch.univ.trieste.it

 © WILEY-VCH Verlag GmbH, D-69451 Weinheim, 2000 1434−1948/00/1111−2351 $ 17.50+.50/0

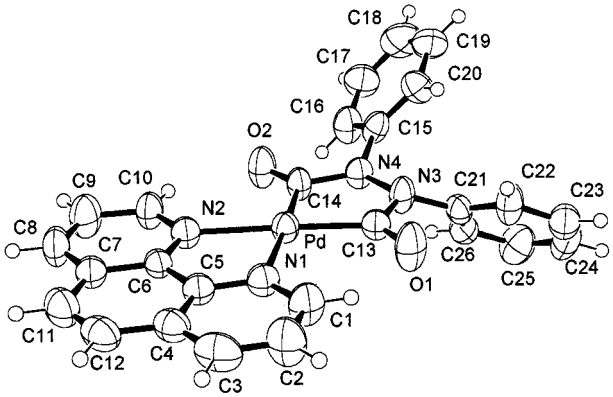


Figure 1. An ORTEP drawing (50% probability thermal ellipsoids) of the metallacycle **2a** with atom numbering scheme; selected bond lengths (Å) and angles (°): Pd−C(14) 1.947(7), Pd−C(13) 1.963(7), Pd−N(2) 2.148(6), Pd−N(1) 2.173(5), N(3)−N(4) 1.419(7); C(14)−Pd−C(13) 81.8(3), C(14)−Pd−N(2) 100.9(3), C(13)−Pd−N(2) 177.3(3), C(14)−Pd−N(1) 177.0(3), C(13)−Pd−N(1) 101.1(3), N(2)−Pd−N(1) 76.2(2), C(1)−N(1)−Pd 126.5(5), C(5)−N(1)−Pd 113.5(5), C(10)−N(2)−Pd 127.5(5), C(6)−N(2)−Pd 114.4(5)

dered over two positions since the phenanthroline and the atoms of the metallacycle Pd*C*(O)NN*C*(O) lie on a crystallographic mirror plane (see Experimental Section). In Figure 1 the rings are represented in a *trans* arrangement, which is the most likely configuration, with their mean planes forming dihedral angles of 48.7 and 45.4° with the crystallographic plane.

The N−N azo bond length of 1.419(7) Å is indicative of considerable single bond character when compared with the value of 1.26−1.27 Å measured in a series of (*E*)-azobenzenes.[7] On the other hand, the nitrogen atoms display a bonding geometry close to planarity, as shown by the summation of the bond angles about them (ca. 355°), and by the value of the torsion angle C(Ph)−N−N−C(Ph) [50.0(6)°], an aspect that may suggest a π delocalization in the azodioxo ring, although packing forces are not to be excluded in driving the observed configuration. In fact, in the crystal structure the [(phen)Pd*C*(O)NN*C*(O)] moieties stack at 3.38 Å (i.e. half of the *b* axis) in a head-to-tail arrangement.

For complexes **2** the IR spectra in the solid state show the typical band of ketonic CO stretching at 1627 cm^{-1}.

Their ^1H NMR spectra in $CDCl_3$ solution present one set of signals for the N-N ligand and one for the *C*(O)N(Ph)N(Ph)*C*(O) moiety. The number of signals of the N-N ligand and their integration confirm the equivalence of the two halves of the ligand in solution, as already observed in the solid state. All the signals of the nitrogen ligand are shifted with respect to those of the free ligand; in particular, the signals attributed to $H^{2,9}$ are deshielded by about 1.00 ppm.

The addition of one equivalent of tm-phen to a solution of [(phen)Pd*C*(O)N(Ph)N(Ph)*C*(O)], **(2a)**, resulted in an exchange of the two ligands at the palladium centre, in agreement with the higher coordinating capability of tm-phen with respect to phen. Indeed, immediately after the dissolution, the spectrum shows the signals of both coordinated and free ligands, indicating that the exchange process is slow on the NMR time scale. Although the frequencies of $H^{2,9}$ of the coordinated phen and tm-phen are quite broad, from their integration it is possible to follow the proceeding of the reaction with time. After five min, 64% of **2a** is transformed into **2b** and the equilibrium is reached after 30 min. The equilibrium mixture is formed from 83% of **2b** with the remainder being unchanged **2a**. Working in the presence of an excess of tm-phen (two equivalents with respect to Pd), the exchange process is accelerated and after five min the phen-metallacycle is completely transformed into the tm-phen derivative. In agreement with this behaviour the metallacycle [(tm-phen)Pd*C*(O)N(Ph)N(Ph)*C*(O)] **(2b)** is easily obtained by a ligand exchange reaction starting from [(phen)Pd*C*(O)N(Ph)N(Ph)*C*(O)], in chloroform, at room temperature.

We have previously reported that the catalytic system formed by $[Pd(phen)_2][PF_6]_2$ in combination with free phen and the acid cocatalyst $[(phen)H][PF_6]$ is very active in the reductive carbonylation of nitroaromatic compounds to the corresponding carbamates.[2b,8] We have now found that the same catalytic system promotes the carbonylation of both azoxy- and azobenzene to urethane (Table 1). The preliminary results reported in Table 1 show that 94% of azobenzene is converted into carbamate in two hours, with aniline as the main by-product. On the other hand, when azoxybenzene is the substrate, azobenzene is the main product. These data indicates that azoxybenzene is transformed in azobenzene, which further reacts to give the carbamate.

Table 1. Carbonylation of azoxy- and azobenzene to carbamate; catalytic system: $[Pd(phen)_2][PF_6]_2$ + phen + $[(phen)H][PF_6]$[a]

Substrate	Conv. (%)	Selectivity (%)			
		Carbamate	Aniline	Azobenzene	Other
Azobenzene	94	80	14		6
Azoxybenzene	75	29	3	41	2

[a] Reaction conditions: n_{Pd} = 0.02 mmol; $n_{free\ phen}$ = 0.08 mmol; $n_{[(phen)H][PF6]}$ = 0.12 mmol; substrate: 2.5 mmol; methanol: V = 8.0 mL; 2,2′-dimethoxypropane: V = 0.4 mL; T = 155 °C; P_{CO} = 40 atm; t = 2 h.

On the basis of the catalytic results and on the isolated metallacycles (**2**) we propose a catalytic cycle (Figure 2) which may be operative contemporary to that of the main reaction.[4] The carbonylated species **A**, which is also supposed to be the active species for the conversion of nitrobenzene to carbamate, reacts with azoxybenzene yielding the metallacycle **B**. From the latter, azobenzene is obtained and the active species **A** is restored. Azoxy- and azobenzene may compete for the intermediate **A**. When azobenzene interacts with **A** the metallacycle **C** is formed. This intermediate can follow two different pathways: in one case it reacts with methanol and protons yielding one equivalent of carbamate and aniline, which was found to be the main by-product. In the other, the insertion of carbon monoxide into the Pd−N bond is possible yielding the metallacycle **D**, which corresponds to **2**. The attack of methanol on this

species generates two equivalents of carbamate and regenerates the active species **A**.[9]

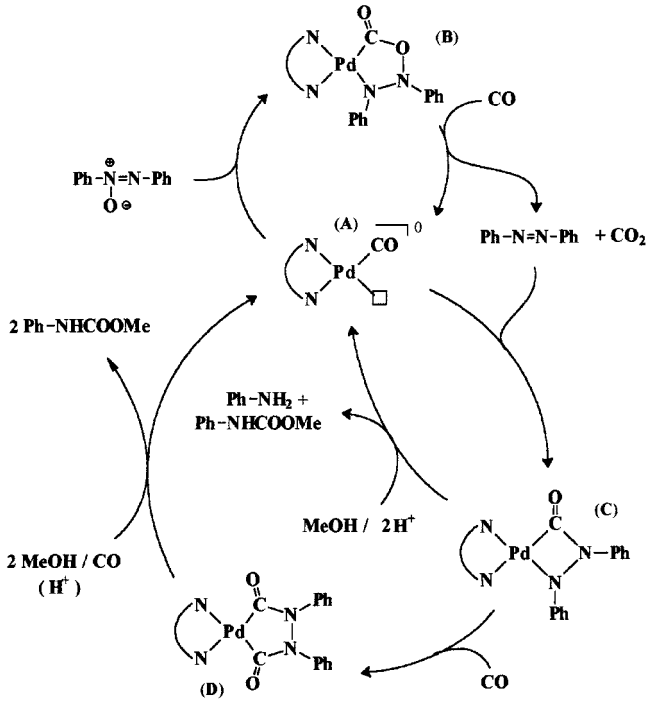


Figure 2. Proposed catalytic cycle

Conclusion

The isolation of the new metallacylic derivatives [(N-N)Pd*C*(O)N(Ph)N(Ph)*C*(O)] has allowed us to propose another catalytic cycle which should be operative contemporary to that of direct conversion of nitrobenzene to carbamate. In agreement with this hypothesis azoxy- and azobenzene are better regarded as intermediates of the reaction rather than by-products.

Moreover, a comparison of the two metallacycles [(phen)Pd*C*(O)N(Ph)O*C*(O)] **(1a)** and [(phen)Pd*C*(O)N-(Ph)N(Ph)*C*(O)] **(2a)** shows that, in the former, the N−O bond of the *C*(O)N(Ph)O*C*(O) moiety is polar, and therefore more likely to be broken than the N−N bond of the *C*(O)N(Ph)N(Ph)*C*(O) fragment of the second one. Therefore, the high amount of azobenzene obtained in the reductive carbonylation of nitrobenzene to urethane might be related to the more difficult formation and reaction of the metallacycles **2** than of **1**. The use of unsymmetrically substituted phenanthrolines, such as 3,4-dimethyl-1,10-phenanthroline, might favour the transformation of the corresponding metallacycle **2** into carbamate, increasing the selectivity of the overall reaction.

Experimental Section

The nitrogen-donor ligands were used as supplied (Aldrich). Azoxybenzene was synthesised from nitrosobenzene (Aldrich) in 0.2 M NaOH ethanolic solution. Azobenzene (Fluka) and methanol (Baker) were used without further purification. Carbon monoxide (CP grade, 99.9%) was supplied by SIAD.

IR spectra were recorded on a Perkin−Elmer 983G spectrometer as KBr pellets.

^{1}H NMR spectra were recorded at 400 MHz on a Jeol EX 400 spectrometer operating in Fourier-transform mode, with tetramethylsilane (TMS) as internal standard.

The GC analyses were conducted on a gas-chromatograph DANI 6800 on a column 10% SE 30 (2 m), equipped with a Carlo Erba DP700 data processor.

Synthesis: The complexes [Pd(N-N)($CH_3COO)_2$], [Pd(N-N)$_2$][PF_6]$_2$ and compounds [(N-N)H][PF_6] were synthesised according to the procedures reported in literature.[10,11]

Synthesis of [(N-N)Pd*C*(O)N(Ph)N(Ph)*C*(O)] [N-N = phen (2a), tmphen (2b)]: The reaction was carried out in a Berghof stainless steel autoclave (100 mL), equipped with a Teflon liner and magnetic stirrer. [Pd(phen)($CH_3COO)_2$] (0.30 g, 0.7 mmol), phen (0.27 g, 1.5 mmol), azobenzene (0.77 g, 4.2 mmol) and methanol (10 mL) were placed in the reactor, which was then pressurised at 40 atm. with CO. The system was stirred at room temperature for 24 h. After releasing the residual gas, the pale-yellow solid was filtered at reduced pressure, washed with methanol and dried under vacuum.

The same procedure was followed for the complex with the tmphen ligand.

2a: Yield: 75 mg, 20%. − $C_{26}H_{18}N_4O_2Pd$ (524.85): calcd. C 59.5, H 3.46, N 10.7; found C 58.5, H 3.26, N 10.2. − IR (KBr): ν(CO) = 1627 cm^{-1}. − ^{1}H NMR ($CDCl_3$): δ = 7.05 (t, 2 H, *p*-Ph), 7.28 (overlapped with $CDCl_3$, *m*-Ph), 7.46 (d, 4 H, *o*-Ph), 7.91 (dd, 2 H, H^{3,8}), 7.95 (s, 2 H, H^{5,6}), 8.47 (d, 2 H, H^{4,7}), 10.25 (d, 2 H, H^{2,9}).

Synthesis of [(tm-phen)Pd*C*(O)N(Ph)N(Ph)*C*(O)] (2b): A chloroform (2.5 mL) solution of [(phen)Pd*C*(O)N(Ph)N(Ph)*C*(O)] (0.05 g, 0.1 mmol) was treated with tm-phen (0.03 g, 0.12 mmol). After stirring for 3 h at room temperature, a few drops of diethyl ether were added. The solid was filtered off, washed with cold chloroform and diethyl ether and dried under vacuum.
Yield: 53 mg, 90%. − $C_{30}H_{26}N_4O_2Pd$ (580.96): calcd. C 62.0, H 4.51, N 9.64; found C 61.5, H 4.26, N 9.52. − IR (KBr): ν(CO) = 1627 cm^{-1}. − ^{1}H NMR ($CDCl_3$): δ = 2.59 (s, 6 H, CH_3 of tm-phen), 2.70 (s, 6 H, CH_3 of tm-phen), 7.05 (t, 2 H, *p*-Ph), 7.28 (overlapped with $CDCl_3$, *m*-Ph), 7.45 (d, 4 H, *o*-Ph), 8.01 (s, 2 H, H^{5,6}), 9.74 (s, 2 H, H^{2,9}).

X-ray Structure Determination: A yellow single crystal of **2a**, prism shaped (0.40 × 0.20 × 0.18 mm) was mounted on an Enraf−Nonius CAD4 diffractometer, equipped with graphite monochromator and Mo-K_α radiation. Unit cell dimensions were obtained from a least-squares fit of the setting angles of 25 reflections in the θ range 10.0−14.5°. Intensity data were corrected for Lorentz-polarisation effects and absorption by an empirical ψ-scan method. The structure was solved by conventional Patterson and Fourier techniques[12] and refined by a full-matrix anisotropic least-squares method.[13] All the calculations were performed using the WinGX System, Ver 1.61.[14]

The choice of space group $P2_1/m$ involves a structural disorder of the phenyl rings, the Pd(phen) moiety being located on a symmetry mirror. On the other hand, an attempted structure solution in the

noncentrosymmetric space group $P2_1$ did not produce satisfactory results (large correlation matrix elements and nonpositive definite thermal ellipsoids for some atoms).

$C_{26}H_{18}N_4O_2Pd$, M = 524.84, monoclinic, space group $P2_1/m$ (No. 11), a = 10.125(5), b = 6.766(2), c = 15.468(3) Å, β = 94.97(2)°, U = 1055.7(6) Å^3, Z = 2, ρ_{calcd} =1.651 g cm^{-3}, μ (Mo-K_α) = 0.912 mm^{-1}, F(000) = 528; 2902 measured reflections at room temperature ($2\theta_{max}$ = 56°, octants $-14 \le h \le 14$; $0 \le k \le 9$; $0 \le l \le 20$), 2783 unique reflections [R(int) = 0.0708], 1568 observed [$I > 2\sigma(I)$], 229 parameters, $R1$ = 0.0524, $wR2$ = 0.0939, GoF = 0.953; hydrogen atoms in idealized geometries; weighting scheme $w = 1/[\sigma^2(F_o^2) + (0.0410P)^2]$, where P = (Max (F_o^2, 0) + $2F_c^2$)/3; max positive and negative peaks in ΔF map 0.460 and −0.909 e Å^{-3}, respectively. Crystallographic data (excluding structure factors) for the structure included in this paper have been deposited with the Cambridge Crystallographic Data Centre as supplementary publication no. CCDC-100492. Copies of the data can be obtained free of charge on application to CCDC, 12 Union Road, Cambridge CB2 1EZ, UK [Fax: (internat.) + 44-1223/336-033; Email: deposit@ccdc.cam.ac.uk].

Catalysis: The carbonylation reactions were carried out in the Berghof reactor (see above). After introducing the catalyst precursor, the ligand and the acid cocatalyst the autoclave was closed. Nitrobenzene, methanol and 2,2′-dimethoxypropane were placed in a two necked flask connected both to the reactor and to the CO bomb through a PTFE tube. This solution was flushed with CO for 20 min and it was then transferred to the reactor. The autoclave was charged at 40 atm. of CO and heated to the proper temperature. At the end of the run the autoclave was cooled and the residual gas vented. The reaction mixture was filtered off over fine paper and analysed by GC.

Acknowledgments

This work was supported by Ministero dell'Università e della Ricerca Scientifica (MURST-Rome) grant N. 9903153427.

[1] [1a] A. M. Tafesh, J. Weiguny, *Chem. Rev.* **1996**, *96*, 2035−2052. − [1b] F. Ragaini, S. Cenini, *J. Mol. Cat.*, **1996**, *109*, 89−91. − [1c] R. Sundermann, H. J. Scholl, *Applied Homogeneous Catalysis with Organometallic Compounds* (Eds.: B. Cornils and W. A. Herrmann), **1996**, VCH, Vol. 2, pg. 1072−1080.

[2] [2a] A. Bontempi, E. Alessio, G. Chanos, G. Mestroni, *J. Mol. Catal.*, **1987**, *42*, 67−80. − [2b] R. Santi, A. M. Romano, F. Panella, G. Mestroni, A. Sessanta o Santi, *J. Mol. Catal. A: Chemical*, **1999**, *144*, 41−45.

[3] [3a] P. Wehman, P. C. J. Kamer, P. W. N. M. van Leeuwen, *Chem. Commun.* **1996**, 217−218. − [3b] P. Wehman, V. E. Kaasjager, W. G. J. de Lange, F. Hartl, P. C. J. Kamer, P. W. N. M. van Leeuwen, J. Fraanje, K. Goubitz, *Organometallics* **1995**, *14*, 3751−3761. − [3c] P. Wehman, G. C. Dol, E. R. Moorman, P. C. J. Kamer, P. W. N. M. van Leeuwen, J. Fraanje, K. Goubitz, *Organometallics* **1994**, *13*, 4856−4869.

[4] [4a] P. Leconte, F. Metz, A. Mortreux, J. A. Osborn, F. Paul, F. Petit, A. Pillot, *J. Chem. Soc., Chem. Commun.* **1990**, 1616−1617. − [4b] F. Paul, J. Fischer, P. Oschsenbein, J. A. Osborn, *Angew. Chem. Int. Ed. Engl.* **1993**, *32*, 1638−1640. − [4c] F. Paul, J. Fischer, P. Ochsenbein, J. A. Osborn, *Organometallics* **1998**, *17*, 2199−2206.

[5] A. Sessanta o Santi, B. Milani, G. Mestroni, E. Zangrando, L. Randaccio, *J. Organomet. Chem.* **1997**, *545−546*, 89−91.

[6] N. Masciocchi, F. Ragaini, S. Cenini, A. Sironi, *Organometallics* **1998**, *17*, 1052−1057.

[7] J. Harada, K. Ogawa, S. Tomoda, *Acta Crystallogr., Sect. B*, **1997**, *53*, 662−672.

[8] A. Sessanta o Santi, Ph. D. Thesis, **1997**, University of Trieste.

[9] When the metallacycle **2a** was treated with methanol, under reflux, in the presence of *p*-toluenesulfonic acid for 2 h, the GC analysis of the solution revealed the presence of the corresponding urethane.

[10] B. Milani, E. Alessio, G. Mestroni, A. Sommazzi, F. Garbassi, E. Zangrando, N. Bresciani-Pahor, L. Randaccio, *J. Chem. Soc., Dalton Trans.* **1994**, 1903−1911.

[11] B. Milani, A. Anzilutti, L. Vicentini, A. Sessanta o Santi, E. Zangrando, S. Geremia, G. Mestroni, *Organometallics* **1997**, *16*, 5064−5075.

[12] G. M. Sheldrick, SHELXS-86, Program for structure solution, *Acta Crystallogr., Sect. A*, **1990**, *46*, 467−473.

[13] G. M. Sheldrick, SHELXL-97, *Program for crystal structure refinement*, University of Göttingen, Germany, **1997**.

[14] WinGX − A Windows Program for Crystal Structure Analysis, L. J. Farrugia, University of Glasgow, Glasgow, **1998**.

Received May 18, 2000
[I00203]

Zinc Complexes of Condensed Phosphates, 2[‡]

Diphosphate−Zinc Complexes with Chelating Coligands

Alexandra Müller-Hartmann[a] and Heinrich Vahrenkamp*[a]

Keywords: Zinc / Phosphates / Organic pyrophosphates / Synthetic methods / Phosphatases

Zinc perchlorate, diorganodiphosphates (POP^{2-}), and chelating ligands L (L = 1,10-phenanthroline, neocuproine, 2,2′-bipyridine, oxinate) yield three types of ternary complexes. Type 1 ($L_2Zn{\cdot}POP$) contains octahedral zinc bound by the diphosphate as an OPOPO chelate ligand. Type 2 (LZn·POP) consists of dimeric complexes containing five-coordinate zinc, with the diphosphates acting as OPOPO chelate ligands for one zinc ion and as OPO bridges between two zinc ions. Type 3 ($L_2Zn_2{\cdot}POP$), observed only for oxinate, is proposed to contain two five-coordinate zinc ions bridged by the diphosphate as a tetradentate ligand.

Introduction

In the chemistry of condensed phosphates, metal ions play an important role with regard to both the stabilization of the phosphate structures in the solid state[2] and in solution[3] and the activation of the phosphates for hydrolytic cleavage, as exemplified by the many enzymes that transfer phosphate units from oligophosphates, e.g. ATPases, kinases, and pyrophosphatases.[4−7] While the typical metal ions for this purpose are magnesium, calcium, and manganese, zinc can also fulfil the role of the former and may be essential in certain enzymes.[8]

This clearly provides a motivation to study the coordination chemistry of oligophosphates, both from a structural and mechanistic standpoint as well as with regard to modeling of the bonding and reactivity patterns of enzymes that act on oligophosphates. Numerous studies have been published in this field, with a considerable emphasis on metal complexes of ATP and cyclic triphosphate.[3,9] There has been comparatively little work on soluble coordination compounds of pyrophosphate,[10−12] although a copper complex of thiamine pyrophosphate has been described.[13] In addition, structure determinations of several enzymes containing metal-bound oligophosphates, e.g. inorganic pyrophosphate,[14] ADP,[15] and thiamine pyrophosphate,[16] have been reported.

In our field, namely the biorelevant coordination chemistry of zinc, information on condensed phosphates as ligands is still scarce. We are not aware of any solution studies or syntheses of species containing zinc coordinated by simple inorganic or organic pyrophosphates or triphosphates. However, the interactions between zinc and nucleotides have been investigated in solution,[2] the species $Zn_3(ADP)_2$ and $Zn_2(ATP)$ have been isolated,[17] and the structures of zinc complexes with H_2ATP^{2-} [18] and $HATP^{3-}$ [19] have been reported. Among the many metal−oligophosphate solid-state compounds, several zinc pyrophosphate species,[2] a zinc triphosphate,[20] and a zinc tetraphosphate[21] have been obtained and structurally characterized.

Our interest in the coordination chemistry of zinc with oligophosphates stems from our observation that our "enzyme models", the pyrazolylborate−zinc hydroxide complexes, are well suited to effect hydrolytic cleavage of tetraorganopyrophosphates.[22] Our mechanistic implications for these and similar hydrolytic reactions with Zn−OH species[23,24] require that the substrate (e.g. the pyrophosphate) is attached to only one zinc ion through only one oxygen donor during the activation step, which is in contrast to common schemes for phosphate hydrolyses[3,8] that imply attachment of zinc to two P−O units or the attachment of two metal ions to one phosphate entity. We therefore embarked on a comprehensive study of the coordination chemistry of zinc with condensed phosphates.

The aim of this study was to gain an understanding of the factors that control the bonding modes (terminal, chelating, bridging) and the hapticity (monodentate to polydentate) of oligophosphates towards zinc. The measures taken to achieve this were a control of the number of available coordination sites on the zinc ion and influence on the number of donor sites on the oligophosphates. The former was accomplished by using nitrogen-containing coligands with varying donor numbers, the latter by using partially esterified oligophosphates. Thus, we used neither inorganic pyrophosphate or triphosphates nor ADP, ATP, or analogues thereof. Our "substrates" were triorgano- or diorgano-diphosphates, -triphosphates, and -methylenediphosphonates. Our coligands were bidentate and tridentate chelators or tridentate and tetradentate tripods. In accordance with the aims of this investigation, conditions favoring

[‡] Part 1: Ref.[1]

[a] Institut für Anorganische und Analytische Chemie der Universität Freiburg,
Albertstraße 21, 79104 Freiburg, Germany
Fax: (internat.) + 49-(0)761/203-6001
E-mail: vahrenka@uni-freiburg.de

 © WILEY-VCH Verlag GmbH, D-69451 Weinheim, 2000 1434−1948/00/1111−2355 $ 17.50+.50/0

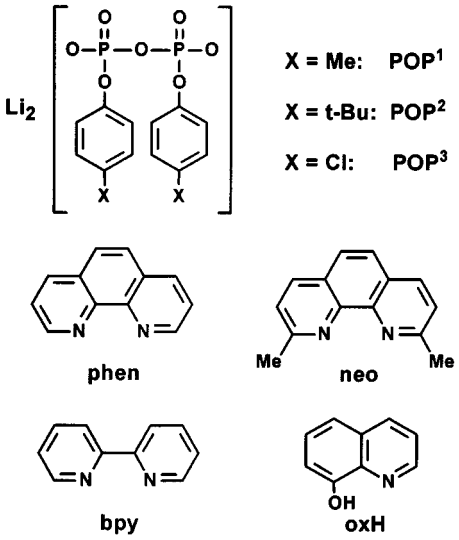
the stoichiometric or catalytic hydrolysis of the oligophosphates were carefully avoided.

This paper describes the results obtained with bidentate coligands. The first paper in this series[1] dealt with oligophosphate complexes of zinc without coligands. The two succeeding papers[25,26] will deal with complexes incorporating coligands of higher donor numbers.

Phosphates and Coligands

The three dilithium diorganodiphosphates $Li_2[POP^1]$, $Li_2[POP^2]$, and $Li_2[POP^3]$ have been described previously by both ourselves[1] and others.[27] They are obtained by condensation of the appropriate organophosphoric acid with the organo(*n*-butylcarbamoyl)phosphate. They undergo hydrolytic cleavage in water only very slowly, but in some cases their reactions with zinc salts give rise to hydrolysis products in the reaction mixtures.

As coligands, we chose the classical examples listed below. Of these, neocuproine could be expected to favor lower coordination numbers than six for zinc, while oxinate, as a negatively charged O,N donor, was likely to produce complexes of a different type compared to the other three coligands.



In the following discussion, the resulting complexes are classified according to product types. Three different stoichiometries corresponding to three different structural types were observed.

Type 1 Complexes: $L_2Zn(POP)$

The complexes of this type, **1** and **2**, were obtained when the *p*-chlorophenyl-substituted diphosphate POP^3 was combined with zinc perchlorate and the coligands phen and bpy. They are the only products in this series for which the octahedral coordination of zinc and the chelating nature of the diphosphate ligands could be predicted from their compositions coupled with the mirror symmetry of the diphosphates and coligands as evidenced by NMR.

$(phen)_2Zn(POP^3)$ **1** $(bpy)_2Zn(POP^3)$ **2**

X-ray structure determinations of **1** and **2** verified their octahedral nature. Inspection of Figure 1 and 2 reveals the similarity of the two structures. Table 1 summarizes the relevant structural features. It is noticeable that the Zn−O bonds are shorter than the Zn−N bonds, indicating good zinc−phosphate bonding, and that the P=O and P−O(Zn) bond lengths are similar, pointing to a highly ionic nature of the zinc−phosphate interactions. The other structural features are normal for these types of ligands, as observed for instance in $(bpy)_2Zn(NO_3)_2$,[28] $[(phen)_2Zn(H_2O)_2]SO_4$,[29] $(NH_3)_4Co(HP_2O_7)$,[30] and $(bpy)Zn(H_2ATP)$.[18] Both structures demonstrate the stress-free attachment of the organodiphosphates as bidentate ligands forming six-membered chelate rings.

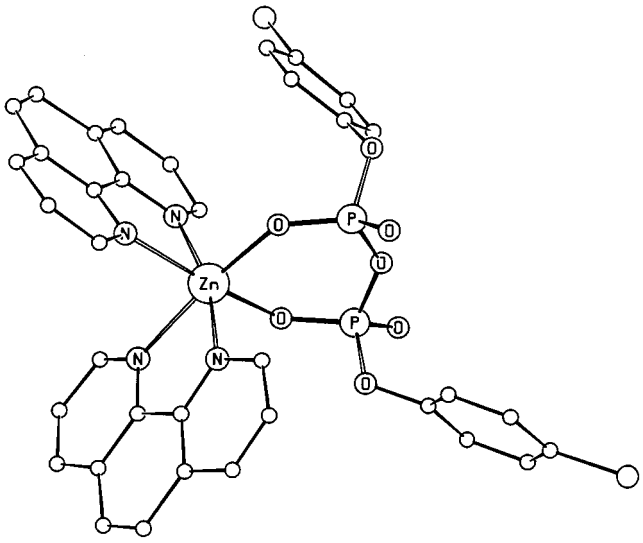


Figure 1. Molecular structure of **1**

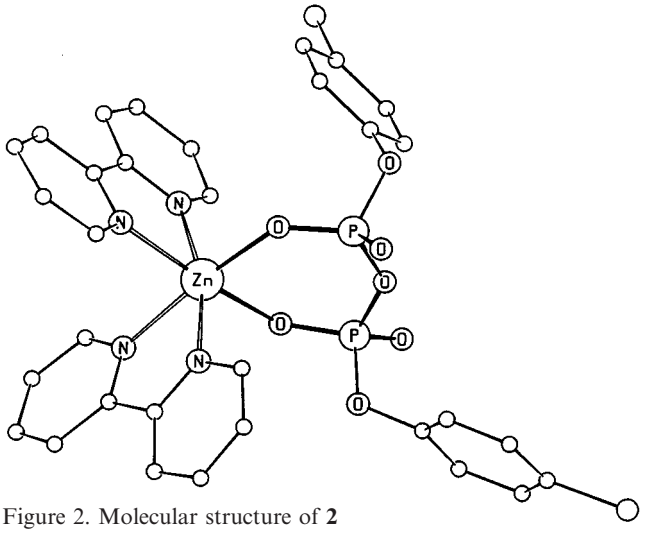


Figure 2. Molecular structure of **2**

Table 1. Bond lengths [Å] and angles [°] in **1** and **2**

	1	**2**
Zn−N	2.12−2.22(1)	2.130−2.214(2)
Zn−O	2.05−2.07(1)	2.057−2.098(2)
P−O(Zn)	1.48−1.49(1)	1.484−1.491(2)
P=O	1.45−1.49(1)	1.468−1.469(2)
P−O(P)	1.59−1.62(1)	1.584−1.615(2)
P−O(C)	1.59−1.62(1)	1.593−1.599(2)
Zn−O−P	130.4−136.0(5)	132.1−137.2(1)
P−O−P	135.5(5)	136.3(1)
O−Zn−O	90.6(3)	89.0(1)

Type 2 Complexes: LZn(POP)

Irrespective of the reaction stoichiometry, all three N,N coligands (phen, neo, bpy) formed 1:1:1 complexes of type 2 with zinc perchlorate and the diphosphates POP^1 and POP^2. In addition, neo also yielded a complex of this type with POP^3. The ^1H NMR data (see Experimental Section) allow a distinction to be made between types 1 and 2, cf. **1**/**3** or **2**/**8**, but they yield no structural information other than that both the diphosphates and the coligands have mirror symmetry. The ^{31}P NMR spectra give the same indications, thereby pointing to a symmetrical bidentate coordination of the diphosphates. This would imply that in solution complex type 2 contains zinc in a tetrahedral ZnN_2O_2 environment.

L·Zn(POP)

L	POP^1	POP^2	POP^3
phen	**3**	**4**	
neo	**5**	**6**	**7**
bpy	**8**	**9**	

Structure determinations of **5** and **6** yielded the surprising information that the compounds are dimeric in the solid state. Figure 3 and 4 show that zinc is five-coordinate in the solid state, its coordination geometry being distorted trigonal-bipyramidal. In both compounds, the two mononuclear fragments are related to each other by an inversion center. Each diphosphate ligand uses two of its terminal oxygen atoms for chelate bonding to one zinc ion and another one to form the bridge linking the two complex halves.

The bonding details (see Table 2) of the coligands and of the chelating diphosphates resemble those of complexes **1** and **2** and may be compared to the same reference compounds (see above). There is, however, a wider spread of bond lengths and angles between **5** and **6** than between **1** and **2**. Overall, the Zn−O and Zn−N bonds in **5** and **6** are shorter, in agreement with the lower coordination number. A notable feature concerns the Zn−O bond lengths in the bridging vs. the chelating mode of the diphosphates. One of the two Zn−O (chelate) bonds is short while the other is 0.10−0.13 Å longer. The latter involves the monophosphate fragment that also provides the bridge bond, thus indicating a weakening of the Zn−O interaction due to the attach-

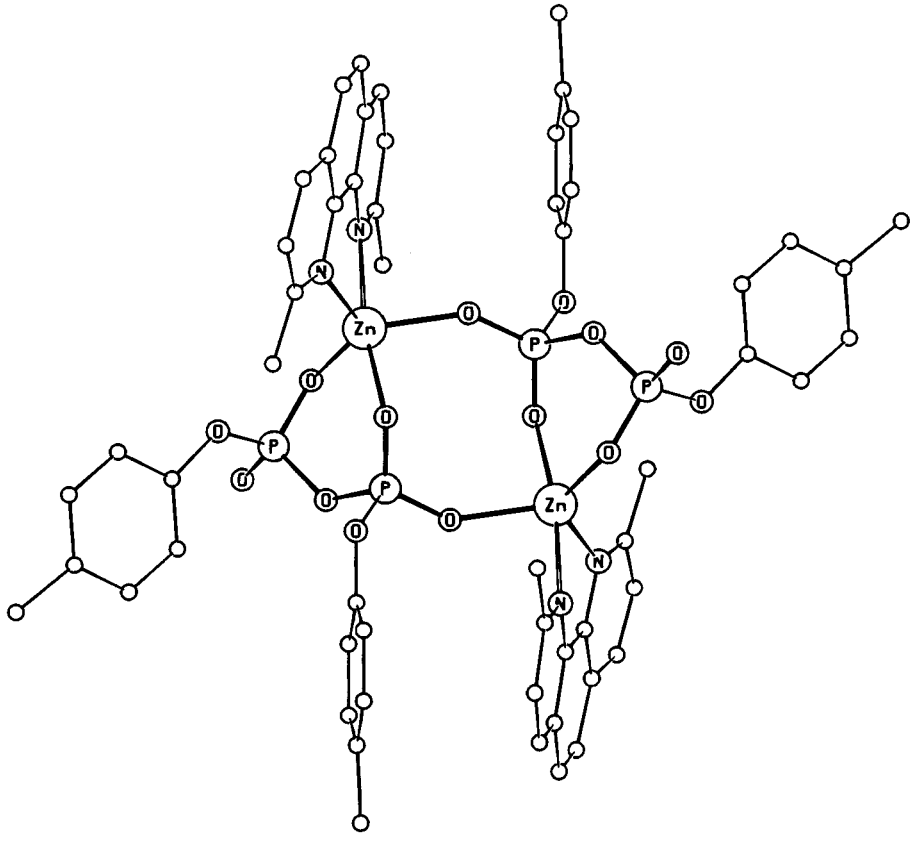


Figure 3. Molecular structure of dimeric **5**

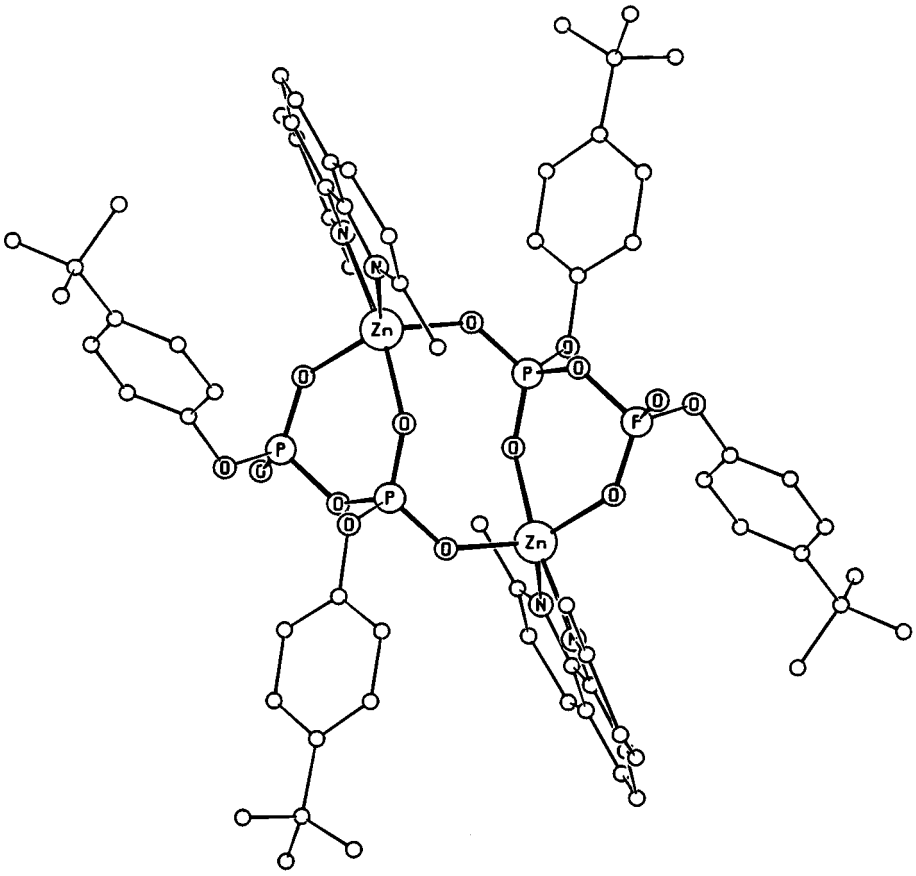


Figure 4. Molecular structure of dimeric **6**

Table 2. Bond lengths [Å] and angles [°] in **5** and **6**

	5	**6**
Zn−N	2.104, 2.141(2)	2.158, 2.173(4)
Zn−O(br)	2.018(2)	1.974(3)
Zn−O(chel)	1.981, 2.078(2)	1.951, 2.082(3)
P−O(br)	1.482(2)	1.530(3)
P−O(chel)	1.478, 1.484(2)	1.534, 1538(3)
P=O	1.470(2)	1.518(4)
P−O(P)	1.601, 1.610(2)	1.602, 1.601(4)
P−O(C)	1.594, 1.600(2)	1.579, 1.587(4)
Zn−O−P(br)	141.9(2)	133.4(2)
Zn−O−P(chel)	128.9, 130.9(2)	137.2, 139.9(2)
P−O−P	129.7(1)	125.8(2)
O−Zn−O(chel)	90.1(7)	83.2(2)
O−Zn−O(br)	87.7, 122.7(8)	93.3, 120.3(2)

ment of a second zinc ion. In contrast, the bridging Zn−O interaction is strong, as indicated by the short bond length. Again, the P−O bond lengths, which are virtually identical for the terminal, bridging, and chelating situations, do not reflect the varying Zn−O interactions in which these P−O functions are involved.

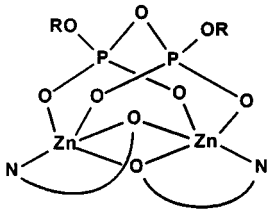
Type 3 Complexes: $L_2Zn_2(POP)$

Only one complex of this type was obtained, and it was also the only complex that could be isolated in a pure state from reactions with oxine. Compound **10** was found to be readily soluble in methanol and hence is unlikely to be a coordination polymer.

$$(ox)_2Zn_2(POP^2)$$

10

The spectra of **10** (see below) again give no information other than that the diphosphate is bound symmetrically. It seems likely that the oxinate oxygen serves as a bridging ligand, as observed for tetrameric bis(oxinato)zinc,[31] and that zinc with oxinate ligands is five- or six-coordinate.[31,32] If one also excludes coordination polymers or solvated species, the number of possible constitutions for **10** becomes small. That depicted below is one of the possibilities, but in view of the lack of spectroscopic support, it can only be regarded as a proposal.



Spectroscopy

The ^{1}H NMR data (see Experimental Section) serve no other purpose than to confirm the compositions of the complexes. In all cases, they indicate that the diphosphates are bound in a symmetrical fashion. As has been shown for **5** and **6**, this is not the case in the solid state. Thus, it must be concluded that the complexes are labile, being characterized by the solution phenomena of solvation and/or fluxionality.

Table 3 lists the IR and ^{31}P NMR spectroscopic data. Coordination of the diphosphates leads to typical features for the very strong IR bands of the PO_2 stretches. In all cases, the two bands due to $\nu_{as}(PO_2)$ are significantly shifted to higher wavenumbers, while the band for $\nu_s(PO_2)$ is shifted by a similar amount to lower wavenumbers. However, as shown by the arrangement in Table 3, similarities within groups of the same POP ligand are more typical than similarities within groups representing the same complex type. Similar conclusions can be drawn from the ^{31}P NMR data. Coordination of the diphosphates is evident from a shift of about 2 ppm to higher field in all cases. However, there are no group trends, and the unsymmetrical nature of the diphosphates in complex type 2 is not reflected in the spectra.

Table 3. IR and ^{31}P NMR data

	$\nu_{as}(PO_2)$[a]	$\nu_s(PO_2)$[a]	$\delta(^{31}P)$[b]
$Li_2[POP^1]$	1270/1230	1140	−15.3
(phen)Zn(POP^1) (**3**)	1288/1228	1115	−17.2
(neo)Zn(POP^1) (**5**)	1289/1241	1118	−17.5
(bpy)Zn(POP^1) (**8**)	1293/1235	1117	−17.2
$Li_2[POP^2]$	1249/1220	1138	−15.5
(phen)Zn(POP^2) (**4**)	1282/1240	1121	−17.2
(neo)Zn(POP^2) (**6**)	1281/1240	1121	−17.4
(bpy)Zn(POP^2) (**9**)	1291/1234	1119	−17.1
$(ox)_2Zn_2(POP^2)$ (**10**)	1274/1230	1119	−17.4
$Li_2[POP^3]$	1254/1223	1155	−16.0
$(phen)_2Zn(POP^3)$ (**1**)	1275/1238	1120	−17.5
(neo)Zn(POP^3) (**7**)	1279/1241	1132	−18.0
$(bpy)_2Zn(POP^3)$ (**2**)	1274/1250	1119	−17.8

[a] In KBr, cm^{-1}. − [b] In DMSO, ppm rel. to H_3PO_4.

Conclusions

In the preceding paper[1] it was shown that reducing the donor capacity of oligophosphates by esterification is not sufficient to produce low molecular weight zinc−oligophosphate complexes. In the present work, we have shown that this can be achieved by reducing the number of coordination sites on zinc through the use of chelating coligands. Complex types **1** and **2**, for which structural information has been obtained, contain one diphosphate ligand per zinc ion, which is bound as an O,O chelate ligand with a six-membered chelate ring. With two N,N coligands, zinc achieves octahedral ZnO_2N_4 coordination. When only one N,N coligand is attached, the diphosphates become tridentate, using one of their P=O functions as a bridging donor. The resulting dinuclear complexes contain zinc in a trigonal-bipyramidal ZnO_3N_2 coordination. Neither a monodentate attachment to one zinc ion nor a bis-monodentate bridging of two zinc ions has been observed. This has prompted us to increase the hapticity of the coligands, leading to the results presented in the two succeeding papers.

Experimental Section

General: For general working and measuring procedures, see ref.[33] The lithium salts of the diphosphates[1,27] were stored under anhydrous conditions. During the course of the reactions, no precautions were taken to prevent the access of moisture. All organic phosphates are potentially toxic and were handled accordingly.

1: A solution of $Li_2[POP^3]$ (100 mg, 0.23 mmol) in boiling methanol (80 mL) was added to a solution of phen (42 mg, 0.23 mmol) and $Zn(ClO_4)_2{\cdot}6H_2O$ (87 mg, 0.23 mmol) in boiling methanol (50 mL). The mixture was filtered while hot, slowly allowed to cool to room temp., and then slowly concentrated to a volume of 20 mL in a desiccator. 30 mg (30%) of **1**, m.p. 168 °C, was precipitated. − $C_{36}H_{24}Cl_2N_4O_7P_2Zn{\cdot}3\,H_2O$ (822.8 + 54.1): calcd. C 49.31, H 3.45, N 6.39, Zn 7.46; found C 48.86, H 3.10, N 6.70, Zn 7.85. − ^{1}H NMR ([D$_6$]DMSO): δ = 6.69 (d, *J* = 8.2 Hz, 4 H, Ph), 6.90 (d, *J* = 8.2 Hz, 4 H, Ph), 7.97 (s, 6 H, phen), 8.25 (s, 6 H, phen), 8.84 (d, *J* = 7.8 Hz, 12 H, phen).

2: Prepared in the same manner as **1** from $Li_2[POP^3]$ (100 mg, 0.23 mmol), bpy (36 mg, 0.23 mmol), and $Zn(ClO_4)_2{\cdot}6H_2O$ (87 mg, 0.23 mmol). After cooling, the mixture was filtered and the filtrate was slowly concentrated to a volume of 8 mL, yielding 35 mg (39%) of **2**; m.p. 261 °C. Water of crystallization (5 H_2O) could be removed by prolonged pumping. − $C_{32}H_{24}Cl_2N_4O_7P_2Zn$ (774.8): calcd. C 49.61, H 3.12, N 7.23, Zn 8.44; found C 48.55, H 2.91, N 6.89, Zn 8.25. − ^{1}H NMR ([D$_6$]DMSO): δ = 7.05 (d, *J* = 8.8 Hz, 4 H, Ph), 7.20 (d, *J* = 8.8 Hz, 4 H, Ph), 7.55 (m, 4 H, bpy), 8.06 (m, 4 H, bpy), 8.45 (m, 4 H, bpy), 8.71 (m, 4 H, bpy).

3: Prepared in the same manner as **1** from $Li_2[POP^1]$ (124 mg, 0.28 mmol) in methanol (25 mL) and phen (50 mg, 0.28 mmol) and $Zn(ClO_4)_2{\cdot}6H_2O$ (103 mg, 0.28 mmol) in methanol (95 mL). Upon cooling, 72 mg (43%) of **3**, m.p. 284 °C, was precipitated. − $C_{26}H_{22}N_2O_7P_2Zn$ (601.8): calcd. C 51.89, H 3.68, N 4.65, Zn 10.86; found C 51.12, H 3.66, N 4.61, Zn 10.76. − ^{1}H NMR ([D$_6$]DMSO): δ = 2.10 (s, 6 H, Me), 6.80 (m, 8 H, Ph), 8.02 (dd, *J* = 6.4, 6.4 Hz, 2 H, phen), 8.19 (s, 2 H, phen), 8.81 (d, *J* = 8.0 Hz, 2 H, phen), 9.11 (d, *J* = 4.2 Hz, 2 H, phen).

4: Prepared in the same manner as **1** from $Li_2[POP^2]$ (92 mg, 0.19 mmol) in methanol (30 mL) and phen (35 mg, 0.19 mmol) and $Zn(ClO_4)_2{\cdot}6H_2O$ (72 mg, 0.19 mmol). Yield 30 mg (23%) of **4**; m.p. 296 °C. − $C_{32}H_{34}N_2O_7P_2Zn$ (686.0): calcd. C 56.03, H 5.00, N 4.08, Zn 9.53; found C 55.43, H 5.01, N 3.89, Zn 9.65. − ^{1}H NMR ([D$_6$]DMSO): δ = 1.19 (s, 18 H, *t*Bu), 6.94 (d, *J* = 8.4 Hz, 4 H, Ph), 7.12 (d, *J* = 8.4 Hz, 4 H, Ph), 8.08 (dd, *J* = 6.4, 6.4 Hz, 2 H, phen), 8.21 (s, 2 H, phen), 8.83 (d, *J* = 8.1 Hz, 2 H, phen), 9.23 (d, *J* = 3.5 Hz, 2 H, phen).

5: Prepared in the same manner as **1** from $Li_2[POP^1]$ (148 mg, 0.33 mmol) in methanol (20 mL) and neo·H_2O (74 mg, 0.33 mmol) and $Zn(ClO_4)_2{\cdot}6H_2O$ (123 mg, 0.33 mmol) in methanol (20 mL). After cooling, the mixture was filtered and the filtrate was slowly concentrated to a volume of 35 mL, yielding 50 mg (24%) of **5**;

m.p. 282 °C. – $C_{28}H_{26}N_2O_7P_2Zn$ (629.9): calcd. C 53.39, H 4.16, N 4.45, Zn 10.38; found C 53.19, H 4.14, N 4.39, Zn 10.40. – ^{1}H NMR ([D$_6$]DMSO): δ = 2.20 (s, 6 H, Me), 2.98 (s, 6 H, Me), 6.91 (m, 8 H, Ph), 7.96 (d, J = 8.6 Hz, 2 H, neo), 8.15 (s, 2 H, neo), 8.80 (d, J = 7.6 Hz, 2 H, neo).

6: Prepared in the same manner as **1** from $Li_2[POP^2]$ (257 mg, 0.54 mmol) in ethanol (150 mL) and neo·H_2O (123 mg, 0.54 mmol) and $Zn(ClO_4)_2$·$6H_2O$ (220 mg, 0.54 mmol) in ethanol (50 mL). After cooling, the mixture was filtered and the filtrate was slowly concentrated to a volume of 150 mL, yielding 171 mg (40%) of **6**; m.p. 294 °C. – $C_{34}H_{38}N_2O_7P_2Zn$·EtOH·H_2O (714.0 + 46.1 + 18.0): calcd. C 55.57, H 5.96, N 3.60, Zn 8.40; found C 55.29, H 5.50, N 3.68, Zn 8.90. – ^{1}H NMR ([D$_6$]DMSO): δ = 1.05 (t, J = 6.9 Hz, 3 H, EtOH), 1.23 (s, 18 H, *t*Bu), 2.99 (s, 6 H, Me), 3.17 (s, 2 H, H_2O), 3.43 (q, J = 6.9 Hz, 2 H, EtOH), 6.95 (d, J = 8.7 Hz, 4 H, Ph), 7.18 (d, J = 8.7 Hz, 4 H, Ph), 7.93 (d, J = 8.1 Hz, 2 H, neo), 8.22 (s, 2 H, neo), 8.73 (d, J = 8.9 Hz, 2 H, neo).

7: Prepared in the same manner as **1** from $Li_2[POP^3]$ (138 mg, 0.32 mmol) in ethanol (100 mL) and neo·H_2O (73 mg, 0.32 mmol) and $Zn(ClO_4)_2$·$6H_2O$ (120 mg, 0.32 mmol) in ethanol (100 mL). Yield 46 mg (21%) of **7**; m.p. 235 °C. – $C_{26}H_{20}Cl_2N_2O_7P_2Zn$ (670.7): calcd. C 46.56, H 3.01, N 4.18, Zn 9.75; found C 47.00, H 3.56, N 3.98, Zn 9.60. – ^{1}H NMR ([D$_6$]DMSO): δ = 3.00 (s, 6 H, Me), 7.04 (d, J = 8.8 Hz, 4 H, Ph), 7.21 (d, J = 8.8 Hz, 4 H, Ph), 7.97 (m, 2 H, neo), 8.16 (s, 2 H, neo), 8.77 (m, 2 H, neo).

8: Prepared in the same manner as **1** from $Li_2[POP^1]$ (105 mg, 0.23 mmol) in methanol (90 mL) and bpy (36 mg, 0.23 mmol) and $Zn(ClO_4)_2$·$6H_2O$ (87 mg, 0.23 mmol) in methanol (10 mL). The mixture was filtered while hot and the filtrate was slowly concentrated to a volume of 50 mL at room temp., yielding 21 mg (16%) of **8**; m.p. 266 °C. – $C_{24}H_{22}N_2O_7P_2Zn$ (577.8): calcd. C 49.89, H 3.84, N 4.85, Zn 11.32; found C 48.82, H 3.64, N 4.76, Zn 11.14. – ^{1}H NMR ([D$_6$]DMSO): δ = 2.18 (s, 6 H, Me), 6.91 (m, 8 H, Ph), 7.71 (m, 2 H, bpy), 8.23 (m, 2 H, bpy), 8.57 (d, J = 7.5 Hz, 2 H, bpy), 8.74 (s, 2 H, bpy).

9: Prepared in the same manner as **1** from $Li_2[POP^2]$ (100 mg, 0.21 mmol) in methanol (90 mL) and bpy (33 mg, 0.21 mmol) and $Zn(ClO_4)_2$·$6H_2O$ (79 mg, 0.21 mmol) in methanol (10 mL). The mixture was filtered while hot and then slowly concentrated to a volume of 50 mL at room temp., yielding 29 mg (20%) of **9**; m.p. 296 °C. – $C_{30}H_{34}N_2O_7P_2Zn$·H_2O (661.9 + 18.0): calcd. C 52.99, H 5.34, N 4.12, Zn 9.62; found C 52.79, H 5.07, N 4.03, Zn 9.45. – ^{1}H NMR ([D$_6$]DMSO): δ = 1.22 (s, 18 H, *t*Bu), 3.17 (s, 2 H, H_2O), 6.97 (d, J = 8.7 Hz, 4 H, Ph), 7.16 (d, J = 8.7 Hz, 4 H, Ph), 7.72 (m, 2 H, bpy), 8.23 (m, 2 H, bpy), 8.58 (d, J = 7.9 Hz, 2 H, bpy), 8.78 (m, 2 H, bpy).

10: Prepared in the same manner as **1** from $Zn(ClO_4)_2$·$6H_2O$ (81 mg, 0.22 mmol) and $Li_2[POP^2]$ (103 mg, 0.22 mmol) in methanol (30 mL) and oxH (32 mg, 0.22 mmol) in methanol (5 mL). The mixture was refluxed for 15 min., filtered while hot, allowed to cool, and then slowly concentrated to a volume of 15 mL, yielding 40 mg (21%) of **10**; m.p. 206 °C. – $C_{38}H_{38}N_2O_9P_2Zn_2$ (859.5): calcd. C 53.11, H 4.46, N 3.26, Zn 15.21; found C 54.27, H 4.87, N 3.20, Zn 14.89. – ^{1}H NMR ([D$_6$]DMSO): δ = 1.23 (s, 18 H, *t*Bu), 7.03 (d, J = 8.5 Hz, 4 H, Ph), 7.08 (s, 2 H, ox), 7.22 (d, J = 8.5 Hz, 4 H, Ph), 7.41 (m, 4 H, ox), 7.56 (dd, J = 6.2, 6.2 Hz, 2 H, ox), 8.35 (d, J = 8.2 Hz, 2 H, ox), 8.83 (s, 2 H, ox).

Structure Determinations:[34] The selected crystals were taken directly from the reaction solutions and used without drying in vacuo. They were immersed in fluorinated polyether oil and immediately placed in the nitrogen stream of the diffractometer's cooling system. Diffraction data were recorded at ca. −100 °C using the ω/2θ technique with a Nonius CAD4 diffractometer fitted with a molybdenum tube (K_α, λ = 0.7107 Å) and a graphite monochromator. Empirical absorption corrections based on ψ scans were applied. The structures were solved by direct methods and refined anisotropically with the SHELX program suite.[35] Hydrogen atoms were included with fixed distances and isotropic temperature factors 1.5 times those of their attached atoms. Parameters were refined against F^2. The R values are defined as $R_1 = \Sigma|F_o - F_c|/\Sigma F_o$ and

Table 4. Crystallographic details

	1	**2**	**5**	**6**
Empirical formula	$C_{36}H_{24}Cl_2N_4O_7P_2Zn$·$3H_2O$	$C_{32}H_{24}Cl_2N_4O_7P_2Zn$·$5H_2O$	$C_{28}H_{26}N_2O_7P_2Zn$·MeOH	$C_{34}H_{38}N_2O_7P_2Zn$·EtOH·H_2O
Molecular mass	822.8 + 36.0	774.8 + 90.1	629.9 + 32.0	714.0 + 46.1 + 18.0
Crystal size [mm]	0.4 × 0.4 × 0.4	0.5 × 0.5 × 0.5	0.5 × 0.4 × 0.3	0.3 × 0.2 × 0.2
Space group	$P2_1$	$P2_1/n$	P-1	$P2_1/c$
Z	4	4	2	4
a [Å]	15.655(1)	15.029(1)	9.868(2)	11.648(2)
b [Å]	15.151(1)	15.499(1)	10.013(2)	29.480(6)
c [Å]	16.737(1)	16.607(1)	15.929(3)	12.255(2)
α [°]	90	90	88.42(3)	90
β [°]	105.54(1)	99.53(1)	72.13(3)	113.70(3)
γ [°]	90	90	75.79(3)	90
V [Å^3]	3824.9(2)	3815.0(1)	1450.2(5)	3853.3(12)
d(calcd.) [gcm^{-3}]	1.43	1.51	1.52	1.29
μ(Mo-K_α) [mm^{-1}]	0.92	0.93	1.01	2.08 (Cu-K_α)
hkl range	h: −20 to 21	h: 0 to 21	h: −12 to 11	h: −13 to 15
	k: −20 to 21	k: 0 to 21	k: −12 to 0	k: −36 to 0
	l: −23 to 21	l: −23 to 23	l: −19 to 19	l: −14 to 0
Measured reflections	12090	11151	6020	8239
Independent reflections	10154	11151	5679	7847
Observed refl. [$I > 2\sigma(I)$]	6493	6325	5120	5542
Parameters	961	478	408	448
Refined reflections	10154	11151	5679	7847
R_1 (obsd. refl.)	0.073	0.040	0.033	0.067
wR_2 (all refl.)	0.206	0.123	0.095	0.220
Residual electron density [e/Å^3]	+0.5	+0.6	+0.8	+0.5
	−0.3	−0.3	−0.5	−0.5

$wR_2 = \{\Sigma[w(F_o^2 - F_c^2)^2]\Sigma[w(F_o^2)^2]\}^{1/2}$. Drawings were produced with SCHAKAL.[36] The crystallographic data are collected in Table 4.

Acknowledgments

This work was supported by the Fonds der Chemischen Industrie. We are indebted to Drs. W. Deck and A. Trösch for help with the structure determinations.

[1] A. Müller-Hartmann, H. Vahrenkamp, *Inorg. Chim. Acta* **2000**, *300–302*, 531–536.
[2] A. Durif, *Crystal Chemistry of Condensed Phosphates*, Plenum Press, New York, **1995**.
[3] H. Sigel, *Chem. Soc. Rev.* **1993**, 255–267.
[4] A. S. Mildvan, C. M. Grisham, *Struct. Bonding* **1974**, *20*, 1–21.
[5] B. S. Cooperman in *Metal Ions in Biological Systems* (Ed.: H. Sigel), Marcel Dekker, New York, **1976**, vol. 5, pp. 79–126.
[6] J. R. Knowles, *Ann. Rev. Biochem.* **1980**, *49*, 877–919.
[7] D. Gani, J. Wilkie, *Chem. Soc. Rev.* **1995**, 55–63.
[8] N. Sträter, W. N. Lipscomb, T. Klabunde, B. Krebs, *Angew. Chem.* **1996**, *108*, 2158–2191; *Angew. Chem. Int. Ed. Engl.* **1996**, *35*, 2024–2052.
[9] The Cambridge Crystallographic Data File contains ten structures each of metal–ATP and metal–P_3O_9 complexes.
[10] N. Herron, D. L. Thorn, R. L. Harlow, G. W. Coulston, *J. Am. Chem. Soc.* **1997**, *119*, 7149–7150.
[11] A. Gharbi, A. Jouini, M. T. Averbuch-Pouchot, A. Durif, *J. Solid State Chem.* **1994**, *111*, 330–337.
[12] L. M. Engelhardt, E. A. Keegan, G. A. Lawrance, A. H. White, *Aust. J. Chem.* **1989**, *42*, 1045–1055.
[13] K. Aoki, H. Yamazaki, *J. Am. Chem. Soc.* **1980**, *102*, 6878–6880.
[14] S. S. Terzyan, A. A. Voronova, E. A. Smirnova, I. P. Harutyunyan, E. H. Harutyunyan, B. K. Vainstein, W. Höhne, G. Hansen, *Bioorg. Khim*. **1984**, *10*, 1469–1482.
[15] F. Takusagawa, S. Kamitori, G. D. Markham, *Biochemistry* **1996**, *35*, 2586–2596.
[16] Y. Lindqvist, G. Schneider, U. Emler, M. Sundström, *EMBO Journal* **1992**, *11*, 2373–2379. F. Dyda, W. Furey, S. Swaminathan, M. Sax, B. Farrenkopf, F. Jordan, *Biochemistry* **1993**, *32*, 6165–6170.
[17] G. Weitzel, T. Spehr, *Hoppe Seyler's Z. Physiol. Chem.* **1958**, *313*, 212–226.
[18] P. Orioli, R. Cini, D. Donati, S. Mangani, *J. Am. Chem. Soc.* **1981**, *103*, 4446–4452.
[19] R. Cini, L. G. Marzilli, *Inorg. Chem.* **1988**, *27*, 1855–1856.
[20] M. T. Averbuch-Pouchot, A. Durif, J. C. Guitel, *Acta Crystallogr., Sect. B* **1977**, *33*, 1427–1431.
[21] M. T. Averbuch-Pouchot, A. Durif, J. C. Guitel, *Acta Crystallogr., Sect. C* **1989**, *45*, 46–49.
[22] K. Weis, H. Vahrenkamp, *Eur. J. Inorg. Chem*. **1998**, 271–274.
[23] M. Rombach, C. Maurer, K. Weis, E. Keller, H. Vahrenkamp, *Chem. Eur. J.* **1999**, *5*, 1013–1027.
[24] H. Vahrenkamp, *Acc. Chem. Res.* **1999**, *32*, 589–596.
[25] F. Groß, A. Müller-Hartmann, H. Vahrenkamp, *Eur. J. Inorg. Chem*. **2000**, 2363–2370, succeeding paper.
[26] A. Müller-Hartmann, H. Vahrenkamp, *Eur. J. Inorg. Chem.* **2000**, 2371–2377, after succeeding paper.
[27] F. Cramer, M. Winter, *Chem. Ber.* **1959**, *92*, 2761–2767.
[28] C. J. Simmons, B. J. Hathaway, K. Amornjarusiri, B. D. Santarisiero, A. Clearfield, *J. Am. Chem. Soc.* **1987**, *109*, 1947–1958.
[29] N.-h. Hu, Y. S. Liu, *Acta Crystallogr., Sect. C* **1991**, *47*, 2324–2326.
[30] E. A. Merritt, M. Sundaralingam, *Acta Crystallogr., Sect. B* **1980**, *36*, 2576–2584.
[31] Y. Kai, M. Morita, N. Yasuoka, N. Kasai, *Bull. Chem. Soc. Jpn.* **1985**, *58*, 1631–1635.
[32] G. J. Palenik, *Acta Crystallogr.* **1964**, *17*, 696–700.
[33] M. Förster, R. Burth, A. K. Powell, T. Eiche, H. Vahrenkamp, *Chem. Ber.* **1993**, *126*, 2643–2648.
[34] Crystallographic data (excluding structure factors) for the structures reported in this paper have been deposited with the Cambridge Crystallographic Data Centre as supplementary publication nos. CCDC-141958 (for **1**), -141959 (for **2**), -141960 (for **5**), and -141961 (for **6**). Copies of these data can be obtained free of charge on application to the CCDC, 12 Union Road, Cambridge CB2 1EZ, U.K. [Fax: (internat.) + 44-1223/336-033; E-mail: deposit@ccdc.cam.ac.uk].
[35] G. M. Sheldrick, *SHELX-86* and *SHELXL-93*, *Programs for Crystal Structure Determination*, Universität Göttingen, **1986** and **1993**.
[36] E. Keller, *SCHAKAL for Windows*, Universität Freiburg, **1999**.
Received March 23, 2000
[I00109]

Zinc Complexes of Condensed Phosphates, 3[‡]

Diphosphate−Zinc Complexes with Tridentate Coligands

Florian Groß,[a] Alexandra Müller-Hartmann,[a] and Heinrich Vahrenkamp*[a]

Keywords: Zinc / Phosphates / Organic pyrophosphates / Methylene diphosphonates / Phosphatases

Diorganodiphosphates (POP^{2-}) and a triorgano-methylenediphosphonate (PCP^{-}) have been combined with zinc salts and the tridentate ligands L [L = bis(benzimidazolylmethyl)amine, bis(2-pyridylmethyl)amine, triazacyclononane, trimethyltriazacyclononane, and (dimethylaminoethyl)(2-pyridylmethyl)amine]. The resulting ternary complexes have been found to contain four-, five-, or six-coordinate zinc. Four-coordinate zinc has been identified in the complex types $[L{\cdot}Zn(PCP)]^{+}$ and $[L{\cdot}Zn(POP)Zn{\cdot}L]^{2+}$, containing monodentate phosphate ligands. Five-coordinate zinc has been found in the complexes [L·Zn(POP)] with chelating diphosphate ligands. Six-coordinate zinc has been observed in the complex type $[L{\cdot}Zn(POP){\cdot}H_2O]$ containing chelating diphosphates and in the complex type $[L{\cdot}Zn(POP)]_2$ in which the diphosphates act as tridentate bridging ligands. In a few cases, hydrolytic cleavage of the diphosphates resulted in the isolation of the trinuclear complexes $[(L{\cdot}Zn)_3(ROPO_3)_2]$ HPO_4 containing triply-bridging monophosphates.

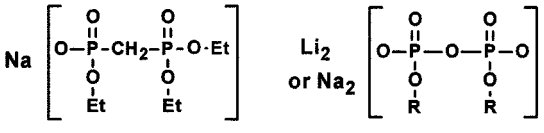
Introduction

In the preceding paper[1] we outlined our motivation for studying the coordination chemistry of zinc with condensed phosphates and the associated scientific background. The main impetus is the importance of metal-containing systems (catalysts, enzymes) in the hydrolytic cleavage of oligophosphates, which is of relevance in the technical as well as in the biological world. Metal catalysis involves coordination of the substrates to the metals, and hence bonding modes of oligophosphates toward metals should provide an insight into possible catalytic pathways for their hydrolysis.

The literature on metal−oligophosphate complexes[1] is largely confined to studies of ATP and inorganic pyrophosphates. Specifically for the biologically important metal zinc, there have been only a few reports and even less structure determinations.[1] We have started to close this gap by carrying out a systematic study, in which the number of available coordination sites at zinc as well as the number of available donor functions on the phosphates have been varied. So far, we have reported on oligophosphate complexes of zinc without coligands[2] and with bidentate coligands.[1] In this paper, we present our results for zinc complexes with tridentate coligands. The succeeding paper[3] will report on systems with encapsulating tripodal coligands.

Phosphates and Coligands

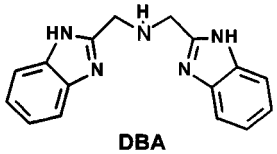
Diphosphates with both P−C−P and P−O−P linkages have been employed. The triethyl methylenediphosphonate PCP[4] was chosen to represent minimal donor qualities since it possesses only one P−O function with a formal negative charge. The diorganodiphosphates POP^1−POP^5 [2,5,6] have two negative charges. They have already[1] been shown to act as chelating bidentate as well as chelating plus bridging tridentate ligands. They could furthermore be expected to act as monodentate or bis-monodentate bridging ligands.



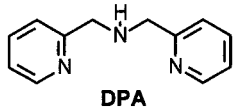
PCP

POP[1]: R = benzyl
POP[2]: R = phenyl
POP[3]: R = p-tolyl
POP[4]: R = p-t-Bu-phenyl
POP[5]: R = p-Cl-phenyl

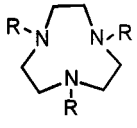
As coligands, we chose tridentate systems containing only nitrogen donors, all of which can be derived from ethylenediamine. DBA,[7] DPA,[8] TACN,[9] and TACN*[10] are well established in coordination chemistry. PDEA was newly prepared by $NaBH_4$ reduction of the corresponding Schiff base.



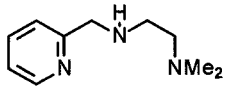
DBA



DPA



TACN: R = H
TACN*: R = Me



PDEA

[‡] Part 2: Ref.[1]

[a] Institut für Anorganische und Analytische Chemie der Universität Freiburg,
Albertstraße 21, 79104 Freiburg, Germany
Fax: (internat.) + 49-(0)761/203-6001
E-mail: vahrenka@uni-freiburg.de

 © WILEY-VCH Verlag GmbH, D-69451 Weinheim, 2000 1434−1948/00/1111−2363 $ 17.50+.50/0

As in the previous paper,[1] we sort the resulting zinc complexes according to product types rather than according to phosphates or coligands. We observed three different product types and one class of decomposition products.

Four-Coordinate Complexes

It was anticipated that the PCP ligand might only bind in a monodentate fashion. Its combination with the coligands DBA and DPA seems to verify this. With zinc perchlorate, the products **1** and **2** were obtained. While the spectroscopic data (see below) of these and all the other complexes yield no other information than the compositions of the products, support for the mononuclear nature of **1** and **2** was obtained from the ESI mass spectrum of **1**, which showed the parent ion.

$[(DBA)Zn(PCP)]ClO_4$ **1** $[(DPA)Zn(PCP)]ClO_4$ **2**

Likewise, a presumably bis-monodentate coordination was found for the POP ligands in three cases. All three involved the pyridine-containing coligands DPA or PDEA. The resulting complexes were **3**, **4**, and **5**. The main evidence for their constitutions was again provided by ESI-MS. The MS of compound **4** showed the parent ion of the dinuclear complex cation.

$[(L)Zn(POP)Zn(L)](ClO_4)_2$

3: L = DPA, POP = POP^3
4: L = DPA, POP = POP^4
5: L = PDEA, POP = POP^1

As none of the compounds proved to be suitable for X-ray structure determination, the structural assignments of **1**–**5** as tetrahedral complexes with ZnN_3O coordination are not unambiguous. As seen before,[1] the diphosphate ligands can be chelating, leading to five-coordinate zinc. They may also be bridging,[1] giving the same result. While there is some likelihood that the PCP ligand in **1** and **2** is indeed bridging, this should not be the case in **3**–**5**. The latter would require that the one POP ligand uses four of its P–O functions to generate two chelate rings. Although we have discussed this previously, it is unrealistic and would produce noticeable ^{31}P NMR shifts. The ^{31}P NMR data of **3**–**5** (see below) are, however, normal, showing the typical small shifts for the attachment of one zinc ion.

Five-Coordinate Complexes

The most typical coordination mode for the POP ligands seems to be the chelating one with six-membered Zn(O-POPO) chelate rings.[1] In combination with the tridentate coligands, this would lead to five-coordinate complexes, a very common coordination motif in zinc chemistry. Surprisingly, this could only be verified for the coligand DBA. In combination with the five POP ligands, it produced the complexes **6**–**10**. Otherwise, only DPA and POP^1 could be combined in this fashion to yield **11**. Proof of the nature of **6**–**11** as monomolecular species in solution and in the gas phase was obtained from the ESI mass spectrum of **10**, which showed a prominent peak attributable to the $[\mathbf{10}Na]^+$ ion.

$(DBA)Zn(POP^n)$ **6**–**10**: n = 1–5 $(DPA)Zn(POP^1)$ **11**

Proof of the monomolecular nature in the solid state was obtained by a structure determination of **8** (see Figure 1). The coordination of zinc in **8** is, to a good approximation, trigonal-bipyramidal; the central N atom of DBA and one O atom occupy the axial positions. While the axial Zn–N distance is typically long, the equatorial and axial Zn–O distances differ by just 0.015 Å. The essentially ionic nature of the Zn–O interactions can again[1] be derived from the fact that the P–O bond lengths for the coordinated and uncoordinated P–O functions are virtually identical. The geometrical parameters of the chelating POP ligand compare well with those in other zinc complexes (see below and ref.[1]). Otherwise, structures of trigonal-bipyramidal complexes of DBA or POP ligands are rare, two examples being the $CuCl_2$ complex of DBA[11] and a Cu complex of thiamine pyrophosphate.[12]

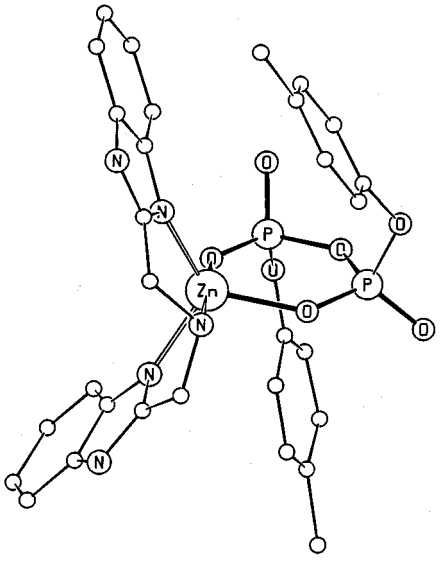


Figure 1. Molecular structure of **8**; selected bond lengths [Å] and angles [°]: Zn–O 2.020(3), 1.987(3), Zn–N 2.018(3), 2.373(3), 2.007(3), P–O(Zn) 1.473(3), 1.494(3), P=O 1.484(4), 1.473(3), P–O(P) 1.602(3), 1.590(3), P–O(C) 1.526(4), 1.594(4); Zn–O–P 134.0(2), 133.1(2), P–O–P 136.5(2), O–Zn–N(axial) 178.4(1)

Six-Coordinate Complexes

The triazacyclononane ligands are well known to form octahedral metal complexes. In this study, they were found to do so without exception. The TACN* coligand could be combined with POP^1, POP^2, and POP^3 in the 1:1:1 zinc complexes **12**–**14**. These were found to be hydrates like **6** and **7**. However, in contrast to these cases, where the water molecules are co-crystallized solvent, the complexes **12**–**14** contain coordinated water. This was shown by an X-ray

structure determination of **12**. In addition, on the basis of slightly different ^{1}H NMR patterns for the POP ligands, complexes **6**–**8** and complexes **12**–**14** can be divided into two separate groups.

$$(TACN^*)Zn(POP^n) \cdot H_2O$$

12–**14**: n = 1–3

The structure of **12** (Figure 2) contains zinc in a slightly distorted octahedral environment. The diphosphate ligand adopts the chelating mode, and all the salient structural details correspond to those discussed already (see above and ref.[1]). The features of the Zn−TACN* coordination correspond to those in the cationic complex $[(TACN^*)_2Zn_2(\mu\text{-}OAc)_2(\mu\text{-}OH)]$.[13]

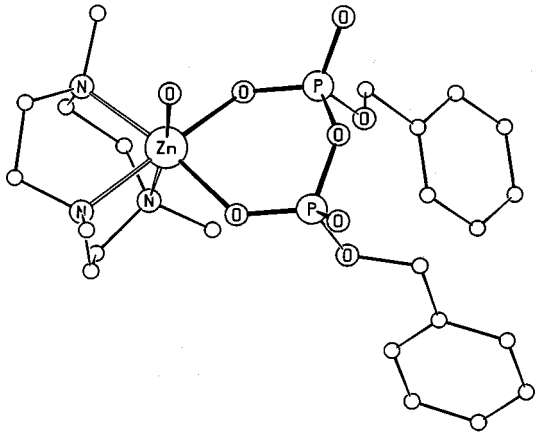


Figure 2. Molecular structure of **12**; selected bond lengths [Å] and angles [°]: Zn−N 2.206, 2.190, 2.178(2), Zn−O(P) 2.055, 2.059(2), Zn−O(H_2O) 2.115(2), P−O(Zn) 1.491, 1.490(2), P=O 1.492, 1.482(2), P−O(P) 1.599, 1.625(2), P−O(C) 1.590, 1.589(2); Zn−O−P 130.4, 131.5(1), P−O−P 131.0(1)

Two other complexes of 1:1:1 composition isolated as hydrates were **15** and **16**. On the basis of their spectral data, these might have been grouped with **12**–**14**. However, their structure determinations showed that in these cases the water molecules are not coordinated to zinc. Instead, the metal achieves octahedral coordination by using a third P−O function of each diphosphate as a bridging donor, thereby linking two molecular units to a dinuclear complex. We have observed this bonding mode before in dinuclear complexes with five-coordinate zinc.[1] It is difficult to explain why the two alternatives of octahedral coordination (coordinated water or diphosphate bridging), both of which exist in the presence of water, are preferred in specific examples.

$$(TACN)Zn(POP^1) \qquad (PDEA)Zn(POP^2)$$

15 **16**

The basic structural features of **15** (Figure 3) and **16** (Figure 4) are very similar, and they also resemble those of the previously reported complexes of this type with five-coordinate zinc.[1] The bridging makes the diphosphates tridentate ligands. The dinuclear entities have inversion centers, hence the zinc−diphosphate chelate rings are arranged in a parallel fashion, and the eight-membered rings created by the dimerization are in the chair conformation. In both cases, the Zn−O bond to the bridging oxygen is significantly shorter than the two Zn−O bonds in the chelate ring. For the diphosphate ligands, there is no noticeable change in their geometrical parameters or bond lengths as compared to the purely chelating mode. The distortion of the ZnO_3N_3 octahedra is comparably small in both the hydrate **12** and the dimers **15** and **16**. Compared to the related five-coordinate zinc complexes (see above and ref.[1]), all the Zn−O and Zn−N bonds are elongated.

Trinuclear Monophosphate Complexes

Although the pyrophosphates used in this study were found to be quite inert towards hydrolytic cleavage, in the presence of zinc salts they sometimes underwent hydrolysis.

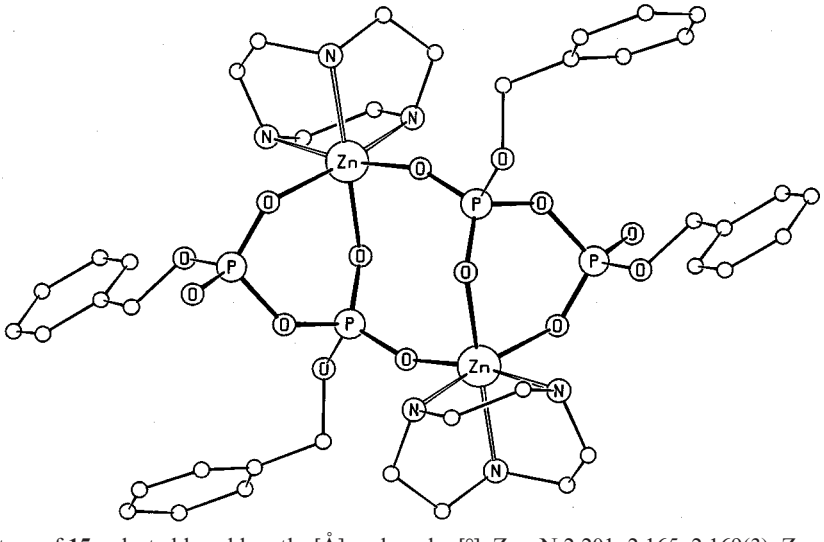


Figure 3. Molecular structure of **15**; selected bond lengths [Å] and angles [°]: Zn−N 2.201, 2.165, 2.169(3), Zn−O(br) 2.027(3), Zn−O(ch) 2.114, 2.099(3), P−O(Zn) 1.476, 1.473, 1.490(3), P=O 1.484(3), P−O(P) 1.612, 1.597(3), P−O(C) 1.600, 1.581(3); Zn−O−P 131.0, 127.8(2), P−O−P 131.5(2)

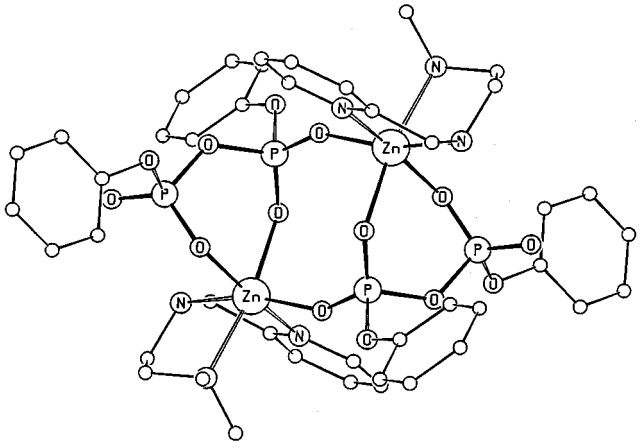


Figure 4. Molecular structure of **16**; selected bond lengths [Å] and angles [°]: Zn−N 2.171, 2.184, 2.221(2), Zn−O(br) 2.016(2), Zn−O(ch) 2.144, 2.112(2), P−O(Zn) 1.485, 1.487, 1.472(2), P=O 1.463(2), P−O(P) 1.609, 1.611(2), P−O(C) 1.603, 1.605(2); Zn−O−P 130.4, 126.1(1), P−O−P 126.8(1)

This normally meant that work-up of the reaction mixtures failed, which is the reason why the series of compounds presented here is incomplete. In two cases, however, the hydrolysis products were isolated as zinc complexes, the trinuclear nature of which was established by structure determinations. Both these complexes, **17** and **18**, were derived from the coligand DPA. They have HPO_4^{2-} counterions, as was verified by ^{31}P NMR spectroscopy.

$[(\mathbf{D}PA{\cdot}Zn)_3(TolOPO_3)_2]\,HPO_4$ **17**

$[(\mathbf{D}PA{\cdot}Zn)_3(ClC_6H_4OPO_3)_2]\,HPO_4$ **18**

Figure 5 depicts the structure of the trinuclear cation of complex **17**. The structure of **18** is quite similar, but will not be discussed here because of its mediocre quality. The $Zn_3(ROPO_3)_2$ units give rise to a structural motif that is seemingly unknown in the coordination chemistry of phosphates. The $P_2(OZnO)_3$ framework, having roughly trigonal symmetry and roughly planar POZnOP wings, is that of bicyclo[3.3.3]undecane. In contrast, the coordination of three metal−ligand units to one phosphate is not uncommon, as exemplified by the zinc complex $\{[(12\text{-ane-}N_4)Zn]_3(ROPO_3)\}^{4+}$.[14] The zinc ions in **17** and **18** are in a severely distorted trigonal-bipyramidal environment. Their Zn−O and Zn−N bond lengths fall in the characteristic ranges for ZnO_2N_3 complexes. The P−O bonds of the P−O−Zn linkages are somewhat longer than in those cases where there is only one zinc ion per phosphate unit (see above). The HPO_4^{2-} ions in the lattice lie beyond the range for coordination to zinc.

Spectroscopy

The ^1H NMR spectra (see Experimental Section) identify the coligands in the complexes and indicate that the POP ligands are bound in a symmetrical fashion in all cases. This does not conform with the solid-state structures of **15** and **16** and suggests that these complexes exist as solvated monomers or are fluxional in solution.

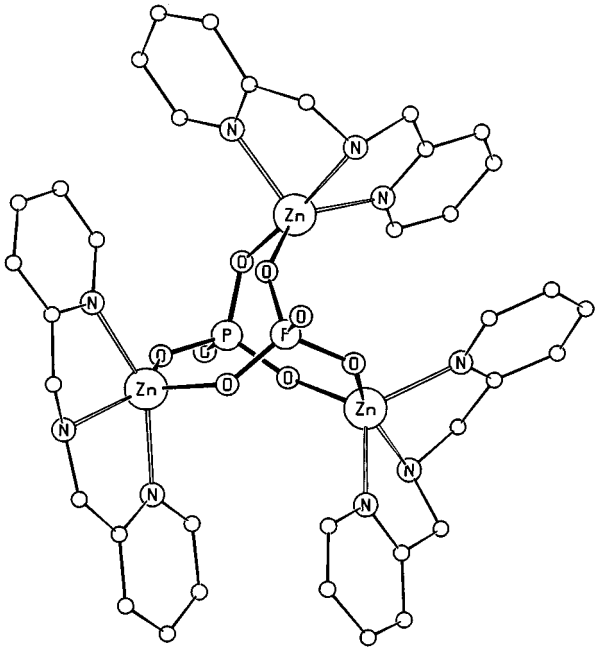


Figure 5. Structure of the zinc complex in **17** (tolyl groups omitted for clarity); important bond lengths [Å] and angles [°]: Zn−O(ax) 1.962−2.002(4), Zn−O(eq) 1.939−1.954(4), Zn−N(ax) 2.148−2.237(6), Zn−N(eq) 2.073−2.149(6), P−O(Zn) 1.493−1.520(4); O−Zn−O 96.8, 105.2, 115.0(2), Zn−O−P 123.5−156.0(3), O−P−O 112.3−114.4(3)

The IR bands in the P−O region show irregular coordination shifts (see Table 1). The $\nu_{as}(PO_2)$ bands are shifted by small amounts to either higher or lower wavenumbers. The $\nu_s(PO_2)$ bands are shifted by 20−30 cm^{-1} to lower wavenumbers. Thus, these bands are only of diagnostic value. More information can be derived from the ^{31}P NMR data. In all cases, an upfield shift is seen upon coordination. Its magnitude is around 1−2 ppm for aryl diphosphates,

Table 1. IR (KBr, cm^{-1}) and ^{31}P NMR (rel. to H_3PO_4) data

	$\nu_{as}(PO_2)$	$\nu_s(PO_2)$	$\delta(^{31}P)$
Na[PCP]	1237	1054	−6.0/26.5 (J = 5.4)
Na_2[POP[1]]	1270/1239	1141	−8.5
Li_2[POP[2]]	1256/1226	1155	−15.9
Li_2[POP[3]]	1270/1230	1140	−15.3
Li_2[POP[4]]	1249/1220	1138	−15.5
Li_2[POP[5]]	1254/1223	1155	−16.0
1 (PCP)	1230	1043	9.6/27.7 (J = 5.0)
2 (PCP)	1233	1048	12.2/26.7 (J = 10.1)
3 (POP^3)	1261/1223	1121	−15.8
4 (POP^4)	1258/1230	1119	−15.9
5 (POP^1)	1254/1222	1121	−10.6
6 (POP^1)	1246/1215	1122	−11.4
7 (POP^2)	1247/1224	1115	−17.5
8 (POP^3)	1253/1222	1112	−17.4
9 (POP^4)	1255/1227	1121	−17.3
10 (POP^5)	1259/1219	1115	−17.8
11 (POP^1)	1256/1224	1121	−10.1
12 (POP^1)	1249/1204	1123	−10.8
13 POP^2)	1263/1224	1126	−16.8
14 (POP^3)	1259/1228	1124	−16.5
15 (POP^1)	1281/1234	1127	−10.4
16 (POP^2)	1289/1247	1120	−16.6
17 ($ROPO_3$)	1155/1096[a]	–	−1.3/−1.0
18 ($ROPO_3$)	1156/1091[a]	–	−1.6/−1.0

[a] PO_3 vibrations.

2−3 ppm for benzyl diphosphate, and 10−15 ppm for triethyl methylenediphosphonate. This proves that the phosphates are coordinated to zinc even in good donor solvents such as DMSO or water.

Conclusions

The reliable tridentate attachment of the coligands in this study and the fact that all the complexes contain just one coligand per zinc ion has allowed the observation of three coordination modes for the diphosphates. Monodentate attachment of PCP and bis-monodentate attachment of the POP ligands seems to yield tetrahedral $ZnON_3$ complexes. The most typical coordination mode of the POP ligands seems to be the chelating one. It has been observed in five- and six-coordinate zinc complexes with the coordination patterns ZnO_2N_3 and ZnO_3N_3. The open-chain tridentate ligands favor five-coordination, while the TACN ligands enforce octahedral coordination.

Two unusual bonding types have been found. In one of these, the POP ligands act as chelators for one zinc ion and as additional donors for the other zinc ion in dinuclear complexes. In the other, organo-monophosphates, which result from hydrolysis, act as triply-bridging ligands in trinuclear $(LZn)_3(phosphate)_2$ complexes.

With regard to the catalytic function of zinc in conventional or biological oligophosphate hydrolyses, the complexes described here and in the preceding papers[1,2] seemingly give no mechanistic information. The chelating mode of the diphosphates seems to provide stabilization rather than activation. Specifically in enzymes, steric restrictions at the active center render a chelating coordination unlikely. We therefore decided to enforce similar steric restrictions through the use of encapsulating ligands for zinc. The succeeding paper[3] describes their application in zinc−diphosphate chemistry.

Experimental Section

General: For general working and measuring procedures, see ref.[15] The lithium and sodium salts of the diphosphates[2,4−6] were stored under anhydrous conditions, as were the hygroscopic coligands.[7−10] During the course of the reactions, no precautions were taken to prevent the access of moisture. All organic phosphates are potentially toxic and were handled accordingly.

Ligand PDEA: The Schiff base PDEI (derived from pyridine-2-carbaldehyde and *N*,*N*-dimethylethylenediamine[16]) (1.50 g, 8.40 mmol) was dissolved in methanol (15 mL). $NaBH_4$ (1.60 g, 42.3 mmol) was then slowly added with stirring. After stirring for 20 h, 2 N HCl (20 mL) was added. The resulting mixture was extracted with dichloromethane (3 × 20 mL). After drying with Na_2SO_4, the combined extracts were concentrated to dryness. Chromatography of the residue on a 2 × 20 cm silica gel column (0.063−0.20 mm) eluting with cyclohexane/ethyl acetate/triethylamine (8:2:1) yielded the product PDEA; R_f = 0.29. 1.02 g (68%) of PDEA was obtained as an orange oil, which was not analytically pure. − $C_{10}H_{17}N_3$ (179.3): calcd. C 67.00, H 9.56, N 23.44; found C 64.22, H 9.30, N 21.88. − ^{1}H NMR (CD_3OD): δ = 2.21 (s, 6 H, Me), 2.39 (t, *J* = 6.7 Hz, 2 H, CH_2), 2.63 (t, *J* = 6.7 Hz, 2 H, CH_2), 3.79 (s, 2 H, py-CH_2), 7.19 (m, 1 H, py), 7.36 (d, *J* = 7.7 Hz, 1 H, py), 7.70 (m, 1 H, py), 8.40 (d, *J* = 4.9 Hz, 1 H, py).

1: Na[PCP] (70 mg, 0.25 mmol) in boiling ethanol (5 mL) was added to a solution of DBA·H_2O (73 mg, 0.25 mmol) and $Zn(ClO_4)_2$·$6H_2O$ (92 mg, 0.25 mmol) in boiling ethanol (20 mL). After refluxing for 15 min., the mixture was filtered while hot, cooled to room temp., and then slowly concentrated to one third of its original volume. 97 mg (55%) of **1** was precipitated as a colorless powder; m.p. 186 °C. − $C_{23}H_{32}ClN_5O_{10}P_2Zn$ (701.3): calcd. C 39.39, H 4.60, N 9.99, Zn 9.32; found C 38.72, H 4.58, N 9.57, Zn 8.99. − ^{1}H NMR ([D_6]DMSO): δ = 1.05 (m, 9 H, CH_3), 2.36 (t, *J* = 19.8 Hz, 2 H, PCH_2P), 3.84 (m, 6 H, CH_2), 4.27 (s, 1 H, NH), 4.36 (s, 4 H, NCH_2), 7.31 (m, 4 H, Ph), 7.58 (m, 2 H, Ph), 8.07 (m, 2 H, Ph), 13.31 (s, 2 H, NH).

2: Prepared in the same manner as **1** from Na[PCP] (108 mg, 0.37 mmol) in methanol (20 mL) and $Zn(ClO_4)_2$·$6H_2O$ (140 mg, 0.37 mmol) and DPA (75 mg, 0.37 mmol) in methanol (20 mL). Yield 117 mg (50%) of **2** as a colorless powder; m.p. 186 °C. − $C_{19}H_{30}ClN_3O_{10}P_2Zn$ (623.2): calcd. C 36.62, H 4.85, N 6.74, Zn 10.49; found C 35.95, H 4.71, N 6.63, Zn 10.72. − ^{1}H NMR (D_2O): δ = 1.20 (m, 9 H, CH_3), 2.33 (t, *J* = 20.2 Hz, 2 H, PCH_2P), 3.86 (dq, *J* = 7.2, 7.3 Hz, 2 H, OCH_2), 4.15 (d, *J* = 16.6 Hz, 2 H, NCH_2), 4.25 (dq, *J* = 7.0, 7.1 Hz, 4 H, OCH_2), 4.53 (d, *J* = 16.6 Hz, 2 H, NCH_2), 7.49 (m, 4 H, Ph), 7.93 (dd, *J* = 8.5, 8.5 Hz, 2 H, Ph), 8.54 (d, *J* = 4.6 Hz, 2 H, Ph).

3: DPA (60 mg, 0.30 mmol) and $Zn(ClO_4)_2$·$6H_2O$ (112 mg, 0.30 mmol) were combined in methanol (12 mL). Li_2[POP^3] (55 mg, 0.15 mmol) in methanol (10 mL) was then added with stirring. After stirring for 15 h, the solvent was removed in vacuo and the residue was taken up in dichloromethane (25 mL). After filtering, *n*-heptane was carefully added to the filtrate until precipitation commenced. Subsequent slow evaporation of the solvent yielded 73 mg (45%) of **3** as colorless microcrystals; m.p. 195 °C. − $C_{38}H_{40}Cl_2N_6O_{15}P_2Zn_2$ (1084.4): calcd. C 42.09, H 3.72, N 7.75, Zn 12.06; found C 40.95, H 3.71, N 7.71, Zn 11.15. − ^{1}H NMR (CD_3OD): δ = 2.14 (s, 6 H, CH_3), 3.81 (d, *J* = 16.5 Hz, 4 H, NCH_2), 4.34 (d, *J* = 16.5 Hz, 4 H, NCH_2), 6.88 (s, 8 H, Ph), 7.38 (m, 4 H, py), 7.48 (d, *J* = 7.9 Hz, 4 H, py), 7.98 (m, 4 H, py), 8.42 (d, *J* = 4.6 Hz, 4 H, py).

4: Prepared in the same manner as **3** from DPA (29 mg, 0.15 mmol), $Zn(ClO_4)_2$·$6H_2O$ (54 mg, 0.15 mmol), and Li_2[POP^4] (34 mg, 0.073 mmol) in methanol (total volume 15 mL). Yield 50 mg (59%) of **4** as a colorless powder; m.p. 150−155 °C. − $C_{44}H_{52}Cl_2N_6O_{15}P_2Zn_2$ (1168.5): calcd. C 45.23, H 4.49, N 7.19, Zn 11.19; found C 44.65, H 4.40, N 7.07, Zn 11.03. − ^{1}H NMR (CD_3OD): δ = 1.25 (s, 18 H, *t*Bu), 3.92 (d, *J* = 16.7 Hz, 4 H, NCH_2), 4.43 (d, *J* = 16.7 Hz, 4 H, NCH_2), 6.99 (d, *J* = 8.7 Hz, 4 H, Ph), 7.21 (d, *J* = 8.7 Hz, 4 H, Ph), 7.49 (m, 8 H, py), 7.99 (m, 4 H, py), 8.62 (d, *J* = 3.9 Hz, 4 H, py).

5: Prepared in the same manner as **3** from PDEA (54 mg, 0.30 mmol), $Zn(ClO_4)_2$·$6H_2O$ (112 mg, 0.30 mmol), and Na_2[POP^1] (60 mg, 0.15 mmol) in methanol (total volume 25 mL); reflux for 2 h. Yield 80 mg (51%) of **5** as a colorless powder; m.p. 95 °C. − $C_{34}H_{48}Cl_2N_6O_{15}P_2Zn_2$ (1044.4): calcd. C 39.10, H 4.63, N 8.05, Zn 12.52; found C 39.75, H 4.65, N 7.77, Zn 11.81. − ^{1}H NMR (CD_3OD): δ = 2.27 (s, 12 H, NMe_2), 2.68 (m, 8 H, C_2H_4), 3.87 (d, *J* = 17.3 Hz, 2 H, NCH_2), 4.20 (d, *J* = 17.3 Hz, 2 H, NCH_2), 4.91 (d, *J* = 7.4 Hz, 4 H, OCH_2), 7.20 (s, 10 H, Ph), 7.38 (m, 4 H, py), 7.93 (m, 2 H, py), 8.62 (d, *J* = 4.4 Hz, 2 H, py).

6: $Na_2[POP^1]$ (272 mg, 0.68 mmol) was dissolved in hot methanol (50 mL) and as much water as necessary to obtain a clear solution. The resulting solution was added to a solution of DBA (200 mg, 0.68 mmol) and $Zn(ClO_4)_2{\cdot}6H_2O$ (252 mg, 0.68 mmol) in hot methanol (50 mL). The mixture was refluxed for 8 h and then stirred at room temp. for 48 h. During this time, 310 mg (65%) of **6** was precipitated as a colorless powder; m.p. 230 °C. − $C_{30}H_{29}N_5O_7P_2Zn{\cdot}H_2O$ (689.9 + 18.0): calcd. C 50.26, H 4.36, N 9.77, Zn 9.12; found C 50.88, H 4.30, N 9.70, Zn 8.67. − ^{1}H NMR ([D$_6$]DMSO): δ = 4.27 (d, *J* = 4.8 Hz, 4 H, NCH_2), 4.83 (dd, *J* = 2.7, 2.7 Hz, 4 H, OCH_2), 7.25 (m, 14 H, Ph + Bz), 7.54 (d, *J* = 8.0 Hz, 2 H, Ph), 8.43 (d, *J* = 8.0 Hz, 2 H, Ph).

7: $Li_2[POP^2]$ (116 mg, 0.34 mmol) in hot methanol (15 mL) was added to a solution of DBA (100 mg, 0.34 mmol) and $Zn(ClO_4)_2{\cdot}6H_2O$ (126 mg, 0.34 mmol) in boiling methanol (15 mL). On cooling, 99 mg (42%) of **7** was precipitated as a colorless powder; m.p. 270 °C. − $C_{28}H_{25}N_5O_7P_2Zn{\cdot}H_2O$ (670.9 + 18.0): calcd. C 48.82, H 3.95, N 10.17, Zn 9.49; found C 48.32, H 3.79, N 9.74, Zn 9.99. − ^{1}H NMR ([D$_6$]DMSO): δ = 4.23 (s, 4 H, NCH_2), 4.91 (s, 1 H, NH), 6.91 (m, 2 H, Ph), 7.08 (m, 8 H, Ph), 7.28 (m, 4 H, Ph), 7.56 (d, *J* = 7.4 Hz, 2 H, Ph), 8.34 (d, *J* = 7.4 Hz, 2 H, Ph), 13.27 (s, 2 H, NH).

8: Prepared in the same manner as **6** from $Li_2[POP^3]$ (94 mg, 0.21 mmol), DBA (62 mg, 0.21 mmol), and $Zn(ClO_4)_2{\cdot}6H_2O$ (78 mg, 0.21 mmol) in methanol (total volume 50 mL). Slow crystallization by evaporation of the solvent yielded 44 mg (30%) of **8** as colorless crystals; m.p. 300 °C. − $C_{30}H_{29}N_5O_7P_2Zn$ (689.9): calcd. C 51.56, H 4.18, N 10.02, Zn 9.35; found C 51.18, H 4.07, N 11.16, Zn 9.37. − ^{1}H NMR ([D$_6$]DMSO): δ = 2.13 (s, 6 H, CH_3), 4.22 (d, *J* = 4.9 Hz, 4 H, NCH_2), 6.82 (d, *J* = 8.5 Hz, 4 H, Ph), 6.94 (d, *J* = 8.5 Hz, 4 H, Ph), 7.26 (m, 4 H, Ph), 7.54 (d, *J* = 7.1 Hz, 2 H, Ph), 8.31 (d, *J* = 7.3 Hz, 2 H, Ph), 13.21 (s, 2 H, NH).

9: Prepared in the same manner as **6** from $Li_2[POP^4]$ (100 mg, 0.21 mmol), DBA (62 mg, 0.21 mmol), and $Zn(ClO_4)_2{\cdot}6H_2O$ (78 mg, 0.21 mmol) in methanol (total volume 20 mL). Yield 156 mg (95%) of **9** as colorless crystals; m.p. 260 °C. − $C_{36}H_{41}N_5O_7P_2Zn$ (783.1): calcd. C 55.22, H 5.28, N 8.94, Zn 8.35; found C 54.22, H 5.23, N 8.60, Zn 8.55. − ^{1}H NMR ([D$_6$]DMSO): δ = 1.19 (s, 18 H, *t*Bu), 4.24 (d, *J* = 4.2 Hz, 4 H, NCH_2), 6.98 (d, *J* = 8.8 Hz, 4 H, Ph), 7.08 (d, *J* = 8.8 Hz, 4 H, Ph), 7.25 (m, 4 H, Ph), 7.54 (d, *J* = 7.2 Hz, 2 H, Ph), 8.38 (d, *J* = 7.2 Hz, 2 H, Ph), 13.27 (s, 2 H, NH).

10: Prepared in the same manner as **6** from $Li_2[POP^5]$ (100 mg, 0.23 mmol), DBA (69 mg, 0.23 mmol), and $Zn(ClO_4)_2{\cdot}6H_2O$ (87 mg, 0.23 mmol) in methanol (total volume 65 mL). Slow crystallization by evaporation of the solvent yielded 76 mg (44%) of **10** as colorless crystals; m.p. 320 °C. − $C_{28}H_{23}Cl_2N_5O_7P_2Zn$ (739.8): calcd. C 45.46, H 3.13, N 9.47, Zn 8.84; found C 44.99, H 3.15, N 9.49, Zn 8.75. − ^{1}H NMR ([D$_6$]DMSO): δ = 4.27 (s, 4 H, NCH_2), 7.06 (m, 8 H, Ph), 7.26 (m, 4 H, Ph), 7.45 (d, *J* = 7.0 Hz, 2 H, Ph), 8.26 (d, *J* = 7.2 Hz, 2 H, Ph), 13.27 (s, 2 H, NH).

11: A solution of $K_2[POP^1]$ (130 mg, 0.70 mmol) in methanol (8 mL) was added to a solution of DPA (60 mg, 0.30 mmol) and $Zn(ClO_4)_2{\cdot}6H_2O$ (112 mg, 0.30 mmol) in methanol (15 mL). After stirring for 15 h, the mixture was filtered and the filtrate was concentrated to dryness. The residue was taken up in dichloromethane and the resulting solution was filtered. Addition of a few mL of *n*-heptane and slow evaporation of the solvents yielded 81 mg (44%) of **11** as colorless crystals; m.p. 170 °C. − $C_{26}H_{27}N_3O_7P_2Zn$ (620.9): calcd. C 50.30, H 4.38, N 6.77, Zn 10.53; found C 49.96, H 4.57, N 6.26, Zn 10.55. − ^{1}H NMR (CD_3OD): δ = 4.27 (d, *J* = 16.6 Hz, 2 H, NCH_2), 4.72 (d, *J* = 16.6 Hz, 2 H, NCH_2), 4.80 (dd, *J* = 3.2, 3.3 Hz, 4 H, OCH_2), 7.10 (s, 10 H, Ph), 7.20 (m, 2 H, py), 7.30 (d, *J* = 7.8 Hz, 2 H, py), 7.79 (m, 2 H, py), 8.68 (d, *J* = 5.5 Hz, 2 H, py).

12: $ZnCl_2$ (51 mg, 0.37 mmol) in acetonitrile/water (10 mL) was treated with TACN* (64 mg, 0.37 mmol) and $Na_2[POP^1]$ (150 mg, 0.37 mmol) in acetonitrile/water (20 mL). After stirring at 80 °C for 15 h, the mixture was slowly concentrated to a volume of 15 mL at room temp. 90 mg (36%) of **12** was precipitated as colorless crystals; m.p. 200 °C. − $C_{23}H_{35}N_3O_7P_2Zn{\cdot}5H_2O$ (592.9 + 90.1): calcd. C 40.45, H 6.64, N 6.15, Zn 9.57; found C 40.46, H 6.63, N 6.10, Zn 9.52. − ^{1}H NMR (CD_3OD): δ = 2.63 (s, 9 H, CH_3), 2.73 (s, 12 H, C_2H_4), 5.03 (dd, *J* = 3.2, 3.2 Hz, 4 H, OCH_2), 7.36 (m, 10 H, Ph).

13: Prepared in the same manner as **11** from $K_2[POP^2]$ (140 mg, 0.30 mmol), TACN* (51 mg, 0.30 mmol), and $Zn(ClO_4)_2{\cdot}6H_2O$ (112 mg, 0.30 mmol). Crystals were obtained by slow evaporation of the solvents from a methanol/water solution. Yield 124 mg (67%) of **13** as colorless crystals; m.p. 185 °C. − $C_{21}H_{31}N_3O_7P_2Zn{\cdot}3H_2O$ (564.8 + 54.0): calcd. C 40.76, H 6.03, N 6.79, Zn 10.57; found C 41.02, H 5.97, N 6.83, Zn 10.19. − ^{1}H NMR (CD_3OD): δ = 2.60 (s, 9 H, CH_3), 2.72 (s, 12 H, C_2H_4), 7.08 (m, 2 H, Ph), 7.25 (m, 8 H, Ph).

14: Prepared in the same manner as **11** from $Li_2[POP^3]$ (110 mg, 0.30 mmol), TACN* (51 mg, 0.30 mmol), and $Zn(ClO_4)_2{\cdot}6H_2O$ (112 mg, 0.30 mmol). Yield 93 mg (50%) of **14** as colorless crystals; m.p. 145 °C. − $C_{23}H_{35}N_3O_7P_2Zn{\cdot}1.5H_2O$ (592.9 + 27.0) calcd. C 44.56, H 6.18, N 6.75, Zn 10.55; found C 44.59, H 6.13, N 6.73, Zn 10.40. − ^{1}H NMR (CD_3OD): δ = 2.28 (s, 6 H, CH_3), 2.59 (s, 9 H, CH_3), 2.73 (s, 12 H, C_2H_4), 7.07 (s, 8 H, Ph).

15: Prepared in the same manner as **11** from $K_2[POP^1]$ (109 mg, 0.25 mmol), TACN (32.2 mg, 0.25 mmol), and $Zn(ClO_4)_2{\cdot}6H_2O$ (93 mg, 0.25 mmol). Yield 36 mg (25%) of **15** as colorless crystals. − $C_{20}H_{29}N_3O_7P_2Zn{\cdot}H_2O$ (550.8 + 18.0): calcd. C 42.23, H 5.49, N 7.39, Zn 11.50; found C 41.09, H 5.29, N 6.76, Zn 11.23. − ^{1}H NMR (CD_3OD): δ = 2.47 (m, 6 H, C_2H_4), 2.97 (m, 6 H, C_2H_4), 5.01 (s, 4 H, OCH_2), 7.34 (m, 10 H, Ph).

16: Prepared in the same manner as **11** from $K_2[POP^2]$ (102 mg, 0.25 mmol), PDEA (45 mg, 0.25 mmol), and $Zn(ClO_4)_2{\cdot}6H_2O$ (93 mg, 0.25 mmol). Yield 51 mg (35%) of **16** as colorless crystals; m.p. 175 °C. − ^{1}H NMR (CD_3OD): δ = 2.38 (s, 6 H, CH_3), 2.76 (m, 4 H, C_2H_4), 3.91 (d, *J* = 17.2 Hz, 1 H, NCH_2), 4.17 (d, *J* = 17.2 Hz, 1 H, NCH_2), 7.02 (m, 2 H, Ph), 7.20 (m, 8 H, Ph), 7.49 (m, 2 H, py), 8.03 (m, 1 H, py), 8.67 (d, *J* = 5.8 Hz, 1 H, py).

17: A solution of $Li_2[POP^3]$ (180 mg, 0.40 mmol) in hot methanol (40 mL) was added to a solution of BPA (160 mg, 0.80 mmol) and $Zn(ClO_4)_2{\cdot}6H_2O$ (299 mg, 0.80 mmol) in boiling methanol (20 mL). After refluxing for 10 min, the mixture was filtered while hot and the filtrate was cooled to −24 °C. 70 mg (32%) of **17** was precipitated as colorless crystals; m.p. 235 °C. − $C_{50}H_{54}N_9O_{12}P_3Zn_3{\cdot}H_2O$ (1262.1 + 18.0): calcd. C 46.91, H 4.41, N 9.85, Zn 15.32; found C 43.01, H 3.85, N 8.96, Zn 14.55. − ^{1}H NMR (CD_3OD): δ = 2.28 (s, 6 H, CH_3), 3.78 (d, *J* = 16.2 Hz, 6 H, NCH_2), 4.33 (d, *J* = 16.2 Hz, 6 H, NCH_2), 7.05 (m, 14 H, Ph, py), 7.41 (d, *J* = 7.8 Hz, 6 H, py), 7.83 (dd, *J* = 7.2, 7.8 Hz, 6 H, py), 8.59 (d, *J* = 4.8 Hz, 6 H, py). − ^{31}P NMR ([D$_6$]DMSO): δ = −1.3 (3 P), −1.0 (1 P).

18: Prepared in the same manner as **17** from $Li_2[POP^5]$ (106 mg, 0.25 mmol), BPA (99 mg, 0.50 mmol), and $Zn(ClO_4)_2{\cdot}6H_2O$

(185 mg, 0.50 mmol) in boiling methanol (total volume 40 mL). Yield 70 mg (32%) of **18** as colorless crystals; m.p. 235 °C. – $C_{48}H_{48}Cl_2N_9O_{12}P_3Zn{\cdot}H_2O$ (1302.9 + 18.0): calcd. C 44.25, H 3.71, N 9.68, Zn 15.05; found C 40.32, H 3.30, N 8.83, Zn 13.73. – ^{1}H NMR (CD_3OD): δ = 3.81 (d, J = 16.2 Hz, 6 H, NCH_2), 4.36 (d, J = 16.2 Hz, 6 H, NCH_2), 7.04 (dd, J = 5.7, 6.1 Hz, 6 H, py), 7.18 (m, 8 H, Ph), 7.43 (d, J = 7.8 Hz, 6 H, py), 7.82 (dd, J = 7.3, 7.4 Hz, 6 H, py), 8.58 (d, J = 4.4 Hz, 6 H, py). – ^{31}P NMR ([D_6]DMSO): δ = −1.6 (3 P), −1.0 (1 P).

Structure Determinations:[17] The selected crystals were taken directly from the reaction solutions and used without drying in vacuo. They were immersed in fluorinated polyether oil and immediately placed in the nitrogen stream of the diffractometer's cooling system. Diffraction data were recorded at ca. −100 °C using the ω/2θ technique on a Nonius CAD4 diffractometer fitted with a molybdenum tube (K_α, λ = 0.7107 Å) and a graphite monochromator. Empirical absorption corrections based on ψ scans were applied. The structures were solved by direct methods and refined anisotropically with the SHELX program suite.[18] Hydrogen atoms were included with fixed distances and isotropic temperature factors 1.5 times those of their attached atoms. Parameters were refined against F^2. The R values are defined as $R_1 = \Sigma|F_o - F_c|/\Sigma F_o$ and $wR_2 = \{\Sigma[w(F_o^2 - F_c^2)^2]\Sigma[w(F_o^2)^2]\}^{1/2}$. Drawings were produced with SCHAKAL.[19] The crystallographic data are collected in Table 2.

Table 2. Crystallographic details

	8	**12**	**15**
Empirical formula	$C_{30}H_{29}N_5O_7P_2Zn$	$C_{23}H_{35}N_3O_7P_2Zn{\cdot}5H_2O$	$C_{20}H_{29}N_3O_7P_2Zn{\cdot}H_2O$
Molecular mass	689.9	592.9 + 90.1	550.8 + 18.0
Crystal size [mm]	1.1 × 1.1 × 1.1	0.3 × 0.2 × 0.2	0.4 × 0.4 × 0.3
Space group	$P2_1/n$	$P\bar{1}$	$P\bar{1}$
Z	4	2	2
a [Å]	10.152(2)	8.911(1)	8.419(2)
b [Å]	16.232(3)	10.135(1)	10.457(2)
c [Å]	19.707(4)	17.751(2)	14.373(2)
α [°]	90	85.44(2)	79.37(3)
β [°]	99.02(3)	80.36(2)	87.62(3)
γ [°]	90	89.14(2)	79.20(3)
V [Å^3]	3207.3(11)	1575.5(4)	1221.6(4)
d(calcd) [gcm^{-3}]	1.47	1.44	1.55
μ(Mo-K_α) [mm^{-1}]	0.92	0.94	1.19
hkl range	h: 0 to 12	h: −11 to 11	h: −9 to 9
	k: 0 to 20	k: −13 to 12	k: −11 to 11
	l: −24 to 24	l: −22 to 23	l: −15 to 15
Measured reflections	6707	13914	7869
Independent reflections	6341	7055	3494
Observed refl. [$I > 2\sigma(I)$]	4633	5902	2749
Parameters	406	370	307
Refined reflections	6341	7055	3494
R_1 (obsd. refl.)	0.055	0.043	0.044
wR_2 (all refl.)	0.155	0.154	0.132
Residual electron density	+1.4	+0.7	+0.7
[e/Å^3]	−0.6	−0.5	−0.5

	16	**17**	**18**
Empirical formula	$C_{22}H_{27}N_3O_7P_2Zn{\cdot}0.5H_2O$	$C_{50}H_{54}N_9O_{12}P_2Zn_3{\cdot}H_2O$	$C_{48}H_{48}Cl_2N_9O_{12}P_3Zn{\cdot}H_2O$
Molecular mass	572.8 + 9.0	1262.1 + 18.0	1302.9 + 18.0
Crystal size [mm]	0.4 × 0.3 × 0.3	0.5 × 0.2 × 0.1	0.3 × 0.2 × 0.2
Space group	$C2/c$	$P4_2/n$	$P4_2/n$
Z	8	8	8
a [Å]	16.611(2)	21.349(3)	21.284(3)
b [Å]	12.503(1)	21.349(3)	21.284(3)
c [Å]	24.954(2)	26.636(5)	26.242(5)
α [°]	90	90	90
β [°]	100.22(2)	90	90
γ [°]	90	90	90
V [Å^3]	5100.4(8)	12140(3)	11888
d(calcd) [gcm^{-3}]	1.51	1.39	1.46
μ(Mo-K_α) [mm^{-1}]	1.14	2.67 (Cu)	1.44
hkl range	h: −21 to 10	h: 0 to 26	h: −22 to 0
	k: −16 to 15	k: 0 to 26	k: −22 to 0
	l: −33 to 31	l: 0 to 33	l: −28 to 0
Measured reflections	15660	13079	7992
Independent reflections	6035	12399	7429
Observed refl. [$I > 2\sigma(I)$]	4021	8410	3173
Parameters	321	698	698
Refined reflections	6035	12399	7429
R_1 (obsd. refl.)	0.033	0.090	0.110
wR_2 (all refl.)	0.075	0.279	0.378
Residual electron density	+0.6	+2.3	+1.4
[e/Å^3]	−0.3	−0.8	−0.6

Acknowledgments

This work was supported by the Fonds der Chemischen Industrie. We are indebted to Drs. W. Deck and A. Trösch for help with the structure determinations.

[1] A. Müller-Hartmann, H. Vahrenkamp, *Eur. J. Inorg. Chem.* **2000**, 2355−2361, preceding paper.
[2] A. Müller-Hartmann, H. Vahrenkamp, *Inorg. Chim. Acta* **2000**, *300−302*, 531−536.
[3] A. Müller-Hartmann, H. Vahrenkamp, *Eur. J. Inorg. Chem.* **2000**, 2371−2377, succeeding paper.
[4] J. A. Stock, *J. Org. Chem.* **1979**, *44*, 3997−3999.
[5] L. Zervas, I. Dilaris, *Chem. Ber.* **1956**, *89*, 925−933.
[6] F. Cramer, M. Winter, *Chem. Ber.* **1959**, *92*, 2761−2767.
[7] H. Adams, N. A. Bailey, J. D. Crane, D. E. Fenton, *J. Chem. Soc., Dalton Trans.* **1990**, 1727−1735.
[8] J. K. Romary, J. E. Bunds, J. D. Berger, *J. Chem. Eng. Data* **1967**, *12*, 224−226.
[9] G. H. Searle, R. J. Geve, *Aust. J. Chem.* **1984**, *37*, 959−970.
[10] M. Ciampolini, N. Nardi, *Inorg. Chem.* **1966**, *5*, 41−44.
[11] D. Wahnon, R. C. Hynes, J. Chin, *J. Chem. Soc., Chem. Commun.* **1994**, 1441−1442.
[12] K. Aoki, H. Yamazaki, *J. Am. Chem. Soc.* **1980**, *102*, 6878−6880.
[13] P. Chaudhuri, C. Stockheim, K. Wieghardt, W. Deck, R. Gregorzik, H. Vahrenkamp, B. Nuber, J. Weiss, *Inorg. Chem.* **1992**, *31*, 1451−1457.
[14] E. Kimura, S. Aoki, T. Koike, M. Shiro, *J. Am. Chem. Soc.* **1997**, *119*, 3068−3076.
[15] M. Förster, R. Burth, A. K. Powell, T. Eiche, H. Vahrenkamp, *Chem. Ber.* **1993**, *126*, 2643−2648.
[16] G. Zakrzewski, E. C. Lingafelter, *Inorg. Chim. Acta* **1970**, *4*, 251−257.
[17] Crystallographic data (excluding structure factors) for the structures reported in this paper have been deposited with the Cambridge Crystallographic Data Centre as supplementary publication nos. CCDC-141962 (for **8**), -141963 (for **12**), -141964 (for **15**), -141965 (for **16**), -141966 (for **17**), and -141967 (for **18**). Copies of the data can be obtained free of charge on application to the CCDC, 12 Union Road, Cambridge CB2 1EZ, U.K. [Fax: (internat.) + 44-1223/336-033; E-mail: deposit@ccdc.cam.ac.uk].
[18] G. M. Sheldrick, *SHELX-86* and *SHELXL-93*, *Programs for Crystal Structure Determination*, Universität Göttingen, **1986** and **1993**.
[19] E. Keller, *SCHAKAL for Windows*, Universität Freiburg, **1999**.
Received March 23, 2000
[I00110]

Zinc Complexes of Condensed Phosphates, 4[‡]

Diphosphate−Zinc Complexes with Encapsulating Tripodal Coligands

Alexandra Müller-Hartmann[a] and Heinrich Vahrenkamp*[a]

Keywords: Zinc / Phosphates / Organic pyrophosphates / Methylene diphosphonates / Phosphatases

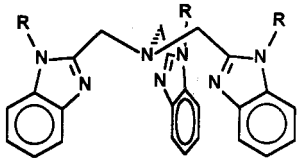
Tris(benzimidazolylmethyl)amine (TBA) and tris(pyrazolyl)borate (Tp) ligands have been used to prepare ternary zinc complexes with triorganodiphosphates (R_3POP^-), triorganomethylenediphosphonates (R_3PCP^-), and diorganodiphosphates (R_2POP^{2-}). The complex types $[(TBA)Zn(R_3POP)]^+$ and $[(TBA)Zn(R_3PCP)]^+$ have been assigned as containing trigonal-bipyramidal zinc with monodentate diphosphate ligands. By X-ray structure determination, the complex type $[(TBA)Zn(R_2POP)]$ has been found to contain the same ZnN_4O coordination pattern, which has also been assigned to the dinuclear complexes $[(TBA)Zn(R_2POP)Zn(TBA)]^{2+}$ incorporating the diphosphates as bis-monodentate bridging ligands. The same monodentate and bis-monodentate attachment of the diphosphates, but with tetrahedral zinc in a ZnN_3O environment, has been identified in the pyrazolylborate complexes $TpZn(R_3POP)$ and $TpZn(R_2POP)ZnTp$.

Introduction

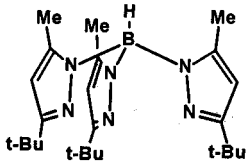
This paper is the fourth and final one in a series on zinc complexes of oligophosphates.[1−3] Our main motivation for this work has stemmed from the importance of metal-containing enzymes in biological phosphate transfer to and from inorganic pyrophosphate, ADP, ATP, and the like, which is among the most frequently observed biological processes. In the first papers of the series,[2,3] we made reference to the biochemical and biostructural background of the work and surveyed the literature on the associated coordination chemistry. While there have been numerous solution studies[4] and structure determinations[5] of metal−ATP species, literature on other metal−oligophosphate compounds is scarce. In the coordination chemistry of zinc, which is of particular interest to us, we are not aware of any studies on soluble complex species other than those of nucleotides.[4,6−8]

Our aim in this field, as before,[9,10] has been to learn about function from structure. We set out to delineate all possible coordination modes between zinc ions and oligophosphate species. In order to avoid typical lattice structures and coordination polymers, which cannot be biorelevant, we reduced the functionality of both the phosphates and the zinc species. The former was achieved by esterification, i.e. rather than pyrophosphate we used diorgano- and triorganodiphosphates. The latter was achieved by reducing the number of available coordination sites at zinc through the use of chelating coligands. We found that bidentate[3] and even tridentate coligands[1] still allow the oligophosphates to become polydentate towards one zinc ion. A further reduction in the functionality at zinc was thus deemed necessary.

In this paper, we describe the use of tripodal coligands for this purpose. As such, we used tris(benzimidazolylmethyl)amine (TBA) and its benzyl derivative TBA*, which we have previously found to be a reliable enforcer of trigonal-bipyramidal coordination in (TBA)Zn−X complexes.[11,12] Likewise, the 3-substituted tris(pyrazolyl)borate (Tp) ligands are known to be tetrahedral enforcers,[13] particularly the *tert*-butyl-substituted Tp*.[14] It thus had to be established whether the enforcing qualities of these tripodal coligands would be sufficiently strong to limit the oligophosphates to monodentate coordination towards one zinc ion.



TBA : R = H
TBA*: R = benzyl



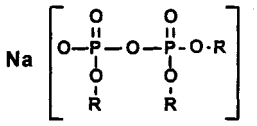
Tp*

The oligophosphates used were the same as those used previously. The methylenediphosphonate PCP and the diphosphates PO^1 and PO^2, both having three organic substituents, were expected to be monofunctional and possibly monodentate. The diorganodiphosphates POP^1−POP^4 were expected to be difunctional, and we know[1,3] that their preferred bonding mode is as OPOPO chelate ligands, which should be unlikely in the presence of the tripodal coligands. Thus, we hoped to limit the oligophosphates to monodentate coordination towards one zinc ion and possibly bis-monodentate coordination as bridging ligands in dinuclear complexes.

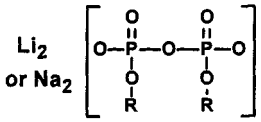
[‡] Part 3: Ref.[1]

[a] Institut für Anorganische und Analytische Chemie der Universität Freiburg,
Albertstraße 21, 79104 Freiburg, Germany
Fax: (internat.) + 49-(0)761/203-6001
E-mail: vahrenka@uni-freiburg.de

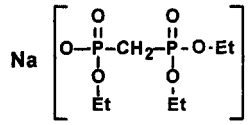
 © WILEY-VCH Verlag GmbH, D-69451 Weinheim, 2000 1434−1948/00/1111−2371 $ 17.50+.50/0



PO[1]: R = benzyl
PO[2]: R = p-Br-benzyl



POP[1]: R = benzyl
POP[2]: R = p-tolyl
POP[3]: R = p-t-Bu-phenyl
POP[4]: R = p-Cl-phenyl

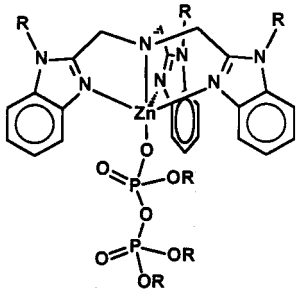


PCP

(TBA)Zn Complexes of Triorganodiphosphates

Both TBA ligands were combined with zinc perchlorate and the three monofunctional phosphates PO^1, PO^2, and PCP. In all six cases, complexes with a 1:1:1 composition, **1**−**6**, were produced as perchlorate salts. While crystals of **1**−**6** suitable for X-ray analysis could not be obtained, FAB mass spectra of **1**, **2**, and **5** and an ESI mass spectrum of **3**, each showing the parent ion of the respective cationic complex as the only prominent peak, supported the assignment of the complexes as monomolecular. This makes it likely that the oligophosphates are monodentate and that the coordination geometry is trigonal-bipyramidal as indicated below.

$[(TBA)Zn(PO^1)]^+$	$[(TBA)Zn(PO^2)]^+$	$[(TBA)Zn(PCP)]^+$
1	**2**	**3**
$[(TBA^*)Zn(PO^1)]^+$	$[(TBA^*)Zn(PO^2)]^+$	$[(TBA^*)Zn(PCP)]^+$
4	**5**	**6**



The IR data for the P−O vibrations (Table 1) show a characteristic shift of the 1100 cm^{-1} band, attributable to $\nu_s(PO_2)$, to lower wavenumbers (cf. refs.[1,3]), but yield no structural information. In contrast, the ^{31}P NMR data are quite informative. All the phosphate ligands in **1**−**6** are unsymmetrical with typical shifts for the ^{31}P nuclei and typical coupling constants. Upon coordination to zinc, one of the two ^{31}P resonances is shifted upfield by 2−5 ppm while the other remains unchanged, and the coupling constants become characteristically smaller. This is in full agreement with the structural assignments. Together with the structure determinations of **8** and **10** (see below), these observations lend support to the statement that in all complexes **1**−**6** the oligophosphate ligands are monodentate.

Table 1. IR data (KBr, cm^{-1}) and ^{31}P NMR data (DMSO, rel. to H_3PO_4, ppm/Hz) of **1**−**6** and their phosphate constituents

	ν(PO)	δ/*J*(^{31}P)
Na[PO^1]	1277 vs, 1136 m	−11.5, −10.9/21.1
Na[PO^2]	1273 vs, 1133 s	−11.6, −11.0/21.1
Na[PCP]	1237 s, 1054 vs	−6.0, +26.5/5.4
[**1**]ClO_4	1277 s, 1110 s	−15.0, −11.5/17.0
[**2**]ClO_4	1279 s, 1120 vs	−14.8, 11.6/16.6
[**3**]ClO_4	1224 s, 1041 vs	−8.1, +24.3/5.1
[**4**]ClO_4	1282 s, 1119 s	−15.1, −11.4/16.4
[**5**]ClO_4	1285 s, 1122 s	−14.8, −11.5/17.1
[**6**]ClO_4	1235 s, 1039 vs	−7.8, +26.1/5.1

(TBA)Zn Complexes of Diorganodiphosphates

Having established that the phosphates can be monodentate in (TBA)Zn complexes, it seemed likely that the bifunctional POP^{2-} ligands would also have this ability, being monodentate in (TBA)Zn(POP) complexes and bis-monodentate in dinuclear $[(TBA)Zn(POP)Zn(TBA)]^{2+}$ complexes. Both alternatives could be realized. Of the eight possibilities in each case, combining the given TBA and POP ligands, four could be realized for the mononuclear complexes and five for the dinuclear complexes. The mononuclear and dinuclear combinations are almost mutually exclusive, i.e. for a given set of TBA and POP only one of the two alternatives seems to be stable.

Mononuclear complexes were isolated only for the unsubstituted coligand TBP, but with all four POP ligands. Compounds **7**−**10** could be unambiguously identified as mononuclear and molecular entities, e.g. by X-ray structure determinations of **8** and **10** and through the FAB mass spectrum of **9**. Among them, **8** and **10** are the only species for which the dinuclear alternative (**11**, **12**, see below) also exists. However, **8** and **10** could not be prepared in suitably pure form from 1:1:1 mixtures of zinc salts, TBA, and $[POP]^{2-}$. They were obtained from solutions of **11** and **12** when these were left to stand for prolonged periods in attempts to obtain crystals of the latter for structure determinations.

(TBA)Zn(POP^n)

7: $n = 1$ **8**: $n = 2$ **9**: $n = 3$ **10**: $n = 4$

In those cases where the syntheses of the dinuclear complexes were successful, they proceeded straightforwardly from 2:2:1 mixtures of zinc perchlorate, the TBA ligand, and the POP salt. Proof of the dinuclear nature of complexes **11**−**15** and disproof of their existence as coordination polymers was obtained from a FAB mass spectrum of **11** and an ESI mass spectrum of **14**, both of which showed the parent ion of the complex cation as the prominent peak.

Attempts to grow crystals of **11**−**15** for structure determinations were unsuccessful.

(TBA)Zn(POP^n)Zn(TBA)

11: $n = 2$ **12**: $n = 4$

(TBA*)Zn(POP^n)Zn(TBA*)

13: $n = 2$ **14**: $n = 3$ **15**: $n = 4$

The IR and ^{31}P NMR spectra of complexes **7**−**15** (Table 2) yield less information than might have been expected. The strong and characteristic IR bands due to the P−O vibrations are shifted by small amounts, as observed previously.[1,3] A typical feature arising from the coordination of the diphosphates is the pronounced decrease in the intensity of the $\nu_s(PO_2)$ band. The ^{31}P NMR signals undergo the usual upfield shifts of 2−4 ppm upon coordination of the phosphates to zinc. Again,[1,3] in those cases where the diphosphates should be unsymmetrical (complexes **7**−**10**), there is only one ^{31}P resonance rather than two. As before, the explanation for this must be that in solution the complexes are labile and undergo rapid exchange of their coordinated and uncoordinated P−O donor functions.

Table 2. IR data (KBr, cm^{-1}) and ^{31}P NMR data (DMSO, rel. to H_3PO_4, ppm) of **7**−**15** and their phosphate constituents

	$\nu_{as}(PO_2)$	$\nu_s(PO_2)$	$\delta(^{31}P)$
Na_2[POP^1]	1270/1239	1141	−8.5
Li_2[POP^2]	1270/1230	1140	−15.3
Li_2[POP^3]	1249/1220	1138	−15.5
Li_2[POP^4]	1254/1223	1155	−16.0
7	1279/1223		−11.0
8	1278/1225	1123	−17.1
9	1263/1230		−16.8
10	1257/1235		−17.6
[**11**]$(ClO_4)_2$	1279/1258		−17.8
[**12**]$(ClO_4)_2$	1279/1265		−19.1
[**13**]$(ClO_4)_2$	1280/1224	1160	−17.8
[**14**]$(ClO_4)_2$	1277		−17.9
[**15**]$(ClO_4)_2$	1282/1236	1161	−19.1

Structure determinations of **8** and **10** were necessary to eliminate any doubts concerning the structural assignments of the complexes in this class. They verified the monodentate coordination of the diphosphates in the 1:1:1 complexes **7**−**10**. By analogy and spectroscopic similarity, they furthermore supported the assignment of bis-monodentate coordination in the 2:2:1 complex cations **11**−**15**. The molecular structures of **8** (Figure 1) and **10** (Figure 2) are quite similar in terms of the environment of the zinc ions. However, they show conformational differences, specifically in the orientation of the phenyl rings at the phosphates. Moreover, in **8** there are two independent complex molecules in the asymmetric unit, which again differ conformationally, most notably in their non-bonding Zn···O(P) distances.

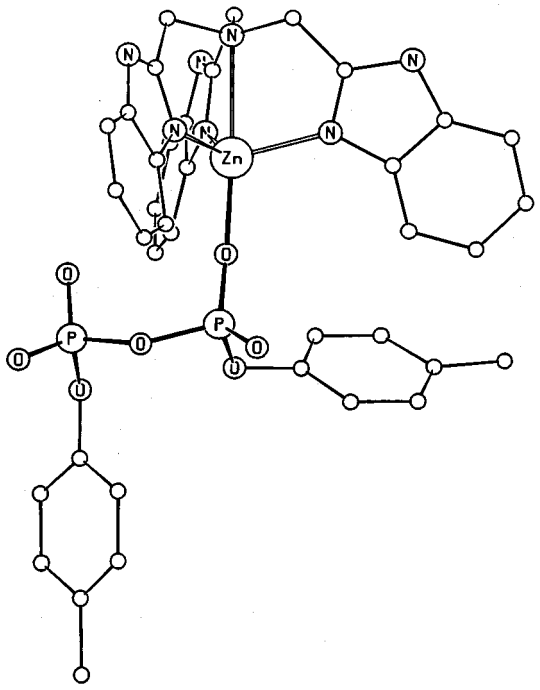


Figure 1. Molecular structure of **8**; selected bond lengths [Å] and angles [°] for both independent molecules: Zn−N(ax) 2.490(4), 2.474(4), Zn−N(eq) 2.030−2.039(4), 2.030−2.044(4), Zn−O 1.969(4), 1.979(4), Zn···O 4.109(4), 3.550(4), P−O(Zn) 1.485(4), 1.480(4), P=O 1.474−1.479(4), 1.475−1.484(4), P−O(P) 1.595−1.617(4), 1.591−1.619(4); Zn−O−P 164.0(3), 156.7(2), P−O−P 136.2(3), 135.7(2)

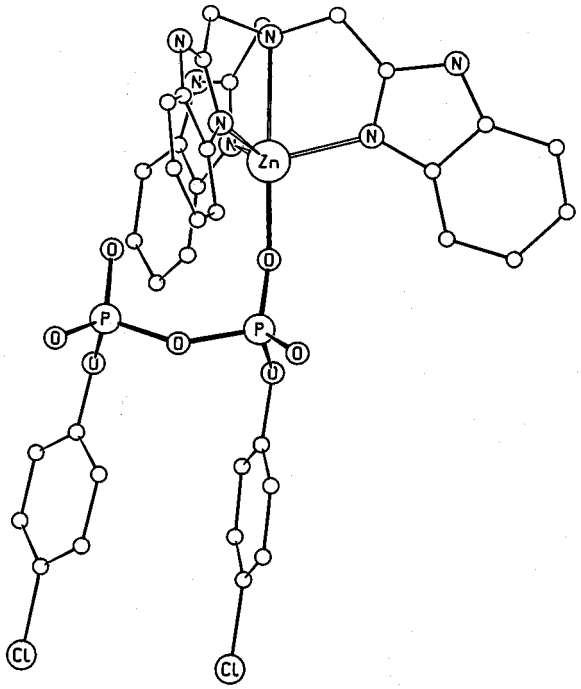


Figure 2. Molecular structure of **10**; selected bond lengths [Å] and angles [°]: Zn−N(ax) 2.49(2), Zn−N(eq) 2.01−2.03(2), Zn−O 1.97(1), Zn···O 3.48(1), P−O(Zn) 1.48(2), P=O 1.44−1.47(2), P−O(P) 1.60, 1.62(2); Zn−O−P 165(1), P−O−P 136(1)

The coordination of the zinc ions in **8** and **10** can be described as trigonal-bipyramidal. As usual for TBA com-

plexes,[11,12] the elongation of the axial Zn−N bond is so pronounced and the equatorial Zn−N bonds are so clearly bent away from the Zn−O bond (102−107°) that a tetrahedral description (ignoring the axial Zn−N interaction) is also appropriate. Accordingly, the Zn−O bond is almost as short as in tetrahedral zinc−phosphate complexes.[15,16] The diphosphates are coordinated to zinc in a clearly monodentate fashion. Although one P−O donor function on the second phosphorus atom is oriented towards the zinc ion, its Zn−O distance (3.5−4.1 Å) is outside the range for bonding. Monodentate coordination of oligophosphates to zinc is unprecedented. There are, however, examples in $(NH_3)_5Co^{III}$−oligophosphate chemistry.[17,18] All bonding parameters of the diphosphates in **8** and **10** correspond to those of the same phosphates in the chelating mode and have been discussed in the preceding papers.[1,3] The most important observation in this respect concerns the formal P=O bond lengths, which do not change when one, two, or three of these P=O units are coordinated to zinc, thus indicating that the Zn−O interactions are quite ionic.

(Tp)Zn Complexes

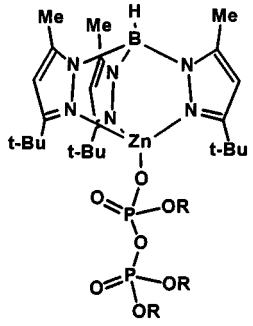
The pyrazolylborate ligand Tp* could be expected to confine the zinc ion to a tetrahedral coordination. The products obtained following condensation reactions of Tp* Zn−OH with the diphosphoric acids $HP_2O_4(OR)_3$ and $H_2P_2O_5(OR)_2$ seemed to confirm this. The monofunctional triorganodiphosphates H[PO^1] and H[PO^2] yielded the mononuclear complexes **16** and **17**, while 2:1 reactions of Tp*Zn−OH with the difunctional diorganodiphosphates led to the dinuclear complexes **18** and **19**.

Tp*Zn(PO^1)	Tp*Zn(PO^2)
16	**17**
Tp*Zn(POP^1)ZnTp*	Tp*Zn(POP^2)ZnTp*
18	**19**

The molecular nature of **16−19** is evident from their solubilities in non-polar solvents. Their nuclearity was confirmed by a FAB mass spectrum of **17** and an ESI mass spectrum of **18**. The IR bands due to the P−O vibrations (Table 3) show little variation as compared to those of the anionic diphosphates (cf. Tables 1 and 2). The most significant information is provided by the ^{31}P NMR spectra recorded in non-polar solvents (Table 3). In all four cases, a considerable upfield shift (7−8 ppm) of the ^{31}P resonance of the zinc-coordinated phosphate unit to higher field is seen, while that of the uncoordinated phosphate unit in **16** and **17** remains practically unchanged. Thus, there is good evidence that the phosphates in **16** and **17** are indeed monodentate and that those in **18** and **19** are bis-monodentate. Together with the evidence from the structure determinations of **8** and **10**, the structural assignments given below for **16** and **17** seem appropriate.

Table 3. IR data (KBr, cm^{-1}) and ^{31}P NMR data ($CDCl_3$, rel. to H_3PO_4, ppm/Hz) of **16−19**

	ν(PO)	δ/J(^{31}P)
16	1290, 1187, 1137	−11.8, −18.3/11.2
17	1279, 1185, 1136	−11.6, −18.3/10.0
18	1278, 1186	−15.3
19	1292, 1187, 1123	−23.6



Conclusions

This paper concludes the series of investigations on the coordination of condensed phosphates to zinc. Throughout the series, phosphates with organic substituents have been employed, such that they have some relation to the most important biological oligophosphates, i.e. nucleotides. The available coordination sites at zinc have been controlled by using "naked" zinc ions,[2] bidentate,[3] tridentate,[1] and encapsulating tripodal coligands (this paper). The oligophosphates have been found to be mono-, di-, tri-, and possibly tetradentate. Three coordination sites at zinc had to be blocked in order to prevent the formation of coordination polymers. Furthermore, considerable steric hindrance had to be enforced to ensure purely monodentate coordination. The most commonly encountered coordination mode is that of an OPOPO chelate ligand.

In terms of the catalytic activation of the oligophosphates by zinc for hydrolytic reactions, the monodentate and chelating bidentate coordination modes seem to be relevant. Both provide one point of attachment per phosphate unit, thereby activating the P−O function, and leave coordination sites at the zinc or space in the coordination sphere for the hydrolytic nucleophile. We favor the monodentate attachment, as we have already presented preparative[15,16] and mechanistic[9,10] evidence in support of it. This paper has proved its existence in the environment of encapsulating ligands, which resembles most closely that in enzymes.

An aim of this series of investigations (refs.[1−3] and this paper) was to provide structural information related to catalytic events. Accordingly, conditions favoring stoichiometric or catalytic hydrolyses of the oligophosphates were carefully avoided. Nevertheless, some hydrolytic decomposition was observed, underlining the reactivity of the intermediate zinc−aqua and zinc−hydroxide species in this respect.

Thus, the natural extension of this work will be catalytic studies, in continuation of our previous work on the hydrolyses of pyrophosphates and sulfonatophosphates.[15]

Experimental Section

General: For general working and measuring procedures, see ref.[19] The lithium and sodium salts and the free acids of the triorgano-[20,21] and diorganodiphosphates,[2,20,22] as well as the TBP[11] coligands and Tp*Zn−OH,[23] were stored under inert conditions. During the course of the reactions no precautions were taken to prevent the access of moisture. All organic phosphates are potentially toxic and were handled accordingly.

1: A solution of TBA (100 mg, 0.245 mmol) and $Zn(ClO_4)_2·6H_2O$ (91 mg, 0.25 mmol) in ethanol (10 mL) was added to a solution of Na[PO^1] (115 mg, 0.245 mmol) in boiling ethanol (30 mL). After stirring for 15 min., the precipitate was filtered off and recrystallized from hot ethanol to yield 151 mg (58%) of [**1**]·ClO_4, m.p. 170 °C. − $C_{45}H_{42}ClN_7O_{11}P_2Zn·2H_2O$ (1019.5 + 36.0): calcd. C 51.20, H 4.39, N 9.29, Zn 6.19; found C 51.51, H 3.97, N 9.17, Zn 5.68. − ^{1}H NMR ([D$_6$]DMSO): δ = 3.32 (s, 4 H, H_2O), 4.53 (s, 6 H, CH_2), 5.08 (d, J = 7.4 Hz, 4 H, CH_2), 5.25 (d, J = 6.4 Hz, 2 H, CH_2), 7.12 (t, J = 8.0 Hz, 3 H, Ph), 7.28 (m, 15 H, Ph), 7.40 (m, 3 H, Ph), 7.56 (d, J = 8.4 Hz, 3 H, Ph), 8.43 (d, J = 8.4 Hz, 3 H, Ph), 14.12 (s, 3 H, NH).

2: Prepared in the same manner as **1** from TBA (58 mg, 0.14 mmol), $Zn(ClO_4)_2·6H_2O$ (53 mg, 0.14 mmol), and Na[PO^2] (100 mg, 0.14 mmol). Yield 107 mg (60%) of [**2**]·ClO_4; m.p. 142 °C. − $C_{45}H_{39}Br_3ClN_7O_{11}P_2Zn$ (1256.3): calcd. C 43.02, H 3.13, N 7.80, Zn 5.20; found C 42.76, H 3.17, N 7.30, Zn 5.30. − ^{1}H NMR ([D$_6$]DMSO): δ = 4.53 (s, 6 H, CH_2), 5.05 (d, J = 7.9 Hz, 4 H, CH_2), 5.18 (d, J = 7.3 Hz, 2 H, CH_2), 7.1−7.5 (m, 18 H, Ph), 7.56 (d, J = 8.1 Hz, 3 H, Ph), 8.38 (d, J = 7.9 Hz, 3 H, Ph), 13.53 (s, 3 H, NH).

3: Prepared in the same manner as **1** from TBA (79 mg, 0.19 mmol), $Zn(ClO_4)_2·6H_2O$ (72 mg, 0.19 mmol), and Na[PCP] (55 mg, 0.19 mmol). Yield 114 mg (72%) of [**3**]·ClO_4; m.p. 156 °C. − $C_{31}H_{38}ClN_7O_{10}P_2Zn$ (831.5): calcd. C 44.78, H 4.61, N 11.79, Zn 7.86; found C 42.90, H 4.57, N 11.02, Zn 6.29. − ^{1}H NMR ([D$_6$]DMSO): δ = 1.13 (m, 9 H, CH_3), 2.47 (m, 2 H, PCH_2P), 3.95 (q, J = 7.2 Hz, 4 H, OCH_2), 4.14 (q, J = 7.2 Hz, 2 H, OCH_2), 4.53 (s, 6 H, CH_2), 7.32 (m, 6 H, Ph), 7.56 (m, 3 H, Ph), 8.52 (m, 3 H, Ph), 13.42 (s, 3 H, NH).

4: Prepared in the same manner as **1** from Na[PO^1] (69 mg, 0.15 mmol), $Zn(ClO_4)_2·6H_2O$ (54 mg, 0.15 mmol), and TBA* (100 mg, 0.15 mmol). Yield 92 mg (48%) of [**4**]·ClO_4; m.p. 110 °C. − $C_{66}H_{60}ClN_7O_{11}P_2Zn·H_2O$ (1290.1 + 18.0): calcd. C 60.60, H 4.78, N 7.50, Zn 5.00; found C 60.13, H 4.31, N 8.16, Zn 4.23. − ^{1}H NMR ([D$_6$]DMSO): δ = 3.31 (s, 2 H, H_2O), 4.61 (s, 6 H, CH_2), 5.06 (d, J = 7.4 Hz, 4 H, OCH_2), 5.27 (d, J = 8.0 Hz, 2 H, OCH_2), 5.53 (s, 6 H, CH_2), 7.30 (m, 36 H, Ph), 7.61 (d, J = 8.8 Hz, 3 H, Ph), 8.46 (d, J = 8.8 Hz, 3 H, Ph).

5: Prepared in the same manner as **1** from Na[PO^2] (104 mg, 0.15 mmol), $Zn(ClO_4)_2·6H_2O$ (55 mg, 0.15 mmol), and TBA* (100 mg, 0.15 mmol). Yield 114 mg (51%) of [**5**]·ClO_4; m.p. 116 °C. − $C_{66}H_{57}Br_3ClN_7O_{11}P_2Zn$ (1526.7): calcd. C 51.92, H 3.76, N 6.42, Zn 4.28; found C 51.49, H 3.87, N 6.39, Zn 4.00. − ^{1}H NMR ([D$_6$]DMSO): δ = 4.60 (s, 6 H, CH_2), 5.03 (d, J = 8.1 Hz, 4 H, OCH_2), 5.18 (d, J = 6.9 Hz, 2 H, OCH_2), 5.51 (s, 6 H, CH_2), 7.1−7.5 (m, 33 H, Ph), 7.60 (d, J = 8.3 Hz, 3 H, Ph), 8.45 (m, 3 H, Ph).

6: Prepared in the same manner as **1** from Na[PCP] (13 mg, 0.05 mmol), $Zn(ClO_4)_2·6H_2O$ (17 mg, 0.05 mmol), and TBP* (31 mg, 0.05 mmol). Yield 40 mg (79%) of [**6**]·ClO_4; m.p. 200 °C. − $C_{52}H_{56}ClN_7O_{10}P_2Zn$ (1101.8): calcd. C 56.68, H 5.12, N 8.90, Zn 5.93; found C 55.72, H 5.58, N 8.62, Zn 5.93. − ^{1}H NMR ([D$_6$]DMSO): δ = 0.83 (t, J = 7.0 Hz, 6 H, CH_3), 1.22 (t, J = 7.9 Hz, 3 H, CH_3), 2.33 (t, J = 20.0 Hz, 2 H, PCH_2P), 3.65 (q, J = 7.2 Hz, 4 H, OCH_2), 4.14 (q, J = 7.0 Hz, 2 H, OCH_2), 4.62 (s, 6 H, CH_2), 5.49 (s, 6 H, CH_2), 7.1−7.3 (m, 21 H, Ph), 7.60 (m, 3 H, Ph), 8.51 (m, 3 H, Ph).

7: A solution of Na_2[POP^1] (30 mg, 0.075 mmol) in boiling methanol (40 mL) was added to a solution of TBA (30 mg, 0.075 mmol) and $Zn(ClO_4)_2·6H_2O$ (28 mg, 0.075 mmol) in boiling methanol (10 mL). The mixture was filtered while hot, slowly allowed to cool to room temp., and kept in a desiccator to allow slow removal of the solvent. 45 mg (71%) of **7**, m.p. 250 °C (dec.), was isolated. − $C_{38}H_{35}N_7O_7P_2Zn·CH_3OH$ (829.1 + 32.0): calcd. C 54.40, H 4.56, N 11.39, Zn 7.59; found C 53.47, H 4.45, N 11.26, Zn 7.50. − ^{1}H NMR ([D$_6$]DMSO): δ = 3.27 (s, 3 H, CH_3OH), 4.40 (s, 6 H, CH_2), 4.90 (m, 4 H, OCH_2), 7.19 (m, 16 H, Ph), 7.50 (d, J = 7.2 Hz, 3 H, Ph), 8.18 (d, J = 7.0 Hz, 3 H, Ph), 13.16 (s, 3 H, NH).

8: **11** (130 mg, 0.084 mmol) in a mixture of acetonitrile (30 mL), water (5 mL), and toluene (3 mL) was kept in a flask fitted with a solvent-permeable plastic seal for 2 months until most of the solvent had evaporated. A single crystal for structure determination was taken from the resulting crude precipitate. After filtration, washing with a small volume of methanol, and drying in vacuo, 85 mg (27%) of impure **8** remained; m.p. 220 °C (dec.). − $C_{38}H_{35}N_7O_7P_2Zn$ (829.1): calcd. C 55.05, H 4.26, N 11.83, Zn 7.89; found C 48.00, H 3.82, N 10.16, Zn 7.29. − ^{1}H NMR ([D$_6$]DMSO): δ = 2.12 (s, 6 H, CH_3), 4.33 (s, 6 H, CH_2), 6.84 (d, J = 8.3 Hz, 4 H, Ph), 6.99 (d, J = 8.3 Hz, 4 H, Ph), 7.22 (m, 6 H, Ph), 7.52 (d, J = 6.9 Hz, 3 H, Ph), 8.10 (d, J = 6.3 Hz, 3 H, Ph).

9: Prepared in the same manner as **7** from Li_2[POP^3] (62 mg, 0.13 mmol), TBA (107 mg, 0.26 mmol), and $Zn(ClO_4)_2·6H_2O$ (98 mg, 0.26 mmol). Yield 29 mg (24%) of **9**; m.p. 240 °C (dec.). − $C_{44}H_{47}N_7O_7P_2Zn$ (913.2): calcd. C 57.87, H 5.19, N 10.74, Zn 7.16; found C 54.32, H 4.99, N 9.57, Zn 7.00. − ^{1}H NMR ([D$_6$]DMSO): δ = 1.15 (s, 18 H, *t*Bu), 4.30 (s, 6 H, CH_2), 7.00 (d, J = 8.8 Hz, 4 H, Ph), 7.08 (d, J = 8.8 Hz, 4 H, Ph), 7.25 (m, 6 H, Ph), 7.52 (m, 3 H, Ph), 8.15 (m, 3 H, Ph).

10: Prepared in the same manner as **8** from **12** (39 mg, 0.025 mmol) within 3 months. Yield 7 mg (32%) of **10**, which, according to NMR analysis, was not pure. − ^{1}H NMR ([D$_6$]DMSO): δ = 4.42 (s, 6 H, CH_2), 7.05 (d, J = 9.1 Hz, 4 H, Ph), 7.11 (d, J = 9.1 Hz, 4 H, Ph), 7.25 (m, 6 H, Ph), 7.53 (m, 3 H, Ph), 8.10 (m, 3 H, Ph), 13.11 (s, 3 H, NH).

11: A solution of Li_2[POP^2] (55 mg, 0.12 mmol) in boiling ethanol (20 mL) was added to a solution of TBA (100 mg, 0.245 mmol) and $Zn(ClO_4)_2·6H_2O$ (91 mg, 0.25 mmol) in boiling ethanol (20 mL). After stirring for 10 min, the clear solution was slowly allowed to cool to room temp. 130 mg (70%) of [**11**]·$(ClO_4)_2$ was precipitated, which was washed with cold ethanol and dried in vacuo; m.p. 260 °C (dec.). − $C_{62}H_{56}Cl_2N_{14}O_{15}P_2Zn_2·3H_2O$ (1500.8 + 54.1): calcd. C 47.89, H 4.02, N 12.61, Zn 8.41; found C 46.94, H 3.63, N 12.18, Zn 7.77. − ^{1}H NMR ([D$_6$]DMSO): δ = 2.12 (s, 6 H, CH_3), 3.37 (s, 6 H, H_2O), 4.48 (s, 12 H, CH_2), 6.85 (d, J = 8.2 Hz, 4 H, Ph),

7.06 (d, J = 8.2 Hz, 4 H, Ph), 7.21 (t, J = 7.4 Hz, 12 H, Ph), 7.49 (d, J = 7.8 Hz, 6 H, Ph), 8.19 (d, J = 7.2 Hz, 6 H, Ph).

12: Prepared in the same manner as **11** from $Li_2[POP^4]$ (16 mg, 0.064 mmol), TBA (52 mg, 0.13 mmol), and $Zn(ClO_4)_2{\cdot}6H_2O$ (48 mg, 0.13 mmol). The precipitate was recrystallized from hot ethanol to yield 39 mg (38%) of **[12]**·$(ClO_4)_2$; m.p. 250 °C (dec.). − $C_{60}H_{50}Cl_4N_{14}O_{15}P_2Zn_2{\cdot}3H_2O$ (1541.7 + 54.1): calcd. C 45.16, H 3.54, N 12.29, Zn 8.19; found C 45.05, H 3.27, N 11.28, Zn 7.57. − ^{1}H NMR ([D$_6$]DMSO): δ = 3.42 (s, 6 H, H_2O), 4.51 (s, 12 H, CH_2), 7.2−6.9 (m, 20 H, Ph), 7.46 (d, J = 8.2 Hz, 6 H, Ph), 8.29 (d, J = 7.4 Hz, 6 H, Ph).

13: Prepared in the same manner as **11** from $Li_2[POP^2]$ (33 mg, 0.074 mmol), TBA* (100 mg, 0.15 mmol), and $Zn(ClO_4)_2{\cdot}6H_2O$ (55 mg, 0.15 mmol). The precipitate was recrystallized from hot ethanol to yield 134 mg (87%) of **[13]**·$(ClO_4)_2$; m.p. 161 °C. − $C_{104}H_{92}Cl_2N_{14}O_{15}P_2Zn_2{\cdot}2H_2O$ (2041.6 + 36.0): calcd. C 60.12, H 4.66, N 9.44, Zn 6.29; found C 59.71, H 4.43, N 9.53, Zn 6.33. − ^{1}H NMR ([D$_6$]DMSO): δ = 2.08 (s, 6 H, CH_3), 3.36 (s, 4 H, H_2O), 4.61 (s, 12 H, CH_2), 5.45 (s, 12 H, CH_2), 6.75 (d, J = 7.7 Hz, 4 H, Ph), 6.88 (d, J = 7.7 Hz, 4 H, Ph), 7.11 (m, 12 H, Ph), 7.23 (m, 30 H, Ph), 7.50 (d, J = 7.7 Hz, 6 H, Ph), 8.23 (d, J = 7.7 Hz, 6 H, Ph).

14: Prepared in the same manner as **11** from $Li_2[POP^3]$ (46 mg, 0.097 mmol), TBA* (132 mg, 0.195 mmol), and $Zn(ClO_4)_2{\cdot}6H_2O$ (73 mg, 0.19 mmol). Yield 105 mg (51%) of **[14]**·$(ClO_4)_2$; m.p. 174 °C. − $C_{110}H_{104}Cl_2N_{14}O_{15}P_2Zn_2$ (2125.7): calcd. C 62.15, H 4.93, N 9.22, Zn 6.15; found C 60.49, H 4.92, N 8.94, Zn 6.45. − ^{1}H NMR ([D$_6$]DMSO): δ = 1.22 (s, 18 H, *t*Bu), 4.60 (s, 12 H, CH_2), 5.46 (s, 12 H, CH_2), 6.9−7.2 (m, 50 H, Ph), 7.51 (d, J = 8.1 Hz, 6 H, Ph), 8.27 (d, J = 8.1 Hz, 6 H, Ph).

15: Prepared in the same manner as **11** from $Li_2[POP^4]$ (15 mg, 0.035 mmol), TBA* (47 mg, 0.070 mmol), and $Zn(ClO_4)_2{\cdot}6H_2O$ (26 mg, 0.070 mmol). Recrystallization from hot ethanol yielded 64 mg (88%) of **[15]**·$(ClO_4)_2$; m.p. 180 °C (dec.). − $C_{102}H_{86}Cl_4N_{14}O_{15}P_2Zn_2$ (2082.5): calcd. C 58.83, H 4.16, N 9.42, Zn 6.28; found C 58.63, H 4.26, N 9.44, Zn 5.62. − ^{1}H NMR ([D$_6$]DMSO): δ = 4.67 (s, 12 H, CH_2), 5.54 (s, 12 H, CH_2), 7.17 (m, 50 H, Ph), 7.53 (m, 6 H, Ph), 8.22 (m, 6 H, Ph).

16: A freshly prepared solution of $H[PO^1]$ (49 mg, 0.12 mmol) in dichloromethane (6 mL) was added to a solution of Tp*Zn−OH (56 mg, 0.12 mmol) in dichloromethane (12 mL). After stirring for 1 d, the mixture was filtered and the filtrate was concentrated to dryness. The residue was taken up in the minimum volume of dichloromethane and this solution was layered with *n*-hexane (25 mL). After a few days at 0 °C, 38 mg (34%) of **16** had separated, which was washed with cold acetonitrile (1 mL); m.p. 42 °C. − $C_{45}H_{61}BN_6O_7P_2Zn$ (936.2): calcd. C 57.74, H 6.57, N 8.98, Zn 6.98; found C 57.85, H 6.15, N 8.89, Zn 6.52. − ^{1}H NMR ($CDCl_3$): δ = 1.29 (s, 27 H, *t*Bu), 2.35 (s, 9 H, CH_3), 5.18 (d, J = 6.2 Hz, 4 H, OCH_2), 5.30 (d, J = 6.4 Hz, 2 H, OCH_2), 5.79 (s, 3 H, pz), 7.30 (m, 15 H, Ph).

17: Prepared in the same manner as **16** from $H[PO^2]$ (102 mg, 0.15 mmol) and Tp*Zn−OH (75 mg, 0.15 mmol). Yield 44 mg (25%) of **17**; m.p. 112 °C. − $C_{45}H_{58}BBr_3N_6O_7P_2Zn$ (1172.9): calcd. C 46.08, H 4.98, N 7.17, Zn 5.57; found C 46.16, H 4.97, N 6.99, Zn 5.60. − ^{1}H NMR ($CDCl_3$): δ = 1.30 (s, 27 H, *t*Bu), 2.38 (s, 9 H, CH_3), 5.12 (m, 4 H, OCH_2), 5.25 (d, J = 6.7 Hz, 2 H, OCH_2), 5.83 (s, 3 H, pz), 7.20 (d, J = 8.5 Hz, 2 H, Ph), 7.26 (d, J = 8.5 Hz, 4 H, Ph), 7.43 (m, 6 H, Ph).

18: Prepared in the same manner as **16** from $H_2[POP^1]$ (36 mg, 0.11 mmol) and Tp*Zn−OH (119 mg, 0.24 mmol). Yield 38 mg (27%) of **18**; m.p. 214 °C. − $C_{62}H_{94}B_2N_{12}O_7P_2Zn_2$ (1333.9): calcd. C 55.83, H 7.10, N 12.60, Zn 9.80; found C 55.99, H 7.05, N 12.17, Zn 9.99. − ^{1}H NMR ($CDCl_3$): δ = 1.30 (s, 54 H, *t*Bu), 2.37 (s, 18 H, CH_3), 5.64 (m, 4 H, OCH_2), 5.78 (s, 6 H, pz), 7.26 (m, 10 H, Ph).

19: Prepared in the same manner as **16** from $H_2[POP^2]$ (77 mg, 0.20 mmol) and Tp*Zn−OH (218 mg, 0.43 mmol). Yield 150 mg (58%) of **19**; m.p. 235 °C. − $C_{62}H_{94}B_2N_{12}O_7P_2Zn_2$ (1333.9): calcd. C 55.83, H 7.10, N 12.60, Zn 9.80; found C 54.97, H 7.09, N 12.19,

Table 4. Crystallographic details

	8	**10**
Empirical formula	$C_{38}H_{35}N_7O_7PZn{\cdot}CH_3CN{\cdot}4H_2O$	$C_{36}H_{29}Cl_2N_7O_7P_2Zn{\cdot}2C_2H_5OH{\cdot}3H_2O$
Molecular mass	829.1 + 82.1 + 72.1	869.9 + 92.1 + 54.1
Crystal size [mm]	0.6 × 0.5 × 0.3	0.3 × 0.3 × 0.3
Space group	$P\bar{1}$	$P\bar{1}$
Z	2	2
a [Å]	13.941(7)	11.560(4)
b [Å]	18.074(6)	13.400(2)
c [Å]	20.522(5)	16.967(4)
α [°]	67.81(2)	72.29(2)
β [°]	73.85(3)	88.00(2)
γ [°]	84.93(4)	67.32(2)
V [Å^3]	4598(3)	2300(1)
d(calcd) [gcm^{-3}]	1.41	1.46
μ(Mo-K_α) [mm^{-1}]	0.67	0.79
hkl range	h: −13 to 0	h: −10 to 9
	k: −17 to 17	k: −12 to 0
	l: −20 to 19	l: −15 to 14
Measured reflections	9473	3477
Independent reflections	8986	3317
Observed refl. [$I > 2\sigma(I)$]	7303	2498
Parameters	722	349
Refined reflections	8980	3317
R_1 (obsd. refl.)	0.049	0.103
wR_2 (all refl.)	0.147	0.374
Residual electron density [e/Å^3]	+0.7	+0.9
	−0.4	−0.9

Zn 10.01. − ^{1}H NMR ($CDCl_3$): δ = 1.34 (s, 54 H, *t*Bu), 2.27 (s, 6 H, CH_3), 2.37 (s, 18 H, CH_3), 5.79 (s, 6 H, pz), 6.99 (d, J = 8.4 Hz, 4 H, Ph), 7.40 (d, J = 8.4 Hz, 4 H, Ph).

Structure Determinations:[24] The selected crystals were taken directly from the reaction solutions and used without drying in vacuo. They were immersed in fluorinated polyether oil and immediately placed in the nitrogen stream of the diffractometer's cooling system. Diffraction data were recorded at ca. −100 °C using the ω/2θ technique with a Nonius CAD4 diffractometer fitted with a molybdenum tube (Mo-K_α, λ = 0.7107 Å) and a graphite monochromator. Empirical absorption corrections based on ψ scans were applied. The structures were solved by direct methods and refined anisotropically with the SHELX program suite.[25] Hydrogen atoms were included with fixed distances and isotropic temperature factors 1.5 times those of their attached atoms. Parameters were refined against F^2. The R values are defined as $R_1 = \Sigma|F_o - F_c|/\Sigma F_o$ and $wR_2 = \{\Sigma[w(F_o^2 - F_c^2)^2]\Sigma[w(F_o^2)^2]\}^{1/2}$. Drawings were produced with SCHAKAL.[26] The crystallographic data are collected in Table 4.

Acknowledgments

This work was supported by the Deutsche Forschungsgemeinschaft and the Fonds der Chemischen Industrie. We are indebted to Mrs. P. Klose and Mrs. F. Bitgül for assistance with the preparative work, Drs. W. Deck and M. Tesmer for recording the NMR spectra, and Drs. M. Ruf, B. Müller, and A. Trösch for help in solving the crystal structures.

[1] F. Groß, A. Müller-Hartmann, H. Vahrenkamp, *Eur. J. Inorg. Chem*. **2000**, 2363−2370, preceding paper.
[2] A. Müller-Hartmann, H. Vahrenkamp, *Inorg. Chim. Acta* **2000**, *300−302*, 531−536.
[3] A. Müller-Hartmann, H. Vahrenkamp, *Eur. J. Inorg. Chem*. **2000**, 2355−2361, before preceding paper.
[4] H. Sigel, *Chem. Soc. Rev.* **1993**, 255−267.
[5] The Cambridge Crystallographic Data File contains ten structures of metal−ATP complexes.
[6] G. Weitzel, T. Spehr, *Hoppe Seyler's Z. Physiol. Chem.* **1958**, *313*, 212−226.
[7] P. Orioli, R. Cini, D. Donati, S. Mangani, *J. Am. Chem. Soc.* **1981**, *103*, 4446−4452.
[8] R. Cini, L. G. Marzilli, *Inorg. Chem.* **1988**, *27*, 1855−1856.
[9] M. Rombach, C. Maurer, K. Weis, E. Keller, H. Vahrenkamp, *Chem. Eur. J.* **1999**, *5*, 1013−1027.
[10] H. Vahrenkamp, *Acc. Chem. Res.* **1999**, *32*, 589−596.
[11] R. Gregorzik, U. Hartmann, H. Vahrenkamp, *Chem. Ber.* **1994**, *127*, 2117−2122.
[12] U. Hartmann, R. Gregorzik, H. Vahrenkamp, *Chem. Ber.* **1994**, *127*, 2123−2127.
[13] S. Trofimenko, *Scorpionates*, Imperial College Press, London, **1999**.
[14] G. Parkin, *Adv. Inorg. Chem*. **1996**, *42*, 291−393.
[15] K. Weis, H. Vahrenkamp, *Eur. J. Inorg. Chem*. **1998**, 271−274.
[16] K. Weis, M. Rombach, M. Ruf, H. Vahrenkamp, *Eur. J. Inorg. Chem*. **1998**, 263−270.
[17] E. A. Merrit, M. Sundaralingam, *Acta Crystallogr.* **1980**, *B36*, 2576−2584.
[18] T. P. Haromy, P. F. Gilletti, R. D. Cornelius, M. Sundaralingam, *J. Am. Chem. Soc.* **1984**, *106*, 2812−2818.
[19] M. Förster, R. Burth, A. K. Powell, T. Eiche, H. Vahrenkamp, *Chem. Ber*. **1993**, *126*, 2643−2648.
[20] L. Zervas, I. Dilaris, *Chem. Ber*. **1956**, *89*, 925−933.
[21] J. A. Stock, *J. Org. Chem*. **1979**, *44*, 3997−3999.
[22] F. Cramer, M. Winter, *Chem. Ber.* **1959**, *92*, 2761−2767.
[23] R. Alsfasser, M. Ruf, S. Trofimenko, H. Vahrenkamp, *Chem. Ber.* **1993**, *126*, 703−710.
[24] Crystallographic data (excluding structure factors) for the structures reported in this paper have been deposited with the Cambridge Crystallographic Data Centre as supplementary publication nos. CCDC-141968 (for **8**) and -141969 (for **10**). Copies of the data can be obtained free of charge on application to the CCDC, 12 Union Road, Cambridge CB2 1EZ, U.K. [Fax: (internat.) + 44-1223/336-033; E-mail: deposit@ccdc.cam.ac.uk].
[25] G. M. Sheldrick, *SHELX-86* and *SHELXL-93, Programs for Crystal Structure Determination*, Universität Göttingen, **1986** and **1993**.
[26] E. Keller, *SCHAKAL for Windows*, Universität Freiburg, **1999**.

Received March 23, 2000
[I00111]

Sulfur Compounds, 213[‡]

Geometries, Acidities, and Dissociation Reactions of the Gaseous Superacids $H_2S_2O_3$, H_2SO_5, HSO_3F, and HSO_3Cl

Ralf Steudel*[a] and André H. Otto[a]

Dedicated to Professor J. Gijs Kuenen, Delft, on the occasion of his 60th birthday

Keywords: Sulfur oxoacids / Acidity / Ab initio calculations / Thermodynamics / Structures

The gas-phase geometries, dipole moments, enthalpies, and Gibbs free energies of thiosulfuric acid $H_2S_2O_3$, peroxosulfuric acid H_2SO_5, fluorosulfuric acid HSO_3F, and chlorosulfuric acid HSO_3Cl as well as of their monoanions have been determined by ab initio MO calculations at various levels of theory. The most stable conformations of the four acid molecules are all of C_1 symmetry. The acidities, defined as $\Delta G°_{298}$ of the deprotonation reaction, obtained by the G2 method are as follows [kJ mol^{-1}]: *H*O–SO_2–SH 1251 and HO–SO_2–S*H* 1276, *H*O–SO(=S)–OH 1241, *H*O–SO_2–OOH 1239, *H*O–SO_2–F 1229, *H*O–SO_2–Cl 1219. Good agreement of the calculated acidities of HSO_3F and HSO_3Cl is observed with the experimental gas-phase acidities, which are the only experimental values available. The OH acidities of all five species are higher than that of sulfuric acid (1268 kJ mol^{-1}). Therefore, these compounds may be termed as superacids. In contrast to the liquid state, chlorosulfuric acid is a stronger proton donor than fluorosulfuric acid in the gas phase. The dissociation of the acid molecules HSO_3X (X = SH, OOH, F, Cl) into SO_3 and HX is endothermic and endergonic in all cases. The same holds for the dissociation of the anions SO_3X^- into SO_3 and X^-. From these dissociation enthalpies and literature data the enthalpies of formation of the mentioned sulfonic acids and their anions are calculated.

Introduction

According to a suggestion by R. J. Gillespie[1] superacids are those nonaqueous systems which are of higher acidity than pure sulfuric acid as far as Brønsted acids are concerned. Using the Hammett acidity scale[2] 100% H_2SO_4 has the acidity $H_o = -12$. Well-known examples of superacids (H_o in parentheses) are disulfuric acid $H_2S_2O_7$ (−14.8), chlorosulfuric acid HSO_3Cl (−13.8), and fluorosulfuric acid HSO_3F (−15.1). A 1:9 mixture of HSO_3F and SbF_5 exhibits the highest known acidity ($H_o = -27$).[3,4] This mixture is called *magic acid* since it protonates and consequently dissolves even saturated hydrocarbons.

The concept of superacids can also be applied to gaseous Brønsted acids again using the acidity of sulfuric acid as a reference value. The acidity of gaseous H_2SO_4 may be defined as the Gibbs free energy change for the deprotonation reaction [Equation (1)].

$$H_2SO_4 \rightarrow H^+ + HSO_4^- \quad (1)$$

It is obvious that this enthalpy change will always be strongly endothermic (> 1200 kJ mol^{-1}). For example, $\Delta G°_{298}$ [Equation (1)] was determined experimentally[5] as 1265±10 kJ mol^{-1} while 1268 kJ mol^{-1} was calculated by high-level ab initio MO methods.[6] As part of a systematic study of the acidities of the sulfur oxo acids we report here a detailed study of the geometries and acidities of the gaseous compounds $H_2S_2O_3$, H_2SO_5, HSO_3F, and HSO_3Cl which are of general formula HO−SO_2−X (X = SH, OOH, F, Cl).

To obtain accurate gas-phase acidities for the above-mentioned species *at identical levels of theory* we have calculated the energies of these acids HA and their corresponding anions A^- at the G2 level of theory, which has been shown to provide reliable acidity data for sulfur compounds, agreeing with the best experimental values within ca. 8 kJ mol^{-1}.[7] In addition, the CBS-Q and G2(MP2) methods were applied to all species since these more economical levels of theory will be used in an upcoming publication on several larger sulfur oxo acid molecules like polythionic acids, $H_2S_nO_6$, and polysulfuric acids, $H_2S_nO_{3n+1}$ ($n > 1$). In this way a comparison of data for different acids as well as a discussion of trends in acidities as a function of molecular structure will be possible. Since the gas-phase acidity has been defined in the literature as either $\Delta G°_{298}$ or $\Delta H°_{298}$ of the deprotonation reaction we also calculated both values for the systems investigated.

Calculations

Ab initio molecular orbital calculations were performed at the CBS-Q,[8] G2(MP2),[9] and G2[10] levels of theory us-

[‡] Part 212: R. Steudel, K. Hassenberg, V. Münchow, O. Schumann, J. Pickardt, *Eur. J. Inorg. Chem.*, **2000**, 921−928.

[a] Institut für Anorganische und Analytische Chemie, Technische Universität Berlin, Sekr. C2,
10623 Berlin, Germany
Fax: (internat.) + 49-30/31426519
E-mail: steudel@schwefel.chem.tu-berlin.de

 © WILEY-VCH Verlag GmbH, D-69451 Weinheim, 2000 1434−1948/00/1111−2379 $ 17.50+.50/0

ing the GAUSSIAN program system.[11] The G2 method essentially implies an energy calculation at the QCISD(T)/6-311+G(3df,2p) level using geometries optimized at the MP2(fu)/6-31G(d) level. Harmonic vibrational wavenumbers were obtained at the HF/6-31G(d) level and were scaled by a factor of 0.893. The G2(MP2) method is a modified version of G2 but uses the second-order Møller–Plesset perturbation theory (MP2) for the basis set extension correction rather than the fourth order (MP4). G2(MP2) is almost as accurate as the G2 method but at a substantially reduced computational expense.

Complete Basis Set (CBS) model chemistries utilize the "dagger" 6-31G† basis set[12] in trying to overcome some deficiencies in the standard 6-31G(d) basis set. While the latter arbitrarily assigns an exponent of 0.8 to all four elements, the former uses the exponents from the d functions in the 6-311G basis set. The CBS models[10] use the asymptotic convergence of pair natural orbital expansion to extrapolate from calculations using a finite basis set to the estimated CBS limit. The CBS method consists of the following steps: geometry optimization at the HF/6-31G† level, thermal corrections using wavenumbers obtained at the same level and scaled by a factor of 0.918, reoptimization at the MP2/6-31G† level followed by energy calculations using a large basis set in combination with HF and MP2. The next steps are MP4(sdq) and QCISD(T) calculations applying medium-size basis sets. Then the CBS extrapolation is made and empirical corrections are added to obtain the final thermodynamic data.

The excellent performance of all of these methods in predicting gas-phase acidities of small molecules is well established.[13]

To obtain reliable geometries of the most stable isomers complete optimizations as well as wavenumber calculations were performed at the MP2/6-311++G(d,p) level.

For details of the quantum chemical methods see ref.[14] All calculations were carried out with a Cray J90 or a Linux workstation. A list of the absolute enthalpies $H°_{298}$ and Gibbs free energies $G°_{298}$ of all species used in this work at the levels CBS-Q, G2(MP2) and G2 is given in the Appendix (Table 12). To allow for the thermal corrections to the Gibbs free energy of the proton a value of −0.010654 hartree (−28 kJ mol^{-1}) was used.

Results and Discussion

Molecular Structures

Thiosulfuric Acid $H_2S_2O_3$

No experimental structures of $H_2S_2O_3$ or its monoanion are known since these species are thermally unstable at temperatures above −20 °C. In fact, the molecule $H_2S_2O_3$ has never been observed although this compound is mentioned in practically all inorganic chemistry textbooks. The anion $HS_2O_3^-$ is contained in the ammonium salt $NH_4[HS_2O_3]$ which is the only hydrogen thiosulfate which has ever been prepared.[15] The low-temperature Raman spectra of this salt and its deuterated derivative demonstrated that the connectivity of the anion is $HS-SO_3^-$ rather than $HO-SO_2(=S)^-$. By ab initio MO calculations at the MP4/6-311G(d,p)//HF/6-311G(d,p) + ZPE level of theory it was shown that the most stable connectivity of thiosulfuric acid is $HO-SO_2-SH$ (**1**) which is 41 kJ mol^{-1} more stable than the alternative $HO-SO(=S)-OH$ (**2**) and that the connectivity $HS-SO_3^-$ (**3**) is 20 kJ mol^{-1} more stable than the tautomer $HO-SO_2(=S)^-$ (**4**).[16] Calculations at the MP2/6-31+G(d)//HF/6-31G(d) level revealed that **1** exists as two conformers **1a** and **1b** (Figure 1).[17] The energy difference between these species was calculated as 4 kJ mol^{-1} (at 0 K) with **1a** as the global minimum.

The geometries of $H_2S_2O_3$ and its monoanion obtained at the MP2/6-311++G(d,p) level are given in Table 1; the numbering of atoms is shown in Figure 1. In accordance with the previous results the thiosulfuric acid molecule is of C_1 symmetry and two conformations **1a** and **1b** exist which differ only by the orientation of the SH and OH groups with respect to the terminal oxygen atoms. The global minimum is the conformer **1a** which has an analogous conformation to the sulfuric acid molecule. The bonds O–H and S–H point in almost opposite directions. The second conformer **1b** and the isomer **2** with two O–H bonds are less stable by 2.9 and 34.7 kJ mol^{-1}, respectively, if $\Delta G°_{298}$ at the G2 level is taken as a measure (Table 2). The anions **3** (SH) and **4** (OH) are of C_s and C_1 symmetry, respectively. The OH species **4** is by 24.7 kJ mol^{-1} less stable than the SH tautomer **3** and therefore has not been considered any further. Very similar thermodynamic data were obtained at the levels CBS-Q and G2(MP2) (see Table 2).

Compared to our previous calculations there are some significant changes in the geometrical parameters. In particular, the S–S bond lengths are now considerably longer and calculated as 210.1 and 222.6 pm for the acid and the anion while 205.7 and 215.5 pm had been obtained at the HF/6-311G(d,p) level.[16]

Peroxosulfuric Acid H_2SO_5

The molecular structure of crystalline peroxosulfuric acid is known from an X-ray diffraction study of single crystals.[18] However, the gas-phase structure seems to be unknown. The crystal structure is characterized by extensive intermolecular hydrogen bonding but there are no intramolecular hydrogen bonds (Table 3). The O–O bond length (146.4 pm) and the S–O–O–H torsion angle (104°) have values typical for covalent peroxides. The molecular symmetry is C_1 (Figure 1). The structure of the monoanion HSO_5^- is known from two independent X-ray crystal structure determinations of the potassium salt $KHSO_5 \cdot H_2O$ (Table 4).[19,20] The anion is of C_1 symmetry with the connectivity $HO-O-SO_3^-$. The O–O distance was determined as 146 pm while the S–O–O–H torsion angle was given as "ca. 90°"[19] and 87°.[20] Again, intermolecular hydrogen bonding is a characteristic feature of the structure. The structure of this anion has also been investigated by ab

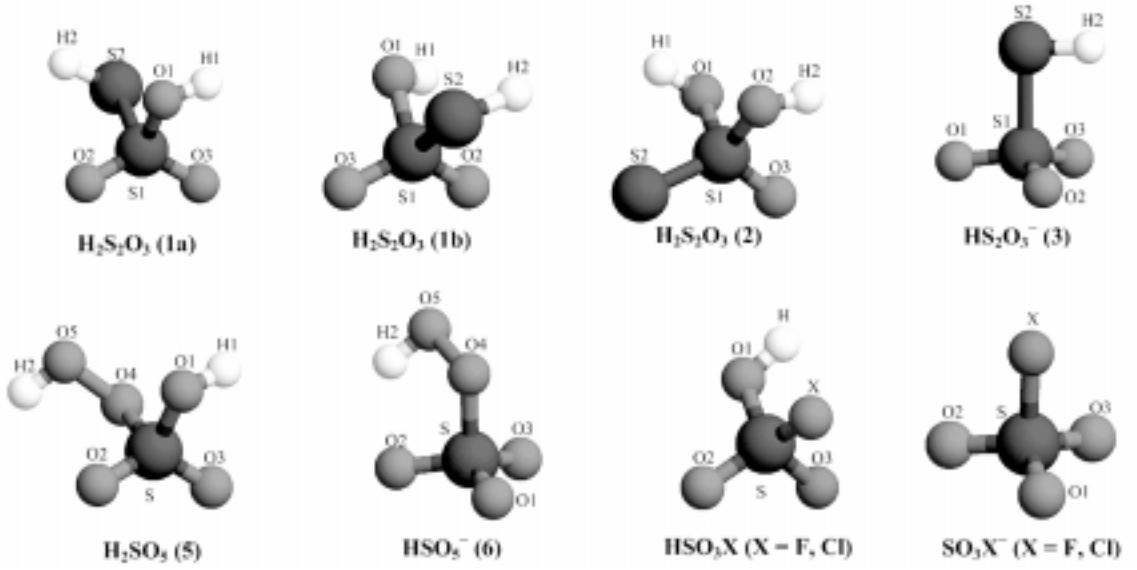


Figure 1. Structures of the acids $H_2S_2O_3$, H_2SO_5, HSO_3F, HSO_3Cl, and of their anions

Table 1. Geometrical parameters of $H_2S_2O_3$ (**1a**, C_1) and $HS_2O_3^-$ (**3**, C_s) calculated at the MP2/6-311++G(d,p) level (internuclear distances in pm, bond angles and torsion angles in °); for numbering of atoms see Figure 1

Parameter	$HO-SO_2-SH$	$HS-SO_3^-$
H1−O1	96.9	−
S1−O1	162.4	146.9
S1−O2	143.6	146.9
S1−O3	144.2	146.7
S1−S2	210.1	222.6
S2−H2	133.9	133.7
H1−O1−S1	108.6	−
O1−S1−O2	104.4	114.4
O1−S1−O3	108.2	115.5
O2−S1−O3	124.0	115.5
O2−S1−S2	110.1	104.0
O3−S1−S2	105.3	100.9
O1−S1−S2	102.9	104.0
S1−S2−H2	92.7	92.8
H1−O1−S1−S2	−78.6	−
O1−S1−S2−H2	−66.0	−60.0
O2−S1−S2−H2	44.7	60.0
O3−S1−S2−H2	−179.3	180.0
O3−S1−O1−H1	32.6	−

Table 2. Relative enthalpies and Gibbs free energies [kJ mol^{-1}] of the isomers of thiosulfuric acid $H_2S_2O_3$ and of their anions $HS_2O_3^-$ at 298 K

Species	CBS-Q		G2(MP2)		G2	
	$\Delta H°_{298}$	$\Delta G°_{298}$	$\Delta H°_{298}$	$\Delta G°_{298}$	$\Delta H°_{298}$	$\Delta G°_{298}$
1a, (HS)(HO)SO_2	0	0	0	0	0	0
1b, (HS)(HO)SO_2	4.5	2.8	3.8	2.6	4.2	2.9
2, $(HO)_2S(=S)O$	34.7	34.4	33.8	33.4	35.1	34.7
3, (HS)SO_3^-	0	0	0	0	0	0
4, (HO)S(=S)O_2^-	23.3	23.4	24.6	24.7	24.6	24.7

initio MO calculations at the MP2/3-21+G(*) level.[21] These data will be discussed below.

As part of the acidity calculation we have optimized the structures of H_2SO_5 (**5**) and HSO_5^- (**6**) with no symmetry restrictions first at the MP2/6-31G(d) level. The vibrational eigenvalues of the structures found were all positive. After the most stable conformations of H_2SO_5 and HSO_5^- had been located on the energy hypersurface these structures were optimized at the MP2/6-311++G(d,p) level. In Table 3 and Table 4 we compare the calculated geometries with the solid-state structures.

Table 3. Structural parameters of H_2SO_5 (C_1) in the gas phase and in the crystal (internuclear distances in pm, bond angles and torsion angles in °); for numbering of atoms see Figure 1

Parameter	MP2/6-311++G(d,p)	X-ray diffraction[a]
H1−O1	96.9	94 (4)
H2−O5	96.9	95.4
O4−O5	144.0	146.4 (3)
S−O1	160.2	152.4 (2)
S−O2	143.0	141.8 (2)
S−O3	144.2	143.2 (2)
S−O4	166.1	160.2
H1−O1−S	109.0	112 (2)
O1−S−O2	105.9	106.8 (1)
O1−S−O3	110.2	112.9 (1)
O1−S−O4	101.7	104.0 (1)
O2−S−O3	125.2	121.4 (2)
O3−S−O4	101.9	101.0 (1)
S−O4−O5	109.5	108.7 (2)
O4−O5−H2	100.6	98 (3)
H1−O1−S−O4	−74.9	−68
O1−S−O4−O5	−63.6	−59.4
S−O4−O5−H2	−95.2	−104

[a] See ref.[18]

There is a remarkably good agreement between the two conformations of H_2SO_5 calculated for the free molecule and found in the crystal. This can be seen from the close agreement of the three torsion angles given in Table 3. The two O−H bonds point into practically opposite directions and the four atoms O3−S−O4−O5 (torsion angle −177.4°) are almost located in a plane. Most of the bond lengths and bond angles agree rather closely with the solid-state

Table 4. Comparison of calculated and crystallographic structure data for the peroxymonosulfate ion HSO_5^- (C_1) (internuclear distances in pm, bond angles and the torsion angle in °); for numbering of atoms see Figure 1

Parameter	Calculated MP2/6-311++G(d,p)	Experimental	
	Schlemper et al.[a]	Flanagan et al.[b]	
H2−O5	97.6	87 (2)	–
O4−O5	145.4	146.3 (1)	146.0 (3)
S−O4	173.2	163.4 (1)	163.2 (2)
S−O2	147.9	145.0 (1)	144.4 (2)
S−O3	146.3	144.6 (1)	143.7 (2)
S−O1	146.0	144.0 (1)	143.5 (2)
H2−O5−O4	99.1	101	–
S−O4−O5	108.2	109.2	109.4
O2−S−O4	100.7	105.7	105.9
O3−S−O4	106.9	106.9	106.8
O1−S−O4	99.2	99.1	99.0
O2−S−O3	114.3	113.1	113.1
O1−S−O2	116.3	115.2	115.2
O1−S−O3	116.2	115.0	115.0
H2−O5−O4−S	43.2	87	ca. 90

[a] $KHSO_5H_2O$: ref.[19] – [b] $KHSO_5H_2O$: ref.[20]

structure. Exceptions are the two S−O single bonds involving O1 and O4 which are calculated to be 6−8 pm longer than observed in the crystal. Since these oxygen atoms do not take part in the hydrogen bonding network we have no explanation for the differing bond lengths. There are no intramolecular hydrogen bonds in **5** since the shortest nonbonded contact distance (O3···H1: 254.1 pm) is about equal to the sum of the van der Waals radii.

The calculated anion structure (Table 4) also agrees quite well with the crystallographically determined structure of $KHSO_5 \cdot H_2O$ despite the fact that the anion is coordinated by six cations and three water molecules. The differing H−O−O−S torsion angles (calcd. 43.2° versus 87°) may be caused by the intermolecular hydrogen bonding in the crystal on one hand and by the intramolecular hydrogen bond in the free ion. The strongest hydrogen bond in the crystal originates from the peroxide hydrogen and ends at the oxygen atom of a neighboring water molecule.[20] In the free ion the same hydrogen atom is linked to the oxygen atom O2 by a weak hydrogen bond of length 200.9 pm. The S−O single bond to the peroxide oxygen atom is calculated much longer (173.2 pm) than observed in the crystal (163.3 pm) which may be caused by the coordination of the peroxomonosulfate ion to the surrounding potassium ions. All other calculated S−O bond lengths agree within 2.6 pm with the solid-state data but the deviations always follow the same trend: The calculated distances are larger than the observed ones. The same type of deviations have been observed when the structure of HSO_5^- was calculated at the MP2/3-21+G(*) level.[21]

Attempts to optimize the structure of the isomeric anion HO_3S-O-O^- failed since its structure always rearranged to the more stable isomer $HO-O-SO_3^-$. Therefore, the acidity of the peroxide proton of H_2SO_5 could not be calculated.

Fluorosulfuric Acid HSO_3F

The molecular structure of gaseous HSO_3F seems to be unknown but the crystalline acid has been studied by X-ray diffraction at 123 K.[22] The HO−SO_2−F molecules form infinite chains via OH···O hydrogen bonds. The site symmetry is C_1. The structural parameters are given in Table 5 together with the results of our calculations at the MP2/6-311++G(d,p) level. Previous geometry calculations had been performed at the HF/6-31+G(d)[23,24] and HF/6-31G(d) levels.[17] The gas-phase symmetry is also C_1. The hydrogen atom shows no tendency to move close to the fluorine atom and there is no intramolecular O···H bond either: The closest O···H distance is 252.3 pm (with O3), which is about identical to the van der Waals distance. There is a fairly good agreement between calculated and observed bond lengths and angles taking the two different phases into account. Besides the OH bond length, which cannot be determined accurately by X-ray diffraction, the largest difference between the calculated and the solid-state structures is found for the S−OH single bond which is calculated to be too long by 8 pm. Next is the S−F bond, which is calculated to be too long by 6.6 pm. However, by comparison with a gaseous derivative of HSO_3F it can been demonstrated that the calculated structure is basically correct. The structure of the methyl ester Me−O−SO_2−F has been determined by microwave spectroscopy and electron diffraction.[25] Assuming identical lengths for the two S=O bonds of the sulfone group the following internuclear distances [pm] and bond angles [°] were obtained: S=O 141.0(2), S−O 155.8(7), S−F 154.5(6), O−S=O 109.5(6), O=S=O 124.4(7), F−S=O 106.8(5). The S−O bond length agrees within 4 pm with our data for HSO_3F while the S−F bond deviates by 6.1 pm. The three bond angles agree within 1.5°. Taking into account the fact that two different, although related molecules are being compared and that ab initio MO methods reproduce S−F and S−O single bond lengths only poorly, the agreement of the data may be considered fairly good.

Table 5. Molecular structure of HSO_3F (C_1) in the gas phase and in the crystal (internuclear distances in pm, bond angles and the torsion angle in °); for numbering of atoms see Figure 1

Parameter	MP2/6-311++G(d,p)	X-ray diffraction[a]
H−O1	96.9	63 (3)
S−O1	59.6	151.4 (2)
S−O2	143.1	142.0 (1)
S−O3	142.3	141.2 (1)
S−F	160.6	154.0 (1)
O1−S−O2	110.2	107.2 (1)
O1−S−O3	107.0	113.1 (1)
O2−S−O3	125.4	120.9 (1)
O1−S−F	98.1	100.7 (1)
O2−S−F	105.7	106.2 (1)
O3−S−F	106.9	106.6 (1)
H−O−S	109.5	–
H−O−S−F	−78.6	–
H−O1−S−O3	31.5	–
H−O1−S−O2	170.8	–

[a] See ref.[22]

The structure of the fluorosulfate anion has been determined, for example, by X-ray crystallography of the lithium salt.[26] The gas-phase symmetry of the anion is C_{3v} but owing to its unsymmetrical coordination by lithium cations in $LiSO_3F$ the site symmetry is C_s. The structural parameters are compared to our calculated data in Table 6. Previous geometry calculations had been performed at the HF/6-31G(d)[17] and HF/6-31+G(d)[23,24] levels.

Table 6. Molecular structure of the anion SO_3F^- in the gas phase (C_{3v}) and in the crystal of $LiSO_3F$ (internuclear distances in pm, bond angles in °); for numbering of atoms see Figure 1

Parameter	MP2/6-311++ G(d, p)	X-ray diffraction[a]
S−O1	146.1	145.5 (6)
S−O2,3	146.1	142.4 (4)
S−F	169.8	155.5 (7)
O1−S−O2	116.0	113.5 (2)
O2−S−O3	116.0	117.4 (4)
O1−S−F	101.7	104.5 (5)
O2−S−F	101.7	102.8 (3)

[a] See ref.[26]

The anion of $LiSO_3F$ is coordinated to eight cations through Li−O contacts. There is no Li−F contact shorter than the sum of the van der Waals radii. Therefore, the S−F bond length should not be influenced too much and should approximately agree with the value calculated for the free molecule. However, at the level MP2/6-311++G(d,p) the agreement is rather poor: the calculated S−F distance is 14.3 pm or 9% too large! The previous uncorrelated calculations with smaller basis sets reproduced the S−F bond length much better although in all cases too long (by 3.5% or more). The larger deviation between calculated and observed solid-state bond lengths, especially in anions, may be partly caused by the coordination of the lithium cations which withdraw electron density and therefore strengthen the S−O and S−F bonds in a manner similar to that what protonation of anions does: The S−F bond of HSO_3F is 9.2 pm or 6% shorter than that of SO_3F^-. Similar effects are observed with the S−Cl bonds in HSO_3Cl and SO_3Cl^-.

Chlorosulfuric Acid HSO_3Cl

The structure of chlorosulfuric acid has never been determined experimentally but a number of theoretical studies have been published. Basch and Hoz[17] as well as Otto et al.[23] and Bencivenni et al.[24] found a structure of C_1 symmetry at the HF/6-31G(d) and HF/6-31+G(d) levels. The conformation is analogous to that of fluorosulfuric acid (see above). Our results obtained for the most stable conformation of this acid and for its anion at the MP2/6-311++G(d,p) level are shown in Table 7. A comparison of these data with the previous results shows once more that the uncorrelated calculations with the smaller basis sets yield shorter internuclear distances for all three types of bonds. The only experimental data available for comparison are the geometrical parameters of the methyl ester of chlorosulfuric acid, the structure of which has been determined by electron diffraction assuming identical S=O bond lengths in the sulfonyl group.[27] The following internuclear distances [pm] and bond angles [°] were obtained: S−O 156.2(4), S=O 141.9(3), S−Cl 202.3(4), O−S=O 108.7(8), O=S=O 122.2(15), Cl−S−O 102.8(14), Cl−S=O 106.4(6). The maximum deviation of the bond lengths from our data for HSO_3Cl amounts to 4.4 pm while the bond angles agree within 2.7°.

Table 7. Molecular structures of chlorosulfuric acid HSO_3Cl and of its anion calculated at the MP2/6-311++G(d,p) level (internuclear distances in pm, bond angles and torsion angles in °); for numbering of atoms see Figure 1

Parameter	HSO_3Cl (C_1)	SO_3Cl^- (C_{3v})
H−O1	97.0	–
S−O1	160.6	146.1
S−O2	142.9	146.1
S−O3	143.7	146.1
S−Cl	206.2	224.2
O1−S−O2	106.0	116.1
O1−S−O3	109.0	116.1
O2−S−O3	124.6	116.1
O1−S−Cl	100.1	101.5
O2−S−Cl	107.7	101.5
O3−S−Cl	106.8	101.5
H−O1−S−Cl	−80.4	–
H−O1−S−O2	167.8	–
H−O1−S−O3	31.5	–

An interesting feature of the two structures shown in Table 7 are the quite different S−Cl bond lengths in HSO_3Cl (206.2 pm) and in its anion (224.2 pm). Obviously, the strengthening of the bond S−O1 on deprotonation is partly due to a simultaneous weakening of the S−Cl bond. The anion may therefore be viewed as an adduct between SO_3 and a chloride anion. Below it will be shown that the thermodynamics of this adduct formation (or of the reverse dissociation) supports this view.

The shortest intramolecular nonbonded O···H contact distance of 250.8 pm (O3···H) corresponds to the sum of the van der Waals radii.

Acidities

The gas-phase acidity data calculated for various sulfonic acids of the type $HO-SO_2-X$ like H_2SO_3,[6] H_2SO_4,[6] $H_2S_2O_3$, H_2SO_5, HSO_3F, and HSO_3Cl are given in Table 8. The acidity is defined here as either $\Delta H°_{298}$ or $\Delta G°_{298}$ of the deprotonation reaction. The Gibbs free energies obtained at the CBS-Q and G2(MP2) levels differ by only 6 kJ mol^{-1} (0.5%) or less from the G2 data.

Table 8. Gas phase acidities [kJ mol^{-1}] of the sulfonic acids $HO-SO_2-X$ (X = H, OH, SH, OOH, F, Cl)

	CBS-Q		G2(MP2)		G2	
	$\Delta H°_{298}$	$\Delta G°_{298}$	$\Delta H°_{298}$	$\Delta G°_{298}$	$\Delta H°_{298}$	$\Delta G°_{298}$
HO−SO_2−H	1303	1275	1310	1282	1307	1279
HO−SO_2−OH	1299	1264	1307	1271	1305	1268
HO−SO_2−SH	1280	1247	1286	1254	1284	1251
HO−SO_2−S*H*	1303	1271	1311	1278	1308	1276
HO−SO_2−OOH	1264	1233	1272	1241	1270	1239
HO−SO_2−F	1256	1223	1263	1232	1260	1229
HO−SO_2−Cl	1243	1213	1252	1222	1249	1219

The OH acidities presented in Table 8 obviously depend on the electronegativity and the charge capacity of the substituent X. Therefore, sulfonic acid HO−SO_2−H (X = H) is the weakest of the mentioned sulfonic acids, followed by sulfuric acid HO−SO_2−OH. Surprisingly, thiosulfuric acid and peroxosulfuric acid are considerably stronger than sulfuric acid and therefore may be termed as *superacids*. Obviously, the charge capacity of the substituents SH and OOH, i.e., the ability to accommodate an additional negative charge in the anion, is larger than that of the OH group in sulfuric acid. For the same reason, gaseous chlorosulfuric acid is stronger than fluorosulfuric acid, in contrast to the pure liquids. The experimental deprotonation enthalpy of HSO_3F at 368 K was reported as $\Delta H°_{368}$ = 1285 kJ mol^{-1} with $\Delta G°_{368}$ = 1255±10 kJ mol^{-1}.[5] Both values deviate by 26 kJ mol^{-1} from our G2 data. This deviation is much smaller than from the previously reported theoretical data[23] obtained using geometries calculated at a much lower level than in this work. It should be pointed out that the experimental acidity of sulfuric acid[5] perfectly agrees with the G2 results cited in Table 8. No experimental acidity data are known for $H_2S_2O_3$ and H_2SO_5. In the case of thiosulfuric acid we also computed the SH acidity ($\Delta G°_{298}$ = 1276 kJ mol^{-1}) which is of course much smaller than the OH acidity (1251 kJ mol^{-1}) of this compound but still comparable to the OH acidity of sulfonic acid (1279 kJ mol^{-1}) which is a tautomer of sulfurous acid. The OH acidity of the metastable tautomer of thiosulfuric acid, HO−SO(=S)−OH **2**, was calculated as $\Delta G°_{298}$ = 1241 kJ mol^{-1} at the G2 level.

The *dipole moments* of the acids calculated at the MP2/6-311++G(d,p) level are as follows (in D): H_2SO_3 3.77, H_2SO_4 3.63, $H_2S_2O_3$ (**1a**) 4.18, H_2SO_5 2.26, HSO_3F 3.15, HSO_3Cl 3.28.

Dissociation Reactions

Sulfonic acid HO−SO_2−H is unstable with respect to dissociation to H_2O and SO_2[6] and a number of the acids investigated in this work also decompose easily either at room temperature ($H_2S_2O_3$) or on heating (H_2SO_5, HSO_3Cl). Even sulfuric acid partly decomposes into H_2O and SO_3 on distillation at ambient pressure. Therefore, we have calculated the reaction enthalpies and Gibbs free reaction energies of the dissociation reactions of the most stable conformers of HO−SO_2−X into SO_3 and HX (X = H, OH, SH, OOH, F, Cl). The results are shown in Table 9.

In contrast to the instability of H_2SO_3 all other decomposition reactions are endothermic and endergonic at 298 K. However, the dissociation of HSO_3Cl requires a Gibbs free energy of only 9.8 kJ mol^{-1}. It is therefore understandable that this compound cannot be purified by distillation. In fact, chlorosulfuric acid is difficult to prepare in a pure state except by fractional crystallization.[28]

We have also studied the dissociation of the related gaseous anions SO_3X^- into X^- and SO_3 (SO_2 in the case of the sulfonate ion). Only the most stable tautomers and conformations were used. As the data in Table 10 demonstrate

Table 11. Enthalpies of formation of the gaseous acids HO−SO_2−X (X = H, OH, SH, OOH, F, Cl) and of their anions [kJ mol^{-1}]. Experimental values in parentheses

Acid	$\Delta_f H°_{298}$	Anion	$\Delta_f H°_{298}$
HO−SO_2−H	−520	H−SO_3^-	−711 (−693±12)
HO−SO_2−OH	−722 (−735)	HO−SO_3^-	−951 (−967±11)
HO−SO_2−SH	−485	HS−SO_3^-	−735/−722
HO−SO_2−OOH	−623	HOO−SO_3^-	−885
HO−SO_2−F	−739 (−753)	SO_3F^-	−1006 (ca. −986)
HO−SO_2−Cl	−538 (−543)	SO_3Cl^-	−822

Table 9. Stabilities of some sulfonic acids HO−SO_2−X with respect to dissociation into HX and SO_3 or SO_2 [kJ mol^{-1}]

	CBS-Q $\Delta H°_{298}$	$\Delta G°_{298}$	G2(MP2) $\Delta H°_{298}$	$\Delta G°_{298}$	G2 $\Delta H°_{298}$	$\Delta G°_{298}$
$H_2SO_3 \rightarrow H_2O + SO_2$	−18	−61	−20	−63	−19	−62
$H_2SO_4 \rightarrow H_2O + SO_3$	88	44	81	37	84	40
$H_2S_2O_3 \rightarrow H_2S + SO_3$	73	30	67	25	69	26
$H_2SO_5 \rightarrow H_2O_2 + SO_3$	94	48	89	43	91	45
$HSO_3F \rightarrow HF + SO_3$	74	34	68	28	71	31
$HSO_3Cl \rightarrow HCl + SO_3$	55	15	48	8.5	50	9.8

Table 10. Stabilities of the anions SO_3X^- with respect to dissociation into HX and SO_3 or SO_2 [kJ mol^{-1}]

	CBS-Q $\Delta H°_{298}$	$\Delta G°_{298}$	G2(MP2) $\Delta H°_{298}$	$\Delta G°_{298}$	G2 $\Delta H°_{298}$	$\Delta G°_{298}$
$HSO_3^- \rightarrow HO^- + SO_2$	287	240	261	214	277	231
$HSO_4^- \rightarrow HO^- + SO_3$	428	390	400	362	418	381
$HS_2O_3^- \rightarrow HS^- + SO_3$	259	220	255	217	258	220
$HSO_5^- \rightarrow HO_2^- + SO_3$	405	355	394	345	395	346
$SO_3F^- \rightarrow F^- + SO_3$	377	343	361	327	362	328
$SO_3Cl^- \rightarrow Cl^- + SO_3$	202	168	196	163	199	165

all reactions are strongly endothermic and endergonic. The reverse reactions are the nucleophilic additions of the Lewis bases X^- to the strong Lewis acid SO_3. By far the lowest reaction energy is that calculated for the addition of chloride anions to SO_3, which is in agreement with the structure of the chlorosulfate anion and its rather weak S−Cl bond as discussed above.

From the G2 enthalpies in Table 9 and 10 and the published enthalpies of formation[29] of SO_2, SO_3, H_2O, H_2S, H_2O_2, HF, HCl, OH^-, OOH^-, SH^-, F^-, and Cl^- we have calculated the enthalpies of formation of the gaseous acids and their monoanions as given in Table 11. Only few experimental data[28] are available for comparison and these are often not very accurate. Nevertheless, the agreement is reasonable. In the case of the hydrogen sulfide anion two slightly different values for the enthalpy of formation have been published.[28] Therefore, two enthalpies are given for $HSSO_3^-$ in Table 11 with the second value probably being more reliable. In the case of HSO_3Cl the enthalpy of formation was calculated from $\Delta_f H°_{298}$ of the liquid substance (−597.5 kJ mol^{-1})[28] and the enthalpy of evaporation at the boiling point (53.6 kJ mol^{-1} at 150°C).[28] The result (−543 kJ mol^{-1}) perfectly agrees with the value found in the present study (−538 kJ mol^{-1}).

Conclusion

The five sulfur oxo acids HO−SO_2−SH, HO−SO(=S)−OH, HO−SO_2−OOH, HO−SO_2−F, and HO−SO_2−Cl, as well as their monoanions, were investigated by ab initio MO calculations at the CBS-Q, G2(MP2), and G2 levels of theory to obtain their structures as well as their enthalpies and Gibbs free energies, from which the thermodynamics of the deprotonation reactions at 298 K were calculated. Unexpectedly, the OH acidities of all spe-

Table 12. Enthalpies $H°$ and Gibbs free energies $G°$ (negative a.u.) of the acids HO−SO_2−X (X = H, OH, SH, OOH, F, Cl), their anions, and the products of decomposition at 298 K

	Species	Symmetry	CBS-Q	G2(MP2)	G2
$H°$	**1a**, (HS)(HO)SO_2	C_1	1022.104627	1022.056003	1022.073874
	1b, (HS)(HO)SO_2	C_1	1022.102887	1022.054539	1022.072275
	2, $(HO)_2S(=S)O$	C_1	1022.091394	1022.043125	1022.060501
	3, (HS)SO_3^-	C_s	1021.619545	1021.568491	1021.587345
	4, (HO)S(=S)O_2^-	C_1	1021.610670	1021.559117	1021.577958
	5, H_2SO_5	C_1	774.555147	774.501182	774.517270
	6, HSO_5^-	C_1	774.076138	774.018928	774.036091
	FSO_3H	C_1	723.531263	723.479661	723.494518
	FSO_3^-	C_{3v}	723.055130	723.000806	723.016835
	$ClSO_3H$	C_1	1083.512145	1083.456827	1083.476593
	$ClSO_3^-$	C_{3v}	1083.041134	1082.982326	1083.003139
	SO_2	$D_{\infty v}$	548.031089	548.003069	548.011734
	SO_3	D_{3h}	623.147303	623.110157	623.120863
	H_2O	C_{2v}	76.332707	76.326223	76.328266
	H_2O_2	C_2	151.371965	151.357146	151.361601
	HO_2^-	C_s	150.774768	150.758876	150.764873
	OH^-	$C_{\infty v}$	75.710924	75.709473	75.706670
	H_2S	C_{2v}	398.929676	398.920280	398.926912
	HS^-	$C_{\infty v}$	398.373711	398.361053	398.368281
	HF	$C_{\infty v}$	100.355756	100.343723	100.346696
	F^-	K_h	99.764381	99.753329	99.758238
	HCl	$C_{\infty v}$	460.343766	460.328319	460.336872
	Cl^-	K_h	459.817037	459.797359	459.806635
$G°$	**1a**, (HS)(HO)SO_2	C_1	1022.140619	1022.092206	1022.110076
	1b, (HS)(HO)SO_2	C_1	1022.139574	1022.091241	1022.108977
	2, $(HO)_2S(=S)O$	C_1	1022.127526	1022.079485	1022.096861
	3, (HS)SO_3^-	C_s	1021.654964	1021.604105	1021.622960
	4, (HO)S(=S)O_2^-	C_1	1021.646045	1021.594713	1021.613555
	5, H_2SO_5	C_1	774.592206	774.538476	774.554564
	6, HSO_5^-	C_1	774.112025	774.054995	774.072158
	FSO_3H	C_1	723.564782	723.513358	723.528215
	FSO_3^-	C_{3v}	723.087758	723.033560	723.049589
	$ClSO_3H$	C_1	1083.547130	1083.491983	1083.511749
	$ClSO_3^-$	C_{3v}	1083.074585	1083.015955	1083.036769
	SO_2	$D_{\infty v}$	548.059176	548.031188	548.039853
	SO_3	D_{3h}	623.176331	623.139258	623.149965
	H_2O	C_{2v}	76.354061	76.347599	76.349642
	H_2O_2	C_2	151.397722	151.382895	151.387350
	HO_2^-	C_s	150.800350	150.784475	150.790471
	OH^-	$C_{\infty v}$	75.730474	75.729025	75.726222
	H_2S	C_{2v}	398.952984	398.943590	398.950222
	HS^-	$C_{\infty v}$	398.394858	398.382201	398.389429
	HF	$C_{\infty v}$	100.375430	100.363410	100.366383
	F^-	K_h	99.780901	99.769848	99.774758
	HCl	$C_{\infty v}$	460.364929	460.349482	460.358035
	Cl^-	K_h	459.834421	459.814742	459.824019

cies are higher than that of sulfuric acid. Therefore, these species may be termed superacids. The OH acidity of acids of type $HO-SO_2-X$ obviously depends on the electronegativity as well as on the charge capacity of the substituent X (X = H, OH, SH, OOH, F, Cl). In addition, the enthalpies and Gibbs free energies of the products of the two dissociation reactions $HO-SO_2-X \rightarrow SO_3 + H-X$ and $SO_3X^- \rightarrow SO_3 + X^-$ were calculated to obtain the reaction enthalpies. All these reactions are endothermic and endergonic. In other words, both the acids and their monoanions are thermodynamically stable species in the gas phase at 298 K. From these dissociation enthalpies and literature data of the dissociation products we have calculated the enthalpies of formation of the gaseous acids H_2SO_3, $H_2S_2O_3$, H_2SO_5, HSO_3F, and HSO_3Cl.

Appendix

Enthalpies $H°$ and Gibbs free energies $G°$ of the acids $HO-SO_2-X$ (X = H, OH, SH, OOH, F, Cl), their anions, and the products of decomposition at 298 K are given in Table 12.

Acknowledgments

This work was supported by the Deutsche Forschungsgemeinschaft, the Verband der Chemischen Industrie, and the Konrad-Zuse-Zentrum für Informationstechnologie Berlin.

[1] R. J. Gillespie, T. E. Peel, *J. Am. Chem. Soc.* **1973**, *95*, 5173−5178.
[2] L. P. Hammett, A. J. Deyrup, *J. Am. Chem. Soc.* **1932**, *54*, 2721−2739.
[3] G. A. Olah, G. K. Surya Prakash, J. Sommer, *Superacids*, Wiley, New York, **1985**.
[4] T. A. O'Donnell, *Superacids and Acidic Melts as Inorganic Chemical Reaction Media*, VCH, New York, **1993**.
[5] A. A. Viggiano, M. J. Henchman, F. Dale, C. A. Deakyne, J. F. Paulson, *J. Am. Chem. Soc.* **1992**, *114*, 4299−4306.
[6] A. H. Otto, R. Steudel, *Eur. J. Inorg. Chem.* **2000**, 617−624.
[7] [7a]B. J. Smith, L. Radom, *J. Phys. Chem.* **1991**, *95*, 10549−10551. − [7b]B. J. Smith, L. Radom, *Chem. Phys. Lett.* **1995**, *245*, 123−128. − [7c]L. A. Curtiss, K. Raghavachari, P. S. Redfern, J. A. Pople, *J. Chem. Phys.* **1997**, *106*, 1063−1079.
[8] J. W. Ochterski, G. A. Petersson and J. A. Montgomery, Jr., *J. Chem. Phys.* **1996**, *104*, 2598−2519.
[9] L. A. Curtiss, K. Raghavachari, J. A. Pople, *J. Chem. Phys.* **1993**, *98*, 1293−1298.
[10] L. A. Curtiss, K. Raghavachari, G. W. Trucks, J. A. Pople, *J. Chem. Phys.* **1991**, *94*, 7221−7230.
[11] M. J. Frisch, G. W. Trucks, H. B. Schlegel, P. M. W. Gill, B. G. Johnson, M. A. Robb, J. R. Cheeseman, T. A. Keith, G. A. Petersson, J. A. Montgomery, K. Raghavachari, M. A. Al-Laham, V. G. Zakrzewski, J. V. Ortiz, J. B. Foresman, J. Cioslowski, B. B. Stefanov, A. Nanayakkara, M. Challacombe, C. Y. Peng, P. Y. Ayala, W. Chen, M. W. Wong, J. L. Andres, E. S. Replogle, R. Gomperts, R. L. Martin, D. J. Fox, J. S. Binkley, D. J. Defrees, J. Baker, J. P. Stewart, M. Head-Gordon, C. Gonzalez, J. A. Pople, *GAUSSIAN 94 Revisions D.2* (Cray) and *E.1* (workstation), Gaussian, Inc., Pittsburgh, PA, **1995**.
[12] 12a G. A. Petersson, A. Bennett, T. G. Tensfeldt, M. A. Al-Laham, W. A. Shirley, J. Mantzaris, *J. Chem. Phys.* **1988**, *89*, 2193−2218. − 12b G. A. Petersson, M. A. Al-Laham, *J. Chem. Phys.* **1991**, *94*, 6081−6090
[13] J. W. Ochterski, G. A. Petersson, K. B. Wiberg, *J. Am. Chem. Soc.* **1995**, *117*, 11299−11308.
[14] J. B. Foresman, A. E. Frisch, *Exploring Chemistry with Electronic Structure Methods*, 2nd ed., Gaussian, Inc., Pittsburgh, PA, **1996**.
[15] R. Steudel, A. Prenzel, *Z. Naturforsch.* **1989**, *B44*, 1499−1502.
[16] K. Miaskiewicz, R. Steudel, *Angew. Chem.* **1992**, *104*, 87−89; *Angew. Int. Ed. Engl.* **1992**, *31*, 58−59.
[17] H. Basch, T. Hoz, in: *The Chemistry of Sulphonic Acids, Esters and their Derivatives* (Eds.: S. Patai, Z. Rappoport), Wiley, New York **1991**, chapter 1, pp. 1−61.
[18] W. Frank, B. Bertsch-Frank, *Angew. Chem.* **1992**, *104*, 469−471; *Angew. Chem. Int. Ed. Engl.* **1992**, *31*, 436−438.
[19] J. Flanagan, W. P. Griffith, A. C. Skapski, *J. Chem. Soc., Chem. Commun.* **1984**, 1574−1575.
[20] E. O. Schlemper, R. C. Thompson, C. K. Fair, F. K. Ross, *Acta Crystallogr.* **1984**, *C40*, 1781−1785.
[21] K. A. Schugart, J. A. Noblet, *J. Mol. Struct. (Theochem)* **1994**, *304*, 13−16.
[22] K. Bartmann, D. Mootz, *Acta Crystallogr.* **1990**, *C46*, 319−320.
[23] A. H. Otto, S. Schrader, T. Steiger, M. Schneider, *J. Chem. Soc., Faraday Trans.* **1997**, *93*, 3927−3930.
[24] L. Bencivenni, R. Caminiti, A. Feltrin, F. Ramondo, C. Sadun, *J. Mol. Struct. (Theochem)* **1992**, *257*, 369−403.
[25] I. Hargittai, R. Seip, K. P. R. Nair, C. O. Britt, J. E. Boggs, B. N. Cyvin, *J. Mol. Struct.* **1977**, *39*, 1−13.
[26] Z. Žák, M. Kosička, *Acta Cryst.* **1978**, *B34*, 38−40.
[27] I. Hargittai, G. Schultz, M. Kolonits, *J. Chem. Soc,. Dalton Trans.* **1977**, 1299−1302.
[28] *Ullmann's Encyclopedia of Industrial Chemistry*, 5th ed., vol. A7, VCH, Weinheim **1986**, pp. 17−21.
[29] National Institute of Standards and Technology, Gaithersburg, USA (http://webbook.nist.gov).

Received March 20, 2000
[I00101]

Synthesis and Characterization of Novel Iodine(III) Compounds; Crystal Structures of Methoxy(trifluoromethyl)iodine(III) Chloride [$CF_3I(Cl)OCH_3$] and Dimethoxy(trifluoromethyl)iodine(III) [$CF_3I(OCH_3)_2$]

Rolf Minkwitz,*[a] Michael Berkei,[a] and Ralf Ludwig[a]

Keywords: Iodine / Structure elucidation / Vibrational spectroscopy

The reactions of $CF_3I(Cl)F$ and CF_3IF_2 with $(CH_3)_3SiOCH_3$ lead to the novel iodine(III) compounds $CF_3I(Cl)OCH_3$ and $CF_3I(OCH_3)_2$, respectively. The crystal structure of $CF_3I(Cl)OCH_3$ confirms that it is a ternary, trifluoromethyl-substituted iodine(III) derivative. $CF_3I(Cl)OCH_3$ crystallizes in the triclinic space group $P\bar{1}$, with four formula units per unit cell with the dimensions $a = 8.164(1)$, $b = 8.802(1)$, $c = 10.237(1)$ Å and angles $\alpha = 97.10(1)°$, $\beta = 91.41(1)°$, $\gamma = 115.00(1)°$. $CF_3I(OCH_3)_2$ crystallizes in the monoclinic space group $P2_1/n$ with four formula units per unit cell with $a = 6.295(1)$, $b = 15.607(1)$, $c = 7.736(1)$ Å, and $\beta = 111.44(1)°$. Both molecules have been additionally characterized by Raman, IR, and NMR spectroscopy and the experimental results are compared with quantum-mechanically calculated parameters.

Introduction

The chemistry of (trifluoromethyl)iodine(III) compounds is a well-explored field of research, although crystal structures have been obtained in only a few cases. The reported structures are limited to compounds having highly electronegative ligands, such as F, Cl, or ONO_2, in the apical positions.[1−3] These compounds are more stable and can be isolated more easily than derivatives having less electronegative ligands. According to Bent's rule, the apical positions are favourably occupied by the most electronegative ligands.[4] These positions are characterized by 3-center-4-electron bonds, in which the negative charge is located at the termini.[5]

Since all attempts to synthesize $CF_3I(OH)_2$ have proven unsuccessful, we became interested in its alkyl-substituted derivatives $CF_3I(OR)_2$. The tendency of iodine to form double bonds with oxygen leads to destabilization of these compounds and favours condensation reactions leading to CF_3IO. Although methanolysis of PhIO leads to $PhI(OCH_3)_2$ and Naumann et al. supposed a similar tendency of CF_3IO to form $CF_3I(OCH_3)_2$, no experimental details of this have yet been reported.[6,7] In 1974, Oates and Winfield described the synthesis of $CF_3IF_{4-n}(OCH_3)_n$ ($n = 1-4$) by reaction of CF_3IF_4 with $(CH_3)_3SiOCH_3$.[8] All the products were identified by their mass and NMR spectra. Since no similar investigation has been carried out in the case of iodine(III), it seemed desirable to study the reaction of CF_3IF_2 with $(CH_3)_3SiOCH_3$. In this reaction, $CF_3I(F)OCH_3$ is expected to be an observable intermediate. In general, ternary iodine(III) compounds are known to decompose by symmetrization in solution, even at low temperatures, and are thus difficult to isolate.[9] In order to obtain ternary iodine(III) compounds, $CF_3I(Cl)F$ represents a good starting material.[9] In this compound, the I−F bond is elongated and the I−Cl bond is shortened. This renders it suitable for exchange reactions in which only the I−F bond is replaced.

In this work, we report the syntheses and crystal structures of $CF_3I(Cl)OCH_3$ and $CF_3I(OCH_3)_2$. As far as we are aware, this constitutes the first report of structural data for (trifluoromethyl)iodine(III) compounds substituted by methoxy groups.

Results and Discussion

Formation of $CF_3I(Cl)OCH_3$ and $CF_3I(OCH_3)_2$

The molecules were obtained by reactions of (methoxy)-trimethylsilane with $CF_3I(Cl)F$ and CF_3IF_2, respectively [Equations (1) and (2)]. This synthesis is analogous to the preparation of $CF_3IF_n(OCH_3)_{4-n}$ ($n = 1-4$) by Oates and Winfield.[8] The driving force behind these reactions is the formation of the thermodynamically favoured Si−F bond at the expense of the Si−O bond.

$$CF_3I(Cl)F + (CH_3)_3SiOCH_3 \xrightarrow{-80°C} CF_3I(Cl)OCH_3 + (CH_3)_3SiF$$

$$CF_3IF_2 + 2(CH_3)_3SiOCH_3 \xrightarrow{-50°C} CF_3I(OCH_3)_2 + 2(CH_3)_3SiF$$

The fine colourless solids proved to be stable for several months at −70 °C under nitrogen, decomposing at about −40 °C. The iodine(III) compounds were found to be soluble in sulfur dioxide at −50 °C. In solution, they start to decompose even at temperatures below −50 °C.

Vibrational Spectra

The observed Raman and IR frequencies of $CF_3I(Cl)OCH_3$ and $CF_3I(OCH_3)_2$ are summarized in

[a] Fachbereich Chemie der Universität Dortmund, 44221 Dortmund, Germany

 © WILEY-VCH Verlag GmbH, D-69451 Weinheim, 2000 1434−1948/00/1111−2387 $ 17.50+.50/0

Table 1. The vibrational spectra are assigned on the basis of C_1 symmetry for the molecules. For $CF_3I(Cl)OCH_3$, 27 fundamental vibrations are to be expected. The strongest line in the Raman spectrum at 509 cm^{-1} corresponds to the I−O stretching mode. The I−Cl stretching mode can be assigned to the line at 304 cm^{-1}. This is in good accordance with assignments made for $CF_3I(Cl)ONO_2$ (326 cm^{-1}) and $CF_3I(Cl)F$ (304 cm^{-1}).[3,9] The asymmetric CF_3 stretching modes are found in the range 1056 to 1209 cm^{-1}, while the symmetric mode is seen at about 1043 cm^{-1}. The corresponding bending modes are observed at 739 cm^{-1} (δ_{as} CF_3), 542 cm^{-1} (δ_s CF_3), and in the range 243 to 265 cm^{-1} (ρ CF_3). In the case of $CF_3I(OCH_3)_2$, the I−O stretching modes can be assigned to the strongest lines in the Raman spectrum at 532 cm^{-1} (ν_{as} IO_2) and 353 cm^{-1} (ν_s IO_2), respectively, while the IO_2 bending is seen at 236 cm^{-1}. For comparison, in $CF_3I(ONO_2)_2$, these vibrational modes are found at 705−734 cm^{-1} (ν_{as} IO_2), 332/346 cm^{-1} (ν_s IO_2), and 182/190 cm^{-1} (δ IO_2).[3] The C−I stretching mode is observed at about 277 cm^{-1}. The vibrational bands of the CF_3 and CH_3 groups were detected in the expected ranges.

Table 1. Vibrational frequencies of $CF_3I(Cl)OCH_3$ and $CF_3I(OCH_3)_2$

$CF_3I(Cl)OCH_3$ Raman $T = -196$ °C	IR[a] $T = -50$ °C	$CF_3I(OCH_3)_2$ Raman $T = -196$ °C	IR[a] $T = -50$ °C	Assignment
2994 (12)[b]		3001 (41)[b]		ν_{as} CH_3
2984 (14)		2965 (29)	2961 w	ν_{as} CH_3
2978 (12)		2947 (33)	2943 w	ν_{as} CH_3
2957 (11)	2960 w	2917 (21)	2918 w	ν_{as} CH_3
2938 (15)				ν_{as} CH_3
2898 (11)		2903 (23)		ν_{as} CH_3
2825 (12)	2821 vw	2838 (41)	2835 w	ν_s CH_3
1929 (8)			1971 vw	
1465 (8)	1461 w	1458 (19)	1457 m	δ_{as} CH_3
1459 (9)				δ_{as} CH_3
1449 (9)				δ_{as} CH_3
1440 (9)			1443 m	δ_{as} CH_3
1437 (9)	1434 w			δ_{as} CH_3
1430 (9)		1416 (9)		δ_{as} CH_3
			1288 w	δ_s CH_3
	1255 m		1255 w	δ_s CH_3
1209 (8)	1201 vs	1210 (9)	1201 vs	ν_{as} CF_3
1196 (8)				ν_{as} CF_3
1194 (8)		1175 (9)	1187 s	ν_{as} CF_3
1165 (9)		1160 (10)		ν_{as} CF_3
1156 (8)		1097 (10)		ν_{as} CF_3
1045 (14)	1042 vs	1075 (14)		ν_s CF_3
		1060 (19)	1054 vs	ν_s CF_3
			1018 m	ν CO
977 (18)	968 m	997 (25)	989 s	ν CO
	844 m		849 w	
	821 sh	817 (29)	820 m	
739 (33)	738 s	745 (59)	740 s	δ_s CF_3
		548 (33)		δ_{as} CF_3
542 (10)		542 (81)		δ_{as} CF_3
530 (10)		532 (100)	536 s	ν_{as} IO_2
		513 (24)	517 m, sh	
508 (100)	510 m			ν IO
		411 (22)	407 m	
		353 (85)	360 s	ν_s IO_2
313 (13)	329 w	329 (31)	324 m	δ ClO
			310 m	
304 (17)	304 m			ν ICl
		290 (36)		
		285 (47)		
278 (18)	279 w	279 (56)	274 m	ν CI
265 (59)	266 w	266 (26)	264 vw	ρ CF_3
243 (35)		254 (26)		ρ CF_3
		236 (15)	238 w	δ IO_2
215 (52)				δ ClCl
		210 (15)		
149 (20)				δ OICl
137 (23)		128 (24)		lattice modes
118 (13)		113 (27)		lattice modes
92 (23)				lattice modes
79 (20)				lattice modes
62 (25)				lattice modes

[a] vs = very strong, s = strong, m = medium, w = weak, vw = very weak, sh = shoulder. − [b] Relative intensities are given in parentheses.

Crystal Structure of $CF_3I(Cl)OCH_3$

$CF_3I(Cl)OCH_3$ crystallizes in the triclinic space group $P\bar{1}$ with four formula units per unit cell. The crystal data are summarized in Table 2. The molecule has a distorted Ψ-trigonal bipyramidal structure with chlorine and the methoxy group in the apical positions and the trifluoromethyl group and two lone pairs in the equatorial positions (Figure 1). This is in accordance with the Gillespie−Nyholm model and the structure can be described as T-shaped.[10,11] Bond lengths and selected bond angles are listed in Table 3.

The unit cell contains two crystallographically independent molecules with slightly different bond lengths. The I−Cl bonds have lengths of 2.578(2) and 2.580(2) Å, about 0.3 Å longer than the sum of the covalent radii, and are 0.1 Å longer than those found in CF_3ICl_2.[2,12] For the I−O bonds, values of 1.969(5) and 1.991(5) Å are observed, these being only slightly longer than the sum of the covalent radii of 1.94 Å.[12] The molecules are arranged in chains, due to strong intermolecular I−Cl contacts. Owing to intermolecular I−O contacts, the chains are arranged in layers, stacked along the *b* axis. All these interactions result in the formation of ribbons of twelve-membered, centrosymmetric rings (Figure 1). In these rings, I−O−I−O parallelograms are spanned by two molecules involving I−O contacts with lengths of 3.235(5) and 3.250(5) Å. On the basis of these contacts, the environment at the iodine atom can be designated as distorted square-pyramidal. Between the layers of molecules, no contacts shorter than the sum of the van der Waals radii are found.

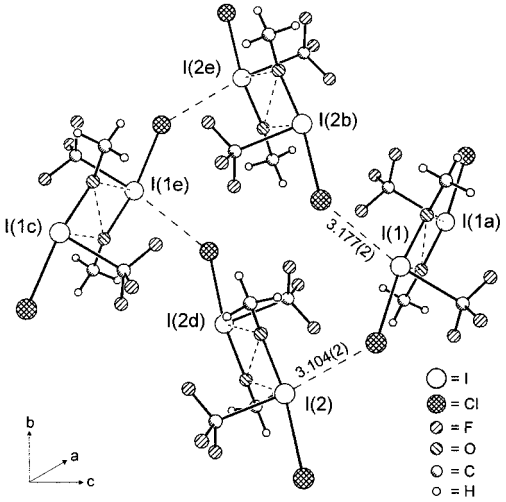


Figure 1. Fragment of the structure of $CF_3I(Cl)OCH_3$; projection of a twelve-membered ring; distances [Å]: I(1)···Cl(2b) 3.177(2), I(1)···O(1a) 3.235(5), O(1)···O(1a) 2.864(5), I(2)···Cl(1) 3.104(2), I(2)···O(2d) 3.250(5), O(2)···O(2d) 2.878(5); symmetry operations: *a*: $-x+2, -y+1, -z+1$; *b*: $x+1, y, z$; *c*: $x, y, z-1$; *d*: $-x+1, -y+1, -z$; *e*: $-x+2, -y+1, -z$

Crystal Structure of $CF_3I(OCH_3)_2$

$CF_3I(OCH_3)_2$ (Figure 2) crystallizes in the monoclinic space group $P2_1/n$ with four formula units per unit cell. The crystal data are summarized in Table 2 and bond lengths and selected angles are listed in Table 3. $CF_3I(OCH_3)_2$ has a T-shaped arrangement with two methoxy groups in apical positions. The I−O bonds have lengths of 2.019(11) Å

Table 2. X-ray diffraction data of $CF_3I(Cl)OCH_3$ and $CF_3I(OCH_3)_2$

	$CF_3I(Cl)OCH_3$	$CF_3I(OCH_3)_2$
Space group	$P\bar{1}$	$P2_1/n$
Crystal system	triclinic	monoclinic
a [Å]	8.164(1)	6.295(1)
b [Å]	8.802(1)	15.607(1)
c [Å]	10.237(1)	7.736(1)
α [°]	97.10(1)	90
β [°]	91.41(1)	111.44(1)
γ [°]	115.00(1)	90
Volume [Å^3]	659.17(13)	707.4(2)
Density (calcd.) [g cm^{-3}]	2.644	2.422
Z	4	4
Molecular mass [g mol^{-1}]	262.39	257.98
Absorption coefficient [mm^{-1}]	5.231	4.516
Temperature [K]	173(2)	173(2)
F(000)	480	480
Wavelength [Å]	0.71069	0.71069
θ range for data collection [°]	$3.41 \le \theta \le 30.24$	$2.61 \le \theta \le 29.28$
Index ranges	$-11 \le h \le 9$ $-9 \le k \le 11$ $-14 \le l \le 11$	$-8 \le h \le 8$ $-19 \le k \le 19$ $-6 \le l \le 7$
Reflections collected/independent	3913/2401 [*R*(int) = 0.0418]	3575/1316 [*R*(int) = 0.1469]
Parameters	145	82
Goodness-of-fit on F^2	1.031	1.015
Final *R* indices [$I > 2\sigma(I)$]	$R1 = 0.0421$ $wR2 = 0.0989$	$R1 = 0.0672$ $wR2 = 0.1549$
R indices (all data)	$R1 = 0.0629$ $wR2 = 0.1087$	$R1 = 0.1372$ $wR2 = 0.1977$
Largest diff. peak and hole [e$^-$ Å^{-3}]	1.757 and −1.619	1.187 and −1.018
Refinement method	full-matrix least squares on F^2	full-matrix least squares on F^2

Table 3. Quantum-mechanically calculated bond lengths [Å] and angles [°] in $CF_3I(Cl)OCH_3$ and $CF_3I(OCH_3)_2$ in comparison with the experimentally observed values

	$CF_3I(Cl)OCH_3$				$CF_3I(OCH_3)_2$		
	exp.	RHF-LANL2DZ	B3LYP-LANL2DZ		exp.	RHF-LANL2DZ	B3LYP-LANL2DZ
I1−Cl1	2.578(2)	2.6559	2.6806	I1−O1	2.019(11)	2.0154	2.1106
I2−Cl2	2.580(2)	2.6559	2.6806	I1−O2	2.087(11)	2.0268	2.1106
I1−O1	1.969(5)	1.9843	2.0996	I1−C3	2.190(12)	2.1846	2.2896
I2−O2	1.991(5)	1.9843	2.0996	O1−C1	1.40(2)	1.4338	1.4580
I1−C1	2.212(8)	2.2054	2.2815	O2−C2	1.38(2)	1.4334	1.4580
I2−C2	2.207(7)	2.2054	2.2815	ø C−F[a]	1.31(2)	1.3569	1.3876
O1−C4	1.443(7)	1.4465	1.4674				
O2−C3	1.450(8)	1.4465	1.4674				
ø C−F[a]	1.311(8)	1.3495	1.3786				
Cl1−I1−O1	171.0(2)	170.06	171.22	O1−I1−O2	166.7(4)	165.28	169.05
Cl2−I2−O2	171.0(2)	170.06	171.22	O1−I1−C3	81.4(5)	86.11	84.61
Cl1−I1−C1	81.7(2)	81.68	83.35	O2−I1−C3	85.3(5)	79.41	84.61
Cl2−I2−C2	82.0(2)	81.68	83.35	C1−O1−I1	115.0(10)	129.95	120.29
C1−I1−O1	89.3(3)	88.43	88.34	C2−O2−I1	117.0(9)	129.01	120.29
C2−I2−O2	89.2(2)	88.43	88.34				
I1−O1−C4	116.4(4)	126.67	119.48				
I2−O2−C3	113.9(4)	126.67	119.48				

[a] For the sake of simplicity, the average C−F bond lengths are shown.

[I(1)−O(1)] and 2.087(11) Å [I(1)−O(2)] and are significantly longer than the sum of the covalent radii of 1.94 Å and the corresponding bonds in $CF_3I(Cl)OCH_3$ [1.969(5) and 1.991(5) Å].[12] The molecules present donors as well as acceptors for each secondary I−O bond, which points to the C−I bond. For iodine, a square-planar environment results. Taking the intermolecular contacts into consideration, the observed difference in I−O bond lengths due to weakening of the I(1)−O(2) bond becomes reasonable. The molecules are arranged in chains along the *c* axis. The CF_3 group and the methoxy group of O(1) are not involved in any intermolecular contacts and occupy the positions of side groups on the chains. A similar arrangement is found in CF_3ICl_2.[2] The C−I distance of 2.190(12) Å is comparable to those in similar compounds such as CF_3IF_2 [2.174(6) Å], CF_3ICl_2 [2.229(10) Å], and $CF_3I(ONO_2)_2$ [2.212(4) Å].[1−3] The CF_3 group is almost tetrahedral with F−C−F angles of about 108° and an average C−F bond length of about 1.31(2) Å.

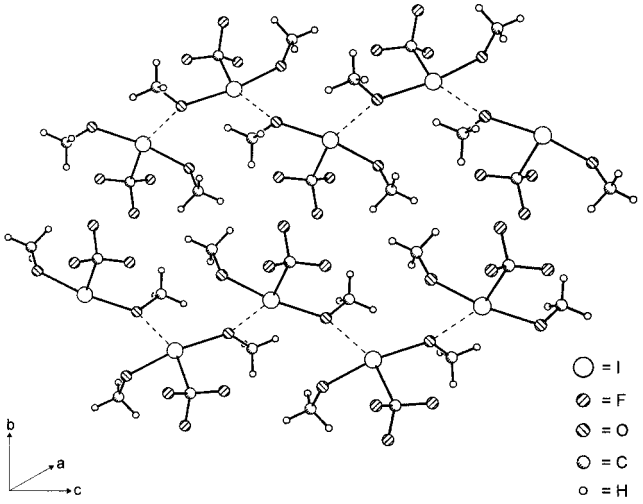


Figure 2. View of the crystal structure of $CF_3I(OCH_3)_2$ in *q* orientation; the intermolecular I−O contacts measure 2.749(9) Å

Quantum-Mechanical Calculations

Ab initio RHF and density functional B3LYP calculations were performed using the Gaussian 98 program.[13] To take relativistic effects into account, calculations were carried out with the LANL2DZ basis set, which includes D95 on first-row atoms, and a Los Alamos ECP, which puts DZ on other atoms.[14−17] Additional calculations with CEP-121G and SDD basis sets not described here yielded similar results.[18−21] To obtain optimized molecular structures, the wavefunctions were analyzed by the natural bond orbital (NBO) method, a standard program option of Gaussian 98.[22]

The optimized geometries for both systems are given in Table 3 and are compared with experimental data. Whereas the HF method overestimates the I−Cl bond length by about 8 pm, the density functional method B3LYP systematically overestimates the lengths of all iodine-containing bonds by about 10 pm. With the chosen basis set, the B3LYP approximation does not yield adequate results for iodine-containing systems. It should also be borne in mind that all calculations were performed for free molecules in the gas phase. Some deviations between the calculated and experimentally observed values can thus be attributed to the strong intermolecular cross-links in the crystalline solid state. In the case of $CF_3I(OCH_3)_2$, we could not find any explanation for the difference in symmetries calculated by the two methods.

For both compounds, NBO analyses for all methods and basis sets were performed.[22] Summarizing the calculated charges on each atom of the various ligands clearly indicates that total negative charges increase in the order: $F_3C > H_3CO > Cl$ (Table 4). The calculated charges support the assumption that the apical ligands are bound by 3-center-4-electron bonds.[5] In 1992, Boyd and Boyd reported group electronegativities calculated by the bond critical model.[23] For the CF_3 and H_3CO groups, values of 2.71 and 3.53, respectively, were calculated.[23] In accordance with Bent's

rule, this explains the apical positions of chlorine and the methoxy group in $CF_3I(Cl)OCH_3$ and of both methoxy groups in $CF_3I(OCH_3)_2$.[4]

Table 4. Calculated and summarized NBO charges of the three different ligands in $CF_3I(Cl)OCH_3$ and $CF_3I(OCH_3)_2$; charges are given in e^-

	$CF_3I(Cl)OCH_3$		$CF_3I(OCH_3)_2$	
	RHF LANL2DZ	B3LYP LANL2DZ	RHF LANL2DZ	B3LYP LANL2DZ
Cl	−0.472	−0.616		
H_3CO	−0.420	−0.545	−0.494	−0.641
F_3C	−0.112	−0.132	−0.210	−0.215

Experimental Section

Caution! $CF_3I(Cl)F$ and CF_3IF_2 are unstable at room temperature and are sensitive to moisture. Skin contact with these compounds should be avoided because their hydrolysis leads to HF or HCl, which cause burns and in some cases irreparable damage. Safety precautions should be taken when using and handling these materials.

All synthetic work and sample handling was performed using a standard glass vacuum line and standard Schlenk techniques. Nonvolatile materials were handled under dry nitrogen. The syntheses of $CF_3I(Cl)F$ and CF_3IF_2 were carried out by treating trifluoromethyl iodide (CF_3I) with trifluoromethyl hypochlorite (CF_3OCl) at −78 °C and −50 °C, respectively, based on literature methods.[1,9] (Methoxy)trimethylsilane [$(CH_3)_3SiOCH_3$] (ABCR) was used as received without any purification. Owing to the low stability of the products, we were unable to obtain reliable elemental analysis results. − The Raman spectra were recorded with a Jobin Yvon T64000 spectrometer using an Ar^+ laser (514.5 nm) from Spectra Physics. The spectra were obtained from samples in a glass cell cooled with liquid N_2.[24] − Infrared spectra were recorded with a Bruker IFS 113v spectrophotometer. Spectra were obtained from samples coated on CsBr plates placed in a low-temperature cell.[25] − NMR spectra in SO_2 solution at −50 °C were recorded with Bruker DPX 300 and Bruker DRX 400 spectrometers. − Single crystals were placed in Lindemann capillaries in a cooled stream of dry nitrogen, and X-ray diffraction data were collected using a Nonius Kappa CCD diffractometer. The crystal structures were solved by the Patterson method and successive difference Fourier syntheses. For refinement, full-matrix least-squares methods were applied. Data reduction, structure solution, and refinement were carried out with programs in the SHELXTL package, PLATON, MISSYM, and PARST.[26−30]

Quantum-Mechanical Calculations: Hartree−Fock and density functional calculations were performed with the program Gaussian 98.[13] In the density functional B3LYP,[31] the 3-parameter exchange functional by Becke[32] and the correlation functional by Lee, Yang, and Parr[33] were used. The LANL2DZ basis set contains a D95 basis[14] for elements of the first period and an effective core potential and a double-zeta basis for elements from sodium to bismuth.[15−17] For the geometry optimization, different starting coordinates were chosen. The calculation of the vibrational frequencies showed whether or not the energy-minimized structures represented stable molecules. All frequencies were positive, indicating that at least local minima on the Born−Oppenheimer hypersurface were found.

Preparation of $CF_3I(Cl)OCH_3$: In a typical reaction, $(CH_3)_3SiOCH_3$ (0.26 g, 2.50 mmol) was condensed onto $CF_3I(Cl)F$ (0.50 g, 2.00 mmol) in a dry glass vessel with greaseless stopcocks (Young). The mixture was then allowed to warm to −80 °C and was maintained at this temperature for 30 min. After removal of the volatile materials in vacuo at −70 °C, the formation of 0.39 g (1.49 mmol, 74%) of methoxy(trifluoromethyl)iodine(III) chloride, $CF_3I(Cl)OCH_3$, was observed. The resulting colourless solid was found to be stable up to −40 °C and sensitive to moisture. − NMR: ^{19}F: δ = −29.68 (s, CF_3). − ^{13}C: δ = 67.47 (s, CH_3), 83.09 (q, ^1J = 344 Hz, CF_3). − ^1H: δ = 4.13 (s, CH_3).

Preparation of $CF_3I(OCH_3)_2$: $(CH_3)_3SiOCH_3$ (0.52 g, 5.00 mmol) was condensed onto CF_3IF_2 (0.47 g, 2.00 mmol) in a dry glass vessel with greaseless stopcocks (Young). The mixture was allowed to warm to −50 °C and was maintained at this temperature for 1 h. After removal of the volatile materials in vacuo at −50 °C, the formation of 0.24 g (0.93 mmol, 48%) of dimethoxy(trifluoromethyl)iodine(III), $CF_3I(OCH_3)_2$, was observed. The resulting colourless solid was found to be stable up to −40 °C and sensitive to moisture. − NMR: ^{19}F: δ = −28.42 (s, CF_3). − ^{13}C: δ = 63.21 (s, CH_3), δ = 81.19 (q, ^1J = 344 Hz, CF_3). − ^1H: δ = 4.36 (s, CH_3).

Acknowledgments

This work was supported by the Fonds der Chemischen Industrie.

[1] R. Minkwitz, M. Berkei, *Inorg. Chem.* **1998**, *37*, 5247−5250.
[2] R. Minkwitz, M. Berkei, *Inorg. Chem.* **1999**, *38*, 5041−5044.
[3] R. Minkwitz, T. Hertel, H. Preut, *Z. Anorg. Allg. Chem.* **1995**, *621*, 1552−1557.
[4] H. A. Bent, *Chem. Rev.* **1961**, *61*, 275−311.
[5] A. Varvoglis, in *The Organic Chemistry of Polycoordinated Iodine*, VCH, Weinheim, **1992**, p. 1−119.
[6] J. F. Kinneary, J. S. Albert, C. J. Burrows, *J. Am. Chem. Soc.* **1988**, *110*, 6124−6129.
[7] D. Naumann, L. Deneken, E. Renk, *J. Fluorine Chem.* **1975**, *5*, 509−519.
[8] G. Oates, J. M. Winfield, *J. Chem. Soc., Dalton Trans.* **1974**, 119−124.
[9] R. Minkwitz, R. Bröchler, M. Schütze, *Z. Anorg. Allg. Chem.* **1995**, *621*, 1727−1730.
[10] R. J. Gillespie, R. S. Nyholm, *Quart. Rev., Chem. Soc.* **1957**, *11*, 339−380.
[11] R. J. Gillespie, *J. Chem. Educ.* **1963**, *40*, 295−301.
[12] A. Bondi, *J. Phys. Chem*. **1964**, *68*, 441−451.
[13] M. J. Frisch, G. W. Trucks, H. B. Schlegel, G. E. Scuseria, M. A. Robb, J. R. Cheeseman, V. G. Zakrzewski, J. A. Montgomery, R. E. Stratmann, J. C. Burant, S. Dapprich, J. M. Millam, A. D. Daniels, K. N. Kudin, M. C. Strain, O. Farkas, J. Tomasi, V. Barone, M. Cossi, R. Cammi, B. Mennucci, C. Pomelli, C. Adamo, S. Clifford, J. Ochterski, G. A. Petersson, P. Y. Ayala, Q. Cui, K. Morokuma, D. K. Malick, A. D. Rabuck, K. Raghavachari, J. B. Foresman, J. Cioslowski, J. V. Ortiz, B. B. Stefanov, G. Liu, A. Liashenko, P. Piskorz, I. Komaromi, R. Gomperts, R. L. Martin, D. J. Fox, T. Keith, M. A. Al-Laham, C. Y. Peng, A. Nanayakkara, C. Gonzalez, M. Challacombe, P. M. W. Gill, B. G. Johnson, W. Chen, M. W. Wong, J. L. Andres, M. Head-Gordon, E. S. Replogle, J. A. Pople, *Gaussian 98 (Revision A.1)*, Gaussian, Inc., Pittsburgh PA, **1998**.
[14] T. H. Dunning, Jr., P. J. Hay, in *Modern Theoretical Chemistry* (Ed.: H. F. Schaefer, III), Plenum, New York, **1976**, p. 1−28.
[15] P. J. Hay, W. R. Wadt, *J. Chem. Phys.* **1985**, *82*, 270−283.
[16] W. R. Wadt, P. J. Hay, *J. Chem. Phys.* **1985**, *82*, 284−298.
[17] P. J. Hay, W. R. Wadt, *J. Chem. Phys.* **1985**, *82*, 299−310.
[18] W. Stevens, H. Basch, J. Krauss, *J. Chem. Phys.* **1984**, *81*, 6026−6033.
[19] W. J. Stevens, J. Krauss, H. Basch, P. G. Jasien, *Can. J. Chem.* **1992**, *70*, 612−630.
[20] T. R. Cundari, W. J. Stevens, *J. Chem. Phys.* **1993**, *98*, 5555−5565.

[21] U. Wedig, M. Dolg, H. Stoll, H. Preuss, in *Quantum Chemistry: The Challenge of Transition Metals and Coordination Chemistry* (Ed.: A. Veillard), Reidel, Dordrecht, **1986**, p. 79.

[22] A. E. Reed, L. A. Curtis, F. Weinhold, *Chem. Rev.* **1988**, *88*, 899−926.

[23] R. J. Boyd, S. L. Boyd, *J. Am. Chem. Soc.* **1992**, *114*, 1652−1655.

[24] A. Werner, Dissertation, University of Dortmund, Germany, **1988**.

[25] L. Bayersdorfer, R. Minkwitz, J. Jander, *Z. Anorg. Allg. Chem.* **1972**, *392*, 137−142.

[26] G. M. Sheldrick, *SHELXTL-PLUS: An Integrated System for Solving, Refining, and Displaying Structures from Diffraction Data*, University of Göttingen, Germany, **1987**.

[27] A. L. Spek, "The EUCLID Package", in *Computational Crystallography* (Ed.: D. Sayre), Clarendon Press, Oxford, **1982**, p. 528.

[28] Y. Le Page, *J. Appl. Crystallogr.* **1987**, *20*, 264−269.

[29] M. Nardelli, *Comput. Chem.* **1983**, *7*, 95−98.

[30] Crystallographic data (excluding structure factors) for the structures reported in this paper have been deposited with the Cambridge Crystallographic Data Centre as supplementary publication nos. CCDC-141229 [$CF_3I(Cl)OCH_3$] and -141228 [$CF_3I(OCH_3)_2$]. Copies of the data can be obtained free of charge on application to the CCDC, 12 Union Road, Cambridge CB2 1EZ, U.K. [Fax: (internat.) + 44-1223/336-033; E-mail: deposit@ccdc.cam.ac.uk].

[31] B. Miehlich, A. Savin, H. Stoll, H. Preuss, *Chem. Phys. Lett.* **1989**, *157*, 200−206.

[32] A. D. Becke, *J. Chem. Phys.* **1993**, *98*, 5648−5652.

[33] C. Lee, W. Yang, R. G. Parr, *Phys. Rev. B* **1988**, *37*, 785−789.

Received March 6, 2000
[I00089]

Reduction of the Phosphododecamolybdate Ion by Phosphonium Ylides and Phosphanes

Vincent Artero[a] and Anna Proust*[a]

Keywords: Polyoxometalates / Molybdenum / Ylides / Phosphanes / Electron transfer / Heteropoly blues

The reaction of phosphonium ylides with $[PMo_{12}O_{40}]^{3-}$ consists of successive single electron transfers leading to the formation of the 1e- and 2e-reduced polyoxomolybdates $[PMo_{12}O_{40}]^{4-}$ and $[PMo_{12}O_{40}]^{5-}$. The ylide is converted into the corresponding phosphonium cation via a radical-cation intermediate. The reaction of phosphanes follows the same pathway but subsequent reactions with residual water produce protons which induce the disproportionation of $[PMo_{12}O_{40}]^{4-}$. Authentic samples of heteropoly blues in different protonation states have been obtained from the reaction of phenyllithium with $[PMo_{12}O_{40}]^{3-}$ and subsequent protonation with triflic acid. On the basis of electrochemical and spectroscopic data, the reaction product of $[PMo_{12}O_{40}]^{3-}$ with triphenylphosphane, which has been previously described as the oxygen-deficient species $[PMo_{12}O_{39}]^{3-}$, is reformulated as $[H_2PMo_{12}O_{40}]^{3-}$.

Introduction

Early transition metals in their highest oxidation states form a large class of oxo−metal cluster anions called polyoxometalates.[1] For the past ten years, our group has been involved in a systematic study of the functionalization of polyoxometalates.[2] One subclass of derivatized polyoxometalates include compounds that derive from parent polyoxometalates through the replacement of terminal oxo ligands by other multiply bonded ligands. The oxo, imido, nitrido and cyclopentadienyl groups are formally six-electron donors. Thus imido,[3] nitrido[4] and cyclopentadienyl[5] derivatives of polyoxometalates are effectively isoelectronic with the parent polyoxometalates. On the other hand, the $[MoO]^{4+}$, $[Mo(NO)]^{3+}$ and $[Mo(NNR)]^{3+}$ groups are isolobal, so that the formation of nitrosyl[6] and diazenido[7] polyoxomolybdates can easily be rationalized. The oxo ligand can also act as a four-electron donor and, as such, is isoelectronic with alkylidene groups. These considerations led us to look for alkylidene derivatives of polyoxometalates. Our aims were threefold: (i) to provide structural and spectroscopic models for metathesis reactions on oxide surfaces; (ii) to identify the reactive species when $[Mo_6O_{19}]^{2-}$ is used as a precatalyst;[8] (iii) to design new metathesis catalysts or precatalysts in a special oxo environment that could be further tuned through size, shape or charge modifications. One strategy for the functionalization of polyoxometalates relies on the analogy between oxometal units and organic functionalities. This has been established by Floriani et al. for oxovanadium groups.[9] The analogy also holds to some extent for oxomolybdenum groups. Indeed, hydrazido[4,7b,10] and imido[3a,11,12] derivatives of polyoxomolybdates have been obtained from the reactions of *N*,*N*-disubstituted hydrazines and iminophosphoranes or isocyanates with polyoxomolybdates. The formation of imido derivatives is reminiscent of the aza Wittig reaction and is thought to proceed by a net [2 + 2] cycloaddition of the P=N and Mo=O bonds.[13] Intermetal exchange of oxo, imido and alkylidene ligands has been shown to occur readily, at least at coordinatively unsaturated metal centres.[14] However, attempts to achieve the replacement of an oxo ligand by an alkylidene ligand have so far failed. For instance, the reaction of *cis*-$[MoO_2(mesityl)_2]$ with Bu_3PCH_2 has afforded the stable betaine-like $[MoO_2(mesityl)_2(CH_2PBu_3)]$.[15] We have investigated the reactions of a number of phosphonium ylides with $(nBu_4N)_3[PMo_{12}O_{40}]$ in acetonitrile and we have found that only 1e- and/or 2e-reduced derivatives of $[PMo_{12}O_{40}]^{3-}$ are formed.

Another route to functionalized polyoxometalates involves lacunary polyoxometalates. This has been widely applied to the rational synthesis of metal-substituted polyoxometalates. On the other hand, polyoxometalates with oxygen vacancies would be potential precursors for the synthesis of ligand-substituted polyoxometalates. The only oxygen-deficient polyoxometalates that have been reported so far are the species $[PMo_{12}O_{40-x}]^{3-}$ (x = 1, 2 or 3) which were obtained by Kawafune et al. by reaction of $[PMo_{12}O_{40}]^{3-}$ with PPh_3 in acetonitrile.[16] However, these results have not been confirmed by Mattes et al., who isolated $[HPMo_{12}O_{40}]^{4-}$ from Kawafune's reaction.[17] Furthermore, Bond et al. have recently shown that the similar reaction of the Dawson-type polyanion $[S_2Mo_{18}O_{62}]^{4-}$ yields plenary reduced species.[18] This led us to revisit the reaction of $[PMo_{12}O_{40}]^{3-}$ with phosphanes. We have shown that only plenary reduced anions are formed in these reactions and that the compound formulated as $(nBu_4N)_3[PMo_{12}O_{39}]$ by Kawafune et al. is actually $(nBu_4N)_3[H_2PMo_{12}O_{40}]$. Identification of the reduced species formed in the reactions of $[PMo_{12}O_{40}]^{3-}$ with phosphonium ylides or phosphanes has been based on the comparison with the samples ob-

[a] Laboratoire de Chimie Inorganique et Matériaux Moléculaires, unité C.N.R.S. 7071, Université Pierre et Marie Curie,
Case Courrier 42, 4 place Jussieu 75252 Paris Cedex 05, France
Fax: (internat.) + 33-1/44273841
E-mail: proust@ccr.jussieu.fr

 © WILEY-VCH Verlag GmbH, D-69451 Weinheim, 2000 1434−1948/00/1111−2393 $ 17.50+.50/0

tained by reduction of $[PMo_{12}O_{40}]^{3-}$ by phenyllithium. Thus this report deals with interrelated studies of the reactions of $[PMo_{12}O_{40}]^{3-}$ with phosphonium ylides, phenyllithium and phosphanes.

Results

From here on, the Keggin anions $[PMo_{12}O_{40}]^{3-}$, $[PMo_{12}O_{40}]^{4-}$ and $[PMo_{12}O_{40}]^{5-}$ will be designated by the numerals **0**, **I** and **II**, respectively, according to their reduction state. Unless otherwise stated, they were isolated as tetrabutylammonium salts. Other cations will be specified when appropriate. Thus, **LiII** refers to $(n\mathrm{Bu_4N})_4\mathrm{Li}[PMo_{12}O_{40}]$ while **H_2II** refers to $(n\mathrm{Bu_4N})_3[H_2PMo_{12}O_{40}]$.

1e- and 2e-Reduced Derivatives of $[PMo_{12}O_{40}]^{3-}$

In nonaqueous solvents, most often MeCN and DMF, 1e- and 2e-reduced derivatives of $[PMo_{12}O_{40}]^{3-}$ have usually been obtained by electrolysis and characterized in situ. Only in a few cases were the reduced derivatives isolated. Phenyllithium proved to be a convenient reagent for the synthesis of **I** and **LiII** from **0** in MeCN. Reduction of **0** by phenyllithium was first recognized when an excess of phenyllithium was inadvertently used in the synthesis of the benzylidene ylide, which was subsequently added to a solution of $(n\mathrm{Bu_4N})_3[PMo_{12}O_4]$ in MeCN. When the reaction of $(n\mathrm{Bu_4N})_3[PMo_{12}O_{40}]$ with PhLi in MeCN was monitored by ^{31}P NMR spectroscopy, it was found that **I** is quantitatively formed upon addition of one equivalent of PhLi, while addition of a second equivalent yields **II**. The reduction does not proceed beyond the 2e-reduced state. The 1e- and 2e-reduced derivatives were readily isolated as $(n\mathrm{Bu_4N})_4[PMo_{12}O_{40}]$ (**I**) and $(n\mathrm{Bu_4N})_4\mathrm{Li}[PMo_{12}O_{40}]$ (**LiII**). Acidification of the solution of **LiII** with triflic acid allowed the isolation of $(n\mathrm{Bu_4N})_4[HPMo_{12}O_{40}]$ (**HII**) and $(n\mathrm{Bu_4N})_3[H_2PMo_{12}O_{40}]$ (**H_2II**). In this way, a full set of spectroscopic data could be obtained for the 1e- and 2e-reduced derivatives of $[PMo_{12}O_{40}]^{3-}$. Indeed, only **0** and **I** had been previously fully characterized by IR,[19] UV/Vis,[20] ^{31}P NMR[3b,21] and (for **I**) by EPR spectroscopy.[20] IR data for **HII** and **H_2II**, UV/Vis data for **II** and **H_2II**, and ^{31}P NMR data for **II** and **H_2II** have now been obtained and are reported herein. ^{31}P NMR data are gathered in Table 1. The electrochemical behaviour of **HII** and **H_2II** in MeCN had been previously studied by Himeno et al.[22] As electrochemical data will be at the centre of the discussion, they were examined further. The results reported in Table 2 are in agreement with those reported by Himeno et al. Solution data for **HII** and **H_2II** were measured both for these species formed in situ by acidification of **LiII** and after isolation of $(n\mathrm{Bu_4N})_4[HPMo_{12}O_{40}]$ and $(n\mathrm{Bu_4N})_3[H_2PMo_{12}O_{40}]$, respectively. No significant discrepancy was observed.

The ^{31}P NMR chemical shift of **II** steadily moves to higher frequency as the proton content increases. The values characteristic of **II**, **HII** and **H_2II** are $\delta = -5.4$, -5.2 and -5.0, respectively, in CH_3CN. **I** undergoes disproportionation upon acidification. Indeed, the ^{31}P NMR spectrum of an equimolecular mixture of **I** and triflic acid displays two signals with equal intensities at $\delta = -2.3$ and -5.0 which can be unambiguously assigned to **0** and **H_2II**, respectively, indicating the full disproportionation of **I** according to Equation (1).

$$2\,[PMo_{12}O_{40}]^{4-} + 2\,H^+ \rightarrow [PMo_{12}O_{40}]^{3-} + [H_2PMo_{12}O_{40}]^{3-} \quad (1)$$

On the other hand, the ^{31}P NMR spectrum of a solution of **I** with half an equivalent of triflic acid displays three signals at $\delta = +1.4$, -2.3 and -5.2, which are respectively assigned to **I**, **0** and **HII**. Further, the same spectrum is obtained for an equimolar solution of **0** and **HII**. This

Table 1. ^{31}P NMR chemical shift of some relevant species, referenced to external 85% H_3PO_4

	$\delta_{(CH_3CN/CD_3CN)}$ [ppm]	$\delta_{(DMSO/[D_6]DMSO)}$ [ppm]		$\delta_{(CH_6CN/CD_6CN)}$ [ppm]
$[PMo_{12}O_{40}]^{3-}$	−2.3	−2.9	$Bu_3PCH_3^+$	33.5
$[PMo_{12}O_{40}]^{4-}$	1.4 [21]	0.8	Bu_3PO	47.5
$[PMo_{12}O_{40}]^{5-}$	−5.4	−5.8	Bu_3P	−30.8
$[HPMo_{12}O_{40}]^{4-}$	−5.2[a]	−	$Ph_3P{=}CHPh$	9.3
$[H_2PMo_{12}O_{40}]^{3-}$	−5.0	−5.5	$Ph_3PCH_2Ph^+$	24.2
			Ph_3PO	27.5
			Ph_3P	−4.5
			Ph_4P^+	24.4

[a] This value aggrees with that reported by Mattes et al. for $[K(18\text{-crown-6})]_2[N(PPh_3)_2]_2[HPMo_{12}O_{40}]$ when locking the value for **0** at −2.3 ppm.[17]

Table 2. Electrochemical data[22] for $[H_xPMo_{12}O_{40}]^{n-}$ species, 1 mM in MeCN, at a platinum electrode

		$E_{1/2}$ [V/SCE]	$1/2(E_{pa}+E_{pc})$	$E_{1/2}$ [V/SCE]	$1/2(E_{pa}+E_{pc})$
$[PMo_{12}O_{40}]^{4-}$	**I**	0.14 ($1e^-$, ox)[a]	0.18 (rev.)[b]	−0.28 ($1e^-$, red)	−0.24 (rev.)
$\{Li[PMo_{12}O_{40}]\}^{4-}$	**LiII**	0.17 ($1e^-$, ox)	0.22 (rev.)	−0.10 ($1e^-$, ox)	−0.11 (rev.)
$[HPMo_{12}O_{40}]^{4-}$	**HII**	0.56 ($1e^-$, ox)	irrev.	0.2 ($1e^-$, ox)	irrev.
$[H_2PMo_{12}O_{40}]^{3-}$	**H_2II**	0.56 ($2e^-$, ox)	irrev.	0.1 ($1e^-$, red)	irrev.

[a] ox and red for oxidation and reduction processes, respectively. − [b] rev. and irrev. for reversible and irreversible processes, respectively.

shows that **0**, **I** and **HII** are in equilibrium according to Equation (2).

$$2\ [PMo_{12}O_{40}]^{4-} + H^+ \leftrightarrows [PMo_{12}O_{40}]^{3-} + [HPMo_{12}O_{40}]^{4-} \quad (2)$$

It follows therefore that $[HPMo_{12}O_{40}]^{3-}$ cannot be isolated. Whether the more positive oxidation wave of $[HPMo_{12}O_{40}]^{4-}$ at 0.56 V/SCE is due to the 1e-oxidation of **HI**, as assumed by Himeno et al.,[22] or to the 2e-oxidation of $\mathbf{H_2II}$ resulting from the disproportionation of **HI**, remains to be established. Indeed, the R.D.E. voltammogram of an equimolar mixture of **I** and triflic acid is identical to that of an equimolar mixture of **0** and $\mathbf{H_2II}$ at the same overall polyanion concentration.

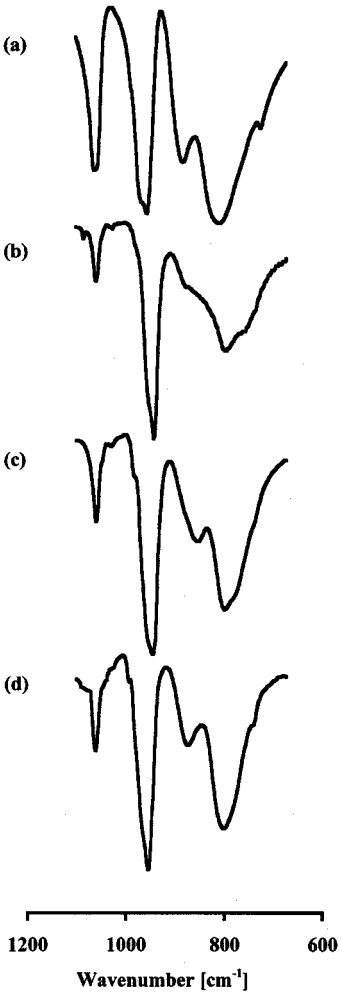


Figure 1. Infrared spectra of $(n\mathrm{Bu_4N})_3[PMo_{12}O_{40}]$ (**0**, a), $Li(n\mathrm{Bu_4N})_4[PMo_{12}O_{40}]$ (**LiII**, b), $(n\mathrm{Bu_4N})_4[HPMo_{12}O_{40}]$ (**HII**, c) and $(n\mathrm{Bu_4N})_3[H_2PMo_{12}O_{40}]$ ($\mathbf{H_2II}$, d)

The IR spectra of **0**, **LiII**, **HII**, and $\mathbf{H_2II}$ (Figure 1 and Table 3) all display the characteristic pattern of α-Keggin anions, with four bands arising from the P−O, Mo=O_t, and Mo−O−Mo stretching vibrations.[23] The progressive decrease in both the intensity and the energy of the P−O and Mo−O−Mo bands upon reduction has been fully discussed in the literature.[17,19] The energy of the Mo=O_t stretching mode also decreases upon reduction. However, the corresponding band shifts to higher frequencies upon protonation so that the values are fortuitously the same for **0** and $\mathbf{H_2II}$.

Reactions of Phosphonium Ylides with $[PMo_{12}O_{40}]^{3-}$

Various phosphonium ylides $R_3P{=}CR^1R^2$ (R = Bu, $R^1 = R^2 = H$; R = Ph, $R^1 = H$, R^2 = Ph, C(O)Me, C(O)N(Me)OMe; R = Ph, $R^1R^2 = (CH_2)_4$; R = Ph, R^1 = Me, R^2 = CHO) were used. In each case, the addition of a phosphonium ylide to a solution of $(n\mathrm{Bu_4N})_3[PMo_{12}O_{40}]$ in MeCN results in the formation of reduced species as evidenced by the strong blue colour of the resulting solutions. However, the reaction proceeds most cleanly with $Bu_3P{=}CH_2$. Immediately after the addition of one equivalent of $Bu_3P{=}CH_2$ to a solution of $(n\mathrm{Bu_4N})_3[PMo_{12}O_{40}]$ in CH_3CN, the ^{31}P NMR spectrum displays two signals, assigned to **I** and to the phosphonium cation $Bu_3PCH_3^+$, respectively (Figure 2). Subsequent addition of a second

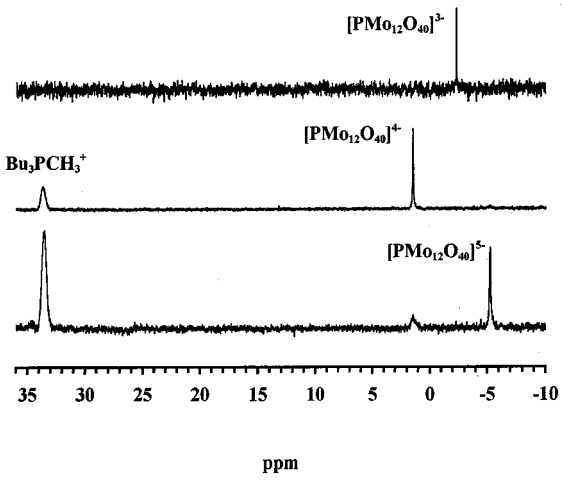


Figure 2. ^{31}P NMR spectra (referenced to external 85% H_3PO_4) in acetonitrile: $(n\mathrm{Bu_4N})_3[PMo_{12}O_{40}]$ (top); $(n\mathrm{Bu_4N})_3[PMo_{12}O_{40}]$ + 1 equiv. $Bu_3P{=}CH_2$ (center); $(n\mathrm{Bu_4N})_3[PMo_{12}O_{40}]$ + 2 equiv. $Bu_3P{=}CH_2$ (bottom)

Table 3. Spectroscopic data for $[H_xPMo_{12}O_{40}]^{n-}$ species

Anion		Electronic λ_{max} (solvent) [nm]	Infrared [cm^{-1}] $10^{-3}\varepsilon$ [$mol^{-1}\cdot L\cdot cm^{-1}$]	ν(PO)	ν(Mo=O)	ν(MoOMo)
$[PMo_{12}O_{40}]^{3-}$ [23]	**0**	–	–	1063	965sh, 956	880, 807
$[PMo_{12}O_{40}]^{4-}$ [19][20]	**I**	800 (DMF)	1.3	1058	952, 942	858, 794
$[LiPMo_{12}O_{40}]^{4-}$	**LiII**	715 (CH_3CN)	3.4	1058	950 sh, 941	860, 794
$[HPMo_{12}O_{40}]^{4-}$ [17]	**HII**	724 (CH_3CN)	3.9	1059	952 sh, 942	852, 800
$[H_2PMo_{12}O_{40}]^{3-}$	$\mathbf{H_2II}$	740 (CH_3CN)	4.5	1061	955	872, 800

equivalent of $Bu_3P{=}CH_2$ leads to the reduction of **I** to **II** with formation of another equivalent of phosphonium cation. The reduction products were further identified as **I** and **II** by R.D.E. measurements. According to ^{31}P NMR and electrochemical analyses, the reactions are quantitative. When $(Ph_4P)_3[PMo_{12}O_{40}]$ was used instead of $(nBu_4N)_3[PMo_{12}O_{40}]$, precipitation of $(Ph_4P)_4[PMo_{12}O_{40}]$ occurred after addition of one equivalent of ylide.

A similar pattern was observed for the reaction of $Ph_3P{=}CHPh$ with $(nBu_4N)_3[PMo_{12}O_{40}]$, with the exception of the initial formation of a green precipitate, which proved to be a mixture of oxidized and reduced phosphodecamolybdates containing lithium, tetrabutylammonium and phosphonium cations. This was followed by the precipitation of $(nBu_4N)_4[PMo_{12}O_{40}]$ which could be recrystallized from DMSO.

Reactions of Phosphanes with $[PMo_{12}O_{40}]^{3-}$

Phosphanes react with $(nBu_4N)_3[PMo_{12}O_{40}]$ in MeCN to yield reduced species, as indicated by the blue colour of the resulting solutions. In a typical experiment, a solution of $(nBu_4N)_3[PMo_{12}O_{40}]$ (510 mg, 0.200 mmol) and PPh_3 (52.5 mg, 0.200 mmol) in distilled MeCN (20 mL) was heated to reflux and samples were periodically analysed by ^{31}P NMR spectroscopy, which showed a progressive decrease in the signals of PPh_3 and $[PMo_{12}O_{40}]^{3-}$ at $\delta = -4.5$ and -2.3, respectively, and a concomitant increase in two new signals, one at $\delta = 27.5$, which is unambiguously assigned to Ph_3PO, the second at $\delta = -5.0$, which is consistent with $[H_2PMo_{12}O_{40}]^{3-}$. These observations are in agreement with those reported by Kawafune et al.[16] However, contrary to these authors, we found that the complete disappearance of $[PMo_{12}O_{40}]^{3-}$ in distilled acetonitrile required more than one equivalent of PPh_3. A pure product with analytical and spectroscopic features identical to those reported by Kawafune et al. for $(nBu_4N)_3[PMo_{12}O_{39}]$, was then isolated after heating a solution of $(nBu_4N)_3[PMo_{12}O_{40}]$ and a 10-fold excess of PPh_3 at reflux for 17 h (see Experimental Section). It was subsequently found that only one equivalent of phosphane is needed if the reaction is carried out in the presence of a sufficient amount of water. Analytical, spectroscopic and electrochemical data for the compounds obtained either in distilled acetonitrile, but in the presence of an excess of PPh_3, or in wet acetonitrile are identical to those of $\mathbf{H_2II}$ as well as to the analytical and spectroscopic data reported by Kawafune for $(nBu_4N)_3[PMo_{12}O_{39}]$. The latter has thus to be reformulated as $(nBu_4N)_3[H_2PMo_{12}O_{40}]$ and the reaction could be thought to proceed according to Equation (3).[24,25]

$$[PMo_{12}O_{40}]^{3-} + PPh_3 + H_2O \rightarrow [H_2PMo_{12}O_{40}]^{3-} + Ph_3PO \quad (3)$$

The reaction of tributylphosphane with $[PMo_{12}O_{40}]^{3-}$ is much faster than that of PPh_3 and proceeds according to a different stoichiometry. The reaction was monitored by ^{31}P NMR spectroscopy (Figure 3). For molar ratios less than 0.5 phosphane per polyanion, three signals are observed, which are unambiguously assigned to $[PMo_{12}O_{40}]^{3-}$ (**0**), $[H_2PMo_{12}O_{40}]^{3-}$ ($\mathbf{H_2II}$) and Bu_3PO. For ratios from 0.5 to ca. 1.0, five signals are observed: The first three are unambiguously assigned to **0**, **I** and Bu_3PO; the fourth, which shifts from $\delta = -5.0$ to $\delta = -5.2$ as the ratio increases, is tentatively assigned to a mixture of **HII** and $\mathbf{H_2II}$; the fifth, which appears as a broad doublet ($\delta = 14-35$, $J_{PH} = 400$ Hz), is assigned to Bu_3PH^+. Its chemical shift varies widely, which might be indicative of proton exchange with other species such as reduced polyoxometalates. Complete disappearance of **0** is observed for ratios in the range 1 to 1.1. Control experiments have shown that the reduction of **I** by PBu_3 is quite slow at room temperature.

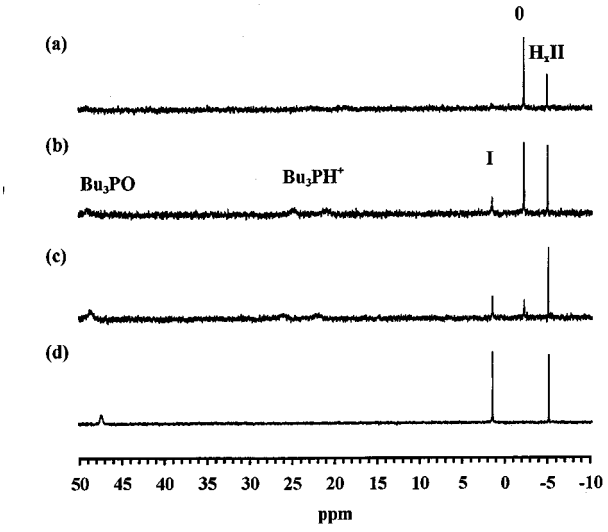


Figure 3. ^{31}P NMR spectra (referenced to external 85% H_3PO_4) in acetonitrile: (a) $(nBu_4N)_3[PMo_{12}O_{40}]$ + 0.5 equiv. PBu_3; (b) $(nBu_4N)_3[PMo_{12}O_{40}]$ + 0.75 equiv. PBu_3; (c) $(nBu_4N)_3[PMo_{12}O_{40}]$ + 1 equiv. PBu_3; (d) $(nBu_4N)_3[PMo_{12}O_{40}]$ + 2 equiv. PBu_3

Discussion

Reactions of Phosphonium Ylides with $[PMo_{12}O_{40}]^{3-}$

The addition of a phosphonium ylide to a solution of $(nBu_4N)_3[PMo_{12}O_{40}]$ in MeCN only results in the formation of reduced species **I** and **II**, whatever ylide is used. We could not obtain any evidence for the formation of an alkylidene derivative of $[PMo_{12}O_{40}]^{3-}$. The more reducing the ylide is, the cleaner the reaction. The reactions of Bu_3PCH_2 with **0** and **I** are fast. Both the reduction of **0** in **I** and that of **I** in **II** involve one equivalent of ylide and yield one equivalent of the parent phosphonium ion. The stoichiometry of the reactions is consistent with Equations (4) and (5).

$$[PMo_{12}O_{40}]^{3-} + R_3P{=}CR^1R^2 \rightarrow [PMo_{12}O_{40}]^{4-} + [R_3P{=}CR^1R^2]^{\bullet+} \quad (4)$$

$$[PMo_{12}O_{40}]^{4-} + R_3P{=}CR^1R^2 \rightarrow [PMo_{12}O_{40}]^{5-} + [R_3P{=}CR^1R^2]^{\bullet+} \quad (5)$$

The formation of ylide-derived radical-cations is known. Indeed, $[Ph_3P{=}CPh_2]^{\bullet+}$ has been obtained and characterized by electrochemical oxidation of $Ph_3P{=}CPh_2$ in MeCN in the probe of an EPR spectrometer.[26] However, direct

evidence for the formation of $[R_3P{=}CR^1R^2]^{\bullet+}$ could not be obtained. Indirect evidence for the formation of a radical is nevertheless provided by the formation of diphenyl disulfide when the reaction was carried out in the presence of thiophenol. Diphenyl disulfide was isolated by extraction with ether and characterized by TLC and IR spectroscopy. Control experiments showed that thiophenol is not oxidized by **0** on the reaction timescale.

The formation of the parent phosphonium ion $[R_3PCHR^1R^2]^+$ by reaction of the ylide with solvent can be excluded since $Ph_3P{=}CHPh$ proved to be stable in the absence of $(n\mathrm{Bu}_4\mathrm{N})_3[\mathrm{PMo}_{12}\mathrm{O}_{40}]$. Indeed, complete "spontaneous" transformation of $Ph_3P{=}CHPh$ into $[Ph_3PCH_2Ph]^+$ requires more than 12 h in MeCN at room temperature. The formation of phosphonium ions in the reactions of various ylides with dioxomolybdenum complexes in CH_2Cl_2 has been observed by Lai et al. and ascribed to transylidation between residual ylide and an oxometallabetaine initially formed.[15] However, such a pathway could not account for the complete transformation of the ylide into the parent phosphonium ion. We have reinvestigated the reactions of various ylides with $[MoO_2(dedtc)_2]$ (dedtc = diethyl dithiocarbamate) in MeCN and we have found that addition of the ylide is followed by the precipation of the purple compound $[Mo_2O_3(dedtc)_4]$. The formation of this complex most probably accounts for the violet colour observed by Lai et al. in their experiments and suggests that a redox pathway also occurs in the reaction of ylides with dioxomolybdenum complexes.

The actual source (XH) of the hydrogen atom in the formation of the phosphonium ion from the ylide-derived radical cation (Equation 6) has not been definitively established.

$$[R_3P{=}CR^1R^2]^{\bullet+} + XH \rightarrow [R_3P{-}CHR^1R^2]^+ + X^{\bullet} \quad (6)$$

It is unlikely that either the ylide or the tetrabutylammonium ion acts as XH. Indeed the ylide is quantitatively transformed into the parent phosphonium ion and the course of the reaction is not altered upon the replacement of tetrabutylammonium by tetraphenylphosphonium, which does not act as an hydrogen donor. Thus XH is most likely MeCN or residual H_2O.

Reactions of Phosphanes with $[PMo_{12}O_{40}]^{3-}$

Reactions of phosphanes with oxomolybdenum complexes have been largely investigated in relation to modelling studies of molybdenum oxotransferases.[27] Oxo transfer reaction from $[MoO_2L_n]$ to PR_3 is initiated by nucleophilic attack on an $Mo^{VI}{=}O$ unit and the formation of a $(\mu\text{-oxo})Mo^V$ dimer $[Mo_2O_3L_{2n}]$ often competes with that of the Mo^{IV} complex $[MoOL_n]$. Kawafune et al. were the first to extend such reactions to polyoxoanions by investigating the reaction of PPh_3 with $(n\mathrm{Bu}_4\mathrm{N})_3[\mathrm{PMo}_{12}\mathrm{O}_{40}]$ in MeCN.[16] They claimed to have obtained the oxygen-deficient reduced species $(n\mathrm{Bu}_4\mathrm{N})_3[\mathrm{PMo}_{12}\mathrm{O}_{40-x}]$ (x = 1, 2 or 3) by successive oxo transfer reactions. Although it is commonly accepted that oxygen-deficient species are formed in the course of heterogeneous catalytic oxidations with polyoxometalates,[28] the formation of such species in solution may be questioned. The reaction has been revisited by Mattes et al. who isolated **HII** by reaction of PPh_3 with $[K(18\text{-crown-6})][N(PPh_3)_2]_2[PMo_{12}O_{40}]$ and subsequent workup.[17] It should also be noted at this point that the UV/Vis and ^{31}P NMR spectra of $[HPMo_{12}O_{40}]^{4-}$ are not in agreement with those reported by Kawafune et al. for the so-called $[PMo_{12}O_{39}]^{3-}$ species. Mattes et al. assumed that $[PMo_{12}O_{39}]^{3-}$, once formed, reacts with residual water. Indeed we found the reaction of PPh_3 with $(n\mathrm{Bu}_4\mathrm{N})_3[\mathrm{PMo}_{12}\mathrm{O}_{40}]$ to be dependent on the residual amount of water in the solvent. The reaction did not go to completion when distilled acetonitrile was used, probably due to kinetically competitive phosphane-consuming side-reactions. Only in the presence of a sufficient amount of water did the reaction go to completion with one equivalent of PPh_3. The product obtained in this way displays all the features reported by Kawafune et al. for $(n\mathrm{Bu}_4\mathrm{N})_3[\mathrm{PMo}_{12}\mathrm{O}_{39}]$ and will be referred to as Kawafune's compound. Analytical data reasonably conform to the formula $(n\mathrm{Bu}_4\mathrm{N})_3[\mathrm{PMo}_{12}\mathrm{O}_{39}]$, but would equally be consistent with either $(n\mathrm{Bu}_4\mathrm{N})_3[\mathrm{HPMo}_{12}\mathrm{O}_{40}]$ or $(n\mathrm{Bu}_4\mathrm{N})_3[\mathrm{H}_2\mathrm{PMo}_{12}\mathrm{O}_{40}]$. IR features are clearly indicative of a reduced Keggin anion by the reduced intensity of P−O and Mo−O−Mo stretching bands. Moreover, the $Mo{-}O_t$ stretching band is almost unaltered with respect to $[PMo_{12}O_{40}]^{3-}$, which suggests that both compounds have the same charge. Again, this would be consistent with any of the three formulas above. In any case, the formation of $[PMo_{12}O_{40}]^{5-}$ (**II**) can be ruled out since this species could not coexist with $[PMo_{12}O_{40}]^{3-}$ in solution. The hypothesis of a 1e-reduced product may also be ruled out since the observed ^{31}P signal is shielded with respect to that of $[PMo_{12}O_{40}]^{3-}$. Neither does the product correspond to $[HPMo_{12}O_{40}]^{4-}$ (**HII**) as described by Mattes et al. Definitive evidence for the true nature of the product is provided by electrochemistry which shows that the behaviour of the product is identical to that of $(n\mathrm{Bu}_4\mathrm{N})_3[\mathrm{H}_2\mathrm{PMo}_{12}\mathrm{O}_{40}]$ (**H_2II**). Indeed the R.D.E. voltammogram (Figure 4) displays a 2e-oxidation wave at +0.56 V/SCE and becomes indistinguishable from those of $[HPMo_{12}O_{40}]^{4-}$ and $[PMo_{12}O_{40}]^{5-}$ upon addition of one and two equivalents of tetrabutylammonium hydroxide, respectively. Finally, electrochemical, ^{31}P NMR, IR and UV/Vis data are identical to those of $(n\mathrm{Bu}_4\mathrm{N})_3[\mathrm{H}_2\mathrm{PMo}_{12}\mathrm{O}_{40}]$. Thus, Kawafune's compound, which was postulated to be $(n\mathrm{Bu}_4\mathrm{N})_3[\mathrm{PMo}_{12}\mathrm{O}_{39}]$, is actually $(n\mathrm{Bu}_4\mathrm{N})_3[\mathrm{H}_2\mathrm{PMo}_{12}\mathrm{O}_{40}]$.

While only **H_2II** was obtained by reaction of PPh_3 with $(n\mathrm{Bu}_4\mathrm{N})_3[\mathrm{PMo}_{12}\mathrm{O}_{40}]$, **I**, **HII** and **$H_2$II** have been characterized from the products of the reaction with PBu_3, depending on the amount of phosphane. This can be explained on the basis of the mechanism postulated by Bond et al. for the reduction of $[S_2Mo_{18}O_{62}]^{4-}$ by phosphanes [Equation (7) to Equation (9)].[18]

$$[PMo_{12}O_{40}]^{3-} + R_3P \rightarrow [PMo_{12}O_{40}]^{4-} + R_3P^{\bullet+} \quad (7)$$

$$R_3P^{\bullet+} + H_2O \rightarrow R_3POH^{\bullet} + H^+ \quad (8)$$

$$[PMo_{12}O_{40}]^{3-} + R_3POH^{\bullet} \rightarrow [PMo_{12}O_{40}]^{4-} + R_3PO + H^+ \quad (9)$$

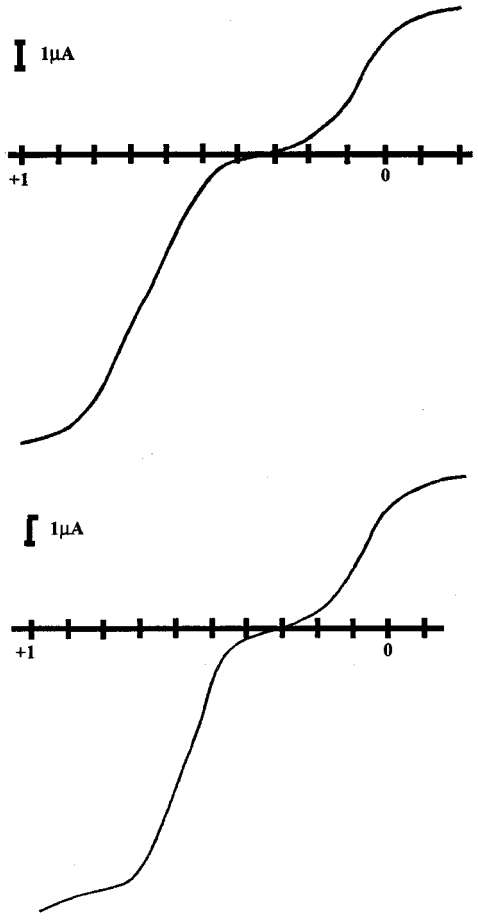


Figure 4. R.D.E. voltammogram of the reaction product of PPh_3 with $(nBu_4N)_3[PMo_{12}O_{40}]$ (top) and $(nBu_4N)_3[H_2PMo_{12}O_{40}]$ (bottom), both 1 mM in MeCN, E in Volt vs. SCE at a platinum electrode

The net reaction can then be written as Equation (10).

$$2\,[PMo_{12}O_{40}]^{3-} + R_3P + H_2O \rightarrow 2\,[PMo_{12}O_{40}]^{4-} + R_3PO + 2\,H^+ \quad (10)$$

As **I** disproportionates in the presence of protons, the final products will depend upon the relative basicities of the different species. When a strong base such as triethylamine is added to the reaction mixture, the reaction stops after addition of half an equivalent of PBu_3 and the ^{31}P NMR spectrum only displays the signal of **I**, in agreement with Equation (11).

$$2\,[PMo_{12}O_{40}]^{3-} + PBu_3 + H_2O + 2\,Et_3N \rightarrow 2\,[PMo_{12}O_{40}]^{4-} + Bu_3PO + 2\,Et_3NH^+ \quad (11)$$

In the absence of any additional base, the products depend on the basicity of the phosphane. PPh_3 is a weak base so that **I** undergoes disproportionation according to Equation (1), and the overall reaction reduces to Equation (3). On the other hand, PBu_3 is more basic than PPh_3 and competes with **I** for protonation. For low phosphane-to-polyanion ratios, $\mathbf{H_2II}$ is the only product observed while a mixture of **I**, $\mathbf{H_2II}$ and/or **HII** is found for higher ratios.

While this mechanism is consistent with the experimental results, the following alternative mechanism [Equation (12) to Equation (15)] might equally account for the stoichiometry of the reaction of $(nBu_4N)_3[PMo_{12}O_{40}]$ with PBu_3 in the presence of NEt_3.

$$[PMo_{12}O_{40}]^{3-} + R_3P \rightarrow [PMo_{12}O_{39}]^{3-} + R_3PO \quad (12)$$

$$[PMo_{12}O_{39}]^{3-} + H_2O \rightarrow [H_2PMo_{12}O_{40}]^{3-} \quad (13)$$

$$[H_2PMo_{12}O_{40}]^{3-} + 2\,NEt_3 \rightarrow [PMo_{12}O_{40}]^{5-} + 2\,Et_3NH^+ \quad (14)$$

$$[PMo_{12}O_{40}]^{3-} + [PMo_{12}O_{40}]^{5-} \rightarrow 2\,[PMo_{12}O_{40}]^{4-} \quad (15)$$

As no evidence could be obtained for either $R_3P^{\bullet+}$ or $[PMo_{12}O_{39}]^{3-}$, it is not possible to discriminate between these two mechanisms.

Concluding Remarks

Phenyllithium and phosphonium ylides act as 1e-reducing reagents towards $[PMo_{12}O_{40}]^{3-}$. The former is a convenient reagent for the millimolar-scale preparation of **I**, **LiII**, **HII** and $\mathbf{H_2II}$, which have been fully characterized. To the best of our knowledge, the only previous mention of the reduction of polyoxometalates by organometallic reagents is the report by McCann et al. of the catalytic norbornene ROMP by a single crystal of $(nBu_4N)_2[Mo_6O_{19}]$, in the presence of $EtAlCl_2$.[8] On the other hand, phosphanes act as 2e-reducing reagents, although it could not be established whether the reactions proceed through oxo transfer or via phosphane-based radical intermediates. Whatever the actual mechanism, the so-called oxygen-deficient compound $(nBu_4N)_3[PMo_{12}O_{39}]$ previously reported by Kawafune is actually $(nBu_4N)_3[H_2PMo_{12}O_{40}]$.

Experimental Section

Reagents and Solvents: Reactions were routinely carried out under inert atmospheres unless otherwise stated. Solvents were dried and freed of oxygen using standard procedures. $(nBu_4N)_3[PMo_{12}O_{40}]\cdot xH_2O$ was prepared as previously described[2,3] and further dried overnight at 80 °C under vacuum; $(Ph_4P)_3[PMo_{12}O_{40}]$ was obtained by a similar procedure, using Ph_4PBr instead of nBu_4NBr. Other chemicals were used as supplied.

Methods and Instrumentation: Infrared spectra were recorded from KBr pellets with a Bio-Rad FT 165 spectrophotometer and electronic absorption spectra on Shimadzu UV-2101 spectrophotometer. – Elemental analyses were performed at the Service Central d'Analyse of the CNRS (Vernaison, France). – ^{31}P NMR spectra (121.5 MHz, external 85% H_3PO_4) were recorded on CH_3CN/CD_3CN or DMSO/[D_6]DMSO solutions (0.3 mL – 0.1 mL) with a Bruker AC300 spectrometer equipped with a QNP probehead. – All electrochemical measurements were carried in 0.1 M $(nBu_4N)BF_4$ CH_3CN solutions under nitrogen at room temperature using a standard three-electrode cell [platinum rotating disk working electrode, auxiliary platinum wire and aqueous KCl saturated double junction calomel electrode (SCE)]. Rotating disk electrode voltammograms were recorded with a Tacussel PRG3 device at the rate of 5 $mV\cdot s^{-1}$. Cyclic voltammograms were recorded with a PAR 273A instrument at the rate of 100 $mV\cdot s^{-1}$.

Ylide Syntheses: Tributyl(methylene)phosphorane $Bu_3P{=}CH_2$ was prepared from tributyl(methyl)phosphonium iodide and butylli-

thium and distilled under vacuum.[29] − A slurry of benzyltriphenylphosphonium bromide (433 mg, 1.00 mmol) in CH_3CN (10 mL) was cooled in an ice bath. Phenyllithium solution (1 equiv.) was then added via syringe. The reaction mixture quickly turned orange and was filtered via canula after stirring for 15 min at 0 °C. The solution of benzylidenetriphenylphosphorane was then directly used in the reaction on $[PMo_{12}O_{40}]^{3-}$.

Reduced Phosphododecamolybdates. − (nBu$_4$N)$_4$[PMo$_{12}$O$_{40}$]: Phenyllithium (1.00 mmol) was added slowly to a solution of (nBu$_4$N)$_3$[PMo$_{12}$O$_{40}$] (2.55 g, 1.00 mmol) in acetonitrile (90 mL). The blue solution was filtered when necessary and (nBu$_4$N)BF$_4$ (320 mg, 1.00 mmol) was added. Cooling to −40 °C afforded a blue-green precipitate coated with a brown oil and was isolated by filtration. Pure (nBu$_4$N)$_4$[PMo$_{12}$O$_{40}$] was obtained by washing the blue-green powder with tetrahydrofuran and methanol until the filtrate was colourless. Further crops of the product can be isolated by successive additions of (nBu$_4$N)BF$_4$ (320 mg, 1.00 mmol) followed by cooling, filtration and washing. The powder can be handled in air and its solutions in MeCN, DMF or DMSO are stable towards oxidation. Yield: 2.1 g (75%). − $C_{64}H_{144}N_4PMo_{12}O_{40}$ (2792.0824): calcd. C 27.53, H 5.2, Mo 41.23, N 2.01, P 1.11; found C 27.57, H 5.23, Mo 40.86, N 2.05, P 1.19. − Recrystallization in DMSO led to dark-blue crystals of (nBu$_4$N)$_4$[PMo$_{12}$O$_{40}$]: tetragonal, $a = b = 18.72(2)$ Å, $c = 14.548(3)$ Å, $V = 5094(2)$ Å^3.[3b]

Li(nBu$_4$N)$_4$[PMo$_{12}$O$_{40}$]: The same procedure with two equivalents of phenyllithium afforded pure Li(nBu$_4$N)$_4$[PMo$_{12}$O$_{40}$]. Yield: 2.3 g (82%). − $C_{64}H_{144}LiMo_{12}N_4O_{40}P$ (2799.0234): calcd. C 27.46, H 5.19, Li 0.25, N 2, P 1.11; found C 27.46, H 5.40, Li 0.21, N 2.22, P 1.14.

(nBu$_4$N)$_4$[HPMo$_{12}$O$_{40}$]: A solution of triflic acid in acetonitrile (1.00 mL, 200 mM) was slowly added to a solution of Li(n-Bu$_4$N)$_4$[PMo$_{12}$O$_{40}$] (560 mg, 0.200 mmol) in acetonitrile (10 mL). Subsequent addition of (nBu$_4$N)BF$_4$ (320 mg, 1.00 mmol) and cooling to −40 °C afforded a blue precipitate of (nBu$_4$N)$_4$[HPMo$_{12}$O$_{40}$], which was washed with THF and dried in vacuum. Yield: 0.42 g (0.15 mmol, 75%). − $C_{64}H_{145}Mo_{12}N_4O_{40}P$ (2793.0903): calcd. C 27.52, H 5.23, Mo 41.22, N 2.01, P 1.11; found C 27.36, H 5.21, Mo 40.20, N 2.07, P 1.22.

(nBu$_4$N)$_3$[H$_2$PMo$_{12}$O$_{40}$]: The same procedure using 2.00 mL of the 200 mM solution of triflic acid in acetonitrile afforded (nBu$_4$N)$_3$[H$_2$PMo$_{12}$O$_{40}$]. Yield: 0.29 mg (57%). − $C_{48}H_{110}Mo_{12}N_3O_{40}P$ (2551.6311): calcd. C 22.59, H 4.35, N 1.65, P 1.21; found C 22.92, H 4.83, N 1.76, P 1.30.

Typical Experiment for the Reaction of (nBu$_4$N)$_3$[PMo$_{12}$O$_{40}$] with Phosphonium Ylide or Tributylphosphane: In a typical experiment, (nBu$_4$N)$_3$[PMo$_{12}$O$_{40}$] (510 mg, 0.200 mmol) was dissolved in acetonitrile (20 mL) or DMSO (5 mL) and the desired amount of reagent was added via syringe or transferred via canula (benzylidenetriphenylphosphorane solution). The reaction mixture was stirred for 10 min at room temperature. A sample (0.3 mL) was then placed in an NMR tube, purged with argon, and CD_3CN (0.1 mL) was added.

(Ph$_4$P)$_4$[PMo$_{12}$O$_{40}$]: To a solution of (Ph$_4$P)$_3$[PMo$_{12}$O$_{40}$] (1.0 g, 0.35 mmol) in acetonitrile (100 mL) was added a slight excess of Bu_3PCH_2 (85 mg, 0.40 mmol) via syringe. The solution turned dark green and a blue precipitate formed immediately. Yield: 0.6 g. Recrystallization in DMF led to dark-blue crystals of composition (Ph$_4$P)$_4$[PMo$_{12}$O$_{40}$]·2DMF: triclinic, $a = 13.973(2)$ Å, $b = 14.378(4)$ Å, $c = 15.193(2)$ Å, $\alpha = 71.17(2)°$, $\beta = 77.97(1)°$, $\gamma = 79.40(2)°$, $V = 2803$ (1) Å^3. − $C_{102}H_{94}Mo_{12}N_2O_{42}P_5$ (3325.9860): calcd. C 36.83, H 2.85, Mo 34.61, N 0.84, P 4.66; found C 37.16, H 2.8, Mo 33.85, N 0.98, P 4.59.

Reaction of (nBu$_4$N)$_3$[PMo$_{12}$O$_{40}$] with Triphenylphosphane: (nBu$_4$N)$_3$[PMo$_{12}$O$_{40}$] (510 mg, 0.200 mmol) and PPh_3 (525 mg, 2.00 mmol) were heated at reflux in acetonitrile (20 mL) for 17 h. The solvent was then evaporated in vacuum and the blue residue washed with ethyl ether and THF until the filtrate was colourless. Yield: 0.40 g (78%). − $C_{48}H_{110}Mo_{12}N_3O_{40}P$ (2551.6311): calcd. C 22.59, H 4.35, Mo 45.12, N 1.65, P 1.21; found C 23.39, H 4.37, Mo 46.45, N 1.64, P 1.26. − ^{31}P NMR (CD_3CN): $\delta = -5.0$. − IR (cm^{-1}): $\tilde{\nu} = 1062$ (m), 955(s), 880(m), 807(s). − UV/Vis (CH_3CN): $\lambda_{max} = 740$ nm ($\varepsilon = 5.4\ 10^3\ mol^{-1}\cdot L\cdot cm^{-1}$).

Acknowledgments

We are very grateful to Prof. P. Gouzerh for fruitful discussions from the very beginning of the experimental search to the final version of this manuscript.

[1] M. T. Pope, in *Hetero- and Isopolyanions*, Springer-Verlag, Berlin, New York, **1983**. − M. T. Pope, A. Müller, *Angew. Chem. Int. Ed. Engl.* **1991**, *30*, 34−48. − *Polyoxometalates: From Platonic Solids to Anti-Retroviral Activity* (Eds.: M. T. Pope, A. Müller), Kluwer Academic Publishers, Dordrecht, **1994**. − Special issue of *Chem. Rev.* **1998**, *98*.

[2] P. Gouzerh, A. Proust, *Chem. Rev.* **1998**, *98*, 77−111.

[3] [3a] A. Proust, R. Thouvenot, M. Chaussade, P. Gouzerh, F. Robert, *Inorg. Chim. Acta* **1994**, ***224***, 81−95. − [3b] A. Proust, S. Taunier, V. Artero, F. Robert, R. Thouvenot, P. Gouzerh, *Chem. Commun.* **1996**, 2437−2438.

[4] H. Kang, J. Zubieta, *J. Chem. Soc., Chem. Commun.* **1988**, 1192−1193.

[5] A. Proust, R. Thouvenot, P. Herson, *J. Chem. Soc., Dalton Trans.* **1999**, 51−55.

[6] P. Gouzerh, Y. Jeannin, A. Proust, F. Robert, *Angew. Chem. Int. Ed. Eng.* **1989**, *28*, 1363−1364. − A. Proust, P. Gouzerh, F. Robert, *Inorg. Chem.* **1993**, *32*, 5291−5298. − A. Proust, R. Thouvenot, F. Robert, P. Gouzerh, *Inorg. Chem.* **1993,** *32*, 5299−5304. − A. Proust, M. Fournier, R. Thouvenot, P. Gouzerh, *Inorg. Chim. Acta* **1994**, *215*, 61−66. − A. Proust, R. Thouvenot, S.-G. Roh, J.-K. Yoo, P. Gouzerh, *Inorg. Chem.* **1995**, *34*, 4106−4112. − A. Proust, F. Robert, P. Gouzerh, Q. Chen, J. Zubieta, *J. Am. Chem. Soc.* **1997**, *119*, 3523−3535. − R. Villanneau, A. Proust, F. Robert, P. Gouzerh, *Chem. Commun.* **1998**, 1491−1492. − R. Villanneau, A. Proust, F. Robert, P. Gouzerh, *J. Chem. Soc., Dalton Trans.* **1999**, 421−426. − R. Villanneau, A. Proust, F. Robert, P. Veillet, P. Gouzerh, *Inorg. Chem.* **1999**, *38*, 4981−4985.

[7] [7a] T.-Z. Hsieh, J. A. Zubieta, *Polyhedron* **1986**, *5*, 1655−1657. − [7b] S. Bank, S. Liu, S. N. Shaikh, X. Sun, J. Zubieta, P. C. Ellis, *Inorg. Chem.* **1988**, *27*, 3535−3543.

[8] M. McCann, D. McDonnell, *J. Chem. Soc., Chem. Commun.* **1993**, 1718−1719.

[9] M. Pasquali, A. Landi, C. Floriani, *Inorg. Chem.* **1979**, *18*, 2397−2400 and references therein.

[10] S. N. Shaikh, J. Zubieta, *Inorg. Chem.* **1986**, *25*, 4615−4616; **1988**, *27*, 1896−1903.

[11] W. Clegg, R. J. Errington, K. A. Fraser, S. A. Holmes, A. Schäfer, *J. Chem. Soc., Chem. Commun.* **1995**, 455−456.

[12] J. B. Strong, R. Ostrander, A. L. Rheingold, E. A. Maatta, *J. Am. Chem. Soc.* **1994**, *116*, 3601−3602. − Y. Du, A. L. Rheingold, E. A. Maatta, *J. Am. Chem. Soc.* **1992**, *114*, 345−346. − J. L. Stark, A. L. Rheingold, E. A. Maatta, *J. Chem. Soc., Chem. Commun.* **1995**, 1165−1166. − J. B. Strong, B. S. Haggerty, A. L. Rheingold, E. A. Maatta, *Chem. Commun.* **1997**, 1137−1138. − J. B. Strong, G. P. A. Yap, R. Ostrander, L. M. Liable-Sands, A. L. Rheingold, R. Thouvenot, P. Gouzerh, E. A. Maatta, *J. Am. Chem. Soc.* **2000**, *122*, 639−649.

[13] P. Jernakoff, G. L. Geoffroy, A. L. Rheingold, S. J. Geib, *J. Chem. Soc., Chem. Commun.* **1987**, 1610−1611. − R. Pilato,

C. E. Housmekenides, P. Jernakoff, D. Rubin, G. L. Geoffroy, A. L. Rheingold, *Organometallics* **1990,** *9*, 2333−2341.
[14] M. Jolly, J. P. Mitchell, V. C. Gibson, *J. Chem. Soc., Dalton Trans.* **1992**, 1331−1332.
[15] R. Lai, S. Le Bot, A. Baldy, M. Pierrot, H. Arzoumanian, *J. Chem. Soc., Chem. Commun.* **1986**, 1208−1209. − H. Arzoumanian, A. Baldy, R. Lai, A. Odreman, J. Metzger, M. Pierrot, *J. Organomet. Chem.* **1985**, *295*, 343−352.
[16] I. Kawafune, *Chem. Lett*. **1986**, 1503−1506; **1989**, 185−188. − I. Kawafune, G. Matsubayashi, *Inorg. Chim. Acta* **1991**, *188*, 33−39; *Chem. Lett.* **1992**, 1869−1872; *Bull. Chem. Soc. Jpn.* **1994**, *67*, 694−698.
[17] R. Neier, C. Trajanovski, R. Mattes, *J. Chem. Soc., Dalton Trans.* **1995**, 2521−2528.
[18] A. M. Bond, J. C. Eklund, V. Tedesco, T. Yu, A. G. Wedd, *Inorg. Chem.* **1998**, *37*, 2366−2372.
[19] M. Fournier, C. Rocchiccioli-Deltcheff, L. P. Kazanskii, *Chem. Phys. Lett.* **1994**, *223*, 297−30.
[20] C. Sanchez, J. Livage, J. P. Launay, M. Fournier, Y. Jeannin, *J. Am. Chem. Soc.* **1982**, *104*, 3194−3202.
[21] L. A. Combs-Walker, C. L. Hill, *Inorg. Chem.* **1991**, *30*, 4016−4026.
[22] K. Maeda, S. Himeno, T. Osakai, A. Saito, T. Hori, *J. Electroanal. Chem.* **1994**, *364*, 149−154. − K. Maeda, H. Katano, T. Osakai, S. Himeno, A. Saito, *J. Electroanal. Chem.* **1995**, *389*, 167−173.
[23] C. Rocchiccioli-Deltcheff, M. Fournier, R. Franck, R. Thouvenot, *Inorg. Chem.* **1983**, *22*, 207−216.
[24] The concentration of water in distilled acetonitrile was about 3.9 10^{-3} mol L^{-1}, as determined by Reichardt's dye method, that is 2.5-fold less than required for Equation (3). Residual water could also be introduced by $(n\mathrm{Bu_4N})_3[\mathrm{PMo_{12}O_{40}}]$ in spite of its thermal treatment, since it initially crystallizes with 0.8 equivalent of water (see ref.[23]). Neither the quality of the solvent nor that of $(n\mathrm{Bu_4N})_3[\mathrm{PMo_{12}O_{40}}]$ were specified by Kawafune et al.
[25] H. Langhals, *Anal. Lett.* **1990**, *23*, 2243−2258.
[26] J.-M. Savéant, S. Khac Binh, *Bull. Soc. Chim. Fr.* **1972**, 3549−3556.
[27] R. H. Holm, J. M. Berg, *Acc. Chem. Res.* **1986**, *19*, 363−376. − R. H. Holm, *Chem. Rev.* **1987**, *87*, 1401−1449. − S. J. Lippard, J. M. Berg, *Principles of Bioinorganic Chemistry*, University Science Books, Mill Valley, **1994**.
[28] N. Mizuno, M. Misono, *Chem. Rev.* **1998**, *98*, 199−217.
[29] H. Schmidbaur, W. Malisch, *Chem. Ber.* **1970**, *103*, 97−103.

Received December 3, 1999
[I99443]

Chiral Recognition Among Tris(diimine)−Metal Complexes, 6[‡]

Racemic Compound Formation *versus* Conglomerate Formation with $[M(bpy)_3](PF_6)_2$ (M = Ni, Zn, Ru); Molecular and Crystal Structures

Josef Breu,*[a] Holger Domel,[a] and Alexander Stoll[a]

Keywords: Molecular recognition / Chiral recognition / Conglomerate crystallization / Self-assembly / Polymorphism

Minor modifications in molecular size and shape induced by variation of the central atom drastically alter the crystallization behaviour of the hexafluorophosphate salts of $[M(bpy)_3]^{2+}$. With M = Ru, racemic solutions crystallize as true racemates in the β-type [$P\bar{3}c1$, a = 10.6453(5), c = 16.2987(9) Å, Z = 2], while for M = Zn the racemic structure cannot be obtained, as spontaneous resolution {γ-type [$P3_1$, a = 10.3873(5), c = 26.1309(16) Å, Z = 3]} is the only crystallization path observed. For $[Ni(bpy)_3](PF_6)_2$, crystals of both structural types can be obtained concomitantly from the same crystallization batch. The γ-phase is systematically twinned by merohedry. The dramatic and unpredictable change in the packing pattern of the very similar building blocks within this series arises from a delicate balance between the intermolecular forces. Distinct intermolecular interactions with different directionalities can be identified in the two structure types. Through careful analysis of the crystal and molecular structures, a trend with respect to molecular size and shape on going from $[Ru(bpy)_3](PF_6)_2$ to $[Zn(bpy)_3](PF_6)_2$ can be established. Even though one might speculate that increasing the size of the molecular cation should destabilize the β-type structure relative to the γ-type, no conclusive rationalization based solely on structural parameters can be given as regards why the relative order of the two local minima on the energy hypersurface should become inverted.

Introduction

Crystal structures of molecular solids are the result of cooperative molecular (chiral) recognition and self-assembly leading to a favourable 3D arrangement. Recognition involves the storage of information at the molecular level and its manifestation at the supramolecular level in a double-complementary fashion, taking into account energetic as well as geometrical requirements.[2,3] However, the ways in which individual noncovalent forces compete with or reinforce one another in complex systems are poorly understood.

Dunitz[4,5] succinctly described the crystal as the "*supramolecule par excellence*". Indeed, each observed packing pattern represents the culmination of highly specific and amazingly precise molecular (chiral) recognition based on noncovalent interactions. Consequently, each crystal structure contains a wealth of valuable information about the ways in which the multitude of noncovalent intermolecular interactions compete and collaborate to achieve their subtle balance.[6] Careful analysis of crystal structures, packing motifs, and distinct differences in intramolecular geometries should make available the inherent information, thereby assisting in the development of a better understanding of the "*grammar of crystal packing*".[7] Besides the more general utility of these rules in the syntheses of designed molecular materials (i.e. for "crystal engineering"), a practical application might be the development of strategies for increasing the likelihood of conglomerate crystallization.

Conglomerate crystallization is defined as the phenomenon whereby a racemic solution or melt produces a mechanical mixture of enantiomorphic, homochiral crystals, i.e. each individual crystal (or at least domain in the case of racemic twinning) contains a single enantiomer.[8,9] The phenomenon of conglomerate crystallization can be utilized for optical resolution by the so-called method of "resolution by entrainment", but it is relatively rare; its frequency has been estimated to be in the range 5−10%.[10]

Tris(chelate)−metal complexes of planar ligands, $[M(L-L)_3]^{n+}$ (e.g. L−L: phen = 1,10-phenanthroline, bpy = 2,2′-bipyridine, bpdz = 3,3′-bipyridazine, bpm = 4,4′-bipyrimidine, bpym = 2,2′-bipyrimidine, bpz = 2,2′-bipyrazine) are especially well suited for studying crystal packing phenomena.[11−13] On the one hand, these propeller-shaped, chiral molecules display a very corrugated molecular form. In Lehn's[2] notation, much information is stored at the molecular level, which will inevitably be manifested at the supramolecular level when neighbouring molecular ions interpenetrate to achieve maximum packing density. Moreover, this molecular recognition will not be obscured by gross intramolecular changes since the molecular ions are rather rigid. On the other hand, such molecular systems are extremely flexible. The central atom and its oxidation state may be varied over a wide range and this allows for a fine, systematic tuning of the component parts. Such alterations should help us to gain further insight into

[‡] Part 5: Ref.[1]

[a] Institut für Anorganische Chemie der Universität Regensburg, 93040 Regensburg, Germany
Fax: (internat.) + 49-(0)941/943-3261
E-mail: josef.breu@chemie.uni-regensburg.de

 © WILEY-VCH Verlag GmbH, D-69451 Weinheim, 2000 1434−1948/00/1111−2401 $ 17.50+.50/0

the relative strengths, directionalities, and structural influences of the various noncovalent forces.

The crystal structures of the true racemate β-[Ru(bpy)$_3$](PF$_6$)$_2$ [14,15] and its closely related low-temperature polymorph α-[Ru(bpy)$_3$](PF$_6$)$_2$ [16] have been known for some time. Of the analogous molecular salts of the first-row transition metals, only the structure of [Fe(bpy)$_3$](PF$_6$)$_2$ has been reported[17] to be isomorphous with that of β-[Ru(bpy)$_3$](PF$_6$)$_2$. All others are absent from the Cambridge Structural Database (CSD),[18] probably because the structures could not be successfully refined. For example, as early as 1983, Ferguson and Herren[19] recognized that in contrast to the Ru analogue, [Zn(bpy)$_3$](PF$_6$)$_2$ undergoes spontaneous resolution upon crystallization. However, they continued: "Attempts to determine the structure by X-ray methods proved fruitless and the difficulties were consistent with perfect multiple twinning." Solution of the crystal structure was claimed in two later publications[20,21] and cell data were given, but the structural details were never published as no satisfactory structure refinement could be accomplished.[22]

After having solved the twinning problem, we are able to report herein the detailed molecular and crystal structures of the enantiomorphic structure type γ-[M(bpy)$_3$](PF$_6$)$_2$ (M = Ni, Zn, Ru) and compare them with those of the true racemate β-[M(bpy)$_3$](PF$_6$)$_2$ (M = Ni, Ru).

Results and Discussion

Braga, Grepioni, and co-workers, who have been at the forefront of developing an organometallic "branch" of crystal engineering, conclude from their experience[23] that "objects of similar shape tend to pack in a similar manner, provided that the type of noncovalent interactions at work are not significantly altered." Contrary to this, we have found that even minor modifications in molecular size and shape induced by variation of the central atom drastically alter the crystallization behaviour of the hexafluorophosphate salts of [M(bpy)$_3$]$^{2+}$. With M = Fe, Ru, the racemic solutions crystallize as true racemates in the β-type, while for M = Zn the racemic structure could not be obtained, as spontaneous resolution (γ-type) is the only crystallization path observed. Interestingly, for [Ni(bpy)$_3$](PF$_6$)$_2$, crystals of both structure types can be obtained concomitantly[24] from the same crystallization batch. Finally, since [Ru(bpy)$_3$]$^{2+}$ is inert towards racemization, the γ-type can be "forced" upon [Ru(bpy)$_3$](PF$_6$)$_2$ by chemical resolution prior to crystallization. Enantiomerically pure [Ru(bpy)$_3$](PF$_6$)$_2$ can no longer crystallize in the centrosymmetric β-type, but must crystallize in an enantiomorphic structure with a space group that contains no improper symmetry operations. The dramatic and unpredictable change in the packing arrangement of the very similar building blocks within this series arises from a delicate balance between the intermolecular forces. The following detailed analysis and interpretation of systematic changes in the molecular shapes and intermolecular parameters of the crystal packings within this series should help to establish trends for these systems and to recover some of the information concerning noncovalent forces encoded in these polymorphic modifications.

Even for these rather rigid units, the geometries observed in the solid state result from the interplay of intra- and intermolecular interactions. To explore the effect of packing forces on the intramolecular geometry, the structure of β-[Ru(bpy)$_3$](PF$_6$)$_2$ was redetermined at a low temperature (200 K) intermediate between those of the prior determinations of the α-type (105 K)[16] and the β-type (294 K).[15]

Finally, the structure of γ-[Ni(bpy)$_3$](PF$_6$)$_2$ was determined twice using two different crystals at the same temperature to get an estimate of the variance in the intermolecular and intramolecular parameters introduced by statistical errors inherent to any structure determination. Not surprisingly, the structural parameters were found to agree within experimental error, but their influence on the packing energies[25] was noticeable.

Comparison of Crystal Structures

Both the β- and γ-type structures are composed of layers of complex cations extending parallel to the *ab* plane, with the anions fully immersed in the layers (Figure 1 and Figure 2). In both structures, the cation layers are homochiral (Figure 3 and Figure 4). However, while in β-[M(bpy)$_3$](PF$_6$)$_2$ layers of complex cations with Λ and Δ configuration alternate along *c*, in the γ-type structure layers of the same chirality are stacked along *c*. The molecular cations are arranged in a hexagonal primitive array in both structures and the distances between the metal atoms in the plane are similar {e.g. 10.3809(7) Å and 10.6453(6) Å in γ- and β-[Ru(bpy)$_3$](PF$_6$)$_2$, respectively; see Table 1}.

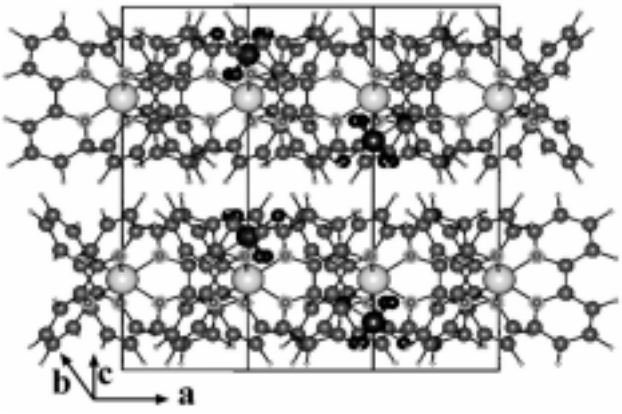


Figure 1. Crystal-packing diagram of β-[M(bpy)$_3$](PF$_6$)$_2$

In the β-phase, the complex cations occupy D_3 sites and are oriented with their C_3 axes exactly perpendicular to the layers and with their C_2 axes extending exactly along the hexagonal axes. In contrast, the cations in the γ-phase are

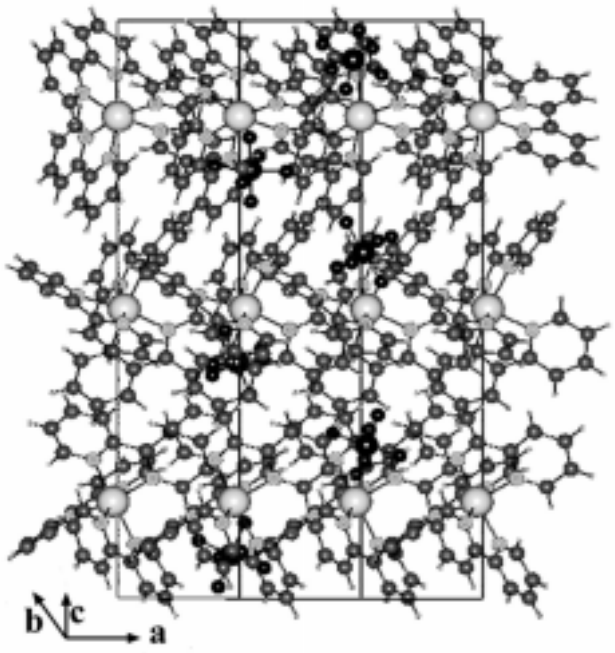


Figure 2. Crystal-packing diagram of γ-$[M(bpy)_3](PF_6)_2$

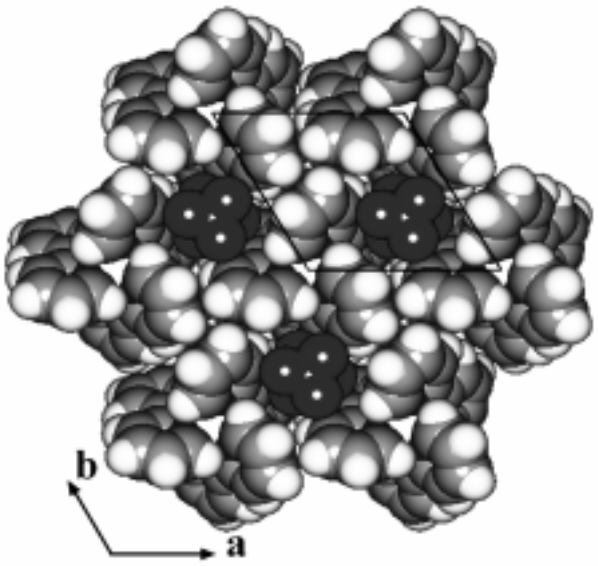


Figure 3. Space-filling packing diagram of the complex cation layer in β-$[M(bpy)_3](PF_6)_2$

effectively "tipped over". Their pseudo C_3 axes lie approximately in the *ab* plane. Moreover, the pseudo C_2 axes are not aligned along the hexagonal axes as would be required in the higher symmetry space group $P3_221$ (or $P3_121$), but rather are inclined towards the *ab* and *ac* planes (for $< C_2|ab$, $< C_2|ac$, see Table 1). The rigorous point symmetry of the cation is C_1 rather than C_2. Presumably, this slight distortion permits a more efficient packing. Furthermore, this induces a small dipole moment in the unit cell in the *c* direction, cancelling out of which might, in turn, be the reason for the systematic twinning of this structure type.

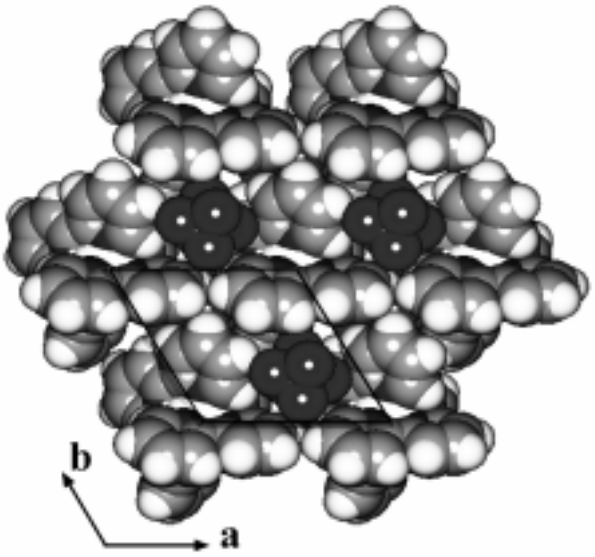


Figure 4. Space-filling packing diagram of the complex cation layer in γ-$[M(bpy)_3](PF_6)_2$

The packing coefficients (Table 1) are similar for both structure types. The absence of improper symmetry elements in the γ-structure does not hamper packing efficiency. This is in line with a study of a larger number of systems, in which no clear trends regarding the densities of true racemates and conglomerates were found either.[26] Despite the corrugated molecular shape, more than one arrangement of almost equal density is possible.

In neither of these close-packed layers do neighbouring complex cations interpenetrate. Instead, the voids are filled with anions. However, the interlocking of the corrugated van der Waals surfaces in the stacking direction (*c*) is notable and very distinct for both structure types. In the β-structure, racemic columns of complex cations with colinear C_3 axes extend along *c*. Along the columns, complexes of opposite chirality are engaged like gearwheels with the tips of the ligands interacting (Figure 5a) and relatively short cation−cation contacts arise {e.g. 8.1494(5) Å for β-$[Ru(bpy)_3](PF_6)_2$; see Table 1}. This stacking results in a T-shaped geometry of adjacent aromatic ligands.[27] In the γ-structure, homochiral columns of cations related by the 3_1 (or 3_2) screw axis are observed. The relative orientation of the C_3 axes of neighbouring cations is therefore reasonably close to the tetrahedral angle, which has been recognized as a preferred mutual orientation for an active pair of propeller-shaped molecules based on van der Waals interactions.[28,29] This mutual arrangement affords two "shifted π-stacks" of adjacent pyridine rings per complex cation (Figure 5c), which are in close contact {8.7601(6) Å for γ-$[Ru(bpy)_3](PF_6)_2$; see Table 1}. The shortest perpendicular distances between the centroid of one bipyridine ring and the plane of the second ring in the diad are, for instance, 3.689 Å and 3.496 Å in γ-$[Ru(bpy)_3](PF_6)_2$.

The intermolecular interactions along the cationic chain for both structure types appear to be controlled by so-called "π−π interactions".[30−32] Lateral interactions of this kind are commonly encountered motifs in the crystal packings

Table 1. Selected intermolecular parameters

	$[Ru(bpy)_3](PF_6)_2$ β_{200}	γ_{200}	$[Ni(bpy)_3](PF_6)_2$ β_{240}	$\gamma_{200}(1)$	$\gamma_{200}(2)$	$[Zn(bpy)_3](PF_6)_2$ γ_{200}
MM_{column} [Å]	8.1494(5)	8.7601(6)	8.2345(5)	8.7158(9)	8.7136(12)	8.7237(6)
MM_{layer} [Å]	10.6453(6)	10.3809(7)	10.6585(6)	10.3534(11)	10.3599(12)	10.3873(8)
MP [Å]	6.4422(5)	6.248(2)	6.4703(6)	6.183(2)	6.184(2)	6.096(2)
		6.249(2)		6.249(2)	6.251(2)	6.163(2)
		6.389(1)		6.397(1)	6.398(1)	6.362(1)
		6.500(2)		6.541(2)	6.551(2)	6.638(2)
		6.802(2)		6.760(2)	6.764(2)	6.850(2)
		6.845(2)		6.815(2)	6.817(2)	6.902(1)
$Cg_{perp.}$ [Å][a]		3.689/3.496		3.713/3.505	3.712/3.502	3.757/3.493
pack. coeff.[b]	0.697	0.685	0.689	0.689	0.690	0.691
$< C_2\|ab$	0.00	1.78	0.00	1.65	1.41	1.67
$< C_2\|ac$	0.00	4.95	0.00	4.63	4.58	6.13

[a] Shortest perpendicular distances between the centroid of one bipyridine ring and the plane of the second ring in the "shifted π-stacks". – [b] Ref.[61]

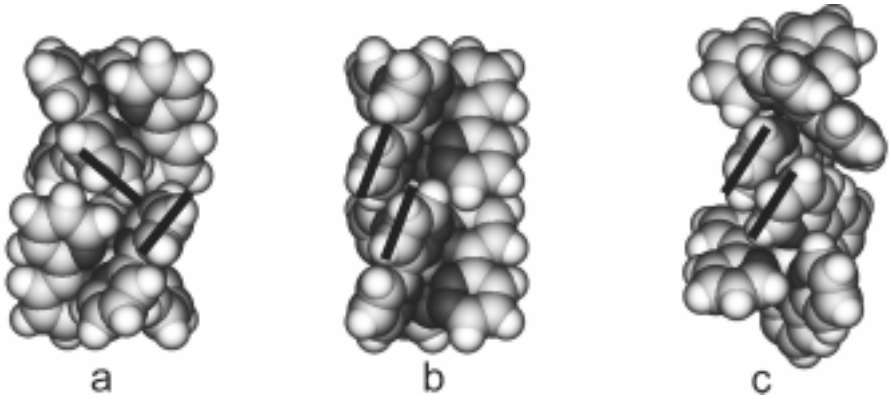


Figure 5. Space-filling packing diagram of the complex cation columns running along *c* in β-$[M(bpy)_3](PF_6)_2$ (a), $[Ni(bpdz)_3](ClO_4)_2$ [49] (b), and γ-$[M(bpy)_3](PF_6)_2$ (c) displaying the interlocking of adjacent cations in the various "π−π interactions"

of aromatic compounds[33,34] and their general importance in molecular recognition has been acknowledged.[35,36] Recent experimental[35,37−39] and theoretical[31,40−42] work has shown that both dispersion forces and electrostatic C−H···π interactions contribute towards the favourable "π−π interactions". The relative importance of these two contributions is a matter of debate,[38,39] especially for the T-shaped arrangement. The inherent polarity of aromatic systems stems from the electron-rich core being surrounded by an electron-poor torus of hydrogen atoms. This electrostatic contribution accounts for the energetic preference of both T-shaped and shifted π-stacked arrangements. Which one is preferred depends on the relative magnitude of the dispersion and C−H···π interactions and therefore on the planar extension of the aromatic system. Even for the simplest system, i.e. the benzene dimer in the gas phase, there is an ongoing dispute as to which local minimum on the potential energy hypersurface represents the more stable configuration.[41,43−47] In the solid state, the two local minima manifest themselves in herringbone and/or π-stacked crystal packing motifs.[33,34,48] These favourable "π−π interactions" may facilitate direct cation−cation contacts. However, with $[M(L-L)_3]^{n+}$, the situation is somewhat more complicated than that with simple aromatic systems since the fixing of three aromatic systems in a rigid mutual orientation imposes certain spatial requirements that also depend on the chirality of these complexes. Racemic pairs with colinear C_3 axes, as in β-$[Ru(bpy)_3](PF_6)_2$, lead to a T-shaped configuration (Figure 5a), for the analogous active pair as observed in $[Ni(bpdz)_3](ClO_4)_2$ [49] a shifted π-stack involving half of a ligand results (Figure 5b), while active pairs with tilted C_3 axes as in the γ-modification yield a shifted π-stack implying a complete ligand.

Despite the spatial restraints imposed by the coordination, "π−π interactions" are frequently observed in crystal structures of neutral {$[Ru(bpy)_3]$[50]} and, more surprisingly, charged propeller-shaped molecules of the type investigated here {$[Ru(bpym)_3](PF_6)_2 \cdot CH_3CN$,[15] $[Ru(phen)_3](PF_6)_2$ [13]}.

The "coordination" of the cations by anions is quite similar in both the γ- and β-type structures. Each cation is surrounded by six PF_6^- anions in a trigonal antiprism and the MP distances are all of comparable magnitude (Table 1). This suggests that the monopole−monopole interaction between cations and anions should be very similar in both structural types (see also ref.[25]).

Grepioni et al.[23] have shown that for hexafluorophosphate organometallic salts C−H···F interactions play a significant role among the various intermolecular interactions when assisted by the charge difference between anions and cations. In both structure types, we find bonds shorter than the van der Waals cut-off distances (Table 2), these being indicative of specific and directional interactions. However,

Table 2. Hydrogen-bonding geometry [Å, °] for $[Ru(bpy)_3](PF_6)_2$

D-H···A[a][b]	H···A	D···A	D-H···A
β-type:			
C4-H4···F1[i]	2.4057	3.126(4)	134.21
γ-type:			
C14-H14···F12[ii]	2.5433	3.153(5)	122.13
C24-H24···F11[iii]	2.4775	3.236(7)	136.83
C33-H33···F16	2.4964	3.199(6)	130.77
C35-H35···F14[iv]	2.4196	3.208(5)	140.35
C36-H36···F12[iv]	2.4785	3.228(5)	135.72
C45-H45···F23[v]	2.3073	3.114(11)	142.39
C55-H55···F22[vi]	2.5350	3.376(11)	147.68
C63-H63···F23[vii]	2.5414	3.316(13)	138.82

[a] D···A < R(D) + R(A) + 0.50 Å, H···A < R(H) + R(A) - 0.12 Å, D-H···A > 100.0°. − [b] Symmetry codes: [i] $y, -x + y, -z$. − [ii] $1 - y, 1 + x - y, 1/3 + z$. − [iii] $-y, x - y, 1/3 + z$. − [iv] $x, -1 + y, z$. − [v] $x, 1 + y, z$. − [vi] $1 - x + y, 1 - x, -1/3 + z$. − [vii] $1 - x + y, -x, -1/3 + z$.

it is impossible to even qualitatively assess their relative energetic significance.

The racemic low-temperature polymorph (α-type) represents just a slight distortion of the packing in the β-type[16,51] and will not be discussed further here.

Comparison of Molecular Structures

The three bpy ligands form a propeller-like trigonal arrangement around the metal atoms. The coordination by the nitrogen atoms is trigonally distorted octahedral owing to the fact that the ligand bite (Figure 6, Table 3) is too short to fit a perfect octahedron. The stereochemistry is completely defined by the normalized bite of the bidentate ligand, b = N···N/M−N, and the angle of twist Θ between the upper and lower triangular faces formed by the N atoms of the bpy ligands (Table 4). The regular octahedron corresponds to Θ = 30° and $b = 2^{1/2}$. Calculations have shown that distortions from D_3 symmetry are increasingly possible as b is decreased.[52] The distortions in the γ-phase are indeed quite substantial, as manifested in variations of more than 3° in the N−M−N angles at the base of the trigonal antiprisms (ν, Figure 6). Moreover, the trigonal faces are no longer parallel and the central atoms are displaced from the midpoint between them (Table 4). Apparently, the coordination sphere is rather flexible and can be adjusted within certain limits to suit packing requirements.

Not even the ligands can be treated as rigid units. Admittedly, the bond lengths and bond angles within the pyridine moieties are consistent within experimental error in the different phases and compounds; the rings are planar, and the maximum deviations from the best planes are smaller than 0.03 Å (Δ_{max} in Table 3). However, the two pyridine rings within a ligand are deflected downwards around the midpoint of the py−py bond. This kink can be quantified by the difference between A and B (Table 3), which decreases on going from $[Ru(bpy)_3](PF_6)_2$ to $[Zn(bpy)_3](PF_6)_2$ while the ligand bite and M−N distance increase accordingly. This trend reflects the size of the central cation. The extent of the kink together with the trigonal twist determines the height of the complex cation along the C_3 axis. The smaller the kink and the trigonal twist, the "taller" the complex

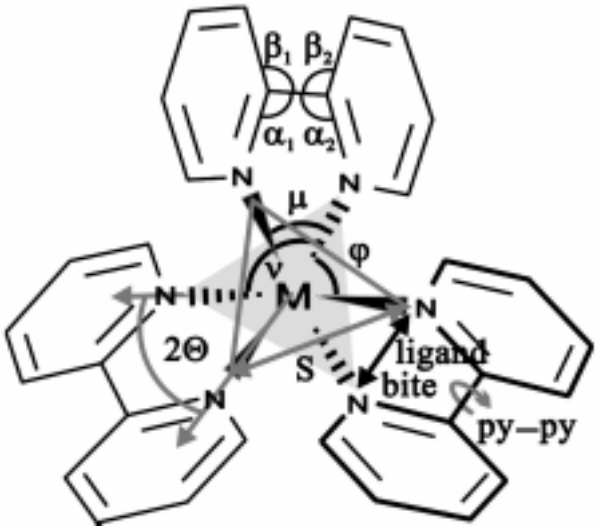


Figure 6. Labelling scheme of the geometrical parameters listed in Tables 3 and 4

Table 3. Selected geometrical data, ligands

	$[Ru(bpy)_3](PF_6)_2$			$[Ni(bpy)_3](PF_6)_2$			$[Zn(bpy)_3](PF_6)_2$
	β_{294}[a]	β_{200}	γ_{200}	β_{240}	$\gamma_{200}(1)$	$\gamma_{200}(2)$	γ_{200}
ligand bite [Å][b]	2.607(3)	2.598(3)	2.631(5)	2.628(3)	2.653(5)	2.641(5)	2.678(5)
			2.612(5)		2.644(4)	2.632(5)	2.677(4)
			2.627(5)		2.645(5)	2.636(5)	2.676(4)
py−py [°][b]	7.90(19)[c]	8.81(13)	12.7(2)	8.37(15)	16.2(2)	16.3(3)	17.2(2)
			6.7(2)		12.9(2)	13.1(2)	17.1(1)
			9.4(3)		10.6(3)	10.9(3)	8.9(3)
$A = \alpha_1 + \alpha_2$ [°][b]	229.4(6)	228.9(4)	230.0(7)	230.5(4)	230.8(7)	229.8(8)	232.3(7)
			229.4(8)		231.1(8)	230.2(8)	232.4(8)
			230.7(7)		231.7(8)	231.6(8)	233.3(6)
$B = \beta_1 + \beta_2$ [°][b]	249.2(6)	247.9(4)	246.4(8)	246.4(4)	244.7(8)	244.0(9)	244.3(8)
			247.7(8)		245.9(8)	246.5(9)	244.2(8)
			246.3(8)		245.9(8)	246.0(9)	245.7(8)
Δ_{max} [Å][d]	0.015(2)	0.019(2)	0.028(4)	0.017(2)	0.020(4)	0.026(5)	0.017(4)

[a] For labelling scheme, see Figure 6. − [b] Ref.[15] − [c] Value given in ref.[15] is erroneous. − [d] Maximum deviation from the best plane within a single pyridine ring.

Table 4. Selected geometrical data, coordination sphere

	$[Ru(bpy)_3](PF_6)_2$			$[Ni(bpy)_3](PF_6)_2$			$[Zn(bpy)_3](PF_6)_2$
	β_{294}	β_{200}	γ_{200}	β_{240}	$\gamma_{200}(1)$	$\gamma_{200}(2)$	γ_{200}
M−N [Å]	2.056(2)	2.048(2)	2.058(4)	2.067(2)	2.074(4)	2.070(4)	2.150(4)
			2.065(3)		2.088(3)	2.083(3)	2.158(3)
			2.066(4)		2.072(3)	2.076(4)	2.147(3)
			2.067(4)		2.093(3)	2.084(4)	2.182(3)
			2.062(3)		2.080(3)	2.075(4)	2.156(3)
			2.063(4)		2.093(4)	2.085(4)	2.182(4)
site symmetry	D_3	D_3	C_1	D_3	C_1	C_1	C_1
ligand bite	78.67(8)	78.74(8)	79.29(12)	78.93(9)	79.21(13)	78.96(13)	78.86(12)
angle, μ [°][a]			78.41(15)		78.82(12)	78.50(16)	76.41(11)
			79.14(12)		78.68(13)	78.64(14)	76.15(11)
[°][a]	89.13(10)	89.51(9)	92.12(16)	90.6(1)	92.53(14)	92.43(16)	94.80(14)
			91.40(12)		93.04(12)	93.09(14)	95.92(11)
			89.36(13)		91.27(13)	91.22(15)	93.13(12)
ν [°][a]	96.29(9)	96.08(9)	94.78(15)	95.49(9)	93.97(13)	94.17(15)	93.79(13)
			95.43(13)		94.72(13)	94.86(15)	96.10(12)
			96.75(13)		95.83(13)	95.99(14)	95.78(12)
			93.43(12)		92.73(12)	92.84(13)	92.65(12)
			94.95(16)		95.10(13)	95.34(16)	95.97(13)
			96.59(12)		96.14(12)	96.04(15)	96.19(11)
b[b]	1.268(3)	1.269(2)	1.271(4)[c]	1.271(3)[c]	1.279(5)[c]	1.268(5)[c]	1.238(4)[c]
2Θ [°][d]	51.9(1)	51.6(1)	50.5(2)[c]	50.8(1)[c]	49.3(2)[c]	49.2(2)[c]	45.5(2)[c]
M−t1 [Å][e]	1.049(2)	1.050(4)	1.068(4)	1.074(2)	1.094(3)	1.089(4)	1.126(3)
M−t2 [Å][e]	1.049(2)	1.050(2)	1.082(4)	1.074(2)	1.104(3)	1.098(4)	1.139(3)
t1−M−t2 [°]	180.00	180.00	179.3(2)	180.00	179.2(3)	179.4(3)	179.4(2)
S [Å][f]	3.063(4)	3.046(3)	3.050[b]	3.060(4)	3.066[b]	3.062[b]	3.191[b]

[a] For labelling scheme, see Figure 6. − [b] Normalized ligand bite. − [c] Averaged in D_3 symmetry. − [d] Trigonal twist. − [e] Distances between the central atom and the centre of gravity of the trigonal faces formed by the N atoms of the bpy ligands. − [f] Edge length of the base of the trigonal antiprism.

cation. Thus, $[Ru(bpy)_3](PF_6)_2$ is shorter than $[Zn(bpy)_3](PF_6)_2$, as indicated by the height of the trigonal antiprisms formed by the N atoms of the bpy ligands (2.100 Å and 2.265 Å, respectively).

The widths of the molecular cations, i.e. their extensions perpendicular to the C_3 axis, are largely determined by the M−N distance since the ligands are pushed further away as the bond lengths increase. The mean lengths of the edges of the bases of the trigonal faces (S, Table 4) increase from 3.046 Å to 3.191 Å on going from $[Ru(bpy)_3](PF_6)_2$ to $[Zn(bpy)_3](PF_6)_2$. This suggests that the height/width ratio changes slightly in the series, with $[Zn(bpy)_3](PF_6)_2$ being relatively larger around the "waist".

Another intramolecular low-energy mode that the cation takes advantage of to adjust to the local packing environment is the torsion about the py−py bond. Lowering the temperature from 294 K to 200 K, thereby shortening the intermolecular distances, results in an increase in the dihedral angle between the two pyridine rings in the ligand from 7.90(19)° to 8.81(13)° for β-$[Ru(bpy)_3](PF_6)_2$ (Table 3) and still further to 9.0(4)−10.3(3)° for α-$[Ru(bpy)_3](PF_6)_2$.[16] The variation in the γ-phase [6.7(2)−12.7(2)°] is even more notable.

Conclusion

In the realm of organic and organometallic compounds, polymorphism has often been associated with torsional degrees of freedom of molecular fragments bound by single bonds, thus making it conformational in nature. Although the system under consideration here utilizes its very limited intramolecular degrees of freedom to optimize packing, the molecular shape of the building blocks is to a first approximation the same. A similar example of a rather rigid coordination compound crystallizing in different polymorphs has been recently found in the case of $[Pd(dmpz)_2(Hdmpz)_2]_2$ (Hdmpz = 3,5-dimethylpyrazole).[53]

The simple fact that there are coexisting polymorphs in the case of $[Ni(bpy)_3](PF_6)_2$ emphasizes the importance of kinetic aspects, but it is nevertheless expected that the non-occurrence of γ-$[Fe(bpy)_3](PF_6)_2$, γ-$[Ru(bpy)_3](PF_6)_2$, or β-$[Zn(bpy)_3](PF_6)_2$ on crystallization from the respective racemic solutions can be attributed to thermodynamic factors. At least it is hard to imagine that nucleation kinetics could be so different for these similar systems. On the one hand, careful analysis of the crystal and molecular structures has established a trend with respect to molecular size and shape (Table 4) on going from $[Ru(bpy)_3](PF_6)_2$ to $[Zn(bpy)_3](PF_6)_2$. On the other hand, distinct intermolecular interactions with different directionalities (T-shaped as opposed to shifted π-stack π−π interactions) have been identified in the two structure types. However, this gives no indication of their relative strengths, and no rationalization can be given as to why the relative order of the two local minima on the energy hypersurface becomes inverted. This requires an analysis of the packing energies, which will be dealt with in a separate paper.[25] Given the molecular structure, little can be said a priori on the likelihood of spontaneous resolution of racemic solutions upon crystallization, even though one might speculate that increasing the size of

the molecular cation should destabilize the β-type relative to the γ-type structure. However, size alone cannot give a satisfactory explanation since $[Ru(bpy)_3](PF_6)_2$ and $[Ni(bpy)_3](PF_6)_2$ are very similar in that respect and yet still display different crystallization behaviour. Evidently, other information at the molecular level, as for instance the molecular electrostatic potential, is also important.

Certainly, the presented case gives a striking example of the sensitivity of crystal packings to even tiny variations in molecular structure. Moreover, the shape of molecular building blocks alone surely does not determine the crystal structure, but rather it is the subtle balance between all the various intermolecular forces. This equilibrium balance of forces embraces many intermolecular interactions; "π−π interactions" are apparent in crystal structures of $[M(bpy)_3](PF_6)_2$ compounds. However, T-shaped and shifted π-stack arrangements compete. Unquestionably, postulation of dominance by a T-shaped arrangement, as in a report by Dance,[27] is not justified. Moreover, solely on the basis of topology, nothing can be said about the relative contributions of dispersion/repulsion forces and electrostatic C−H···π interactions to these "π−π interactions".

Experimental Section

Synthesis: All $[M(bpy)_3](PF_6)_2$ salts were obtained by metathesis of the corresponding chloride, sulfate, or bromide salts, in turn prepared according to literature procedures.[54,55] − Optical resolution of $[Ru(bpy)_3]^{2+}$, which did not occur spontaneously, was achieved by a modification of the procedure of Dwyer and Gyarfas using potassium antimonyl tartrate.[56] − Concomitant crystallization of β- and γ-$[Ni(bpy)_3](PF_6)_2$ could be achieved by slow evaporation of the solvents from an acetone/water (2:1) solution at ambient temperature. β-$[Ru(bpy)_3](PF_6)_2$ could be crystallized from the same solvent mixture, but from ethanol/water (2:1) more suitable single crystals were obtained. The best crystals of γ-$[Ru(bpy)_3](PF_6)_2$ and γ-$[Zn(bpy)_3](PF_6)_2$ were obtained by recrystallization from acetone/ethanol (5:1).

Crystal Structure Analyses: Relevant crystallographic data and details of the data collection and structure refinement are listed in Table 5. Structure solution and refinement of the β-type structures was straightforward.

All compounds crystallizing in the γ-phase are affected by systematic twinning due to merohedry. This is indicated by a gritty appearance of the crystal faces. The twin antisymmetry space group is $P3_22'1$ (or $P3_12'1$).[57] Structure solution in this space group proved impossible. In $P3_1$ (and its enantiomorphic space group $P3_2$), direct methods yielded a partial structure model, which could be completed by successive difference Fourier syntheses. However, anisotropic refinement was not feasible until the correct twinning law ([110]) was introduced. The absolute structure was assigned on the basis of the Flack *x* parameter,[58] where *x* is the fractional contribution of the inverted component of a "racemic twin". It is expected to be zero for the correct structure, unity for the inverted structure, and somewhere in between if racemic twinning is present. For the chemically resolved γ-$[Ru(bpy)_3](PF_6)_2$, the assignment is in agreement with the observed specific rotation. Surprisingly, while for γ-$[Zn(bpy)_3](PF_6)_2$ each singular crystal seems to be homochiral, for γ-$[Ni(bpy)_3](PF_6)_2$ general and racemic twinning has to be refined simultaneously.

Table 5. Crystallographic data and details of the structure determination

	$[Ru(bpy)_3](PF_6)_2$ β_{200}	γ_{200}	$[Ni(bpy)_3](PF_6)_2$ β_{240}	$\gamma_{200}(1)$	$\gamma_{200}(2)$	$[Zn(bpy)_3](PF_6)_2$ γ_{200}
Empirical formula	$C_{30}H_{24}RuN_6{\cdot}2(F_6P)$	$C_{30}H_{24}RuN_6{\cdot}2(F_6P)$	$C_{30}H_{24}NiN_6{\cdot}2(F_6P)$	$C_{30}H_{24}NiN_6{\cdot}2(F_6P)$	$C_{30}H_{24}NiN_6{\cdot}2(F_6P)$	$C_{30}H_{24}NiN_6{\cdot}2(F_6P)$
Molecular mass	859.56	859.56	817.18	817.18	817.18	823.88
Crystal system	trigonal	trigonal	trigonal	trigonal	trigonal	trigonal
Space group	$P\bar{3}c1$ (No. 165)	$P3_1$ (No. 144)	$P\bar{3}c1$ (No. 165)	$P3_1$ (No. 144)	$P3_1$ (No. 144)	$P3_1$ (No. 144)
a [Å]	10.6453(5)	10.3809(4)	10.6585(6)	10.3534(4)	10.3599(5)	10.3873(5)
c [Å]	16.2987(9)	26.2576(13)	16.4690(10)	26.1231(14)	26.1163(13)	26.1309(16)
V [Å^3]	1599.56(14)	2450.51(18)	1620.28(16)	2425.05(19)	2427.5(2)	2441.7(2)
Z	2	3	2	3	3	3
D_x [g/cm^3]	1.785	1.747	1.675	1.679	1.677	1.681
F(000)	856	1284	824	1236	1236	1242
μ [cm^{-1}]	6.9	6.8	8.0	8.0	8.0	9.6
Crystal size [mm]	0.40 × 0.18 × 0.18	0.52 × 0.30 × 0.24	0.70 × 0.26 × 0.26	0.50 × 0.18 × 0.17	0.30 × 0.16 × 0.15	0.48 × 0.30 × 0.30
Crystal shape	hexagonal prism	hexagonal needle	hexagonal prism	hexagonal needle	hexagonal needle	hexagonal needle
Crystal colour	dark orange	dark orange	light brown	light red	light red	colourless
Temperature [K]	200	200	240	200	200	200
Radiation [Å]	Mo-K_α 0.71069	Mo-K_α 0.71069	Mo-K_α 0.71069	Mo-K_α 0.71069	Mo-K_α 0.71069	Mo-K_α 0.71069
θ range [°]	2.2−25.6	2.4−25.2	2.2−25.5	2.4−25.6	2.3−25.6	2.4−25.6
h	−11/12	−12/10	−12/12	−12/12	−12/12	−12/12
k	−12/11	−10/12	−12/11	−11/5	−12/12	−12/12
l	−19/19	−31/31	−16/19	−27/30	−28/27	−24/31
Tot. no. of reflections	7163	10150	5510	8836	12038	10839
Unique reflections	1006	5669	996	5317	5700	5317
R_{int}	0.034	0.022	0.026	0.019	0.028	0.021
Observed reflections	820 [$I_o > 2\sigma(I_o)$]	5645 [$I_o > 2\sigma(I_o)$]	844 [$I_o > 2\sigma(I_o)$]	5172 [$I_o > 2\sigma(I_o)$]	5253 [$I_o > 2\sigma(I_o)$]	5248 [$I_o > 2\sigma(I_o)$]
Refined parameters	78	461	78	463	463	461
*R*1[a]	0.0261	0.0242	0.0415	0.0278	0.0311	0.0261
*wR*2(all)[b]	0.0668	0.0622	0.1260	0.0682	0.0608	0.0690
S[c]	0.98	1.03	1.07	1.02	0.95	1.04
d, *e*[d]	0.0495, 0.0	0.0528, 0.0597	0.0844, 0.5662	0.0494, 0.0	0.0315, 0.0	0.0569, 0.0
Flack *x* parameter[e]	−	−0.01(3)	−	0.505(9)	0.520(9)	0.00(1)
$\Delta\rho_{min}$, $\Delta\rho_{max}$.[e$^-$/ Å^3]	−0.39, 0.37	−0.35, 0.44	−0.40, 0.47	−0.22, 0.35	−0.20, 0.28	−0.22, 0.31

[a] $R1 = \Sigma||F_o| - |F_c||/\Sigma|F_o|$. − [b] $wR2 = \{\Sigma[w(F_o^2 - F_c^2)^2]/\Sigma[w(F_o^2)^2]\}^{1/2}$. − [c] $S = \{\Sigma[w(F_o^2 - F_c^2)^2]/(n - p)\}^{1/2}$, where *n* = no. of refl. and *p* = total no. of parameters refined. − [d] $w = 1/[\sigma^2(F_o^2) + (dP)^2 + eP]$, where $P = [2F_c^2 + \mathrm{Max}(F_o^2,0)]/3$. − [e] Ref.[58]

All structures were refined in a consistent manner employing the SHELX-97 program package.[59] SHELX refines against F^2 and all data were used in the full-matrix least-squares refinement. H atoms were placed in idealized positions and were refined with fixed isotropic displacement parameters of $1.2U_{eq}$ (parent C). All other atoms were refined anisotropically. The weighting scheme recommended by the program was used and refinement was continued until complete convergence (maximum shift/esd < 0.001) was achieved. Graphics and geometrical parameters were generated using the PLATON package.[60]

Crystallographic data (excluding structure factors) for the structures reported in this paper have been deposited with the Cambridge Crystallographic Data Centre as supplementary publication nos. CCDC-101675 {β_{200}-[Ru(bpy)$_3$](PF$_6$)$_2$}, -101676 {γ_{200}-[Ru(bpy)$_3$](PF$_6$)$_2$}, -101677 {β_{240}-[Ni(bpy)$_3$](PF$_6$)$_2$}, -101678 {γ_{200}(1)-[Ni(bpy)$_3$](PF$_6$)$_2$}, -101679 {γ_{200}(2)-[Ni(bpy)$_3$](PF$_6$)$_2$}, and -101680 {γ_{200}-[Zn(bpy)$_3$](PF$_6$)$_2$}. Copies of the data can be obtained free of charge on application to the CCDC, 12 Union Road, Cambridge CB2 1EZ, U.K. [Fax: (internat.) + 44-1223/336-033; E-mail: deposit@ccdc.cam.ac.uk].

Since submission of the manuscript we have been informed that the structure of γ-[Zn(bpy)$_3$](PF$_6$)$_2$ has meanwhile also been solved by Bernal's group; the manuscript will soon be submitted to *J. Chem. Soc., Dalton Trans.*[62]

Acknowledgments

We would like to thank Prof. Dr. K.-J. Range for making equipment available and for support in various areas, the Fonds der Chemischen Industrie, and the DFG for financial support. Furthermore, we thank the Degussa AG for a donation of $RuCl_3 \cdot 3H_2O$.

[1] J. Breu, N. Raj, C. R. A. Catlow, *J. Chem. Soc., Dalton Trans.* **1999**, 835−845.
[2] J. M. Lehn, *Pure Appl. Chem.* **1994**, *66*, 1961−1966.
[3] J. M. Lehn, in *Lock-and-Key Principle* (Ed.: J. P. Behr), John Wiley & Sons Ltd., **1994**.
[4] J. D. Dunitz, *Acta Crystallogr. B* **1995**, *51*, 619−631.
[5] J. D. Dunitz, in *The Crystal as a Supramolecular Entity* (Ed.: G. R. Desiraju), John Wiley & Sons Ltd., **1996**.
[6] C. B. Aakeröy, *Acta Crystallogr. B* **1997**, *53*, 569−586.
[7] C. P. Brock, J. D. Dunitz, *Chem. Mater.* **1994**, *6*, 1118−1127.
[8] I. Bernal, J. Cetrullo, J. Myrczek, J. W. Cai, W. T. Jordan, *J. Chem. Soc., Dalton Trans.* **1993**, 1771−1776.
[9] Z. Bocskei, D. Kozma, K. Simon, E. Fogassy, *J. Chem. Res. (S)* **1995**, 160−161.
[10] J. Jacques, A. Collet, S. H. Wilen, *Enantiomers, Racemates, and Resolution*, John Wiley & Sons, New York, **1981**.
[11] H. Lai, D. S. Jones, D. C. Schwind, D. P. Rillema, *J. Crystallogr. Spectrosc. Res.* **1990**, *20*, 321−325.
[12] J. Breu, P. Belser, H. Yersin, *Acta Crystallogr. C* **1996**, *52*, 858−861.
[13] J. Breu, A. J. Stoll, *Acta Crystallogr. C* **1996**, *52*, 1174−1177.
[14] D. P. Rillema, D. J. Jones, *J. Chem. Soc., Chem. Commun.* **1979**, 849−851.
[15] D. P. Rillema, D. S. Jones, C. Woods, H. A. Levy, *Inorg. Chem.* **1992**, *31*, 2935−2938.
[16] M. Biner, H.-B. Bürgi, A. Ludi, C. Rohr, *J. Am. Chem. Soc.* **1992**, *114*, 5197−5203.
[17] S. Dick, *Z. Kristallogr. New Cryst. Struct.* **1998**, *213*, 356.
[18] F. H. Allen, O. Kennard, *Chem. Des. Autom. News* **1993**, *8*, 31−37.
[19] J. Ferguson, F. Herren, *Chem. Phys.* **1983**, *76*, 45−59.
[20] J. Ferguson, E. Krausz, *Inorg. Chem.* **1987**, *26*, 1383−1386.
[21] E. Krausz, G. Moran, *J. Luminesc.* **1988**, *42*, 21−27.
[22] I. Bernal, private communication, **1994**.
[23] F. Grepioni, G. Cojazzi, S. M. Draper, N. Scully, D. Braga, *Organometallics* **1998**, *17*, 296−307.
[24] J. Bernstein, R. J. Davey, J.-O. Henck, *Angew. Chem.* **1999**, *111*, 3646−3669; *Angew. Chem. Int. Ed.* **1999**, *38*, 3440−3461.
[25] J. Breu, H. Domel, *Eur. J. Inorg. Chem.* **2000**, 2409−2419, subsequent paper.
[26] C. P. Brock, W. B. Schweizer, J. D. Dunitz, *J. Am. Chem. Soc.* **1991**, *113*, 9811−9820.
[27] I. Dance, M. Scudder, *J. Chem. Soc., Dalton Trans.* **1998**, 1341−1350.
[28] R. Kuroda, S. F. Mason, C. D. Rodger, R. H. Seal, *Mol. Phys.* **1981**, *42*, 33−50.
[29] R. Kuroda, P. Biscarini, *Mol. Cryst. Liq. Cryst. Sci. Tech. A* **1996**, *278*, A275−A284.
[30] T. Liljefors, I. Petterssen, *J. Comput. Chem.* **1987**, *8*, 1139−1145.
[31] W. L. Jorgensen, D. L. Severance, *J. Am. Chem. Soc.* **1990**, *112*, 4768−4774.
[32] C. A. Hunter, in *From Simplicity to Complexity in Chemistry − and Beyond* (Ed.: A. Müller), Vieweg, Braunschweig, **1996**.
[33] G. R. Desiraju, A. Gavezzotti, *Acta Crystallogr. B* **1989**, *45*, 473−482.
[34] J. D. Dunitz, A. Gavezzotti, *Acc. Chem. Res.* **1999**, *32*, 677−684.
[35] C. A. Hunter, *Angew. Chem.* **1993**, *105*, 1653−1655; *Angew. Chem. Int. Ed.* **1993**, *32*, 1584−1586.
[36] C. A. Hunter, *Phil. Trans. R. Soc. London, A* **1993**, *345*, 77−85.
[37] H. Adams, K. D. M. Harris, G. A. Hembury, C. A. Hunter, D. Livingstone, J. F. McCabe, *Chem. Commun.* **1996**, 2531−2532.
[38] C. S. Wilcox, E. Kim, S. Paliwal, *J. Am. Chem. Soc.* **1998**, *120*, 11192−11193.
[39] C. S. Wilcox, S. Paliwal, S. Geib, *J. Am. Chem. Soc.* **1994**, *116*, 4497−4498.
[40] G. Karlström, P. Linse, A. Wallqvist, B. Jönsson, *J. Am. Chem. Soc.* **1983**, *105*, 3777−3782.
[41] P. Hobza, H. L. Selzle, E. W. Schlag, *J. Phys. Chem.* **1996**, *100*, 18790−18794.
[42] P. Hobza, V. Spirko, H. L. Selzle, E. W. Schlag, *J. Phys. Chem. A* **1998**, *102*, 2501−2504.
[43] P. Hobza, H. L. Selzle, E. W. Schlag, *J. Phys. Chem.* **1993**, *97*, 3937−3938.
[44] W. Scherzer, O. Kratzschmar, H. L. Selzle, E. W. Schlag, *Z. Naturforsch., A* **1992**, *47*, 1248−1252.
[45] V. A. Venturo, P. M. Felker, *J. Chem. Phys.* **1993**, *99*, 748−751.
[46] E. Arunan, H. S. Gutowsky, *J. Chem. Phys.* **1993**, *98*, 4294−4296.
[47] J. A. Niesse, H. R. Mayne, *J. Phys. Chem.* **1997**, *101*, 9137−9137.
[48] A. Gavezzotti, *Chem. Phys. Lett.* **1989**, *161*, 67−72.
[49] D. Onggo, A. D. Rae, H. A. Goodwin, *Inorg. Chim. Acta* **1990**, *178*, 151−163.
[50] E. Perez-Cordero, C. Campana, L. Echegoyen, *Angew. Chem.* **1997**, *109*, 85−88; *Angew. Chem. Int. Ed. Engl.* **1997**, *36*, 137−140.
[51] J. Breu, C. Kratzer, H. Yersin, *J. Am. Chem. Soc.*, in print.
[52] D. L. Kepert, *Inorganic Chemistry*, Springer Verlag, Berlin, **1982**.
[53] N. Masciocchi, G. A. Ardizzoia, G. La Monica, M. Moret, A. Sironi, *Inorg. Chem.* **1997**, *36*, 449−454.
[54] F. M. Jaeger, J. A. van Dijk, *Z. Anorg. Allg. Chem.* **1936**, *227*, 273−327.
[55] M. M. T. Khan, R. C. Bhardwaj, C. Bhardwaj, *Polyhedron* **1990**, *9*, 1243−1248.
[56] V. Joshi, P. K. Ghosh, *J. Am. Chem. Soc.* **1989**, *111*, 5604−5612.
[57] T. Araki, *Z. Kristallogr.* **1991**, *194*, 161−191.
[58] H. D. Flack, *Acta Crystallogr. A* **1983**, *39*, 876−881.
[59] G. M. Sheldrick, *SHELX-97*, University of Göttingen, **1997**.
[60] A. L. Spek, *Acta Crystallogr. A* **1990**, *46*, C34.
[61] A. I. Kitajgorodski, *Molecular Crystals and Molecules*, Academic Press, New York, **1973**.
[62] I. Bernal, private communication, **2000**.

Received February 8, 2000
[I00042]

Chiral Recognition Among Trisdiimine−Metal Complexes, 7[‡]

Racemic Compound Formation *versus* Conglomerate Formation with $[M(bpy)_3](PF_6)_2$ (M = Ni, Zn, Ru); Lattice Energy Minimisations and Implications for Structure Prediction

Josef Breu,*[a] Holger Domel,[a] and Per-Ola Norrby[b]

Keywords: Molecular recognition / Chiral recognition / Conglomerate crystallisation / Crystal structure prediction / Polymorphism

Polymorphism observed with $[M(bpy)_3](PF_6)_2$ (M = Ru, Ni, Zn) offers a unique opportunity to study the impact of different intermolecular packing motifs on lattice energies. Additionally, it allows us to test the accuracy of empirical intermolecular potentials, because these compounds represent an example of a system where a small change in molecular geometry already induces a qualitatively different crystal packing. Lattice energy minimisations for these three compounds applying both, rigid body and flexible body approaches, are reported. The calculations quite reasonably reproduce the crystallisation behaviour observed in this heteropolymorphic series. We conclude that the state-of-the-art approach and all four tested empirical intermolecular potentials are adequate for these organometallic compounds. However, it is crucial to input the most accurate molecular structures. Molecular structures determined by X-ray analysis need to be corrected for the apparent bond shrinkage due to librational motion. When these molecular structures are to be obtained by Molecular Mechanics or Quantum Mechanics methods the highest possible accuracy is required. Our results suggest that routine polymorph prediction may be more severely hampered by inaccuracies in molecular structures than by inadequacies in the intermolecular potentials. The key to a successful structure prediction is therefore the input of reliable molecular structures.

Introduction

The last few years have seen an increasing interest in the prediction of crystal structures for various reasons. The two main motives are, on the one hand, structure solution in real space (solving the phase problem), where interpretation of the powder diffraction intensities in reciprocal space has proved impossible;[2−5] on the other hand, exploration of the lattice energy hypersurface is driven by the need for so-far-unknown polymorphs with desired properties (shelf life, solubility, bioavailability, morphology, etc.),[6−13] or even perhaps for patenting and registration purposes.

The vast majority of search engines employ lattice energies based on some empirical intermolecular atom−atom pair potentials as the cost function,[14,15] and the systems most frequently investigated are neutral organic molecules. The basic experience is that, often, many theoretical polymorphs are identified within a lattice energy range of 10 kJ/mol[16] and that the experimentally observed structure — where known — is indeed close to the global minimum. This suggests that phase space is thoroughly covered by the different search engines, but even the most elaborate and presumably accurate potentials often fail to give the experimental crystal structure always with the lowest lattice energy as would be expected for thermodynamic product control. Observation of polymorphism at the same *p,T* conditions or even in the same crystal crop indicates that, for some substances, there may indeed be a range of energetically accessible structures, and that the kinetics and thermodynamics of nucleation — about which little is known — are responsible for selecting those which will be found experimentally. However, contrary to the experience in theoretical predictions, in the experimental world polymorphism seems to be much less pervasive.[17] No one has, for instance, ever seen acetylsalicylic acid polymorphs[18] despite the large quantities of aspirin tablets manufactured.

Polymorphs may be considered as conformers of the supramolecule which is the crystal structure itself.[19] Crystal polymorphism for any one compound is therefore already a valuable and informative phenomenon with regard to supramolecular chemistry and crystal engineering. Polymorphs are the result of the same cohesive forces and therefore they should provide better information on intermolecular forces. Moreover, since it is not expected that nucleation-induced metastability is very pronounced when growing

[‡] Part 6: Ref.[1]

[a] Institut für Anorganische Chemie der Universität Regensburg, D-93040 Regensburg, Germany
Fax: (internat.) + 49-941/943-3261
E-mail: josef.breu@chemie.uni-regensburg.de
[b] Department of Medical Chemistry, Royal Danish School of Pharmacy,
Universitetsparken 2, DK-2100 Copenhagen, Denmark
Fax: (internat.) + 45-35/372-209
E-mail: peo@dfh.dk

Supporting information for this article is available on the WWW under http://www.wiley-vch.de/home/eurjic or from the author.

 © WILEY-VCH Verlag GmbH, D-69451 Weinheim, 2000 1434−1948/00/1111−2409 $ 17.50+.50/0

crystals at room temperature, polymorphism may also help to assess the quality of different empirical intermolecular potentials used in structure prediction. In that respect, it is very useful if polymorphism can be tailored and/or the crystallisation of unstable polymorphs can be enforced on the system, for example, by taking advantage of chirality or tailor-made additives. In such a way, a wider lattice-energy range should be accessible experimentally. Furthermore, it is helpful if the molecule has few internal degrees of freedom that would require a balanced and accurate treatment of intra- and intermolecular parts of a force field.

The preceding paper[1] describes such a system. With $[M(bpy)_3](PF_6)_2$ (M = Ni, Zn, Ru) three different polymorphs are observed. α-$[M(bpy)_3](PF_6)_2$ is just a slight distortion of β-$[M(bpy)_3](PF_6)_2$ and the phase transition is induced upon cooling, but the packing in the γ-polymorph is drastically different: while the α- and β-form are true racemates the γ-structure is an enantiomorph.

We have performed lattice-energy minimisations of the three compounds in the different structure types, both within the rigid body and the flexible body framework. The results are analysed with regard to the self-organisation of such propeller-shaped molecules. Additionally, more general conclusions regarding the mentioned problems in structure prediction are discussed on the basis of calculated lattice energies.

Results and Discussion

When studying the relative importance of different intermolecular contributions during the self-assembly of crystals, organometallic compounds display significant advantages over organic compounds since structural molecular parameters may be tuned to a much finer degree. With $[M(bpy)_3](PF_6)_2$ the size of the complex cations and the molecular electrostatic potential (MEP) may be delicately varied by substitution of the central atom. Moreover, this variation leads to different polymorphs, and it is possible to switch between the polymorphs by choosing the right metal. With M = Fe,[20] M = Ru,[21,22] or M = Os[23,24] the racemic solutions crystallize as true racemates in the β-type. This β-type undergoes a phase transition to the closely related low temperature α-polymorph.[25,26] For M = Zn this racemic structure is not accessible experimentally. Instead, the enantiomorphous γ-type is the only modification observed. For M = Ni, crystals of both structure types are obtained concomitantly in the very same crystallization batch. Finally, since $[Ru(bpy)_3]^{2+}$ is inert towards racemisation the γ-type can be "forced" upon $[Ru(bpy)_3](PF_6)_2$ by chemical resolution prior to crystallization.

According to thermodynamics, polymorphic modifications can be at equilibrium only at the phase-transition temperature where the ΔG curves cross. The likelihood of choosing exactly this temperature for crystallization is rather slim.[27] Moreover, Gavezzotti & Filippini[17] have shown in their systematic study of crystal polymorphism that entropy differences between polymorphs of differing packing topology are never large enough to have $300\Delta S$ exceed ΔH (Note that ΔH is also dependant on temperature). They conclude that relative stability among polymorphs at room temperature can be judged on the basis of packing energy (enthalpy) alone. Consequently, it is obvious that kinetics must have a certain impact when concomitant crystallization of two polymorphs is observed at the same temperature, in the same solvent, and at the same supersaturation level. For this to happen the nucleation rates of both modifications must be similar. However, concomitantly crystallizing polymorphic modifications as observed with $[Ni(bpy)_3](PF_6)_2$ must nevertheless have energetically equivalent structures.[27] Generally, it is thought that even polymorphs obtainable at varying crystallization conditions (solvent, temperature, supersaturation) have lattice energies within 4−12 kJ/mol.[18] It is expected that for concomitantly crystallizing polymorphs this range is even smaller. Therefore, already $[Ni(bpy)_3](PF_6)_2$ provides an excellent and very demanding benchmark for the validation of interatomic potentials as they must reproduce the near equivalency of the crystal energetics. The crystallization behaviour of the heteropolymorphic series of $[M(bpy)_3](PF_6)_2$ structures as a whole is even better suited to test the accuracy of empirical intermolecular atom−atom pair potentials: It is anticipated that the calculated lattice energies for β-$[Ni(bpy)_3](PF_6)_2$ and for γ-$[Ni(bpy)_3](PF_6)_2$ are very similar, irrespective of the unknown absolute value. For $[Ru(bpy)_3](PF_6)_2$ the racemic β-type, and for $[Zn(bpy)_3](PF_6)_2$ the enantiomorphic γ-type, should be preferred energetically.

Rigid-Body Minimisations

Lattice-energy minimisations for these three compounds applying the rigid body code MPA[9] (Molecular Packing Analysis) in combination with four popular sets of intermolecular potentials, CFF91,[28] Williams,[29] UNI,[30] and MM3,[31] yield very satisfying results (Tables 1−4).

In a first approximation, the quality of a set of intermolecular atom−atom pair potentials for crystal structure calculations can be judged by relaxing the experimental structures in the force field. When the experimental structure does not change much upon minimising, the intermolecular potentials are considered adequate. For a high quality set of potentials small shifts of 1−2% in the cell edges are reasonable, since this is the typical range of thermal expansion. Judging by this criterion, all experimentally observed crystal structures (EXPTL crystal model) of both structure types are satisfactorily reproduced by any of the four sets of intermolecular potentials. The maximum relative error in cell lengths is 2.2% (Table 1−4). Because our calculations neglect thermal vibrations, a shrinkage of cell lengths would have been expected. Actually, we observe quite a few cell expansions upon relaxation. This is due to the fact that, with the exception of β_{294}-$[Ru(bpy)_3](PF_6)_2$, all crystal structures were determined at low temperatures. Nevertheless, with "true 0 K" empirical intermolecular potentials, a shrinkage due to the effect of thermal expansion would still be expected, since the experimental temperatures are always

Table 1. Rigid-body lattice-energy minimisations, CFF91[28] potentials

	$[Ru(bpy)_3](PF_6)_2$				$[Ni(bpy)_3](PF_6)_2$			$[Zn(bpy)_3](PF_6)_2$	
	α_{105}[a]	β_{294}[b]	β_{200}[c]	γ_{200}[c]	β_{240}[c]	$\gamma_{200}(1)$[c]	$\gamma_{200}(2)$[c]	β[d]	γ_{200}[c]
EXPTL crystal model:									
$(a-a_{exp})/a_{exp}$ [%]	−0.6	−1.6	−1.0	−0.4	−1.3	−0.4	−0.4	–	−0.6
$(c-c_{exp})/c_{exp}$ [%]	+1.5	−1.0	+0.7	−0.2	0.0	−0.8	−0.5	–	0.0
$(V-V_{exp})/V_{exp}$ [%]	+0.3	−4.2	−1.3	−1.0	−2.6	−1.6	−1.3	–	−1.1
$E_{Inter.}$[kJ/mol][e]	−1287.3	−1291.4	−1289.4	−1278.2	−1288.5	−1285.6	−1286.0	−1261.1	−1279.9
CORR crystal model:									
$(a-a_{exp})/a_{exp}$ [%]	−0.6	−1.6	−1.0	−0.1	−1.2	+0.0	0.0	–	−0.1
$(c-c_{exp})/c_{exp}$ [%]	+1.9	0.2	+1.2	0.3	+0.6	−0.1	−0.1	–	+0.1
$(V-V_{exp})/V_{exp}$ [%]	+0.6	−3.1	−0.8	0.1	−1.8	−0.1	0.0	–	+0.0
$E_{Inter.}$[kJ/mol][e]	−1284.2	−1280.2	−1283.1	−1266.3	−1280.2	−1274.8	−1274.0	−1255.1	−1270.0

[a] Ref.[25] – [b] Ref.[21,22] – [c] Ref.[1] – [d]Hypothetical. – [e] Per mol $[M(bpy)_3](PF_6)_2$.

Table 2. Rigid-body lattice-energy minimisations, Williams[29][78] potentials

	$[Ru(bpy)_3](PF_6)_2$				$[Ni(bpy)_3](PF_6)_2$			$[Zn(bpy)_3](PF_6)_2$	
	α_{105}[a]	β_{294}[b]	β_{200}[c]	γ_{200}[c]	β_{240}[c]	$\gamma_{200}(1)$[c]	$\gamma_{200}(2)$[c]	β[d]	γ_{200}[c]
EXPTL crystal model:									
$(a-a_{exp})/a_{exp}$ [%]	0.3	−0.8	−0.1	−0.1	−0.5	0.0	0.0	–	0.0
$(c-c_{exp})/c_{exp}$ [%]	1.5	−1.1	0.4	0.1	−0.2	−0.1	−0.2	–	0.0
$(V-V_{exp})/V_{exp}$ [%]	2.1	−2.6	0.2	0.0	−1.2	0.0	−0.1	–	0.0
$E_{Inter.}$[kJ/mol][e]	−1165.6	−1170.2	−1168.3	−1166.1	−1167.9	−1173.0	−1173.5	−1146.8	−1168.5
CORR crystal model:									
$(a-a_{exp})/a_{exp}$ [%]	0.3	−0.6	0.0	0.4	−0.3	0.4	0.4	–	0.3
$(c-c_{exp})/c_{exp}$ [%]	1.7	−0.2	1.0	0.4	0.4	0.0	0.2	–	0.3
$(V-V_{exp})/V_{exp}$ [%]	2.4	−1.5	1.0	1.2	−0.2	0.7	1.0	–	0.9
$E_{Inter.}$[kJ/mol][e]	−1162.8	−1160.2	−1162.7	−1156.4	−1160.6	−1163.7	−1163.1	−1141.4	−1160.0

[a] Ref.[25] – [b] Ref.[21,22] – [c] Ref.[1] – [d] Hypothetical. – [e] Per mol $[M(bpy)_3](PF_6)_2$.

Table 3. Rigid-body lattice-energy minimisations, UNI[30] potentials

	$[Ru(bpy)_3](PF_6)_2$				$[Ni(bpy)_3](PF_6)_2$			$[Zn(bpy)_3](PF_6)_2$	
	α_{105} [a]	β_{294}[b]	β_{200}[c]	γ_{200}[c]	β_{240}[c]	$\gamma_{200}(1)$[c]	$\gamma_{200}(2)$[c]	β[d]	γ_{200}[c]
EXPTL crystal model:									
$(a-a_{exp})/a_{exp}$ [%]	0.7	−0.3	0.4	0.8	0.1	0.9	1.0	–	0.7
$(c-c_{exp})/c_{exp}$ [%]	2.2	−0.4	0.9	0.6	0.2	0.3	0.2	–	0.8
$(V-V_{exp})/V_{exp}$ [%]	3.7	−1.0	1.7	2.2	0.4	2.2	2.1	–	2.3
$E_{Inter.}$[kJ/mol][e]	−1151.1	−1155.0	−1153.5	−1148.2	−1153.1	−1155.3	−1155.7	−1132.7	−1151.2
CORR crystal model:									
$(a-a_{exp})/a_{exp}$ [%]	0.8	−0.1	0.6	1.2	0.2	1.3	1.3	–	1.2
$(c-c_{exp})/c_{exp}$ [%]	2.3	0.2	1.3	0.9	0.9	0.7	0.7	–	0.8
$(V-V_{exp})/V_{exp}$ [%]	4.0	0.0	2.5	3.4	1.3	3.2	3.3	–	3.1
$E_{Inter.}$[kJ/mol][e]	−1148.5	−1145.5	−1148.1	−1138.9	−1146.2	−1146.5	−1145.9	−1127.5	−1143.2
$\Delta E_{Coul.}$ [kJ/mol]			11.6		13.9			16.5	
$\Delta E_{d/r}$ [kJ/mol]			−20.8		−14.0			−0.8	

[a] Ref.[25] – [b] Ref.[21,22] – [c] Ref.[1] – [d] Hypothetical. – [e] Per mol $[M(bpy)_3](PF_6)_2$.

Table 4. Rigid-body lattice-energy minimisations, MM3[31] potentials

	$[Ru(bpy)_3](PF_6)_2$				$[Ni(bpy)_3](PF_6)_2$			$[Zn(bpy)_3](PF_6)_2$	
	α_{105}[a]	β_{294}[b]	β_{200}[c]	γ_{200}[c]	β_{240}[c]	$\gamma_{200}(1)$[c]	$\gamma_{200}(2)$[c]	β[d]	γ_{200}[c]
EXPTL crystal model:									
$(a-a_{exp})/a_{exp}$ [%]	0.6	−0.3	0.4	0.6	0.0	0.7	0.8	0.4	0.7
$(c-c_{exp})/c_{exp}$ [%]	1.7	−1.2	0.3	−0.1	−0.2	−0.2	−0.1	3.5	0.1
$(V-V_{exp})/V_{exp}$ [%]	2.9	−1.8	1.1	1.2	−0.1	1.3	1.4	4.3	1.5
$E_{Inter.}$[kJ/mol][e]	−1101.8	−1105.2	−1104.3	−1101.4	−1099.4	−1102.2	−1102.7	−1082.1	−1097.1
CORR crystal model:									
$(a-a_{exp})/a_{exp}$ [%]	0.6	−0.1	0.4	1.0	0.1	1.1	1.1	0.5	0.8
$(c-c_{exp})/c_{exp}$ [%]	2.0	−0.4	0.8	0.4	0.5	0.0	0.3	3.7	0.6
$(V-V_{exp})/V_{exp}$ [%]	3.2	−0.6	−1.6	2.4	0.6	2.1	2.5	4.8	2.3
$E_{Inter.}$[kJ/mol][e]	−1099.7	−1097.4	−1099.9	−1094.2	−1093.8	−1095.4	−1095.1	−1077.9	−1090.7

[a] Ref.[25] – [b] Ref.[21,22] – [c] Ref.[1] – [d] Hypothetical. – [e] Per mol $[M(bpy)_3](PF_6)_2$.

well above 0 K. However, although temperature is not explicitly considered, some thermal effects have been subsumed into the interatomic potentials during their fitting to experimental observables which were mostly determined at room temperature. As discussed in more detail by Gale,[32] modern-day potentials correspond to an effective temperature which is a weighted average of the temperatures at which the different pieces of data were measured. The simulations therefore should rather be called athermal, and this might explain the observed cell expansions upon relaxation.

The lattice energies calculated for the three compounds $[M(bpy)_3](PF_6)_2$ (M = Ru, Ni, Zn) in the two basic structure types (β and γ) cover only a small energy range despite the drastically differing packing topology. This result, in combination with the uncertainty in the model potential would render it impossible to estimate the relative stability of the two polymorphs of any singular compound and the reliability of such a conclusion without further evidence. However, we can take advantage of the additional observation that only the Ni compound crystallizes concomitantly in both structure types. Therefore, for $[Ni(bpy)_3](PF_6)_2$ both structure types are expected to be energetically equivalent, while for $[Zn(bpy)_3](PF_6)_2$ the γ-type, and for $[Ru(bpy)_3](PF_6)_2$ the β-type, should be energetically favoured. It is a very fortunate coincidence that, within this series of complexes, it is possible to switch between the two topologically different polymorphs by simply substituting the central metal atom. If this experimentally observed crystallization behaviour within this unique heteropolymorphic series of $[M(bpy)_3](PF_6)_2$ (M = Ru, Ni, Zn) compounds is reflected in the predicted relative stability of the two polymorphs, even small lattice-energy differences may be regarded as significant. Furthermore, since the transition between the α- and the β-structure for $[Ru(bpy)_3](PF_6)_2$ is driven by cooling and therefore by entropy, a "0 K" static lattice energy minimisation should predict the α-structure to be more stable.

Judging by this energy criterion all four sets of empirical intermolecular potentials perform well again. The maximum energy difference between the γ- and the β-structure for the Ni compound is observed with the Williams potentials (5.1 kJ/mol, Table 1−4, EXPTL crystal model). Also, all four potential sets predict the relative stability of the two polymorphs for the Ru and the Zn compound correctly. However, for the Williams, the UNI, and the MM3 potential sets, the β- and γ-structures for $[Ru(bpy)_3](PF_6)_2$ are getting almost as close in energy as for $[Ni(bpy)_3](PF_6)_2$. None of the intermolecular potential sets predicts α-$[Ru(bpy)_3](PF_6)_2$ to be lower in energy than β-$[Ru(bpy)_3](PF_6)_2$.

Although all four intermolecular force fields have been calibrated by using some experimentally determined sublimation enthalpies, the absolute values for the calculated lattice energies differ considerably (up to 15%).

It is difficult to quantify precisely the uncertainties associated with this rigid body approach. The lattice energies as defined by the intermolecular interactions are rather sensitive to the particular rigid molecular structures (see also next two sections) that are put into the starting configuration. These molecular structures may vary due to experimental errors and, more importantly, due to tiny conformational changes induced by the interplay of intramolecular and intermolecular forces, which in turn is dependant on temperature. To explore the effect of such methodical uncertainties in the molecular structures on the results of the lattice energy minimisations, the lattice energy for γ-$[Ni(bpy)_3](PF_6)_2$ was calculated for two starting structures which were determined at the same temperature (200 K) using two data sets sampled on different crystals [$\gamma_{200}(1)$ and $\gamma_{200}(2)$[1]]. The lattice energies for these two starting structures determined at the same temperature differ by less than 0.5 kJ/mol. To investigate minor modifications in the molecular shapes induced by temperature-dependant packing requirements the lattice energy for the racemic $[Ru(bpy)_3](PF_6)_2$ structures was not only calculated for the α-type (105 K, α_{105})[25] and the β-structure determined by Rillema at 294 K (β_{294}),[22] but also for a structure determined at an intermediate temperature (200 K, β_{200}),[1] that is still well above the onset of the phase transition to the low-temperature modification. The variation of the calculated lattice energies increases by up to 2 kJ/mol. Since the lattice energies are compared for structures determined at different temperatures, this may be regarded as the error in the intermolecular lattice energy inherent in this rigid body approximation.

Influence of Systematic Errors in Molecular Structures

Next, the effect of a systematic error on lattice energies calculated within the rigid body approach shall be taken into account which is contained in input molecular structures determined by X-ray structure analysis. Cruishank noted as early as 1956 that rotational oscillations of rigid molecules or moieties in crystals cause the apparent atomic positions to be slightly displaced from the true position towards the rotation axis.[33] X-ray analysis locates the centroids of atomic distributions that are undergoing vibrations. Distances calculated from these mean positions are shorter and cannot be interpreted directly as interatomic distances.

Approximately spherical molecules like $[PF_6]^-$ are especially prone to be affected by this systematic error. When comparing Ru−N distances as determined by different structure determinations of $[Ru(bpy)_3](PF_6)_2$ with the corresponding P−F bond lengths (Table 5) it is striking that the variation in bond length is up to an order of magnitude larger in the complex anion than in the cation.

From the principal axis directions and mean-square libration amplitudes (eigenvectors and eigenvalues of $\boldsymbol{L}$) calculated from the anisotropic displacement parameters reported for $LiPF_6$ [34] a true experimental bond length of 1.61 Å can be estimated for the P−F bond in $[PF_6]^-$. From a comparison with the uncorrected values a considerable shrinkage effect due to librational motion is evident. The apparent shortening of the P−F bond as observed in structure determinations of $[Ru(bpy)_3](PF_6)_2$ can be up to 0.08 Å. Thus the molecular dimension of the hexafluorophosphate anion obtained by X-ray crystal structure analysis is considerably in error unless corrected for the effect of mo-

Table 5. Variance of Ru−N and P−F distances in different structure determinations of $[Ru(bpy)_3](PF_6)_2$

Structure type	β_{294}[a]	β_{200}[b]	α_{105}[c]			γ_{200} [b]
Site symmetry	D_3	D_3	C_3			C_1
Independ. site			A	B	C	
Ru−N [Å]	2.056	2.048	2.052 2.053	2.053 2.053	2.053 2.053	2.049 – 2.069
P−F [Å]	1.549 1.568	1.570 1.593		1.583 – 1.618		1.527 – 1.614

[a] Ref.[21,22] – [b] Ref.[1]. – [c] Ref.[25]

lecular libration. Since the complex cations are effected to a much lesser extent by molecular libration, no corrections were applied to their molecular shape. When expanding the P−F vector in the starting structures to a reasonable value of 1.61 Å (CORR crystal model) considerable shifts in the calculated lattice energies are observed (Table 1−4). The maximum shift as compared to the EXPTL crystal model is observed for γ-$[Ru(bpy)_3](PF_6)_2$ in connection with the CFF91 potentials and amounts to 11.9 kJ/mol. When recalling that 10 kJ/mol is an energy range within which, usually, many theoretical polymorphs are predicted, it becomes obvious that correction of the observed molecular structure does indeed matter and should not be neglected.

Also, calculated lattice energies are in much better agreement with the observed crystallization behaviour for the CORR crystal model than for the EXPTL crystal model. The energy differences between β-$[Ni(bpy)_3](PF_6)_2$ and $\gamma_{200}(1)$-$[Ni(bpy)_3](PF_6)_2$ become 5.4 kJ/mol, 3.1 kJ/mol, 0.3 kJ/mol and 1.6 kJ/mol for the CFF91, Williams, UNI, and MM3 potentials, respectively. All four sets of empirical intermolecular potentials predict the γ-type to be significantly lower in energy than the β-type for $[Zn(bpy)_3](PF_6)_2$. β-$[Ru(bpy)_3](PF_6)_2$ is not only predicted to be more stable than γ-$[Ru(bpy)_3](PF_6)_2$, the energy gap between the two structure types also increases after applying the correction. Moreover, the CFF91, Williams, and UNI potentials even predict α-$[Ru(bpy)_3](PF_6)_2$ to be slightly more stable (100−400 J) than β_{200}-$[Ru(bpy)_3](PF_6)_2$.

Although the dispersion/repulsion parameters used with the four tested intermolecular force fields have not been optimised for this class of organometallic compounds, the potentials yield an excellent agreement with experiment. The atom centred monopoles give an accurate enough description of the electrostatic potential, and even anisotropic electrostatic interactions, such as the important π−π interactions, are satisfactorily represented. Quadrupole−quadrupole interactions from the π electrons are not explicitly included into the electrostatic model, but they get subsumed into the monopole−monopole interactions. Also, the assumed isotropic atom−atom form for the repulsion appears to be adequate to describe the stacking of aromatic rings as observed in the γ-structure[1] even though the charge density in these regions is known not to be spherical.[35]

This satisfying result encourages further interpretation with respect to crystal engineering. Recognition of special interactions and recurring intermolecular motifs in molecular crystals offers the opportunity of classification, but quantifying the interaction strengths provides a deeper understanding than sheer geometry — there is no such thing as a pure and simple structure-defining interaction. With respect to the intermolecular interaction patterns the β- and γ-structure differ most significantly in the particular C−H···π-interaction realised. In the β-modification T-shaped π−π interaction[36−38] contacts along the racemic columns with colinear C_3 axes are observed, while in the γ-type shifted π-stacks occur along the complex cation columns running along *c* (Figure 5a and 5c in ref.[1] respectively). Since these two mutual arrangements also allow for an effective penetration of adjacent molecules, it cannot even be decided from geometry alone whether these C−H···π-interactions have to be realised or just happen to be there because of the complementarity of molecular surfaces and thus packing efficiency. It is unclear whether the dispersion/repulsion- or the electrostatic C−H···π-interactions are predominantly responsibly for these two intermolecular interaction patterns. As the implied energies are small, a sound proof of this cannot be given without quantitative calculations. The calculated lattice energies may therefore be used to examine the relative strength, energetics and structural influence of these two different intermolecular interactions.

A comparison of the relative size of the dispersion/repulsion ($\Delta E_{d/r}$) and the electrostatic ($\Delta E_{Coul.}$) contribution to the total lattice energy is revealing with respect to the relative significance of the C−H···π-interactions (Table 3, CORR crystal model). On one hand, the Coulomb energy would prefer the γ-structure for all three compounds. This is not provoked by the arrangement of the ions, which in fact is very similar in both structures and would actually give a larger Coulomb energy for the β-arrangement: putting charges of +2 and −1 at the corresponding positions of the Ru and the P atom gives Madelung energies of −1000.4 kJ/mol and −998.0 kJ/mol for the β_{200}- and γ-arrangement, respectively. Consequently, the electrostatic preference of the γ-type must be founded in local electrostatic contributions, i.e. C−H···π- or C−H···F-interactions. Unfortunately, these two cannot be further separated. The differing MEPs for the three cations contribute towards the observed differences in $\Delta E_{Coul.}$. On the other hand, the dispersion/repulsion contribution to the total lattice energy favours the β-type for all three compounds. The differing size of the complex cations is subsumed into this energy term via the repulsion. While $\Delta E_{Coul.}$ increases moderately when going from $[Ru(bpy)_3](PF_6)_2$ to $[Ni(bpy)_3](PF_6)_2$ and to $[Zn(bpy)_3](PF_6)_2$, $\Delta E_{d/r}$ drops sharply. With large cations (e.g. M = Zn) only the γ-type, and with small cations (e.g. M = Fe, Ru) only the β-type, is observed. By chance the differences happen to cancel with M = Ni and consequently both structures crystallize concomitantly. Although the

C−H···π- and C−H···F-contributions to the Coulomb energy cannot be separated, these results indicate that C−H···π-interactions have a larger relative weight in the concert of intermolecular interactions in the shifted π-stack geometry realised in the γ-structure than in the T−shaped (edge-to-face) arrangement in the β-structure. This result contradicts the importance assigned by Dance[39] to such concerted T-shaped arrangements with regard to the molecular recognition between $[M(bpy)_3]^{n+}$. This supramolecular motif was even given a distinct name, "sextuple aryl embrace". Instead, our lattice energy calculations are in line with the experimental evidence presented by Wilcox[40,41] that suggests that the electrostatic potential of the aromatic ring is *not* a dominant aspect of the edge-to-face aryl−aryl interaction, but that London dispersion forces should be the predominant driving force for this type of interaction.

However, it should be kept in mind that the experimental crystal structures cannot be explained by a single type of interaction but result from an interplay between all the different interactions, both weak and strong.

Flexible Body Minimisations

From a comparison of the lattice energies calculated for β_{200}-$[Ru(bpy)_3](PF_6)_2$ and β_{294}-$[Ru(bpy)_3](PF_6)_2$ it is already evident that even the very limited conformational flexibility inherent in $[M(bpy)_3]^{2+}$ does play some role and that the subtle interplay between the molecular structure and the crystal structure may be significant even for these rather rigid molecules. When molecules are conformationally flexible, the intramolecular energy difference between the two solid phases has to be included in the total energy, since the crystal structure molecular conformers are not necessarily the lowest energy conformers.[42,43] However, this requires an accurate balance between inter- and intramolecular potentials.

To get an idea of the significance of the intramolecular term, we have performed single-point density-functional calculations, although there are justified concerns about calculating the relative stability of conformers using ab initio methods on molecules with a fixed geometry.[42] Such single-point calculations are very sensitive to slight errors in the experimental bond lengths and angles. These errors may be of varying magnitude for different structure determinations and, consequently, this will bias the results in an unpredictable way. However, α-$[Ru(bpy)_3](PF_6)_2$ offers the rare opportunity of three crystallographically independent complex cation sites with slightly varying molecular shapes (see intramolecular parameters given in Table 6), which should be of comparable accuracy. These three sites differ most significantly in the torsional angles around the pyridine−pyridine bond (py−py). The ab initio energies for the three different crystallographic sites in the gas phase already differ by 5.3 kJ/mol which is of similar magnitude to the lattice-energy differences observed in the rigid body approach. This result suggests that one might have to worry about intramolecular contributions even though $[M(bpy)_3]^{2+}$ cations display only very limited conformational flexibility.

Unfortunately, reliable molecular mechanics parameters for Ru^{II}−polypyridyl coordination compounds have up to now only been developed within the context of the MM3* force field in MacroModel.[44] However, this package does not allow lattice-energy calculations with accelerated convergence techniques. Therefore, we derived molecular mechanics parameters within the context of the CFF91 force

Table 6. Molecular geometries and (cluster) energies of the independent cation sites in α-$[Ru(bpy)_3](PF_6)_2$ [25]

Independent site	A	B	C
M−N [Å]	2.052	2.053	2.053
	2.053	2.053	2.053
μ [°][a]	78.65	78.56	78.59
[°][a]	89.51	89.88	89.90
ν [°][a]	95.05	96.56	96.77
	97.18	95.44	95.17
np_{xyz}−cpp−cpp−np_{xyz} [°][a]	6.02	4.61	8.39
cp−cpp−cpp−cp [°][a]	11.53	13.07	6.74
py−py [°][a]	9.73	10.26	9.01
ligand bite [Å][a]	2.601	2.599	2.601
b[b]	1.267	1.266	1.267
2Θ [°][c]	51.2	51.1	51.5
μ−t1 [Å][d]	1.074	1.067	1.026
μ−t2 [Å][d]	1.036	1.041	1.075
t1−M−t2 [°]	180.0	180.0	180.0
S [Å][e]	3.051[f]	3.051[f]	3.053[f]
$A = \alpha_1 + \alpha_2$ [°][a]	228.7	228.7	228.6
$B = \beta_1 + \beta_2$ [°][a]	247.6	246.9	247.7
Δ_{max} [Å][g]	0.037	0.037	0.018
E(DMol) [kJ/mol]	−29618.8	−29618.8	−29624.1
$E_{rel.}$(DMol) [kJ/mol]	5.3	5.3	0
E(CFF91) [kJ/mol]	118.8	118.4	117.6
$E_{rel.}$(CFF91) [kJ/mol]	1.2	0.8	0

[a] For labelling scheme see Figure 1. − [b] Normalised ligand bite. − [c] Trigonal twist. − [d] Distances between the central atom and the centre of gravity of the trigonal faces formed by N atoms of the bpy ligands. − [e] Edge length of the basis of the trigonal antiprism. − [f] Averaged in D_3−symmetry. − [g] Maximum deviation from the best plane within a single pyridine ring.

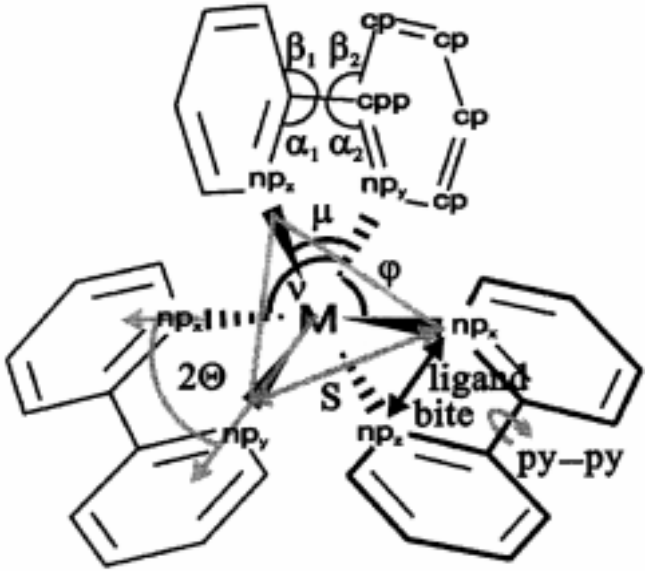


Figure 1. Labelling scheme of geometrical parameters and atom types listed in the Tables

field, which subsequently permits lattice energy minimisations employing Cerius−OFF.[45] This program uses Ewald summation methods for evaluation of the electrostatic- and the dispersion term yielding lattice energies of the same precision as obtained by MPA in the rigid body approach.

In order to accurately reproduce structures and energies by a molecular mechanics force field, information about the exact shape of the intramolecular potential energy surface (PSE) has to be used in the fitting of the force field.[46] Mass weighted Hessian elements calculated by Quantum Mechanics (QM) supply a wealth of information about the PSE and can be included very efficiently in parametrizations. However, it is important to realise that systematic errors in the QM method will be reproduced by the force field. This may be counteracted by simultaneous use[44,46−49] of structural information contained in experimentally determined molecular structures. Here, it should be kept in mind that these structures might be influenced by crystal packing[50] and by systematic errors caused by thermal motion, as discussed earlier. The relative weighting factors for QM and experimental "observables" employed in the fitting of the Ru force field parameters (Table S8) and the optimised parameters (Tables S9−S12) are given in the supporting information.

Unfortunately, there are not enough reliable experimental parameters available in the literature that could be used in the parametrization of the anion (see discussion in the previous section). Furthermore, density functional methods applied to $[PF_6]^-$ in the gas phase give equilibrium bond lengths that are longer (1.648 Å) than the values observed in crystal structures. Therefore, the equilibrium bond length has to be shifted after fitting (r_0 = 1.61 Å). The optimised force-field parameters for $[PF_6]^-$ are also listed in the supporting information (Table S13).

The ab initio energies calculated for the three independent sites in α-$[Ru(bpy)_3](PF_6)_2$ may be used as a first benchmark that might confirm the accuracy of the derived force field. DMol[53] and CFF91 energies are indeed consistent (Table 6), suggesting that, to a first approximation, the intramolecular potential energy landscape is adequately described by the force field. Structural overlays of molecular structures as observed in the two crystal structures and as minimised in the context of the force field show only minor deviations (Figure 2) and indicate that intra- and intermolecular interactions are quite satisfactorily balanced.

Nevertheless, the flexible-body model fails to produce the correct order in lattice energies for β_{200}-$[Ru(bpy)_3](PF_6)_2$ and γ-$[Ru(bpy)_3](PF_6)_2$. The energy difference between the γ- and the β-type drops from 16.8 kJ/mol to −8.5 kJ/mol when going from the rigid body to the flexible body model (Table 1, CORR crystal model and Table 7). At first glance the optimised unit-cell dimensions are still in satisfying agreement with those determined by experiment. Also, the experimental intramolecular parameters listed in Table 8 are well reproduced. There is only one py−py torsion in the γ-modification that stands out by differing by 8.1° from the experimental value. The valence terms of the energies are

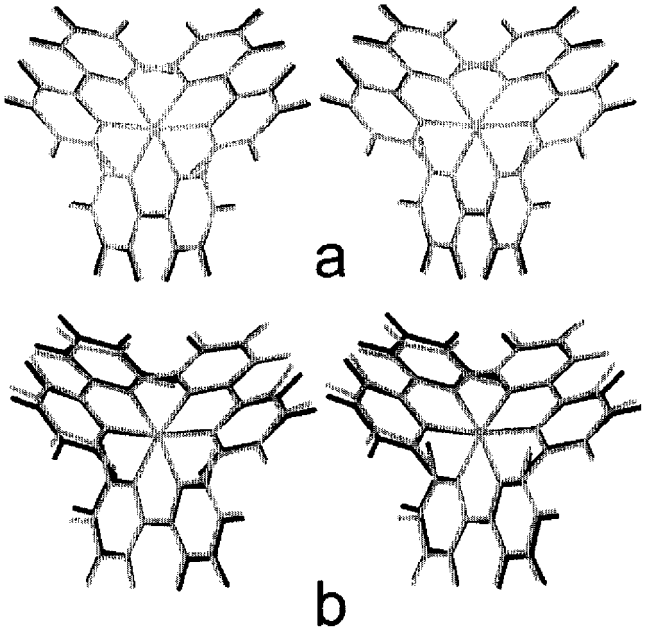


Figure 2. Stereo view of overlayed experimental (black) and molecular mechanics minimised (grey) molecular structures of $[M(bpy)_3]^{2+}$ in the β- (a) and γ-modification (b), respectively

Table 7. Flexible-body lattice-energy minimisations, CFF91 potentials

	β_{200}	γ_{200}
$(a - a_{exp})/a_{exp}$ [%]	−0.5	+0.4
$(c - c_{exp})/c_{exp}$ [%]	2.6	−2.2
$(V - V_{exp})/V_{exp}$ [%]	+1.7	−1.4
E_{Total} [kJ/mol][a]	−857.7	−866.2
$E_{Coul.}$[kJ/mol][a]	−544.2	−558.2
$E_{Disp./Rep.}$[kJ/mol][a]	−349.6	−344.3
$E_{Valence}$[kJ/mol][a]	36.1	36.3
$E_{Inter.}$[kJ/mol][a] [b]	−1280.4	−1290.8

[a] Per mol $[M(bpy)_3](PF_6)_2$. − [b] Calculated employing MPA.

actually very similar in both polymorphs (36.1 kJ/mol and 36.3 kJ/mol for β- and γ-type, respectively).

The decisive change when going from the rigid- to the flexible-body model happens in the intermolecular energy [note that the nonbonding energies calculated in the molecular mechanics approach (Table 7) contain intramolecular contributions!]. While the intermolecular lattice energy as calculated with MPA for the flexible body minimised β_{200}-$[Ru(bpy)_3](PF_6)_2$ structure is very similar to the one observed in the rigid body approach (−1280.4 kJ/mol versus −1283.1 kJ/mol), it changes considerably for flexible body minimised γ-$[Ru(bpy)_3](PF_6)_2$ (−1290.8 kJ/mol versus −1266.3 kJ/mol). When taking a closer look at both the intra- and the intermolecular parameter differences (Table 8 and 9), an interesting correlation becomes evident. In comparison to the experimentally observed molecular structure in the γ-type, the relaxed cation is somewhat higher along the pseudo−C_3 axis as indicated by the M−t1 and M−t2 distances (1.102 Å and 1.103 Å) and slightly thinner perpendicular to it (S = 3.012 Å). In other words, the cation is stretched out along the pseudo-C_3 axis. Since the pseudo-

Table 8. Comparison of experimental (exp.) and flexible-body-minimised (fmin., CFF91 force field, Cerius−OFF) intramolecular geometrical parameters for $[Ru(bpy)_3](PF_6)_2$

	β_{200}^{exp}	β_{200}^{fmin}	$\gamma\cong_{200}^{exp}$	$\gamma\cong_{200}^{fmin}$
M−N [Å]	2.048(2)	2.045	2.058(4)	2.057
			2.065(3)	2.061
			2.066(4)	2.060
			2.067(4)	2.060
			2.061(3)	2.061
			2.063(4)	2.057
μ [°][a]	78.74(8)	80.29	79.29(12)	80.16
			78.41(15)	79.85
			79.14(12)	80.17
[°][a]	89.51(9)	90.44	92.12(16)	93.37
			91.40(12)	92.17
			89.36(13)	92.17
ν [°][a]	96.08(9)	94.82	94.78(15)	93.51
			95.43(13)	92.56
			96.75(13)	95.93
			93.43(12)	92.55
			94.95(16)	93.51
			96.59(12)	95.93
ligand bite[Å][a]	2.598(3)	2.637	2.631(5)	2.651
			2.612(5)	2.644
			2.627(5)	2.651
b[b]	1.269(2)	1.289	1.271(4)[c]	1.286[c]
2Θ [°][d]	51.6(1)	51.9	50.5(2)[c]	49.9[c]
μ−t1 [Å][e]	1.050(4)	1.077	1.068(4)	1.102
μ−t2 [Å][e]	1.050(2)	1.077	1.082(4)	1.103
t1−M−t2 [°]	180.0	180.0	179.3(2)	179.3
S [Å][f]	3.046(3)	3.011	3.050[c]	3.012[c]
py−py [°][a]	8.81(13)	10.58	6.7(2)	14.8
			9.4(2)	8.1
			12.7(3)	14.8
$\alpha_1 + \alpha_2$ [°][a]	228.9(4)	233.0	230.0(7)	233.7
			229.4(8)	233.5
			230.7(7)	233.7
$\beta_1 + \beta_2$[°][a]	247.9(4)	244.2	246.4(8)	242.4
			247.7(8)	243.4
			246.3(8)	242.5
Δ_{max} [Å][g]	0.019(2)	0.032	0.028(4)	0.028

[a] For labelling scheme see Figure 1. − [b] Normalised ligand bite. − [c] Averaged in D_3−symmetry. − [d] Trigonal twist. − [e] Distances between the central atom and the centre of gravity of the trigonal faces formed by N atoms of the bpy ligands. − [f] Edge length of the basis of the trigonal antiprism. − [g] Maximum deviation from the best plane within a single pyridine ring.

C_3 axes of the complex cations in the γ-type lie approximately in the *ab* plane, the *a* and *b* axes expand upon minimisation in the context of the flexible body force field, while the *c* axis shrinks relative to the experimental values. In the rigid-body minimisation it is the other way around. As a consequence the cation−cation distance along the columns is too short by 0.2 Å (Table 9). The prominent change in one of the py−py torsions is probably the outgrowth of an intramolecular adjustment to this alteration in intermolecular geometry. Even though other small distortions occur to the molecular shape upon minimisation, it appears that changing this critical molecular parameter of relative height by a tiny amount of a few hundredths of an angström already induces a different ranking of the two polymorphs. As a consequence, one has to realize that a successful crystal structure prediction requires an accuracy in the determination of the underlying molecular shape that certainly overtaxes the best force fields and even QM methods currently available. Apparently, some force constants for intramolecular distortions are predicted to be too weak in the DFT calculations. Consequently, errors are introduced in the MM force field, since the force field cannot give better results than the data that went into its derivation. It should be noted that, due to its corrugated shape, $[Ru(bpy)_3]^{2+}$ displays quite a few intramolecular inter-ligand contacts which are less than the van der Waals separation. Therefore, the electron-density distribution in these rather remote inter-ligand regions needs to be represented accurately in order to get a realistic picture of nonbonding intramolecular contributions to the PES, which in turn greatly influence the relative positions of the ligands. It is a well-known fact that present day DFT is struggling with the long-range behaviour of the electron density.[54,55]

Table 9. Comparison of experimental (exp.), rigid-body- (rmin., CFF91 force-field, MPA), and flexible-body-minimised (fmin., CFF91 force-field, Cerius-OFF) intermolecular geometrical parameters for $[Ru(bpy)_3](PF_6)_2$

	β_{200}^{exp}	β_{200}^{rmin}	β_{200}^{fmin}	$\gamma\cong_{200}^{exp}$	$\gamma\cong_{200}^{rmin}$	$\gamma\cong_{200}^{fmin}$
M···M_{column} [Å]	8.1494(5)	8.247	8.363	8.7601(6)	8.782	8.559
M···M_{layer} [Å]	10.6453(6)	10.542	10.596	10.3809(7)	10.373	10.427
M···P [Å]	6.4422(5)	6.365	6.431	6.281(2)	6.279	6.445
				6.249(2)	6.248	6.445
				6.389(1)	6.387	6.621
				6.500(2)	6.498	6.332
				6.802(2)	6.800	6.332
				6.845(2)	6.843	6.621

Conclusions

Polymorphism may be of considerable benefit to crystal engineering. Polymorphic systems provide unique opportunities to study the competition between different intermolecular interaction patterns and correlations between changes in molecular structure and crystal packing. This is especially true if concomitant crystallization is observed.

Our calculations reproduce quite reasonably the crystallization behaviour observed in this heteropolymorphic system of $[M(bpy)_3](PF_6)_2$ (M = Ru, Ni, Zn). We conclude that the state-of-the-art approach and all four tested sets of empirical intermolecular atom−atom pair potentials are adequate for this class of organometallic compounds. When starting with the most accurate crystal structures, determined at low temperature and corrected for apparent bond shrinkage due to librational motion, significantly lower lattice energies are calculated for the experimentally observed packing topologies. Where two polymorphs crystallize concomitantly, similar lattice energies result for both structures. However, since the rigid body approach requires molecular geometries from crystal structure determinations it involves no predictive power.

A comparison of the relative size of the dispersion/repulsion ($\Delta E_{d/r}$) and the electrostatic ($\Delta E_{Coul.}$) contribution to the total lattice energy suggests that the electrostatic potential of the aromatic ring is *not* a dominant aspect of the edge-to-face aryl−aryl interaction. Certainly, concerted T-

shaped arrangements are not the electrostatically favoured molecular recognition motif between $[M(bpy)_3]^{n+}$.

The essence of the crystal structure prediction difficulties is the close proximity of several possible crystal structures for the same compound. The investigated compounds represent a good example of a system where a small change in molecular geometry already induces a qualitatively different crystal packing. Changing the M−N bond length by a few hundredths of an angström is therefore relevant. Even modest changes in molecular size or shape, which only induce slightly different intermolecular distances, have a drastically amplified effect on the lattice energy in these molecular salts due to the long range interactions.

Implications to crystal structure and polymorph prediction strategies are considerable, since either known molecular structures determined by XRD or gas phase structures optimised at various levels of theory are employed as input to the packing and search algorithms used. These results suggest that routine polymorph prediction may be more severely hampered by inaccuracies in molecular structures than by inadequacies in the empirical intermolecular potentials. The key to a successful structure prediction is therefore input of the most accurate molecular structures.

In this respect it cannot be stressed too strongly that molecular dimensions obtained by X-ray crystal structure analysis in general may be considerably in error unless corrected for the effect of libration. In extreme cases, like for spherical molecular ions such as hexafluorophosphate, the bond length errors due to this effect may exceed 0.1 Å. Of course, errors of such magnitude in the molecular shape and/or size matter when trying to predict the relative stability of polymorphs.

Furthermore, X-ray structures used for deriving inter- and intramolecular force fields should be carefully checked. Low temperature determination may be given a higher weighting factor, while structures that suffer from any kind of disorder should be excluded. In the generation of molecular structures for polymorph prediction even high level ab initio calculations may not be accurate enough. Certainly, the extreme sensitivity of the lattice energy to the molecular shape in such molecular salts tests the limits of current day intramolecular force fields. Even with molecules of very limited conformational flexibility, a balanced description of intra- and intermolecular interactions proves to be a difficult task. The situation gets still more difficult with more flexible molecules where a precise balance between intra- and intermolecular interactions is required.

Aside from the problems inherent in the accuracy of input molecular structures and force fields, the purely thermodynamic approach ignores the fact that the kinetics of crystal nucleation may be actually responsible for selecting those polymorphs that will be found experimentally. This will require a deeper understanding of molecular recognition and self-organisation in the polymolecular subcritical nuclei present in supersaturated solutions[56,57] and the effect of solvent−solute interactions on nucleation.[58] It is reassuring that the presented results give confidence that modern day intermolecular potentials should be accurate enough to realistically model nucleation kinetics for these organometallic compounds.

Experimental Section

Computational Methods

Crystal Structure Models: Two types of crystal models were constructed for each polymorph of $[M(bpy)_3](PF_6)_2$ (M = Ru, Ni, Zn) using different molecular structures. The EXPTL crystal model used the experimental structures as reported in the literature and the preceding paper,[1,21,22,25] but corrected for well-recognised inadequacies of X-ray determination by positioning the hydrogen atoms at a bond length of 1.09 Å. Secondly, in the CORR crystal model the P−F bond length was also corrected for the apparent shortening caused by librational motion of the almost spherical anion. Applying the PLATON package[59] the principal axes and eigenvalues of the molecular libration tensor ***L*** and of the translation tensor ***T*** were estimated together with components of a tensor ***S*** that allows for the quadratic correlation between librational and translational motion[60] from the atomic displacement parameters (ADPs or U_{ij} tensor components). Since the polymorphs of $[M(bpy)_3](PF_6)_2$ are affected to a different extent by static and dynamic disorder, this TLS analysis was applied instead to $LiPF_6$ for which a very precise structure determination has been reported in the literature.[34]

The hypothetical starting structure for β-$[Zn(bpy)_3](PF_6)_2$, which is inaccessible experimentally, was obtained by averaging the molecular parameters of $[Zn(bpy)_3]^{2+}$ as observed in γ-$[Zn(bpy)_3](PF_6)_2$ in D_3-symmetry and importing this molecular structure into the structure of the Ru−analogue.

Electrostatic Model: The MEPs of the complex anions and cations were represented by point charges positioned at the nucleus of the atoms. As most widely used, point charges were fitted to the quantum mechanically calculated MEP[61] employing the program POL.[62] The net charge was constrained using a Lagrange multiplicator and least-squares fits were performed for points given on a rectangular grid (0.2 Å spacing) in a 0.7 Å thick layer outside the van der Waals surface. For the cation, the charge of the well-buried central atom was fixed to its Hirshfeld partition value.[63] Symmetry-equivalent atoms were averaged. The partial charges listed in the supporting information (Tables S1 and S2) reproduce the MEPs quite well, as indicated by the low relative root-mean-square values (< 3% for cations and 5.1% for $[PF_6]^-$) for the fits and should be well suited to represent the electrostatic interactions. The MEPs were calculated applying the density functional code DMol.[53] Molecular geometries for the single-point calculations were taken from X-ray structures with H atoms recalculated at idealised positions (C−H = 1.09 Å) and no symmetry restrictions were applied. We used DNP basis sets with inner cores frozen, a FINE integration grid, and the Vosko, Wilk, Nusair[64] parametrization of the correlation energy in the homogenous electron gas. The local spin-density approximation was used in SCF iterations and gradient corrections were added in a pertubative approach using the functionals proposed by Perdew and Wang[65] and Becke[66] for the correlation and exchange, respectively. The same approach was used for the single point energy calculations given in Table 6.

Rigid Body Minimisations: Within the rigid-body approach, molecules were considered to be rigid. The lattice energy was expressed as being purely intermolecular, and was calculated as the sum of intermolecular coulombic, dispersion and repulsion interactions between individual atom sites.

Applying the code MPA[9] the starting crystal models were relaxed using the method of static lattice energy minimisation with periodic boundary condition, which calculates the structure corresponding to the nearest energy minimum[9][67−69] in the context of a given set of interatomic potentials. The crystal structure was specified by six unit cell constants, three molecular rotation angles, and three *xyz* coordinates specifying the molecular centre. The site symmetry of molecules consequently needs to be lowered to C_1. Parameters related by space group or symmetry are connected by constraints.

The program calculates first (gradient) and second (Hessian) derivatives with respect to the above-mentioned variables. To remove imaginary modes from the Hessian, the program automatically selects energy minimisation by the OREM (off-ridge eigenvector minimisation[70]) method. If the Hessian is positive definite the NR (Newton−Raphson) method is used.

For evaluation of the slowly converging electrostatic and dispersion terms, accelerated convergence techniques are applied,[71] while the repulsion term is summed in real space (cut-off 15 Å).

It is a well-known fact that the lattice energy of a polar crystal, where the unit cell has a non-zero dipole moment, depends in principle on the external shape of the crystal.[72] Consequently, the lattice energy of the polar γ-modification cannot be given precisely unless the form of the crystals is specified. However, the γ-structure displays only a very small dipole moment {(e.g. −0.8008 eÅ for $\gamma_{200}(1)-[Ni(bpy)_3](PF_6)_2$}. Using the correction term derived by Smith[73] with the assumption of a spherical crystal ($2\pi p^2/3V$, with p and V being the dipole moment and the volume of the unit cell) a minor correction of 0.26 kJ/mol would apply for the total lattice energy. Therefore, no correction was applied to the values given in the Tables.

Four popular sets of empirical intermolecular potentials, CFF91,[28] Williams,[29], UNI,[30] and MM3,[31] were tested. It should be mentioned that all but the MM3 set are lacking some parameters and needed to be supplemented with parameters from other sources. Also, MPA will not allow the use of explicit parameters for mixed interactions, but instead uses combination rules to deduce these. Further, the combination rules are restricted to the common terms, $A_{ij} = (A_iA_j)^{1/2}$, $B_{ij} = (B_iB_j)^{1/2}$, $C_{ij} = (C_i + C_j)/2$, more elaborate rules as implemented in the CFF91 force field could not be used. Explicit values and details are given in the supporting information (Table S3).

Flexible Body Minimizations: The parametrization was performed according to the new method developed by Norrby and Liljefors with simultaneous use of experimental and quantum mechanical data.[44,46−49] A slightly modified *penalty function*[51] from the one used for the MM3* parametrization[44] was applied. Inverse distances were utilised instead of bond and torsion angles. The weighting factors employed are given in the supporting information (Table S8). Starting with the MM3* values, the stretching, bending, and torsional parameters involving ruthenium were optimised by minimising the penalty function using numerical NR techniques.[47] The same mass-weighted Hessian elements and structural data applied in the previous derivation of the MM3* parameters were used in the fit. Starting values involving the coordinating N−atom types (np_x, np_y, np_z) were taken from the CFF91[28] force field (np). The subscript is needed in order to be able to differentiate between *cis* and *trans* configurations in the angle-bending term, otherwise the atom types are equivalent and they are abbreviated np_{xyz}. Furthermore, the original CFF91 force field contains no appropriate atom type for the pyridyl−pyridyl bridge (cpp). This new atom type was also included in the fitting procedure. The starting values were taken from the corresponding atom type for biphenyl as contained in CFF95 (cpb).[74]

Parameters for the anion $[PF_6]^-$ were derived in a consistent way. The geometry was fully optimised in O_h symmetry, whereupon the Hessian was calculated numerically. The mass-weighted Hessian elements were used in the parametrization. Calculations employed the Gaussian94[75] program. The B3LYP[76][77] hybrid functional was used together with the 6−31G* basis set. The quantum mechanically determined P−F distance in the gas phase is much longer (1.648 Å) than the experimentally observed value in the solid state. This was noted before[52] by others even with better basis sets and is not a shortcoming of the ab initio method, but is due to the lack of an embedding environment as anions are very sensitive to this. Ideally, a perfect force field should be able to reproduce the bond shortening that will occur upon incorporation of the anion into the crystal field. Since the force field failed to fully match this appreciable bond shortening when going into the solid state the problem was "fixed" by shifting the r_0 value derived in the fitting procedure to the *TLS* corrected value (1.61 Å). Since there are not enough reliable experimental values available for the anion only QM information could be utilised in the parametrization. In the fitting procedure the same partial charges were used as in the lattice minimisations.

Supporting information for this article (Tables S1 and S2 with partial charges, Table S3 with intermolecular potentials, Tables S4−S7 with the contributions to the total lattice energy, Table S8 with waiting factors used for the penalty function, and Tables S9−S13 with intramolecular potential parameters) is available on the WWW under http://www.wiley-vch.d/home/eurjic or from the corresponding author.

Acknowledgments

We would like to thank Prof. Dr. K. -J. Range for making equipment available and for miscellaneous support, the Fonds der Chemischen Industrie, and the DFG for financial support. Also, we are grateful to Professor Caroline Röhr for kindly providing the atomic coordinates and U_{ij} values for $LiPF_6$. Furthermore, we thank the Degussa AG for a donation of $RuCl_3 \cdot 3H_2O$.

[1] J. Breu, H. Domel, A. J. Stoll, *Eur. J. Inorg. Chem.* **2000**, 2401−2408, preceeding paper.
[2] M. Tremayne, P. Lightfoot, C. Glidewell, K. D. M. Harris, K. Shankland, C. J. Gilmore, G. Bricogne, P. G. Bruce, *J. Mater. Chem.* **1992**, *2*, 1301−1302.
[3] T. S. Bush, C. R. A. Catlow, P. D. Battle, *J. Mater. Chem.* **1995**, *5*, 1269−1272.
[4] B. M. Kariuki, H. Serrano-Gonzalez, R. L. Johnston, K. D. M. Harris, *Chem. Phys. Lett.* **1997**, *280*, 189−195.
[5] Y. G. Andreev, P. G. Bruce, *J. Chem. Soc., Dalton Trans.* **1998**, 4071−4080.
[6] H. R. Karfunkel, F. J. J. Leusen, R. J. Gdanitz, *J. Computer-Aided Mater. Design* **1993**, *1*, 177−185.
[7] A. Gavezzotti, G. Filippini, *J. Am. Chem. Soc.* **1996**, *118*, 7153−7157.
[8] A. M. Chaka, R. Zaniewski, W. Youngs, C. Tessier, G. Klopman, *Acta Cryst. B* **1996**, *52*, 165−183.
[9] D. E. Williams, *Acta Cryst. A* **1996**, *52*, 326−328.
[10] D. M. Hofmann, T. Lengauer, *J. Mol. Model.* **1998**, *4*, 132−144.
[11] W. T. M. Mooij, B. P. van Eijck, S. L. Price, P. Verwer, J. Kroon, *J. Comput. Chem.* **1998**, *19*, 459−474.
[12] B. P. van Eijck, J. Kroon, *J. Comput. Chem.* **1999**, *20*, 799−812.
[13] M. Jansen, J. C. Schön, *Z. Anorg. Allg. Chem.* **1998**, *624*, 533−540.
[14] R. J. Gdanitz, in *Theoretical Aspects and Computer Modeling*

of the Molecular Solid State (Ed.: A. Gavezzotti). John Wiley Sons, Chichester, **1997**.
[15] P. Verwer, F. J. J. Leusen, in *Reviews in Computational Chemistry* (Eds.: K. B. Lipkowitz, D. B. Boyd), Wiley-VCH, New York, **1998**.
[16] A. Gavezzotti, *Crystallography Reviews* **1998**, *7*, 5−121.
[17] A. Gavezzotti, G. Filippini, *J. Am. Chem. Soc.* **1995**, *117*, 12299−12305.
[18] R. S. Payne, R. C. Rowe, R. J. Roberts, M. H. Charlton, R. Docherty, *J. Comput. Chem.* **1999**, *20*, 262−273.
[19] J. D. Dunitz, in *The Crystal as a Supramolecular Entity* (Ed.: G. R. Desiraju), John Wiley & Sons Ltd., **1996**.
[20] S. Dick, *Z. Kristallogr. New Crystal Structures* **1998**, *213*, 356.
[21] D. P. Rillema, D. J. Jones, *J. Chem. Soc., Chem. Commun.* **1979**, 849−851.
[22] D. P. Rillema, D. S. Jones, C. Woods, H. A. Levy, *Inorg. Chem.* **1992**, *31*, 2935−2938.
[23] E. C. Constable, P. R. Raithby, D. N. Smit, *Polyhedron* **1989**, *8*, 367−369.
[24] M. M. Richter, B. Scott, K. J. Brewer, R. D. Willett, *Acta Cryst. C* **1991**, *47*, 2443−2444.
[25] M. Biner, H.-B. Bürgi, A. Ludi, C. Rohr, *J. Am. Chem. Soc.* **1992**, *114*, 5197−5203.
[26] J. Breu, C. Kratzer, H. Yersin, *J. Am. Chem. Soc.* **2000**, *122,* 2548−2555.
[27] J. Bernstein, R. J. Davey, J.-O. Henck, *Angew. Chem.* **1999**, *111*, 3646−3669; *Angew. Chem. Int. Ed.* **1999**, *38*, 3440−3461.
[28] CFF91 force field. Molecular Simulation. (December 1991): 9658 Scranton Road, San Diego, CA 92121−2777, USA: MSI. (1991).
[29] D. E. Williams, D. J. Houpt, *Acta Cryst. B* **1986**, *42*, 286−295.
[30] G. Filippini, A. Gavezzotti, *Acta Cryst. B* **1993**, *49*, 868−880.
[31] N. L. Allinger, X. Zhou, J. Bergsma, *J. Mol. Struc.* **1994**, *312*, 69−83.
[32] J. D. Gale, *Phil. Mag. B* **1996**, *73*, 3−19.
[33] D. W. J. Cruickshank, *Acta Cryst.* **1956**, *9*, 754−756.
[34] C. Röhr, R. Kniep, *Z. Naturforsch. (B)* **1994**, *49*, 650−654.
[35] C. B. Aakeröy, M. Nieuwenhuyzen, S. L. Price, *J. Am. Chem. Soc.* **1998**, *120*, 8986−8993.
[36] T. Liljefors, I. Petterssen, *J. Comput. Chem.* **1987**, *8*, 1139−1145.
[37] W. L. Jorgensen, D. L. Severance, *J. Am. Chem. Soc.* **1990**, *112*, 4768−4774.
[38] C. A. Hunter, in *From Simplicity to Complexity in Chemistry − and beyond* (Ed.: A. Müller), Vieweg, Braunschweig, **1996**.
[39] I. Dance, M. Scudder, *J. Chem. Soc., Dalton Trans.* **1998**, 1341−1350.
[40] C. S. Wilcox, E. Kim, S. Paliwal, *J. Am. Chem. Soc.* **1998**, *120*, 11192−11193.
[41] C. S. Wilcox, S. Paliwal, S. Geib, *J. Am. Chem. Soc.* **1994**, *116*, 4497−4498.
[42] D. Buttar, M. H. Charlton, R. Docherty, J. Starbuck, *J. Chem. Soc., Perkin Trans. 2* **1998**, 763−772.
[43] J. Starbuck, R. Docherty, M. H. Charlton, D. Buttar, *J. Chem. Soc., Perkin Trans. 2* **1999**, 677−691.
[44] P. Brandt, T. Norrby, B. Åkermark, P.-O. Norrby, *Inorg. Chem.* **1998**, *37*, 4120−4127.
[45] Cerius-OFF. Molecular Simulation. (2 3.5): 9658 Scranton Road, San Diego, CA 92121−2777, USA: MSI. (1996).
[46] P.-O. Norrby, P. Brandt, *Coord. Chem. Rev.* **2000**, in print.
[47] P.-O. Norrby, T. Liljefors, *J. Comput. Chem.* **1998**, *19*, 1146−1166.
[48] P.-O. Norrby, T. Rasmussen, J. Haller, T. Strassner, K. N. Houk, *J. Am. Chem. Soc.* **1999**, *121*, 10186−10192.
[49] P.-O. Norrby, in *Computational Organometallic Chemistry* (Ed.: T. Cundari), Marcel Dekker, New York, **2000**.
[50] U. Burkert, N. L. Allinger, *Molecular Mechanics*, American Chemical Society, **1982**.
[51] C. Breen, J. S. Brooks, S. Forder, J. C. E. Hamer, *J. Mater. Chem.* **1996**, *6*, 849−859.
[52] B. I. Robinson, S. A. Johnson, T. H. Tang, R. J. Gillespie, *Inorg. Chem. 36,* **1997**, *14*, 3022−3030.
[53] B. Delley, *J. Chem. Phys.* **1990**, *92*, 508−517.
[54] G. R. Parr, W. Yang, in *Density-Functional Theory of Atoms and Molecules*, Oxford University Press, Oxford, **1989**.
[55] R. J. Boyd, J. Wang, in *Recent Advances in Density Functional Methods* (Ed.: D. P. Chong), World Scientific, Singapore, **1995**.
[56] A. Gavezzotti, G. Filippini, *J. Chem. Soc.,Chem. Commun.* **1998**, 287−294.
[57] A. Gavezzotti, *Chem. Eur. J.* **1999**, *5*, 567−576.
[58] N. Bladgen, R. J. Davey, H. F. Liebermann, L. Williams, R. Payne, R. Roberts, R. Rowe, R. Docherty, *J. Chem. Soc., Faraday Trans.* **1998**, *94*, 1035−1044.
[59] A. L. Spek, *Acta Cryst. A* **1990**, *46*, C34.
[60] V. Schomaker, K. N. Trueblood, *Acta Cryst. B* **1968**, *24*, 63−76.
[61] E. Sigfridsson, U. Ryde, *J. Comput. Chem.* **1998**, *19*, 377−395.
[62] POL − Program for Derivation of Molecular Electrostatic Properties from DMOL DFT Calculations. Grochowski,P. Warsaw University: (**1995**).
[63] F. L. Hirshfeld, *Theoret. Chim. Acta* **1977**, *44*, 129−138.
[64] S. H. Vosko, L. Wilk, M. Nusair, *Can. J. Phys.* **1980**, *58*, 1200−1211.
[65] J. P. Perdew, Y. Wang, *Phys. Rev. B* **1992**, *45*, 13244−13249.
[66] A. D. Becke, *J. Chem. Phys.* **1988**, *88*, 2547−2553.
[67] J. D. Gale, *J. Chem. Soc., Faraday Trans.* **1997**, *93*, 629−637.
[68] C. R. A. Catlow, L. Ackermann, R. G. Bell, F. Cora, D. H. Gay, M. A. Nygren, J. C. Pereira, G. Sastre, B. Slater, P. E. Sinclair, *Faraday Discuss.* **1997**, 1−40.
[69] G. W. Watson, P. Tschaufeser, A. Wall, R. A. Jackson, S. C. Parker, in *Computer Modelling in Inorganic Crystallography* (Ed.: C. R. A. Catlow), Academic Press Inc., San Diego, **1997**.
[70] D. E. Williams, *Chem. Phys. Lett.* **1992**, *192*, 538−543.
[71] D. E. Williams, in *International Tables for Crystallography, Vol. B, Reciprocal Space* (Ed.: U. Shmueli) Kluwer Academic Publishers, Dordrecht, **1993**.
[72] B. P. van Eijck, J. Kroon, *J. Phys. Chem. B* **1997**, *101*, 1096−1100.
[73] E. R. Smith, *Proc. Royal Soc. A* **1981**, *375*, 475−505.
[74] CFF95 force field. Molecular Simulation. (December 1998): 9658 Scranton Road, San Diego, CA 92121−2777, USA: MSI. (1995).
[75] M. J. Frisch, G. W. Trucks, H. B. Schlegel, P. M. W. Gill, P. G. Johnson, M. A. Robb, J. R. Cheesemen, T. A. Keith, J. A. Petersson, J. A. Montgomery, K. Raghavachari, L. A. Al-Laham, V. G. Zakrzewski, J. V. Ortiz, J. B. Foresman, J. Cioslowski, B. B. Stefanov, A. Nanayakkara, M. Challacombe, C. Y. Peng, P. Y. Ayala, W. Chen, M. W. Wong, J. L. Andres, E. S. Replogle, R. Gomperts, R. L. Martin, D. J. Fox, J. S. Binkley, D. J. DeFrees, J. Baker, J. J. P. Stewart, M. Head-Gordon, C. Gonzales, J. A. Pople, *Gaussian 94*, Gaussian, Inc., Pittsburgh, PA, **1995**.
[76] C. Lee, W. Yang, R. G. Parr, *Phys. Rev. B* **1988**, *37*, 785−789.
[77] A. D. Becke, *J. Chem. Phys.* **1993**, *98*, 5648−5652.
[78] D. E. Williams, *Acta Cryst. A* **1972**, *28*, 84−88.
[79] N. L. Allinger, J. H. Yuh, J. H. Lii, *J. Am. Chem. Soc.* **1989**, *111*, 8551−8566.
[80] S. L. Mayo, B. D. Olafson, W. A. Goddard, *J. Phys. Chem.* **1990**, *94*, 8897−8909.

Received February 8, 2000
[I00043]

Binary [Hydrotris(indazol-1-yl)borato]metal Complexes, $M(Tp^{4Bo})_2$ with M = Fe, Co, Ni, Cu, and Zn: Electronic Properties and Solvent-Dependent Framework Structures through C−H···π Interactions

Christoph Janiak,* Savaş Temizdemir, Sebastian Dechert, Werner Deck, Frank Girgsdies, Jürgen Heinze, Mario J. Kolm, Tobias G. Scharmann, and Oliver M. Zipffel

Eur. J. Inorg. Chem. **2000**, 1229−1241

We regret that in Table 3 on page 1232 the isomer shifts at 290 K were given incorrectly. Also Γ/2 is actually Γ. The correct Table is shown below. Changes are highlighted in ***bold****.*

Table 3. Parameters of ^{57}Fe-Mössbauer spectra for the iron complex **4** (cf. Figure 3)

T/K [θ/°C]	N_{lin} [a]	$\delta^{\alpha\text{-Fe}}$ [b] /mm s^{-1}	Γ [c] /mm s^{-1}	ΔE_Q [d] /mm s^{-1}	A_r/% [e] (A/A_Σ)
290 [17] [f]	3	**0.35**	0.28	0.15	60
		0.39	0.61	1.02	28
		1.06	0.71	2.70	13
523 [250]	2	0.20	0.79	0.00	82
		0.20	0.38	1.21	18
473 [200]	2	0.21	0.54	−0.23	62
		0.24	0.56	1.16	38
287 [14]	1	0.34	0.26	0.16	100

[a] Number of lines used to fit the spectrum. − [b] Isomer shift referred to α-iron at room temperature. − [c] **Full width at half height.** − [d] Quadrupole splitting. − [e]Line area relative to total area. − [f] The spectrum was measured after heating the sample to 523 K and may contain some decomposition product.

C. Janiak
[C I99436]

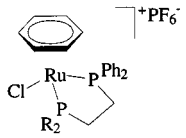
 © WILEY-VCH Verlag GmbH, D-69451 Weinheim, 2000 1434−1948/00/1111−2421 $ 17.50+.50/0

Mononuclear Ruthenium and Hetero-Tetranuclear Ruthenium-Silver Complexes Containing the Unsymmetrical Bidentate Ligands $R_2P(CH_2)_nER'_2$ (n = 1, 2; E = P, As) as Chelating or Bridging Units

Guido Fries, Birgit Weberndörfer, Kerstin Ilg, and Helmut Werner*

Eur. J. Inorg. Chem. **2000**, 1651−1656

In Scheme 1 on page 1652 the compound designations of the right-hand product have inadvertently been omitted. This product with complete designations is depicted below.



rac-
R = *i*Pr **7**, Cy **8**

The Editors
[C I00040]

 © WILEY-VCH Verlag GmbH, D-69451 Weinheim, 2000 1434−1948/00/1111−2423 $ 17.50+.50/0

Phosphaalkenes with Inverse Electron Density

Lothar Weber[a]

Keywords: Phosphaalkenes / Electron density / Synthetic methods / Phosphorus

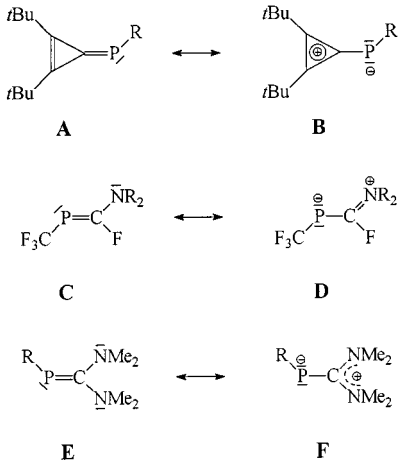
This review gives an account of the syntheses, structures, and properties of phosphaalkenes $R^1P{=}CR^2R^3$ with an inverse electron distribution at the P–C double bond ($P^{\delta-}C^{\delta+}$). The chemical reactivity of compounds of this type is novel and quite surprising compared to the chemistry of "classically polarized" phosphaalkenes ($P^{\delta+}C^{\delta-}$).

1. Introduction

The chemistry of compounds with low-coordinate phosphorus atoms involved in phosphorus−carbon multiple bonding has rapidly developed since the discovery of HC≡P by Gier in 1961.[1,2] The formal replacement of one methylene group in alkenes $R^2R^3C{=}CR^4R^5$ by the phosphanediyl unit R^1P affords the class of phosphaalkenes $R^1P{=}CR^2R^3$. Numerous papers on phosphaalkenes have highlighted the remarkable ability of phosphorus to mimic the chemistry of carbon.[3] The vast majority of phosphaalkenes feature an electron distribution $P^{\delta+}C^{\delta-}$ at the P−C double bond, as would be anticipated from the different electronegativities of carbon (2.5) and phosphorus (2.1).

About ten years ago inversely polarized phosphaalkenes were independently discovered by several research groups. Regitz et al. synthesized the first 2,3-di-*tert*-butylcyclopropylidene phosphanes and pointed out that these phosphatriafulvenes have an inverse π-electron distribution at the exocyclic P=C double bond, as depicted in the zwitterionic limiting structure **B**.[4]

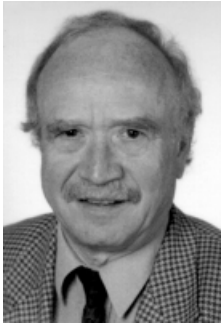
A similar polarization of the π-bond was inferred from the ^{31}P NMR spectra of phosphaalkenes such as $F_3CP{=}C(F)NR_2$ (R = Me, Et, *i*Pr; NR_2 = pyrrolidino, piperidino, 2-methylpiperidino, 3-methylpiperidino, *N*-methylanilino),[5] $F_3CP{=}C(OR)NR'_2$ (R, R′ = Me, Et),[6] or $HP{=}C(Me)NMe_2$[7] where unusual high-field resonances for the dicoordinate phosphorus atom were observed (Scheme 1).



Scheme 1. Resonance structures of phosphaalkenes with an inverse π-electron density

This polarization is even more pronounced in phosphaalkenes with two amino substituents at the carbon atom of the double bond, such as $RP{=}C(NMe_2)_2$ (R = H,[8] Me_3Si,[9] alkyl,[7] aryl[10]) (Scheme 1).

[a] Fakultät für Chemie der Universität Bielefeld, Universitätsstraße 25, 33615 Bielefeld, Germany



Lothar Weber was born in 1944 in Langenöls in Schlesien. He studied at the Universität Marburg and received his doctorate there under the direction of Professor Günter Schmid in 1973. Afterwards, he carried out post-doctoral studies with Professor Barry M. Trost at the University of Wisconsin in Madison, USA. On his return to Marburg, he began the experimental work leading to his Habilitation, which was completed in 1982 at the Universität Essen. His work centered on the coordination chemistry of sulfur ylides. In 1985, he became a C2 Professor and then joined the Fakultät für Chemie der Universität Bielefeld. His research interests include the chemistry of compounds with low-coordinate elements of the fifth main group, the synthesis of homo- and heterocycles with heavy elements, new aspects in boron chemistry, and metal complex catalyzed reactions of multiply bonded systems.

MICROREVIEWS: This feature introduces the readers to the authors' research through a concise overview of the selected topic. Reference to important work from others in the field is included.

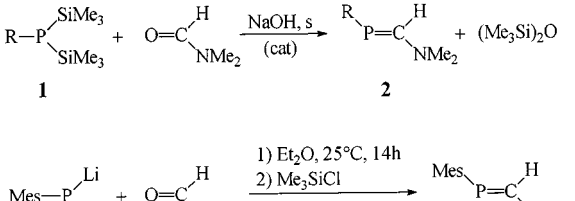
2. Syntheses

Basically, phosphaalkenes with an inverse π-electron density are available by the same synthetic methods which have been developed for phosphaalkenes with a normal π-electron distribution ($P^{\delta+}C^{\delta-}$). The most useful approaches to inversely polarized phosphaalkenes, however, involve condensations or substitution reactions at the P=C skeleton of appropriate precursors.

2.1. Condensation

Among condensation processes the Peterson olefination plays a prominent role in the construction of P=C double bonds.

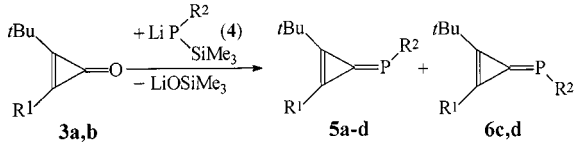
Thus, condensation of neat organobis(trimethylsilyl)phosphanes $RP(SiMe_3)_2$ (**1a**: R = Mes; **b**: Ph; **c**: *t*Bu) with excess *N*,*N*-dimethylformamide to afford the yellow phosphaalkenes $RP{=}C(H)NMe_2$ (**2a–c**, Scheme 2) was achieved in the presence of catalytic amounts of solid sodium hydroxide.[11] Without the catalyst, the reaction takes several weeks for completion.[12] An alternative high-yield synthesis of $MesP{=}C(H)NMe_2$ makes use of lithium phosphanide $LiP(Mes)(SiMe_3)$ as a starting material. Here the $LiOSiMe_3$ byproduct must be treated with Me_3SiCl prior to work up.[11]



1, 2	a	b	c
R	Mes	Ph	*t*Bu

Scheme 2. Synthesis of *C*-(dimethylamino)phosphaalkenes **2a–c**

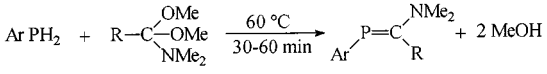
Analogously, treatment of cyclopropenones **3a**,**b** with lithium (trimethylsilyl)phosphanides **4** led to the formation of the cyclopropanylidene phosphanes **5a–d** and **6c**,**d** (Scheme 3).[4]



5, 6	R1	R2
a	*t*Bu	Me_3Si
b	*t*Bu	Mes
c	1-Ad	Me_3Si
d	1-Ad	Mes

Scheme 3. Synthesis of cyclopropenylidenephosphanes **5** and **6**

Another effective route to the *P*-arylated phosphaalkenes **2a**,**b**,**d–f** makes use of the ready condensation of carboxylic amide acetals with primary arylphosphanes at 60 °C. The products were isolated as dark yellow oils, which in some cases solidified to give light yellow crystals (Scheme 4).

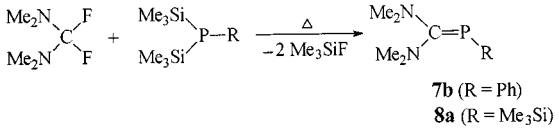


	2a	2b	2d	2e	2f
Ar	Mes	Ph	Ph	Mes*	Mes*
R	H	H	Me	H	Me

Scheme 4. Reaction of carboxylic amide acetals with arylphosphanes

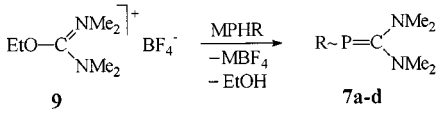
It is worth mentioning that primary alkylphosphanes do not react with these acetals.

Geminal difluorides are useful precursors for the preparation of *C*-amino-functionalized phosphaalkenes. Thus, [bis(dimethylamino)methylene](phenyl)phosphane (**7b**) and [bis(dimethylamino)methylene](trimethylsilyl)phosphane (**8a**) were obtained by gentle heating of an equimolar mixture of 1,1-difluoro-*N*,*N*,*N*′,*N*′-tetramethyldiaminomethane and either $PhP(SiMe_3)_2$ or $(Me_3Si)_3P$, respectively (Scheme 5).[9]



Scheme 5. Synthesis of **7b** and **8a**

Aryl bis(dimethylamino)methylene phosphanes such as $RP{=}C(NMe_2)_2$ [R = Mes (**7a**), Ph (**7b**)] are also conveniently accessible by combination of the carbenium salt $[EtOC(NMe_2)_2]^+BF_4^-$ (**9**) with the respective alkali metal arylphosphanide in diethyl ether[10] (Scheme 6).



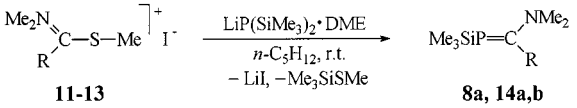
7	a	b	c	d
R	Mes	Ph	*t*Bu	H
M	Li	Na	Li	K

Scheme 6. Reaction of carbenium salts with alkali metal phosphanides

This approach, however, is of only limited value, and usually fails with the more basic alkali metal alkylphosphanides. Only $tBuP{=}C(NMe_2)_2$ (**7c**) could be prepared in 30% yield from lithium *tert*-butylphosphanide and **9**.[7] A comparable yield of the phosphaalkene **7d** was achieved when the carbenium salt **9** was allowed to react with KPH_2 in THF at ambient temperature.[7]

Spontaneous condensation occurred upon mixing of lithium bis(trimethylsilyl)phosphanide · DME with the methylthiocarbenium iodides **11–13** in *n*-pentane. The

phosphaalkenes **8**, **14a**, and **14b** were formed as orange-yellow oils in moderate to good yields (Scheme 7).[15,16]



11-13 **8a, 14a,b**

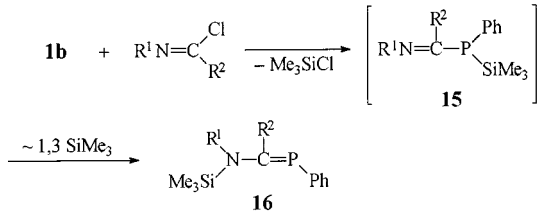
	R
8a, 11	NMe_2
12, 14a	Ph
13, 14b	*t*Bu

Scheme 7. Synthesis of *P*-silylphosphaalkenes **8a** (R = NMe_2), **14a** (R = Ph), and **14b** (R = *t*Bu)

2.2. Condensation and 1,3-Trimethylsilyl Migration

The transformation of organodisilylphosphanes to amino-substituted phosphaalkenes such as **16** with imidoyl chlorides formally parallels the synthesis of the oxygen-functionalized analogues $R^1P{=}C(OSiMe_3)R^2$. Thus, heating a 1:1 mixture of phenylbis(trimethylsilyl)phosphane **1b** with imidoyl chlorides at 150−160 °C led to compounds **16a−k** in 23−85% yield. Intermediates of the type **15** could not be detected by ^{31}P NMR spectroscopy.[17]

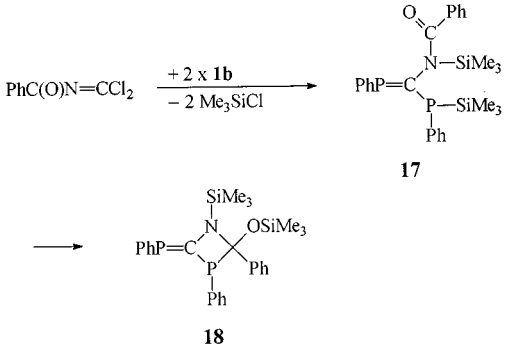
The content of Scheme 8 has to be regarded critically, as not all the phosphaalkenes **16** exhibit an inverse π-electron distribution, and in line with this, significantly shielded ^{31}P NMR absorptions. In keeping with Scheme 1, only those species where the limiting structure **D** is possible are regarded as inverse phosphaalkenes. Whenever, for steric reasons, the amino group and the C−C=P−C skeleton cannot be accommodated in the same plane, π-conjugation between the lone pair of electrons and the P=C-π bond will be precluded and the molecule will behave as a normally polarized phosphaalkene. This point will be discussed in more detail in Chapter 3 of this account.



15, 16	R^2	R^1
a	Ph	Ph
b	*t*Bu	Ph
c	Ph	Me
d	Mes	Ph
e	Ph	2,6-$Et_2C_6H_3$
f	Ph	*c*-C_6H_{11}
g	*p*-ClC_6H_4	Ph
h	*p*-$MeOC_6H_4$	Ph
i	Ph	*p*-ClC_6H_4
k	Ph	*p*-$MeOC_6H_4$

Scheme 8. Synthesis of phosphaalkenes **16** from imidoyl chlorides

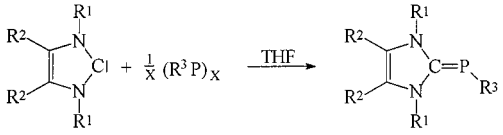
Condensation with subsequent silatropy was also effected with *N*-(dichloromethylene)amides. Consistently, interaction of **1b** with *N*-(dichloromethylene)benzamide afforded phosphaalkene **17**, which in polar solvents at elevated temperatures underwent a rapid intramolecular insertion of the carbonyl unit into the P−Si bond with the formation of **18** (Scheme 9).[18]



Scheme 9. Reaction of *N*-(dichloromethylene)benzamide with $PhP(SiMe_3)_2$

2.3. Carbene Addition

Adducts **20** formed between imidazol-2-ylidenes **19** and phenylphosphinidene or (trifluoromethyl)phosphinidine also exhibit the structural features of phosphaalkenes with an inverse π-electron distribution (Scheme 10). They were easily synthesized from suitable stable carbenes and pentaphenylcyclopentaphosphane, or tetrakis(trifluoromethyl)cyclotetraphosphane as the sources of the phosphinidene fragments.[19,20]



19a-c **20a-c**

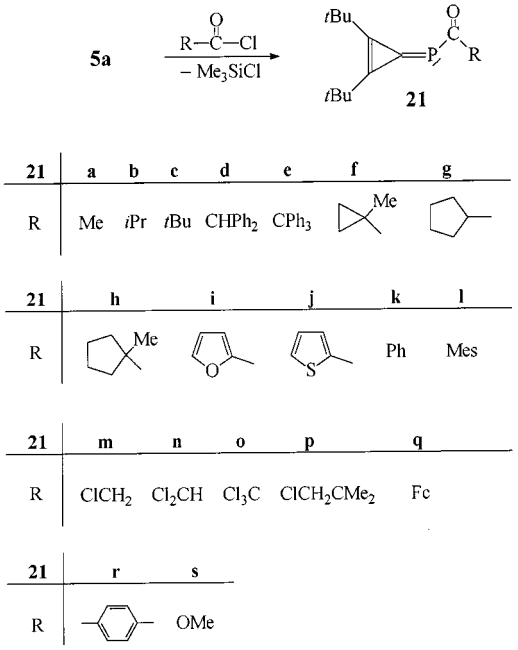
20	R^1	R^2	R^3
a	Me	Me	Ph
b	Mes	H	Ph
c	Mes	H	CF_3

Scheme 10. Synthesis of **20a−c** by carbene addition to phosphinidenes

2.4. Substitution

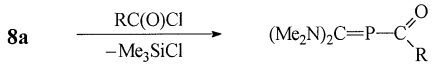
Substitution reactions at the P=C skeleton of inversely polarized phosphaalkenes represent a valuable approach to many of the compounds under discussion. In particular, *P*-silylated phosphaalkenes proved to be appropriate targets for further functionalization.

The reaction of phosphatriafulvene **5a** with carboxylic chlorides in diethyl ether afforded the *P*-acylphosphatriafulvenes **21** in yields of 40−87% (Scheme 11).[4b]



Scheme 11. Acylation of **5a**

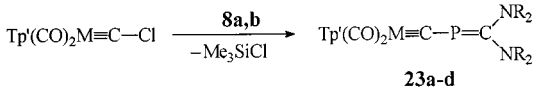
Similarly $Me_3SiP{=}C(NMe_2)_2$ (**8**) was transformed into the *P*-acyl derivatives **22a** and **22b** when allowed to react with an equimolar amount of pivaloyl or benzoyl chloride, respectively (Scheme 12).[21]



22a (R = *t*Bu)
22b (R = Ph)

Scheme 12. Acylation of **8a** by *t*BuC(O)Cl and PhC(O)Cl

Reaction of the chlorocarbyne complexes $Tp'(CO)_2M{\equiv}C{-}Cl$ [M = Mo, W; Tp′ = HB(3,5-$Me_2C_3HN_2)_3$] with two molar equivalents of **8a** in CH_2Cl_2 led to the precipitation of the red carbyne complex functionalized phosphaalkenes **23a**,**b** within 2 h (Scheme 13). The analogous conversion of the chlorocarbyne complexes into **23c**,**d** by treatment with $Me_3SiP{=}C(NEt_2)_2$ (**8b**) required 15−18 h to reach completion.[22]

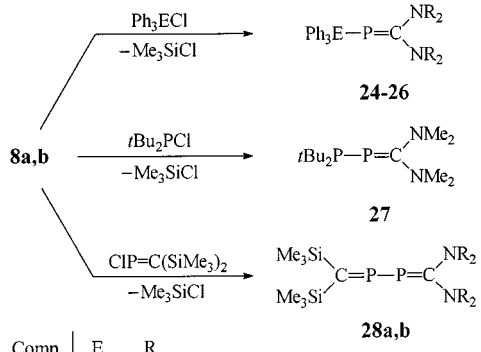


23	a	b	c	d
M	Mo	W	Mo	W
R	Me	Me	Et	Et

Scheme 13. Condensation of chlorocarbyne complexes with **8a** and **8b**

Bis(amino)methylene(trimethylsilyl)phosphane **8a** underwent transsilylation when treated with equimolar amounts of chlorotriphenylsilane in benzene at 20 °C for 3 h.[23]

In contrast to this, the reactions of the phosphaalkenes with trialkylchlorosilanes were reversible as indicated by the action of $(Et_2N)_2C{=}PSiMe_3$ (**8b**) with 1.2 equiv. of $Me_2EtSiCl$ at 20 °C, which led to an 1:2 equilibrium mixture of starting material and $(Et_2N)_2C{=}PSiMe_2Et$. Treatment of **8b** with equimolar amounts of Ph_3GeCl and Ph_3SnCl in benzene at 40 °C irreversibly afforded $Ph_3GeP{=}C(NEt_2)_2$ (**25**) and $Ph_3SnP{=}C(NEt_2)_2$ (**26**), respectively (Scheme 14).[23] The replacement of the silyl function in **8a** by a di-*tert*-butylphosphanyl group with formation of $tBu_2P{-}P{=}C(NMe_2)_2$ (**27**) was effected with an equimolar amount of tBu_2PCl in diethyl ether.[9b]

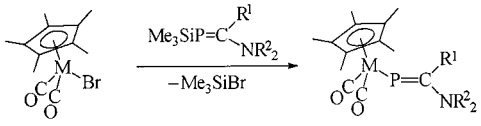


Comp.	E	R
24	Si	Me
25	Ge	Et
26	Sn	Et
28a		Me
28b		Et

Scheme 14. Reaction of **8a**,**b** with Ph_3ECl (E = Si, Ge, Sn), tBu_2PCl, and $ClP{=}C(SiMe_3)_2$

Reactions of *P*-silylphosphaalkenes **8a**,**b** with *P*-chlorophosphaalkenes are a valuable route to compounds **28a**,**b** with a diphosphadiene system (92−93% yield)[24] (Scheme 14).

The transition metal functionalized phosphaalkenes **29a−e** were obtained as crystalline products from the condensation of *P*-silylphosphaalkenes with $[(\eta^5\text{-}C_5Me_5)(CO)_2FeBr]$ and $[(\eta^5\text{-}C_5Me_5)(CO)_2RuBr]$[16,25] (Scheme 15).

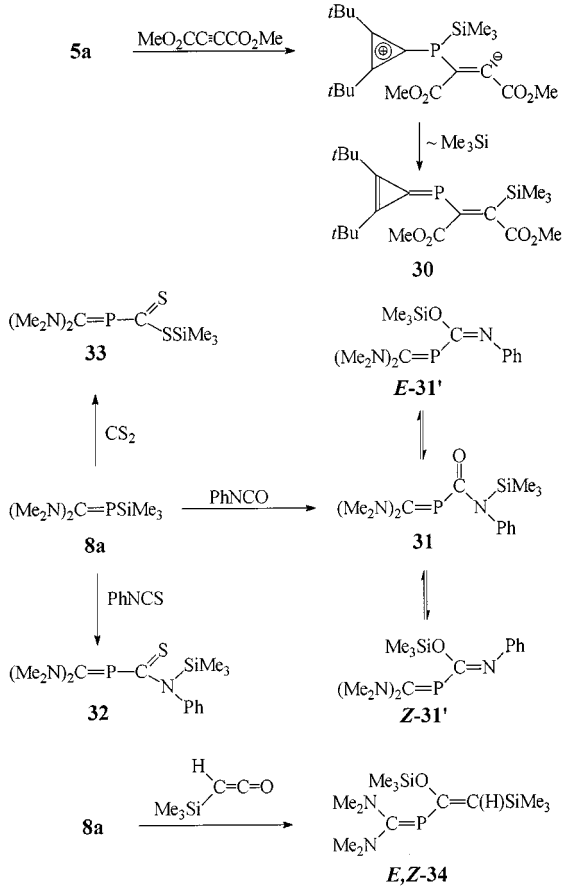


29	M	R1	R2
a	Fe	NMe_2	Me
b	Fe	NEt_2	Et
c	Fe	Ph	Me
d	Fe	*t*Bu	Me
e	Ru	NMe_2	Me

Scheme 15. Synthesis of metallophosphaalkenes **29a−e**

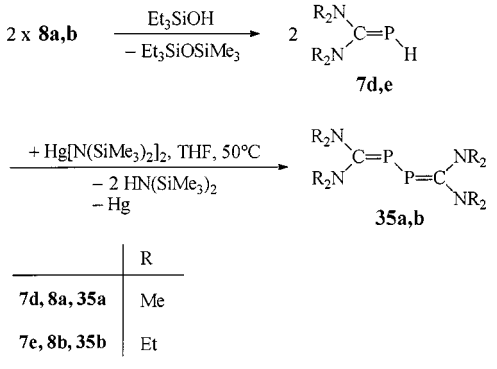
The P−Si bond of **5a** and **8a**,**b** tends to undergo 1,2 addition to the multiple bonds in alkynes and heterocumulenes

to yield compounds **30**–**34** as yellow to red crystalline solids[4,21,26] (Scheme 16).



Scheme 16. Reaction of **5a** and **8a** with $MeO_2C-C{\equiv}C-CO_2Me$ and heterocumulenes

Triethylsilanol selectively cleaved the P–Si bond in *P*-silylphosphaalkenes **8a**,**b** without affecting the P=C bond. This transformation constitutes a convenient method for the preparation of **7d** and **7e**,[27] which can be further transformed into the yellow liquid 2,3-diphosphabutadienes **35a**,**b** by treatment with $Hg[N(SiMe_3)_2]_2$ (Scheme 17).[28]

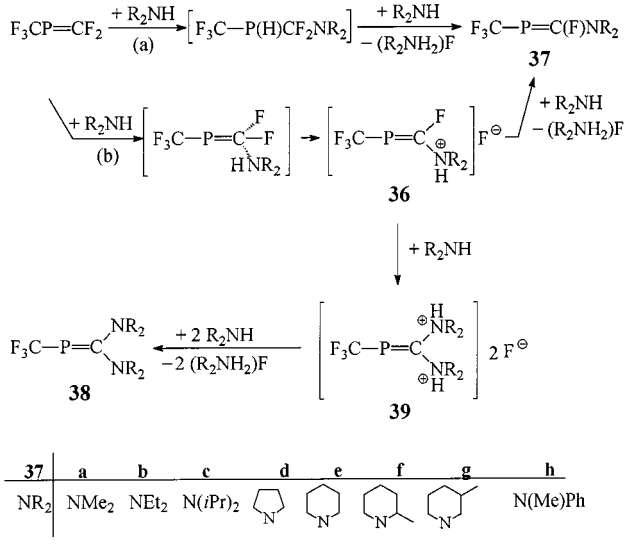


Scheme 17. Preparation of 2,3-diphosphabutadienes from **7d**,**e**

It is also possible to synthesize *C*-amino-functionalized phosphaalkenes by replacement of a fluorine substituent in phosphaalkenes such as $F_3CP{=}CF_2$ or $HP{=}CF_2$.

Perfluoro-2-phosphapropene reacted quantitatively with secondary amines in the molar ratio 1:2 at low temperature to yield the (*Z*)-configured phosphaalkenes $F_3CP{=}C(F)NR_2$ **37a**–**h**.[5]

Two possible mechanisms were discussed in rationalizing this result. In path (a) the addition of the NH function to the P=C bond was rapidly followed by the base-assisted 1,2-elimination of HF. In route (b) one molar equivalent of amine was added to the positively polarized carbon atom of the P=C bond prior to fluoride extrusion to give intermediate **36**, which was subsequently deprotonated by a second equivalent of amine (Scheme 18). During the course of this reaction small amounts of the disubstituted products $F_3CP{=}C(NR_2)_2$ (**38**) were also generated, which was explained by a second competing fluoride displacement from intermediate **36** by amine and a twofold deprotonation of the resulting dication **39**.



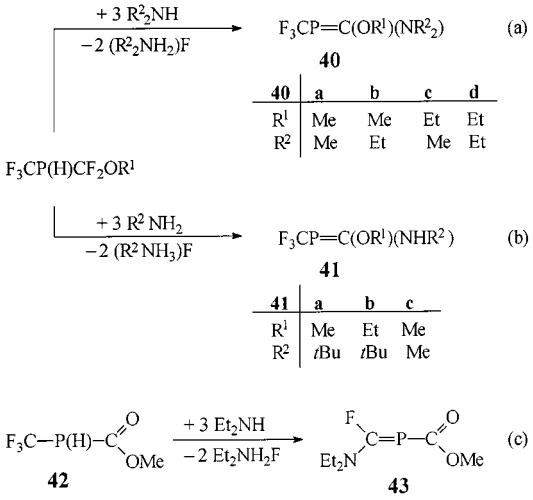
Scheme 18. Preparation of $F_3CP{=}C(F)NR_2$ and $F_3CP{=}C(NR_2)_2$ from $F_3C-P{=}CF_2$

Alternatively, the monoamino products **37** were accessible by treatment of bis(trifluoromethyl)phosphane with the secondary amine in a molar ratio of 1:3 at −40 °C via transient $F_3CP{=}CF_2$. This approach has the advantages of a one-pot reaction and the easy availability of the precursor $(CF_3)_2PH$.[5]

This synthetic principle was extended to the preparation of the yellow liquid phosphaalkenes $HP{=}C(F)NR_2$ [R = Me (**a**), Et (**b**), *i*Pr (**c**)] by the utilization of CF_3PH_2 as a starting material.[29]

Similarly, compounds $F_3CP{=}C(F)(OR^1)$ were subjected to reaction with secondary amines to yield the stable inversely polarized phosphaalkenes $F_3CP{=}C(NR^2_2)(OR^1)$ (**40a**–**d**).[6] Again it was advantageous to generate the phosphaalkene precursors $F_3CP{=}C(F)(OR^1)$ in situ from PH-functionalized phosphanes $F_3CP(H)CF_2OR^1$ by amine-induced HF elimination[6] [Scheme 19 (a)].

The employment of primary amines gave rise to the thermolabile compounds **41a**–**c**, which in CH_2Cl_2 solution at 20 °C completely decomposed within a few hours[30] [Scheme 19, (b)].



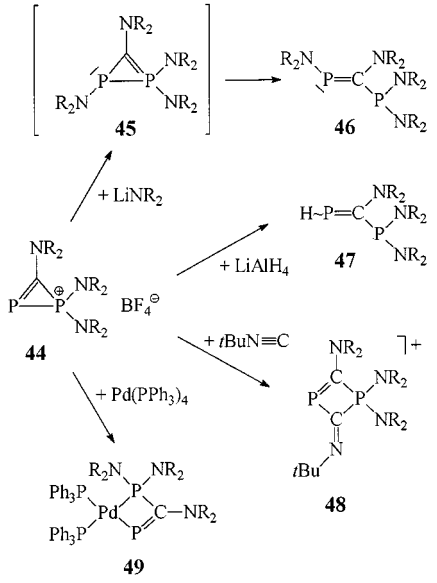
Scheme 19. Preparation of $F_3CP{=}C(OR^1)(NR^2_2)$, $F_3CP{=}C(OR^1)(NHR^2)$ and **43**

The very interesting *P*-methoxycarbonyl-functionalized phosphaalkene **43** resulted as a final product from the combination of phosphane **42** with an excess of diethylamine at −40 °C by a sequence of elimination and addition steps [Scheme 19, (c)].

The product was isolated as a yellow thermally stable oil in 65% yield.[30]

2.5. Miscellaneous

Ring opening reactions occurred when the readily available diphosphirenium salt **44** was treated with nucleophiles. After combination of a THF solution of **44** with a stoichiometric amount of lithium diisopropylamide at −78 °C, phosphaalkene **46** was isolated in 85% yield. The formation of **46** was explained by the nucleophilic attack of the lithium salt at the dicoordinate phosphorus atom of **44**, leading to a transient $\lambda^3\sigma^3,\lambda^5\sigma^4$-diphosphirene **45**, which was stabilized by ring opening[31] (Scheme 20). In a similar manner, addition of one equivalent of lithium aluminium hydride to a THF solution of **44** afforded the corresponding *P*-hydrophosphaalkene **47** as a 50:50 mixture of (*Z*) and (*E*) isomers.[32] Ring expansion of **44** was achieved by the addition of *tert*-butyl isocyanide[31] or $Pd(PPh_3)_4$[32c] to the cation. In both cases diphosphacyclobutenes with the structural features of inversely polarized phosphaalkenes were obtained.

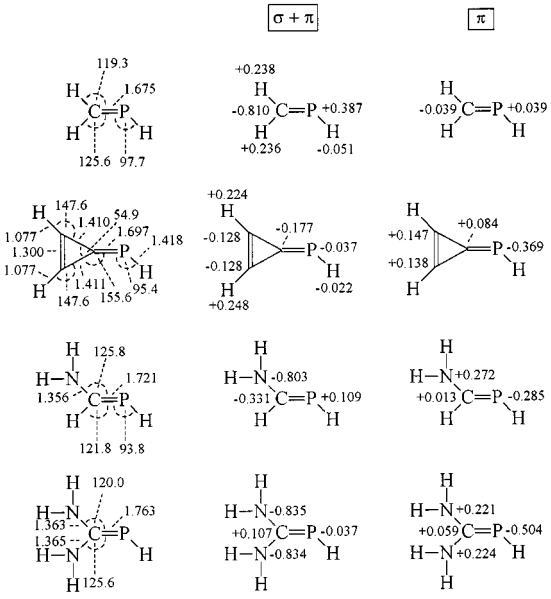


Scheme 20. Nucleophilic ring opening and ring expansion of **44**

3. Structure and Bonding

3.1. Theoretical Studies

Quantum chemical calculations were performed on the parent methylenephosphane and its amino-substituted derivatives (B3LYP/6-31g* level)[33] to substantiate the presence of an inverse π-electron density in the molecules (Scheme 21). The parent compound $HP{=}CH_2$ has a σ+π NBO charge of +0.387 e at the phosphorus and of −0.810 e at the carbon atom, whereas its P−C π-bond is essentially nonpolar (+0.030 e at P; −0.039 e at C). This agrees well with previous ab initio calculations based on Mulliken charges and a different basis set.[34a] By comparison, in the cyclopropylidenephosphane a σ+π Mulliken charge of −0.037 e at the phosphorus and of −0.177 e at the carbon atom of the exocyclic double bond were calculated (at the RHF approximation utilizing an ab initio wavefunction with a double-zeta basis set).[4] Here the P−C π-bond is clearly polarized towards the phosphorus atom as the negative end of the dipole with an excess of 0.369 e at the P atom and a deficiency of 0.084 electron at the C atom. The positive charge is stabilized by incorporation into the Hückel aromatic cyclopropenium unit. Quantum chemical calculations on the *C*-amino-substituted phosphaalkenes (B3LYP/6-31g*) predict a strong polarization of the π-bond. Only one, and to a greater extent, two amino



Scheme 21. Geometric parameters and charge distribution of $HP{=}CH_2$, cyclopropylidenephosphane, $HP{=}C(NH_2)H$ and $HP{=}C(NH_2)_2$

groups at the carbon atom induce an inverse electron density distribution at the π-bond, the charge at the phosphorus is increased in comparison to parent methylenephosphane. Alternatively, an amino group at the phosphorus atom has an opposite effect; it enhances the π-electron density at the methylene carbon atom. One may note that polarization of the P−C π-bond by amino substituents had been proposed some time ago.[34b] The quantum chemical investigations are based on the results of C_s symmetry imposed structures.[33] The calculations reveal that this holds true for the monoamino-substituted derivatives but for the *C*,*C*-diamino-substituted methylenephosphane, weak pyramidalization at the nitrogen atoms is predicted which causes a structural relaxation by 2.5 kcal/mol. However, the principal result of polarization of the P−C π-bond by the amino groups is retained.

Rotation of the amino groups lifts the π-conjugation ability of the amino group and causes a shrinking of the P−C bond. In other words the bonding features resemble more closely those of the parent methylenephosphane. Actually, the following structural parameters were obtained for the geometries with one orthogonal amino group (B3LYP/6-31g*) level:[34c] *cis*-(*trans*-)*C*-aminomethylenephosphane, P−C = 1.686 (1.686), C−N = 1.439 (1.441) Å.

3.2. Molecular Structures

Elongation of the P=C bond is the most noticeable structural change that classical phosphaalkenes undergo on replacement of one or two organic substituents at the tricoordinate carbon atom of the P=C double bond by one or two functionalities which are capable of π-donation. The P=C double bond length in nonconjugated phosphaalkenes ranges from 1.65−1.67 Å[2] whereas in *C*-amino-functionalized phosphaalkenes P−C distances of 1.70−1.76 Å are frequently measured[8] as is illustrated in **29a** [1.709(5) Å],[25] **29c** [1.717(4) Å] [Figure 1, (c)],[16] **7d** [1.740(1) Å],[5b] and **37a** [1.744(2) Å][21] [Figure 1, (a)]. A prerequisite for this bond lengthening is an effective π-interaction with (nearly) coplanar dialkylamino groups. In keeping with this, the atomic distances between the trigonal planar carbon atom and the nitrogen atoms are significantly shorter than the standard value for the C(sp^2)−N(sp^2) single bond (1.45 Å). Compound **29d**[16] represents a good example where, presumably for steric reasons, such a heteroallylic π-electron delocalization does not occur [Figure 1, (d)]. Here the P=C bond length of 1.697(3) Å is smaller and resembles that of the "classical" phosphaalkenes (η^5-C_5Me_5)$(CO)_2$Fe−P=C($SiMe_3$)Ph [1.665(6) Å][16] and (η^5-C_5Me_5)$(CO)_2$FeP=C($SiMe_3$)$_2$ [1.680(9) Å].[35] The atomic distance between the planar atom C(13) and the slightly pyramidalized nitrogen atom N(1) of 1.448(4) Å is clearly that of a single bond. The ferriophosphaalkenes with an inverse π-electron density about the P=C bond **29a** and **29c** feature significantly longer Fe−P bonds [2.325(2) and 2.316(1) Å] than **29d** [2.276(1) Å]. The latter value compares well with that of (η^5-C_5Me_5)$(CO)_2$FeP=C($SiMe_3$)$_2$ [2.269(2) Å] or (η^5-

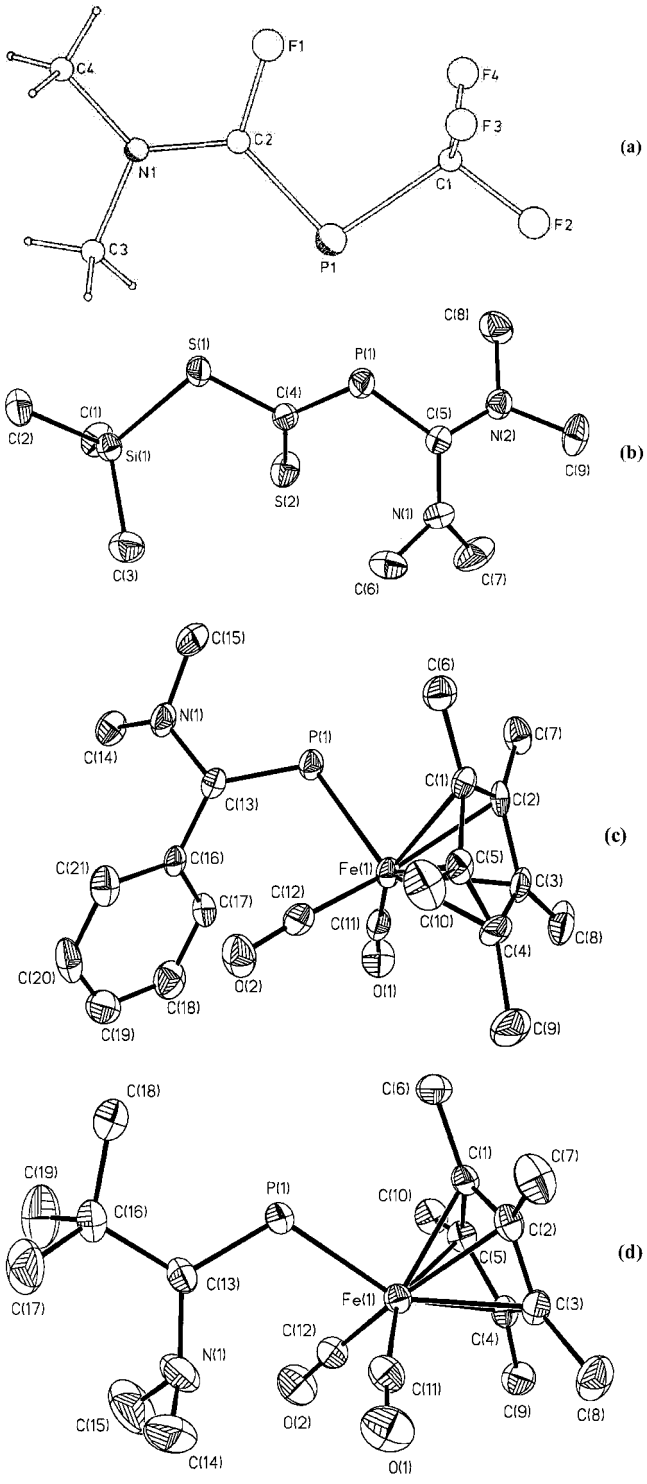


Figure 1. Molecular structures in the crystal of the phosphaalkenes **37a**, **33**, **29c**, and **29d**; selected bond lengths [Å] and angles [°]: (a) **37a**: P(1)−C(1) 1.862(2), P(1)−C(2) 1.744(2), C(2)−N(1) 1.311(2), C(1)−P(1)−C(2) 97.0(1), ΣN(1) 359.3(1); (b) **33**: P(1)−C(4) 1.748(2), P(1)−C(5) 1.826(2), C(4)−S(1) 1.801(2), C(4)−S(2) 1.673(2), C(5)−N(1) 1.341(2), C(5)−N(2) 1.338(2), N(1)−C(6) 1.458(2), C(4)−P(1)−C(5) 101.89(7), ΣN(1) 358.81(15), ΣN(2) 359.18(14); (c) **29c**: P(1)−C(13) 1.717(4), P(1)−Fe(1) 2.316(1), C(13)−N(1) 1.399(4), N(1)−C(14) 1.452(5), Fe(1)−P(1)−C(13) 118.9(1), ΣN(1) 352.6(3); (d) **29d**: P(1)−C(13) 1.697(3), Fe(1)−P(1) 2.276(1), C(13)−N(1) 1.448(4), N(1)−C(14) 1.447(5), Fe(1)−P(1)−C(13) 117.0(1), ΣN(1) 348.2(3)

$C_5Me_5)(CO)_2FeP{=}C(SiMe_3)_2$ [2.256(2) Å]. The bond lengthening in **29a** and **29c** presumably results from an electronic repulsion between the electron-rich iron atom and the negatively polarized P atom of the P=C bond. In the light of these observations the ferriophosphaalkenes **29a** and **29c** have to be considered as inversely polarized phosphaalkenes, whereas compound **29d** displays the characteristics of a normally polarized P=C bond. The molecular structure of **33** is particularly interesting [Figure 1, (b)]. Here a dithiocarboxy function successfully competes for the negative charge accumulated at the P atom of an inversely polarized phosphaalkene. Charge delocalization into the C−S double bond is evident by the bond shortening of P(1)−C(4) to 1.748(2) Å and concomitant elongation of the C=S bond to 1.673(2) Å. By comparison, a P−C single bond and a localized C=S double bond show bond lengths of 1.85 and 1.62 Å, respectively. Consistent with this, the former P−C double bond P(1)−C(5) is lengthened to 1.826(2) Å and the nearly planar nitrogen atoms N(1) and N(2) provide multiple bonding to carbon atom C(5) [N(1)−C(5) = 1.341(2) Å, N(2)−C(5) = 1.338(2) Å]. The bond angles at the P atom in **37a** [97.0(1)°], **7d** [103(1)°], and **33** [101.89(7)°] are comparable to that of the parent molecule $HP{=}CH_2$ (97.4°),[36] whereas steric congestion in **29a**, **29b**, and **29d** accounts for the more obtuse angle of ca. 118°. Thus, the valence angle at the P atom of phosphaalkenes does not reflect the polarity of the P=C π-bond.

3.3. Spectra

3.3.1. NMR Spectra

The characteristic ^{31}P and ^{13}C NMR shifts for selected compounds are summarized in Table 1. Generally, the ^{31}P NMR chemical shifts of phosphaalkenes vary in the wide range between δ = −99.9 for (*Z*)-H−P=C(F)NMe_2[29] and δ = 740.5 in the nickel complex [Cp*(PEt_3)Ni−P=$C(SiMe_3)_2$].[37] The ^{31}P NMR data of compounds containing low-coordinate phosphorus are compiled in several reviews.[2d,38,39] In spite of the large problems associated with the theoretical collation and interpretation of these large differences in shift, which generally occur for compounds containing two-coordinate phosphorus, some trends can be discerned for phosphaalkenes in general and for such representatives with an inverse π-electron density in particular. Basically, there are two major contributions to the ^{31}P chemical shift, namely a diamagnetic contribution reflecting the electron density associated with the low-coordinate P atom and another contribution, which is determined by the HOMO−LUMO gap of the molecule. Small HOMO−LUMO gaps in *P*-metallophosphaalkenes such as the aforementioned nickel compound or the complex [Cp*$(CO)_2FeP{=}C(SiMe_3)_2$] (δ = 641.5)[37] give rise to significant low-field shifts. The large valence angle at phosphorus [126.2(6)°] in the iron complex indicates that the energy of the nonbonding orbital as the HOMO is raised by sp^2-hy-

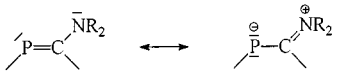
Table 1. ^{13}C and ^{31}P NMR spectroscopic data of selected phosphaalkenes with an inverse π-electron distribution

Compound		$\delta^{31}P$	$^1J_{P,H}$/Hz	$\delta^{13}C$	$^1J_{P,C}$/Hz	Ref.
(*E*)−Mes−P=C(H)NMe_2	**2a**	58.8		187.4	49.0	[11]
(*E*)−*t*Bu−P=C(H)NMe_2	**2c**	119.0		187.5	48.0	[11]
$Me_3Si-P=C^a-C^b(tBu){=}C^c(tBu)(C^a-C^c)$	**5a**	−74.1		174.6	102.5	[4b]
$Mes-P=C^a-C^b(tBu){=}C^c(tBu)(C^a-C^c)$	**5b**	−23.2		163.7	85.6	[4b]
Ph−P=$C(NMe_2)_2$	**7b**	28.4		198.8	67.1	[10]
*t*Bu−P=$C(NMe_2)_2$	**7c**	91.9		199.0	72.7	[7]
H−P=$C(NMe_2)_2$	**7d**	−62.6	158.7	207.5	70.6	[7]
$Me_3Si-P=C(NMe_2)_2$	**8a**	−47.1		204.0	85.0	[9b]
$Ph_3Si-P=C(NMe_2)_2$	**24a**	−85.1				[23]
[Cp*$(CO)_2Fe-P=C(NMe_2)_2$]	**29a**	135.5		202.4	97.0	[25]
(*E*)−$Me_3SiP{=}C(Ph)NMe_2$	**14a**	54.3		204.7	65.2	[16]
(*Z*)−$Me_3SiP{=}C(tBu)NMe_2$	**14b**	68.7		219.7	94.1	[16]
(*E*)−Ph−P=C(Ph)N(Ph)$SiMe_3$	(*E*)-**16a**	144		205	50	[17]
(*Z*)−Ph−P=C(Ph)N(Ph)$SiMe_3$	(*Z*)-**16a**	225		193	47	[17]
$Ph-P^a{=}C^a-N(SiMe_3)C(OSiMe_3)(Ph)P^bPh(C^a-P^b)$	**18**	112.7		197.3	60.6	[18]
$PhP{=}C^aN^a(Me)C(Me){=}C(Me)N^b(Me)(C^a-N^b)$	**20a**	−53.5		169	97.6	[19]
$tBuC(O)-P=C^a-C^b(tBu){=}C^c(tBu)(C^a-C^c)$	**21c**	9.7		174.7	89.2	[4b]
$Tp'(CO)_2Mo{\equiv}C-P=C(NMe_2)_2$	**23a**	62.3		202.7	89.0	[22]
$(Me_3Si)_2C^2{=}P^2-P^1{=}C^1(NMe_2)_2$	**27a**	P^1: 99.7 P^2: 455.4[a]		C^1: 201.2 C^2: 172.0	86.8 87.7	[24]
[(*E*)-Cp*$(CO)_2Fe-P=C(Ph)NMe_2$]	**29c**	232.0		199.8	84.3	[16]
[(*Z*)-Cp*$(CO)_2Fe-P=C(tBu)NMe_2$]	**29d**	409.0		217.3	75.3	[16]
$(Me_2N)_2C=P-C(S)N(Ph)SiMe_3$	**32**	82.8		198.1	72.1	[21]
$(Me_2N)_2C=P-C(S)SSiMe_3$	**33**	145		193.7	87.2	[21]
$F_3C-P=C(F)NMe_2$	**37a**	−9.0		200.5	94.0	[5]
(*E,Z*)−H~P=C(F)NMe_2	(*E,Z*)-**39a**	(*E*): −99.0 (*Z*): −99.9	166.0 178.0	200.6 199.6	65.1 87.7	[29]
(*Z*)−$F_3C-P=C(OMe)NMe_2$	**40a**	17.3		205.8	77.3	[6]
$MeO_2C-P=C(F)NMe_2$	**43**	−23.4		198.7	100.8	[30]

[a] $J_{P1,P2}$ = 403 Hz.

bridization, whereas the energy of the LUMO, which is the π* orbital, remains roughly unaffected. The electronic nature of the substituent at the phosphorus atom also markedly influences the chemical shift. In η^1-Cp*P=$C(SiMe_3)_2$[40] the valence angle at phosphorus was determined to be 118.7(2)°, which also agrees with sp^2-hybridization, but the ^{31}P NMR resonance appears at only δ = 370.6. The substituents at the C atom of the P=C bond in "normal" phosphaalkenes also determine the ^{31}P NMR chemical shift as evident in ClP=C(Ph)$SiMe_3$ (δ = 273) and ClP=$C(SiMe_3)_2$ (δ = 342).[2d]

In several amino- and bis(amino)-substituted representatives where π-conjugation of the nitrogen lone pair with the P=C double bond operates in addition to the paramagnetic contribution, a second component to the ^{31}P NMR shift has to be considered. As a consequence of the three-center four-π-electron system, the phosphorus atom β to the nitrogen atom experiences additional negative charge, which causes a pronounced high-field shift.



This is evident in compounds (*E*)-**16a** ($\delta^{31}P$ = 144) and (*Z*)-**16a** ($\delta^{31}P$ = 225), where presumably for steric reasons only the (*E*) isomer achieves the planar geometry required for a three-center four-electron arrangement in an inversely polarized phosphaalkene.[17]

The influence of the substituent at phosphorus on the ^{31}P chemical shift may be studied in molecules of the type X−P=$C(NMe_2)_2$. Here the compound with the highest degree of shielding at phosphorus is $Ph_3SiP=C(NMe_2)_2$ (δ = −85.1).[23] An increasing low-field shift as a function of X is observed as follows: **7d** (X = H; $\delta^{31}P$ = −62.6) > **8a** (Me_3Si; −47.1) > **23a** [Tp′$(CO)_2$Mo≡C; 62.3] > **7c** (*t*Bu; 91.9) > **29a** [Cp*$(CO)_2$Fe; 135.5]. Particularly interesting is the replacement of the hydrogen atom at phosphorus by functional groups, which are able to withdraw electron density from phosphorus by π-delocalization as observed in $MeO_2CP=C(F)NMe_2$ (**43**) ($\delta^{31}P$ = −23.4)[30] vs. (*E*,*Z*)-HP=$C(F)NMe_2$ (**39a**) ($\delta^{31}P$ = −90.0 and −99.9)[29] or in $(Me_2N)C=P-C(S)SSiMe_3$ (**32**) ($\delta^{31}P$ = 145)[21] vs. **7d**.

The introduction of a bulky and electron-releasing substituent at the phosphorus atom, such as the [Cp*$(CO)_2$Fe] group in **29a**, causes a strong low-field shift which may be due to the small HOMO−LUMO gap discussed above. Further deshielding was achieved by replacing one amino group by a phenyl ring in **29c** ($\delta^{31}P$ = 232.0), which is oriented orthogonally to the NCP four-π-electron unit. In contrast to (*E*)-**29c** in complex (*Z*)-**29d** a planar three-center four-electron arrangement is not possible for steric reasons, and consequently this compound behaves as a normal phosphaalkene with a low-field ^{31}P NMR signal at δ = 409.0.[16]

The ^{13}C NMR spectra of phosphaalkenes show characteristic doublets for the tricoordinate carbon atom of the P−C double bond at δ = 160−220. The cyclopropenylidenephosphanes are found at the lower range ranging from $\delta^{13}C$ = 163.7 (d, $^1J_{P,C}$ = 85.6 Hz) in **5b** to $\delta^{13}C$ = 178.5 (d, $^1J_{P,C}$ = 96.1 Hz) for $Cl_3C-C(O)-P=C^a-C^b(tBu)=C^c(tBu)$($C^a-C^c$) (**21o**). These values are quite typical for the cyclopropenylium system. In the cyclopropenium cation the corresponding resonances appear at δ = 176.8 whereas in the dipolar di-*tert*-butylcyclopropenone a chemical shift of δ = 159.4 was determined for the heteroatom-substituted ring carbon atom.[41] For the methylene carbon atoms of bis(amino)phosphaalkenes $XP=C(NMe_2)_2$ doublets were observed between δ = 197.0 (d, $^1J_{P,C}$ = 68.4 Hz) in **7a** (X = Mes)[10] and δ = 207.5 (d, $^1J_{P,C}$ = 70.6 Hz) in **7d** (X = H).[7] The signals of the monoamino-functionalized inverse phosphaalkenes $XP=C(R)NMe_2$ range from δ = 184.0 (d, $^1J_{P,C}$ = 54.5 Hz) for the P−C carbon atom in **2c** (X = *t*Bu; R = H) to δ = 219.7 (d, $^1J_{P,C}$ = 94.1 Hz) in **14b** (X = Me_3Si; R = *t*Bu).

3.3.2. IR Spectra

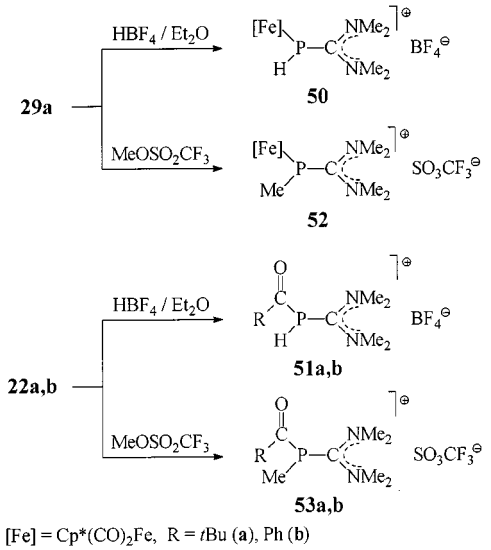
Valuable information about the polarity of the P=C bond in *P*-acylated phosphaalkenes is provided by IR spectroscopy. In *t*BuC(O)P=C$(OSiMe_3)$*t*Bu an intense band at $\tilde{\nu}$ = 1663 cm^{-1} was assigned to the IR stretching mode.[42] This value falls within the 1630−1690 cm^{-1} range usually encountered in acylphosphanes, where no electron delocalization from the phosphorus lone pair into the CO group is present. In the IR spectra of the inversely polarized phosphaalkenes **22a** and **22b**, strong bands at $\tilde{\nu}$ = 1563 and 1546 cm^{-1} respectively, indicate pronounced π-delocalization of electron density into the carbonyl group.[21] In $MeO_2C-P=C(F)NMe_2$ the ν(CO) vibration is observed at $\tilde{\nu}$ = 1685 cm^{-1} and thus at a lower wavenumber than in $MeO_2CP(H)CF_3$ [ν(CO) = 1738 cm^{-1}].[30] The CO frequencies of **21** are also bathochromically shifted (1590−1640 cm^{-1}) in comparison with monoacylated phosphanes.[4b]

4. Reactivity of Inversely Polarized Phosphaalkenes

4.1. Protonation

The ferriophosphaalkene **29a** was protonated at the P atom by ethereal HBF_4 (54%) in diethyl ether at −50 to 20 °C to afford the yellow salt **50** in high yield.[43] Similarly, the reaction of the *P*-acylphosphaalkenes **22a** and **22b** with equimolar amounts of ethereal HBF_4 at −50 °C led to the formation of the phosphanyl carbenium salts $[RC(O)P(H)C(NMe_2)_2]BF_4$ **51a** (R = *t*Bu) and **51b** (R = Ph)[33] (Scheme 22).

Upon protonation, the ^{31}P NMR signal of **29a** (δ = 135.5 in C_6D_6) was shifted upfield and appeared in **50** as a broad singlet at δ = −78.4. In the ^1H NMR spectrum of **50** a doublet at δ = 2.82 ($^1J_{P,H}$ = 205.0 Hz) was attributed to the PH functionality. Interestingly, protonation of the normally polarized phosphaalkene $Cp(CO)_3W-P=C(SiMe_3)_2$ ($\delta^{31}P$ = 505.2) to give $[Cp(CO)_3WP(H)C(SiMe_3)_2]^+$ ($\delta^{31}P$ = 187.0) resulted in even stronger shielding and a much larger PH coupling ($^1J_{P,H}$ = 367 Hz),[44] which agrees with a tri-



Scheme 22. Reaction of **22a**,**b** and **29a** with HBF_4 and $MeOSO_2CF_3$

gonal-planar P atom in this cation. By analogy with the structures of the alkylated products (vide infra) it is clear that the P atom in **50** has a trigonal-pyramidal geometry. In the ^{31}P NMR spectrum, the protonated products **51a**,**b** display doublets at $\delta = -53.7$ ($^1J_{P,H} = 245$ Hz) and $\delta = -46.6$ ($^1J_{P,H} = 257.7$ Hz) which are significantly shifted to high field with respect to the corresponding signals in **22a** ($\delta = 26.4$) and **22b** ($\delta = 31.3$). In the ^1H NMR spectrum a doublet at $\delta = 6.02$ ($^1J_{P,H} = 245$ Hz) (**51a**) and at $\delta = 6.23$ ($^1J_{P,H} = 257.7$ Hz) (**51b**) accounts for the PH unit.[34]

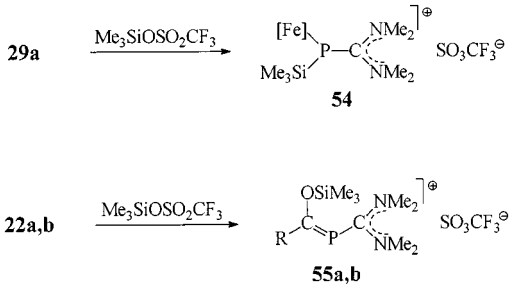
4.2. Alkylation

Alkylation of **29a** and **22a**,**b** was achieved by treatment with equimolar amounts of methyl trifluoromethanesulfonate (triflate) in diethyl ether at −60 °C. Compounds **52** and **53a**,**b** spontaneously precipitated and were isolated in good yield as orange or yellow powders[43,33] (Scheme 22).

Methylation at the phosphorus center of **22a**,**b** and **29a** was accompanied by marked shifts of the P NMR resonances to high field (**52**: $\delta = -26.4$ s; **53a**: −3.8 s; **53b**: −2.3 s). An X-ray structure analysis of the cation $[Cp^*(CO)_2FeAs(Me)C(NMe_2)_2]^+$ displayed a trigonal-pyramidal arsenic atom, analogously to **52**. From the analogous analytical and spectroscopic data it was inferred that **52** also contains a pyramidal pnicogen center.

4.3. Silylation

Reaction of **29a** with trimethylsilyl triflate in diethyl ether at −70 °C caused the precipitation of **54** as a yellow solid in 92% yield (Scheme 23). In the ^{31}P NMR spectrum of **54** a singlet was observed at $\delta = -78.4$. Here it seems appropriate to describe the cation as a η^1-complex of the phosphaalkene $Me_3SiP{=}C(NMe_2)_2$ (**8a**) ($\delta^{31}P = -47.1$) with the 16VE fragment $[(\eta^5\text{-}C_5Me_5)(CO)_2Fe]^+$. Coordination of **8a** caused a high field shift of its ^{31}P NMR signal, which in fact has been frequently encountered in the coordination chemistry of inversely polarized phosphaalkenes (vide infra).

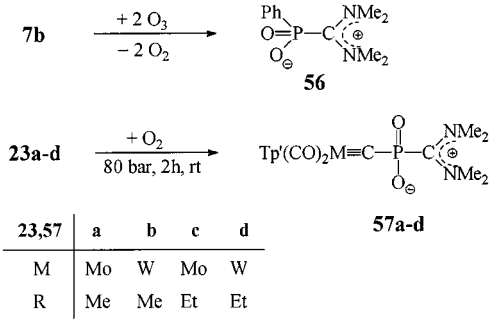


Scheme 23. Silylation of **22a**,**b** and **29a**

The silylation of **22a**,**b** with trimethylsilyl triflate in diethyl ether gave the extremely air- and moisture-sensitive salts **55a**,**b**. Here, in contrast to the protonation and methylation of **22a**,**b**, deshielding of the ^{31}P NMR resonances [$\delta = 109.2$ (**55a**) and $\delta = 101.0$ (**55b**)] was observed. This situation is best explained by an attack of the hard acid "Me_3Si" at the hard oxygen center of the carbonyl group with the generation of Si−O and P=C bonds. The products can be described as salts with unsymmetrical phosphaallyl cations or, alternatively, as phosphaalkenyl-functionalized carbocations.[45] Thus, the main spectroscopic evidence for an electrophilic attack at the P or O atom of *P*-acylphosphaalkenes with inverse electron density is from the direction in which the ^{31}P NMR resonances of the product are shifted.

4.4. Reaction with Chalcogens

Phosphaalkene **7b** reacted directly with ozone at ambient temperature with formation of the amidiniophosphinate **56** (Scheme 24). Compound **7b** always incorporates two atoms of oxygen. Intermediates in this process could not be detected. Product **56** appears to be inert towards excess O_3.[46]



23,57	a	b	c	d
M	Mo	W	Mo	W
R	Me	Me	Et	Et

Scheme 24. Oxidation of **7b** and **23a−d**

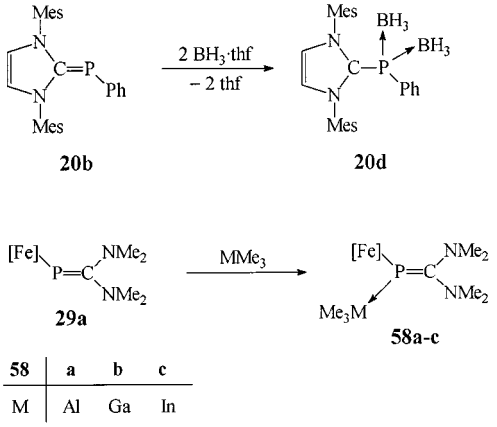
The related carbyne complex functionalized α-carbenium phosphinates **57** were obtained when crystalline samples of the complexes **23c** and **23d** (R = Et) were exposed to air for two weeks, whereupon a color change from deep red to orange-red occurred.

Similarly, compounds **23a** and **23b** (R = Me) were rapidly oxidized under O_2 pressure, whereas in air complete oxidation took about three weeks.[47]

4.5. Reaction with Group 13 Electrophiles

Treatment of carbene **20b** with $BH_3 \cdot THF$ in toluene resulted in exclusive formation of the bis(borane) adduct **20g**.[20b] The ^{31}P NMR signal is shifted from $\delta = -23.0$ to $\delta = 4$. The P−C bond in **20b** [1.763(6) Å] lengthens to 1.856(2) Å in the adduct.[20b]

Combination of **29a** with equimolar amounts of $AlMe_3$, $GaMe_3$, and $InMe_3$ in *n*-pentane in the temperature range −78 °C to 20 °C afforded the trimethylmetal adducts **58a−c** as air- and moisture-sensitive solids, whereas the phosphaalkene appeared to be inert towards $Al\textit{i}Pr_3$[48] (Scheme 25).



Scheme 25. Reaction of **20b** with $BH_3 \cdot THF$, and of **29a** with $AlMe_3$, $GaMe_3$ and $InMe_3$

The ^{31}P NMR spectra of the adducts **58a−c** are characterized by singlets at $\delta = -12.1$, 14.5, and 22.2, which are strongly deshielded with respect to **29a** ($\delta = 135.5$).

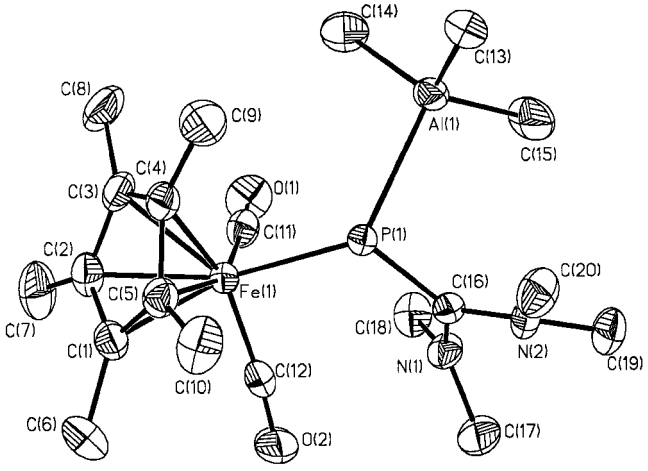
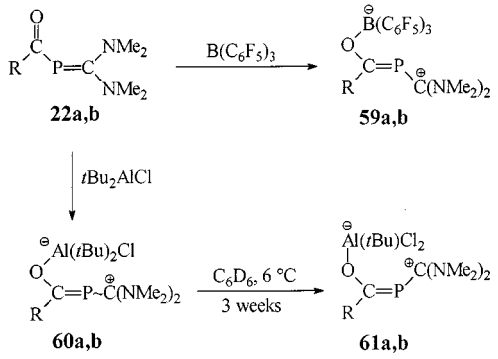


Figure 2. Molecular structure of **58a** in the crystal; selected bond lengths [Å] and angles [°]: Fe(1)−P(1) 2.317(1), Al(1)−P(1) 2.508(1), P(1)−C(16) 1.779(3), Fe(1)−P(1)−Al(1) 124.13(4), Al(1)−P(1)−C(16) 99.4(1), Fe(1)−P(1)−C(16) 116.5(1)

The X-ray structural analysis of **58a** (Figure 2) shows that coordination of **29a** to trimethylaluminium through the phosphorus lone pair results in significant distortion of the organophosphorus ligand. The P atom is now coordinated in a trigonal-pyramidal fashion (sum of angles 340.0°) and forms single bonds to the atoms Fe, Al, and C(16).

In comparison with **29a** the P−C bond is elongated from 1.709(5) to 1.779(3) Å. As in precursor **29a** the methylene carbon atom C(16) is trigonal planar.

In view of the electrophilic attack of Me_3Si at the carbonyl oxygen atom of **22a**,**b** we focused our interest on the reactivity of the phosphaalkene towards the hard Lewis acids $B(C_6F_5)_3$, $t\text{Bu}_2\text{AlCl}$, and $(AlMe_3)_2$. Combination of **22a** or **22b** with tris(pentafluorophenyl)borane in toluene solution at 20 °C gave the adducts **59a** and **59b** as yellow solids (Scheme 26). Low-field shifted singlets in the $^{31}P\{^1H\}$ NMR spectra at $\delta = 68.3$ (**59a**) ($\Delta\delta = 41.9$) and 72.6 (**59b**) ($\Delta\delta = 41.5$), and the absence of ν(C=O) bands in the IR spectra of the adducts agree with the phosphaalkenes attaching to the electron-deficient boron center via the oxygen atom.[34]



Scheme 26. Reaction of **22a**,**b** with $B(C_6F_5)_3$ and $t\text{Bu}_2\text{AlCl}$

The X-ray structural analysis of **59b** confirmed the presence of a tetracoordinate boron atom, which is linked to the carbonyl group via a B−O single bond of 1.506(3) Å (Figure 3). Delocalization of the negative charge into the C=O bond is clear by its elongation from 1.240(2) Å (as measured in **22b**)[49] to 1.315(3) Å, and by the bond length P(1)−C(1) of 1.735(2) Å, which is similar to the P=C bond length in $HP{=}C(NMe_2)_2$ (**7d**) [1.740(1) Å]. The PC(N) bond in **22b** [1.800(1) Å] is lengthened to 1.838(3) Å in **59b**. The very bulky $B(C_6F_5)_3$ moiety is directed towards the P atom of the P−C multiple bond, giving rise to torsion angles B(1)−O(1)−C(1)−P(1) and B(1)−O(1)−C(1)−C(41) of 2.5° and −179.4°, respectively.

Di-*tert*-butylaluminium chloride reacted smoothly with equimolar amounts of **22a** or **22b** in toluene at −30 C° to yield the adducts **60a**,**b** as extremely moisture-sensitive orange solids. Attempts to grow crystals of **60a** and **60b** from C_6D_6 solutions at 6 C over a period of 3 weeks led to the formation of crystals of the dismutation products **61a** and **61b** instead. The $^{31}P\{^1H\}$ NMR resonances of both adducts, which appeared at lower field (**60a**: $\delta = 72.9$ s; **60b**: $\delta = 78.2$ s) than in the precursors are diagnostic for the mode of coordination, and the presence of dative Al−O bonds in the products was inferred.

The X-ray structural analysis of the dismutation product **61b** showed a (*Z*)-configured phosphaalkene with a P=C double bond of 1.728(2) Å between the phosphorus atom and the carbonyl carbon atom. The carbonyl bond is lengthened to 1.309(2) Å. The trigonal-planar amino-sub-

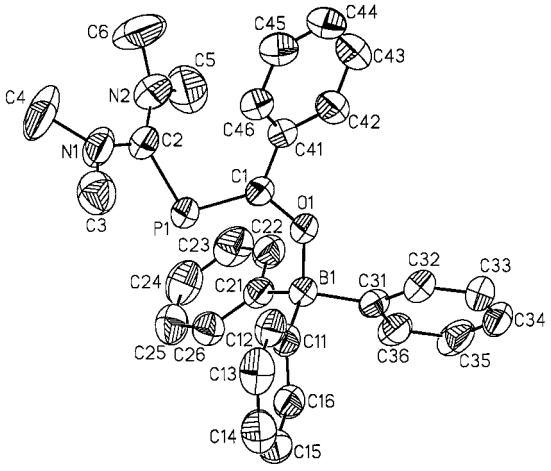
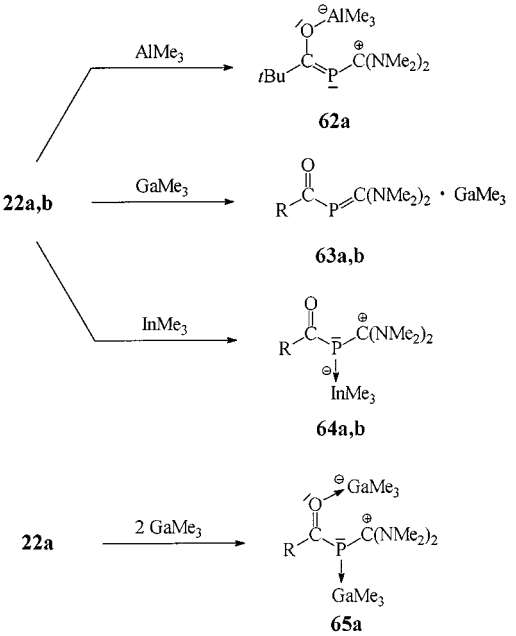


Figure 3. Molecular structure of **59b** in the crystal (fluorine atoms at the borane unit are omitted for clarity); selected bond lengths [Å] and angles [°]: P(1)−C(1) 1.735(2), P(1)−C(2) 1.838(3), O(1)−C(1) 1.315(3), O(1)−B(1) 1.506(3), C(1)−P(1)−C(2) 102.3(1), C(1)−O(1)−B(1) 130.2(2)

stituted carbon atom forms a single bond of 1.844(2) Å with the P atom.

Reaction of equimolar amounts of **22a** and trimethylaluminium in *n*-pentane yielded adduct **62a** as a pale yellow moisture-sensitive oil. The $^{31}P\{^1H\}$ NMR spectrum of the product displayed a singlet at $\delta = 62.7$, which is deshielded by $\Delta\delta = 36.3$ with respect to free **22a**. Thus, the aluminium atom is attached to the oxygen atom of the carbonyl group, as it is in the case of the adducts **60** and **61**.

Under analogous conditions one equivalent of trimethylgallium was added to **22a** and **22b** with formation of yellow **63a** and **63b**[34] (Scheme 27).



Scheme 27. Reaction of **22a**,**b** with $AlMe_3$, $GaMe_3$, and $InMe_3$

Broad singlets in the $^{31}P\{^1H\}$ NMR spectra at $\delta = 38.7$ (**63a**) or $\delta = 48.1$ (**63b**) did not allow for an unambiguous assignment of the structure, and crystals suitable for an X-ray study were not available. However, it was possible to grow yellow crystals of the 1:2 adduct **65a** from a concentrated mixture of **22a** and excess $GaMe_3$ in *n*-pentane at −30 °C. The NMR spectra of **65a** did not differ significantly from those determined for **63a**. All the three adducts **63a**,**b** and **65a** easily lose the ligated $GaMe_3$ in vacuo.

The crystal structure analysis of **65a** sheds some light in the nature of the 1:2 adduct (Figure 4). The backbone of the molecule is constituted by a *P*-acyl unit with a trigonal-pyramidal P atom (sum of angles 333.26°), which is connected to the atoms C(4), C(12), and Ga(2) via single bonds. The bond length P(1)−C(4) [1.784(3) Å] is shorter than P(1)−C(12) [1.831(3) Å]. The latter bond length was determined to be 1.800(1) Å in **22b**. A pronounced strengthening of the $P-C_{(CO)}$ bond, as observed in **59b** and **61b**, did not occur. The C−O bond length of the carbonyl group [1.249(3) Å] is similar to that of the *P*-acyl function in **2b** [1.240(2) Å]. Both $GaMe_3$ units are only weakly attached to the organophosphorus ligand as is evident from the long atomic distances Ga(2)−P [2.635(2) Å] and Ga(1)−O(1) [2.109(2) Å].

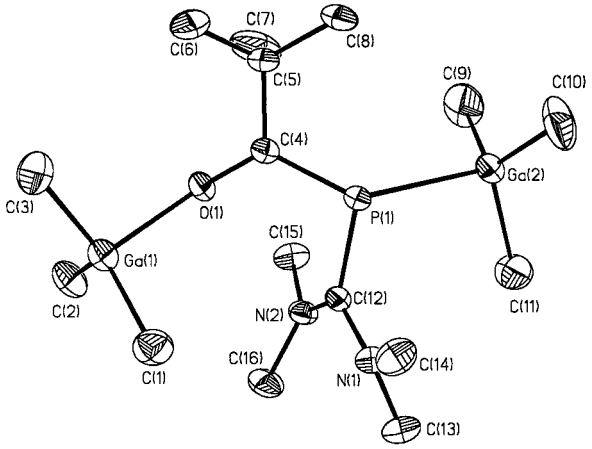


Figure 4. Molecular structure of **65a** in the crystal; selected bond lengths [Å] and angles [°]: P(1)−C(4) 1.784(3), P(1)−C(12) 1.831(3), P(1)−Ga(2) 2.635(2), O(1)−C(4) 1.249(3), O(1)−Ga(1) 2.109(2), C(4)−P(1)−C(12) 102.9(1), C(4)−P(1)−Ga(2) 127.7(1), Ga(2)−P(1)−C(12) 102.6(1)

The coordination chemistry of **22a** and **22b** towards the "soft" acid $InMe_3$ is more straightforward (Scheme 27). The adducts **64a** and **64b** display singlets in their $^{31}P\{^1H\}$ NMR spectra at $\delta = 15.6$ and 36.8. A high-field coordination shift of $\Delta\delta = 10.8$ for **64a**, and a low-field shift of $\Delta\delta = 5.5$ are consistent with In−P contact rather than with the alternative In−O ligation. In the IR spectrum of **64a** strong ν(CO) bands appear at $\tilde{\nu} = 1594$ and 1546 cm^{-1}, and in the spectrum of **64b** a ν(CO) band of medium intensity at 1540 cm^{-1} with a shoulder at 1597 cm^{-1} was observed.

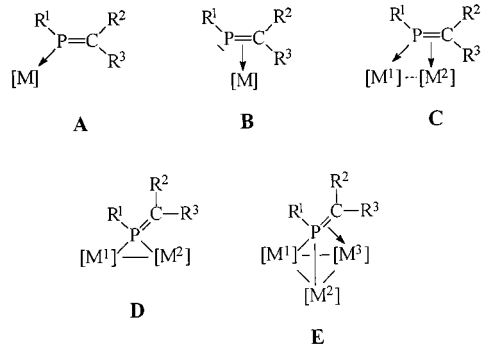
The X-ray structural analysis of **64a** features a *P*-acylphosphaalkene with a trigonal-pyramidal P atom, which is coordinated to the indium atom by a single bond of 2.774(4) Å.

The environment around the carbonyl carbon atom is trigonal-planar; a C=O double bond [1.238(10) Å] and a

single bond to the P atom [1.851(9) Å] clearly exclude π-conjugation of the carbonyl group with the lone pair on phosphorus in **64a**. The bond between the phosphorus atom and the amino-substituted carbon atom of 1.823(8) Å is elongated with respect to the precursor.[34]

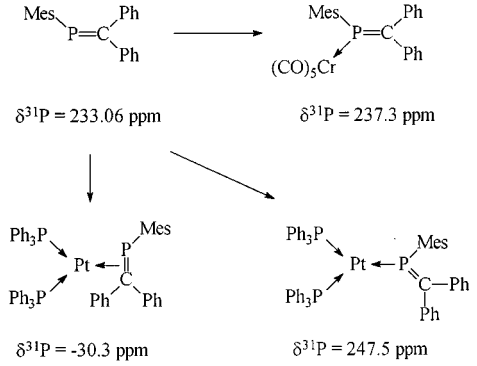
4.6. Transition Metal Complexes

Normally polarized phosphaalkenes are versatile ligands in transition metal coordination chemistry. At least five different fundamental modes of coordination of phosphaalkene ligands are known to date (Scheme 28).



Scheme 28. Modes of coordination in phosphaalkene complexes

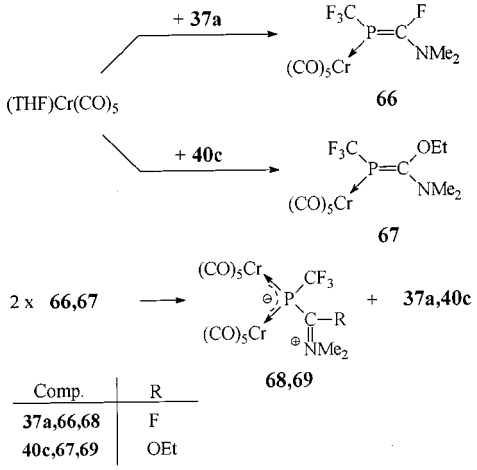
The most frequently observed types are η^1-coordination via the lone pair at phosphorus (**A**) and η^2-ligation **B**, which resembles that of alkenes in their transition metal π-complexes. In all of these complexes **A**−**E** the structural integrity of the phosphaalkene ligand is generally preserved. This particularly applies in case **A**. Here the P atom has a trigonal-planar geometry with a nearly unchanged P=C bond length with respect to the free ligand.[50] In η^2-complexes of the type **B** the P−C bond is usually elongated beyond 1.80 Å. While in η^1-complexes the ^{31}P NMR signals usually exert small coordination shifts (mostly to low field), in η^2-complexes strong high-field shifts are observed[50−52] (Scheme 29).



Scheme 29. Coordination shifts in phosphaalkene complexes

The coordination chemistry of inversely polarized phosphaalkenes is somewhat different. Pentacarbonylchromium complexes of the phosphaalkenes $CF_3P{=}C(F)NMe_2$ (**37a**)[5b] and $CF_3P{=}C(OEt)NMe_2$ (**40c**)[6] are available by treatment with equimolar amounts of $(THF)Cr(CO)_5$ in THF.

In organic solvents ($CDCl_3$, [D_8]toluene) complexes **66** and **67** were dismutated into to the binuclear complexes **68** and **69** and the free ligands **37** and **40c**, respectively (Scheme 30).

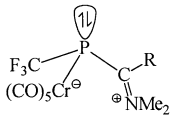


Scheme 30. Formation of the complexes **66**, **67**, **68**, and **69**

The coordination of **37a** ($\delta^{31}P = -9.0$) to one or two $[Cr(CO)_5]$ fragments via the phosphorus atom was accompanied by deshielding of the ^{31}P NMR signal to δ = 3.94 (**66**) and δ = 98.8 (**68**). On going from $CF_3P{=}C(OEt)NMe_2$ to **67** and **69** the ^{31}P NMR resonance is shifted to δ = 13.4 (**67**) and δ = 89.9 (**69**).

The molecular structures of **66**[5b] and **68**[53] are particularly interesting (Figure 5). The P=C bond length is markedly elongated from 1.744(2) Å in **37a** to 1.805(3) Å in **66** and 1.859(5) Å in **68**.

Those atomic distances are close to the average value of 1.85 Å for a P−C single bond. At the same time, the C−N separation in **66** [1.288(3) Å] and **68** [1.278(6) Å] indicates multiple bonding. In contrast with the situation in $[(CO)_5Cr]$ complexes of normally polarized phosphaalkenes having trigonal-planar P atoms, a trigonal-pyramidal phosphorus atom is observed in **66** (sum of angles: 304.8°). These observations favor a zwitterionic description of the complexes and rationalize the binding of a second $[Cr(CO)_5]$ unit at the phosphorus center.



The transfer of negative charge onto the $[Cr(CO)_5]$ building block is also reflected in bathochromically shifted CO stretching bands [**66**: $\tilde{\nu}$ = 2055 w, 1985 w, 1940 vs, 1930 s, 1912 s cm^{-1}] relative to $[(CO)_5Cr\{P(Mes){=}CPh_2\}]$ [ν(CO) ($CHCl_3$): 2068, 1955 cm^{-1}].[50a] The mode of coordination in **68** is unprecedented. Reaction of ferriophosphaalkene **29a** with an excess of $[Ni(CO)_4]$ led to the tricarbonylnickel adduct **70**.[54] This process was accompanied by a strong high-field shift of the $^{31}P\{^1H\}$ NMR signals from δ = 135.5 in **29** to δ = 15.0. A similar observation was made during the preparation of complex **71** from **29a** and [(*Z*)-

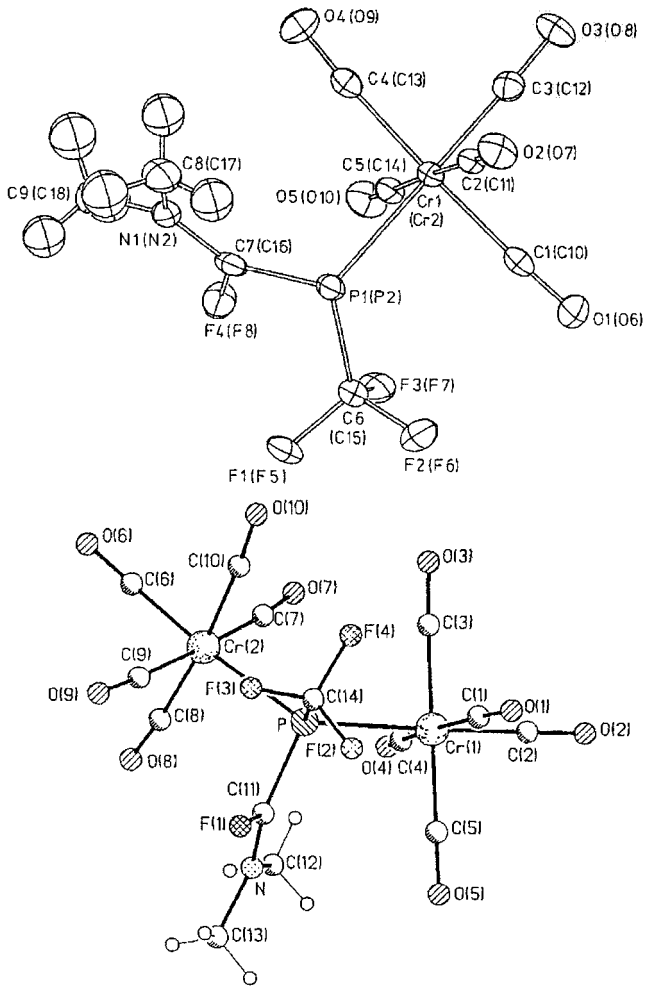
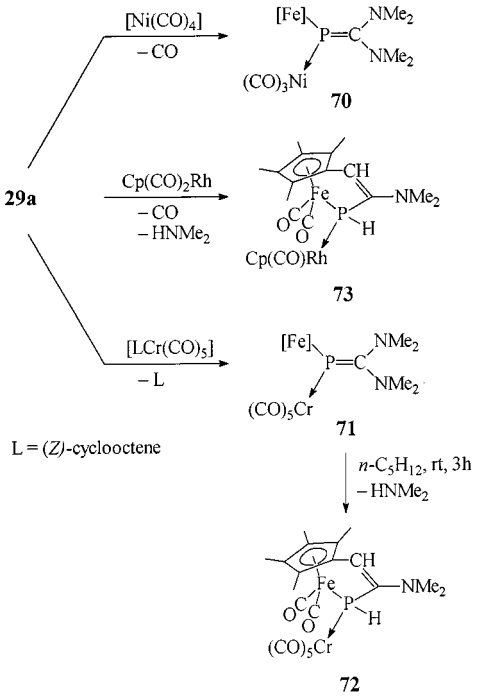


Figure 5. Molecular structures in the crystal of **66** (top) and **68** (bottom); selected bond lengths [Å] and angles[°]: **66**: Cr(1)−P(1) 2.454(1), P(1)−C(7) 1.805(1), N(1)−C(7) 1.288(3); Cr(1)−P(1)−C(6) 108.3(1), Cr(1)−P(1)−C(7) 102.4(1), C(6)−P(1)−C(7) 94.1(1); **68**: Cr(1)−P 2.459(2), Cr(2)−P 2.457(2), P−C(11) 1.859(5), C(11)−N 1.278(6); Cr(1)−P−Cr(2) 127.5(1)

cyclooctene]$Cr(CO)_5$ in *n*-pentane. The dark violet complex ($\delta^{31}P = -1.0$) was, however, not stable. Upon prolonged stirring of the slurry in *n*-pentane it underwent condensation to give **72** and free dimethylamine.[54] A condensation product analogous to **72** resulted from the treatment of **29a** with [η^5-$Cp(CO)_2Rh$][55] in *n*-pentane. No intermediates in this transformation could be detected (Scheme 31).

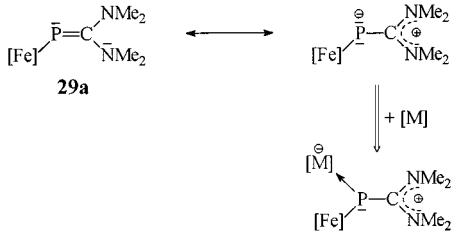
The formation of **72** and **73** is remarkable as one of the five methyl groups of the C_5Me_5 ligand behaves as a CH-acidic species which is involved in a Knoevenagel-type condensation. Usually Cp* ligands are ideal spectator ligands and insertions of metal atoms in one or more C−H bonds of methyl substituents are only observed with coordinatively and electronically unsaturated complexes.

The IR spectra of **70** and **71** display carbonyl stretching bands at remarkably low wavenumbers [e.g. **70**: ν(CO) = 2034, 1957, 1950 cm^{-1}] in comparison with [Mes*P=C=Ph_2]$Ni(CO)_3$ [ν(CO) = 2080, 2020, 1990 cm^{-1}],[56] indicating a considerable transfer of charge from the ligand onto the $[Ni(CO)_3]$ unit.



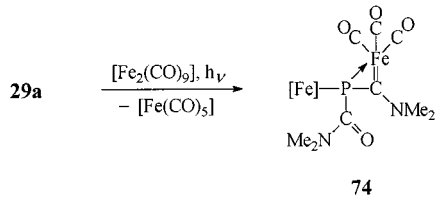
Scheme 31. Conversion of **29a** into the complexes **70**, **71**, **72**, and **73**

According to X-ray diffraction studies, the complexation of **29a** to an $[Ni(CO)_3]$ or $[Cr(CO)_5]$ fragment[57] leads to a severe distortion of the metallophosphaalkene skeleton (Scheme 32). Whereas the Fe(1)−P(1) distance in **70** and **71** [2.329(2) and 2.325(2) Å] remains nearly unaffected when compared with **29a** [Fe(1)−P(1) = 2.325(2) Å] the P−C bond in both complexes is significantly lengthened [**70**: 1.770(5); **71**: 1.793(5) Å. The P atoms have trigonal-pyramidal geometries with sum of angles of 335.9° (**70**) and 346.1° (**71**). In contrast to this, the carbon atom of the former P=C bond is trigonal-planar with relatively short C−N bonds [1.352(6) − 1.373(6) Å]. The electronic ground state of **29a** may be expressed by means of two canonical formulae, the which the zwitterionic form is obviously stabilized by coordination to metal fragments.



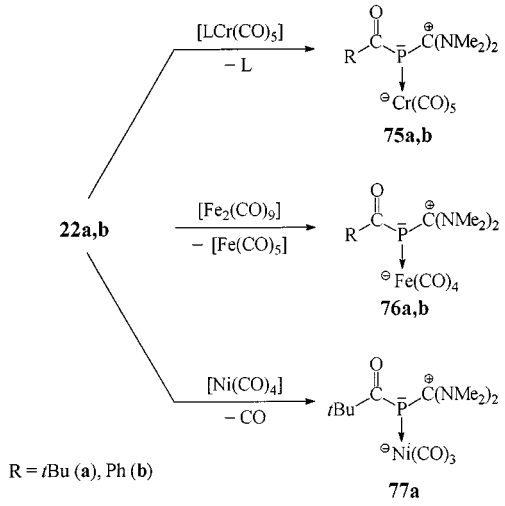
Scheme 32. Resonance structures of **29a** and its complexes

The photochemical reaction of **29a** with $[Fe_2(CO)_9]$ in *n*-pentane took a completely different course. Instead of the anticipated $[Fe(CO)_4]$ adduct, the phosphanylcarbene complex **74** was isolated as black crystals (Scheme 33).



Scheme 33. Formation of **74**

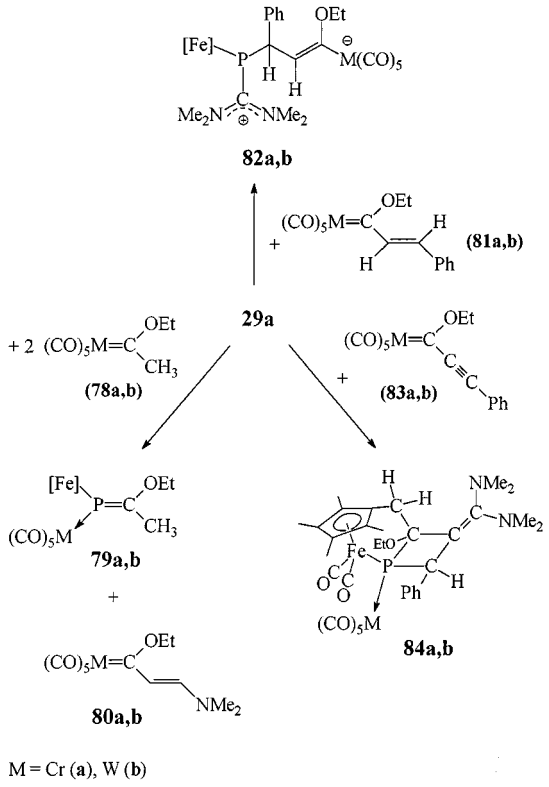
The reaction of **22a** and **22b** with carbonyl compounds of transition metals would be expected to lead to coordination compounds with metal−phosphorus bonds by the hard-soft acid-base concept (Scheme 34).



Scheme 34. Syntheses of complexes **75a**,**b**, **76a**,**b**, and **77a**

The high-field shifts of the $^{31}P\{^{1}H\}$ NMR singlets of complexes **75a**,**b**, **76a**,**b** and **77a**, in the range $\delta = -26.4$ to 1.9, agree with metal−phosphorus ligation. The X-ray structural analysis of **75a** unambiguously confirms coordination to $[Cr(CO)_5]$ of the trigonal-pyramidal phosphorus atom (sum of angles = 332.9°) with a P−Cr bond of 2.516(1) Å, which is at the upper end of P−Cr single bonds in low-valent carbonylchromium−phosphorus systems. The phosphorus−carbon distances [1.848(2) and 1.833(2) Å] are indicative of single bonds. Within the organophosphorus ligand, a localized C−O double bond of 1.225(2) Å was found.[34]

Having obtained some insight into the coordination behavior of inversely polarized phosphaalkenes toward trialkyl- and carbonylmetal compounds, the question of its reactivity towards Fischer carbene complexes became relevant. Compound **29a** was allowed to react with two molar equivalents of carbene complexes **78a** and **78b** in ether, forming the novel ferriophosphaalkene complexes **79a**,**b** and β-aminoalkenyl(ethoxy)carbene complexes **80a**,**b**[58] (Scheme 35).



Scheme 35. Reaction of **29a** with Fischer carbene complexes

The X-ray structural analysis of **79b** (Figure 6) shows an (*E*)-configured, classically polarized phosphaalkene, which is η^1-coordinated to the $[W(CO)_5]$ fragment via a remarkably long W−P bond [2.567(3) Å].[59] The P−C bond of 1.689(10) Å is typical for a P=C bond with an oxygen substituent, and the coordination geometry about P(1) and C(1) is trigonal planar. Interestingly the Fe(1)−P(1) dis-

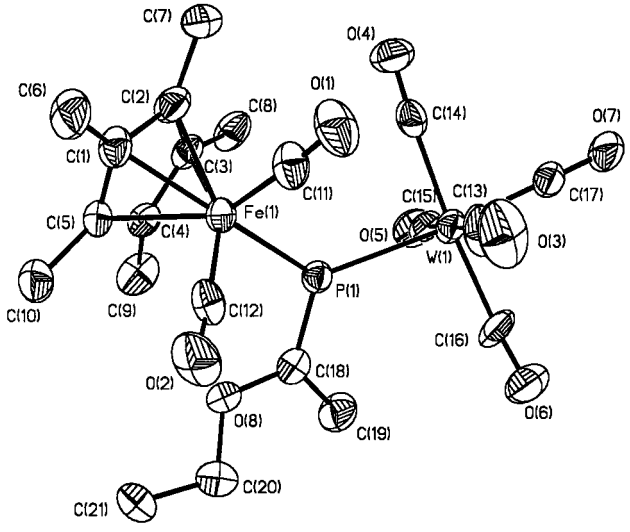


Figure 6. Molecular structure of **79b** in the crystal; selected bond lengths [Å] and angles [°]: W(1)−P(1) 2.567(3), Fe(1)−P(1) 2.262(3), P(1)−C(18) 1.689(10); Fe(1)−P(1)−C(18) 112.8(3)

tance of 2.262(3) Å is significantly shorter than in the carbonylmetal complexes of **29a**.

Combination of **29a** and the alkenylcarbene complexes **81a**,**b** in a mixture of *n*-pentane diethyl ether at −30 °C led to the precipitation of the orange zwitterionic Michael-type adducts **82a**,**b** (Scheme 35).

In sharp contrast to the synthesis of **79a**,**b** and **82a**,**b**, treatment of **29a** with an equimolar amount of the ethynyl(phenyl)carbene complexes **83a**,**b** in *n*-pentane at −60 °C afforded the yellow pentacarbonylmetal adducts **84a**,**b** of a 1-ferriophosphetane as the only tractable phosphorus-containing products (ca. 20% yield). (Scheme 35)

From the diversity of the product patterns the reactions of inversely polarized phosphaalkenes with carbene complexes display, it is clear that exploration of this fruitful area is only just beginning.

5. Conclusions and Perspectives

The "peculiarities" in the chemistry of *C*-amino-substituted phosphaalkenes, as discussed by Markovskii et al.[8] can be explained by their inverse distribution of π-electron density ($P^{\delta-}C^{\delta+}$) in comparison to the normal polarization ($C^{\delta-}P^{\delta+}$) in classical phosphaalkenes. Considering a growing body of evidence, the inverse π-electron density in a phosphaalkene may be detected from the following experimental features:

• The ^{31}P NMR signals of such molecules occur at unusually high field, whereas in normally polarized phosphaalkenes low-field ^{31}P NMR resonances are typical.

• These ^{31}P NMR signals may even be more shielded in transition metal complexes having inversely polarized η^1-phosphaalkene ligands. In η^1-complexes of normally polarized phosphaalkenes, coordination shifts to low field are usually observed.

• In η^1-complexes with inversely polarized phosphaalkene ligands, the phosphorus atom is pyramidal and the P−C bond is significantly elongated, in some cases attaining a bond order of unity, whereas in complexes with normally polarized phosphaalkenes the bond length between the trigonal planar atoms P and C is nearly unaffected upon coordination.

• The introduction of electron-withdrawing substituents at the P atom of inversely polarized phosphaalkenes results in delocalization of negative charge from the P−C unit into the substituent.

It is clear that classically and inversely polarized phosphaalkenes differ in their chemical reactivity. The latter are pronounced nucleophiles via their P atom and the systematic investigation of their synthetic potentials has just commenced. An interesting question still to be answered concerns Wittig-type reactivity of inversely polarized phosphaalkenes with organic carbonyl compounds. Little information is available on transformations with compounds which tend to liberate electron-sextet species, such as organic azides, diazoalkanes, carbenoid species etc.

The electronic situation present in inversely polarized phosphaalkenes should also be studied by electrochemical methods.

[1] T. E. Gier, *J. Am. Chem. Soc.* **1961**, *83*, 1769−1770.

[2] Reviews: [2a]*Multiple Bonds and Low Coordination in Phosphorus Chemistry* (Eds.: M. Regitz, O. J. Scherer), Thieme, Stuttgart **1990**. − [2b]R. Appel, F. Knoll, *Adv. Inorg. Chem.* **1989**, *33*, 259−361. − [2c]L. N. Markovskii, V. D. Romanenko, *Tetrahedron* **1989**, *45*, 6019−6090. − [2d]R. Appel, F. Knoll, I. Ruppert, *Angew. Chem.* **1981**, *93*, 771−784; *Angew. Chem. Int. Ed. Engl.* **1981**, *20*, 731.

[3] K. B. Dillon, F. Mathey, J. F. Nixon, *Phosphorus: The Carbon Copy*, Wiley, Chichester, **1998**.

[4] [4a]E. P. O. Fuchs, H. Heydt, M. Regitz, W. W. Schoeller, T. Busch, *Tetrahedron Lett.* **1989**, *30*, 5111−5114. − [4b]E. Fuchs, B. Breit, H. Heydt, W. Schoeller, T. Busch, C. Krüger, P. Betz, M. Regitz, *Chem. Ber.* **1991**, *124*, 2843−2855.

[5] [5a]J. Grobe, D. Le Van, J. Nientiedt, *Z. Naturforsch. Teil B* **1986**, *41b*, 149−161. − [5b]J. Grobe, D. Le Van, J. Nientiedt, B. Krebs, M. Dartmann, *Chem. Ber.* **1988**, *121*, 655−664.

[6] J. Grobe, D. Le Van, U. Althoff, B. Krebs, M. Dartmann, R. Gleiter, *Heteroatom Chem.* **1991**, *2*, 385−394.

[7] K. Issleib, E. Leißring, M. Riemer, *Z. Chem.* **1983**, *23*, 99−100.

[8] A. N. Chernega, A. V. Ruban, V. D. Romanenko, L. N. Markovskii, A. A. Korkin, M. Y. Antipin, Y. T. Struchkov, *Heteroatom Chem.* **1991**, *2*, 229−241.

[9] [9a]L. N. Markovskii, V. D. Romanenko, T. I. Pidvarko, *Zh. Obshch. Khim.* **1982**, *52*, 1925−1926; *Chem. Abstr.* **1982**, *97*, 216330h. − [9b]M. I. Povolotskii, V. V. Negrebetskii, V. D. Romanenko, V. I. Ivanchenko, T. V. Sarina, L. N. Markovskii, *Zh. Obshch. Khim.* **1990**, *60*, 2238−2244; *Chem. Abstr.* **1991**, *115*, 8934w.

[10] H. Oehme, E. Leißring, H. Meyer, *Z. Chem.* **1981**, *21*, 407−408 and references cited herein.

[11] G. Becker, W. Uhl, H.-J. Wessely, *Z. Anorg. Allg. Chem.* **1981**, *479*, 41−56.

[12] G. Becker, O. Mundt, *Z. Anorg. Allg. Chem.* **1980**, *462* 130−142.

[13] H. Oehme, E. Leissring, H. Meyer, *Tetrahedron Lett.* **1980**, *21*, 1141−1144.

[14] J. Navech, J. P. Majoral, R. Kraemer, *Tetrahedron Lett.* **1983**, *24*, 5885−5886.

[15] L. Weber, O. Kaminski, *Synthesis* **1995**, 158.

[16] L. Weber, S. Kleinebekel, A. Rühlicke, H.-G. Stammler, B. Neumann, *Eur. J. Inorg. Chem.* **2000**, 1185−1191.

[17] K. Issleib, H. Schmidt, H. Meyer, *J. Organomet. Chem.* **1978**, *160*, 47−57.

[18] R. Appel, M. Halstenberg, F. Knoch, H. Kunze, *Chem. Ber.* **1982**, *115*, 2371−2373.

[19] A. J. Arduengo III, H. V. R. Dias, J. C. Calabrese, *Chem. Lett.* **1997**, 143−144.

[20] [20a] A. J. Arduengo III, J. C. Calabrese, A. H. Cowley, H. V. R. Dias, J. R. Goerlich, W. J. Marshall, B. Riegel, *Inorg. Chem.* **1997**, *36*, 2151−2158. − [20b] A. J. Arduengo III, C. J. Carmalt, J. A. C. Clyburne, A. H. Cowley, R. Pyati, *Chem. Commun.* **1997**, 981−982.

[21] L. Weber, S. Uthmann, H. Bögge, A. Müller, H.-G. Stammler, B. Neumann, *Organometallics* **1998**, *17*, 3593−3598.

[22] L. Weber, G. Dembeck, R. Boese, D. Bläser, *Chem Ber./Recueil* **1997**, *130*, 1305−1308.

[23] L. N. Markovskii, V. D. Romanenko, T. V. Sarina-Pidvarko, M. I. Povolotskii, *Zh. Obshch. Khim.* **1985**, *55*, 221−222; *Chem. Abstr.* **1985**, *103*, 6462u.

[24] L. N. Markovskii, V. D. Romanenko, L. S. Kachkovskaya, M. I. Povolotskii, I. I. Patsanovskii, Yu. Z. Stepanova, E. A. Ismayeva, *Zh. Obshch. Khim.* **1987**, *57*, 901−907; *Chem. Abstr.* **1988**, *108*, 204691j.

[25] L. Weber, O. Kaminski, H.-G. Stammler, B. Neumann, V. D. Romanenko, *Z. Naturforsch., Teil B* **1993**, *48b*, 1784−1794.

[26] L. N. Markovskii, V. D. Romanenko, I. V. Pidvarko, *Zh. Obshch. Khim.* **1983**, *53*, 1672−1673; *Chem. Abstr.* **1983**, *99*, 195100g.

[27] V. D. Romanenko, T. V. Sarina, N. V. Kolotilo, L. N. Markov-

skii, *Zh. Obshch. Khim.* **1985**, *55*, 1188−1190; *Chem. Abstr.* **1986**, *104*, 5933g.
[28] V. D. Romanenko, L. S. Kachkovskaya, L. N. Markovskii, *Zh. Obshch. Khim.* **1985**, *55*, 2140−2141; *Chem. Abstr.* **1985**, *103*, 6424h.
[29] J. Grobe, D. Le Van, B. Lüth, M. Hegemann, *Chem. Ber.* **1990**, *123*, 2317−2320.
[30] J. Grobe, D. Le Van, G. Lange, *Z. Naturforsch., Teil B* **1983**, *48b*, 58−67.
[31] M. Soleilhavoup, A. Baceiredo, F. Dahan, G. Bertrand, *J. Chem. Soc., Chem. Commun.* **1994**, 337−338.
[32] [32a] D. Bourissou, Y. Canac, M. I. Collado, A. Baceiredo, G. Bertrand, *Chem. Commun.* **1997**, 2399−2400. − [32b] D. Bourissou, Y. Canac, H. Gornitzka, C. J. Marsden, A. Baceiredo, G. Bertrand, *Eur. J. Inorg. Chem.* **1999**, 1479−1488. − [32c] Y. Canac, M. Soleilhavoup, L. Ricard, A. Baceirdo, G. Bertrand, *Organometallics* **1995**, *14*, 3614−3616
[33] L. Weber, S. Uthmann, H.-G. Stammler, B. Neumann, W. W. Schoeller, R. Boese, D. Bläser, *Eur. J. Inorg. Chem.* **1999**, 2369−2381.
[34] [34a] W. W. Schoeller, *J. Chem. Soc., Chem. Commun.* **1985**, 334−335. − [34b] W. W. Schoeller, E. Niecke, *J. Chem. Soc., Chem. Commun.* **1982**, 569−570. − [34c] W. W. Schoeller, A. Rozhenko, unpublished results.
[35] D. Gudat, E. Niecke, A. M. Arif, A. H. Cowley, S. Quashie, *Organometallics* **1986**, *5*, 593−595.
[36] W. W. Schoeller, in ref.[2a], p. 5−32.
[37] E. Niecke, H.-J. Metternich, M. Nieger, D. Gudat, P. Wenderoth, W. Malisch, C. Hahner, W. Reich, *Chem. Ber.* **1993**, *126*, 1299−1309.
[38] [38a] S. Lochschmidt, A. Schmidpeter, *Phosphorus Sulfur* **1986**, *29*, 73−109. − [38b] K. Karaghiosoff, A. Schmidpeter, *Phosphorus Sulfur* **1988**, *36*, 217−259. − [38c] S. Karaghiosoff in ref.[2a], p. 463−471 and refs. cited therein.
[39] [39a] L. Weber, *Chem. Rev.* **1992**, *92*, 1839−1906. − [39b] L. Weber, *Angew. Chem.* **1996**, *108*, 292−310; *Angew. Chem. Int. Ed. Engl.* **1996**, *35*, 271−288.
[40] D. Gudat, E. Niecke, B. Krebs, M. Dartmann, *Chimia* **1985**, *39*, 277−279.
[41] H.-O. Kalinowski, S. Berger, S. Braun, *^{13}C NMR Spektroskopie*, p. 122 ff, Thieme, Stuttgart, **1984**.
[42] G. Becker, *Z. Anorg. Allg. Chem.* **1977**, *430*, 66−76.
[43] L. Weber, M. H. Scheffer, H. G. Stammler, B. Neumann, W. W. Schoeller, A. Sundermann, K. K. Laali, *Organometallics* **1999**, *18*, 4216−4221.
[44] D. Gudat, E. Niecke, W. Malisch, U. Hofmockel, S. Quashie, A. H. Cowley, A. M. Arif, B. Krebs, M. Dartmann, *J. Chem. Soc., Chem. Commun.* **1985**, 1687−1689.
[45] For symmetrical phosphaallyl cations see: [45a] Ref.[4b] and [45b] R. O. Day, A. Willhalm, J. M. Holmes, R. R. Holmes, A. Schmidpeter, *Angew. Chem.* **1985**, *97*, 775−777; *Angew. Chem. Int. Ed. Engl.* **1985**, *24*, 764.
[46] A. Schmidpeter, K.-H. Zirzow, A. Willhalm, J. M. Holmes, R. O. Day, R. R. Holmes, *Angew. Chem.* **1986**, *98*, 471−472; *Angew. Chem. Int. Ed. Engl.* **1986**, *25*, 457.
[47] L. Weber, G. Dembeck, H.-G. Stammler, B. Neumann, *Eur. J. Inorg. Chem.* **1998**, 579−582.
[48] L. Weber, M. H. Scheffer, H.-G. Stammler, A. Stammler, *Eur. J. Inorg. Chem.* **1999**, 1607−1611.
[49] L. Weber, S. Uthmann, H.-G. Stammler, B. Neumann, A. Stammler, unpublished results.
[50] [50a] T. C. Klebach, R. Lourens, F. Bickelhaupt, C. H. Stam, A. van Herk, *J. Organomet. Chem.* **1981**, *210*, 211−221. − [50a] Th. A. van der Knaap, F. Bickelhaupt, H. van der Poel, G. van Koten, C. H. Stam, *J. Am. Chem. Soc.* **1982**, *104*, 1756−1757.
[51] T. A. van der Knaap, L. W. Jenneskens, H. J. Meeuwissen, F. Bickelhaupt, D. Walther, E. Dinjus, E. Uhlig, A. L. Spek, *J. Organomet. Chem.* **1983**, *254*, C33−C36.
[52] T. A. van der Knaap, F. Bickelhaupt, J. G. Kraaykamp, G. van Koten, J. P. C. Bernards, H. T. Edzes, W. S. Veeman, E. de Boer, E. J. Baerends, *Organometallics* **1984**, *3*, 1804−1811.
[53] J. Grobe, D. Le Van, B. Krebs, R. Fröhlich, A. Schiemann, *J. Organomet. Chem.* **1990**, *380*, C29−C33.
[54] L. Weber, O. Kaminski, B. Quasdorff, H.-G. Stammler, B. Neumann, *J. Organomet. Chem.* **1997**, *529*, 329−341.
[55] L. Weber, M. H. Scheffer, H.-G. Stammler, B. Neumann, *Inorg. Chim. Acta* **1999**, *291*, 311−316.
[56] R. Appel, F. Knoch, V. Winkhaus, *J. Organomet. Chem.* **1986**, *307*, 93−95.
[57] B. Quasdorff, PhD Thesis, University of Bielefeld, **1977**.
[58] L. Weber, B. Quasdorff, H.-G. Stammler, B. Neumann, *Chem. Eur. J.* **1998**, *4*, 469−475.
[59] W−P distances in (phosphaalkene)$W(CO)_5$ and (phosphinine)$W(CO)_5$ complexes amount to ca. 2.46 Å.[59a] A. Marinetti, S. Bauer, L. Ricard, F. Mathey, *J. Chem. Soc., Dalton Trans.* **1991**, 597−602. − [59b] P. Le Floch, L. Ricard, F. Mathey, *Polyhedron* **1990**, *9*, 991−997.

Received March 24, 2000
[I00117]

Thiomolybdates — Simple but Very Versatile Reagents

Stuart H. Laurie

Keywords: Copper / Molybdenum / Sulfur / Redox chemistry / Bioinorganic chemistry / EPR spectroscopy / Exafs spectroscopy

A large number of thiometallate anions, $MO_xS_{4-x}^{n-}$, and some of the seleno analogues, are known in which M is a transition metal in a high oxidation state. They are characterised by their strong colours arising from low energy S(Se)→M charge transfer transitions, by unusual redox properties and by their ability to act as ligands to produce a wide range of heterometal complexes. This review outlines some of these properties associated with the thiometallate anions of molybdenum(VI). These anions are prepared by passing H_2S through an alkaline molybdate solution, giving a sequential replacement of O atoms by S and ultimately MoS_4^{2-} (TTM) as product. The thiomolybdates, particularly TTM, have been the most intensively studied because of their ease of preparation, their relatively greater thermal and hydrolytic stabilities and their biological roles. Unusual redox changes which involve internal electron transfer have been shown by reaction with organic disulfides and with Cu^{II}. In the latter case insoluble polymeric products are readily formed which, from EPR and EXAFS studies, involve S-bridged reduced Cu and Mo centres. Reaction of TTM with Cu^{I}, on the other hand, produces a range of complexes in which from 1 to 6 Cu ions add across the tetrahedral faces of TTM with no redox changes. Further Cu^{I} ions can be added to the $[Cu_6(MoS_4)]$ moiety to produce cluster ions. This illustrates the ability of the thiometallates to act as building blocks for a very wide range of heterometal complexes ranging from simple linear ions to complex clusters, a prime example of the latter being the FeMo cofactor of the enzyme nitrogenase. TTM was identified sometime ago as the reactive intermediate in the Mo-induced Cu-deficiency that afflicts ruminants with serious consequences. Subsequently TTM, as its ammonium salt, has been successfully used in removing the excess Cu and then controlling the Cu levels of patients of Wilson's disease. It appears to act by blocking the intestinal absorption of Cu and by converting Cu into a metabolically inert form, and in these respects is different to the mode of action of chelating agents which can be used for treating this disease.

1. Introduction

There exists a number of thiometallate anions of general formula $MO_xS_{4-x}^{n-}$ in which M is a transition metal and $x = 0-3$ (Table 1). Because of their strong colours (mainly yellow to red) compounds of these ions have attracted attention since the very early studies by Berzelius in the 19th century. For some of these the corresponding selenide anions are also known − although generally less well studied. All these chalcogenide anions form a remarkably reactive series whose chemistry has still not been fully explored.

A full assignment of the UV/Vis and IR bands of these tetrahedral anions has been given by Müller and his coworkers.[1,2] Two remarkable features are first, all the metal centres are in their highest oxidation states — despite being

[a] Department of Chemistry, De Montfort University, The Gateway, Leicester, LE1 9BH, UK



Professor Stuart Laurie obtained his BSc(Hons) and PhD degrees in chemistry at the University College of Wales, Aberystwyth. He then spent several years as a research worker, first at Washington State University and subsequently at the Protein Chemistry Division of the CSIRO, Australia. It was at the latter institute that he first developed his research interests in bioinorganic chemistry. He then spent two years as a Senior Research Fellow with professor R. D. Gillard's bio-inorganic group at the Univerity of Kent at Canterbury. In 1969 he joined the staff of De Montfort University (then Leicester Polytechnic) as a lecturer, subsequently being promoted to Senior Lecturer and then Reader and Professor of Inorganic Chemistry. During the time at DMU he has spent sabbatical periods at the Biochemistry Division, Hospital for Sick Children, Toronto, working with Professors B. Sarkar and (the late) A. Sass-Kortsak on Wilson's Disease therapy and, more recently, at the Marine Sciences Laboratory, University of South Florida, with Professor R. H. Byrne working on aspects of aqueous metal speciation. His current research interests are still focussed on coordination chemistry with particular reference to ternary metal chalcogenides and the recovery of metals from industrial wastes.

MICROREVIEWS: This feature introduces the readers to the authors' research through a concise overview of the selected topic. Reference to important work from others in the field is included.

 © WILEY-VCH Verlag GmbH, D-69451 Weinheim, 2000 1434−1948/00/1212−2443 $ 17.50+.50/0

Table 1. Known thio- and selenometallates

VS_4^{3-}	VOS_3^{3-}	$VO_2S_2^{3-}$	
VSe_4^{3-}	$VOSe_3^{3-}$	$VO_2Se_2^{3-}$	
NbS_4^{3-}			
TaS_4^{3-}			
MoS_4^{2-}	$MoOS_3^{2-}$	$MoO_2S_2^{2-}$	MoO_3S^{2-}
$MoSe_4^{2-}$	$MoOSe_3^{2-}$	$MoO_2Se_2^{2-}$	MoO_3Se^{2-}
WS_4^{2-}	WOS_3^{2-}	$WO_2S_2^{2-}$	WO_3S^{2-}
WSe_4^{2-}	$WOSe_3^{2-}$	$WO_2Se_2^{2-}$	WO_3Se^{2-}
ReS_4^{-}	$ReOS_3^{-}$	$ReO_2S_2^{-}$	ReO_3S^{-}

coordinated to the strongly reductive S^{2-} ions. Second, the M−S bond lengths that have been determined are all very similar, 2.15−2.18 Å. The first feature accounts for their strong colours as the S→M charge transfer bands are of relatively low energy and lie in the visible region. Linear relationships in fact have been established between the energy of the longest wavelength electronic transition with the M−S stretching force constant and with the optical electronegativity of the metal centre (for closely related species). In the latter case the transition energy increases as the χ_{opt} value decreases — consistent with charge transfer being in the S→M direction.[2]

The second feature points towards some π character in the M−S bonds — as also suggested from MO calculations.[1] Electron delocalisation through π bonding also explains why these anions do not undergo a spontaneous internal redox reaction.

Of this series it is the Mo^{VI} anions, particularly MoS_4^{2-} (TTM), which have been the most studied — this can be attributed to their ease of formation and conversion into other dimolybdenum-thiol species, their greater thermal and hydrolytic stabilities and their implication and use in biological systems.

2. Preparation and Properties of the Thiomolybdates

TTM can be most easily prepared as its ammonium salt by passing H_2S through an ammoniacal molybdate solution. [3] In 15−20 minutes $(NH_4)_2MoS_4$ precipitates from the reaction mixture as red crystals of high purity and in high yield — a chemist's dream! The Na^+ and K^+ salts [3,4] are also known but are more difficult to prepare (and keep). Attempts to prepare the Ca^{2+} salt for medical use (vide infra) have been unsuccessful.[5] Alkylammonium and phosphonium salts are particularly important for studying reactions in non-aqueous media and as starting materials for many of the known heterometal complexes. The $[R_4N]_2MoS_4$ salts can be readily prepared from aqueous solutions of the ammonium salt by elimination of the ammonium ion as ammonia. $[PPh_4]_2MoS_4$ is a particularly useful starting material for dimolybdenum compounds and is readily precipitated from aqueous solutions of $[NH_4]_2MoS_4$ by the simple addition of $[PPh_4]Cl$.[6] Preparation of salts of the intermediate oxythio anions, $MoO_xS_{4-x}^{2-}$ (x = 1−3), have all been reported — these all involve passage of H_2S but require more strictly controlled conditions in order to avoid contamination with neighbouring thiomolybdates.[1,3,7]

Formation of TTM from MoO_4^{2-} clearly proceeds via successive replacement of oxygen, as evidenced from the colour sequence change in solution: MoO_4^{2-}(colourless) → MoO_3S^{2-}(yellow) → $MoO_2S_2^{2-}$(orange) → $MoOS_3^{2-}$(orange-red) → MoS_4^{2-}(red). This colour sequence is shown in the aesthetic UV/Vis absorbance spectrum of the reaction between MoO_4^{2-} and S^{2-} as a function of time, as shown in Figure 1.

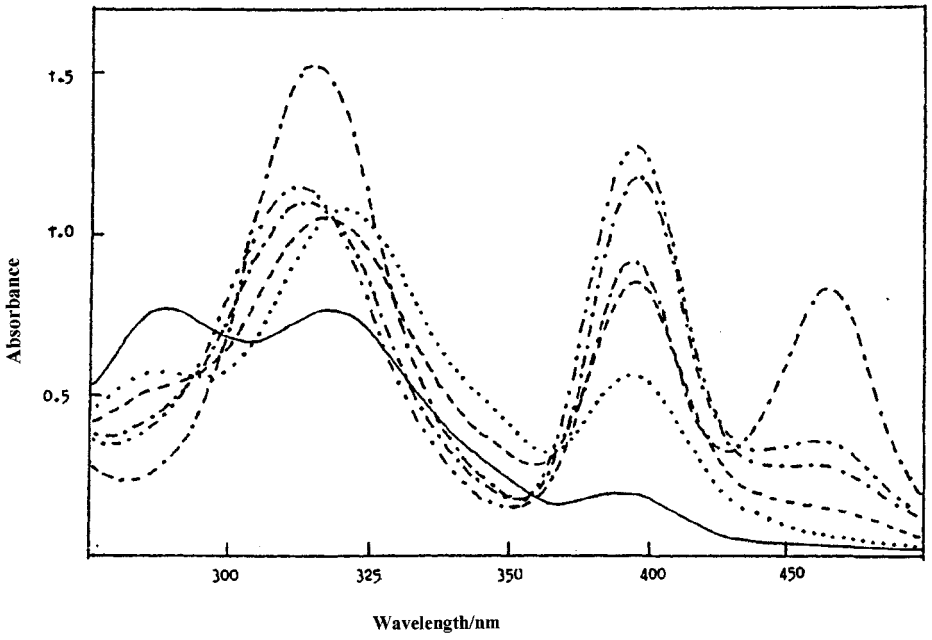


Figure 1. Formation of thiomolydate anions as a function of time (initial MoO_4^{2-} 1.3×10^{-4} M, S^{2-} 2.9×10^{-3} M, pH 7.0, 37 °C): after ——— 1 min., ····· 6 min., - - - - - - 21 min., ·-·-·-·-·- 60 min., ··-··-··-··- 110 min., --·--·--·--·--19 h; see Table 2 for assignment of the absorbance peaks)

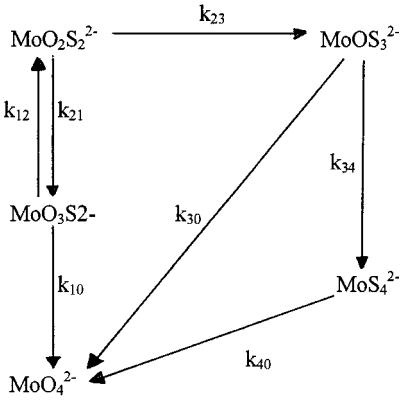
The strong UV/Vis and IR absorption bands are particularly useful diagnostic tools in determining the purity of the thiomolybdates and in following their reactions. These spectral details are given in Table 2.

Table 2. UV/Vis and IR bands of the thiomolybdate anions[a]

	UV/Vis λ/nm[b] (ε)[c]	IR[d] λ/cm^{-1} Mo−S	Mo−O
MoS_4^{2-}	316 (1.76), 465 (1.24)	476	-
$MoOS_3^{2-}$	315 (0.84), 398 (0.81), 465 (0.14)	470	860
$MoO_2S_2^{2-}$	288 (0.39), 320 (0.64), 394 (0.29)	460	860, 840
MoO_3S^{2-}	288 (−), 390 (−)[e]	476	880, 860, 840

[a] From measurements made in this laboratory. − [b] In pH 7 buffered aqueous solutions, ±2 nm. − [c] 10^4 dm^3 mol^{-1} cm^{-1}. − [d] Peak positions vary depending on the nature of the solvent and cation. − [e] Difficult to obtain accurate values.

The distinctive UV/Vis spectra of TTM and the oxythiomolybdate anions (Figure 1) have been used [8] to determine the rate constants for the formation (pseudo-first order with S^{2-} in excess) and hydrolysis of the ions as in Scheme 1.



Scheme 1

The rate constants for the thiol formation reactions follow the order:

$k_{12} > k_{23} > k_{34}$

Whilst that for the hydrolysis reactions is:

$k_{10} > k_{21} \approx k_{30} > k_{40}$

All the rates increase linearly with increase in H^+ concentration. Two important results with regard to TTM formation and existence in biological systems are that its complete formation in aqueous media requires a high S:Mo ratio and that its known increasing hydrolysis rate with increasing H^+ concentration proceeds without detectable formation of the intermediate oxythio ions in the above scheme.[8]

Earlier claims that, like MoO_4^{2-}, polymerisation of TTM occurs in lower pH solutions have not been substantiated. However, treatment with polysulfide produces dimeric and trimeric species in which the Mo centres have been reduced to oxidation states V and IV respectively,[9−11] e.g. to $(NH_4)_2[Mo_2^V(S_2)_6]\cdot 2H_2O$ and $(NH_4)_2[Mo_3^{IV}S(S_2)_6]$. Cyclic voltammetry of TTM in aqueous solution shows an irreversible reduction wave at −1.08 V,[12] whilst in dimethylformamide a reversible reduction potential of −2.50 V is observed.[13]

3. Thiomolybdates as Ligands

By far the most important property of the thiomolybdates, in particular TTM, is their role as ligands in a range of complexes, In these the $MoO_xS_{4-x}^{2-}$ moieties are mostly retained. It is the sulfide ions that play the key role as bridging ligands in which they can bridge two, three or four metal centres. The complexes formed range from simple linear structures, to small cubanes (Figure 2) to more complex clusters. In these cases the thiometallate anions act as the building blocks.

These compounds have received an enormous amount of attention over recent years because of their structural diversity and potential applications, e.g. as nonlinear optical materials, industrial catalysts and as models for the active Fe−Mo−S cluster site in the metalloenzyme nitrogenase. Consequently, they have been well reviewed.[2,14−17] Mention will be made here of only the much-studied system R/$Cu^I/MoO_xS_{4-x}^{2-}$, where R typically is a phosphane PR_3, halide (Cl^- or Br^-) or CN^-. In the absence of R, polymeric products are obtained, as in $(NH_4)CuMoS_4$ and Cu_2MoS_4, which feature alternate S-linked Cu^I and Mo^{VI} centres. In the presence of the R ligands, which preferentially occupy Cu^I sites, a range of discrete complexes can be obtained

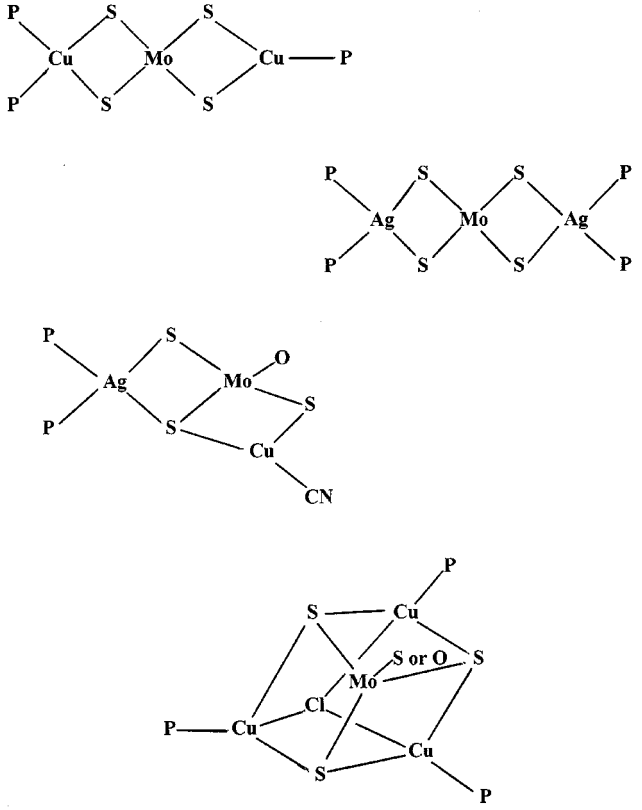


Figure 2. Some simple linear and cubane structures in schematic form illustrating the ability of thiomolybdate anions to act as ligands and as building blocks for more complex structures (P = triphenylphosphane)

depending on the reaction conditions (some examples are given in Table 3), the structures of many of these are known. Compounds have been reported from the reaction of CuCl with MoS_4^{2-} in which 1 to 6 Cu atoms occupy the six edges of the tetrahedral MoS_4^{2-} ion, i.e. of the form $[MoS_4(CuL)_n]$ ($n = 1-6$). A number of clusters with larger Cu:Mo ratios have also been synthesised, e.g. the anion $[MoS_4Cu_{10}\ Cl_{12}]^{4-}$ in which the central MoS_4^{2-} ion has six bridging Cu^I ions along its tetrahedral faces (as in the $n = 6$ case above) with the remaining four Cu^I ions forming an outer tetrahedral array linked by Cl^- bridges.[18] The formation of this latter complex from $(NH_4)_2MoS_4$ and CuCl illustrates how important the ratios of the starting reactants and the nature of the solvent are in terms of the final product(s) obtained. The structures of many of these heterometal compounds are known and illustrate the wide range of structural forms that they can exhibit.[19] Spectroscopic studies show that the IR ν(Mo−S) absorption modes in the 415−500 cm^{-1} region are diagnostic of the number of coordinated Cu^I ions.[20] For the diamagnetic heterometal complexes, ^{95}Mo NMR spectroscopy appears to provide a sensitive probe of the Mo environment;[21,22] for $[NPr_4]_2[Pt(MoS_4)_2]$ in DMF solution the observation of Pt−Mo coupling implies significant M−Mo interactions in these compounds.

Table 3. Examples of compounds isolated from R + Cu^I + (a) MoS_4^{2-}, + (b) $MoOS_3^{2-}$ or + (*c*) $MoO_2S_2^{2-}$

(*a*) $[Cl(PPh_3)_3Cu_3MoS_4]$	(*a*) $(PPh_3)_3[Cu_2(MoS_4)].0.8CH_2Cl_2$
(*a*) $(Bu_4N)_4[Cu_{12}(MoS_4)_8]$	(*b*) $(Bu_4N)_4[Mo_4Cu_{10}S_{16}O_3].H_2O$
(*a*) $(Me_4N)_5[MoS_4(CuCl)_6Cl_3]$	(*c*) $(Et_4N)_4[Mo_4Cu_4S_{12}O_4]$

A variation on the above is to use S^{2-} as the additional ligand leading to a further variation in structural types such as, $[Mo_4Cu_4S_{12}O_4]^{4-}$ (square type), $[Mo_8Cu_{12}S_{28}E_4]^{4-}$ E = S,O (cage), $[Mo_6Cu_6S_{19}O_6]^{2-}$ (cage).[23]

4. Redox Activity

Both the metal centres and the S ligands are redox active — either acting separately or, of more interest, acting in concert.[24] Oxidation of S^{2-} can result in a number of species with oxidation states ranging up to VI, e.g. S_2^{2-}, S_4^{2-}, S_8, SO_2, SO_3 as well as the various oxyanions. All of these are also potential ligands. As mentioned above, the occurrence of high metal oxidation state Mo^{VI} and low S state makes the occurrence and stability of the thiometallate ions somewhat surprising, especially for the thiomolybdate ions as the Mo and S redox potentials are fairly close. The potential redox activity has been realised in a number of reactions, e.g. in the reaction between TTM and organic disulfides elucidated by Stiefel and co-workers.[25,26]

$$2\ MoS_4^{2-} + RSSR \rightarrow Mo_2S_8^{2-} + 2\ RS^- \quad (1)$$

In this reaction the disulfide *oxidant* appears to have caused reduction of the Mo^{VI} centres to Mo^V! The required four electron donation in fact comes from the conversion of sulfides to persulfides:

$$4\ S^{2-} \rightarrow 2\ S_2^{2-} + 4e^- \quad (2)$$

The sulfide ion oxidation proceeds without M−S bond cleavage as X-ray analysis shows the persulfide ions to be coordinated to the Mo centres (Figure 3).

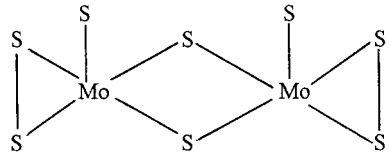


Figure 3. Structure of the anion $[Mo_2^VS_4(S_2)_2]^{2-}$ showing the coordinated persulfide ions (from ref. 25)

Under the same conditions WS_4^{2-} was found not to undergo metal reduction, but only a ligand redox reaction.[25] However, induced internal electron transfer has been observed with other tetrathiometallates. Stiefel[25] has pointed to a correlation between the ease of internal redox reactions and the lowest energy ligand-to-metal charge-transfer band (LMCT) and points to the position of the LMCT band being a "spectroscopic indicator" for such reactions. The LMCT bands in question are: ReS_4^-, 19800 cm^{-1}; MoS_4^{2-}, 21300 cm^{-1}; WS_4^{2-}, 25300 cm^{-1}. Of these ions, WS_4^{2-}, with the highest energy LMCT transition, undergoes internal redox changes the least easily. A similar intramolecular redox reaction has been reported by Coucouvanis et al.[27] involving the reaction between the oxy- and tetrathiomolybdates with elemental sulfur: under *oxidising* conditions the Mo centres were reduced to Mo^{IV} complexes with the formation of coordinated S_4^{2-} ions.

We have reported a similar redox reaction between TTM and salts and complexes of Cu^{II}, a black insoluble compound of composition $Cu_{1.6}MoS_4X_y$ was obtained (X = Cl^-, Br^-, $y = 1$; X = SO_4^{2-}, $y = 0.5$) when the Cu^{II} halide or sulfate salts were reacted with TTM in aqueous solutions.[28,29] EPR spectroscopy showed no Cu^{II} but the presence of Mo^V with a small (ca. 10%) contribution to the spectrum from an S radical species.[29] Presumably, the one electron reduction of each of the metal centres arises mainly from sulfide oxidation to persulfide, as in reactions (1) and (2) above. Some sulfide oxidation must also lead to the S radicals that were observed. EXAFS spectroscopy at the Cu and Mo K-edges show the Mo coordination to have been reduced to a trigonal MoS_3 moiety whilst the Cu is most likely a mixture of CuS_3 and CuS_4 coordination. Without some knowledge of the S species present it is difficult to predict the likely structure of this fascinating material; its insolubility does, however, suggest a multi-S bridged polymer. A further, surprising, finding was the observation that the solid irreversibly absorbs up to 2 mol O_2, with no change in either the EPR or EXAFS spectra, which suggests oxygenation at the S atoms. These EXAFS spectra are shown in Figure 4. We also found WS_4^{2-},despite its reported greater redox stability, to react with Cu^{II} identically to TTM in its reaction stoichiometry, redox changes and oxygenation.

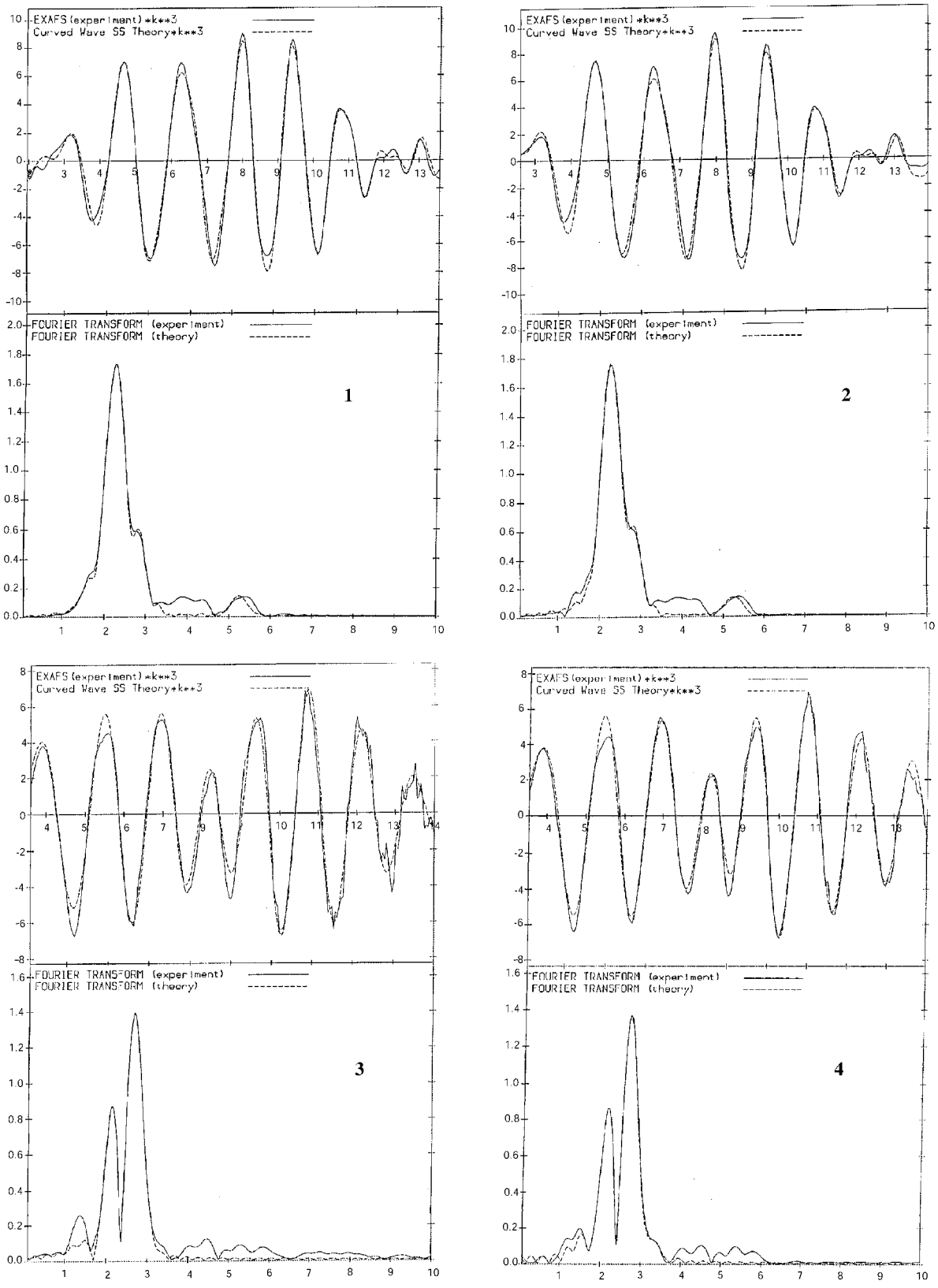


Figure 4. EXAFS spectra and Fourier transforms of $[Cu_{1.6}MoS_4Cl]$ showing retention of the metal coordination sites after O_2 uptake; **1** Cu k-edge, **2** Cu k-edge of oxygenated sample, **3** Mo k-edge, **4** Mo k-edge after oxygenation

Recently, Noble et al.[30] have shown that S coordinated at a dimolybdenum centre can undergo conversion into coordinated SO (sulfoxide) and coordinated SO_2 (sulfone). Similar oxygen capture reactions have been reported for Ni thiolates.[31] It would appear that this is a reaction with unexplored potential.

The Cu:Mo ratio in the above product is very close to that in the discrete anion $[Cu_{12}Mo_8S_{32}]^{4-}$, formed from the reaction in the solid state between TTM and CuCN. Surprisingly, the CN^- ligand is not retained in this case.[31] This anion, one of the largest known of its type, contains slightly distorted $Mo^{VI}S_4$ units linking tetrahedral Cu^IS_4 centres. A fuller description is given in reference 32 and in the review by Dance and Fisher.[15]

Reaction with the oxythioanions $MoO_xS_{4-x}^{2-}$ (x = 1,2; M = Mo, W) with Cu^{II} has also been found to lead to mutual metal reduction to Cu^I and Mo^V from the EPR spectra of the products. However, the stoichiometry in these cases is close to 1:1 Cu:Mo rather than the 1.6:1 observed with TTM.[33] Preliminary analysis of the EXAFS Cu spectra of these compounds shows a consistent trigonal CuS_3 coordination in all samples (Cu−S 2.5−2.7 Å) and a Mo atom at 2.67−2.70 Å. The EXAFS Mo spectra are consistent with $MoOS_3$ and $MoOS_2$ environments, the latter suggesting, rather surprisingly, the cleavage of one O atom from the $MoO_2S_2^{2-}$ reactant; the presence of Mo−O bonds is also evident from the strong IR absorption in the 800−900 cm^{-1} region. As with the Cu K-edge spectra there is also one neighbouring Cu atom observed in the Mo spectra at 2.67−2.70 Å. Our preliminary studies also show an oxygenation reaction occurs without any change in either the EPR or the EXAFS spectra.

5. Biological Properties

The Copper−Molybdenum Antagonism

Both Cu and Mo are well-known essential elements occurring in a range of metalloenzymes. Although their enzymatic functions primarily involve redox processes there is no evidence of any direct biological interactions between them as there is, for example, between Cu and Zn and Cu and Fe; this would be as expected from their different coordination chemistry behaviour and from their very different naturally occurring forms. However, there is one exception to this, and that is the well documented Mo-induced Cu deficiency that can afflict ruminants; more correctly this should be expressed as a Mo−S−Cu interaction.

The first component of the complex digestive system of ruminants (e.g. cattle and sheep), the rumen, has a high microbial content and is anaerobic, under these conditions both inorganic and organic sulfur are reduced to sulfide. Rumen sulfide levels of up to 6.0 ppm have been observed. High dietary Mo levels have been found to inhibit sulfide production.[34] It was recognised over 50 years ago that ruminant animals grazing pastures of high Mo content (ca. ≥2 mg/kg) develop symptoms characteristic of copper deficiency, i.e. a decline in weight gain, diarrhoea, rough and discoloured coats, and skeletal abnormalities.[35] Much research on this widespread antagonism has subsequently shown that although the dietary Cu levels may be sufficient this was indeed an induced Cu deficiency. High Mo levels themselves do not necessarily induce Cu deficiency — the Mo-induced Cu deficiency also requires a high dietary S intake. Several reviews cover this earlier work.[36−38] Mills and his co-workers subsequently showed that TTM forms from molybdate ion in rumen cultures.[39] Laboratory simulation of rumen conditions also showed that the oxythiomolybdate ions and subsequently TTM can form.[40] However, because of the low natural concentrations of molybdate in the rumen it has not been possible to directly observe the presence of any thiomolybdate within a rumen.

Addition of Cu^{II} to a solution of TTM in strained rumen contents resulted in the loss of the TTM UV/Vis spectrum, with a complete loss of spectrum at an approximately 1:1 Cu:Mo ratio.[39] Our own studies[40,41] have confirmed that a rapid reaction occurs between Cu^{II} ions and its complexes with TTM and with the oxythiomolybdates: in fact, taking into account the rapidity of the reaction and the rumen concentrations it was concluded that the oxythiomolybdate ions $MoO_xS_{x-4}^{2-}$ (x = 1,2) were the more likely reactants.[41] Studies by Mason and co-workers show that the di-, tri-, and tetrathiomolybdates all have an effect on Cu metabolism when given intravenously to ruminants and have a reversible inhibitory effect on caeruloplasmin oxidase.[42]

Despite these latter observations the majority of studies on the biological effects of the thiomolybdate ions have concentrated on TTM because of its greater aqueous stability. The Cu depletion caused by TTM appears to result from a decreased absorption from the diet and the formation of a non-bioabsorbable form. The latter has been identified as a ternary Cu−Mo protein form in both blood plasma and in liver cells, the proteins involved being albumin and metallothionein, respectively. Molybdenum-95 NMR spectroscopy shows that TTM can bind to serum albumin protein.[43] Our own studies, using membrane filtration and UV/Vis spectroscopy, suggest this association to be a relatively weak, mainly ionic, binding between albumin and TTM, there was certainly no evidence of any S cross-linking. With Cu-albumin, however, there was rapid formation of a ternary TTM-Cu-Albumin complex with similar characteristics to the polymeric compound that we isolated in vitro, i.e. EPR evidence of Cu^I and Mo^V centres.[41] While we could find no evidence of any interaction between the Zn-thionein protein and TTM, with Cu^I-thionein TTM was strongly bound; the other thiomolybdates were found to behave in a similar manner.[41]

Administration of TTM to nonruminants such as rats causes dramatic changes to the Cu distribution within plasma and reduction in the catalytic activity of the Cu enzymes, caeruloplasmin, ascorbate oxidase, superoxide dismutase and tyrosinase. The oxythiomolybdates were found to have less marked effects. From these studies it is evident that TTM may have potential as an antidote in acute Cu intoxication, animal studies have confirmed this and showed that it could also act as an antidote against Zn and Ni toxicity but not against other metals.[44]

TTM in the Treatment of Wilson′s Disease

Wilson′s disease is a relatively rare human disease first described by Kinnear Wilson in 1912 as progressive lenti-

cular degeneration, a familial disease occurring in young people. It is progressive and invariably fatal — unless treated early.[45] The cause of the disease is an accumulation of Cu resulting from a genetic defect which impairs the body′s normal excretion of dietary copper. As stated by Wilson, the disease is progressive, with severe neurological and liver deterioration. Unless treated early on, patients invariably die in their late teens or early twenties. The high Cu concentrations in the liver, low caeuloplasmin levels and Cu deposits in the cornea of the eyes (Kayser-Fleischer rings) are typical clinical symptoms used in the diagnosis of the disease. At the molecular level, free Cu ions are well-known enzyme poisons because of their potential to bind strongly to the many coordinating sites present in protein molecules. In fact, the body has well-established mechanisms for maintaining very low concentrations of free metal ions. This capacity is obviously exceeded in Wilson′s disease and the excess Cu ions are transported into the brain, the central nervous system and the liver, as well as other tissues.

Treatment of the disease is normally with chelating agents which can (a) rapidly excrete the excess Cu, and (b) over the rest of the patient′s life keep him/her in a low Cu balance. The two chelating agents of choice are D-penicillamine and triethylenetetraamine (trientine). The former is the more effective and is the usual first choice; however, penicillamine does have toxic side-effects and some patients become intolerant, in which case trientine is then used. Treatment with zinc salts has also been claimed to be beneficial, although not as effective as the above chelating agents. Another compound which is finding increasing use is TTM.

The usual criteria for successful chelation therapy is that the chelate must be nontoxic, be water soluble, resistant to metabolic degeneration, and have selective and adequate chelating ability at physiological pH. The agents and their metal chelates must be rapidly excreted by the kidneys. As shown above, TTM is very effective at removing Cu from animal tissues — even when the Cu is at normal levels — but it would not seem to fit many of the criteria for chelation therapy; it has nevertheless become another useful reagent for treating this disease. A useful summary of the prognosis of this disease and its therapy together with the related copper disorder, Menkes Disease, has recently been given by Sarkar.[46]

TTM was first used by Dr John Walshe, then at Addenbrookes Hospital, Cambridge, in 1982 on a patient who had become intolerant of all the other available treatments. She was initially treated with 50 mg twice a day, this was subsequently reduced to 30 mg twice a day and she was maintained on this regime until her death from other causes 16 years later; the longest recorded successful treatment to-date with TTM. She was initially treated with D-penicillamine but became intolerant of this, following this she responded well to trientine which reduced her liver Cu level to 90 units (ug/g wet tissue weight) but then became intolerant of this as well. She was then put on $ZnSO_4$ but after one year developed gastric problems, at this time her liver Cu level was 155 units. After a further 10 months without treatment she had deteriorated and her liver Cu level was up to 408 units. It was at this time that she was put on TTM, her health then improved and her liver Cu level decreased to 130 units. The initial follow up studies on this patient and others were reported in 1986 by Walshe.[47] TTM appears to act by blocking the intestinal absorption of Cu and by converting Cu into a metabolically inert form. The latter is most likely an S-linked Cu−Mo protein ternary complex as found in the earlier animal studies and our laboratory studies mentioned above and, more recently, in the TTM application to a rat strain that models Wilson′s disease.[48] The salt used then, and now, is the ammonium salt. Although there was some initial concern about the prolonged use of the ammonium ion there appears to have been no related adverse effect. It would have been preferable to use salts with cations such as Na^+, K^+ or Ca^{2+}, but, as noted above, these are difficult to prepare (most commercially available materials we have found to be impure, the major impurity being the highly insoluble MoS_3). The sodium salt has been found to be less toxic in rat studies than the ammonium form, LD_{50} 537 mg/kg and 176 mg/kg, respectively.[44] TTM has been successfully used by others:[44,50] in particular, a detailed study by Brewer et al. showed very promising results on using TTM as an initial treatment both to reduce Cu levels and improve neurological functions, followed by zinc administration for long term maintenance.[44] However, because of the lack of clinical data the use of TTM must still be treated as an experimental therapy. Additionally, there have been reports of it having toxic side effects,[48,49,51] although in two of these studies[48,49] the dosages used on a mg/kg body weight basis were considerably higher than those used successfully by Walshe on his patients. The applicability of some of the animal studies as models for the treatment of Wilson′s disease is also questionable. However, it is clear that continuous monitoring of a patient′s Cu and Mo tissue levels and other related clinical testing is needed during treatment with TTM.

6. Conclusions

We have shown that the unusual redox reaction between thiomolybdates and Cu^{II} occurs for a wide range of different forms of Cu^{II}. The question then arises as to how extensive this reaction is in terms of other thioanions, as listed in Table 1, and other reducible metal ions, and how common is the oxygenation reaction? I suspect that many similar reactions have previously gone undetected. Unpublished studies in our laboratory show that the thioanions of W, $WO_xS_{4-x}^{2-}$ ($x = 0-2$) undergo the same reactions with Cu^{II} as do the Mo analogues. A solid-state redox reaction between Cu^{II} and VS_4^{3-} has also been observed. The combination of EPR and EXAFS measurements has proved particularly valuable in these studies. As regards other potentially reducible metal ions to-date we have only carried out some preliminary studies with Fe^{III}. In this latter case, redox reactions have been observed but no well-defined

products have been obtained. A further area worthy of investigation is to carry out the reactions with Cu^{II} in the presence of Cu^{I} ligands so as to produce more tractable molecular species. There is also still much to be learnt about the metabolic properties of TTM and the nature of the ternary Cu-TTM-protein complex formed in the application of TTM in treating Wilson′s disease.

[1] E. Diemann, A. Müller, *Coord. Chem. Rev.* **1973**, *10*, 79, and references therein.
[2] A. Müller, E. Diemann, in *Comprehensive Coordination Chemistry* (Eds.: G. Wilkinson, R. D. Gillard, J. A. McCleverty), Pergamon Press, Oxford, **1987**, *vol. 2*, p.559.
[3] J. W. Mellor, *A Comprehensive Treatise on Inorganic and Theoretical Chemistry*, Longmans, London, **1943**, *vol. 11*, p.650.
[4] S. H. Laurie, D. E. Pratt, J. H. L. Yong, *Inorg. Chim. Acta* **1984**, *93*, L57.
[5] S. H. Laurie, unpublished observations.
[6] A. I. Hadjikyriacou, D. Coucouvanis, *Inorg. Synth*. **1990**, *27*, 39.
[7] A. Müller, H. Dornfeld, H. Schultze, R. C. Sharma, *Z. Anorg. Allgem. Chem*. **1980**, *468*, 193.
[8] N. J. Clarke, S. H. Laurie, M. J. Blandamer, J. Burgess, A. Hakin, *Inorg. Chim. Acta* **1987**, *130*, 79.
[9] A. Müller, S. Sarkar, R. G. Bhattacharrya, S. Pohl, M. Dartmann, *Angew. Chem. Int. Ed*. **1978**, *17*, 535.
[10] A. Müller, W. O. Nolte, B. Krebs, *Inorg. Chem.* **1980**, *19*, 2835.
[11] D. Coucouvanis, A. J. Hadjikyriacou, *Inorg. Chem.* **1986**, *25*, 4317.
[12] J. You, D. Wu, H. Liu, *Polyhedron*, **1984**, *5*, 535.
[13] D. E. Pratt, S. H. Laurie. R. H. Dahm, *Inorg. Chim. Acta* **1987**, *135*, L21.
[14] B. W. Eichhorn, *Prog. Inorg. Chem.* **1994**, *42*, 139.
[15] I. Dance, K. Fisher, *Prog. Inorg. Chem.* **1991**, *41*, 637.
[16] H.-W Hou, X.-Q Xin, S Shi, *Coord. Chem. Rev.* 1996, **153**, 5.
[17] X. Wu, Q. Huang, Q. Wang, T. Sheng, J. Lu, in *Transition Metal Sulfur Chemistry*: *Biological and Industrial Significance* (Eds.: E. I. Stiefel, K. Matsumoto), American Chemical Society Symposium series, Washington, **1996**, pp282.
[18] D. Wu, M. Hong, R. Cao, H. Liu, *Inorg. Chem.* **1996**, *35*, 1080.
[19] Y. Jeannin, F. Scheresse, S. Bernes, F. Roberts, *Inorg. Chim. Acta* **1992**, *200*, 493.
[20] R. J. H. Clarke, S. Joss, M. Zvagulis, C. D. Garner, J. R. Nicholson, *J. Chem. Soc*., *Dalton Trans.* **1986**, 1595.
[21] M. Minelli, J. H. Enemark, R. T. C. Brownlee, M. J. O′Connor, A. G. Wedd, *Coord. Chem. Rev.* **1986**, *68*, 169.
[22] M. J. Toohey, C. D. Scattergood, C. D. Garner, *Inorg. Chim. Acta* **1987**, *129*, L19.
[23] J. Guo, T. Sheng, W. Zhang, X. Wu, P. Lin, Q. Wang, J. Lu, *Inorg. Chem.* **1998**, *37*, 3689 and references therein.
[24] E I Stiefel, *ref. 17*, pp 2.
[25] W.-H. Pan, M. A. Harmer, T. R. Halbert, E. I. Stiefel, *J. Am. Chem. Soc.* **1984**, *106*, 459.
[26] W.-H. Pan, T. R. Halbert, L. L. Hutchings, E. I. Stiefel, *J. Chem. Soc., Chem. Commun*. **1985**, 927.
[27] D. Coucouvanis, A. Toupadakis, S.-M. Koo, A. Hadjikyriacou, *Polyhedron*, **1989**, *8*, 1705.
[28] S. H. Laurie, D. E. Pratt, J. B. Raynor, *Inorg. Chim. Acta* **1986**, *123*, 193.
[29] T. Ecclestone, I. Harvey, S. H. Laurie, M. C. R. Symons, F. A. Taiwo, *Inorg. Chem. Commun*., **1998**, *1*, 460.
[30] R. Wang, M. S. Mashuta, J. F. Richardson, M. E. Noble, *Inorg. Chem.* **1996**, *35*, 3022.
[31] C. A. Grapperhaus, M. Y. Darensburg, *Acc. Chem. Res.* **1998**, *31*, 451.
[32] L. Jiguo, X. Xinquan, Z. Zhongyuan, Y. Kaibei, *J. Chem. Soc., Chem. Commun.* **1991**, 249.
[33] T. Ecclestone, S. H. Laurie, unpublished observations.
[34] N. F. Suttle, in *Sulphur in Forages*, An Foras Taluntais, Dublin, **1978**, p.197.
[35] W. S. Ferguson, A. L. Lewis, S. J. Watson, *J. Agric. Sci*. **1943**, *33*, 44.
[36] C. F. Mills, *Proc. Nutr. Soc*. **1960**, *19*, 162.
[37] N. F. Suttle, in *Trace Element Metabolism in Animals* (Eds.: W. G. Hoekstra, J. W. Suttie, H. E. Ganther, W. Mertz), Buttersworths, London, **1974**, p.612.
[38] C. F. Mills, *Proc. Roy. Soc*., *B.* **1979**, *288*, 53.
[39] T. T. El-Gallad, C. F. Mills, I. Bremner, R Summers, *J. Inorg. Biochem*. **1983**, *18*, 323.
[40] N. J. Clarke, S. H, Laurie, *J. Inorg. Biochem*. **1980**, *12*, 37.
[41] N. J. Clarke, S. H. Laurie, D. E. Pratt, *Inorg. Chim. Acta* **1987**, *138*, 103.
[42] B. Lannon, J. Mason, *J. Inorg. Biochem*. **1986**, *26*, 107, and references therein.
[43] S. Bristow, C. D. Garner, S. K. Haygard, G. A. Morris, J. R. Nicholson, C. F. Mills, *J. Chem. Soc. Chem. Commun*. **1985**, 479
[44] S. H. Laurie, M. A. Basinger, M. M. Jones, *Inorg. Chim. Acta* **1984**, *91*, 121.
[45] S. A. K. Wilson, *Brain* **1912,** *34*, 295.
[46] B. Sarkar, *Chem. Rev.***1999**, *99*, 2535.
[47] J. M. Walshe, in *Orphan Diseases and Orphan Drugs* (Eds.: I. H. Scheinberg, J. M. Walshe), Manchester Univ. Press, **1986**, p.76.
[48] Y. Ogra, K. T. Suzuki, *J. Inorg. Biochem*. **1998**, *70*, 49.
[49] G. J. Brewer, R. D. Dick, V. Yuzbasiyan-Gurkin, R. Tankanow, A. B. Young, K. J. Kluin, *Arch. Neurol*. **1991**, *48*, 42.
[50] D. M. Danks, *Eur. J Pediatr*. **1991**, *150*, 142.
[51] P. L. Harper, J. M. Walshe, *Br. J. Haematol*. **1986**, *64*, 851.

Received January 13, 2000
[I00010]

Electron Density and Charge Distribution around the Metal Atom in [Cp*Fe(η^5-As_5)]

Rolfe H. Herber*[a] and Otto J. Scherer[b]

Keywords: Sandwich complexes / Iron / Arsenic / Moessbauer spectroscopy / Calorimetry

^{57}Fe Mössbauer effect spectroscopy has been used to study the charge density, charge distribution, and lattice dynamics in the ferrocene-related compound [Cp*Fe(η^5-As_5)]. The isomer shift (at 90 K) is significantly more positive than that observed for the related η^5-P_5 homologue reported earlier, while the quadrupole hyperfine interaction is essentially the same in both compounds, but only about a quarter of that observed in related ferrocenes with only carbon atoms in the ring structure. The temperature dependence of the recoil-free fraction evidences a discontinuity centered at about 213 K, which is also observed in the DSC data. These data are compared to related results acquired for homologous ferrocenes with variable ring substitution.

Introduction

Due to its centrality in the development of organometallic chemistry over the past several decades, ferrocene [(η^5)$(Cp)_2$Fe] has been the subject of a multitude of physical and chemical characterizations, and is, undoubtedly, among the best characterized organometallic compounds in the chemical literature.[1] Among these characterizations have been temperature-dependent ^{57}Fe Mössbauer effect studies[2,3] designed to explore the charge density and symmetry of the charge distribution around the metal atom, and to relate these to a satisfactory description of the bonding and dynamics in this compound. In a recent study,[4] these investigations have been extended to [Cp*FeP_5] (**1**) and [$Cp^R FeP_5$] (**2**) [Cp* = $C_5(CH_3)_5$, Cp^R = $C_5(CH_3)_4(C_2H_5)$] and it was noted that the replacement of five $C(CH_3)$ ring components by the isoelectronic P atom resulted in a marked change in both the isomer shift (IS) and quadrupole splitting (QS) parameters over the temperature range $90 \leq T \leq 340$ K, compared to the parent ferrocene homologues. The recently reported synthesis[5a] and manifold chemistry[5b] of the corresponding [Cp*Fe (η^5-As_5)] (**3**) has made it possible to extend these studies to the arsenic congener, and the details of this study are the subject of the present communication. The structure of the related homologue of **3,** with Cp^R instead of Cp*[5a] is shown in Figure 1.

To overcome the pronounced nonresonant scattering by arsenic of the 14.4 keV gamma radiation accompanying the Mössbauer transition, the recent availability of strong (≈ 100 mCi) sources of ^{57}Co radiation, and the use of fast detector electronics, has made possible studies of arsenic containing iron organometallics which to date have been very limited.[6] The experimental details governing these measurements are briefly described below.

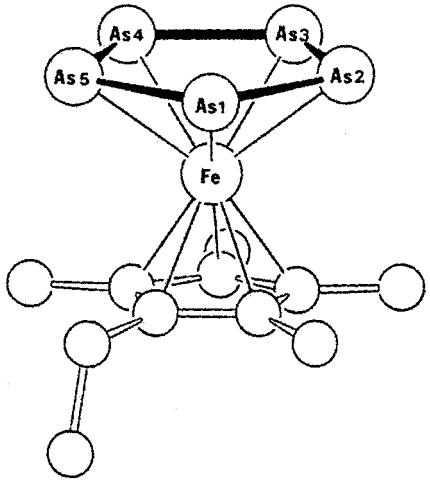


Figure 1. Structure of Cp^RFe(η^5-As_5) at 298 K; the X-ray structure of **3** with Cp* instead of Cp^R has not yet been reported

Results and Discussion

The ^{57}Fe Mössbauer spectra of all the compounds reported here consist of well-resolved doublets, and a typical spectrum is shown in Figure 2.

The IS, QS, and related parameters at 90 K are summarized in Table 1. A number of features of these data are worthy of comment. Compared to the corresponding data[4] for **1** and **2**, the IS of **3** is significantly more positive, and has nearly the same value as that of the parent ferrocene without ring substituents **6**, but is significantly smaller than that reported for [Cp*FeCp][7,8] and [Cp^*_2Fe], indicating a reduction of the s-electron density at the metal center. It is well-known that changes in the Cp ring substituents which are bonded to the carbon atoms by σ bonds have relatively little effect on the electron density at the iron atom since

[a] Racah Institute of Physics, The Hebrew University, 91904 Jerusalem, Israel
E-mail: herber@vms.huji.ac.il
[b] Fachbereich Chemie, Universität Kaiserslautern, 67653 Kaiserslautern, Germany

 © WILEY-VCH Verlag GmbH, D-69451 Weinheim, 2000 1434−1948/00/1212−2451 $ 17.50+.50/0

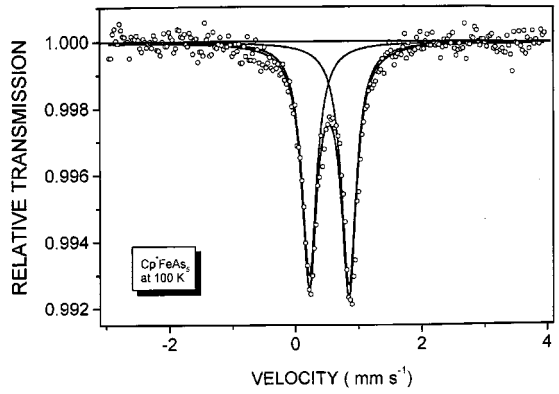


Figure 2. ^{57}Fe Mössbauer spectrum of **3** at 90 K; the velocity scale is with respect to the centroid of an α-Fe spectrum at 300 K; the small effect magnitude (even at 100 K) is a reflection of the presence of large amounts of arsenic in the sample, as discussed in the text

the latter is bonded primarily by overlap between the metal atom d-orbitals and the π density associated with the carbon atoms of the ring structure. Clearly, the effect of the presence of the electron-donating methyl groups is offset by the larger size of the As atoms constituting the ring, and presumably arises from the increase in shielding by the presence of 10 d-electrons in As compared to P and CH. This shielding reduces the s-electron density at the Fe nucleus and thus leads to the observed increase in the IS parameter. The temperature dependence of the IS is well represented by a linear regression over the range $90 \leq T \leq 273.2$ K: IS = $0.592 - (3.66 \pm 0.13) \times 10^{-4}$ T mm s^{-1}, with a correlation coefficient of 0.986 for 25 data points. This temperature dependence corresponds to an M_{eff} [9] of 113 daltons, reflecting the covalency of the metal-ligand bonding interaction.

Turning next to the QS interaction, it is seen (Table 1) that the numerical value of this parameter is essentially identical to that observed in **1** and **2**; that is, about a quarter of the size of that observed in complexes with Cp_2, Cp^*_2 and CpCp*[7] ligands. The likely explanation of this observation in the case of **1** and **2** has been discussed earlier.[4] It is to be noted, however, that going from the 3s,3p orbitals of P to the 4s,4p (and 3d) orbitals of As does not result in a further diminution of the QS. Again, it can be inferred that the electron density in the metal−ring atom overlap in latter case is − due to greater delocalization and the effect of the intervening 3d orbitals − essentially equivalent to that in the case of the P atoms, keeping in mind that the covalent atomic radii in the two cases are nearly identical (2.19 and 2.18 Å). The temperature dependence of the QS is essentially zero within the error limits of the present measurements, in contrast to the small positive value of d (QS)/ d T observed[4] for **1** and **2**. Due to the unavailability of well-formed single crystals of **3**, it is not possible to infer the sign of the QS from the presently available data (compare the intensity asymmetry shown in Figure 2 to that reported earlier for **1** at 90 K), and such an inference — in the absence of single crystal samples — would have to be based on measurements in high magnetic fields[10] to remove the (magnetic) degeneracy of the ±3/2 and ±1/2 spin levels observed in the present study.

Turning next to the dynamics of the metal atom motion in **3**, this characteristic is most clearly revealed in the temperature dependence of the area (A) under the resonance curve, which (for a thin absorber) scales directly with the recoil-free fraction, and hence with the mean-square amplitude of the metal atom relative to the center of symmetry of the molecule as a whole. It is amply clear from the temperature insensitivity of the intensity ratio R [= A(+)/ A(−)] that there is no resolvable Gol'danskii−Karyagin asymmetry[11] of the metal atom motion in this compound despite the presence of the five heavy As atoms. The temperature dependence of A over the range $90 \leq T \leq 273.2$ K is summarized graphically in Figure 3, in which the open and closed points refer to data accumulated in the warming and cooling modes, respectively, and illustrate the reversibility of these data. It is clear that there are two distinct regimes in this plot separated by a transition region centered at about 213 K. The slopes in the two regions are nearly identical [$-(7.79 \pm 0.36) \times 10^{-3}$ and $-(8.58 \pm 0.78) \times 10^{-3}$ K^{-1} in the ranges $90 \leq T \leq 205$ and $220 \leq T \leq 273.2$ K, respectively] and are very similar to the behavior reported[4] for **1** in which the mid-point of the discontinuity was observed at 195 K. As in the earlier study, the identification of this discontinuity is supported by the DSC data summarized in Figure 4.

The relatively broad endotherm at 217 K, observed at a warming rate of five degrees per minute, is in reasonable agreement (midpoint about 213 K) with the data summarized in Figure 3, which show Mössbauer data accumulated over a period of several hours at each temperature. It is tempting to identify this transition with the lambda point

Table 1. Summary of Mössbauer data for the compounds discussed in the text [Cp = η^5-C_5H_5, Cp* = η^5-$C_5(CH_3)_5$, Cp^R = η^5-$C_5(CH_3)_4(C_2H_5)$ P_5 = η^5-P_5, As_5 = η^5-As_5]

Compd.	**1**	**2**	**3**	**4**	**5**	**6**	Units
	Cp^*FeP_5	Cp^RFeP_5	Cp^*FeAs_5	Cp*FeCp	Cp*FeCp*	CpFeCp	
IS(90)	0.468(4)	0.456(20)	0.559(1)	0.499(5)	0.492(3)	0.525(5)	mm s^{-1}
QS(90)	0.624(1)	0.652(1)	0.626(21)	2.436(1)	2.473(2)	2.388(1)	mm s^{-1}
$-$d lnA/dT	8.09(26)[a] 11.20(29)[e]		7.79(36)[b] 8.58(78)[f]	7.55(10)	7.97(40)[c]	6.23(23)[d] 7.20(23)[g]	$K^{-1}\cdot10^3$

[a] $90 \leq T \leq 170$ K. − [b] $90 \leq T \leq 205$ K. − [c] Below 273 K. − [d] Below λ-point. − [e] $195 \leq T \leq 340$ K. − [f] $220 \leq T \leq 273.2$ K. − [g] Above λ-point.

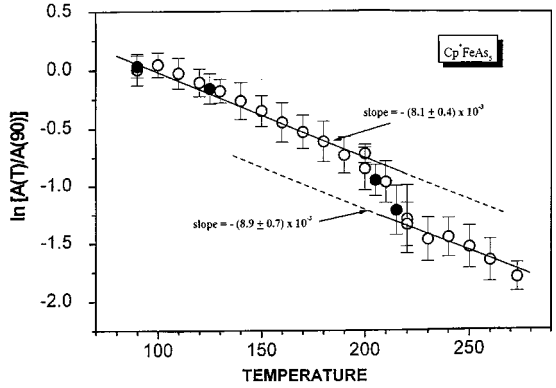


Figure 3. Temperature dependence of the area under the resonance curve for **3**; the open and closed points refer to data acquired during warming and cooling regimes, respectively

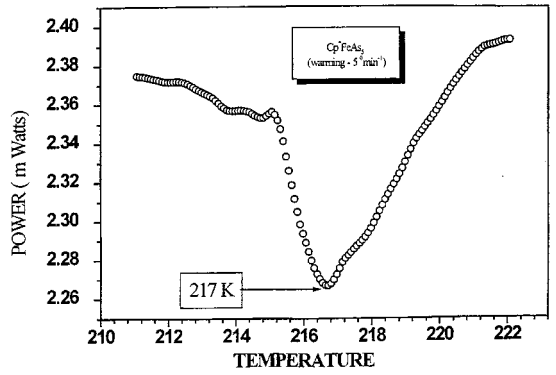


Figure 4. Portion of the differential scanning calorimetry data for **3**, showing the endotherm at about 217 K

(at 169 K) reported for ferrocene, which is related[12] to a change from the triclinic (low *T*, nearly eclipsed rings) to the orthorhombic/monoclinic (high *T*, staggered rings) form, but additional support for this identification cannot be extracted from the presently available data. The gas phase (473 K) structure of [Cp*FeP_5] has been reported by Blom et al.,[13] and consists of a staggered conformation of the two five-membered rings. No comparable data for **3** have been reported to date, although the X-ray diffraction data for [Cp^RFeAs_5] have been summarized by Scherer et al.[5a]

Experimental Section

A sample of **3** was synthesized as described earlier,[5a] and, because of its (slight) light and air sensitivity, quickly mixed in subdued light with an equal weight of BN to optimize random crystallite orientation. This sample was then mounted in a standard plastic sample holder and immediately cooled to 78 K before transferring to the Mössbauer spectrometer. The other compounds cited in this study were obtained as described previously.[4]

For the gamma ray resonance measurements, a strong (≈100 mCi) ^{57}Co/Rh source was used at room temperature in connection with a fast proportional counter able to handle input rates in excess of 10^5 Hz. The problem of the efficient detection of the resonantly scattered 14.4 keV gamma radiation in the presence of As is, of course, exacerbated by the reduction in the recoil-free fraction with increasing temperature. To obtain reasonably reliable data, in excess of 5×10^7 counts per channel were scaled at the higher temperatures indicated above. Temperature control was maintained by use of a regulated proportional feedback circuit, and temperatures maintained at better than ±0.2 degrees over the data collection interval. Spectrometer calibration was effected before and after the data collection period, using a standard α-Fe foil at room temperature, and all IS values are quoted with reference to the centroids of these spectra. Data reduction was effected as detailed earlier.[3,4]

The DSC data were acquired using a Mettler Toledo Model DSC30 differential scanning calorimeter at heating and cooling rates of 2 and 5 degrees per minute over the temperature interval $173 \leq T \leq 308$ K.

Acknowledgments

The authors are indebted to Ms. Sigalit Gura of Bar Ilan University for the DSC measurements, and to Prof. I. Nowik for helpful discussions concerning data reduction. This research was supported in part by the Israel National Academy of Science.

[1] *Gmelin Handbuch der Anorg. Chemie*, Springer Verlag, Berlin **1974**, vol. 14, and references therein.
[2] T. C. Gibb, *J. Chem. Soc., Dalton Trans.***1976**, 1237−42.
[3] R. H. Herber, K. Temple, I. Manners, M. Buretea, T. D. Tilley, *Inorg. Chim. Acta* **1999**, *287*, 152−8.
[4] R. H. Herber, O. J. Scherer, *Inorg. Chim. Acta* (in press).
[5] [5a] O. J. Scherer, C. Blath, G. Wolmershäuser, *J. Organomet. Chem.***1990**, *387*, C21−24. − [5b] O. J. Scherer, *Acc. Chem. Res.* **1999**, *32*, 751−762.
[6] For Mössbauer studies of inorganic Fe/As compounds, see for example: A. M. van der Kraan, K. H. J. Buschow, *Physica B+C*,**1986**, *138*, 55−62; S. K. Kulshreshta, *Phys. Stat. Solidii b* **1990**, *160*, 313−20; F. Grandjean, A. Gerard, R. Sobry. *J. Magn. and Magn. Mater.* **1975**, *1*, 64−72 **1972**, *3*, 1; K. Venugopalan, R. Chandra, J. Varma, D. R. S. Somayajulu, *Chem. Abstr.* **1985**, *102*, 157432q; L. Haeggstroem, A. Gustavsson-Seidel, H. Fjellvaeg, *Europhys. Letters,***1989**, *9*, 87−91.
[7] R. H. Herber, to be published. See also K. L. Cunningham, D. R. McMillin, *Polyhedron* **1996**, *15*, 1673−75.
[8] L. Phillips, A. R. Lacey, M. K. Cooper, *J. Chem. Soc., Dalton Trans.* **1988**, 1383−91, and references therein.
[9] R. H. Herber, *Chemical Mössbauer Spectroscopy* (Ed.: R. H. Herber), Plenum Press, New York, **1984**, 203−4.
[10] R. L. Collins, *J. Chem. Phys.* **1965**, *42*, 1072−1080.
[11] N. N. Greenwood, T. C. Gibb, in *Mössbauer Spectroscopy*, Chapman and Hall, London, **1971**, pp 74−66; V. I. Gol'danskii, E. F. Makarov, in *Chemical Applications of Mössbauer Spectroscopy* (Eds.: V. I. Gol'danskii and R. H. Herber), Academic Press, New York, **1968**, pp 102−7 and references therein.
[12] M. Naruse, M. Sorai, M. Sakiyama, *Molec. Cryst. Liq. Cryst.* **1983**, *101*, 219−34; E. Maverick, J. D. Dunitz, *Molecular Physics*, **1987**, *62*, 451; P. Seiler, J. D. Dunitz, *Acta Cryst.* **1979**, *B35*, 1068−74; F. Takusagawa, T. F. Koetzle, *Acta Cryst.* **1979**, *B35*, 1074−81; *J.* W. Edwards, G. L. Kington, R. Mason, *Trans. Farad. Soc.***1960**, *56*, 660−67.
[13] R. Blom, Th. Brück, O. J. Scherer, *Acta Chem. Scand.* **1989**, *43*, 458−62.

Received June 5, 2000
[I00226]

Alkane Hydroxylation by Cytochrome P450: Is Kinetic Isotope Effect a Reliable Probe of Transition State Structure?

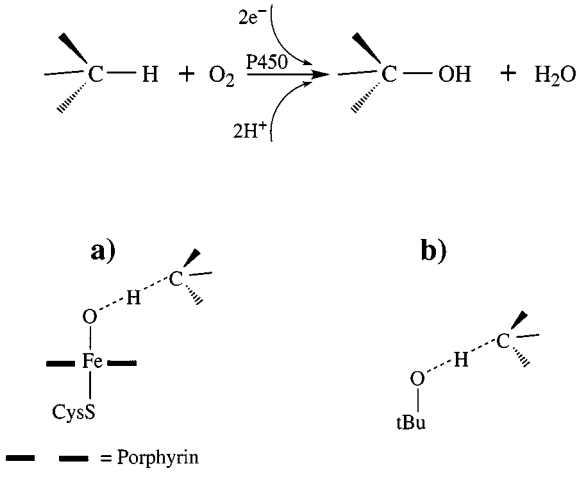
François Ogliaro,[a] Michael Filatov,[a] and Sason Shaik*[a]

Keywords: Density functional calculations / Isotope effects / Cytochrome P450 / Hydroxylation / Metalloenzymes

Computed kinetic isotope effect (*KIE*) values for methane hydroxylation by Cytochrome P450, in both high- and low-spin states, compare well with *KIE*'s for model hydrogen abstraction reactions, thereby demonstrating the utility of *KIE* as a mechanistic probe and supporting a two-state-rebound mechanism.

Introduction

Kinetic Isotope Effect (*KIE*) has been used extensively as a mechanistic probe in alkane hydroxylation by Cytochrome P450, Scheme 1.[1−5] In view of the importance of the process, and the questions which still surround its mechanism, it is deemed essential to establish the mechanistic significance of *KIE* by theoretical means in a manner that can be related to experimental measurements and mechanistic questions.



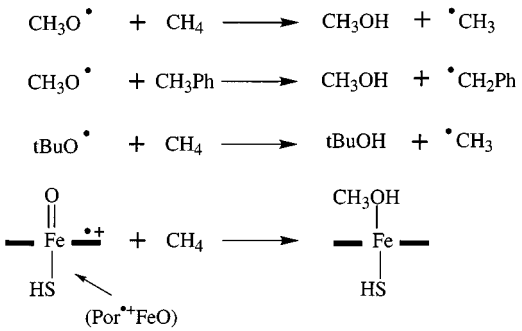
Scheme 1. Alkane hydroxylation by Cytochrome P450: **a**) and **b**) describe the proposed isostructural transition states based on kinetic isotope effect studies[6]

Let us first mention experimental data which form the primary motivation for this study. Thus, Dinnocenzo-Jones and co-workers have investigated the *intrinsic* $KIE_{H/D}$, for C−H vs. C−D hydroxylation[6] in a series of substrates undergoing P450 hydroxylation vis à vis hydrogen abstraction by the tertiary butoxyl radical. The $KIE_{H/D}$ data for the two processes were found to exhibit a good linear correlation as well as a virtual identity of the individual $KIE_{H/D}$ values for hydrogen abstraction and P450 oxidation of each substrate. These findings suggest, in agreement with earlier conclusions by Meunier et al.,[4] that the transition state for the bond activation step of P450 hydroxylation possesses a structure with a co-linear O−H−C moiety, as in a hydrogen abstraction process (**a** and **b**, Scheme 1). This structural feature of the transition state supports the "rebound" mechanism of alkane hydroxylation by P450.[1] However, since the rebound mechanism has been questioned by recent mechanistic investigations,[7,8] theoretical calculations are necessary to assess the mechanistic utility of the Dinnocenzo-Jones concept as a means to probe transition state structure.

To tackle this problem, we carried out density functional calculations of $KIE_{H/D}$ in the model hydroxylation reaction, Scheme 2, where methane is used as a substrate and the ferryl-oxene oxidant ($Por^{\bullet+}FeO$) carries a simplified thiolate ligand.[9,10] These $KIE_{H/D}$ values are compared with three model hydrogen abstraction processes by methoxyl and tertiary-butoxyl radicals, using methane and toluene as substrates. The mechanism for methane hydroxylation by ferryl-oxene was determined in recent work,[9,11] and the results are schematized in Figure 1. It was found that hydroxylation proceeds by a two-state-rebound mechanism of the high-spin (HS) quartet state and the low-spin (LS) doublet state, both nascent from the corresponding states of ferryl-oxene.[9,11] The processes exhibit two-phases with distinct atomic rearrangements; C−H bond activation and rebound. The bond activation takes place via two closely lying transition states ($^{4,2}TS_H$). Subsequently, the HS reaction proceeds to form an iron-hydroxo intermediate and a $CH_3^{\cdot}$ radical with a significant barrier for rebound. On the other hand, the ^2TS_H transition state collapses to alcohol products in a virtually barrier-free fashion, making the LS process effectively concerted.[9,11] In the present study we determine $KIE_{H/D}$ values for both HS and LS surfaces. These results are compared with the corresponding $KIE_{H/D}$ values of the radical abstraction reactions (Scheme 2), and enable us to assess the Dinnocenzo-Jones method,[6] and answer the title question.

[a] Department of Organic Chemistry and The Lise Meitner-Minerva Center for Computational Quantum Chemistry, Hebrew University,
91904 Jerusalem, Israel
Fax: (internat.) +972-2/658-4680
E-mail: sason@yfaat.ch.huji.ac.il

 © WILEY-VCH Verlag GmbH, D-69451 Weinheim, 2000 1434−1948/00/1212−2455 $ 17.50+.50/0



Scheme 2. Model reactions for kinetic isotope effect calculations

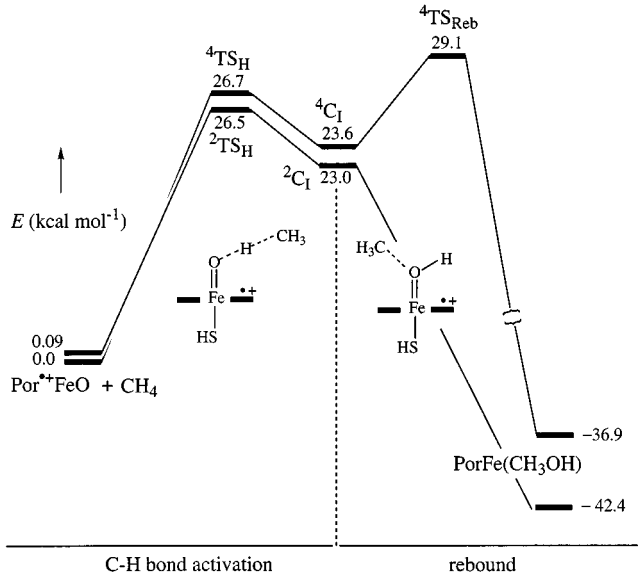


Figure 1. Calculated two-state rebound mechanism for methane hydroxylation by a model ferryl-oxene

Results and Discussion

All calculations were done with the GAUSSIAN98 package of programs.[12] The hybrid (HF/DFT) density functional UB3LYP calculations[13] was used. The Los Alamos effective core potential coupled with the double-zeta LACVP basis set[14] on iron and the 6−31G basis[12] for the rest of the atoms (hence, ECP+LACVP-6−31G). Geometries for all the species were fully optimized without symmetry constraints.[9,11] Here, the reactants, transition states, intermediates and alcohol products for all processes in Scheme 2 were ascertained by frequency calculations. Possible dependence of the KIE on the basis set was tested for the model hydrogen abstraction reaction by the alkoxyl radicals. Semiclassical *KIE* values[15] were determined from the Eyring equation using free energies of activation. Tunneling corrections[15] of the semiclassical *KIE* values were examined using three different models: the asymmetrical Eckart potential model,[15,16] the Bell model[15,16] and the Wigner model.[15,16]

Figure 2 shows essential features of the O−H−C portions of the transition states for the HS and LS bond activation, $^{4,2}TS_H$, and the model transition states for hydrogen abstraction by methoxyl and tertiary butoxyl radicals, $^2TS_{MeO}$, $^2TS_{Tol}$, and $^2TS_{tBuO}$. The latter three transition states are seen to be slightly more "central" than the P450 transition states, but otherwise the four transition states are similar. In all the structures, C−H cleavage is significant and the O−H−C portion is close to being linear. A negative spin density on the hydrogen flanked by positive densities on the heavy atoms is a mark of three-electron delocalization over three centers. The observation of such a feature in the transition states shows that all of them involve three electrons delocalized in the O−H−C portion, thereby emphasizing the common electronic structure shared by these transition states. This similarity supports the concept of Dinnocenzo-Jones and co-workers[6] that the hydrogen abstraction reaction by *t*BuO· models the bond activation in C−H hydroxylation by Cytochrome P450.

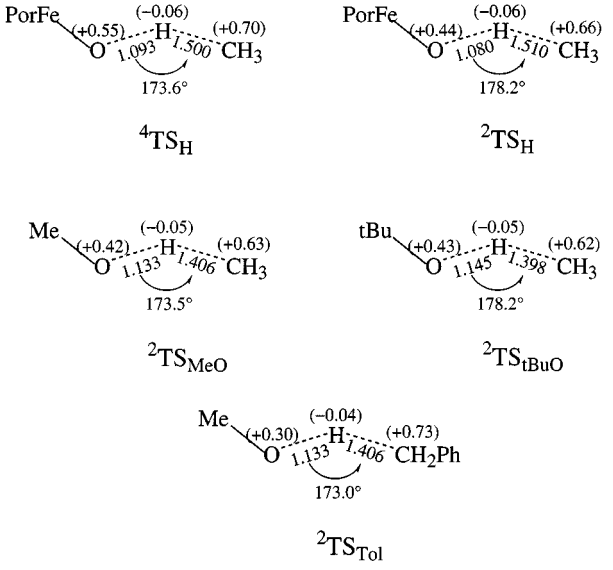


Figure 2. Transition state structures for the model reactions in Scheme 2; data in parentheses correspond to group spin densities; the spin densities on the oxygen atom P450 transition states ($^{2,4}TS_H$) are atomic spin densities and do not include the density on the rest of the species (hence the sum is not unity)

Table 1 shows computed $KIE_{H/D}$ for the four reactions; semiclassical values (3rd line), as well as tunneling corrected ones (fourth, fifth and sixth lines). As can be seen from the semiclassical values for the alkoxyl radicals, improvement of the basis set increases the $KIE_{H/D}$ values by less than 5%. Changing the substrate from methane to toluene has a small effect too (*ca* 15%). Due to the size of the problem, we cannot upgrade the frequency calculations for the P450 reactions, but the preceding comparisons indicate that the ECP+LACVP-6−31G results can be regarded with credence.

As shown in Table 1, the approximate tunneling corrections are extremely sensitive to the imaginary frequency of the transition state. All three different types of tunneling corrections agree with one another for the imaginary fre-

Table 1. Imaginary frequencies (cm^{-1}) in the transition states (TS) of the four processes (Figure 2), and calculated *KIE* values at T = 298.15 K; the Eckart correction for the doublet state is calculated with parameters for an effectively concerted process

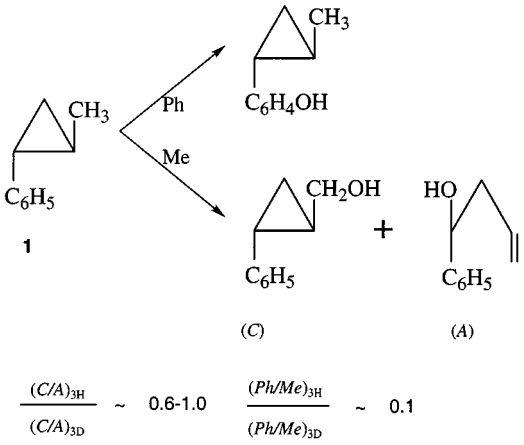
	^2TS_H [a]	^4TS_H [a]	$^2TS_{MeO}$ [a][b]	$^2TS_{tBuO}$ [a][b]	$^2TS_{Tol}$ [a]
ν_H	*i*703	*i*942	*i*1337 [*i*1648]	*i*1458 [*i*1709]	*i*1002
ν_D	*i*604	*i*764	*i*1006 [*i*1216]	*i*1090 [*i*1261]	*i*787
$KIE_{H/D}$					
semi-classical	5.10	5.87[c]	6.17 [6.36]	6.46 [6.47]	5.28
Wigner	5.57	6.97	8.51 [9.49]	9.19 [9.75]	6.51
Eckart	5.95	7.53	11.26 [21.55]	15.15 [28.22]	8.44
Bell	5.94	9.13	63.76 [2.39]	11.51 [1.04]	9.61

[a] Out of brackets are results of the ECP+LACVP-6−31G (for the P450 reactions) and 6−31G (for alkoxyl reactions) basis sets. − [b] In square brackets 6−31G* results. − [c] At T = 278 K the semi-classical $KIE_{H/D}$ for P450 is 6.95, close to the maximum limit.[4]

quencies below ca. 1000 cm^{-1}, but show strong basis set- and model dependence for higher frequencies. Apparently, such situations cannot be adequately treated by the one-dimensional tunneling corrections. Unfortunately, the size of the P450 species does not allow us to perform sophisticated calculations of the tunneling. However, for P450 situations, the tunneling correction for the three models, changes the $KIE_{H/D}$ values by less than 20% (see Table 1). Thus, tunneling has a modest effect on the $KIE_{H/D}$ values, and the semiclassical $KIE_{H/D}$ values may be used for comparison with the experiment.[6] A similar estimation of the role of tunneling in this reaction has been done by Meunier et al.[4]

The Dinnocenzo-Jones[6] $KIE_{H/D}$ values for hydrogen abstraction from toluene and *p*-xylene by *t*BuO$^{\cdot}$ are 6.0 ± 0.2 and 6.3 ± 0.3, respectively, compared with 5.9 ± 0.35 and 6.4 ± 0.90 for the corresponding P450 hydroxylations. The average computed $KIE_{H/D}$ for P450 hydroxylation is only 5−15% lower than the corresponding values for the hydrogen abstraction by alkoxyl radicals. Considering the spread of the experimental values, of 10−15%, our computed results exhibit a reasonable match between the $KIE_{H/D}$ values for hydrogen abstraction by alkoxyl groups and those for the bond activation step in P450 hydroxylation. The common features of transition state structures, discussed in Figure 2, and the similarity of $KIE_{H/D}$ values support, therefore, the mechanistic conclusion of Dinnocenzo and Jones[6] based on $KIE_{H/D}$ profiles of P450 C−H hydroxylation vis à vis a model hydrogen-abstraction reaction. The results indicate that the kinetic isotope effect can serve as a reliable probe of the transition state structure in P450 hydroxylation, and support the rebound mechanism.[1]

It is interesting to apply these results on the $KIE_{H/D}$ profiles to another situation where the deuterium substitution comes into play. Recently, Newcomb and co-workers[17−19] have shown that a substitution of the CH_3 group of **1**, Scheme 3, by CD_3, changes the regioselectivity by an order of magnitude, from a methyl to a phenyl oxidation ("metabolic switching"). However, the amount of rearrangement due to C−H hydroxylation of **1**, measured by the ratio of cyclic to acyclic products (*C*/*A*), exhibits a small isotope effect, if any.[17,18] The metabolic switching implies a large *KIE* on the C−H hydroxylation in agreement with independent measurements[1−5] of internal *KIE* values. What could then be the mechanistic significance of a small product isotope effect on the *C*/*A* ratio? Is it always going to be small, or will it change, and if so what factors govern its change?



Scheme 3. Results of oxidation of probe **1** by Cytochrome P450 [17−19]

From mutation studies, Newcomb[19] has concluded that probe **1** undergoes C−H hydroxylation mostly, if not exclusively, by ferryl-oxene. If the hydroxylation occurs by the classical rebound mechanism with a single oxidant species, where the oxidant participates with a single reactive state and produces free radicals in the first step of the reaction, a constant *C*/*A* value (subject only to secondary isotope effects) will always result. However, as already mentioned, this scenario faces difficulties to account for the trend of radical lifetimes and for the incomplete scrambling often observed.[7,8]

These difficulties can be circumvented in the two-state-rebound mechanism. In this scenario (Figure 1), rearrangement occurs only on the HS surface which exhibits a barrier for the radical rebound.[9,11] In the event where the ferryl-oxene oxidant engages primarily or exclusively in C−H hydroxylation,[20,21] the isotope effect on the *C*/*A* ratio of a probe like **1** will be gauged by the ratio of the isotope effects for the HS and LS processes.[20,21] In the extreme situations, where the kinetic isotope effects for the HS and LS processes are very different, i.e., either $(KIE_{H/D})^{HS} >> (KIE_{H/D})^{LS}$ or $(KIE_{H/D})^{HS} << (KIE_{H/D})^{LS}$, replacement of the methyl group by deuteriomethyl will considerably slow down either the HS or the LS processes, thereby causing the $(C/A)_{3D}$ ratio to either increase or decrease dramatically relative to $(C/A)_{3H}$. Thus, a significant product isotope effect is expected under such conditions. In contrast, identical $KIE_{H/D}$ values for the HS and the LS processes can lead to a constant *C*/*A* ratio (neglecting secondary isotope effect).[20] The $KIE_{H/D}$ values in Table 1 for the HS and the LS processes are not identical, however they differ by only 15% of each other. If these *KIE* results are relevant to the probe substrate **1** in Scheme 2, they would predict a small

isotope effect on the *C*/*A* ratio,[21] as is found experimentally.[17]

It is important to emphasize that the near equality, $(KIE_{H/D})^{HS} \approx (KIE_{H/D})^{LS}$, in our calculation arises due to the structural similarity of the corresponding transition-state structures for the two states (Figure 2). The HS and LS transition structures have been predicted before to depend on the donor ability of the substrate (probe) and on the binding capability of the cysteinato ligand which can introduce structural variations between the two paths.[9,11] Thus, the two-state-reactivity scenario predicts some dependence of the product isotope effect on the *C*/*A* ratio on these factors, as well as on the rates of rearrangement and rebound of the free radical clock.[20] No such dependencies will be expected when the rebound mechanism proceeds on a single state surface and with a single oxidant.

Conclusions

In summary, the combination of a small isotope effect on the *C*/*A* ratio in P450 hydroxylation, along with the match of *KIE* values to model hydrogen-abstraction reactions have jointly a clear mechanistic significance in terms of two-state reactivity.[22,23] Other scenarios are possible; for example, a large product isotope effect on the *C*/*A* ratio will indicate either a more complex mechanistic scheme of two state reactivity,[21] or two-oxidants which participate in C−H hydroxylation.[7,8] It is hoped that this work will form the incentive to further articulate the various models and elucidate the mechanistic significance of *KIE* in P450 hydroxylation.

Acknowledgments

This research was sponsored by The Israeli Science Foundation (ISF) and in part by the Volkswagen Stiftung and The Israel Ministry of Science. F. O. thanks the EU for a Marie Curie Fellowship. Helpful discussions with J. P. Dinnocenzo, J. T. Groves, J. P. Jones, M. Newcomb and B. Meunier are acknowledged.

[1] J. T. Groves, Y.-Z. Hang, in Cytochrome P450: Structure, Mechanisms and Biochemistry, (Ed.: P. R. Ortiz de Montellano), Plenum Press, NY, *2nd ed.* **1995**, p 3−48.
[2] W.-D. Woggon, *Top. Curr. Chem.* **1996**, *184*, 40−96.
[3] M. Sono, M. P. Roach, E. D. Coulter, J. H. Dawson, *Chem. Rev.* **1996**, *96*, 2841−2887.
[4] A. Sorokin, A. Robert, R. Meunier, *J. Am. Chem. Soc.* **1993**, *115*, 7293−7299.
[5] C. Audergon, K. R. Iyer, J. P. Jones, J. F. Darbyshire, W. F. Trager, *J. Am. Chem. Soc.* **1999**, *121*, 41−47.
[6] J. I. Manchester, J. P. Dinnocenzo, L. A. Higgins, J. P. Jones, *J. Am. Chem. Soc.* **1997** *119*, 5069−5070.
[7] M. Newcomb, R. Shen, S.-Y. Choi, P. H. Toy, P. F. Hollenberg, A. D. N. Vaz, M. J. Coon, *J. Am. Chem. Soc.* **2000**, *122*, 2677−2686.
[8] M. Newcomb, M.-H. Le Tadic, D. A. Putt, P. F. Hollenberg, *J. Am. Chem. Soc.* **1995**, *117*, 3312−3313.
[9] N. Harris, S. Cohen, F. Ogliaro, M. Filatov, S. Shaik, *Angew. Chem. Int. Ed.* **2000**, *39*, 2003−2007.
[10] The HS^- ligand was shown to be a good mimic of the full cysteinato ligand, and better than CH_3S^-, by criteria of bond energy and energy spread of the state manifold. See: F. Ogliaro, S. Cohen, N. Harris, S. de Visser, M. Filatov, S. Shaik, *Angew. Chem.*, in press.
[11] F. Ogliaro, S. Cohen, N. Harris, S. de Visser, M. Filatov, S. Shaik, *J. Am. Chem. Soc.* **2000**, *122*, 8977−8989.
[12] *GAUSSIAN98*, Gaussian, Inc., Pittsburgh PA, **1998**.
[13] P. J. Stevens, F. J. Devlin, C. F. Chablowski, M. J. Frisch, *J. Phys. Chem.* **1994**, *98*, 11623−11627.
[14] LACVP: J. P. Hay, W. R. Wadt, *J. Chem. Phys.* **1985**, *82*, 299−308.
[15] L. Mellander, W. H. Saunders, Jr., *Reaction Rates of Isotopic Molecules*, Wiley Interscience, N. Y., **1980**, Ch. 1−2.
[16] Our program can calculate Bell corrections [ref. 15], Wigner corrections [ref. 15], and Eckart corrections. The latter correction uses the description in, H. S. Johnston, J. Heicklen, *J. Chem. Phys.* **1962**, *66*, 532−533.
[17] J. K. Atkinson, P. F. Hollenberg, C. Johnson, M.-H. Le Tadic, M. Newcomb, D. A. Putt, *Biochemistry* **1994**, *33*, 10630−10637. [1.04 ± 0.24 for racemic mixture of the probe, and 0.6−0.7 (±0.1) for the pure enatiomers (*R,R*)-**1** and (*S,S*)-**1**].The data seem to show an apparent discrepancy between the *C*/*A* ratios for the racemic mixture vis à vis the pure enantiomers. However, the uncertainties of the data are of the same order as the discrepancy.
[18] The *KIE* on the *C*/*A* ratio is more reliable than the KIE values on the methyl/phenyl oxidation ratios which may reflect selective binding [ref. 5].
[19] P. H. Toy, M. Newcomb, M. J. Coon, A. D. N. Vaz, *J. Am. Chem. Soc.* **1998**, *120*, 9718−9719.
[20] Using a simple two-state C−H hydroxylation scheme[11] with spin-state crossing leads to an equal partition of the HS and LS paths, one gets the following expression for the product isotope effect on the *C*/*A* ratio, $(C/A)_{3H}/(C/A)_{3D} = (KIE_{H/D})^{LS}/(KIE_{H/D})^{HS}\{[1+\xi_H]/[1+\xi_D]\}$, where $\xi_H = (k_{HS}{}^H/k_{LS}{}^H)[k_{OH}/(k_r+k_{OH})]$ and $\xi_D = (k_{HS}{}^D/k_{LS}{}^D)[k_{OH}/(k_r+k_{OH})]$. The various terms refer to Figure 1, as follows: k_{OH}: the rebound rate on the HS surface; k_r: the rate of free radical rearrangement on the HS surface. k_{HS} and k_{LS} are the rate constants of the bond activation of the HS and LS surfaces, where the superscripts H and D refer to the hydrogenic and deuterio isotopomers. The situation in which $\xi_H \approx \xi_D$ means, necessarily, that $(KIE_{H/D})^{LS} \approx (KIE_{H/D})^{HS}$, and leads to $(C/A)_H/(C/A)_D \approx (KIE_{H/D})^{LS}/(KIE_{H/D})^{HS} \approx 1$.
[21] If, however, ferryl oxene is engaged significantly also in phenyl oxidation, the kinetic expression becomes more complex. Then the $(C/A)_{3H}/(C/A)_{3D}$ ratio can be significantly different than unity, even if the *KIE's* are the same for the HS and LS path. We thank J. P. Jones for communicating this point.
[22] D. Schröder, S. Shaik, H. Schwarz, *Acc. Chem. Res.* **2000**, *35*, 139−145.
[23] N. Harris, S. Shaik, D. Schröder, H. Schwarz, *Helv. Chem. Acta* **1999**, *82*, 1784−1797.

Received August 18, 2000
[I00324]

Cobalt-Assisted Condensation of 2-Butanone Oxime and Acetone: Synthesis and X-ray Structure of the Novel Acetaldiimine Complex $[CoI_2\{((CH_3CH_2)(CH_3)C{=}NO)_2C(CH_3)_2\}]$

Jean-Cyrille Hierso,[a] Dianne D. Ellis,[b] Anthony L. Spek,[b] Elisabeth Bouwman,*[a] and Jan Reedijk[a]

Keywords: Cobalt / Ketoximes / Ketones / Template synthesis / Metallacycles / Acetaldiimine

The synthesis of the first acetaldiimine cobalt complex and its full characterisation are reported. The nitrogen-bonded chelate complex $[CoI_2\{((CH_3CH_2)(CH_3)C{=}NO)_2C(CH_3)_2\}]$ is obtained in high yield from the reaction of 2-butanone oxime with cobalt iodide dihydrate in acetone, in the presence of trimethyl orthoformate as dehydrating agent. A single-crystal X-ray structure determination, infrared spectroscopy and mass spectrometry analyses confirm the formation of a new ligand in situ from the addition of an acetone molecule to two oximato species. This cobalt-mediated reaction provides an indirect proof for the existence in solution of monodentate *N*-bonded cobalt–ketoxime species.

Introduction

The chemistry of oxime/oximato transition metal complexes is rich and has shown a great variety of reactivity modes, as demonstrated in the review by Kukushkin et al.[1] Simple oxime complexes[2] (or mono-oximes as opposed to chelating dioximes) are known to form with palladium, nickel[3] or platinum, for which they have been thoroughly studied.[4] These compounds display generally a strict monodentate coordination to the metal by bonding through the nitrogen centre. To date, the analogous cobalt-ketoxime complexes still remain unknown, and only a single cobalt-aldoxime complex has been reported which displays monodentate coordination.[5] Thus, although several hundred complexes of cobalt-dioximes have been identified, the stabilisation and proper description of cobalt mono-ketoxime complexes, especially monodentate ones (either N- or O-bonded), still remains challenging. In the course of our attempts to isolate new cobalt species with simple ketoxime ligands from cobalt halide salts,[6] we have identified an as-yet-unknown reactivity of cobalt allowing the addition of 2-butanone oxime to acetone.

Results and Discussion

The title compound $[CoI_2\{((CH_3CH_2)(CH_3)C{=}NO)_2C(CH_3)_2\}]$ (**1**) was prepared from the reaction of $CoI_2{\cdot}2H_2O$ with a solution of $(CH_3CH_2)(CH_3)C{=}NOH$ in acetone, in the presence of trimethyl orthoformate. The new compound was characterised by infrared spectroscopy, elemental analysis, mass spectrometry and single-crystal X-ray crystallography. A fully labelled representation of the molecular structure of the complex is given in Figure 1. The cobalt(II) atom is surrounded by two iodide and two nitrogen atoms in a distorted tetrahedral environment. The two nitrogen atoms linked to cobalt are part of a novel chelating ligand, which has been formed in situ from two 2-butanone oxime molecules bridged by a $-C(CH_3)_2-$ unit. The six-membered ring formed by the acetaldiimine ligand at cobalt forces the N(1)−Co(2)−N(2) angle to contract to 96.31(13)°, whilst the angle I(1)−Co(1)−I(2) opens to 117.32(2)°, resulting in a distorted tetrahedron around Co. The Co−I distances [Co(1)−I(1) 2.5508(7), Co(1)−I(2) 2.5802(6) Å] are in the range of values reported for CoI_2 in a tetrahedral environment.[7] The bond distances in the acetaldiimine ligand are in very good agreement with those of the related compound previously described in the crystallographic literature [1,1-bis(1-phenylethylidenaminooxy)-ethyl]benzene.[8] The six-membered Co(1)−N(1)−O(1)−C(2)−O(2)−N(2) ring adopts a flattened boat conformation at the temperature of measurement. The chair-like conformation for this kind of metal−ligand rings is common,[9] whereas boat forms are rarely observed.[10]

The infrared measurements confirmed the chelating cyclization of the 2-butanone oxime molecules by both the disappearance of the oxime OH stretching vibration at 3214 cm^{-1}, and the large shift of the C=N stretching vibration from 1664 cm^{-1} in the free simple oxime to 1620 cm^{-1} in the bound acetaldiimine. From electrospray mass spectrometry experiments on **1**, the parent peak has been found at m/z = 215; this value corresponds to the ionic fragment $[H(CH_3CH_2)(CH_3)C{=}NO)_2C(CH_3)_2]^+$, which confirms not only the formation but also the stability of the acetaldiimine ligand.[11] Our attempts to isolate the cobalt chloride and cobalt bromide analogues of **1** have failed, producing sticky

[a] Leiden Institute of Chemistry, Gorlaeus Laboratories, Leiden University,
PO Box 9502, 2300 RA Leiden, The Netherlands
[b] Bijvoet Center for Biomolecular Research, Crystal and Structural Chemistry, Utrecht University,
Padualaan 8, 3584 CH Utrecht, The Netherlands
E-mail: Bouwman@chem.leidenuniv.nl
Tel: (internat.) +31-71/527-4459

 © WILEY-VCH Verlag GmbH, D-69451 Weinheim, 2000 1434−1948/00/1212−2459 $ 17.50+.50/0

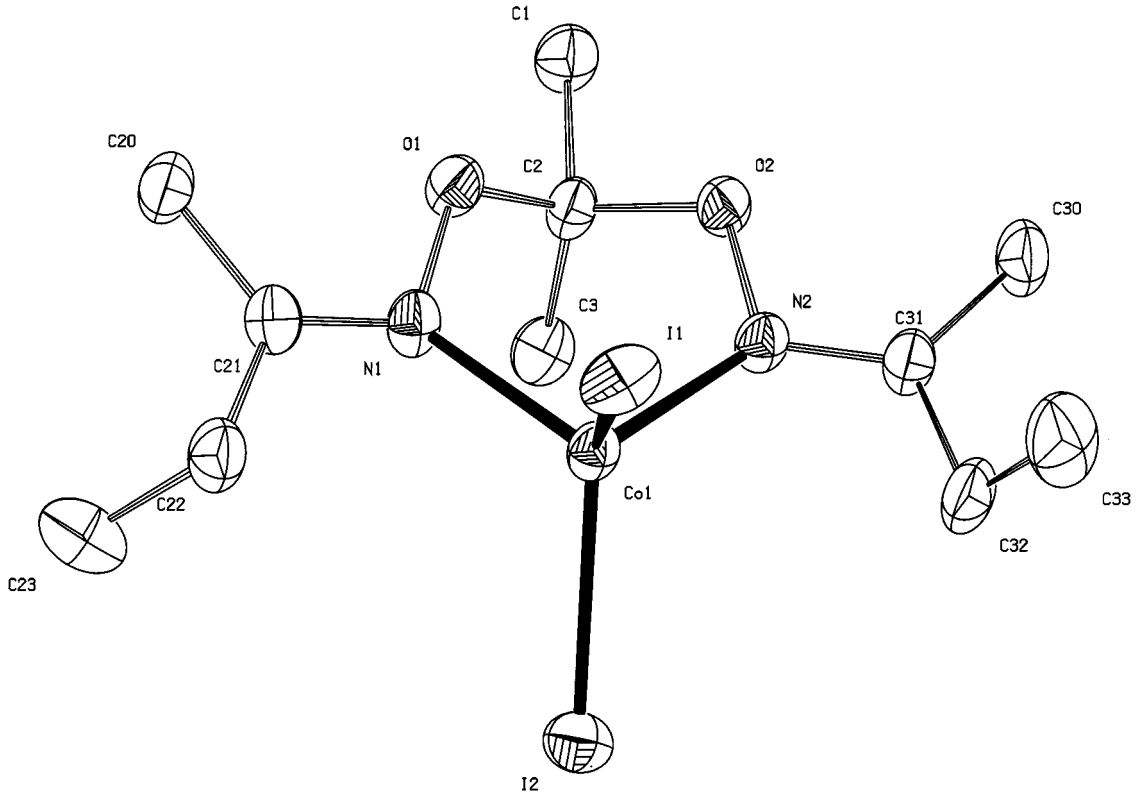


Figure 1. Ortep view at 50% probability level of the molecular structure of **1**; selected bond lengths [Å] and bond angles [°]: Co(1)−I(1) 2.5508(7), Co(1)−I(2) 2.5802(6), Co(1)−N(1) 2.029(3), Co(1)−N(2) 2.035(3), N(1)−C(21) 1.281(5), N(2)−C(31) 1.286(5), O(1)−N(1) 1.422(4), O(2)−N(2) 1.421(4); I(1)−Co(1)−I(2) 117.32(2), I(1)−Co(1)−N(1) 105.46, I(1)−Co(1)−N(2) 109.68(10), I(2)−Co(1)−N(1) 114.61(10), I(2)−Co(1)−N(2) 111.34(10), N1−Co(1)−N(2) 96.31(13), N(1)−O(1)−C(2) 113.9(3), N(2)−O(2)−C(2) 114.2(3), Co(1)−N(1)−O(1) 115.83(18), Co(1)−N(2)−O(2) 119.3(2), O(1)−C(2)−O(2) 110.6(4)

oils which are difficult to characterise. The van der Waals volume of the iodide ions, which is considerable larger than those of the smaller halide analogues, possibly permits the crystallisation of the complex. The tetrahedral geometry around cobalt is confirmed by Vis-NIR spectroscopy (typical broad band split in three, centred around 7000 cm^{-1} and a more intense band around 15000 cm^{-1}).

The global equation for the reaction leading to the acetaldiimine can be written as:

$$2\ RR'C{=}N{-}OH + (CH_3)_2C{=}O \rightleftarrows H_2O + RR'C{=}N{-}O{-}C(CH_3)_2{-}O{-}N{=}CR'R$$

The use of trimethyl orthoformate, which reacts readily with water molecules to form methanol and methyl formate,[12] displaces the above equilibrium to the right toward the formation of the adduct. Experiments with 2-butanone oxime and acetone (four equivalents) refluxed at 80 °C for three hours in either an acidic (pH = 3), neutral, or basic (pH = 12) medium, in the absence of the cobalt salt, do not show any changes in the infrared and ^1H NMR spectra of the mixture. Similar attempts conducted in the presence of trimethyl orthoformate also failed to yield the acetaldiimine, showing the need for cobalt in order to perform the condensation of the oxime and acetone.

Oximes, being weak oxygen acids, can react with bases and undergo deprotonation. Literature reports state that the nitrogen coordination of oxime ligands to a metal centre leads to a large increase in their acidic character, and the formation of oximato ligands is favourable upon coordination. It has also been shown that oximes behave as nucleophiles towards other unsaturated species such as olefins, arenes or ketones involving nucleophilic addition by either the O or the N atom.[1] From these data the following hypothesis can be proposed concerning the global mechanism of formation of the ligand and the complex: (i) the 2-butanone oxime molecules could coordinate to the cobalt centre giving a strong acidic character at their OH hydrogen atoms, (ii) the electrophilic attack of an acetone molecule towards the activated oxygens in the coordination sphere of the metal could then take place, the formation of the adduct being favoured by the progressive consumption of water by reaction with trimethyl orthoformate (without this reactant no compound has been isolated). Following this idea, the formation of the complex should be favoured in alkaline medium and disfavoured in acidic medium. Indeed, the synthesis conducted with addition of 0.1 mL of 1 M NaOH solution in water leads to **1** precipitating quickly as a fine powder, whereas from an acidic medium (addition of 0.1 mL of HCl in water at pH = 2), compound **1** could not be isolated. It is worthwhile to note that conventional acetal formation is acid-catalysed and does not proceed under alkaline conditions, contrary to this metal-mediated reaction. The qualitative observations reported above support the

formation in solution of intermediary N-bonded monodentate cobalt-ketoxime species, explaining the OH acidic activation towards the oximato species. However, these N-bonded monodentate cobalt-ketoxime complexes still have to be isolated.

Only a few other examples of the metal-assisted addition of oximes to compounds containing double or triple bonds are described in the literature.[13,14] Amongst these the most notable one was described by Kukushkin et al.:[15] from the reaction of the platinum(II) complex $[PtCl_2((CH_3)_2C{=}NOH)_2]$ with *m*-chloroperoxybenzoic acid in acetone the *N*,*O*-chelating complex $[PtCl_2\{OC(CH_3)_2ON{=}C(CH_3)_2\}_2]$ was obtained which contains two five-membered Pt−N−O−C−O rings. The most likely explanation for the formation of the product was proposed to be the coordination of acetone molecules at vacant sites on platinum, followed by ring closure with neighbouring N-coordinated monodentate oxime ligands. Here, the isolated platinum bis(ketoxime) species is the starting product, and, similarly, a cobalt-ketoxime compound is assumed to be an intermediate in the formation of **1**.

In conclusion, this work describes a novel template reaction of acetone with two ketoxime molecules, forming a symmetric chelating diimine ligand with an acetal backbone. Applications of this template reactivity in syntheses of new diimine ligands can be of interest in comparison to the "organic" routes reported so far,[16] and might be further explored.

Experimental Section

Acetone was distilled, dried and degassed over molecular sieves under an argon atmosphere. Other reactants and solvents were used as received from commercial sources. Vis-NIR spectra were obtained on a Perkin−Elmer Lambda 900 spectrophotometer using the diffuse reflectance technique with MgO as a reference. Infrared spectra were obtained on a Perkin−Elmer Paragon 1000 FTIR spectrophotometer equipped with a Golden Gate ATR device, using the reflectance technique (4000−500 cm^{-1}, res. 4 cm^{-1}). NMR measurements were performed at 300.13 MHz on a Bruker 300 DPX spectrometer. Mass spectrometry and elemental analyses were performed in the analytical service department of the Gorlaeus laboratories.

IR of 2-Butanone Oxime: Selected bands (cm^{-1}): $\tilde{\nu}$ = 923 vs/br, 975 vs; 1072 s, 1096 s, CC stretching; 1368 s, 1458 s, CH bending; 1664 m, C=N stretching; 2880 m, 2972 m, sh, CH stretching; 3214 s, br, OH stretching.

Synthesis of $[Co\{((CH_3CH_2)(CH_3)C{=}NO)_2C(CH_3)_2\}I_2]$ (1): $CoI_2{\cdot}2H_2O$ (0.65 g, 1.9 mmol) in an Erlenmeyer flask was covered by 2.5 mL of trimethyl orthoformate and then dissolved in 10 mL of dry acetone to give a bright deep green solution. An excess of 2-butanone oxime (0.60 g, 7.3 mmol) in 15 mL of dry acetone was prepared. The two solutions were boiled and mixed, the mixture was boiled for 5−6 minutes to reduce the volume to approximately 10 mL. After 24 h standing in air, almost all the residual solvent was evaporated and bright green needles were formed. The crystals were washed with a minimum of acetone, and quickly with 2 × 1 mL of diethyl ether, then with pentane, resulting in 0.78 g of complex (yield 80%) as single crystals suitable for X-ray diffraction measurements. $C_{11}H_{22}CoI_2N_2O_2$ (527.04): calcd. C 25.07, H 4.21, N 5.32, Co 11.18; found C 24.94, H 3.96, N 5.32, Co 11.42. − IR (cm^{-1}): $\tilde{\nu}$ = 891 vs, 933 vs; 1148 s, CO stretching; 1366 s, 1377 s, 1456 s, CH bending; 1620 s, C=N stretching; 2972 m, sh, CH stretching. Vis-NIR (solid state, cm^{-1}): $\tilde{\nu}$ = 6900, 7400, 9600, 14900, 28000.

X-ray Crystal Structure Analysis of 1: $C_{11}H_{22}CoI_2N_2O_2$, M = 527.04, dark green needles (0.21 × 0.09 × 0.09 mm^3), monoclinic, $P2_1/c$ (no. 14), a = 10.9678(3), b = 12.0102(4), c = 15.7274(4) Å, β = 119.924(2)°, V = 1795.52(10) $Å^3$, Z = 4, D_c = 1.950 $g{\cdot}cm^{-3}$, $F(000)$ = 1004, μ(Mo-K_α) = 4.392 mm^{-1}, 11288 reflections measured, 4509 independent, R_{int} = 0.036. Data were collected on a Nonius Kappa CCD area detector with rotating anode, λ(Mo-K_α) = 0.71073 Å, T = 150 K, using a graphite monochromator. Absorption corrections based on multiple measured equivalent reflections were applied. The structure was solved by Patterson techniques (DIRDIF-99[17]) and refined using full-matrix least-squares on F^2 (SHELXL-97[18]). All non-hydrogen atoms were refined with anisotropic displacement parameters, hydrogen atoms were located at calculated positions and refined riding on their carrier atoms. Refinement converged at $R1$ = 0.0331 [for 3929 reflections with $F_o > 4\sigma(F_o)$], $wR2$ value of 0.0740 (S = 1.193). Geometric calculations and molecular graphics were performed with PLATON.[19] One of the butane moieties is disordered due to an exchange of the methyl, C(30), and ethyl, C(32)−C(33), groups (major site occupancy 80% is shown in Figure 1).

Crystallographic data (excluding structure factors) for the structure in this paper have been deposited at the Cambridge Crystallographic Data Centre as supplementary publication no. CCDC-144112. Copies of the data can be obtained free of charge on application to CCDC, 12 Union Road, Cambridge CB2 1EZ, UK [Fax:+44-1223/336-033; E-mail: deposit@ccdc.cam.ac.uk].

Acknowledgments

Thanks are due to Dr. P. Gamez, Dr. J. G. Haasnoot, Mr. G. A. van Albada, Dr. W. Buijs (DSM, Geleen) and Mr. J. ter Borg and Dr. J. Bieleman (Condea Servo, Delden) for helpful discussions. The Dutch Ministry of Economic Affairs (project BTS 98141) has provided financial support. This work was supported in part (DDE, ALS) by the Council for Chemical Sciences of the Netherlands Foundation for Scientific Research (CW-NWO).

[1] V. Y. Kukushkin, D. Tudela, A. J. L. Pombeiro, *Coord. Chem. Rev.* **1996**, *156*, 333−362; V. Y. Kukushkin, A. J. L. Pombeiro, *Coord. Chem. Rev.* **1999**, *181*, 147−175.

[2] See R. C. Mehrotra, in *Comprehensive Coordination Chemistry* (Eds.: G. Wilkinson, R. D. Gillard, J. A. McCleverty), Pergamon Press, Oxford U. K., **1987**; vol. 2 pp. 276−279, and references therein.

[3] Y. Kitano, K. Kobori, M. Tanimura, Y. Kinoshita, *Bull. Chem. Soc. Jpn.* **1974**, *47*, 2969−2971; M. E. Stone, B. E. Robertson, E. Stanley, *J. Chem. Soc. (A)*, **1971**, 3632−3636.

[4] V. Y. Kukushkin, V. K. Belsky, E. A. Aleksandrova, V. E. Konovalov, G. A. Kirakosyan, *Inorg. Chem.* **1992**, *31*, 3836−3840; V. Y. Kukushkin, T. Nishioka, D. Tudela, K. Isobe, I. Kinoshita, *Inorg. Chem.* **1997**, *36*, 6157−6165.

[5] B. Norén, Å. Oskarsson, K. C. Dash, M. Mohapatra, *Acta Crystallogr.* **1990**, *C46*, 2093−2095.

[6] J.-C. Hierso, D. D. Ellis, A. L. Spek, E. Bouwman, J. Reedijk, *Chem. Commun.* **2000**, 1359−1360.

[7] See for example: M. Bonamico, G. Dessy, V. Fares, L. Scaramuzza, *Cryst. Struct. Comm.*, **1975**, *4*, 629−632; S. Gorter, W.

Hinrichs, J. Reedijk, J. Rimbault, J. C. Pierrard, R. P. Hugel, *Inorg. Chim. Acta*, **1985**, *105*, 181−186; S. Jin, M. Nieuwenhuyzen, W. T. Robinson, C. J. Wilkins, *Acta Cryst.*, **1992**, *C48*, 274−279.

[8] A. Gieren, V. Lamm, *Acta Crystallogr.* **1978**, *B34*, 3837−3840.

[9] M. Kojima, J. Fujita, *Bull. Chem. Soc. Jpn.* **1977**, *50*, 3237−3244 and references therein.

[10] T. Hosokawa, T. Ohta, S.-I. Murahashi, M. Kido, *J. Organomet. Chem.* **1982**, *228*, C55−C58.

[11] Mass spectrometry under soft conditions can give useful indications on stability of compounds, see: J.-C. Hierso, R. Feurer, P. Kalck, *Chem. Mater.* **2000**, *12*, 390−399.

[12] P. W. M. N. van Leeuwen, W. L. Groeneveld, *Inorg. Nucl. Chem. Letters.* **1967**, *3*, 145−146.

[13] J. Grigg, D. Collison, C. D. Garner, M. Helliwell, P. A. Tasker, J. M. Thorpe, *J. Chem. Soc., Chem. Commun.* **1993**, 1807−1809.

[14] R. Baker, M. S. Nobbs, *Tetrahedron Lett.* **1977**, 3759−3760.

[15] V. Y. Kukushkin, V. K. Belsky, D. Tudela, *Inorg. Chem.* **1996**, *35*, 510−513.

[16] M. G. Voronkov, N. A. Keiko, Y. A. Shuvashev, I. D. Kalikhman, V. V. Keiko, *J. Org. Chem. USSR, Eng. Transl.* **1987**, *23*, 49−52. The closely related compound acetone *O*,*O*′−2-propylidene(dioxime) was obtained in a 10.64% yield, as a by-product from the reaction of acetone oxime with butoxyethene in presence of *p*-toluenesulfonic acid.

[17] P. T. Beurskens, G. Admiraal, G. Beurskens, W. P. Bosman, S. Garcia-Granda, R. O. Gould, J. M. M. Smits, C. Smykalla, DIRDIF-99 Program System, Technical Report. Crystallography Laboratory, University of Nijmegen, The Netherlands, **1999**.

[18] G. M. Sheldrick, *SHELXL-97*. Program for crystal structure refinement. University of Göttingen, Germany, **1997**.

[19] A. L. Spek, *PLATON*. A multipurpose crystallographic tool. Utrecht University, The Netherlands, **2000**.

Received May 12, 2000
[I00199]

Influence of Charge Distribution on the Properties of Keggin- and Dawson-Type Heteropolyanions

Bineta Keita,[a] Yu Wei Lu,[a] Louis Nadjo,*[a] and Roland Contant[b]

Keywords: Polyoxometalates / Polyanions / Lacunary species / Cyclic voltammetry / Charge distribution / Acid-base equilibria

The cyclic voltammetric behavior of selected Keggin- and Dawson-type heteropolyanions has been studied as a function of electrolyte composition. The buffer capacity of the electrolyte is shown to be an important parameter that can be used to reveal the symmetry or dissymetry in charge distribution within each oxometalate. A fully symmetrical heteropolyanion like $[P_2W_{18}O_{62}]^{6-}$ exhibits a uniform protonability, while its α_1 and α_2 lacunary derivatives present a donor set of hard oxide ions with stepwise acid-base equilibria. The behavior of these sites is revealed readily in unbuffered or poorly buffered media at pH = 3, and is ascribed to the change in symmetry of charge distribution in the molecules. It is shown that cations other than the proton, even in very high excess, fail to give rise to the classical voltammograms of lacunary heteropolyanions. The same behavior also appears in $\alpha_2[Mo_2P_2W_{15}O_{61}]^{10-}$, $\alpha[PW_{11}O_{39}]^{7-}$, $\alpha[SiW_{11}O_{39}]^{8-}$, $[H_2P_2W_{12}O_{48}]^{12-}$, and, to a lesser extent, in $\alpha_2[Ni(H_2O)P_2W_{17}O_{61}]^{8-}$ and $\alpha_2[Zn(H_2O)P_2W_{17}O_{61}]^{8-}$. The analogy in the cyclic voltammograms of most dication-substituted heteropolyanions with those of the precursor lacunary species could thus be explained.

Introduction

Interest in the study of oxometalates remains at a high level due to their wide range of properties in several fields.[1−3] In particular, the main results from electrochemistry investigations by this group and from others, which establish unambiguously the existence of catalytic properties for heteropolyanions towards numerous chemicals in solution, have been reviewed recently.[4] New results concern the ability of one- and two-electron reduced heteropolyanions of the Keggin and Dawson series to convert quantitatively NO into N_2O in acidic aqueous media.[5] Unsubstituted and lacunary as well as transition metal cation substituted heteropolyanions of these two groups prove active for this purpose. Such achievements have stimulated our interest in the synthesis of heterometal-substituted heteropolyanions of these two families, with the aim of investigating their new electrocatalytic behavior.[6−10] Furthermore, the electrochemical characterization of these compounds reveals that most of them cannot be considered as "saturated" species and that the appropriate comparison remains between the cyclic voltammograms of the metal ion-substituted and the lacunary precursor oxometalates.[6,8−10] In the course of these comparisons, a strong sensitivity of the shapes, peak potential locations, and current intensities of the cyclic voltammograms to changes in the electrolyte was observed. On further scrutiny it was found that the influence appears to increase as the nominal charge of the heteropolyanion increases. Various lines of experimental evidence confirm the very low surface charge density, at least for symmetrical saturated Keggin- and Dawson-type heteropolyanions.[11−14] For example, a simple linear variation of the first reduction potentials of $\alpha[XW_{12}O_{40}]^{n-}$ with the anion charge is observed under conditions without protonation.[2] Extension of the preceding remarks to the corresponding lacunary species and to their first transition metal ion-substituted derivatives do not seem straightforward, possibly owing to the change in symmetry of the charge distribution in the molecules in conjunction with the increase in the overall negative charge. The lacunary heteropolyanions are known to exhibit "a donor set of hard oxide ions, while the adjacent d^0 (Mo^{VI}, W^{VI}) atoms provide acceptor orbitals".[1,15,16] In contrast, the classical symmetrical heteropolyacids like $H_6P_2W_{18}O_{62}$, $H_6Mo_3P_2W_{15}O_{62}$, $H_3PW_{12}O_{40}$, and $H_4SiW_{12}O_{40}$, which can be considered as the precursors of the species under investigation, are strong acids with a uniform acidity.[17]

The aim of the present paper is to illustrate the behavior, in cyclic voltammetry, of selected representative lacunary heteropolyanions and of the corresponding metal ion substituted species in the presence of various electrolytes.

[a] Laboratoire de Physicochimie des Rayonnements, UMR 8610, CNRS, Electrochimie et Photoélectrochimie, Université Paris-Sud,
Bâtiment 420, 91405 Orsay Cedex France
Fax: (internat.) + 33-1/69154328
E-mail: nadjo@icmo.u-psud.fr
[b] Laboratoire de Chimie Inorganique et Matériaux Moléculaires, UPRESA 7071, CNRS, Université Paris VI,
4, place Jussieu, 75252 Paris Cedex 05, France

Results

The Selection of Experimental Conditions

The following heteropolyanions were used: $\alpha[P_2W_{18}O_{62}]^{6-}$ (abbreviated as P_2W_{18}); α_1- and $\alpha_2[P_2W_{17}O_{61}]^{10-}$ (α_1- and $\alpha_2P_2W_{17}$); $\alpha[Mo_3P_2W_{15}O_{62}]^{6-}$ ($P_2W_{15}Mo_3$); $\alpha_2[Mo_2P_2$-

 © WILEY-VCH Verlag GmbH, D-69451 Weinheim, 2000 1434−1948/00/1212−2463 $ 17.50+.50/0

$W_{15}O_{61}]^{10-}$ ($\alpha_2P_2W_{15}Mo_2$); $\alpha[PW_{11}O_{39}]^{7-}$ (PW_{11}); $\alpha[SiW_{11}O_{39}]^{8-}$ (SiW_{11}); $[H_2P_2W_{12}O_{48}]^{12-}$ (P_2W_{12}); $\alpha_2[Zn(H_2O)P_2W_{17}O_{61}]^{8-}$ ($\alpha_2P_2W_{17}Zn$); $\alpha_2[Ni(H_2O)P_2W_{17}O_{61}]^{8-}$ ($\alpha_2P_2W_{17}Ni$). The preparation and characterization of these materials have already been described in detail.[6,8,9,18–21]

A priori, at least two antagonist influences due to the supporting electrolyte can be anticipated during the reduction of heteropolyanions: on the one hand, protonation and/or ion-pair formation with other cations, which might enhance the reduction kinetics; on the other hand, the anions of the electrolyte might counteract these reduction kinetics. It is desirable to maintain one of these influences constant for the study of the second one. First, sodium salts or, occasionally, lithium salts were used to maintain a constant cation concentration [M] = 0.4 M. In the cases in which the results are known, these two cations are not completely without action on the oxidized forms of several heteropolyanions; however, the stability constants of the corresponding complexes are rather small.[18] Even if a stronger association could be anticipated with the reduced forms of the heteropolyanions, the experiments described in the following pages indicate, as anticipated, that the interaction does not depend to an appreciable extent on the nature of these alkaline cations. This observation leaves room for the identification of other effects. Furthermore, the compounds under scrutiny in this work are sensitive to the concentration of protons. The corresponding saturated species react mostly by ECE- or EEC-type processes, with the C step usually being a protonation. Therefore, a constant pH = 3 value was selected throughout; in the present work we found this proton level high enough, in sulfate media, to favor the protonation of the reduced oxometalates over their ion-pairing with Na^+ or Li^+ cations, at least as far as the first redox system of the studied heteropolyanions is concerned. A detailed examination of the competition between protonation and ion-pairing of the reduced heteropolyanions is beyond the scope of this paper. Finally, our usual experimental conditions have been maintained in the present work, which is aimed first at confirming and expanding previous observations: This point essentially concerns the glassy carbon working electrode, which we have demonstrated to be suitable for the study of the electrochemical and electrocatalytic behaviors of heteropolyanions under a variety of experimental conditions.[5–10,22,23] Indeed, the present knowledge of the interfacial properties of glassy carbon is, at best, qualitative, even though several papers suggest that this electrode material could be used for kinetic studies.[11,24,25] Gold and platinum are well characterized but cannot be used throughout in experiments spanning a large potential domain in the relatively acidic media necessary for our studies.

Voltammetric Behavior of Selected Heteropolyanions in Several pH = 3 Media

Two lacunary heteropolyanions, $\alpha_2P_2W_{15}Mo_2$ and $\alpha_2P_2W_{17}$, were selected to illustrate the basic observations. Figure 1 (1A and 1B) shows the evolution of the corresponding cyclic voltammograms for $5\cdot10^{-4}$ M heteropolyanion in the presence of appropriate concentrations of Na_2SO_4, $NaClO_4$, $NaNO_3$, and NaCl as supporting electrolytes.

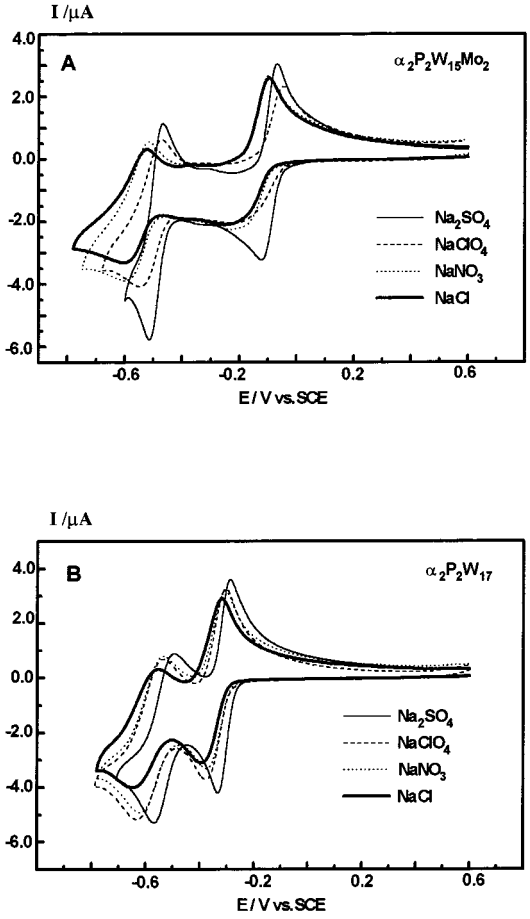


Figure 1. Cyclic voltammograms of a $5\cdot10^{-4}$ M solution of the relevant heteropolyanion in several pH = 3 media containing 0.4 M Na^+; scan rate: 10 mVs^{-1}; working electrode: glassy carbon

The potential domain is restricted to encompass the first two redox systems for each oxometalate. Figure 1 speaks for itself and only brief comments are necessary. However, the distortion is more marked in the cyclic voltammogram of $\alpha_2P_2W_{15}Mo_2$ than that of $\alpha_2P_2W_{17}$, even though qualitatively identical effects are observed. We note that the two waves are modified: taking the voltammogram in the sulfate medium as a reference, those in the presence of other salts show drawn out shapes, with smaller current intensities and peak potentials that are pushed in the negative direction. The concentration of Na^+ is 800 times that of the oxometalate. In this situation the ionic strength of the solution cannot be suspected to induce the observed phenomena. The nature of the anions of the supporting electrolyte is thus proposed as the relevant parameter. Furthermore, as these observations are made in the presence of a large excess of supporting electrolyte, it can be concluded that the effect of cations other than the proton is minimal in the reduction processes of these systems or largely counteracted by some anion effect. An attempt can be made to rationalize the difference in behavior between the two lacunary heteropolyanions by considering their respective basicities. The first

two-electron wave for $\alpha_2P_2W_{15}Mo_2$ in the sulfate medium (taken as a reference) features Mo-centered redox processes while that for $\alpha_2P_2W_{17}$ is W-centered. A report in the literature[26] suggests the reduced Mo-substituted site to be the stronger base of the two compounds. As a consequence, protonation and/or ion-pairing are easier in Mo-substituted complexes. Correlatively, a higher sensitivity of the latter compound to possible anion effects is not expected, a situation in contrast to that actually observed. Provisionally, comparison between α_1 and $\alpha_2P_2W_{17}$ shows the two compounds to behave in exactly the same way. However, not much work was carried out with the α_1 isomer due to its known relative instability under most of the conditions used in the present investigation. Further discussion of this system is postponed until the main parameters of this study emerge clearly.

Figure 2 and Figure 3 are helpful in this issue. Figure 2 shows the observations pertaining to three other lacunary species and to a Zn-substituted Dawson-type complex in the two electrolytes that give the most contrasting behavior.

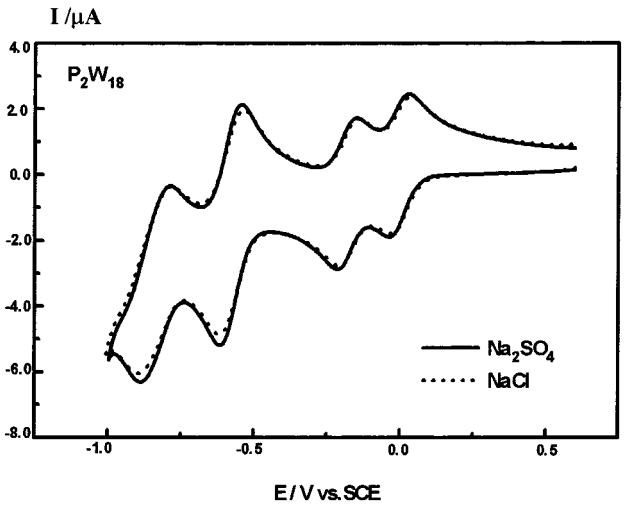


Figure 3. Cyclic voltammograms of a $5\cdot10^{-4}$ M $[P_2W_{18}O_{62}]^{6-}$ in two pH = 3 media containing 0.4 M Na^+; scan rate: 10 mVs^{-1}; working electrode: glassy carbon

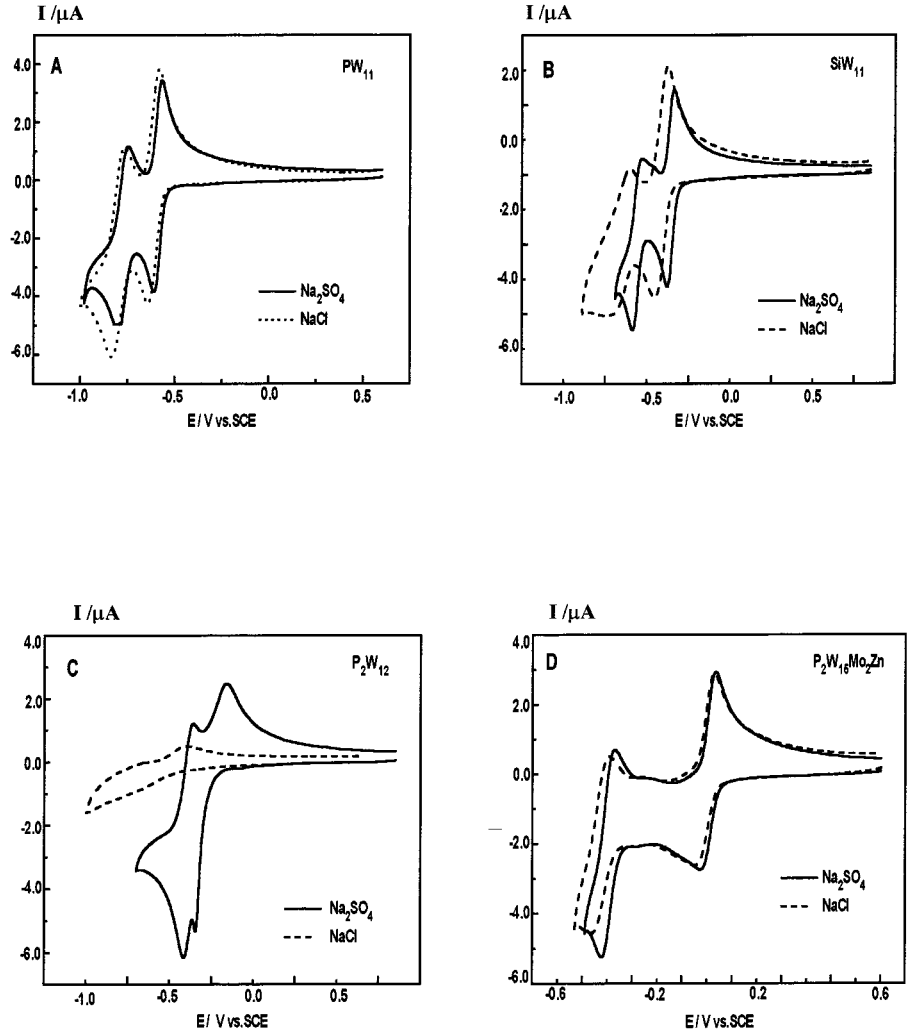


Figure 2. Cyclic voltammograms of a $5\cdot10^{-4}$ M solution of the relevant heteropolyanion in two pH = 3 media containing 0.4 M Na^+; scan rate: 10 mVs^{-1}; working electrode: glassy carbon

The previously observed effect also exists in this group, which contains two Keggin-type species. Even though the surface charge density varies from one component to the next, the structure of the heteropolyanion does not seem to constitute a relevant parameter. Strikingly, the intensity of the effect is greater as the nominal negative charge of the anion under scrutiny becomes larger. At least two details are worth noting and these will be elaborated in the following discussion: (i) the cyclic voltammogram of $[H_2P_2W_{12}O_{48}]^{12-}$ in NaCl solution vanishes almost completely; (ii) the behavior of $\alpha_2P_2W_{17}Zn$ also deserves emphasis in that as the volume increases, the nominal charge remains the same as SiW_{11} and a slightly smaller first peak potential shift is observed. Figure 3 compares the behaviors of P_2W_{18} in sulfate and chloride media and shows that no difference is observed. The same observation holds for $P_2W_{15}Mo_3$. This result is in agreement with the previously known behaviors of saturated heteropolyanions. Even though P_2W_{18} and $P_2W_{15}Mo_3$ are the less charged of the complexes in the present series, the main characteristic likely to bring about the difference in behavior in comparison with the others is the symmetry of the charge distribution in the saturated species.

The observations discussed above all converge to indicate the total nominal charge of each anion on the one hand and its distribution on the other, as two of the parameters that govern the shape and potential location of cyclic voltammetric waves. A second conclusion concerns the particular role of protons in the presence of large amounts of other cations, which failed to counteract the suggested anion effect. Could these observations be rationalized in the framework of the double layer theory? Some complementary experiments seem to contradict this possibility. For example, in a pH = 3 medium containing 0.1 M Na_2SO_4 + 0.2 M NaCl, the classical cyclic voltammograms known in sulfate media for $\alpha_2P_2W_{15}Mo_2$, $\alpha_2P_2W_{17}$, or P_2W_{12} are obtained almost exactly. More strikingly, upon addition of 0.1 M Na_2SO_4 to pH = 3 solutions containing 0.2, 0.3, or 1 M NaCl, the vanishingly small and drawn-out cyclic voltammogram of P_2W_{12} is immediately replaced by a well-defined pattern. In addition, the cyclic voltammograms depend on the concentration of the relevant heteropolyanion in solution. This behavior suggests a preeminent role for the proton and deserves further investigations, which are described in the following section.

Influence of the Proton to Heteropolyanion Concentration Ratio

To highlight the influence of this parameter, the following experiments were carried out with a proton to heteropolyanion concentration ratio from 4 down to 0.22 in most cases. Typically, the pH = 3 supporting electrolyte contains 0.2 M Na_2SO_4 and the concentration of the appropriate heteropolyanion varied from $0.25\cdot10^{-3}$ to $4.5\cdot10^{-3}$ M. Figure 4 and Figure 5 pertain to $\alpha_2P_2W_{15}Mo_2$ and $\alpha_2P_2W_{17}$, respectively. For the sake of clarity each figure is split into three parts.

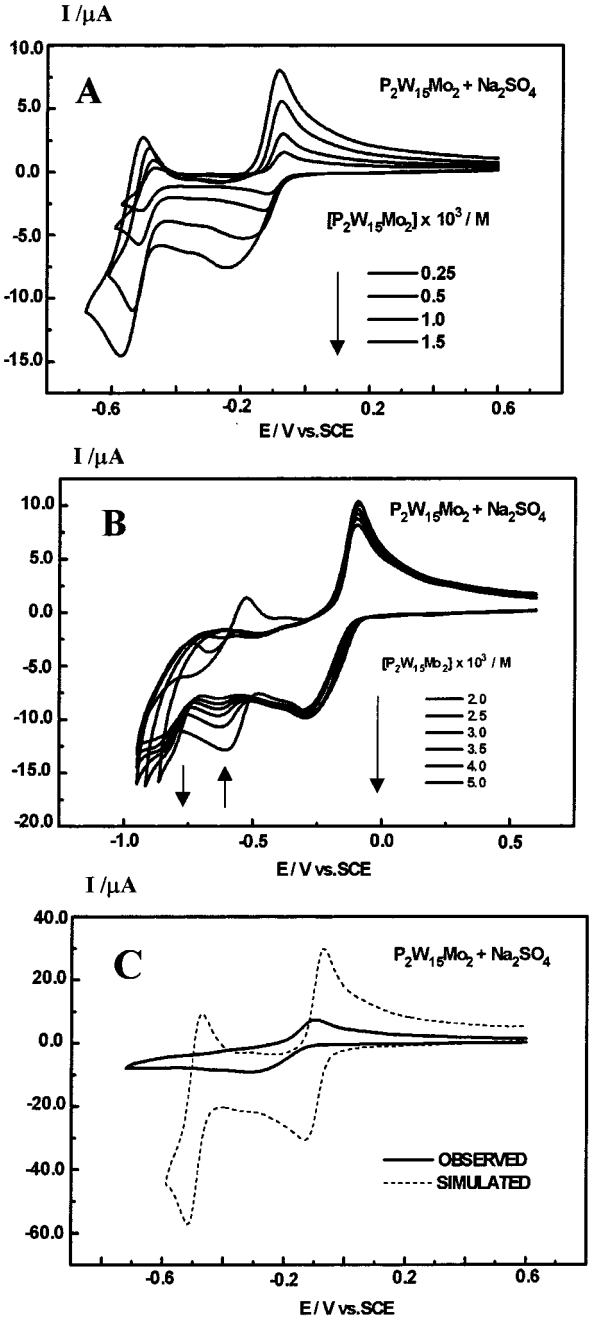


Figure 4. Cyclic voltammograms of several increasing concentrations of $\alpha_2[Mo_2P_2W_{15}O_{61}]^{10-}$ in 0.2 M Na_2SO_4 + H_2SO_4 (pH = 3 before addition of heteropolyanion); scan rate: 10 mVs^{-1}; working electrode: glassy carbon; A and B: the appropriate concentrations are indicated in the sketches; C: observed and simulated cyclic voltammograms for a concentration of $4.5\cdot10^{-3}$M $\alpha_2[Mo_2P_2W_{15}O_{61}]^{10-}$ in the initially pH = 3 medium; scan rate: 10 mVs^{-1}; working electrode: glassy carbon; for further details, see text

In Figure 4A the peak current intensities are strictly proportional to the analytical concentration of the heteropolyanion. This concentration domain is narrow, despite the presence of a high concentration of cations in the solution. Details in Figure 4B deserve particular attention. Upon in-

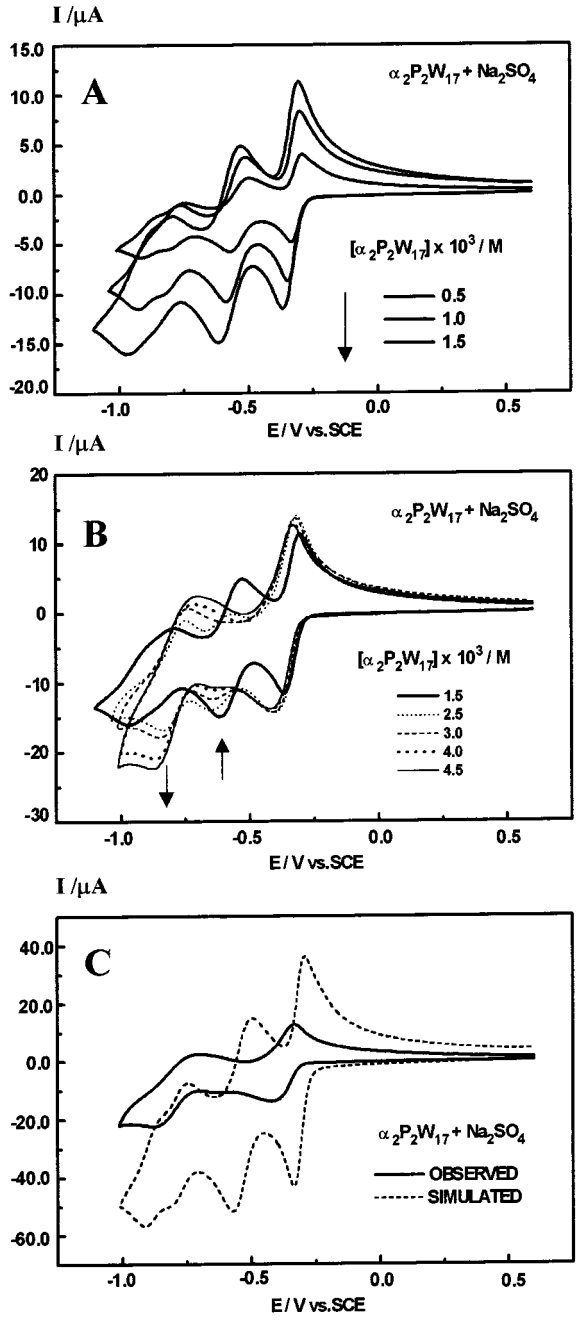


Figure 5. Cyclic voltammograms of several increasing concentrations of $\alpha_2[P_2W_{17}O_{61}]^{10-}$ in 0.2 M Na_2SO_4 + H_2SO_4 (pH = 3 before addition of heteropolyanion); scan rate: 10 mVs^{-1}; working electrode: glassy carbon; A and B: the appropriate concentrations are indicated in the sketches; C: observed and simulated cyclic voltammograms for a concentration of $4.5\cdot10^{-3}$ M $\alpha_2[P_2W_{17}O_{61}]^{10-}$ in the initially pH = 3 medium; scan rate: 10 mVs^{-1}; working electrode: glassy carbon; for further details, see text

creasing the heteropolyanion concentration, the first wave becomes roughly constant in intensity and the peak potential continues its slight shift in the negative direction; the current intensity of the second wave decreases until it becomes vanishingly small; concomitantly, a new wave appears at a more negative potential than the former second wave and grows at its expense. Figure 4 C shows a comparison between the final voltammogram observed for $4.5\cdot10^{-3}$ M $\alpha_2P_2W_{15}Mo_2$ and the voltammogram simulated from that corresponding to the lowest concentration of complex on the assumption that the peak current intensities maintain the expected proportionality and peak potentials remain constant. Figure 5 shows analogous observations for $\alpha_2P_2W_{17}$. Apart from the difference in wave shapes, which is the incentive for showing both Figure 4 and 5, exactly the same comments are applicable to the two complexes and will not be repeated.

In contrast, the addition of potassium hydrogen phthalate, which increases the buffer strength of the sulfate solution, improves drastically the observed phenomena. Figure 6 compares the observed and simulated cyclic voltammograms for $\alpha_2P_2W_{15}Mo_2$ and $\alpha_2P_2W_{17}$, respectively, under these experimental conditions.

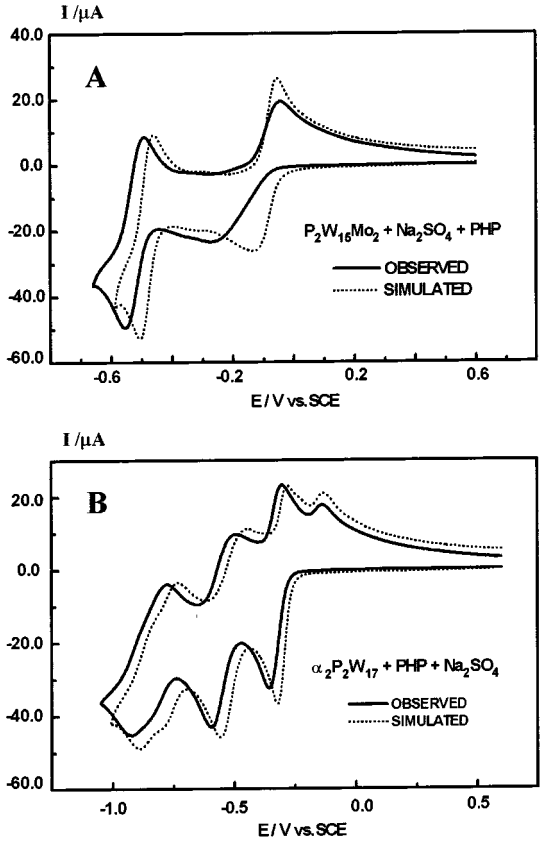


Figure 6. Observed and simulated cyclic voltammograms for $5\cdot10^{-3}$ M of the relevant heteropolyanion in 0.175 M Na_2SO_4 + $5\cdot10^{-2}$ M PHP (initial pH = 3); scan rate: 10 mVs^{-1}; working electrode: glassy carbon; for further details, see text; A: $\alpha_2[Mo_2P_2W_{15}O_{61}]^{10-}$; B: $\alpha_2[P_2W_{17}O_{61}]^{10-}$

Even with modest concentrations of the phthalate, the "expected" cyclic voltammograms are almost completely restored, as can be seen in Figure 6. Such an observation underscores the influence of the buffer capacity of the electrolyte and the special participation of the proton in the electrochemistry of the selected oxometalates. Also, comparison of the behavior of the two complexes in the same medium confirms the difference in basicity between their reduced forms.

Finally, complementary experiments were carried out. Figure 7 indicates for two metal ion substituted heteropolyanions, $\alpha_2P_2W_{17}Ni$ and $\alpha_2P_2W_{17}Zn$ selected as representative examples, the same trends as obtained for the precursor lacunary species, albeit to a lesser extent.

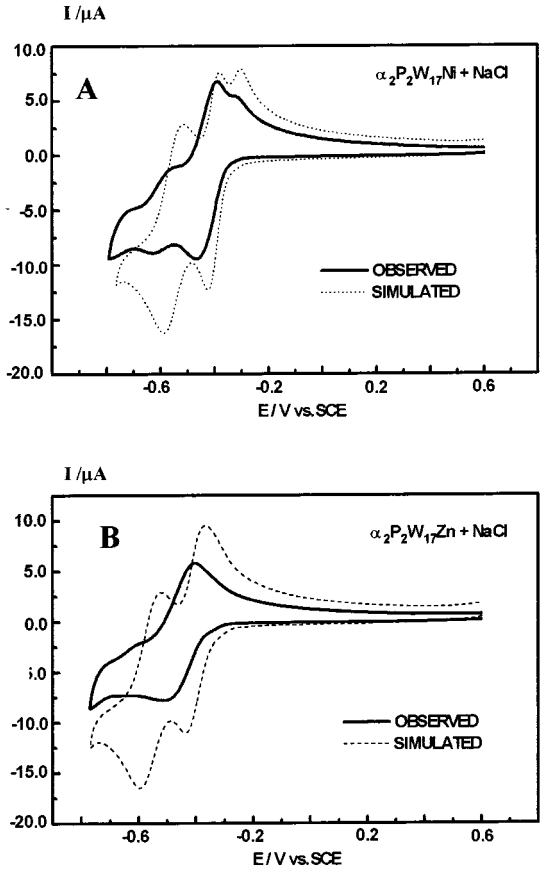


Figure 7. Observed and simulated cyclic voltammograms for $5 \cdot 10^{-3}$ M of the relevant heteropolyanion in 0.4 M NaCl + HCl (initial pH = 3); scan rate: 10 mVs^{-1}; working electrode: glassy carbon; for further details, see text; A: $\alpha_2[NiP_2W_{17}O_{61}]^{8-}$; B: $\alpha_2[ZnP_2W_{17}O_{61}]^{8-}$

Substitution of Na^+ by Li^+ in the supporting electrolyte does not change the general behavior observed for lacunary as well as for metal cation substituted heteropolyanions. Figure 8 summarizes the evolution, with the heteropolyanion concentration, of the current intensity ratio of the observed and simulated first voltammetric waves as defined previously.

It is also clear from Figure 8 that there is a slower decrease of this ratio when the ionic strength of the electrolyte increases.

With a proton-to-heteropolyanion ratio smaller than 2, all the observations suggest a reaction pathway in which two main species are in equilibrium in the solution, with their reduction featured respectively by the first and the second voltammetric waves. In this issue, it can be hypothesized that the first wave should correspond to the reduction of a protonated form of the heteropolyanion and the second wave to another protonated or to an unprotonated form.

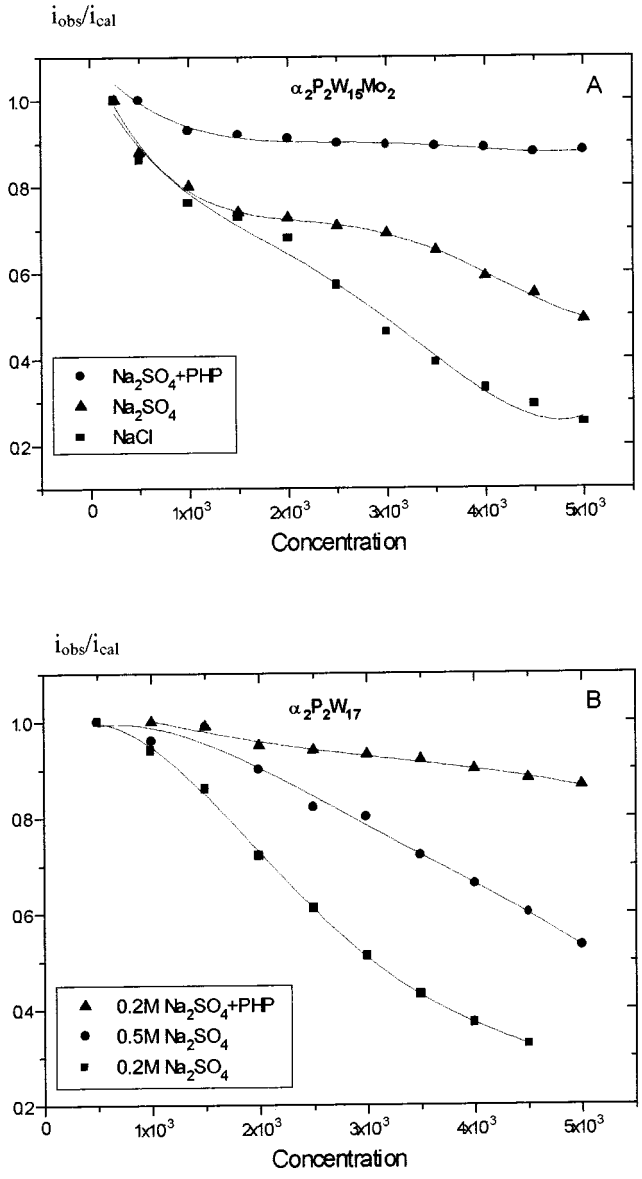


Figure 8. Normalized first reduction peak current intensity as a function of heteropolyanion concentration [M], using the calculated diffusion current as a reference; for further details, see text; A: $\alpha_2[Mo_2P_2W_{15}O_{61}]^{10-}$; B: $\alpha_2[P_2W_{17}O_{61}]^{10-}$

This distinction stems from the failure of large amounts of sodium or lithium cation to assume the role of protons and from the known polybasic behavior of $\alpha_2P_2W_{17}$,[18] which is also anticipated for $\alpha_2P_2W_{15}Mo_2$.

Acid−Base Equilibria

An attempt to rationalize the observations discussed above demands complementary experiments that can support or invalidate the basic hypothesis. The study is restricted to $\alpha_2P_2W_{15}Mo_2$ and $\alpha_2P_2W_{17}$.

Typically, several experiments were performed by starting the measurements with a pH = 3 solution containing the appropriate concentration of Na_2SO_4 + PHP, Na_2SO_4, or NaCl, which are the most representative supporting electrolytes used in this work. The pH of such solutions was then monitored accurately as a function of the added concentra-

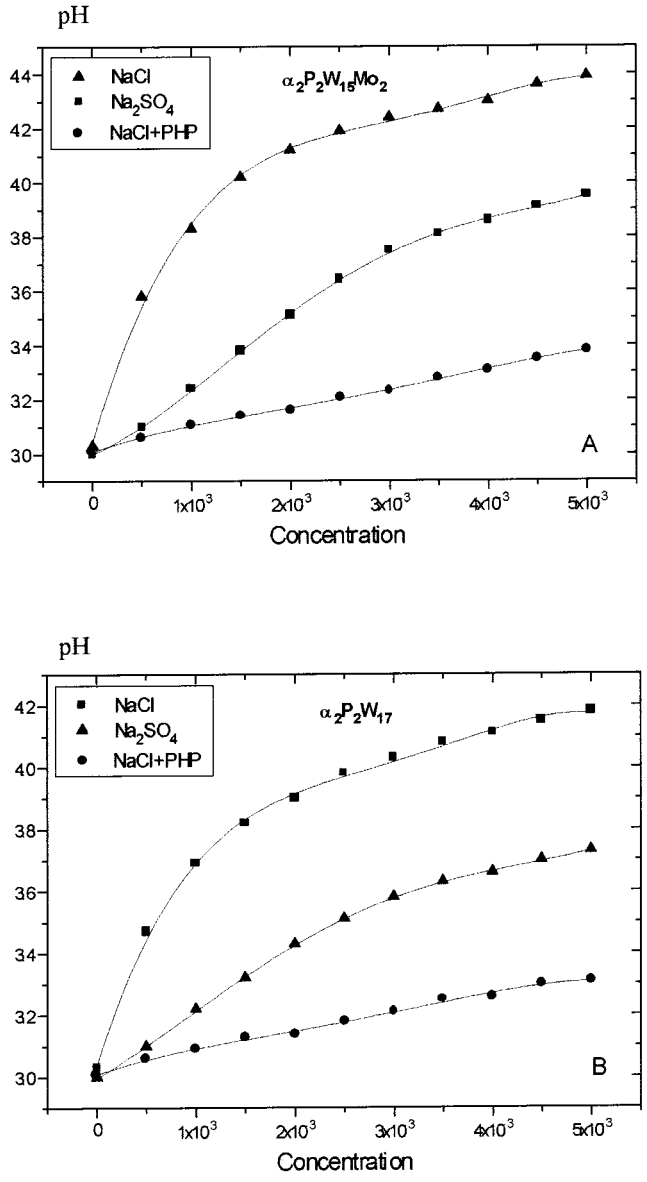


Figure 9. Variation of pH as a function of the concentration of heteropolyanion added to an initially pH = 3 solution; the composition of the electrolyte is indicated on each curve; A: $\alpha_2[Mo_2P_2W_{15}O_{61}]^{10-}$; B: $\alpha_2[P_2W_{17}O_{61}]^{10-}$

tion of the relevant heteropolyanion. The results are shown in Figure 9 and are enlightening.

Even with the smallest concentration of oxometalate used in this work, proton consumption occurs. Clearly, for both heteropolyanions, at least one of their pK_a values falls in the pH domain of the supporting electrolyte. The differences observed between the various media are easily explained in terms of their buffer capacity. The chloride medium has no buffer capacity and the consumption of protons by the heteropolyanion results in a rapid increase in the pH value. In the pure sulfate medium, $[HSO_4]^-$ is a proton donor, the presence of which confers some buffer capacity to the electrolyte. By following a literature procedure,[27] the initial concentration of hydrogen sulfate in the pH = 3 solution containing 0.2 M Na_2SO_4 can be evaluated and was found to be roughly $1.54 \cdot 10^{-2}$ M. Incidentally, it is worth noting that the increase of hydrogen sulfate species in 0.5 M Na_2SO_4 ($3.85 \cdot 10^{-2}$ M) and, to a lesser extend, the increase of cations, participate in the observed influence of ionic strength in Figure 8A. Finally, two proton donors are present in the mixture of sulfate and PHP, which can explain the small variation of pH with the concentration of heteropolyanion in that medium.

As far as the acid-base equilibria of the heteropolyanions are concerned, each of the present Dawson-type lacunary compounds is theoretically expected to fix ten protons. In fact, previous work on $\alpha_2P_2W_{17}$[18] and the present experiments on the two species under investigation indicate that the consumption of only three protons occurs. A detailed account of the accurate pK_a determinations for these compounds, as well as for several other species in the Dawson and Keggin series, under various experimental conditions will be given elsewhere along with the distribution of the various possible species in equilibrium at a given pH value.[28]

Discussion

The classical picture encountered so far in our studies for the reduction of lacunary heteropolyanions in pH = 2 or 3 media with a large enough proton-to-heteropolyanion ratio,[6–10,29] begins with two two-electron waves. At least the first peak current intensity is proportional to the analytical concentration of the oxometalate. Most, but not all, first transition metal ion substituted heteropolyanions behave similarly and show a system of two-electron waves at practically the same potential locations as those of the precursor lacunary species.[6–10,29] Hence the conclusion that most of these systems cannot actually be considered as "saturated" compounds.

Several observations in the experiments described above deserve further specific discussion. Emphasis will be placed on an attempt at the rationalization of the influence of the overall negative charge of the heteropolyanion, the partial localization of this charge, and the role of various counterions present in the solution, with particular attention paid to the remarkable behavior of the proton.

In the pH domain explored and with the heteropolyanion concentrations used in this work, the lacunary as well as the substituted compounds are stable. As a matter of fact, regardless of the starting situation, addition of acid to obtain a large proton-to-heteropolyanion ratio restores immediately the classical cyclic voltammograms with a first two-electron wave, the current intensity of which is proportional to the analytical concentration of the oxometalate. The extremely high speed of this restoration might rule out association phenomena as the origin of the observed behavior.

We consider first the situation in Figure 1 through 3. With the sulfate medium chosen as a reference, the electrolyte composition seems suitable to ensure classical behavior for the oxometalates described in this work. For this same pH but in the presence of other anions, a general negative shift in the peak potential locations is obtained with a con-

comitant decrease of the peak currents. Such behavior spans a large potential domain, roughly from +0.6 to −1 V in the present experiments. Provisionally, it must be noted that this domain encompasses two two-electron waves of the fully symmetrical heteropolyanion P_2W_{18}, and that the whole cyclic voltammogram for this compound remains unaltered by the change in anion in the supporting electrolyte. On the reasonable assumption that the added electrons are delocalized in the equatorial region or that the charge distribution remains symmetrical in the first few reduced forms of P_2W_{18}, this cyclic voltammogram would indicate that the overall charge by itself is not a main parameter in the observed behavior. In contrast, substituted heteropolyanions are sensitive to the change of anions, which lends support to the conclusion that they behave much like the precursor lacunary species. The idea emerges that charge localization is of prime importance to induce the behaviors of lacunary and lacunary-like species. The larger this charge localization, the larger the effects. It has also been confirmed by UV/Vis spectroscopy that decomposition of the oxometalates does not occur. Given this information we are left with an explanation involving anion effects and/or local pH effects. The most striking or complex behaviors are encountered with $\alpha_2P_2W_{15}Mo_2$ and P_2W_{12}. Work is still in progress on the latter compound. Therefore, focus is placed on the first compound. The anion effect in electrochemistry has been known for some time and is rationalized in terms of adsorption and double layer effects.[30−35] More specifically, the anion effect in the reduction of chromate ions has been described in detail by Gierst and co-workers.[36,37]

However, examination of Figure 8A. and Figure 9A, indicates that $\alpha_2P_2W_{15}Mo_2$ and its reduced species should fix protons irreversibly, thus raising the pH value in the reaction layer. As a consequence, the peak current intensity could be lowered and the peak potential driven in the negative direction. This possibility might appear difficult to separate from the pure double layer effect, but the present observations rule out any preeminent anion effect.

The second issue of importance concerns the role of counter cations in the reaction mixture. Even though they are active in ensuring the overall electroneutrality of the solutions, their behavior is particularly prominent when the proton to heteropolyanion ratio is low. In these circumstances, it is observed that the high cation-to-heteropolyanion ratio cannot counteract the pH variation effect. This conclusion is confirmed in Figure 4 and 5, in which it can be seen that cations other than the proton also fail to give rise to the classical cyclic voltammograms of lacunary heteropolyanions. In contrast, the efficiency of protons in these circumstances is clearly highlighted, in particular through the buffer capacity of the supporting electrolyte. The facts in this particular case are clear although their complete rationalization seems difficult at present. Therefore, the following discussion represents an attempt to sum up the main questions raised by the present observations, with an indication of the tentative ways in which these questions could be solved. At least two questions arise: (i) the extent, if any, of ion-pairing of cations with the outer surface of heteropolyanions, more specifically in the reduced states; (ii) the compensation by cations of the localized charges of the vacancy corresponding to the missing moiety. Complexation and/or ion-pairing of the lacunary[18] and the substituted[18,38,39] heteropolyanions with alkali metal cations were demonstrated and seem to be associated with the dissymetry of the molecules.[12,40] This remark suggests charge localization to some extent. As a consequence, we focus on the atoms in and around the vacancy. The complexation stability constants, in the cases in which they were measured,[18,28] have sizeable values. It can be assumed that the corresponding reduced species should be even more strongly complexed by alkali metal cations. Then, the particular role played by protons should be tentatively attributed to either or both of the following possibilities: the very fast protonation kinetics, in agreement with the p*K* values, and/or some restricted accessibility of protonable/complexable sites. This last assumption might be supported by the known bulkiness of solvated alkali metal cations:[41,42] the ionic radii are 2.35 Å for solvated Na^+, 2.08 Å for solvated Li^+, while the value of 0.74 Å for W^{6+} is generally accepted to represent also the radius of the vacancy. A new problem now arises concerning the actual state (i.e. whether they are solvated, partially solvated or unsolvated) of the cations that participate in the neutralization of the charges around the vacancy. It is known[18,28] that, among the five protonable sites, only the four outer sites have a good accessibility and that three are protonable. It is likely that solvated cations can only complex these sites in a fairly loose manner. Work in progress is aimed at clarifying several of these problems.

Concluding Remarks

The observations made for the electrochemical behavior of the oxometalates studied in this work show evidence for the influence of electrolyte composition. Despite the variety of Dawson- and Keggin-type structures, the conclusion emerges that lacunary as well as their divalent cation substituted species are sensitive mainly to the buffer capacity of the electrolytes. This influence pushes the peak potentials in the negative direction and, as a whole, increases the reduction overvoltage of the oxometalate. The intensity of the influence decreases smoothly from the lacunary species to their divalent cation substituted derivatives, and vanishes completely in the precursor-saturated compound. Furthermore, the importance of this influence turns out to follow smoothly the nominal negative charge borne by each molecule. This observation confirms and reinforces the conclusion that most divalent cation substituted heteropolyanions are not actually "saturated" compounds and that their electrochemistry should be compared with that of the corresponding lacunary species. This behavior reveals, in fact, some dissymmetry in the charge distribution in the molecules, as evidenced by the comparative study with P_2W_{18} or $P_2W_{15}Mo_3$. The possible further interference of local pH changes during reduction processes must also be considered. Thus, one remarkable outcome of this work is the pos-

sibility that electrochemical behavior governed by electrolyte composition can serve as probes of charge distribution in oxometalates.

Another issue of interest concerns the very modest role played by cations other than the proton in the electrochemical behavior of oxometalates. The series of questions raised by this observation can be partly answered by considering qualitatively the charge localization on hard oxide ions around the vacancy and the bulkiness of solvated alkali cations in competition with proton hopping. Also, the pK_a value of the various sites in the oxidized as well as in the reduced forms must be considered. These explanations cannot be extended to the known specificity of several cations in the synthesis of lacunary heteropolyanions. Work in progress aims at answering several such questions.

Experimental Section

Pure water from a Milli-RO_4 unit followed by a Millipore Q purification set was used throughout. All chemicals were of high-purity grade and were used as received. H_2SO_4, Li_2SO_4, Na_2SO_4, LiCl, NaCl, HCl, $NaClO_4$, $NaNO_3$, $C_8H_5O_4K$ (potassium hydrogen phthalate, abbreviated as PHP), CH_3COOH, CH_3COONa (Prolabo) were commercial products. In the present comparative study, only pH = 3 media were used. The heteropolyanions used in this work have been cited previously, along with appropriate abbreviations and preparations.[6,8,9,18–21] The stability of these compounds was checked in a 0.2 M Na_2SO_4 + H_2SO_4 medium (pH = 3) by UV/Vis spectroscopy over a period of at least 24 h. The solutions were deaerated thoroughly for at least 30 min with pure argon and kept under a positive pressure of this gas during the experiments.

The source, mounting and polishing of the glassy carbon (GC, Le Carbone Lorraine, France, 3 mm diameter) have been described.[5,6] The electrochemical set-up was an EG & G 273 A driven by a PC with the corresponding 270 software. Potentials are quoted against a saturated calomel electrode (SCE) in a compartment separated from the test solution by a fine-porosity glass frit. The counter electrode was platinum gauze of large surface area in a separated compartment with a medium-porosity glass frit. The UV/Vis spectra were recorded with a Perkin–Elmer Lambda 19 spectrophotometer. Experiments were performed at 23 ± 1 °C.

Acknowledgments

This work was supported by the CNRS (Laboratoire de Chimie Physique, UMR 8000 CNRS and UPRESA 7071) and the Universities Paris XI and Paris VI. The help of Sabrina Guilly is gratefully acknowledged.

[1] C. L. Hill (Guest Ed.), *Chem. Rev.* **1998**, *98*, 1–389.
[2] M. T. Pope, *Heteropoly and Isopoly Oxometalates*, Springer-Verlag, Berlin, **1983**.
[3] *Polyoxometalates: From Platonic Solids to Antiretroviral Activity* (Eds.: M. T. Pope, A. Muller), Kluwer Academic Publications, Dordrecht, **1994**.
[4] M. Sadakane, E. Steckhan, *Chem. Rev.* **1998**, *98*, 219–237.
[5] A. Belhouari, B. Keita, L. Nadjo, R. Contant, *New J. Chem.* **1998**, 83–86.
[6] R. Contant, M. Abbessi, J. Canny, A. Belhouari, B. Keita, L. Nadjo, *Inorg. Chem.* **1997**, *36*, 4961–4967.
[7] B. Keita, L. Nadjo, R. Contant, *J. Electroanal. Chem.* **1998**, *443*, 168–174.
[8] R. Contant, M. Abbessi, J. Canny, B. Keita, A. Belhouari, L. Nadjo, *Eur. J. Inorg. Chem.*, in press.
[9] B. Keita, Y. W. Lu, L. Nadjo, R. Contant, M. Abbessi, J. Canny, M. Richet, *J. Electroanal. Chem.* **1999**, *477*, 146–157.
[10] B. Keita, F. Girard, L. Nadjo, R. Contant, J. Canny, M. Richet, *J. Electroanal. Chem.* **1999**, *478*, 76–82.
[11] B. Keita, L. Nadjo, *J. Electroanal. Chem.* **1987**, *219*, 355–363.
[12] B. Keita, T. Lucas, L. Nadjo, *J. Electroanal. Chem.* **1986**, *208*, 343–356.
[13] L. Barcza, M. T. Pope, *J. Phys. Chem.* **1973**, *77*, 1795–1796.
[14] L. Barcza, M. T. Pope, *J. Phys. Chem.* **1975**, *79*, 92–93.
[15] C. Rong, M. T. Pope, *J. Am. Chem. Soc.* **1992**, *114*, 2932–2938.
[16] P. Souchay, *Ions Minéraux Condensés*, Masson, Paris, **1969**.
[17] B. Keita, L. Nadjo, *J. Electroanal. Chem.* **1987**, *227*, 77–98.
[18] R. Contant, J. P. Ciabrini, *J. Chem. Res. (S)* **1982**, 50–51; *J. Chem. Res. (M)* **1982**, 641–660.
[19] R. Contant, *Inorg. Synth.* **1990**, *27*, 104–111.
[20] M. Abbessi, R. Contant, R. Thouvenot, G. Hervé, *Inorg. Chem.* **1991**, *30*, 1695–1702.
[21] R. Contant, *J. Chem. Res. (S)* **1984**, 120–121; *J. Chem. Res. (M)* **1984**, 1063–1081.
[22] B. Keita, L. Nadjo, *Mater. Chem. Phys.* **1989**, *22*, 77–103.
[23] B. Keita, L. Nadjo, *Cur. Top. Electrochem.* **1993**, *2*, 77–106.
[24] D. C. Thornton, K. T. Kosby, V. A. Spendel, J. Jordan, A. Robbat, D. J. Rutstrom, M. Gross, G. Ritzler, *Anal. Chem.* **1985**, *57*, 150–155.
[25] O. Opallo, B. Behr, A. Kapturkiewicz, *J. Electroanal. Chem.* **1985**, *182*, 427–432.
[26] E. Papaconstantinou, M. T. Pope, *Inorg. Chem.* **1967**, *6*, 1152–1155.
[27] M. I. Florit, M. E. Martins, A. J. Arvia, *J. Electroanal. Chem.* **1983**, *151*, 209–226.
[28] Y. W. Lu, B. Keita, L. Nadjo, R. Contant, to be published.
[29] B. Keita, A. Belhouari, L. Nadjo, R. Contant, *J. Electroanal. Chem.* **1998**, *442*, 49–57.
[30] A. N. Frumkin, *Z. Phys. Chem.* **1933**, *164 A*, 121–133.
[31] A. N. Frumkin, *Z. Elektrochem.* **1955**, *59*, 807–822.
[32] A. N. Frumkin, *J. Electrochem. Soc.* **1960**, *107*, 461–472.
[33] A. N. Frumkin, N. V. Nikolajeva, *J. Chem. Phys.* **1957**, *26*, 1552–1553.
[34] P. Delahay, *Double Layer and Electrode Kinetics*, Interscience Publishers, New York, **1965**.
[35] S. G. Mairanovskii, *Catalytic and Kinetic Waves in Polarography*, Plenum Press, New York, **1968**.
[36] J. J. Tondeur, A. Dombret, L. Gierst, *J. Electroanal. Chem.* **1962**, *3*, 225–262.
[37] L. Gierst, J. Tondeur, E. Nicolas, *J. Electroanal. Chem.* **1965**, *10*, 397–415.
[38] J. E. Toth, F. C. Anson, *J. Electroanal. Chem.* **1988**, *256*, 361–370.
[39] J. F. Kirby, L. C. W. Baker, *Inorg. Chem.* **1998**, *37*, 5537–5549.
[40] B. Keita, L. Nadjo, *J. Electroanal. Chem.* **1987**, *230*, 267–271.
[41] Y. Marcus, *Chem. Rev.* **1988**, *88*, 1475–1498.
[42] H. Ohtaki, T. Radnai, *Chem. Rev.* **1993**, *93*, 1157–1204.

Received April 7, 2000
[I00140]

Hyperfine Shifts in Low-Spin Iron(III) Hemes: A Ligand Field Analysis

Ivano Bertini,*[a,b] Claudio Luchinat,[a,c] and Giacomo Parigi[a,c]

Keywords: Magnetic properties / Anisotropy / Iron / Heme proteins / Low-spin complexes / Partial orientation

The hyperfine shifts of heme nuclei in low-spin iron(III) porphyrins of known geometry are predicted from: (i) a ligand field analysis, and (ii) the Kurland and McGarvey theory (R. J. Kurland, B. R. McGarvey, *J. Magn. Reson.* **1970**, *2*, 286–301). The ligand field parameters are optimized to reproduce the experimentally available *g* values and magnetic susceptibility anisotropy, the latter being obtained from the analysis of pseudo-contact shifts. Simple known geometric relationships (I. Bertini, C. Luchinat, G. Parigi, F. A. Walker, *J. Biol. Inorg. Chem.* **1999**, *4*, 515–519; N. V. Shokhirev, F.A. Walker, *J. Biol. Inorg. Chem.* **1998**, *3*, 581–594), are used to relate the contact shifts to the various heme positions. The systems investigated are: metMyoglobin cyanide, cytochrome b_5 and cytochrome *c*. It is shown that the contact hyperfine coupling constants recalculated from this approach are different to those obtained through the simple and generally used McConnell equation, and that the deviation can be more or less severe, depending on the position on the heme and on the orientation of the axial ligands. The contact shift tensor is highly anisotropic and therefore the shift is dependent on the orientation of the molecule in a magnetic field. This theoretical analysis is necessary to interpret ENDOR spectra and NMR spectra in partially oriented systems.

Introduction

Contact shifts are generally and incorrectly assumed to be isotropic because the hyperfine coupling constant is isotropic.[1−4] However, contact shifts depend on the induced electron magnetic moment at the nucleus, and such magnetic moments are orientation-dependent because spin-orbit coupling causes anisotropy in the expected value of S_z, $<S_z>$. This effect is well-known[5] but does not show up in solution where the anisotropy is averaged out.[1−4]

Dipolar shifts due to the electron-nucleus coupling are known to be anisotropic.[2−6] They have an average value of zero in the absence of spin-orbit coupling and if all the orientations in solution are equally probable. In the presence of spin-orbit coupling, *g* and the magnetic susceptibility χ become anisotropic and the average dipolar coupling is different from zero. This effect gives rise to the well-known pseudo-contact shift.[2−6]

The interest here is in low-spin iron(III) heme systems. The *g* values of the ground state are available from EPR spectroscopy.[7−10] The magnetic susceptibility anisotropy, $\Delta\chi$, is available from the analysis of the ^{1}H pseudo-contact shifts, which are easily obtained for heme proteins [11−24]. Indeed, protons separated from the metal ion by several chemical bonds experience only pseudo-contact shifts, which then provide both magnetic susceptibility anisotropy and the principal directions of the magnetic susceptibility tensor. By fitting the *g* and $\Delta\chi$ values and directions with any ligand-field approach, the proper wave functions of the three lowest orbital levels are obtained, which are the basis set for the Kurland and McGarvey approach to determine: (i) the contact shifts for each orientation of the molecule in the external magnetic field, and (ii) the average value of isotropic rotation. The calculated contact shifts are then compared to the contact shifts of the heme methyl protons, which are estimated from the experimental hyperfine shifts by subtracting the calculated pseudo-contact shifts from the known magnetic susceptibility anisotropy tensor. Here, a simple analytical approach[9,25−29] is used. The contact shifts along the heme positions are predicted by assuming a $\sin^2\theta$ dependence for the ground state and a $\cos^2\theta$ dependence for the first excited state, where θ is the angle between the iron-proton vector and the direction of the (average) p-orbital nodal plane(s) of the π-bonding axial ligand(s)[21,30]. The analysis of the experimental contact shifts on the basis of this theoretical approach is quite instructive. The systems analyzed are: cyanometmyoglobin, rat microsomal cytochrome b_5 and horse heart cytochrome *c*.

Finally, since the technology of partial orientation is rapidly developing,[31−39] we want to address the problem of the effect of partial, but extensive, orientation on the contact (and pseudo-contact) shifts. This prediction is extremely important for the analysis of ENDOR spectroscopy and is not yet available in the literature, whereas extensive orientation in solution is not yet obtainable without severe broadening of the NMR lines.

Theory

Contact Shift

The Fermi contact contribution to the paramagnetic NMR shift can be calculated by using the Kurland and

[a] CERM, Magnetic Resonance Center, University of Florence, Via L. Sacconi, 6, 50019 Sesto Fiorentino, Italy
Fax: (internat.) +39-055/420-9271
E-mail: bertini@cerm.unifi.it
[b] Department of Chemistry, University of Florence
E-mail: luchinat@cerm.unifi.it
parigi@cerm.unifi.it
[c] Department of Soil Science and Plant Nutrition, University of Florence

 © WILEY-VCH Verlag GmbH, D-69451 Weinheim, 2000 1434−1948/00/1212−2473 $ 17.50+.50/0

McGarvey equation,[5] as it depends on the thermally populated electronic states:

$$\delta_i^{con} = \frac{1}{kT\sum_{\Gamma n} e^{-\varepsilon_\Gamma/kT}}\left(\sum_{\Gamma n,\Gamma m} e^{-\varepsilon_\Gamma/kT} < \Gamma n \mid \mu_i \mid \Gamma m >< \Gamma m \mid A_{Fi} \mid \Gamma n > + \right. \quad (1)$$

$$\left. - kT \sum_{\Gamma n,\Gamma m\,(\Gamma \neq \Gamma')} \frac{e^{-\varepsilon_\Gamma/kT} - e^{-\varepsilon_{\Gamma'}/kT}}{\varepsilon_\Gamma - \varepsilon_{\Gamma'}} < \Gamma n \mid \mu_i \mid \Gamma' m >< \Gamma' m \mid A_{Fi} \mid \Gamma n > \right)$$

Here i represents any of the principal directions of the molecular axes, $|\Gamma n>$ are the eigenstates of the electronic multiplets, ε_Γ is the energy of each multiplet state $|\Gamma>$, k is the Boltzmann constant and T is the temperature. Furthermore,

$$\mu_i = -\mu_B(L_i + 2S_i)$$

$$A_F = \frac{8\pi g_e \mu_B}{3}\delta(r)S$$

where δ indicates the Dirac δ operator, μ_B is the electron Bohr magneton, g_e is the electron g factor and L and S are the electron-orbital and spin operators. The eigenstates $|\Gamma n>$ can be provided by a ligand-field analysis.[9,25–29]

A pictorial scheme of the electronic levels of low-spin iron(III) heme proteins[26] is shown in Figure 1. On the left-hand side, the splitting of the d_{xy}, d_{yz}, d_{xz} orbitals (with energies E_0, E_1, E_2) is provided by the low symmetry, whereas on the right-hand side the effect of spin-orbit coupling is shown (and the orbital energy levels are labeled E'_0, E'_1, E'_2). The figure also shows the energy of the excited states, ε_1 and ε_2.

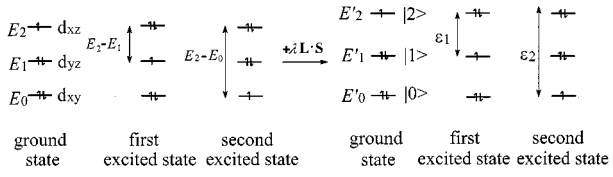


Figure 1. The low-symmetry splitting of the orbitally degenerate $^2T_2$ ground state and first and second excited states of low-spin iron(III)

This simple three-state analysis provides the g values for the ground state and the molecular χ values as follows [9,25–29]:

$$g_x = 2[2\xi_0\zeta_0 - \eta_0^2 - \sqrt{2}\eta_0(\xi_0 - \zeta_0)]$$

$$g_y = 2[-2\xi_0\zeta_0 - \eta_0^2 - \sqrt{2}\eta_0(\xi_0 + \zeta_0)] \quad (2)$$

$$g_z = 2[-2\xi_0^2 + \eta_0^2]$$

$$\chi_{ii} = -\frac{\mu_0\mu_B^2}{4\sum_{\Gamma n} e^{-\varepsilon_\Gamma/kT}}\sum_{\Gamma n}\sum_{\Gamma' m}(g_{\Gamma\Gamma'})_i^2 \frac{e^{-\varepsilon_\Gamma/kT} - e^{-\varepsilon_{\Gamma'}/kT}}{\varepsilon_\Gamma - \varepsilon_{\Gamma'}} \quad (3)$$

where μ_0 is the vacuum permeability, $(g_{\Gamma\Gamma'})_i$ are the electron g values in the ith direction[29] and ξ, η, and ζ are the coefficients of the ground and the two excited-state Kramer doublets, given by the following linear combination of the $|m_l, m_s>$ states:

$$|\Gamma,+> = \xi_\Gamma|1,-1/2> + \eta_\Gamma|0,1/2> + \zeta_\Gamma|-1,-1/2>$$

$$|\Gamma,-> = \xi_\Gamma|-1,1/2> + \eta_\Gamma|0,-1/2> + \zeta_\Gamma|1,1/2> \quad (4)$$

for $\Gamma = 0$, 1 and 2.

The fitting of the experimental data requires E_1 and E_2 of Figure 1 and the spin-orbit coupling constant. The orbital reduction parameter is taken to be 1.

By performing the calculations of Equation (1) with $|\Gamma n>$ provided by the three Kramer doublets, for external magnetic field directions along the principal directions of the g (or χ) tensor, the following components of the contact shift tensor are obtained:

$$\delta_x^{con} = a_x A_0/h + b_x A_1/h + c_x A_2/h$$

$$\delta_y^{con} = a_y A_0/h + b_y A_1/h + c_y A_2/h \quad (5)$$

$$\delta_z^{con} = a_z A_0/h + b_z A_1/h + c_z A_2/h$$

The a, b and c coefficients derive from the specific $|\Gamma n>$ functions weighted by the Boltzmann population, and $A_{0,1,2}/h$ are the hyperfine coupling constants (expressed in MHz; $\frac{A_i}{h} = \frac{\gamma_N}{2\pi}\frac{8\pi g_e\mu_B}{3}K_i$, where γ_N is the proton magnetogyric ratio and K_i represents the proportionality constant between the orbital-spin density and the electron-spin density at the nucleus[5]) for the ground and excited levels, respectively. In fact, since the hyperfine contact constants A are different for the different electronic states, three such terms are needed. The functional form of these terms has been extensively studied in previous works for the particular case of low-spin iron(III) heme systems,[17,21,30,41–49] and will be summarized below.

The average contact shift in solution is obtained by averaging over all orientations,

$$\delta_{av}^{con} = \frac{1}{3}\left[\delta_x^{con} + \delta_y^{con} + \delta_z^{con}\right] \quad (6)$$

For completeness, the equation for the average dipolar shift, which is the pseudo-contact shift, is also reported:[5,40]

$$\delta^{pc} = \frac{1}{24\pi}\frac{1}{r^3}\left\{\left[2\chi_{zz} - (\chi_{xx} + \chi_{yy})\right](3n^2 - 1) + 3(\chi_{xx} - \chi_{yy})(l^2 - m^2)\right\} \quad (7)$$

where χ_{ii} is the magnetic susceptibility of the molecule in the i direction, r is the distance of the observed nucleus from the atom bearing the unpaired electron spin, and l, m and n are the direction cosines of the metal-nucleus vector with respect to the principal directions of the χ-tensor.

Functional Form of A_0, A_1 and A_2

In low-spin heme complexes, A_0 and A_1 for heme methyl substituents are a function of the angle between the metal-pyrrole II direction and the direction of the (average) p-orbital nodal plane(s) of the π-bonding axial ligand(s)(Figure 2).[17,21,41−43] A_0 depends on the spin density according to[30]

$$A_0 = a\sin^2(\gamma_i - \varphi) \quad (8)$$

where a is a proportionality constant which depends on the amount of orbital-spin density and γ_i is the angle between the metal-*i*th-proton direction and the metal-pyrrole II axis (equal to 112.5, 22.5, 292.5 and 157.5 for methyls 1, 3, 5 and 8, respectively).

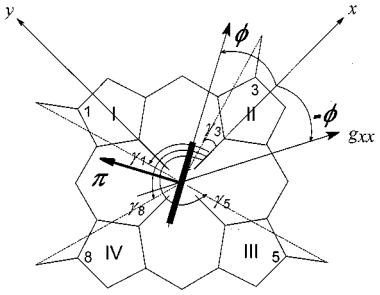


Figure 2. Schematic representation of the heme moiety; the γ_i angles for the four methyl groups are defined as the angles between the metal−methyl *i*th vector and the metal−pyrrole II direction; the Φ angle defines the direction of the average p-orbital nodal plane of the π-bonding axial ligand(s), and the -Φ angle the resulting direction of the g_{xx} and χ_{xx} axis

The second A value, A_1, is related to the heme spin-density pattern originating from the excited π-MO. It has been assumed that A_1 is equal to A_0, but shifted by 90°, and thus[30]

$$A_1 = a\cos^2(\gamma_i - \varphi) \quad (9)$$

The third A value, A_2, is related to the spin density on a MO to which iron contributes mostly with the d_{xy} orbital. Its value is given by a constant owing to the symmetry of the d_{xy} orbital. Furthermore, its contribution is small as found in those systems with a d_{xy} ground state.[44−49]

Results and Discussion

The simultaneous reproduction of the observed g values and the anisotropy of the magnetic susceptibility values, $\Delta\chi$, was obtained with the parameters reported in Table 1 for cyanometmyoglobin, cytochromes b_5 and c. The values of E_1, E_2, and λ are somewhat different to those calculated by fitting the g values only,[9,26] but the overall picture is the same. The values of E_1 and E_2 vary by about 10% when calculated through an angular overlap approach, which takes into consideration all the excited levels (program CAMMAG [50,51]). This provides a difference in the calculated contact shifts of about 5%, which is considered negligible. Therefore, the three-orbital approximation is sufficient.

In cyanometmyoglobin, the electron energy levels are 0, 692, and 915 cm^{-1} for the lowest three orbitals, d_{xy}, d_{yz}, and d_{xz}, respectively, so that the difference in energy between the ground and the two excited states is 223 and 915 cm^{-1}. These states are perturbed by spin-orbit coupling (with spin-orbit coupling constant $\lambda = 240$ cm^{-1})[52] to 0, 348, and 1023 cm^{-1} (Figure 1). These energy values provide $g_x = 0.93$, $g_y = 1.86$, $g_z = 3.40$ (see Table 1), in good agreement with the experimental values,[8,53] and $\chi_x = 3.12\cdot10^{-32}$, $\chi_y = 4.15\cdot10^{-32}$, $\chi_z = 7.35\cdot10^{-32}$ m^3, at 298 K, which provide $\Delta\chi_{ax} = 3.71\cdot10^{-32}$ m^3 and $\Delta\chi_{rh} = -1.03\cdot10^{-32}$ m^3, again in good agreement with the experimental values (see Table 1). The values of $\delta^{con}_{x,y,z}$, for external magnetic field directions along the principal directions of the g (or χ) tensor, have thus been calculated (in ppm):

$$\delta_x^{con} = 14.7A_0/h + 9.9A_1/h + 0.5A_2/h$$

$$\delta_y^{con} = 19.9A_0/h + 7.7A_1/h + 0.6A_2/h$$

$$\delta_z^{con} = 36.3A_0/h + 0.7A_1/h + 0.9A_2/h$$

at 298 K, where $A_{0,1,2}/h$ are expressed in MHz. Since A_2 is reasonably much smaller than A_0 and A_1,[44−49] and since the coefficients for the second excited state are usually smaller than the others, we will neglect the second excited state contribution hereafter.

The average solution values of the calculated contact and pseudo-contact shifts for the methyl protons, found by setting a fixed value for the a parameter in Equations (8) and (9), are reported in Table 2. It can be seen that the shift pattern is well reproduced for both the contact and the pseudo-contact contributions. For cyanometmyoglobin, for instance, the calculated contact shifts for the 1, 3, 5, and 8 methyl protons are 21.5, 8.2, 26.3, and 12.0 ppm, respectively, in comparison with the experimental values 18.4, 6.7, 27.8, and 15.8 ppm, and the calculated pseudo-contact shifts for the 1, 3, 5, and 8 methyl protons are −3.0, −5.8, −3.0, and −5.6 ppm, respectively, in comparison with the experimental values −3.4, −5.7, −3.3, and −6.5 ppm.[12] It should be noted that the angular dependence of the contact constants is of the same type as that of the pseudo-contact shift. Therefore, the sum of contact and pseudo-contact shifts is provided by an equation which contains the linear combination of $\sin^2$ and $\cos^2$ terms. This justifies the use of a recently proposed heuristic equation.[30]

Similarly, satisfactory results were obtained for cytochrome b_5 and cytochrome c (Table 2). In cytochromes b_5 and c the φ angle in Equations (8) and (9)[43] is determined by the presence of two histidines or a histidine and a methionine as axial ligands.[54] The a values needed to best reproduce the experimental shifts are within ±25% from those found for MetMbCN.

A comparison between the contact hyperfine constants calculated with the Kurland and McGarvey equation and the McConnell equation is reported in Table 3. It is interesting to compare the analysis of the contact shifts through

Table 1. Energy values of the excited orbitals, E_1 and E_2, obtained by fitting the experimental g and χ values of MetMbCN, cytochrome b_5 and cytochrome c. ε_1 and ε_2 are the energies of the excited states; the energy values are expressed in cm^{-1}, the values of the magnetic susceptibility are expressed in m^3; the a, b, and c coefficients of Equation (5) are provided for the three proteins;[a] the experimental data are from: MetMbCN, for g see ref.[8,53] and for $\Delta\chi$ see ref.[18]; cytochrome b_5: for g see ref.[9] and for $\Delta\chi$ see ref.[20]; cytochrome c:for g see ref.[26] and for $\Delta\chi$ see ref.[19,21]

MetMbCN		Experimental	Calculated	Experimental	Calculated			
$E_1 = 692$	$\varepsilon_1 = 348$	$g_x = 0.93$	$g_x = 0.93$	$\Delta\chi_{ax} = 3.78\cdot10^{-32}$	$\Delta\chi_{ax} = 3.71\cdot10^{-32}$	$a_x = 14.7$	$b_x = 9.9$	$c_x = 0.5$
$E_2 = 915$	$\varepsilon_2 = 1023$	$g_y = 1.89$	$g_y = 1.86$	$\Delta\chi_{rh} = -1.01\cdot10^{-32}$	$\Delta\chi_{rh} = -1.03\cdot10^{-32}$	$a_y = 19.9$	$b_y = 7.7$	$c_y = 0.6$
		$g_z = 3.45$	$g_z = 3.40$			$a_z = 36.3$	$b_z = 0.7$	$c_z = 0.9$
Cytochrome b_5		Experimental	Calculated	Experimental	Calculated			
$E_1 = 554$	$\varepsilon_1 = 483$	$g_x = 1.43$	$g_x = 1.43$	$\Delta\chi_{ax} = 2.83\cdot10^{-32}$	$\Delta\chi_{ax} = 2.83\cdot10^{-32}$	$a_x = 17.2$	$b_x = 6.1$	$c_x = 0.4$
$E_2 = 963$	$\varepsilon_2 = 1050$	$g_y = 2.23$	$g_y = 2.23$	$\Delta\chi_{rh} = -1.06\cdot10^{-32}$	$\Delta\chi_{rh} = -1.52\cdot10^{-32}$	$a_y = 23.7$	$b_y = 3.8$	$c_y = 0.6$
		$g_z = 3.03$	$g_z = 2.99$			$a_z = 32.7$	$b_z = 0.7$	$c_z = 0.9$
Cytochrome c		Experimental	Calculated	Experimental	Calculated			
$E_1 = 437$	$\varepsilon_1 = 441$	$g_x = 1.25$	$g_x = 1.25$	$\Delta\chi_{ax} = 2.68\cdot10^{-32}$	$\Delta\chi_{ax} = 2.99\cdot10^{-32}$	$a_x = 16.9$	$b_x = 7.6$	$c_x = 0.6$
$E_2 = 791$	$\varepsilon_2 = 895$	$g_y = 2.25$	$g_y = 2.25$	$\Delta\chi_{rh} = -1.25\cdot10^{-32}$	$\Delta\chi_{rh} = -1.73\cdot10^{-32}$	$a_y = 25.0$	$b_y = 4.4$	$c_y = 1.0$
		$g_z = 3.06$	$g_z = 3.06$			$a_z = 35.0$	$b_z = 0.5$	$c_z = 1.4$

[a] In the present work, the theoretical treatment always results in labeling g_x as the smallest of the three g-tensor components (in absolute value). The same holds for the χ-tensor components. Therefore, $\Delta\chi_{rh}$ values are always negative.

Table 2. Calculated and experimental contact and pseudo-contact shifts for MetMbCN [12], cytochrome b_5 [20] and cytochrome c;[19] the shifts (in ppm) are reported for methyl protons 1, 3, 5, and 8; the methyl proton shifts were corrected for an average higher shift value of the protons of methyls 5 and 8 and an average lower shift value of the protons of methyls 1 and 3 (±1 and ±2.4 ppm for cytochrome c and for cytochrome b_5 and MetMbCN, respectively);[30,43] the empirical a values in Equations (8) and (9) are 1.2, 0.9 and 1.4 for MetMbCN, cytochrome b_5 and cytochrome c, respectively

	Contact shift calculated	experimental	Pseudo-contact shift calculated	experimental
MetMbCN	21.5/8.2/26.3/12.0	18.4/6.7/27.8/15.8	−3.0/−5.8/−3.0/−5.6	−3.4/−5.7/−3.3/−6.5
Cytochrome b_5	6.3/13.5/11.2/6.2	8.6/16.0/17.7/2.0	−0.9/−5.9/−0.9/−2.3	−1.5/−4.7/−1.5/−2.8
Cytochrome c	9.9/29.6/11.9/33.0	7.7/30.1/11.0/35.4	−5.9/−1.2/−5.9/−1.6	−4.4/−1.1/−4.9/−1.9

the Kurland and McGarvey approach and the McConnell approach. In the latter case, the contact shift is given by[1]

$$\delta^{con} = \frac{g_e \mu_B S(S+1)}{3kT\gamma_N}\frac{A'}{\hbar} \quad (10)$$

where A' is the McConnell hyperfine coupling constant. The data reported in Table 3 show that the value of A'/h is not directly correlated to the values of A_0/h and A_1/h, and the deviation is different for the different methyl protons. Data reported in Table 3 provide an indication of the error inherent in use of the simple McConnell equation. If the difference in energy between the ground and excited states increases, the spin-orbit coupling does not efficiently mix the different d orbitals, the g anisotropy decreases and A' approaches A_0. It should be noted that A' differs from A_0 even in the limits of zero and infinite temperatures (Table 3). In the first case, this is because $<S_z>$ contains an orbital contribution which makes it different from the Curie value used in the McConnell equation. In the second case, the contact coupling constants of each level differ from one another. Only in a case where $A_0 = A_1 = A_2$, which is unrealistic for methyl protons in heme porphyrins, would A' coincide with A_0.

Figure 3 shows how anisotropic the contact shift of methyl protons in cyanometmyoglobin is predicted to be. The contact shift is reported for different orientations of the external magnetic field in either the xy, xz, or yz planes. NMR experimentalists of low-spin hemeproteins have always ignored this anisotropy, because they are dealing with an averaged shift in solution and only the average contact contribution to the hyperfine interaction is obtained. It is obvious, however, that in the case of partially oriented systems, the average should be calculated by providing a different weighting in the different directions, and therefore anisotropy must be considered.

In Table 4 the contributions to the contact shift along the three main directions have been reported for the methyl protons. Data show that the anisotropy can be very large, so that such an effect must be taken into account in the presence of partial orientation. Appropriate equations are reported in the Appendix.

It should be noted that, since contact shifts are usually larger than pseudo-contact shifts, the effects originating from the anisotropy in the contact term are similarly expected to be larger than those related to the anisotropies in the dipolar term. Therefore, such dependencies should be carefully considered in ENDOR spectroscopy, where any

Table 3. Contact shifts of the methyl protons, δ^{con}, of MetMbCN, cytochrome b_5 and cytochrome c, obtained with the Kurland and McGarvey equation with the values of A_0/h and A_1/h calculated from Equations (8, 9) and the resulting coupling constant A'/h back-calculated from the values of δ^{con} and from the McConnell equation, for three different temperatures; A/h values are expressed in MHz, and the shifts in ppm; note that in the table the heuristic correction made in Table 2, and suggested in ref.[43] was not made

MetMbCN								
	δ^{con} 298 K	A'/h (McConnell)	A_0/h (McGarvey)	A_1/h (McGarvey)	δ^{con} 1 K	A'/h (McConnell)	δ^{con} 3130 K	A'/h (McConnell)
1-CH_3	23.9	0.902	0.960	0.199	6306	0.799	1.440	0.571
3-CH_3	10.6	0.400	0.199	0.960	1316	0.167	0.941	0.373
5-CH_3	23.9	0.902	0.960	0.199	6306	0.799	1.440	0.571
8-CH_3	9.6	0.362	0.142	1.017	941	0.119	0.904	0.358
Cytochrome b_5								
	δ^{con} 313 K	A'/h (McConnell)	A_0/h (McGarvey)	A_1/h (McGarvey)	δ^{con} 1 K	A'/h (McConnell)	δ^{con} 3130 K	A'/h (McConnell)
1-CH_3	8.7	0.345	0.267	0.610	2066	0.262	0.805	0.319
3-CH_3	15.9	0.630	0.610	0.267	4714	0.597	0.998	0.396
5-CH_3	8.7	0.345	0.267	0.610	2066	0.262	0.805	0.319
8-CH_3	3.8	0.151	0.035	0.842	271	0.034	0.674	0.133
Cytochrome c								
	δ^{con} 293 K	A'/h (McConnell)	A_0/h (McGarvey)	A_1/h (McGarvey)	δ^{con} 1 K	A'/h (McConnell)	δ^{con} 3130 K	A'/h (McConnell)
1-CH_3	10.9	0.404	0.239	1.152	1764	0.223	1.154	0.457
3-CH_3	30.6	1.135	1.152	0.239	8475	1.073	1.681	0.666
5-CH_3	10.9	0.404	0.239	1.152	1764	0.223	1.154	0.457
8-CH_3	32.0	1.187	1.221	0.171	8980	1.137	1.720	0.682

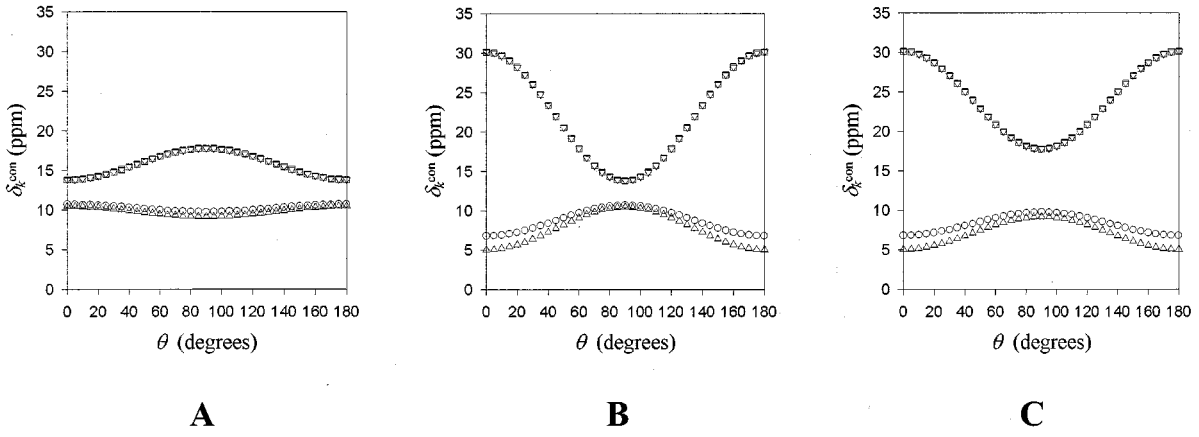


Figure 3. Contact shift calculated for different k orientations of the molecule in a magnetic field for the four methyl protons (□ = 1-CH_3, ○ = 3-CH_3, ▽ = 5-CH_3, Δ = 8-CH_3); panel A shows the shifts for the magnetic field B_0 in the xy plane, where θ is the angle between B_0 and the metal-pyrrole(II) direction; in panels B and C, θ is the angle between B_0 and the z axis, with B_0 in the xz (B) or yz (C) planes; φ is set to −2°, as found experimentally for MetMbCN[60,61]

angular dependence is usually ascribed to the dipolar interaction, and assuming an isotropic contact contribution would be erroneous.

Concluding Remarks and Perspectives

The McConnell equation (Equation 10) is generally used to analyze contact shift patterns. As outlined on several occasions,[5,55] such an equation only holds for one unpaired electron in a single orbital with g near to 2. Low-spin Ru^{III} and Fe^{III} have g values very different from 2, and also have low-lying excited levels.[28,29,53] In these cases a much more complex analysis is needed. In the case of heme proteins, the hyperfine shifts are provided by both contact and pseudocontact contributions. The latter are absolutely dominant for protons several bonds away from the metal ion, and allow for the determination of magnetic susceptibility anisotropies (according to Equation 7) together with the

Table 4. Anisotropic contributions to the contact shifts (in ppm), calculated for MetMbCN, cytochrome b_5, and cytochrome *c*

Methyl		MetMbCN[12,59]	Cytochrome b_5[20]	Cytochrome *c*[19,21]
1-CH_3	*x*	12.3	8.2	9.0
	y	15.9	8.5	7.8
	z	27.0	9.1	6.3
	average	18.4	8.6	7.7
3-CH_3	*x*	7.9	12.2	21.0
	y	7.2	15.6	29.4
	z	5.0	20.2	39.9
	average	6.7	16.0	30.1
5-CH_3	*x*	18.6	16.8	12.9
	y	24.0	17.6	11.1
	z	40.7	18.7	9.0
	average	27.8	17.7	11.0
8-CH_3	*x*	20.1	3.0	24.3
	y	17.6	2.1	34.6
	z	9.8	0.9	47.3
	average	15.8	2.0	35.4

principal direction of the χ tensor and a refinement of the solution structure.[19,20,40,56] From the knowledge of the *g* and Δχ values, the contact shift of the heme protons can be estimated. A ligand-field analysis, together with the Kurland and McGarvey approach, allows for a detailed and instructive analysis of the contributions of the various electronic levels. Such an analysis is absolutely necessary when the hyperfine coupling is analyzed by ENDOR spectroscopy and when proton hyperfine shifts are analyzed in partially oriented systems.

Finally, magnetically anisotropic molecules in a high magnetic field experience partial orientation, which should result in a variation in the hyperfine shifts due to residual dipolar coupling between the unpaired electron(s) and the resonating nucleus. When the contact shift is anisotropic, there is also a variation in the contact contribution. This is the first time that such an effect has been accurately calculated for heme proteins, although dipolar coupling in those systems is well known in ENDOR spectroscopy.[57] When contact shift occurs, its anisotropy also contributes to the change in hyperfine shifts in partially oriented systems. This has always been neglected in ENDOR and NMR spectroscopy, despite the warnings of McGarvey,[5,55] which have largely been ignored.

Residual electron-nucleus dipolar couplings are a new class of structural constraints and may become significant when systems with $S > 1/2$ and/or more efficient orienting solvents are used. When the contact interaction is operative, further details of the electronic structure of the systems under investigation become available.

Appendix

In the presence of partial orientation, an orientational *D* tensor should be defined, with principal components D_x, D_y, and D_z. The residual contact shift, i.e. the difference between the averaged contact shift in the absence and in the presence of partial orientation, $\Delta\delta^{con}$, is given by

$$\Delta\delta^{con} = \tilde{\delta}_x^{con} D_x + \tilde{\delta}_y^{con} D_y + \tilde{\delta}_z^{con} D_z \qquad (A.2)$$

In general, the *D* and *g* tensors are not diagonal in the same frame. Therefore, the shifts must be calculated by evaluating the weighted average between the shifts along the main directions of the orientational *D* tensor, so that in Equation A.1

$$\tilde{\delta}_i^{con} = \delta_x^{con} \sin^2\alpha\cos^2\beta + \delta_y^{con} \sin^2\alpha\sin^2\beta + \delta_z^{con} \cos^2\alpha \qquad (A.2)$$

where $\tilde{\delta}_i^{con}$ are provided by Equation (5), with α and β equal to the polar angles that define the position of the $i = x, y, z$ axes of the *D* tensor in the frame of the *g* tensor.

Analogously, the residual dipolar shift contribution is provided by the following equation

$$\Delta\delta^{dip} = \tilde{\delta}_x^{dip} D_x + \tilde{\delta}_y^{dip} D_y + \tilde{\delta}_z^{dip} D_z \qquad (A.3)$$

with[4]

$$\tilde{\delta}_i^{dip} = \frac{1}{4\pi r^3}\left[3\left(\chi_{zz}\cos\alpha\cos\vartheta + \chi_{xx}\sin\alpha\cos\beta\sin\vartheta\cos\varphi + \chi_{yy}\sin\alpha\sin\beta\sin\vartheta\sin\varphi\right)\right.$$
$$\left(\cos\alpha\cos\vartheta + \sin\alpha\cos\beta\sin\vartheta\cos\varphi + \sin\alpha\sin\beta\sin\vartheta\sin\varphi\right) - \qquad (A.4)$$
$$\left.\left(\chi_{zz}\cos^2\alpha + \chi_{xx}\sin^2\alpha\cos^2\beta + \chi_{yy}\sin^2\alpha\sin^2\beta\right)\right]$$

where α and β are the polar angles that define the position of the main axis *i* of the *D* tensor in the frame where χ is diagonal, and are the polar angles that define the position of the electron−proton direction in the same frame (see Figure 4). Integration of Equation (A.4) over all space gives Equation (7). Equations (A.1−A.2) and (A.3−A.4) may prove useful whenever extensive orientation in solution

without too severe broadening in the NMR lines is obtained.

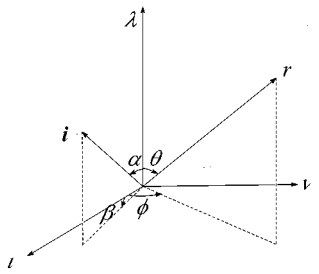


Figure 4. Schematic representation in the χ frame of the α and β polar angles defining the position of the *i* direction and of the θ and φ polar angles defining the proton-electron *r* direction

For completeness, we mention the limit values of Equations (A.1−A.2) and (A.3−A.4) when the *D*, *g* and χ tensors are diagonal in the same frame. This may be the case for molecules experiencing partial orientation in a field as a result of the anisotropy of the χ tensor itself.[58] For the residual contact shift, $\tilde{\delta}_i^{\mathrm{con}}$ in Equation (A.1) are provided by Equation (5). For the residual dipolar shifts, $\tilde{\delta}_i^{\mathrm{dip}}$ in Equation (A.3) reduce to:

$$\tilde{\delta}_x^{\mathrm{dip}} = \frac{\chi_{xx}\left(3l^2-1\right)}{4\pi r^3} \qquad \tilde{\delta}_y^{\mathrm{dip}} = \frac{\chi_{yy}\left(3m^2-1\right)}{4\pi r^3} \qquad \tilde{\delta}_z^{\mathrm{dip}} = \frac{\chi_{zz}\left(3n^2-1\right)}{4\pi r^3}$$

In the axial case and in the hypothesis that the components of the *D* tensor are proportional to those of the χ tensor, the following relationships can be derived:

$$D_{\parallel} = \frac{1+\frac{B_0^2}{2\mu_0 kT}\chi_{\parallel}}{3+\frac{B_0^2}{2\mu_0 kT}\chi_{\parallel}+2\frac{B_0^2}{2\mu_0 kT}\chi_{\perp}} \qquad D_{\perp} = \frac{1+\frac{B_0^2}{2\mu_0 kT}\chi_{\perp}}{3+\frac{B_0^2}{2\mu_0 kT}\chi_{\parallel}+2\frac{B_0^2}{2\mu_0 kT}\chi_{\perp}}$$

so that $D_{\parallel} + 2D_{\perp} = 1$. Substituting into Equation (A.3) provides the pseudo-contact shift

$$\delta^{\mathrm{pc}} = \frac{1}{3+\frac{B_0^2}{2\mu_0 kT}\chi_{\parallel}+2\frac{B_0^2}{2\mu_0 kT}\chi_{\perp}} \cdot \frac{1}{4\pi r^3}\left[\left(3\chi_{\parallel}\cos^2\theta-\chi_{\parallel}\right)\left(1+\frac{B_0^2}{2\mu_0 kT}\chi_{\parallel}\right)+2\left(\frac{3}{2}\chi_{\perp}\sin^2\theta-\chi_{\perp}\right)\left(1+\frac{B_0^2}{2\mu_0 kT}\chi_{\perp}\right)\right]$$

where θ is the angle between *r* and $\chi_{\parallel}$. To first order, the above equation can be approximated as

$$\delta^{\mathrm{pc}} = \frac{(3\cos^2\theta-1)(\chi_{\parallel}-\chi_{\perp})}{12\pi r^3}\left(1+\frac{B_0^2}{6\mu_0 kT}(2\chi_{\parallel}+\chi_{\perp})\right) \quad (A.5)$$

A similar equation has already been reported.[58] A remarkable feature of this equation is that the correction to the pseudo-contact shifts owing to orientation $\left(\frac{B_0^2}{6\mu_0 kT}(2\chi_{\parallel}+\chi_{\perp})\right)$ depends on the magnitude of the magnetic susceptibility but is independent of its anisotropy.

Acknowledgments

We thank Professor Bruce McGarvey for the enlightening discussions on the factors determining the anisotropy of contact shift during his stay as visiting professor in Florence in 1998. He has given us the correct perception of the importance of such effects. For financial support, we thank Murst ex 40%, Italy, the European Union, TMR-LSF contract ERB FMGE CT950033, and CNR, Progetto Finalizzato Biotecnologie, Italy.

[1] H. M. McConnell, D. B. Chesnut, *J. Chem. Phys.* **1958**, *28*, 107−117.
[2] *NMR of Paramagnetic Molecules* (Eds.: G. N. La Mar, W. De. W. Horrocks, Jr., R. H. Holm), Academic Press, New York, **1973**.
[3] I. Bertini, C. Luchinat, *NMR of paramagnetic molecules in biological systems*, Benjamin/Cummings, Menlo Park, CA, **1986**.
[4] I. Bertini, C. Luchinat, *NMR of paramagnetic substances, Coord. Chem. Rev. 150*, Elsevier, Amsterdam, **1996**.
[5] R. J. Kurland, B. R. McGarvey, *J. Magn. Reson.* **1970**, *2*, 286−301.
[6] H. M. McConnell, R. E. Robertson, *J. Chem. Phys.* **1958**, *29*, 1361−1365.
[7] W. E. Blumberg, J. Peisach, B. A. Wittenberg, J. B. Wittenberg, *J. Biol. Chem.* **1968**, *243*, 1854−1862. B. A. Wittenberg, L. Kampa, J. G. Wittenberg, W. E. Blumberg, J. Peisach, *J. Biol. Chem.* **1968**, *243*, 1863−1870.
[8] H. Hori, *Biochim. Biophys. Acta* **1971**, *251*, 227−235.
[9] C. P. S. Taylor, *Biochim. Biophys. Acta* **1977**, *491*, 137−149.
[10] J. C. Ferrer, P. Turano, L. Banci, I. Bertini, I. K. Morris, K. M. Smith, M. Smith, A. G. Mauk, *Biochemistry* **1994**, *33*, 7819−7829.
[11] G. Williams, N. J. Clayden, G. R. Moore, R. J. P. Williams, *J. Mol. Biol.* **1985**, *183*, 447−460.
[12] S. D. Emerson, G. N. La Mar, *Biochemistry* **1990**, *29*, 1556−1566.
[13] Y. Q. Feng, H. Roder, S. W. Englander, *Biochemistry* **1990**, *29*, 3494−3504.
[14] K. Rajarathnam, G. N. La Mar, M. L. Chiu, S. G. Sligar, *J. Am. Chem. Soc.* **1992**, *114*, 9048−9058.
[15] D. L. Turner, *Eur. J. Biochem.* **1993**, *211*, 563−568.
[16] M. Gochin, H. Roder, *Protein Sci.* **1995**, *4*, 296−305.
[17] D. L. Turner, *Eur. J. Biochem.* **1995**, *227*, 829−837.
[18] L. Banci, R. Pierattelli, D. L. Turner, *Eur. J. Biochem.* **1995**, *232*, 522−527.
[19] L. Banci, I. Bertini, H.B. Gray, C. Luchinat, T. Reddig, A. Rosato, P. Turano, *Biochemistry* **1997**, *36*, 9867−9877.
[20] F. Arnesano, L. Banci, I. Bertini, I. C. Felli, *Biochemistry* **1998**, *37*, 173−184.
[21] L. Banci, I. Bertini, C. Luchinat, R. Pierattelli, N. V. Shokhirev, F. A. Walker, *J. Am. Chem. Soc.* **1998**, *120*, 8472−8479.
[22] J. Boyd, C. M. Dobson, A. S. Morar, R. J. P. Williams, G. J. Pielak, *J. Am. Chem. Soc.* **1999**, *121*, 9247−9248.
[23] P. Tsan, M. Caffrey, M. L. Daku, M. Cusanovich, D. Marion, P. Gans, *J. Am. Chem. Soc.* **1999**, *121*, 1795−1805.
[24] L. Banci, I. Bertini, C. Luchinat, P. Turano, in *The Porphyrin Handbook* (Eds.: K. M. Kadish, K. M. Smith, R. Guilard), Academic Press, San Diego, CA, **2000**, pp 323−350.
[25] J. S. Griffith, *Proc. Roy. Soc. London* **1956**, *235*, 23−36.
[26] W. D. Horrocks, Jr., E. S. Greenberg, *Biochim. Biophys. Acta* **1973**, *322*, 38−44.
[27] T. L. Bohan, *J. Magn. Reson.* **1977**, *26*, 109−118.
[28] B. R. McGarvey, *Coord. Chem. Rev.* **1998**, *170*, 75−92.
[29] B. R. McGarvey, N. C. Batista, C. W. B. Bezerra, M. S. Schultz, D. W. Franco, *Inorg. Chem.* **1998**, *37*, 2865−2872.

[30] I. Bertini, C. Luchinat, G. Parigi, F. A. Walker, *JBIC* **1999**, *4*, 515−519.
[31] J. A. Losonczi, J. H. Prestegard, *J. Biomol. NMR* **1998**, *12*, 447−451.
[32] B. W. Koenig, H. Jin-Shan, M. Ottiger, S. Bose, R. W. Hendler, A. Bax, *J. Am. Chem. Soc.* **1999**, *121*, 1385−1386.
[33] G. M. Clore, M. R. Starich, A. M. Gronenborn, *J. Am. Chem. Soc.* **1998**, *120*, 10571−10572.
[34] M. R. Hansen, M. Rance, A. Pardi, *J. Am. Chem. Soc.* **1998**, *120*, 11210−11211.
[35] M. Ottiger, A. Bax, *J. Biomol. NMR* **1998**, *12*, 361−372.
[36] H. Wang, M. Eberstadt, E. T. Olejniczak, R. P. Meadows, S. W. Fesik, *J. Biomol. NMR* **1998**, *12*, 443−446.
[37] N. Tjandra, S. Grzesiek, A. Bax, *J. Am. Chem. Soc.* **1996**, *118*, 6264−6272.
[38] J. R. Tolman, J. M. Flanagan, M. A. Kennedy, J. H. Prestegard, *Proc. Natl. Acad. Sci. USA* **1995**, *92*, 9279−9283.
[39] A. A. Bothner-By, in *Encyclopedia of Nuclear Magnetic Resonance* (Eds.: D. M. Grant, R. K. Harris), John Wiley and Sons: Chichester, **1996**; pp 2932−2938.
[40] L. Banci, I. Bertini, K. L. Bren, M. A. Cremonini, H. B. Gray, C. Luchinat, P. Turano, *JBIC* **1996**, *1*, 117−126.
[41] I. Bertini, A. Dikiy, C. Luchinat, R. Macinai, M. S. Viezzoli, *Inorg. Chem.* **1998**, *37*, 4814−4821.
[42] M. Karplus, G. K. Fraenkel, *J. Chem. Phys.* **1961**, *35*, 1312−1323.
[43] N. V. Shokhirev, F. A. Walker, *JBIC* **1998**, *3*, 581−594.
[44] G. N. La Mar, J. del Gaudio, J. S. Frye, *Biochim. Biophys. Acta* **1977**, *498*, 422−432.
[45] G. Simonneaux, F. Hindre, M. Le Plouzennec, *Inorg. Chem.* **1989**, *28*, 823−825.
[46] F. A. Walker, H. Nasri, I. Turowska-Tyrk, K. Mohanrao, C. T. Watson, N. V. Shokhirev, P. G. Debrunner, W. R. Scheidt, *J. Am. Chem. Soc.* **1996**, *118*, 12109−12118.
[47] M. Nakamura, T. Ikeue, H. Fujii, T. Yoshimura, *J. Am. Chem. Soc.* **1997**, *119*, 6284−6291.
[48] J. Wojaczynski, L. Latos-Grazynski, P. J. Chmielewski, P. Van Calcar, A. L. Balch, *Inorg. Chem.* **1999**, *38*, 3040−3050.
[49] F. A. Walker, in *The Porphyrin Handbook* (Eds.: K. M. Kadish, K. M. Smith, R. Guilard), Academic Press, San Diego, CA, **2000**, pp 81−183.
[50] D. A. Cruse, J. E. Davies, M. Gerloch, J. H. Harding, D. J. Macking, R. F. McMeecking, *CAMMAG, a FORTRAN computing package*, University Chemical Laboratory, Cambridge, **1979**.
[51] H. Stratemeier, M. A. Hitchman, P. Comba, P. V. Bernhardt, M. J. Riley, *Inorg. Chem.* **1991**, *30*, 4088−4093.
[52] Values of λ in the range 240−400 cm^{-1} can be considered reasonable, see refs. [20, 26, 62].
[53] L. Banci, A. Rosato, P. Turano, *JBIC* **1996**, *1*, 364−367.
[54] R. O. Louro, I. J. Correia, L. Brennan, I. B. Coutinho, A. V. Xavier, D. L. Turner, *J. Am. Chem. Soc.* **1998**, *120*, 13240−13247.
[55] B. R. McGarvey, *J. Am. Chem. Soc.* **1972**, *95*, 1103−1110. B. R. McGarvey, *J. Chem. Phys.* **1976**, *65*, 962−971. B. R. McGarvey, *Inorg. Chem.* **1988**, *27*, 4691−4698. B. R. McGarvey, *Inorg. Chem.* **1995**, *34*, 6000−6007.
[56] L. Banci, I. Bertini, K. L. Bren, H. B. Gray, P. Sompornpisut, P. Turano, *Biochemistry* **1997**, *36*, 8992−9001.
[57] H. Reinhard, R. Kappl, J. Huttermann, M. S. Viezzoli, *J. Phys. Chem.* **1994**, *98*, 8806−8812.
[58] I. Bertini, I. C. Felli, C. Luchinat, *J. Magn. Reson.* **1998**, *134*, 360−364.
[59] L. Banci, I. Bertini, R. Pierattelli, A. J. Vila, *Inorg. Chem.* **1994**, *33*, 4338−4343.
[60] S. D. Emerson, G. N. La Mar, *Biochemistry* **1990**, *29*, 1545−1556.
[61] K. Vyas, K. Rajarathnam, L. P. Lu, S. D. Emerson, G. N. La Mar, R. Krishnamoorthi, H. Mizukami, *J. Biol. Chem.* **1993**, *268*, 14826−14835.
[62] D. L. Turner, R. J. P. Williams, *Eur. J. Biochem.* **1993**, *211*, 555−562.

Received January 20, 2000
[I00022]

Diastereospecific Control in the Synthesis of Enantiomerically Pure Bis-Equatorial Rhodium(II) Catalysts by Chiral Phosphanes

Pascual Lahuerta,*[a] Eduardo Moreno,[a] Angeles Monge,[b] Guillermo Muller,[c] Julia Pérez- Prieto,*[d] Mercedes Sanaú,[a] and Salah-Eddine Stiriba[a][‡]

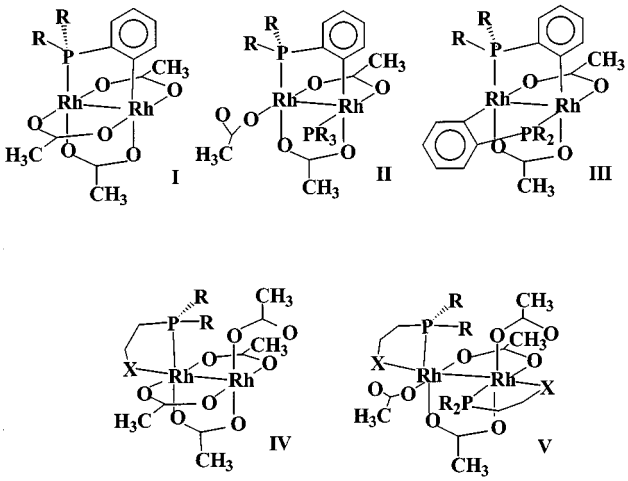
Keywords: Carboxylato complexes / Chirality / Diazo compounds / P ligands / Rhodium

The reaction of $Rh_2(O_2CR)_4$ [R = CH_3, CF_3] with the chiral phosphane (1*S*,2*S*,5*R*)-(2-hydroxy-5-isopropenyl-2-methylcyclohexyl)(diphenyl)phosphane, (+)PPh_2(CH–R*–OH) or its enantiomer (1*R*,2*R*,5*S*)-(2-hydroxy-5-isopropenyl-2-methylcyclohexyl)(diphenyl)phosphane, (–)-PPh_2(CH–R*–OH), results in the specific formation of the products (*P*)-$Rh_2(\mu\text{-}O_2CR)_2(\eta^1\text{-}O_2CR)_2\{\eta^2\text{-}(+)PPh_2(CH–R^*–OH)\}_2$ [**P(+)1**, R = CH_3; **P(+)2** R = CF_3] and (*M*)-$Rh_2(\mu\text{-}O_2CR)_2(\eta^1\text{-}O_2CR)_2\{\eta^2\text{-}(–)PPh_2(CH–R^*–OH)\}_2$ [**M(–)1**, R = CH_3; **M(–)2**, R = CF_3] in a high yield. Their synthesis, characterisation and catalytic behaviour in metal–carbenoid reactions are reported. X-ray analysis of **P(+)2** and **M(–)2** shows, in each case, a Rh_2^{4+} unit supported by two bridging and two monodentate trifluoroacetates; two phosphanes, (+)PPh_2(CH–R*–OH) or (–)PPh_2(CH–R*–OH) respectively, acting as chelating equatorial (P) and axial (O) donor ligands, complete the coordination sphere. These compounds are a pair of enantiomers. The crystallographic parameters are as follow: for **P(+)2**, space group $P3_121$ (trigonal) with $a = b = 13.0366(8)$, $c = 29.756(2)$ Å, $Z = 6$ and $R = 0.0499$; for **M(–)2** space group $P3_2$ (trigonal) with $a = b = 12.9751(9)$, $c = 29.685(3)$ Å, $Z = 3$ and $R = 0.0747$.

Introduction

The current interest in the development of rhodium(II) compounds recently observed[1] is due to their applications in catalytic metal−carbene transformations.[2] Most rhodium(II) compounds are formulated as $[Rh_2(ABC)_4L_2]$ and have the lantern-type structure characteristic of dimetal tetracarboxylate compounds.[1a] Cotton[3] and others[4] have reported that rhodium(II) carboxylate compounds with arylphosphanes afford compounds of the type $[Rh_2(\mu\text{-}O_2CR)_{4-x}(\mu\text{-PC})_x]$ (x = 1,2; R = CH_3 or CF_3; PC = metalated arylphosphane).

The great variety of these structures[3,4] and the possibility of modifying these compounds for specific purposes ensure continued emphasis on synthesis, characterisation and catalytic studies.[5] Cyclometalated rhodium(II) compounds with structures of type **I**−**III** (Scheme 1) have been characterised by X-ray methods,[3a][4a][4b] and some of them have shown chemoselectivity in diazo transformations.[4f]



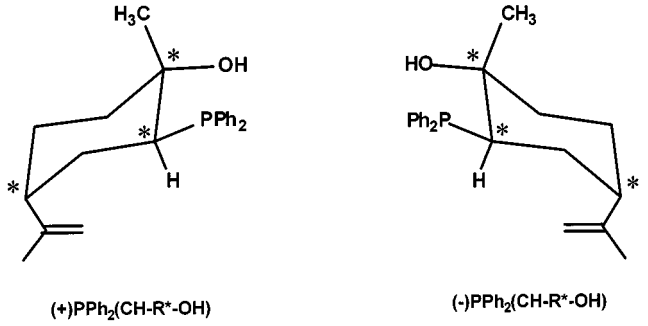
Scheme 1. Rhodium compounds type **I**−**V**

Related compounds with *ortho*-functionalised phosphanes and structures **IV**[6] and **V**, [5] have also been reported. It should be noted that structures **III** and **V** have C_2 symmetry and consequently are inherently chiral. Compounds with the formula $Rh_2(O_2CCH_3)_2[(C_6H_4)P(C_6H_5)_2]_2$, with structure **III**, have been isolated as pure enantiomers by conventional resolution methods.[7] The resolved enanti-

[a] Dep. de Química Inorgánica, Facultad de Químicas, Universidad de Valencia,
Dr. Moliner 50, 46100 Burjassot-Valencia, Spain
Fax: (internat.) + 34-96/386-4322
E-mail: pascual.lahuerta@uv.es
[b] Instituto de Ciencia de Materiales de Madrid, CSIC 28949, Cantoblanco, Madrid, Spain
[c] Dep. de Química Inorgánica, Universidad de Barcelona, Diagonal 647, 08028, Barcelona, Spain
[d] Dep. de Química Orgánica, Facultad de Farmacia, Universidad de Valencia,
Av. Vicent A. Estelles, s/n, 46100, Burjassot-Valencia, Spain
Fax: (internat.) + 34-96/386-4939
E-mail: julia.perez@uv.es
[‡] Present address: UMR 7513, Laboratoire de Chimie Organométallique et de Catalyse, Institut le Bel, Universite Louis Pasteur, rue Blaise Pascal, 67007, Strasbourg-cedex, France.

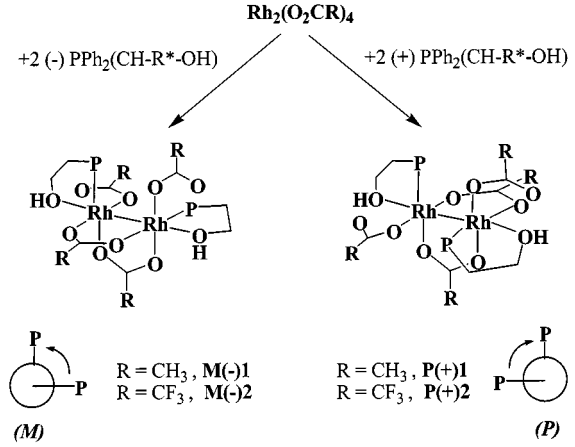
omers induce moderate enantioselectivity in a C−H insertion reaction.

Compounds of type **V**, with acetate groups and X = Cl, OCH_3, have shown catalytic activity in cyclopropanation reactions.[5] Considering the potential interest of these type of compounds as pure enantiomers, we explored their selective synthesis by using the chiral phosphanes (*1S*,2*S*,5*R*)-(2-hydroxy-5-isopropenyl-2-methylcyclohexyl)(diphenyl)-phosphane, (+)-PPh_2(CH−R*−OH)[8] or its enantiomer (1*R*,2*R*,5*S*)-(2-hydroxy-5-isopropenyl-2-methylcyclohexyl)(diphenyl)-phosphane, (−)-PPh_2(CH−R*−OH) (Scheme 2).



Scheme 2. (1*S*,2*S*,5*R*)-(2-hydroxy-5-isopropenyl-2-methylcyclohexyl)(diphenyl)phosphane (+)PPh_2(CH−R*−OH) and its enantiomer, (−)PPh_2(CH−R*−OH)

We describe in this paper the diastereospecific synthesis of compounds **P(+)1** and **P(+)2** from the reaction of (+)-PPh_2(CH−R*−OH) with rhodium acetate or trifluoroacetate (Scheme 3). Similar reactions with the phosphane (−)-PPh_2(CH−R*−OH) produced **M(−)1** and **M(−)2**. We also report on the X-ray structure of the trifluoroacetate derivatives **P(+)2** and **M(−)2**, as well as the catalytic behaviour of several of these compounds.



Scheme 3. Synthesis of bis equatorial rhodium(II) catalysts by reaction of chiral phosphanes with rhodium tetracarboxylates

Results

Synthetic Aspects

Addition of 2 equivalents of (+)-PPh_2(CH−R*−OH) to a solution of $Rh_2(O_2CCH_3)_4$·2MeOH in refluxing toluene/acetic acid (3:1), resulted in the formation of a green solution from which the complex (*P*)-$Rh_2(\mu\text{-}O_2CCH_3)_2(\eta\text{-}O_2CCH_3)_2\{\eta^2\text{-}(+)\text{-}PPh_2(CH-R^*-OH)\}_2$ **[P(+)1]** was easily isolated in a high yield. The same reaction with the phosphane (−)-PPh_2(CH−R*−OH) yielded the corresponding enantiomer (*M*)-$Rh_2(\mu\text{-}O_2CCH_3)_2(\eta\text{-}O_2CCH_3)_2\{\eta^2\text{-}(-)\text{-}PPh_2(CH-R^*-OH)\}_2$ **[M(−)1]**.

Addition of 2 equiv. of (+)-PPh_2(CH−R*−OH) to a solution of $Rh_2(O_2CCF_3)_4$ in diethyl ether at room temperature, yielded the complex (*P*)-$Rh_2(\mu\text{-}O_2CCF_3)_2(\eta\text{-}O_2CCF_3)_2\{\eta^2\text{-}(+)\text{-}PPh_2(CH-R^*-OH)\}_2$ **[P(+)2]** in a high yield. The same reaction with the phosphane (−)-PPh_2(CH−R*−OH) yielded the corresponding enantiomer (*M*)-$Rh_2(\mu\text{-}O_2CCF_3)_2(\eta\text{-}O_2CCF_3)_2\{\eta^2\text{-}(-)\text{-}PPh_2(CH-R^*-OH)\}_2$ **[M(−)2]**.

X-ray Analysis

The crystal structures for compounds **P(+)2** and **M(−)2** have been determined by X-ray procedures. ORTEP diagrams, with the corresponding atom-labelling schemes are shown in Figure 1 and 2 for both the compounds together with selected bond lengths and angles.

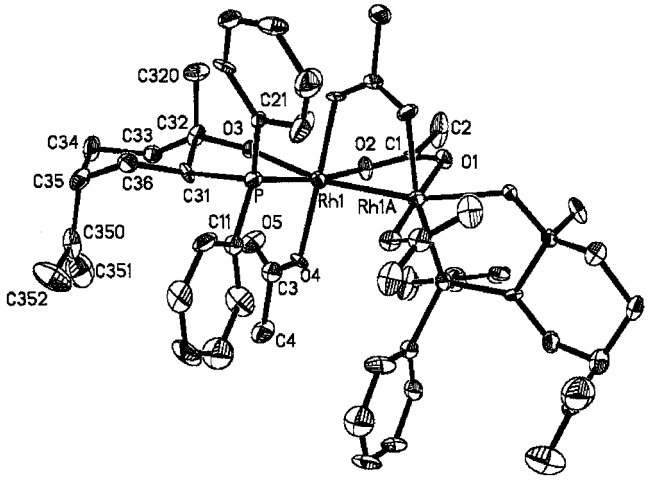


Figure 1. ORTEP diagram of the complex (*P*)-$Rh_2(\mu\text{-}O_2CCF_3)_2(\eta^1\text{-}O_2CCF_3)_2\{\eta^2\text{-}(+)PPh_2(CH-R^*-OH)\}_2$ **[P(+)2]** with the F and H atoms omitted for clarity; selected bond lengths [Å] and angles [°]: Rh1−Rh1A 2.5873(13), Rh1−O3 2.250(5), Rh1−P 2.252(3), Rh1−O2 2.148(8); O1−Rh1−O4 176.4(3), O2−Rh1−P 168.9(2), O3−Rh1−Rh1A 165.8(2), O4−Rh1−P 92.6(2)

The structure of **P(+)2** consists of an Rh_2^{4+} unit supported by two bridging and two monodentate trifluoroacetates; two (+)PPh_2(CH−R*−OH) phosphanes, acting as chelating equatorial (P) and axial (O) donor ligands, complete the coordination sphere around the metal atoms.

The two bridging trifluoroacetate groups are in a *cisoid* configuration and the phosphorous atoms exhibit a (*P*) configuration.

The Rh−Rh bond length, 2.5873(13) Å, is slightly longer than the distance [2.5605(11) Å] found in a structurally related compound with the formula $[Rh_2(\mu\text{-}O_2CCH_3)_2(\eta\text{-}Cl)_2\{\eta^2\text{-}(o\text{-}CH_3OC_6H_4)P(C_6H_5)_2\}_2]$.[5]

One interesting feature of **P(+)2** is that the axial Rh−O bond length, 2.250(5) Å, is shorter than that observed in the analogous $[Rh_2(\mu\text{-}O_2CCH_3)_2(\eta\text{-}Cl)_2\{\eta^2\text{-}(o\text{-}CH_3\text{-}$

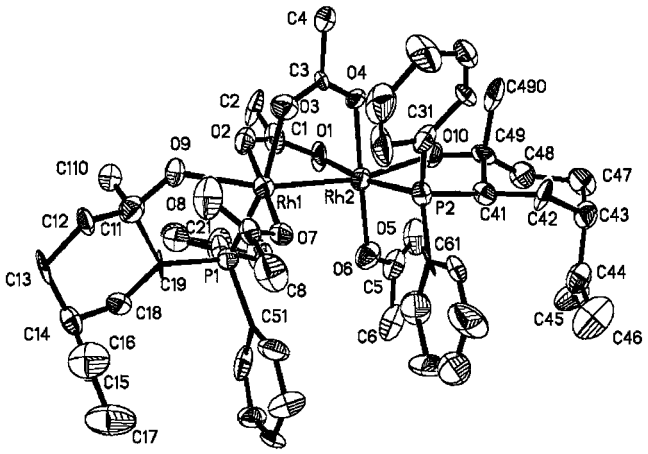


Figure 2. ORTEP diagram of the complex $(Rh_2(\mu\text{-}O_2CCF_3)_2(\eta^1\text{-}O_2CCF_3)_2\ \{\eta^2\text{-}(-)PPh_2(CH-R^*-OH)\}_2$ [**M(−)2**] with the F and H atoms omitted for clarity; selected bond lengths [Å] and angles [°]: Rh1−Rh2 2.6011(18), Rh1−O9 2.255(13), Rh1−P1 2.246(5), Rh1−O3 2.170(12); O2−Rh1−O7 176.0(5), O3−Rh1−P 169.1(4), O9−Rh1−Rh2 166.6(3), O7−Rh1−P 93.0(3)

$OC_6H_4)P(C_6H_5)_2\}_2$, 2.342(7) Å].[5] This distance is also shorter than the average Rh−O distance observed for rhodium(II) bis-adduct complexes with oxygen donor ligands.[1a][3a,4]

Compound **M(−)2** has the same overall structure as **P(+)2**, but has an (*M*) configuration. The Rh−Rh distance of 2.602(8) Å, is typical for such a type of species.

NMR-Spectroscopic Data

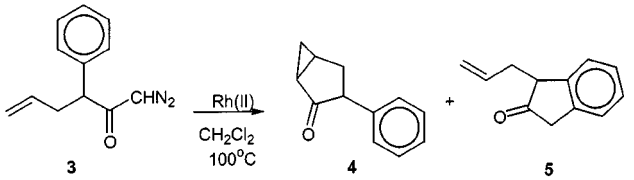
The spectroscopic data recorded for all the isolated compounds, support that the solid-state structure is maintained in solution. The ^{31}P NMR spectra show a second-order signal, with a very similar chemical shift for all the isolated compounds ($\delta \approx 46$), that corresponds to the AA′ part of an AA′XX′ system. This high value of the chemical shift is characteristic of nonmetalated phosphanes in an equatorial coordination.[5] The signals from the protons of the OH groups of the phosphanes appear at a remarkable low field, ($\delta \approx 10-12$), in agreement with the axial Rh−O coordination observed in the X-ray data. In particular, the homonuclear shift correlated 2D NMR spectrum of **P(+)2** confirms the coupling between the proton of the OH group (at 10.1 ppm) with the CH_3 group at $\delta = 1.4$ ppm, and also the coupling between the olefinic protons ($\delta = 4.2$ and 4.6) and the methyl group ($\delta = 1.1$).

The NMR-spectroscopic data also confirms the existence of two different types of carboxylate groups in each compound. Thus, compounds **P(+)2** and **M(−)2**, with trifluoroacetate groups, show two resonance signals in the corresponding ^{19}F NMR spectra. For the corresponding compounds with acetate groups, **P(+)1** and **M(−)1**, the ^1H NMR spectra show four resonance signals of equal intensity; two of these signals, at $\delta = 1.4$ and 1.1, correspond to the phosphane while the others, at $\delta = 1.0$ and 1.2, correspond to the acetate groups.

Catalytic Studies

The X-ray structural analysis provides evidence for the relatively strong coordination of the OH groups of the phosphanes to the axial site of the rhodium centre. This data suggests a low reactivity of these rhodium dimers toward diazo compounds; in order to confirm this assumption, control experiments were performed. Thus, the reaction of ethyl diazoacetate with compound **P(+)2** in dichloromethane, was carried out in a sealed tube at different temperatures in the 45−100 °C temperature range. We only observed a transformation of the diazo compound at temperatures close to 100 °C; at lower temperatures the substrate was recovered unchanged after extensive heating. ^{31}P and ^1H NMR spectra confirm that no decomposition of the rhodium compound occurred during this heating.

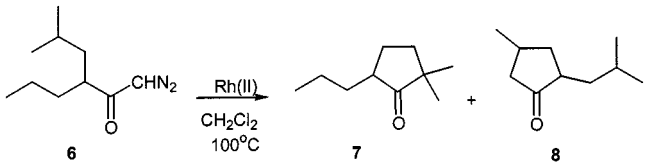
Studies of chemo- and regioselectivity of compounds **P(+)1** and **P(+)2** in diazo compound transformation were performed by using model substrates. Diazo ketone **3**[9] was used to study the competition between the cyclopropanation reaction and aromatic substitution (Scheme 4), while diazo ketone **6**[10] was used for similar studies in tertiary versus secondary C−H insertion reaction (Scheme 5). It is remarkable that these compounds led to a similar selectivity as rhodium acetate. Not surprisingly, these rhodium compounds exhibited poor enantioselectivity in the cyclopropanation of 1-diazo-5-phenyl-2-pentanone[11] (enantiomeric excess less than 6%).



3 **4** **5**

Complex	Yield(%)	4	5
1	75	69	31
2	74	60	40
$Rh_2(O_2CCH_3)_4$	92	63	27

Scheme 4. Cyclopropanation vs. aromatic substitution



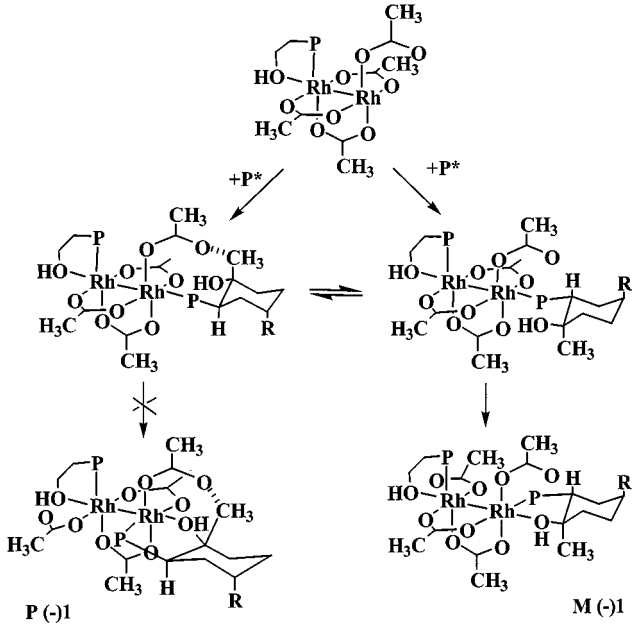
6 **7** **8**

Complex	Yield(%)	7	8
1	85	73	27
2	80	76	24
$Rh_2(O_2CCH_3)_4$	84	79	21

Scheme 5. Aliphatic tertiary vs. secondary C−H insertion

Discussion

The above results confirm that it is possible to induce diastereospecificity in the synthesis of compounds of type **V**, $Rh_2(\mu\text{-}O_2CR)_2(\eta\text{-}O_2CR)_2(\eta\text{-}P{-}X)_2$, using the OH-functionalised chiral phosphanes (+)PPh_2(CH−R*−OH) and (−)PPh_2(CH−R*−OH). As the formation of these compounds occurs by coordination of the phosphane to one axial coordination site, followed by migration from the axial to the equatorial position, this highly chiral induction could be rationalised in terms of the steric effects in some of the steps of this process. Thus, in Scheme 6 the reaction intermediate is represented with the axial ligand (−)PPh_2(CH−R*−OH) in the two extreme orientations leading to each diastereoisomer. It also shows how the repulsive interaction between the methyl group of the entering phosphane and the monodentate carboxylate group is especially important in the intermediate that leads to the diastereoisomer **P(−)1**, justifying the selective formation of the **M (−)1** isomer. The same applies to the reaction with the phosphane (+)PPh_2(CH−R*−OH), where the only isomer formed is **P(+)1**.



R = isopropenyl
P*= (-)PPh_2(CH-R*-OH)

Scheme 6. Proposed origin of the diastereospecificity

The low activity and selectivity of these catalysts must be a consequence of the relatively strong Rh−O axial ligation. The high temperature needed to reach catalytic activity suggests that, under such thermal conditions, Rh−O bond dissociation can take place supplying free active catalytic sites.

The high temperature needed to liberate the active catalytic site produces the carbene transfer reaction in relatively drastic conditions and precludes the selective diazo transformation. In fact, the selectivities shown by these compounds are similar to those reported for the poorly selective rhodium acetate.[9]

Conclusion

These results confirm the ability of a functionalised chiral phosphane, to induce diastereospecificity in the synthesis of chiral rhodium(II) compounds. The above described catalytic results prove that the relatively strong axial Rh−O coordination lowers the activity of the synthesised species of structural type **V**. In general, this strong axial coordination must be considered as a negative effect in the design of a catalyst. However, we suggest that this property might be used in a beneficial way in the case of complexes of type **II**. In this case the functionalised phosphane could be used to block one axial coordination site, leaving the other metal centre open for interaction with the diazo compound. Thus, the use of this sort of functionalised phosphanes in the synthesis of chiral complexes of type **II**, appears as a useful strategy for obtaining enantiomerically pure species with only one available position for catalytic purposes.

Experimental Section

General Considerations: Commercially available $Rh_2(O_2CCH_3)_4{\cdot}2MeOH$ was purchased from Pressure Chemical Com. $Rh_2(O_2CCF_3)_4$ $2(Me_2CO)$,[12] the phosphanes (+)PPh_2(CH−R*−OH),[8] and (−)PPh_2(CH−R*−OH)[8] and the diazo compounds **3**,[9] **6**,[10] and **9**[11] were prepared according to literature procedures. − Solvents were distilled prior to use. − ^1H, $^{13}C\{^1H\}$, $^{31}P\{^1H\}$ and ^{19}F NMR spectra were recorded with a Varian−300 Unity and with a Bruker AM-250 instrument; spectra were obtained as solutions in $CDCl_3$. − Elemental analyses were performed at Centro de Microanálisis Elemental (Universidad Complutense de Madrid). − Optical rotations were measured with a Perkin−Elmer 241 polarimeter at the Na-D line in 10-cm quartz cuvettes. − The UV/Vis measurements were performed with a Varian Cary 1 spectrophotometer.

X-ray Crystallographic Procedures: Single crystals of compounds **P(+)2** or **M(−)2** were obtained by slow diffusion of hexane into an ethyl ether solution of each compound at room temperature. X-ray diffraction experiments were carried out with a Siemens Smart diffractometer with a CCD detector using Mo-K_α radiation. Unit cell dimensions were determined by a least fit of 50 reflections, ($2.73° < \theta < 23.31°$). All calculations were done using SMART software for data collection.[13] Empirical absorption correction was applied on compound **P(+)2**. The structures were solved by direct methods, and refined on F^2 with the program SHELXTL.[14] The positions of the remaining atoms were located after an alternating series of least-squares cycles and difference Fourier maps. Anisotropic displacement parameters were assigned to all nonhydrogen atoms, except to C51 on **M(−)2**, which was refined isotropically. Hydrogen atoms were placed in geometrically generated positions and refined riding on the carbon atom to which they are attached. Crystal Data: **P(+)2**: $C_{26}H_{26}F_6O_5PRh{\cdot}1/2CHCl_3$, M = 728.05, trigonal, $a = b = 13.0366(8)$, $c = 29.756(2)$ Å, V = 4379.6(5) Å^3, T = 293 K, space group $P3_121$, Z = 6, μ(Mo-K_α) = 0.851 mm^{-1}, 6335 reflections measured, 2615 unique (R_{int} = 0.0426) which were used in all calculations. Data/parameters

2615:351. The final R was 0.0499 ($wR2$ = 0.098). − **M(−)2**: $C_{52}H_{52}F_{12}O_{10}P_2Rh_2{\cdot}2H_2O$, M = 1358.69, trigonal $a = b$ = 12.9751(9), c = 29.685(3) Å, V = 4328.0(6) Å^3, T = 173 K, space group $P3_2$, Z = 3, μ(Mo-K_α) = 0.723 mm^{-1}, 6662 reflections measured, 4751 unique (R_{int} = 0.0547) which were used in all calculations. Data/parameters 4751:715. The final R was 0.0747($wR2$ = 0.1762). − Crystallographic data (excluding structure factors) for the structures reported in this paper have been deposited with the Cambridge Crystallographic Data Centre as supplementary publications nos. CCDC-139657 **[P(+)2]** and CCDC-139658 **[M(−)2]**. Copies of the data can be obtained free of charge on application to CCDC, 12 Union Road, Cambridge CB2 1EZ, UK [Fax: (internat.) + 44-1223/336-033; E-mail: deposit@ccdc.cam.ac.uk].

General Procedure for Rhodium(II)-Catalysed Reactions of Diazo Compounds: The rhodium(II) compound (1%) was added under argon to a solution containing a diazo compound (0.5 mmol) in dry dichloromethane (4 mL). The mixture was heated at 100 °C in a sealed tube. The extent of reaction was monitored by TLC, using hexane/ethyl acetate as the eluent, until the diazo starting material was consumed. The solution was filtered through a 1-cm plug of silica gel, followed by washing with CH_2Cl_2 (20 mL). The filtrate was concentrated in vacuum and the residue was directly chromatographed with a mixture of hexane/ethyl acetate (10:1).

(*P*)-Rh$_2$(μ-O$_2$CCH$_3$)$_2$(η^1-O$_2$CCH$_3$)$_2${η^2-(+)PPh$_2$(CH−R*−OH)}$_2$ [P(+)1]: $Rh_2(O_2CH_3)_4{\cdot}2$(MeOH) (0.15 g, 0.3 mmol) was refluxed with (+)PPh$_2$(CH−R*−OH) (0.22 g, 0.65 mmol) in toluene/acetic acid (3:1) (30 mL) for 1 h. The resulting green solution was concentrated to dryness to yield a green solid that was crystallised from CH_2Cl_2/hexane giving **P(+)1** (0.30 g, 80%). − $[\alpha]_D$ = −39 (c = 0.125, $CHCl_3$). −^{1}H NMR ($CDCl_3$): δ = 12.0 (s, 2 H, OH), 7.8 (m, 4 H, aromatic protons), 7.0−7.5 (m, 16 H, aromatics), 4.5 (s, 2 H, HC=C), 4.0 (s, 2 H, HC=C), 2.6 (m, 2 H, HC−P), 2.3−1.5 (m, 14 H, cyclohexyl protons), 1.4 (s, 6 H, CH_3), 1.2 (s, 6 H, acetate), 1.1 (s, 6 H, CH_3), 1.0 (s, 6 H, acetate). − ^{13}C{^{1}H} NMR ($CDCl_3$): δ = 21.6 (CH_3C=C), 23.0 (CH_3, acetate), 23.7 (CH_3COH), 26.2, 29.6, 38.3, 38.6 (cyclohexyl carbons), 55.1 (HC−P), 75.3 (COH), 111.5 (CH_2=C), 127.4, 127.7, 129.5, 129.9, 132.7, 134.5 (aromatic carbons), 143.9 (C=CH_2), 184.6 (OOC acetate), 188.5 (O_2C acetate). − ^{31}P{^{1}H} NMR ($CDCl_3$): δ = 46 ($^1J_{Rh-P}$ = 163 Hz, $^2J_{Rh-P}$ = −5 Hz, J_{Rh-Rh} = 20 Hz). − UV/Vis ($CHCl_3$): $\lambda_{max}(\varepsilon)$ = 321 nm (41690), 258 nm (32370). − $C_{52}H_{66}O_{10}P_2Rh_2$ (1118.94): calcd. C 55.80, H 5.95; found C 55.49, H 5.58.

(*P*)-Rh$_2$(μ-O$_2$CCF$_3$)$_2$(η^1-O$_2$CCF$_3$)$_2${η^2-(+)PPh$_2$(CH−R*−OH)}$_2$ [P(+)2]: (0.08 g, 0.25 mmol,) of solid (+)PPh$_2$(CH−R*−OH) was added to a solution of $Rh_2(O_2CCF_3)_4{\cdot}2(Me_2CO)$ (0.07 g, 0.1 mmol) in diethyl ether (15 mL). The resulting brown-red solution was stirred overnight. The solvent was removed, the residue was crystallised from CH_2Cl_2/hexane to give **P(+)2** (0.14 g, 86%). − $[\alpha]_D$ = −61 (c = 0.06 in $CHCl_3$). − ^{1}H NMR ($CDCl_3$): δ = 10.1 (s, 2 H, COH), 7.7 (m, 4 H, aromatic protons), 7.2−7.6 (m, 16 H, aromatics), 4.6 (s, 2 H, HC=C), 4.2 (s, 2 H, HC=C), 2.7 (m, 2 H, HC−P), 2.3−1.8 (m, 14 H, cyclohexyl protons), 1.4 (s, 6 H, CH_3), 1.1 (s, 6 H, CH_3). − ^{13}C{^{1}H} NMR ($CDCl_3$): δ = 21.5 (CH_3C=C), 23.2 (CH_3COH), 26.2, 29.7, 38.4, 38.6 (cyclohexyl carbons), 55.1 (HC−P), 74.5 (COH), 112.4 (CH_2=C), 126.0, 128.1, 128.3, 130.7, 131.5, 134.0, 134.2 (aromatic carbons), 143.2 (C=CH_2), 168.0 (OOC), 168.8 (OOC). − ^{31}P{^{1}H} NMR ($CDCl_3$): δ = 45.7 ($^1J_{Rh-P}$ = 154.57 Hz, $^2J_{Rh-P}$ = 10.6 Hz). − ^{19}F{^{1}H} NMR ($CDCl_3$): δ = −75.6 (s, 6 F), −75.0 (s, 6 F). − UV/Vis ($CHCl_3$): $\lambda_{max}(\varepsilon)$ = 442 nm (2470), 335 nm (3807), 248 nm (23480). − $C_{52}H_{54}F_{12}O_{10}P_2Rh_2{\cdot}2H_2O$ (1370.86): calcd. C 45.56, H 4.27; found C 45.17, H 3.96.

Acknowledgments

We thank the DGICYT (Project PB94−988) and the European Human Capital and Mobility Program (CONTRACT No. CT-0091) for financial support. S. E. S. thanks the Ministerio de Educación y Ciencia (Spain) for a grant.

[1] [1a] F. A.Cotton, R. A. Walton, *Multiple Bonds between Metal atoms*; Clarendon Press, Oxford, England, **1993**. − [1b] E. B. Boyar, S. D. Robinson, *Coord. Chem. Rev.* **1983**, *50*, 109. − [1c] T. R. Felthouse, *Prog. Inorg. Chem*. **1982**, *29*, 73.

[2] For general reviews on metal-carbenoid see: [2a] M. P. Doyle, in *Comprehensive Organometallic Chemistry* (Ed.: L. S. Hegedus), Pergamon, New York, **1995**, vol. 12, chapter 5.1. − [2b] T. Ye, M. A. McKervey, *Chem. Rev.* **1994**, *94*, 587. − [2c] E. J. Corey, A. Guzmán-Pérez, *Angew. Chem. Int. Ed.* **1998**, *37*, 388.

[3] [3a] A. R. Chakravarty, F. A. Cotton, D. A. Tocher, J. H. Tocher, *Organometallics* **1985**, *4*, 8. − [3b] F. Barceló, F. A. Cotton, P. Lahuerta, R. Llusar, M. Sanaú, W. Schwotzer, M. A. Ubeda, *Organometallics* **1986**, *5,* 808. − [3c] F. Barceló, F. A. Cotton, P. Lahuerta, M. Sanaú, W. Schwotzer, M. A. Ubeda, *Organometallics* **1987**, *6,* 1105. − [3d] F. A. Cotton, F. Barceló, P. Lahuerta, R. Llusar, J. Payá, M. A. Ubeda, *Inorg. Chem.* **1988**, *27*, 1010.

[4] [4a] P. Lahuerta, J. Payá, J. Solans, M. A. Ubeda, *Inorg. Chem.* **1992**, *31*, 385. − [4b] P. Lahuerta, J. Payá, A. Tiripicchio, M. Tiripicchio, *Inorg. Chem*. **1992**, *31*, 1224. − [4c] P. Lahuerta, M. A. Ubeda, J. Payá, S. García-Granda, F. Gómez-Beltrán, A. Anillo, *Inorg. Chim. Acta* **1993**, *205*, 91. − [4d] F. Estevan, P. Lahuerta, E. Peris, M. A. Ubeda, S. García-Granda,; F. Gómez-Beltrán, G. González, E. Pérez-Carreño, M. Martinez, *Inorg. Chim. Acta* **1994**, *218*, 189. − [4e] García-Bernabé, A. P. Lahuerta, M. A. Ubeda, S. Granda-García, P. Pertierra, *Inorg. Chim. Acta*. **1995**, *229*, 203. − [4f] F. Estevan, P. Lahuerta, J. Pérez-Prieto, M. Sanaú, S. E. Stiriba, M. A. Ubeda, *Organometallics* **1997**, *16*, 880.

[5] F. Estevan, A. García-Bernabé, S. García-Granda, P. Lahuerta, E. Moreno, J. Perez-Prieto, M. Sanaú, M. A. Ubeda, *J. Chem. Soc., Dalton Trans.* **1999**, 3493.

[6] P. Lahuerta, E. Peris, M. A. Ubeda, S. García-Granda, F. Gómez-Beltran, R. Díaz, *J. Organomet. Chem*. **1993**, *455*, C10.

[7] D. F. Taber, S. C. Malcolm, S. K. Bieger, P. Lahuerta, S.-E. Stiriba, J. Pérez-Prieto, M. Sanaú, M. A. Monje, *J. Am. Chem. Soc.* **1999**, *121*, 860.

[8] G. Muller, D. Sainz, *J. Organomet. Chem*. **1995**, *495*, 103.

[9] A. Padwa, D. J. Austin, A. T. Price, M. A. Semones, M. P. Doyle, M. N. Protopopova, W. R. Winchester, A. Tran, *J. Am. Chem. Soc*. **1993**, *115*, 8669.

[10] F. Estevan, P. Lahuerta, I. Pereíra, J. Pérez-Prieto, S.-E. Stiriba, *Organometallics* **1998**, *17*, 3342.

[11] B. G. Christensen, L. D. Cama, R. N. Guthikonda, *J. Am. Chem. Soc.* **1974**, *96*, 7584.

[12] S. A. Johnson, H. R. Hunt, H. M. Neumann, *Inorg. Chem.* **1963**, *2*, 960.

[13] Siemens, *Data Collection and Procedure − Software for the SMART System*, Siemens Analytical X-ray Instruments, Inc., Wisconsin, USA, **1995**.

[14] *SHELXTL Version 5.05*, AXS Siemens, **1996**.

Received March 9, 2000
[I00091]

Organometallic Complexes of Uracil and Orotic Acid Derivatives: Coordination Mode, Structure, and Reactivity

Donald J. Darensbourg,*[a] Brian J. Frost,[a] David L. Larkins,[a] and Joseph H. Reibenspies[a]

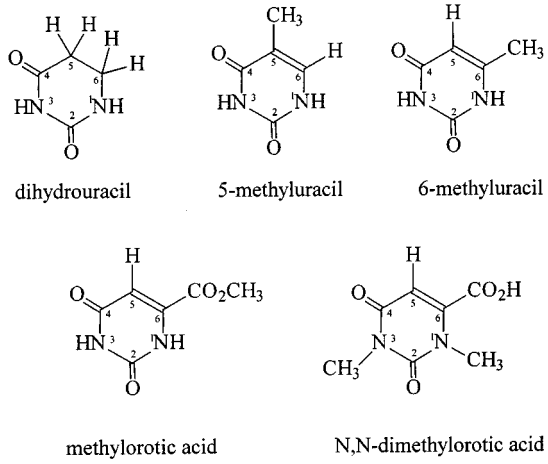
Keywords: Carbonyl complexes / Uracil / Pyrimidines / Kinetics

Carbonyltungsten derivatives of uracilates and orotates, where the metal center is bound to a nitrogen atom of the pyrimidine ring, are described. There organometallic complexes were synthesized by the reaction of either $W(CO)_5THF$ or $W(CO)_5MeOH$ with the tetraethylammonium salt of the deprotonated monoanion of dihydrouracil (**1**), 5-methyluracil (**2**), 6-methyluracil (**3**), methylorotic acid (**4**), and *N*,*N*-dimethylorotic acid (**5**). The complexes were all characterized in solution by IR and ^{13}C NMR spectroscopy, and in select instances in the solid-state by X-ray crystallography. The structures of complexes **1** and **3** consist of octahedrally coordinated anions of pentacarbonyltungsten uracilate, where the uracilate ligand is bound to the metal center by the N3 atom of the pyrimidine ring, and the tetraethylammonium cation for charge balance. In contrast, the anion of complex **2** reveals that the uracilate ligand is bound to the $W(CO)_5$ fragment by the N1 atom of the pyrimidine ring. The ν(CO) vibrational modes and ^{13}C NMR chemical shifts for the carbonyl ligands of complexes **1** and **3** indicate that the metal centers are more electron-rich than those of complex **2**. This conclusion is further substantiated by the rates of intermolecular CO exchange in these carbonylmetal anions with ^{13}CO. The facile CO exchange observed in complexes **1** and **3** is faster than that seen in complex **2**. The rapid CO dissociation process measured in these derivatives is attributed to the π-donation of electron density from the pyrimidine ring to the tungsten center in the transition state as the M–CO bond is broken.

Introduction

The coordination chemistry of pyrimidine bases has been a subject of interest for many years, and has been studied from a variety of perspectives by many different research groups.[1−4] Pyrimidine derivatives of thymine and uracil, such as AZT (3′-azido-3′-deoxythymidine), have been shown to be effective antiviral drugs.[5,6] Metal complexes of pyrimidines have been shown to be useful as biological carriers for some of these drugs such as AZT,[7−10] others have demonstrated anti-cancer/tumor activity.[11,12] Despite the plethora of coordination complexes of pyrimidines, the organometallic chemistry involving these ligands has received limited attention, with most efforts coming from the laboratory of Beck and co-workers.[13,14] Recently, we have examined the coordination modes of uracils and orotic acid derivatives to zero-valent group-6 carbonylmetal compounds, focusing our studies on the ability of the ring nitrogen atoms to serve as π-donor ligands and to facilitate CO dissociation.[15,16] Previously, investigations of the coordination chemistry of uracils have revealed a wide range of metal-dependent binding modes, including via N1, N3, the exocyclic oxygen atoms,[1,2] both an endocyclic nitrogen and an exocyclic oxygen (or sulfur) atom,[15,17] and finally, though less common, through C5.[18]

Herein, we wish to communicate a continuation of our studies of organometallic derivatives of uracils and orotic acid derivatives. Specifically, this study will examine the various coordination modes and π-donor abilities of a series of tungsten-bound uracilate and orotate derivatives, in particular dihydrouracil, 5-methyluracil (thymine), 6-methyluracil, methylorotic acid, and *N*,*N*-dimethylorotic acid (Scheme 1). Also discussed are the electronic effects of different pyrimidine derivatives as examined by IR and ^{13}C NMR spectroscopy, and CO exchange kinetics.



Scheme 1

Results and Discussion

A series of $[Et_4N][W(CO)_5L]$ complexes, where L = dihydrouracilate (**1**), 5-methyluracilate (**2**), 6-methyluracilate (**3**), methylorotate (**4**), and *N*,*N*-dimethylorotate (**5**), were synthesized in good yields by the labile-ligand displacement of THF or methanol from $W(CO)_5(THF)$ or $W(CO)_5(MeOH)$

[a] Texas A&M University, Department of Chemistry, College Station, Texas 77843, USA

 © WILEY-VCH Verlag GmbH, D-69451 Weinheim, 2000 1434−1948/00/1212−2487 $ 17.50+.50/0

Table 1. Stretching frequencies of the carbonyl ligands in complexes **1**−**5**, and other related complexes

Complex[a][b]	ν(CO) [cm^{-1}]			ν(CO_2) [cm^{-1}]	
$[W(CO)_5$(dihydrouracilate)]$^-$ (**1**)	2057.9 (w)	1910.4 (vs)	1839.0 (m)	1660.6	1597.9
$[W(CO)_5$(5-methyluracilate)]$^-$ (**2**)	2064.7 (w)	1915.2 (vs)	1855.4 (m)	1660.6	1637.5
$[W(CO)_5$(6-methyluracilate)]$^-$ (**3**)	2058.9 (w)	1912.3 (vs)	1840.0 (m)	1663.5	1571.9
$[W(CO)_5$(methylorotate)]$^-$ (**4**)	2059.9 (w)	1914.2 (vs)	1845.8 (m)	1665.4	1644.2
$[W(CO)_5$(*N*,*N*-dimethylorotate)]$^-$ (**5**)	2067.6 (w)	1920.9 (vs)	1853.5 (m)	1661.5	1647.1
$[W(CO)_5$(uracilate)]$^-$	2065.6 (w)	1917.1 (vs)	1858.3 (m)	1668.3	1637.5[c]

[a] As the tetraethylammonium salt. − [b] Spectra determined in CH_3CN. − [c] Ref.[15]

[prepared in situ by photolysis of $W(CO)_6$ in THF or meth-1anol] by the tetraethylammonium salt of the deprotonated monoanion of the corresponding uracil or orotic acid derivative. All complexes were characterized by IR and ^{13}C NMR spectroscopy in the carbonyl region, elemental analysis, and X-ray crystallography for complexes **1**−**3**. In addition, the product of the reaction of **1** with methanol, $[Et_4N]_2[W_2(CO)_8(OMe)_2]$ (**6**), was also characterized by X-ray crystallographic analysis and ^{13}C NMR spectroscopy.

The IR spectra in the ν(CO) stretching region of complexes **1**−**5** consist of three bands of the appropriate intensity pattern for a $W(CO)_5$ fragment of C_{4v} local symmetry. Table 1 contains the ν(CO) values for these, and closely related, derivatives. Since the ν(CO) stretching vibrational modes are such good probes of the electron-donating ability of the ancillary ligands bound to the metal center in the carbonylmetal derivatives, it is clear from a close scrutiny of the ν(CO) spectra of complexes **2** and **3** (Figure 1) that the uracilate ligands are coordinated differently in these instances. That is, there is a significant difference in the low-frequency A_1 modes of these two derivatives, where the electronic effects of the uracilate-binding mode should be most evident. Similarly, the pyrimidine carbonyl stretches are also quite different, with the $\Delta\nu(CO_2)$ for the asymmetric and symmetric vibrations being 23 and 92 cm^{-1} for **2** and **3**, respectively. Furthermore, based on the similarity of the ν(CO) spectra of complexes **1**, **3**, and **4**, it is reasonable to suggest that in these derivatives the pyrimidine ligands are bonded in a similar fashion. It is also evident from the ν(CO) IR data listed in Table 1 that complex **2** and the structurally characterized $[Et_4N][W(CO)_5$(uracilate)] derivative[15] share a common structure. The *N*,*N*′-dimethylorat-

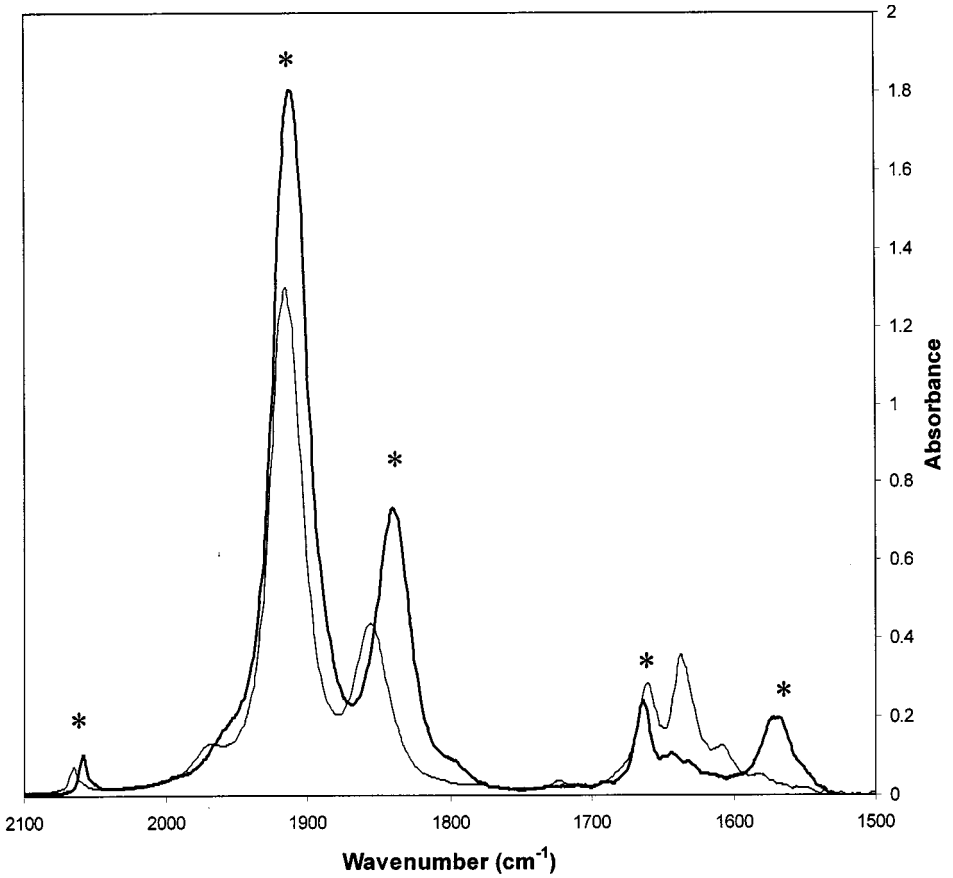


Figure 1. Infrared spectra in the ν(CO) and ν(CO_2) regions of $[Et_4N][W(CO)_5$(5-methyluracilate)] (**2**) and $[Et_4N][W(CO)_5$(6-methyluracilate) (**3**) in acetonitrile solvent; peaks marked with asterisks are those due to complex **3**

ate derivative, complex **5**, exhibits ν(CO) IR bands typical of carboxylates bound in a monodentate fashion containing electron-withdrawing substituents in anionic complexes of the type $W(CO)_5$(carboxylate)$^-$. For example, the $W(CO)_5(O_2CCF_3)^-$ anion has ν(CO) vibrational modes at 2066, 1916, and 1857 cm^{-1} in THF solution.[19]

^{13}C NMR spectroscopic data for the carbonyl ligands were compiled for complexes **1**−**6**, and are listed in Table 2. Complexes **1**−**5** exhibit the anticipated two ^{13}C resonances of intensity ratio 1:4, with the more intense upfield signal corresponding to that of the four *cis* carbonyl ligands. Complex **2** displays ^{13}C NMR signals for the equatorial and axial CO ligands at δ = 200.6 and 205.7, respectively, which are quite similar to values previously reported for the carbonyl ligands of the $W(CO)_5$(uracilate)$^-$ anion.[15] On the other hand, complexes **1**, **3**, and **4** exhibit ^{13}C NMR resonances which are measurably different from complex **2** and $[Et_4N][W(CO)_5$(uracilate)], again suggesting a different coordination mode for these latter two pyrimidine derivatives.

Table 2. ^{13}C NMR data for the carbonyl ligands in complexes **1**−**6**

Complex[a]	^{13}C resonance, δppm ($^1J_{W-C}$ [Hz]) CO (equatorial)	CO (axial)
$[W(CO)_5$(dihydrouracilate)]$^-$ (**1**)	203.0 (130)	208.5 (149)[b]
$[W(CO)_5$(5-methyluracilate)]$^-$ (**2**)	200.7 (131)	205.8[c]
$[W(CO)_5$(6-methyluracilate)]$^-$ (**3**)	202.0 (131)	204.8[c]
$[W(CO)_5$(methylorotate)]$^-$ (4)	201.7 (131)	207.9[c]
$[W(CO)_5$(*N*,*N*-dimethylorotate)]$^-$ (**5**)	200.7	205.8[c]
$[W_2(CO)_8(OMe)_2]^{2-}$ (**6**)	208.5	220.1[d]
$[W_2(CO)_6(OMe)_3]^{3-}$	234.1[d]	

[a] As the tetraethylammonium salt. − [b] Spectrum determined in THF/CD_3CN. − [c] Spectrum determined in CD_3CN. − [d] Spectrum determined in [D_4]methanol.

In order to address the question of the coordination modes of the pyrimidines definitively, the structures of complexes **1**−**3** were determined in the solid state by X-ray crystallography. The structures of all three derivatives are quite similar with five of the octahedral coordination sites occupied by carbonyl ligands and the sixth position occupied by a pseudo-amido donor from the pyrimidine base. Indeed, the differences in these structures lie in the pyrimidine ring/coordination mode. That is, in complexes **1** and **3** the pyrimidine ligand is bound through the deprotonated N3 nitrogen atom of the pyrimidine ring. In contrast, complex **2** contains a pyrimidine ring bound to the tungsten center through the deprotonated N1 nitrogen atom in a manner analogous to that previously reported for the $W(CO)_5$(uracilate)$^-$ anion.[15] Coordination through the N3 nitrogen atom of the pyrimidine ring places the exocyclic oxygen atoms in close proximity to the metal center, thereby assisting in the loss of a CO ligand with concomitant formation of a tetracarbonyl derivative containing a chelating uracilate ligand. For example, the tetracarbonyl derivative of complex **3** has been characterized by ν(CO) IR: 1991(w), 1865(s), 1840(m), and 1808(m) in THF; and by ^{13}C NMR: δ = 208.1 (2 *C*O), 217.7 (1 *C*O), and 218.3 (1 *C*O) in CD_3CN.

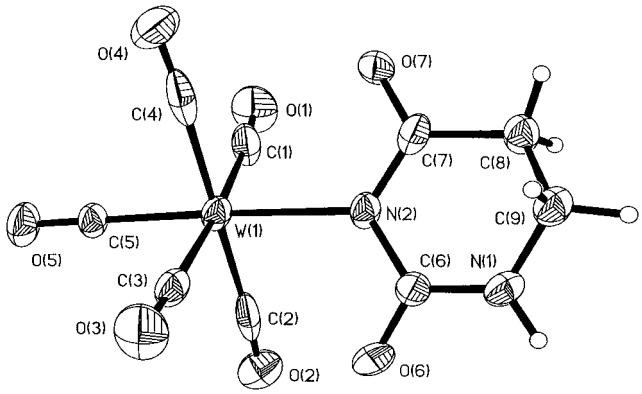


Figure 2. Thermal ellipsoid representation of the anion of complex **1**, $W(CO)_5$(dihydrouracilate)$^-$

Crystals of complex **1** suitable for X-ray analysis were obtained by the slow diffusion of hexane into a THF solution of the complex maintained at 0 °C. A thermal ellipsoid drawing of the monoanion, $W(CO)_5$(dihydrouracilate)$^-$, is depicted in Figure 2 along with the atomic numbering scheme. Selected bond lengths and bond angles are listed in Table 3. The crystal lattice of complex **1** contains a tetraethylammonium cation (for charge balance), as well as a diethyl ether molecule of solvation. The octahedral environment about the tungsten center consists of a dihydrouracilate anion bound to the metal center through the N3 atom of the pyrimidine ring at a distance of 2.263(8) Å. This bond length compares well with other related W−N bond lengths which are summarized in Table 4.[20−22] The *trans*-CO ligand exhibits a slightly shorter W−C bond length [1.967(10) Å] than the average W−C distance for the four *cis*-CO ligands [2.061(16) Å]. As anticipated, the pyrimidine ring in complex **1** is non-planar (Figure 3), unlike those in complexes **2** and **3** (vide supra) where the ring is pseudoaromatic.

The solid-state structure of complexes **2** and **3** were determined by crystallographic analysis on crystals obtained from the slow diffusion of hexane into a THF solution of the respective complex at ambient temperature. Thermal ellipsoid drawings of the anions of complexes **2** and **3** are shown in Figure 4 and Figure 5, respectively. Table 5 and Table 6 compile selected bond lengths and bond angles for these derivatives.

In complex **2**, the pyrimidine ligand is bound through the deprotonated N1 position of the ring like that observed in the parent $W(CO)_5$(uracilate)$^-$ anion.[15] On the other hand, the $[W(CO)_5]$ fragment in complex **3** is bound through the deprotonated N3 position of the pyrimidine ring, much like that seen in complex **1**. The choice of binding modes appears to be mainly a consequence of steric interactions. As is apparent from the space-filling models for the anions of complexes **2** and **3** (Figure 6), the methyl substituent on the pyrimidine ring precludes binding at the N1 site in complex **3**.

On the other hand, for all other structures we have determined herein and elsewhere,[15] binding occurs at the N1

Table 3. Selected bond lengths [Å] and angles [°] for **1**; estimated standard deviations are given in parentheses

W1−C5	1.967(10)	W1−C4	2.07(2)
W1−C1	2.045(12)	W1−C2	2.07(2)
W1−C3	2.059(12)	W1−N2	2.263(8)
O1−C1	1.134(14)	N1−C9	1.447(14)
O5−C5	1.149(13)	C7−C8	1.513(14)
O2−C2	1.16(2)	C8−C9	1.512(14)
O3−C3	1.136(15)	N2−C7	1.365(14)
O4−C4	1.16(2)	N2−C6	1.413(13)
O7−C7	1.222(13)	N1−C6	1.334(14)
O6−C6	1.238(13)		
C5−W1−C1	88.0(4)	O1−C1−W1	174.6(10)
C5−W1−C3	88.8(4)	O5−C5−W1	179.7(12)
C1−W1−C3	175.9(4)	O2−C2−W1	175.6(10)
C5−W1−C4	90.2(4)	O3−C3−W1	177.3(10)
C1−W1−C4	85.9(5)	O4−C4−W1	175.1(10)
C3−W1−C4	91.7(5)	O7−C7−N2	121.1(9)
C5−W1−C2	88.6(4)	O7−C7−C8	119.5(10)
C1−W1−C2	90.9(5)	N2−C7−C8	119.2(9)
C3−W1−C2	91.5(5)	C9−C8−C7	112.5(9)
C4−W1−C2	176.6(4)	N1−C9−C8	107.5(9)
C5−W1−N2	177.1(3)	O6−C6−N1	120.1(9)
C1−W1−N2	94.7(4)	O6−C6−N2	119.2(9)
C3−W1−N2	88.5(4)	N1−C6−N2	120.7(9)
C4−W1−N2	90.9(4)	C7−N2−W1	120.8(6)
C2−W1−N2	90.4(4)	C6−N2−W1	120.4(6)
C7−N2−C6	118.9(8)	C6−N1−C9	123.1(9)

Table 4. W−N bond lengths for complexes **1−3**, as well as other similar complexes

Complex[a]	W−N [Å]	Ref.
$[W(CO)_5$(dihydrouracilate)$]^-$ (**1**)	2.263(8)	this work
$[W(CO)_5$(5-methyluracilate)$]^-$ (**2**)	2.236(15)	this work
$[W(CO)_5$(6-methyluracilate)$]^-$ (**3**)	2.276(4)	this work
$[W(CO)_5$(uracilate)$]^-$	2.281(8)	[15]
$[W(CO)_4$(orotate)$]^{2-}$	2.258(9)	[15]
$[W(CO)_4$(dihydroorotate)$]^{2-}$	2.231(13)	[15]
$[W(CO)_4$(glycinate)$]^-$	2.328(22)	[20]
$W(CO)_5$(piperidine)	2.331(5)	[21]
$W(CO)_5$(pyridine)	2.26(1)	[22]

[a] As the tetraethylammonium salt.

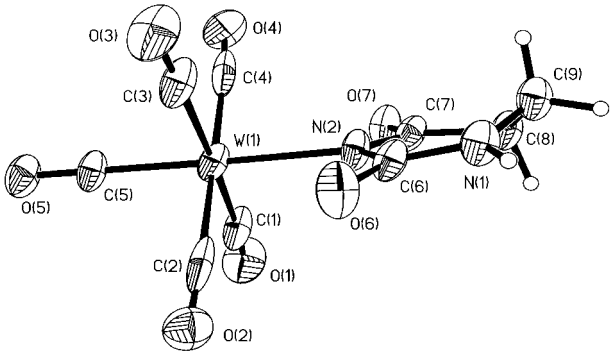


Figure 3. Thermal ellipsoid drawing of the anion of complex **1**, $W(CO)_5$(dihydrouracilate)$^-$, illustrating the puckering of the dihydrouracilate ring

site in the absence of steric hindrance. This is consistent as well with the prediction based on spectroscopic data that suggest complex **4** to be bound at the N3 site. In this instance the steric bulk of $-CO_2CH_3$ would inhibit binding at

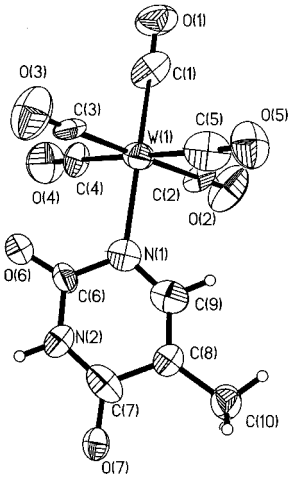


Figure 4. Thermal ellipsoid representation of the anion of complex **2**, $W(CO)_5$(5-methyluracilate)$^-$

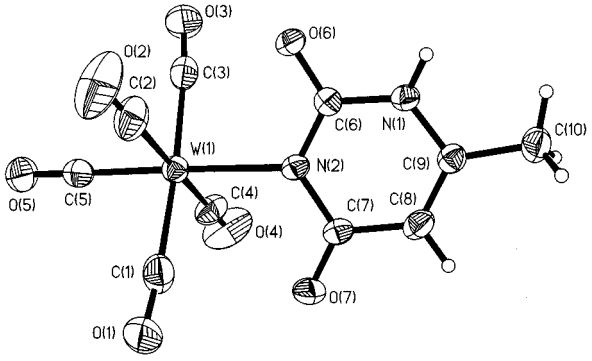


Figure 5. Thermal ellipsoid representation of the anion of complex **3**, $W(CO)_5$(6-methyluracilate)$^-$

Table 5. Selected bond lengths [Å] and angles [°] for **2**; estimated standard deviations are given in parentheses

W(1)−C(5)	1.98(2)	C(1)−O(1)	1.12(2)
W(1)−C(2)	2.006(19)	N(1)−C(9)	1.33(2)
W(1)−C(3)	2.05(2)	N(1)−C(6)	1.39(2)
W(1)−C(4)	2.07(2)	C(6)−O(6)	1.18(2)
W(1)−C(1)	2.05(3)	C(6)−N(2)	1.37(2)
W(1)−N(1)	2.236(15)	N(2)−C(7)	1.33(3)
C(5)−O(5)	1.14(2)	C(7)−O(7)	1.29(2)
C(2)−O(2)	1.11(2)	C(7)−C(8)	1.46(2)
C(4)−O(4)	1.15(2)	C(8)−C(9)	1.36(2)
C(3)−O(3)	1.11(2)	C(8)−C(10)	1.51(2)
C(1)−W(1)−C(2)	89.5(8)	O(3)−C(3)−W(1)	174.8(18)
C(1)−W(1)−C(4)	88.9(8)	O(4)−C(4)−W(1)	178(2)
C(2)−W(1)−C(4)	90.0(9)	O(5)−C(5)−W(1)	175.5(19)
C(1)−W(1)−C(3)	89.4(7)	C(9)−N(1)−C(6)	115.6(17)
C(2)−W(1)−C(3)	178.7(7)	C(9)−N(1)−W(1)	124.6(12)
C(4)−W(1)−C(3)	89.2(8)	C(6)−N(1)−W(1)	119.8(13)
C(1)−W(1)−C(5)	90.6(8)	O(6)−C(6)−N(2)	117.1(16)
C(2)−W(1)−C(5)	89.5(9)	O(6)−C(6)−N(1)	126.0(18)
C(4)−W(1)−C(5)	179.3(8)	N(2)−C(6)−N(1)	116.7(18)
C(3)−W(1)−C(5)	91.2(9)	C(7)−N(2)−C(6)	127.3(16)
C(1)−W(1)−N(1)	179.3(6)	O(7)−C(7)−N(2)	124.5(17)
C(2)−W(1)−N(1)	91.0(6)	O(7)−C(7)−C(8)	118(2)
C(4)−W(1)−N(1)	91.6(7)	N(2)−C(7)−C(8)	117.2(18)
C(3)−W(1)−N(1)	90.1(6)	C(9)−C(8)−C(7)	111.3(18)
C(5)−W(1)−N(1)	88.9(7)	C(9)−C(8)−C(10)	124.4(18)
O(1)−C(1)−W(1)	178.1(18)	C(7)−C(8)−C(10)	124.2(18)
O(2)−C(2)−W(1)	175.5(19)	N(1)−C(9)−C(8)	131.4(19)

Table 6. Selected bond lengths [Å] and angles [°] for **3**; estimated standard deviations are given in parentheses

W1−C5	1.952(5)	N1−C6	1.373(5)
W1−C2	2.028(6)	N2−C6	1.354(6)
W1−C3	2.039(6)	N2−C7	1.398(5)
W1−C4	2.045(6)	N1−C9	1.373(6)
W1−C1	2.046(6)	O6−C6	1.248(5)
W1−N2	2.276(4)	C10−C9	1.493(6)
O1−C1	1.144(7)	C7−O7	1.234(5)
O2−C2	1.151(8)	C7−C8	1.450(6)
O3−C3	1.148(7)	C8−C9	1.347(7)
O4−C4	1.137(7)	O5−C5	1.170(6)
C5−W1−C2	88.1(2)	C7−N2−W1	120.3(3)
C5−W1−C3	87.4(2)	C9−N1−C6	123.3(4)
C2−W1−C3	88.9(2)	O7−C7−N2	121.1(4)
C5−W1−C4	89.4(2)	O7−C7−C8	121.3(4)
C2−W1−C4	176.1(2)	N2−C7−C8	117.6(4)
C3−W1−C4	88.0(2)	C9−C8−C7	121.2(4)
C5−W1−C1	88.3(2)	C8−C9−N1	117.7(4)
C2−W1−C1	92.0(3)	C8−C9−C10	125.7(4)
C3−W1−C1	175.5(2)	N1−C9−C10	116.6(4)
C4−W1−C1	90.9(2)	O6−C6−N2	122.2(4)
C5−W1−N2	177.9(2)	O6−C6−N1	118.0(4)
C2−W1−N2	93.9(2)	N2−C6−N1	119.8(4)
C3−W1−N2	93.0(2)	O3−C3−W1	174.9(5)
C4−W1−N2	88.6(2)	O4−C4−W1	177.1(5)
C1−W1−N2	91.4(2)	O5−C5−W1	178.9(4)
O1−C1−W1	173.5(5)	C6−N2−C7	120.1(4)
O2−C2−W1	175.3(5)	C6−N2−W1	119.5(3)

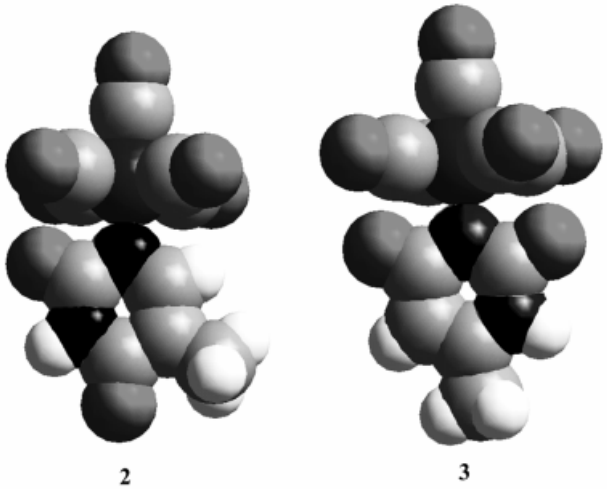


Figure 6. Space-filling models of the anions of complex **2** (left) and **3** (right)

N1. The tungsten−nitrogen distances are 2.236(15) Å and 2.276(4) Å, respectively, in complexes **2** and **3**. The W−C distances in the two derivatives are similar as expected, with both exhibiting a *trans* effect. That is, the W−C distance *trans* to the pyrimidine ligand is shorter than the average W−C distance *cis* to the pyrimidine ligand. For example, in complex **3**, the W−C *trans* distance is 1.952(5) Å, whereas the average W−C *cis* bond length is 2.040(6) Å. The packing diagrams of complexes **1**−**3** reveal that there is substantial amount of hydrogen bonding that is prevalent in the crystal structures of these complexes, as might be anticipated for pyrimidine derivatives. This is illustrated in Figure 7, which depicts the base-pairing observed in complex **3**, where the average O···N distance is 2.754 Å.

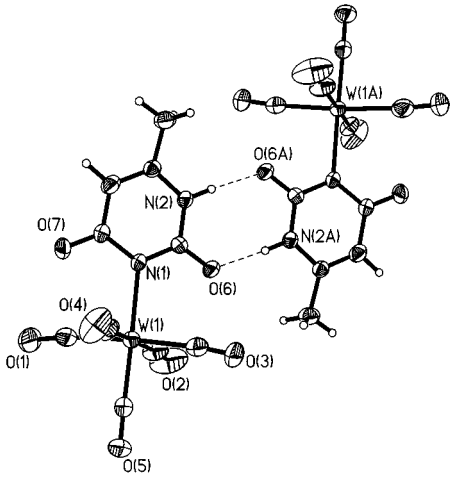


Figure 7. Thermal ellipsoid representation of the anions of complex **3**, $W(CO)_5$(6-methyluracilate)$^-$, showing the hydrogen-bonding motif between base pairs

These pyrimidine derivatives of carbonyltungsten are unstable in protic solvents. For example, on dissolving complex **1** in methanol the solution rapidly underwent a color change from orange to bright red and back to orange. Crystals of complex **6**, $[Et_4N]_2[W(CO)_4OMe]_2$ were isolated from a sample of **1** dissolved in CD_3OD in an NMR tube. We have characterized this derivative in the solid state by X-ray crystallography and in solution by ^{13}C NMR spectroscopy (δ = 208.5 and 220.1), thereby demonstrating that it is identical to the methoxide-bridged dimer we reported previously.[23] Presumably, this complex results from pro-

Table 7. Observed first-order rate constants for the CO exchange kinetics in complexes **1**−**4** as a function of temperature

Complex[a]	Temp [°C]	k [s^{-1}] × 10^4
1[b]	35.0	2.750
	40.0	4.617
	45.0	12.97
	50.0	22.35
	57.0	53.13
2[c]	20.0	0.1167
	30.0	0.5000
	40.0	1.567
	50.0	4.733
3[c]	5.0	0.0833
	15.0	0.4500
	30.0	2.600
	40.0	6.133
4[c]	20.0	0.119
	35.0	0.497
	41.3	0.987
	45.0	1.033
	50.0	1.991

[a] Kinetic data on all complexes were obtained as Et_4N^+ salts to avoid significant ion-pairing effects (M. W. Payne, D. L. Leussing, S. G. Shore, *Organometallics* **1991**, *10*, 574). − [b] In THF. − [c] In CH_3CN.

tonation of the dihydrouracilate ligand by methanol to initially afford the $W(CO)_5OMe^-$ anion. This methoxide derivative has been shown to readily undergo CO dissociation and aggregation to the anions $[W(CO)_4(OMe)]_2^{2-}$ and $[W_2(CO)_6(OMe)_3]^{3-}$, or $[W(CO)_3OMe]_4^{4-}$.[23]

The CO lability in complexes **1**−**5** was examined by monitoring CO exchange (Equation 1) using in situ spectroscopy in the ν(CO) region. The decrease in absorbance of the highest frequency ν(CO) band was measured as a function of time with an IR probe inserted directly into an acetonitrile solution of the respective complex maintained at constant temperature with a thermostated water bath. The reactions were performed in the presence of a large excess of ^{13}CO in order to avoid having to consider the reverse process. Table 7 compiles the first-order rate constants for the CO exchange for the various complexes as a function of temperature. Table 8 lists the derived activation parameters for these processes obtained from the data in Table 7 and Figure 8, along with the corresponding values for the $W(CO)_5(uracilate)^-$ anion previously reported.

$$W(CO)_5(uracilate)^- + n^{13}CO \underset{k_2}{\overset{k_1}{\rightleftharpoons}} W(CO)_{5-n}(^{13}CO)_n(uracilate)^- + nCO \quad (1)$$

As is evident from the Eyring plots in Figure 8 for ^{13}CO exchange in complex **1**−**3** and the parent uracilate derivative, there are two distinct regions, one for the N1-bound complexes (**2** and the parent uracilate) and one for the N3-bound derivatives (**1** and **3**). The two complexes bound through the deprotonated N3 center are slightly more reactive towards CO exchange than the two complexes ligated by way of the deprontonated N1 group. Furthermore, within each grouping the presence of an electron-donating methyl substituent in the pyrimidine ring results in a somewhat enhanced rate (factor of 2−3) of CO lability. In other words, this facile CO exchange is attributed to π-donation of electron density from the deprotonated N1 or N3 atoms of the uracilate ligands, thereby stabilizing the developing 5-coordinate metal intermediate. Previously, we have demonstrated for the uracilate derivative that it is the *cis*-carbonyl ligands that are selectively exchanged. Nevertheless, these pyrimidine ligands bound through their endocyclic ni-

Table 8. Activation parameters for CO exchange reactions

Complex[a]	$\Delta H^‡$ [kJ/mol]	$\Delta S^‡$ [J/mol K]	k [s^{-1}][b]
$[W(CO)_5$(dihydrouracilate)$]^-$ (**1**)	114.4 ± 6	57.3 ± 18.8[c]	$5.83\cdot10^{-5}$
$[W(CO)_5$(5-methyluracilate)$]^-$ (**2**)	94.0 ± 2.8	−18.4 ± 9.0[d]	$2.41\cdot10^{-5}$
$[W(CO)_5$(6-methyluracilate)$]^-$ (**3**)	86.0 ± 5.9	−31.0 ± 20.0[d]	$13.3\cdot10^{-5}$
$[W(CO)_5$(uracilate)$]^-$	106.9 ± 4.3	16.3 ± 13.7[d] [e]	$0.86\cdot10^{-5}$

[a] As Et_4N^+ salt. − [b] Computed at 25.0 °C. − [c] In THF. − [d] In CH_3CN. − [e] Ref.[15]

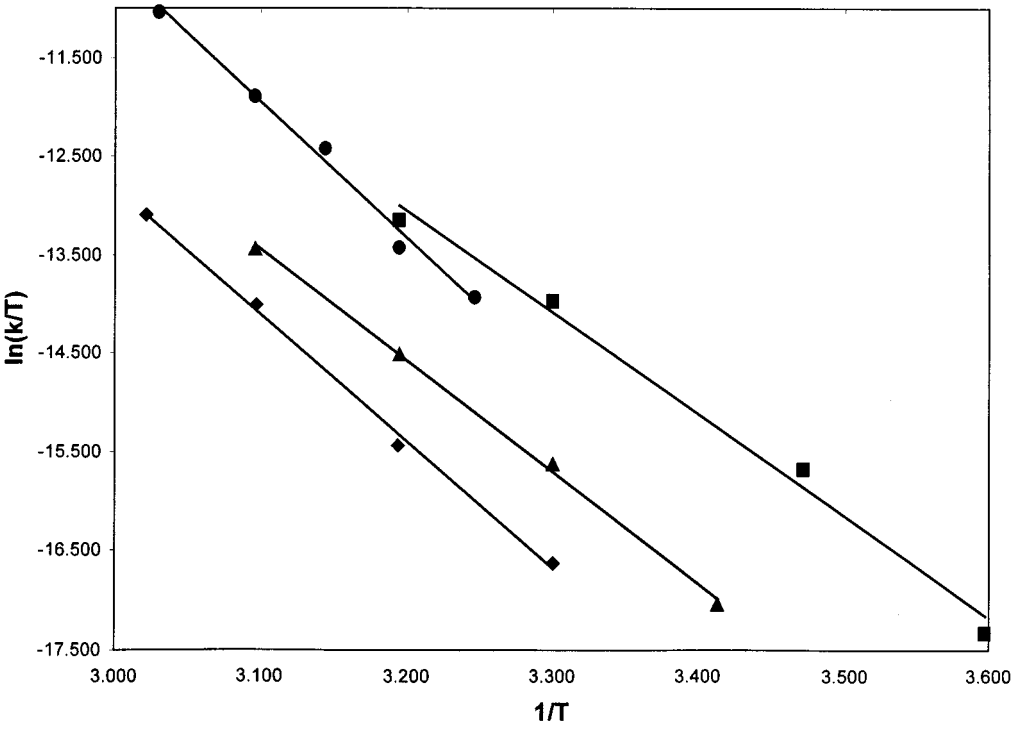


Figure 8. Eyring plots for the first-order CO exchange process involving the $W(CO)_5L^-$ anions and ^{13}CO [L = dihydrouracilate (◆), 6-methyluracilate (●), 5-methyluracilate (▲), and uracilate (■)]

trogen atoms are *considerably less* CO-labilizing than the good π-donating phenolate ligands,[23] and *slightly less* CO-labilizing than the Cl^- ion or the exocyclic sulfur donors in thiouracilate derivatives.[16,23]

The rate constant for CO exchange ($1.88 \cdot 10^{-5}$ s^{-1} at 25 °C) in complex **4**, the closely related methylorotate derivative, is similar to those determined for the other pyrimidine complexes examined herein. The corresponding activation parameters, $\Delta H^{\neq} = 69.6 \pm 3.6$ kJ/mol and $\Delta S^{\neq} = -101.8 \pm 11.6$ J/molK, were derived from the temperature-dependent rate constant data. On the other hand, attempts to determine the kinetic parameters for intermolecular CO exchange in the carboxylate-bound derivative, $[Et_4N][W(CO)_5(N,N\text{-dimethylorotate})]$ (**5**), lead to extensive ligand loss with the formation of ^{13}CO-labeled $W(CO)_6$. Concomitantly, when the substitution reaction was carried out with $P(OEt)_3$ as an incoming ligand the principal product was the neutral complex $W(CO)_5P(OEt)_3$, resulting from displacement of the carboxylate ligand.

Conclusion

Stable tetraethylammonium salts of pentacarbonyltungsten anions of pyrimidine bases have been synthesized from the reactions of $W(CO)_5$(solvent), where solvent = THF or MeOH, with the deprotonated monoanion of the corresponding uracil or orotic acid derivative. Crystal structures of $[Et_4N][W(CO)_5$(dihydrouracilate)] (**1**) and $[Et_4N][W(CO)_5$(6-methyluracilate)] (**3**) reveal that the uracilate ligands are bonded to the tungsten center through the deprotonated N3 atom, whereas $[Et_4N][W(CO)_5$(5-methyluracilate)] (**2**) is bound to the metal fragment by the deprotonated N1 nitrogen atom of the ring. This disparity in binding mode appears to be dictated by steric considerations. In the absence of steric hindrance preferential binding at the N1 position is anticipated.

This difference in metal-binding sites is evident as well, by both IR and ^{13}C NMR spectroscopy. The ν(CO) and $\nu(CO_2)$ vibrational modes of complexes **1** and **3** are quite similar and occur at lower frequencies than the corresponding parameters of complex **2**. This is indicative of a less electron-donating nitrogen center in the latter derivative. This conclusion is also consistent with the more downfield positions of the ^{13}C resonances for the carbonyl ligands in complexes **1** and **3**.

Concomitantly the rates of CO dissociation in the complexes ligated through the deprotonated N3 center (complexes **1** and **3**), are slightly more facile than the corresponding rate in the N1 ligated derivative (complex **2**). This facile CO exchange with labeled ^{13}CO, which is comparable to that seen in the $W(CO)_5Cl^-$ anion but less than that observed in the alkoxide or aryloxide analogs, is attributed to π-donation of electron density from the nitrogen atom of the pyrimidine bases to the tungsten center in the transition state as the CO bond is broken.

Experimental Section

Methods and Materials: All manipulations were performed in a double manifold Schlenk vacuum line under argon or in an argon-filled glovebox. Solvents were freshly distilled under nitrogen from sodium/benzophenone ketyl (tetrahydrofuran, hexane, diethyl ether), magnesium iodide (methanol), or phosphorous pentoxide followed by calcium hydride (acetonitrile). − Photolysis experiments were performed using a mercury arc 450-W UV immersion lamp purchased from Ace Glass Co. − Routine IR spectra were recorded with a Matteson 6022 spectrometer with DTGS and MCT detectors, using a 0.10-mm CaF_2 cell. − Kinetic measurements were monitored with an ASI REACT IR™ 1000 system equipped with an MCT detector and 30 bounce SiCOMP™ in situ probe. − ^{13}C NMR spectra were obtained with a Varian Unity XL-300 spectrometer. − ^{13}CO was purchased from Cambridge Isotopes and used as received. $W(CO)_6$ was purchased from Fluka, and used without further purification. Dihydrouracil, 6-methyluracil, 5-methyluracil, and orotic acid methyl ester were purchased from Aldrich Chemical and used as received. 1,3-dimethylorotic acid was synthesized according to a previously published procedure.[24] − Microanalyses were performed by Canadian Microanalytical Service, Ltd., Delta, B.C.

Synthesis of $[NEt_4][W(CO)_5$(dihydrourcilate)] (1): In a typical synthesis dihydrouracil (0.163 g, 1.43 mmol) was placed in a Schlenk flask with a 25% w/w Et_4NOH solution in methanol (0.85 g, 1.44 mmol), along with 10 mL of THF. This solution was stirred for 45 min and concentrated for about 12 h to provide a white solid. $W(CO)_5THF$ was prepared by photolysis of $W(CO)_6$ (0.50 g, 1.44 mmol) in 60 mL of THF for 45 min. This yellow solution was then transferred to the $[Et_4N]$[diydrouracilate] and 1.5 mL methanol was added to dissolve the salt. The solution turned dark orange red on addition of the methanol. The solution was stirred for 10 min and concentrated to dryness leaving an orange powder. This powder was dissolved in CH_3CN and filtered through Celite leaving a clear orange solution, which was washed with 2 × 20 mL of hexane to remove excess $W(CO)_6$, and a white solid (unchanged $[Et_4N]$[diydrouracilate]). The product was precipitated with diethyl ether and vacuum-dried yielding 0.61 g (75% yield) of an analytically pure orange powder. − $C_{17}H_{25}O_7N_3W$ (567.3): calcd. C 36.00, H 4.44, N 7.41; found C 35.22, H 4.48, N 7.38. − IR (CH_3CN): $\tilde{\nu}$ = 2058 (w), 1911 (s), 1838 (m) cm^{-1}. − ^{13}C NMR (CD_3CN): δ = 202.3 (4 *cis*-CO), 208.0 (*trans*-CO). − Orange block crystals of **1** were obtained by slow diffusion of hexane into a THF solution of $[Et_4N][W(CO)_5(C_4H_5N_2O_2)]$ at 0° C.

Synthesis of $[NEt_4][W(CO)_5$(5-methyluracilate)] (2): In a typical synthesis 5-methyluracil (thymine) (0.179 g, 1.42 mmol) was placed in a Schlenk flask with tetraethylammonium hydroxide (25% w/w in methanol) (0.842 g, 1.43 mmol) and 10 mL of methanol. This solution was stirred for 1 h and vacuum-dried for about 12 h, yielding a white solid. $W(CO)_5THF$ (1.44 mmol), generated as in **1**, was added to this white solid, and 3 mL of methanol was also added to aid in the solubility of the salt. This yellow solution was stirred for 1 h and concentrated to dryness. The resulting yellow/brown solid was redissolved in THF and filtered through Celite leaving a yellow solution and a brown solid. The remaining yellow solution was layered with hexane and 0.49 g (57% yield) of an analytically pure bright yellow powder was obtained. − $C_{18}H_{25}O_7N_3W$ (579.3): calcd. C 37.32, H 4.35, N 7.25; found C 37.39, H 4.38, N 7.19. − IR (CH_3CN): $\tilde{\nu}$ = 2065 (w), 1915 (s), 1855(m) cm^{-1}. − ^{13}C NMR (CD_3CN): δ = 200.7 (4 *cis*-COs), 205.8 (*trans*-CO). − Yellow crystals of **2** were obtained by slow diffusion of hexane into a THF solution of **2** at room temperature over 4 d.

Synthesis of [NEt$_4$][W(CO)$_5$(6-methyluracilate)] (3): The synthesis of **3** was carried out in a manner analogous to that of **2**. 6-methyluracil (0.181 g, 1.44 mmol) was placed in a Schlenk flask with 1 equiv. of tetraethylammonimum hydroxide (25% w/w in methanol), and 10 mL of methanol. This solution was stirred for 2 h and vacuum dried for about 12 h, yielding a white solid. W(CO)$_5$THF (1.44 mmol), generated photochemically, was added to this and 2 mL of methanol was added to aid in its solubility. The resulting cloudy orange solution was filtered through Celite, leaving a clear orange solution. This solution was layered with hexane yielding 0.58 g (66% yield) of an analytically pure yellow powder. − $C_{18}H_{25}O_7N_3W$ (579.3): calcd. C 37.32, H 4.35, N 7.25; found C 37.39, H 4.35, N 7.25. − IR (CH_3CN): $\tilde{\nu}$ = 2059 (w), 1912 (s), 1840 (m) cm^{-1}. − ^{13}C NMR (CD_3CN): δ = 202.0 (4 *cis*-CO), 204.8 (*trans*-CO) cm^{-1}. − Yellow diffraction-quality crystals of **3** were grown by slow diffusion of hexane into a THF solution of **3** at room temperature over 3 d.

Synthesis of [Et$_4$N][W(CO)$_5$(methylorotate)] (4): In a typical synthesis a Schlenk flask was charged with the methyl ester of orotic acid (0.242 g, 1.44 mmol), slurried in 10 mL of THF and deprotonated with a 25% w/w Et$_4$NOH solution in methanol (0.85 g, 1.44 mmol). This solution was stirred for 30 min and the solvent was removed under vacuum, leaving a pale yellow solid. W(CO)$_5$THF was prepared photochemically, starting with W(CO)$_6$ (0.50 g, 1.44 mmol) in 60 mL of THF. This was photolyzed for 45 min. The resulting yellow solution was transferred via a cannula into the flask containing the deprotonated ester. The resulting solution changed color from yellow to a dark yellow-brown. The solution was stirred for 45 min and then concentrated to dryness overnight. The resulting solid was dissolved in CH_3CN and filtered through Celite affording a clear brownish-yellow solution which was washed with hexane to remove any residual W(CO)$_6$. The product was obtained in < 80% yield by the removal of solvent under reduced pressure to give a sticky brown solid. − $C_{19}H_{25}N_3O_9W$ (623.2712): calcd. C 36.61, H 4.04, N 6.74; found C 35.72, H 3.94, N 6.88. − IR (CH_3CN): $\tilde{\nu}$ = 2060 (w), 1914 (s), 1846 (m) cm^{-1}.

Synthesis of [Et$_4$N][W(CO)$_5$(*N*,*N*-dimethylorotate)] (5): A Schlenk flask was charged with *N*,*N*-dimethylorotic acid (0.261 g, 1.44 mmol), slurried in 10 mL of THF and deprotonated with a 25% w/w Et$_4$NOH solution in methanol (0.85 g, 1.44 mmol). This solution was stirred for 30 min and the solvent was removed under vacuum, leaving a white solid. W(CO)$_5$THF was prepared photochemically, starting with W(CO)$_6$ (0.50 g, 1.44 mmol) in 60 mL of THF. This was photolyzed for 45 min. The resulting yellow solution was transferred via a cannula into the flask containing the deprotonated acid. The resulting solution changed color from yellow to a dark orange-yellow. The solution was stirred for 45 min and then concentrated to dryness overnight. The sticky solid was dissolved in CH_3CN and filtered through Celite affording a clear brownish-orange solution which was washed with hexane to remove any residual W(CO)$_6$. The product was obtained in < 80% yield by the removal of solvent under reduced pressure to give a brown-orange solid. − $C_{20}H_{27}N_3O_9W$ (637.3): calcd. C 37.69, H 4.27, N 6.59; found C 37.65, H 4.56, N 6.62. − IR (CH_3CN): $\tilde{\nu}$ = 2067 (w), 1920 (s), 1853 (m) cm^{-1}.

Reaction of 1 with Methanol: Approximately 0.05 g of **1** was placed in an NMR tube with 1 mL of CD_3OD. The orange solution was then placed under ^{13}CO and inserted into an NMR probe. On removal of the tube from the NMR spectrometer, red block crystals of [Et$_4$N]$_2$[W(CO)$_4$(OMe)]$_2$ (**6**) were found. − ^{13}C NMR (CD_3OD): δ = 208.5 (4 *cis*-CO), 220.1 (4 *trans*-CO).

X-ray Crystallography

[Et$_4$N][W(CO)$_5$(dihydrouracilate)] (1): Crystal data and details of data collection are given in Table 9. An orange block of **1** was mounted on a glass fiber with epoxy cement, at room temperature. Preliminary examination and data collection were performed with a Rigaku AFC5R X-ray diffractometer (Cu-K_α, λ = 1.54178 Å radiation) for **1**. Cell parameters were calculated from the least-squares fitting of the setting angles for 24 reflections; ω scans for several intense reflections indicated acceptable crystal quality. Data were collected for 7.62° ≤ 2θ ≤ 120.12°. Three control reflections, collected every 97 reflections, showed no significant trends. Background measurements by stationary-crystal and stationary-counter techniques were taken at the beginning and end of each scan for half of the total scan time. Lorentz and polarization corrections were applied to 3873 reflections for **1**. A semiempirical absorption correction was applied to **1**. A total of 3873 unique reflections with $|I| \geq 2.0\sigma(I)$ were used in further calculations. The structure of **1** was solved by direct methods (SHELXS program package, Sheldrick, **1993**). Full-matrix least-squares anisotropic refinement for all non-hydrogen atoms yielded R = 0.0598, R_w = 0.0634, and S = 1.085 for **1**. Hydrogen atoms were placed in idealized positions with

Table 9. Crystallographic data for complexes **1**−**3** and **6**

	1	**2**	**3**	**6**
Empirical formula	$C_{21}H_{35}N_3O_8W$	$C_{20}H_{30}N_3O_{7.5}W$	$C_{18}H_{25}N_3O_7W$	$C_{19.5}H_{34.5}N_{1.5}O_{7.5}W_{1.5}$
Molecular mass	641.37	614.30	579.26	685.76
Space group	$P\bar{1}$	$C2/c$	$P\bar{1}$	$P\bar{1}$
V [Å^3]	1301.5(5)	4865(8)	1108.1(2)	2450.6(8)
Z	2	8	2	4
$d_{calcd.}$ [g/cm^3]	1.637	1.677	1.736	1.859
a [Å]	10.994(2)	19.76(3)	9.8884(13)	10.216(2)
b [Å]	14.336(3)	21.014(8)	10.4293(12)	11.680(2)
c [Å]	10.922(2)	12.485(11)	11.5381(12)	21.247(4)
α [°]	112.12(3)	−	78.120(9)	97.49(3)
β [°]	110.88(3)	110.18(10)	75.314(10)	95.29(3)
γ [°]	106.69(3)	−	77.158(10)	100.88(3)
T [K]	298(2)	163(2)	173(2)	173(2)
μ(Mo-K$_\alpha$) [mm^{-1}]	8.630	9.195	5.254	7.087
Wavelength [Å]	1.541 78	1.541 78	0.710 73	0.710 73
R_F[a] (%)	5.98	6.65	2.79	4.73
R_{wF} [b] (%)	6.34	14.66	7.04	7.06

[a] $R_F = \Sigma|F_o - F_c|/\Sigma F_o$. − [b] $R_{wF} = \{[\Sigma w(F_o^2 - F_c^2)^2]/(\Sigma wF_o^2)\}^{1/2}$.

the isotropic thermal parameters fixed at 0.08. Neutral-atom scattering factors and anomalous scattering correction terms were taken from the *International Tables for X-ray Crystallography.* Crystallographic data (excluding structure factors) for the structure(s) reported in this paper have been deposited with the Cambridge Crystallographic Data Centre as supplementary publication no. CCDC-148932 (**1**), -148933 (**3**), -148934 (**6**), and -148935 (**2**). Copies of the data can be obtained free of charge on application to CCDC, 12 Union road, Cambridge CB2 1EZ, UK [Fax: (internat.) + 44-1223/336-033; E-mail: deposit@ccdc.cam.ac.uk].

$[Et_4N][W(CO)_5(L)]$ [L = 5-Methyluracilate (2), 6-Methyluracilate (3)]: Crystal data and details of data collection are given in Table 9. A yellow needle of **2** and a yellow block of **3** were mounted on a glass fiber with epoxy cement at room temperature, and cooled in a cold stream of liquid nitrogen. Preliminary examination and data collection were performed with a Rigaku AFC5R X-ray diffractometer (Cu-K_α, λ = 1.54178 Å radiation) for **2**, and a Siemens P4 X-ray diffractometer (Mo-K_α, λ = 0.71073 Å radiation) for **3**. Data collection and parameters are identical to those described for complex **1**. Data were collected for $6.36° \leq 2\theta \leq 100.00°$ for **2** and $4.06° \leq 2\theta \leq 50.00°$ for **3**. Lorentz and polarization corrections were applied to 2437 reflections for **2** and 3887 reflections for **3**. A total of 2437 unique reflections for **2** and 3886 unique reflections for **3** were used in further calculations. Anisotropic refinement for all non-hydrogen atoms yielded R = 0.0665, R_w = 0.1466, and S = 0.920 for **2**, and R = 0.0274, R_w = 0.0704, and S = 0.786 for **3**.

$[Et_4N]_2[W_2(CO)_8(OMe)_2]$ (6): Crystal data and details of data collection are given in Table 9. A red block of **6** was mounted on a glass fiber with epoxy cement at room temperature, and cooled in a cold stream of liquid nitrogen. Preliminary examination and data collection were performed with a Siemens P4 X-ray diffractometer (Mo-K_α, λ = 0.710 73 Å radiation). Data collection and parameters are identical to that described for complex **1**. Data were collected for $4.08° \leq 2\theta \leq 50.00°$ for **6**. Lorentz and polarization corrections were applied to 8614 reflections. A total of 8614 unique reflections were used in further calculations. Anisotropic refinement for all non-hydrogen atoms yielded R = 0.0473, R_w = 0.0706, and S = 1.006.

Kinetic Measurements: The rates of ^{13}CO exchange in complexes **1**−**5** were determined at a variety of temperatures; ^{13}CO was placed over the solution of 0.1 g of the complex in 15 mL of THF or CH_3CN, which was situated in a thermostated temperature bath. The solutions were magnetically stirred and placed in a temperature bath at a variety of temperatures for **1** (35.0, 40.0, 45.0, 50.0, 57.0 °C), **2** (20.0, 30.0, 40.0, 50.0 °C), **3** (5.0, 15.0, 30.0, 40.0 °C), **4** (20, 35, 41, 45, 50 °C), and **5** (30, 40, 50 °C). The kinetics were monitored using ASI ReactIR in situ IR probe, by following the decrease in absorbance of the highest frequency A_1 band in the ν(CO) region of the IR spectrum as a function of time.

Acknowledgments

Financial support from the National Science Foundation (CHE99-10342 and CHE98-07975 for the purchase of X-ray equipment) and the Robert A. Welch Foundation is greatly appreciated.

[1] M. Goodgame, D. A. Jakubovic, *Coord. Chem. Rev.* **1987**, *79*, 97.
[2] I. Mutikainen, *Ann. Acad. Sci. Fenn, Ser. A. II. Chem.* **1988**, 217, and references therein.
[3] J. R. Lusty (Ed.), *CRC Handbook of Nucleobase Complexes: Transition Metal Complexes of Naturally Occurring Nucleobases and Their Derivatives*; CRC Press, Boca Raton, FL, **1990**, vol. 1, pp. 9−99.
[4] M. J. Bloemink, J. Reedijk, in: *Interaction of Metal Ions with Nucleotides, Nucleic Acids and Their Derivatives* (Eds. A. Sigel, H. Sigel), Marcel Dekker, New York, **1996**, pp. 641−685.
[5] D. M. Huryn, M. Okabe, *Chem. Rev.* **1992**, *92*, 1745−1768.
[6] E. DeClercq, *J. Med. Chem.* **1995**, *38*, 2491−2517.
[7] M. Shionoya, E. Kimura, M. Shiro, *J. Am. Chem. Soc.* **1993**, *115*, 6730−6737.
[8] M. Shionoya, T. Ikeda, E. Kimura, M. Shiro, *J. Am. Chem. Soc.* **1994**, *116*, 3848−3859.
[9] S. Aoki, Y. Honda, E. Kimura, *J. Am. Chem. Soc.* **1998**, *120*, 10018−10026.
[10] S. Aoki, C. Sugimura, E. Kimura, *J. Am. Chem. Soc.* **1998**, *120*, 10094−10102.
[11] P. D. Cookson, E. R. T. Tiekink, M. W. Whitehouse, *Aust. J. Chem.* **1994**, *47*, 577.
[12] E. R. T. Tiekink, P. D. Cookson, B. M. Linahan, L. K. Webster, *Metal Based Drugs* **1994**, 299.
[13] W. Beck, N. Kottmair, *Chem. Ber.* **1976**, *109*, 970.
[14] N. Kottmair, W. Beck, *Inorg. Chim. Acta* **1979**, *34*, 134−144.
[15] D. J. Darensbourg, J. D. Draper, D. L. Larkins, B. J Frost, J. H. Reibenspies, *Inorg. Chem.* **1998**, *37*, 2538.
[16] D. J. Darensbourg, B. J. Frost, A. Derecskei-Kovacs, J. H. Reibenspies, *Inorg. Chem.* **1999**, *38*, 4715.
[17] M. Ruf, K Weis, H. Vahrenkamp, *Inorg. Chem.* **1997**, *36*, 2130.
[18] G. W. Hunt, E. A. H. Griffith, E. L. Amma, *Inorg. Chem.* **1976**, *15*, 2993−2997.
[19] D. J. Darensbourg, J. A. Joyce, C. J. Bischoff, J. H. Reibenspies, *Inorg. Chem.* **1991**, *30*, 1137−1142.
[20] D. J. Darensbourg, E. V. Atnip, K. K. Klausmeyer, J. H. Reibenspies, *Inorg. Chem.* **1994**, *33*, 5230−5237.
[21] C. Moralejo, C. H. Langford, P. H. Bird, *Can. J. Chem.* **1991**, *69*, 2033.
[22] [22a] L. Tutt, J. I. Zink, *J. Am. Chem. Soc.* **1986**, *108*, 5830. − [22b] U. Klement, *Z. Kristallogr.* **1993**, *208*, 111.
[23] D. J. Darensbourg, K. K. Klausmeyer, J. D. Draper, J. A. Chojnacki, J. H. Reibenspies, *Inorg. Chim. Acta* **1998**, *270*, 405−413.
[24] P. Beak, B. Siegel, *J. Am. Chem. Soc.* **1976**, *98*, 3601.

Received April 7, 2000
[I00137]

Investigation of the Structure of New Gallium Phosphonate Based Hybrid Materials by ^{31}P, ^{71}Ga, and ^{1}H Solid-State NMR

Martine Bujoli-Doeuff,[a] Michel Evain,[a] Franck Fayon,[b] Bruno Alonso,[b] Dominique Massiot,[b] and Bruno Bujoli*[c]

Keywords: Phosphonate complexes / Gallium / NMR spectroscopy / Homonuclear proton decoupling

Modern high-resolution solid-state NMR is a powerful tool for probing the structure of phosphonate-based hybrid materials, in the organic as well as in the inorganic region. This is illustrated in the case of a series of new gallium phosphonates [$Ga(OH)(O_3PCH_3) \cdot x\,H_2O$ [x = 1 (**1**); x = 0 (**1′**)] and $Ga(OH)(O_3PCH_2C_6H_5)$ (**2**)], that were characterized by X-ray diffraction and FTIR, and then studied using ^{71}Ga, ^{31}P, and ^{1}H NMR.

Introduction

Metal phosphonates are organic-inorganic hybrid materials in which the structure can be tuned by the choice of the organic moiety covalently bonded to the inorganic portion.[1] These materials are attracting increasing interest because of the large variety of applications they can offer, among which supported catalysis has particularly attracted our attention.[2] For a better understanding of the structure/property relationships in these solids, modern high-resolution solid-state NMR offers a wide variety of methods that can selectively examine the inorganic part, the organic part, and their connection, provided NMR-observable nuclei are present. In this paper we describe a new series of gallium phosphonates and their study by recently developed experimental NMR techniques which demonstrate the potential of these methods to give access to detailed structural information. Layered phosphonates are now well documented,[1] but to date, only one example of the gallium series has been reported;[3] in this study, two new layered gallium phosphonates [$Ga(OH)(O_3PCH_3) \cdot H_2O$ (**1**) and $Ga(OH)(O_3PCH_2C_6H_5)$ (**2**)] were prepared under hydrothermal conditions. The metal/PO_3 arrangement within the slabs of compound **1** can be described as edge-sharing octahedra (made of four phosphonate oxygen atoms and two μ-2 hydroxide groups) forming infinite chains parallel to the *b* axis.

These chains are connected via the PO_3 groups, thus leading to a 2D network (Figure 1), with the methyl substituents oriented perpendicular to the layers, and the non-coordinated water molecules located between the sheets, weakly hydrogen-bonded to some phosphonate and hydroxide oxygen atoms (Figure 2).

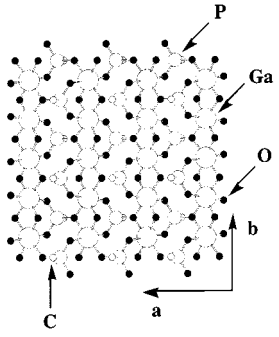


Figure 1. Schematic representation of a $Ga(OH)(O_3PCH_3) \cdot H_2O$ (**1**) layer viewed down the *c* axis; selected interatomic distances [Å]: Ga−O: 1.967(3) [X 2], 2.006(3) [X 2], 1.941(3) [X 2−OH]

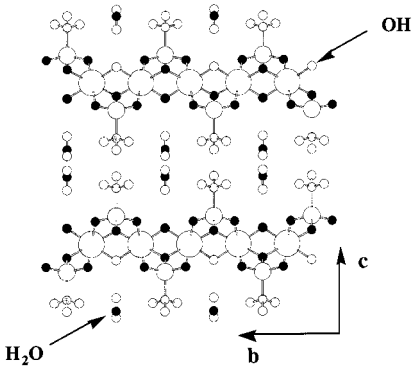


Figure 2. Schematic representation of the layered arrangement of **1** shown perpendicular to the *a* axis

No modification of the inorganic network occurs after the loss of the water molecule [performed by heating **1** at 100 °C for 1 h to yield **1′**] since the infrared spectrum is not modified, except in the ν(OH) region. As FTIR is very sensitive to the metal−O_3P arrangement in metal phosphonates, the strong similarities observed in the IR data

[a] Institut des Matériaux Jean Rouxel, UMR CNRS 6502, 2 Rue de la Houssinière, B. P. 92208, 44322 Nantes Cedex 03, France
[b] CRMHT, UPR CNRS 4212, 1D Avenue de la Recherche Scientifique, 45071 Orléans Cedex 02, France
[c] Laboratoire de Synthèse Organique, UMR CNRS 6513, 2 Rue de la Houssinière, B. P. 92208, 44322 Nantes Cedex 03, France
Fax: (internat.) + 33-2/51125412
E-mail: bujoli@chimie.univ-nantes.fr

 © WILEY-VCH Verlag GmbH, D-69451 Weinheim, 2000 1434−1948/00/1212−2497 $ 17.50+.50/0

collected for **2** and **1′** (for the OH and PO_3 absorptions − see Experimental Section) give clear evidence that the structural features in these three products are quite similar.

As far as the inorganic component in these materials is concerned, the six-coordinate nature of the gallium atoms is clearly evident from the isotropic chemical shift measured from the ^{71}Ga VOCS NMR[3,4] spectra [$\delta_{iso} = -13 \pm 10$ for **1** and **1′**, and 10 ± 10 for **2**] shown in Figure 3.

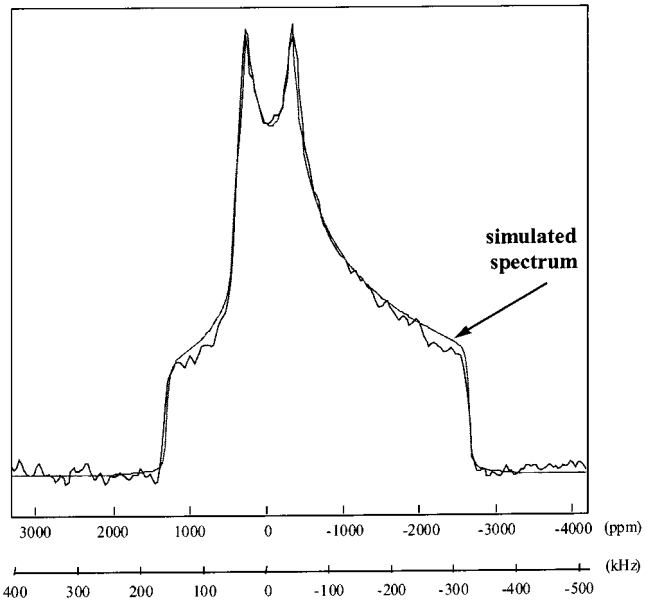


Figure 3. Experimental ^{71}Ga static NMR spectrum of **1**, and simulated spectrum with second-order quadrupolar broadened shape, according to parameters described in Table 1

On the other hand, as previously demonstrated in the case of zinc phosphonates,[5] it appears that the connectivity of the PO_3 groups (i.e. the number of metal atoms connected to each of the three oxygen atoms bound to the phosphorus atom) can be deduced from the ^{31}P MAS NMR spectra, by the chemical shift asymmetry parameter κ (skew) of the individual phosphorus sites (reported in Table 1). Interestingly, in the previously described gallium phosphonate $Ga(OH)(O_3PC_2H_4CO_2H) \cdot H_2O$[3] (and more generally in the case of aluminum phosphonates with well-established structures[6]) the highest connectivity observed for the PO_3 groups was (111) and the range of variation of the κ value for the P sites was then [−0.3, −0.5]. As evidenced by the X-ray structure of **1**, a (112) connectivity is found for the first time in such compounds, with a markedly different κ value observed for the P sites: $\kappa = 0$ for **1** and +0.2 for **1′** and for **2**.

Resolved ^1H NMR solid-state spectra cannot be obtained using simple acquisition sequences, due to dominant homonuclear couplings between the protons. We acquired 2D $\{^1H\}$-^1H correlation spectra using the Phase Modulated Lee−Goldburg (PMLG) experiment recently proposed by Vinogradov and co-workers.[7] In this experiment a better resolved proton (homonuclear decoupled under Lee−Goldburg excitation) spectrum is obtained in the indirect dimension of a 2D experiment and is correlated with the usual low-resolution MAS spectrum.

The resulting 2D spectrum of **1** is presented in Figure 4. We observe two resolved signals at $\delta = 4.6$ and 1.5 in **1** in a ca. 1:1 ratio. The most deshielded signal ($\delta = 4.6$) is ascribed to water molecules and hydroxide groups (H_2O + OH) and the signal at $\delta = 1.5$ to CH_3 units. In the case of the water-free compound **1′**, these signals at $\delta = 4.5$ and 1.7 are in a ca. 1:3 ratio and correspond to hydroxide and methyl groups respectively, in agreement with the stoichiometry. Under similar acquisition conditions, the broad MAS spectrum of **2** splits in two resolved contributions ascribed to (OH + CH_2) at $\delta = 4.5$ and C_6H_5 at $\delta = 7$.

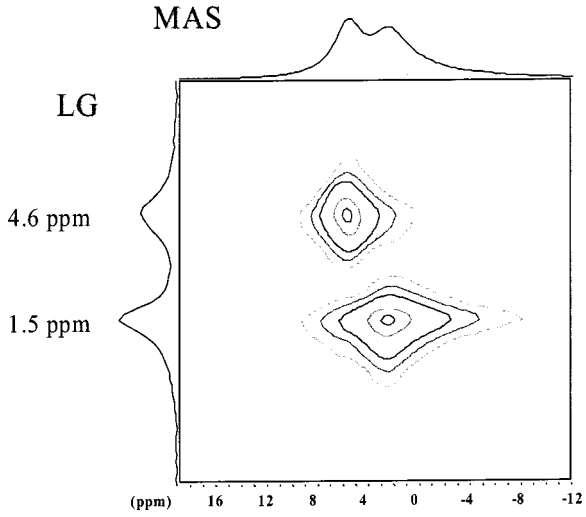


Figure 4. 2D PMLG/MAS $\{^1H\}/^1H$ spectrum of **1**

Table 1. Experimental values for ^{71}Ga chemical shift and electric field gradient, and for ^{31}P chemical shift tensor, for compounds **1**, **1′**, and **2**

$Ga(OH)(O_3PCH_3) \cdot H_2O$ (**1**)	^{71}Ga ^{31}P	δ_{iso}[a] = −13 δ_{iso}[d] = 32.2	C_Q[b] = 16.2 MHz Ω[e] = 60.4	η_Q[c] = 0.8 κ[f] = 0
$Ga(OH)(O_3PCH_3)$ (**1′** from dehydration of **1**)	^{71}Ga ^{31}P	Same values as for **1** δ_{iso}[d] = 30.5	 Ω[e] = 69.7	 κ[f] = 0.2
$Ga(OH)(O_3PCH_2C_6H_5)$ (**2**)	^{71}Ga ^{31}P	δ_{iso}[a] = 10 δ_{iso}[d] = 25.6	C_Q[b] = 17.5 MHz Ω[e] = 89.4	η_Q[c] = 0.8 κ[f] = 0.2

[a] Chemical shifts are referenced to ^{71}Ga resonance in a 1 M gallium nitrate solution; error in the measured value: ±10 ppm. − [b] Quadrupolar coupling constant ($C_Q = e^2qQ/h$); error in the measured value: ±0.25 MHz. − [c] Asymmetry factor. − [d] Chemical shifts are referenced to ^{31}P resonance in 85% H_3PO_4. − [e] Chemical shift span defined as $\delta_{11} - \delta_{33}$ with $\delta_{11} \geq \delta_{22} \geq \delta_{33}$. − [f] Chemical shift skew defined as $3(\delta_{22} - \delta_{iso})/\Omega$.

In conclusion, solid-state NMR appears to be an efficient tool to provide accurate insights into the local environments of P, Ga, and H present in these hybrid (organic/inorganic) compounds. Work is in progress to investigate a wider range of model gallium phosphonate compounds which should allow us to establish a stronger correlation between NMR parameters and local structure: δ_{iso} and skew of chemical shift anisotropy of ^{31}P, δ_{iso} and quadrupolar tensor of ^{71}Ga and δ_{iso} for resolved ^{1}H. This approach should easily be transferred to the case of aluminum phosphonates using the recently established correlation between ^{27}Al and ^{71}Ga NMR parameters.[4] The improved resolution obtained in the Lee−Goldburg decoupled ^{1}H spectra opens the possibility of exploring the whole material on different scales using spin diffusion between protons with possible encoding through the other NMR active nuclei. These experiments are expected to be very fruitful in the case of polycrystalline or amorphous materials involving phase-separated domains as well as organic/inorganic interfaces.

Experimental Section

Syntheses of 1 and 2: A mixture of gallium nitrate (1 mmol) and methylphosphonic (**1**) or benzylphosphonic (**2**) acid (10 mmol) in water (20 mL) was placed in the PTFE cell of an autoclave, which was sealed and kept at 160 °C (**1**) or 170 °C (**2**) in a drying oven for 8 (**1**) or 5 d (**2**). Compound **1** was obtained in 32% yield (64 mg) as white crystals, used for the X-ray structure determination, while **2** was isolated as a white powder in 45% yield (115 mg). − **1:** CH_6GaPO_5 (198.7): calcd. C 6.04, H 3.04, P 15.58; found C 6.12, H 2.94, P 15.29. − FTIR (KBr): $\tilde{\nu}$ = 3589 m, 3512 s, 3453 m, 3382 m, 1324 m, 1099 vs, 1058 vs, 995 vs, 912 s cm^{-1}. − TGA (25−300 °C): 8.90% (calcd. 9.05%; $-H_2O$, 35 °C). − After dehydration of **1** (performed by heating at 100 °C for 1 h to yield **1′**), the infrared spectrum was unchanged, except in the ν(OH) region where only a strong (3515 cm^{-1}) and a broad band (3400 cm^{-1}) remained. − **2:** $C_7H_8GaPO_4$ (256.8): calcd. C 32.73, H 3.14, P 12.06; found C 32.89, H 3.10, P 12.18. − FTIR (KBr): $\tilde{\nu}$ = 3519 s, 3400 b, 1151 m, 1100 vs, 1060 vs, 990 vs, 910 s cm^{-1}. − TGA (25−300 °C): 0%.

Solid-State NMR Experiments: NMR solid-state spectra of ^{71}Ga, ^{31}P, and ^{1}H have been acquired with a Bruker DSX400 spectrometer operating at 9.4 T. The wide ^{71}Ga spectra extend over several hundreds of kHz and have been acquired in static following the VOCS protocol[8] (Magic Angle Spinning would not provide any gain in resolution). The ^{31}P spectra have been acquired using CP-MAS $\{^{1}H\}$-^{31}P excitation, as previously described[3] with a typical contact time of 1.5 ms and 1 s of recycle time. The Lee−Goldburg/MAS $\{^{1}H\}/^{1}H$ correlation spectra have been acquired using the Phase Modulated Lee−Goldburg decoupling scheme[7] with a ^{1}H radio-frequency field of 50 kHz. The two-dimensional spectra were typically obtained within 10 mins with two transients per slice and up to 256 slices, depending on resolution. Spectra were simulated using a modified version of the Bruker Winfit program.[9]

Structure Determination of 1: Data collection was carried out with a single crystal approximately 0.3×0.2×0.04 mm in size with a STOE Imaging Plate Diffraction System,[10] using graphite-monochromatized Mo-K-$L_{2,3}$ radiation (λ = 0.71073 Å). Data intensities were corrected for Lorentz polarization and absorption (Gaussian analytical correction) and subsequently merged according to the *mmm* point group (R_{int} = 0.051), giving rise to a set of 409 independent reflections at a 2σ level. Although the systematic extinctions suggested *Pnmn* as the most probable space group, *Pnma* was found to be the correct space group, both at the residue factor and the structure coherence level. A starting model was found with the Shelxtl V5.0 direct method program[11] and refined (F^2, all reflections included) with the Jana2000 program.[12] All subsequent calculations were carried out with the Jana2000 program package. Missing atoms, including hydrogen atoms, were found in difference Fourier synthesis maps. Non-hydrogen atoms were refined with anisotropic displacement parameters and hydrogen atoms were kept at fixed positions with a common fixed isotropic displacement parameter. At the last stage of the refinement, a secondary extinction coefficient[13] was introduced and the residue factor smoothly converged with R/R_w = 0.0303/0.0681 for 409 reflections with $I/\sigma(I) > 2$ and 47 parameters. − Crystal Data: $Ga(OH)(O_3PCH_3) \cdot H_2O$; orthorhombic *Pnma*; a = 4.5193(7), b = 5.9965(7), c = 19.556(2) Å, V = 530.0(2) $Å^3$ from 3096 reflections collected with the STOE IPDS; monochromatized Mo-K-$L_{2,3}$ radiation; Z = 4; M = 198.75; $\rho_{calcd.}$ = 2.490 $g \cdot cm^3$; μ = 54.25 cm^{-1}; residual electron density [−0.84/+0.62] $e \cdot Å^3$. Crystallographic data (excluding structure factors) for the structure reported in this paper have been deposited with the Cambridge Crystallographic Data Centre as supplementary publication no.CCDC-142094. Copies of the data can be obtained free of charge on application to CCDC, 12 Union Road, Cambridge CB2 1EZ, UK [Fax: (internat.) + 44-1223/336-033; E-mail: deposit@ccdc.cam.ac.uk].

[1] See for example: A. Clearfield, in: *Progress in Inorganic Chemistry*, vol. 47 (Ed.: K. D. Karlin), John Wiley & Sons, Inc., New York, **1998**, pp. 371−510. F. Fredoueil, M. Evain, M. Bujoli-Doeuff, B. Bujoli, *Eur. J. Inorg. Chem.* **1999**, 1077−1079, and references therein.

[2] D. Deniaud, B. Schöllhorn, D. Mansuy, J. Rouxel, P. Battioni, B. Bujoli, *Chem. Mater.* **1995**, *7*, 995−1000. D. Deniaud, G. A. Spyroulias, J. F. Bartoli, P. Battioni, D. Mansuy, C. Pinel, F. Odobel, B. Bujoli, *New J. Chem.* **1998**, *22*, 901−905.

[3] F. Fredoueil, D. Massiot, D. Poojary, M. Bujoli-Doeuff, A. Clearfield, B. Bujoli, *Chem Commun.* **1998**, 175−176.

[4] D. Massiot, T. Vosegaard, N. Magneron, D. Trumeau, V. Montouillout, P. Berthet, T. Loiseau, B. Bujoli, *Solid State NMR* **1999**, *15*, 159−169.

[5] D. Massiot, S. Drumel, P. Janvier, M. Bujoli-Doeuff, B. Bujoli, *Chem. Mater.* **1997**, *9*, 6−7.

[6] K. Maeda, J. Akimoto, Y. Kiyozumi, F. Mizukami, *J. Chem. Soc., Chem. Commun.* **1995**, 1033−1034. K. Maeda, J. Akimoto, Y. Kiyozumi, F. Mizukami, *Angew. Chem. Int. Ed. Engl.* **1995**, *34*, 1199−1201. L. J. Sawers, V. J. Carter, A. R. Armstrong, P. G. Bruce, P. A. Wright, B. E. Gore, *J. Chem. Soc., Dalton Trans.* **1996**, 3159−3161. G. B. Hix, V. J. Carter, D. S. Wragg, R. E. Morris, P. A. Wright, *J. Mater. Chem* **1999**, *9*, 179−185. A. Cabeza, M. A. G. Aranda, S. Bruque, D. M. Poojary, A. Clearfield, J. Sanz, *Inorg. Chem.* **1998**, *37*, 4168−4178.

[7] E. Vinogradov, P. K. Madhu, S. Vega, *Chem. Phys. Letters* **1999**, *314*, 443−450.

[8] D. Massiot, I. Farnan, N. Gautier, D. Trumeau, A. Trokiner, J. P. Coutures, *Solid State NMR* **1995**, *4*, 241−248.

[9] D. Massiot, H. Thiele, A. Germanus, *Bruker Report* **1994**, *140*, 43−46.

[10] IPDS software, STOE & Cie GmbH, Darmstadt, Germany, **1996**.

[11] G. M. Sheldrick, *SHELXTL V5.0*, Analytical X-ray Instruments Inc., Madison, WI, USA, **1995**.

[12] V. Petricek, M. Dusek, *JANA2000, programs for modulated and composite crystals*, Institute of Physics, Praha, Czech Republic, **2000**.

[13] P. J. Becker, P. Coppens, *Acta Crystallogr. A* **1974**, *30*, 129−147.

Received April 12, 2000
[I00142]

Organoamido- and Aryloxo-Lanthanoids, 23[‡]

Aryl Ether C−O Bond Activation by Organoamidolanthanoid(II) Complexes

Glen B. Deacon,*[a] Craig M. Forsyth,[a] and Natalie M. Scott[a]

Dedicated to Prof. Dr. Herbert Schumann on the occasion of his 65th birthday

Keywords: N ligands / Ytterbium / C−O activation / O ligands / Lanthanoids

The reaction of ytterbium metal, $HgPh_2$ and *N*-(2-methoxyphenyl)-*N*-(trimethylsilyl)amine (L^1H) or *N*-(2-phenoxyphenyl)-*N*-(trimethylsilyl)amine (L^2H) in tetrahydrofuran (thf) unexpectedly yielded the ytterbium(III) complexes $[Yb(L^1)_2(\mu\text{-OMe})]_2$ **(1)** and $[Yb(L^2)_2(OPh)(thf)]$ **(2)**, the structures of which were established by X-ray crystallography. These are considered to be derived from C–O bond cleavage of the ligand aryl ether moiety by an initially formed Yb^{II} species, e.g. the thermally unstable, but crystallographically authenticated $[Yb(L^1)_2(thf)_2]$ **(3)**, which was independently prepared from $[Yb\{N(SiMe_3)_2\}_2(thf)_2]$ and L^1H.

Introduction

Divalent lanthanoid complexes react with a number of oxygen-containing substrates due to the oxophilicity of these metals and the large $Ln^{3+} \rightarrow Ln^{2+}$ reduction potentials (Ln = Yb,Sm).[2] For example, tetrahydrofuran (thf) solutions of SmI_2 have found extensive applications in organic synthesis as a selective reducing agent for ketones.[2−4] Other LnL_2 species are capable of stoichiometric reactions with ketones, forming metal-bound ketyl radical anions,[5,6] and the reductive coupling of carbon dioxide by $Sm(C_5Me_5)_2$ complexes has been reported.[7] Whilst $Sm(C_5Me_5)_2$-induced deoxygenation of epoxides is facile, yielding $[Ln(C_5Me_5)_2(\mu\text{-O})]_2$,[8] transformations of unstrained carbon−oxygen single bonds occur only under unusual circumstances. For example, thermolytic cleavage of diethyl ether by very low coordinate ytterbium(II) complexes has been reported[9,10] and photolysis of 1,2-dimethoxyethane (dme) solutions of YbI_2 gives the methoxide complex $[YbI_2(\mu\text{-OMe})(dme)]_2$.[11] Furthermore, cleavage of dme by highly novel La^{II} or Ce^{II} organometallic complexes was recently reported.[12−14] These few examples of C−O cleavage of alkyl ethers contrast the numerous stable coordination complexes of divalent lanthanoids with these ligands.[15,16]

In this contribution, we report the unexpected cleavage of the aryl ether C−O single bond of the anionic bidentate N,O-ligands L^1, L^2 [L^1 = $N(SiMe_3)C_6H_4$-2-OMe, L^2 = $N(SiMe_3)C_6H_4$-2-OPh] by a ytterbium(II) centre and the characterisation of the lanthanoid(III) products $[Yb(L^1)_2(\mu\text{-OMe})]_2$ **(1)** and $[Yb(L^2)_2(OPh)(thf)]$ **(2)**. The latter is the first structurally authenticated lanthanoid complex with an unsubstituted phenoxide ligand; surprisingly, for a sterically undemanding ligand, it is nonbridging. The synthesis and characterisation of the thermally unstable, proposed ytterbium(II) precursor $[Yb(L^1)_2(thf)_2]$ **(3)** are also described.

Results and Discussion

We initially attempted to prepare novel ytterbium(II) complexes of the bidentate N,O-ligands L^1 and L^2 (for preparations and the X-ray crystal structure of L^1H see Experimental Section) by a redox transmetallation/ligand exchange reaction (Equation 1).

$$Ln^0 + HgPh_2 + 2LH \longrightarrow Ln(L)_2 + 2PhH + Hg^0 \quad (L = L^1 \text{ or } L^2) \qquad (1)$$

This route has previously been utilised for the preparation of $Ln(NRR')_2$ species including $[Ln\{N(SiMe_3)Ar\}_2(thf)_2]$ (Ar = C_6H_3-2,6-*i*Pr_2, Ln = Sm, Yb).[17] The current reactions afford moderate to low yields of red-orange crystals after workup. The presence of L^1 or L^2 was evident from the infrared spectra, but the products were shown to contain Yb^{III} by the observation of *f*←*f* transitions near 1000 nm[18] in the electronic spectra. Furthermore, the analytical data did not fit the compositions $Yb(L^1)_3$ or $Yb(L^2)_3$ and thus the formation of heteroleptic Yb^{III} species was indicated. X-ray crystallography subsequently revealed that the products were the alkoxide and aryloxide complexes $[Yb(L^1)_2(\mu\text{-OMe})]_2$ **(1)** and $[Yb(L^2)_2(OPh)(thf)]$ **(2)** (Figure 1 and 2).

Complex **1** crystallises as two virtually identical, but independent, dimers each having two bridging methoxide ligands, chelating L^1 coordination and hexacoordinate ytterbium atoms of an irregular geometry. Both molecules are sited on crystallographic twofold axes through the methox-

[‡] Part 22: Ref.[1]

[a] School of Chemistry, Monash University, Victoria 3800, Australia
E-mail: glen.deacon@sci.monash.edu.au

 © WILEY-VCH Verlag GmbH, D-69451 Weinheim, 2000 1434−1948/00/1212−2501 $ 17.50+.50/0

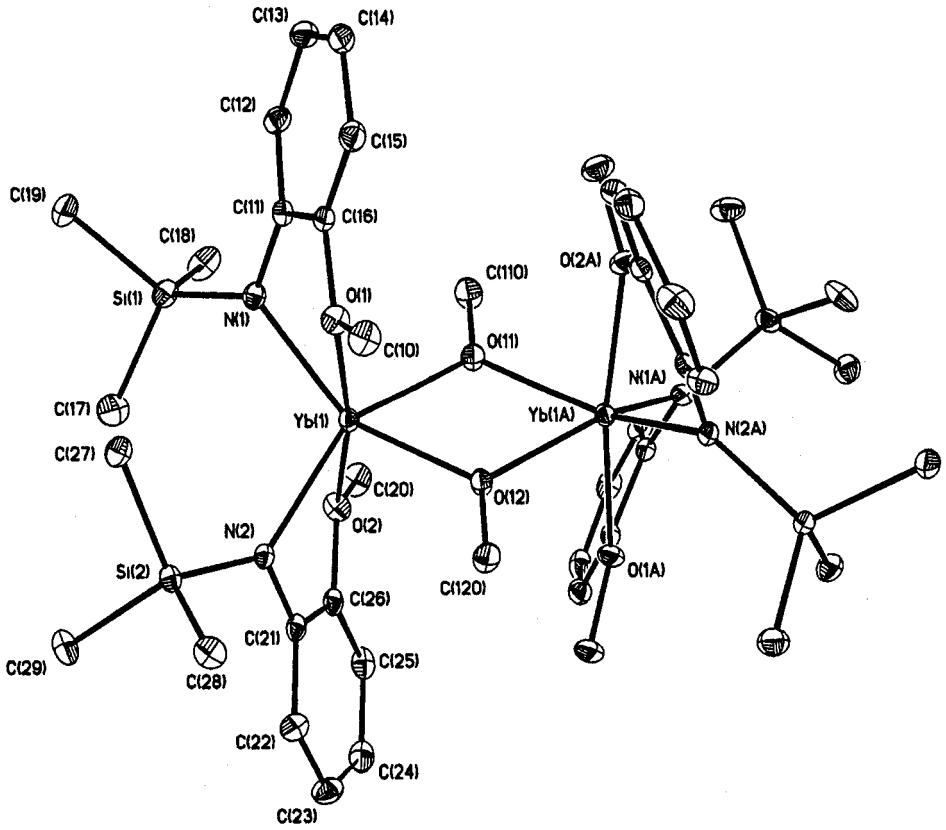


Figure 1. ORTEP view of one molecule of $[Yb(L^1)_2(\mu\text{-}OMe)]_2$ **(1)** drawn with 30% thermal ellipsoids; hydrogen atoms have been omitted for clarity; selected bond lengths (Å) and angles (°): Yb(1)−O(1) 2.346(2), Yb(1)−O(2) 2.355(2), Yb(1)−N(1) 2.250(3), Yb(1)−N(2) 2.245(3), Yb(1)−O(11) 2.221(2), Yb(1)−O(12) 2.217(2); O(1)−Yb(1)−O(2) 171.09(8), N(1)−Yb(1)−N(2) 112.7(1), N(2)−Yb(1)−O(1) 106.24(9), N(1)−Yb(1)−(O2) 102.03(9), N(2)−Yb(1)−O(2) 71.16(9), N(1)−Yb(1)−O(1) 70.80(9), O(12)−Yb(1)−O(11) 72.5(1), O(12)−Yb(1)−N(2) 91.12(9), O(11)−Yb(1)−N(2) 147.90(7), O(12)−Yb(1)−N(1) 149.79(8), O(11)−Yb(1)−N(1) 93.2(1), O(12)−Yb(1)−O(1) 85.27(6), O(11)−Yb(1)−O(1) 99.85(6), O(12)−Yb(1)−O(2) 103.17(6), O(11)−Yb(1)−O(2) 85.60(6), Yb(1)−O(11)−Yb(1A) 107.4(1), Yb(1)−O(12)−Yb(1A) 107.6(1); symmetry transformation: −x, y, −z + 3/2

ide ligands, hence the four-membered Yb_2O_2 rings are planar. The geometry of the methoxide bridges, with larger O−Yb−O than Yb−O−Yb angles is virtually identical to that of $[CeCp''_2(\mu\text{-}OMe)]_2$ [Cp" = $\eta\text{-}C_5H_3\text{-}1,3\text{-}(SiMe_3)_2$].[12] The near equal Yb−OMe distances are comparable with the *longer* of the two Yb−OMe distances 2.210(6), 2.152(4) Å,[11] in $[YbI_2(\mu\text{-}OMe)(dme)]_2$, where the Yb−OMe bond lengthening was attributed to the *trans* influence of the iodide ligand.[11] In **1**, the two methoxide ligands have the same relative dispositions to the amide nitrogens. One nitrogen is *transoid* to each methoxide and hence exerts a *trans* influence. However, the present lengthening may also be attributed to steric crowding, since the Yb−O(ether) distances approach values expected for crowded systems.[19] The ether oxygen atoms of the L^1 ligands are approximately *trans*, with Yb−O bond lengths somewhat larger than those of the dme ligands in $[\{YbI_2(\mu\text{-}OMe)(dme)\}_2]$, 2.317(6) and 2.308(5) Å.[11] Surprisingly, the angle between the nitrogens of the bulky aryl(trimethylsilyl)amide groups is *cisoid* [c.f. *transoid* O(ether)−Yb−O(ether)], although this is consistent with the *fac*-coordination of the alkyl(trimethylsilyl)amide groups in tris(*N*,*N*-dimethyl-*N'*-trimethylsilylethane-1,2-diaminato)lanthanoid(III) complexes.[20] In a similar manner, the bulky carbazolate (cbz) ligands are *cisoid* in six coordinate $[Ln(cbz)_2(thf)_4]$ (Ln = Yb and Sm).[21,22] The Yb−N distances are nearly identical with those of six coordinate $[YbL_2(\mu\text{-}Cl)_2Li(thf)_2]$ [L = $Me_2Si(OtBu)(NtBu)$], 2.247(5) and 2.225(5) Å,[23] implying a similar steric congestion.

In contrast to **1**, complex **2** crystallises as discrete monomers with two independent, but similar, molecules comprising the asymmetric unit, one being displayed in Figure 2. The ytterbium atoms are hexacoordinate, each with an irregular coordination sphere provided by two chelating L^2 ligands, a terminal phenoxide and a coordinated thf. The relative orientation of the L^2 ligands, with the ether-OPh groups coordinated in an approximately *cis* arrangement, is different from that of L^1 in **1**. One of the Yb−O(ether) bond lengths is significantly longer than the other, attributable to its *trans* disposition relative to the phenoxide oxygen. A meaningful *trans*-influence for aryloxide ligands in lanthanoid complexes has been reported.[19] Both the shorter Yb−O(ether) and the Yb−O(thf) bond lengths are of a similar magnitude to the mutually *trans* Yb−O(ether) distances in **1**. As with **1**, the bulky silylamide groups are *cisoid*, and whilst the N−Yb−N angle is marginally smaller than in **1**, there is no significant change in the Yb−N distances. The Yb−OPh distance is comparable to, albeit marginally smaller than, those of terminal 2,6-disubstituted aryloxide ligands bound to six coordinate ytterbium(III) {e.g.

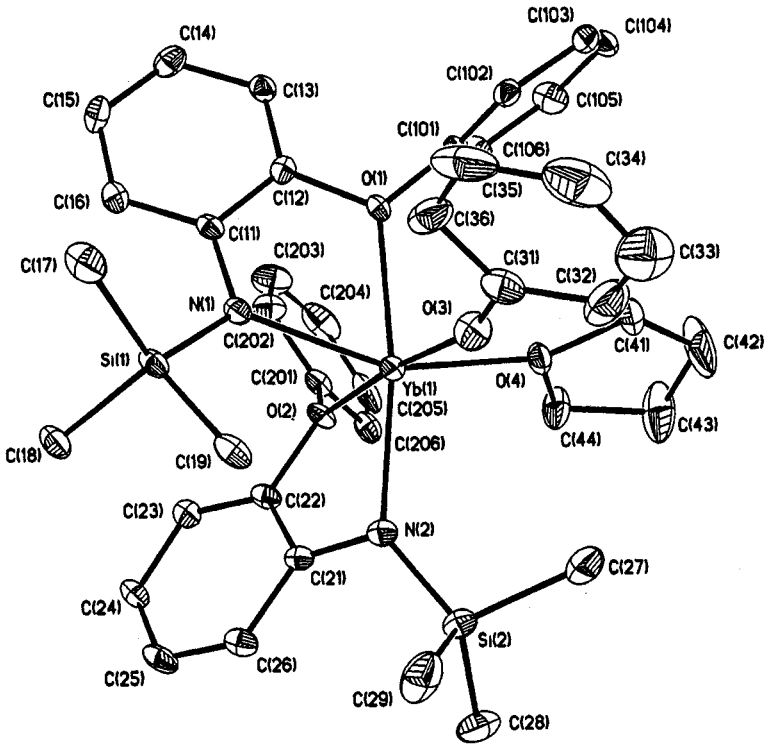


Figure 2. ORTEP view of one molecule of $[Yb(L^2)_2(OPh)(thf)]$ **(2)** drawn with 30% thermal ellipsoids; hydrogen atoms have been omitted for clarity; selected bond lengths (Å) and angles (°): Yb(1)−O(1) 2.380(4), Yb(1)−O(2) 2.459(5); Yb(1)−O(3) 2.023(6), Yb(1)−O(4) 2.357(4), Yb(1)−N(1) 2.250(5), Yb(1)−N(2) 2.247(5), O(3)−Yb(1)−N(2) 108.4(2), O(3)−Yb(1)−N(1) 104.3(2), N(2)−Yb(1)−N(1) 107.0(2), O(3)−Yb(1)−O(4) 86.1(2), N(2)−Yb(1)−O(4) 95.6(2), N(1)−Yb(1)−O(4) 150.3(2), O(3)−Yb(1)−O(1) 95.9(2), N(2)−Yb(1)−O(1) 155.2(2), N(1)−Yb(1)−O(1) 70.7(2), O(4)−Yb(1)−O(1) 80.7(2), O(3)−Yb(1)−O(2) 173.2(2), N(2)−Yb(1)−O(2) 69.9(2), N(1)−Yb(1)−O(2) 82.5(2), O(4)−Yb(1)−O(2) 87.5(2), O(1)−Yb(1)−O(2) 85.4(2)

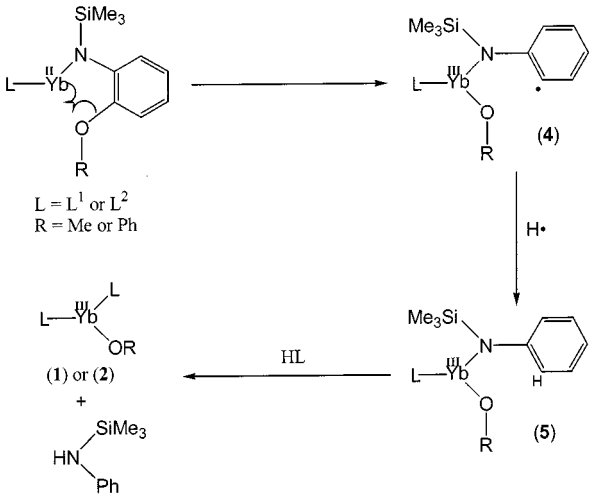
in $[Yb(MeC_5H_4)(OAr)_2(thf)]$, 2.040(4) and 2.078(4) Å[24] and $[Yb(OAr)Cl_2(thf)_3]$, 2.083(5) Å;[25] Ar = C_6H_2–2,6-tBu$_2$-4-Me}, consistent with reduced crowding in **2**. The structure of **2** is novel as the first authenticated example of an unsubstituted phenoxide bound to a lanthanoid centre.[16,26] There must be a fine balance between formation of a six coordinate μ-OPh (thf-free) species and the observed thf-coordinated structure **2**, since OPh is only marginally bulkier than thf.[27]

The methoxide and phenoxide groups in **1** and **2** are derived from the ligands L^1 and L^2, respectively. There was some ambiguity arising from the use of dme as a recrystallisation solvent in our initial isolation of **1**, since dme could be a OMe source.[11−14] However, the same product is formed in similar yield in the absence of dme (Experimental Section), i.e. where the crude product of the redox transmetallation/ligand exchange was treated with diethyl ether and recrystallised from hexane. We propose that the formation of **1** and **2** occurs by a one-electron transfer from Yb^{II} to an L^1 or L^2 ligand, Ar−O bond cleavage, formation of a Yb^{III}−OR (R = Me or Ph) bond, and then protolysis of the intermediate **5** by L^1H or L^2H (Scheme 1) present as reactants (Equation 1). In confirmation, we have shown that $[Yb(L^1)_2(thf)_2]$ **(3)** (see below) is converted into **1** in the presence of an excess of L^1H in hexane (see Experimental Section). A GC-MS analysis of the hydrolysed filtrate after the isolation of **2** showed the presence of phenol, *o*-phenoxyaniline and aniline, the last consistent with hydrolysis of the proposed product $HNPh(SiMe_3)$ and hence with prior proton abstraction (probably from the solvent[28]) by the aryl radical **4** (Scheme 1). The first two are the expected products of hydrolysis of the isolated $[Yb(L^2)_2(OPh)(thf)]$ **(2)**. Instability of *N*-trimethylsilylamines to hydrolysis in the present systems was established by partial conversion of L^1H into *o*-methoxyaniline on exposure to air. Whilst a mechanism involving reduction of the aryl ether by ytterbium metal (analogous to alkali metal cleavage of ethers)[29] may also be plausible, it would seem less likely since, under similar conditions, we have previously utilised methoxy-substituted aryloxide ligands in the presence of Yb metal without detection of ether cleavage.[30]

We have also prepared the thermally unstable divalent ytterbium complex $[Yb(L^1)_2(thf)_2]$ (**3**), by a ligand exchange reaction of $[Yb\{N(SiMe_3)_2\}_2(thf)_2]$[17] with L^1H in toluene at −78 °C (Equation 2).

$$Yb\{N(SiMe_3)_2\}_2 + 2L^1H \longrightarrow Yb(L^1)_2 + HN(SiMe_3)_2 \quad (2)$$

The divalent complex **3** was characterised by spectroscopic methods and a single crystal structure determination. Satisfactory elemental analyses were not obtained, even for single crystals, presumably due to the instability of the complex, but the ^1H NMR spectrum is consistent with the proposed composition. The structure of **3** (Figure 3), determined at 123 K, shows a monomeric complex with the ytterbium atom situated on a twofold axis and surrounded



Scheme 1

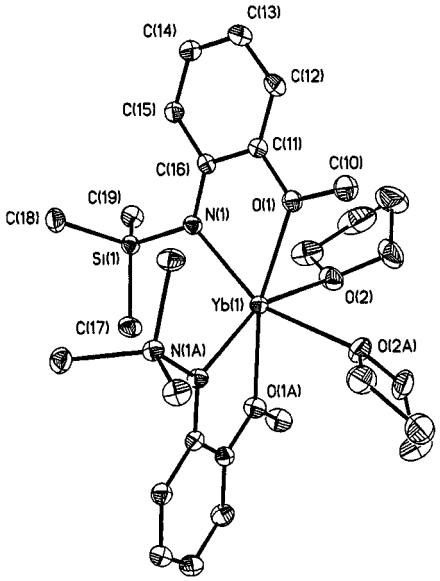


Figure 3. ORTEP view of $[Yb(L^1)_2(thf)_2]$ **(3)** drawn with 30% thermal ellipsoids; hydrogen atoms have been omitted for clarity; selected bond lengths (Å) and angles (°): Yb(1)−O(1) 2.458(2), Yb(1)−O(2) 2.494(2); Yb(1)−N(1) 2.386(2), N(1A)−Yb(1)−N(1) 108.81(12), N(1A)−Yb(1)−O(1) 121.79(8), N(1)−Yb(1)−O(1) 67.71(8), N(1)−Yb(1)−O(1A) 121.79(8), O(1)−Yb(1)−O(1A) 165.43(11), N(1A)−Yb(1)−O(2) 154.33(9), N(1)−Yb(1)−O(2) 89.45(9), O(1)−Yb(1)−O(2) 81.36(9), O(1A)−Yb(1)−O(2) 87.48(8), N(1A)−Yb(1)−O(2A) 89.48(8), O(1A)−Yb(1)−O(2A) 81.35(9), O(2)−Yb(1)−O(2A) 80.01(14); symmetry transformation: −x + 1, y, −z + 3/2

by two chelating L^1 ligands and two *cis* thf molecules with an irregular six-coordinate geometry. The orientation of the L^1 ligands is similar to that found in **1** above, with comparable *transoid* O(ether)−Yb−O(ether) and *cisoid* N−Yb−N angles (Figure 3). The Yb−N distance of **3** is comparable with or shorter than those of $[Yb(cbz)_2(thf)_2(dme)]$ [2.43(3), 2.45(2) Å][30] and **3** has a similar N−Yb−N angle to that of the unidentate carbazolyl ligands (107.3(7) °).[31] The Yb−O(thf) distance is longer than <Yb−O(thf)> of the six coordinate complex $[Yb\{PhC(NSiMe_3)_2\}_2(thf)_2]$ (2.415 Å)[32] which has *trans* thf ligands since each thf oxygen of **3** is *transoid* to an amide nitrogen. Further, the *cis* thf coordination geometry in **3** is similar to that of $[Yb(cbz)_2(thf)_2(dme)]$ [Yb−O(thf) 2.41(2), 2.48(2) Å; O(thf)−Yb−O(thf) 87.6(6) °].[31] It is noteworthy that there are only a few examples of bidentate, ether supported, amide ligands attached to a divalent lanthanoid, e.g. deprotonated 4,13-diaza-18-crown-6[33] and $Me_2Si(O\textit{t}\text{-}Bu)(N\textit{t}Bu)$.[23]

Compounds **1** and **2** are unique examples of the products of O−C(Ar) bond activation by a lanthanoid(II) centre. The ligands L^1 and L^2 also show the ability to stabilise heteroleptic lanthanoid(III) complexes with sterically undemanding co-ligands e.g. OMe, OPh.

Experimental Section

All reactions were carried out under dry nitrogen using dry box and standard Schlenk techniques. Solvents were dried by distillation from sodium wire/benzophenone. IR data (4000−650 cm^{-1}) were recorded for Nujol mulls sandwiched between NaCl plates with a Perkin−Elmer 1600 FTIR spectrometer. NMR spectra were obtained with a Bruker AC 300 MHz (^{1}H) spectrometer. The ytterbium(III) complexes gave unresolvable, uninterpretable, broadened spectra. Mass spectra were recorded with a VG Trio-1 GC mass spectrometer. Each listed *m*/*z* value for Yb-containing ions is the most intense peak of a cluster pattern in good agreement with the calculated pattern. GC-MS measurements were carried out using helium as a carrier gas and run on a Hewlett-Packard 5890A instrument interfaced to a VG Trio-1 GC mass spectrometer using a XTI-5 column (30m, 0.32 mm id) (bonded 5% phenyl − 95% dimethylpolysiloxane). The temperature program started at 50 °C (2 min) and then was increased by 10 °C/min to 280 °C. Retention times are measured in minutes from injection. Elemental analyses (C,H,N) were determined by the Campbell Microanalytical Service, University of Otago, New Zealand. Ytterbium analyses of digested samples were by complexiometric titration with $[Na_2EDTA]$.[1,34] $[Yb\{N(SiMe_3)_2\}_2(thf)_2]$ was prepared according to a reported procedure.[17] Commercial $HgPh_2$ (Aldrich) and lanthanoid powders (Rhône-Poulenc) were used as received.

[L^1H]: To a stirred solution of *o*-methoxyaniline (18 mL, 0.16 mol) in ether (100mL) at 0 °C was slowly added *n*BuLi (100 mL, 0.16 mol). After complete addition a white solid was obtained which was stirred and warmed to room temperature (ca. 1 h). Following cooling to 0 °C, Me_3SiCl (18.5 mL, 0.16 mol) was slowly added and the reaction mixture was allowed to warm to room temperature (ca. 1 h). The solvent volume was then reduced in vacuo until a residual oil remained which was vacuum distilled and upon cooling formed a colourless moisture-sensitive (see below) crystalline solid (26.7 g, 85%). − m.p. 25−27 °C − IR: $\tilde{\nu}$ = 3401 vs, 3043 s, 2956 vs, 2901 s, 2884 s, 1599 vs, 1504 vs, 1460 s, 1446 s, 1386 vs, 1322 vs, 1289 vs, 1238 vs, 1215 vs, 1174 s, 1113 vs, 1050 s, 1031 vs, 902 vs, 842 vs, 776 s, 735 vs, 689 s, 620 w, 590 w cm^{-1}. − MS: *m*/*z* (%) = 195 (80) [M^+], 180 (50) [$(L^1)^+$ − Me], 165 (100) [$(L^1)^+$ − 2Me], 150 (60) [$(L^1)^+$ − 3Me], 135 (45) [$C_6H_5ONSi^+$], 108 (19) [$C_6H_4OMe^+$], 73 (75) [$SiMe_3^+$], 58 [$SiMe_2^+$]. − ^{1}H NMR (300 MHz, C_6D_6, 298 K): δ = 0.16 [s, 9 H, $Si(CH_3)_3$], 3.31 [s, 3 H, OCH_3], 4.26 [br s, 1 H, N*H*], 6.57 [dd, ^3J = 7.4 Hz, ^4J = 1.1 Hz, 1 H, H-6], 6.74 [ddd, 1 H, H-5], 6.88 [m, 2 H, H-3, H-4]. − $C_{10}H_{17}NOSi$, (195.34): calcd. C 61.49, H 8.77, N 7.17; found C 61.66, H 8.89, N 7.29.

A sample of L^1H was exposed to air for 5 h, diluted with $CHCl_3$, and analysed by GC-MS: R_t (rel. int.) = 9.73 (100), *m*/*z* (%) = 123

(90) [$CH_3OC_6H_4NH_2^+$]; R_t = 12.51 (25), *m/z* (%) = 195 (20) [L^1H^+]; no $SiMe_3$-containing decomposition products, e.g. Me_3SiOH, were observed.

[L^2H]: As for L^1H above, 16.9 mL of a solution of *n*BuLi (1.6 M in hexanes) was added dropwise to a stirred solution of *o*-phenoxyaniline (5 g, 27 mmol) in ether (50 mL) at 0 °C. After complete addition a white solid was obtained which was stirred and warmed to room temperature (ca. 1 h) and Me_3SiCl (3.5 mL, 27 mmol) was slowly added. The reaction mixture was stirred for another 5 h. The reaction solution was decanted from the LiCl formed and the solvent volume was then reduced in vacuo until a residual oil remained. This was vacuum distilled and upon cooling formed a colourless moisture-sensitive crystalline solid (5.3 g, 76%). − m.p. 33−35 °C − IR: $\tilde{\nu}$ = 3401 vs, 1606 vs, 1589 s, 1583 s, 1499 s, 1307 vs, 1253 vs, 1240 vs, 1217 s, 1161 s, 1099 vs, 1072 s, 1038 s, 912 vs, 841 s, 750 vs, 689 vs. cm^{-1}. − MS: *m/z* (%) = 257 (60) [M^+], 242 (61) [$(L^2)^+ - Me$], 226 (15) [$(L^2)^+ - Me_2H$], 211 (5) [$(L^2)^+ - Me_3H$], 165 (100) [$OC_6H_4NHSiMe_2^+$], 150 (40) [$C_6H_4ONHSiMe^+$], 135 (30) [$C_6H_4OSiNH^+$], 73 (35) [$SiMe_3^+$], 58 (10) [$SiMe_2^+$]. − ^{1}H NMR (300 MHz, C_6D_6, 298 K): δ = 0.07 [s, 9 H, $Si(CH_3)_3$], 4.14 [br s, 1 H, NH], 6.57−6.63 [ddd, 1 H, H-4], 6.76−6.80 [tt, 1 H, H-5], 6.82−6.88 [dd, 1 H, H-3], 6.90−7.02 [m, 6 H, H-6, H-2′,H-3′,H-4′,H-5′,H-6′] − $C_{15}H_{19}NOSi$ (257.41): calcd. C 69.99, H 7.44, N 5.44; found C 69.98, H 7.57, N 5.60.

[$Yb(L^1)_2(\mu\text{-}OMe)]_2$ (1): Method 1. A mixture of ytterbium powder (0.69 g, 4.0 mmol), $HgPh_2$ (0.71 g, 2.0 mmol) and L^1H (0.82 g, 4.0 mmol) in thf (60 mL) was stirred and heated at 60 °C for 24 h. Evaporation to dryness of the filtered reaction mixture gave a red oil. Treatment of the residue with dme (20 mL), evaporation to dryness, and then treatment with hexane (15 mL) afforded red/orange crystals of **1** on standing (0.45 g, 19%). − IR (Nujol): $\tilde{\nu}$ = 1590 vs, 1560 vs, 1314 w, 1287 s, 1242 s, 1204 vs, 1160 vs, 1115 vs, 1050 vs, 1033 vs, 1005 vs, 916 br s, 843 s, 832 s, 782 vs, 768 vs, 723 s, 670 s, 642 vs, 596 vs cm^{-1}. − Vis/near IR (dme): λ_{max} (ε) = 431 (304), 911 (22), 978 (63) nm (dm^3mol^{-1}). − MS: *m/z* (%) = 990 (<1) [$M^+ - L^1$], 368 (<1) [$(YbL^1)^+$]. − $C_{42}H_{70}N_4O_6Si_4Yb_2$ (1185.47): calcd. C 42.55, H 5.95, N 4.73; found C 42.55, H 5.68, N 4.91.

Method 2: From a similar reaction [with Yb (0.30 g, 1.7 mmol), $HgPh_2$ (0.35 g, 1.0 mmol) and L^1H (0.41 g, 2.0 mmol)], the resulting red oil was treated with diethyl ether instead of dme. Evaporation and recrystallisation of the residue from hexane (20 mL) gave **1** (0.22 g, 23%). The spectroscopic and X-ray properties were identical with those of the product from Method 1.

[$Yb(L^2)_2(OPh)(thf)$] (2): A mixture of ytterbium powder (0.17 g, 1.0 mmol), $HgPh_2$ (0.35 g, 1.0 mmol) and L^2H (0.51 g, 2.0 mmol) in thf (40 mL) was stirred and heated at 60 °C for 24 h. The resulting mixture was filtered and the dark red filtrate evaporated to dryness. Recrystallisation from toluene (20 mL) and standing overnight gave orange crystals (0.18 g, 21%). − IR (Nujol): $\tilde{\nu}$ = 1718 w, 1621 s, 1588 vs, 1554 s, 1307 vs, 1288 s, 1241 s, 1190 vs, 1158 vs, 1101 vs, 1070 vs, 1045 vs, 863 m, 830 br m, 807 m, 786 m, 756 s, 736 s, 706 s, 695 vs, 630 vs, 602 s, 594 s cm^{-1}. − Vis/near IR (dme): λ_{max} (ε) = 416 (401), 919 (31), 982 (73) nm (dm^3mol^{-1}). − MS: *m/z* (%) = 779 (<1) [$M^+ - thf$], 686 (<1) [$(YbL_2^2)^+$], 613 (<1) [$(YbL_2^2)^+ - SiMe_3$], 430 (<1) [$(YbL^2)^+$]. − $C_{40}H_{49}N_2O_4Si_2Yb$ (851.03): calcd. C 56.45, H 5.80, N 3.29; found C 56.41, H 5.77, N 3.59. The reaction filtrate of **2** was hydrolysed with H_2O (15 mL) and this mixture extracted with $CHCl_3$ (30 mL) which was then reduced under vacuum to 5 mL and analysed by GC-MS. − GC-MS: R_t (rel. int.) = 2.62 (80), *m/z* (%) = 93 (10) [$C_6H_5NH_2^+$]; R_t = 7.12 (5), *m/z* (%) = 94 (100) [$C_6H_5OH^+$]; R_t = 17.35 (95), *m/z* (%) = 185 (100) [$C_6H_5OC_6H_4NH_2^+$].

[$Yb(L^1)_2(thf)_2$] (3): A toluene solution (5 mL) of L^1H (0.31 g, 2.0 mmol) was added to a toluene solution (40 mL) of [$Yb(N(SiMe_3)_3)_2(thf)_2$] (0.65 g, 1.0 mmol) at −78 °C. The reaction mixture was warmed to −20 °C and dark red crystals formed overnight (0.54 g, 76%). − IR (Nujol): $\tilde{\nu}$ = 1584 vs, 1552 vs, 1320 sh s, 1296 br s, 1251 s, 1203 vs, 1162 vs, 1116 vs, 1054 vs, 1010 vs, 934 br s, 831 br s, 765 s, 723 s, 668 s, 617 vs, 593 vs cm^{-1}. − Vis/near IR (dme): λ_{max} (ε) = 487 sh (201) nm (dm^3mol^{-1}). − ^{1}H NMR (300 MHz, C_6D_6, 298 K): δ = 0.44 [s, 18 H, $Si(CH_3)_3$], 1.19 [br s, 8 H, β-*H* (thf)], 3.35 [s, 8 H, α-*H* (thf)], 3.47 [s, 6 H, OCH_3], 6.54−6.59 [m (br), 4 H, Ar], 7.03 [s (br), 4 H, Ar]. − $C_{28}H_{48}N_2O_4Si_2Yb$ (705.90): calcd. C 47.64, H 6.85, N 3.97, Yb, 24.51; found C 41.75, H 5.90, N 4.63, Yb, 25.59. A sample of diamagnetic **3** in

Table 1. Crystal data and refinement parameters

Compound	L^1H[a]	**1**	**2**	**3**
Formula	$C_{10}H_{17}NOSi$	$C_{42}H_{70}N_4O_6Si_4Yb_2$	$C_{40}H_{49}N_2O_4Si_2Yb$	$C_{28}H_{48}N_2O_4Si_2Yb$
M	195.34	1185.47	851.03	705.90
Crystal system	tetragonal	monoclinic	monoclinic	monoclinic
Space group	*P*4/*n*	*C*2/*c*	*P*2(1)/n	C2/*c*
a (Å)	25.5964(5)	24.1340(4)	24.3109(3)	15.5139(2)
b (Å)		19.1294(3)	15.0605(2)	11.3411(2)
c (Å)	7.0684(2)	23.6252(4)	24.5560(2)	19.2898(3)
β (°)		112.150(1)	118.833(1)	112.368(1)
V (Å^3)	4631.0(13)	10102.1(3)	7876(3)	3138.6(11)
Z	16	4	8	4
ρ_{calcd} (g.cm^{-3})	1.121	1.559	1.435	1.494
μ (cm^{-1})	1.69	38.20	24.76	30.89
F(000)	1696	4752	3464	1440
$2\theta_{max}$ (°)	55.8	60.06	55.8	60.04
N_{total}	18145	35621	97744	22197
N, N_o	5497, 4209	14634, 12012	17146, 12246	4212, 3947
$A^*_{min, max}$		0.524, 0.714	0.754, 0.784	0.906, 1.11
R, R_w [$I>2\sigma(I)$]	0.039, 0.090	0.028, 0.067	0.054, 0.122	0.029, 0.083
R, R_w (all data)	0.060, 0.098	0.044, 0.089	0.100, 0.165	0.033, 0.084
Goodness of Fit	1.037	1.151	1.118	1.039

[a] The asymmetric unit comprises two independent, similar, well separated (no H-bonding), molecules. Bond lengths and angles were as expected,[36] and the details are available in the supplementary data.

C_6D_6 was shown to convert into a paramagnetic species upon heating at 60 °C for 24h by ^1H NMR spectroscopy.

To **3** (0.47 g, 0.66 mmol) in hexane (30 mL) was added L^1H (0.13 g, 0.66 mmol). The resulting mixture was heated to 60 °C for 12h. The reaction mixture was then allowed to stand for 3 weeks at room temperature and the solvent volume was reduced to 3 mL under vacuum giving crystals of **1** which was identified by a unit cell determination and an IR spectrum.

X-ray Crystal Structure Analysis: Crystals were mounted under viscous oil onto a glass fibre. Low temperature (≈123 K) data were collected on an Enraf−Nonius CCD area-detector diffractometer (Mo-K_α radiation, λ = 0.71073 Å, frames comprised 1.0° increments in φ and ω yielding a sphere of data) using proprietary software (Nonius B.V., 1998). Each data set was merged (R_{int} as quoted) to N unique reflections and the structures were solved by conventional methods and refined, with anisotropic thermal parameter forms for the non-hydrogen atoms, by full-matrix least-squares on all F^2 data using the SHELX 97 software package.[35] Hydrogen atoms were included in calculated positions and allowed to ride on the parent carbon atom with isotropic thermal parameters. For **1**, the methoxide carbon atoms lie on crystallographic twofold axes and therefore two sets of hydrogens atoms, each with occupancies of 0.5, were placed on each carbon, disordered about the axes. Crystal and refinement data are listed in Table 1.

Crystallographic data (excluding structure factors) for the structures reported in this paper have been deposited with the Cambridge Crystallographic Data Centre as supplementary publication nos. CCDC-146332 (L^1H), -143939 **(1)**, -143940 **(2)**, -143941 **(3)**. Copies of the data can be obtained free of charge on application to CCDC, 12 Union Road, Cambridge CB2 1EZ, UK [Fax: (internat.) + 44-1223/336-033; E-mail: deposit@ccdc.cam.ac.uk].

Acknowledgments

We acknowledge the financial support of the Australian Research Council and an Australian Postgraduate Award to N. M. S.

[1] G. B. Deacon, T. Feng, C. M. Forsyth, A. Gitlits, D. C. R. Hockless, Q. Shen, B. W. Skelton, A. H. White, *J. Chem. Soc., Dalton Trans.* **2000**, 961−966.
[2] H. B Kagan, J. L. Namy, *Handbook on the Physics and Chemistry of Rare Earths,* (Eds.: K. A. Gschneidner, L. Eyring), North-Holland Amsterdam,**1984**, vol. 6, chapter 50.
[3] G. A. Molander, C. R. Harris, *Chem. Rev.* **1996**, *96*, 307−338; G. A. Molander, *Chem. Rev.* **1992**, *92*, 29−68.
[4] T. Imamoto, *Lanthanides in Organic Synthesis,* Academic Press, **1994**.
[5] W. Clegg, C. Eaborn, K. Izod, P. O′Shaughnessy, J. D. Smith, *Angew. Chem. Int. Ed. Engl.* **1997**, *36*, 2815−2817.
[6] Z. Hou, A. Fujita, Y. Zhang, T. Miyano, H. Yamazaki, Y. Wakatsuki, *J. Am. Chem. Soc.* **1998**, *120*, 754−766.
[7] W. J. Evans, C. A. Seibel, J. W. Ziller, *Inorg. Chem.* **1998**, *37*, 770−776.
[8] W. J. Evans, J. W. Grate, I. Bloom, W. E. Hunter, J. L. Atwood, *J. Am. Chem. Soc.* **1985**, *107*, 405−409.
[9] J. R. van den Hende, P. A. Hitchcock, S. A. Holmes, M. F. Lappert, W.-P. Leung, T. C. W. Mak, S. Prashar, *J. Chem. Soc., Dalton Trans.* **1995**, 1427− 1433.
[10] C. Eaborn, P. B. Hitchcock, K. Izod, Z.-G. Lu. J. D. Smith, *Organometallics* **1996**, *15*, 4783−4790.
[11] D. J. Duncalf, P. B. Hitchcock, G. A. Lawless, *Chem. Commun.* **1996**, 269− 271.
[12] Yu. K. Gun′ko, P. B. Hitchcock, M. F. Lappert, *J. Organomet. Chem.* **1995**, *499*, 213−219.
[13] M. C. Cassani, M. F. Lappert, F. Laschi, *Chem. Commun.* **1997**, 1563−1564.
[14] M. C. Cassani, D. J Duncalf, M. F. Lappert, *J. Am. Chem. Soc.* **1998**, *120*, 12958−12959.
[15] F. T. Edelmann, in *Comprehensive Organometallic Chemistry II*, (Eds.: G. Wilkinson, F. G. A. Stone, E. W. Abel), Pergamon, Oxford, **1995**, vol. 3, chapter 2.
[16] M. N. Bochkarev, L. N. Zacharov, G. S. Kalinina, *Organoderivatives of the Rare Earth Elements*, Kluwer Academic, Dordrecht, **1995**.
[17] G. B. Deacon, G. D. Fallon, C. M. Forsyth, H. Schumann, R. Weimann, *Chem. Ber.* **1997**, *130*, 409−415.
[18] F. Calderazzo, R. Pappalardo, S. Losi, *J. Inorg. Nucl. Chem.*, **1966**, *28*, 987−999.
[19] G. B. Deacon, T. Feng, B. W. Skelton, A. H. White, *Aust. J. Chem.,* **1995**, *48*, 741−756.
[20] G. B. Deacon, C. M. Forsyth, P. C. Junk, B. W. Skelton, A. H. White, *J. Chem. Soc., Dalton Trans.* **1998**, 1381−1387.
[21] G. B. Deacon, C. M. Forsyth, B. M. Gatehouse, P. A. White, *Aust. J. Chem*., **1990**, *43*, 795−806.
[22] W. J. Evans, G. W. Rabe, J. W. Ziller, *Organometallics* **1994**, *13*, 1641−1645.
[23] A. Recknagel, A. Steiner, S. Brooker, D. Stalke, F. T. Edelmann, *J. Organomet. Chem.* **1991**, *415*, 315−326.
[24] Y. Yao, Q. Shen, J. Sun, F. Xue, *Acta Crystallogr., Sect. C*, **1998**, *54*, 625−627.
[25] Y. Yao, Q. Shen, J. Sun, *Polyhedron*, **1998**, *17*, 519−522.
[26] R. C. Mehrotra, A. Singh, U. M. Tripathi, *Chem. Rev.* **1991**, *91*, 1287−1303.
[27] J. Marcalo, A. P. De Matos, *Polyhedron*, **1989**, *8*, 2431−2437.
[28] G. B. Deacon, P. I. MacKinnon, T. D. Tuong, *Aust. J. Chem.*, **1983**, *36*, 43−53.
[29] A. Maercker, *Angew. Chem. Int. Ed. Engl.* **1987**, *26*, 972−989.
[30] S. C. Harris, *PhD Thesis*, Monash University, **1999**; G. Zelesny, *Dr der Math.-Natur. Fakultat Thesis*, Universität zu Köln, **1998**.
[31] C. T. Abrahams, G. B. Deacon, B. M. Gatehouse, G. N. Ward, *Acta Crystallogr., Sect. C*, **1994**, *50*, 504−507.
[32] M. Wedler, M. Notlemeyer, U. Pieper, H.-G. Schmidt, D. Stalke, F. T. Edelmann, *Angew. Chem. Int. Ed. Engl.* **1990**, *29*, 894−896.
[33] L. Lee, D. J. Berg, G. W. Bushnell, *Inorg. Chem.* **1994**, *33*, 5302−5308.
[34] J. L. Atwood, W. E. Hunter, A. L. Wayda, W. J. Evans, *Inorg. Chem.* **1981**, *20*, 4115−4118.
[35] G. M. Sheldrick, *SHELX97*, *Program for Crystal Structure Determination,* Universität Göttingen, **1997.**
[36] *Interatomic Distances*, Special Publication II, The Chemical Society, London, **1958**.

Received May 3, 2000
[I00174]

Thermally Robust Metal Coordination Polymers: The Cobalt, Nickel, and Zinc Pyrimidin-2-olate Derivatives

Norberto Masciocchi,*[a,b] G. Attilio Ardizzoia,*[b,c] Girolamo LaMonica,[b,c] Angelo Maspero,[b,c] and Angelo Sironi[a]

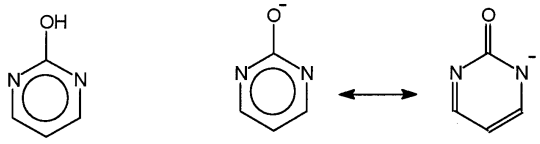
Keywords: X-ray powder diffraction / Coordination chemistry / Nitrogen heterocycles / Polymers

A number of coordination polymers of the pymo ligand (Hpymo = 2-hydroxypyrimidine) have been prepared and fully characterized by chemical, spectroscopic, and thermal analyses. Their complete crystal structures have been solved ab initio from laboratory X-ray powder diffraction data and ultimately refined by the Rietveld method. The $M(pymo)_2$ species (M = Co, Ni, Zn) consist of structurally related three-dimensional frameworks of very high thermal stability (decomposing under N_2 only at $T > 550$ °C), with the metal atoms, linked by μ_2-η^1-η^1 (*N*;*N*′) (Co, Zn) or μ_2-η^2-η^1 (*N*,*O*;*N*′) bridges, about 5.4–5.7 Å apart. The hydrated species $Ni(pymo)_2(H_2O)_{2.5}$ is based on a two-dimensional array of $Ni(pymo)_2$ stoichiometry, containing both coordinated and clathrated water molecules, and can be selectively transformed into $Ni(pymo)_2$ by thermal treatment, through an amorphous intermediate, recrystallizing at $T > 315$ °C. In contrast, one dimensional chains are found in the three hydrazine adducts, $M(pymo)_2(N_2H_4)_2$, which show unique bis(μ_2-hydrazine) bridges (M···M ca. 4.0 Å) and terminally *O*-bonded pymo ligands.

Introduction

Coordination polymers containing metal ions in their backbones have been widely investigated, and found to possess a variety of interesting electrical, electrochemical and optical properties.[1] In particular, metal polymers containing azoles and azolates have very recently shown remarkable magnetic,[2] anticorrosion,[3] and even antimicrobial[4] activity. In order to design stable, coordinatively saturated systems, a number of metal ions have been therefore treated with polydentate ligands, either neutral (such as 4,4′-bipyridine or longer spacers[5]) or negatively charged. In the latter group, pyrazolates[6,7] and imidazolates[8] have been found to afford binary species which could be structurally characterized only by X-ray powder diffraction (XRPD) methods.

Recently, we have shifted our interests to the less known pyrimidin-2-olate (pymo) ligand (Scheme 1), which afforded, with silver(I) ions, one-dimensional (hydrated) polymeric species[9] and cyclic hexamers,[10] and, with copper(I) ions, a surprising crystal phase containing, simultaneously, hexamers and infinite helical polymers.[11] In our search for polymers of higher dimensionality and higher thermal stability, we focused on cobalt(II), nickel(II), and zinc(II) ions, i.e. on metals with different electronic requirements, larger coordination numbers and lower redox propensities than copper and silver.



Hpymo pymo

Scheme 1

Therefore, in this paper we report on the syntheses, thermal, and spectroscopic characterization of a number of polymeric species of the M/pymo type (outlined below), which have been structurally characterized by the newly emerging ab initio XRPD technique,[12] pioneered by us in the field of coordination chemistry, from conventional laboratory equipment.[13] The following numbering scheme has been used throughout the paper: **1a** = $Co(pymo)_2$; **1b** = $Ni(pymo)_2$; **1c** = $Zn(pymo)_2$; **2b** = $Ni(pymo)_2(H_2O)_{2.5}$; **3a** = $Co(pymo)_2(N_2H_4)_2$; **3b** = $Ni(pymo)_2(N_2H_4)_2$; **3c** = $Zn(pymo)_2(N_2H_4)_2$.

Results

Syntheses

The reaction of 2-hydroxy-pyrimidine with cobalt, nickel, and zinc dichlorides in water, in the presence of a base such as NH_3, affords, in high yield, the corresponding metal pyrimidinolate derivatives $Co(pymo)_2$, **1a**, $Ni(pymo)_2(H_2O)_{2.5}$,

[a] Dipartimento di Chimica Strutturale e Stereochimica Inorganica e Centro CNR, Università di Milano, Via Venezian 21, 20133 Milano, Italy
Fax: (internat.) +39-02/7063-5288,
E-mail: norbert@csmtbo.mi.cnr.it
[b] Dipartimento di Scienze Chimiche, Fisiche e Matematiche, Università dell'Insubria, via Valleggio 11, 22100 Como, Italy
[c] Dipartimento di Chimica Inorganica, Metallorganica ed Analitica e Centro CNR, Università di Milano, Via Venezian 21, 20133 Milano, Italy

 © WILEY-VCH Verlag GmbH, D-69451 Weinheim, 2000 1434–1948/00/1212–2507 $ 17.50+.50/0

2b, and $Zn(pymo)_2$, **1c**. The water content in complex **2b** has been verified by TGA analyses, which indicated that all the water molecules are lost in a one-step process at relatively low temperature (200 °C, vide infra) giving rise to the anhydrous species $Ni(pymo)_2$, **1b**.

The synthesis of the hydrazine derivatives $M(pymo)_2(NH_2NH_2)_2$ (M = Ni, Co, Zn) originally derives from the failure in attempting the synthesis of cobalt(I) species by one electron reduction of cobalt(II) in the $Co(pymo)_2$ derivative **1a** with NH_2NH_2. The formation of the unexpected $Co(pymo)_2(NH_2NH_2)_2$ species, **3a**, prompted us to thoroughly investigate this complex and to verify if such a reaction could also occur for the nickel and zinc pyrimidin-2-olate derivatives. Consistently, all three species $M(pymo)_2$ easily react with NH_2NH_2 in acetonitrile, giving rise to derivatives of general formula $M(pymo)_2(NH_2NH_2)_2$ (M = Co, **3a**; Ni, **3b**; Zn, **3c**).

Crystal Structures of $Co(pymo)_2$ (1a) and $Zn(pymo)_2$ (1c)

The isomorphous crystals of **1a** and **1c** contain tetrahedrally coordinated metal(II) ions (lying on a −4 symmetry site, *a* in Wyckoff notation), which are linked to four nitrogen atoms of distinct pymo ligands [Co−N = 2.032(4) Å, Zn−N = 2.086(4) Å]. A schematic drawing of the crystal packing, viewed approximately down [001], is shown in Figure 1. As already observed in several group 11 derivatives, pymo ligands coordinate in the common *N,N′*-exobidentate mode (μ_2-η^1-η^1 coordination), bridging metal atoms which are 5.65 (Co) or 5.70 Å (Zn) apart.[14] In the crystals, all ligands lie about twofold axes (*d* in Wyckoff notation), passing through the C=O vector and parallel to *a* (and *b*).

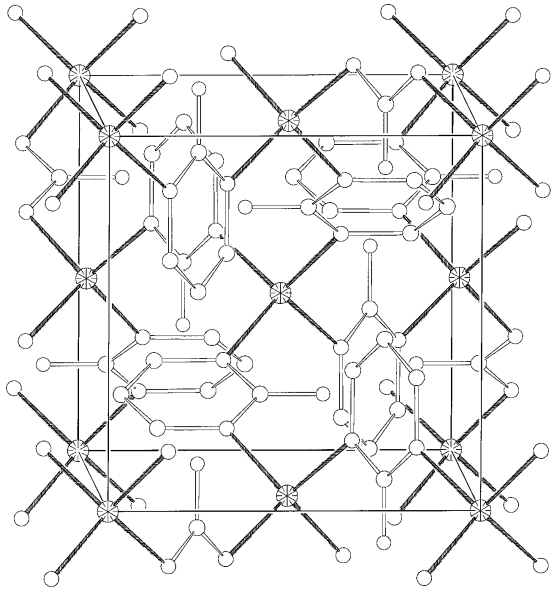


Figure 1. Crystal packing of species **1a**, viewed approximately down [001]; metal atoms are cross-hatched

Disregarding the actual shape of the ligands, the topology of the overall connectivity is far from unusual, since a non-interpenetrated diamond-like framework can be easily recognized. However, it is rather surprising that simple(r) metal diazolates, which contain tetrahedral ions and N,N′ exobidentate C_{2v} anionic heterocycles (i.e. ligands of similar steric, electronic, and symmetry requirements) do not afford the highly symmetric structure found for **1a**; indeed, up to eight crystallographically independent imidazolate (imz) ligands (average Co−N distance: 1.984 Å) are found in $Co(imz)_2$.[15] Similarly, cobalt and zinc pyrazolates (pz), where much shorter M···M contacts are present,[16] do not afford three-dimensional diamondoid structures, but, albeit maintaining tetrahedral coordination, only exist as linear chain (1-D) polymers. However, it must be noted that many of these species are prone to extended polymorphism [see for example Cu(pz),[6] Ag(pz),[6] $Cu(imz)_2$[17] and $Pt(pz)_2$[18]], and that the occurrence of one crystal phase cannot rule out the possibility of a different polymorph.

Crystal Structure of $Ni(pymo)_2$ (1b)

A schematic drawing of the crystal packing of **1b**, viewed down [001] is shown in Figure 2. Bearing in mind that a body-centered tetragonal cell can be always described by a F-centered tetragonal lattice with twice the volume, one can see that the structure of **1b**, in the observed *Fdd*2 space group (after axis relabelling) bears a proper subgroup relation to that of **1a**, (*I*-42*d*) and, therefore, suggests that **1b** can be obtained by removing a symmetry element (in this case, the −4 improper rotation) from the highly symmetric crystals of **1a**. Indeed, crystals of **1b** contain nickel(II) ions (lying on twofold axes, *a* in Wyckoff notation) connected to four distinct pymo ligands, with Ni−N values of 2.135(4) and 2.172(4) Å. The removal of the −4 symmetry element is here tentatively explained by the higher tendency of nickel(II), vs. cobalt(II), to hexacoordination,[19] which distorts the original tetrahedral geometry found in **1a** to a NiN_4 fragment of approximate saw-horse geometry [*trans* N−Ni−N value: 150.3(9)°], leaving two open coordination sites, now occupied by oxygen atoms of two already coordinated pymo ligands [Ni−O 2.288(6)Å]. Thus, while maintaining the overall (diamondoid) three-dimensional topology found in **1a**, pymo ligands are here found in the *new* μ_2-η^1-η^2 coordination mode, i.e. N,O chelating on one side, and purely N donor on the other; the Ni···Ni interatomic distance, bridged by such a tridentate pymo ligand, is only 5.46 Å. The overall coordination geometry of each nickel ion is, therefore, best described by *cis*-NiN_4O_2 pseudooctahedral fragments, their refined bond lengths and angles being reported in the caption of Figure 2. It is noteworthy that the coexistence of N and η^2-*N,O* coordination at the same metal has been previously found for the $[Cu(Hpymo)_4]^{2+}$ cation,[20] with the notable difference that, although maintaining crystallographically imposed C_2 symmetry, the oxygen atoms in the latter occupy *trans*, rather than *cis*, positions.

Crystal Structure of $Ni(pymo)_2(H_2O)_{2.5}$ (2b)

Crystals of **2b** contain octahedrally coordinated nickel(II) ions (lying on a crystallographic −1 site symmetry position, *e* in Wyckoff notation), bonded to four nitrogen atoms of four distinct pymo ligands and two mutually *trans* water

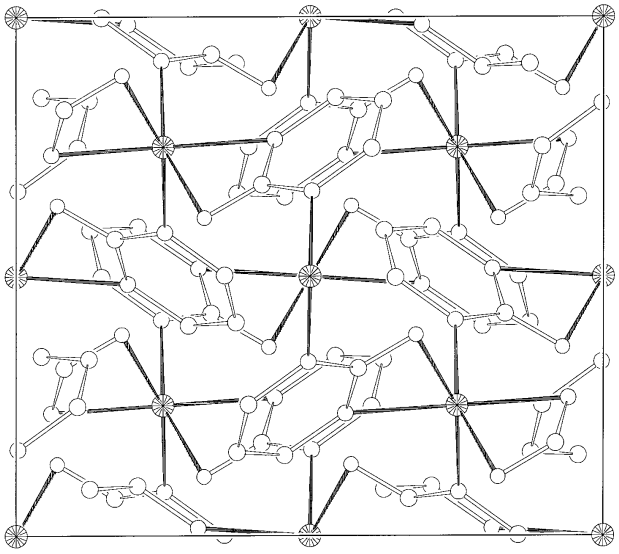


Figure 2. Crystal packing of species **1b**, viewed down [001]; metal atoms are cross-hatched

molecules. Additional water molecules, not involved in metal coordination [lying on *2m m* . (Wyckoff's *c*) positions] fill the cavities of the whole framework. Therefore, species **2b** is best represented by the $Ni(pymo)_2(H_2O)_2 \cdot {}^1/_2H_2O$ formulation. A schematic drawing of the crystal packing, viewed approximately down [1−49] is shown in Figure 3. As depicted therein, the pymo ligands act in the *N*,*N*′-exobidentate mode, connecting Ni ions which are 6.33 Å apart (inter alia, the largest distance ever found within such a class of compounds).

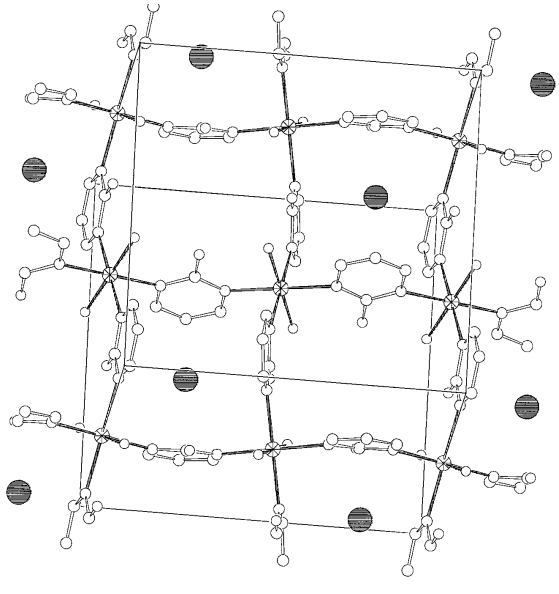


Figure 3. Crystal packing of species **2b**, viewed approximately down [1−49]; metal atoms are cross-hatched, while non-coordinated water molecule are depicted by solid black circles; hydrogen bonds are present, with O···O distances of 2.506(5) and 2.576(3) Å

Neglecting terminally bonded and non-framework water molecules, the overall topology of **2b** can be described by a stack (along *c*) of *two-dimensional* arrays of $Ni(pymo)_2$ squares, thus intrinsically different from the $Co(pymo)_2$ 3-D array described above for **1a**. Interestingly, loosely H-bonded water molecules (O···O >3.0 Å) occupy the cavities of the framework, while much stronger (intralayer, thus "intramolecular") C=O···H−O−H bonds (O···O 2.51−2.58 Å), connecting the pymo oxygens to the coordinated water molecule, are found [and reflected by the significant lowering of the ν(CO) absorption frequency, vide infra].

Crystal Structures of $Co(pymo)_2(N_2H_4)_2$ (3a), $Ni(pymo)_2(N_2H_4)_2$ (3b), and $Zn(pymo)_2(N_2H_4)_2$ (3c)

Species **3a**, **3b**, and **3c** are strictly isomorphous and contain octahedrally coordinated metal ions. A schematic drawing of the crystal packing, viewed approximately down [108] is shown in Figure 4. Each metal(II) ion lies on a crystallographic *2/m* position (*a* in Wyckoff notation) and is bonded to two (mutually *trans*) oxygen atoms of *mono*dentate (μ_1-η^1) pymo ligands (slightly off the mirror plane, see Experimental Section) and, equatorially, to four nitrogen atoms of four distinct hydrazine molecules, which bridge metal atoms separated by ca. 4.0 Å (the *b* vector). It is notable that such M···M distances correlate well with the shrinking of the apparent ionic radii on passing from cobalt(II) to zinc(II) ions.

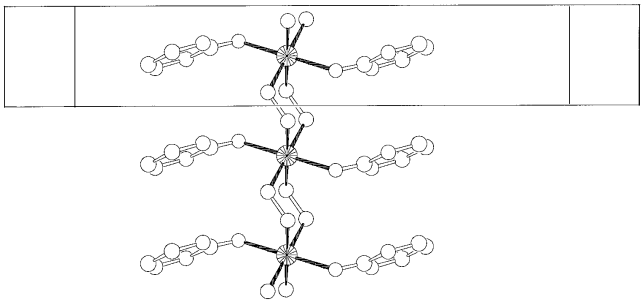


Figure 4. Crystal packing of species **3b**, viewed approximately down [108]; metal atoms are cross-hatched; relevant bond lengths [Å] and angles [°]: Ni−N 2.105(6)−2.111(5), Ni−O 2.208(25); N−Ni−N 89.7(6)−90.3(6), N−Ni−O 89.7(11)−90.3(8)

With reference to Figure 4, one can envisage the existence of linear chains of metal(II) atoms, doubly bridged by μ_2-N_2H_4 molecules (in the very same manner as the pyrazolate anion does) and bearing axial monodentate ligands: such a structural pattern is well-known in coordination chemistry, and accounts for a large portion of the known MX_2L_2 structures, where M = an octahedrally coordinated dication, X = a bridging anionic ligand (halide, hydroxide, azide) and L = a nitrogen donor neutral ligand.[21]

The most interesting structural features of these species are the monodentate nature of the pymo ligand and the unexpected poly(hydrazine) bridges, which, apparently successfully compete with the propensity of pymo to act as a strong *exo*-bidentate ligand. While the first of these anomalies can be partially understood upon analyzing in detail the environment of the "swinging" end of pymo, for which a number of (weak) N···H−N(hydrazine) bonds is detected (see caption to Figure 4), the formation (and stability) of the μ_2-N_2H_4 bridges need more subtle comments.

Hydrazine is known to afford μ_2-bridges, mostly with second and third row transition metals (Ru, Mo, W, Pt), the only structurally characterized species containing a lighter metal being for Fe^{III}.[22] Among the known species, a *transoid* form (ideal value of the M−N−N−M torsion angle of 180°) is by far the most commonly observed one. On the other hand, *cis*-M−N−N−M forms are likely to be disfavored by the presence of eclipsed H···H contacts, even if isosteric (and isoelectronic) peroxo fragments bridging octahedrally coordinated metal atoms at distances as low as 4.01 Å are known.[23] These observations, therefore, seem to suggest that there should not be anything special in the formation of a *staggered* M−N−N−M bridge, either *trans* or *gauche* (like in the present case, with a torsion angle near 77°). The peculiar feature in species **3abc** is, however, the presence of an unprecedented[24] bis-dihydrazine link, leading to six-membered M−N−N−M−N−N− *spiro*-rings with chair-like conformation.

Thermal Stability of Cobalt Derivatives

Powders of **1a** are rather stable and, if heated in a nitrogen atmosphere, only decompose at T > 500 °C, a strongly endothermic peak being observed in the DSC trace near 560 °C. This behaviour is clearly in good agreement with the three-dimensional nature of such coordination polymer, as well as with the negligible tendency of cobalt(II) to display solid-state redox chemistry. In contrast, the much poorer coordination strength of hydrazine speaks for a labile product: indeed, powders of **3a** lose N_2H_4 ($t_{1/2}$ a few hours at room temp.), and, surprisingly, quantitatively transform, in the solid, into polycrystalline **1a**. Note that, as discussed below, such transformation requires a dramatic change in the coordination mode of the pymo ligand with heavy shifts (several Å's) of the metal atom locations; nevertheless, it appears to occur without the formation of an (XRPD detectable) intermediate crystalline, or amorphous, material.

Thermal Stability of Nickel Derivatives

Powders of **2b** lose all water molecules upon heating to almost 200 °C, in a single, nonstructured event, affording a turquoise amorphous powder. Further heating promotes its crystallization (exothermic DSC peak with onset near 315 °C, ca. 26 kJ mol^{-1}), forming **1b** in a quantitative manner. Thus the loss of water leaves empty coordination sites and is not immediately accompanied by the 2-D to 3-D structural rearrangement (**2b** => **1b**) which requires extra energy. Interestingly, this transformation leads, from (originally) centrosymmetric crystals, to a conglomerate of enantiomorphic, acentric crystals. Obviously, additional cooling and heating cycles of powders of **1b** (in the 50−400 °C range), did not show any of the aforementioned features. Heating of **1b** at ca. 450 °C in vacuum promotes a *reversible* change of color (green to brown), which may be associated to the formation of tetrahedral nickel(II) ions by labilization of the Ni−O contacts, possibly leading to a tetragonal high-temperature crystal phase isomorphous to **1a** and **1c**, through an easy crystal-to-crystal phase transformation (vide infra).

Species **3b** is rather stable and can be stored under nitrogen indefinitely at room temperature. Contrasting the cobalt analogue, when heated for several hours at 150 °C, **3b** slowly transforms, with hydrazine loss, into a green amorphous material and *does not* form the binary species **1b**, which is, however, restored, as described above for **2b**, upon heating above 320 °C.

Thermal Stability of Zinc Derivatives

Very similarly to **1a**, and sharing the same crystal structure, species **1c**, upon heating, is rather stable and decomposes near 570 °C, a slightly higher temperature than **1a**. In contrast, species **3c** is rather labile and very rapidly loses N_2H_4 ($t_{1/2}$ < 15 min at room temp.) and, as observed for the cobalt analogue, transforms into polycrystalline **1c**. Consistently, this fast loss of hydrazine resulted in an

Table 1. Relevant structural features for compounds **1abc**, **2b**, and **3abc** (e.s.d.'s in parentheses)

Compound	**1a**	**1b**	**1c**	**2b**	**3a**	**3b**	**3c**
Species	$Co(pymo)_2$	$Ni(pymo)_2$	$Zn(pymo)_2$	$Ni(pymo)_2(H_2O)_{2.5}$	$Co(pymo)_2(N_2H_4)_2$	$Ni(pymo)_2(N_2H_4)_2$	$Zn(pymo)_2(N_2H_4)_2$
Site symmetry of M	−4	2	−4	−1	−1[a]	−1	−1
Site symmetry of pymo	2	1	2	*m*	1[a]	1	1
M···M [Å]	5.655	5.462	5.696	6.327	4.0558(2)	4.0070(3)	3.928(2)
M−N [Å]	2.032(4)	2.172(4) 2.135(4)	2.086(4)	2.137(6) 2.189(1)	n.a.[b]	2.105(6)[c] 2.111(5)[c]	n.a.[b]
M−O [Å]		2.288(6)		2.01(1)		2.208(25)	
O···O [Å]				2.506(5) 2.576(3)			
N−M−N [°]	107.2(1) 114.0(3)	150.3(9), *trans* 96.8(5)−109.8(2), *cis*	108.0(1) 112.5(2)			89.5(5) 90.5(5)	
Coordination mode of pymo	μ_2-η^1-η^1(*N*,*N'*)	μ_2-η^2-η^1[(*N*,*O*),*N'*)]	μ_2-η^1-η^1(*N*,*N'*)	μ_2-η^1-η^1(*N*,*N'*)	η^1(*O*)	η^1(*O*)	η^1 (O)
ν(CO) [cm^{-1}]	1630	1586	1633	1605		1223	
Color	pink (fuchsia)	green	white	turquoise	pale pink	pale violet	white

[a] For **3abc**, the site symmetry of an *ideally ordered* crystal phase is quoted (see *Experimental*). − [b] Structures not refined (isomorphous with **3b**). − [c] Subjected to restraints.

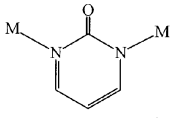
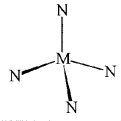
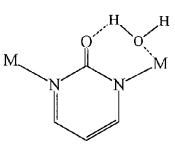
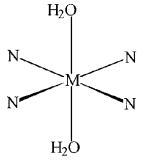
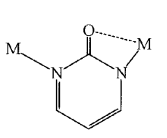
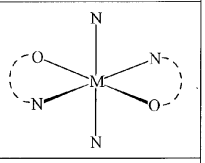
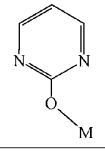
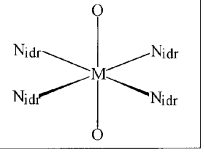
XRPD pattern of low(er) quality, for it shows a multiphase system (evolving with time), measured, in order to avoid complete decomposition, over a short time.

Infrared Spectroscopy

Infrared spectra of complexes **1abc**, **2b**, and **3abc** display the versatility of the coordination features of the pymo ligand. In particular, the position of the ν(CO) band of the lactamic form can be employed as a useful diagnostic tool in order to establish the coordination mode of the ligand (see Table 1).

Derivatives **1a** and **1c** show ν(CO) absorptions at relatively high wavenumbers (1630 and 1633 cm^{-1}, respectively), in agreement with the *N*,*N* coordination of the pyrimidin-2-olate ligand and the absence of any interaction between the exocyclic oxygen and the metal centers.[25] Complex **2b** exhibits such a ν(CO) absorption at 1605 cm^{-1}. The shift can be justified by the presence of strong hydrogen-bonds between coordinated water and the carbonyl moiety. Moreover, complex **2b** also shows two strong and broad absorptions centered at 2900 and 2250 cm^{-1}. These bands are often found in species possessing strong *intra-* or *inter*-molecular hydrogen bonds, e.g. in a large series of pyrazole/pyrazolate derivatives.[26] After removal of coordinated and clathrated water from **2b** (obtaining **1b)**, the aforementioned bands disappear and the ν(CO) absorption shifts at 1586 cm^{-1}, in agreement with the presence of the M···O=C interaction depicted above.

Given the poor stability at ambient conditions of species **3a** and **3c**, only the hydrazine adduct of the Ni(pymo)$_2$ species can give spectroscopic information about the coordination mode of pymo. Indeed, in **3b**, the aforementioned ν(C=O) bands near 1600 cm^{-1} are absent, while a strong absorption, not present in **1abc** or **2b**, is found at 1223 cm^{-1}, which can be attributed to the C−O stretching (of single-bond character) of the pymo ligand coordinating as a phenolate (vide supra).

METAL (M)	ENVIRONMENT AROUND THE METAL		
Co, (**1a**) Zn, (**1c**)	$M(N)_4$		
Ni, (**2b**)	$M(N)_4(O_W)_2$		
Ni, (**1b**)	$M(N,O)_2(N)_2$		
Co, (**3a**) Ni, (**3b**) Zn, (**3c**)	$M(O)_2(N_{idr})_4$		

Scheme 2

Finally, complex **3b** shows a ν(CO) absorption at 1223 cm^{-1}, which is typical of the C−O stretching of a phenolate group, in agreement with the coordination mode of the pymo ligand.

A schematic summary of the structural and spectroscopic information discussed above is pictorially drawn in Scheme 2.

Discussion

All M(pymo)$_2$ phases presented above crystallize in non-centrosymmetric space groups and contain aromatic *dipolar* fragments of idealized C_{2v} symmetry with highly delocalized π electrons. Therefore, in agreement with recent studies on C_{2v} DCM laser dye derivatives[27] and diazaaromatic metal complexes,[28] they are ideal candidates for testing NLO properties, such as second harmonic generation activity.[29] Preliminary measurements (λ_{exc} = 1064 nm) by the Kurtz−Perry technique[30] have indeed shown SHG efficiencies of about 5, 8, and 0.2% (urea as standard) for **1a**, **1b**, and **1c**, respectively.

In addition, they all display rather stable three-dimensional frameworks, which do not decompose or melt upon heating at 500 °C; compared to the other known metal(II) diazolates, they show the highest stabilities: indeed, only Zn(pz)$_2$ was found to sustain rather high temperatures (although decomposing near 440 °C to crystalline zinc dicyanide, with selective CH_3CN extrusion), while accessibility to redox reactions [such as cyanogen formation for Cd(pz)$_2$ or ring mercuriation for Hg(pz)$_2$] dramatically lowers the thermal stability of such species,[16b] including Cu(4X-pz)$_2$. (X = H, Br, Cl, CH_3)[31] and Cu(imz)$_2$.[17] That pymo ligands form rather stable metal adducts was already observed for copper(I) and silver(I) ions: indeed, Cu(pymo)[32] decomposes 70 °C higher than α-Cu(pz)[33] (dec. 270 °C) and *hexameric* Ag(pymo) is stable up to 300 °C,[34] about 40 °C higher than the Ag(pz)[33] and Ag(imz)[35] *polymers*.

Interestingly, while in the previously known silver and copper pyrimidinolates, the pymo ligand was exclusively found to coordinate in the μ_2-η^1-η^1 (*N*,*N*′) mode, the structures reported in this paper demonstrate its coordination versatility. Indeed, within a homogeneous class of compounds, pymo acts either as a (μ_1-η^1-*O*) monodentate or as a (*N*,*N*′) polydentate ligand, with (μ_2-η^2-η^1) or without (μ_2-η^1-η^1) ancillary oxygen coordination.[36] In contrast, the isostructural pyrimidin-2-thiolato ligand, which, owing to the biological importance of its derivatives,[37] has been extensively characterized in a large number of metal complexes, has never been found in the pure μ_2-η^1-η^1 (*N*,*N*′) mode, but, in the rare cases where both N atoms were involved in metal coordination,[38] the (larger and softer) sulfur atom was invariably found in the coordination sphere of one metal.

The different bridging modes of the pymo ligand also influence the distances at which nearest M···M contacts are found: they surprisingly range from 5.46 to 5.70 Å for the binary species up to ca. 6.33 Å for the octahedrally coordinated nickel(II) ions in the hydrated species **2b**. Consistently, the flexibility of such links affects not only the different

connectivity patterns described above, but also the actual values of the M−N and M−N−C bond lengths and angles (see Table 1).

Conclusions

In this paper we have demonstrated that reaction of metal ions with deprotonated diazaaromatic ligands can afford rather stable coordination polymers, which can be heated without decomposition up to ca. 550 °C. When pymo and Co, Ni, and Zn ions are employed, three-dimensional diamondoid networks are formed, in contrast with the 1-D nature of all known $M(pz)_2$ polymers (M = Cu, Zn, Cd, Hg). Such stereochemical features, together with the low(er) propensity of Co, Ni and, particularly, Zn toward redox reactions, are thought to heavily influence the stability of such crystal phases. In the process of developing suitable syntheses for such species, a number of water and hydrazine adducts have been prepared, the structural characterization of which showed the extreme versatility of the pymo ligands, as well as the formation of 2-D (for **2b**) and 1-D (**3abc**) polymers.

Since all these species could only be obtained as microcrystalline samples, their full structural analyses was performed through the ab initio XRPD technique (see Appendix); as recently shown by us in the field of coordination chemistry for metal pyrazolates and metal diazaaromatic halides, this method has become a powerful laboratory tool for the complete characterization of *entire* classes of compounds and not only, as often appeared in the recent literature, for fortunate, isolated or benchmark cases bearing methodologically important aspects.

Experimental Section

General: 2-Hydroxypyrimidine hydrochloride and metal salts were used as supplied (Aldrich Chemical Co.). − Infrared spectra were recorded on a BIO RAD FTIR 7 instrument. − Thermogravimetric analyses were performed on a Perkin−Elmer TGA-7 system. DSC traces were obtained with the aid of a Perkin−Elmer DSC 7 calorimeter. − X-ray powder diffraction was used to characterize the phases formed upon heating the powders in the DSC furnace. − Elemental analyses (C, H, N) were carried out at Microanalytical Laboratory of the University of Milan.

Synthesis of Cobalt(II), Nickel(II), and Zinc(II) Derivatives: Complexes **1a**, **2b**, and **1c** have been prepared following the same synthetic route: ten mmol of the appropriate metal chloride ($CoCl_2{\cdot}6H_2O$, 2.38 g, $NiCl_2{\cdot}6H_2O$, 2.38 g and $ZnCl_2$, 1.36 g) were dissolved in distilled water (30 mL) and 2-hydroxypyrimidine hydrochloride (3.31 g, M/Hpymo ratio = 1:2.5) was added under stirring. The clear solutions were kept at room temperature for about 20 min., then the temperature was raised to 90 °C and aqueous ammonia (25% w/w) was added dropwise, adjusting the pH of the solution to a value near 10. The pink $Co(pymo)_2$, **1a**, and the white $Zn(pymo)_2$ species, **1c**, suddenly precipitate, whereas turquoise $Ni(pymo)_2(H_2O)_{2.5}$, **2b**, separates from a deep blue solution in about 10 minutes. The suspensions were stirred at 90 °C for an additional half hour, the solids were then filtered, washed with hot water and dried under vacuum.

Anhydrous $Ni(pymo)_2$, 1b, (amorphous phase) was obtained upon heating the hydrated $Ni(pymo)_2(H_2O)_{2.5}$ species **2b** at 200 °C for 10 min under vacuum. A microcrystalline powder of **1b**, suitable for the XRPD study (vide infra), was obtained after over-heating the solid at ca. 550 °C under vacuum. All preparations gave quantitative (>95%) yields. Analyses: **1a**: $C_8H_6CoN_4O_2$: calcd. C 38.57, H 2.41, N 22.49; found C 38.51, H 2.47, N 22.41; **1b**: $C_8H_6N_4NiO_2$: calcd. C 38.60, H 2.41, N 22.52; found C 38.53, H 2.45, N 22.45; **1c**: $C_8H_6N_4O_2Zn$: calcd. C 37.59, H 2.35, N 21.93; found C 37.47, H 2.43, N 21.86; **2b**: $C_8H_{11}N_4NiO_{4.5}$: calcd. C 32.69, H 3.75, N 19.07; found C 31.91, H 3.85, N 18.85.

Synthesis of the Hydrazine Adducts: Complexes **1a** (or **1b/1c**) (500 mg, about 2 mmol) were suspended in acetonitrile (7 mL) and hydrazine (160 μL, 80% water solution) was added with stirring. A rapid change in color was observed when cobalt or nickel pyrimidin-2-olate derivatives were employed (from pink to white and from turquoise to very light violet, respectively). The suspensions were stirred for 4 h, the solids were then filtered under nitrogen (to avoid atmospheric moisture) and dried under a flow of dry nitrogen. The nickel derivative $Ni(pymo)_2(N_2H_4)_2$, can also be obtained employing $Ni(pymo)_2(H_2O)_{2.5}$ in place of $Ni(pymo)_2$. A longer reaction time is in this case required (about 12 h). Analysis for **3b**: $C_8H_{14}N_8NiO_2$: calcd. C 30.70, H 4.48, N 35.82; found C 30.77, H 4.41, N 35.73; due to thermal instability, the chemical analyses for **3a** and **3c** are erratic (see text).

X-ray Powder Diffraction Analysis of 1abc, 2b, and 3abc: The powders were gently ground in an agate mortar, than cautiously deposited in the hollow of an aluminium holder equipped with a zero background plate (supplied by The Gem Dugout, State College, PA) with the aid of glass slide. Diffraction data (Cu-K_α, λ = 1.5418 Å) were collected on a vertical scan Philips PW1820 diffractometer, equipped with parallel (Soller) slits, a secondary beam curved graphite monochromator, a Na(Tl)I scintillation detector and pulse height amplifier discrimination. The generator was operated at 40 KV and 40 mA. Slits used: divergence 1.0°, antiscatter 1.0° and receiving 0.2 mm. Nominal resolution for the present setup is 0.12° 2θ (FWHM) for the Si(111) peak at 28.44° (2θ). Long overnight scans were performed for **1abc**, **2b**, and **2c** with $5<2\theta<95°$, with t = 10 s and $\Delta 2\theta$ = 0.02°, while the low stability of the zinc hydrazine adduct required a much faster scan ($5<2\theta<35°$, t = 1s, approximately 30 min long).

Indexing, using TREOR,[39] of the low angle peaks suggested, for **1a** and **2b**, tetragonal unit cells of approximate dimensions a = 7.39, c = 17.03 Å for **1a** [M(20)[40] = 19; F(20)[41] = 25 (0.016, 51), I-centered] and a = 12.62, c = 14.54 Å for **2b** [M(10) = 32; F(10) = 38 (0.012, 22), primitive]; in contrast, the unit cell determination of **3a** lead to a triclinic cell [a = 4.04, b = 6.04, c = 15.42 Å, α = 64.3, β = 113.3 and γ = 90.4°; M(13) = 24; F(13) = 35 (0.015, 24)], which could be successfully transformed into a C-centered monoclinic lattice with a = 25.04, b = 4.04, c = 6.04 Å, β = 92.8°; indexing of **1b** suggested, as probable unit cell, an orthorhombic lattice with a = 11.02, b = 9.60 Å, c = 16.21, [M(11) = 23; F(11) = 29 (0.006, 67); F-centered]. Systematic absences indicated (among others) *I−42d*, *C2/m*, *$P4_2$/nmc*, and *Fdd2* as the probable space group, for **1a**, **3a**, **2b**, and **1b**, respectively, later confirmed by successful solution and refinement; **3b** and **3c** were found to be strictly isomorphous with **3a** (and **1c** to **1a**), and, therefore, not solved ab initio.

Structure solutions of **1a**, **1b**, and **2b** were initiated by EXPO[42] [108 ($2\theta<85°$), 147 and 84 ($2\theta < 65°$) independent F_o's, respectively]

which afforded all metal and N atom locations, as well as the positions of a few other light atoms. With the help of difference Fourier syntheses and geometrical modeling, approximate coordinates for the remaining non-hydrogen atoms were easily obtained. Approximate lattice constants and atomic coordinates for **1c** were taken from those of the isomorphous species **1a**.

In contrast, the structure of **3abc** could not solved by this method; therefore, we resorted to the ′brutal force′ program ESPOIR,[43] which combines direct space search and a reverse Monte Carlo algorithm; rather efficiently, using 134 F_o's extracted by EXPO, this program succeeded in finding the Ni atom in **3b** and approximate location and orientation of the (crystallographically unique) pymo ligand. Difference Fourier and geometric modeling later afforded the location of μ_2-bridging hydrazine. However, the original location of the pymo and hydrazine ligands, bisected by crystallographic mirror planes, afforded reasonable profile agreement factors (wR_p and R_p: 0.175 and 0.132, respectively), but a poor R_F value (0.184) and a rather strained hydrazine molecule, possessing an implausible *eclipsed* conformation and N−N−Co angles near 135°. Therefore, we suspected the presence of local disorder of the hydrazine bridges and simulated the diffraction pattern for ordered and disordered C-1 and C2 models. Comparison of the Rietveld refinements, of the resulting stereochemistries and evaluation of the overall (intramolecular + packing) steric energy by a locally developed molecular mechanics programs (based on the MM3 force field and capable of dealing with crystal lattices and polymeric systems[44]), revealed that *disordered* bis-hydrazine bridges, with M−N−N−M−N−N rings in chair conformation, and pymo ligands slightly off the mirror plane, are present, with the strict stereochemical condition that, within each polymeric chain, a rather perfect order is maintained, and that the average *C2/m* space group symmetry stems from the order loss in the lateral packing of chains. Therefore, the final model described in the following, as well in Table 1 and Table 2, Figure 5 and in the Supporting Information, show split ligands with atomic fractional occupancy of 0.5.

The final refinements were performed with the aid of the GSAS suite of programs,[45] by imposing steric restraints to chemically stiff and known fragments: pymo rings were idealized with average literature values (C−C and C−N: 1.38 Å; C=O: 1.25 Å; all angles set at 120°). A soft restraint was also applied to hydrazine N−N distance [1.44(1) Å in **3b**]. The peak shapes were best described by the Thompson/Cox/Hastings formulation[46] of the pseudo Voigt function, with GV and LY set to zero. The experimental background was modeled by a cosine Fourier series, while systematic errors were corrected with the aid of a sample-displacement angular shift. Metal atoms were given a refinable isotropic displacement parameter [U_{iso}(M)], while lighter atoms *U*'s were arbitrarily given [U_{iso}(M) + 0.02] Å^2 values. The contribution of the hydrogen atoms to the scattered intensity was neglected. Scattering factors, corrected for real and imaginary anomalous dispersion terms, were taken from the internal library of GSAS. Final R_p, R_{wp}, and R_F agreement factors, together with details of the data collections and analyses for the seven crystal phases can be found in Table 2. Figure 5 shows the final Rietveld refinement plots. The multiphase nature *and* the variable composition of the XRPD data for species **3a** and **3c** prevented a full structural refinement; therefore, the data reported in Table 2 refer to a LeBail (**3a**) and multiple peak positions (**3c**), rather than Rietveld, fit. Final fractional coordinates and full lists of bond lengths and angles are supplied as Supporting Information. Crystallographic data (excluding structure factors) for the structures reported in this paper have been deposited with the Cambridge Crystallographic Data Centre as supplementary publication no. CCDC-141485−141489. Copies of the data can be obtained free of charge on application to CCDC, 12 Union Road, Cambridge CB2 1EZ, UK [fax: (+44)1223 336−033; E-mail: deposit@ccdc.cam.ac.uk].

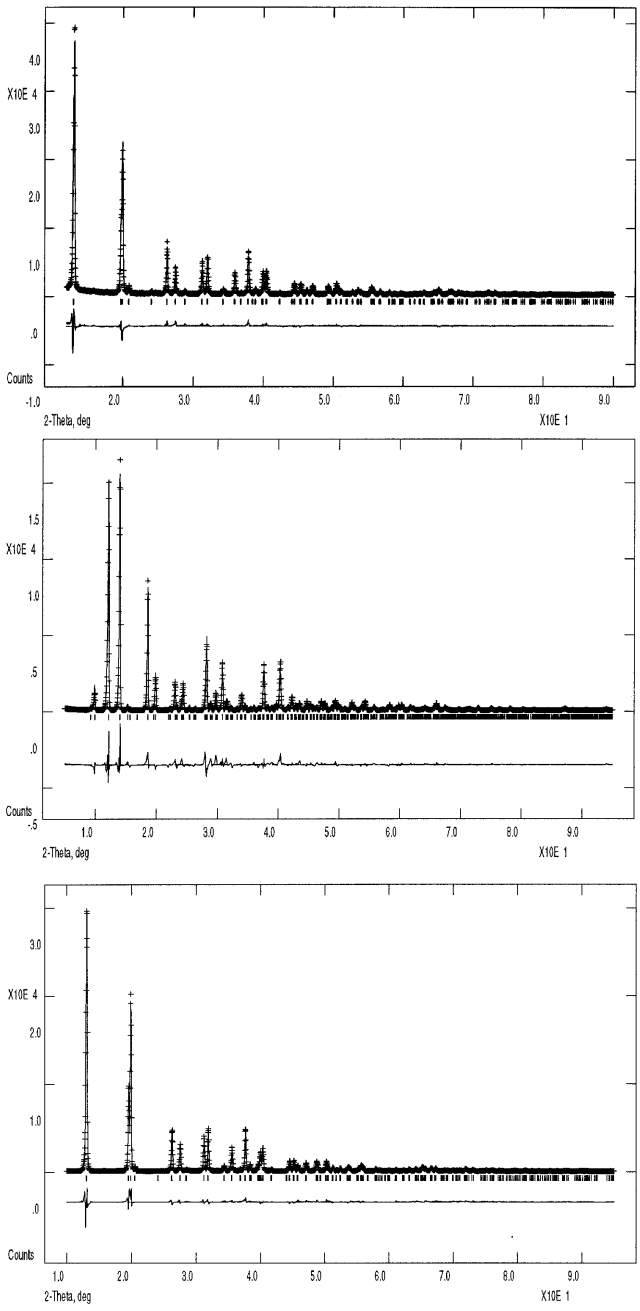
Appendix

X-ray powder diffraction is known to afford very good estimates of the lattice parameters, but only approximate values for atomic position and thermal displacement parameters. Also, in the formulation of the ′correct′ structural model for complex structures, *external* knowledge, such as chemical composition and stereochemical rules, must be introduced by the sagacious use of restraints. We

Table 2. Crystal data and refinement parameters for compounds **1abc**, **2b**, and **3abc** (e.s.d.'s in parentheses)

Compound	**1a**	**1b**	**1c**	**2b**	**3a**	**3b**	**3c**
Species	$Co(pymo)_2$	$Ni(pymo)_2$	$Zn(pymo)_2$	$Ni(pymo)_2(H_2O)_{2.5}$	$Co(pymo)_2(N_2H_4)_2$	$Ni(pymo)_2(N_2H_4)_2$	$Zn(pymo)_2(N_2H_4)_2$
Formula	$C_8H_6CoN_4O_2$	$C_8H_6N_4NiO_2$	$C_8H_6N_4O_2Zn$	$C_8H_{11}N_4NiO_{4.5}$	$C_8H_{14}CoN_8O_2$	$C_8H_{14}N_8NiO_2$	$C_8H_{14}N_8O_2Zn$
Fw [g mol^{-1}]	249.09	248.87	255.33	293.91	313.18	312.97	319.62
Crystal system	Tetragonal	Orthorhombic	Tetragonal	Tetragonal	Monoclinic	Monoclinic	Monoclinic
Space Group	*I*-42*d*	*Fdd*2	*I*-42*d*	$P4_2/nmc$	*C*2/*m*	*C*2/*m*	*C*2/*m*
a [Å]	7.4114(3)	11.0361(6)	7.3919(2)	12.6531(4)	25.139(2)	25.237(5)	25.40(1)[b]
b [Å]	7.4114(3)	9.6611(8)	7.3919(2)	12.6531(4)	4.0558(2)	4.0070(4)	3.928(2)
c [Å]	17.0879(7)	16.1935(8)	17.3389(6)	14.5844(9)	6.0752(4)	6.0580(7)	6.163(3)
α [°]	90	90	90	90	90	90	90
β [°]	90	90	90	90	92.813(4)	93.156(9)	93.06(4)
γ [°]	90	90	90	90	90	90	90
V [Å^3]	938.63(6)	1726.6(2)	947.39(5)	2335.0(2)	618.66(8)	611.7(2)	614.2(6)
Z	4	8	4	8	2	2	2
ρ_{calc} [g cm^{-3}]	1.763	1.915	1.791	1.669	1.681	1.704	1.729
μ(Cu-K_α) [cm^{-1}]	149.4	31.0	35.4	25.4	115.5	24.1	29.5
Diffractometer	Philips PW 1820	Philips PW 1820	Philips PW 1820	Philips PW 1820	Philips PW 1820	Philips PW 1820	Philips PW 1820
T [K]	298	298	298	298	298	298	298
2θ range °	12−90	10−95	10−95	5−95	5−65	5−65	5−35
N_{obs}	3900	4250	4250	4500	3000	3000	1500
N_{refl}	120	204	135	600	131	142	n.a.
R_p, R_p	0.103, 0.078	0.090. 0.066	0.121, 0.088	0.199, 0.142	0.100, 0.072[a]	0.125, 0.089	n.a.
R_F, χ	0.076, 2.92	0.051, 1.55	0.096, 2.54	0.129, 3.67	n.a.	0.069, 2.86	n.a.

[a] From a model-independent LeBail fit. − [b] From 14 single-peak locations, using UNITCELL (Toraya, H.; Kitamura, M.; *J. Appl. Crystallogr.*, **1990**, *23*, 282.)



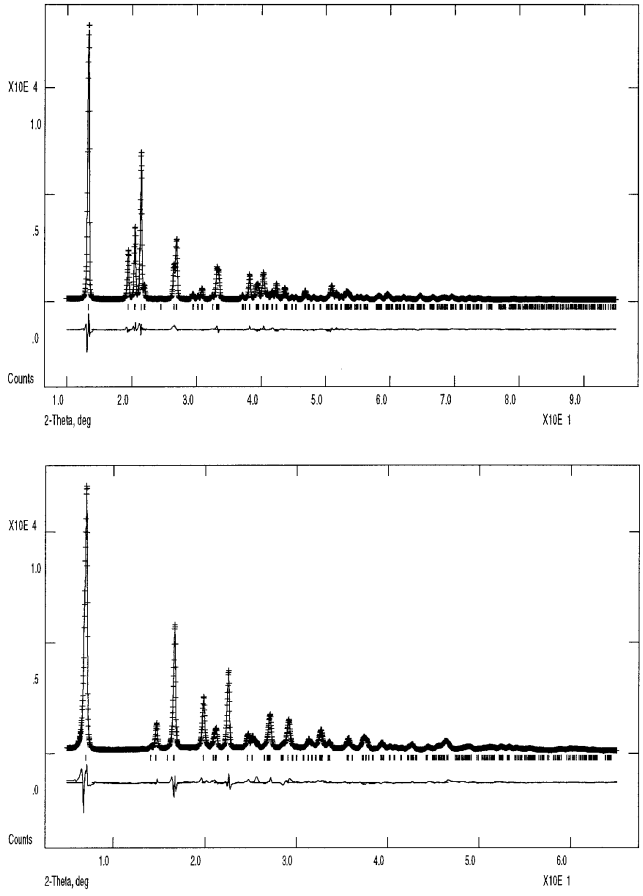


Figure 5. Rietveld Refinement plots for species **1a**, **1b**, **1c**, **2b**, and **3b** (top to bottom, left to right), respectively; peak markers and difference plot at the bottom

have recently demonstrated that packing energy evaluation within the crystal lattice may discriminate among similar models, thus acting as a lens for rescuing subtle details at spatial resolution higher that that affordable by XRPD data alone.[47] Accordingly, the final structural model for species **3b** has been derived after *overall* steric energy minimization, stereochemical considerations and a number of parallel refinements had been performed, with the aim of identifying the most likely (i.e. correct?) structural model. While the figures reported hereafter in Table 3 cannot be straightforwardly used as in standard single-crystal diffractometry (apart from the "unobservable" R_F value), it is only their internal comparison and the stereochemical features associated to the different cases that guarantee successful results even from XRPD data.

Acknowledgments

We thank the Italian Consiglio Nazionale delle Ricerche and MURST for funding. We also acknowledge financial support from

Table 3. Comparison of Rietveld refinements for **3b**, in the 5−65° (2θ) range (fixed cell)

	Model	S.G.	$N_{parameters}$	$N_{restraints}$	wR_p	R_p	R_F	N_{ref}
1	ordered	*C*−1	40	19	0.139	0.105	0.108	222
2	ordered	*C*2	40	19	0.141	0.104	0.092	141
3	ordered (N−N free)	*C*2/*m*	30	16	0.146	0.108	0.162	141
4	as 3 (N−N 1.44 Å)	*C*2/*m*	30	17	0.175	0.132	0.184	141
5	disordered	*C*2/*m*	40	19	0.126	0.093	0.082	141

ICDD − International Centre for Diffraction Data. The help of E. Cariati for the SHG measurements is also acknowledged.

[1] J. E. Mark, H. R. Allcock, R. West, *Inorganic Polymers*, Prentice-Hall Inc., Englewood Cliffs, NJ, **1992**; *Inorganic and Organometallic Polymers II* (Eds. P. Wisian-Neilson, H. R. Allcock, K. J. Wynne), ACS Symposium Series 572, American Chemical Society, Washington, DC, **1994**.

[2] O. Kahn, C. Jay Martinez, *Science* **1998**, *279*, 44−48 and references therein.

[3] I. V. Tsarenko, A. V. Makarevich, T. P. Kofman, *Russian J. Electrochem.* **1997**, *33*, 1092−1097; W. N. Richmond, P. W. Faguy, S. C. Weibel, *J. Electroan. Chem.* **1998**, *448*, 237−244; I. V. Tsarenko, S. A. Chizhik, A. V. Makarevich, *Protect. Met.* **1999**, *35*, 81−84.

[4] K. Nomiya, K. Tsuda, T. Sudoj, M. Oda, *J. Inorg. Biochem.* **1997**, *68*, 39−44; K. Nomiya, K. Tsuda, N. C. Kasuga, *J. Chem. Soc., Dalton Trans.* **1998**, 1653−1659.

[5] A. J. Blake, N. R. Champness, P. Hubberstey, W. S. Li, M. A. Withersby, M. Schröder, *Coord. Chem. Rev.* **1999**, *183*, 117−138.

[6] N. Masciocchi, M. Moret, P. Cairati, A. Sironi, G. A. Ardizzoia, G. LaMonica, S. Cenini, *J. Am. Chem. Soc.* **1994**, *116*, 7668−7676.

[7] [7a]N. Masciocchi, G. A. Ardizzoia, G. LaMonica, M. Moret, A. Sironi, *Inorg. Chem.* **1997**, *36*, 449−454. − [7b] N. Masciocchi, P. Cairati, A. Sironi, *Powder Diffr.* **1998**, *13*, 35−40. − [7c] G. A. Ardizzoia, S. Cenini, G. LaMonica, N. Masciocchi, A. Maspero, M. Moret, *Inorg. Chem.* **1998**, *37*, 4284−4292.

[8] N. Masciocchi, M. Moret, P. Cairati, A. Sironi, G. A. Ardizzoia, G. La Monica, *J. Chem. Soc., Dalton Trans.* **1995**, 1671−1675.

[9] M. Quiros, *Acta Crystallogr.* **1994**, *C50*, 1236−1238.

[10] N. Masciocchi, E. Corradi, M. Moret, G. A. Ardizzoia, A. Maspero, G. LaMonica, A. Sironi, *Inorg. Chem.* **1997**, *36*, 5648−5650.

[11] N. Masciocchi, G. A. Ardizzoia, G. LaMonica, A. Maspero, A. Sironi, *Angew. Chem. Int. Ed.* **1998**, *37*, 3366−3369.

[12] K.D.M. Harris, M. Tremayne, *Chem. Mater.* **1996**, *8*, 2554−2570; J. I. Langford, D. Louër, *Rep. Prog. Phys.* **1996**, *59*, 131−234; D. M. Poojary, A. Clearfield, *Acc. Chem. Res.* **1997**, *30*, 414−422.

[13] N. Masciocchi, A. Sironi, *J. Chem. Soc., Dalton Trans.* **1997**, 4643−4650.

[14] In contrast to that observed in previous XRPD studies, all M···M separations reported in this paper are rather accurately estimated, since, owing to the special location of the metal atoms, they only depend on the lattice metrics which, from PD experiments, typically possess e.s.d.'s lower than in conventional single-crystal diffractometry.

[15] M. Sturm, F. Brandl, D. Engel, W. Hoppe, *Acta Crystallogr.* **1975**, *B31*, 2369−2378.

[16] [16a]M. Ehlert, A. Storr, R. C. Thompson, *Can. J. Chem.* **1989**, *67*, 1412−1424. − [16b] N. Masciocchi, G. A. Ardizzoia, A. Maspero, G. LaMonica, A. Sironi, *Inorg. Chem.* **1999**, *38*, 3657−3664.

[17] M. Inoue, M. Kishita, M. Kubo, *Inorg. Chem.* **1965**, *4*, 626−628.

[18] W. Bürger, J. Strähle, *Z. Allg. Anor. Chem.* **1985**, *529*, 111−117.

[19] F. A. Cotton, G. Wilkinson, C. A. Murillo, M. Bochmann, *Advanced Inorganic Chemistry*, 6th Edition, Wiley, New York, **1999**, p. 817.

[20] B. A. Cartwright, C. D. Reynolds, A. J. Skapski, *Acta Crystallogr.,* **1977**, *B33*, 1883−1887.

[21] See for example: B. J. Hathaway, *Comprehensive Coordination Chemistry* (Ed.: G. Wikinson), Pergamon, **1987**, vol. 5, p. 599.

[22] D. Sellmann, P. Kreutzer, G. Huttner, A. Frank, *Z. Naturforsch. B* **1978**, *33*, 1341−1346.

[23] K. Kim, S. J. Lippard, *J. Am. Chem. Soc.* **1996**, *118*, 4914−4915.

[24] A very brief report of a ruthenium complex bridged by one disulfide and two hydrazine links has however recently appeared (K. Matsumoto, H. Uemura, M. Kawano, *Chem. Lett.* **1994**, 1215−1218).

[25] For comparison, the ν(CO) of the free Hpymo (lactamic form) is found at 1647 cm^{-1} in the solid state and 1644 cm^{-1} in water solution (A. Albert, E. Spinner, *J. Chem. Soc. A* **1960**, 1221−1226).

[26] G. A. Ardizzoia, G. LaMonica, A. Maspero, M. Moret, N. Masciocchi, *Eur. J. Inorg. Chem.* **1998**, 1503−1512 and references therein.

[27] C. R. Moylan, S. Ermer, S. M. Lovejoy, I.-H. McComb, D. S. Leung, R. Wortmann, P. Krdmer, R. J. Twieg, *J. Am. Chem. Soc.* **1996**, *118*, 12950−12955.

[28] H. Le Bozec, T. Renouard, *Eur. J. Org. Chem.* **2000**, 229−239.

[29] Indeed, a closely related species, 5-nitrouracil (a substituted 2-hydroxypyrimidine), was among the most thoroughly studied crystal phases, with NLO properties similar, or higher in magnitude, than KDP or $LiNbO_3$ [J. F. Nicoud, R. J. Twieg, in *Nonlinear Optical Properties of Organic Molecules and Liquid Crystals* (Eds.: D. S. Chemla, F. Zyss), Academic Press, **1987**, p. 268].

[30] S. K. Kurtz, T. T. Perry, *J. Appl. Phys.* **1968**, *39*, 3798−3813.

[31] M. K. Ehlert, S. J. Rettig, A. Storr, R. C. Thompson, J. Trotter, *Can. J. Chem.* **1989**, *67*, 1970−1974; M. K. Ehlert, A. Storr, R. C. Thompson, F. W. B. Einstein, R. J. Batchelor, *Can. J. Chem.* **1993**, *71*, 331−334; M. K. Ehlert, S. J. Rettig, A. Storr, R. C. Thompson, J. Trotter, *Can. J. Chem.* **1991**, *69*, 432−439.

[32] N. Masciocchi, G. A. Ardizzoia, G. La Monica, A. Maspero, A. Sironi, *Angew. Chem. Int. Ed. Engl.* **1998**, *37*, 3366−3369.

[33] N. Masciocchi, M. Moret, P. Cairati, A. Sironi, G. A. Ardizzoia, G. La Monica, *J. Am. Chem. Soc.* **1994**, *116*, 7668−7676.

[34] N. Masciocchi, E. Corradi, M. Moret, G. A. Ardizzoia, A. Maspero, G. La Monica, A. Sironi, *Inorg. Chem.* **1997**, *36*, 5648−5650.

[35] N. Masciocchi, M. Moret, P. Cairati, A. Sironi, G. A. Ardizzoia, G. La Monica, *J. Chem. Soc., Dalton Trans.* **1995**, 1671−1675.

[36] That pymo ligands could bind also via the oxygen atom was also proposed, from UV/Vis spectroscopic measurements, in: D. M. L. Goodgame, I. Jeeves, *Inorg. Chim. Acta* **1979**, *32*, 157−162.

[37] See for example: J. A. Carbon, L. Hung, D. S. Jones, *Proc. Nat. Acad. Sci.* **1965**, *53*, 979−986; J. A. Carbon, H. David, M. H. Studier, *Science* **1968**, *161*, 1146−1147.

[38] D. R. Corbin, L. C. Francesconi, D. N. Hendrickson, G. D. Stucky, *Inorg. Chem.* **1979**, *18*, 3069−3074; M. L. Godino-Salido, M. D. Gutierrez-Valero, R. Lopez-Garzon, J. M. Moreno-Sanchez, *Inorg. Chim. Acta* **1994**, *221*, 177−181.

[39] P. E. Werner, L. Eriksson, M. Westdahl, *J. Appl. Crystallogr.* **1985**, *18*, 367−370.

[40] P. M. De Wolff, *J. Appl. Crystallogr.* **1968**, *1*, 108−113.

[41] G. S. Smith, R. L. Snyder, *J. Appl. Crystallogr.* **1979**, *12*, 60−65.

[42] A. Altomare, M. C. Burla, G. Cascarano, G. Giacovazzo, A. Guagliardi, A. G. G. Moliterni, G. Polidori, *J. Appl. Crystallogr.* **1995**, *28*, 842−846; A. Altomare, M. C. Burla, M. Camalli, B. Carrozzini, G. L. Cascarano, C. Giacovazzo, A. Guagliardi, A. G. G. Moliterni, G. Polidori, R. Rizzi, *J. Appl. Crystallogr.* **1999**, *32*, 339−340.

[43] A. Le Bail, "http://fluo.univ-lemans.fr:8001/sdpd/espoir/index.html".

[44] P. L. Mercandelli, M. Moret, A. Sironi, *Inorg. Chem.* **1998**, *37*, 2563−2569.

[45] A. C. Larson, R. B. Von Dreele, LANSCE, MS-H805, Los Alamos National Laboratory, New Mexico, **1990**.

[46] P. Thompson, D. E. Cox, J. B. Hastings, *J. Appl. Crystallogr.* **1987**, *20*, 79−83.

[47] N. Masciocchi, F. Ragaini, S. Cenini, A. Sironi, *Organometallics* **1998**, *17*, 1052−1057; N. Masciocchi, A. Sironi, *Adv. X-ray Anal.* **1999**, *42*, 366−372.

Received May 24, 2000
[I00214]

Synthesis and Structure of Siloxy-Substituted ZnO Aggregates Having $(ZnO)_n$ (n = 2, 4) and Zn_3O_4 Cores

Matthias Driess,*[a] Klaus Merz,[a] and Stefan Rell[a]

Keywords: Clusters / Metal oxides / Siloxides / Zinc

Convenient syntheses and X-ray crystallographic characterizations of the first bis(trimethylsilyl)amido-, methyl-, and iodozinc triorganosiloxide aggregates **1**–**5** are described. They are accessible by the simple reaction of ZnR'_2 [R = Me, $N(SiMe_3)_2$] with the respective silanols R_3SiOH (R = Me, Et, *i*Pr), which affords the dimeric $[(Me_3Si)_2NZnOSiR_3]_2$ (**1a**: R = *i*Pr; **1b**: R = Et), trinuclear $[(MeZn)_2Zn(OSi{\it i}Pr_3)_4]$ (**2a**), $\{[(Me_3Si)_2NZn]_2Zn(OSiR_3)_4\}$ (**2b**: R = Et; **2c**: R = Me), and tetranuclear heterocubanes $[MeZnOSiR_3]_4$ (**3a**: R = Me; **3b**: R = Et), respectively. The latter were oxidized with four equivalents of elemental iodine to form the tetraiodo derivatives $[IZnOSiR_3]_4$ (**4a**: R = Me; **4b**: R = Et) in 82 and 88% yield, respectively. Due to the higher polarity of the Zn–I vs. Zn–C σ-bond, the Zn–O distances of the almost regular Zn_4O_4 core in **4a** are 2–6 pm shorter than those observed in the less Lewis-acidic cluster **3b**. However, the Zn–O distances in **3b** and **4a** are ca. 10–15 pm longer than those in **1a**, **2a**, and **2c**, due to different coordination numbers at Zn and the effects of ring strain. Remarkably, the iodo derivatives **4a**,**b** undergo dissociation in THF to give the respective dimeric THF solvates $[IZn(THF)OSiR_3]_2$ (**5a**: R = Me; **5b**: R = Et), whereas the Zn_4O_4 cores in **3a** and **3b** are retained even in aprotic polar solvents.

Introduction

Molecular single-source precursors for the formation of metal oxides such as metal alkoxides and siloxides[1] have attracted wide interest in the fields of material science and catalysis. While many fascinating applications have been developed in the series of homo- and heterometallic alkoxides and siloxides[1,2] relating to most s-, p-, d-, and f-block elements, the precursor chemistry of molecular zinc alkoxide aggregates[3] and related systems (siloxides, phosphonates)[4] has received much less attention. Remarkably, in contrast to molecular zinc thiolate/sulfide clusters, which consist of structural subunits of sphalerite with six-membered Zn_3S_3 rings comprised of alternating zinc and sulfur atoms,[5] zinc alkoxide aggregates possess single or edge-fused, four-membered Zn_2O_2 cores. This is evident from the rare examples of structurally characterized Zn_4O_4 heterocubanes, edge-shared Zn_7O_8 double-cubanes, and spirobicyclic Zn_3O_4 aggregates.[3] The formation of other types of aggregates or substitution of the exocyclic organic ligands at zinc without degradation of the Zn_xO_y framework seems very limited, due to the high polarity of the Zn−O bond. Since the degree of aggregation and reactivity of such clusters is strongly influenced by the steric and electronic properties of the substituents at oxygen, siloxy-substituted derivatives can be expected to be even more versatile building blocks than their alkoxide analogues due to the convenient leaving-group properties of silyl groups. Whereas only two types of siloxy-substituted ZnO aggregates have been described previously, 35 years ago by Schmidbaur et al.,[6] no information is yet available concerning the influence of the size of the triorganosilyl group at O or of the substituent at Zn on the degree of aggregation of molecular zinc siloxides. We report herein on the synthesis and structural characterization of the siloxy-substituted di-, tri-, and tetranuclear ZnO clusters **1**, **2**, and **3**, which represent potentially useful precursors for the synthesis of ZnO nanoparticles. Remarkably, the methyl groups at Zn in **3a**,**b** can easily be replaced by iodine atoms, ultimately leading to the respective tetraiodides **4a**,**b**, which are promising starting materials for the synthesis of other nonorgano-substituted (Zn−X) Zn_4O_4 heterocubanes.

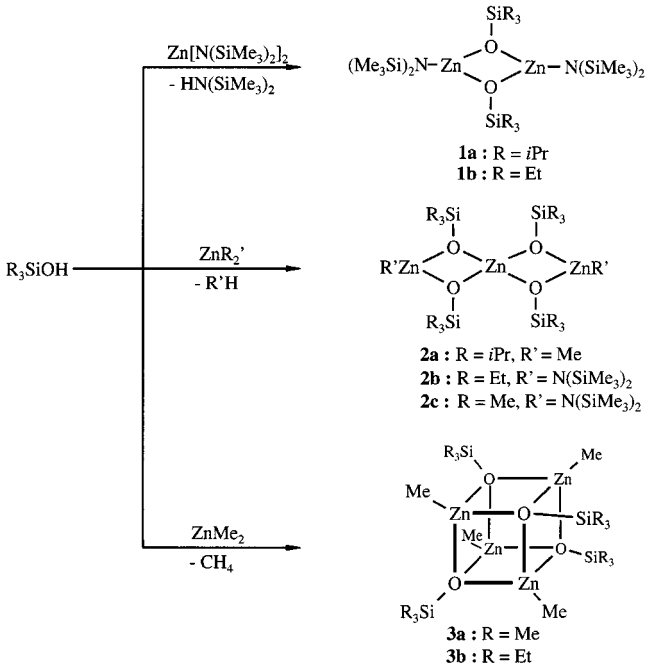
Results and Discussion

Different siloxy-substituted ZnO aggregates are accessible simply by the Brønsted acid/base reaction of triorganosilanols with dialkyl- and diamidozinc compounds. Thus, conversion of the triorganosilanols R_3SiOH (R = Me, Et, *i*Pr) with the zinc bases ZnR_2' [R′ = Me, $N(SiMe_3)_2$] furnishes, depending on the steric demand of the substituents, di-, tri-, and tetranuclear ZnO aggregates of types **1**−**3**. Reaction of the sterically congested silanol iPr_3SiOH with $ZnMe_2$ leads exclusively to the trinuclear, spirobicyclic Zn_3O_4 aggregate **2a** in 76% yield, while its analogous conversion with the bulky zinc diamide $Zn[N(SiMe_3)_2]_2$ affords only the dimer **1a** in 84% yield (Scheme 1). However, reaction of Et_3SiOH with $Zn[N(SiMe_3)_2]_2$ furnishes a 1:1 mixture of the dimeric and trinuclear species **1b** and **2b**, respectively. Apparently, the size of the silyl group has a stronger influence on the rate of deprotonation and the degree of

[a] Lehrstuhl für Anorganische Chemie I: Molekül- und Koordinationschemie, Ruhr-Universität Bochum, Universitätsstraße 150, 44780 Bochum, Germany
Fax: (internat.) + 49-(0)234/3214378
E-mail: matthias.driess@ac1.ruhr-uni-bochum.de

 © WILEY-VCH Verlag GmbH, D-69451 Weinheim, 2000 1434−1948/00/1212−2517 $ 17.50+.50/0

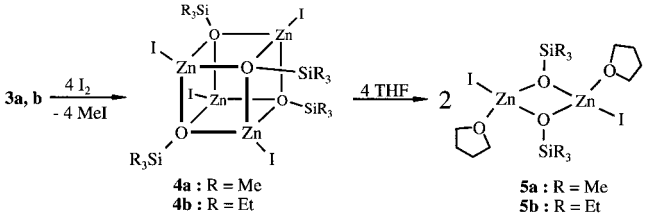
aggregation than the steric or electronic situation at the zinc center.



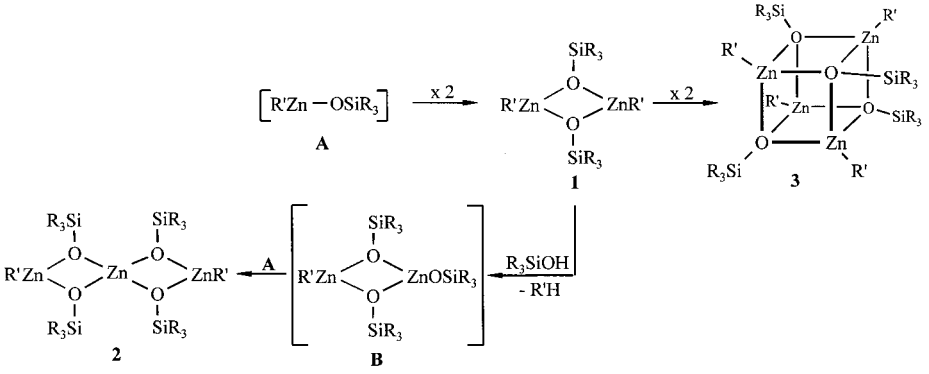
Scheme 1. Synthesis of **1**–**3**

Consequently, a higher degree of aggregation can be expected by employing sterically less congested silyl groups. This is confirmed by the reaction of R_3SiOH (R = Me, Et) with Me_2Zn, which leads to the tetranuclear heterocubanes **3a** and **3b**, respectively, in > 90% yield. Compound **3a** has already been prepared and structurally characterized by Schmidbaur et al.[6] The formation of tetrameric ZnO heterocubanes has also been observed for a few appropriate alkoxides, but in these cases the zinc atoms bore relatively bulky organo groups implying a relatively low reactivity of the cluster.[5] Although the mechanism of aggregation is still unknown, we propose that the initial step of the reaction of R_3SiOH with ZnR'_2 involves the formation of monomeric $R'ZnOSiR_3$ moieties **A**, which subsequently dimerize to a derivative of type **1** (Scheme 2).

$R'ZnOSiR_3$. Appropriate substitution favors dimerization of **1** to **3**, while additional Brønsted acid/base reaction (siloxylation) with one molecule R_3SiOH affords the polar, coordinatively unsaturated intermediate **B**. The latter can either undergo a rearrangement or association with **A** to form derivatives of type **2**. The siloxy derivatives **1**–**3** were found to be well soluble on warming in aliphatic and aromatic solvents, and their structures were also found to be retained in aprotic polar solvents such as ethers and tertiary amines. The relatively high stability of the Zn_4O_4 core in **3a** and **3b** permits oxidative exchange of the substituents at the zinc centers. While attempts to achieve Me/X exchange (X = halogen) at zinc on the intact Zn_4O_4 skeleton in **3a**,**b** with Ph_2PX as a potential halogenating agent failed,[7] we obtained the colorless, crystalline tetraiodo derivatives **4a** and **4b** in 88 and 82% yield, respectively, through direct iodination of **3a**,**b** with four molar equivalents of I_2 in toluene. This iodination was found to proceed in a stepwise manner, the rate of the reaction decreasing with increasing number of iodine atoms in the reaction intermediates, and complete conversion required about 48 h.



While **4b** is only sparingly soluble even in boiling toluene, **4a** dissolves in hexane and toluene at room temperature without dissociation. Because of the greater polarity of the terminal Zn–X bonds in the heterocubane core of **4a**,**b** (X = I) compared to those in **3a**,**b** (X = C), the Zn_4O_4 core in **4a**,**b** decomposes in aprotic polar solvents or in the presence of donor molecules, affording two molar equivalents of solvated Zn_2O_2 dimers. Thus, the dimers **5a** and **5b**



Scheme 2. Proposed mechanism for the formation of **1**–**3** via **A** and **B**

Apparently, the fate of **1** depends decisively on the steric demand of the substituents and the reactivity of the terminal Zn–X bond (X = C, N) toward R_3SiOH and

are formed quantitatively in THF solution. The compositions of compounds **1**–**5** have been verified by correct combustion analyses, whereas mass spectrometric analyses (EI,

FAB) resulted only in the detection of fragment ions. Since most of the compounds discussed here give rise to relatively simple ^{1}H NMR spectra, their structures could only be unequivocally corroborated by single-crystal X-ray diffraction analysis, as discussed below.

Structural Descriptions

The dinuclear aggregate **1a** crystallizes in the monoclinic space group *C*2/*c* and consists of a planar Zn_2O_2 core (Figure 1). The coordination of the Zn and O centers is trigonal-planar with uniform Zn−O distances that resemble the values observed in other dimers.[5b] Due to the steric requirements of the *i*Pr$_3$Si and amino groups, the N(SiMe$_3$)$_2$ groups at Zn cannot be oriented in a coplanar fashion in relation to the Zn_2O_2 plane. However, this configuration permits significant Zn−O π-interactions, which lower the high Zn−O σ-bond polarity (difference in Pauling electronegativities = 1.78).

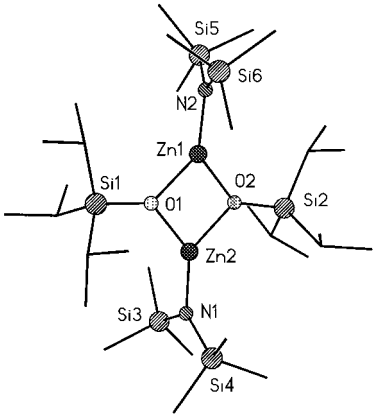


Figure 1. Solid-state structure of **1a**; H atoms are omitted for clarity

The average Zn−N distance of 1.871 Å is practically identical to values found for analogous dinuclear systems bearing terminal N(SiMe$_3$)$_2$ substituents,[7,8] but is significantly shorter than in the tris(amido) complex anion Zn[N(SiMe$_3$)$_2$]$_3^-$ (1.957 and 1.985 Å).[9] The topologically identical spirobicyclic Zn_3O_4 aggregates **2a** and **2c** crystallize in monoclinic (*C*2/*c*) and orthorhombic (*Pbcn*) space groups, respectively, and consist of an almost linear array of three Zn centers bridged by four siloxide ligands. The coordination of both the two terminal Zn and the O centers is trigonal-planar, whereas the central zinc atom has a distorted tetrahedral geometry (Figure 2 and Figure 3). Similar to the situation in **1a**, the amido groups at Zn in **2c** are almost perpendicularly oriented with respect to the Zn_2O_2 planes. Although the terminal and central Zn atoms have different coordination numbers, their respective Zn−O distances are almost uniform (Table 1), reflecting a relatively strong Zn−O σ-bond polarity within the Zn_3O_4 backbone.

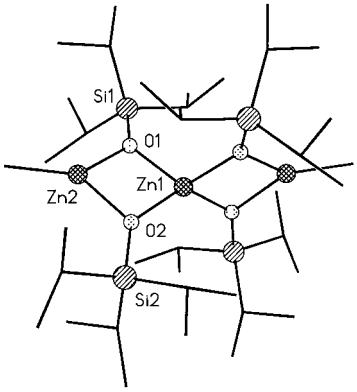


Figure 2. Molecular structure of **2a**; H atoms are omitted for clarity

In contrast, the Zn−O distances in the tetrameric ZnO aggregates **3b** and **4a**, which crystallize in monoclinic space groups (*C*2/*c* and *P*2$_1$/*n*, respectively) are, for steric reasons, ca. 10−15 pm longer than those in **1a**, **2a**, and **2c** (see Table 1). It is noteworthy that the Zn−O distances in the tetraiodo derivative **4a** are ca. 2−6 pm shorter than those in **3b**, probably because of the greater polarity of the Zn−I bond compared to the Zn−C bond. The heterocubane Zn_4O_4 cores in **3b** and **4a** (Figure 4 and Figure 5) are almost regular and therefore resemble very closely the structures observed for related Zn_4O_4 derivatives.[5b,6]

The Zn−I distances in **4a** are almost identical and are unremarkable, comparing well with the values observed for other iodozinc complexes.[7c,10] Slightly longer Zn−I distances, and concomitantly shorter endocyclic Zn−O1 distances are observed, as expected, in the THF solvate **5b**, which crystallizes in the orthorhombic space group *Pbca* (Figure 6). The terminal Zn−O2 distance, i.e. that between the zinc atom and the oxygen center of the THF ligand, is 10 pm longer than the endocyclic Zn−O1 distance, while the elongation of the Zn−I distance is caused by the stabilizing dative Zn−O(THF) bond. Apparently, the driving force behind the facile decomposition of heterocubanes **4a**,**b** in polar solvents can be interpreted in terms of coordination effects and the release of ring strain. Finally, it is worthy of note that the structures of the Zn(OSiR$_3$) aggregates **1**−**4** show a striking similarity to those of the isoelectronic Zn(NPR$_3$) clusters (phosphoraneimidinato complexes).[7] However, the Zn centers in the latter are much more electronically stabilized by π-donation from the N=P moiety and therefore, in contrast to **4a** and **4b**, the aggregates resist degradation even in donor solvents.

Experimental Section

General Remarks: All reactions were performed under anaerobic conditions using modified Schlenk techniques. Solvents were freshly distilled from Na and saturated with Ar prior to use. − ^{1}H NMR spectra were recorded at 250 MHz, ^{13}C NMR spectra at 63 MHz, and ^{29}Si NMR spectra at 50 MHz with samples in C_6D_6

Table 1. Selected bond lengths [Å] and angles [°] in **1a**, **2a**, **2c**, **3b**, **4a**, and **5b**

Zn_2O_2 (**1a**)			
Zn1−O1	1.962(1)	Zn1−N2	1.871(2)
Zn1−O2	1.943(1)	Zn2−N1	1.872(2)
Zn2−O2	1.950(1)	Si2−O2	1.665(1)
Zn2−O2	1.956(1)	Si2−O2	1.667(1)
N2−Zn1−O2	137.09(6)	Si1−O1−Zn2	131.93(8)
N2−Zn1−O1	138.22(6)	Si1−O1−Zn1	132.93(8)
O2−Zn1−O1	84.67(6)	Zn2−O1−Zn1	95.14(6)
Zn_3O_4 (**2a**)			
Zn1−O1	1.979(2)	Zn2−O1	1.968(2)
Zn1−O1A	1.979(2)	Zn2−O2	1.982(2)
Zn1−O2	1.966(2)	Zn−C	1.946(3)
Zn1−O2A	1.966(2)	Si1−O1	1.651(2)
O2−Zn1−O2A	130.9(1)	C−Zn2−O1	140.0(1)
O2−Zn1−O1	86.51(8)	C−Zn2−O2	133.6(1)
O2A−Zn1−O1	119.53(8)	O1−Zn2−O2	86.37(8)
O2−Zn1−O1A	119.52(8)	C−Zn2−Zn1	175.1(1)
Zn_3O_4 (**2c**)			
Zn1−O1	1.951(2)	Zn2−N1	1.855(3)
Zn1−O2	1.947(3)	Si1−O1	1.639(3)
Zn2−O1	1.933(3)	Si2−O2	1.636(3)
Zn2−O2	1.936(3)	Si3−N1	1.704(5)
O2−Zn1−O2A	1.228(2)	N1−Zn2−O1	136.8(2)
O2−Zn1−O1	85.3(1)	N1−Zn2−O2	137.0(2)
O2A−Zn1−O1	122.7(1)	O1−Zn2−O2	86.2(1)
O1−Zn1−O1A	122.6(2)	N1−Zn2−Zn1	179.8(2)
Zn_4O_4 (**3b**)			
Zn1−O1	2.104(4)	Zn1−C	1.959(6)
Zn1−O2	2.078(4)	Zn2−C	1.965(7)
Zn2−O1	2.085(4)	Si1−O1	1.675(4)
Zn2−O1	2.091(4)	Si2−O2	1.674(4)
C−Zn1−O2	127.8(3)	C−Zn2−O1	129.0(3)
C−Zn1−O2A	128.3(3)	C−Zn2−O2	130.3(3)
O2−Zn1−O1	85.9(2)	O1−Zn2−O2	86.1(2)
O2A−Zn1−O1	85.5(2)	O1A−Zn2−O2	85.8(2)
Zn_4O_4 (**4a**)			
Zn1−O1	87.0(5)	Zn2−O1	2.037(12)
Zn1−O2	86.7(5)	Zn2−O3	2.057(12)
Zn1−O3	126.6(3)	Zn2−O4	2.054(12)
Zn1−I1	128.9(3)	Zn2−I2	2.433(3)
O1−Zn1−O2	87.0(5)	O1−Zn2−O4	86.2(5)
O2−Zn1−O3	86.7(5)	O1−Zn2−O3	86.1(5)
O2−Zn1−I1	126.6(3)	O1−Zn2−I2	131.3(4)
O3 Zn1−I1	128.9(3)	O4−Zn2−I2	125.9(3)
Zn_2O_2·2THF (**5b**)			
Zn1−O1	1.945(6)	O1−Zn1−O2	105.1(3)
Zn1−O2	2043(5)	O1A−Zn1−O2	103.8(2)
Zn1−I1	2.498(1)	O1−Zn1−I1	126.4(1)
Si1−O1	1.658(6)	Si1−O1−Zn1A	133.2(3)

solution with a Bruker WP250 spectrometer; chemical shifts are quoted in δ values relative to $SiMe_4$ as an internal standard.

$[(Me_3Si)_2NZnOSi\mathit{i}Pr_3]_2$ (1a): A solution of $Zn[N(SiMe_3)_2]_2$ (Aldrich) (1.43 g, 3.71 mmol) in toluene (30 mL) was allowed to react with $\mathit{i}Pr_3SiOH$ (0.65 g, 3.71 mmol) at −78 °C. After stirring, the clear mixture for 6 h at room temperature, the volatile components were removed under reduced pressure (10^{-3} Torr, 40 °C) and the residue was redissolved by gently heating in a small volume of hexane. Colorless crystals of **1a** were deposited at room temperature. Yield: 1.24 g (1.55 mmol, 84%); m.p. 186−189 °C (decomp.). − ^{1}H NMR (C_6D_6): δ = 0.42 (s, 36 H, SiMe), 1.29 (sept, 6 H, C*H*Me$_2$), 1.35 (d, 36 H, CH*Me*$_2$). − ^{13}C NMR (C_6D_6): δ = 5.7 [q, 12 C, $SiMe_3$, ^1J(C,H) = 117 Hz], 16.3 [d, 6 C, *C*HMe$_2$, ^1J(C,H) = 116 Hz], 19.3 [q, 12 C, CH*Me*$_2$, ^1J(C,H) = 126 Hz]. − ^{29}Si NMR (C_6D_6): δ = −1.5 [dec, 4 Si, $SiMe_3$, ^2J(Si,H) = 3.8 Hz], 15.3 (m, 2 Si, Si$\mathit{i}Pr_3$). − $C_{30}H_{78}N_2O_2Si_6Zn_2$ (798.2): calcd. C 45.14, H 9.85; found C 44.98, H 9.83.

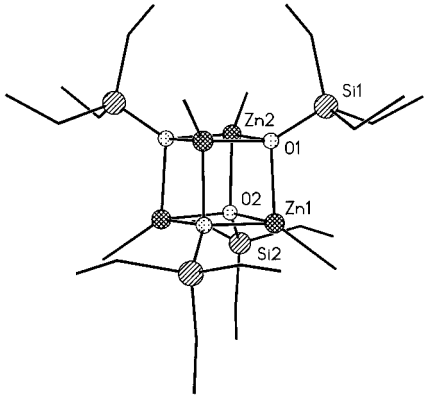


Figure 4. Molecular structure of **3b**; H atoms are omitted for clarity

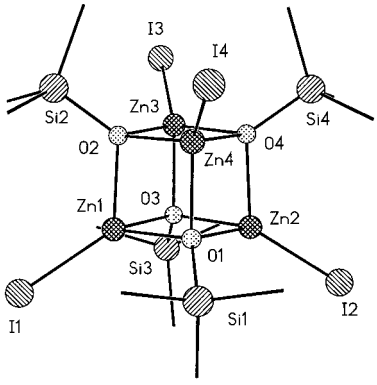


Figure 5. Solid-state structure of **4a**

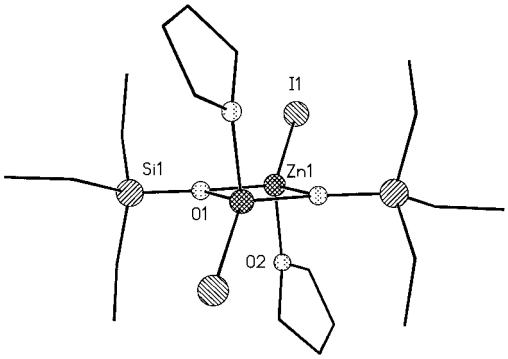


Figure 6. Molecular structure of **5b**; H atoms are omitted for clarity

$[(Me_3Si)_2NZnOSiEt_3]_2$ (1b), $\{[(Me_3Si)_2NZn]_2Zn(OSiEt_3)_4\}$ (2b): The product **1b** was prepared in a similar manner as **1a**. However, from common organic solvents, **1b** could only be crystallized in the form of a 1:1 mixture with **2b**. Reaction of a solution of zinc diamide (1.37 g, 3.55 mmol) in toluene (20 mL) with Et_3SiOH (0.47 g, 3.55 mmol) afforded colorless plates. Yield: 1.03 g; m.p. 167−170

Table 2. Details of the crystal structure determinations of **1a**, **2a**, **2c**, **3b**, **4a**, and **5b**

Compound	**1a**	**2a**	**2c**	**3b**	**4a**	**5b**
Crystal colour	transparent	transparent	transparent	transparent	transparent	transparent
Crystal size [mm]	0.1 × 0.2 × 0.1	0.2 × 0.2 × 0.2	0.3 × 0.1 × 0.1	0.2 × 0.3 × 0.3	0.1 × 0.1 × 0.1	0.2 × 0.2 × 0.2
Empirical formula	$C_{30}H_{78}N_2O_2Si_6Zn_2$	$C_{38}H_{90}O_4Si_4Zn_3$	$C_{24}H_{72}N_2O_4Si_8Zn_3$	$C_{28}H_{72}O_4Si_4Zn_4$	$C_{12}H_{36}I_4O_4Si_4Zn_4$	$C_{20}H_{46}I_2O_4Si_2Zn_2$
Formula mass	798.22	919.57	873.67	846.70	1125.96	791.28
Temperature [K]	203	203	203	203	203	203
Radiation (graphite-monochromated)	Mo-K_α	Mo-K_α	Mo-K_α	Mo-K_α	Mo-K_α	Mo-K_α
Wavelength [Å]	0.71073	0.71073	0.71073	0.71073	0.71073	0.71073
Crystal system, space group	monoclinic, *C*2/*c*	monoclinic, *C*2/*c*	orthorhombic, *Pbcn*	monoclinic, *C*2/*c*	monoclinic, $P2_1/c$	orthorhombic, *Pbca*
Unit cell no. reflections	77	74	75	68	62	68
θ range [°]	3.45 to 19.40	3.85 to 19.20	3.55 to 18.65	4.10 to 19.50	4.05 to 20.05	4.05 to 18.95
a [Å]	30.8683(7)	21.200(5)	11.686(2)	21.419(7)	18.484(7)	14.360(6)
b [Å]	14.2321(3)	11.738(3)	17.920(3)	11.630(4)	10.982(8)	14.656(6)
c [Å]	20.5578(5)	22.367(4)	23.539(4)	20.149(7)	21.932(2)	15.006(6)
α [°]	90	90	90	90	90	90
β [°]	96.220(1)	115.330(1)	90	119.850(2)	111.91(5)	90
γ [°]	90	90	90	90	90	90
Volume [Å^3]	8978.3(4)	5031(2)	4929.2(15)	4353(3)	4130(5)	3158(2)
Z, $D_{calcd.}$ [Mg m^{-3}]	8, 1.181	4, 1.214	4, 1.177	4, 1.292	4, 1.936	4, 1.660
Abs. coeff. μ [mm^{-1}]	1.254	1.546	1.668	2.313	5.420	3.570
Diffractometer	Bruker axs SMART 1000	Bruker axs SMART 1000	Bruker axs SMART 1000	Bruker axs SMART 1000	Bruker axs SMART 1000	Bruker axs SMART 1000
Scan	ω-scan	ω-scan	ω-scan	ω-scan	ω-scan	ω-scan
F(000)	3456	1984	1856	1792	2280	1560
θ range for data collection [°]	1.58 to 34.04	2.01 to 25.00	1.73 to 25.19	2.07 to 27.50	1.91 to 25.23	2.41 to 25.00
Index range	$-48 \le h \le 37$ $-21 \le k \le 22$ $-32 \le l \le 31$	$0 \le h \le 22$ $0 \le k \le 13$ $-26 \le l \le 24$	$-13 \le h \le 13$ $-21 \le k \le 12$ $-28 \le l \le 27$	$0 \le h \le 17$ $0 \le k \le 15$ $-26 \le l \le 22$	$-22 \le h \le 14$ $-13 \le k \le 12$ $-23 \le l \le 26$	$-11 \le h \le 9$ $-17 \le k \le 3$ $-17 \le l \le 9$
Refl. collected/unique [R_{int}]	49725/17292 [0.0587]	4423/4295 [0.0601]	24024/4400 [0.0481]	4187/4057 [0.0598]	20856/7408 [0.1166]	4578/1946 [0.0743]
Refl. observed ($[I_0 > 2\sigma(I_0)]$)	13670	3483	3285	1670	6155	1511
Data/restraints/parameters	17292/0/379	4295/0/223	4400/0/186	4057/3/183	7408/6/297	1946/0/137
Goodness-of-fit on F^2	1.115	0.975	1.030	0.745	1.069	1.051
Final *R*1, *wR*2 [$I > 2\sigma(I)$]	0.0482, 0.0990	0.0365, 0.0928	0.0451, 0.1226	0.0536, 0.1243	0.0674, 0.1684	0.0498, 0.1391
*R*1, *wR*2 (all data)	0.0715, 0.1117	0.0449, 0.0947	0.0643, 0.1411	0.1241. 0.1372	0.0780, 0.1790	0.0650, 0.1530
Extinction coefficient	–	0.00203	–	0.0003	0.0014	0.0028
Diff. peak and hole [e Å^{-3}]	0.963 and −1.230	0.547 and −0.940	0.672 and −0.470	0.392 and −0.545	1.908 and −1.924	0.651 and −0.846

°C (decomp.). The structure of this mixture was established by X-ray crystallography, which confirmed the presence of equimolar amounts of **1b** and **2b**. The moderate crystal quality did not permit a satisfactory refinement of the data.

[(MeZn)$_2$Zn(OSi*i*Pr$_3$)$_4$] (2a): At −78 °C, a solution of $ZnMe_2$ (1.44 g, 15.2 mmol, 2 M solution in toluene; Aldrich) in toluene (ca. 100 mL) was slowly treated with a solution of *i*Pr$_3$SiOH (3.52 g, 20.3 mmol) in toluene (10 mL), which resulted in the immediate evolution of methane. The solution was then allowed to warm to room temperature and all volatiles were removed in vacuo (10^{-3} Torr). Colorless plates were obtained after recrystallization of the residue from a small volume of hexane at 25 °C. Yield: 3.53 g (3.84 mmol, 76%); m.p. 211−214 °C (decomp.). − ^{1}H NMR (C_6D_6): δ = −0.05 (s, 6 H, ZnMe), 1.12 [sept, 12 H, C*H*Me$_2$, ^3J(H,H) = 6.8 Hz], 1.20 [d, 72 H, CH*Me*$_2$, ^3J(H,H) = 6.8 Hz]. − ^{13}C{1H} NMR (C_6D_6): δ = −11.9 (s, 2 C, ZnMe), 15.6 (s, 12 C, *C*HMe$_2$), 19.2 (s, 24 C, CH*Me*$_2$). − ^{29}Si{^{1}H} NMR (C_6D_6): δ = 14.9 (s). − $C_{38}H_{90}O_4Si_4Zn_3$ (919.6): calcd. C 49.63, H 9.86; found C 49.19, H 9.85.

{[(Me$_3$Si)$_2$NZn]$_2$Zn(OSiMe$_3$)$_4$} (2c): Product **2c** was prepared in a similar manner as **2a**, starting from Zn[N(SiMe$_3$)$_2$]$_2$ (1.01 g, 2.62 mmol) and Me$_3$SiOH (0.31 g, 3.49 mmol). Recrystallization of the residue from hexane (10 mL) afforded colorless cubes. Yield: 0.60 g (0.069 mmol, 79%); m.p. 218−222 °C (decomp.). − ^{1}H NMR (C_6D_6): δ = 0.31 (s, 36 H, OSiMe), 0.44 (s, 36 H, NSiMe), 1.27 (sept, 6 H, C*H*Me$_2$), 1.34 (d, 36 H, CH*Me*$_2$). − ^{13}C{^{1}H} NMR (C_6D_6): δ = 3.1 (s, 12 C, OSiMe$_3$), 5.7 (s, 12 C, NSiMe$_3$), 16.0 (s, 6 C, *C*HMe$_2$), 19.4 (s, 12 C, CH*Me*$_2$). − ^{29}Si{^{1}H} NMR (C_6D_6): δ = −1.5 (s, 4 Si, NSiMe$_3$), 19.6 (s, 4 Si, OSiMe$_3$). − $C_{24}H_{72}N_2O_4Si_8Zn_3$ (873.6): calcd. C 32.99, H 8.30; found C 32.34, H 8.28.

[MeZnOSiMe$_3$]$_4$ (3a): This compound was prepared and characterized according to a literature procedure.[6]

[MeZnOSiEt$_3$]$_4$ (3b): At −78 °C, a solution of $ZnMe_2$ (0.90 g, 11.11 mmol, 2 M solution in toluene; Aldrich) in toluene (ca. 80 mL) was treated with Et$_3$SiOH (1.46 g, 11.11 mmol). After methane evolution had ceased, the clear solution was concentrated to dryness in vacuo. Recrystallization of the residue from hexane afforded colorless plates. Yield: 2.23 g (2.63 mmol, 95%). − ^{1}H NMR (C_6D_6): δ = 0.01 (s, 12 H, ZnMe), 0.96 [q, 24 H, CH_2Me, ^3J(H,H) = 7 Hz], 1.08 [t, 36 H, CH_2*Me*, ^3J(H,H) = 7 Hz]. − ^{13}C{^{1}H} NMR (C_6D_6): δ = −8.30 (s, 4 C, ZnMe), 7.97 (s, 12 C, CH$_2$*Me*), 8.70 (s, 12 C, *C*H$_2$Me). − ^{29}Si{^{1}H} NMR (C_6D_6): δ = 23.8 (s). − $C_{28}H_{72}O_4Si_4Zn_4$ (846.7): calcd. C 39.71, H 8.57; found C 39.11, H 8.50.

$[IZnOSiMe_3]_4$ (4a): A solution of **3a** (1.37 g, 2.02 mmol) was treated with I_2 (4.90 g, 8.08 mmol) at room temperature. The violet color of the mixture slowly disappeared in the course of about 48 h. Evaporation of all volatile components in vacuo (10^{-3} Torr) afforded a solid residue, which was redissolved by gently heating in a small volume of hexane. The product **4a** crystallized in the form of colorless cubes. Yield: 2.00 g (1.70 mmol, 88%). – ^{1}H NMR (C_6D_6): δ = 0.62 (s, SiMe). – ^{13}C NMR (C_6D_6): δ = 4.20 [q, SiMe, ^1J(C,H) = 119 Hz]. – ^{29}Si{^{1}H} NMR (C_6D_6): δ = 37.7 (s). – $C_{12}H_{36}I_4O_4Si_4Zn_4$ (1126): calcd. C 12.80, H 3.22; found C 12.47, H 3.19.

$[IZnOSiEt_3]_4$ (4b): Derivative **4b** was prepared in a similar manner as **4a**, starting from **3b** (1.01 g, 1.19 mmol) and I_2 (1.21 g, 4.76 mmol). Recrystallization of the residue from hot benzene afforded colorless cubes. Yield: 1.15 g (0.97 mmol, 82%). – ^{1}H NMR (C_6D_6): δ = 0.91 [q, C*H*$_2$Me, ^3J(H,H) = 7 Hz], 1.01 [t, CH$_2$*Me*, ^3J(H,H) = 7 Hz]. – ^{13}C{^{1}H} NMR (C_6D_6): δ = 7.97 (s, CH$_2$*Me*), 8.70 (s, *C*H$_2$Me). – ^{29}Si{^{1}H} NMR (C_6D_6): δ = 23.2 (s). – $C_{24}H_{60}I_4O_4Si_4Zn_4$ (1294): calcd. C 22.27, H 4.67; found C 22.04, H 4.61.

$[IZn(THF)OSiMe_3]_2$ (5a) and $[IZn(THF)OSiEt_3]_2$ (5b): The heterocubanes **4a** (1.00 g, 0.88 mmol) and **4b** (1.10 g, 0.93 mmol) were dissolved in THF at room temperature. Complete evaporation of the solvent in vacuo (10^{-3} Torr) and recrystallization of the residue from hexane afforded colorless cubes in quantitative yield. – **5a:** ^{1}H NMR (C_6D_6): δ = 0.65 (s, 18 H, SiMe), 1.32 (m, 8 H, THF), 3.50 (m, 8 H, THF). – ^{29}Si{^{1}H} NMR (C_6D_6): δ = 36.7 (s). – $C_{14}H_{34}I_2O_4Si_2Zn_2$ (707.1): calcd. C 23.78, H 4.84; found C 23.23, H 4.80. – **5b:** ^{1}H NMR (C_6D_6): δ = 0.99 [q, 12 H, C*H*$_2$Me, ^3J(H,H) = 7 Hz], 1.01 [t, 18 H, CH$_2$*Me*, ^3J(H,H) = 7 Hz], 1.28 (m, 8 H, THF), 3.44 (m, 8 H, THF). – ^{29}Si{1H} NMR (C_6D_6): δ = 23.7 (s). – $C_{20}H_{46}O_4I_2Si_2Zn_2$ (791.3): calcd. C 30.35, H 5.86; found C 30.11, H 5.84.

X-ray Structure Determinations: Experimental details relating to the X-ray crystal structure determinations of **1a**, **2a**, **2c**, **3b**, **4a**, and **5b** are listed in Table 2. The intensities were measured with a Bruker-axs-SMART 1000 diffractometer. The structures were solved by direct methods (SHELXS-97). Refinements were carried out using the SHELXL-97 package. All nonhydrogen atoms were refined with anisotropic temperature factors. The hydrogen atoms were placed in calculated positions and refined isotropically in riding mode. All refinements were made by full-matrix least-squares methods on F^2. Crystallographic data (excluding structure factors) for the structures reported in this paper have been deposited with the Cambridge Crystallographic Data Centre as supplementary publication nos. CCDC-143075 (**1a**), -143076 (**2c**), -143077 (**4a**), -143078 (**2a**), -143079 (**5b**), and -143080 (**3b**). Copies of the data can be obtained free of charge on application to the CCDC, 12 Union Road, Cambridge CB2 1EZ, U.K. [Fax: (internat.) + 44-1223/336-033; E-mail: deposit@ccdc.cam.ac.uk].

Acknowledgments

We thank the Deutsche Forschungsgemeinschaft, the Fonds der Chemischen Industrie, and the Ministerium für Wissenschaft, Schule, und Weiterbildung, Nordrhein-Westfalen (Germany), for support.

[1] [1a] K. G. Coulton, L. G. Hubert-Pfalzgraf, *Chem. Rev.* **1990**, *90*, 969. –[1b] C. D. Chandler, C. Roger, M. J. Hampden-Smith, *Chem. Rev.* **1993**, *93*, 1205. –[1c] D. J. Teff, J. C. Huffman, K. G. Coulton, *J. Am. Chem. Soc.* **1996**, *118*, 4030. –[1d] P. O'Brien, *Precursors for Electronic Materials* in *Inorganic Materials* (Eds.: D. W. Bruce, D. O'Hare), Wiley, New York, **1996**, p. 525.

[2] [2a] K. W. Terry, T. D. Tilley, *Chem. Mater.* **1991**, *3*, 1001. –[2b] K. W. Terry, K. Su, T. D. Tilley, A. L. Rheingold, *Polyhedron* **1998**, *5–6*, 891.

[3] [3a] H. M. M. Shearer, C. B. Spencer, *Chem. Commun.* **1966**, 194. –[3b] H. M. M. Shearer, C. B. Spencer, *Acta Crystallogr., Sect. B* **1980**, *B36*, 2046. –[3c] M. L. Ziegler, J. Weiss, *Angew. Chem.* **1970**, *82*, 931. –[3d] J. Boersma, A. L. Spek, J. G. Noltes, *J. Organomet. Chem.* **1974**, *81*, 7. –[3e] M. Ishimori, T. Hagiwara, T. Tsuruta, Y. Kai, N. Yasuoka, N. Kasai, *Bull. Chem. Soc. Jpn.* **1976**, *49*, 1165.

[4] [4a] T. D. Tilley, K. Su, M. J. Sailor, *J. Am. Chem. Soc.* **1996**, *118*, 3459. –[4b] M. G. Walawalkar, H. W. Roesky, *Acc. Chem. Res.* **1999**, *32*, 117. –[4c] C. G. Lugmair, T. D. Tilley, *Inorg. Chem.* **1998**, *37*, 6304.

[5] [5a] I. G. Dance, A. Choy, M. L. Scudder, *J. Am. Chem. Soc.* **1984**, *106*, 6285. –[5b] M. M. Olmstead, P. P. Power, S. C. Shoner, *J. Am. Chem. Soc.* **1991**, *113*, 3379.

[6] [6a] F. Schindler, H. Schmidbaur, U. Krüger, *Angew. Chem.* **1965**, *77*, 865. –[6b] F. Schindler, H. Schmidbaur, *Angew. Chem.* **1967**, *79*, 697.

[7] [7a] M. Krieger, R. O. Gould, B. Neumüller, K. Harms, K. Dehnicke, *Z. Anorg. Allg. Chem.* **1998**, *624*, 1434. –[7b] M. Driess, K. Merz, S. Rell, unpublished. –[7c] S. Abram, U. Abram, R. Meyer zu Köck, K. Dehnicke, *Z. Anorg. Allg. Chem.* **1996**, *622*, 867.

[8] S. C. Goel, M. Y. Chiang, W. F. Buhro, *Inorg. Chem.* **1990**, *29*, 4646.

[9] M. A. Putzer, B. Neumüller, K. Dehnicke, *Z. Anorg. Allg. Chem.* **1997**, *623*, 539.

[10] [10a] B. Müller, H. Vahrenkamp, *Eur. J. Inorg. Chem.* **1999**, 129. –[10b] G. Sawitzki, H. G. von Schnering, *Chem. Ber.* **1974**, *107*, 3266.

Received April 17, 2000
[I00147]

η^1- and η^3-Allylpalladium(II) Complexes Bearing Potentially Tridentate Ligands: Synthesis, Solution Dynamics, and Crystal Structures

Laurent Barloy,[a] Shailesh Ramdeehul,[a] John A. Osborn,*[a][†] Claire Carlotti,[b] Francis Taulelle,[b] André De Cian,[c] and Jean Fischer[c]

Keywords: Palladium / Allyl complexes / Tridentate ligands / Fluxionality

The potentially tridentate ligands 2,2′:6′,2"-terpyridine (terpy) and 2,6-bis(diphenylphosphanylmethyl)pyridine (PNP) have been used to prepare novel palladium–allyl complexes of general formula [(terpy)Pd(CH_2CHCRR')](BF_4) [R = R′ = H (**1**); R = H, R′ = Me (**2**); R = R′ = Me (**3**)] and [(PNP)Pd(CH_2CHCRR')](BF_4) [R = R′ = H (**4**); R = H, R′ = Me (**5**); R = R′ = Me (**6**)], which were characterized by elemental analysis, IR spectroscopy, and ^{13}C, ^{31}P and variable-temperature ^1H NMR spectroscopy. The low-temperature ^1H NMR spectra show that the configuration of the complexes in solution depends strongly on the nature of the ligand. The terpy complexes **1**–**3** are η^3-allyl species, where terpy is dihapto and one pyridine ring remains uncoordinated, whereas the PNP complexes **4**–**6** occur as η^1-allyl compounds with a trihapto PNP ligand. All complexes are fluxional through η^3-η^1 exchange processes. Energy barriers of 47.5–48.6 kJ·mol^{-1} (243–262 K) are reported for the interconversion of terminal allylic protons (complexes **2**–**4**). $\Delta G^{\ddagger}$ is higher (71.1 kJ·mol^{-1} at 350 K) for the interconversion of the methyl groups in complex **6**. A lower-barrier oscillatory mechanism involving terpy ($\Delta G^{\ddagger}$ = 43.9 kJ·mol^{-1} at 231 K) is also involved in complex **1**. The X-ray structures of complexes [(η^3-terpy)Pd(η^1-C_5H_9)](BF_4) (**3a**) and [(η^3-PNP)Pd(η^1-C_4H_7)](BF_4) (**5a**) are reported; the structure of **3a** corresponds to a species that is not observed in solution.

Introduction

Palladium−allyl complexes have been much studied in the last thirty years, and have recently attracted even more attention because of their importance as intermediates in palladium-catalyzed allylic substitution (e.g. alkylation) reactions. Attack of the nucleophile on a cationic palladium η^3-allyl complex is at present conventionally accepted as the crucial step in the catalytic cycle.[1] One major goal in allylic alkylation catalysis is to achieve regio-, stereo- or enantioselectivity, especially by modifying the nature of the spectator ligand. Up to now, few examples have been reported concerning the use of potentially meridional tridentate ligands in palladium allyl chemistry[2−5] or in palladium-catalyzed allylic alkylation.[5,6] This type of ligand is prone to stabilize a η^1-allyl palladium complex, which was proposed in some cases as another possible intermediate in allylic substitution.[7]

We have lately been interested in the use of potentially tridentate ligands, such as the mixed-P,N-donor ligand 2,6-(diphenylphosphanylmethyl)pyridine (PNP) and its derivatives, in coordination chemistry and catalysis.[8] We have also reported preliminary results in palladium allyl chemistry with 2,2′:6′,2"-terpyridine (terpy).[9] Therefore we decided to investigate the influence of the nature of the tridentate ligand and the allyl ligand on the structure of the corresponding complex.

We report here the synthesis and complete characterization, especially by X-ray diffraction analysis and variable-temperature NMR spectroscopy, of palladium allyl complexes bearing the terpy and PNP ligands.

Results and Discussion

The complexes **1**−**6** were prepared in good chemical yields (73−92%) by abstraction of Cl^- from the corresponding chloride-bridged allylpalladium dimers with a silver salt, followed by coordination of palladium(II) with the appropriate ligand (Table 1). They were obtained as air-

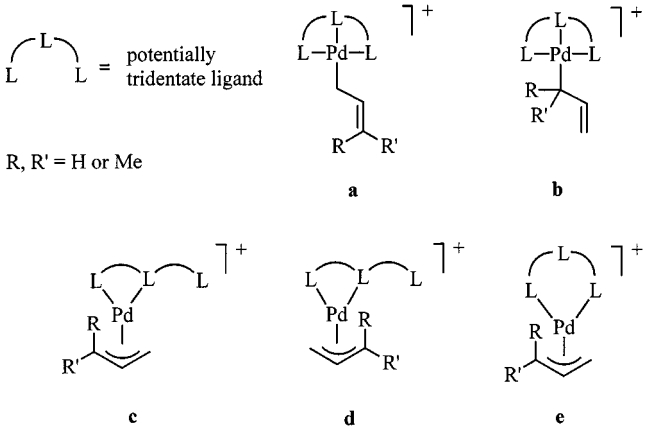
Table 1. Synthesized palladium complexes [(ligand)-Pd(CH_2CHCRR')](BF_4)

Complex	Ligand	R	R′
1	terpy	H	H
2	terpy	H	Me
3	terpy	Me	Me
4	PNP	H	H
5	PNP	H	Me
6	PNP	Me	Me

[a] Laboratoire de Chimie des Métaux de Transition et de Catalyse, UMR 7513 CNRS, Institut Le Bel, Université Louis Pasteur, 4 rue Blaise Pascal, 67070 Strasbourg Cedex, France
Fax: (internat.) +33-388/416-171
E-mail: barloy@chimie.u-strasbg.fr
[†] Deceased April 23, 2000. Send further correspondence to L. Barloy.
[b] RMN et Chimie du Solide, UMR 7510 CNRS, Institut Le Bel, Université Louis Pasteur, 4 rue Blaise Pascal, 67070 Strasbourg Cedex, France
[c] Laboratoire de Cristallochimie et Chimie Structurale, UMR 7513 CNRS, Institut Le Bel, Université Louis Pasteur, 4 rue Blaise Pascal, 67070 Strasbourg Cedex, France
Supporting information for this article is available on the WWW under http://www.wiley-vch.de/home/eurjic or from the author.

 © WILEY-VCH Verlag GmbH, D-69451 Weinheim, 2000 1434−1948/00/1212−2523 $ 17.50+.50/0

stable, yellow to red powders, which were soluble in dichloromethane or acetonitrile. If we assume that these palladium complexes are square planar, we can consider that they can adopt five possible configurations (Scheme 1). It is the purpose of our study to determine which configuration is adopted by each complex in solution and/or in the solid state.



Scheme 1. Potential isomeric forms of complexes **1**–**6**

Variable-Temperature ^{1}H NMR Spectroscopy

The room-temperature ^{1}H NMR spectra of most of the synthesized complexes show some broad resonances, which is a hint that they are fluxional. Variable-temperature NMR analysis indicates that this is actually the case for all of them. It was necessary to record the spectra at low temperature (184–200 K) in order to detect the frozen species, except for complex **6**. Selected ^{1}H signals and H-H or H-P coupling constants of complexes **1**–**6** at low temperature and high or room temperature are given in Table 2 and Table 3.

The low-temperature ^{1}H NMR spectra of complexes **1**, **2**, and **3** display eleven terpy signals and five signals belonging to the allylic moiety. This pattern is characteristic of η^3-allylpalladium complexes with an unsymmetrical terpy ligand, of which only two nitrogen atoms coordinate to the metal center, viz. under the form **c** or **d** (Scheme 1). A thorough analysis shows that the actual configuration is **c**, which is also the less sterically constrained one (Scheme 2;

Table 2. ^{1}H NMR spectroscopic data for the terpy ligand in complexes **1**–**3**

Complex	T [K]	H^4/H^{18} [a]	H^5/H^{17}	H^6/H^{16}	H^7/H^{15}	H^{10}/H^{12}	H^{11}
1	298	8.81 (dt, 5.1, 1.3[b][c])	7.63 (ddd, 5.1, 7.1, 2.0[b])	8.13 (m)	8.13 (m)	8.24 (d, 7.3)	8.35 (t, 7.9)
	188	8.76 (m)	7.56 (app t, 5.9, H^{17}) 7.66 (app t, 6.1, H^5)	7.96 (m, H^{16}) 8.22 (app t, 7.6, H^6)	7.81 (d, 6.3, H^{15}) 8.40 (m, H^7)	7.96 (m, H^{12}) 8.40 (m, H^{10})	8.32 (app t, 7.9)
2	298	8.75 (d, 4.3)	7.66 (app t, 6.1)	8.13 (app t, 7.5)	8.18 (d, 8)	8.27 (d, 7.8)	8.34 (t, 7.8)
	191	8.56 (d, 5.4, H^4) 8.75 (d, 4.6, H^{18})	7.55 (app t, 6.3, H^{17}) 7.73 (app t, 6.3, H^5)	7.94 (app t, 7.8, H^{16}) 8.23 (app t, 7.9, H^6)	7.85 (br, H^{15}) 8.36 (d, 8.6, H^7)	8.01 (d, 7.2, H^{12}) 8.40 (d, 8.3, H^{10})	8.31 (app t, 7.8)
3	298	8.72 (d, 4.8)	7.69 (ddd, 5.3, 6.9, 1.4[b])	8.15 (m)	8.15 (m)	8.26 (d, 7.8)	8.34 (t, 7.8)
	200	8.54 (d, 4.8, H^4) 8.78 (d, 4.3, H^{18})	7.56 (app t, 6.0, H^{17}) 7.76 (app t, 6.3, H^5)	7.96 (app t, 7.1, H^{16}) 8.24 (app t, 7.6, H^6)	7.85 (br, H^{15}) 8.37 (d, 8.6, H^7)	8.01 (d, 7.8, H^{12}) 8.39 (d, 8.3, H^{10})	8.30 (app t, 7.8)

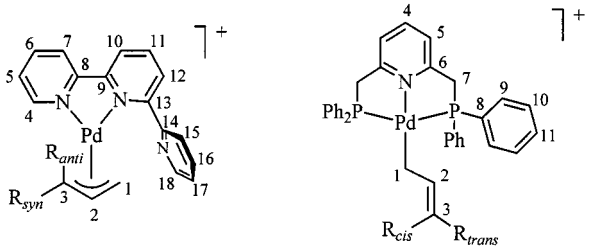
[a] Chemical shift data (ppm) of spectra recorded in CD_2Cl_2 on a 300 MHz (**1**) or a 400 MHz (**2**, **3**) spectrometer. For the adopted numbering scheme, see Scheme 2. Multiplicity: d = doublet, t = triplet, m = multiplet, br = broad signal, app = apparent. Numbers in parentheses are coupling constants (Hz) ($^3J_{HH}$ unless otherwise stated). – [b] $^4J_{HH}$. – [c] $^5J_{HH}$.

Table 3. ^{1}H NMR spectroscopic data for the allyl ligands in complexes **1**–**6**

Complex	T [K]	H^{2}[a]	H^1	R, R′
1	298	5.55 (quintuplet, 9.8)	3.14 (d, 9.6)	
	188	5.47 (app tt, 12.6, 6.8)	2.13 (d, 6.3, H^{syn}) 2.51 (d, 12.2, H^{anti})	3.35 (d, 12.3, H^{3anti}) 4.06 (d, 6.3, H^{3syn})
2	336[b]	5.36 (app q, 10.0)	2.83 (d, 9.1)	1.20 (d, 6.2, Me) 4.01 (dq, 10.8, 6.0, H^3)
	191[c]	5.16 (d app t, 7.0, 12.3)	2.11 (br, H^{syn})[d] 2.30 (br, H^{anti})[d]	1.40 (d, 5.9, Me) 3.86 (br, H^3)
3	298[c]	5.08 (t, 10.4)	2.51 (d, 10.2)	1.58 (s), 1.22 (s)
	200[c]	4.98 (dd, 13.1, 7.5)	2.15 (d, 6.4, H^{syn}) 2.57 (d, 13.1, H^{anti})	1.53 (s), 1.14 (s)
4	325[e]	5.67 (quintuplet t, 11.0, 1.3[f])	3.55 (d, 10.2)	
	184	5.63 (ddt, 16.3, 9.8, 8.8)	2.62 (dt, 8.4, 5.3[f])	4.18 (d, 16.4, H^{3cis}) 4.28 (d, – [g], H^{3trans})
5	325[e]	5.29 (dttq[h], 14.3, 8.4, 1.5[f], 1.5[i])	2.72 (dt, 8.6, 5.1[f])	1.12 (d, 5.5, Me) 4.83 (dq, 14.0, 5.5, H^3)
	220[j]	5.22 (dt, 14.7, 8.2)	2.62 (dt, 7.8, 5.5[f])	1.13 (d, 5.1, Me) 4.63 (dq, 14.7, 6.0, H^3)
6	298[e]	5.04 (t, 9.0)	2.70 (dt, 8.6, 4.4[f])	1.13 (s), 0.96 (s)

[a] Chemical shift data (ppm) of spectra recorded in CD_2Cl_2 on a 300 MHz spectrometer unless otherwise stated. For the adopted numbering scheme, see Scheme 2. Multiplicity: d = doublet, t = triplet, q = quadruplet, br = broad signal, app = apparent. Numbers in parentheses are coupling constants (Hz) ($^3J_{HH}$ unless otherwise stated). – [b] Solvent CD_3CN. – [c] Recorded at 400 MHz. – [d] Sharper signals at 210 K indicate J = ca. 11 Hz for H^{anti} and J = ca. 6 Hz for H^{syn}. – [e] Solvent $CDCl_3$. – [f] J_{HP} – [g] Overlap with the H^7 signal. – [h] apparent dt sextuplet. – [i] $^4J_{HH}$. – [j] Major species.

vide infra). No traces of other isomeric compounds (especially **a**) were detected at any temperature.



Scheme 2. Complexes present in solution according to low-temperature NMR spectroscopic data

The assignment of all signals could be made with the help of proton-decoupling experiments and/or NOE and scalar-coupling cross-peaks in 2D-ROESY NMR experiments. In fact, the aromatic pattern presents close similarities concerning both multiplicities and chemical shifts to the spectra of other bidentate terpy metal complexes analyzed in detail in the literature (Table 2, Figure 1).[10,11] The aromatic signals of complexes **1**−**3** generally appear at the same chemical shift within ±0.02 ppm at 190−200 K (Table 2). However, two protons do not follow this trend; the chemical shift of H^4 and, to a lesser extent, of H^5 are affected by the nature of the substituents R and R′. For instance, H^4 is shielded by 0.22 ppm and H^5 is deshielded by 0.1 ppm when one changes from **1** (R = R′ = H) to **3** (R = R′ = Me). This can be explained by their proximity to the R and R′ groups.

At 188 K, the H^{1anti} and H^{15} signals of **1** appear broadened; this is probably the result of a fluxional process with a very low energy barrier, i.e. the restricted rotation of the dangling pyridine. In comparison, both analogous frozen rotamers could be clearly observed by low-temperature NMR spectroscopy in the (η^2-terpy)$PtIMe_3$ complex,[10b] where the rotation is more hindered than in complex **1**. The H^1 and H^{15} signals of complexes **2** and **3** undergo the same broadening when the temperature is decreased (see Figure 1 and Figure 2); furthermore, the H^1 protons are shielded by the pendant pyridine (δ = 2.11−2.57) as they are in complex **1**.[9] These observations allow us to rule out the form **d** in favor of form **c** for the terpy complexes (Scheme 1). In the case of complex **2**, the value of the H^2-H^3 coupling constant (12.3 Hz) infers that the methyl group is in the *syn* position, which is common in η^3-allyl palladium complexes.[12]

With an increase in temperature, most of the NMR signals of complexes **1**−**3** broaden, then sharpen to give simplified spectra at or above ambient temperature. We observe the coalescence of pairs of aromatic signals H^4/H^{18}, H^5/H^{17}, H^6/H^{16}, H^7/H^{15}, and H^{10}/H^{12} characteristic of the exchange between the uncoordinating and the coordinating lateral pyridines of terpy (Table 2, Figure 1). The corresponding energy barriers were estimated from the coalescence of the clearly distinguishable H^5 and H^{17} with the help of the Eyr-

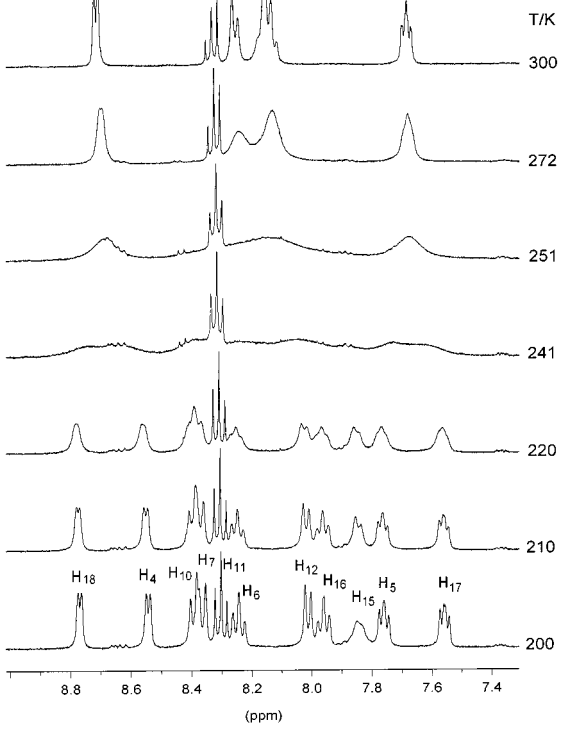


Figure 1. 400 MHz ^{1}H NMR spectra (aromatic region) of [(terpy)$Pd(CH_2CHCMe_2)$](BF_4) **(3)** in CD_2Cl_2 in the range 200−300 K; see Scheme 2 for hydrogen labelling

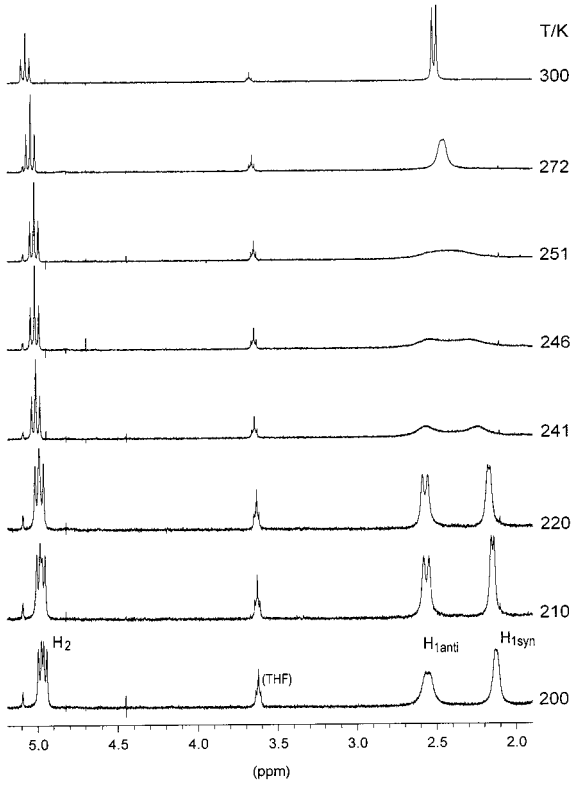


Figure 2. 400 MHz ^{1}H NMR spectra (allylic region) of [(terpy)$Pd(CH_2CHCMe_2)$](BF_4) **(3)** in CD_2Cl_2 in the range 200−300 K; see Scheme 2 for hydrogen labelling

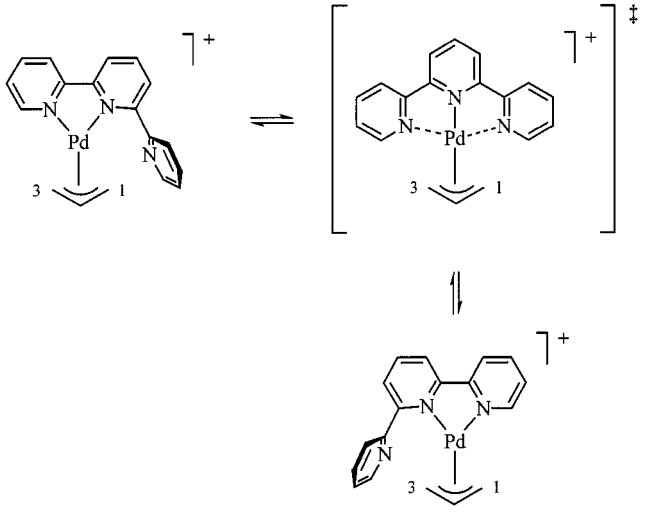
ing equation (see Experimental Section), and are given in Table 4.

Table 4. Variable-temperature ^{1}H NMR spectroscopic data and calculated activation free enthalpies for fluxional processes in complexes **1**−**4** and **6**

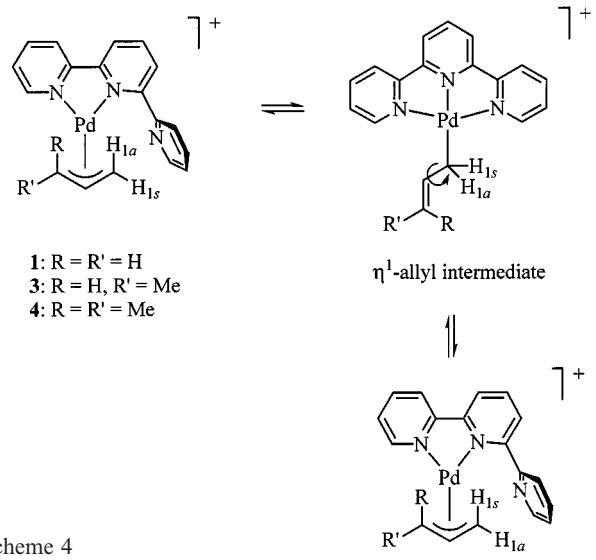
Complex	Δν [Hz]	T_c [K]	$\Delta G^{\ddagger}$ [kJ·mol^{-1}]	Interchanging groups[a]
1[b]	29	210	43.5	H^5/H^{17}
	251	231	43.9	H^{1anti}/H^{3anti}
2[c]	72	243	48.8	H^5/H^{17}
	78	243	48.6	H^{1syn}/H^{1anti}
3[c]	81	243	48.6	H^5/H^{17}
	166	250	48.5	H^{1syn}/H^{1anti}
4[d]	807[e]	262	47.5	$H^1/(H^{3cis} + H^{3trans})$
6[f]	78	350	71.1	Me^{cis}/Me^{trans}

[a] For the adopted numbering scheme, see Scheme 2. − [b] Spectra recorded in CD_2Cl_2 at 300 MHz. − [c] Spectra recorded in CD_2Cl_2 at 400 MHz. − [d] Spectra recorded in CD_2Cl_2 at 500 MHz. − [e] Difference between the average chemical shift of H^{3cis} and H^{3trans}, and the chemical shift of H^1. − [f] Spectra recorded in [D$_6$]DMSO at 400 MHz.

The four signals corresponding to the terminal allylic protons of complex **1** coalesce into one doublet with an average coupling constant of 9.6 Hz.[9] A close examination of the NMR spectra on raising the temperature first shows a coalescence of the H^{1syn} and H^{3syn} signals and another coalescence of the H^{1anti} and H^{3anti} signals, related to a fast chemical exchange between both ends of the allyl moiety. This leads to two very large superimposed signals, which then sharpen into a doublet through a slower *syn-anti* chemical exchange. From the coalescence of both H^{anti} signals, a $\Delta G^{\ddagger}$ value of 43.9 kJ·mol^{-1} can be estimated for the first exchange; this infers that it is concerted with the exchange of the terpy hydrogens (43.5 kJ·mol^{-1}; see Table 4). This is explained by the oscillatory or "tick-tock" twist fluxional motion (Scheme 3), which was introduced by Orrell et al. for similar terpy metallic complexes[10,11] and has been the object of thorough studies and discussions.[13] In the second process, the *syn* and *anti* protons exchange through a classical η^3-η^1-η^3 mechanism,[1b] where the intermediate is probably the form **a** (Scheme 4).



Scheme 3



Scheme 4

A phase-sensitive 2D NMR ROESY spectrum of **1** recorded at 200 K confirms our analysis (Figure 3). Strong H^{1syn}/H^{3syn} and H^{1anti}/H^{3anti} exchange positive cross-peaks are displayed, whereas H^{syn}/H^{anti} exchange cross-peaks are not observed, perhaps because they are hidden under the geminal H^{syn}/H^{anti} NOE cross-peaks of the opposite sign. Thus the *syn*/*anti* exchanges must be slower than the *syn*/*syn* and *anti*/*anti* exchanges, otherwise the corresponding cross-peaks would probably have appeared on the ROESY spectrum in spite of the NOE effect.

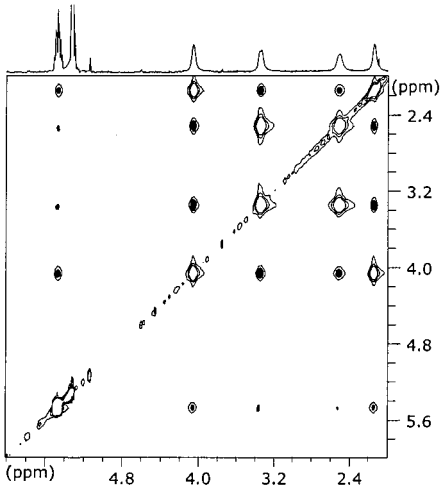


Figure 3. Section of the ^{1}H phase-sensitive ROESY spectrum of [(terpy)Pd(CH_2CHCH_2)](BF_4) **1** (CD_2Cl_2, 200 K, 500 MHz), showing exchange cross peaks and NOE (darkened) cross peaks within the allyl signals

In the spectra of complexes **2** and **3**, the two upfield H^{1syn} and H^{1anti} signals coalesce into a doublet with an average coupling constant; the H^2 signal changes from a doublet of doublets to a triplet (Figure 2). This *syn*/*anti* interconversion also takes place through the mechanism given in Scheme 4 and the corresponding energy barriers agree with the values calculated for the terpy signals (Table 4). These barriers are roughly the same for both complexes (ca.

48.6 kJ·mol^{-1}). This is not surprising if we consider that the number of substituents on the C^3 allylic carbon does not modify the steric hindrance in the intermediate involved in the fluxional process (Scheme 2). It ensues that the energy barrier of the *syn*/*anti* exchange in **1** is very likely to be approximately the same, and thus superior to the "tick-tock" barrier.

The methyl signal of **2** also undergoes some modifications over this temperature range: it broadens and sharpens several times, and this is an indication of additional fluxional processes. We believe that there are equilibria between the major isomer **c** (Me *syn*) and minor ones: isomer **c** (Me *anti*) (via the intermediate **b**) and/or isomer **d** (through the "tick-tock" mechanism) (Scheme 1). Yet the small methyl signals corresponding to these minor isomers could not be clearly distinguished in the NMR spectra. On the contrary, the methyl signals of **3** do not undergo any modification up to 340 K.

The ^{1}H NMR pattern of the PNP ligand in complexes **4**−**6** does not vary with temperature and is indicative of a tridentate coordinating mode. Apart from the aromatic signals, the methylene signal appears as a virtual triplet at δ = 4.3−4.7 (depending on the solvent and the temperature) with a $|^2J_{HP} + {}^4J_{HP'}|$ value of approximately 9 Hz. Such virtual triplets are commonly observed in the same region for other PNP palladium complexes in which the phosphorus atoms are mutually *trans*.[14,15,16]

In contrast to the terpy complexes, the allyl ligand in the frozen complexes **4**−**6** is η^1 (form **a**; see Scheme 1) according to their low-temperature (**4**,**5**) or room-temperature (**6**) NMR spectroscopic data (Table 3, Figure 4). The NMR spectra display four signals for the allyl ligand at the expected chemical shifts that one would expect by comparison with other η^1-allyl palladium complexes reported in the literature.[3,17,18] The value of the H^2-H^3 coupling constant (14.7 Hz) in complex **5** at 220 K indicates that the C−C double bond is in the thermodynamically preferred *trans* form. However, we detect a small methyl doublet at δ = 0.83 at that temperature which probably belongs to the *cis* isomer (ca. 10% according to the signal integration).

When the temperature is increased from 184 K to 325 K, the three allyl signals H^1, H^{3cis} and H^{3trans} of complex **4** coalesce into a doublet at δ = 3.55 (Figure 4). This results from a η^1-η^3-η^1 fluxional process, with an energy barrier of 47.5 kJ·mol^{-1} comparable to the ones estimated for the terpy complexes (Table 4). In complex **5**, the coalescence of the two methyl signals (T_c = 281 K) reveals that the *trans* and *cis* isomers are in equilibrium. The energy barrier calculated for the *trans* to *cis* transformation following the Shanan-Atidi and Bar-Eli method[19] reaches 60.8 kJ·mol^{-1}. We note that at high temperatures, the H^2-H^3 coupling constant is not significantly modified (ca 14 Hz, see Table 3), which suggests that the *cis* form is still minor. The methyl groups of complex **6** also exchange to give rise to a singlet at δ = 1.07 in [D_6]DMSO at high temperature; the coalescence temperature and the energy barrier are then higher (350 K and 71.1 kJ·mol^{-1}, respectively). We propose that η^3-allyl complexes and the η^1-allyl form **b** are involved as intermediates in the chemical exchanges of both complexes (see the mechanism depicted in Scheme 5). The progression of the energy barriers from **4** to **5** and **6** reflects the increasing steric hindrance within the intermediates of the fluxional processes, owing to the proximity of the methyl group(s) and the coordination sphere.

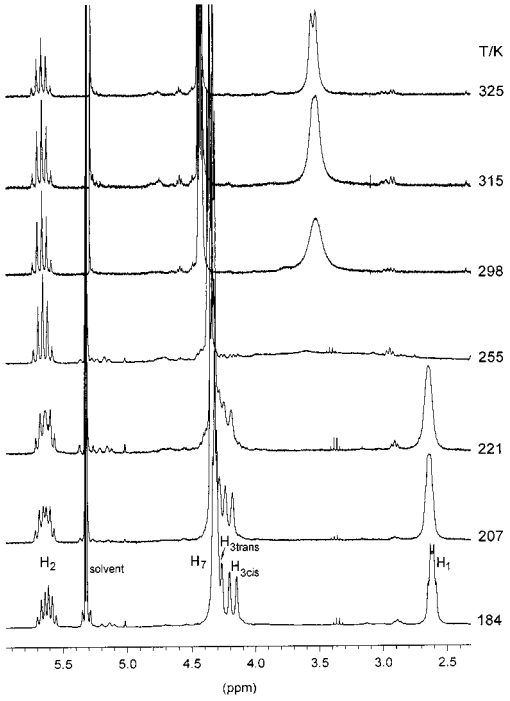
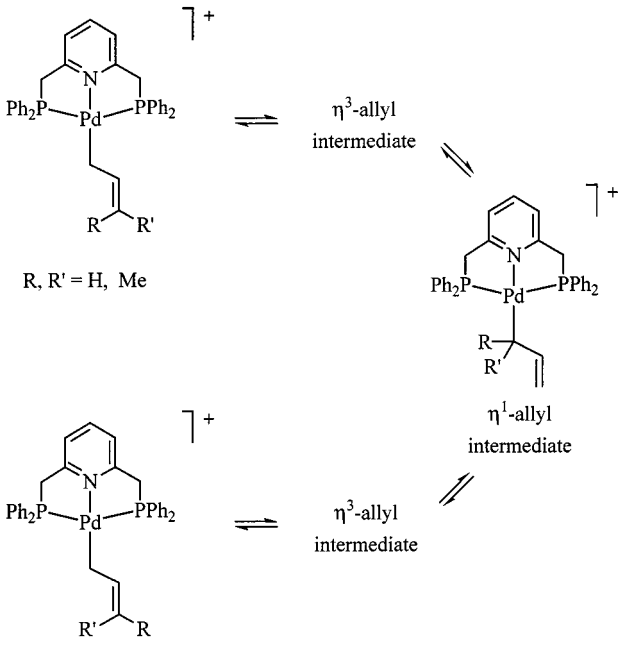


Figure 4. 300 MHz ^{1}H NMR spectra (allylic region) of [(PNP)Pd(CH_2CHCH_2)](BF_4) **(4)** (range 188−255 K: solvent CD_2Cl_2; range 298−325 K: solvent $CDCl_3$); see Scheme 2 for hydrogen labelling



Scheme 5

Table 5. $^{13}C\{^1H\}$ NMR spectroscopic data for the complexes **1**−**6**

Complex	Me[a]	C^1/C^3	C^2	C^4/C^{18}	C^5/C^{17} + C^7/C^{15} + C^{10}/C^{12}	C^6/C^{16}	C^8/C^{14} + C^9/C^{13}	C^{11}
1		63.7	118.4	152.1	124.6, 125.3, 126.7	139.4	157.2, 158.3	141.8
2	17.1	61.3 (C^1), 81.6 (C^3)	− [b]	152.3	125.8, 126.2, 127.6	140.5	157.5, 158.3	142.5
3	26.1 22.0	58.1 (C^1), 93.5 (C^3)	112.1	150.2	124.8, 125.2, 126.8	139.5	157.3, 158.0	141.8

	Me	C^1	C^2	C^3	C^4	C^5	C^6	C^7	C^8	C^9	C^{10}	C^{11}
4[c]		− [b]	142.8	− [b]	141.5	123.8 (9)	159.5	44.6 (27)	129.2 (44)	134.3 (12)	130.5 (10)	132.9
5	18[d]	18[d]	136.0	121.4	141.5	123.8 (9)	159.4	44.7 (28)	129.5 (43)	134.4 (13)	130.5 (10)	132.9
6	17.9 (*cis*) 26.2 (*trans*)	16.1	131.5	133.5	141.4	123.7 (8)	159.2	44.7 (28)	129.7 (43)	134.3 (13)	130.4 (10)	132.8

[a] Chemical shift data (ppm) of spectra recorded at 298 K at a 50 MHz frequency (unless otherwise stated) in CD_2Cl_2 (**1**, **3**) or CD_3CN (**2**, **4**−**6**). For the adopted numbering scheme, see Scheme 2. Numbers in parentheses are coupling constants $|J_{CP} + J_{CP'}|$ (Hz) for virtual triplets. − [b] Signal not detected. − [c] 75 MHz frequency. − [d] Broad signal.

^{13}C and ^{31}P NMR Spectroscopy

In general, the proton-decoupled ^{31}P and ^{13}C NMR spectra recorded at room temperature are in agreement with the room-temperature ^1H NMR spectra, i.e. that of dynamic species (except for **6**). The ^{31}P NMR spectra of complexes **4**−**6** exhibit singlets at δ = 26.0, 25.2, and 25.1, respectively. These values are close to that found by Vasapollo and coworkers for $(PNP)PdCl_2$ (δ = 24.35), and are therefore consistent with the form **a**.[16] The room-temperature ^{13}C NMR spectroscopic data are given in Table 5. The rapidly exchanging C^1 and C^3 nuclei of **1** show a common signal at δ = 63.7. The chemical shifts for **1**, **2**, and **3** are typical of palladium η^3-allyl complexes with nitrogen-donor ligands.[20] In contrast, the vinylic carbons of the η^1-allyl complexes **4**−**6** are deshielded (δ = 121.4−142.8), whereas the C^1 signal (δ = 16.1−18) is typical of a metal-bonded carbon atom.[3c][17f] We can probably not detect the C^1/C^3 signal of **4** because the corresponding temperature of coalescence is very close to room temperature. Besides, the values found for the ^{13}C chemical shifts of the PNP ligand are consistent with the assignment proposed by Taube et al.[15]

Solid-State Analysis

We have previously reported the X-ray structures of the isomeric $[(\eta^3\text{-terpy})Pd(\eta^1\text{-}C_3H_5)]^+$ and $[(\eta^2\text{-terpy})Pd(\eta^3\text{-}C_3H_5)]^+$ cations.[9] Single crystals of **3** and **5** suitable for X-ray diffraction analysis were obtained under a nitrogen atmosphere from dichloromethane solutions by vapor-phase diffusion of diethyl ether (**3**) or pentane (**5**). Their solid-state structures are depicted in Figure 5 and Figure 6, respectively, and selected bond lengths and angles are given in Table 6 and Table 7. They crystallize as monocationic, square-planar palladium complexes and separate noncoordinating anions, and appear as the forms **3a** and **5a**, where the terpy or PNP ligand is tridentate and the allyl ligand monohapto. On the contrary, we note that the X-ray structure of the complex $[(SNS)Pd(CH_2CHCMe_2)]^+$ (SNS = 2,6-bis(dimethylthiomethyl)pyridine), resolved by Canovese et al., reveals a η^3-allyl complex with a noncoordinating sulfur.[4a] We observe a striking resemblance between the structures of $[(\eta^3\text{-terpy})Pd(\eta^1\text{-}C_3H_5)]^+$ and **3a**, which are nearly mirror images of each other, except for the C19 and C20 atoms of **3a**. The bond lengths and bond angles within the (terpy)Pd fragment are of the same order of magnitude, as well as the Pd−C16 bond length.

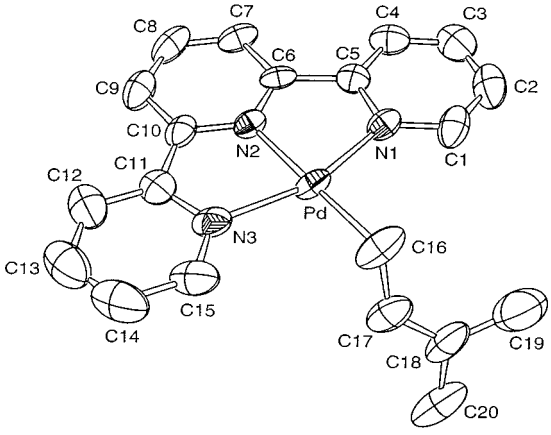


Figure 5. ORTEP drawing of **3a** showing 50% probability thermal ellipsoids and the atom-numbering scheme; hydrogen atoms and the BF_4^- anion are omitted for clarity

Two structures of **5a** are drawn in Figure 6; as long as crystallographic disorder is observed in the allyl ligand, the vinylic carbons C33 and C34 occupy two positions each. However, in both cases the allyl is in the *trans* configuration, which is also the case in the major isomer detected in solution by NMR spectroscopy (vide supra). The dihedral angles P1−Pd−C32−C33 and P1−Pd−C32−C33′ are −115.5° and −79.8°, respectively. Furthermore, the N−Pd−P1 and N−Pd−P2 bond angles are smaller than 90° [81.41(6)° and 81.61(6)°, respectively], owing to the constrained five-membered metallacycles. The palladium, nitrogen and phosphorus atoms are all nearly coplanar, with deviations of less than 0.04 Å. In general, the bond lengths and angles related to PNP and Pd compare well with the data reported for complexes $[(PNP)Pd(PEt_3)](BF_4)_2$[14] and $[(PNP)Pd(styrene)](BF_4)_2$,[15] except for the Pd−N bond length which is longer [2.137(2) Å vs. 2.107(4) and 2.058(4)

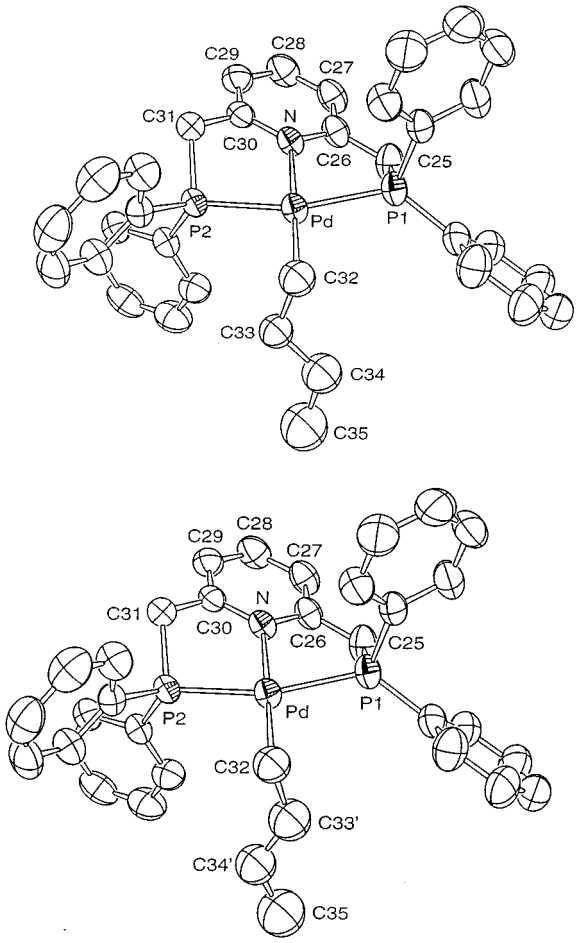


Figure 6. ORTEP drawings of both forms of **5a** showing 50% probability thermal ellipsoids and the atom-numbering scheme, the occupancy ratios for (C33, C34) and (C33′, C34′) being 50%/50%; hydrogen atoms and the BF_4^- anion are omitted for clarity

Table 6. Selected bond lengths [Å] and bond angles [°] for **3a**

Pd−N1	2.083(4)	C16−C17	1.430(9)
Pd−N2	2.017(4)	C17−C18	1.366(9)
Pd−N3	2.076(4)	C18−C19	1.49(1)
Pd−C16	2.054(6)	C18−C20	1.44(1)
N1−Pd−N2	78.6(2)	Pd−N2−C6	118.8(3)
N1−Pd−N3	158.1(2)	Pd−N2−C10	118.2(4)
N1−Pd−C16	102.1(2)	Pd−N3−C11	112.9(3)
N2−Pd−N3	79.5(2)	Pd−N3−C15	127.8(4)
N2−Pd−C16	178.2(2)	Pd−C16−C17	108.2(4)
N3−Pd−C16	99.8(2)	C16−C17−C18	131.7(7)
Pd−N1−C1	128.9(4)	C17−C18−C19	123.0(7)
Pd−N1−C5	113.7(3)	C17−C18−C20	120.5(7)

Å] because of the strong *trans* influence of the η^1-allyl ligand.[21]

The bonds lengths and bond angles of the η^1-allyl fragments of **3a** and **5a** are comparable to other examples of transition metal η^1-allyl complexes.[22] The palladium−carbon bond lengths (2.036−2.075 Å) agree with the moderate *trans* influence of pyridine.[23] We also note that the angle between the plane defined by the three allylic carbons and the coordination plane (mean plane defined by the four coordinating atoms) is roughly the same

Table 7. Selected bond lengths [Å] and bond angles [°] for **5a**

Pd−P1	2.3017(7)	C32−C33′	1.53(1)
Pd−P2	2.2894(7)	C33−C34	1.49(1)
Pd−N	2.137(2)	C34−C35	1.49(1)
Pd−C32	2.075(4)	C35−C34′	1.43(1)
C32−C33	1.425(8)	C33′−C34′	1.32(1)
P1−Pd−P2	162.76(3)	Pd−P1−C25	97.57(4)
P1−Pd−N	81.41(6)	Pd−P2−C31	98.20(3)
P1−Pd−C32	99.5(1)	Pd−C32−C33	109.8(1)
P2−Pd−N	81.61(6)	Pd−C32−C33′	106.8(2)
P2−Pd−C32	97.4(1)	C32−C33−C34	117.3(7)
N−Pd−C32	179.0(1)	C33−C34−C35	121.0(8)
Pd−N−C26	119.26(8)	C32−C33′−C34′	128.7(9)
Pd−N−C30	120.07(8)	C35−C34′−C33′	121.4(9)

for both complexes [**3a**: 109.6(6)°; **5a**: 111.9(2)° and 109.1(3)°].

Finally, a distinct medium-intensity $\nu_{C=C}$ band can be detected at approximately 1630 cm^{-1} in the IR spectra of both dimethylallyl complexes (**3**: 1629 cm^{-1}; **6**: 1634 cm^{-1}), which is characteristic of an η^1-allyl complex.[17c,24] This is consistent with the results depicted above for **6** from NMR analysis, and for **3** from X-ray diffraction studies. In addition, two bands are observed at 1599 and 1565 cm^{-1} in the spectra of complexes **4**−**6**; this confirms that the nitrogen atom of PNP actually coordinates with the palladium atom in the solid state.[25]

Conclusion

According to low-temperature NMR spectra, the complexes **1**−**3** are η^2-terpy, η^3-allyl complexes (form **c**) and the complexes **4**−**6** η^3-PNP, η^1-allyl complexes (form **a**). In no case were both forms detected together in solution (although a solution of $[(terpy)Pd(C_3H_5)]^+$ led to monocrystals of each form[9]). In comparison, Werner et al. have reported that the two isomers $[(\eta^5\text{-Cp})Pd(\eta^1\text{-}C_3H_5)]$ and $[(\eta^1\text{-Cp})Pd(\eta^3\text{-}C_3H_5)]$ coexist in solution.[18] On the basis of the six complexes studied here, the existence of one form or the other depends solely on the nature of the ancillary, potentially tridentate ligand. In contrast, whether the allyl ligand bears two, one or no methyl groups makes no difference for a given ancillary ligand.

Vrieze et al. found that $[(terpy)Pd(allyl)]^+$ adopts form **a** when the allyl bears an acetyl group in the 2 position,[3a] and that it is also the case for the (PNN)Pd(allyl) cationic complex.[3b][3c] The latter can be compared with our PNP complexes **4**−**6**, where both phosphanyl groups also show a good coordinating ability towards palladium. The presence of the form **c** is rather unexpected for our terpy complexes because of the rigidity of this ligand.[26] Indeed, the steric constraints within $[(\eta^2\text{-terpy})Pd(\eta^3\text{-}C_3H_5)]^+$ are important,[9] as indicated by various data taken from the X-ray diffraction study; thus steric factors do not seem to play a major role in the predominance of one isomeric form or another.

All complexes proved to be fluxional, as indicated by variable-temperature NMR experiments, either through a "tick-tock" mechanism or through the η^3-allyl/η^1-allyl

mechanism, which is well-known in palladium allyl chemistry. The latter reflects the competition between one donor atom of the tridentate ligand and the allylic C=C double bond to coordination to the palladium center. In our complexes, the energy barriers associated with H^{syn}/H^{anti} exchanges are lower than 50 kJ·mol^{-1}, whereas it has generally been found to be higher for allyl palladium complexes bearing mono- or bidentate ligands.[27] This is probably the effect of the tridentate nature of the ligand.

We note that only the η^3-allyl forms **1c** and **3c** could be seen in solution at 200 K, whereas the corresponding η^1-allyl isomers **1a** and **3a** were only intermediates involved in the fluxional processes. However, those intermediates can indeed be isolated in the solid state, as shown by their X-ray structures.

Experimental Section

General Remarks: All experiments were carried out under a nitrogen or argon atmosphere, using a vacuum line or Vacuum Atmospheres glovebox equipped with Dri-Train HE-493 inert gas purifier. Pentane and diethyl ether were distilled with sodium and benzophenone, and dichloromethane with calcium hydride under nitrogen immediately before use. Bis[(η^3-allyl)chloropalladium],[28] bis[(η^3-1-methylallyl)chloropalladium],[28] bis[(η^3-1,1-dimethylallyl)chloropalladium],[28] and 2,6-bis(diphenylphosphanylmethyl)pyridine[25] were prepared as described in the literature. 2,2′:6′,2"-terpyridine was purchased from Aldrich and used as received. − The NMR spectra were obtained at room temperature (unless otherwise indicated) on Bruker spectrometers, at a concentration of ca 0.02 M. ^{1}H NMR spectra were recorded at 300.16 MHz (AC-300 instrument), 400.13 MHz (AM-400) or 500.13 MHz (ARX-500) and referenced to $SiMe_4$. ^{13}C NMR{^{1}H} (broadband decoupled) spectra were recorded at 50.32 MHz (AC-200) or 75.48 MHz (AC-300) and referenced to $SiMe_4$. ^{31}P{^{1}H} (broadband decoupled) spectra were recorded at 121.51 MHz (AC-300) and referenced to 85% aqueous H_3PO_4. The assignments given are supported by irradiations or 2D NMR analysis, and/or were in agreement with ref.[29] For variable-temperature spectra, the probe temperature was controlled (±1 K) by a B-VT 2000 unit calibrated with a methanol (low-temperature) or ethylene glycol (high-temperature) NMR tube. The $\Delta G^{\ddagger}$ values were calculated with the Eyring equation[30] $\Delta G^{\ddagger} = RT_c(22.96 + \ln T_c/\Delta\nu)$ [J·mol^{-1}] where T_c (K) is the temperature of coalescence of two given signals and $\Delta\nu$ (Hz) is the difference in their chemical shifts at low exchange temperature; the error is estimated to be ±0.4 kJ·mol^{-1}. The ^{1}H phase-sensitive 2D-ROESY spectrum[31] was recorded on the ARX-500 spectrometer using a mixing time of 0.3 s. − FT-IR spectra were recorded on a Perkin−Elmer 1600 Series spectrometer on KBr pellets. − FAB MS spectra and elemental analyses were carried out by the respective facilities at the Centre de Recherche de Chimie, Université Louis Pasteur, Strasbourg.

Preparation of Complexes 1−6. Typical Procedure: To a solution of $[Pd(\eta^3\text{-}C_3H_5)Cl]_2$ (100 mg, 0.273 mmol) in CH_2Cl_2 (10 mL) was added dropwise under nitrogen and in the dark a solution of $AgBF_4$ (2.1 equiv.) in CH_2Cl_2 (2 mL). The resulting suspension was stirred at room temperature for 15 min, then filtered through celite. A solution of terpy (2.1 equiv.) in CH_2Cl_2 (2 mL) was added to the filtrate, after which the solution turned from yellow to orange. After stirring at room temperature for 15 min, the solution was evaporated to dryness and the resulting complex **1** recrystallized from CH_2Cl_2/diethyl ether as an air-stable solid.

The other complexes were prepared in a similar manner starting from the corresponding allylpalladium chloride dimer (100 mg), replacing terpy with PNP (**4**−**6**, in which case the color changed from yellow to red upon addition of the ligand) and CH_2Cl_2 with CH_3CN (**2**, **4**, **5**).

[(terpy)Pd(CH_2CHCH_2)](BF_4) (1): Orange crystals; yield 232 mg (91%). − $C_{18}H_{16}BF_4N_3Pd$ (467.55): calcd. C 46.24, H 3.45, N 8.99, found C 46.45, H 3.23, N 9.07. − MS (FAB$^+$, NBA matrix); *m/z* (%): 380.0 (100) [$M^+ - BF_4$], 339.0 (54) [$M^+ - BF_4 - C_3H_5$], 234.1 (61) terpy [$M^+ + 1$].

[(terpy)Pd($CH_2CHCHCH_3$)](BF_4) (2): Orange crystals; yield 225 mg (92%). − $C_{19}H_{18}BF_4N_3Pd{\cdot}1.3CH_2Cl_2$ (591.99): calcd. C 41.19, H 3.51, N 7.10, found C 41.42, H 3.43, N 6.96.

[(terpy)Pd($CH_2CHC(CH_3)_2$)](BF_4) (3): Red crystals; yield 172 mg (73%). − $C_{20}H_{20}BF_4N_3Pd$ (495.61): calcd. C 48.47, H 4.07, N 8.48, found C 48.71, H 3.90, N 8.40.

[(PNP)Pd(CH_2CHCH_2)](BF_4) (4): Orange crystals; yield 333 mg (86%). − $C_{34}H_{32}BF_4NP_2Pd$ (709.79): calcd. C 57.53, H 4.54, N 1.97, P 8.73, found C 56.35, H 4.50, N 2.07, P 8.54. − ^{31}P{^{1}H} NMR (CD_3CN, 298 K) δ = 26.0 (s). − ^{1}H NMR (300 MHz, $CDCl_3$, 325 K) δ = 4.45 (virtual t, $|^2J_{HP} + {}^4J_{HP'}|$ = 9.3 Hz, 4 H, H^7), 7.4−7.8 (m, 23 H, H^{arom}); allyl ligand signals: see Table 3.

[(PNP)Pd($CH_2CHCHCH_3$)](BF_4) (5): Yellow-orange crystals; yield 290 mg (79%). − $C_{35}H_{34}BF_4NP_2Pd$ (723.82): calcd. C 58.08, H 4.73, N 1.94, found C 57.87, H 4.77, N 2.15. − ^{31}P{^{1}H} NMR (CD_3CN, 298 K) δ = 25.2 (s). − ^{1}H NMR (300 MHz, $CDCl_3$, 325 K) δ = 4.43 (virtual t, $|^2J_{HP} + {}^4J_{HP'}|$ = 9.3 Hz, 4 H, H^7), 7.4−8.0 (m, 23H, H^{arom}); allyl ligand signals: see Table 3.

[(PNP)Pd($CH_2CHC(CH_3)_2$)](BF_4) (6): Orange crystals; yield 287 mg (82%). − $C_{36}H_{36}BF_4NP_2Pd$ (737.85): calcd. C 58.60, H 4.92, N 1.90, found C 59.14, H 4.70, N 1.77. − MS (FAB$^+$, NBA matrix); *m/z* (%): 650.1 (100) [$M^+ - BF_4$], 581.1 (81) [$M^+ - BF_4 - C_5H_9$], 504.0 (12) [$M^+ - BF_4 - C_5H_9 - Ph$]. − ^{31}P{^{1}H} NMR ([D$_6$]DMSO, 298 K) δ = 25.1 (s). − ^{1}H NMR (300 MHz, $CDCl_3$, 298 K) δ = 4.55 (virtual t, $|^2J_{HP} + {}^4J_{HP'}|$ = 9.2 Hz, 4 H, H^7), 7.4−7.8 (m, 23 H, H^{arom}); allyl ligand signals: see Table 3.

Collection of the X-ray Data and Structure Determination for 3a and 5a: For compound **3a**, a Philips PW100/16 diffractometer was used with Cu-K_α graphite monochromated radiation (λ = 1.5418 Å). For compound **5a**, the data were collected on a Nonius CAD4 or MACH3 diffractometer using Mo-K_α graphite monochromated radiation (λ = 0.7107 Å). The structures were solved by direct methods and refined against |*F*|. Hydrogen atoms were introduced as fixed contributors. Absorption corrections were derived from psi scans of 7 reflections. For all computations, the Nonius OpenMoleN package[32] was used. The crystal and refinement data are summarized in Table 8. The C32, C33, C33′, C34, C34′, and C35 atoms of **5a** were refined isotropically. Crystallographic data (excluding structure factors) for the structures reported in this paper have been deposited with the Cambridge Crystallographic Data Centre as supplementary publication no. CCDC-140659 (**3a**) and -140660 (**5a**). Copies of the data can be obtained free of charge on application to CCDC, 12 Union Road, Cambridge CB2 1EZ, UK [Fax: (internat.) + 44-1223/336-033; E-mail: deposit@ccdc.cam.ac.uk).

Table 8. Crystal and refinement data for **3a** and **5a**

Compound	**3a**	**5a**
Formula	$C_{20}H_{20}BN_3F_4Pd$	$C_{35}H_{34}BNF_4P_2Pd$
Mol wt	495.6	723.8
Color	red	yellow
Crystal system	monoclinic	triclinic
a (Å)	15.680(4)	9.763(2)
b (Å)	17.430(4)	10.532(3)
c (Å)	7.077(3)	17.085(5)
α (deg)		97.03(2)
β (deg)	90.42(2)	104.26(2)
γ (deg)		101.55(2)
V (Å^3)	1934.1	1640.7
Z	4	2
D_{calc} (g cm^{-3})	1.70	1.465
Wavelength (A)	1.54184	0.7107
μ (cm^{-1})	81.82	7.001
Space group	P 1 2_1/n 1	P−1
Diffractometer	Philips PW1100/16	Nonius Mach3
Crystal dimensions (mm)	0.30 × 0.30 × 0.25	0.40 × 0.35 × 0.35
Temperature (K)	173	293
Radiation	Cu-*Kα*, graphite monochromated	Mo-*Kα*, graphite monochromated
Mode	θ/2θ	θ/2θ
Scan speed (deg s^{-1})	0.020	variable
Scan width (deg)	0.80 + 0.14 tan θ	0.81 + 0.34 tan θ
Octants	±h+k+l	+h±k±l
θ min/max (deg)	3/54	2/30
No. of data collected	2645	10391
No. of data with $I>3\sigma(I)$	2056	6616
No. of variables	262	385
Abs min/max	0.83/1.45	0.95/1.00
R (F)	0.041	0.041
R_w (F)	0.059	0.062
Largest peak in final difference (e Å^{-3})	0.628	0.872
GOF	1.187	1.194

Acknowledgments

We thank Jean Pierre Le Ny and Alain Dedieu for helpful discussions, Roland Graff for 2D NMR analysis and Nathalie Kyritsakas for X-ray analysis. We are grateful to the Centre National de la Recherche Scientifique for supporting this work. S. R. is indebted to the Ministère de l'Education et de la Recherche Scientifique for a grant.

[1] [1a] J. Tsuji, *Tetrahedron* **1986**, *42*, 4361. – [1b] G. Consiglio, R. M. Waymouth, *Chem. Rev.* **1989**, *89*, 257. – [1c] S. A. Godleski, in: *Comprehensive Organic Synthesis* (Eds.: B. M. Trost, I. Fleming), Pergamon Press, Oxford, U. K., **1991**, vol. 4, p. 585. – [1d] C. G. Frost, J. Howarth, J. M. J. Williams, *Tetrahedron: Asymmetry* **1992**, *3*, 1089. – [1e] B. M. Trost, D. L. Van Vranken, *Chem. Rev.* **1996**, *96*, 395.

[2] P. K. Byers, A. J. Canty, *J. Chem. Soc., Chem. Commun.* **1988**, 639.

[3] [3a] R. E. Rülke, D. Kliphuis, C. J. Elsevier, J. Fraanje, K. Goubitz, P. W. N. M. van Leeuwen, K. Vrieze, *J. Chem. Soc., Chem. Commun.* **1994**, 1817. – [3b] P. Wehman, R. E. Rülke, V. E. Kaasjager, P. C. J. Kamer, H. Kooijman, A. L. Spek, C. J. Elsevier, K. Vrieze, P. W. N. M. van Leeuwen, *J. Chem. Soc., Chem. Commun.* **1995**, 331. – [3c] R. E. Rülke, V. E. Kaasjager, P. Wehman, C. J. Elsevier, P. W. N. M. van Leeuwen, K. Vrieze, J. Fraanje, K. Goubitz, A. Spek, *Organometallics* **1996**, *15*, 3022.

[4] [4a] L. Canovese, F. Visentin, P. Uguagliati, V. Lucchini, G. Bandoli, *Inorg. Chim. Acta* **1998**, *277*, 247. – [4b] L. Canovese, F. Visentin, G. Chessa, A. Niero, P. Uguagliati, *Inorg. Chim. Acta* **1999**, *293*, 44.

[5] G. Zhu, M. Terry, X. Zhang, *Tetrahedron Lett.* **1996**, *37*, 4475.

[6] [6a] J. M. Longmire, X. Zhang, *Tetrahedron Lett.* **1997**, *38*, 1725. – [6b] G. Chelucci, V. Caria, A. Saba, *J. Mol. Catal. A* **1998**, *130*, 51.

[7] [7a] B. Åkermark, G. Åkermark, L. Hegedus, K. Zetterberg, *J. Am. Chem. Soc.* **1983**, *103*, 3037. – [7b] J. C. Fiaud, J. L. Malleron, *Tetrahedron Lett.* **1981**, *22*, 1399.

[8] [8a] R. Sablong, C. Newton, P. Dierkes, J. A. Osborn, *Tetrahedron Lett.* **1996**, *37*, 4933. – [8b] R. Sablong, J. A. Osborn, *Tetrahedron Lett.* **1996**, *37*, 4937. – [8c] L. Barloy, S. Y. Ku, J. A. Osborn, A. De Cian, J. Fischer, *Polyhedron* **1997**, *16*, 291. – [8d] N. Rahmouni, J. A. Osborn, A. De Cian, J. Fischer, A. Ezzamarty, *Organometallics* **1998**, *17*, 2470.

[9] S. Ramdeehul, L. Barloy, J. A. Osborn, A. De Cian, J. Fischer, *Organometallics* **1996**, *15*, 5442.

[10] [10a] E. R. Civitello, P. S. Dragovitch, T. B. Karpishin, S. G. Novick, G. Bierach, J. F. O'Connell, T. D. Westmoreland, *Inorg. Chem.* **1993**, *32*, 237. – [10b] E. W. Abel, V. S. Dimitrov, N. J. Long, K. G. Orrell, A. G. Osborne, V. Sik, M. B. Hursthouse, M. A. Mazid, *J. Chem. Soc., Dalton Trans.* **1993**, 291. – [10c] E. W. Abel, V. S. Dimitrov, N. J. Long, K. G. Orrell, A. G. Osborne, H. M. Pain, V. Sik, M. B. Hursthouse, M. A. Mazid, *J. Chem. Soc., Dalton Trans.* **1993**, 597. – [10d] E. W. Abel, K. G. Orrell, A. G. Osborne, H. M. Pain, V. Sik, M. B. Hursthouse, K. M. Abdul Malik, *J. Chem. Soc., Dalton Trans.* **1994**, 3441.

[11] [11a] E. W. Abel, N. J. Long, K. G. Orrell, A. G. Osborne, H. M. Pain, V. Sik, *J. Chem. Soc., Chem. Commun.* **1992**, 303. – [11b] E. W. Abel, K. G. Orrell, A. G. Osborne, H. M. Pain, V. Sik, *J. Chem. Soc., Dalton Trans.* **1994**, 111.

[12] A. Vitagliano, B. Åkermark, S. Hansson, *Organometallics* **1991**, *10*, 2592.

[13] [13a] E. Rotondo, G. Giordano, D. Minniti, *J. Chem. Soc., Dalton Trans.* **1996**, 253. – [13b] E. W. Abel, K. G. Orrell, A. G. Osborne, H. M. Pain, V. Sik, M. B. Hursthouse, K. M. Abdul Malik, *J. Chem. Soc., Dalton Trans.* **1996**, 253. – [13c] E. W. Abel, A. Gelling, K. G. Orrell, A. G. Osborne, V. Sik, *Chem. Commun.* **1996**, 2329. – [13d] A. Gelling, K. G. Orrell, A. G. Osborne, V. Sik, *J. Chem. Soc., Dalton Trans.* **1998**, 937.

[14] B. D. Steffey, A. Miedaner, M. L. Maciejewski-Farmer, P. R. Bernatis, A. M. Herring, V. S. Allured, V. Carperos, D. L. DuBois, *Organometallics* **1994**, *13*, 4844.

[15] C. Hahn, A. Vitagliano, F. Giordano, R. Taube, *Organometallics* **1998**, *17*, 2060.

[16] G. Vasapollo, C. F. Nobile, A. Sacco, *J. Organomet. Chem.* **1985**, *296*, 435.

[17] [17a] J. Powell, B. L. Shaw, *J. Chem. Soc (A)* **1967**, 1839. – [17b] D. J. Tune, H. Werner, *Helv. Chim. Acta* **1975**, *58*, 2240. – [17c] S. Numata, R. Okawara, H. Kurosawa, *Inorg. Chem.* **1977**, *16*, 1737. – [17d] B. Henc, P. W. Jolly, R. Salz, S. Stobbe, G. Wilke, R. Benn, R. Mynott, K. Seevogel, R. Goddard, C. Krüger, *J. Organomet. Chem.* **1980**, *191*, 449. – [17e] H. Werner, G. T. Crisp, P. W. Jolly, H.-J. Kraus, C. Krüger, *Organometallics* **1983**, *2*, 1369. – [17f] R. Benn, P. W. Jolly, R. Mynott, B. Raspel, G. Schenker, K.-P. Schick, G. Schroth, *Organometallics* **1985**, *4*, 1945. – [17g] J. Krause, W. Bonrath, K. R. Pörschke, *Organometallics* **1992**, *11*, 1158.

[18] [18a] H. Werner, A. Kühn, *Angew. Chem. Int. Ed. Engl.* **1979**, *18*, 416. – [18b] H. Werner, A. Kühn, C. Burschka, *Chem. Ber.* **1980**, *113*, 2291.

[19] H. Shanan-Atidi, K. H. Bar-Eli, *J. Phys. Chem.* **1970**, *74*, 961.

[20] [20a] J. Herrmann, P. S. Pregosin, R. Salzmann, A. Albinati, *Organometallics* **1995**, *14*, 3311. – [20b] B. Akermark, B. Krakenberger, S. Hansson, A. Vitagliano, *Organometallics* **1987**, *6*, 620.

[21] T. G. Appleton, H. C. Clark, L. E. Manzer, *Coord. Chem. Rev.* **1973**, *10*, 335.

[22] [22a] F. Dahan, C. Agami, J. Levisalles, F. Rose-Munch, *J. Chem. Soc., Chem. Commun.* **1974**, 505. – [22b] F. Dahan, *Acta Cryst.* **1976**, *B32*, 1941. – [22c] M. A. Bennett, R. N. Johnson, G. B. Robertson, I. B. Tomkins, P. O. Whimp, *J. Am. Chem. Soc.* **1976**, *98*, 3514. – [22d] H. M. Büch, P. Binger, R. Benn, C. Krüger, A. Rufinska, *Angew. Chem. Int. Ed. Engl.* **1983**, *22*, 774. – [22e] P. W. Jolly, *Angew. Chem. Int. Ed. Engl.* **1985**, *24*, 283. – [22f] A. Döhring, R. Goddard, G. Hopp, P. W. Jolly, N. Kokel, C. Krüger, *Inorg. Chim. Acta* **1994**, *222*, 179. – [22g] T. Sone, S. Ozaki, N. C. Kasuga, A. Fukuoka, S. Komiya, *Bull. Chem. Soc. Jpn.* **1995**, *68*, 1523.

[23] B. A. Markies, D. Kruis, M. H. P. Rietveld, K. A. N. Verkerk,

J. Boersma, H. Kooijman, M. T. Lakin, A. L. Spek, G. van Koten, *J. Am. Chem. Soc.* **1995**, *117*, 5263.

[24] [24a] L. J. Bellamy, *The Infra-Red Spectra of Complex Molecules*, Methuen, London, U. K., **1964**, p. 35. – [24b] C. Sourisseau, B. Pasquier, *J. Organomet. Chem.* **1972**, *39*, 51.

[25] W. V. Dahlhoff, S. M. Nelson, *J. Chem. Soc. (A)* **1971**, 2184.

[26] R. E. Rülke, I. M. Han, C. J. Elsevier, K. Vrieze, P. W. N. M. van Leeuwen, C. F. Roobeek, M. C. Zoutberg, Y. F. Wang, C. H. Stam, *Inorg. Chim. Acta* **1990**, *169*, 5.

[27] [27a] J. W. Faller, M. E. Thomsen, M. J. Mattina, *J. Am. Chem. Soc.* **1971**, *93*, 2642. – [27b] S. Hansson, P.-O. Norrby, M. P. T. Sjögren, B. Akermark, M. E. Cucciolito, F. Giordano, A. Vitagliano, *Organometallics* **1993**, *12*, 4940. – [27c] C. Breutel, P. S. Pregosin, R. Salzmann, A. Togni, *J. Am. Chem. Soc.* **1994**, *116*, 4067. – [27d] B. Crociani, S. Antonaroli, M. Paci, F. Di Bianca, L. Canovese, *Organometallics* **1997**, *16*, 384.

[28] [28a] W. T. Dent, R. Long, A. J. Wilkinson, *J. Chem. Soc.* **1964**, 1585. – [28b] P. R. Auburn, P. B. Mackenzie, B. Bosnich, *J. Am. Chem. Soc.* **1985**, *107*, 2046.

[29] R. M. Silverstein, F. X. Webster, *Spectrometric Identification of Organic Compounds*, J. Wiley & Sons, New-York, U. S. A., **1998**.

[30] H. Günther, *La Spectroscopie de RMN*, Masson, Paris, France, **1993**.

[31] D. G. Davis, A. Bax, *J. Magn. Res.* **1985**, *64*, 533.

[32] C. K. Fair in *MolEN. "An Interactive Intelligent System for Crystal Structure Analysis"* Nonius, Delft, The Netherlands, **1990**.

Received February 18, 2000
[I00068]

Coordination Chemistry of SCS Pd^{II} Pincer Systems

Henk-Jan van Manen,[a] Kazuaki Nakashima,[a,b] Seiji Shinkai,[b] Huub Kooijman,[c] Anthony L. Spek,[c][‡] Frank C. J. M. van Veggel,*[a] and David N. Reinhoudt*[a]

Keywords: Coordination chemistry / N ligands / P ligands / Palladium / Tridentate ligands

We have studied the coordination of substituted pyridines, and phosphorus- and sulfur-containing ligands to an SCS Pd^{II} pincer system. These ligands coordinate to Pd^{II} (*trans* to the cyclopalladated aryl group) by quantitative substitution of the labile acetonitrile ligand in complex **1**. Competition experiments showed that both electronic and steric effects influence the strength of coordination to the Pd^{II} pincer of the substituted pyridines. A quantitative analysis of the substituent effect was achieved by a Hammett correlation. Phosphorus-containing ligands also coordinate to this SCS Pd^{II} motif, as evidenced by NMR spectroscopy and single-crystal X-ray diffraction studies. They are much stronger ligands than the pyridines. The coordination strength of the thioureas falls in between those of the pyridines and phosphanes/phosphites. Our results lead therefore to the following order of ligand strength towards Pd^{II} in SCS Pd^{II} pincers: $PR_3 > P(OR)_3 > N,N'$-disubstituted thiourea > (substituted) pyridines > MeCN.

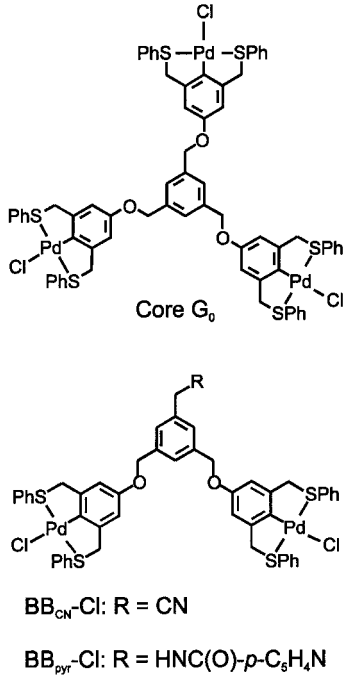
Introduction

meta-Xylene derivatives in which the two methylene groups carry suitable donor atoms (e.g. N, P, or S), so-called pincer ligands,[1] are used for the complexation of a wide range of transition metals.[2] Cyclometallation gives rise to a variety of systems displaying rich coordination chemistry.

A number of stable Pd^{II} complexes containing SCS pincer systems have been reported to date,[3] with recent examples mainly related to supramolecular chemistry.[4] We have been exploiting the SCS Pd^{II} pincer motif in the noncovalent synthesis of nanosize metallodendrimers.[5] Representative dendritic building blocks used in our investigations are depicted in Scheme 1.

Controlled metallodendrimer assembly up to generation 5 has been achieved by *divergently* growing from the core $\mathbf{G_0}$.[6] In these metallodendritic structures, the coordination of nitrile ligands is used as the assembling principle. Large self-assembled hyperbranched organopalladium spheres (100−400 nm) have also been synthesized divergently by an uncontrolled one-pot strategy.[7]

By employing ligands of different coordination strengths, it is also possible to synthesize metallodendrimers in a *convergent* manner.[8] This growth strategy commences by coordinating the strongest ligands first (at the periphery). Subsequent growth proceeds inwards using building blocks of decreasing coordination strength. This order is imperative in preventing ligand scrambling. We have demonstrated this type of growth in the synthesis of a third generation metallodendrimer containing cyano- and pyridine-based building blocks. In order to broaden the scope of this metallodendrimer synthetic method, other ligands with different binding strengths are needed. Therefore, we have studied the relative coordination strengths of a series of ligands towards



Scheme 1. Representative building blocks that have been employed to assemble metallodendrimers, see refs.[6−8]

[a] Laboratory of Supramolecular Chemistry and Technology, MESA+Research Institute, University of Twente, P. O. Box 217, 7500 AE, Enschede, The Netherlands
Fax: (internat.) + 31-53/4894645
E-mail: smct@ct.utwente.nl
[b] Chemotransfiguration Project, Japan Science and Technology Corporation, 2432 Aikawa, Kurume, Fukuoka 839-0861, Japan
[c] Bijvoet Center for Biomolecular Research, Department of Crystal and Structural Chemistry, Utrecht University, Padualaan 8, 3584 CH Utrecht, The Netherlands
[‡] To whom correspondence pertaining to crystallographic studies should be addressed (E-mail: a.l.spek@chem.uu.nl)

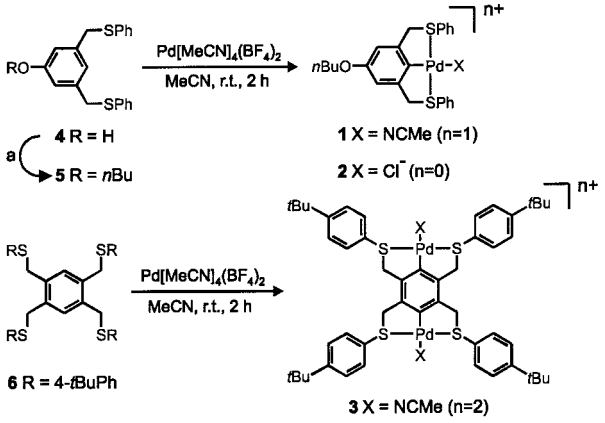
 © WILEY-VCH Verlag GmbH, D-69451 Weinheim, 2000 1434−1948/00/1212−2533 $ 17.50+.50/0

the SCS Pd^{II} pincer system. We report here our results for the parent Pd^{II} pincer. Moreover, a dipincer has been synthesized which could be used as a new rigid core for metallodendrimer synthesis.

Results and Discussion

Synthesis and Characterization of Model SCS Pd^{II} Pincer Complexes

The SCS Pd^{II} complexes **1** and **2** were prepared in two and three steps, respectively (Scheme 2). After alkylation of the previously reported[7b] SCS pincer ligand **4** with *n*-butyl bromide (77% yield), cyclopalladation of the resulting ligand **5** was achieved by reaction with $[Pd(CH_3CN)_4][BF_4]_2$.



Scheme 2. Synthesis of SCS Pd^{II} pincer complexes; a) *n*BuBr, *t*BuOK, CH_3CN

The cationic acetonitrile complex **1** (containing the noncoordinating BF_4^- counter anion) was obtained in 90% yield by precipitation with Et_2O from CH_3CN solution after completion of the cyclopalladation. The neutral chloro complex **2** was isolated (in 94% yield) by stirring a solution of **1** in CH_2Cl_2/CH_3CN with saturated NaCl, followed by column chromatography.

Similarly, dipincer **3** was prepared in two steps from 1,2,4,5-tetrakis(bromomethyl)benzene by first allowing the benzyl bromides to react with *tert*-butylthiophenol using K_2CO_3 as base and 18-crown-6 as catalyst (81% yield), followed by cyclopalladation of the resulting dipincer ligand **6** using $[Pd(CH_3CN)_4][BF_4]_2$ in CH_3CN. The bis(acetonitrile) complex was purified by precipitation from CH_3CN solution with Et_2O (60% yield). Complexes **1**, **2** and **3** were isolated as air- and moisture-stable yellow solids. All spectroscopic and analytical data are consistent with cyclopalladation. Compared to the free ligands **5** and **6**, the ^1H NMR resonances for the diastereotopic CH_2S protons in the palladium complexes are shifted downfield by ca. 0.5 ppm and are broadened due to slow conformational interconversion of the Pd^{II}-containing five-membered rings. At lower temperatures the coupling of the two diastereotopic CH_2S protons results in the broad signal splitting into a pair of doublets (vide infra). Further, the signals for the *ortho*-protons at $\delta = 6.80$ (in **5**) or $\delta = 6.92$ (in **6**) are absent from the ^1H NMR spectra, indicating complete cyclopalladation. In the ^{13}C NMR spectra of the acetonitrile complexes **1** and **3**, the signal of the carbon atom directly linked to Pd^{II} is too weak to be observed (probably due to long relaxation times), whereas in the chloro complex **2** it is present at $\delta = 150.9$ (30 ppm downfield compared to ligand **5**). In the positive FAB-MS spectrum of **2**, a signal corresponding to $[M - Cl + H]^+$ ($m/z = 499.6$) is present, whereas in the negative FAB-MS spectrum the chloride ion remains coordinated to Pd^{II}, resulting in a signal at $m/z = 533.7$ ($[M]^+$). Loss of the acetonitrile ligand is observed in both the positive and negative FAB-MS spectra of **1**, resulting in signals corresponding to $[M - MeCN - BF_4]^+$ ($m/z = 499.0$) and $[M - MeCN + BF_4]^-$ ($m/z = 671.6$) respectively, while both acetonitriles are lost in the positive FAB-MS spectrum of **3** ($m/z = 1001.1$ for $[M - 2MeCN - 2BF_4 + H]^+$).

X-ray Structure of 1

Besides the analytical evidence discussed above, structural proof of the acetonitrile complex **1** is provided by an X-ray analysis. A drawing of the acetonitrile complex **1** is shown in Figure 1. The following bond lengths for the atoms bonded to Pd^{II} have been obtained: Pd−S(1) 2.2992(8) Å, Pd−S(2) 2.2961(9) Å, Pd−N 2.110(2) Å, Pd−C(1) 1.975(2) Å.

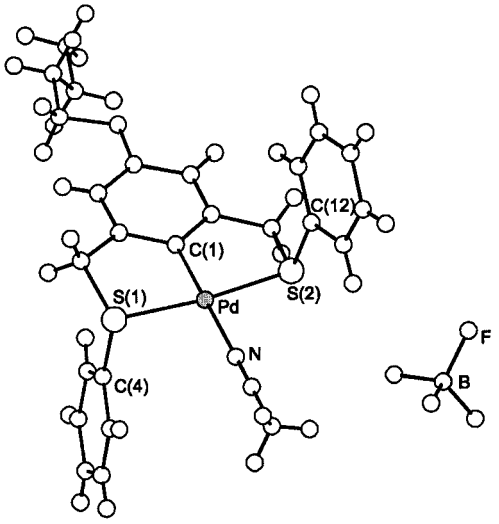


Figure 1. Structure of the acetonitrile complex **1**

The Pd atom adopts a slightly distorted square-planar geometry [S(1)−Pd−S(2) 171.11(2)° and N−Pd−C(1) 178.26(11)°] and the two five-membered chelate rings possess somewhat distorted envelope conformations in which the two phenyl rings (oriented *anti* with respect to the square plane) are in axial positions [Pd−S(1)−C(4) 100.51(9)° and Pd−S(2)−C(12) 103.17(9)°]. It should be noted that complex **1** is chiral in the solid state (prepared as a racemate) due to the lack of symmetry elements.

Substitution of the Labile MeCN Ligand by Pyridine

Substitution of the labile acetonitrile ligand of complex **1** by stronger ligands such as pyridine is facile. Upon treat-

ment of **1** with 1 equiv. of pyridine (in $CDCl_3$), fast and quantitative substitution was observed. In the ^1H NMR spectrum of the pyridine adduct, the resonance of the pyridine α-protons is shifted *upfield* from δ = 8.60 (free pyridine) to δ = 8.15 (coordinated pyridine). This is different from the pyridine complexes of SCS Pd^{II} pincers reported by Loeb and co-workers[9] for which a *downfield* shift of the pyridine α-protons was observed upon coordination. This difference must be due to the presence of the phenyl rings attached to the sulfur atoms in our system. The ring current of these aromatic rings will have a shielding effect on the pyridine protons (mostly the α-protons). The α-proton signal is also considerably broadened, indicating hindered rotation of the pyridine ligands with respect to the plane of coordination. The CH_2S proton signal shifts downfield by 0.15 ppm, and the aromatic proton signal by 0.05 ppm, upon substitution of MeCN by pyridine. The greater coordination strength of the pyridine ligand as compared to acetonitrile is also evident from the positive FAB-MS spectrum, in which a small, but significant peak corresponding to the molecular ion $[M - BF_4]^+$ is observed at *m*/*z* = 578.4, in addition to a large signal at *m*/*z* = 499.2 from $[M - pyr - BF_4]^+$.

Upon adding excess pyridine, two separate NMR signals for free and bound pyridine are observed. This observation can be explained by either slow exchange of pyridine on the NMR timescale or a kinetically stable pyridine complex. Exchange of pyridine was indeed evidenced by treatment of the pyridine complex with an excess (5 equiv.) of $[D_5]$pyridine. The signal at δ = 8.15 disappeared and a new peak appeared at δ = 8.6, indicating free pyridine. This kinetic lability is consistent with other pyridine−Pd^{II} complexes.[10]

The pyridine exchange rate is dependent on the solvent. In $CDCl_3$ two separate signals for bound and free pyridine were observed up to 50 °C. However, when acetonitrile complex **1** was treated with 2 equiv. of pyridine in $[D_6]$DMSO, a coordinating solvent, only one broad signal for the pyridine α-protons was observed in the ^1H NMR spectrum, indicating fast exchange on the NMR timescale. When $[D_6]$DMSO was titrated into a $CDCl_3$ solution of the pyridine complex containing 1 equiv. of excess pyridine (Figure 2), the rate of pyridine exchange varied with the concentration of $[D_6]$DMSO.

It is known that the kinetics of substitution in d^8 square-planar complexes depends on two factors, one related to direct ligand attack (associative-dissociative mechanism) and the other to an associative solvolysis pathway, in which the leaving group is first displaced by a solvent molecule and which is subsequently substituted by the incoming ligand (dissociative-associative mechanism).[11] The observed pyridine exchange rate can be rationalized in this way. With increasing $[D_6]$DMSO concentration, the pyridine exchange increasingly follows the solvolysis pathway. In $CDCl_3$ this pathway is not possible and only slow direct pyridine attack occurs.

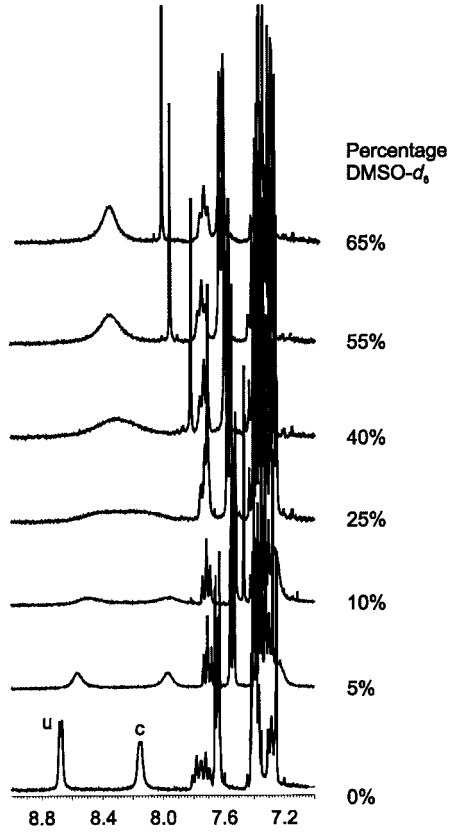
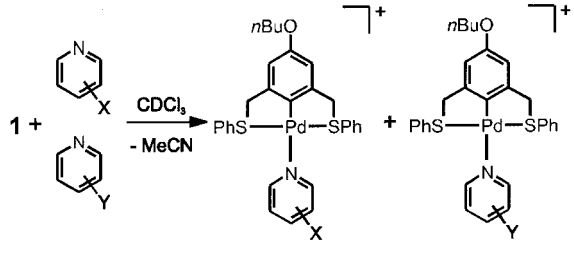


Figure 2. ^1H NMR spectra (298 K) of the titration of $[D_6]$DMSO to a $CDCl_3$ solution of the pyridine complex of the SCS Pd^{II} pincer system containing an excess of 1 equiv. pyridine; the designations u and c correspond to the pyridine α-proton signals of uncoordinated and coordinated pyridine, respectively

Substituent Effects on Pyridine Complex Stability

Within a series of substituted pyridines, we anticipated that subtle differences in nitrogen electron density would control the coordination strength towards Pd^{II}. When two different pyridines (each 1 equiv.) were mixed with 1 equiv. of the acetonitrile complex **1** in $CDCl_3$ (Scheme 3), the α-proton signals of the two pyridines in the ^1H NMR spectra were used as a probe to determine the extent of coordination of each pyridine (e.g. see Figure 3).



Scheme 3. Competition experiments between substituted pyridines

Table 1 shows that electron-donating pyridines bind more strongly than pyridine, whereas electron-withdrawing pyridines are weaker ligands than pyridine. The stability of these pyridine complexes follows the Hammett equation using the σ^+ constant of Brown and Okamoto.[13] This modified substituent constant applies to reactions in which strong ac-

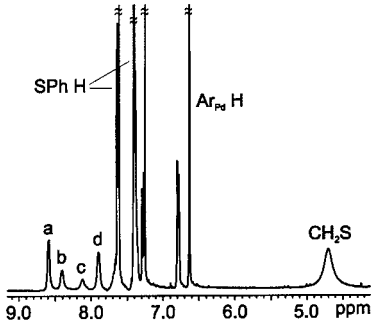


Figure 3. Part of the ^{1}H NMR spectrum ($CDCl_3$, 298 K) for a competition experiment between pyridine and 4-methoxypyridine. The designated signals correspond to the pyridine α-proton signals of: a) free pyridine, b) free 4-methoxypyridine, c) bound pyridine, d) bound 4-methoxypyridine

ceptor character develops at the aromatic ring, e.g. solvolysis of tertiary halides in which ionization is rate-determining. Using the selectivities reported in Table 1 (only the data of the 4-substituted pyridines are analyzed), a Hammett plot as shown in Figure 4 is obtained with a ρ^+ value of -1.0.

Table 1. Results of coordination competition experiments between substituted pyridines

X	Y	% bound pyr−X/pyr−Y	Selectivity[a]
4-H	4-NH_2	17:83	4.88
4-H	4-MeO	32:68	2.13
4-H	4-*t*Bu	40:60	1.50
4-H	4-Me	45:55	1.22
4-H	4-Ph	44:56	1.27
4-H	4-Ac	62:38	0.61
4-H	4-CO_2Me	64:36	0.56
2-Me	4-Me	43:57	1.33
2-Me	3-Me	57:43	0.75

[a] Ratio of bound pyridine−Y over bound pyridine−X.

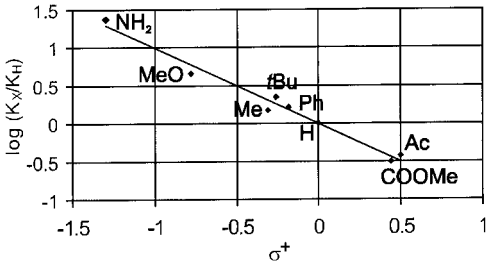


Figure 4. Hammett plot of the stability of 4-substituted pyridine complexes with the SCS Pd^{II} pincer system against the Brown−Okamoto σ^+ substituent constant

Usually in systems obeying the Brown−Okamoto equation, the values of ρ^+ are much more negative. However, in those cases a full positive charge develops in the rate-determining step instead of the partial positive charge developing on nitrogen in pyridine−Pd^{II} coordination.

The effect of steric hindrance was investigated in the picoline series. On the basis of electronic effects alone, it would be expected that 2-picoline would bind stronger than 3-picoline. However, as the reverse is found experimentally, it must be concluded that steric hindrance between the 2-methyl group and the aryl groups of the Pd^{II} pincer system overrules electronic effects in this case.

Coordination of Triphenylphosphane to Pd^{II}

The coordination of phosphorus-containing ligands to SCS Pd^{II} pincers has, to the best of our knowledge, not been investigated. Only phosphanes coordinated to transition metal pincer systems of the PCP[14] and NCN[15] type, and a phosphane coordinated to an SCS Pt^{II} pincer[3] have been reported. Upon addition of 1 equiv. of PPh_3 to **1**, several distinct spectroscopic features evidenced phosphane coordination to Pd^{II}. Firstly, in the ^{1}H NMR spectrum a broad peak corresponding to the CH_2S protons is present. The signal is sharper and is shifted downfield (± 0.25 ppm) when compared to the MeCN complex. Furthermore, the signal from the aromatic protons is a doublet (J = 2.9 Hz) due to proton-phosphorus coupling. In the ^{31}P NMR spectrum, the phosphorus signal shifts from δ = −5.6 (free PPh_3) to δ = 13.6 upon coordination. These combined results prove the coordination of PPh_3 *trans* to the cyclometallated aryl group. Opening of the S−Pd chelate ring, as suggested by Shaw et al.,[16] does not occur.

X-ray Structure of 3·$(PPh_3)_2$

The *dipincer* complex **3**, which is more soluble in organic solvents than reported dipincers[17] due to its *tert*-butyl groups, was mixed with 2 equiv. of PPh_3. Crystals were grown by vapor diffusion of diethyl ether into a $CHCl_3$ solution of the bis(PPh_3) complex (Figure 5).

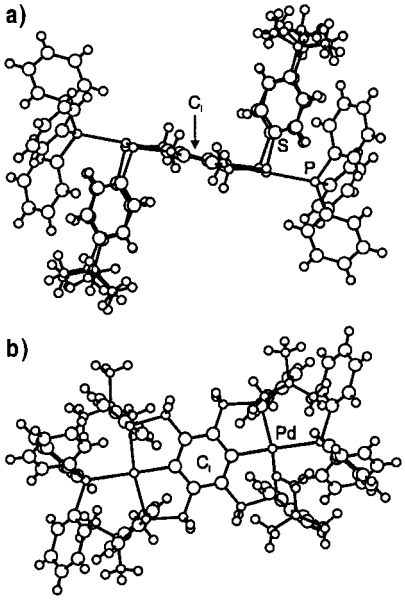


Figure 5. Structure of 3·$(PPh_3)_2$; a) side view, b) top view

In the bis(triphenylphosphane) complex, the Pd atoms are in a distorted square-planar environment: S(1)−Pd(1)−S(2) 167.15(3)° and P(1)−Pd(1)−C(1) 178.53(9)°. The following bond lengths for the atoms bon-

ded to Pd^{II} were obtained: Pd−S(1) 2.3075(10) Å, Pd−S(2) 2.3057(9) Å, Pd−P 2.3785(9) Å, Pd−C(1) 2.032(3) Å. The Pd^{II}−C bond is substantially longer than in complex **1** (2.03 vs. 1.98 Å). The complex has C_i symmetry (inversion point at the center of the bispalladated ring) in which the two *tert*-butyl phenyl groups attached to the metal-bound sulfur atoms of the same SCS Pd^{II} pincer moiety are oriented towards the same side of the square plane.

Stability of Coordinated PPh_3 Complexes

In transition metal inorganic complexes, PPh_3 is in general a stronger ligand than pyridine. This is expressed in their respective nucleophilicity parameters, for example, which differ substantially (n^0_{Pt} = 3.19 for pyridine and 8.93 for PPh_3, respectively).[11] In the ^1H NMR spectrum of a mixture of 1 equiv. of PPh_3 and the pyridine complex of compound **1** (Scheme 2: X = pyridine), quantitative substitution of pyridine by PPh_3 is shown. The spectrum is a superposition of the spectra of free pyridine and the PPh_3 complex. Heating the PPh_3 complex in refluxing $CHCl_3$ with a 10-fold excess of pyridine did not result in any detectable exchange.

As mentioned before, ring opening of the S−Pd chelate by PPh_3 has been suggested. Upon adding 5 equiv. of PPh_3 to *acetonitrile* complex **1**, no changes were observed in either the ^1H or ^{31}P NMR spectra. The situation was different when PPh_3 was added to the *chloro* complex **2**. Increasing amounts (0.25, 0.5, 1.0, 1.5, 2.5 and 5.0 equiv.) of PPh_3 were added to **2**. The ^1H and ^{31}P NMR spectra show that an equilibrium is established after each addition because in every case two signals are observed in the ^{31}P NMR spectrum, one corresponding to free PPh_3 ($\delta = -5.6$), and the other indicating coordination of PPh_3 *different from that described for the substitution of acetonitrile above* because the signal of coordinated PPh_3 now appears at $\delta = 21.9$ instead of $\delta = 13.6$. In the ^1H NMR spectrum a signal appears that corresponds to "free" CH_2S protons. This means that *the S−Pd chelate ring opens upon PPh_3 addition*. It also seems that both chelate rings open together, as the opening of only one would destroy the symmetry of the system. Substitution of the chloro ligand by PPh_3 is also unlikely, as can be inferred from the ^{31}P NMR spectra (i.e. no signal observed at $\delta = 13.6$). Therefore it is concluded that 2 molecules of PPh_3 displace the sulfur atoms as ligands. This only occurs quantitatively with a large excess (> 4−5 equiv.) of PPh_3.

Coalescence Temperatures of Different SCS Pd^{II} Pincer Complexes

The two five-membered chelate rings of the cyclopalladated pincer system display slow conformational interconversion, which is reflected in the ^1H NMR spectrum by the broadening of the CH_2S proton signal of the pincer complexes. Different ligands have a different influence on the conformational interconversion of the chelate rings. This phenomenon is reflected in the coalescence temperature T_c where the two *separate* signals of the CH_2S protons coalesce into a broad singlet.

As can be seen from Table 2, the coalescence temperature decreases in the order acetonitrile > pyridine > chloride > triphenylphosphane. For the neutral ligands this order corresponds to the lone pair electron donation (the nucleophilicity) towards Pd^{II}. In the case of PPh_3, no unambiguous coalescence temperature could be observed. NMR experiments at low temperatures reveal multiple signals for the CH_2S protons for all the complexes mentioned above. On one hand, freezing out the ring puckering results in loss of the apparent C_{2v} symmetry of the complex that exists at higher temperatures in solution. On the other hand, in the PPh_3 complex one very broad signal is observed, ranging from $\delta = 4.3$ to $\delta = 5.2$ at −10 °C. Splitting of the signal into two doublets is not observed, suggesting that besides lowering the rate of ring interconversion, rotation of the bulky PPh_3 ligand around the Pd^{II}−P bond is also restricted, leading to different conformational isomers. Moreover a long range coupling to ^{31}P cannot be excluded a priori.

Table 2. Coalescence temperatures and free energies of activation for ring interconversion of SCS Pd^{II} pincer complexes

Ligand X	Coalescence temperature T_c [K]	Free energy of activation $\Delta G^{\ddagger}_c$ [kJ/mol] at T_c
MeCN	289 ± 2	57.5 ± 0.3
Pyridine	286 ± 2	56.5 ± 0.3
Cl^-	271 ± 2	54.8 ± 0.5
PPh_3	< 268[a]	−

[a] No unambiguous coalescence temperature was observed, see also text.

From the coalescence temperature the free energy of activation for ring puckering can be estimated.[12] The free energies of activation for ring puckering vary between 55 and 58 kJ/mol in the ligand order chloride < pyridine < acetonitrile. From Table 2 it is evident that higher coalescence temperatures correspond to higher free energies of activation at T_c for ring puckering in this system.

Coordination of Other Phosphorus-Containing Ligands

Besides triphenylphosphane other phosphorus-containing ligands were investigated as ligands for the SCS Pd^{II} pincer system. Coordination of these ligands to Pd^{II} was shown by ^1H and ^{31}P NMR spectroscopy and by FAB mass spectrometry (Table 3).

As with the substituted pyridines competition experiments were employed, establishing that the relative coordination strengths of these ligands increase in the order $PCy_3 > PPh_3 > P(OMe_3) > P(OPh)_3$. The relative differences in coordination strengths are quite high, as in all cases [PCy_3 vs. PPh_3, PPh_3 vs. $P(OMe)_3$ and $P(OMe)_3$ vs. $P(OPh)_3$] the selectivity exceeds a 4:1 ratio. Further competition experiments revealed that all the phosphorus containing ligands coordinate much more strongly than pyrid-

Table 3. Complexes of phosphorus-containing ligands with the SCS Pd^{II} pincer system

Complex **1** with X =	^{1}H NMR Ar H[a] (ppm)/*J* (Hz)	^{31}P NMR coord/free ligand (ppm)	FAB-MS $[M]^+$ found/calcd
$P(OMe)_3$	6.72/4.8	122.7/141.0	623.2/623.1
$P(OPh)_3$	6.64/5.1	114.7/127.9	809.1/809.1
PCy_3	6.66/2.9	24.0/11.5	779.5/779.3

[a] Aromatic protons of cyclopalladated ring.

ine. Only a minor amount of pyridine complex was found in competition experiments with the weakest phosphite ligand [$P(OPh_3)$].

In the case of PCy_3 and $P(OPh)_3$, addition of excess ligand to their respective phosphane or phosphite complexes had no effect on the complex stability, as was the case for PPh_3 (vide supra). However, upon addition of excess $P(OMe)_3$ to complex **1** [X = $P(OMe)_3$], the SPh ligands were substituted by $P(OMe)_3$ to form a complex containing three phosphite ligands. This was evidenced by ^{1}H (the CH_2S protons give a sharp signal at $\delta = 4.2$) and ^{31}P NMR spectroscopy (the two *trans* phosphite ligands couple to the *cis* phosphite ligand and vice versa to give one triplet and one doublet, $J = 73$ Hz). In the other cases the presence of one bulky ligand apparently prevents the coordination of additional ligands.

The observed order of phosphorus ligand strengths matches the order of χ_i values [$\chi_i = 0.1$ (Cy), 4.3 (Ph), 7.7 (OMe) and 9.7 (OPh)], which is regarded as a parameter measuring substituent contribution to the σ donor and π acceptor abilities of phosphorus-containing ligands.[18] On the other hand, the cone angle θ (the ligand bulkiness) increases in the order $P(OMe)_3$ (107°) < $P(OPh)_3$ (128°) < PPh_3 (145°) < PCy_3 (170°).[18] Obviously in our case steric effects can be ignored, as the ligand strength order is the same as the electronic parameter χ_i and not the steric parameter θ.

Coordination of Sulfur-Containing Ligands

Finally, we have investigated the coordination of sulfur-containing ligands to the SCS Pd^{II} pincer. Thioureas have high nucleophilicity values ($n^0_{Pt} = 7.17$ for unsubstituted thiourea),[11] so they are possible ligands.[19] *N*-Benzyl-*N'*-butylthiourea was prepared from butyl isothiocyanate and benzylamine. Upon addition of this thiourea to the acetonitrile complex **1**, the ^{1}H NMR spectrum indicated thiourea coordination. Firstly, the acetonitrile signal was present at $\delta = 1.99$, indicating the release of acetonitrile (coordinated MeCN gives rise to a signal at $\delta = 2.08$). Secondly, significant changes in the chemical shifts of the thiourea NH protons and the adjacent CH_2 protons were observed. Finally, the broad signals of the SPh protons of the pincer and essentially all protons of the thiourea indicated restricted thiourea rotation. Moreover, the FAB-MS spectrum displayed an intense signal at $m/z = 721.2$ corresponding to the thiourea complex.

From their n^0_{Pt} values we can expect that thioureas are stronger ligands than pyridine but weaker ligands than phosphanes. This was confirmed experimentally by competition experiments. The ^{1}H NMR spectra show that the ratio of coordinated thiourea to coordinated pyridine is higher than 95:5. In the presence of PPh_3 the thiourea did not coordinate significantly, as was inferred from ^{1}H and ^{31}P NMR spectroscopy. FAB mass spectrometry only showed the PPh_3 complex of the SCS Pd^{II} pincer system in such mixtures. This means that the order of ligand strength is PPh_3 > thiourea > pyridine.

Conclusions

In this paper, a study of the coordination strengths of various ligands towards a SCS Pd^{II} pincer system has been reported. Several *para*-substituted pyridines have been coordinated to this pincer system, and the differences in coordination strengths found to arise from electronic and steric effects. The effect of *para* substituents was quantitatively analyzed by correlation with the Brown−Okamoto σ^+ substituent constants. Moreover, it was demonstrated that phosphorus- and sulfur-containing ligands are stronger ligands than pyridines. These results allow for the *convergent* metallodendrimer assembly methodology to be extended. Investigations concerning these topics are currently underway and the results will be described elsewhere.

Experimental Section

General: Melting points were determined with a Reichert melting point apparatus and are uncorrected. CH_2Cl_2 and hexane were freshly distilled from $CaCl_2$. CH_3CN (p.a. from Merck) was stored over molecular sieves (4 Å). Other solvents (EtOH, $CHCl_3$, acetone) were used as received (p.a. from Merck). All reagents were purchased from Aldrich and used without further purification. Solutions containing phosphanes or phosphites were degassed prior to use. − NMR spectra were recorded in $CDCl_3$ (unless stated otherwise) at 298 K with a Varian Unity 300 locked to the deuterated solvent. Chemical shifts are given relative to tetramethylsilane (TMS). − FAB-MS spectra were recorded with a Finnigan MAT 90 spectrometer with *m*-nitrobenzyl alcohol (NBA) as the matrix. − Elemental analyses were performed using a Carlo Erba EA1106. − Column chromatography was performed using silica gel (SiO_2, E. Merck, 0.040−0.063 mm, 230−240 mesh).

1-(*n*-Butoxy)-3,5-bis(phenylthiomethyl)benzene (5): To a solution of 3,5-bis(phenylthiomethyl)phenol (**4**) (1.40 g, 4.1 mmol) in CH_3CN (200 mL) was added *t*BuOK (0.93 g, 8.3 mmol) and the resulting mixture was stirred at room temperature for 1 h. A solution of *n*-butyl bromide (0.44 mL, 4.1 mmol) in CH_3CN (20 mL) was added

dropwise, and the mixture was stirred overnight at 40 °C. After evaporation of the solvent in vacuo, the residue was taken up in CH_2Cl_2 (100 mL), washed with 1 M HCl (100 mL), saturated $NaHCO_3$ (100 mL) and brine (100 mL). The dried ($MgSO_4$) organic layer was concentrated to dryness and the crude product was purified by column chromatography (SiO_2; eluent: CH_2Cl_2/hexane, 1:1, v/v) to afford a colorless oil. Yield: 1.26 g (77%). − ^{1}H NMR: δ = 0.94 (t, J = 7.3 Hz, 3 H, CH_3), 1.36−1.51 (m, 2 H, CH_2CH$_3$), 1.63−1.74 (m, 2 H, OCH$_2$CH_2), 3.83 (t, J = 6.6 Hz, 2 H, OCH$_2$), 4.01 (s, 4 H, CH_2S), 6.68 (s, 2 H, Ar H), 6.80 (s, 1 H, Ar H), 7.12−7.29 (m, 10 H, SPh). − ^{13}C NMR: δ = 13.3, 18.7, 30.7, 38.5, 67.1, 113.4, 121.1, 125.8, 128.3, 129.4, 135.8, 138.5, 158.8. − FAB-MS; *m/z*: 395.1 [M + H]$^+$, calcd. for $C_{24}H_{26}OS_2$: 395.1.

Acetonitrile Complex of Pd Pincer 1: Ligand **5** (233 mg, 0.6 mmol) was dissolved in CH_3CN (50 mL) and the solution was placed under argon. Pd[MeCN]$_4$(BF$_4$)$_2$ (262 mg, 0.6 mmol) was added in one portion, and the mixture was stirred at room temperature for 2 h. After evaporation of the solvent in vacuo, the yellow paste was taken up in CH_3CN (3 mL) and the product was precipitated by dropwise addition of diethyl ether. Yield: 334 mg (90%). − M.p. 68−70 °C. − ^{1}H NMR: δ = 0.95 (t, J = 7.3 Hz, 3 H, CH_3), 1.37−1.52 (m, 2 H, CH_2CH$_3$), 1.67−1.76 (m, 2 H, OCH$_2$CH_2), 2.08 (s, 3 H, CH_3CN), 3.88 (t, J = 6.4 Hz, 2 H, OCH$_2$), 4.57 (br s, 4 H, CH_2S), 6.59 (s, 2 H, Ar H), 7.48−7.50 (m, 6 H, SPh), 7.77−7.81 (m, 4 H, SPh). − ^{13}C NMR (CD_3CN): δ = 13.6, 19.4, 31.4, 50.3, 68.2, 110.2, 130.6, 131.3, 131.5, 132.1, 151.8, 158.2. − FAB-MS; *m/z*: 499.0 [M − BF_4 − CH_3CN]$^+$, calcd. 499.0. − $C_{26}H_{28}BF_4NOPdS_2$·H_2O: calcd. C 48.35, H 4.68, N 2.17, S 9.93; found C 48.18, H 4.50, N 2.25, S 9.92.

Chloro Complex of Pd Pincer 2: Acetonitrile complex **1** (0.75 g, 1.2 mmol) was dissolved in a mixture of CH_2Cl_2 (75 mL) and CH_3CN (25 mL). After the addition of brine (100 mL), the mixture was stirred vigorously overnight. After separation of the layers, the organic phase was concentrated in vacuo and the residue was purified by column chromatography (SiO_2; eluent: CH_2Cl_2/Et_2O, 95:5, v/v) to afford a yellow solid. Yield: 0.60 g (94%). − M.p. 63−64 °C. − ^{1}H NMR: δ = 0.94 (t, J = 7.3 Hz, 3 H, CH_3), 1.40−1.48 (m, 2 H, CH_2CH$_3$), 1.66−1.75 (m, 2 H, OCH$_2$CH_2), 3.85 (t, J = 6.4 Hz, 2 H, OCH$_2$), 4.53 (br s, 4 H, CH_2S), 6.56 (s, 2 H, Ar H), 7.32−7.37 (m, 6 H, SPh), 7.78−7.83 (m, 4 H, SPh). − ^{13}C NMR: δ = 13.3, 18.7, 30.8, 51.2, 67.3, 108.3, 129.1, 129.2, 130.9, 131.9, 149.6, 150.9, 156.5. − FAB-MS; *m/z*: 499.6 [M − Cl + H]$^+$, calcd. 500.0. − $C_{24}H_{25}ClOPdS_2$: calcd. C 53.83, H 4.71, S 11.98; found C 53.90, H 4.70, S 11.88.

Dipincer Ligand 6: A mixture of 1,2,4,5-tetrakis(bromomethyl)benzene (3.00 g, 6.7 mmol), 4-*tert*-butylthiophenol (5.00 g, 30.1 mmol), K_2CO_3 (9.20 g, 66.6 mmol) and 18-crown-6 (1.80 g, 6.8 mmol) in acetone (150 mL) was heated at reflux overnight under argon. After evaporation of the solvent, the residue was taken up in CH_2Cl_2 (250 mL) and washed with brine (250 mL). After drying the organic layer with $MgSO_4$ and evaporation of the solvent in vacuo, the crude product was recrystallized from EtOH/$CHCl_3$ to afford a white solid. Yield: 4.30 g (81%). − M.p. 185−186 °C. − ^{1}H NMR:

Table 4. Crystallographic data for **1** and **3**·(PPh$_3$)$_2$

	1	**3**·(PPh$_3$)$_2$
Empirical formula	$C_{26}H_{28}NOPdS_2$·BF_4	$C_{86}H_{90}P_2Pd_2S_4$·2BF_4·2$CHCl_3$
Molecular mass	627.86	1939.07
Crystal system	monoclinic	triclinic
Space group	$P2_1/c$ (No. 14)	$P\bar{1}$ (No. 2)
a [Å]	17.9797(16)	10.2613(12)
b [Å]	8.7315(12)	11.807(2)
c [Å]	20.390(5)	19.428(3)
α [°]	90	97.598(8)
β [°]	122.084(12)	94.227(10)
γ [°]	90	103.319(10)
V [Å^3]	2712.1(9)	2257.1(6)
$D_{calcd.}$ [g cm^{-3}]	1.538	1.426
Z	4	1
F (000)	1272	990
μ [mm^{-1}] (Mo-K_α)	0.9	0.8
Crystal colour	yellow	pale yellow
Crystal size [mm]	0.15 × 0.25 × 0.40	0.05 × 0.15 × 0.15
Data collection:		
θ_{min}, θ_{max} [°]	1.6, 27.5	0.9, 25.4
X-ray exposure [h]	1.5	4
Data set	−23:23, −11:9, −23:26	−12:12, −14:13, −18:23
Total data	21995	15846
Total unique data	6192	8259
R_{int}	0.0396	0.0601
R_σ	0.0370	0.0757
Absorption corr. range	0.953, 1.027 [MULTI-SCAN][a]	−
Refinement:		
No. of refined parameters	409	415
Final $R1$[b]	0.0291 [5013 $I > 2\sigma(I)$]	0.0442 [6653 $I > 2\sigma(I)$]
Final $wR2$[c]	0.0823	0.1171
Goodness of fit	1.075	1.021
w^{-1}[d]	$\sigma^2(F^2) + (0.0327P)^2 + 1.81P$	$\sigma^2(F^2) + (0.0589P)^2$
$(\Delta/\sigma)_{av}$, $(\Delta/\sigma)_{max}$	< 0.001, 0.001	< 0.001, 0.001
Min. and max. residual density [e$^-$ Å^{-3}]	−0.50, 0.64	−0.52, 0.83

[a] Incorporated in PLATON.[22] − [b] $R1 = \Sigma||F_o| - |F_c||/\Sigma|F_o|$. − [c] $wR2 = [\Sigma[w(F_o^2 - F_c^2)^2]/\Sigma[w(F_o^2)^2]]^{1/2}$. − [d] $P = [\mathrm{Max}(F_o^2, 0) + 2F_c^2]/3$.

δ = 1.29 [s, 36 H, $C(CH_3)_3$], 4.04 (s, 8 H, CH_2S), 6.92 (s, 2 H, Ar H), 7.19 (d, *J* = 8.6 Hz, 8 H, SAr), 7.27 (d, *J* = 8.6 Hz, 8 H, SAr). − ^{13}C NMR: δ = 31.3, 34.5, 36.7, 130.8, 132.4, 132.8, 134.9, 150.1. − FAB-MS; *m/z*: 625.2 [M − SAr]$^+$, calcd. 625.3. − $C_{50}H_{62}S_4$·0.5H_2O: calcd. C 75.04, H 7.93, S 16.03; found C 75.01, H 7.86, S 15.90.

Bis(acetonitrile) Complex of Pd Dipincer 3: Dipincer ligand **6** (213 mg, 0.3 mmol) was dissolved in CH_3CN (40 mL) and the solution was placed under argon. $Pd[MeCN]_4(BF_4)_2$ (240 mg, 0.6 mmol) was added in one portion, and the mixture was heated at reflux overnight. After evaporation of the solvent, the crude product was taken up in CH_3CN (5 mL) and precipitated by dropwise addition of Et_2O. Yield: 203 mg (60%). − M.p. > 280 °C (dec.). − ^{1}H NMR (CD_3CN): δ = 1.33 [s, 36 H, $C(CH_3)_3$], 4.61 (br s, 8 H, CH_2S), 7.56 (d, *J* = 8.8 Hz, 8 H, SAr H), 7.74 (d, *J* = 8.8 Hz, 8 H, SAr H). − ^{13}C NMR (CD_3CN): δ = 30.8, 35.2, 50.0, 127.8, 127.9, 132.0, 145.8, 155.2. − FAB-MS; *m/z*: 1001.1 [M − 2MeCN − 2BF_4 + H]$^+$, calcd. 1001.2. − $C_{52}H_{65}B_2F_8NOPd_2S_4$·2$H_2O$: calcd. C 49.15, H 5.47, N 1.10 S 10.09; found C 48.86, H 5.14, N 1.25, S 10.00 (the found values for the elemental composition correspond to the substitution of one acetonitrile ligand by water, which probably occurs upon prolonged standing).

Crystal Structure Determinations of 1 and 3·$(PPh_3)_2$: Crystals suitable for X-ray structure determination were mounted on a Lindemann-glass capillary and transferred into the cold nitrogen stream of the diffractometer. Data were collected with a Nonius Kappa CCD diffractometer on rotating anode (Mo-K_α radiation, graphite monochromator, λ = 0.71073 Å, *T* = 150 K, φ and ω scans). Pertinent data for the structure determinations are collected in Table 4. Structures were solved with automated Patterson and subsequent difference Fourier methods for structure **1** and direct methods for structure **3**·$(PPh_3)_2$, using SHELXS86[20] for both structures. Full-matrix refinement on F^2 was performed with SHELXL-97−2.[21] The hydrogen atoms of structure **1** were located on a difference Fourier map and their coordinates were included as parameters in the refinement; the hydrogen atoms of **3**·$(PPh_3)_2$ were included in the refinement on calculated positions riding on their carrier atoms. The nonhydrogen atoms were refined with anisotropic displacement parameters. The hydrogen atoms were refined with a fixed isotropic displacement parameter related to the value of the equivalent isotropic displacement parameter of their carrier atoms. The *t*Bu groups of **3**·$(PPh_3)_2$ were refined with a disorder model involving two sites. The BF_4^- counteranions and the chloroform solvent molecules of this compound were also disordered. Since no satisfactory disorder model could be obtained the contribution of the disordered region to the structure factors was taken into account using the SQUEEZE procedure as incorporated in PLATON.[22] A total of 219 e^- were found in a cavity of 537 Å^3, located at the inversion center on (0,0,0). Neutral atom scattering factors and anomalous dispersion corrections were taken from the International Tables for Crystallography.[23] Geometrical calculations were performed with PLATON.[22] Crystallographic data (excluding structure factors) for the structures reported in this paper have been deposited with the Cambridge Crystallographic Data Centre as supplementary publication nos. CCDC-141832 [for **3** · $(PPh_3)_2$] and -141833 (for **1**). Copies of the data can be obtained free of charge on application to CCDC, 12 Union Road, Cambridge CB2 1EZ, UK [Fax: (internat.) + 44-1223/336-033; E-mail: deposit@ccdc.cam.ac.uk].

Acknowledgments

Financial support of this research by the Council for the Chemical Sciences of the Netherlands Organization for Scientific Research (CW-NWO) is gratefully acknowledged.

[1] These tridentate ligands are usually abbreviated as NCN, PCP and SCS ligands.
[2] [2a] A. Weisman, M. Gozin, H.-B. Kraatz, D. Milstein, *Inorg. Chem.* **1996**, *35*, 1792, and references cited therein. − [2b] P. Steenwinkel, R. A. Gossage, G. van Koten, *Chem. Eur. J.* **1998**, *4*, 759, and references cited therein.
[3] Only one Pt^{II} SCS pincer complex has been reported: G. S. Hanan, J. E. Kickham, S. J. Loeb, *J. Chem. Soc., Chem. Commun.* **1991**, 893.
[4] [4a] J. E. Kickham, S. J. Loeb, S. L. Murphy, *Chem. Eur. J.* **1997**, *3*, 1203 − [4b] J. R. Hall, S. J. Loeb, G. K. H. Shimizu, G. P. A. Yap, *Angew. Chem. Int. Ed.* **1998**, *37*, 121.
[5] Recent reviews on metallodendrimers: [5a] G. R. Newkome, E. He, C. N. Moorefield, *Chem. Rev.* **1999**, *99*, 1689 − [5b] M. A. Hearshaw, J. R. Moss, *Chem. Commun.* **1999**, 1. − [5c]C. Gorman, *Adv. Mater.* **1998**, *10*, 295.
[6] W. T. S. Huck, F. C. J. M. van Veggel, D. N. Reinhoudt, *Angew. Chem. Int. Ed. Engl.* **1996**, *35*, 1213.
[7] [7a] W. T. S. Huck, F. C. J. M. van Veggel, B. L. Kropman, D. H. A. Blank, E. G. Keim, M. M. A. Smithers, D. N. Reinhoudt, *J. Am. Chem. Soc.* **1995**, *117*, 8293. − [7b] W. T. S. Huck, F. C. J. M. van Veggel, D. N. Reinhoudt, *J. Mater. Chem.* **1997**, *7*, 1213.
[8] W. T. S. Huck, L. J. Prins, R. H. Fokkens, N. M. M. Nibbering, F. C. J. M. van Veggel, D. N. Reinhoudt, *J. Am. Chem. Soc.* **1998**, *120*, 6240.
[9] J. E. Kickham, S. J. Loeb, *Inorg. Chem.* **1994**, *33*, 4351.
[10] For example, see: M. Fujita, F. Ibukuro, H. Hagihara, K. Ogura, *Nature* **1994**, *367*, 720.
[11] M. L. Tobe, J. Burgess, *Inorganic Reaction Mechanisms*, Longman, Essex, **1999**.
[12] M. Oki, "Applications of Dynamic NMR Spectroscopy to Organic Chemistry", *Methods in Stereochemical Analysis*, vol. 4, VCH, Weinheim, **1985**.
[13] H. C. Brown, Y. Okamoto, *J. Am. Chem. Soc.* **1958**, *80*, 4979.
[14] M. Gozin, A. Weisman, Y. Ben-David, D. Milstein, *Nature* **1993**, *364*, 699.
[15] R. A. T. M. Abbenhuis, I. Del Río, M. M. Bergshoef, J. Boersma, N. Veldman, A. L. Spek, G. van Koten, *Inorg. Chem.* **1998**, *37*, 1749.
[16] J. Errington, W. S. McDonald, B. L. Shaw, *J. Chem. Soc., Dalton Trans.* **1980**, 2312.
[17] S. J. Loeb, G. K. H. Shimizu, *J. Chem. Soc., Chem. Commun.* **1993**, 1395.
[18] C. A. Tolman, *Chem. Rev.* **1977**, *77*, 313.
[19] Isothiocyanates were found to be too weak to displace the acetonitrile from complex **1**. In the ^{1}H NMR spectrum ($CDCl_3$), the diagnostic signal shift from δ = 2.08 (coordinated CH_3CN) to δ = 1.99 (uncoordinated CH_3CN) was not observed upon addition of butyl isothiocyanate to the acetonitrile complex **1**. FT-IR spectroscopy also failed to demonstrate the coordination of isothiocyanate to Pd^{II}.
[20] G. M. Sheldrick, *SHELXS86 Program for crystal structure determination*, University of Göttingen, Germany, **1986**.
[21] G. M. Sheldrick, *SHELXL-97−2 Program for crystal structure refinement*, University of Göttingen, Germany, **1997**.
[22] A. L. Spek, *PLATON, A multi-purpose crystallographic tool*, Utrecht University, The Netherlands, **2000**; Internet: http://www.cryst.chem.uu.nl/platon/
[23] A. J. C. Wilson (Ed.), *International Tables for Crystallography*, vol. C, Kluwer Academic Publishers, Dordrecht, The Netherlands, **1992**.

Received March 21, 2000
[I00103]

Binuclear Nickel(II) Complexes Based on Bridging Oxalate and Pseudohalides as Peripheral Ligands: Synthesis, Crystal Structure, DFT Calculations and Magnetic Properties of $[\{Ni(X)(dien)\}_2(\mu\text{-ox})]\cdot n H_2O$ Complexes ($X = N_3^-$, NCS^-, $n = 0$; NCO^-, $n = 1$)

Iñaki Muga,[a] Juan M. Gutiérrez-Zorrilla,*[a] Pablo Vitoria,[a] Antonio Luque,[a] Maite Insausti,[a] Pascual Román,[a] and Francesc Lloret[b]

Keywords: Nickel / Binuclear complexes / Density functional calculations / Structure elucidation / Magnetic properties

Nickel(II) molecular complexes were obtained by water displacement reactions of $[\{Ni(dien)(H_2O)\}_2(\mu\text{-ox})]Cl_2$ and the corresponding pseudohalide. The three nickel(II) compounds $[\{Ni(N_3)(dien)\}_2(\mu\text{-ox})]$ (**1**), $[\{Ni(NCO)(dien)\}_2(\mu\text{-ox})]\cdot H_2O$ (**2**) and $[\{Ni(NCS)(dien)\}_2(\mu\text{-ox})]$ (**3**) are almost isostructural. The structure determinations reveal the presence of a binuclear complex with C_{2h} symmetry, where the oxalate ligand is coordinated in a bis(bidentate) fashion to the twofold related nickel atoms. The distorted octahedral environment of each nickel atom is completed by the three nitrogen atoms of the diethylenetriamine ligand in a *fac* arrangement and one nitrogen atom from a pseudohalide ligand. Magnetic susceptibility data in the temperature range 4.2–300 K shows intramolecular antiferromagnetic coupling.

Introduction

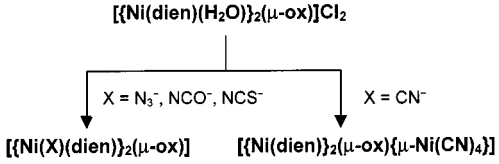
The design and synthesis of molecular magnetic compounds has attracted increasing attention over the past two decades or so.[1] A significant amount of magnetostructural research work during the last twenty five years has been devoted to analysing the remarkable ability of the oxalate bridge to mediate exchange coupling between first-row transition metal ions separated by more than 5 Å in both homo- and heteropolynuclear compounds.[2] The simple binuclear geometry involving symmetric, in-plane bridging with a single oxalate ion binding through two oxygen atoms to each of two metal centres has been observed in the chemistry of copper,[3] nickel,[4] and less frequently, the remaining first transition series metal ions.[5] Magnetostructural data of oxalato-bridged Ni^{II} complexes have revealed that J varies from -22 to -39 cm^{-1}.[6] This value is strongly dependent on the nature of the donor atoms in the peripheral ligands. The present contribution is devoted to the analysis of this factor in oxalato-bridged octahedral nickel(II) complexes with an NiN_4O_2 environment. We have succeeded in synthesising a related series of nickel(II) complexes of general formulation $[\{Ni(X)(dien)\}_2(\mu\text{-ox})]\cdot n H_2O$ ($X = N_3^-$, NCS^-, $n = 0$; $X = NCO^-$, $n = 1$). This work has allowed us to study the influence of the water of crystallization on the crystal packing and thermal behaviour of these compounds.

[a] Departamento de Química Inorgánica, Facultad de Ciencias, Universidad del País Vasco,
Apartado 644, 48080 Bilbao, Spain
E-mail: qipguloj@lg.ehu.es
[b] Departament de Química Inorgànica, Facultat de Química, Universitat de València,
Dr. Moliner 50, 46100 Burjassot, València, Spain

Results and Discussion

Synthesis

In the synthesis of the three molecular compounds, the binuclear complex $[\{Ni(dien)(H_2O)\}_2(\mu\text{-ox})]Cl_2$[2c] was used as a precursor owing to the lability of its water molecules, which may be substituted by pseudohalide ligands. The preparation of the compound was performed as follows: the sodium or potassium salt of the corresponding pseudohalide dissolved in a small amount of water was added to a hot aqueous solution of $[\{Ni(dien)(H_2O)\}_2(\mu\text{-ox})]Cl_2$. When we used cyanide as pseudohalide, a neutral trinuclear complex was obtained where the two water molecules were replaced by two cyano groups belonging to a square planar $[Ni(CN)_4]^{2-}$ unit,[7] (Scheme 1).



Scheme 1

Description of the Crystal Structures

The three compounds crystallize in the same monoclinic space group $C2/m$ and could be considered almost isostructural. Single crystal structure analyses were performed for the neutral $[\{Ni(N_3)(dien)\}_2(\mu\text{-ox})]$ (**1**) and $[\{Ni(NCO)(dien)\}_2(\mu\text{-ox})]\cdot H_2O$ (**2**) complexes. These analyses reveal the presence of a binuclear complex of C_{2h} symmetry, with nickel atoms and pseudohalide ligands contained in the symmetry plane. The twofold axis is defined by the C−C bond of the oxalate ligand which is coordinated in a bis(bidentate) fashion to the twofold related nickel atoms.

 © WILEY-VCH Verlag GmbH, D-69451 Weinheim, 2000 1434−1948/00/1212−2541 $ 17.50+.50/0

The distorted octahedral environment of each nickel atom is completed by three nitrogen atoms from a diethylenetriamine ligand in a *fac* arrangement and one nitrogen atom from a pseudohalide ligand (Figure 1). The Ni−oxalato−Ni fragments adopt a chair conformation with a Ni−Ni distance of 5.397 Å for **1** and 5.491 Å for **2**. The nickel atoms are displaced by 0.021 Å for **1** and 0.198 Å for **2** out of the oxalate plane towards the N atom of the pseudohalide. The dihedral angle between the oxalato group and the equatorial mean plane is 2.37° for **1** and 3.98° for **2**. Bond lengths and angles involving non-hydrogen atoms are listed in Table 1. The Ni−O (oxalate) distances are 2.081 Å for **1** and 2.108 Å for **2**, whereas the Ni−N bonds vary in the range 2.08−2.16 Å. These distances agree with those observed in other oxalato-bridged nickel(II) complexes.

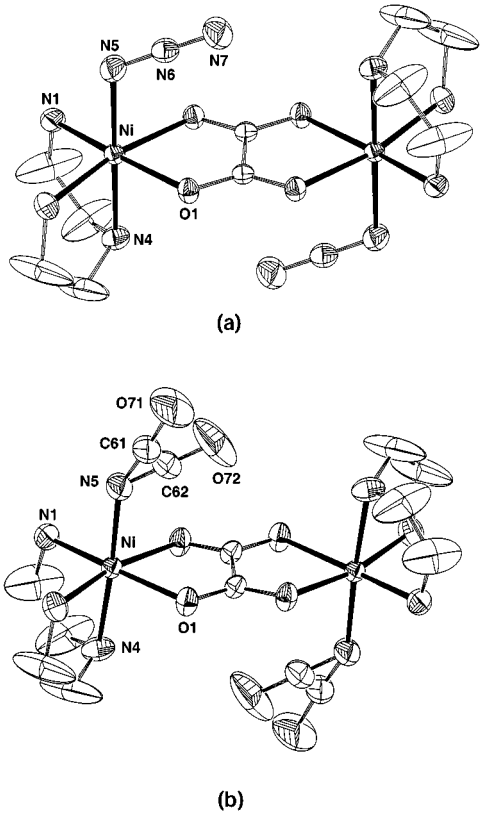


Figure 1. ORTEP views of compound **1** (a) and compound **2** (b) with atom labelling

The thermal analysis of the compound **2** confirms the presence of one water molecule, which is found to be disordered around an inversion centre in the crystal structure determination.

The different coordination modes of the pseudohalide ligands are remarkable. In compound **1** the azide ligand coordinates with an Ni−N5−N6 angle of 113.3°, while in compound **2** the cyanate ligand shows two coordination modes, with different values of the Ni−N5−C6 angle, 152.0° (64%) and 121.4° (36%). In order to check if this behaviour is due to electronic or packing effects, theoretical calculations were performed on a mononuclear model compound of general formula $[Ni(X)(NH_3)_3(CH_2O_2)]^+$ where $X = N_3^-$, NCO^-. Both structures were fully optimised and only one minimum was found for each, with a coordination angle of 109.9° for the azide and 124.8° for the cyanate ligand. Both values agree quite well with experimental ones. As there is no energy minimum with (quasi)linear coordination of the cyanate ligand, the experimental value of 152° observed for 64% of the molecules in the crystal must be due to the formation of hydrogen bonds with the water molecule present in compound **2** but absent in compound **1** (vide infra). The water molecule plays an important role in the thermal behaviour of this compound. Just before the end of the dehydration process (210 °C) the heat flow curve shows a sharp endothermic peak superimposed on the broad peak associated with water loss (Figure 2). Preliminary studies indicate a disorder-order phase transition. The loss of the water molecule destabilises the cyanate coordination mode having the higher angle and all cyanate ligands should coordinate with an angle of ≈120°.

Table 1. Selected experimental and theoretical (obtained using BPW91 optimizations) bond lengths [Å] and angles [°] for compounds **1** and **2**

Compounds	**1**		**2**		
Ni environment	Experimental	*BPW91*	Experimental		*BPW91*
Ni1−O1	2.081 (2)	2.029	2.108 (2)		2.036
Ni1−N1	2.079 (2)	2.067	2.082 (2)		2.070
N1−N4	2.106 (3)	2.102	2.122 (4)		2.102
NI1−N5	2.154 (4)	2.004	2.091 (4)		2.001
O1−Ni1−O1′	80.8 (1)	84.4	79.2 (1)		84.0
O1−Ni1−N5	89.3 (1)	91.6	91.9 (1)		92.4
N1−Ni1−N4	83.5 (1)	84.3	83.0 (1)		84.1
N1−Ni1−N5	96.9 (1)	96.8	94.8 (1)		96.4
N4−Ni1−N5	180.0 (1)	178.1	176.5 (2)		179.2
Oxalate ligand					
C1−C1′	1.553 (5)	1.556	1.552 (3)		1.558
C1−O1	1.252 (2)	1.268	1.260 (2)		1.269
N_3^- ligand					
N5−N6	1.179 (4)	1.211			
N6−N7	1.180 (5)	1.188			
Ni1−N5−N6	113.3 (2)	117.0			
N5−N6−N7	178.9 (4)	179.6			
NCO^- ligand			X = 1	X = 2	
N5−C6X			1.126 (7)	1.191 (2)	1.217
C6X−O7X			1.20 (1)	1.20 (3)	1.223
Ni1−N5−C6X			152.0 (6)	121.4 (9)	120.4
N5−N6X−O7X			176 (1)	179 (2)	179.6

Based on the high accuracy of the above-mentioned DFT calculations on model monomers, the geometry of the dimers has been optimized at the same level. The combination of the BPW91 functional with the 6-31G* basis set seems a good choice for studies of coordination compounds.[8] A summary comparison of the experimental and theoretical geometrical parameters is given in Table 1, which show good agreement.

In both compounds the dinuclear units are held together by means of an extensive two-dimensional hydrogen bonding network, involving the amino groups as donors and the oxygen atoms of the oxalate ligand and nitrogen atoms of the pseudohalide ligand as acceptors, such that each dimeric unit is connected to its neighbours through eight N1−H11···O1 and eight N1−H12···N5 hydrogen bonds

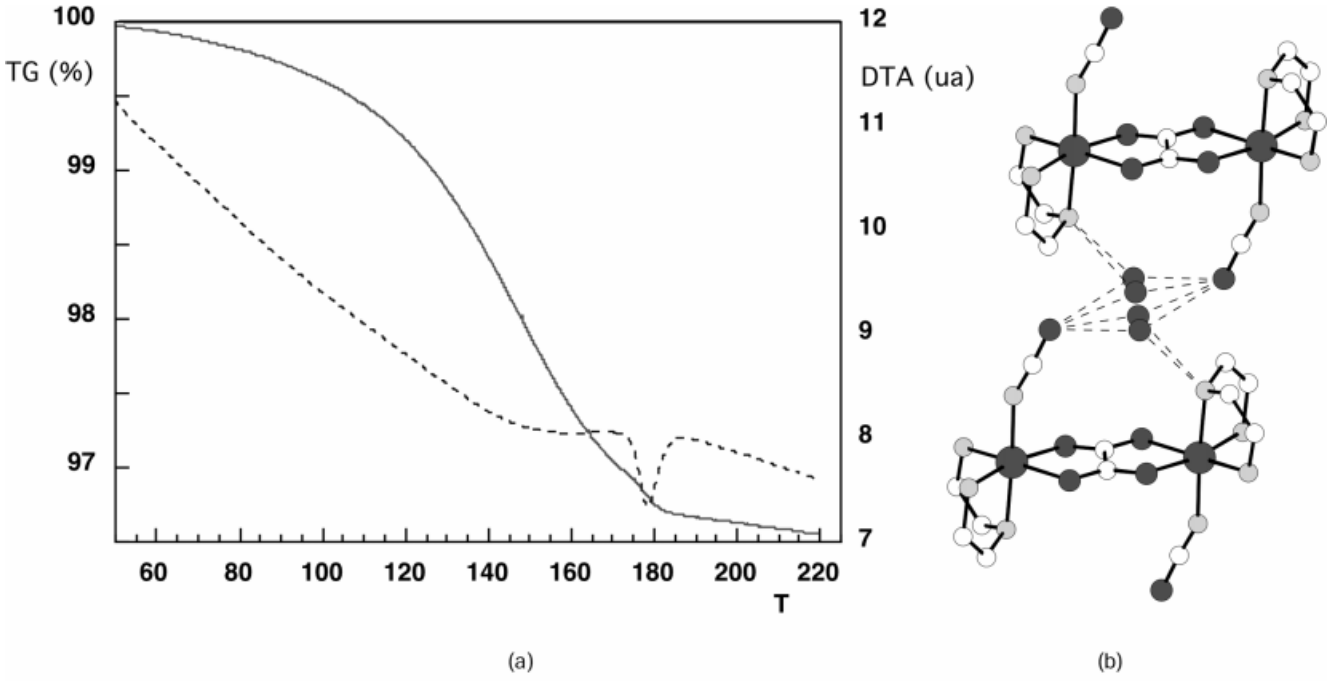


Figure 2. (a) Thermal analysis of the dehydration process and (b) disordered water molecule environment in compound **2**

(Table 2), leading to an infinite two-dimensional arrangement along the *xy* plane (Figure 3). However, they differ in the connections between layers, which in compound **1** are held together through hydrophobic interactions involving the CH_2 groups of dien ligand, but in compound **2** such connections are through hydrogen bonding of the water molecule, the oxygen atom of NCO^- and the secondary nitrogen atom of the dien ligand (Figure 2b). The presence of this water molecule in the structure causes an increase of about 1 Å in the value of the unit cell *c* parameter with respect to that of compound **1**, corresponding with the layer packing direction.

Besides these intermolecular hydrogen bonds, two intramolecular N4−H41···N7 interactions are also present in compound **1**.

Magnetic Properties

The molar magnetic susceptibility, χ_M, vs. temperature curves for compounds **1−3** are depicted in Figure 4. The susceptibility curve for these complexes increases when the compound is cooled until a maximum is reached (T_{max} = 46.4, 42.0 and 48.7 K, for **1−3**, respectively) and then decreases very quickly. The ground state of nickel(II) ion in an octahedral environment is orbitally nondegenerate, and as such, it is possible to represent the intradimer magnetic interaction, *J*, with the isotropic spin Hamiltonian $H = -JS_A \cdot S_B$. The molar magnetic susceptibility for a nickel(II) dimer (local spins $S_A = S_B = 1$) may be expressed by Equation 1, where *N*, β, *k*, *g* and *T* have their usual meaning.

$$\chi_M = \frac{2N\beta^2 g^2}{kT} \times \frac{\exp(J/kT) + 5\exp(3J/kT)}{1 + 3\exp(J/kT) + 5\exp(3J/kT)}$$

Table 2. Hydrogen bonding contacts

Type	D−H [Å]	D···A [Å]	H···A [Å]	<D−H···A [°]
Compound **1**				
N1−H11···N5[a][b]	0.91 (5)	3.130 (4)	2.28 (5)	155 (4)
N1−H12···O1[c]	0.83 (4)	3.062 (3)	2.23 (5)	172 (4)
N4−H41···N7[d][e](intra)	0.91 (5)	3.130 (4)	2.28 (5)	155 (4)
N4−H41···N7 (BPW91)	*1.04*	*3.25*	*2.22*	*175.4*
Compound **2**				
N1−H11···N5[a][b]	0.87 (8)	3.267 (4)	2.49 (9)	149 (8)
N1−H12···O1[c]	0.89 (4)	3.060 (3)	2.19 (5)	168 (8)
N4−H41···Ow1[f]	0.80 (9)	2.97 (2)	2.25 (9)	149.2 (5)
Ow1···O71[d][e]		2.68 (2)		
Ow1···O71[g][h]		2.89 (2)		
Ow1···O72[g][h]		2.73 (3)		

Symmetry codes: [a] 1 − *x*, −*y*, −*z*. − [b] 1 − *x*, *y*, −*z*. − [c] 1/2 − *x*, 1/2 − *y*, −*z*. − [d] −*x*, −*y*, −*z*. − [e] −*x*, *y*, −*z*. − [f] *x*, −*y*, *z*. − [g] *x*, *y*, 1 + *z*. − [h] *x*, −*y*, 1 + *z*.

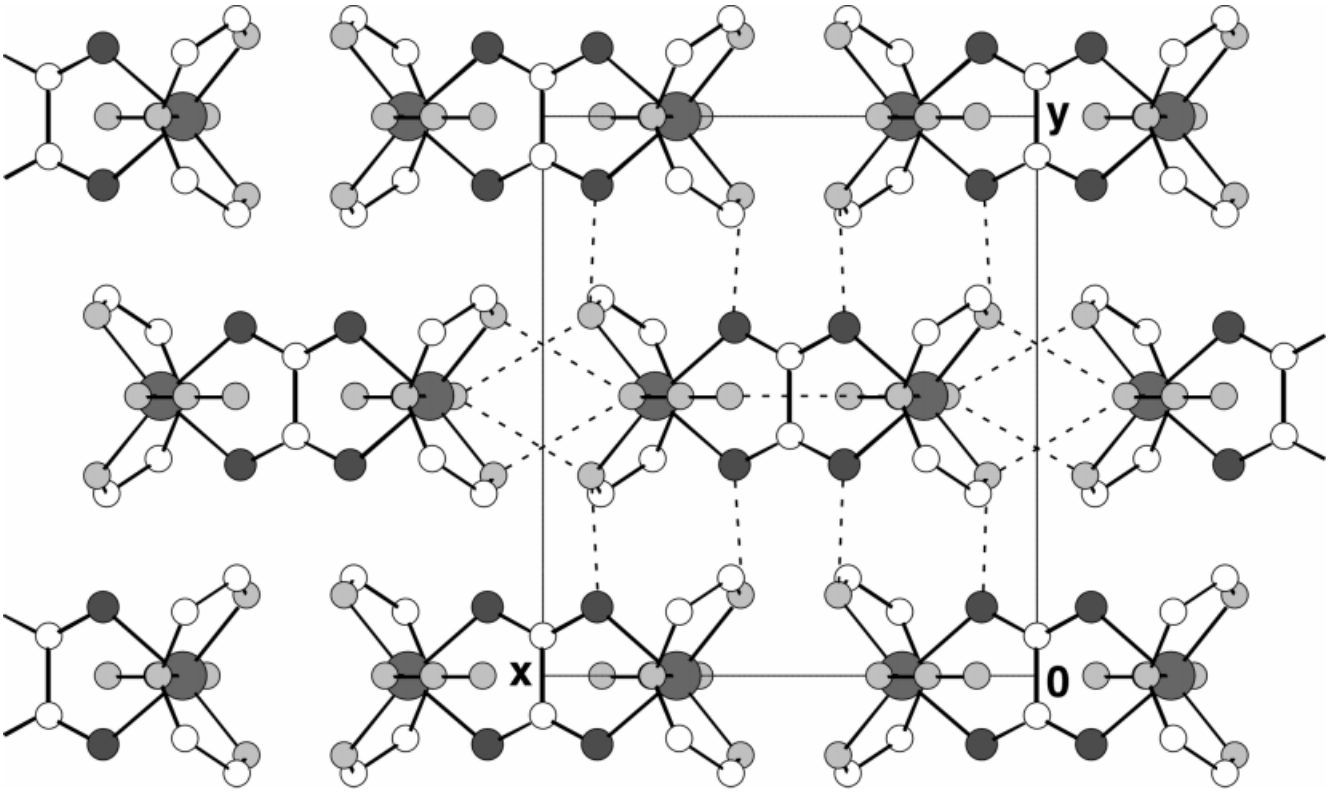


Figure 3. Two dimensional arrangement along the *xy* plane; dotted lines mean all hydrogen bonds of one binuclear unit

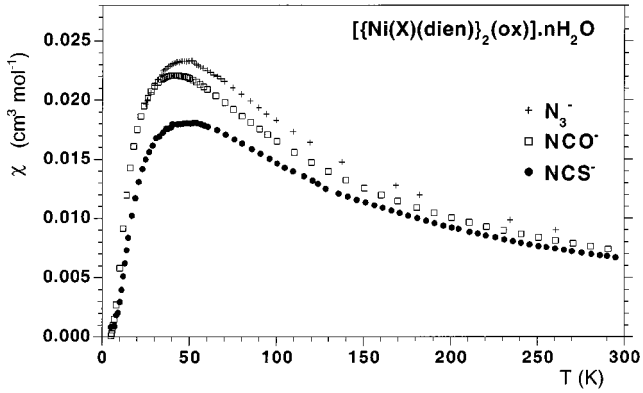


Figure 4. Thermal dependence of the molar magnetic susceptibility for compounds **1**−**3**

Although nickel(II) with axial symmetry can have a large zero-field splitting *D*, the magnetic behaviour of nickel(II) dimers closely follows Equation 1 when a relatively strong antiferromagnetic interaction is operative.[9] This is the case for complexes **1**−**3** where least-squares analysis of the experimental data with Equation 1 leads to $J = -31.4$ cm^{-1}, $g = 2.25$ and $R = 1{\cdot}10^{-4}$ for **1**; $J = -28.5$ cm^{-1}, $g = 2.14$ and $R = 5{\cdot}10^{-5}$ for **2**; $J = -33.0$ cm^{-1}, $g = 2.08$ and $R = 1.6{\cdot}10^{-5}$ for **3**. *R* is the agreement factor defined as $R = \Sigma(\chi_M^{obs} - \chi_M^{calc})^2/\Sigma(\chi_M^{obs})^2$. Previously reported *J* values for μ-oxalato bridged nickel(II) binuclear complexes are close to those of compounds **1**−**3**. This information is summarized in Table 3 for dinuclear Ni^{II}-oxalato systems in an NiO_2N_4 environment. It is well known that structural distortions (distance Ni−O_{ox}, bite angle O−Ni−O, deviation from the planarity of the nickel ion respect to mean plane of the oxalate bridging ligand) can play a key role in the fine-tuning of exchange coupling and the influence of apical pseudohalide ligands on the *J* values is similar in the three compounds since all are N-donor ligands.

A graphical representation of the four DFT magnetic orbitals of compound **2** is given in Figure 5, with those for compound **1** being very similar. As expected for the case of octahedral nickel centres, the unpaired electrons are mainly located in the d_{z^2} and d_{xy} orbitals, with a noticeable contribution to the d_{z^2} magnetic orbital of the pseudohalide orbital.

Conclusions

The reaction between pseudohalogen species and the cationic complex $[\{Ni(dien)(H_2O)\}_2(\mu\text{-ox})]^{2+}$ results in water displacement when the pseudohalides are N_3^-, NCO^-, and NCS^-, leading to the corresponding neutral binuclear complexes. However, in the case of cyanide anion, the trinuclear species $[\{Ni(dien)\}_2(\mu\text{-ox})\{\mu\text{-}Ni(CN)_4\}]$ is obtained due to the high stability of the $[Ni(CN)_4]^{2-}$ complex which is initially formed when the cyanide salt is added. The tetracyanonickelate(II) acts a template for the formation of the trinuclear unit.

The three compounds are almost isostructural, but differ in the degree of hydration. Compound **2** is monohydrated

Table 3. Selected magnetostructural parameters [Å,°] for dinuclear nickel(II) oxalato systems in an NiO_2N_4 environment

Compound[a]	$-J$[b]	g	d(Ni−O)[c]	d(Ni−N_{eq})[d]	D(Ni−N_{ap})[e]	d(Ni···Ni)[f]	O−Ni−O[g]	h(Ni)[h]	ref.
[{Ni(cth)}$_2$(μ-ox)](ClO_4)$_2$	36.8	2.19							[4a]
[{Ni(trien)}$_2$(μ-ox)](ClO_4)$_2$	35.2	2.20							[4a]
[{Ni(en)$_2$}$_2$(μ-ox)](ClO_4)$_2$	36.8	2.27	2.091 / 2.093	2.12	2.15	5.488	81.05	0.106	[5d]
[{Ni(en)$_2$}$_2$(μ-ox)](NO_3)$_2$	32.0	2.19	2.094 / 2.098	2.09	2.10	5.420	79.71	0.037	[3a]
[{Ni(tn)$_2$}$_2$(μ-ox)](ClO_4)$_2$	36.4	2.18	2.080−2.162	2.09	2.09	5.481 / 5.492	78.05−79.33	0.032−0.101	[4g]
[{Ni(cyclam)}$_2$(μ-ox)](NO_3)$_2$	39.0	2.33	2.070 / 2.071	2.09	2.10	5.395	80.75	0.040	[4f]
[{Ni(cyclen)}$_2$(μ-ox)](NO_3)$_2$	35.0	2.15							[4j]
[{Ni(Me_2cyclen)}$_2$(μ-ox)](ClO_4)$_2$	34.0	2.30	2.095 / 2.102	2.05	2.15	5.465	79.28	0.021	[4j]
[{Ni(323-tet)}$_2$(μ-ox)](ClO_4)$_2$	28.9	2.17	2.115 / 2.124	2.11	2.11	5.506	78.88	0.073	[4m]
[{Ni(tren)$_2$}$_2$(μ-ox)](ClO_4)$_2$	28.8	2.16	2.050 / 2.112	2.07	2.13	5.413	80.43	0.044	[4p]
[{Ni(dien)$_2$}$_2$(μ-ox){μ-Ni($CN)_4$}]	31.2	2.15	2.088	2.08	2.09	5.324	80.30	0.391	[7]
[{Ni(N_3)(dien)$_2$}$_2$(μ-ox)]	31.4	2.25	2.081	2.08	2.13	5.397	80.77	0.021	Compound **1**
[{Ni(NCO)(dien)$_2$}$_2$(μ-ox)]	28.5	2.14	2.108	2.08	2.11	5.491	79.18	0.198	Compound **2**
[{Ni(NCS)(dien)$_2$}$_2$(μ-ox)]	33.0	2.08							Compound **3**

[a] Abbreviations used: cth = 2,4,4,9,9,11-hexamethyl-1,5,8,12-tetraazacyclotetradecane; trien = triethylenetetramine; en = ethylenediamine; tn = 1,3-diaminopropane; cyclam = 1,4,8,11-tetraazacyclotetradecane; cyclen = 1,4,7,10-tetraazacyclododecane; Me_2cyclen = 1,7-dimethyl-1,4,7,10-tetraazacyclododecane, 323-tet = *N,N′*-bis(3-aminopropyl)-1,2-ethenediamine; tren = tris(2-aminoethyl)amine; dien = diethylenetriamine. − [b] J in cm^{-1}. − [c] d(Ni−O): distance Ni−O(oxalato). − [d] d(Ni−N_{eq}): mean distance Ni−N(equatorial). − [e] d(Ni−N_{ap}): mean distance Ni−N(apical). − [f] d(Ni···Ni): nickel−nickel separation across the oxalato ligand. − [g] O−Ni−O: bite angle. − [h] h(Ni): metal height from the oxalato mean plane.

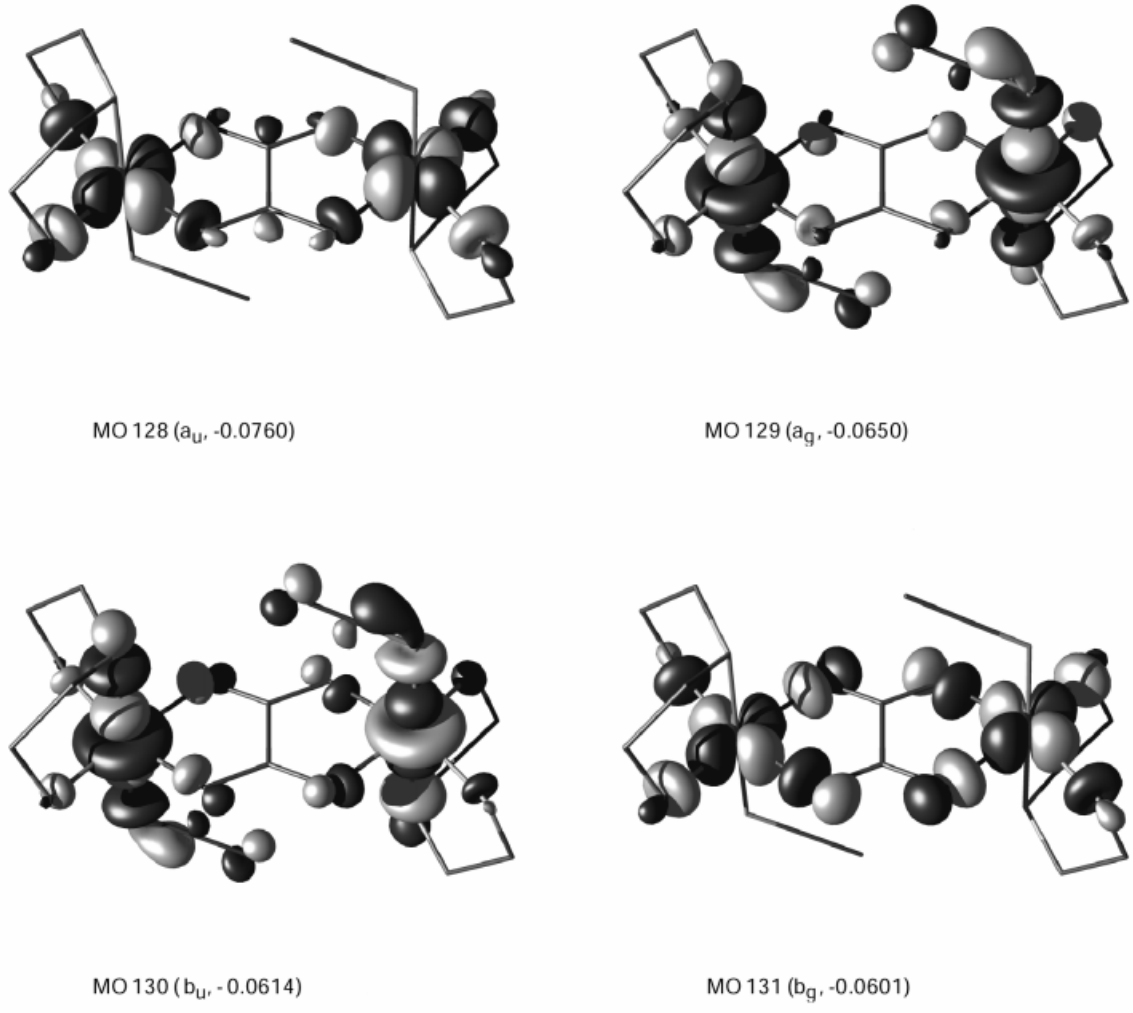


Figure 5. Magnetic orbitals for compound **2** (symmetry, energy)

but compound **1** and **3** are anhydrous. Although the dinuclear units in both compounds are held together by means of an extensive two-dimensional hydrogen bonding network, they differ in the connection between layers. In anhydrous compound **1** the layers are held together through hydrophobic interactions, but in hydrated compound **2** such connections are via hydrogen bonding involving the water molecule. This fact confirms that hydrogen bonds of type O−H···O are stronger than possible O−H···N or O−H···S ones, and are strong enough to force 64% of NCO^- ligands to adopt a coordination fashion which according to the DFT calculations is less stable.

DFT calculations on the binuclear complexes confirm the nature of the magnetic orbital previously reported in these kinds of compounds,[2c] although the energetic order is different.

Experimental Section

General: Microanalyses of carbon, nitrogen, hydrogen, and sulfur were performed on a LECO CHNS-932 analyser. −IR: NICOLET 740 FT-IR. − TG: SETARAM TAG 24 S16. The thermal experiments were performed in synthetic dry air atmosphere (100 $mL{\cdot}min^{-1}$) and a heating rate of 2 $°C{\cdot}min^{-1}$ in the temperature range 25−250 °C. All chemicals were procured commercially and used without subsequent purification.

Synthesis of [{Ni(N_3)(dien)}$_2$(μ-ox)] (1): Obtained from [{Ni(dien)(H_2O)}$_2$(μ-ox)]Cl_2 (0.360 g, 0.707 mmol) in water (40 mL) and NaN_3 (0.114 g, 2.25 mmol) in water (5 mL), as blue crystals in 60% yield (0.210 g, 0.424 mmol). − $C_{10}H_{26}N_{12}Ni_2O_4$ (495.80): calcd. C 24.23; H 5.29; N 33.90; found C 24.2; H 5.4; N 34.0. − IR (KBr): $\tilde{\nu}$ = 2036 cm^{-1} (N_3^-).

Synthesis of [{Ni(NCO)(dien)}$_2$(μ-ox)]·H_2O (2): [{Ni(dien)(H_2O)}$_2$(μ-ox)]Cl_2 (0.231 g, 0.448 mmol) in water (70 mL) and NaNCO (0.110 g, 1.69 mmol), as blue crystals in 55% yield (0.120 g, 0.244 mmol). $C_{12}H_{26}N_8Ni_2O_6{\cdot}H_2O$ (513.81): calcd. C 28.05; H 5.49; N 21.81; found C 28.1; H 5.6; N 21.9. − IR (KBr): $\tilde{\nu}$ = 2210, 2169 cm^{-1} (NCO^-).

Synthesis of [{Ni(NCS)(dien)}$_2$(μ-ox)] (3): [{Ni(dien)(H_2O)}$_2$(μ-ox)]Cl_2 (0.230 g, 0.440 mmol) in water (50 mL) and KSCN (0.115 g, 1.18 mmol), as blue spherulites in 75% yield (0.174 g, 0.330 mmol). − $C_{12}H_{26}N_8Ni_2O_4S_2$ (527.91): calcd. C 27.30; H 4.96; N 21.23; found C 27.3; H 4.96; N 21.23. − IR (KBr): $\tilde{\nu}$ = 2049 cm^{-1} (NCS^-).

Magnetic Susceptibility Measurements: Magnetic susceptibility measurements were carried out on polycrystalline samples in the temperature range 4.2−300 K, with a pendulum type susceptometer/magnetometer (Manicsd DSM8) equipped with a helium continuous flow cryostat. The diamagnetic contribution was calculated from Pascal's constants.

X-ray Crystallographic Studies: Data collection for the prismatic blue single crystals of **1** and **2** was performed on an Enraf−Nonius CAD4 and a Philips PW1100 diffractometer, respectively, with graphite monochromated Mo-K_α radiation (λ = 0.71069 Å). Intensities were collected by the ω-2θ scan technique. A Lorentz-polarization (Lp) correction was applied. The experimental details and crystal data are listed in Table 4. The atomic scattering factors were taken from the International Tables for X-ray Crystallography.[10] The structures were solved by direct methods (DIRDIF92[11]). The non-hydrogen atoms were anisotropically refined by the full-matrix least-squares method. In compound **2**, C

Table 4. Crystallographic data for [{Ni(N_3)(dien)}$_2$(μ-ox)] (**1**), [{Ni(NCO)(dien)}$_2$(μ-ox)]·H_2O (**2**) and [{Ni(NCS)(dien)}$_2$(μ-ox)] (**3**)

Compound	**1**	**2**	**3**
Formula	$C_{10}H_{26}N_{12}Ni_2O_4$	$C_{12}H_{26}N_8Ni_2O_6 \cdot H_2O$	$C_{12}H_{26}N_8Ni_2O_4S_2$
Formula weight	495.80	513.81	527.91
Crystal system	monoclinic	monoclinic	monoclinic
Space group	*C* 2/*m*	*C* 2/*m*	*C* 2/*m*
a [Å]	9.681 (4)	9.911 (2)	9.606 (1)
b [Å]	10.938 (3)	10.787 (2)	10.631 (1)
c [Å]	9.050 (2)	9.978 (2)	10.175 (1)
β [°]	92.90 (2)	96.97 (2)	98.55 (2)
V [$Å^3$]	957.2 (5)	1058.9 (4)	1027.6 (2)
Z	2	2	2
$D_{calcd.}$ [g/cm^3]	1.728	1.608	1.706
Crystal source	H_2O	H_2O	
Crystal size [mm]	0.70×0.50×0.25	0.60×0.50×0.20	
Diffractometer	Enraf Nonius CAD 4	Philips PW 1100	Stoe Darmstad
Radiation	Mo-K_α	Mo-K_α	Cu-$K_{\alpha1}$
μ [mm^{-1}]	2.021	1.829	
θ limits [°]	2−30	2−35	2.5−35
h, *k*, *l* range	0−13	−15−15	
	0−15	0−17	
	−12−12	0−16	
No. of unique reflns.	1457	2424	
No. of obsd. data	1358 [$I > 3\sigma(I)$]	2137 [$I > 3\sigma(I)$]	100
No. of parameters	83	104	
R_1 (obsd. rflns)	0.043	0.051	
wR_2 (all rflns)	0.058	0.066	
$\Delta\rho_{max}/\Delta\rho_{min}$ [$e/Å^3$]	+0.8 / −0.5	+0.9 / −0.9	
R_p			0.217
R_{wp}			0.229
R_{Bragg}			0.060
R_F			0.034

and O pseudohalide atoms were found to be distributed over two positions. Hydrogen atoms bonded to nitrogen atoms were located in a difference Fourier synthesis and refined isotropically. Most calculations were performed using XRAY76 System.[12]

For compound **3** the powder X-ray diffraction pattern was collected on a STOE diffractometer using Cu-$K_{\alpha 1}$ radiation (λ = 1.54059 Å). Data were collected by scanning in the 2θ range 5−70° with increments of 0.02°. The structure was refined by the Rietveld method using the FULLPROF program.[13]

Crystallographic data (excluding structure factors) for the structures reported in this paper have been deposited with the Cambridge Crystallographic Data Centre as supplementary publication no. CCDC-140558 (**1**), -140559 (**2**). Copies of the data can be obtained free of charge on application to CCDC, 12 Union Road, Cambridge CB2 1EZ, UK (E-mail: deposit@ccdc.cam.ac.uk).

Acknowledgments

This work was supported by the Gobierno Vasco (Grant PI-96/69) and Ministerio de Educación y Cultura, DGESIC (Grant PB98-0238). P.V. acknowledges financial support from MEC (Grant AP95 30650377).

[1] [1a]D. Gatteschi, O. Khan, J. S. Miller, F. Palacio, *Magnetic Molecular Materials*, Kluwer, Dordrecht, **1991**. − [1b]*Inorganic Materials* (Eds.: Q. W. Bruce, D. O'Hare), Wiley, Chichester, **1992**. − [1c]O. Khan, *Molecular Magnetism*, VCH, New York, **1993**.

[2] [2a]P. J. Hay, J. C. Thibeault, R. Hoffmann, *J. Am. Chem. Soc.* **1975**, *97*, 4884. − [2b] S. Alvarez, M. Julve, M. Verdaguer, *Inorg. Chem.* **1990**, *29*, 4500. − [2c] P. Román, C. Guzmán-Miralles, A. Luque, J. I. Beitia, J. Cano, F. Lloret, M. Julve, S. Alvarez, *Inorg. Chem.* **1996**, *35*, 3741. − [2d] J. Cano, E. Ruiz, P. Alemany, F. Lloret, S. Alvarez, *J. Chem. Soc., Dalton Trans.* **1999**, 1669.

[3] [3a]N. F. Curtis, I. R. N. McCormick, T. N. Waters, *J. Chem. Soc., Dalton Trans.* **1973**, 1537. − [3b] M. Julve, M. Verdaguer, O. Kahn, A. Gleizes, M. Philoche-Levisalles, *Inorg. Chem.* **1983**, *22*, 368. − [3c] J. Sletten, *Acta Chem. Scand. Ser. A* **1983**, *37*, 569. − [3d] M. Julve, M. Verdaguer, A. Gleizes, M. Philoche-Levisalles, O. Kahn, *Inorg. Chem.* **1984**, *23*, 3808. − [3e] M. Julve, J. Faus, M. Verdaguer, A. Gleizes, *J. Am. Chem. Soc.* **1984**, *106*, 8306. − [3f] A. Bencini, A. C. Fabretti, C. Zanchini, P. Zannini, *Inorg. Chem.* **1987**, *26*, 1445. − [3g] J. A. Real, J. Borras, X. Solans, M. Font-Altaba, *Transition Met. Chem.* **1987**, *12*, 254. − [3h] L. Soto, J. Garcia, E. Escriva, J.-P. Legros, J.-P. Tuchagues, F. Dahan, A. Fuertes, *Inorg. Chem.* **1989**, *28*, 3378. − [3i] I. Castro, J. Faus, M. Julve, M. Mollar, A. Monge, E. Gutiérrez-Puebla, *Inorg. Chim. Acta* **1989**, *161*, 97. − [3j] I. Castro, J. Faus, M. Julve, M. C. Munoz, W. Diaz, X. Solans, *Inorg. Chim. Acta* **1991**, *179*, 59. − [3k] I. Castro, J. Faus, M. Julve, A. Gleizes, *J. Chem. Soc., Dalton Trans.* **1991**, 1937. − [3l] L. S. Tuero, J. Garcia-Lozano, E. E. Monto, M. B. Borja, F. Dahan, J.-P. Tuchagues, J.-P. Legros, *J. Chem. Soc., Dalton Trans.* **1991**, 2619. − [3m] A. Gleizes, M. Julve, M. Verdaguer, J. A. Real, J. Faus, X. Solans, *J. Chem. Soc., Dalton Trans.* **1992**, 3209. − [3n] C. George, A. Purdy, *Acta Crystallogr., Sect. C* **1992**, *48*, 155. − [3o] P. E. Kruger, K. S. Murray, E. R. T. Tienkink, *Z. Kristallogr.* **1994**, *209*, 624. − [3p] J. Li, J. Sun, P. Chen, X. Wu, *Cryst. Res. and Technol.* **1995**, *30*, 353. − [3q] S. Warzeska, R. Kramer, *Chem. Ber.* **1995**, *128*, 115. − [3r] R. Vicente, A. Escuer, J. Ferretjans, H. Stoeckli-Evans, X. Solans, M. Font-Bardia, *J. Chem. Soc., Dalton Trans.* **1997**, 167. − [3s] M. K. Saha, S. Sen, P. Kundu, T. Gupta, V. Gramlich, S. Mitra, *Z. Naturforsch., Teil B* **1998**, *53*, 1281. − [3t] Z. Smekal, Z. Travnicek, M. Nadvornik, Z. Sindelar, R. Klicka, J. Marek, *Collect. Czech. Chem. Commun.* **1998**, *63*, 783. − [3u] O. Castillo, I. Muga, A. Luque, J. M. Gutiérrez-Zorrilla, J. Sertucha, P. Vitoria, P. Román, *Polyhedron* **1999**, *18*, 1235.

[4] [4a]D. M. Duggan, E. K. Barefield, D. N. Hendrickson, *Inorg. Chem.* **1973**, *12*, 985. − [4b] J. Kopf, U. Behrens, M. Kastner, G. Klar, *J. Inorg. Nucl. Chem.* **1977**, *39*, 889. − [4c] A. R. Davis, F. W. B. Einstein, A. C. Willis, *Acta Crystallogr., Sect. B* **1982**, *38*, 443. − [4d] N. W. Alcock, P. Moore, H. A. A. Omar, *Acta Crystallogr., Sect. C* **1987**, *43*, 2074. − [4e] H.-F. Klein, T. Wiemer, M.-J. Menu, M. Dartiguenave, Y. Dartiguenave, *Inorg. Chim. Acta* **1988**, *154*, 21. − [4f] L. P. Battaglia, A. Bianchi, A. B. Corradi, E. Garcia-España, M. Micheloni, M. Julve, *Inorg. Chem.* **1988**, *27*, 4174. − [4g] J. Ribas, M. Monfort, C. Díaz, X. Solans, *Anal. Quim.* **1988**, *84*, 186. − [4h] M. I. Arriortua, R. Cortes, T. Rojo, J. Via, X. Solans, *Eur. J. Solid State Inorg. Chem.* **1989**, *26*, 91. − [4i] A. Bencini, A. Bianchi, P. Paoli, E. Garcia-España, M. Julve, V. Marcelino, *J. Chem. Soc., Dalton Trans.* **1990**, 2213. − [4j] A. Bencini, A. Bianchi, E. Garcia-España, Y. Jeannin, M. Julve, V. Marcelino, M. Philoche-Levisalles, *Inorg. Chem.* **1990**, *29*, 963. − [4k] K. Yamada, Y. Fukuda, T. Kawamoto, Y. Kushi, W. Mori, K. Unoura, *Bull. Chem. Soc. Jpn.* **1993**, *66*, 2758. − [4l] A. Escuer, R. Vicente, J. Ribas, J. Jaud, B. Raynaud, *Inorg. Chim. Acta* **1994**, *216*, 139. − [4m] A. Escuer, R. Vicente, M. S. El Fallah, J. Jaud, *Inorg. Chim. Acta* **1995**, *232*, 151. − [4n] M. Hagiwara, K. Kobayashi, T. Chihara, *J. Phys. Soc. Jpn.* **1997**, *66*, 1702. − [4o] Z. Travnicek, Z. Smekal, J. Marek, *Z. Kristallogr.* **1997**, *212*, 123. − [4p] I. Castro, M. L. Calatayud, J. Sletten, F. Lloret, M. Julve, *J. Chem. Soc., Dalton Trans.* **1997**, 811.

[5] [5a]M. G. B. Drew, G. W. A. Fowles, D. F. Lewis, *J. Chem. Soc. D.* **1969**, 876. − [5b] N. F. Curtis, I. R. N. McCormick, T. N. Waters, *J. Chem. Soc., Dalton Trans.* **1973**, 1537. − [5c] A. E. Shvelashvili, L. M. Chanturia, N. I. Pirtskhalava, M. G. Tavberidze, A. I. Kvitashvili, B. M. Shchedrin, *Soob. Akad. Nauk Gruz. SSR* **1974**, *75*, 597. − [5d] A. E. Shvelashvili, M. A. Porai-Koshits, A. I. Kvitashvili, B. M. Shchedrin, *Zh. Strukt. Khim.* **1974**, *15*, 310. − [5e] I. F. Bourshteyn, A. E. Shvelashvili, B. M. Shchedrin, *Kristallokhim. Neorg. Soedin* **1976**, 163. − [5f] F. Bottomley, I. J. B. Lin, P. S. White, *J. Organomet. Chem.* **1981**, *212*, 341. − [5g] A. Penicaud, P. Batail, K. Bechgaard, J. Sala-Pala, *Synthetic Metals* **1988**, *22*, 201. − [5h] M. Ohba, H. Tamaki, N. Matsumoto, H. Okawa, *Inorg. Chem.* **1993**, *32*, 5385. − [5i] R. Cortés, M. K. Urtiaga, L. Lezama, M. I. Arriortua, T. Rojo, *Inorg. Chem.* **1994**, *33*, 829. − [5j] M. I. Khan, Yuan-Da Chang, Qin Chen, J. Salta, Y.-S. Lee, C. J. O'Connor, J. Zubieta, *Inorg. Chem.* **1994**, *33*, 6340. − [5k] J. Glerup, P. A. Goodson, D. J. Hodgson, K. Michelsen, *Inorg. Chem.* **1995**, *34*, 6255. − [5l] J. Salta, C. J. O'Connor, S. Li, J. Zubieta, *Inorg. Chim. Acta* **1996**, *250*, 303. − [5m] M. Andruh, R. Melanson, C. V. Stager, F. D. Rochon, *Inorg. Chim. Acta* **1996**, *251*, 309. − [5n] M. Feist, S. Troyanov, E. Kemnitz, *Inorg. Chem.* **1996**, *35*, 3067. − [5o] K. Heinze, G. Huttner, L. Zsolnai, A. Jacobi, P. Schober, *Eur. J. Chem.* **1997**, *3*, 732. − [5p] Xinjian Lei, Maoyu Shang, T. P. Fehlner, *Organometallics* **1997**, *16*, 5289. − [5q] Li-Min Zheng, H. W. Schmalle, S. Ferlay, S. Decurtins, *Acta Crystallogr., Sect. C* **1998**, *54*, 1435. − [5r] V. M. Masters, C. A. Sharrad, P. V. Bernhardt, L. R. Gahan, B. Moubaraki, K. S. Murray, *J. Chem. Soc., Dalton Trans.* **1998**, 413.

[6] Refs. [2c], [4m].

[7] I. Muga, J. M. Gutiérrez-Zorrilla, A. Luque, P. Román, F. Lloret, *Inorg. Chem.* **1997**, *36*, 743.

[8] V. Rodríguez, J. M. Gutiérrez-Zorrilla, P. Vitoria, A. Luque, P. Román, M. Martínez-Ripoll, *Inorg. Chim. Acta* **1999**, *290*, 57.

[9] G. De Munno, M. Julve, F. Lloret, A. Derory, *J. Chem. Soc., Dalton Trans.* **1993**, 1179.

[10] *International Tables for X-ray Crystallography*, Vol. 4, Kynoch, Birmingham, UK, **1974**, pp 55, 99, and 149.

[11] P. T. Beurskens, G. Admiraal, G. Beurskens, W. P. Bosman, S. Garcia-Grande, R. O. Gould, J. M. M. Smits, C. Smykalla, *The DIRDIF92 program system*, Technical Report of the Crystallography Laboratory, University of Nijmegen, The Netherlands, **1992**.

[12] J. M. Stewart, P. A. Machin, C. W. Dickinson, H. L. Ammon, H. Heck, H. Flack, *The X-ray 76 system*, Technical report tr-446, Computer Science Center, University of Maryland, College Park, **1976**.

[13] J. Rodríguez-Carvajal, *Physica B* **1992**, *192*, 55.

Received March 27, 2000
[I00104]

Syntheses and Structures of Silver and Copper Coordination Polymers with 4,4′-Azopyridine − Effect of Counter Anions and π−π Interactions on the Network Systems

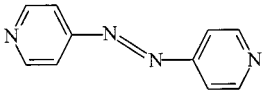
Cheng He,[a] Bing-Guang Zhang,[b] Chun-ying Duan,*[a] Ji-hui Li,[a] and Qing-Jin Meng*[a]

Keywords: Anions / Stacking interactions / Polymers / Silver / Copper

The syntheses and structures of $[Ag(azpy)](NO_3)(H_2O)(CH_3OH)$ (**1**), $[Cu(azpy)_2](ClO_4)$ (**2**), $[Cu(azpy)_2(H_2O)_2](NO_3)_2(H_2O)_2$ (**3**) and $[Cu(azpy)_2(H_2O)_2](ClO_4)_2(C_2H_5OH)_2$ (**4**), where azpy = trans-4,4′-azopyridine, are reported to test the dependence of network topology on counter anions and π–π interactions. Complex **1** contains pairs of linear chains of alternating Ag^I ions and azpy ligands, resembling a ladder structure in which the ligands form π–π interactions (with a distance of 3.53 Å) and AgAg interactions (with a distance of 3.30 Å). Complex **2** exists as a 3D adamantoid polymer in which each Cu^I center is coordinated to four azpy ligands in a tetrahedral geometry, the ligands are in turn coordinated to four other Cu^I centers. The cavities are filled with four other adamantoid units forming five interpenetrating networks. Complexes **3** and **4** are composed of two-dimensional sheets in which the Cu^{II} atom is coordinated in an octahedral geometry to two water molecules and four ligands. The ligands are in turn coordinated to four other Cu^{II} centers. While the sheets in complex **3** display inclined 2D interpenetration, the sheets in complex **4** are all parallel and isolated, with an intersheet separation of ca. 4.7 Å.

Introduction

Much interest at present is focused on the deliberate construction of coordination polymers by self-assembly of the component metal complexes. These solid materials with well-defined, discrete network topologies are attractive to chemists not only for aesthetic reasons, but also for their potential applications in many areas.[1−3] A large amount of these research works have used the 4,4′-bipyridine (4,4′-bipy) ligand and its analogues.[4−5] The coordination polymers observed can be predicted to a certain extent and this led to the development of a wide variety of architectures related to common models such as the honeycomb,[6] ladder,[7] grid,[8] and adamantoid network,[9] or to less common ones exhibiting different degrees of interpenetrations.[1b,10] Although the overall structure is predominantly controlled by the coordination preferences of the transition metal and the ligand building blocks, more subtle effects such as anion control[11] and π−π stacking interactions[12] have been seen to have a profound effect upon network topology. Here we report on the syntheses of some silver and copper complexes, by reaction of the potentially bridging ligand 4,4′-azopyridine (Scheme 1) and metal salts with different anions. A few compounds which exhibit quite novel structures with this ligand have been reported.[13−15] As a result of the different conformations exhibited by this type of ligand, its capability of forming hydrogen bonds with the anions and solvent molecules, as well as the potential π−π stacking interactions between ligands, it was anticipated that the products would present interesting structural features.



Scheme 1. 4,4′-Azopyridine

[a] Coordination Chemistry Institute, The State Key Laboratory of Coordination Chemistry, Nanjing University, Nanjing 210093, P. R. China
[b] Department of Chemistry, Wuhan University, Wuhan 430072, P. R. China

Results and Discussion

Structure of $[Ag(azpy)](NO_3)\cdot(CH_3OH)\cdot(H_2O)$

The structure contains pairs of linear chains (Figure 1) of alternating Ag^I ions and azpy ligands, resembling a ladder structure in which the ligands form π−π interactions (with a distance of 3.53 Å) and weak AgAg interaction (with a distance of 3.30 Å). Each Ag^I ion coordinates to two azpy ligands in a linear arrangement [Ag(1)−N(1) 2.147(8) Å, Ag(1)−N(4A) (A: 1 + *x*, *y*, 1 + *z*) 2.180(9) Å, N(1)−Ag(1)−N(4A) 173.0(3)°], giving an infinite chain of alternating Ag^I separated by 14.65 Å, and azpy ligands which align themselves along the (101) direction. The pairs of chains are linked together by π−π interactions between the azpy ligands and in which the ligands lie parallel to each other at a distance of 3.36 Å forming a two-dimensional sheet. Chains, ladders and sheets of (bipyridine)silver(I) complexes have been reviewed by A. J. Blake et. al.[2a] It is said that the π−π stacking interaction had a profound effect upon the solid-state packing of Ag−bipyridine chains. From the simple linear chains of [Ag(4,4′-bipy)](BF_4), to the ladders of [Ag(pybut)](PO_2F_2) [pybut = 1,4-bis(4-pyridyl)butadiyne],[2a] and to the 2D sheets of [Ag(diaz)](BF_4) (diaz = 2,7-diazapyrene[10b]), it can be seen

 © WILEY-VCH Verlag GmbH, D-69451 Weinheim, 2000 1434−1948/00/1212−2549 $ 17.50+.50/0

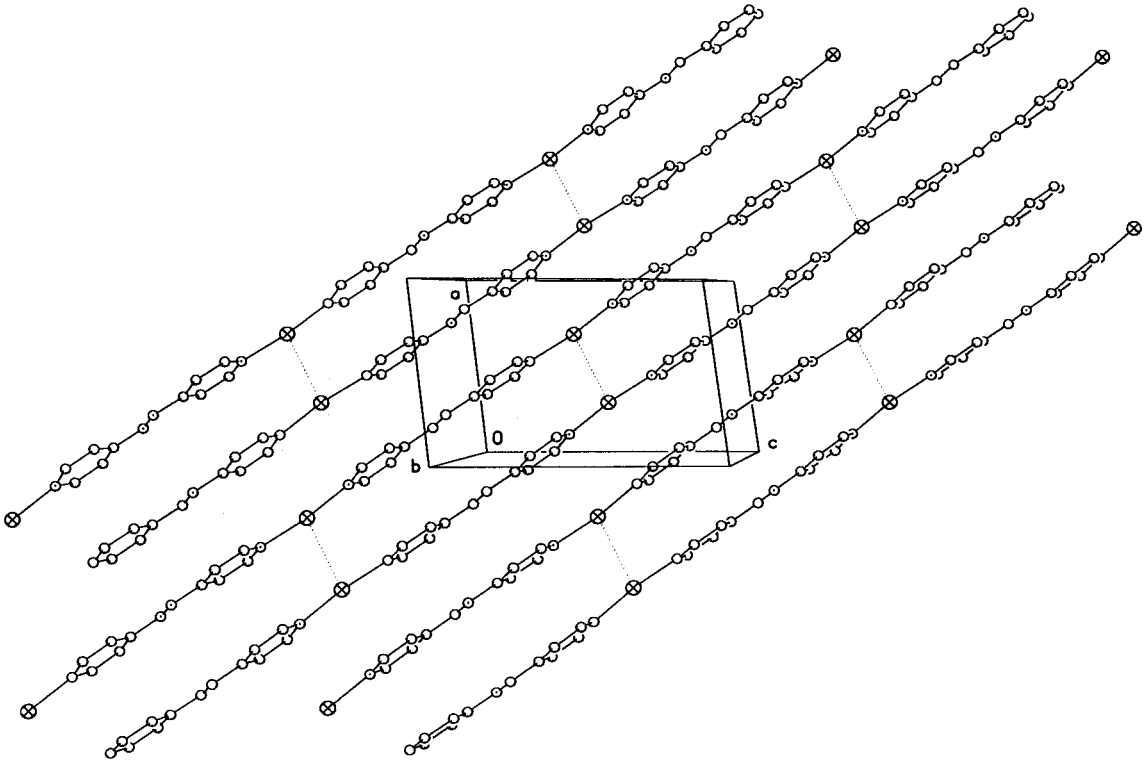


Figure 1. View of the pairs of linear chains observed in complex **1**, in which the ligands form π−π interactions (with a distance of 3.53 Å) and AgAg interactions (with a distance of 3.30 Å)

that by increasing the ability of the ligand to form π−π interactions, the construction of long-range arrays is be encouraged. The increased ability of azpy to form π−π interactions compared with 4,4′-bipy and pybut, encourages not only the formation of pairs of chains, or ladders, but also the formation of a sheet structure with extended π−π stacking interactions.

Structure of $[Cu(azpy)_2]ClO_4$

The reaction of $[Cu(MeCN)_4]ClO_4$ with azpy in MeCN/CH_2Cl_2 affords black crystal suitable for X-ray analysis. The crystal structure shows that the complex exists as a three-dimensional adamantoid polymer in which each Cu^I is coordinated in a tetrahedral geometry to four azpy ligands, which are in turn coordinated to four other Cu^I centers, Cu(1)-N, 2.054(7) Å, Cu(2)-N, 2.025(10) Å. The 3D structure is built through the formation of edge-sharing adamantoid units. The CuCu separation is 12.98 Å creating large cavities within this first 3D lattice. These cavities are filled with four other $[Cu(azpy)_2]^+$ lattices so that a total of five independent adamantoid lattices, related by translation symmetry, interpenetrate throughout the 3D structure, as illustrated in a simplified form by the five adamantoid units (Figure 2).

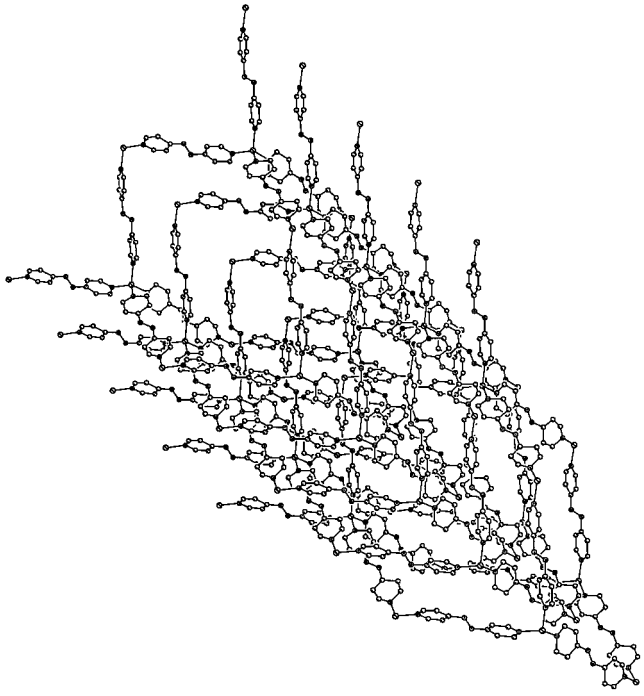


Figure 2. The five independent interpenetrating adamantoid lattices of complex **2**

The channels running through the structure are parallel to the translation vector relating the five networks and accommodate the ClO_4^- counter anions (Figure 3).

Adamantoid networks based on bifunctional linear ligands have been studied for some Cu^I and Ag^I complexes. In general, the lengths of the bridging ligands and the lateral bulk of the ligands are possible factors in controlling the degree and type of interpenetration in adamantoid lattices. Comparing this structure with two other isomorphous structures $[Cu(bpe)_2](BF_4)\cdot 0.5CH_2Cl_2$[9b] and $[Cu(bpe)_2](BF_4)(CH_3CN)$[16] [bpe = *trans*-1,2-bis(4-pyridyl)ethene], it

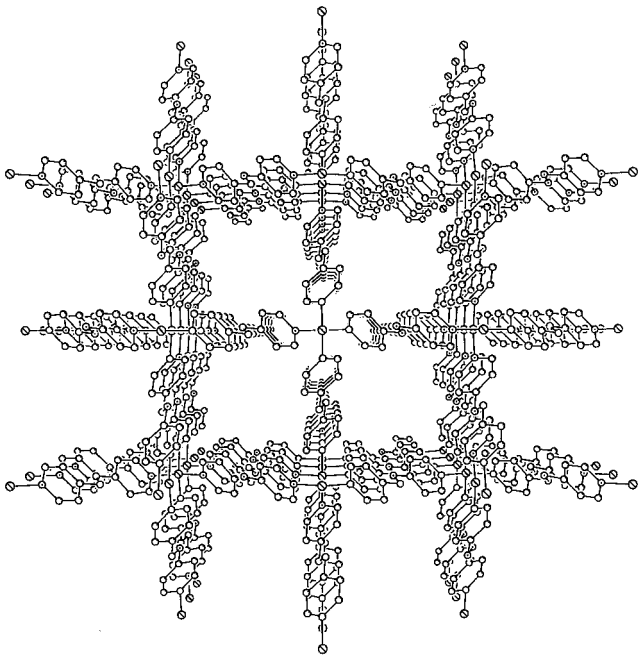


Figure 3. View of the complex **2** network illustrating the channels that run through the accommodating counter ions

is interesting to find that the structure remains essentially the same with different ligands and anions. The implications of this are that the solvent and the counter anion have little or no templating effects.

Structures of $[Cu(azpy)_2(H_2O)_2](NO_3)_2\cdot 2H_2O$ and $[Cu(azpy)_2(H_2O)_2](ClO_4)_2\cdot 2EtOH$

The Cu^{II} complexes **3** and **4** are obtained as large black crystals by treating $Cu(NO_3)_2$ or $Cu(ClO_4)_2$ in water with the azpy ligand in an ethanol solution in a 1:2 molar ratio. One of the aims of this research was to compare the behavior of azpy with that of the shorter 4,4′-bipyridine ligand. These ligands give both interpenetrated[17] and noninterpenetrated structures when treated with $ZnSiF_6$.[8a] Another aim was to assess the effect of the counter anion on the crystal packing of the sheets.

The structure of **3** contains two-dimensional layers of squares (Figure 4). The Cu^{II} atoms are octahedrally coordinated to four equatorial azpy ligands (Cu−N distance ca. 2.02 Å) and two axial water molecules (Cu−O distance ca. 2.50 Å). Each azpy unit is attached to two copper centers to form an infinite sheet. The Cu^{II} cations within a sheet are coplanar and form a grid of edge-shared squares, the average CuCu distance along the edge is ca. 12.95 Å. Parallel sheets, stacked on top of each other, are laterally displaced so that the copper centers of the first sheet, viewed in the horizontal plane, are vertically above those of the 3rd, 5th, 7th etc. sheets, and are vertically above the midpoints of the Cu_4 squares of the 2nd, 4th, 6th etc. sheets. An equivalent stack of sheets is found in planes perpendicular to the first, giving rise to the interpenetrating pattern represented in Figure 5. Hydrogen bonds are apparent between the coordinated water molecules and the disordered NO_3^- anions.

The structure of **3** is isomorphous with the structure of $[Zn(azpy)_2(H_2O)_2]\ SiF_6\cdot H_2O$,[13b] the size of the cavity is almost equivalent (166 vs. 165 Å^2). An interesting feature of this structure is the fact that the structure remains essentially unchanged whether the metal center is Cu^{II} or Zn^{II} and the anion is SiF_6^{2-} or NO_3^-. The implications of this are that either SiF_6^{2-} and NO_3^- behave similarly as templates for the interpenetrating structure, or they have little or no template effect. In both structures the counter anions and water molecules are contained in the tetrahedral channels, although there is twice as much NO_3^- included as there is SiF_6^{2-}. It was anticipated that when the perchlorate counter anion was used instead of the nitrate counter anion, the expected structure would be similar to that proposed for **3** and $[Zn(azpy)_2(H_2O)_2]SiF_6\cdot H_2O$. However, after synthesizing and studying the crystal structure of the perchlorate salt of **3** (i.e. **4**), it was surprising to find that the structure of **4** is quite different.

Compound **4** crystallizes in the tetragonal space group $P4_2/mnm$ with $Z = 2$. The skeleton structure of the two-dimensional sheet 2 (in **4**) is the same as that in **3** (CuCu distance along the edge is 13.06 Å, and the Cu−N, Cu−O distances ca. 2.02 Å, 2.68 Å, respectively). However, the sheets subsequently stack along *c* in a close-packed staggered manner, as described above, with interplane separations 4.7 Å. Such short inter-plane separations certainly

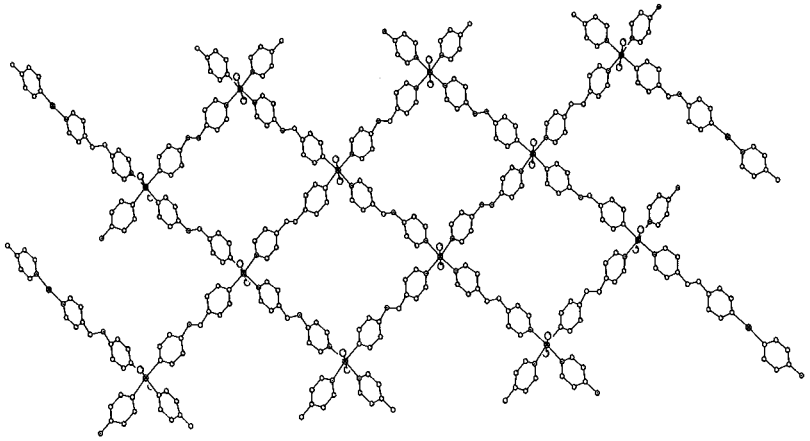


Figure 4. View of the two-dimensional sheets of complex **3**

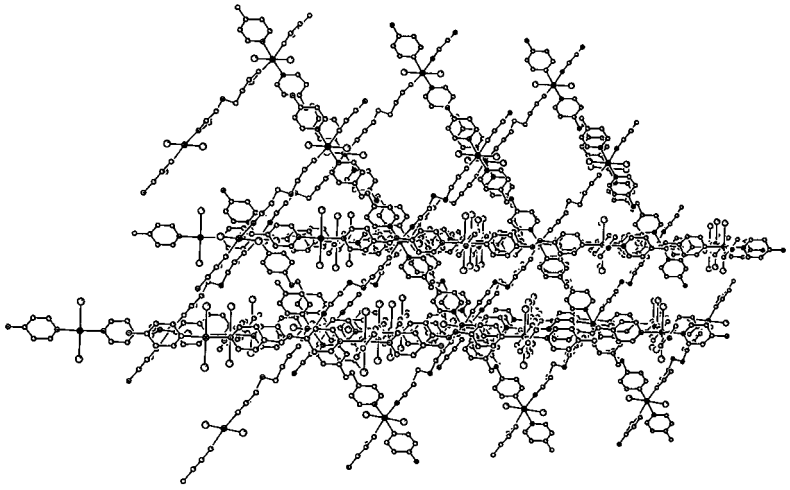


Figure 5. A schematic view of the interpenetration of the layers, showing its inclined nature, and the channels of complex **3**; the anions and the solvent molecules are omitted for clarity

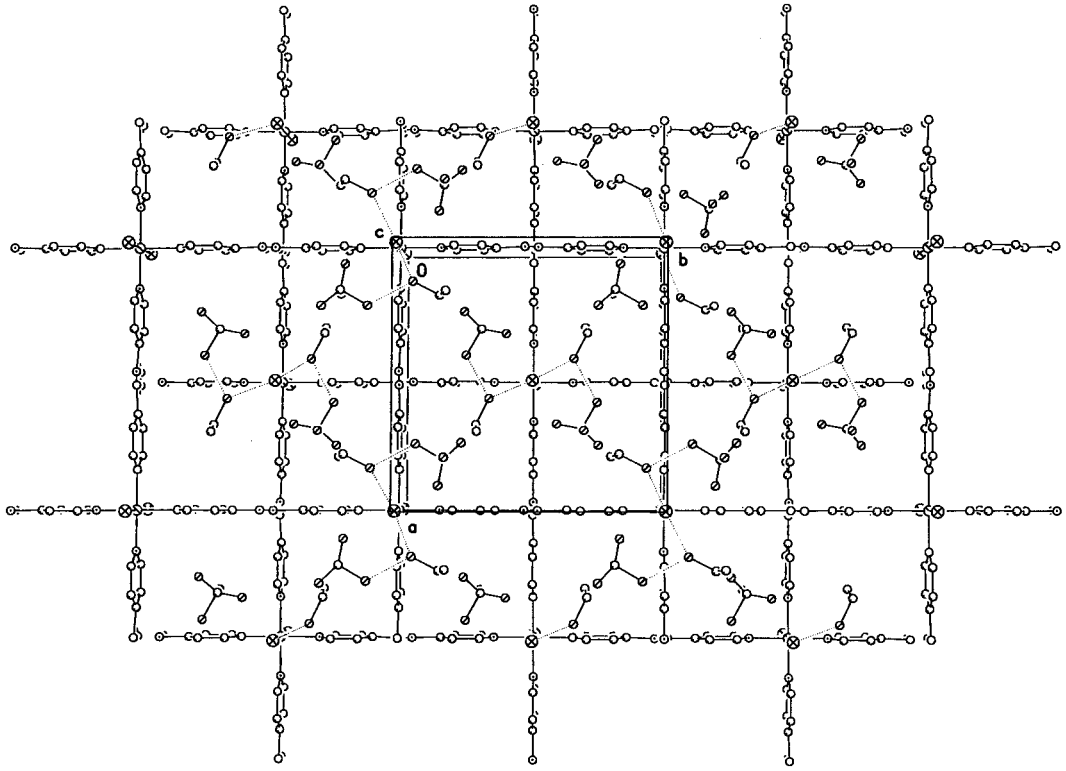


Figure 6. View of the square cavities of a single sheet in complex **4**, showing the ClO_4^- anions and ethanol molecules in the clathrates

preclude the possibility of interpenetration. The square cavities are enclosed by the azpy ligands. Two ClO_4^- anions and two ethanol molecules occupy the square cavity within the clathrate (Figure 6). There is significant hydrogen bonding between the ethanol molecules and the ClO_4^- anions.

It is interesting to find that the water molecules coordinated to the Cu^{II} atom extend to the center of the cavity on the adjacent layer and interact with the two ethanol molecules in the clathrate by hydrogen bonding, to form one-dimensional chains along the *c* axis (Figure 7).

The fact that the counter anions can influence the final structure of coordinated complexes has been noted. It is clearly indicated that noncoordinating counter anions can play an important role in the crystal engineering of coordination complexes. The result of this study illustrates the fine balance between interpenetrated and noninterpenet-

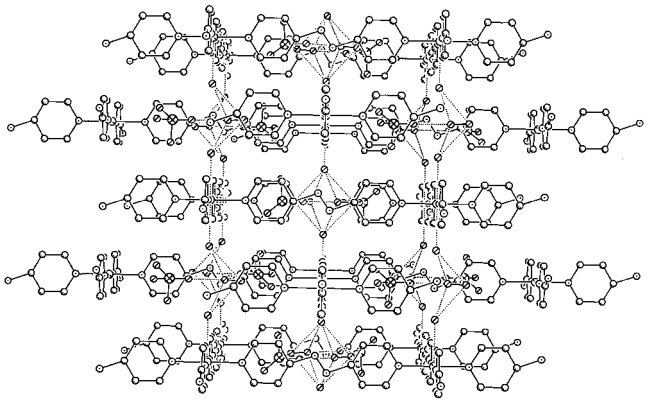


Figure 7. View through the *ac* plane in complex **4**, showing the one-dimensional hydrogen-bonding chains on the *c* axis

rated structures. Although the mechanism of the structural change is unpredictable, understanding the features may be a clue to the design of self-assembly network compounds.

Experimental Section

General: All starting materials were purchased from Aldrich and used as received. The ligand 4,4′-azopyridine[18] and $Cu(MeCN)_4ClO_4$[19] were prepared by literature procedures. − The IR spectra were recorded with a Nicolet 170SX FT-IR spectrophotometer with KBr pellet in the 4000−400cm^{-1} region. − ^{1}H NMR spectra were recorded with Am5600 Bruker spectrometers at 298 K using TMS as an internal standard.

[Ag(azpy)](NO$_3$)(CH$_3$OH): A solution of $AgNO_3$ (0.10 g, 0.59 mmol) in water (5 mL) was added to a stirred solution of azpy (0.11 g, 0.60 mmol) in methanol (10 mL). A pale red precipitate formed and was filtered off and dried under vacuum(0.16 g, yield 69%). − $C_{11}H_{12}AgN_5O_4$ (386.1133): calcd. C 34.2, H 3.1, N 18.1; found C 34.7, H 2.7, N 18.2. − ^{1}H NMR [$(CD_3)_2SO$]: δ = 8.88 (d, J = 5.0 Hz, 4 H, py], 7.84 [d, J = 5.6 Hz, 4 H, py]. − IR (KBr): $\tilde{\nu}$ = 1594 cm^{-1} (m), 1587 (m), 1565 (m), 1486 (w), 1414 (s), 1384 (s), 1317 (m), 1238 (w), 1222 (m), 1051 (w), 1006 (w), 989 (w) and 836 (s). Crystals were obtained by slow concentration of an acetonitrile/ethanol solution at ambient temperature.

[Cu(azpy)$_2$](ClO$_4$): Solutions of $Cu(CH_3CN)_4ClO_4$ (0.10 g, 0.31 mmol) in CH_2Cl_2 (10 mL) and azpy (0.12 g, 0.65 mmol) in CH_3CN (10 mL) were mixed. After concentrating the solution to a small volume, black crystals of **2** were obtained and were filtered off (0.09 g, yield 55%). − $C_{20}H_{16}ClCuN_8O_4$ (531.3950): calcd. C 45.2, H 3.0, N 21.1; found C 45.6, H 3.2, N 21.3. − IR (KBr): $\tilde{\nu}$ = 1595 (s), 1563 (m), 1486 (m), 1467 (w), 1416 (s), 1324 (w), 1241 (w), 1224 (m), 1101 (s), 1083 (s), 1051 (s), 1010 (m), 962 (m), 932 (w), 867 (w), 846 (s), 831 (s).

[Cu(azpy)$_2$(H$_2$O)$_2$](NO$_3$)$_2$2H$_2$O: Solutions of $Cu(NO_3)_26H_2O$ (0.10 g, 0.33 mmol) in water (10 mL) and azpy (0.12 g, 0.65 mmol) in ethanol (10 mL) were mixed. After slow concentration of the solution to a small volume, black crystals were formed and were filtered off. − IR (KBr): $\tilde{\nu}$ = 3431 (w), 3102 (w), 1608 (s), 1570 (w), 1513 (m), 1480 (s), 1424 (s), 1384 (s), 1352 (s), 1327 (m), 1293 (s), 1274 (s), 1231 (m), 1194 (m), 1094 (w), 1051 (m), 1034 (w), 1013 (m), 995 (m), 850 (s), 803 (m) .

[Cu(azpy)$_2$(H$_2$O)$_2$](ClO$_4$)$_2$2CH$_3$CH$_2$OH: Solutions of $Cu(ClO_4)_26H_2O$ (0.10 g, 0.27 mmol) in water (10 mL) and azpy (0.10 g, 0.54 mmol) in ethanol (10 mL) were mixed. Black crystals were obtained by slowly concentrating the solution in air. They were filtered off. − IR (KBr): $\tilde{\nu}$ = 3449 (w), 3111 (w), 1609 (s), 1568 (w), 1494 (w), 1423 (s), 1229 (m), 1184 (s), 1043 (s), 989 (m), 928 (m), 846 (s), 621 (s).

X-ray Crystallography: Parameters for data collection and refinement of the crystals are summarized in Table 1. Intensities were collected with a Siemens P4 four-circle diffractometer with graphite-monochromated Mo-K_α radiation (λ = 0.71073 Å) using the ω-2θ scan mode. Data were corrected for Lorentz polarization effects during data reduction using XSCANS,[20] and a semi-empirical absorption correction from ψ scans was applied. The structures were solved by direct methods and refined on F^2 by full-matrix least-squares methods using SHELXTL version 5.0.[21] Anisotropic thermal parameters were refined for the non-hydrogen atoms. For complex **1**, the nitrate anion, and the H_2O and CH_3OH molecules were found to be disordered into two occupied sites. The site occupancy factor (SOF) of the atoms of the NO_3^- anion were refined using

Table 1. X-ray crystal data of compounds **1−4**

	1	**2**	**3**	**4**
Molecular formula	$C_{11}H_{14}AgN_5O_5$	$C_{20}H_{16}ClCuN_8O_4$	$C_{20}H_{24}CuN_{10}O_{10}$	$C_{24}H_{32}Cl_2CuN_8O_{12}$
M	404.14	531.40	628.03	759.02
Crystal system	triclinic	tetragonal	orthorhombic	tetragonal
Space group	$P\bar{1}$	$I\bar{4}$	$Pbcm$	$P4_2/mnm$
a [Å]	7.691(2)	17.765(9)	12.314(6)	13.063(1)
b [Å]	9.176(3)	17.765(9)	11.134(7)	13.063(1)
c [Å]	11.601(3)	7.567(6)	19.875(7)	9.401(2)
α [°]	105.18(2)			
β [°]	96.53(2)			
γ [°]	100.41(3)			
V/Å^3	792.7(4)	2388(2)	2725(2)	1604.2(3)
Z	2	4	4	2
T [K]	293(2)	293(2)	293(2)	293(2)
μ [mm^{-1}]	1.301	1.069	0.873	0.920
No. reflections measured	2970	1553	5854	2017
No. unique reflections	2752 (R_{int} = 0.035)	1447 (R_{int} = 0.058)	2485 (R_{int} = 0.075)	799 (R_{int} = 0.046)
R1	0.069	0.074	0.0670	0.0779
wR2(all data)	0.180 (0.202)	0.170 (0.221)	0.174 (0.209)	0.216 (0.257)
Goodness of fit	1.037	1.039	1.108	1.044

free variables, the SOF of the atoms in the methanol molecules, however, were fixed at 0.5. To assist in the refinement, several restraints were applied for the nitrate anion: 1) all N-O bonded and all OO nonbonded distances were restrained to be similar; 2) thermal parameters on adjacent atoms were restrained to be similar for the disordered pairs. For complex **2**, the perchlorate anion was disordered with the SOF of the atoms fixed at 0.5. The ClO_4^- was refined to the idealized tetrahedron with Cl−O distance fixed at 1.43(1) Å, and OO separation fixed at 2.32(2) Å. For complex **3**, hydrogen atoms of the water molecules were found from the difference Fourier maps, however, they were refined using the riding model. The ligands were disordered along the direction of the Cu−azpy−Cu chains, the ligands and the nitrate anions were also affected. The SOF was fixed at 0.5 for each ligand. In order to make the refinement stable, many restrains such as distance restrains on the atoms in the ligands and thermal parameter restrains were used in the refinement of the nitrate anions. For complex **4** the oxygen atoms of the perchlorate anion were found to be disordered, the site occupancy factors for them were fixed at 0.25. The atoms of the ethanol molecules were also found to be disordered, the SOF for them were also fixed at 0.25, the C−O and C−C distances were fixed at 1.45(1) Å. Crystallographic data for the structures reported in this paper have been deposited with the Cambridge Crystallographic Data Center: CCDC-145343 (**1**), CCDC-145344 (**2**), CCDC-145346 (**3**), CCDC-145345 (**4**). Copies of the data can be obtained free of charge and by application to CCDC, 12 Union Road, Cambridge CB2 1EZ, UK [Fax: (internat.) + 44−1223/336−033; E-mail: deposit@ccdc.cam.ac.uk].

Acknowledgments

We gratefully thank the National Natural Science Foundation of China for their financial help.

[1] [1a] R. Robson, in *Comprehensive Supramolecular Chemistry* (Eds.: J. L Atwood, J. E. D. Davies, D. D. MacNicol, F. Vortle, J. M. Lehn), Pergamon, Oxford, **1997**, vol. 6, ch. 22, pp. 733−755. − [1b] S. R. Batten, R. Robson, *Angew. Chem. Int. Ed.* **1998**, 37, 1460−1494.

[2] [2a] A. J. Blake, N. R. Champness, P. Hubberstey, W-S. Li, M. A. Withersby, M. Schröder, *Coord. Chem. Rev.* **1999**, *183*, 117−138. − [2b] N. R. Champness, M. Schröder, *Curr. Opin. Solid. State Mater. Sci.* **1998**, *3*, 419−424.

[3] [3a] L. Carlucci, G. Ciani, P. Macchi, D. M. Proserpoo, S. Rizzato, *Chem. Eur J.* **1999**, *5*, 237−243. − [3b] M. Munakata, L. P. Wu, T. Kuroda-Sowa, *Adv. Inorg. Chem.* **1998**, *46*, 173−303.

[4] [4a] M. Fujata, K. Ogura, *Coord. Chem. Rev.* **1996**, *148*, 249. − [4b] P. J. Hagrman, D. Hagrman, J. Zubieta, *Angew. Chem. Int. Ed.* **1999**, *38*, 2638−2684.

[5] [5a] B. Olcnyuk, A. Fechtenkotter, P. J. Stang, *J. Chem. Soc., Dalton Trans.* **1998**, 1707−1728. − [5b] P. J. Stang, *Chem. Eur J.* **1998**, *4*, 19−27.

[6] [6a] G. B. Gardner, D. Venkataraman, J. S. Moore, S. Lee, *Nature* **1995**, *374*, 792−795. − [6b] L. R. MacGillivray, S. Subramanan, M. J. Zaworotko, *J. Chem. Soc., Chem. Commun.* **1994**, 1325−1326.

[7] [7a] M. Fujita, O. Sasaki, K. Watanabe, K. Ogura, K. Yamaguchi, *New. J. Chem*. **1998**, 189−191. − [7b] A. J. Blake, N. R. Champness, A. Khlobystov, D. A. Lemenovskii, W-S. Li, M. Schroder, *Chem. Commun.* **1997**, 2027−2028.

[8] [8a] S. Subramanian, M. J. Zaworotko, *Angew. Chem. Int. Ed. Engl.* **1995**, *34*, 2127−2129. − [8b] M. Fujita, Y. J. Kwon, S. Washizu, K. Ogura, *J. Am Chem. Soc.* **1994**, *226*, 1151−1152.

[9] [9a] M. J. Zaworotko, *Chem. Soc. Rev.* **1994**, 283−288. − [9b] A. J. Blake, N. R. Champness, S. S. M. Chung, W-S. Li, M. Schroder, *Chem. Commun.* **1997**, 1005−1006.

[10] [10a] K. A. Hirsch, S. R. Wilson, J. S. Moore, *Chem. Eur. J.* **1997**, *3*, 765−771. − [10b] A. J. Blake, N. R. Champness, A. N. Khlobystov, D. A. Lemenovski, W-S. Li, M. Schroder, *Chem. Commun.* **1997**, 1339−1340.

[11] [11a] D. M. P. Mingos, A. L. Rohl, *Inorg. Chem.* **1991**, *30*, 3769−3771. − [11b] K. A. Hirsch, S. R. Wilson, J. S. Moore, *Inorg. Chem.* **1997**, *36*, 2960−2968.

[12] [12a] K. Biradha, K. V. Domasevitch, B. Moulton, C. Seward, M. J. Zaworotko, *Chem Commun*. **1999**, 1327−1328. − [12b] M. A. Withersby, A. J. Blake, N. R. Champness, P. Hubberstey, W −S. Li, M. Schroder, *Angew. Chem. Int. Ed. Engl.* **1997**, *36*, 2327−2329.

[13] [13a] L. Carlucci, G. Ciani, D. M. Proserpio, *J. Chem. Soc., Dalton Trans.* **1999**, 1799−1804. − [13b] L. Carlucci, G. Ciani, D. M. Proserpio, *New. J. Chem*. **1998**, 1319−1321.

[14] [14a] S. Noro, M. Kondo, T. Ishii, S. Kitagawa, H. Matsuzaka, *J. Chem. Soc., Dalton Trans.* **1999**, 1569−1574. − [14b] M. Kondo, M. Shimamura, S. Noro. T. Yoshitomi, S. Minakoshi, S. Kitagawa, *Chem Lett.* **1999**, 285−286.

[15] [15a] N. Molinear, M. C. Munoz, J. A. Real, *Inorg. Chem. Commun.* **1999**, *2*, 25−27. − [15b] M. A. Withersby, P. A. Cooke, A. J. Blake, N. R. Champness, P. Hubberstey, M. Schroder, *New. J. Chem*. **1999**, 573−576.

[16] S. R. Batten, J. C. Jeffery, M. D. Ward, *Inorg. Chem. Acta* **1999**, *292*, 231−237.

[17] R. W. Gable, B. F. Hoskins, R. Robson, *J. Chem. Soc., Chem. Commun.* **1990**, 1677−1678.

[18] J.-P. Launay, M. Tourrel-Pagis, J.-F. Lipskier, V. Marvaud, C. Joachim, *Inorg. Chem.***1991**, *30*, 1033−1038.

[19] B. J. Hathaway, D.G. Holah, J. D. Postlethwaite, *J. Chem. Soc*. **1961**, 3215−3218.

[20] *XSCANS, Version 2.1*, Siemens Analytical X-ray Instruments, Inc., Madison, WI, **1994**.

[21] Siemens, *SHELXTL, Version 5.0*, Siemens Industrial Automation, Inc. Analytical Instrumentation, Madison, WI, **1995**.

Received March 28, 2000
[I00112]

Neutral and Cationic Methyl Complexes of Platinum(II) with 6-Substituted 2,2′-Bipyridines: Synthesis, Characterisation and Reactivity with Carbon Monoxide − Molecular Structures of [PtCl(methyl)(6-ethyl-2,2′-bipyridine)] and of [Pt(methyl)(acetonitrile)(6-ethyl-2,2′-bipyridine)][BF_4]

Angelino Doppiu,[a] Maria Agostina Cinellu,[a] Giovanni Minghetti,*[a] Sergio Stoccoro,[a] Antonio Zucca,[a] Mario Manassero,*[b] and Mirella Sansoni[b]

Keywords: Platinum / N ligands / Methyl complexes / Crystal structure / Hydrogen bonds

The complex *trans*-[PtCl(Me)(SMe_2)$_2$] reacts with 6-R-substituted 2,2′-bipyridine, HL^n (n = 1, R = H; n = 2, R = Me; n = 3, R = Et; n = 4, R = *i*Pr; n = 5, R = CH_2Ph; n = 7, R = Ph), to afford the neutral complexes [PtCl(Me)(HL^n)]. Only one isomer is formed (R *cis* to Cl) with all the ligands, but one (R = Ph). When R = $C(Me)_2Ph$ (HL^6), only an (N–N–C) cyclometallated species is formed. The stereoselectivity observed is interpreted in terms of the nature of the substituent R, and of the hydrogen bond formed between H–C(α) of the R substituent and the chloride ion bound to the platinum center. The molecular structure of [PtCl(Me)(HL^3)] has been resolved by an X-ray analysis and shows that the above-mentioned hydrogen bond length is 2.28 Å. The reactivity of three representative complexes (R = H, Et, CH_2Ph) with carbon monoxide has been studied. The reaction affords the ionic species [Pt(Me)(CO)(HL^n)]$^+$[$PtCl_2$(Me)(CO)]$^-$ and the free ligand. There is evidence of the formation of an acyl species, which does not contain the bipyridine ligand, only when working at high pressures of CO. The above cations are also obtained by direct carbonylation of the solvent species, [Pt(Me)(MeCN)(HL^n)][BF_4], achieve by halide abstraction from the neutral complexes. The molecular structure of [Pt(Me)(MeCN)(HL^3)][BF_4] has been resolved by an X-ray analysis.

Introduction

Palladium complexes [PdX(R)(N−N)], where X is a halide, R an alkyl or aryl group and (N−N) a bidentate nitrogen ligand, have been widely studied because of their potential in organic syntheses.[1] Many studies have focused their attention on the reaction of these Pd complexes with carbon monoxide. This is of fundamental interest in industrial processes, e.g., hydroformylation and copolymerisation of olefins and carbon monoxide.[2] As a result, there is a lot of experimental and theoretical data available on the insertion of carbon monoxide, as well as of alkenes, into the palladium−carbon σ bonds.[3] The analogous platinum complexes [PtX(R)(N−N)] also have been the subject of many studies concerning intra- and intermolecular C−H activation,[4] oxidative addition reactions[5] and addition of neutral ligands to give coordinatively saturated 18-electron species.[6] Great efforts have been devoted to the electronic and steric requirements which could stabilise pentacoordinated derivatives: in this context, in the case of bipyridine or phenanthroline derivatives, reactions with olefins have been widely investigated.[7] Surprisingly, reactions with CO, as well as the related migratory−insertion reactions into metal−carbon σ bonds, have been less investigated in spite of the extensively developed chemistry of alkylplatinum(II) and -platinum(IV) compounds[8] with nitrogen donors and being interesting as models for the catalytic species in the palladium systems.

Herein we report the synthesis and the spectroscopic characterisation of a series of alkylplatinum(II) derivatives of the type: [PtX(Me)(HL^n)] (X = Cl or I, HL^n = unsymmetric 2,2′-bipyridine 6-alkyl-, benzyl- or aryl-substituted), as well as their reactivity with carbon monoxide. Furthermore, some X-ray structural determinations are given.

Results and Discussion

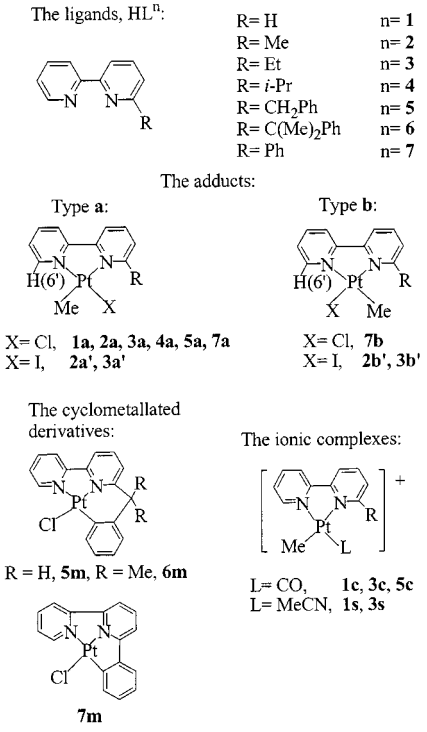
Synthesis of the Adduct Species

The ligands HL^n and the platinum complexes are depicted in Scheme 1; the index n indicates the ligand.

The complex **1a** (HL^1 = 2,2′-bipyridine) is well known, it can be prepared in an almost quantitative yield by reaction of [PtCl(Me)(COD)] (COD = 1,5-cyclooctadiene) with HL^1 in CH_2Cl_2.[9] The 6-substituted-2,2′-bipyridines HL^{2-7} show a different reactivity, in spite of several attempts under a variety of experimental conditions, we were unable to achieve displacement of COD. Nevertheless, the adducts of all the ligands but one (HL^6, see later), can easily be obtained by reaction of *trans*-[PtCl(Me)(SMe_2)$_2$], an intermediate used in the synthesis of other species with (N−N) ligands.[5b,7b] The adducts can be isolated in good yields, they

[a] Dipartimento di Chimica, Università di Sassari,
via Vienna 2, 07100 Sassari, Italy
Fax: (internat.) + 39-(0)79/212069
E-mail: mingh@ssmain.uniss.it
[b] Dipartimento di Chimica Strutturale e Stereochimica Inorganica, Università di Milano,
Centro CNR, 20133 Milano, Italy
E-mail: m.manassero@csmtbo.mi.cnr.it

 © WILEY-VCH Verlag GmbH, D-69451 Weinheim, 2000 1434−1948/00/1212−2555 $ 17.50+.50/0



Scheme 1

are stable in the solid state and in all cases but one (**5a**) also in solutions of chlorinated solvents at room temperature. They are not electrolytes in acetone. Owing to the ligand asymmetry, two stereoisomers are possible (Scheme 1).

In the case of the alkyl- or benzyl-substituted ligands HL^{2-5} only one isomer is formed. ^1H NMR spectroscopic data are consistent with isomer **a**; in particular the assessment relies on the chemical shift of H(6′) proton and its coupling constant to ^{195}Pt. The resonance is known to be influenced by the neighbouring ligands,[10] halides having a stronger deshielding effect than a methyl ligand. The values observed for **2a**−**5a** and **7a** (see Table 1) indicate that the methyl group is in close proximity to H(6′). This is supported by NOE difference experiments on **2a** and **3a** ($CDCl_3$ solution), irradiation of the H(6′) resonance gives enhancement of the signal of the methyl group bound to the platinum center, and vice versa. The extent of the coupling between H(6′) and ^{195}Pt is related to the nature of the ligand *trans* to the nitrogen atom N(1) of the unsubstituted pyridine ring. The relatively high values of $^3J_{Pt-H}$ indicate that the ligand has a low *trans* influence, like a chloride ligand.[11] It is worth noting that in **1a**, one H(6) is close to the chloride ion and the other to the methyl group. Indeed, one of the resonances is strongly deshielded ($\delta = 9.65$) with $^3J_{Pt-H} \approx 17$ Hz, whereas the other one ($\delta = 9.23$) has a larger $^3J_{Pt-H}$ value (60.3 Hz). The latter values are very similar to those found for **2a**−**5a** and **7a**.

As stated above, two stereoisomers **7a** and **7b** (ca. 1:1) are formed, only in the case of the ligand HL[7]. Evidence for the formation of two isomers is given by ^1H NMR spectra. There are two methyl signals at $\delta = 1.26$ ($^2J_{Pt-H} = 82.3$ Hz) and $\delta = 0.32$ ($^2J_{Pt-H} = 77.2$ Hz) and two H(6′) resonances. The upfield methyl signal can be assigned to **7b**, taking into account the anisotropic shielding effect of the phenyl substituent. The H(6′) resonance in **7b** ($\delta = 9.58$) is, as expected, more deshielded than in **7a** ($\delta = 9.10$); the extent of the $^{195}Pt-^1H$ coupling reflects the difference in the *trans* influence between the chloride ($^3J_{Pt-H(6')} = 60.0$ Hz, **7a**) and the methyl group (coupling not observable, **7b**). One of the isomers, **7b**, can be isolated in a pure form from the mixture by column chromatography, the other one is converted during elution through the column to the cyclometallated species **7m** (see later). The structure of **3a** has been resolved by an X-ray analysis.

Molecular Structure of [PtCl(Me)(HL^3)] (3a)

The structure consists of the packing of discrete [PtCl(Me)(HL^3)] molecules. An ORTEP[12] view of the molecule is shown in Figure 1. Selected bond lengths and angles are reported in Table 2.

Table 1. ^1H NMR spectroscopic data of the adduct and the cyclometallated species, room temperature, solvent $CDCl_3$ unless otherwise stated, coupling constants in Hz, J_{Pt-H} in brackets, J_{H-H} in parentheses, chemical shift in ppm from internal TMS.

	Pt−Me	Me	CH_2 or CH	H(6′)	Other Aromatics
1a	1.23 s [76.9]			9.23 d (5.6) [60.3] H(6′) 9.65 d (5.9) [ca. 17] H(6)	7.5−8.2 {6 H}
2a	1.37 s [80.8]	3.17 s		9.09 d (5.4) [61.5]	7.4−8.1 {6 H}
3a	1.37 s [81.3]	1.41 t (7.6)	3.73 q (7.6)[a]	9.06 d (6.1) [62.8]	7.4−8.1 {6 H}
4a	1.39 s [82.3]	1.36 d (6.9)	5.02 m (6.9)[b]	9.07 dd (5.4) [61.8]	7.4−8.2 {6 H}
5a	1.42 s [80.8]		5.17 s[a]	9.10 dd (5.1) [61.8]	7.2−8.2 {11 H}
7a	1.26 s [82.3]			9.10 d (6.3) [60.0]	7.4−8.2 {11 H}
7b	0.32 s [77.2]			9.58 d (6.0)	7.4−8.2 {11 H}
2a′	1.44 s [78.1]	3.28 s		8.92 d (5.7) [59.3]	7.4−8.4 {6 H}
2b′	1.48 s [78.6]	2.87 s [ca. 6]		9.90 dd (5.4) [ca. 23]	7.4−8.4 {6 H}
3a′	1.45 s [77.2]	1.37 t (7.6)	3.80 q (7.6)[a]	8.90 d (5.4) [58.8]	7.4−8.2 {6 H}
3b′	1.45 s [77.0]	1.35 t (7.6)	3.30 q (7.6)[a]	9.87 dd (5.1) [ca. 20]	7.4−8.2 {6 H}
5m			4.29 s[a]	9.55 d (5.4)	7.0−8.1 {10 H}
6m[c]		2.13 s		9.60 dd (7.1)	6.9−8.2 {10 H}
7m				9.01 dd (6.1) [ca. 18]	7.0−8.1 {10 H}

[a] CH_2. − [b] CH. − [c] Solvent CD_2Cl_2.

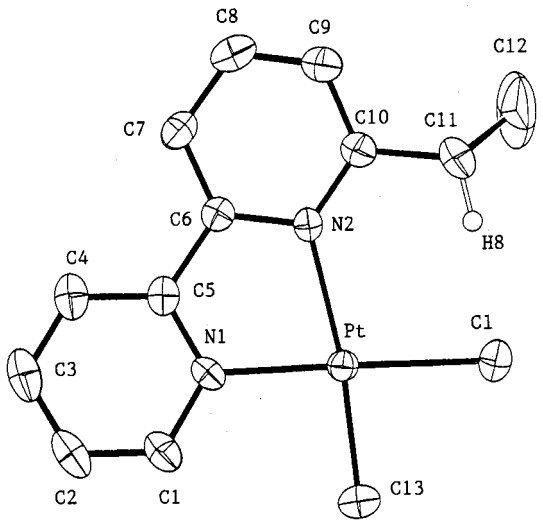


Figure 1. ORTEP view of compound **3a**; ellipsoids are drawn at the 30% probability level

Table 2. Selected bond lengths [Å] and angles [°] with e.s.d.s in parentheses for compound **3a**

Pt−Cl	2.299(2)	Pt−N1	2.022(4)
Pt−N2	2.188(4)	Pt−C13	2.043(6)
Cl···H8	2.28		
Cl−Pt−N1	176.1(1)	Cl−Pt−N2	103.1(1)
Cl−Pt−C13	83.8(2)	N1−Pt−N2	78.7(2)
N1−Pt−C13	94.4(2)	N2−Pt−C13	173.0(2)
C11−H8···Cl	160.4		

The platinum atom displays a square-planar coordination with a slight square-pyramidal distortion; maximum deviations from the best plane are +0.033(1) and −0.034(4) Å for Pt and N1, respectively. The Pt−Cl and Pt−N1 bond lengths, 2.299(2) and 2.022(4) Å, respectively, are normal and in good agreement with the corresponding values, 2.289(2) and 2.030(6) Å found in $[PtCl_2(HL)]$[13] [HL = diphenyl(2-pyridylmethyl)phosphane oxide]. The Pt−N2 distance, 2.188(4) Å, is rather long even after taking into account the *trans* influence of the Me ligand; compare Pt−N1 = 2.117(7) Å in [PtCl(L)][14] (HL = 6-*tert*-butyl-2,2′-bipyridine), where the pyridine N atom is *trans* to an alkyl group. The Pt−C13 bond length, 2.043(6) Å, is in good agreement with the corresponding value, 2.037(3) Å, found in $[Pt\{HOB(C_6F_5)_3\}(Me)(HL)]$[8b] (HL = 4,4′-di-*tert*-butyl-2,2′-bipyridine). The Cl−Pt−N2 angle, 103.1(1)°, is very large and is probably a result of the steric hindrance of the ethyl substituent on the bipyridine ligand. However, it must be observed that there is a clear intramolecular hydrogen bond between H8, bonded to C11, and the Cl atom (see Figure 1, Cl···H8 = 2.28 Å, C11−H8···Cl angle = 160.4°). The two pyridine rings are strictly planar and are twisted 9.8(2)° with respect to each other. A rather short distance (2.78 Å) between the chlorine atom of one molecule and the hydrogen atom H2, bonded to C2, of a neighbouring molecule, suggests the possibility of a weak intermolecular hydrogen bond.

The isolation of only one isomer (type **a**) for the adducts of the ligands HL^{1-5} deserves comments. Several factors can play a role in making isomer **a** the preferred one: *i*) in **a**, the Me group, more bulky than Cl, is far away from the R substituent; *ii*) owing to the higher *trans* influence of the methyl group with respect to the chloride ion, a methyl group *trans* to N2 can lengthen the Pt−N2 bond, thus relieving the steric effects of the R substituent; *iii*) the **a**-type isomer can be more stable due to the hydrogen bond between the chloride ion and the hydrogen atom on C(α) of the R substituent. The hydrogen bond could be responsible, at least in part, also for the deshielding of the α-hydrogen signals observed in the solution ^1H NMR: $[\delta_{complex} - \delta_{ligand}]$ = 0.54 (**2a**, 3 α-H), 0.82 (**3a**, 2 α-H), 1.92 (**4a**, 1 α-H), 0.92 (**5a**, 2 α-H).

The ligand HL^7 (R = Ph) lacks α-hydrogen atoms on the substituent, thus preventing the formation of a hydrogen bond with the chloride ion. Furthermore, the phenyl ring is sterically less demanding, owing to the ability of setting itself perpendicular to the coordination plane. Indeed, in this case both isomers **a** and **b** are formed in about a 1:1 ratio.

In order to obtain an insight into the role of the α-hydrogen atoms in driving the reaction selectively towards isomer **a**, several attempts were carried out to obtain the adduct of the *tert*-butyl-substituted ligand. No adduct was isolated and no evidence was provided by ^1H NMR spectra for its existence in solution. Actually, the reaction affords an unusual C(3)-metallated (C−N) species, $[PtCl(SMe_2)(L)]$ (HL = 6-*tert*-butyl-2,2′-bipyridine), with the loss of methane. The X-ray structure of this complex has recently been reported.[15]

Replacement of the chloride by an iodide ion has been carried out on **2a** and **3a** by reaction with LiI. Alternatively, these products can be obtained by reaction of the ligands HL^2 and HL^3 with *trans*-$[PtI(Me)(SMe_2)_2]$. The two procedures give the same products, the latter one in lower yield. Both isomers are obtained, **2a′**, **2b′** and **3a′**, **3b′**, the **a**-type isomers being the major products (77% for **2a′** and 79% for **3a′**). Therefore, it seems that both *α*-hydrogen atoms and a chloride ligand are required to make isomer **a** the more favoured isomer.

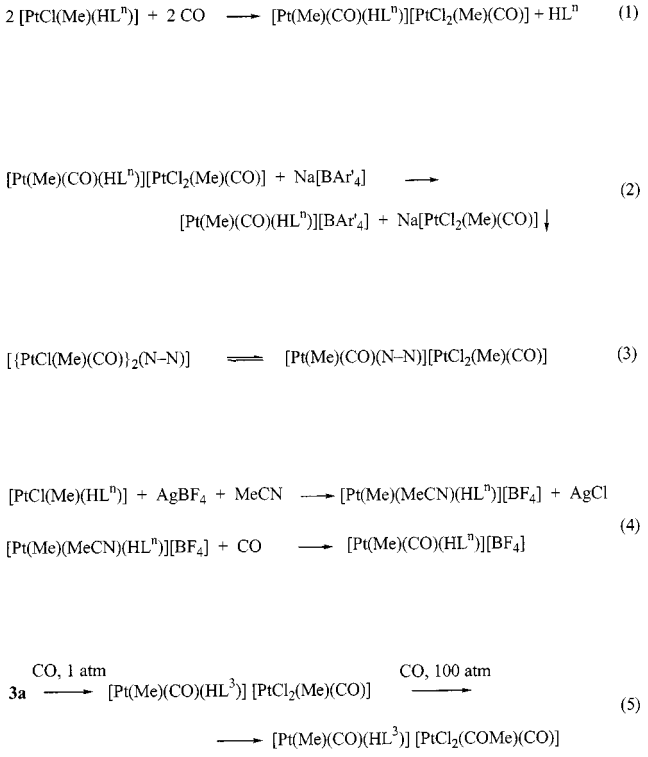
Cyclometallated Species

The synthesis of the adduct species is straightforward with all the ligands but HL^6 (R = $C(Me)_2Ph$). It behaves like an (N−N−C) tridentate ligand, affording only the cyclometallated species **6m** which arises from aromatic C−H activation and elimination of methane. Similar cyclometallated species are also obtained with HL^5 and HL^7 (Scheme 1). The adduct **5a** is not stable in chlorinated solvents, and slowly converts at room temperature to the cyclometallated species **5m**; **7m** is formed during the chromatographic separation of the mixture of isomers **7a** and **7b**.

Reaction with Carbon Monoxide

The reaction of the neutral adducts **1a**, **3a** and **5a** with carbon monoxide (p_{CO} = 1 atm) did not afford the corres-

ponding acyl derivatives, either at room temperature, or in refluxing chloroform. Only when working under high pressures of CO (ca. 100 atm) there is some evidence for slow formation of an acyl species (see later). Under mild conditions, the reaction proceeds to give the ionic species in accordance with Equation (1) of Scheme 2.



Scheme 2

The free ligand was recovered almost quantitatively from the reaction mixture. The ionic nature of the products was confirmed, by conductivity measurements in dichloromethane and acetone, and by FAB mass spectroscopy (positive and negative ions). The IR spectra show two strong absorptions at ca. 2100 and 2060 cm^{-1} due to the stretching vibrations of the terminal carbonyl groups (Table 3). The lower frequency can be assigned to the CO ligand of the anionic complex. The ^1H NMR spectra (Table 3) show two methyl signals; the more shielded one at $\delta = 0.87$ [$(CD_3)_2CO$ solution] is assigned to the anion and is unaffected by the type of the cation (**1c**, **3c**, **5c**), further supporting the hypothesis of two independent ions, one of which does not contain the (N−N) ligand. Indeed, the cations **1c**, **3c** and **5c** could be isolated as $[BAr'_4]^-$ salts {$[BAr'_4]^-$ = tetrakis[3,5-bis(trifluoromethyl)phenyl]borate} by exchange with Na[BAr'_4] [Equation (2), Scheme 2] in CH_2Cl_2 solution. The sodium salt of the anion could not be isolated owing to rapid decomposition.

It is worth noting that [**1c**] $[PtCl_2(Me)(CO)]$ is obtained in two forms that differ in colour, one is yellow and the other one red. Analytical and spectroscopic (^1H NMR, IR and MS) data support their identical composition, while UV spectra ($CHCl_3$ solution) show that the colour difference is due to an absorption at 410 nm (λ_{max}, $\varepsilon \approx 1500$ M^{-1} cm^{-1}) present in the red form. The absorption is concentration-dependent and disappears upon dilution, thus supporting stacking interactions between the anion and the cation and leading to charge-transfer phenomena.[16] Unfortunately, in spite of several attempts, we were unable to grow crystals suitable for X-ray determinations.

Tetraalkylammonium salts of $[PtCl_2(Me)(CO)]^-$ have previously been described[17] as having a *cis* configuration for the anion and our experimental data confirm this arrangement. In particular, the IR spectra show two Pt−Cl stretching frequencies at ca. 320 and 260 cm^{-1}.

A behaviour somewhat reminiscent of that observed in our complexes is described in the literature.[18] In the case of a complex with a 6-R-pyridine-2-carbaldehyde imine, carbonylation of pentacoordinated [PtCl(Me)(ethylene)-(N−N)] (N−N = 6-Me-py-2-CH=NPh) gave a mixture of products, in which free (N−N) and square-planar mono- and dinuclear complexes were detected. The main species is described as a dinuclear complex having a bridging (N−N) ligand; it is not an electrolyte in chloroform, but does dissociate in nitromethane according to the equilibrium shown in Equation (3), Scheme 2.

Cationic Species

The cationic complexes $[Pt(Me)(CO)(HL^n)]^+$ can also be obtained by halide abstraction from the neutral complexes with $AgBF_4$ and subsequent carbonylation of the solvent species [Equation (4), Scheme 2].

The ^1H NMR spectra of the cations obtained in this way are "exactly" superimposable on the spectra of the products obtained by direct carbonylation of the neutral complexes (Table 3), except for the methyl resonance of the anion $[PtCl_2(Me)(CO)]^-$. Although two isomers are possible for **3c** and **5c**, the carbonylation reaction is stereospecific affording only the **a**-type isomer, as confirmed by NOE difference experiment on **3c**[BF_4] (CD_3CN solution). Irradiation of H(6′) at $\delta = 8.90$ gives enhancement of the signal at $\delta = 1.40$ (Me) and vice versa. The linear structure of CO, which does not cause steric hindrance, most likely favours isomer **a**. The solvent species are obtained in good yields and can be isolated and characterised in the solid state. The structure of **3s**[BF_4] has been resolved by an X-ray analysis.

Molecular Structure of [Pt(Me)(MeCN)(HL^3)][BF_4] (**3s**[BF_4])

The structure consists of the packing of $[Pt(Me)(MeCN)(HL^3)]^+$ cations and $[BF_4]^-$ anions in the molar ratio 1:1. An ORTEP view of the molecule is shown in Figure 2. Selected bond lengths and angles are reported in Table 4.

The platinum atom displays a square-planar coordination with a slight square-pyramidal distortion; maximum deviations from the best plane are +0.011(1) and −0.005(4) Å for atoms Pt and C13, respectively. The Pt−N1, Pt−N2 and Pt−C13 bond lengths, 2.013(2), 2.173(3) and 2.036(4) Å, respectively, are very similar to the corresponding values, discussed above, observed in **3a**, 2.022(4), 2.188(4) and 2.043(6) Å. The Pt−N3 distance, 1.971(3) Å, can be com-

Table 3. ^{1}H NMR and selected IR data [cm^{-1}] of the ionic species

Cation	Anion	Solvent	MeCN	^{1}H NMR[a] Pt−Me	Me	CH_2	H(6′)	Other aromatics	IR (CO)
1c	$[BF_4]$	$(CD_3)_2CO$		1.35 s [68.1]			9.15 d (5.8) [40] 9.25 d (5.1) [20]	8.0−8.9	2119 vs[b]
1c	$[BAr'_4]$	$CDCl_3$		1.27 s [67.1]			8.68 dd (5.4) [20] 8.78 dd (5.7) [42]	7.5−8.0	2100 vs[b]
		$(CD_3)_2CO$		1.35 s [68.1]			9.10−9.30 b {2 H}	7.7−9.0	
1c	$[PtCl_2(Me)(CO)]$	$(CD_3)_2CO$		0.87 s [78.4] 1.35 s [68.1]			9.20 b {2 H}	8.0−8.9	2104 vs, 2060 vs[c] 2093 vs, 2045 vs[b]
1s	$[BF_4]$	CD_3CN	2.61 s [14.7]	0.99 s [76.4]			8.88 dd (5.1) [15] 8.92 d (6.6) [60]	7.6−8.4	
3c	$[BF_4]$	$(CD_3)_2CO$		1.48 s [68.9]	1.54 t (7.6)	3.33 q (7.6)	9.17 dd (5.6) [43]	8.0−8.9	2100 vs[c] 2109 vs[b]]
3c	$[BAr'_4]$	$(CD_3)_2CO$		1.48 s [68.9]	1.54 t (7.5)	3.34 q (7.5)	9.18 d (5.6) [43]	7.6−8.9	2100 vs[b]
3c	$[PtCl_2(Me)(CO)]$	$(CD_3)_2CO$		0.87 s [78.6] 1.48 s [68.9]	1.54 t (7.5)	3.34 q (7.5)	9.17 d (5.4) [42]	8.0−8.9	2099 vs, 2059 vs[c] 2084 vs, 2043 vs[b]
3s	$[BF_4]$	CD_3CN	2.58 s [15.6]	1.15 s [77.9]	1.41 t (7.6)	3.13 q (7.6)	8.90 dd (5.4) [63]	7.6−8.3	
5c	$[PtCl_2(Me)(CO)]$	$(CD_3)_2CO$		0.87 s [78.6] 1.45 s [68.9]		4.80 s	9.18 dd (5.6) [42]	7.3−8.9	2100 vs, 2060 vs[c] 2081 vs, 2055 vs[b]

[a] Room temperature, coupling constants in Hz, J_{Pt-H} in square brackets, J_{H-H} in round brackets, chemical shift in ppm from internal TMS. − [b] Nujol mull. − [c] CH_2Cl_2 solution.

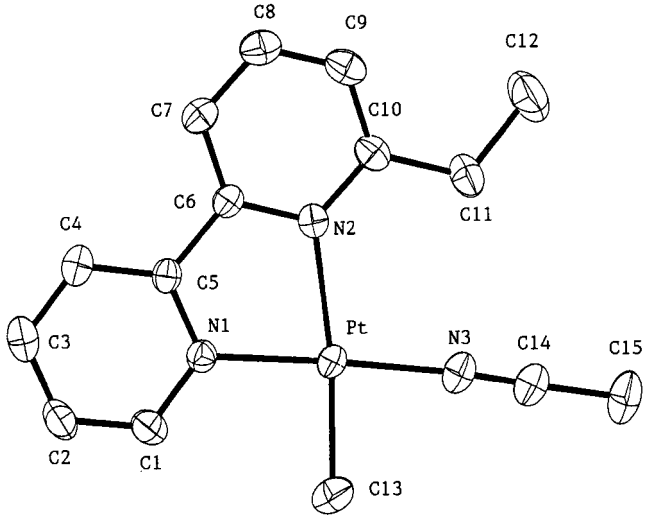


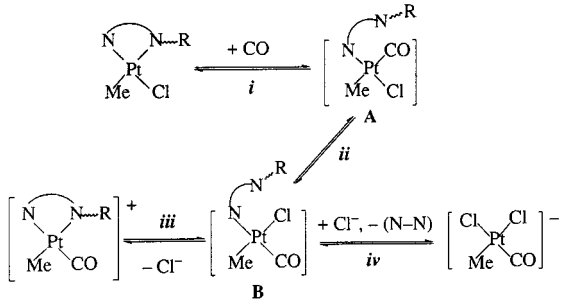
Figure 2. ORTEP view of the cation in compound **3s**$[BF_4]$; ellipsoids as in Figure 1

Table 4. Selected bond lengths [Å] and angles [°] with e.s.d.s in parentheses for compound **3s**$[BF_4]$

Pt−N1	2.013(2)	Pt−N2	2.173(3)
Pt−N3	1.971(3)	Pt−C13	2.036(4)
N3−C14	1.128(5)	C14−C15	1.456(6)
N1−Pt−N2	79.0(1)	N1−Pt−N3	177.2(1)
N1−Pt−C13	93.7(1)	N2−Pt−N3	103.7(1)
N2−Pt−C13	172.6(1)	N3−Pt−C13	83.7(2)
Pt−N3−C14	175.5(4)	N3−C14−C15	178.0(4)

pared with the Pt−NCMe bond length, 1.955(4) Å, found in the cation $[Pt(Me)(MeCN)(Ar_2DAB)]^+$ [19] (Ar_2DAB = diaryldiazabutadiene). It is interesting also to observe that the N2−Pt−N3 angle, 103.7(1)°, is very similar to the N2−Pt−Cl angle, 103.1(1)°, found in **3a**, thus confirming the hypothesis that it is a result of the bulkiness of the ethyl substituent on the bipyridine ligand. The existence of intramolecular hydrogen bonds in this cation is more dubious, because the two hydrogen atoms bonded to C11 are 2.51 and 2.72 Å apart from atom N3, whereas one of the hydrogen atoms bonded to C13 lies 2.35 Å from N3. The two pyridine rings are strictly planar and are twisted 3.9(1.2)° with respect to each other. Four rather short interionic F···H interactions in the range 2.41−2.48 Å suggest the possibility of weak interionic hydrogen bonds.

A plausible reaction pathway that accounts for Equation (1) is shown in Scheme 3. The reaction implies (*i*) Addition of CO with displacement of a coordinated nitrogen and (*ii*) isomerisation of **A** to species **B**, having the chloride *trans* to the methyl group. Isomer **B** can re-establish the pentacycle with the bipyridine (*iii*) loosing a chloride ion or (*iv*) detach completely the bipyridine in the presence of chloride produced in step *iii*. Partial evidence for the formation of the



Scheme 3

cation **nc** and the anion $[PtCl_2(Me)(CO)]^-$ through **B** is provided by the reaction of **3c**$[BF_4]$ with LiCl in acetone, monitored by NMR spectroscopy. With excess LiCl, the ^1H NMR spectrum shows the total conversion of **3c** into $[PtCl_2(Me)(CO)]^-$ and free ligand, in an equimolecular ratio. If the reaction is carried out in the absence of excess LiCl, only the stoichiometric amount of **3c** reacts and there is no evidence of the presence of the species **B**, which seems to be very labile.

High-Pressure Carbonylation

As stated previously, we observe formation of an acyl species only when working under high pressures of CO. The acylation is indeed very slow, for example, in the case of complex **3a**, partial conversion (ca. 80%) of the ionic intermediate to an acyl species is obtained after 20 d [$p_{CO} \approx 100$ atm, Equation (5), Scheme 2].

The ^1H NMR spectra ($CDCl_3$ solution) clearly indicate that only the anion is involved in the acylation. In fact, the signals due to the cation species are not changed, while the intensity of the methyl signal (of the anion) is reduced and a new signal with satellites ($^3J_{Pt-H} = 10.3$ Hz) appears at $\delta = 2.49$; the intensities of the latter two resonances integrate to 3 protons. The IR spectra, in addition to strong bands in the region of terminal carbonyl groups, show a strong absorption at 1650 cm^{-1} and a new Pt−Cl stretch at 347 cm^{-1}.

Experimental Section

General: The unsymmetric 6-R-2,2′-bipyridine HL^{3-7} ligands were obtained through not trivial syntheses according to a procedure previously described,[20] the ligand HL^2 according to Kauffmann et al.[21] The compounds *trans*-$[PtCl(Me)(SMe_2)_2]$,[22] *trans*-$[PtI(Me)(SMe_2)_2]$[22] and $Na[BAr'_4]$[23] {sodium tetrakis[3,5-bis(trifluoromethyl)phenyl]borate} were prepared as reported elsewhere. All solvents were freshly distilled prior to use. Reactions with CO under pressure were performed with a Pyrex bottle in a stainless steel autoclave. − Elemental analyses were performed with a Perkin−Elmer Elemental Analyzer 240B by Mr A. Canu (Dipartimento di Chimica, Università di Sassari). − Conductivities were measured with a Philips PW 9505 conductimeter. − Infrared spectra (Nujol mull or CH_2Cl_2 solution) were recorded in the range 4000−180 cm^{-1} with a Perkin−Elmer 983 spectrophotometer. − UV spectra ($CHCl_3$ solution) were determined with a Hitachi 2010 spectrophotometer. − ^1H NMR spectra were recorded with a Varian VXR 300 spectrometer operating at 299.9 MHz and the selected data are collected in Table 1 and Table 3; the chemical shifts are given in ppm relative to internal TMS and were determined by reference to the residual ^1H solvent peaks. − Mass spectra were obtained with a VG 7070EQ instrument operating under FAB conditions with 3-nitrobenzyl alcohol as a supporting matrix.

[PtCl(Me)(HL^1)] (1a): A solution of the ligand (46.4 mg, 0.297 mmol) in CH_2Cl_2 (10 mL) was added to a solution of *trans*-$[PtClMe(SMe_2)_2]$ (100.0 mg, 0.270 mmol), in the same solvent (20 mL). The solution was stirred for 3 h and then concentrated under vacuum to a small volume, hexane was added dropwise affording a yellow solid adduct. Yield 102.0 mg (94%); m.p. 250 °C. − $C_{11}H_{11}ClN_2Pt$: calcd. C 32.88, H 2.77, N 6.97; found C 32.55, H 2.89, N 6.72. − FAB-MS; *m/z*: 401 $[M]^+$, 386 $[M - Me]^+$, 366 $[M - Cl]^+$, 351 $[M - Cl - Me]^+$. − IR (Nujol): $\tilde{\nu}$ = 1599 s, 1555 m, 333 s cm^{-1}.

The other adduct species were obtained according to the same procedure but with different reaction times.

[PtCl(Me)(HL^2)] (2a): 30 min, orange. Yield 97%, m.p. 176−177 °C. − $C_{12}H_{13}ClN_2Pt$: calcd. C 34.66, H 3.16, N 6.74; found C 34.43, H 3.05, N 6.38. − FAB-MS; *m/z*: 415 $[M]^+$, 400 $[M - Me]^+$, 380 $[M - Cl]^+$, 365 $[M - Cl - Me]^+$. − IIR (Nujol): $\tilde{\nu}$ = 1600 s, 1556 m, 320 s cm^{-1}.

[PtI(Me)(HL^2)] (2a′+2b′): LiI (43.4 mg, 0.325 mmol) was added to a solution of **2a** (45.0 mg, 0.108 mmol) in acetone (20 mL). The solution was stirred for 20 h at room temperature. It was then concentrated to dryness and the residue dissolved in CH_2Cl_2, filtered and concentrated to a small volume. Addition of hexane gave an orange analytical sample. Yield 45.0 mg (82%); m.p. 134−136 °C (mixture). The reaction between *trans*-$[PtIMe(SMe_2)_2]$ and the ligand in CH_2Cl_2 gave the products in 32% yield. − $C_{12}H_{13}ClN_2Pt$: calcd. C 28.41, H 2.59, N 5.52; found C 28.25, H 2.35, N 5.30. − IR (Nujol): $\tilde{\nu}$ = 1597 s, 1556 m cm^{-1}.

[PtCl(Me)(HL^3)] (3a): 30 min, yellow. Yield 84%; m.p. 142−144 °C. − $C_{13}H_{15}ClN_2Pt$: calcd. C 36.32, H 3.52, N 6.52; found C 35.95, H 3.64, N 6.27. − FAB-MS; *m/z*: 414 $[M - Me]^+$, 379 $[M - Cl - Me]^+$. − IR (Nujol): $\tilde{\nu}$ = 1599 s, 1565 m, 321 s cm^{-1}.

[PtI(Me)(HL^3)] (3a′ + 3b′): The title compounds were prepared according to the two procedures described for **2a′** and **2b′**. Orange. Yields: 80−40%; m.p. 97−100 °C (dec., mixture). − $C_{13}H_{15}IN_2Pt$: calcd. C 29.95, H 2.91, N 5.38; found C 30.08, H 2.76, N 5.32. − IR (Nujol): $\tilde{\nu}$ = 1595 s, 1556 m cm^{-1}.

[PtCl(Me)(HL^4)] (4a): 4.5 h. Pale yellow. Yield 68%; m.p. 85−89 °C (dec. with gas evolution). − $C_{14}H_{17}ClN_2Pt$: calcd. C 37.88, H 3.87, N 6.31; found C 37.60, H 3.55, N 5.95. − FAB-MS; *m/z*: 443 $[M]^+$, 428 $[M - Me]^+$, 393 $[M - Cl - Me]^+$. − IR (Nujol): $\tilde{\nu}$ = 1599 s, 1562 m, 317 s cm^{-1}.

[PtCl(Me)(HL^5)] (5a): 30 min. Orange. Yield 73%; m.p. 147−150 °C. − $C_{18}H_{17}ClN_2Pt$: calcd. C 43.95, H 3.49, N 5.70; found C 43.69, H 3.38, N 5.52. − FAB-MS; *m/z*: 476 $[M - Me]^+$, 456 $[M - Cl]^+$, 441 $[M - Cl - Me]^+$. − IR (Nujol): $\tilde{\nu}$ = 1596 s, 1562 m, 702 s, 322 s cm^{-1}.

[PtCl(L^5)] (5m): A solution of **5a** in CH_2Cl_2 was stirred at room temperature for 4 d. It was then concentrated under vacuum to a small volume and diethyl ether was added dropwise, affording the title complex in a quantitative yield. The product was a yellow solid; m.p. 247−249 °C. − $C_{17}H_{13}ClN_2Pt$: calcd. C 42.91, H 2.76, N 5.89; found C 42.71, H 2.51, N 5.67. − FAB-MS; *m/z*: 475 $[M]^+$, 440 $[M - Cl]^+$. − IR (Nujol): $\tilde{\nu}$ = 1600 s, 340 s, 319 s cm^{-1}.

[PtCl(L^6)] (6m): A solution of the ligand (89.8 mg, 0.327 mmol) in CH_2Cl_2 (10 mL) was added to a solution of *trans*-[PtClMe(SMe_2)$_2$] (110.0 mg, 0.297 mmol), in the same solvent (20 mL). The solution was stirred for 2 h and then concentrated under vacuum to a small volume. Hexane was added dropwise to afford the cyclometallated species as an orange solid. Yield 94.4 mg (63%);. m.p. stable at 280 °C. − $C_{19}H_{17}ClN_2Pt$: calcd. C 45.28, H 3.41, N 5.56; found C 45.00, H 3.51, N 5.34. − FAB-MS; *m/z*; 503 $[M]^+$, 468 $[M - Cl]^+$. − IR (Nujol): $\tilde{\nu}$ = 1595 s, 1568 m, 339 s cm^{-1}.

[PtCl(Me)(HL^7)] (7a + 7b): 4 h. Orange. Yield 84%; m.p. 258 °C (mixture). − $C_{17}H_{15}ClN_2Pt$: calcd. C 42.72, H 3.17, N 5.86; found C 42.45, H 3.07, N 5.71. − IR (Nujol): $\tilde{\nu}$ = 1595 s, 1573 s, 697 s, 337 s cm^{-1}.

[PtCl(L^7)] (7m): The two isomers, **7a + 7b**, were separated by chromatography on neutral Al_2O_3 (activity II) by elution with dichloromethane. **7b** was recovered in the first fraction, whereas **7a** underwent a decomposition affording the cyclometallated species **7m**: red-orange; m.p. stable at 280 °C. − $C_{16}H_{11}ClN_2Pt$: calcd. C 41.61, H 2.41, N 6.07; found C 41.53, H 2.33, N 6.08. − IR (Nujol): $\tilde{\nu}$ = 1590 s, 1570 m, 328 s cm^{-1}.

1c[PtCl$_2$(Me)(CO)]: CO was bubbled through a stirred orange solution of **1a** (110.0 mg, 0.274 mmol) in CH_2Cl_2 (20 mL) at room temperature. After 2.5 h, the solution became pale yellow. It was concentrated under vacuum to a small volume, diethyl ether was then added dropwise affording a yellow solid which was filtered and collected (67.0 mg, m.p. 149 °C). The filtrate was concentrated to dryness and the oily residue washed with diethyl ether several times to give a red solid which was recrystallised from CH_2Cl_2/diethyl ether (14.0 mg, m.p. 148 °C). Yield 81.0 mg (84%). From the mother liquor, some ligand was recovered (20.0 mg, 0.128 mmol). − $C_{14}H_{14}Cl_2N_2O_2Pt_2$: calcd. C 23.91, H 2.01, N 3.98; found C 23.75, H 2.12, N 4.36. (the microanalysis refers to the yellow form, the one of the red form is very similar). − FAB-MS; *m/z*: 394 $[M]^+$, 379 $[M - Me]^+$, 366 $[M - CO]^+$, 351 $[M - Me - CO]^+$, 308 $[N]^-$, 293 $[N-Me]^-$, 280 $[N-CO]^-$, 265 $[N-Me-CO]^-$. − IR (CH_2Cl_2): $\tilde{\nu}$ = 2104 vs, 2060 vs; (Nujol) 2093 vs, 2045 vs, 1602 s, 318 m, 262 m cm^{-1}(the spectroscopic data are identical for the yellow and the red form). − UV ($CHCl_3$): λ_{max} (yellow form) = 335 nm ($c = 10^{-3}$ M); red form: 335 nm, 410 nm ($c = 10^{-3}$ M), 300 nm ($c = 2{\cdot}10^{-5}$ M).

1s[BF$_4$]: A solution of $AgBF_4$ (48.5 mg, 0.249 mmol) in MeCN (5 mL) was added dropwise to a stirred orange solution of **1a** (100.0 mg, 0.249 mmol) in CH_2Cl_2 (10 mL). The mixture was stirred in the absence of light for 0.5 h at room temperature, it was then filtered through a Celite filter aid, affording a yellow filtrate. The solvent was removed in vacuo to give an orange-yellow solid, which was recrystallised from CH_2Cl_2/diethyl ether, affording a brick-red solid. Yield 110.7 mg (90%); m.p. 218−226 °C (dec.). − $C_{13}H_{14}BF_4N_3Pt$: calcd. C 31.60, H 2.86, N 8.50; found C 31.49, H 2.81, N 8.25. − FAB-MS; *m/z*: 407 $[M]^+$, 392 $[M - Me]^+$, 366 $[M - MeCN]^+$, 351 $[M - Me - MeCN]^+$. − IR (Nujol): $\tilde{\nu}$ = 2359−2303 vw, 1600 m, 1058 vs cm^{-1}.

1c[BF$_4$]: CO was bubbled through a stirred orange solution of **1s**[BF_4] (200.0 mg, 0.405 mmol) in CH_2Cl_2 (50 mL) at room temperature. After 20 h, the solution was lemon-yellow, it was concentrated under vacuum to a small volume and diethyl ether was then added dropwise, affording a pale yellow solid in a quantitative yield (193.7 mg); m.p. 260−270 °C (dec.). − $C_{12}H_{11}BF_4N_2OPt$: calcd. C 29.95, H 2.31, N 5.82; found C 29.60, H 2.11, N 5.59. − IR (Nujol): $\tilde{\nu}$ = 2119 vs, 1598 s, 1060 vs cm^{-1}.

1c[BAr′$_4$]: Na[BAr′$_4$] (62.9 mg, 0.071 mmol) was added to a stirred solution of **1c**[$PtCl_2$(Me)(CO)] (50.9 mg, 0.072 mmol) in CH_2Cl_2 (5 mL). After a few minutes, the solution was filtered through a Celite filter aid, concentrated to dryness and then dried in vacuo. The off-white solid was recrystallised from CH_2Cl_2/hexane. Yield 89.3 mg (quantitative). m.p. 139−141 °C. − $C_{44}H_{23}BF_{24}N_2OPt$: calcd. C 42.02, H 1.85, N 2.23; found C 41.70, H 1.67, N 2.38. − FAB-MS; *m/z*: 394 $[M]^+$, 379 $[M - Me]^+$, 366 $[M - CO]^+$, 351 $[M - Me - CO]^+$, 863 $[N]^-$. − IR (Nujol): $\tilde{\nu}$ = 2100 s, 1600 m, 1120 vs cm^{-1}.

3c[PtCl$_2$(Me)(CO)]: CO was bubbled through a deep yellow solution of **3a** (52.0 mg, 0.121 mmol) in CH_2Cl_2 (20 mL) at room temperature. After 1 h, the resulting pale yellow solution was concentrated to dryness and the oily residue washed with diethyl ether to afford a pale-yellow solid which was recrystallised from CH_2Cl_2/diethyl ether. The free ligand (9.9 mg, 0.054 mmol) was recovered from the mother liquor. Yield 41.1 mg (93%). m.p. 153 °C (dec.). − $C_{16}H_{18}Cl_2N_2O_2Pt_2$: calcd. C 26.27, H 2.48, N 3.83; found C 26.37, H 2.16, N 3.64. − FAB-MS; *m/z*: 422 $[M]^+$, 407 $[M - Me]^+$, 379 $[M - Me - CO]^+$, 308 $[N]^-$, 293 $[N-Me]^-$, 280 $[N-CO]^-$, 265 $[N-Me-CO]^-$, 258 $[N-Me-Cl]^-$. − IR (CH_2Cl_2): $\tilde{\nu}$ = 2099 vs, 2059 vs; (Nujol) 2084 vs, 2043 vs, 1601 s, 1568 m, 320 s, 262 m cm^{-1}.

3s[BF$_4$]: The title complex was prepared in the same manner as **1s**[BF_4]. A bright-yellow solid was obtained (the dropwise addition of diethyl ether caused the precipitation of a bright-red solid which was rapidly converted into a bright-yellow one). Yield 81%. m.p. 215 °C (dec.). − $C_{15}H_{18}BF_4N_3Pt$: calcd. C 34.49, H 3.48, N 8.05; found C 34.41, H 3.32, N 7.97. − FAB-MS; *m/z*: 435 $[M]^+$, 420 $[M - Me]^+$, 394 $[M - MeCN]^+$, 379 $[M - Me - MeCN]^+$. − IR (Nujol): $\tilde{\nu}$ = 2358−2332 vw, 1600 m, 1563 m, 1052 vs cm^{-1}

3c[BF$_4$]: The title complex was prepared in the same manner as **1c**[BF_4]. 10 h, colourless solution. Quantitative yield; m.p. 235−238 °C. − $C_{14}H_{15}BF_4N_2OPt$: calcd. C 33.02, H 2.98, N 5.50; found C 32.74, H 2.60, N 5.39. − FAB-MS; *m/z*: 422 $[M]^+$, 407 $[M - Me]^+$, 394 $[M - CO]^+$, 379 $[M - Me - CO]^+$. − IR (CH_2Cl_2): $\tilde{\nu}$ = 2100 vs, (Nujol) 2109 vs, 1599 s, 1566 m, 1057 vs cm^{-1}.

3c[BAr′$_4$]: The title complex was prepared in the same manner as **1c**[BAr′$_4$]. Yield: quantitative; m.p. 129 °C. − $C_{46}H_{27}BF_{24}N_2OPt$: calcd. C 42.97, H 2.12, N 2.18; found C 42.64, H 2.02, N 2.38. − FAB-MS; *m/z*: 422 $[M]^+$, 407 $[M - Me]^+$, 394 $[M - CO]^+$, 379 $[M - Me - CO]^+$. − IR (Nujol): $\tilde{\nu}$ = 2100 s, 1600 m, 1120 vs cm^{-1}.

5c[PtCl$_2$(Me)(CO)]: The title complex was prepared in the same manner as **3c**[$PtCl_2$(Me)(CO)]. Pale-yellow. Yield 90%; m.p. 154−158 °C (dec.). − $C_{21}H_{20}Cl_2N_2O_2Pt_2$: calcd. C 31.78, H 2.54, N 3.53; found C 32.04, H 2.29, N 3.74. − FAB-MS; *m/z*: 484 $[M]^+$, 468 $[M - CH_4]^+$, 440 $[M - CH_4 - CO]^+$, 308 $[N]^-$, 293 $[N-Me]^-$, 280 $[N-CO]^-$, 265 $[N-Me-CO]^-$, 258 $[N-Me-Cl]^-$. − IR (CH_2Cl_2): $\tilde{\nu}$ = 2100 vs, 2060 vs; (Nujol) 2081 vs, 2055 vs, 1605 s, 1568 m, 702 s, 323 s, 274 s cm^{-1}.

X-ray Data Collections and Structure Determinations: Crystal data and other experimental details are summarised in Table 5. The diffraction experiments were carried out with a Siemens SMART CCD area detector diffractometer at room temperature using Mo-K_α radiation (λ = 0.71073 Å) with a graphite crystal monochromator in the incident beam. Cell parameters and orientation matrices were obtained from the least-squares refinement of 83 (for **3a**) and 52 (for **3s**[BF_4]) reflections measured in three different sets of 15 frames each, in the range $3° < \theta < 23°$. At the end of the data collections the first 50 frames, containing 251 (for **3a**) and 180 (for **3s**[BF_4]) reflections, were recollected in order to monitor the crystal

Table 5. Crystallographic data

Compound	**3a**	**3s**[BF_4]
Empirical formula	$C_{13}H_{15}ClN_2Pt$	$C_{15}H_{18}BF_4N_3Pt$
M	429.82	522.23
Colour	yellow	Yellow
Crystal system	orthorhombic	Triclinic
Space group	$P2_12_12_1$ (no. 19)	$P\bar{1}$ (no.2)
a [Å]	6.984(1)	8.223(1)
b [Å]	9.860(1)	8.969(1)
c [Å]	19.111(2)	12.936(1)
α [°]		103.29(1)
β [°]		105.87(1)
γ [°]		102.68(1)
V [Å^3]	1316.0(3)	851.5(2)
Z	4	2
F(000)	808	496
$D_{calcd.}$ [g cm^{-3}]	2.17	2.03
T [K]	293	293
Crystal size [mm]	0.11 × 0.23 × 0.25	0.11 × 0.23 × 0.39
μ (Mo-K_α) [cm^{-1}]	109.6	83.6
Min. and max. transm. factors	0.50−1.00	0.50−1.00
Scan mode	ω	ω
Frame width [°]	0.30	0.30
Time per frame [s]	15	20
No. of frames	2450	2450
Detector−sample distance [cm]	5.00	5.00
θ range [°]	3−26	3−26
Reciprocal space explored (*h*, *k*, *l*)	±9, ±13, ±24	±10, ±12, ±17
No. of reflections (total; independent)	15516; 3192	9996; 3987
R_{int}	0.051	0.033
Final R_2 and R_{2w} indices[a] (F^2, all reflections)	0.042, 0.054	0.035, 0.044
Conventional R_1 index [$I > 2\sigma(I)$]	0.024	0.020
Reflections with $I > 2\sigma(I)$	2735	3265
No. of variables	154	217
Goodness of fit[b]	1.06	0.95

[a] $R_2 = [\Sigma(|F_o^2 - kF_c^2|)/\Sigma F_o^2]$, $R_{2w} = [\Sigma w(F_o^2 - kF_c^2)^2/\Sigma w(F_o^2)^2]^{1/2}$. − [b] $[\Sigma w(F_o^2 - kF_c^2)^2/(N_o - N_v)]^{1/2}$, where $w = 4F_o^2/\sigma(F_o^2)^2$, $\sigma(F_o^2) = [\sigma^2(F_o^2) + (0.04F_o^2)^2]^{1/2}$, N_o is the number of observations and N_v the number of variables.

decay, which was not observed, so that no time-decay correction was needed. The 2450 (for both **3a** and **3s**[BF_4]) collected frames were processed with the software SAINT,[24] and an empirical absorption correction was applied (SADABS[25]) to the 15516 collected reflections of **3a**, 3192 of which are unique with $R_{int} = 0.051$ ($R_{int} = \Sigma|F_o^2 - F_{mean}^2|/\Sigma F_o^2$), and to the 9996 collected reflections of **3s**[BF_4], 3987 of which are unique with $R_{int} = 0.033$. Scattering factors and anomalous dispersion corrections were taken from ref.[26] The calculations were performed with an AST Power Premium 486/33 computer using the Personal Structure Determination Package[27] and the physical constants tabulated therein. The structures were solved by Patterson and Fourier methods and refined by full-matrix least squares, using all reflections and minimising the function $\Sigma w(F_o^2 - k|F_c^2|)^2$ (refinement on F^2). Anisotropic thermal factors were refined for all the non-hydrogen atoms. The hydrogen atoms of the methyl group bonded to the platinum center and those of the methyl group belonging to the acetonitrile ligand were detected in the final Fourier maps and not refined. All the other hydrogen atoms were placed in their ideal positions (C−H = 0.97 Å, *B* 1.10 times that of the carbon atom to which they are attached) and not refined. For the noncentrosymmetric compound **3a**, full refinement of the reported structure model led to $R_2 = 0.042$ and $R_{2w} = 0.054$, full refinement of the structure enantiomorph led to $R_2 = 0.056$ and $R_{2w} = 0.094$. The final Fourier maps show maximum residuals of 1.7(4) e/Å^3 at 0.85 Å from Pt for **3a**, and of 0.88(30) e/Å^3 at 1.06 Å from Pt for **3s**[BF_4]. Crystallographic data (excluding structure factors) for the structures reported in this paper have been deposited with the Cambridge Crystallographic Data Centre as supplementary publication no. CCDC-142180 (**3a**) and -142181 (**3s**[BF_4]). Copies of the data can be obtained free of charge on application to CCDC, 12 Union Road, Cambridge CB2 1EZ, UK [Fax: (internat.) + 44-1223/336-033; E-mail: deposit@ccdc.cam.ac.uk].

Acknowledgments

We thank the Università di Sassari and Consiglio Nazionale delle Ricerche for financial support. A. D. thanks the Regione Autonoma della Sardegna for a research fellowship.

[1] [1a] R. van Asselt, E. E. C. G. Gielens, R. E. Rülke, C. J. Elsevier, *J. Chem. Soc., Chem. Commun.* **1993**, 1203−1205. − [1b] B. A. Markies, M. H. P. Rietveld, J. Boersma, A. L. Spek, G. van Koten, *J. Organomet. Chem*. **1992**, *424*, C12−C16. − [1c] P. L. Alsters, J. Boersma, W. J. J. Smeets, A. Spek, G. van Koten, *Organometallics* **1993**, *12*, 1639−1647. − [1d] M. A. Cinellu, S. Gladiali, G. Minghetti, *J. Organomet. Chem.* **1989**, *363*, 401−408. − [1e] J. Vicente, J. A. Abad, J. Gil-Rubio, P. G. Jones, E. Bembenek, *Organometallics* **1993**, *12*, 4151−4160. − [1f] J. Vicente, J. A. Abad, R. Fernandez de Bobadilla, P. G. Jones, M. C. Ramirez de Arellano, *Organometallics* **1996**, *15*, 24−34. − [1g] J. A. Abad, *Gazz. Chim. Ital.* **1997**, *127*, 119−130. − [1h] J. Vicente, J. A. Abad, E. Martinez-Viviente, M. C. Ramirez de Arellano, P. G. Jones, *Organometallics* **2000**, *19*, 752−760.

[2] [2a] E. Drent, J. A. M. van Broekhaven, M. J. Doyle, *J. Organomet. Chem*. **1991**, *417*, 235−251. − [2b] A. Sen, *Acc. Chem. Res.* **1993**, *26*, 303. − [2c]R. van Asselt, E. E. C. G. Gielens, R. E. Rülke, K. Vrieze, C. J. Elsevier, *J. Am. Chem. Soc.* **1994**, *116*, 977−985.

[3] [3a] K. J. Cavell, *Coord. Chem. Rev.* **1996**, *155*, 209−243 and

references therein. – [3b] F. C. Rix, M. Brookhart, P. S. White, *J. Am. Chem. Soc.* **1996**, *118*, 4746–4764.

[4] [4a] M. W. Holtcamp, J. A. Labinger, J. E. Bercaw, *J. Am. Chem. Soc.* **1997**, *119*, 848–849. – [4b] M. W. Holtcamp, L. M. Henling, M. W. Day, J. A. Labinger, J. E. Bercaw, *Inor. Chim. Acta* **1998**, *270*, 467–478. – [4c] M. Crespo, X. Solans, M. Font-Bardia, *Organometallics* **1995**, *14*, 355–364.

[5] [5a] M. Crespo, R. J. Puddephatt, *Organometallics* **1987**, *6*, 2548–2550. – [5b] S. Achar, R. J. Puddephatt, J. D. Scott, *Polyhedron* **1996**, *15*, 2363–2368. – [5c] V. G. Albano, C. Castellari, M. Monari, V. De Felice, A. Panunzi, F. Ruffo, *Organometallics* **1996**, *15*, 4012–4019.

[6] [6a] V. De Felice, M. L. Ferrara, F. Giordano, F. Ruffo, *Gazz. Chim. Ital.* **1994**, *124*, 117–119. – [6b] M. L. Ferrara, I. Orabona, F. Ruffo, V. De Felice, *J. Organomet. Chem.* **1996**, *519*, 75–82.

[7] [7a] F. P. Fanizzi, L. Maresca, G. Natile, M. Lanfranchi, A. Tiripicchio, G. Pacchioni, *J. Chem. Soc., Chem. Commun.* **1992**, 333–335. – [7b] M. E. Cucciolito, V. De Felice, A. Panunzi, A. Vitagliano, *Organometallics* **1989**, *8*, 1180–1187. – [7c] V. G. Albano, C. Castellari, M. Monari, V. De Felice, A. Panunzi, F. Ruffo, *Organometallics* **1992**, *11*, 3665–3669. – [7d] M. E. Cucciolito, F. Giordano, A. Panunzi, F. Ruffo, V. De Felice, *J. Chem. Soc., Dalton Trans.* **1993**, 3421–3426.

[8] [8a] G. S. Hill, L. M. Rendina, R.J. Puddephatt, *J. Chem. Soc., Dalton Trans.* **1996**, 1809–1813. – [8b] G. S. Hill, L. Manojlovic-Muir, K. W. Muir, R. J. Puddephatt, *Organometallics* **1997**, *16*, 525–530. – [8c] T. G. Appleton, J. R. Hall, M. A. Williams, *J. Organomet. Chem.* **1986**, *303*, 139–149 and references therein. – [8d] C. R. Baar, M. C. Jennings, R. J. Puddephatt, K. W. Muir, *Organometallics* **1999**, *18*, 4373–4379.

[9] H. C. Clark, L. E. Manzer, *J. Organomet. Chem.* **1973**, *59*, 411–428.

[10] P. K. Byers, A. J. Canty, *Organometallics* **1990**, *9*, 210–220.

[11] T. G. Appleton, H. C. Clark, L. E. Manzer, *Coord. Chem. Rev.* **1973**, *10*, 335- 422.

[12] C. K. Johnson, *ORTEP*, Report ORNL-5138. Oak Ridge National Laboratory, Oak Ridge, TN, **1976**.

[13] G. Minghetti, S. Stoccoro, M. A. Cinellu, A. Zucca, M. Manassero, M. Sansoni, *J. Chem. Soc., Dalton Trans.* **1998**, 4119–4126.

[14] G. Minghetti, M. A. Cinellu, S. Stoccoro, A. Zucca, M. Manassero, *J. Chem. Soc., Dalton Trans.* **1995**, 777–781.

[15] G. Minghetti, A. Doppiu, A. Zucca, S. Stoccoro, M. A. Cinellu, M. Manassero, M. Sansoni, *Chem. Heterocycl. Comp. (Russ. Ed.)* **1999**, *386*, 1127–1137; *Chem. Abstr.* **2000**, *132*, 293871d.

[16] [16a] R. H. Herber, M. Croft, M. J. Coyer, B. Bilash, A. Sahiner, *Inorg. Chem.* **1994**, *33*, 2422–2426. – [16b] G. Arena, G. Calogero, S. Campagna, L. Monsù Scolaro, V. Ricevuto, R. Romeo, *Inorg. Chem.* **1998**, *37*, 2763–2769. – [16c] R. Büchner, C. T. Cunningham, J. S. Field, R. J. Haines, D. R. McMillin, G. C. Summerton, *J. Chem. Soc., Dalton. Trans.* **1999**, 711–717.

[17] J. Browning, P. L. Goggin, R. J. Goodfellow, N. W. Hurst, L. G. Mallison, M. Murray, *J. Chem. Soc., Dalton. Trans.* **1978**, 872–876.

[18] V. De Felice, A. De Renzi, M. L. Ferrara, A. Panunzi, *J. Organomet. Chem* **1996**, *513*, 97–104.

[19] P. J. Albietz, Jr., K. Yang, R. Eisenberg, *Organometallics* **1999**, *18*, 2747- 2749.

[20] [20a] U. Azzena, G. Chelucci, G. Delogu, S. Gladiali, M. Marchetti, F. Soccolini, C. Botteghi, *Gazz. Chim. Ital.* **1986**, *116*, 307–315. – [20b] C. Botteghi, G. Chelucci, G. Chessa, G. Delogu, S. Gladiali, F. Soccolini, *J. Organomet. Chem* **1986**, *304*, 217–225.

[21] T. Kauffmann, J. König, A. Woltermann, *Chem. Ber.* **1976**, *109*, 3864–3868.

[22] J. D. Scott, R. J. Puddephatt, *Organometallics* **1983**, *2*, 1643–1648.

[23] M. Brookhart, B. Grant, A. F. Volpe, Jr., *Organometallics* **1992**, *11*, 3920- 3922.

[24] *SAINT, Reference Manual*, Siemens Energy and Automation, Madison, WI, **1994–1996**.

[25] G. M. Sheldrick, *SADABS, Empirical Absorption Correction Program*, University of Göttingen, **1997**.

[26] *International Tables for X-ray Crystallography*, Kynoch Press, Birmingham, **1974**, vol. 4.

[27] [27a] B. A. Frenz, *Comput. Phys.* **1988**, *2*, 42. – [27b] B. A. Frenz, *Crystallographic Computing 5*, Oxford University Press, Oxford, U.K., **1991**, chapter 11, p. 126.

Received March 31, 2000
[I00126]

Syntheses of Phosphinine-Based Tripodal Ligands

Ute Rhörig,[a] Nicolas Mézailles,[a] Nicole Maigrot,[a] Louis Ricard,[a] François Mathey,*[a] and Pascal Le Floch*[a]

Keywords: Phosphorus heterocycles / Phosphinines / Cycloadditions / Tungsten / Tripodal ligands

The syntheses of several tripodal phosphinine-based ligands are presented. 1,3,2-Diazaphosphinine **(1)** undergoes Diels–Alder reactions with tris-(propynyl)phenylsilane to yield tris-(1,2-azaphosphinine)phenylsilane **6**. This intermediate serves as precursor for the preparation of two tripodal ligand. First, tris(phosphinine)phenylsilane **(7)** is obtained from the reaction with trimethylsilylacetylene. Under more drastic conditions, compound **6** reacts with 4-octyne to yield the tripodal ligand **8** containing six *n*-propyl groups. Reaction of **8** with $[W(CO)_5(THF)]$ affords the corresponding $W(CO)_3$ complex **9** whose structure was confirmed by an X-ray crystallographic study. The synthesis of two extended tripodal ligands **12** and **13** containing three phosphinine units each connected to the same CH linker by dimethylsilyl groups was also studied. As a prerequisite, the precursor tris(propynyldimethylsilyl)methane **(10)** was synthesized by reaction of three equivalents of propynyllithium with tris(bromodimethylsilyl)methane. Reaction of excess **1** with **10** yielded the corresponding tris(dimethylsilyl-1,2-azaphosphinine)methane **(11)** as an intermediate. The formation of ligands **12** and **13** was achieved by reacting **11** with trimethylsilylacetylene or 4-octyne, respectively, in excess. The reaction of ligand **13** with $[W(CO)_5(THF)]$ in toluene yielded the corresponding $W(CO)_3$ complex **14** which was structurally characterized.

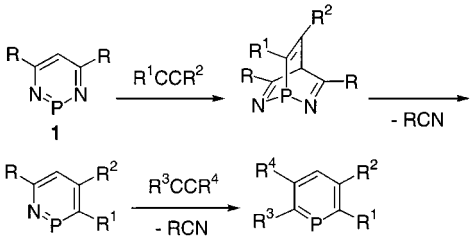
Introduction

Polydentate phosphane ligands continue to attract a lot of interest from both coordination and organometallic chemists. This is mainly due to their unique structural and electronic properties which allow the stabilization of many metallic centers with various oxidation states and geometries.[1] Furthermore, transition metal complexes of such ligands have shown an interesting potential in many catalytic processes of importance. Indeed, tripodal systems have been successfully used in the hydrogenation of alkynes, alkenes and nitriles, hydroformylation and isomerization reactions of alkenes, oligomerization and polymerization of alkynes,[2] C−H activation of unsaturated substrates[3] and, very recently, Bianchini et al. have reported the use of soluble metal complexes for hydrogenation, hydrogenolysis and desulfurization of thiophenic substrates.[4] For synthetic reasons most of these ligands usually bear *P*-alkyl or *P*-aryl groups as binding sites and tripodal structures incorporating strong π-acceptor phosphane groups are still rather rare.[5]

In the course of our studies on phosphinines we became interested in synthesizing analogs of these tripodal ligands. Phosphinines are known to be excellent π-acceptor ligands which significantly increase the Lewis-acidity of the metal centers to which they are coordinated.[6] Furthermore, they have shown a strong ability to stabilize very electron-rich metallic centers,[7] and recently, the synthesis of a remarkably stable gold(0) complex in which a phosphinine-based macrocycle acts like a "CO matrix" was reported.[8] Though some sp^2-based tridentate ligands with phosphaalkenes[9] and phosphinines[10] are known, tri- or tetrapodal ligands including P=C bonds are still unknown. Herein we wish to report on a simple synthetic methodology which allows the assembly of these phosphinine-based tripodal structures.

Results and Discussion

Synthetic approaches allowing the connection of phosphinines are rare and often require multi-step sequences. To circumvent this limitation, we developed a simple strategy relying on the reactivity of 1,3,2-diazaphosphinines.[11] As shown below, these heterocycles react with one equivalent of alkyne to give 1,2-azaphosphinines, which can subsequently be transformed into phosphinines at higher temperatures when a second equivalent of alkyne is reacted (Scheme 1). These thermally promoted transformations involve two successive [4+2] cycloaddition/cycloreversion sequences with the concomitant release of two molecules of nitrile. In a series of articles we showed that this approach was indeed particularly efficient for building sophisticated



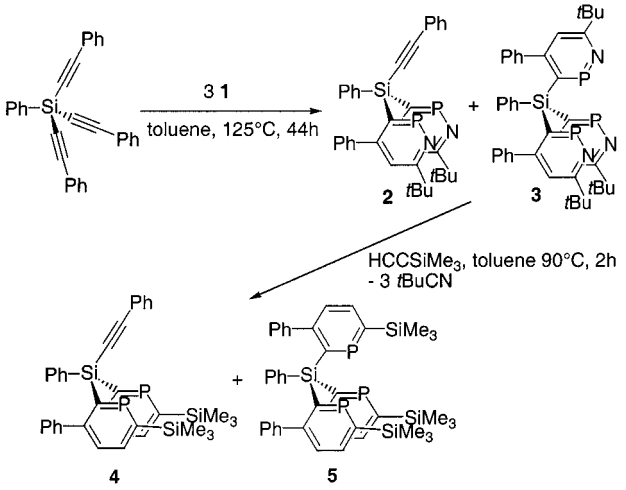
Scheme 1. Reactivity of 1,3,2-di- and 1,2-azaphosphinines towards alkynes

[a] Laboratoire "Héteroéléments et Coordination", UMR CNRS 7653, Ecole Polytechnique,
91128 Palaiseau Cedex, France
E-mail: lefloch@poly.polytechnique.fr

 © WILEY-VCH Verlag GmbH, D-69451 Weinheim, 2000 1434−1948/00/1212−2565 $ 17.50+.50/0

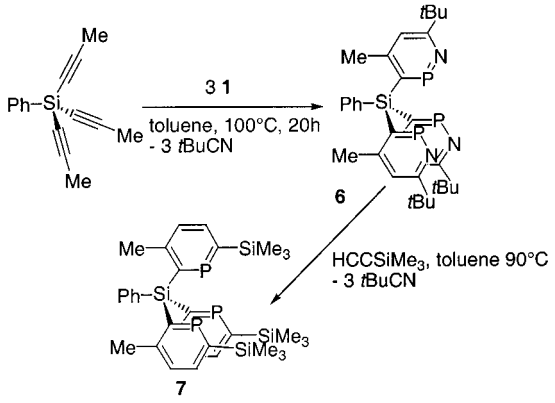
structures such as 2,3,5,6-tetrafunctionalized rings,[10] bis- and tris-phosphinines and phosphinine-based macrocycles.[12]

Quite logically we attempted to see whether this method could be transferred to the synthesis of tripodal structures with triynes. In all our experiments, the readily available 4,6-di-*tert*-butyl-1,3,2-diazaphosphinine **(1)** was used as precursor.[11] As the regioselectivity in the cycloaddition reaction can be a problem, we focused on silyl-substituted alkynes which usually react regiospecifically. Previous studies have indeed shown that the silyl-substituted carbon atom of the alkyne reacts exclusively at phosphorus, and therefore the silicon group is always located at the α-carbon atom in the final compound.[10–12] A first series of experiments demonstrated that the bulkiness of the alkyne is of utmost importance. Thus, the reaction of tris(phenylethynyl)phenylsilane with four equivalents of **1** in toluene at 125 °C yields a mixture of two compounds whose structures were ascribed, on the basis of their ^{31}P NMR spectroscopic data, to the bis(1,2-azaphosphinine)silane **(2)** (80%) (δ = 308.3) and the expected tris(1,2-azaphosphinine)silane **(3)** (20%) (δ = 307.5). Whatever the experimental conditions used (temperature, ratio of precursors, heating time), the formation of **3** never exceeded 20%: the presence of a phenyl group at the β-position of the phosphinine very likely hampers the third cycloaddition leading to **3**. To confirm our hypothesis about the structures of **2** and **3**, trimethylsilylacetylene was reacted with the mixture of compounds. After two hours of heating at 90 °C in toluene, the bis(phosphinine)phenylethynylsilane **(4)**, the desired tripodal ligand **5** and traces of the 2,6-bis(trimethylsilyl)phosphinine[11] resulting from the reaction of the excess of **1** with the alkyne were formed. Whereas this latter could easily be eliminated by chromatographic purification, complete separation of **4** and **5** turned out to be impossible and only compound **4** was isolated in pure form. Nevertheless, mass spectroscopy measurements carried out on a mixture of both compounds allowed us to confirm the proposed structure for ligand **5** {*m*/*z* (%) = 823 (10) [M]} (Scheme 2).



Scheme 2. Synthesis of ligands **4** and **5**

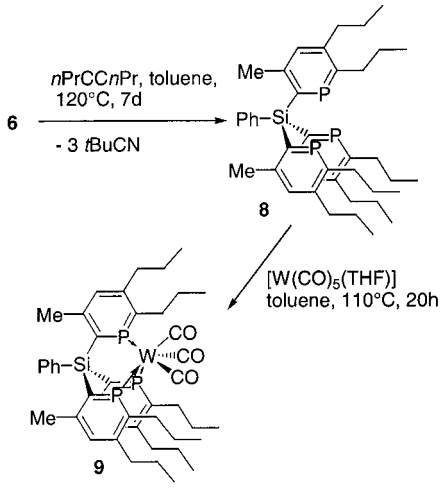
Better results were obtained simply by replacing the phenyl group of the alkyne moiety by a methyl group. Tris(propynyl)phenylsilane reacts with four equivalents of **1** to yield, after 20 hours at 100 °C, a mixture of **1** and a compound which gives a singlet in the ^{31}P NMR spectrum at δ = 308.0. On the basis of this chemical shift, which compares well with those of other 3-silyl-substituted-1,2-azaphosphinines, its formula was ascribed to that of the expected intermediate, the tris(1,2-azaphosphinine)phenylsilane **(6)**. In a subsequent step, **6** was reacted with trimethylsilylacetylene in excess. After 2 hours at 90 °C, the tripodal ligand **7** was formed together with traces of the 2,6-bis(trimethylsilyl)phosphinine.[11] The formulation of **7** was elucidated by conventional NMR spectroscopy and mass spectrometry. A significant piece of information is found in the ^{13}C NMR spectrum of **7**: the signal of the C2-carbon atom appears as a doublet of triplets due to the coupling to the neighboring P atom (^1J = 87.5 Hz) and to the two other magnetically equivalent P atoms of the other rings (^3J = 5.5 Hz) (Scheme 3).



Scheme 3. Synthesis of ligand **7**

Unfortunately, although somewhat predictably, the presence of three peripheral silyl groups in ligand **7** preclude complexation to non-sterically demanding $M(CO)_3$ fragments {M = Cr, Mo, W, with $[Cr(CO)_4(CH_3CN)_2]$, $[Mo(CO)_4(nbd)]$, $[W(CO)_5(THF)]$ or $[W(CO)_4(CH_3CN)_2]$ as precursors}. To alleviate the steric bulk around the cavity, we therefore decided to replace these silyl substituents by alkyl groups. To avoid the formation of many isomers, we decided to use the symmetrical 4-octyne. As previously observed, the use of a nonpolar alkyne dramatically decreases the rate of the reaction and seven days of heating at 120 °C were necessary to ensure the complete formation of ligand **8**, which was isolated as a yellow oil in 76% yield (Scheme 4).

Unequivocal evidence for the proposed structures were provided by NMR spectroscopy and mass spectrometry. As a result of alkyl substitution, the ^{31}P NMR chemical shift of **8** appears at rather high field (δ = 247.0) compared to that of phosphinine **7** (δ = 272.6). As postulated, the introduction of smaller groups at the α-positions frees the access to the cavity and complexation can now be achieved. Reaction of $[W(CO)_5(THF)]$ with **8** yields the expected $W(CO)_3$



Scheme 4. Synthesis of ligand **8** and complex **9**

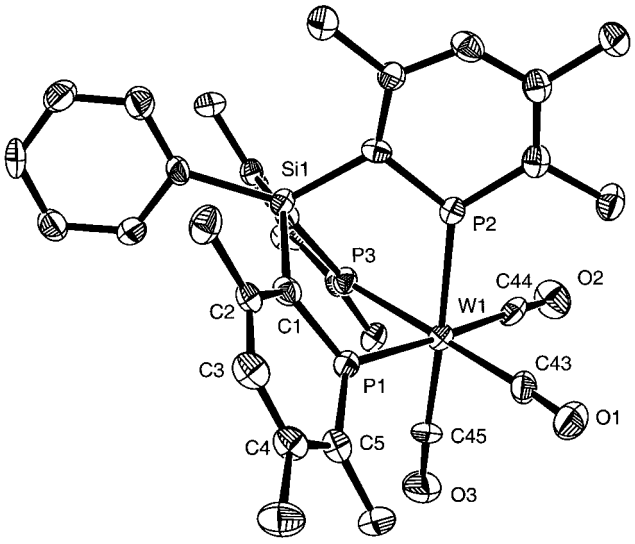
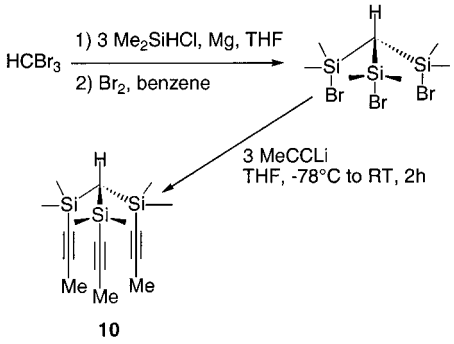


Figure 1. ORTEP drawing of **9** as determined by a single-crystal X-ray diffraction analysis; ellipsoids are drawn to enclose 50% of the electron density; the hydrogen atoms of the CH_2CH_3 grouping of the *n*-propyl substituent have been omitted for clarity[a]
[a] Selected bond lengths [Å] and angles [°]: W−P1 2.437(2), W−P2 2.502(2), W−P3, 2.427(2), W−C43, 2.00(1), W−C44, 2.02(1), W−C45 1.998(8), Si1−C1, 1.907(8), P1−C1 1.723(8), C1−C3, 1.40(1), C2−C3, 1.39(1), C3−C4 1.39(1), C4−C5 1.38(1), C5−P1 1.733(8), P1−W−P2, 84.76(7), P1−W−P3 84.56(7), P3−W−P1, 88.47(6), P1−W−C44 176.8(2), P2−W−C45 177.3(3), P3−W−C43 179.3(3), C5−P1−C1, 107.4(4), C6−C16 131.24(3), C1−C16, 100.93(3), C11−C16 101.62(3)

complex **9** after refluxing for 20 hours in toluene (Scheme 4).

Complex **9** was characterized by conventional NMR techniques, IR spectroscopy and elemental analysis. As frequently observed with phosphinines, coordination to a tungsten carbonyl fragment induces a significant upfield shift ($\delta = 213.1$, $\Delta\delta = -34$). In the ^{13}C NMR spectrum, the very characteristic doublet of triplets at $\delta = 210$, assignable to three magnetically equivalent carbonyl ligands, is found. Indeed, each carbonyl group is located *trans* to one phosphorus atom ($^2J = 29.0$ Hz) and *cis* to the other two ($^2J = 7.0$ Hz). Finally, as expected for strong π-acceptor ligands, the bands in the IR spectrum are shifted towards higher frequencies (1950 and 1875 cm^{-1}) than for "analogous" phosphane complexes[13a] {1930 and 1834 in $[MeC(CH_2PPh)_3W(CO)_3]$}.[13b] Slow diffusion of methanol (or pentane) into a dichloromethane solution of **9** furnished crystals suitable for an X-ray study. An ORTEP view of the structure is shown in Figure 1. The crystallographic labelling used is arbitrary and differs from the numbering utilized for NMR spectral assignments. As expected from NMR and IR spectroscopic data, the tripodal ligand occupies one face of the octahedron leaving three structurally equivalent carbonyls ligands. As previously observed in the X-ray structure of $[W(CO)_3$(silacalix-3-phosphinine)],[12a] a strain is found in the coordination sphere of tungsten, and the P−W−P angles are slightly smaller than the ideal value of 90° [ranging from 84.46(7) to 88.47(6)]. On the other hand, the internal bond lengths in the three phosphinine subunits are close to those recorded for free 2-substituted silylphosphinines,[12] thus indicating that aromaticity is not significantly perturbed. A similar observation has been made for $[W(CO)_5$(2-chlorophosphinine)].[14] The most surprising feature concerns the geometry around the silicon atom, where a significant deviation from the ideal tetrahedral geometry can be observed. Whereas four C−Si−C angles are "normal" [100.9(3) to 103.2(3)°], C1−Si1−C6 [119.3 (3)°] and C16−Si1−C11 [131.2(3)°] are strongly widened. This phenomenon very likely reflects a strong steric crowding between the hydrogen atoms of the phenyl substituent and those of the three methyl groups which point towards the top of the ligand. With this particular arrangement, the shortest through-space H(phenyl)−H(methyl) interaction measured is 2.29 Å.

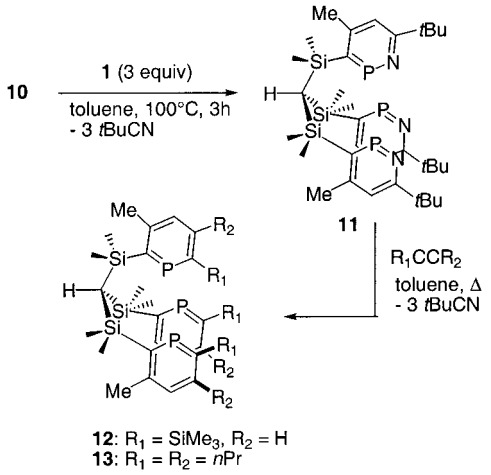
Being encouraged by these first results, we then attempted to enlarge the scope of our method to the preparation of more sophisticated polydentate species, such as extended tripodal ligands. We selected tris(propynyldimethylsilane)methane **(10)** as the starting material. Preparation of this molecule was readily achieved by reaction of three equivalents of propynyllithium with one equivalent of tris(bromodimethylsilyl)methane, whose synthesis was reported by Gade and Becker (Scheme 5).[15]



Scheme 5. Synthesis of triyne **10**

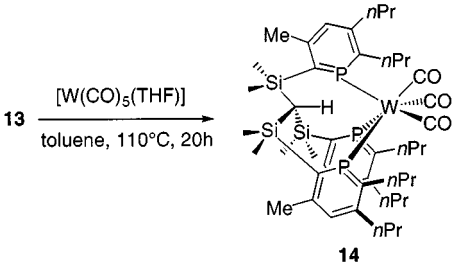
Reaction of this precursor with an excess of **1** for 30 hours at 100 °C yields intermediate **11**, which was characterized by ^{31}P NMR spectroscopy only ($\delta = 305.8$). Subsequent reaction with trimethylsilylacetylene in a large ex-

cess then led to the desired ligand **12** which was formed together with the 2,6-bis(trimethylsilyl)phosphinine as by-product. These two compounds were readily separated by column chromatography, and **12** was isolated as a white solid. All NMR spectroscopic data, as well as mass spectrometry, confirm the proposed structure. Despite the extension of each arm of the tripod resulting, supposedly, both in a larger size of the cavity and a greater flexibility, ligand **12** has the same coordinating behavior as **7**: the three $SiMe_3$ groups prevent the approach of $M(CO)_3$ fragments. Following the above-mentioned strategy we investigated the replacement of bulky $SiMe_3$ groups by linear alkyl groups. As shown in Scheme 6, the intermediate **11** can be reacted with 4-octyne in excess to yield ligand **13**. Heating at 120 °C for 13 days was necessary to ensure complete consumption of **11**. This very long heating period was somewhat detrimental to the overall yield (35%). All NMR spectroscopic data, as well as mass spectroscopy, confirm the proposed structure. The ^{31}P NMR chemical shift is found at δ = 242.6 as expected for an α-alkyl-substituted phosphinine.



Scheme 6. Syntheses of ligands **12** and **13**

As expected, the reaction of this extended tripod with $[W(CO)_5(THF)]$ in toluene at 110 °C for 20 h yield complex **14** as a red oil which slowly crystallizes (Scheme 7). Coordination to tungsten is obvious in the ^{31}P NMR spectrum. Coupling of ^{183}W (14% abundance) with three magnetically equivalent phosphorus atoms gives rise to the expected satellites at δ = 211.6 ($^1J_{P,W}$ = 227.7 Hz). In the ^{13}C NMR, the signal of the three carbonyl ligands appears as a "doublet of triplets" because each CO couples with one *trans* ($^2J_{P,C}$ = 21.2 Hz) and two *cis* ($^2J_{P,C}$ = 9.2 Hz) phosphorus atoms. The most surprising feature is found in the ^1H NMR spectrum. Whereas the signal for the H−C in the free ligand appears at about δ = 0 as a broad singlet, it is found in the complex at δ = +6 as a quadruplet ($^4J_{H,P}$ = 8.5 Hz). Surprisingly, no such effect in the chemical shift of the C−H was observed in the ^{13}C NMR spectrum. It thus seems that the strong downfield shift of the hydrogen results from a geometrical constraint. This hydrogen must be located in the anisotropy cone created by the three aromatic phosphinine moieties. This blocked conformation is also responsible for the magnetic inequivalence of the two methyl groups of the $SiMe_2$ linkers. The difference in their chemical shift of 0.5 ppm clearly shows that they have a very different electronic environment. In order to verify these assumptions, an X-ray crystal study was carried out.



Scheme 7. Complexation of ligand **13** with $[W(CO)_5(THF)]$

The complex crystallized as red blocks of almost millimeter size from a diffusion of MeOH into a chloroform solution of **14**. An ORTEP plot of the structure is shown in Figure 2. A number of very peculiar features are found in the structure. First, the apex carbon appears very flattened. The three Si−C−Si angles range between 114.93 and 118.17°. The sum of these angles at C (349.76°) is much closer to a C sp^2 hybridized than expected. Second, confirming the NMR findings, the hydrogen atom is located inside the cavity. This very peculiar arrangement prompted us to have a closer look at the bond lengths between C−H and H···W. In fact the C−H bond length is not elongated (0.979 Å) and the H···W distance of 2.683 Å indicates only a weak interaction between the metal center and the hydrogen. As expected for a coordinatively saturated metallic center there is no indication of an agostic interaction.

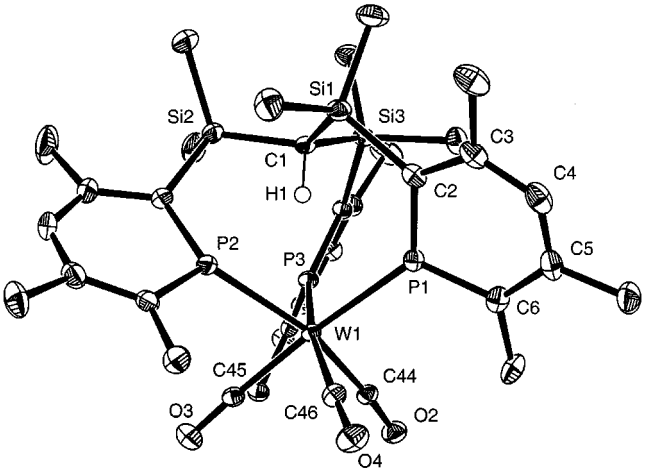


Figure 2. ORTEP drawing of **14** as determined by a single-crystal X-ray diffraction analysis; ellipsoids are drawn to enclose 50% of the electron density; the hydrogen atoms of the CH_2CH_3 grouping of the *n*-propyl substituents have are omitted for clarity[a]
[a] Selected bond lengths [Å] and angles [°]: W1−P1 2.5551(8), W1−P2 2.559(1), W1−P3 2.5700(8), W1−C44 1.967(2), W1−C45 1.975(3), W1−C46 1.970(2), P1−C2 1.741(3), C2−C3 1.408(3), C3−C4 1.398(4), C4−C5 1.389(4), C5−C6 1.403(3), C6−P1 1.747(3), C2−Si1 1.903(3), Si1−C1 1.871(3), C1−Si2 1.878(2), C1−Si3 1.881(3), C1−H1 0.979; P1−W1−P2 98.18(2), P2−W1−P3 98.63(3), P3−W1−P1, 99.15(3), P1−W1−C44 97.22(7), P1−W1−C46 80.46(8), P1−W1−C45 165.57(7), C6−P1−C2 106.7(1), P1−C2−Si1 119.1(1), Si1−C1−Si3 116.7(1), Si3−C1−Si2 114.9(1), Si1−C1−Si2 118.2(1)

Therefore the particularities of the structure are just a consequence of the coordination. The value of the dihedral angles $C_{ring}-C_{ring}-P-W$ (for example $C_3-C_2-P_1-W$ = 154.2°) should be 180° and they are found between 145 and 160° in the structure. As it appears in the ORTEP plot, the three phosphinine rings do not experience this strain and are not significantly distorted (if one excepts small deviations from planarity). This phenomenon is obvious from the ORTEP plot and this confirms the strain in the complex.

In conclusion, we have developed a simple access to the first phosphinine-based tripodal ligands using a "one pot sequence" from 1,3,2-diazaphosphinines. This simple synthetic scheme seems to be flexible enough to allow the introduction of various functional groups on phosphinines and should provide an access to more sophisticated cavities incorporating, for example, other heteroatom-based ligands which can serve as a hemilabile moiety. These developments as well as those concerning the coordinating behavior of ligands such as **8** and **13** and are currently under investigation and will be reported in due course.

Experimental Section

General: All reactions were routinely performed under nitrogen using Schlenk techniques and dry, oxygen-free solvents. Dry toluene and hexane were obtained by distillation from sodium/benzophenone and dry CH_2Cl_2 was obtained by distillation from P_2O_5. Dry celite was used for filtration. − NMR: Bruker AC-200 SY operating at 200.12 MHz for ^1H, 50.32 MHz for ^{13}C, and 81.01 MHz for ^{31}P; chemical shifts (ppm) are relative to TMS (^1H and ^{13}C) or 85% H_3PO_4 (^{31}P). List of abbreviations used: s, singlet, d, doublet, t, triplet, q, quadruplet, p, pseudo, m, multiplet. − Elemental analyses: "Service d'analyse du CNRS", Gif-sur-Yvette, France. Phosphinine **1** was prepared according to a published method.[11]

Synthesis of Ligand 4: A solution of diazaphosphinine **1** (0.63 g, 3.0 mmol) and tris(phenylethynyl)phenylsilane (0.29 g, 0.7 mmol) in toluene (25 mL) was heated at 125 °C for 44 hours. After this period, ^{31}P NMR analysis showed the presence of intermediates **2** and **3**. Trimethylsilylacetylene (0.78 g, 7.9 mmol) was then added and the resulting reaction mixture was heated at 90 °C for 2 hours. After cooling the flask to room temperature, celite (0.5 g) was added and the volatiles were evaporated. The resulting brown powder was then poured onto the top of a silica-gel column for chromatography. A first fraction, eluted with hexane, yielded the 2,6-bis(trimethylsilyl)phosphinine which is formed as a by-product. A second fraction, eluted with a mixture of toluene/hexane (70:30), yielded ligand **4**. The tripodal ligand **5** was recovered (mixture with **4**) in an additional fraction with a mixture of toluene/hexane (65:35). After evaporation of solvents, **4** was recovered as a yellow oil (0.19 g, 40% based on silane). − ^1H NMR ($CDCl_3$): δ = 0.30 (s, 18 H, $SiMe_3$), 6.90−7.50 (m, 20 H, C_6H_5), 7.73−8.20 (dd, 4 H, H-5 and H-4). − ^{13}C NMR ($CDCl_3$): δ = 0.7 (s, $SiMe_3$), 92.8 (s, C*C*−Si), 110.8 (s, C*C*−Ph), 125.0−135.0 (m, C_6H_5), 137.4 (s, C-5), 138.6 (d, ^3J = 5.0 Hz, C-4), 145.6 (s, Cq of C_6H_5), 154.7 (d, ^2J = 8.6 Hz, C-3), 162.2 (dd, ^1J = 91.5 Hz, ^3J = 7.8 Hz, C-2), 167.1 (d, ^1J = 84.5 Hz, C-6). − ^{31}P NMR ($CDCl_3$): δ = 269.6 (s). − MS ; *m/z* (%): 692 (100) [M]. − $C_{42}H_{42}P_2Si_3$ (693.0): calcd. C 72.79, H 6.11; found C 72.95, H 6.20.

Synthesis of Ligand 7: A solution of diazaphosphinine **1** (0.63 g, 3.0 mmol) and tris(propynyl)phenylsilane (0.16 g, 0.7 mmol) in toluene (25 mL) was heated at 100 °C for 20 hours. After this period a ^{31}P NMR control indicated the complete formation of intermediate **6**. Trimethylsilyacetylene (0.78 g, 7.9 mmol) was then added and the resulting reaction mixture was heated at 90 °C for 3.5 hours. After cooling the flask to room temperature, celite (0.5 g) was added and volatiles were evaporated. The resulting brown powder was then poured on to the top of a silica-gel column for chromatography. A first fraction, eluted with hexane, yielded the 2,6-bis(trimethylsilyl)phosphinine formed as a by-product. A second fraction, eluted with a mixture of toluene/hexane (70:30), yielded ligand **7**. After evaporation of solvents, **7** was recovered as a yellow oil (0.32 g, 70% based on the silane). − ^1H NMR ($CDCl_3$): δ = 0.20 (s, 27 H, $SiMe_3$), 2.16 (s, 9 H, Me of phosphinine), 7.07−7.27 (m, 5 H, C_6H_5), 7.53 (d, ^3J = 6.5 Hz, 3 H, H-4), 7.84−7.93 (m, 3 H, H-5). − ^{13}C NMR ($CDCl_3$): δ = 0.7 (d, ^3J = 4.0 Hz, $SiMe_3$), 29.9 (s, Me of phosphinine), 126.0−129.7 (C_6H_5), 131.1 (d, ^3J = 25.0 Hz, C-4), 138.4 (s, Cq of C_6H_5), 139.3 (d, ^2J = 10.0 Hz, C-5), 151.9 (d, ^2J = 10.5 Hz, C-3), 163.6 (td, ^1J = 87.50 Hz, ^3J = 5.5 Hz, C-2), 166.7 (d, ^1J = 83.0 Hz, C-6). − ^{31}P NMR ($CDCl_3$): δ = 272.5 (s). − MS ; *m/z* (%): 648 [M] (100), 575 (31) [M − $SiMe_3$]. − $C_{33}H_{47}P_3Si_4$ (649.0): calcd. C 61.07, H 7.30; found C 61.25, H 7.28.

Synthesis of Ligand 8: A solution of intermediate **6** in toluene (20 mL), prepared as described above from diazaphosphinine **1** (0.50 g, 2.40 mmol) and tris(propynyl)phenylsilane (0.12 g, 0.56 mmol), was heated with 4-octyne (1.10 g, 10 mmol) at 120 °C for one week. Celite (0.5 g) was then added and toluene and the excess of alkyne were evaporated yielding a brown solid, which was purified by chromatography. A fraction eluted with a mixture of hexane/toluene (50:50) yielded **8** which was isolated as a brown oil after evaporation of solvents (0.29 g, 76% based on the silane). − ^1H NMR ($CDCl_3$): δ = 0.92−1.03 (m, 18 H, 6 C*H*$_3$−CH$_2$), 1.52−1.71 (m, 12 H, 6 CH$_3$−C*H*$_2$), 2.17 (s, 9 H, Me of phosphinine), 2.61−2.68 (m, 6 H, CH$_2$−C-5), 2.79−2.91 (m, 6 H, CH$_2$−C-6), 7.16−7.32 (m, 5 H, C_6H_5), 7.62 (d, ^3J = 8.0 Hz, 3 H, H-4). − ^{13}C NMR ($CDCl_3$): δ = 15.0 and 15.1 (2s, 2 Me of *n*-propyl groups), 25.3 (s, Me of phosphinine), 27.7 (d, ^3J = 8.0 Hz, *C*H$_2$−CH$_2$−C-6), 29.1 (s, *C*H$_2$−CH$_2$−C-5), 36.9 (s, *C*H$_2$−C-5), 37.6 (d, ^2J = 36.5 Hz, *C*H$_2$−C-6), 126.0−129.7 (C_6H_5), 135.2 (d, ^3J = 19.0 Hz, C-4), 138.4 (s, Cq of C_6H_5), 147.3 (d, ^2J = 10.0 Hz, C-5), 149.5 (d, ^2J = 12.5 Hz, C-3), 161.3 (dt, ^1J = 76.0 Hz, ^3J = 5.5 Hz, C-2), 167.8 (d, ^1J = 60.0 Hz, C-6). − ^{31}P NMR ($CDCl_3$): δ = 247.0 (s). − MS ; *m/z* (%): 685 (92) [M + 1], 491 (100) [M − $C_{12}H_{18}P$], 299 (37) [M − 2 $C_{12}H_{18}P$]. − $C_{42}H_{59}P_3Si$ (684.9): calcd. C 73.65, H 8.68; found C 73.80, H 8.82.

Synthesis of Complex 9: A solution of ligand **8** (0.27 g, 0.39 mmol) in toluene (5 mL) was added to a solution of [W(CO)$_5$(THF)] (0.31 g, 0.78 mmol) in toluene (10mL). The resulting mixture was then heated at 110 °C for 20 hours. After cooling to room temperature, celite (0.5 g) was added and the mixture was evaporated to dryness yielding a brown powder which was purified by chromatography over silica gel. A first fraction, eluted with hexane, yielded traces of $W(CO)_6$. A second fraction, eluted with a mixture of hexane/toluene (80:20), yielded complex **9** as a red oil after evaporation of solvents (0.20 g, 56% based on the ligand). Microcrystals suitable for an X-ray analysis study were obtained by slow diffusion of methanol in a toluene solution of the complex. − ^1H NMR ($CDCl_3$): δ = 0.77−1.18 (m, 18 H, 6 C*H*$_3$−CH$_2$), 1.71−1.84 (m, 12 H, 6 CH$_3$−C*H*$_2$), 2.08 (s, 9 H, Me−C-3), 2.47 (t, ^3J = 7.9 Hz, 6 H, C*H*$_2$−C-5), 2.80−2.99 (m, 6 H, CH$_2$−C-6), 7.17−7.31 (m, 5

H, C_6H_5), 7.80−7.84 (m, 3 H, H_4). − ^{13}C NMR ($CDCl_3$): δ = 15.1 (s, 2 CH_3CH_2), 25.5 (s, *Me*−C-3), 27.4 (d, ^3J = 6.0 Hz, CH_2−CH_2−C-5), 29.9 (d, ^4J = 7.5 Hz, CH_2−CH_2−C6), 25.3 (d, ^2J = 23.5 Hz, CH_2−C-6), 37.3 (d, ^2J = 3.0 Hz, CH_2−C-5), 128.6−129.7 (C_6H_5), 131.0 (d, ^3J = 27.0 Hz, C-4), 136.7 (s, Cq of C_6H_5), 148.4 (d, ^2J = 9.0 Hz, C-5), 149.7 (d, ^2J = 15.0 Hz, C-3), 149.7 (signal of C-2 which is partially masked), 157.3 (s, C-6), 210.4 (dt, ^2J = 29.0 Hz, ^2J = 7.0 Hz, CO). − ^{31}P NMR ($CDCl_3$): δ = 213.1 (s). − IR (KBr): ν (CO) = 1950, 1875 cm^{-1}. − $C_{45}H_{59}0_3P_3SiW$ (952.8): calcd. C 56.73, H 6.24; found C 56.70, H 6.20.

Synthesis of Triyne 10: Tris(bromodimethylsilyl)methane was synthesized following a reported procedure.[15] This compound (4.55g, 10.6 mmol) was added to three equivalents of MeCCLi (1.47g, 32.0 mmol) suspended in THF (60 mL) cooled to −78 °C. The mixture was stirred at −78 °C for 30 minutes and at room temperature for an additional two hours. After evaporation of the volatiles, the mixture was purified by column chromatography on silica gel with hexanes as eluent. The title compound was obtained as a viscous oil in 55% yield (nonoptimized). − ^{1}H NMR ($CDCl_3$): δ = −0.50 (s, 1 H, CH), 0.34 (s, 18 H, 3 $SiMe_2$), 1.87 (s, 9 H, Me). − ^{13}C NMR ($CDCl_3$): δ = 3.1 (s, $SiMe_2$), 3.2 (s, CH), 5.6 (s, C−Me), 86.4 (s, C−Si), 104.3 (s, *C*−Me). − MS (CI, NH_3); *m*/*z* (%): 306 (10) [M + 1], 291 (15) [M − CH_3+1].

Synthesis of Ligand 12: A solution of diazaphosphinine **1** (0.53 g, 2.5 mmol) and ligand **10** (0.17 g, 0.56 mmol) in toluene (20 mL) was heated at 100 °C for 30 hours. After this period a ^{31}P NMR control indicated the complete formation of intermediate **11**. Trimethylsilylacetylene (0.99 g, 10 mmol) was then added and the resulting reaction mixture was heated at 90 °C for 5 hours. After cooling the flask to room temperature, celite (0.5 g) was added and the volatiles were evaporated. The resulting brown powder was then purified by column chromatography on silica gel. A first fraction, eluted with hexane, yielded the 2,5-bis(trimethylsilyl)phosphinine as by-product. A second fraction, eluted with a mixture of hexane/CH_2Cl_2 (90:10), yielded ligand **12**. After evaporation of solvents, **12** was recovered as a white solid (0.32 g, 75% based on the silane). − ^{1}H NMR ($CDCl_3$): δ = 0.06 (br. s, 1 H, CH), 0.30 (s, 18 H, $SiMe_2$), 0.50 (d, ^4J = 2.0 Hz, 27 H, $SiMe_3$), 2.36 (s, 9 H, Me of phosphinine), 6.93 (d, ^3J = 8.1 Hz, 3 H, H-4), 7.78 (dd, ^3J = 8.1 Hz, 3 H, H-5). − ^{13}C NMR ($CDCl_3$): δ = 0.8 (d, ^3J = 5.5 Hz, $SiMe_3$), 3.0 (br. s, CH), 5.0 (d, ^3J = 16.5 Hz, $SiMe_2$), 27.1 (s, Me of phosphinine), 130.2 (d, ^3J = 25.0 Hz, C-4), 138.7 (d, ^2J = 11.5 Hz, C-5), 149.3 (d, ^2J = 12.5 Hz, C-3), 166.0 (d, ^1J = 83.5 Hz, C-2), 168.9 (d, ^1J = 89.0 Hz, C-6). − ^{31}P NMR ($CDCl_3$): δ = 263.0 (s). − MS ; *m*/*z* (%): 731 (8) [M], 549 (100) [M − phosphinine]. − $C_{34}H_{61}P_3Si_6$ (731.3): calcd. C 55.84, H 8.41; found C 55.69, H 8.38.

Synthesis of Ligand 13: A solution of diazaphosphinine **1** (0.69 g, 3.25 mmol) and ligand **10** (0.22 g, 0.72 mmol) in toluene (20 mL) was heated at 100 °C for 30 hours. After this period a ^{31}P NMR control indicated the complete formation of intermediate **11**. 4-Octyne (1.20 g, 11 mmol) was then added and the resulting reaction mixture was heated at 120 °C for 13 days. After cooling the flask to room temperature, celite (0.5 g) was added and the volatiles were evaporated. The resulting brown powder was then purified by column chromatography on silica gel. A first fraction, eluted with hexane, yielded the 2,3,4,5-tetrapropylphosphinine as by-product. A second fraction, eluted with a mixture of hexane/toluene (50:50), yielded ligand **13**. After evaporation of solvents, **13** was recovered as a viscous oil (0.18 g, 35% based on the silane). − ^{1}H NMR ($CDCl_3$): δ = 0.08 (br. s, 1 H, CH), 0.45 (d, ^4J = 2.0 Hz, 18 H, $SiMe_2$), 0.95−1.05 (m, 18 H, 6 CH_3−CH_2), 1.56−1.65 (m, 12 H, 6 CH_3−CH_2), 2.35 (s, 9 H, Me of phosphinine), 2.52−2.58 (m, 6 H, CH_2−C-5), 2.72−2.90 (m, 6 H, CH_2−C-6), 6.77 (d, ^4J = 1.3 Hz, 3 H, H-4). − ^{13}C NMR ($CDCl_3$): δ = 3.0 (br. s, CH), 4.7 (d, ^3J = 15.3 Hz, $SiMe_2$), 15.0 (s, Me), 25.3 (s, C-5−CH_2−CH_2−CH_3), 26.5 (s, Me of phosphinine), 27.6 (d, ^3J = 10.0 Hz, C-6−CH_2−CH_2−CH_3), 36.8 (s, CH_2−C-5), 37.6 (d, ^2J = 34.5 Hz, CH_2−C-6), 134.4 (d, ^3J = 20.0 Hz, C-4), 146.5 (d, ^2J = 11.5 Hz, C-5 or C-3), 147.2 (d, ^2J = 14.5 Hz, C-3 or C-5), 166.4 (d, ^1J = 78.0 Hz, C-2 or C-6), 166.8 (d, ^1J = 58.3 Hz, C-6 or C-2). − ^{31}P NMR ($CDCl_3$): δ = 242.6 (s). − MS ; *m*/*z* (%): 767 (8) [M], 573 (100) [M − phosphinine]. − $C_{43}H_{73}P_3Si_3$ (767.2): calcd. C 67.32, H 9.59; found C 67.45, H 9.70.

Synthesis of Complex 14: A solution of ligand **13** (0.15 g, 0.20 mmol) in toluene (5 mL) was added to a solution of [$W(CO)_5$(THF)] (0.16 g, 0.40 mmol) in toluene (10mL). The resulting mixture was then heated at 110 °C for 20 hours. After completion, celite (0.5 g) was added and the mixture was evaporated to dryness,yielding a red-brown powder, which was purified by chromatography over silica gel. A first fraction, eluted with hexane, yielded traces of $W(CO)_6$. A second fraction, eluted with a mixture of hexane/toluene (80:20), yielded complex **14** as a red oil after evaporation of solvents (0.11 g, 56% based on **13**). This oil turned into a red solid after trituration in methanol. − ^{1}H NMR ($CDCl_3$): δ = 0.00 (s, 9 H, CH_3 of $SiMe_2$), 0.50 (s, 9 H, CH_3 of $SiMe_2$), 0.86 (t, ^3J = 7.3 Hz, 9 H, 3 CH_3−CH_2), 0.97 (t, ^3J = 7.3 Hz, 9 H, 3 CH_3−CH_2), 1.40 (m, 6 H, 3 CH_3−CH_2−CH_2), 1.63 (m, 6 H, 3

Table 1. Crystal data of **9** and **14**

Compound	**9**	**14**
Molecular formula	$C_{45}H_{59}O_3P_3SiW$	$C_{46}H_{73}O_3P_3Si_3W$
Molecular weight	952.77	1035.07
Crystal habit	red cube	red cube
Crystal dimensions(mm)	0.22×0.22×0.22	0.18×0.18×0.18
Crystal system	Tetragonal	Monoclinic
Space group	P-42_1c	$P2_1/n$
a (Å)	18.2250(2)	13.389(5)
b (Å)	18.2250(2)	25.355(5)
c (Å)	26.4180(4)	14.643(5)
β (°)		91.190(5)
V (Å^3)	8774.75(19)	4970(3)
Z	8	4
d (g.cm^{-3})	1.442	1.383
*F*000	3888	2136
μ (cm^{-1})	2.807	2.530
T (K)	148.0(1)	150.0(1)
Maximum θ	26.36	30.03
hkl ranges	0 22; 0 16; 0 32	−14 18; −35 34; −20 17
Reflections measured	4882	32691
Independent reflections	4882	13911
R_{int}	0.0000	0.0791
Reflections used	4487	11094
Criterion	>2sigma(*I*)	>2sigma(*I*)
Refinement type	Fsqd	Fsqd
Hydrogen atoms	mixed	mixed
Parameters refined	487	524
Reflections / parameter	9	21
*wR*2	0.1026	0.0776
*R*1	0.0379	0.0295
Flack′s parameter	0.422(10)	not applicable
Weighs *a*, *b*[a]	0.0633; 17.81	0.0339; 0.1547
GoF	1.054	1.022
difference peak/hole (eÅ^{-3})	1.302(0.122)/ −0.718(0.122)	0.945(0.147)/ −1.531(0.147)

[a] $w = 1/[\sigma^2(F_o^2)+(aP)^2+ bP]$, where $P = (F_o^2+2F_c^2)/3$; *R*1 is the conventional *R* factor as defined in SHELXL-97.[16]

$CH_3-CH_2-CH_2$), 2.41 (s, 9 H, Me of phosphinine), 2.46−3.40 (m, 12 H, 6 $CH_3-CH_2-CH_2$), 6.87 (br. s, 3 H, H-4), 6.03 (q, ^4J = 8.5 Hz, 1 H, CH). − ^{13}C NMR ($CDCl_3$): δ = 1.4 (q, ^3J = 15.6 Hz, *C*H), 4.7 (s, $SiMe_2$), 5.0 (s, $SiMe_2$), 14.1 (s, CH_3), 14.9 (s, CH_3), 25.5 (s, C-5−$CH_2-CH_2-CH_3$), 27.2 (s, Me of phosphinine), 27.6 (s, C-6−$CH_2-CH_2-CH_3$), 35.3 (AXY_2, Σ *J* = 16.0 Hz, CH_2−C-6), 38.1 (s, *C*H_2−C-5), 132.5 (AXY_2, Σ *J* = 28.7 Hz, C-4), 149.2 (AXY_2, Σ *J* = 19.3 Hz, C-5 or C-3), 149.7 (AXY_2, Σ *J* = 10.3 Hz, C-3 or C-5), 160.0 (AXY_2, Σ *J* = 30.8 Hz, C-6), 162.0 (s, C-2), 213.7 (dt, ^2J = 21.2 Hz, ^2J = 9.2 Hz, CO). − ^{31}P NMR ($CDCl_3$): δ = 211.6 (^1J = 227.7 Hz). − IR (KBr): ν (CO) = 1950, 1875 cm^{-1}. − MS; *m*/*z* (%): 1007 (8) [M − CO], 979 (90) [M − 2 CO], 951 (25) [M − 3 CO], 767 (20) [M − $W(CO)_3$]. − $C_{46}H_{73}O_3P_3Si_3W$ (1035.1): calcd. C 53.38, H 7.11; found C 53.42, H 7.18.

X-Ray Structural Analysis: For compounds **9** and **14**, data were collected on a KappaCCD diffractometer. Mo-K_α (λ = 0.71073 Å) radiation and a graphite monochromator were used in all cases. The crystal structures were solved and refined using SIR-97[16a] and refined with SHELXL-97.[16b] Other experimental details are given in Table 1. The ORTEP drawings reported in this article were generated using the winGX program created by Professor L. J. Farrugia (ORTEP III for Windows, available on the internet as a freeware at louis@chem.gla.ac.uk, Department of Chemistry at the University of Glasgow).

Crystallographic Data (excluding structure factors) for the structures reported have been deposited with the Cambridge Data Centre as supplementary publication nos. CCDC-142208 (**9**) and CCDC-142209 (**14**). Copies of the data can be obtained free of charge on application to CCDC, 12 Union Road, Cambridge CB2 1EZ, UK [Fax: (internat.) + 44-1223/336-033; E-mail: deposit@ccdc.cam.ac.uk].

Acknowledgments

The authors thank the *CNRS* and the *Ecole Polytechnique* for support of this work.

[1] [1a] D. W. Meek, in *Homogeneous Catalysis with Metal Phosphine Complexes* (Ed.: L. H. Pignolet), Plenum Press, New York, **1983**. − [1b] C. Bianchini, C. Mealli, A. Meli, M. Sabat, in *Stereochemistry of Organometallic and Inorganic Compounds* (Ed.: I. Bernal), Elsevier, Amsterdam, **1986**; *Vol. 1*, p 146. − [1c] C. Bianchini, *Comments Inorg. Chem.* **1988**, *8*, 27−43.

[2] Leading references in these different areas are quoted in the following reference: C. Bianchini, A. Meli, M. Peruzzini, F. Vizza, *Organometallics* **1990**, *9*, 226−240.

[3] C. Bianchini, P. Barbaro, A. Meli, M. Peruzzini, A. Vacca, F. Vizza, *Organometallics* **1993**, *12*, 2505−2514.

[4] [4a] C. Bianchini, D. Fabbri, S. Gladiali, A. Meli, W. Pohl, F. Vizza, *Organometallics* **1996**, *15*, 4604−4611. − [4b] C. Bianchini, A. Meli, *Acc. Chem. Res.* **1998**, *31*, 109−116.

[5] F. A. Cotton, B. Hong, in *Progress in Inorganic Chemistry* (Ed.: S. J. Lippard), John Wiley and Sons, Inc., **1992**; *Vol. 40*, p 180.

[6] [6a] C. Elschenbroich, M. Nowotny, A. Behrendt, W. Massa, S. Wocadlo, *Angew. Chem. Int. Ed. Engl.* **1992**, *104*, 1343−1345. − [6b] N. Mézailles, N. Avarvari, L. Ricard, F. Mathey, P. Le Floch, *Inorg. Chem.* **1998**, *37*, 5313−5316. − [6c] P. Rosa, L. Ricard, P. Le Floch, F. Mathey, G. Sini, O. Eisenstein, *Inorg. Chem.* **1998**, *37*, 3154−3158.

[7] F. Mathey, P. Le Floch, *Chem. Ber.* **1996**, *129*, 263−268.

[8] N. Mézailles, N. Avarvari, N. Maigrot, L. Ricard, F. Mathey, P. Le Floch, L. Cataldo, T. Berclaz, M. Geoffroy, *Angew. Chem. Int. Ed.* **1999**, *38*, 3194−3197.

[9] [9a] A. Jouaiti, M. Geoffroy, G. Bernardinelli, *Tetrahedron Lett.* **1992**, *33*, 5071−5074. − [9b] A. Jouaiti, M. Geoffroy, G. Terron, G. Bernardinelli, *J. Am. Chem. Soc.* **1995**, *117*, 2251−2258. − [9c] M. van de Sluis, V. Beverwijk, A. Termaten, E. Gavrilova, F. Bickelhaupt, H. Kooijman, N. Veldman, *Organometallics* **1997**, *16*, 1144−152.

[10] [10a] N. Avarvari, P. Le Floch, L. Ricard, F. Mathey, *Organometallics* **1997**, *16*, 4089−4098. − [10b] N. Avarvari, P. Rosa, F. Mathey, P. Le Floch, *J. Organomet. Chem.* **1998**, *567*, 151−155.

[11] N. Avarvari, P. Le Floch, F. Mathey, *J. Am. Chem. Soc.* **1996**, *118*, 11978−11979.

[12] [12a] N. Avarvari, N. Mézailles, L. Ricard, P. le Floch, F. Mathey, *Science* **1998**, *280*, 1587−1589. − [12b] N. Avarvari, N. Maigrot, L. Ricard, F. Mathey, P. Le Floch, *Chem. Eur. J.* **1999**, *5*, 2109−2118.

[13] [13a] F. A. Cotton, C. S. Kraihanzel, *J. Am. Chem. Soc.* **1962**, *84*, 4432. − [13b] J. Chatt, H. R. Watson, *J. Chem. Soc.* **1961**, 4980.

[14] P. Le Floch, L. Ricard, F. Mathey, *Polyhedron* **1990**, *9*, 991.

[15] L. H. Gade, C. Becker, *Inorg. Chem.* **1993**, *32*, 2308.

[16] [16a] SIR97, an integrated package of computer programs for the solution and refinement of crystal structures using single crystal data: Altomare, A.; Burla, M. C.; Camalli, M.; Cascarano, G.; Giacovazzo, C.; Guagliardi, A.; Moliterni, A. G. G.; Polidori, G.; Spagna, R. − [16b] G. M. Sheldrick, *SHELXL-97*, Universität Göttingen, Germany, **1997**.

Received April 3, 2000
[I00127]

Multinuclear NMR Study and Crystal Structure of *trans*-[$PtCl_2(PHtBu_2)_2$]

Roberto Giannandrea,[a] Piero Mastrorilli,*[a] Mariangela Palma,[a] Francesco Paolo Fanizzi,[b] Ulli Englert,[c] and Cosimo Francesco Nobile[a]

Keywords: Platinum / Phosphanes / Bridging ligands / Force field calculations / Conformational equilibrium

trans-[$PtCl_2(PHtBu_2)_2$] **(1)** was thoroughly characterised by ^1H, $^{31}P\{^1H\}$ and $^{195}Pt\{^1H\}$ NMR spectroscopy. Two rotational conformers were found to be stable in solution at room temperature. Force field calculations confirmed that these two conformers are very similar in energy. They co-crystallise in the tetragonal space group *P*4bar as revealed by X-ray diffraction studies. The dynamics of *trans*-[$PtCl_2(PHtBu_2)_2$] is here reported together with spectroscopic evidence of a phosphido-bridged reduction product.

Introduction

As part of our continuing interest in the chemistry of low-valent transition metal complexes, we recently became interested in the coordination chemistry of metals with secondary bulky phosphanes, such as $PHtBu_2$, $PHCy_2$ and $PHPh_2$, in phosphorus-bridged binuclear systems.[1]

With the aim of investigating the behaviour of platinum(II) complexes towards alkali metal-promoted reduction we have synthesised *trans*-[$PtCl_2(PHtBu_2)_2$] (**1**) and reacted it with metallic sodium.

Results and Discussion

trans-[$PtCl_2(PHtBu_2)_2$] **(1)** was first prepared by Shaw et al. who extracted the main NMR features of the $[AMX_{18}]_2$ system from its ^1H spectrum.[2] Moreover, it was noticed that **1** exists in solution as a mixture of two conformational isomers even at room temperature[2] (Figure 1).

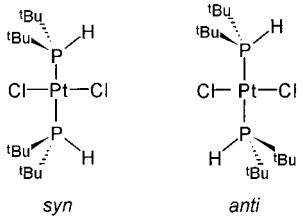


Figure 1

More recently, Goel and Ogini[3] claimed a new synthesis of **1** (as a white solid) from the reaction of K_2PtCl_4 with $PtBu_3$ in a 1:3 ratio in refluxing DMF. Contrary to Shaw's findings they observed only a broad peak (with satellites) in the $^{31}P\{^1H\}$ NMR spectrum at ambient temperature (δ = 56.8, CH_2Cl_2) which was resolved into two peaks at 183 K.

By reaction of $PtCl_2(PhCN)_2$ with $PHtBu_2$ in a Pt:P ratio of 1:2 we have obtained **1** as a pale yellow solid. Its ^1H NMR spectrum is consistent with that reported by Shaw[2] and shows two overlapped spin systems of the $[AMX_{18}]_2$ type, where A is the phosphorus atom, M is the hydrogen directly bound to the phosphorus, X_{18} are the *tert*-butyl hydrogens. Figure 2 shows the M part of this spectrum. The analysis of such a system, developed by Mann,[4] allowed us to obtain the spectroscopic features reported in Table 1 along with ^1H, ^{31}P, ^{13}C and ^{195}Pt chemical shifts.

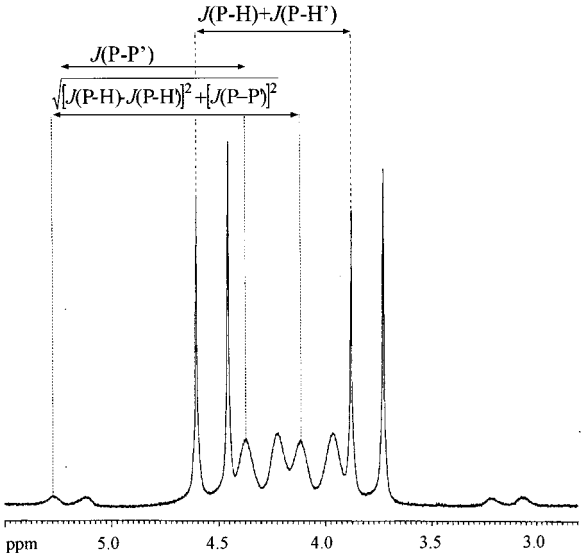


Figure 2. P-H region of the ^1H NMR spectrum of *syn* and *anti* conformers of complex **1** ($CDCl_3$, 295 K); see ref.[4] for the analysis of the $[AMX_{18}]_2$ spin system

[a] Centro C.N.R. M.I.S.O. and Istituto di Chimica del Politecnico di Bari,
via E. Orabona 4, 70125 Bari, Italy
[b] Dipartimento Farmaco-Chimico, Università di Bari,
via E. Orabona 4, 70125 Bari, Italy
and
Consortium C.A.R.S.O. Cancer Research Center,
70010 Valenzano − Bari, Italy
[c] Institut für Anorganische Chemie der RWTH,
Prof.-Pirlet-Str. 1, 52074 Aachen, Germany

 © WILEY-VCH Verlag GmbH, D-69451 Weinheim, 2000 1434−1948/00/1212−2573 $ 17.50+.50/0

Table 1. NMR spectroscopic data of complex 1 ($CDCl_3$, 295 K)

	syn isomer	*anti* isomer
δ(*t*Bu)	1.49	1.48
δ(**H**−P)	4.20	4.05
^1J(P−H)	362 Hz	368 Hz
^3J(P−H′)	1.5 Hz	−5 Hz
^2J(P−P′)	450 Hz	450 Hz
^3J(P−*t*Bu)	13 Hz	11 Hz
^5J(P−*t*Bu′)	1.6 Hz	1.7 Hz
δ(**P**−H)	49.4	56.5
^1J(P−Pt)	2429 Hz	2421 Hz
δ(**C**H_3)[a]	31.3	31.3
δ(**C**−P)[a]	34.9	34.9
^1J(P−C)[a]	24 Hz	24 Hz
^2J(P−C)[a]	12 Hz	12 Hz
δ(Pt)	−3738	−3767

[a] Solvent C_6D_6, 298 K.

The $^{31}P\{^1H\}$ NMR spectrum of **1** recorded in $CDCl_3$ at ambient temperature shows the presence of two signals with satellites at δ = 49.4 and 56.5 ascribable to the *syn* and *anti* conformers of **1**. Their *anti*/*syn* ratio, as assessed by the integrals in the ^{31}P NMR spectrum, was found to be equal to 1.2.

The $^{31}P\{^1H\}$ dynamic NMR spectrum shows the expected broadening of the signals with increasing temperature (Figure 3). A line-shape analysis[5] allowed an estimation of a lower limit of ΔG for the interconversion of the conformers equal to 18 ± 2 kcal/mol.

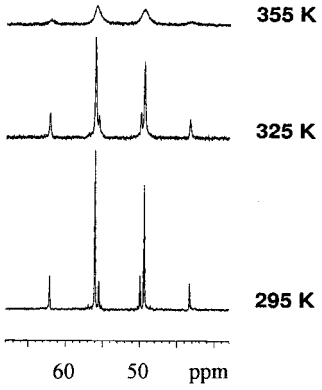


Figure 3. Variable temperature $^{31}P\{^1H\}$ NMR spectra of complex **1** ([D_8]toluene)

The $^{195}Pt\{^1H\}$ spectrum (Figure 4) shows the expected two triplets with Pt-P direct couplings of 2429 Hz (*syn* isomer) and 2421 Hz (*anti* isomer).

The resonance of the methyl carbons in the $^{13}C\{^1H\}$ NMR spectrum was found as a doublet ($^2J_{P-C}$ = 12 Hz) centred at δ = 31.3. The quaternary carbons of the coordinated phosphanes give a pseudotriplet arising from the AXX′ system (A = ^{13}C; X,X′ = ^{31}P) when $J_{XX'} >> J_{AX}$.[6] The chemical shift is δ = 34.9, and the value of $|^1J_{P-C} + {}^3J_{P-C}|$ directly obtainable from the spectrum is 23.4 Hz.

In order to gain insight into the structure of the two (or at least of the most stable) conformers we probed the energy hypersurface with respect to the torsional position of the phosphane ligands. Molecular mechanics calculations were

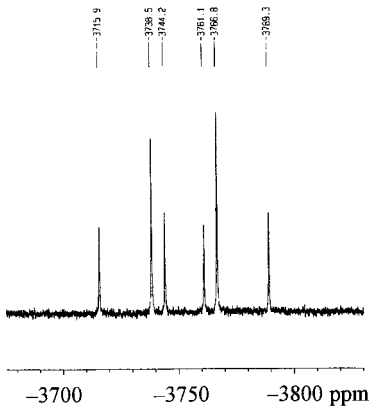


Figure 4. $^{195}Pt\{^1H\}$ NMR spectrum of complex **1** ($CDCl_3$, 295 K)

performed with an augmented MM2[7] force field. The torsion angles between the Cl−Pt and the P−H bonds in the P*H*$t$$Bu_2$ ligands were independently varied in steps of three degrees, and for each step all other intramolecular degrees of freedom were allowed to relax. The energy profile and four selected conformers are shown in Figure 5. The two geometries with both PH groups in the coordination plane of the metal centre, i.e. the *anti* (A) and the *syn* isomer (D), have almost the same energy, whereas the geometries with one (B) or two (C) P−H bonds perpendicular to the plane of coordination are energetically less favourable.

In addition to the force field calculations a crystallographic analysis was undertaken. X-ray diffraction studies were carried out on three single crystals of **1**. A ^1H NMR analysis of these crystals redissolved in $CDCl_3$ showed the immediate presence of both conformers.

The X-ray diffraction study revealed that **1** crystallises in the space group $P\bar{4}$ with the metal atom on the twofold axis (Wyckoff position 2*g*) and a fractional *z* coordinate of approximately 0.25**.** Due to this position of the most prom-

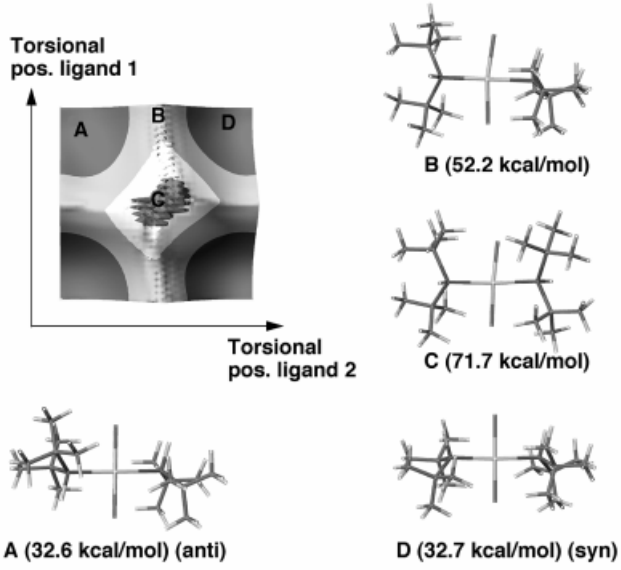


Figure 5. Profile of the energy hypersurface of **1** as a function of the torsional orientation of the phosphane ligands and the geometry of four selected conformers

inent scatterer, the intensity statistics resemble that of an *I* centred lattice: over 95% of the scattered intensity may be attributed to reflections of the type *hkl*, $h + k + l = 2n$.

Location of the metal, chlorine, and phosphorus atoms was straightforward. After refinement of this initial model a Fourier-difference synthesis showed electron density above and below the Pt coordination plane attributable to the carbon atoms of the phosphane ligands. Two alternative strategies were followed to deal with the electron density above and below this plane:

a) Tentative refinement as carbon positions resulted in highly anisotropic displacement parameters. Rigid bond and distance restraints had to be applied to ensure physically and chemically reasonable refinement results. In view of the site symmetry of the Pt central atom this procedure necessarily leads to an *anti* geometry although the NMR spectrum suggested the presence of both conformers in the crystal. Furthermore, the resulting angles around phosphorus were much larger than expected and in conflict with both the above mentioned force-field results and comparable structures of the $PHtBu_2$ ligand[8] drawn from the CSD database.[9]

b) It was observed that the electron density closely matched the situation depicted in Figure 6 and could be explained by superposition of *anti* and *syn* (shaded) conformers, corresponding to geometries A and D, respectively, in Figure 5.

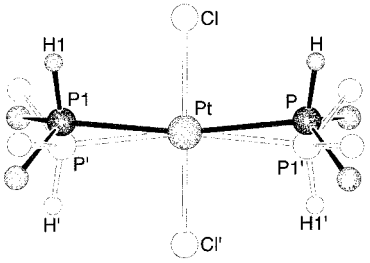


Figure 6. SCHAKAL[12] representation of the alternative orientations of **1** in the crystal; all methyl groups have been omitted, primed atoms are related to unprimed ones by the symmetry operation $1 - x, -y, z$; a possible *syn* conformer has been emphasized by shading

The $PHtBu_2$ ligand geometry was extracted from the molecular mechanics model and introduced as a rigid group in two alternative orientations. In addition to the parameters regarding Pt, Cl, and P only two overall isotropic displacement parameters for the methyl C and the phosphorus-bonded carbon atoms were refined. Despite the much smaller number of variables this second approach gave better convergence results. Figure 7 shows a PLATON view of the

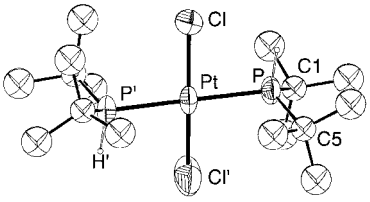


Figure 7. PLATON[13] view of the *anti* conformer of **1** with selected bond lengths [Å] and angles [deg.]: Pt−Cl 2.266(5), Pt−P 2.317(11), Pt−P−C1 112.1(7), Pt−P−C5 113.9(7), C1−P−C5 117.4

anti conformer and lists selected interatomic angles and distances.

trans-[$PtCl_2(PHtBu_2)_2$] was reacted with excess sodium metal to obtain a complex mixture of compounds as revealed by ^{31}P NMR spectroscopy. Among the signals present in the ^{31}P NMR spectrum of the reaction solution a triplet centred at $\delta = 278.7$ with satellites ($J_{P-P} = 43$ Hz; $J_{P-Pt} = 2588$ Hz) was clearly evident in the low field region (Figure 8). The values of the chemical shift and coupling constants are typical for *tert*-butyl phosphides bridging two platinum(I) atoms linked by a metal−metal bond.[7a] The presence, in the region of terminally bonded phosphanes, of a sharp triplet centred at $\delta = 62.0$, with a coupling constant as high as 43 Hz, strongly suggests the formation of the binuclear phosphido-bridged platinum(I) complex [Pt(μ-$PtBu_2$)($PHtBu_2$)]$_2$ **(2)**.

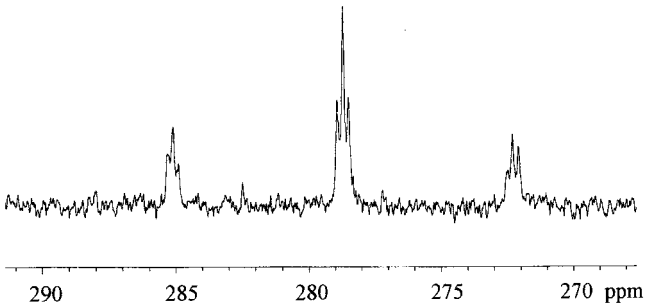


Figure 8. Phosphide resonance in the $^{31}P\{^1H\}$ NMR spectrum of complex **2** ([D_8]toluene, 295 K)

The synthesis of **2** has already been reported by Leoni, Pasquali et al. by hydride abstraction from [Pt(μ-$PtBu_2$)(H)($PtBu_2H$)]$_2$ but no NMR spectroscopic data were reported, due to its low solubility.[8a] Prolonged reaction times of **1** with sodium led to decomposition into free phosphane, NaCl and platinum metal.

Experimental Section

General: All manipulations were carried out under a pure dinitrogen atmosphere, using freshly distilled and oxygen-free solvents. Di-*tert*-butylphosphane was purchased from Fluka and used as received.

Infrared spectra were recorded on a Perkin−Elmer 883 spectrometer. Elemental analyses were carried out by using a Carlo Erba model EA 1108 elemental analyser.

NMR spectra were recorded on a Bruker Avance DRX500 spectrometer; chemical shifts are referenced to Me_4Si (^1H and ^{13}C), 85% H_3PO_4 (^{31}P), and H_2PtCl_6 (^{195}Pt).

***trans*-Bis(di-*tert*-butylphosphane)dichloroplatinum(II) (1):** A suspension of [$PtCl_2(PhCN)_2$][10] (1.3 g, 2.8 mmol) and di-*tert*-butylphosphane (0.88 g, 6.0 mmol) in toluene (20 cm^3) was stirred at 70 °C. After a few minutes a clear yellow solution was obtained, which was cooled to room temperature and concentrated in vacuo. It was then filtered and washed three times with petroleum ether and dried in vacuo (1.3 g, 85% yield). − IR (nujol mull): $\tilde{\nu}_{max} = 2351$m (P−H), 1365vs, 1181vs, 1023s, 901s, 813vs, 468s, 333vs (Pt−Cl) cm^{-1}. − UV/Vis (CH_2Cl_2, 1.61×10^{-4} mol dm^{-3}): λ_{max} (ε/dm^3 mol^{-1} cm^{-1}) = 240.0 (6180), 267 (8260) and 301.0 (sh) nm.

Crystallography

Crystals of compound **1** were obtained by crystallisation from toluene. Intensity data were collected with Mo-K_α radiation (λ = 0.71073 Å, graphite monochromator) on an ENRAF-Nonius CAD4 diffractometer at 243 K on a crystal of approximate dimensions 0.13 × 0.13 × 0.13 mm.

Crystal data: a = 8.906(1), c = 14.337(4) Å; V = 1137.2(4) Å^3, Z = 2, d(calcd.) = 1.63 g·cm^{-3}, μ = 6.605 mm^{-1}, F(000) = 552. 3977 Reflections were collected with the $\omega-2\theta$ scan method in the range $3.2 < \theta < 25.1$ deg. After merging symmetry equivalent data [R(int) = 0.062], 2032 independent reflections remained for structure solution by direct methods.[11] The final structure model was based on rigid-group refinement of the force field optimised PHtBu$_2$ ligand in two alternative orientations with full-matrix least-squares on F^2.[10] Convergence was reached for 2032 reflections and 50 variables at agreement factors of $wR2$ = 0.0997 (all data), $R1$ = 0.0431 [observations with $I > 2\sigma(I)$]. Max. and min. from a final Fourier map were 1.506 and −0.461 e·Å^{-3}.

Crystallographic data (excluding structure factors) for the structure reported in this paper have been deposited with the Cambridge Crystallographic Data Centre as supplementary publication no. CCDC-141698. Copies of the data can be obtained free of charge on application to The Director, CCDC 12 Union Road, Cambridge CB2 1EZ, U.K. [Fax: (internat.) +44-1223/336-033; E-mail: deposit@ccdc.cam.ac.uk].

Reduction of 1 with Sodium: A suspension of *trans*-[PtCl$_2$(PHtBu$_2$)$_2$] (0.5 g, 0.9 mmol) and sodium sand (0.3 g, 13 mmol) in toluene (10 cm^3) was vigorously stirred at room temperature until a dark green suspension was obtained (about 10 h). Unreacted metallic sodium, NaCl and small amount of platinum metal were filtered off and the solution concentrated in vacuo and used for ^{31}P NMR analysis. The ^{31}P{^{1}H} NMR spectrum of the obtained orange solution showed two triplets with satellites [^{31}P{^{1}H} NMR ([D$_8$]toluene): δ = 62.0 (t, J_{P-P} = 43 Hz, J_{P-Pt} = 4775 Hz, P$_t$), 278.7 (t, J_{P-P} = 43 Hz, J_{P-Pt}= 2588 Hz, P$_\mu$), along with less-intense signals ascribable to uncharacterised species.

[1] [1a] R. Giannandrea, P. Mastrorilli, C. F. Nobile, U. Englert, *J. Chem. Soc., Dalton Trans.* **1997**, 1355. – [1b] R. Giannandrea, P. Mastrorilli, C.F. Nobile, *Inorg. Chim. Acta* **1999**, 116.

[2] A. Bright, B. E. Mann, C. Masters, B. L. Shaw, R. M. Slade, R. E.Steinbank, *J. Chem. Soc. A* **1971**, 1826.

[3] R. G. Goel, W. O. Ogini, *Organometallics* **1982**, *1*, 654.

[4] B. E. Mann, *J. Chem. Soc. A* **1970**, 3050.

[5] J. H. Brown, C. H. Bushweller, *Quantum Chemistry Program Exchange*, Program N. QCPE 633.

[6] P. S. Pregosin, R. K. Kunz, *^{31}P and ^{13}C NMR of Transition Metal Phosphane Complexes, NMR Basic Principles and Progress* (Eds.: P. Diehl, E. Fluck, R. Kosfeld), vol. 16, Springer-Verlag, Berlin, **1979**.

[7] [7a] N. L. Allinger, *J. Am. Chem. Soc.* **1977**, *99*, 8127. – [7b] CAChe Version 4.0 for Power Macintosh, Oxford Molecular: Oxford, United Kingdom, **1996**.

[8] [8a] P. Leoni, G. Chiaradonna, M. Pasquali, F. Marchetti, *Inorg. Chem.* **1999**, *38*, 253–259. – [8b] P. Leoni, M. Pasquali, A. Fortunelli, G. Germano, A. Albinati, *J. Am. Chem. Soc.* **1998**, *120*, 9564. – [8c] P. Leoni, G. Chiaradonna, M. Pasquali, F. Marchetti, A. Fortunelli, G. Germano, *Inorg. Chim. Acta*, **1997**, *264*, 185.

[9] F. H. Allen,; J. E. Davies, J. J. Gallogy, E. M. Mitchell, G. F. Mitchell, J. M Smith, D. G. Watson, *J. Chem. Inf. Comput. Sci.,* **1991**, *31*, 187.

[10] P. Braunstein, R. Bender, J. Jud, *Inorg. Synth*. **1992**, *29*, 341.

[11] G. M. Sheldrick, *SHELX97*, Program for Crystal Structure Determination, University of Göttingen, **1997**.

[12] E. Keller, *SCHAKAL88* − a FORTRAN Program for the Graphic Representation of Molecular and Crystallographic Models, Freiburg, Germany, **1988**.

[13] A. L. Spek, *PLATON-98*, University of Utrecht, The Netherlands, **1998**.

Received April 6, 2000
[I00135]

Structural Patterns and Forms of Aggregation of Metallated Diamido Donor Ligands upon Going from Lithium to Thallium(I)

Christian H. Galka,[a] Dominique J. M. Trösch,[a] Martin Schubart,[b] Lutz H. Gade,*[a] Sanja Radojevic,[c] Ian J. Scowen,[c] and Mary McPartlin[c]

Dedicated to Professor Max Schmidt on the occasion of his 75th birthday

Keywords: Lithium / Amides / Thallium / N ligands / Structure elucidation

Two polyfunctional lithium amides, $[(2\text{-}C_5H_4N)C(CH_3)\{CH_2N(Li)SiMe_2R\}_2]_2$ [R = Me (**3**), *t*Bu (**4**)], have been synthesized and structurally characterized by X-ray crystallography. They were found to have dimeric structures containing ladder-type Li–N arrangements in which the form of aggregation and thus folding of the ladder appears to be influenced by the steric demand of the *N*-bonded silyl groups. Substitution of the lithium ions by thallium(I) was achieved in two steps, yielding the mixed metal amide $[(2\text{-}C_5H_4N)C(CH_3)\{CH_2N(Li)SiMe_3\}\{CH_2N(Tl)SiMe_3\}]_2$ (**5**) and the thallium(I) diamide $[(2\text{-}C_5H_4N)C(CH_3)\{CH_2N(Tl)SiMe_3\}_2]_2$ (**6**). X-ray diffraction studies of both compounds revealed a dimeric ring structure through Li–N links for the former, while the latter is monomeric and only weakly aggregated in the crystal structure through a short, unsupported thallium(I)–thallium(I) contact of 3.500(2) Å.

Introduction

Alkali metal amides derived from polyfunctional amines display molecular structures and forms of aggregation which are largely dictated by the relative orientation of the functional groups joined by the ligand framework.[1,2] This reduction of the structural degrees of freedom may lead to patterns of aggregation which are different from those of simple monofunctional amides.[3,4] More significantly, the integration of several functional groups within a ligand system enables systematic control of their role in the assembly of metallated derivatives. This provides an alternative to the well-established co-aggregation of alkali metal amides and neutral ligands or donor solvents.[1,2]

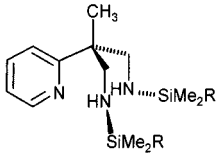
We recently reported the synthesis of a novel dianionic tripodal ligand in which two amido functions are combined with a neutral pyridyl unit.[5,6] This ligand system provides the key to stabilizing a whole range of early transition metal complexes, among these a series of imido complexes.[7,8] Whereas the role of this polydentate ligand in transition metal chemistry is clearly the protection of a large part of the coordination sphere around the metal centre and the masking of potentially accessible coordination sites by the displaceable neutral pyridyl function, the latter may play the part of a "capping" functionality in aggregates of its main group derivatives. While the structures of the group-1 metal amides may be viewed as resulting from primarily ionic interactions between the N-functions and the metal cations,[1] we and others have previously shown that monovalent thallium amides display structures which are markedly different.[9–12]

In this paper we present a systematic study of the forms of aggregation adopted by the lithium amides containing the ligand $[(2\text{-}C_5H_4N)C(CH_3)(CH_2NR)_2]^{2-}$, their thallium analogues and the mixed lithium–thallium species. It will be shown that stepwise replacement of the alkali metal ions by thallium(I) is feasible under appropriate reaction conditions, thus enabling the synthesis of a mixed metal species. The aim will be not only to demonstrate how the ligand enforces the relative arrangement of the metal atoms but also to elucidate the way interactions between the monovalent metal ions themselves determine the structural patterns.

Results and Discussion

Synthesis and Structural Characterization of $[(2\text{-}C_5H_4N)C(CH_3)\{CH_2N(Li)SiMe_2R\}_2]_2$ [R = Me (3), *t*Bu (4)]

Reaction of the pyridyl diamines $(2\text{-}C_5H_4N)C(CH_3)(CH_2NHSiMe_2R)_2$ [R = Me (**1**), *t*Bu (**2**)] with two



R = Me : **1**
*t*Bu : **2**

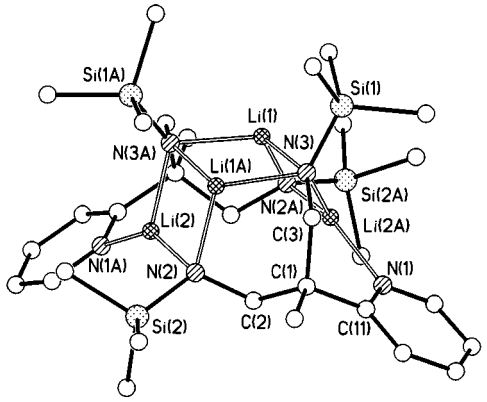
[a] Laboratoire de Chimie Organométallique et de Catalyse (UMR 7513), Institut Le Bel, Université Louis Pasteur, 4, rue Blaise Pascal, 67070 Strasbourg, France
Fax: (internat.) + 33-3/88416045
E-mail: gade@chimie.u-strasbg.fr
[b] Institut für Anorganische Chemie der Universität Würzburg, Am Hubland, 97074 Würzburg, Germany
[c] School of Applied Chemistry, University of North London, Holloway Road, London N7 8DB, UK

 © WILEY-VCH Verlag GmbH, D-69451 Weinheim, 2000 1434–1948/00/1212–2577 $ 17.50+.50/0

molar equivalents of *n*-butyllithium and subsequent workup yields the corresponding lithium amides. Whereas the ^{1}H, ^{13}C, ^{29}Si, and ^{7}Li NMR spectra of **4** in C_6D_6 display structural patterns consistent with a C_s-symmetric monomeric structure, the NMR spectra of **3** indicate aggregation of the lithium amide. The inequivalence of the signals assigned to the methyl groups of the $SiMe_3$ substituents and the patterns of the signals from the protons and carbon nuclei in the ligand framework indicate dimerization of the lithium amide and thus reduction of the local symmetry of the diamidopyridine ligand. This postulated dimerization is supported by a cryoscopic study of **3** in benzene, which also indicated a degree of aggregation lower than two for the analogous compound **4** containing the bulkier ligand periphery. It is assumed that the solution NMR data of the latter are those of the monomeric species. In order to obtain more specific information of the structures of the aggregates, an X-ray crystallographic study of both complexes was clearly essential.

Large colourless single crystals of **3** and **4** were obtained by cooling solutions of the lithiated amines in toluene and pentane, respectively. X-ray structure analyses of both compounds established their dimeric structures in the solid state, which are depicted in Figure 1 and 2 along with selected lengths and inter-bond angles.

The only available crystals of **4** diffracted poorly, leading to relatively high ESDs for all parameters in this structure, but although bond lengths have to be treated with caution, the overall structure is well established and it is interesting to compare the ladder arrangement in the two dimeric molecules. The dilithium diamide units are aggregated in both structures forming four-rung ladders which are terminated by coordination of the neutral pyridyl functions. In compound **3** this lithium amide ladder adopts a boat-type arrangement which is derived from the $(LiN)_4$ cube previously observed in difunctional lithium amides such as $[CH_2\{CH_2N(Li)SiMe_3\}_2]_2$,[13] $[\{t\text{BuN(Li)}\}_2SiMe_2]_2$ [14] and $[\{rac\text{-N}(t\text{Bu})\text{CH(Me)CH(Me)N}t\text{Bu}\}\text{Li}]_2$.[15] Coordination of the neutral donor function has led to opening of one face of the cubic structure to generate the ladder arrangement with crystallographic C_2 symmetry. In **3**, the three Li_2N_2 parallelograms are each planar to within 0.006 Å, and the two symmetry-related outer Li_2N_2 units are folded by 62.3° towards cubic from a possible co-planar arrangement with the central unit. In contrast, in the dimeric ag-



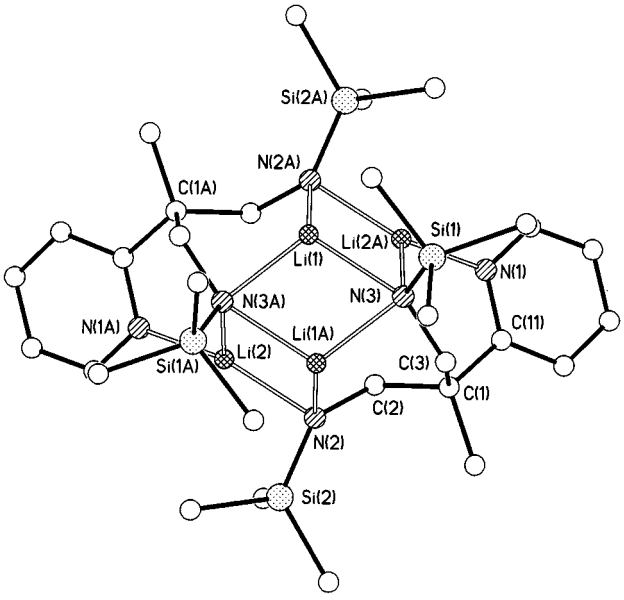


Figure 1. a) (top) Molecular structure of **3** showing the boat-type arrangement of the lithium amide ladder; b) (bottom) the same molecule viewed along the twofold crystallographic axis; selected bond lengths [Å] and angles [°]: Li(1)−N(3) 2.111(8), Li(1)−N(3A) 2.038(8), Li(1)−N(2A) 1.964(8), Li(2)−N(1A) 1.985(8), Li(2)−N(2) 2.023(7), Li(2)−N(3A) 1.984(7); Li(1)−N(3)−Li(1A) 70.9(3), Li(1)−N(3)−Li(2A) 69.9(3), N(3A)−Li(1)−N(3) 109.0(3), N(2A)−Li(1)−N(3A) 111.0(4), N(2A)−Li(1)−N(3) 107.6(4), Li(1A)−N(2)−Li(2) 72.1(3), Li(2A)−N(3)−Li(1A) 106.3(3)

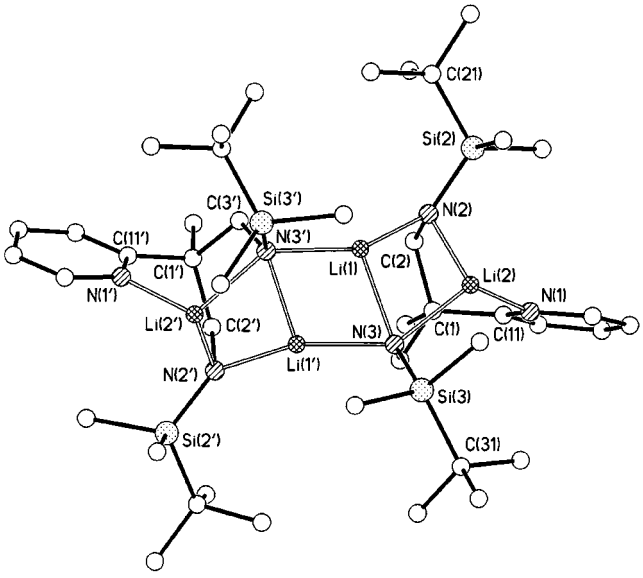


Figure 2. Molecular structure of **4**, which has virtual C_2 symmetry, showing the almost linear arrangement of the lithium amide ladder; mean values of selected bond lengths [Å] and angles [°]: Li(1)−N(2) 1.93(1), Li(1)−N(3) 2.11(1), Li(1)−N(3′) 2.11(2), Li(2)−N(1) 1.85(1), Li(2)−N(2) 1.97(1); N(1′)−Li(1)−N(2) 151(1), N(2)−Li(1)−N(3) 94(1), N(3)−Li(1)−N(3′) 109(1), N(2)−Li(2)−N(3) 105(1), N(3)−Li(2)−N(1) 109(1), N(3)−Li(2)−N(2) 97(1), Li(1)−N(2)−Li(2) 79(1), Li(2)−N(3)−Li(1) 71(1), Li(2)−N(3)−Li(1′) 140 (1)

gregate of compound **4**, unlike the arrangement in **3**, the lithium amide ladder is stepped in the normal way (Figure 2). Six atoms of the Li_4N_4 ladder in **4** show only a small "bowing" from planarity [maximum deviations: Li(1), Li(1′): 0.19 Å and Li(2), Li(2′): −0.19 Å], but the two outer amido nitrogen atoms, N(2) and N(2′), each lie out of this plane by 1.0 Å in the same direction. The mean dihedral angle between the best planes of the inner and each of the outer Li_2N_2 unit, which fold towards each other, is only 20.5° in **4**.

Compound **3** has exact C_2 symmetry, and although compound **4** has only virtual C_2 symmetry, all chemically equivalent bond lengths and angles are equal within experimental error, so the mean values are used (with the atomic symbols for one half of the molecule) in the caption to Figure 2 and in the following discussion. The two lithium atoms in each half of the molecules of **3** and **4** are three-coordinate with Li(1) connected to three amido functions, and Li(2) to two amide groups and one pyridyl group. The amido−N−Li distances of 1.964(8)−2.111(8) Å in **3**, and 1.93(1)−2.11(1) Å in **4**, lie in the expected range for lithium amides.[16] The structure of **4** is readily envisaged as two similar dinuclear monomeric units in which Li(1) and Li(2) are bridged by both amido groups N(2) and N(3) of one ligand, with a third bond from N(3) to a lithium atom, Li(1′), of the second dinuclear unit forming the only bridge between the virtually identical monomer units. In contrast the structure of **3** is intrinsically tetranuclear with the two amido groups of each ligand spanning all four lithium atoms, so that N(2) bridges Li(2) and Li(1A) and N(3) bridges Li(1) and Li(2A) and also forms a bridge to Li(1A) to complete the ladder arrangement. These solid-state structural features are consistent with the observed differences in the NMR spectra of these two compounds, **4** giving a C_s spectrum characteristic of the dinuclear monomer, and **3** giving the less symmetric spectrum characteristic of the Li_4 aggregate. The more linear arrangement in **4** leads to a greater spatial separation of the silyl groups, which are considerably bulkier than those in **3**. It is probable that steric interaction of the peripheral *N*-bound substituents in **4** favours the more open form of aggregation.

Synthesis and Structural Characterization of [(2-C_5H_4N)-$C(CH_3)\{CH_2N(Li)SiMe_3\}\{CH_2N(Tl)SiMe_3\}]_2$ (5) and [(2-C_5H_4N)$C(CH_3)\{CH_2N(Tl)SiMe_3\}_2]_2$ (6)

We have recently established the crystal structures of several polyfunctional thallium(I) amides and found patterns of aggregation which differ markedly from those of the alkali metal derivatives.[11,12] A polyfunctional system containing both neutral and anionic donor atoms has not been studied to date. In view of the results described above, it was of interest to find out how the analogous thallium(I) amides aggregate in the solid.

Reaction of $[(2\text{-}C_5H_4N)C(CH_3)\{CH_2N(Li)SiMe_3\}_2]_2$ (**3**) with two molar equivalents of TlCl (per monomeric unit) in pentane over a period of four days led to the exchange of the lithium ions by Tl^+. After workup, two types of crystalline solid, **5** and **6**, were obtained by cooling the pentane solution of the reaction product(s). Colourless crystals (**5**) were collected along with a deep orange crystalline solid (**6**) and were separated by hand. Whereas the orange product did not contain any lithium and was analyzed as the dithallium(I) diamide $[(2\text{-}C_5H_4N)C(CH_3)\{CH_2N(Tl)SiMe_3\}_2]_2$ (**6**) the colourless product was found to be a mixed lithium−thallium amide and was formulated as $[(2\text{-}C_5H_4N)C(CH_3)\{CH_2N(Li)SiMe_3\}\{CH_2N(Tl)SiMe_3\}]_2$ (**5**). Repeated runs of this metal exchange under the same reaction conditions gave both compounds in every case as described above whereas use of 1,4-dioxane as solvent exclusively led to formation of the dithallium(I) diamide **6**.

In order to establish their patterns of aggregation in the solid single-crystal X-ray structure analyses of both compounds were carried out. Their molecular structures are displayed in Figure 3 and 4 along with selected bond lengths and angles.

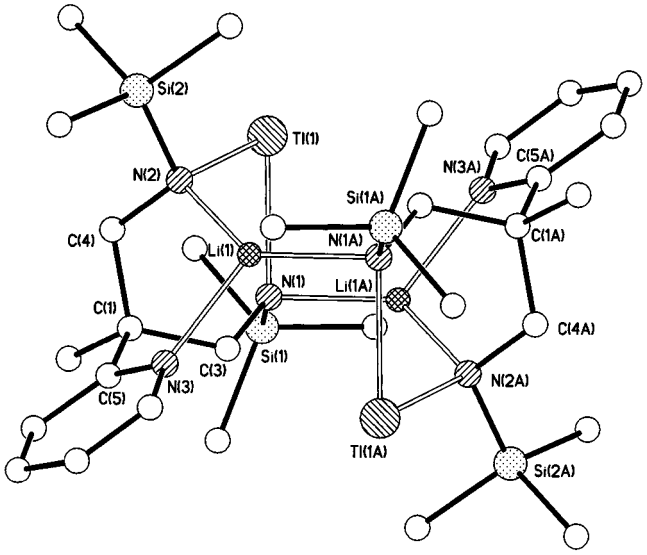


Figure 3. Molecular structure of **5**; selected bond lengths [Å] and angles [°]: Li(1)−N(1A) 2.044(12), Li(1)−N(2) 1.998(12), Li(1)−N(3) 2.102(12), Tl(1)−N(1) 2.483(5), Tl(1)−N(2) 2.455(5); N(2)−Li(1)−N(1A) 135.0(6), N(2)−Li(1)−N(3) 99.3(5), Tl(1)−N(2)−Li(1) 111.4(4), Li(1A)−N(1)−Tl(1) 88.9(3), N(1)−Tl(1)−N(2) 83.29(17), N(3)−Li(1)−N(1A) 123.1(6)

The structural centrepiece of **5** is a $Li_2Tl_2N_4$ macrocycle in which the thallium atoms occupy intramolecular bridging positions and the lithium atoms link the two metallated diamidopyridine ligands. The centre of this cyclic structure coincides with a crystallographic centre of inversion which relates the two halves of the molecule. Whereas the dicoordinate thallium centres adopt the typically exposed positions, the lithium atoms are three-coordinate due to additional bonding of the pyridyl units. The Tl−N distances of Tl(1)−N(2) [2.455(5) Å] and Tl(1)−N(1) [2.483(5) Å] lie in the usual range observed for thallium(I) amides.[10−12,17] The amido-N−Li bond lengths of Li(1)−N(2) [1.998(12) Å] and Li(1)−N(1A) [2.044(12) Å] are significantly shorter than the corresponding value for the pyridyl-N−Li bond of 2.102(12) Å.

In contrast to the dimeric mixed metal amide **5**, the homometallic species $[(2\text{-}C_5H_4N)C(CH_3)\{CH_2N(Tl)$-

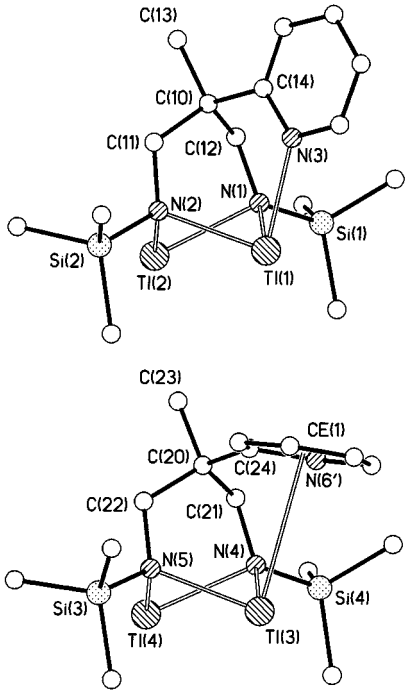


Figure 4. Molecular structure of the monomeric dithallium compound **6**: a) (top) fully ordered monomer unit of **6**, which is one half of the asymmetric unit in the crystal; b) (bottom) second isomer **6′**, present as a 30% component disordered in the second "molecule" of the asymmetric unit of **6**; selected bond lengths [Å] and angles [°]: Tl(1)−N(1) 2.470(14), Tl(1)−N(2) 2.406(15), Tl(1)−N(3) 2.468(15), Tl(2)−N(1) 2.445(13), Tl(2)−N(2) 2.434(14); N(2)−Tl(1)−N(1) 72.4(5), N(3)−Tl(1)−N(1) 80.0(5), N(3)−Tl(1)−N(2) 84.1(5), Tl(1)−N(3)−C(18) 119.2(14), Tl(1)−N(3)−C(14) 121.8(11), Tl(1)−N(2)−Tl(2) 90.4(5), Tl(1)−N(1)−Tl(2) 88.6(4)

$SiMe_3\}_2]_2$ (**6**) is monomeric in the solid state with two independent molecules in the asymmetric unit. The structure of the first molecule, which is fully ordered, is shown in Figure 4 (a); disorder present in the second molecular unit involves two orientations of the pyridyl ring which corresponds to 30% occupancy by a second isomer [Figure 4 (b)], in which rotation of the pyridyl ring gives a π-interaction of this ring with a thallium atom [Tl(3)−centroid: 3.524 Å]. The ordered monomer unit of **6** has one three-coordinate [Tl(1)] and one two-coordinate thallium centre [Tl(2)] and possesses almost exact molecular mirror symmetry, the virtual mirror plane containing the pyridyl ring, the ligand backbone atoms C(10) and C(13) as well as the two thallium atoms Tl(1) and Tl(2). With respect to Tl(1), the ligand adopts the typical tripod arrangement previously established for the early transition metal derivatives of this system.[6−8] Remarkably, the Tl−N distances to Tl(1) of the two anionic amido functions [Tl(1)−N(1) 2.470(14) Å and Tl(1)−N(2) 2.406(15) Å] and the neutral pyridyl function [Tl(1)−N(3) 2.468(15) Å] lie in the same range and thus do not allow for differentiation between the two types of metal−ligand interactions.

The orientation of the two monomeric units in the crystal corresponds to a weak association to dimeric aggregates

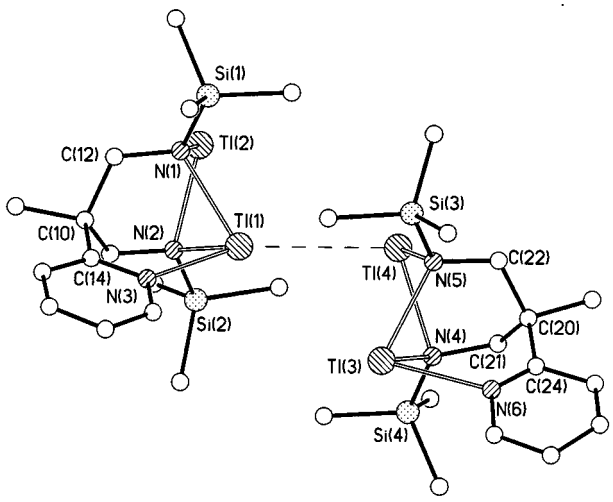


Figure 5. The asymmetric unit of **6** showing the aggregation of the two monomers via weak Tl−Tl interactions [Tl(1)Tl(4) 3.500(2) Å]

(Figure 5) of the type previously established for several other thallium amides, with an unsupported Tl−Tl contact.[9−12] This involves the three-coordinate thallium centre of one monomer and the two-coordinate metal atom of a neighbouring molecule ("head-to-tail" arrangement). The intermetallic distance of Tl(1)−Tl(4) [3.500(2) Å] is significantly shorter than the sum of the van der Waals radii (ca. 4.0 Å) and is thought to reflect a weakly attractive dispersive interaction between the metal centres.

Comparison of the Crystal Structures of 3−6: Variation of the Patterns of Aggregation upon Replacement of Lithium by Thallium(I)

The progression from the lithium amides via the mixed metal amide **5** to the homometallic thallium species **6** may be viewed as a gradual opening of a molecular cage. This is best represented if the cubic dimeric structure of the simple dilithium diamide $[CH_2\{CH_2N(Li)SiMe_3\}_2]$, which we reported recently,[13] is added to the series (Figure 6). If we begin with the cube, addition of the neutral pyridyl units first leads to an opening to form a ladder structure, either of the boat-type arrangement found in **3** or the stepped arrangement found for **4**. Replacement of lithium by thallium leads to a reduction in the nitrogen−metal interaction and breakdown of the dimer to give the weakly associated structure found for the thallium complex **6**.

Conclusions

In this study we have presented the first systematic structural investigation of lithium and thallium(I) derivatives of a polydentate amido donor ligand. The combination of these two different metal monocations leads to disparate forms of aggregation in the solid, ranging from the principally electrostatic amido−metal interaction in the alkali metal derivatives to the weakly dispersive metal attraction found for the thallium complex. Current work is aimed at extending the structural chemistry of mixed alkali

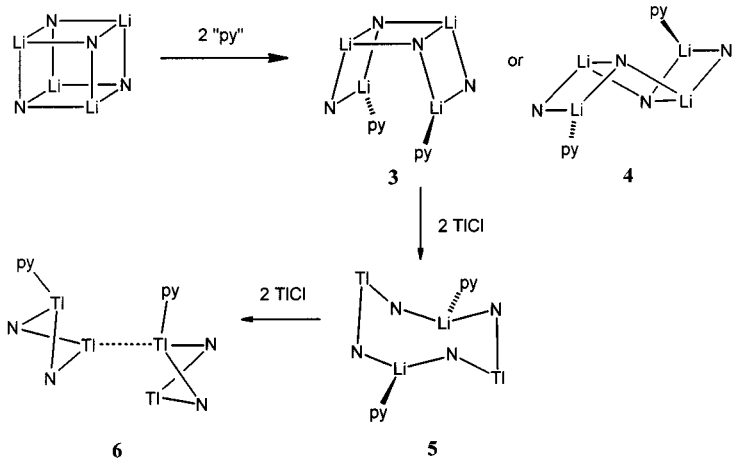


Figure 6. Opening of the heterocubane structure of bidentate lithium amides upon integration of neutral donors and substitution of lithium by thallium(I)

metal−thallium amides in order to gain further insight into the interactions defining their aggregation in the solid state.

Experimental Section

All manipulations were performed under dried argon in standard (Schlenk) glassware, which was flame-dried with a Bunsen burner prior to use. Solvents were dried according to standard procedures and saturated with Ar. The deuterated solvents used for the NMR-spectroscopic measurements were degassed by three successive "freeze-pump-thaw" cycles and dried over 4-Å molecular sieves. − The ^{1}H, ^{13}C, ^{29}Si, and ^{7}Li NMR spectra were recorded with a Bruker AC 200 spectrometer equipped with a B-VT-2000 variable-temperature unit (at 200.13, 50.32, 39.76, and 77.77 MHz, respectively) with tetramethylsilane or LiI/H_2O (1 M) as reference. − The IR spectra were recorded with a Bruker IFS 25 FT-IR spectrometer. − Elemental analyses were carried out in the microanalytical laboratory of the chemistry department at Würzburg. − The compounds (2-C_5H_4N)$C(CH_3)(CH_2NH_2)_2$ and (2-C_5H_4N)$C(CH_3)$-$(CH_2NHSiMe_3)_2$ (**1**) were prepared as reported previously.[6] All other chemicals used as starting materials were obtained commercially and used without further purification.

Preparation of (2-C_5H_4N)$C(CH_3)(CH_2NHSiMe_2tBu)_2$ (2): To a stirred solution of of (2-C_5H_4N)$C(CH_3)(CH_2NH_2)_2$ (9.01 g, 54.5 mmol) in thf (250 mL), NEt_3 (16.0 mL, 114.8 mmol), and then *t*$BuMe_2SiCl$ (16.4 g, 109.0 mmol) in thf (50 mL) was added in small portions at 0 °C. The mixture was warmed to room temperature and stirred for 3 h. After filtration, the solvent was removed under reduced pressure. Compound **2** was obtained as a colourless liquid after distillation under reduced pressure (yield: 20.6 g, 96%). − B.p.: 150 °C/3 mbar. − ^{1}H NMR (200.13 MHz, C_6D_6, 295 K): δ = −0.3, −0.1 [s, 12 H, $Si(CH_3)_2$], 0.73 (m, 2 H, NH), 0.91 [s, 18 H, $SiC(CH_3)_3$], 1.33 [s, 3 H, $C(CH_3)$], 3.09 {dd, 2 H, $^{2}J_{HH}$ = 12.5 Hz, $^{3}J_{HH}$ = 8.5 Hz, C[C*H*HNHSi$(CH_3)_2]_2$}, 3.31 {dd, 2 H, $^{3}J_{HH}$ = 8.1 Hz, C[CH*H*NHSi$(CH_3)_2]_2$}, 6.58 (m, 1 H, H^5, C_5H_4N), 7.06 (m, 1 H, H^3, C_5H_4N), 7.10 (m, 1 H, H^4, C_5H_4N), 8.46 (m, 1 H, H^6, C_5H_4N). − $\{^{1}H\}^{13}C$ NMR (50.32 MHz, C_6D_6, 295 K): δ = −4.8, −4.7 [$Si(CH_3)_3$], 18.7 [$SiC(CH_3)_3$], 21.2 [$C(CH_3)$], 26.8 [$SiC(CH_3)_3$], 48.6 [$C(CH_3)$], 51.2 {C[$CH_2NHSi(CH_3)_2]_2$}, 120.9 (CH, C^5, C_5H_4N), 121.9 (CH, C^4, C_5H_4N), 135.7 (CH, C^3, C_5H_4N), 149.2 (CH, C^6, C_5H_4N), 166.4 (C, C^2, C_5H_4N). − $\{^{1}H\}^{29}Si$ NMR (39.76 MHz, C_6D_6, 295 K): δ = 8.3. − IR (film): $\tilde{\nu}$ = 3396 w, 2952 vs, 2927 vs, 2982 s, 2854 vs, 1588 s, 1569 w, 1471 vs, 1431 s, 1401 vs, 1360 s, 1254 vs, 1110 vs, 1084 vs, 1006 s, 829 vs, 811 s, 777 s, 746 s, 662 s cm^{-1}. − $C_{21}H_{43}N_3Si_2$ (393.8): calcd. C 64.06, H 11.01, N 10.67; found C 63.73, H 10.79, N 10.78.

Preparation of [(2-C_5H_4N)$C(CH_3)\{CH_2N(Li)SiMe_3\}_2]_2$ (3) and [(2-C_5H_4N)$C(CH_3)\{CH_2N(Li)SiMe_2tBu\}_2]_2$ (4): To a stirred solution of **1** (1.01 g, 3.26 mmol) or **2** (1.28 g, 3.26 mmol) in *n*-pentane (20 mL), a 2.5 M solution of *n*BuLi in *n*-hexane (2.61 mL = 6.52 mmol) was added at −30 °C. The mixture was warmed to room temperature and stirred for 16 h. After concentration to 5 mL, the solution was stored at −35 °C. Compounds **3** and **4** were obtained as colourless, highly crystalline solids (yields: **3**: 880 mg, 84%; **4**: 1.01 g, 77%).

3: ^{1}H NMR (200.13 MHz, C_6D_6, 295 K): δ = 0.24, 0.46 [s, 18 H, $Si(CH_3)_3$], 1.40 [s, 3 H, $C(CH_3)$], 3.10, 3.17 {d, 2 H, $^{2}J_{HH}$ = 13.8 Hz, C[C*H*HNSi$(CH_3)_3$]}, 3.48, 3.72 {d, 2 H, C[CH*H*NSi$(CH_3)_3$]}, 6.47 (ddd, 1 H, $^{3}J_{H5H4}$ = 6.9 Hz, $^{3}J_{H5H6}$ = 5.1 Hz, $^{4}J_{H5H3}$ = 1.7 Hz, H^5, C_5H_4N), 6.95−7.11 (m, 2 H, H^3/H^4, C_5H_4N), 8.34 (ddd, 1 H, $^{4}J_{H4H6}$ = 1.8 Hz, $^{5}J_{H3H6}$ = 1.1 Hz, H^6, C_5H_4N). − $\{^{1}H\}^{13}C$ NMR (50.32 MHz, C_6D_6, 295 K): δ = 0.2, 4.4 [$Si(CH_3)_3$], 24.4 [$C(CH_3)$], 50.7 {*C*[$CH_2NSi(CH_3)_3]_2$}, 55.4, 58.6 {C[*C*$H_2NSi(CH_3)_3]_2$}, 120.9, 121.7 (CH, C^3/C^5, C_5H_4N), 137.7 (CH, C^4, C_5H_4N), 147.3 (CH, C^6, C_5H_4N), 169.6 (C, C^2, C_5H_4N). − $\{^{1}H\}^{7}Li$ NMR (77.77 MHz, C_6D_6, 295 K): δ = 0.16, 0.88. − $\{^{1}H\}^{29}Si$ NMR (39.76 MHz, C_6D_6, 295 K): δ = −7.6, −4.4. − $C_{30}H_{58}Li_4N_6Si_4$ (642.9): calcd. C 56.04, H 9.09, N 13.07; found C 55.69, H 9.38, N 12.82.

4: ^{1}H NMR (200.13 MHz, C_6D_6, 295 K): δ = −0.04, 0.03 [s, 12 H, $Si(CH_3)_2$], 1.01 [s, 18 H, $SiC(CH_3)_3$], 1.22 [s, 3 H, $C(CH_3)$], 3.60 {d, 2 H, $^{2}J_{HH}$ = 12.0 Hz, C[C*H*HNSi$(CH_3)_2]_2$}, 3.80 {d, 2 H, C[CH*H*NSi$(CH_3)_2]_2$}, 6.59 (m, 1 H, H^5, C_5H_4N), 6.91 (m, 1 H, H^3, C_5H_4N), 7.10 (m, 1 H, H^4, C_5H_4N), 8.02 (m, 1 H, H^6, C_5H_4N). − $\{^{1}H\}^{13}C$ NMR (50.32 MHz, C_6D_6, 295 K): δ = −2.3, −2.4 [$Si(CH_3)_3$], 20.1 [$SiC(CH_3)_3$], 25.8 [$C(CH_3)$], 28.4 [$SiC(CH_3)_3$], 47.7 [$C(CH_3)$], 62.5 {C[$CH_2NSi(CH_3)_2]_2$}, 120.7 (CH, C^5, C_5H_4N), 121.2 (CH, C^4, C_5H_4N), 137.4 (CH, C^3, C_5H_4N), 146.1 (CH, C^6, C_5H_4N), 168.6 (C, C^2, C_5H_4N). − $\{^{1}H\}^{7}Li$ NMR (77.77 MHz, C_6D_6, 295 K): δ = 0.08, 0.79. − $C_{42}H_{82}Li_4N_6Si_4$ (811.3): calcd. C 62.18, H 10.19, N 10.36; found C 61.97, H 10.21, N 10.25.

Preparation of [(2-C_5H_4N)$C(CH_3)\{CH_2N(Li)SiMe_3\}\{CH_2N(Tl)$-$SiMe_3\}]_2$ (5) and [(2-C_5H_4N)$C(CH_3)\{CH_2N(Tl)SiMe_3\}_2]_2$ (6): Solid TlCl (720 mg, 3.00 mmol) was added to a stirred solution of

482 mg (1.50 mmol) **3** in *n*-pentane (25 mL) at −55 °C. After the mixture was warmed to room temperature and stirred for 94 h, the LiCl formed in the reaction was removed by centrifugation and the yellow solution was stored at −35 °C. Compound **5** was obtained as a colourless, and compound **6** as an orange, highly crystalline solid (yield: **5**: 83 mg, 10%; **6**: 579 mg, 54%).

5: ^{1}H NMR (200.13 MHz, C_6D_6, 295 K): δ = 0.02 [s, 18 H, $Si(CH_3)_3$], 1.34 [s, 3 H, $C(CH_3)$], 2.96, 3.02 {d, 2 H, $^2J_{HH}$ = 8.4 Hz, $C[CHHNSi(CH_3)_3]_2$}, 3.27, 3.33 {d, 2 H, $C[CHHNSi(CH_3)_3]_2$}, 6.59 (ddd, 1 H, $^3J_{H4H5}$ = 6.6 Hz, $^3J_{H5H6}$ = 4.8 Hz, $^4J_{H3H5}$ = 1.8 Hz, H^5, C_5H_4N), 7.02−7.10 (m, 2 H, H$^{3/4}$, C_5H_4N), 8.50 (ddd, 1 H, $^3J_{H5H6}$ = 4.8 Hz, $^4J_{H4H6}$ = 1.8 Hz, $^5J_{H3H6}$ = 1.1 Hz, H^6, C_5H_4N). − {^{1}H}^{13}C NMR (50.32 MHz, C_6D_6, 295 K): δ = 0.3 [$Si(CH_3)_3$], 21.0 [$C(CH_3)$], 48.4, 50.7 {$C[CH_2NSi(CH_3)_3]_2$}, 65.1 {$C[CH_2NSi(CH_3)_3]_2$}, 120.8, 122.0 (CH, C$^{3/5}$, C_5H_4N), 135.6 (CH, C^4, C_5H_4N), 149.2 (CH, C^6, C_5H_4N), 166.5 (C, C^2, C_5H_4N). − $C_{15}H_{29}LiN_3Si_2Tl \cdot 0.5\,C_5H_{12}$ (555.0): calcd. C 37.87, H 6.36, N 7.57, Tl 36.83; found C 37.38, H 6.11, N 7.28, Tl 36.72.

6: ^{1}H NMR (200.13 MHz, C_6D_6, 295 K): δ = 0.17 [br s, 18 H, $Si(CH_3)_3$], 1.08 [s, 3 H, $C(CH_3)$], 3.70 {br m, 1 H, $C[CH_2NSi(CH_3)_3]_2$}, 4.30 {br m, 3 H, $C[CH_2NSi(CH_3)_3]_2$}, 6.48 (ddd, 1 H, $^3J_{H4H5}$ = 7.8 Hz, $^3J_{H5H6}$ = 4.9 Hz, $^4J_{H3H5}$ = 1.0 Hz, H^5, C_5H_4N), 7.05 (td, 1 H, $^3J_{H3H4}$ = 7.8 Hz, $^4J_{H4H6}$ = 2.1 Hz, H^4, C_5H_4N), 7.27 (dt, 1 H, $^3J_{H3H4}$ = 7.8 Hz, $^4J_{H3H5}$ = 1.0 Hz, H^3, C_5H_4N), 8.25 (ddd, 1 H, $^3J_{H5H6}$ = 4.9 Hz, $^4J_{H4H6}$ = 2.1 Hz, $^5J_{H3H6}$ = 1.0 Hz, H^6, C_5H_4N). − {^{1}H}^{13}C NMR (50.32 MHz, C_6D_6, 295 K): δ = 1.0 [dd, $^3J_{TlC}$ = 56 Hz, $^3J_{TlC}$ = 106 Hz, $Si(CH_3)_3$], 27.8 [br, $C(CH_3)$], 55.6 [d, $^3J_{TlC}$ = 143 Hz, $C(CH_3)$], 60.2 {dd, $^2J_{TlC}$ = 60 Hz, $^2J_{TlC}$ = 115 Hz, $C[CH_2NSi(CH_3)_3]_2$}, 121.3 (CH, C$^{3/5}$, C_5H_4N), 121.6 (d, $^3J_{TlC}$ = 27 Hz, CH, C$^{3/5}$, C_5H_4N), 137.6 (d, $^4J_{TlC}$ = 28 Hz, CH, C^4, C_5H_4N), 149.4 (d, $^2J_{TlC}$ = 91 Hz, CH, C^6, C_5H_4N), 169.4 (d, $^2J_{TlC}$ = 15 Hz, C, C^2, C_5H_4N). − $C_{15}H_{29}N_3Si_2Tl_2$ (716.4): calcd. C 25.15, H 4.08, N 5.87, Tl 57.06; found C 24.66, H 3.98, N 5.53, Tl 56.31.

X-ray Crystallographic Study of 3−6: Data of **3** and **4** were collected using a Siemens P4 diffractometer at a temperature of 198(2) K (**3**) and 305(2) K (**4**), respectively, with oil-coated crystals mounted in Lindemann tubes. Data of **5** and **6** were collected using an Enraf−Nonius CAD4 diffractometer at a temperature of 133(2) K (**5**) and 193(2) K (**6**), respectively, with oil-coated shock-cooled crystals[18] mounted on the top of a glass pin under nitrogen. Crystal data and experimental details for the crystals of **3−6** are given in Table 1. All data for the structures **5** and **6** were corrected for absorption using Ψ-scans. No absorption correction was applied for structure **3** and **4**. Structure **5** was solved by Patterson methods, structures **3**, **4**, and **6** by direct methods (SHELXS-86: **3**, **5**, **6**; SHELXS-97: **4**) and refined on F^2 (SHELXL-93: **3**; SHELXL-97: **4−6**).[19] The comparatively high residual electron density in **5** and **6** was in the vicinity of the thallium atoms. Due to extremely poor diffraction by the only crystals of **4** available, data was collected in a very limited θ range (θ < 18°) and the chemically equivalent bond lengths in the two halves of the molecule were constrained in the refinement to be equal within an esd of 0.03 Å, because of the shortage of data. In the case of **5** a solvent molecule (*n*-pentane) was disordered across the inversion centre. In the case of **6**, disorder of the pyridine ring in one molecule in the asymmetric unit corre-

Table 1. Crystal data and structure refinement for **3−6**

	3	**4**	**5**	**6**
Empirical formula	$C_{30}H_{58}Li_4N_6Si_4$	$C_{42}H_{82}Li_4N_6Si_4$	$C_{30}H_{58}Li_2N_6Si_4Tl_2{\cdot}C_5H_{12}$	$C_{15}H_{29}N_3Si_2Tl_2$
*M*r	642.94	811.26	1109.94	716.33
Temperature	198(2) K	305(2) K	133(2) K	193(2) K
Wavelength	0.71073 Å	0.71073 Å	0.71073 Å	0.71073 Å
Crystal system	monoclinic	triclinic	triclinic	triclinic
Space group	*C*2/*c* (no. 15)	$P\bar{1}$ (no. 2)	$P\bar{1}$ (no. 2)	$P\bar{1}$ (no. 2)
Z	4	2	1	4
Unit cell dimensions	*a* = 22.366(2) Å *b* = 9.3954(8) Å *c* = 19.404(3) Å β = 104.874(10)°	*a* = 10.369(3) Å *b* = 13.142(4) Å *c* = 20.092(12) Å α = 94.72(3)° β = 102.09(3)° γ = 91.03(2)°	*a* = 9.7249(19) Å *b* = 12.065(2) Å *c* = 12.181(2) Å α = 119.59(3)° β = 95.59(3)° γ = 106.03(3)°	*a* = 11.755(5) Å *b* = 13.480(6) Å *c* = 15.149(6) Å α = 99.51(2)° β = 97.41(3)° γ = 109.34(2)°
Volume	3940.9(7) Å^3	2666.4(19) Å^3	1146.8(4) Å^3	2190.1(16) Å^3
$D_{calcd.}$	1.084 g cm^{-3}	1.010 g cm^{-3}	1.607 g cm^{-3}	2.173 g cm^{-3}
Absorption coefficient	0.177 mm^{-1}	0.143 mm^{-1}	7.151 mm^{-1}	0.202 mm^{-1}
F(000)	1392	888	546	1320
Crystal size	0.2 × 0.36 × 0.42 mm	0.35 × 0.38 × 0.4 mm	0.2 × 0.2 × 0.2 mm	0.2 × 0.2 × 0.2 mm
Scan method	ω/2θ scan	θ/2θ scan	ω scan	ω/θ scan
θ range for data collection	1.88−25.00°	1.95−18.00°	2.00−24.99°	2.10−22.46°
Limiting indices	−26 ≤ *h* ≤ 26, −11 ≤ *k* ≤ 11, −23 ≤ *l* ≤ 23	−9 ≤ *h* ≤ 1, −11 ≤ *k* ≤ 11, 17 ≤ *l* ≤ 17	−11 ≤ *h* ≤ 1, −14 ≤ *k* ≤ 14, −14 ≤ *l* ≤ 14	−12 ≤ *h* ≤ 0, −13 ≤ *k* ≤ 14, −16 ≤ *l* ≤ 16
Reflections collected	7110	4193	4394	9655
Independent reflections	3472	3420	4051	5708
Refinement method	full-matrix least squares on F^2	full-matrix least squares on F^2	full-matrix least squares on F^2	full-matrix least squares on F^2
Data/restraints/parameters	3472/0/206	3420/349/505	4051/0/243	5708/245/457
$T_{max/min}$	−/−	−/−	0.9993/0.7767	0.9981/0.7297
Goodness-of-fit on F^2	1.003	0.839	1.056	1.055
Final *R* indices [$I > 2\sigma(I)$]	R_1 = 0.0652, wR_2 = 0.1036	R_1 = 0.0962, wR_2 = 0.2346	R_1 = 0.0342, wR_2 = 0.0777	R_1 = 0.0524, WR_2 = 0.0907
R indices (all data)	R_1 = 0.1609, wR_2 = 0.1335	R_1 = 0.2563, wR_2 = 0.3347	R_1 = 0.0407, wR_2 = 0.0813	R_1 = 0.0877, wR_2 = 0.1076
Largest diff. peak/hole	0.292/−0.287 e Å^{-3}	0.252/−0.321 e Å^{-3}	2.656/−1.795 e Å^{-3}	1.285/−1.073 e Å^{-3}

sponds to a random distribution at this site, throughout the crystal, of two isomers **6** and **6′** (differing only in the orientation of this pyridine ring) in a 70:30% ratio. In the final cycles of refinement all non-hydrogen atoms of **3**−**6** were assigned anisotropic displacement parameters. Hydrogen atoms were included in idealized positions riding on the parent atoms and were assigned isotropic displacement parameters of 1.2 U_{eq} (=CH, CH_2) and 1.5 U_{eq} (CH_3) of the parent atom. Crystallographic data (excluding structure factors) for the structures reported in this paper have been deposited with the Cambridge Crystallographic Data Centre as supplementary publication nos. CCDC-142874 (**3**), -142875 (**4**), -142876 (**5**), -142877 (**6**). Copies of the data can be obtained free of charge on application to CCDC, 12 Union Road, Cambridge CB2 1EZ, UK [Fax: (internat.) + 44-1223/336-033; E-mail: deposit@ccdc.cam.ac.uk].

Acknowledgments

We thank the Deutsche Forschungsgemeinschaft, the CNRS (France), the EPSRC (UK), and the Fonds der Chemischen Industrie for financial support.

[1] [1a] K. Gregory, P. v. Ragué Schleyer, R. Snaith, *Adv. Inorg. Chem.* **1991**, *37*, 47. – [1b] R. E. Mulvey, *Chem. Soc. Rev.* **1991**, *20*, 167.
[2] M. F. Lappert, P. P. Power, A. R. Sanger, R. C. Srivastava, *Metal and Metalloid Amides*, Ellis-Horwood-Wiley, Chichester, **1980**.
[3] L. H. Gade, N. Mahr, *J. Chem. Soc., Dalton Trans.* **1993**, 489.
[4] L. H. Gade, C. Becker, J. W. Lauher, *Inorg. Chem.* **1993**, *32*, 2308.
[5] S. Friedrich, L. H. Gade, A. J. Edwards, M. McPartlin, *J. Chem. Soc., Dalton Trans.* **1993**, 2861.
[6] S. Friedrich, M. Schubart, L. H. Gade, I. J. Scowen, A. J. Edwards, M. McPartlin, *Chem. Ber./Recueil* **1997**, *130*, 1751.
[7] A. J. Blake, P. E. Collier, L. H. Gade, M. McPartlin, P. Mountford, M. Schubart, I. J. Scowen, *Chem. Commun.* **1997**, 1555.
[8] A. Bashall, P. E. Collier, L. H. Gade, M. McPartlin, P. Mountford, D. J. M. Trösch, *Chem. Commun.* **1998**, 2555.
[9] [9a] *Unkonventionelle Wechselwirkungen in der Chemie metallischer Elemente* (Ed. B. Krebs), VCH, Weinheim, **1992**. – [9b] P. Pyykkö, *Chem. Rev.* **1997**, *97*, 597. – [9c] C. Janiak, *Coord. Chem. Rev.* **1997**, *163*, 107.
[10] [10a] M. Veith, A. Spaniol, J. Pöhlmann, F. Gross, V. Huch, *Chem. Ber.* **1993**, *126*, 2625. – [10b] S. D. Waezsada, T. Belgardt, M. Noltemeyer, H. W. Roesky, *Angew. Chem.* **1994**, *106*, 1413; *Angew. Chem. Int. Ed. Engl.* **1994**, *33*, 1351.
[11] [11a] K. W. Hellmann, L. H. Gade, I. J. Scowen, M. McPartlin, *Chem. Commun.* **1996**, 2515. – [11b] K. W. Hellmann, L. H. Gade, R. Fleischer, D. Stalke, *Chem. Commun.* **1997**, 527. – [11c] K. W. Hellmann, C. H. Galka, L. H. Gade, A. Steiner, D. S. Wright, T. Kottke, D. Stalke, *Chem. Commun.* **1998**, 549.
[12] [12a] K. W. Hellmann, L. H. Gade, A. Steiner, D. Stalke, F. Möller, *Angew. Chem.* **1997**, *109*, 99; *Angew. Chem. Int. Ed. Engl.* **1997**, *36*, 160. – [12b] K. W. Hellmann, L. H. Gade, R. Fleischer, T. Kottke, *Chem. Eur. J.* **1997**, *3*, 1801. – [12c] C. H. Galka, L. H. Gade, *Inorg. Chem.* **1999**, *38*, 1038.
[13] K. W. Hellmann, A. Bergner, L. H. Gade, I. J. Scowen, M. McPartlin, *J. Organomet. Chem.* **1999**, *573*, 156.
[14] D. J. Brauer, H. Bürger, G. R. Liewald, *J. Organomet. Chem.* **1986**, *308*, 119.
[15] M. G. Gardiner, C. L. Raston, *Inorg. Chem.* **1995**, *34*, 4206.
[16] [16a] M. F. Lappert, M. J. Slade, A. Singh, J. L. Atwood, R. D. Rogers, R. Shakir, *J. Am. Chem. Soc.* **1983**, *105*, 302. – [16b] D. Barr, W. Clegg, R. E. Mulvey, D. Reed, R. Snaith, *Angew. Chem.* **1985**, *97*, 322; *Angew. Chem. Int. Ed. Engl.* **1985**, *24*, 328. –[16c] D. J. Brauer, H. Bürger, G. R. Liewald, J. Wilke, *J. Organomet. Chem.* **1985**, *287*, 305. – [16d] L. M. Engelhardt, G. E. Jacobsen, P. C. Junk, C. L. Raston, B. W. Skelton, A. H. White, *J. Chem. Soc., Dalton Trans.* **1988**, 1011. – [16e] M. Veith, F. Goffing, V. Huch, *Chem. Ber.* **1988**, *121*, 943. – [16f] B.-J. Deelman, M. F. Lappert, H.-K. Lee, T. C. W. Mak, W.-P. Leung, P.-R. Wei, *Organometallics* **1997**, *16*, 1247. – [16g] M. Veith, M. Zimmer, P. Kosse, *Chem. Ber.* **1994**, *127*, 2099. – [16h] I. Hemme, B. Tecklenburg, M. Noltemeyer, U. Klingebiel, *Chem. Ber.* **1995**, *128*, 351.
[17] K. W. Klinkhammer, S. Henkel, *J. Organomet. Chem.* **1994**, *480*, 167.
[18] [18a] T. Kottke, D. Stalke, *J. Appl. Crystallogr.* **1993**, *26*, 615. – [18b] T. Kottke, R. J. Lagow, D. Stalke, *J. Appl. Crystallogr.* **1996**, *29*, 465. – [18c] D. Stalke, *Chem. Soc. Rev.* **1998**, *27*, 171.
[19] [19a] G. M. Sheldrick, *SHELXS-86, Program for Crystal Structure Solution*, Universität Göttingen, **1986**. – [19b] G. M. Sheldrick, *Acta Crystallogr., Sect. A* **1990**, *46*, 467. – [19c] G. M. Sheldrick, *SHELXL-93, Program for Crystal Structure Refinement*, Universität Göttingen, **1993**. – [19d] G. M. Sheldrick, *SHELXL-97, Program for Crystal Structure Refinement*, Universität Göttingen, **1997**.

Received April 10, 2000
[I00138]

Synthesis and Properties of Novel Metal-Linked P_n Ligand Complexes

Perumal Sekar,[a] Shubhangi Umbarkar,[a] Manfred Scheer,*[a] Andreas Voigt,[b] and Reinhard Kirmse[b]

Dedicated to Professor Herbert Schumann on the occasion of his 65th birthday

Keywords: Phosphorus / Chromium / Molybdenum / Cyclopentadienes / Sandwich complexes

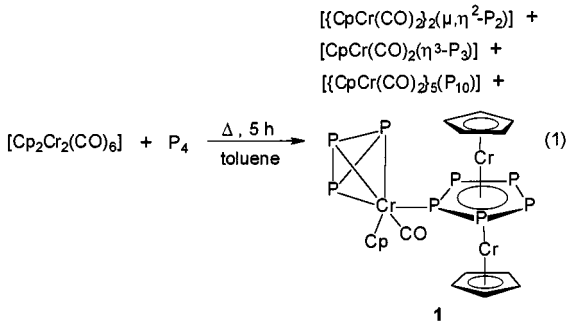
The reaction of $[CpCr(CO)_3]_2$ with P_4 in toluene at 90 °C for 5 h affords the triple-decker sandwich complex $[CpCr(CO)(\eta^3\text{-}P_3)(CpCr)_2(\mu,\eta^1\text{:}\eta^5\text{:}\eta^5\text{-}P_5)]$ (**1**) as a new product, along with the previously described products with P_2, P_3, and P_{10} units. The structure of the paramagnetic complex **1** has been established by single-crystal X-ray diffraction methods. A novel complex $[\{CpCr(CO)_2\}_2(\mu,\eta^1\text{:}\eta^1\text{:}\eta^2\text{-}P_2)\{Mo(CO)_4\}_2\{(\mu,\eta^1\text{:}\eta^1\text{:}\eta^5\text{:}\eta^5\text{-}P_5)(CpCr)_2\}]$ (**2**) has been obtained from the reaction of $[\{CpCr(CO)_2\}_2(\mu,\eta^2\text{-}P_2)]$ with $[Mo(CO)_4(NBD)]$ (NBD = norbornadiene). The X-ray structure of **2** reveals a six-membered Mo_2P_4 ring combining a Cr_2P_2 tetrahedral core and a triple-decker sandwich Cr_2P_5 moiety. The EPR spectra of the paramagnetic ($S' = 1/2$) complexes **1** and **2** are reported. A noticeable hyperfine interaction with two ^{31}P nuclei is observed for **2**.

Introduction

Research in the area of complexes with "naked" Group-15 elements as ligands has recently undergone a dynamic and exciting development.[1] The majority of publications in this field deal with the synthesis and structural features of E_n (E = P, As, Sb, Bi) containing complexes. However, during the last decade, various groups[2–5] have started to investigate the reactivities of such species, especially those of P_n ligand complexes. In continuation of our activities aimed at exploring unusual reactivity features of E_n-containing complexes, we have focussed our interest on studying the reactivity pattern of $[\{CpCr(CO)_2\}_2(\mu,\eta^2\text{-}P_2)]$, which was first obtained by Goh et al.[6] In one of our projects in this field, our interest lies in the synthesis of oligomers of such P_2 ligand complexes linked by transition metal moieties. In this context, we tried to obtain an Mo-bridged dimer of $[\{CpCr(CO)_2\}_2(\mu,\eta^2\text{-}P_2)]$ tetrahedral units by using the lone pairs of the phosphorus atoms. The surprising results are reported herein.

Results and Discussion

Goh et al. have described the isolation of $[\{CpCr(CO)_2\}_2(\mu,\eta^2\text{-}P_2)]$, $[CpCr(CO)_2(\eta^3\text{-}P_3)]$, $[(CpCr)_2(\mu,\eta^5\text{:}\eta^5\text{-}P_5)]$, and $[\{CpCr(CO)_2\}_5(P_{10})]$ from the thermolysis of $[CpCr(CO)_3]_2$ with P_4.[6] Additionally, from the same reaction we have obtained $[CpCr(CO)(\eta^3\text{-}P_3)(CpCr)_2(\mu,\eta^1\text{:}\eta^5\text{:}\eta^5\text{-}P_5)]$ (**1**) as a new product in good yields by stirring the reaction mixture for 5 h at 90 °C [Equation (1)].



Complex **1** was isolated along with $[\{CpCr(CO)_2\}_2(\mu,\eta^2\text{-}P_2)]$, $[CpCr(CO)_2(\eta^3\text{-}P_3)]$, and $[\{CpCr(CO)_2\}_5(P_{10})]$ after column chromatographic work-up. The ^{31}P NMR spectrum of the crude reaction mixture showed no signal attributable to the complex $[(CpCr)_2(\mu,\eta^5\text{:}\eta^5\text{-}P_5)]$. On the basis of this observation, one may speculate that **1** is formed by the subsequent reaction of $[CpCr(CO)_2(\eta^3\text{-}P_3)]$ with $[(CpCr)_2(\mu,\eta^5\text{:}\eta^5\text{-}P_5)]$, which are initially formed in the reaction of $[CpCr(CO)_3]_2$ with P_4. Complex **1** is insoluble in *n*-hexane but moderately soluble in toluene, CH_2Cl_2, and THF. Its infrared spectrum shows a broad absorption at 1897 cm^{-1} attributable to a terminal CO group. Due to the paramagnetic nature of **1**, no signal could be detected in its ^{31}P NMR spectrum. The mass spectrum of **1** shows peaks due to the parent ions $[CpCr(CO)(\eta^3\text{-}P_3)]$ and $[(CpCr)_2(\mu,\eta^5\text{:}\eta^5\text{-}P_5)]$ and fragmentation products thereof.

The molecular structure of **1** is shown in Figure 1. It consists of a triple-decker sandwich with a *cyclo*-P_5 middle deck, of which one of the P atoms coordinates to the Cr atom of the distorted $[CpCr(CO)(\eta^3\text{-}P_3)]$ tetrahedral moiety. The P–P distances in the P_5 middle deck fall into long [2.331(2) and 2.437(2) Å] and short [2.180(3) and 2.198(3) Å] categories, reflecting a lengthening of the P–P bonds around the atom P(4) due to its additional coordination to the Cr atom of the CrP_3 unit. This also leads to a slight

[a] Institut für Anorganische Chemie der Universität Karlsruhe, 76128 Karlsruhe, Germany
Fax: (internat.) + 49-(0)721/661921
E-mail: mascheer@achibm6.chemie.uni-karlsruhe.de
[b] Institut für Anorganische Chemie der Universität Leipzig, Johannisallee 29, 04103 Leipzig, Germany

 © WILEY-VCH Verlag GmbH, D-69451 Weinheim, 2000 1434–1948/00/1212–2585 $ 17.50+.50/0

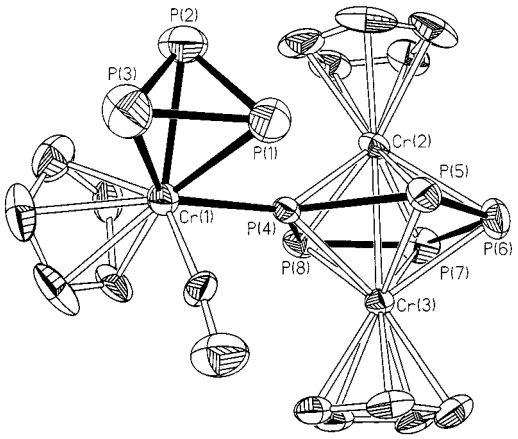
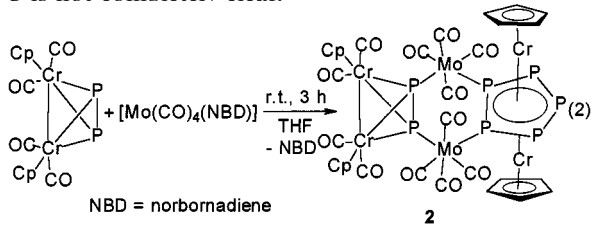


Figure 1. Molecular structure of **1** (ellipsoids drawn at a 50% probability level, H atoms of the Cp ligands are omitted for clarity); selected bond lengths [Å] and angles [°]: Cr(1)−P(1) 2.483(2), Cr(1)−P(2) 2.420(2), Cr(1)−P(3) 2.431(2), Cr(1)−P(4) 2.309(2), Cr(2)−Cr(3) 2.727(13), P(1)−P(2) 2.138(3), P(2)−P(3) 2.169(3), P(3)−P(1) 2.132(3), P(4)−P(5) 2.331(2), P(5)−P(6) 2.180(3), P(6)−P(7) 2.197(3), P(7)−P(8) 2.198(3), P(8)−P(4) 2.437(2); Cr(1)−P(4)−Cr(2) 141.18(8), P(4)−Cr(1)−P(1) 77.82(7), P(4)−Cr(2)−Cr(3) 53.54(5), P(1)−P(2)−P(3) 59.63(10)

shortening of the other P−P bonds within the *cyclo*-P_5 ring as compared to those in the *cyclo*-P_5 unit in $[(CpCr)_2(\mu,\eta^5{:}\eta^5\text{-}P_5)]$ [*d*(P−P) = 2.276(2)−2.206(3) Å],[6b] which is not additionally coordinated. In contrast, the P−P bond lengths in the *cyclo*-P_3 unit in **1** are slightly longer [2.132(3)−2.169(3) Å] than those in the *cyclo*-P_3 unit in $[CpCr(CO)_2(\eta^3\text{-}P_3)]$[6a] [2.118(3)−2.127(3) Å]. Due to this effect, a shortening of the Cr−P bond lengths in the tetrahedral CrP_3 unit of **1** is observed. These Cr−P bond lengths are in the range 2.420(2)−2.483(2) Å, thus making them slightly shorter than the corresponding distances observed in the complex $[CpCr(CO)_2(\eta^3\text{-}P_3)]$ [2.432(2)−2.494(1) Å]. The Cr−Cr distance in **1** [2.727(3) Å] is very similar to those in other triple-decker complexes reported in the literature, e.g. $[(CpCr)_2(\mu,\eta^5{:}\eta^5\text{-}P_5)]$ [2.738(1) Å] and $[(Cp^*Cr)_2(\mu,\eta^5{:}\eta^5\text{-}P_5)]$ [2.727(5) Å].[7]

Reactivity of $[\{CpCr(CO)_2\}_2(\mu,\eta^2\text{-}P_2)]$

Reaction of $[\{CpCr(CO)_2\}_2(\mu,\eta^2\text{-}P_2)]$ with one equivalent of $[Mo(CO)_4(NBD)]$ in THF at room temperature and subsequent column chromatographic work-up led to the isolation of $[\{CpCr(CO)_2\}_2(\mu,\eta^1{:}\eta^1{:}\eta^2\text{-}P_2)\{Mo(CO)_4\}_2\text{-}\{(\mu,\eta^1{:}\eta^1{:}\eta^5{:}\eta^5\text{-}P_5)(CpCr)_2\}]$ (**2**). In a further fraction, a paramagnetic complex − referred as **3** − was isolated as a minor product. In the mass spectrum of **3**, a small peak attributable to $[\{CpCr(CO)_2\}(\mu,\eta^1{:}\eta^1{:}\eta^3\text{-}P_3)\{Mo(CO)_4\}_2\text{-}\{(\mu,\eta^1{:}\eta^1{:}\eta^5{:}\eta^5\text{-}P_5)(CpCr)_2\}]$ was detected. All attempts to isolate suitable crystals for X-ray structure analysis failed, thus with only the mass spectral data available the nature of **3** is not completely clear.



The reddish-brown complex **2** was found to be insoluble in *n*-hexane but soluble in CH_2Cl_2. Its ^{31}P NMR spectrum features only a singlet at δ = 61.7, which can be assigned to the Cr_2P_2 part of the molecule.

The molecular structure of **2** is shown in Figure 2. It consists of a triple-decker sandwich and a tetrahedral Cr_2P_2 core bridged by two $[Mo(CO)_4]$ moieties, which results in a planar, six-membered Mo_2P_4 ring. Each Mo atom resides in a sixfold coordination environment made up of two P atoms, one from each of the $[\{CpCr(CO)_2\}_2(\mu,\eta^2\text{-}P_2)]$ and $[(CpCr)_2(\mu,\eta^5{:}\eta^5\text{-}P_5)]$ fragments, along with four carbonyl groups. This molecule represents the first example of a complex containing a tetrahedron as well as both five- and six-membered rings. The P_4Mo_2 and *cyclo*-P_5 moieties are coplanar and are connected by a shared P_2 edge. Scherer et al. have reported the complex $[\{[CpMo(CO)_2]_2(\mu,\eta^2{:}\eta^1{:}\eta^1\text{-}P_2)\}_2\{Re(CO)_3Br\}_2]$,[8] in which the two Re atoms and the P_2 units of two tetrahedral $[\{CpMo(CO)_2\}_2(\mu,\eta^2\text{-}P_2)]$ fragments form a planar six-membered ring. Due to the coordination to the $[Mo(CO)_4]$ moieties in **2**, the P(2)−P(2A) distance [2.438(5) Å] in the P_5 ring is lengthened as compared to those in $[(CpCr)_2(\mu,\eta^5{:}\eta^5\text{-}P_5)]$ [*d*(P−P) = 2.276(2)−2.206(3) Å]. The bond lengths and angles in the coordinated Cr_2P_2 tetrahedron in **2** differ very little from those in the uncoordinated molecule. The Mo−P bond lengths in **2** [2.517(2) and 2.541(2) Å] are slightly longer than that in $[\{CpCr(CO)_2\}_2(\mu,\eta^2{:}\eta^1{:}\eta^1\text{-}P_2)\{Mo(CO)_5\}_2]$ (2.506 Å).[9]

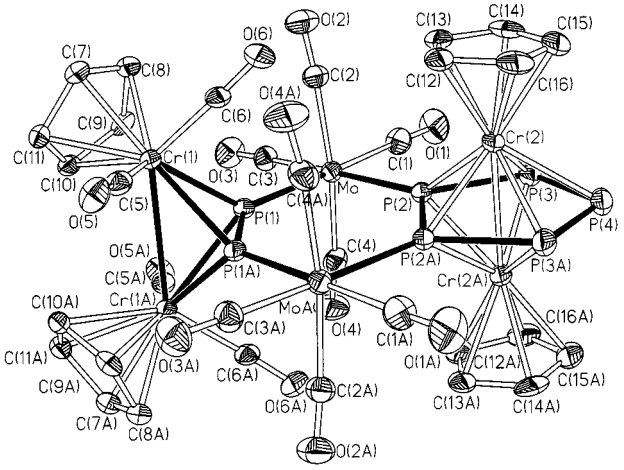


Figure 2. Molecular structure of **2** (ellipsoids drawn at a 30% probability level, H atoms of the Cp ligands are omitted for clarity); selected bond lengths [Å] and angles [°]: Mo−P(1) 2.517(2), Mo−P(2) 2.541(2), Cr(1)−Cr(1A) 3.019(1), Cr(2)−Cr(2A) 2.728(3), Cr(1)−P(1) 2.329(2), Cr(1)−P(1A) 2.514(2), Cr(1A)−P(1) 2.514(2), Cr(1A)−P(1A) 2.329(2), P(1)−P(1A) 2.087(4), P(2)−P(2A) 2.438(5), P(2)−P(3) 2.276(3), P(3)−P(4) 2.206(3), P(4)−P(3A) 2.206(3), P(4)−P(2A) 2.276(3); P(1)−Mo−P(2) 88.39(7), Cr(1)−P(1)−Mo 137.54(9), Cr(2)−P(2)−Mo 144.33(9), P(1A)−P(1)−Mo 138.87(5), P(2A)−P(2)−Mo 132.66(5)

EPR Investigations

The room-temperature X-band EPR spectrum of a CH_2Cl_2 solution of **1** consists of one line with a linewidth of $\Delta B_{pp} \approx 5$ mT and shows no hyperfine interactions. At low temperatures (T = 130 K), an EPR spectrum character-

ized by an axially symmetric $\boldsymbol{g}$ tensor is observed. Again, no hyperfine interactions can be detected. This spectrum is reproduced in Figure 3. The g values detected are given in Table 1.

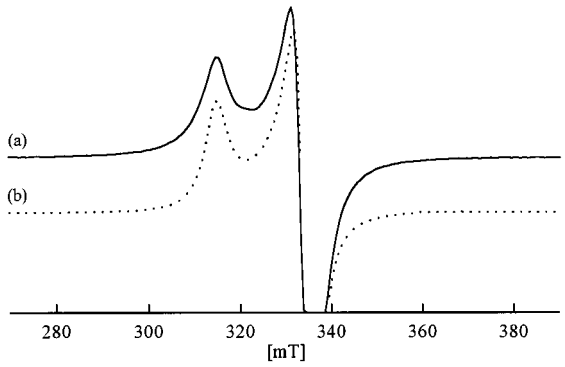


Figure 3. Experimental (a) and simulated (b) X-band EPR spectrum of **1** in CH_2Cl_2 at $T = 130$ K

Table 1. EPR parameters of **1** and **2**; hyperfine coupling constants are given in [10^{-4} cm^{-1}]

	1[a]		**2**[a]
$g_\perp$	2.018	g_1	1.991
$g_\parallel$	2.145	g_2	2.021
g_{av}[b]	2.060	g_3	2.048
g_0	2.073	g_{av}[c]	2.020
A^P_1	[d]	A^P_1	17.2
A^P_2	[d]	A^P_2	16.0
A^P_3	[d]	A^P_3	24.6
$A^P{}_{av}$[c]	–	$A^P{}_{av}$[c]	19.3

[a] Experimental error: $g_i \pm 0.003$; $A^P{}_i \pm 1.0$. – [b] $g_{av} = (2g_\perp + g_\parallel)/3$. – [c] $g_{av} = (g_1 + g_2 + g_3)/3$; $A^P{}_{av} = (A^P{}_1 + A^P{}_2 + A^P{}_3)/3$. – [d] Not resolved.

For compound **2**, the EPR spectrum recorded in THF at room temperature shows a 1:2:1 triplet of lines (the linewidth of $\Delta B_{pp} \approx 0.5$ mT is considerably smaller than that observed in the case of **1**), as expected for the interaction of one unpaired electron with two $I = 1/2$ nuclei (^{31}P). The derived isotropic parameters are: $g_0 = 2.022 \pm 0.002$ and $a^P_0 = (18.0 \pm 1.0) \times 10^{-4}$ cm^{-1}. The frozen-solution EPR spectrum of **2** is given in Figure 4 together with its simulation. For the simulation, the aforementioned isotropic parameters were taken into account. The main features of the spectrum can be rationalized by assuming a spin system consisting of one unpaired electron and its interaction with two equivalent ^{31}P nuclei. The derived parameters are listed in Table 1. However, the spectrum also shows some smaller splittings, possibly due to hyperfine interactions with neighbouring protons or phosphorus nuclei. Since no other signals could be detected in the accessible spectral range (neither for **1** nor for **2**), the spectra as described above were interpreted with the following "effective" spin Hamiltonian [Equation (3)].

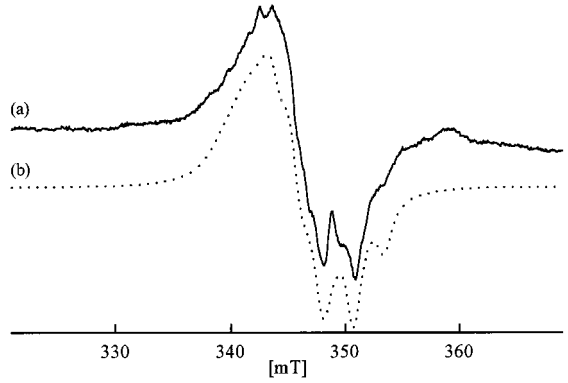


Figure 4. Experimental (a) and simulated (b) X-band EPR spectrum of **2** in THF at $T = 130$ K

$$\boldsymbol{H}_{sp} = \mu_B \cdot \boldsymbol{g} \cdot \boldsymbol{B}_0 \cdot \boldsymbol{S}' + \boldsymbol{S}' \cdot \boldsymbol{A}^P \cdot \boldsymbol{I}^P \quad (3)$$

In Equation (3), S' denotes $S = 1/2$; for compound **2**, two equivalent ^{31}P nuclei were taken into account. It should be noted that in spite of the aforementioned ^{31}P hyperfine interactions, no other hyperfine interactions (e.g. ^{53}Cr, $^{95,97}Mo$) could be detected.

The ^{31}P hyperfine parameters derived for **2** can be used to estimate the spin density on these nuclei. For this, the isotropic component A^P_{av} and the dipolar component b^P ($b^P = A^P_\perp - A^P_{av}$) of the ^{31}P coupling are needed. According to the nearly axially symmetric ^{31}P hyperfine tensor, A^P_1 and A^P_2 can be averaged to $A^P_\perp = 16.6 \cdot 10^{-4}$ cm^{-1}. Using the previously reported procedure[2c,10,11] and the atomic parameters calculated by Morton and Preston,[10] 0.5% and 2.2% of the spin density was calculated to reside in the 3s and 3p orbitals of P, respectively. Thus, 5.4% of the overall spin density is located on the two P atoms observed in the spectra. Since no other hyperfine interactions (e.g. $^{95,97}Mo$) could be successfully analysed for the $Cr_4Mo_2P_7$ unit of **2**, the bulk of the electron spin density seems to be localized in a $Cp_2Cr_2P_2$ unit, thereby accounting for the observed ^{31}P hyperfine interactions with the bridging P atoms of the P_5 ring.

Conclusions

Although the initial goal of the synthesis of a metal-linked dimer of tetrahedral Cr_2P_2 complexes has not been achieved, the interesting reactivity of [{$CpCr(CO)_2$}$_2$(μ,η^2-P_2)] has led to the generation of the unexpected product **2**. The formation of **1** and **2** under mild conditions is suggestive of preferential transformation to a triple-decker sandwich complex [$(CpCr)_2$(μ,η^5:η^5-P_5)], even when this forms a part of more complex molecules, giving rise to novel structural features. This characteristic has previously been observed in the reaction of [{$CpCr(CO)_2$}$_2$(μ,η^2-P_2)] with $LiBEt_3H$, where the complex [{[$CpCr(CO)_2$]$_2$(μ-PH)}{$(CpCr)_2$(μ,η^1:η^1:η^5:η^5-P_5)}] [2c] was formed as a side-product. In contrast to the situation in the analogous tetrahedral M_2P_2 ligand complexes of molybdenum and tungsten, the weaker Cr–Cr bond in [{$CpCr(CO)_2$}$_2$(μ,η^2-P_2)]

has been shown to be largely responsible for the unusual reactivity behaviour of this species. The formation of a triple-decker sandwich complex in **2** is one of its consequences. This effect is also observed in the reactions of $[\{CpCr(CO)_2\}_2(\mu,\eta^2\text{-}P_2)]$ with ECl_3 (E = P, As, Sb), which furnish the corresponding mixed *cyclo*-P_2E ligand complexes under elimination of $[CpCrCl_2]_2$.[2d] Further investigation of this interesting behaviour of $[\{CpCr(CO)_2\}_2(\mu,\eta^2\text{-}P_2)]$ is part of our ongoing research.

Experimental Section

General Techniques: All reactions and manipulations were performed under dry argon using standard Schlenk techniques. Solvents were dried and distilled under argon prior to use, toluene and THF with Na/benzophenone, hexane with $LiAlH_4$, dichloromethane with P_2O_5. – IR spectra were recorded with a Bruker IFS 28 FT-IR spectrometer, mass spectra with a Finnigan MAT 711 spectrometer at 70 eV. Satisfactory elemental analyses were obtained with an Elementar Vario EL at the Institute of Inorganic Chemistry, University of Karlsruhe.

Reaction of $[\{CpCr(CO)_3\}_2]$ with P_4: Dry P_4 (0.92 g, 7.45 mmol) was added to a deep-green solution of $[\{CpCr(CO)_3\}_2]$ (3.0 g, 7.45 mmol) in toluene (75 mL) and the resulting mixture was stirred at 90 °C for 5 h. The reddish-brown solution was then filtered through silica gel and the filtrate was concentrated to dryness in vacuo. The unchanged P_4 was removed by sublimation prior to chromatography. Chromatographic workup on a silica gel column (40 × 3.0 cm) eluting with *n*-hexane yielded a trace amount of unchanged P_4 followed by a yellowish-brown fraction containing $[CpCr(CO)_2(\eta^3\text{-}P_3)]$ (0.3 g, 1.13 mmol, 7.5%). Elution with *n*-hexane/toluene (2:1) gave a yellow fraction that turned brown, from which black crystals of $[CpCr(CO)(\eta^3\text{-}P_3)(CpCr)_2(\mu,\eta^1{:}\eta^5{:}\eta^5\text{-}P_5)]$ (**1**) (1.0 g, 1.59 mmol, 33% yield) crystallized. Using *n*-hexane/toluene (1:1) as eluent, a magenta-coloured fraction containing $[\{CpCr(CO)_2\}_2(\mu,\eta^2\text{-}P_2)]$ (1.1 g, 2.69 mmol, 36%) followed by a golden-brown fraction containing $[\{CpCr(CO)_2\}_5P_{10}]$ (1.2 g, 1.02 mmol, 7%) were obtained (yields are calculated on the basis of $[\{CpCr(CO)_3\}_2]$).

1: IR [KBr, ν(CO)/cm^{-1}]: 1897 (s, br). – ^{1}H NMR (250.13 MHz, CD_2Cl_2, TMS, 301 K): δ = 4.21 (br. s, $CpCrP_3$), 19.48 [br. s, $(CpCr)_2P_5$]. – EI-MS (70 eV, 150 °C): *m*/*z* (%) = 389 (100) $[Cp_2Cr_2P_5]$, 327 (86) $[Cp_2Cr_2P_3]$, 262 (6) $[CpCr_2P_3]$, 238 (24) $[CpCr(CO)P_3]$, 210 (59) $[CpCrP_3]$, 200 (12) $[CpCr_2P]$, 182 (74) $[CrCp_2]$, 135 (6) $[Cp_2Cr]$, 124 (33) $[P_4]$, 117 (60) [CrCp]. – $C_{16}H_{15}Cr_3OP_8$ (627.1): calcd. C 30.65, H 2.41; found C 30.05, H 2.61.

Reaction of $[\{CpCr(CO)_2\}_2(\mu,\eta^2\text{-}P_2)]$ with $[Mo(CO)_4(NBD)]$: $[\{CpCr(CO)_2\}_2(\mu,\eta^2\text{-}P_2)]$ (100 mg, 0.245 mmol) and $[Mo(CO)_4(NBD)]$ (74 mg, 0.245 mmol) were dissolved in THF (40 mL) and the resulting mixture was stirred at room temperature for 3 h. The solvent was then removed in vacuo. Chromatographic workup on a silica gel column (35 × 2.5 cm) eluting with *n*-hexane/CH_2Cl_2 (1:1) gave a magenta-coloured solution of unchanged $[\{CpCr(CO)_2\}_2(\mu,\eta^2\text{-}P_2)]$ (25 mg, 25%), a trace amount of $[Mo(CO)_4(NBD)]$, followed by a reddish-brown fraction containing $[\{CpCr(CO)_2\}_2(\mu,\eta^1{:}\eta^1{:}\eta^2\text{-}P_2)\{Mo(CO)_4\}_2\{(\mu,\eta^1{:}\eta^1{:}\eta^5{:}\eta^5\text{-}P_5)(CpCr)_2\}]$ (**2**) (50 mg, 34%). Elution with *n*-hexane/CH_2Cl_2 (1:3) yielded a dark-brown fraction containing **3** (20 mg).

2: IR [CH_2Cl_2, ν(CO)/cm^{-1}]: 2070 (w), 2023 (w), 1942 (s, br). – ^{31}P NMR (101.256 MHz, C_6D_6, 85% H_3PO_4): δ = 61.7 (s). – ^{1}H NMR (250.13 MHz, CD_2Cl_2, TMS, 301 K): δ = 3.38 (br. s, Cr_2P_2). – EI-MS (70 eV, 350 °C): *m*/*z* (%) = 989 (1) $[M^+ - 8CO]$, 840 (5) $[M^+ - Cp - 11CO]$, 676 (2) $[Cp_3Cr_4P_7(CO)_2]$. – **3**: IR [CH_2Cl_2, ν(CO)/cm^{-1}]: 2072 (w), 2020 (s), 1977 (s), 1940 (vs, br). – ^{31}P NMR (101.256 MHz, C_6D_6, 85% H_3PO_4): δ = −58.9 (s). – EI-MS (70 eV, 370 °C): *m*/*z* (%) = 1071 (0.02) $[Cp_3Cr_3P_8Mo_2(CO)_8]$,

Table 2. Crystallographic data for **1** and **2**

	1	**2** · 5 CH_2Cl_2
Empirical formula	$C_{16}H_{15}Cr_3OP_8$	$C_{37}H_{30}Cl_{10}Cr_4Mo_2O_{12}P_7$
M_w	627.04	1637.78
Crystal size [mm]	0.30 × 0.08 × 0.01	0.22 × 0.19 × 0.04
T [K]	200(1)	200(1)
Space group	monoclinic	monoclinic
Crystal system	$P2_1/n$	$C2/c$
a [Å]	15.995(3)	25.086(5)
b [Å]	7.2200(14)	19.073(4)
c [Å]	20.321(4)	15.341(3)
β [°]	112.38(3)	127.70(3)
V [Å^3]	1490.7(5)	5808(2)
Z	4	4
d_c [g/cm^3]	1.919	1.873
μ_c [mm^{-1}]	2.073	1.846
F(000)	1244	3212
diffractometer	STOE IPDS	STOE IPDS
2Θ range [°]	4.34 ≤ 2Θ ≤ 47.92	2.96 ≤ 2Θ ≤ 47.92
hkl range	−18 ≤ *h* ≤ 18	−28≤ *h* ≤ 27
	−7 ≤ *k* ≤ 8	−20 ≤ *k* ≤ 21
	−23 ≤ *l* ≤ 23	−17 ≤ *l* ≤ 17
Data/restraints/parameters	3150/0/253	4406/18/339
Independent reflections [$I > 2\sigma(I)$]	2283 (R_{int} = 0.0689)	2567 (R_{int} = 0.1052)
Goodness-of-fit on F^2	0.972	0.900
R_1,[a] wR_2 [b] [$I > 2\sigma(I)$]	0.0493, 0.1180	0.0630, 0.1447
R_1,[a] wR_2 [b] [all data]	0.0715, 0.1261	0.1042, 0.1627
largest diff. peak/hole [e Å^{-3}]	1.012, −0.524	1.291, −0.802

[a] $R = |F_o| - |F_c||/|F_o|$. – [b] $wR_2 = [\omega(F_o^2 - F_c^2)^2]/[(F_o^2)^2]^{1/2}$

857 (29) [$Cp_2Cr_3P_5Mo_2(CO)_8$], 844 (24) [$Cp_3Cr_3Mo_2P_7(CO)_3$], 502 (13) [$Cr_3P_5Mo_2$].

X-ray Structure Determination and Details of the Refinement: Data were collected with a STOE IPDS area detector diffractometer using Mo-K_α (λ = 0.71069 Å) radiation. Machine parameters, crystal data, and data collection parameters are summarized in Table 2. The structures were solved by direct methods using SHELXS-86[12a] and refined by full-matrix least-squares methods on F^2 using SHELXL-93[12b] with anisotropic displacement factors for non-H atoms; hydrogen atoms were placed in idealized positions and refined isotropically according to the riding model. Crystallographic data (excluding structure factors) for the structures reported in this paper have been deposited with the Cambridge Crystallographic Data Centre as supplementary publication nos. CCDC-142655 and -142656. Copies of the data can be obtained free of charge on application to CCDC, 12 Union Road, Cambridge CB2 1EZ, U.K. [Fax: (internat.) + 44-1223/336-033; E-mail: deposit@ccdc.cam.ac.uk.

EPR Measurements: EPR spectra were recorded in the X-band ($\nu \approx 9.5$ GHz) with a Bruker ESP 300E spectrometer in the temperature range 295−130 K using ca. 10^{-2}−10^{-3} M solutions of **1** (CH_2Cl_2) and **2** (THF). After cooling the samples, the formation of a good "glass" was proven. The EPR parameters were obtained using a modified version of the computer program written by White and Belford.[13,14]

Acknowledgments

The authors thank the Deutsche Akademische Austauschdienst (S. U.), the Deutsche Forschungsgemeinschaft, and the Fonds der Chemischen Industrie for comprehensive financial support.

[1] Reviews: [1a] M. Scheer, E. Herrmann, *Z. Chem.* **1990**, *30*, 41−55. − [1b] O. J. Scherer, *Angew. Chem.* **1990**, *102*, 1137−1155; *Angew. Chem. Int. Ed. Engl.* **1990**, *29*, 1104. − [1c] M. Di Vaira, P. Stoppioni, *Coord. Chem. Rev.* **1992**, *120*, 259−279. − [1d] K. H. Whitmire, *Adv. Organomet. Chem.* **1998**, *42*, 1−145.

[2] [2a] M. Scheer, M. Dargatz, P. G. Jones, *J. Organomet. Chem.* **1993**, *447*, 259−264. − [2b] M. Scheer, U. Becker, *Phosphorus Sulfur Silicon* **1994**, *93−94*, 257−260. − [2c] P. Sekar, M. Scheer, A. Voigt, R. Kirmse, *Organometallics* **1999**, *18*, 2833−2837. − [2d] S. Umbarkar, P. Sekar, M. Scheer, *J. Chem. Soc., Dalton Trans.* **2000**, 1135−1137.

[3] [3a] M. Di Vaira, P. Stoppioni, M. Peruzzini, *J. Chem. Soc., Dalton Trans.* **1990**, 109−113. − [3b] M. Di Vaira, D. Rovai, P. Stoppioni, *Polyhedron* **1990**, *9*, 2477−2481. − [3c] M. Di Vaira, P. Stoppioni, S. Midollini, F. Laschi, P. Zanello, *Polyhedron* **1991**, *10*, 2123−2129. − [3d] G. Cappozzi, L. Chiti, M. Di Vaira, M. Peruzzini, P. Stoppioni, *J. Chem. Soc., Chem. Commun.* **1986**, 1799−1800. − [3e] M. Peruzzini, J. A. Ramirez, F. Vizza, *Angew. Chem.* **1998**, *110*, 2376−2378; *Angew. Chem. Int. Ed.* **1998**, *37*, 2255−2257. − [3f] P. Barbaro, M. Peruzzini, A. J. Ramirez, F. Vizza, *Organometallics* **1999**, *18*, 4237−4240.

[4] [4a] O. J. Scherer, G. Berg, G. Wolmershäuser, *Chem. Ber.* **1995**, *128*, 635−639. − [4b] M. Detzel, T. Mohr, O. J. Scherer, G. Wolmershäuser, *Angew. Chem.* **1994**, *106*, 1142−1144; *Angew. Chem. Int. Ed. Engl.* **1994**, *33*, 1110−1112. − [4c] M. Detzel, G. Friedrich, O. J. Scherer, G. Wolmershäuser, *Angew. Chem.* **1995**, *107*, 1454−1456; *Angew. Chem. Int. Ed. Engl.* **1995**, *34*, 1321−1323. − [4d] O. J. Scherer, S. Weigel, G. Wolmershäuser, *Chem. Eur. J.* **1998**, *4*, 1910−1916.

[5] [5a] J. E. Davies, M. J. Mays, P. R. Raithby, G. P. Shields, P. K. Tompkin, *Chem. Commun.* **1997**, 361−362. − [5b] J. E. Davies, L. C. Kerr, M. J. Mays, P. R. Raithby, P. K. Tompkin, A. D. Woods, *Angew. Chem.* **1998**, *110*, 1473−1475; *Angew. Chem. Int. Ed.* **1998**, *37*, 1428−1429. − [5c] J. E. Davies, M. C. Klunduk, M. J. Mays, P. R. Raithby, G. P. Shields, P. K. Tompkin, *J. Chem. Soc., Dalton Trans.* **1997**, 715−719. − [5d] K. V. Adams, N. Choi, G. Conole, J. E. Davies, J. D. King, M. J. Mays, M. McPartlin, P. R. Raithby, *J. Chem. Soc., Dalton Trans.* **1999**, 3679−3686. − [5e] J. E. Davies, N. Feeder, M. J. Mays, P. K. Tompkin, A. D. Woods, *Organometallics* **2000**, *19*, 984−993.

[6] [6a] L. Y. Goh, C. K. Chu, R. C. S. Wong, T. W. Hambley, *J. Chem. Soc., Dalton Trans.* **1989**, 1951−1956. − [6b] L. Y. Goh, R. C. S. Wong, C. K. Chu, T. W. Hambley, *J. Chem. Soc., Dalton Trans.* **1990**, 977−982. − [6c] L. Y. Goh, R. C. S. Wong, E. Sinn, *Organometallics* **1993**, *12*, 888−894.

[7] A. K. Hughes, V. J. Murphy, D. O'Hare, *J. Chem. Soc., Chem. Commun.* **1994**, 163−164.

[8] O. J. Scherer, H. Sitzmann, G. Wolmershäuser, *Angew. Chem.* **1984**, *96*, 979−980; *Angew. Chem. Int. Ed. Engl.* **1984**, *23*, 931−932.

[9] L. Y. Goh, R. C. S. Wong, W. Ru-Ji, T. C. W. Mak, *Jiegou Huaxue* **1991**, *10*, 89−92.

[10] J. R. Morton, K. F. Preston, *J. Magn. Reson.* **1978**, *30*, 577.

[11] R. Kirmse, J. Stach, *ESR-Spektroskopie-Anwendungen in der Chemie*, Akademie-Verlag, Berlin, **1985**, p. 86−95.

[12] [12a] G. M. Sheldrick, *SHELXS-86*, University of Göttingen, **1986**. − [12b] G. M. Sheldrick, *SHELXL-93*, University of Göttingen, **1993**.

[13] L. K. White, R. L. Belford, *J. Am. Chem. Soc.* **1976**, *98*, 4428.

[14] L. K. White, Dissertation, Urbana, IL, **1975**; revised version written by K. Köhler and R. Böttcher, University of Leipzig, **1990**.

Received April 11, 2000
[I00141]

Novel Main Group-Transition Metal Cluster Compounds Incorporating Antimony, Iron and Cobalt

Thomas Gröer,[a] Tobias Palm,[a] and Manfred Scheer*[a]

Dedicated to Professor Herbert W. Roesky on the occasion of his 65th birthday

Keywords: Antimony / Iron / Cobalt / Cluster / Polyhedra

The reaction of [{$Cp^x(CO)_2Fe$}$SbCl_2$] [**1a**: $Cp^x = \eta^5$-$C_5H_3tBu_2$-1,3 (Cp"); **1b**: $Cp^x = \eta^5$-C_5Me_5 (Cp*)] with $Na_2[Fe(CO)_4]$ or $K[Co(CO)_4]$ affords the novel antimony-transition metal cluster compounds [{μ_3-$SbFe(CO)_2Cp"$}$_3${$Fe(CO)_3$}$_4$] **(2)**, [{$Fe_3(CO)_9$}{μ_3-$SbFe(CO)_2Cp"$}$_2$] **(3)** and [{μ_4-$SbFe(CO)_2$-Cp^*}$_2${$Co_4(CO)_{10}(\mu$-CO)}] **(4)**. All products were characterised by X-ray structure analyses and other methods. Cluster **2** reveals a novel Sb_3Fe_4 core, which does not follow the Wade–Mingos rules. Cluster **3** forms a square-pyramidal *nido*-cluster. The Sb_2Co_4 cluster core of **4** derives from a pentagonal bipyramid and consists of apical Sb and equatorial Co atoms with one missing pentagonal core atom.

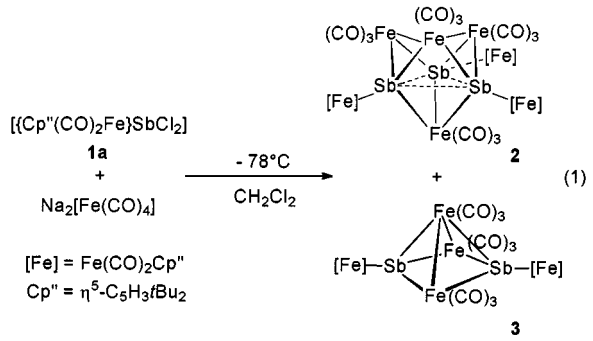
Introduction

Clusters which incorporate main group elements and transition metals together in a core framework have been of wide interest in the last years.[1] We are particularly interested in complexes which contain the heavy group 15 elements Sb and Bi. Amongst those, only a few examples of antimony-rich complexes have been prepared, e.g. [{$Mo(CO)_3Cp^x$}$_2$(μ,η^2-Sb_2)] (Cp^x = Cp,[2] Cp*[3]) [(μ,η^2-Sb_2){$W(CO)_5$}$_3$],[4] and [{$Mo(CO)_2Cp^x$}(η^3-Sb_3)][3] (Cp^x = Cp, Cp*). The synthetic approach to these clusters is versatile: they can be prepared either by metalation of $SbCl_3$, reaction of elemental antimony with transition metal complexes or from cyclic organo-antimony precursors.

Even though there is a large variety of synthetic methods to yield these cluster compounds, a rational way of preparing them is still missing. Recently, we reported the synthesis and structure of transition metal-substituted dichlorides of antimony and bismuth of the formula [{$Cp"(CO)_2Fe$}ECl_2] [E = Sb **(1a)**, Bi].[5] These complexes have interesting properties for the building-up of main group element-transition metal clusters of varying composition in a straightforward manner. This might be feasible by either using reducing agents (e.g. Mg) to yield (μ_3-E) bridged binary compounds[5] or by incorporating other transition metals from a reaction with metalates. This latter reaction was successfully used to prepare phosphorus rich complexes starting from $[Cp(CO)_3WPCl_2]$.[6] We herein report the synthesis and structures of novel antimony-containing main group-transition metal cluster compounds.

Results and Discussion

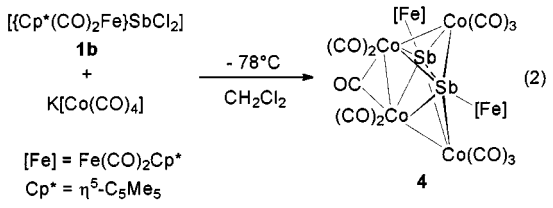
The reaction of [{$Cp"(CO)_2Fe$}$SbCl_2$] **(1a)** with $Na_2[Fe(CO)_4]$ yields the novel cluster compound [{μ_3-$SbFe(CO)_2Cp"$}$_3${$Fe(CO)_3$}$_4$] **(2)** as the main product and smaller amounts of [{μ_3-$SbFe(CO)_2Cp"$}$_2${$Fe_3(CO)_9$}] **(3)** [Equation (1)]. While it was possible to isolate **2** as a pure compound by fractional crystallisation, the minor product **3** always co-crystallises with **2**. Attempts to separate these mixtures by column chromatography on silica gel or aluminium oxide failed due to the decomposition of the products. The complex [{$Cp^*(CO)_2Fe$}$SbCl_2$] **(1b)** reacts with two equivalents of $K[Co(CO)_4]$ to form [{μ_4-$SbFe(CO)_2$-Cp^*}$_2${$Co_4(CO)_{10}(\mu$-CO)}] **(4)** [Equation (2)] and some $[Cp^*(CO)Fe(\mu\text{-}CO)_2Co(CO)_3]$ **(5)**. The occurrence of **5** is a hint that, as a side-reaction, a metal-antimony bond cleavage occurs — as it was also reported for the reaction of **1a** with magnesium.[5] Complex **5** has already been structurally characterised,[7] and our X-ray[8] and spectroscopic data are similar to the reported values.



All complexes were isolated as red crystalline compounds, which are readily soluble in *n*-hexane or toluene. In the IR spectra of compounds **2**–**4**, the CO stretching frequencies for terminal CO groups are detected, whereas for cluster **4** an addition band at 1779 cm^{-1} for a bridging

[a] Institut für Anorganische Chemie der Universität Karlsruhe, 76128 Karlsruhe, Germany
Fax: (internat.) +49-721/661-921
E-mail: mascheer@achibm6.chemie.uni-karlsruhe.de

 © WILEY-VCH Verlag GmbH, D-69451 Weinheim, 2000 1434–1948/00/1212–2591 $ 17.50+.50/0



CO group is found. In the ^{1}H NMR spectrum of **2** at ambient temperature the *t*Bu groups and the protons on the Cp" rings are inequivalent. At a temperature of 368 K the two signals of the methyl protons coalesce indicating the free rotation of the Cp" ligands. The free activation enthalpy of this process at the coalescence temperature (T_c = 368 K) is calculated to be $\Delta G^{\#}_{Tc}$ = 80 kJ/mol.

An X-ray structure analysis of **2** reveals a central Sb_3Fe tetrahedron, the Sb_3 and two Sb_2Fe planes of which are capped by three $Fe(CO)_3$ groups (Figure 1). The Fe atom of the tetrahedron additionally coordinates to three carbonyl ligands, whereas each antimony atom binds to an $Fe(CO)_2Cp"$ fragment. Within the Sb_3 unit two different kinds of Sb···Sb distances are observed: long distances are found around the Sb(3) atom [3.2412(9) and 3.2574(10) Å] and are much longer than known Sb−Sb single bonds as, for example, in Sb_7^{3-} [2.717(2)−2.906(2) Å],[9] $[\{Mo(CO)_2Cp^*\}(\eta^3\text{-}Sb_3)]$[3] [2.7397(9)−2.7682(8) Å], (*t*BuSb)$_4$ [2.822(1)−2.878(1) Å[10a]] or in $[(Me_3Si)_2CHSb]_3$ [2.8188(6)−2.8453(6) Å].[10b] However, the shortest distance in **2** [Sb(1)−Sb(2) = 3.0259(9) Å] is still within the range of long, bonding Sb−Sb distances as found in the compound $[\{Cp(CO)_2Fe\}\{Cr(CO)_5\}SbBr]_2$,[11] possessing the longest known Sb−Sb single bond length of 3.069(6) Å. Intermolecular Sb···Sb distances within the structure of **2** are in the range of 3.678(1)−4.271(1) Å, as found for Me_4Sb_2 [12] and $[(\eta^3\text{-}Sb_3)\{Mo(CO)_2Cp^x\}]$ (Cp^x = Cp, Cp*).[3]

The Sb_3Fe_4 cluster core of **2** is close to C_s symmetry with the symmetry plane defined by the atoms Sb(3), Fe(6) and Fe(7), which becomes evident by the similarity in the bond lengths of Fe(6)−Sb(1) and Fe(6)−Sb(2) [2.6686(14) vs. 2.6672(15) Å], and Fe(6)−Fe(5) and Fe(6)−Fe(4) [2.844(2) vs. 2.8466(18) Å] (Figure 2). Due to the steric hindrance of the bulky Cp" ligands, the molecule might not be able to adopt an overall C_s symmetry. Describing the Sb_3Fe_4 cluster core of the 20 skeletal electrons by the Wade−Mingos rules does not lead to a satisfactory explanation of the adopted polyhedron. An explanation can be given using the concept of "Topological Electron Counting" (TEC), as suggested by Teo[13] for the relation between cluster geometry and valence electrons in transition metal clusters. Using this relation with mixed transition metal-main group element clusters, the number of bonding orbitals (CVMO) will count to $CVMO = 8X + 3N - F + 2$ (X = number of transition elements; N = number of main group elements; F = number of polyhedral faces). In the case of the cluster core in compound **2** this results in a CVMO of 34 on assuming bonding Sb−Sb interactions. Calculating the number of cluster electrons by EAN rules leads to 68, which fits with the number of bonding cluster orbitals. To the best of our knowledge this polyhedron is so far unique for a main group transition metal cluster.

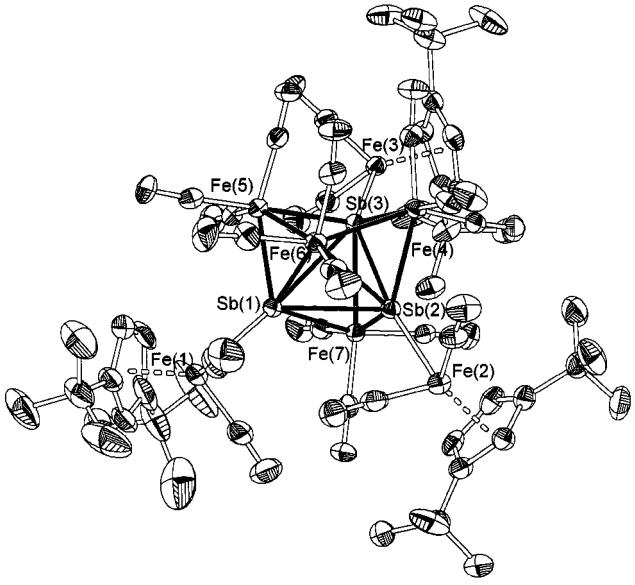


Figure 1. Molecular structure of $[\{\mu_3\text{-}SbFe(CO)_2Cp"\}_3\{Fe(CO)_3\}_4]$ **(2)** showing 30% probability ellipsoids; hydrogen atoms are omitted for clarity; selected bond lengths [Å]: Sb(1)−Sb(2) 3.0259(9), Sb(1)−Sb(3) 3.2412(9), Sb(2)−Sb(3) 3.2574(10), Sb(1)−Fe(1) 2.5917(14), Sb(1)−Fe(5) 2.5170(14), Sb(1)−Fe(6) 2.6686(14), Sb(1)−Fe(7) 2.6337(13), Sb(2)−Fe(2) 2.5921(16), Sb(2)−Fe(4) 2.5311(13), Sb(2)−Fe(6) 2.6672(15), Sb(2)−Fe(7) 2.6076(14), Sb(3)−Fe(3) 2.6415(14), Sb(3)−Fe(4) 2.6312(14), Sb(3)−Fe(5) 2.6157(13), Sb(3)−Fe(7) 2.6833(12), Fe(6)−Fe(5) 2.844(2), Fe(6)−Fe(4) 2.8466(18)

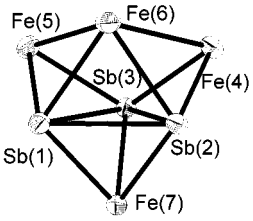


Figure 2. Sb_3Fe_4 cluster core in **2**

The structure of the compound $[\{\mu_3\text{-}SbFe(CO)_2Cp"\}_2\{Fe_3(CO)_9\}]$ **(3)** is built up of a tetragonal pyramid of three Fe and two Sb atoms, with the two Sb and two of the Fe atoms alternately building the base square (Figure 3). The third Fe atom is at the top of the pyramid. Each Sb atom is additionally bound to a $Fe(CO)_2Cp"$ moiety. On using the Wade−Mingos rules on the Sb_2Fe_3 cluster core, an electron count comes to 14 skeletal electrons, which is the same number as in *nido*-pentaborane B_5H_9, which also forms a square pyramid. A similar cluster framework has been found for the lighter congeners of Sb within $[\{Fe_3(CO)_9\}\{\mu_3\text{-}PFe(CO)_2Cp\}_2]$[14] and $[\{Fe_3(CO)_9\}\{\mu_3\text{-}AsMo(CO)_3Cp\}_2]$.[15] The Fe−Fe distances within the $Fe_3(CO)_9$ fragment in **3** are 2.823(2) Å and 2.814(2) Å. The Fe−Fe bond length is dependent on the atomic radius of the pnicogenido atom, and decreases from **3** through $[\{Fe_3(CO)_9\}\{\mu_3\text{-}AsMo(CO)_3Cp\}_2]$ [2.726(2) and 2.750(2) Å] to $[\{Fe_3(CO)_9\}\{\mu_3\text{-}PFe(CO)_2Cp\}_2]$ [2.704(3) and 2.718(4) Å]. In compound **3** there is no bonding interaction

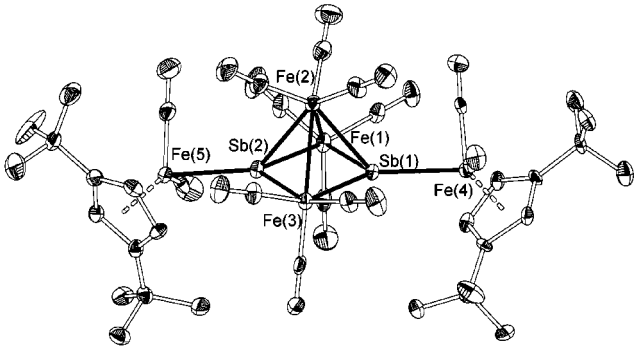


Figure 3. Molecular structure of $[\{\mu_3\text{-SbFe}(CO)_2Cp''\}_2\{Fe_3(CO)_9\}]$ **(3)** showing 30% probability ellipsoids; hydrogen atoms are omitted for clarity; selected bond lengths [Å] and angles [°]: Sb(1)−Fe(1) 2.5075(19), Sb(1)−Fe(2) 2.543(2), Sb(1)−Fe(3) 2.530(2), Sb(1)−Fe(4) 2.5518(19), Sb(2)−Fe(1) 2.512(2), Sb(2)−Fe(3) 2.5240(18), Sb(2)−Fe(2) 2.5529(18), Sb(2)−Fe(5) 2.5607(18), Sb(1)···Sb(2) 3.1705(15), Fe(1)−Fe(2) 2.823(2), Fe(2)−Fe(3), 2.814(2); Fe(1)−Sb(1)−Fe(3) 101.94(7), Fe(1)−Sb(2)−Fe(3) 101.97(7), Sb(1)−Fe(1)−Sb(2) 78.34(6), Sb(2)−Fe(3)−Sb(1) 77.71(6), Fe(1)−Sb(1)−Fe(4) 121.74(6), Fe(3)−Sb(1)−Fe(4) 136.28(6), Fe(2)−Sb(1)−Fe(4) 128.54(6), Fe(1)−Sb(2)−Fe(5) 125.27(6), Fe(2)−Sb(2)−Fe(5) 135.23(7), Fe(3)−Sb(2)−Fe(5) 131.87(6), Fe(3)−Fe(2)−Fe(1) 87.92(7)

between Fe(1) and Fe(3) [Fe(1)···Fe(3) = 3.913(2) Å]. All Sb−Fe bond lengths are within the small range of 2.5075(19) [Sb(1)−Fe(1)] and 2.5607(18) Å [Sb(2)−Fe(5)] and are therefore shorter than the Sb−Fe bond lengths in **2**. The Sb···Sb distance is 3.1705(15) Å. The folding angle between the two planes defined by Sb(1), Fe(1) and Sb(2), and Sb(1), Fe(3) and Sb(2), respectively, is 178.29(2)° and hence close to planarity. It is similar to that of the dianionic *nido*-cluster $[\{Fe_3(CO)_9\}(\mu_3\text{-SbFe}(CO)_4)_2]^{2-}$ [174.54(3)°].[16a] At first sight, the structures of this compound and of its homologues $[\{Fe_3(CO)_9\}(\mu_3\text{-EFe}(CO)_4)_2]^{2-}$ (E = As,[16b] Bi[16c]) seem to be similar to **3**; however, in these dianionic complexes the lone pair of the pnicogens coordinates to an exocyclic $Fe(CO)_4$ group,[16d] whereas in **3** a σ-bond exists to exocyclic $CpFe(CO)_2$ moieties.

The X-ray structure analysis of **4** (Figure 4) shows a central Sb_2Co_2 tetrahedron, two planes of which are capped by one $Co(CO)_3$ group each. The Co−Co edge of the tetrahedron is bridged by a carbonyl ligand. Each antimony atom additionally binds to an $Fe(CO)_2Cp^*$ fragment. The Sb−Sb distance in **4** is 2.986(2) Å and hence is shorter than the distances in compound **2** [3.0259(9)−3.2574(10) Å]. The Sb−Co bond lengths [2.605(4)−2.651(3) Å] are in the known range for single bonds [2.480(1)−2.690(1) Å].[17−19]

The anionic cluster compounds $[E_2Co_4(CO)_{10}(\mu\text{-CO})]^{n-}$ (E = Sb, Bi; n = 1, 2), possessing a E_2Co_4 core similar to **4**, were first described by Whitmire[20] and Martinengo,[21] respectively. In contrast to these compounds, compound **4** is uncharged, and the electrons of the charges in the former compounds are in **4** formally located in the Sb−Fe bonds to the $Fe(CO)_2Cp^*$ fragments. This results in a longer Sb−Sb distance in **4** [2.986(2) Å] than that in $[Sb_2Co_4(CO)_{10}(\mu\text{-CO})]^{2-}$ [2.882(2) Å] and a concomitant shortening of the Co−Co bond lengths within the cluster core [2.598(5)−2.683(4) Å] compared to those in

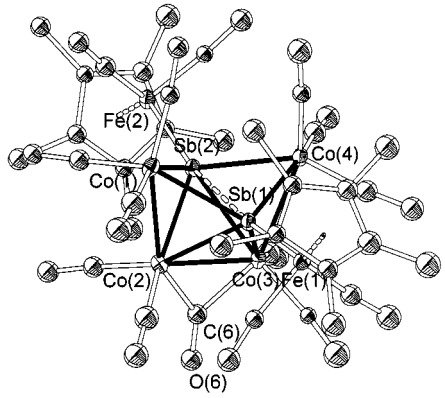


Figure 4. Molecular structure of $[\{\mu_4\text{-SbFe}(CO)_2\text{-}Cp^*\}_2\{Co_4(CO)_{10}(\mu\text{-CO})\}]$ **(4)** showing 30% probability ellipsoids; hydrogen atoms are omitted for clarity; selected bond lengths [Å] and angles [°]: Sb(1)−Sb(2) 2.986(2), Sb(1)−Fe(1) 2.599(4), Sb(2)−Fe(2) 2.606(3), Co(1)−Co(2) 2.658(5), Co(2)−Co(3) 2.598(5), Co(3)−Co(4) 2.683(4), Sb(1)−Co(1) 2.628(3), Sb(1)−Co(2) 2.653(4), Sb(1)−Co(3) 2.605(4), Sb(1)−Co(4) 2.608(4), Sb(2)−Co(1) 2.611(4), Sb(2)−Co(2) 2.614(3), Sb(2)−Co(3) 2.651(3), Sb(2)−Co(4) 2.621(4), Co(2)−C(6) 1.84(3), Co(3)−C(6) 1.93(3), C(6)−O(6) 1.20(3); Sb(1)−Co(2)−Sb(2) 69.07(9), Sb(1)−Co(3)−Sb(2) 69.23(10), Co(1)−Co(2)−Co(3) 104.78(15), Co(2)−Co(3)−Co(4) 104.47(15)

$[Sb_2Co_4(CO)_{10}(\mu\text{-CO})]^{2-}$ [2.645(5)−2.717(5) Å]. The same tendency is visible for the Sb−Co bond lengths [2.605(4)−2.653(4) Å in **4** compared to 2.616(4)−2.676(4) Å]. The Sb−Sb bond length in the monoanionic compound $[Sb_2Co_4(CO)_{10}(\mu\text{-CO})]^-$ [2.911(1) Å][20] is still shorter than in **4**, whereas the Co−Co distances in $[Sb_2Co_4(CO)_{10}(\mu\text{-CO})]^-$ tend to fall in a wider range [2.510(3)−2.725(3) Å], as do Sb−Co distances [2.605(2)−2.692(2) Å]. As for the Sb_3Fe_4 polyhedron in **2**, a description of the Sb_2Co_4 cluster core of **4** following the Wade−Mingos rules fails. A thorough MO-theoretical discussion of charged 18-electron clusters of this type and a discussion as to whether $[E_2Co_4(CO)_{10}(\mu\text{-CO})]^{2-}$ clusters are best expressed as a bicapped tetrahedron or derived from a pentagonal bipyramid was previously described by Whitmire and co-workers.[20] On this basis, for **4** we tend towards the explanation of the pentagonal bipyramid with a missing pentagonal core atom. Assuming that the structure of **4** derives from a bicapped tetrahedron, angles of 109.5° are expected, whereas only 108° is necessary for a pentagonal bipyramid. Angles of 104.78(15) and 104.47(15) for Co(1)−Co(2)−Co(3) and Co(2)−Co(3)−Co(4), respectively, are found within **4** and are even smaller than necessary, whereas the angles of the tetrahedral faces Sb(1)−Co(2)−Sb(2) [69.07(9)°] and Sb(1)−Co(3)−Sb(2) [69.23(10)°] are larger than the expected 60° for a bicapped tetrahedron.

Conclusions

In contrast to reactions of $[\{Cp^x(CO)_2Fe\}SbCl_2]$ [Cp^x = Cp" **(1a)**; Cp^x = Cp* **(1b)**] with magnesium, which yield (μ_3-Sb) bridged binary antimony-transition metal complexes, these compounds react with transition metalates

with incorporation of a main group element moiety within a transition metal cluster framework. Only a small tendency to Sb−Sb bond formation was observed, as found for the complexes **2** and **4**. For similar reactions of phosphorus-containing starting materials of the formula $[L_nMPCl_2]$,[6] a higher tendency of P−P bond formation was discovered. The reason for this can probably be found in the stronger metallic character of Sb, and hence in the higher tendency of element−metal bond formation.

Generally, the compounds **1a,b** open a facile and rational way to generate novel main group-transition metal clusters. Starting from halogenated main group elements which already bear a transition metal function, they might even serve as a good starting point for preparing cluster compounds with different main group elements and different transition metals in a specific manner.

Experimental Section

General Techniques: All manipulations were performed under an atmosphere of dry Ar using standard Schlenk techniques. All solvents were dried by common methods and freshly distilled prior to use. NMR spectra were recorded on a Bruker AC 250 using TMS as external standard. Mass spectra were done with a Varian MAT 711. IR spectra were recorded on a Bruker IFS 28 FT-IR spectrometer. Elemental analyses were performed on a Elementar Vario EL of the institute.

Reagents: $K[Co(CO)_4]$[22] and $Na_2[Fe(CO)_4]$[23] were prepared according to literature methods. The synthesis of $[\{Cp^x(CO)_2Fe\}SbCl_2]$ (**1a:** $Cp^x = \eta^5$-$C_5H_3tBu_2$-1,3; **1b:** $Cp^x = \eta^5$-C_5Me_5) has been described previously.[5]

Synthesis of $[\{\mu_3$-$SbFe(CO)_2Cp''\}_3\{Fe(CO)_3\}_4]$ (2) and $[\{\mu_3$-$SbFe(CO)_2Cp''\}_2\{Fe_3(CO)_9\}]$ (3). To a solution of $[\{Cp''(CO)_2Fe\}SbCl_2]$ **(1a)** (0.42 g, 0.87 mmol) in 50 mL of THF at −78 °C was added $Na_2[Fe(CO)_4]$ (0.19 g, 0.87 mmol in one portion). After one hour, the solution was allowed to warm up to room temperature. The solvent was then evaporated in vacuo. Subsequently, the brown residue was dissolved in 50 mL of hexane and filtered through a column of dry SiO_2 (10 cm × 2 cm). The solution was concentrated to 30 mL and red crystals of **2** (120 mg, 23%) were obtained at 0 °C. Further concentration of the solution to 10 mL gave a mixture of **2** and **3** (457 mg).

2: IR (KBr): ν̃(CO) = 2012(m), 1997(vs), 1985(s), 1961(m), 1942(m), 1932(m), 1925(m), 1911 (m), 1897(m), 1879(s). − ^{1}H NMR (C_7D_8, 300 K): δ = 1.05 (s, 9 H), 1.10 (s, 9 H), 4.10 (dd, J = 1.9 Hz, 1 H) 5.17 (dd, J = 1.9 Hz, 1 H), 5.53 (dd, J = 1.9 Hz, 1 H); 368 K: 1.10 (s, 9 H), 4.20 (br, 1 H) 5.13 (br, 1 H), 5.30 (br, 1 H). − $C_{57}H_{63}Fe_7O_{18}Sb_3$ (1792.30): calcd. C 38.20, H 3.54; found C 37.94, H 3.23.

Synthesis of $[\{\mu_4$-$SbFe(CO)_2Cp^*\}_2\{Co_4(CO)_{10}(\mu$-$CO)\}]$ ($Cp^* = \eta^5$-C_5Me_5) (4): To a solution of $[\{Cp^*(CO)_2Fe\}SbCl_2]$ **(1b)** (0.44 g, 1 mmol) in 50 mL of THF at −78 °C was added $K[Co(CO)_4]$ (0.42 g, 2 mmol) at one go. After 1 h of stirring at this temperature the solution was allowed to warm up to room temperature. After another hour of stirring at room temperature all volatiles were evaporated in vacuo. The brown residue was dissolved in 20 mL of CH_2Cl_2 and subsequently filtered through a column of dry SiO_2 (10 cm × 2 cm). The resulting solution was reduced in vacuo to 10 mL. At 0 °C red crystals of **4** were obtained. Isolated yield: 860 mg (67%, based on **1b**). After reducing the solution to a volume of 2 mL 50 mg of $[Cp^*(CO)Fe(\mu$-$CO)_2Co(CO)_3]$ **(5)** was isolated.

4: IR (KBr): ν̃(CO) = 2004(vs), 1971(s), 1949(sh), 1779(m). − ^{1}H NMR ($CDCl_3$, 300 K): δ = 1.90 (s, 15 H). − EI-MS (70 eV): *m/z* (%) = 1281.6 (1.4) [M^+], 494.1 (10.6) [$Cp^*_2Fe_2(CO)_4^+$], 341.0 (3.3)

Table 1. Crystallographic Data for 2−4

	2	**3**	**4**
empirical formula	$C_{57}H_{63}Fe_7O_{18}Sb_3$	$C_{39}H_{42}Fe_5O_{13}Sb_2$	$C_{35}H_{30}Co_4Fe_2O_{15}Sb_2$
M_r	1792.27	1241.48	1281.51
T [K]	200(1)	200(1)	200(1)
Crystal size	0.30 × 0.20 × 0.16	0.20 × 0.08 × 0.01	0.10 × 0.10 × 0.02
Space group	$P2_1/c$	$P\bar{1}$	$P\bar{1}$
Crystal system	monoclinic	triclinic	triclinic
a [Å]	10.319(2)	9.6577(19)	10.928(2)
b [Å]	26.876(5)	9.793(2)	14.194(2)
c [Å]	26.411(5)	27.484(6)	15.792(3)
α [°]	92.67(3)	82.57(3)	67.62(3)
β [°]	90	80.45(3)	73.45(3)
γ [°]	90	63.76(3)	69.31(3)
V [Å^{-3}]	7316(3)	2294.8(8)	2086.7(7)
Z	4	2	2
d_c [g cm^{-3}]	1.627	1.797	2.040
μ_c [mm^{-1}]	2.491	2.753	3.562
2θ range [°]	4.24 ≤ 2θ ≤ 51.68	4.52 ≤ 2θ ≤ 51.82	3.56 ≤ 2θ ≤ 51.68
hkl range	−11 ≤ *h* ≤ 12	−11 ≤ *h* ≤ 11	−13 ≤ *h* ≤ 8
	−33 ≤ *k* ≤ 32	−11 ≤ *k* ≤ 11	−17 ≤ *k* ≤ 17
	−30 ≤ *l* ≤ 29	−33 ≤ *l* ≤ 30	−19 ≤ *l* ≤ 17
Data/restraints/parameters	48806/0/784	16159/0/544	8128/0/283
No. of unique data	13250 (R_{int} = 0.0986)	8252 (R_{int} = 0.1204)	6059 (R_{int} = 0.1721)
Independent reflections [$I > 2\sigma(I)$]	9503	3820	2100
Goodness-of fit on F^2	1.047	0.771	0.781
R_1,[a] wR_2[b] [$I > 2\ \sigma(I)$]	0.0609, 0.1537	0.0540, 0.0909	0.0835, 0.1828
R_1,[a] wR_2 [b] [all data]	0.0849, 0.1667	0.1356, 0.1110	0.2006, 0.2311
Largest diff. peak/hole [e·Å^{-3}]	1.059, −0.637	0.805, −1.273	1.174, −1.817

[a] $R = |F_0| - |F_c||/|F_0|$. − [b] $wR_2 = [\omega(F_0^2 - F_c^2)^2]/[(F_0^2)^2]^{1/2}$.

$[Co_2(CO)_8^+]$, 134.1 (100) [Cp*$^+$]. – $C_{35}H_{30}Co_4Fe_2O_{15}Sb_2$ (1281.54): calcd. C 32.80, H 2.36; found C 32.09, H 2.44.

X-ray Structure Determination and Details of Refinement: Data were collected on a STOE IPDS area-detector diffractometer using Mo-K_α (λ = 0.71069 Å) radiation. Machine parameters, crystal data and data collection parameters are summarised in Table 1. The structures were solved by direct methods using SHELXS-86,[24a] full-matrix least-squares refinement on F^2 in SHELXL-97[24b] with anisotropic displacement for non-H atoms (**2** and **3**), hydrogen atoms placed in idealised positions and refined isotropically according to the riding model. Due to the low crystal quality of **4**, only the heavy atoms Fe, Co and Sb were anisotropically refined, which causes relatively large values for R_1 and wR_2.

Crystal Data for [Cp*(CO)Fe(μ-CO)$_2$Co(CO)$_3$] (5): Cell dimensions: a = 8.1836(16) Å, b = 9.1759(18) Å, c = 12.139(2) Å, α = 90.51(3)°, β = 90.67(3)°, γ = 110.50(3)°, V = 853.7(3) Å^3, Z = 2, $d_{calcd.}$ = 1.626 g cm^{-3}, μ = 1.848 mm^{-1}, space group $P\bar{1}$, 6655 reflection collected, of which 3082 independent (R_{int} = 0.0389), 2656 with $I > 2\sigma(I)$. $R1$ = 0.0289, $wR2$ = 0.0789, max./min. residual electron densities 0.455 and −0.496 e Å^{-3}.

Crystallographic data (excluding structure factors) for the structures reported in this paper have been deposited with the Cambridge Crystallographic Data Centre as supplementary publication no. CCDC-143869 to -143871 (**2**–**4**) and CCDC-143985 for **5**. Copies of the data can be obtained free of charge on application to CCDC, 12 Union Road, Cambridge CB2 1EZ, UK [Fax: (internat.) + 44-1223/336-033; E-mail: deposit@ccdc.cam.ac.uk].

Acknowledgments

The authors thank the Deutsche Forschungsgemeinschaft and the Fonds der Chemischen Industrie for comprehensive financial support of this work.

[1] For reviews see: W. A. Herrmann, *Angew. Chem. Int. Ed. Engl.* **1986**, *25*, 56–76; D. Fenske, J. Ohmer, J. Hachgenei, K. Merzweiler, *Angew. Chem. Int. Ed. Engl.* **1988**, *27*, 1277–1297; M. Scheer, E. Herrmann, *Z. Chem.* **1990**, *30*, 41–55; O. J. Scherer, *Angew. Chem. Int. Ed. Engl.* **1990**, *29*, 1104–1132; O. J. Scherer, *Acc. Chem. Res.* **1999**, *32*, 751–762; K. H. Whitmire, *Adv. Organomet. Chem.* **1998**, *42*, 1–145.

[2] J. R. Harper, A. L. Rheingold, *J. Organomet. Chem.* **1990**, *390*, C36–C38.

[3] H. J. Breunig, R. Rösler, E. Lork, *Angew. Chem. Int. Ed. Engl.* **1997**, *36*, 2819–2820.

[4] G. Huttner, U. Weber, B. Sigwarth, O. Scheidsteger, *Angew. Chem. Int. Ed. Engl.* **1982**, *21*, 215–216; G. Huttner, U. Weber, L. Zsolnai, *Z. Naturforsch.* **1982**, *37B*, 707–721.

[5] T. Gröer, M. Scheer, *J. Chem. Soc., Dalton Trans.* **2000**, 647–653.

[6] T. Gröer, M. Scheer, *Z. Anorg. Allg. Chem*. **2000**, *626*, 1211–1216.

[7] M. Akita, M. Terada, N. Ishii, H. Hirakawa, Y. Moro-oka *J. Organomet. Chem*. **1994**, *473*, 175–186.

[8] We solved the structure of [Cp*(CO)Fe(μ-CO)$_2$Co(CO)$_3$] **(5)** with different cell dimensions than for the reported X-ray structure of **5** (ref.[7]).

[9] S. C. Chritchlow, J. D. Corbett, *Inorg. Chem.* **1984**, *23*, 770–774.

[10] [10a] O. Mundt, G. Becker, H.-J. Wessely, H.-J. Breunig, H. Kischkel, *Z. Anorg. Allg. Chem.* **1982**, *486*, 70–89. – [10b] H. J. Breunig, R. Rösler, E. Lork, *Organometallics* **1998**, *17*, 5594–5595.

[11] U. Weber, L. Zsolnai, G. Huttner, *Z. Naturforsch.* **1985**, *40B*, 1430–1436.

[12] O. Mundt, H. Riffel, G. Becker, A. Simon, *Z. Naturforsch.* **1984**, *39B*, 317–322; A. J. Ashe III, E. G. Lugwig, J. Oleksyszyn, J. C. Huffman, *Organometallics* **1984**, *3*, 337–338.

[13] B. K. Teo, *Inorg. Chem.* **1984**, *23*, 1251–1257; D. P. Mingos, *Inorg. Chem.* **1985**, *24*, 114–115; B. K. Teo, *Inorg. Chem.* **1985**, *24*, 115–116.

[14] M. T. Bautista, P. S. White, C. K. Schauer, *J. Am. Chem. Soc.* **1991**, *113*, 8963–8965.

[15] M. Gorzellik, B. Nuber, M. L. Ziegler, *J. Organomet. Chem.* **1992**, *436*, 207–222.

[16] [16a] K. H. Whitmire, J. S Leigh, S. Luo, M. Shieh, M. D. Fabiano, A. L. Rheingold, *New J. Chem.* **1988**, *12*, 397. – [16b] R. E. Bachman, S. K. Miller, K. H. Whitmire, *Organometallics* **1995**, *14*, 796–803. – [16c] K. H. Whitmire, K. S. Raghuveer, M. R. Churchill, J. C. Fettinger, R. F. See, *J. Am. Chem. Soc*. **1986**, *108*, 2778–2779. – [16d] J. R. Eveland, J-Y Saillard, K. H. Whitmire, *Inorg. Chem*. **1997**, *36*, 330–334.

[17] N. C. Norman, P. M. Webster, L. J. Farrugia, *J. Organomet. Chem.* **1992**, *430*, 205–219.

[18] A. S. Foust, L. F. Dahl, *J. Am. Chem. Soc.* **1970**, *92*, 7337–7338.

[19] G. Gilli, M. Sacerdoti, P. Domiano, *Acta Crystallogr. Sect. B* **1974**, *30*, 1485.

[20] T. A. Albright, K. A. Yee, J.-Y. Saillard, S. Kahlal, J.-F.Halet, J. S. Leigh, K. H. Whitmire, *Inorg. Chem.* **1991**, *30*, 1179–1190.

[21] For $[Bi_2Co_4(CO)_{10}(\mu\text{-}CO)]^-$ compare: S. Martinengo, G. Ciani, *J. Chem. Soc., Chem. Commun.* **1987**, 1589–1591.

[22] J. E. Ellis, E. A. Flom, *J. Organomet. Chem.* **1975**, *99*, 263.

[23] H. Strong, P. J. Krusic, J. San Filippo Jr., *Inorg. Synth.* **1986**, *24*, 157–161.

[24] [24a] G. M. Sheldrick, *SHELXS-86*, University of Göttingen, **1986**. – [24b] G. M. Sheldrick, *SHELXL-97*, University of Göttingen, **1997**.

Received May 5, 2000
[I00181]

Six-Coordinate Ruthenium(II) Complexes Containing Unsymmetrical 1,2-Bis(phosphanyl)ethanes and 1-Arsanyl-2-phosphanylethanes as Ligands

Guido Fries,[a] Kerstin Ilg,[a] Matthias Pfeiffer,[a] Dietmar Stalke,[a] and Helmut Werner*[a]

Dedicated to Professor Herbert Schumann on the occasion of his 65th birthday

Keywords: Acetylacetonato complexes / Allyl complexes / Ruthenium / Chelates / Phosphorus / Arsenic

The bis(η^3-2-methallyl)ruthenium(II) complexes [Ru(η^3-2-MeC_3H_4)$_2$(κ^2-$Ph_2PCH_2CH_2PR_2$)] [R = *i*Pr (**2**), Cy (**3**)] were prepared from the cycloocta-1,5-diene derivative [Ru(η^3-2-MeC_3H_4)$_2$(η^4-C_8H_{12})] (**1**) and the unsymmetrical 1,2-bis(phosphanyl)ethanes $Ph_2PCH_2CH_2PR_2$. The As,P analogue [Ru(η^3-2-MeC_3H_4)$_2$(κ^2-$Ph_2PCH_2CH_2AstBu_2$)] (**4**) was obtained by the same route. The reaction of **2** with hexafluoroacetylacetone afforded the chelate compound [Ru(κ^2-[F_6]-acac)$_2$(κ^2-*i*$Pr_2PCH_2CH_2PPh_2$)], whereas treatment of **2** and **3** with pentachlorophenol gave the related, more labile complexes [Ru(κ^2-*O*,*Cl*-OC_6Cl_5)$_2$(κ^2-$R_2PCH_2CH_2PPh_2$)] [R = *i*Pr (**6**), Cy (**7**)]. Preparation of the parent bis(acac) compound [Ru(κ^2-acac)$_2$(κ^2-*i*$Pr_2PCH_2CH_2PPh_2$)] (**8**), which could not be obtained from **2** and acacH, was achieved by ligand exchange of **6** and acetylacetone. The molecular structures of **2** and **6** were determined by X-ray crystallography.

Introduction

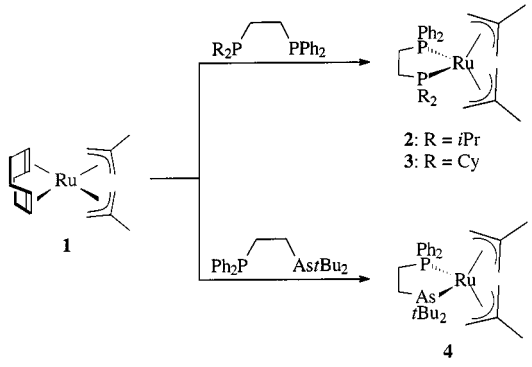
By attempting to modify the donor/acceptor properties of bidentate ligands with P, As, and Sb as donor atoms, we recently described two new synthetic methodologies for unsymmetrical bis(phosphanyl)methanes and 1,2-bis(phosphanyl)ethanes as well as for their As,P analogues.[1,2] While the methane derivatives $R_2PCH_2ER'_2$ were prepared from the stannylated phosphanes $R_2PCH_2SnR''_3$ by metalation with MeLi or PhLi in the presence of tetramethylethylenediamine followed by treatment with R'_2PCl or R'_2AsCl,[1] the corresponding disubstituted ethanes $R_2PCH_2CH_2ER'_2$ were obtained in a one-pot reaction from the cyclic sulfate $C_2H_4O_2SO_2$ by stepwise addition of R'_2ELi and R_2PLi, respectively. The latter method is also suitable for the preparation of *chiral* bidentate P,P donors of the general composition $R_2PCH_2CH(Me)PPh_2$ and $R_2PCH_2CH_2CH(Me)PPh_2$ where the substituent R is a bulky alkyl or cycloalkyl group such as *i*Pr, *t*Bu, or C_6H_{11}.[2,3]

In the initial phase of these studies, we tested the coordination properties of the new ligands toward rhodium(I) and isolated a series of square-planar and half-sandwich-type complexes including [Rh(η^4-C_8H_{12})(κ^2-*R*-$Ph_2PCH(Me)CH_2PCy_2$)]PF_6[3] and [(η^6-C_6H_5R)Rh(κ^2-$Cy_2PCH_2Pi Pr_2$)]PF_6 (R = H, Me).[1] In this paper we report the synthesis of a series of ruthenium(II) compounds with both $Ph_2PCH_2CH_2PR_2$ and $Ph_2PCH_2CH_2AstBu_2$ as chelating ligands and η^3-2-methallyl, pentachlorphenolate, and acetylacetonates as ancillary bidentate units. Some preliminary results of this work have already been communicated.[2]

[a] Institut für Anorganische Chemie der Universität Würzburg, Am Hubland, 97074 Würzburg, Germany

Results and Discussion

The preparation of the chelate complexes **2** and **3** (Scheme 1) followed the route which was used by Holle, Jolly, and Kuhnigk to obtain the related bis(η^3-allyl)ruthenium(II) compounds with $iPr_2P(CH_2)_nPiPr_2$ (n = 1, 2, and 3) as ligands.[4] The reaction proceeds in hexane under reflux conditions and affords the products as yellow solids in about 70% isolated yield. Compounds **2** and **3** are only slightly air-sensitive and, apart from pentane and ether, readily soluble in most common organic solvents. The ^{31}P NMR spectra of both **2** and **3** display two sharp doublets for the nonequivalent phosphorus nuclei with ^{31}P-^{31}P coupling constants of 8.5 and 7.6 Hz, respectively. Due to the presence of the unsymmetrical 1.2-bis(phosphanyl)ethane ligand, the ^1H NMR spectra of **2** and **3** are rather complex, thus making an exact assignment of the signals for the CH_2 allyl protons difficult.



Scheme 1

The molecular structure of compound **2**, of which single crystals were obtained from a saturated solution in hexane, was determined by X-ray crystallography. The molecular

 © WILEY-VCH Verlag GmbH, D-69451 Weinheim, 2000 1434–1948/00/1212–2597 $ 17.50+.50/0

diagram (Figure 1) reveals that the coordination geometry around the metal center can be described as a distorted tetrahedron with the two phosphorus atoms P1 and P2 and the two central carbon atoms C40 and C50 of the allylic moieties at the corners of the tetrahedron. The bond lengths Ru−C40 and Ru−C50 are somewhat shorter than those from the ruthenium center to the terminal carbon atoms of the 2-methallyl ligands. This results in dihedral angles of 37.7(1)° and 34.9(1)° between the planes [C40,C41,C42] and [C50,C51,C52] of the π-allyl units and the plane of the five-membered chelate ring [Ru,P1,C2,C1,P2]. The distances Ru−P1 and Ru−P2 differ only slightly to those in similar phosphaneruthenium(II) complexes[5−7] while the bite angle P1−Ru−P2 of 85.32(3)° is nearly identical to that in $[Ru(\eta^3\text{-}2\text{-}MeC_3H_4)_2(\kappa^2\text{-}Cy_2PCH_2CH_2PCy_2)]$ [85.03(4)°].[5]

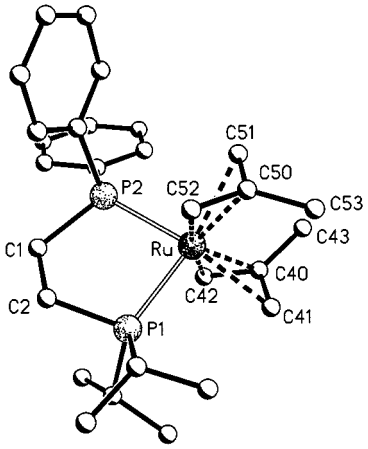
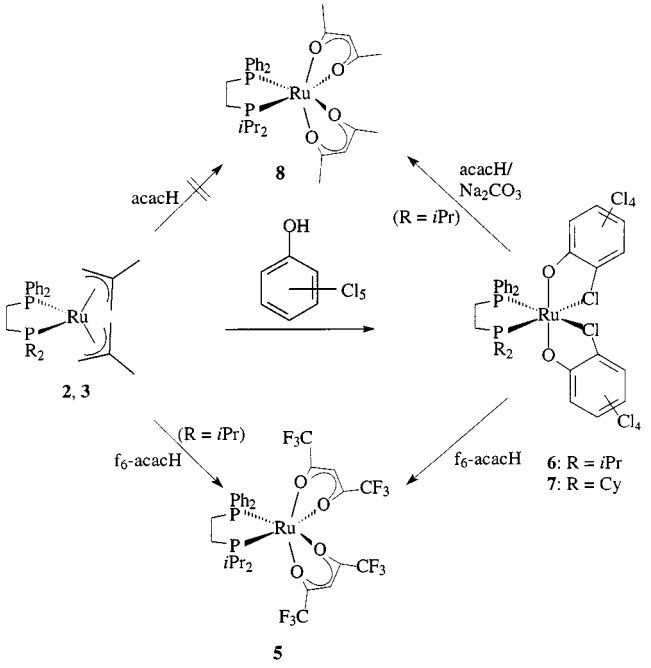


Figure 1. Molecular structure of compound **2**; selected bond lengths [Å] and angles [°]: Ru−P1 2.3278(9), Ru−P2 2.2981(8), Ru−C40 2.178(3), Ru−C41 2.237(4), Ru−C42 2.232(4), Ru−C50 2.181(3), Ru−C51 2.247(3), Ru−C52 2.230(4), P1−C2 1.854(3), P2−C1 1.851(3); P1−Ru−P2 85.32(3), C1−P2−Ru 110.07(11), C2−P1−Ru 107.03(11), C1−C2−P1 111.9(2), C2−C1−P2 110.1(2), C41−C40−C42 116.4(3), C51−C50−C52 117.9(3)

In contrast to $iPr_2PCH_2AstBu_2$, which does not react with the starting material **1** by substitution of the cyclooctadiene ligand,[3] the reaction of the ethane derivative $Ph_2PCH_2CH_2AstBu_2$ with **1** affords the chelate complex **4** (see Scheme 1) as a yellow solid in 51% isolated yield. While the ^{31}P NMR spectrum of **4** displays, in agreement with the proposed structure, a single resonance at δ = 79.4, the ^1H NMR spectrum is very complex and shows several overlapping signals between δ = 2.95 and 0.51, which originate from the allyl, the *tert*-butyl and the CH_2 protons of the coordinated As,P donor unit. In the ^{13}C NMR spectrum of **4**, the CH_2 carbon atoms of the 2-methallyl units give rise to four doublets at δ = 39.6, 36.9, 36.3, and 33.4, thus confirming the presence of an additional unsymmetrical bidentate ligand.

Similarly to the starting material **1**, the substituted compounds **2** and **3** are also quite reactive towards Brönsted acids. However, in contrast to **1** which reacts cleanly with CF_3CO_2H to give $[Ru(\eta^4\text{-}C_8H_{12})(\mu\text{-}O_2CCF_3)_2]_2$,[8] treatment of **2** or **3** with trifluoroacetic acid leads to a mixture of products which could not be separated by conventional techniques.

The reaction of **2** with two equivalents of hexafluoracetylacetone affords, by protonation of both 2-methallyl ligands (and elimination of isobutene), the chelate complex **5** (Scheme 2) as a red air-stable solid in almost quantitative yield. Due to the coordination of the unsymmetrical 1,2-bis(phosphanyl)ethane, the two [F_6]acac units are nonequivalent and therefore the ^{13}C NMR as well as the ^{19}F NMR spectrum of **5** display four resonances for the carbon and fluorine nuclei of the CF_3 groups. The appearance of four quadruplets for the CF_3CO and of two singlets for the $COCHCO$ carbon atoms equally illustrates the stereochemical nonequivalence of the [F_6]acac ligands.



Scheme 2

In contrast to the hexafluoro derivative [F_6]acacH, the parent compound acacH does not react, even in refluxing toluene, with the starting material **2**. The lower acidity of acetylacetone (pK_a = 9.0) compared to the hexafluoro analogue (pK_a = 5.3)[9] presumably causes the difference in the reactivity of the two diketones toward the η³-2-methallylruthenium(II) complex **2**.

However, the bis(acac) compound **8** is accessible in a stepwise route via the intermediate bis(pentachlorophenolato) complex **6**. Both **6** and **7** are obtained in excellent yield as orange, moderately air-sensitive solids upon treatment of **2** and **3** with two equivalents of C_6Cl_5OH in toluene at room temperature. With regard to the spectroscopic data of **6** and **7**, the interesting feature is that the ^{13}C NMR spectra (in [D_8]toluene) display at both 295 K and 188 K only one signal for the *ortho*- and one signal for the *meta*-carbon atoms of the OC_6Cl_5 units. This observation indicates that a fluxional process takes place in solution, which involves (on the NMR time scale) rapid coordination/decoordination of the chlorine atoms in *ortho* position of the six-membered rings to the metal center. There is good reason to believe that the stability of the chelating bonding mode (via

oxygen and chlorine) of the pentachlorophenolato ligands to the ruthenium center depends significantly on the coordination sphere since the tris(chelate) complexes [Ru(κ^2-OC_6Cl_5)$_2$(κ^2-$Ph_2PCH_2PR_2$)] (R = *i*Pr, Cy) are fluxional at 295 K but rigid at 188 K,[10] while the hydrido compound [RuH(κ^2-OC_6Cl_5)(CO)(P*i*Pr$_3$)$_2$] is nonfluxional on the NMR timescale even at room temperature.[11]

The X-ray crystal structure analysis of **6** (Figure 2) confirms the existence of weak Ru−Cl interactions comparable to those between transition metals and other C−Cl bonds.[12] The Ru−Cl distances of 2.498(1) Å and 2.524(1) Å are significantly longer than in *trans*-[RuCl$_2$(κ^2-$Ph_2PCH_2CH_2PPh_2$)$_2$] [2.4325(12) Å][13] and *trans*-[RuCl$_2$(κ^2-$Ph_2PCH_2PPh_2$)$_2$] [2.426(1) Å,[14] where "normal" covalent Ru−Cl bonds are present. The coordination geometry around the metal center in **6** is a distorted octahedron with a bite angle P1−Ru−P2 of 84.32(5)° that is almost identical to that in compound **2**. The bond angles Ru−O1−C1 [120.6(3)°] and Ru−O2−C7 [119.3(3)°] are considerably smaller than in the hydrido complex *trans*-[RuH(OC_6H_4-4-Me)(κ^2-$Me_2PCH_2CH_2PMe_2$)$_2$] [137.58(16)°][15] where no additional interaction between the C−H units of the phenolato ligand and the metal exists.

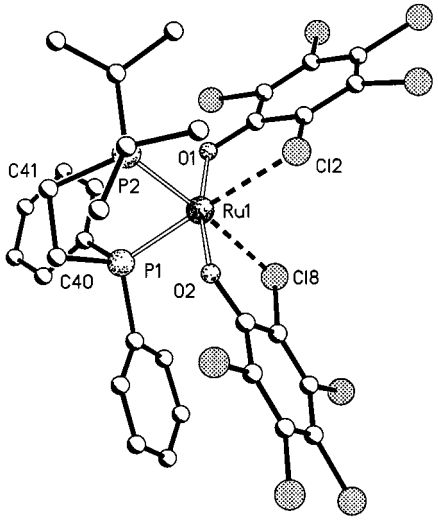


Figure 2. Molecular structure of compound **6**; the THF molecule is omitted for clarity; selected bond lengths [Å] and angles [°]: Ru−P1 2.2341(13), Ru−P2 2.2578(13), Ru−O1 2.088(3), Ru−O2 2.078(3), Ru−Cl2 2.5240(13), Ru−Cl8 2.4978(13); P1−Ru−P2 84.32(5), P1−Ru−O1 99.45(9), P1−Ru−O2 89.24(9), P1−Ru−Cl2 176.70(4), P1−Ru−Cl8 94.03(5), P2−Ru−O1 94.51(9), P2−Ru−O2 93.00(8), P2−Ru−Cl2 98.90(5), P2−Ru−Cl8 174.32(4), O1−Ru−O2 169.03(11), O1−Ru−Cl2 79.60(9), O1−Ru−Cl8 91.12(9), O2−Ru−Cl2 91.34(9), O2−Ru−Cl8 81.53(8), Cl2−Ru−Cl8 82.85(4)

In contrast to **2**, compound **6** reacts with acetylacetone in the presence of Na_2CO_3 to afford the bis(acac) complex **8** as a yellow air-stable solid in 89% isolated yield. Moreover, the bis(pentachlorophenolato) derivative **6** affords the bis([F$_6$]acac) complex **5** almost instantaneously upon treatment with [F$_6$]acacH in toluene. This pattern of reactivity indicates that **6** (and equally **7**) could be considered as a masked 14-electron species in which the additional interaction between the chlorine atoms in *ortho* position of the OC_6Cl_5 units and the metal center prevents a subsequent oligomerization or decomposition process. We note that quite recently Baratta et al. reported another example of a ruthenium(II) complex with a formal 14-electron configuration; in this case two strong agostic RuHC interactions relieve part of the electronic unsaturation at the metal center.[16]

Experimental Section

All operations were carried out under argon using Schlenk techniques. The starting material **1**[17] as well as the ligands $Ph_2PCH_2CH_2PR_2$ (R = *i*Pr, Cy) and $Ph_2PCH_2CH_2AstBu_2$[2,3] were prepared as described in the literature. − IR: Perkin−Elmer 1320. − NMR: Bruker AC 200 and AMX 400. − Melting points determined by DTA.

1. Preparation of [Ru(η^3-2-MeC_3H_4)$_2$(κ^2-$Ph_2PCH_2CH_2P$*i*Pr_2)] (2): A suspension of **1** (261 mg, 0.8 mmol) in hexane (8 mL) was treated with $Ph_2PCH_2CH_2P$*i*Pr_2 (252 mg, 0.8 mmol) and heated at reflux for 12 h. After cooling to room temperature, the solvent was evaporated in vacuo, the residue was washed with pentane (10 mL) and dried. A yellow microcrystalline solid was obtained; yield 308 mg (72%); m.p. 114 °C. − ^{1}H NMR (400 MHz, C_6D_6): δ = 7.96 (m, 2 H, C_6H_5), 7.30 (m, 4 H, C_6H_5), 7.00 (m, 4 H, C_6H_5), 2.93 (br m, 1 H, one H of PCH_2), 2.48, 2.25 (both s, 3 H each, CH_3 of 2-MeC_3H_4), 2.42−2.15 (br m, 5 H, PCH_2 and CH_2 of 2-MeC_3H_4), 2.10 [sept, 2 H, *J*(PH) = 1.7 Hz, PC*H*CH$_3$], 1.73−1.52 (br m, 4 H, CH_2 of 2-MeC_3H_4), 1.47 [dd, 3 H, *J*(PH) = 14.2, *J*(HH) = 7.2 Hz, PCHC*H*$_3$], 1.24 [dd, 3 H, *J*(PH) = 11.3, *J*(HH) = 7.2 Hz, PCHC*H*$_3$], 1.13 [dd, 1 H, *J*(PH) = 15.1, *J*(HH) = 4.8 Hz, one H of 2-MeC_3H_4], 0.92 [dd, 3 H, *J*(PH) = 9.4, *J*(HH) = 7.3 Hz, PCHC*H*$_3$], 0.89 [dd, 3 H, *J*(PH) = 9.6, *J*(HH) = 7.3 Hz, PCHC*H*$_3$], 0.50 [d, 1 H, *J*(PH) = 13.5 Hz, one H of 2-MeC_3H_4]. − ^{13}C NMR (100.6 MHz, C_6D_6): δ = 140.5 [d, *J*(PC) = 40.5 Hz, *ipso*-C of C_6H_5], 138.9 [d, *J*(PC) = 21.0 Hz, *ipso*-C of C_6H_5], 133.8 [d, *J*(PC) = 10.5 Hz, *ortho*-C of C_6H_5], 131.3 [d, *J*(PC) = 6.7 Hz, *ortho*-C of C_6H_5], 129.2 [d, *J*(PC) = 1.9 Hz, *para*-C of C_6H_5], 126.9 (s, *para*-C of C_6H_5), 126.7 [d, *J*(PC) = 8.6 Hz, *meta*-C of C_6H_5], 126.3 [d, *J*(PC) = 7.6 Hz, *meta*-C of C_6H_5], 95.2 (s, *C*CH$_3$ of 2-MeC_3H_4), 94.2 [d, *J*(PC) = 1.9 Hz, *C*CH$_3$ of 2-MeC_3H_4], 41.6 [dd, *J*(P^{1}C) = 19.1, *J*(P^{2}C) = 1.9 Hz, CH_2 of 2-MeC_3H_4], 38.0, 36.8 (both m, CH_2 of 2-MeC_3H_4), 34.2, 34.0 [both d, *J*(PC) = 1.9 Hz, C*C*H$_3$ of 2-MeC_3H_4], 32.7 [dd, *J*(P^{1}C) = 25.3, *J*(P^{2}C) = 18.1 Hz, PCH_2], 31.1 [dd, *J*(P^{1}C) = *J*(P^{2}C) = 21.9 Hz, PCH_2], 26.8 [d, *J*(PC) = 28.6 Hz, P*C*HCH$_3$], 26.6 [d, *J*(PC) = 18.6 Hz, P*C*HCH$_3$], 21.2 [d, *J*(PC) = 4.8 Hz, PCH*C*H$_3$], 20.7, 19.8 (both s, PCH*C*H$_3$), 19.6 [d, *J*(PC) = 2.9 Hz, PCH*C*H$_3$]. − ^{31}P NMR (162.0 MHz, C_6D_6): δ = 81.4 [d, *J*(PP) = 8.5 Hz, *i*Pr$_2$P], 73.9 [d, *J*(PP) = 8.5 Hz, Ph_2P]. − $C_{28}H_{42}P_2Ru$ (541.4): calcd. C 62.09, H 7.82; found C 61.81, H 8.07.

2. Preparation of [Ru(η^3-2-MeC_3H_4)$_2$(κ^2-$Ph_2PCH_2CH_2PCy_2$)] (3): Analogous to the procedure described for **2**, using **1** (152 mg, 0.5 mmol) and $Ph_2PCH_2CH_2PCy_2$ (189 mg, 0.5 mmol) as starting materials. Yellow microcrystalline solid; yield 308 mg (70%); m.p. 108 °C. − ^{1}H NMR (200 MHz, C_6D_6): δ = 7.76−6.66 (br m, 10 H, C_6H_5), 3.25−0.43 (br m, 40 H, PCH_2, CH_2 and CH_3 of 2-MeC_3H_4 and C_6H_{11}). − ^{13}C NMR (50.3 MHz, C_6D_6): δ = 134.8 [d, *J*(PC) = 13.2 Hz, *ipso*-C of C_6H_5], 134.6 [d, *J*(PC) = 9.0 Hz, *ipso*-C of C_6H_5], 133.7 [d, *J*(PC) = 14.2 Hz, *ortho*-C of C_6H_5], 131.4 [d, *J*(PC) = 8.3 Hz, *ortho*-C of C_6H_5], 129.5, 128.1 [both d, *J*(PC) = 1.9 Hz, *para*-C of C_6H_5], 128.3 [d, *J*(PC) = 7.5 Hz, *meta*-C of C_6H_5], 127.7 [d, *J*(PC) = 8.5 Hz, *meta*-C of C_6H_5], 95.4, 94.6 (both

s, *C*CH$_3$ of 2-MeC$_3$H$_4$), 43.0 [dd, *J*(P^{1}C) = 10.3, *J*(P^{2}C) = 6.1 Hz, CH of C$_6$H$_{11}$], 39.4 [d, *J*(PC) = 3.4 Hz, CH$_2$ of 2-MeC$_3$H$_4$], 38.8 [d, *J*(PC) = 4.2 Hz, CH$_2$ of 2-MeC$_3$H$_4$], 38.6 [d, *J*(PC) = 5.1 Hz, CH of C$_6$H$_{11}$], 36.1, 36.0 [both d, *J*(PC) = 4.0 Hz, CH$_2$ of 2-MeC$_3$H$_4$], 33.1 [dd, *J*(P^{1}C) = 24.7, *J*(P^{2}C) = 16.9 Hz, PCH$_2$], 31.1 [dd, *J*(P^{1}C) = 22.7, *J*(P^{2}C) = 18.9 Hz, PCH$_2$], 30.4, 30.2 (both s, CH$_2$ of C$_6$H$_{11}$), 30.6 [d, *J*(PC) = 4.0 Hz, CH$_2$ of C$_6$H$_{11}$], 29.3 [d, *J*(PC) = 3.1 Hz, CH$_2$ of C$_6$H$_{11}$], 28.5 [d, *J*(PC) = 12.2 Hz, CH$_2$ of C$_6$H$_{11}$], 27.6 [d, *J*(PC) = 9.2 Hz, CH$_2$ of C$_6$H$_{11}$], 27.5 [d, *J*(PC) = 7.3 Hz, CH$_2$ of C$_6$H$_{11}$], 27.1 [d, *J*(PC) = 10.1 Hz, CH$_2$ of C$_6$H$_{11}$], 26.8, 26.7 (both s, CH$_2$ of C$_6$H$_{11}$), 26.6, 25.9 (both s, C*C*H$_3$ of 2-MeC$_3$H$_4$). – ^{31}P NMR (81.0 MHz, C$_6$D$_6$): δ = 81.5 [d, *J*(PP) = 7.6 Hz, Cy$_2$P], 66.6 [d, *J*(PP) = 7.6 Hz, Ph$_2$P]. – C$_{34}$H$_{50}$P$_2$Ru (621.8): calcd. C 65.68, H 8.11; found C 65.57, H 7.82.

3. Preparation of [Ru(η^3-2-MeC$_3$H$_4$)$_2$(κ^2-Ph$_2$PCH$_2$CH$_2$As*t*Bu$_2$)] (4): Analogous to the procedure described for **2**, using **1** (281 mg, 0.9 mmol) and Ph$_2$PCH$_2$CH$_2$As*t*Bu$_2$ (355 mg, 0.88 mmol) as starting materials. Yellow microcrystalline solid; yield 275 mg (51%); m.p. 99 °C. – ^{1}H NMR (400 MHz, C$_6$D$_6$): δ = 7.89 (m, 2 H, C$_6$H$_5$), 7.22–7.09 (br m, 4 H, C$_6$H$_5$), 6.87 (m, 4 H, C$_6$H$_5$), 2.95–0.51 (br m, 36 H, CH$_2$ and CH$_3$ of 2-MeC$_3$H$_4$, PCH$_2$, and AsCCH$_3$). – ^{13}C NMR (100.6 MHz, C$_6$D$_6$): δ = 140.4 [d, *J*(PC) = 37.2 Hz, *ipso*-C of C$_6$H$_5$], 139.3 [d, *J*(PC) = 22.9 Hz, *ipso*-C of C$_6$H$_5$], 134.1 [d, *J*(PC) = 11.4 Hz, *ortho*-C of C$_6$H$_5$], 131.7 [d, *J*(PC) = 6.7 Hz, *ortho*-C of C$_6$H$_5$], 129.2 [d, *J*(PC) = 1.9 Hz, *para*-C of C$_6$H$_5$], 126.9 (s, *para*-C of C$_6$H$_5$), 126.5 [d, *J*(PC) = 9.5 Hz, *meta*-C of C$_6$H$_5$], 126.3 [d, *J*(PC) = 6.7 Hz, *meta*-C of C$_6$H$_5$], 95.0, 91.2 (both s, *C*CH$_3$ of 2-MeC$_3$H$_4$), 39.6, 36.3 [both d, *J*(PC) = 2.9 Hz, CH$_2$ of 2-MeC$_3$H$_4$], 39.1, 39.0 (both s, As*C*CH$_3$), 36.9 [d, *J*(PC) = 4.8 Hz, CH$_2$ of 2-MeC$_3$H$_4$], 33.4 [d, *J*(PC) = 2.3 Hz, CH$_2$ of 2-MeC$_3$H$_4$], 32.8 [d, *J*(PC) = 24.8 Hz, PCH$_2$], 32.2, 31.5 (both s, AsC*C*H$_3$), 25.9, 25.7 (both s, C*C*H$_3$ of 2-MeC$_3$H$_4$), 21.6 [d, *J*(PC) = 20.2 Hz, AsCH$_2$]. – ^{31}P NMR (162.0 MHz, C$_6$D$_6$): δ = 79.4 (s). – C$_{30}$H$_{46}$AsPRu (613.7): calcd. C 58.72, H 7.56; found C 58.37, H 7.06.

4. Preparation of [Ru(κ^2-[F$_6$]acac)$_2$(κ^2-Ph$_2$PCH$_2$CH$_2$P*i*Pr$_2$)] (5): a) A solution of **2** (104 mg, 0.2 mmol) in toluene (5 mL) was treated at –78 °C with hexafluoroacetylacetone (88 μL, 0.4 mmol), which led to a rapid change of color from yellow to dark red. After warming to room temperature and stirring the solution for 20 min, the solvent was evaporated in vacuo and the residue was dissolved in pentane (2 mL). The solution was chromatographed on Al$_2$O$_3$ (basic, activity grade I, height of column 10 cm). With pentane a red fraction was eluted, from which a dark red microcrystalline solid was obtained upon removal of the solvent; yield 147 mg (92%). – b) A solution of **6** (164 mg, 0.2 mmol) in toluene (5 mL) was treated with hexafluoroacetylacetone (71 μL, 0.4 mmol), which led to a rapid change of color from orange to dark red. The solvent was evaporated in vacuo, the residue was washed with pentane (5 mL, –20 °C) and dried. Orange microcrystalline solid; yield 133 mg (93%); m.p. 148 °C. – IR (CH$_2$Cl$_2$): ν([F$_6$]acac) = 1611, 1522 cm^{-1}. – ^{1}H NMR (400 MHz, CDCl$_3$): δ = 7.97 (m, 2 H, C$_6$H$_5$), 7.63 (m, 3 H, C$_6$H$_5$), 7.46–7.34 (br m, 3 H, C$_6$H$_5$), 7.18 (m, 2 H, C$_6$H$_5$), 6.37, 5.67 (both s, 1 H each, CH of acac-f$_6$), 3.40–2.76 (br m, 2 H, PCH$_2$), 2.64–2.52 (br m, 1 H, PC*H*CH$_3$), 2.48–2.34 (br m, 2 H, PCH$_2$), 2.28–2.12 (br m, 1 H, PC*H*CH$_3$), 1.49 [dd, 3 H, *J*(PH) = 9.4, *J*(HH) = 7.0 Hz, PCHC*H*$_3$], 1.45 [dd, 3 H, *J*(PH) = 10.4, *J*(HH) = 7.2 Hz, PCHC*H*$_3$], 1.18 [dd, 3 H, *J*(PH) = 14.1, *J*(HH) = 7.0 Hz, PCHC*H*$_3$], 1.07 [dd, 3 H, *J*(PH) = 14.2, *J*(HH) = 7.2 Hz, PCHC*H*$_3$]. – ^{13}C NMR (100.6 MHz, CDCl$_3$): δ = 175.1, 174.0, 172.1, 171.3 [all q, *J*(FC) = 34.3 Hz, CO of acac-f$_6$], 134.9 [d, *J*(PC) = 42.9 Hz, *ipso*-C of C$_6$H$_5$], 133.3 [d, *J*(PC) = 10.5 Hz, *ortho*-C of C$_6$H$_5$], 132.0 [d, *J*(PC) = 43.9 Hz, *ipso*-C of C$_6$H$_5$], 130.6 [d, *J*(PC) = 9.5 Hz, *ortho*-C of C$_6$H$_5$], 129.2 [d, *J*(PC) = 2.9 Hz, *para*-C of C$_6$H$_5$], 128.3 [d, *J*(PC) = 9.5 Hz, *meta*-C of C$_6$H$_5$], 118.5, 117.7, 116.3, 116.1 [all q, *J*(FC) = 284.2 Hz, CF$_3$], 91.2, 89.9 (both s, CH of acac-f$_6$), 27.8 [dd, *J*(P^{1}C) = 34.3, *J*(P^{2}C) = 8.6 Hz, PCH$_2$], 25.3 [d, *J*(PC) = 22.9 Hz, P*C*HCH$_3$], 25.0 [d, *J*(PC) = 23.8 Hz, P*C*HCH$_3$], 23.9 [dd, *J*(P^{1}C) = 38.6, *J*(P^{2}C) = 12.4 Hz, PCH$_2$], 18.3, 18.3, 18.2, 18.0 (all s, PCH*C*H$_3$). – ^{19}F NMR (376.5 MHz, CDCl$_3$): δ = –75.7, –75.4, –74.6, –74.2 (all s). – ^{31}P NMR (162.0 MHz, CDCl$_3$): δ = 90.4 [d, *J*(PP) = 25.4 Hz, *i*Pr$_2$P], 79.1 [d, *J*(PP) = 25.4 Hz, Ph$_2$P]. – C$_{30}$H$_{30}$F$_{12}$O$_4$P$_2$Ru (845.6): calcd. C 42.61, H 3.58; found C 42.30 H 3.22.

5. Preparation of [Ru(κ^2-*O*,*Cl*-OC$_6$Cl$_5$)$_2$(κ^2-Ph$_2$PCH$_2$CH$_2$P*i*Pr$_2$)] (6): A solution of **2** (135 mg, 0.3 mmol) in toluene (5 mL) was treated at –30 °C with a solution of pentachlorophenol (133 mg, 0.5 mmol) in toluene (5 mL). After warming to room temperature and stirring for 10 min, the solvent was evaporated in vacuo. The residue was washed with pentane (5 mL) and dried. An orange microcrystalline solid was obtained; yield 221 mg (92%); m.p. 165 °C. – ^{1}H NMR (400 MHz, C$_6$D$_6$): δ = 8.09 (m, 2 H, C$_6$H$_5$), 7.19 (m, 3 H, C$_6$H$_5$), 6.87 (m, 2 H, C$_6$H$_5$), 6.69 (m, 3 H, C$_6$H$_5$), 2.17–1.96 (br m, 2 H, PCH$_2$), 1.72 (m, 1 H, PC*H*CH$_3$), 1.60–1.49 (br m, 2 H, PCH$_2$), 1.43–1.29 (br m, 1 H, PC*H*CH$_3$), 1.21 [dd, 3 H, *J*(PH) = 14.1, *J*(HH) = 7.0 Hz, PCHC*H*$_3$], 1.15 [dd, 3 H, *J*(PH) = 13.9, *J*(HH) = 7.7 Hz, PCHC*H*$_3$], 0.60 [dd, 3 H, *J*(PH) = 11.4, *J*(HH) = 7.0 Hz, PCHC*H*$_3$], 0.56 [dd, 3 H, *J*(PH) = 11.7, *J*(HH) = 7.0 Hz, PCHC*H*$_3$]. – ^{13}C NMR (100.6 MHz, C$_6$D$_6$): δ = 163.6, 162.7 (both s, *ipso*-C of C$_6$Cl$_5$), 134.6 [d, *J*(PC) = 10.5 Hz, *ortho*-C of C$_6$H$_5$], 133.8 [d, *J*(PC) = 47.7 Hz, *ipso*-C of C$_6$H$_5$], 132.6 [d, *J*(PC) = 45.8 Hz, *ipso*-C of C$_6$H$_5$], 131.7 [d, *J*(PC) = 8.6 Hz, *ortho*-C of C$_6$H$_5$], 131.3, 129.4 [both d, *J*(PC) = 1.9 Hz, *para*-C of C$_6$H$_5$], 128.6 [d, *J*(PC) = 10.5 Hz, *meta*-C of C$_6$H$_5$], 127.5 [d, *J*(PC) = 9.5 Hz, *meta*-C of C$_6$H$_5$], 125.7, 125.4, 118.0, 117.8, 116.4, 115.6 (all s, C$_6$Cl$_5$), 28.1 [dd, *J*(P^{1}C) = 36.2, *J*(P^{2}C) = 7.2 Hz, PCH$_2$], 26.7, 26.2 [both d, *J*(PC) = 24.8 Hz, P*C*HCH$_3$], 20.9 [dd, *J*(P^{1}C) = 30.0, *J*(P^{2}C) = 11.0 Hz, PCH$_2$], 19.3, 18.5, 18.1, 18.0 (all s, PCH*C*H$_3$). – ^{31}P NMR (162.0 MHz, C$_6$D$_6$): δ = 99.2 [d, *J*(PP) = 28.8 Hz, *i*Pr$_2$P], 84.8 [d, *J*(PP) = 28.8 Hz, Ph$_2$P]. – C$_{32}$H$_{28}$Cl$_{10}$O$_2$P$_2$Ru (962.2): calcd. C 39.95 H 2.91; found C 40.04 H 3.22.

6. Preparation of [Ru(κ^2-*O*,*Cl*-OC$_6$Cl$_5$)$_2$(κ^2-Ph$_2$PCH$_2$CH$_2$PCy$_2$)] (7): Analogous to the procedure described for **6**, using **3** (246 mg, 0.5 mmol) and pentachlorophenol (245 mg, 1.0 mmol) as starting materials. Orange microcrystalline solid; yield 221 mg (92%); m.p. 208 °C. – ^{1}H NMR (200 MHz, C$_6$D$_6$): δ = 8.10–6.60 (br m, 10 H, C$_6$H$_5$), 2.32–0.38 (br m, 26 H, PCH$_2$ and C$_6$H$_{11}$). – ^{13}C NMR (50.3 MHz, C$_6$D$_6$): δ = 162.6, 162.5 (both s; *ipso*-C of C$_6$Cl$_5$), 135.1 [d, *J*(PC) = 43.2 Hz, *ipso*-C of C$_6$H$_5$], 134.8 [d, *J*(PC) = 39.8 Hz, *ipso*-C of C$_6$H$_5$], 133.8 [d, *J*(PC) = 14.1 Hz, *ortho*-C of C$_6$H$_5$], 131.3 [d, *J*(PC) = 8.0 Hz, *ortho*-C of C$_6$H$_5$], 129.9, 128.0 [both d, *J*(PC) = 1.9 Hz, *para*-C of C$_6$H$_5$], 128.4, 127.3 [both d, *J*(PC) = 7.1 Hz, *meta*-C of C$_6$H$_5$], 125.6, 125.4, 118.7, 118.0, 116.7, 116.1 (all s, C$_6$Cl$_5$), 43.3 [dd, *J*(P^{1}C) = 12.1, *J*(P^{2}C) = 5.8 Hz, CH of C$_6$H$_{11}$], 38.4 [d, *J*(PC) = 6.1 Hz, CH of C$_6$H$_{11}$], 32.5 [dd, *J*(P^{1}C) = 24.2, *J*(P^{2}C) = 16.7 Hz, PCH$_2$], 31.0 [dd, *J*(P^{1}C) = 22.5, *J*(P^{2}C) = 18.9 Hz, PCH$_2$], 30.8, 30.0, 26.5, 26.4 (all s, CH$_2$ of C$_6$H$_{11}$), 30.4, 29.9 [both d, *J*(PC) = 4.3 Hz, CH$_2$ of C$_6$H$_{11}$], 29.0 [d, *J*(PC) = 9.7 Hz, CH$_2$ of C$_6$H$_{11}$], 26.9 [d, *J*(PC) = 9.4 Hz, CH$_2$ of C$_6$H$_{11}$], 26.8 [d, *J*(PC) = 6.9 Hz, CH$_2$ of C$_6$H$_{11}$], 26.7 [d, *J*(PC) = 10.6 Hz, CH$_2$ of C$_6$H$_{11}$]. – ^{31}P NMR (81.0 MHz, C$_6$D$_6$): δ = 91.3 [d, *J*(PP) = 28.7 Hz, Cy$_2$P], 85.4 [d, *J*(PP) = 28.7 Hz, Ph$_2$P]. – C$_{38}$H$_{36}$Cl$_{10}$O$_2$P$_2$Ru (1042): calcd. C 43.78 H 3.48; found C 44.08 H 3.45.

7. Preparation of [Ru(κ²-acac)₂(κ²-Ph₂PCH₂CH₂P*i*Pr₂)] (8): A solution of **6** (189 mg, 0.2 mmol) in toluene (8 mL) was treated with acetylacetone (55 mg, 0.6 mmol) and Na_2CO_3 (69 mg, 0.7 mmol) and then heated for 1 h at 65 °C. After cooling to room temperature, the solvent was evaporated in vacuo. The residue was dissolved in pentane (5 mL), the solution filtered and the filtrate was brought to dryness in vacuo. A yellow microcrystalline solid was obtained; yield 112 mg (89%); m.p. 157 °C. – IR (CH_2Cl_2): ν(acac) = 1580, 1518 cm^{-1}. – ^1H NMR (200 MHz, $CDCl_3$): δ = 7.88–7.76 (br m, 2 H, C_6H_5), 7.30–6.95 (br m, 8 H, C_6H_5), 5.14, 4.55 (both s, 1 H each, CH of acac), 2.62–2.50, 2.24–2.12 (both br m, 2H each, PCH_2), 1.99–1.83 (br m, 2 H, PC*H*CH_3), 1.86, 1.68, 1.62, 1.20 (all s, 3H each, CH_3 of acac), 1.24–1.18 (br m, 6 H, PCHC*H*$_3$), 0.86–0.76 (br m, 6 H, PCHC*H*$_3$). – ^{13}C NMR (100.6 MHz, $CDCl_3$): δ = 184.7, 183.9, 183.3, 182.7 (all s, CO of acac), 138.6 [d, *J*(PC) = 37.6 Hz, *ipso*-C of C_6H_5], 136.3 [d, *J*(PC) = 36.6 Hz, *ipso*-C of C_6H_5], 134.0, 131.1 [both d, *J*(PC) = 8.1 Hz, C_6H_5], 129.1, 127.7, 127.3 (all s, C_6H_5), 127.2 [d, *J*(PC) = 8.4 Hz, C_6H_5], 97.1, 96.6 (both s, CH of acac), 27.9 [dd, $J(P^1C)$ = 34.8, $J(P^2C)$ = 8.6 Hz, PCH_2], 27.8, 27.6, 27.3, 27.1 (all s, CH_3 of acac), 25.2 [d, *J*(PC) = 18.9 Hz, P*C*HCH$_3$], 25.0 [d, *J*(PC) = 23.8 Hz, P*C*HCH$_3$], 22.9 [dd, $J(P^1C)$ = 29.6, $J(P^2C)$ = 10.4 Hz, PCH_2], 18.4, 18.3, 18.2, 18.0 (all s, PCH*C*H$_3$). – ^{31}P NMR (81.0 MHz, $CDCl_3$): δ = 91.2 [d, *J*(PP) = 23.4 Hz, *i*Pr_2P], 82.5 [d, *J*(PP) = 23.4 Hz, Ph_2P]. – $C_{30}H_{42}O_4P_2Ru$ (629.7): calcd. C 57.22 H 6.73; found C 56.89 H 7.03.

X-ray Structure Determination of Compounds 2 and 6:[18] Single crystals of **2** were grown from hexane at 25 °C and those of **6** from THF at 25 °C. Crystal data collection parameters for these structures are presented in Table 1. The data were collected with an Enraf–Nonius CAD4 diffractometer using monochromated Mo-K_α radiation (λ = 0.71073 Å). Intensity data were corrected for Lorentz and polarization effects. An empirical absorption correction was applied for both structures [Ψ scans; T_{min} = 0.90, T_{max} = 1.00 (**2**); T_{min} = 0.59, T_{max} = 0.80 (**6**)]. The structures were solved by Patterson methods with SHELXS-97.[19] All structures were refined by full-matrix least-squares procedures on F^2, using SHELXL-97.[20] The positions of all hydrogen atoms were calculated according to ideal geometry and refined by employing the riding method, except for H41a, H41b, H42a, H42b, H51a, H51b, H52a, and H52b of **2**, which were found in a differential Fourier synthesis and refined without restraints.

Table 1. Crystal data for complexes **2** and **6**

	2	**6** · C_4H_8O
Empirical formula	$C_{27}H_{42}P_2Ru$	$C_{36}H_{36}Cl_{10}O_3P_2Ru$
M	541.38	1034.16
Crystal system	monoclinic	triclinic
Space group	*C*2/*c* (no. 15)	*P*$\bar{1}$ (no. 2)
a [Å]	22.795(2)	12.381(4)
b [Å]	10.982(1)	13.088(2)
c [Å]	23.162(3)	14.374(4)
α [°]	–	66.69(2)
β [°]	112.856(5)	80.19(2)
γ [°]	–	71.57(2)
V [Å³]	5342.8(10)	2027.7(7)
Z	8	2
D_c [g cm^{-3}]	1.314	1.695
Temperature [K]	193(2)	193(2)
μ [mm^{-1}]	0.718	1.162
No. reflections measured	4814	7185
No. unique reflections (R_{int})	4682 (0.0241)	5269 (0.0245)
$R1$[a]	0.034	0.035
$wR2$[b]	0.072	0.083

[a] $R1 = \Sigma|F_o - F_c|/\Sigma F_o$ [for $F_o > 2\sigma(F_o)$]. – [b] $wR2 = [\Sigma w(F_o^2 - F_c^2)^2/\Sigma w(F_o^2)^2]^{1/2}$.

Acknowledgments

This work was supported by the Deutsche Forschungsgemeinschaft (SFB 347) and the Fonds der Chemischen Industrie. We are grateful to the latter in particular for a Ph.D. scholarship (to K. I.). We also thank Dr. W. Buchner and Mrs. M.-L. Schäfer for NMR measurements, Mrs. R. Schedl and Mr. C. P. Kneis for elemental analysis and DTA measurements. Generous support by the BASF AG and the Degussa-Hüls AG is also gratefully acknowledged.

[1] J. Wolf, M. Manger, U. Schmidt, G. Fries, D. Barth, B. Weberndörfer, D. A. Vice, W. D. Jones, H. Werner, *J. Chem. Soc., Dalton. Trans.* **1999**, 1867–1875.
[2] G. Fries, J. Wolf, M. Pfeiffer, D. Stalke, H. Werner, *Angew. Chem.* **2000**, *112*, 575–578; *Angew. Chem. Int. Ed. Engl.* **2000**, *39*, 564–566.
[3] G. Fries, Dissertation, Universität Würzburg, **2000**.
[4] S. Holle, P. W. Jolly, J. Kuhnigk, *J. Organomet. Chem.* **1997**, *543*, 255–258.
[5] C. Six, B. Gabor, H. Görls, R. Mynott, P. Philipps, W. Leitner, *Organometallics* **1999**, *18*, 3316–3326.
[6] J. P. Genet, X. Pfister, V. Ratovelomanana-Vidal, C. Pinel, J. A. Laffitte, S. Malort, M. C. Cano de Andrade, *Tetrahedron*: *Asymm.* **1994**, *5*, 665–674.
[7] H. Werner, T. Braun, T. Daniel, O. Gevert, M. Schulz, *J. Organomet. Chem.* **1997**, *541*, 127–141.
[8] B. Heiser, E. A. Broger, Y. Crameri, *Tetrahedron*: *Asymmetry* **1991**, *2*, 51–62.
[9] J. R. Jones, S. P. Patel, *J. Am. Chem. Soc.* **1974**, *96*, 574–575.
[10] H. Werner, G. Fries, B. Weberndörfer, *J. Organomet. Chem.*, in press.
[11] M. A. Tena, O. Nürnberg, H. Werner, *Chem. Ber.* **1993**, *126*, 1597–1602.
[12] [12a] M. F. Richardson, G. Wulfsberg, R. Marlow, S. Zaghonni, D. McCorkle, K. Shadid, J. Gagliardi, Jr., B. Farris, *Inorg. Chem.* **1993**, *32*, 1913–1919. – [12b] W. Beck, K. Schloter, *Z. Naturforsch., B* **1978**, *33*, 1214–1222. – [12c] R. J. Kulawiec, R. H. Crabtree, *Coord. Chem. Rev.* **1990**, *99*, 89–115.
[13] C.-W. Chang, P.-C. Ting, Y.-C. Lin, G.-H. Lee, Y. Wang, *J. Organomet. Chem.* **1998**, *553*, 417–425.
[14] A. R. Chakravarty, F. A. Cotton, W. Schwotzer, *Inorg. Chim. Acta* **1984**, *84*, 179–185.
[15] M. J. Burn, M. G. Fickes, F. J. Hollander, R. G. Bergman, *Organometallics* **1995**, *14*, 137–150.
[16] W. Baratta, E. Herdtweck, P. Rigo, *Angew. Chem.* **1999**, *111*, 1733–1735; *Angew. Chem. Int. Ed. Engl.* **1999**, *38*, 1629–1631.
[17] M. O. Albers, E. Singleton, Y. E. Yates, *Inorg. Synth.* **1989**, *26*, 253–254.
[18] Crystallograhic data (excluding structure factors) for the structures of **2** and **6** have been deposited with the Cambridge Crystallograhic Data Centre as supplementary publication no. CCDC-143547 (**2**) and -133284 (**6**). Copies of the data can be obtained free of charge on application to CCDC, 12 Union Road, Cambridge CB2 1EZ, UK [Fax: (internat.) + 44-1223/336-033; E-mail: deposit@ccdc.cam.ac.uk].
[19] G. M. Sheldrick, *Acta Crystallogr., Sect. A* **1990**, *46*, 467–473.
[20] G. M. Sheldrick, *Program for crystal structure refinement*, Universität Göttingen, **1996**.

Received April 17, 2000
[I00149]

2-[Ethyl-(2-methallyl)amino]indenyllithium: Structural Characterization of a Base-Free Oligomeric Supersandwich Indenyllithium Compound

Jean-Luc Fauré,[a] Gerhard Erker,*[a] Roland Fröhlich,[a][+] and Klaus Bergander[a][++]

Keywords: Lithium / Sandwich complexes / Polymers / 2-Aminoindenyllithium

Treatment of the enamine **2**, formed by condensation of 2-indanone and ethyl(2-methallyl)amine, with *n*-butyllithium yields 2-[ethyl(2-methallyl)amino]indenyllithium (**3**), whose structure was determined by X-ray single crystal diffraction. Complex **3** exhibits an oligomeric supersandwich structure in the solid state, characterized by a linear string of alternating μ-η^5:η^5-indenyl anion and lithium cation moieties along which the substituents are found attached in a helical conformational arrangement.

Introduction

The alkali metal cyclopentadienides and their benzoanellated analogues are important reagents in organic and organometallic synthesis, but have also attracted a great deal of interest in themselves due to their unique structural properties. The high electrostatic component of the carbon−alkali metal bond[1] has made a variety of specific structural arrangements possible for the family of the ^{R}CpM^{I} systems, ranging from neutral (^{R}Cp)ML$_n$ monomers to cationic [M−^{R}Cp−M^{+}, "inverse sandwich"] and anionic [^{R}Cp−M−^{R}Cp^{-}, sandwich] arrangements, and to neutral-ligand-capped dimeric [^{R}Cp−M−^{R}Cp−ML$_n$] or oligomeric [^{R}Cp−M−^{R}Cp−M]$_n$ "supersandwich" structures.[2] The latter polymers are frequently encountered in ^{R}Cp sodium or potassium chemistry, but so far the lithium analogues have seldom been unambiguously characterized. The first example, [($C_5H_4SiMe_3$)Li]$_n$, was only recently described,[3−6] and its structure was solved by a single crystal X-ray diffraction analysis. Oligomeric (CpLi)$_n$ was recently characterized by high resolution X-ray powder diffraction.[7] The same technique was used for the determination of the oligomeric supersandwich structure of (η^5-indenyl-Li)$_n$ in the solid state [with Li-indenyl five-membered ring distances ranging between 2.304(3) Å and 2.350(3) Å].[8] Oligomeric (indenyl-Li)$_n$, characterized by X-ray powder diffraction, exhibits local internal C_s-symmetry. We describe here the structure of a related (2-aminoindenyl)Li reagent (**3**), whose oligomeric supersandwich structure was determined by single crystal X-ray diffraction.

[a] Organisch-Chemisches Institut der Universität Münster, Corrensstraße 40, 48149 Münster, Germany
Fax: (internat.) +49-(0)251/833-6503
E-mail: erker@uni-muenster.de
[+] X-ray crystal structure analysis
[++] NMR spectroscopy

Results and Discussion

Preparation and Structure of the 2-[Ethyl(2-methallyl)-amino]indenyllithium Oligomer

The title compound **3** was prepared in the following way: 2-indanone was treated with a ca. threefold excess of ethyl(2-methallyl)amine in toluene in the presence of 3 Å molecular sieves to yield the corresponding enamine **2** (85% isolated).[9] Treatment of **2** with *n*-butyllithium in toluene/hexane resulted in the formation of the amino-substituted indenyllithium compound **3** in almost quantitative yield. The NMR spectra of **3** in [D_8]THF solution show the signals of a conformationally averaged, 2-substituted indenyl ligand (1-/3-H NMR signal at δ = 5.35; arene resonances at δ = 6.35 and 7.05). Single crystals of this specifically substituted indenyllithium example were obtained by slowly concentrating a solution of **3** in a mixture of toluene/ether (90:10) in a stream of argon at −20 °C during 48 h. The obtained single crystals of **3** were free of the donor ligand and suitable for characterization by an X-ray crystal structure analysis.

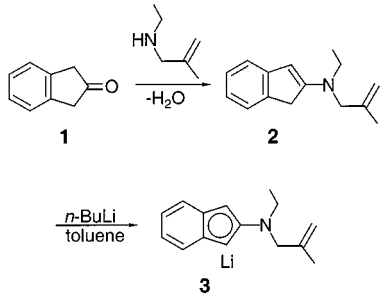
In the crystal the indenyllithium compound **3** adopts a polymeric supersandwich structure composed of alternating η^5-(2-aminoindenyl) units and intercalating lithium atoms. There are three crystallographically independent Li(R_2N-indenyl) subunits present in the solid, which represent chemically equivalent moieties. The planes of the individual 2-[ethyl(2-methallyl)amino]indenyl units are oriented almost parallel to each other [angles between the individual Cp planes: 15.9° ("Cp1"/"Cp21"), 16.6° ("Cp21"/"Cp41"), and 10.3° ("Cp41"/"Cp1")]. The lithium atoms are symmetrically η^5-coordinated from either side of the indenyl five-membered ring systems. Within all three independent subunits the minimum/maximum Li−C indenyl values amount to 2.237(7) Å (Li3−C1$^{\#}$) and 2.389(7) Å (Li1−C8). The Li1−C1,2,7−9(av.) values, averaged over the three inde-

 © WILEY-VCH Verlag GmbH, D-69451 Weinheim, 2000 1434−1948/00/1212−2603 $ 17.50+.50/0

pendent molecules, are within a narrow range between 2.288(7) and 2.321(7) Å; the corresponding Li1−C21,22,27−29(av.) values are found between 2.284(7) and 2.313(7) Å. The overall averaged Li−C bond lengths to either side of the Cp sections of the indenyl ligands in the supersandwich structure amount to 2.305 Å [Σ Li1−C1,2,7−9(av.)/5] and 2.297 Å [Σ Li1−C21,22,27−29(av.)/5], which illustrates the symmetrical bonding of the lithium atoms between adjacent η^5-indenyl ligands along the oligomeric chain in the crystal of **3** (see Figure 1). Both these averaged Li−C(av.) distances of **3** are smaller than the respective value determined in the recent X-ray powder diffraction study of $(\text{indenyl-Li})_n$ (2.320 Å).[8] The Li−C(av.) values found for **3** are close to the average Li−C(Cp) values obtained from the X-ray powder diffraction study of the parent $(\text{CpLi})_n$ oligomer (2.307 Å).[7]

The framework of the 2-[ethyl(2-methallyl)amino]indenyl ligand in **3** is completely planar (sum of averaged C−C−C bond angles inside the five-membered ring: 539.9°; inside the six-membered ring: 720.0°). The C−C bond lengths inside the five-membered ring are in a narrow range between 1.439(5) Å (C2−C7) and 1.411(5) (C8−C9)/1.413(4) (C1−C9). The pronounced contact of the lithium atoms to all five carbon atoms of the indenyl five-membered ring has a marked influence on the bonding features of the anellated planar arene system, which exhibits a marked bond alternation: the C3−C4(av.) [1.364(5) Å] and C5−C6(av.) [1.367(5) Å] bonds (see Figure 1) are noticeably shorter than the adjacent C4−C5(av.) [1.400(5) Å] bonds, as expected for an overall bonding situation of **3** as indicated in Scheme 1.

The coordination geometry of the nitrogen atom N10 in **3** is very close to trigonal planar (sum of C−N−C bond angles: 356.7°), and the amino-substituent is oriented in the central ligand plane. The C9−N10(av.) linkage is short {1.387(4) Å, the adjacent N10−C11(av.) [1.450(4) Å] and N10−C13(av.) [1.444(5) Å] bonds being much longer}, which indicates an enamine-like interaction at the aminoin-



Scheme 1

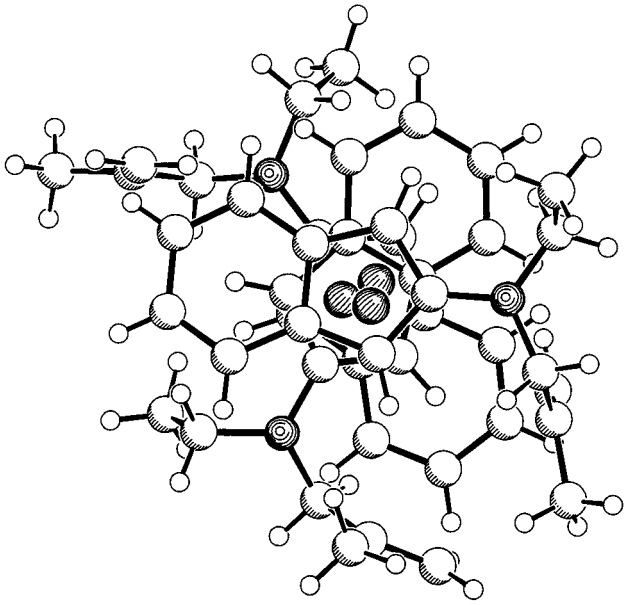


Figure 2. Top view of the arrangement of the three independent molecules of **3**

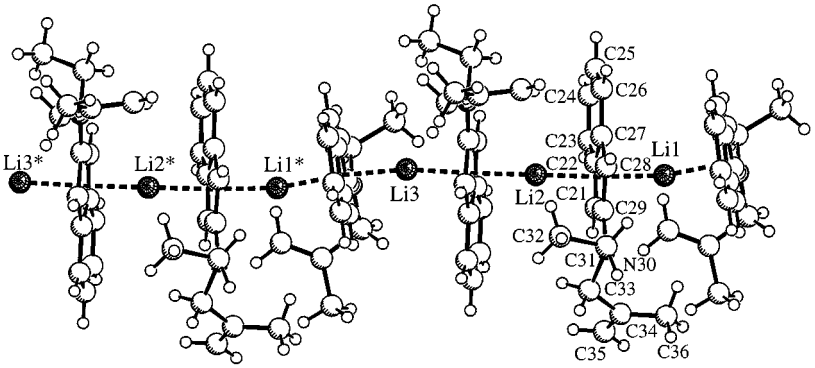


Figure 1. Side view of the oligomeric supersandwich chain of **3** with unsymmetrical atom numbering scheme, containing two pairs of the set of three independent monomeric subunits found in the crystal; averaged (av.) bond lengths (Å) and angles (°): Li1−C1(av.) = (Li1−C1 + Li2−C21 + Li3−C41)/3 = 2.289(7), Li1−C2(av.) 2.288(7), Li1−C7(av.) 2.317(7), Li1−C8(av.) 2.321(7), Li1−C9(av.) 2.308(7), Li1−C21(av.) 2.285(7), Li1−C22(av.) 2.284(7), Li1−C27(av.) 2.297(7), Li1−C28(av.) 2.313(7), Li1−C29(av.) 2.306(7), C1−C2(av.) 1.424(5), C1−C9 1.413(4), C2−C7(av.) 1.439(5), C7−C8(av.) 1.423(5), C8−C9(av.) 1.411(5), C2−C3(av.) 1.412(5), C3−C4(av.) 1.364(5), C4−C5(av.) 1.400(5), C5−C6(av.) 1.367(5), C6−C7(av.) 1.406(5), C9−N10(av.) 1.387(4), N10−C11(av.) 1.450(4), C11−C12(av.) 1.523(6), N10−C13(av.) 1.444(5), C13−C14(av.) 1.480(6), C14−C15(av.) 1.330(6); C9−C1−C2(av.) 108.2(3), C1−C2−C3(av.) 133.1(3), C1−C2−C7(av.) 107.5(3), C3−C2−C7(av.) 119.3(3), C2−C3−C4(av.) 119.4(3), C3−C4−C5(av.) 121.3(4), C4−C5−C6(av.) 121.3(4), C5−C6−C7(av.) 119.5(4), C6−C7−C8(av.) 133.5(3), C6−C7−C2(av.) 119.2(3), C2−C7−C8(av.) 107.3(3), C7−C8−C9(av.) 108.5(3), C8−C9−C1(av.) 108.4(3), C8−C9−N10(av.) 125.8(3), C1−C9−N10(av.) 125.7(3), C9−N10−C11(av.) 119.8(3), C9−N10−C13(av.) 119.2(3), C11−N10−C13(av.) 117.7(3), N10−C13−C14(av.) 115.2(4), C13−C14−C15(av.) 120.8(4), C13−C14−C16(av.) 117.0(3), C15−C14−C16(av.) 122.1(6)

denyl unit,[10] probably resulting in an increased electron density at carbon inside this anionic ligand system.

The conformational arrangement of the indenyl anions along the $[-Li-Cp(centroid)-]_n$ vector is such that the amino substituents are arranged almost ideally staggered along the chain (see Figure 2) which is characterized by dihedral angles of close to 120° between the corresponding N−C(Cp) vectors. There are subtle differences in the conformational arrangement of the rather large methallyl substituents at the three independent Li−2-[ethyl(2−methallyl)amino]indenyl subunits [one $-CH_2-C(CH_3)=CH_2$ group pointing "up", one "down" and one being arranged in the ligand plane] that lead to the observed marginal deviation of the overall chain from ideal linearity (see Figure 1).

Conclusions

We conclude that compound **3** seems to represent the first example of a base-free oligomeric (μ-η^5:η^5-indenyl) lithium supersandwich system that was characterized by an X-ray single crystal structure analysis. The amino-functionalized (η^5-indenyl)Li structure **(3)** exhibits shorter bonds between the lithium atom and the carbon atoms of the indenyl five-membered ring than in the recent high resolution X-ray powder diffraction analysis of the (η^5-indenyl-Li) structure.[8] Like the parent $(indenyl\text{-}Li)_n$, the amino-substituted compound **3** exhibits an organometallic oligomeric structure in the solid state. The 2-[ethyl(2-methallyl)amino]indenyllithium polymer **(3)** is characterized by a regularly alternating arrangement of η^5-aminoindenyl anion moieties and lithium cations, probably formed by dominant electrostatic metal−carbon interactions. The helical conformational arrangement of the substituents at the resulting oligomeric chain indicates that such systems possess well-defined stereochemical features in the crystal. The use of such substituted indenyllithium reagents is currently being studied in our laboratory.

Experimental Section

All reactions were carried out under argon using Schlenk-type glassware or in a glovebox. Solvents (including deuterated solvents used for the NMR spectroscopic characterization) were dried and distilled under argon prior to use. For additional general information see ref.[4] and ref.[5a] NMR experiments were carried out on a Varian Unity Plus 600 NMR spectrometer. The ^1H and ^{13}C NMR assignments were confirmed by GCOSY, GHSQC, GHMBC and DPFGSE-NOE experiments. The $\delta(^{15}N)$ determination was performed by indirect detection by the $^1H,^{15}N$-GHMBC experiment [preparation delay: $1/(2J) = 0.1$ s)]. Compound **2** was synthesized in analogy to a literature method.[9]

Preparation of 2-[Ethyl(2-methallyl)amino]indene (2): 2-Indanone (**1**, 3.2 g, 24.2 mmol) was added to a stirred suspension (3 g) of activated 3 Å molecular sieves in 40 mL of toluene. Ethyl(2-methallyl)amine (7.02 g, 72.6 mmol) was added, and the reaction mixture was stirred for 1 day at 70 °C. The mixture was filtered and the remaining molecular sieves washed with toluene (20 mL). Volatiles were removed from the combined organic solutions in vacuo to yield **2** as a liquid (4.31 g, 85%). HRMS (ESI): calcd. for $C_{15}H_{19}NH^+$: m/z = 214.1596; found m/z = 214.1572. − ^1H NMR (599.1 MHz, [D$_8$]toluene, 298 K): indene: δ = 7.04 (dd, 1 H, 5-H), 7.01 (d, 1 H, 7-H), 6.93 (d, 1 H, 4-H), 6.76 (dd, 1 H, 6-H), 5.19 (s, 1 H, 3-H), 3.00 (s, 2 H, 1-H); 2-methallyl: δ = 4.66 (s, 2 H, $=CH_2$), 3.28 (s, 2 H, CH_2), 1.43 (s, 3 H, CH_3); ethyl: δ = 2.87 (q, 2 H, CH_2), 0.85 (t, 3 H, CH_3). − ^{13}C NMR (150.7 MHz, [D$_8$]toluene, 298 K): indene: δ = 156.0 (C2), 148.7 (C3a), 136.8 (C7a), 126.9 (C5), 122.8 (C7), 119.9 (C6), 116.9 (C4), 96.6 (C3); 2-methallyl: δ = 142.0 (quat.-C), 111.3 ($=CH_2$), 56.1 (CH_2), 56.1 (CH_2), 19.9 (CH_3); ethyl: δ = 45.1 (CH_2), 12.0 (CH_3). − ^{15}N NMR (60.7 MHz, [D$_8$]toluene, 298 K): δ = −306.

Preparation of 2-[Ethyl(2-methallyl)amino]indenyllithium (3): *n*-Butyllithium (17.0 mmol, 9.8 mL of a 1.75 M solution in hexane) was slowly added at −78 °C to a stirred solution of 2-[ethyl(2-methallyl)amino]indene (**2**, 3.46 g, 16 mmol) in toluene (30 mL). The reaction mixture was allowed to warm to room temperature and then stirred for 16 h. The resulting solid was recovered from the suspension by filtration, washed with pentane (2 × 10 mL) and dried in vacuo to yield 3.50 g (98%) of **3** as a white solid. ^1H NMR (599.1 MHz, [D$_8$]THF, 298 K): indene: δ = 7.02 (m, 2 H, 4-H, 7-H), 6.31 (m, 2 H, 5-H, 6-H), 5.33 (s, 2 H, 3 H); 2-methallyl: δ = 4.91 (s, 1 H) and 4.76 (s, 1 H, $=CH_2$), 3.74 (s, 2 H, CH_2), 1.73 (s, 3 H, CH_3); ethyl: δ = 3.26 (2 H, CH_2), 1.08 (t, 3 H, CH_3). − ^{13}C NMR (150.7 MHz, [D$_8$]THF, 298 K): indene: δ = 151.1 (C2), 131.5 (C3a, C7a), 119.2 (C4, C7), 115.5 (C5, C6), 80.5 (C1, C3); 2-methallyl: δ = 148.7 (quat.-C), 113.5 ($=CH_2$), 61.3 (CH_2) 23.5 (CH_3); ethyl: δ = 48.5 (CH_2), 14.8 (CH_3). − ^{15}N NMR (60.7 MHz, [D$_8$]THF, 298 K): δ = −326.

X-ray Crystal Structure Analysis of 3: Single crystals were obtained from a toluene/ether (9:1) solution, that was concentrated under argon at −20 °C. $C_{15}H_{18}NLi$, M = 219.24, a = 16.447(1), b = 11.611(1), c = 21.706(1) Å, β = 101.01(3)°, V = 4068.8(5) Å^3, μ = 0.61 cm^{-1}, Z = 12, monoclinic, space group $P2_1/c$ (No. 14), λ = 0.71073 Å, T = 198 K, 9655 reflections collected ($\pm h$, $\pm k$, $\pm l$), 5336 independent (R_{int} = 0.075) and 2864 observed reflections [$I \geq 2\,\sigma(I)$], R = 0.065, wR^2 = 0.139. The data set was collected with a Nonius KappaCCD diffractometer, equipped with a rotating anode generator Nonius FR591. Programs used: data collection COLLECT (Nonius B.V., 1998), data reduction Denzo-SMN (Z. Otwinowski, W. Minor, *Methods Enzymol.* **1997**, *276*, 307−326), absorption correction SORTAV (R. H. Blessing, *Acta Crystallogr.* **1995**, *A51*, 33−37; R. H. Blessing, *J. Appl. Crystallogr.* **1997**, *30*, 421−426), structure solution SHELXS-97 (G. M. Sheldrick, *Acta Crystallogr.* **1990**, *A46*, 467−473), structure refinement SHELXL-97 (G. M. Sheldrick, Universität Göttingen, 1997), graphics SCHAKAL (E. Keller, Universität Freiburg, 1997). − Crystallographic data (excluding structure factors) for the structure reported in this paper have been deposited with the Cambridge Crystallographic Data Centre as supplementary publication CCDC-144456. Copies of the data can be obtained free of charge on application to The Director, CCDC, 12 Union Road, Cambridge CB2 1EZ, UK [Fax: (internat.) +44-1223/336−033; E-mail: deposit@ccdc.cam.ac.uk].

Acknowledgments

Financial support from the Fonds der Chemischen Industrie, the Deutsche Forschungsgemeinschaft, and the Alexander von Humboldt-Stiftung (stipend to J.-L. F.) is gratefully acknowledged.

[1] *Lithium Chemistry, A Theoretical and Experimental Overview* (Eds.: A.-M. Sapse, P. v. R. Schleyer), Wiley, New York **1995**, and references cited therein.

[2] Reviews: P. Jutzi, *J. Organomet. Chem.* **1990**, *400*, 1−17; D. Stalke, *Angew. Chem.* **1994**, *106*, 2256−2259; *Angew. Chem. Int. Ed. Engl.* **1994**, *33*, 2168−2171; P. Jutzi, N. Burford, *Chem. Rev.* **1999**, *99*, 969−990.

[3] W. J. Evans, T. J. Boyle, J. W. Ziller, *Organometallics* **1992**, *11*, 3903−3907; see also: W.-P. Leung, F.-Q. Song, F. Xue, T. C. W. Mak, *J. Chem. Soc., Dalton Trans.* **1997**, 4307−4311.

[4] For an oligomeric $[(fluorenyl)Li(OEt_2)]_n$ example see: M. Könemann, G. Erker, R. Fröhlich, E.-U. Würthwein, *J. Am. Chem. Soc*. **1997**, *119*, 11155−11164.

[5] [5a] For a related cyclooligomeric structure see: M. Könemann, G. Erker, M. Grehl, R. Fröhlich, E.-U. Würthwein, *J. Am. Chem. Soc*. **1995**, *117*, 11215−11219. − [5b] See for a comparison: C. Üffing, R. Köppe, H. Schnöckel, *Organometallics* **1998**, *17*, 3512−3515.

[6] For structures of ligand stabilized monomeric indenyllithium systems see e.g.: W. E. Rhine, G. D. Stucky, *J. Am. Chem. Soc*. **1975**, *97*, 737−743; E. Weiss, *Angew. Chem*. **1993,** *105*, 1565−1587; *Angew. Chem. Int. Ed. Engl*. **1993**, *32*, 1501−1523 and references cited therein; I. Hoppe, M. Marsch, K. Harms, G. Boche, D. Hoppe, *Angew. Chem*. **1995**, *107*, 2328−2330; *Angew. Chem. Int. Ed. Engl.* **1995**, *34*, 2158−2160. For a related monomeric $[(fluorenyl)lithium(OEt_2)_2]$ structure see: M. Håkansson, C.-H. Ottosson, A. Boman, D. Johnels, *Organometallics* **1998**, *17*, 1208−1214.

[7] R. E. Dinnebier, U. Behrens, F. Olbrich, *Organometallics* **1997**, *16*, 3855−3858; R. E. Dinnebier, M. Schneider, S. van Smaalen, F. Olbrich, U. Behrens, *Acta Cryst*. **1999**, *B55*, 35−44.

[8] R. E. Dinnebier, S. Neander, U. Behrens, F. Olbrich, *Organometallics* **1999**, *18*, 2915−2918.

[9] H. Plenio, D. Burth, *Z. Anorg. Allg. Chem*. **1996**, *622*, 225−230; *J. Organomet. Chem.* **1996**, *519*, 269−272.

[10] D. Kowalski, R. Fröhlich, G. Erker, *Z. Naturforsch*. **1996**, *51b*, 1053−1059; K. L. Brown, L. Damm, J. D. Dunitz, A. Eschenmoser, R. Hobi, C. Kratky, *Helv. Chim. Acta* **1978**, *61*, 3108−3135.

Received May 5, 2000
[I00183]

Structural and Theoretical Studies of *ortho*-Substituted Triphenylphosphane Ligands and Their Rhodium(I) Complexes

Pekka Suomalainen,[a] Sirpa Jääskeläinen,[a] Matti Haukka,[a] Riitta H. Laitinen,[b] Jouni Pursiainen,[b] and Tapani A. Pakkanen*[a]

Keywords: Structure elucidation / P ligands / Rhodium / Molecular modeling

The triarylphosphanes, (*o*-thiomethylphenyl)diphenylphosphane (SP, **1**), (*o*-*N*,*N*′-dimethylaminophenyl)diphenylphosphane (NP, **2**), and (*o*-methoxyphenyl)diphenylphosphane (OP, **3**) have been structurally characterized. Detailed information on the stereochemistry of the ligands was gathered by spectroscopic (^{1}H, ^{31}P, ^{13}C NMR) and X-ray crystallographic studies. Molecular modeling methods for investigation of the structures were also applied. It is shown that the geometrical optimization of the ligand can be performed accurately by the ab initio Hartree–Fock method. Furthermore, the steric contribution of the coordinated ligands can be estimated by studying the different conformational states of the free ligands. The coordination abilities of the ligands were studied in reactions with the rhodium compounds $Rh_2(CO)_4Cl_2$ and $Rh(NO_3)_3$ under different reaction conditions. The SP and NP ligands yielded mononuclear chelate complexes, while the OP ligand coordinated solely in a monodentate fashion through the phosphorus atom. The crystal structures of the ligands **1**–**3** and the rhodium(I) complexes [RhCl(CO)(NP)] (**5**) and [RhCl(CO)(OP)$_2$] (**6**) are reported.

Introduction

Increasing research is being done to rationalize the design of homogeneous catalysts for specific industrial applications. The demand for higher selectivity of the several homogenous catalytic reactions has inspired research on the effects of modifying the metal sphere with various ligands. The development of tertiary phosphane ligands began with Wilkinson′s catalyst.[1] Since then, many sterically and electronically enhanced PX_3 ligands have been investigated, and useful tools have been developed for measuring the properties of these ligands.[2,3] Polydentate phosphorus ligands have attracted much interest in the field of homogeneous catalysis. Mixed ligands containing phosphorus together with oxygen, nitrogen or sulfur have been studied in a number of applications including polymerization and oligomerization of olefins,[4] carbonylation of methanol,[5] and hydroformylation of olefins.[6] With the possible hemilabile character of these ligands, a more weakly coordinated donor site may appear between the coordinated/uncoordinated equilibrium, allowing an interesting setup for catalytic reactions. Hemilabile character has earlier been reported for several mixed heteroatom-phosphorus ligands, including ether-phosphanes,[7] hydroxyphenyl phosphanes,[8] phosphonate-phosphanes,[9] and amido-diphosphanes.[10] The fluxional behavior of this type of ligand around the metal center is considered to activate CO and H_2 molecules, thus improving the oxo-reactions such as carbonylation and hydroformylation. Recently, Reinius et al. studied the hydroformylation of methyl methacrylate (MMA) in the presence of SP, NP, and OP ligands. Exceptional selectivity towards branched methyl-α-formylisobutyrate was found when the SP ligand was used in situ with $Rh(NO_3)_3$.[11]

This paper describes structural and complexation studies on three *ortho*-substituted triphenylphosphane derivatives: (*o*-thiomethylphenyl)diphenylphosphane (SP, **1**), (*o*-*N*,*N*′-dimethylaminophenyl)diphenylphosphane (NP, **2**), and (*o*-methoxyphenyl)diphenylphosphane (OP, **3**). In addition to spectroscopic and crystallographic studies, theoretical investigations of the ligand structures have been carried out to obtain a better understanding of the stereochemistry. We were particularly interested to know whether the steric requirements of the coordinated ligands could be estimated by ab initio calculations of the ligands in the gas phase. The coordination modes of the ligands were studied in reactions with the rhodium compounds $Rh_2(CO)_4Cl_2$ and $Rh(NO_3)_3$. Syntheses at a higher synthesis gas pressure and temperature were carried out to investigate the behavior of the ligands in a catalytic environment.

Results and Discussion

Synthesis and Characterization of Substituted Triarylphosphane Ligands

The mono-substituted triphenylphosphane derivatives SP, NP, and OP were prepared according to literature methods.[11–13] The X-ray crystal structures of the ligands are reported for the first time. Crystallographic data are given in Table 1. Figure 1 shows an Ortep drawing of the SP ligand. Selected bond parameters for ligands **1**–**3** are compiled in Table 2. The labeling scheme for the NP and OP ligands is the same as for the SP ligand.

[a] Department of Chemistry, University of Joensuu, P. O. Box 111, 80101 Joensuu, Finland
E-mail: pekka.suomalainen@joensuu.fi
[b] Department of Chemistry, University of Oulu, Linnanmaa, 90570 Oulu, Finland

 © WILEY-VCH Verlag GmbH, D-69451 Weinheim, 2000 1434–1948/00/1212–2607 $ 17.50+.50/0

Table 1. Crystallographic data for SP, NP, OP, [Rh(CO)Cl(NP)] (**5**), and [Rh(CO)Cl(OP)$_2$] (**6**)

	SP	NP	OP	**5**	**6**
Empirical formula	$C_{19}H_{17}PS$	$C_{20}H_{20}NP$	$C_{19}H_{17}OP$	$C_{21}H_{20}ClNOPRh$	$C_{39}H_{34}ClO_3P_2Rh$
Mol wt	308.36	305.34	292.30	471.71	750.96
Crystal size, mm	0.3 × 0.2 × 0.2	0.1 × 0.1 × 0.4	0.3 × 0.1 × 0.1	0.3 × 0.2 × 0.1	0.6 × 0.4 × 0.3
Cryst. syst.	Monoclinic	Orthorhombic	Monoclinic	Monoclinic	Monoclinic
Space group	*P*2(1)/*c*	*Pbca*	*C*2/*c*	*P*2(1)/*n*	*Pn*
λ, Å	0.71073	0.71073	0.71073	0.71073	0.71073
a, Å	11.320(2)	16.481(3)	31.324(6)	9.3518(19)	12.826(3)
b, Å	16.151(3)	12.281(2)	7.2730(10)	18.394(4)	10.298(2)
c, Å	9.673(2)	16.932(3)	28.698(6)	11.693(2)	13.296(3)
β, deg	109.44(3)	90	90.66(3)	101.74(3)	106.15(3)
V, Å^3	1667.7(5)	3427.1(10)	6538(2)	1969.3(7)	1686.7(6)
Z	4	8	16	4	2
D_{calc}, g/cm^3	1.228	1.184	1.188	1.591	1.479
μ mm^{-1}	0.281	0.157	0.164	1.094	0.718
T °C	293(2)	293(2)	293(2)	120(2)	120(2)
θ range, deg	3.16 to 26.48	2.98 to 25.00	2.88 to 25.00	2.84 to 27.48	1.98 to 27.47
No. of unique rflns	3405	2991	5289	4446	7493
No. of obsd. data[a]	2755	1359	2289	3939	7268
No. of params	242	200	380	315	419
R_1	0.0380	0.0605	0.0713	0.0231	0.0241
*wR*2	0.0987	0.0907	0.1683	0.0549	0.0557
Largest diff. Peak and hole, e Å^{-3}	0.154 −0.186	0.228 −0.208	0.702 −0.215	0.421 −0.875	0.588 −0.516

[a] $I > 2\sigma$.

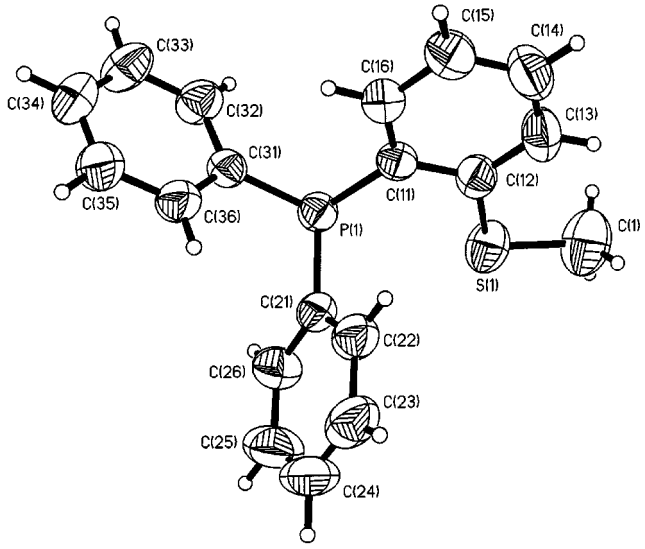


Figure 1. Ortep drawing of the SP ligand with thermal ellipsoids at 50% level

Table 2. Selected bond lengths, angles, and torsional angles for the SP, NP, and OP ligands

Atoms[a]	SP (1)	NP (2)	OP (3)
Bond lengths (Å)			
P(1)−C(11)	1.833 (2)	1.828 (3)	1.830 (5)
P(1)−C(21)	1.830 (2)	1.831 (3)	1.838 (5)
P(1)−C(31)	1.829 (2)	1.824 (3)	1.828 (5)
X(1)−C(1)	1.783 (3)	1.467 (4)	1.429 (6)
X(1)−C(2)	-	1.462 (4)	-
C(12)−X(1)	1.767 (2)	1.439 (4)	1.375 (6)
P(1A)−C(11A)	-	-	1.838 (5)
P(1A)−C(21A)	-	-	1.839 (5)
P(1A)−C(31A)	-	-	1.818 (5)
	Bond angles (deg)		
C(31)−P(1)−C(21)	101.8 (7)	101.1 (2)	102.1 (2)
C(31)−P(1)−C(11)	102.8 (7)	102.0 (2)	100.9 (2)
C(21)−P(1)−C(11)	102.1 (7)	101.5 (2)	100.9 (2)
C(12)−X(1)−C(1)	103.1 (1)	112.0 (3)	118.7 (5)
C(12)−X(1)−C(2)	-	113.5 (3)	-
C(12A)−O(1A)−C(1A)	-	-	121.4 (7)

[a] X = S, N or O.

Table 3. Low lying conformations and corresponding cone angles of ligands

Conformation	Δ*E* (kJ/mol)/Θ (deg) SP		OP		NP	
Conf 1*	0	158	0	166	0	180
Conf 2	2.55	158	8.94	156	27.40	153
Conf 3	23.78	155	12.61	153		
Conf 4	32.13	153				

* Global minimum.

Conformational Flexibility of the Ligands

The equilibrium geometries of the SP, OP, and NP ligands were first determined by optimizing the structures with the ab initio Hartree−Fock method using a 3−21G* basis set. Starting from the initial geometries, a conformational analysis was carried out by rotating the torsional angles of the three phenyl rings. Several local minima were identified and subsequently optimized with the HF/3−21G* method. The energies of the minima relative to the ground state are shown in Table 3.

The steric crowding of the free ligands was measured using Tolman's semi-cone angle concept.[2] The cone angles of the free ligands were calculated for the ground states and for low lying conformations. As shown in Table 3, the cone angles are widest for the ground states and narrow for the higher energy conformers, giving an indication of the en-

ergy demands of the steric repulsion. In the lowest energy conformations, the maximum semi-cone angles are always determined by the *m*-hydrogen atoms of the phenyl rings and by one of the hydrogen atoms in the -XCH_3 group. In this manner, the ligands can be arranged in decreasing order of bulkiness: SP = OP < NP. For the higher energy conformations of the ligands, the cone angles diminish because the substituted phenyl ring(s) rotates in such a way that the -XCH_3 group becomes located inside the cone and no longer directly affects the maximum semi-cone angle. This eventually leads to identical values of cone angles.

Synthesis and Characterization of Rhodium Phosphane Complexes

Two different rhodium sources, $Rh_2(CO)_4Cl_2$ and $Rh(NO_3)_3$, were used to prepare the complexes. Variations in atmosphere, temperature, pressure, and solvent, were introduced to clarify the various possibilities for the reaction pathways, and to proceed step-by-step from milder reaction conditions to a more severe, actual catalytic environment. At room temperature, the syntheses were carried out in an atmosphere of either nitrogen or carbon monoxide. Conditions nearer to a catalytic environment were obtained when the reactions were carried out in autoclaves that were heated to 100 °C and pressurized to 20 bar with carbon monoxide or synthesis gas (CO/H_2). The reaction time in the pressurized synthesis reactions was 4 h, after which the autoclaves were allowed to cool to room temperature.

Reactions With the SP Ligand

A yellow precipitate was isolated after $Rh_2(CO)_4Cl_2$ and the SP ligand were allowed to react in a methanol solution at room temperature and under an atmosphere of nitrogen. The product was identified crystallographically as the square-planar rhodium compound [Rh(CO)Cl(SP)] **(4)** with the SP ligand chelating through the sulfur and phosphorus atoms. The IR spectrum of **4** shows a CO stretching vibration at 2010 cm^{-1}, while the ^{31}P NMR spectrum gives a doublet at $\delta = 67.2$ with $J_{Rh-P} = 152$ Hz. Dilworth et al.[14] have previously reported the synthesis of a brown precipitate, which they proposed on the basis of spectroscopic investigation to be compound **4**. More recently, Steeg et al.[15] published a crystallographic characterization of the same compound, which was, however, reached by a different route.

Compound **4** was again formed under an atmosphere of carbon monoxide in toluene solution. Likewise the formation of **4** was observed under syngas pressure (CO/H_2 20bar) and at high temperature (100 °C), but another doublet in the ^{31}P NMR spectrum was found at $\delta = 48.9$ with a smaller coupling constant of 77 Hz. This new signal was assigned to an isomeric form of complex **4** with the carbonyl group *trans* to phosphorus, since such coordination gives a lower shift and coupling constant than the corresponding orientation with phosphorus *trans* to chloride.[16]

The reaction between $Rh(NO_3)_3 \cdot 2H_2O$ and SP in a catalytic environment gave peaks at 2034 and 1873 cm^{-1} in the IR spectrum, as well as a broad line at $\delta = 28$ in the ^{31}P NMR spectrum. Resemblance of the spectroscopic data to those of the rhodium diphosphane compounds $HRh(CO)_x(P)_y$ prepared under similar reaction conditions can be seen.[17] In addition, the fluctuation of the SP coordination is possible. Furthermore, the formation of polynuclear carbonyl compounds is possible as a result of degradation of the ligand under severe reaction conditions.[18]

Reactions With the NP Ligand

Methanol solutions of $Rh_2(CO)_4Cl_2$ and NP were mixed at room temperature under an atmosphere of nitrogen to form a yellow precipitate. The product was identified crystallographically as the monometallic chelate species, [Rh(CO)Cl(NP)] (**5**), bonded through nitrogen and phosphorus (Figure 2). The structure shows a planar geometry around the rhodium atom with a slight deviation from ideal. The largest discrepancy is along the axis P(1)−Rh(1)−Cl(1) where the angle is 174.7 (2) Å. A shorter Rh−C(4) distance than in complex **4** indicates the stronger

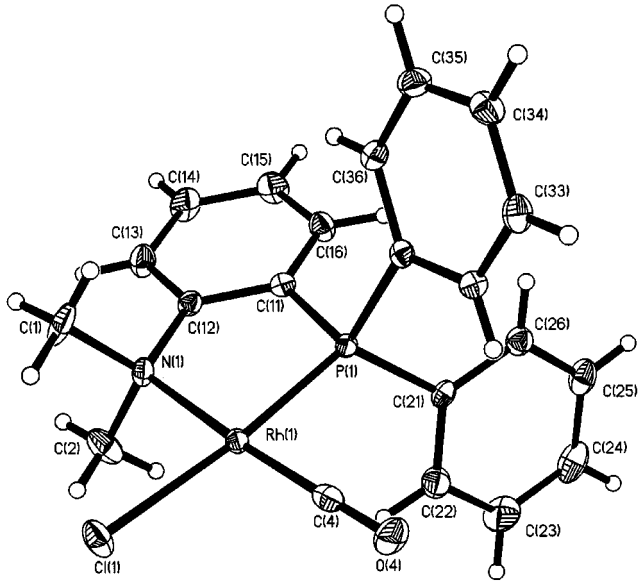


Figure 2. Ortep drawing of Rh(CO)ClNP with thermal ellipsoids at 50% level

Table 4. Selected bond angles and distances for Rh(CO)Cl(NP) (**5**)

Atoms	Bond lengths (Å)
Rh(1)−P(1)	2.3308(10)
Rh(1)−P(2)	2.3335(10)
Rh(1)−Cl(1)	2.4131(10)
Rh(1)−C(4)	1.827(5)
C(4)−O(4)	0.989(5)
Atoms	**Bond angles (deg)**
C(4)−Rh(1)−P(1)	87.26(10)
C(4)−Rh(1)−P(2)	92.21(9)
P(1)−Rh(1)−P(2)	179.39(4)
C(4)−Rh(1)−Cl(1)	178.40(11)
P(1)−Rh(1)−Cl(1)	92.89(3)
P(2)−Rh(1)−Cl(1)	87.63(3)

electron-donor character of the NP ligand. The flow of electron density to the rhodium increases π-back donation to the carbonyl. This is further observed in the CO stretching frequencies of 2010 cm^{-1} and 1995 cm^{-1} for **4** and **5**, respectively. The ^{31}P spectrum of **5** shows a doublet at δ = 56.8 with a Rh−P coupling of 171 Hz.

When the same reactants were allowed to react in the autoclave (toluene, 100 °C, 20 bar CO, 4 hours), species **5** was again isolated and characterized by its IR stretching vibration and elemental analysis. The same product was observed when a CO/H_2 atmosphere was applied to the reaction. An IR absorption at 1995 cm^{-1} was found, but also an additional peak at 2071 cm^{-1} appeared in the spectrum, suggesting the formation of a $Rh_6(CO)_{16}$ cluster. The synthesis and stereochemistry of **5** has previously been discussed by Roundhill et al.[19,20]

The strong chelating ability of the NP ligand was also observed in the reaction with $Rh(NO_3)_3 \cdot 2H_2O$ at room temperature under a CO atmosphere. From the assignment of a doublet at δ = 57.9 (141 Hz) in the ^{31}P NMR spectrum and an IR absorption at 1995 cm^{-1}, we deduced that a chelate compound was formed with the NP ligand. Under more severe reaction conditions, the product from the reaction with $Rh(NO_3)_3 \cdot 2H_2O$ and NP afforded similar spectroscopic data to those obtained with the SP ligand, suggesting corresponding species.

Reactions With the OP Ligand

$Rh_2(CO)_4Cl_2$ and the OP ligand were allowed to react under nitrogen at room temperature in a methanol solution to form a yellow precipitate. The compound, *trans*-[Rh(CO)-$Cl(OP)_2$] (**6**), was characterized crystallographically as a tetracoordinate monocarbonyl complex with two phosphorus ligands bonded in a monodentate fashion (Figure 3). Analogous $[RhX(CO)(PAr_3)_2]$ (X = Cl, I, Br) structures have been reported previously.[21−23] Compound **6** gives a strong CO stretching vibration at 1974 cm^{-1} and the ^{31}P NMR spectrum shows a doublet at δ = 23.2 with a Rh−P coupling constant of 129 Hz. The crystallographic data for **6** are given in Table 1. Selected bond lengths and angles are given in Table 5. Under similar reaction conditions in dichloromethane, the reaction proceeds differently, resulting in strong IR absorptions at 2090 and 2010 cm^{-1}, characteristic of either monometallic *cis*-dicarbonyl or dimeric, doubly five-coordinated phosphane derivatives.[24] At an elevated pressure and temperature, complex **6** was again the main product.

Table 5. Selected bond angles and distances for $Rh(CO)Cl(OP)_2$ (**6**)

Atoms	Bond lengths (Å)
Rh(1)−C(4)	1.807(2)
Rh(1)−P(1)	2.1947(6)
Rh(1)−N(1)	2.1865(2)
Rh(1)−Cl(1)	2.3867(7)
C(4)−O(4)	1.150(2)
P(1)−C(21)	1.824(2)
P(1)−C(31)	1.8216(2)
P(1)−C(11)	1.815(2)
N(1)−C(12)	1.477(2)
N(1)−C(1)	1.496(3)
N(1)−C(2)	1.487(3)
Atoms	**Bond angles (deg)**
C(4)−Rh(1)−P(1)	91.24(7)
C(4)−Rh(1)−N(1)	176.26(7)
P(1)−Rh(1)−N(1)	85.03(5)
C(4)−Rh(1)−Cl(1)	92.62(7)
P(1)−Rh(1)−Cl(1)	174.696(2)
X(1)−Rh(1)−Cl(1)	91.11(5)
O(4)−C(4)−Rh(1)	178.94(2)

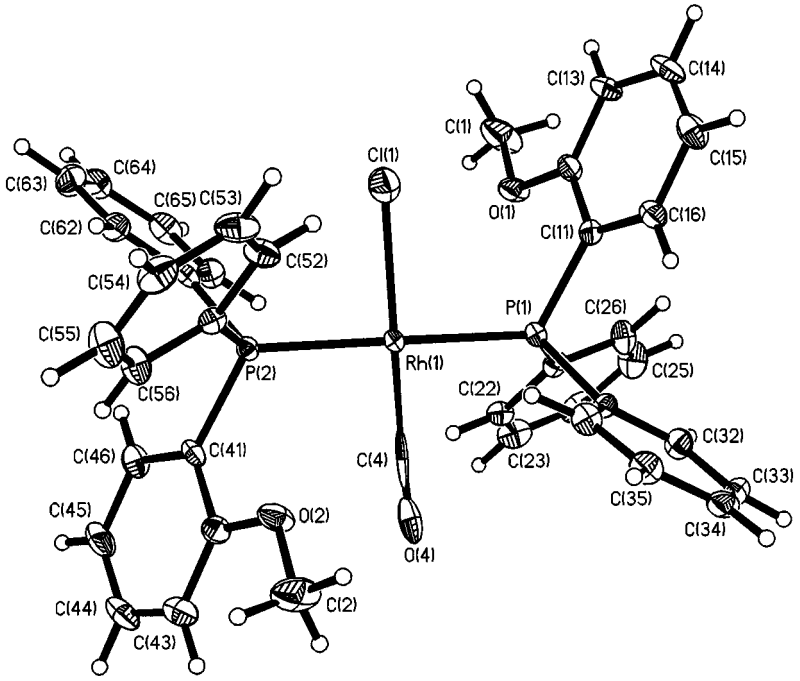


Figure 3. Ortep drawing of $Rh(CO)Cl(OP)_2$ with thermal ellipsoids at 50% level

The reaction between $Rh(NO_3)_3 \cdot 2H_2O$ and the OP ligand in a methanol solution under an atmosphere of CO resulted in a greenish-yellow solid. This compound gives a strong IR absorbance at 1974 cm^{-1}, indicating a geometry similar to that of complex **6**. Crystallization from dichloromethane led to a mixture of yellow and green crystals. The yellow crystals turned out to be species **6**, evidently formed through exchange of an NO_3 group for the chlorine atom. The green crystals have a linear P−Rh−P skeleton, as in complex **6**, with a bidentate NO_3 ligand attached by two oxygen atoms. However, the remaining ligands were disordered, and crystallization of two different species also seemed probable. In the ^{31}P NMR spectrum, the green crystals give rise to a doublet at $\delta = 20.2$ with $J_{Rh-P} = 153$ Hz.

The presence of **6** was again observed at elevated temperature and 20 bar syngas pressure. Additional absorptions were detected at 2034 and 1873 cm^{-1} in the IR spectrum, and there is a broad line at $\delta = 28$ in the ^{31}P NMR spectrum. Similar species as observed with the SP and NP ligands are proposed.

No evidence was found for the chelating character of the OP ligand. The monodentate binding mode of the OP ligand has also been observed by Trzeciak et.al.[8] However, they found that substitution of a methoxy group for a hydroxyl group changes the reactivity of the ligand, resulting in stable chelate complexes.

Comparison Between Solid State and Calculated Structures

Reliable predictions of ligand geometries were obtained using the Hartree−Fock method. The geometries of the ground-state structures and the X-ray structures of the ligands deviate by only a few hundredths of an angstrom in bond lengths and one degree in bond angles. The cone angle values based on the solid state structures of the free ligands fall within the cone angle range measured for the different gas-phase conformers. Only the SP ligand was found to have a greater angle in the solid state. The cone angle data for the ligands are shown in Table 6. A closer investigation of the coordinated OP ligand in complex **6** revealed a similar geometry to its lowest energy conformation. Being in the *trans* position to each other, the two OP ligands can lie near the low energy conformation. We can assume that the phosphane does not encounter a significant amount of steric interaction from the CO or Cl ligands. A comparison of the structures of the free and bonded OP ligand is shown in Figure 4. The presence of a bidentate coordination mode in compounds **4** and **5** makes a similar examination of these compounds more difficult.

Table 6. Cone angle values based on different structural data

Ligand	Free ligand (X-ray)	Flexibility range (HF 3−21G*)	Coordinated ligands (X-ray) $Rh(CO)Cl(L)_2$ **(6)**
SP	164	153−158	-
NP	176	153−180	-
OP	162	153−166	154, 155

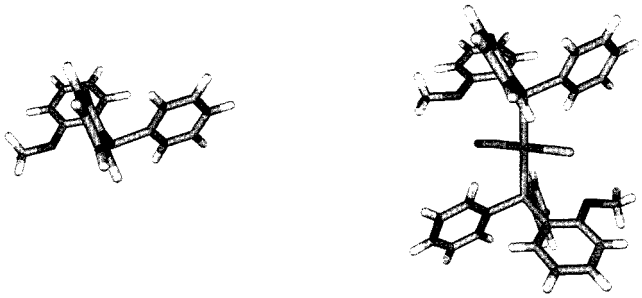


Figure 4. Comparison of the lowest energy conformations of (*o*-methoxyphenyl)diphenylphosphane and the coordinated ligand

Conclusion

Through a detailed examination of the conformational variations of the free ligand structures in the gas phase, we were able to estimate the steric requirements of the solid-state structures of the free and coordinated ligands. However, the multiple binding sites of the ligands may lead to highly strained conformations, which are hard to predict on the basis of the free ligand structures.

The coordination preference of the ligand in the prepared rhodium complexes was influenced by the type of donor atom in the *ortho* position of the phenyl ring. The strong σ-donor ligands, SP and NP, both yielded chelate species independently of the reaction conditions. In contrast, the OP ligand was found to coordinate in a monodentate fashion.

Experimental Section

General: All the syntheses were carried out using standard Schlenk techniques under an atmosphere of nitrogen. Other gases, carbon monoxide and synthesis gas (CO/H_2), were of high purity grade (99.997%) and were purchased from AGA and MG, respectively. The solvents, methanol and toluene (p.a. grade), were deoxygenated with nitrogen prior to use. $Rh_2(CO)_4Cl_2$ was prepared according to a literature method[25] and $Rh(NO_3)_3 \cdot 2H_2O$ was purchased from Alfa. NMR spectra were recorded on a Bruker AM250 spectrometer. ^{31}P spectra were referenced to 85% H_3PO_4. Elemental analyses were done with a Perkin−Elmer 2400 Series II CHNS/O analyzer. High-pressure synthesis reactions were conducted in 100 mL Berghof autoclaves with a 60 mL Teflon liner. In a typical run, the autoclave was charged in a glovebox with the rhodium compound, ligand, and solvent (toluene). The autoclaves were then sealed and pressurized with either H_2/CO (1:1) or CO to 20 bar. The autoclaves were heated to 100 °C, with the temperature controlled and monitored by an internal thermocouple. After four hours reaction time, the autoclaves were cooled slowly and brought to normal atmospheric pressure. The Gaussian 94[26]and Sybyl[27] programs were used in modeling. The 3−21G* basis set was used for geometric optimizations at the Hartree−Fock level. In the conformational analyses, the single point energies were calculated with the grid-search method of Sybyl, and the final geometries were determined with the HF/3−21G* method. The phenyl rings were rotated 180° and the substituted phenyl ring was rotated 360° in increments of 20°. For cone angle determinations, the metal−phosphorus distance was fixed at 2.28 Å. A dummy atom was used for free ligands.

Rh(CO)ClSP (4): $Rh_2(CO)_4Cl_2$ (25 mg, 0.064 mol) and SP (40 mg, 0.129 mol) were dissolved in methanol in separate flasks. The ligand solution was added dropwise to the solution of the rhodium compound. The yellow precipitate that formed was filtered, washed with methanol, and quickly dried under vacuum. Yellow crystals for X-ray studies were crystallized from CH_2Cl_2. – $C_{20}H_{17}ClPRhS$ (474.73): calcd. C 50.60, H 3.61, S 6.75; found C 50.67, H 3.62, S 6.89. – IR (CH_2Cl_2): ν(CO) = 2010cm^{-1}. – ^{31}P NMR: δ = 67.5 [d, J(Rh–P) = 152 Hz].

Rh(CO)ClNP (5): $Rh_2(CO)_4Cl_2$ (100 mg, 0.257 mol) and NP (80 mg, 0.262 mol) were dissolved in methanol in separate Schlenk flasks. The ligand solution was added dropwise to the solution of the rhodium compound. Rapid formation of a yellow precipitate was observed and the reaction was allowed to continue for 2 hours. The precipitate was filtered, washed with methanol and dried under vacuum. Yellow crystals for X-ray studies were obtained from a CH_2Cl_2/hexane solution. – $C_{21}H_{20}ClPRhS$: calcd. C 53.47, H 4.27, N 2.97; found C 53.27, H 4.31, N 3.14. – IR (CH_2Cl_2): ν(CO) = 1995cm^{-1}. – ^{31}P NMR: δ = 56.8 [d, J(Rh–P) = 171 Hz].

Rh(CO)Cl(OP)$_2$ (6). Method 1: $Rh_2(CO)_4Cl_2$ (100 mg, 0.257 mol) and OP (150 mg, 0.3763 mol) were dissolved in methanol in separate flasks. The ligand solution was added dropwise to the precursor solution. The yellow precipitate that formed was filtered, washed with methanol, and quickly dried under vacuum. Yellow crystals for X-ray studies were crystallized from a CH_2Cl_2/hexane solution. – $C_{39}H_{34}ClO_3P_2Rh$: calcd. C 62.37, H 4.56; found C 62.07, H 4.54. – IR (CH_2Cl_2): ν(CO) = 1974cm^{-1}. – ^{31}P NMR: δ = 23.5 [d, J(Rh–P) = 130 Hz].
Method 2: $Rh_2(CO)_4Cl_2$ (25 mg, 0.064 mol) and OP (55 mg, 0.3763 mol) were packed into the autoclave together with 5 mL of toluene. The autoclave was pressurized to 20 bar (CO/H_2) and heated to 100 °C. After four hours the autoclave was cooled and brought to normal atmospheric pressure. The yellow precipitate that formed was filtered, washed with toluene, and dried under vacuum.

X-ray Crystallographic Study: X-ray diffraction data were collected with a Nonius KappaCCD diffractometer using Mo-K_α radiation (λ = 0.71073 Å) and φ-scan or combined φ/ω-scan data collection mode with a Collect[28] data collection program. The Denzo and Scalepack[29] programs were used for cell refinements and data reduction. All structures were solved by direct methods using the SHELXS97[30] program with the WinGX[31] graphical user interface or by using the SHELXTL v5.1[32] program package. The structure refinements were carried out with SHELXL97.[33] For compounds OP, NP, Rh(CO)Cl(SP), and Rh(CO)Cl(OP)$_2$, hydrogen atoms were constrained to ride on their parent atom. [aromatic hydrogens: C–H = 0.93Å, U_{iso} = 1.2(C_{eq}) at 293 K and C–H = 0.95Å, U_{iso} = 1.2(C_{eq}) at 120 K; methyl hydrogens: C–H = 0.96 Å, U_{iso} = 1.5(C_{eq}) at 293 K and C–H = 0.95Å, U_{iso} = 1.2(C_{eq}) at 120 K]. For compound **5** and SP, all atoms were located from the difference Fourier map. In the former case, the hydrogen atoms were refined isotropically, and in the latter case with constant U_{iso} = 0.08. The structure of [Rh(CO)Cl(OP)$_2$] (**6**) was solved as a racemic twin (Flack parameter 0.48952) in the acentric space group *Pn*.

Crystallographic data are summarized in Table 1 and selected bond lengths and angles for the ligands are presented in Table 2, Table 4 and Table 5.

Crystallographic data (excluding structure factors) for the structure(s) reported in this paper have been deposited with the Cambridge Crystallographic Data Centre as supplementary publication no. CCDC-140374 **(3)**, -140375 **(1)**, -140376 **(2)**, -140377 **(6)**, -140378 **(5)**. Copies of the data can be obtained free of charge on application to CCDC, 12 Union Road, Cambridge CB2 1EZ, UK [Fax: (internat.) + 44–1223/336–033; E-mail: deposit@ccdc.cam.ac.uk].

[1] D. Evans, J. A. Osborn, G. Wilkinson, *J. Chem. Soc.* **1968** 3133.
[2] C. A. Tolman, *Chem. Rev.* **1977**, *77*, 313.
[3] C. P. Casey, G. T. Whiteker, *Isr. J. Chem*. **1990**, *30*, 299.
[4] G. Braca, A. M. Raspolli Galletti, M. Di Girolamo, G. Sbrana, R. Silla, P. Ferrarini, *J. Mol. Cat.* **1995**, *96*, 203.
[5] A. Bader, E. Lindner, *Coord. Chem. Rev.* **1991**, *108*, 27.
[6] C. Abu-Gnim, I. Amer, *J. Mol. Cat.* **1993**, *85*, L275.
[7] E. Lindner, K. Gierling, B. Keppeler, H. A. Mayer, *Organometallics* **1997**, *16*, 3531.
[8] A. M. Trzeciak, J. J. Ziolkowski, T. Lis, R. Choukroun, *J. Organom. Chem.* **1999**, *575*, 87.
[9] S. Bischoff, A. Weight, H. Miessner, B. Lucke, *Energy & Fuels* **1996**, *10*, 520.
[10] K. K. Hii, M. Thornton-Pett, A. Jutand, R. P. Tooze, *Organometallics* **1999**, *18*, 1887.
[11] H. K. Reinius, R. H. Laitinen, A. O. I. Krause, J. T. Pursiainen, Catal. Lett. **1999**, *60*, 65.
[12] D. W. Meek, G. Dyer, M. O. Workman, *Inorganic Syntheses* **1976**, *16*, 168.
[13] E. Meintjies, E. Singleton, R. Schmutzler, M. Sell, *S. Afr. J. Chem*. **1985**, *38*, 115.
[14] J. R. Dilworth, J. R. Miller, N. Wheatley, M. J. Baker, J. G. Sunley, *J. Chem. Soc., Chem. Commun.* **1995**, 1579.
[15] N. Steeg, R. Kramolowsky, *Z. Kristallogr*. **1997**, *212*, 273.
[16] J. F. Nixon and A. Pidcock, *Phosphorus-31 NMR Spectra of Coordination Compounds*, Annu. Rev. NMR Spectrosc., **1969**, *2*, 345.
[17] A. Castellanos-Paez, S. Castillion, C. Claver, *Organometallics* **1998**, *17*, 2543.
[18] G. J. H Buisman, E. J. Vos, P. C. J. Kamer, P. W. N. M van Leeuwen, *J. Chem. Soc., Dalton Trans.* **1995**, 409.
[19] D. M. Roundhill, R. A. Bechtold, S. G. N. Roundhill, *Inorg. Chem*. **1980**, *19*, 284.
[20] T. B. Rauchfuss, D. M. Roundhill, *J. Am. Chem. Soc*. **1973**, 3098.
[21] A. Ceriotti, G. Ciani, A. Sironi, *J. Organomet. Chem*. **1983**, *247*, 345.
[22] F. R. Hartley, S. G. Murray, D. M. Potter, *J. Organomet. Chem*. **1983**, *254*, 119.
[23] R. H. Laitinen, J. Soininen, P. Suomalainen, T. A. Pakkanen, M. Ahlgren, J. Pursiainen, *Acta Chem. Scand.* **1999**, *53*, 53.
[24] [24a] R. Poilblanc, *J. Organomet. Chem*. **1975**, *94*, 241. – [24b] P. Uguagliati, G. Deganello, U. Belluco, *Inorg. Chim. Acta* **1974**, *9*, 203. – [24c] R. Poilblanc, J. Gallay, *J. Organomet. Chem*. **1971**, *27*, C53.
[25] J. A. Cleverty, G. Wilkinson, *Inorganic Syntheses*, Vol. 8, McGraw-Hill, New-York, **1966**, p.211
[26] M. J. Frisch, G. W. Trucks, H. B. Schlegel, P. M. W. Gill, B. G. Johnson, M. A. Robb, J. R. Cheeseman, T. Keith, G. A. Petersson, J. A. Montgomery, K. Raghavachari, M. A. Al-Lahman, V. G. Zakrzewski, J. V. Ortiz, J. B. Foresman, J. Cioslowski, B. B. Stefanov, A. Nanayakkara, M. Challacombe, C. Y. Peng, P. Y. Ayala, W. Chen, M. W. Wong, J. L. Andres, E. S. Replogle, R. Gomperts, R. L. Martin, D. J. Fox, J. S. Binkley, D. J. Defrees, J. Baker, J. P. Stewart, M. Head-Gordon, C. Gonzales, J. A. Pople, Gaussian, Inc., Pittsburgh PA, 1995
[27] Sybyl 6.03; Tripos Associates, 1699 S. Hanley Road, Suite 303, St. Louis, MO 63144.
[28] Collect: Data Collection Software, Enraf–Nonius, Delft, The Netherlands, **1999**.
[29] Z. Otwinowski, W. Minor, *Processing of X-ray Diffraction Data Collected in Oscillation Mode, Methods in Enzymology, Volume 276, Macromolecular Crystallography, Part A*, C. W. Carter, Jr. and R. M. Sweet, Eds., Academic Press, **1997**, p. 307–326.
[30] G. M. Sheldrick, SHELXS97, Program for Crystal Structure Determination, University of Göttingen, Germany, **1997**.

[31] L. J. Farrugia, WinGX v1.61 − A Windows Program for Crystal Structure Analysis, University of Glasgow, Glasgow, **1998**.
[32] G. M. Sheldrick, SHELXTL Version 5.1, Bruker Analytical X-ray Systems, Bruker AXS, Inc. Madison, Wisconsin, USA, **1998**.
[33] G. M. Sheldrick, SHELXL97, Program for Crystal Structure Refinement, University of Göttingen, Germany, **1997**.

Received February 15, 2000
[I00242]

Metal Complexes with Tetrapyrrole Ligands, LXXV[‡]

Osmium Complexes of the 5,10,15,20-Tetrakis(4-phosphonomethylphenyl)-porphyrin Anion, A New Water-Soluble Tetraphenylporphyrinate System

Johann W. Buchler[a] and Joachim R. Simon*[b]

Keywords: Osmium / Porphyrinates / Anions / Autoxidation / Electrophoresis

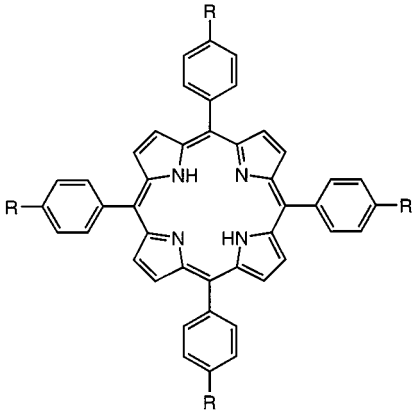
The synthesis of a new class of water-soluble osmium tetraphenylporphyrinates, complexes of the tetrakis(4-phosphonomethylphenyl)porphyrin anion $[H_2(tP_4O_8\{OH\}_4mpp)]^{4-}$ **(5)**, is described. Starting from OsCO(tmecpp)thf **(1a)** and OsO_2(tmecpp) **(1b)**, the new complexes **5a–c** were synthesized by a four-step reaction with Os(t{OH}$_4$mpp)LL′ **(2a–b)**, Os(tBr_4mpp)LL′ **(3a–b)**, and Os(tP_4O_4{OEt}$_8$mpp)LL′ **(4a–c)** as intermediates. The new complexes were characterized by UV/Vis, IR, ^{1}H NMR, and ^{31}P NMR spectroscopy, as well as by cyclic voltammetry and electrophoresis.

Introduction

Only a few water-soluble porphyrin systems with anionic functional groups are known. Besides the tetrakis(4-sulfonatophenyl)porphyrin anion $[H_2(tpps_4)]^{4-}$ **(6)**, tetrakis(4-carboxyphenyl)porphyrin $H_2(tH_4cpp)$[2] **(7)**, and tetrakis(4-boronatophenyl)porphyrin **(8)**[3] are mentioned exclusively. Additionally, the tetrakis(4-phosphonophenyl)porphyrin is reported,[4] however, its synthesis is difficult. As compared with **6**, **7** and **8** are soluble only in alkaline media. All in all the tetrakis(4-sulfonatophenyl)porphyrin anion **6** is the only water-soluble porphyrin system that can be synthesized easily, and is soluble in aqueous media over the full pH range.

Anionic porphyrin systems are very interesting, due to their behaviour.[5–11] As the number of these porphyrins are limited, researchers look out for further possibilities of synthesizing new porphyrin systems with anionic functional groups. By a four-step reaction starting from H_2(tmecpp) **(1)**, Katzenmeier[12] was able to extend the number of anionic porphyrin systems. A new porphyrin, the tetra-sodium salt of 5,10,15,20-tetrakis(4-phosphonomethylphenyl)porphyrin anion $[H_2(tP_4O_8\{OH\}_4mpp)]^{4-}$ **(5)** was described. Like tetrakis(4-sulfonatophenyl)porphyrin anion **(6)**, compound **5** shows no reactions in alkaline or acidic media. The excellent solubility over almost the full pH-range must be noted.

With the exception of complexes with carbonic[13a,13b] or sulfonic[13] functional groups, no other water-soluble osmium porphyrin complexes are known. Attempts to synthesize cationic osmium porphyrin complexes have been described,[13b] although it was not possible to obtain the desirable products.



No.	R	Formula
1	COOMe	H_2(tmecpp)
2	CH_2OH	H_2(t{OH}$_4$mpp)
3	CH_2Br	H_2(tBr_4mpp)
4	$CH_2PO(OEt)_2$	$H_2(tP_4O_4\{OEt\}_8mpp)$
5	$CH_2PO_3H^-$	$[H_2(tP_4O_8\{OH\}_4mpp)]^{4-}$
6	SO_3^-	$[H_2(tpps_4)]^{4-}$
7	COOH	$H_2(tH_4cpp)$
8	$B(OH)_2$	$H_2(tB_4\{OH\}_4pp)$

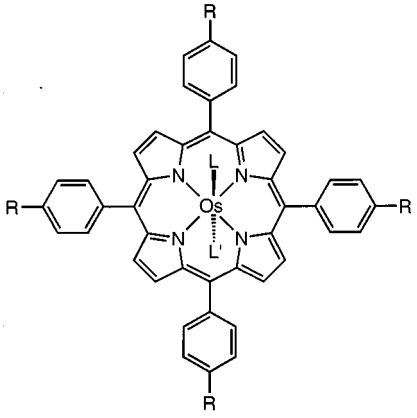
Water-soluble osmium(II) porphyrinates with sulfonate groups in the *para*-position of the phenyl rings can undergo reversible redox reactions,[13] and because of this behaviour are good cytochrome models. The aim of this work was to prove whether other hydrophilic osmium(II) porphyrinates show the same redox behaviour. Based on the results of Katzenmeier,[12] we were able to synthesize a new class of

[‡] Part LXXIII: Ref.[1]

[a] Institut für Anorganische Chemie, Technische Universität Darmstadt,
Petersenstraße 18, 64287 Darmstadt, Germany
[b] Dr. Theodor Schuchardt & Co.
Eduard-Buchner-Str. 14–20, 85662 Hohenbrunn, Germany
Fax: (internat.) +49-8102/802-207

 © WILEY-VCH Verlag GmbH, D-69451 Weinheim, 2000 1434–1948/00/1212–2615 $ 17.50+.50/0

water-soluble osmium tetraphenylporphyrinates, the osmium complexes of the tetrakis(4-phosphonomethylphenyl)porphyrin anion $[Os(tP_4O_8\{OH\}_4mpp)LL']^{4-}$ **(5a–d)** and extend the number of water-soluble osmium porphyrin complexes. Synthesis and results are reported below.



No.	R	Formula
1a–b	COOMe	Os(tmecpp)LL'
2a–b	CH_2OH	Os(t{OH}$_4$mpp)LL'
3a–d	CH_2Br	Os(tBr_4mpp)LL'
4a–d	$CH_2PO(OEt)_2$	Os(tP_4O_4{OEt}$_8$mpp)LL'
5a–d	$CH_2PO_3OH^-$	$[Os(tP_4O_8\{OH\}_4mpp)LL']^{4-}$

Synthesis

As shown previously,[13b] water-soluble osmium(II) porphyrin complexes cannot be synthesized directly by reaction of K_2OsCl_6 with the ionic porphyrin system: they must be synthesized by a four-step reaction with water-insoluble osmium porphyrin complexes as intermediates. Based on these results we decided to synthesize the osmium complexes of the tetrakis(4-phosphonomethylphenyl)porphyrin anion $[H_2(tP_4O_8\{OH\}_4mpp)]^{4-}$ **(5)** by metallation of $H_2(tP_4O_4\{OEt\}_8mpp)$ **(4)**, followed by saponification. Unfortunately, we were not able to obtain the product by the method described for metallation of H_2(tmecpp).[13] Indeed, complete metallation was confirmed by UV/Vis spectroscopy. However, some ester groups were saponified during the reaction. Also, several experiments in the presence of EtOH yielded only the diester $A_2[OsCO(tP_4O_6\{OEt\}_2\{OH\}_4mpp)thf]$ **(4d)**, as seen in the ^1H NMR spectra. Compound **4d** was saponified, for standardization. Neither saponification with CH_3SiBr/KOH,[12,14,15] nor KOH (4%)[13b,16] yielded the expected product, but instead a water-soluble residue was characterized as $K_2[OsCO(tP_4O_6\{OEt\}_2\{OH\}_4mpp)thf]$ **(5d)** by NMR spectroscopy and elemental analysis. Reaction of **5d** with 1-methylimidazole or MeOH, resulted in the axial ligand (thf) being substituted to yield $K_2[OsCO(tP_4O_6\{OEt\}_2\{OH\}_4mpp)MEOH]$ **(5e)** or $K_2[OsCO(tP_4O_6\{OEt\}_2\{OH\}_4mpp)(1\text{-meim})]$ **(5f)**, respectively. The new axial ligands were established by IR spectroscopy.

In agreement with Künzel,[13b] it was not possible to synthesize the water-soluble osmochromes $K_4[Os(tP_4O_8\{OH\}_4mpp)LL']$ **(5h)** by oxidation of **5d** or by the reduction of the intermediate dioxo complex **5g**. As shown by the UV/Vis and IR spectra, either no reaction was observed, or **5g** was contaminated with decomposition compounds that could not be separated by chromatography or ultrafiltration. As a result, a different method of synthesis of **5h** was sought. The most important reference was given by the retro-synthetic work of Katzenmeier.[12] He was able to show that the tetrakis(4-phosphonomethylphenyl)porphyrin anion $[H_2(tP_4O_8\{OH\}_4mpp)]^{4-}$ **(5)** can be synthesized in a four-step reaction starting from the well-known tetrakis(4-methoxycarbonylphenyl)porphyrin H_2(tmecpp) **(1)**. Indeed, the corresponding osmium complexes are well-known too.[13b,16] We decided to synthesize the osmochromes $[Os(tP_4O_8\{OH\}_4mpp)LL']^{4-}$ **(5h)**, starting from **1a** and **1b**, by substitution in the porphyrin periphery.

Reduction of [OsCO(tmecpp)thf] **(1a)** or $[OsO_2$(tmecpp)] **(1b)** with $LiAlH_4$ in anhydrous THF yielded the complexes **2a** and **2b**. During this procedure only the ester groups in the porphyrin periphery were reduced, and the osmium was not affected. This is shown by the characteristic Os=O oscillation of **2b** at 834 cm^{-1}. Partial reduction of the hydroxyl to the methyl groups was prevented by the thin layer chromatography control and hydrolysis of excess $LiAlH_4$.[17] Compound **2a** was transformed into $[OsCO(tBr_4mpp)thf]$ **(3a)** by nucleophilic substitution with PBr_3. The highest yields were obtained with CH_2Cl_2 as the solvent, whereas reactions in $CHCl_3$ mainly led to polymerization and decomposition products. Reaction of $[OsO_2(t\{OH\}_4mpp)]$ **(2b)** with PBr_3 did not yield the expected dioxo-complex $[OsO_2(tBr_4mpp)]$ **(3c)**, but the paramagnetic bis(bromo) complex $[Os(tBr_4mpp)Br_2]$ **(3b)**. Hitherto analogous bis(-bromo)osmium(IV)porphyrin complexes were synthesized exclusively by reaction of bis(ligand)osmium(II)porphyrin complexes with CCl_4.[18] Presumably, the osmium is reduced from the +6 to the +4 oxidation state by the H_3PO_3 formed from the reaction with PBr_3. Reaction of **3b** in the presence of 1-methylimidazole yielded the osmichrome $[Os(tBr_4mpp)(Br)(1\text{-meim})]$ **(3c)**. During this procedure the substitution of Br^- by 1-meim is followed by a reduction step with 1-methylimidazole as the reducing agent. Attempts to synthesize the analogous bis(1-methylimidazole) complex $[Os(tBr_4mpp)(1\text{-meim})_2]$ **(3d)** by adding further amounts of $N_2H_4{\cdot}H_2O$ and 1-methylimidazole were not successful.

Following the Michaelis–Arbuzov-reaction,[19,20] compounds **3a** and **3b** were transformed into the tetrakis(4-diethylphosphonomethylphenyl)porphyrin complexes by adding $P(OEt)_3$. As shown by the NMR and IR spectra, the substitution in the porphyrin periphery occurred in conjunction with the substitution of the axial ligands. Reaction of **3a** with $P(OEt)_3$ yielded $[Os(tP_4O_4\{OEt\}_8mpp)\{P(OEt)_3\}_2]$ **(4a)**. Presumably, the weakly

bound thf ligand is displaced by $P(OEt)_3$. Furthermore, back-bonding from the *trans*-CO ligand is weakened by this π-acceptor ligand and CO is finally displaced by $P(OEt)_3$. Satisfactory observations were made by Kokisch[21] for the osmium porphyrin complexes $[Os(oep)\{P(OMe)_3\}_2]$ and $[OsCO(oep)\{P(OMe)_3\}_2]$. As for **3b**, the ligand substitution is followed by reduction of osmium from the +4 to +3 oxidation state with $P(OEt)_3$ as the reducing agent,[22] to yield $[Os(tP_4O_4\{OEt\}_8mpp)\{P(OEt)_3\}Br]$ **(4b)**, which can be transformed into $[Os(tP_4O_4\{OEt\}_8mpp)\{P(OEt)_3\}(1\text{-meim})]$ **(4c)** by reaction with 1-methylimidazole in the presence of $N_2H_4{\cdot}H_2O$. Compound **4c** can also be obtained by ligand substitution of **4a** with 1-methylimidazole.

The tetrakis(4-phosphonomethylphenyl)porphyrin complexes **5a−c** were synthesized as described for **5**,[12] by saponification of the complexes **4a−c** by silylation with CH_3SiBr and subsequent addition of KOH (4%). The new water-soluble osmium porphyrin anions $[Os(tP_4O_8\{OH\}_4mpp)\{P(OEt)_3\}_2]^{4-}$ **(5a)**, $[Os(tP_4O_8\{OH\}_4mpp)\{P(OEt)_3\}Br]^{4-}$ **(5b)** and $[Os(tP_4O_8\{OH\}_4mpp)\{P(OEt)_3\}(1\text{-meim})]^{4-}$ **(5c)** were obtained in good yields. Indeed, **5c** can be obtained by reaction of **5a** and **5b** with 1-methylimidazole in the presence of $N_2H_4{\cdot}H_2O$.

Analytical Characterization

All compounds were identified by UV/Vis, IR, and ^1H NMR spectroscopy. The phosphorous containing complexes were also characterized by ^{31}P NMR spectroscopy (for individual data, see protocols 1−11). The new water-soluble complexes **5a−d** were also characterized by cyclic voltammetry and electrophoresis.

UV/Vis Spectra

A special feature of the lipophilic osmochromes is their acid-induced autoxidation, which has been shown to proceed via superoxide formation.[21,23] Contrary to these results, compound **4c,** as well as the water-soluble complexes **5a** and **5c,** are oxidized to the osmichrome salts [**4c**, **5a**, **5c**]$^+$, also in the absence of acid (Equation 1, Figure 1, and Table 1). Indeed, the osmochromes can be restored by adding small amounts of $N_2H_4{\cdot}H_2O$ to the solution. As **4c**, **5a**, **5c** can perform this reversible redox reaction, these osmochromes are cytochrome models under these spectroscopic and functional aspects.[24]

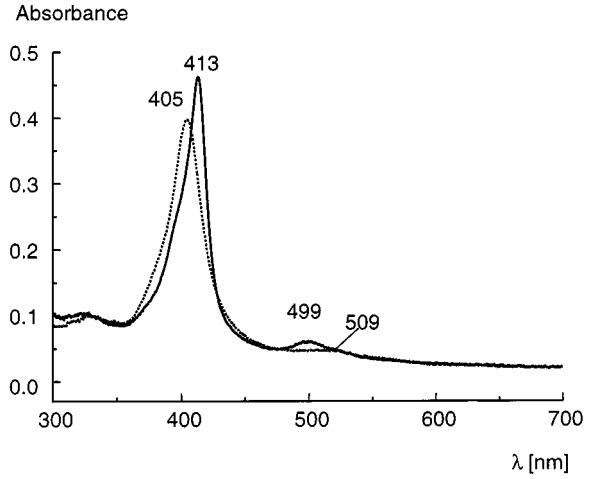


Figure 1. UV/Vis spectra of $[Os(tP_4O_8\{OH\}_4mpp)\{P(OEt)_3\}(1\text{-meim})]^{4-}$ (**5c**$^-$) (full line) and $[Os(tP_4O_8\{OH\}_4mpp)\{P(OEt)_3\}(1\text{-meim})]^{3-}$ (**5c**) (dotted line) in H_2O

Table 1. UV/Vis spectroscopic data (λ_{max} [nm], lg ε in parentheses, at 25 °C in H_2O) of the osmochromes **5a** and **5c** (n = +2) and the osmichromes (n = +3) formed by autoxidation

	n	B (Soret)	Q and others
5a	+2	414 (5.19)	322 (4.42), 499 (4.16)
	+3	403 (5.10)	329 (4.41), 511 (4.00), 555 (3.82)
5c	+2	413 (5.07)	326 (4.34), 499 (4.04)
	+3	405 (5.01)	327 (4.34), 509 (3.94), 560 (3.75)

$$[Os(tP_4O_8\{OH\}_4mpp)LL']^{4-} \xrightarrow{O_2} [Os(tP_4O_8\{OH\}_4mpp)LL']^{3-}$$
$$L = P(OEt)_3,\quad L' = P(OEt)_3,\ 1\text{-meim}$$

Cyclic Voltammetry

In the voltage range from −1.5 to +1.5 V, osmochromes usually show two reversible oxidations (E_1 and E_2), both occurring at the metal centre and producing the osmium(III) and the osmium(IV) porphyrin complex, respectively.[13,21,22] Contrary to this result we observed only one quasi-reversible redox step (E_1) when studying the complexes **4a** and **4c** by cyclic voltammetry. In comparison with analogous complexes of the type Os(tmecpp)LL′,[25] the redox potentials of **4a** and **4c** are shifted to lower potentials, hence the $(tP_4O_4\{OEt\}_8mpp)$ system is characterized as a weaker π-acceptor ligand (Table 2).

Table 2. Comparison of the redox potentials of the complexes **4a**, **4c**, **5a**, and **5c** [**4a**, **4c**: CH_2Cl_2; **5a**, **5c**: DMF/H_2O (9:1); 25 °C, NBu_4PF_6 as supporting electrolyte, potentials versus saturated calomel electrode (SCE)]

Complex	No.	E_1 [V]	E_2 [V]
$Os(tP_4O_4\{OEt\}_8mpp)\{P(OEt)_3\}_2$	**4a**	0.147[a]	1.123[b]
$Os(tP_4O_4\{OEt\}_8mpp)\{P(OEt)_3\}(1\text{-meim})$	**4c**	0.027[a]	–
$[Os(tP_4O_8\{OH\}_4mpp)\{P(OEt)_3\}_2]^{3-}$	**5a**	0.078[a]	–
$[Os(tP_4O_8\{OH\}_4mpp)\{P(OEt)_3\}(1\text{-meim})]^{3-}$	**5c**	[c]	–

[a] Quasireversible. – [b] Irreversible. – [c] Not analyzable.

Indeed, analysis of the complexes **5a** and **5c** by cyclic voltammetry was difficult. The complexes were completely insoluble in DMF and as a result the addition of small amounts of water to the suspension was necessary. To our disappointment, only broad quasi-reversible voltammograms (E_1) were seen under these conditions. Thus, a comparison with the redox potentials of water-soluble osmium porphyrin complexes published elsewhere[1,13,25] was neither sensible, nor possible.

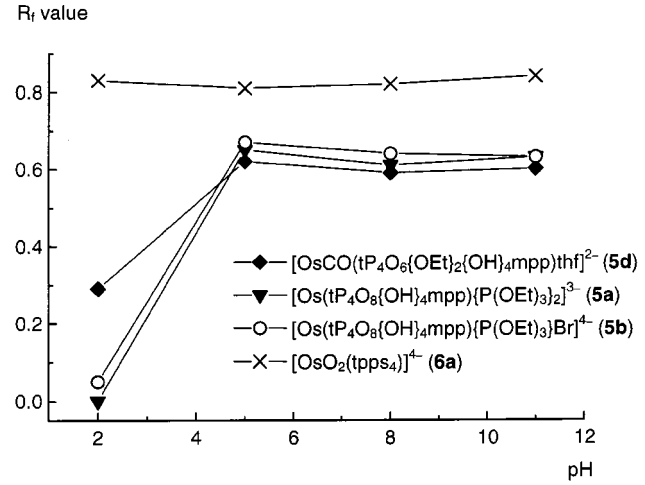


Figure 2. R_f values of the osmium porphyrin complexes $[Os(tP_4O_8\{OH\}_4mpp)LL']^{n-}$ **5a−5d** and their pH dependence {agarose gel, R_f values versus $K_4[InS_4]$ (R_f = 1)}

Electrophoresis

In accordance with the results of Katzenmeier,[12] **5a−d** showed no dependence on pH in the range from pH 3 to pH 11 (see Figure 2). Electrophoretic measurements at pH 12 could not be observed. This is due to the change of the total charge of the benzylphosphonate groups from −4 to −8.[12]

Compared with $[OsO_2(tpps_4)]^{4-}$ **(6a)** as an internal standard, we observed much smaller R_f values for the osmichromes **5a** and **5c**. This effect can be explained by the formation of a so called "inner salt".[13b] In accordance with the complexes of the type $[Os(tpps_4)LL']^{3-}$, the positive charge of the osmium(III) ion is neutralized by one of the four anionic benzylphosphonate groups.

To our surprise, the R_f values of **5a−d** were not influenced by a change in the effective charge n of the osmium porphyrin complexes (Table 3). As demonstrated in Figure 2, compounds **5a−d** showed similar R_f values in the pH range from 3 to 11, although the effective charges varied from n = −4 **(5b)** to n = −2 **(5d)**.

Table 3. R_f Values of the osmium porphyrin complexes $[Os(tP_4O_8\{OH\}_4mpp)LL']^{n-}$ **5a−5d** and their pH dependence {agarose gel, R_f values versus $K_4[InS_4]$ (R_f = 1)}

Ligands L	L′	n	No.	R_f values pH 2	pH 5	pH 8	pH 11
CO	thf[a]	2−	**5d**	0.29	0.62	0.59	0.60
$P(OEt)_3$	$P(OEt)_3$	3−	**5a**	0.00	0.65	0.61	0.63
$P(OEt)_3$	1-meim	3−	**5c**	0.00	0.64	0.61	0.62
$P(OEt)_3$	Br^-	4−	**5b**	0.05	0.67	0.64	0.63
O	O[b]	4−	**6a**	0.83	0.81	0.82	0.84

[a] Diester $[OsCO(tP_4O_6\{OEt\}_2\{OH\}_4mpp)thf]^{2-}$. − [b] *trans*-Dioxoosmium(VI) porphyrin complex $[OsO_2(tpps_4)]^{4-}$ [13b,25] as internal standard.

At pH < 3 the benzylphosphonate groups are protonated, hence no electrophoretic measurements were obtained for **5a−c** at pH 2. A broad spot was observed for $[OsCO(tP_4O_6\{OEt\}_2\{OH\}_4mpp)thf]^{2-}$ **(4d)** at 0.29. Satisfactory observations were made by Katzenmeier[12] for $[H_2(tP_4O_8\{OH\}_4mpp)]^{4-}$ **(4)**.

Experimental Section

Methods and Materials: UV/Vis: spectrometers Hewlett-Packard HP 8451A "Diode Array" and Bruins-Instruments Omega 10, programme SPECTRA CALC (Galactic Industries Corporation). − IR: Nicolet IMPACT 400 FT-IR-spectrometer, (KBr, 4000−400 cm^{-1}), programme Omnic (Nicolet Analytical Instruments). − NMR: spectrometers Bruker WM 300 and Bruker AM 200. − MS: Varian MAT 311 A, field desorption method. − Elemental analyses: Analytical Laboratories, P.O.B. 1106, D-51779 Lindlar. − Electrochemistry: Princeton Applied Research potentiostat M 173 controlled by an interface 175 with the software M 270/250; conditions: 25 °C, redox potentials versus SCE (Ingold), working electrode: platinum electrode (Beckman), reference electrode: platinum (Metrohm). − Ultrafiltration: Stirred cell 8400 and Diaflow ultrafiltration membranes YM1 from Amicon. − Electrophoresis: horizontal slab gel system type Desaphor HE 200 (Desaga), voltage multiplier Pherograph type 74 (Vetter KG). − Conductivity measurements: conductometer type CD 78 with cell CM 0.5/88 G from Tacussel, France. − K_2OsCl_6 was obtained from Degussa-Hüls; potassium indigo 5,5′,7,7′-tetrasulfonate ($K_4[InS_4]$) from Aldrich; Agarose, Tris, Glycin, DEGE, HCOOH 100%, $N_2H_4{\cdot}H_2O$, DMF, DMSO, $LiAlH_4$, PBr_3, $P(OEt)_3$, KBr p.a., CH_3SiBr from Fluka; DEGE from Acros; all other chemicals and solvents from Merck or Merck Schuchardt. − Al_2O_3 W 200 neutral (super I) was obtained from ICN Biomedicals, the lower activity grades were adjusted by adding adequate portions of water. − Analytical thin layer chromatography was performed on commercial aluminium sheets coated with silica gel 60 F_{254}, alumina 60 F_{254} Typ E and alumina RP-18F_{254s} (Merck). − 1,2,4-Trichlorobenzene (TCB) from Fluka was chromatographed on an alumina column (activity grade super I, basic, 40 × 3 cm) before use. All other solvents were distilled before use. − DMF for electrochemistry was prepared by a literature method.[26] 5,10,15,20-Tetrakis(4-methoxycarbonylphenyl)porphyrin (**1**)[27], as well as **1a** and **1b**[13b,25] were prepared by literature methods.

Protocol 1: General Procedure of Synthesis of Bis(ligand)-[5,10,15,20-tetrakis(4-hydroxymethylphenyl)porphyrinato]-osmium (2a, 2b): $LiAlH_4$ (325 mg, 8563 μmol) was added in small portions to a solution of **1a** (299 mg, 263 μmol) or **1b** (233 mg, 218 μmol) in 200 mL of anhydrous THF, and the solutions were stirred for 30 min at 20 °C. Addition of 40 mL of hydrous THF destroyed the excess $LiAlH_4$ and the resulting slurry strained with silica gel. The silica gel containing residues of the product was put in an Twisselmannaufsatz and allowed to reflux in 70 mL of anhydrous THF for 2 h. After cooling the solvent of the combined filtrates was evaporated and the residue dried at 80 °C. The products $[OsCO(t\{OH\}_4mpp)thf]$ **(2a)**, and $[OsO_2(t\{OH\}_4mpp)]$ **(2b)** were isolated as blue-violet powders.

Carbonyl(tetrahydrofuran)[5,10,15,20-tetrakis(4-hydroxymethylphenyl)porphyrinato]osmium(II) (2a): 239 mg (89%). − UV/Vis (DMSO): λ_{max} (lg ε) = 411 nm (5.34), 521 (4.06), 594 (3.71). − IR (KBr): $\tilde{\nu}$ = 1899 cm^{-1} (CO), 1351, 1074 (thf), 1351, 1203, 1043 (CH_2OH). − ^1H NMR ([D_6]DMSO): δ = 1.42 (m, 4 H, OH), 4.41 (m, 4 H, thf), 4.84 (m, 8 H, CH_2R), 5.53 (m, 4 H, thf), 7.71 (m, 8 H, phenyl-H), 7.98 (m, 4 H, phenyl-H), 8.14 (m, 4 H, phenyl-H), 8.46 (s, 8 H, pyrrole-H). − MS (FD); *m/z* (%): 947 (100) [M^+ − thf, − 3 H].

***trans*-Dioxo[5,10,15,20-tetrakis(4-hydroxymethylphenyl)porphyrinato]osmium(VI) (2b):** 138 mg (66%). − UV/Vis (DMSO): λ_{max} (lg ε) = 399 nm (4.80), 513 (3.91), 584 (3.67), 638 (3.45). − IR (KBr): $\tilde{\nu}$ = 834 cm^{-1} (Os=O), 1205, 1131, 1051 (CH_2OH). − ^1H NMR ([D_6]DMSO): δ = 1.42 (m, 4 H, OH), 4.92 (s, 8 H, CH_2R), 7.85 (m, 8 H, *m*-phenyl-H), 8.30 (m, 8 H, *o*-phenyl-H), 9.17 (m, 8 H, pyrrole-H).

Protocol 2: Carbonyl(tetrahydrofuran)[5,10,15,20-tetrakis(4-bromomethylphenyl)porphyrinato]osmium(II) (3a): PBr_3 (1.2 mL, 12.72 mmol) was added dropwise to a suspension of [OsCO(t{OH}$_4$mpp)thf] **(2a)** (361 mg, 352 μmol) in 700 mL of $CHCl_3$, and the suspension was refluxed for 1 h. After cooling and neutralization with saturated aqueous sodium carbonate solution the suspension was washed three times with 100 mL of water and dried by adding sodium sulfate. Evaporation of the solvent in vacuo and drying at 40 °C yielded 290 mg (65%) of **3a** as a blue-violet powder. − UV/Vis (CH_2Cl_2): λ_{max} (lg ε) = 409 nm (5.11), 520 (4.11). − IR (KBr): $\tilde{\nu}$ = 1898 cm^{-1} (CO), 1350, 1073 (thf), 608 (CH_2Br). − ^1H NMR ($CDCl_3$): δ = 4.10 (m, 4 H, thf), 4.80 (s, 8 H, CH_2R), 5.62 (m, 4 H, thf), 7.67 (m, 8 H, phenyl-H), 7.93 (m, 4 H, phenyl-H), 8.18 (m, 4 H, phenyl-H), 8.49 (m, 8 H, pyrrole-H).

Protocol 3: Dibromo[5,10,15,20-tetrakis(4-bromomethylphenyl)porphyrinato]osmium(IV) (3b): PBr_3 (0.9 mL, 9540 μmol) was added dropwise to a suspension of [OsO_2(t{OH}$_4$mpp)] **(2b)** (250 mg, 261 μmol) in 400 mL of CH_2Cl_2, and the suspension was allowed to reflux for 1 h. After cooling and neutralization with saturated aqueous sodium carbonate solution the suspension was washed three times with 100 mL water and dried by adding sodium sulfate. Evaporation of the solvent in vacuo and drying at 40 °C in high vacuo yielded 143 mg (41%) of **3b** as a green-black powder. − UV/Vis (CH_2Cl_2): λ_{max} (lg ε) = 332 nm (4.01), 407 (4.58), 453 (3.99), 514 (3.69), 605 (3.38). − IR (KBr): $\tilde{\nu}$ = 619 cm^{-1}, 600 (CH_2Br).

Protocol 4: [5,10,15,20-Tetrakis(4-diethylphosphonomethylphenyl)-porphyrinato]bis(triethyl phosphite)osmium(II) (4a): A solution of [OsCO(tBr_4mpp)thf] **(3a)** (242 mg, 189 μmol) in 30 mL of $P(OEt)_3$ was allowed to reflux for 6 h. After standing without stirring for 24 h, the solvent was removed in vacuo. 257 mg (78%) of **4a** was obtained as a blue-violet powder after chromatography on an alumina column (activity grade III, neutral, 10 × 2.5 cm, isolation of the first brown-red fraction) with CH_2Cl_2/EtOH (9:1). − UV/Vis (CH_2Cl_2): λ_{max} (lg ε) = 328 nm (4.44), 421 (5.26), 509 (4.12). − IR (KBr): $\tilde{\nu}$ = 2978 cm^{-1}, 1528, 1028, 772, 727, 536 {$P(OEt)_3$}, 1260 (P=O), 1052 (P−O−R). − ^1H NMR (CD_2Cl_2): δ = 0.01 (m, 12 H, P{OCH_2CH_3}$_3$), 1.16 (m, 18 H, P{OCH_2CH_3}$_3$), 1.35 (m, 24 H, CH_3), 3.40 (m, 8 H, CH_2P), 4.14 (m, 16 H, OCH_2), 7.57−7.88 (m, 24 H, phenyl-H and pyrrole-H). − ^{31}P NMR ($CDCl_3$): δ = 25.44 (s), 27.56 (s). − MS (FD); *m/z* (%): 1734 (100) [M^+].

Protocol 5: Bromo[5,10,15,20-tetrakis(4-diethylphosphonomethylphenyl)porphyrinato](triethyl phosphite)osmium(III) (4b): A solution of [Os(tBr_4mpp)Br_2] **(3b)** (124 mg, 92 μmol) in 25 mL of $P(OEt)_3$ was allowed to reflux for 7 h. After standing without stirring for 10 h, the solvent was removed in vacuo. The remaining oil was treated with 15 mL of THF and the product isolated by adding 60 mL of water. Drying at 60 °C in high vacuo yielded 51 mg (33%) of **4b** as a red-violet powder. − UV/Vis (CH_2Cl_2): λ_{max} (lg ε) = 330 nm (4.29), 406 (5.03), 515 (3.88). − IR (KBr): $\tilde{\nu}$ = 2980 cm^{-1}, 1525, 1026, 771, 736, 556 {$P(OEt)_3$}, 1234 (P=O), 1051 (P−O−R). − ^1H NMR (CD_2Cl_2, + N_2H_4·H_2O): δ = −0.07 (m, 6 H, P{OCH_2CH_3}$_3$), 1.16 (m, 9 H, P{OCH_2CH_3}$_3$), 1.26 (m, 24 H, -CH_3), 3.41 (m, 8 H, -CH_2P), 4.19 (m, 16 H, OCH_2-), 7.58 (m, 8 H, *m*-phenyl-H), 7.94 (m, 8 H, *o*-phenyl-H), 8.06 (m, 8 H, pyrrole-H). − ^{31}P NMR ($CDCl_3$): δ = 25.25 (s), 27.24 (s).

Protocol 6: (1-Methylimidazole)[5,10,15,20-tetrakis(4-diethylphosphonomethylphenyl)porphyrinato](triethyl phosphite)osmium(II) (4c): A) Reaction of 4a with 1-Methylimidazole: A solution of [Os(tP_4O_4{OEt}$_8$mpp){$P(OEt)_3$}$_2$] **(4a)** (50 mg, 28 μmol) in 25 mL of CH_2Cl_2 and 1 mL of 1-methylimidazole were allowed to reflux under argon for 15 min. After standing without stirring for 12 h, the solvent was removed in high vacuo. The residue was treated with 10 mL of CH_2Cl_2 and chromatographed on an alumina column (activity grade III, neutral, 8 × 2.5 cm). Fractions were obtained as follows: with CH_2Cl_2 the red fraction of [Os(tP_4O_4{OEt}$_8$mpp){$P(OEt)_3$}(1-meim)] **(4c)** and with CH_2Cl_2/EtOH (2:1) the orange fraction of the oxidized complex [Os(tP_4O_4{OEt}$_8$mpp){$P(OEt)_3$}(1-meim)]$^+$ **(4c$^+$)**. N_2H_4·H_2O (0.1 mL) was added to the combined fractions and the solution stirred for 15 min at 20 °C. Evaporation of the solvent and drying at 50 °C in high vacuo yielded 41 mg (85%) of **4c** as a blue-violet powder.

B) Reaction of 4b with 1-Methylimidazole: N_2H_4·H_2O (0.1 mL) was added to a solution of Os(tP_4O_4{OEt}$_8$mpp){$P(OEt)_3$}Br (**4b**) (15 mg, 9 μmol) in 15 mL of CH_2Cl_2 and 1 mL of 1-methylimidazole, at 60 °C. After stirring for 4 h at 60 °C, the solution was cooled and the solvent removed in high vacuo. Drying at 50 °C in high vacuo yielded 9 mg (60%) of **4c** as a blue-violet powder. − UV/Vis (CH_2Cl_2): λ_{max} (lg ε) = 328 nm (4.03), 416 (4.82), 501 (3.81). − IR (KBr): $\tilde{\nu}$ = 2963 cm^{-1}, 1529, 1024, 737 {$P(OEt)_3$}, 3124, 1529, 1399, 1095 (1-meim), 1261 (P=O), 1052 (P−O−R). − ^1H NMR (CD_2Cl_2 and N_2H_4·H_2O): δ = 0.06 (m, 6 H, P{OCH_2CH_3}$_3$), 1.27 (m, 9 H, P{OCH_2CH_3}$_3$), 1.36 (m, 24 H, CH_3), 1.91 (s, 1-meim), 2.32 (m, 1-meim), 3.45 (m, 8 H, CH_2P), 3.67 (s, 1-meim), 4.15 (m, 16 H, OCH_2), 7.58−8.05 (m, 24 H, phenyl-H and pyrrole-H). − ^{31}P NMR ($CDCl_3$): δ = 25.83 (s), 27.33 (s).

Protocol 7: General Procedure of Saponification of Bis(ligand)-[5,10,15,20-tetrakis(4-diethylphosphonomethylphenyl)porphyrinato]osmium (4a,4b): CH_3SiBr (0.25 mL, 1950 μmol) was added to a solution of **4a** (50 mg, 28 μmol) or **4b** (28 mg, 16 μmol) in 25 mL of anhydrous CH_2Cl_2, and the mixture was stirred for 14 h at 20 °C. After neutralization with 25 mL of KOH (4%) the aqueous phase was washed twice with 40 mL of CH_2Cl_2, separated and cleaned via ultrafiltration. Evaporation of the solvent in vacuo and drying at 60 °C yielded the complexes K_3[Os(tP_4O_8{OH}$_4$mpp){$P(OEt)_3$}$_2$] **(5a-K)** and K_4[Os(tP_4O_8{OH}$_4$mpp){$P(OEt)_3$}Br] **(5b-K)** as blue-violet powders.

Tripotassium [{5,10,15,20-Tetrakis(4-phosphonomethylphenyl)-porphyrinato}bis(triethyl phosphite)osmate(III)], K_3[Os(tP_4O_8{OH}$_4$mpp){$P(OEt)_3$}$_2$] (5a-K): 40 mg (86%). − UV/Vis (H_2O): λ_{max} (lg ε) = 329 nm (4.41), 403 (5.10), 511 (4.00), 555 (3.82). − IR (KBr): $\tilde{\nu}$ = 2978 cm^{-1}, 1043, 776, 552 {$P(OEt)_3$}, 1181, 1164 (P=O). − ^1H NMR (CD_3OD, + N_2H_4·H_2O): δ = 0.01 (m, 12 H, P{OCH_2CH_3}$_3$), 1.24 (m, 18 H, P{OCH_2CH_3}$_3$), 3.92 (m, 8 H, CH_2P), 7.59 (m, 8 H, phenyl-H), 7.81 (m, 8 H, phenyl-H), 8.01 (m, 4 H, pyrrole-H), 8.08 (m, 4 H, pyrrole-H). − ^{31}P NMR (CD_3OD): δ = 16.98 (s), 18.17 (s).

Tetrapotassium [(Bromo){5,10,15,20-tetrakis(4-phosphonomethylphenyl)porphyrinato}(triethyl phosphite)osmate(III)], K_4[Os(tP_4O_8{OH}$_4$mpp){$P(OEt)_3$}Br] (5b-K): 22 mg (82%). − UV/Vis (H_2O): λ_{max} (lg ε) = 329 nm (4.36), 403 (5.06), 511 (3.91), 557 (3.74). − IR (KBr): $\tilde{\nu}$ = 2978 cm^{-1}, 1522, 1048, 776, 553 {$P(OEt)_3$}, 1181, 1161 (P=O). − ^1H NMR (CD_3OD, + N_2H_4·H_2O): δ = 0.01 (m, 6 H, P{OCH_2CH_3}$_3$), 1.28 (m, 9 H, P{OCH_2CH_3}$_3$), 3.96 (m, 8 H, CH_2P), 7.68−8.11 (m, 24 H, phenyl-H and pyrrole-H). − ^{31}P NMR (CD_3OD): δ = 16.54 (s), 18.08 (s).

Protocol 8: Tripotassium [(1-Methylimidazole){5,10,15,20-tetrakis(4-phosphonomethylphenyl)porphyrinato}(triethyl phosphite)-osmate(III)] (5c-K): A) Saponification of 4c: CH_3SiBr (0.3 mL, 2340 μmol) was added to a solution of **4c** (30 mg, 18 μmol) in 25 mL of anhydrous CH_2Cl_2, and the mixture was stirred for 10 h at 20 °C. After neutralization with 25 mL of KOH (4%) the aqueous phase was washed twice with 40 mL of CH_2Cl_2, separated and cleaned by ultrafiltration. Evaporation of the solvent in vacuo and drying at 60 °C in high vacuo yielded 19 mg (68%) of $K_3[Os(tP_4O_8\{OH\}_4mpp)\{P(OEt)_3\}(1\text{-meim})]$ **(5c-K)** as a red-violet powder.

B) Reaction of 5a-K with 1-Methylimidazole: $N_2H_4{\cdot}H_2O$ (0.1 mL) was added to a solution of $K_3[Os(tP_4O_8\{OH\}_4mpp)\{P(OEt)_3\}_2]$ **(5a-K)** (19 mg, 11 μmol) in 15 mL of Glycin-buffer pH 11[12,24] and 1 mL of 1-methylimidazole, at 70 °C. The solution was stirred for 4 h at 70 °C. After cooling, the solution was cleaned via ultrafiltration. Evaporation of the solvent in vacuo and drying at 60 °C in high vacuo yielded 17 mg (94%) of **5c-K** as a red-violet powder.

C) Reaction of 5b-K with 1-Methylimidazole: A solution of $K_4[Os(tP_4O_8\{OH\}_4mpp)\{P(OEt)_3\}Br]$ **(5b-K)** (3 mg, 1.9 μmol) in 5 mL of H_2O and 0.5 mL of 1-methylimidazole was stirred for 2 h at 60 °C. After cooling, the solvent was removed in vacuo. Drying at 120 °C in high vacuo yielded 2 mg (69%) of **5c-K** as a orange-red powder. – UV/Vis (H_2O): λ_{max} (lg ε) = 327 nm (4.34), 405 (5.01), 509 (3.94), 560 (3.75). – IR (KBr): $\tilde{\nu}$ = 2973 cm^{-1}, 1048, 734, 552 {$P(OEt)_3$}, 3129, 1539, 1403, 1096 (1-meim), 1181, 1161 (P=O). – ^1H NMR (CD_3OD, + $N_2H_4{\cdot}H_2O$): δ = 0.05 (m, 6 H, $P\{OCH_2CH_3\}_3$), 1.25 (m, 9 H, $P\{OCH_2CH_3\}_3$), 1.90 (m, 1-meim), 3.70 (s, 1-meim), 3.96 (m, 8 H, CH_2P), 5.46 (m, 1-meim), 6.99–8.10 (m, 24 H, phenyl-H and pyrrole-H). – ^{31}P NMR (CD_3OD): δ = 17.17 (s), 18.28 (s).

Protocol 9: Reaction of K_2OsCl_6 with 5,10,15,20-Tetrakis(4-diethylphosphonomethylphenyl)porphyrin (4): A solution of K_2OsCl_6 (66 mg, 132 μmol) in 10 mL formic acid was allowed to reflux under argon for 4 h. After cooling, the solvent was removed in high vacuo. The remaining residue was dissolved in 8 mL of TCB and 30 mL of DEGE, $H_2(tP_4O_4\{OEt\}_8mpp)$ **(4)** (122 mg, 100 μmol) was added and the solution was refluxed under CO for 18 h. After cooling, the solvent was removed in high vacuo and the residue dried in vacuo for 2 h at 80 °C.

As shown by the analytical thin layer chromatography, the ester groups of the porphyrin were partially saponified during metallation. For standardization, the residue was dissolved in an anhydrous mixture of 30 mL of CH_2Cl_2/THF/EtOH (1:1:1). After adding CH_3SiBr (0.7 mL, 5460 μmol), the solution was stirred for 15 h at 25 °C. A further 50 mL of KOH (4%) was added and the aqueous phase was washed twice with 70 mL of CH_2Cl_2. The aqueous phase was separated and cleaned via ultrafiltration. Evaporation of the solvent in vacuo and drying at 60 °C yielded 141 mg (97%) of $K_2[OsCO(tP_4O_6\{OEt\}_2\{OH\}_4mpp)thf]{\cdot}2\ H_2O$ **(5d-K)** as a blue-violet powder. – UV/Vis (0.01 N NaOH): λ_{max} (lg ε) = 409 nm (5.18), 5.21 (4.01), 555 (3.74), 589 (3.55), 644 (3.38). – IR (KBr): $\tilde{\nu}$ = 1897 cm^{-1} (CO), 1351, 1070 (thf), 1206, 1188 (P=O). – ^1H NMR (CD_3OD): δ = 1.40 (m, 6 H, $-CH_3$), 3.17 (m, 4 H, thf), 3.56 (m, 8 H, $-CH_2P$), 4.10 (m, 4 H, thf), 4.21 (m, 4 H, OCH_2-), 7.78–8.88 (m, 24 H, phenyl-H and pyrrole-H). – ^{31}P NMR (CD_3OD): δ = 19.83 (m), 27.47 (m). – $C_{57}H_{54}K_2N_4O_{14}OsP_4$ (1411.36): calcd. C 48.60, H 4.93, N 4.08, P 8.86, K 5.72; found C 48.51, H 3.86, N 3.97, P 8.78, K 5.54.

Protocol 10: Reaction of $K_2[OsCO(tP_4O_6\{OEt\}_2\{OH\}_4mpp)thf]$ (5d-K) with MeOH: A solution of $K_2[OsCO(tP_4O_6\{OEt\}_2\{OH\}_4mpp)thf]$ **(8d-K)** (60 mg, 41 μmol) in 15 mL of MeOH was stirred for 2 h at 60 °C. Evaporation of the solvent in vacuo and drying at 60 °C yielded 50 mg (81%) of $K_2[OsCO(tP_4O_6\{OEt\}_2\{OH\}_4mpp)MeOH]$ **(5e-K)** as a blue-violet powder. The new axial ligand MeOH was confirmed by IR spectroscopy. – UV/Vis (0.01 N NaOH): λ_{max} (lg ε) = 4.11 nm (5.06), 521 (3.96), 555 (3.67), 589 (3.46), 646 (3.32). – IR (KBr): $\tilde{\nu}$ = 1889 cm^{-1} (CO), 1352 (MeOH), 1205, 1186 (P=O).

Protocol 11: Reaction of $K_2[OsCO(tP_4O_6\{OEt\}_2\{OH\}_4mpp)thf]$ (5d-K) with 1-Methylimidazole: A solution of $K_2[OsCO(tP_4O_6\{OEt\}_2\{OH\}_4mpp)thf]$ **(5d-K)** (86 mg, 59 μmol) in 10 mL H_2O and 2 mL 1-methylimidazole were stirred for 2 h at 80 °C. Evaporation of the solvent in vacuo and drying at 120 °C in high vacuo yielded 63 mg (69%) $K_2[OsCO(tP_4O_6\{OEt\}_2\{OH\}_4mpp)(1\text{-meim})]$ **(5f-K)** as a blue-violet powder. The new axial ligand 1-methylimidazole was confirmed by IR spectroscopy. – UV/Vis (0.01 N NaOH): λ_{max} (lg ε) = 411 nm (5.02), 5.22 (3.92), 555 (3.68), 588 (3.48), 646 (3.31). – IR (KBr): $\tilde{\nu}$ = 1899 cm^{-1} (CO), 3127, 1527, 1401, 1097 (1-meim), 1239, 1211, 1186 (P=O).

Acknowledgments

Financial support by the BASF AG, Bayer AG, Hoechst AG, Aventis AG, Fonds der Chemischen Industrie, and the Deutsche Forschungsgemeinschaft is gratefully acknowledged. The authors thank Prof. Dr. J. J. Veith and Mr. M. Fischer for performing mass spectra, Dr. S. Braun, K. Jungk, K.-O. Runzheimer, Dr. U. Möller, and J. Wendlig for performing NMR spectra.

[1] Part LXXIII: J. W. Buchler, T. Dippell, *Eur. J. Inorg. Chem.* **1998**, 445–449.

[2] Abbreviations used: $(oep)^{2-}$, $(tmecpp)^{2-}$, $(t\{OH\}_4mpp)^{2-}$, $(tBr_4mpp)^{2-}$, $(tP_4O_4\{OEt\}_8mpp)^{2-}$: dianions of 2,3,7,8,12,13,17,18-octaethylporphyrin, 5,10,15,20-tetrakis(4-methoxycarbonylphenyl)porphyrin (**1**), 5,10,15,20-tetrakis(4-hydroxymethylphenyl)porphyrin (**2**), 5,10,15,20-tetrakis(4-bromomethylphenyl)porphyrin (**3**), 5,10,15,20-tetrakis(4-diethylphosphonomethylphenyl)porphyrin (**4**); $(tP_4O_8\{OH\}_4mpp)^{6-}$, $(tpps_4)^{6-}$, $(tcpp)^{6-}$: hexaanions of 5,10,15,20-tetrakis(4-phosphonomethylphenyl)porphyrin (**5**), 5,10,15,20-tetrakis(4-sulfonatophenyl)porphyrin (**6**), 5,10,15,20-tetrakis(4-carboxyphenyl)porphyrin (**7**); 1-meim, 1-methylimidazole; DEGE, diethyleneglycolmonomethylether; DMF, dimethylformamide; DMSO, dimethyl sulfoxide; L, L′, axial ligands; SCE, saturated calomel electrode; TCB, trichlorobenzene; THF, thf, tetrahydrofuran.

[3] [3a]H. Murakamai, T. Nagasaki, I. Hamachi, S. Shinkai, *Tetrahedron Lett.* **1993**, *34*, 6273–6276; H. Murakamai, T. Nagasaki, I. Hamachi, S. Shinkai, *J. Chem. Soc., Perkin Trans. 2* **1994**, 975–981. – [3b] M. Takeuchi, Y. Chin, T. Imada, S. Shinkai, *Chem. Commun.* **1996**, 1867–1868. – [3c] H. Toi, Y. Nagai, Y. Aoyama, H. Kawabe, K. Aizawa, H. Ogoshi, *Chem. Lett.* **1993**, 1043–1046.

[4] [4a] S. B. Ungashe, W. L. Wilson, H. E. Katz, G. R. Scheller, T. M. Putvinski, *J. Am. Chem. Soc.* **1992**, *114*, 8717–8719. – [4b] D. Deniaud, B. Schollorn, D. Mansuy, J. Rouxel, P. Battioni, B. Bujoli, *Chem. Mater.* **1995**, *7*, 995–1000.

[5] H. Hennig, J. Behling, R. Meusinger, L. Weber, *Chem. Ber.* **1995**, *128*, 229–234.

[6] B. Meunier, *Chem. Rev.* **1992**, *92*, 1411–1456.

[7] J. Lahiri, G. D. Fate, S. B. Ungashe, J. T. Groves, *J. Am. Chem. Soc.* **1996**, *118*, 2347–2358.

[8] E. Tsuchida, T. Komatsu, K. Arai, K. Yamada, H. Nishide, C. Böttcher, J.-H. Fuhrhop, *J. Chem. Soc., Chem. Commun.* **1995**, *20*, 1063–1064.

[9] H. Brunner, H. Obermeier, *Angew. Chem.* **1994**, *106*, 2305–2306; *Angew. Chem. Int. Ed. Engl.* **1994**, *33*, 2214–2215.

[10] C. S. Chow, J. P. Whitehead, S. J. Lippard, *Biochemistry* **1994**, *33*, 15124–15130.

[11] K. Bockhorst, M. Hoehn-Berlage, *Tetrahydron* **1994**, *50*, 8657–8660.

[12] H. W. Katzenmeier, Ph. D. Dissertation, Technische Hochschule Darmstadt, **1996**.
[13] [13c] J. W. Buchler, F. M. Künzel, *Z. Anorg. Allg. Chem.* **1994**, *620*, 888−897. – [13b] F. M. Künzel, Ph. D. Dissertation, Technische Hochschule Darmstadt, **1992**. – [13c] J. W. Buchler, J. R. Simon, *Z. Anorg. Allg. Chem.* **2000**, *626*, 1731−1732.
[14] [14a] R. Rabinowitz, *J. Org. Chem.* **1963**, *28*, 2975−2978. – [14b] T. Morita, Y. Okamoto, H. Sakurai, *Tetrahedron Lett.* **1978**, *19*, 2523−2526. – [14c] Y. Machida, S. Nomoto, I. Saito, *Synth. Commun.* **1979**, *9*, 97−102.
[15] [15a] J. Chojnowski, M. Cypryk, J. Michalski, *Synthesis* **1978**, *10*, 777−779. – [15b] H. Schmidbaur, R. Seeber, *Chem. Ber.* **1974**, *107*, 1731−1738. – [15c] C. E. McKenna, M. T. Higa, N. H. Cheung, M.-C. McKenna, *Tetrahedron Lett.* **1977**, *18*, 155−158. – [15d] A. J. Rudinskas, T. L. Hullar, *J. Org. Chem.* **1977**, *42*, 2771−2776. – [15e] J. R. Knowles, *Aldrichim. Acta* **1989**, *22*, 59−66.
[16] J. R. Simon, Diploma Thesis, Technische Hochschule Darmstadt, **1994**.
[17] F. M. Künzel, unpublished results.
[18] [18a] J. W. Buchler, W. Kokisch, P. D. Smith, B. Tonn, *Z. Naturforsch.* **1978**, *33b*, 1371−1380. – [18b] P. D. Smith, Ph. D. Dissertation, RWTH Aachen, **1976**. – [18c] Z. Gross, A. Mahammed, *Inorg. Chem.* **1996**, *35*, 7260−7263.
[19] M. Arbuzov, *Pure Appl. Chem.* **1964**, *9*, 307−335.
[20] [20a] A. J. Kirby, S. G. Warren, in: *Reaction Mechanisms in Organic Chemistry* (Eds.: C. Eaborn, N. B. Chapman), Elsevier, Amsterdam, **1967**, Monograph 5. – [20b] J. I. G. Cadogan, in: *Organophosphorus Reagents in Organic Synthesis* (Ed.: J. I. G. Cadogan), Academic Press, London, **1979**, chapter 1.
[21] W. Kokisch, Ph. D. Dissertation, RWTH Aachen, **1979**.
[22] K. Oesten, Ph. D. Dissertation, Technische Hochschule Darmstadt, **1984**.
[23] [23a] J. Billecke, W. Kokisch, J. W. Buchler, *J. Am. Chem. Soc.* **1980**, *102*, 3622−3624. – [23b] J. W. Buchler, J. Billecke, W. Kokisch, in: *Chemical and Biochemical Aspects of Superoxide and Superoxide Dismutase* (Eds.: J. V. Bannister, H. A. O. Hill), Elsevier/North Holland, New York, **1980**, 45−55.
[24] J. W. Buchler, *Comments Inorg. Chem.* **1987**, *6*, 175−191.
[25] J. R. Simon, Ph. D. Dissertation, Technische Hochschule Darmstadt, **1997**.
[26] J. F. Cotzze, in: *Recommended Methods for Purification of Solvents*, Pergamon Press, Oxford, **1982**.
[27] N. Datta-Gupta, T. J. Bardos, *J. Heterocycl. Chem.* **1966**, *3*, 495−502.

Received February 11, 2000
[I00048]

Asymmetric Halogeno-Bridged Complexes of the Late Transition Metals − A Computational and Experimental Study

Margarita Öhm,[a] Axel Schulz,*[a] and Kay Severin*[a]

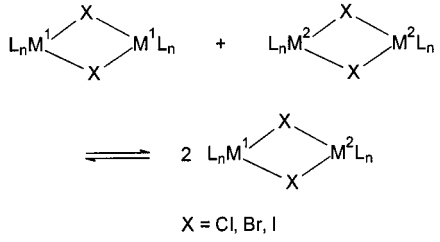
Keywords: Density functional calculations / Dinuclear complexes / Bridging ligands / Transition metals / halides

Metathesis reactions of dinuclear halo-bridged complexes of the late transition metals have been studied by NMR. For selected combinations of 15 different complexes, it has been shown that asymmetric complexes are formed in a dynamic equilibrium. The equilibrium constants have been calculated and the trends therein are discussed. A theoretical analysis of halo-bridged complexes containing $(C_3H_5)MX$, $(H_3P)MX_2$, $[(H_3P)_2MX]^+$, and $(ppy)_2RhCl$ fragments (M = Pd, Pt; X = Cl, Br, I; ppy = anion of 2-phenylpyridine) has been carried out to gain further insight into (i) the influence of the bridging halogen atoms on the equilibrium, (ii) the electron transfer, (iii) the thermodynamic stability and the dynamic equilibrium behaviour, and (iv) structural differences between symmetric and asymmetric halo-bridged complexes.

Introduction

Dinuclear complexes in which two identical metal fragments are connected through halo bridges are versatile starting materials in organometallic chemistry. They readily react with neutral or anionic ligands to form mononuclear complexes. Due to their intrinsic reactivity, they are often used as catalyst precursors. Asymmetric complexes on the other hand, i.e. complexes in which two different metal fragments are joined through halo bridges, have been described only rarely.[1] The reactivity of this class of compounds has just started to be explored. Grubbs and co-workers have reported that asymmetric complexes such as **1** are extremely active catalysts for alkene metathesis, being more active than the original "Grubbs catalyst" $[(PCy_3)_2Ru(=CHPh)Cl_2]$.[2] Furthermore, it has been shown that the activity is modulated by the second metal fragment, which itself is catalytically inactive. Similar results have been obtained by Herrmann and co-workers, who have investigated catalysts such as **2**.[3] These findings clearly show that asymmetric chloro-bridged complexes are an interesting class of compounds, among which highly active catalysts showing co-operative effects between the two metal centres can be found.

In previous publications, we have reported that in some cases heterobimetallic and mixed-valence chloro-bridged complexes can be obtained in almost quantitative yield by metathesis reactions of the appropriate symmetrical complexes.[4] This kind of reaction has provided easy access to a variety of different complexes, several of which have been structurally characterized. In this paper, we provide experimental evidence that halo-bridged complexes of the late transition metals generally undergo metathesis reactions with one another. In chlorinated organic solvents, an equilibrium between symmetrical and asymmetrical halo-bridged complexes is rapidly established (Scheme 1). Factors determining the position of this equilibrium are discussed herein. The experimental results have been supplemented by a computational study, performed to gain further insight into the stabilities, electronic character, and structural features of asymmetric halo-bridged complexes.



Scheme 1

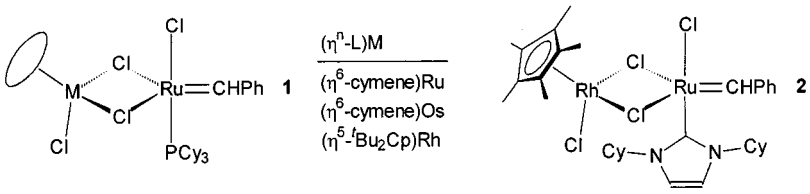
Results and Discussion

NMR Studies

The mixed-valence complex $[(azb)_2Rh(\mu\text{-}Cl)_2Rh(CO)_2]$ (azb = *ortho*-metallated azobenzene) (**3**) was among the first asymmetric chloro-bridged complexes to be isolated[5] and structurally characterized.[6] Although other methods of preparation were initially investigated, it was realized that this compound could also be obtained by metathesis of $[(azb)_2Rh(\mu\text{-}Cl)]_2$ with $[(OC)_2Rh(\mu\text{-}Cl)]_2$.[5c] The first systematic analysis concerning the dynamic behaviour of chloro-bridge metathesis was carried out by Masters and co-workers.[7] They studied the reaction of $[(R_3P)ClPd(\mu\text{-}Cl)]_2$ with $[(R_3P)ClPt(\mu\text{-}Cl)]_2$ (R = Pr, Bu) in chloroform by means of ^{31}P NMR. The two symmetrical complexes were shown to be in a dynamic equilibrium with the heterobimetallic compound $[(R_3P)ClPd(\mu\text{-}Cl)_2PtCl(PR_3)]$. In contrast to the above-mentioned rhodium complex, only a slight thermodynamic preference for the asymmetric complex was observed (K = 5.3 for R = Bu). These results were later confirmed by Clark and co-workers, who also carried

[a] Institut für Anorganische Chemie der Ludwig-Maximilians-Universität,
Butenandtstraße 5−13, 81377 München, Germany
E-mail: kse@cup.uni-muenchen.de
lex@cup.uni-muenchen.de

 © WILEY-VCH Verlag GmbH, D-69451 Weinheim, 2000 1434−1948/00/1212−2623 $ 17.50+.50/0



out a crystal structure analysis of $[(Et_3P)ClPd(\mu\text{-}Cl)_2PtCl(PEt_3)]$.[8] In recent publications, we have reported on investigations of the reactions of $[(C_{10}H_{16})ClRu(\mu\text{-}Cl)]_2$, $[(R_3P)_2M(\mu\text{-}Cl)]_2(BF_4)_2$ (M = Pd, Pt), and $[(\text{“N}-\text{C”})_2M(\mu\text{-}Cl)]_2$ (M = Rh, Ir; “N−C” = 2-phenylpyridine anion, benzo[*h*]quinoline anion) with various chloro-bridged complexes of the late transition metals.[4] In almost all cases, the corresponding asymmetric complexes were found to be formed in virtually quantitative yields ($K > 100$). In order to gain further insight into the scope and limitations of metathesis as a method for preparing asymmetric dinuclear complexes, we have now performed a comprehensive NMR study with selected combinations of 15 different halo-bridged complexes of the late transition metals.[9] Equimolar amounts of two symmetrical complexes were dissolved in $CDCl_3$ or CD_2Cl_2. An approximation of the equilibrium constant was then determined by integration of suitable NMR signals. The results, supplemented by data from the literature, are summarized in Table 1.

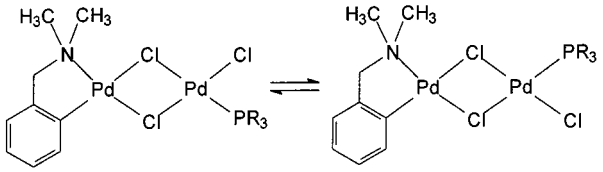
In all cases, asymmetric halo-bridged complexes could be detected by NMR. Side reactions or mononuclear species were not observed. The temperature-independent equilibrium distribution was reached within seconds and remained constant thereafter. For some complexes, dynamic behaviour led to significant line broadening at room temperature. Therefore, the spectra were generally recorded at temperatures below 0 °C. Depending on the symmetry of the dinuclear product, two different dynamic processes responsible for line broadening can be distinguished. Firstly, the complexes $[(dmb)Pd(\mu\text{-}Cl)_2MCl(PBu_3)]$ (M = Pd, Pt; Table 1, Entries 5 and 11) exist as mixtures of two isomers. For $[(dmb)Pd(\mu\text{-}Cl)_2PdCl(PBu_3)]$, the interconversion of these isomers is fast compared to the NMR time scale (Scheme 2). From the coalescence temperature T_c and the difference in chemical shifts of the ^{31}P NMR signals, a $\Delta G^{\ddagger}$ value of 14.0 (± 0.2) kcal/mol was calculated.[10] Interestingly, for the corresponding platinum complex $[(dmb)Pd(\mu\text{-}Cl)_2PtCl(PBu_3)]$, a coalescence of the ^{31}P NMR signals was

Table 1. Equilibrium constants together with selected NMR data for asymmetric halo-bridged complexes

Entry	Complex	^{31}P NMR [ppm]	Temp. [°C]	K
1	$[(C_3H_5)Pd(\mu\text{-}I)_2PdI(PEt_3)]$	46.23	−40	$0.2\cdot10^{-1}$
2	$[(C_3H_5)Pd(\mu\text{-}Br)_2PdBr(PEt_3)]$	42.60	−40	$0.8\cdot10^{-1}$
3	$[(C_3H_5)Pd(\mu\text{-}Cl)_2PdCl(PEt_3)]$	46.00	−40	$1.2\cdot10^{-1}$
4	$[(cod)Rh(\mu\text{-}Cl)_2PdCl(PBu_3)]$[a]	38.70	−40	$1.5\cdot10^{-1}$
5	$[(dmb)Pd(\mu\text{-}Cl)_2PdCl(PBu_3)]$[b]	37.50; 37.66 (10:16)	−40	$2.4\cdot10^{-1}$
6	$[Cp^*ClIr(\mu\text{-}Cl)_2Pd(C_3H_5)]$	–	−40	$2.7\cdot10^{-1}$
7	$[Cp^*ClRh(\mu\text{-}Cl)_2Pd(C_3H_5)]$	–	−40	$4.8\cdot10^{-1}$
8	$[(cymene)ClRu(\mu\text{-}Cl)_2Pd(C_3H_5)]$	–	−40	$5.1\cdot10^{-1}$
9	$[(C_3H_5)Pd(\mu\text{-}Cl)_2PtCl(PEt_3)]$	6.61	−40	$8.8\cdot10^{-1}$
10	$[(C_3H_5)_2Rh(\mu\text{-}Cl)_2PdCl(PBu_3)]$	35.01	−40	1.2
11	$[(dmb)Pd(\mu\text{-}Cl)_2PtCl(PBu_3)]$[b]	0.15 ($^1J_{PtP}$ = 3728 Hz) 0.38 ($^1J_{PtP}$ = 3686 Hz) (15:10)	−40	1.3
12	$[(cod)Rh(\mu\text{-}Cl)_2PtCl(PBu_3)]$[a]	1.17 ($^1J_{PtP}$ = 3733 Hz)	−40	1.7
13	$[(Et_3P)ClPd(\mu\text{-}Cl)_2PtCl(PEt_3)]$[8]	50.4 9.6 ($^1J_{PtP}$ = 3864 Hz)	25	4.8
14	$[(C_{10}H_{16})ClRu(\mu\text{-}Cl)_2RuCl(cymene)]$[4c]	–	25	7.0
15	$[(C_{10}H_{16})ClRu(\mu\text{-}Cl)_2RhClCp^*]$[4c]	–	−20	9.0
16	$[(C_{10}H_{16})ClRu(\mu\text{-}Cl)_2IrClCp^*]$[4c]	–	−20	$4.0\cdot10^{1}$
17	$[(C_3H_5)_2Rh(\mu\text{-}Cl)_2PtCl(PBu_3)]$	−1.97 ($^1J_{PtP}$ = 3687 Hz)	−40	$8.8\cdot10^{1}$
18	$[(ppy)_2Rh(\mu\text{-}Cl)_2PtCl(PBu_3)]$[4b]	−2.80 ($^1J_{PtP}$ = 3489 Hz)	25	$> 10^2$
19	$[(ppy)_2Rh(\mu\text{-}Cl)_2Rh(cod)]$[4b]	–	25	$> 10^2$
20	$[(C_{10}H_{16})ClRu(\mu\text{-}Cl)_2PtCl(PBu_3)]$[4c]	−0.07 ($^1J_{PtP}$ = 3770 Hz)	25	$> 10^2$
21	$[(C_3H_5)Pd(\mu\text{-}Cl)_2Pt(PBu_3)_2](BF_4)$[4a]	5.75 ($^1J_{PtP}$ = 3598 Hz)	25	$> 10^2$

[a] cod = 1,5-cyclooctadiene. – [b] dmb = *ortho*-metallated dimethylbenzylamine.

not observed under similar conditions. A "*cis*−*trans*" isomerization has also been observed for heterodimeric complexes with a significantly higher equilibrium constant, such as $[(ppy)_2Rh(\mu\text{-}Cl)_2PtCl(PBu_3)_2]$ (Table 1, Entry 18), or for symmetrical complexes such as $[(Ph_3P)(CO)Rh(\mu\text{-}Cl)]_2$.[11] Recently, the same fluxional process was detected for mixed-valence rhodium complexes of the formula $[(Ph_3P)_2H_2Rh(\mu\text{-}X)_2Rh(CO)(PPh_3)]$ (X = Cl, I).[12] A plausible mechanism for this isomerization is a dissociative opening of one halide bridge, followed by rotation about the remaining bridge and subsequent reformation of the second one.



Scheme 2

Secondly, the metathesis reaction itself can be fast compared to the NMR time scale. If this is the case, a coalescence of the signals due to the symmetrical and asymmetrical complexes is observed. Such behaviour was found for $[(C_3H_5)Pd(\mu\text{-}Cl)_2PdCl(PEt_3)]$ (Table 1, Entry 3). At −40 °C, the ^{31}P NMR spectrum shows two distinct signals due to $[(Et_3P)PdCl(\mu\text{-}Cl)]_2$ and $[(C_3H_5)Pd(\mu\text{-}Cl)_2PdCl(PEt_3)]$ in a ratio of 100:34 ($K = 1.2 \cdot 10^{-1}$). At temperatures above 20 °C, on the other hand, only one broad signal is detected (Figure 1).

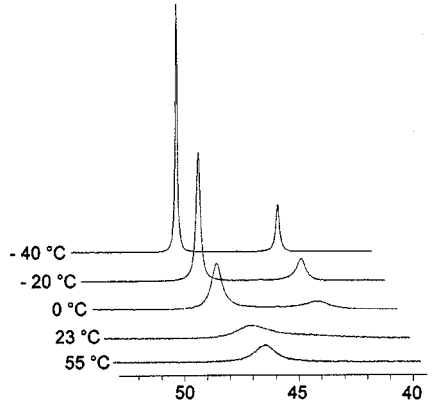
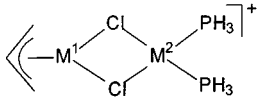


Figure 1. ^{31}P NMR spectra of $[(C_3H_5)Pd(\mu\text{-}Cl)_2PdCl(PEt_3)]$ (in $CDCl_3$) at various temperatures

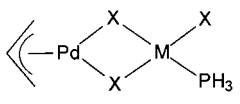
From the data summarized in Table 1, some trends regarding the stabilities of the asymmetric complexes can be deduced. In all cases investigated, the metathesis reaction between two d^8 complexes gave equilibrium constants close to $K = 1.0$, the value expected for a statistical distribution. Complexes with $(R_3P)PtCl$ fragments generally proved to be more stable than those with $(R_3P)PdCl$ fragments (Table 1, Entries 3/9, 4/12, 10/17). The nature of the halo bridge is seen to have only a small effect on the position of the equilibrium with $K_{Cl} > K_{Br} > K_I$ (Table 1, Entries 1−3). The highest equilibrium constants were found for complexes containing metals in different oxidation states such as Ru^{IV}, Rh^{III}, or Ir^{III} in combination with metal ions in oxidation state II, or for complexes with positively charged metal fragments such as $[(R_3P)_2PtCl]^+$. Other asymmetric halo-bridged complexes not synthesized by metathesis and for which an equilibrium with the corresponding homodimeric complexes has not been discussed, such as **3** ($Rh^{III}-Rh^{I}$),[5,6] **4** ($Ir^{III}-Pd^{II}$),[13] **5** ($Pt^{IV}-Pt^{II}$),[14] and **6** (a combination of formally negative and positive fragments),[15] share the same characteristic.

Computational Study

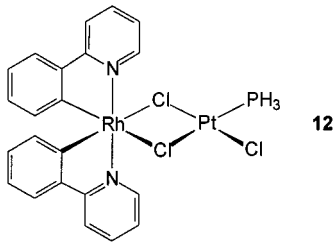
To complement the experimental results, a computational study was carried out on five different asymmetric complexes (**7**−**11**) together with the corresponding symmetrical complexes using density functional theory at the B3LYP level with effective core potentials for the heavy metals. Complexes **7**−**11** were chosen because structural, vibrational, and NMR data are available for several closely related chloro compounds (in the computational model species, PH_3 was used instead of PR_3). These data were used to validate the computational results.[16]



	M^1	M^2	X
7	Pd	Pt	Cl, Br, I
8	Pt	Pt	Cl
9	Pd	Pd	Cl



	M	X
10	Pt	Cl, Br, I
11	Pd	Cl, Br, I



12

In Table 2, selected structural data for some of the computed species are compared with the experimental data. The molecular structures of all the species were fully optimized at the B3LYP level and characterized as minima by a frequency analysis. For $[(H_3P)MCl(\mu\text{-}Cl)]_2$ (M = Pd, Pt), two different isomers (*cis* and *trans*) were obtained. The *trans* isomer was found to be stabilized by ca. 3 kcal/mol at the HF and B3LYP levels. This is in agreement with the experimental results, which show that the *trans* isomer is favoured both in solution as well as in the crystal.[27,46,48] An exception is the triphenylphosphane complex $[(Ph_3P)PtCl(\mu\text{-}Cl)]_2$, for which the *cis* form can be isolated.[17] Two isomers were also found for the allyl complexes $[(C_3H_5)M(\mu\text{-}Cl)]_2$ (M = Pd, Pt): a planar *trans* isomer with a centre of symmetry and a *cis* form with a bent chloro bridge (Pt: θ = 157.4°; Pd: θ = 167.5°). The pairs of isomers are very similar in energy [$\Delta E_{B3LYP}(Pt_{cis/trans}) = -2.60$ kcal/mol; $\Delta E_{B3LYP}(Pd_{cis/trans}) = +0.04$ kcal/mol]. This result is confirmed by the observation that both isomeric forms have been reported for substituted allylpalladium complexes.[18]

Table 2. Selected structural data for all computed species at the B3LYP level in comparison with experimental data

Entry	Complex	calcd./ref.	M−Cl^1 [Å]	M−Cl^2 [Å]	M^1−M^2 [Å]	Cl^1−M^1−Cl^2 [°]	Cl^1−M^2−Cl^2 [°]	θ [°]
1	$[(C_3H_5)Pt(\mu\text{-}Cl)]_2$[a]	calcd.	2.47	2.47	3.68	83.5	83.5	180.0
2	$[(C_3H_5)Pd(\mu\text{-}Cl)]_2$[a]	calcd.	2.45	2.45	3.52	88.2	88.2	180.0
3	$[(C_3H_5)Pd(\mu\text{-}Cl)]_2$	ref.[44]	2.41	2.41	3.48	88.3	88.3	180.0
4	$[(H_3P)_2Pt(\mu\text{-}Cl)]_2^{2+}$	calcd.	2.46	2.46	3.65	84.1	84.1	180.0
5	$[(dppb)_2Pt(\mu\text{-}Cl)]_2^{2+}$ [b]	ref.[45]	2.41	2.41	3.75	77.3	77.3	180.0
6	*trans*-$[(H_3P)PtCl(\mu\text{-}Cl)]_2$	calcd.	2.46[c]	2.41[d]	3.60	84.7	84.7	180.0
7	*trans*-$[(Et_3P)PtCl(\mu\text{-}Cl)]_2$	ref.[46]	2.43[c]	2.32[d]	3.54	83.5	83.5	180.0
8	$[(H_3P)_2Pd(\mu\text{-}Cl)]_2^{2+}$	calcd.	2.43	2.43	3.55	86.2	86.2	180.0
9	$[(Ph_3P)_2Pd(\mu\text{-}Cl)]_2^{2+}$	ref.[47]	2.39	2.35	3.50	84.9	84.9	176.2
10	*trans*-$[(H_3P)PdCl(\mu\text{-}Cl)]_2$	calcd.	2.44[c]	2.39[d]	3.52	86.5	86.5	180.0
11	*trans*-$[(Bu_3P)PdCl(\mu\text{-}Cl)]_2$	ref.[48]	2.44[c]	2.31[d]	3.48	85.7	85.7	180.0
12	$[(C_3H_5)Pd(\mu\text{-}Cl)_2Pt(PH_3)_2]^+$ (**7**)	calcd.	2.52[e]	2.41[f]	3.59	83.0[e]	87.4[f]	164.3
13	$[(C_3H_5)Pd(\mu\text{-}Cl)_2Pt(PBu_3)_2]^+$	ref.[4a]	2.40[e]	2.40[f]	3.57	83.0[e]	83.0[f]	167.9
14	$[(C_3H_5)Pt(\mu\text{-}Cl)_2Pt(PH_3)_2]^+$ (**8**)	calcd.	2.53[e]	2.47[f]	3.59	80.7[e]	85.5[f]	152.4
15	$[(C_3H_5)Pd(\mu\text{-}Cl)_2Pd(PH_3)_2]^+$ (**9**)	calcd.	2.51[e]	2.38[f]	3.54	83.7[e]	89.4[f]	164.7
16	$[(C_3H_5)Pd(\mu\text{-}Cl)_2PtCl(PH_3)]$ (**10**)	calcd.	2.47[e]	2.41[f]	3.56	85.3[e]	86.6[f]	171.4
17	$[(C_3H_5)Pd(\mu\text{-}Cl)_2PdCl(PH_3)]$ (**11**)	calcd.	2.47[e]	2.40[f]	3.52	86.0[e]	88.1[f]	174.3

[a] (C_3H_5) *trans* to (C_3H_5). − [b] dppb = 1,4-bis(diphenylphosphanyl)butane. − [c] Cl *trans* to PR_3. − [d] Cl *trans* to Cl. − [e] M = $M(C_3H_5$. − [f] M = $M(PR_3)$.

A more complicated situation is encountered with the rhodium complex $[(ppy)_2Rh(\mu\text{-}Cl)]_2$ (**12**). Not only the size of the ligands (as a consequence of which only the HF method was utilized) but also different isomers of the complexes need to be considered. Since the rhodium atoms are stereogenic centres, diastereoisomers are observed: the homochiral complexes ΔΔ and ΛΛ, as well as the *meso* complex ΔΛ. The homochiral complexes are energetically favoured by 7.77 kcal/mol at Hartree−Fock level. On the basis of molecular modelling studies of $[(ppy)_2Rh(\mu\text{-}Cl)]_2$[19] and closely related complexes,[20] it has previously been suggested that the *meso* form is less stable due to interligand steric repulsion. Accordingly, for this class of compounds only ΔΔ/ΛΛ complexes have been structurally characterized.[20,21]

A common feature of all the symmetrical complexes is a planar $M(\mu\text{-}Cl)_2M$ unit (Table 2, Entries 1−11), the only exception being $[(PPh_3)_2Pd(\mu\text{-}Cl)]_2^{2+}$, which displays a slightly bent chloro bridge in the crystal. This characteristic is also observed for most other halo-bridged complexes of d^8 transition metal ions.[22] For all asymmetric complexes, on the other hand, a bent chloro bridge (θ = 152−174°) and two significantly different Cl^1M^1 and Cl^1M^2 bond lengths are found (Table 2, Entries 12−17). This striking property is in agreement with the experimental results; e.g. a bent chloro bridge (θ = 164°) was found for the optimized structure of **7** and an angle of 168° was observed for $[(C_3H_5)Pd(\mu\text{-}Cl)_2Pt(PBu_3)_2](BF_4)$ in the crystal. To determine the energy difference between the planar and bent forms, the bending potentials of **7** in the range 230° to 130° were investigated. Apparently, the potential is very flat [$\Delta E(180°-164°) \approx 0.1$ kcal/mol] and, as expected, is not symmetrical (Figure 2). The bent chloro bridges observed for asymmetric complexes are thus a direct consequence of the reduced symmetry of these compounds. Moreover, the very flat bending potential indicates that Coulomb and packing forces may be of great relevance to the structure upon crystallization.

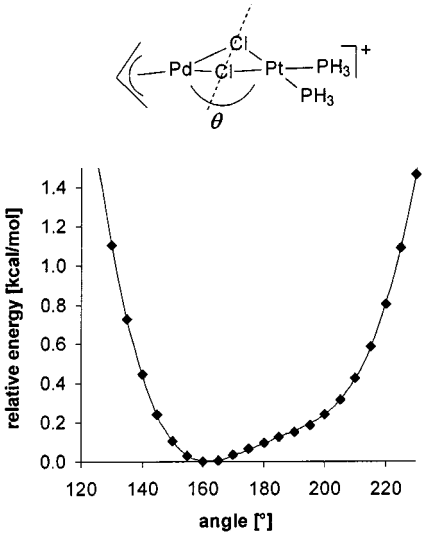


Figure 2. Relative energy of $[(C_3H_5)Pd(\mu\text{-}Cl)_2Pt(PH_3)_2]^+$ as a function of the bending angle θ

Overall, the calculated structural parameters are in good agreement with the experimental data. It should be noted that the computation was carried out for single, isolated (gas-phase) molecules with PH_3 ligands instead of bulky PR_3 ligands. Therefore, small differences between the gas-phase and solid-state data are to be expected.

In a second step of our investigation, the thermodynamics of the equilibrium reactions (Scheme 1) of the asymmetric complexes **7**−**11** was studied. The total energies and zero-point vibrational energies, the molecular free enthalpies, and the equilibrium constants of all the reactions are summarized in Table 3. From these data, and in excellent agreement with the experimental findings, it can be stated that in the case of equilibrium reactions with the mono-

cationic phosphane complexes **7**−**9**, only the metathesis products should be observed. These reactions are fairly exothermic (−65 to −75 kcal/mol) and therefore have very large equilibrium constants associated with them. Apparently, the nature of the metal ion (Pd or Pt) has only a very small influence on the energetics. Thus, formation of the homodimeric Pt complex **8** is only slightly more exothermic than that of the corresponding Pd complex **9**. The situation changes dramatically when neutral d^8 complexes undergo the same reaction (**10** and **11**). Here, the free enthalpy of the metathesis lies on the borderline between exothermic and endothermic reactions. Therefore, the formation of the asymmetric complexes (regardless of whether they are homo- or heterodinuclear) represents an observable equilibrium with a very small equilibrium constant (compared to the formation of **7**−**9**). Again, this fact represents a nice agreement between experiment and theory. Furthermore, we looked at the influence of the bridging halo ligand. Like the effect of the metal centre, changing the halogen was found to have only a small influence on the thermodynamic stabilities of the asymmetric complexes, the equilibrium constants increasing in the order $K_{Cl} < K_{Br} \approx K_I$ (Table 3).

The entropy terms of all the considered metathesis reactions are fairly small (Table 3). Consequently, the temperature is found not to have any great influence on the equilibrium. This finding is in agreement with our NMR studies.

Finally, the metathesis reaction of $[(ppy)_2Rh(\mu\text{-}Cl)]_2$ with $[(PH_3)(Cl)Pt(\mu\text{-}Cl)]_2$ was investigated. Although this reaction results in a neutral product complex, it is essentially quantitative (Table 1, Entry 18). At HF level, we were able to confirm this experimental observation. For the homochiral rhodium complex an equilibrium constant of ca. 10^{29} ($\Delta E = -39.9$ kcal/mol) was estimated, while that for the *meso* complex was estimated to be ca. 10^{23} ($\Delta E = -32.1$ kcal/mol).

In order to investigate the electronic situation in the asymmetric complexes **7**−**11**, we calculated the partial charges[16] as well as the charge transfer that occurs upon metathesis (Table 3). The total amount of charge transfer, q_{ct}, lies in the range 0.20 to 0.17e for the cationic complexes **7**−**9** and 0.06 to 0.10e for the neutral complexes **10** and **11**. It is interesting to note that a considerable proportion of the values for **7**−**9** stems from the allyl ligand and is mainly "received" by the PH_3 ligand, e.g. for **7** 0.162e is donated by the allyl ligand and 0.150e is accepted by the two PH_3 ligands (0.075e per PH_3) with a total electron transfer of 0.203e between the two different monomers. As the allyl ligand acts as a donor and therefore possesses a much smaller negative charge in the metathesis product, a dramatic change in the chemical reaction behaviour towards nucleophilic attack on the allyl group is to be expected. This is especially interesting since allylpalladium complexes are versatile catalysts for allylic substitutions.[23]

Investigation of the reaction of $[(ppy)_2Rh(\mu\text{-}Cl)]_2$ with $[(PH_3)(Cl)Pt(\mu\text{-}Cl)]_2$ leading to **12** supports the hypothesis that charge transfer within the complex upon metathesis plays an important role with regard to the thermodynamic stability of such metathesis complexes. For this reaction, a large charge transfer was found (0.268e), even though only neutral complexes are involved.[24] The phenylpyridine ligand system constitutes a very good electron donor, but the PH_3 group does not act as the main electron acceptor (0.061e). Most of the redistributed charge density is transferred to the chloro bridge (0.103e) and to the central platinum atom (0.074e).

Table 3. Total energies (E_{tot}/a.u.), zero-point vibrational energies (zpe/kcal mol^{-1}), enthalpies (ΔH_{298}/kcal mol^{-1}), free enthalpies (ΔG_{298}/kcal mol^{-1}), equilibrium constants (K), and charge transfer (Δq_{ct}/e; negative sign means acceptor, positive sign means donor)

	X	ΔE_0	ΔH_{298}	ΔG_{298}	K	ΔqM(PH_3)	ΔqM(C_3H_5)	Δq(Cl_b)[a][b]	Δq(C_3H_5)	Δq(PH_3)	Δq(Cl_t)[a]	Δq_{ct}[c]
7	Cl	−74.64	−74.31	−72.78	$2\cdot10^{53}$	−0.0052	−0.0532	+0.0938	+0.1625	−0.0752	−	+0.2031
7	Br	−74.33	−73.37	−74.36	$3\cdot10^{54}$	−	−	−	−	−	−	−
7	I	−72.81	−71.88	−73.45	$6\cdot10^{53}$	−	−	−	−	−	−	−
8	Cl	−72.17	−71.82	−71.62	$3\cdot10^{52}$	−0.0098	−0.03614	+0.0557	+0.1436	−0.0710	−	+0.1631
9	Cl	−68.86	−68.50	−66.56	$6\cdot10^{48}$	−0.0090	−0.0576	+0.0707	+0.1619	−0.0695	−	+0.1750
10	Cl	−1.03	−1.00	−1.99	29	+0.0106	−0.0168	+0.0808	+0.0403	−0.0342	−0.0058	+0.1042
10	Br	−0.69	−0.10	−3.06	173	−	−	−	−	−	−	−
10	I	0.09	0.66	−2.97	148	−	−	−	−	−	−	−
11	Cl	−0.10	−0.09	−0.90	5	+0.0132	−0.0061	+0.0491	+0.0175	−0.0224	−0.0060	+0.0605
11	Br	−0.12	−0.13	0.21	1	−	−	−	−	−	−	−
11	I	0.25	0.82	−2.86	124	−	−	−	−	−	−	−

[a] b = bridging, t = terminal. − [b] $\Delta q(Cl_b) = [q_1(Cl_b, \text{product}) + q_2(Cl_b, \text{product})]*0.5 - q(Cl_b, \text{starting material})$. − [c] $\Delta q_{ct} = [\Delta q(C_3H_5) + \Delta q\text{M}(C_3H_5) + \Delta q(Cl_b)] = \Delta q_{ct}(\text{fragment 1}) = -\Delta q_{ct}(\text{fragment 2})$

Overall, a correlation between q_{ct} and the exothermicity of the metathesis reaction is evident for the reactions investigated. The often discussed linear relationship between ΔG and q_{ct} for Lewis acid−Lewis base complexes arises from a model in which charge transfer is only allowed between donor and acceptor centres and the effects of charge redistribution and changes in structure are ignored.[25] This may account for the observed differences.

Conclusions

The NMR data presented in this paper indicate that in organic solvents such as chloroform, halo-bridged complexes of the late transition metals generally undergo metathesis reactions to form asymmetric homo- or heterobimet-

allic complexes. This hypothesis is wholly consistent with previously published results relating to this class of compounds.[26] The possibility that asymmetric halo-bridged complexes are in dynamic equilibrium with the corresponding symmetric complexes should therefore be considered even if the relevant compounds have not been prepared by metathesis reactions (e.g. **1**, **2**, and **4−6**). Due to the high lability of the halo bridge, the metathesis reaction is very fast, in some cases even fast compared to the NMR time scale. The position of the equilibrium strongly depends on the nature of the participating metal fragments. For combinations of two neutral d^8 complexes, only small equilibrium constants close to the statistical value of $K = 1.0$ have been observed. For charged metal fragments or complexes in different oxidation states, however, the equilibrium may lie completely on the side of the asymmetric complex.

These findings have been confirmed by the results of theoretical investigations. Interestingly, the difference between the metathesis reactions of neutral complexes vs. cationic complexes or complexes with different oxidation states is to some extent correlated with the charge redistribution that occurs upon metathesis. The charge transfer has consequences regarding the reactivities of compounds of this class, which are expected to differ from those of the corresponding symmetrical complexes. We are currently investigating possible applications of asymmetric halo-bridged complexes in homogeneous catalysis and the first results will be reported in due course.

Experimental Section

General Remarks: NMR spectra were recorded with JEOL EX 400 or GSX 270 spectrometers taking the solvent signal as an internal standard. The complexes $[(PR_3)MX(\mu\text{-}X)]_2$ (M = Pd, Pt; R = Et, Bu; X = Cl, Br, I),[27] $[(cod)Rh(\mu\text{-}Cl)]_2$,[28] $[(cod)Ir(\mu\text{-}Cl)]_2$,[29] $[Cp^*MCl(\mu\text{-}Cl)]_2$ (M = Rh, Ir),[30] $[(cymene)RuCl(\mu\text{-}Cl)]_2$,[31] $[(C_3H_5)_2Rh(\mu\text{-}Cl)_2]_2$,[32] $[(dmb)Pd(\mu\text{-}Cl)]_2$,[33] and $[(C_3H_5)Pd(\mu\text{-}Cl)_2]_2$ [34] were prepared according to literature procedures.

NMR Experiments: $CDCl_3$ or CD_2Cl_2 (600 μL) was added to equimolar amounts (30 μmol each) of two different halo-bridged complexes. Once the compounds had dissolved, the solution was transferred to an NMR tube. Spectra were recorded at −40 °C, except where otherwise indicated.

Computational Details: The structural and vibrational data of the species under consideration were calculated by means of density functional theory using the program package Gaussian 98.[35] For Br and I (I: ECP46MWB; Br: ECP28MWB)[36] as well as for Pt and Pd (Pd: ECP28MWB; Pt: ECP60MWB),[37] quasi-relativistic pseudopotentials of the Stuttgart group[38] were utilized. The use of this pseudopotential facilitates the treatment of major relativistic effects such as Darwin and mass velocity terms. Spin-orbit interaction is not included. For H, C, P, and Cl, a standard 6-31G(d,p) basis set was used, for Br and I a (5s5p1d)/[3s3p1d] DZ+P basis set,[39] and for Pt and Pd an (8s7p6d)/[6s5p3d] basis set.[36] − The computations were carried out at the HF level (pre-optimization) and at the DFT level using the hybrid method B3LYP, which includes a mixture of Hartree−Fock exchange with DFT exchange correlation. Becke's 3-parameter functional, where the non-local correlation is provided by the LYP expression (Lee, Yang, Parr correlation functional), was used as implemented in Gaussian 98. For a concise definition of the B3LYP functional, see ref.[40] − The theoretically predicted vibrational frequencies[16] for all the species were calculated with the harmonic approximation. It was found that the deviation from the experimentally obtained frequencies could be partly be compensated by using scaling factors. The frequencies may also be different for various vibrational modes accessible to the molecules.[41] − The metathesis energies were corrected for zero-point vibrational energies obtained at the same level of theory from unscaled harmonic vibrational frequencies. Thermal corrections were also made to allow estimation of the molecular free enthalpies of metathesis and equilibrium constants. Atomic charges (NPA) and the extent of charge transfer were determined by means of NBO analysis.[42,43] It should be emphasized that the computation was carried out for a single, isolated (gas-phase) molecule. There may well be significant differences between gas-phase and solid-state data. In addition, to save CPU time PH_3 was used instead of PPh_3 in our model species.

Acknowledgments

K. S. and A. S. thank Prof. Dr. W. Beck (LMU München) and Prof. Dr. T. M. Klapötke (LMU München) for their generous support and E. Karaghiosoff for technical assistance. Financial funding from the Bayerischer Habilitations-Förderpreis (K. S.) is gratefully acknowledged. We also wish to thank the Leibniz Rechenzentrum (München) for a generous allocation of CPU time.

[1] [1a] *Comprehensive Organometallic Chemistry* (Eds.: G. Wilkinson, F. G. A. Stone), vols. 4−6 and 8, Pergamon Press, Oxford, **1982**. − [1b] *Comprehensive Organometallic Chemistry II* (Eds.: E. W. Abel, F. G. A. Stone, G. Wilkinson), vols. 7−9 and 12, Pergamon Press, Oxford, **1995**.

[2] E. L. Dias, R. H. Grubbs, *Organometallics* **1998**, *17*, 2758. Structurally related allenylidene complexes have been described: A. Fürstner, A. F. Hill, M. Liebl, J. D. E. T. Wilton-Ely, *Chem. Commun.* **1999**, 601.

[3] T. Weslamp, F. J. Kohl, W. Hieringer, D. Gleich, W. Herrmann, *Angew. Chem.* **1999**, *111*, 2573−2576; *Angew. Chem. Int. Ed.* **1999**, *38*, 2416.

[4] [4a] K. Polborn, K. Severin, J. Chem. Soc., *Dalton Trans.* **1999**, 759. − [4b] K. Polborn, K. Severin, *Eur. J. Inorg. Chem.* **1998**, 1187. − [4c] K. Severin, S. Mihan, W. Beck, *Inorg. Chim. Acta* **1995**, *240*, 339.

[5] [5a] M. I. Bruce, B. L. Goodall, M. Z. Iqbal, F. G. A. Stone, *J. Chem. Soc., Chem. Commun.* **1971**, 661. − [5b] A. R. M. Craik, G. R. Knox, P. L. Pauson, R. J. Hoare, O. S. Mills, *J. Chem. Soc., Chem. Commun.* **1971**, 168. − [5c] M. I. Bruce, M. Z. Iqbal, F. G. A. Stone, *J. Organomet. Chem.* **1972**, *40*, 393.

[6] R. J. Hoare, O. S. Mills, *J. Chem. Soc., Dalton Trans.* **1972**, 2141.

[7] [7a] C. Masters, J. P. Visser, *J. Chem. Soc., Chem. Commun.* **1974**, 932. − [7b] A. A. Kiffen, C. Masters, J. P. Visser, *J. Chem. Soc., Dalton Trans.* **1975**, 1311.

[8] H. C. Clark, G. Ferguson, V. K. Jain, M. Parvez, *Inorg. Chem.* **1985**, *24*, 1477.

[9] Asymmetric complexes have been detected for other combinations but due to poor separation of the corresponding NMR signals an accurate determination of the equilibrium constant was not possible.

[10] H. Friebolin, *Ein- und zweidimensionale NMR-Spektroskopie*, VCH, Weinheim, **1992**, p. 285.

[11] G. Giordano, E. Rotondo, *Polyhedron* **1994**, *13*, 2507.

[12] P. D. Morran, S. B. Duckett, P. R. Howe, J. E. McGrady, S. A. Colebrooke, R. Eisenberg, M. G. Partridge, J. A. B. Lohman, *J. Chem. Soc., Dalton Trans.* **1999**, 3949.

[13] C. E. Briant, K. A. Rowland, C. T. Webber, D. M. P. Mingos, *J. Chem. Soc., Dalton Trans.* **1981**, 1515.

[14] E. J. Parsons, R. D. Larsen, P. W. Jennings, *J. Am. Chem. Soc.* **1985**, *107*, 1793.
[15] 15a G. López, G. García, G. Sánchez, C. de Haro, M. D. Santana, J. Casabó, M. Caldés, M. Mejías, E. Molins, C. Miravitlles, *J. Chem. Soc., Dalton Trans.* **1991**, 3311. − 15b G. López, G. García, C. de Haro, G. Sánchez, J. García, *J. Organomet. Chem.* **1986**, *317*, C23.
[16] Supplementary data are available on request (total energies, frequencies, NBO partial charges, HF data).
[17] 17a N. M. Boag, M. S. Ravetz, *J. Chem. Soc., Dalton Trans.* **1995**, 3473. − 17b F. R. Hartley, G. W. Searle, *Inorg. Chem.* **1973**, *12*, 1949.
[18] J.-M. Rosset, M. P. Glenn, J. D. Cotton, A. C. Willis, C. H. L. Kennard, K. A. Byriel, B. H. Riches, W. Kitching, *Organometallics* **1998**, *17*, 1968.
[19] S. Sprouse, K. A. King, P. J. Spellane, R. J. Watts, *J. Am. Chem. Soc.* **1984**, *106*, 6647.
[20] L. Ghizdavu, B. Kolp, A. v. Zelewsky, H. Stoeckli-Evans, *Eur. J. Inorg. Chem.* **1999**, 1271.
[21] 21a P. J. Steel, *J. Organomet. Chem.* **1991**, *408*, 395. − 21b F. O. Garces, K. Dedeian, N. L. Keder, R. J. Watts, *Acta Cryst.* **1993**, *C49*, 1117.
[22] G. Aullón, G. Ujaque, A. Lledós, S. Alvarez, P. Alemany, *Inorg. Chem.* **1998**, *37*, 804.
[23] A. Heumann, in: *Transition Metals for Organic Synthesis*, vol. 1 (Eds.: M. Beller, C. Bolm), Wiley-VCH, Weinheim, **1998**, p. 251.
[24] Only the HF density was used here.
[25] 25a A. Y. Timoshkin, A. V. Suvorov, H. F. Bettinger, H. F. Schaefer III, *J. Am. Chem. Soc.* **1999**, *121*, 5687. − 25b V. Jonas, G. Frenking, M. T. Reetz, *J. Am. Chem. Soc.* **1994**, *116*, 8741. − [25c] E. N. Gurjanova, I. P. Goldstein, I. P. Romm, *Donor−Acceptor Bond*, Wiley, New York, **1975**.
[26] Only in some rare cases have side reactions such as ligand transfer been observed; see ref.[4a]
[27] 27a W. Baratta, P. S. Pregosin, *Inorg. Chim. Acta* **1993**, *209*, 85. − 27b F. R. Hartley, *Organomet. Chem. Rev. A* **1970**, *6*, 119.
[28] G. Giordano, R. H. Crabtree, *Inorg. Synth.* **1990**, *28*, 88.
[29] J. L. Herde, J. C. Lambert, C. V. Senoff, *Inorg. Synth.* **1974**, *15*, 18.
[30] J. W. Kang, K. Moseley, P. M. Maitlis, *J. Am. Chem. Soc.* **1969**, *91*, 5970.
[31] M. A. Bennett, T.-N. Huang, T. W. Matheson, A. K. Smith, *Inorg. Synth.* **1982**, *21*, 74.
[32] J. Powell, B. L. Shaw, *J. Chem. Soc. A* **1968**, 583.
[33] A. C. Cope, E. C. Friedrich, *J. Am. Chem. Soc.* **1968**, *90*, 909.
[34] M. Sakakibara, Y. Takahashi, S. Sakai, Y. Ishii, *J. Chem. Soc., Chem. Commun.* **1969**, 396−397.
[35] M. J. Frisch, G. W. Trucks, H. B. Schlegel, G. E. Scuseria, M. A. Robb, J. R. Cheeseman, V. G. Zakrzewski, J. A. Montgomery, Jr., R. E. Stratmann, J. C. Burant, S. Dapprich, J. M. Millam, A. D. Daniels, K. N. Kudin, M. C. Strain, O. Farkas, J. Tomasi, V. Barone, M. Cossi, R. Cammi, B. Mennucci, C. Pomelli, C. Adamo, S. Clifford, J. Ochterski, G. A. Petersson, P. Y. Ayala, Q. Cui, K. Morokuma, D. K. Malick, A. D. Rabuck, K. Raghavachari, J. B. Foresman, J. Cioslowski, J. V. Ortiz, B. B. Stefanov, G. Liu, A. Liashenko, P. Piskorz, I. Komaromi, R. Gomperts, R. L. Martin, D. J. Fox, T. Keith, M. A. Al-Laham, C. Y. Peng, A. Nanayakkara, C. Gonzalez, M. Challacombe, P. M. W. Gill, B. Johnson, W. Chen, M. W. Wong, J. L. Andres, C. Gonzalez, M. Head-Gordon, E. S. Replogle, J. A. Pople, *Gaussian 98, Revision A.6*, Gaussian, Inc., Pittsburgh, PA, **1998**.
[36] P. Schwertfeger, M. Dolg, W. H. E. Schwarz, G. A. Bowmaker, P. D. W. Boyd, *J. Chem. Phys.* **1989**, *91*, 1762.
[37] D. Andrae, U. Haeussermann, M. Dolg, H. Stoll, H. Preuss, *Theor. Chim. Acta* **1990**, *77*, 123.
[38] http://www.theochem.uni-stuttgart.de/
[39] M. Kaupp, P. v. R. Schleyer, H. Stoll, H. Preuss, *J. Am. Chem. Soc.* **1991**, *113*, 1602.
[40] 40a C. W. Bauschlicher, H. Partridge, *Chem. Phys. Lett.* **1994**, *231*, 277. − 40b A. D. Becke, *J. Chem. Phys.* **1993**, *98*, 5648. − 40c A. D. Becke, *Phys. Rev. A* **1988**, *38*, 3098. − 40d C. Lee, W. Yang, R. G. Parr, *Phys. Rev. B* **1988**, *37*, 785. − 40e S. H. Vosko, L. Wilk, M. Nusair, *Can. J. Phys.* **1980**, *58*, 1200.
[41] [41a] W. Hehre, L. Radom, P. v. R. Schleyer, J. A. Pople, *Ab Initio Molecular Orbital Theory*, Wiley & Sons, New York, **1986**, p. 236. − [41b] T. M. Klapötke, A. Schulz, *Quantenchemische Methoden in der Hauptgruppenchemie*, Spektrum, Heidelberg, **1996**; English version: T. M. Klapötke, A. Schulz, *Quantum Chemical Methods in Main-Group Chemistry* with an invited chapter by R. D. Harcourt, Wiley & Sons, Chichester, **1998**. − 41c M. Otto, S. D. Lotz, G. Frenking, *Inorg. Chem.* **1992**, *31*, 3647.
[42] A. E. Reed, L. A. Curtiss, F. Weinhold, *Chem. Rev.* **1988**, *88*, 899.
[43] A. E. Reed, R. B. Weinstock, F. Weinhold, *J. Chem. Phys.* **1985**, *83*, 735.
[44] A. E. Smith, *Acta Crystallogr.* **1965**, *18*, 331.
[45] S. A. Litster, L. Mole, A. D. Redhouse, J. L. Spencer, *Acta Crystallogr.* **1992**, *C48*, 913.
[46] A. J. Blake, R. O. Gould, A. M. Marr, D. W. H. Rankin, M. Schröder, *Acta Crystallogr.* **1989**, *C45*, 1218.
[47] S. Ganguly, E. M. Georgiev, J. T. Mague, D. M. Roundhill, *Acta Crystallogr.* **1993**, *C49*, 1168.
[48] P. A. Chaloner, S. Z. Dewa, P. B. Hitchcock, *Acta Crystallogr.* **1995**, *C51*, 232.

Received March 13, 2000
[I00093]

Transition-Metal-Promoted C−N Bond-Formation Processes − Low-Spin Fe^{III}, Fe^{II}, and Ni^{II} Complexes of 2-[(Arylamido)phenylazo]pyridine − X-ray Structure, Redox- and Spectroelectrochemistry

Amrita Saha,[a] Partha Majumdar,[a] Shie-Ming Peng,[b] and Sreebrata Goswami*[a]

Dedicated to Professor Animesh Chakravorty on the occasion of his 65th birthday

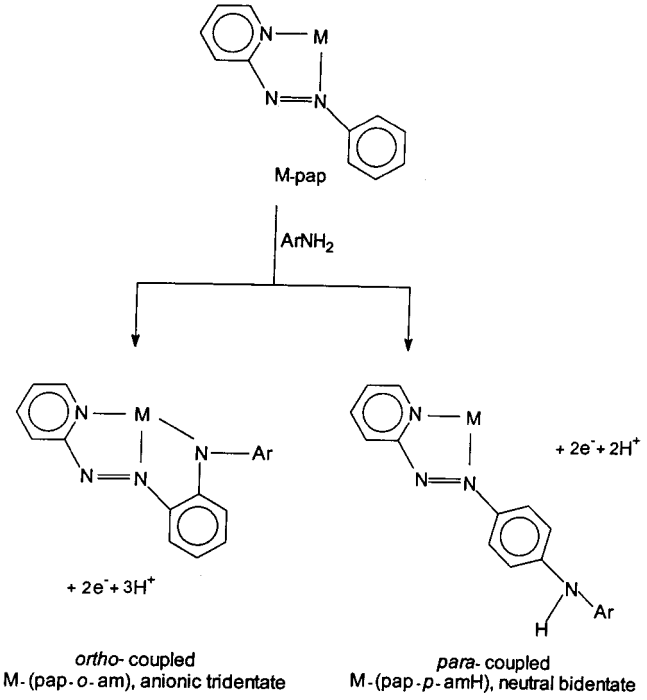
Keywords: Transition-metal-promoted reactions / Aminations / Iron / Nickel / Electrochemistry / N ligands

The metal-promoted amination of an aromatic ring of coordinated L^1 [L^1, pap = 2-(phenylazo)pyridine] is described. Whereas the labile cobalt complex $[Co(L^1)_3]^{2+}$ prefers *ortho*-amination, yielding L^2H {2-[2-(arylamino)phenylazo]-pyridine}, the corresponding $[Fe(L^1)_3]^{2+}$ complex produces the *para*-aminated product L^3H {2-[4-(arylamino)-phenylazo]pyridine}. Both L^2H and L^3H have been isolated in the pure state and were fully characterised. They have low pK_a values, for example pK_a(L^{2a}H) = 8.5 ± 1 and pK_a(L^{3a}H) = 9.1 ± 1. Upon deprotonation, the ligand L^2H behaves as a potential tridentate N,N,N donor. It reacts with anhydrous $FeCl_3$ and $NiCl_2{\cdot}6H_2O$ to produce cationic $[Fe(L^2)_2]^+$ (**1**$^+$) and neutral $[Ni(L^2)_2]$ (**2**), respectively. The cationic ferric complex has been isolated as its perchlorate salt, which is paramagnetic with one unpaired electron (1.66 μ_B). It shows a rhombic EPR spectrum with g_1 = 2.11, g_2 = 2.08, g_3 = 1.93. The room-temperature magnetic moment of the nickel complex is 2.89 μ_B, which confirms the presence of two unpaired electrons. The representative X-ray structures of [**1**]ClO_4 and **2** are reported. In both cases the azo nitrogen atoms of the coordinated ligand, $[L^2]^-$ approach the metal centres more closely, and there is a significant degree of ligand backbone conjugation. The complexes display multiple redox responses. Chemical reduction of **1**$^+$ with dilute hydrazine affords the corresponding ferrous complex $[Fe(L^2)_2]$ (**1**) in almost quantitative yield. The spectral changes upon electrolysis of the above couples have been recorded in an OTTLE cell.

Introduction

Reactions of coordinated ligands belong to an important class of chemical transformations,[1−5] as they provide facile synthetic routes for the formation of many novel molecules that are otherwise difficult, or even impossible, to synthesise by conventional synthetic procedures. We are interested in the aromatic ring amination of coordinated azoarene ligands. In this respect, we have recently described[6,7] cobalt- and rhodium-promoted amination processes of the coordinated 2-(phenylazo)pyridine ligand (pap, L^1). Upon coordination, the phenyl ring of the ligand L^1 is activated, and as a result, both *ortho*- and *para*-amination processes were observed (Scheme 1). The *ortho*-aminated product L^2H can act as a monoanionic tridentate N,N,N donor with the dissociation of the amine proton.

The *para*-aminated product L^3H, on the other hand, binds as a neutral bidentate N,N-donor.[6] The tridentate ligand $[L^2]^-$ has a unique combination of hard as well as soft donor sites. The strong acceptor ability of the azopyridine moiety[8] is capable of stabilising low oxidation states of the metal centre, while the strong electron donor



Scheme 1. Amination of the coordinated ligand 2-(phenylazo)pyridine

[a] Department of Inorganic Chemistry, Indian Association for the Cultivation of Science,
Calcutta 700032, India
Fax: (internat.) + 91-33/473-2805
E-mail: icsg@mahendra.iacs.res.in
[b] Department of Chemistry, National Taiwan University,
Taipei, Taiwan, Republic of China
Supporting information for this article is available on the WWW under http://www.wiley-vch.de/home/eurjic or from the author.

 © WILEY-VCH Verlag GmbH, D-69451 Weinheim, 2000 1434−1948/00/1212−2631 $ 17.50+.50/0

amido part is expected to stabilise the high-valent metal centre. Thus, tunable donor-acceptor properties of this ligand that depend on the oxidation state of the metal centre may be found. It should be noted here that the anionic ligand $[L^2]^-$ reacts readily with the respective metal salts to produce[9] octahedral low-spin complexes of Mn^{II} and Co^{III}.

Two interrelated aspects, viz. metal-promoted reactions of the coordinated azopyridine ligand and the coordination chemistry thereof, are of great interest in this area. As a logical continuation of this project, we report here the first isolation of the *para*-aminated ligand L^3H, together with the coordination chemistry of $[L^2]^-$ involving low-spin Fe^{II} and Fe^{III} ions, and Ni^{II} ion. It may be worth noting that examples of stable and structurally characterised low-spin ferric complexes are rare in the literature.[10–12]

Results and Discussion

Iron- and Nickel-Promoted Aromatic Ring Amination of Coordinated 2-(Phenylazo)pyridine (L^1)

The neutral ligand, L^1 is known to form cationic tris(chelates) of the type $[M(L^1)_3]^{2+}$ (M = Co^{II}, Fe^{II}, and Ni^{II}) with the respective metal ions.[13] The labile cobalt complex $[Co(L^1)_3]^{2+}$ reacts smoothly with primary aromatic amines ($ArNH_2$), without solvent, to produce[6] green, crystalline complexes $[Co^{III}(L^2)_2]^+$. The free ligand $[L^2H]$ has been isolated[9] by the removal of the metal ion from $[Co(L^2)_2]^+$ (Scheme 2). Similarly, the corresponding Fe^{II} and Ni^{II} complexes $[M(L^1)_3]^{2+}$ react with $ArNH_2$ to produce blue or blue-violet mixtures. Unfortunately, these compounds could not be purified. They decompose rapidly in solution and give inconsistent analyses. The blue iron intermediate is diamagnetic, but the nickel compound is paramagnetic. The iron intermediate is thus an Fe^{II} complex. However, the transformed organic ligands can be isolated from these crude mixtures by the removal of the metal ions (Scheme 3).

$$[Co^{II}(L^1)_3]^{2+} \xrightarrow{ArNH_2} [Co^{III}(L^2)_2]^+ \xrightarrow{N_2H_4/(NH_4)_2S_x} [L^2H] + CoS + \text{Other products}$$
Brown Green Orange

Scheme 2. Preparation of the ligand L^2H

$$[Fe^{II}(L^1)_3]^{2+} \xrightarrow{ArNH_2} [\text{Intermediate}] \xrightarrow{\text{aq. } NH_3} [L^3H] + Fe_2O_3.nH_2O + \text{Other products}$$
Blue Deep blue Yellow

$$[Ni^{II}(L^1)_3]^{2+} \xrightarrow{ArNH_2} [\text{Intermediate}] \xrightarrow{(NH_4)_2S_x} [L^2H] + [L^3H] + NiS + \text{Other products}$$
Green Blue-violet Organge Yellow

Scheme 3. Isolation of the ligands L^2H and L^3H

While only *ortho*-amination was observed in the case of $[Co(L^1)_3]^{2+}$, the *para*-aminated ligand L^3H is the only product obtained from $[Fe(L^1)_3]^{2+}$. In contrast, the corresponding nickel compound $[Ni(L^1)_3]^{2+}$ produced a mixture of $[L^2H]$ and $[L^3H]$ in almost equal proportions. The actual reasons for the regioselectivity of these amination processes are yet to be established. It has been shown, however, that prior coordination of the amine residue to the metal centre is an important prerequisite for an *ortho*-amination process of the above type, which is favoured in the case of a labile metal complex.[6] Of the three (pap)metal complexes mentioned above, $[Co(pap)_3]^{2+}$ is kinetically most labile and readily dissociates one pap moiety in solution. These amination reactions are ($2\,e^- + 2\,H^+$) transfer processes and occur in the presence of air, which is the source of the oxidising agent.

Isolation and Characterisation of $[L^3H]$

A methanolic solution of the blue mixture obtained from the reaction of $[Fe(L^1)_3]^{2+}$ and $ArNH_2$ on treatment with NH_3(aq.) precipitated brown hydrated ferric oxide and the solution became yellow. Upon work-up $[L^3H]$ was obtained as orange crystals (Scheme 3). Two such compounds viz. $[L^{3a}H]$ and $[L^{3b}H]$ ($L^{3a}H$: $ArNH_2$ = aniline and $L^{3b}H$: $ArNH_2$ = *p*-toluidine) were isolated. Both the ligands show highly resolved ^1H NMR spectra in $CDCl_3$. The N–H resonance appears as a broad singlet at $\delta = 6.12$. This is in marked contrast to the corresponding *ortho* ligand, where the N–H resonates at $\delta = 10.58$. In the *ortho* isomer, intramolecular hydrogen bonding is expected which is absent in the *para* isomer. For the ^1H NMR spectrum of $[L^{3b}H]$ see Supporting Information. The reagent ammoniacal polysulfide was used to decompose the nickel intermediate.

The ligand $[L^{3a}H]$ formed crystals suitable for a single-crystal X-ray structure determination. The structure confirms the formation of $[L^{3a}H]$ from coordinated L^1 and aniline. The ORTEP and atom numbering scheme are shown in Figure 1. The geometry of this ligand is *trans* about the diazo fragment. The N–N distance is 1.264(2) Å, which is indicative of a double bond. For comparison, this distance[14] in $[L^1H]ClO_4$ is 1.258(5) Å. All other bond lengths are within the range of normally observed values. The pyridyl ring, diazo function, phenyl ring, and amine nitrogen atoms are all coplanar. The terminal phenyl group is out of this plane by ca. 44°. The tetrahedral nature of the amine

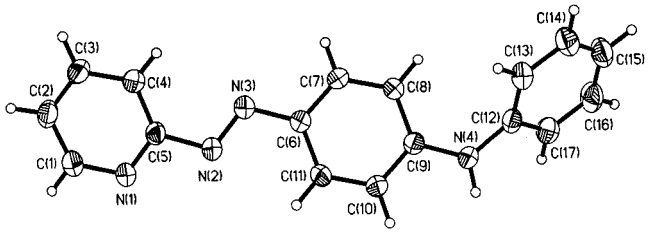
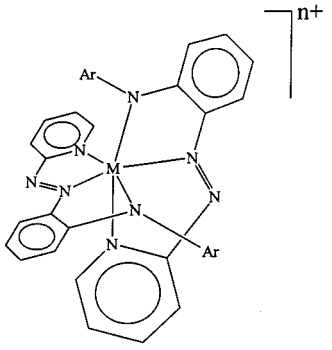


Figure 1. Molecular structure and atom numbering scheme for $[L^{3a}H]$; selected bond lengths [Å]: N(1)–C(5) 1.337(2), N(2)–C(5) 1.427(2), N(2)–N(3) 1.264(2), N(3)–C(6) 1.408(2), C(6)–C(10) 1.394(3), C(10)–C(11) 1.370(2), C(9)–C(10) 1.401(2), N(4)–C(9) 1.383(2), N(4)–C(12) 1.405(2), C(12)–C(13) 1.382(3)

nitrogen atom N(4) may be assessed by the nonplanarity of the two phenyl rings attached to it.

The Iron and Nickel Complexes of $[L^2]^-$

The 1:2 reaction of anhydrous $FeCl_3$ with $[L^2H]$ in methanol in the presence of dilute NEt_3 produced a brown solution at room temperature. Subsequent addition of dilute aqueous $NaClO_4$ afforded crystalline $[Fe(L^2)_2]ClO_4$, **[1]**ClO_4 in excellent yields. The green nickel(II) complexes, $[Ni(L^2)_2]$ (**2**) were obtained directly from the reaction of hydrated nickel(II) chloride with $[L^2H]$ in the presence of dilute NEt_3 (Scheme 4).



$M = Fe^{III}$; $n = 1$

$M = Ni^{II}$; $n = 0$

Scheme 4. Schematic diagram of the metal complexes, $[M(L^2)_2]^{n+}$

In solution, the bivalent nickel complex behaves as a non-electrolyte, whereas the complex $[Fe(L^2)_2]ClO_4$ is a 1:1 electrolyte[15] (Λ = 135−140 $\Omega^{-1}cm^2M^{-1}$ in MeCN). The room-temperature (298 K) magnetic moments of solid $[Fe(L^2)_2]ClO_4$ and $[Ni(L^2)_2]$ lie in the ranges 1.66−1.73 μ_B and 2.89−2.93 μ_B, respectively. Thus, the iron compound is in a low-spin state, $t_2^5(Fe^{III})$. For comparison, the magnetic moments of the corresponding low-spin manganese(II) complex $[Mn(L^2)_2]$ are observed[9] in the range 1.65−1.70 μ_B. In frozen (77 K) dichloromethane/toluene solution the ferric complexes display rhombic spectra with g_1 = 2.11, g_2 = 2.08, and g_3 = 1.93. The rhombic nature of EPR spectra in the present case indicates the asymmetry of the electronic environment around Fe^{III}. The spectrum may be considered as pseudo-axial, consisting of a rather isolated signal g_3 (g_{II} in the true axial case) and two relatively close signals g_1 and g_2 (rhombic components of $g_\perp$). Accordingly, the axial distortion (Δ) that splits the t_2 levels into a and e components is expected to be larger[16] than the rhombic distortion (V) that splits e. The EPR spectral pattern further confirms[11] the low-spin state of iron in $[Fe(L^2)_2]^+$.

Structures

Figure 2 and Figure 3 show the ORTEP and atom numbering schemes for **[1a]**$^+$ and **2a**, respectively.

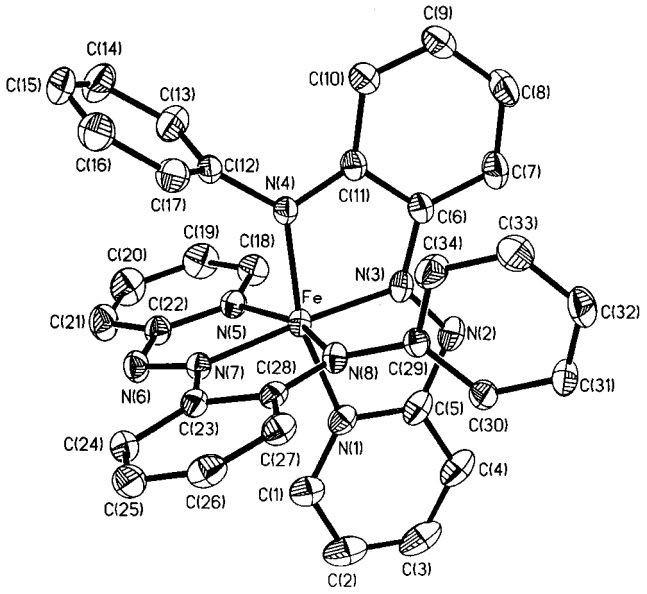


Figure 2. Molecular structure and atom numbering scheme for $[Fe(L^{2a})_2]^+$ cation in $[Fe(L^{2a})_2]$ ClO_4; selected bond lengths [Å]: Fe−N(1) 1.962(2), Fe−N(3) 1.885(2), Fe−N(4) 1.914(2), Fe−N(5) 1.969(2), Fe−N(7) 1.880(2), Fe−N(8) 1.921(2), N(1)−C(5) 1.366(3), N(2)−C(5) 1.379(3), N(2)−N(3) 1.304(2), N(3)−C(6) 1.373(3), C(6)−C(11) 1.425(3), N(4)−C(11) 1.355(3), N(4)−C(12) 1.432(2)

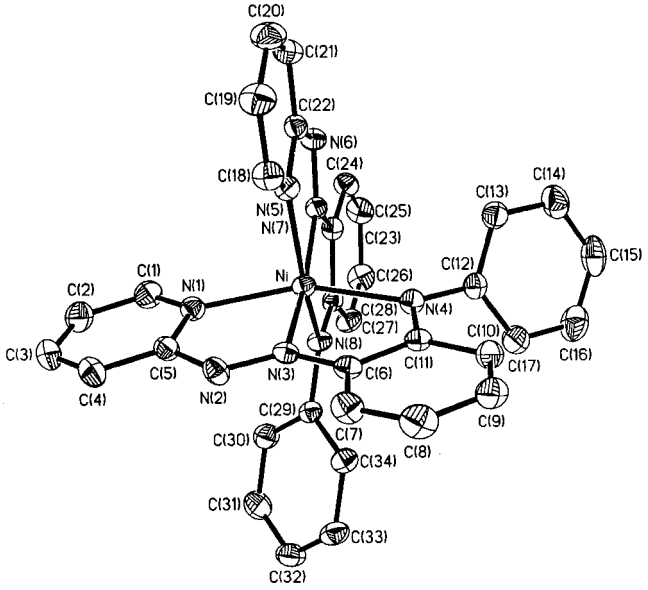


Figure 3. Molecular structure and atom numbering scheme for $[Ni(L^{2a})_2]$; selected bond lengths [Å]: Ni−N(1) 2.099(2), Ni−N(3) 2.002(2), Ni−N(4) 2.079(2), Ni−N(5) 2.103(2), Ni−N(7) 1.989(2), Ni−N(8) 2.078(2), N(1)−C(5) 1.346(3), N(2)−C(5) 1.394(3), N(2)−N(3) 1.301(3), N(3)−C(6) 1.348(3), C(6)−C(11) 1.447(3), N(4)−C(11) 1.318(3), N(4)−C(12) 1.418(3)

The structural analysis of cationic $[Fe(L^{2a})_2]^+$ reveals the presence of two ligands, each of which acts as an N,N,N-tridentate donor with deprotonation of the amine nitrogens, viz. N(4) and N(8). Its geometry is meridional and the Fe atom sits on an imposed C_2 axis bisecting the angles

N(1)−Fe−N(5) and N(4)−Fe−N(8). The two azo nitrogen atoms of the anionic tridentate ligands approach the metal centre more closely [Fe−N(3)/N(7) ≈ 1.88 Å] than the other four Fe−N bonds. There is an indication of significant backbone conjugation in the coordinated anionic ligand. Notably, the N=N azo distances in these complexes are appreciably elongated. For example, this bond length in [**1a**]ClO_4 (1.299 Å) is much longer than in $L^{3a}H$ (1.264 Å). This change is reflected in the reduction of $\nu_{N=N}$ in [**1a**]ClO_4, which appears at 1370 cm^{-1}. In the infrared spectrum of $L^{2a}H$, the $\nu_{N=N}$ stretching is observed at 1420 cm^{-1}. Moreover, the bond length N(azo)−C(phenyl) (1.377 Å) is shorter than the value of 1.421 Å found for the corresponding distance[14] in the salt [Hpap]ClO_4. Similarly, the amido nitrogen atom of $[L^{2a}]^-$ binds to the phenyl group of pap at a shorter distance than is observed for a N−C(phenyl) single bond. These are all in agreement with the notion of extensive electron delocalisation along the ligand backbone. Some degree of conjugation along the ligand backbone of this bis(chelate) system could be implicated in the shortening of Fe−N(azo) bonds, either through an increase in the electron density on N(azo) and a concomitant increased basicity or through an enhanced π-bonding capability of the more conjugated ligand.

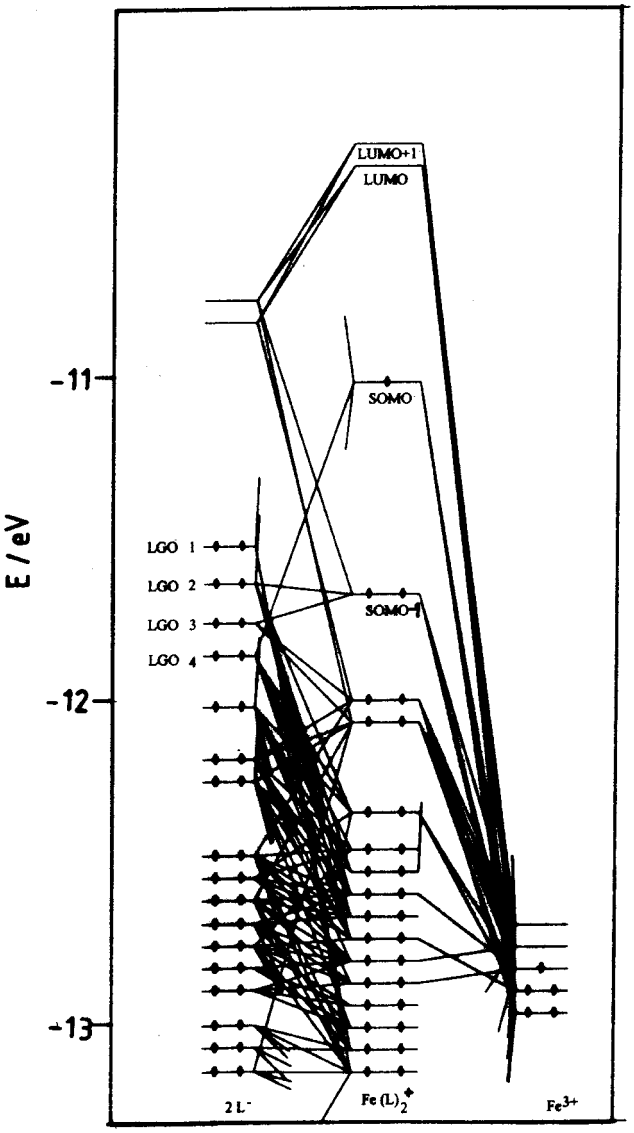


Figure 4. Partial energy level diagram of $[Fe(L^{2a})_2]^+$; for pictorial representations of the ligand group orbitals (LGO) see Supporting Information

The main features of the structure of the molecular complex $[Ni(L^{2a})_2]$ (**2a**) are very similar to those for **1a**$^+$. The two anionic ligands $[L^{2a}]^-$ bind the metal ion in an N_6 fashion using pairs of pyridyl-N, azo-N, and deprotonated arylamido-N atoms. The relative orientations within the pairs are *cis*, *trans*, and *cis*, respectively. The chelate bite angles are dissimilar, and are considerably less than the ideal octahedral value (90°). Extensive electron delocalization along the ligand backbone has also been observed in this case. As a result, the N−N(diazo) distances are longer than the usual N=N distance, and the average of the two Ni−N(azo) distances is shorter than the other Ni−N distances in this molecule.

From the crystallographic data it is obvious that the metal complexes under consideration may best be described as delocalised systems. In order to have some insight into the nature of redox and spectroscopically relevant orbitals, a standard extended Hückel MO calculation using the crystallographic parameters was performed on $[Fe(L^{2a})_2]^+$ using the CACAO programme by Mealli and Proserpio.[17] A partial energy level scheme for $[Fe(L^{2a})_2]^+$ is shown in Figure 4. In this complex the SOMO is strongly delocalised. It has 40% metal d-character with significant contributions from both amide and azo functions. The next lower orbital, SOMO-1, is a ligand orbital where the metal contribution is only 11%. There are two closely spaced LUMO and LUMO+1 orbitals which are predominantly ligand π-acceptor orbitals (−N=N− + phenyl rings) with an admixture of 18−19% metal d-character. For pictorial presentation of the above four MOs see Supporting Information.

Redox Properties and Behaviour

The redox properties of the iron and nickel complexes have been studied by cyclic voltammetry (CV) with a platinum working electrode. Voltammetric data are collected in Table 1 and representative voltammograms are displayed in

Table 1. Cyclic voltammetric data

Compound	Oxidation $E_{1/2}$ [V][a]	Reduction $E_{1/2}$ [V][a]
$[Fe(L^{2a})_2]ClO_4$	1.1, 1.75[b]	0.18, −0.97, −1.45
$[Fe(L^{2b})_2]ClO_4$	1.05, 1.73[b]	0.16, −1.01, −1.49
$[Ni(L^{2a})_2]$	0.56, 0.85[c], 1.48[b]	−1.10, −1.26[d]
$[Ni(L^{2b})_2]$	0.54, 0.84[c], 1.45[b]	−1.13, −1.28[d]
$L^{2a}H$	1.00,[b] 1.30[b]	−1.15

[a] Experiments were carried out in CH_3CN at 298 K using TEAP as supporting electrolyte. The reported data corresponds to a scan rate of 50 mVs^{-1}. − [b] Irreversible anodic response, the potential corresponds to E_{pa}. − [c] $i_{pa} > i_{pc}$. − [d] Irreversible cathodic response, the potential corresponds to E_{pc}.

Figure 5. In all cases acetonitrile was used as solvent. The nature of the voltammograms of the complexes under consideration do not change in dichloromethane. However, due to the relatively limited potential window of dichloromethane, acetonitrile was commonly used for voltammetric studies.

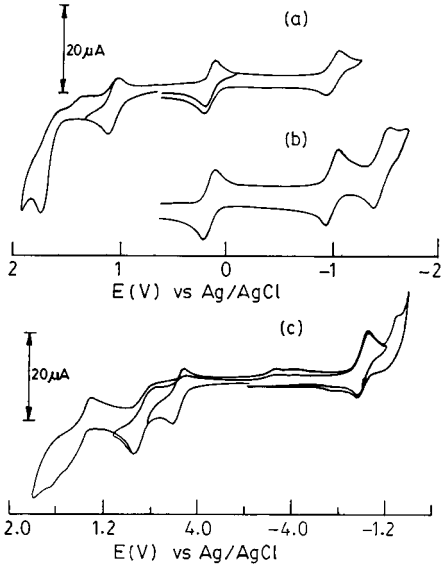


Figure 5. Cyclic voltammograms (scan rate 50 mVs^{-1}, solvent CH_3CN, 0.1 M TEAP) of (a) $[Fe(L^{2a})_2]ClO_4$ (platinum), (b) $[Fe(L^{2a})_2]ClO_4$ (glassy carbon), and (c) $Ni(L^{2a})_2$ (platinum)

The ferric complexes show four responses in the range +1.5 to −1.6 V. Three of these are cathodic, while the fourth one, occurring at ca. 1.0 V, is an anodic response. The free ligand $L^{2a}H$ displays[9] two irreversible anodic responses and a reversible cathodic response at 1.00, 1.30, and −1.15 V, respectively. The cathodic response in free $L^{2a}H$ is due to the reduction of the diazo function. For comparison, the parent ligand pap undergoes two successive step reductions at −1.31 and −1.57 V. Thus, the two cathodic responses in $\mathbf{1}^+$ at −0.97 and −1.45 V may be logically assigned to ligand reductions, centred mainly at the azoamide chromophore. The reductive response at +0.18 V and the oxidative response at 1.1 V both occur presumably at SOMO, which has almost equal metal and ligand contributions. These two responses may formally be assigned to Fe^{III}/Fe^{II} and Fe^{III}/Fe^{IV} couples. Presence of a hard donor site like $[ArN]^-$ in the deprotonated $[L^2]^-$ ligand helps in stabilisation of higher valent states of iron. For comparison, the ferrous state is highly stabilised in the parent $[Fe(pap)_3]^{2+}$ complex. The irreversible anodic response in $[\mathbf{1}]^+$ at > 1.7 V mainly concerns the oxidation of the amido function (SOMO-1).

Such low potentials for the Fe^{III}/Fe^{II} couple in $\mathbf{1}^+$ persuaded us to try and isolate the corresponding ferrous complex **1** in the pure state. Fortunately, with hydrazine as the reducing agent, we were able to isolate pink **1** in almost quantitative yield. This compound is thermally stable, but air-sensitive and is slowly reoxidised to $\mathbf{1}^+$ in the presence of air. In solution, the ferrous complex is a nonelectrolyte and is diamagnetic. Diamagnetism in this case confirms a low-spin state (t_2^6), which shows a highly resolved ^1H NMR spectrum. The nature of the ^1H NMR spectrum is similar to that observed for $[Co^{III}(L^2)_2]^+$.[6] The most notable feature in the infrared spectrum of **1a** is a large shift of $\nu_{N=N}$ to lower wavenumber (1300 cm^{-1}), indicating very strong $d_\pi - p_\pi$ interactions between the metal and ligand orbitals. For comparison, this vibration in the corresponding $[Fe(pap)_3]^{2+}$ complex is observed at 1350 cm^{-1}.[13] Our attempts to isolate the oxidized product, $[Fe(L^2)_2]^{2+}$ have so far been unsuccessful. Multiple electron-transfer responses are also the main features for the nickel complexes. These show two adjacent oxidative responses at ca. 0.56 and 0.85 V. The first one of these is reversible and the second one is only partly chemically reversible ($i_{pa} > i_{pc}$). Another high potential ligand-based irreversible oxidation process at > 1.4 V was also observed. The isolation of corresponding cationic $[\mathbf{2}]^+$ by chemical oxidation has been unsuccessful.

Spectroelectrochemistry

In order to study the spectra of the parent as well as other stable members of the redox series, two representative examples viz. $[Fe(L^{2a})_2]ClO_4$, $[\mathbf{1a}]ClO_4$, and $[Ni(L^{2a})_2]$ (**2a**) were chosen for spectroelectrochemical studies. These were performed in an OTTLE cell.[18] In both cases dichloromethane was used as solvent to take advantage of the higher solubilities of the complexes. The spectral data are collected in Table 2.

Figure 6 shows the solution spectra of the parent $\mathbf{1a}^+$ along with electrogenerated $\mathbf{1a}^{2+}$, **1a**, and $\mathbf{1a}^-$. The starting complex $\mathbf{1a}^+$ shows a very broad transition at 2125 nm (ε = 1070 $M^{-1}cm^{-1}$) in the NIR region. There are also two ill-defined shoulders at 1170 and 1055 nm. High-intensity multiple CT transitions ($\varepsilon \geq 10{,}000$ $M^{-1}cm^{-1}$) in the visible and UV range are the characteristics of all the above spectra. Upon oxidation, $\mathbf{1a}^+ \rightarrow \mathbf{1a}^{2+}$, the above broad NIR transition in $\mathbf{1a}^+$ is shifted to 2050 nm (ε = 2950 $M^{-1}cm^{-1}$), which is associated with a less-intense transition at 1635 nm (ε = 535 $M^{-1}cm^{-1}$). The intensities of NIR transitions for the present examples are too intense for a d−d transition. The lowest energy transition in $\mathbf{1a}^{2+}$ presumably involves two molecular orbitals that are ligand (SOMO-1, donor) and metal-ligand (SOMO, acceptor) orbitals. Hence, this transition is formally a ligand-to-metal charge-transfer (LMCT) transition. Notably, the corresponding Mn complex, $[Mn(L^{2a})_2]^+$, also shows[9] a similar transition at 2250 nm. The NIR region transitions in the case of **1a** appear at 1240 and 1440 nm. Upon further reduction to $\mathbf{1a}^-$, the NIR transitions completely disappear. The highly intense visible-range transitions may be due to SOMO→LUMO transitions. The rest of the high-energy transitions are assigned as intra-ligand transitions. It should be noted here that the free ligand $L^{2a}H$ shows[9] an intense transition at 490 nm, which is due to amido→azo charge transfer. All the above redox processes viz. $\mathbf{1a}^+ \rightleftarrows \mathbf{1a}^{2+}$, $\mathbf{1a}^+ \rightleftarrows \mathbf{1a}$ and $\mathbf{1a} \rightleftarrows \mathbf{1a}^-$ are reversible, and the spectrum of each of them

Table 2. Electronic spectral data

Compound	Absorption[a] λ_{max} [nm (ε [$M^{-1}cm^{-1}$])]
$[Fe(L^{2a})_2]ClO_4$	2125 (1070), 1170[b] (1610), 1055[b] (1600), 860[b] (6960), 760 (8300), 570[b] (9640), 510 (13120), 360[b] (17680)
$[Fe(L^{2a})_2]^{2+}$[c]	2050 (2950), 1635[b] (540), 860[b] (4280), 660[b] (9910), 610[b] (13120), 560[b] (13400), 380[b] (23800), 320[b] (20600)
$[Fe(L^{2a})_2]$[c]	1440[b] (1070), 1240[b] (1060), 820[b] (7230), 740(9640),670 (9100), 570(15260), 480[b] (10200), 340(19010), 300[b] (29200)
$[Fe(L^{2a})_2]^-$ [c]	770[b] (7770), 580(7770), 400(18750), 340[b] (19300)
$[Fe(L^{2b})_2]ClO_4$	760[b] (5900), 580[b] (6000), 510(9300), 420[b] (9540), 360[b] (13200)
$[Ni(L^{2a})_2]$	720[b] (20400), 680[b] (21340), 400(15380), 300[b] (28560), 250[b] (35460)
$[Ni(L^{2a})_2]^+$ [c]	1570[b] (1570), 1210[b] (1260), 700[b] (13200), 360 (19000), 260 (31400)
$[Ni(L^{2b})_2]$	730[b] (19500), 680[b] (17000), 400[b] (14300), 360[b] (12300), 250[b] (46900), 230 (51520)

[a] Data obtained from absorption spectra. – [b] Shoulder. – [c] Spectroelectrochemically generated compound in an OTTLE cell (see text).

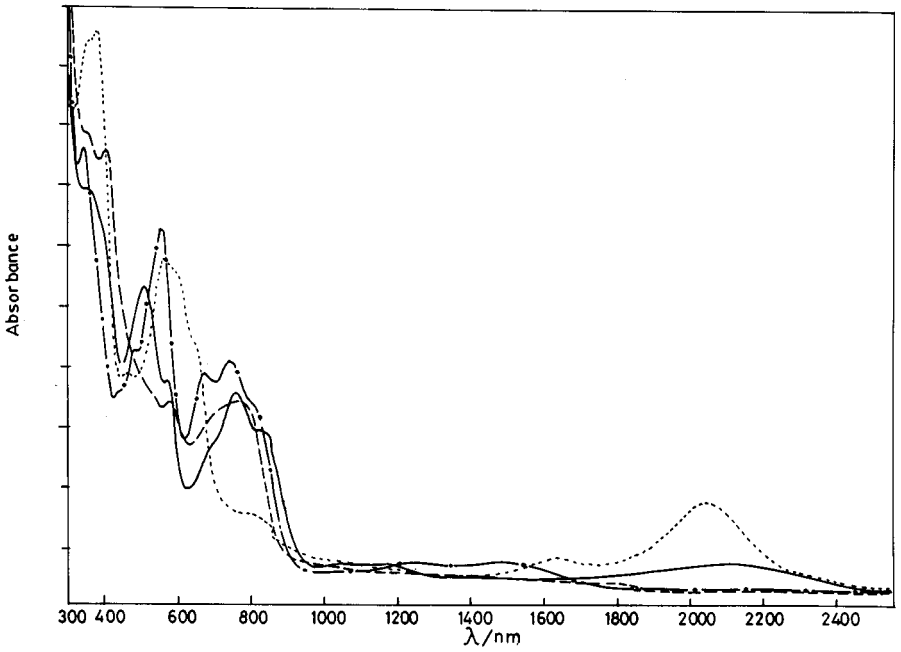


Figure 6. Solution spectra of $[Fe(L^{2a})_2]^+$ (—), $[Fe(L^{2a})_2]^{2+}$ (·····), $[Fe(L^{2a})_2]$ (– · – · –), and $[Fe(L^{2a})_2]^-$ (- - - - -).

may be quantitatively generated by application of the appropriate potential.

A spectroelectrochemical study on $[Ni(L^{2a})_2]$ (**2a**) was confined only to one reversible oxidation process, viz. **2a** $\rightleftarrows$ $\mathbf{2a}^+$ (see Supporting Information). The other redox processes are not chemically reversible, and these are not reported. Like the other transition metal complexes of this ligand system, the starting nickel(II) complex **2a** also shows multiple allowed CT transitions in the visible and UV region. Upon oxidation of the complex to $\mathbf{2a}^+$ the two low-energy transitions at 1570 and 1210 nm appear.

Conclusions

Metal-promoted amination of the pendant aromatic ring of a coordinated diazo ligand together with the chemistry of the transformed ligands involving iron and nickel are the two major aspects of this report. This work further demonstrates that, upon coordination, the ligand pap is susceptible to a fascinating metal-mediated chemical transformations. Earlier it was demonstrated that the pendant phenyl group of pap can be hydroxylated[4a] and thiolated[4b] by C–H activation. In the present study we have been able to isolate the aminated ligands that show interesting modifications of properties as ligands. The *ortho* fusion of the above type results in the formation of a potent N,N,N donor, which stabilises the rare low-spin state of both Fe^{III} and Fe^{II}. This anionic ligand has a unique combination of hard and soft donor sites. Extensive charge delocalisation plays a crucial role in the stabilization of low-spin state of the iron(III) complex. The study of coordination chemistry of both L^2H and L^3H involving heavier transition elements is in progress.

Experimental Section

Materials: The starting complexes $[Co(L^1)_3](ClO_4)_2$, $[Fe(L^1)_3](ClO_4)_2$, $[Ni(L^1)_3](ClO_4)_2$, and L^2H were prepared by reported

methods.[9,20] The solvents and chemicals used for synthesis were of analytical grade. The supporting electrolyte tetraethylammonium perchlorate (TEAP) and solvents for electrochemical work were obtained as before.[21]

Caution: Perchlorate salts of metal complexes were generally explosive. Although no detonation tendencies have been observed, care is advised and handling of only small quantities is recommended.

Physical Measurements: A Shimadzu UV 2100 UV/Vis spectrophotometer was used to record electronic spectra. − The IR spectra were recorded with a Perkin-Elmer 783 spectrophotometer. − ^{1}H NMR spectra in $CDCl_3$ were recorded with a Bruker Avance DPX300 spectrophotometer. $SiMe_4$ was used as an internal standard. − A Perkin−Elmer 240C elemental analyser was used to collect microanalytical data (C,H,N). − Electrochemical measurements were performed under dry nitrogen with an EG&G PARC Model 273A Potentiostat/Galvanostat based electrochemistry system. All potentials reported in this work are referenced to the Ag/AgCl electrode and are uncorrected for junction contribution. − The pH measurements were made with a μ-pH system 361 Systronics pH meter, standardised with buffers of pH = 7.0 and 9.2. − Electrical conductivities were measured by using a Systronics Direct Reading Conductivity meter 304. The pK_a values of the ligands were determined pH-metrically as described before.[21] − EPR measurements were made with a Varian 109C E-line X-band spectrometer fitted with a flat cell. Spectra were calibrated with the help of DPPH (g = 2.0037). − Magnetic moment measurements were carried out by using a PAR 155 vibrating sample magnetometer fitted with a Walker Scientific L75FBAL magnet. − Spectroelectrochemical studies were carried out in an OTTLE cell mounted in the sample compartment of a Perkin−Elmer Lambda 19 spectrophotometer, as described earlier.[18]

Isolation of 2-[4-(Arylamino)phenyl]azopyridine, L^3H: The reaction of neat $ArNH_2$ ($ArNH_2$ = aniline or *p*-toluidine) with $[Fe(L^1)_3](ClO_4)_2$ produced a blue mixture from which no pure product could be isolated. However, this crude product was used to isolate L^3H in the pure state. Details are given below. − The above crude product (0.10 g, $ArNH_2$ = aniline) was dissolved in methanol (30 mL) and NH_3(aq) (5 mL) was added. The mixture was then stirred for 30 min at a room temperature. The resulting yellow solution was concentrated to dryness under vacuum. The residue was then extracted with benzene and subjected to column chromatography on a silica gel (1 × 15 cm) column. A yellow band of $L^{3a}H$ was eluted with a benzene/chloroform mixture (3:1, v/v). The yellow extract was taken to dryness under vacuum. X-ray quality crystals were obtained at room temperature by slow diffusion of a benzene solution of the compound into hexane. Yield:0.06 g (60%). − UV/Vis (CH_2Cl_2): λ_{max} (ε, $M^{-1}cm^{-1}$) = 270 (10400), 415 (20800), 545(sh) nm. − IR (KBr): $\tilde{\nu}$ = 1575 (C=N), 1450 cm^{-1} (N=N). − ^{1}H NMR ($CDCl_3$): δ = 6.12 (s, N−H), 7.02 (d, J = 8.92 Hz, 2 H, 9-H and 11-H), 7.16 (4 H, 14-H,18-H and 15-H,17-H), 7.29 (t, J = 8.36 and 7.39 Hz, 1 H, 5-H), 7.72 (d, J = 8.0 Hz, 1 H, 3-H), 7.80 (t, J = 8.06 and 7.20 Hz, 1 H, 4-H), 7.93 (d, J = 8.86 Hz, 2 H, 8-H and 12-H), 8.64 (d, J = 4.73 Hz, 1 H, 6-H) (Figure 7). − pK_a = 9.1 ± 1. − $C_{17}H_{14}N_4$ (274.32): calcd. C 74.37, H 5.10, N 20.41; found C 74.02, H 5.63, N 20.04. − Similarly $L^{3b}H$ ($ArNH_2$ = *p*-toluidine) was isolated as orange needles following the above procedure. Yield: 58%. − UV/Vis (CH_2Cl_2): λ_{max} (ε, $M^{-1}cm^{-1}$) = 275 (11400), 410 (19000), 550(sh) nm. − IR (KBr): $\tilde{\nu}$ = 1595 (C=N), 1455 cm^{-1} (N=N). − ^{1}H NMR ($CDCl_3$): δ = 6.09 (s, N−H), 7.02 (d, J = 8.90 Hz, 2 H, 9-H and 11-H), 7.17 (4 H, 14-H,18-H and 15-H,17-H), 7.35 (t, J = 7.85 and 7.12 Hz, 1 H, 5-H), 7.79 (d, J = 7.94 Hz, 1 H, 3-H), 7.85 (t, J = 8.06 and 7.16 Hz, 1 H, 4-H), 7.97 (d, J = 8.85 Hz, 2 H, 8-H and 12-H), 8.70 (d, J = 3.67 Hz, 1 H, 6-H). − pK_a = 9.5 ± 1. − $C_{18}H_{16}N_4$ (288.32): calcd. C 74.92, H 5.55, N 19.42; found C 75.38, H 5.68, N 19.49.

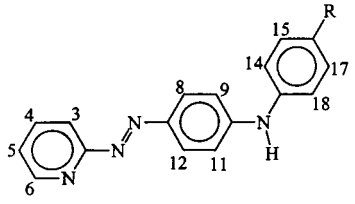


Figure 7. Numbering scheme for the protons of ligand L^3H

Synthesis of Bis[2-(2-phenylamido)phenyl)azopyridine]iron(III) Perchlorate, $[Fe(L^{2a})_2]ClO_4$, [1a]ClO_4: The ligand $L^{2a}H$ (0.11 g, 0.41 mmol) was dissolved in 25 mL of methanol and 1−2 drops of triethylamine were added. To this deprotonated ligand solution was added a methanolic solution of anhydrous $FeCl_3$ (0.03 g, 0.20 mmol) and the mixture was stirred for 1 h at a room temperature. The colour of the solution changed from orange yellow to reddish brown. The resulting solution was filtered and 5 mL of a dilute aqueous solution of $NaClO_4$ (ca. 1 M) was added. X-ray quality crystals were obtained at room temperature by slow diffusion of a dichloromethane solution of the compound into hexane. Yield: 0.12 g (85%). − IR (KBr): $\tilde{\nu}$ = 1595 (C=N), 1370 (N=N), 1100, 625 cm^{-1} (ClO_4^-). − Λ_M = 135 $\Omega^{-1}cm^2mol^{-1}$ (1 × 10^{-3} M in CH_3CN). − μ_{eff} (298 K) = 1.66 μ_B. − $C_{34}H_{26}ClFeN_8O_4$(701.93): calcd. C 58.13, H 3.70, N 15.96; found C 58.53, H 3.94, N 15.17. − Similarly, anhydrous $FeCl_3$ was treated with $L^{2b}H$ in a 1:2 ratio in methanolic solution in the presence of 1−2 drops of triethylamine as base. Subsequent addition of aqueous $NaClO_4$ to the reaction mixture produced crystalline $[Fe(L^{2b})_2]ClO_4$ (**1b**). Yield: 80%. − IR (KBr): $\tilde{\nu}$ = 1595 (C=N), 1365 (N=N), 1100, 625 cm^{-1} (ClO_4^-). − Λ_M = 140 Ω^{-1} cm^2mol^{-1} ($1{\cdot}10^{-3}$ M in CH_3CN). − μ_{eff} (298 K) = 1.68 μ_B. − $C_{36}H_{30}ClFeN_8O_4$ (729.93): calcd. C 59.18, H 4.11, N 15.34; found C 59.32, H 4.45, N 15.98.

Chemical Reduction of $[Fe^{III}(L^{2a})_2]ClO_4$ {[1a]ClO_4} to $[Fe^{II}(L^{2a})_2]$ {[1a]}: A dichloromethane solution of [**1a**]ClO_4 (0.10 g in 20 mL) was stirred with 5 mL of dilute aqueous hydrazine solution at room temperature for 30 min. The colour of the solution changed from reddish-brown to pink. The above mixture was extracted with dichloromethane (2 × 10 mL), which was then dried with anhydrous sodium sulfate. The dried solution was concentrated to half of its initial volume. Slow addition of hexane to the above pink solution precipitated dark microcrystals of **1a**. This was further crystallised from a dichloromethane/hexane solvent mixture. The compound is diamagnetic. Yield: 95%. − IR (KBr): $\tilde{\nu}$ = 1595 (C=N), 1300 cm^{-1} (N=N). − $C_{34}H_{26}FeN_8$ (602.43): calcd. C, 67.73, H 4.32, N 18.59; found C 67.46, H 4.73, N 18.30.

Synthesis of Bis[2-{2-(phenylamido)phenyl}azopyridine]nickel(II), $[Ni(L^{2a})_2]$, [2a]: The ligand $L^{2a}H$, (0.20 g, 0.74 mmol) was dissolved in 25 mL of methanol and 1−2 drops of triethylamine were added. To the deprotonated ligand solution was added a methanolic solution of $NiCl_2{\cdot}6H_2O$ (0.09 g, 0.37 mmol), and the mixture was stirred for 1 h at room temperature. The colour of the solution changed from orange yellow to green. The resultant mixture was filtered and the solvent was evaporated under vacuum. The compound thus obtained was finally crystallised from a dichlorome-

Table 3. Crystallographic data collection parameters for complexes

	[1a]ClO_4	2a	$L^{3a}H$
Empirical formula	$C_{34}H_{26}ClFeN_8O_4$	$C_{34}H_{26}N_8Ni$	$C_{17}H_{14}N_4$
Molecular mass	701.93	605.34	274.32
Temperature [K]	295(2)	295(2)	295(2)
Crystal system	triclinic	monoclinic	monoclinic
Space group	$P\bar{1}$	$P2_1/n$	$P2_1/c$
a [Å]	9.1859(1)	10.4656(12)	13.3331(6)
b [Å]	10.3559(1)	16.215(2)	9.8123(5)
c [Å]	17.2478(1)	16.821(2)	11.8449(5)
α [°]	103.887(1)	90	90
β [°]	91.143(1)	90.575(10)	114.595(1)
γ [°]	93.850(1)	90	90
V [Å^3]	1588.10(2)	2854.5(6)	1409.05(11)
Z	2	4	4
$D_{calcd.}$ [Mg/m^3]	1.468	1.409	1.293
Crystal dimensions [mm]	0.40 × 0.20 × 0.15	0.50 × 0.50 × 0.50	0.40 × 0.25 × 0.16
θ range for data collection [°]	1.22−26.37	1.74−25.00	1.68−25.00
GOF	1.001	1.033	1.048
Wavelength [Å]	0.71073	0.71073	0.71073
Reflections collected	18996	5037	6832
Unique reflections	6502	5037	2482
Largest difference between peak and hole [eÅ^{-3}]	0.364, −0.371	0.280, −0.274	0.162, −0.147
Final R indices [$I > 2\sigma(I)$]	$R1$ = 0.0370 $wR2$ = 0.1018	$R1$ = 0.0334 $wR2$ = 0.0783	$R1$ = 0.0469 $wR2$ = 0.0994

thane/hexane mixture. X-ray quality crystals were obtained at room temperature by slow diffusion of a dichloromethane solution of the compound into hexane. Yield: 0.19 g (85%). − IR (KBr): $\tilde{\nu}$ = 1595 (C=N), 1370 cm^{-1} (N=N). − μ_{eff} (298 K) = 2.89 μ_B. − $C_{34}H_{26}N_8Ni$ (605.34): calcd. C 67.40, H 4.30, N 18.50; found C 67.67, H 4.80, N 18.32. − Similarly, $NiCl_2{\cdot}6H_2O$ was treated with $L^{2b}H$ in a 1:2 ratio in methanolic solution in the presence of 1−2 drops of triethylamine as base to produce crystalline [Ni(L^{2b})$_2$] (**2b**). Yield: 80%. − IR (KBr): $\tilde{\nu}$ = 1595 (C=N), 1375 cm^{-1} (N=N). − μ_{eff} (298 K) = 2.92 μ_B. − $C_{36}H_{30}N_8Ni$ (633.34): C 68.21, H 4.74, N 17.68; found C 68.92, H 5.03, N 17.53.

Crystal Structure Determination: The crystallographic data for the compounds $L^{3a}H$, Fe(L^{2a})$_2ClO_4$, [**1a**]ClO_4, and Ni(L^{2a})$_2$ (**2a**) are collected in Table 3. The data were corrected for Lorentz and polarisation effects. All the structures were solved by using SHELXS-86 package of programme.[22] These revealed the positions of all non-hydrogen atoms and refined by full-matrix least-squares techniques against F^2 (SHELXL-93).[23] Absorption corrections were made with the SADABS package of programs. Hydrogen atoms were placed at the calculated positions. Crystallographic data (excluding structure factors) for the structures reported in this paper have been deposited with the Cambridge Crystallographic Data Centre as supplementary publication no. CCDC-141470, -141471, -141472. Copies of the data can be obtained free of charge on application to CCDC, 12 Union Road, Cambridge CB2 1EZ, UK [Fax: (internat.) + 44-1223/336-033; E-mail: deposit@ccdc.cam.ac.uk].

Acknowledgments

Financial support received from the Department of Science and Technology, New Delhi, is acknowledged. We are grateful to Professor J. A. McCleverty, Dr. M. D. Ward, University of Bristol, and Dr. S. Bhattacharya for their help. S. G. thanks the RSC for its financial support, which allowed him to visit the University of Bristol. We are thankful to the referees for suggestions.

[1] D. St. C. Black, *Comprehensive Coordination Chemistry* (Eds: R. D. Gillard, J. A. McCleverty), Pergamon Press, **1987**, vol. 1, p. 415; vol. 6, p. 155.
[2] L. S. Hegedus, *Coord. Chem. Rev.* **1998**, *168*, 49; L. S. Hegedus, *Coord. Chem. Rev.* **1998**, *175*, 159.
[3] K. N. Mitra, S.-M. Peng, S. Goswami, *Chem. Commun.* **1998**, 1685.
[4] [4a] P. Bandyopadhyay, D. Bandyopadhyay, A. Chakravorty, F. A. Cotton, L. R. Falvello, S. Han, *J. Am. Chem. Soc.* **1983**, *105*, 6327. − [4b] B. K. Santra, G. A. Thakur, P. Ghosh, A. Pramanik, G. K. Lahiri, *Inorg. Chem.* **1996**, *35*, 3050. − [4c] G. K. Lahiri, S. Goswami, L. R. Falvello, A. Chakravorty, *Inorg. Chem.* **1987**, *13*, 1714.
[5] [5a] J. F. Hartwig, *Angew. Chem. Int. Ed. Engl.* **1998**, *37*, 2046. − [5b] M. Bruncko, T.-A. V. Khoung, K. B. Sharpless, *Angew. Chem. Int. Ed. Engl.* **1996**, *35*, 454. − [5c] S. D. Gray, J. L. Thorman, V. A. Adamian, K. M. Kadish, K. L. Woo, *Inorg. Chem.* **1998**, *37*, 1. − [5d] Z. Li, R. W. Quan, E. N. Jacobsen, *J. Am. Chem. Soc.* **1995**, *117*, 5889.
[6] A. Saha, A. K. Ghosh, P. Majumdar, K. N. Mitra, S. Mondal, K. K. Rajak, L. R. Falvello, S. Goswami, *Organometallics* **1999**, *18*, 3772.
[7] A. K. Ghosh, P. Majumdar, L. R. Falvello, G. Mostafa, S. Goswami, *Organometallics* **1999**, *18*, 5086.
[8] [8a] S. Goswami, R. N. Mukherjee, A. Chakravorty, *Inorg. Chem.* **1983**, *22*, 2825. − [8b] B. K. Ghosh, A. Mukhopadhyay, S. Goswami, S. Ray, A. Chakravorty, *Inorg. Chem.* **1984**, *23*, 4633. − [8c] M. N. Ackermann, C. R. Barton, C. J. Deodene, E. M. Specht, S. C. Keill, W. E. Schreibet, M. Kim, *Inorg. Chem.* **1989**, *28*, 397.
[9] A. Saha, P. Majumdar, S. Goswami, *J. Chem. Soc., Dalton Trans.* **2000**, 1703.
[10] M. Ray, D. Ghosh, Z. Shirin, R. Mukherjee, *Inorg. Chem.* **1997**, *36*, 3568 and references therein.
[11] S. Karmakar, S. B. Choudhury, A. Chakravorty, *Inorg. Chem.* **1994**, *33*, 6148.
[12] [12a]S. Wolowiec, L. Latos-Grazynski, M. Mazzanti, J. C. Marchen, *Inorg. Chem.* **1997**, *36*, 5761. − [12b] C. Morice, P. L. Maux, G. Simonneaux, *Inorg. Chem.* **1998**, *37*, 6100.
[13] B. S. Raghavendra, A. Chakravorty, *Indian J. Chem., Sect. A* **1976**, *14A*, 166.
[14] P. Majumdar, S.-M. Peng, S. Goswami, *J. Chem. Soc., Dalton Trans.* **1998**, 1569.

[15] W. J. Greary, *Coord. Chem. Rev.* **1971**, *7*, 81.
[16] W. P. Griffith, *Coord. Chem. Rev.* **1975**, *17*, 177.
[17] C. Mealli, D. M. Proserpio, *J. Chem. Educ.* **1990**, *67*, 399.
[18] S.-M. Lee, M. Marcaccio, J. A. McCleverty, M. D. Ward, *Chem. Mater.* **1998**, *10*, 3272.
[19] A. K. Mahapatra, Ph. D. Thesis, Jadavpur University, India, **1989**.
[20] S. Choudhury, A. K. Deb, S. Goswami, *J. Chem. Soc., Dalton Trans.* **1994**, 1305.
[21] P. Ghosh, A. Chakravorty, *J. Chem. Soc., Dalton Trans.* **1985**, 361.
[22] G. M. Sheldrick, *SHELXS-86, Program for the solution of crystal structures*, University of Göttingen, **1990**.
[23] G. M. Sheldrick, *SHELXL-93, Program for the solution of crystal structures*, University of Göttingen, **1993**.

Received December 21, 1999
[I99464]